

**INTERNATIONAL JOURNAL OF MODERN
ENGINEERING RESEARCH (IJMER)**

ISSN : 2249-6645



Volume 2 - Issue 4

Web : www.ijmer.com

Email : ijmer.editor@gmail.com

International Journal of Modern Engineering Research (IJMER)

Editorial Board

Executive Managing Editor

Prof. Shiv Kumar Sharma
India

Editorial Board Member

Dr. Jerry Van
Department of Mechanical, USA

Dr. George Dyrud
Research centre dy. Director of Civil Engineering, New Zealand

Dr. Masoud Esfal
R& D of Chemical Engineering, Australia

Dr. Nouby Mahdy Ghazaly
Minia University, Egypt

Dr. Stanley John
Department of Textile Engineering, United Kingdom

Dr. Valfitaf Rasoul
Professor and HOD of Electromechanical, Russian

Dr. Mohammed Ali Hussain
HOD, Sri Sai Madhavi Institute of Science & Technology, India

Dr. Manko dora
Associate professor of Computer Engineering, Poland

Dr. Ahmed Nabih Zaki Rashed
Menoufia University, Egypt

Ms. Amani Tahat
Ph.D physics Technical University of Catalonia-Spain

Associate Editor Member

Dr. Mohd Nazri Ismail
University of Kuala Lumpur (UniKL), Malaysia

Dr. Kamaljit I. Lakhtaria
Sir Padmapat Singhaniya University, Udaipur

Dr. Rajesh Shrivastava
Prof. & Head Mathematics & computer Deptt. Govt. Science & commerce College Benazir. M.P

Dr. Asoke Nath
Executive Director, St. Xavier's College, West Bengal, India

Prof. T. Venkat Narayana Rao
Head, CSE, HITAM Hyderabad

Dr. N. Balasubramanian
Ph. D (Chemical Engg), IIT Madras

Jasvinder Singh Sadana
M. TECH, USIT/GGSIPU, India

Dr. Bharat Raj Singh

Associate Director, SMS Institute of Technology, Lucknow

DR. RAVINDER RATHEE

C. R. P, Rohtak, Haryana

Dr. S. Rajendran

Research Supervisor, Corrosion Research Centre Department of Chemistry, GTN Arts College, Dindigul

Mohd Abdul Ahad

Department of Computer Science, Faculty of Management and Information Technology, Jamia Hamdad, New Delhi

Kunjai Mankad

Institute of Science & Technology for Advanced Studies & Research (ISTAR)

NILANJAN DEY

JIS College of Engineering, Kalyani, West Bengal

Dr. Hawz Nwayu

Victoria Global University, UK

Prof. Plewin Amin

Crewe and Alsager College of Higher Education, UK

Dr. (Mrs.) Annifer Zalic

London Guildhall University, London

Dr. (Mrs.) Malin Askiy

Victoria University of Manchester

Dr. ABSALOM

Sixth form College, England

Dr. Nimrod Nivek

London Guildhall University, London

Facial Expression Recognition for Security

Mrs. Ayesha Butalia, Dr. Maya Ingle, Dr. Parag Kulkarni

Abstract: Facial expressions play an important role in interpersonal relations as well as for security purposes. The malicious intentions of a thief can be recognized with the help of his gestures, facial expressions being its major part. This is because humans demonstrate and convey a lot of evident information visually rather than verbally. Although humans recognize facial expressions virtually without effort or delay, reliable expression recognition by machine remains a challenge.

A picture portrays much more than its equivalent textual description. Along this theory, we assert that although verbal and gestural methods convey valuable information, facial expressions are unparalleled in this regard.

In sustenance to this idea, a facial expression is considered to consist of deformations of facial components and their spatial relations, along with changes in the pigmentation of the same. This paper envisages the detection of faces, localization of features thus leading to emotion recognition in images.

Key Terms: Facial Gestures, Action Units, Neural Networks, Fiducial Points, Feature Contours.

INTRODUCTION

Facial expression recognition is a basic process performed by every human every day. Each one of us analyses the expressions of the individuals we interact with, to understand best their response to us. The malicious intentions of a thief or a person to be interviewed can be recognized with the help of his gestures, facial expressions being its major part. In this paper we have tried to highlight the facial expressions for security reasons.

In the next step to Human-Computer interaction, we endeavor to empower the computer with this ability — to be able to discern the emotions depicted on a person's visage. This seemingly effortless task for us needs to be broken down into several parts for a computer to perform. For this purpose, we consider a facial expression to represent fundamentally, a deformation of the original features of the face.

On a day-to-day basis, humans commonly recognize emotions by characteristic features displayed as part of a facial expression. For instance, happiness is undeniably associated with a smile, or an upward movement of the corners of the lips. This could be accompanied by upward movement of the cheeks and wrinkles directed outward from the outer corners of the eyes. Similarly, other emotions are characterized by other deformations typical to the particular expression.

More often than not, emotions are depicted by subtle changes in some facial elements rather than their obvious contortion to represent its typical expression as is defined. In order to detect these slight variations induced, it is important to track fine-grained changes in the facial features.

The general trend of comprehending observable components of facial gestures utilizes the FACS, which is also a commonly used psychological approach. This system, as described by Ekman^[12], interprets facial information in terms of *Action Units*, which isolate localized changes in features such as eyes, lips, eyebrows and cheeks.

The actual process is akin to a divide-and-conquer approach, a step-by-step isolation of facial features, and then recombination of the interpretations of the same in order to finally arrive at a conclusion about the emotion depicted.

RELATED WORK

Visually conveyed information is probably the most important communication mechanism used for centuries, and even today. As mentioned by Mehrabian^[8], upto 55% of the communicative message is understood through facial expressions. This understanding has sparked an enormous amount of speculation in the field of facial gestural analysis over the past couple of decades. Many different techniques and approaches have been proposed and implemented in order to simplify the way computers comprehend and interact with their users.

The need for faster and more intuitive Human-Computer Interfaces is ever increasing with many new innovations coming to the forefront.^[1]

Azcarate et al.^[11] used the concept of *Motion Units* (MUs) as input to a set of classifiers in their solution to the facial emotion recognition problem. Their concept of MUs is similar to "Action Units" as described by Ekman.^[12] Chibelushi and Bourel^[3] propose the use of GMM (Gaussian Mixture Model) for pre-processing and HMM (Hidden Markov Model) with Neural Networks for AU identification.

Lajevardi and Hussain^[15] suggest the idea of dynamically selecting a suitable subset of Gabor filters from the available 20 (called Adaptive Filter Selection), depending on the kind of noise present. Gabor Filters have also been used by Patil et al.^[16]. Lucey et al.^[17] have devised a method to detect expressions invariant of registration using Active Appearance Models (AAM). Along with multi-class SVMs, they have used this method to identify expressions that are more generalized and independent of image processing constraints such as pose and illumination.

Noteworthy is the work of Theo Gevers et al.^[21] in this field. Their facial expression recognition approach enhances the AAMs mentioned above, as well as MUs. Tree-augmented Bayesian Networks (TAN), Native Bayes (NB) Classifiers and Stochastic Structure Search (SSS) algorithms are used to effectively classify motion detected in the facial structure dynamically.

Similar to the approach adopted in our system, P. Li et al have utilized *fiducial points* to measure feature deviations and OpenCV detectors for face and feature detection.

Moreover, their geometric face model orientation is akin to our approach of polar transformations for processing faces rotated within the same plane (i.e. for tilted heads).

SYSTEM ARCHITECTURE

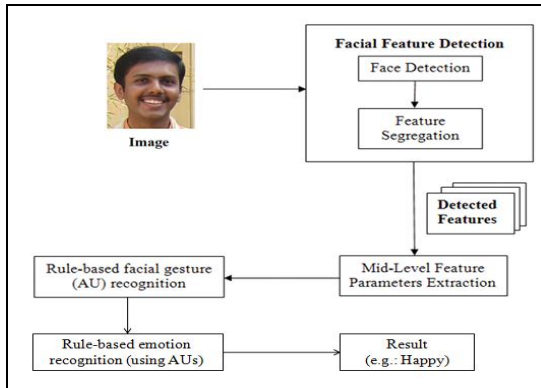


Fig. 1: Block Diagram of the Facial Recognition System

The task of automatic facial expression recognition from face image sequences is divided into the following sub-problem areas: detecting prominent facial features such as eyes and mouth, representing subtle changes in facial expression as a set of suitable midlevel feature parameters, and interpreting this data in terms of facial gestures.

As described by Chibelushi and Bourel^[3], facial expression recognition shares a generic structure similar to that of facial recognition. While facial recognition requires that the face be independent of deformations in order to identify the individual correctly, facial expression recognition measures deformations in the facial features to classify them. Although the face and feature detection stages are shared by these techniques, their eventual aim is different.

Face detection is widely applied through the HSV segmentation technique. This step narrows the region of interest of the image down to the facial region, eliminating unnecessary information for faster processing.

Analyzing this region (facial) helps in locating the predominant seven regions of interest (ROIs), viz. two eyebrows, two eyes, nose, mouth and chin. Each of these regions is then filtered to obtain the desired facial features. Following up this step, to spatially sample the contour of a certain permanent facial feature, one or more facial-feature detectors are applied to the pertinent ROI. For example, the contours of the eyes are localized in the ROIs of the eyes by using a single detector representing an adapted version of a hierarchical-perception feature location method^[13]. We have performed feature extraction by a method that extracts features based on Haar-like features, and classifies them using a tree-like decision structure. This is similar to the process described by Borsboom et. al^[7].

The contours of the facial features, generated by the facial feature detection method, are utilized for further analysis of shown facial expressions. Similar to the approach taken by Pantic and Rothkrantz^[2], we carry out feature points' extraction under the assumption that the face images are non-occluded and in frontal view. We extract 22 fiducial points, which constitute the action units, once grouped by the ROI they belong to. The last stage

employs the FACS, which is still the most widely used method to classify facial deformations.

The output of the above stage is a set of detected action units. Each emotion is the equivalent of a unique set of action units, represented as rules in first-order logic. These rules are utilized to interpret the most probable emotion depicted by the subject.

The rules can be described in first-order predicate logic or propositional logic in the form:

Gesture (surprise):- **eyebrows** (raised) ^ **eyes** (wide-open) ^ **mouth** (open).

For instance, the following diagram shows all the fiducial points marked on the human face. And for a particular emotion, a combination of points are affected and monitored. Like for surprise, the following action units are considered:

- Opening of mouth indicated by pt 19 and pt 18
- Widening of eyes shown by pt 13, pt14, pt 9 and pt 10.
- Raised eyebrows using pt 2 and pt 5

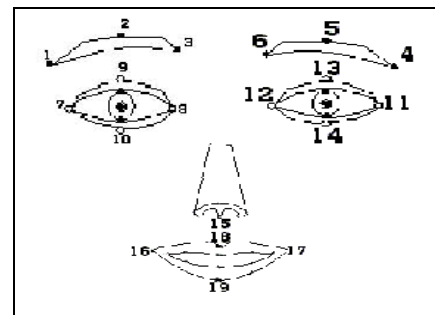


Fig. 2: Facial Points used for the distances definition^[13]

Both face and feature localization are challenging because of the face/features manifold owing to the high inter-personal variability (e.g. gender and race), the intrapersonal changes (e.g. pose, expression, presence/absence of glasses, beard, mustaches), and the acquisition conditions (e.g. illumination and image resolution).

Artificial Neural Networks and Fuzzy Sets

We observed that other applications used an ANN^[13] with one hidden layer^[1] to implement recognition of gestures for a single facial feature (lips) alone. Hence it is but obvious that one such ANN will be necessary for each independent feature or *Action Unit* that will be interpreted for emotion analysis. We intend to utilize the concept of Neural Networks to assist the system to learn (in a semi-supervised manner) how to customize its recognition of expressions for different specialized cases or environments.

Fuzzy logic^[22] (and fuzzy sets) is a form of multi-valued logic derived from fuzzy set theory to deal with reasoning that is approximate rather than accurate. Pertaining to facial expressions, fuzzy logic comes into picture when a certain degree of deviation is to be made permissible from the expected set of values for a particular facial expression.

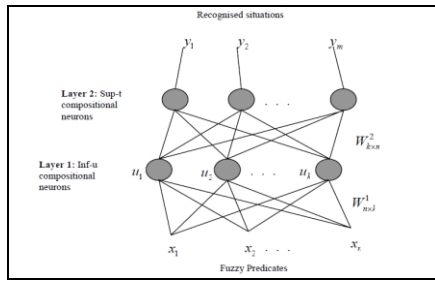


Fig. 3: The Two-Layer Neurofuzzy Architecture ^[13]

This is necessary because each person's facial muscles contort in slightly different ways while showing similar emotions. Thus the deviated features may have slightly different coordinates, yet still the algorithm should work irrespective of these minor differences. Fuzzy logic is used to increase the success rate of the process of recognition of facial expressions across different people. A neuro-fuzzy architecture incorporates both the techniques, merging known values and rules with variable conditions, as shown in Fig. 3. Chatterjee and Shi ^[18] have also utilized the neuro-fuzzy concept to classify expressions, as well as to assign weights to facial features depending on their importance to the emotion detection process.

POTENTIAL ISSUES

Geographical Versatility

One of the fundamental problems faced by any software that accepts images of the user as an input is that it needs to account for the geographical variations bound to occur in it. Though people coming from one geographical area share certain physiological similarities, they tend to be distinct from those who belong to another region. However, these physical differences will create a lot of inconsistencies in the input obtained.

To tackle this issue, the software must employ a technique that helps increase the scale of deviations occurring, so that divergence to a certain degree can be rounded off and the corresponding feature recognized. Support Vector Machines ^[10] help the software do this.

Fundamentally, a set of SVMs will be used to specify and incorporate rules for each facial feature and related possible gestures. The more the rules for a particular feature, the greater will be the degree of accuracy for even the smallest of micro-expressions and for the greater resolution images.

Originally designed for binary classification, there are currently two types of approaches ^[10] for multi-class SVMs. The first approach is to construct and combine several binary classifiers (also called "one-per-class" method) while the other is to consider all data in one optimization formulation named one-one way. Also, SVMs can be used to form slightly customized rules for drastically different geographical populations. Once the nativity of the subject is identified, the appropriate multi-class SVM can be used for further analysis and processing.

Thus, this method uses SVMs to take care of the differences and inconsistencies due to the environmental variations.

Personalization and Calibration

The process of emotion detection can be further enhanced to train the system using semi-supervised learning. Since past data about a particular subject's emotive expression can be stored and be made available to the system later, it may serve to improve the machines 'understanding' and be used as a base for inferring more about a person's emotional state from a more experienced perspective.

One approach to supervised learning is on inception of the system, for AU and gesture mapping. Here, the user will give feedback to the system with respect to his/her images flashed on the screen in the form of gesture name. This calibration process may be allowed approximately a minute or two to complete. In this way the user is effectively tutoring the system to recognize basic gestures so that it can build up on this knowledge in a semi-supervised manner later on. This feedback will be stored in a database along with related entries for the parameters extracted from the region of interest (ROI) of the image displayed. The same feedback is also fed into the neuro-fuzzy network structure which performs the translation of the input parameters to obtain the eventual result. It is used to shift the baseline for judging the input parameters and classifying them as part of the processing involved in the system. Now, for further input received, the neural network behaves in tandem with its new, personalized rule set.

The user can also request for training examples to be gathered at discrete time intervals and provide a label for each. This can be combined with the displacements output by the feature extraction phase and added as a new example to the training set. Another way to increase the personalized information is to maintain an active history of the user, similar to a session. This data is used further on to implement a context-based understanding of the user, and predict the likelihoods of emotions that may be felt in the near future.

Calibration and Personalization would further increase the recognition performance and allow a tradeoff between generality and precision to be made. By applying these methods, the system in focus will be able to recognize the user's facial gestures with very high accuracy; this approach is highly suitable for developing a personalized, user-specific application.

Dealing with Missing Values

The uncontrolled conditions of the real world and the numerous methods that can be employed to obtain the information for processing can cause extensive occlusions and create a vast scope for missing values in the input. Back in the history of linear PCA, the problem of missing values has long been considered as an essential issue and investigated in depth. ^{[24][25]} Thus in this paper the problem of missing values is tackled by taking into consideration the facial symmetry of the subject.

Though the human faces aren't exactly symmetrical for most expressions, we create perfectly symmetrical faces using the left or right (depending on which one is clearer) side of the face. Let's call it the reference image. The creation of the Reference image is shown below using the left and right sides of the face respectively.



Fig 4: Left: original face, Centre: Symmetrical face created using the right side, Right: Symmetrical face created using the left side.

Now the original image is first scanned for the occluded or blank areas in the face, that constitute the set of missing values. After all the locations of blockages have been identified, the Reference image is super-imposed on this scanned image. During the superimposition the facial symmetry is therefore utilized to complete the input values wherever necessary, and the missing values taken care of.

Overcoming Time Constraints

The main challenge in analyzing the face, for the expression being portrayed, is the amount of processing time required. This becomes a bottleneck in real time scenarios. One way of overcoming this time constraints is dividing the image into various regions of interest and analyzing each in parallel independently. For instance, the face can be divided into regions of the mouth; chin, eyes, eyebrows etc. and the parallel analysis of these can be combined to get the final result. This approach will guarantee a gain in the throughput of the system.

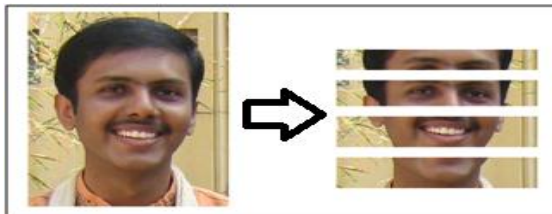


Fig. 5: Delegation of Image Components to Parallel Processors

RESULTS

In this section we present the resulting effectiveness of our systems facial expression recognition capability as well as subsequent emotion classification. The Confusion Matrix below shows that for a dataset of images depicting a particular emotion, how many were identified correctly, and how many were confused with other emotions. The dataset comprised images taken of an expert user, having knowledge of what a typical emotion is expected to show as per universal norms described by Ekman [12]. Our dataset comprised 60 images of Indian faces, with 15 each depicting Joy, Sorrow, Surprise and Neutral emotive states.

Total Accuracy: 71.7%

Table 1: Person-dependent Confusion Matrix for training and test data supplied by an expert user

Expression	Joy	Sorrow	Neutral	Surprise	Overall
Joy	11	1	1	2	73.3%
Sorrow	2	10	2	1	66.7%
Neural	3	2	10	0	66.7%
Surprise	2	0	1	12	80.0%

As is evident from Table 1, our system shows greater accuracy for Joy and Surprise with 73.3% and 80.0% accuracy rates respectively. The average accuracy of our system is 71.7%.

These results can be further improved by personalizing the system as discussed in the previous section. A personalized system is tuned to its user's specific facial actions, and hence, after a calibration period, can be expected to give an average accuracy of up to 90%.

FUTURE SCOPE AND APPLICATIONS

As human facial expression recognition is a very elementary process, it is useful to evaluate the mood or emotional state of a subject under observation. As such, tremendous potential lies untapped in this domain. The basic idea of a machine being able to comprehend the human emotive state can be put to use in innumerable scenarios, a few of which we have mentioned here.

- The ability to detect and track a user's state of mind has the potential to allow a computing system to offer relevant information when a user needs help – not just when the user requests help, for instance, the change in the Room Ambience by judging the mood of the person entering it.
- Help people in emotion-related research to improve the processing of emotion data.
- Applications in surveillance and security. For instance, computer models obtained up to 71% correct classification of innocent or guilty participants based on the macro features extracted from the video camera footage.
- In this regard, lie detection amongst criminal suspects during interrogation is also a useful aspect in which this system can form a base. It is proven that facial cues more often than not can give away a lie to the trained eye.
- Patient Monitoring in hospitals to judge the effectiveness of prescribed drugs is one application to the Health Sector. In addition to this, diagnosis of diseases that alter facial features and psychoanalysis of patient mental state are further possibilities.
- Clever Marketing is feasible using emotional knowledge of a patron and can be done to suit what a patron might be in need of based on his/her state of mind at any instant.
- Detecting symptoms such as drowsiness, fatigue, or even inebriation can be done using this system. Thus, by helping in the process of Driver Monitoring, this system can play an integral role in reducing road mishaps to a great extent.

Also noteworthy of mention is the advantage of reading emotions through facial cues, as our system does, over reading them through study of audio data of human voices. Not only does the probability of noise affecting and distorting the input reduce for our system, but also there are fewer ways to disguise or misread from visual information as opposed to audio data, as is also stated by Busso et. al [23]. Hence facial expressions would form a vital part of a multimodal system for emotion analysis as well.

CONCLUSION

As is quite evident after plenty of research and deliberation, gaining insight on what a person may be feeling is very valuable for many reasons. The future scope of this field is visualized to be practically limitless, with more futuristic applications visible on the horizon especially in the field of Security.

Our facial expression recognition system, utilizing neuro-fuzzy architecture is 71.7% accurate, which is approximately the level of accuracy expected from a support vector machine approach as well. Every system has its limitations. Although this particular implementation of facial expression recognition may perform less than entirely accurate as per the end users' expectations, it is envisioned to contribute significantly to the field, upon which similar work can be furthered and enhanced. Our aim in forming such a system is to form a standard protocol that may be used as a component in many of the applications that will no doubt require an emotion-based HCI.

Empowering computers in this way has the potential of changing the very way a machine "thinks". It gives them the ability to understand humans as 'feelers' rather than 'thinkers'. This in mind, this system can even be implemented in the context of Artificial Intelligence. As part of the relentless efforts of many to create intelligent machines, facial expressions and emotions have and always will play a vital role.

REFERENCES

- [1] Piotr Dalka, Andrzej Czyzewski, "Human-Computer Interface Based on Visual Lip Movement and Gesture Recognition", International Journal of Computer Science and Applications, ©Technomathematics Research Foundation Vol. 7 No. 3, pp. 124 - 139, 2010
- [2] M. Pantic, L.J.M. Rothkrantz, "Facial Gesture Recognition in face image sequences: A study on facial gestures typical for speech articulation" Delft University of Technology.
- [3] Claude C. Chibelushi, Fabrice Bourel, "Facial Expression Recognition: A Brief Overview", 1-5 ©2002.
- [4] Aysegul Gunduz, Hamid Krim "Facial Feature Extraction Using Topological Methods" © IEEE, 2003
- [5] Kyungnam Kim, "Face Recognition Using Principal Component Analysis"
- [6] Abdallah S. Abdallah, A. Lynn Abbott, and Mohamad Abou El-Nasr, "A New Face Detection Technique using 2D DCT and Self Organizing Feature Map", World Academy of Science, Engineering and Technology 27 2007
- [7] Sander Borsboom, Sanne Korzec, Nicholas Piel, "Improvements on the Human Computer Interaction Software: Emotion", Methodology, 2007, 1-8.
- [8] A. Mehrabian, Communication without Words, Psychology Today 2 (4) (1968) 53-56.
- [9] M. Pantic, L.J.M. Rothkrantz, "Expert System for Automatic for Automatic Analysis of Facial Expressions" Image and Vision Computing 18 (2000) 881-905.
- [10] Li Chaoyang, Liu Fang, Xie Yinxiang, "Face Recognition using Self-Organizing Feature Maps and Support Vector Machines", Proceedings of the Fifth ICCIMA, 2003.
- [11] Aitor Azcarate, Felix Hageloh, Koen van de Sande, Roberto Valenti, "Automatic Facial Emotion Recognition" University of Amsterdam, 1-10, June 2005
- [12] P. Ekman "Strong evidence for universals in Facial Expressions" Psychol. Bull., 115(2): 268-287, 1994.
- [13] A. Raouzaoui et. Al, "A Hybrid Intelligence System for Facial Expression Recognition" EUNITE 2002 482-490.
- [14] Y. Liu et. al, "Facial Asymmetry Quantification for Expression Invariant Human Identification"
- [15] Seyed Mehdi Lajevardi, Zahir M. Hussain "A Novel Gabor Filter Selection Based on Spectral Difference and Minimum Error Rate for Facial Expression Recognition" 2010 Digital Image Computing: Techniques and Applications, 137-140.
- [16] Ketki K. Patil et. Al, "Facial Expression Recognition and Head Tracking in Video Using Gabor Filtering", Third International Conference on Emerging Trends in Engineering and Technology, 152-157.
- [17] Patrick Lucey, Simon Lucey, Jeffrey Cohn, "Registration Invariant Representations for Expression Detection" 2010 Digital Image Computing: Techniques and Applications, 255-261.
- [18] Suvam Chatterjee, Hao Shi, "A Novel Neuro-Fuzzy Approach to Human Emotion Determination" 2010 Digital Image Computing: Techniques and Applications, 282-287.
- [19] P. Li et. al, "Automatic Recognition of Smiling and Neutral Facial Expressions" 2010 Digital Image Computing: Techniques and Applications, 581-586.
- [20] Irfan A. Essa, "Coding, Analysis, Interpretation and Recognition of Facial Expressions" IEEE Transactions on Pattern Recognition and Machine Intelligence, July 1997, 757-763.
- [21] Roberto Valenti, Nicu Sebe, Theo Gevers, "Facial Expression Recognition: A Fully Integrated Approach" ICIAPW '07 Proceedings of the 14th International Conference of Image Analysis and Processing, 2007, 125-130.
- [22] L. A. Zadeh, "Fuzzy Sets" Information and Control 8, 1965, 338-353.
- [23] Carlos Busso et. al, "Analysis of Emotion Recognition using Facial Expressions, Speech and Multimodal Information", ACM 2004.
- [24] N.F Troje et al, "How is bilateral symmetry of human faces used for recognition of novel views", Vision Research 1998, 79-89
- [25] R Thornhill et al, "Facial Attractiveness", Trans. In Cognitive Sciences, December 1999.

3d Heat Transfer Analysis and Numerical Modeling of LENSTM Process for One End Stepped Cylindrical Wall by Using Stainless Steel 304

Chirag P. Patel¹, Prof. R. I. Patel²

^{1,2}(Department Of Mechanical Engineering, Government Engineering College, Dahod/ GTU, India

Abstract : Laser Engineered Net Shaping (LENSTM) is a rapid-manufacturing process that involves complex thermal, mechanical, and metallurgical interactions. Due to process input parameter such as laser power, laser scanning velocity and feed rate, the effect on solidification of component to be produced must be understood. The finite element method (FEM) may be used to accurately model this process and solidification behavior by varying parameters. In this study the commercial FEM code ANSYS is used to predict the thermal histories, residual stresses, total deformation generated in One end stepped cylindrical wall and substrate of stainless steel 304. The computational results are compared with experimental measurements for validation.

Keywords: Laser engineering net shaping, FEM, Residual stresses, Total deformation, One end stepped Cylindrical wall, Element birth and death technique

I. Introduction

Laser Engineered Net Shaping (LENSTM) is a rapid manufacturing technology developed by Sandia National Laboratories (SNL) that combines features of powder injection and laser welding toward component fabrication. Several aspects of LENSTM are similar to those of single-step laser cladding. However, whereas laser cladding is primarily used to bond metallic coatings to the surfaces of parts that have already been produced with traditional methods^[1], LENSTM involves the complete fabrication of three-dimensional, solid metallic components through layer by layer deposition of melted powder metal. In this process, a laser beam is directed onto the surface of a metallic substrate to create a molten pool. Powder metal is then propelled by an inert gas, such as argon or nitrogen through converging nozzles into the molten pool.

Depending upon the alignment of the nozzle focal point with respect to that of laser, then powder is then melted either mid-stream or as it enters the pool. As the laser source moves away, the molten material then quickly cools by conduction through the substrate, leaving a solidified deposit. The substrate is located on a 3 or 5-axis stage capable of translating in the X and Y-directions. Initially, a 3-D CAD model is created to represent the geometry of a desired component. The CAD model is then converted to a faceted geometry composed of multiple slices used to direct the movement of the X-Y stage where each slice represents a single layer of deposition. During the build, the powder-nozzle/laser/stage system first traces a 2-D outline of the cross section represented by each slice in the X-Y plane and then proceeds to fill this area with an operator-specified rastering pattern.

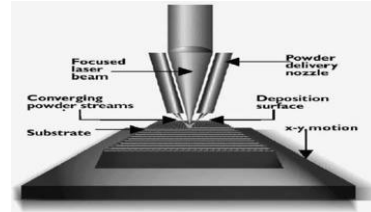


Figure 1 : Schematic Of LENSTM Deposition Process

The laser/nozzle assembly then ascends in the Z-direction so that the next layer can be added. This process is repeated for consecutive layers, until completion of the 3-D component^[2]. This feature is illustrated schematically in Figure 1.

II. Literature Review

Keicher *et al.*^[5] evaluated the effects of process parameters on multi-layer deposition of laser-melted powder Inconel® 625 in a process similar to both laser cladding and LENSTM. The group initially examined various parameters, including laser irradiance, stage translation speed, powder flow rate, powder particle size, and the size of each Z-directional increment between layers and their effect on heat affected zone (HAZ) size generated during the build. The HAZ was defined in this study as the melted region below the surface of the substrate and was examined post-build via metallographic analysis. Khaleel and Kar^[10] performed an investigation into the effects of several parameters on the resulting yield strength of AISI 304 stainless steel thin plates in process identical to LENSTM termed laser-aided direct rapid manufacturing (LADRM). This team sought to generate a range of input parameter values within which components with acceptable mechanical properties could be deposited. Their approach involved using the Buckingham II-Theorem to express the process variables associated with heat transfer and powder mass flux in terms of 14 dimensionless parameters. Rangaswamy *et al.*^[11,12] sought to experimentally measure residual stresses in LENSTM deposits using the neutron diffraction method, the details of which are discussed in next Section. The measurements were performed on LENSTM-produced rectangular plates of AISI 316. The neutron data was collected at several points methodically distributed within the geometry of the samples, to provide a map of the stress distribution then calculated the axial components of residual stress through Hooke's law. Each stress component was then plotted against position within the plate, first, along the height (Z direction) on the sample vertical centerline, and next, along the width (Y-direction) on the plate horizontal centre line. Wang and Felicelli^[15] next performed a parametric study similar to that done by Hofmeister *et al.*^[8] to determine if the same trends in

cooling rates and thermal gradients were observable for different laser power. He repeated the previous simulation using five power intensity values, revealing that the temperature gradient at the edge of the molten pool increases substantially with laser power, while the cooling rate decreases. Neela and De^[16] to study the effects of translation speed and laser power on the resulting temperature profiles using the general purpose FE package, ABAQUS® 6.6. The researchers used an element Activation/deactivation similar to those previously to model the deposition of a thin plate of AISI 316 with temperature-dependent thermal conductivity and specific heat according to a liner, and quadratic relation, respectively. Deus and Mazumder^[17] attempted to predict the residual stresses resulting from a laser cladding deposition of C95600 copper alloy onto an AA333 aluminium alloy substrate. Since residual stresses would be generated by the heterogeneous

thermal expansions of the deposited and substrate materials, accurate stress calculations would also require accurate prediction of the temperature fields created during the build. Labudovic *et al.*^[18] to predict residual stresses in a process identical to LENSTM termed the direct laser metal powder deposition process. A 3-D coupled model was implemented through the FE package ANSYS® for the deposition of a 50 mm x 20 mm x 10 mm thin plate of MONEL 400 onto a substrate of AISI 1006. The deposition was modelled with an ANSYS® element activation option similar to those already presented. Energy input density was modelled as a moving Gaussian distribution through the ANSYS® Parametric Design Language subroutine. The constitutive model was a temperature-dependent viscoplastic model, in which viscous effects were neglected by ignoring it the associated term in the equation of state.

III. CAD MODEL

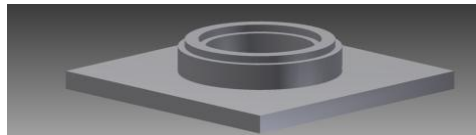


Figure 2 : Cad model for one end stepped cylindrical wall

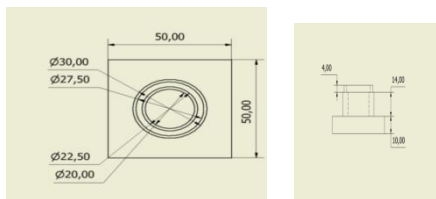


Figure 3 : Dimension for one end stepped cylindrical wall

The cylindrical wall model is created in the cylindrical coordinate system. x and y coordinates are defined as the radial and angular directions, respectively, while the z coordinate is defined in the vertical direction. A model for LENS process is built. As shown in Figure 3, Substrate : 50 x 50 x 10 mm. The example under consideration cylindrical wall upper cylinder has outer diameter 27.50 mm, inner diameter 22.50 mm and thickness 5 mm. the lower cylinder has outer diameter 30 mm, inner diameter 20 mm and thickness 10 mm. the total height $H=18$ mm. The 20 layers in the cylindrical wall height here each layer is assumed of equal 0.9 mm height .

IV. FINITE ELEMENT MODEL

The general purpose FE package ANSYS is used for both the thermal and stress analyses performed sequentially with an appropriate combination of elements. The main features of the 3D model are the moving heat input, the element birth-and-death technique, the heat loss, the temperature-dependent material properties, and the application of ANSYS parametric design language (APDL) to model the moving heat source and adaptive boundary conditions. The element types used in the thermal and structural analyses are SOLID70 and SOLID45, respectively. Both of them are the 8-noded brick elements that are compatible and can be automatically converted to each other during the solution process. The meshes used for

both simulations (thermal and structural) are the same. As shown in Figure 4, a total of 88919 nodes, and 44321 elements are generated to accomplish this simulation.

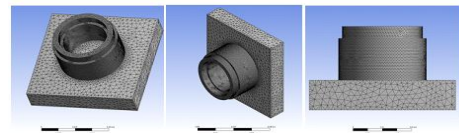


Figure 4: Meshing model for one end stepped cylindrical wall

V. THERMAL STRESS ANALYSIS

The first iteration in the solution procedure solves the system of equations at an assumed starting temperature (298 K), and the subsequent iterations use temperatures from previous iterations to calculate the thermal conductivity and specific heat matrices. The first born element is positioned onto the substrate with a set of initial and boundary conditions. For the subsequent elements, the model uses there results from the previous step as the initial condition for the birth of each new set of elements. This process is repeated for all the birthing events until the geometry is completed. After the structure has been built up the iterative process continues for some time required for the deposit to reach room temperature (the cooling sequence). Once the thermal simulation is done, the data regarding the temperature distribution in the buildup structure during the process is stored to a database. That data is used in the next step (structural analysis) as the only load that is applied as the body force. The structural simulation consists of the same steps during the building and cooling sequences as in the case of the thermal simulation. So, the temperature distribution scheme from some specific load step in the thermal analysis is applied to the corresponding load step in the structural analysis. It is

necessary to define the boundary conditions in the structural analysis to prevent a rigid body motion. Also, the intention is to allow substrate bending and reduce the influence of the rigid substrate on the stress development in the buildup as much as it possible. For these reasons, displacement of the substrate side surface, perpendicular to the wall depositing direction, is assumed to be zero.

VI. RESULT AND DISCUSSION

Since the cylindrical wall doesn't have free edges, the temperature distribution is different the higher average temperature is present along the circular path. Also at the start-end point of each layer, the laser beam dwells for some short time during the z-direction incremental movement. At that time, the heat input per distance moved along the wall length is increased, and the molten pool penetrates deeper into the previous deposit. Consequently the temperature is higher. As shown in figure 5 the inside surface lower cylinder has least deformation of value between 0.04075 to 0.034934mm. and the outer surface has maximum deformation of value between 0.052383 to 0.046566 mm. The all surface of lower cylinder and top of substrate has normal stress of value between 0.12365 to -0.076904 Mpa. and the side surface of substrate has normal stress of value between -1.8819 to -2.0824 Mpa. As shown in figure 6 the top surface lower cylinder has maximum deformation of value between 0.077006 to 0.068877mm. and the bottom surface has intermediate deformation of value between 0.033668 to 0.02893

mm. and the side of substrate has minimum value of total deformation between 0.0052402 to 0.00050218 mm. The all surface of lower cylinder and all surface of substrate has normal stress of value between 153.54 and -53.541 Mpa. and maximum value of normal stress is 774.71 Mpa at contacting area of substrate and first layer of cylinder. As shown in figure 7 the top surface lower cylinder has maximum deformation of value between 0.086938 to 0.080775 mm. and the bottom surface has intermediate deformation of value between 0.056124 to 0.049961 mm. the top and all sides of substrate has minimum value of total deformation between 0.0068224 to 0.00065973 mm. The all surface of lower cylinder and all surface of substrate has normal stress of value between 74.086 to -137.53 Mpa. and maximum value of normal stress is 708.93 Mpa at contacting area of substrate and first layer of cylinder. As shown in figure 8 the top surface upper cylinder has maximum deformation of value between 0.090096 to 0.097008 mm. and the top and bottom surface of lower cylinder has intermediate deformation of value between 0.07627 to 0.034795 mm. The top and all sides of substrate has minimum value of total deformation between 0.014058 to 0.00023262 mm. The all surface of upper and lower cylinder and all surface of substrate has normal stress of value between 49.817 to -169.59 Mpa. and maximum value of normal stress is 708.03 Mpa at contacting area of substrate and first layer of cylinder.

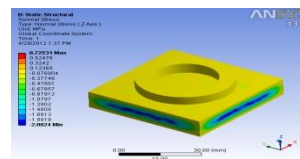
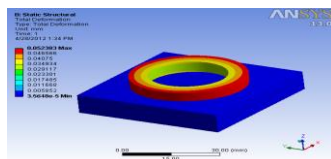


Figure 5 : Total deformation and Normal stress(σ_z) for 5 layers one end stepped cylindrical wall

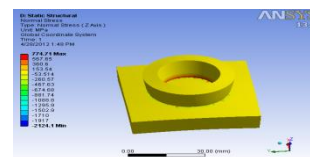
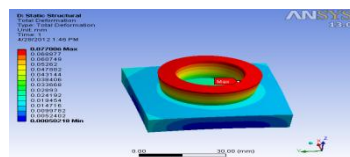


Figure 6 : Total deformation and Normal stress(σ_z) for 10 layers one end stepped cylindrical wall

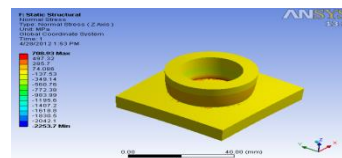
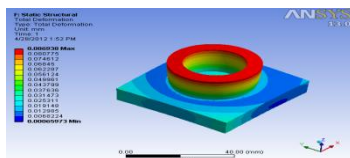


Figure 7 : Total deformation and Normal stress(σ_z) for 15 layers one end stepped cylindrical wall

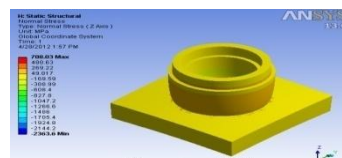
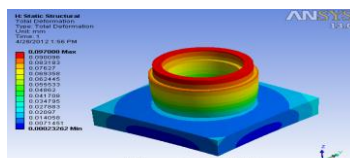


Figure 8 : Total deformation and Normal stress(σ_z) for 20 layers one end stepped cylindrical wall

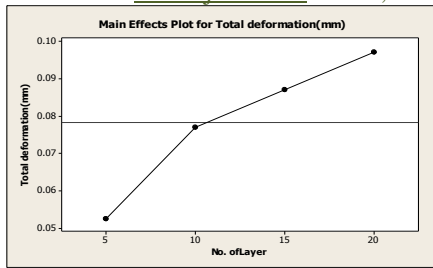


Figure 9: Graphical representation of total deformation for all layers

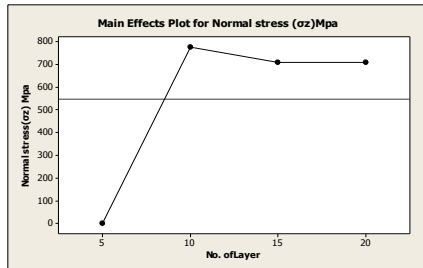


Figure 10: Graphical representation of Normal stress (σ_z) for all layers

As shown in figure 9 the cylindrical wall doesn't have free edges, the total deformation is different for 5, 10, 15, 20 layers. That difference means that the higher average deformation is present along the circular path which cause the higher deformation. Also at the start-end point of each layer, the laser beam dwells for some short time during the z-direction incremental movement. At that time, the heat input per distance moved along the wall length is increased, and the molten pool penetrates deeper into the previous deposit. Consequently the total deformation is higher, but it is still lower than at the free edges because of the larger volume of the heat sink. Generally speaking, the one-directional deposited wall has stress values slightly higher than the cylindrical deposited wall which is expected according to lower temperature differences during deposition. Also, the high localized stress above the tensile strength observed at the corners. Because of the deposition strategy, the stress close to the free edges is not symmetric. The tensile stress is higher at the ending free edge. Some differences of the stress distribution between the cylindrical deposited walls can be observed at the free edges. Since, there is no laser beam reverse in the one-direction deposition strategy, the compressive stress in the z-direction has lower values. The lower residual stress is expected more in the cylindrical wall, which is proved by the analysis. The maximum residual stress is obtained at the bottom of the cylinder and the value is lower than the material yield strength. The stress distribution along at the inner surface is uniform except at the free end and the bottom of the cylinder where the stress behaviour is complex. If this result is compared with the stress distribution along the same line at the outer surface, that is also uniform, it is obvious that the axial stress σ_z and hoop stress σ_y at the inner surface is tensile while the stress at the outer surface is compressive. The radial stress σ_x across the thickness of the wall changes the sign too, but it is much lower than the axial and hoop stress. As shown in figure 10 distribution of the stress causes a bending effect across the wall thickness.

VII. CONCLUSION

The total deformation at the layers 5, 10, 15, 20 indicate that the pre-defined location is heated up when the laser beam passes over, and the negative peaks indicate that the pre-defined location cools down after the laser beam passes by, from the initial layer to subsequent layer depositions. At the first layer, the cooling rate decreases when the subsequent layers are deposited. After the third layer is deposited, the first layer still receives a maximum cooling rate. The maximum cooling rate for each pass decreases as more layers are deposited, which is due to the integrated heat of the substrate and previous layers. The maximum residual stress is obtained at the bottom of cylinder and contacting area of substrate and first cylindrical layer. The inner surface is tensile and the outer surface is compressive in terms of stress distribution and this distribution of stresses causes the bending effect across the thickness direction. The distribution of residual stress in cylindrical wall is uniform. There is no immediate crack observed maximum residual stress accumulated at the substrate center region. The stress in a cylindrical wall is seen to have maximum value at the top, with this value increasing with an increase in the number of layers in a wall, reaching a value of -298 Mpa at the top of a 20-layer wall.

VIII. ACKNOWLEDGEMENTS

I would like to express my deep sense of gratitude and respect to my guide Prof. R.I.Patel sir for his excellent guidance, suggestions and constructive criticism. I consider myself extremely lucky to be able to work under the guidance of such a dynamic personality. I am also thankful to A.H.Makwana sir for his co-operation throughout the semester.

REFERENCES

- [1] Vilar, R. J. Laser Cladding. Laser Appl. Vol 11. No 2. 1999. Pp. 64-79.
- [2] Atwood, C., Griffith, M., Harwell, D., Reckaway, D., Ensz, M., Keicher, D., Schlienger, M., Romero, M., Oliver, M., Jeanette, F., Smurgesky, J. Laser Spray Fabrication for Net-Shape Rapid Product Realization LDRD. Sandia Report.1999.
- [3] Sandia National Laboratories website.
- [4] Griffith, M., Ensz, M., Puskar, J., Robino, C., Brooks, J., Philliber, J., Smurgesky, J., Hofmeister, W. Understanding the microstructures and properties of components fabricated by laser engineered net shaping (LENS). Mat. Res. Soc. Symp. Proc. Vol 625. Warrendale, PA. 2000. Pp. 9-21.
- [5] Keicher, D. Jellison, J., Schanwald, L., Romero, J. Towards a reliable laser spray powder deposition system through process characterization. 27th Int. Tech. Conf. Soc. Adv. Mat. Pro. Eng. Albuquerque, NM. 1995. Pp. 1009-1018.
- [6] Hofmeister, W., Wert, M., Smurgesky, J., Philliber, J., Griffith M., Ensz, M. Investigating solidification with the laser-engineering net shaping (LENS™) process. JOM-e.
- [7] Hofmeister, W., Griffith, M., Ensz, M., Smurgesky, J. Solidification in direct metal deposition by LENS processing. JOM. Vol.53. No 9. 2001. Pp. 30-34.

- [8] Hofmeister, W., MacCalum, D., Knorovsky, G. Video monitoring and control of the LENS process. American Welding Society 9th International Conference of Computer Technology in Welding. Detroit, MI. 1998. Pp. 187–196.
- [9] Smugeresky, J., Keicher, D., Romero, J., Griffith, M., Harwell, L. Laser engineered net shaping (LENSTM) process: optimization of surface finish and microstructural properties Proc. of the World Congress on Powder Metallurgy and Particulate Materials. Princeton, NJ. 1997. Part 21.
- [10] Kahlen, F.-J., Kar, A. J. Tensile strengths for laser-fabricated parts and similarity parameters for rapid manufacturing. Manuf. Sci. Eng. Vol 123. No 1. 2001. Pp. 38-44.
- [11] Rangaswamy, P., Holden, T., Rogge, R., Griffith, L. J. Residual stresses in components formed by the laser-engineered net shaping (LENS®) process. Strain Analysis. Vol 38. No 6. 2003. Pp. 519-528.
- [12] Rangaswamy, P. Griffith, M., Prime, M., Holden, T., Rogge, R., Edwards, J., Sebring, R. Residual stresses in LENS® components using neutron diffraction and contour method. Mat. Sci. Eng. A. Vol 399. 2005. Pp. 72-83.
- [13] Riqing, Y., Smugeresky, J., Zheng, B., Zhou, Y., Lavernia, E. Numerical modeling of the thermal behavior during the LENS® process. Mat. Sci. Eng. A. Vol 428. 2006. Pp. 47-53.
- [14] Lindgren, L.-E. Finite element modeling and simulation of welding part : increased complexity. Journal of Thermal Stresses. Vol 24. 2001. Pp. 195-231.
- [15] Wang, L., Felicelli, S. Analysis of thermal phenomena in LENS™ deposition. Mater. Sci. Eng. A. Vol 435-436. 2006. Pp. 625-631.
- [16] Neela, V., De, A. Numerical modeling of LENS™ process using special element features. 2007 Abaqus India Regional Users' Meeting. 2007.
- [17] Deus, A., Mazumder, J. Two-dimensional thermo-mechanical finite element model for laser cladding. Proc. ICALEO. Duley, W., Shibata, K., Poprawe, R., eds. Orlando, FL. Laser Institute of America. 1996. Pp. B/174-B/183.
- [18] Labudovic, M., Hu, D., Kovacevic, R. A three dimensional model for direct laser metal powder deposition and rapid prototyping. J. Mat. Sci. Vol 38. 2003. Pp. 35-49.

Experimental Investigation of Cotton Seed Oil and Neem Methyl Esters as Biodiesel On Ci Engine

K.Dilip Kumar¹ P.Ravindra Kumar²

^{1,2}Dept.of Mechanical Engineering,
L.B.Reddy College of Engineering, Mylavaram-521230, JNTU, KAKINADA
A.P, India

Abstract: In a modern day world alternative source of energy are given importance due to gradual depletion of fossil fuels reserves vegetable oils can be used as an alternative to diesel in CI engines. The use of vegetable oils in CI engine results in low CO and HC emissions compared to conventional diesel fuel. The present study covers the various aspects of biodiesels fuel derived from cottonseed oil. Cottonseed oil is converted to cottonseed oil methyl esters by transesterification process

An experimental investigations were carried out on C.I. engine with Bio Diesel blends of cotton seed Methyl Esters and Neem Oil Methyl Esters. The engine used for the experiments was single cylinder Four Stroke water cooled, constant speed diesel engine. Cotton seed Methyl ester (CSOME) and Neem oil methyl ester (NOME) are derived through transesterification process and parameters of transesterification were optimized. The blends of various proportions of the CSOME & NOME with diesel were prepared, analyzed and compared with diesel fuel, and comparison was made to suggest the better option among the bio diesel.

Various Tests have been carried out to examine properties, performance of different blends (C05, C10, C15, and C20) of CSOME and NOME in comparison to diesel. From the experimental Results it is indicated that C20 have closer performance to diesel. However, its diesel blends showed reasonable efficiencies. From the experimental results it is observed that cotton seed methyl ester gives better performance compared to Neem methyl esters and also the emissions and smoke for these diesel blends are less as compare to the pure diesel.

Keywords: Bio-diesel, Properties, Transesterification, Optimization, cottonseed oil methyl Ester (CSOME), Neem oil methyl ester (NOME)

I. Introduction

Energy is key input for technological, industrial, social and economical development of a nation. Five generations (125 years) ago, wood supplied up to 90% of our energy needs. Due to the convenience and low prices of fossil fuels wood use has fallen globally. The present energy scenario now is heavily biased towards the conventional energy sources such as petroleum products, coal, atomic energy etc, which are finite in nature besides causing environmental pollution. Of the available energy, the present energy utilization pattern is heavily biased for meeting the high energy requirement in urban and metropolitan cities. There are different types of BioDiesels are available such as Sunflower, Soyabean, Cottonseed, Linseed, Mahua, Jatropha, Pongamia, etc. [3]. The vegetable oils can be used in Diesel engines by various techniques such as fuel modifications by Transesterification, Diesel Vegetable blends and Vegetable oil heating etc. [4]. The present work was to investigate the evolution of Cotton seed and Neem seed oils with Diesel. Experiments were carried out at constant speed 1500 rpm and at different loads with different blends.

1.1 Fuel Modification

The alternative diesel fuels must be technically and environmentally acceptable and economically competitive. From the view point s of requirements, triglycerides (vegetable oils or animal fats) and their derivatives may be considered as viable alternative for diesel fuels [5]. The problems with substituting triglycerides for diesel fuels are mostly associated with high viscosity, low volatility and poly un-saturated character. The problems have been mitigated by developing vegetable oil derivatives that approximate the properties and performance and make them compatible with the hydro carbon based diesel fuels by following methods: Dilution (blending), Pyrolysis (cracking), Micro-emulsification [7] and Transesterification.

1.1.1 Transesterification:

Transesterification is the reaction of vegetable oil or animal fat with an alcohol, in most cases methanol, to form esters and glycerol. The transesterification reaction is affected by alcohol type, molar ratio of glycerides to alcohol, type and amount of catalyst, reaction temperature, reaction time and free fatty acids and water content of vegetable oils or animal fats. The transesterification reaction proceeds with or without a catalyst by using primary or secondary monohydric aliphatic alcohols having 1–8 carbon atoms as follows:

Triglycerides + Alcohol Glycerin + Mono-alkyl esters

Generally, the reaction temperature near the boiling point of the alcohol is recommended. Nevertheless, the reaction may be carried out at room temperature. The reactions take place at low temperatures (~65°C) and at modest pressures (2 atm, 1 atm = 101.325 kPa). Bio-diesel is further purified by washing and evaporation to remove any remaining methanol. The oil (87%), alcohol (9%), and catalyst (1%) are the inputs in the production of bio-diesel (86%), the main output. Pre-treatment is not required if the reaction is carried out under high pressure (9000 kPa) and high temperature (~240°C), where

simultaneous esterification and transesterification take place with maximum yield obtained at temperatures ranging from 60 to 80°C at a molar ratio of 6:1. The alcohols employed in the transesterification are generally short chain alcohols such as methanol, ethanol, propanol, and butanol. It was reported that when transesterification of soybean oil using methanol, ethanol and butanol was performed, 96–98% of ester could be obtained after 1 h of reaction.

Table 1. Properties of Diesel and Crude Oils

S.NO	PROPERTY	DIESEL	COTTONSEED	NEEMSEED
1	Calorific Value	43,000 kJ/kg	39,648kJ/kg	35,125 kJ/kg
2	Flash Point	44 ⁰ C	234 ⁰ C	178 ⁰ C
3	Fire Point	49 ⁰ C	192 ⁰ C	209 ⁰ C
4	Viscosity	0.278 poise	2.52 poise	1.864 poise
5	Density	835 kg/m ³	850 kg/m ³	928 kg/m ³

Table 1.1 Blending percentage of fuel

NOTATION	FUEL QUANTITY (Liters)	BIO-DIESEL QUANTITY (ml)	DIESEL QUANTITY (ml)
C10	1	100	900
C20	1	200	800
C30	1	300	700

Table 1.2 Properties of Pure Diesel, Cottonseed oil With Neem oil

Property	Diesel	Cottonseed Methyl Ester	C10	C20	C30
Heating value (kJ/kg)	43000	39648	42308	42116	41834
Carbon residue (% by weight)	<0.35	0.42	0.39	0.38	0.36
Density (g/cc)	0.815	0.850	0.830	0.852	0.862
Kinematic Viscosity(cSt)	3.5	6.0	4.68	4.87	5.05

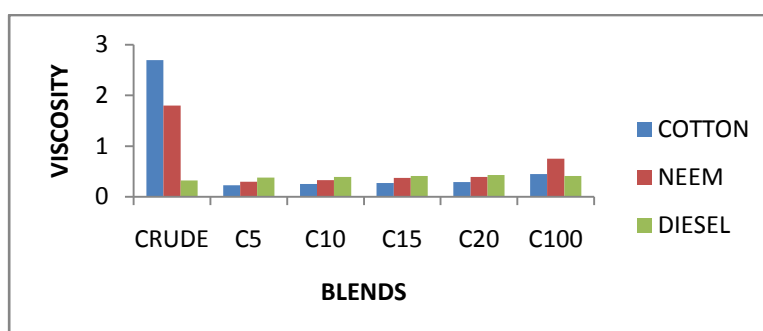


Fig. 1. Variation of viscosity of biodiesel blends and diesel

II. Experimental set up

The experimental set up used in this investigation is shown in Fig. 2. It consists of a single cylinder, four stroke, constant speed, water cooled, variable compression ratio, direct injection compression ignition engine with hemispherical open combustion chamber. The fuel injection system of the engine comprised of a plunger type pump with an injector having three spray holes, each 0.28 mm diameter. The injector needle lift pressure and fuel injection timing of the engine are 210 bar and 27° before TDC respectively. The specifications of the engine are shown in Table 2.

A single cylinder four stroke water cooled diesel engine was coupled to an eddy current dynamometer with a load cell. The In-cylinder pressure was measured by piezoelectric pressure transducer (Kistler) fitted on the engine cylinder head. A crank angle encoder was used to sense the crank position. Exhaust gas analysis was performed using five gas exhaust analyzer (Netel Make). A Hartridge smoke meter was attached to exhaust pipe to measure smoke levels.

3.1 FUEL PROPERTY MEASUREMENT

The improvement in the performance of the CI engines, over the past century, has resulted from the complimentary refinement of the engine design and fuel properties. Calculate the fuel properties like flash point, fire point, specific gravity, calorific value for different oils for different blends using the suitable equipment. Some of the fuel properties include are

- Flash point
- Fire point
- Specific gravity
- Calorific value
- Viscosity
- Carbon residue

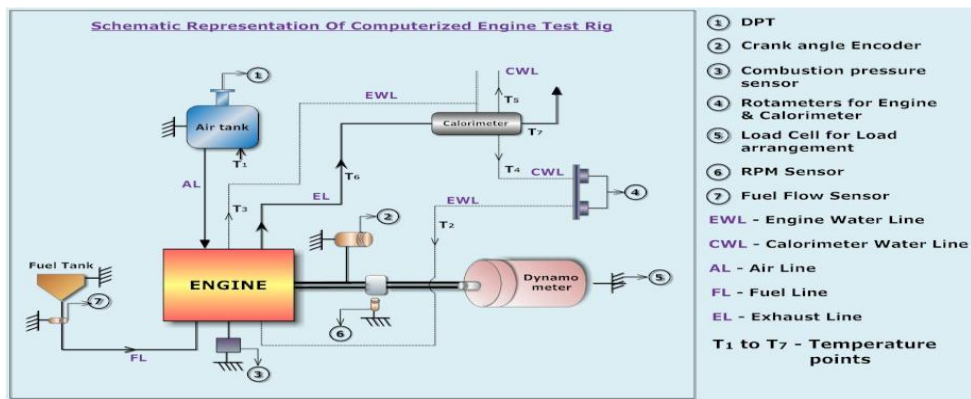


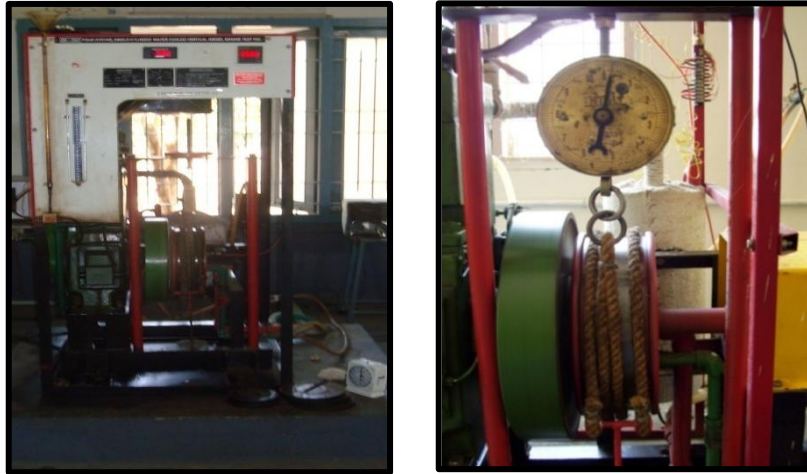
Fig. 2: Four Stroke Single Cylinder Diesel Engine setup

Table 2: Engine specifications

Manufacturer	Kirloskar engines Ltd, Pune, India
Engine Type	Four stroke, single cylinder, constant speed, compression ignition engine
Rated power	3.7 kW at 1500 RPM
Bore	80 mm
Stroke	110 mm
Swept volume	553 cc
Compression Ratio	12.5 to 21.5
Mode of injection	Direct injection
Cooling system	Water
Dynamometer	Eddy current dynamometer

Table 3: Properties of diesel fuel

Cetane number	53
Density at 30 °C	836 kg/m ³
Viscosity at 40°C	2.68 mm ² /s
Calorific value	42500 KJ/ Kg



(a) (b)
 Fig.3(a) 4- Stroke diesel engine (b) Dynamometer

III. PERFORMANCE

The performance test was conducted on Single cylinder 4-stroke Diesel Engine with water cooling, constant speed which is coupled to Rope brake dynamometer. Initially the engine was tested with Pure Diesel and later on with different blends of the LSOME and NOME with Diesel were prepared, analyzed and compared with Diesel Fuel, and comparison was made to suggest the better option among Bio Diesel blend, however its Diesel blends showed reasonable efficiencies. Different engine performance parameters like Brake Power, Brake Thermal Efficiency, bsfc, IP, CV, Mechanical Efficiency etc were determined and results were plotted with respect to load.

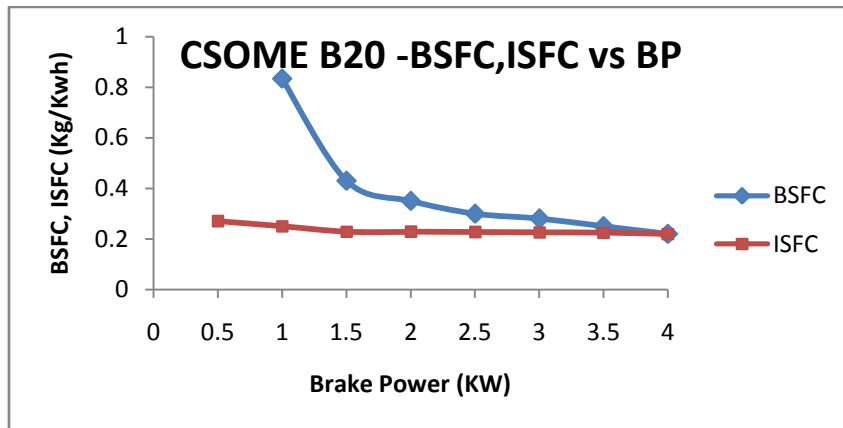


Fig. 3: Variations of CSOME C20-BSFC, ISFC Vs BP

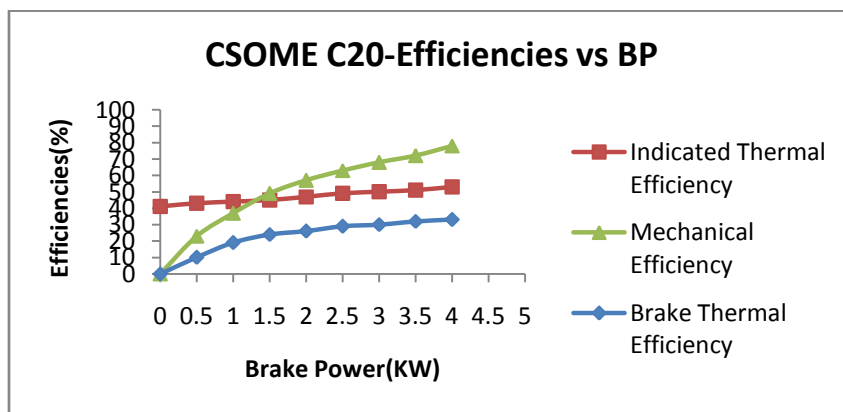


Fig 4: Variations of CSOME B20-EFFICIENCIES Vs BP

IV. RESULTS AND DISCUSSION

From the results obtained from experiments of Diesel and its blends the graphs were plotted with respect to load.

5.1 FUEL CONSUMPTION

The fuel consumption characteristics of an engine are generally expressed in terms of specific fuel consumption in kilograms of fuel per kilowatt-hour. It is an important parameter that reflects how good the engine performance is. It is inversely proportional to the thermal efficiency of the engine.

- Sfc = Specific fuel consumption per unit time/power

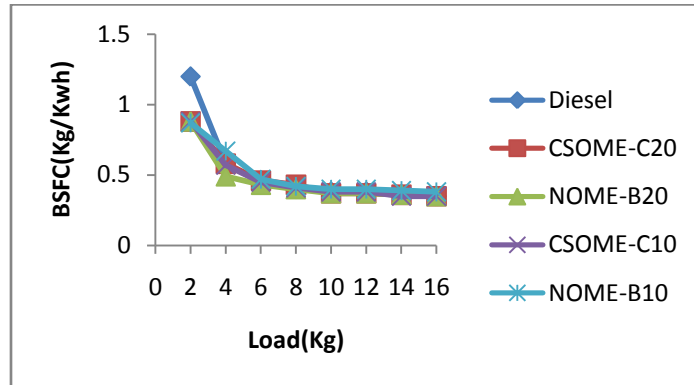


Fig 5: Variations of BSFC vs Load of CSOME & NOME blends with Diesel

From the above plot, it is observed that the brake specific fuel consumption (bsfc) for CSOME and NOME with Diesel are decreasing and these blends were giving better values as compared to the diesel fuel.

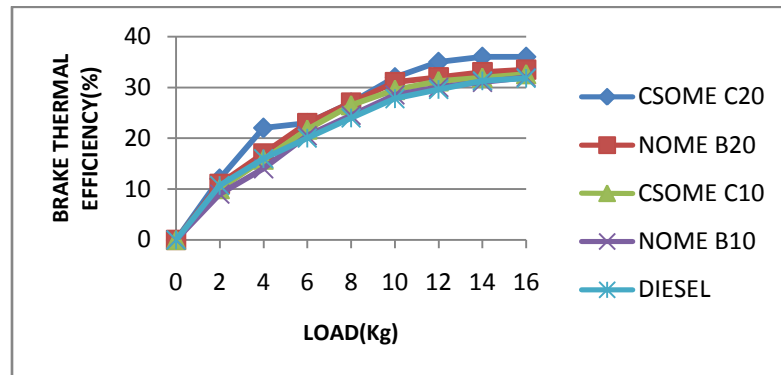


Fig 6: Variations of Brake Thermal Efficiency vs Load of CSOME & NOME with Diesel

From the plot, it is indicated that the Brake Thermal efficiencies of CSOME and NOME are slightly higher values as compared the Diesel because of complete combustion.

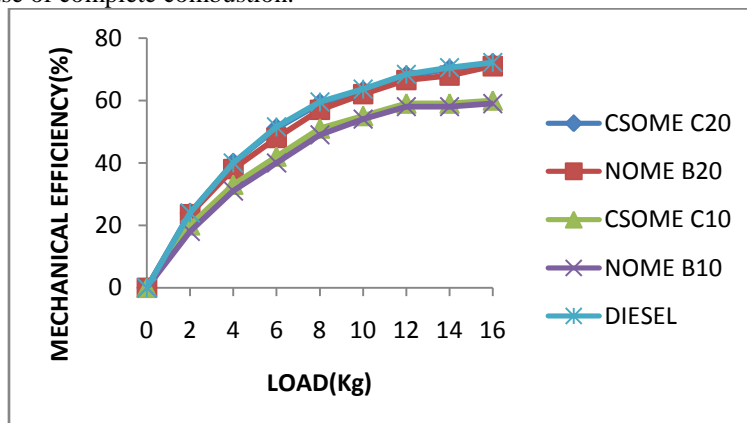


Fig 7: Variations of Mechanical Efficiency vs. Load of LSOME & NOME with Diesel

From the plot it is observed that Mechanical efficiency in case of Diesel with CSOME & NOME blends has been found that the mechanical efficiency is on par when compared to Diesel but a slight drop of efficiency was found with methyl esters (bio-diesel) when compared with diesel. This drop in thermal efficiency must be attributed to the poor combustion characteristics of methyl esters due to high viscosity. It was observed that the brake thermal efficiency of C10

and C20 are very close to brake thermal efficiency of diesel. C20 methyl ester had equal efficiency with diesel. So C20 can be suggested as best blend for bio-diesel preparation.

V. CONCLUSION

In the current investigation, it has confirmed that COTTONSEED and NEEM oil may be used as resource to obtain the bio diesel. The methyl esters of Cottonseed and Neem seed along with diesel may reduce the environmental impacts of transportation and also reduce the dependency on crude oil imports, and also provide employments in agricultural field. The conclusions are summarized as follows.

1. There was increase in Brake Thermal Efficiency of CSOME –C20 as compared to Pure Diesel because of complete combustion.
2. It was observed that the smoke and emissions for the blends of CSOME and NOME are less as compared to Pure Diesel.
3. Properties of the 20% blend of LSOME are nearer to the Diesel Fuel.
4. Thus the above investigations suggest that blend of CSOME – C20 is the optimum blend which can produce better values with Pure Diesel for Diesel engines as far as performance and emissions were considered.

References

- [1] Srinivasa rao. P, Gopialakrishna KV. “Esterified oils as fuels in diesel engines”, 11th national conference on IC Engines, IIT Madras, India, 1983.
- [2] Tomasevic AV, Marinkovic SS “Methanolysis of used frying oil”. Fuel process technology 2003; 81:1-6.
- [3] A.S Ramadhas, S.Jayaraj, C Muraleedharan, “use of vegetable oils as IC engine fuels A review”, Renewable energy, Vol.29,203,727-742.
- [4] Canakci and Vam Geroen (2003) “A pilot plant to produce biodiesel form high free fatty acid feedstock”, American society of agricultural engineers, 46(4), PP: 945-954
- [5] Jon H. Van Gerpen, Charles L. Peterson, Carroll E. Goering, Biodiesel: An Alternative Fuel for Compression Ignition Engines, For presentation at the 2007 Agricultural Equipment Technology Conference Louisville, Kentucky, USA 11-14 February 2007.
- [6] ASTM. 2002. D 6751 – Standard specification for biodiesel fuel (B100) blend stock for distillate fuels. West Conshohocken, Penn: ASTM International..
- [7] Rupinder Sing, Biodiesel Production from Jatropha (Source- Kurukshetra, volume-55, No-4, February- Prof. (Dr.) R. K. Khotoliya, Dr. Harinder Kaur &2007).
- [8] Knothe, G. 2005b. Cetane numbers—the history of vegetable oil-based diesel fuels. Chapter 2 in G. Knothe, J. Van Gerpen, and J. Krahl, eds. *The Biodiesel Handbook*. Champaign, Ill.: American Oil Chemists’ Society Press.
- [9] Peterson, C.L. 1980. Vegetable oils—Renewable fuels for diesel engines. ASAE Paper No. PNW 80- 105. St. Joseph, Mich.: ASAE.
- [10] Dizge N, Aydine C, Imer DY, Bayramoglu M, Tanriseven A, Keskinler B. Biodiesel production from sunflower, soybean and waste cooking oils by transesterification using lipase immobilized onto a novel microporous polymer. bioresour technol 2009;100:1983-91
- [11] NBB. Biodiesel production and quality. Fuel fact sheets. Usa: National Biodiesel board:2007
- [12] Bondioli p, Gasparoli A, Lanzani A, Fedeli E, veronese S, Sala M. storage stability of biodiesel. J Am oil chem soc 1995; 72:699-702.
- [13] Bhattacharya S and Reddy CS (1994) Vegetable oils as fuels for internal combustion engines: a review, Instt.57, 157-166.
- [14] Srivastava A and Prasad R (2000) Triglycerides –based diesel fuels, Renewable & Sustainable Energy Rev.4,111-133.
- [15] Ayhan Demirbas , “ A Survey of Bio Diesel fuels from vegetable oils via Catalytic and Non Catalytic Alcohol Transesterifications and other methods” Journal of Energy Conversion and Management , September 2002.

Enhancing Security in a Video Copy Detection System Using Content Based Fingerprinting

E. Meenachi¹, G. Selva Vinayagam², C. Vinothini³

1. PG Student, Dept of IT, SNS College Technology, Coimbatore

2. Assistant Professor, Dept of IT, SNS College of Technology, Coimbatore

3. PG Student, Dept of IT, SNS College Technology, Coimbatore

Abstract: Information Security means protecting information and information systems from unauthorized access, use, disclosure, disruption, modification, inspection, recording or destruction. The "Video Copy Detection" system is based on detecting video copies from a video sample to avoid copyright violations. To identify video sequences, Content Based Copy Detection (CBCD) presents an alternative to the watermarking approach. Content based Video fingerprinting methods extract several unique features of a digital video that can be stored as a fingerprint of the video content. Video copy detection system aims at deciding whether a query video segment is a copy of a video from the indexed dataset or not. The evaluation and identification of video content is then performed by comparing the extracted video fingerprints. The search algorithm searches the fingerprints that are stored in the database to find closest match with the fingerprints of the query video. The Interest point Matching algorithm is implemented to make the fingerprint robust against content changing attacks such as changing the background of the video. The proposed algorithm is tested on videos which are affected by the distortions like noise, changes in brightness/contrast, rotation, time shift and changes in background. The results give the high average true positive rate and low average false positive rate. The results demonstrate that the fingerprint extracted using this algorithm is robust. Video fingerprinting system is important for the applications like Digital Rights Management (DRM) area, particularly regarding the distribution of unauthorized content on the internet.

Index Terms: Content-Based Fingerprinting, Video Copy Detection, Video Copy Retrieval, Interest points

I. INTRODUCTION

The widespread availability of video content and services and the rapid diffusion of broadband platforms have brought new challenges to content owners, publishers and distributors. Video copy detection is a recent research domain which has emerged largely in response to this technological trend. The goal of video copy detection is to develop automated video analysis procedure to identify the original and modified copies of a video among the large amount of video data for the purposes of copyright control, monitoring and structuring large video databases.

A. Content Based Video Copy Detection

Content-Based Copy Detection (CBCD) schemes are an alternative to the watermarking approach for persistent identification of images and video clips. The primary concept of content-based copy detection (CBCD) is "the media itself is the watermark," i.e., the media (video, audio, image) contains enough unique information that can be used for detecting copies. Content-based copy detection schemes extract signatures from the original media and store it in a database. The same signatures are extracted from the test media stream and compared to the original media signature which is already extracted and stored in a database to determine if the test stream contains a copy of the original media. The signatures that are extracted from the media are termed as 'fingerprints'.

B. Fingerprint

Fingerprints are compact content-based signature that summarizes a video signal or another media signal. These signatures are feature vectors that uniquely characterize specific signal. Video fingerprinting is a proven and commercially available technique that can be used for content based copy detection. The task of a video-fingerprinting system is to detect whether a particular segment of video is (partly) based on the same original video as video footage in a database of reference videos.

The fingerprint of a video should be *robust* to the content-preserving distortions i.e., the changes made to the videos unintentionally or intentionally by the users of video sharing websites. It determines the tolerance of the system to different encoding processing that give rise to several distortions. Fingerprint should also be *discriminant* to make sure that different videos has distinguishable fingerprints. It should also be *secure* so that it is difficult for an adversary to generate similar fingerprints for different videos and manipulate the video copy detection systems.

C. Type of Fingerprints

Existing video fingerprints can be classified into four groups: spatial, temporal, colour and spatio-temporal fingerprints. A *spatial fingerprint* characterizes spatial features of a video frame and is computed independent of other

frames. These approaches are based on intensity statistics such as mean, variance, centroid, and other higher order moments of the spatial content of the different frames of the video. The frames are divided into subsections and for each section, the features are calculated. This approach allows uniform spatial processing over the entire frame. However it is less robust to geometrical operations like rotation and scaling. Examples of spatial features include luminance patterns, differential luminance or gradient patterns, and edges.

The *temporal fingerprint* describes temporal features of a video and is computed between two frames in the temporal direction. This involves comparing each frame against the previous frame. Differences between the two are flagged as motion. This is done by comparing macro-blocks of a pre-determined size. Motion is detected as a change in the color between frames within a macro-block, while the magnitude of the motion is deduced from the difference in color. A measure of the amount of motion of each frame relative to the preceding frame is calculated by summing the differences in color between these frames for all macro blocks. This results in a series of features, each indicative of a measure of motion between two adjacent frames over time. Consequently, the size of the motion fingerprints is dependent on the amount of motion that has been detected. Examples of temporal features include frame difference measures, motion vector patterns, and shot durations.

A *color fingerprint* captures color characteristics of a video frame and is computed in a color space such as RGB or YUV. Color-space-based fingerprints are among the first feature extraction methods used for video fingerprinting. They are mostly derived from the histograms of the colors in specific regions in time and/or space within the video. Since color features changes with different video formats these features have not been popular. Another drawback of the color features is that they are not applicable to black and white videos.

A *spatio-temporal fingerprints* contains both spatial and temporal informations about the video. They perform better than the fingerprints that use only spatial or temporal fingerprints. To capture relevant information from both temporal and spatial domain they apply temporal and spatial differentiation in the feature space. They take the differences of corresponding features extracted from subsequent blocks from one frame, and from subsequent frames in the temporal direction. This feature extraction is robust to global changes in luminance, also robust to luminance and contrast variations because only the signs of the difference are retrained. Their experimental results show that the method is also robust against MPEG compression and median filtering. Different types of fingerprints are combined to form a video fingerprint.

II. LITERATURE REVIEW

Hye-Jeong Cho et al.[6] proposed the hierarchical video copy detection method which estimates similarity using statistical characteristics between original video and its spatial variations. The target video is transformed by various spatial variations such as blurring, contrast change, zoom in, and zoom out. Zheng Cao et al.[15] computed a video signature based on ordinal measurement of video spatio-temporal distribution feature. The video similarity is measured by the computation of the distance of video signature. The duplicate videos are generated by spatio and temporal changes. Juan Chen[7] extracted key frames from the video sequences to save the computing time and storage space. Candidate descriptors are then determined in the local context by applying Harris point detection. The descriptors are invariant to spatial deformations like shifting, cropping and change of ratio.

Coskun et al. proposed a hash function [3] to extract a fingerprint based on signal processing operations. Two robust hash algorithms for video were implemented in this paper. Discrete Cosine Transform (DCT) based on classical basis set and Discrete Cosine Transform (DCT) based on a novel randomized basis set (RBT). The video here is considered as the 3D matrix. DCT transformations are applied to extract the coefficients and hashing was performed. The 3D transformations extract both spatial and temporal coefficients. The fingerprint is robust against signal processing modifications and channel transformations. Does not robust against malicious attacks. Security measures are not solved thoroughly in RBT [9].

Malekesmaeili.M et al generates fingerprints of a video sequence that carries both temporal and spatial information's [5]. This algorithm is applied for a 2D data. Gaussian filtering is applied to the video signals to prevent aliasing. Then the video signals are pre-processed (re-sampling and spatial resizing) to get the fixed frame size and frame rate. Then the video is divided into frames and weighted average of the frames is taken to obtain TIRI (Temporally Informative and Representative Images). DCT based hashing is applied which results in equal number of 0's and 1's. The fingerprint is robust to time shift, frame dropping, added Gaussian noise. But the performance is low for rotation and shift attacks. Hampapur et al uses a combination of feature based matching and inverted index files to detect copies of video clips [3].

CBCD does not modify the video stream and hence can be applied to find copies of media in circulation. The Reference Signature extract a set of signatures for the original media (M). The Test Signature extract the same set of signatures from the test media (T). Then the distance between the test and reference signatures are measured to compare both the signatures. If distance is lesser than a threshold, then it is a copied video. A set of representative frames are selected from each video item in the collection. The corresponding representative frames from each set are represented by an inverted image index table. Once a inverted image index has been created, it can be used to match a query image against the collection [3].

III. EXTRACTION OF FINGERPRINT

A fingerprint is a content-based signature which is derived from a video (or other form of a multimedia asset) so that it specifically represents the video or asset. To find a copy of a query video in a video database, one can search for a close match of its fingerprint in the corresponding fingerprint database[10].

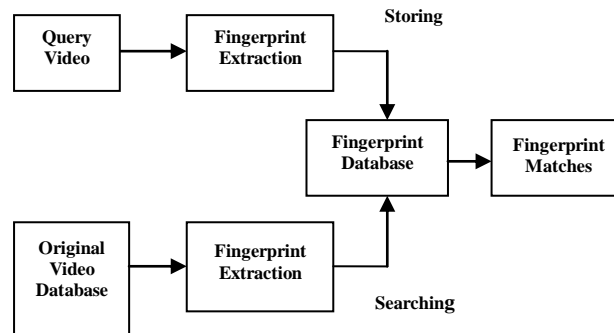


Fig.1. A complete Fingerprinting system

A. Tiri-Dct Algorithm

The existing algorithm for extracting the fingerprint is TIRI-DCT (Temporally Informative Representative Images). This method calculates a weighted average of the frames to generate representative images. This sequence will carry the temporal as well as spatial informations. The image is then divided into blocks. Then the first horizontal and the first vertical DCT coefficients (features) are then extracted from each block. The value of the features from all the blocks is concatenated to form the feature vector.[10] Each feature is then compared to a threshold (which is the median value of the feature vector) and then a binary fingerprint is generated.

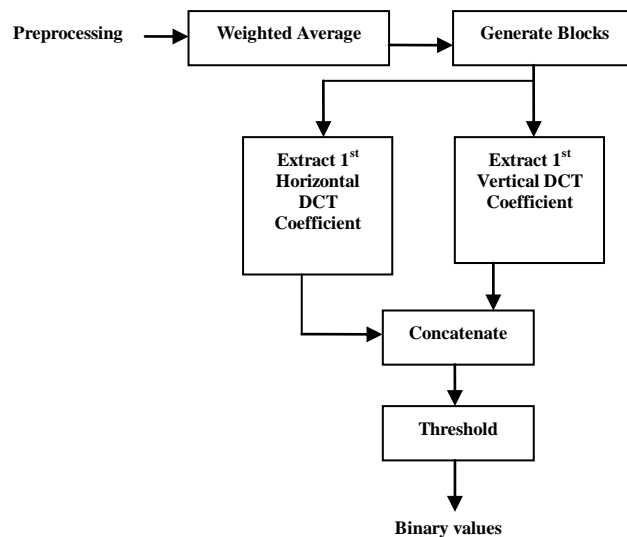


Fig.2Finger Print Algorithm Preprocessing Steps

In order to determine whether a query video is an attacked version of a video in a database or not, its fingerprint is first extracted. The fingerprint database (previously created from the videos in the video database) is then searched for the closest fingerprint to the extracted query fingerprint.

Two searching techniques are implemented:

- Inverted-File-Based Similarity Search
- Cluster-Based Similarity Search

1). Inverted-File-Based Similarity Search

The search method is based on the idea that for two fingerprints which are similar enough to be considered as matches, the probability of an exact match between smaller sub-blocks of those fingerprints is high. Divide each fingerprint into small non overlapping blocks of bits. [10]The horizontal dimension of this table refers to the position of a word inside a fingerprint, and the vertical direction corresponds to possible values of the word. The query is then compared to all the fingerprints that start with the same word. The Hamming distance between these fingerprints and the query is then

calculated. If a fingerprint has a Hamming distance of less than some predefined threshold, it will be announced as the match. When no match is found in the end, it is stated that the query does not belong to the database.

2). Cluster-Based Similarity Search

Clustering is used to reduce the number of queries that are examined within the database. By assigning each fingerprint to one and only one cluster (out of K clusters), the fingerprints in the database will be clustered into K non overlapping groups. To do so, a centroid is chosen for each cluster, termed the cluster head.[10]

A fingerprint will be assigned to a cluster if it is closest to this cluster's head. To determine if a query fingerprint matches a fingerprint in the database, the cluster head closest to the query is found. All the fingerprints (of the videos in the database) belonging to this cluster are then searched to find a match, i.e., the one which has the minimum Hamming distance (of less than a certain threshold) from the query. This process continues until a match is found or the farthest cluster is examined. If no match is found, the query is declared to be out of the database.

B. Problem Description

In existing system the fingerprint which is extracted using TIRI-DCT algorithm is not robust against the content changing attacks such as changing the background of the video or replacing picture in picture and the performance of the system is low in the presence of some other attacks, such as cropping, and logo insertion. The security of the fingerprint can be achieved only with the fingerprints of smaller length. Larger fingerprints results in a decrease in detection speed as they require more computation in calculating the hamming distance between the fingerprints. Also performance of the detection speed gets reduced when there are a large number of fingerprints in the database

IV. INTEREST POINT MATCHING ALGORITHM

Corner detection is an approach used to extract certain kinds of features and infer the contents of an image. Corner detection is frequently used in motion detection, image registration and video tracking. Corner detection overlaps with the topic of Interest point detection. An interest point is a point in an image which has a well defined position in an image and can be robustly detected. A good interest point detector has the following three properties:(1)The interest points are repeatable, (2)the descriptors produced from them are unique, (3) they are well-distributed spatially. An Interest point in an image has a clear, mathematically well-founded definition and has an well defined position in an image. It is stable under local and global distortions in an image domain. To increase the robustness of the fingerprint against the content changing attacks such as changing the background of the video an Interest point Matching algorithm is proposed. The conceptual basis of this algorithm is the detection of "super points," those points which have the greatest interest strength (i.e., which represent the most prominent features) and the subsequent construction of a control network. Sufficient spatial information is then available to reduce the ambiguity and avoid false matches.

The algorithm proposed in this paper includes two parts: A) Interest-point detection;B) interest-point matching.

A. Interest-Point Detection

The Harris detector is a well-known interest-point detection algorithm[17] to detect and extract the interest points. The Harris algorithm determines whether a point is a corner based on the Harris matrix A at the point $P(x, y)$. The interest strength is determined based on the magnitudes of the eigenvalues (γ_1 and γ_2) of A . The following function Mc was suggested as the interest strength:

$Mc = \det(A) - \kappa \text{trace}^2(A)$. The value of κ has to be determined empirically, and in the literature, values in the range of 0.04–0.06. If $Mc > 0$, it is a corner; otherwise, it is not a corner. Obviously, the corner should be the point with the local maximum value of Mc . By calculating the interest strength Mc over the whole image, an image which shows the interest strength can be obtained[17]

B. Interest-Point Matching

After the detection of interest points, a control network is constructed with the correspondences. Correspondences are defined as those interest points with the minimum difference in position and angle. Then the control network of each frame is compared.

If the location of the points are same then it is marked as 1 else it is marked as 0. Thus the binary sequences that are obtained are stored as the fingerprint.

V. EXPERIMENTAL RESULTS

To evaluate the performance of the proposed algorithm the videos are collected and stored in the database. TIRI-DCT and Interest-point matching algorithm were separately applied to each video in the database. A fingerprint database is formed for each algorithm and the extracted fingerprints are stored. Then, videos in the database were attacked(disorted) to generate query videos. The attacks include added Gaussian noise, changes in brightness/contrast, time shift, rotation and changes in background of the video. True Positive Rate and False Positive Rate are calculated for each algorithm. Let true positives (TP) be positive examples correctly labelled as positives

$$TPR = TP/P$$

False positives (*FP*) be negative examples incorrectly labelled as positives.

$$FPR = FP/N$$

F-Score is calculated to measure the accuracy of the system. If the value of the F-Score is low then it represents the poor system in terms of both robustness and discrimination. It considers both the precision *p* and the recall *r* of the test to compute the score

p is the number of correct results divided by the number of all returned results.

$$P = TP / (TP + FN)$$

and *r* is the number of correct results divided by the number of results that should have been returned.

$$R = TP / (TP + FP)$$

The F_1 score can be interpreted as a weighted average of the precision and recall, where an F_1 score reaches its best value at 1 and worst score at 0.

$$F = (1 + \beta^2) (\text{precision} \cdot \text{Recall}) / (\beta^2 \text{ precision} + \text{recall})$$

β value is chosen as 0.5 to give precision twice the importance of recall. Following table shows the F-score for different attack parameters: noise addition, change in brightness, contrast, rotation, time shift and changes in background.

TABLE I
COMPARING TIRI-DCT AND INTEREST-POINT-MATCHING ALGORITHM

Attacks	TIRI-DCT			INTEREST-POINT-MATCHING		
	TPR(%)	FPR(%)	F-SCORE	TPR(%)	FPR(%)	F-SCORE
Noise	91.9724	8.0276	0.8542	97.7549	2.2451	0.9049
Brightness	91.9500	8.0500	0.8615	97.7523	2.2477	0.9023
Contrast	91.2927	8.7073	0.8623	97.6701	2.3299	0.9021
Time shift	91.8374	8.1626	0.8587	97.6856	2.3144	0.9058
Rotate	92.1669	7.8331	0.8583	97.7106	2.2894	0.9023
Background Changed	91.5541	8.4459	0.8582	97.4372	2.5628	0.9057
Average	91.7955	8.204	0.8585	97.6684	2.3315	0.9038

The proposed Interest-Point-matching algorithm shows the higher F-score value than the existing algorithms. It maintains higher performance for all the attacks such as noise addition, change in brightness, contrast, rotation, time shift and changes in background. The algorithm maintains a high True Positive Rate of 97.66% and low False Positive Rate of 2.33%.

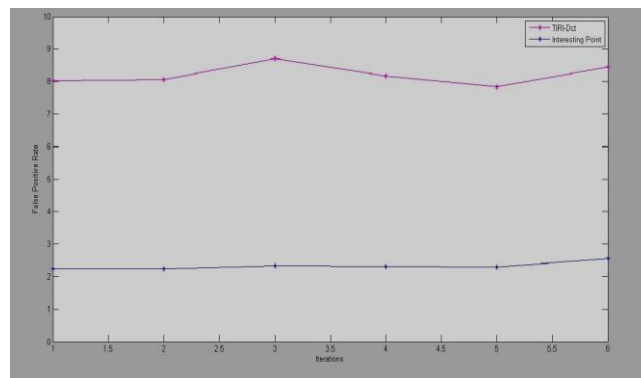


Fig .3. False Positive Rate of TIRI-DCT and Interest Point- Matching algorithm for different attack parameters from Table I

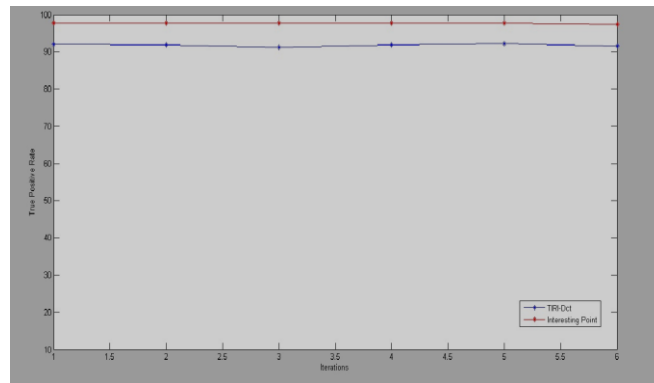


Fig .4. True Positive Rate of TIRI-DCT and Interest-Point-Matching algorithm for different attack parameters from Table I

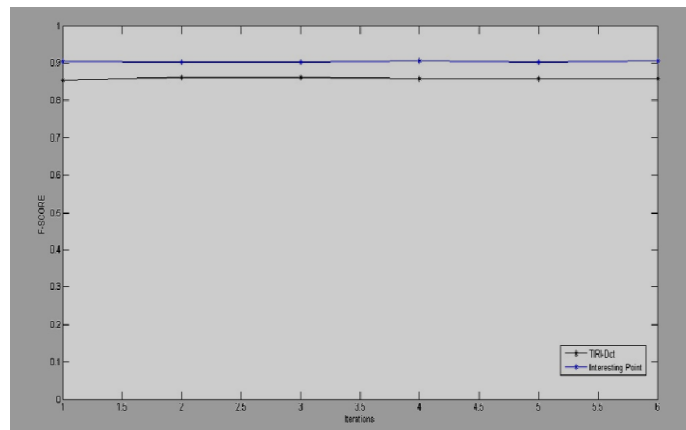


Fig.5. F-Score value of TIRI-DCT and Insert-Point-Matching algorithm for different attack parameters from Table I

VI. CONCLUSION AND FUTURE WORK

The fingerprinting system is proposed for video copy detection system. It can be used for copyright management and indexing applications. The system consists of a fingerprint extraction algorithm followed by an approximate search method. The proposed fingerprinting algorithm which is Interest point Matching Algorithm extracts robust, discriminate and compact fingerprints from videos in a fast and reliable fashion. The fingerprint extracted using this algorithm maintains a good performance for attacks such as noise addition, changes in brightness or contrast rotation, time shift, and changes in background. Two fast searching methods: Inverted file based searching and cluster based similarity search are implemented for efficient searching in the fingerprint database.

Future work includes enhancing the security to the fingerprint. It also includes the study of the performance of the system in the presence of some other attacks, such as large geometric attacks like cropping or inserting some logo. Comparing to the other fingerprinting methods our system will reduce the searching time so it improves to faster searching methods.

REFERENCES

- [1] Christoph Strecha, Alexander M. Bronstein, Member, IEEE, Michael M. Bronstein, Senior Member, IEEE, and Pascal Fua, Senior Member, IEEE (Jan 2012) "LDAHash: Improved Matching with Smaller Descriptors" IEEE Transactions On Pattern Analysis And Machine Intelligence, Vol. 34, No. 1
- [2] Cordelia Schmid, Roger Mohr and Christian Bauckhage (2000) "Evaluation of Interest Point Detectors" International Journal of Computer Vision 37(2), 151-172
- [3] Coskun, B, B. Sankur, and N. Memon, (Dec. 2006) "Spatiotemporal transform based video hashing," IEEE Trans. Multimedia, vol. 8, no. 6, pp. 1190-1208
- [4] Gerhard Roth, Robert Laganiere, Patrick Lambert, Ilias Lakhmiri, and Tarik Janati (2010) "A simple but effective approach to video copy detection" Canadian conference computer and robot vision
- [5] Hampapur and R. M. Bolle, Videogrep(2001) "Video copy detection using inverted file indices" IBM Research Division Thomas. J. Watson Research Center, Tech. Rep.
- [6] Hye-Jeong Cho, Yeo-Song Lee, Chae-Bong Sohn, Kwang-Sue Chung, and Seoung-Jun Oh(2009) "A novel video copy detection method based on statistical analysis"
- [7] Juan Chen(2010) "Detection Of Video Copies Based On Robust Descriptors" 978-1-4244-8026-5/10/\$26.00 ©2010 IEEE

- [8] Law-To.J, L. Chen, A. Joly, I. Laptev, O. Buisson, V. Gouet-Brunet, N. Boujemaa, and F. Stentiford,(2007) “Video copy detection: A comparative study,” in Proc. ACM Int. Conf. Image and Video Retrieval, New York, NY, pp. 371–378, ACM.
- [9] Malekesmaeili.M, M. Fatourehchi, and R. K.Ward,(Dec. 2009) “Video copy detection using temporally informative representative images,” in Proc. Int. Conf. Machine Learning and Applications , pp. 69–74.
- [10] Mani Malek Esmaeili,Mehrdad Fatourehchi and Rabab Kreidieh Ward(March 2011) “A Robust and Fast Video Copy Detection System Using Content-Based Fingerprinting” IEEE Transactions on Information Forensics and Security, vol 6,No1
- [11] Radhakrishnan.R and C. Bauer, (Oct. 2007)“Content-based video signatures based on projections of difference images,” in Proc. MMSP, pp. 341–344.
- [12] Roopalakshmi.R, Ram Mohana Reddy.G(2010) “Recent Trends in Content-Based Video Copy Detection” 978-1-4244-5967-4/10/\$26.00 ©2010 IEEE
- [13] Shikui Wei, Yao Zhao, Member, IEEE, Ce Zhu, Senior Member, IEEE,(Jan 2011) “Frame Fusion for Video Copy Detection” IEEE Transactions On Circuits And Systems For Video Technology, Vol. 21, No. 1
- [14] Swaminathan, Y. Mao, and M. Wu,(Jun. 2006.) “Robust and secure image hashing,” IEEE Trans. Inf. Forensics Security, vol. 1, no. 2, pp.215–230,
- [15] Zheng Cao, and Ming Zhu (Aug 2009) “An efficient video copy detection method based on video signature” Proceedings of the IEEEInternational Conference on Automation and Logistics Shenyang, China
- [16] Yoshiaki Itoh , Masahiro Erokumae, Kazunori Kojima, Masaaki Ishigame, Kazuyo Tanaka(2010) “Time-space Acoustical Feature for Fast Video Copy Detection” 978-1-4244-8112-5/10/\$26.00 ©2010 IEEE
- [17] Zhen Xiong and Yun Zhang ,(December. 2009) “A Novel Interest-Point-Matching Algorithm for High-Resolution Satellite Images” IEEE Trans. on Geoscience and Remote Sensing, Vol. 47, No. 12,

The Effects of Different Temperatures and Temperature Cycling On Breakdown Voltages of Tantalum Capacitors

Johanna Virkki

Department of Electronics/Tampere University of Technology, Finland

Abstract : This study focuses on the effects of different temperatures and temperature cycling on breakdown voltages of tantalum capacitors. High and low temperature tests and temperature cycling tests were done. In all tests the used temperatures were inside component's operating temperature limits. After the tests, capacitors were tested for their breakdown voltage. According to results of this research, high or low temperature testing inside component's operating temperature limits does not have an effect on the breakdown voltage of tantalum capacitors. However, temperature cycling inside component's operating temperature limits can lower the breakdown voltage of tantalum capacitors.

Keywords: accelerated testing, reliability, tantalum capacitors, temperature, temperature cycling

I. INTRODUCTION

In today's competitive market, it is important for a company to know the reliability of its products and to be able to control it for continued production at optimum reliability. Sometimes there is a need to examine the performance of a specific electronic component: it may be radically redesigned, or there may be an individual reliability specification for that component. That is why reliability testing of components has become a concern for electronics manufacturers. Also, in many cases, component-level reliability testing is undertaken to begin characterizing a product's reliability when full system-level test units are unavailable.

Electronic components are often stored and used at high or low temperatures, and sometimes temperature can change radically during component's lifetime. Temperature and temperature changes can have various, often unpredictable effects on components. Reliability tests seek to simulate the component's use environment in order to find the effects of environmental stresses. Because such testing is very time-consuming, accelerated testing becomes necessary. Accelerated testing is a procedure in which conditions are intensified to cut down the time required to obtain a weakening effect similar to one encountered in normal service conditions [1].

High Temperature Storage Life (HTSL), JESD22-A103C, and Low Temperature Storage Life (LTSL), JESD22-A119, tests "are applicable for evaluation, screening, monitoring, and/or qualification of all solid state devices and typically used to determine the effect of time and temperature, under storage conditions, for thermally activated failure mechanisms of solid state electronic devices [2, 3]." The standard HTSL test is run for 1000 hours (42 days) and the standard LTSL test for 168 hours (7 days) [2, 3]. During the tests, increased/reduced temperatures (test conditions) are used without electrical stress.

Temperature cycling, according to the standard JESD22-A104D, "is conducted to determine the ability of components and solder interconnects to withstand mechanical stresses induced by alternating high- and low-temperature extremes. Permanent changes in electrical and/or physical characteristics can result from these mechanical stresses [4]." This standard test includes numerous temperature cycling conditions. The test usually lasts 500 or 1000 cycles.

These standard accelerated tests are commonly used for testing reliability of electronics and were used in this research. The object of this research was to test the effects of low temperature, high temperature, and the effects of temperature cycling on tantalum capacitors.

II. TANTALUM CAPACITORS

Surface mount solid tantalum capacitors (henceforth referred to as "tantalum capacitors", shown in Fig. 1) of a maximum voltage of 50V, a capacitance of 10 μ F, and an operating and non-operating temperature of -55°C to 125°C were used in this research. The structure of these capacitors is presented more detailed in Fig 2.



Figure 1. Bottom side of a surface mount tantalum capacitor used in this research.

A. Structure of tantalum capacitors

A tantalum capacitor (structure shown in Fig. 2) consists of three main elements: anode, cathode, and a dielectric layer of tantalum pentoxide that separates them. The capacitor contains an embedded tantalum pellet (anode), surrounded by a tantalum pentoxide, amorphous dielectric layer. The cathode is a semiconductor, manganese dioxide. This pellet is coated with carbon and then with silver to provide the final connecting layer to the cathode terminal. The tantalum wire passes through these layers and connects the positive termination to the tantalum pellet. The negative termination of the capacitor is attached with a silver adhesive to the silver paint layer. Next sections focus on possible failure mechanisms caused by temperature and changes in it.

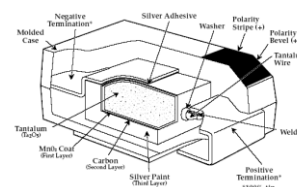


Figure 2. Structure of a tantalum capacitor [5].

B. Effects of temperature and temperature cycling on tantalum capacitors

Temperature, whether generated externally or internally, degrades the performance and reliability of tantalum capacitors. The use of tantalum capacitors at high temperatures has been studied, and manufacturing tantalum capacitors for high-temperature applications is found to be challenging [6, 7]. Mechanical stresses related to the temperature changes during reflow-manufacturing and use of surface mount tantalum capacitors at high temperatures affect their performance and reliability and can account for their breakdowns. Due to mismatch of the coefficients of thermal expansion between the constituent materials, significant mechanical stresses develop in the bulk of materials and at the interfaces. During heating, shear forces are exerted on the anode wire. The molded case pushes on the lead frame in one direction and the pellet in another, generating forces that pull the wire away from the anode structure. Once the device has passed through high temperatures and its elements are shrinking while cooling, they may not fit together as they did before the expansion. Compressive forces may appear on the pellet structure and produce fractures. In addition, these stresses may cause cracking in the tantalum pentoxide dielectric and/or delaminations at the interfaces, resulting in different failure modes of the components. A crack in the dielectric at a corner or edge, when exposed to high stress, may lead to failure [9-11]. The cracking increases leakage current, decreases breakdown voltage, and may cause short-circuits. On the other hand, delaminations can raise the effective series resistance and thus increase power dissipation and temperature of the capacitor, which can decrease its reliability. Severe delaminations may result in intermittent contacts and open-circuit failures of the components [11]. Temperature has also a specific effect inside a tantalum capacitor, known as crystal growth [12-14]. The tantalum pentoxide dielectric is considered an amorphous material. An amorphous state tends to order and crystallize to reduce its internal energy. Surface impurities can induce direct growth of tantalum pentoxide crystals and any imperfection in the dielectric structure is a potential site for crystals to grow. Once the dielectric crystallizes, conductivity and leakage current increase. The presence of impurities is not the only mechanism that may lead to a growth of crystals; Crystal growth can also be initiated in small areas of crystalline order in the dielectric. The conductivity of the crystallized structure has been reported to be higher than that of a dielectric in an amorphous state [14]. However, the latest findings suggest that the crystals themselves are good insulators with very limited conductivity [12, 13]. The exact conductivity mechanism related to the crystal phase is not yet fully understood. The increase in leakage current may still be caused by other mechanisms accelerated by the crystal growth. However, studies show that field crystallization may have only a limited impact on the end use of tantalum capacitors [12].

The temperature cycling of tantalum capacitors has been studied before [11, 15] with capacitors subjected to temperature cycling in a range from -40°C to 85°C [15], -65°C to 125°C, and -65°C to 150°C [11]. Results indicate that tantalum capacitors are capable of withstanding up to 500 cycles of temperature ranging from -65°C to 150°C. However, different lots show different robustness under

cycling conditions, and though parts may not fail formally by exceeding specified limits, a significant degradation in the leakage current and breakdown voltages indicates an increased propensity of some lots to failure after temperature cycling. Cracking in the tantalum pentoxide dielectric, which develops during temperature cycling, results not only in increased leakage current, but also increases the probability of scintillation breakdowns [11]. The results suggested that a harmful temperature cycling effect can be achieved in a much shorter time than in 500 cycles [15].

III. RELIABILITY TESTING

Testing was divided into five tests, hereafter called Tests A, B, C, D, and E. Test A was a low temperature test in -40°C temperature and lasted for 168h. Tests B and C were high temperature tests, Test B was done in 85°C and Test C was done in 125°C. Both tests lasted for 1000h. Tests D and E were temperature cycling tests. Both tests lasted for 500 cycles and one cycle lasted for 0.5h. In test D, the temperature changed between -40°C and 85°C and in Test E, temperature changed between -40°C and 125°C. In all tests, 18 capacitors were tested. Because the capacitors were rated for an operating and non-operating temperature of -55°C to 125°C, they were tested here within their operating limits. This was done in order to get information on their usability in such field conditions and to compare the effects of different temperatures and temperature cycling. All tests and their conditions can be seen in Table 1.

Table 1. All tests and their test conditions.

Test	A	B	C	D	E
Stresses	-40°C	85°C	125°C	-40°C 85°C	-40°C 125°C
Time	168h	1000h	1000h	500 0,5h	* 500* 0,5h

After all temperature tests, capacitors were tested for their breakdown voltage. The capacitors were tested for voltage that was slowly increased (rate of voltage increase: 1V per second) from 0V to 93V provided no failure occurred. The voltage range was chosen because of equipment limitations. The accuracy of measurement was 1V

IV. RESULTS AND DISCUSSION

Table 2 shows breakdown voltages for capacitors without testing and in Tests A-E. Accordingly, capacitors not submitted to any kind of temperature testing did not fail at voltages below 93V. This means that the capacitors can be expected to withstand voltages of over 93V.

Table 2. Failure voltages for capacitors without testing and in Tests A-E.

No Test	Test A	Test B	Test C	Test D	Test E
>93	>93	>93	86	50	57
>93	>93	>93	>93	79	63
>93	>93	>93	>93	81	72
>93	>93	>93	>93	84	72
>93	>93	>93	>93	91	89
>93	>93	>93	>93	>93	>93

Synthesis, Characterization Ac Conductivity of Ni²⁺ Doped In Magnesium Ferrite

Pathan Amjadkhan Noorkhan¹ and Sangshetty Kalayne^{2*}

¹Department of Physics, Singhania University, Pachheri- Bari, Jhunjunu, Rajasthan

^{2*}Department of Physics, Rural Engineering College, Bhalki, Bidar, Karnataka, India.

Abstract: Magnesium nickel ferrites were synthesized by employing sol gel technique at 1473 K sintering temperature. A critical Rietveld analysis of XRD reveals that the presence of a very small amount of NiO phase along with the ferrite phase. It indicates that almost a stoichiometric (Mg,Ni)-ferrite phase has been obtained at 1473 K. SEM image shows that of (MgNi) ferrite is regular in shape have granular in structure, compact and well connected grain to each others. The ac conductivity increases with increase in applied frequency. The magnesium nickel ferrite (MnNiFe₂O₄) shows σ_{ac} conductivity of 1.2×10^{-4} S/cm. This is may be attributed to the dipole polarization i.e., the rotation of dipoles between two equivalent equilibrium positions is involved. The high value of dielectric constant of the sample MnNiFe₂O₄ may be the structural changes associated with the magnesium nickel ferrite when the grain size is reduced. Therefore, this ferrites material is attracted to use in many science and technological applications.

Keywords: Ac conductivity, (MgNi) ferrite, dielectric constant, Impedance spectra, X-ray diffraction.

I. INTRODUCTION

Small ferrimagnetic oxides, technically known as ferrites have attracted considerable attention not only from a fundamental scientific interest but also from a practical point of view for growing applications in the magnetic, electronic and microwave fields [1-3]. Simultaneous presence of magnetic and dielectric nature of ferrites is vastly exploited in a variety of applications at different frequencies. The special feature of these materials is that the properties can be tailored over wide ranges by appropriate substitution of various ions in the chemical formula unit and control of processing procedures. Ferrites are extensively used in magnetic recording, information storage, colour imaging, bio-processing, magnetic refrigeration and in magneto optical devices [4, 5].

Ferrites also have great promise for atomic engineering of materials with functional magnetic properties. The formation of corrosion product on the out of core surfaces in pressurized heavy water reactors (PHWRs) are major problem. Ferrite having spinal structure such as magnetic and nickel etc play a major role to prevent such problem. Thus attempts are being made to study the various ferrites to evaluate the impact of substitution of the divalent metal ions to modify the properties of these oxides [6-8].

In the present study authors, report synthesis, characterization and dielectric studies of MgNiFe₂O₄. A critical Rietveld analysis of XRD reveals that the presence of a very small amount of NiO phase along with the ferrite phase. It indicates that almost a stoichiometric (Mg,Ni)-ferrite phase has been obtained at 1473 K. SEM image shows that of (MgNi) ferrite is regular in shape have granular in structure, compact and well connected grain to each others. The ac conductivity increases with increase in applied frequency and dielectric constant decreases. Therefore, this ferrites material is attracted to use in many science and technological applications.

II. Experimental

All Chemicals used were analytical grade (AR). The magnesium chloride, nickel chloride (purity 99.99%) and dehydrated ferric chloride were procured and were used as received.

1.1 Synthesis Of Magnesium Nickel Ferrite

The chloride salts of magnesium, nickel chloride and ferric chloride are mixed in calculated stoichiometric with oxalic acid in equimolar ratio so as to form nickel ferric oxalate precursor. The precursor is then filtered and dried at 323K to achieve constant weight. The precursor is mixed with polyethylene glycol (PEG) in the ratio 1:5 and is ignited. The combustion propagates throughout the precursor. After completion of combustion nickel ferrite (MgNiFe₂O₄) is formed. The MgNi-ferrite is sonicated in acetone media for 20min and then calcinated at 1473 K to remove the impurities. Finally, fine graded nanosized nickel ferrite particles are formed [9, 10].

The pellets of 10 mm diameter are prepared with thickness varying up to 2 mm by applying pressure of 10 Tons in a UTM – 40 (40 Ton Universal testing machine). For temperature dependent conductivity and sensor studies, the pellets are coated with silver paste on either side of the surfaces to obtain better contacts.

1.2 CHARACTERIZATION

The X-ray diffraction (XRD) pattern of the MgNiFe₂O₄ was recorded at room temperature by employing an x-ray powder diffractometer (Rigaku Miniflex) with CuK α radiation ($\lambda=1.5405\text{\AA}$) in the 2θ (Bragg angles) range ($2^{\circ} \leq 2\theta \leq 10^{\circ}$) at a scan speed of $0.5^{\circ} \text{ minute}^{-1}$.

The percentage transmittances for the entire sample are measured from 300 to 4000 cm^{-1} . The SEM images of MgNiFe₂O₄ were recorded using Philips XL-30 (ESEM) scanning electron microscopy. The set up used for measuring ac conductivity is Hioki 3050 impedance analyzer, which is in turn interfaced to the computer.

III. RESULTS AND DISCUSSION

2.1 X-RAYS DIFFRACTION

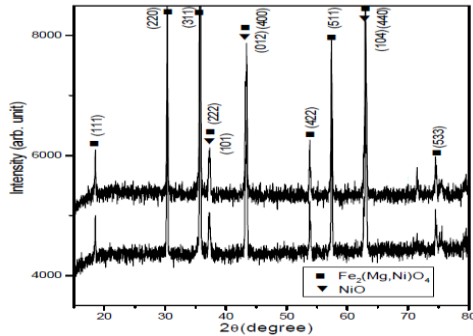


Figure 1 shows the XRD patterns of Mg,Ni)-ferrite annealed at temperature 1473 K.

It seems that the (Mg,Ni)-ferrite phase is formed completely after this heat-treatment. However, a critical rietveld analysis reveals the presence of a very small amount of NiO phase along with the ferrite phase. It indicates that almost a stoichiometric (Mg,Ni)-ferrite phase has been obtained at 1473 K. This indicates that the amount of ferrite phase formation is dependent of annealing time. By measuring particle size we actually measure the coherently diffracting zone of a grain. The particle or crystallites re separated from each other by grain boundaries and the grain boundaries are nothing but bulk crystal imperfections in a crystal [11]. The size of the crystallite in the nanometer range. As can be seen from the experiment, annealing the sample increases the size of the particles. Heat energy helps to annihilate the deformations in the crystals. As a result of grain boundaries started to vanish during annealing and the small crystallites agglomerate together to form larger particles due to intra-grain diffusion.

2.2 SCANNING ELECTRON MICROSCOPY

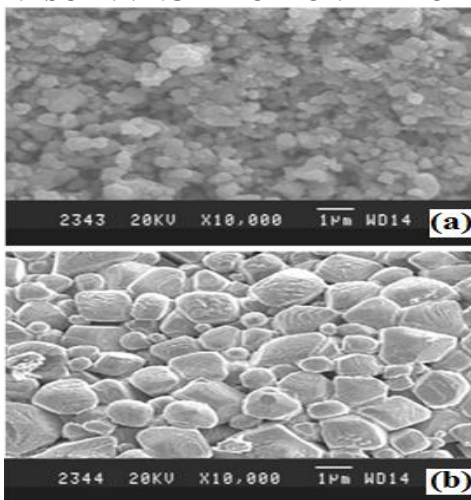


Figure 2 shows the SEM image of (a) NiO and (b) MgNi-ferrite at 1473 K.

Figure 2 (a) shows that SEM image of nickel oxide. It is clearly observed from the image they are agglomerated, highly branched and porous in nature. The

average grain size was calculated by using line intercept formula and it is found to be 0.21µm.

Figure 2 (c) shows that SEM image of (MgNi) ferrite. It is found that the image is regular in shape have granular in structure, compact and well connected grain to each others. The average grain size was calculated by using line intercept formula and it is found to be 0.7µm.

2.3 AC CONDUCTIVITY

The variation of σ_{ac} of $MnNiFe_2O_4$ as a function of frequency as shown in figure 3. The conductivity of nickel ferrites is increases with increase in frequency. The magnesium nickel ferrite ($MnNiFe_2O_4$) shows σ_{ac} conductivity of 1.2×10^{-4} S/cm.

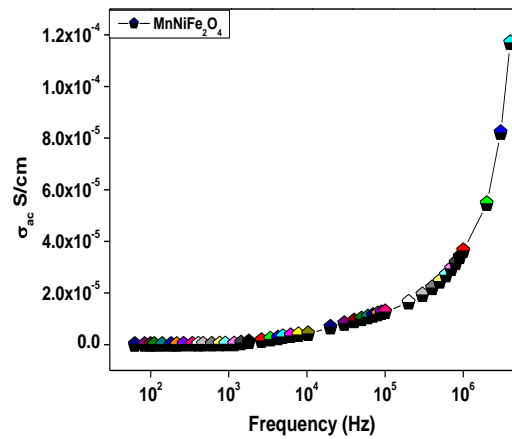


Figure 3 shows the variation of σ_{ac} of $MnNiFe_2O_4$ as a function of frequency.

This is may be attributed to the dipole polarization i.e., the rotation of dipoles between two equivalent equilibrium positions is involved. It is the spontaneous alignment of dipoles in one of the equilibrium positions that give rise to the nonlinear polarization behavior of this composition.

This behaviour of $MnNiFe_2O_4$ obeys the universal power law, $\sigma(\omega) = \sigma_0 + A\omega^n$ (the solid line is the fit to the expression), where σ_0 is the dc conductivity (frequency independent plateau in the low frequency region), A is the pre-exponential factor, and n is the fractional exponent between 0 and 1 [12]. On crystallization, the conductivity spectrum remains similar as that of the nickel ferrite except dispersion in the low frequency region, where the deviation from σ_{dc} (plateau region) is more prominent. The deviation from σ_{dc} (plateau region) value in the conductivity spectrum (in the low frequency region) is due to the electrode polarization effect. The values of σ_0 , A, and n were obtained by fitting the $\sigma(\omega)$ to $\sigma(\omega) = \sigma_0 + A\omega^n$. The overall behavior of σ_{ac} follows the universal dynamic response, which has widely been observed in disordered materials like ionically conducting glasses and also doped crystalline solids, and is generally believed to be reflected in the mechanism of charge transport behavior of charge carriers.

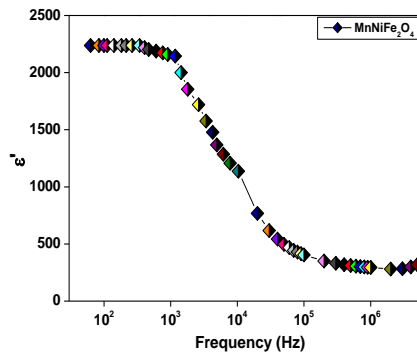


Figure 4 shows the variation real permittivity (ϵ') of nickel ferrite as a function of frequency.

Figure 4 shows the variation real permittivity (ϵ') of nickel ferrite of various composition as a function of logarithmic frequency. It is found that in all these nickel ferrite compositions, as frequency increases, dielectric constant decreases up to the frequency range of 10^3 Hz and after that it remains constant for further increasing in frequency [13]. The strong frequency dispersion of permittivity is observed in the low frequency region followed by a nearly frequency independent behaviour above 10^3 Hz. It is observed that Debye type relaxation mechanism is responsible for higher value of $\text{MnNiFe}_2\text{O}_4$.

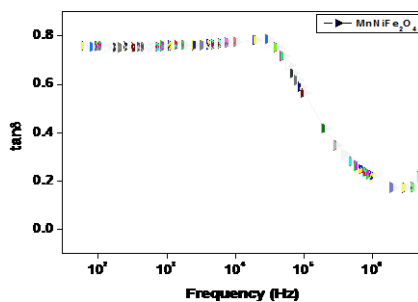


Figure 5 shows the variation of dielectric constant as a function of frequency of $\text{MnNiFe}_2\text{O}_4$

Figure 5 shows the variation of dielectric constant as a function of frequency for $\text{MnNiFe}_2\text{O}_4$. The high value of dielectric constant of the sample $\text{MnNiFe}_2\text{O}_4$ may be explained on the basis of the structural changes associated with the magnesium nickel ferrite when the grain size is reduced. Magnesium nickel ferrite crystallizes into a cubic close-packed arrangement of oxygen ions. It belongs to the class of ferrites with an inverse spinel structure having structural formula, $\text{Fe}^{3+}[\text{Mg}^{2+}\text{Ni}^{3+}]\text{O}_4$. The metal ions given in the square bracket are called octahedral (B site) ions and that outside the square bracket are called tetrahedral (A site) ions. The nickel ions (Ni^{2+}) together with half of the iron ions (Fe^{3+}) occupy the B site and the Mg^{2+} occupy the remaining half of the iron ions reside in A site. The presence of Mg^{2+} and Ni^{3+} ions gives rise to p-type carriers (holes) whereas Fe^{2+} and Fe^{3+} ions produce n-type carriers (electrons). Therefore, both electrons and holes that are present in the B sites are due to the presence of Mg and Ni ions. Since Mg ions are present in A sites, electrons are the carriers in A sites. The distance between the ions in A sites (0.357 nm) is larger than the distance between the ions in B site (0.292 nm) [14-16]. Also, the

degree of covalency for the A site ions is higher than that of the B site ions. All the above factors result in a high activation energy for the A sites compared to the B sites. Hence, in ordinary magnesium nickel ferrite with an inverse spinel structure the electron movement in B sites dominates compared to that in A sites.

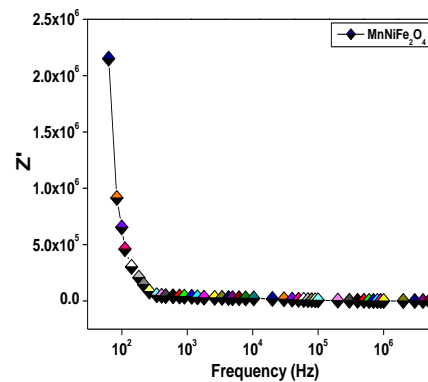


Figure 6 the variation of real part of impedance as a function of frequency

The variation of real part of impedance of $\text{MnNiFe}_2\text{O}_4$ is shown in figure 6 as a function of increasing frequency. It is observed that the real part of impedance decreases with increase in frequency. The initial decrease in impedance value due to the increase in conductivity at lower frequency region up to 10^3 Hz and further increases in applied frequency, the impedance value remains constant. This indicates that after 10^3 Hz the ferrite acts as lossless materials. Therefore, these ferrites can be used in many technological applications such as memory device, microwave, sensor, transducer, solar cell etc.

IV. CONCLUSION

Sol-gel technique was employed to prepare the magnesium nickel ferrites were at 1473 K sintering temperature. A critical Rietveld analysis of XRD reveals that the presence of a very small amount of NiO phase along with the ferrite phase. It indicates that almost a stoichiometric (Mg,Ni)-ferrite phase has been obtained at 1473 K. SEM image shows that of (MgNi) ferrite is regular in shape have granular in structure, compact and well connected grain to each others. The ac conductivity increases with increase in applied frequency. The magnesium nickel ferrite ($\text{MnNiFe}_2\text{O}_4$) shows σ_{ac} conductivity of 1.2×10^{-4} S/cm. This is may be attributed to the dipole polarization i.e., the rotation of dipoles between two equivalent equilibrium positions is involved. The high value of dielectric constant of the sample $\text{MnNiFe}_2\text{O}_4$ may be the structural changes associated with the magnesium nickel ferrite when the grain size is reduced. It is observed that the real part of impedance decreases with increase in frequency. The initial decrease in impedance value due to the increase in conductivity at lower frequency region up to 10^3 Hz and further increases in applied frequency, the impedance value remains constant. Therefore, this ferrites material is attracted to use in many science and technological applications.

REFERENCE

- [1] I. Anton, I. D. Dabata and L. Vekas, "Application Orientated Researches on Magnetic Fluids," *Journal of Magnetism and Magnetic Materials*, 85 (1), 1990, 219-226.
- [2] R. D. McMickael, R. D. Shull, L. J. Swartzendruber, L. H. Bennett and R. E. Watson, "Magnetocaloric Effect in Superparamagnets," *Journal of Magnetism and Magnetic Materials*, 111(1), 1992, 29-33.
- [3] D. L. Leslie-Pelecky and R. D. Rieke, "Magnetic Properties of Nanostructures Materials," *Chemistry of Materials*, 8 (8), 1996, 1770-1783.
- [4] T. Hirai, J. Kobayashi and I. Koasawa, "Preparation of Acicular Ferrite Fine Particles Using an Emulsion Liquid Membrane System," *Langmuir*, 15 (19), 1999, 6291-6298.
- [5] R. H. Kodama, "Magnetic Nanoparticles," *Journal of Magnetism and Magnetic Materials*, 200 (1), 1999, 359-372.
- [6] K. V. P. M. Shafi, Y. Koltypin, A. Gedanken, R. Prozorov, J. Balogh, J. Lendvai and I. Felner, "Sonochemical Preparation of Nanosized Amorphous NiFe₂O₄ Particles," *The Journal of Physical Chemistry B*, 101 (33), 1996, 6409-6414.
- [7] D. Niznansky, M. Drillon and J. L. Renspinger, "Preparation of Magnetic Nanoparticles (γ -Fe₂O₃) in the Silica Matrix," *IEEE Transaction on Magnetics*, 30 (2), 1994, 821-823.
- [8] J. M. Yang, W. J. Tsuo and F. S. J. Yen, "Preparation of Ultrafine Nickel Ferrite Powder Using Ni and Fe Tartrates," *Journal of Solid State Chemistry*, 145(1), 1999, 50-57.
- [9] Y. Shi, J. Ding, X. Liu and J. Wang, "NiFe₂O₄ Ultrafine Particles Prepared by Co- Precipitation / Mechanical Alloying," *Journal of Magnetism and Magnetic Materials*, 205 (2), 1999, 249-254.
- [10] P. Druska, U. Steinike and V. Sepelak, "Surface Structure of Mechanically Activated and of Mechano-synthesized Zinc Ferrite," *Journal of Solid State Chemistry*, 146 (1), 1999, 13-21.
- [11] V. Sepelak, K. Tkacova, V. V. Boldyrev and U. Steinike, "Crystal Structure Refinement of the Mechanically Activated Spinel-Ferrite," *Materials Science Forum*, 228, 1996, 783-788.
- [12] V. Sepelak, A. Yu, U. Rogachev, D. Steinike, C. Uecker, S. Wibmann and K. D. Becker, "Structure of Nanocrystalline Spinel Ferrite Produced by High Energy Ballmilling Method," *Acta Crystallographica A*, 52, 1996, C367.
- [13] V. Sepelak, U. Steinike, D. C. Uecker, S. Wibmann and K. D. Becker, "Structural Disorder in Mechano-synthesized by Zinc Ferrite," *Journal of Solid State Chemistry*, 135 (1), 1998, 52-58.
- [14] H. M. Rietveld, "Line Profile of Neutron Powder Diffraction Peaks for Structure Refinement," *Acta Crystallographica*, 22, 1967, 151-152.
- [15] H. M. Rietveld, "A Profile Refinement Method for Nuclear and Magnetic Structures," *Journal of Applied Crystallography*, 2, 1969, 65-71.
- [16] L. Lutterotti, P. Scardi and P. Maistrelli, "LSI-a Computer Program for Simultaneous Refinement of Material Structure and Microstructure," *Journal of Applied Crystallography*, 25 (3), 1992, 459-462.

Event, Cause, Space-Time and Quantum Memory Register- A Forty Two Storey Augmentation-Arrondissement Model

¹Dr. K. N. Prasanna Kumar, ²Prof. B. S. Kiranagi, ³Prof. C. S. Bagewadi

ABSTRACT: We study a consolidated system of event; cause and n Qubit register which makes computation with n Qubits. Model extensively dilates upon systemic properties and analyses the systemic behaviour of the equations together with other concomitant properties. Inclusion of event and cause, we feel enhances the "Quantum ness" of the system holistically and brings out a relevance in the Quantum Computation on par with the classical system, in so far as the analysis is concerned. Additional VARIABLES OF Space Time provide bastion for the quantum space time studies.-

I. INTRODUCTION:

EVENT AND ITS VINDICATION:

There definitely is a sense of compunction, contrition, hesitation, regret, remorse, hesitation and reservation to the **acknowledgement of** the fact that there is a personal **relation to** what **happens to** oneself. Louis de Broglie said that the events have already happened and it **shall disclose** to the people **based on** their level of consciousness. So there is destiny to start with! Say I am undergoing some seemingly insurmountable problem, which has hurt my sensibilities, susceptibilities and sentimentalities that I refuse to accept that that event was waiting for me to happen. In fact this is the statement of stoic philosophy which is referred to almost as bookish or abstract. Wound is there; it **had to happen** to me. So I was wounded. Stoics tell us that the wound **existed** before me; I was born **to embody** it. It is the question of consummation, consolidation, concretization, consubstantiation, that of this, that **creates an** "event" in us; thus you have **become a quasi cause for** this wound. For instance, my feeling to **become an** actor made me to behave with such perfectionism everywhere, that people's expectations rose and when I did not come up to them I **fell**; thus the 'wound' was waiting for me and 'I' was waiting for the wound! One fellow professor used to say like you are searching for ideas, ideas also searching for you. Thus the wound **possesses in itself** a nature which is "impersonal and preindividual" in character, beyond general and particular, the collective and the private. It is the question **of becoming** universalistic and holistic in your outlook. Unless this fate had not befallen you, the "**grand design**" would not have taken place in its entire entirety. It had to happen. And the concomitant ramifications and pernicious or positive **implications**. Everything is in order **because the** fate befell you. It is not as if the wound had to get something that is best from me or that I am a chosen by God to face the event. As said earlier 'the grand design' would have **been altered**. And **it cannot alter**. You got to play your part and go; there is just no other way. The legacy must go on. You shall be torch bearer and you shall hand over the torch to somebody. This is the name of the game in totalistic and holistic way.

When it comes to ethics, I would say it makes no sense if any obstreperous, obstreperous, ululations, serenading, tintinnabulations are made for the event has happened to me. It means to say that you are unworthy of the fate that has befallen you. To feel that what happened to you was unwarranted and not autonomous, telling the world that you are aggressively iconoclastic, veritably resentful, and volitionally resentient, is choosing the cast of allegation aspersions and accusations at the Grand Design. What is immoral is to invoke the name of god, because some event has **happened to** you. Cursing him is immoral. Realize that it is all "grand design" and you are playing **a part**. Resignation, renunciation, revocation is only one form of resentment. Willing the event is primarily **to release** the eternal truth; in fact you cannot release an event despite the fact everyone tries all ways and means they pray god; they prostrate for others destitution, poverty, penury, misery. But **releasing an** event is something like an "action at a distance" which only super natural power can do.

Here we are face to face with volitional intuition and repetitive transmutation. Like a premeditated skirmisher, **one quarrel** with one self, with others, with god, and finally the accuser **leaves** this world in despair. Now look at this sentence which was quoted by I think Bousquet "if there is a **failure of** will", "I will **substitute a** longing for death" for that shall be apotheosis, a perpetual and progressive glorification of the will.

EVENT AND SINGULARITIES IN QUANTUM SYSTEMS:

What is an event? Or for that matter an ideal event? An event **is a** singularity or rather a set of singularities or set of singular points **characterizing a** mathematical curve, a physical state of affairs, a psychological person or a moral person. Singularities are turning points and points of inflection: they are bottle necks, foyers and centers; they are points of fusion; condensation and boiling; points of tears and joy; sickness and health; hope and anxiety; they are so to say "sensitive" points; such singularities should not be confused or confounded, aggravated or exacerbated with personality of a system expressing itself; or the individuality and idiosyncrasies of a system which is designated with a proposition. They should also **not be fused** with the generalizational concept or universalistic axiomatic predications and postulation alcovishness, or the dipsomaniac flageolet dirge of a concept. Possible a concept could be signified by a figurative representation or a schematic configuration. "Singularity is essentially, pre individual, and has no personalized bias in it, or for that matter a prejudice or

pre circumspection of a conceptual scheme. It is in this sense **we can define a** "singularity" as being neither affirmative nor non affirmative. It can be positive or negative; it can **create or destroy**. On the other hand it must be noted that singularity is different both in its thematic discursive from the run of the mill day to day musings and mundane drooling. They are in that sense "extra-ordinary".

Each singularity is a **source and resource**, the origin, reason and raison d'être of a mathematical series, it could be any series any type, and that is interpolated or extrapolated to the structural location of the **destination of** another singularity. This according to this standpoint, there are different. It can be positive or negative; it can create or destroy. On the other hand it must be noted that singularity is different both in its thematic discursive from the run of the mill day to day musings and mundane drooling. There are in that sense "extra-ordinary".

This according to the widely held standpoint, there are different, multifarious, myriad, series IN A structure. In the eventuality of the fact that we conduct an unbiased and prudent examination of the series belonging to different "singularities" we can come to indubitable **conclusions** that the "singularity" of one system is different from the "other system" in the subterranean realm and ceratoid dualism of comparison and contrast

EPR experiment derived that there exists a communications between two particles. We go a further step to say that there **exists a channel** of communication however slovenly, inept, clumpy, between the two singularities. It is also possible the communication exchange could be one of belligerence, cantankerousness, tempestuousness, astutely truculent, with ensorcelled frenzy. That does not matter. All we are telling is that singularities communicate with each other.

Now, how do find **the reaction** of systems to these singularities. You do the same thing a boss does for you. "Problematize" the events and see how you behave. I will resort to "pressure tactics". "intimidation of deriding report", or "cut in the increment" to make you undergo trials, travails and tribulations. I am happy to see if you improve your work; but may or may not be sad if you succumb to it and hang yourself! We do the same thing with systems. systems show conducive response, felicitous reciprocation or behave erratically with inner roil, eponymous radicalism without and with blitzy conviction say like a solipsist nature of bellicose and blustering particles, or for that matter coruscation, trepidational **motion in** fluid flows, or seemingly perfidious incendiaries in gormandizing fellow elementary particles, abnormal ebullitions, surcharged calumniation and unwarranted(you think so but the system does not!) unrighteous fulminations.

So the point that is made here is "like we problematize the "events" to understand the human behaviour we have to "problematize" the events of systems to understand their behaviour.

This statement is made in connection to the fact that there shall be **creation or destruction** of particles or complete obliteration of the system (blackhole evaporation) or obfuscation of results. Some systems are like "inside traders" they will not put signature at all! How do you find they did it! Anyway, there are possibilities of a CIA finding out as they recently did! So we can do the same thing with systems to. This is accentuation, corroboration, fortification, .fomentatory notes to explain the various coefficients we have used in the model as also the dissipations called for

In the Bank example we have clarified that various systems are individually conservative, and their conservativeness extends holistically too. that one law is universal does not mean there is complete adjudication of **nonexistence of** totality or global or holistic figure. Total always exists and "individual" systems always exist, if we do not bring Kant in to picture! For the time being let us not! Equations would become more enuretic and frenzied..

Various, myriad, series in a structure. In the eventuality of the fact that we conduct an unbiased and prudent examination of the series belonging to different "singularities" we can come to indubitable conclusions that the "singularity" of one system is different from the "other system" in the subterranean realm and ceratoid dualism of comparison and contrast.

CONSERVATION LAWS:

Conservation laws bears ample testimony ,infallible observatory, and impeccable demonstration to the fact that the essential predications, character constitutions, ontological consonances remain unchanged with evolution despite the system's astute truculence, serenading whimsicality, assymetric disposition or on the other hand anachronistic dispensation ,eponymous radicality, entropic entrepotishness or the subdued ,relationally contributive, diverse parametrisizational, conducive reciprocity to environment, unconventional behaviour, enuretic nonlinear frenetic ness ,ensorcelled frenzy, abnormal ebullitions, surcharged fulminations , or the inner roil. And that holds well with the evolution with time. We present a model of the generalizational conservation of the theories. A theory of all the conservation theories. That all conservation laws hold and there is no relationship between them is bête noir. We shall on this premise build a 36 storey model that deliberates on various issues, structural, dependent, thematic and discursive,

Note THAT The classification is executed on systemic properties and parameters. And everything that is known to us measurable. We do not know "intangible". Nor we accept or acknowledge that. All laws of conservation must hold. Hence the holistic laws must hold. Towards that end, interrelationships must exist. All science like law wants evidence and here we shall provide one under the premise that for all conservations laws to hold each must be interrelated to the other, lest the very conception is a fricative contremps. And we live in "Measurement" world.

QUANTUM REGISTER:

Devices that **harness and explore** the fundamental axiomatic predications of Physics has wide ranging amplitudinal **ramification** with its essence of locus and focus on information processing that outperforms their classical counterparts, and for unconditionally secure communication. However, in particular, implementations **based on** condensed-matter systems face the challenge of short coherence times. Carbon materials, particularly diamond, however, are suitable **for hosting** robust solid-state quantum registers, **owing to** their spin-free lattice and weak spin-orbit **coupling**. Studies with the structurally notched criticism and schizoid fragments of manifestations of historical perspective of diamond hosting quantum register

have borne ample testimony and, and at differential and determinate levels have articulated the generalized significations and manifestations of quantum logic elements can **be realized** by exploring long-range magnetic dipolar coupling between individually addressable single electron spins **associated with** separate colour centres in diamond. The strong distance dependence of this coupling was used to characterize the separation of single qubits ($98 \pm 3 \text{ \AA}$) with accuracy close to the value of the crystal-lattice spacing. Coherent **control over** electron spins, **conditional** dynamics, selective readout as well as switchable **interaction** should rip open glittering façade for a prosperous and scintillating irreducible affirmation of open the way towards a viable room-temperature solid-state quantum register. As both electron spins are optically **addressable**, this solid-state quantum device **operating at** ambient conditions **provides a** degree of **control** that is at present available only for a few systems at low temperature (See for instance P. Neumann, R. Kolesov, B. Naydenov, J. Bec F. Rempp, M. Steiner V. Jacques,, G. Balasubramanian, M. L. Markham,, D. J. Twitchen,, S. Pezzagna,, J. Meijer, J. Twamley, F. Jelezko & J. Wrachtrup)-

CAUSE AND EVENT:

MODULE NUMBERED ONE-
NOTATION :

G_{13} : CATEGORY ONE OF CAUSE
 G_{14} : CATEGORY TWO OF CAUSE
 G_{15} : CATEGORY THREE OF CAUSE
 T_{13} : CATEGORY ONE OF EVENT
 T_{14} : CATEGORY TWO OF EVENT
 T_{15} : CATEGORY THREE OF EVENT

FIRST TWO CATEGORIES OF QUBITS COMPUTATION:
MODULE NUMBERED TWO:

G_{16} : CATEGORY ONE OF FIRST SET OF QUBITS
 G_{17} : CATEGORY TWO OF FIRST SET OF QUBITS
 G_{18} : CATEGORY THREE OF FIRST SET OF QUBITS
 T_{16} : CATEGORY ONE OF SECOND SET OF QUBITS
 T_{17} : CATEGORY TWO OF SECOND SET OF QUBITS
 T_{18} : CATEGORY THREE OF SECOND SET OF QUBITS

THIRD SET OF QUBITS AND FOURTH SET OF QUBITS:
MODULE NUMBERED THREE:

G_{20} : CATEGORY ONE OF THIRD SET OF QUBITS
 G_{21} : CATEGORY TWO OF THIRD SET OF QUBITS
 G_{22} : CATEGORY THREE OF THIRD SET OF QUBITS
 T_{20} : CATEGORY ONE OF FOURTH SET OF QUBITS
 T_{21} : CATEGORY TWO OF FOURTH SET OF QUBITS
 T_{22} : CATEGORY THREE OF FOURTH SET OF QUBITS

FIFTH SET OF QUBITS AND SIXTH SET OF QUBITS
: MODULE NUMBERED FOUR:

G_{24} : CATEGORY ONE OF FIFTH SET OF QUBITS
 G_{25} : CATEGORY TWO OF FIFTH SET OF QUBITS
 G_{26} : CATEGORY THREE OF FIFTH SET OF QUBITS
 T_{24} : CATEGORY ONE OF SIXTH SET OF QUBITS
 T_{25} : CATEGORY TWO OF SIXTH SET OF QUBITS
 T_{26} : CATEGORY THREE OF SIXTH SET OF QUBITS

SEVENTH SET OF QUBITS AND EIGHTH SET OF QUBITS:
MODULE NUMBERED FIVE:

G_{28} : CATEGORY ONE OF SEVENTH SET OF QUBITS
 G_{29} : CATEGORY TWO OF SEVENTH SET OF QUBITS
 G_{30} : CATEGORY THREE OF SEVENTH SET OF QUBITS
 T_{28} : CATEGORY ONE OF EIGHTH SET OF QUBITS
 T_{29} : CATEGORY TWO OF EIGHTH SET OF QUBITS
 T_{30} : CATEGORY THREE OF EIGHTH SET OF QUBITS

(n-1)TH SET OF QUBITS AND nTH SET OF QUBITS :
MODULE NUMBERED SIX:

G_{32} : CATEGORY ONE OF (n-1)TH SET OF QUBITS
 G_{33} : CATEGORY TWO OF (n-1)TH SET OF QUBITS
 G_{34} : CATEGORY THREE OF (N-1)TH SET OF QUBITS
 T_{32} : CATEGORY ONE OF n TH SET OF QUBITS
 T_{33} : CATEGORY TWO OF n TH SET OF QUBITS
 T_{34} : CATEGORY THREE OF n TH SET OF QUBITS

GLOSSARY OF MODULE NUMBERED SEVEN

G_{36} : CATEGORY ONE OF TIME
 G_{37} : CATEGORY TWO OF TIME
 G_{38} : CATEGORY THREE OF TIME
 T_{36} : CATEGORY ONE OF SPACE
 T_{37} : CATEGORY TWO OF SPACE
 T_{38} : CATEGORY THREE OF SPACE

$(a_{13})^{(1)}, (a_{14})^{(1)}, (a_{15})^{(1)}, (b_{13})^{(1)}, (b_{14})^{(1)}, (b_{15})^{(1)}, (a_{16})^{(2)}, (a_{17})^{(2)}, (a_{18})^{(2)}, (b_{16})^{(2)}, (b_{17})^{(2)}, (b_{18})^{(2)}$;
 $(a_{20})^{(3)}, (a_{21})^{(3)}, (a_{22})^{(3)}, (b_{20})^{(3)}, (b_{21})^{(3)}, (b_{22})^{(3)}$
 $(a_{24})^{(4)}, (a_{25})^{(4)}, (a_{26})^{(4)}, (b_{24})^{(4)}, (b_{25})^{(4)}, (b_{26})^{(4)}, (b_{28})^{(5)}, (b_{29})^{(5)}, (b_{30})^{(5)}, (a_{28})^{(5)}, (a_{29})^{(5)}, (a_{30})^{(5)}$;
 $(a_{32})^{(6)}, (a_{33})^{(6)}, (a_{34})^{(6)}, (b_{32})^{(6)}, (b_{33})^{(6)}, (b_{34})^{(6)}$

are Accentuation coefficients

$(a'_{13})^{(1)}, (a'_{14})^{(1)}, (a'_{15})^{(1)}, (b'_{13})^{(1)}, (b'_{14})^{(1)}, (b'_{15})^{(1)}, (a'_{16})^{(2)}, (a'_{17})^{(2)}, (a'_{18})^{(2)}, (b'_{16})^{(2)}, (b'_{17})^{(2)}, (b'_{18})^{(2)}$
 $, (a'_{20})^{(3)}, (a'_{21})^{(3)}, (a'_{22})^{(3)}, (b'_{20})^{(3)}, (b'_{21})^{(3)}, (b'_{22})^{(3)}$
 $(a'_{24})^{(4)}, (a'_{25})^{(4)}, (a'_{26})^{(4)}, (b'_{24})^{(4)}, (b'_{25})^{(4)}, (b'_{26})^{(4)}, (b'_{28})^{(5)}, (b'_{29})^{(5)}, (b'_{30})^{(5)}, (a'_{28})^{(5)}, (a'_{29})^{(5)}, (a'_{30})^{(5)}$;
 $(a'_{32})^{(6)}, (a'_{33})^{(6)}, (a'_{34})^{(6)}, (b'_{32})^{(6)}, (b'_{33})^{(6)}, (b'_{34})^{(6)}$

are Dissipation coefficients-

CAUSE AND EVENT: MODULE NUMBERED ONE

The differential system of this model is now (Module Numbered one)-1

$$\begin{aligned} \frac{dG_{13}}{dt} &= (a_{13})^{(1)}G_{14} - [(a'_{13})^{(1)} + (a''_{13})^{(1)}(T_{14}, t)]G_{13} -2 \\ \frac{dG_{14}}{dt} &= (a_{14})^{(1)}G_{13} - [(a'_{14})^{(1)} + (a''_{14})^{(1)}(T_{14}, t)]G_{14} -3 \\ \frac{dG_{15}}{dt} &= (a_{15})^{(1)}G_{14} - [(a'_{15})^{(1)} + (a''_{15})^{(1)}(T_{14}, t)]G_{15} -4 \\ \frac{dT_{13}}{dt} &= (b_{13})^{(1)}T_{14} - [(b'_{13})^{(1)} - (b''_{13})^{(1)}(G, t)]T_{13} -5 \\ \frac{dT_{14}}{dt} &= (b_{14})^{(1)}T_{13} - [(b'_{14})^{(1)} - (b''_{14})^{(1)}(G, t)]T_{14} -6 \\ \frac{dT_{15}}{dt} &= (b_{15})^{(1)}T_{14} - [(b'_{15})^{(1)} - (b''_{15})^{(1)}(G, t)]T_{15} -7 \\ + (a''_{13})^{(1)}(T_{14}, t) &= \text{First augmentation factor} -8 \\ - (b''_{13})^{(1)}(G, t) &= \text{First detritions factor} - \end{aligned}$$

FIRST TWO CATEGORIES OF QUBITS COMPUTATION:
MODULE NUMBERED TWO:

The differential system of this model is now (Module numbered two)-9

$$\begin{aligned} \frac{dG_{16}}{dt} &= (a_{16})^{(2)}G_{17} - [(a'_{16})^{(2)} + (a''_{16})^{(2)}(T_{17}, t)]G_{16} -10 \\ \frac{dG_{17}}{dt} &= (a_{17})^{(2)}G_{16} - [(a'_{17})^{(2)} + (a''_{17})^{(2)}(T_{17}, t)]G_{17} -11 \\ \frac{dG_{18}}{dt} &= (a_{18})^{(2)}G_{17} - [(a'_{18})^{(2)} + (a''_{18})^{(2)}(T_{17}, t)]G_{18} -12 \\ \frac{dT_{16}}{dt} &= (b_{16})^{(2)}T_{17} - [(b'_{16})^{(2)} - (b''_{16})^{(2)}((G_{19}), t)]T_{16} -13 \\ \frac{dT_{17}}{dt} &= (b_{17})^{(2)}T_{16} - [(b'_{17})^{(2)} - (b''_{17})^{(2)}((G_{19}), t)]T_{17} -14 \\ \frac{dT_{18}}{dt} &= (b_{18})^{(2)}T_{17} - [(b'_{18})^{(2)} - (b''_{18})^{(2)}((G_{19}), t)]T_{18} -15 \\ + (a''_{16})^{(2)}(T_{17}, t) &= \text{First augmentation factor} -16 \\ - (b''_{16})^{(2)}((G_{19}), t) &= \text{First detritions factor} -17 \end{aligned}$$

**THIRD SET OF QUBITS AND FOURTH SET OF QUBITS:
 MODULE NUMBERED THREE**

The differential system of this model is now (Module numbered three)-18

$$\begin{aligned} \frac{dG_{20}}{dt} &= (a_{20})^{(3)}G_{21} - [(a'_{20})^{(3)} + (a''_{20})^{(3)}(T_{21}, t)]G_{20} -19 \\ \frac{dG_{21}}{dt} &= (a_{21})^{(3)}G_{20} - [(a'_{21})^{(3)} + (a''_{21})^{(3)}(T_{21}, t)]G_{21} -20 \\ \frac{dG_{22}}{dt} &= (a_{22})^{(3)}G_{21} - [(a'_{22})^{(3)} + (a''_{22})^{(3)}(T_{21}, t)]G_{22} -21 \\ \frac{dT_{20}}{dt} &= (b_{20})^{(3)}T_{21} - [(b'_{20})^{(3)} - (b''_{20})^{(3)}(G_{23}, t)]T_{20} -22 \\ \frac{dT_{21}}{dt} &= (b_{21})^{(3)}T_{20} - [(b'_{21})^{(3)} - (b''_{21})^{(3)}(G_{23}, t)]T_{21} -23 \\ \frac{dT_{22}}{dt} &= (b_{22})^{(3)}T_{21} - [(b'_{22})^{(3)} - (b''_{22})^{(3)}(G_{23}, t)]T_{22} -24 \\ + (a''_{20})^{(3)}(T_{21}, t) &= \text{First augmentation factor-} \\ - (b''_{20})^{(3)}(G_{23}, t) &= \text{First detritions factor -25} \end{aligned}$$

**FIFTH SET OF QUBITS AND SIXTH SET OF QUBITS
 : MODULE NUMBERED FOUR**

The differential system of this model is now (Module numbered Four)-26

$$\begin{aligned} \frac{dG_{24}}{dt} &= (a_{24})^{(4)}G_{25} - [(a'_{24})^{(4)} + (a''_{24})^{(4)}(T_{25}, t)]G_{24} -27 \\ \frac{dG_{25}}{dt} &= (a_{25})^{(4)}G_{24} - [(a'_{25})^{(4)} + (a''_{25})^{(4)}(T_{25}, t)]G_{25} -28 \\ \frac{dG_{26}}{dt} &= (a_{26})^{(4)}G_{25} - [(a'_{26})^{(4)} + (a''_{26})^{(4)}(T_{25}, t)]G_{26} -29 \\ \frac{dT_{24}}{dt} &= (b_{24})^{(4)}T_{25} - [(b'_{24})^{(4)} - (b''_{24})^{(4)}(G_{27}, t)]T_{24} -30 \\ \frac{dT_{25}}{dt} &= (b_{25})^{(4)}T_{24} - [(b'_{25})^{(4)} - (b''_{25})^{(4)}(G_{27}, t)]T_{25} -31 \\ \frac{dT_{26}}{dt} &= (b_{26})^{(4)}T_{25} - [(b'_{26})^{(4)} - (b''_{26})^{(4)}(G_{27}, t)]T_{26} -32 \\ + (a''_{24})^{(4)}(T_{25}, t) &= \text{First augmentation factor-33} \\ - (b''_{24})^{(4)}(G_{27}, t) &= \text{First detritions factor -34} \end{aligned}$$

**SEVENTH SET OF QUBITS AND EIGHTH SET OF QUBITS:
 MODULE NUMBERED FIVE**

The differential system of this model is now (Module number five)-35

$$\begin{aligned} \frac{dG_{28}}{dt} &= (a_{28})^{(5)}G_{29} - [(a'_{28})^{(5)} + (a''_{28})^{(5)}(T_{29}, t)]G_{28} -36 \\ \frac{dG_{29}}{dt} &= (a_{29})^{(5)}G_{28} - [(a'_{29})^{(5)} + (a''_{29})^{(5)}(T_{29}, t)]G_{29} -37 \\ \frac{dG_{30}}{dt} &= (a_{30})^{(5)}G_{29} - [(a'_{30})^{(5)} + (a''_{30})^{(5)}(T_{29}, t)]G_{30} -38 \\ \frac{dT_{28}}{dt} &= (b_{28})^{(5)}T_{29} - [(b'_{28})^{(5)} - (b''_{28})^{(5)}(G_{31}, t)]T_{28} -39 \\ \frac{dT_{29}}{dt} &= (b_{29})^{(5)}T_{28} - [(b'_{29})^{(5)} - (b''_{29})^{(5)}(G_{31}, t)]T_{29} -40 \\ \frac{dT_{30}}{dt} &= (b_{30})^{(5)}T_{29} - [(b'_{30})^{(5)} - (b''_{30})^{(5)}(G_{31}, t)]T_{30} -41 \\ + (a''_{28})^{(5)}(T_{29}, t) &= \text{First augmentation factor -42} \\ - (b''_{28})^{(5)}(G_{31}, t) &= \text{First detritions factor -43} \end{aligned}$$

**n-1)TH SET OF QUBITS AND nTH SET OF QUBITS :
 MODULE NUMBERED SIX:**

The differential system of this model is now (Module numbered Six)-44

$$\begin{aligned} 45 \\ \frac{dG_{32}}{dt} &= (a_{32})^{(6)}G_{33} - [(a'_{32})^{(6)} + (a''_{32})^{(6)}(T_{33}, t)]G_{32} -46 \\ \frac{dG_{33}}{dt} &= (a_{33})^{(6)}G_{32} - [(a'_{33})^{(6)} + (a''_{33})^{(6)}(T_{33}, t)]G_{33} -47 \\ \frac{dG_{34}}{dt} &= (a_{34})^{(6)}G_{33} - [(a'_{34})^{(6)} + (a''_{34})^{(6)}(T_{33}, t)]G_{34} -48 \\ \frac{dT_{32}}{dt} &= (b_{32})^{(6)}T_{33} - [(b'_{32})^{(6)} - (b''_{32})^{(6)}(G_{35}, t)]T_{32} -49 \\ \frac{dT_{33}}{dt} &= (b_{33})^{(6)}T_{32} - [(b'_{33})^{(6)} - (b''_{33})^{(6)}(G_{35}, t)]T_{33} -50 \end{aligned}$$

$$\frac{dT_{34}}{dt} = (b_{34})^{(6)}T_{33} - [(b'_{34})^{(6)} - (b''_{34})^{(6)}((G_{35}), t)]T_{34} - 51$$

$$+(a''_{32})^{(6)}(T_{33}, t) = \text{First augmentation factor-52}$$

SPACE AND TIME:GOVERNING EQUATIONS:

The differential system of this model is now (SEVENTH MODULE)

$$\frac{dG_{36}}{dt} = (a_{36})^{(7)}G_{37} - [(a'_{36})^{(7)} + (a''_{36})^{(7)}(T_{37}, t)]G_{36} - 54$$

$$\frac{dG_{37}}{dt} = (a_{37})^{(7)}G_{36} - [(a'_{37})^{(7)} + (a''_{37})^{(7)}(T_{37}, t)]G_{37} - 55$$

$$\frac{dG_{38}}{dt} = (a_{38})^{(7)}G_{37} - [(a'_{38})^{(7)} + (a''_{38})^{(7)}(T_{37}, t)]G_{38} - 56$$

$$\frac{dT_{36}}{dt} = (b_{36})^{(7)}T_{37} - [(b'_{36})^{(7)} - (b''_{36})^{(7)}((G_{39}), t)]T_{36} - 57$$

$$\frac{dT_{37}}{dt} = (b_{37})^{(7)}T_{36} - [(b'_{37})^{(7)} - (b''_{37})^{(7)}((G_{39}), t)]T_{37} - 58$$

$$\frac{dT_{38}}{dt} = (b_{38})^{(7)}T_{37} - [(b'_{38})^{(7)} - (b''_{38})^{(7)}((G_{39}), t)]T_{38} - 60$$

$$+(a''_{36})^{(7)}(T_{37}, t) = \text{First augmentation factor -61}$$

$$-(b_{36})^{(7)}((G_{39}), t) = \text{First detritions factor}$$

FIRST MODULE CONCATENATION:

$$\frac{dG_{13}}{dt} = (a_{13})^{(1)}G_{14} - \left[\begin{array}{c} (a'_{13})^{(1)} + (a''_{13})^{(1)}(T_{14}, t) + (a''_{16})^{(2,2)}(T_{17}, t) + (a''_{20})^{(3,3)}(T_{21}, t) \\ + (a''_{24})^{(4,4,4,4)}(T_{25}, t) + (a''_{28})^{(5,5,5,5)}(T_{29}, t) + (a''_{32})^{(6,6,6,6)}(T_{33}, t) \\ + (a''_{36})^{(7)}(T_{37}, t) \end{array} \right] G_{13}$$

$$\frac{dG_{14}}{dt} = (a_{14})^{(1)}G_{13} - \left[\begin{array}{c} (a'_{14})^{(1)} + (a''_{14})^{(1)}(T_{14}, t) + (a''_{17})^{(2,2)}(T_{17}, t) + (a''_{21})^{(3,3)}(T_{21}, t) \\ + (a''_{25})^{(4,4,4,4)}(T_{25}, t) + (a''_{29})^{(5,5,5,5)}(T_{29}, t) + (a''_{33})^{(6,6,6,6)}(T_{33}, t) \\ + (a''_{37})^{(7)}(T_{37}, t) \end{array} \right] G_{14}$$

$$\frac{dG_{15}}{dt} = (a_{15})^{(1)}G_{14} - \left[\begin{array}{c} (a'_{15})^{(1)} + (a''_{15})^{(1)}(T_{14}, t) + (a''_{18})^{(2,2)}(T_{17}, t) + (a''_{22})^{(3,3)}(T_{21}, t) \\ + (a''_{26})^{(4,4,4,4)}(T_{25}, t) + (a''_{30})^{(5,5,5,5)}(T_{29}, t) + (a''_{34})^{(6,6,6,6)}(T_{33}, t) \\ + (a''_{38})^{(7)}(T_{37}, t) \end{array} \right] G_{15}$$

Where $(a''_{13})^{(1)}(T_{14}, t)$, $(a''_{14})^{(1)}(T_{14}, t)$, $(a''_{15})^{(1)}(T_{14}, t)$ are first augmentation coefficients for category 1, 2 and 3
 $(a''_{16})^{(2,2)}(T_{17}, t)$, $(a''_{17})^{(2,2)}(T_{17}, t)$, $(a''_{18})^{(2,2)}(T_{17}, t)$ are second augmentation coefficient for category 1, 2 and 3
 $(a''_{20})^{(3,3)}(T_{21}, t)$, $(a''_{21})^{(3,3)}(T_{21}, t)$, $(a''_{22})^{(3,3)}(T_{21}, t)$ are third augmentation coefficient for category 1, 2 and 3
 $(a''_{24})^{(4,4,4,4)}(T_{25}, t)$, $(a''_{25})^{(4,4,4,4)}(T_{25}, t)$, $(a''_{26})^{(4,4,4,4)}(T_{25}, t)$ are fourth augmentation coefficient for category 1, 2 and 3
 $(a''_{28})^{(5,5,5,5)}(T_{29}, t)$, $(a''_{29})^{(5,5,5,5)}(T_{29}, t)$, $(a''_{30})^{(5,5,5,5)}(T_{29}, t)$ are fifth augmentation coefficient for category 1, 2 and 3
 $(a''_{32})^{(6,6,6,6)}(T_{33}, t)$, $(a''_{33})^{(6,6,6,6)}(T_{33}, t)$, $(a''_{34})^{(6,6,6,6)}(T_{33}, t)$ are sixth augmentation coefficient for category 1, 2 and 3
 $(a''_{36})^{(7)}(T_{37}, t)$, $(a''_{37})^{(7)}(T_{37}, t)$, $(a''_{38})^{(7)}(T_{37}, t)$ ARE SEVENTH AUGMENTATION COEFFICIENTS

$$\frac{dT_{13}}{dt} = (b_{13})^{(1)}T_{14} - \left[\begin{array}{c} (b'_{13})^{(1)} - (b''_{16})^{(1)}(G, t) - (b''_{36})^{(7)}(G_{39}, t) - (b''_{20})^{(3,3)}(G_{23}, t) \\ - (b''_{24})^{(4,4,4,4)}(G_{27}, t) - (b''_{28})^{(5,5,5,5)}(G_{31}, t) - (b''_{32})^{(6,6,6,6)}(G_{35}, t) \\ - (b''_{36})^{(7)}(G_{39}, t) \end{array} \right] T_{13}$$

$$\frac{dT_{14}}{dt} = (b_{14})^{(1)}T_{13} - \left[\begin{array}{c} (b'_{14})^{(1)} - (b''_{14})^{(1)}(G, t) - (b''_{17})^{(2,2)}(G_{19}, t) - (b''_{21})^{(3,3)}(G_{23}, t) \\ - (b''_{25})^{(4,4,4,4)}(G_{27}, t) - (b''_{29})^{(5,5,5,5)}(G_{31}, t) - (b''_{33})^{(6,6,6,6)}(G_{35}, t) \\ - (b''_{37})^{(7)}(G_{39}, t) \end{array} \right] T_{14}$$

$$\frac{dT_{15}}{dt} = (b_{15})^{(1)}T_{14} - \left[\begin{array}{c} (b'_{15})^{(1)} - (b''_{15})^{(1)}(G, t) - (b''_{18})^{(2,2)}(G_{19}, t) - (b''_{22})^{(3,3)}(G_{23}, t) \\ - (b''_{26})^{(4,4,4,4)}(G_{27}, t) - (b''_{30})^{(5,5,5,5)}(G_{31}, t) - (b''_{34})^{(6,6,6,6)}(G_{35}, t) \\ - (b''_{38})^{(7)}(G_{39}, t) \end{array} \right] T_{15}$$

Where $-(b_{13}^{(1)}(G, t))$, $-(b_{14}^{(1)}(G, t))$, $-(b_{15}^{(1)}(G, t))$ are first detritions coefficients for category 1, 2 and 3
 $-(b_{16}^{(2,2)}(G_{19}, t))$, $-(b_{17}^{(2,2)}(G_{19}, t))$, $-(b_{18}^{(2,2)}(G_{19}, t))$ are second detritions coefficients for category 1, 2 and 3
 $-(b_{20}^{(3,3)}(G_{23}, t))$, $-(b_{21}^{(3,3)}(G_{23}, t))$, $-(b_{22}^{(3,3)}(G_{23}, t))$ are third detritions coefficients for category 1, 2 and 3
 $-(b_{24}^{(4,4,4,4)}(G_{27}, t))$, $-(b_{25}^{(4,4,4,4)}(G_{27}, t))$, $-(b_{26}^{(4,4,4,4)}(G_{27}, t))$ are fourth detritions coefficients for category 1, 2 and 3
 $-(b_{28}^{(5,5,5,5)}(G_{31}, t))$, $-(b_{29}^{(5,5,5,5)}(G_{31}, t))$, $-(b_{30}^{(5,5,5,5)}(G_{31}, t))$ are fifth detritions coefficients for category 1, 2 and 3
 $-(b_{32}^{(6,6,6,6)}(G_{35}, t))$, $-(b_{33}^{(6,6,6,6)}(G_{35}, t))$, $-(b_{34}^{(6,6,6,6)}(G_{35}, t))$ are sixth detritions coefficients for category 1, 2 and 3
 $-(b_{36}^{(7)}(G_{39}, t))$, $-(b_{36}^{(7)}(G_{39}, t))$, $-(b_{36}^{(7)}(G_{39}, t))$ ARE SEVENTH DETRITION COEFFICIENTS

62

$$\frac{dT_{15}}{dt} = (b_{15}^{(1)})T_{14} - \left[\begin{array}{c} (b_{15}^{(1)})-(b_{15}^{(1)}(G, t))-(b_{18}^{(2,2)}(G_{19}, t))-(b_{22}^{(3,3)}(G_{23}, t)) \\ -(b_{26}^{(4,4,4,4)}(G_{27}, t))-(b_{30}^{(5,5,5,5)}(G_{31}, t))-(b_{34}^{(6,6,6,6)}(G_{35}, t)) \end{array} \right] T_{15} \quad 63$$

Where $-(b_{13}^{(1)}(G, t))$, $-(b_{14}^{(1)}(G, t))$, $-(b_{15}^{(1)}(G, t))$ are first detrition coefficients for category 1, 2 and 3
 $-(b_{16}^{(2,2)}(G_{19}, t))$, $-(b_{17}^{(2,2)}(G_{19}, t))$, $-(b_{18}^{(2,2)}(G_{19}, t))$ are second detritions coefficients for category 1, 2 and 3
 $-(b_{20}^{(3,3)}(G_{23}, t))$, $-(b_{21}^{(3,3)}(G_{23}, t))$, $-(b_{22}^{(3,3)}(G_{23}, t))$ are third detritions coefficients for category 1, 2 and 3
 $-(b_{24}^{(4,4,4,4)}(G_{27}, t))$, $-(b_{25}^{(4,4,4,4)}(G_{27}, t))$, $-(b_{26}^{(4,4,4,4)}(G_{27}, t))$ are fourth detritions coefficients for category 1, 2 and 3
 $-(b_{28}^{(5,5,5,5)}(G_{31}, t))$, $-(b_{29}^{(5,5,5,5)}(G_{31}, t))$, $-(b_{30}^{(5,5,5,5)}(G_{31}, t))$ are fifth detritions coefficients for category 1, 2 and 3
 $-(b_{32}^{(6,6,6,6)}(G_{35}, t))$, $-(b_{33}^{(6,6,6,6)}(G_{35}, t))$, $-(b_{34}^{(6,6,6,6)}(G_{35}, t))$ are sixth detritions coefficients for category 1, 2 and 3 64

SECOND MODULE CONCATENATION

$$\frac{dG_{16}}{dt} = (a_{16}^{(2)})G_{17} - \left[\begin{array}{c} (a_{16}^{(2)})+(a_{16}^{(2)}(T_{17}, t))+(a_{13}^{(1,1)}(T_{14}, t))+(a_{20}^{(3,3,3)}(T_{21}, t)) \\ +(a_{24}^{(4,4,4,4,4)}(T_{25}, t))+(a_{28}^{(5,5,5,5,5)}(T_{29}, t))+(a_{32}^{(6,6,6,6,6)}(T_{33}, t)) \\ +(a_{36}^{(7,7)}(T_{37}, t)) \end{array} \right] G_{16} \quad 66$$

$$\frac{dG_{17}}{dt} = (a_{17}^{(2)})G_{16} - \left[\begin{array}{c} (a_{17}^{(2)})+(a_{17}^{(2)}(T_{17}, t))+(a_{14}^{(1,1)}(T_{14}, t))+(a_{21}^{(3,3,3)}(T_{21}, t)) \\ +(a_{25}^{(4,4,4,4,4)}(T_{25}, t))+(a_{29}^{(5,5,5,5,5)}(T_{29}, t))+(a_{33}^{(6,6,6,6,6)}(T_{33}, t)) \\ +(a_{37}^{(7,7)}(T_{37}, t)) \end{array} \right] G_{17} \quad 67$$

$$\frac{dG_{18}}{dt} = (a_{18}^{(2)})G_{17} - \left[\begin{array}{c} (a_{18}^{(2)})+(a_{18}^{(2)}(T_{17}, t))+(a_{15}^{(1,1)}(T_{14}, t))+(a_{22}^{(3,3,3)}(T_{21}, t)) \\ +(a_{26}^{(4,4,4,4,4)}(T_{25}, t))+(a_{30}^{(5,5,5,5,5)}(T_{29}, t))+(a_{34}^{(6,6,6,6,6)}(T_{33}, t)) \\ +(a_{38}^{(7,7)}(T_{37}, t)) \end{array} \right] G_{18} \quad 68$$

Where $+(a_{16}^{(2)}(T_{17}, t))$, $+(a_{17}^{(2)}(T_{17}, t))$, $+(a_{18}^{(2)}(T_{17}, t))$ are first augmentation coefficients for category 1, 2 and 3
 $+(a_{13}^{(1,1)}(T_{14}, t))$, $+(a_{14}^{(1,1)}(T_{14}, t))$, $+(a_{15}^{(1,1)}(T_{14}, t))$ are second augmentation coefficient for category 1, 2 and 3
 $+(a_{20}^{(3,3,3)}(T_{21}, t))$, $+(a_{21}^{(3,3,3)}(T_{21}, t))$, $+(a_{22}^{(3,3,3)}(T_{21}, t))$ are third augmentation coefficient for category 1, 2 and 3
 $+(a_{24}^{(4,4,4,4,4)}(T_{25}, t))$, $+(a_{25}^{(4,4,4,4,4)}(T_{25}, t))$, $+(a_{26}^{(4,4,4,4,4)}(T_{25}, t))$ are fourth augmentation coefficient for category 1, 2 and 3
 $+(a_{28}^{(5,5,5,5,5)}(T_{29}, t))$, $+(a_{29}^{(5,5,5,5,5)}(T_{29}, t))$, $+(a_{30}^{(5,5,5,5,5)}(T_{29}, t))$ are fifth augmentation coefficient for category 1, 2 and 3
 $+(a_{32}^{(6,6,6,6,6)}(T_{33}, t))$, $+(a_{33}^{(6,6,6,6,6)}(T_{33}, t))$, $+(a_{34}^{(6,6,6,6,6)}(T_{33}, t))$ are sixth augmentation coefficient for category 1, 2 and 3 -69

70

$+(a_{36}^{(7,7)}(T_{37}, t))$, $+(a_{37}^{(7,7)}(T_{37}, t))$, $+(a_{38}^{(7,7)}(T_{37}, t))$ ARE SEVENTH DETRITION COEFFICIENTS-71

$$\frac{dT_{16}}{dt} = (b_{16}^{(2)})T_{17} - \left[\begin{array}{c} (b_{16}^{(2)})-(b_{16}^{(2)}(G_{19}, t))-(b_{13}^{(1,1)}(G, t))-(b_{20}^{(3,3,3)}(G_{23}, t)) \\ -(b_{24}^{(4,4,4,4,4)}(G_{27}, t))-(b_{28}^{(5,5,5,5,5)}(G_{31}, t))-(b_{32}^{(6,6,6,6,6)}(G_{35}, t)) \\ -(b_{36}^{(7,7)}(G_{39}, t)) \end{array} \right] T_{16} \quad 72$$

$$\frac{dT_{17}}{dt} = (b_{17}^{(2)})T_{16} - \left[\begin{array}{c} (b_{17}^{(2)})-(b_{17}^{(2)}(G_{19}, t))-(b_{14}^{(1,1)}(G, t))-(b_{21}^{(3,3,3)}(G_{23}, t)) \\ -(b_{25}^{(4,4,4,4,4)}(G_{27}, t))-(b_{29}^{(5,5,5,5,5)}(G_{31}, t))-(b_{33}^{(6,6,6,6,6)}(G_{35}, t)) \\ -(b_{37}^{(7,7)}(G_{39}, t)) \end{array} \right] T_{17} \quad 73$$

$$\frac{dT_{18}}{dt} = (b_{18}^{(2)})T_{17} - \left[\begin{array}{c} (b_{18}^{(2)})-(b_{18}^{(2)}(G_{19}, t))-(b_{15}^{(1,1)}(G, t))-(b_{22}^{(3,3,3)}(G_{23}, t)) \\ -(b_{26}^{(4,4,4,4,4)}(G_{27}, t))-(b_{30}^{(5,5,5,5,5)}(G_{31}, t))-(b_{34}^{(6,6,6,6,6)}(G_{35}, t)) \\ -(b_{38}^{(7,7)}(G_{39}, t)) \end{array} \right] T_{18} \quad 74$$

where $-(b_{16}^{(2)}(G_{19}, t))$, $-(b_{17}^{(2)}(G_{19}, t))$, $-(b_{18}^{(2)}(G_{19}, t))$ are first detrition coefficients for category 1, 2 and 3

$-(b''_{13})^{(1,1,1)}(G, t)$, $-(b''_{14})^{(1,1,1)}(G, t)$, $-(b''_{15})^{(1,1,1)}(G, t)$ are second detrition coefficients for category 1,2 and 3
 $-(b''_{20})^{(3,3,3)}(G_{23}, t)$, $-(b''_{21})^{(3,3,3)}(G_{23}, t)$, $-(b''_{22})^{(3,3,3)}(G_{23}, t)$ are third detrition coefficients for category 1,2 and 3
 $-(b''_{24})^{(4,4,4,4,4)}(G_{27}, t)$, $-(b''_{25})^{(4,4,4,4,4)}(G_{27}, t)$, $-(b''_{26})^{(4,4,4,4,4)}(G_{27}, t)$ are fourth detritions coefficients for category 1,2 and 3
 $-(b''_{28})^{(5,5,5,5,5)}(G_{31}, t)$, $-(b''_{29})^{(5,5,5,5,5)}(G_{31}, t)$, $-(b''_{30})^{(5,5,5,5,5)}(G_{31}, t)$ are fifth detritions coefficients for category 1,2 and 3
 $-(b''_{32})^{(6,6,6,6,6)}(G_{35}, t)$, $-(b''_{33})^{(6,6,6,6,6)}(G_{35}, t)$, $-(b''_{34})^{(6,6,6,6,6)}(G_{35}, t)$ are sixth detritions coefficients for category 1,2 and 3
 $-(b''_{36})^{(7,7,7)}(G_{39}, t)$, $-(b''_{37})^{(7,7,7)}(G_{39}, t)$, $-(b''_{38})^{(7,7,7)}(G_{39}, t)$ are seventh detrition coefficients

THIRD MODULE CONCATENATION:-75

$$\begin{aligned}
 \frac{dG_{20}}{dt} &= (a_{20})^{(3)}G_{21} - \left[\begin{array}{l} (a'_{20})^{(3)} + (a''_{20})^{(3)}(T_{21}, t) + (a''_{16})^{(2,2,2)}(T_{17}, t) + (a''_{13})^{(1,1,1)}(T_{14}, t) \\ + (a''_{24})^{(4,4,4,4,4)}(T_{25}, t) + (a''_{28})^{(5,5,5,5,5)}(T_{29}, t) + (a''_{32})^{(6,6,6,6,6)}(T_{33}, t) \\ + (a''_{36})^{(7,7,7)}(T_{37}, t) \end{array} \right] G_{20} \quad -76 \\
 \frac{dG_{21}}{dt} &= (a_{21})^{(3)}G_{20} - \left[\begin{array}{l} (a'_{21})^{(3)} + (a''_{21})^{(3)}(T_{21}, t) + (a''_{17})^{(2,2,2)}(T_{17}, t) + (a''_{14})^{(1,1,1)}(T_{14}, t) \\ + (a''_{25})^{(4,4,4,4,4)}(T_{25}, t) + (a''_{29})^{(5,5,5,5,5)}(T_{29}, t) + (a''_{33})^{(6,6,6,6,6)}(T_{33}, t) \\ + (a''_{37})^{(7,7,7)}(T_{37}, t) \end{array} \right] G_{21} \quad -77 \\
 \frac{dG_{22}}{dt} &= (a_{22})^{(3)}G_{21} - \left[\begin{array}{l} (a'_{22})^{(3)} + (a''_{22})^{(3)}(T_{21}, t) + (a''_{18})^{(2,2,2)}(T_{17}, t) + (a''_{15})^{(1,1,1)}(T_{14}, t) \\ + (a''_{26})^{(4,4,4,4,4)}(T_{25}, t) + (a''_{30})^{(5,5,5,5,5)}(T_{29}, t) + (a''_{34})^{(6,6,6,6,6)}(T_{33}, t) \\ + (a''_{38})^{(7,7,7)}(T_{37}, t) \end{array} \right] G_{22} \quad -78
 \end{aligned}$$

$+(a''_{20})^{(3)}(T_{21}, t)$, $+(a''_{21})^{(3)}(T_{21}, t)$, $+(a''_{22})^{(3)}(T_{21}, t)$ are first augmentation coefficients for category 1, 2 and 3
 $+(a''_{16})^{(2,2,2)}(T_{17}, t)$, $+(a''_{17})^{(2,2,2)}(T_{17}, t)$, $+(a''_{18})^{(2,2,2)}(T_{17}, t)$ are second augmentation coefficients for category 1, 2 and 3
 $+(a''_{13})^{(1,1,1)}(T_{14}, t)$, $+(a''_{14})^{(1,1,1)}(T_{14}, t)$, $+(a''_{15})^{(1,1,1)}(T_{14}, t)$ are third augmentation coefficients for category 1, 2 and 3
 $+(a''_{24})^{(4,4,4,4,4)}(T_{25}, t)$, $+(a''_{25})^{(4,4,4,4,4)}(T_{25}, t)$, $+(a''_{26})^{(4,4,4,4,4)}(T_{25}, t)$ are fourth augmentation coefficients for category 1, 2 and 3
 $+(a''_{28})^{(5,5,5,5,5)}(T_{29}, t)$, $+(a''_{29})^{(5,5,5,5,5)}(T_{29}, t)$, $+(a''_{30})^{(5,5,5,5,5)}(T_{29}, t)$ are fifth augmentation coefficients for category 1, 2 and 3
 $+(a''_{32})^{(6,6,6,6,6)}(T_{33}, t)$, $+(a''_{33})^{(6,6,6,6,6)}(T_{33}, t)$, $+(a''_{34})^{(6,6,6,6,6)}(T_{33}, t)$ are sixth augmentation coefficients for category 1, 2 and 3 -79

80

$+(a''_{36})^{(7,7,7)}(T_{37}, t)$, $+(a''_{37})^{(7,7,7)}(T_{37}, t)$, $+(a''_{38})^{(7,7,7)}(T_{37}, t)$ are seventh augmentation coefficient-81

$$\begin{aligned}
 \frac{dT_{20}}{dt} &= (b_{20})^{(3)}T_{21} - \left[\begin{array}{l} (b'_{20})^{(3)} - (b''_{20})^{(3)}(G_{23}, t) - (b''_{36})^{(7,7,7)}(G_{19}, t) - (b''_{13})^{(1,1,1)}(G, t) \\ - (b''_{24})^{(4,4,4,4,4)}(G_{27}, t) - (b''_{28})^{(5,5,5,5,5)}(G_{31}, t) - (b''_{32})^{(6,6,6,6,6)}(G_{35}, t) \\ - (b''_{36})^{(7,7,7)}(G_{39}, t) \end{array} \right] T_{20} \quad -82 \\
 \frac{dT_{21}}{dt} &= (b_{21})^{(3)}T_{20} - \left[\begin{array}{l} (b'_{21})^{(3)} - (b''_{21})^{(3)}(G_{23}, t) - (b''_{17})^{(2,2,2)}(G_{19}, t) - (b''_{14})^{(1,1,1)}(G, t) \\ - (b''_{25})^{(4,4,4,4,4)}(G_{27}, t) - (b''_{29})^{(5,5,5,5,5)}(G_{31}, t) - (b''_{33})^{(6,6,6,6,6)}(G_{35}, t) \\ - (b''_{37})^{(7,7,7)}(G_{39}, t) \end{array} \right] T_{21} \quad -83 \\
 \frac{dT_{22}}{dt} &= (b_{22})^{(3)}T_{21} - \left[\begin{array}{l} (b'_{22})^{(3)} - (b''_{22})^{(3)}(G_{23}, t) - (b''_{18})^{(2,2,2)}(G_{19}, t) - (b''_{15})^{(1,1,1)}(G, t) \\ - (b''_{26})^{(4,4,4,4,4)}(G_{27}, t) - (b''_{30})^{(5,5,5,5,5)}(G_{31}, t) - (b''_{34})^{(6,6,6,6,6)}(G_{35}, t) \\ - (b''_{38})^{(7,7,7)}(G_{39}, t) \end{array} \right] T_{22} \quad -84
 \end{aligned}$$

$-(b''_{20})^{(3)}(G_{23}, t)$, $-(b''_{21})^{(3)}(G_{23}, t)$, $-(b''_{22})^{(3)}(G_{23}, t)$ are first detritions coefficients for category 1, 2 and 3
 $-(b''_{16})^{(2,2,2)}(G_{19}, t)$, $-(b''_{17})^{(2,2,2)}(G_{19}, t)$, $-(b''_{18})^{(2,2,2)}(G_{19}, t)$ are second detritions coefficients for category 1, 2 and 3
 $-(b''_{13})^{(1,1,1)}(G, t)$, $-(b''_{14})^{(1,1,1)}(G, t)$, $-(b''_{15})^{(1,1,1)}(G, t)$ are third detrition coefficients for category 1,2 and 3
 $-(b''_{24})^{(4,4,4,4,4)}(G_{27}, t)$, $-(b''_{25})^{(4,4,4,4,4)}(G_{27}, t)$, $-(b''_{26})^{(4,4,4,4,4)}(G_{27}, t)$ are fourth detritions coefficients for category 1, 2 and 3
 $-(b''_{28})^{(5,5,5,5,5)}(G_{31}, t)$, $-(b''_{29})^{(5,5,5,5,5)}(G_{31}, t)$, $-(b''_{30})^{(5,5,5,5,5)}(G_{31}, t)$ are fifth detritions coefficients for category 1, 2 and 3
 $-(b''_{32})^{(6,6,6,6,6)}(G_{35}, t)$, $-(b''_{33})^{(6,6,6,6,6)}(G_{35}, t)$, $-(b''_{34})^{(6,6,6,6,6)}(G_{35}, t)$ are sixth detritions coefficients for category 1, 2 and 3 -85
 $-(b''_{36})^{(7,7,7)}(G_{39}, t)$, $-(b''_{37})^{(7,7,7)}(G_{39}, t)$, $-(b''_{38})^{(7,7,7)}(G_{39}, t)$ are seventh detritions coefficients

FOURTH MODULE CONCATENATION:-86

$$\frac{dG_{24}}{dt} = (a_{24})^{(4)} G_{25} - \left[\begin{array}{c} (a'_{24})^{(4)} + (a''_{24})^{(4)}(T_{25}, t) \quad + (a''_{28})^{(5,5)}(T_{29}, t) \quad + (a''_{32})^{(6,6)}(T_{33}, t) \\ + (a''_{13})^{(1,1,1,1)}(T_{14}, t) \quad + (a''_{16})^{(2,2,2,2)}(T_{17}, t) \quad + (a''_{20})^{(3,3,3,3)}(T_{21}, t) \\ + (a''_{36})^{(7,7,7,7)}(T_{37}, t) \end{array} \right] G_{24} \quad -87$$

$$\frac{dG_{25}}{dt} = (a_{25})^{(4)} G_{24} - \left[\begin{array}{c} (a'_{25})^{(4)} + (a''_{25})^{(4)}(T_{25}, t) \quad + (a''_{29})^{(5,5)}(T_{29}, t) \quad + (a''_{33})^{(6,6)}(T_{33}, t) \\ + (a''_{14})^{(1,1,1,1)}(T_{14}, t) \quad + (a''_{17})^{(2,2,2,2)}(T_{17}, t) \quad + (a''_{21})^{(3,3,3,3)}(T_{21}, t) \\ + (a''_{37})^{(7,7,7,7)}(T_{37}, t) \end{array} \right] G_{25} \quad -88$$

$$\frac{dG_{26}}{dt} = (a_{26})^{(4)} G_{25} - \left[\begin{array}{c} (a'_{26})^{(4)} + (a''_{26})^{(4)}(T_{25}, t) \quad + (a''_{30})^{(5,5)}(T_{29}, t) \quad + (a''_{34})^{(6,6)}(T_{33}, t) \\ + (a''_{15})^{(1,1,1,1)}(T_{14}, t) \quad + (a''_{18})^{(2,2,2,2)}(T_{17}, t) \quad + (a''_{22})^{(3,3,3,3)}(T_{21}, t) \\ + (a''_{38})^{(7,7,7,7)}(T_{37}, t) \end{array} \right] G_{26} \quad -89$$

Where $(a'_{24})^{(4)}(T_{25}, t)$, $(a'_{25})^{(4)}(T_{25}, t)$, $(a'_{26})^{(4)}(T_{25}, t)$ are first augmentation coefficients for category 1,2 and 3
 $(a''_{28})^{(5,5)}(T_{29}, t)$, $(a''_{29})^{(5,5)}(T_{29}, t)$, $(a''_{30})^{(5,5)}(T_{29}, t)$ are second augmentation coefficient for category 1,2 and 3
 $(a''_{32})^{(6,6)}(T_{33}, t)$, $(a''_{33})^{(6,6)}(T_{33}, t)$, $(a''_{34})^{(6,6)}(T_{33}, t)$ are third augmentation coefficient for category 1,2 and 3
 $(a''_{13})^{(1,1,1,1)}(T_{14}, t)$, $(a''_{14})^{(1,1,1,1)}(T_{14}, t)$, $(a''_{15})^{(1,1,1,1)}(T_{14}, t)$ are fourth augmentation coefficients for category 1, 2, and 3
 $(a''_{16})^{(2,2,2,2)}(T_{17}, t)$, $(a''_{17})^{(2,2,2,2)}(T_{17}, t)$, $(a''_{18})^{(2,2,2,2)}(T_{17}, t)$ are fifth augmentation coefficients for category 1, 2, and 3
 $(a''_{20})^{(3,3,3,3)}(T_{21}, t)$, $(a''_{21})^{(3,3,3,3)}(T_{21}, t)$, $(a''_{22})^{(3,3,3,3)}(T_{21}, t)$ are sixth augmentation coefficients for category 1, 2, and 3
 $(a''_{36})^{(7,7,7,7)}(T_{37}, t)$, $(a''_{37})^{(7,7,7,7)}(T_{37}, t)$, $(a''_{38})^{(7,7,7,7)}(T_{37}, t)$ ARE SEVENTH augmentation coefficients

$$\frac{dT_{24}}{dt} = (b_{24})^{(4)} T_{25} - \left[\begin{array}{c} (b'_{24})^{(4)} - (b''_{24})^{(4)}(G_{27}, t) \quad - (b''_{28})^{(5,5)}(G_{31}, t) \quad - (b''_{32})^{(6,6)}(G_{35}, t) \\ - (b''_{13})^{(1,1,1,1)}(G, t) \quad - (b''_{16})^{(2,2,2,2)}(G_{19}, t) \quad - (b''_{20})^{(3,3,3,3)}(G_{23}, t) \\ - (b''_{36})^{(7,7,7,7)}(G_{39}, t) \end{array} \right] T_{24} \quad -93$$

$$\frac{dT_{25}}{dt} = (b_{25})^{(4)} T_{24} - \left[\begin{array}{c} (b'_{25})^{(4)} - (b''_{25})^{(4)}(G_{27}, t) \quad - (b''_{29})^{(5,5)}(G_{31}, t) \quad - (b''_{33})^{(6,6)}(G_{35}, t) \\ - (b''_{14})^{(1,1,1,1)}(G, t) \quad - (b''_{17})^{(2,2,2,2)}(G_{19}, t) \quad - (b''_{21})^{(3,3,3,3)}(G_{23}, t) \\ - (b''_{37})^{(7,7,7,7)}(G_{39}, t) \end{array} \right] T_{25} \quad -94$$

$$\frac{dT_{26}}{dt} = (b_{26})^{(4)} T_{25} - \left[\begin{array}{c} (b'_{26})^{(4)} - (b''_{26})^{(4)}(G_{27}, t) \quad - (b''_{30})^{(5,5)}(G_{31}, t) \quad - (b''_{34})^{(6,6)}(G_{35}, t) \\ - (b''_{15})^{(1,1,1,1)}(G, t) \quad - (b''_{18})^{(2,2,2,2)}(G_{19}, t) \quad - (b''_{22})^{(3,3,3,3)}(G_{23}, t) \\ - (b''_{38})^{(7,7,7,7)}(G_{39}, t) \end{array} \right] T_{26} \quad -95$$

Where $(b'_{24})^{(4)}(G_{27}, t)$, $(b'_{25})^{(4)}(G_{27}, t)$, $(b'_{26})^{(4)}(G_{27}, t)$ are first detrition coefficients for category 1,2 and 3
 $(b''_{28})^{(5,5)}(G_{31}, t)$, $(b''_{29})^{(5,5)}(G_{31}, t)$, $(b''_{30})^{(5,5)}(G_{31}, t)$ are second detrition coefficients for category 1,2 and 3
 $(b''_{32})^{(6,6)}(G_{35}, t)$, $(b''_{33})^{(6,6)}(G_{35}, t)$, $(b''_{34})^{(6,6)}(G_{35}, t)$ are third detrition coefficients for category 1,2 and 3
 $(b''_{13})^{(1,1,1,1)}(G, t)$, $(b''_{14})^{(1,1,1,1)}(G, t)$, $(b''_{15})^{(1,1,1,1)}(G, t)$ are fourth detrition coefficients for category 1,2 and 3
 $(b''_{16})^{(2,2,2,2)}(G_{19}, t)$, $(b''_{17})^{(2,2,2,2)}(G_{19}, t)$, $(b''_{18})^{(2,2,2,2)}(G_{19}, t)$ are fifth detrition coefficients for category 1,2 and 3
 $(b''_{20})^{(3,3,3,3)}(G_{23}, t)$, $(b''_{21})^{(3,3,3,3)}(G_{23}, t)$, $(b''_{22})^{(3,3,3,3)}(G_{23}, t)$ are sixth detrition coefficients for category 1,2 and 3
 $(b''_{36})^{(7,7,7,7)}(G_{39}, t)$, $(b''_{37})^{(7,7,7,7)}(G_{39}, t)$, $(b''_{38})^{(7,7,7,7)}(G_{39}, t)$ ARE SEVENTH DETRITION COEFFICIENTS-96-97

FIFTH MODULE CONCATENATION

$$\frac{dG_{28}}{dt} = (a_{28})^{(5)} G_{29} - \left[\begin{array}{c} (a'_{28})^{(5)} + (a''_{28})^{(5)}(T_{29}, t) \quad + (a''_{24})^{(4,4)}(T_{25}, t) \quad + (a''_{32})^{(6,6,6)}(T_{33}, t) \\ + (a''_{13})^{(1,1,1,1,1)}(T_{14}, t) \quad + (a''_{16})^{(2,2,2,2,2)}(T_{17}, t) \quad + (a''_{20})^{(3,3,3,3,3)}(T_{21}, t) \\ + (a''_{36})^{(7,7,7,7,7)}(T_{37}, t) \end{array} \right] G_{28} \quad -99$$

$$\frac{dG_{29}}{dt} = (a_{29})^{(5)} G_{28} - \left[\begin{array}{l} (a'_{29})^{(5)} + (a''_{29})^{(5)}(T_{29}, t) + (a''_{25})^{(4,4)}(T_{25}, t) + (a''_{33})^{(6,6,6)}(T_{33}, t) \\ + (a''_{14})^{(1,1,1,1,1)}(T_{14}, t) + (a''_{17})^{(2,2,2,2,2)}(T_{17}, t) + (a''_{21})^{(3,3,3,3,3)}(T_{21}, t) \\ + (a''_{37})^{(7,7,7,7,7)}(T_{37}, t) \end{array} \right] G_{29} -100$$

$$\frac{dG_{30}}{dt} = (a_{30})^{(5)} G_{29} - \left[\begin{array}{l} (a'_{30})^{(5)} + (a''_{30})^{(5)}(T_{29}, t) + (a''_{26})^{(4,4)}(T_{25}, t) + (a''_{34})^{(6,6,6)}(T_{33}, t) \\ + (a''_{15})^{(1,1,1,1,1)}(T_{14}, t) + (a''_{18})^{(2,2,2,2,2)}(T_{17}, t) + (a''_{22})^{(3,3,3,3,3)}(T_{21}, t) \\ + (a''_{38})^{(7,7,7,7,7)}(T_{37}, t) \end{array} \right] G_{30} -101$$

Where $(a'_{28})^{(5)}(T_{29}, t)$, $(a'_{29})^{(5)}(T_{29}, t)$, $(a'_{30})^{(5)}(T_{29}, t)$ are first augmentation coefficients for category 1,2 and 3
 And $(a''_{24})^{(4,4)}(T_{25}, t)$, $(a''_{25})^{(4,4)}(T_{25}, t)$, $(a''_{26})^{(4,4)}(T_{25}, t)$ are second augmentation coefficient for category 1,2 and 3
 $(a''_{32})^{(6,6,6)}(T_{33}, t)$, $(a''_{33})^{(6,6,6)}(T_{33}, t)$, $(a''_{34})^{(6,6,6)}(T_{33}, t)$ are third augmentation coefficient for category 1,2 and 3
 $(a''_{13})^{(1,1,1,1,1)}(T_{14}, t)$, $(a''_{14})^{(1,1,1,1,1)}(T_{14}, t)$, $(a''_{15})^{(1,1,1,1,1)}(T_{14}, t)$ are fourth augmentation coefficients for category 1,2, and 3
 $(a''_{16})^{(2,2,2,2,2)}(T_{17}, t)$, $(a''_{17})^{(2,2,2,2,2)}(T_{17}, t)$, $(a''_{18})^{(2,2,2,2,2)}(T_{17}, t)$ are fifth augmentation coefficients for category 1,2, and 3
 $(a''_{20})^{(3,3,3,3,3)}(T_{21}, t)$, $(a''_{21})^{(3,3,3,3,3)}(T_{21}, t)$, $(a''_{22})^{(3,3,3,3,3)}(T_{21}, t)$ are sixth augmentation coefficients for category 1,2, 3 -102
 -103

$$\frac{dT_{28}}{dt} = (b_{28})^{(5)} T_{29} - \left[\begin{array}{l} (b'_{28})^{(5)} - (b''_{28})^{(5)}(G_{31}, t) - (b''_{24})^{(4,4)}(G_{23}, t) - (b''_{32})^{(6,6,6)}(G_{35}, t) \\ - (b''_{13})^{(1,1,1,1,1)}(G, t) - (b''_{16})^{(2,2,2,2,2)}(G_{19}, t) - (b''_{20})^{(3,3,3,3,3)}(G_{23}, t) \\ - (b''_{36})^{(7,7,7,7,7)}(G_{38}, t) \end{array} \right] T_{28} -104$$

$$\frac{dT_{29}}{dt} = (b_{29})^{(5)} T_{28} - \left[\begin{array}{l} (b'_{29})^{(5)} - (b''_{29})^{(5)}(G_{31}, t) - (b''_{25})^{(4,4)}(G_{27}, t) - (b''_{33})^{(6,6,6)}(G_{35}, t) \\ - (b''_{14})^{(1,1,1,1,1)}(G, t) - (b''_{17})^{(2,2,2,2,2)}(G_{19}, t) - (b''_{21})^{(3,3,3,3,3)}(G_{23}, t) \\ - (b''_{37})^{(7,7,7,7,7)}(G_{38}, t) \end{array} \right] T_{29} -105$$

$$\frac{dT_{30}}{dt} = (b_{30})^{(5)} T_{29} - \left[\begin{array}{l} (b'_{30})^{(5)} - (b''_{30})^{(5)}(G_{31}, t) - (b''_{26})^{(4,4)}(G_{27}, t) - (b''_{34})^{(6,6,6)}(G_{35}, t) \\ - (b''_{15})^{(1,1,1,1,1)}(G, t) - (b''_{18})^{(2,2,2,2,2)}(G_{19}, t) - (b''_{22})^{(3,3,3,3,3)}(G_{23}, t) \\ - (b''_{38})^{(7,7,7,7,7)}(G_{38}, t) \end{array} \right] T_{30} -106$$

where $-(b''_{28})^{(5)}(G_{31}, t)$, $-(b''_{29})^{(5)}(G_{31}, t)$, $-(b''_{30})^{(5)}(G_{31}, t)$ are first detrition coefficients for category 1,2 and 3
 $-(b''_{24})^{(4,4)}(G_{27}, t)$, $-(b''_{25})^{(4,4)}(G_{27}, t)$, $-(b''_{26})^{(4,4)}(G_{27}, t)$ are second detrition coefficients for category 1,2 and 3
 $-(b''_{32})^{(6,6,6)}(G_{35}, t)$, $-(b''_{33})^{(6,6,6)}(G_{35}, t)$, $-(b''_{34})^{(6,6,6)}(G_{35}, t)$ are third detrition coefficients for category 1,2 and 3
 $-(b''_{13})^{(1,1,1,1,1)}(G, t)$, $-(b''_{14})^{(1,1,1,1,1)}(G, t)$, $-(b''_{15})^{(1,1,1,1,1)}(G, t)$ are fourth detrition coefficients for category 1,2, and 3
 $-(b''_{16})^{(2,2,2,2,2)}(G_{19}, t)$, $-(b''_{17})^{(2,2,2,2,2)}(G_{19}, t)$, $-(b''_{18})^{(2,2,2,2,2)}(G_{19}, t)$ are fifth detrition coefficients for category 1,2, and 3
 $-(b''_{20})^{(3,3,3,3,3)}(G_{23}, t)$, $-(b''_{21})^{(3,3,3,3,3)}(G_{23}, t)$, $-(b''_{22})^{(3,3,3,3,3)}(G_{23}, t)$ are sixth detrition coefficients for category 1,2, and 3 -107

SIXTH MODULE CONCATENATION-108

$$\frac{dG_{32}}{dt} = (a_{32})^{(6)} G_{33} - \left[\begin{array}{l} (a'_{32})^{(6)} + (a''_{32})^{(6)}(T_{33}, t) + (a''_{28})^{(5,5,5)}(T_{29}, t) + (a''_{24})^{(4,4,4)}(T_{25}, t) \\ + (a''_{13})^{(1,1,1,1,1,1)}(T_{14}, t) + (a''_{16})^{(2,2,2,2,2,2)}(T_{17}, t) + (a''_{20})^{(3,3,3,3,3,3)}(T_{21}, t) \\ + (a''_{36})^{(7,7,7,7,7,7)}(T_{37}, t) \end{array} \right] G_{32} -109$$

$$\frac{dG_{33}}{dt} = (a_{33})^{(6)} G_{32} - \left[\begin{array}{l} (a'_{33})^{(6)} + (a''_{33})^{(6)}(T_{33}, t) + (a''_{29})^{(5,5,5)}(T_{29}, t) + (a''_{25})^{(4,4,4)}(T_{25}, t) \\ + (a''_{14})^{(1,1,1,1,1,1)}(T_{14}, t) + (a''_{17})^{(2,2,2,2,2,2)}(T_{17}, t) + (a''_{21})^{(3,3,3,3,3,3)}(T_{21}, t) \\ + (a''_{37})^{(7,7,7,7,7,7)}(T_{37}, t) \end{array} \right] G_{33} -110$$

$$\frac{dG_{34}}{dt} = (a_{34})^{(6)} G_{33} - \left[\begin{array}{l} (a'_{34})^{(6)} + (a''_{34})^{(6)}(T_{33}, t) + (a''_{30})^{(5,5,5)}(T_{29}, t) + (a''_{26})^{(4,4,4)}(T_{25}, t) \\ + (a''_{15})^{(1,1,1,1,1,1)}(T_{14}, t) + (a''_{18})^{(2,2,2,2,2,2)}(T_{17}, t) + (a''_{22})^{(3,3,3,3,3,3)}(T_{21}, t) \\ + (a''_{38})^{(7,7,7,7,7,7)}(T_{37}, t) \end{array} \right] G_{34} -111$$

$(a'_{32})^{(6)}(T_{33}, t)$, $(a'_{33})^{(6)}(T_{33}, t)$, $(a'_{34})^{(6)}(T_{33}, t)$ are first augmentation coefficients for category 1,2 and 3
 $(a''_{28})^{(5,5,5)}(T_{29}, t)$, $(a''_{29})^{(5,5,5)}(T_{29}, t)$, $(a''_{30})^{(5,5,5)}(T_{29}, t)$ are second augmentation coefficients for category 1,2 and 3
 $(a''_{24})^{(4,4,4)}(T_{25}, t)$, $(a''_{25})^{(4,4,4)}(T_{25}, t)$, $(a''_{26})^{(4,4,4)}(T_{25}, t)$ are third augmentation coefficients for category 1,2 and 3
 $(a''_{13})^{(1,1,1,1,1,1)}(T_{14}, t)$, $(a''_{14})^{(1,1,1,1,1,1)}(T_{14}, t)$, $(a''_{15})^{(1,1,1,1,1,1)}(T_{14}, t)$ - are fourth augmentation coefficients
 $(a''_{16})^{(2,2,2,2,2,2)}(T_{17}, t)$, $(a''_{17})^{(2,2,2,2,2,2)}(T_{17}, t)$, $(a''_{18})^{(2,2,2,2,2,2)}(T_{17}, t)$ - fifth augmentation coefficients

$\boxed{+(a_{20}'')^{(3,3,3,3,3)}(T_{21}, t)}$, $\boxed{+(a_{21}'')^{(3,3,3,3,3)}(T_{21}, t)}$, $\boxed{+(a_{22}'')^{(3,3,3,3,3)}(T_{21}, t)}$ sixth augmentation coefficients
 $\boxed{+(a_{36}'')^{(7,7,7,7,7)}(T_{37}, t)}$, $\boxed{+(a_{36}'')^{(7,7,7,7,7)}(T_{37}, t)}$, $\boxed{+(a_{36}'')^{(7,7,7,7,7)}(T_{37}, t)}$ ARE SEVENTH AUGMENTATION COEFFICIENTS-112

-113

$$\frac{dT_{32}}{dt} = (b_{32})^{(6)}T_{33} - \left[\begin{array}{l} \boxed{(b_{32}')^{(6)} - \boxed{(b_{32}'')^{(6)}(G_{35}, t) - \boxed{(b_{28}'')^{(5,5,5)}(G_{31}, t) - \boxed{(b_{24}'')^{(4,4,4)}(G_{27}, t)} \\ \boxed{-(b_{13}'')^{(1,1,1,1,1)}(G, t) - \boxed{(b_{16}'')^{(2,2,2,2,2)}(G_{19}, t) - \boxed{(b_{20}'')^{(3,3,3,3,3)}(G_{23}, t)} \\ \boxed{-(b_{36}'')^{(7,7,7,7,7)}(G_{39}, t)} \end{array} \right] T_{32} \text{ -114}$$

$$\frac{dT_{33}}{dt} = (b_{33})^{(6)}T_{32} - \left[\begin{array}{l} \boxed{(b_{33}')^{(6)} - \boxed{(b_{33}'')^{(6)}(G_{35}, t) - \boxed{(b_{29}'')^{(5,5,5)}(G_{31}, t) - \boxed{(b_{25}'')^{(4,4,4)}(G_{27}, t)} \\ \boxed{-(b_{14}'')^{(1,1,1,1,1)}(G, t) - \boxed{(b_{17}'')^{(2,2,2,2,2)}(G_{19}, t) - \boxed{(b_{21}'')^{(3,3,3,3,3)}(G_{23}, t)} \\ \boxed{-(b_{37}'')^{(7,7,7,7,7)}(G_{39}, t)} \end{array} \right] T_{33} \text{ -115}$$

$$\frac{dT_{34}}{dt} = (b_{34})^{(6)}T_{33} - \left[\begin{array}{l} \boxed{(b_{34}')^{(6)} - \boxed{(b_{34}'')^{(6)}(G_{35}, t) - \boxed{(b_{30}'')^{(5,5,5)}(G_{31}, t) - \boxed{(b_{26}'')^{(4,4,4)}(G_{27}, t)} \\ \boxed{-(b_{15}'')^{(1,1,1,1,1)}(G, t) - \boxed{(b_{18}'')^{(2,2,2,2,2)}(G_{19}, t) - \boxed{(b_{22}'')^{(3,3,3,3,3)}(G_{23}, t)} \\ \boxed{-(b_{38}'')^{(7,7,7,7,7)}(G_{39}, t)} \end{array} \right] T_{34} \text{ -116}$$

$\boxed{-(b_{32}'')^{(6)}(G_{35}, t)}$, $\boxed{-(b_{33}'')^{(6)}(G_{35}, t)}$, $\boxed{-(b_{34}'')^{(6)}(G_{35}, t)}$ are first detrition coefficients for category 1, 2 and 3
 $\boxed{-(b_{28}'')^{(5,5,5)}(G_{31}, t)}$, $\boxed{-(b_{29}'')^{(5,5,5)}(G_{31}, t)}$, $\boxed{-(b_{30}'')^{(5,5,5)}(G_{31}, t)}$ are second detrition coefficients for category 1, 2 and 3
 $\boxed{-(b_{24}'')^{(4,4,4)}(G_{27}, t)}$, $\boxed{-(b_{25}'')^{(4,4,4)}(G_{27}, t)}$, $\boxed{-(b_{26}'')^{(4,4,4)}(G_{27}, t)}$ are third detrition coefficients for category 1, 2 and 3
 $\boxed{-(b_{13}'')^{(1,1,1,1,1)}(G, t)}$, $\boxed{-(b_{14}'')^{(1,1,1,1,1)}(G, t)}$, $\boxed{-(b_{15}'')^{(1,1,1,1,1)}(G, t)}$ are fourth detrition coefficients for category 1, 2, and 3
 $\boxed{-(b_{16}'')^{(2,2,2,2,2)}(G_{19}, t)}$, $\boxed{-(b_{17}'')^{(2,2,2,2,2)}(G_{19}, t)}$, $\boxed{-(b_{18}'')^{(2,2,2,2,2)}(G_{19}, t)}$ are fifth detrition coefficients for category 1, 2, and 3
 $\boxed{-(b_{20}'')^{(3,3,3,3,3)}(G_{23}, t)}$, $\boxed{-(b_{21}'')^{(3,3,3,3,3)}(G_{23}, t)}$, $\boxed{-(b_{22}'')^{(3,3,3,3,3)}(G_{23}, t)}$ are sixth detrition coefficients for category 1, 2, and 3
 $\boxed{-(b_{36}'')^{(7,7,7,7,7)}(G_{39}, t)}$, $\boxed{-(b_{36}'')^{(7,7,7,7,7)}(G_{39}, t)}$, $\boxed{-(b_{36}'')^{(7,7,7,7,7)}(G_{39}, t)}$ ARE SEVENTH DETRITION COEFFICIENTS-117

-118

SEVENTH MODULE CONCATENATION:-119

$$\frac{dG_{36}}{dt} = (a_{36})^{(7)}G_{37} - \left[\boxed{(a_{36}')^{(7)}} + \boxed{(a_{36}'')^{(7)}(T_{37}, t)} + \boxed{(a_{16}'')^{(7)}(T_{17}, t)} + \boxed{(a_{20}'')^{(7)}(T_{21}, t)} + \boxed{(a_{24}'')^{(7)}(T_{23}, t)}G_{36} + a_{28}''7T_{29,t} + a_{32}''7T_{33,t} + a_{13}''7T_{14,t} \right] G_{36-120}$$

121

$$\frac{dG_{37}}{dt} = (a_{37})^{(7)}G_{36} - \left[\boxed{(a_{37}')^{(7)}} + \boxed{(a_{37}'')^{(7)}(T_{37}, t)} + \boxed{(a_{14}'')^{(7)}(T_{14}, t)} + \boxed{(a_{21}'')^{(7)}(T_{21}, t)} + \boxed{(a_{17}'')^{(7)}(T_{17}, t)} + a_{25}''7T_{25,t} + a_{33}''7T_{33,t} + a_{29}''7T_{29,t} \right] G_{37}$$

-122

$$\frac{dG_{38}}{dt} = (a_{38})^{(7)}G_{37} - \left[\boxed{(a_{38}')^{(7)}} + \boxed{(a_{38}'')^{(7)}(T_{37}, t)} + \boxed{(a_{15}'')^{(7)}(T_{14}, t)} + \boxed{(a_{22}'')^{(7)}(T_{21}, t)} + \boxed{(a_{18}'')^{(7)}(T_{17}, t)} + a_{26}''7T_{25,t} + a_{34}''7T_{33,t} + a_{30}''7T_{29,t} \right] G_{38}$$

-123
124

125

$$\frac{dT_{36}}{dt} = \left[\boxed{(b_{36}')^{(7)}} - \boxed{(b_{36}'')^{(7)}(G_{39}, t)} - \boxed{(b_{16}'')^{(7)}(G_{19}, t)} - \boxed{(b_{13}'')^{(7)}(G_{14}, t)} - \boxed{(b_{20}'')^{(7)}(G_{231}, t)} - b_{24}''7G_{27,t} - b_{28}''7G_{31,t} - b_{32}''7G_{35,t} \right] T_{36}$$

-126

$$\frac{dT_{37}}{dt} = (b_{37})^{(7)}T_{36} - \left[\boxed{(b_{36}'')^{(7)}(G_{39}, t)} - \boxed{(b_{17}'')^{(7)}(G_{19}, t)} - \boxed{(b_{19}'')^{(7)}(G_{14}, t)} - \boxed{(b_{21}'')^{(7)}(G_{231}, t)} - \boxed{(b_{25}'')^{(7)}(G_{27}, t)} - \boxed{(b_{29}'')^{(7)}(G_{31}, t)} - \boxed{(b_{33}'')^{(7)}(G_{35}, t)} \right] T_{37}$$

-127

Where we suppose

(A) $(a_i)^{(1)}, (a'_i)^{(1)}, (a''_i)^{(1)}, (b_i)^{(1)}, (b'_i)^{(1)}, (b''_i)^{(1)} > 0,$
 $i, j = 13, 14, 15$

(B) The functions $(a''_i)^{(1)}, (b''_i)^{(1)}$ are positive continuous increasing and bounded.

Definition of $(p_i)^{(1)}, (r_i)^{(1)}$:

$$(a''_i)^{(1)}(T_{14}, t) \leq (p_i)^{(1)} \leq (\hat{A}_{13})^{(1)}$$

$$(b''_i)^{(1)}(G, t) \leq (r_i)^{(1)} \leq (b'_i)^{(1)} \leq (\hat{B}_{13})^{(1)}$$

(C) $\lim_{T_2 \rightarrow \infty} (a''_i)^{(1)}(T_{14}, t) = (p_i)^{(1)}$
 $\lim_{G \rightarrow \infty} (b''_i)^{(1)}(G, t) = (r_i)^{(1)}$

Definition of $(\hat{A}_{13})^{(1)}, (\hat{B}_{13})^{(1)}$:

Where $(\hat{A}_{13})^{(1)}, (\hat{B}_{13})^{(1)}, (p_i)^{(1)}, (r_i)^{(1)}$ are positive constants
 and $i = 13, 14, 15$

They satisfy Lipschitz condition:

$$|(a''_i)^{(1)}(T'_{14}, t) - (a''_i)^{(1)}(T_{14}, t)| \leq (\hat{k}_{13})^{(1)} |T'_{14} - T_{14}| e^{-(\hat{M}_{13})^{(1)}t}$$

$$|(b''_i)^{(1)}(G', t) - (b''_i)^{(1)}(G, T)| < (\hat{k}_{13})^{(1)} ||G - G'| e^{-(\hat{M}_{13})^{(1)}t}$$

With the Lipschitz condition, we place a restriction on the behavior of functions $(a''_i)^{(1)}(T'_{14}, t)$ and $(a''_i)^{(1)}(T_{14}, t)$. (T'_{14}, t) and (T_{14}, t) are points belonging to the interval $[(\hat{k}_{13})^{(1)}, (\hat{M}_{13})^{(1)}]$. It is to be noted that $(a''_i)^{(1)}(T_{14}, t)$ is uniformly continuous. In the eventuality of the fact, that if $(\hat{M}_{13})^{(1)} = 1$ then the function $(a''_i)^{(1)}(T_{14}, t)$, the **first augmentation coefficient** attributable to terrestrial organisms, would be absolutely continuous.

Definition of $(\hat{M}_{13})^{(1)}, (\hat{k}_{13})^{(1)}$:

(D) $(\hat{M}_{13})^{(1)}, (\hat{k}_{13})^{(1)}$, are positive constants

$$\frac{(a_i)^{(1)}}{(\hat{M}_{13})^{(1)}}, \frac{(b_i)^{(1)}}{(\hat{M}_{13})^{(1)}} < 1$$

Definition of $(\hat{P}_{13})^{(1)}, (\hat{Q}_{13})^{(1)}$:

(E) There exists two constants $(\hat{P}_{13})^{(1)}$ and $(\hat{Q}_{13})^{(1)}$ which together with $(\hat{M}_{13})^{(1)}, (\hat{k}_{13})^{(1)}, (\hat{A}_{13})^{(1)}$ and $(\hat{B}_{13})^{(1)}$ and the constants $(a_i)^{(1)}, (a'_i)^{(1)}, (b_i)^{(1)}, (b'_i)^{(1)}, (p_i)^{(1)}, (r_i)^{(1)}, i = 13, 14, 15,$ satisfy the inequalities

$$\frac{1}{(\hat{M}_{13})^{(1)}} [(a_i)^{(1)} + (a'_i)^{(1)} + (\hat{A}_{13})^{(1)} + (\hat{P}_{13})^{(1)} (\hat{k}_{13})^{(1)}] < 1$$

$$\frac{1}{(\hat{M}_{13})^{(1)}} [(b_i)^{(1)} + (b'_i)^{(1)} + (\hat{B}_{13})^{(1)} + (\hat{Q}_{13})^{(1)} (\hat{k}_{13})^{(1)}] < 1$$

$\frac{dT_{38}}{dt} = (b_{38})^{(7)}T_{37} - [(b'_{38})^{(7)} - \boxed{(b''_{38})^{(7)}((G_{39}, t))} - \boxed{(b''_{18})^{(7)}((G_{19}, t))} - \boxed{(b''_{20})^{(7)}((G_{14}, t))}] -$	128
$b_{22}''7G_{23}, t - b_{26}''7G_{27}, t - b_{30}''7G_{31}, t - b_{34}''7G_{35}, t$	129
T_{38}	130
	131
	132

$+(a''_{36})^{(7)}(T_{37}, t) =$ **First augmentation factor** 134

$(1)(a_i)^{(2)}, (a'_i)^{(2)}, (a''_i)^{(2)}, (b_i)^{(2)}, (b'_i)^{(2)}, (b''_i)^{(2)} > 0, i, j = 16, 17, 18$ 135

(F) (2) The functions $(a''_i)^{(2)}, (b''_i)^{(2)}$ are positive continuous increasing and bounded. 136

Definition of $(p_i)^{(2)}, (r_i)^{(2)}$:	137
$(a_i'')^{(2)}(T_{17}, t) \leq (p_i)^{(2)} \leq (\hat{A}_{16})^{(2)}$	138
$(b_i'')^{(2)}(G_{19}, t) \leq (r_i)^{(2)} \leq (b_i')^{(2)} \leq (\hat{B}_{16})^{(2)}$	139
(G) (3) $\lim_{T_2 \rightarrow \infty} (a_i'')^{(2)}(T_{17}, t) = (p_i)^{(2)}$	140
$\lim_{G \rightarrow \infty} (b_i'')^{(2)}(G_{19}, t) = (r_i)^{(2)}$	141
Definition of $(\hat{A}_{16})^{(2)}, (\hat{B}_{16})^{(2)}$:	142
Where $(\hat{A}_{16})^{(2)}, (\hat{B}_{16})^{(2)}, (p_i)^{(2)}, (r_i)^{(2)}$ are positive constants and $i = 16, 17, 18$	
They satisfy Lipschitz condition:	143
$ (a_i'')^{(2)}(T_{17}', t) - (a_i'')^{(2)}(T_{17}, t) \leq (\hat{k}_{16})^{(2)} T_{17}' - T_{17} e^{-(\hat{M}_{16})^{(2)}t}$	144
$ (b_i'')^{(2)}((G_{19})', t) - (b_i'')^{(2)}((G_{19}), t) < (\hat{k}_{16})^{(2)} (G_{19})' - (G_{19}) e^{-(\hat{M}_{16})^{(2)}t}$	145
With the Lipschitz condition, we place a restriction on the behavior of functions $(a_i'')^{(2)}(T_{17}', t)$ and $(a_i'')^{(2)}(T_{17}, t)$. (T_{17}', t) and (T_{17}, t) are points belonging to the interval $[(\hat{k}_{16})^{(2)}, (\hat{M}_{16})^{(2)}]$. It is to be noted that $(a_i'')^{(2)}(T_{17}, t)$ is uniformly continuous. In the eventuality of the fact, that if $(\hat{M}_{16})^{(2)} = 1$ then the function $(a_i'')^{(2)}(T_{17}, t)$, the SECOND augmentation coefficient would be absolutely continuous.	146
Definition of $(\hat{M}_{16})^{(2)}, (\hat{k}_{16})^{(2)}$:	147
(H) (4) $(\hat{M}_{16})^{(2)}, (\hat{k}_{16})^{(2)}$, are positive constants	148
$\frac{(a_i)^{(2)}}{(\hat{M}_{16})^{(2)}}, \frac{(b_i)^{(2)}}{(\hat{M}_{16})^{(2)}} < 1$	
Definition of $(\hat{P}_{16})^{(2)}, (\hat{Q}_{16})^{(2)}$:	149
There exists two constants $(\hat{P}_{16})^{(2)}$ and $(\hat{Q}_{16})^{(2)}$ which together with $(\hat{M}_{16})^{(2)}, (\hat{k}_{16})^{(2)}, (\hat{A}_{16})^{(2)}$ and $(\hat{B}_{16})^{(2)}$ and the constants $(a_i)^{(2)}, (a_i')^{(2)}, (b_i)^{(2)}, (b_i')^{(2)}, (p_i)^{(2)}, (r_i)^{(2)}, i = 16, 17, 18$, satisfy the inequalities	
$\frac{1}{(\hat{M}_{16})^{(2)}} [(a_i)^{(2)} + (a_i')^{(2)} + (\hat{A}_{16})^{(2)} + (\hat{P}_{16})^{(2)} (\hat{k}_{16})^{(2)}] < 1$	150
$\frac{1}{(\hat{M}_{16})^{(2)}} [(b_i)^{(2)} + (b_i')^{(2)} + (\hat{B}_{16})^{(2)} + (\hat{Q}_{16})^{(2)} (\hat{k}_{16})^{(2)}] < 1$	151
Where we suppose	152
(I) (5) $(a_i)^{(3)}, (a_i')^{(3)}, (a_i'')^{(3)}, (b_i)^{(3)}, (b_i')^{(3)}, (b_i'')^{(3)} > 0, i, j = 20, 21, 22$	153
The functions $(a_i'')^{(3)}, (b_i'')^{(3)}$ are positive continuous increasing and bounded.	
Definition of $(p_i)^{(3)}, (r_i)^{(3)}$:	
$(a_i'')^{(3)}(T_{21}, t) \leq (p_i)^{(3)} \leq (\hat{A}_{20})^{(3)}$	
$(b_i'')^{(3)}(G_{23}, t) \leq (r_i)^{(3)} \leq (b_i')^{(3)} \leq (\hat{B}_{20})^{(3)}$	
$\lim_{T_2 \rightarrow \infty} (a_i'')^{(3)}(T_{21}, t) = (p_i)^{(3)}$	154
$\lim_{G \rightarrow \infty} (b_i'')^{(3)}(G_{23}, t) = (r_i)^{(3)}$	155
Definition of $(\hat{A}_{20})^{(3)}, (\hat{B}_{20})^{(3)}$:	156
Where $(\hat{A}_{20})^{(3)}, (\hat{B}_{20})^{(3)}, (p_i)^{(3)}, (r_i)^{(3)}$ are positive constants and $i = 20, 21, 22$	
They satisfy Lipschitz condition:	157
$ (a_i'')^{(3)}(T_{21}', t) - (a_i'')^{(3)}(T_{21}, t) \leq (\hat{k}_{20})^{(3)} T_{21}' - T_{21} e^{-(\hat{M}_{20})^{(3)}t}$	158
$ (b_i'')^{(3)}(G_{23}', t) - (b_i'')^{(3)}(G_{23}, t) < (\hat{k}_{20})^{(3)} G_{23}' - G_{23} e^{-(\hat{M}_{20})^{(3)}t}$	159
With the Lipschitz condition, we place a restriction on the behavior of functions $(a_i'')^{(3)}(T_{21}', t)$ and $(a_i'')^{(3)}(T_{21}, t)$. (T_{21}', t) and (T_{21}, t) are points belonging to the interval $[(\hat{k}_{20})^{(3)}, (\hat{M}_{20})^{(3)}]$. It is to be noted that $(a_i'')^{(3)}(T_{21}, t)$ is uniformly continuous. In the eventuality of the fact, that if $(\hat{M}_{20})^{(3)} = 1$ then the function $(a_i'')^{(3)}(T_{21}, t)$, the THIRD augmentation coefficient, would be absolutely continuous.	160
Definition of $(\hat{M}_{20})^{(3)}, (\hat{k}_{20})^{(3)}$:	161
(J) (6) $(\hat{M}_{20})^{(3)}, (\hat{k}_{20})^{(3)}$, are positive constants	
$\frac{(a_i)^{(3)}}{(\hat{M}_{20})^{(3)}}, \frac{(b_i)^{(3)}}{(\hat{M}_{20})^{(3)}} < 1$	
There exists two constants $(\hat{P}_{20})^{(3)}$ and $(\hat{Q}_{20})^{(3)}$ which together with $(\hat{M}_{20})^{(3)}, (\hat{k}_{20})^{(3)}, (\hat{A}_{20})^{(3)}$ and $(\hat{B}_{20})^{(3)}$ and the constants $(a_i)^{(3)}, (a_i')^{(3)}, (b_i)^{(3)}, (b_i')^{(3)}, (p_i)^{(3)}, (r_i)^{(3)}, i = 20, 21, 22$, satisfy the inequalities	162
$\frac{1}{(\hat{M}_{20})^{(3)}} [(a_i)^{(3)} + (a_i')^{(3)} + (\hat{A}_{20})^{(3)} + (\hat{P}_{20})^{(3)} (\hat{k}_{20})^{(3)}] < 1$	163
$\frac{1}{(\hat{M}_{20})^{(3)}} [(b_i)^{(3)} + (b_i')^{(3)} + (\hat{B}_{20})^{(3)} + (\hat{Q}_{20})^{(3)} (\hat{k}_{20})^{(3)}] < 1$	164
Where we suppose	165
(K) $(a_i)^{(4)}, (a_i')^{(4)}, (a_i'')^{(4)}, (b_i)^{(4)}, (b_i')^{(4)}, (b_i'')^{(4)} > 0, i, j = 24, 25, 26$	166
	167
	168
	169

(L) (7) The functions $(a_i'')^{(4)}, (b_i'')^{(4)}$ are positive continuous increasing and bounded.

Definition of $(p_i)^{(4)}, (r_i)^{(4)}$:

$$\begin{aligned} (a_i'')^{(4)}(T_{25}, t) &\leq (p_i)^{(4)} \leq (\hat{A}_{24})^{(4)} \\ (b_i'')^{(4)}((G_{27}), t) &\leq (r_i)^{(4)} \leq (b_i')^{(4)} \leq (\hat{B}_{24})^{(4)} \end{aligned}$$

170

(M) (8) $\lim_{T_2 \rightarrow \infty} (a_i'')^{(4)}(T_{25}, t) = (p_i)^{(4)}$

$$\lim_{G \rightarrow \infty} (b_i'')^{(4)}((G_{27}), t) = (r_i)^{(4)}$$

Definition of $(\hat{A}_{24})^{(4)}, (\hat{B}_{24})^{(4)}$:

Where $(\hat{A}_{24})^{(4)}, (\hat{B}_{24})^{(4)}, (p_i)^{(4)}, (r_i)^{(4)}$ are positive constants and $i = 24, 25, 26$

171

They satisfy Lipschitz condition:

$$\begin{aligned} |(a_i'')^{(4)}(T_{25}, t) - (a_i'')^{(4)}(T_{25}, t)| &\leq (\hat{k}_{24})^{(4)} |T_{25} - T_{25}'| e^{-(\hat{M}_{24})^{(4)}t} \\ |(b_i'')^{(4)}((G_{27}), t) - (b_i'')^{(4)}((G_{27}), t)| &\leq (\hat{k}_{24})^{(4)} |(G_{27}) - (G_{27})'| e^{-(\hat{M}_{24})^{(4)}t} \end{aligned}$$

With the Lipschitz condition, we place a restriction on the behavior of functions $(a_i'')^{(4)}(T_{25}', t)$ and $(a_i'')^{(4)}(T_{25}, t)$

172

(T_{25}', t) and (T_{25}, t) are points belonging to the interval $[(\hat{k}_{24})^{(4)}, (\hat{M}_{24})^{(4)}]$. It is to be noted that

$(a_i'')^{(4)}(T_{25}, t)$ is uniformly continuous. In the eventuality of the fact, that if $(\hat{M}_{24})^{(4)} = 4$ then the function

173

$(a_i'')^{(4)}(T_{25}, t)$, the **FOURTH augmentation coefficient WOULD** be absolutely continuous.

Definition of $(\hat{M}_{24})^{(4)}, (\hat{k}_{24})^{(4)}$:

174

(N) $(\hat{M}_{24})^{(4)}, (\hat{k}_{24})^{(4)}$, are positive constants

(O)

$$\frac{(a_i)^{(4)}}{(\hat{M}_{24})^{(4)}} + \frac{(b_i)^{(4)}}{(\hat{M}_{24})^{(4)}} < 1$$

Definition of $(\hat{P}_{24})^{(4)}, (\hat{Q}_{24})^{(4)}$:

175

(P) (9) There exists two constants $(\hat{P}_{24})^{(4)}$ and $(\hat{Q}_{24})^{(4)}$ which together with

$(\hat{M}_{24})^{(4)}, (\hat{k}_{24})^{(4)}, (\hat{A}_{24})^{(4)}$ and $(\hat{B}_{24})^{(4)}$ and the constants $(a_i)^{(4)}, (a_i')^{(4)}, (b_i)^{(4)}, (b_i')^{(4)}, (p_i)^{(4)}, (r_i)^{(4)}, i = 24, 25, 26$,

satisfy the inequalities

$$\frac{1}{(\hat{M}_{24})^{(4)}} [(a_i)^{(4)} + (a_i')^{(4)} + (\hat{A}_{24})^{(4)} + (\hat{P}_{24})^{(4)} (\hat{k}_{24})^{(4)}] < 1$$

$$\frac{1}{(\hat{M}_{24})^{(4)}} [(b_i)^{(4)} + (b_i')^{(4)} + (\hat{B}_{24})^{(4)} + (\hat{Q}_{24})^{(4)} (\hat{k}_{24})^{(4)}] < 1$$

Where we suppose

176

(Q) $(a_i)^{(5)}, (a_i')^{(5)}, (a_i'')^{(5)}, (b_i)^{(5)}, (b_i')^{(5)}, (b_i'')^{(5)} > 0, i, j = 28, 29, 30$

177

(R) (10) The functions $(a_i'')^{(5)}, (b_i'')^{(5)}$ are positive continuous increasing and bounded.

Definition of $(p_i)^{(5)}, (r_i)^{(5)}$:

$$\begin{aligned} (a_i'')^{(5)}(T_{29}, t) &\leq (p_i)^{(5)} \leq (\hat{A}_{28})^{(5)} \\ (b_i'')^{(5)}((G_{31}), t) &\leq (r_i)^{(5)} \leq (b_i')^{(5)} \leq (\hat{B}_{28})^{(5)} \end{aligned}$$

178

(S) (11) $\lim_{T_2 \rightarrow \infty} (a_i'')^{(5)}(T_{29}, t) = (p_i)^{(5)}$

$$\lim_{G \rightarrow \infty} (b_i'')^{(5)}(G_{31}, t) = (r_i)^{(5)}$$

Definition of $(\hat{A}_{28})^{(5)}, (\hat{B}_{28})^{(5)}$:

Where $(\hat{A}_{28})^{(5)}, (\hat{B}_{28})^{(5)}, (p_i)^{(5)}, (r_i)^{(5)}$ are positive constants and $i = 28, 29, 30$

179

They satisfy Lipschitz condition:

$$\begin{aligned} |(a_i'')^{(5)}(T_{29}', t) - (a_i'')^{(5)}(T_{29}, t)| &\leq (\hat{k}_{28})^{(5)} |T_{29} - T_{29}'| e^{-(\hat{M}_{28})^{(5)}t} \\ |(b_i'')^{(5)}((G_{31}), t) - (b_i'')^{(5)}((G_{31}), t)| &\leq (\hat{k}_{28})^{(5)} |(G_{31}) - (G_{31})'| e^{-(\hat{M}_{28})^{(5)}t} \end{aligned}$$

With the Lipschitz condition, we place a restriction on the behavior of functions $(a_i'')^{(5)}(T_{29}', t)$ and $(a_i'')^{(5)}(T_{29}, t)$

180

(T_{29}', t) and (T_{29}, t) are points belonging to the interval $[(\hat{k}_{28})^{(5)}, (\hat{M}_{28})^{(5)}]$. It is to be noted that

$(a_i'')^{(5)}(T_{29}, t)$ is uniformly continuous. In the eventuality of the fact, that if $(\hat{M}_{28})^{(5)} = 5$ then the function

$(a_i'')^{(5)}(T_{29}, t)$, the **FIFTH augmentation coefficient** attributable would be absolutely continuous.

181

Definition of $(\hat{M}_{28})^{(5)}, (\hat{k}_{28})^{(5)}$:

(T) $(\hat{M}_{28})^{(5)}, (\hat{k}_{28})^{(5)}$, are positive constants

$$\frac{(a_i)^{(5)}}{(\hat{M}_{28})^{(5)}} + \frac{(b_i)^{(5)}}{(\hat{M}_{28})^{(5)}} < 1$$

Definition of $(\hat{P}_{28})^{(5)}, (\hat{Q}_{28})^{(5)}$:

182

(U) There exists two constants $(\hat{P}_{28})^{(5)}$ and $(\hat{Q}_{28})^{(5)}$ which together with

$(\hat{M}_{28})^{(5)}, (\hat{k}_{28})^{(5)}, (\hat{A}_{28})^{(5)}$ and $(\hat{B}_{28})^{(5)}$ and the constants $(a_i)^{(5)}, (a_i')^{(5)}, (b_i)^{(5)}, (b_i')^{(5)}, (p_i)^{(5)}, (r_i)^{(5)}, i =$

28,29,30, satisfy the inequalities

$$\frac{1}{(\hat{M}_{28})^{(5)}} [(a_i)^{(5)} + (a'_i)^{(5)} + (\hat{A}_{28})^{(5)} + (\hat{P}_{28})^{(5)} (\hat{k}_{28})^{(5)}] < 1$$

$$\frac{1}{(\hat{M}_{28})^{(5)}} [(b_i)^{(5)} + (b'_i)^{(5)} + (\hat{B}_{28})^{(5)} + (\hat{Q}_{28})^{(5)} (\hat{k}_{28})^{(5)}] < 1$$

Where we suppose

$$(a_i)^{(6)}, (a'_i)^{(6)}, (a''_i)^{(6)}, (b_i)^{(6)}, (b'_i)^{(6)}, (b''_i)^{(6)} > 0, \quad i, j = 32, 33, 34$$

(12) The functions $(a''_i)^{(6)}, (b''_i)^{(6)}$ are positive continuous increasing and bounded.

Definition of $(p_i)^{(6)}, (r_i)^{(6)}$:

$$(a''_i)^{(6)}(T_{33}, t) \leq (p_i)^{(6)} \leq (\hat{A}_{32})^{(6)}$$

$$(b''_i)^{(6)}((G_{35}), t) \leq (r_i)^{(6)} \leq (b'_i)^{(6)} \leq (\hat{B}_{32})^{(6)}$$

$$(13) \lim_{T_2 \rightarrow \infty} (a''_i)^{(6)}(T_{33}, t) = (p_i)^{(6)}$$

$$\lim_{G \rightarrow \infty} (b''_i)^{(6)}((G_{35}), t) = (r_i)^{(6)}$$

Definition of $(\hat{A}_{32})^{(6)}, (\hat{B}_{32})^{(6)}$:

Where $(\hat{A}_{32})^{(6)}, (\hat{B}_{32})^{(6)}, (p_i)^{(6)}, (r_i)^{(6)}$ are positive constants and $i = 32, 33, 34$

They satisfy Lipschitz condition:

$$|(a''_i)^{(6)}(T'_{33}, t) - (a''_i)^{(6)}(T_{33}, t)| \leq (\hat{k}_{32})^{(6)} |T'_{33} - T_{33}| e^{-(\hat{M}_{32})^{(6)}t}$$

$$|(b''_i)^{(6)}((G'_{35}), t) - (b''_i)^{(6)}((G_{35}), t)| < (\hat{k}_{32})^{(6)} ||G'_{35} - G_{35}'|| e^{-(\hat{M}_{32})^{(6)}t}$$

With the Lipschitz condition, we place a restriction on the behavior of functions $(a''_i)^{(6)}(T'_{33}, t)$ and $(a''_i)^{(6)}(T_{33}, t)$

(T'_{33}, t) and (T_{33}, t) are points belonging to the interval $[(\hat{k}_{32})^{(6)}, (\hat{M}_{32})^{(6)}]$. It is to be noted that

$(a''_i)^{(6)}(T_{33}, t)$ is uniformly continuous. In the eventuality of the fact, that if $(\hat{M}_{32})^{(6)} = 6$ then the function

$(a''_i)^{(6)}(T_{33}, t)$, the SIXTH **augmentation coefficient** would be absolutely continuous.

Definition of $(\hat{M}_{32})^{(6)}, (\hat{k}_{32})^{(6)}$:

$(\hat{M}_{32})^{(6)}, (\hat{k}_{32})^{(6)}$, are positive constants

$$\frac{(a_i)^{(6)}}{(\hat{M}_{32})^{(6)}}, \frac{(b_i)^{(6)}}{(\hat{M}_{32})^{(6)}} < 1$$

Definition of $(\hat{P}_{32})^{(6)}, (\hat{Q}_{32})^{(6)}$:

There exists two constants $(\hat{P}_{32})^{(6)}$ and $(\hat{Q}_{32})^{(6)}$ which together with $(\hat{M}_{32})^{(6)}, (\hat{k}_{32})^{(6)}, (\hat{A}_{32})^{(6)}$ and $(\hat{B}_{32})^{(6)}$

and the constants $(a_i)^{(6)}, (a'_i)^{(6)}, (b_i)^{(6)}, (b'_i)^{(6)}, (p_i)^{(6)}, (r_i)^{(6)}, i = 32, 33, 34$,

satisfy the inequalities

$$\frac{1}{(\hat{M}_{32})^{(6)}} [(a_i)^{(6)} + (a'_i)^{(6)} + (\hat{A}_{32})^{(6)} + (\hat{P}_{32})^{(6)} (\hat{k}_{32})^{(6)}] < 1$$

$$\frac{1}{(\hat{M}_{32})^{(6)}} [(b_i)^{(6)} + (b'_i)^{(6)} + (\hat{B}_{32})^{(6)} + (\hat{Q}_{32})^{(6)} (\hat{k}_{32})^{(6)}] < 1$$

Theorem 1: if the conditions IN THE FOREGOING above are fulfilled, there exists a solution satisfying the conditions

Definition of $G_i(0), T_i(0)$:

$$G_i(t) \leq (\hat{P}_{13})^{(1)} e^{(\hat{M}_{13})^{(1)}t}, \quad G_i(0) = G_i^0 > 0$$

$$T_i(t) \leq (\hat{Q}_{13})^{(1)} e^{(\hat{M}_{13})^{(1)}t}, \quad T_i(0) = T_i^0 > 0$$

Definition of $G_i(0), T_i(0)$

$$G_i(t) \leq (\hat{P}_{16})^{(2)} e^{(\hat{M}_{16})^{(2)}t}, \quad G_i(0) = G_i^0 > 0$$

$$T_i(t) \leq (\hat{Q}_{16})^{(2)} e^{(\hat{M}_{16})^{(2)}t}, \quad T_i(0) = T_i^0 > 0$$

$$G_i(t) \leq (\hat{P}_{20})^{(3)} e^{(\hat{M}_{20})^{(3)}t}, \quad G_i(0) = G_i^0 > 0$$

$$T_i(t) \leq (\hat{Q}_{20})^{(3)} e^{(\hat{M}_{20})^{(3)}t}, \quad T_i(0) = T_i^0 > 0$$

Definition of $G_i(0), T_i(0)$:

$$G_i(t) \leq (\hat{P}_{24})^{(4)} e^{(\hat{M}_{24})^{(4)}t}, \quad G_i(0) = G_i^0 > 0$$

$$T_i(t) \leq (\hat{Q}_{24})^{(4)} e^{(\hat{M}_{24})^{(4)}t}, \quad T_i(0) = T_i^0 > 0$$

Definition of $G_i(0), T_i(0)$:

$$G_i(t) \leq (\hat{P}_{28})^{(5)} e^{(\mathcal{M}_{28})^{(5)}t}, \quad \boxed{G_i(0) = G_i^0 > 0}$$

$$T_i(t) \leq (\hat{Q}_{28})^{(5)} e^{(\mathcal{M}_{28})^{(5)}t}, \quad \boxed{T_i(0) = T_i^0 > 0}$$

198
199

Definition of $G_i(0), T_i(0)$:

$$G_i(t) \leq (\hat{P}_{32})^{(6)} e^{(\mathcal{M}_{32})^{(6)}t}, \quad \boxed{G_i(0) = G_i^0 > 0}$$

$$T_i(t) \leq (\hat{Q}_{32})^{(6)} e^{(\mathcal{M}_{32})^{(6)}t}, \quad \boxed{T_i(0) = T_i^0 > 0}$$

=====

Definition of $G_i(0), T_i(0)$:

$$G_i(t) \leq (\hat{P}_{36})^{(7)} e^{(\mathcal{M}_{36})^{(7)}t}, \quad \boxed{G_i(0) = G_i^0 > 0}$$

$$T_i(t) \leq (\hat{Q}_{36})^{(7)} e^{(\mathcal{M}_{36})^{(7)}t}, \quad \boxed{T_i(0) = T_i^0 > 0}$$

Proof: Consider operator $\mathcal{A}^{(1)}$ defined on the space of sextuples of continuous functions $G_i, T_i: \mathbb{R}_+ \rightarrow \mathbb{R}_+$ which satisfy 200

$$G_i(0) = G_i^0, T_i(0) = T_i^0, G_i^0 \leq (\hat{P}_{13})^{(1)}, T_i^0 \leq (\hat{Q}_{13})^{(1)}, \quad 201$$

$$0 \leq G_i(t) - G_i^0 \leq (\hat{P}_{13})^{(1)} e^{(\mathcal{M}_{13})^{(1)}t} \quad 202$$

$$0 \leq T_i(t) - T_i^0 \leq (\hat{Q}_{13})^{(1)} e^{(\mathcal{M}_{13})^{(1)}t} \quad 203$$

By 204

$$\bar{G}_{13}(t) = G_{13}^0 + \int_0^t \left[(a_{13})^{(1)} G_{14}(s_{(13)}) - \left((a'_{13})^{(1)} + a''_{13}(s_{(13)}, s_{(13)}) \right) G_{13}(s_{(13)}) \right] ds_{(13)}$$

$$\bar{G}_{14}(t) = G_{14}^0 + \int_0^t \left[(a_{14})^{(1)} G_{13}(s_{(13)}) - \left((a'_{14})^{(1)} + a''_{14}(s_{(13)}, s_{(13)}) \right) G_{14}(s_{(13)}) \right] ds_{(13)} \quad 205$$

$$\bar{G}_{15}(t) = G_{15}^0 + \int_0^t \left[(a_{15})^{(1)} G_{14}(s_{(13)}) - \left((a'_{15})^{(1)} + a''_{15}(s_{(13)}, s_{(13)}) \right) G_{15}(s_{(13)}) \right] ds_{(13)} \quad 206$$

$$\bar{T}_{13}(t) = T_{13}^0 + \int_0^t \left[(b_{13})^{(1)} T_{14}(s_{(13)}) - \left((b'_{13})^{(1)} - b''_{13}(s_{(13)}, s_{(13)}) \right) T_{13}(s_{(13)}) \right] ds_{(13)} \quad 207$$

$$\bar{T}_{14}(t) = T_{14}^0 + \int_0^t \left[(b_{14})^{(1)} T_{13}(s_{(13)}) - \left((b'_{14})^{(1)} - b''_{14}(s_{(13)}, s_{(13)}) \right) T_{14}(s_{(13)}) \right] ds_{(13)} \quad 208$$

$$\bar{T}_{15}(t) = T_{15}^0 + \int_0^t \left[(b_{15})^{(1)} T_{14}(s_{(13)}) - \left((b'_{15})^{(1)} - b''_{15}(s_{(13)}, s_{(13)}) \right) T_{15}(s_{(13)}) \right] ds_{(13)} \quad 209$$

Where $s_{(13)}$ is the integrand that is integrated over an interval $(0, t)$ 210

if the conditions IN THE FOREGOING above are fulfilled, there exists a solution satisfying the conditions

Definition of $G_i(0), T_i(0)$:

$$G_i(t) \leq (\hat{P}_{36})^{(7)} e^{(\mathcal{M}_{36})^{(7)}t}, \quad \boxed{G_i(0) = G_i^0 > 0}$$

$$T_i(t) \leq (\hat{Q}_{36})^{(7)} e^{(\mathcal{M}_{36})^{(7)}t}, \quad \boxed{T_i(0) = T_i^0 > 0}$$

Consider operator $\mathcal{A}^{(7)}$ defined on the space of sextuples of continuous functions $G_i, T_i: \mathbb{R}_+ \rightarrow \mathbb{R}_+$ which satisfy

$$G_i(0) = G_i^0, T_i(0) = T_i^0, G_i^0 \leq (\hat{P}_{36})^{(7)}, T_i^0 \leq (\hat{Q}_{36})^{(7)},$$

$$0 \leq G_i(t) - G_i^0 \leq (\hat{P}_{36})^{(7)} e^{(\mathcal{M}_{36})^{(7)}t}$$

$$0 \leq T_i(t) - T_i^0 \leq (\hat{Q}_{36})^{(7)} e^{(\mathcal{M}_{36})^{(7)}t}$$

By

$$\bar{G}_{36}(t) = G_{36}^0 + \int_0^t \left[(a_{36})^{(7)} G_{37}(s_{(36)}) - \left((a'_{36})^{(7)} + a''_{36}(s_{(36)}, s_{(36)}) \right) G_{36}(s_{(36)}) \right] ds_{(36)}$$

$$\bar{G}_{37}(t) = G_{37}^0 +$$

$$\int_0^t \left[(a_{37})^{(7)} G_{36}(s_{(36)}) - \left((a'_{37})^{(7)} + a''_{37}(s_{(36)}, s_{(36)}) \right) G_{37}(s_{(36)}) \right] ds_{(36)}$$

$$\bar{G}_{38}(t) = G_{38}^0 +$$

$$\int_0^t \left[(a_{38})^{(7)} G_{37}(s_{(36)}) - \left((a'_{38})^{(7)} + (a''_{38})^{(7)} (T_{37}(s_{(36)}), s_{(36)}) \right) G_{38}(s_{(36)}) \right] ds_{(36)}$$

$$\bar{T}_{36}(t) = T_{36}^0 + \int_0^t \left[(b_{36})^{(7)} T_{37}(s_{(36)}) - \left((b'_{36})^{(7)} - (b''_{36})^{(7)} (G(s_{(36)}), s_{(36)}) \right) T_{36}(s_{(36)}) \right] ds_{(36)}$$

$$\bar{T}_{37}(t) = T_{37}^0 + \int_0^t \left[(b_{37})^{(7)} T_{36}(s_{(36)}) - \left((b'_{37})^{(7)} - (b''_{37})^{(7)} (G(s_{(36)}), s_{(36)}) \right) T_{37}(s_{(36)}) \right] ds_{(36)}$$

$$\bar{T}_{38}(t) = T_{38}^0 +$$

$$\int_0^t \left[(b_{38})^{(7)} T_{37}(s_{(36)}) - \left((b'_{38})^{(7)} - (b''_{38})^{(7)} (G(s_{(36)}), s_{(36)}) \right) T_{38}(s_{(36)}) \right] ds_{(36)}$$

Where $s_{(36)}$ is the integrand that is integrated over an interval $(0, t)$

Consider operator $\mathcal{A}^{(2)}$ defined on the space of sextuples of continuous functions $G_i, T_i: \mathbb{R}_+ \rightarrow \mathbb{R}_+$ which satisfy - 211

$$G_i(0) = G_i^0, T_i(0) = T_i^0, G_i^0 \leq (\hat{P}_{16})^{(2)}, T_i^0 \leq (\hat{Q}_{16})^{(2)}, -212$$

$$0 \leq G_i(t) - G_i^0 \leq (\hat{P}_{16})^{(2)} e^{(M_{16})^{(2)}t} -213$$

$$0 \leq T_i(t) - T_i^0 \leq (\hat{Q}_{16})^{(2)} e^{(M_{16})^{(2)}t} -214$$

By

$$\bar{G}_{16}(t) = G_{16}^0 + \int_0^t \left[(a_{16})^{(2)} G_{17}(s_{(16)}) - \left((a'_{16})^{(2)} + a''_{16}^{(2)} (T_{17}(s_{(16)}), s_{(16)}) \right) G_{16}(s_{(16)}) \right] ds_{(16)} -215$$

$$\bar{G}_{17}(t) = G_{17}^0 + \int_0^t \left[(a_{17})^{(2)} G_{16}(s_{(16)}) - \left((a'_{17})^{(2)} + (a''_{17})^{(2)} (T_{17}(s_{(16)}), s_{(17)}) \right) G_{17}(s_{(16)}) \right] ds_{(16)} -216$$

$$\bar{G}_{18}(t) = G_{18}^0 + \int_0^t \left[(a_{18})^{(2)} G_{17}(s_{(16)}) - \left((a'_{18})^{(2)} + (a''_{18})^{(2)} (T_{17}(s_{(16)}), s_{(16)}) \right) G_{18}(s_{(16)}) \right] ds_{(16)} -217$$

$$\bar{T}_{16}(t) = T_{16}^0 + \int_0^t \left[(b_{16})^{(2)} T_{17}(s_{(16)}) - \left((b'_{16})^{(2)} - (b''_{16})^{(2)} (G(s_{(16)}), s_{(16)}) \right) T_{16}(s_{(16)}) \right] ds_{(16)} -218$$

$$\bar{T}_{17}(t) = T_{17}^0 + \int_0^t \left[(b_{17})^{(2)} T_{16}(s_{(16)}) - \left((b'_{17})^{(2)} - (b''_{17})^{(2)} (G(s_{(16)}), s_{(16)}) \right) T_{17}(s_{(16)}) \right] ds_{(16)} -219$$

$$\bar{T}_{18}(t) = T_{18}^0 + \int_0^t \left[(b_{18})^{(2)} T_{17}(s_{(16)}) - \left((b'_{18})^{(2)} - (b''_{18})^{(2)} (G(s_{(16)}), s_{(16)}) \right) T_{18}(s_{(16)}) \right] ds_{(16)}$$

Where $s_{(16)}$ is the integrand that is integrated over an interval $(0, t)$ -220

Consider operator $\mathcal{A}^{(3)}$ defined on the space of sextuples of continuous functions $G_i, T_i: \mathbb{R}_+ \rightarrow \mathbb{R}_+$ which satisfy -221

$$G_i(0) = G_i^0, T_i(0) = T_i^0, G_i^0 \leq (\hat{P}_{20})^{(3)}, T_i^0 \leq (\hat{Q}_{20})^{(3)}, -222$$

$$0 \leq G_i(t) - G_i^0 \leq (\hat{P}_{20})^{(3)} e^{(M_{20})^{(3)}t} -223$$

$$0 \leq T_i(t) - T_i^0 \leq (\hat{Q}_{20})^{(3)} e^{(M_{20})^{(3)}t} -224$$

By

$$\bar{G}_{20}(t) = G_{20}^0 + \int_0^t \left[(a_{20})^{(3)} G_{21}(s_{(20)}) - \left((a'_{20})^{(3)} + a''_{20}^{(3)} (T_{21}(s_{(20)}), s_{(20)}) \right) G_{20}(s_{(20)}) \right] ds_{(20)} -225$$

$$\bar{G}_{21}(t) = G_{21}^0 + \int_0^t \left[(a_{21})^{(3)} G_{20}(s_{(20)}) - \left((a'_{21})^{(3)} + (a''_{21})^{(3)} (T_{21}(s_{(20)}), s_{(20)}) \right) G_{21}(s_{(20)}) \right] ds_{(20)} -226$$

$$\bar{G}_{22}(t) = G_{22}^0 + \int_0^t \left[(a_{22})^{(3)} G_{21}(s_{(20)}) - \left((a'_{22})^{(3)} + (a''_{22})^{(3)} (T_{21}(s_{(20)}), s_{(20)}) \right) G_{22}(s_{(20)}) \right] ds_{(20)} -227$$

$$\bar{T}_{20}(t) = T_{20}^0 + \int_0^t \left[(b_{20})^{(3)} T_{21}(s_{(20)}) - \left((b'_{20})^{(3)} - (b''_{20})^{(3)} (G(s_{(20)}), s_{(20)}) \right) T_{20}(s_{(20)}) \right] ds_{(20)} -228$$

$$\bar{T}_{21}(t) = T_{21}^0 + \int_0^t \left[(b_{21})^{(3)} T_{20}(s_{(20)}) - \left((b'_{21})^{(3)} - (b''_{21})^{(3)} (G(s_{(20)}), s_{(20)}) \right) T_{21}(s_{(20)}) \right] ds_{(20)} -229$$

$$\bar{T}_{22}(t) = T_{22}^0 + \int_0^t \left[(b_{22})^{(3)} T_{21}(s_{(20)}) - \left((b'_{22})^{(3)} - (b''_{22})^{(3)} (G(s_{(20)}), s_{(20)}) \right) T_{22}(s_{(20)}) \right] ds_{(20)}$$

Where $s_{(20)}$ is the integrand that is integrated over an interval $(0, t)$ -230

Consider operator $\mathcal{A}^{(4)}$ defined on the space of sextuples of continuous functions $G_i, T_i: \mathbb{R}_+ \rightarrow \mathbb{R}_+$ which satisfy -231

$$G_i(0) = G_i^0, T_i(0) = T_i^0, G_i^0 \leq (\hat{P}_{24})^{(4)}, T_i^0 \leq (\hat{Q}_{24})^{(4)}, -232$$

$$0 \leq G_i(t) - G_i^0 \leq (\hat{P}_{24})^{(4)} e^{(M_{24})^{(4)}t} -233$$

$$0 \leq T_i(t) - T_i^0 \leq (\hat{Q}_{24})^{(4)} e^{(M_{24})^{(4)}t} -234$$

By

$$\bar{G}_{24}(t) = G_{24}^0 + \int_0^t \left[(a_{24})^{(4)} G_{25}(s_{(24)}) - \left((a'_{24})^{(4)} + a''_{24}^{(4)} (T_{25}(s_{(24)}), s_{(24)}) \right) G_{24}(s_{(24)}) \right] ds_{(24)} -235$$

$$\bar{G}_{25}(t) = G_{25}^0 + \int_0^t \left[(a_{25})^{(4)} G_{24}(s_{(24)}) - \left((a'_{25})^{(4)} + (a''_{25})^{(4)} (T_{25}(s_{(24)}), s_{(24)}) \right) G_{25}(s_{(24)}) \right] ds_{(24)} -236$$

$$\bar{G}_{26}(t) = G_{26}^0 + \int_0^t \left[(a_{26})^{(4)} G_{25}(s_{(24)}) - \left((a'_{26})^{(4)} + (a''_{26})^{(4)} (T_{25}(s_{(24)}), s_{(24)}) \right) G_{26}(s_{(24)}) \right] ds_{(24)} -237$$

$$\bar{T}_{24}(t) = T_{24}^0 + \int_0^t \left[(b_{24})^{(4)} T_{25}(s_{(24)}) - \left((b'_{24})^{(4)} - (b''_{24})^{(4)} (G(s_{(24)}), s_{(24)}) \right) T_{24}(s_{(24)}) \right] ds_{(24)} -238$$

$$\bar{T}_{25}(t) = T_{25}^0 + \int_0^t \left[(b_{25})^{(4)} T_{24}(s_{(24)}) - \left((b'_{25})^{(4)} - (b''_{25})^{(4)} (G(s_{(24)}), s_{(24)}) \right) T_{25}(s_{(24)}) \right] ds_{(24)} \quad -239$$

$$\bar{T}_{26}(t) = T_{26}^0 + \int_0^t \left[(b_{26})^{(4)} T_{25}(s_{(24)}) - \left((b'_{26})^{(4)} - (b''_{26})^{(4)} (G(s_{(24)}), s_{(24)}) \right) T_{26}(s_{(24)}) \right] ds_{(24)}$$

Where $s_{(24)}$ is the integrand that is integrated over an interval $(0, t)$ -240

Consider operator $\mathcal{A}^{(5)}$ defined on the space of sextuples of continuous functions $G_i, T_i: \mathbb{R}_+ \rightarrow \mathbb{R}_+$ which satisfy

$$242$$

$$G_i(0) = G_i^0, T_i(0) = T_i^0, G_i^0 \leq (\hat{P}_{28})^{(5)}, T_i^0 \leq (\hat{Q}_{28})^{(5)}, \quad -243$$

$$0 \leq G_i(t) - G_i^0 \leq (\hat{P}_{28})^{(5)} e^{(\hat{M}_{28})^{(5)}t} \quad -244$$

$$0 \leq T_i(t) - T_i^0 \leq (\hat{Q}_{28})^{(5)} e^{(\hat{M}_{28})^{(5)}t} \quad -245$$

By

$$\bar{G}_{28}(t) = G_{28}^0 + \int_0^t \left[(a_{28})^{(5)} G_{29}(s_{(28)}) - \left((a'_{28})^{(5)} + a''_{28}^{(5)} (T_{29}(s_{(28)}), s_{(28)}) \right) G_{28}(s_{(28)}) \right] ds_{(28)} \quad -246$$

$$\bar{G}_{29}(t) = G_{29}^0 + \int_0^t \left[(a_{29})^{(5)} G_{28}(s_{(28)}) - \left((a'_{29})^{(5)} + (a''_{29})^{(5)} (T_{29}(s_{(28)}), s_{(28)}) \right) G_{29}(s_{(28)}) \right] ds_{(28)} \quad -247$$

$$\bar{G}_{30}(t) = G_{30}^0 + \int_0^t \left[(a_{30})^{(5)} G_{29}(s_{(28)}) - \left((a'_{30})^{(5)} + (a''_{30})^{(5)} (T_{29}(s_{(28)}), s_{(28)}) \right) G_{30}(s_{(28)}) \right] ds_{(28)} \quad -248$$

$$\bar{T}_{28}(t) = T_{28}^0 + \int_0^t \left[(b_{28})^{(5)} T_{29}(s_{(28)}) - \left((b'_{28})^{(5)} - (b''_{28})^{(5)} (G(s_{(28)}), s_{(28)}) \right) T_{28}(s_{(28)}) \right] ds_{(28)} \quad -249$$

$$\bar{T}_{29}(t) = T_{29}^0 + \int_0^t \left[(b_{29})^{(5)} T_{28}(s_{(28)}) - \left((b'_{29})^{(5)} - (b''_{29})^{(5)} (G(s_{(28)}), s_{(28)}) \right) T_{29}(s_{(28)}) \right] ds_{(28)} \quad -250$$

$$\bar{T}_{30}(t) = T_{30}^0 + \int_0^t \left[(b_{30})^{(5)} T_{29}(s_{(28)}) - \left((b'_{30})^{(5)} - (b''_{30})^{(5)} (G(s_{(28)}), s_{(28)}) \right) T_{30}(s_{(28)}) \right] ds_{(28)}$$

Where $s_{(28)}$ is the integrand that is integrated over an interval $(0, t)$ -251

Consider operator $\mathcal{A}^{(6)}$ defined on the space of sextuples of continuous functions $G_i, T_i: \mathbb{R}_+ \rightarrow \mathbb{R}_+$ which satisfy -252

$$G_i(0) = G_i^0, T_i(0) = T_i^0, G_i^0 \leq (\hat{P}_{32})^{(6)}, T_i^0 \leq (\hat{Q}_{32})^{(6)}, \quad -253$$

$$0 \leq G_i(t) - G_i^0 \leq (\hat{P}_{32})^{(6)} e^{(\hat{M}_{32})^{(6)}t} \quad -254$$

$$0 \leq T_i(t) - T_i^0 \leq (\hat{Q}_{32})^{(6)} e^{(\hat{M}_{32})^{(6)}t} \quad -255$$

By

$$\bar{G}_{32}(t) = G_{32}^0 + \int_0^t \left[(a_{32})^{(6)} G_{33}(s_{(32)}) - \left((a'_{32})^{(6)} + a''_{32}^{(6)} (T_{33}(s_{(32)}), s_{(32)}) \right) G_{32}(s_{(32)}) \right] ds_{(32)} \quad -256$$

$$\bar{G}_{33}(t) = G_{33}^0 + \int_0^t \left[(a_{33})^{(6)} G_{32}(s_{(32)}) - \left((a'_{33})^{(6)} + (a''_{33})^{(6)} (T_{33}(s_{(32)}), s_{(32)}) \right) G_{33}(s_{(32)}) \right] ds_{(32)} \quad -257$$

$$\bar{G}_{34}(t) = G_{34}^0 + \int_0^t \left[(a_{34})^{(6)} G_{33}(s_{(32)}) - \left((a'_{34})^{(6)} + (a''_{34})^{(6)} (T_{33}(s_{(32)}), s_{(32)}) \right) G_{34}(s_{(32)}) \right] ds_{(32)} \quad -258$$

$$\bar{T}_{32}(t) = T_{32}^0 + \int_0^t \left[(b_{32})^{(6)} T_{33}(s_{(32)}) - \left((b'_{32})^{(6)} - (b''_{32})^{(6)} (G(s_{(32)}), s_{(32)}) \right) T_{32}(s_{(32)}) \right] ds_{(32)} \quad -259$$

$$\bar{T}_{33}(t) = T_{33}^0 + \int_0^t \left[(b_{33})^{(6)} T_{32}(s_{(32)}) - \left((b'_{33})^{(6)} - (b''_{33})^{(6)} (G(s_{(32)}), s_{(32)}) \right) T_{33}(s_{(32)}) \right] ds_{(32)} \quad -260$$

$$\bar{T}_{34}(t) = T_{34}^0 + \int_0^t \left[(b_{34})^{(6)} T_{33}(s_{(32)}) - \left((b'_{34})^{(6)} - (b''_{34})^{(6)} (G(s_{(32)}), s_{(32)}) \right) T_{34}(s_{(32)}) \right] ds_{(32)}$$

Where $s_{(32)}$ is the integrand that is integrated over an interval $(0, t)$ -261-262

(a) The operator $\mathcal{A}^{(1)}$ maps the space of functions satisfying GLOBAL EQUATIONS into itself .Indeed it is obvious that

$$G_{13}(t) \leq G_{13}^0 + \int_0^t \left[(a_{13})^{(1)} \left(G_{14}^0 + (\hat{P}_{13})^{(1)} e^{(\hat{M}_{13})^{(1)}s_{(13)}} \right) \right] ds_{(13)} =$$

$$\left(1 + (a_{13})^{(1)} t \right) G_{14}^0 + \frac{(a_{13})^{(1)} (\hat{P}_{13})^{(1)}}{(\hat{M}_{13})^{(1)}} \left(e^{(\hat{M}_{13})^{(1)}t} - 1 \right) \quad -263$$

From which it follows that

$$(G_{13}(t) - G_{13}^0) e^{-(\hat{M}_{13})^{(1)}t} \leq \frac{(a_{13})^{(1)}}{(\hat{M}_{13})^{(1)}} \left[\left((\hat{P}_{13})^{(1)} + G_{14}^0 \right) e^{\left(-\frac{(\hat{P}_{13})^{(1)} + G_{14}^0}{\hat{M}_{13}^{(1)}} \right)} + (\hat{P}_{13})^{(1)} \right]$$

(G_i^0) is as defined in the statement of theorem 1-264

Analogous inequalities hold also for $G_{14}, G_{15}, T_{13}, T_{14}, T_{15}$ -265

The operator $\mathcal{A}^{(2)}$ maps the space of functions satisfying GLOBAL EQUATIONS into itself .Indeed it is obvious that-266

$$G_{16}(t) \leq G_{16}^0 + \int_0^t \left[(a_{16})^{(2)} \left(G_{17}^0 + (\hat{P}_{16})^{(2)} e^{(\hat{M}_{16})^{(2)}s_{(16)}} \right) \right] ds_{(16)} = \left(1 + (a_{16})^{(2)} t \right) G_{17}^0 + \frac{(a_{16})^{(2)} (\hat{P}_{16})^{(2)}}{(\hat{M}_{16})^{(2)}} \left(e^{(\hat{M}_{16})^{(2)}t} - 1 \right)$$

-267

From which it follows that

$$(G_{16}(t) - G_{16}^0) e^{-(\hat{M}_{16})^{(2)}t} \leq \frac{(a_{16})^{(2)}}{(\hat{M}_{16})^{(2)}} \left[\left((\hat{P}_{16})^{(2)} + G_{17}^0 \right) e^{\left(-\frac{(\hat{P}_{16})^{(2)} + G_{17}^0}{\hat{M}_{16}^{(2)}} \right)} + (\hat{P}_{16})^{(2)} \right] \quad -268$$

Analogous inequalities hold also for $G_{17}, G_{18}, T_{16}, T_{17}, T_{18}$ -269

(a) The operator $\mathcal{A}^{(3)}$ maps the space of functions satisfying GLOBAL EQUATIONS into itself .Indeed it is obvious that

$$G_{20}(t) \leq G_{20}^0 + \int_0^t \left[(a_{20})^{(3)} \left(G_{21}^0 + (\hat{P}_{20})^{(3)} e^{(\hat{M}_{20})^{(3)} s_{(20)}} \right) \right] ds_{(20)} =$$

$$(1 + (a_{20})^{(3)} t) G_{21}^0 + \frac{(a_{20})^{(3)} (\hat{P}_{20})^{(3)}}{(\hat{M}_{20})^{(3)}} \left(e^{(\hat{M}_{20})^{(3)} t} - 1 \right) -270$$

From which it follows that

$$(G_{20}(t) - G_{20}^0) e^{-(\hat{M}_{20})^{(3)} t} \leq \frac{(a_{20})^{(3)}}{(\hat{M}_{20})^{(3)}} \left[\left((\hat{P}_{20})^{(3)} + G_{21}^0 \right) e^{-\frac{(\hat{P}_{20})^{(3)} + G_{21}^0}{G_{21}^0}} + (\hat{P}_{20})^{(3)} \right] -271$$

Analogous inequalities hold also for $G_{21}, G_{22}, T_{20}, T_{21}, T_{22}$ -272

(b) The operator $\mathcal{A}^{(4)}$ maps the space of functions satisfying GLOBAL EQUATIONS into itself. Indeed it is obvious that

$$G_{24}(t) \leq G_{24}^0 + \int_0^t \left[(a_{24})^{(4)} \left(G_{25}^0 + (\hat{P}_{24})^{(4)} e^{(\hat{M}_{24})^{(4)} s_{(24)}} \right) \right] ds_{(24)} =$$

$$(1 + (a_{24})^{(4)} t) G_{25}^0 + \frac{(a_{24})^{(4)} (\hat{P}_{24})^{(4)}}{(\hat{M}_{24})^{(4)}} \left(e^{(\hat{M}_{24})^{(4)} t} - 1 \right) -273$$

From which it follows that

$$(G_{24}(t) - G_{24}^0) e^{-(\hat{M}_{24})^{(4)} t} \leq \frac{(a_{24})^{(4)}}{(\hat{M}_{24})^{(4)}} \left[\left((\hat{P}_{24})^{(4)} + G_{25}^0 \right) e^{-\frac{(\hat{P}_{24})^{(4)} + G_{25}^0}{G_{25}^0}} + (\hat{P}_{24})^{(4)} \right]$$

(G_i^0) is as defined in the statement of theorem 1-274

(c) The operator $\mathcal{A}^{(5)}$ maps the space of functions satisfying GLOBAL EQUATIONS into itself. Indeed it is obvious that

$$G_{28}(t) \leq G_{28}^0 + \int_0^t \left[(a_{28})^{(5)} \left(G_{29}^0 + (\hat{P}_{28})^{(5)} e^{(\hat{M}_{28})^{(5)} s_{(28)}} \right) \right] ds_{(28)} =$$

$$(1 + (a_{28})^{(5)} t) G_{29}^0 + \frac{(a_{28})^{(5)} (\hat{P}_{28})^{(5)}}{(\hat{M}_{28})^{(5)}} \left(e^{(\hat{M}_{28})^{(5)} t} - 1 \right) -275$$

From which it follows that

$$(G_{28}(t) - G_{28}^0) e^{-(\hat{M}_{28})^{(5)} t} \leq \frac{(a_{28})^{(5)}}{(\hat{M}_{28})^{(5)}} \left[\left((\hat{P}_{28})^{(5)} + G_{29}^0 \right) e^{-\frac{(\hat{P}_{28})^{(5)} + G_{29}^0}{G_{29}^0}} + (\hat{P}_{28})^{(5)} \right]$$

(G_i^0) is as defined in the statement of theorem 1-276

(d) The operator $\mathcal{A}^{(6)}$ maps the space of functions satisfying GLOBAL EQUATIONS into itself. Indeed it is obvious that

$$G_{32}(t) \leq G_{32}^0 + \int_0^t \left[(a_{32})^{(6)} \left(G_{33}^0 + (\hat{P}_{32})^{(6)} e^{(\hat{M}_{32})^{(6)} s_{(32)}} \right) \right] ds_{(32)} =$$

$$(1 + (a_{32})^{(6)} t) G_{33}^0 + \frac{(a_{32})^{(6)} (\hat{P}_{32})^{(6)}}{(\hat{M}_{32})^{(6)}} \left(e^{(\hat{M}_{32})^{(6)} t} - 1 \right) -277$$

From which it follows that

$$(G_{32}(t) - G_{32}^0) e^{-(\hat{M}_{32})^{(6)} t} \leq \frac{(a_{32})^{(6)}}{(\hat{M}_{32})^{(6)}} \left[\left((\hat{P}_{32})^{(6)} + G_{33}^0 \right) e^{-\frac{(\hat{P}_{32})^{(6)} + G_{33}^0}{G_{33}^0}} + (\hat{P}_{32})^{(6)} \right]$$

(G_i^0) is as defined in the statement of theorem 1

Analogous inequalities hold also for $G_{25}, G_{26}, T_{24}, T_{25}, T_{26}$ -278
-279-280

It is now sufficient to take $\frac{(a_i)^{(1)}}{(\hat{M}_{13})^{(1)}}, \frac{(b_i)^{(1)}}{(\hat{M}_{13})^{(1)}} < 1$ and to choose

$$\frac{(a_i)^{(1)}}{(\hat{M}_{13})^{(1)}} \left[\left((\hat{P}_{13})^{(1)} + \left((\hat{P}_{13})^{(1)} + G_j^0 \right) e^{-\frac{(\hat{P}_{13})^{(1)} + G_j^0}{G_j^0}} \right) \right] \leq (\hat{P}_{13})^{(1)} -283$$

$$\frac{(b_i)^{(1)}}{(\hat{M}_{13})^{(1)}} \left[\left((\hat{Q}_{13})^{(1)} + T_j^0 \right) e^{-\frac{(\hat{Q}_{13})^{(1)} + T_j^0}{T_j^0}} + (\hat{Q}_{13})^{(1)} \right] \leq (\hat{Q}_{13})^{(1)} -284$$

In order that the operator $\mathcal{A}^{(1)}$ transforms the space of sextuples of functions G_i, T_i satisfying GLOBAL EQUATIONS into itself-285

The operator $\mathcal{A}^{(1)}$ is a contraction with respect to the metric

$$d \left((G^{(1)}, T^{(1)}), (G^{(2)}, T^{(2)}) \right) =$$

$$\sup_i \left\{ \max_{t \in \mathbb{R}_+} |G_i^{(1)}(t) - G_i^{(2)}(t)| e^{-(\hat{M}_{13})^{(1)} t}, \max_{t \in \mathbb{R}_+} |T_i^{(1)}(t) - T_i^{(2)}(t)| e^{-(\hat{M}_{13})^{(1)} t} \right\} -286$$

Indeed if we denote

Definition of \tilde{G}, \tilde{T} :

$$(\tilde{G}, \tilde{T}) = \mathcal{A}^{(1)}(G, T)$$

It results

$$|\tilde{G}_{13}^{(1)} - \tilde{G}_i^{(2)}| \leq \int_0^t (a_{13})^{(1)} |G_{14}^{(1)} - G_{14}^{(2)}| e^{-(\hat{M}_{13})^{(1)} s_{(13)}} e^{(\hat{M}_{13})^{(1)} s_{(13)}} ds_{(13)} +$$

$$\int_0^t \{ (a'_{13})^{(1)} |G_{13}^{(1)} - G_{13}^{(2)}| e^{-(\bar{M}_{13})^{(1)}s_{(13)}} e^{-(\bar{M}_{13})^{(1)}s_{(13)}} + (a''_{13})^{(1)} (T_{14}^{(1)}, s_{(13)}) |G_{13}^{(1)} - G_{13}^{(2)}| e^{-(\bar{M}_{13})^{(1)}s_{(13)}} e^{(\bar{M}_{13})^{(1)}s_{(13)}} + G_{13}^{(2)} | (a''_{13})^{(1)} (T_{14}^{(1)}, s_{(13)}) - (a''_{13})^{(1)} (T_{14}^{(2)}, s_{(13)}) | e^{-(\bar{M}_{13})^{(1)}s_{(13)}} e^{(\bar{M}_{13})^{(1)}s_{(13)}} \} ds_{(13)}$$

Where $s_{(13)}$ represents integrand that is integrated over the interval $[0, t]$

From the hypotheses it follows-287

$$|G^{(1)} - G^{(2)}| e^{-(\bar{M}_{13})^{(1)}t} \leq \frac{1}{(\bar{M}_{13})^{(1)}} \left((a_{13})^{(1)} + (a'_{13})^{(1)} + (\bar{A}_{13})^{(1)} + (\bar{P}_{13})^{(1)} (\hat{k}_{13})^{(1)} \right) d \left((G^{(1)}, T^{(1)}; G^{(2)}, T^{(2)}) \right)$$

And analogous inequalities for G_i and T_i . Taking into account the hypothesis the result follows-288

Remark 1: The fact that we supposed $(a''_{13})^{(1)}$ and $(b''_{13})^{(1)}$ depending also on t can be considered as not conformal with the reality, however we have put this hypothesis in order that we can postulate condition necessary to prove the uniqueness of the solution bounded by $(\bar{P}_{13})^{(1)} e^{(\bar{M}_{13})^{(1)}t}$ and $(\bar{Q}_{13})^{(1)} e^{(\bar{M}_{13})^{(1)}t}$ respectively of \mathbb{R}_+ .

If instead of proving the existence of the solution on \mathbb{R}_+ , we have to prove it only on a compact then it suffices to consider that $(a''_i)^{(1)}$ and $(b''_i)^{(1)}$, $i = 13, 14, 15$ depend only on T_{14} and respectively on G (and not on t) and hypothesis can be replaced by a usual Lipschitz condition.-289

Remark 2: There does not exist any t where $G_i(t) = 0$ and $T_i(t) = 0$

From 19 to 24 it results

$$G_i(t) \geq G_i^0 e^{-\int_0^t \{ (a'_i)^{(1)} - (a''_i)^{(1)} (T_{14}(s_{(13)}), s_{(13)}) \} ds_{(13)}} \geq 0$$

$$T_i(t) \geq T_i^0 e^{-(b'_i)^{(1)}t} > 0 \text{ for } t > 0 \text{-290}$$

291

Definition of $(\bar{M}_{13})^{(1)}_1$, and $(\bar{M}_{13})^{(1)}_3$:

Remark 3: if G_{13} is bounded, the same property have also G_{14} and G_{15} . indeed if

$G_{13} < (\bar{M}_{13})^{(1)}$ it follows $\frac{dG_{14}}{dt} \leq ((\bar{M}_{13})^{(1)})_1 - (a'_{14})^{(1)} G_{14}$ and by integrating

$$G_{14} \leq ((\bar{M}_{13})^{(1)})_2 = G_{14}^0 + 2(a_{14})^{(1)} ((\bar{M}_{13})^{(1)})_1 / (a'_{14})^{(1)}$$

In the same way, one can obtain

$$G_{15} \leq ((\bar{M}_{13})^{(1)})_3 = G_{15}^0 + 2(a_{15})^{(1)} ((\bar{M}_{13})^{(1)})_2 / (a'_{15})^{(1)}$$

If G_{14} or G_{15} is bounded, the same property follows for G_{13} , G_{15} and G_{13} , G_{14} respectively.-292

Remark 4: If G_{13} is bounded, from below, the same property holds for G_{14} and G_{15} . The proof is analogous with the preceding one. An analogous property is true if G_{14} is bounded from below.-293

Remark 5: If T_{13} is bounded from below and $\lim_{t \rightarrow \infty} ((b'_i)^{(1)}(G(t), t)) = (b'_{14})^{(1)}$ then $T_{14} \rightarrow \infty$.

Definition of $(m)^{(1)}$ and ε_1 :

Indeed let t_1 be so that for $t > t_1$

$$(b_{14})^{(1)} - (b'_i)^{(1)}(G(t), t) < \varepsilon_1, T_{13}(t) > (m)^{(1)} \text{-294}$$

Then $\frac{dT_{14}}{dt} \geq (a_{14})^{(1)}(m)^{(1)} - \varepsilon_1 T_{14}$ which leads to

$$T_{14} \geq \left(\frac{(a_{14})^{(1)}(m)^{(1)}}{\varepsilon_1} \right) (1 - e^{-\varepsilon_1 t}) + T_{14}^0 e^{-\varepsilon_1 t} \text{ If we take } t \text{ such that } e^{-\varepsilon_1 t} = \frac{1}{2} \text{ it results}$$

$$T_{14} \geq \left(\frac{(a_{14})^{(1)}(m)^{(1)}}{2} \right), t = \log \frac{2}{\varepsilon_1} \text{ By taking now } \varepsilon_1 \text{ sufficiently small one sees that } T_{14} \text{ is unbounded. The same property}$$

holds for T_{15} if $\lim_{t \rightarrow \infty} (b''_{15})^{(1)}(G(t), t) = (b'_{15})^{(1)}$

We now state a more precise theorem about the behaviors at infinity of the solutions -295

-296

It is now sufficient to take $\frac{(a_i)^{(2)}}{(\bar{M}_{16})^{(2)}}, \frac{(b_j)^{(2)}}{(\bar{M}_{16})^{(2)}} < 1$ and to choose

$(\hat{P}_{16})^{(2)}$ and $(\hat{Q}_{16})^{(2)}$ large to have-297

$$\frac{(a_i)^{(2)}}{(\bar{M}_{16})^{(2)}} \left[(\hat{P}_{16})^{(2)} + ((\hat{P}_{16})^{(2)} + G_j^0) e^{-\left(\frac{(\hat{P}_{16})^{(2)} + G_j^0}{G_j^0} \right)} \right] \leq (\hat{P}_{16})^{(2)} \text{-298}$$

$$\frac{(b_j)^{(2)}}{(\bar{M}_{16})^{(2)}} \left[((\hat{Q}_{16})^{(2)} + T_j^0) e^{-\left(\frac{(\hat{Q}_{16})^{(2)} + T_j^0}{T_j^0} \right)} + (\hat{Q}_{16})^{(2)} \right] \leq (\hat{Q}_{16})^{(2)} \text{-299}$$

In order that the operator $\mathcal{A}^{(2)}$ transforms the space of sextuples of functions G_i, T_i satisfying -300

The operator $\mathcal{A}^{(2)}$ is a contraction with respect to the metric

$$d \left(((G_{19})^{(1)}, (T_{19})^{(1)}), ((G_{19})^{(2)}, (T_{19})^{(2)}) \right) =$$

$$\sup_i \{ \max_{t \in \mathbb{R}_+} |G_i^{(1)}(t) - G_i^{(2)}(t)| e^{-(\bar{M}_{16})^{(2)}t}, \max_{t \in \mathbb{R}_+} |T_i^{(1)}(t) - T_i^{(2)}(t)| e^{-(\bar{M}_{16})^{(2)}t} \} \text{-301}$$

Indeed if we denote

Definition of $\widetilde{G}_{19}, \widetilde{T}_{19} : (\widetilde{G}_{19}, \widetilde{T}_{19}) = \mathcal{A}^{(2)}(G_{19}, T_{19})$ -302

It results

$$|\widetilde{G}_{16}^{(1)} - \widetilde{G}_i^{(2)}| \leq \int_0^t (a_{16})^{(2)} |G_{17}^{(1)} - G_{17}^{(2)}| e^{-(\overline{M}_{16})^{(2)}s_{(16)}} e^{(\overline{M}_{16})^{(2)}s_{(16)}} ds_{(16)} + \int_0^t \{ (a_{16}')^{(2)} |G_{16}^{(1)} - G_{16}^{(2)}| e^{-(\overline{M}_{16})^{(2)}s_{(16)}} e^{-(\overline{M}_{16})^{(2)}s_{(16)}} + (a_{16}'')^{(2)} (T_{17}^{(1)}, s_{(16)}) |G_{16}^{(1)} - G_{16}^{(2)}| e^{-(\overline{M}_{16})^{(2)}s_{(16)}} e^{(\overline{M}_{16})^{(2)}s_{(16)}} + G_{16}^{(2)} | (a_{16}'')^{(2)} (T_{17}^{(1)}, s_{(16)}) - (a_{16}'')^{(2)} (T_{17}^{(2)}, s_{(16)}) | e^{-(\overline{M}_{16})^{(2)}s_{(16)}} e^{(\overline{M}_{16})^{(2)}s_{(16)}} \} ds_{(16)} -303$$

Where $s_{(16)}$ represents integrand that is integrated over the interval $[0, t]$

From the hypotheses it follows-304

$$|(G_{19})^{(1)} - (G_{19})^{(2)}| e^{-(\overline{M}_{16})^{(2)}t} \leq \frac{1}{(\overline{M}_{16})^{(2)}} ((a_{16})^{(2)} + (a_{16}')^{(2)} + (\widehat{A}_{16})^{(2)} + (\widehat{P}_{16})^{(2)} (\widehat{k}_{16})^{(2)}) d((G_{19})^{(1)}, (T_{19})^{(1)}; (G_{19})^{(2)}, (T_{19})^{(2)}) -305$$

And analogous inequalities for G_i and T_i . Taking into account the hypothesis the result follows-306

Remark 1: The fact that we supposed $(a_{16}'')^{(2)}$ and $(b_{16}'')^{(2)}$ depending also on t can be considered as not conformal with the reality, however we have put this hypothesis, in order that we can postulate condition necessary to prove the uniqueness of the solution bounded by $(\widehat{P}_{16})^{(2)} e^{(\overline{M}_{16})^{(2)}t}$ and $(\widehat{Q}_{16})^{(2)} e^{(\overline{M}_{16})^{(2)}t}$ respectively of \mathbb{R}_+ .

If instead of proving the existence of the solution on \mathbb{R}_+ , we have to prove it only on a compact then it suffices to consider that $(a_i'')^{(2)}$ and $(b_i'')^{(2)}$, $i = 16, 17, 18$ depend only on T_{17} and respectively on (G_{19}) (and not on t) and hypothesis can be replaced by a usual Lipschitz condition.-307

Remark 2: There does not exist any t where $G_i(t) = 0$ and $T_i(t) = 0$

From 19 to 24 it results

$$G_i(t) \geq G_i^0 e^{-\int_0^t \{ (a_i')^{(2)} - (a_i'')^{(2)} (T_{17}(s_{(16)}), s_{(16)}) \} ds_{(16)}} \geq 0$$

$$T_i(t) \geq T_i^0 e^{-(b_i'')^{(2)}t} > 0 \text{ for } t > 0 -308$$

Definition of $(\overline{M}_{16})^{(2)}_1, (\overline{M}_{16})^{(2)}_2$ and $(\overline{M}_{16})^{(2)}_3$:

Remark 3: if G_{16} is bounded, the same property have also G_{17} and G_{18} . indeed if

$$G_{16} < (\overline{M}_{16})^{(2)} \text{ it follows } \frac{dG_{17}}{dt} \leq ((\overline{M}_{16})^{(2)})_1 - (a_{17}')^{(2)} G_{17} \text{ and by integrating}$$

$$G_{17} \leq ((\overline{M}_{16})^{(2)})_2 = G_{17}^0 + 2(a_{17})^{(2)} ((\overline{M}_{16})^{(2)})_1 / (a_{17}')^{(2)}$$

In the same way, one can obtain

$$G_{18} \leq ((\overline{M}_{16})^{(2)})_3 = G_{18}^0 + 2(a_{18})^{(2)} ((\overline{M}_{16})^{(2)})_2 / (a_{18}')^{(2)}$$

If G_{17} or G_{18} is bounded, the same property follows for G_{16} , G_{18} and G_{16} , G_{17} respectively.-309

310

Remark 4: If G_{16} is bounded, from below, the same property holds for G_{17} and G_{18} . The proof is analogous with the preceding one. An analogous property is true if G_{17} is bounded from below.-311

Remark 5: If T_{16} is bounded from below and $\lim_{t \rightarrow \infty} ((b_i'')^{(2)} ((G_{19})(t), t)) = (b_{17}')^{(2)}$ then $T_{17} \rightarrow \infty$.

Definition of $(m)^{(2)}$ and ε_2 :

Indeed let t_2 be so that for $t > t_2$

$$(b_{17})^{(2)} - (b_i'')^{(2)} ((G_{19})(t), t) < \varepsilon_2, T_{16}(t) > (m)^{(2)} -312$$

Then $\frac{dT_{17}}{dt} \geq (a_{17})^{(2)} (m)^{(2)} - \varepsilon_2 T_{17}$ which leads to

$$T_{17} \geq \left(\frac{(a_{17})^{(2)} (m)^{(2)}}{\varepsilon_2} \right) (1 - e^{-\varepsilon_2 t}) + T_{17}^0 e^{-\varepsilon_2 t} \text{ If we take } t \text{ such that } e^{-\varepsilon_2 t} = \frac{1}{2} \text{ it results -313}$$

$$T_{17} \geq \left(\frac{(a_{17})^{(2)} (m)^{(2)}}{2} \right), t = \log \frac{2}{\varepsilon_2} \text{ By taking now } \varepsilon_2 \text{ sufficiently small one sees that } T_{17} \text{ is unbounded. The same property}$$

holds for T_{18} if $\lim_{t \rightarrow \infty} (b_{18}'')^{(2)} ((G_{19})(t), t) = (b_{18}')^{(2)}$

We now state a more precise theorem about the behaviors at infinity of the solutions -314

-315

It is now sufficient to take $\frac{(a_i)^{(3)}}{(\overline{M}_{20})^{(3)}}, \frac{(b_i)^{(3)}}{(\overline{M}_{20})^{(3)}} < 1$ and to choose

$(\widehat{P}_{20})^{(3)}$ and $(\widehat{Q}_{20})^{(3)}$ large to have-316

$$\frac{(a_i)^{(3)}}{(\overline{M}_{20})^{(3)}} \left[(\widehat{P}_{20})^{(3)} + ((\widehat{P}_{20})^{(3)} + G_j^0) e^{-\left(\frac{(\overline{P}_{20})^{(3)} + G_j^0}{G_j^0} \right)} \right] \leq (\widehat{P}_{20})^{(3)} -317$$

$$\frac{(b_i)^{(3)}}{(\overline{M}_{20})^{(3)}} \left[((\widehat{Q}_{20})^{(3)} + T_j^0) e^{-\left(\frac{(\overline{Q}_{20})^{(3)} + T_j^0}{T_j^0} \right)} + (\widehat{Q}_{20})^{(3)} \right] \leq (\widehat{Q}_{20})^{(3)} -318$$

In order that the operator $\mathcal{A}^{(3)}$ transforms the space of sextuples of functions G_i, T_i into itself-319

The operator $\mathcal{A}^{(3)}$ is a contraction with respect to the metric

$$d\left(\left((G_{23})^{(1)}, (T_{23})^{(1)}\right), \left((G_{23})^{(2)}, (T_{23})^{(2)}\right)\right) = \sup_i \left\{ \max_{t \in \mathbb{R}_+} |G_i^{(1)}(t) - G_i^{(2)}(t)| e^{-(\bar{M}_{20})^{(3)}t}, \max_{t \in \mathbb{R}_+} |T_i^{(1)}(t) - T_i^{(2)}(t)| e^{-(\bar{M}_{20})^{(3)}t} \right\} - 320$$

Indeed if we denote

Definition of $\widetilde{G}_{23}, \widetilde{T}_{23} : \left((\widetilde{G}_{23}), (\widetilde{T}_{23}) \right) = \mathcal{A}^{(3)}\left((G_{23}), (T_{23}) \right)$ -321

It results

$$\begin{aligned} |\widetilde{G}_{20}^{(1)} - \widetilde{G}_i^{(2)}| &\leq \int_0^t (a_{20})^{(3)} |G_{21}^{(1)} - G_{21}^{(2)}| e^{-(\bar{M}_{20})^{(3)}s_{(20)}} e^{(\bar{M}_{20})^{(3)}s_{(20)}} ds_{(20)} + \\ &\int_0^t \left\{ (a_{20}')^{(3)} |G_{20}^{(1)} - G_{20}^{(2)}| e^{-(\bar{M}_{20})^{(3)}s_{(20)}} e^{-(\bar{M}_{20})^{(3)}s_{(20)}} + \right. \\ &(a_{20}'')^{(3)} (T_{21}^{(1)}, s_{(20)}) |G_{20}^{(1)} - G_{20}^{(2)}| e^{-(\bar{M}_{20})^{(3)}s_{(20)}} e^{(\bar{M}_{20})^{(3)}s_{(20)}} + \\ &\left. G_{20}^{(2)} |(a_{20}'')^{(3)} (T_{21}^{(1)}, s_{(20)}) - (a_{20}'')^{(3)} (T_{21}^{(2)}, s_{(20)})| e^{-(\bar{M}_{20})^{(3)}s_{(20)}} e^{(\bar{M}_{20})^{(3)}s_{(20)}} \right\} ds_{(20)} \end{aligned}$$

Where $s_{(20)}$ represents integrand that is integrated over the interval $[0, t]$

From the hypotheses it follows-322

323

$$|G^{(1)} - G^{(2)}| e^{-(\bar{M}_{20})^{(3)}t} \leq \frac{1}{(\bar{M}_{20})^{(3)}} \left((a_{20})^{(3)} + (a_{20}')^{(3)} + (\bar{A}_{20})^{(3)} + (\bar{P}_{20})^{(3)} (\bar{k}_{20})^{(3)} \right) d\left(\left((G_{23})^{(1)}, (T_{23})^{(1)}\right); \left((G_{23})^{(2)}, (T_{23})^{(2)}\right)\right)$$

And analogous inequalities for G_i and T_i . Taking into account the hypothesis the result follows-324

Remark 1: The fact that we supposed $(a_{20}'')^{(3)}$ and $(b_{20}'')^{(3)}$ depending also on t can be considered as not conformal with the reality, however we have put this hypothesis, in order that we can postulate condition necessary to prove the uniqueness of the solution bounded by $(\bar{P}_{20})^{(3)} e^{(\bar{M}_{20})^{(3)}t}$ and $(\bar{Q}_{20})^{(3)} e^{(\bar{M}_{20})^{(3)}t}$ respectively of \mathbb{R}_+ .

If instead of proving the existence of the solution on \mathbb{R}_+ , we have to prove it only on a compact then it suffices to consider that $(a_i'')^{(3)}$ and $(b_i'')^{(3)}$, $i = 20, 21, 22$ depend only on T_{21} and respectively on (G_{23}) (and not on t) and hypothesis can be replaced by a usual Lipschitz condition.-325

Remark 2: There does not exist any t where $G_i(t) = 0$ and $T_i(t) = 0$

From 19 to 24 it results

$$G_i(t) \geq G_i^0 e^{-\int_0^t \{(a_i')^{(3)} - (a_i'')^{(3)}\} (T_{21}(s_{(20)}), s_{(20)}) ds_{(20)}} \geq 0$$

$$T_i(t) \geq T_i^0 e^{-(b_i')^{(3)}t} > 0 \text{ for } t > 0 \text{-326}$$

Definition of $((\bar{M}_{20})^{(3)})_1, ((\bar{M}_{20})^{(3)})_2$ and $((\bar{M}_{20})^{(3)})_3$:

Remark 3: if G_{20} is bounded, the same property have also G_{21} and G_{22} . indeed if

$$G_{20} < (\bar{M}_{20})^{(3)} \text{ it follows } \frac{dG_{21}}{dt} \leq ((\bar{M}_{20})^{(3)})_1 - (a_{21}')^{(3)} G_{21} \text{ and by integrating}$$

$$G_{21} \leq ((\bar{M}_{20})^{(3)})_2 = G_{21}^0 + 2(a_{21})^{(3)} ((\bar{M}_{20})^{(3)})_1 / (a_{21}')^{(3)}$$

In the same way, one can obtain

$$G_{22} \leq ((\bar{M}_{20})^{(3)})_3 = G_{22}^0 + 2(a_{22})^{(3)} ((\bar{M}_{20})^{(3)})_2 / (a_{22}')^{(3)}$$

If G_{21} or G_{22} is bounded, the same property follows for G_{20} , G_{22} and G_{20} , G_{21} respectively.-327

Remark 4: If G_{20} is bounded, from below, the same property holds for G_{21} and G_{22} . The proof is analogous with the preceding one. An analogous property is true if G_{21} is bounded from below.-328

Remark 5: If T_{20} is bounded from below and $\lim_{t \rightarrow \infty} ((b_i'')^{(3)}) ((G_{23})(t), t) = (b_{21}')^{(3)}$ then $T_{21} \rightarrow \infty$.

Definition of $(m)^{(3)}$ and ε_3 :

Indeed let t_3 be so that for $t > t_3$

$$(b_{21}')^{(3)} - (b_i'')^{(3)} ((G_{23})(t), t) < \varepsilon_3, T_{20}(t) > (m)^{(3)} \text{-329}$$

330

Then $\frac{dT_{21}}{dt} \geq (a_{21})^{(3)} (m)^{(3)} - \varepsilon_3 T_{21}$ which leads to

$$T_{21} \geq \left(\frac{(a_{21})^{(3)} (m)^{(3)}}{\varepsilon_3} \right) (1 - e^{-\varepsilon_3 t}) + T_{21}^0 e^{-\varepsilon_3 t} \text{ If we take } t \text{ such that } e^{-\varepsilon_3 t} = \frac{1}{2} \text{ it results}$$

$$T_{21} \geq \left(\frac{(a_{21})^{(3)} (m)^{(3)}}{2} \right), t = \log \frac{2}{\varepsilon_3} \text{ By taking now } \varepsilon_3 \text{ sufficiently small one sees that } T_{21} \text{ is unbounded. The same property}$$

holds for T_{22} if $\lim_{t \rightarrow \infty} ((b_{22}'')^{(3)}) ((G_{23})(t), t) = (b_{22}')^{(3)}$

We now state a more precise theorem about the behaviors at infinity of the solutions -331

-332

It is now sufficient to take $\frac{(a_i)^{(4)}}{(\bar{M}_{24})^{(4)}}, \frac{(b_i)^{(4)}}{(\bar{M}_{24})^{(4)}} < 1$ and to choose

$(\bar{P}_{24})^{(4)}$ and $(\bar{Q}_{24})^{(4)}$ large to have-333

$$\frac{(a_i)^{(4)}}{(\bar{M}_{24})^{(4)}} \left[(\bar{P}_{24})^{(4)} + ((\bar{P}_{24})^{(4)} + G_j^0) e^{-\left(\frac{(\bar{P}_{24})^{(4)} + G_j^0}{G_j^0} \right)} \right] \leq (\bar{P}_{24})^{(4)} \text{-334}$$

$$\frac{(b_i)^{(4)}}{(\widehat{M}_{24})^{(4)}} \left[((\widehat{Q}_{24})^{(4)} + T_j^0) e^{-\left(\frac{(\widehat{Q}_{24})^{(4)} + T_j^0}{T_j^0}\right)} + (\widehat{Q}_{24})^{(4)} \right] \leq (\widehat{Q}_{24})^{(4)} - 335$$

In order that the operator $\mathcal{A}^{(4)}$ transforms the space of sextuples of functions G_i, T_i satisfying IN to itself-336
 The operator $\mathcal{A}^{(4)}$ is a contraction with respect to the metric

$$d\left(((G_{27})^{(1)}, (T_{27})^{(1)}), ((G_{27})^{(2)}, (T_{27})^{(2)}) \right) = \sup_i \{ \max_{t \in \mathbb{R}_+} |G_i^{(1)}(t) - G_i^{(2)}(t)| e^{-(\widehat{M}_{24})^{(4)}t}, \max_{t \in \mathbb{R}_+} |T_i^{(1)}(t) - T_i^{(2)}(t)| e^{-(\widehat{M}_{24})^{(4)}t} \}$$

Indeed if we denote

$$\text{Definition of } (\widehat{G}_{27}), (\widehat{T}_{27}) : ((\widehat{G}_{27}), (\widehat{T}_{27})) = \mathcal{A}^{(4)}((G_{27}), (T_{27}))$$

It results

$$\begin{aligned} |\widehat{G}_{24}^{(1)} - \widehat{G}_{24}^{(2)}| &\leq \int_0^t (a_{24})^{(4)} |G_{25}^{(1)} - G_{25}^{(2)}| e^{-(\widehat{M}_{24})^{(4)}s(24)} e^{(\widehat{M}_{24})^{(4)}s(24)} ds(24) + \\ &\int_0^t \{ (a'_{24})^{(4)} |G_{24}^{(1)} - G_{24}^{(2)}| e^{-(\widehat{M}_{24})^{(4)}s(24)} e^{-(\widehat{M}_{24})^{(4)}s(24)} + \\ &(a''_{24})^{(4)} (T_{25}^{(1)}, s(24)) |G_{24}^{(1)} - G_{24}^{(2)}| e^{-(\widehat{M}_{24})^{(4)}s(24)} e^{(\widehat{M}_{24})^{(4)}s(24)} + \\ &G_{24}^{(2)} |(a''_{24})^{(4)} (T_{25}^{(1)}, s(24)) - (a''_{24})^{(4)} (T_{25}^{(2)}, s(24))| e^{-(\widehat{M}_{24})^{(4)}s(24)} e^{(\widehat{M}_{24})^{(4)}s(24)} \} ds(24) \end{aligned}$$

Where $s(24)$ represents integrand that is integrated over the interval $[0, t]$

From the hypotheses it follows-337

38

$$|(G_{27})^{(1)} - (G_{27})^{(2)}| e^{-(\widehat{M}_{24})^{(4)}t} \leq \frac{1}{(\widehat{M}_{24})^{(4)}} ((a_{24})^{(4)} + (a'_{24})^{(4)} + (\widehat{A}_{24})^{(4)} + (\widehat{P}_{24})^{(4)} (\widehat{k}_{24})^{(4)}) d\left(((G_{27})^{(1)}, (T_{27})^{(1)}); ((G_{27})^{(2)}, (T_{27})^{(2)}) \right)$$

And analogous inequalities for G_i and T_i . Taking into account the hypothesis the result follows-339

Remark 1: The fact that we supposed $(a''_{24})^{(4)}$ and $(b''_{24})^{(4)}$ depending also on t can be considered as not conformal with the reality, however we have put this hypothesis, in order that we can postulate condition necessary to prove the uniqueness of the solution bounded by $(\widehat{P}_{24})^{(4)} e^{(\widehat{M}_{24})^{(4)}t}$ and $(\widehat{Q}_{24})^{(4)} e^{(\widehat{M}_{24})^{(4)}t}$ respectively of \mathbb{R}_+ .

If instead of proving the existence of the solution on \mathbb{R}_+ , we have to prove it only on a compact then it suffices to consider that $(a_i'')^{(4)}$ and $(b_i'')^{(4)}$, $i = 24, 25, 26$ depend only on T_{25} and respectively on (G_{27}) (and not on t) and hypothesis can be replaced by a usual Lipschitz condition.-340

Remark 2: There does not exist any t where $G_i(t) = 0$ and $T_i(t) = 0$

From GLOBAL EQUATIONS it results

$$G_i(t) \geq G_i^0 e^{-\int_0^t \{ (a_i')^{(4)} - (a_i'')^{(4)} (T_{25}(s(24)), s(24)) \} ds(24)} \geq 0$$

$$T_i(t) \geq T_i^0 e^{-(b_i')^{(4)}t} > 0 \text{ for } t > 0 -341$$

Definition of $((\widehat{M}_{24})^{(4)})_1, ((\widehat{M}_{24})^{(4)})_2$ and $((\widehat{M}_{24})^{(4)})_3$:

Remark 3: if G_{24} is bounded, the same property have also G_{25} and G_{26} . indeed if

$$G_{24} < (\widehat{M}_{24})^{(4)} \text{ it follows } \frac{dG_{25}}{dt} \leq ((\widehat{M}_{24})^{(4)})_1 - (a_{25}')^{(4)} G_{25} \text{ and by integrating}$$

$$G_{25} \leq ((\widehat{M}_{24})^{(4)})_2 = G_{25}^0 + 2(a_{25})^{(4)} ((\widehat{M}_{24})^{(4)})_1 / (a_{25}')^{(4)}$$

In the same way, one can obtain

$$G_{26} \leq ((\widehat{M}_{24})^{(4)})_3 = G_{26}^0 + 2(a_{26})^{(4)} ((\widehat{M}_{24})^{(4)})_2 / (a_{26}')^{(4)}$$

If G_{25} or G_{26} is bounded, the same property follows for G_{24} , G_{26} and G_{24} , G_{25} respectively.-342

Remark 4: If G_{24} is bounded, from below, the same property holds for G_{25} and G_{26} . The proof is analogous with the preceding one. An analogous property is true if G_{25} is bounded from below.-343

Remark 5: If T_{24} is bounded from below and $\lim_{t \rightarrow \infty} ((b_i'')^{(4)} ((G_{27})(t), t)) = (b_{25}')^{(4)}$ then $T_{25} \rightarrow \infty$.

Definition of $(m)^{(4)}$ and ε_4 :

Indeed let t_4 be so that for $t > t_4$

$$(b_{25}')^{(4)} - (b_i'')^{(4)} ((G_{27})(t), t) < \varepsilon_4, T_{24}(t) > (m)^{(4)} - 344$$

Then $\frac{dT_{25}}{dt} \geq (a_{25}')^{(4)} (m)^{(4)} - \varepsilon_4 T_{25}$ which leads to

$$T_{25} \geq \left(\frac{(a_{25}')^{(4)} (m)^{(4)}}{\varepsilon_4} \right) (1 - e^{-\varepsilon_4 t}) + T_{25}^0 e^{-\varepsilon_4 t} \text{ If we take } t \text{ such that } e^{-\varepsilon_4 t} = \frac{1}{2} \text{ it results}$$

$$T_{25} \geq \left(\frac{(a_{25}')^{(4)} (m)^{(4)}}{2} \right), t = \log \frac{2}{\varepsilon_4} \text{ By taking now } \varepsilon_4 \text{ sufficiently small one sees that } T_{25} \text{ is unbounded. The same property}$$

holds for T_{26} if $\lim_{t \rightarrow \infty} (b_{26}')^{(4)} ((G_{27})(t), t) = (b_{26}')^{(4)}$

We now state a more precise theorem about the behaviors at infinity of the solutions ANALOGOUS inequalities hold also for $G_{29}, G_{30}, T_{28}, T_{29}, T_{30}$ -345

-346

It is now sufficient to take $\frac{(a_i)^{(5)}}{(\overline{M}_{28})^{(5)}}, \frac{(b_i)^{(5)}}{(\overline{M}_{28})^{(5)}} < 1$ and to choose $(\widehat{P}_{28})^{(5)}$ and $(\widehat{Q}_{28})^{(5)}$ large to have
 -347

$$\frac{(a_i)^{(5)}}{(\overline{M}_{28})^{(5)}} \left[(\widehat{P}_{28})^{(5)} + ((\widehat{P}_{28})^{(5)} + G_j^0) e^{-\left(\frac{(\widehat{P}_{28})^{(5)} + G_j^0}{G_j^0}\right)} \right] \leq (\widehat{P}_{28})^{(5)} \quad -348$$

$$\frac{(b_i)^{(5)}}{(\overline{M}_{28})^{(5)}} \left[((\widehat{Q}_{28})^{(5)} + T_j^0) e^{-\left(\frac{(\widehat{Q}_{28})^{(5)} + T_j^0}{T_j^0}\right)} + (\widehat{Q}_{28})^{(5)} \right] \leq (\widehat{Q}_{28})^{(5)} \quad -349$$

In order that the operator $\mathcal{A}^{(5)}$ transforms the space of sextuples of functions G_i, T_i into itself-350

The operator $\mathcal{A}^{(5)}$ is a contraction with respect to the metric

$$d \left(((G_{31})^{(1)}, (T_{31})^{(1)}), ((G_{31})^{(2)}, (T_{31})^{(2)}) \right) = \sup \left\{ \max_{t \in \mathbb{R}_+} |G_i^{(1)}(t) - G_i^{(2)}(t)| e^{-(\overline{M}_{28})^{(5)}t}, \max_{t \in \mathbb{R}_+} |T_i^{(1)}(t) - T_i^{(2)}(t)| e^{-(\overline{M}_{28})^{(5)}t} \right\}$$

Indeed if we denote

$$\text{Definition of } (\overline{G}_{31}), (\overline{T}_{31}) : ((\overline{G}_{31}), (\overline{T}_{31})) = \mathcal{A}^{(5)}((G_{31}), (T_{31}))$$

It results

$$\begin{aligned} |\overline{G}_{28}^{(1)} - \overline{G}_{28}^{(2)}| &\leq \int_0^t (a_{28})^{(5)} |G_{29}^{(1)} - G_{29}^{(2)}| e^{-(\overline{M}_{28})^{(5)}s_{(28)}} e^{(\overline{M}_{28})^{(5)}s_{(28)}} ds_{(28)} + \\ &\int_0^t \{ (a_{28}')^{(5)} |G_{28}^{(1)} - G_{28}^{(2)}| e^{-(\overline{M}_{28})^{(5)}s_{(28)}} e^{-(\overline{M}_{28})^{(5)}s_{(28)}} + \\ &(a_{28}'')^{(5)} (T_{29}^{(1)}, s_{(28)}) |G_{28}^{(1)} - G_{28}^{(2)}| e^{-(\overline{M}_{28})^{(5)}s_{(28)}} e^{(\overline{M}_{28})^{(5)}s_{(28)}} + \\ &G_{28}^{(2)} | (a_{28}'')^{(5)} (T_{29}^{(1)}, s_{(28)}) - (a_{28}'')^{(5)} (T_{29}^{(2)}, s_{(28)}) | e^{-(\overline{M}_{28})^{(5)}s_{(28)}} e^{(\overline{M}_{28})^{(5)}s_{(28)}} \} ds_{(28)} \end{aligned}$$

Where $s_{(28)}$ represents integrand that is integrated over the interval $[0, t]$

From the hypotheses it follows-351

352

$$\begin{aligned} |(G_{31})^{(1)} - (G_{31})^{(2)}| e^{-(\overline{M}_{28})^{(5)}t} &\leq \\ \frac{1}{(\overline{M}_{28})^{(5)}} &((a_{28})^{(5)} + (a_{28}')^{(5)} + (\overline{A}_{28})^{(5)} + (\widehat{P}_{28})^{(5)} (\widehat{k}_{28})^{(5)}) d \left(((G_{31})^{(1)}, (T_{31})^{(1)}); (G_{31})^{(2)}, (T_{31})^{(2)} \right) \end{aligned}$$

And analogous inequalities for G_i and T_i . Taking into account the hypothesis (35,35,36) the result follows-353

Remark 1: The fact that we supposed $(a_{28}'')^{(5)}$ and $(b_{28}'')^{(5)}$ depending also on t can be considered as not conformal with the reality, however we have put this hypothesis, in order that we can postulate condition necessary to prove the uniqueness of the solution bounded by $(\widehat{P}_{28})^{(5)} e^{(\overline{M}_{28})^{(5)}t}$ and $(\widehat{Q}_{28})^{(5)} e^{(\overline{M}_{28})^{(5)}t}$ respectively of \mathbb{R}_+ .

If instead of proving the existence of the solution on \mathbb{R}_+ , we have to prove it only on a compact then it suffices to consider that $(a_i'')^{(5)}$ and $(b_i'')^{(5)}, i = 28, 29, 30$ depend only on T_{29} and respectively on (G_{31}) (and not on t) and hypothesis can be replaced by a usual Lipschitz condition.-354

Remark 2: There does not exist any t where $G_i(t) = 0$ and $T_i(t) = 0$

From GLOBAL EQUATIONS it results

$$G_i(t) \geq G_i^0 e^{-\int_0^t \{ (a_i')^{(5)} - (a_i'')^{(5)} (T_{29}(s_{(28)}), s_{(28)}) \} ds_{(28)}} \geq 0$$

$$T_i(t) \geq T_i^0 e^{-(b_i')^{(5)}t} > 0 \text{ for } t > 0 \quad -355$$

Definition of $(\overline{M}_{28})^{(5)}_1, (\overline{M}_{28})^{(5)}_2$ and $(\overline{M}_{28})^{(5)}_3$:

Remark 3: if G_{28} is bounded, the same property have also G_{29} and G_{30} . indeed if

$$G_{28} < (\overline{M}_{28})^{(5)} \text{ it follows } \frac{dG_{29}}{dt} \leq ((\overline{M}_{28})^{(5)})_1 - (a_{29}')^{(5)} G_{29} \text{ and by integrating}$$

$$G_{29} \leq ((\overline{M}_{28})^{(5)})_2 = G_{29}^0 + 2(a_{29})^{(5)} ((\overline{M}_{28})^{(5)})_1 / (a_{29}')^{(5)}$$

In the same way, one can obtain

$$G_{30} \leq ((\overline{M}_{28})^{(5)})_3 = G_{30}^0 + 2(a_{30})^{(5)} ((\overline{M}_{28})^{(5)})_2 / (a_{30}')^{(5)}$$

If G_{29} or G_{30} is bounded, the same property follows for G_{28}, G_{30} and G_{28}, G_{29} respectively.-356

Remark 4: If G_{28} is bounded, from below, the same property holds for G_{29} and G_{30} . The proof is analogous with the preceding one. An analogous property is true if G_{29} is bounded from below.-357

Remark 5: If T_{28} is bounded from below and $\lim_{t \rightarrow \infty} ((b_i'')^{(5)} ((G_{31})(t), t)) = (b_{29}')^{(5)}$ then $T_{29} \rightarrow \infty$.

Definition of $(m)^{(5)}$ and ε_5 :

Indeed let t_5 be so that for $t > t_5$

$$(b_{29})^{(5)} - (b_i'')^{(5)} ((G_{31})(t), t) < \varepsilon_5, T_{28}(t) > (m)^{(5)} \quad -358$$

359

Then $\frac{dT_{29}}{dt} \geq (a_{29})^{(5)}(m)^{(5)} - \varepsilon_5 T_{29}$ which leads to

$$T_{29} \geq \left(\frac{(a_{29})^{(5)}(m)^{(5)}}{\varepsilon_5} \right) (1 - e^{-\varepsilon_5 t}) + T_{29}^0 e^{-\varepsilon_5 t}$$

If we take t such that $e^{-\varepsilon_5 t} = \frac{1}{2}$ it results

$$T_{29} \geq \left(\frac{(a_{29})^{(5)}(m)^{(5)}}{2} \right), \quad t = \log \frac{2}{\varepsilon_5}$$

By taking now ε_5 sufficiently small one sees that T_{29} is unbounded. The same property holds for T_{30} if $\lim_{t \rightarrow \infty} (b_{30}'')^{(5)}((G_{31})(t), t) = (b_{30}')^{(5)}$

We now state a more precise theorem about the behaviors at infinity of the solutions

Analogous inequalities hold also for $G_{33}, G_{34}, T_{32}, T_{33}, T_{34}$ -360

-361

It is now sufficient to take $\frac{(a_i)^{(6)}}{(\bar{M}_{32})^{(6)}}, \frac{(b_i)^{(6)}}{(\bar{M}_{32})^{(6)}} < 1$ and to choose

$(\hat{P}_{32})^{(6)}$ and $(\hat{Q}_{32})^{(6)}$ large to have -362

$$\frac{(a_i)^{(6)}}{(\bar{M}_{32})^{(6)}} \left[(\hat{P}_{32})^{(6)} + ((\hat{P}_{32})^{(6)} + G_j^0) e^{-\left(\frac{(\hat{P}_{32})^{(6)} + G_j^0}{G_j^0} \right)} \right] \leq (\hat{P}_{32})^{(6)} \quad -363$$

$$\frac{(b_i)^{(6)}}{(\bar{M}_{32})^{(6)}} \left[((\hat{Q}_{32})^{(6)} + T_j^0) e^{-\left(\frac{(\hat{Q}_{32})^{(6)} + T_j^0}{T_j^0} \right)} + (\hat{Q}_{32})^{(6)} \right] \leq (\hat{Q}_{32})^{(6)} \quad -364$$

In order that the operator $\mathcal{A}^{(6)}$ transforms the space of sextuples of functions G_i, T_i into itself -365

The operator $\mathcal{A}^{(6)}$ is a contraction with respect to the metric

$$d \left(((G_{35})^{(1)}, (T_{35})^{(1)}), ((G_{35})^{(2)}, (T_{35})^{(2)}) \right) =$$

$$\sup_i \{ \max_{t \in \mathbb{R}_+} |G_i^{(1)}(t) - G_i^{(2)}(t)| e^{-(\bar{M}_{32})^{(6)}t}, \max_{t \in \mathbb{R}_+} |T_i^{(1)}(t) - T_i^{(2)}(t)| e^{-(\bar{M}_{32})^{(6)}t} \}$$

Indeed if we denote

$$\text{Definition of } (\widehat{G_{35}}, \widehat{T_{35}}) : (\widehat{G_{35}}, \widehat{T_{35}}) = \mathcal{A}^{(6)}((G_{35}), (T_{35}))$$

It results

$$\begin{aligned} |\widehat{G}_{32}^{(1)} - \widehat{G}_{32}^{(2)}| &\leq \int_0^t (a_{32})^{(6)} |G_{33}^{(1)} - G_{33}^{(2)}| e^{-(\bar{M}_{32})^{(6)}s_{(32)}} e^{(\bar{M}_{32})^{(6)}s_{(32)}} ds_{(32)} + \\ &\int_0^t \{ (a_{32}')^{(6)} |G_{32}^{(1)} - G_{32}^{(2)}| e^{-(\bar{M}_{32})^{(6)}s_{(32)}} e^{-(\bar{M}_{32})^{(6)}s_{(32)}} + \\ &(a_{32}'')^{(6)} (T_{33}^{(1)}, s_{(32)}) |G_{32}^{(1)} - G_{32}^{(2)}| e^{-(\bar{M}_{32})^{(6)}s_{(32)}} e^{(\bar{M}_{32})^{(6)}s_{(32)}} + \\ &G_{32}^{(2)} |(a_{32}'')^{(6)} (T_{33}^{(1)}, s_{(32)}) - (a_{32}'')^{(6)} (T_{33}^{(2)}, s_{(32)})| e^{-(\bar{M}_{32})^{(6)}s_{(32)}} e^{(\bar{M}_{32})^{(6)}s_{(32)}} \} ds_{(32)} \end{aligned}$$

Where $s_{(32)}$ represents integrand that is integrated over the interval $[0, t]$

From the hypotheses it follows -366

367

$$(1) \quad (a_i')^{(1)}, (a_i'')^{(1)}, (b_i)^{(1)}, (b_i')^{(1)}, (b_i'')^{(1)} > 0, \\ i, j = 13, 14, 15$$

(2) The functions $(a_i'')^{(1)}, (b_i'')^{(1)}$ are positive continuous increasing and bounded.

Definition of $(p_i)^{(1)}, (r_i)^{(1)}$:

$$(a_i'')^{(1)}(T_{14}, t) \leq (p_i)^{(1)} \leq (\hat{A}_{13})^{(1)}$$

$$(b_i'')^{(1)}(G, t) \leq (r_i)^{(1)} \leq (b_i')^{(1)} \leq (\hat{B}_{13})^{(1)}$$

$$(3) \lim_{T_2 \rightarrow \infty} (a_i'')^{(1)}(T_{14}, t) = (p_i)^{(1)}$$

$$\lim_{G \rightarrow \infty} (b_i'')^{(1)}(G, t) = (r_i)^{(1)}$$

Definition of $(\hat{A}_{13})^{(1)}, (\hat{B}_{13})^{(1)}$:

Where $(\hat{A}_{13})^{(1)}, (\hat{B}_{13})^{(1)}, (p_i)^{(1)}, (r_i)^{(1)}$ are positive constants

and $i = 13, 14, 15$

They satisfy Lipschitz condition:

$$|(a_i'')^{(1)}(T_{14}, t) - (a_i'')^{(1)}(T_{14}, t)| \leq (\hat{k}_{13})^{(1)} |T_{14} - T'_{14}| e^{-(\hat{M}_{13})^{(1)}t}$$

$$|(b_i'')^{(1)}(G', t) - (b_i'')^{(1)}(G, T)| < (\hat{k}_{13})^{(1)} \|G - G'\| e^{-(\hat{M}_{13})^{(1)}t}$$

With the Lipschitz condition, we place a restriction on the behavior of functions $(a_i'')^{(1)}(T'_{14}, t)$ and $(a_i'')^{(1)}(T_{14}, t)$. (T'_{14}, t) and (T_{14}, t) are points belonging to the interval $[(\hat{k}_{13})^{(1)}, (\hat{M}_{13})^{(1)}]$. It is to be noted that $(a_i'')^{(1)}(T_{14}, t)$ is uniformly continuous. In the eventuality of the fact, that if $(\hat{M}_{13})^{(1)} = 1$ then the function $(a_i'')^{(1)}(T_{14}, t)$, the **first augmentation coefficient** attributable to terrestrial organisms, would be absolutely continuous.

Definition of $(\hat{M}_{13})^{(1)}, (\hat{k}_{13})^{(1)}$:

(V) $(\hat{M}_{13})^{(1)}, (\hat{k}_{13})^{(1)}$, are positive constants

$$\frac{(a_i)^{(1)}}{(\hat{M}_{13})^{(1)}}, \frac{(b_i)^{(1)}}{(\hat{M}_{13})^{(1)}} < 1$$

Definition of $(\hat{P}_{13})^{(1)}, (\hat{Q}_{13})^{(1)}$:

(W) There exists two constants $(\hat{P}_{13})^{(1)}$ and $(\hat{Q}_{13})^{(1)}$ which together with $(\hat{M}_{13})^{(1)}, (\hat{k}_{13})^{(1)}, (\hat{A}_{13})^{(1)}$ and $(\hat{B}_{13})^{(1)}$ and the constants $(a_i)^{(1)}, (a_i')^{(1)}, (b_i)^{(1)}, (b_i')^{(1)}, (p_i)^{(1)}, (r_i)^{(1)}, i = 13, 14, 15$, satisfy the inequalities

$$\frac{1}{(\hat{M}_{13})^{(1)}} [(a_i)^{(1)} + (a_i')^{(1)} + (\hat{A}_{13})^{(1)} + (\hat{P}_{13})^{(1)} (\hat{k}_{13})^{(1)}] < 1$$

$$\frac{1}{(\hat{M}_{13})^{(1)}} [(b_i)^{(1)} + (b_i')^{(1)} + (\hat{B}_{13})^{(1)} + (\hat{Q}_{13})^{(1)} (\hat{k}_{13})^{(1)}] < 1$$

$$|(G_{35})^{(1)} - (G_{35})^{(2)}| e^{-(\hat{M}_{32})^{(6)}t} \leq \frac{1}{(\hat{M}_{32})^{(6)}} ((a_{32})^{(6)} + (a'_{32})^{(6)} + (\hat{A}_{32})^{(6)} + (\hat{P}_{32})^{(6)} (\hat{k}_{32})^{(6)}) d((G_{35})^{(1)}, (T_{35})^{(1)}; (G_{35})^{(2)}, (T_{35})^{(2)}) \quad 368$$

And analogous inequalities for G_i and T_i . Taking into account the hypothesis the result follows

NOTE: SIMILAR ANALYSIS FOLLOWS FOR MODULE SEVEN

Remark 1: The fact that we supposed $(a_{32}'')^{(6)}$ and $(b_{32}'')^{(6)}$ depending also on t can be considered as not conformal with the reality, however we have put this hypothesis, in order that we can postulate condition necessary to prove the uniqueness of the solution bounded by $(\hat{P}_{32})^{(6)} e^{(\hat{M}_{32})^{(6)}t}$ and $(\hat{Q}_{32})^{(6)} e^{(\hat{M}_{32})^{(6)}t}$ respectively of \mathbb{R}_+ . 369

If instead of proving the existence of the solution on \mathbb{R}_+ , we have to prove it only on a compact then it suffices to consider that $(a_i'')^{(6)}$ and $(b_i'')^{(6)}, i = 32, 33, 34$ depend only on T_{33} and respectively on (G_{35}) (and not on t) and hypothesis can be replaced by a usual Lipschitz condition.

Remark 2: There does not exist any t where $G_i(t) = 0$ and $T_i(t) = 0$ 370

From GLOBAL EQUATIONS it results

$$G_i(t) \geq G_i^0 e^{-\int_0^t \{(a_i')^{(6)} - (a_i'')^{(6)}(T_{33}(s_{(32)}), s_{(32)})\} ds_{(32)}} \geq 0$$

$$T_i(t) \geq T_i^0 e^{-(b_i')^{(6)}t} > 0 \text{ for } t > 0$$

Definition of $(\hat{M}_{32})^{(6)}_1, (\hat{M}_{32})^{(6)}_2$ and $(\hat{M}_{32})^{(6)}_3$: 371

Remark 3: if G_{32} is bounded, the same property have also G_{33} and G_{34} . indeed if

$$G_{32} < (\hat{M}_{32})^{(6)} \text{ it follows } \frac{dG_{33}}{dt} \leq ((\hat{M}_{32})^{(6)})_1 - (a'_{33})^{(6)} G_{33} \text{ and by integrating}$$

$$G_{33} \leq ((\hat{M}_{32})^{(6)})_2 = G_{33}^0 + 2(a_{33})^{(6)} ((\hat{M}_{32})^{(6)})_1 / (a'_{33})^{(6)}$$

In the same way, one can obtain

$$G_{34} \leq ((\hat{M}_{32})^{(6)})_3 = G_{34}^0 + 2(a_{34})^{(6)} ((\hat{M}_{32})^{(6)})_2 / (a'_{34})^{(6)}$$

If G_{33} or G_{34} is bounded, the same property follows for G_{32} , G_{34} and G_{32} , G_{33} respectively.

Remark 4: If G_{32} is bounded, from below, the same property holds for G_{33} and G_{34} . The proof is analogous with the preceding one. An analogous property is true if G_{33} is bounded from below. 372

Remark 5: If T_{32} is bounded from below and $\lim_{t \rightarrow \infty} ((b_i'')^{(6)}((G_{35})(t), t)) = (b_{33}')^{(6)}$ then $T_{33} \rightarrow \infty$. 373

Definition of $(m)^{(6)}$ and ε_6 :

Indeed let t_6 be so that for $t > t_6$

$$(b_{33})^{(6)} - (b_i'')^{(6)}((G_{35})(t), t) < \varepsilon_6, T_{32}(t) > (m)^{(6)}$$

374
375

Then $\frac{dT_{33}}{dt} \geq (a_{33})^{(6)}(m)^{(6)} - \varepsilon_6 T_{33}$ which leads to

$$T_{33} \geq \left(\frac{(a_{33})^{(6)}(m)^{(6)}}{\varepsilon_6} \right) (1 - e^{-\varepsilon_6 t}) + T_{33}^0 e^{-\varepsilon_6 t} \text{ If we take } t \text{ such that } e^{-\varepsilon_6 t} = \frac{1}{2} \text{ it results}$$

$$T_{33} \geq \left(\frac{(a_{33})^{(6)}(m)^{(6)}}{2} \right), \quad t = \log \frac{2}{\varepsilon_6} \text{ By taking now } \varepsilon_6 \text{ sufficiently small one sees that } T_{33} \text{ is unbounded. The}$$

same property holds for T_{34} if $\lim_{t \rightarrow \infty} ((b_{34}'')^{(6)}((G_{35})(t), t(t), t)) = (b_{34}')^{(6)}$

We now state a more precise theorem about the behaviors at infinity of the solutions

(e) The operator $\mathcal{A}^{(7)}$ maps the space of functions satisfying 37,35,36 into itself .Indeed it is obvious that 376

$$G_{36}(t) \leq G_{36}^0 + \int_0^t \left[(a_{36})^{(7)} \left(G_{37}^0 + (\hat{P}_{36})^{(7)} e^{(\hat{M}_{36})^{(7)} s_{(36)}} \right) \right] ds_{(36)} = \\ (1 + (a_{36})^{(7)} t) G_{37}^0 + \frac{(a_{36})^{(7)} (\hat{P}_{36})^{(7)}}{(\hat{M}_{36})^{(7)}} \left(e^{(\hat{M}_{36})^{(7)} t} - 1 \right)$$

377

From which it follows that

$$(G_{36}(t) - G_{36}^0) e^{-(\hat{M}_{36})^{(7)} t} \leq \frac{(a_{36})^{(7)}}{(\hat{M}_{36})^{(7)}} \left[((\hat{P}_{36})^{(7)} + G_{37}^0) e^{-\left(\frac{(\hat{P}_{36})^{(7)} + G_{37}^0}{G_{37}^0} \right)} + (\hat{P}_{36})^{(7)} \right]$$

(G_i^0) is as defined in the statement of theorem 1

Analogous inequalities hold also for $G_{37}, G_{38}, T_{36}, T_{37}, T_{38}$

378

It is now sufficient to take $\frac{(a_i)^{(7)}}{(\hat{M}_{36})^{(7)}}, \frac{(b_i)^{(7)}}{(\hat{M}_{36})^{(7)}} < 1$ and to choose

$(\hat{P}_{36})^{(7)}$ and $(\hat{Q}_{36})^{(7)}$ large to have

$$\frac{(a_i)^{(7)}}{(\hat{M}_{36})^{(7)}} \left[(\hat{P}_{36})^{(7)} + ((\hat{P}_{36})^{(7)} + G_j^0) e^{-\left(\frac{(\hat{P}_{36})^{(7)} + G_j^0}{G_j^0} \right)} \right] \leq (\hat{P}_{36})^{(7)}$$

379

$$\frac{(b_i)^{(7)}}{(\hat{M}_{36})^{(7)}} \left[((\hat{Q}_{36})^{(7)} + T_j^0) e^{-\left(\frac{(\hat{Q}_{36})^{(7)} + T_j^0}{T_j^0} \right)} + (\hat{Q}_{36})^{(7)} \right] \leq (\hat{Q}_{36})^{(7)}$$

380

In order that the operator $\mathcal{A}^{(7)}$ transforms the space of sextuples of functions G_i, T_i satisfying GLOBAL EQUATIONS AND ITS CONCOMITANT CONDITIONALITIES into itself 381

The operator $\mathcal{A}^{(7)}$ is a contraction with respect to the metric

382
383

$$d \left(((G_{39})^{(1)}, (T_{39})^{(1)}), ((G_{39})^{(2)}, (T_{39})^{(2)}) \right) = \\ \sup_i \left\{ \max_{t \in \mathbb{R}_+} |G_i^{(1)}(t) - G_i^{(2)}(t)| e^{-(\hat{M}_{36})^{(7)} t}, \max_{t \in \mathbb{R}_+} |T_i^{(1)}(t) - T_i^{(2)}(t)| e^{-(\hat{M}_{36})^{(7)} t} \right\}$$

Indeed if we denote

Definition of $(\widetilde{G}_{39}), (\widetilde{T}_{39})$:

$$((\widetilde{G}_{39}), (\widetilde{T}_{39})) = \mathcal{A}^{(7)}((G_{39}), (T_{39}))$$

It results

$$|\tilde{G}_{36}^{(1)} - \tilde{G}_i^{(2)}| \leq \int_0^t (a_{36})^{(7)} |G_{37}^{(1)} - G_{37}^{(2)}| e^{-(\bar{M}_{36})^{(7)} s_{(36)}} e^{(\bar{M}_{36})^{(7)} s_{(36)}} ds_{(36)} + \int_0^t \{ (a'_{36})^{(7)} |G_{36}^{(1)} - G_{36}^{(2)}| e^{-(\bar{M}_{36})^{(7)} s_{(36)}} e^{-(\bar{M}_{36})^{(7)} s_{(36)}} + (a''_{36})^{(7)} (T_{37}^{(1)}, s_{(36)}) |G_{36}^{(1)} - G_{36}^{(2)}| e^{-(\bar{M}_{36})^{(7)} s_{(36)}} e^{(\bar{M}_{36})^{(7)} s_{(36)}} + G_{36}^{(2)} | (a''_{36})^{(7)} (T_{37}^{(1)}, s_{(36)}) - (a''_{36})^{(7)} (T_{37}^{(2)}, s_{(36)}) | e^{-(\bar{M}_{36})^{(7)} s_{(36)}} e^{(\bar{M}_{36})^{(7)} s_{(36)}} \} ds_{(36)}$$

Where $s_{(36)}$ represents integrand that is integrated over the interval $[0, t]$

From the hypotheses it follows

384

$$|(G_{39})^{(1)} - (G_{39})^{(2)}| e^{-(\bar{M}_{36})^{(7)} t} \leq \frac{1}{(\bar{M}_{36})^{(7)}} ((a_{36})^{(7)} + (a'_{36})^{(7)} + (\bar{A}_{36})^{(7)} + (\bar{P}_{36})^{(7)} (\bar{k}_{36})^{(7)}) d((G_{39})^{(1)}, (T_{39})^{(1)}; (G_{39})^{(2)}, (T_{39})^{(2)})$$

And analogous inequalities for G_i and T_i . Taking into account the hypothesis (37,35,36) the result follows

Remark 1: The fact that we supposed $(a''_{36})^{(7)}$ and $(b''_{36})^{(7)}$ depending also on t can be considered as not conformal with the reality, however we have put this hypothesis, in order that we can postulate condition necessary to prove the uniqueness of the solution bounded by $(\bar{P}_{36})^{(7)} e^{(\bar{M}_{36})^{(7)} t}$ and $(\bar{Q}_{36})^{(7)} e^{(\bar{M}_{36})^{(7)} t}$ respectively of \mathbb{R}_+ . 385

If instead of proving the existence of the solution on \mathbb{R}_+ , we have to prove it only on a compact then it suffices to consider that $(a''_i)^{(7)}$ and $(b''_i)^{(7)}$, $i = 36, 37, 38$ depend only on T_{37} and respectively on (G_{39}) (and not on t) and hypothesis can be replaced by a usual Lipschitz condition. 386

Remark 2: There does not exist any t where $G_i(t) = 0$ and $T_i(t) = 0$

From CONCATENATED GLOBAL EQUATIONS it results

$$G_i(t) \geq G_i^0 e^{-\int_0^t \{ (a'_i)^{(7)} - (a''_i)^{(7)} (T_{37}(s_{(36)}), s_{(36)}) \} ds_{(36)}} \geq 0$$

$$T_i(t) \geq T_i^0 e^{-(b'_i)^{(7)} t} > 0 \text{ for } t > 0$$

Definition of $((\bar{M}_{36})^{(7)})_1, ((\bar{M}_{36})^{(7)})_2$ and $((\bar{M}_{36})^{(7)})_3$: 387

Remark 3: if G_{36} is bounded, the same property have also G_{37} and G_{38} . indeed if

$$G_{36} < (\bar{M}_{36})^{(7)} \text{ it follows } \frac{dG_{37}}{dt} \leq ((\bar{M}_{36})^{(7)})_1 - (a'_{37})^{(7)} G_{37} \text{ and by integrating}$$

$$G_{37} \leq ((\bar{M}_{36})^{(7)})_2 = G_{37}^0 + 2(a_{37})^{(7)} ((\bar{M}_{36})^{(7)})_1 / (a'_{37})^{(7)}$$

In the same way, one can obtain

$$G_{38} \leq ((\bar{M}_{36})^{(7)})_3 = G_{38}^0 + 2(a_{38})^{(7)} ((\bar{M}_{36})^{(7)})_2 / (a'_{38})^{(7)}$$

If G_{37} or G_{38} is bounded, the same property follows for G_{36} , G_{38} and G_{36} , G_{37} respectively.

Remark 7: If G_{36} is bounded, from below, the same property holds for G_{37} and G_{38} . The proof is analogous with the preceding one. An analogous property is true if G_{37} is bounded from below. 388

Remark 5: If T_{36} is bounded from below and $\lim_{t \rightarrow \infty} ((b'_i)^{(7)} ((G_{39})(t), t)) = (b'_{37})^{(7)}$ then $T_{37} \rightarrow \infty$. 389

Definition of $(m)^{(7)}$ and ε_7 :

Indeed let t_7 be so that for $t > t_7$

$$(b_{37})^{(7)} - (b'_i)^{(7)} ((G_{39})(t), t) < \varepsilon_7, T_{36}(t) > (m)^{(7)}$$

Then $\frac{dT_{37}}{dt} \geq (a_{37})^{(7)} (m)^{(7)} - \varepsilon_7 T_{37}$ which leads to 390

$$T_{37} \geq \left(\frac{(a_{37})^{(7)} (m)^{(7)}}{\varepsilon_7} \right) (1 - e^{-\varepsilon_7 t}) + T_{37}^0 e^{-\varepsilon_7 t} \text{ If we take } t \text{ such that } e^{-\varepsilon_7 t} = \frac{1}{2} \text{ it results}$$

$$T_{37} \geq \left(\frac{(a_{37})^{(7)} (m)^{(7)}}{2} \right), \quad t = \log \frac{2}{\varepsilon_7} \text{ By taking now } \varepsilon_7 \text{ sufficiently small one sees that } T_{37} \text{ is unbounded. The}$$

same property holds for T_{38} if $\lim_{t \rightarrow \infty} (b''_{38})^{(7)} ((G_{39})(t), t) = (b'_{38})^{(7)}$

We now state a more precise theorem about the behaviors at infinity of the solutions

$$-(\sigma_2)^{(2)} \leq -(a'_{16})^{(2)} + (a'_{17})^{(2)} - (a''_{16})^{(2)}(T_{17}, t) + (a''_{17})^{(2)}(T_{17}, t) \leq -(\sigma_1)^{(2)} \quad 391$$

$$-(\tau_2)^{(2)} \leq -(b'_{16})^{(2)} + (b'_{17})^{(2)} - (b''_{16})^{(2)}(G_{19}, t) - (b''_{17})^{(2)}(G_{19}, t) \leq -(\tau_1)^{(2)} \quad 392$$

Definition of $(v_1)^{(2)}, (v_2)^{(2)}, (u_1)^{(2)}, (u_2)^{(2)}$: 393

By $(v_1)^{(2)} > 0, (v_2)^{(2)} < 0$ and respectively $(u_1)^{(2)} > 0, (u_2)^{(2)} < 0$ the roots 394

(a) of the equations $(a_{17})^{(2)}(v^{(2)})^2 + (\sigma_1)^{(2)}v^{(2)} - (a_{16})^{(2)} = 0$ 395

and $(b_{14})^{(2)}(u^{(2)})^2 + (\tau_1)^{(2)}u^{(2)} - (b_{16})^{(2)} = 0$ and 396

Definition of $(\bar{v}_1)^{(2)}, (\bar{v}_2)^{(2)}, (\bar{u}_1)^{(2)}, (\bar{u}_2)^{(2)}$: 397

By $(\bar{v}_1)^{(2)} > 0, (\bar{v}_2)^{(2)} < 0$ and respectively $(\bar{u}_1)^{(2)} > 0, (\bar{u}_2)^{(2)} < 0$ the 398

roots of the equations $(a_{17})^{(2)}(v^{(2)})^2 + (\sigma_2)^{(2)}v^{(2)} - (a_{16})^{(2)} = 0$ 399

and $(b_{17})^{(2)}(u^{(2)})^2 + (\tau_2)^{(2)}u^{(2)} - (b_{16})^{(2)} = 0$ 400

Definition of $(m_1)^{(2)}, (m_2)^{(2)}, (\mu_1)^{(2)}, (\mu_2)^{(2)}$:- 401

(b) If we define $(m_1)^{(2)}, (m_2)^{(2)}, (\mu_1)^{(2)}, (\mu_2)^{(2)}$ by 402

$$(m_2)^{(2)} = (v_0)^{(2)}, (m_1)^{(2)} = (v_1)^{(2)}, \text{ if } (v_0)^{(2)} < (v_1)^{(2)} \quad 403$$

$$(m_2)^{(2)} = (v_1)^{(2)}, (m_1)^{(2)} = (\bar{v}_1)^{(2)}, \text{ if } (v_1)^{(2)} < (v_0)^{(2)} < (\bar{v}_1)^{(2)}, \quad 404$$

and $(v_0)^{(2)} = \frac{G_{16}^0}{G_{17}^0}$

$$(m_2)^{(2)} = (v_1)^{(2)}, (m_1)^{(2)} = (v_0)^{(2)}, \text{ if } (\bar{v}_1)^{(2)} < (v_0)^{(2)} \quad 405$$

and analogously 406

$$(\mu_2)^{(2)} = (u_0)^{(2)}, (\mu_1)^{(2)} = (u_1)^{(2)}, \text{ if } (u_0)^{(2)} < (u_1)^{(2)}$$

$$(\mu_2)^{(2)} = (u_1)^{(2)}, (\mu_1)^{(2)} = (\bar{u}_1)^{(2)}, \text{ if } (u_1)^{(2)} < (u_0)^{(2)} < (\bar{u}_1)^{(2)},$$

and $(u_0)^{(2)} = \frac{T_{16}^0}{T_{17}^0}$

$$(\mu_2)^{(2)} = (u_1)^{(2)}, (\mu_1)^{(2)} = (u_0)^{(2)}, \text{ if } (\bar{u}_1)^{(2)} < (u_0)^{(2)} \quad 407$$

Then the solution satisfies the inequalities 408

$$G_{16}^0 e^{(S_1)^{(2)} - (p_{16})^{(2)}t} \leq G_{16}(t) \leq G_{16}^0 e^{(S_1)^{(2)}t}$$

$(p_i)^{(2)}$ is defined 409

$$\frac{1}{(m_1)^{(2)}} G_{16}^0 e^{(S_1)^{(2)} - (p_{16})^{(2)}t} \leq G_{17}(t) \leq \frac{1}{(m_2)^{(2)}} G_{16}^0 e^{(S_1)^{(2)}t} \quad 410$$

$$\left(\frac{(a_{18})^{(2)} G_{16}^0}{(m_1)^{(2)}((S_1)^{(2)} - (p_{16})^{(2)} - (S_2)^{(2)})} \left[e^{(S_1)^{(2)} - (p_{16})^{(2)}t} - e^{-(S_2)^{(2)}t} \right] + G_{18}^0 e^{-(S_2)^{(2)}t} \right) \leq G_{18}(t) \leq \quad 411$$

$$\frac{(a_{18})^{(2)} G_{16}^0}{(m_2)^{(2)}((S_1)^{(2)} - (a_{18})^{(2)})} \left[e^{(S_1)^{(2)}t} - e^{-(a_{18})^{(2)}t} \right] + G_{18}^0 e^{-(a_{18})^{(2)}t}$$

$$\boxed{T_{16}^0 e^{(R_1)^{(2)}t} \leq T_{16}(t) \leq T_{16}^0 e^{((R_1)^{(2)} + (r_{16})^{(2)})t} \quad 412$$

$$\frac{1}{(\mu_1)^{(2)}} T_{16}^0 e^{(R_1)^{(2)}t} \leq T_{16}(t) \leq \frac{1}{(\mu_2)^{(2)}} T_{16}^0 e^{((R_1)^{(2)} + (r_{16})^{(2)})t} \quad 413$$

$$\frac{(b_{18})^{(2)} T_{16}^0}{(\mu_1)^{(2)}((R_1)^{(2)} - (b_{18})^{(2)})} \left[e^{(R_1)^{(2)}t} - e^{-(b_{18})^{(2)}t} \right] + T_{18}^0 e^{-(b_{18})^{(2)}t} \leq T_{18}(t) \leq \quad 414$$

$$\frac{(a_{18})^{(2)} T_{16}^0}{(\mu_2)^{(2)}((R_1)^{(2)} + (r_{16})^{(2)} + (R_2)^{(2)})} \left[e^{((R_1)^{(2)} + (r_{16})^{(2)})t} - e^{-(R_2)^{(2)}t} \right] + T_{18}^0 e^{-(R_2)^{(2)}t}$$

Definition of $(S_1)^{(2)}, (S_2)^{(2)}, (R_1)^{(2)}, (R_2)^{(2)}$:- 415

Where $(S_1)^{(2)} = (a_{16})^{(2)}(m_2)^{(2)} - (a'_{16})^{(2)}$ 416

$$(S_2)^{(2)} = (a_{18})^{(2)} - (p_{18})^{(2)}$$

$$(R_1)^{(2)} = (b_{16})^{(2)}(\mu_2)^{(2)} - (b'_{16})^{(2)} \quad 417$$

$$(R_2)^{(2)} = (b_{18})^{(2)} - (r_{18})^{(2)}$$

Behavior of the solutions 418

If we denote and define 419

Definition of $(\sigma_1)^{(3)}, (\sigma_2)^{(3)}, (\tau_1)^{(3)}, (\tau_2)^{(3)}$:

(a) $\sigma_1^{(3)}, \sigma_2^{(3)}, \tau_1^{(3)}, \tau_2^{(3)}$ four constants satisfying

$$-(\sigma_2)^{(3)} \leq -(a'_{20})^{(3)} + (a'_{21})^{(3)} - (a''_{20})^{(3)}(T_{21}, t) + (a''_{21})^{(3)}(T_{21}, t) \leq -(\sigma_1)^{(3)}$$

$$-(\tau_2)^{(3)} \leq -(b'_{20})^{(3)} + (b'_{21})^{(3)} - (b''_{20})^{(3)}(G, t) - (b''_{21})^{(3)}(G_{23}, t) \leq -(\tau_1)^{(3)}$$

Definition of $(v_1)^{(3)}, (v_2)^{(3)}, (u_1)^{(3)}, (u_2)^{(3)}$: 420

(b) By $(v_1)^{(3)} > 0, (v_2)^{(3)} < 0$ and respectively $(u_1)^{(3)} > 0, (u_2)^{(3)} < 0$ the roots of the equations

$$(a_{21})^{(3)}(v^{(3)})^2 + (\sigma_1)^{(3)}v^{(3)} - (a_{20})^{(3)} = 0$$

and $(b_{21})^{(3)}(u^{(3)})^2 + (\tau_1)^{(3)}u^{(3)} - (b_{20})^{(3)} = 0$ and

By $(\bar{v}_1)^{(3)} > 0, (\bar{v}_2)^{(3)} < 0$ and respectively $(\bar{u}_1)^{(3)} > 0, (\bar{u}_2)^{(3)} < 0$ the

roots of the equations $(a_{21})^{(3)}(v^{(3)})^2 + (\sigma_2)^{(3)}v^{(3)} - (a_{20})^{(3)} = 0$

and $(b_{21})^{(3)}(u^{(3)})^2 + (\tau_2)^{(3)}u^{(3)} - (b_{20})^{(3)} = 0$

Definition of $(m_1)^{(3)}, (m_2)^{(3)}, (\mu_1)^{(3)}, (\mu_2)^{(3)}$:- 421

(c) If we define $(m_1)^{(3)}, (m_2)^{(3)}, (\mu_1)^{(3)}, (\mu_2)^{(3)}$ by
 $(m_2)^{(3)} = (v_0)^{(3)}, (m_1)^{(3)} = (v_1)^{(3)}$, **if** $(v_0)^{(3)} < (v_1)^{(3)}$
 $(m_2)^{(3)} = (v_1)^{(3)}, (m_1)^{(3)} = (\bar{v}_1)^{(3)}$, **if** $(v_1)^{(3)} < (v_0)^{(3)} < (\bar{v}_1)^{(3)}$,

and $(v_0)^{(3)} = \frac{G_{20}^0}{G_{21}^0}$

$(m_2)^{(3)} = (v_1)^{(3)}, (m_1)^{(3)} = (v_0)^{(3)}$, **if** $(\bar{v}_1)^{(3)} < (v_0)^{(3)}$
 and analogously 422

$(\mu_2)^{(3)} = (u_0)^{(3)}, (\mu_1)^{(3)} = (u_1)^{(3)}$, **if** $(u_0)^{(3)} < (u_1)^{(3)}$

$(\mu_2)^{(3)} = (u_1)^{(3)}, (\mu_1)^{(3)} = (\bar{u}_1)^{(3)}$, **if** $(u_1)^{(3)} < (u_0)^{(3)} < (\bar{u}_1)^{(3)}$, and $(u_0)^{(3)} = \frac{T_{20}^0}{T_{21}^0}$

$(\mu_2)^{(3)} = (u_1)^{(3)}, (\mu_1)^{(3)} = (u_0)^{(3)}$, **if** $(\bar{u}_1)^{(3)} < (u_0)^{(3)}$

Then the solution satisfies the inequalities

$G_{20}^0 e^{((S_1)^{(3)} - (p_{20})^{(3)})t} \leq G_{20}(t) \leq G_{20}^0 e^{(S_1)^{(3)}t}$ 423

$(p_i)^{(3)}$ is defined 424
 $\frac{1}{(m_1)^{(3)}} G_{20}^0 e^{((S_1)^{(3)} - (p_{20})^{(3)})t} \leq G_{21}(t) \leq \frac{1}{(m_2)^{(3)}} G_{20}^0 e^{(S_1)^{(3)}t}$

$\left(\frac{(a_{22})^{(3)} G_{20}^0}{(m_1)^{(3)}((S_1)^{(3)} - (p_{20})^{(3)} - (S_2)^{(3)})} \left[e^{((S_1)^{(3)} - (p_{20})^{(3)})t} - e^{-(S_2)^{(3)}t} \right] + G_{22}^0 e^{-(S_2)^{(3)}t} \right) \leq G_{22}(t) \leq$ 425

$\frac{(a_{22})^{(3)} G_{20}^0}{(m_2)^{(3)}((S_1)^{(3)} - (a'_{22})^{(3)})} \left[e^{(S_1)^{(3)}t} - e^{-(a'_{22})^{(3)}t} \right] + G_{22}^0 e^{-(a'_{22})^{(3)}t}$
 $\left[T_{20}^0 e^{(R_1)^{(3)}t} \leq T_{20}(t) \leq T_{20}^0 e^{((R_1)^{(3)} + (r_{20})^{(3)})t} \right]$ 426

$\frac{1}{(\mu_1)^{(3)}} T_{20}^0 e^{(R_1)^{(3)}t} \leq T_{20}(t) \leq \frac{1}{(\mu_2)^{(3)}} T_{20}^0 e^{((R_1)^{(3)} + (r_{20})^{(3)})t}$ 427

$\frac{(b_{22})^{(3)} T_{20}^0}{(\mu_1)^{(3)}((R_1)^{(3)} - (b_{22})^{(3)})} \left[e^{(R_1)^{(3)}t} - e^{-(b_{22})^{(3)}t} \right] + T_{22}^0 e^{-(b_{22})^{(3)}t} \leq T_{22}(t) \leq$ 428

$\frac{(a_{22})^{(3)} T_{20}^0}{(\mu_2)^{(3)}((R_1)^{(3)} + (r_{20})^{(3)} + (R_2)^{(3)})} \left[e^{((R_1)^{(3)} + (r_{20})^{(3)})t} - e^{-(R_2)^{(3)}t} \right] + T_{22}^0 e^{-(R_2)^{(3)}t}$ 429

Definition of $(S_1)^{(3)}, (S_2)^{(3)}, (R_1)^{(3)}, (R_2)^{(3)}$:-

Where $(S_1)^{(3)} = (a_{20})^{(3)}(m_2)^{(3)} - (a'_{20})^{(3)}$

$(S_2)^{(3)} = (a_{22})^{(3)} - (p_{22})^{(3)}$

$(R_1)^{(3)} = (b_{20})^{(3)}(\mu_2)^{(3)} - (b'_{20})^{(3)}$

$(R_2)^{(3)} = (b_{22})^{(3)} - (r_{22})^{(3)}$

430

431

432

If we denote and define

Definition of $(\sigma_1)^{(4)}, (\sigma_2)^{(4)}, (\tau_1)^{(4)}, (\tau_2)^{(4)}$:

(d) $(\sigma_1)^{(4)}, (\sigma_2)^{(4)}, (\tau_1)^{(4)}, (\tau_2)^{(4)}$ four constants satisfying

$-(\sigma_2)^{(4)} \leq -(a'_{24})^{(4)} + (a'_{25})^{(4)} - (a''_{24})^{(4)}(T_{25}, t) + (a''_{25})^{(4)}(T_{25}, t) \leq -(\sigma_1)^{(4)}$

$-(\tau_2)^{(4)} \leq -(b'_{24})^{(4)} + (b'_{25})^{(4)} - (b''_{24})^{(4)}((G_{27}), t) - (b''_{25})^{(4)}((G_{27}), t) \leq -(\tau_1)^{(4)}$

Definition of $(v_1)^{(4)}, (v_2)^{(4)}, (u_1)^{(4)}, (u_2)^{(4)}, v^{(4)}, u^{(4)}$: 433

(e) By $(v_1)^{(4)} > 0, (v_2)^{(4)} < 0$ and respectively $(u_1)^{(4)} > 0, (u_2)^{(4)} < 0$ the roots of the equations

$(a_{25})^{(4)}(v^{(4)})^2 + (\sigma_1)^{(4)}v^{(4)} - (a_{24})^{(4)} = 0$

and $(b_{25})^{(4)}(u^{(4)})^2 + (\tau_1)^{(4)}u^{(4)} - (b_{24})^{(4)} = 0$ and

Definition of $(\bar{v}_1)^{(4)}, (\bar{v}_2)^{(4)}, (\bar{u}_1)^{(4)}, (\bar{u}_2)^{(4)}$: 434

435

By $(\bar{v}_1)^{(4)} > 0, (\bar{v}_2)^{(4)} < 0$ and respectively $(\bar{u}_1)^{(4)} > 0, (\bar{u}_2)^{(4)} < 0$ the

roots of the equations $(a_{25})^{(4)}(v^{(4)})^2 + (\sigma_2)^{(4)}v^{(4)} - (a_{24})^{(4)} = 0$

and $(b_{25})^{(4)}(u^{(4)})^2 + (\tau_2)^{(4)}u^{(4)} - (b_{24})^{(4)} = 0$

Definition of $(m_1)^{(4)}, (m_2)^{(4)}, (\mu_1)^{(4)}, (\mu_2)^{(4)}, (v_0)^{(4)}$:- 436

(f) If we define $(m_1)^{(4)}, (m_2)^{(4)}, (\mu_1)^{(4)}, (\mu_2)^{(4)}$ by

$$(m_2)^{(4)} = (v_0)^{(4)}, (m_1)^{(4)} = (v_1)^{(4)}, \text{ if } (v_0)^{(4)} < (v_1)^{(4)}$$

$$(m_2)^{(4)} = (v_1)^{(4)}, (m_1)^{(4)} = (\bar{v}_1)^{(4)}, \text{ if } (v_4)^{(4)} < (v_0)^{(4)} < (\bar{v}_1)^{(4)},$$

$$\text{and } \boxed{(v_0)^{(4)} = \frac{G_{24}^0}{G_{25}^0}}$$

$$(m_2)^{(4)} = (v_4)^{(4)}, (m_1)^{(4)} = (v_0)^{(4)}, \text{ if } (\bar{v}_4)^{(4)} < (v_0)^{(4)}$$

and analogously 437

$$(\mu_2)^{(4)} = (u_0)^{(4)}, (\mu_1)^{(4)} = (u_1)^{(4)}, \text{ if } (u_0)^{(4)} < (u_1)^{(4)}$$

$$(\mu_2)^{(4)} = (u_1)^{(4)}, (\mu_1)^{(4)} = (\bar{u}_1)^{(4)}, \text{ if } (u_1)^{(4)} < (u_0)^{(4)} < (\bar{u}_1)^{(4)},$$

$$\text{and } \boxed{(u_0)^{(4)} = \frac{T_{24}^0}{T_{25}^0}}$$

$(\mu_2)^{(4)} = (u_1)^{(4)}, (\mu_1)^{(4)} = (u_0)^{(4)}, \text{ if } (\bar{u}_1)^{(4)} < (u_0)^{(4)}$ where $(u_1)^{(4)}, (\bar{u}_1)^{(4)}$ are defined respectively 438

Then the solution satisfies the inequalities 439

$$G_{24}^0 e^{((S_1)^{(4)} - (p_{24})^{(4)})t} \leq G_{24}(t) \leq G_{24}^0 e^{(S_1)^{(4)}t}$$

where $(p_j)^{(4)}$ is defined 440

$$\frac{1}{(m_1)^{(4)}} G_{24}^0 e^{((S_1)^{(4)} - (p_{24})^{(4)})t} \leq G_{25}(t) \leq \frac{1}{(m_2)^{(4)}} G_{24}^0 e^{(S_1)^{(4)}t}$$

$$\left(\frac{(a_{26})^{(4)} G_{24}^0}{(m_1)^{(4)} ((S_1)^{(4)} - (p_{24})^{(4)} - (S_2)^{(4)})} \left[e^{((S_1)^{(4)} - (p_{24})^{(4)})t} - e^{-(S_2)^{(4)}t} \right] + G_{26}^0 e^{-(S_2)^{(4)}t} \right) \leq G_{26}(t) \leq (a_{26})^{(4)} G_{24}^0 e^{(S_1)^{(4)}t} + G_{26}^0 e^{-(S_2)^{(4)}t}$$

$$\boxed{T_{24}^0 e^{(R_1)^{(4)}t} \leq T_{24}(t) \leq T_{24}^0 e^{((R_1)^{(4)} + (r_{24})^{(4)})t}}$$

$$\frac{1}{(\mu_1)^{(4)}} T_{24}^0 e^{(R_1)^{(4)}t} \leq T_{24}(t) \leq \frac{1}{(\mu_2)^{(4)}} T_{24}^0 e^{((R_1)^{(4)} + (r_{24})^{(4)})t}$$

$$\frac{(b_{26})^{(4)} T_{24}^0}{(\mu_1)^{(4)} ((R_1)^{(4)} - (b'_{26})^{(4)})} \left[e^{(R_1)^{(4)}t} - e^{-(b'_{26})^{(4)}t} \right] + T_{26}^0 e^{-(b'_{26})^{(4)}t} \leq T_{26}(t) \leq$$

$$\frac{(a_{26})^{(4)} T_{24}^0}{(\mu_2)^{(4)} ((R_1)^{(4)} + (r_{24})^{(4)} + (R_2)^{(4)})} \left[e^{((R_1)^{(4)} + (r_{24})^{(4)})t} - e^{-(R_2)^{(4)}t} \right] + T_{26}^0 e^{-(R_2)^{(4)}t}$$

Definition of $(S_1)^{(4)}, (S_2)^{(4)}, (R_1)^{(4)}, (R_2)^{(4)}$:- 442

Where $(S_1)^{(4)} = (a_{24})^{(4)}(m_2)^{(4)} - (a'_{24})^{(4)}$

$$(S_2)^{(4)} = (a_{26})^{(4)} - (p_{26})^{(4)}$$

$$(R_1)^{(4)} = (b_{24})^{(4)}(\mu_2)^{(4)} - (b'_{24})^{(4)}$$

$$(R_2)^{(4)} = (b'_{26})^{(4)} - (r_{26})^{(4)} 453$$

Behavior of the solutions

454

If we denote and define

Definition of $(\sigma_1)^{(5)}, (\sigma_2)^{(5)}, (\tau_1)^{(5)}, (\tau_2)^{(5)}$:

(g) $(\sigma_1)^{(5)}, (\sigma_2)^{(5)}, (\tau_1)^{(5)}, (\tau_2)^{(5)}$ four constants satisfying

$$-(\sigma_2)^{(5)} \leq -(a'_{28})^{(5)} + (a'_{29})^{(5)} - (a''_{28})^{(5)}(T_{29}, t) + (a''_{29})^{(5)}(T_{29}, t) \leq -(\sigma_1)^{(5)}$$

$$-(\tau_2)^{(5)} \leq -(b'_{28})^{(5)} + (b'_{29})^{(5)} - (b''_{28})^{(5)}((G_{31}), t) - (b''_{29})^{(5)}((G_{31}), t) \leq -(\tau_1)^{(5)}$$

Definition of $(v_1)^{(5)}, (v_2)^{(5)}, (u_1)^{(5)}, (u_2)^{(5)}, v^{(5)}, u^{(5)}$:

455

(h) By $(v_1)^{(5)} > 0, (v_2)^{(5)} < 0$ and respectively $(u_1)^{(5)} > 0, (u_2)^{(5)} < 0$ the roots of the equations

$$(a_{29})^{(5)}(v^{(5)})^2 + (\sigma_1)^{(5)}v^{(5)} - (a_{28})^{(5)} = 0$$

$$\text{and } (b_{29})^{(5)}(u^{(5)})^2 + (\tau_1)^{(5)}u^{(5)} - (b_{28})^{(5)} = 0 \text{ and}$$

Definition of $(\bar{v}_1)^{(5)}, (\bar{v}_2)^{(5)}, (\bar{u}_1)^{(5)}, (\bar{u}_2)^{(5)}$:

456

By $(\bar{v}_1)^{(5)} > 0, (\bar{v}_2)^{(5)} < 0$ and respectively $(\bar{u}_1)^{(5)} > 0, (\bar{u}_2)^{(5)} < 0$ the

roots of the equations $(a_{29})^{(5)}(v^{(5)})^2 + (\sigma_2)^{(5)}v^{(5)} - (a_{28})^{(5)} = 0$

and $(b_{29})^{(5)}(u^{(5)})^2 + (\tau_2)^{(5)}u^{(5)} - (b_{28})^{(5)} = 0$

Definition of $(m_1)^{(5)}, (m_2)^{(5)}, (\mu_1)^{(5)}, (\mu_2)^{(5)}, (v_0)^{(5)}$:-

(i) If we define $(m_1)^{(5)}, (m_2)^{(5)}, (\mu_1)^{(5)}, (\mu_2)^{(5)}$ by

$$(m_2)^{(5)} = (v_0)^{(5)}, (m_1)^{(5)} = (v_1)^{(5)}, \text{ if } (v_0)^{(5)} < (v_1)^{(5)}$$

$$(m_2)^{(5)} = (v_1)^{(5)}, (m_1)^{(5)} = (\bar{v}_1)^{(5)}, \text{ if } (v_1)^{(5)} < (v_0)^{(5)} < (\bar{v}_1)^{(5)},$$

$$\text{and } (v_0)^{(5)} = \frac{a_{28}^0}{a_{29}^0}$$

$$(m_2)^{(5)} = (v_1)^{(5)}, (m_1)^{(5)} = (v_0)^{(5)}, \text{ if } (\bar{v}_1)^{(5)} < (v_0)^{(5)}$$

and analogously

457

$$(\mu_2)^{(5)} = (u_0)^{(5)}, (\mu_1)^{(5)} = (u_1)^{(5)}, \text{ if } (u_0)^{(5)} < (u_1)^{(5)}$$

$$(\mu_2)^{(5)} = (u_1)^{(5)}, (\mu_1)^{(5)} = (\bar{u}_1)^{(5)}, \text{ if } (u_1)^{(5)} < (u_0)^{(5)} < (\bar{u}_1)^{(5)},$$

$$\text{and } (u_0)^{(5)} = \frac{T_{28}^0}{T_{29}^0}$$

$(\mu_2)^{(5)} = (u_1)^{(5)}, (\mu_1)^{(5)} = (u_0)^{(5)}, \text{ if } (\bar{u}_1)^{(5)} < (u_0)^{(5)}$ where $(u_1)^{(5)}, (\bar{u}_1)^{(5)}$ are defined respectively

Then the solution satisfies the inequalities

458

$$G_{28}^0 e^{((S_1)^{(5)} - (p_{28})^{(5)})t} \leq G_{28}(t) \leq G_{28}^0 e^{(S_1)^{(5)}t}$$

where $(p_i)^{(5)}$ is defined

$$\frac{1}{(m_5)^{(5)}} G_{28}^0 e^{((S_1)^{(5)} - (p_{28})^{(5)})t} \leq G_{29}(t) \leq \frac{1}{(m_2)^{(5)}} G_{28}^0 e^{(S_1)^{(5)}t}$$

459

$$\left(\frac{(a_{30})^{(5)} G_{28}^0}{(m_1)^{(5)} ((S_1)^{(5)} - (p_{28})^{(5)}) - (S_2)^{(5)}} \right) \left[e^{((S_1)^{(5)} - (p_{28})^{(5)})t} - e^{-(S_2)^{(5)}t} \right] + G_{30}^0 e^{-(S_2)^{(5)}t} \leq G_{30}(t) \leq (a_{30})^{(5)} G_{28}^0 (m_2)^{(5)} (S_1)^{(5)} - (a_{30})^{(5)} 5e^{(S_1)^{(5)}t} - e^{-(a_{30})^{(5)}t} + G_{30}^0 e^{-(a_{30})^{(5)}t}$$

460

461

$$\boxed{T_{28}^0 e^{(R_1)^{(5)}t} \leq T_{28}(t) \leq T_{28}^0 e^{((R_1)^{(5)}+(r_{28})^{(5)})t}} \quad 462$$

$$\frac{1}{(\mu_1)^{(5)}} T_{28}^0 e^{(R_1)^{(5)}t} \leq T_{28}(t) \leq \frac{1}{(\mu_2)^{(5)}} T_{28}^0 e^{((R_1)^{(5)}+(r_{28})^{(5)})t} \quad 463$$

$$\frac{(b_{30})^{(5)} T_{28}^0}{(\mu_1)^{(5)}((R_1)^{(5)}-(b_{30})^{(5)})} \left[e^{(R_1)^{(5)}t} - e^{-(b_{30})^{(5)}t} \right] + T_{30}^0 e^{-(b_{30})^{(5)}t} \leq T_{30}(t) \leq \quad 464$$

$$\frac{(a_{30})^{(5)} T_{28}^0}{(\mu_2)^{(5)}((R_1)^{(5)}+(r_{28})^{(5)}+(R_2)^{(5)})} \left[e^{((R_1)^{(5)}+(r_{28})^{(5)})t} - e^{-(R_2)^{(5)}t} \right] + T_{30}^0 e^{-(R_2)^{(5)}t}$$

Definition of $(S_1)^{(5)}, (S_2)^{(5)}, (R_1)^{(5)}, (R_2)^{(5)}$:- 465

Where $(S_1)^{(5)} = (a_{28})^{(5)}(m_2)^{(5)} - (a'_{28})^{(5)}$

$$(S_2)^{(5)} = (a_{30})^{(5)} - (p_{30})^{(5)}$$

$$(R_1)^{(5)} = (b_{28})^{(5)}(\mu_2)^{(5)} - (b'_{28})^{(5)}$$

$$(R_2)^{(5)} = (b'_{30})^{(5)} - (r_{30})^{(5)}$$

Behavior of the solutions 466

If we denote and define

Definition of $(\sigma_1)^{(6)}, (\sigma_2)^{(6)}, (\tau_1)^{(6)}, (\tau_2)^{(6)}$:

(j) $(\sigma_1)^{(6)}, (\sigma_2)^{(6)}, (\tau_1)^{(6)}, (\tau_2)^{(6)}$ four constants satisfying

$$-(\sigma_2)^{(6)} \leq -(a'_{32})^{(6)} + (a'_{33})^{(6)} - (a''_{32})^{(6)}(T_{33}, t) + (a''_{33})^{(6)}(T_{33}, t) \leq -(\sigma_1)^{(6)}$$

$$-(\tau_2)^{(6)} \leq -(b'_{32})^{(6)} + (b'_{33})^{(6)} - (b''_{32})^{(6)}((G_{35}), t) - (b''_{33})^{(6)}((G_{35}), t) \leq -(\tau_1)^{(6)}$$

Definition of $(v_1)^{(6)}, (v_2)^{(6)}, (u_1)^{(6)}, (u_2)^{(6)}, v^{(6)}, u^{(6)}$: 467

(k) By $(v_1)^{(6)} > 0, (v_2)^{(6)} < 0$ and respectively $(u_1)^{(6)} > 0, (u_2)^{(6)} < 0$ the roots of the equations

$$(a_{33})^{(6)}(v^{(6)})^2 + (\sigma_1)^{(6)}v^{(6)} - (a_{32})^{(6)} = 0$$

$$\text{and } (b_{33})^{(6)}(u^{(6)})^2 + (\tau_1)^{(6)}u^{(6)} - (b_{32})^{(6)} = 0 \text{ and}$$

Definition of $(\bar{v}_1)^{(6)}, (\bar{v}_2)^{(6)}, (\bar{u}_1)^{(6)}, (\bar{u}_2)^{(6)}$: 468

By $(\bar{v}_1)^{(6)} > 0, (\bar{v}_2)^{(6)} < 0$ and respectively $(\bar{u}_1)^{(6)} > 0, (\bar{u}_2)^{(6)} < 0$ the

roots of the equations $(a_{33})^{(6)}(v^{(6)})^2 + (\sigma_2)^{(6)}v^{(6)} - (a_{32})^{(6)} = 0$

$$\text{and } (b_{33})^{(6)}(u^{(6)})^2 + (\tau_2)^{(6)}u^{(6)} - (b_{32})^{(6)} = 0$$

Definition of $(m_1)^{(6)}, (m_2)^{(6)}, (\mu_1)^{(6)}, (\mu_2)^{(6)}, (v_0)^{(6)}$:-

(l) If we define $(m_1)^{(6)}, (m_2)^{(6)}, (\mu_1)^{(6)}, (\mu_2)^{(6)}$ by

$$(m_2)^{(6)} = (v_0)^{(6)}, (m_1)^{(6)} = (v_1)^{(6)}, \text{ if } (v_0)^{(6)} < (v_1)^{(6)}$$

$$(m_2)^{(6)} = (v_1)^{(6)}, (m_1)^{(6)} = (\bar{v}_6)^{(6)}, \text{ if } (v_1)^{(6)} < (v_0)^{(6)} < (\bar{v}_1)^{(6)},$$

$$\text{and } \boxed{(v_0)^{(6)} = \frac{a_{32}^0}{a_{33}^0}}$$

470

$$(m_2)^{(6)} = (v_1)^{(6)}, (m_1)^{(6)} = (v_0)^{(6)}, \text{ if } (\bar{v}_1)^{(6)} < (v_0)^{(6)}$$

and analogously 471

$$(\mu_2)^{(6)} = (u_0)^{(6)}, (\mu_1)^{(6)} = (u_1)^{(6)}, \text{ if } (u_0)^{(6)} < (u_1)^{(6)}$$

$$(\mu_2)^{(6)} = (u_1)^{(6)}, (\mu_1)^{(6)} = (\bar{u}_1)^{(6)}, \text{ if } (u_1)^{(6)} < (u_0)^{(6)} < (\bar{u}_1)^{(6)},$$

and $(u_0)^{(6)} = \frac{T_{32}^0}{T_{33}^0}$

$(\mu_2)^{(6)} = (u_1)^{(6)}, (\mu_1)^{(6)} = (u_0)^{(6)}, \text{ if } (\bar{u}_1)^{(6)} < (u_0)^{(6)}$ where $(u_1)^{(6)}, (\bar{u}_1)^{(6)}$ are defined respectively

Then the solution satisfies the inequalities

472

$$G_{32}^0 e^{((S_1)^{(6)} - (p_{32})^{(6)})t} \leq G_{32}(t) \leq G_{32}^0 e^{(S_1)^{(6)}t}$$

where $(p_i)^{(6)}$ is defined

$$\frac{1}{(m_1)^{(6)}} G_{32}^0 e^{((S_1)^{(6)} - (p_{32})^{(6)})t} \leq G_{33}(t) \leq \frac{1}{(m_2)^{(6)}} G_{32}^0 e^{(S_1)^{(6)}t}$$

473

$$\left(\frac{(a_{34})^{(6)} G_{32}^0}{(m_1)^{(6)} ((S_1)^{(6)} - (p_{32})^{(6)} - (S_2)^{(6)})} \right) \left[e^{((S_1)^{(6)} - (p_{32})^{(6)})t} - e^{-(S_2)^{(6)}t} \right] + G_{34}^0 e^{-(S_2)^{(6)}t} \leq G_{34}(t) \leq (a_{34})^{(6)} G_{32}^0 (m_2)^{(6)} (S_1)^{(6)} - (a_{34}')^{(6)} e^{(S_1)^{(6)}t} + G_{34}^0 e^{-(a_{34}')^{(6)}t}$$

474

$$T_{32}^0 e^{(R_1)^{(6)}t} \leq T_{32}(t) \leq T_{32}^0 e^{((R_1)^{(6)} + (r_{32})^{(6)})t}$$

475

$$\frac{1}{(\mu_1)^{(6)}} T_{32}^0 e^{(R_1)^{(6)}t} \leq T_{32}(t) \leq \frac{1}{(\mu_2)^{(6)}} T_{32}^0 e^{((R_1)^{(6)} + (r_{32})^{(6)})t}$$

476

$$\frac{(b_{34})^{(6)} T_{32}^0}{(\mu_1)^{(6)} ((R_1)^{(6)} - (b_{34})^{(6)})} \left[e^{(R_1)^{(6)}t} - e^{-(b_{34}')^{(6)}t} \right] + T_{34}^0 e^{-(b_{34}')^{(6)}t} \leq T_{34}(t) \leq$$

477

$$\frac{(a_{34})^{(6)} T_{32}^0}{(\mu_2)^{(6)} ((R_1)^{(6)} + (r_{32})^{(6)} + (R_2)^{(6)})} \left[e^{((R_1)^{(6)} + (r_{32})^{(6)})t} - e^{-(R_2)^{(6)}t} \right] + T_{34}^0 e^{-(R_2)^{(6)}t}$$

Definition of $(S_1)^{(6)}, (S_2)^{(6)}, (R_1)^{(6)}, (R_2)^{(6)}$:-

478

Where $(S_1)^{(6)} = (a_{32})^{(6)} (m_2)^{(6)} - (a'_{32})^{(6)}$

$$(S_2)^{(6)} = (a_{34})^{(6)} - (p_{34})^{(6)}$$

$$(R_1)^{(6)} = (b_{32})^{(6)} (\mu_2)^{(6)} - (b'_{32})^{(6)}$$

$$(R_2)^{(6)} = (b'_{34})^{(6)} - (r_{34})^{(6)}$$

479

If we denote and define

Definition of $(\sigma_1)^{(7)}, (\sigma_2)^{(7)}, (\tau_1)^{(7)}, (\tau_2)^{(7)}$:

(m) $(\sigma_1)^{(7)}, (\sigma_2)^{(7)}, (\tau_1)^{(7)}, (\tau_2)^{(7)}$ four constants satisfying

$$-(\sigma_2)^{(7)} \leq -(a'_{36})^{(7)} + (a'_{37})^{(7)} - (a''_{36})^{(7)} (T_{37}, t) + (a''_{37})^{(7)} (T_{37}, t) \leq -(\sigma_1)^{(7)}$$

$$-(\tau_2)^{(7)} \leq -(b'_{36})^{(7)} + (b'_{37})^{(7)} - (b''_{36})^{(7)} (G_{39}, t) - (b''_{37})^{(7)} (G_{39}, t) \leq -(\tau_1)^{(7)}$$

Definition of $(v_1)^{(7)}, (v_2)^{(7)}, (u_1)^{(7)}, (u_2)^{(7)}, v^{(7)}, u^{(7)}$:

480

(n) By $(v_1)^{(7)} > 0, (v_2)^{(7)} < 0$ and respectively $(u_1)^{(7)} > 0, (u_2)^{(7)} < 0$ the roots of the equations

$$(a_{37})^{(7)} (v^{(7)})^2 + (\sigma_1)^{(7)} v^{(7)} - (a_{36})^{(7)} = 0$$

481

$$\text{and } (b_{37})^{(7)} (u^{(7)})^2 + (\tau_1)^{(7)} u^{(7)} - (b_{36})^{(7)} = 0 \text{ and}$$

Definition of $(\bar{v}_1)^{(7)}, (\bar{v}_2)^{(7)}, (\bar{u}_1)^{(7)}, (\bar{u}_2)^{(7)}$:

482

By $(\bar{v}_1)^{(7)} > 0, (\bar{v}_2)^{(7)} < 0$ and respectively $(\bar{u}_1)^{(7)} > 0, (\bar{u}_2)^{(7)} < 0$ the

roots of the equations $(a_{37})^{(7)} (v^{(7)})^2 + (\sigma_2)^{(7)} v^{(7)} - (a_{36})^{(7)} = 0$

and $(b_{37})^{(7)} (u^{(7)})^2 + (\tau_2)^{(7)} u^{(7)} - (b_{36})^{(7)} = 0$

Definition of $(m_1)^{(7)}, (m_2)^{(7)}, (\mu_1)^{(7)}, (\mu_2)^{(7)}, (v_0)^{(7)}$:-

(o) If we define $(m_1)^{(7)}, (m_2)^{(7)}, (\mu_1)^{(7)}, (\mu_2)^{(7)}$ by

$$(m_2)^{(7)} = (v_0)^{(7)}, (m_1)^{(7)} = (v_1)^{(7)}, \text{ if } (v_0)^{(7)} < (v_1)^{(7)}$$

$$(m_2)^{(7)} = (v_1)^{(7)}, (m_1)^{(7)} = (\bar{v}_1)^{(7)}, \text{ if } (v_1)^{(7)} < (v_0)^{(7)} < (\bar{v}_1)^{(7)},$$

$$\text{and } \boxed{(v_0)^{(7)} = \frac{G_{36}^0}{G_{37}^0}}$$

$(m_2)^{(7)} = (v_1)^{(7)}, (m_1)^{(7)} = (v_0)^{(7)}, \text{ if } (\bar{v}_1)^{(7)} < (v_0)^{(7)}$
 and analogously

483

$$(\mu_2)^{(7)} = (u_0)^{(7)}, (\mu_1)^{(7)} = (u_1)^{(7)}, \text{ if } (u_0)^{(7)} < (u_1)^{(7)}$$

$$(\mu_2)^{(7)} = (u_1)^{(7)}, (\mu_1)^{(7)} = (\bar{u}_1)^{(7)}, \text{ if } (u_1)^{(7)} < (u_0)^{(7)} < (\bar{u}_1)^{(7)},$$

$$\text{and } \boxed{(u_0)^{(7)} = \frac{T_{36}^0}{T_{37}^0}}$$

$(\mu_2)^{(7)} = (u_1)^{(7)}, (\mu_1)^{(7)} = (u_0)^{(7)}, \text{ if } (\bar{u}_1)^{(7)} < (u_0)^{(7)}$ where $(u_1)^{(7)}, (\bar{u}_1)^{(7)}$
 are defined respectively

Then the solution satisfies the inequalities

484

$$G_{36}^0 e^{((S_1)^{(7)} - (p_{36})^{(7)})t} \leq G_{36}(t) \leq G_{36}^0 e^{(S_1)^{(7)}t}$$

where $(p_i)^{(7)}$ is defined

$$\frac{1}{(m_7)^{(7)}} G_{36}^0 e^{((S_1)^{(7)} - (p_{36})^{(7)})t} \leq G_{37}(t) \leq \frac{1}{(m_2)^{(7)}} G_{36}^0 e^{(S_1)^{(7)}t}$$

485
486

$$\left(\frac{(a_{38})^{(7)} G_{36}^0}{(m_1)^{(7)} ((S_1)^{(7)} - (p_{36})^{(7)} - (S_2)^{(7)})} \left[e^{((S_1)^{(7)} - (p_{36})^{(7)})t} - e^{-(S_2)^{(7)}t} \right] + G_{38}^0 e^{-(S_2)^{(7)}t} \leq G_{38}(t) \leq \frac{(a_{38})^{(7)} G_{36}^0}{(m_2)^{(7)} ((S_1)^{(7)} - (a'_{38})^{(7)})} \left[e^{(S_1)^{(7)}t} - e^{-(a'_{38})^{(7)}t} \right] + G_{38}^0 e^{-(a'_{38})^{(7)}t} \right)$$

487

$$\boxed{T_{36}^0 e^{(R_1)^{(7)}t} \leq T_{36}(t) \leq T_{36}^0 e^{((R_1)^{(7)} + (r_{36})^{(7)})t}$$

488

$$\frac{1}{(\mu_1)^{(7)}} T_{36}^0 e^{(R_1)^{(7)}t} \leq T_{36}(t) \leq \frac{1}{(\mu_2)^{(7)}} T_{36}^0 e^{((R_1)^{(7)} + (r_{36})^{(7)})t}$$

489

$$\frac{(b_{38})^{(7)} T_{36}^0}{(\mu_1)^{(7)} ((R_1)^{(7)} - (b'_{38})^{(7)})} \left[e^{(R_1)^{(7)}t} - e^{-(b'_{38})^{(7)}t} \right] + T_{38}^0 e^{-(b'_{38})^{(7)}t} \leq T_{38}(t) \leq$$

490

$$\frac{(a_{38})^{(7)} T_{36}^0}{(\mu_2)^{(7)} ((R_1)^{(7)} + (r_{36})^{(7)} + (R_2)^{(7)})} \left[e^{((R_1)^{(7)} + (r_{36})^{(7)})t} - e^{-(R_2)^{(7)}t} \right] + T_{38}^0 e^{-(R_2)^{(7)}t}$$

Definition of $(S_1)^{(7)}, (S_2)^{(7)}, (R_1)^{(7)}, (R_2)^{(7)}$:-

491

Where $(S_1)^{(7)} = (a_{36})^{(7)}(m_2)^{(7)} - (a'_{36})^{(7)}$

$$(S_2)^{(7)} = (a_{38})^{(7)} - (p_{38})^{(7)}$$

$$(R_1)^{(7)} = (b_{36})^{(7)}(\mu_2)^{(7)} - (b'_{36})^{(7)}$$

$$(R_2)^{(7)} = (b'_{38})^{(7)} - (r_{38})^{(7)}$$

From GLOBAL EQUATIONS we obtain

492

$$\frac{dv^{(7)}}{dt} = (a_{36})^{(7)} - \left((a'_{36})^{(7)} - (a'_{37})^{(7)} + (a''_{36})^{(7)}(T_{37}, t) \right) -$$

$$(a_{37}'')^{(7)}(T_{37}, t)v^{(7)} - (a_{37})^{(7)}v^{(7)}$$

Definition of $v^{(7)}$:-
$$v^{(7)} = \frac{G_{36}}{G_{37}}$$

It follows

$$-\left((a_{37})^{(7)}(v^{(7)})^2 + (\sigma_2)^{(7)}v^{(7)} - (a_{36})^{(7)} \right) \leq \frac{dv^{(7)}}{dt} \leq -\left((a_{37})^{(7)}(v^{(7)})^2 + (\sigma_1)^{(7)}v^{(7)} - (a_{36})^{(7)} \right)$$

From which one obtains

Definition of $(\bar{v}_1)^{(7)}, (v_0)^{(7)}$:-

(a) For $0 < \boxed{(v_0)^{(7)} = \frac{G_{36}^0}{G_{37}^0}} < (v_1)^{(7)} < (\bar{v}_1)^{(7)}$

$$v^{(7)}(t) \geq \frac{(v_1)^{(7)} + (C)^{(7)}(v_2)^{(7)} e^{[-(a_{37})^{(7)}(v_1)^{(7)} - (v_0)^{(7)}]t}}{1 + (C)^{(7)} e^{[-(a_{37})^{(7)}(v_1)^{(7)} - (v_0)^{(7)}]t}}, \quad \boxed{(C)^{(7)} = \frac{(v_1)^{(7)} - (v_0)^{(7)}}{(v_0)^{(7)} - (v_2)^{(7)}}$$

it follows $(v_0)^{(7)} \leq v^{(7)}(t) \leq (v_1)^{(7)}$

In the same manner , we get

493

$$v^{(7)}(t) \leq \frac{(\bar{v}_1)^{(7)} + (\bar{C})^{(7)}(\bar{v}_2)^{(7)} e^{[-(a_{37})^{(7)}(\bar{v}_1)^{(7)} - (\bar{v}_2)^{(7)}]t}}{1 + (\bar{C})^{(7)} e^{[-(a_{37})^{(7)}(\bar{v}_1)^{(7)} - (\bar{v}_2)^{(7)}]t}}, \quad \boxed{(\bar{C})^{(7)} = \frac{(\bar{v}_1)^{(7)} - (v_0)^{(7)}}{(v_0)^{(7)} - (\bar{v}_2)^{(7)}}$$

From which we deduce $(v_0)^{(7)} \leq v^{(7)}(t) \leq (\bar{v}_1)^{(7)}$

(b) If $0 < (v_1)^{(7)} < (v_0)^{(7)} = \frac{G_{36}^0}{G_{37}^0} < (\bar{v}_1)^{(7)}$ we find like in the previous case,

494

$$(v_1)^{(7)} \leq \frac{(v_1)^{(7)} + (C)^{(7)}(v_2)^{(7)} e^{[-(a_{37})^{(7)}(v_1)^{(7)} - (v_2)^{(7)}]t}}{1 + (C)^{(7)} e^{[-(a_{37})^{(7)}(v_1)^{(7)} - (v_2)^{(7)}]t}} \leq v^{(7)}(t) \leq$$

$$\frac{(\bar{v}_1)^{(7)} + (\bar{C})^{(7)}(\bar{v}_2)^{(7)} e^{[-(a_{37})^{(7)}(\bar{v}_1)^{(7)} - (\bar{v}_2)^{(7)}]t}}{1 + (\bar{C})^{(7)} e^{[-(a_{37})^{(7)}(\bar{v}_1)^{(7)} - (\bar{v}_2)^{(7)}]t}} \leq (\bar{v}_1)^{(7)}$$

(c) If $0 < (v_1)^{(7)} \leq (\bar{v}_1)^{(7)} \leq \boxed{(v_0)^{(7)} = \frac{G_{36}^0}{G_{37}^0}}$, we obtain

495

$$(v_1)^{(7)} \leq v^{(7)}(t) \leq \frac{(\bar{v}_1)^{(7)} + (\bar{C})^{(7)}(\bar{v}_2)^{(7)} e^{[-(a_{37})^{(7)}(\bar{v}_1)^{(7)} - (\bar{v}_2)^{(7)}]t}}{1 + (\bar{C})^{(7)} e^{[-(a_{37})^{(7)}(\bar{v}_1)^{(7)} - (\bar{v}_2)^{(7)}]t}} \leq (v_0)^{(7)}$$

And so with the notation of the first part of condition (c) , we have

Definition of $v^{(7)}(t)$:-

$$(m_2)^{(7)} \leq v^{(7)}(t) \leq (m_1)^{(7)}, \quad \boxed{v^{(7)}(t) = \frac{G_{36}(t)}{G_{37}(t)}}$$

In a completely analogous way, we obtain

Definition of $u^{(7)}(t)$:-

$$(\mu_2)^{(7)} \leq u^{(7)}(t) \leq (\mu_1)^{(7)}, \quad \boxed{u^{(7)}(t) = \frac{T_{36}(t)}{T_{37}(t)}}$$

Now, using this result and replacing it in GLOBAL EQUATIONS we get easily the result stated in the theorem.

Particular case :

If $(a''_{36})^{(7)} = (a''_{37})^{(7)}$, then $(\sigma_1)^{(7)} = (\sigma_2)^{(7)}$ and in this case $(v_1)^{(7)} = (\bar{v}_1)^{(7)}$ if in addition $(v_0)^{(7)} = (v_1)^{(7)}$ then $v^{(7)}(t) = (v_0)^{(7)}$ and as a consequence $G_{36}(t) = (v_0)^{(7)}G_{37}(t)$ **this also defines $(v_0)^{(7)}$ for the special case .**

Analogously if $(b''_{36})^{(7)} = (b''_{37})^{(7)}$, then $(\tau_1)^{(7)} = (\tau_2)^{(7)}$ and then $(u_1)^{(7)} = (\bar{u}_1)^{(7)}$ if in addition $(u_0)^{(7)} = (u_1)^{(7)}$ then $T_{36}(t) = (u_0)^{(7)}T_{37}(t)$ This is an important consequence of the relation between $(v_1)^{(7)}$ and $(\bar{v}_1)^{(7)}$, **and definition of $(u_0)^{(7)}$.**

We can prove the following

If $(a''_i)^{(7)}$ and $(b''_i)^{(7)}$ are independent on t , and the conditions

$$(a'_{36})^{(7)}(a'_{37})^{(7)} - (a_{36})^{(7)}(a_{37})^{(7)} < 0$$

$$(a'_{36})^{(7)}(a'_{37})^{(7)} - (a_{36})^{(7)}(a_{37})^{(7)} + (a_{36})^{(7)}(p_{36})^{(7)} + (a'_{37})^{(7)}(p_{37})^{(7)} + (p_{36})^{(7)}(p_{37})^{(7)} > 0$$

$$(b'_{36})^{(7)}(b'_{37})^{(7)} - (b_{36})^{(7)}(b_{37})^{(7)} > 0,$$

$$(b'_{36})^{(7)}(b'_{37})^{(7)} - (b_{36})^{(7)}(b_{37})^{(7)} - (b'_{36})^{(7)}(r_{37})^{(7)} - (b'_{37})^{(7)}(r_{37})^{(7)} + (r_{36})^{(7)}(r_{37})^{(7)} < 0$$

with $(p_{36})^{(7)}, (r_{37})^{(7)}$ as defined are satisfied, then the system WITH THE SATISFACTION OF THE FOLLOWING PROPERTIES HAS A SOLUTION AS DERIVED BELOW.

Particular case :

If $(a''_{16})^{(2)} = (a''_{17})^{(2)}$, then $(\sigma_1)^{(2)} = (\sigma_2)^{(2)}$ and in this case $(v_1)^{(2)} = (\bar{v}_1)^{(2)}$ if in addition $(v_0)^{(2)} = (v_1)^{(2)}$ then $v^{(2)}(t) = (v_0)^{(2)}$ and as a consequence $G_{16}(t) = (v_0)^{(2)}G_{17}(t)$

Analogously if $(b''_{16})^{(2)} = (b''_{17})^{(2)}$, then $(\tau_1)^{(2)} = (\tau_2)^{(2)}$ and then

$(u_1)^{(2)} = (\bar{u}_1)^{(2)}$ if in addition $(u_0)^{(2)} = (u_1)^{(2)}$ then $T_{16}(t) = (u_0)^{(2)}T_{17}(t)$ This is an important consequence of the relation between $(v_1)^{(2)}$ and $(\bar{v}_1)^{(2)}$

From GLOBAL EQUATIONS we obtain

$$\frac{dv^{(3)}}{dt} = (a_{20})^{(3)} - \left((a'_{20})^{(3)} - (a'_{21})^{(3)} + (a''_{20})^{(3)}(T_{21}, t) \right) - (a''_{21})^{(3)}(T_{21}, t)v^{(3)} - (a_{21})^{(3)}v^{(3)}$$

Definition of $v^{(3)}$:-
$$v^{(3)} = \frac{G_{20}}{G_{21}}$$

It follows

$$- \left((a_{21})^{(3)}(v^{(3)})^2 + (\sigma_2)^{(3)}v^{(3)} - (a_{20})^{(3)} \right) \leq \frac{dv^{(3)}}{dt} \leq - \left((a_{21})^{(3)}(v^{(3)})^2 + (\sigma_1)^{(3)}v^{(3)} - (a_{20})^{(3)} \right)$$

From which one obtains

(a) For $0 < (v_0)^{(3)} = \frac{G_{20}^0}{G_{21}^0} < (v_1)^{(3)} < (\bar{v}_1)^{(3)}$

$$v^{(3)}(t) \geq \frac{(v_1)^{(3)} + (C)^{(3)}(v_2)^{(3)} e^{[-(a_{21})^{(3)}(v_1)^{(3)} - (v_0)^{(3)}]t}}{1 + (C)^{(3)} e^{[-(a_{21})^{(3)}(v_1)^{(3)} - (v_0)^{(3)}]t}}, \quad (C)^{(3)} = \frac{(v_1)^{(3)} - (v_0)^{(3)}}{(v_0)^{(3)} - (v_2)^{(3)}}$$

it follows $(v_0)^{(3)} \leq v^{(3)}(t) \leq (v_1)^{(3)}$

In the same manner, we get

$$v^{(3)}(t) \leq \frac{(\bar{v}_1)^{(3)} + (\bar{C})^{(3)}(\bar{v}_2)^{(3)} e^{[-(a_{21})^{(3)}(\bar{v}_1)^{(3)} - (\bar{v}_2)^{(3)}]t}}{1 + (\bar{C})^{(3)} e^{[-(a_{21})^{(3)}(\bar{v}_1)^{(3)} - (\bar{v}_2)^{(3)}]t}}, \quad (\bar{C})^{(3)} = \frac{(\bar{v}_1)^{(3)} - (v_0)^{(3)}}{(v_0)^{(3)} - (\bar{v}_2)^{(3)}}$$

Definition of $(\bar{v}_1)^{(3)}$:-

From which we deduce $(v_0)^{(3)} \leq v^{(3)}(t) \leq (\bar{v}_1)^{(3)}$

(b) If $0 < (v_1)^{(3)} < (v_0)^{(3)} = \frac{G_{20}^0}{G_{21}^0} < (\bar{v}_1)^{(3)}$ we find like in the previous case,

$$(v_1)^{(3)} \leq \frac{(v_1)^{(3)} + (C)^{(3)}(v_2)^{(3)} e^{[-(a_{21})^{(3)}(v_1)^{(3)} - (v_2)^{(3)}]t}}{1 + (C)^{(3)} e^{[-(a_{21})^{(3)}(v_1)^{(3)} - (v_2)^{(3)}]t}} \leq v^{(3)}(t) \leq \frac{(\bar{v}_1)^{(3)} + (\bar{C})^{(3)}(\bar{v}_2)^{(3)} e^{[-(a_{21})^{(3)}(\bar{v}_1)^{(3)} - (\bar{v}_2)^{(3)}]t}}{1 + (\bar{C})^{(3)} e^{[-(a_{21})^{(3)}(\bar{v}_1)^{(3)} - (\bar{v}_2)^{(3)}]t}} \leq (\bar{v}_1)^{(3)}$$

(c) If $0 < (v_1)^{(3)} \leq (\bar{v}_1)^{(3)} \leq (v_0)^{(3)} = \frac{G_{20}^0}{G_{21}^0}$, we obtain 505

$$(v_1)^{(3)} \leq v^{(3)}(t) \leq \frac{(\bar{v}_1)^{(3)} + (\bar{C})^{(3)} (\bar{v}_2)^{(3)} e^{[-(a_{21})^{(3)} (\bar{v}_1)^{(3)} - (\bar{v}_2)^{(3)}] t}}{1 + (\bar{C})^{(3)} e^{[-(a_{21})^{(3)} (\bar{v}_1)^{(3)} - (\bar{v}_2)^{(3)}] t}} \leq (v_0)^{(3)}$$

And so with the notation of the first part of condition (c), we have

Definition of $v^{(3)}(t)$:-

$$(m_2)^{(3)} \leq v^{(3)}(t) \leq (m_1)^{(3)}, \quad v^{(3)}(t) = \frac{G_{20}(t)}{G_{21}(t)}$$

In a completely analogous way, we obtain

Definition of $u^{(3)}(t)$:-

$$(\mu_2)^{(3)} \leq u^{(3)}(t) \leq (\mu_1)^{(3)}, \quad u^{(3)}(t) = \frac{T_{20}(t)}{T_{21}(t)}$$

Now, using this result and replacing it in GLOBAL EQUATIONS we get easily the result stated in the theorem.

Particular case :

If $(a_{20}'')^{(3)} = (a_{21}'')^{(3)}$, then $(\sigma_1)^{(3)} = (\sigma_2)^{(3)}$ and in this case $(v_1)^{(3)} = (\bar{v}_1)^{(3)}$ if in addition $(v_0)^{(3)} = (v_1)^{(3)}$ then $v^{(3)}(t) = (v_0)^{(3)}$ and as a consequence $G_{20}(t) = (v_0)^{(3)} G_{21}(t)$

Analogously if $(b_{20}'')^{(3)} = (b_{21}'')^{(3)}$, then $(\tau_1)^{(3)} = (\tau_2)^{(3)}$ and then

$(u_1)^{(3)} = (\bar{u}_1)^{(3)}$ if in addition $(u_0)^{(3)} = (u_1)^{(3)}$ then $T_{20}(t) = (u_0)^{(3)} T_{21}(t)$ This is an important consequence of the relation between $(v_1)^{(3)}$ and $(\bar{v}_1)^{(3)}$

: From GLOBAL EQUATIONS we obtain

$$\frac{dv^{(4)}}{dt} = (a_{24})^{(4)} - \left((a_{24}')^{(4)} - (a_{25}')^{(4)} + (a_{24}'')^{(4)} (T_{25}, t) \right) - (a_{25}'')^{(4)} (T_{25}, t) v^{(4)} - (a_{25})^{(4)} v^{(4)}$$

Definition of $v^{(4)}$:-

$$v^{(4)} = \frac{G_{24}}{G_{25}}$$

It follows

$$- \left((a_{25})^{(4)} (v^{(4)})^2 + (\sigma_2)^{(4)} v^{(4)} - (a_{24})^{(4)} \right) \leq \frac{dv^{(4)}}{dt} \leq - \left((a_{25})^{(4)} (v^{(4)})^2 + (\sigma_4)^{(4)} v^{(4)} - (a_{24})^{(4)} \right)$$

From which one obtains

Definition of $(\bar{v}_1)^{(4)}, (v_0)^{(4)}$:-

(d) For $0 < \frac{G_{24}^0}{G_{25}^0} < (v_1)^{(4)} < (\bar{v}_1)^{(4)}$

$$v^{(4)}(t) \geq \frac{(v_1)^{(4)} + (C)^{(4)} (v_2)^{(4)} e^{[-(a_{25})^{(4)} ((v_1)^{(4)} - (v_0)^{(4)}) t]}}{4 + (C)^{(4)} e^{[-(a_{25})^{(4)} ((v_1)^{(4)} - (v_0)^{(4)}) t]}} , \quad (C)^{(4)} = \frac{(v_1)^{(4)} - (v_0)^{(4)}}{(v_0)^{(4)} - (v_2)^{(4)}}$$

it follows $(v_0)^{(4)} \leq v^{(4)}(t) \leq (v_1)^{(4)}$

In the same manner, we get

$$v^{(4)}(t) \leq \frac{(\bar{v}_1)^{(4)} + (\bar{C})^{(4)} (\bar{v}_2)^{(4)} e^{[-(a_{25})^{(4)} ((\bar{v}_1)^{(4)} - (\bar{v}_2)^{(4)}) t]}}{4 + (\bar{C})^{(4)} e^{[-(a_{25})^{(4)} ((\bar{v}_1)^{(4)} - (\bar{v}_2)^{(4)}) t]}} , \quad (\bar{C})^{(4)} = \frac{(\bar{v}_1)^{(4)} - (v_0)^{(4)}}{(v_0)^{(4)} - (\bar{v}_2)^{(4)}}$$

From which we deduce $(v_0)^{(4)} \leq v^{(4)}(t) \leq (\bar{v}_1)^{(4)}$

(e) If $0 < (v_1)^{(4)} < (v_0)^{(4)} = \frac{G_{24}^0}{G_{25}^0} < (\bar{v}_1)^{(4)}$ we find like in the previous case, 510

$$(v_1)^{(4)} \leq \frac{(v_1)^{(4)} + (C)^{(4)} (v_2)^{(4)} e^{[-(a_{25})^{(4)} ((v_1)^{(4)} - (v_2)^{(4)}) t]}}{1 + (C)^{(4)} e^{[-(a_{25})^{(4)} ((v_1)^{(4)} - (v_2)^{(4)}) t]}} \leq v^{(4)}(t) \leq$$

$$\frac{(\bar{v}_1)^{(4)} + (\bar{C})^{(4)} (\bar{v}_2)^{(4)} e^{[-(a_{25})^{(4)} ((\bar{v}_1)^{(4)} - (\bar{v}_2)^{(4)}) t]}}{1 + (\bar{C})^{(4)} e^{[-(a_{25})^{(4)} ((\bar{v}_1)^{(4)} - (\bar{v}_2)^{(4)}) t]}} \leq (\bar{v}_1)^{(4)}$$

(f) If $0 < (v_1)^{(4)} \leq (\bar{v}_1)^{(4)} \leq \boxed{(v_0)^{(4)} = \frac{G_{24}^0}{G_{25}^0}}$, we obtain

$$(v_1)^{(4)} \leq v^{(4)}(t) \leq \frac{(\bar{v}_1)^{(4)} + (C)^{(4)}(\bar{v}_2)^{(4)} e^{[-(a_{25})^{(4)}(\bar{v}_1)^{(4)} - (\bar{v}_2)^{(4)}]t}}{1 + (C)^{(4)} e^{[-(a_{25})^{(4)}(\bar{v}_1)^{(4)} - (\bar{v}_2)^{(4)}]t}} \leq (v_0)^{(4)}$$

And so with the notation of the first part of condition (c), we have

Definition of $v^{(4)}(t)$:-

$$(m_2)^{(4)} \leq v^{(4)}(t) \leq (m_1)^{(4)}, \quad \boxed{v^{(4)}(t) = \frac{G_{24}(t)}{G_{25}(t)}}$$

In a completely analogous way, we obtain

Definition of $u^{(4)}(t)$:-

$$(\mu_2)^{(4)} \leq u^{(4)}(t) \leq (\mu_1)^{(4)}, \quad \boxed{u^{(4)}(t) = \frac{T_{24}(t)}{T_{25}(t)}}$$

Now, using this result and replacing it in GLOBAL EQUATIONS we get easily the result stated in the theorem.

Particular case :

If $(a_{24}'')^{(4)} = (a_{25}'')^{(4)}$, then $(\sigma_1)^{(4)} = (\sigma_2)^{(4)}$ and in this case $(v_1)^{(4)} = (\bar{v}_1)^{(4)}$ if in addition $(v_0)^{(4)} = (v_1)^{(4)}$ then $v^{(4)}(t) = (v_0)^{(4)}$ and as a consequence $G_{24}(t) = (v_0)^{(4)}G_{25}(t)$ **this also defines $(v_0)^{(4)}$ for the special case .**

Analogously if $(b_{24}'')^{(4)} = (b_{25}'')^{(4)}$, then $(\tau_1)^{(4)} = (\tau_2)^{(4)}$ and then $(u_1)^{(4)} = (\bar{u}_4)^{(4)}$ if in addition $(u_0)^{(4)} = (u_1)^{(4)}$ then $T_{24}(t) = (u_0)^{(4)}T_{25}(t)$ This is an important consequence of the relation between $(v_1)^{(4)}$ and $(\bar{v}_1)^{(4)}$, **and definition of $(u_0)^{(4)}$.**

From GLOBAL EQUATIONS we obtain

$$\frac{dv^{(5)}}{dt} = (a_{28})^{(5)} - \left((a'_{28})^{(5)} - (a'_{29})^{(5)} + (a''_{28})^{(5)}(T_{29}, t) \right) - (a''_{29})^{(5)}(T_{29}, t)v^{(5)} - (a_{29})^{(5)}v^{(5)}$$

Definition of $v^{(5)}$:- $\boxed{v^{(5)} = \frac{G_{28}}{G_{29}}}$

It follows

$$- \left((a_{29})^{(5)}(v^{(5)})^2 + (\sigma_2)^{(5)}v^{(5)} - (a_{28})^{(5)} \right) \leq \frac{dv^{(5)}}{dt} \leq - \left((a_{29})^{(5)}(v^{(5)})^2 + (\sigma_1)^{(5)}v^{(5)} - (a_{28})^{(5)} \right)$$

From which one obtains

Definition of $(\bar{v}_1)^{(5)}, (v_0)^{(5)}$:-

(g) For $0 < \boxed{(v_0)^{(5)} = \frac{G_{28}^0}{G_{29}^0}} < (v_1)^{(5)} < (\bar{v}_1)^{(5)}$

$$v^{(5)}(t) \geq \frac{(v_1)^{(5)} + (C)^{(5)}(v_2)^{(5)} e^{[-(a_{29})^{(5)}(v_1)^{(5)} - (v_0)^{(5)}]t}}{5 + (C)^{(5)} e^{[-(a_{29})^{(5)}(v_1)^{(5)} - (v_0)^{(5)}]t}}, \quad \boxed{(C)^{(5)} = \frac{(v_1)^{(5)} - (v_0)^{(5)}}{(v_0)^{(5)} - (v_2)^{(5)}}$$

it follows $(v_0)^{(5)} \leq v^{(5)}(t) \leq (v_1)^{(5)}$

In the same manner, we get

$$v^{(5)}(t) \leq \frac{(\bar{v}_1)^{(5)} + (\bar{c})^{(5)} (\bar{v}_2)^{(5)} e^{[-(a_{29})^{(5)} (\bar{v}_1)^{(5)} - (\bar{v}_2)^{(5)}] t}}{5 + (\bar{c})^{(5)} e^{[-(a_{29})^{(5)} (\bar{v}_1)^{(5)} - (\bar{v}_2)^{(5)}] t}} , \quad \boxed{(\bar{c})^{(5)} = \frac{(\bar{v}_1)^{(5)} - (v_0)^{(5)}}{(v_0)^{(5)} - (\bar{v}_2)^{(5)}}$$

From which we deduce $(v_0)^{(5)} \leq v^{(5)}(t) \leq (\bar{v}_5)^{(5)}$

(h) If $0 < (v_1)^{(5)} < (v_0)^{(5)} = \frac{G_{28}^0}{G_{29}^0} < (\bar{v}_1)^{(5)}$ we find like in the previous case, 517

$$(v_1)^{(5)} \leq \frac{(v_1)^{(5)} + (\bar{c})^{(5)} (v_2)^{(5)} e^{[-(a_{29})^{(5)} (v_1)^{(5)} - (v_2)^{(5)}] t}}{1 + (\bar{c})^{(5)} e^{[-(a_{29})^{(5)} (v_1)^{(5)} - (v_2)^{(5)}] t}} \leq v^{(5)}(t) \leq \frac{(\bar{v}_1)^{(5)} + (\bar{c})^{(5)} (\bar{v}_2)^{(5)} e^{[-(a_{29})^{(5)} (\bar{v}_1)^{(5)} - (\bar{v}_2)^{(5)}] t}}{1 + (\bar{c})^{(5)} e^{[-(a_{29})^{(5)} (\bar{v}_1)^{(5)} - (\bar{v}_2)^{(5)}] t}} \leq (\bar{v}_1)^{(5)}$$

(i) If $0 < (v_1)^{(5)} \leq (\bar{v}_1)^{(5)} \leq \boxed{(v_0)^{(5)} = \frac{G_{28}^0}{G_{29}^0}}$, we obtain 518

$$(v_1)^{(5)} \leq v^{(5)}(t) \leq \frac{(\bar{v}_1)^{(5)} + (\bar{c})^{(5)} (\bar{v}_2)^{(5)} e^{[-(a_{29})^{(5)} (\bar{v}_1)^{(5)} - (\bar{v}_2)^{(5)}] t}}{1 + (\bar{c})^{(5)} e^{[-(a_{29})^{(5)} (\bar{v}_1)^{(5)} - (\bar{v}_2)^{(5)}] t}} \leq (v_0)^{(5)}$$

519

And so with the notation of the first part of condition (c), we have

Definition of $v^{(5)}(t)$:-

$$(m_2)^{(5)} \leq v^{(5)}(t) \leq (m_1)^{(5)}, \quad \boxed{v^{(5)}(t) = \frac{G_{28}(t)}{G_{29}(t)}}$$

In a completely analogous way, we obtain

Definition of $u^{(5)}(t)$:-

$$(\mu_2)^{(5)} \leq u^{(5)}(t) \leq (\mu_1)^{(5)}, \quad \boxed{u^{(5)}(t) = \frac{T_{28}(t)}{T_{29}(t)}}$$

Now, using this result and replacing it in GLOBAL EQUATIONS we get easily the result stated in the theorem.

Particular case :

If $(a_{28}^{''})^{(5)} = (a_{29}^{''})^{(5)}$, then $(\sigma_1)^{(5)} = (\sigma_2)^{(5)}$ and in this case $(v_1)^{(5)} = (\bar{v}_1)^{(5)}$ if in addition $(v_0)^{(5)} = (v_5)^{(5)}$ then $v^{(5)}(t) = (v_0)^{(5)}$ and as a consequence $G_{28}(t) = (v_0)^{(5)} G_{29}(t)$ **this also defines $(v_0)^{(5)}$ for the special case .**

Analogously if $(b_{28}^{''})^{(5)} = (b_{29}^{''})^{(5)}$, then $(\tau_1)^{(5)} = (\tau_2)^{(5)}$ and then $(u_1)^{(5)} = (\bar{u}_1)^{(5)}$ if in addition $(u_0)^{(5)} = (u_1)^{(5)}$ then $T_{28}(t) = (u_0)^{(5)} T_{29}(t)$ This is an important consequence of the relation between $(v_1)^{(5)}$ and $(\bar{v}_1)^{(5)}$, **and definition of $(u_0)^{(5)}$.**

we obtain

520
521

$$\frac{dv^{(6)}}{dt} = (a_{32})^{(6)} - \left((a'_{32})^{(6)} - (a'_{33})^{(6)} + (a''_{32})^{(6)}(T_{33}, t) \right) - (a''_{33})^{(6)}(T_{33}, t)v^{(6)} - (a_{33})^{(6)}v^{(6)}$$

Definition of $v^{(6)}$:- $\boxed{v^{(6)} = \frac{G_{32}}{G_{33}}}$

It follows

$$- \left((a_{33})^{(6)} (v^{(6)})^2 + (\sigma_2)^{(6)} v^{(6)} - (a_{32})^{(6)} \right) \leq \frac{dv^{(6)}}{dt} \leq - \left((a_{33})^{(6)} (v^{(6)})^2 + (\sigma_1)^{(6)} v^{(6)} - (a_{32})^{(6)} \right)$$

From which one obtains

Definition of $(\bar{v}_1)^{(6)}, (v_0)^{(6)}$:-

(j) For $0 < \boxed{(v_0)^{(6)} = \frac{G_{32}^0}{G_{33}^0}} < (v_1)^{(6)} < (\bar{v}_1)^{(6)}$

$$v^{(6)}(t) \geq \frac{(v_1)^{(6)} + (C)^{(6)}(v_2)^{(6)} e^{[-(a_{33})^{(6)}(v_1)^{(6)} - (v_0)^{(6)}]t}}{1 + (C)^{(6)} e^{[-(a_{33})^{(6)}(v_1)^{(6)} - (v_0)^{(6)}]t}}, \quad \boxed{(C)^{(6)} = \frac{(v_1)^{(6)} - (v_0)^{(6)}}{(v_0)^{(6)} - (v_2)^{(6)}}$$

it follows $(v_0)^{(6)} \leq v^{(6)}(t) \leq (v_1)^{(6)}$

In the same manner , we get

$$v^{(6)}(t) \leq \frac{(\bar{v}_1)^{(6)} + (\bar{C})^{(6)}(\bar{v}_2)^{(6)} e^{[-(a_{33})^{(6)}(\bar{v}_1)^{(6)} - (\bar{v}_2)^{(6)}]t}}{1 + (\bar{C})^{(6)} e^{[-(a_{33})^{(6)}(\bar{v}_1)^{(6)} - (\bar{v}_2)^{(6)}]t}}, \quad \boxed{(\bar{C})^{(6)} = \frac{(\bar{v}_1)^{(6)} - (v_0)^{(6)}}{(v_0)^{(6)} - (\bar{v}_2)^{(6)}}$$

522

523

From which we deduce $(v_0)^{(6)} \leq v^{(6)}(t) \leq (\bar{v}_1)^{(6)}$

(k) If $0 < (v_1)^{(6)} < (v_0)^{(6)} = \frac{G_{32}^0}{G_{33}^0} < (\bar{v}_1)^{(6)}$ we find like in the previous case,

524

$$(v_1)^{(6)} \leq \frac{(v_1)^{(6)} + (C)^{(6)}(v_2)^{(6)} e^{[-(a_{33})^{(6)}(v_1)^{(6)} - (v_2)^{(6)}]t}}{1 + (C)^{(6)} e^{[-(a_{33})^{(6)}(v_1)^{(6)} - (v_2)^{(6)}]t}} \leq v^{(6)}(t) \leq$$

$$\frac{(\bar{v}_1)^{(6)} + (\bar{C})^{(6)}(\bar{v}_2)^{(6)} e^{[-(a_{33})^{(6)}(\bar{v}_1)^{(6)} - (\bar{v}_2)^{(6)}]t}}{1 + (\bar{C})^{(6)} e^{[-(a_{33})^{(6)}(\bar{v}_1)^{(6)} - (\bar{v}_2)^{(6)}]t}} \leq (\bar{v}_1)^{(6)}$$

(l) If $0 < (v_1)^{(6)} \leq (\bar{v}_1)^{(6)} \leq \boxed{(v_0)^{(6)} = \frac{G_{32}^0}{G_{33}^0}}$, we obtain

525

$$(v_1)^{(6)} \leq v^{(6)}(t) \leq \frac{(\bar{v}_1)^{(6)} + (\bar{C})^{(6)}(\bar{v}_2)^{(6)} e^{[-(a_{33})^{(6)}(\bar{v}_1)^{(6)} - (\bar{v}_2)^{(6)}]t}}{1 + (\bar{C})^{(6)} e^{[-(a_{33})^{(6)}(\bar{v}_1)^{(6)} - (\bar{v}_2)^{(6)}]t}} \leq (v_0)^{(6)}$$

And so with the notation of the first part of condition (c) , we have

Definition of $v^{(6)}(t)$:-

$$(m_2)^{(6)} \leq v^{(6)}(t) \leq (m_1)^{(6)}, \quad \boxed{v^{(6)}(t) = \frac{G_{32}(t)}{G_{33}(t)}}$$

In a completely analogous way, we obtain

Definition of $u^{(6)}(t)$:-

$$(\mu_2)^{(6)} \leq u^{(6)}(t) \leq (\mu_1)^{(6)}, \quad \boxed{u^{(6)}(t) = \frac{T_{32}(t)}{T_{33}(t)}}$$

Now, using this result and replacing it in GLOBAL EQUATIONS we get easily the result stated in the theorem.

Particular case :

If $(a''_{32})^{(6)} = (a''_{33})^{(6)}$, then $(\sigma_1)^{(6)} = (\sigma_2)^{(6)}$ and in this case $(v_1)^{(6)} = (\bar{v}_1)^{(6)}$ if in addition $(v_0)^{(6)} = (v_1)^{(6)}$ then $v^{(6)}(t) = (v_0)^{(6)}$ and as a consequence $G_{32}(t) = (v_0)^{(6)}G_{33}(t)$ **this also defines $(v_0)^{(6)}$ for the special case .**

Analogously if $(b''_{32})^{(6)} = (b''_{33})^{(6)}$, then $(\tau_1)^{(6)} = (\tau_2)^{(6)}$ and then $(u_1)^{(6)} = (\bar{u}_1)^{(6)}$ if in addition $(u_0)^{(6)} = (u_1)^{(6)}$ then $T_{32}(t) = (u_0)^{(6)}T_{33}(t)$ This is an important consequence of the relation between $(v_1)^{(6)}$ and $(\bar{v}_1)^{(6)}$, **and definition of $(u_0)^{(6)}$.**

526

527

528

We can prove the following

Theorem 3: If $(a''_i)^{(1)}$ and $(b''_i)^{(1)}$ are independent on t , and the conditions

$(a'_{13})^{(1)}(a'_{14})^{(1)} - (a_{13})^{(1)}(a_{14})^{(1)} < 0$	
$(a'_{13})^{(1)}(a'_{14})^{(1)} - (a_{13})^{(1)}(a_{14})^{(1)} + (a_{13})^{(1)}(p_{13})^{(1)} + (a'_{14})^{(1)}(p_{14})^{(1)} + (p_{13})^{(1)}(p_{14})^{(1)} > 0$	
$(b'_{13})^{(1)}(b'_{14})^{(1)} - (b_{13})^{(1)}(b_{14})^{(1)} > 0$,	
$(b'_{13})^{(1)}(b'_{14})^{(1)} - (b_{13})^{(1)}(b_{14})^{(1)} - (b'_{13})^{(1)}(r_{14})^{(1)} - (b'_{14})^{(1)}(r_{14})^{(1)} + (r_{13})^{(1)}(r_{14})^{(1)} < 0$	
with $(p_{13})^{(1)}, (r_{14})^{(1)}$ as defined, then the system	529
If $(a''_i)^{(2)}$ and $(b''_i)^{(2)}$ are independent on t , and the conditions	530.
$(a'_{16})^{(2)}(a'_{17})^{(2)} - (a_{16})^{(2)}(a_{17})^{(2)} < 0$	531
$(a'_{16})^{(2)}(a'_{17})^{(2)} - (a_{16})^{(2)}(a_{17})^{(2)} + (a_{16})^{(2)}(p_{16})^{(2)} + (a'_{17})^{(2)}(p_{17})^{(2)} + (p_{16})^{(2)}(p_{17})^{(2)} > 0$	532
$(b'_{16})^{(2)}(b'_{17})^{(2)} - (b_{16})^{(2)}(b_{17})^{(2)} > 0$,	533
$(b'_{16})^{(2)}(b'_{17})^{(2)} - (b_{16})^{(2)}(b_{17})^{(2)} - (b'_{16})^{(2)}(r_{17})^{(2)} - (b'_{17})^{(2)}(r_{17})^{(2)} + (r_{16})^{(2)}(r_{17})^{(2)} < 0$	534
with $(p_{16})^{(2)}, (r_{17})^{(2)}$ as defined are satisfied, then the system	
If $(a''_i)^{(3)}$ and $(b''_i)^{(3)}$ are independent on t , and the conditions	535
$(a'_{20})^{(3)}(a'_{21})^{(3)} - (a_{20})^{(3)}(a_{21})^{(3)} < 0$	
$(a'_{20})^{(3)}(a'_{21})^{(3)} - (a_{20})^{(3)}(a_{21})^{(3)} + (a_{20})^{(3)}(p_{20})^{(3)} + (a'_{21})^{(3)}(p_{21})^{(3)} + (p_{20})^{(3)}(p_{21})^{(3)} > 0$	
$(b'_{20})^{(3)}(b'_{21})^{(3)} - (b_{20})^{(3)}(b_{21})^{(3)} > 0$,	
$(b'_{20})^{(3)}(b'_{21})^{(3)} - (b_{20})^{(3)}(b_{21})^{(3)} - (b'_{20})^{(3)}(r_{21})^{(3)} - (b'_{21})^{(3)}(r_{21})^{(3)} + (r_{20})^{(3)}(r_{21})^{(3)} < 0$	
with $(p_{20})^{(3)}, (r_{21})^{(3)}$ as defined are satisfied, then the system	
If $(a''_i)^{(4)}$ and $(b''_i)^{(4)}$ are independent on t , and the conditions	536
$(a'_{24})^{(4)}(a'_{25})^{(4)} - (a_{24})^{(4)}(a_{25})^{(4)} < 0$	
$(a'_{24})^{(4)}(a'_{25})^{(4)} - (a_{24})^{(4)}(a_{25})^{(4)} + (a_{24})^{(4)}(p_{24})^{(4)} + (a'_{25})^{(4)}(p_{25})^{(4)} + (p_{24})^{(4)}(p_{25})^{(4)} > 0$	
$(b'_{24})^{(4)}(b'_{25})^{(4)} - (b_{24})^{(4)}(b_{25})^{(4)} > 0$,	
$(b'_{24})^{(4)}(b'_{25})^{(4)} - (b_{24})^{(4)}(b_{25})^{(4)} - (b'_{24})^{(4)}(r_{25})^{(4)} - (b'_{25})^{(4)}(r_{25})^{(4)} + (r_{24})^{(4)}(r_{25})^{(4)} < 0$	
with $(p_{24})^{(4)}, (r_{25})^{(4)}$ as defined are satisfied, then the system	
If $(a''_i)^{(5)}$ and $(b''_i)^{(5)}$ are independent on t , and the conditions	537
$(a'_{28})^{(5)}(a'_{29})^{(5)} - (a_{28})^{(5)}(a_{29})^{(5)} < 0$	
$(a'_{28})^{(5)}(a'_{29})^{(5)} - (a_{28})^{(5)}(a_{29})^{(5)} + (a_{28})^{(5)}(p_{28})^{(5)} + (a'_{29})^{(5)}(p_{29})^{(5)} + (p_{28})^{(5)}(p_{29})^{(5)} > 0$	
$(b'_{28})^{(5)}(b'_{29})^{(5)} - (b_{28})^{(5)}(b_{29})^{(5)} > 0$,	
$(b'_{28})^{(5)}(b'_{29})^{(5)} - (b_{28})^{(5)}(b_{29})^{(5)} - (b'_{28})^{(5)}(r_{29})^{(5)} - (b'_{29})^{(5)}(r_{29})^{(5)} + (r_{28})^{(5)}(r_{29})^{(5)} < 0$	
with $(p_{28})^{(5)}, (r_{29})^{(5)}$ as defined satisfied, then the system	
If $(a''_i)^{(6)}$ and $(b''_i)^{(6)}$ are independent on t , and the conditions	538
$(a'_{32})^{(6)}(a'_{33})^{(6)} - (a_{32})^{(6)}(a_{33})^{(6)} < 0$	
$(a'_{32})^{(6)}(a'_{33})^{(6)} - (a_{32})^{(6)}(a_{33})^{(6)} + (a_{32})^{(6)}(p_{32})^{(6)} + (a'_{33})^{(6)}(p_{33})^{(6)} + (p_{32})^{(6)}(p_{33})^{(6)} > 0$	
$(b'_{32})^{(6)}(b'_{33})^{(6)} - (b_{32})^{(6)}(b_{33})^{(6)} > 0$,	
$(b'_{32})^{(6)}(b'_{33})^{(6)} - (b_{32})^{(6)}(b_{33})^{(6)} - (b'_{32})^{(6)}(r_{33})^{(6)} - (b'_{33})^{(6)}(r_{33})^{(6)} + (r_{32})^{(6)}(r_{33})^{(6)} < 0$	539
with $(p_{32})^{(6)}, (r_{33})^{(6)}$ as defined are satisfied, then the system	
$(a_{13})^{(1)}G_{14} - [(a'_{13})^{(1)} + (a''_{13})^{(1)}(T_{14})]G_{13} = 0$	540
$(a_{14})^{(1)}G_{13} - [(a'_{14})^{(1)} + (a''_{14})^{(1)}(T_{14})]G_{14} = 0$	541
$(a_{15})^{(1)}G_{14} - [(a'_{15})^{(1)} + (a''_{15})^{(1)}(T_{14})]G_{15} = 0$	542
$(b_{13})^{(1)}T_{14} - [(b'_{13})^{(1)} - (b''_{13})^{(1)}(G)]T_{13} = 0$	543
$(b_{14})^{(1)}T_{13} - [(b'_{14})^{(1)} - (b''_{14})^{(1)}(G)]T_{14} = 0$	544
$(b_{15})^{(1)}T_{14} - [(b'_{15})^{(1)} - (b''_{15})^{(1)}(G)]T_{15} = 0$	545
has a unique positive solution, which is an equilibrium solution for the system	546
$(a_{16})^{(2)}G_{17} - [(a'_{16})^{(2)} + (a''_{16})^{(2)}(T_{17})]G_{16} = 0$	547
$(a_{17})^{(2)}G_{16} - [(a'_{17})^{(2)} + (a''_{17})^{(2)}(T_{17})]G_{17} = 0$	548
$(a_{18})^{(2)}G_{17} - [(a'_{18})^{(2)} + (a''_{18})^{(2)}(T_{17})]G_{18} = 0$	549
$(b_{16})^{(2)}T_{17} - [(b'_{16})^{(2)} - (b''_{16})^{(2)}(G_{19})]T_{16} = 0$	550
$(b_{17})^{(2)}T_{16} - [(b'_{17})^{(2)} - (b''_{17})^{(2)}(G_{19})]T_{17} = 0$	551
$(b_{18})^{(2)}T_{17} - [(b'_{18})^{(2)} - (b''_{18})^{(2)}(G_{19})]T_{18} = 0$	552
has a unique positive solution, which is an equilibrium solution for	553
$(a_{20})^{(3)}G_{21} - [(a'_{20})^{(3)} + (a''_{20})^{(3)}(T_{21})]G_{20} = 0$	554
$(a_{21})^{(3)}G_{20} - [(a'_{21})^{(3)} + (a''_{21})^{(3)}(T_{21})]G_{21} = 0$	555
$(a_{22})^{(3)}G_{21} - [(a'_{22})^{(3)} + (a''_{22})^{(3)}(T_{21})]G_{22} = 0$	556
$(b_{20})^{(3)}T_{21} - [(b'_{20})^{(3)} - (b''_{20})^{(3)}(G_{23})]T_{20} = 0$	557
$(b_{21})^{(3)}T_{20} - [(b'_{21})^{(3)} - (b''_{21})^{(3)}(G_{23})]T_{21} = 0$	558
$(b_{22})^{(3)}T_{21} - [(b'_{22})^{(3)} - (b''_{22})^{(3)}(G_{23})]T_{22} = 0$	559
has a unique positive solution, which is an equilibrium solution	560

$(a_{24})^{(4)}G_{25} - [(a'_{24})^{(4)} + (a''_{24})^{(4)}(T_{25})]G_{24} = 0$	561
$(a_{25})^{(4)}G_{24} - [(a'_{25})^{(4)} + (a''_{25})^{(4)}(T_{25})]G_{25} = 0$	563
$(a_{26})^{(4)}G_{25} - [(a'_{26})^{(4)} + (a''_{26})^{(4)}(T_{25})]G_{26} = 0$	564
$(b_{24})^{(4)}T_{25} - [(b'_{24})^{(4)} - (b''_{24})^{(4)}((G_{27}))]T_{24} = 0$	565
$(b_{25})^{(4)}T_{24} - [(b'_{25})^{(4)} - (b''_{25})^{(4)}((G_{27}))]T_{25} = 0$	566
$(b_{26})^{(4)}T_{25} - [(b'_{26})^{(4)} - (b''_{26})^{(4)}((G_{27}))]T_{26} = 0$	567
has a unique positive solution , which is an equilibrium solution for the system	568
$(a_{28})^{(5)}G_{29} - [(a'_{28})^{(5)} + (a''_{28})^{(5)}(T_{29})]G_{28} = 0$	569
$(a_{29})^{(5)}G_{28} - [(a'_{29})^{(5)} + (a''_{29})^{(5)}(T_{29})]G_{29} = 0$	570
$(a_{30})^{(5)}G_{29} - [(a'_{30})^{(5)} + (a''_{30})^{(5)}(T_{29})]G_{30} = 0$	571
$(b_{28})^{(5)}T_{29} - [(b'_{28})^{(5)} - (b''_{28})^{(5)}(G_{31})]T_{28} = 0$	572
$(b_{29})^{(5)}T_{28} - [(b'_{29})^{(5)} - (b''_{29})^{(5)}(G_{31})]T_{29} = 0$	573
$(b_{30})^{(5)}T_{29} - [(b'_{30})^{(5)} - (b''_{30})^{(5)}(G_{31})]T_{30} = 0$	574
has a unique positive solution , which is an equilibrium solution for the system	575
$(a_{32})^{(6)}G_{33} - [(a'_{32})^{(6)} + (a''_{32})^{(6)}(T_{33})]G_{32} = 0$	576
$(a_{33})^{(6)}G_{32} - [(a'_{33})^{(6)} + (a''_{33})^{(6)}(T_{33})]G_{33} = 0$	577
$(a_{34})^{(6)}G_{33} - [(a'_{34})^{(6)} + (a''_{34})^{(6)}(T_{33})]G_{34} = 0$	578
$(b_{32})^{(6)}T_{33} - [(b'_{32})^{(6)} - (b''_{32})^{(6)}(G_{35})]T_{32} = 0$	579
$(b_{33})^{(6)}T_{32} - [(b'_{33})^{(6)} - (b''_{33})^{(6)}(G_{35})]T_{33} = 0$	580
$(b_{34})^{(6)}T_{33} - [(b'_{34})^{(6)} - (b''_{34})^{(6)}(G_{35})]T_{34} = 0$	584
has a unique positive solution , which is an equilibrium solution for the system	582
$(a_{36})^{(7)}G_{37} - [(a'_{36})^{(7)} + (a''_{36})^{(7)}(T_{37})]G_{36} = 0$	583
$(a_{37})^{(7)}G_{36} - [(a'_{37})^{(7)} + (a''_{37})^{(7)}(T_{37})]G_{37} = 0$	584
$(a_{38})^{(7)}G_{37} - [(a'_{38})^{(7)} + (a''_{38})^{(7)}(T_{37})]G_{38} = 0$	585
$(b_{36})^{(7)}T_{37} - [(b'_{36})^{(7)} - (b''_{36})^{(7)}(G_{39})]T_{36} = 0$	586
	587

$$(b_{37})^{(7)}T_{36} - [(b'_{37})^{(7)} - (b''_{37})^{(7)}(G_{39})]T_{37} = 0 \quad 588$$

$$(b_{38})^{(7)}T_{37} - [(b'_{38})^{(7)} - (b''_{38})^{(7)}(G_{39})]T_{38} = 0 \quad 589$$

has a unique positive solution , which is an equilibrium solution for the system (79 to 36) 560

(a) Indeed the first two equations have a nontrivial solution G_{36}, G_{37} if

$$F(T_{39}) = (a'_{36})^{(7)}(a'_{37})^{(7)} - (a_{36})^{(7)}(a_{37})^{(7)} + (a'_{36})^{(7)}(a''_{37})^{(7)}(T_{37}) + (a'_{37})^{(7)}(a''_{36})^{(7)}(T_{37}) + (a''_{36})^{(7)}(T_{37})(a''_{37})^{(7)}(T_{37}) = 0$$

Definition and uniqueness of T_{37}^* :- 561

After hypothesis $f(0) < 0, f(\infty) > 0$ and the functions $(a''_i)^{(7)}(T_{37})$ being increasing, it follows that there exists a unique T_{37}^* for which $f(T_{37}^*) = 0$. With this value , we obtain from the three first equations

$$G_{36} = \frac{(a_{36})^{(7)}G_{37}}{[(a'_{36})^{(7)} + (a''_{36})^{(7)}(T_{37}^*)]} , \quad G_{38} = \frac{(a_{38})^{(7)}G_{37}}{[(a'_{38})^{(7)} + (a''_{38})^{(7)}(T_{37}^*)]}$$

(f) By the same argument, the equations 92,93 admit solutions G_{36}, G_{37} if

$$\varphi(G_{39}) = (b'_{36})^{(7)}(b'_{37})^{(7)} - (b_{36})^{(7)}(b_{37})^{(7)} - [(b_{36})^{(7)}(b''_{37})^{(7)}(G_{39}) + (b_{37})^{(7)}(b''_{36})^{(7)}(G_{39})] + (b''_{36})^{(7)}(G_{39})(b''_{37})^{(7)}(G_{39}) = 0$$

Where in $(G_{39})(G_{36}, G_{37}, G_{38}), G_{36}, G_{38}$ must be replaced by their values from 96. It is easy to see that φ is a decreasing function in G_{37} taking into account the hypothesis $\varphi(0) > 0, \varphi(\infty) < 0$ it follows that there exists a unique G_{37}^* such that $\varphi(G^*) = 0$ 562

Finally we obtain the unique solution of 89 to 97

G_{37}^* given by $\varphi((G_{39})^*) = 0, T_{37}^*$ given by $f(T_{37}^*) = 0$ and

$$G_{36}^* = \frac{(a_{36})^{(7)}G_{37}^*}{[(a'_{36})^{(7)} + (a''_{36})^{(7)}(T_{37}^*)]} , \quad G_{38}^* = \frac{(a_{38})^{(7)}G_{37}^*}{[(a'_{38})^{(7)} + (a''_{38})^{(7)}(T_{37}^*)]} \\ T_{36}^* = \frac{(b_{36})^{(7)}T_{37}^*}{[(b_{36})^{(7)} - (b_{36})^{(7)}(G_{39})^*]} , \quad T_{38}^* = \frac{(b_{38})^{(7)}T_{37}^*}{[(b_{38})^{(7)} - (b_{38})^{(7)}(G_{39})^*]} \quad 563$$

Definition and uniqueness of T_{21}^* :- 564

After hypothesis $f(0) < 0, f(\infty) > 0$ and the functions $(a''_i)^{(1)}(T_{21})$ being increasing, it follows that there exists a unique T_{21}^* for which $f(T_{21}^*) = 0$. With this value , we obtain from the three first equations

$$G_{20} = \frac{(a_{20})^{(3)}G_{21}}{[(a'_{20})^{(3)} + (a''_{20})^{(3)}(T_{21}^*)]} , \quad G_{22} = \frac{(a_{22})^{(3)}G_{21}}{[(a'_{22})^{(3)} + (a''_{22})^{(3)}(T_{21}^*)]} \quad 565$$

Definition and uniqueness of T_{25}^* :- 566

After hypothesis $f(0) < 0, f(\infty) > 0$ and the functions $(a''_i)^{(4)}(T_{25})$ being increasing, it follows that there exists a unique T_{25}^* for which $f(T_{25}^*) = 0$. With this value , we obtain from the three first equations

$$G_{24} = \frac{(a_{24})^{(4)}G_{25}}{[(a'_{24})^{(4)} + (a''_{24})^{(4)}(T_{25}^*)]} , \quad G_{26} = \frac{(a_{26})^{(4)}G_{25}}{[(a'_{26})^{(4)} + (a''_{26})^{(4)}(T_{25}^*)]}$$

Definition and uniqueness of T_{29}^* :- 567

After hypothesis $f(0) < 0, f(\infty) > 0$ and the functions $(a''_i)^{(5)}(T_{29})$ being increasing, it follows that there exists a unique T_{29}^* for which $f(T_{29}^*) = 0$. With this value , we obtain from the three first equations

$$G_{28} = \frac{(a_{28})^{(5)}G_{29}}{[(a'_{28})^{(5)} + (a''_{28})^{(5)}(T_{29}^*)]} , \quad G_{30} = \frac{(a_{30})^{(5)}G_{29}}{[(a'_{30})^{(5)} + (a''_{30})^{(5)}(T_{29}^*)]}$$

Definition and uniqueness of T_{33}^* :- 568

After hypothesis $f(0) < 0, f(\infty) > 0$ and the functions $(a''_i)^{(6)}(T_{33})$ being increasing, it follows that there exists a unique T_{33}^* for which $f(T_{33}^*) = 0$. With this value , we obtain from the three first equations

$$G_{32} = \frac{(a_{32})^{(6)}G_{33}}{[(a'_{32})^{(6)} + (a''_{32})^{(6)}(T_{33}^*)]} , \quad G_{34} = \frac{(a_{34})^{(6)}G_{33}}{[(a'_{34})^{(6)} + (a''_{34})^{(6)}(T_{33}^*)]}$$

- (g) By the same argument, the equations 92,93 admit solutions G_{13}, G_{14} if 569

$$\varphi(G) = (b'_{13})^{(1)}(b'_{14})^{(1)} - (b_{13})^{(1)}(b_{14})^{(1)} - [(b'_{13})^{(1)}(b''_{14})^{(1)}(G) + (b'_{14})^{(1)}(b''_{13})^{(1)}(G)] + (b''_{13})^{(1)}(G)(b''_{14})^{(1)}(G) = 0$$
 Where in $G(G_{13}, G_{14}, G_{15}), G_{13}, G_{15}$ must be replaced by their values from 96. It is easy to see that φ is a decreasing function in G_{14} taking into account the hypothesis $\varphi(0) > 0, \varphi(\infty) < 0$ it follows that there exists a unique G_{14}^* such that $\varphi(G^*) = 0$
- (h) By the same argument, the equations 92,93 admit solutions G_{16}, G_{17} if 570

$$\varphi(G_{19}) = (b'_{16})^{(2)}(b'_{17})^{(2)} - (b_{16})^{(2)}(b_{17})^{(2)} - [(b'_{16})^{(2)}(b''_{17})^{(2)}(G_{19}) + (b'_{17})^{(2)}(b''_{16})^{(2)}(G_{19})] + (b''_{16})^{(2)}(G_{19})(b''_{17})^{(2)}(G_{19}) = 0$$
 Where in $(G_{19})(G_{16}, G_{17}, G_{18}), G_{16}, G_{18}$ must be replaced by their values from 96. It is easy to see that φ is a decreasing function in G_{17} taking into account the hypothesis $\varphi(0) > 0, \varphi(\infty) < 0$ it follows that there exists a unique G_{14}^* such that $\varphi((G_{19})^*) = 0$ 571
- (i) By the same argument, the concatenated equations admit solutions G_{20}, G_{21} if 572

$$\varphi(G_{23}) = (b'_{20})^{(3)}(b'_{21})^{(3)} - (b_{20})^{(3)}(b_{21})^{(3)} - [(b'_{20})^{(3)}(b''_{21})^{(3)}(G_{23}) + (b'_{21})^{(3)}(b''_{20})^{(3)}(G_{23})] + (b''_{20})^{(3)}(G_{23})(b''_{21})^{(3)}(G_{23}) = 0$$
 Where in $G_{23}(G_{20}, G_{21}, G_{22}), G_{20}, G_{22}$ must be replaced by their values from 96. It is easy to see that φ is a decreasing function in G_{21} taking into account the hypothesis $\varphi(0) > 0, \varphi(\infty) < 0$ it follows that there exists a unique G_{21}^* such that $\varphi((G_{23})^*) = 0$ 573
- (j) By the same argument, the equations of modules admit solutions G_{24}, G_{25} if 574

$$\varphi(G_{27}) = (b'_{24})^{(4)}(b'_{25})^{(4)} - (b_{24})^{(4)}(b_{25})^{(4)} - [(b'_{24})^{(4)}(b''_{25})^{(4)}(G_{27}) + (b'_{25})^{(4)}(b''_{24})^{(4)}(G_{27})] + (b''_{24})^{(4)}(G_{27})(b''_{25})^{(4)}(G_{27}) = 0$$
 Where in $(G_{27})(G_{24}, G_{25}, G_{26}), G_{24}, G_{26}$ must be replaced by their values from 96. It is easy to see that φ is a decreasing function in G_{25} taking into account the hypothesis $\varphi(0) > 0, \varphi(\infty) < 0$ it follows that there exists a unique G_{25}^* such that $\varphi((G_{27})^*) = 0$
- (k) By the same argument, the equations (modules) admit solutions G_{28}, G_{29} if 575

$$\varphi(G_{31}) = (b'_{28})^{(5)}(b'_{29})^{(5)} - (b_{28})^{(5)}(b_{29})^{(5)} - [(b'_{28})^{(5)}(b''_{29})^{(5)}(G_{31}) + (b'_{29})^{(5)}(b''_{28})^{(5)}(G_{31})] + (b''_{28})^{(5)}(G_{31})(b''_{29})^{(5)}(G_{31}) = 0$$
 Where in $(G_{31})(G_{28}, G_{29}, G_{30}), G_{28}, G_{30}$ must be replaced by their values from 96. It is easy to see that φ is a decreasing function in G_{29} taking into account the hypothesis $\varphi(0) > 0, \varphi(\infty) < 0$ it follows that there exists a unique G_{29}^* such that $\varphi((G_{31})^*) = 0$
- (l) By the same argument, the equations (modules) admit solutions G_{32}, G_{33} if 578

$$\varphi(G_{35}) = (b'_{32})^{(6)}(b'_{33})^{(6)} - (b_{32})^{(6)}(b_{33})^{(6)} - [(b'_{32})^{(6)}(b''_{33})^{(6)}(G_{35}) + (b'_{33})^{(6)}(b''_{32})^{(6)}(G_{35})] + (b''_{32})^{(6)}(G_{35})(b''_{33})^{(6)}(G_{35}) = 0$$
579
580
581
 Where in $(G_{35})(G_{32}, G_{33}, G_{34}), G_{32}, G_{34}$ must be replaced by their values It is easy to see that φ is a decreasing function in G_{33} taking into account the hypothesis $\varphi(0) > 0, \varphi(\infty) < 0$ it follows that there exists a unique G_{33}^* such that $\varphi(G^*) = 0$
- Finally we obtain the unique solution of 89 to 94 582
 G_{14}^* given by $\varphi(G^*) = 0, T_{14}^*$ given by $f(T_{14}^*) = 0$ and

$$G_{13}^* = \frac{(a_{13})^{(1)}G_{14}^*}{[(a'_{13})^{(1)} + (a''_{13})^{(1)}(T_{14}^*)]}, \quad G_{15}^* = \frac{(a_{15})^{(1)}G_{14}^*}{[(a'_{15})^{(1)} + (a''_{15})^{(1)}(T_{14}^*)]}$$

$$T_{13}^* = \frac{(b_{13})^{(1)}T_{14}^*}{[(b'_{13})^{(1)} - (b''_{13})^{(1)}(G^*)]}, \quad T_{15}^* = \frac{(b_{15})^{(1)}T_{14}^*}{[(b'_{15})^{(1)} - (b''_{15})^{(1)}(G^*)]}$$
 Obviously, these values represent an equilibrium solution
- Finally we obtain the unique solution 583
 G_{17}^* given by $\varphi((G_{19})^*) = 0, T_{17}^*$ given by $f(T_{17}^*) = 0$ and 584

$$G_{16}^* = \frac{(a_{16})^{(2)}G_{17}^*}{[(a'_{16})^{(2)} + (a''_{16})^{(2)}(T_{17}^*)]}, \quad G_{18}^* = \frac{(a_{18})^{(2)}G_{17}^*}{[(a'_{18})^{(2)} + (a''_{18})^{(2)}(T_{17}^*)]}$$
585

$$T_{16}^* = \frac{(b_{16})^{(2)}T_{17}^*}{[(b'_{16})^{(2)} - (b''_{16})^{(2)}((G_{19})^*)]}, \quad T_{18}^* = \frac{(b_{18})^{(2)}T_{17}^*}{[(b'_{18})^{(2)} - (b''_{18})^{(2)}((G_{19})^*)]}$$
586
 Obviously, these values represent an equilibrium solution 587
 Finally we obtain the unique solution 588
 G_{21}^* given by $\varphi((G_{23})^*) = 0, T_{21}^*$ given by $f(T_{21}^*) = 0$ and

$$G_{20}^* = \frac{(a_{20})^{(3)}G_{21}^*}{[(a'_{20})^{(3)} + (a''_{20})^{(3)}(T_{21}^*)]}, \quad G_{22}^* = \frac{(a_{22})^{(3)}G_{21}^*}{[(a'_{22})^{(3)} + (a''_{22})^{(3)}(T_{21}^*)]}$$

$$T_{20}^* = \frac{(b_{20})^{(3)}T_{21}^*}{[(b'_{20})^{(3)} - (b''_{20})^{(3)}(G_{23}^*)]}, \quad T_{22}^* = \frac{(b_{22})^{(3)}T_{21}^*}{[(b'_{22})^{(3)} - (b''_{22})^{(3)}(G_{23}^*)]}$$

Obviously, these values represent an equilibrium solution

Finally we obtain the unique solution

G_{25}^* given by $\varphi(G_{27}) = 0$, T_{25}^* given by $f(T_{25}^*) = 0$ and

$$G_{24}^* = \frac{(a_{24})^{(4)} G_{25}^*}{[(a'_{24})^{(4)} + (a''_{24})^{(4)} (T_{25}^*)]} , G_{26}^* = \frac{(a_{26})^{(4)} G_{25}^*}{[(a'_{26})^{(4)} + (a''_{26})^{(4)} (T_{25}^*)]}$$

$$T_{24}^* = \frac{(b_{24})^{(4)} T_{25}^*}{[(b'_{24})^{(4)} - (b''_{24})^{(4)} ((G_{27})^*)]} , T_{26}^* = \frac{(b_{26})^{(4)} T_{25}^*}{[(b'_{26})^{(4)} - (b''_{26})^{(4)} ((G_{27})^*)]}$$

Obviously, these values represent an equilibrium solution

Finally we obtain the unique solution

G_{29}^* given by $\varphi((G_{31})^*) = 0$, T_{29}^* given by $f(T_{29}^*) = 0$ and

$$G_{28}^* = \frac{(a_{28})^{(5)} G_{29}^*}{[(a'_{28})^{(5)} + (a''_{28})^{(5)} (T_{29}^*)]} , G_{30}^* = \frac{(a_{30})^{(5)} G_{29}^*}{[(a'_{30})^{(5)} + (a''_{30})^{(5)} (T_{29}^*)]}$$

$$T_{28}^* = \frac{(b_{28})^{(5)} T_{29}^*}{[(b'_{28})^{(5)} - (b''_{28})^{(5)} ((G_{31})^*)]} , T_{30}^* = \frac{(b_{30})^{(5)} T_{29}^*}{[(b'_{30})^{(5)} - (b''_{30})^{(5)} ((G_{31})^*)]}$$

Obviously, these values represent an equilibrium solution

Finally we obtain the unique solution

G_{33}^* given by $\varphi((G_{35})^*) = 0$, T_{33}^* given by $f(T_{33}^*) = 0$ and

$$G_{32}^* = \frac{(a_{32})^{(6)} G_{33}^*}{[(a'_{32})^{(6)} + (a''_{32})^{(6)} (T_{33}^*)]} , G_{34}^* = \frac{(a_{34})^{(6)} G_{33}^*}{[(a'_{34})^{(6)} + (a''_{34})^{(6)} (T_{33}^*)]}$$

$$T_{32}^* = \frac{(b_{32})^{(6)} T_{33}^*}{[(b'_{32})^{(6)} - (b''_{32})^{(6)} ((G_{35})^*)]} , T_{34}^* = \frac{(b_{34})^{(6)} T_{33}^*}{[(b'_{34})^{(6)} - (b''_{34})^{(6)} ((G_{35})^*)]}$$

Obviously, these values represent an equilibrium solution

ASYMPTOTIC STABILITY ANALYSIS

Theorem 4: If the conditions of the previous theorem are satisfied and if the functions $(a_i'')^{(1)}$ and $(b_i'')^{(1)}$ belong to $C^{(1)}(\mathbb{R}_+)$ then the above equilibrium point is asymptotically stable.

Proof: Denote

Definition of G_i, T_i :-

$$G_i = G_i^* + \mathbb{G}_i , T_i = T_i^* + \mathbb{T}_i$$

$$\frac{\partial (a_i'')^{(1)}}{\partial T_{14}} (T_{14}^*) = (q_{14})^{(1)} , \frac{\partial (b_i'')^{(1)}}{\partial G_j} (G^*) = s_{ij}$$

Then taking into account equations (global) and neglecting the terms of power 2, we obtain

$$\frac{dG_{13}}{dt} = -((a'_{13})^{(1)} + (p_{13})^{(1)})G_{13} + (a_{13})^{(1)}G_{14} - (q_{13})^{(1)}G_{13}^*T_{14}$$

$$\frac{dG_{14}}{dt} = -((a'_{14})^{(1)} + (p_{14})^{(1)})G_{14} + (a_{14})^{(1)}G_{13} - (q_{14})^{(1)}G_{14}^*T_{14}$$

$$\frac{dG_{15}}{dt} = -((a'_{15})^{(1)} + (p_{15})^{(1)})G_{15} + (a_{15})^{(1)}G_{14} - (q_{15})^{(1)}G_{15}^*T_{14}$$

$$\frac{dT_{13}}{dt} = -((b'_{13})^{(1)} - (r_{13})^{(1)})T_{13} + (b_{13})^{(1)}T_{14} + \sum_{j=13}^{15} (s_{(13)(j)})T_{13}^*G_j$$

$$\frac{dT_{14}}{dt} = -((b'_{14})^{(1)} - (r_{14})^{(1)})T_{14} + (b_{14})^{(1)}T_{13} + \sum_{j=13}^{15} (s_{(14)(j)})T_{14}^*G_j$$

$$\frac{dT_{15}}{dt} = -((b'_{15})^{(1)} - (r_{15})^{(1)})T_{15} + (b_{15})^{(1)}T_{14} + \sum_{j=13}^{15} (s_{(15)(j)})T_{15}^*G_j$$

If the conditions of the previous theorem are satisfied and if the functions $(a_i'')^{(2)}$ and $(b_i'')^{(2)}$ belong to $C^{(2)}(\mathbb{R}_+)$ then the above equilibrium point is asymptotically stable

Denote

Definition of G_i, T_i :-

$$G_i = G_i^* + \mathbb{G}_i , T_i = T_i^* + \mathbb{T}_i$$

$$\frac{\partial (a_i'')^{(2)}}{\partial T_{17}} (T_{17}^*) = (q_{17})^{(2)} , \frac{\partial (b_i'')^{(2)}}{\partial G_j} ((G_{19})^*) = s_{ij}$$

taking into account equations (global) and neglecting the terms of power 2, we obtain

$$\frac{dG_{16}}{dt} = -((a'_{16})^{(2)} + (p_{16})^{(2)})G_{16} + (a_{16})^{(2)}G_{17} - (q_{16})^{(2)}G_{16}^*T_{17}$$

$$\frac{dG_{17}}{dt} = -((a'_{17})^{(2)} + (p_{17})^{(2)})G_{17} + (a_{17})^{(2)}G_{16} - (q_{17})^{(2)}G_{17}^*T_{17}$$

$$\frac{dG_{18}}{dt} = -((a'_{18})^{(2)} + (p_{18})^{(2)})G_{18} + (a_{18})^{(2)}G_{17} - (q_{18})^{(2)}G_{18}^*T_{17}$$

$$\frac{dT_{16}}{dt} = -((b'_{16})^{(2)} - (r_{16})^{(2)})T_{16} + (b_{16})^{(2)}T_{17} + \sum_{j=16}^{18} (s_{(16)(j)})T_{16}^*G_j$$

$$\frac{dT_{17}}{dt} = -((b'_{17})^{(2)} - (r_{17})^{(2)})T_{17} + (b_{17})^{(2)}T_{16} + \sum_{j=16}^{18} (s_{(17)(j)})T_{17}^*G_j$$

$$\frac{dT_{18}}{dt} = -((b'_{18})^{(2)} - (r_{18})^{(2)})T_{18} + (b_{18})^{(2)}T_{17} + \sum_{j=16}^{18} (s_{(18)(j)})T_{18}^*G_j$$

If the conditions of the previous theorem are satisfied and if the functions $(a_i'')^{(3)}$ and $(b_i'')^{(3)}$ belong to $C^{(3)}(\mathbb{R}_+)$ then the above equilibrium point is asymptotically stable

Denote

Definition of G_i, T_i :-

$$G_i = G_i^* + \mathbb{G}_i , T_i = T_i^* + \mathbb{T}_i$$

$$\frac{\partial (a_{21}''^{(3)})}{\partial T_{21}} (T_{21}^*) = (q_{21})^{(3)}, \quad \frac{\partial (b_i''^{(3)})}{\partial G_j} ((G_{23})^*) = s_{ij}$$

Then taking into account equations (global) and neglecting the terms of power 2, we obtain

$$\frac{dG_{20}}{dt} = -((a'_{20})^{(3)} + (p_{20})^{(3)})G_{20} + (a_{20})^{(3)}G_{21} - (q_{20})^{(3)}G_{20}^* T_{21}$$

$$\frac{dG_{21}}{dt} = -((a'_{21})^{(3)} + (p_{21})^{(3)})G_{21} + (a_{21})^{(3)}G_{20} - (q_{21})^{(3)}G_{21}^* T_{21}$$

$$\frac{dG_{22}}{dt} = -((a'_{22})^{(3)} + (p_{22})^{(3)})G_{22} + (a_{22})^{(3)}G_{21} - (q_{22})^{(3)}G_{22}^* T_{21}$$

$$\frac{dT_{20}}{dt} = -((b'_{20})^{(3)} - (r_{20})^{(3)})T_{20} + (b_{20})^{(3)}T_{21} + \sum_{j=20}^{22} (s_{(20)(j)})T_{20}^* G_j$$

$$\frac{dT_{21}}{dt} = -((b'_{21})^{(3)} - (r_{21})^{(3)})T_{21} + (b_{21})^{(3)}T_{20} + \sum_{j=20}^{22} (s_{(21)(j)})T_{21}^* G_j$$

$$\frac{dT_{22}}{dt} = -((b'_{22})^{(3)} - (r_{22})^{(3)})T_{22} + (b_{22})^{(3)}T_{21} + \sum_{j=20}^{22} (s_{(22)(j)})T_{22}^* G_j$$

If the conditions of the previous theorem are satisfied and if the functions $(a_i'')^{(4)}$ and $(b_i'')^{(4)}$ belong to $C^{(4)}(\mathbb{R}_+)$ then the above equilibrium point is asymptotically stable

Denote

Definition of G_i, T_i :-

$$G_i = G_i^* + G_i, \quad T_i = T_i^* + T_i$$

$$\frac{\partial (a_{25}''^{(4)})}{\partial T_{25}} (T_{25}^*) = (q_{25})^{(4)}, \quad \frac{\partial (b_i''^{(4)})}{\partial G_j} ((G_{27})^*) = s_{ij}$$

Then taking into account equations (global) and neglecting the terms of power 2, we obtain

$$\frac{dG_{24}}{dt} = -((a'_{24})^{(4)} + (p_{24})^{(4)})G_{24} + (a_{24})^{(4)}G_{25} - (q_{24})^{(4)}G_{24}^* T_{25}$$

$$\frac{dG_{25}}{dt} = -((a'_{25})^{(4)} + (p_{25})^{(4)})G_{25} + (a_{25})^{(4)}G_{24} - (q_{25})^{(4)}G_{25}^* T_{25}$$

$$\frac{dG_{26}}{dt} = -((a'_{26})^{(4)} + (p_{26})^{(4)})G_{26} + (a_{26})^{(4)}G_{25} - (q_{26})^{(4)}G_{26}^* T_{25}$$

$$\frac{dT_{24}}{dt} = -((b'_{24})^{(4)} - (r_{24})^{(4)})T_{24} + (b_{24})^{(4)}T_{25} + \sum_{j=24}^{26} (s_{(24)(j)})T_{24}^* G_j$$

$$\frac{dT_{25}}{dt} = -((b'_{25})^{(4)} - (r_{25})^{(4)})T_{25} + (b_{25})^{(4)}T_{24} + \sum_{j=24}^{26} (s_{(25)(j)})T_{25}^* G_j$$

$$\frac{dT_{26}}{dt} = -((b'_{26})^{(4)} - (r_{26})^{(4)})T_{26} + (b_{26})^{(4)}T_{25} + \sum_{j=24}^{26} (s_{(26)(j)})T_{26}^* G_j$$

If the conditions of the previous theorem are satisfied and if the functions $(a_i'')^{(5)}$ and $(b_i'')^{(5)}$ belong to $C^{(5)}(\mathbb{R}_+)$ then the above equilibrium point is asymptotically stable

Denote

Definition of G_i, T_i :-

$$G_i = G_i^* + G_i, \quad T_i = T_i^* + T_i$$

$$\frac{\partial (a_{29}''^{(5)})}{\partial T_{29}} (T_{29}^*) = (q_{29})^{(5)}, \quad \frac{\partial (b_i''^{(5)})}{\partial G_j} ((G_{31})^*) = s_{ij}$$

Then taking into account equations (global) and neglecting the terms of power 2, we obtain

$$\frac{dG_{28}}{dt} = -((a'_{28})^{(5)} + (p_{28})^{(5)})G_{28} + (a_{28})^{(5)}G_{29} - (q_{28})^{(5)}G_{28}^* T_{29}$$

$$\frac{dG_{29}}{dt} = -((a'_{29})^{(5)} + (p_{29})^{(5)})G_{29} + (a_{29})^{(5)}G_{28} - (q_{29})^{(5)}G_{29}^* T_{29}$$

$$\frac{dG_{30}}{dt} = -((a'_{30})^{(5)} + (p_{30})^{(5)})G_{30} + (a_{30})^{(5)}G_{29} - (q_{30})^{(5)}G_{30}^* T_{29}$$

$$\frac{dT_{28}}{dt} = -((b'_{28})^{(5)} - (r_{28})^{(5)})T_{28} + (b_{28})^{(5)}T_{29} + \sum_{j=28}^{30} (s_{(28)(j)})T_{28}^* G_j$$

$$\frac{dT_{29}}{dt} = -((b'_{29})^{(5)} - (r_{29})^{(5)})T_{29} + (b_{29})^{(5)}T_{28} + \sum_{j=28}^{30} (s_{(29)(j)})T_{29}^* G_j$$

$$\frac{dT_{30}}{dt} = -((b'_{30})^{(5)} - (r_{30})^{(5)})T_{30} + (b_{30})^{(5)}T_{29} + \sum_{j=28}^{30} (s_{(30)(j)})T_{30}^* G_j$$

If the conditions of the previous theorem are satisfied and if the functions $(a_i'')^{(6)}$ and $(b_i'')^{(6)}$ belong to $C^{(6)}(\mathbb{R}_+)$ then the above equilibrium point is asymptotically stable

Denote

Definition of G_i, T_i :-

$$G_i = G_i^* + G_i, \quad T_i = T_i^* + T_i$$

$$\frac{\partial (a_{33}''^{(6)})}{\partial T_{33}} (T_{33}^*) = (q_{33})^{(6)}, \quad \frac{\partial (b_i''^{(6)})}{\partial G_j} ((G_{35})^*) = s_{ij}$$

Then taking into account equations (global) and neglecting the terms of power 2, we obtain

$$\frac{dG_{32}}{dt} = -((a'_{32})^{(6)} + (p_{32})^{(6)})G_{32} + (a_{32})^{(6)}G_{33} - (q_{32})^{(6)}G_{32}^* T_{33}$$

$$\frac{dG_{33}}{dt} = -((a'_{33})^{(6)} + (p_{33})^{(6)})G_{33} + (a_{33})^{(6)}G_{32} - (q_{33})^{(6)}G_{33}^* T_{33}$$

$$\frac{dG_{34}}{dt} = -((a'_{34})^{(6)} + (p_{34})^{(6)})G_{34} + (a_{34})^{(6)}G_{33} - (q_{34})^{(6)}G_{34}^* T_{33}$$

$$\begin{aligned} \frac{dT_{32}}{dt} &= -((b'_{32})^{(6)} - (r_{32})^{(6)})T_{32} + (b_{32})^{(6)}T_{33} + \sum_{j=32}^{34} (s_{(32)(j)})T_{32}^* G_j & 648 \\ \frac{dT_{33}}{dt} &= -((b'_{33})^{(6)} - (r_{33})^{(6)})T_{33} + (b_{33})^{(6)}T_{32} + \sum_{j=32}^{34} (s_{(33)(j)})T_{33}^* G_j & 649 \\ \frac{dT_{34}}{dt} &= -((b'_{34})^{(6)} - (r_{34})^{(6)})T_{34} + (b_{34})^{(6)}T_{33} + \sum_{j=32}^{34} (s_{(34)(j)})T_{34}^* G_j & 650 \end{aligned}$$

Obviously, these values represent an equilibrium solution of 79,20,36,22,23, 651

If the conditions of the previous theorem are satisfied and if the functions $(a''_i)^{(7)}$ and $(b''_i)^{(7)}$ belong to $C^{(7)}(\mathbb{R}_+)$ then the above equilibrium point is asymptotically stable.

Proof: Denote

Definition of G_i, T_i :- 652

$$G_i = G_i^* + G_i \quad , \quad T_i = T_i^* + T_i \quad 653$$

$$\frac{\partial (a''_{37})^{(7)}}{\partial T_{37}} (T_{37}^*) = (q_{37})^{(7)} \quad , \quad \frac{\partial (b''_i)^{(7)}}{\partial G_j} ((G_{39})^{**}) = s_{ij}$$

Then taking into account equations(SOLUTIONAL) and neglecting the terms of power 2, we obtain 654

$$\frac{dG_{36}}{dt} = -((a'_{36})^{(7)} + (p_{36})^{(7)})G_{36} + (a_{36})^{(7)}G_{37} - (q_{36})^{(7)}G_{36}^* T_{37} \quad 655$$

$$\frac{dG_{37}}{dt} = -((a'_{37})^{(7)} + (p_{37})^{(7)})G_{37} + (a_{37})^{(7)}G_{36} - (q_{37})^{(7)}G_{37}^* T_{37} \quad 657$$

$$\frac{dG_{38}}{dt} = -((a'_{38})^{(7)} + (p_{38})^{(7)})G_{38} + (a_{38})^{(7)}G_{37} - (q_{38})^{(7)}G_{38}^* T_{37} \quad 658$$

$$\frac{dT_{36}}{dt} = -((b'_{36})^{(7)} - (r_{36})^{(7)})T_{36} + (b_{36})^{(7)}T_{37} + \sum_{j=36}^{38} (s_{(36)(j)})T_{36}^* G_j \quad 659$$

$$\frac{dT_{37}}{dt} = -((b'_{37})^{(7)} - (r_{37})^{(7)})T_{37} + (b_{37})^{(7)}T_{36} + \sum_{j=36}^{38} (s_{(37)(j)})T_{37}^* G_j \quad 660$$

$$\frac{dT_{38}}{dt} = -((b'_{38})^{(7)} - (r_{38})^{(7)})T_{38} + (b_{38})^{(7)}T_{37} + \sum_{j=36}^{38} (s_{(38)(j)})T_{38}^* G_j \quad 661$$

2. The characteristic equation of this system is

$$\begin{aligned} & \left((\lambda)^{(1)} + (b'_{15})^{(1)} - (r_{15})^{(1)} \right) \left\{ \left((\lambda)^{(1)} + (a'_{15})^{(1)} + (p_{15})^{(1)} \right) \right. \\ & \left[\left((\lambda)^{(1)} + (a'_{13})^{(1)} + (p_{13})^{(1)} \right) (q_{14})^{(1)} G_{14}^* + (a_{14})^{(1)} (q_{13})^{(1)} G_{13}^* \right] \\ & \left((\lambda)^{(1)} + (b'_{13})^{(1)} - (r_{13})^{(1)} \right) s_{(14),(14)} T_{14}^* + (b_{14})^{(1)} s_{(13),(14)} T_{14}^* \\ & + \left((\lambda)^{(1)} + (a'_{14})^{(1)} + (p_{14})^{(1)} \right) (q_{13})^{(1)} G_{13}^* + (a_{13})^{(1)} (q_{14})^{(1)} G_{14}^* \\ & \left((\lambda)^{(1)} + (b'_{13})^{(1)} - (r_{13})^{(1)} \right) s_{(14),(13)} T_{14}^* + (b_{14})^{(1)} s_{(13),(13)} T_{13}^* \\ & \left((\lambda)^{(1)} \right)^2 + \left((a'_{13})^{(1)} + (a'_{14})^{(1)} + (p_{13})^{(1)} + (p_{14})^{(1)} \right) (\lambda)^{(1)} \\ & \left((\lambda)^{(1)} \right)^2 + \left((b'_{13})^{(1)} + (b'_{14})^{(1)} - (r_{13})^{(1)} + (r_{14})^{(1)} \right) (\lambda)^{(1)} \\ & + \left((\lambda)^{(1)} \right)^2 + \left((a'_{13})^{(1)} + (a'_{14})^{(1)} + (p_{13})^{(1)} + (p_{14})^{(1)} \right) (\lambda)^{(1)} (q_{15})^{(1)} G_{15} \\ & + (\lambda)^{(1)} + (a'_{13})^{(1)} + (p_{13})^{(1)} \left((a_{15})^{(1)} (q_{14})^{(1)} G_{14}^* + (a_{14})^{(1)} (a_{15})^{(1)} (q_{13})^{(1)} G_{13}^* \right) \\ & \left. \left((\lambda)^{(1)} + (b'_{13})^{(1)} - (r_{13})^{(1)} \right) s_{(14),(15)} T_{14}^* + (b_{14})^{(1)} s_{(13),(15)} T_{13}^* \right\} = 0 \end{aligned}$$

+

$$\left((\lambda)^{(2)} + (b'_{18})^{(2)} - (r_{18})^{(2)} \right) \left\{ \left((\lambda)^{(2)} + (a'_{18})^{(2)} + (p_{18})^{(2)} \right) \right.$$

$$\left[\left((\lambda)^{(2)} + (a'_{16})^{(2)} + (p_{16})^{(2)} \right) (q_{17})^{(2)} G_{17}^* + (a_{17})^{(2)} (q_{16})^{(2)} G_{16}^* \right] \\
\left((\lambda)^{(2)} + (b'_{16})^{(2)} - (r_{16})^{(2)} \right) s_{(17),(17)} T_{17}^* + (b_{17})^{(2)} s_{(16),(17)} T_{17}^* \\
+ \left((\lambda)^{(2)} + (a'_{17})^{(2)} + (p_{17})^{(2)} \right) (q_{16})^{(2)} G_{16}^* + (a_{16})^{(2)} (q_{17})^{(2)} G_{17}^* \\
\left((\lambda)^{(2)} + (b'_{16})^{(2)} - (r_{16})^{(2)} \right) s_{(17),(16)} T_{17}^* + (b_{17})^{(2)} s_{(16),(16)} T_{16}^* \\
\left((\lambda)^{(2)} \right)^2 + \left((a'_{16})^{(2)} + (a'_{17})^{(2)} + (p_{16})^{(2)} + (p_{17})^{(2)} \right) (\lambda)^{(2)} \\
\left((\lambda)^{(2)} \right)^2 + \left((b'_{16})^{(2)} + (b'_{17})^{(2)} - (r_{16})^{(2)} + (r_{17})^{(2)} \right) (\lambda)^{(2)} \\
+ \left((\lambda)^{(2)} \right)^2 + \left((a'_{16})^{(2)} + (a'_{17})^{(2)} + (p_{16})^{(2)} + (p_{17})^{(2)} \right) (\lambda)^{(2)} (q_{18})^{(2)} G_{18} \\
+ (\lambda)^{(2)} + (a'_{16})^{(2)} + (p_{16})^{(2)} \left((a_{18})^{(2)} (q_{17})^{(2)} G_{17}^* + (a_{17})^{(2)} (a_{18})^{(2)} (q_{16})^{(2)} G_{16}^* \right) \\
\left((\lambda)^{(2)} + (b'_{16})^{(2)} - (r_{16})^{(2)} \right) s_{(17),(18)} T_{17}^* + (b_{17})^{(2)} s_{(16),(18)} T_{16}^* \} = 0$$

+

$$\left((\lambda)^{(3)} + (b'_{22})^{(3)} - (r_{22})^{(3)} \right) \left\{ (\lambda)^{(3)} + (a'_{22})^{(3)} + (p_{22})^{(3)} \right\} \\
\left[\left((\lambda)^{(3)} + (a'_{20})^{(3)} + (p_{20})^{(3)} \right) (q_{21})^{(3)} G_{21}^* + (a_{21})^{(3)} (q_{20})^{(3)} G_{20}^* \right] \\
\left((\lambda)^{(3)} + (b'_{20})^{(3)} - (r_{20})^{(3)} \right) s_{(21),(21)} T_{21}^* + (b_{21})^{(3)} s_{(20),(21)} T_{21}^* \\
+ \left((\lambda)^{(3)} + (a'_{21})^{(3)} + (p_{21})^{(3)} \right) (q_{20})^{(3)} G_{20}^* + (a_{20})^{(3)} (q_{21})^{(3)} G_{21}^* \\
\left((\lambda)^{(3)} + (b'_{20})^{(3)} - (r_{20})^{(3)} \right) s_{(21),(20)} T_{21}^* + (b_{21})^{(3)} s_{(20),(20)} T_{20}^* \\
\left((\lambda)^{(3)} \right)^2 + \left((a'_{20})^{(3)} + (a'_{21})^{(3)} + (p_{20})^{(3)} + (p_{21})^{(3)} \right) (\lambda)^{(3)} \\
\left((\lambda)^{(3)} \right)^2 + \left((b'_{20})^{(3)} + (b'_{21})^{(3)} - (r_{20})^{(3)} + (r_{21})^{(3)} \right) (\lambda)^{(3)} \\
+ \left((\lambda)^{(3)} \right)^2 + \left((a'_{20})^{(3)} + (a'_{21})^{(3)} + (p_{20})^{(3)} + (p_{21})^{(3)} \right) (\lambda)^{(3)} (q_{22})^{(3)} G_{22} \\
+ (\lambda)^{(3)} + (a'_{20})^{(3)} + (p_{20})^{(3)} \left((a_{22})^{(3)} (q_{21})^{(3)} G_{21}^* + (a_{21})^{(3)} (a_{22})^{(3)} (q_{20})^{(3)} G_{20}^* \right) \\
\left((\lambda)^{(3)} + (b'_{20})^{(3)} - (r_{20})^{(3)} \right) s_{(21),(22)} T_{21}^* + (b_{21})^{(3)} s_{(20),(22)} T_{20}^* \} = 0$$

+

$$\left((\lambda)^{(4)} + (b'_{26})^{(4)} - (r_{26})^{(4)} \right) \left\{ (\lambda)^{(4)} + (a'_{26})^{(4)} + (p_{26})^{(4)} \right\} \\
\left[\left((\lambda)^{(4)} + (a'_{24})^{(4)} + (p_{24})^{(4)} \right) (q_{25})^{(4)} G_{25}^* + (a_{25})^{(4)} (q_{24})^{(4)} G_{24}^* \right] \\
\left((\lambda)^{(4)} + (b'_{24})^{(4)} - (r_{24})^{(4)} \right) s_{(25),(25)} T_{25}^* + (b_{25})^{(4)} s_{(24),(25)} T_{25}^* \\
+ \left((\lambda)^{(4)} + (a'_{25})^{(4)} + (p_{25})^{(4)} \right) (q_{24})^{(4)} G_{24}^* + (a_{24})^{(4)} (q_{25})^{(4)} G_{25}^* \\
\left((\lambda)^{(4)} + (b'_{24})^{(4)} - (r_{24})^{(4)} \right) s_{(25),(24)} T_{25}^* + (b_{25})^{(4)} s_{(24),(24)} T_{24}^* \\
\left((\lambda)^{(4)} \right)^2 + \left((a'_{24})^{(4)} + (a'_{25})^{(4)} + (p_{24})^{(4)} + (p_{25})^{(4)} \right) (\lambda)^{(4)} \\
\left((\lambda)^{(4)} \right)^2 + \left((b'_{24})^{(4)} + (b'_{25})^{(4)} - (r_{24})^{(4)} + (r_{25})^{(4)} \right) (\lambda)^{(4)} \\
+ \left((\lambda)^{(4)} \right)^2 + \left((a'_{24})^{(4)} + (a'_{25})^{(4)} + (p_{24})^{(4)} + (p_{25})^{(4)} \right) (\lambda)^{(4)} (q_{26})^{(4)} G_{26} \\
+ (\lambda)^{(4)} + (a'_{24})^{(4)} + (p_{24})^{(4)} \left((a_{26})^{(4)} (q_{25})^{(4)} G_{25}^* + (a_{25})^{(4)} (a_{26})^{(4)} (q_{24})^{(4)} G_{24}^* \right) \\
\left((\lambda)^{(4)} + (b'_{24})^{(4)} - (r_{24})^{(4)} \right) s_{(25),(26)} T_{25}^* + (b_{25})^{(4)} s_{(24),(26)} T_{24}^* \} = 0$$

+

$$\begin{aligned} & \left((\lambda)^{(5)} + (b'_{30})^{(5)} - (r_{30})^{(5)} \right) \left\{ \left((\lambda)^{(5)} + (a'_{30})^{(5)} + (p_{30})^{(5)} \right) \right. \\ & \left[\left((\lambda)^{(5)} + (a'_{28})^{(5)} + (p_{28})^{(5)} \right) (q_{29})^{(5)} G_{29}^* + (a_{29})^{(5)} (q_{28})^{(5)} G_{28}^* \right] \\ & \left((\lambda)^{(5)} + (b'_{28})^{(5)} - (r_{28})^{(5)} \right) s_{(29),(29)} T_{29}^* + (b_{29})^{(5)} s_{(28),(29)} T_{29}^* \\ & + \left((\lambda)^{(5)} + (a'_{29})^{(5)} + (p_{29})^{(5)} \right) (q_{28})^{(5)} G_{28}^* + (a_{28})^{(5)} (q_{29})^{(5)} G_{29}^* \\ & \left((\lambda)^{(5)} + (b'_{28})^{(5)} - (r_{28})^{(5)} \right) s_{(29),(28)} T_{29}^* + (b_{29})^{(5)} s_{(28),(28)} T_{28}^* \\ & \left((\lambda)^{(5)} \right)^2 + \left((a'_{28})^{(5)} + (a'_{29})^{(5)} + (p_{28})^{(5)} + (p_{29})^{(5)} \right) (\lambda)^{(5)} \\ & \left((\lambda)^{(5)} \right)^2 + \left((b'_{28})^{(5)} + (b'_{29})^{(5)} - (r_{28})^{(5)} + (r_{29})^{(5)} \right) (\lambda)^{(5)} \\ & + \left((\lambda)^{(5)} \right)^2 + \left((a'_{28})^{(5)} + (a'_{29})^{(5)} + (p_{28})^{(5)} + (p_{29})^{(5)} \right) (\lambda)^{(5)} (q_{30})^{(5)} G_{30} \\ & + (\lambda)^{(5)} + (a'_{28})^{(5)} + (p_{28})^{(5)} \left((a_{30})^{(5)} (q_{29})^{(5)} G_{29}^* + (a_{29})^{(5)} (a_{30})^{(5)} (q_{28})^{(5)} G_{28}^* \right) \\ & \left. \left((\lambda)^{(5)} + (b'_{28})^{(5)} - (r_{28})^{(5)} \right) s_{(29),(30)} T_{29}^* + (b_{29})^{(5)} s_{(28),(30)} T_{28}^* \right\} = 0 \end{aligned}$$

+

$$\begin{aligned} & \left((\lambda)^{(6)} + (b'_{34})^{(6)} - (r_{34})^{(6)} \right) \left\{ \left((\lambda)^{(6)} + (a'_{34})^{(6)} + (p_{34})^{(6)} \right) \right. \\ & \left[\left((\lambda)^{(6)} + (a'_{32})^{(6)} + (p_{32})^{(6)} \right) (q_{33})^{(6)} G_{33}^* + (a_{33})^{(6)} (q_{32})^{(6)} G_{32}^* \right] \\ & \left((\lambda)^{(6)} + (b'_{32})^{(6)} - (r_{32})^{(6)} \right) s_{(33),(33)} T_{33}^* + (b_{33})^{(6)} s_{(32),(33)} T_{33}^* \\ & + \left((\lambda)^{(6)} + (a'_{33})^{(6)} + (p_{33})^{(6)} \right) (q_{32})^{(6)} G_{32}^* + (a_{32})^{(6)} (q_{33})^{(6)} G_{33}^* \\ & \left((\lambda)^{(6)} + (b'_{32})^{(6)} - (r_{32})^{(6)} \right) s_{(33),(32)} T_{33}^* + (b_{33})^{(6)} s_{(32),(32)} T_{32}^* \\ & \left((\lambda)^{(6)} \right)^2 + \left((a'_{32})^{(6)} + (a'_{33})^{(6)} + (p_{32})^{(6)} + (p_{33})^{(6)} \right) (\lambda)^{(6)} \\ & \left((\lambda)^{(6)} \right)^2 + \left((b'_{32})^{(6)} + (b'_{33})^{(6)} - (r_{32})^{(6)} + (r_{33})^{(6)} \right) (\lambda)^{(6)} \\ & + \left((\lambda)^{(6)} \right)^2 + \left((a'_{32})^{(6)} + (a'_{33})^{(6)} + (p_{32})^{(6)} + (p_{33})^{(6)} \right) (\lambda)^{(6)} (q_{34})^{(6)} G_{34} \\ & + (\lambda)^{(6)} + (a'_{32})^{(6)} + (p_{32})^{(6)} \left((a_{34})^{(6)} (q_{33})^{(6)} G_{33}^* + (a_{33})^{(6)} (a_{34})^{(6)} (q_{32})^{(6)} G_{32}^* \right) \\ & \left. \left((\lambda)^{(6)} + (b'_{32})^{(6)} - (r_{32})^{(6)} \right) s_{(33),(34)} T_{33}^* + (b_{33})^{(6)} s_{(32),(34)} T_{32}^* \right\} = 0 \end{aligned}$$

+

$$\begin{aligned} & \left((\lambda)^{(7)} + (b'_{38})^{(7)} - (r_{38})^{(7)} \right) \left\{ \left((\lambda)^{(7)} + (a'_{38})^{(7)} + (p_{38})^{(7)} \right) \right. \\ & \left[\left((\lambda)^{(7)} + (a'_{36})^{(7)} + (p_{36})^{(7)} \right) (q_{37})^{(7)} G_{37}^* + (a_{37})^{(7)} (q_{36})^{(7)} G_{36}^* \right] \\ & \left((\lambda)^{(7)} + (b'_{36})^{(7)} - (r_{36})^{(7)} \right) s_{(37),(37)} T_{37}^* + (b_{37})^{(7)} s_{(36),(37)} T_{37}^* \\ & + \left((\lambda)^{(7)} + (a'_{37})^{(7)} + (p_{37})^{(7)} \right) (q_{36})^{(7)} G_{36}^* + (a_{36})^{(7)} (q_{37})^{(7)} G_{37}^* \\ & \left((\lambda)^{(7)} + (b'_{36})^{(7)} - (r_{36})^{(7)} \right) s_{(37),(36)} T_{37}^* + (b_{37})^{(7)} s_{(36),(36)} T_{36}^* \\ & \left((\lambda)^{(7)} \right)^2 + \left((a'_{36})^{(7)} + (a'_{37})^{(7)} + (p_{36})^{(7)} + (p_{37})^{(7)} \right) (\lambda)^{(7)} \\ & \left((\lambda)^{(7)} \right)^2 + \left((b'_{36})^{(7)} + (b'_{37})^{(7)} - (r_{36})^{(7)} + (r_{37})^{(7)} \right) (\lambda)^{(7)} \\ & + \left((\lambda)^{(7)} \right)^2 + \left((a'_{36})^{(7)} + (a'_{37})^{(7)} + (p_{36})^{(7)} + (p_{37})^{(7)} \right) (\lambda)^{(7)} (q_{38})^{(7)} G_{38} \\ & + (\lambda)^{(7)} + (a'_{36})^{(7)} + (p_{36})^{(7)} \left((a_{38})^{(7)} (q_{37})^{(7)} G_{37}^* + (a_{37})^{(7)} (a_{38})^{(7)} (q_{36})^{(7)} G_{36}^* \right) \end{aligned}$$

$$\left\{ \left((\lambda)^{(7)} + (b'_{36})^{(7)} - (r_{36})^{(7)} \right) s_{(37),(38)} T_{37}^* + (b_{37})^{(7)} s_{(36),(38)} T_{36}^* \right\} = 0$$

REFERENCES

- =====
- [1]. A HAIMOVICI: "On the growth of a two species ecological system divided on age groups". Tensor, Vol 37 (1982), Commemoration volume dedicated to Professor Akitsugu Kawaguchi on his 80th birthday
- [2]. (2)FRTJOF CAPRA: "The web of life" Flamingo, Harper Collins See "Dissipative structures" pages 172-188
- [3]. (3)HEYLIGHEN F. (2001): "The Science of Self-organization and Adaptivity", in L. D. Kiel, (ed) . Knowledge Management, Organizational Intelligence and Learning, and Complexity, in: The Encyclopedia of Life Support Systems ((EOLSS), (Eolss Publishers, Oxford) [http://www.eolss.net
- [4]. (4)MATSUI, T, H. Masunaga, S. M. Kreidenweis, R. A. Pielke Sr., W.-K. Tao, M. Chin, and Y. J Kaufman (2006), "Satellite-based assessment of marine low cloud variability associated with aerosol, atmospheric stability, and the diurnal cycle", J. Geophys. Res., 111, D17204, doi:10.1029/2005JD006097
- [5]. (5)STEVENS, B, G. Feingold, W.R. Cotton and R.L. Walko, "Elements of the microphysical structure of numerically simulated nonprecipitating stratocumulus" J. Atmos. Sci., 53, 980-1006
- [6]. (6)FEINGOLD, G, Koren, I; Wang, HL; Xue, HW; Brewer, WA (2010), "Precipitation-generated oscillations in open cellular cloud fields" *Nature*, 466 (7308) 849-852, doi: 10.1038/nature09314, Published 12-Aug 2010
- [7]. (7)HEYLIGHEN F. (2001): "The Science of Self-organization and Adaptivity", in L. D. Kiel, (ed) . Knowledge Management, Organizational Intelligence and Learning, and Complexity, in: The Encyclopedia of Life Support Systems ((EOLSS), (Eolss Publishers, Oxford) [http://www.eolss.net
- [8]. (8)MATSUI, T, H. Masunaga, S. M. Kreidenweis, R. A. Pielke Sr., W.-K. Tao, M. Chin, and Y. J Kaufman (2006), "Satellite-based assessment of marine low cloud variability associated with aerosol, atmospheric stability, and the diurnal cycle", J. Geophys. Res., 111, D17204, doi:10.1029/2005JD006097
- (8A) STEVENS, B, G. Feingold, W.R. Cotton and R.L. Walko, "Elements of the microphysical structure of numerically simulated nonprecipitating stratocumulus" J. Atmos. Sci., 53, 980-1006
- (8B) FEINGOLD, G, Koren, I; Wang, HL; Xue, HW; Brewer, WA (2010), "Precipitation-generated oscillations in open cellular cloud fields" *Nature*, 466 (7308) 849-852, doi: 10.1038/nature09314, Published 12-Aug 2010
- [9]. (9)^{a b c} Einstein, A. (1905), "Ist die Trägheit eines Körpers von seinem Energieinhalt abhängig?", *Annalen der Physik* **18**: 639 Bibcode 1905AnP...323..639E, DOI:10.1002/andp.19053231314. See also the English translation.
- [10]. ^{a b} Paul Allen Tipler, Ralph A. Llewellyn (2003-01), *Modern Physics*, W. H. Freeman and Company, pp. 87-88, ISBN 0-7167-4345-0
- [11]. ^{a b} Rainville, S. et al. World Year of Physics: A direct test of E=mc². *Nature* 438, 1096-1097 (22 December 2005) | doi: 10.1038/4381096a; Published online 21 December 2005.
- [12]. ^a In F. Fernflores. The Equivalence of Mass and Energy. Stanford Encyclopedia of Philosophy
- [13]. ^a Note that the relativistic mass, in contrast to the rest mass m_0 , is not a relativistic invariant, and that the velocity is not a Minkowski four-vector, in contrast to the quantity dx^μ , where dx^μ is the differential of the proper time. However, the energy-momentum four-vector is a genuine Minkowski four-vector, and the intrinsic origin of the square-root in the definition of the relativistic mass is the distinction between $d\tau$ and dt .
- [14]. ^a Relativity DeMystified, D. McMahon, Mc Graw Hill (USA), 2006, ISBN 0-07-145545-0
- [15]. ^a Dynamics and Relativity, J.R. Forshaw, A.G. Smith, Wiley, 2009, ISBN 978-0-470-01460-8
- [16]. ^a Hans, H. S.; Puri, S. P. (2003). *Mechanics* (2 ed.). Tata McGraw-Hill. p. 433. ISBN 0-07-047360-9., Chapter 12 page 433
- [17]. ^a E. F. Taylor and J. A. Wheeler, **Spacetime Physics**, W.H. Freeman and Co., NY. 1992. ISBN 0-7167-2327-1, see pp. 248-9 for discussion of mass remaining constant after detonation of nuclear bombs, until heat is allowed to escape.
- [18]. ^a Mould, Richard A. (2002). *Basic relativity* (2 ed.). Springer. p. 126. ISBN 0-387-95210-1., Chapter 5 page 126
- [19]. ^a Chow, Tail L. (2006). *Introduction to electromagnetic theory: a modern perspective*. Jones & Bartlett Learning. p. 392. ISBN 0-7637-3827-1., Chapter 10 page 392
- [20]. ^a [2] Cockcroft-Walton experiment
- [21]. ^{a b c} Conversions used: 1956 International (Steam) Table (IT) values where one calorie \equiv 4.1868 J and one BTU \equiv 1055.05585262 J. Weapons designers' conversion value of one gram TNT \equiv 1000 calories used.
- [22]. ^a Assuming the dam is generating at its peak capacity of 6,809 MW.
- [23]. ^a Assuming a 90/10 alloy of Pt/Ir by weight, a C_p of 25.9 for Pt and 25.1 for Ir, a Pt-dominated average C_p of 25.8, 5.134 moles of metal, and 132 J.K⁻¹ for the prototype. A variation of ± 1.5 picograms is of course, much smaller than the actual uncertainty in the mass of the international prototype, which are ± 2 micrograms.
- [24]. ^a [3] Article on Earth rotation energy. Divided by c^2 .
- [25]. ^{a b} Earth's gravitational self-energy is 4.6×10^{30} that of Earth's total mass, or 2.7 trillion metric tons.

Citation: *The Apache Point Observatory Lunar Laser-Ranging Operation (APOLLO)*, T. W. Murphy, Jr. et al. University of Washington, Dept. of Physics (132 kB PDF, here.).

- [26]. [^] There is usually more than one possible way to define a field energy, because any field can be made to couple to gravity in many different ways. By general scaling arguments, the correct answer at everyday distances, which are long compared to the quantum gravity scale, should be *minimal coupling*, which means that no powers of the curvature tensor appear. Any non-minimal couplings, along with other higher order terms, are presumably only determined by a theory of quantum gravity, and within string theory, they only start to contribute to experiments at the string scale.
- [27]. [^] G. 't Hooft, "Computation of the quantum effects due to a four-dimensional pseudoparticle", *Physical Review D* 14:3432–3450 (1976).
- [28]. [^] A. Belavin, A. M. Polyakov, A. Schwarz, Yu. Tyupkin, "Pseudoparticle Solutions to Yang Mills Equations", *Physics Letters* 59B:85 (1975).
- [29]. [^] F. Klinkhammer, N. Manton, "A Saddle Point Solution in the Weinberg Salam Theory", *Physical Review D* 30:2212.
- [30]. [^] Rubakov V. A. "Monopole Catalysis of Proton Decay", *Reports on Progress in Physics* 51:189–241 (1988).
- [31]. [^] S.W. Hawking "Black Holes Explosions?" *Nature* 248:30 (1974).
- [32]. [^] Einstein, A. (1905), "Zur Elektrodynamik bewegter Körper." (PDF), *Annalen der Physik* 17: 891–921, Bibcode 1905AnP...322...891E, DOI:10.1002/andp.19053221004. English translation.
- [33]. [^] See e.g. Lev B. Okun, *The concept of Mass*, *Physics Today* 42 (6), June 1969, p. 31–36, http://www.physicstoday.org/vol-42/iss-6/vol42no6p31_36.pdf
- [34]. [^] Max Jammer (1999), *Concepts of mass in contemporary physics and philosophy*, Princeton University Press, p. 51, ISBN 0-691-01017-X
- [35]. [^] Eriksen, Erik; Vøyenli, Kjell (1976), "The classical and relativistic concepts of mass", *Foundations of Physics* (Springer) 6: 115–124, Bibcode 1976FoPh....6..115E, DOI:10.1007/BF00708670
- [36]. [^] Jannsen, M., Mecklenburg, M. (2007), *From classical to relativistic mechanics: Electromagnetic models of the electron.*, in V. F. Hendricks, et al., , *Interactions: Mathematics, Physics and Philosophy* (Dordrecht: Springer): 65–134
- [37]. [^] Whittaker, E.T. (1951–1953), 2. Edition: *A History of the theories of aether and electricity, vol. 1: The classical theories / vol. 2: The modern theories 1900–1926*, London: Nelson
- [38]. [^] Miller, Arthur I. (1981), *Albert Einstein's special theory of relativity. Emergence (1905) and early interpretation (1905–1911)*, Reading: Addison–Wesley, ISBN 0-201-04679-2
- [39]. [^] Darrigol, O. (2005), "The Genesis of the theory of relativity." (PDF), *Séminaire Poincaré* 1: 1–22
- [40]. [^] Philip Ball (Aug 23, 2011). "Did Einstein discover $E = mc^2$?" *Physics World*.
- [41]. [^] Ives, Herbert E. (1952), "Derivation of the mass-energy relation", *Journal of the Optical Society of America* 42 (8): 540–543, DOI:10.1364/JOSA.42.000540
- [42]. [^] Jammer, Max (1961/1997). *Concepts of Mass in Classical and Modern Physics*. New York: Dover. ISBN 0-486-29998-8.
- [43]. [^] Stachel, John; Torretti, Roberto (1982), "Einstein's first derivation of mass-energy equivalence", *American Journal of Physics* 50 (8): 760–763, Bibcode1982AmJPh..50..760S, DOI:10.1119/1.12764
- [44]. [^] Ohanian, Hans (2008), "Did Einstein prove $E=mc^2$?", *Studies In History and Philosophy of Science Part B* 40 (2): 167–173, arXiv:0805.1400, DOI:10.1016/j.shpsb.2009.03.002
- [45]. [^] Hecht, Eugene (2011), "How Einstein confirmed $E_0=mc^2$ ", *American Journal of Physics* 79 (6): 591–600, Bibcode 2011AmJPh..79..591H, DOI:10.1119/1.3549223
- [46]. [^] Rohrlich, Fritz (1990), "An elementary derivation of $E=mc^2$ ", *American Journal of Physics* 58 (4): 348–349, Bibcode 1990AmJPh..58..348R, DOI:10.1119/1.16168
- [47]. (1996). *Lise Meitner: A Life in Physics*. California Studies in the History of Science. 13. Berkeley: University of California Press. pp. 236–237. ISBN 0-520-20860-

- [48]. ^ UIBK.ac.at
[49]. ^ J. J. L. Morton; *et al.* (2008). "Solid-state quantum memory using the ^{31}P nuclear spin". *Nature* **455** (7216): 1085–1088. Bibcode 2008Natur.455.1085M.DOI:10.1038/nature07295.
[50]. ^ S. Weisner (1983). "Conjugate coding". *Association of Computing Machinery, Special Interest Group in Algorithms and Computation Theory* **15**: 78–88.
[51]. ^ A. Zeilinger, *Dance of the Photons: From Einstein to Quantum Teleportation*, Farrar, Straus & Giroux, New York, 2010, pp. 189, 192, ISBN 0374239665
[52]. ^ B. Schumacher (1995). "Quantum coding". *Physical Review A* **51** (4): 2738–2747. Bibcode 1995PhRvA..51.2738S. DOI:10.1103/PhysRevA.51.2738.
-

Acknowledgments:

The introduction is a collection of information from various articles, Books, News Paper reports, Home Pages Of authors, Journal Reviews, Nature 's Letters, Article Abstracts, Research papers, Abstracts Of Research Papers, Stanford Encyclopedia, Web Pages, Ask a Physicist Column, Deliberations with Professors, the internet including Wikipedia. We acknowledge all authors who have contributed to the same. In the eventuality of the fact that there has been any act of omission on the part of the authors, we regret with great deal of compunction, contrition, regret, trepidation and remorse. As Newton said, it is only because erudite and eminent people allowed one to piggy ride on their backs; probably an attempt has been made to look slightly further. Once again, it is stated that the references are only illustrative and not comprehensive

First Author: ¹**Mr. K. N.Prasanna Kumar** has three doctorates one each in Mathematics, Economics, Political Science. Thesis was based on Mathematical Modeling. He was recently awarded D.litt. for his work on 'Mathematical Models in Political Science'--- Department of studies in Mathematics, Kuvempu University, Shimoga, Karnataka, India Corresponding

Second Author: ²**Prof. B.S Kiranagi** is the Former Chairman of the Department of Studies in Mathematics, Manasa Gangotri and present Professor Emeritus of UGC in the Department. Professor Kiranagi has guided over 25 students and he has received many encomiums and laurels for his contribution to Co homology Groups and Mathematical Sciences. Known for his prolific writing, and one of the senior most Professors of the country, he has over 150 publications to his credit. A prolific writer and a prodigious thinker, he has to his credit several books on Lie Groups, Co Homology Groups, and other mathematical application topics, and excellent publication history.-- UGC Emeritus Professor (Department of studies in Mathematics), Manasagangotri, University of Mysore, Karnataka, India

Third Author: ³**Prof. C.S. Bagewadi** is the present Chairman of Department of Mathematics and Department of Studies in Computer Science and has guided over 25 students. He has published articles in both national and international journals. Professor Bagewadi specializes in Differential Geometry and its wide-ranging ramifications. He has to his credit more than 159 research papers. Several Books on Differential Geometry, Differential Equations are coauthored by him--- Chairman, Department of studies in Mathematics and Computer science, Jnanasahyadri Kuvempu University, Shankarghatta, Shimoga district, Karnataka, India

A New Three Phase Seven Level Asymmetrical Inverter with Hybrid Carrier and Third Harmonic Reference

Johnson Uthayakumar R. *, Natarajan S.P. **, Padmathilagam.V. ***

*Department of Electronics and Instrumentation Engineering, Annamalai University, India

** Department of Electronics and Instrumentation Engineering, Annamalai University, India

*** Department of Electrical and Electronics Engineering, Annamalai University, India

ABSTRACT: Carrier based techniques have been used widely for switching of multilevel inverters due to their simplicity, flexibility and reduced computational requirements compared to Space Vector Modulation (SVM). A novel carrier based Pulse Width Modulation (PWM) technique for three phase Asymmetrical Multi Level Inverter (AMLI) with Third Harmonic Injection (THI) reference is proposed in this paper. The technique is based on the combination of the Control Freedom Degrees (CFD). The combination of inverted sine carrier and triangular carrier is used as hybrid carrier in order to produce pulses for the power switches used in the proposed seven level three phase cascaded inverter. This paper investigates the potentials of hybrid carrier based cascaded multilevel inverter in the development of medium power AC power supplies with specific emphasis on Power Conditioning Systems (PCS) for alternate sources of energy. The performance of chosen inverter is evaluated based on MATLAB/ SIMULINK simulation. The performance indices used are Total Harmonic Distortion (THD), RMS value of output voltage and DC bus utilization. It is observed that Carrir over lapping PWM provides better DC bus utilization and Phase opposition Disposition (POD) technique creates less distortion for $m_a=0.7-1$

Keywords: APOD, COPWM, PD, POD, ISPWM

I. INTRODUCTION

In recent years, multi-level Voltage Source Inverters (VSIs) are widely used as static power converter for high-power applications. MLIs can operate at both fundamental switching frequency and high switching frequency PWM. The topologies of MLIs are classified into three types: the flying capacitor inverter, the diode clamped inverter and the modular H-bridge inverter. Seyezhai and Mathur [1] have described a technique that combines the advantage of inverted rectified sine wave and variable frequency carriers for a seven level inverter for balancing the switch utilization and have also stated that the switching losses for the chosen modulation scheme is very less. Chandra and Kumar in [2] presented an automatic switching pattern generation for multilevel cascaded H-Bridge inverters with equal DC voltage sources based on the Space Vector Pulse Width Modulation (SVPWM) technique. Seyezhai and Mathur [3,4] have done a comparative evaluation between hybrid modulation strategy and the conventional Phase Disposition (PD) PWM method in terms of output voltage quality, power circuitry complexity, Distortion Factor (DF) and THD. Jeevananthan et al [5] have proposed an Inverted Sine Carrier PWM (ISCPWM) method which used the

conventional sinusoidal reference signal and an inverted sine carrier to produce better spectral quality and a higher fundamental component compared to the conventional Sinusoidal PWM (SPWM) without any pulse dropping. A survey of topologies, controls and applications of MLIs has been carried out by Rodriguez et al [6]. The common topology is the cascaded inverter shown in Fig.1 for three phase structure. The three multilevel modulation methods most discussed in the literature include multilevel carrier-based PWM, multilevel space-vector PWM and selective harmonic elimination [6]. Analysis of multicarrier PWM methods for a single phase five level inverter was proposed by Calais Borle and Agelidis [7]. A novel clew for the research on carrier based PWM methods for multilevel inverters is proposed by Wu et al [8] based on the concept of combination of the Control Freedom Degrees (CFD). Sun [9] have presented a new asymmetrical multilevel inverter topology. The new topology can improve the number of output voltage levels greatly using a bidirectional auxiliary switch. Further they have proposed multicarrier PWM method for the asymmetrical inverter [9]. Taleb et al [10] have proposed a neural implementation of a Harmonic Elimination Strategy (HES) to control a Uniform Step Asymmetrical Multilevel Inverter (USAMI). Mihalache [11] has proposed an asymmetrical PWM modulation technique which is known to offer lower harmonic content as compared to the symmetrical modulation. Nami et al [12] have optimized asymmetrical arrangement compared with a conventional four level inverter and found that it exhibits lesser switching losses and lesser harmonics. In some application with different DC input sources such as electric vehicles, a modular H-bridge asymmetrical inverter can be used to drive a traction motor from a set of solar cells or fuel cells. A seven level output voltage is achieved with two bridges in asymmetrical inverter whereas only five level output voltage will be achieved with three bridges in case of conventional cascaded MLI. In AMLI with lesser number switches more voltage levels can be achieved. Fig.1. shows the chosen asymmetrical three phase inverter. Each cell has two pairs of complementary switches S1 and S3 and S2 and S4. There are six cells used in the three phase inverter each leg containing two cells each. Since the carrier based method have good CFD, this paper focusses on the hybrid carrier arrangement using triangular carrier in the positive side and inverted sine carrier waveform in the negative side with Phase Disposition (PD), Phase Opposition Disposition (POD), Alternate Phase Opposition Disposition (APOD), Carrier Overlapping (CO) and Inverted Sine (IS) strategies. Fig.2. shows a sample SIMULINK model developed for PWM strategy of a three phase inverter.

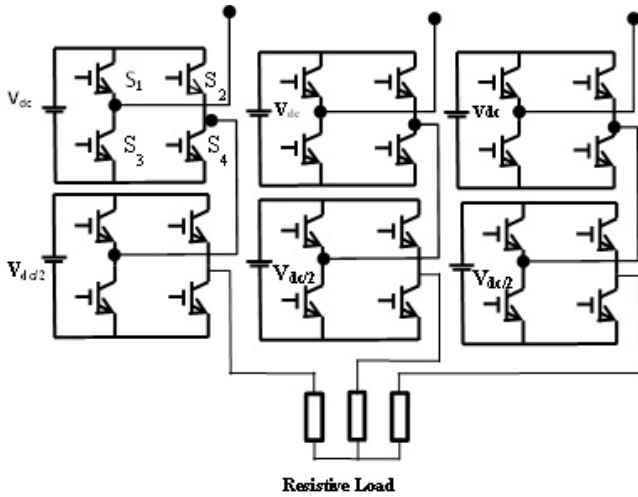


Fig.1. A three phase asymmetrical cascaded seven level inverter

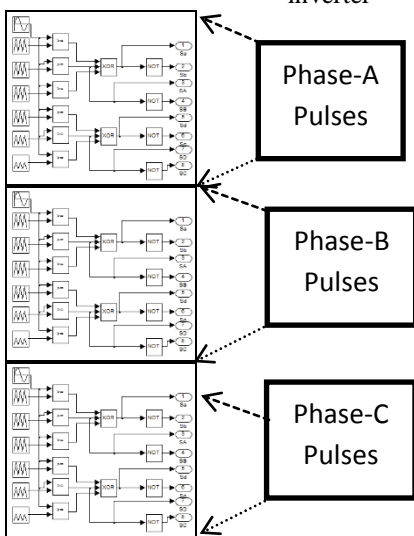


Fig.2. A sample SIMULINK model developed for PWM strategy of a three phase inverter

II. HYBRID CARRIER BASED BIPOLAR MODULATION SCHEMES WITH THI REFERENCE

The maximum modulation index of a three phase inverter can be increased by including a common mode third harmonic term into the target reference waveform of each phase leg. In this method, the modulation index m_a can be increased beyond $m_a=1.0$ without moving into over modulation.

II (a) PDPWM hybrid carrier strategy

This technique employs $(m-1)$ carriers which are all in phase for a m level inverter. In seven level converter all the six carrier waves are in phase with each other across all the bands as described in Fig.3 for a phase leg of a seven level cascaded structure with $m_a = 0.8$.

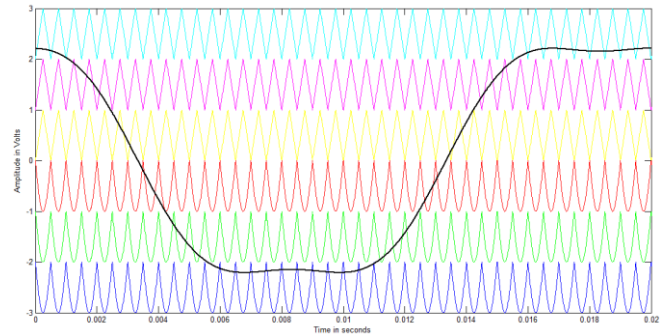


Fig.3. Carrier arrangements for PDPWM hybrid carrier strategy

II (b) PODPWM hybrid carrier

This technique employs $(m-1)$ carriers which are all in phase above and below the zero reference. In seven level converters all the six carrier waves above zero reference are phase shifted by 180 degrees with the ones below zero reference. The PODPWM is explained in the Fig.4 in which all the carriers above the zero reference are in phase and carriers below the zero reference are also in phase but are phase shifted by 180 degree with respect to that above zero reference. Fig.4 illustrates the POD PWM hybrid carrier and THI reference arrangements for a phase leg of a three phase seven level cascaded structure with $m_a = 0.8$.

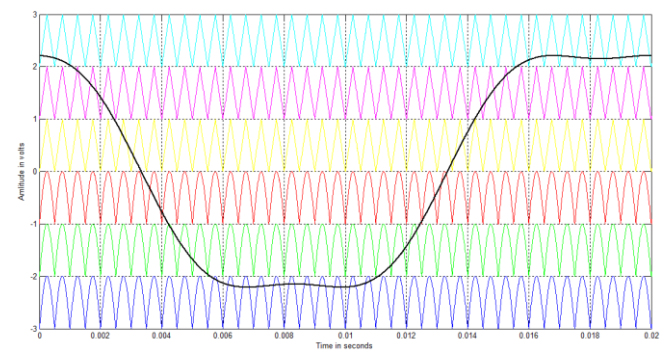


Fig.4. Carrier arrangements for PODPWM hybrid carrier strategy

II (c) APODPWM hybrid carrier strategy

This technique requires each of the $m-1$ carrier waveforms for an m -level phase waveform to be phase displaced from each other by 180 degrees alternatively. In The APOD hybrid carrier and THI reference arrangements for a phase leg of a three phase seven level cascaded structure with $m_a=0.8$ are illustrated in Fig.5.

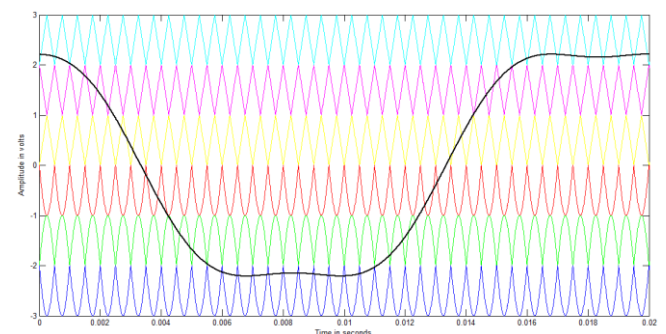


Fig.5. Carrier arrangements for APODPWM hybrid carrier strategy

II (d) COPWM hybrid carrier

For an m-level inverter using carrier overlapping technique, (m-1) carriers with the same frequency (f_c) and same peak-to-peak amplitude (A_c) are disposed such that the bands they occupy overlap each other; the overlapping vertical distance between each carrier is $0.5A_c$. The reference waveform has amplitude of A_m and frequency of f_m and it is centered in the middle of the carrier signals.

Fig.6 shows the COPWM hybrid carrier and THI reference arrangements for a phase leg of a three phase seven level cascaded structure with $m_a=0.8$.

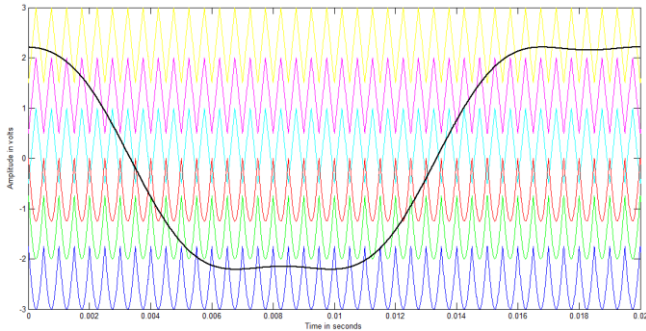


Fig.6. Carrier arrangements for COPWM hybrid carrier strategy

II (e) VFPWM hybrid carrier strategy

Fig.7 illustrates the VFPWM hybrid carrier and THI reference arrangements for a phase leg of a seven level three phase cascaded structure with $m_a = 0.8$.

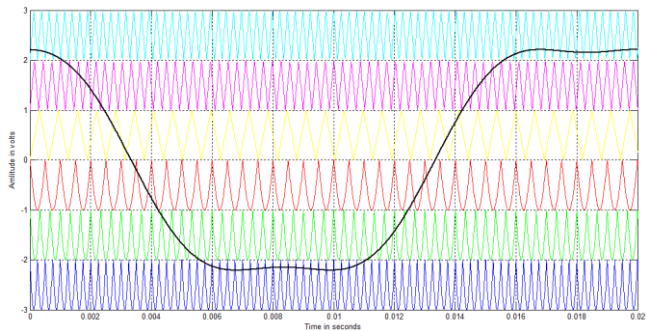


Fig.7. Carrier arrangements for VFPWM hybrid carrier strategy

The frequency modulation index

$$m_f = f_c / f_m$$

The amplitude modulation index

$$m_a = 2A_m / (m-1) A_c$$

where

f_c – Frequency of the carrier signal

f_m – Frequency of the reference signal

A_m – Amplitude of the reference signal

A_c – Amplitude of the carrier signal

$$m_a = A_m / (m / 4) * A_c \text{ (COPWM)}$$

III. SIMULATION RESULTS

Simulation results have been obtained by using MATLAB/SIMULINK power system toolbox software. The

input DC sources are asymmetrical i.e one of the cascaded bridge is fed with V_{dc2} and other by V_{dc} . Figs.8-12 illustrate the output voltages of three phase asymmetrical cascaded seven level multilevel inverter for $m_a=0.8$ only. The Root Mean Square (RMS) value, Total Harmonic Distortion (THD) and Form Factor (FF) of output voltage are evaluated with suitable formula and for various hybrid modulation schemes such as PD, POD, APOD, COPWM, VFPWM strategies for various m_a (0.7-1) as in Tables I-III. Fig.13-18 display the frequency spectra and %THD for chosen strategies. It is found that the DC bus utilisation of the three phase seven level cascaded multilevel inverter is much better in case of COPWM as in Table II. POD technique is formed to create less distortion. It is seen that 3rd,37th, 39th harmonics are dominant in PD and POD PWM where as 3rd,27th,31st,33rd,35th,37th,39th harmonics are dominant in APOD PWM. VFPWM creates only 3rd harmonic dominant energy where as in COPWM 3rd,35th,37th,39th harmonics are dominant. The following parameter values are used simulation: $V_{dc1} = 100V$, $V_{dc2} = 50V$, $A_c=1$, $m_f=40$ and $R(\text{load}) = 100$ ohms for each phase.

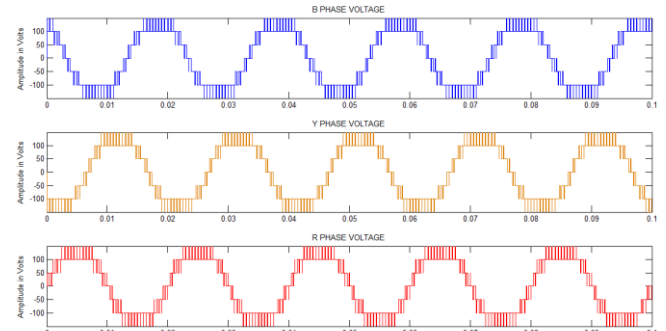


Fig.8. Output voltage of hybrid carrier THI-PDPWM strategy

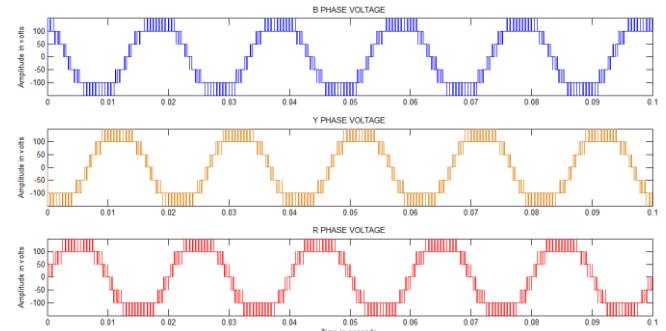


Fig.9. Output voltage of hybrid carrier THI-PODPWM strategy

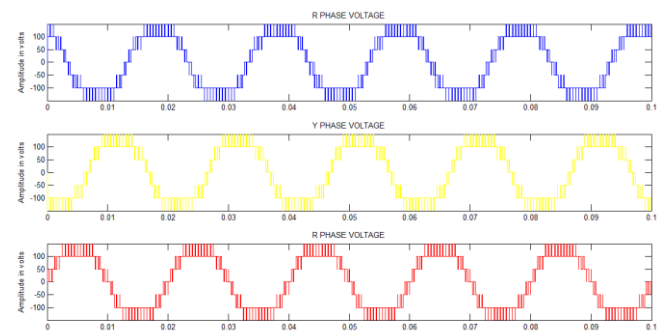


Fig.10. Output voltage of hybrid carrier THI-APODPWM strategy

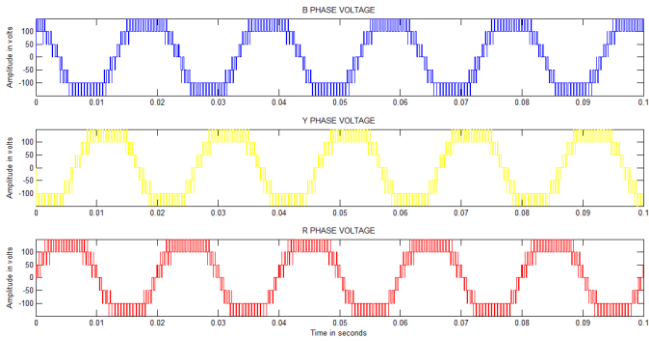


Fig.11. Output voltage of hybrid carrier THI-COPWM strategy

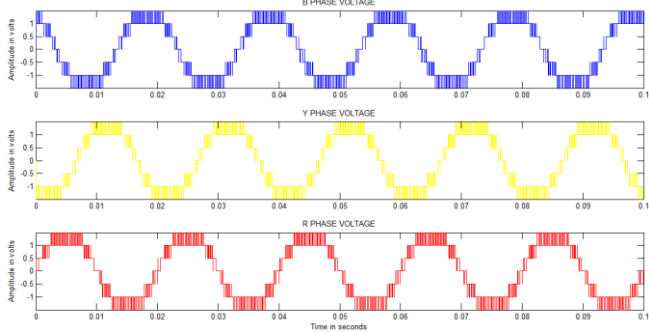


Fig.12. Output voltage of hybrid carrier THI-VFPWM strategy

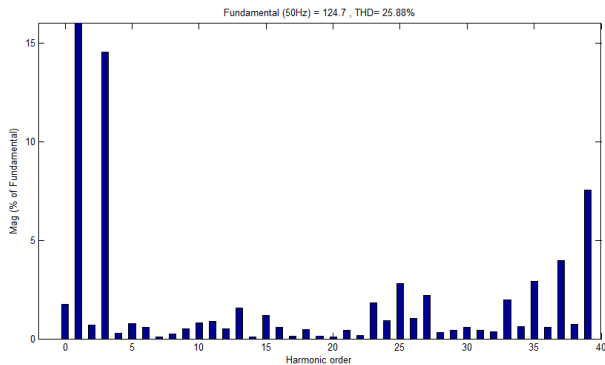


Fig.13. FFT spectrum for hybrid PDPWM strategy for $m_a=0.8$ $m_f=40$ with THI reference

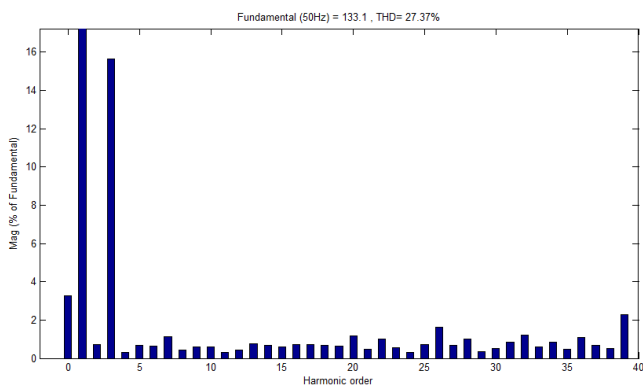


Fig.14. FFT spectrum for hybrid PODPWM strategy for $m_a=0.8$ and $m_f=40$ with THI reference

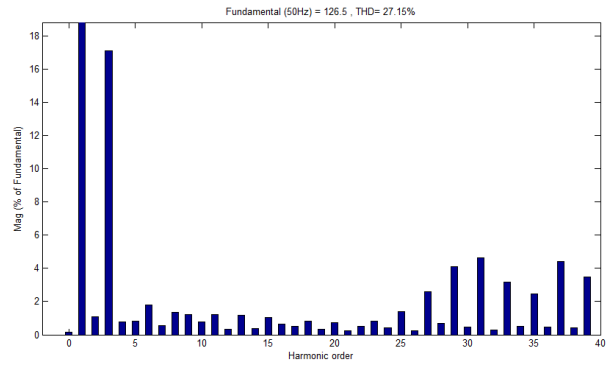


Fig.15. FFT spectrum for hybrid APODPWM strategy for $m_a=0.8$ and $m_f=40$ with THI reference

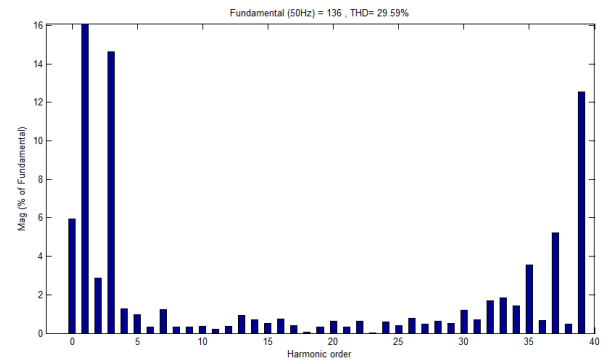


Fig.16. FFT spectrum for hybrid COPWM strategy for $m_a=0.8$ and $m_f=40$ with THI reference

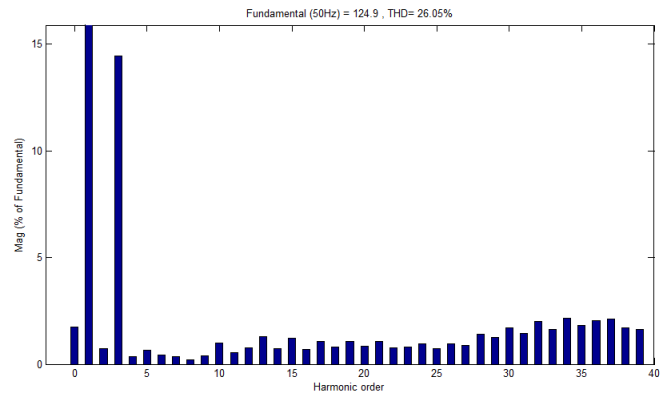


Fig.17. FFT spectrum for hybrid VFPWM strategy for $m_a=0.8$ $m_f=40$ with THI reference

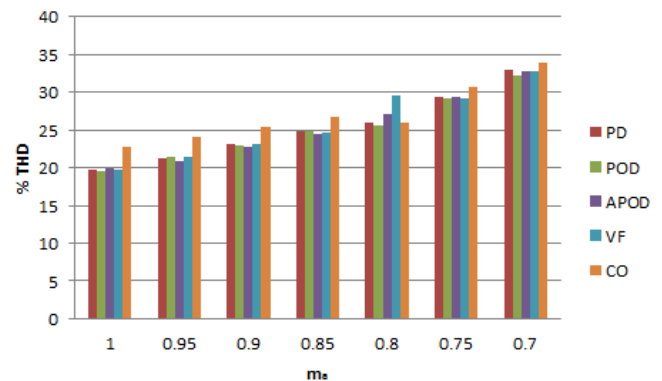


Fig.18. %THD Vs m_a for all strategies.

Table-I

%THD of output voltage of AMLI for various values of m_a

m_a	PD	POD	APOD	VF	CO
1	19.69	19.6	19.9	19.67	22.72
0.95	21.3	21.48	20.89	21.46	24.07
0.9	23.07	22.95	22.75	23.1	25.38
0.85	24.82	24.84	24.49	24.72	26.78
0.8	25.88	27.37	27.15	26.05	29.59
0.75	29.29	29.27	29.4	29.21	30.67
0.7	32.9	32.27	32.8	32.86	33.98

Table-II

RMS(Fundamental) value of output voltage of AMLI for different PWM strategies and various values of m_a

m_a	PD	POD	APOD	VF	CO
1	160.2	160.1	160.1	160	168.6
0.95	154	153.6	153.9	153.6	164
0.9	147.4	147.6	147.7	147.2	158.1
0.85	140.3	140.3	140.5	140.4	153.8
0.8	133.1	133.1	133	133	147.9
0.75	125.2	125.1	125.2	125.4	141.4
0.7	116.4	116	116.4	116.3	133.8

Table-III

FF of output voltage of AMLI for different PWM strategies and various values of m_a

m_a	PD	POD	APOD	VF	CO
1	432.97	1.6E+09	1.6E+09	2286	337.2
0.95	389.87	1.6E+09	1.6E+09	903.5	117.43
0.9	1179.2	1.6E+09	1.6E+09	320	2.08E+09
0.85	7936	1.6E+09	1.6E+09	322.8	2197.14
0.8	1064	1.6E+09	1.6E+09	682.1	870
0.75	1001.6	1.6E+09	1.6E+09	928.9	523.7
0.7	280.48	1.6E+09	1.6E+09	422.9	557.5

IV. CONCLUSION

A new hybrid modulation strategy is proposed for a three phase AMLI which achieves improvement in line to line voltage harmonics compared to the conventional modulation techniques. It is observed that COPWM provides better DC bus utilization and POD technique creates less distortion for $m_a=0.7-1$.

REFERENCES

- [1] R.Seyezhai, B.L.Mathur "Implementation and Control of Variable Frequency ISPWM Technique for an Asymmetric Multilevel Inverter" *European Journal of Scientific Research ISSN 1450-216X Vol.39 No.4 (2010), pp.558-568*
- [2] K.Chandra, J.Kumar, A Simple and Generalized Space Vector PWM Control of Cascaded H-Bridge Multilevel Inverters. *IEEE Trans. on Industrial Electronics, (2006).*
- [3] R. Seyezhai "Investigation of Performance Parameters For Asymmetric Multilevel Inverter" Using Hybrid Modulation Technique. *International Journal of Engineering Science and Technology (IJEST) (2011), 3(12), 8430-8443.*
- [4] R. Seyezhai, B.L.Mathur "Hybrid Multilevel Inverter using ISPWM Technique for Fuel Cell Applications" *International Journal of Computer Applications (0975 – 8887) Volume 9– No.1, November 2010*
- [5] S.Jeevananthan, R.Nandhakumar and P.Dananjayan, "Inverted Sine Carrier for Fundamental Fortification in PWM Inverters and FPGA Based Implementations", *Serbian Journal of Electrical Engineering, Vol. 4, No. 2(2007), pp. 171-187.*
- [6] J.Rodriguez, J.S.Lai, and F.Z.Peng, "Multilevel Inverter: A Survey of Topologies, Controls and Applications", *IEEE Trans. on Industrial Electronics, Vol. 49 (2000), No. 4 pp. 724-738 .*
- [7] Calais, M., Borle, L. J. and Agelidis, V. G. (2001) "Analysis of Multicarrier PWM Methods for a Single-phase Five Level Inverter", in *Proc. 32nd IEEE Power Electronics Specialists Conference, pp. 1351-1356.*
- [8] H. Wu, Y. Deng, Y. Liu, and X. He, "A New Clew For Research on PWM Methods of Multilevel Inverters: Principle and Applications," vol. 2, no. 1, 4-12 *IEEE Trans. Industry Applications, pp. 1251-1256, 2002.*
- [9] X. Sun, "Hybrid Control Strategy for A Novel Asymmetrical Multilevel Inverter," *IEEE Transactions on Industrial Electronics pp. 5-8, 2010.*
- [10] R. Taleb, A. Meroufel, and P. Wira, "Neural Network Control of Asymmetrical Multilevel Converters," *Leonardo Journal of Sciences, no. 15, pp. 53-70, 2009.*
- [11] L. Mihalache, "Asymmetrical PWM Technique for A Three-Level Hybrid Inverter," *Leonardo Journal of Sciences, pp. 609-615, 2007.*

Performance of Symmetrical and Asymmetrical Multilevel Inverters

K. Lakshmi Ganesh , U. Chandra Rao

^{1,2}(Department of Electrical and Electronics Engineering, Sri Vasavi Engineering College, India

Abstract: Distributed Energy Resources (DER) are systems that produce electrical power at the site where the power is needed. If only electrical power is used then the technology is called Distributed Generation (DG). The objective of this paper is to study a novel more than five level multistring inverter topology for DERs based DC/AC conversion system. The distributed energy resource based single-phase inverter is usually adopted in the microgrid system. In order to reduce the conversion losses, the key is to saving costs and size by removing any kind of transformer as well as reducing the power switches. In this study, a high step-up converter is introduced as a front-end stage to improve the conversion efficiency of conventional boost converters and to stabilize the output DC voltage of various DERs such as photovoltaic for use with the simplified multilevel inverter. In addition, two active switches are operated under line frequency. In this project a novel asymmetrical configuration is proposed. The proposed asymmetrical configuration uses less number of switches to get more levels. It will reduce the cost, reduce the number of sources, complexity, losses and improves reliability. The proposed converter is simulated by Matlab/Simulink software and simulation results are presented.

Key words: DC/AC power conversion, multilevel inverter, harmonic analysis and Total Harmonic Distortion (THD).

I. INTRODUCTION

The continuous economic development of many countries and the environmental issues (gas emissions and the green house effect) observed in the last decades forced an intense research in renewable energy sources. Distributed energy resources are small, modular, energy generation and storage technologies that provide electric capacity or energy where you need it. Typically producing less than 10 megawatts (MW) of power, DER systems can usually be sized to meet your particular needs and installed on site.

DER technologies include wind turbines, photo voltaic (PV), fuel cells, micro turbines, reciprocating engines, Hydro, combustion turbines and energy storage systems are the most explored technologies due to their considerable advantages [1],[2], such as reliability, reasonable installation and energy production costs, low environmental impact, capability to support micro grid [3].

The renewable energy resources consists of photovoltaic, fuel cells are generate the voltage are dc voltage. But I want the ac voltage because of mostly used the loads are ac loads. So we are convert the dc power to ac

powerprocessing interface is required and is Commercial, homes, factories and utility grid standards [4],[7].

Differing converter topographies have been acquired DERs establish effectual power flow control performance of DERs. DER systems may be either connected to the local electric power grid or isolated from the grid in stand-alone applications [7], [10].

The dc-dc converters are two types. They are without galvanic isolation and with galvanic isolation (high frequency transformer).The with galvanic isolation converter (high power applications) are used corresponding to size, weight, expense reduces. So low and medium power applications without galvanic isolation means make no use of transformers corresponding to reduces the size, weight expense [7], [8].

The next procedure the output voltage level increases of the inverter output then automatically harmonic component of the output voltage of inverter reduces and also corresponding to small size of filters are used simultaneously the cost reduces. The differing multilevel topographies are usually characterizing by strong reduction of switching power losses and electromagnetic interference (EMI) [6], [7], [8].

A new simplified single-phase multistring five-level multilevel inverter topography of dc/ac power conversion with auxiliary circuit proposed [8], [9]. This topography are used, the number of switching devices and output harmonics are reduced. The THD of the multistring five-level inverter is much less than the conventional multistring three-level inverter because of additional auxiliary circuit has high switching losses [9].

The objective of this paper is to study a newly constructed transformerless five level multistring inverter topology for DERS. In this letter aforesaid GZV-based inverter is reduced to a multistring multilevel inverter topography that require only 6 active switches instead of existing cascaded H-bridge multilevel inverter have eight switches[10].Multi string multilevel inverter have six active switches. They are middle two switches are operated fundamental frequency and remaining four switches are operated switching frequency. A high efficiency dc-dc boost converter reduction of transformer and device voltage and current stresses with continuous input current leakage inductance energy recovery, and avoiding the use of electrolytic capacitor due to reduced ripple current[13]. Operation of the system configuration of operation is shown below. The performance of symmetrical and asymmetrical single phase multilevel inverter with respect to harmonics content and number of switches and input voltage source is DC is simulated by MATLAB/Simulink. A detailed harmonic

analysis is done on the multilevel inverter by considering up to 23rd harmonics for 7 levels to 13 levels operation.

II. SYSTEM CONFIGURATION OF OPERATION PRINCIPLES

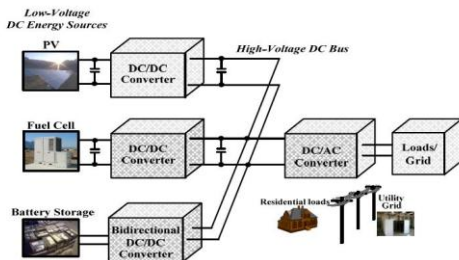


Fig.1 Different type of DERs are system configuration of Multistring Inverter

The above Fig.1 shows the DERs have photovoltaics or Fuel cell inverter are taken as [14]. The individual dc/dc boost converter are connected to the photovoltaic modules or Fuel cell. The bidirectional (buck-boost) dc/dc converter is connected to the only for battery storage. The individual dc/dc boost converter is connected to the multistring inverter. These common inverter for interface with all dc/dc converters of DERs [15]. The two modes of operation above Fig.1. They are standalone mode and grid connected mode. In grid connected mode, the battery storage energy is not connected to the grid. In standalone operation, the battery storage energy is connected to the load.

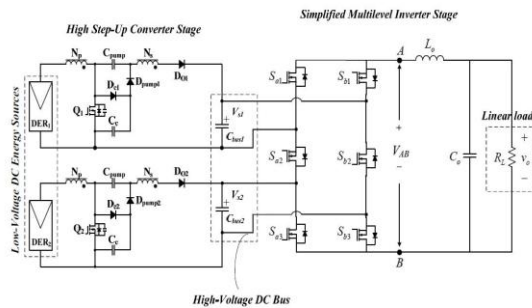


Fig.2 Single phase simplified multistring five-level inverter topology for high stepup converter from DERs

The above Fig.2 shows DER module-1 is connected to the high step up dc/dc converter and DER module-2 is connected to high step up dc/dc converter. These two converters are connected to their individual dc-bus capacitor and a simplified multilevel inverter. The resistive load is connected output of the simplified multilevel inverter from DER through high step up dc/dc converter. The input sources of DERs are photovoltaic or Fuel cells. The basic circuit have eight switches of cascaded H-bridge Multilevel inverter (CHB) with phase shift carrier pulse width modulation scheme are used. The simplified multilevel inverter have six switches then best merits of improved output waveforms, reduced the filter size, low EMI and THD [11],[12]. It should be noted that, by using independent voltage regulation control of the individual high step-up converter, voltage balance control for the two bus capacitors C_{bus1} , C_{bus2} can be achieved normally.

2.1. High Step-Up Converter Stage

In this study, High Efficiency Converter with Charge Pump and Coupled Inductor for Wide Input Photovoltaic AC Module Applications [13]. This simplified multilevel inverter combines the behavior of three different converter topologies: boost, flyback and charge pump. The flyback aspect of the topology allows the design to be optimized in terms of the transformer turns-ratio, allowing for much higher voltage gains than would be possible with a boost converter. However, flyback converters are notoriously inefficient and are very sensitive to leakage inductance, which can cause undue voltage-stress on switches and diodes. By using a clamp-circuit- identical to the output of a boost-converter-after the main switch, much of the efficiency issues can be resolved and the transformer design becomes less complicated. Finally, adding a charge-pump capacitor across the primary and secondary windings of the transformers gives higher converter voltage-gain and reduced peak current stress by allowing the current of the primary-windings to continuous.

The equivalent circuit of the proposed converter is shown in Fig.3. The coupled inductor is modeled as a magnetizing inductor L_m an ideal transformer with a turn's ratio of $N_s : N_p$ primary leakage inductor L_{Lk1} and secondary leakage inductor L_{Lk2} . C_c is the clamp capacitor, S is the Active switch, D_0 is the output diode C_{pump} is the charge pump capacitor. According to voltage-seconds balance condition of the magnetizing inductor, the voltage of the primary winding can be derived as

$$V_{pri} = V_{in} \frac{D}{1-D} \tag{1}$$

Where V_{in} represents each the low-voltage dc energy input sources and voltage of the secondary winding is

$$V_{sec} = \frac{N_s}{N_p} \cdot V_{pri} = \frac{N_s}{N_p} \cdot V_{in} \frac{D}{1-D} \tag{2}$$

Similar to that of the boost converter, the voltage of the charge-pump capacitor C_{pump} and clamp capacitor C_c can be expressed as

$$V_{C_{pump}} = V_{C_c} = V_{in} \cdot \frac{1}{1-D} \tag{3}$$

Hence, the voltage conversion ratio of the high step-up converter, named input voltage to bus voltage ratio, can be derived as [13].

$$\frac{V_0}{V_{in}} = \frac{\left(2 + \frac{N_s}{N_p} \cdot D\right)}{1-D} \tag{4}$$

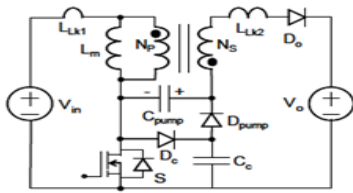


Fig.3. Equivalent circuit of the high step-up boost converter

2.2 Simplified Multilevel Inverter Stage

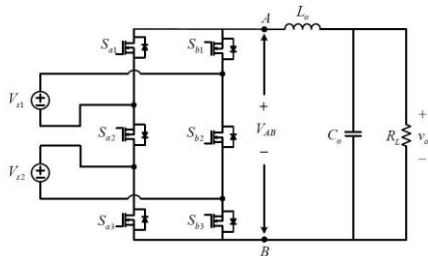


Fig.4 Basic Five-level inverter Circuitry of six switches

The simplified multilevel inverter is the conventional circuit of five level inverter Fig.4 shows above. A new single phase multistring topography, as a new basic circuitry in Fig.4. Referring to Fig.2, it is should be assumed that, in this configuration, the two capacitors in the capacitive voltage divider are connected directly across the dc bus and all switching combinations are activated in an output cycle. The dynamic voltage balance between the two capacitors is automatically controlled by the preceding high step-up converter stage. Then, we can assume $V_{s1} = V_{s2} = V_s$.

This circuit has six power switches compare the basic circuit of cascaded H-bridge has eight power switches which drastically reduces the power circuit complexity and simplifies modulation circuit design and implementation. The phase disposition (PD) pulse width modulation (PWM) control scheme is introduced to generate switching signals and to produce five output voltage levels: $0, V_s, 2V_s, -V_s$ and $2V_s$.

This inverter topology uses two carrier signals and one reference signal to generate the PWM signals for the switches the modulation strategy and its implemented logic scheme in Fig.5 (a) and (b) area widely used alternative for Phase disposition modulation. With the exception of an offset value equivalent to the carrier signal amplitude. Two comparators are used in this scheme with identical carrier signals V_{tri1} and V_{tri2} to provide high-frequency switching signals for S_{a1}, S_{b1}, S_{a3} and S_{b3} . Another comparator is used for zero-crossing detection to provide line-frequency switching signals for switches S_{a2} and S_{b2} .

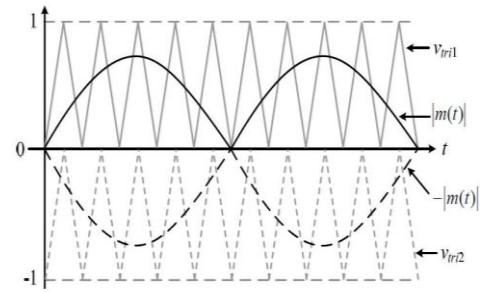
For Fig.4 the switching function of the switch defined as follows.

$$S_{aj} = 1, S_{aj} \text{ ON}$$

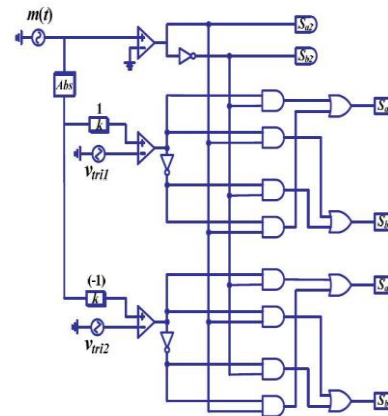
$$S_{aj} = 0, S_{aj} \text{ OFF for } j=1, 2, 3$$

$$S_{bj} = 1, S_{bj} \text{ ON}$$

$$S_{bj} = 0, S_{bj} \text{ OFF for } j=1, 2, 3$$



(a)



(b)

Fig.5. Modulation strategy a) Carrier/reference signals (b) modulation logic

Table-I

Simplified Five Level Inverter Switching Combination

S_{a1}	S_{a2}	S_{a3}	S_{b1}	S_{b2}	S_{b3}	V_{AB}
0	1	0	1	0	1	$2V_s$
0	1	1	1	0	0	V_s
1	1	0	0	0	1	V_s
1	1	1	0	0	0	0
0	0	0	1	1	1	0
1	0	0	0	1	1	$-V_s$
0	0	1	1	1	0	$-V_s$
1	0	1	0	1	0	$-2V_s$

Table-I lists switching combinations that generate the required five output levels. The corresponding operation modes of the simplified multilevel inverter stage are described clearly as follows.

- 1) Maximum positive output voltage ($2V_s$): Active switches S_{a2}, S_{b3} and S_{b1} are ON. The voltage applied to the LC output filter is $2V_s$.
- 2) Half level positive output voltage ($+V_s$): The two switching combinations are there. One switching combination

is that active switches S_{a2} , S_{a3} and S_{b1} are ON, the other is active switches S_{a2} , S_{a1} and S_{b3} are ON. During this operating stage, the voltage applied to the LC output filter $+V_S$.

3) Zero Output, (0): This output condition either one of the leg are left or right all switches are ON. The load is short-circuited, and the voltage applied to the load terminals zero.

4) Half level negative output voltage ($-V_S$): the two switching combinations are there. One switching combination is such that active switches S_{a1} , S_{b2} and S_{b3} are ON, the other switching is active switches S_{b2} , S_{b1} and S_{a3} .

5) Maximum negative output ($-2V_S$): During this stage, active switches S_{a1} , S_{a3} and S_{b2} are ON, and the output voltage applied to the LC output filter $-2V_S$.

In these circuit operations, it can be observed that the open voltage stress of the active power switches S_{a1} , S_{b1} , S_{a3} and S_{b3} is equal to input voltage V_S and the main active switches S_{a2} and S_{b2} are operated at the line frequency. Hence, the switching losses are reduced in the new topology and the overall conversion efficiency is improved.

In Fig.5 control circuit diagram as shown, $m(t)$ is the sinusoidal modulation signal. Both V_{tri1} and V_{tri2} are two carrier signals. The magnitude value and frequency of the sinusoidal modulation signal are given as $m_{peak}=0.7$ and $f_m=60\text{Hz}$. The peak to peak value of the triangular modulation signals is equal to 1 and the switching frequency f_{tri1} and f_{tri2} are both given as 18.06 kHz.

The two input voltage sources feeding from the high step up converter is controlled at 100V that is $V_{s1} = V_{s2} = 100\text{V}$. The five level output of the phase voltage of the simulation waveform is shown in Fig.6.

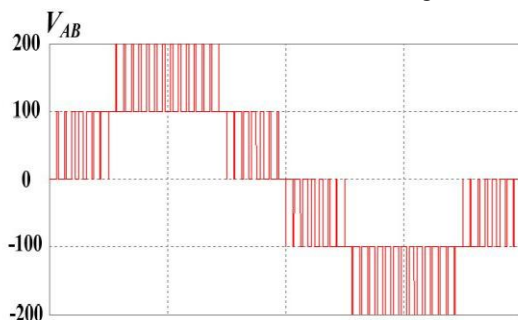


Fig.6 Simplified multilevel five level output phase voltage of simulation waveform V_{AB}

2.3 Basic circuit of Cascaded H-Bridge (CHB) Inverter

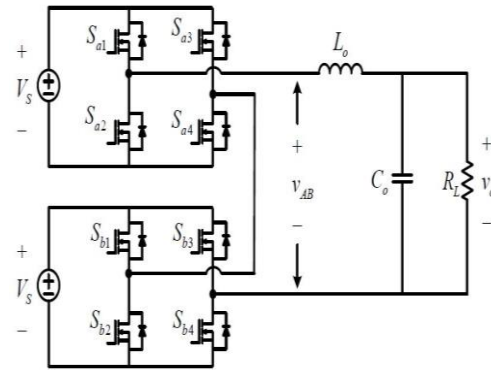


Fig.7 Basic circuit of five-level inverter topology of CHB inverter have eight switches

The above figure shows the Basic circuit of five level inverter CCHB inverter have eight switches. The carrier based sinusoidal phase shift carrier pulse width modulations are used in the basic circuit of CHB inverter. The eight switches are operated of the switching frequency. The CHB inverter are operate at the switching frequency is same as 18.06kHz the same modulation index $m_a=0.7$.

The simplified multilevel inverter and Cascaded H-bridge inverter are operated the same switching frequency and same modulation index m_a , the same input voltage $V_S=100\text{V}$ and output L-C filter, $L_o=20\text{mH}$, $C_o=200\mu\text{F}$, R-load $=10\Omega$. Table VII and Table VIII shows the harmonic component and THD Cascaded H-Bridge Inverter and Simplified multilevel inverter. The simplified multilevel inverter have the lesser THD compare to the Cascaded H-bridge inverter. So the low values of LC filter.

The symmetrical multilevel inverters are Cascaded H-bridge inverter and Simplified multilevel inverter. These are taken the equal voltage values. The symmetrical multilevel inverters above are operated with PWM method. The Proposing methods of asymmetrical multilevel inverters are repeating sequence is used for Seven, Nine, Eleven and Thirteen levels. The seven level have 6switches and Nine, Eleven and Thirteen level have 8 switches. The Seven, Nine, Eleven and Thirteen levels are get by using 12,16,20,24 switches are necessity in symmetrical configuration of Cascaded H-bridge inverter. So the less number of switches are in asymmetrical configuration to get more number of voltage levels, lesser the THD, low cost, reducing the DC sources, reduce the complexity and driving circuits.

III. PROPOSED SYTEM

3.1Seven Level Multi Level Inverter (MLI)

Table- II
Seven Level Multilevel Inverter (MLI)

S_{a1}	S_{a2}	S_{a3}	S_{b1}	S_{b2}	S_{b3}	V_0
0	1	0	1	0	1	$3V_s$
1	1	0	0	0	1	$2V_s$
0	1	1	1	0	0	V_s
1	1	1	0	0	0	0
0	0	0	1	1	1	0
1	0	0	0	1	1	$-V_s$
0	0	1	1	1	0	$-2V_s$
1	0	1	0	1	0	$-3V_s$

The above Table II is shows the active switches operation of seven level, 1 means the switch is ON, the 0 means the switch is OFF. Then we will get the seven level output voltage from the six switches only.

3.2Nine Level Multi Level Inverter (MLI)

Table- III
Nine level Multilevel (MLI)

S_1	S_2	S_3	S_4	S_5	S_6	S_7	S_8	V_0
0	1	0	1	1	0	1	0	$4V_s$
1	1	0	1	0	0	1	0	$3V_s$
0	0	0	1	1	1	1	0	$2V_s$
0	1	1	1	1	0	0	0	V_s
1	1	1	1	0	0	0	0	0
0	0	0	0	1	1	1	1	0
1	0	0	0	0	1	1	1	$-V_s$
1	1	1	0	0	0	0	1	$-2V_s$
0	0	1	0	1	1	0	1	$-3V_s$
1	0	1	0	0	1	0	1	$-4V_s$

The above Table III is shows the active switches operation of eight switches with nine level, 1 means the switch is ON, the 0 means the switch is OFF. Then we will get the nine level output voltage from the eight switches only.

3.3Eleven Level Multilevel inverter (MLI)

Table- IV
Eleven level multilevel Inverter (MLI)

S_1	S_2	S_3	S_4	S_5	S_6	S_7	S_8	V_0
0	1	0	1	1	0	1	0	$5V_s$
1	1	0	1	0	0	1	0	$4V_s$
0	1	0	0	1	0	1	1	$3V_s$
1	1	0	0	0	0	1	1	$2V_s$
0	1	1	1	1	0	0	0	V_s
1	1	1	1	0	0	0	0	0
0	0	0	0	1	1	1	1	0
1	0	0	0	0	1	1	1	$-V_s$
0	0	1	1	1	1	0	0	$-2V_s$
1	0	1	1	0	1	0	0	$-3V_s$
0	0	1	0	1	1	0	1	$-4V_s$
1	0	1	0	0	1	0	1	$-5V_s$

The above Table VI is shows the active switches operation of eight switches with eleven level, 1 means the switch is ON, the 0 means the switch is OFF. Then we will get the eleven level output voltage from the eight switches only.

3.4 Thirteen Level multi Level inverter

Table-V
Thirteen level multi level inverter (MLI)

S_1	S_2	S_3	S_4	S_5	S_6	S_7	S_8	V_0
0	1	0	1	1	0	1	0	$6V_s$
0	1	0	0	1	0	1	1	$5V_s$
1	1	0	1	0	0	1	0	$4V_s$
1	1	0	0	0	0	1	1	$3V_s$
0	1	1	1	1	0	0	0	$2V_s$
0	0	0	1	1	1	1	0	V_s
1	1	1	1	0	0	0	0	0
0	0	0	0	1	1	1	1	0
1	1	1	0	0	0	0	1	$-V_s$
1	0	0	0	0	1	1	1	$-2V_s$
0	0	1	1	1	1	0	0	$-3V_s$
0	0	1	0	1	1	0	1	$-4V_s$
1	0	1	1	0	1	0	0	$-5V_s$
1	0	1	0	0	1	0	1	$-6V_s$

The above Table V is shows the active switches operation of eight switches with thirteen level, 1 means the switch is ON, the 0 means the switch is OFF. Then we will get the thirteen level output voltage from the eight switches only.

3.5 Different voltages are taken as the source voltages of the asymmetrical multilevel inverters

TABLE VI
 DIFFEERENT VOLTAGES

No of levels	No of Switches	V1	V2	V3	Output Voltage in V
7	6	V_S	$2V_S$	-	$3V_S$
9	8	V_S	V_S	$2V_S$	$4V_S$
11	8	V_S	$2V_S$	$2V_S$	$5V_S$
13	8	V_S	$2V_S$	$3V_S$	$6V_S$

The seven level output voltage are get only from six switches only. The nine level, eleven level and thirteen level output voltage are get only from eight switches corresponding to respective voltage sources are taken.

The above table VI shows different voltages are taken for asymmetrical multilevel inverters. The asymmetrical multilevel inverters are simulated the output voltage are designed by using 200V. The seven level output voltage are get by using $V1=66.66V$, $V2=133.33V$. The nine level output voltage are get by using $V1=50V$, $V2=50V$, $V3=100V$. The eleven level output voltage are get by using $V1=40V$, $V2=80V$, $V3=80V$. The thirteen level output voltage are get by using $V1=66.66V$, $V2=99.99V$, $V3=33.33V$. The asymmetrical multilevel inverters are simulate the above written voltage values.

IV. MATLAB/SIMULATION RESULTS

4.1 Basic circuit of Cascaded H-Bridge five level Inverter

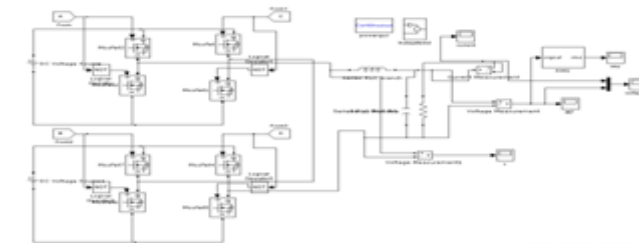


Fig.8 shows the five level inverter CHB simulink circuit

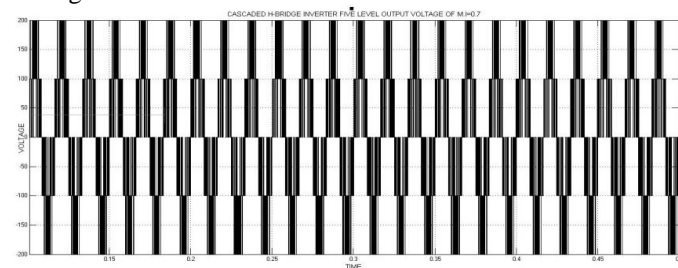


Fig.9 shows the five level output voltage CHB inverter without LC of M.I=0.7

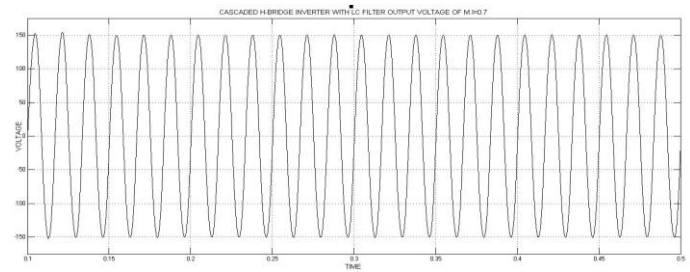


Fig.10 shows the output voltage with LC filter of CHB inverter of M.I=0.7

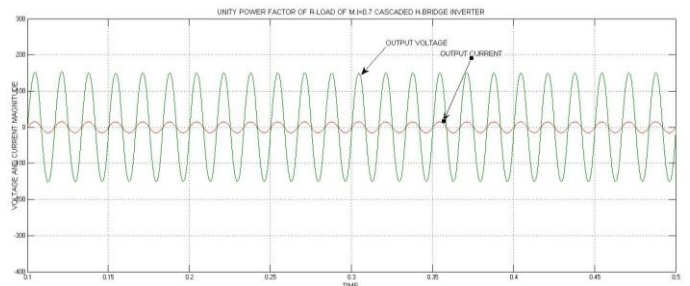


Fig.11 shows the unity power factor at the R-Load with LC filter of CHB inverter of M.I=0.7

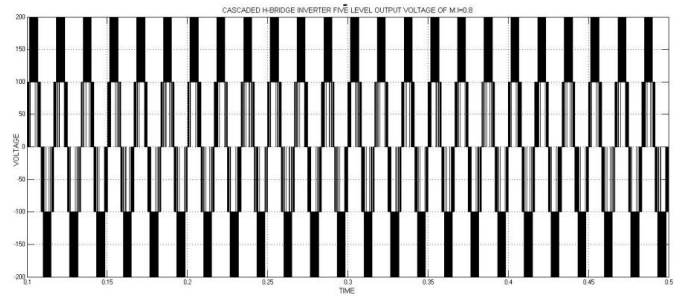


Fig.12 shows the five level output voltage CHB inverter without LC of M.I=0.8

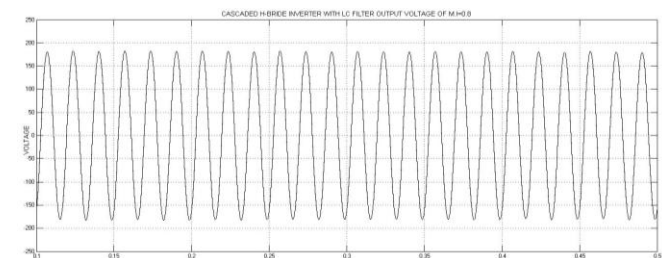


Fig.13 shows the output voltage with LC filter of CHB inverter of M.I=0.8



Fig.14 shows the unity power factor at the R-Load with LC filter of CHB inverter of M.I=0.8

Table-VII
 Harmonics of CHB Inverter with and without LC

The Table VII shows the CHB inverter operating two modulation indexes. They are 0.7 and 0.8 without and with LC filter.

4.2 Simplified Five level Inverter

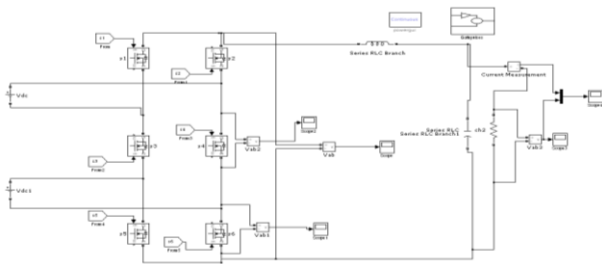


Fig.15. The simulink of simplified five level multilevel inverter

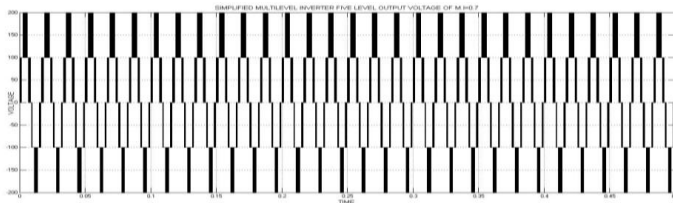


Fig.16 shows the five level output voltage of simplified five level inverter without LC of M.I=0.7

Harmonics	$m_a = 0.7$	$m_a = 0.8$
Fundamental 1	154.02	183.84
h3	2.40	3.31
h5	1.19	0.11
h7	0.24	0.07
h9	0.05	0.20
h11	0.02	0.09
%THD WITHOUT LC	0.146	0.114
%THD WITH LC	0.015	0.013

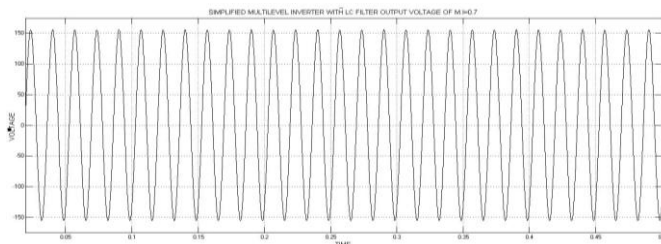


Fig.17 shows the output voltage with LC filter of simplified five level inverter of M.I=0.7

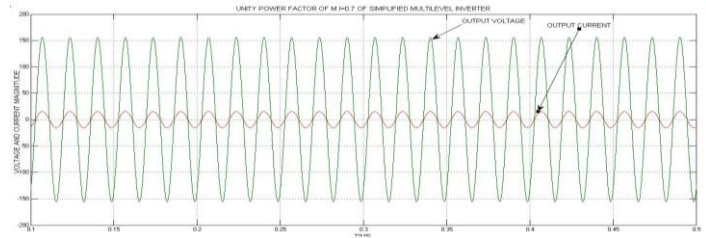


Fig.18 shows the unity power factor at the R-Load with LC filter of simplified five level inverter of M.I=0.7

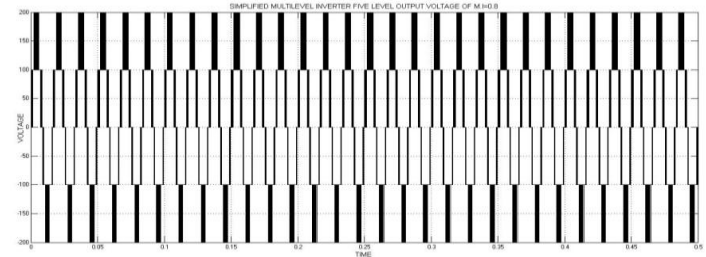


Fig.19 shows the five level output voltage simplified five level inverter without LC of M.I=0.8

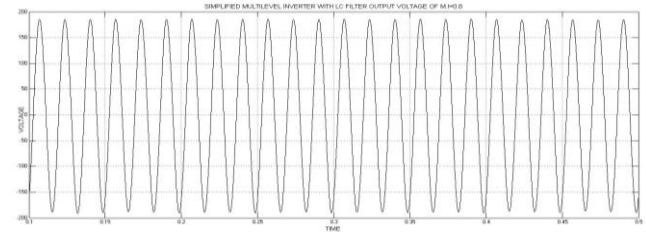


Fig.20 shows the output voltage with LC filter of simplified five level inverter of M.I=0.8

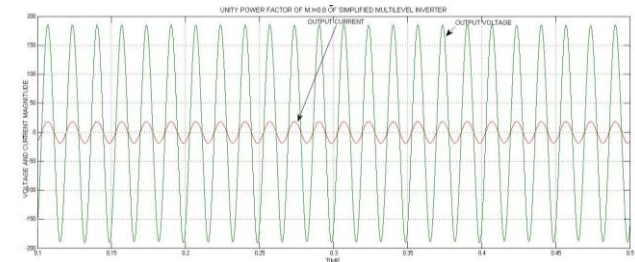


Fig.21 shows the unity power factor at the R-Load with LC filter simplified five level inverter of M.I=0.8

Table-VIII
 Harmonics of Simplified Five Level Inverter with and without LC

Harmonics	$m_a = 0.7$	$m_a = 0.8$
Fundamental 1	157.77	185.66
h3	0.81	1.98
h5	0.25	0.17
h7	0.17	0.32
h9	0.06	0.06
h11	0.07	0.05
%THD WITHOUT LC	0.0701	0.0684
%THD WITH LC	0.005	0.003

The Table VIII shows the simplified five level inverter operating two modulation indexes. They are 0.7 and 0.8 without and with LC filter.

The modulating frequency (Switching frequency) is 18060Hz.

The CHB five level inverter operated with $m_a=0.7$ and $m_a=0.8$ with phase shift carrier pulse width modulation technique then I would get the fundamental component voltage increases and THD value decreases when modulation index $m_a=0.8$ compare to the $m_a=0.7$. The simplified five level inverter operated the same modulation index with phase disposition pulse width modulation technique then I would get the fundamental component voltage increases and THD value decreases compare to the CHB inverter. After clearly understand reduce the number of switches, improved output waveforms, smaller filter size and lower EMI of simplified multistring five level inverter compared to the CHB inverter.

4.3 Proposing system of Seven Level multilevel inverter

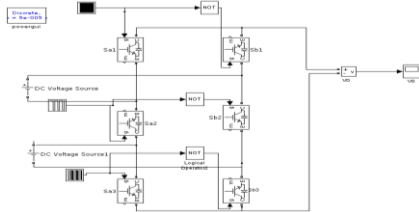


Fig.22 Simulink of the seven level multilevel inverter

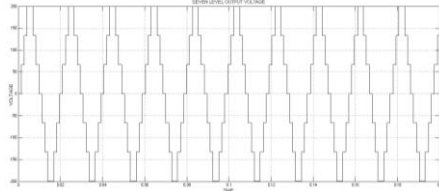


Fig.23 Seven level multilevel Inverter output voltage

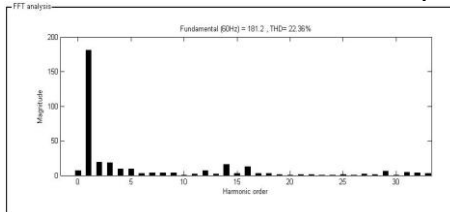


Fig.24 THD value of the Seven level multilevel inverter using FFT analysis

4.4 Proposing System of Nine Level multilevel inverter

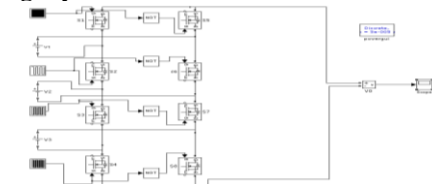


Fig.25 .Simulink of the nine, eleven and thirteen level multilevel inverter

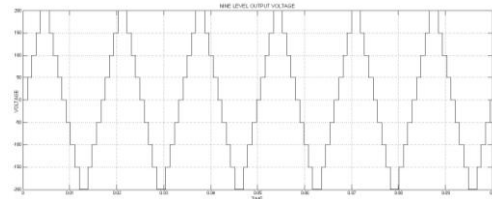


Fig.26 Nine level multilevel Inverter output voltage

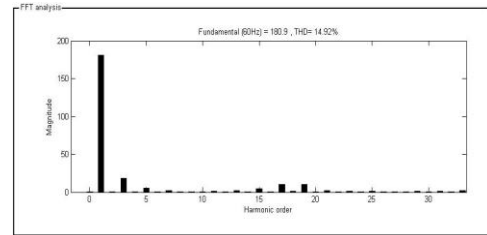


Fig.27 THD value of the nine level multilevel inverter using FFT analysis

4.4 Proposing System of Eleven Level multilevel inverter

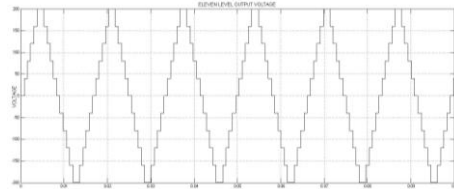


Fig.28 Eleven level multilevel Inverter output voltage

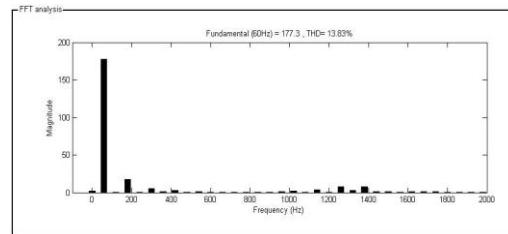


Fig. 29 THD value of the eleven level multilevel inverter using FFT analysis

4.5 Proposing System of Thirteen Level multilevel inverter

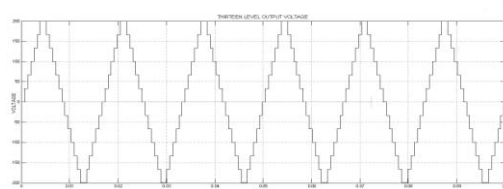


Fig.30 Thirteen level multilevel Inverter output voltage

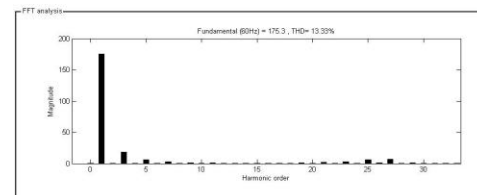


Fig.31 THD value of the thirteen level multilevel inverter using FFT analysis

Table-IX
 Fundamental Component and THD value of the Multilevel inverter of Various Values

Magnitude of individual Harmonic content	No of Levels			
	7	9	11	13
Fundamental	181.25	180.90	177.34	175.34
h3	17.99	17.93	17.68	18.18
h5	9.11	5.21	5.43	5.79
h7	3.45	2.09	3.11	2.66
h9	3.71	0.05	1.23	1.21
h11	1.68	1.24	0.40	0.83
h13	2.32	2.19	0.79	0.07
h15	2.59	4.12	0.73	0.24
h17	2.81	10.16	2.08	0.79
h19	1.23	9.78	3.55	1.10
h21	0.86	2.17	7.70	1.69
h23	0.46	1.06	7.32	2.97
(%THD)	22.36 %	14.92%	13.83%	13.33%

Table-X
 Dominant Harmonics in Various Multilevel inverters

Various Multilevel Inverter	Dominant Harmonics
Seven Level	3 rd , 5 th , 9 th , 7 th
Nine Level	3 rd , 17 th , 19 th , 5 th
Eleven Level	3 rd , 21 st , 23 rd , 5 th , 19 th
Thirteen Level	3 rd , 5 th

V. CONCLUSION

This work reports a Performance analysis of symmetrical and asymmetrical multilevel inverters, so reduce the number of switching devices, reduce the number of DC sources, driving circuits and cost reduces and also THD decreases.

Multistring multilevel inverters have low stress, high conversion efficiency and can also be easily interfaced with renewable energy sources (PV, Fuel cell). Asymmetrical multilevel inverter uses least number of devices to produce higher voltage level. As number of level increases, the THD content approaches to small value as expected. Thus it eliminates the need for filter. Though, THD decreases with increase in number of levels, some lower or higher harmonic contents remain dominant in each level. These will be more dangerous in induction drives.

Hence the future work may be focused to determine the pwm techniques of seven to thirteen level asymmetrical multilevel inverters.

REFERENCES

- [1] Key world energy statistics-2009",International Energy Agency(IEA),2009.Available at:http://www.iea.org.
- [2] F. Kininger, "Photovoltaic systems technology". Kassel, Germany: *Universitat Kassel, Institute for Rationelle Energiewandlung*, 2003. Available at:www.uni-Kassel.de/re.
- [3] M. Liserre. T.Sauter. J.Y. Hung, "Future energy systems: integrating renewable energy sources into the smart power grid through industrial electronics," *IEEE Industrial Electronics Magazine*, vol.4,no.1,pp.18-37,Mar.2010.
- [4] C. L. Chen, Y. Wang, J. S.Lai, Y.S. Lee and D. Martin, "Design of parallel inverters for smooth mode transfer microgrid applications," *IEEE Trans.Power Electronics*, Vol. 25, no.1, pp.6-16, Jan.2010
- [5] F. Blaabjerg, Z. Chen and S. B. Kjaer, "Power electronics as efficient interface in dispersed power generation systems," *IEEE Trans. Power Electronics*, vol. 19, no.5, pp.1184- 1194, Sep.2004.
- [6] D. G. Infield, P. Onions, A. D. Simmons and G. A. Smith, "Power quality from multiple grid-connected single-phase inverters," *IEEE Trans. Power Delivery*, vol. 19, no.4, PP. 1983- 1989, Oct. 2004.
- [7] T. Kerkes. R. Teoderescu and U. Borup. "Transformerless photovoltaic inverters connected to the grid," *IEEE Applied Power Electronics Conference. 2007* PP.1733-1737.
- [8] G.Ceglia V.Guzman, C.Sanchez, F.Ibanez, J. Walter, and M. I. Gimenez " A new simplified multilevel inverter topology for DC-AC conversion," *IEEE Trans. Power Electronics*, vol.21, n0.5, pp.1311-1319, Sep.2006.
- [9] N.A. Rahim and J. Selvaraj, "Multistring five-level inverter with novel PWM control scheme for PV application," *IEEE Trans. Power Electronics*, vol.57 no.6 pp. 2111-2123, Jun.2010.
- [10] S. Vazquez, J.I.Leon, J.M.Carrasco, L.G. Franquelo, E. Galvan, M. Reyes, J.A. Sanchez, and E. Dominguez, "Analysis of the power balance in the cells of multilevel Cascaded H-bridge converter," *IEEE Trans. Industrial Electronics*, vol.57, no.7, PP.2287-2296, Jul.2010.
- [11] S. Kouro, J. Rebolledo, and J.Rodriguez, "Reduced switching-frequency modulation algorithm for high-power multilevel inverter," *IEEE Trans. Industrial Electronics*, vol.54, no.5, PP.2894-2901, Oct.2007.
- [12] Y. Liu, H.Hong, and A. Q. Huang, "Real-time calculation of switching angles minimizing THD for multilevel inverters with step modulation," *IEEE Trans. Industrial Electronics*, vol. 56, no.2, pp.285-293, FEB.2009.
- [13] W.Yu. C. Hutchens, J.S.Lai, J. Zhang, G.Lisi, A. Djabbari, G.Smith, and T. Hegarty, "High Efficiency Converter with Charge Pump and Coupled Inductor for Wide Input Photovoltaic AC Module Applications," *IEEE Energy Conversion Congress and Exposition*, PP.3895-3900, 2009.
- [14] S. Daher, J.Schmid and F.L.M. Antunes, "Multilevel inverter topologies for Stand-alone PV systems," *IEEE Trans. Industrial Electronics*, Vol.55, no.7, PP.2703-2712, Jul.2008
- [15] M. Meinhardt and G.Cramer, "Past, present and future of grid-connected photovoltaic and hybrid-power systems," *IEEE-PES Summer Meeting*, PP.1283-1288,2000

Internal Differentiation, Comparative Variability, Structural Morphology, Normative Aspect of Prognostication of Ipse Dixit NP Hard Problems-A Totalistic Paradigmatic Statement

¹Dr. K. N. Prasanna Kumar, ²Prof. B. S. Kiranagi, ³Prof. C. S. Bagewadi

ABSTRACT: We develop a progressive comparable to Bank's General Ledger, and call it a General Theory of all the problems under the head of NP hard problems. Problems have their variables. For instance "Travelling Sales man problem" can have various different cities. Based upon parameters classification is done and stability analysis, asymptotic stability and Solutional behaviour of the equations are investigated We eschew from stating any primary predications, coextensive representations, predicational anteriority of the Problems attributed to space constraints. In consideration to the parametric based classification and there is both ontological consonance, primordial exactitude, and phenomenological testimony as one finds in Bank's ledgers. General Ledger is in fact the statement of all inflows and outflows and such a one as that occurs in problems and theories in some conditions, like for example the conservation of energy breaking down in Hawking's radiation. Emphasis is laid on the fact that for instance a travelling salesman makes some move and then retracts to redress his move or starts another move to further his final destination. And this destination is General Ledger.-The General Theory Of all the NP (hard) problems. .It is a journey, a journey to find the final balance which probably never ends like an account never closes. So we are on to the journey.....

I. INTRODUCTION

As stated in abstract we will not give any introduction, inconsideration to the leviathans' material and humungous literature on each subject matter for fear of missing woods for trees. On the other hand, for the interested reader the literature provides a rich receptacle, repository and treasure-trove of knowledge. And also because of space constraints. We note that the NP (HARD) problems are classified as follows:

- 1) Boolean satisfiability Problem
- 2) N Puzzle
- 3) Knapsack Problem
- 4) Hamiltonian Path problem
- 5) Travelling Salesman Problem
- 6) Sub graph Isomorphism Problem
- 7) Subset Sum problem
- 8) Clique Problem
- 9) Vertex Cover Problem
- 10) Independent Set problem
- 11) Dominating set problem.
- 12) Graph Coloring Problem

As in a Bank, various parameters are there for an account like balance standing, rate of interest, implications of inflation, money depression, depreciation of the currency, implications of Policies, philosophies and programmes of the Government, each problem has certain parameters. That Gravity is constant does not mean it does not depend upon the masses of individual particles and there is no total gravity. Stratification is done based on the parameters of each problem and then consummated with the other to form a monolithic diaspora for building the Model, which essentially as said is a progressive, nay a General Theory Of all the ways and means in which the problem can be solved be it by invocation or by abnegation and revocation of the action. Everything is recorded in the Computer and we draw up a Final General Ledger-nay The General Theory Of all NP (HARD) Problems. Essentially a prediction model, it as said analyses various other facets too.

GLOSSARY OF THE SYSTEME BOOLEAN SATISFIABILITY PROBLEM AND N PUZZLE

NOTATION :

- G_{13} : Category One Of Boolean Satisfiability Problem
 G_{14} : Category Two Of Boolean Satisfiability Problem
 G_{15} : Category Three Of Boolean Satisfiability Problem
 T_{13} : Category One Of N Puzzle
 T_{14} :Category Two Of N Puzzle
 T_{15} :Category Three Of N Puzzle

GLOSSARY OF THE SYSTEM KNAPSACK PROBLEM AND HAMILTONIAN PATH PROBLEM:

- G_{16} : Category One Of Knapsack Problem
 G_{17} : Category Two Of Knapsack Problem
 G_{18} : Category Three Of Knapsack Problem
 T_{16} : Category One Of Hamiltonian Path Problem
 T_{17} : Category Two Of Hamiltonian Path Problem
 T_{18} : Category Three Of Hamiltonian Path Problem

GLOSSARY OF THE SYSTEM: TRAVELLING SALESMAN PROBLEM AND SUBGRAPH ISOMERISM PROBLEM

- G_{20} : Category One Of Travelling Salesman Problem
 G_{21} : Category Two Of Travelling Salesman Problem
 G_{22} : Category Three Of Travelling Salesman Problem
 T_{20} : Category One Of Sub graph Isomerism Problem
 T_{21} : Category Two Of Sub graph Isomerism Problem
 T_{22} : Category Three Of Sub graph Isomerism Problem

GLOSSARY FOR THE SYSTEM: SUBSET SUM PROBLEM AND CLIQUE PROBLEM

- G_{24} : Category One Of Subset Sum Problem
 G_{25} : Category Two Of Subset Sum Problem
 G_{26} : Category Three Of Subset Sum Problem
 T_{24} : Category One Of Clique Problem
 T_{25} : Category Two Of Clique Problem
 T_{26} : Category Three Of Clique Problem

GLOSSARY FOR THE SYSTEM: VERTEX COVER PROBLEM AND INDEPENDENT SET PROBLEM

- G_{28} : Category One Of Vertex Cover Problem
 G_{29} : Category Two Of Vertex Cover Problem
 G_{30} : Category Three Of Vertex Cover Problem
 T_{28} : Category One Of Independent Set Problem
 T_{29} : Category Two Of Independent Set Problem
 T_{30} : Category Three Of Independent Set Problem

GLOSSARY OF THE SYSTEM: DOMINATING SET PROBLEM AND GRAPH COLORING PROBLEM

- G_{32} : Category One Of Dominating Set Problem
 G_{33} : Category Two Of Dominating Set Problem
 G_{34} : Category Three Of Dominating Set Problem
 T_{32} : Category One Of Graph Coloring Problem
 T_{33} : Category Two Of Graph Coloring Problem
 T_{34} : Category Three Of Graph Coloring Problem

ACCENTUATION COEFFICIENTS AND DISSIPATION COEFFICIENTS

$(a_{13})^{(1)}, (a_{14})^{(1)}, (a_{15})^{(1)}, (b_{13})^{(1)}, (b_{14})^{(1)}, (b_{15})^{(1)}, (a_{16})^{(2)}, (a_{17})^{(2)}, (a_{18})^{(2)}, (b_{16})^{(2)}, (b_{17})^{(2)}, (b_{18})^{(2)}$;
 $(a_{20})^{(3)}, (a_{21})^{(3)}, (a_{22})^{(3)}, (b_{20})^{(3)}, (b_{21})^{(3)}, (b_{22})^{(3)}$
 $(a_{24})^{(4)}, (a_{25})^{(4)}, (a_{26})^{(4)}, (b_{24})^{(4)}, (b_{25})^{(4)}, (b_{26})^{(4)}, (b_{28})^{(5)}, (b_{29})^{(5)}, (b_{30})^{(5)}, (a_{28})^{(5)}, (a_{29})^{(5)}, (a_{30})^{(5)}$;
 $(a_{32})^{(6)}, (a_{33})^{(6)}, (a_{34})^{(6)}, (b_{32})^{(6)}, (b_{33})^{(6)}, (b_{34})^{(6)}$

$(a'_{13})^{(1)}, (a'_{14})^{(1)}, (a'_{15})^{(1)}, (b'_{13})^{(1)}, (b'_{14})^{(1)}, (b'_{15})^{(1)}, (a'_{16})^{(2)}, (a'_{17})^{(2)}, (a'_{18})^{(2)}, (b'_{16})^{(2)}, (b'_{17})^{(2)}, (b'_{18})^{(2)}$;
 $(a'_{20})^{(3)}, (a'_{21})^{(3)}, (a'_{22})^{(3)}, (b'_{20})^{(3)}, (b'_{21})^{(3)}, (b'_{22})^{(3)}$
 $(a'_{24})^{(4)}, (a'_{25})^{(4)}, (a'_{26})^{(4)}, (b'_{24})^{(4)}, (b'_{25})^{(4)}, (b'_{26})^{(4)}, (b'_{28})^{(5)}, (b'_{29})^{(5)}, (b'_{30})^{(5)}, (a'_{28})^{(5)}, (a'_{29})^{(5)}, (a'_{30})^{(5)}$;
 $(a'_{32})^{(6)}, (a'_{33})^{(6)}, (a'_{34})^{(6)}, (b'_{32})^{(6)}, (b'_{33})^{(6)}, (b'_{34})^{(6)}$

GOVERNING EQUATIONS OF THE SYSTEM BOOLEAN SATISFIABILITY PROBLEM AND N PUZZLE

The differential system of this model is now

$\frac{dG_{13}}{dt} = (a_{13})^{(1)}G_{14} - [(a'_{13})^{(1)} + (a''_{13})^{(1)}(T_{14}, t)]G_{13}$	1
$\frac{dG_{14}}{dt} = (a_{14})^{(1)}G_{13} - [(a'_{14})^{(1)} + (a''_{14})^{(1)}(T_{14}, t)]G_{14}$	2
$\frac{dG_{15}}{dt} = (a_{15})^{(1)}G_{14} - [(a'_{15})^{(1)} + (a''_{15})^{(1)}(T_{14}, t)]G_{15}$	3
$\frac{dT_{13}}{dt} = (b_{13})^{(1)}T_{14} - [(b'_{13})^{(1)} - (b''_{13})^{(1)}(G, t)]T_{13}$	4
$\frac{dT_{14}}{dt} = (b_{14})^{(1)}T_{13} - [(b'_{14})^{(1)} - (b''_{14})^{(1)}(G, t)]T_{14}$	5
$\frac{dT_{15}}{dt} = (b_{15})^{(1)}T_{14} - [(b'_{15})^{(1)} - (b''_{15})^{(1)}(G, t)]T_{15}$	6
$+(a''_{13})^{(1)}(T_{14}, t) =$ First augmentation factor	7
$-(b'_{13})^{(1)}(G, t) =$ First detritions factor	8

GOVERNING EQUATIONS:OF THE SYSTEM KANPSACK PROBLEM AND HAMILTONIAN PATH PROBLEM

=====

The differential system of this model is now

$\frac{dG_{16}}{dt} = (a_{16})^{(2)}G_{17} - [(a'_{16})^{(2)} + (a''_{16})^{(2)}(T_{17}, t)]G_{16}$	9
$\frac{dG_{17}}{dt} = (a_{17})^{(2)}G_{16} - [(a'_{17})^{(2)} + (a''_{17})^{(2)}(T_{17}, t)]G_{17}$	10
$\frac{dG_{18}}{dt} = (a_{18})^{(2)}G_{17} - [(a'_{18})^{(2)} + (a''_{18})^{(2)}(T_{17}, t)]G_{18}$	11
$\frac{dT_{16}}{dt} = (b_{16})^{(2)}T_{17} - [(b'_{16})^{(2)} - (b''_{16})^{(2)}((G_{19}), t)]T_{16}$	12
$\frac{dT_{17}}{dt} = (b_{17})^{(2)}T_{16} - [(b'_{17})^{(2)} - (b''_{17})^{(2)}((G_{19}), t)]T_{17}$	13
$\frac{dT_{18}}{dt} = (b_{18})^{(2)}T_{17} - [(b'_{18})^{(2)} - (b''_{18})^{(2)}((G_{19}), t)]T_{18}$	14
$+(a''_{16})^{(2)}(T_{17}, t) =$ First augmentation factor	15
$-(b'_{16})^{(2)}((G_{19}), t) =$ First detritions factor	16

GOVERNING EQUATIONS: FO THE SYSTEM TRAVELLING SALESMAN PROBLEM AND SUBGRAPH ISOMERISM PROBLEM:

=====

The differential system of this model is now

$\frac{dG_{20}}{dt} = (a_{20})^{(3)}G_{21} - [(a'_{20})^{(3)} + (a''_{20})^{(3)}(T_{21}, t)]G_{20}$	17
$\frac{dG_{21}}{dt} = (a_{21})^{(3)}G_{20} - [(a'_{21})^{(3)} + (a''_{21})^{(3)}(T_{21}, t)]G_{21}$	18
$\frac{dG_{22}}{dt} = (a_{22})^{(3)}G_{21} - [(a'_{22})^{(3)} + (a''_{22})^{(3)}(T_{21}, t)]G_{22}$	19
$\frac{dT_{20}}{dt} = (b_{20})^{(3)}T_{21} - [(b'_{20})^{(3)} - (b''_{20})^{(3)}(G_{23}, t)]T_{20}$	20
$\frac{dT_{21}}{dt} = (b_{21})^{(3)}T_{20} - [(b'_{21})^{(3)} - (b''_{21})^{(3)}(G_{23}, t)]T_{21}$	21
$\frac{dT_{22}}{dt} = (b_{22})^{(3)}T_{21} - [(b'_{22})^{(3)} - (b''_{22})^{(3)}(G_{23}, t)]T_{22}$	22
$+(a''_{20})^{(3)}(T_{21}, t) =$ First augmentation factor	23
$-(b'_{20})^{(3)}(G_{23}, t) =$ First detritions factor	24

GOVERNING EQUATIONS:OF THE SYSTEM SUBSET SUM PROBLEM AND CLIQUE PROBLEM

=====

The differential system of this model is now

$\frac{dG_{24}}{dt} = (a_{24})^{(4)}G_{25} - [(a'_{24})^{(4)} + (a''_{24})^{(4)}(T_{25}, t)]G_{24}$	25
$\frac{dG_{25}}{dt} = (a_{25})^{(4)}G_{24} - [(a'_{25})^{(4)} + (a''_{25})^{(4)}(T_{25}, t)]G_{25}$	26
$\frac{dG_{26}}{dt} = (a_{26})^{(4)}G_{25} - [(a'_{26})^{(4)} + (a''_{26})^{(4)}(T_{25}, t)]G_{26}$	27
$\frac{dT_{24}}{dt} = (b_{24})^{(4)}T_{25} - [(b'_{24})^{(4)} - (b''_{24})^{(4)}((G_{27}), t)]T_{24}$	28
$\frac{dT_{25}}{dt} = (b_{25})^{(4)}T_{24} - [(b'_{25})^{(4)} - (b''_{25})^{(4)}((G_{27}), t)]T_{25}$	29
$\frac{dT_{26}}{dt} = (b_{26})^{(4)}T_{25} - [(b'_{26})^{(4)} - (b''_{26})^{(4)}((G_{27}), t)]T_{26}$	30
$+(a''_{24})^{(4)}(T_{25}, t) =$ First augmentation factor	31
$-(b'_{24})^{(4)}((G_{27}), t) =$ First detritions factor	32

GOVERNING EQUATIONS:OF THE SYSTEM VERTEX COVER PROBLEM AND INDEPENDENT SET

PROBLEM

The differential system of this model is now

$$\begin{aligned} \frac{dG_{28}}{dt} &= (a_{28})^{(5)}G_{29} - [(a'_{28})^{(5)} + (a''_{28})^{(5)}(T_{29}, t)]G_{28} & 33 \\ \frac{dG_{29}}{dt} &= (a_{29})^{(5)}G_{28} - [(a'_{29})^{(5)} + (a''_{29})^{(5)}(T_{29}, t)]G_{29} & 34 \\ \frac{dG_{30}}{dt} &= (a_{30})^{(5)}G_{29} - [(a'_{30})^{(5)} + (a''_{30})^{(5)}(T_{29}, t)]G_{30} & 35 \\ \frac{dT_{28}}{dt} &= (b_{28})^{(5)}T_{29} - [(b'_{28})^{(5)} - (b''_{28})^{(5)}((G_{31}), t)]T_{28} & 36 \\ \frac{dT_{29}}{dt} &= (b_{29})^{(5)}T_{28} - [(b'_{29})^{(5)} - (b''_{29})^{(5)}((G_{31}), t)]T_{29} & 37 \\ \frac{dT_{30}}{dt} &= (b_{30})^{(5)}T_{29} - [(b'_{30})^{(5)} - (b''_{30})^{(5)}((G_{31}), t)]T_{30} & 38 \\ + (a''_{28})^{(5)}(T_{29}, t) &= \text{First augmentation factor} & 39 \\ - (b''_{28})^{(5)}((G_{31}), t) &= \text{First detritions factor} & 40 \end{aligned}$$

GOVERNING EQUATIONS: OF THE DOMINATING SET PROBLEM AND GRAPH COLORING

PROBLEM:

The differential system of this model is now

$$\begin{aligned} \frac{dG_{32}}{dt} &= (a_{32})^{(6)}G_{33} - [(a'_{32})^{(6)} + (a''_{32})^{(6)}(T_{33}, t)]G_{32} & 42 \\ \frac{dG_{33}}{dt} &= (a_{33})^{(6)}G_{32} - [(a'_{33})^{(6)} + (a''_{33})^{(6)}(T_{33}, t)]G_{33} & 43 \\ \frac{dG_{34}}{dt} &= (a_{34})^{(6)}G_{33} - [(a'_{34})^{(6)} + (a''_{34})^{(6)}(T_{33}, t)]G_{34} & 44 \\ \frac{dT_{32}}{dt} &= (b_{32})^{(6)}T_{33} - [(b'_{32})^{(6)} - (b''_{32})^{(6)}((G_{35}), t)]T_{32} & 45 \\ \frac{dT_{33}}{dt} &= (b_{33})^{(6)}T_{32} - [(b'_{33})^{(6)} - (b''_{33})^{(6)}((G_{35}), t)]T_{33} & 46 \\ \frac{dT_{34}}{dt} &= (b_{34})^{(6)}T_{33} - [(b'_{34})^{(6)} - (b''_{34})^{(6)}((G_{35}), t)]T_{34} & 47 \\ + (a''_{32})^{(6)}(T_{33}, t) &= \text{First augmentation factor} & 48 \\ - (b''_{32})^{(6)}((G_{35}), t) &= \text{First detritions factor} & 49 \end{aligned}$$

FINAL CONCATENATED GOVERNING EQUATIONS OF THE SYSTEM:

- (1) BOOLEAN SATISFIABILITY PROBLEM
- (2) N PUZZLE
- (3) KNAPSACK PROBLEM
- (4) HAMILTONIAN PATH PROBLEM
- (5) TRAVELLING SALESMAN PROBLEM
- (6) SUB GRAPH ISOMERISM PROBLEM
- (7) SUBSET SUM PROBLEM
- (8) CLIQUE PROBLEM
- (9) VERTEX COVER PROBLEM
- (10) INDEPENDENT SET PROBLEM
- (11) DOMINATING SET PROBLEM
- (12) GRAPH COLORING RPOBLEM

$$\begin{aligned} \frac{dG_{13}}{dt} &= (a_{13})^{(1)}G_{14} - \left[\begin{array}{|c|c|c|c|} \hline (a'_{13})^{(1)} & + (a''_{13})^{(1)}(T_{14}, t) & + (a''_{16})^{(2,2)}(T_{17}, t) & + (a''_{20})^{(3,3)}(T_{21}, t) \\ \hline \end{array} \right] G_{13} & 50 \\ & - \left[\begin{array}{|c|c|c|c|} \hline + (a''_{24})^{(4,4,4,4)}(T_{25}, t) & + (a''_{28})^{(5,5,5,5)}(T_{29}, t) & + (a''_{32})^{(6,6,6,6)}(T_{33}, t) & \\ \hline \end{array} \right] \\ \frac{dG_{14}}{dt} &= (a_{14})^{(1)}G_{13} - \left[\begin{array}{|c|c|c|c|} \hline (a'_{14})^{(1)} & + (a''_{14})^{(1)}(T_{14}, t) & + (a''_{17})^{(2,2)}(T_{17}, t) & + (a''_{21})^{(3,3)}(T_{21}, t) \\ \hline \end{array} \right] G_{14} & 51 \\ & - \left[\begin{array}{|c|c|c|c|} \hline + (a''_{25})^{(4,4,4,4)}(T_{25}, t) & + (a''_{29})^{(5,5,5,5)}(T_{29}, t) & + (a''_{33})^{(6,6,6,6)}(T_{33}, t) & \\ \hline \end{array} \right] \\ \frac{dG_{15}}{dt} &= (a_{15})^{(1)}G_{14} - \left[\begin{array}{|c|c|c|c|} \hline (a'_{15})^{(1)} & + (a''_{15})^{(1)}(T_{14}, t) & + (a''_{18})^{(2,2)}(T_{17}, t) & + (a''_{22})^{(3,3)}(T_{21}, t) \\ \hline \end{array} \right] G_{15} & 52 \\ & - \left[\begin{array}{|c|c|c|c|} \hline + (a''_{26})^{(4,4,4,4)}(T_{25}, t) & + (a''_{30})^{(5,5,5,5)}(T_{29}, t) & + (a''_{34})^{(6,6,6,6)}(T_{33}, t) & \\ \hline \end{array} \right] \end{aligned}$$

Where $\boxed{(a''_{13})^{(1)}(T_{14}, t)}$, $\boxed{(a''_{14})^{(1)}(T_{14}, t)}$, $\boxed{(a''_{15})^{(1)}(T_{14}, t)}$ are first augmentation coefficients for category 1, 2 and 3

$\boxed{+(a''_{16})^{(2,2)}(T_{17}, t)}$, $\boxed{+(a''_{17})^{(2,2)}(T_{17}, t)}$, $\boxed{+(a''_{18})^{(2,2)}(T_{17}, t)}$ are second augmentation coefficient for category 1, 2 and 3

$\boxed{+(a''_{20})^{(3,3)}(T_{21}, t)}$, $\boxed{+(a''_{21})^{(3,3)}(T_{21}, t)}$, $\boxed{+(a''_{22})^{(3,3)}(T_{21}, t)}$ are third augmentation coefficient for category 1, 2 and 3

$\boxed{+(a''_{24})^{(4,4,4,4)}(T_{25}, t)}$, $\boxed{+(a''_{25})^{(4,4,4,4)}(T_{25}, t)}$, $\boxed{+(a''_{26})^{(4,4,4,4)}(T_{25}, t)}$ are fourth augmentation coefficient for

category 1, 2 and 3

$\boxed{+(a''_{28})^{(5,5,5,5)}(T_{29}, t)}$, $\boxed{+(a''_{29})^{(5,5,5,5)}(T_{29}, t)}$, $\boxed{+(a''_{30})^{(5,5,5,5)}(T_{29}, t)}$ are fifth augmentation coefficient for

category 1, 2 and 3

$\boxed{+(a''_{32})^{(6,6,6,6)}(T_{33}, t)}$, $\boxed{+(a''_{33})^{(6,6,6,6)}(T_{33}, t)}$, $\boxed{+(a''_{34})^{(6,6,6,6)}(T_{33}, t)}$ are sixth augmentation coefficient for

category 1, 2 and 3

$$\frac{dT_{13}}{dt} = (b_{13})^{(1)}T_{14} - \left[\begin{array}{ccc} \boxed{(b'_{13})^{(1)} \boxed{-(b''_{13})^{(1)}(G, t)} \boxed{-(b''_{16})^{(2,2)}(G_{19}, t)} \boxed{-(b''_{20})^{(3,3)}(G_{23}, t)}} & & \\ \boxed{-(b''_{24})^{(4,4,4,4)}(G_{27}, t)} \boxed{-(b''_{28})^{(5,5,5,5)}(G_{31}, t)} \boxed{-(b''_{32})^{(6,6,6,6)}(G_{35}, t)} & & \end{array} \right] T_{13} \quad 60$$

$$\frac{dT_{14}}{dt} = (b_{14})^{(1)}T_{13} - \left[\begin{array}{ccc} \boxed{(b'_{14})^{(1)} \boxed{-(b''_{14})^{(1)}(G, t)} \boxed{-(b''_{17})^{(2,2)}(G_{19}, t)} \boxed{-(b''_{21})^{(3,3)}(G_{23}, t)}} & & \\ \boxed{-(b''_{25})^{(4,4,4,4)}(G_{27}, t)} \boxed{-(b''_{29})^{(5,5,5,5)}(G_{31}, t)} \boxed{-(b''_{33})^{(6,6,6,6)}(G_{35}, t)} & & \end{array} \right] T_{14} \quad 61$$

$$\frac{dT_{15}}{dt} = (b_{15})^{(1)}T_{14} - \left[\begin{array}{ccc} \boxed{(b'_{15})^{(1)} \boxed{-(b''_{15})^{(1)}(G, t)} \boxed{-(b''_{18})^{(2,2)}(G_{19}, t)} \boxed{-(b''_{22})^{(3,3)}(G_{23}, t)}} & & \\ \boxed{-(b''_{26})^{(4,4,4,4)}(G_{27}, t)} \boxed{-(b''_{30})^{(5,5,5,5)}(G_{31}, t)} \boxed{-(b''_{34})^{(6,6,6,6)}(G_{35}, t)} & & \end{array} \right] T_{15} \quad 62$$

Where $\boxed{-(b''_{13})^{(1)}(G, t)}$, $\boxed{-(b''_{14})^{(1)}(G, t)}$, $\boxed{-(b''_{15})^{(1)}(G, t)}$ are first detrition coefficients for category 1, 2 and 3 63

$\boxed{-(b''_{16})^{(2,2)}(G_{19}, t)}$, $\boxed{-(b''_{17})^{(2,2)}(G_{19}, t)}$, $\boxed{-(b''_{18})^{(2,2)}(G_{19}, t)}$ are second detrition coefficients for category 1, 2 64

and 3 65

$\boxed{-(b''_{20})^{(3,3)}(G_{23}, t)}$, $\boxed{-(b''_{21})^{(3,3)}(G_{23}, t)}$, $\boxed{-(b''_{22})^{(3,3)}(G_{23}, t)}$ are third detrition coefficients for category 1, 2 and 66

3 67

$\boxed{-(b''_{24})^{(4,4,4,4)}(G_{27}, t)}$, $\boxed{-(b''_{25})^{(4,4,4,4)}(G_{27}, t)}$, $\boxed{-(b''_{26})^{(4,4,4,4)}(G_{27}, t)}$ are fourth detrition coefficients for 68

category 1, 2 and 3

$\boxed{-(b''_{28})^{(5,5,5,5)}(G_{31}, t)}$, $\boxed{-(b''_{29})^{(5,5,5,5)}(G_{31}, t)}$, $\boxed{-(b''_{30})^{(5,5,5,5)}(G_{31}, t)}$ are fifth detrition coefficients for category 69

1, 2 and 3 70

$\boxed{-(b''_{32})^{(6,6,6,6)}(G_{35}, t)}$, $\boxed{-(b''_{33})^{(6,6,6,6)}(G_{35}, t)}$, $\boxed{-(b''_{34})^{(6,6,6,6)}(G_{35}, t)}$ are sixth detrition coefficients for category 71

1, 2 and 3 72

$$\frac{dG_{16}}{dt} = (a_{16})^{(2)}G_{17} - \left[\begin{array}{ccc} \boxed{(a'_{16})^{(2)} \boxed{+(a''_{16})^{(2)}(T_{17}, t)} \boxed{+(a''_{13})^{(1,1)}(T_{14}, t)} \boxed{+(a''_{20})^{(3,3,3)}(T_{21}, t)}} & & \\ \boxed{+(a''_{24})^{(4,4,4,4,4)}(T_{25}, t)} \boxed{+(a''_{28})^{(5,5,5,5,5)}(T_{29}, t)} \boxed{+(a''_{32})^{(6,6,6,6,6)}(T_{33}, t)} & & \end{array} \right] G_{16} \quad 69$$

$$\frac{dG_{17}}{dt} = (a_{17})^{(2)}G_{16} - \left[\begin{array}{ccc} \boxed{(a'_{17})^{(2)} \boxed{+(a''_{17})^{(2)}(T_{17}, t)} \boxed{+(a''_{14})^{(1,1)}(T_{14}, t)} \boxed{+(a''_{21})^{(3,3,3)}(T_{21}, t)}} & & \\ \boxed{+(a''_{25})^{(4,4,4,4,4)}(T_{25}, t)} \boxed{+(a''_{29})^{(5,5,5,5,5)}(T_{29}, t)} \boxed{+(a''_{33})^{(6,6,6,6,6)}(T_{33}, t)} & & \end{array} \right] G_{17} \quad 70$$

$$\frac{dG_{18}}{dt} = (a_{18})^{(2)}G_{17} - \left[\begin{array}{ccc} \boxed{(a'_{18})^{(2)} \boxed{+(a''_{18})^{(2)}(T_{17}, t)} \boxed{+(a''_{15})^{(1,1)}(T_{14}, t)} \boxed{+(a''_{22})^{(3,3,3)}(T_{21}, t)}} & & \\ \boxed{+(a''_{26})^{(4,4,4,4,4)}(T_{25}, t)} \boxed{+(a''_{30})^{(5,5,5,5,5)}(T_{29}, t)} \boxed{+(a''_{34})^{(6,6,6,6,6)}(T_{33}, t)} & & \end{array} \right] G_{18} \quad 71$$

Where $\boxed{+(a''_{16})^{(2)}(T_{17}, t)}$, $\boxed{+(a''_{17})^{(2)}(T_{17}, t)}$, $\boxed{+(a''_{18})^{(2)}(T_{17}, t)}$ are first augmentation coefficients for category 1, 7273

2 and 3 74

$\boxed{+(a''_{13})^{(1,1)}(T_{14}, t)}$, $\boxed{+(a''_{14})^{(1,1)}(T_{14}, t)}$, $\boxed{+(a''_{15})^{(1,1)}(T_{14}, t)}$ are second augmentation coefficient for category 1, 75

2 and 3 76

$\boxed{+(a''_{20})^{(3,3,3)}(T_{21}, t)}$, $\boxed{+(a''_{21})^{(3,3,3)}(T_{21}, t)}$, $\boxed{+(a''_{22})^{(3,3,3)}(T_{21}, t)}$ are third augmentation coefficient for category 77

1, 2 and 3 78

$\boxed{+(a''_{24})^{(4,4,4,4,4)}(T_{25}, t)}$, $\boxed{+(a''_{25})^{(4,4,4,4,4)}(T_{25}, t)}$, $\boxed{+(a''_{26})^{(4,4,4,4,4)}(T_{25}, t)}$ are fourth augmentation coefficient for 79

category 1, 2 and 3 80

$\boxed{+(a''_{28})^{(5,5,5,5,5)}(T_{29}, t)}$, $\boxed{+(a''_{29})^{(5,5,5,5,5)}(T_{29}, t)}$, $\boxed{+(a''_{30})^{(5,5,5,5,5)}(T_{29}, t)}$ are fifth augmentation coefficient for 81

category 1, 2 and 3 82

$\boxed{+(a''_{32})^{(6,6,6,6,6)}(T_{33}, t)}$, $\boxed{+(a''_{33})^{(6,6,6,6,6)}(T_{33}, t)}$, $\boxed{+(a''_{34})^{(6,6,6,6,6)}(T_{33}, t)}$ are sixth augmentation coefficient for 83

category 1, 2 and 3 84

$$\frac{dT_{16}}{dt} = (b_{16})^{(2)}T_{17} - \left[\begin{array}{|c|c|c|} \hline (b'_{16})^{(2)} & -(b''_{16})^{(2)}(G_{19}, t) & -(b''_{13})^{(1,1)}(G, t) & -(b''_{20})^{(3,3,3)}(G_{23}, t) \\ \hline \end{array} \right] T_{16} \tag{79}$$

$$\frac{dT_{17}}{dt} = (b_{17})^{(2)}T_{16} - \left[\begin{array}{|c|c|c|} \hline (b'_{17})^{(2)} & -(b''_{17})^{(2)}(G_{19}, t) & -(b''_{14})^{(1,1)}(G, t) & -(b''_{21})^{(3,3,3)}(G_{23}, t) \\ \hline \end{array} \right] T_{17} \tag{80}$$

$$\frac{dT_{18}}{dt} = (b_{18})^{(2)}T_{17} - \left[\begin{array}{|c|c|c|} \hline (b'_{18})^{(2)} & -(b''_{18})^{(2)}(G_{19}, t) & -(b''_{15})^{(1,1)}(G, t) & -(b''_{22})^{(3,3,3)}(G_{23}, t) \\ \hline \end{array} \right] T_{18} \tag{81}$$

where $-(b''_{16})^{(2)}(G_{19}, t)$, $-(b''_{17})^{(2)}(G_{19}, t)$, $-(b''_{18})^{(2)}(G_{19}, t)$ are first detrition coefficients for category 1, 2 and 3 82

$-(b''_{13})^{(1,1)}(G, t)$, $-(b''_{14})^{(1,1)}(G, t)$, $-(b''_{15})^{(1,1)}(G, t)$ are second detrition coefficients for category 1,2 and 3
 $-(b''_{20})^{(3,3,3)}(G_{23}, t)$, $-(b''_{21})^{(3,3,3)}(G_{23}, t)$, $-(b''_{22})^{(3,3,3)}(G_{23}, t)$ are third detrition coefficients for category 1,2 and 3

$-(b''_{24})^{(4,4,4,4,4)}(G_{27}, t)$, $-(b''_{25})^{(4,4,4,4,4)}(G_{27}, t)$, $-(b''_{26})^{(4,4,4,4,4)}(G_{27}, t)$ are fourth detrition coefficients for category 1,2 and 3

$-(b''_{28})^{(5,5,5,5,5)}(G_{31}, t)$, $-(b''_{29})^{(5,5,5,5,5)}(G_{31}, t)$, $-(b''_{30})^{(5,5,5,5,5)}(G_{31}, t)$ are fifth detrition coefficients for category 1,2 and 3

$-(b''_{32})^{(6,6,6,6,6)}(G_{35}, t)$, $-(b''_{33})^{(6,6,6,6,6)}(G_{35}, t)$, $-(b''_{34})^{(6,6,6,6,6)}(G_{35}, t)$ are sixth detrition coefficients for category 1,2 and 3

$$\frac{dG_{20}}{dt} = (a_{20})^{(3)}G_{21} - \left[\begin{array}{|c|c|c|} \hline (a'_{20})^{(3)} & +(a''_{20})^{(3)}(T_{21}, t) & +(a''_{16})^{(2,2,2)}(T_{17}, t) & +(a''_{13})^{(1,1,1)}(T_{14}, t) \\ \hline \end{array} \right] G_{20} \tag{83}$$

$$\frac{dG_{21}}{dt} = (a_{21})^{(3)}G_{20} - \left[\begin{array}{|c|c|c|} \hline (a'_{21})^{(3)} & +(a''_{21})^{(3)}(T_{21}, t) & +(a''_{17})^{(2,2,2)}(T_{17}, t) & +(a''_{14})^{(1,1,1)}(T_{14}, t) \\ \hline \end{array} \right] G_{21} \tag{84}$$

$$\frac{dG_{22}}{dt} = (a_{22})^{(3)}G_{21} - \left[\begin{array}{|c|c|c|} \hline (a'_{22})^{(3)} & +(a''_{22})^{(3)}(T_{21}, t) & +(a''_{18})^{(2,2,2)}(T_{17}, t) & +(a''_{15})^{(1,1,1)}(T_{14}, t) \\ \hline \end{array} \right] G_{22} \tag{85}$$

$+(a''_{20})^{(3)}(T_{21}, t)$, $+(a''_{21})^{(3)}(T_{21}, t)$, $+(a''_{22})^{(3)}(T_{21}, t)$ are first augmentation coefficients for category 1, 2 and 3 86

$+(a''_{16})^{(2,2,2)}(T_{17}, t)$, $+(a''_{17})^{(2,2,2)}(T_{17}, t)$, $+(a''_{18})^{(2,2,2)}(T_{17}, t)$ are second augmentation coefficients for category 1, 2 and 3

$+(a''_{13})^{(1,1,1)}(T_{14}, t)$, $+(a''_{14})^{(1,1,1)}(T_{14}, t)$, $+(a''_{15})^{(1,1,1)}(T_{14}, t)$ are third augmentation coefficients for category 1, 2 and 3

$+(a''_{24})^{(4,4,4,4,4)}(T_{25}, t)$, $+(a''_{25})^{(4,4,4,4,4)}(T_{25}, t)$, $+(a''_{26})^{(4,4,4,4,4)}(T_{25}, t)$ are fourth augmentation coefficients for category 1, 2 and 3

$+(a''_{28})^{(5,5,5,5,5)}(T_{29}, t)$, $+(a''_{29})^{(5,5,5,5,5)}(T_{29}, t)$, $+(a''_{30})^{(5,5,5,5,5)}(T_{29}, t)$ are fifth augmentation coefficients for category 1, 2 and 3

$+(a''_{32})^{(6,6,6,6,6)}(T_{33}, t)$, $+(a''_{33})^{(6,6,6,6,6)}(T_{33}, t)$, $+(a''_{34})^{(6,6,6,6,6)}(T_{33}, t)$ are sixth augmentation coefficients for category 1, 2 and 3

$$\frac{dT_{20}}{dt} = (b_{20})^{(3)}T_{21} - \left[\begin{array}{|c|c|c|} \hline (b'_{20})^{(3)} & -(b''_{20})^{(3)}(G_{23}, t) & -(b''_{16})^{(2,2,2)}(G_{19}, t) & -(b''_{13})^{(1,1,1)}(G, t) \\ \hline \end{array} \right] T_{20} \tag{87}$$

$$\frac{dT_{21}}{dt} = (b_{21})^{(3)}T_{20} - \left[\begin{array}{|c|c|c|} \hline (b'_{21})^{(3)} & -(b''_{21})^{(3)}(G_{23}, t) & -(b''_{17})^{(2,2,2)}(G_{19}, t) & -(b''_{14})^{(1,1,1)}(G, t) \\ \hline \end{array} \right] T_{21} \tag{89}$$

$$\frac{dT_{22}}{dt} = (b_{22})^{(3)}T_{21} - \left[\begin{array}{|c|c|c|} \hline (b'_{22})^{(3)} & -(b''_{22})^{(3)}(G_{23}, t) & -(b''_{18})^{(2,2,2)}(G_{19}, t) & -(b''_{15})^{(1,1,1)}(G, t) \\ \hline \hline \hline \end{array} \right] T_{22} \tag{90}$$

$-(b''_{20})^{(3)}(G_{23}, t), -(b''_{21})^{(3)}(G_{23}, t), -(b''_{22})^{(3)}(G_{23}, t)$ are first detrition coefficients for category 1, 2 and 3 91
 $-(b''_{16})^{(2,2,2)}(G_{19}, t), -(b''_{17})^{(2,2,2)}(G_{19}, t), -(b''_{18})^{(2,2,2)}(G_{19}, t)$ are second detrition coefficients for category 1, 2 and 3

$-(b''_{13})^{(1,1,1)}(G, t), -(b''_{14})^{(1,1,1)}(G, t), -(b''_{15})^{(1,1,1)}(G, t)$ are third detrition coefficients for category 1, 2 and 3
 $-(b''_{24})^{(4,4,4,4,4)}(G_{27}, t), -(b''_{25})^{(4,4,4,4,4)}(G_{27}, t), -(b''_{26})^{(4,4,4,4,4)}(G_{27}, t)$ are fourth detrition coefficients for category 1, 2 and 3

$-(b''_{28})^{(5,5,5,5,5)}(G_{31}, t), -(b''_{29})^{(5,5,5,5,5)}(G_{31}, t), -(b''_{30})^{(5,5,5,5,5)}(G_{31}, t)$ are fifth detrition coefficients for category 1, 2 and 3
 $-(b''_{32})^{(6,6,6,6,6)}(G_{35}, t), -(b''_{33})^{(6,6,6,6,6)}(G_{35}, t), -(b''_{34})^{(6,6,6,6,6)}(G_{35}, t)$ are sixth detrition coefficients for category 1, 2 and 3 92

$$\frac{dG_{24}}{dt} = (a_{24})^{(4)}G_{25} - \left[\begin{array}{|c|c|c|} \hline (a'_{24})^{(4)} & +(a''_{24})^{(4)}(T_{25}, t) & +(a''_{28})^{(5,5)}(T_{29}, t) & +(a''_{32})^{(6,6)}(T_{33}, t) \\ \hline \hline \hline \end{array} \right] G_{24} \tag{93}$$

$$\frac{dG_{25}}{dt} = (a_{25})^{(4)}G_{24} - \left[\begin{array}{|c|c|c|} \hline (a'_{25})^{(4)} & +(a''_{25})^{(4)}(T_{25}, t) & +(a''_{29})^{(5,5)}(T_{29}, t) & +(a''_{33})^{(6,6)}(T_{33}, t) \\ \hline \hline \hline \end{array} \right] G_{25} \tag{94}$$

$$\frac{dG_{26}}{dt} = (a_{26})^{(4)}G_{25} - \left[\begin{array}{|c|c|c|} \hline (a'_{26})^{(4)} & +(a''_{26})^{(4)}(T_{25}, t) & +(a''_{30})^{(5,5)}(T_{29}, t) & +(a''_{34})^{(6,6)}(T_{33}, t) \\ \hline \hline \hline \end{array} \right] G_{26} \tag{95}$$

Where $(a''_{24})^{(4)}(T_{25}, t), (a''_{25})^{(4)}(T_{25}, t), (a''_{26})^{(4)}(T_{25}, t)$ are first augmentation coefficients for category 1, 2 and 3
 $+(a''_{28})^{(5,5)}(T_{29}, t), +(a''_{29})^{(5,5)}(T_{29}, t), +(a''_{30})^{(5,5)}(T_{29}, t)$ are second augmentation coefficient for category 1, 2 and 3
 $+(a''_{32})^{(6,6)}(T_{33}, t), +(a''_{33})^{(6,6)}(T_{33}, t), +(a''_{34})^{(6,6)}(T_{33}, t)$ are third augmentation coefficient for category 1, 2 and 3
 $+(a''_{13})^{(1,1,1,1)}(T_{14}, t), +(a''_{14})^{(1,1,1,1)}(T_{14}, t), +(a''_{15})^{(1,1,1,1)}(T_{14}, t)$ are fourth augmentation coefficients for category 1, 2, and 3
 $+(a''_{16})^{(2,2,2,2)}(T_{17}, t), +(a''_{17})^{(2,2,2,2)}(T_{17}, t), +(a''_{18})^{(2,2,2,2)}(T_{17}, t)$ are fifth augmentation coefficients for category 1, 2, and 3
 $+(a''_{20})^{(3,3,3,3)}(T_{21}, t), +(a''_{21})^{(3,3,3,3)}(T_{21}, t), +(a''_{22})^{(3,3,3,3)}(T_{21}, t)$ are sixth augmentation coefficients for category 1, 2, and 3

$$\frac{dT_{24}}{dt} = (b_{24})^{(4)}T_{25} - \left[\begin{array}{|c|c|c|} \hline (b'_{24})^{(4)} & -(b''_{24})^{(4)}(G_{27}, t) & -(b''_{28})^{(5,5)}(G_{31}, t) & -(b''_{32})^{(6,6)}(G_{35}, t) \\ \hline \hline \hline \end{array} \right] T_{24} \tag{96}$$

$$\frac{dT_{25}}{dt} = (b_{25})^{(4)}T_{24} - \left[\begin{array}{|c|c|c|} \hline (b'_{25})^{(4)} & -(b''_{25})^{(4)}(G_{27}, t) & -(b''_{29})^{(5,5)}(G_{31}, t) & -(b''_{33})^{(6,6)}(G_{35}, t) \\ \hline \hline \hline \end{array} \right] T_{25} \tag{97}$$

$$\frac{dT_{26}}{dt} = (b_{26})^{(4)}T_{25} - \left[\begin{array}{|c|c|c|} \hline (b'_{26})^{(4)} & -(b''_{26})^{(4)}(G_{27}, t) & -(b''_{30})^{(5,5)}(G_{31}, t) & -(b''_{34})^{(6,6)}(G_{35}, t) \\ \hline \hline \hline \end{array} \right] T_{26} \tag{98}$$

Where $-(b''_{24})^{(4)}(G_{27}, t), -(b''_{25})^{(4)}(G_{27}, t), -(b''_{26})^{(4)}(G_{27}, t)$ are first detrition coefficients for category 1, 2 and 3 100
 $-(b''_{28})^{(5,5)}(G_{31}, t), -(b''_{29})^{(5,5)}(G_{31}, t), -(b''_{30})^{(5,5)}(G_{31}, t)$ are second detrition coefficients for category 1, 2 and 3

$-(b''_{32})^{(6,6,6)}(G_{35}, t)$, $-(b''_{33})^{(6,6,6)}(G_{35}, t)$, $-(b''_{34})^{(6,6,6)}(G_{35}, t)$ are third detrition coefficients for category 1, 2 and 3

$-(b''_{13})^{(1,1,1,1)}(G, t)$, $-(b''_{14})^{(1,1,1,1)}(G, t)$, $-(b''_{15})^{(1,1,1,1)}(G, t)$ are fourth detrition coefficients for category 1, 2 and 3

$-(b''_{16})^{(2,2,2,2)}(G_{19}, t)$, $-(b''_{17})^{(2,2,2,2)}(G_{19}, t)$, $-(b''_{18})^{(2,2,2,2)}(G_{19}, t)$ are fifth detrition coefficients for category 1, 2 and 3

$-(b''_{20})^{(3,3,3,3)}(G_{23}, t)$, $-(b''_{21})^{(3,3,3,3)}(G_{23}, t)$, $-(b''_{22})^{(3,3,3,3)}(G_{23}, t)$ are sixth detrition coefficients for category 1, 2 and 3

$$\frac{dG_{28}}{dt} = (a_{28})^{(5)}G_{29} - \left[\begin{array}{ccc} (a'_{28})^{(5)} + (a''_{28})^{(5)}(T_{29}, t) & + (a''_{24})^{(4,4)}(T_{25}, t) & + (a''_{32})^{(6,6,6)}(T_{33}, t) \\ + (a''_{13})^{(1,1,1,1,1)}(T_{14}, t) & + (a''_{16})^{(2,2,2,2,2)}(T_{17}, t) & + (a''_{20})^{(3,3,3,3,3)}(T_{21}, t) \end{array} \right] G_{28} \quad 101$$

$$\frac{dG_{29}}{dt} = (a_{29})^{(5)}G_{28} - \left[\begin{array}{ccc} (a'_{29})^{(5)} + (a''_{29})^{(5)}(T_{29}, t) & + (a''_{25})^{(4,4)}(T_{25}, t) & + (a''_{33})^{(6,6,6)}(T_{33}, t) \\ + (a''_{14})^{(1,1,1,1,1)}(T_{14}, t) & + (a''_{17})^{(2,2,2,2,2)}(T_{17}, t) & + (a''_{21})^{(3,3,3,3,3)}(T_{21}, t) \end{array} \right] G_{29} \quad 102$$

$$\frac{dG_{30}}{dt} = (a_{30})^{(5)}G_{29} - \left[\begin{array}{ccc} (a'_{30})^{(5)} + (a''_{30})^{(5)}(T_{29}, t) & + (a''_{26})^{(4,4)}(T_{25}, t) & + (a''_{34})^{(6,6,6)}(T_{33}, t) \\ + (a''_{15})^{(1,1,1,1,1)}(T_{14}, t) & + (a''_{18})^{(2,2,2,2,2)}(T_{17}, t) & + (a''_{22})^{(3,3,3,3,3)}(T_{21}, t) \end{array} \right] G_{30} \quad 103$$

Where $+(a''_{28})^{(5)}(T_{29}, t)$, $+(a''_{29})^{(5)}(T_{29}, t)$, $+(a''_{30})^{(5)}(T_{29}, t)$ are first augmentation coefficients for category 1, 2 and 3 104

And $+(a''_{24})^{(4,4)}(T_{25}, t)$, $+(a''_{25})^{(4,4)}(T_{25}, t)$, $+(a''_{26})^{(4,4)}(T_{25}, t)$ are second augmentation coefficient for category 1, 2 and 3 105

$+(a''_{32})^{(6,6,6)}(T_{33}, t)$, $+(a''_{33})^{(6,6,6)}(T_{33}, t)$, $+(a''_{34})^{(6,6,6)}(T_{33}, t)$ are third augmentation coefficient for category 1, 2 and 3 106

$+(a''_{13})^{(1,1,1,1,1)}(T_{14}, t)$, $+(a''_{14})^{(1,1,1,1,1)}(T_{14}, t)$, $+(a''_{15})^{(1,1,1,1,1)}(T_{14}, t)$ are fourth augmentation coefficients for category 1, 2, and 3

$+(a''_{16})^{(2,2,2,2,2)}(T_{17}, t)$, $+(a''_{17})^{(2,2,2,2,2)}(T_{17}, t)$, $+(a''_{18})^{(2,2,2,2,2)}(T_{17}, t)$ are fifth augmentation coefficients for category 1, 2, and 3

$+(a''_{20})^{(3,3,3,3,3)}(T_{21}, t)$, $+(a''_{21})^{(3,3,3,3,3)}(T_{21}, t)$, $+(a''_{22})^{(3,3,3,3,3)}(T_{21}, t)$ are sixth augmentation coefficients for category 1, 2, 3 107

$$\frac{dT_{28}}{dt} = (b_{28})^{(5)}T_{29} - \left[\begin{array}{ccc} (b'_{28})^{(5)} - (b''_{28})^{(5)}(G_{31}, t) & - (b''_{24})^{(4,4)}(G_{27}, t) & - (b''_{32})^{(6,6,6)}(G_{35}, t) \\ - (b''_{13})^{(1,1,1,1,1)}(G, t) & - (b''_{16})^{(2,2,2,2,2)}(G_{19}, t) & - (b''_{20})^{(3,3,3,3,3)}(G_{23}, t) \end{array} \right] T_{28} \quad 108$$

$$\frac{dT_{29}}{dt} = (b_{29})^{(5)}T_{28} - \left[\begin{array}{ccc} (b'_{29})^{(5)} - (b''_{29})^{(5)}(G_{31}, t) & - (b''_{25})^{(4,4)}(G_{27}, t) & - (b''_{33})^{(6,6,6)}(G_{35}, t) \\ - (b''_{14})^{(1,1,1,1,1)}(G, t) & - (b''_{17})^{(2,2,2,2,2)}(G_{19}, t) & - (b''_{21})^{(3,3,3,3,3)}(G_{23}, t) \end{array} \right] T_{29} \quad 109$$

$$\frac{dT_{30}}{dt} = (b_{30})^{(5)}T_{29} - \left[\begin{array}{ccc} (b'_{30})^{(5)} - (b''_{30})^{(5)}(G_{31}, t) & - (b''_{26})^{(4,4)}(G_{27}, t) & - (b''_{34})^{(6,6,6)}(G_{35}, t) \\ - (b''_{15})^{(1,1,1,1,1)}(G, t) & - (b''_{18})^{(2,2,2,2,2)}(G_{19}, t) & - (b''_{22})^{(3,3,3,3,3)}(G_{23}, t) \end{array} \right] T_{30} \quad 110$$

where $-(b''_{28})^{(5)}(G_{31}, t)$, $-(b''_{29})^{(5)}(G_{31}, t)$, $-(b''_{30})^{(5)}(G_{31}, t)$ are first detrition coefficients for category 1, 2 and 3 111

$-(b''_{24})^{(4,4)}(G_{27}, t)$, $-(b''_{25})^{(4,4)}(G_{27}, t)$, $-(b''_{26})^{(4,4)}(G_{27}, t)$ are second detrition coefficients for category 1, 2 and 3

$-(b''_{32})^{(6,6,6)}(G_{35}, t)$, $-(b''_{33})^{(6,6,6)}(G_{35}, t)$, $-(b''_{34})^{(6,6,6)}(G_{35}, t)$ are third detrition coefficients for category 1, 2 and 3

$-(b''_{13})^{(1,1,1,1,1)}(G, t)$, $-(b''_{14})^{(1,1,1,1,1)}(G, t)$, $-(b''_{15})^{(1,1,1,1,1)}(G, t)$ are fourth detrition coefficients for category 1, 2, and 3

$-(b''_{16})^{(2,2,2,2,2)}(G_{19}, t)$, $-(b''_{17})^{(2,2,2,2,2)}(G_{19}, t)$, $-(b''_{18})^{(2,2,2,2,2)}(G_{19}, t)$ are fifth detrition coefficients for category

1,2, and 3

$-(b''_{20})^{(3,3,3,3,3)}(G_{23}, t)$, $-(b''_{21})^{(3,3,3,3,3)}(G_{23}, t)$, $-(b''_{22})^{(3,3,3,3,3)}(G_{23}, t)$ are sixth detrition coefficients for category 1,2, and 3

$$\frac{dG_{32}}{dt} = (a_{32})^{(6)}G_{33} - \left[\begin{array}{ccc} (a'_{32})^{(6)} + (a''_{32})^{(6)}(T_{33}, t) & + (a''_{28})^{(5,5,5)}(T_{29}, t) & + (a''_{24})^{(4,4,4)}(T_{25}, t) \\ + (a''_{13})^{(1,1,1,1,1,1)}(T_{14}, t) & + (a''_{16})^{(2,2,2,2,2,2)}(T_{17}, t) & + (a''_{20})^{(3,3,3,3,3,3)}(T_{21}, t) \end{array} \right] G_{32} \tag{112}$$

$$\frac{dG_{33}}{dt} = (a_{33})^{(6)}G_{32} - \left[\begin{array}{ccc} (a'_{33})^{(6)} + (a''_{33})^{(6)}(T_{33}, t) & + (a''_{29})^{(5,5,5)}(T_{29}, t) & + (a''_{25})^{(4,4,4)}(T_{25}, t) \\ + (a''_{14})^{(1,1,1,1,1,1)}(T_{14}, t) & + (a''_{17})^{(2,2,2,2,2,2)}(T_{17}, t) & + (a''_{21})^{(3,3,3,3,3,3)}(T_{21}, t) \end{array} \right] G_{33} \tag{113}$$

$$\frac{dG_{34}}{dt} = (a_{34})^{(6)}G_{33} - \left[\begin{array}{ccc} (a'_{34})^{(6)} + (a''_{34})^{(6)}(T_{33}, t) & + (a''_{30})^{(5,5,5)}(T_{29}, t) & + (a''_{26})^{(4,4,4)}(T_{25}, t) \\ + (a''_{15})^{(1,1,1,1,1,1)}(T_{14}, t) & + (a''_{18})^{(2,2,2,2,2,2)}(T_{17}, t) & + (a''_{22})^{(3,3,3,3,3,3)}(T_{21}, t) \end{array} \right] G_{34} \tag{114}$$

$+(a''_{32})^{(6)}(T_{33}, t)$, $+(a''_{33})^{(6)}(T_{33}, t)$, $+(a''_{34})^{(6)}(T_{33}, t)$ are first augmentation coefficients 115

for category 1, 2 and 3

$+(a''_{28})^{(5,5,5)}(T_{29}, t)$, $+(a''_{29})^{(5,5,5)}(T_{29}, t)$, $+(a''_{30})^{(5,5,5)}(T_{29}, t)$ are second augmentation coefficients for category 1, 2 and 3

$+(a''_{24})^{(4,4,4)}(T_{25}, t)$, $+(a''_{25})^{(4,4,4)}(T_{25}, t)$, $+(a''_{26})^{(4,4,4)}(T_{25}, t)$ are third augmentation coefficients for category 1, 2 and 3

$+(a''_{13})^{(1,1,1,1,1,1)}(T_{14}, t)$, $+(a''_{14})^{(1,1,1,1,1,1)}(T_{14}, t)$, $+(a''_{15})^{(1,1,1,1,1,1)}(T_{14}, t)$ - are fourth augmentation coefficients

$+(a''_{16})^{(2,2,2,2,2,2)}(T_{17}, t)$, $+(a''_{17})^{(2,2,2,2,2,2)}(T_{17}, t)$, $+(a''_{18})^{(2,2,2,2,2,2)}(T_{17}, t)$ - fifth augmentation coefficients

$+(a''_{20})^{(3,3,3,3,3,3)}(T_{21}, t)$, $+(a''_{21})^{(3,3,3,3,3,3)}(T_{21}, t)$, $+(a''_{22})^{(3,3,3,3,3,3)}(T_{21}, t)$ sixth augmentation coefficients 116

$$\frac{dT_{32}}{dt} = (b_{32})^{(6)}T_{33} - \left[\begin{array}{ccc} (b'_{32})^{(6)} - (b''_{32})^{(6)}(G_{35}, t) & - (b''_{28})^{(5,5,5)}(G_{31}, t) & - (b''_{24})^{(4,4,4)}(G_{27}, t) \\ - (b''_{13})^{(1,1,1,1,1,1)}(G, t) & - (b''_{16})^{(2,2,2,2,2,2)}(G_{19}, t) & - (b''_{20})^{(3,3,3,3,3,3)}(G_{23}, t) \end{array} \right] T_{32} \tag{117}$$

$$\frac{dT_{33}}{dt} = (b_{33})^{(6)}T_{32} - \left[\begin{array}{ccc} (b'_{33})^{(6)} - (b''_{33})^{(6)}(G_{35}, t) & - (b''_{29})^{(5,5,5)}(G_{31}, t) & - (b''_{25})^{(4,4,4)}(G_{27}, t) \\ - (b''_{14})^{(1,1,1,1,1,1)}(G, t) & - (b''_{17})^{(2,2,2,2,2,2)}(G_{19}, t) & - (b''_{21})^{(3,3,3,3,3,3)}(G_{23}, t) \end{array} \right] T_{33} \tag{118}$$

$$\frac{dT_{34}}{dt} = (b_{34})^{(6)}T_{33} - \left[\begin{array}{ccc} (b'_{34})^{(6)} - (b''_{34})^{(6)}(G_{35}, t) & - (b''_{30})^{(5,5,5)}(G_{31}, t) & - (b''_{26})^{(4,4,4)}(G_{27}, t) \\ - (b''_{15})^{(1,1,1,1,1,1)}(G, t) & - (b''_{18})^{(2,2,2,2,2,2)}(G_{19}, t) & - (b''_{22})^{(3,3,3,3,3,3)}(G_{23}, t) \end{array} \right] T_{34} \tag{119}$$

$-(b''_{32})^{(6)}(G_{35}, t)$, $-(b''_{33})^{(6)}(G_{35}, t)$, $-(b''_{34})^{(6)}(G_{35}, t)$ are first detrition coefficients 120

for category 1, 2 and 3

$-(b''_{28})^{(5,5,5)}(G_{31}, t)$, $-(b''_{29})^{(5,5,5)}(G_{31}, t)$, $-(b''_{30})^{(5,5,5)}(G_{31}, t)$ are second detrition coefficients for category 1, 2 and 3

$-(b''_{24})^{(4,4,4)}(G_{27}, t)$, $-(b''_{25})^{(4,4,4)}(G_{27}, t)$, $-(b''_{26})^{(4,4,4)}(G_{27}, t)$ are third detrition coefficients for category 1,2 and 3

coefficients for category 1,2 and 3

$-(b''_{13})^{(1,1,1,1,1,1)}(G, t)$, $-(b''_{14})^{(1,1,1,1,1,1)}(G, t)$, $-(b''_{15})^{(1,1,1,1,1,1)}(G, t)$ are fourth detrition coefficients for category 1, 2, and 3

$-(b''_{16})^{(2,2,2,2,2,2)}(G_{19}, t)$, $-(b''_{17})^{(2,2,2,2,2,2)}(G_{19}, t)$, $-(b''_{18})^{(2,2,2,2,2,2)}(G_{19}, t)$ are fifth detrition coefficients for category 1, 2, and 3

$-(b''_{20})^{(3,3,3,3,3,3)}(G_{23}, t)$, $-(b''_{21})^{(3,3,3,3,3,3)}(G_{23}, t)$, $-(b''_{22})^{(3,3,3,3,3,3)}(G_{23}, t)$ are sixth detrition coefficients for category 1, 2, and 3

Where we suppose 121

(A) $(a_i)^{(1)}, (a'_i)^{(1)}, (a''_i)^{(1)}, (b_i)^{(1)}, (b'_i)^{(1)}, (b''_i)^{(1)} > 0$,
 $i, j = 13, 14, 15$ 122

(B) The functions $(a_i)^{(1)}, (b_i)^{(1)}$ are positive continuous increasing and bounded. 123

Definition of $(p_i)^{(1)}, (r_i)^{(1)}$:

$$(a_i'')^{(1)}(T_{14}, t) \leq (p_i)^{(1)} \leq (\hat{A}_{13})^{(1)} \quad 124$$

$$(b_i'')^{(1)}(G, t) \leq (r_i)^{(1)} \leq (b_i')^{(1)} \leq (\hat{B}_{13})^{(1)}$$

$$(C) \quad \lim_{T_2 \rightarrow \infty} (a_i'')^{(1)}(T_{14}, t) = (p_i)^{(1)} \quad 125$$

$$\lim_{G \rightarrow \infty} (b_i'')^{(1)}(G, t) = (r_i)^{(1)}$$

Definition of $(\hat{A}_{13})^{(1)}, (\hat{B}_{13})^{(1)}$:

Where $(\hat{A}_{13})^{(1)}, (\hat{B}_{13})^{(1)}, (p_i)^{(1)}, (r_i)^{(1)}$ are positive constants and $i = 13, 14, 15$

They satisfy Lipschitz condition: 126

$$|(a_i'')^{(1)}(T_{14}', t) - (a_i'')^{(1)}(T_{14}, t)| \leq (\hat{k}_{13})^{(1)} |T_{14}' - T_{14}| e^{-(\hat{M}_{13})^{(1)}t} \quad 127$$

$$|(b_i'')^{(1)}(G', t) - (b_i'')^{(1)}(G, t)| \leq (\hat{k}_{13})^{(1)} \|G - G'\| e^{-(\hat{M}_{13})^{(1)}t} \quad 128$$

With the Lipschitz condition, we place a restriction on the behavior of functions 129

$(a_i'')^{(1)}(T_{14}, t)$ and $(a_i')^{(1)}(T_{14}, t)$. (T_{14}', t) and (T_{14}, t) are points belonging to the interval $[(\hat{k}_{13})^{(1)}, (\hat{M}_{13})^{(1)}]$. It

is to be noted that $(a_i'')^{(1)}(T_{14}, t)$ is uniformly continuous. In the eventuality of the fact, that if $(\hat{M}_{13})^{(1)} = 1$ then the function $(a_i'')^{(1)}(T_{14}, t)$, the first augmentation coefficient would be absolutely continuous.

Definition of $(\hat{M}_{13})^{(1)}, (\hat{k}_{13})^{(1)}$:

(D) $(\hat{M}_{13})^{(1)}, (\hat{k}_{13})^{(1)}$, are positive constants 130

$$\frac{(a_i)^{(1)}}{(\hat{M}_{13})^{(1)}}, \frac{(b_i)^{(1)}}{(\hat{M}_{13})^{(1)}} < 1$$

Definition of $(\hat{P}_{13})^{(1)}, (\hat{Q}_{13})^{(1)}$:

(E) There exists two constants $(\hat{P}_{13})^{(1)}$ and $(\hat{Q}_{13})^{(1)}$ which together with $(\hat{M}_{13})^{(1)}, (\hat{k}_{13})^{(1)}, (\hat{A}_{13})^{(1)}$ and 131

$(\hat{B}_{13})^{(1)}$ and the constants $(a_i)^{(1)}, (a_i')^{(1)}, (b_i)^{(1)}, (b_i')^{(1)}, (p_i)^{(1)}, (r_i)^{(1)}, i = 13, 14, 15,$ 132

satisfy the inequalities 133

$$\frac{1}{(\hat{M}_{13})^{(1)}} [(a_i)^{(1)} + (a_i')^{(1)} + (\hat{A}_{13})^{(1)} + (\hat{P}_{13})^{(1)} (\hat{k}_{13})^{(1)}] < 1 \quad 134$$

$$\frac{1}{(\hat{M}_{13})^{(1)}} [(b_i)^{(1)} + (b_i')^{(1)} + (\hat{B}_{13})^{(1)} + (\hat{Q}_{13})^{(1)} (\hat{k}_{13})^{(1)}] < 1 \quad 135$$

Where we suppose

(F) $(a_i)^{(2)}, (a_i')^{(2)}, (a_i'')^{(2)}, (b_i)^{(2)}, (b_i')^{(2)}, (b_i'')^{(2)} > 0, i, j = 16, 17, 18$ 136

(G) The functions $(a_i'')^{(2)}, (b_i'')^{(2)}$ are positive continuous increasing and bounded. 137

Definition of $(p_i)^{(2)}, (r_i)^{(2)}$: 138

$$(a_i'')^{(2)}(T_{17}, t) \leq (p_i)^{(2)} \leq (\hat{A}_{16})^{(2)} \quad 139$$

$$(b_i'')^{(2)}(G_{19}, t) \leq (r_i)^{(2)} \leq (b_i')^{(2)} \leq (\hat{B}_{16})^{(2)} \quad 140$$

$$(H) \quad \lim_{T_2 \rightarrow \infty} (a_i'')^{(2)}(T_{17}, t) = (p_i)^{(2)} \quad 141$$

$$\lim_{G \rightarrow \infty} (b_i'')^{(2)}(G_{19}, t) = (r_i)^{(2)} \quad 142$$

Definition of $(\hat{A}_{16})^{(2)}, (\hat{B}_{16})^{(2)}$: 143

Where $(\hat{A}_{16})^{(2)}, (\hat{B}_{16})^{(2)}, (p_i)^{(2)}, (r_i)^{(2)}$ are positive constants and $i = 16, 17, 18$ 144

They satisfy Lipschitz condition: 145

$$|(a_i'')^{(2)}(T_{17}', t) - (a_i'')^{(2)}(T_{17}, t)| \leq (\hat{k}_{16})^{(2)} |T_{17}' - T_{17}| e^{-(\hat{M}_{16})^{(2)}t} \quad 146$$

$$|(b_i'')^{(2)}(G_{19}', t) - (b_i'')^{(2)}(G_{19}, t)| \leq (\hat{k}_{16})^{(2)} \|G_{19}' - G_{19}\| e^{-(\hat{M}_{16})^{(2)}t} \quad 147$$

With the Lipschitz condition, we place a restriction on the behavior of functions $(a_i'')^{(2)}(T_{17}', t)$ and $(a_i'')^{(2)}(T_{17}, t)$ 148

. (T_{17}', t) and (T_{17}, t) are points belonging to the interval $[(\hat{k}_{16})^{(2)}, (\hat{M}_{16})^{(2)}]$. It is to be noted that $(a_i'')^{(2)}(T_{17}, t)$

is uniformly continuous. In the eventuality of the fact, that if $(\hat{M}_{16})^{(2)} = 1$ then the function $(a_i'')^{(2)}(T_{17}, t)$, the SECOND augmentation coefficient would be absolutely continuous.

Definition of $(\hat{M}_{16})^{(2)}, (\hat{k}_{16})^{(2)}$:

(I) $(\hat{M}_{16})^{(2)}, (\hat{k}_{16})^{(2)}$, are positive constants 149

$$\frac{(a_i)^{(2)}}{(\hat{M}_{16})^{(2)}}, \frac{(b_i)^{(2)}}{(\hat{M}_{16})^{(2)}} < 1 \quad 150$$

Definition of $(\hat{P}_{16})^{(2)}, (\hat{Q}_{16})^{(2)}$:

There exists two constants $(\hat{P}_{16})^{(2)}$ and $(\hat{Q}_{16})^{(2)}$ which together with $(\hat{M}_{16})^{(2)}, (\hat{k}_{16})^{(2)}, (\hat{A}_{16})^{(2)}$ and $(\hat{B}_{16})^{(2)}$ 151

and the constants $(a_i)^{(2)}, (a_i')^{(2)}, (b_i)^{(2)}, (b_i')^{(2)}, (p_i)^{(2)}, (r_i)^{(2)}, i = 16, 17, 18,$

satisfy the inequalities

$$\frac{1}{(\hat{M}_{16})^{(2)}} [(a_i)^{(2)} + (a_i')^{(2)} + (\hat{A}_{16})^{(2)} + (\hat{P}_{16})^{(2)} (\hat{k}_{16})^{(2)}] < 1 \quad 152$$

$$\frac{1}{(\hat{M}_{16})^{(2)}} [(b_i)^{(2)} + (b_i')^{(2)} + (\hat{B}_{16})^{(2)} + (\hat{Q}_{16})^{(2)} (\hat{k}_{16})^{(2)}] < 1 \quad 153$$

Where we suppose

(J) $(a_i)^{(3)}, (a_i')^{(3)}, (a_i'')^{(3)}, (b_i)^{(3)}, (b_i')^{(3)}, (b_i'')^{(3)} > 0, \quad i, j = 20, 21, 22$

The functions $(a_i'')^{(3)}, (b_i'')^{(3)}$ are positive continuous increasing and bounded.

Definition of $(p_i)^{(3)}, (r_i)^{(3)}$:

$$(a_i'')^{(3)}(T_{21}, t) \leq (p_i)^{(3)} \leq (\hat{A}_{20})^{(3)}$$

$$(b_i'')^{(3)}(G, t) \leq (r_i)^{(3)} \leq (b_i')^{(3)} \leq (\hat{B}_{20})^{(3)}$$

$\lim_{T_2 \rightarrow \infty} (a_i'')^{(3)}(T_{21}, t) = (p_i)^{(3)}$

$\lim_{G \rightarrow \infty} (b_i'')^{(3)}(G, t) = (r_i)^{(3)}$

Definition of $(\hat{A}_{20})^{(3)}, (\hat{B}_{20})^{(3)}$:

Where $(\hat{A}_{20})^{(3)}, (\hat{B}_{20})^{(3)}, (p_i)^{(3)}, (r_i)^{(3)}$ are positive constants and $i = 20, 21, 22$

They satisfy Lipschitz condition:

$$|(a_i'')^{(3)}(T_{21}, t) - (a_i'')^{(3)}(T_{21}, t)| \leq (\hat{k}_{20})^{(3)} |T_{21} - T_{21}'| e^{-(\hat{M}_{20})^{(3)}t}$$

$$|(b_i'')^{(3)}(G', t) - (b_i'')^{(3)}(G, T)| < (\hat{k}_{20})^{(3)} \|G - G'\| e^{-(\hat{M}_{20})^{(3)}t}$$

With the Lipschitz condition, we place a restriction on the behavior of functions $(a_i'')^{(3)}(T_{21}, t)$ and $(a_i'')^{(3)}(T_{21}, t)$. (T_{21}', t) and (T_{21}, t) are points belonging to the interval $[(\hat{k}_{20})^{(3)}, (\hat{M}_{20})^{(3)}]$. It is to be noted that

$(a_i'')^{(3)}(T_{21}, t)$ is uniformly continuous. In the eventuality of the fact, that if $(\hat{M}_{20})^{(3)} = 1$ then the function $(a_i'')^{(3)}(T_{21}, t)$, the third augmentation coefficient would be absolutely continuous.

Definition of $(\hat{M}_{20})^{(3)}, (\hat{k}_{20})^{(3)}$:

(K) $(\hat{M}_{20})^{(3)}, (\hat{k}_{20})^{(3)}$, are positive constants

$$\frac{(a_i)^{(3)}}{(\hat{M}_{20})^{(3)}} + \frac{(b_i)^{(3)}}{(\hat{M}_{20})^{(3)}} < 1$$

There exists two constants There exists two constants $(\hat{P}_{20})^{(3)}$ and $(\hat{Q}_{20})^{(3)}$ which together with $(\hat{M}_{20})^{(3)}, (\hat{k}_{20})^{(3)}, (\hat{A}_{20})^{(3)}$ and $(\hat{B}_{20})^{(3)}$ and the constants $(a_i)^{(3)}, (a_i')^{(3)}, (b_i)^{(3)}, (b_i')^{(3)}, (p_i)^{(3)}, (r_i)^{(3)}, i = 20, 21, 22,$

satisfy the inequalities

$$\frac{1}{(\hat{M}_{20})^{(3)}} [(a_i)^{(3)} + (a_i')^{(3)} + (\hat{A}_{20})^{(3)} + (\hat{P}_{20})^{(3)} (\hat{k}_{20})^{(3)}] < 1$$

$$\frac{1}{(\hat{M}_{20})^{(3)}} [(b_i)^{(3)} + (b_i')^{(3)} + (\hat{B}_{20})^{(3)} + (\hat{Q}_{20})^{(3)} (\hat{k}_{20})^{(3)}] < 1$$

Where we suppose

(L) $(a_i)^{(4)}, (a_i')^{(4)}, (a_i'')^{(4)}, (b_i)^{(4)}, (b_i')^{(4)}, (b_i'')^{(4)} > 0, \quad i, j = 24, 25, 26$

(M) The functions $(a_i'')^{(4)}, (b_i'')^{(4)}$ are positive continuous increasing and bounded.

Definition of $(p_i)^{(4)}, (r_i)^{(4)}$:

$$(a_i'')^{(4)}(T_{25}, t) \leq (p_i)^{(4)} \leq (\hat{A}_{24})^{(4)}$$

$$(b_i'')^{(4)}((G_{27}), t) \leq (r_i)^{(4)} \leq (b_i')^{(4)} \leq (\hat{B}_{24})^{(4)}$$

(N) $\lim_{T_2 \rightarrow \infty} (a_i'')^{(4)}(T_{25}, t) = (p_i)^{(4)}$

$\lim_{G \rightarrow \infty} (b_i'')^{(4)}((G_{27}), t) = (r_i)^{(4)}$

Definition of $(\hat{A}_{24})^{(4)}, (\hat{B}_{24})^{(4)}$:

Where $(\hat{A}_{24})^{(4)}, (\hat{B}_{24})^{(4)}, (p_i)^{(4)}, (r_i)^{(4)}$ are positive constants and $i = 24, 25, 26$

They satisfy Lipschitz condition:

$$|(a_i'')^{(4)}(T_{25}, t) - (a_i'')^{(4)}(T_{25}, t)| \leq (\hat{k}_{24})^{(4)} |T_{25} - T_{25}'| e^{-(\hat{M}_{24})^{(4)}t}$$

$$|(b_i'')^{(4)}((G_{27})', t) - (b_i'')^{(4)}((G_{27}), T)| < (\hat{k}_{24})^{(4)} \|(G_{27}) - (G_{27}')\| e^{-(\hat{M}_{24})^{(4)}t}$$

With the Lipschitz condition, we place a restriction on the behavior of functions $(a_i'')^{(4)}(T_{25}, t)$ and $(a_i'')^{(4)}(T_{25}, t)$. (T_{25}', t) and (T_{25}, t) are points belonging to the interval $[(\hat{k}_{24})^{(4)}, (\hat{M}_{24})^{(4)}]$. It is to be noted that $(a_i'')^{(4)}(T_{25}, t)$

is uniformly continuous. In the eventuality of the fact, that if $(\hat{M}_{24})^{(4)} = 4$ then the function $(a_i'')^{(4)}(T_{25}, t)$, the fourth augmentation coefficient would be absolutely continuous.

Definition of $(\hat{M}_{24})^{(4)}, (\hat{k}_{24})^{(4)}$:

(O) $(\hat{M}_{24})^{(4)}, (\hat{k}_{24})^{(4)}$, are positive constants

$$\frac{(a_i)^{(4)}}{(\hat{M}_{24})^{(4)}} + \frac{(b_i)^{(4)}}{(\hat{M}_{24})^{(4)}} < 1$$

Definition of $(\hat{P}_{24})^{(4)}, (\hat{Q}_{24})^{(4)}$:

(Q) There exists two constants $(\hat{P}_{24})^{(4)}$ and $(\hat{Q}_{24})^{(4)}$ which together with $(\hat{M}_{24})^{(4)}, (\hat{k}_{24})^{(4)}, (\hat{A}_{24})^{(4)}$ and $(\hat{B}_{24})^{(4)}$ and the constants $(a_i)^{(4)}, (a_i')^{(4)}, (b_i)^{(4)}, (b_i')^{(4)}, (p_i)^{(4)}, (r_i)^{(4)}, i = 24, 25, 26,$

satisfy the inequalities

$$\frac{1}{(\hat{M}_{24})^{(4)}} [(a_i)^{(4)} + (a'_i)^{(4)} + (\hat{A}_{24})^{(4)} + (\hat{P}_{24})^{(4)} (\hat{k}_{24})^{(4)}] < 1$$

$$\frac{1}{(\hat{M}_{24})^{(4)}} [(b_i)^{(4)} + (b'_i)^{(4)} + (\hat{B}_{24})^{(4)} + (\hat{Q}_{24})^{(4)} (\hat{k}_{24})^{(4)}] < 1$$

Where we suppose

$$(R) \quad (a_i)^{(5)}, (a'_i)^{(5)}, (a''_i)^{(5)}, (b_i)^{(5)}, (b'_i)^{(5)}, (b''_i)^{(5)} > 0, \quad i, j = 28, 29, 30$$

(S) The functions $(a''_i)^{(5)}, (b''_i)^{(5)}$ are positive continuous increasing and bounded.

Definition of $(p_i)^{(5)}, (r_i)^{(5)}$:

$$(a''_i)^{(5)}(T_{29}, t) \leq (p_i)^{(5)} \leq (\hat{A}_{28})^{(5)}$$

$$(b''_i)^{(5)}(G_{31}, t) \leq (r_i)^{(5)} \leq (b'_i)^{(5)} \leq (\hat{B}_{28})^{(5)}$$

$$(T) \quad \lim_{T_2 \rightarrow \infty} (a''_i)^{(5)}(T_{29}, t) = (p_i)^{(5)}$$

$$\lim_{G \rightarrow \infty} (b''_i)^{(5)}(G_{31}, t) = (r_i)^{(5)}$$

Definition of $(\hat{A}_{28})^{(5)}, (\hat{B}_{28})^{(5)}$:

Where $(\hat{A}_{28})^{(5)}, (\hat{B}_{28})^{(5)}, (p_i)^{(5)}, (r_i)^{(5)}$ are positive constants and $i = 28, 29, 30$

They satisfy Lipschitz condition:

$$|(a''_i)^{(5)}(T'_{29}, t) - (a''_i)^{(5)}(T_{29}, t)| \leq (\hat{k}_{28})^{(5)} |T'_{29} - T_{29}| e^{-(\hat{M}_{28})^{(5)}t}$$

$$|(b''_i)^{(5)}((G'_{31}), t) - (b''_i)^{(5)}((G_{31}), (T_{31}))| < (\hat{k}_{28})^{(5)} |(G'_{31}) - (G_{31})'| e^{-(\hat{M}_{28})^{(5)}t}$$

With the Lipschitz condition, we place a restriction on the behavior of functions $(a''_i)^{(5)}(T'_{29}, t)$ and $(a''_i)^{(5)}(T_{29}, t)$. (T'_{29}, t) and (T_{29}, t) are points belonging to the interval $[(\hat{k}_{28})^{(5)}, (\hat{M}_{28})^{(5)}]$. It is to be noted that $(a''_i)^{(5)}(T_{29}, t)$ is uniformly continuous. In the eventuality of the fact, that if $(\hat{M}_{28})^{(5)} = 5$ then the function $(a''_i)^{(5)}(T_{29}, t)$, the fifth **augmentation coefficient** would be absolutely continuous.

Definition of $(\hat{M}_{28})^{(5)}, (\hat{k}_{28})^{(5)}$:

(U) $(\hat{M}_{28})^{(5)}, (\hat{k}_{28})^{(5)}$, are positive constants

$$\frac{(a_i)^{(5)}}{(\hat{M}_{28})^{(5)}}, \frac{(b_i)^{(5)}}{(\hat{M}_{28})^{(5)}} < 1$$

Definition of $(\hat{P}_{28})^{(5)}, (\hat{Q}_{28})^{(5)}$:

(V) There exists two constants $(\hat{P}_{28})^{(5)}$ and $(\hat{Q}_{28})^{(5)}$ which together with $(\hat{M}_{28})^{(5)}, (\hat{k}_{28})^{(5)}, (\hat{A}_{28})^{(5)}$ and $(\hat{B}_{28})^{(5)}$ and the constants $(a_i)^{(5)}, (a'_i)^{(5)}, (b_i)^{(5)}, (b'_i)^{(5)}, (p_i)^{(5)}, (r_i)^{(5)}, i = 28, 29, 30$, satisfy the inequalities

$$\frac{1}{(\hat{M}_{28})^{(5)}} [(a_i)^{(5)} + (a'_i)^{(5)} + (\hat{A}_{28})^{(5)} + (\hat{P}_{28})^{(5)} (\hat{k}_{28})^{(5)}] < 1$$

$$\frac{1}{(\hat{M}_{28})^{(5)}} [(b_i)^{(5)} + (b'_i)^{(5)} + (\hat{B}_{28})^{(5)} + (\hat{Q}_{28})^{(5)} (\hat{k}_{28})^{(5)}] < 1$$

Where we suppose

$$(a_i)^{(6)}, (a'_i)^{(6)}, (a''_i)^{(6)}, (b_i)^{(6)}, (b'_i)^{(6)}, (b''_i)^{(6)} > 0, \quad i, j = 32, 33, 34$$

(W) The functions $(a''_i)^{(6)}, (b''_i)^{(6)}$ are positive continuous increasing and bounded.

Definition of $(p_i)^{(6)}, (r_i)^{(6)}$:

$$(a''_i)^{(6)}(T_{33}, t) \leq (p_i)^{(6)} \leq (\hat{A}_{32})^{(6)}$$

$$(b''_i)^{(6)}(G_{35}, t) \leq (r_i)^{(6)} \leq (b'_i)^{(6)} \leq (\hat{B}_{32})^{(6)}$$

$$(X) \quad \lim_{T_2 \rightarrow \infty} (a''_i)^{(6)}(T_{33}, t) = (p_i)^{(6)}$$

$$\lim_{G \rightarrow \infty} (b''_i)^{(6)}(G_{35}, t) = (r_i)^{(6)}$$

Definition of $(\hat{A}_{32})^{(6)}, (\hat{B}_{32})^{(6)}$:

Where $(\hat{A}_{32})^{(6)}, (\hat{B}_{32})^{(6)}, (p_i)^{(6)}, (r_i)^{(6)}$ are positive constants and $i = 32, 33, 34$

They satisfy Lipschitz condition:

$$|(a''_i)^{(6)}(T'_{33}, t) - (a''_i)^{(6)}(T_{33}, t)| \leq (\hat{k}_{32})^{(6)} |T'_{33} - T_{33}| e^{-(\hat{M}_{32})^{(6)}t}$$

$$|(b''_i)^{(6)}((G'_{35}), t) - (b''_i)^{(6)}((G_{35}), (T_{35}))| < (\hat{k}_{32})^{(6)} |(G'_{35}) - (G_{35})'| e^{-(\hat{M}_{32})^{(6)}t}$$

With the Lipschitz condition, we place a restriction on the behavior of functions $(a''_i)^{(6)}(T'_{33}, t)$ and $(a''_i)^{(6)}(T_{33}, t)$. (T'_{33}, t) and (T_{33}, t) are points belonging to the interval $[(\hat{k}_{32})^{(6)}, (\hat{M}_{32})^{(6)}]$. It is to be noted that $(a''_i)^{(6)}(T_{33}, t)$ is uniformly continuous. In the eventuality of the fact, that if $(\hat{M}_{32})^{(6)} = 6$ then the function $(a''_i)^{(6)}(T_{33}, t)$, the sixth **augmentation coefficient** would be absolutely continuous.

Definition of $(\hat{M}_{32})^{(6)}, (\hat{k}_{32})^{(6)}$:

$(\hat{M}_{32})^{(6)}, (\hat{k}_{32})^{(6)}$, are positive constants

$$\frac{(a_i)^{(6)}}{(\hat{M}_{32})^{(6)}}, \frac{(b_i)^{(6)}}{(\hat{M}_{32})^{(6)}} < 1$$

Definition of $(\hat{P}_{32})^{(6)}, (\hat{Q}_{32})^{(6)}$:

There exists two constants $(\hat{P}_{32})^{(6)}$ and $(\hat{Q}_{32})^{(6)}$ which together with $(\hat{M}_{32})^{(6)}$, $(\hat{k}_{32})^{(6)}$, $(\hat{A}_{32})^{(6)}$ and $(\hat{B}_{32})^{(6)}$ and the constants $(a_i)^{(6)}$, $(a'_i)^{(6)}$, $(b_i)^{(6)}$, $(b'_i)^{(6)}$, $(p_i)^{(6)}$, $(r_i)^{(6)}$, $i = 32, 33, 34$, satisfy the inequalities

$$\frac{1}{(\hat{M}_{32})^{(6)}} [(a_i)^{(6)} + (a'_i)^{(6)} + (\hat{A}_{32})^{(6)} + (\hat{P}_{32})^{(6)} (\hat{k}_{32})^{(6)}] < 1$$

$$\frac{1}{(\hat{M}_{32})^{(6)}} [(b_i)^{(6)} + (b'_i)^{(6)} + (\hat{B}_{32})^{(6)} + (\hat{Q}_{32})^{(6)} (\hat{k}_{32})^{(6)}] < 1$$

Theorem 1: if the conditions (A)-(E) (first five conditions related to the system Boolean satisfiability problem) above are fulfilled, there exists a solution satisfying the conditions

Definition of $G_i(0), T_i(0)$:

$$G_i(t) \leq (\hat{P}_{13})^{(1)} e^{(\hat{M}_{13})^{(1)}t}, \quad \boxed{G_i(0) = G_i^0 > 0}$$

$$T_i(t) \leq (\hat{Q}_{13})^{(1)} e^{(\hat{M}_{13})^{(1)}t}, \quad \boxed{T_i(0) = T_i^0 > 0}$$

If the conditions of second module pertaining to Knapsack problem and Hamiltonian Path Problem above are fulfilled, there exists a solution satisfying the conditions

Definition of $G_i(0), T_i(0)$

$$G_i(t) \leq (\hat{P}_{16})^{(2)} e^{(\hat{M}_{16})^{(2)}t}, \quad G_i(0) = G_i^0 > 0$$

$$T_i(t) \leq (\hat{Q}_{16})^{(2)} e^{(\hat{M}_{16})^{(2)}t}, \quad T_i(0) = T_i^0 > 0$$

If the conditions pertaining to the third module Sub graph Isomorphism problem and Subset sum problem above are fulfilled, there exists a solution satisfying the conditions

$$G_i(t) \leq (\hat{P}_{20})^{(3)} e^{(\hat{M}_{20})^{(3)}t}, \quad G_i(0) = G_i^0 > 0$$

$$T_i(t) \leq (\hat{Q}_{20})^{(3)} e^{(\hat{M}_{20})^{(3)}t}, \quad T_i(0) = T_i^0 > 0$$

If the conditions of the fourth module Subset Sum Problem and Clique problem above are fulfilled, there exists a solution satisfying the conditions

Definition of $G_i(0), T_i(0)$:

$$G_i(t) \leq (\hat{P}_{24})^{(4)} e^{(\hat{M}_{24})^{(4)}t}, \quad \boxed{G_i(0) = G_i^0 > 0}$$

$$T_i(t) \leq (\hat{Q}_{24})^{(4)} e^{(\hat{M}_{24})^{(4)}t}, \quad \boxed{T_i(0) = T_i^0 > 0}$$

If the conditions pertaining to the module five namely Vertex Cover Problem and Independent Set problem are fulfilled, there exists a solution satisfying the conditions

Definition of $G_i(0), T_i(0)$:

$$G_i(t) \leq (\hat{P}_{28})^{(5)} e^{(\hat{M}_{28})^{(5)}t}, \quad \boxed{G_i(0) = G_i^0 > 0}$$

$$T_i(t) \leq (\hat{Q}_{28})^{(5)} e^{(\hat{M}_{28})^{(5)}t}, \quad \boxed{T_i(0) = T_i^0 > 0}$$

If the conditions pertaining to Dominating set problem and Graph Coloring Problem above are fulfilled, there exists a solution satisfying the conditions

Definition of $G_i(0), T_i(0)$:

$$G_i(t) \leq (\hat{P}_{32})^{(6)} e^{(\hat{M}_{32})^{(6)}t}, \quad \boxed{G_i(0) = G_i^0 > 0}$$

$$T_i(t) \leq (\hat{Q}_{32})^{(6)} e^{(\hat{M}_{32})^{(6)}t}, \quad \boxed{T_i(0) = T_i^0 > 0}$$

Proof:

Consider operator $\mathcal{A}^{(1)}$ defined on the space of sextuples of continuous functions $G_i, T_i: \mathbb{R}_+ \rightarrow \mathbb{R}_+$ which satisfy

$$G_i(0) = G_i^0, T_i(0) = T_i^0, G_i^0 \leq (\hat{P}_{13})^{(1)}, T_i^0 \leq (\hat{Q}_{13})^{(1)},$$

$$0 \leq G_i(t) - G_i^0 \leq (\hat{P}_{13})^{(1)} e^{(\hat{M}_{13})^{(1)}t}$$

$$0 \leq T_i(t) - T_i^0 \leq (\hat{Q}_{13})^{(1)} e^{(\hat{M}_{13})^{(1)}t}$$

By

$$\bar{G}_{13}(t) = G_{13}^0 + \int_0^t [(a_{13})^{(1)} G_{14}(s_{13}) - ((a'_{13})^{(1)} + a''_{13})^{(1)} (T_{14}(s_{13}), s_{13})) G_{13}(s_{13})] ds_{13}$$

$$\bar{G}_{14}(t) = G_{14}^0 + \int_0^t [(a_{14})^{(1)} G_{13}(s_{13}) - ((a'_{14})^{(1)} + (a''_{14})^{(1)} (T_{14}(s_{13}), s_{13})) G_{14}(s_{13})] ds_{13}$$

$$\bar{G}_{15}(t) = G_{15}^0 + \int_0^t [(a_{15})^{(1)} G_{14}(s_{13}) - ((a'_{15})^{(1)} + (a''_{15})^{(1)} (T_{14}(s_{13}), s_{13})) G_{15}(s_{13})] ds_{13}$$

$$\bar{T}_{13}(t) = T_{13}^0 + \int_0^t [(b_{13})^{(1)} T_{14}(s_{13}) - ((b'_{13})^{(1)} - (b''_{13})^{(1)} (G(s_{13}), s_{13})) T_{13}(s_{13})] ds_{13}$$

$$\bar{T}_{14}(t) = T_{14}^0 + \int_0^t [(b_{14})^{(1)} T_{13}(s_{13}) - ((b'_{14})^{(1)} - (b''_{14})^{(1)} (G(s_{13}), s_{13})) T_{14}(s_{13})] ds_{13}$$

$$\bar{T}_{15}(t) = T_{15}^0 + \int_0^t \left[(b_{15})^{(1)} T_{14}(s_{(13)}) - \left((b'_{15})^{(1)} - (b''_{15})^{(1)} (G(s_{(13)}), s_{(13)}) \right) T_{15}(s_{(13)}) \right] ds_{(13)} \quad 213$$

Where $s_{(13)}$ is the integrand that is integrated over an interval $(0, t)$

214
215

Consider operator $\mathcal{A}^{(2)}$ defined on the space of sextuples of continuous functions $G_i, T_i: \mathbb{R}_+ \rightarrow \mathbb{R}_+$ which satisfy

$$G_i(0) = G_i^0, T_i(0) = T_i^0, G_i^0 \leq (\hat{P}_{16})^{(2)}, T_i^0 \leq (\hat{Q}_{16})^{(2)}, \quad 216$$

$$0 \leq G_i(t) - G_i^0 \leq (\hat{P}_{16})^{(2)} e^{(\hat{M}_{16})^{(2)}t} \quad 217$$

$$0 \leq T_i(t) - T_i^0 \leq (\hat{Q}_{16})^{(2)} e^{(\hat{M}_{16})^{(2)}t} \quad 218$$

By 219

$$\bar{G}_{16}(t) = G_{16}^0 + \int_0^t \left[(a_{16})^{(2)} G_{17}(s_{(16)}) - \left((a'_{16})^{(2)} + a''_{16}(2)(T_{17}(s_{(16)}), s_{(16)}) \right) G_{16}(s_{(16)}) \right] ds_{(16)} \quad 220$$

$$\bar{G}_{17}(t) = G_{17}^0 + \int_0^t \left[(a_{17})^{(2)} G_{16}(s_{(16)}) - \left((a'_{17})^{(2)} + (a''_{17})^{(2)} (T_{17}(s_{(16)}), s_{(17)}) \right) G_{17}(s_{(16)}) \right] ds_{(16)} \quad 221$$

$$\bar{G}_{18}(t) = G_{18}^0 + \int_0^t \left[(a_{18})^{(2)} G_{17}(s_{(16)}) - \left((a'_{18})^{(2)} + (a''_{18})^{(2)} (T_{17}(s_{(16)}), s_{(16)}) \right) G_{18}(s_{(16)}) \right] ds_{(16)} \quad 222$$

$$\bar{T}_{16}(t) = T_{16}^0 + \int_0^t \left[(b_{16})^{(2)} T_{17}(s_{(16)}) - \left((b'_{16})^{(2)} - (b''_{16})^{(2)} (G(s_{(16)}), s_{(16)}) \right) T_{16}(s_{(16)}) \right] ds_{(16)} \quad 223$$

$$\bar{T}_{17}(t) = T_{17}^0 + \int_0^t \left[(b_{17})^{(2)} T_{16}(s_{(16)}) - \left((b'_{17})^{(2)} - (b''_{17})^{(2)} (G(s_{(16)}), s_{(16)}) \right) T_{17}(s_{(16)}) \right] ds_{(16)} \quad 224$$

$$\bar{T}_{18}(t) = T_{18}^0 + \int_0^t \left[(b_{18})^{(2)} T_{17}(s_{(16)}) - \left((b'_{18})^{(2)} - (b''_{18})^{(2)} (G(s_{(16)}), s_{(16)}) \right) T_{18}(s_{(16)}) \right] ds_{(16)} \quad 224$$

Where $s_{(16)}$ is the integrand that is integrated over an interval $(0, t)$

225

Consider operator $\mathcal{A}^{(3)}$ defined on the space of sextuples of continuous functions $G_i, T_i: \mathbb{R}_+ \rightarrow \mathbb{R}_+$ which satisfy

$$G_i(0) = G_i^0, T_i(0) = T_i^0, G_i^0 \leq (\hat{P}_{20})^{(3)}, T_i^0 \leq (\hat{Q}_{20})^{(3)}, \quad 226$$

$$0 \leq G_i(t) - G_i^0 \leq (\hat{P}_{20})^{(3)} e^{(\hat{M}_{20})^{(3)}t} \quad 227$$

$$0 \leq T_i(t) - T_i^0 \leq (\hat{Q}_{20})^{(3)} e^{(\hat{M}_{20})^{(3)}t} \quad 228$$

By 229

$$\bar{G}_{20}(t) = G_{20}^0 + \int_0^t \left[(a_{20})^{(3)} G_{21}(s_{(20)}) - \left((a'_{20})^{(3)} + a''_{20}(3)(T_{21}(s_{(20)}), s_{(20)}) \right) G_{20}(s_{(20)}) \right] ds_{(20)} \quad 230$$

$$\bar{G}_{21}(t) = G_{21}^0 + \int_0^t \left[(a_{21})^{(3)} G_{20}(s_{(20)}) - \left((a'_{21})^{(3)} + (a''_{21})^{(3)} (T_{21}(s_{(20)}), s_{(20)}) \right) G_{21}(s_{(20)}) \right] ds_{(20)} \quad 231$$

$$\bar{G}_{22}(t) = G_{22}^0 + \int_0^t \left[(a_{22})^{(3)} G_{21}(s_{(20)}) - \left((a'_{22})^{(3)} + (a''_{22})^{(3)} (T_{21}(s_{(20)}), s_{(20)}) \right) G_{22}(s_{(20)}) \right] ds_{(20)} \quad 232$$

$$\bar{T}_{20}(t) = T_{20}^0 + \int_0^t \left[(b_{20})^{(3)} T_{21}(s_{(20)}) - \left((b'_{20})^{(3)} - (b''_{20})^{(3)} (G(s_{(20)}), s_{(20)}) \right) T_{20}(s_{(20)}) \right] ds_{(20)} \quad 233$$

$$\bar{T}_{21}(t) = T_{21}^0 + \int_0^t \left[(b_{21})^{(3)} T_{20}(s_{(20)}) - \left((b'_{21})^{(3)} - (b''_{21})^{(3)} (G(s_{(20)}), s_{(20)}) \right) T_{21}(s_{(20)}) \right] ds_{(20)} \quad 234$$

$$\bar{T}_{22}(t) = T_{22}^0 + \int_0^t \left[(b_{22})^{(3)} T_{21}(s_{(20)}) - \left((b'_{22})^{(3)} - (b''_{22})^{(3)} (G(s_{(20)}), s_{(20)}) \right) T_{22}(s_{(20)}) \right] ds_{(20)} \quad 234$$

Where $s_{(20)}$ is the integrand that is integrated over an interval $(0, t)$

Proof: Consider operator $\mathcal{A}^{(4)}$ defined on the space of sextuples of continuous functions $G_i, T_i: \mathbb{R}_+ \rightarrow \mathbb{R}_+$ which satisfy 235

$$G_i(0) = G_i^0, T_i(0) = T_i^0, G_i^0 \leq (\hat{P}_{24})^{(4)}, T_i^0 \leq (\hat{Q}_{24})^{(4)}, \quad 236$$

$$0 \leq G_i(t) - G_i^0 \leq (\hat{P}_{24})^{(4)} e^{(\hat{M}_{24})^{(4)}t} \quad 237$$

$$0 \leq T_i(t) - T_i^0 \leq (\hat{Q}_{24})^{(4)} e^{(\hat{M}_{24})^{(4)}t} \quad 238$$

By 239

$$\bar{G}_{24}(t) = G_{24}^0 + \int_0^t \left[(a_{24})^{(4)} G_{25}(s_{(24)}) - \left((a'_{24})^{(4)} + a''_{24}(4)(T_{25}(s_{(24)}), s_{(24)}) \right) G_{24}(s_{(24)}) \right] ds_{(24)} \quad 240$$

$$\bar{G}_{25}(t) = G_{25}^0 + \int_0^t \left[(a_{25})^{(4)} G_{24}(s_{(24)}) - \left((a'_{25})^{(4)} + (a''_{25})^{(4)} (T_{25}(s_{(24)}), s_{(24)}) \right) G_{25}(s_{(24)}) \right] ds_{(24)} \quad 241$$

$$\bar{G}_{26}(t) = G_{26}^0 + \int_0^t \left[(a_{26})^{(4)} G_{25}(s_{(24)}) - \left((a'_{26})^{(4)} + (a''_{26})^{(4)} (T_{25}(s_{(24)}), s_{(24)}) \right) G_{26}(s_{(24)}) \right] ds_{(24)} \quad 242$$

$$\bar{T}_{24}(t) = T_{24}^0 + \int_0^t \left[(b_{24})^{(4)} T_{25}(s_{(24)}) - \left((b'_{24})^{(4)} - (b''_{24})^{(4)} (G(s_{(24)}), s_{(24)}) \right) T_{24}(s_{(24)}) \right] ds_{(24)} \quad 243$$

$$\bar{T}_{25}(t) = T_{25}^0 + \int_0^t \left[(b_{25})^{(4)} T_{24}(s_{(24)}) - \left((b'_{25})^{(4)} - (b''_{25})^{(4)} (G(s_{(24)}), s_{(24)}) \right) T_{25}(s_{(24)}) \right] ds_{(24)} \quad 243$$

$$\bar{T}_{26}(t) = T_{26}^0 + \int_0^t \left[(b_{26})^{(4)} T_{25}(s_{(24)}) - \left((b'_{26})^{(4)} - (b''_{26})^{(4)} (G(s_{(24)}), s_{(24)}) \right) T_{26}(s_{(24)}) \right] ds_{(24)} \quad 244$$

Where $s_{(24)}$ is the integrand that is integrated over an interval $(0, t)$

Consider operator $\mathcal{A}^{(5)}$ defined on the space of sextuples of continuous functions $G_i, T_i: \mathbb{R}_+ \rightarrow \mathbb{R}_+$ which satisfy 245
246

$$G_i(0) = G_i^0, T_i(0) = T_i^0, G_i^0 \leq (\hat{P}_{28})^{(5)}, T_i^0 \leq (\hat{Q}_{28})^{(5)}, \quad 247$$

$$0 \leq G_i(t) - G_i^0 \leq (\hat{P}_{28})^{(5)} e^{(\hat{M}_{28})^{(5)}t} \quad 248$$

$$0 \leq T_i(t) - T_i^0 \leq (\hat{Q}_{28})^{(5)} e^{(\hat{M}_{28})^{(5)}t} \quad 249$$

By 250

$$\bar{G}_{28}(t) = G_{28}^0 + \int_0^t \left[(a_{28})^{(5)} G_{29}(s_{(28)}) - \left((a'_{28})^{(5)} + a''_{28}(T_{29}(s_{(28)}), s_{(28)}) \right) G_{28}(s_{(28)}) \right] ds_{(28)} \quad 251$$

$$\bar{G}_{29}(t) = G_{29}^0 + \int_0^t \left[(a_{29})^{(5)} G_{28}(s_{(28)}) - \left((a'_{29})^{(5)} + (a''_{29})^{(5)} (T_{29}(s_{(28)}), s_{(28)}) \right) G_{29}(s_{(28)}) \right] ds_{(28)} \quad 252$$

$$\bar{G}_{30}(t) = G_{30}^0 + \int_0^t \left[(a_{30})^{(5)} G_{29}(s_{(28)}) - \left((a'_{30})^{(5)} + (a''_{30})^{(5)} (T_{29}(s_{(28)}), s_{(28)}) \right) G_{30}(s_{(28)}) \right] ds_{(28)} \quad 253$$

$$\bar{T}_{28}(t) = T_{28}^0 + \int_0^t \left[(b_{28})^{(5)} T_{29}(s_{(28)}) - \left((b'_{28})^{(5)} - (b''_{28})^{(5)} (G(s_{(28)}), s_{(28)}) \right) T_{28}(s_{(28)}) \right] ds_{(28)} \quad 254$$

$$\bar{T}_{29}(t) = T_{29}^0 + \int_0^t \left[(b_{29})^{(5)} T_{28}(s_{(28)}) - \left((b'_{29})^{(5)} - (b''_{29})^{(5)} (G(s_{(28)}), s_{(28)}) \right) T_{29}(s_{(28)}) \right] ds_{(28)} \quad 255$$

$$\bar{T}_{30}(t) = T_{30}^0 + \int_0^t \left[(b_{30})^{(5)} T_{29}(s_{(28)}) - \left((b'_{30})^{(5)} - (b''_{30})^{(5)} (G(s_{(28)}), s_{(28)}) \right) T_{30}(s_{(28)}) \right] ds_{(28)} \quad 256$$

Where $s_{(28)}$ is the integrand that is integrated over an interval $(0, t)$ 257

Consider operator $\mathcal{A}^{(6)}$ defined on the space of sextuples of continuous functions $G_i, T_i: \mathbb{R}_+ \rightarrow \mathbb{R}_+$ which satisfy

$$G_i(0) = G_i^0, T_i(0) = T_i^0, G_i^0 \leq (\hat{P}_{32})^{(6)}, T_i^0 \leq (\hat{Q}_{32})^{(6)}, \quad 258$$

$$0 \leq G_i(t) - G_i^0 \leq (\hat{P}_{32})^{(6)} e^{(\hat{M}_{32})^{(6)}t} \quad 259$$

$$0 \leq T_i(t) - T_i^0 \leq (\hat{Q}_{32})^{(6)} e^{(\hat{M}_{32})^{(6)}t} \quad 260$$

By 261

$$\bar{G}_{32}(t) = G_{32}^0 + \int_0^t \left[(a_{32})^{(6)} G_{33}(s_{(32)}) - \left((a'_{32})^{(6)} + a''_{32}(T_{33}(s_{(32)}), s_{(32)}) \right) G_{32}(s_{(32)}) \right] ds_{(32)} \quad 262$$

$$\bar{G}_{33}(t) = G_{33}^0 + \int_0^t \left[(a_{33})^{(6)} G_{32}(s_{(32)}) - \left((a'_{33})^{(6)} + (a''_{33})^{(6)} (T_{33}(s_{(32)}), s_{(32)}) \right) G_{33}(s_{(32)}) \right] ds_{(32)} \quad 263$$

$$\bar{G}_{34}(t) = G_{34}^0 + \int_0^t \left[(a_{34})^{(6)} G_{33}(s_{(32)}) - \left((a'_{34})^{(6)} + (a''_{34})^{(6)} (T_{33}(s_{(32)}), s_{(32)}) \right) G_{34}(s_{(32)}) \right] ds_{(32)} \quad 264$$

$$\bar{T}_{32}(t) = T_{32}^0 + \int_0^t \left[(b_{32})^{(6)} T_{33}(s_{(32)}) - \left((b'_{32})^{(6)} - (b''_{32})^{(6)} (G(s_{(32)}), s_{(32)}) \right) T_{32}(s_{(32)}) \right] ds_{(32)} \quad 265$$

$$\bar{T}_{33}(t) = T_{33}^0 + \int_0^t \left[(b_{33})^{(6)} T_{32}(s_{(32)}) - \left((b'_{33})^{(6)} - (b''_{33})^{(6)} (G(s_{(32)}), s_{(32)}) \right) T_{33}(s_{(32)}) \right] ds_{(32)} \quad 266$$

$$\bar{T}_{34}(t) = T_{34}^0 + \int_0^t \left[(b_{34})^{(6)} T_{33}(s_{(32)}) - \left((b'_{34})^{(6)} - (b''_{34})^{(6)} (G(s_{(32)}), s_{(32)}) \right) T_{34}(s_{(32)}) \right] ds_{(32)} \quad 266$$

Where $s_{(32)}$ is the integrand that is integrated over an interval $(0, t)$ 267

(a) The operator $\mathcal{A}^{(1)}$ maps the space of functions satisfying into itself .Indeed it is obvious that 268

$$G_{13}(t) \leq G_{13}^0 + \int_0^t \left[(a_{13})^{(1)} \left(G_{14}^0 + (\hat{P}_{13})^{(1)} e^{(\hat{M}_{13})^{(1)}s_{(13)}} \right) \right] ds_{(13)} =$$

$$\left(1 + (a_{13})^{(1)}t \right) G_{14}^0 + \frac{(a_{13})^{(1)}(\hat{P}_{13})^{(1)}}{(\hat{M}_{13})^{(1)}} \left(e^{(\hat{M}_{13})^{(1)}t} - 1 \right)$$

From which it follows that 269

$$(G_{13}(t) - G_{13}^0) e^{-(\hat{M}_{13})^{(1)}t} \leq \frac{(a_{13})^{(1)}}{(\hat{M}_{13})^{(1)}} \left[\left((\hat{P}_{13})^{(1)} + G_{14}^0 \right) e^{\left(-\frac{(\hat{P}_{13})^{(1)} + G_{14}^0}{\hat{M}_{13}^{(1)}} \right)t} + (\hat{P}_{13})^{(1)} \right]$$

(G_i^0) is as defined in the statement of theorem 1

Analogous inequalities hold also for $G_{14}, G_{15}, T_{13}, T_{14}, T_{15}$ 270

(b) The operator $\mathcal{A}^{(2)}$ maps the space of functions satisfying into itself .Indeed it is obvious that 271

$$G_{16}(t) \leq G_{16}^0 + \int_0^t \left[(a_{16})^{(2)} \left(G_{17}^0 + (\hat{P}_{16})^{(2)} e^{(\hat{M}_{16})^{(2)}s_{(16)}} \right) \right] ds_{(16)} = \quad 272$$

$$\left(1 + (a_{16})^{(2)}t \right) G_{17}^0 + \frac{(a_{16})^{(2)}(\hat{P}_{16})^{(2)}}{(\hat{M}_{16})^{(2)}} \left(e^{(\hat{M}_{16})^{(2)}t} - 1 \right)$$

From which it follows that 273

$$(G_{16}(t) - G_{16}^0) e^{-(\hat{M}_{16})^{(2)}t} \leq \frac{(a_{16})^{(2)}}{(\hat{M}_{16})^{(2)}} \left[\left((\hat{P}_{16})^{(2)} + G_{17}^0 \right) e^{\left(-\frac{(\hat{P}_{16})^{(2)} + G_{17}^0}{\hat{M}_{16}^{(2)}} \right)t} + (\hat{P}_{16})^{(2)} \right]$$

Analogous inequalities hold also for $G_{17}, G_{18}, T_{16}, T_{17}, T_{18}$ 274

(a) The operator $\mathcal{A}^{(3)}$ maps the space of functions satisfying into itself .Indeed it is obvious that 275

$$G_{20}(t) \leq G_{20}^0 + \int_0^t \left[(a_{20})^{(3)} \left(G_{21}^0 + (\hat{P}_{20})^{(3)} e^{(\hat{M}_{20})^{(3)}s_{(20)}} \right) \right] ds_{(20)} =$$

$$\left(1 + (a_{20})^{(3)}t \right) G_{21}^0 + \frac{(a_{20})^{(3)}(\hat{P}_{20})^{(3)}}{(\hat{M}_{20})^{(3)}} \left(e^{(\hat{M}_{20})^{(3)}t} - 1 \right)$$

From which it follows that

$$(G_{20}(t) - G_{20}^0)e^{-(M_{20})^{(3)}t} \leq \frac{(a_{20})^{(3)}}{(M_{20})^{(3)}} \left[((\hat{P}_{20})^{(3)} + G_{21}^0)e^{-\frac{(\hat{P}_{20})^{(3)} + G_{21}^0}{G_{21}^0}} + (\hat{P}_{20})^{(3)} \right] \quad 276$$

Analogous inequalities hold also for $G_{21}, G_{22}, T_{20}, T_{21}, T_{22}$ 278

(b) The operator $\mathcal{A}^{(4)}$ maps the space of functions satisfying into itself. Indeed it is obvious that 279

$$G_{24}(t) \leq G_{24}^0 + \int_0^t \left[(a_{24})^{(4)} \left(G_{25}^0 + (\hat{P}_{24})^{(4)} e^{(M_{24})^{(4)}s} \right) \right] ds_{(24)} =$$

$$(1 + (a_{24})^{(4)}t)G_{25}^0 + \frac{(a_{24})^{(4)}(\hat{P}_{24})^{(4)}}{(M_{24})^{(4)}} \left(e^{(M_{24})^{(4)}t} - 1 \right)$$

From which it follows that

$$(G_{24}(t) - G_{24}^0)e^{-(M_{24})^{(4)}t} \leq \frac{(a_{24})^{(4)}}{(M_{24})^{(4)}} \left[((\hat{P}_{24})^{(4)} + G_{25}^0)e^{-\frac{(\hat{P}_{24})^{(4)} + G_{25}^0}{G_{25}^0}} + (\hat{P}_{24})^{(4)} \right] \quad 280$$

(G_i^0) is as defined in the statement of theorem 4

(c) The operator $\mathcal{A}^{(5)}$ maps the space of functions satisfying 35,35,36 into itself. Indeed it is obvious that 281

$$G_{28}(t) \leq G_{28}^0 + \int_0^t \left[(a_{28})^{(5)} \left(G_{29}^0 + (\hat{P}_{28})^{(5)} e^{(M_{28})^{(5)}s} \right) \right] ds_{(28)} =$$

$$(1 + (a_{28})^{(5)}t)G_{29}^0 + \frac{(a_{28})^{(5)}(\hat{P}_{28})^{(5)}}{(M_{28})^{(5)}} \left(e^{(M_{28})^{(5)}t} - 1 \right)$$

From which it follows that

$$(G_{28}(t) - G_{28}^0)e^{-(M_{28})^{(5)}t} \leq \frac{(a_{28})^{(5)}}{(M_{28})^{(5)}} \left[((\hat{P}_{28})^{(5)} + G_{29}^0)e^{-\frac{(\hat{P}_{28})^{(5)} + G_{29}^0}{G_{29}^0}} + (\hat{P}_{28})^{(5)} \right] \quad 282$$

(G_i^0) is as defined in the statement of theorem 1

(d) The operator $\mathcal{A}^{(6)}$ maps the space of functions satisfying 34,35,36 into itself. Indeed it is obvious that 283

$$G_{32}(t) \leq G_{32}^0 + \int_0^t \left[(a_{32})^{(6)} \left(G_{33}^0 + (\hat{P}_{32})^{(6)} e^{(M_{32})^{(6)}s} \right) \right] ds_{(32)} =$$

$$(1 + (a_{32})^{(6)}t)G_{33}^0 + \frac{(a_{32})^{(6)}(\hat{P}_{32})^{(6)}}{(M_{32})^{(6)}} \left(e^{(M_{32})^{(6)}t} - 1 \right)$$

From which it follows that

$$(G_{32}(t) - G_{32}^0)e^{-(M_{32})^{(6)}t} \leq \frac{(a_{32})^{(6)}}{(M_{32})^{(6)}} \left[((\hat{P}_{32})^{(6)} + G_{33}^0)e^{-\frac{(\hat{P}_{32})^{(6)} + G_{33}^0}{G_{33}^0}} + (\hat{P}_{32})^{(6)} \right] \quad 284$$

(G_i^0) is as defined in the statement of theorem 1

Analogous inequalities hold also for $G_{25}, G_{26}, T_{24}, T_{25}, T_{26}$

It is now sufficient to take $\frac{(a_i)^{(1)}}{(M_{13})^{(1)}}, \frac{(b_i)^{(1)}}{(M_{13})^{(1)}} < 1$ and to choose

$(\hat{P}_{13})^{(1)}$ and $(\hat{Q}_{13})^{(1)}$ large to have

$$\frac{(a_i)^{(1)}}{(M_{13})^{(1)}} \left[(\hat{P}_{13})^{(1)} + \left((\hat{P}_{13})^{(1)} + G_j^0 \right) e^{-\frac{(\hat{P}_{13})^{(1)} + G_j^0}{G_j^0}} \right] \leq (\hat{P}_{13})^{(1)} \quad 288$$

$$\frac{(b_i)^{(1)}}{(M_{13})^{(1)}} \left[((\hat{Q}_{13})^{(1)} + T_j^0) e^{-\frac{(\hat{Q}_{13})^{(1)} + T_j^0}{T_j^0}} + (\hat{Q}_{13})^{(1)} \right] \leq (\hat{Q}_{13})^{(1)} \quad 289$$

In order that the operator $\mathcal{A}^{(1)}$ transforms the space of sextuples of functions G_i, T_i into itself

The operator $\mathcal{A}^{(1)}$ is a contraction with respect to the metric

$$d\left((G^{(1)}, T^{(1)}), (G^{(2)}, T^{(2)}) \right) =$$

$$\sup_i \left\{ \max_{t \in \mathbb{R}_+} |G_i^{(1)}(t) - G_i^{(2)}(t)| e^{-(M_{13})^{(1)}t}, \max_{t \in \mathbb{R}_+} |T_i^{(1)}(t) - T_i^{(2)}(t)| e^{-(M_{13})^{(1)}t} \right\}$$

Indeed if we denote

Definition of \tilde{G}, \tilde{T} :

$$(\tilde{G}, \tilde{T}) = \mathcal{A}^{(1)}(G, T)$$

It results

$$|\tilde{G}_{13}^{(1)} - \tilde{G}_i^{(2)}| \leq \int_0^t (a_{13})^{(1)} |G_{14}^{(1)} - G_{14}^{(2)}| e^{-(M_{13})^{(1)}s} e^{(M_{13})^{(1)}s} ds_{(13)} +$$

$$\int_0^t \left\{ (a_{13})^{(1)} |G_{13}^{(1)} - G_{13}^{(2)}| e^{-(M_{13})^{(1)}s} e^{-(M_{13})^{(1)}s} + \right.$$

$$(a_{13}'')^{(1)}(T_{14}^{(1)}, s_{(13)}) |G_{13}^{(1)} - G_{13}^{(2)}| e^{-(M_{13})^{(1)}s} e^{(M_{13})^{(1)}s} +$$

$$\left. G_{13}^{(2)} |(a_{13}'')^{(1)}(T_{14}^{(1)}, s_{(13)}) - (a_{13}'')^{(1)}(T_{14}^{(2)}, s_{(13)})| e^{-(M_{13})^{(1)}s} e^{(M_{13})^{(1)}s} \right\} ds_{(13)}$$

Where $s_{(13)}$ represents integrand that is integrated over the interval $[0, t]$

From the hypotheses it follows

$$|G^{(1)} - G^{(2)}| e^{-(\widehat{M}_{13})^{(1)}t} \leq \frac{1}{(\widehat{M}_{13})^{(1)}} ((a_{13})^{(1)} + (a'_{13})^{(1)} + (\widehat{A}_{13})^{(1)} + (\widehat{P}_{13})^{(1)}(\widehat{k}_{13})^{(1)}) d((G^{(1)}, T^{(1)}; G^{(2)}, T^{(2)})) \quad 293$$

And analogous inequalities for G_i and T_i . Taking into account the result follows

Remark 1: The fact that we supposed $(a''_{13})^{(1)}$ and $(b''_{13})^{(1)}$ depending also on t can be considered as not conformal with the reality, however we have put this hypothesis, in order that we can postulate condition necessary to prove the uniqueness of the solution bounded by $(\widehat{P}_{13})^{(1)} e^{(\widehat{M}_{13})^{(1)}t}$ and $(\widehat{Q}_{13})^{(1)} e^{(\widehat{M}_{13})^{(1)}t}$ respectively of \mathbb{R}_+ . 294

If instead of proving the existence of the solution on \mathbb{R}_+ , we have to prove it only on a compact then it suffices to consider that $(a''_i)^{(1)}$ and $(b''_i)^{(1)}$, $i = 13, 14, 15$ depend only on T_{14} and respectively on G (and not on t) and hypothesis can be replaced by a usual Lipschitz condition.

Remark 2: There does not exist any t where $G_i(t) = 0$ and $T_i(t) = 0$ 295

From the governing equations of the holistic system it results

$$G_i(t) \geq G_i^0 e^{-\int_0^t \{(a'_i)^{(1)} - (a''_i)^{(1)}(T_{14}(s_{(13)}), s_{(13)})\} ds_{(13)}} \geq 0$$

$$T_i(t) \geq T_i^0 e^{-(b'_i)^{(1)}t} > 0 \text{ for } t > 0$$

Definition of $((\widehat{M}_{13})^{(1)})_1, ((\widehat{M}_{13})^{(1)})_2$ and $((\widehat{M}_{13})^{(1)})_3$: 296

Remark 3: if G_{13} is bounded, the same property have also G_{14} and G_{15} . indeed if

$G_{13} < (\widehat{M}_{13})^{(1)}$ it follows $\frac{dG_{14}}{dt} \leq ((\widehat{M}_{13})^{(1)})_1 - (a'_{14})^{(1)}G_{14}$ and by integrating

$$G_{14} \leq ((\widehat{M}_{13})^{(1)})_2 = G_{14}^0 + 2(a_{14})^{(1)}((\widehat{M}_{13})^{(1)})_1 / (a'_{14})^{(1)}$$

In the same way, one can obtain

$$G_{15} \leq ((\widehat{M}_{13})^{(1)})_3 = G_{15}^0 + 2(a_{15})^{(1)}((\widehat{M}_{13})^{(1)})_2 / (a'_{15})^{(1)}$$

If G_{14} or G_{15} is bounded, the same property follows for G_{13} , G_{15} and G_{13} , G_{14} respectively.

Remark 4: If G_{13} is bounded, from below, the same property holds for G_{14} and G_{15} . The proof is analogous with the preceding one. An analogous property is true if G_{14} is bounded from below. 297

Remark 5: If T_{13} is bounded from below and $\lim_{t \rightarrow \infty} ((b''_i)^{(1)}(G(t), t)) = (b'_{14})^{(1)}$ then $T_{14} \rightarrow \infty$. 298

Definition of $(m)^{(1)}$ and ε_1 :

Indeed let t_1 be so that for $t > t_1$

$$(b_{14})^{(1)} - (b''_i)^{(1)}(G(t), t) < \varepsilon_1, T_{13}(t) > (m)^{(1)}$$

Then $\frac{dT_{14}}{dt} \geq (a_{14})^{(1)}(m)^{(1)} - \varepsilon_1 T_{14}$ which leads to 299

$$T_{14} \geq \left(\frac{(a_{14})^{(1)}(m)^{(1)}}{\varepsilon_1} \right) (1 - e^{-\varepsilon_1 t}) + T_{14}^0 e^{-\varepsilon_1 t} \text{ If we take } t \text{ such that } e^{-\varepsilon_1 t} = \frac{1}{2} \text{ it results}$$

$T_{14} \geq \left(\frac{(a_{14})^{(1)}(m)^{(1)}}{2} \right)$, $t = \log \frac{2}{\varepsilon_1}$ By taking now ε_1 sufficiently small one sees that T_{14} is unbounded. The same property holds for T_{15} if $\lim_{t \rightarrow \infty} (b''_{15})^{(1)}(G(t), t) = (b'_{15})^{(1)}$

We now state a more precise theorem about the behaviors at infinity of the solutions of equations solution to the governing equations of the global system

It is now sufficient to take $\frac{(a_i)^{(2)}}{(\widehat{M}_{16})^{(2)}}, \frac{(b_i)^{(2)}}{(\widehat{M}_{16})^{(2)}} < 1$ and to choose 300
301

$(\widehat{P}_{16})^{(2)}$ and $(\widehat{Q}_{16})^{(2)}$ large to have

$$\frac{(a_i)^{(2)}}{(\widehat{M}_{16})^{(2)}} \left[(\widehat{P}_{16})^{(2)} + ((\widehat{P}_{16})^{(2)} + G_j^0) e^{-\left(\frac{(\widehat{P}_{16})^{(2)} + G_j^0}{G_j^0} \right)} \right] \leq (\widehat{P}_{16})^{(2)} \quad 302$$

$$\frac{(b_i)^{(2)}}{(\widehat{M}_{16})^{(2)}} \left[((\widehat{Q}_{16})^{(2)} + T_j^0) e^{-\left(\frac{(\widehat{Q}_{16})^{(2)} + T_j^0}{T_j^0} \right)} + (\widehat{Q}_{16})^{(2)} \right] \leq (\widehat{Q}_{16})^{(2)} \quad 303$$

In order that the operator $\mathcal{A}^{(2)}$ transforms the space of sextuples of functions G_i, T_i into itself 306

The operator $\mathcal{A}^{(2)}$ is a contraction with respect to the metric 307

$$d(((G_{19})^{(1)}, (T_{19})^{(1)}), ((G_{19})^{(2)}, (T_{19})^{(2)})) =$$

$$\sup_i \left\{ \max_{t \in \mathbb{R}_+} |G_i^{(1)}(t) - G_i^{(2)}(t)| e^{-(\widehat{M}_{16})^{(2)}t}, \max_{t \in \mathbb{R}_+} |T_i^{(1)}(t) - T_i^{(2)}(t)| e^{-(\widehat{M}_{16})^{(2)}t} \right\}$$

Indeed if we denote 308

Definition of $\widetilde{G}_{19}, \widetilde{T}_{19}$: $(\widetilde{G}_{19}, \widetilde{T}_{19}) = \mathcal{A}^{(2)}(G_{19}, T_{19})$

It results 309

$$|\widetilde{G}_{16}^{(1)} - \widetilde{G}_{16}^{(2)}| \leq \int_0^t (a_{16})^{(2)} |G_{17}^{(1)} - G_{17}^{(2)}| e^{-(\widehat{M}_{16})^{(2)}s_{(16)}} e^{(\widehat{M}_{16})^{(2)}s_{(16)}} ds_{(16)} +$$

$$\int_0^t \{ (a'_{16})^{(2)} |G_{16}^{(1)} - G_{16}^{(2)}| e^{-(\bar{M}_{16})^{(2)} s_{(16)}} e^{-(\bar{M}_{16})^{(2)} s_{(16)}} + (a''_{16})^{(2)} (T_{17}^{(1)}, s_{(16)}) |G_{16}^{(1)} - G_{16}^{(2)}| e^{-(\bar{M}_{16})^{(2)} s_{(16)}} e^{(\bar{M}_{16})^{(2)} s_{(16)}} + G_{16}^{(2)} | (a'_{16})^{(2)} (T_{17}^{(1)}, s_{(16)}) - (a''_{16})^{(2)} (T_{17}^{(2)}, s_{(16)}) | e^{-(\bar{M}_{16})^{(2)} s_{(16)}} e^{(\bar{M}_{16})^{(2)} s_{(16)}} \} ds_{(16)}$$

310

Where $s_{(16)}$ represents integrand that is integrated over the interval $[0, t]$
 From the hypotheses it follows

$$|(G_{19})^{(1)} - (G_{19})^{(2)}| e^{-(\bar{M}_{16})^{(2)} t} \leq \frac{1}{(\bar{M}_{16})^{(2)}} \left((a_{16})^{(2)} + (a'_{16})^{(2)} + (\hat{A}_{16})^{(2)} + (\hat{P}_{16})^{(2)} (\hat{k}_{16})^{(2)} \right) d \left(((G_{19})^{(1)}, (T_{19})^{(1)}), (G_{19})^{(2)}, (T_{19})^{(2)} \right)$$

311

And analogous inequalities for G_i and T_i . Taking into account the hypothesis (34,35,36) the result follows

312

Remark 1: The fact that we supposed $(a'_{16})^{(2)}$ and $(b''_{16})^{(2)}$ depending also on t can be considered as not conformal with the reality, however we have put this hypothesis, in order that we can postulate condition necessary to prove the uniqueness of the solution bounded by $(\hat{P}_{16})^{(2)} e^{(\bar{M}_{16})^{(2)} t}$ and $(\hat{Q}_{16})^{(2)} e^{(\bar{M}_{16})^{(2)} t}$ respectively of \mathbb{R}_+ .

If instead of proving the existence of the solution on \mathbb{R}_+ , we have to prove it only on a compact then it suffices to consider that $(a_i)^{(2)}$ and $(b_i)^{(2)}$, $i = 16, 17, 18$ depend only on T_{17} and respectively on (G_{19}) (and not on t) and hypothesis can be replaced by a usual Lipschitz condition.

Remark 2: There does not exist any t where $G_i(t) = 0$ and $T_i(t) = 0$
 From 19 to 24 it results

314

$$G_i(t) \geq G_i^0 e^{-\int_0^t \{ (a_i)^{(2)} - (a_i)^{(2)} (T_{17}(s_{(16)}), s_{(16)}) \} ds_{(16)}} \geq 0$$

$$T_i(t) \geq T_i^0 e^{-(b_i)^{(2)} t} > 0 \quad \text{for } t > 0$$

Definition of $((\bar{M}_{16})^{(2)})_1$, $((\bar{M}_{16})^{(2)})_2$ and $((\bar{M}_{16})^{(2)})_3$:

315

Remark 3: if G_{16} is bounded, the same property have also G_{17} and G_{18} . indeed if $G_{16} < ((\bar{M}_{16})^{(2)})$ it follows $\frac{dG_{17}}{dt} \leq ((\bar{M}_{16})^{(2)})_1 - (a'_{17})^{(2)} G_{17}$ and by integrating $G_{17} \leq ((\bar{M}_{16})^{(2)})_2 = G_{17}^0 + 2(a_{17})^{(2)} ((\bar{M}_{16})^{(2)})_1 / (a'_{17})^{(2)}$

In the same way, one can obtain $G_{18} \leq ((\bar{M}_{16})^{(2)})_3 = G_{18}^0 + 2(a_{18})^{(2)} ((\bar{M}_{16})^{(2)})_2 / (a'_{18})^{(2)}$

If G_{17} or G_{18} is bounded, the same property follows for G_{16} , G_{18} and G_{16} , G_{17} respectively.
Remark 4: If G_{16} is bounded, from below, the same property holds for G_{17} and G_{18} . The proof is analogous with the preceding one. An analogous property is true if G_{17} is bounded from below.

316

Remark 5: If T_{16} is bounded from below and $\lim_{t \rightarrow \infty} ((b_i)^{(2)} ((G_{19})(t), t)) = (b'_{17})^{(2)}$ then $T_{17} \rightarrow \infty$.

317

Definition of $(m)^{(2)}$ and ε_2 :
 Indeed let t_2 be so that for $t > t_2$
 $(b_{17})^{(2)} - (b_i)^{(2)} ((G_{19})(t), t) < \varepsilon_2$, $T_{16}(t) > (m)^{(2)}$
 Then $\frac{dT_{17}}{dt} \geq (a_{17})^{(2)} (m)^{(2)} - \varepsilon_2 T_{17}$ which leads to

318

$$T_{17} \geq \left(\frac{(a_{17})^{(2)} (m)^{(2)}}{\varepsilon_2} \right) (1 - e^{-\varepsilon_2 t}) + T_{17}^0 e^{-\varepsilon_2 t} \quad \text{If we take } t \text{ such that } e^{-\varepsilon_2 t} = \frac{1}{2} \text{ it results}$$

$$T_{17} \geq \left(\frac{(a_{17})^{(2)} (m)^{(2)}}{2} \right), \quad t = \log \frac{2}{\varepsilon_2} \quad \text{By taking now } \varepsilon_2 \text{ sufficiently small one sees that } T_{17} \text{ is unbounded. The same property holds for } T_{18} \text{ if } \lim_{t \rightarrow \infty} (b''_{18})^{(2)} ((G_{19})(t), t) = (b'_{18})^{(2)}$$

319

We now state a more precise theorem about the behaviors at infinity of the solutions of equations 37 to 42

320

It is now sufficient to take $\frac{(a_i)^{(3)}}{(\bar{M}_{20})^{(3)}} , \frac{(b_i)^{(3)}}{(\bar{M}_{20})^{(3)}} < 1$ and to choose

321

$(\hat{P}_{20})^{(3)}$ and $(\hat{Q}_{20})^{(3)}$ large to have

$$\frac{(a_i)^{(3)}}{(\bar{M}_{20})^{(3)}} \left[(\hat{P}_{20})^{(3)} + ((\hat{P}_{20})^{(3)} + G_j^0) e^{-\left(\frac{(\hat{P}_{20})^{(3)} + G_j^0}{G_j^0} \right)} \right] \leq (\hat{P}_{20})^{(3)}$$

322

$$\frac{(b_i)^{(3)}}{(\bar{M}_{20})^{(3)}} \left[((\hat{Q}_{20})^{(3)} + T_j^0) e^{-\left(\frac{(\hat{Q}_{20})^{(3)} + T_j^0}{T_j^0} \right)} + (\hat{Q}_{20})^{(3)} \right] \leq (\hat{Q}_{20})^{(3)}$$

323

In order that the operator $\mathcal{A}^{(3)}$ transforms the space of sextuples of functions G_i, T_i into itself
 The operator $\mathcal{A}^{(3)}$ is a contraction with respect to the metric

324

$$d \left(((G_{23})^{(1)}, (T_{23})^{(1)}), ((G_{23})^{(2)}, (T_{23})^{(2)}) \right) = \sup_i \{ \max_{t \in \mathbb{R}_+} |G_i^{(1)}(t) - G_i^{(2)}(t)| e^{-(\bar{M}_{20})^{(3)} t}, \max_{t \in \mathbb{R}_+} |T_i^{(1)}(t) - T_i^{(2)}(t)| e^{-(\bar{M}_{20})^{(3)} t} \}$$

Indeed if we denote

Definition of $\widetilde{G}_{23}, \widetilde{T}_{23} : ((\widetilde{G}_{23}), (\widetilde{T}_{23})) = \mathcal{A}^{(3)}((G_{23}), (T_{23}))$

326

It results

$$|\widetilde{G}_{20}^{(1)} - \widetilde{G}_i^{(2)}| \leq \int_0^t (a_{20})^{(3)} |G_{21}^{(1)} - G_{21}^{(2)}| e^{-(\overline{M}_{20})^{(3)}s_{(20)}} e^{(\overline{M}_{20})^{(3)}s_{(20)}} ds_{(20)} + \int_0^t \{(a'_{20})^{(3)} |G_{20}^{(1)} - G_{20}^{(2)}| e^{-(\overline{M}_{20})^{(3)}s_{(20)}} e^{-(\overline{M}_{20})^{(3)}s_{(20)}} + (a''_{20})^{(3)} (T_{21}^{(1)}, s_{(20)}) |G_{20}^{(1)} - G_{20}^{(2)}| e^{-(\overline{M}_{20})^{(3)}s_{(20)}} e^{(\overline{M}_{20})^{(3)}s_{(20)}} + G_{20}^{(2)} |(a''_{20})^{(3)} (T_{21}^{(1)}, s_{(20)}) - (a''_{20})^{(3)} (T_{21}^{(2)}, s_{(20)})| e^{-(\overline{M}_{20})^{(3)}s_{(20)}} e^{(\overline{M}_{20})^{(3)}s_{(20)}}\} ds_{(20)}$$

327

Where $s_{(20)}$ represents integrand that is integrated over the interval $[0, t]$

From the hypotheses it follows

$$|G^{(1)} - G^{(2)}| e^{-(\overline{M}_{20})^{(3)}t} \leq \frac{1}{(\overline{M}_{20})^{(3)}} ((a_{20})^{(3)} + (a'_{20})^{(3)} + (\widehat{A}_{20})^{(3)} + (\widehat{P}_{20})^{(3)} (\widehat{k}_{20})^{(3)}) d(((G_{23})^{(1)}, (T_{23})^{(1)}); (G_{23})^{(2)}, (T_{23})^{(2)}))$$

328

And analogous inequalities for G_i and T_i . Taking into account the hypothesis the result follows

Remark 1: The fact that we supposed $(a''_{20})^{(3)}$ and $(b''_{20})^{(3)}$ depending also on t can be considered as not conformal with the reality, however we have put this hypothesis in order that we can postulate condition necessary to prove the uniqueness of the solution bounded by $(\widehat{P}_{20})^{(3)} e^{(\overline{M}_{20})^{(3)}t}$ and $(\widehat{Q}_{20})^{(3)} e^{(\overline{M}_{20})^{(3)}t}$ respectively of \mathbb{R}_+ .

329

If instead of proving the existence of the solution on \mathbb{R}_+ , we have to prove it only on a compact then it suffices to consider that $(a''_i)^{(3)}$ and $(b''_i)^{(3)}$, $i = 20, 21, 22$ depend only on T_{21} and respectively on (G_{23}) (and not on t) and hypothesis can be replaced by a usual Lipschitz condition.

Remark 2: There does not exist any t where $G_i(t) = 0$ and $T_i(t) = 0$

330

From 19 to 24 it results

$$G_i(t) \geq G_i^0 e^{-\int_0^t \{(a'_i)^{(3)} - (a''_i)^{(3)}\} (T_{21}(s_{(20)}), s_{(20)}) ds_{(20)}} \geq 0$$

$$T_i(t) \geq T_i^0 e^{-(b'_i)^{(3)}t} > 0 \text{ for } t > 0$$

Definition of $((\widehat{M}_{20})^{(3)})_1, ((\widehat{M}_{20})^{(3)})_2$ and $((\widehat{M}_{20})^{(3)})_3$:

331

Remark 3: if G_{20} is bounded, the same property have also G_{21} and G_{22} . indeed if

$G_{20} < (\widehat{M}_{20})^{(3)}$ it follows $\frac{dG_{21}}{dt} \leq ((\widehat{M}_{20})^{(3)})_1 - (a'_{21})^{(3)} G_{21}$ and by integrating

$$G_{21} \leq ((\widehat{M}_{20})^{(3)})_2 = G_{21}^0 + 2(a_{21})^{(3)} ((\widehat{M}_{20})^{(3)})_1 / (a'_{21})^{(3)}$$

332

In the same way, one can obtain

$$G_{22} \leq ((\widehat{M}_{20})^{(3)})_3 = G_{22}^0 + 2(a_{22})^{(3)} ((\widehat{M}_{20})^{(3)})_2 / (a'_{22})^{(3)}$$

If G_{21} or G_{22} is bounded, the same property follows for G_{20} , G_{22} and G_{20} , G_{21} respectively.

Remark 4: If G_{20} is bounded, from below, the same property holds for G_{21} and G_{22} . The proof is analogous with the preceding one. An analogous property is true if G_{21} is bounded from below.

333

Remark 5: If T_{20} is bounded from below and $\lim_{t \rightarrow \infty} ((b'_i)^{(3)} ((G_{23})(t), t)) = (b'_{21})^{(3)}$ then $T_{21} \rightarrow \infty$.

334

Definition of $(m)^{(3)}$ and ε_3 :

Indeed let t_3 be so that for $t > t_3$

$$(b_{21})^{(3)} - (b'_i)^{(3)} ((G_{23})(t), t) < \varepsilon_3, T_{20}(t) > (m)^{(3)}$$

Then $\frac{dT_{21}}{dt} \geq (a_{21})^{(3)} (m)^{(3)} - \varepsilon_3 T_{21}$ which leads to

335

$$T_{21} \geq \left(\frac{(a_{21})^{(3)} (m)^{(3)}}{\varepsilon_3} \right) (1 - e^{-\varepsilon_3 t}) + T_{21}^0 e^{-\varepsilon_3 t} \text{ If we take } t \text{ such that } e^{-\varepsilon_3 t} = \frac{1}{2} \text{ it results}$$

$$T_{21} \geq \left(\frac{(a_{21})^{(3)} (m)^{(3)}}{2} \right), t = \log \frac{2}{\varepsilon_3} \text{ By taking now } \varepsilon_3 \text{ sufficiently small one sees that } T_{21} \text{ is unbounded. The same}$$

property holds for T_{22} if $\lim_{t \rightarrow \infty} ((b''_{22})^{(3)} ((G_{23})(t), t)) = (b'_{22})^{(3)}$

We now state a more precise theorem about the behaviors at infinity of the solutions:

336

It is now sufficient to take $\frac{(a_i)^{(4)}}{(\widehat{M}_{24})^{(4)}}, \frac{(b_i)^{(4)}}{(\widehat{M}_{24})^{(4)}} < 1$ and to choose

337

$(\widehat{P}_{24})^{(4)}$ and $(\widehat{Q}_{24})^{(4)}$ large to have

$$\frac{(a_i)^{(4)}}{(\widehat{M}_{24})^{(4)}} \left[(\widehat{P}_{24})^{(4)} + ((\widehat{P}_{24})^{(4)} + G_j^0) e^{-\left(\frac{(\widehat{P}_{24})^{(4)} + G_j^0}{G_j^0} \right)} \right] \leq (\widehat{P}_{24})^{(4)}$$

338

$$\frac{(b_i)^{(4)}}{(\widehat{M}_{24})^{(4)}} \left[((\widehat{Q}_{24})^{(4)} + T_j^0) e^{-\left(\frac{(\widehat{Q}_{24})^{(4)} + T_j^0}{T_j^0} \right)} + (\widehat{Q}_{24})^{(4)} \right] \leq (\widehat{Q}_{24})^{(4)}$$

339

In order that the operator $\mathcal{A}^{(4)}$ transforms the space of sextuples of functions G_i, T_i into itself 340

The operator $\mathcal{A}^{(4)}$ is a contraction with respect to the metric 341

$$d\left(\left((G_{27})^{(1)}, (T_{27})^{(1)}\right), \left((G_{27})^{(2)}, (T_{27})^{(2)}\right)\right) = \sup_{t \in \mathbb{R}_+} \left\{ \max_i |G_i^{(1)}(t) - G_i^{(2)}(t)| e^{-(\overline{M}_{24})^{(4)}t}, \max_i |T_i^{(1)}(t) - T_i^{(2)}(t)| e^{-(\overline{M}_{24})^{(4)}t} \right\}$$

Indeed if we denote 342

Definition of $(\overline{G_{27}}), (\overline{T_{27}}) : ((\overline{G_{27}}), (\overline{T_{27}})) = \mathcal{A}^{(4)}((G_{27}), (T_{27}))$

It results

$$\begin{aligned} |\overline{G_{24}}^{(1)} - \overline{G_{24}}^{(2)}| &\leq \int_0^t (a_{24})^{(4)} |G_{25}^{(1)} - G_{25}^{(2)}| e^{-(\overline{M}_{24})^{(4)}s_{(24)}} e^{(\overline{M}_{24})^{(4)}s_{(24)}} ds_{(24)} + \\ &\int_0^t \{ (a'_{24})^{(4)} |G_{24}^{(1)} - G_{24}^{(2)}| e^{-(\overline{M}_{24})^{(4)}s_{(24)}} e^{-(\overline{M}_{24})^{(4)}s_{(24)}} + \\ &(a''_{24})^{(4)} (T_{25}^{(1)}, s_{(24)}) |G_{24}^{(1)} - G_{24}^{(2)}| e^{-(\overline{M}_{24})^{(4)}s_{(24)}} e^{(\overline{M}_{24})^{(4)}s_{(24)}} + \\ &G_{24}^{(2)} | (a''_{24})^{(4)} (T_{25}^{(1)}, s_{(24)}) - (a''_{24})^{(4)} (T_{25}^{(2)}, s_{(24)}) | e^{-(\overline{M}_{24})^{(4)}s_{(24)}} e^{(\overline{M}_{24})^{(4)}s_{(24)}} \} ds_{(24)} \end{aligned}$$

Where $s_{(24)}$ represents integrand that is integrated over the interval $[0, t]$

From the hypotheses it follows

$$|(G_{27})^{(1)} - (G_{27})^{(2)}| e^{-(\overline{M}_{24})^{(4)}t} \leq \frac{1}{(\overline{M}_{24})^{(4)}} \left((a_{24})^{(4)} + (a'_{24})^{(4)} + (\widehat{A}_{24})^{(4)} + (\widehat{P}_{24})^{(4)} (\widehat{k}_{24})^{(4)} \right) d\left(\left((G_{27})^{(1)}, (T_{27})^{(1)}\right); (G_{27})^{(2)}, (T_{27})^{(2)}\right) \quad 343$$

And analogous inequalities for G_i and T_i . Taking into account the hypothesis the result follows

Remark 1: The fact that we supposed $(a''_{24})^{(4)}$ and $(b''_{24})^{(4)}$ depending also on t can be considered as not conformal with the reality, however we have put this hypothesis, in order that we can postulate condition necessary to prove the uniqueness of the solution bounded by $(\widehat{P}_{24})^{(4)} e^{(\overline{M}_{24})^{(4)}t}$ and $(\widehat{Q}_{24})^{(4)} e^{(\overline{M}_{24})^{(4)}t}$ respectively of \mathbb{R}_+ . 344

If instead of proving the existence of the solution on \mathbb{R}_+ , we have to prove it only on a compact then it suffices to consider that $(a''_i)^{(4)}$ and $(b''_i)^{(4)}$, $i = 24, 25, 26$ depend only on T_{25} and respectively on (G_{27}) (and not on t) and hypothesis can be replaced by a usual Lipschitz condition.

Remark 2: There does not exist any t where $G_i(t) = 0$ and $T_i(t) = 0$ 345

From 19 to 24 it results

$$G_i(t) \geq G_i^0 e^{-\int_0^t \{ (a'_i)^{(4)} - (a''_i)^{(4)} (T_{25}(s_{(24)}), s_{(24)}) \} ds_{(24)}} \geq 0$$

$$T_i(t) \geq T_i^0 e^{-(b'_i)^{(4)}t} > 0 \text{ for } t > 0$$

Definition of $((\overline{M}_{24})^{(4)})_1, ((\overline{M}_{24})^{(4)})_2$ and $((\overline{M}_{24})^{(4)})_3$: 346

Remark 3: if G_{24} is bounded, the same property have also G_{25} and G_{26} . indeed if

$$G_{24} < (\overline{M}_{24})^{(4)} \text{ it follows } \frac{dG_{25}}{dt} \leq ((\overline{M}_{24})^{(4)})_1 - (a'_{25})^{(4)} G_{25} \text{ and by integrating}$$

$$G_{25} \leq ((\overline{M}_{24})^{(4)})_2 = G_{25}^0 + 2(a_{25})^{(4)} ((\overline{M}_{24})^{(4)})_1 / (a'_{25})^{(4)}$$

In the same way, one can obtain

$$G_{26} \leq ((\overline{M}_{24})^{(4)})_3 = G_{26}^0 + 2(a_{26})^{(4)} ((\overline{M}_{24})^{(4)})_2 / (a'_{26})^{(4)}$$

If G_{25} or G_{26} is bounded, the same property follows for G_{24} , G_{26} and G_{24} , G_{25} respectively.

Remark 4: If G_{24} is bounded, from below, the same property holds for G_{25} and G_{26} . The proof is analogous with the preceding one. An analogous property is true if G_{25} is bounded from below. 347

Remark 5: If T_{24} is bounded from below and $\lim_{t \rightarrow \infty} ((b''_i)^{(4)}((G_{27})(t), t)) = (b'_{25})^{(4)}$ then $T_{25} \rightarrow \infty$. 348

Definition of $(m)^{(4)}$ and ε_4 :

Indeed let t_4 be so that for $t > t_4$

$$(b_{25})^{(4)} - (b''_i)^{(4)}((G_{27})(t), t) < \varepsilon_4, T_{24}(t) > (m)^{(4)}$$

Then $\frac{dT_{25}}{dt} \geq (a_{25})^{(4)}(m)^{(4)} - \varepsilon_4 T_{25}$ which leads to 349

$$T_{25} \geq \left(\frac{(a_{25})^{(4)}(m)^{(4)}}{\varepsilon_4} \right) (1 - e^{-\varepsilon_4 t}) + T_{25}^0 e^{-\varepsilon_4 t} \text{ If we take } t \text{ such that } e^{-\varepsilon_4 t} = \frac{1}{2} \text{ it results}$$

$$T_{25} \geq \left(\frac{(a_{25})^{(4)}(m)^{(4)}}{2} \right), \quad t = \log \frac{2}{\varepsilon_4} \text{ By taking now } \varepsilon_4 \text{ sufficiently small one sees that } T_{25} \text{ is unbounded. The same}$$

property holds for T_{26} if $\lim_{t \rightarrow \infty} (b''_{26})^{(4)}((G_{27})(t), t) = (b'_{26})^{(4)}$

We now state a more precise theorem about the behaviors at infinity of the solutions ;

Analogous inequalities hold also for $G_{29}, G_{30}, T_{28}, T_{29}, T_{30}$

350

It is now sufficient to take $\frac{(a_i)^{(5)}}{(\overline{M}_{28})^{(5)}}, \frac{(b_i)^{(5)}}{(\overline{M}_{28})^{(5)}} < 1$ and to choose $(\widehat{P}_{28})^{(5)}$ and $(\widehat{Q}_{28})^{(5)}$ large to have

351

$$\frac{(a_i)^{(5)}}{(\widehat{M}_{28})^{(5)}} \left[(\widehat{P}_{28})^{(5)} + ((\widehat{P}_{28})^{(5)} + G_j^0) e^{-\left(\frac{(\widehat{P}_{28})^{(5)} + G_j^0}{G_j^0}\right)} \right] \leq (\widehat{P}_{28})^{(5)} \tag{352}$$

$$\frac{(b_i)^{(5)}}{(\widehat{M}_{28})^{(5)}} \left[((\widehat{Q}_{28})^{(5)} + T_j^0) e^{-\left(\frac{(\widehat{Q}_{28})^{(5)} + T_j^0}{T_j^0}\right)} + (\widehat{Q}_{28})^{(5)} \right] \leq (\widehat{Q}_{28})^{(5)} \tag{353}$$

In order that the operator $\mathcal{A}^{(5)}$ transforms the space of sextuples of functions G_i, T_i into itself 354

The operator $\mathcal{A}^{(5)}$ is a contraction with respect to the metric 355

$$d \left(((G_{31})^{(1)}, (T_{31})^{(1)}), ((G_{31})^{(2)}, (T_{31})^{(2)}) \right) = \sup_i \left\{ \max_{t \in \mathbb{R}_+} |G_i^{(1)}(t) - G_i^{(2)}(t)| e^{-(\widehat{M}_{28})^{(5)}t}, \max_{t \in \mathbb{R}_+} |T_i^{(1)}(t) - T_i^{(2)}(t)| e^{-(\widehat{M}_{28})^{(5)}t} \right\}$$

Indeed if we denote **Definition of** $(\widehat{G}_{31}), (\widehat{T}_{31}) : ((\widehat{G}_{31}), (\widehat{T}_{31})) = \mathcal{A}^{(5)}((G_{31}), (T_{31}))$ 356

It results

$$\begin{aligned} |\widehat{G}_{28}^{(1)} - \widehat{G}_i^{(2)}| &\leq \int_0^t (a_{28})^{(5)} |G_{29}^{(1)} - G_{29}^{(2)}| e^{-(\widehat{M}_{28})^{(5)}s_{(28)}} e^{(\widehat{M}_{28})^{(5)}s_{(28)}} ds_{(28)} + \\ &\int_0^t \{ (a'_{28})^{(5)} |G_{28}^{(1)} - G_{28}^{(2)}| e^{-(\widehat{M}_{28})^{(5)}s_{(28)}} e^{-(\widehat{M}_{28})^{(5)}s_{(28)}} + \\ &(a''_{28})^{(5)} (T_{29}^{(1)}, s_{(28)}) |G_{28}^{(1)} - G_{28}^{(2)}| e^{-(\widehat{M}_{28})^{(5)}s_{(28)}} e^{(\widehat{M}_{28})^{(5)}s_{(28)}} + \\ &G_{28}^{(2)} |(a'_{28})^{(5)} (T_{29}^{(1)}, s_{(28)}) - (a'_{28})^{(5)} (T_{29}^{(2)}, s_{(28)})| e^{-(\widehat{M}_{28})^{(5)}s_{(28)}} e^{(\widehat{M}_{28})^{(5)}s_{(28)}} \} ds_{(28)} \end{aligned}$$

Where $s_{(28)}$ represents integrand that is integrated over the interval $[0, t]$

From the hypotheses it follows

$$\begin{aligned} |(G_{31})^{(1)} - (G_{31})^{(2)}| e^{-(\widehat{M}_{28})^{(5)}t} &\leq \\ \frac{1}{(\widehat{M}_{28})^{(5)}} \{ (a_{28})^{(5)} + (a'_{28})^{(5)} + (\widehat{A}_{28})^{(5)} + (\widehat{P}_{28})^{(5)} (\widehat{k}_{28})^{(5)} \} &d \left(((G_{31})^{(1)}, (T_{31})^{(1)}); (G_{31})^{(2)}, (T_{31})^{(2)} \right) \end{aligned} \tag{357}$$

And analogous inequalities for G_i and T_i . Taking into account the hypothesis (35,35,36) the result follows

Remark 1: The fact that we supposed $(a'_{28})^{(5)}$ and $(b'_{28})^{(5)}$ depending also on t can be considered as not conformal with the reality, however we have put this hypothesis, in order that we can postulate condition necessary to prove the uniqueness of the solution bounded by $(\widehat{P}_{28})^{(5)} e^{(\widehat{M}_{28})^{(5)}t}$ and $(\widehat{Q}_{28})^{(5)} e^{(\widehat{M}_{28})^{(5)}t}$ respectively of \mathbb{R}_+ . 358

If instead of proving the existence of the solution on \mathbb{R}_+ , we have to prove it only on a compact then it suffices to consider that $(a''_i)^{(5)}$ and $(b''_i)^{(5)}$, $i = 28, 29, 30$ depend only on T_{29} and respectively on (G_{31}) (and not on t) and hypothesis can be replaced by a usual Lipschitz condition.

Remark 2: There does not exist any t where $G_i(t) = 0$ and $T_i(t) = 0$ 359

$$G_i(t) \geq G_i^0 e^{-\int_0^t \{ (a'_i)^{(5)} - (a''_i)^{(5)} (T_{29}(s_{(28)}), s_{(28)}) \} ds_{(28)}} \geq 0$$

$$T_i(t) \geq T_i^0 e^{-(b'_i)^{(5)}t} > 0 \text{ for } t > 0$$

Definition of $((\widehat{M}_{28})^{(5)})_1, ((\widehat{M}_{28})^{(5)})_2$ and $((\widehat{M}_{28})^{(5)})_3 :$ 360

Remark 3: if G_{28} is bounded, the same property have also G_{29} and G_{30} . indeed if

$$G_{28} < (\widehat{M}_{28})^{(5)} \text{ it follows } \frac{dG_{29}}{dt} \leq ((\widehat{M}_{28})^{(5)})_1 - (a'_{29})^{(5)} G_{29} \text{ and by integrating}$$

$$G_{29} \leq ((\widehat{M}_{28})^{(5)})_2 = G_{29}^0 + 2(a_{29})^{(5)} ((\widehat{M}_{28})^{(5)})_1 / (a'_{29})^{(5)}$$

In the same way, one can obtain

$$G_{30} \leq ((\widehat{M}_{28})^{(5)})_3 = G_{30}^0 + 2(a_{30})^{(5)} ((\widehat{M}_{28})^{(5)})_2 / (a'_{30})^{(5)}$$

If G_{29} or G_{30} is bounded, the same property follows for G_{28}, G_{30} and G_{28}, G_{29} respectively.

Remark 4: If G_{28} is bounded, from below, the same property holds for G_{29} and G_{30} . The proof is analogous with the preceding one. An analogous property is true if G_{29} is bounded from below. 361

Remark 5: If T_{28} is bounded from below and $\lim_{t \rightarrow \infty} ((b'_i)^{(5)}((G_{31})(t), t)) = (b'_{29})^{(5)}$ then $T_{29} \rightarrow \infty$. 362

Definition of $(m)^{(5)}$ and $\varepsilon_5 :$

Indeed let t_5 be so that for $t > t_5$

$$(b_{29})^{(5)} - (b''_i)^{(5)}((G_{31})(t), t) < \varepsilon_5, T_{28}(t) > (m)^{(5)}$$

Then $\frac{dT_{29}}{dt} \geq (a_{29})^{(5)}(m)^{(5)} - \varepsilon_5 T_{29}$ which leads to 363

$$T_{29} \geq \left(\frac{(a_{29})^{(5)}(m)^{(5)}}{\varepsilon_5} \right) (1 - e^{-\varepsilon_5 t}) + T_{29}^0 e^{-\varepsilon_5 t} \text{ If we take } t \text{ such that } e^{-\varepsilon_5 t} = \frac{1}{2} \text{ it results}$$

$$T_{29} \geq \left(\frac{(a_{29})^{(5)}(m)^{(5)}}{2} \right), t = \log \frac{2}{\varepsilon_5} \text{ By taking now } \varepsilon_5 \text{ sufficiently small one sees that } T_{29} \text{ is unbounded. The same}$$

property holds for T_{30} if $\lim_{t \rightarrow \infty} (b''_{30})^{(5)}((G_{31})(t), t) = (b'_{30})^{(5)}$

We now state a more precise theorem about the behaviors at infinity of the solutions;

Analogous inequalities hold also for $G_{33}, G_{34}, T_{32}, T_{33}, T_{34}$

364

It is now sufficient to take $\frac{(a_i)^{(6)}}{(\overline{M}_{32})^{(6)}}, \frac{(b_i)^{(6)}}{(\overline{M}_{32})^{(6)}} < 1$ and to choose

365

$(\widehat{P}_{32})^{(6)}$ and $(\widehat{Q}_{32})^{(6)}$ large to have

$$\frac{(a_i)^{(6)}}{(\overline{M}_{32})^{(6)}} \left[(\widehat{P}_{32})^{(6)} + ((\widehat{P}_{32})^{(6)} + G_j^0) e^{-\left(\frac{(\widehat{P}_{32})^{(6)} + G_j^0}{G_j^0}\right)} \right] \leq (\widehat{P}_{32})^{(6)}$$

366

$$\frac{(b_i)^{(6)}}{(\overline{M}_{32})^{(6)}} \left[((\widehat{Q}_{32})^{(6)} + T_j^0) e^{-\left(\frac{(\widehat{Q}_{32})^{(6)} + T_j^0}{T_j^0}\right)} + (\widehat{Q}_{32})^{(6)} \right] \leq (\widehat{Q}_{32})^{(6)}$$

367

In order that the operator $\mathcal{A}^{(6)}$ transforms the space of sextuples of functions G_i, T_i into itself

368

The operator $\mathcal{A}^{(6)}$ is a contraction with respect to the metric

369

$$d\left(\left((G_{35})^{(1)}, (T_{35})^{(1)}\right), \left((G_{35})^{(2)}, (T_{35})^{(2)}\right)\right) =$$

$$\sup_i \left\{ \max_{t \in \mathbb{R}_+} |G_i^{(1)}(t) - G_i^{(2)}(t)| e^{-(\overline{M}_{32})^{(6)}t}, \max_{t \in \mathbb{R}_+} |T_i^{(1)}(t) - T_i^{(2)}(t)| e^{-(\overline{M}_{32})^{(6)}t} \right\}$$

Indeed if we denote

$$\underline{\text{Definition of}} \left(\overline{(G_{35})}, \overline{(T_{35})}\right) : \left(\overline{(G_{35})}, \overline{(T_{35})}\right) = \mathcal{A}^{(6)}\left((G_{35}), (T_{35})\right)$$

It results

$$\begin{aligned} |\widetilde{G}_{32}^{(1)} - \widetilde{G}_i^{(2)}| &\leq \int_0^t (a_{32})^{(6)} |G_{33}^{(1)} - G_{33}^{(2)}| e^{-(\overline{M}_{32})^{(6)}s_{(32)}} e^{(\overline{M}_{32})^{(6)}s_{(32)}} ds_{(32)} + \\ &\int_0^t \{(a_{32}')^{(6)} |G_{32}^{(1)} - G_{32}^{(2)}| e^{-(\overline{M}_{32})^{(6)}s_{(32)}} e^{-(\overline{M}_{32})^{(6)}s_{(32)}} + \\ &(a_{32}'')^{(6)} (T_{33}^{(1)}, s_{(32)}) |G_{32}^{(1)} - G_{32}^{(2)}| e^{-(\overline{M}_{32})^{(6)}s_{(32)}} e^{(\overline{M}_{32})^{(6)}s_{(32)}} + \\ &G_{32}^{(2)} |(a_{32}'')^{(6)} (T_{33}^{(1)}, s_{(32)}) - (a_{32}'')^{(6)} (T_{33}^{(2)}, s_{(32)})| e^{-(\overline{M}_{32})^{(6)}s_{(32)}} e^{(\overline{M}_{32})^{(6)}s_{(32)}}\} ds_{(32)} \end{aligned}$$

370

Where $s_{(32)}$ represents integrand that is integrated over the interval $[0, t]$

From the hypotheses it follows

$$|(G_{35})^{(1)} - (G_{35})^{(2)}| e^{-(\overline{M}_{32})^{(6)}t} \leq$$

371

$$\frac{1}{(\overline{M}_{32})^{(6)}} \left((a_{32})^{(6)} + (a_{32}')^{(6)} + (\widehat{A}_{32})^{(6)} + (\widehat{P}_{32})^{(6)} (\widehat{k}_{32})^{(6)} \right) d\left(\left((G_{35})^{(1)}, (T_{35})^{(1)}\right); (G_{35})^{(2)}, (T_{35})^{(2)}\right)$$

And analogous inequalities for G_i and T_i . Taking into account the hypothesis the result follows

Remark 1: The fact that we supposed $(a_{32}'')^{(6)}$ and $(b_{32}'')^{(6)}$ depending also on t can be considered as not conformal with the reality, however we have put this hypothesis in order that we can postulate condition necessary to prove the uniqueness of the solution bounded by $(\widehat{P}_{32})^{(6)} e^{(\overline{M}_{32})^{(6)}t}$ and $(\widehat{Q}_{32})^{(6)} e^{(\overline{M}_{32})^{(6)}t}$ respectively of \mathbb{R}_+ .

372

If instead of proving the existence of the solution on \mathbb{R}_+ , we have to prove it only on a compact then it suffices to consider that $(a_i'')^{(6)}$ and $(b_i'')^{(6)}, i = 32, 33, 34$ depend only on T_{33} and respectively on (G_{35}) (and not on t) and hypothesis can be replaced by a usual Lipschitz condition.

Remark 2: There does not exist any t where $G_i(t) = 0$ and $T_i(t) = 0$

373

From governing equations it results

$$G_i(t) \geq G_i^0 e^{-\int_0^t \{(a_i')^{(6)} - (a_i'')^{(6)}(T_{33}(s_{(32)}), s_{(32)})\} ds_{(32)}} \geq 0$$

$$T_i(t) \geq T_i^0 e^{-(b_i')^{(6)}t} > 0 \text{ for } t > 0$$

Definition of $((\widehat{M}_{32})^{(6)})_1, ((\widehat{M}_{32})^{(6)})_2$ and $((\widehat{M}_{32})^{(6)})_3$:

374

Remark 3: if G_{32} is bounded, the same property have also G_{33} and G_{34} . indeed if

$$G_{32} < (\widehat{M}_{32})^{(6)} \text{ it follows } \frac{dG_{33}}{dt} \leq ((\widehat{M}_{32})^{(6)})_1 - (a_{33}')^{(6)} G_{33} \text{ and by integrating}$$

$$G_{33} \leq ((\widehat{M}_{32})^{(6)})_2 = G_{33}^0 + 2(a_{33})^{(6)} ((\widehat{M}_{32})^{(6)})_1 / (a_{33}')^{(6)}$$

In the same way, one can obtain

$$G_{34} \leq ((\widehat{M}_{32})^{(6)})_3 = G_{34}^0 + 2(a_{34})^{(6)} ((\widehat{M}_{32})^{(6)})_2 / (a_{34}')^{(6)}$$

If G_{33} or G_{34} is bounded, the same property follows for G_{32}, G_{34} and G_{32}, G_{33} respectively.

Remark 4: If G_{32} is bounded, from below, the same property holds for G_{33} and G_{34} . The proof is analogous with the preceding one. An analogous property is true if G_{33} is bounded from below.

375

Remark 5: If T_{32} is bounded from below and $\lim_{t \rightarrow \infty} ((b_i'')^{(6)}((G_{35})(t), t)) = (b_{33}')^{(6)}$ then $T_{33} \rightarrow \infty$.

376

Definition of $(m)^{(6)}$ and ε_6 :

Indeed let t_6 be so that for $t > t_6$

$$(b_{33})^{(6)} - (b_i'')^{(6)}((G_{35})(t), t) < \varepsilon_6, T_{32}(t) > (m)^{(6)}$$

Then $\frac{dT_{33}}{dt} \geq (a_{33})^{(6)}(m)^{(6)} - \varepsilon_6 T_{33}$ which leads to 377

$$T_{33} \geq \left(\frac{(a_{33})^{(6)}(m)^{(6)}}{\varepsilon_6} \right) (1 - e^{-\varepsilon_6 t}) + T_{33}^0 e^{-\varepsilon_6 t}$$

If we take t such that $e^{-\varepsilon_6 t} = \frac{1}{2}$ it results

$$T_{33} \geq \left(\frac{(a_{33})^{(6)}(m)^{(6)}}{2} \right), \quad t = \log \frac{2}{\varepsilon_6}$$

By taking now ε_6 sufficiently small one sees that T_{33} is unbounded. The same

property holds for T_{34} if $\lim_{t \rightarrow \infty} (b_{34})''^{(6)}((G_{35})(t), t(t), t) = (b_{34}')^{(6)}$

We now state a more precise theorem about the behaviors at infinity of the solutions 378

Behavior of the solutions 379

Theorem 2: If we denote and define

Definition of $(\sigma_1)^{(1)}, (\sigma_2)^{(1)}, (\tau_1)^{(1)}, (\tau_2)^{(1)}$:

- (a) $(\sigma_1)^{(1)}, (\sigma_2)^{(1)}, (\tau_1)^{(1)}, (\tau_2)^{(1)}$ four constants satisfying
- $$-(\sigma_2)^{(1)} \leq -(a'_{13})^{(1)} + (a'_{14})^{(1)} - (a''_{13})^{(1)}(T_{14}, t) + (a''_{14})^{(1)}(T_{14}, t) \leq -(\sigma_1)^{(1)}$$
- $$-(\tau_2)^{(1)} \leq -(b'_{13})^{(1)} + (b'_{14})^{(1)} - (b''_{13})^{(1)}(G, t) - (b''_{14})^{(1)}(G, t) \leq -(\tau_1)^{(1)}$$

Definition of $(v_1)^{(1)}, (v_2)^{(1)}, (u_1)^{(1)}, (u_2)^{(1)}, v^{(1)}, u^{(1)}$:

- (b) By $(v_1)^{(1)} > 0, (v_2)^{(1)} < 0$ and respectively $(u_1)^{(1)} > 0, (u_2)^{(1)} < 0$ the roots of the equations
- $$(a_{14})^{(1)}(v^{(1)})^2 + (\sigma_1)^{(1)}v^{(1)} - (a_{13})^{(1)} = 0 \text{ and } (b_{14})^{(1)}(u^{(1)})^2 + (\tau_1)^{(1)}u^{(1)} - (b_{13})^{(1)} = 0$$

Definition of $(\bar{v}_1)^{(1)}, (\bar{v}_2)^{(1)}, (\bar{u}_1)^{(1)}, (\bar{u}_2)^{(1)}$:

- By $(\bar{v}_1)^{(1)} > 0, (\bar{v}_2)^{(1)} < 0$ and respectively $(\bar{u}_1)^{(1)} > 0, (\bar{u}_2)^{(1)} < 0$ the roots of the equations
- $$(a_{14})^{(1)}(v^{(1)})^2 + (\sigma_2)^{(1)}v^{(1)} - (a_{13})^{(1)} = 0 \text{ and } (b_{14})^{(1)}(u^{(1)})^2 + (\tau_2)^{(1)}u^{(1)} - (b_{13})^{(1)} = 0$$

Definition of $(m_1)^{(1)}, (m_2)^{(1)}, (\mu_1)^{(1)}, (\mu_2)^{(1)}, (v_0)^{(1)}$:-

- (c) If we define $(m_1)^{(1)}, (m_2)^{(1)}, (\mu_1)^{(1)}, (\mu_2)^{(1)}$ by
- $$(m_2)^{(1)} = (v_0)^{(1)}, (m_1)^{(1)} = (v_1)^{(1)}, \text{ if } (v_0)^{(1)} < (v_1)^{(1)}$$
- $$(m_2)^{(1)} = (v_1)^{(1)}, (m_1)^{(1)} = (\bar{v}_1)^{(1)}, \text{ if } (v_1)^{(1)} < (v_0)^{(1)} < (\bar{v}_1)^{(1)},$$

and $(v_0)^{(1)} = \frac{\sigma_{13}^0}{\sigma_{14}^0}$

$(m_2)^{(1)} = (v_1)^{(1)}, (m_1)^{(1)} = (v_0)^{(1)}, \text{ if } (\bar{v}_1)^{(1)} < (v_0)^{(1)}$

and analogously 383

$(\mu_2)^{(1)} = (u_0)^{(1)}, (\mu_1)^{(1)} = (u_1)^{(1)}, \text{ if } (u_0)^{(1)} < (u_1)^{(1)}$
 $(\mu_2)^{(1)} = (u_1)^{(1)}, (\mu_1)^{(1)} = (\bar{u}_1)^{(1)}, \text{ if } (u_1)^{(1)} < (u_0)^{(1)} < (\bar{u}_1)^{(1)},$

and $(u_0)^{(1)} = \frac{\tau_{13}^0}{\tau_{14}^0}$

$(\mu_2)^{(1)} = (u_1)^{(1)}, (\mu_1)^{(1)} = (u_0)^{(1)}, \text{ if } (\bar{u}_1)^{(1)} < (u_0)^{(1)}$ where $(u_1)^{(1)}, (\bar{u}_1)^{(1)}$ are defined above

Then the solution satisfies the inequalities 384

$$G_{13}^0 e^{((S_1)^{(1)} - (p_{13})^{(1)})t} \leq G_{13}(t) \leq G_{13}^0 e^{(S_1)^{(1)}t}$$

where $(p_i)^{(1)}$ is defined above

$$\frac{1}{(m_1)^{(1)}} G_{13}^0 e^{((S_1)^{(1)} - (p_{13})^{(1)})t} \leq G_{14}(t) \leq \frac{1}{(m_2)^{(1)}} G_{13}^0 e^{(S_1)^{(1)}t}$$

$$\left(\frac{(a_{15})^{(1)} G_{13}^0}{(m_1)^{(1)}((S_1)^{(1)} - (p_{13})^{(1)} - (S_2)^{(1)})} \left[e^{((S_1)^{(1)} - (p_{13})^{(1)})t} - e^{-(S_2)^{(1)}t} \right] + G_{15}^0 e^{-(S_2)^{(1)}t} \right) \leq G_{15}(t) \leq$$

$$\frac{(a_{15})^{(1)} G_{13}^0}{(m_2)^{(1)}((S_1)^{(1)} - (a'_{15})^{(1)})} \left[e^{(S_1)^{(1)}t} - e^{-(a'_{15})^{(1)}t} \right] + G_{15}^0 e^{-(a'_{15})^{(1)}t}$$

$$\boxed{T_{13}^0 e^{(R_1)^{(1)}t} \leq T_{13}(t) \leq T_{13}^0 e^{((R_1)^{(1)} + (r_{13})^{(1)})t}$$

$$\frac{1}{(\mu_1)^{(1)}} T_{13}^0 e^{(R_1)^{(1)}t} \leq T_{13}(t) \leq \frac{1}{(\mu_2)^{(1)}} T_{13}^0 e^{((R_1)^{(1)} + (r_{13})^{(1)})t}$$

$$\frac{(b_{15})^{(1)} T_{13}^0}{(\mu_1)^{(1)}((R_1)^{(1)} - (b'_{15})^{(1)})} \left[e^{(R_1)^{(1)}t} - e^{-(b'_{15})^{(1)}t} \right] + T_{15}^0 e^{-(b'_{15})^{(1)}t} \leq T_{15}(t) \leq$$

$$\frac{(a_{15})^{(1)} T_{13}^0}{(\mu_2)^{(1)}((R_1)^{(1)} + (r_{13})^{(1)} + (R_2)^{(1)})} \left[e^{((R_1)^{(1)} + (r_{13})^{(1)})t} - e^{-(R_2)^{(1)}t} \right] + T_{15}^0 e^{-(R_2)^{(1)}t}$$

Definition of $(S_1)^{(1)}, (S_2)^{(1)}, (R_1)^{(1)}, (R_2)^{(1)}$:- 389

Where $(S_1)^{(1)} = (a_{13})^{(1)}(m_2)^{(1)} - (a'_{13})^{(1)}$

$$(S_2)^{(1)} = (a_{15})^{(1)} - (p_{15})^{(1)}$$

$$(R_1)^{(1)} = (b_{13})^{(1)}(\mu_2)^{(1)} - (b'_{13})^{(1)}$$

$$(R_2)^{(1)} = (b'_{15})^{(1)} - (r_{15})^{(1)}$$

Behavior of the solutions 390

Theorem 2: If we denote and define

Definition of $(\sigma_1)^{(2)}, (\sigma_2)^{(2)}, (\tau_1)^{(2)}, (\tau_2)^{(2)}$:

391

(d) $\sigma_1^{(2)}, (\sigma_2)^{(2)}, (\tau_1)^{(2)}, (\tau_2)^{(2)}$ four constants satisfying
 $-(\sigma_2)^{(2)} \leq -(a'_{16})^{(2)} + (a'_{17})^{(2)} - (a''_{16})^{(2)}(T_{17}, t) + (a''_{17})^{(2)}(T_{17}, t) \leq -(\sigma_1)^{(2)}$ 392
 $-(\tau_2)^{(2)} \leq -(b'_{16})^{(2)} + (b'_{17})^{(2)} - (b''_{16})^{(2)}(G_{19}, t) - (b''_{17})^{(2)}(G_{19}, t) \leq -(\tau_1)^{(2)}$ 393

Definition of $(v_1)^{(2)}, (v_2)^{(2)}, (u_1)^{(2)}, (u_2)^{(2)}$: 394

By $(v_1)^{(2)} > 0, (v_2)^{(2)} < 0$ and respectively $(u_1)^{(2)} > 0, (u_2)^{(2)} < 0$ the roots 395

(e) of the equations $(a_{17})^{(2)}(v^{(2)})^2 + (\sigma_1)^{(2)}v^{(2)} - (a_{16})^{(2)} = 0$ 396

and $(b_{14})^{(2)}(u^{(2)})^2 + (\tau_1)^{(2)}u^{(2)} - (b_{16})^{(2)} = 0$ and 397

Definition of $(\bar{v}_1)^{(2)}, (\bar{v}_2)^{(2)}, (\bar{u}_1)^{(2)}, (\bar{u}_2)^{(2)}$: 398

By $(\bar{v}_1)^{(2)} > 0, (\bar{v}_2)^{(2)} < 0$ and respectively $(\bar{u}_1)^{(2)} > 0, (\bar{u}_2)^{(2)} < 0$ the 399

roots of the equations $(a_{17})^{(2)}(v^{(2)})^2 + (\sigma_2)^{(2)}v^{(2)} - (a_{16})^{(2)} = 0$ 400

and $(b_{17})^{(2)}(u^{(2)})^2 + (\tau_2)^{(2)}u^{(2)} - (b_{16})^{(2)} = 0$ 401

Definition of $(m_1)^{(2)}, (m_2)^{(2)}, (\mu_1)^{(2)}, (\mu_2)^{(2)}$:- 402

(f) If we define $(m_1)^{(2)}, (m_2)^{(2)}, (\mu_1)^{(2)}, (\mu_2)^{(2)}$ by 403

$(m_2)^{(2)} = (v_0)^{(2)}, (m_1)^{(2)} = (v_1)^{(2)}$, **if** $(v_0)^{(2)} < (v_1)^{(2)}$ 404

$(m_2)^{(2)} = (v_1)^{(2)}, (m_1)^{(2)} = (\bar{v}_1)^{(2)}$, **if** $(v_1)^{(2)} < (v_0)^{(2)} < (\bar{v}_1)^{(2)}$, 405

and $(v_0)^{(2)} = \frac{G_{16}^0}{G_{17}^0}$ 406

$(m_2)^{(2)} = (v_1)^{(2)}, (m_1)^{(2)} = (v_0)^{(2)}$, **if** $(\bar{v}_1)^{(2)} < (v_0)^{(2)}$ 407

and analogously

$(\mu_2)^{(2)} = (u_0)^{(2)}, (\mu_1)^{(2)} = (u_1)^{(2)}$, **if** $(u_0)^{(2)} < (u_1)^{(2)}$

$(\mu_2)^{(2)} = (u_1)^{(2)}, (\mu_1)^{(2)} = (\bar{u}_1)^{(2)}$, **if** $(u_1)^{(2)} < (u_0)^{(2)} < (\bar{u}_1)^{(2)}$,

and $(u_0)^{(2)} = \frac{T_{16}^0}{T_{17}^0}$

$(\mu_2)^{(2)} = (u_1)^{(2)}, (\mu_1)^{(2)} = (u_0)^{(2)}$, **if** $(\bar{u}_1)^{(2)} < (u_0)^{(2)}$ 408

Then the solution satisfies the inequalities 409

$G_{16}^0 e^{(S_1)^{(2)} - (p_{16})^{(2)}t} \leq G_{16}(t) \leq G_{16}^0 e^{(S_1)^{(2)}t}$

$(p_i)^{(2)}$ is defined by equation above 410

$\frac{1}{(m_1)^{(2)}} G_{16}^0 e^{(S_1)^{(2)} - (p_{16})^{(2)}t} \leq G_{17}(t) \leq \frac{1}{(m_2)^{(2)}} G_{16}^0 e^{(S_1)^{(2)}t}$ 411

$\left(\frac{(a_{18})^{(2)} G_{16}^0}{(m_1)^{(2)}((S_1)^{(2)} - (p_{16})^{(2)} - (S_2)^{(2)})} \left[e^{(S_1)^{(2)} - (p_{16})^{(2)}t} - e^{-(S_2)^{(2)}t} \right] + G_{18}^0 e^{-(S_2)^{(2)}t} \right) \leq G_{18}(t) \leq$ 412

$\frac{(a_{18})^{(2)} G_{16}^0}{(m_2)^{(2)}((S_1)^{(2)} - (a'_{18})^{(2)})} \left[e^{(S_1)^{(2)}t} - e^{-(a'_{18})^{(2)}t} \right] + G_{18}^0 e^{-(a'_{18})^{(2)}t}$

$\frac{T_{16}^0 e^{(R_1)^{(2)}t} \leq T_{16}(t) \leq T_{16}^0 e^{((R_1)^{(2)} + (r_{16})^{(2)})t}$ 413

$\frac{1}{(\mu_1)^{(2)}} T_{16}^0 e^{(R_1)^{(2)}t} \leq T_{16}(t) \leq \frac{1}{(\mu_2)^{(2)}} T_{16}^0 e^{((R_1)^{(2)} + (r_{16})^{(2)})t}$ 414

$\frac{(b_{18})^{(2)} T_{16}^0}{(\mu_1)^{(2)}((R_1)^{(2)} - (b'_{18})^{(2)})} \left[e^{(R_1)^{(2)}t} - e^{-(b'_{18})^{(2)}t} \right] + T_{18}^0 e^{-(b'_{18})^{(2)}t} \leq T_{18}(t) \leq$ 415

$\frac{(a_{18})^{(2)} T_{16}^0}{(\mu_2)^{(2)}((R_1)^{(2)} + (r_{16})^{(2)} + (R_2)^{(2)})} \left[e^{((R_1)^{(2)} + (r_{16})^{(2)})t} - e^{-(R_2)^{(2)}t} \right] + T_{18}^0 e^{-(R_2)^{(2)}t}$

Definition of $(S_1)^{(2)}, (S_2)^{(2)}, (R_1)^{(2)}, (R_2)^{(2)}$:- 416

Where $(S_1)^{(2)} = (a_{16})^{(2)}(m_2)^{(2)} - (a'_{16})^{(2)}$ 417

$(S_2)^{(2)} = (a_{18})^{(2)} - (p_{18})^{(2)}$

$(R_1)^{(2)} = (b_{16})^{(2)}(\mu_2)^{(1)} - (b'_{16})^{(2)}$ 418

$(R_2)^{(2)} = (b'_{18})^{(2)} - (r_{18})^{(2)}$

419

420

Behavior of the solutions

Theorem 2: If we denote and define

Definition of $(\sigma_1)^{(3)}, (\sigma_2)^{(3)}, (\tau_1)^{(3)}, (\tau_2)^{(3)}$:

(a) $\sigma_1^{(3)}, (\sigma_2)^{(3)}, (\tau_1)^{(3)}, (\tau_2)^{(3)}$ four constants satisfying

$-(\sigma_2)^{(3)} \leq -(a'_{20})^{(3)} + (a'_{21})^{(3)} - (a''_{20})^{(3)}(T_{21}, t) + (a''_{21})^{(3)}(T_{21}, t) \leq -(\sigma_1)^{(3)}$

$-(\tau_2)^{(3)} \leq -(b'_{20})^{(3)} + (b'_{21})^{(3)} - (b''_{20})^{(3)}(G, t) - (b''_{21})^{(3)}(G_{23}, t) \leq -(\tau_1)^{(3)}$

Definition of $(v_1)^{(3)}, (v_2)^{(3)}, (u_1)^{(3)}, (u_2)^{(3)}$: 421

(b) By $(v_1)^{(3)} > 0, (v_2)^{(3)} < 0$ and respectively $(u_1)^{(3)} > 0, (u_2)^{(3)} < 0$ the roots of the equations

$(a_{21})^{(3)}(v^{(3)})^2 + (\sigma_1)^{(3)}v^{(3)} - (a_{20})^{(3)} = 0$

and $(b_{21})^{(3)}(u^{(3)})^2 + (\tau_1)^{(3)}u^{(3)} - (b_{20})^{(3)} = 0$ and

By $(\bar{v}_1)^{(3)} > 0, (\bar{v}_2)^{(3)} < 0$ and respectively $(\bar{u}_1)^{(3)} > 0, (\bar{u}_2)^{(3)} < 0$ the

roots of the equations $(a_{21})^{(3)}(v^{(3)})^2 + (\sigma_2)^{(3)}v^{(3)} - (a_{20})^{(3)} = 0$
 and $(b_{21})^{(3)}(u^{(3)})^2 + (\tau_2)^{(3)}u^{(3)} - (b_{20})^{(3)} = 0$

Definition of $(m_1)^{(3)}, (m_2)^{(3)}, (\mu_1)^{(3)}, (\mu_2)^{(3)}$:- 422

(c) If we define $(m_1)^{(3)}, (m_2)^{(3)}, (\mu_1)^{(3)}, (\mu_2)^{(3)}$ by
 $(m_2)^{(3)} = (v_0)^{(3)}, (m_1)^{(3)} = (v_1)^{(3)}$, **if** $(v_0)^{(3)} < (v_1)^{(3)}$
 $(m_2)^{(3)} = (v_1)^{(3)}, (m_1)^{(3)} = (\bar{v}_1)^{(3)}$, **if** $(v_1)^{(3)} < (v_0)^{(3)} < (\bar{v}_1)^{(3)}$,

and $(v_0)^{(3)} = \frac{G_{20}^0}{G_{21}^0}$

$(m_2)^{(3)} = (v_1)^{(3)}, (m_1)^{(3)} = (v_0)^{(3)}$, **if** $(\bar{v}_1)^{(3)} < (v_0)^{(3)}$

and analogously 423

$(\mu_2)^{(3)} = (u_0)^{(3)}, (\mu_1)^{(3)} = (u_1)^{(3)}$, **if** $(u_0)^{(3)} < (u_1)^{(3)}$

$(\mu_2)^{(3)} = (u_1)^{(3)}, (\mu_1)^{(3)} = (\bar{u}_1)^{(3)}$, **if** $(u_1)^{(3)} < (u_0)^{(3)} < (\bar{u}_1)^{(3)}$, and $(u_0)^{(3)} = \frac{T_{20}^0}{T_{21}^0}$ 424

$(\mu_2)^{(3)} = (u_1)^{(3)}, (\mu_1)^{(3)} = (u_0)^{(3)}$, **if** $(\bar{u}_1)^{(3)} < (u_0)^{(3)}$

Then the solution satisfies the inequalities

$$G_{20}^0 e^{(S_1)^{(3)} - (p_{20})^{(3)}t} \leq G_{20}(t) \leq G_{20}^0 e^{(S_1)^{(3)}t}$$

$(p_i)^{(3)}$ is defined by equation above

$$\frac{1}{(m_1)^{(3)}} G_{20}^0 e^{(S_1)^{(3)} - (p_{20})^{(3)}t} \leq G_{21}(t) \leq \frac{1}{(m_2)^{(3)}} G_{20}^0 e^{(S_1)^{(3)}t} \quad 425$$

$$\left(\frac{(a_{22})^{(3)} G_{20}^0}{(m_1)^{(3)}((S_1)^{(3)} - (p_{20})^{(3)}) - (S_2)^{(3)}} \left[e^{(S_1)^{(3)} - (p_{20})^{(3)}t} - e^{-(S_2)^{(3)}t} \right] + G_{22}^0 e^{-(S_2)^{(3)}t} \right) \leq G_{22}(t) \leq \quad 426$$

$$\frac{(a_{22})^{(3)} G_{20}^0}{(m_2)^{(3)}((S_1)^{(3)} - (a_{22})^{(3)})} \left[e^{(S_1)^{(3)}t} - e^{-(a'_{22})^{(3)}t} \right] + G_{22}^0 e^{-(a'_{22})^{(3)}t}$$

$$\boxed{T_{20}^0 e^{(R_1)^{(3)}t} \leq T_{20}(t) \leq T_{20}^0 e^{((R_1)^{(3)} + (r_{20})^{(3)})t}} \quad 427$$

$$\frac{1}{(\mu_1)^{(3)}} T_{20}^0 e^{(R_1)^{(3)}t} \leq T_{20}(t) \leq \frac{1}{(\mu_2)^{(3)}} T_{20}^0 e^{((R_1)^{(3)} + (r_{20})^{(3)})t} \quad 428$$

$$\frac{(b_{22})^{(3)} T_{20}^0}{(\mu_1)^{(3)}((R_1)^{(3)} - (b_{22})^{(3)})} \left[e^{(R_1)^{(3)}t} - e^{-(b'_{22})^{(3)}t} \right] + T_{22}^0 e^{-(b'_{22})^{(3)}t} \leq T_{22}(t) \leq \quad 429$$

$$\frac{(a_{22})^{(3)} T_{20}^0}{(\mu_2)^{(3)}((R_1)^{(3)} + (r_{20})^{(3)} + (R_2)^{(3)})} \left[e^{((R_1)^{(3)} + (r_{20})^{(3)})t} - e^{-(R_2)^{(3)}t} \right] + T_{22}^0 e^{-(R_2)^{(3)}t}$$

Definition of $(S_1)^{(3)}, (S_2)^{(3)}, (R_1)^{(3)}, (R_2)^{(3)}$:- 430

Where $(S_1)^{(3)} = (a_{20})^{(3)}(m_2)^{(3)} - (a'_{20})^{(3)}$

$$(S_2)^{(3)} = (a_{22})^{(3)} - (p_{22})^{(3)}$$

$$(R_1)^{(3)} = (b_{20})^{(3)}(\mu_2)^{(3)} - (b'_{20})^{(3)}$$

$$(R_2)^{(3)} = (b_{22})^{(3)} - (r_{22})^{(3)}$$

431

432

433

Behavior of the solutions

If we denote and define

Definition of $(\sigma_1)^{(4)}, (\sigma_2)^{(4)}, (\tau_1)^{(4)}, (\tau_2)^{(4)}$:

(d) $(\sigma_1)^{(4)}, (\sigma_2)^{(4)}, (\tau_1)^{(4)}, (\tau_2)^{(4)}$ four constants satisfying

$$-(\sigma_2)^{(4)} \leq -(a'_{24})^{(4)} + (a'_{25})^{(4)} - (a''_{24})^{(4)}(T_{25}, t) + (a''_{25})^{(4)}(T_{25}, t) \leq -(\sigma_1)^{(4)}$$

$$-(\tau_2)^{(4)} \leq -(b'_{24})^{(4)} + (b'_{25})^{(4)} - (b''_{24})^{(4)}((G_{27}), t) - (b''_{25})^{(4)}((G_{27}), t) \leq -(\tau_1)^{(4)}$$

Definition of $(v_1)^{(4)}, (v_2)^{(4)}, (u_1)^{(4)}, (u_2)^{(4)}, v^{(4)}, u^{(4)}$: 434

(e) By $(v_1)^{(4)} > 0, (v_2)^{(4)} < 0$ and respectively $(u_1)^{(4)} > 0, (u_2)^{(4)} < 0$ the roots of the equations

$$(a_{25})^{(4)}(v^{(4)})^2 + (\sigma_1)^{(4)}v^{(4)} - (a_{24})^{(4)} = 0$$

and $(b_{25})^{(4)}(u^{(4)})^2 + (\tau_1)^{(4)}u^{(4)} - (b_{24})^{(4)} = 0$ and 435

Definition of $(\bar{v}_1)^{(4)}, (\bar{v}_2)^{(4)}, (\bar{u}_1)^{(4)}, (\bar{u}_2)^{(4)}$: 436

By $(\bar{v}_1)^{(4)} > 0, (\bar{v}_2)^{(4)} < 0$ and respectively $(\bar{u}_1)^{(4)} > 0, (\bar{u}_2)^{(4)} < 0$ the roots of the equations $(a_{25})^{(4)}(v^{(4)})^2 + (\sigma_2)^{(4)}v^{(4)} - (a_{24})^{(4)} = 0$ and $(b_{25})^{(4)}(u^{(4)})^2 + (\tau_2)^{(4)}u^{(4)} - (b_{24})^{(4)} = 0$

Definition of $(m_1)^{(4)}, (m_2)^{(4)}, (\mu_1)^{(4)}, (\mu_2)^{(4)}, (v_0)^{(4)}$:-

(f) If we define $(m_1)^{(4)}, (m_2)^{(4)}, (\mu_1)^{(4)}, (\mu_2)^{(4)}$ by

$$(m_2)^{(4)} = (v_0)^{(4)}, (m_1)^{(4)} = (v_1)^{(4)}, \text{ if } (v_0)^{(4)} < (v_1)^{(4)}$$

$$(m_2)^{(4)} = (v_1)^{(4)}, (m_1)^{(4)} = (\bar{v}_1)^{(4)}, \text{ if } (v_4)^{(4)} < (v_0)^{(4)} < (\bar{v}_1)^{(4)},$$

and $(v_0)^{(4)} = \frac{G_{24}^0}{G_{25}^0}$

$$(m_2)^{(4)} = (v_4)^{(4)}, (m_1)^{(4)} = (v_0)^{(4)}, \text{ if } (\bar{v}_4)^{(4)} < (v_0)^{(4)}$$

and analogously

437
438

$$(\mu_2)^{(4)} = (u_0)^{(4)}, (\mu_1)^{(4)} = (u_1)^{(4)}, \text{ if } (u_0)^{(4)} < (u_1)^{(4)}$$

$$(\mu_2)^{(4)} = (u_1)^{(4)}, (\mu_1)^{(4)} = (\bar{u}_1)^{(4)}, \text{ if } (u_1)^{(4)} < (u_0)^{(4)} < (\bar{u}_1)^{(4)},$$

and $(u_0)^{(4)} = \frac{T_{24}^0}{T_{25}^0}$

$(\mu_2)^{(4)} = (u_1)^{(4)}, (\mu_1)^{(4)} = (u_0)^{(4)}, \text{ if } (\bar{u}_1)^{(4)} < (u_0)^{(4)}$ where $(u_1)^{(4)}, (\bar{u}_1)^{(4)}$ are defined

Then the solution satisfies the inequalities

439
440
441

$$G_{24}^0 e^{((S_1)^{(4)} - (p_{24})^{(4)})t} \leq G_{24}(t) \leq G_{24}^0 e^{(S_1)^{(4)}t}$$

where $(p_i)^{(4)}$ is defined by equation above

$$\frac{1}{(m_1)^{(4)}} G_{24}^0 e^{((S_1)^{(4)} - (p_{24})^{(4)})t} \leq G_{25}(t) \leq \frac{1}{(m_2)^{(4)}} G_{24}^0 e^{(S_1)^{(4)}t}$$

442

$$\left(\frac{(a_{26})^{(4)} G_{24}^0}{(m_1)^{(4)} ((S_1)^{(4)} - (p_{24})^{(4)} - (S_2)^{(4)})} \left[e^{((S_1)^{(4)} - (p_{24})^{(4)})t} - e^{-(S_2)^{(4)}t} \right] + G_{26}^0 e^{-(S_2)^{(4)}t} \right) \leq G_{26}(t) \leq (a_{26})^{(4)} G_{24}^0 (m_2)^{(4)} (S_1)^{(4)} - (a_{26}')^{(4)} 4e^{(S_1)^{(4)}t} - e^{-(a_{26}')^{(4)}t} + G_{26}^0 e^{-(a_{26}')^{(4)}t}$$

443

$$\boxed{T_{24}^0 e^{(R_1)^{(4)}t} \leq T_{24}(t) \leq T_{24}^0 e^{((R_1)^{(4)} + (r_{24})^{(4)})t}}$$

444

$$\frac{1}{(\mu_1)^{(4)}} T_{24}^0 e^{(R_1)^{(4)}t} \leq T_{24}(t) \leq \frac{1}{(\mu_2)^{(4)}} T_{24}^0 e^{((R_1)^{(4)} + (r_{24})^{(4)})t}$$

445

$$\frac{(b_{26})^{(4)} T_{24}^0}{(\mu_1)^{(4)} ((R_1)^{(4)} - (b_{26})^{(4)})} \left[e^{(R_1)^{(4)}t} - e^{-(b_{26}')^{(4)}t} \right] + T_{26}^0 e^{-(b_{26}')^{(4)}t} \leq T_{26}(t) \leq$$

446

$$\frac{(a_{26})^{(4)} T_{24}^0}{(\mu_2)^{(4)} ((R_1)^{(4)} + (r_{24})^{(4)} + (R_2)^{(4)})} \left[e^{((R_1)^{(4)} + (r_{24})^{(4)})t} - e^{-(R_2)^{(4)}t} \right] + T_{26}^0 e^{-(R_2)^{(4)}t}$$

447

Definition of $(S_1)^{(4)}, (S_2)^{(4)}, (R_1)^{(4)}, (R_2)^{(4)}$:-

448

Where $(S_1)^{(4)} = (a_{24})^{(4)} (m_2)^{(4)} - (a_{24}')^{(4)}$

$$(S_2)^{(4)} = (a_{26})^{(4)} - (p_{26})^{(4)}$$

$$(R_1)^{(4)} = (b_{24})^{(4)} (\mu_2)^{(4)} - (b_{24}')^{(4)}$$

$$(R_2)^{(4)} = (b'_{26})^{(4)} - (r_{26})^{(4)}$$

Behavior of the solutions

449

If we denote and define

Definition of $(\sigma_1)^{(5)}, (\sigma_2)^{(5)}, (\tau_1)^{(5)}, (\tau_2)^{(5)}$:

(g) $(\sigma_1)^{(5)}, (\sigma_2)^{(5)}, (\tau_1)^{(5)}, (\tau_2)^{(5)}$ four constants satisfying

$$-(\sigma_2)^{(5)} \leq -(a'_{28})^{(5)} + (a'_{29})^{(5)} - (a''_{28})^{(5)}(T_{29}, t) + (a''_{29})^{(5)}(T_{29}, t) \leq -(\sigma_1)^{(5)}$$

$$-(\tau_2)^{(5)} \leq -(b'_{28})^{(5)} + (b'_{29})^{(5)} - (b''_{28})^{(5)}((G_{31}), t) - (b''_{29})^{(5)}((G_{31}), t) \leq -(\tau_1)^{(5)}$$

Definition of $(v_1)^{(5)}, (v_2)^{(5)}, (u_1)^{(5)}, (u_2)^{(5)}, v^{(5)}, u^{(5)}$:

450

(h) By $(v_1)^{(5)} > 0, (v_2)^{(5)} < 0$ and respectively $(u_1)^{(5)} > 0, (u_2)^{(5)} < 0$ the roots of the equations

$$(a_{29})^{(5)}(v^{(5)})^2 + (\sigma_1)^{(5)}v^{(5)} - (a_{28})^{(5)} = 0$$

$$\text{and } (b_{29})^{(5)}(u^{(5)})^2 + (\tau_1)^{(5)}u^{(5)} - (b_{28})^{(5)} = 0 \text{ and}$$

Definition of $(\bar{v}_1)^{(5)}, (\bar{v}_2)^{(5)}, (\bar{u}_1)^{(5)}, (\bar{u}_2)^{(5)}$:

451

By $(\bar{v}_1)^{(5)} > 0, (\bar{v}_2)^{(5)} < 0$ and respectively $(\bar{u}_1)^{(5)} > 0, (\bar{u}_2)^{(5)} < 0$ the roots of the equations $(a_{29})^{(5)}(v^{(5)})^2 + (\sigma_2)^{(5)}v^{(5)} - (a_{28})^{(5)} = 0$

$$\text{and } (b_{29})^{(5)}(u^{(5)})^2 + (\tau_2)^{(5)}u^{(5)} - (b_{28})^{(5)} = 0$$

Definition of $(m_1)^{(5)}, (m_2)^{(5)}, (\mu_1)^{(5)}, (\mu_2)^{(5)}, (v_0)^{(5)}$:-

(i) If we define $(m_1)^{(5)}, (m_2)^{(5)}, (\mu_1)^{(5)}, (\mu_2)^{(5)}$ by

$$(m_2)^{(5)} = (v_0)^{(5)}, (m_1)^{(5)} = (v_1)^{(5)}, \text{ if } (v_0)^{(5)} < (v_1)^{(5)}$$

$$(m_2)^{(5)} = (v_1)^{(5)}, (m_1)^{(5)} = (\bar{v}_1)^{(5)}, \text{ if } (v_1)^{(5)} < (v_0)^{(5)} < (\bar{v}_1)^{(5)},$$

$$\text{and } (v_0)^{(5)} = \frac{G_{28}^0}{G_{29}^0}$$

$$(m_2)^{(5)} = (v_1)^{(5)}, (m_1)^{(5)} = (v_0)^{(5)}, \text{ if } (\bar{v}_1)^{(5)} < (v_0)^{(5)}$$

and analogously

452

$$(\mu_2)^{(5)} = (u_0)^{(5)}, (\mu_1)^{(5)} = (u_1)^{(5)}, \text{ if } (u_0)^{(5)} < (u_1)^{(5)}$$

$$(\mu_2)^{(5)} = (u_1)^{(5)}, (\mu_1)^{(5)} = (\bar{u}_1)^{(5)}, \text{ if } (u_1)^{(5)} < (u_0)^{(5)} < (\bar{u}_1)^{(5)},$$

$$\text{and } (u_0)^{(5)} = \frac{T_{28}^0}{T_{29}^0}$$

453

$(\mu_2)^{(5)} = (u_1)^{(5)}, (\mu_1)^{(5)} = (u_0)^{(5)}$, if $(\bar{u}_1)^{(5)} < (u_0)^{(5)}$ where $(u_1)^{(5)}, (\bar{u}_1)^{(5)}$ are defined respectively

Then the solution satisfies the inequalities

454

$$G_{28}^0 e^{((s_1)^{(5)} - (p_{28})^{(5)})t} \leq G_{28}(t) \leq G_{28}^0 e^{(s_1)^{(5)}t}$$

where $(p_i)^{(5)}$ is defined by equation above

$$\frac{1}{(m_5)^{(5)}} G_{28}^0 e^{((s_1)^{(5)} - (p_{28})^{(5)})t} \leq G_{29}(t) \leq \frac{1}{(m_2)^{(5)}} G_{28}^0 e^{(s_1)^{(5)}t}$$

455

$$\left(\frac{(a_{30})^{(5)} G_{28}^0}{(m_1)^{(5)} (S_1)^{(5)} - (p_{28})^{(5)} - (S_2)^{(5)}} \right) \left[e^{((S_1)^{(5)} - (p_{28})^{(5)})t} - e^{-(S_2)^{(5)}t} \right] + G_{30}^0 e^{-(S_2)^{(5)}t} \leq G_{30}(t) \leq (a_{30})^{(5)} G_{28}^0 (m_2)^{(5)} (S_1)^{(5)} - (a_{30}')^{(5)} e^{(S_1)^{(5)}t} - e^{-(a_{30}')^{(5)}t} + G_{30}^0 e^{-(a_{30}')^{(5)}t} \tag{456}$$

$$\boxed{T_{28}^0 e^{(R_1)^{(5)}t} \leq T_{28}(t) \leq T_{28}^0 e^{((R_1)^{(5)} + (r_{28})^{(5)})t}} \tag{457}$$

$$\frac{1}{(\mu_1)^{(5)}} T_{28}^0 e^{(R_1)^{(5)}t} \leq T_{28}(t) \leq \frac{1}{(\mu_2)^{(5)}} T_{28}^0 e^{((R_1)^{(5)} + (r_{28})^{(5)})t} \tag{458}$$

$$\frac{(b_{30})^{(5)} T_{28}^0}{(\mu_1)^{(5)} ((R_1)^{(5)} - (b_{30}')^{(5)})} \left[e^{(R_1)^{(5)}t} - e^{-(b_{30}')^{(5)}t} \right] + T_{30}^0 e^{-(b_{30}')^{(5)}t} \leq T_{30}(t) \leq \tag{459}$$

$$\frac{(a_{30})^{(5)} T_{28}^0}{(\mu_2)^{(5)} ((R_1)^{(5)} + (r_{28})^{(5)} + (R_2)^{(5)})} \left[e^{((R_1)^{(5)} + (r_{28})^{(5)})t} - e^{-(R_2)^{(5)}t} \right] + T_{30}^0 e^{-(R_2)^{(5)}t}$$

Definition of $(S_1)^{(5)}, (S_2)^{(5)}, (R_1)^{(5)}, (R_2)^{(5)}$:- 460

Where $(S_1)^{(5)} = (a_{28})^{(5)} (m_2)^{(5)} - (a_{28}')^{(5)}$

$$(S_2)^{(5)} = (a_{30})^{(5)} - (p_{30})^{(5)}$$

$$(R_1)^{(5)} = (b_{28})^{(5)} (\mu_2)^{(5)} - (b_{28}')^{(5)}$$

$$(R_2)^{(5)} = (b_{30}')^{(5)} - (r_{30})^{(5)}$$

Behavior of the solutions 461

If we denote and define

Definition of $(\sigma_1)^{(6)}, (\sigma_2)^{(6)}, (\tau_1)^{(6)}, (\tau_2)^{(6)}$:

(j) $(\sigma_1)^{(6)}, (\sigma_2)^{(6)}, (\tau_1)^{(6)}, (\tau_2)^{(6)}$ four constants satisfying

$$-(\sigma_2)^{(6)} \leq -(a_{32}')^{(6)} + (a_{33}')^{(6)} - (a_{32}'')^{(6)} (T_{33}, t) + (a_{33}'')^{(6)} (T_{33}, t) \leq -(\sigma_1)^{(6)}$$

$$-(\tau_2)^{(6)} \leq -(b_{32}')^{(6)} + (b_{33}')^{(6)} - (b_{32}'')^{(6)} ((G_{35}), t) - (b_{33}'')^{(6)} ((G_{35}), t) \leq -(\tau_1)^{(6)}$$

Definition of $(v_1)^{(6)}, (v_2)^{(6)}, (u_1)^{(6)}, (u_2)^{(6)}, v^{(6)}, u^{(6)}$: 462

(k) By $(v_1)^{(6)} > 0, (v_2)^{(6)} < 0$ and respectively $(u_1)^{(6)} > 0, (u_2)^{(6)} < 0$ the roots of the equations

$$(a_{33})^{(6)} (v^{(6)})^2 + (\sigma_1)^{(6)} v^{(6)} - (a_{32})^{(6)} = 0$$

and $(b_{33})^{(6)} (u^{(6)})^2 + (\tau_1)^{(6)} u^{(6)} - (b_{32})^{(6)} = 0$ and 463

Definition of $(\bar{v}_1)^{(6)}, (\bar{v}_2)^{(6)}, (\bar{u}_1)^{(6)}, (\bar{u}_2)^{(6)}$: 464

By $(\bar{v}_1)^{(6)} > 0, (\bar{v}_2)^{(6)} < 0$ and respectively $(\bar{u}_1)^{(6)} > 0, (\bar{u}_2)^{(6)} < 0$ the

roots of the equations $(a_{33})^{(6)} (v^{(6)})^2 + (\sigma_2)^{(6)} v^{(6)} - (a_{32})^{(6)} = 0$

and $(b_{33})^{(6)} (u^{(6)})^2 + (\tau_2)^{(6)} u^{(6)} - (b_{32})^{(6)} = 0$

Definition of $(m_1)^{(6)}, (m_2)^{(6)}, (\mu_1)^{(6)}, (\mu_2)^{(6)}, (v_0)^{(6)}$:-

(l) If we define $(m_1)^{(6)}, (m_2)^{(6)}, (\mu_1)^{(6)}, (\mu_2)^{(6)}$ by

$$(m_2)^{(6)} = (v_0)^{(6)}, (m_1)^{(6)} = (v_1)^{(6)}, \text{ if } (v_0)^{(6)} < (v_1)^{(6)}$$

$$(m_2)^{(6)} = (v_1)^{(6)}, (m_1)^{(6)} = (\bar{v}_6)^{(6)}, \text{ if } (v_1)^{(6)} < (v_0)^{(6)} < (\bar{v}_1)^{(6)},$$

and $\boxed{(v_0)^{(6)} = \frac{G_{32}^0}{G_{33}^0}}$

$$(m_2)^{(6)} = (v_1)^{(6)}, (m_1)^{(6)} = (v_0)^{(6)}, \text{ if } (\bar{v}_1)^{(6)} < (v_0)^{(6)}$$

and analogously

465

$$(\mu_2)^{(6)} = (u_0)^{(6)}, (\mu_1)^{(6)} = (u_1)^{(6)}, \text{ if } (u_0)^{(6)} < (u_1)^{(6)}$$

$$(\mu_2)^{(6)} = (u_1)^{(6)}, (\mu_1)^{(6)} = (\bar{u}_1)^{(6)}, \text{ if } (u_1)^{(6)} < (u_0)^{(6)} < (\bar{u}_1)^{(6)},$$

$$\text{and } (u_0)^{(6)} = \begin{matrix} T_{32}^0 \\ T_{33}^0 \end{matrix}$$

$(\mu_2)^{(6)} = (u_1)^{(6)}, (\mu_1)^{(6)} = (u_0)^{(6)}, \text{ if } (\bar{u}_1)^{(6)} < (u_0)^{(6)}$ where $(u_1)^{(6)}, (\bar{u}_1)^{(6)}$ are defined respectively

Then the solution satisfies the inequalities

466

$$G_{32}^0 e^{((S_1)^{(6)} - (p_{32})^{(6)})t} \leq G_{32}(t) \leq G_{32}^0 e^{(S_1)^{(6)}t}$$

where $(p_i)^{(6)}$ is defined by equation above

$$\frac{1}{(m_1)^{(6)}} G_{32}^0 e^{((S_1)^{(6)} - (p_{32})^{(6)})t} \leq G_{33}(t) \leq \frac{1}{(m_2)^{(6)}} G_{32}^0 e^{(S_1)^{(6)}t} \quad 467$$

$$\left(\frac{(a_{34})^{(6)} G_{32}^0}{(m_1)^{(6)} ((S_1)^{(6)} - (p_{32})^{(6)} - (S_2)^{(6)})} \left[e^{((S_1)^{(6)} - (p_{32})^{(6)})t} - e^{-(S_2)^{(6)}t} \right] + G_{34}^0 e^{-(S_2)^{(6)}t} \right) \leq G_{34}(t) \leq (a_{34})^{(6)} G_{32}^0 (m_2)^{(6)} (S_1)^{(6)} - (a_{34}')^{(6)} 6e^{(S_1)^{(6)}t} - e^{-(a_{34}')^{(6)}t} + G_{34}^0 e^{-(a_{34}')^{(6)}t} \quad 468$$

$$T_{32}^0 e^{(R_1)^{(6)}t} \leq T_{32}(t) \leq T_{32}^0 e^{((R_1)^{(6)} + (r_{32})^{(6)})t} \quad 469$$

$$\frac{1}{(\mu_1)^{(6)}} T_{32}^0 e^{(R_1)^{(6)}t} \leq T_{32}(t) \leq \frac{1}{(\mu_2)^{(6)}} T_{32}^0 e^{((R_1)^{(6)} + (r_{32})^{(6)})t} \quad 470$$

$$\frac{(b_{34})^{(6)} T_{32}^0}{(\mu_1)^{(6)} ((R_1)^{(6)} - (b_{34})^{(6)})} \left[e^{(R_1)^{(6)}t} - e^{-(b_{34}')^{(6)}t} \right] + T_{34}^0 e^{-(b_{34}')^{(6)}t} \leq T_{34}(t) \leq \quad 471$$

$$\frac{(a_{34})^{(6)} T_{32}^0}{(\mu_2)^{(6)} ((R_1)^{(6)} + (r_{32})^{(6)} + (R_2)^{(6)})} \left[e^{((R_1)^{(6)} + (r_{32})^{(6)})t} - e^{-(R_2)^{(6)}t} \right] + T_{34}^0 e^{-(R_2)^{(6)}t}$$

Definition of $(S_1)^{(6)}, (S_2)^{(6)}, (R_1)^{(6)}, (R_2)^{(6)}$:-

472

473

Where $(S_1)^{(6)} = (a_{32})^{(6)}(m_2)^{(6)} - (a'_{32})^{(6)}$

$$(S_2)^{(6)} = (a_{34})^{(6)} - (p_{34})^{(6)}$$

$$(R_1)^{(6)} = (b_{32})^{(6)}(\mu_2)^{(6)} - (b'_{32})^{(6)}$$

$$(R_2)^{(6)} = (b'_{34})^{(6)} - (r_{34})^{(6)}$$

474

475

Proof : From Governing equations we obtain

$$\frac{dv^{(1)}}{dt} = (a_{13})^{(1)} - \left((a'_{13})^{(1)} - (a'_{14})^{(1)} + (a''_{13})^{(1)}(T_{14}, t) \right) - (a''_{14})^{(1)}(T_{14}, t)v^{(1)} - (a_{14})^{(1)}v^{(1)}$$

Definition of $v^{(1)}$:-
$$v^{(1)} = \begin{matrix} G_{13} \\ G_{14} \end{matrix}$$

It follows

$$- \left((a_{14})^{(1)}(v^{(1)})^2 + (\sigma_2)^{(1)}v^{(1)} - (a_{13})^{(1)} \right) \leq \frac{dv^{(1)}}{dt} \leq - \left((a_{14})^{(1)}(v^{(1)})^2 + (\sigma_1)^{(1)}v^{(1)} - (a_{13})^{(1)} \right)$$

From which one obtains

Definition of $(\bar{v}_1)^{(1)}, (v_0)^{(1)}$:-

(a) For $0 < \begin{matrix} G_{13}^0 \\ G_{14}^0 \end{matrix} < (v_0)^{(1)} < (v_1)^{(1)} < (\bar{v}_1)^{(1)}$

$$v^{(1)}(t) \geq \frac{(v_1)^{(1)} + (C)^{(1)}(v_2)^{(1)} e^{[-(a_{14})^{(1)}(v_1)^{(1)} - (v_0)^{(1)}]t}}{1 + (C)^{(1)} e^{[-(a_{14})^{(1)}(v_1)^{(1)} - (v_0)^{(1)}]t}}, \quad \boxed{(C)^{(1)} = \frac{(v_1)^{(1)} - (v_0)^{(1)}}{(v_0)^{(1)} - (v_2)^{(1)}}$$

it follows $(v_0)^{(1)} \leq v^{(1)}(t) \leq (v_1)^{(1)}$

In the same manner, we get

$$v^{(1)}(t) \leq \frac{(\bar{v}_1)^{(1)} + (\bar{C})^{(1)}(\bar{v}_2)^{(1)} e^{[-(a_{14})^{(1)}(\bar{v}_1)^{(1)} - (\bar{v}_2)^{(1)}]t}}{1 + (\bar{C})^{(1)} e^{[-(a_{14})^{(1)}(\bar{v}_1)^{(1)} - (\bar{v}_2)^{(1)}]t}}, \quad \boxed{(\bar{C})^{(1)} = \frac{(\bar{v}_1)^{(1)} - (v_0)^{(1)}}{(v_0)^{(1)} - (\bar{v}_2)^{(1)}}$$

From which we deduce $(v_0)^{(1)} \leq v^{(1)}(t) \leq (\bar{v}_1)^{(1)}$

(b) If $0 < (v_1)^{(1)} < (v_0)^{(1)} = \frac{G_{13}^0}{G_{14}^0} < (\bar{v}_1)^{(1)}$ we find like in the previous case,

$$(v_1)^{(1)} \leq \frac{(v_1)^{(1)} + (C)^{(1)}(v_2)^{(1)} e^{[-(a_{14})^{(1)}(v_1)^{(1)} - (v_2)^{(1)}]t}}{1 + (C)^{(1)} e^{[-(a_{14})^{(1)}(v_1)^{(1)} - (v_2)^{(1)}]t}} \leq v^{(1)}(t) \leq \frac{(\bar{v}_1)^{(1)} + (\bar{C})^{(1)}(\bar{v}_2)^{(1)} e^{[-(a_{14})^{(1)}(\bar{v}_1)^{(1)} - (\bar{v}_2)^{(1)}]t}}{1 + (\bar{C})^{(1)} e^{[-(a_{14})^{(1)}(\bar{v}_1)^{(1)} - (\bar{v}_2)^{(1)}]t}} \leq (\bar{v}_1)^{(1)}$$

(c) If $0 < (v_1)^{(1)} \leq (\bar{v}_1)^{(1)} \leq \frac{G_{13}^0}{G_{14}^0}$, we obtain

$$(v_1)^{(1)} \leq v^{(1)}(t) \leq \frac{(\bar{v}_1)^{(1)} + (\bar{C})^{(1)}(\bar{v}_2)^{(1)} e^{[-(a_{14})^{(1)}(\bar{v}_1)^{(1)} - (\bar{v}_2)^{(1)}]t}}{1 + (\bar{C})^{(1)} e^{[-(a_{14})^{(1)}(\bar{v}_1)^{(1)} - (\bar{v}_2)^{(1)}]t}} \leq (v_0)^{(1)}$$

And so with the notation of the first part of condition (c), we have

Definition of $v^{(1)}(t)$:-

$$(m_2)^{(1)} \leq v^{(1)}(t) \leq (m_1)^{(1)}, \quad \boxed{v^{(1)}(t) = \frac{G_{13}(t)}{G_{14}(t)}}$$

In a completely analogous way, we obtain

Definition of $u^{(1)}(t)$:-

$$(\mu_2)^{(1)} \leq u^{(1)}(t) \leq (\mu_1)^{(1)}, \quad \boxed{u^{(1)}(t) = \frac{T_{13}(t)}{T_{14}(t)}}$$

Now, using this result and replacing it in concatenated equations of global system we get easily the result stated in the theorem.

Particular case :

If $(a_{13}^{(1)})'' = (a_{14}^{(1)})''$, then $(\sigma_1)^{(1)} = (\sigma_2)^{(1)}$ and in this case $(v_1)^{(1)} = (\bar{v}_1)^{(1)}$ if in addition $(v_0)^{(1)} = (v_1)^{(1)}$ then $v^{(1)}(t) = (v_0)^{(1)}$ and as a consequence $G_{13}(t) = (v_0)^{(1)}G_{14}(t)$ this also defines $(v_0)^{(1)}$ for the special case Analogously if $(b_{13}^{(1)})'' = (b_{14}^{(1)})''$, then $(\tau_1)^{(1)} = (\tau_2)^{(1)}$ and then $(u_1)^{(1)} = (\bar{u}_1)^{(1)}$ if in addition $(u_0)^{(1)} = (u_1)^{(1)}$ then $T_{13}(t) = (u_0)^{(1)}T_{14}(t)$ This is an important consequence of the relation between $(v_1)^{(1)}$ and $(\bar{v}_1)^{(1)}$, and definition of $(u_0)^{(1)}$.

Proof : From the concatenated set of global governing equations we obtain

$$\frac{dv^{(2)}}{dt} = (a_{16})^{(2)} - \left((a'_{16})^{(2)} - (a'_{17})^{(2)} + (a''_{16})^{(2)}(T_{17}, t) \right) - (a''_{17})^{(2)}(T_{17}, t)v^{(2)} - (a_{17})^{(2)}v^{(2)}$$

Definition of $v^{(2)}$:- $\boxed{v^{(2)} = \frac{G_{16}}{G_{17}}}$

It follows

$$- \left((a_{17})^{(2)}(v^{(2)})^2 + (\sigma_2)^{(2)}v^{(2)} - (a_{16})^{(2)} \right) \leq \frac{dv^{(2)}}{dt} \leq - \left((a_{17})^{(2)}(v^{(2)})^2 + (\sigma_1)^{(2)}v^{(2)} - (a_{16})^{(2)} \right)$$

From which one obtains

Definition of $(\bar{v}_1)^{(2)}, (v_0)^{(2)}$:-

(d) For $0 < (v_0)^{(2)} = \frac{G_{16}^0}{G_{17}^0} < (v_1)^{(2)} < (\bar{v}_1)^{(2)}$

$$v^{(2)}(t) \geq \frac{(v_1)^{(2)} + (C)^{(2)}(v_2)^{(2)} e^{[-(a_{17})^{(2)}(v_1)^{(2)} - (v_0)^{(2)}]t}}{1 + (C)^{(2)} e^{[-(a_{17})^{(2)}(v_1)^{(2)} - (v_0)^{(2)}]t}}, \quad \boxed{(C)^{(2)} = \frac{(v_1)^{(2)} - (v_0)^{(2)}}{(v_0)^{(2)} - (v_2)^{(2)}}$$

it follows $(v_0)^{(2)} \leq v^{(2)}(t) \leq (v_1)^{(2)}$

In the same manner, we get

$$v^{(2)}(t) \leq \frac{(\bar{v}_1)^{(2)} + (\bar{C})^{(2)}(\bar{v}_2)^{(2)} e^{[-(a_{17})^{(2)}(\bar{v}_1)^{(2)} - (\bar{v}_2)^{(2)}]t}}{1 + (\bar{C})^{(2)} e^{[-(a_{17})^{(2)}(\bar{v}_1)^{(2)} - (\bar{v}_2)^{(2)}]t}}, \quad \boxed{(\bar{C})^{(2)} = \frac{(\bar{v}_1)^{(2)} - (v_0)^{(2)}}{(v_0)^{(2)} - (\bar{v}_2)^{(2)}}$$

From which we deduce $(v_0)^{(2)} \leq v^{(2)}(t) \leq (\bar{v}_1)^{(2)}$

(e) If $0 < (v_1)^{(2)} < (v_0)^{(2)} = \frac{G_{16}^0}{G_{17}^0} < (\bar{v}_1)^{(2)}$ we find like in the previous case,

$$\begin{aligned}
 (v_1)^{(2)} &\leq \frac{(v_1)^{(2)} + (C)^{(2)}(v_2)^{(2)} e^{[-(a_{17})^{(2)}(v_1)^{(2)} - (v_2)^{(2)}]t}}{1 + (C)^{(2)} e^{[-(a_{17})^{(2)}(v_1)^{(2)} - (v_2)^{(2)}]t}} \leq v^{(2)}(t) \leq \\
 &\frac{(\bar{v}_1)^{(2)} + (\bar{C})^{(2)}(\bar{v}_2)^{(2)} e^{[-(a_{17})^{(2)}(\bar{v}_1)^{(2)} - (\bar{v}_2)^{(2)}]t}}{1 + (\bar{C})^{(2)} e^{[-(a_{17})^{(2)}(\bar{v}_1)^{(2)} - (\bar{v}_2)^{(2)}]t}} \leq (\bar{v}_1)^{(2)}
 \end{aligned}$$

(f) If $0 < (v_1)^{(2)} \leq (\bar{v}_1)^{(2)} \leq (v_0)^{(2)} = \frac{G_{16}^0}{G_{17}^0}$, we obtain 487

$$(v_1)^{(2)} \leq v^{(2)}(t) \leq \frac{(\bar{v}_1)^{(2)} + (\bar{C})^{(2)}(\bar{v}_2)^{(2)} e^{[-(a_{17})^{(2)}(\bar{v}_1)^{(2)} - (\bar{v}_2)^{(2)}]t}}{1 + (\bar{C})^{(2)} e^{[-(a_{17})^{(2)}(\bar{v}_1)^{(2)} - (\bar{v}_2)^{(2)}]t}} \leq (v_0)^{(2)}$$

And so with the notation of the first part of condition (c), we have

Definition of $v^{(2)}(t)$:- 488

$$(m_2)^{(2)} \leq v^{(2)}(t) \leq (m_1)^{(2)}, \quad \boxed{v^{(2)}(t) = \frac{G_{16}(t)}{G_{17}(t)}}$$

In a completely analogous way, we obtain 489

Definition of $u^{(2)}(t)$:-

$$(\mu_2)^{(2)} \leq u^{(2)}(t) \leq (\mu_1)^{(2)}, \quad \boxed{u^{(2)}(t) = \frac{T_{16}(t)}{T_{17}(t)}}$$

Now, using this result and replacing it in global equations we get easily the result stated in the theorem. 490

Particular case : 491

If $(a_{16}^{''})^{(2)} = (a_{17}^{''})^{(2)}$, then $(\sigma_1)^{(2)} = (\sigma_2)^{(2)}$ and in this case $(v_1)^{(2)} = (\bar{v}_1)^{(2)}$ if in addition $(v_0)^{(2)} = (v_1)^{(2)}$ then $v^{(2)}(t) = (v_0)^{(2)}$ and as a consequence $G_{16}(t) = (v_0)^{(2)}G_{17}(t)$

Analogously if $(b_{16}^{''})^{(2)} = (b_{17}^{''})^{(2)}$, then $(\tau_1)^{(2)} = (\tau_2)^{(2)}$ and then

$(u_1)^{(2)} = (\bar{u}_1)^{(2)}$ if in addition $(u_0)^{(2)} = (u_1)^{(2)}$ then $T_{16}(t) = (u_0)^{(2)}T_{17}(t)$ This is an important consequence of the relation between $(v_1)^{(2)}$ and $(\bar{v}_1)^{(2)}$ 492

Proof : From Global equations we obtain 493

$$\frac{dv^{(3)}}{dt} = (a_{20})^{(3)} - \left((a_{20}')^{(3)} - (a_{21}')^{(3)} + (a_{20}'')^{(3)}(T_{21}, t) \right) - (a_{21}'')^{(3)}(T_{21}, t)v^{(3)} - (a_{21})^{(3)}v^{(3)}$$

Definition of $v^{(3)}$:- 494

$$\boxed{v^{(3)} = \frac{G_{20}}{G_{21}}}$$

It follows

$$- \left((a_{21})^{(3)}(v^{(3)})^2 + (\sigma_2)^{(3)}v^{(3)} - (a_{20})^{(3)} \right) \leq \frac{dv^{(3)}}{dt} \leq - \left((a_{21})^{(3)}(v^{(3)})^2 + (\sigma_1)^{(3)}v^{(3)} - (a_{20})^{(3)} \right)$$

From which one obtains 495

$$(a) \quad \text{For } 0 < (v_0)^{(3)} = \frac{G_{20}^0}{G_{21}^0} < (v_1)^{(3)} < (\bar{v}_1)^{(3)}$$

$$v^{(3)}(t) \geq \frac{(v_1)^{(3)} + (C)^{(3)}(v_2)^{(3)} e^{[-(a_{21})^{(3)}(v_1)^{(3)} - (v_0)^{(3)}]t}}{1 + (C)^{(3)} e^{[-(a_{21})^{(3)}(v_1)^{(3)} - (v_0)^{(3)}]t}}, \quad \boxed{(C)^{(3)} = \frac{(v_1)^{(3)} - (v_0)^{(3)}}{(v_0)^{(3)} - (v_2)^{(3)}}}$$

it follows $(v_0)^{(3)} \leq v^{(3)}(t) \leq (v_1)^{(3)}$

In the same manner, we get 497

$$v^{(3)}(t) \leq \frac{(\bar{v}_1)^{(3)} + (\bar{C})^{(3)}(\bar{v}_2)^{(3)} e^{[-(a_{21})^{(3)}(\bar{v}_1)^{(3)} - (\bar{v}_2)^{(3)}]t}}{1 + (\bar{C})^{(3)} e^{[-(a_{21})^{(3)}(\bar{v}_1)^{(3)} - (\bar{v}_2)^{(3)}]t}}, \quad \boxed{(\bar{C})^{(3)} = \frac{(\bar{v}_1)^{(3)} - (v_0)^{(3)}}{(v_0)^{(3)} - (\bar{v}_2)^{(3)}}}$$

Definition of $(\bar{v}_1)^{(3)}$:-

From which we deduce $(v_0)^{(3)} \leq v^{(3)}(t) \leq (\bar{v}_1)^{(3)}$

(b) If $0 < (v_1)^{(3)} < (v_0)^{(3)} = \frac{G_{20}^0}{G_{21}^0} < (\bar{v}_1)^{(3)}$ we find like in the previous case, 498

$$\begin{aligned}
 (v_1)^{(3)} &\leq \frac{(v_1)^{(3)} + (C)^{(3)}(v_2)^{(3)} e^{[-(a_{21})^{(3)}(v_1)^{(3)} - (v_2)^{(3)}]t}}{1 + (C)^{(3)} e^{[-(a_{21})^{(3)}(v_1)^{(3)} - (v_2)^{(3)}]t}} \leq v^{(3)}(t) \leq \\
 &\frac{(\bar{v}_1)^{(3)} + (\bar{C})^{(3)}(\bar{v}_2)^{(3)} e^{[-(a_{21})^{(3)}(\bar{v}_1)^{(3)} - (\bar{v}_2)^{(3)}]t}}{1 + (\bar{C})^{(3)} e^{[-(a_{21})^{(3)}(\bar{v}_1)^{(3)} - (\bar{v}_2)^{(3)}]t}} \leq (\bar{v}_1)^{(3)}
 \end{aligned}$$

(c) If $0 < (v_1)^{(3)} \leq (\bar{v}_1)^{(3)} \leq (v_0)^{(3)} = \frac{G_{20}^0}{G_{21}^0}$, we obtain 499

$$(v_1)^{(3)} \leq v^{(3)}(t) \leq \frac{(\bar{v}_1)^{(3)} + (\bar{C})^{(3)}(\bar{v}_2)^{(3)} e^{[-(a_{21})^{(3)}(\bar{v}_1)^{(3)} - (\bar{v}_2)^{(3)}]t}}{1 + (\bar{C})^{(3)} e^{[-(a_{21})^{(3)}(\bar{v}_1)^{(3)} - (\bar{v}_2)^{(3)}]t}} \leq (v_0)^{(3)}$$

And so with the notation of the first part of condition (c), we have

Definition of $v^{(3)}(t)$:-

$$(m_2)^{(3)} \leq v^{(3)}(t) \leq (m_1)^{(3)}, \quad v^{(3)}(t) = \frac{G_{20}(t)}{G_{21}(t)}$$

In a completely analogous way, we obtain

Definition of $u^{(3)}(t)$:-

$$(\mu_2)^{(3)} \leq u^{(3)}(t) \leq (\mu_1)^{(3)}, \quad u^{(3)}(t) = \frac{T_{20}(t)}{T_{21}(t)}$$

Now, using this result and replacing it in Global Equations we get easily the result stated in the theorem.

Particular case :

If $(a_{20})^{(3)} = (a_{21})^{(3)}$, then $(\sigma_1)^{(3)} = (\sigma_2)^{(3)}$ and in this case $(v_1)^{(3)} = (\bar{v}_1)^{(3)}$ if in addition $(v_0)^{(3)} = (v_1)^{(3)}$ then $v^{(3)}(t) = (v_0)^{(3)}$ and as a consequence $G_{20}(t) = (v_0)^{(3)}G_{21}(t)$

500

Analogously if $(b_{20})^{(3)} = (b_{21})^{(3)}$, then $(\tau_1)^{(3)} = (\tau_2)^{(3)}$ and then

$(u_1)^{(3)} = (\bar{u}_1)^{(3)}$ if in addition $(u_0)^{(3)} = (u_1)^{(3)}$ then $T_{20}(t) = (u_0)^{(3)}T_{21}(t)$ This is an important consequence of the relation between $(v_1)^{(3)}$ and $(\bar{v}_1)^{(3)}$

Proof : From Global equations we obtain

$$\frac{dv^{(4)}}{dt} = (a_{24})^{(4)} - \left((a'_{24})^{(4)} - (a'_{25})^{(4)} + (a''_{24})^{(4)}(T_{25}, t) \right) - (a''_{25})^{(4)}(T_{25}, t)v^{(4)} - (a_{25})^{(4)}v^{(4)}$$

Definition of $v^{(4)}$:-

$$v^{(4)} = \frac{G_{24}}{G_{25}}$$

It follows

$$- \left((a_{25})^{(4)}(v^{(4)})^2 + (\sigma_2)^{(4)}v^{(4)} - (a_{24})^{(4)} \right) \leq \frac{dv^{(4)}}{dt} \leq - \left((a_{25})^{(4)}(v^{(4)})^2 + (\sigma_4)^{(4)}v^{(4)} - (a_{24})^{(4)} \right)$$

From which one obtains

Definition of $(\bar{v}_1)^{(4)}, (v_0)^{(4)}$:-

(d) For $0 < \left(v_0 \right)^{(4)} = \frac{G_{24}^0}{G_{25}^0} < (v_1)^{(4)} < (\bar{v}_1)^{(4)}$

$$v^{(4)}(t) \geq \frac{(v_1)^{(4)} + (C)^{(4)}(v_2)^{(4)} e^{- (a_{25})^{(4)}(v_1)^{(4)} - (v_0)^{(4)} t}}{4 + (C)^{(4)} e^{- (a_{25})^{(4)}(v_1)^{(4)} - (v_0)^{(4)} t}}, \quad (C)^{(4)} = \frac{(v_1)^{(4)} - (v_0)^{(4)}}{(v_0)^{(4)} - (v_2)^{(4)}}$$

it follows $(v_0)^{(4)} \leq v^{(4)}(t) \leq (v_1)^{(4)}$

In the same manner , we get

501

$$v^{(4)}(t) \leq \frac{(\bar{v}_1)^{(4)} + (\bar{C})^{(4)}(\bar{v}_2)^{(4)} e^{- (a_{25})^{(4)}(\bar{v}_1)^{(4)} - (\bar{v}_2)^{(4)} t}}{4 + (\bar{C})^{(4)} e^{- (a_{25})^{(4)}(\bar{v}_1)^{(4)} - (\bar{v}_2)^{(4)} t}}, \quad (\bar{C})^{(4)} = \frac{(\bar{v}_1)^{(4)} - (v_0)^{(4)}}{(v_0)^{(4)} - (\bar{v}_2)^{(4)}}$$

From which we deduce $(v_0)^{(4)} \leq v^{(4)}(t) \leq (\bar{v}_1)^{(4)}$

(e) If $0 < (v_1)^{(4)} < (v_0)^{(4)} = \frac{G_{24}^0}{G_{25}^0} < (\bar{v}_1)^{(4)}$ we find like in the previous case,

502

$$(v_1)^{(4)} \leq \frac{(v_1)^{(4)} + (C)^{(4)}(v_2)^{(4)} e^{- (a_{25})^{(4)}(v_1)^{(4)} - (v_2)^{(4)} t}}{1 + (C)^{(4)} e^{- (a_{25})^{(4)}(v_1)^{(4)} - (v_2)^{(4)} t}} \leq v^{(4)}(t) \leq$$

$$\frac{(\bar{v}_1)^{(4)} + (\bar{C})^{(4)}(\bar{v}_2)^{(4)} e^{- (a_{25})^{(4)}(\bar{v}_1)^{(4)} - (\bar{v}_2)^{(4)} t}}{1 + (\bar{C})^{(4)} e^{- (a_{25})^{(4)}(\bar{v}_1)^{(4)} - (\bar{v}_2)^{(4)} t}} \leq (\bar{v}_1)^{(4)}$$

503

(f) If $0 < (v_1)^{(4)} \leq (\bar{v}_1)^{(4)} \leq \left(v_0 \right)^{(4)} = \frac{G_{24}^0}{G_{25}^0}$, we obtain

504

$$(v_1)^{(4)} \leq v^{(4)}(t) \leq \frac{(\bar{v}_1)^{(4)} + (\bar{C})^{(4)}(\bar{v}_2)^{(4)} e^{- (a_{25})^{(4)}(\bar{v}_1)^{(4)} - (\bar{v}_2)^{(4)} t}}{1 + (\bar{C})^{(4)} e^{- (a_{25})^{(4)}(\bar{v}_1)^{(4)} - (\bar{v}_2)^{(4)} t}} \leq (v_0)^{(4)}$$

And so with the notation of the first part of condition (c) , we have

Definition of $v^{(4)}(t)$:-

505

$$(m_2)^{(4)} \leq v^{(4)}(t) \leq (m_1)^{(4)}, \quad \boxed{v^{(4)}(t) = \frac{G_{24}(t)}{G_{25}(t)}}$$

In a completely analogous way, we obtain

Definition of $u^{(4)}(t)$:-

$$(\mu_2)^{(4)} \leq u^{(4)}(t) \leq (\mu_1)^{(4)}, \quad \boxed{u^{(4)}(t) = \frac{T_{24}(t)}{T_{25}(t)}}$$

Now, using this result and replacing it in Global equations we get easily the result stated in the theorem.

Particular case :

If $(a''_{24})^{(4)} = (a''_{25})^{(4)}$, then $(\sigma_1)^{(4)} = (\sigma_2)^{(4)}$ and in this case $(v_1)^{(4)} = (\bar{v}_1)^{(4)}$ if in addition $(v_0)^{(4)} = (v_1)^{(4)}$ then $v^{(4)}(t) = (v_0)^{(4)}$ and as a consequence $G_{24}(t) = (v_0)^{(4)}G_{25}(t)$ **this also defines $(v_0)^{(4)}$ for the special case .**

Analogously if $(b''_{24})^{(4)} = (b''_{25})^{(4)}$, then $(\tau_1)^{(4)} = (\tau_2)^{(4)}$ and then $(u_1)^{(4)} = (\bar{u}_1)^{(4)}$ if in addition $(u_0)^{(4)} = (u_1)^{(4)}$ then $T_{24}(t) = (u_0)^{(4)}T_{25}(t)$ This is an important consequence of the relation between $(v_1)^{(4)}$ and $(\bar{v}_1)^{(4)}$, **and definition of $(u_0)^{(4)}$.**

506

Proof : From concatenated set of equations we obtain

$$\frac{dv^{(5)}}{dt} = (a_{28})^{(5)} - \left((a'_{28})^{(5)} - (a'_{29})^{(5)} + (a''_{28})^{(5)}(T_{29}, t) \right) - (a''_{29})^{(5)}(T_{29}, t)v^{(5)} - (a_{29})^{(5)}v^{(5)}$$

Definition of $v^{(5)}$:- $\boxed{v^{(5)} = \frac{G_{28}}{G_{29}}}$

It follows

$$- \left((a_{29})^{(5)}(v^{(5)})^2 + (\sigma_2)^{(5)}v^{(5)} - (a_{28})^{(5)} \right) \leq \frac{dv^{(5)}}{dt} \leq - \left((a_{29})^{(5)}(v^{(5)})^2 + (\sigma_1)^{(5)}v^{(5)} - (a_{28})^{(5)} \right)$$

From which one obtains

Definition of $(\bar{v}_1)^{(5)}, (v_0)^{(5)}$:-

(g) For $0 < \boxed{(v_0)^{(5)} = \frac{G_{28}^0}{G_{29}^0}} < (v_1)^{(5)} < (\bar{v}_1)^{(5)}$

$$v^{(5)}(t) \geq \frac{(v_1)^{(5)} + (C)^{(5)}(v_2)^{(5)} e^{[-(a_{29})^{(5)}(v_1)^{(5)} - (v_0)^{(5)}]t}}{5 + (C)^{(5)} e^{[-(a_{29})^{(5)}(v_1)^{(5)} - (v_0)^{(5)}]t}}, \quad \boxed{(C)^{(5)} = \frac{(v_1)^{(5)} - (v_0)^{(5)}}{(v_0)^{(5)} - (v_2)^{(5)}}$$

it follows $(v_0)^{(5)} \leq v^{(5)}(t) \leq (v_1)^{(5)}$

In the same manner , we get

507

$$v^{(5)}(t) \leq \frac{(\bar{v}_1)^{(5)} + (\bar{C})^{(5)}(\bar{v}_2)^{(5)} e^{[-(a_{29})^{(5)}(\bar{v}_1)^{(5)} - (\bar{v}_2)^{(5)}]t}}{5 + (\bar{C})^{(5)} e^{[-(a_{29})^{(5)}(\bar{v}_1)^{(5)} - (\bar{v}_2)^{(5)}]t}}, \quad \boxed{(\bar{C})^{(5)} = \frac{(\bar{v}_1)^{(5)} - (v_0)^{(5)}}{(v_0)^{(5)} - (\bar{v}_2)^{(5)}}$$

From which we deduce $(v_0)^{(5)} \leq v^{(5)}(t) \leq (\bar{v}_5)^{(5)}$

508

(h) If $0 < (v_1)^{(5)} < (v_0)^{(5)} = \frac{G_{28}^0}{G_{29}^0} < (\bar{v}_1)^{(5)}$ we find like in the previous case,

509

$$(v_1)^{(5)} \leq \frac{(v_1)^{(5)} + (C)^{(5)}(v_2)^{(5)} e^{[-(a_{29})^{(5)}(v_1)^{(5)} - (v_2)^{(5)}]t}}{1 + (C)^{(5)} e^{[-(a_{29})^{(5)}(v_1)^{(5)} - (v_2)^{(5)}]t}} \leq v^{(5)}(t) \leq$$

$$\frac{(\bar{v}_1)^{(5)} + (C)^{(5)}(\bar{v}_2)^{(5)} e^{[-(a_{29})^{(5)}(\bar{v}_1)^{(5)} - (\bar{v}_2)^{(5)}]t}}{1 + (C)^{(5)} e^{[-(a_{29})^{(5)}(\bar{v}_1)^{(5)} - (\bar{v}_2)^{(5)}]t}} \leq (\bar{v}_1)^{(5)}$$

(i) If $0 < (v_1)^{(5)} \leq (\bar{v}_1)^{(5)} \leq \boxed{(v_0)^{(5)} = \frac{G_{28}^0}{G_{29}^0}}$, we obtain

510

$$(v_1)^{(5)} \leq v^{(5)}(t) \leq \frac{(\bar{v}_1)^{(5)} + (C)^{(5)}(\bar{v}_2)^{(5)} e^{[-(a_{29})^{(5)}(\bar{v}_1)^{(5)} - (\bar{v}_2)^{(5)}]t}}{1 + (C)^{(5)} e^{[-(a_{29})^{(5)}(\bar{v}_1)^{(5)} - (\bar{v}_2)^{(5)}]t}} \leq (v_0)^{(5)}$$

And so with the notation of the first part of condition (c), we have

Definition of $v^{(5)}(t)$:-

$$(m_2)^{(5)} \leq v^{(5)}(t) \leq (m_1)^{(5)}, \quad \boxed{v^{(5)}(t) = \frac{G_{28}(t)}{G_{29}(t)}}$$

In a completely analogous way, we obtain

Definition of $u^{(5)}(t)$:-

$$(\mu_2)^{(5)} \leq u^{(5)}(t) \leq (\mu_1)^{(5)}, \quad \boxed{u^{(5)}(t) = \frac{T_{28}(t)}{T_{29}(t)}}$$

Now, using this result and replacing it in global equations we get easily the result stated in the theorem.

Particular case :

If $(a_{28}^{''})^{(5)} = (a_{29}^{''})^{(5)}$, then $(\sigma_1)^{(5)} = (\sigma_2)^{(5)}$ and in this case $(v_1)^{(5)} = (\bar{v}_1)^{(5)}$ if in addition $(v_0)^{(5)} = (v_5)^{(5)}$ then $v^{(5)}(t) = (v_0)^{(5)}$ and as a consequence $G_{28}(t) = (v_0)^{(5)}G_{29}(t)$ **this also defines $(v_0)^{(5)}$ for the special case .**

Analogously if $(b_{28}^{''})^{(5)} = (b_{29}^{''})^{(5)}$, then $(\tau_1)^{(5)} = (\tau_2)^{(5)}$ and then $(u_1)^{(5)} = (\bar{u}_1)^{(5)}$ if in addition $(u_0)^{(5)} = (u_1)^{(5)}$ then $T_{28}(t) = (u_0)^{(5)}T_{29}(t)$ This is an important consequence of the relation between $(v_1)^{(5)}$ and $(\bar{v}_1)^{(5)}$, **and definition of $(u_0)^{(5)}$.**

511
512

Proof : From Global equations we obtain

$$\frac{dv^{(6)}}{dt} = (a_{32})^{(6)} - \left((a'_{32})^{(6)} - (a'_{33})^{(6)} + (a''_{32})^{(6)}(T_{33}, t) \right) - (a''_{33})^{(6)}(T_{33}, t)v^{(6)} - (a_{33})^{(6)}v^{(6)}$$

Definition of $v^{(6)}$:- $\boxed{v^{(6)} = \frac{G_{32}}{G_{33}}}$

It follows

$$- \left((a_{33})^{(6)}(v^{(6)})^2 + (\sigma_2)^{(6)}v^{(6)} - (a_{32})^{(6)} \right) \leq \frac{dv^{(6)}}{dt} \leq - \left((a_{33})^{(6)}(v^{(6)})^2 + (\sigma_1)^{(6)}v^{(6)} - (a_{32})^{(6)} \right)$$

From which one obtains

Definition of $(\bar{v}_1)^{(6)}, (v_0)^{(6)}$:-

513

(j) For $0 < \boxed{(v_0)^{(6)} = \frac{G_{32}^0}{G_{33}^0}} < (v_1)^{(6)} < (\bar{v}_1)^{(6)}$

$$v^{(6)}(t) \geq \frac{(v_1)^{(6)} + (C)^{(6)}(v_2)^{(6)} e^{[-(a_{33})^{(6)}(v_1)^{(6)} - (v_0)^{(6)}]t}}{1 + (C)^{(6)} e^{[-(a_{33})^{(6)}(v_1)^{(6)} - (v_0)^{(6)}]t}}, \quad \boxed{(C)^{(6)} = \frac{(v_1)^{(6)} - (v_0)^{(6)}}{(v_0)^{(6)} - (v_2)^{(6)}}$$

it follows $(v_0)^{(6)} \leq v^{(6)}(t) \leq (v_1)^{(6)}$

In the same manner , we get

514

$$v^{(6)}(t) \leq \frac{(\bar{v}_1)^{(6)} + (\bar{C})^{(6)} (\bar{v}_2)^{(6)} e^{[-(a_{33})^{(6)} (\bar{v}_1)^{(6)} - (\bar{v}_2)^{(6)}] t}}{1 + (\bar{C})^{(6)} e^{[-(a_{33})^{(6)} (\bar{v}_1)^{(6)} - (\bar{v}_2)^{(6)}] t}} , \quad \boxed{(\bar{C})^{(6)} = \frac{(\bar{v}_1)^{(6)} - (v_0)^{(6)}}{(v_0)^{(6)} - (\bar{v}_2)^{(6)}}$$

From which we deduce $(v_0)^{(6)} \leq v^{(6)}(t) \leq (\bar{v}_1)^{(6)}$

(k) If $0 < (v_1)^{(6)} < (v_0)^{(6)} = \frac{G_{32}^0}{G_{33}^0} < (\bar{v}_1)^{(6)}$ we find like in the previous case, 515

$$(v_1)^{(6)} \leq \frac{(v_1)^{(6)} + (C)^{(6)} (v_2)^{(6)} e^{[-(a_{33})^{(6)} (v_1)^{(6)} - (v_2)^{(6)}] t}}{1 + (C)^{(6)} e^{[-(a_{33})^{(6)} (v_1)^{(6)} - (v_2)^{(6)}] t}} \leq v^{(6)}(t) \leq$$

$$\frac{(\bar{v}_1)^{(6)} + (\bar{C})^{(6)} (\bar{v}_2)^{(6)} e^{[-(a_{33})^{(6)} (\bar{v}_1)^{(6)} - (\bar{v}_2)^{(6)}] t}}{1 + (\bar{C})^{(6)} e^{[-(a_{33})^{(6)} (\bar{v}_1)^{(6)} - (\bar{v}_2)^{(6)}] t}} \leq (\bar{v}_1)^{(6)}$$

(l) If $0 < (v_1)^{(6)} \leq (\bar{v}_1)^{(6)} \leq \boxed{(v_0)^{(6)} = \frac{G_{32}^0}{G_{33}^0}}$, we obtain 516

$$(v_1)^{(6)} \leq v^{(6)}(t) \leq \frac{(\bar{v}_1)^{(6)} + (\bar{C})^{(6)} (\bar{v}_2)^{(6)} e^{[-(a_{33})^{(6)} (\bar{v}_1)^{(6)} - (\bar{v}_2)^{(6)}] t}}{1 + (\bar{C})^{(6)} e^{[-(a_{33})^{(6)} (\bar{v}_1)^{(6)} - (\bar{v}_2)^{(6)}] t}} \leq (v_0)^{(6)}$$

And so with the notation of the first part of condition (c) , we have

Definition of $v^{(6)}(t)$:-

$$(m_2)^{(6)} \leq v^{(6)}(t) \leq (m_1)^{(6)} , \quad \boxed{v^{(6)}(t) = \frac{G_{32}(t)}{G_{33}(t)}}$$

In a completely analogous way, we obtain

Definition of $u^{(6)}(t)$:-

$$(\mu_2)^{(6)} \leq u^{(6)}(t) \leq (\mu_1)^{(6)} , \quad \boxed{u^{(6)}(t) = \frac{T_{32}(t)}{T_{33}(t)}}$$

Now, using this result and replacing it in global equations we get easily the result stated in the theorem.

Particular case :

If $(a''_{32})^{(6)} = (a''_{33})^{(6)}$, then $(\sigma_1)^{(6)} = (\sigma_2)^{(6)}$ and in this case $(v_1)^{(6)} = (\bar{v}_1)^{(6)}$ if in addition $(v_0)^{(6)} = (v_1)^{(6)}$ then $v^{(6)}(t) = (v_0)^{(6)}$ and as a consequence $G_{32}(t) = (v_0)^{(6)} G_{33}(t)$ **this also defines $(v_0)^{(6)}$ for the special case .**

Analogously if $(b''_{32})^{(6)} = (b''_{33})^{(6)}$, then $(\tau_1)^{(6)} = (\tau_2)^{(6)}$ and then

$(u_1)^{(6)} = (\bar{u}_1)^{(6)}$ if in addition $(u_0)^{(6)} = (u_1)^{(6)}$ then $T_{32}(t) = (u_0)^{(6)} T_{33}(t)$ This is an important consequence of the relation between $(v_1)^{(6)}$ and $(\bar{v}_1)^{(6)}$, **and definition of $(u_0)^{(6)}$.**

517
518
519

We can prove the following

Theorem 3: If $(a_i'')^{(1)}$ and $(b_i'')^{(1)}$ are independent on t , and the conditions

$$(a'_{13})^{(1)} (a'_{14})^{(1)} - (a_{13})^{(1)} (a_{14})^{(1)} < 0$$

$$(a'_{13})^{(1)} (a'_{14})^{(1)} - (a_{13})^{(1)} (a_{14})^{(1)} + (a_{13})^{(1)} (p_{13})^{(1)} + (a'_{14})^{(1)} (p_{14})^{(1)} + (p_{13})^{(1)} (p_{14})^{(1)} > 0$$

$$(b'_{13})^{(1)} (b'_{14})^{(1)} - (b_{13})^{(1)} (b_{14})^{(1)} > 0 ,$$

$$(b'_{13})^{(1)} (b'_{14})^{(1)} - (b_{13})^{(1)} (b_{14})^{(1)} - (b'_{13})^{(1)} (r_{14})^{(1)} - (b'_{14})^{(1)} (r_{14})^{(1)} + (r_{13})^{(1)} (r_{14})^{(1)} < 0$$

with $(p_{13})^{(1)}$, $(r_{14})^{(1)}$ as defined are satisfied , then the system

If $(a_i'')^{(2)}$ and $(b_i'')^{(2)}$ are independent on t , and the conditions

$$(a'_{16})^{(2)} (a'_{17})^{(2)} - (a_{16})^{(2)} (a_{17})^{(2)} < 0$$

$$(a'_{16})^{(2)} (a'_{17})^{(2)} - (a_{16})^{(2)} (a_{17})^{(2)} + (a_{16})^{(2)} (p_{16})^{(2)} + (a'_{17})^{(2)} (p_{17})^{(2)} + (p_{16})^{(2)} (p_{17})^{(2)} > 0$$

$$(b'_{16})^{(2)} (b'_{17})^{(2)} - (b_{16})^{(2)} (b_{17})^{(2)} > 0 ,$$

$$(b'_{16})^{(2)} (b'_{17})^{(2)} - (b_{16})^{(2)} (b_{17})^{(2)} - (b'_{16})^{(2)} (r_{17})^{(2)} - (b'_{17})^{(2)} (r_{17})^{(2)} + (r_{16})^{(2)} (r_{17})^{(2)} < 0$$

with $(p_{16})^{(2)}$, $(r_{17})^{(2)}$ as defined are satisfied , then the system

: If $(a_i'')^{(3)}$ and $(b_i'')^{(3)}$ are independent on t , and the conditions

$$(a'_{20})^{(3)} (a'_{21})^{(3)} - (a_{20})^{(3)} (a_{21})^{(3)} < 0$$

520
521
522
523
524
525

$(a'_{20})^{(3)}(a'_{21})^{(3)} - (a_{20})^{(3)}(a_{21})^{(3)} + (a_{20})^{(3)}(p_{20})^{(3)} + (a'_{21})^{(3)}(p_{21})^{(3)} + (p_{20})^{(3)}(p_{21})^{(3)} > 0$ $(b'_{20})^{(3)}(b'_{21})^{(3)} - (b_{20})^{(3)}(b_{21})^{(3)} > 0$, $(b'_{20})^{(3)}(b'_{21})^{(3)} - (b_{20})^{(3)}(b_{21})^{(3)} - (b'_{20})^{(3)}(r_{21})^{(3)} - (b'_{21})^{(3)}(r_{21})^{(3)} + (r_{20})^{(3)}(r_{21})^{(3)} < 0$ with $(p_{20})^{(3)}, (r_{21})^{(3)}$ as defined are satisfied, then the system	526
We can prove the following	
If $(a''_i)^{(4)}$ and $(b''_i)^{(4)}$ are independent on t , and the conditions $(a'_{24})^{(4)}(a'_{25})^{(4)} - (a_{24})^{(4)}(a_{25})^{(4)} < 0$ $(a'_{24})^{(4)}(a'_{25})^{(4)} - (a_{24})^{(4)}(a_{25})^{(4)} + (a_{24})^{(4)}(p_{24})^{(4)} + (a'_{25})^{(4)}(p_{25})^{(4)} + (p_{24})^{(4)}(p_{25})^{(4)} > 0$ $(b'_{24})^{(4)}(b'_{25})^{(4)} - (b_{24})^{(4)}(b_{25})^{(4)} > 0$, $(b'_{24})^{(4)}(b'_{25})^{(4)} - (b_{24})^{(4)}(b_{25})^{(4)} - (b'_{24})^{(4)}(r_{25})^{(4)} - (b'_{25})^{(4)}(r_{25})^{(4)} + (r_{24})^{(4)}(r_{25})^{(4)} < 0$ with $(p_{24})^{(4)}, (r_{25})^{(4)}$ as defined are satisfied, then the system	527
If $(a''_i)^{(5)}$ and $(b''_i)^{(5)}$ are independent on t , and the conditions $(a'_{28})^{(5)}(a'_{29})^{(5)} - (a_{28})^{(5)}(a_{29})^{(5)} < 0$ $(a'_{28})^{(5)}(a'_{29})^{(5)} - (a_{28})^{(5)}(a_{29})^{(5)} + (a_{28})^{(5)}(p_{28})^{(5)} + (a'_{29})^{(5)}(p_{29})^{(5)} + (p_{28})^{(5)}(p_{29})^{(5)} > 0$ $(b'_{28})^{(5)}(b'_{29})^{(5)} - (b_{28})^{(5)}(b_{29})^{(5)} > 0$, $(b'_{28})^{(5)}(b'_{29})^{(5)} - (b_{28})^{(5)}(b_{29})^{(5)} - (b'_{28})^{(5)}(r_{29})^{(5)} - (b'_{29})^{(5)}(r_{29})^{(5)} + (r_{28})^{(5)}(r_{29})^{(5)} < 0$ with $(p_{28})^{(5)}, (r_{29})^{(5)}$ as defined are satisfied, then the system	528
If $(a''_i)^{(6)}$ and $(b''_i)^{(6)}$ are independent on t , and the conditions $(a'_{32})^{(6)}(a'_{33})^{(6)} - (a_{32})^{(6)}(a_{33})^{(6)} < 0$ $(a'_{32})^{(6)}(a'_{33})^{(6)} - (a_{32})^{(6)}(a_{33})^{(6)} + (a_{32})^{(6)}(p_{32})^{(6)} + (a'_{33})^{(6)}(p_{33})^{(6)} + (p_{32})^{(6)}(p_{33})^{(6)} > 0$ $(b'_{32})^{(6)}(b'_{33})^{(6)} - (b_{32})^{(6)}(b_{33})^{(6)} > 0$, $(b'_{32})^{(6)}(b'_{33})^{(6)} - (b_{32})^{(6)}(b_{33})^{(6)} - (b'_{32})^{(6)}(r_{33})^{(6)} - (b'_{33})^{(6)}(r_{33})^{(6)} + (r_{32})^{(6)}(r_{33})^{(6)} < 0$ with $(p_{32})^{(6)}, (r_{33})^{(6)}$ as defined are satisfied, then the system Boolean satisfiability problem and N puzzle	529
$(a_{13})^{(1)}G_{14} - [(a'_{13})^{(1)} + (a''_{13})^{(1)}(T_{14})]G_{13} = 0$	530
$(a_{14})^{(1)}G_{13} - [(a'_{14})^{(1)} + (a''_{14})^{(1)}(T_{14})]G_{14} = 0$	531
$(a_{15})^{(1)}G_{14} - [(a'_{15})^{(1)} + (a''_{15})^{(1)}(T_{14})]G_{15} = 0$	532
$(b_{13})^{(1)}T_{14} - [(b'_{13})^{(1)} - (b''_{13})^{(1)}(G)]T_{13} = 0$	533
$(b_{14})^{(1)}T_{13} - [(b'_{14})^{(1)} - (b''_{14})^{(1)}(G)]T_{14} = 0$	534
$(b_{15})^{(1)}T_{14} - [(b'_{15})^{(1)} - (b''_{15})^{(1)}(G)]T_{15} = 0$	535
has a unique positive solution, which is an equilibrium solution for the system	536
$(a_{16})^{(2)}G_{17} - [(a'_{16})^{(2)} + (a''_{16})^{(2)}(T_{17})]G_{16} = 0$	537
$(a_{17})^{(2)}G_{16} - [(a'_{17})^{(2)} + (a''_{17})^{(2)}(T_{17})]G_{17} = 0$	538
$(a_{18})^{(2)}G_{17} - [(a'_{18})^{(2)} + (a''_{18})^{(2)}(T_{17})]G_{18} = 0$	539
$(b_{16})^{(2)}T_{17} - [(b'_{16})^{(2)} - (b''_{16})^{(2)}(G_{19})]T_{16} = 0$	540
$(b_{17})^{(2)}T_{16} - [(b'_{17})^{(2)} - (b''_{17})^{(2)}(G_{19})]T_{17} = 0$	541
$(b_{18})^{(2)}T_{17} - [(b'_{18})^{(2)} - (b''_{18})^{(2)}(G_{19})]T_{18} = 0$	542
has a unique positive solution, which is an equilibrium solution for the system	543
$(a_{20})^{(3)}G_{21} - [(a'_{20})^{(3)} + (a''_{20})^{(3)}(T_{21})]G_{20} = 0$	544
$(a_{21})^{(3)}G_{20} - [(a'_{21})^{(3)} + (a''_{21})^{(3)}(T_{21})]G_{21} = 0$	545
$(a_{22})^{(3)}G_{21} - [(a'_{22})^{(3)} + (a''_{22})^{(3)}(T_{21})]G_{22} = 0$	546
$(b_{20})^{(3)}T_{21} - [(b'_{20})^{(3)} - (b''_{20})^{(3)}(G_{23})]T_{20} = 0$	547
$(b_{21})^{(3)}T_{20} - [(b'_{21})^{(3)} - (b''_{21})^{(3)}(G_{23})]T_{21} = 0$	548
$(b_{22})^{(3)}T_{21} - [(b'_{22})^{(3)} - (b''_{22})^{(3)}(G_{23})]T_{22} = 0$	549
has a unique positive solution, which is an equilibrium solution for the system	550
$(a_{24})^{(4)}G_{25} - [(a'_{24})^{(4)} + (a''_{24})^{(4)}(T_{25})]G_{24} = 0$	551
$(a_{25})^{(4)}G_{24} - [(a'_{25})^{(4)} + (a''_{25})^{(4)}(T_{25})]G_{25} = 0$	552
$(a_{26})^{(4)}G_{25} - [(a'_{26})^{(4)} + (a''_{26})^{(4)}(T_{25})]G_{26} = 0$	553
$(b_{24})^{(4)}T_{25} - [(b'_{24})^{(4)} - (b''_{24})^{(4)}((G_{27}))]T_{24} = 0$	554
$(b_{25})^{(4)}T_{24} - [(b'_{25})^{(4)} - (b''_{25})^{(4)}((G_{27}))]T_{25} = 0$	555
$(b_{26})^{(4)}T_{25} - [(b'_{26})^{(4)} - (b''_{26})^{(4)}((G_{27}))]T_{26} = 0$	556

has a unique positive solution , which is an equilibrium solution for the system 557

$$(a_{28})^{(5)}G_{29} - [(a'_{28})^{(5)} + (a''_{28})^{(5)}(T_{29})]G_{28} = 0 \quad 558$$

$$(a_{29})^{(5)}G_{28} - [(a'_{29})^{(5)} + (a''_{29})^{(5)}(T_{29})]G_{29} = 0 \quad 559$$

$$(a_{30})^{(5)}G_{29} - [(a'_{30})^{(5)} + (a''_{30})^{(5)}(T_{29})]G_{30} = 0 \quad 560$$

$$(b_{28})^{(5)}T_{29} - [(b'_{28})^{(5)} - (b''_{28})^{(5)}(G_{31})]T_{28} = 0 \quad 561$$

$$(b_{29})^{(5)}T_{28} - [(b'_{29})^{(5)} - (b''_{29})^{(5)}(G_{31})]T_{29} = 0 \quad 562$$

$$(b_{30})^{(5)}T_{29} - [(b'_{30})^{(5)} - (b''_{30})^{(5)}(G_{31})]T_{30} = 0 \quad 563$$

has a unique positive solution , which is an equilibrium solution for the system 564

$$(a_{32})^{(6)}G_{33} - [(a'_{32})^{(6)} + (a''_{32})^{(6)}(T_{33})]G_{32} = 0 \quad 565$$

$$(a_{33})^{(6)}G_{32} - [(a'_{33})^{(6)} + (a''_{33})^{(6)}(T_{33})]G_{33} = 0 \quad 566$$

$$(a_{34})^{(6)}G_{33} - [(a'_{34})^{(6)} + (a''_{34})^{(6)}(T_{33})]G_{34} = 0 \quad 567$$

$$(b_{32})^{(6)}T_{33} - [(b'_{32})^{(6)} - (b''_{32})^{(6)}(G_{35})]T_{32} = 0 \quad 568$$

$$(b_{33})^{(6)}T_{32} - [(b'_{33})^{(6)} - (b''_{33})^{(6)}(G_{35})]T_{33} = 0 \quad 569$$

$$(b_{34})^{(6)}T_{33} - [(b'_{34})^{(6)} - (b''_{34})^{(6)}(G_{35})]T_{34} = 0 \quad 570$$

has a unique positive solution , which is an equilibrium solution for the system 571

Proof: 572

(a) Indeed the first two equations have a nontrivial solution G_{13}, G_{14} if 573

$$F(T) = (a'_{13})^{(1)}(a'_{14})^{(1)} - (a_{13})^{(1)}(a_{14})^{(1)} + (a'_{13})^{(1)}(a''_{14})^{(1)}(T_{14}) + (a'_{14})^{(1)}(a''_{13})^{(1)}(T_{14}) + (a''_{13})^{(1)}(T_{14})(a''_{14})^{(1)}(T_{14}) = 0 \quad 574$$

(a) Indeed the first two equations have a nontrivial solution G_{16}, G_{17} if

$$F(T_{19}) = (a'_{16})^{(2)}(a'_{17})^{(2)} - (a_{16})^{(2)}(a_{17})^{(2)} + (a'_{16})^{(2)}(a''_{17})^{(2)}(T_{17}) + (a'_{17})^{(2)}(a''_{16})^{(2)}(T_{17}) + (a''_{16})^{(2)}(T_{17})(a''_{17})^{(2)}(T_{17}) = 0 \quad 575$$

(a) Indeed the first two equations have a nontrivial solution G_{20}, G_{21} if

$$F(T_{23}) = (a'_{20})^{(3)}(a'_{21})^{(3)} - (a_{20})^{(3)}(a_{21})^{(3)} + (a'_{20})^{(3)}(a''_{21})^{(3)}(T_{21}) + (a'_{21})^{(3)}(a''_{20})^{(3)}(T_{21}) + (a''_{20})^{(3)}(T_{21})(a''_{21})^{(3)}(T_{21}) = 0 \quad 576$$

(a) Indeed the first two equations have a nontrivial solution G_{24}, G_{25} if

$$F(T_{27}) = (a'_{24})^{(4)}(a'_{25})^{(4)} - (a_{24})^{(4)}(a_{25})^{(4)} + (a'_{24})^{(4)}(a''_{25})^{(4)}(T_{25}) + (a'_{25})^{(4)}(a''_{24})^{(4)}(T_{25}) + (a''_{24})^{(4)}(T_{25})(a''_{25})^{(4)}(T_{25}) = 0$$

(a) Indeed the first two equations have a nontrivial solution G_{28}, G_{29} if
 $F(T_{31}) =$
 $(a'_{28})^{(5)}(a'_{29})^{(5)} - (a_{28})^{(5)}(a_{29})^{(5)} + (a'_{28})^{(5)}(a''_{29})^{(5)}(T_{29}) + (a'_{29})^{(5)}(a''_{28})^{(5)}(T_{29}) +$
 $(a''_{28})^{(5)}(T_{29})(a''_{29})^{(5)}(T_{29}) = 0$

(a) Indeed the first two equations have a nontrivial solution G_{32}, G_{33} if
 $F(T_{35}) =$
 $(a'_{32})^{(6)}(a'_{33})^{(6)} - (a_{32})^{(6)}(a_{33})^{(6)} + (a'_{32})^{(6)}(a''_{33})^{(6)}(T_{33}) + (a'_{33})^{(6)}(a''_{32})^{(6)}(T_{33}) +$
 $(a''_{32})^{(6)}(T_{33})(a''_{33})^{(6)}(T_{33}) = 0$

Definition and uniqueness of T_{14}^* :-

After hypothesis $f(0) < 0, f(\infty) > 0$ and the functions $(a_i'')^{(1)}(T_{14})$ being increasing, it follows that there exists a unique T_{14}^* for which $f(T_{14}^*) = 0$. With this value, we obtain from the three first equations

$$G_{13} = \frac{(a_{13})^{(1)}G_{14}}{[(a'_{13})^{(1)} + (a''_{13})^{(1)}(T_{14}^*)]} , \quad G_{15} = \frac{(a_{15})^{(1)}G_{14}}{[(a'_{15})^{(1)} + (a''_{15})^{(1)}(T_{14}^*)]}$$

Definition and uniqueness of T_{17}^* :-

After hypothesis $f(0) < 0, f(\infty) > 0$ and the functions $(a_i'')^{(2)}(T_{17})$ being increasing, it follows that there exists a unique T_{17}^* for which $f(T_{17}^*) = 0$. With this value, we obtain from the three first equations

$$G_{16} = \frac{(a_{16})^{(2)}G_{17}}{[(a'_{16})^{(2)} + (a''_{16})^{(2)}(T_{17}^*)]} , \quad G_{18} = \frac{(a_{18})^{(2)}G_{17}}{[(a'_{18})^{(2)} + (a''_{18})^{(2)}(T_{17}^*)]}$$

Definition and uniqueness of T_{21}^* :-

After hypothesis $f(0) < 0, f(\infty) > 0$ and the functions $(a_i'')^{(1)}(T_{21})$ being increasing, it follows that there exists a unique T_{21}^* for which $f(T_{21}^*) = 0$. With this value, we obtain from the three first equations

$$G_{20} = \frac{(a_{20})^{(3)}G_{21}}{[(a'_{20})^{(3)} + (a''_{20})^{(3)}(T_{21}^*)]} , \quad G_{22} = \frac{(a_{22})^{(3)}G_{21}}{[(a'_{22})^{(3)} + (a''_{22})^{(3)}(T_{21}^*)]}$$

Definition and uniqueness of T_{25}^* :-

After hypothesis $f(0) < 0, f(\infty) > 0$ and the functions $(a_i'')^{(4)}(T_{25})$ being increasing, it follows that there exists a unique T_{25}^* for which $f(T_{25}^*) = 0$. With this value, we obtain from the three first equations

$$G_{24} = \frac{(a_{24})^{(4)}G_{25}}{[(a'_{24})^{(4)} + (a''_{24})^{(4)}(T_{25}^*)]} , \quad G_{26} = \frac{(a_{26})^{(4)}G_{25}}{[(a'_{26})^{(4)} + (a''_{26})^{(4)}(T_{25}^*)]}$$

Definition and uniqueness of T_{29}^* :-

After hypothesis $f(0) < 0, f(\infty) > 0$ and the functions $(a_i'')^{(5)}(T_{29})$ being increasing, it follows that there exists a unique T_{29}^* for which $f(T_{29}^*) = 0$. With this value, we obtain from the three first equations

$$G_{28} = \frac{(a_{28})^{(5)}G_{29}}{[(a'_{28})^{(5)} + (a''_{28})^{(5)}(T_{29}^*)]} , \quad G_{30} = \frac{(a_{30})^{(5)}G_{29}}{[(a'_{30})^{(5)} + (a''_{30})^{(5)}(T_{29}^*)]}$$

Definition and uniqueness of T_{33}^* :-

After hypothesis $f(0) < 0, f(\infty) > 0$ and the functions $(a_i'')^{(6)}(T_{33})$ being increasing, it follows that there exists a unique T_{33}^* for which $f(T_{33}^*) = 0$. With this value, we obtain from the three first equations

$$G_{32} = \frac{(a_{32})^{(6)}G_{33}}{[(a'_{32})^{(6)} + (a''_{32})^{(6)}(T_{33}^*)]} , \quad G_{34} = \frac{(a_{34})^{(6)}G_{33}}{[(a'_{34})^{(6)} + (a''_{34})^{(6)}(T_{33}^*)]}$$

(e) By the same argument, the equations of global system admit solutions G_{13}, G_{14} if

$$\varphi(G) = (b'_{13})^{(1)}(b'_{14})^{(1)} - (b_{13})^{(1)}(b_{14})^{(1)} -$$

$$[(b'_{13})^{(1)}(b''_{14})^{(1)}(G) + (b'_{14})^{(1)}(b''_{13})^{(1)}(G)] + (b''_{13})^{(1)}(G)(b''_{14})^{(1)}(G) = 0$$

Where in $G(G_{13}, G_{14}, G_{15}), G_{13}, G_{15}$ must be replaced by their values from 96. It is easy to see that φ is a decreasing function in G_{14} taking into account the hypothesis $\varphi(0) > 0, \varphi(\infty) < 0$ it follows that there exists a unique G_{14}^* such that $\varphi(G^*) = 0$

(f) By the same argument, the equations 92,93 admit solutions G_{16}, G_{17} if

$$\varphi(G_{19}) = (b'_{16})^{(2)}(b'_{17})^{(2)} - (b_{16})^{(2)}(b_{17})^{(2)} -$$

$$[(b'_{16})^{(2)}(b''_{17})^{(2)}(G_{19}) + (b'_{17})^{(2)}(b''_{16})^{(2)}(G_{19})] + (b''_{16})^{(2)}(G_{19})(b''_{17})^{(2)}(G_{19}) = 0$$

Where in $(G_{19})(G_{16}, G_{17}, G_{18}), G_{16}, G_{18}$ must be replaced by their values from 96. It is easy to see that φ is a decreasing function in G_{17} taking into account the hypothesis $\varphi(0) > 0, \varphi(\infty) < 0$ it follows that there exists a unique G_{14}^* such that $\varphi((G_{19})^*) = 0$

(g) By the same argument, the equations of the global system admit solutions G_{20}, G_{21} if

$$\varphi(G_{23}) = (b'_{20})^{(3)}(b'_{21})^{(3)} - (b_{20})^{(3)}(b_{21})^{(3)} -$$

$$[(b'_{20})^{(3)}(b''_{21})^{(3)}(G_{23}) + (b'_{21})^{(3)}(b''_{20})^{(3)}(G_{23})] + (b''_{20})^{(3)}(G_{23})(b''_{21})^{(3)}(G_{23}) = 0$$

Where in $G_{23}(G_{20}, G_{21}, G_{22}), G_{20}, G_{22}$ must be replaced by their values from 96. It is easy to see that φ is a decreasing function in G_{21} taking into account the hypothesis $\varphi(0) > 0, \varphi(\infty) < 0$ it follows that there exists a unique G_{21}^* such that $\varphi((G_{23})^*) = 0$

(h) By the same argument, the equations of the global system admit solutions G_{24}, G_{25} if 592

$$\varphi(G_{27}) = (b'_{24})^{(4)}(b'_{25})^{(4)} - (b_{24})^{(4)}(b_{25})^{(4)} - [(b'_{24})^{(4)}(b''_{25})^{(4)}(G_{27}) + (b'_{25})^{(4)}(b''_{24})^{(4)}(G_{27})] + (b''_{24})^{(4)}(G_{27})(b''_{25})^{(4)}(G_{27}) = 0$$

Where in $(G_{27})(G_{24}, G_{25}, G_{26}), G_{24}, G_{26}$ must be replaced by their values. It is easy to see that φ is a decreasing function in G_{25} taking into account the hypothesis $\varphi(0) > 0, \varphi(\infty) < 0$ it follows that there exists a unique G_{25}^* such that $\varphi((G_{27})^*) = 0$

(i) By the same argument, the global equations admit solutions G_{28}, G_{29} if 593

$$\varphi(G_{31}) = (b'_{28})^{(5)}(b'_{29})^{(5)} - (b_{28})^{(5)}(b_{29})^{(5)} - [(b'_{28})^{(5)}(b''_{29})^{(5)}(G_{31}) + (b'_{29})^{(5)}(b''_{28})^{(5)}(G_{31})] + (b''_{28})^{(5)}(G_{31})(b''_{29})^{(5)}(G_{31}) = 0$$

Where in $(G_{31})(G_{28}, G_{29}, G_{30}), G_{28}, G_{30}$ must be replaced by their values from 96. It is easy to see that φ is a decreasing function in G_{29} taking into account the hypothesis $\varphi(0) > 0, \varphi(\infty) < 0$ it follows that there exists a unique G_{29}^* such that $\varphi((G_{31})^*) = 0$

(j) By the same argument, the global equations admit solutions G_{32}, G_{33} if 594

$$\varphi(G_{35}) = (b'_{32})^{(6)}(b'_{33})^{(6)} - (b_{32})^{(6)}(b_{33})^{(6)} - [(b'_{32})^{(6)}(b''_{33})^{(6)}(G_{35}) + (b'_{33})^{(6)}(b''_{32})^{(6)}(G_{35})] + (b''_{32})^{(6)}(G_{35})(b''_{33})^{(6)}(G_{35}) = 0$$

Where in $(G_{35})(G_{32}, G_{33}, G_{34}), G_{32}, G_{34}$ must be replaced by their values from 96. It is easy to see that φ is a decreasing function in G_{33} taking into account the hypothesis $\varphi(0) > 0, \varphi(\infty) < 0$ it follows that there exists a unique G_{33}^* such that $\varphi(G^*) = 0$

Finally we obtain the unique solution of the global system: 598

G_{14}^* given by $\varphi(G^*) = 0, T_{14}^*$ given by $f(T_{14}^*) = 0$ and

$$G_{13}^* = \frac{(a_{13})^{(1)}G_{14}^*}{[(a'_{13})^{(1)} + (a''_{13})^{(1)}(T_{14}^*)]}, \quad G_{15}^* = \frac{(a_{15})^{(1)}G_{14}^*}{[(a'_{15})^{(1)} + (a''_{15})^{(1)}(T_{14}^*)]}$$

$$T_{13}^* = \frac{(b_{13})^{(1)}T_{14}^*}{[(b'_{13})^{(1)} - (b''_{13})^{(1)}(G^*)]}, \quad T_{15}^* = \frac{(b_{15})^{(1)}T_{14}^*}{[(b'_{15})^{(1)} - (b''_{15})^{(1)}(G^*)]} \quad \text{599}$$

Obviously, these values represent an equilibrium solution 600

Finally we obtain the unique solution 601

G_{17}^* given by $\varphi((G_{19})^*) = 0, T_{17}^*$ given by $f(T_{17}^*) = 0$ and 602

$$G_{16}^* = \frac{(a_{16})^{(2)}G_{17}^*}{[(a'_{16})^{(2)} + (a''_{16})^{(2)}(T_{17}^*)]}, \quad G_{18}^* = \frac{(a_{18})^{(2)}G_{17}^*}{[(a'_{18})^{(2)} + (a''_{18})^{(2)}(T_{17}^*)]} \quad \text{603}$$

$$T_{16}^* = \frac{(b_{16})^{(2)}T_{17}^*}{[(b'_{16})^{(2)} - (b''_{16})^{(2)}((G_{19})^*)]}, \quad T_{18}^* = \frac{(b_{18})^{(2)}T_{17}^*}{[(b'_{18})^{(2)} - (b''_{18})^{(2)}((G_{19})^*)]} \quad \text{604}$$

Obviously, these values represent an equilibrium solution 605

Finally we obtain the unique solution 606

G_{21}^* given by $\varphi((G_{23})^*) = 0, T_{21}^*$ given by $f(T_{21}^*) = 0$ and

$$G_{20}^* = \frac{(a_{20})^{(3)}G_{21}^*}{[(a'_{20})^{(3)} + (a''_{20})^{(3)}(T_{21}^*)]}, \quad G_{22}^* = \frac{(a_{22})^{(3)}G_{21}^*}{[(a'_{22})^{(3)} + (a''_{22})^{(3)}(T_{21}^*)]}$$

$$T_{20}^* = \frac{(b_{20})^{(3)}T_{21}^*}{[(b'_{20})^{(3)} - (b''_{20})^{(3)}(G_{23}^*)]}, \quad T_{22}^* = \frac{(b_{22})^{(3)}T_{21}^*}{[(b'_{22})^{(3)} - (b''_{22})^{(3)}(G_{23}^*)]}$$

Obviously, these values represent an equilibrium solution

Finally we obtain the unique solution 607

G_{25}^* given by $\varphi(G_{27}) = 0, T_{25}^*$ given by $f(T_{25}^*) = 0$ and

$$G_{24}^* = \frac{(a_{24})^{(4)}G_{25}^*}{[(a'_{24})^{(4)} + (a''_{24})^{(4)}(T_{25}^*)]}, \quad G_{26}^* = \frac{(a_{26})^{(4)}G_{25}^*}{[(a'_{26})^{(4)} + (a''_{26})^{(4)}(T_{25}^*)]}$$

$$T_{24}^* = \frac{(b_{24})^{(4)}T_{25}^*}{[(b'_{24})^{(4)} - (b''_{24})^{(4)}((G_{27})^*)]}, \quad T_{26}^* = \frac{(b_{26})^{(4)}T_{25}^*}{[(b'_{26})^{(4)} - (b''_{26})^{(4)}((G_{27})^*)]} \quad \text{608}$$

Obviously, these values represent an equilibrium solution

Finally we obtain the unique solution 609

G_{29}^* given by $\varphi((G_{31})^*) = 0, T_{29}^*$ given by $f(T_{29}^*) = 0$ and

$$G_{28}^* = \frac{(a_{28})^{(5)}G_{29}^*}{[(a'_{28})^{(5)} + (a''_{28})^{(5)}(T_{29}^*)]}, \quad G_{30}^* = \frac{(a_{30})^{(5)}G_{29}^*}{[(a'_{30})^{(5)} + (a''_{30})^{(5)}(T_{29}^*)]}$$

$$T_{28}^* = \frac{(b_{28})^{(5)}T_{29}^*}{[(b'_{28})^{(5)} - (b''_{28})^{(5)}((G_{31})^*)]}, \quad T_{30}^* = \frac{(b_{30})^{(5)}T_{29}^*}{[(b'_{30})^{(5)} - (b''_{30})^{(5)}((G_{31})^*)]} \quad \text{610}$$

Obviously, these values represent an equilibrium solution

Finally we obtain the unique solution 611

G_{33}^* given by $\varphi((G_{35})^*) = 0, T_{33}^*$ given by $f(T_{33}^*) = 0$ and

$$G_{32}^* = \frac{(a_{32})^{(6)}G_{33}^*}{[(a'_{32})^{(6)} + (a''_{32})^{(6)}(T_{33}^*)]}, \quad G_{34}^* = \frac{(a_{34})^{(6)}G_{33}^*}{[(a'_{34})^{(6)} + (a''_{34})^{(6)}(T_{33}^*)]}$$

$$T_{32}^* = \frac{(b_{32})^{(6)}T_{33}^*}{[(b_{32})^{(6)} - (b_{32})^{(6)}((G_{35})^*)]} , T_{34}^* = \frac{(b_{34})^{(6)}T_{33}^*}{[(b_{34})^{(6)} - (b_{34})^{(6)}((G_{35})^*)]} \quad 612$$

Obviously, these values represent an equilibrium solution

ASYMPTOTIC STABILITY ANALYSIS 613

Theorem 4: If the conditions of the previous theorem are satisfied and if the functions $(a_i'')^{(1)}$ and $(b_i'')^{(1)}$ Belong to $C^{(1)}(\mathbb{R}_+)$ then the above equilibrium point is asymptotically stable.

Proof: Denote

Definition of G_i, T_i :-

$$G_i = G_i^* + G_i , T_i = T_i^* + T_i$$

$$\frac{\partial (a_{14}'')^{(1)}}{\partial T_{14}}(T_{14}^*) = (q_{14})^{(1)} , \frac{\partial (b_i'')^{(1)}}{\partial G_j}(G^*) = s_{ij}$$

Then taking into account equations of global system neglecting the terms of power 2, we obtain

$$\frac{dG_{13}}{dt} = -((a_{13}')^{(1)} + (p_{13})^{(1)})G_{13} + (a_{13})^{(1)}G_{14} - (q_{13})^{(1)}G_{13}^*T_{14} \quad 614$$

$$\frac{dG_{14}}{dt} = -((a_{14}')^{(1)} + (p_{14})^{(1)})G_{14} + (a_{14})^{(1)}G_{13} - (q_{14})^{(1)}G_{14}^*T_{14} \quad 615$$

$$\frac{dG_{15}}{dt} = -((a_{15}')^{(1)} + (p_{15})^{(1)})G_{15} + (a_{15})^{(1)}G_{14} - (q_{15})^{(1)}G_{15}^*T_{14} \quad 616$$

$$\frac{dT_{13}}{dt} = -((b_{13}')^{(1)} - (r_{13})^{(1)})T_{13} + (b_{13})^{(1)}T_{14} + \sum_{j=13}^{15} (s_{(13)(j)})T_{13}^*G_j \quad 617$$

$$\frac{dT_{14}}{dt} = -((b_{14}')^{(1)} - (r_{14})^{(1)})T_{14} + (b_{14})^{(1)}T_{13} + \sum_{j=13}^{15} (s_{(14)(j)})T_{14}^*G_j \quad 618$$

$$\frac{dT_{15}}{dt} = -((b_{15}')^{(1)} - (r_{15})^{(1)})T_{15} + (b_{15})^{(1)}T_{14} + \sum_{j=13}^{15} (s_{(15)(j)})T_{15}^*G_j \quad 619$$

$$\frac{dT_{15}}{dt} = -((b_{15}')^{(1)} - (r_{15})^{(1)})T_{15} + (b_{15})^{(1)}T_{14} + \sum_{j=13}^{15} (s_{(15)(j)})T_{15}^*G_j \quad 620$$

If the conditions of the previous theorem are satisfied and if the functions $(a_i'')^{(2)}$ and $(b_i'')^{(2)}$ Belong to $C^{(2)}(\mathbb{R}_+)$ then the above equilibrium point is asymptotically stable 621

Denote 622

Definition of G_i, T_i :-

$$G_i = G_i^* + G_i , T_i = T_i^* + T_i \quad 623$$

$$\frac{\partial (a_{17}'')^{(2)}}{\partial T_{17}}(T_{17}^*) = (q_{17})^{(2)} , \frac{\partial (b_i'')^{(2)}}{\partial G_j}(G_{19}^*) = s_{ij} \quad 624$$

taking into account equations (global) and neglecting the terms of power 2, we obtain 625

$$\frac{dG_{16}}{dt} = -((a_{16}')^{(2)} + (p_{16})^{(2)})G_{16} + (a_{16})^{(2)}G_{17} - (q_{16})^{(2)}G_{16}^*T_{17} \quad 626$$

$$\frac{dG_{17}}{dt} = -((a_{17}')^{(2)} + (p_{17})^{(2)})G_{17} + (a_{17})^{(2)}G_{16} - (q_{17})^{(2)}G_{17}^*T_{17} \quad 627$$

$$\frac{dG_{18}}{dt} = -((a_{18}')^{(2)} + (p_{18})^{(2)})G_{18} + (a_{18})^{(2)}G_{17} - (q_{18})^{(2)}G_{18}^*T_{17} \quad 628$$

$$\frac{dT_{16}}{dt} = -((b_{16}')^{(2)} - (r_{16})^{(2)})T_{16} + (b_{16})^{(2)}T_{17} + \sum_{j=16}^{18} (s_{(16)(j)})T_{16}^*G_j \quad 629$$

$$\frac{dT_{17}}{dt} = -((b_{17}')^{(2)} - (r_{17})^{(2)})T_{17} + (b_{17})^{(2)}T_{16} + \sum_{j=16}^{18} (s_{(17)(j)})T_{17}^*G_j \quad 630$$

$$\frac{dT_{18}}{dt} = -((b_{18}')^{(2)} - (r_{18})^{(2)})T_{18} + (b_{18})^{(2)}T_{17} + \sum_{j=16}^{18} (s_{(18)(j)})T_{18}^*G_j \quad 631$$

If the conditions of the previous theorem are satisfied and if the functions $(a_i'')^{(3)}$ and $(b_i'')^{(3)}$ Belong to $C^{(3)}(\mathbb{R}_+)$ then the above equilibrium point is asymptotically stable. 632

Denote

Definition of G_i, T_i :-

$$G_i = G_i^* + G_i , T_i = T_i^* + T_i$$

$$\frac{\partial (a_{21}'')^{(3)}}{\partial T_{21}}(T_{21}^*) = (q_{21})^{(3)} , \frac{\partial (b_i'')^{(3)}}{\partial G_j}(G_{23}^*) = s_{ij}$$

Then taking into account equations (global) and neglecting the terms of power 2, we obtain 633

$$\frac{dG_{20}}{dt} = -((a_{20}')^{(3)} + (p_{20})^{(3)})G_{20} + (a_{20})^{(3)}G_{21} - (q_{20})^{(3)}G_{20}^*T_{21} \quad 634$$

$$\frac{dG_{21}}{dt} = -((a_{21}')^{(3)} + (p_{21})^{(3)})G_{21} + (a_{21})^{(3)}G_{20} - (q_{21})^{(3)}G_{21}^*T_{21} \quad 635$$

$$\frac{dG_{22}}{dt} = -((a_{22}')^{(3)} + (p_{22})^{(3)})G_{22} + (a_{22})^{(3)}G_{21} - (q_{22})^{(3)}G_{22}^*T_{21} \quad 636$$

$$\frac{dT_{20}}{dt} = -((b_{20}')^{(3)} - (r_{20})^{(3)})T_{20} + (b_{20})^{(3)}T_{21} + \sum_{j=20}^{22} (s_{(20)(j)})T_{20}^*G_j \quad 637$$

$$\frac{dT_{21}}{dt} = -((b_{21}')^{(3)} - (r_{21})^{(3)})T_{21} + (b_{21})^{(3)}T_{20} + \sum_{j=20}^{22} (s_{(21)(j)})T_{21}^*G_j \quad 638$$

$$\frac{dT_{22}}{dt} = -((b_{22}')^{(3)} - (r_{22})^{(3)})T_{22} + (b_{22})^{(3)}T_{21} + \sum_{j=20}^{22} (s_{(22)(j)})T_{22}^*G_j \quad 639$$

If the conditions of the previous theorem are satisfied and if the functions $(a_i'')^{(4)}$ and $(b_i'')^{(4)}$ Belong to $C^{(4)}(\mathbb{R}_+)$ then the above equilibrium point is asymptotically stable. 640

Denote

Definition of G_i, T_i :- 641

$$G_i = G_i^* + G_i , T_i = T_i^* + T_i$$

$$\frac{\partial (a_{25}'')^{(4)}}{\partial T_{25}}(T_{25}^*) = (q_{25})^{(4)} , \frac{\partial (b_i'')^{(4)}}{\partial G_j}(G_{27}^*) = s_{ij}$$

Then taking into account equations (global) and neglecting the terms of power 2, we obtain

$$\begin{aligned} \frac{dG_{24}}{dt} &= -((a'_{24})^{(4)} + (p_{24})^{(4)})G_{24} + (a_{24})^{(4)}G_{25} - (q_{24})^{(4)}G_{24}^* T_{25} & 642 \\ \frac{dG_{25}}{dt} &= -((a'_{25})^{(4)} + (p_{25})^{(4)})G_{25} + (a_{25})^{(4)}G_{24} - (q_{25})^{(4)}G_{25}^* T_{25} & 643 \\ \frac{dG_{26}}{dt} &= -((a'_{26})^{(4)} + (p_{26})^{(4)})G_{26} + (a_{26})^{(4)}G_{25} - (q_{26})^{(4)}G_{26}^* T_{25} & 645 \\ \frac{dT_{24}}{dt} &= -((b'_{24})^{(4)} - (r_{24})^{(4)})T_{24} + (b_{24})^{(4)}T_{25} + \sum_{j=24}^{26} (s_{(24)(j)})T_{24}^* G_j & 646 \\ \frac{dT_{25}}{dt} &= -((b'_{25})^{(4)} - (r_{25})^{(4)})T_{25} + (b_{25})^{(4)}T_{24} + \sum_{j=24}^{26} (s_{(25)(j)})T_{25}^* G_j & 647 \\ \frac{dT_{26}}{dt} &= -((b'_{26})^{(4)} - (r_{26})^{(4)})T_{26} + (b_{26})^{(4)}T_{25} + \sum_{j=24}^{26} (s_{(26)(j)})T_{26}^* G_j & 648 \end{aligned}$$

If the conditions of the previous theorem are satisfied and if the functions $(a_i'')^{(5)}$ and $(b_i'')^{(5)}$ belong to $C^{(5)}(\mathbb{R}_+)$ then the above equilibrium point is asymptotically stable. 649

Denote

Definition of G_i, T_i :- 650

$$G_i = G_i^* + G_i, T_i = T_i^* + T_i$$

$$\frac{\partial (a_{29})^{(5)}}{\partial T_{29}}(T_{29}^*) = (q_{29})^{(5)}, \frac{\partial (b_i'')^{(5)}}{\partial G_j}((G_{31})^*) = s_{ij}$$

Then taking into account equations(global) and neglecting the terms of power 2, we obtain

$$\begin{aligned} \frac{dG_{28}}{dt} &= -((a'_{28})^{(5)} + (p_{28})^{(5)})G_{28} + (a_{28})^{(5)}G_{29} - (q_{28})^{(5)}G_{28}^* T_{29} & 651 \\ \frac{dG_{29}}{dt} &= -((a'_{29})^{(5)} + (p_{29})^{(5)})G_{29} + (a_{29})^{(5)}G_{28} - (q_{29})^{(5)}G_{29}^* T_{29} & 652 \\ \frac{dG_{30}}{dt} &= -((a'_{30})^{(5)} + (p_{30})^{(5)})G_{30} + (a_{30})^{(5)}G_{29} - (q_{30})^{(5)}G_{30}^* T_{29} & 653 \\ \frac{dT_{28}}{dt} &= -((b'_{28})^{(5)} - (r_{28})^{(5)})T_{28} + (b_{28})^{(5)}T_{29} + \sum_{j=28}^{30} (s_{(28)(j)})T_{28}^* G_j & 654 \\ \frac{dT_{29}}{dt} &= -((b'_{29})^{(5)} - (r_{29})^{(5)})T_{29} + (b_{29})^{(5)}T_{28} + \sum_{j=28}^{30} (s_{(29)(j)})T_{29}^* G_j & 655 \\ \frac{dT_{30}}{dt} &= -((b'_{30})^{(5)} - (r_{30})^{(5)})T_{30} + (b_{30})^{(5)}T_{29} + \sum_{j=28}^{30} (s_{(30)(j)})T_{30}^* G_j & 656 \end{aligned}$$

If the conditions of the previous theorem are satisfied and if the functions $(a_i'')^{(6)}$ and $(b_i'')^{(6)}$ belong to $C^{(6)}(\mathbb{R}_+)$ then the above equilibrium point is asymptotically stable. 658

Denote

Definition of G_i, T_i :- 659

$$G_i = G_i^* + G_i, T_i = T_i^* + T_i$$

$$\frac{\partial (a_{33})^{(6)}}{\partial T_{33}}(T_{33}^*) = (q_{33})^{(6)}, \frac{\partial (b_i'')^{(6)}}{\partial G_j}((G_{35})^*) = s_{ij}$$

Then taking into account equations(global) and neglecting the terms of power 2, we obtain

$$\begin{aligned} \frac{dG_{32}}{dt} &= -((a'_{32})^{(6)} + (p_{32})^{(6)})G_{32} + (a_{32})^{(6)}G_{33} - (q_{32})^{(6)}G_{32}^* T_{33} & 660 \\ \frac{dG_{33}}{dt} &= -((a'_{33})^{(6)} + (p_{33})^{(6)})G_{33} + (a_{33})^{(6)}G_{32} - (q_{33})^{(6)}G_{33}^* T_{33} & 661 \\ \frac{dG_{34}}{dt} &= -((a'_{34})^{(6)} + (p_{34})^{(6)})G_{34} + (a_{34})^{(6)}G_{33} - (q_{34})^{(6)}G_{34}^* T_{33} & 662 \\ \frac{dT_{32}}{dt} &= -((b'_{32})^{(6)} - (r_{32})^{(6)})T_{32} + (b_{32})^{(6)}T_{33} + \sum_{j=32}^{34} (s_{(32)(j)})T_{32}^* G_j & 663 \\ \frac{dT_{33}}{dt} &= -((b'_{33})^{(6)} - (r_{33})^{(6)})T_{33} + (b_{33})^{(6)}T_{32} + \sum_{j=32}^{34} (s_{(33)(j)})T_{33}^* G_j & 664 \\ \frac{dT_{34}}{dt} &= -((b'_{34})^{(6)} - (r_{34})^{(6)})T_{34} + (b_{34})^{(6)}T_{33} + \sum_{j=32}^{34} (s_{(34)(j)})T_{34}^* G_j & 665 \end{aligned}$$

The characteristic equation of this system is

$$\begin{aligned} &((\lambda)^{(1)} + (b'_{15})^{(1)} - (r_{15})^{(1)})\{((\lambda)^{(1)} + (a'_{15})^{(1)} + (p_{15})^{(1)}) \\ &[\{((\lambda)^{(1)} + (a'_{13})^{(1)} + (p_{13})^{(1)})(q_{14})^{(1)}G_{14}^* + (a_{14})^{(1)}(q_{13})^{(1)}G_{13}^*\}] \\ &((\lambda)^{(1)} + (b'_{13})^{(1)} - (r_{13})^{(1)})s_{(14),(14)}T_{14}^* + (b_{14})^{(1)}s_{(13),(14)}T_{14}^* \\ &+ ((\lambda)^{(1)} + (a'_{14})^{(1)} + (p_{14})^{(1)})(q_{13})^{(1)}G_{13}^* + (a_{13})^{(1)}(q_{14})^{(1)}G_{14}^* \\ &((\lambda)^{(1)} + (b'_{13})^{(1)} - (r_{13})^{(1)})s_{(14),(13)}T_{14}^* + (b_{14})^{(1)}s_{(13),(13)}T_{13}^* \\ &((\lambda)^{(1)2} + ((a'_{13})^{(1)} + (a'_{14})^{(1)} + (p_{13})^{(1)} + (p_{14})^{(1)}) (\lambda)^{(1)}) \\ &((\lambda)^{(1)2} + ((b'_{13})^{(1)} + (b'_{14})^{(1)} - (r_{13})^{(1)} + (r_{14})^{(1)}) (\lambda)^{(1)}) \\ &+ ((\lambda)^{(1)2} + ((a'_{13})^{(1)} + (a'_{14})^{(1)} + (p_{13})^{(1)} + (p_{14})^{(1)}) (\lambda)^{(1)}) (q_{15})^{(1)}G_{15} \\ &+ ((\lambda)^{(1)} + (a'_{13})^{(1)} + (p_{13})^{(1)}) ((a_{15})^{(1)}(q_{14})^{(1)}G_{14}^* + (a_{14})^{(1)}(a_{15})^{(1)}(q_{13})^{(1)}G_{13}^*) \\ &((\lambda)^{(1)} + (b'_{13})^{(1)} - (r_{13})^{(1)})s_{(14),(15)}T_{14}^* + (b_{14})^{(1)}s_{(13),(15)}T_{13}^*\} = 0 \end{aligned}$$

+

$$\begin{aligned}
& ((\lambda)^{(2)} + (b'_{18})^{(2)} - (r_{18})^{(2)}) \{ ((\lambda)^{(2)} + (a'_{18})^{(2)} + (p_{18})^{(2)}) \\
& \left[((\lambda)^{(2)} + (a'_{16})^{(2)} + (p_{16})^{(2)}) (q_{17})^{(2)} G_{17}^* + (a_{17})^{(2)} (q_{16})^{(2)} G_{16}^* \right] \\
& \left(((\lambda)^{(2)} + (b'_{16})^{(2)} - (r_{16})^{(2)}) s_{(17),(17)} T_{17}^* + (b_{17})^{(2)} s_{(16),(17)} T_{17}^* \right) \\
& + \left(((\lambda)^{(2)} + (a'_{17})^{(2)} + (p_{17})^{(2)}) (q_{16})^{(2)} G_{16}^* + (a_{16})^{(2)} (q_{17})^{(2)} G_{17}^* \right) \\
& \left(((\lambda)^{(2)} + (b'_{16})^{(2)} - (r_{16})^{(2)}) s_{(17),(16)} T_{17}^* + (b_{17})^{(2)} s_{(16),(16)} T_{16}^* \right) \\
& \left(((\lambda)^{(2)})^2 + ((a'_{16})^{(2)} + (a'_{17})^{(2)} + (p_{16})^{(2)} + (p_{17})^{(2)}) (\lambda)^{(2)} \right) \\
& \left(((\lambda)^{(2)})^2 + ((b'_{16})^{(2)} + (b'_{17})^{(2)} - (r_{16})^{(2)} + (r_{17})^{(2)}) (\lambda)^{(2)} \right) \\
& + \left(((\lambda)^{(2)})^2 + ((a'_{16})^{(2)} + (a'_{17})^{(2)} + (p_{16})^{(2)} + (p_{17})^{(2)}) (\lambda)^{(2)} \right) (q_{18})^{(2)} G_{18} \\
& + ((\lambda)^{(2)} + (a'_{16})^{(2)} + (p_{16})^{(2)}) ((a_{18})^{(2)} (q_{17})^{(2)} G_{17}^* + (a_{17})^{(2)} (a_{18})^{(2)} (q_{16})^{(2)} G_{16}^*) \\
& \left(((\lambda)^{(2)} + (b'_{16})^{(2)} - (r_{16})^{(2)}) s_{(17),(18)} T_{17}^* + (b_{17})^{(2)} s_{(16),(18)} T_{16}^* \right) \} = 0 \\
& + \\
& ((\lambda)^{(3)} + (b'_{22})^{(3)} - (r_{22})^{(3)}) \{ ((\lambda)^{(3)} + (a'_{22})^{(3)} + (p_{22})^{(3)}) \\
& \left[((\lambda)^{(3)} + (a'_{20})^{(3)} + (p_{20})^{(3)}) (q_{21})^{(3)} G_{21}^* + (a_{21})^{(3)} (q_{20})^{(3)} G_{20}^* \right] \\
& \left(((\lambda)^{(3)} + (b'_{20})^{(3)} - (r_{20})^{(3)}) s_{(21),(21)} T_{21}^* + (b_{21})^{(3)} s_{(20),(21)} T_{21}^* \right) \\
& + \left(((\lambda)^{(3)} + (a'_{21})^{(3)} + (p_{21})^{(3)}) (q_{20})^{(3)} G_{20}^* + (a_{20})^{(3)} (q_{21})^{(3)} G_{21}^* \right) \\
& \left(((\lambda)^{(3)} + (b'_{20})^{(3)} - (r_{20})^{(3)}) s_{(21),(20)} T_{21}^* + (b_{21})^{(3)} s_{(20),(20)} T_{20}^* \right) \\
& \left(((\lambda)^{(3)})^2 + ((a'_{20})^{(3)} + (a'_{21})^{(3)} + (p_{20})^{(3)} + (p_{21})^{(3)}) (\lambda)^{(3)} \right) \\
& \left(((\lambda)^{(3)})^2 + ((b'_{20})^{(3)} + (b'_{21})^{(3)} - (r_{20})^{(3)} + (r_{21})^{(3)}) (\lambda)^{(3)} \right) \\
& + \left(((\lambda)^{(3)})^2 + ((a'_{20})^{(3)} + (a'_{21})^{(3)} + (p_{20})^{(3)} + (p_{21})^{(3)}) (\lambda)^{(3)} \right) (q_{22})^{(3)} G_{22} \\
& + ((\lambda)^{(3)} + (a'_{20})^{(3)} + (p_{20})^{(3)}) ((a_{22})^{(3)} (q_{21})^{(3)} G_{21}^* + (a_{21})^{(3)} (a_{22})^{(3)} (q_{20})^{(3)} G_{20}^*) \\
& \left(((\lambda)^{(3)} + (b'_{20})^{(3)} - (r_{20})^{(3)}) s_{(21),(22)} T_{21}^* + (b_{21})^{(3)} s_{(20),(22)} T_{20}^* \right) \} = 0 \\
& + \\
& ((\lambda)^{(4)} + (b'_{26})^{(4)} - (r_{26})^{(4)}) \{ ((\lambda)^{(4)} + (a'_{26})^{(4)} + (p_{26})^{(4)}) \\
& \left[((\lambda)^{(4)} + (a'_{24})^{(4)} + (p_{24})^{(4)}) (q_{25})^{(4)} G_{25}^* + (a_{25})^{(4)} (q_{24})^{(4)} G_{24}^* \right] \\
& \left(((\lambda)^{(4)} + (b'_{24})^{(4)} - (r_{24})^{(4)}) s_{(25),(25)} T_{25}^* + (b_{25})^{(4)} s_{(24),(25)} T_{25}^* \right) \\
& + \left(((\lambda)^{(4)} + (a'_{25})^{(4)} + (p_{25})^{(4)}) (q_{24})^{(4)} G_{24}^* + (a_{24})^{(4)} (q_{25})^{(4)} G_{25}^* \right) \\
& \left(((\lambda)^{(4)} + (b'_{24})^{(4)} - (r_{24})^{(4)}) s_{(25),(24)} T_{25}^* + (b_{25})^{(4)} s_{(24),(24)} T_{24}^* \right) \\
& \left(((\lambda)^{(4)})^2 + ((a'_{24})^{(4)} + (a'_{25})^{(4)} + (p_{24})^{(4)} + (p_{25})^{(4)}) (\lambda)^{(4)} \right) \\
& \left(((\lambda)^{(4)})^2 + ((b'_{24})^{(4)} + (b'_{25})^{(4)} - (r_{24})^{(4)} + (r_{25})^{(4)}) (\lambda)^{(4)} \right) \\
& + \left(((\lambda)^{(4)})^2 + ((a'_{24})^{(4)} + (a'_{25})^{(4)} + (p_{24})^{(4)} + (p_{25})^{(4)}) (\lambda)^{(4)} \right) (q_{26})^{(4)} G_{26} \\
& + ((\lambda)^{(4)} + (a'_{24})^{(4)} + (p_{24})^{(4)}) ((a_{26})^{(4)} (q_{25})^{(4)} G_{25}^* + (a_{25})^{(4)} (a_{26})^{(4)} (q_{24})^{(4)} G_{24}^*) \\
& \left(((\lambda)^{(4)} + (b'_{24})^{(4)} - (r_{24})^{(4)}) s_{(25),(26)} T_{25}^* + (b_{25})^{(4)} s_{(24),(26)} T_{24}^* \right) \} = 0 \\
& + \\
& ((\lambda)^{(5)} + (b'_{30})^{(5)} - (r_{30})^{(5)}) \{ ((\lambda)^{(5)} + (a'_{30})^{(5)} + (p_{30})^{(5)}) \\
& \left[((\lambda)^{(5)} + (a'_{28})^{(5)} + (p_{28})^{(5)}) (q_{29})^{(5)} G_{29}^* + (a_{29})^{(5)} (q_{28})^{(5)} G_{28}^* \right] \\
& \left(((\lambda)^{(5)} + (b'_{28})^{(5)} - (r_{28})^{(5)}) s_{(29),(29)} T_{29}^* + (b_{29})^{(5)} s_{(28),(29)} T_{29}^* \right) \\
& + \left(((\lambda)^{(5)} + (a'_{29})^{(5)} + (p_{29})^{(5)}) (q_{28})^{(5)} G_{28}^* + (a_{28})^{(5)} (q_{29})^{(5)} G_{29}^* \right) \\
& \left(((\lambda)^{(5)} + (b'_{28})^{(5)} - (r_{28})^{(5)}) s_{(29),(28)} T_{29}^* + (b_{29})^{(5)} s_{(28),(28)} T_{28}^* \right) \\
& \left(((\lambda)^{(5)})^2 + ((a'_{28})^{(5)} + (a'_{29})^{(5)} + (p_{28})^{(5)} + (p_{29})^{(5)}) (\lambda)^{(5)} \right) \\
& \left(((\lambda)^{(5)})^2 + ((b'_{28})^{(5)} + (b'_{29})^{(5)} - (r_{28})^{(5)} + (r_{29})^{(5)}) (\lambda)^{(5)} \right) \\
& + \left(((\lambda)^{(5)})^2 + ((a'_{28})^{(5)} + (a'_{29})^{(5)} + (p_{28})^{(5)} + (p_{29})^{(5)}) (\lambda)^{(5)} \right) (q_{30})^{(5)} G_{30} \\
& + ((\lambda)^{(5)} + (a'_{28})^{(5)} + (p_{28})^{(5)}) ((a_{30})^{(5)} (q_{29})^{(5)} G_{29}^* + (a_{29})^{(5)} (a_{30})^{(5)} (q_{28})^{(5)} G_{28}^*) \\
& \left(((\lambda)^{(5)} + (b'_{28})^{(5)} - (r_{28})^{(5)}) s_{(29),(30)} T_{29}^* + (b_{29})^{(5)} s_{(28),(30)} T_{28}^* \right) \} = 0
\end{aligned}$$

$$\begin{aligned}
 &+ \\
 &((\lambda)^{(6)} + (b'_{34})^{(6)} - (r_{34})^{(6)})\{((\lambda)^{(6)} + (a'_{34})^{(6)} + (p_{34})^{(6)}) \\
 &[\{((\lambda)^{(6)} + (a'_{32})^{(6)} + (p_{32})^{(6)})(q_{33})^{(6)}G_{33}^* + (a_{33})^{(6)}(q_{32})^{(6)}G_{32}^*\}] \\
 &((\lambda)^{(6)} + (b'_{32})^{(6)} - (r_{32})^{(6)})s_{(33),(33)}T_{33}^* + (b_{33})^{(6)}s_{(32),(33)}T_{33}^* \\
 &+ ((\lambda)^{(6)} + (a'_{33})^{(6)} + (p_{33})^{(6)})(q_{32})^{(6)}G_{32}^* + (a_{32})^{(6)}(q_{33})^{(6)}G_{33}^* \\
 &((\lambda)^{(6)} + (b'_{32})^{(6)} - (r_{32})^{(6)})s_{(33),(32)}T_{33}^* + (b_{33})^{(6)}s_{(32),(32)}T_{32}^* \\
 &((\lambda)^{(6)})^2 + ((a'_{32})^{(6)} + (a'_{33})^{(6)} + (p_{32})^{(6)} + (p_{33})^{(6)}) (\lambda)^{(6)} \\
 &((\lambda)^{(6)})^2 + ((b'_{32})^{(6)} + (b'_{33})^{(6)} - (r_{32})^{(6)} + (r_{33})^{(6)}) (\lambda)^{(6)} \\
 &+ ((\lambda)^{(6)})^2 + ((a'_{32})^{(6)} + (a'_{33})^{(6)} + (p_{32})^{(6)} + (p_{33})^{(6)}) (\lambda)^{(6)} (q_{34})^{(6)}G_{34} \\
 &+ ((\lambda)^{(6)} + (a'_{32})^{(6)} + (p_{32})^{(6)}) ((a_{34})^{(6)}(q_{33})^{(6)}G_{33}^* + (a_{33})^{(6)}(a_{34})^{(6)}(q_{32})^{(6)}G_{32}^*) \\
 &((\lambda)^{(6)} + (b'_{32})^{(6)} - (r_{32})^{(6)})s_{(33),(34)}T_{33}^* + (b_{33})^{(6)}s_{(32),(34)}T_{32}^* \} = 0
 \end{aligned}$$

And as one sees, all the coefficients are positive. It follows that all the roots have negative real part, and this proves the theorem.

Acknowledgments:

The introduction is a collection of information from various articles, Books, News Paper reports, Home Pages Of authors, Journal Reviews, the internet including Wikipedia. We acknowledge all authors who have contributed to the same. In the eventuality of the fact that there has been any act of omission on the part of the authors, We regret with great deal of compunction, contrition, and remorse. As Newton said, it is only because erudite and eminent people allowed one to piggy ride on their backs; probably an attempt has been made to look slightly further. Once again, it is stated that the references are only illustrative and not comprehensive

REFERENCES

- [1] Garey, Michael R.; Johnson, D. S. (1979). Victor Klee. Ed. Computers and Intractability: A Guide to the Theory of NP-Completeness. A Series of Books in the Mathematical Sciences. W. H. Freeman and Co... pp. x+338. ISBN 0-7167-1045-5. MR 519066.
- [2] Agrawal, M.; Allender, E.; Rudich, Steven (1998). "Reductions in Circuit Complexity: An Isomorphism Theorem and a Gap Theorem". Journal of Computer and System Sciences (Boston, MA: Academic Press) 57 (2): 127–143. DOI:10.1006/jcss.1998.1583. ISSN 1090-2724
- [3] Agrawal, M.; Allender, E.; Impagliazzo, R.; Pitassi, T.; Rudich, Steven (2001). "Reducing the complexity of reductions". Computational Complexity (Birkhäuser Basel) 10 (2): 117–138. DOI:10.1007/s00037-001-8191-1. ISSN 1016-3328
- [4] Don Knuth, Tracy Larrabee, and Paul M. Roberts, Mathematical Writing § 25, MAA Notes No. 14, MAA, 1989 (also Stanford Technical Report, 1987).
- [5] Knuth, D. F. (1974). "A terminological proposal". SIGACT News 6 (1): 12–18. DOI:10.1145/1811129.1811130. Retrieved 2010-08-28.
- [6] See the poll, or [1].
- [7] <http://www.nature.com/news/2000/000113/full/news000113-10.html>
- [8] Garey, M.R.; Johnson, D.S. (1979). Computers and Intractability: A Guide to the Theory of NP-Completeness. New York: W.H. Freeman. ISBN 0-7167-1045-5. This book is a classic, developing the theory, and then cataloguing many NP-Complete problems.
- [9] Cook, S.A. (1971). "The complexity of theorem proving procedures". Proceedings, Third Annual ACM Symposium on the Theory of Computing, ACM, New York. pp. 151–158. DOI:10.1145/800157.805047.
- [10] Dunne, P.E. "An annotated list of selected NP-complete problems". COMP202, Dept. of Computer Science, University of Liverpool. Retrieved 2008-06-21.
- [11] Crescenzi, P.; Kann, V.; Halldórsson, M.; Karpinski, M.; Woeginger, G. "A compendium of NP optimization problems". KTH NADA, Stockholm. Retrieved 2008-06-21.
- [12] Dahlke, K. "NP-complete problems". Math Reference Project. Retrieved 2008-06-21.
- [13] Karlsson, R. "Lecture 8: NP-complete problems" (PDF). Dept. of Computer Science, Lund University, Sweden. Retrieved 2008-06-21. [dead link]
- [14] Sun, H.M. "The theory of NP-completeness" (PPT). Information Security Laboratory, Dept. of Computer Science, National Tsing Hua University, Hsinchu City, Taiwan. Retrieved 2008-06-21.
- [15] Jiang, J.R. "The theory of NP-completeness" (PPT). Dept. of Computer Science and Information Engineering, National Central University, Jhongli City, Taiwan. Retrieved 2008-06-21.
- [16] Cormen, T.H.; Leiserson, C.E.; Rivest, R.L.; Stein, C. (2001). Introduction to Algorithms (2nd ed.). MIT Press and McGraw-Hill. Chapter 34: NP-Completeness, pp. 966–1021. ISBN 0-262-03293-7.
- [17] Sipser, M. (1997). Introduction to the Theory of Computation. PWS Publishing. Sections 7.4–7.5 (NP-

completeness, Additional NP-complete Problems), pp. 248–271. ISBN 0-534-94728-X.

[18] Papadimitriou, C. (1994). Computational Complexity (1st ed.). Addison Wesley. Chapter 9 (NP-complete problems), pp. 181–218. ISBN 0-201-53082-1.

[19] Computational Complexity of Games and Puzzles

First Author: ¹**Mr. K. N.Prasanna Kumar** has three doctorates one each in Mathematics, Economics, Political Science. Thesis was based on Mathematical Modeling. He was recently awarded D.litt., for his work on ‘Mathematical Models in Political Science’--- Department of studies in Mathematics, Kuvempu University, Shimoga, Karnataka, India

Second Author: ²**Prof. B.S Kiranagi** is the Former Chairman of the Department of Studies in Mathematics, Manasa Gangotri and present Professor Emeritus of UGC in the Department. Professor Kiranagi has guided over 25 students and he has received many encomiums and laurels for his contribution to Co homology Groups and Mathematical Sciences. Known for his prolific writing, and one of the senior most Professors of the country, he has over 150 publications to his credit. A prolific writer and a prodigious thinker, he has to his credit several books on Lie Groups, Co Homology Groups, and other mathematical application topics, and excellent publication history.-- UGC Emeritus Professor (Department of studies in Mathematics), Manasangotri, University of Mysore, Karnataka, India

Third Author: ³**Prof. C.S. Bagewadi** is the present Chairman of Department of Mathematics and Department of Studies in Computer Science and has guided over 25 students. He has published articles in both national and international journals. Professor Bagewadi specializes in Differential Geometry and its wide-ranging ramifications. He has to his credit more than 159 research papers. Several Books on Differential Geometry, Differential Equations are coauthored by him--- Chairman, Department of studies in Mathematics and Computer science, Jnanasahyadri Kuvempu University, Shankarghatta, Shimoga district, Karnataka, India

=====

Shape Recognition Based On Features Matching Using Morphological Operations

Shikha Garg¹, Gianetan Singh Sekhon²

¹(Student, M.Tech Department of Computer Engineering, YCOE, Punjabi University, Patiala, India)

²(Assistant Professor, M.Tech Department of Computer Engineering, YCOE, Punjabi University, Patiala, India)

Abstract: This paper presents the implementation of method of shape recognition among different regular geometrical shapes using morphological operations. Many algorithms have been proposed for this problem but the major issue that has been enlightened in this paper is over segmentation dodging among different objects. After an introduction to shape recognition concept, we describe the process of extracting the boundaries of objects in order to avoid over segmentation. Then, a shape recognition approach is proposed. It is based on some mathematical formulae. Our new algorithm detects the shapes in the following cases when (i) There are distinct objects in the given image. (ii) The objects are touching in the given image. (iii) The objects are overlapping in the given image. (iv) One object is contained in the other in the given image. Then with the help of boundaries concentrate and shape properties, classification of the shapes is done.

Keywords: Edge detection, geometrical shapes, morphological operations, over segmentation, Shape recognition.

I. Introduction

In an image, shape plays a significant role. Shape of an image is one of the key information when an eye recognizes an object. Shape of an image does not change when colour of image is changed. Shape recognition finds its applications in robotics, fingerprint analysis, handwriting mapping, face recognition, remote sensors etc [6]. In pattern recognition shape is one of the significant research areas. Main focus of the pattern recognition is the classification between objects.

In a computer system, shape of an object can be interpreted as a region encircled by an outline of the object. The important job in shape recognition is to find and represent the exact shape information. Many algorithms for shape representation have been proposed so far.

Many methods for 2D shape representation and recognition have been reported. Curvature scale space (CSS), dynamic programming, shape context, Fourier descriptor, and wavelet descriptor are as the example of these approaches [8]. There are two methods for shape recognition, area based and boundary based technique. In area based technique, all pixels within the region of image are taken into consideration to get shape representation. Common area based technique uses moment descriptors to depict the shape. Whereas boundary based technique focuses mainly on object boundary. Boundary based technique represents shape feature of object more clearly as compared to area based technique. It is fast in processing and needs less computation than area based technique. Due to fast processing and easy computation it is widely used in

real time and practical applications. In this paper we consider just the boundary based technique.

In the previous work of shape recognition, object detection approaches based on color/texture segmentation or image binarization and foreground extraction is proposed, which can be used in this case. Other shape detection solutions are based on edge-detection, sliding-windows or generalized Hough transforms. The identified image objects are then recognized by their shapes. The focus of this paper is shape recognition by edge detection using morphological operations. In this paper the problem of over segmentation among different objects has been taken into consideration for shape recognition. The different objects in the given image are processed one by one and then they are clustered together to form the output image. This process is executed in two stages: firstly, the image is read in from the user and objects which are touching one another are segmented. Then we will match the features of the current object with the preloaded features in the database or we can say training set for recognition.

II. Materials and methods

The computation of proposed method can be briefly summarised in 2 steps (1) Avoidance of over segmentation among different objects like circle, rectangle, square etc with the use of morphological operations (2) Labelling the objects after recognition of various objects within the image.

2.1 Over segmentation avoidance

The proposed method is trying to prevent the over segmentation and segment some overlapping areas to extract the boundaries of various objects within the image. For this, read the RGB image in from the user and convert the RGB (coloured) image to gray scale and then to binary image. Invert the binary image in order to speed up the time of processing. Then morphological operation is implemented so that all the objects are eroded from all the sides and then the boundaries of small radius are enhanced along the edges of the objects.

```
se = strel('disk', 1);  
dummy1=imerode(dummy,se);
```

SE = strel('disk', R,) creates a flat, disk-shaped structuring element, where R specifies the radius. R must be a nonnegative integer. Here the value of R is 1. Imerode performs binary erosion; otherwise it performs gray scale erosion. If SE is an array of structuring element objects, imerode performs multiple erosions of the input image, using each structuring element in SE in succession.

2.2 Recognition and labelling of objects

In this algorithm when the objects are being segmented from each other, the final stage is to identify the shape of the objects. This is done by using filtering technique. Some properties like centroid and corners of the objects are needed to predict the shapes of varying objects. Then with these mathematical parameters, objects of input image are matched with the preloaded features of the objects in the database or we can say training set and thus we can recognize the shape of the objects.

CIRCLE > Number of corners = 0 > Absolute difference b/w length and breadth < 25 > Sensitivity Factor = 0.24	TRIANGLE > Number of corners = 3 > Sensitivity Factor = 0.24	SQUARE > Number of corners = 4 > Absolute difference b/w length and breadth < 10 > Sensitivity Factor = 0.24
--	---	--

RECTANGLE > Number of corners = 4 > Absolute difference b/w length and breadth > 10 > Sensitivity Factor = 0.24	POLYGON > Number of corners = 4 > Absolute difference b/w length and breadth < 10 > Sensitivity Factor = 0.2
---	--

Table.1 filters used to distinguish objects

III. Experiments

We have performed numerous experiments using the described shape recognition approach. The proposed technique has been tested on various image datasets and satisfactory results have been obtained. A high recognition rate, of approximately 95 %, is achieved by our method. It represents a better rate than those of many other object recognition approaches.

An indexed image consists of an array and a colormap matrix. The pixel values in the array are direct indices into a colormap. An indexed image uses direct mapping of pixel values to colormap values. The color of each image pixel is determined by using the corresponding value of X as an index. As RGB image is having an index value of 255 therefore we set this parameter to a scalar between 250 and 0 and in loop this scalar value go on decrementing with a value 5. As this scalar value matches with the index value of object, the particular object is identified. The image is then converted in the binary form, then the binary image is processed using some morphological operations, to eliminate the over segmented area and retain only the important image regions.

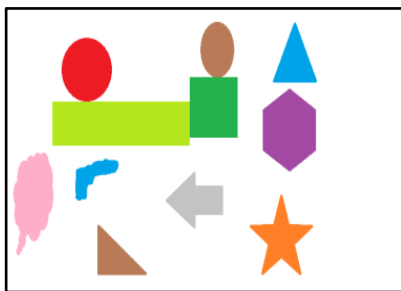


Fig.1 Image containing several objects

A shape recognition example is described in the next figures. Thus, in Fig.2 there is a displayed image containing objects which are segmented. Each object is marked with the obj_i value in the picture, $i = 2 \dots, 12$.

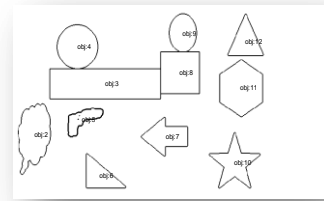


Fig.2 segmented objects

The connected components of the enhanced binary image are detected, thus the image foreground, containing the main objects, being extracted. The feature extraction process is then applied on the detected shapes. The obtained shapes are then classified using the presented shape recognition algorithm. The shape names corresponding to the image from Fig. 1 are represented in Fig. 3. As one can see in that figure, each object is labelled with the name matched with its features. The final recognition results are, circle {obj4,obj6}, square {obj8}, rectangle {obj3}, triangle {obj5,obj12}, polygon {obj11}.

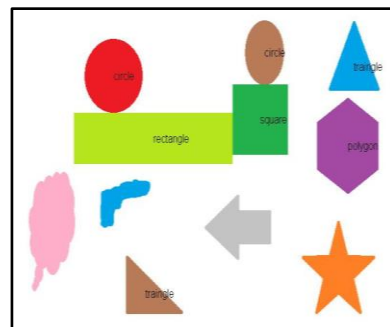


Fig.3 The resulted labelled objects

IV. Conclusion

In this study, a new method of shape recognition is proposed which takes into account the problem of over segmentation. By integrating the structural features like distance measure and centroid, the proposed method extracts the structural information of shapes. Based on those properties, various shapes can be recognized. The identification of the appropriate name of shape clusters automatizes the classification method, which represents a very important thing. That means our recognition technique can be used successfully for very large sets of images, containing a high number of shapes.

Experiments have shown that this method produces accurate and fast results with different images provided. The results of this provided recognition technique can be applied successfully in important domains, such as object recognition and segmentation.

References

- [1] S. W.Chen, S. T. Tung, and C. Y. Fang, Extended Attributed String Matching for Shape Recognition, *COMPUTER VISION AND IMAGE UNDERSTANDING*, Vol. 70, No. 1, April, pp. 36–50, 1998.
- [2] Sajjad Baloch, Object Recognition Through Topo-Geometric Shape Models Using Error-Tolerant Subgraph Isomorphism, *IEEE TRANSACTIONS ON IMAGE PROCESSING*, VOL. 19, NO. 5, 1191, 2010.
- [3] Rong Wang, Fanliang Bu, Hua Jin, Lihua Li, TOE SHAPE RECOGNITION ALGORITHM BASED ON FUZZY NEURAL NETWORKS, *Third International Conference on Natural Computation (ICNC 2007)*,0-7695-2875-9/07, © 2007.
- [4] Ruixia Song , Zhaoxia Zhao, Yanan Yanan Li, Qiaoxia Zhang, Xi Chen, The Method of Shape Recognition Based on V-system, *Fifth International Conference on Frontier of Computer Science and Technology*, China, 100144,2010.
- [5] S.Thilagamani, N.Shanthi, A Novel Recursive Clustering Algorithm for Image algorithm, *European Journal of Scientific Research*, ISSN 1450-216X, Vol.52, No.3, 2011.
- [6] Ehsan Moomivand, A Modified Structural Method for Shape Recognition, *IEEE Symposium on Industrial Electronics and Applications (ISIEA2011)*, September 25-28, Langkawi, Malaysia, 2011.
- [7] Jon Almaz'an, Alicia Forn' Third es, Ernest Valveny, A Non-Rigid Feature Extraction Method for Shape Recognition, *International Conference on Document Analysis and Recognition*, Spain, 2011.
- [8] Kosorl Thourn and Yuttana Kitjaidure, Multi-View Shape Recognition Based on Principal Component Analysis, *International Conference on Advanced Computer Control Department of Electronics*, Bangkok, 10520, 2008.
- [9] Sen Wang, Yang Wang, Miao Jin, Xian feng David Gu, and Dimitris Samaras, Conformal Geometry and Its Applications on 3D Shape Matching, Recognition, and Stitching, *IEEE TRANSACTIONS ON PATTERN ANALYSIS AND MACHINE INTELLIGENCE*, VOL. 29, NO. 7, JULY 2007.
- [10] REN Honge, ZHONG Qiubo, KANG Junfen, Object Recognition Algorithm Research Based on Variable Illumination, *Proceedings of the IEEE International Conference on Automation and Logistics Shenyang*, 150040, China, 2009.

Modeling and Analysis of Laminated Composite Leaf Spring under the Static Load Condition by using FEA

M. Raghavedra¹, Syed Altaf Hussain², V. Pandurangadu³, K. PalaniKumar⁴

*(PG student, School of Mechanical Engineering RGM College of Engg. & Technology, Nandyal-518501, India.)

** (School of Mechanical Engineering, RGM College of Engineering & Technology, Nandyal-518501, India)

*** (Department of Mechanical Engineering, JNTU College of Engineering, Anantapur, Anantapur-512002, India)

**** (Department of Mechanical Engineering, Sri Sai Ram Institute of Technology, Chennai-44, Tamilnadu, India)

ABSTRACT: This paper describes design and analysis of laminated composite mono leaf spring. Weight reduction is now the main issue in automobile industries. In the present work, the dimensions of an existing mono steel leaf spring of a Maruti 800 passenger vehicle is taken for modeling and analysis of a laminated composite mono leaf spring with three different composite materials namely, E-glass/Epoxy, S-glass/Epoxy and Carbon/Epoxy subjected to the same load as that of a steel spring. The design constraints were stresses and deflections. The three different composite mono leaf springs have been modeled by considering uniform cross-section, with unidirectional fiber orientation angle for each lamina of a laminate. Static analysis of a 3-D model has been performed using ANSYS 10.0. Compared to mono steel leaf spring the laminated composite mono leaf spring is found to have 47% lesser stresses, 25%~65% higher stiffness, 27%~67% higher frequency and weight reduction of 73%~80% is achieved.

Keywords: Laminated Composite leaf spring (LCLS), Static analysis, E- Glass/Epoxy, S-glass/Epoxy, Carbon/Epoxy,

I. INTRODUCTION

In order to conserve natural resources and economize energy, weight reduction has been the main focus of automobile manufacturers in the present scenario.

Weight reduction can be achieved primarily by the introduction of better material, design optimization and better manufacturing processes. The suspension leaf spring is one of the potential items for weight reduction in automobiles as it accounts for 10% - 20% of the unstrung weight. This achieves the vehicle with more fuel efficiency and improved riding qualities. The introduction of composite materials was made it possible to reduce the weight of the leaf spring without any reduction on load carrying capacity and stiffness.

Since, the composite materials have more elastic strain energy storage capacity and high strength to weight ratio as compared with those of steel, multi- leaf steel springs are being replaced by mono- leaf composite laminated springs. The composite material offer opportunities for substantial weight saving but not always are cost-effective over their steel counter parts. The leaf spring should absorb the vertical vibrations and impacts due to road irregularities by means of vibrations in the spring deflection so that the potential energy is stored in spring as strain energy and then released slowly. So,

increasing the energy storage capability of a leaf spring ensures a more compliant suspension system. According to the studies made a material with maximum strength and minimum modulus of elasticity in the longitudinal direction is the most suitable material for a leaf spring. Fortunately, composites have these characteristics. In the present work, an attempt is made to replace the existing mono steel leaf spring used in maruti 800 passenger car with a laminated composite mono steel leaf spring made of three different composite materials viz., E-glass/epoxy, S-glass/epoxy and Carbon/epoxy composites. Dimensions and the number of leaves for both steel leaf spring and laminated composite leaf springs are considered to be the same.

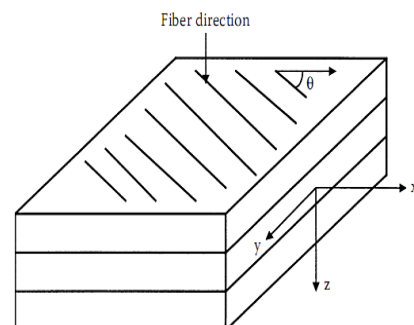


Fig. No.1 Schematic diagram of a laminate.

II. LITERATURE REVIEW

The review mainly focuses on replacement of steel leaf spring with the composite leaf spring made of glass fibre reinforced polymer (GFRP) and majority of the published work applies to them.

Mouleswaran et al. [1] describes static and fatigue analysis of steel leaf spring and composite multi leaf spring made up of glass fibre reinforced polymer using life datanalysis. The dimensions of an existing conventional steel leaf spring of a light commercial vehicle are taken and are verified by design calculations. Static analysis of 2-D model of conventional leaf spring is also performed using ANSYS 7.1 and compared with experimental results.

Al-Qureshi et al. [2] has described a single leaf, variable thickness spring of glass fiber reinforced plastic (GFRP) with similar mechanical and geometrical properties to the multi leaf spring, was designed, fabricated and tested.

Rajendran I, et al.[3] investigated the formulation and solution technique using genetic algorithms (GA) for

design optimization of composite leaf springs. Gulur Siddaramanna et al. [4] explain the automobile industry has shown interest in the replacement of steel spring with fibreglass composite leaf spring due to high strength to weight ratio.

Peiyong et al. [5] describes that the leaf spring design was mainly based on simplified equations and trail and error methods. The simplified equation models were limited to the three-link mechanism assumption and linear beam method. This work presents detailed finite element modeling and analysis of a two stage multi leaf spring, a leaf spring assembly, and a Hotchkiss suspension using ABAQUS.

III. SPECIFICATION OF THE PROBLEM

The objective of the present work is to design and analyses, of mono steel leaf spring and also laminated composite leaf spring made of three different composite materials viz., E-glass/epoxy, S-glass/ epoxy and Carbon/epoxy composites. Laminated composite leaf of four layers with uni-directional fiber orientation angle i.e., 0° is considered. A virtual model of both steel and laminated mono composite leaf spring was created in Pro-E. Model is imported in ANSYS 10.0 for analysis by applying normal load conditions. After analysis a comparison is made between existing conventional steel leaf spring and laminated mono composite leaf spring viz., e-glass/epoxy, s-glass/epoxy, carbon/epoxy in terms of deflections and stresses, to choose the best one.

IV. LEAF SPRINGS

Leaf springs also known as flat spring are made up of flat plates. Leaf springs are designed in two ways: 1. Multi leaf 2. Mono leaf. The importance of leaf spring is to carry bump loads (i.e due to road irregularities), brake torque, driving torque, etc... in addition to shocks.

The multi-leaf spring is made up of several steel plates of different length stacked together, while mono-leaf spring is made up of single steel plate. During normal operation, the spring compresses to absorb road shock. The leaf spring bend and slide on each other allowing suspension movement.

IV.I Materials for Leaf springs :

The material used for leaf springs is usually a plain carbon steel having 0.90 to 1.0% carbon. The leaves are heat treated after the forming process. After the heat treatment process spring steel products gets greater strength and therefore greater load capacity, greater range of deflection and better fatigue properties.

IV.II Theoretical calculations of conventional steel leaf spring:

In the present analysis the maximum deflection of the mono leaf spring is limited to 34mm, then the allowable load on the spring is given by

Deflection

$$\delta = \frac{12 \cdot W \cdot L^3}{E \cdot b \cdot t^3 \cdot (2n_G + 3n_F)}$$

$$34 = \frac{12 \cdot W \cdot L^3}{E \cdot b \cdot t^3 \cdot (2n_G + 3n_F)}$$

$$W = 794.5N$$

Stress

$$\sigma = \frac{6 \cdot W \cdot L}{n \cdot b \cdot t^2}$$

$$= \frac{6 \cdot 794.5 \cdot 482.5}{1 \cdot 50 \cdot 10^2}$$

$$= 460.038Mpa.$$

V. COMPOSITE MATERIALS:

A composite material is defined as a material composed of two or more constituents combined on a macroscopic scale by mechanical and chemical bonds.

Composites are combinations of two materials in which one of the material is called the “matrix phase” is in the form of fibers, sheets, or particles and is embedded in the other material called the “reinforcing phase”.

Many composite materials offer a combination of strength and modulus that are either comparable to or better than any traditional metallic metals. Because of their low specific gravities, the strength to weight-ratio and modulus to weight-ratios of these composite materials are markedly superior to those of mettalic materials.

The fatigue strength weight ratios as well as fatigue damage tolerances of many composite laminates are excellent. For these reasons, fiber composite have emerged as a major class of structural material and are either used or being considered as substitutions for metal in many weight-critical components in aerospace, automotive and other industries.

Another unique characteristic of many fiber reinforced composites is their high interal damping capacity. This leads to better vibration energy absorption within the material and results in reduced transmission of noise to neighboring structures.

High damping capacity of composite materials can be beneficial in many automotive applications in which noise, vibration, and hardness is a critical issue for passenger comfort.

VI. SPECIFICATION OF EXISTING LEAF SPRING:

Table 1 shows the specifications of a mono leaf steel spring of a maruti 800 passenger vehicle. The typical chemical composition of the material is 0.565C, 1.8% Si, 0.7% Mn, 0.045%P and 0.045% S.

Table: 1 Specifications of Mono leaf steel spring

S.No	Parameters	Value
1.	Total length of the spring(Eye to Eye)	965 mm
2.	Free camber (At no load condition)	68 mm
3.	No.of full length leave (Master Leaf)	01
4.	Thickness of leaf	10 mm
5.	Width of leaf spring	50 mm
6.	Maximum load given on spring	794.54 N
7.	Young's Modulus of leaf spring	2.1e5 N/mm ²

VII. FINITE ELEMENT ANALYSIS OF LAMINATED COMPOSITE LEAF SPRING

Dimensions of Laminated composite leaf spring (LCLS) are taken as that of the conventional steel leaf spring (SLS). Laminated composite leaf spring (LCLS) is assumed to have 4 lamina of 0° degree fiber orientation angle (thickness of each lamina of 2.5mm). Width of the leaf is 50mm. Since the properties of LCLS vary with directions of fiber, a 3-D model of leaf spring is used for analysis in ANSYS 10.0. The loading conditions are assumed to be static. The element chosen for the analysis is SHELL 99, which is a layered version of the 8-node structural shell model. The element has six degrees of freedom at each node : translations in the nodal x, y, and z directions and rotations about the nodal x, y, and z-axes. The element allows up to 250 layers. The finite element analysis is carried out on mono steel leaf spring as well as on three different types of laminated composite mono leaf spring. From the analysis the equivalent stress (Von-mises stress) and displacements were determined and are shown in figure 1-9. Table 2 shows the comparative analysis of mono leaf steel spring and laminated composite mono leaf spring of three different materials. Figure 10-11 shows the variation of deflections and stresses induced in steel spring and laminated composite leaf spring with respect to the variation of load.



Fig. No.1- Stacking sequence of laminate.

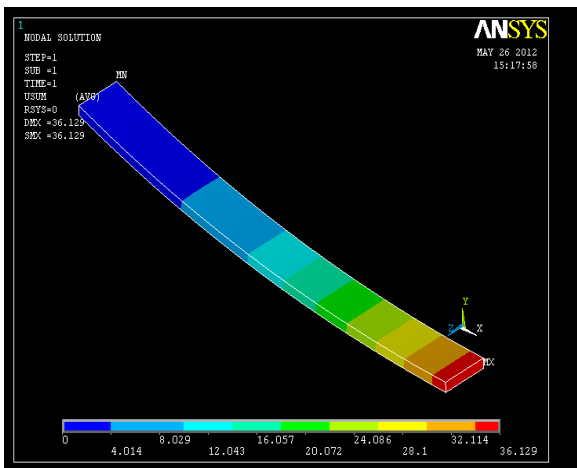


Fig. No.2- Displacement pattern for steel leaf spring

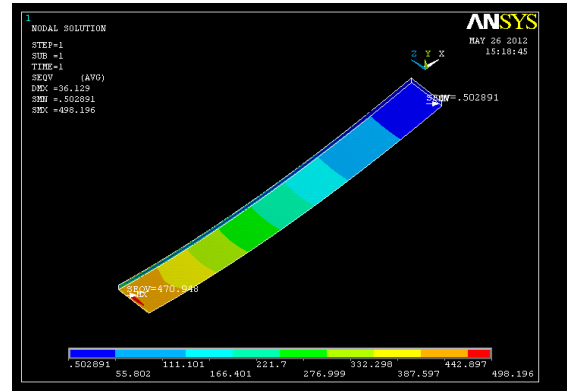


Fig. No.3- Stress distribution for steel leaf spring

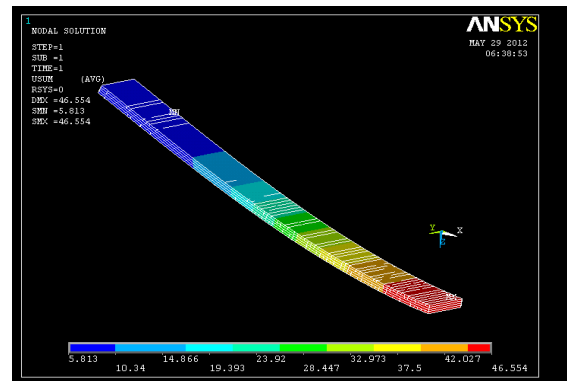


Fig. No. 4- Displacement pattern for E-glass/epoxy laminated composite leaf spring

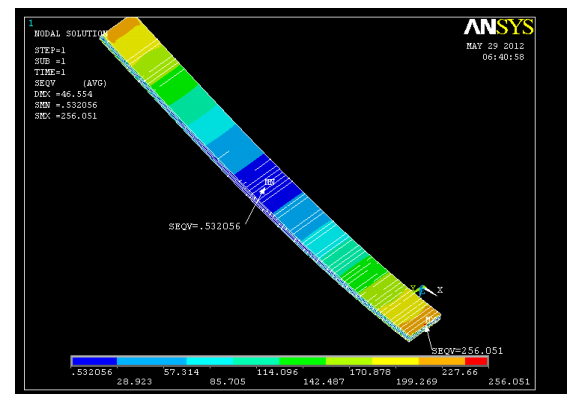


Fig. No.5- Stress distribution for E-glass/epoxy laminated composite leaf spring.

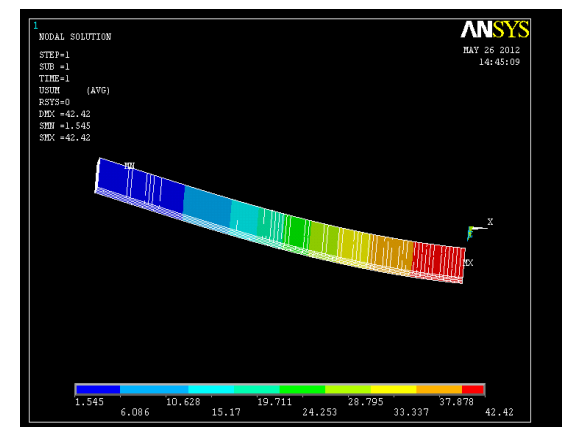


Fig. No.6- Displacement pattern for S-glass/epoxy laminated composite leaf spring.

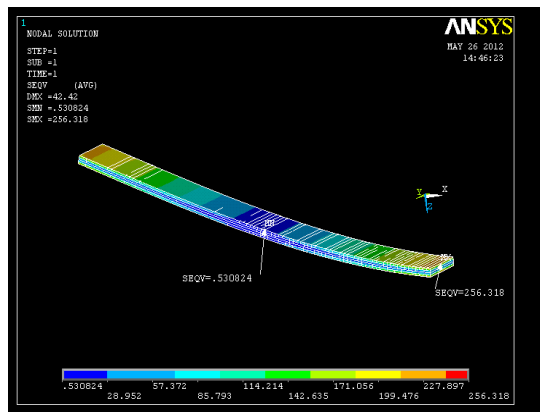


Fig. No.7-Stress distribution for S-glass/epoxy laminated composite leaf spring.

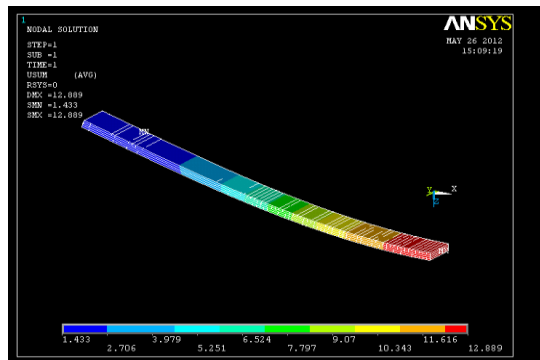


Fig. No. 8-Displacement pattern for carbon/epoxy laminated composite leaf spring.

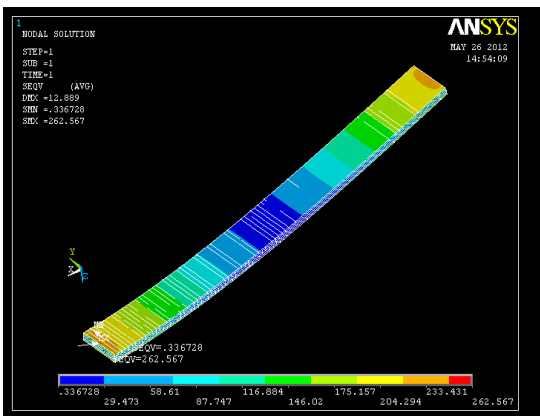


Fig. No. 9- Stress distribution for carbon/epoxy laminated composite leaf spring.

Table 2. Comparative Analysis of mono leaf steel spring and laminated composite mono leaf spring.

S.No	parameter	steel spring	Laminated composite leaf spring		
			Comp:1	Comp:2	Comp:3
1	Weight (kg)	3.79	1.01	0.965	0.762
2	Stress (N/mm ²)	498.19	256.05	256.32	262.56

Comp:1- E-glass/Epoxy, Comp:2-S-glass/Epoxy, Comp:3- Carbon/Epoxy

Graphs:

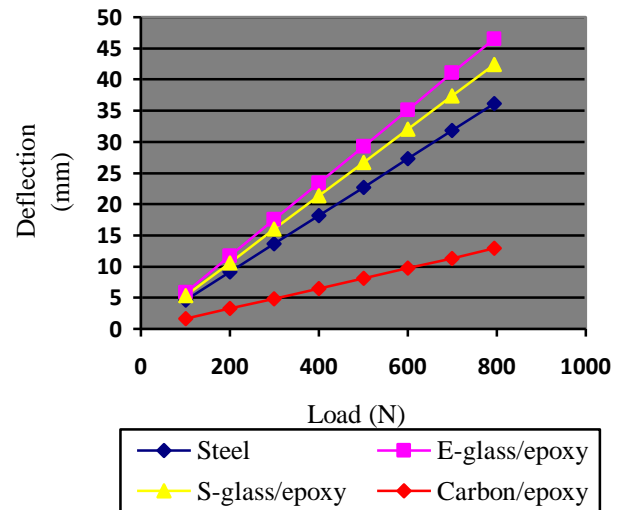


Fig. No. 10- Load - Deflection curves for Steel and Laminated composite leaf spring

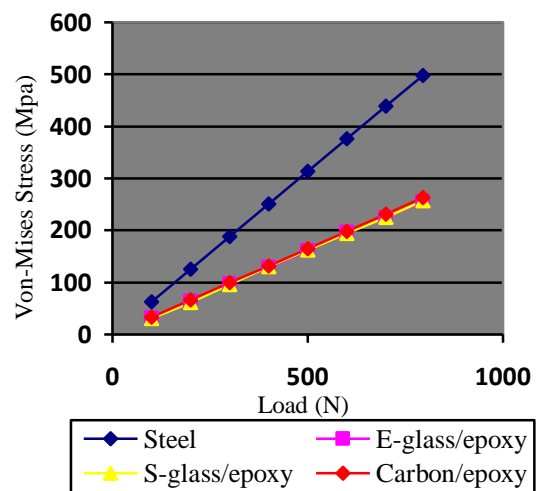


Fig. No. 11- Load - Von-Mises stress for Steel and Laminated Composite leaf spring

VIII. CONCLUSIONS

A comparative study has been made between laminated composite leaf spring and steel leaf spring with respect to weight, stiffness and strength.

By employing a composite leaf spring for the same load carrying capacity, there is a reduction in weight of 73%~80%, natural frequency of composite leaf springs are 27%~67% higher than steel leaf spring and 23~65% stiffer than the steel spring.

Based on the results, it was inferred that carbon/epoxy laminated composite mono leaf spring has superior strength and stiffness and lesser in weight compared to steel and other composite materials considered in this investigation.

From the results, it is observed that the laminated composite leaf spring is lighter and more economical than the conventional steel spring with similar design specifications.

REFERENCES

9.1 Journals Papers:

- [1] Mouleeswaran Senthil kumar, sabapathy vijayarangam; Analytical and Experimental Studies on Fatigue Life Prediction of Steel and Composite Multi-leaf Spring for Light Passenger Vehicles Using Life Data Analysis *Materials Science*, 13(2), 2007, 141-146.
- [2] H.A. AL-Qureshi, Automobile Leaf springs from composite materials”, *Journal of Material Processing Technology*, 118, 2001, 58-61.
- [3] I Rajendran, S. Vijayarangan, “Design and Analysis of a Composite Leaf spring”, *Journal of Institute of Engineers India*, 82, 2002, 180-187
- [4] Gulur Siddaramanna Shiva Shankar, Sambagam Vjayarangan; “Mono Composite Leaf Spring for Light Weight Vehicle Design, End Joint Analysis”. and Testing *Materials Science*, 12 (3), 2006, 220-225.
- [5] Peiyong Qin, Glenn Dental, and Mikhail Mesh “Multi-Leaf Spring and Hotchkiss Suspension”, *ABAQUS Users’ Conference, 2002*.

9.2 Books:

- [6] Nitin S. Gokhale- *Practical Finite Element Analysis*.
- [7] R.S. Khurmi, J.K. Gupta. *A Text book of Machine Design, 2007*.
- [8] Zafer Gurdal, Raphael T. Haftka, Prabhat Hajela. *Design and Optimization of Laminated Composite Materials*.
- [9] Autar K. Kaw. *Mechanics of Composite Materials*. 2e, Taylor & Francis Group, LLC, 2006.

Tribological Investigation of Detonation Sprayed Ni-Cr And Al₂O₃ 13TiO₂ Coatings On Grey Cast Iron To Enhance Its Wear Resistance

¹Harjot Singh Gill, ²J. P. Singla ³Dr. N.K. Grover

¹ HOD, Mechanical Department DTC, Ferozepur

² Assistant Professor, Mechanical Department SBSCET, Ferozepur

³HOD, Mechanical Department SBSCET, Ferozepur

Abstract: This paper is concerned with the investigation of the capability of Detonation sprayed Ni-Cr And Al₂O₃ 13TiO₂ coatings to improve the tribological and mechanical properties of grey cast iron. The present study describes and compares the mechanical and tribological properties of NiCr and Al₂O₃ 13TiO₂ D-Sprayed coatings deposited on two different substrates (GI250 and GIHC). Experiments using a tribometer (pin on disc) is performed in order to evaluate the wear properties. The coating microstructures were characterised by SEM and EDAX. Cumulative weight analysis is done to compare the wear loss in weight and its concluded Al₂O₃ 13TiO₂ form a good bond with GI250 using Detonation spray process.

Keywords: Al₂O₃ 13TiO₂, Detonation, EDAX, Ni-Cr, SEM.

I. Introduction

Surface engineering is an economic method for the production of materials, tools and machine parts with required surface properties, such as wear and corrosion resistance [1]. Since many types of attack such as corrosion, friction, wear, heat, radiation occur on the surface of a component, or transferred via the surface into the component, surface protection is of a considerable significance as regards modern materials technology.

The purpose of surface technology including thermal spraying is to produce functionally effective surfaces [2]. The wear resistance in the case of brake disc rotors, wire drawing pulleys etc. can be improved by a wide range of coatings.

Thermal spray is a technique that produces a wide range of coatings for diverse applications. The principle of thermal spray is to melt material feedstock (wire or powder), to accelerate the melt to impact on a substrate where rapid solidification and deposit build-up occurs[3].

To reduce the wear problem, wear resistant coatings are deposited on the grey irons. Standard test methods for wear testing with pin-on disc apparatus are employed to study the wear behavior of the uncoated and coated grey irons as well. Thermal spray processes that have been considered to deposit the coatings are enlisted as: (1) Flame spraying with a powder or wire, (2) Electric arc wire spraying, (3) Plasma spraying, (4) Spray and fuse, (5) High Velocity Oxyfuel (HVOF) spraying, (6) Detonation Gun.

Among the commercially available thermal spray coating techniques, detonation spray (DS) is chosen to get hard, dense and consequently wear resistant coatings

II. Experimental Procedure

Two types of gray irons were studied: one Grade 250 (GI250), one high-carbon (GIHC), whose chemical compositions and basic mechanical properties are shown in Table 1.

Table 1
Chemical composition (wt.%) and mechanical properties of irons

	GI250	GIHC
C	3.54	3.73
Si	2.15	2.07
Mn	0.51	0.78
P	0.054	0.058
S	0.1	0.085
Ti	0.012	0.014
Cu	0.69	0.56
Cr	0.034	0.27
Sn	0.061	0.039
Hardness(HB)	195 ± 5	180 ± 5

Samples of cylindrical shape, with diameter 8mm and length 30mm were casted with the components of GI250 and GIHC. The casted samples were marked accordingly with sample numbers and The grinding of end faces (to be coated) of the pins is done using emery papers of five different grades 220, 400, 600, 800, 1000 in the same order. Grinding was followed by polishing with 1/0, 2/0, 3/0 and 4/0 grades polishing papers. Two types of coating powders namely (1)Ni-Cr (2) Al₂O₃-13TiO₂ are selected for Detonation Spray Coating Process after the literature survey. Powder Ni-Cr and Al₂O₃-13TiO₂ form hard dense and excellent bonded coatings on the samples. The wear tests were performed in a machine (Wear and Friction Monitor Tester TR-201) conforming to ASTM G 99 standard. The wear tests for coated as well as uncoated specimens were conducted under three normal loads of 30 N, 40 N and 50 N and a fixed sliding velocity of 1 m/s. A track diameter of D=40 mm, sliding speed v=1 m/s is kept. Wear tests have been carried out for a total sliding distance of 5400 m (6 cycles of 5min, 5min, 10min, 10min, 20min, 40min duration),so that only top coated surface was exposed for each detonation sprayed sample. Weight losses for pins were measured after each cycle to determine the wear loss.

The weight was measured by a micro balance to an accuracy of 0.0001 gm. The coefficient of friction has been determined from the friction force and the normal loads in all

the cases. The wear tracks produced in the coating were studied by SEM (FEI Quanta 200F), and The EDAX genesis software indicates the elemental compositions (weight %) present at point/area of interest. The results of coating volume loss are reported.

III. Results and Discussion

Cumulative weight loss for samples are compared in Figure 1 and The FE-SEM micrograph for Detonation sprayed Ni-Cr and Al₂O₃-13TiO₂ coatings on GI250 and GIHC along with micrograph for uncoated sample are shown in Figure 2.

Cumulative weight loss figure shows the loss in weight for each sample after a cycle of 5400m at a load of 40N. From the table it is clear that weight loss in case of coated samples is very less as compared to uncoated samples. In case of first and second sample (Ni-Cr coating on GIHC) and (Ni-Cr coating on GI250) if we compare it is found that weight loss in case of first sample is higher than the later, this means Ni-Cr coating is more

compatible with GI250 but coated GI250 and GIHC sample as compared to uncoated samples clearly illustrates that wear is negligible. In case of third and fourth sample (Al₂O₃ 13TiO₂ coating on GIHC) and (Al₂O₃ 13TiO₂ coating on GI250) it is predicted that Al₂O₃ 13TiO₂ is good wear resistant as it shows negligible wear as compared to uncoated GI250 and GIHC samples.

And if uncoated samples are compared it is found that GI250 is more wear resistant than GIHC mainly due to its higher hardness than GIHC

The FE-SEM micrographs in general indicate that the coatings are uniform, homogeneous and free from surface cracks. The Al₂O₃-13TiO₂ coatings have small size splats whereas the splats are coarse for Ni-Cr coating. More surface roughness is visible on micrographs of uncoated samples of GI250 and GIHC.

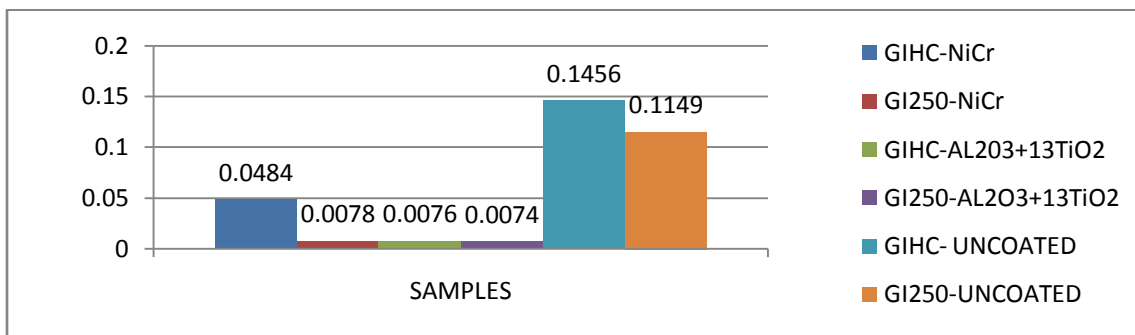
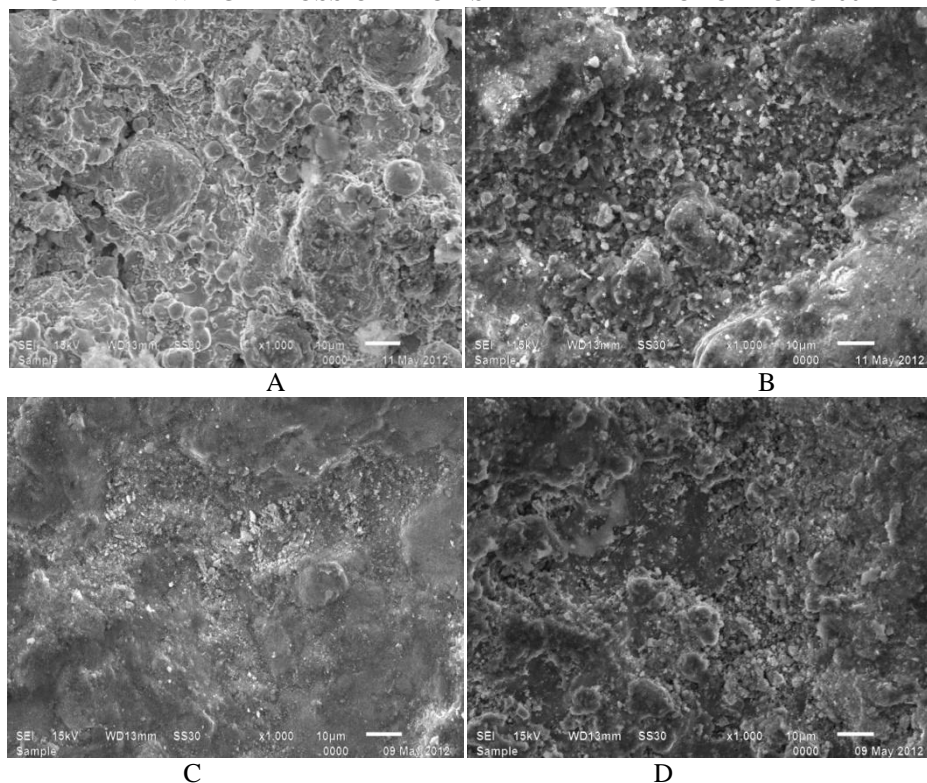


Figure 1: CUMMULATIVE WEIGHT LOSS OF EACH SAMPLE AFTER CYCLE OF 5400M AT 40 N LOADS.



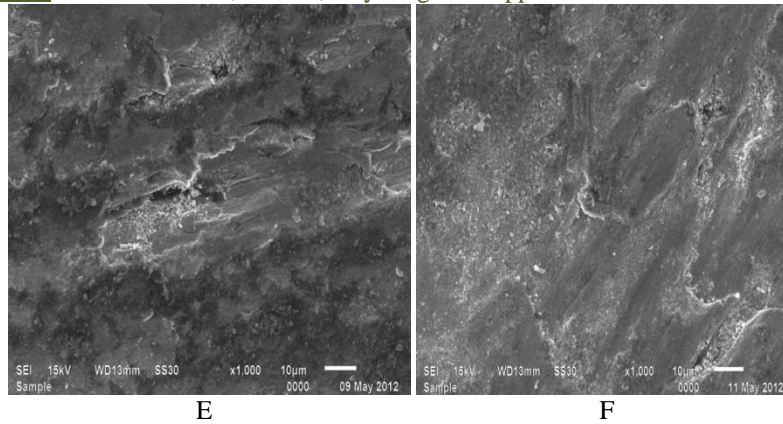


Fig. 2.: SEM Micrographs Of Worn Out Samples Of (A) Ni-Cr Coating On GIHC (B) $Al_2O_3+13TiO_2$ Coating On GIHC (C) Ni-Cr Coating On GI250 (D) $Al_2O_3+13TiO_2$ Coating On GI250 (E) Uncoated GIHC Sample (F) Uncoated GI250 Sample At 40N Load

As reported by Astakhov, (2008) [4] that it is possible to deposit almost any material on any substrate without change in the properties of base material by D-gun spray process to considerably extend the life of parts, it is observed in the present study that the NiCr, $Al_2O_3-13TiO_2$ coatings powders have been successfully deposited on GI250 and GIHC substrates by the detonation spray process. It was further confirmed by characterization of coatings using EDAX analysis of as coated specimens. obtained in the study have been supported by the findings of Mohanty et al., (1996)[5]; Sahraoui et al., (2003)[6] and Bolelli et al.,(2006). [7]

The detonation sprayed NiCr, $Al_2O_3-13TiO_2$ coated GI250 and GIHC specimens showed significantly lower cumulative weight loss (Figure 1) as compared to bare GI250 and GIHC materials under the normal load of 40N. It was investigated with the help of Pin-on-Disk Wear Test Rig according to ASTM G99-03 Standard. There are many studies ; Murthy & Venkataraman (2006)[8], Sundarajan et al.(2005)[9] which support the above finding that Detonation sprayed coatings reduces the wear loss.

IV. Conclusion

- Detonation Sprayed NiCr, $Al_2O_3-13TiO_2$ coatings have successfully been deposited on GI250 and GIHC grades of grey cast iron.
- The detonation sprayed NiCr, $Al_2O_3-13TiO_2$ coated GI250 and GIHC specimens showed significantly lower cumulative weight loss as compared to uncoated GI250 and GIHC materials.
- Cumulative weight loss for detonation sprayed NiCr, $Al_2O_3-13TiO_2$ coated as well as bare GI250 and GIHC specimens increases with increase in load.
- The Cumulative weight loss for $Al_2O_3-13TiO_2$ coating was observed to be minimum in the present study.
- The $Al_2O_3-13TiO_2$ GI250 coating substrate combination has shown minimum Cumulative weight loss among all the combinations. The wear resistance for coating-substrate combinations in their decreasing order (at

40N) is $Al_2O_3-13TiO_2-GI250 > Al_2O_3-13TiO_2-GIHC > NiCr-GI250 > NiCr-GIHC > Uncoated GI250 > Uncoated GIHC$

References

- [1] Iordanova I, Surtchev M, Forcey KS. Metallographic and SEM investigation of the thermally sprayed coatings on steel substrate. Surf Coat Technol 2001;139:118 –126.
- [2] Kahraman, N, Gulenc, B, Investigation of the coating thickness effect on the surface roughness and hardness of powder flame spraying coated specimens, Powder Metallurgy Science and Technology, Second International Conference on Powder Metallurgy, Ro PM 2000, Technical University of Cluj, 2000, Romania.
- [3] Herman H, Sampath S. In: Stern KH, editor. Thermal spray coatings, metallurgical and ceramic protective coatings. London, UK: Chapman & Hall; 1996. p. 261–89
- [4] 325-347, 2008. Astakhov . Editorial: Tribology at the forefront of study and research on metal cutting, International Journal of Machining and Machinability of materials.
- [5] Mohanty M, R W Smith, M De Bonte, LP Celis, E Lugscheider (1996), “Sliding wear behavior of thermally sprayed 75/25 $Cr_3C_2/NiCr$ wear resistant coatings” Wear, vol 198, pp 251-266.
- [6] Murthy J K N, Venkataraman B (2006), “Abrasive wear behaviour of WC–CoCr and $Cr_3C_2-20NiCr$ deposited by HVOF and detonation spray processes” Surface & Coatings Technology, vol 200 , pp 2642– 2652
- [7] Bolelli G, Cannillo V, Lusvardi L, Manfredini T (2006),” Wear behaviour of thermally sprayed ceramic oxide coatings” Wear, vol 261, pp 1298–1315
- [8] Murthy J K N, Venkataraman B (2006), “Abrasive wear behaviour of WC–CoCr and $Cr_3C_2-20NiCr$ deposited by HVOF and detonation spray processes” Surface & Coatings Technology, vol 200 , pp 2642– 2652
- [9] Sundararajan G, Sen D, G Sivakumar (2005), “The tribological behaviour of detonation sprayed coatings: the importance of coating process parameters” Wear, vol 258, pp 377–391

Drought Investigation for Crop Planning in Gagar Watershed in Kumaon Region of Uttarakhand

P. D. Aher¹, K. K. Singh², H. C. Sharma²

¹Junior Research Fellow, Department of Irrigation & Drainage Engineering, G.B. Pant University of Agriculture and Technology, Pantnagar-263145, Uttarakhand, India

²Professor, Department of Irrigation & Drainage Engineering, G.B. Pant University of Agriculture and Technology, Pantnagar-263145, Uttarakhand, India

ABSTRACT: Water scarcity is a burning problem for the hill agrarians, as the same is limited particularly during dry period and no irrigation facilities are available except in the valleys where it is possible with perennial water sources. Usually, downstream reaches of the hilly region faces the flood during the monsoon season and drought during the non-monsoon season due to the available topographical variation. Therefore, in this region rainfall amount, variability and distribution pattern plays a vital role in pragmatic planning and management of natural resources. Considering all points and the indispensable role of water in domestic purpose, agriculture, horticulture, animal husbandry, fisheries and forestry, etc., drought analysis of Gagar watershed located in Nainital district of Uttarakhand, have been statistically accomplished. Weekly rainfall data was observed to be more useful for planning of irrigation schemes, cropping patterns, design of natural resources conservation and management measures so as to mitigate situations like flood, and managing harvested rainfall in drought conditions.

Key words: Rainfall behaviour, Drought Investigation, Kumaon region, Crop planning, Watershed management

I. INTRODUCTION

Rainfall plays significant role in deciding the severity of drought prone area in a particular region. In a rainfed farming region, the crop irrigation scheduling is also preferred by analysing the pattern of rainfall in a season. Various water conservation techniques such as rain water harvesting, rainfall cistern system, etc. are all rainfall dependent. Therefore, for implementation of preferential conservation measures, it is essential to study rainfall behaviour in terms of information on rainfall amount, duration and intensity of drought. Rainfall trend analysis performed from past records of rainfall can be used to generate future scenarios of rainfall occurrence and could be useful particularly in rainfed farming areas.

Sharma et al. (1979) analysed annual, seasonal, monthly and weekly rainfall data of Pantnagar. They reported that weekly data of rainfall was found to be more useful than monthly, seasonal or annual data for planning of cropping programme as well as for water management practices Bertoni et al. (1992) studied on rainfall-based real-time flood forecasting. A conceptual rainfall-runoff model (IPH-II) for real time flood forecasting and a simplified stochastic model. The methods were tested using data from a small watershed (the river Ray at Grendon Underwood, UK), for which 17 years of records were available. The results showed that a simple method used to forecast rain falling during the next few hours, might help to improve real-time discharge estimates. Suresh et al. (1993) conducted a study at Pusa (Bihar) for rainfall data of 26 years (1969-1985) by including characteristics and variation in rainfall with respect to normal, abnormal and drought months in a year by using Weibull's method and reported that at 90 per cent probability level the expected annual rainfall obtained was below the drought level and during Rabi season there was hazardous distribution of rainfall. Subudhi et al. (1996) analysed 28 years' rainfall data at Phulbani and based on probability analysis, suggested the crop varieties with growing period of four months from June to September for Phulbani under rainfed conditions. In this paper an attempt has been made to carry out the probability drought analysis on the basis of weekly rainfall data for Gagar watershed of Uttarakhand.

II. MATERIALS AND METHODS

Drought is the period of abnormal dry weather condition / deficit rainfall resulting in moisture stress condition and hydrological disparity of the system It is one of the important parameter for planning and management of various sectors such as agriculture, industrial, domestic, etc. particularly, in rainfed and water scarce region. In this research an attempt has been made to investigate the drought over the Gagar watershed located in Kumaon region of Uttarakhand.

A. Study Area

The study area i.e. Gagar watershed consists the Research Station of Govind Ballabh Pant University of Agriculture and Technology, Pantnagar and nearby area, forming the watershed, which is located near Bhowali in Nainital district of Uttarakhand state in India as shown in Fig 1. The watershed, covering an area of 603.02 ha is located between 79° 31' 43" E to 79° 33' 24" E longitude and 29° 24' 38" N to 29° 26' 43" N latitude. The elevation varied from 1413 to 2380 m above mean sea level (MSL).

Slope, drainage, shade cast etc. are the important elements of topography. There was a lot of variation in the topography of the study area. In conformity with the dramatic altitudinal and climatic differences, the region supported variety of forest ecosystems. Mixed forests predominated in the area. The land slope varied from 2 to 75%. The soils of the Gagar watershed varied from extremely acidic to medium acidic with high organic matter content. These soils were fairly

deep and moderately permeable. Very strongly acidic to medium acidic soils were also found at higher elevations, where rainfall was high and strong enough to leach down the bases from the soil minerals under temperate climatic conditions.

The climate of the region was humid temperate but variations existed which largely depend upon the altitude and geological differences. The most common factors which lead to the development of microclimate were altitude, aspect, slope, drainage condition, vegetation etc. The valleys were hot in summer and cold in winter. The minimum temperature of the area was found to be -4°C in the month of January and maximum temperature was 41°C in the month of May. The average rainfall in the study area was found to be 1040 mm, of which 70 to 80 per cent was received between June to September. With further increase in elevation, rainfall tended to decrease.

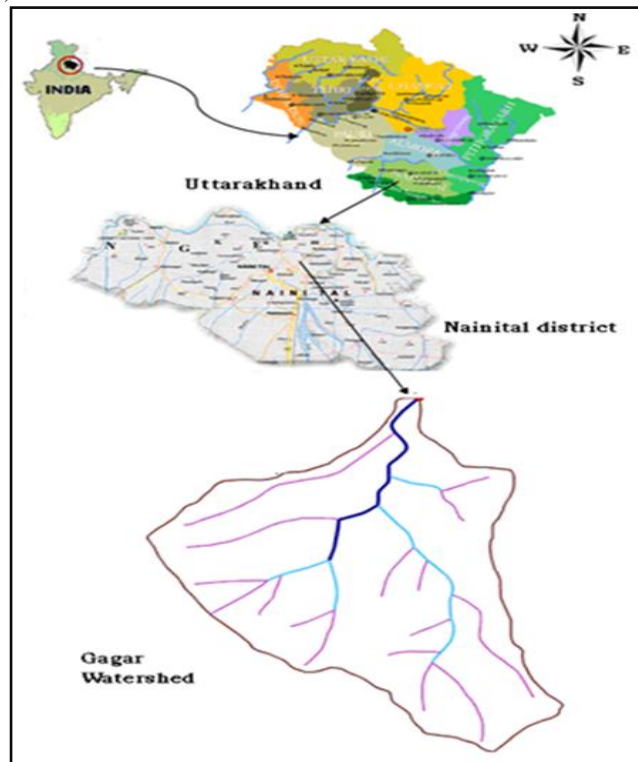


Fig. 1. Drought-rainfall distribution at Gagar watershed

Directional aspect played very important role in the development of vegetation, particularly at higher altitudes. Southern aspect was exposed to more insolation. The insolation on southern aspect was about 1.5 to 2.4 times higher than that of northern aspect. East and west aspects though received an equal amount of insolation; eastern aspect received the highest insolation during morning, before the air temperature becomes fully warm. Western aspects were comparatively hotter and drier than eastern aspects. The difference in the temperature on different aspects of the hills was the result of difference in insolation. The southern aspect was warmest and northern aspect was the coolest. Aspect plays an important role in receiving the rainfall and snowfall. Soil formation is also effected by it.

Drought Analysis

Rainfall data were collected from Agro meteorological Observatory of G. B. Pant University of Agriculture and Technology located at Gagar, Nainital, Uttarakhand which covers the study region of Gagar watershed. The data were organized in to 52 standard meteorological weeks in which each year, 8 days were counted in 52nd meteorological week and in 9th meteorological week in case of leap years and analysed for their yearly, monthly and weekly behaviour.

In this research, the monthly and yearly total rainfall was determined for each year. The monthly and yearly events were then classified as drought, normal and surplus using the following criteria.

- **Drought Month:** The month was classified as drought month in which precipitation received was less than 50 per cent of average monthly rainfall.
- **Surplus Month:** The month was classified as surplus month in which precipitation received was more than twice of average monthly rainfall.
- **Normal Month:** The month was classified as normal month in which precipitation received was in between 50 per cent and 200 per cent of average monthly rainfall.
- **Drought Year:** The year was classified as drought year in which precipitation received was less than or equal to $\bar{x} - \sigma$, where \bar{x} is mean annual precipitation and σ is standard deviation.

- Surplus Year: The year was classified as surplus year in which precipitation received was more than or equal to $\bar{x} + \sigma$.
- Normal Year: The year was classified as normal year in which precipitation received was $\bar{x} \pm \sigma$, i.e. in between $\bar{x} - \sigma$ and $\bar{x} + \sigma$.

To study the drought proneness of area and likely extend of drought following definitions were used. According to Ministry of Agriculture (1976), agricultural drought is an occasion when the rainfall in the week is half of the normal rainfall and normal rainfall should be 5 mm or more. If there are four such consecutive weeks in rainy season, the area may be classified as drought affected. According to Irrigation Commission (1972).

RESULTS AND DISCUSSION

A. Drought, Normal and Surplus Months

On the basis of definitions outlined earlier, the rainfall for a month to be normal, surplus and drought with the average rainfall are given in Table 1. There was very less rainfall in the month of November (average rainfall of 2.19 mm) for the period of study and overall 7 months of November out of 10 months were observed as drought months, therefore, November was categorized as drought month.

Table 1. Monthly rainfall to be drought, surplus and normal month with average rainfall at gagar watershed

Month	Avg. rainfall (mm)	Drought (less than)	Surplus (more than)	Normal (in between)
January	61.05	30.52	122.10	30.52 - 122.1
February	90.94	45.47	180.08	45.47 - 180.08
March	75.99	37.99	151.99	37.99 - 151.99
April	47.08	23.54	94.17	23.54 - 94.17
May	77.56	38.78	155.11	38.77 - 155.11
June	112.86	56.43	225.72	56.43 - 225.72
July	272.19	136.09	544.38	136.09 - 544.38
August	251.83	125.91	503.66	125.91 - 503.66
September	144.33	72.17	288.66	72.165 - 288.66
October	41.54	20.77	83.09	20.72 - 83.09
November	10.04	5.02	20.08	5.02 - 20.08
December	32.56	16.27	65.12	16.27 - 65.12

Month wise and year wise distribution of number of months to be drought, surplus and normal are shown in Table 2 and 3, respectively.

Table 2. Month wise distribution of number of months to be drought, surplus and normal at gagar watershed

Month	Drought Month	Normal Month	Surplus Month
January	5	4	1
February	3	5	2
March	4	5	1
April	2	6	2
May	4	5	1
June	1	9	0
July	1	9	0
August	2	8	0
September	4	5	1
October	5	2	3
November	7	0	3
December	4	4	2
Total	42	62	16

From the Table 2 and 3, it can be observed that about 51.67 per cent months were normal months during the period of 10 years (1998 to 2007). It was observed that during this 10 years period, 35.00 per cent months were drought months. Maximum number of normal months in a year was found to be 9, which accounted for only 20 per cent of total years. Most of the drought months had occurred in the post and pre-monsoon periods i.e. October to May having highest frequency for November (7 drought months out of 10 months).

Table 3. Year wise distribution of number of months to be drought, surplus and normal at gagar watershed

Year	Drought Month	Normal Month	Surplus Month
1998	2	9	1
1999	8	3	1
2000	4	7	1
2001	7	5	0
2002	4	7	1
2003	2	10	0
2004	4	6	2
2005	3	7	2
2006	5	6	1
2007	3	5	4
Total	42	65	13

It was also observed that, frequency of occurrence of normality was highest in the month of June and July followed by August, April, February - March – May – September, January and December. It can also be seen that during monsoon, the percentage distribution of drought months was, 40.00, 20.00, 10.00 per cent for, September, August, July-June, respectively, which indicated the assured rainfall during these months. The maximum number of surplus months in a year was 3, occurred during 20.00 per cent of the total years. Normality for the month of June-July was found to be 90.00 per cent followed by August (80%), April (60%), February-March-May-September (50%), January-December (40%) and October (20%). During the monsoon period (June to October), 66 per cent of the total months were normal, 26 per cent under drought and rest 8 per cent were surplus, while for the other period the normality was 41.43 per cent.

During the Rabi season i.e. October to February, out of total 50 months, the number of drought months was worked out to be 24, which was accounted for 48 per cent of the total rabi months. This indicated the likelihood of failure of Rabi crops under rainfed conditions. The percentage distribution of drought months during Rabi season was 70.00, 40.00, 30.00, and 50.00 percent during November, October-December, February and January, respectively.

B. Drought, Normal and Surplus Years

The average or mean annual rainfall was 1040.39 mm and standard deviation for the study region was found to be 302.62 mm. Therefore, any year receiving the rainfall less than or equal to 737.77 mm will be a drought year. Thus, as per the definition for drought year, described in previous chapter, 20.00 per cent of years (1999 and 2001) received rainfall less than 949.54 mm, would be drought years. Distribution of drought years is shown in Fig. 2.

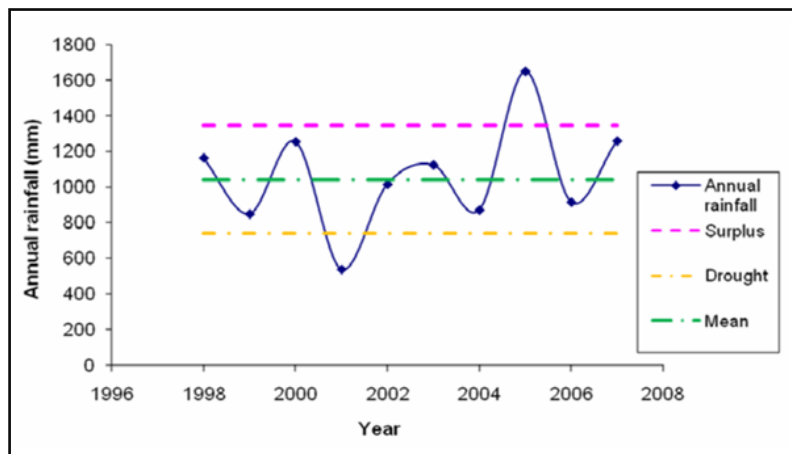


Fig. 2. Drought-rainfall distribution at Gagar watershed

Any year receiving the rainfall equal to or more than 1343.01 mm will be the surplus year, therefore, 10.00 per cent of the year which received rainfall equal to or more than 1343.01 mm (2005) was the surplus year for the period under study. Years receiving rainfall between 737.77 mm and 1343.01 mm would be the normal year. Therefore, remaining 70.00 per cent of years (1998, 2000, 2002, 2003, 2004, 2006 and 2007) were normal years for the period of analysis. Thus, it was inferred from the study that, there were about 70 per cent chance of year to have normal rainfall, 20 per cent chance of year to be the drought year and very less chance of year to be surplus (10%).

III. CONCLUSION

Drought analysis based on rainfall data of Gagar watershed was computed based on weekly rainfall. The analysis indicated the likelihood of failure of Rabi crops under rainfed conditions. It can be seen that during monsoon, the percentage distribution of normal, drought, surplus months was 66, 26, and 8 percent, respectively. It was also inferred from the study that, there was about 70 per cent chance to have normal rainfall year, 20 per cent chance to be the drought year and very less chance to be surplus year (10%). The paradigm developed from analysis of normal, surplus and drought months/years will be useful for planning of various agricultural operations such as sowing, irrigation scheduling schemes, etc. for the area.

REFERENCES

- [1] Bertoni, J. C., Tucci, C. E. and Clarke, R. T. (1992). Rainfall- based real- time flood forecasting. *Journal of Hydrology*, **131**, 313-339.
- [2] Ministry of Agriculture. (1976). Agricultural commission report. Government of India, New Delhi
- [3] Ministry of Irrigation. (1972). Irrigation commission report. Government of India, New Delhi.
- [4] Sharma, H. C., Chauhan, H. S. and Sewa Ram. (1979). Probability analysis of rainfall for crop planning. *Journal of Agricultural Engineering*, **16(3)**, 87-94.
- [5] Subudhi, C. R., Pradhan, P. C., Behara, B., Senapati, P. C. and Singh, G. S. (1996). Rainfall characteristics at Phulani. *Indian Journal of Soil Conservation*, **24 (1)**, 41-43.
- [6] Suresh, R., Singh, N. K. and Prasad, P. (1993). Rainfall analysis for drought study at Pusa, Bihar. *Indian Journal of Agricultural Engineering*, **3 (1-2)**, 77-82.

Use of IEEE 802.11e to Ensure the Quality of Service (QoS) For Multimedia Streaming

V. REVATHI¹, S. VANITHA²

¹ PG Student, Department of ECE, SNS College of technology, India

² Assistant Professor, Department of ECE, SNS College of technology, India

ABSTRACT: Multimedia streaming is a key service provided by certain home appliances. A home network helps to control home appliances, to connect the internet and to use data in home server. A large bandwidth and real time operations are required for multimedia streaming services that consist of large amount of data and require sufficient bandwidth and delay variation to achieve the good quality of service. It is difficult for WLAN to guarantee a high QoS with respect to bandwidth and delay. Hence 802.11e standard is designed to solve this problem. It has Hybrid Coordination Function (HCF) and Enhanced Distributed Coordination Function (EDCF) to support QoS that could not be supported in the 802.11 standard. The Hop-Based Priority (HBP) technique using 802.11e is used for ensuring a good QoS for multimedia streaming. In HBP technique, the multimedia streaming data packets are assigned a higher priority after every hop. So that each packet increases the priority and minimizes the contention between the packets. We propose HBP technique in Adhoc mesh network. The wireless mesh network has been an emerging technology, since many routes may randomly exist and some routes have a lower priority than other routes at cross route node and cannot obtain the channel. For this, label switching routing protocol is used for the efficient transmission to reduce the delay and improve the throughput.

Keywords: Multimedia streaming, 802.11e EDCF, Hop-based priority technique, label switching routing protocol.

I. INTRODUCTION

Networks have evolved from wired to wireless. Recently, users of wireless LAN (WLAN) like laptop computer, PDA, mobile internet devices are increasing rapidly. WLAN supports scalability, flexibility and ubiquity, and these features make WLAN more popular. Especially, wireless multi-hop network has overcome the limit of WLAN's communication range. The applications and services of wired and wireless networks are not different. Quality of Service (QoS) is a key problem of today's IP networks.

In wireless environments, bandwidth is scarce and channel conditions are time-varying and sometimes highly lossy. Although IEEE 802.11 Wireless LAN (WLAN) is the most widely used WLAN standard today, it cannot provide QoS support for the increasing number of multimedia applications. Since multimedia streaming services have to be played in real-time, a large bandwidth is required. Services that need a good Quality of Service (QoS) like Voice over IP (VoIP) and multimedia streaming can be provided through wireless networks. However, WLAN cannot provide good QoS with respect to bandwidth and delay. High collision rate and frequent retransmissions cause unpredictable delays and jitter, which degrade the quality of real-time voice and video transmission. So IEEE 802.11e is the MAC enhancement standard used for providing QoS for the real-time applications. In this paper we analyze the Hop-Based Priority technique in multicast network and propose a solution for it.

II. IEEE 802.11E OVERVIEW

The upcoming IEEE 802.11e wireless LAN standard is the MAC enhancement standard for providing QoS capabilities in the emerging wireless local area networks. For achieving QoS, IEEE 802.11e uses multiple queues for the prioritized and separate handling of different traffic categories (TCs). IEEE 802.11e introduces the Enhanced Distributed Coordination Function (EDCF) and the Hybrid Coordination Function (HCF).

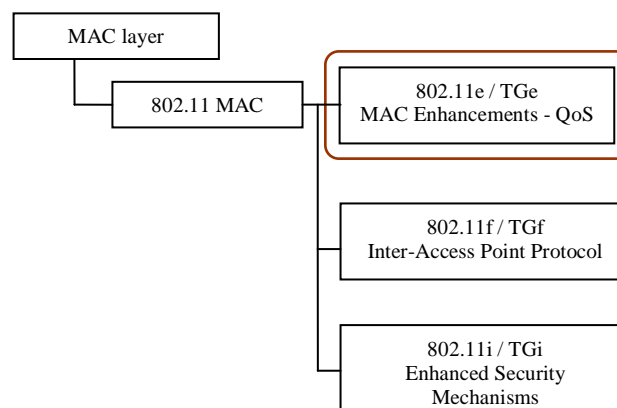


Figure 1 802.11 MAC

The 802.11e MAC is based on both center controlled channel access and contention-based channel access mechanisms. Figure 1 specifies the legacy 802.11 MAC with MAC enhancement scheme for supporting QoS. The 802.11e enhances the Distributed Coordination Function (DCF) and Point Coordination Function (PCF) both the

2.1. Hybrid Coordination Function (HCF)

HCF is the queue based service which extends the Point Coordination Function (PCF) to support the immediate sending of data. An Access Point (AP)-based infrastructure mode is used in HCF. HCF uses QoS-Enhanced Access Point (QAP) as a traffic director for different queues. HCF uses two modes of operation: HCF Controlled Channel Access (HCCA) is contention free, Enhanced Distributed Channel Access (EDCA) is contention based access mechanism. The HCF is the basis for the EDCF and controls both the contention free period (CFP) and contention period (CP). Therefore one enhanced station must be responsible for the management of the medium access. His station is denoted as Hybrid Coordinator (HC). The HC is normally co-located to the access point (AP).

III. Enhanced Distributed Coordination Function (EDCF)

EDCF supports priority upon DCF. EDCF introduces the concept of traffic categories. EDCF provides differentiated, distributed channel accesses for frames with eight different priorities (from 0 to 7) by enhancing DCF as specified in Table 1.

Table 1 User traffic priorities mapped to access categories

User Priority	Access Category	IEEE 802.11E Service Type
1	AC_BK	Background
2	AC_BK	Background
0	AC_BE	Best Effort
3	AC_BE	Video
4	AC_VI	Video
5	AC_VI	Video
6	AC_VO	Voice
7	AC_VO	Voice

EDCF establishes a probabilistic priority mechanism to allocate bandwidth based on traffic categories. Distinct from the legacy DCF, the EDCF is not a separate coordination function rather, it is a part of HCF of 802.11e MAC. Each frame from the higher layer arrives at the MAC along with the specific priority value. Then, each QoS data frame carries its specific priority value in the MAC header frame. 802.11e station implements four access categories where an access category is an enhanced variant of DCF 0.

The EDCF enhances the 802.11 DCF by introducing an own backoff instance with a separate backoff parameter set for each priority queue. Each TC on a station contends for a transmission opportunity (TXOP). A TXOP is defined as "an interval of time when a station has the right to initiate transmissions, defined by a starting time and the maximum duration".

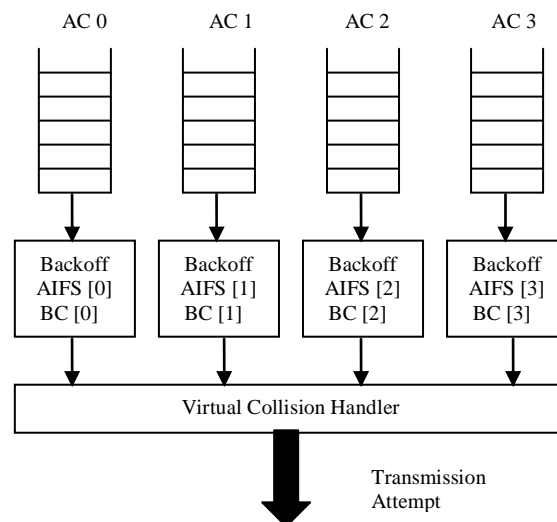


Figure 2 Four access categories for EDCF

Figure 2 shows the four transmission queues of 802.11e MAC, where each queue has its own AIFS and maintains its own backoff counter [12]. Each queue contends for Transmission Opportunity (TXOP) to send the packets. When more than one access categories compete for the backoff at the same time then collision is handled virtually. It means, the highest priority frame among the colliding frames is transmitted and the other frames perform a backoff.

An access category uses AIFSD [AC], CWmin [AC] and CWmax [AC] instead of DIFS, CWmin and CWmax of DCF respectively for the contention process to transmit the frame. AIFSD [AC] is given by,

$$\text{AIFSD [AC]} = \text{SIFS} + \text{AIFS [AC]} * \text{SlotTime}$$

Where AIFS [AC] is an integer greater than 0. The EDCF channel access mechanism is shown in Figure 3.

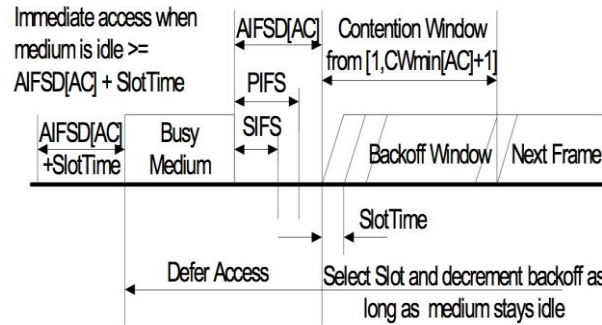


Figure 3 IEEE 802.11e EDCF channel access

EDCF => Enhanced Distributed Channel Access (EDCA).

IV. HOP-BASED PRIORITY TECHNIQUE

The Hop-Based Priority (HBP) technique using 802.11e EDCF is used for minimizing the contention between the hops. A previous packet contends with a next packet when packets try to transmit to a destination through a route. If the previous packet and next packet have the same priority and contend with each other by a fair condition which means the probability of gain of each packet in the channel is 50%. The effect that the next packet cannot get the channel by contention with the previous packet is small. If the next packet wins the previous packet and transmits one more hop, it cannot transmit more hops until the previous packet transmits. This causes the delay to decrease and bandwidth to increase. So the previous packet has a highest priority than the next packet every time.

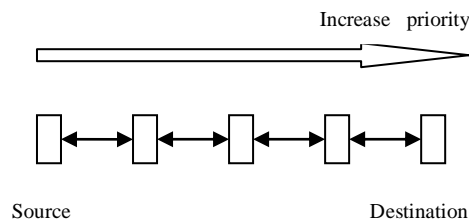


Figure 4 Hop-by-hop increases in priority

In order to avoid this contention between the previous and next packets Hop-based priority technique is used. In HBP, each packet increases the priority after every hop and minimizes the contention between the packets as specified in Figure 5. In other words, a priority is assigned to each hop and a packet is assigned a higher priority after each hop. The inter-packet delay is constant in HBP. The HBP technique uses 802.11e EDCF which can control the channel gain on the basis of priority.

V. RELATED WORK

Most of the previous work on wireless LAN specifies the QoS using various mechanisms.

In [2], A. Ksentini et al. introduced a new cross-layer architecture that ensures H.264 video transmission over IEEE 802.11-based wireless networks. This architecture achieves better performances in terms of delays and loss rate than actual WLAN standard and QoS enhancement mechanism and increases the video quality.

In [3], Q.Zhang et al. proposed a new multimedia streaming TCP-friendly protocol (MSTFP) and a novel quality-adaptation resource allocation scheme to periodically estimate the available bandwidth using MSTFP. It achieves the improvement in end-to-end QoS.

In [4], H. Gharavi et al. proposed a cross-layer feedback mechanism with a rate control approach. This method effectively controls the packet-loss rate by avoiding excessive packet drops, which could affect the resynchronization process at the decoder.

In [5], Antonio Grilo et al. presented a scheduling algorithm- Scheduling Based on Estimated Transmission Times—Earliest Due Date (SETT—EDD) for QoS provisioning in IEEE 802.11e WLANs. SETT-EDD achieves better performance in the transmission of streamed video.

VI. PRIOR WORK

The main objective of this paper is to improve the Quality of Service(QoS) for multimedia streaming services in IEEE 802.11e standard using Hop Based Priority(HBP) technique. The Hop Based Priority(HBP) technique is used in IEEE 802.11E Standard. IEEE 802.11 Wireless LAN(WLAN) is one of the most deployed wireless technologies in all over the world and is likely to play a major role in next generation wireless communication networks. The IEEE 802.11 wireless LAN has simple and robust WLAN which offers time-bounded and asynchronous services.

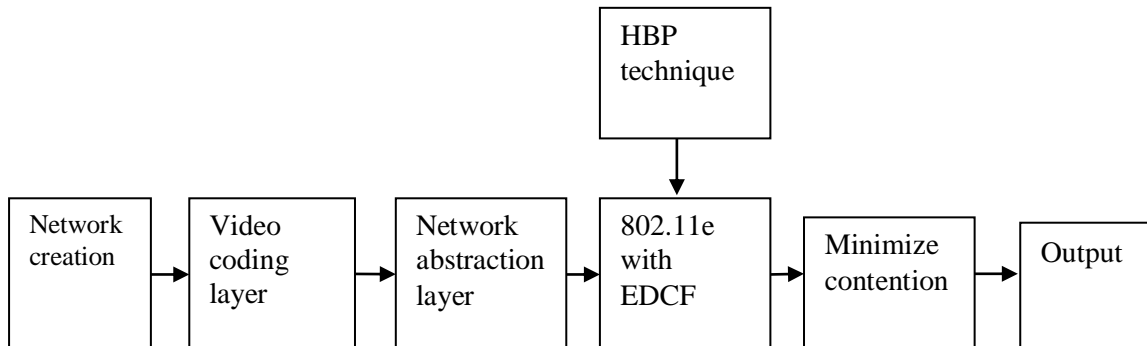


Figure 5 Block diagram of HBP with mesh network

5.1 Wireless network creation

The network topology in an ad-hoc network is highly dynamic due to the movement of nodes; hence an on-going session suffers frequent path breaks. Disruption occurs, either due to the movement of intermediate nodes in the path or due to the movement of end nodes. Such situations do not arise because of reliable links in wired networks where all the nodes are stationary. Even though wired network provides high reliability with low cost but the Quality of Service (QoS) is not provided in the better way. So the wireless ad-hoc networks must be used able to perform efficient and effective mobility management. The simulation time required to create wireless network is 15M. The following two parameters stand for the physical terrain in which the nodes are being simulated. For example, the following represents an area of size 100 meters by 100 meters. All range parameters are in terms of meters.

TERRAIN – DIMENSIONS (800,800)

The following parameter represents the number of nodes being simulated.

NUMBER-OF-NODES 10

5.2 Video coding packet

Requirements of multimedia streaming are different from those of a general file transfer. Bandwidth is the most important factor in a file transfer. A large bandwidth leads to a short transfer time and guarantees a good QoS. However, streaming has variable requirements with respect to the type of streaming service. Bandwidth is important in multimedia streaming. Multimedia data size typically ranges from a few megabytes to a few gigabytes. These large amounts of data require sufficient bandwidth to minimize buffering. If sufficient bandwidth is not guaranteed, then multimedia streaming service must have periodic buffering or download all multimedia data before play. Therefore, bandwidth is an important factor for multimedia streaming. Another important requirement for multimedia streaming is the delay variation or jitter. Buffering for multimedia streaming is decided by the delay variation. When the delay variation is large, the buffering time increases considerably in order to minimize the effect of delay. Delay is determined upon the initialization of multimedia streaming. If a delay spike occurs after initialization, additional buffering is required and a low quality of multimedia is experienced. In ad-hoc network, Ad-hoc On-demand Distance Vector (AODV) protocol maintains a routing table for an entry (destination) with a hop count (number of hops from source to destination) and a sequence number. This can be used by the application to control the transmission rate in accordance with the hop count. If a route change is the consequence of a link breakage, any intermediate node (between the source and the destination) detecting the link breakage (to the next hop) will send the route error (RERR) message back to the source node. Therefore, the source node may use the reception of RERR as an indication of a link breakage. As soon as a new route is established, the application layer, upon receiving the hop-count information from the routing layer, can adjust its bit rates in accordance with the permissible transmission rate. In the case of video communications, the bit rates can be adjusted by changing the value of the Quantization Parameter (QP). This parameter has been specifically defined in the syntax structure by all video coding standards as a means to control the video transmission rate. Here, a new video-coding standard such as H.264 Advanced Video Coding (AVC) is used. H.264 AVC is a standard capable of providing good video quality at substantially lower bit rates than previous standards (H.263 or MPEG-4), without increasing the complexity of design so much that it would be impractical or excessively expensive to implement. An additional goal was to provide enough flexibility to allow the standards to be applied to a wide variety of applications on a wide variety of networks and systems, including low and high bit rates, low and high resolution video, broadcast and ITU-T multimedia telephony systems.

5.3 Network abstraction layer

Cross-layer architecture is designed for H.264 AVC. Such a cross-layer architecture is based on two main interactions with 802.11e. First, a top-down cross-layer interaction allows the H.264 network abstraction layer (NAL) video delivery module to transmit the QoS information related to the video fragment priority to the network layer. Second, a second top-down cross-layer interaction allows the network layer, in turn, to express the same QoS exigencies to an EDCA-BASED MAC layer.

5.4 Hop-based priority

Multimedia streaming services require sufficient bandwidth and delay variation to achieve the good Quality of Service (QoS). Previous ad-hoc networks could not satisfy these requirements since 802.11 requires an ad-hoc wireless network with 802.11 to have a contention between the previous and next hops. This leads to delay fluctuation and additional back-off time due to collision. These, in turn, decrease the network bandwidth. The Hop-based priority (HBP) technique using 802.11e is used for minimizing the contention between hops. A previous packet contends with a next packet or a later sent packet when the packets try to transmit to a destination through a route. The previous packet and the next packet have the same priority and contend with each other by a fair condition. It brings the probability of the gain of each packet in the channel to 50%. The effect that the next packet cannot get the channel by contention with the previous packet is small. If the next packet wins the previous packet and transmits one more hop, it cannot transmit more hops until the previous packet transmits. In other words, winning of the previous packet from the next packet causes the delay to decrease and the bandwidth to increase. Therefore, the previous packet has a higher priority than the next packet every time. Hence, HBP technique is used to avoid the contention between the previous and the next packets. In other techniques, every packet has a fixed priority, and the previous packet and the next packet contend with each other. In HBP, each packet increases the priority after every hop and minimizes the contention between the packets.

5.5 Comparison

The performance of the proposed Hop-based priority technique using 802.11e is measured by the throughput and delay. The throughput comparison is made based on the delay variation between various IEEE 802.11 standard with 802.11e standard. First the analysis of delay in 802.11 WLAN is made. The delay in 1-hop transmission is denoted as

$$T_{trans} = T_{bas} + T_{cont} + T_{col} \quad (3.1)$$

T_{trans} denotes the time of 1-hop transmission. T_{bas} is the basic transmission time. T_{cont} and T_{col} are the additional delay caused by the loosening of contention and collision. T_{bas} is the total sum of the DCF interframe space (T_{dif}), random backoff (T_{ran}), transmission data (T_{data}), short interframe space (T_{sifs}) and transmission acknowledgement (T_{ack}) time.

$$T_{bas} = T_{dif} + T_{ran} + T_{data} + T_{sifs} + T_{ack} \quad (3.2)$$

T_{ran} is based on the size of the contention windows (CWs) and can be calculated.

$$T_{ran} = (CW_{max} + CW_{min}) * slot_time / 2 \quad (3.3)$$

T_{const} has a probability related to the loosening for contention (P_{loose})

$$T_{const} = P_{loose} * (T_{dif} + T_{data} + T_{sifs} + T_{ack}) \quad (3.4)$$

When a collision occurs, 802.11 operates the random backoff and attempts to transmit the data.

The total delay can be calculated by $T_{tran} * (\text{number of hops})$. In 802.11e with HBP, the total delay has to be calculated because the priority changes at every hop.

VII. PROPOSED WORK

In the previous work, HBP technique is used in wireless multi-hop networks to avoid the contention between the packets. 802.11e EDCF supports eight priorities, which implies that HBP technique has a limit of eight hops. We propose a Wireless Mesh Networks (WMN) using HBP technique which has a number of features that distinguish from wireless multi-hop networks. First, the positions of nodes of a WMN are relatively fixed it means any change of position is limited within certain range. The implication of this is that routing paths can be created that are likely to be stable. This reduces the need for routing packet overhead. Second, unlike pure ad-hoc networks, where the traffic flows between arbitrary pairs of nodes, in WMN, all traffic is either to or from a designated gateway, which connects the wireless mesh network to the Internet. The relevance of this point is that the traffic may be split over multiple gateways, so as to reduce the load within any given portion of the network. Third, the nodes will typically have access to a power source, and so power consumption is not a critical issue.

Packet delay is caused by various reasons, including collision resolution during packet forwarding, packet buffering, and different scheduling algorithms [13]. However, the most critical cause is packet delay in WMN is path length. Under the same traffic intensity, a smaller number of hops would lead to less packet delay. For two nodes, S (x_S, y_S) and D (x_D, y_D), in a grid network, their shortest distance is given in equation,

$$d = |x_S - x_D| + |y_S - y_D| \quad \dots\dots\dots(1)$$

To minimize the packet delay, the shortest path is used. However, this must be done in the context of minimizing collisions, since highly-contended paths that are shortest are not necessarily ideal. In Label switching protocol (LSP) each packet is associated with labels. Each packet is associated with the labels. It reduces the complexity of network operation. LSP always select the shortest path. Label switching protocol is used in MPLS (Multiprotocol label switching).

5.1 Wireless mesh network

Wireless mesh networks have the potential to play a critical role as an alternative technology for last-mile broadband internet access. The positions of different nodes of a WMN are relatively fixed. It can be viewed as a special case of wireless multihop Adhoc networks, in which each node operates both as a host and as a router.

Wireless mesh networks are as with pure Adhoc networks easy to install. The setup cost for internet service providers is only gateway installation and configuration.

The most commonly used topology for wireless mesh network is a grid layout of buildings. Since each node would communicate with the gateway. In that mesh network label switching protocol is used to find the shortest path.

5.2 Label switching protocol

In Label switching protocol(LSP) each packet is associated with labels. Each packet is associated with the labels. It reduces the complexity of network operation. LSP always select the shortest path. Label switching protocol is used in MPLS(Multiprotocol label switching).

The label switching protocol(LSP) is used in the Multi protocol label switching(MPLS). It provides a foundation that supports the deployment of advanced routing services because it solves a number of complex problems:

- It addresses the scalability issues associated with the currently deployed IP over ATM overlay model.
- It reduces the complexity of the network operation.
- It facilitates the delivery of new routing capabilities that enhance conventional IP routing techniques.
- It also offers a standards based solution that promotes multivendor interoperability.

VIII. RESULTS AND IMPLEMENTATION

To validate our analysis, we have to implement the Hop-Based Priority (HBP) technique in 802.11e for wireless mesh network (WMN) in a simulator and by performing a series of simulation based experiments to test its effectiveness. Glomosim simulator is used for the simulation purpose and the simulation parameters are,

Simulation parameters

Simulation time		15M
Number of nodes	25	
Node placement		Grid
MAC protocol		802.11
Routing protocol	AODV	

We have compared the throughput of 802.11 alone the data sending rate from 800 Kbps to 1500 Kbps range. With these we are going to add HBP technique and compare the results with the current 802.11e, same as we have compared the delay of 802.11 with adding HBP technique and compare the results with current 802.11e. Then the delay and throughput comparison is made. Under the consideration for the transmission of multimedia data, the Hop-Based Priority (HBP) technique has to be implemented in 802.11e.

Table 2 Comparison table for Throughput values

DATA SENDING RATE	IEEE 802.11 VALUES	IEEE 802.11E VALUES	IEEE 802.11E WITH MESH NETWORK
800	950	950	960
900	1089	972	1102
1000	1198	1024	1223
1100	1238	1031	1298
1200	1342	1045	1395
1300	1457	1052	1564
1400	1476	1064	1599
1500	1498	1071	1612

Table 3 Comparison table for Delay values

DATA SENDING RATE	IEEE 802.11 VALUES	IEEE 802.11E VALUES	IEEE 802.11E WITH MESH NETWORK
800	0	0	0
900	0.05	0.001	0.003

1000	0.07	0.02	0.016
1100	0.04	0.018	0.03
1200	0.035	0.015	0.03
1300	0.032	0.014	0.03
1400	0.039	0.014	0.029
1500	0.034	0.015	0.0275

7.1 Simulation Results

In the first module the creation of the nodes is done. The simulation time required to create wireless environment is 15M. The following two parameters (800,800) required to stand for the physical terrain in which the nodes are being simulated. The numbers of nodes being simulated are 10. The packets are transmitted from the source node (5,7) to the destination (1,3) respectively in which normal transmission of packets takes place. Since the video packet is also considered as the ordinary data packet, the transmission of the video packet takes more time which increases the delay so the throughput decreases.

7.1.1. Screenshots

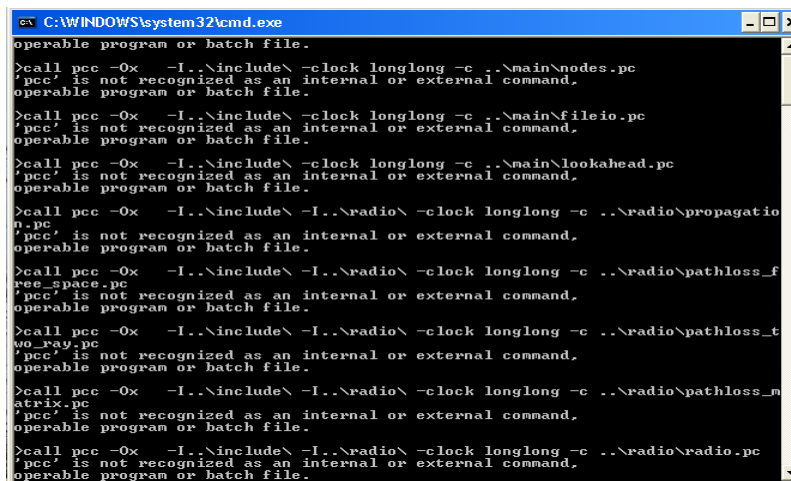


Figure 7.1.1 Compilation steps

Figure 7.1.1 shows compilation for all layers like physical layer, data link layer, network layer, radio layer.

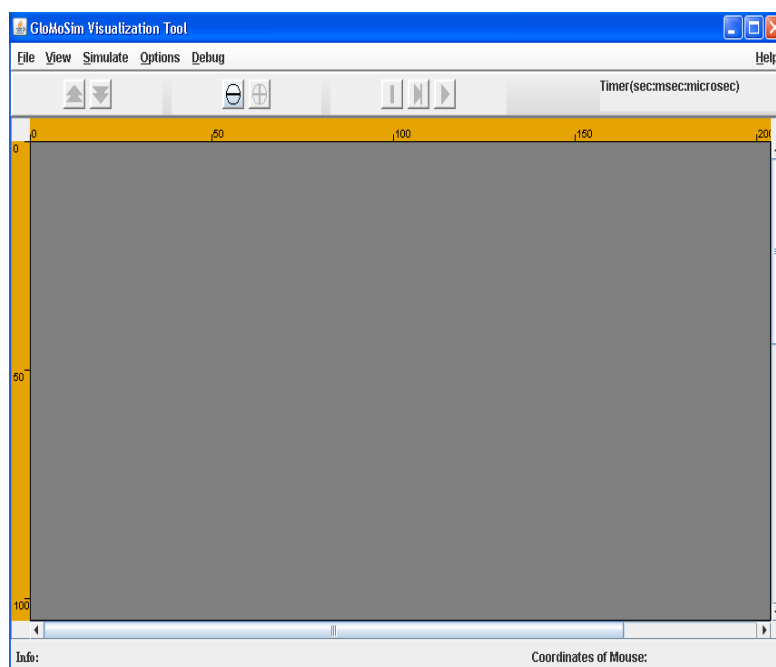


Figure 7.1.2 Glomosim Visualization

Figure 7.1.2 shows the glomosim visualization tool. Global Mobile Information System Simulator (GloMoSim) is a scalable simulation environment for large wireless and wire line communication networks. GloMoSim uses a parallel discrete-event simulation capability provided by Parsec. GloMoSim simulates networks with up to thousand nodes linked by a heterogeneous communications capability that includes multicast, asymmetric communications using direct satellite broadcasts, multi-hop wireless communications using ad-hoc networking, and traditional Internet protocols.

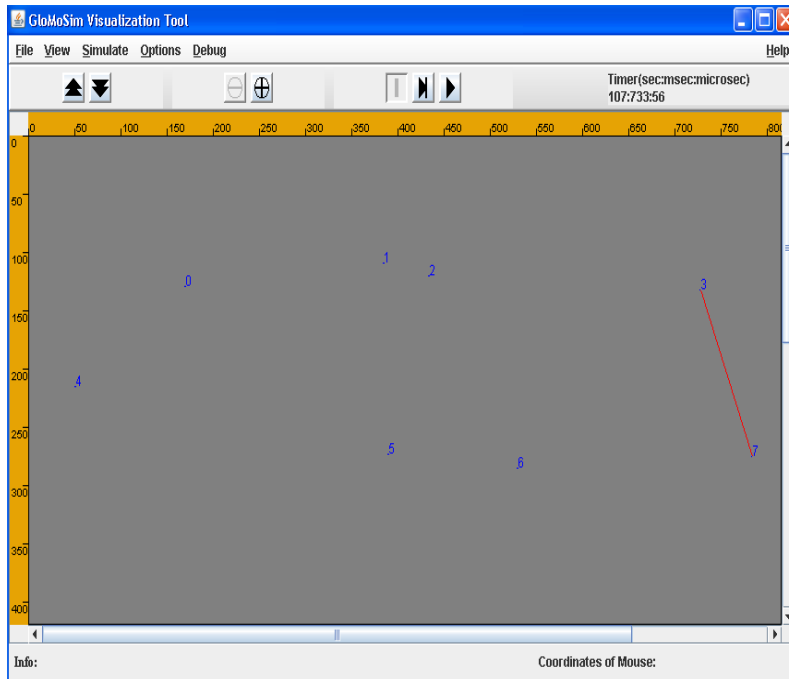


Figure 7.1.3 Transmission of Packets

Figure 7.1.3 shows the transmission of packets. Here the packets are transmitted from the source node (5,7) to the destination (1,3) respectively in which normal transmission of packets takes place.

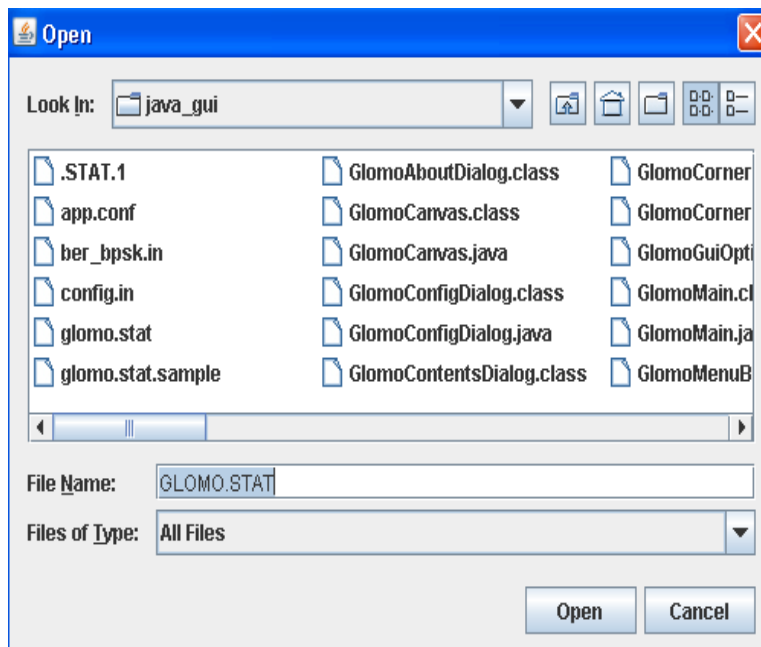


Figure 7.1.4 Glomo.stat file view

Figure 7.1.4 shows the GLOMO.STAT file is produced at the end of the simulation and contains all the statistics generated.

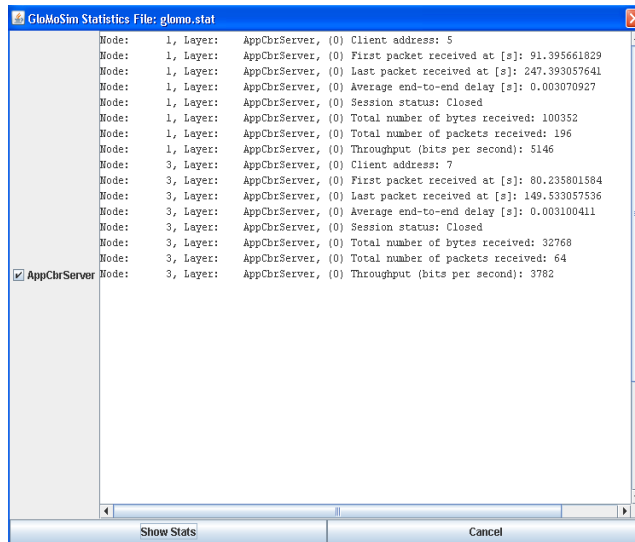


Figure 7.1.5 Viewing the stat file in visualization tool

Figure 7.1.5 shows the stat file in visualization tool for viewing the throughput and delay values of each packets.

IX. Output of throughput and delay

Comparing the throughput and delay values of 802.11(WLAN), 802.11e with HBP, HBP with mesh network. Here the HBP with mesh network throughput is high compare to the other throughputs. But the HBP with mesh network delay is constant(low) compare to the others delays.

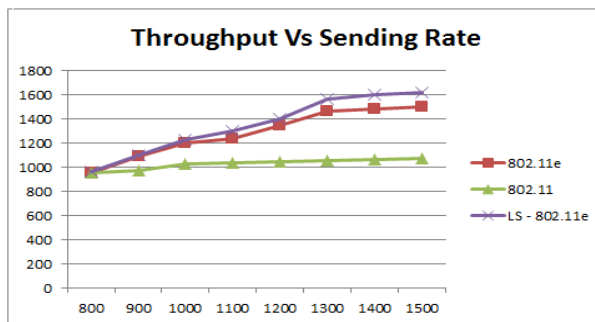


Figure 6 Throughput comparison

Figure 6 shows the throughput waveform of wireless network, x-axis shows the data sending rate in kilo bits per second(kbps), y-axis shows the throughput values IEEE 802.11, IEEE 802.11E with HBP technique and IEEE 802.11E with HBP mesh network, in kilo bits per second(kbps).

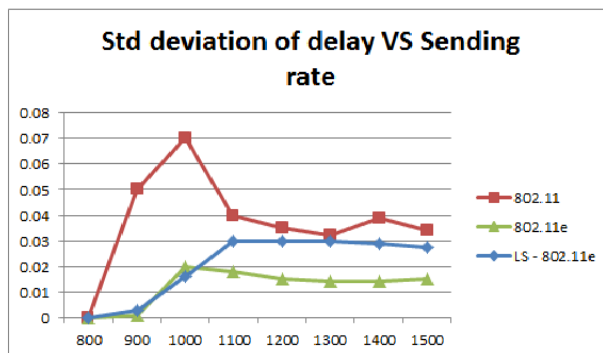


Figure 7 Delay comparison

Figure 7 shows the throughput waveform of wireless network, x-axis shows the data sending rate in kilo bits per second(kbps), y-axis shows the delay values of IEEE 802.11, IEEE 802.11E with HBP technique and IEEE 802.11E with HBP mesh network, in seconds(sec).

VIII. CONCLUSION

The usage of multimedia streaming in the wireless network is an open problem and deserves more research work. In this paper, we have analyzed the usage of multimedia streaming data packets in 802.11e using wireless mesh networks and presented the objectives that need to be achieved. Here we have shown that it is easy for the transmission of multimedia packets using hop-based priority technique in adhoc mesh networks so that the contention between the transmissions of packets is reduced with the improvement in the throughput. Which in turn increases the channel usage for the various other data transmission for the improvement in the Quality of Service (QoS). Since security is the main challenging issue, that has to be implemented in future.

REFERENCES

- [1] ShinHyoung Lee and Chuck Yoo, "Hop-Based Priority Technique Using 802.11e for Multimedia Streaming," IEEE Transactions on Consumer Electronics, Vol. 56, No.1, Feb. 2010.
- [2] A. Ksentini, M. Naimi, and A.Gueroui, "Toward an improvement of H.264 video transmission over IEEE 802.11e through a cross-layer architecture," IEEE Communication Magazine, vol. 44, issue 1, pp.107-114, Jan. 2006.
- [3] Q.Zhang, W.Zhu, and Y.Zhang, "Resource allocation for multimedia streaming over the Internet," IEEE Transaction on Multimedia, vol. 3, no.3, pp.339-355, Sept. 2001.
- [4] H. Gharavi and K.Ban, "Rate adaptive video transmission over ad-hoc networks," Electron Lett., vol. 40,no. 19,pp.1177-1178, Sept.2004.
- [5] Antonio Grilo, Mario Macedo, and Maria Nunes, "A scheduling Algorithm for QoS Support in IEEE 802.11E Networks," IEEE Wireless Communications, June 2003.
- [6] Joe Naoum-Sawaya, Bissam Ghaddar, Sami Khawan, Haidar Safa, Hassan Artail, and Zaher Dawy, "Adaptive Approach for QoS Support in IEEE 802.11e Wireless LAN,".
- [7] Mayank Mishra and Anirudha Sahoo, "An 802.11 based MAC protocol for providing QoS to real time applications,".
- [8] Yoon-Sik Yoo, Jung-Rae Kim, You-Jin Kim, and Jae-Doo Huh, "Analysis of EDCA MAC throughput for the IEEE 802.11e WLANs," International Conference on Convergence Information Technology, 2007.
- [9] Stefan Mangold, Sunghyun Choi, Guido R.Hiertz, and Ole Klein, "Analysis of IEEE 802.11e for QoS Support in Wireless LANs," IEEE Wireless Communications, Dec.2003.
- [10] Simone MiLANi, and Pamela Zontone, "Cross-layer optimization Strategies for video transmission over IEEE 802.11e networks,".
- [11] Dimitris Vassis, and George Kormentzas, "Delay performance analysis and evaluation of IEEE 802.11e EDCA in finite load conditions," IEEE Wireless Personal Communications 2005.
- [12] Byung Joon Oh and Chang Wen Chen, "Energy efficient H.264 video transmission over wireless ad-hoc networks based on adaptive 802.11E EDCA MAC protocol," ICME 2008.
- [13] Ann Lee and Paul A.S. Ward, "A Study of routing algorithms in wireless mesh networks,".
- [14] Sven Wietholter, Christian Hoene, "Design and Verification of an IEEE 802.11e EDCF Simulation Model in ns-2.26," Telecommunication Networks Group, Technische Universitat Berlin, Nov. 2003.

Authors

1. Revathi.V received the BE degree in electronics & communication engineering from V.S.B Engineering college from Anna University, Chennai in 2010. Currently, she is a ME student in SNS college of technology under Anna University, Coimbatore, India. Her research interests are in Wireless networks and wireless communication.

2. Prof.S.Vanitha received the BE. Degree in electronics and communication engineering from the Government college of Engineering under Anna University, Chennai. She received the ME. Degree in communication systems from Kumaraguru college of technology, under Anna University, Coimbatore. Currently, She is a Assistant professor at SNS College of Technology, Coimbatore, India. Her research interest includes Wireless technologies and digital image processing.

Air Brake Proportional to Load

Saeed Abu Alyazeed Albatlan

*Department of Mechanical Engineering (Automotive-Branch)
 Higher Technological Institute, 10th of Ramadan City- 6th October Branch – Cairo-Egypt*

Abstract : The brake system is the primary system in an automobile which ensures its safety on the road. The ideal brake system should operate with the least effort from the driver and should stop the vehicle within the minimum possible distance without losing controllability. This paper deals with the air brake system combination valve experimental performance. The work focuses on different parameters which would affect valve characteristics. Experimental investigation of the valve characteristics under these parameters is performed and analyzed.

Keywords: Air brake; relay valve; combination valve; performance; characteristics.

I. INTRODUCTION

A brake system must ensure the safe control of a vehicle during its normal operation and must bring the vehicle to a smooth stop within the shortest possible distance under emergency conditions [1, 2]. The air brake system currently used in commercial vehicles can be broadly divided into a pneumatic subsystem and a mechanical subsystem. One of the main components in the pneumatic subsystem is the relay valve which operates the brakes on the rear axles of a tractor and the axles of a trailer. A relay valve has different modes of operation and the pressure response of the relay valve can be naturally described as the response of a hybrid system [3]. An air brake system for truck and trailer combinations comprises a vehicle load sensing valve to control brake pressure of the vehicle axles [4]. A vehicle load responsive brake control device for adjusting the braking force according to the varying load of the vehicle in each braking range; the purpose of the brake control device is to adjust the braking forces in accordance with the static and dynamic shifting of the axle loads [5]. For vehicles without electronic control of brake pressure, there is need to vary the control pressure for different load conditions. This is done in order to avoid the instability that would occur if wheels lock (start skidding) in an unsuitable order. This device is called a load sensing valve [6]. In [7] new generations of mechanical and pneumatic load sensing valves are developed with an integrated relay valve and connection to ABS to meet the requirements for modern commercial vehicles. Natarajan et al. [8] showed complete mathematical model governing the response of the relay valve in an air brake system. The development of an electropneumatic brake which would decrease the response time of the air brake system there by providing a reduced stopping distance can be found in [9]. Zhang et al. [10] developed a new modeling and simulation methodology for a pneumatic brake system with ABS widely used in commercial vehicle. The construction and operation of load sensing relay valve which is described in [11] and illustrated Fig. 1. The present paper deals with experimental investigation of performance characteristics of the combination valve at different operating conditions. A

test rig is designed and built for the study purpose, and the analysis of test results is performed.

II. MATHEMATICAL MODEL

The combination valve mathematical model can be represented in two stages according to air charged in each chamber.

2.1 Stage (1)

During apply and hold phases, when the pressure in chamber (B) increases to a level where it balances the primary piston force and the inlet valve (3) is closed.

$$A_A \times P_P = P_B (A_A + A_V) \quad (1)$$

$$P_B = P_P \times \frac{A_A}{(A_A + A_V)} \quad (2)$$

$$A_V = \frac{A_A (P_P - P_B)}{P_B} \quad (3)$$

Where:

P_B = pressure in chamber (B), bar

P_P = treadle valve pressure, bar

A_A = chamber (A) surface area = $784.37 \times 10^{-6} \text{ m}^2$

A_V = variable area, m^2

2.2 Stage (2)

During hold phase, when compressed air from the storage reservoir flows into chamber (C) and brake chamber.

$$P_B \times A_P - F_S = P_C \times A_P \quad (4)$$

$$P_C = P_B - \frac{F_S}{A_P} \quad (5)$$

Where:

F_S = spring force = 203 N

P_C = pressure in chamber (c) = brake chamber pressure, bar

A_P = primary piston surface area, m^2

Mathematical model of the load sensing relay valve constructed on Matlab /Simulink. Details about this mathematical model are given in [11].

III. Experimental Work

The objective of the experimental work is to test the air brake system with load sensing relay valve under different operation conditions, and to measure the behavior of brake pressure line. The experimental data were used to evaluate their performance characteristics.

Figure 2 shows a general layout of the test rig, which can be divided, into three main groups: test rig main components, the measuring instruments and data acquisition systems [DAQs]. The detail of each group is given below.

3.1 Test Rig Main Components

The test rig is designed and built to simulate the vehicle air brake system; the rig uses actual air brake system units and components. It allows testing different types of pressure regulator valves. The air brake system includes an air compressor (1) coupled with electric motor (2), an air reservoir (3), brake foot valve (treadle valve) (4), combination valve (5), rear brake chamber (6), rear axle wheel and hoses (7) which connect different components, as shown in Fig. 3. Air compressor actuating mechanism showed in Fig. 3 (a) consists of electric motor and V- belt connecting air compressor with motor pulley. To have a wide range of rear axle load, the load sensing lever indexing plate (8) is provided with holes which are corresponding to deflections due to different loads on the rear axle.

3.2 The Measuring Instruments

Test rig is equipped with several measuring instruments, which are necessary for performing the tests. The measuring instruments, shown in Fig. 2 include:

3.2.1 Pressure transducers

A pressure transducer is mounted at the entrance of each of the combination valve (9) from brake foot valve (treadle valve), entrance to combination valve (10) from the air tank, and output of the combination valve (11) by means of a custom designed and fabricated pitot tube fixture. The purpose of this measurement is to evaluate their performance characteristics of the valve.

3.3 Data Acquisition Systems [DAQs]

All the transducers are interfaced with a connector block through shielded cables. The connector block is connected to a DAQ board [12], (connect with computer by USB cable) that collects the data during experimental test runs. This DAQ board can measure (16-channel single ended inputs or 8 channel differential inputs) and can provide two analog output signals. The DAQ board discretizes the analog input signals using an analog-to-digital (A/D) converter (12) and the resulting digital signals are stored in the computer. An application program written in Labview is used to collect and store the data in the computer [13]. DC supply (13) is used to provide pressure sensors with the required electrical volts. All the transducers are interfaced to a lap top computer (14), through an amplifier and signal conditioning devices.

IV. Results And Discussion:

This section presents experimental results obtained in two cases. Case (I) when the valve with rear axle chamber and case (II) when the valve without rear axle chamber. The main objectives to be considered are to

evaluate the performance characteristics of the valve, study the effect of pedal travel rate on its performance and to evaluate the delay time of the valve.

4.1 Model Validation

The model is validated by comparing its performance to experimental results obtained from the test rig undergoing different load conditions with model simulation results. Figures 4, 5 show the reservoir pressure, treadle valve pressure (relay pressure) and chamber brake line pressure, plotted against the brake time, for experimental and simulation results in different cases covering the whole loading conditions range of the vehicle. The results show a good agreement between simulation and experimental results. Details about this result are given in [11].

4.2 Evaluating the Performance Characteristics of Valve.

Figures from 6 to 9 show the experimental results of the relationship between treadle valve pressure (P_1), chamber brake line pressure (P_2), and reservoir pressure (P_3), plotted against the brake time in different operation conditions. Fig. 5 represents the behavior of treadle valve pressure, and brake chamber line pressure at the same operation conditions but at different reservoir pressure in two cases, where three stages can be noticed as follows:

4.2.1 Stage (1):

During this stage the brake line pressure increases up to the required pressure whose value depends on the loading condition of the vehicle. This stage is called the apply phase, which depends on pedal travel rate and required braking force.

4.2.2 Stage (2):

The brake line pressure during this stage is constant. This stage is called the hold phase, affected by reservoir pressure, relay valve parameters and required braking force.

4.2.3 Stage (3):

This stage is called the released stage, affected by pedal release rate. Figures from 6 to 10 show lag time for the chamber brake line pressure with respect to treadle valve pressure, the values of lag time in case (I) and case (II) are 0.101, 0.15, 0.199, 0.25 and 0.049, 0.05, 0.098, 0.1 (sec.) respectively, due to increase delay period of brake system, i. e. increasing the response time of the air brake system there by a increasing stopping distance. One of the important parameters which affect the delay period of air brake system is the brake chamber conditions and pedal travel rate. From these values we can conclude that lag time increases in case (I) and variable pedal travel and decreases in case (II) and slow pedal travel. Results shown in Fig. 6 show the operation pressure of treadle valve and combination valve affected by reservoir pressure.

From Figs 6 to 10 it can be noted that:

1-The brake chamber pressure changes in proportion to loading conditions and treadle valve pressure changes according to reservoir pressure.

2-There is a lag time for the outlet pressure of valve with respect to the treadle valve pressure affected by pedal travel rate and brake chamber conditions?

4.3 Effect of cam on Air Brake System performance

Figure 11 shows the experimental result in different positions covering the whole loading condition of the vehicle at slow rate pedal travel, and indicates that the performance of valve effected by shape of cam; load sensing cam (10) in Fig. (1).

From Fig. 11 it can be noted that performance characteristics of valve affected by the shape of load sensing cam

4.4 Effect of leak on Air Brake System performance

Figure 12 represents the performance behavior of valve at one position of load, and indicates that the performance of valve is affected by any leak in air brake system, due to decrease in the pressure of each reservoir (P_3), treadle valve (P_1), and chamber brake line (P_2). This means that brake force applied is not proportional to its load due to unstable brake balance [14].

From Fig 12 it can be noted that the performance characteristics of valve affected by the leak in air brake system pressure.

V. CONCLUSIONS:

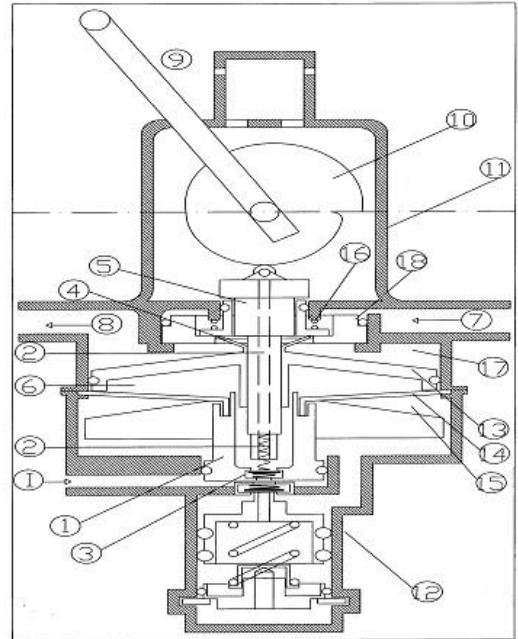
The measurements performed on the valve using the developed test rig show

1. The brake chamber pressure changes in proportion to loading conditions and treadle valve pressure according to reservoir pressure.
2. There is a lag time for the outlet pressure of valve with respect to the treadle valve pressure affected by pedal travel rate and brake chamber conditions.
3. Performance characteristics of valve are affected by
 - a- Shape of load sensing cam
 - b- Leak in air brake system pressure.

VI. REFERNCES

1. T. K. Garrett, K. Newton, and W. Steed, the Motor Vehicle, 13rd ed. Warrendale, Pennsylvania: Society of Automotive Engineers, 2001.
2. R. Limpert, Brake Design and Safety, 2nd ed. Warrendale, Pennsylvania: Society of Automotive Engineers, 1999.
3. Darbha et al." A Diagnostic System for Air Brakes in Commercial Vehicles", Intelligent Transportation Systems, IEEE Transactions on Volume 7, PP. 360 – 376, Issue 3, Sept. 2006.
4. Truck and trailer braking systems. <http://www.freepatentsonline.com/4078844.html>
5. Load-dependent braking force control device. <http://www.patentgenius.com/image/4223955-3.html>
6. Brake Calculation Software for Commercial Vehicles. 1998. <http://www.vehicular.isy.liu.se>.
7. Mechanical Load – Sensing Valve with Relay Valve http://www.wabcoauto.com/products_and_systems/products-systems-valves.
8. Natarajan et al, "Model of The Relay Valve Used In an Air Brake System" Department of Mechanical Engineering, Texas A&M University, January 2007.
9. Subramanian et al, "Development and modeling of an electropneumatic brake system", Intelligent Vehicles Symposium, IEEE, June 2009.
10. Zhang et al, "Modeling and simulation of a pneumatic brake system", Intelligent Vehicles Symposium, IEEE, June 2009.

11. National Instruments "Data Acquisition systems" <http://www.ni.com/digitalio/>
12. G. W. Johnson and R. Jennings, Labview Graphical Programming, 3rd NewYork: McGraw-Hill, 2008.
13. Nosseir et al, "Proper Utilization of Load Sensing Valve to Improve Brake Performance", Ain Shams University. Faculty of Engineering, Vol. 40, No.2, PP. 823-843, June 30, 2005.



1- Inlet port from treadle valve
 2- Primary piston
 3- Inlet from treadle valve
 4- Atmospheric control valve
 5- Regulating rod
 6- Chamber (B)
 7- Inlet port from reservoir
 8- Outlet to brake wheel chamber
 9- Load sensing cam lever
 10- Load sensing cam
 11- Upper valve body
 12- Lower valve body
 13- Relay piston
 14- Variable area diaphragm
 15- Variable area diaphragm disc
 16- Coil spring
 17- Chamber (C)
 18- Inlet valve seat

Figure 1 Load sensing relay valve (combination valve) main parts [11].

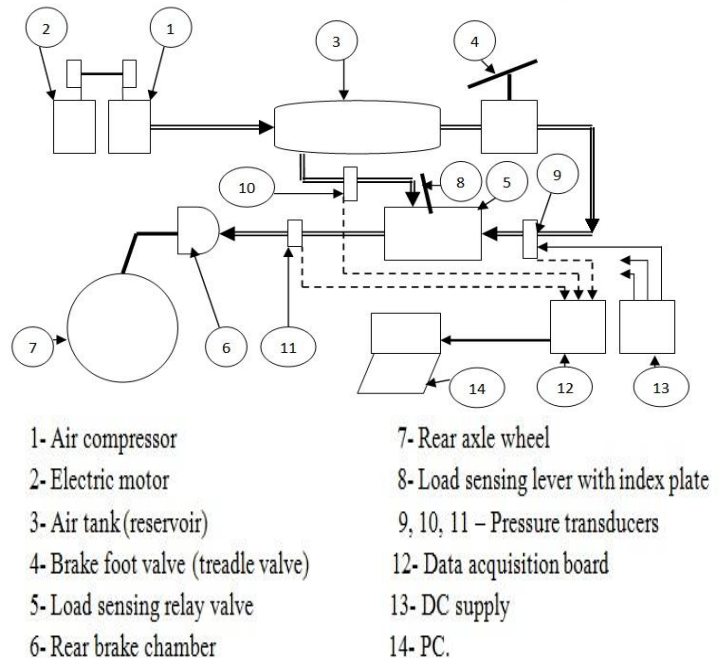
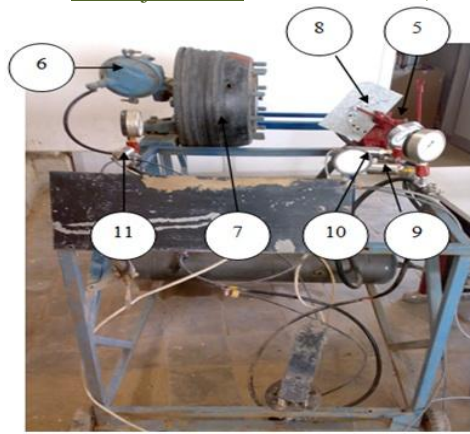


Figure 2 Layout of test rig [11]



a- Air brake system components

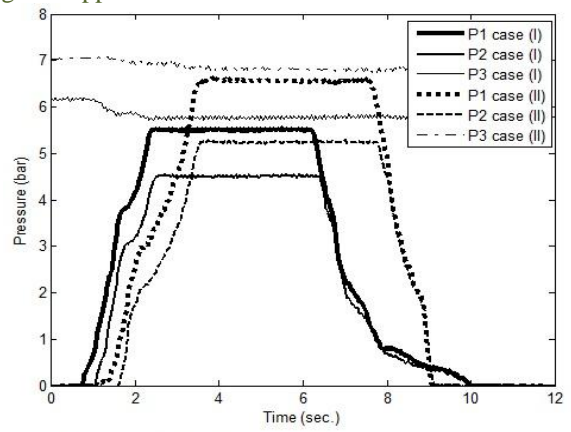


Figure 6 Air line brake pressure at half-load in two cases



b- Air brake system components
Figure 3 Test rig

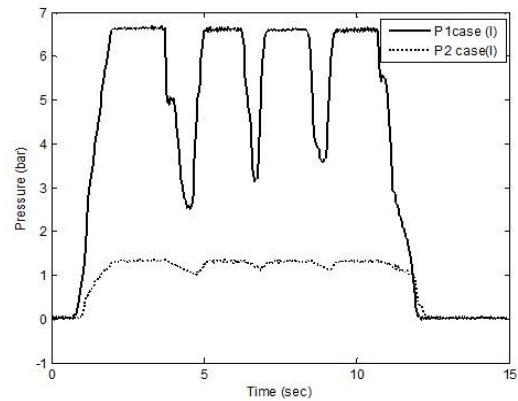


Figure 7 Air line brake pressure at (1/3) load in case (I) at variable pedal travel

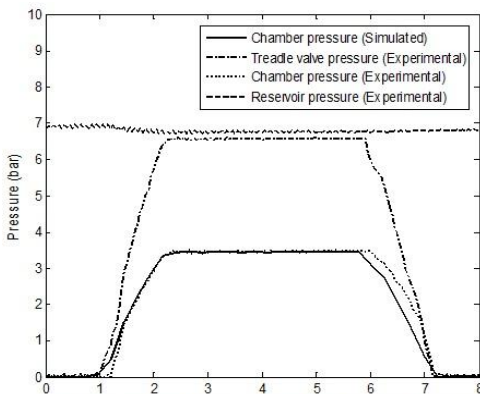


Figure 4 Simulated and experimental air brake pressure at no-load

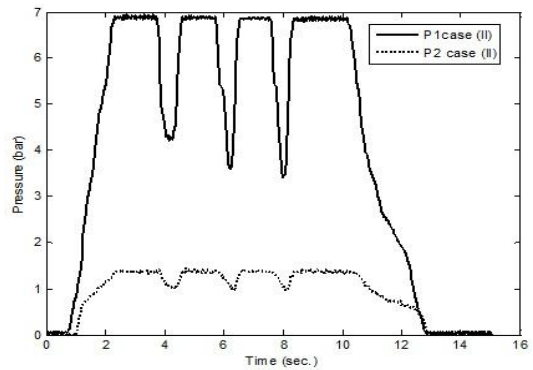


Figure 8 Air line brake pressure at (1/3) load in case (II) at variable pedal travel

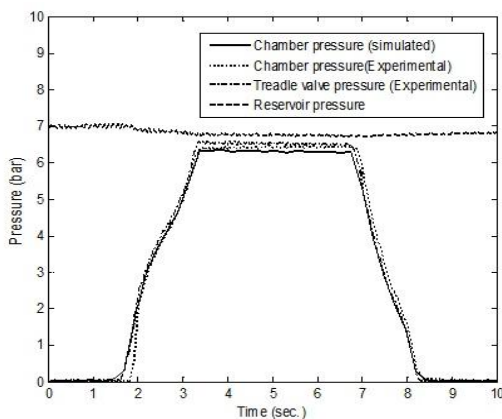


Figure 5 Simulated and experimental air brake pressure at full-load

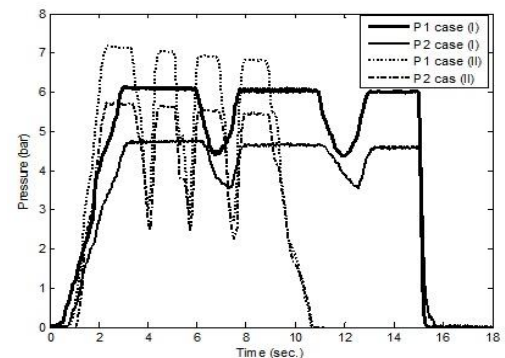


Figure 9 Air line brake pressure at half load in two cases at variable pedal travel

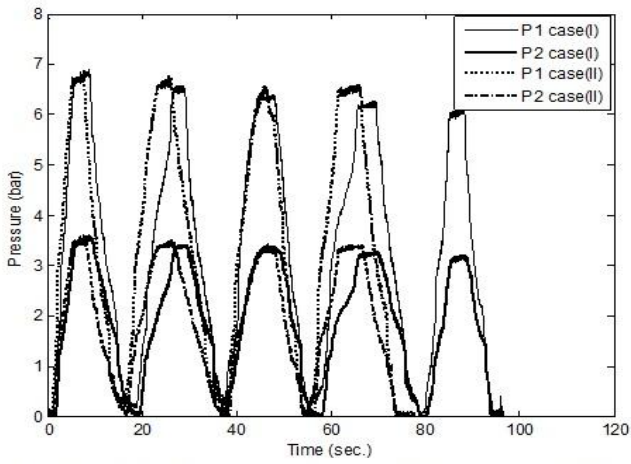


Figure 10 Air line brake pressure at no- load in two cases at variable pedal travel

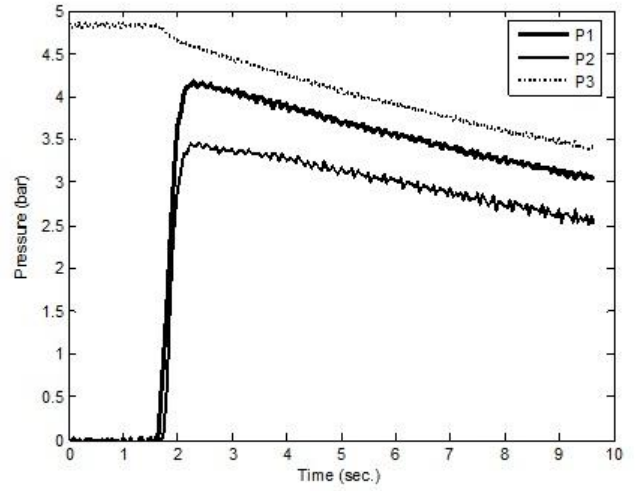


Figure 12 Effect of leak in air brake pressure

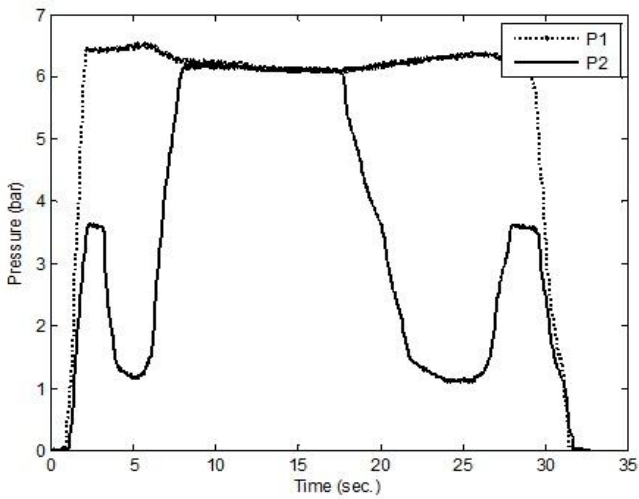


Figure 11 Wheel chamber air brake pressure at different loading conditions

Multilevel Converter for Ac–Dc Harmonic Immunity in VSC HvdC Transmission

¹Polisetty Hema Sundar, ²Aswani Kumar Eedara

¹Mtech Student Scholar Department of Electrical and Electronics Engineering, SASI Inst. Of Technology and Engg. , Tadepalligudem, W.G.Dist., A.P, India.

²Head of the Dept. of Electrical & Electronics Engg.,

SASI Inst. of Technology and Engg. Tadepalligudem, W.G.Dist., A.P, India

Email: ¹hemasundar10@gmail.com, ²aswani@sasi.ac.in

Abstract: The concept of multilevel inverters, introduced about 20 years ago entails performing power conversion in multiple voltage steps to obtain improved power quality, lower switching losses, better electromagnetic compatibility, and higher voltage capability. The benefits are especially clear for medium-voltage drives in industrial applications and are being considered for future naval ship propulsion systems. Several topologies for multilevel inverters have been proposed over the years; the most popular cascaded H-bridge apart from other multilevel inverters is the capability of utilizing different dc voltages on the individual H-bridge cells which results in splitting the power conversion amongst higher-voltage lower-frequency and lower-voltage higher-frequency inverters. Control methods based on selective harmonic elimination pulse-width modulation (SHE-PWM) techniques offer the lowest possible number of switching transitions. This feature also results in the lowest possible level of converter switching losses. For this reason, they are very attractive techniques for the voltage-source-converter-(VSC) based high-voltage dc (HVDC) power transmission systems. The paper discusses optimized modulation patterns which offer controlled harmonic immunity between the ac and dc side. The application focuses on the conventional two-level converter when its dc-link voltage contains a mix of low-frequency harmonic components. Simulation and experimental results are presented to confirm the validity of the proposed switching patterns. Finally a five level Multilevel converter topology is applied for this application

Keywords-Amplitude modulation (AM), dc-ac power conversion, harmonic control, HVDC, insulated-gate bipolar transistor (IGBT), power electronics, power transmission system, pulse-width modulation, voltage-source converter (VSC).

I. INTRODUCTION

The continuous growth of electricity demand and ever increasing society awareness of climate change issues directly affect the development of the electricity grid infrastructure. The utility industry faces continuous pressure to transform the way the electricity grid is managed and operated. On one hand, the diversity of supply aims to increase the energy mix and accommodate more and various sustainable energy sources. On the other hand, there is a clear need to improve the efficiency, reliability, energy security, and quality of supply. With the breadth of benefits that the smart grid can deliver, the improvements in technology capabilities, and the reduction in technology

cost, investing in smart grid technologies has become a serious focus for utilities [1].

Advanced technologies, such as flexible alternating current transmission system (FACTS) and voltage-source converter (VSC)-based high-voltage dc (HVDC) power transmission systems, are essential for the restructuring of the power systems into more automated, electronically controlled smart grids. An overview of the recent advances of HVDC based on VSC technologies is offered in [2]. The most important control and modeling methods of VSC-based HVDC systems and the list of existing installations are also available in [2]

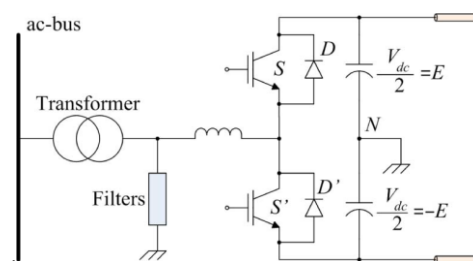


Fig. 1. Phase of the two-level VSC for the HVDC power transmission system[7].

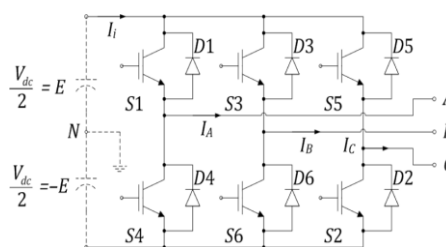


Fig. 2. Three-phase two-level VSC.

The first generation of utility power converters is based on current-source converter (CSC) topologies [3], [4]. Today, many projects still use CSCs due to their ultra-high power capabilities. With the invention of fully controlled power semiconductors, such as insulated-gate bipolar transistors (IGBTs) and integrated gate-commutated thyristors (IGCTs) [5], the VSC topologies are more attractive due to their four-quadrant power-flow characteristics [6]. A typical configuration of the VSC-based HVDC power transmission system is shown in Fig. 1 as it is shown in [7] and [8].

With the advancement of power electronics and emergence of new multilevel converter topologies, it is possible to work at voltage levels beyond the classic semiconductor limits. The multilevel converters achieve high-voltage switching by means of a series of voltage steps, each of which lies within the ratings of the individual

power devices. Among the multilevel Converters [1-4], the cascaded H-bridge topology (CHB) is particularly attractive in high-voltage applications, because it requires the least number of components to synthesize the same number of voltage levels.

Additionally, due to its modular structure, the hardware implementation is rather simple and the maintenance operation is easier than alternative multilevel converters. The multilevel voltage source inverter is recently applied in many industrial applications such as ac power supplies, static VAR compensators, drive systems, etc. One of the significant advantages of multilevel configuration is the harmonic reduction in the output waveform without increasing switching frequency or decreasing the inverter power output [5-11]. The output voltage waveform of a multilevel inverter is composed of the number of levels of voltages, typically obtained from capacitor voltage sources. The so-called multilevel starts from three levels. As the number of levels reach infinity, the output THD approaches zero. The number of the achievable voltage levels, however, is limited by voltage unbalance problems voltage clamping requirement, circuit layout, and packaging constraints.

On the other hand, optimized modulation methods offer many advantages toward tight control of converter-generated harmonics [19]. A minimization method to find the complete set of solutions by solving the SHE-PWM equations for two-level inverters is discussed in [20]. In this paper, the dc-link voltage is assumed to be constant. In [10], a method is proposed to prevent the dc-link ripple voltage from creating low-order harmonics on the ac side of fixed and variable frequency inverters. However, only one of the multiple SHE-PWM sets [20] of solutions is reported.

An investigation of the harmonic interaction between the ac and dc side for STATCOM is presented in [21] including the so-called dynamic SHE-PWM scheme based on precalculated angles for better THD. However, the dynamic SHE-PWM scheme is applied only for a three-level converter and can be applied only for known magnitude and frequency of the ripple. Another method for improving the harmonic performance of a two-level VSC with SHE-PWM is studied in [22]. However, only one set of SHE-PWM solutions is considered for the method of [22] which requires the exact values of magnitude, phase, and frequency of the ripple in order to be implemented.

Control strategies to compensate unbalances are reported in the literature. Mild imbalances caused by unbalanced loads of the ac side are regulated by using separate control loops for the positive- and negative-sequence components of the voltage as proposed in [23]. Efficient control of unbalanced compensator currents can be achieved by a control algorithm based on the D-STATCOM model [24]. D-STATCOM allows separate control of positive- and negative-sequence currents and decoupled current control of the d-q frame. An advanced strategy based on direct power control under unbalanced grid voltage conditions has been recently presented for a doubly fed induction generator [25]. To take the full advantages of VSCs for HVDC power transmission systems, an auxiliary controller is added to the main controller which is conventionally implemented in the positive-sequence d-q frame [26]. To compensate for unbalanced ac-side loads,

the auxiliary controller is implemented in the negative-sequence d-q frame.

The objective of this paper is to discuss the effectiveness of optimized modulation based on precalculated SHE-PWM in a two-level three-phase VSC to make the ac side immune from the fluctuations of the dc link without the use of passive components. However, since the VSC studied here does not include a closed-loop controller, strategies to compensate unbalances are not addressed in this paper.

This paper is organized in the following way. In Section II, a brief analysis of the VSC and the modulation method is provided. Section III contains the characteristics of the method on a VSC with dc-side ripple voltage. Section IV provides extensive experimental results to support the theoretical arguments. Conclusions are documented in Section V.

II. Analysis Of The Pwm Converter And She-Pwm

The optimized SHE-PWM technique is investigated on a two level three-phase VSC topology with IGBT technology, shown in Fig. 2. A typical periodic two-level SHE-PWM waveform is shown in Fig. 3.

The waveforms of the line-to-neutral voltages can be expressed as follows:

$$V_{LN} = \begin{bmatrix} V_{AN} \\ V_{BN} \\ V_{CN} \end{bmatrix} = V_{dc} \begin{bmatrix} \sum_{n=1}^{\infty} A_n \sin n\omega_0 t \\ \sum_{n=1}^{\infty} A_n \sin n \left(\omega_0 t - \frac{2\pi}{3} \right) \\ \sum_{n=1}^{\infty} A_n \sin n \left(\omega_0 t + \frac{2\pi}{3} \right) \end{bmatrix} \quad (1)$$

When ω_0 is the operating frequency of the ac, and V_{dc} is the dc-link voltage.

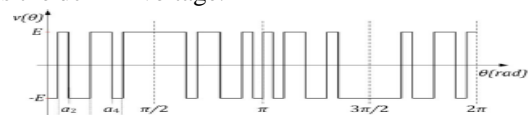


Fig. 3. Typical two-level PWM switching waveform with five angles per quarter cycle.

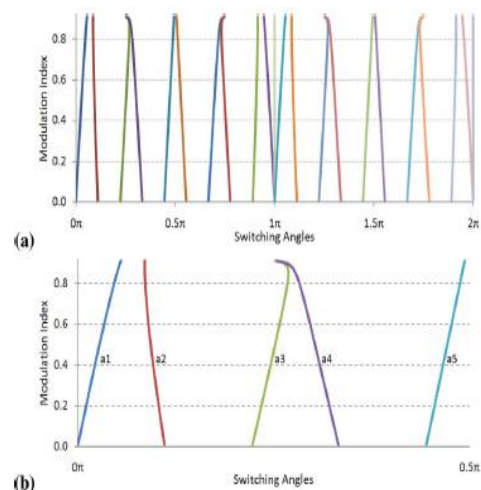


Fig. 4. Solution trajectories. (a) Per-unit modulation index over a complete periodic cycle. (b) Five angles in radians.

Thus, the line-to-line voltages are given by

$$V_{LL} = \begin{bmatrix} V_{AB} \\ V_{BC} \\ V_{CA} \end{bmatrix} = \sqrt{3} \cdot V_{dc} \begin{bmatrix} \sum_{n=1}^{\infty} A_n \sin n \left(\omega_0 t + \frac{\pi}{6} \right) \\ \sum_{n=1}^{\infty} A_n \sin n \left(\omega_0 t - \frac{\pi}{2} \right) \\ \sum_{n=1}^{\infty} A_n \sin n \left(\omega_0 t + \frac{5\pi}{6} \right) \end{bmatrix} \quad (2)$$

The SHE-PWM method offers numerical solutions which are calculated through the Fourier series expansion [20] of the waveform

$$M = 1 + 2 \sum_{i=1,2,3,..}^{N+1} (-1)^i \cos(\alpha_i)$$

$$0 = 1 + 2 \sum_{i=1,2,3,..}^{N+1} (-1)^i \cos(k\alpha_i) \quad (3)$$

Where N+1 are the angles that need to be found.

Using five switching angles per quarter-wave in (N=4)SHE-PWM, k= 5, 7, 11, 13 to eliminate the 5th, 7th, 11th, and 13th harmonics. During the case of a balanced load, the third and all other harmonics that are multiples of three are cancelled, due to the 120 symmetry of the switching function of the three-phase converter. The even harmonics are cancelled due to the half-wave quarter-wave symmetry of the angles, being constrained by

$$0 < \alpha_1 < \alpha_2 < \dots < \alpha_{N+1} < \pi/2$$

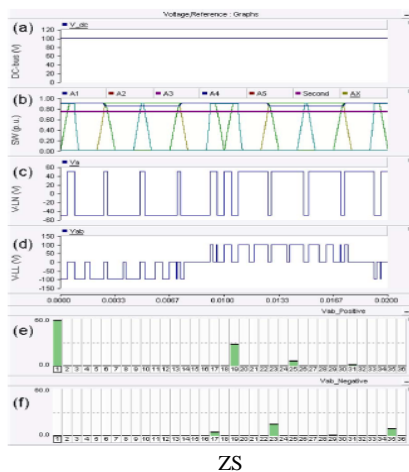


Fig. 5. Simulation results for SHE-PWM eliminating 5th, 7th, 11th, and 13th harmonics. (a) DC-link voltage. (b) Solution trajectories to eliminate harmonics and intersection points with the modulating signal (M=0.75). (c) Line-to-neutral voltage. (d) Line-to-line voltage. (e) and (f) Positive- and negative-sequence line-to-line voltage spectra, respectively.

III. Cascaded H-Bridge Multilevel Converter

2.1 Full H-Bridge

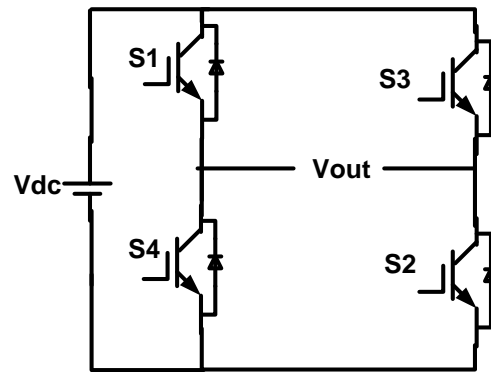


Figure. 6 Full H-Bridge

Switches Turn ON	Voltage Level
S1,S2	Vdc
S3,S4	-Vdc
S4,D2	0

Table 1. Switching table for H-Bridge

Fig.6 shows the Full H-Bridge Configuration. By using single H-Bridge we can get 3 voltage levels. The number output voltage levels of cascaded Full H-Bridge are given by 2n+1 and voltage step of each level is given by Vdc/n. Where n is number of H-bridges connected in cascaded. The switching table is given in Table 1 and 2.

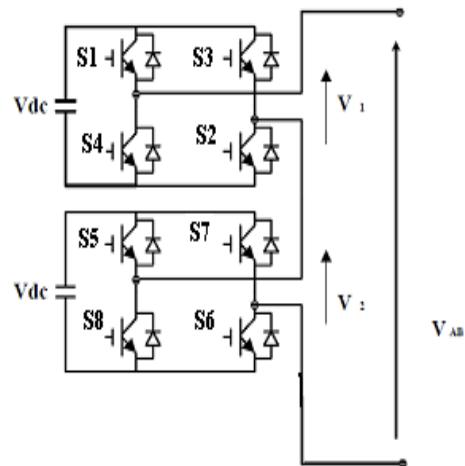


Table 2. Switching table for Cascaded H-Bridge

Switches Turn On	Voltage Level
S1, S2	Vdc
S1,S2,S5,S6	2Vdc
S4,D2,S8,D6	0
S3,S4	-Vdc
S3,S4,S7,S8	-2Vdc

IV. SIMULATION RESULTS

4.1 Modeling of Cascaded H-Bridge Multilevel Converter

Fig.7 shows the Matlab/Simulink Model of five level Cascaded H-Bridge multilevel converter. Each H-bridge DC voltage is 50 V. In order to generate three phase output such legs are connected in star/delta. Each leg gating pulses are displaced by 120 degrees.

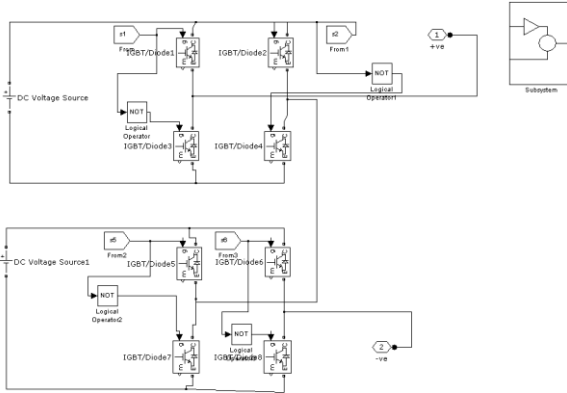


Figure. 7 Matlab/Simulink Model of CHB

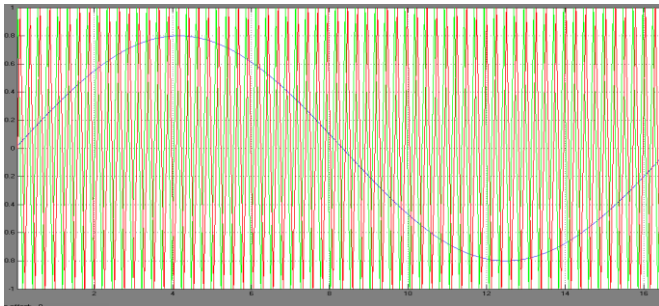


Figure. 8 Carrier Signals of Phase Shifted Carrier PWM

Fig.8 shows the Phase shifted Carrier PWM wave form. Here four carriers each are phase shifted by 90 degrees are compared with sine wave.

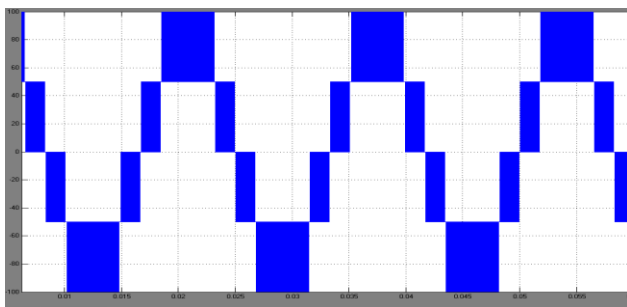


Figure. 9 Five Level output

Fig.9 shows the phase voltage of phase shifted carrier PWM CHB inverter. Fig.10 shows the line voltage of phase shifted carrier PWM CHB inverter. Here phase voltage has five voltage levels where as line voltage has nine voltage levels.

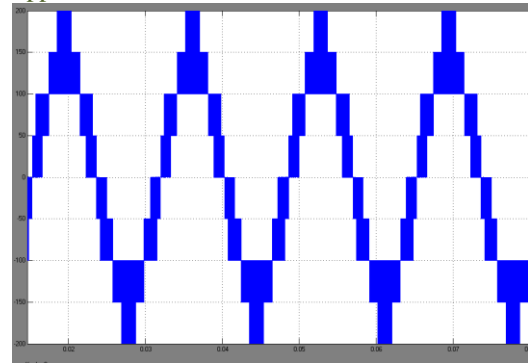


Figure. 10 Nine Level Line Voltage

Fig.10 shows the Level shifted Carrier PWM wave form. Here four carriers each are level shifted by 0.5 in positive and negative side are compared with sine wave.

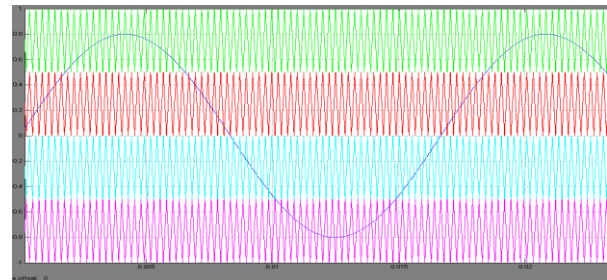


Figure. 11 Carrier Signals of Level Shifted PWM

Fig.11 shows the phase voltage of level shifted carrier PWM CHB inverter. Fig.12&13 shows the phase and line voltage of level shifted carrier PWM CHB inverter. Here phase voltage has five voltage levels where as line voltage has nine voltage levels.

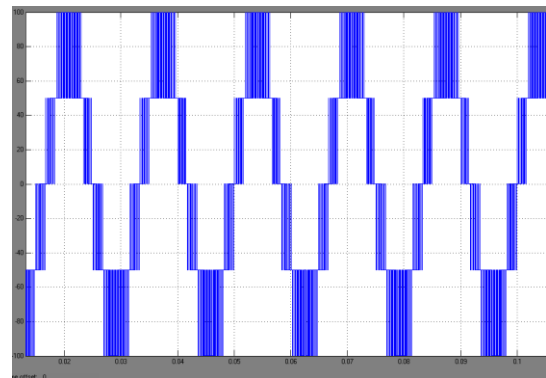


Figure. 12 Five Level Phase Voltage

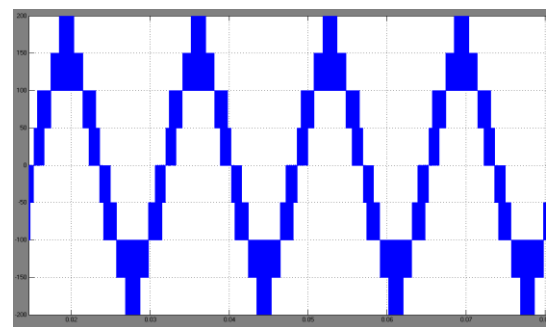


Figure. 13 Nine Level Line Voltage

V. CONCLUSIONS

This paper presents Novel Hybrid H-Bridge multilevel converter. The proposed converter produces more voltage levels with less number of switches compared to H- bridge configuration. This will reduce number of gate drivers and protection circuits which in turn reduces the cost and complexity of the circuit. Finally a five level single H-bridge is proposed. A SIMULINK based model is developed and Simulation results are presented.

References

- [1] J. McDonald, "Leader or follower [The business scene]," *IEEE Power Energy Mag.*, vol. 6, no. 6, pp. 18–90, Nov. 2008.
- [2] N. Flourentzou, V. G. Agelidis, and G. D. Demetriades, "VSC-based HVDC power transmission systems: An overview," *IEEE Trans. Power Electron.*, vol. 24, no. 3, pp. 592–602, Mar. 2009.
- [3] A. A. Edris, S. Zelingher, L. Gyugyi, and L. J. Kovalsky, "Squeezing more power from the grid," *IEEE Power Eng. Rev.*, vol. 22, no. 6, pp. 4–6, Jun. 2002.
- [4] B. K. Perkins and M. R. Iravani, "Dynamic modeling of high power static switching circuits in the dq-frame," *IEEE Trans. Power Syst.*, vol. 14, no. 2, pp. 678–684, May 1999.
- [5] P. Steimer, O. Apeldoorn, E. Carroll, and A. Nagel, "IGCT technology baseline and future opportunities," in *Proc. IEEE Transmi. Distrib. Conf. Expo.*, Oct. 2001, vol. 2, pp. 1182–1187.
- [6] V. G. Agelidis and G. Joos, "On applying graph theory toward a unified analysis of three-phase PWM inverter topologies," in *Proc. IEEE Power Electronics Specialists Conf.*, Seattle, WA, Jun. 1993, pp. 408–415.
- [7] J. Arrillaga, Y. H. Liu, and N. RWatson, *Flexible Power Transmission: The HVDC options*. Hoboken, NJ: Wiley, 2007.
- [8] G. Asplund, "Application of HVDC light to power system enhancement," in *Proc. IEEE Power Eng. Soc. Winter Meeting*, Singapore, Jan. 2000, vol. 4, pp. 2498–2503.
- [9] P. N. Enjeti, P. D. Ziogas, and M. Ehsani, "UnbalancedPWMconverter analysis and corrective measures," in *Proc. IEEE Industry Applications Soc. Annu. Meet.*, San Diego, CA, Oct. 1989, pp. 861–870.
- [10] P. N. Enjeti and W. Shireen, "A new technique to reject dc-link voltage ripple for inverters operating on programmedPWM waveforms," *IEEE Trans. Power Electron.*, vol. 7, no. 1, pp. 171–180, Jan. 1992.
- [11] J. Y. Lee and Y. Y. Sun, "Adaptive harmonic control in PWM inverters with fluctuating input voltage," *IEEE Trans. Ind. Electron.*, vol. IE-33, no. 1, pp. 92–98, Feb. 1986.
- [12] S. Funabiki and Y. Sawada, "Computative decision of pulse width in three-phase PWM inverter," in *Proc. IEEE Industry Applications Soc. Annu. Meet.*, Pittsburgh, PA, Oct. 1988, pp. 694–699.
- [13] T. Kato, "Precise PWM waveform analysis of inverter for selected harmonic elimination," in *Proc. IEEE Industry Appl. Soc. Annu. Meeting*, Piscataway, NJ, Sep. 1986, vol. 1, pp. 611–616.
- [14] B. P. McGrath and D. G. Holmes, "A general analytical method for calculating inverter dc-link current harmonics," in *Proc. IEEE Ind. Appl. Soc. Annu. Meeting*, Edmonton, AB, Canada, Oct. 2008, pp. 1–8.
- [15] A. M. Cross, P. D. Evans, and A. J. Forsyth, "DC link current in PWM inverters with unbalanced and nonlinear loads," *Proc. Inst. Elect. Eng., Elect. Power Appl.*, vol. 146, no. 6, pp. 620–626, Nov. 1999.
- [16] M. H. Bierhoff and F. W. Fuchs, "DC-link harmonics of three-phase voltage-source converters influenced by the pulsewidth-modulation strategy—An analysis," *IEEE Trans. Ind. Electron.*, vol. 55, no. 5, pp. 2085–2092, May 2008.
- [17] M. N. Anwar and M. Teimor, "An analytical method for selecting dc-link-capacitor of a voltage stiff inverter," in *Proc. 37th IAS Annu.Meeting IEEE Industry Applications Conf.*, Dearborn, MI, Oct. 2002, vol. 2, pp. 803–810.
- [18] F. D. Kieferndorf, M. Forster, and T. A. Lipo, "Reduction of dc-bus capacitor ripple current with PAM/PWM converter," *IEEE Trans. Ind. Appl.*, vol. 40, no. 2, pp. 607–614, Mar. 2004.
- [19] P. N. Enjeti, P. D. Ziogas, and J. F. Lindsay, "Programmed PWM techniques to eliminate harmonics: A critical evaluation," *IEEE Trans. Ind.Appl.*, vol. 26, no. 2, pp. 302–316, Mar. 1990.
- [20] V. G. Agelidis, A. Balouktsis, I. Balouktsis, and C. Cossar, "Multiple sets of solutions for harmonic elimination PWM bipolar waveforms: Analysis and experimental verification," *IEEE Trans. Power Electron.*, vol. 21, no. 2, pp. 415–421, Mar. 2006.
- [21] L. Ran, L. Holdsworth, and G. A. Putrus, "Dynamic selective harmonic elimination of a three-level inverter used for static VAR compensation," *Proc. Inst. Elect. Eng., Gen., Transm. Distrib.*, vol. 149, no. 1, pp. 83–89, Jan. 2002.
- [22] S. Filizadeh and A. M. Gole, "Harmonic performance analysis of an OPWM-controlled STATCOM in network applications," *IEEE Trans. Power Del.*, vol. 20, no. 2, pt. 1, pp. 1001–1008, Apr. 2005.
- [23] C. Hochgraf and R. H. Lasseter, "Statcom controls for operation with unbalanced voltages," *IEEE Trans. Power Del.*, vol. 13, no. 2, pp. 538–544, Apr. 1998.
- [24] B. Blazic and I. Papic, "Improved D-STATCOM control for operation with unbalanced currents and voltages," *IEEE Trans. Power Del.*, vol. 21, no. 1, pp. 225–233, Jan. 2006.



P. HEMA SUNDAR, pursuing M.Tech in SASI institute of Technology and Engineering with the specialization Power Electronics. I completed my under graduation in the stream of Electrical and Electronics Engineering in SASI institute of Technology and

Engineering, Tadepalligudem, Andhra Pradesh. My areas of interest are Power Electronic drive systems, Harmonic studies in power systems.



ASWANI KUMAR EEDARA received the B.Tech. degree in Electrical and Electronics Engineering from the JNTU college of Engineering Hyderabad, India in 2005 and the M.E. degree in Power Systems from the University

College of Engineering Osmania university Hyderabad in 2008. He worked as Project Trainee at GE-consumer and Industrial Hyderabad for one year. He has been on the faculty of SASI Institute of Technology and Engineering at Tadepalligudem as an Assistant Professor in Department of Electrical and Electronics Engineering Since 2008. He has been working as Head of the Department of E.E.E. since MAY 2012. He is member of IAENG .He has one international journal publication. He is presently doing his research in the area of Power Electronics applications in Power systems at JNTUK. His areas of interest are FACTS Controllers, Evolutionary algorithms, Modeling and simulation of Power Electronics and Power Systems.

Performance Evaluation of Single Phase H-Bridge Type Diode Clamped Five Level Inverter

E.Sambath¹, S.P. Natarajan², C.R.Balamurugan³

^{1,2}Department of EIE, Annamalai University, Chidambaram, Tamilnadu, India

³Department of EEE, Arunai Engineering College, Thiruvannamalai, Tamilnadu, India

ABSTRACT

The Diode Clamped Multilevel Inverter (DCMLI) is an attractive type multilevel inverter due to its robustness. This paper discusses new modulation strategies for a single phase five level H-bridge type DCMLI with reduced components as compared to conventional DCMLI. The chosen multi level inverter is controlled with multicarrier based Sinusoidal Pulse Width Modulation (SPWM) technique with Variable Frequency (VF), Phase Shift (PS), Carrier Overlapping (CO), Phase Opposition and Disposition (POD), Alternative Opposition and Disposition (APOD) and Phase Disposition (PD) PWM techniques. The performance of proposed strategies are evaluated through MATLAB-SIMULINK/POWER SYSTEM BLOCKSET / POWER GUL. The variation of Total Harmonic Distortion (THD), V_{RMS} (fundamental), Form Factor (FF), Crest Factor (CF) and Distortion Factor (DF) are observed for various modulation indices. The simulation results indicates that sinusoidal reference with PODPWM/APODPWM provides output with relatively low distortion. It is also seen that COPWM strategy is found to perform better since it provides relatively higher fundamental RMS output voltage.

Keywords : COPWM , DCMLI, DF, SH PWM, THD

I. INTRODUCTION

A Multi Level Inverter (MLI) can switch either its input or output nodes (or both) between multiple (more than two) levels of voltage or current. As the number of levels reaches infinity, the output THD approaches zero. The number of the achievable voltage levels however is limited by voltage imbalance problems, voltage clamping requirements, circuit layout and packaging constraints, complexity of the controller and of course, capital and maintenance costs. Three different major multilevel inverter structures have been applied in industrial applications: Cascaded H-bridge inverter with Separate DC sources(SDCS), diode clamped inverter and flying capacitors inverter. Yuan and Barbi [1] proposed fundamentals of a new diode clamping multilevel inverter. Anshuman Shukla et al [2] introduced control schemes for equalization of DC capacitor voltage in diode clamped multilevel inverter. Deepthi and Saxena [3] have discussed variation of THD in a diode clamped multilevel inverter with respect to modulation index and control strategy. NagaHaskar Reddy et al [4] have proposed a advanced modulating technique for diode clamped multilevel inverter fed induction motor. Jose Rodriguez et al [5] have presented a survey of multilevel inverters topologies, controls and applications. Yu Liu et al [6] found

a new clew for research on realtime algorithm for minimizing THD in multilevel inverters with unequal or varying voltage steps under staircase modulation. Hinago and Koizumi [7] proposed single phase multilevel inverter using switched series/parallel DC voltage sources. Xue and Manjrekar [8] developed a new class of single phase multilevel inverter. Farokhnia et al [9] made a comparison between approximate and accurate line voltage THD of multilevel inverter with equal DC sources. Farokhnia et al [10] also made a comparison between approximate and accurate calculation of line voltage THD in multilevel inverters with unequal DC sources. Rahim and Selvaraj [11] proposed multistring five level inverter with novel PWM control scheme for photo voltaic application. Shanthy and Natarajan [12] have described that the multilevel inverter triggered by the developed unipolar PWM strategies exhibits reduced harmonics and higher DC bus utilisation. PWM strategies developed are implemented in real time using dSPACE/Real Time Interface (RTI).Seyezhai [13] presented carrier overlapping PWM methods for asymmetrical multi level inverter. This literature survey reveals few papers only on various PWM techniques and DCMLI. Hence this work presents a new approach for controlling the harmonics of output voltage of chosen DCMLI fed resistive load employing sinusoidal switching reference. Simulations are performed using MATLAB-SIMULINK.

II. MULTILEVEL INVERTER

The operation of a multilevel inverter can be described as an optional stacking of a number of DC voltage source stages dependent on a certain time of operation that one stage is stacked (forward or reverse) or bypassed. MLIs also have some issues, such as requiring a big number of semiconductor switches which increases as the number of steps/levels increases and complex design for synchronous gate drivers for different levels. There are many types of multilevel inverter topologies in its history, starting from the series H-bridge design, followed by the diode-clamped, which utilizes a bank of capacitors to split the DC bus voltage and then the switched flying capacitor (or capacitor clamped) topology. An inverter design can also cascade these fundamental topologies to make hybrid topologies to improve power quality.

II. (a) Conventional DCMLI

The main concept of this inverter is to use diodes to limit the voltage stress on power devices. A DCMLI typically consists of (m-1) capacitors on the DC bus where m is the total number of positive, negative and zero levels in the output voltage. The order of numbering of the switches is S1, S2, S3, S4, S1', S2', S3' and S4'. The DC bus consists of four capacitors C1, C2, C3 and C4 acting as

voltage divider. For a DC bus voltage V_{dc} , the voltage across each capacitor is $V_{dc}/4$ and voltage stress on each device is limited to $V_{dc}/4$ through clamping diode. The middle point of the four capacitors 'n' can be defined as the neutral point. The principle of diode clamping to DC link voltages can be extended to any number of voltage levels. Since the voltages across the semiconductor switches are limited by conduction of the diodes connected to the various DC levels, the inverter is called DCMLI. The switches are arranged into 4 pairs (S1,S1'), (S2,S2'), (S3,S3') and (S4,S4'). If one switch of the pair is turned ON, the complementary switch of the same pair must be OFF. The output voltage V_{an} has five states: $V_{dc}/2$, $V_{dc}/4$, 0, $-V_{dc}/4$ and $-V_{dc}/2$. Four switches are triggered at any point of time to select the desired level in the five level DCMLI. Fig.1 shows a conventional single phase one leg five level DCMLI.

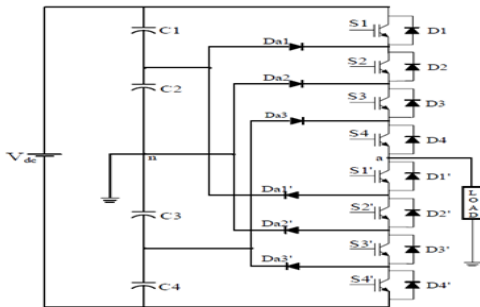


Figure 1 Conventional single phase five level DCMLI

II. (b) Chosen DCMLI

Two important issues in multilevel inverter control are obtaining near sinusoidal output voltage waveform and the elimination of the lower order harmonics. In this paper, a H-bridge type diode clamped inverter is used to propose a modified switching technique in such a way that the THD and number of components is minimized. Table 1 shows that comparisons of components used in conventional as well as chosen DCMLI. Fig.2 shows a configuration of single phase five level H-bridge type DCMLI. Here also the same output voltage states exist : $V_{dc}/2$, $V_{dc}/4$, 0, $-V_{dc}/4$ and $-V_{dc}/2$. The gate signals used for five level H-bridge type DCMLI are simulated using MATLAB – SIMULINK / POWER SYSTEM BLOCKSET / POWER GUI. The gating pulses for the inverter are generated for various values of modulation index m_a and for various PWM techniques. The chosen DCMLI is investigated with multicarrier SPWM for modulation indices ranging from 0.6-1.

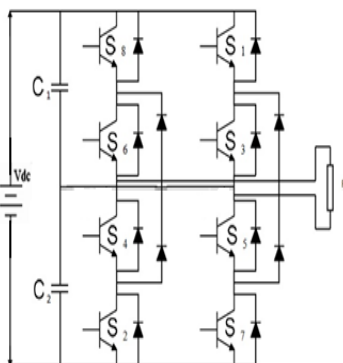


Figure 2 Chosen single phase H-bridge type five level DCMLI

TABLE-1

Comparison between conventional DCMLI and chosen DCMLI

Type of MLI	Conventional DCMLI	Chosen DCMLI
Main power devices	8	8
Main diodes	8	8
Clamping diodes	6	4
DC bus capacitors	4	2
Balancing capacitors	0	0
No. of leg	1	2

III. MODULATION TECHNIQUE FOR SWITCHES

In this paper a control technique of carrier based SPWM strategy is present. Number of triangular waveforms is compared with a controlled sinusoidal modulating signal. The number of carriers required to produce the m- level output is m-1. All the carriers have the same peak to peak amplitude A_{cpp} . The reference is continuously compared with each of the carrier signals and whenever the reference is greater then the carrier signal, the pulse is generated. The switching rules for the switches are decided by the intersection of the carrier waves with the modulating signal. The frequency modulation index $m_f=f_c/f_o$ where f_c is the frequency of the carrier signal and f_o is the frequency of the modulating signal. The amplitude modulation index is m_a where A_0 is the amplitude of the modulating signal and A_{cpp} is the peak to peak value of the carrier (triangular) signal. The amplitude modulation indices are :

$$SHPWM \text{ and } VFPWM = 2A_o/(m-1).A_{cpp}$$

$$COPWM = A_o/(m/4).A_{cpp}$$

$$PSPWM = A_o/(A_{cpp}/2)$$

Multiple degrees of freedom are available in carrier based multilevel PWM. The principle of the carrier based PWM strategy is to use m-1 different carriers with a reference signal for a m level inverter. Differences of carriers includes carrier's frequency, carrier's amplitude, carrier's phases, carrier's DC offset and multiple third harmonic content of reference signal. This paper uses different modulation strategies that all well known carrier based multilevel PWM strategies such as PDPWM, PODPWM, APODPWM, COPWM, PSPWM and VFPWM. Fig.3 shows the sample SIMULINK model developed for PSPWM technique for chosen inverter.

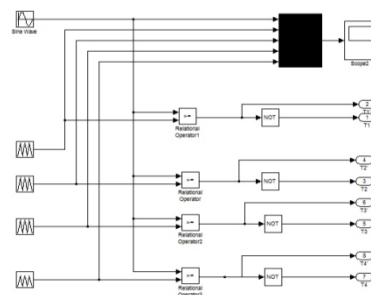


Figure 3 Sample SIMULINK model developed for chosen single phase inverter for PSPWM technique

III. (a) Phase Disposition PWM (PDPWM) Strategy

In this method all carriers have the same frequency, amplitude and phases but they are just different in DC offset to occupy contiguous bands. Since all carriers are selected with the same phase, the method is known as PD strategy. The carrier arrangement for this strategy is shown in Fig.4.

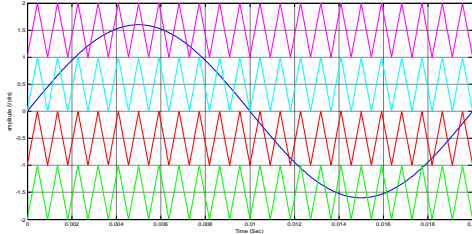


Figure 4 Modulating and carrier waveforms for PDPWM strategy ($m_a=0.8$ and $m_f=22$)

III. (b) Phase Opposition Disposition PWM (PODPWM) Strategy

The PODPWM strategy is having the carriers above the zero line of reference voltage out of phase with those of below the line by 180 degrees as shown in Fig.5.

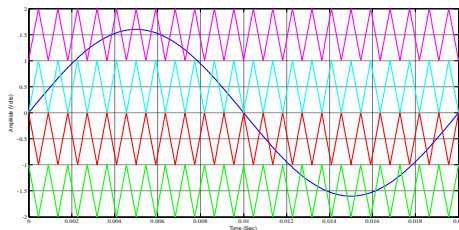


Figure 5 Modulating and carrier waveforms for PODPWM strategy ($m_a=0.8$ and $m_f=22$)

III. (c) Alternative Phase Opposition and Disposition PWM (APODPWM) Strategy

In APOD strategy each carrier is phase shifted by 180 degrees from its adjacent one as shown in Fig.6.

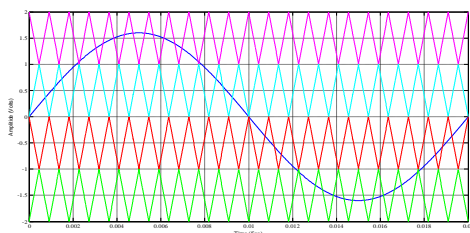


Figure 6 Modulating and carrier waveforms for APODPWM strategy ($m_a=0.8$ and $m_f=22$)

III. (d) Phase Shift PWM (PSPWM) Strategy

In this strategy all carrier signals have the same amplitude and frequency but they are phase shifted by 90 degrees to each other as shown in Fig.7.

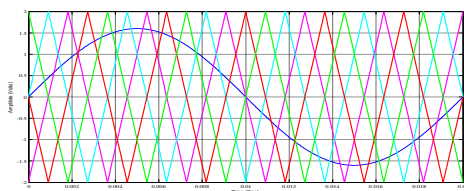


Figure 7 Modulating and carrier waveforms for PSPWM strategy ($m_a=0.8$ and $m_f=22$)

III. (e) Carrier Overlapping PWM (COPWM) Strategy

For an m-level inverter, m-1 carriers with the same frequency f_c and same peak to peak amplitude A_{cpp} are disposed such that the bands they occupy overlap each other. The overlapping vertical distance between each carrier is $A_{cpp}/2$ which is shown in Fig.8. The reference waveform has amplitude of A_o and frequency f_o and it is centred in the middle of the carrier signals.

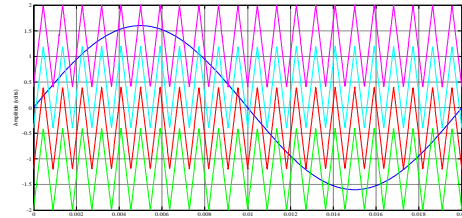


Figure 8 Modulating and carrier waveforms for COPWM strategy ($m_a=0.8$ and $m_f=22$)

III. (f) Variable Frequency PWM (VF PWM) Strategy

The number of switchings for upper and lower devices of chosen MLI is much more than that of intermediate switches in PDPWM using constant frequency carriers. In order to equalize the number of switchings for all the switches, variable frequency PWM strategy is used as illustrated in Fig.9 in which the carrier frequency of the intermediate switches is properly increased to balance the number of switchings for all the switches.

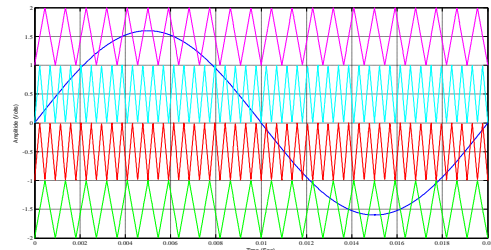


Figure 9 Modulating and carrier waveforms for VF PWM strategy ($m_a=0.8$ and $m_f=22$ for upper and lower switches)

IV. SIMULATION RESULTS

Simulation studies are performed by using MATLAB-SIMULINK to verify the proposed PWM strategies for chosen single phase H- bridge type diode clamped five level inverter for various values of m_a ranging from 0.6 – 1 and corresponding %THD values are measured using FFT block and they are shown in Table 2. Table 3 shows the V_{RMS} of fundamental of inverter output for the same modulation indices. Figs.10-21 show the simulated output voltage of chosen DCMLI and the corresponding FFT plots with different strategies but only for one sample value of $m_a=0.8$ and $m_f=22$. Fig.10 shows the five level output voltage generated by PDPWM strategy and its FFT plot is shown in Fig.16. From Fig.16, it is observed that the PDPWM strategy produces significant 12th,14th,18th and 20th harmonic energy. Fig.11 shows the five level output voltage generated by PODPWM strategy and its FFT plot is shown in Fig.17. From Fig.17, it is observed that the PODPWM strategy produces significant 15th,17th and 21th harmonic energy. Fig.12 shows the five level output voltage generated by APODPWM strategy and its FFT plot is shown in Fig.18.

From Fig.18, it is observed that the APODPWM strategy produces significant 17th,19th and 21th harmonic energy. Fig.13 shows the five level output voltage generated by PSPWM strategy and its FFT plot is shown in Fig.19. From Fig.19, it is observed that the PSPWM strategy produces significant 11th,17th, 19th and 21th harmonic energy. Fig.14 shows the five level output voltage generated by COPWM strategy and its FFT plot is shown in Fig.20. From Fig.20, it is observed that the COPWM strategy produces significant 3rd and 20th harmonic energy. Fig.15 shows the five level output voltage generated by VFPWM strategy and its FFT plot is shown in Fig.21. From Fig.21, it is observed that the VFPWM strategy produces significant 16th and 20th harmonic energy.

The following parameter values are used for simulation : $V_{DC}=440V$, $f_c=1100Hz$ and $R(load)=100\text{ ohms}$.

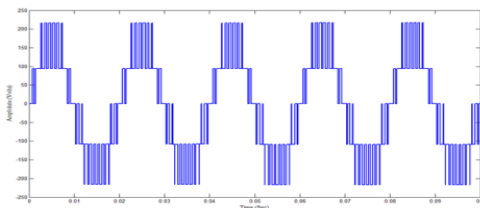


Figure 10 Simulated output voltage generated by PDPWM technique for R load

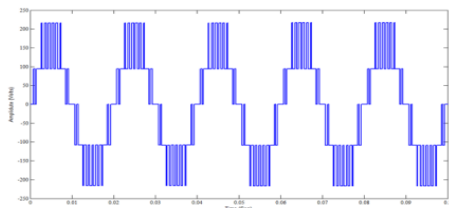


Figure 11 Simulated output voltage generated by PODPWM technique for R load

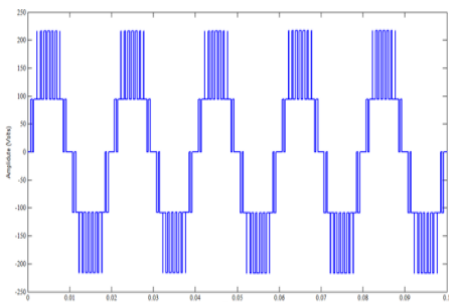


Figure 12 Simulated output voltage generated by APODPWM technique for R load

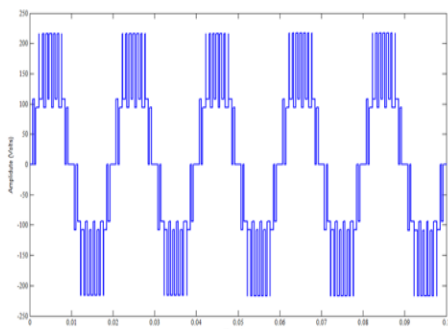


Figure 13 Simulated output voltage generated by PSPWM technique for R load

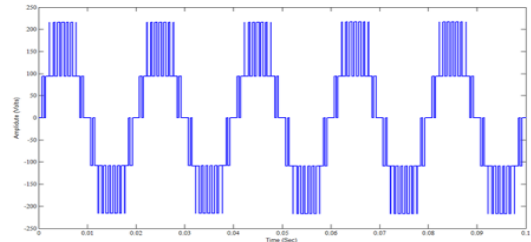


Figure 14 Simulated output voltage generated by COPWM technique for R load

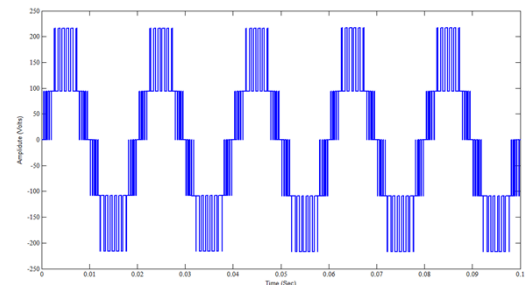


Figure 15 Simulated output voltage generated by VFPWM technique for R load

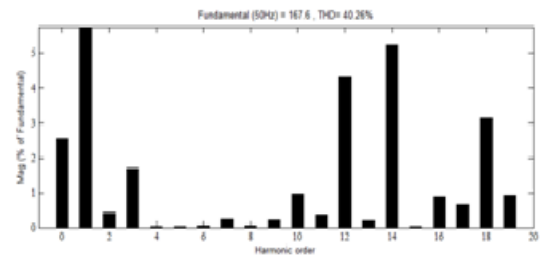


Figure 16 FFT spectrum for PDPWM technique

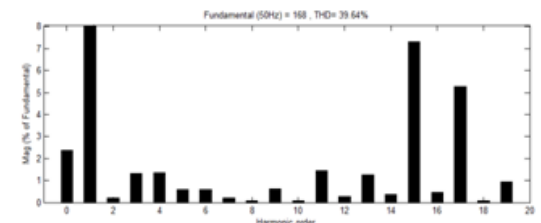


Figure 17 FFT spectrum for PODPWM technique

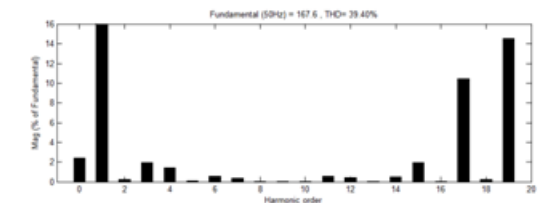


Figure 18 FFT spectrum for APODPWM technique

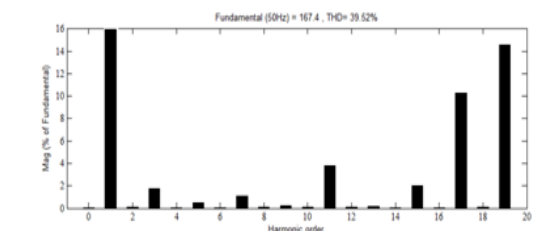


Figure 19 FFT spectrum for PSPWM technique

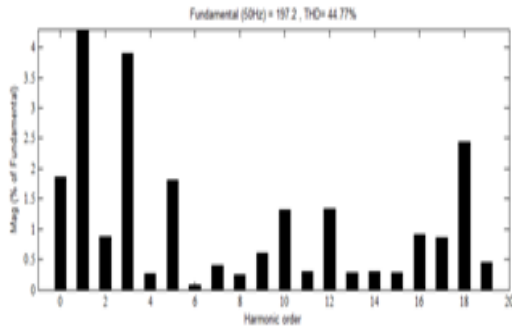


Figure 20 FFT spectrum for COPWM technique

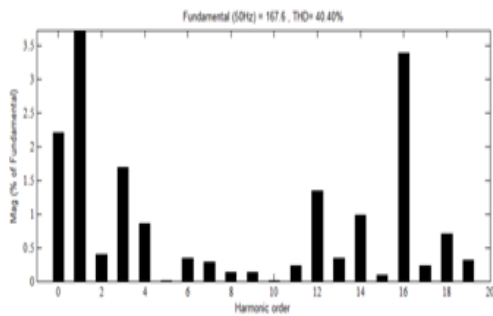


Figure 21 FFT spectrum for VFPWM technique

TABLE-2

%THD of output voltage of chosen DCMLI for various values of m_a

m_a	PD	POD	APOD	VF	CO	PS
1	27.91	27.66	27.70	27.94	34.03	27.70
0.9	34.69	34.38	34.94	34.96	39.09	35.03
0.8	40.26	39.64	39.40	40.40	44.77	39.52
0.7	44.04	43.60	43.60	44.09	51.22	43.81
0.6	45.87	44.87	44.51	46.05	60.50	44.84

TABLE-6

DF of output voltage of chosen DCMLI for various values of m_a

m_a	PD	POD	APOD	VF	CO	PS
1	0.45	0.3329	0.2783	0.3345	0.82	1.998
0.9	0.4251	0.3152	0.2199	0.3191	0.722	0.1944
0.8	0.2372	0.1923	0.2485	0.2255	0.5211	0.212
0.7	0.3923	0.3043	0.3003	0.317	0.4181	0.1689
0.6	0.329	0.5077	0.5171	0.4156	0.4604	0.1283

V. CONCLUSION

Single phase H-bridge type diode clamped five level inverter employing different multi carrier single reference modulation schemes has been investigated. It is found from Table 2 that PODPWM /APODPWM techniques provide output with relatively low distortion. COPWM technique is observed to perform better since it provides relatively higher fundamental RMS output voltage (Table 3). Table 4 shows crest factor, Table 5 provide FF and Table 6 shows DF for all modulation indices.

TABLE-3

RMS (fundamental) of output voltage of chosen DCMLI for various values of m_a

m_a	PD	POD	APOD	VF	CO	PS
1	150.9	150.4	151	151	162.3	150.9
0.9	134.9	134.1	135	134.8	151.4	135
0.8	118.5	118.8	118.5	118.5	139.4	118.4
0.7	102.7	102.5	102.9	102.6	126.6	102.9
0.6	87.1	87.57	87.17	87.12	111.9	87.14

TABLE-4

CF of output voltage of chosen DCMLI for various values of m_a

m_a	PD	POD	APOD	VF	CO	PS
1	1.4141	1.414	1.4139	1.413	1.414	1.414
0.9	1.4143	1.414	1.414	1.413	1.414	1.414
0.8	1.4143	1.414	1.4144	1.414	1.414	1.413
0.7	1.4138	1.413	1.4139	1.414	1.414	1.413
0.6	1.4144	1.413	1.4144	1.414	1.414	1.413

TABLE-5

FF of output voltage of chosen DCMLI for various values of m_a

m_a	PD	POD	APOD	VF	CO	PS
1	79.421	113.93	21.3	98.69	174.51	5030
0.9	50.14	73.68	75.84	60.72	127.22	4500
0.8	46.47	49.707	49.37	53.86	74.54	2960
0.7	29.511	33.27	33.73	32.06	59.15	3430
0.6	22.5	23.004	22.7	21.78	48.23	4357

REFERENCES

- [1] X. Yuan and I. Barbi, "Fundamentals of a New Diode Clamping Multilevel Inverter", *IEEE Transactions on Power Electronics*, Vol. 15, No. 4, 2000, pp. 711-718.
- [2] Anshuman Shukla, Arindam Ghosh and Avinash Joshi, "Control Schemes for DC Capacitor Voltages Equalization in Diode-Clamped Multilevel", *IEEE Trans. on Power Delivery*, Vol. 23, No. 2, 2008, pp. 1139-1149.

- [3] Janyavula Deepthi and S.N. Saxena, "Study of Variation of THD in a Diode Clamped Multilevel Inverter with respect to Modulation Index and Control Strategy", *2nd International Conference and workshop on Emerging Trends in Technology 2011*, pp 37-42.
- [4] V. NagaHaskar Reddy, Ch.Sai.Babu and K.Suresh, "Advanced Modulating Techniques for Diode Clamped Multilevel Inverter Fed Induction Motor", *ARPV Journal of Engineering and Applied Sciences, Vol.6, No.1, January 2011*, pp 90-99.
- [5] Jose Rodriguez, Jih-Sheng Lai and Fang Zheng, "Multilevel Inverters: A Survey of Topologies, Controls, and Applications", *IEEE Transactions on Power Electronics, Vol.49, No.4, 2002*, pp.724-738.
- [6] Yu Liu, Hoon Hong and Alex Q.Huang, "Real-Time Algorithm for Minimizing THD in Multilevel Inverters With Unequal or Varying Voltage Steps Under Staircase Modulation", *IEEE Transactions on Industrial Electronics, Vol.56, No.6, 2009*, pp 2249-2258.
- [7] Youhei Hinago and Hiroataka Koizumi, "A Single Phase Multilevel Inverter Using Switched Series/Parallel DC Voltage sources", *IEEE Transactions on Industrial Electronics, Vol.57, No.8, August 2010*, pp2643-2650.
- [8] Yaosuo Xue and Madhav Manjrekar, "A New Class of Single-Phase Multilevel Inverter", *2nd IEEE International Symposium on Power Electronics for Distributed Generation Systems, 2010*, pp 565-571.
- [9] N.Farokhnia, H.Vadizadeh, F.Anvari asl and F.Kadkhoda, "Comparison between Approximate and Accurate Line Voltage THD, Case II: Multilevel Inverter with Equal DC Sources", *2nd IEEE International Symposium on Power Electronics for Distributed Generation Systems, 2010*, pp 246-251.
- [10] N.Farokhnia, S.H.Fathi, H.Vadizadeh and H.Toodeji, "Comparison between Approximate and Accurate Calculation of Line Voltage THD in Multilevel Inverters with Unequal DC Sources", *5th IEEE Conference on Industrial Electronics and Applications, 2010*, pp 1034-1039.
- [11] Nasrudin A.Rahim and Jeyraj Selvaraj, "Multistring Five-Level Inverter with Novel PWM Control Scheme for PV Application", *IEEE Transactions on Industrial Electronics, Vol.57, No.6, 2010*, pp. 2111-2123.
- [12] B.Shanthi and S.P. Natarajan, "Comparative Study on Various Unipolar PWM Strategies for Single Phase Five-Level Cascaded Inverter", *Int.J. Power Electronics*, Vol. 2, No. 1, 2010, pp. 36-50.
- [13] R.Seyezhai, "Carrier Overlapping PWM Methods for Asymmetrical Inverter", *International Journal of Engineering Science and Technology (IJEST)*, Vol. 3, No. 8, 2011, pp. 6630-6639.

DESIGN OF RING ROAD FOR ERODE DISTRICT USING GIS

T.SUBRAMANI¹ P.MALAISAMY²

¹Professor & Dean, Department of Civil Engineering, VMKV Engg. College, Vinayaka Missions University,

²PG Student of Environmental Engineering, Department of Civil Engineering,
VMKV Engg. College, Vinayaka Missions University, Salem, India

Abstract: Design of ring road deals with the development of a comprehensive plan for Construction and operation of transportation facilities. In order to develop efficient and better transport facility, it is necessary to have a proper procedure transport movement. This ring road helps to a great extent in improving the safe and fast movement of both human and goods traffic, thereby increasing the economy of the City. This improved economy contributes the growth of the country. The first and foremost step is reducing the traffic for the particular route by diverting the density of the vehicles to enhance the safe transport and environmental pollution. This project deals with the traffic problem of the erode city and provides better transportation. In this project GIS is used for surveying, for preparing Contour maps, for developing three dimensional Digital Elevation Models, for various types of route alignments and for estimation of cutting and filling volumes.

The purpose of this study was to develop a tool to locate a suitable less route between two points. The GIS approach using ground parameters and spatial analysis provided to achieve this goal. Raster based map analysis provide a wealth of capabilities for incorporating terrain information surrounding linear infrastructure. Costs resulting from terrain, geomorphology, land use, drainage and elevation resulting low cost estimation for implementing the shortest routes for the study area. Finally Ring road for Erode city of 22 kms all around which connect the major roads of bypass was formulated.

Keywords: Design, ring road, Erode district, Using gis

I. INTRODUCTION

Determining the best route through an area is one of the oldest spatial problems. This problem has recently been solved effectively using GIS and Remote Sensing technologies. During the last decade, a few attempts have been made to automate the route-planning process using GIS technology. A review of a number of papers suggests that the methodology is still at an exploratory stage (Saha et al., 2005). A number of research have already been performed in pipeline route design using GIS which include optimal routing for pipeline selection of best route for expansion and road network, this will achieve by using high resolution remote sensing image. In this context, physical, environmental, political, social, economical and legal processes was considered and implemented for road and pipeline routing determination (Rylsky 2004, Saha, V.D 2005, Delevar and Naghibi 2003, Yusof and Baban 2004, Glasgow vd. 2004, Berry 2000, Çevik and Topal 2003, Luettingearve Clark 2005). Multiple factors were considered using GIS techniques for road, highway, forest

roads and bike roads routing determination (Mackenzie and Walker 2004, Malpica ve Pedraza 2001). GIS based route determination for railway (Ashish and Dhingra 2005, Kov vd. 2005, Gipps vd. 2001), irrigation/drainage channels (Yusof and Baban 2000, Smith 2006), power line (Cheng and Chang 2001) have already been implemented.

The present study was initiated to demonstrate the use of various data from different sources, GIS analysis and raster network analysis techniques for developing a least cost pathway for linear civil engineering structures. This is probably the most asked question posed to those in the Geographic Information Systems (GIS) field and is probably the hardest to answer in a succinct and clear manner.

1.2 SOFTWARE

Different software packages are important for GIS. Central to this is the GIS application package. Such software is essential for creating, editing and analyzing spatial and attribute data, therefore these packages contain a myriad of GIS functions inherent to them. Extensions or add-ons are software that extends the capabilities of the GIS software package. Component GIS software is the opposite of application software. Component GIS seeks to build software applications that meet a specific purpose and thus are limited in their spatial analysis capabilities. Utilities are stand-alone programs that perform a specific function. For example, a file format utility that converts from one type of GIS file to another. There is also web GIS software that helps serve data through Internet browsers.

1.2.1 Data

Data is the core of any GIS. There are two primary types of data that are used in GIS. A geodatabase is a database that is in some way referenced to locations on the earth. Geodatabases are grouped into two different types: vector and raster. Vector data is spatial data represented as points, lines and polygons. Raster data is cell-based data such as aerial imagery and digital elevation models. Coupled with this data is usually data known as attribute data. Attribute data generally defined as additional information about each spatial feature housed in tabular format. Documentation of GIS datasets is known as metadata. Metadata contains such information as the coordinate system, when the data was created, when it was last updated, who created it and how to contact them and definitions for any of the code attribute data.

1.2.2 Remote sensing system

With the background treatise on remote sensing we have made so far, it would now be easier make an analysis of the different stages in remote sensing.

- Origin of electromagnetic energy.

- Transmission of energy
- Intervening of energy or self emission
- Detection of energy
- Transmission or coding of the sensor output
- Collection of ground truth
- Data analysis and interpretation

1.2.3 Remote sensors

The instrument used to measure electromagnetic radiation reflected or emitted by the radiation either emitted or reflected from the earth is called passive sensors, sensors which carry electromagnetic radiation to illuminates the earth's surface are called active sensors.

1.2.4 Platforms

Sensor system need to be placed on suitable observation platforms and need to be a pre-defined altitude .Platforms can be stationary or mobile depending on the needs of the observation mission and the constraints. Geo-stationary ,which are about 3600km above earth second is sun synchronous satellites which are nearer to earth.

1.2.5 Digital Processing Techniques

Digital facilitates quantitative analysis, make use of full spectral information and avoid individual bias. Simultaneous analysis of multi-temporal and multi sensor facilitated in digital methods. The computer analysis the signature ,so as to associates each pixel with a particular feature of imagery.

1.2.6 Generation of DEM and slope

Slope map was generated using the elevation information derived from ancillary topographical and GIS techniques. ARCGIS's TOPOGRID functions were used to generate DEM and slope maps. A sampling method was used to extract representative points to build a surface model that approximates the actual surface. The contour map, was prepared from the SOI topographic.

1.2.7 Shortest Path Analysis

The inputs required for shortest path analysis are a source and a destination raster, cost raster surface, cost weighted distance, direction raster. After preparing all the required inputs Spatial Analyst is used to generate the shortest path and the results for analysis.

1.2.8 Global Positioning System

The **Global Positioning System (GPS)** is a space-based global navigation satellite system (GNSS) that provides reliable location and time information in all weather and at all times and anywhere on or near the Earth when and where there is an unobstructed line of sight to four or more GPS satellites. It is maintained by the United States government and is freely accessible by anyone with a GPS receiver. The GPS project was started in 1973 to overcome the limitations of previous navigation systems,^[1] integrating ideas from several predecessors, including a number of classified engineering design studies from the 1960s. GPS was created and realized by the U.S. Department of Defense (USDOD) and was originally run with 24 satellites. It became fully operational in 1994. In addition to GPS, other systems are in use or under development. The Russian global navigation Satellite

System (GLONASS) was in use by the Russian military only until it was made fully available to civilians in 2007. There are also the planned Chinese Compass navigation system and the European Union's Galileo positioning system.

1.2.9 How GPS Work

The Global Positioning System (GPS) is a technical marvel made possible by a group of satellites in earth orbit that transmit precise signals, allowing GPS receivers to calculate and display accurate location, speed, and time information to the user. By capturing the signals from three or more satellites (among a constellation of 31 satellites available), GPS receivers are able to use the mathematical principle of **trilateration** to pinpoint your location. With the addition of computing power, and data stored in memory such as road maps, points of interest, topographic information, and much more, GPS receivers are able to convert location, speed, and time information into a useful display format. GPS was originally created by the United States Department of Defense (DOD) as a military application. The system has been active since the early 1980s, but began to become useful to civilians in the late 1990s. Consumer GPS has since become a multi-billion dollar industry with a wide array of products, services, and Internet-based utilities. GPS works accurately in all weather conditions, day or night, around the clock, and around the globe. There is no subscription fee for use of GPS signals. GPS signals may be blocked by dense forest, canyon walls, or skyscrapers, and they don't penetrate indoor spaces well, so some locations may not permit accurate GPS navigation.

1.2.10 Types of GPS for Driving, Outdoors, Sports

Imagine never being lost or needing to ask for directions as you drive. Imagine going out for a run or bike ride and capturing all of your speed, distance, elevation change and heart rate data and uploading it to a training log or an online map you can share. Imagine going hiking and always knowing the way back to camp. Imagine playing golf and always knowing the exact distance to the pin. These scenarios and many more are reality with the use of Global Positioning System (GPS) receivers.

II. Aim And Scope Of Investigation

- To establish shortest path for road network.
- To minimize the traffic in the city.
- To provide a better and comfortable for updating the traffic and other related information in road administration.
- To reduce travelling time.
- To prepare various thematic maps.
- To find paths /routes/places for laying eco-friendly ring road.
- To reduce the pollution rate in the city.

III. Study Area - Erode City

Erode is a city, a municipal corporation and the headquarters of Erode district in the South Indian state of Tamil Nadu. It is situated at the centre of the South Indian Peninsula, about 400 kilometres (249 mi) southwest from the state capital Chennai and on the banks of the rivers Cauvery and Bhavani, between 11° 19.5" and 11° 81.05"

North latitude and $77^{\circ} 42.5''$ and $77^{\circ} 44.5''$ East longitude. As per Census 2011 alignments. It has population around 156,953. Erode Local planning Area extends up to 54sq.km. Within the city, and will be extended to 109 km². The roadway connects all the parts of the state and nearby states such as Kerala, Karnataka and Andhra Pradesh with the city. The City has both local (City) and mofussil (city-to-city) bus services with connections to nearby towns and villages. Plenty of city buses are ply to connect all parts of the city. One can get buses from Erode to almost any part of the state. NH connecting Salem – Coimbatore – Cochin passes through Erode and Bypasses the city via Bhavani (Lakshminagar by-pass), Chithode, Perundurai, which is the major National Highway connectivity for the city. SH 79 connecting Rasipuram - Tiruchengode - Pallipalayam – Erode. SH-15 connecting Erode – Gobi – Sathy – Ooty. NH-67A connecting Karur – Erode – Sathy – Mysore. Another planned from Erode (Bhavani) – Anthiyur – Bangalore. Figure.1 shows the study area details.

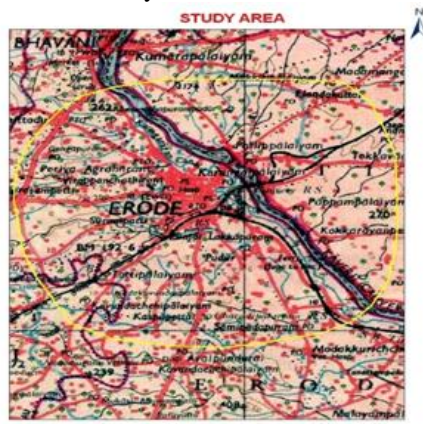


FIGURE.1 ERODE CITY MAP

IV. Data Base Generation

4.1 DATA COLLECTION

Survey of India Toposheet No. 58 E /12

4.2 LAND SAT (MSS) DATA 2007

Maps, field work and remote sensing techniques are necessary for proposed road design and construction. Topographic maps, geomorphology, Land use/Land Cover, Drainage, DEM, road, Slope and Contour maps were used for this proposed route. The favorable path analysis, using various data and GIS analysis, was intended to confirm the best transport route within this site.

4.3 DATA PROCESS AND ANALYSIS

In this implementation, the best route is found for a new road. The steps to find possible path are outlined below. Path is identified by using ArcGIS 9.1 Spatial Analysis Module.

Create Source, Destination and Datasets

Generate different Thematic Maps (Classify and Weight age)

Perform Weighted Distance

Create Direction Datasets

Identified Shortest Path with Distance and Direction Datasets

Figure.2 shows Satellite Image For Erode

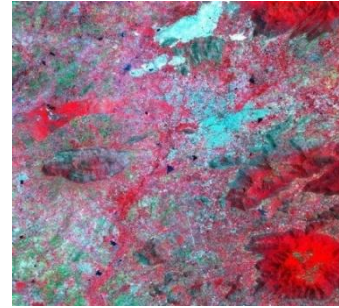


FIGURE.2 SATELLITE IMAGE FOR ERODE

V. Design Guide Lines

5.1 PLANNING OF ROAD IN PLAIN AREAS

Planning of roads in plain area is somewhat different from hill areas. In hill areas alignment of roads has to be circuitous and is primarily governed by the topography. In the plain area we should find the elevation and depression by the survey. The elevation areas should be leveled by removing the upper surface of the earth and this soil can be used for filling up the low lying areas. The roads in our country in plain areas, they have been classified as National Highways, State Highways, Major District Roads, Other District Roads and Village Roads according to specification, traffic needs, and socio-economic, administrative or strategic consideration. Some National Highways are point to point which will connect the state boundaries. State Highways will connect all the National Highways. Major District roads will connect all the State Highways. Other District Roads and Village Roads will connect the Major District Roads however from topographical considerations; these can be broadly divided into arterial roads and link roads. Arterial roads will include national/state highways and major district roads. Link roads take off from arterial roads to link villages/production areas in small/sub-valleys. These will comprise other district roads and village roads.

5.2 HIGHWAY ALIGNMENT

The position or layout of the centre line of the highway on the ground is called alignment. In general the alignment is of two types,

- Horizontal alignment
- Vertical alignment

5.2.1 Requirements

The basic requirements of ideal alignments between two terminal stations are

- Short – A straight line alignment would be the, though there may be several practical considerations which would cause the deviation from the shortest path.
- Easy – The alignment should be such that it is easy to construct and maintain with minimum problems.
- Safe – The alignment should be safe enough for construction and maintenance from the view point of stability of natural hill slopes, embankments, cut slopes.
- Economical – The alignment is considered economical only if the total cost including the initial cost, maintenance cost.

5.2.2 Factors controlling alignment

For an alignment to be shortest, it should be straight between two terminals which are not always possible due to practical difficulties such as intermediate obstructions and topography. A shortest route may have very steep gradients and hence not easy for operations. Similarly there will be construction and maintenance problems along the route which may be otherwise short and easy. Canals are often deviated from the shortest route in order to cater for intermediate places of importance or obligatory points.

5.2.3 Obligatory points

These are control points governing the alignment of a canal. These control points may be broadly divided into two categories,

- Points through which the alignment is to pass.
- Points through which alignment should not pass.

Obligatory points through which alignment has to pass may cause alignment to often deviate from the shortest or easiest path.

5.2.4 Geometric design

Geometric design factors gradient, radius of curvature govern the final alignment. As far as possible while aligning a canal, the gradient should be gradually increasing. It may be necessary to make adjustments in horizontal alignment of canal keeping in view the minimum radius of curvature and the gradient.

5.2.5 Slope stability

While aligning canal, special care should be taken to align along the side of the hill which is stable. A problem in doing this is that of the landslides. The cutting and filling to construct the canal on the hill side causes steepening of existing slopes and effects its stability

5.2.6 Engineering surveys for Highway Alignment

Before canal alignment, engineering surveys are to be carried out. The surveys may be completed in four stages; first three stages consider all possible alternate alignment keeping in

view the various requirements. Four stages of engineering surveys are,

- Map study
- Reconnaissance
- Preliminary survey
- Final location and detailed survey

5.2.7 Horizontal Alignment

The horizontal alignment should be fluent and blend well with the surrounding topography. The horizontal alignment should be co-ordinate carefully with the longitudinal profile. Breaks in horizontal alignments at cross drainage structure and sharp curves at the end of long tangents/straight sections should be avoided. Short curves gives appearance of kinks, particularly for small deflections angles should be avoided. The curves should be sufficiently long and have suitable transitions to provide pleasing appearances. Curve length should be at least 150m for a deflection angle of 5 degrees and this should be increased by 30m for each degree deflection angle. Reverse curves may be needed in difficult t

errain by very sparingly used. It should be ensured that there is sufficient length between the two curves for introduction of requisite curves. Curves in same direction separated by short tangents, known as broken back curves, should be avoided as far as possible in the interest of aesthetics and replaced by a single curve.

5.2.8 Minimum Curve Radii

On a horizontal, the centrifugal force is balanced by the combined effect of super elevation and side friction. Basic equation for this condition of equilibrium is as follows:

$$v^2/g R=e + f$$

$$R=v^2/127(e + f)$$

Where v = vehicle speed in meter/second

V = vehicle speed in km/hr

g = acceleration due to gravity in meter/s²

e = super elevation in meter

f = coefficient of side friction between vehicle type and pavements (taken as 0.15)

r = radius in meter

5.2.9 Vertical Alignment

Broken back grade lines, i.e. two vertical curves in the same direction separated by a short tangent, should be avoided due to poor appearance, and preferably replaced by a single curve. Decks of small cross drainage structures should follow the same profile as the flanking road section with no break in the grade line.

5.2.10 Co-ordination of Horizontal and Vertical Alignment

The overall appearance of a highway can be enhanced considerably by judicious combination of horizontal and vertical alignment. Plan and profile of the road should not be designed independently but in unison so as to produce appropriate three dimensional effect.

VI. Methodology

The base (study area) map, Drainage, Slope and Contour maps were prepared with help of SOI Toposheet (on 1:50,000 scale). High resolution LANSAT satellite data of 2007 was used and by using Digital Image Processing techniques the following thematic maps such as geomorphology, Land use / Land Cover were generated. The Digital Elevation Model (DEM) was generated using various GIS based analysis, such as overlay, raster network analysis. The DEM is used in order to understand the terrain condition, environmental factors and social economic status in this study area. Finally, possible / feasible route was identified based on various physical and cultural parameters and their inherent properties. The cost reduction analysis was also done for substantiating the formation of ring road. Figure.3. Shows the flow diagram.

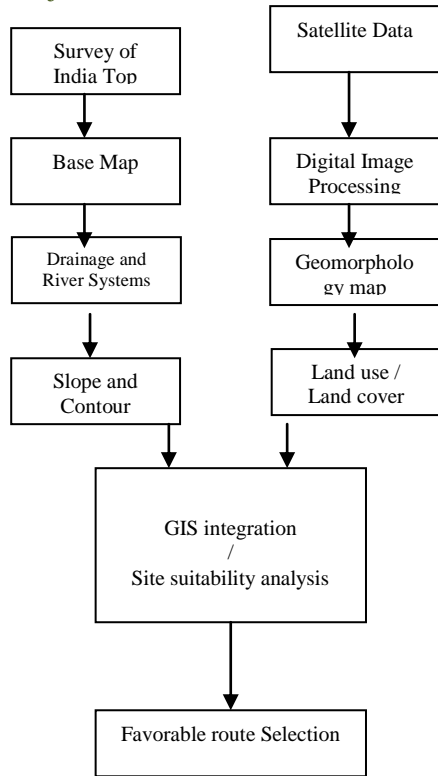


FIGURE.3 FLOW DIAGRAM

VII. TOPOGRAPHY

Topographic and geologic data of the proposed road network area were prepared in a GIS ready format and used as input to the GIS database. The locations of roads, railways, wetland, forests and drainage features were derived from the topographic map layer. The map that produced by SOI is the base for national topographic database and has a number of features for instance location of roads, railways ,wetland ,forests , drainage features, elevation points (Figure. 4). In this proposed project, digital elevation model (DEM) was prepared from the elevation data. It was used as input to the least cost and shortest pathway analysis.

VIII. Geomorphology

Different landforms present in the area are depicted in Figure.5. This geomorphic unit were extracted from the satellite image by digital data interpretation and incorporated into the GIS database. These geomorphic units were classified into Plateau, Scarp face, Debris slope, bazada, residual hill and pediments (deep, shallow & moderate).



FIGURE.4 TOPOSHEET 58 E/12

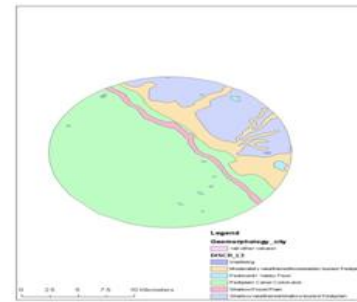


FIGURE.5 GEOMORPHOLOGY MAP

IX. DRAINAGE PATTERN

Erode district is drained by Cauvery and Ponnaiyar river basin. The Cauvery River forms the western and south-western boundary of the district. The domestic and industrial usage of water is being satisfied by Cauvery river water. As far as the drainage fabrication of the study area is concerned, it is covered by third order and fifth order streams in the North and Northeast part.. These streams are seasonal and become dry during summer season and the main stream which is passing through this area of interest is Thirumanimuttar (Figure.6)

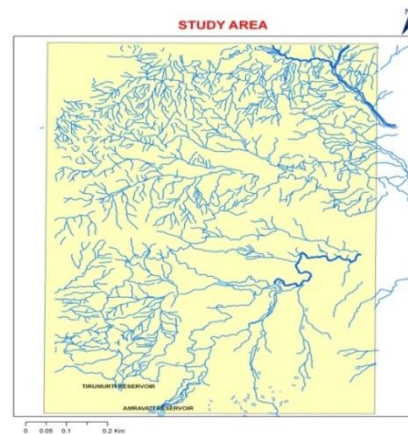


FIGURE.6 DRAINAGE PATTERN

X. LOCATION FOR BRIDGES

In the study area, it is advisable that to construct necessary bridges in the study area where there is crossing of streams that are higher order (more than 3rd order). And the culvert is used for the streams that are lower order (less than 3rd order) (Figure.7).

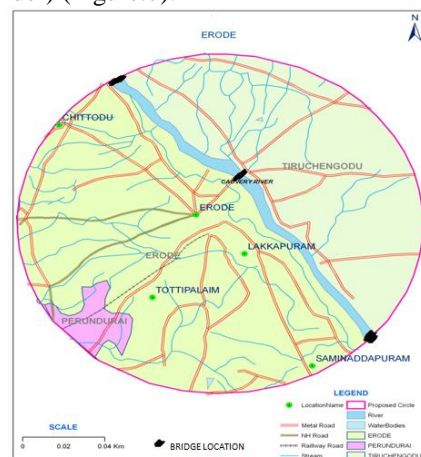


FIGURE.7. LOCATION FOR BRIDGES

XI. LAND USE / LAND COVER

The land use map was prepared from Digital LANDSAT 2007 satellite data and the features were classified as per Integrated Mission for Sustainable Development (NRS, 1995) classification system and following land use patterns were identified as agricultural land, forests, mining area, water body, plantations, barren rock area and urban areas. Most of the area is being occupied by fallow land. Hills/barren rocky area is located in the northern and southern part of the study area. Besides these two major categories, the crop land is also sporadically distributed in the study area. (Figure.8).



FIGURE.8. LAND USE / LAND COVER

XII. OVERVIEW OF SOFTWARE- Arcgis

ArcGIS is a suite consisting of a group of geographic information system (GIS) software products produced by Esri. There are also server-based ArcGIS products, as well as ArcGIS products for PDAs. Extensions can be purchased separately to increase the functionality of ArcGIS.

ArcGIS 8.x

In late 1999, Esri released ArcGIS 8.0, which ran on the Microsoft Windows operating system. ArcGIS combined the visual user-interface aspect of ArcView GIS 3.x interface with some of the power from the Arc/INFO version 7.2 workstation. This pairing resulted in a new software suite called ArcGIS, which included the command-line ArcInfo workstation (v8.0) and a new graphical user interface application called ArcMap (v8.0) incorporating some of the functionality of ArcInfo with a more intuitive interface, as well as an ArcGIS file management application called ArcCatalog (v8.0). The release of the ArcGIS suite constituted a major change in Esri's software offerings, aligning all their client and server products under one software architecture known as ArcGIS, developed using Microsoft Windows COM standards. One major difference is the programming (scripting) languages available to customize or extend the software to suit particular user needs.

In the transition to ArcGIS, Esri dropped support of its application-specific scripting languages, Avenue and the ARC MacroLanguage (AML), in favor of Visual Basic for Applications scripting and open access to ArcGIS components using the Microsoft COM standards. ArcGIS is designed to store data in a proprietary RDBMS format, known as geodatabase. ArcGIS 8.x introduced other new

features, including on-the-fly map projections, and annotation in the database. Updates of ArcView 3.x extensions, including 3D Analyst and Spatial Analyst, came later with release of ArcGIS 8.1, which was unveiled at the Esri International User Conference in 2000.

XIII. CONCLUSION

The purpose of this study was to develop a tool to locate a suitable less route between two points. The GIS approach using ground parameters and spatial analysis provided to



FIGURE.9 FINAL RING ROAD FOR ERODE CITY

achieve this goal. Raster based map analysis provide a wealth of capabilities for incorporating terrain information surrounding linear infrastructure. Costs resulting from terrain, geomorphology, land use, drainage and elevation resulting low cost estimation for implementing the shortest routes for the study area. The Figure.9 shows the final ring road for Erode city of 22 kms all around which connect the major roads of bypass.

Reference

- [1]. Ashish, V., Dhinga, S., L., 2005, Integrated Framework Using Geographical Information System, Journal of urban planning and development, urban public transportation world Review: challenges and innovations. Vol: 131 no: 2, pp: 98-111
- [2]. Berry, K., J., 2000, Optimal Path Analysis and Corridor Routing: Infusing Stakeholder Perspective in Calibration and Weighting of Model Criteria.
- [3]. Cheng, M., Y., Chang, G., L., 2001, Automating Utility Route Design and Planning Through GIS, Vol: 10, N: 4, pp. 507-516(10).
- [4]. Çevik, E., Topal T., 2003, GIS-Based Landslide Susceptibility Mapping for a Problematic Segment of the Natural Gas Pipeline, Hendek (Turkey), Environmental Geology, and Vol: 44, pp: 949-962.
- [5]. Delevar, R., M., Naghibi, F., 2003, Pipeline Routing Using Geospatial Information System Analysis.
- [6]. Gipps, G., P., Kevin, Q., G., Held, A., Barnett, G., 2001, New Technologies for Transport Route Selection, Transportation Research Part C, Vol: 9 pp:135-154..
- [7]. Glasgow, J., French, S., Zwick, P., Kramer, L., Richardson, S., Berry, K., J., 2004, A Consensus Method Finds Preferred Routing.
- [8]. Kov, K., C., Chowdhury, R., Flentje, P., 2005, Hazard and Risk Assessment of Rainfall-Induced Land sliding Along a Railway Line.

Study of a Parabolic Leaf Spring by Finite Element Method & Design of Experiments

Manas Patnaik¹, Narendra Yadav², Ritesh Dewangan³,

^{1,2,3}(Department of Mechanical Engineering, Rungta College of Engineering & Technology, Raipur-492001-India)

Abstract : This work is carried out on a mono parabolic leaf spring of a mini loader truck, which has a loading capacity of 1 Tonnes. The modelling of the leaf spring has been done in CATIA V5 R20. And for finite element analysis the model was imported in the static structural analysis workbench of CATIA V5 R20. The finite element analysis of the leaf spring has been carried out by initially discretising the model and then applying the relevant boundary conditions. Max Von Mises stress and Max Displacement are the output parameters of this analysis. In order to study the behaviour of parabolic leaf spring, Design of experiments has been implemented. In DOE, input parameters such as Eye Distance & Depth of camber have been varied and their affect on output parameters have been plotted.

Keywords: Computer Aided Design (CAD), Camber, Design of Experiments (DOE), Eye Distance, Finite Element Analysis (FEA), Parabolic Leaf Spring (PLS).

I. INTRODUCTION

Parabolic Leaf springs are essential suspension elements used on mini loader trucks necessary to minimize the vertical vibrations, impacts and bumps due to road irregularities and to ensure safety of the loaded cargo. Parabolic Leaf springs are widely used for automobiles. The Parabolic leaf spring absorbs the vertical vibrations and impacts due to road irregularities by means of variations in the spring deflection so that the potential energy is stored in spring as strain energy and then gradually released to maintain comfort. The finite element analysis (FEA) is a computing technique that is used to obtain approximate solutions to the boundary value problems in engineering. It uses a numerical technique called the finite element method (FEM). It is now accepted by major industries across the world and a company that is able to verify a proposed design will be able to perform to the clients specifications prior to manufacturing or construction. In the present work, leaf spring has been analyzed for static strength and deflection using 3D finite element analysis. CATIA V5 R20 has been utilized in the creation of the three dimensional model and its static structural workbench for analysis when subjected to vertical loads. The variation of bending stress and displacement values are computed. To add on the different combinations of input parameters (camber & eye distance) have been taken into account & its influence on bending stress and max deflection has been studied.

II. Parabolic Leaf Spring & Dimensions

A more modern implementation of old leaf springs is the parabolic leaf spring for automobiles. The new innovative design is characterized by the use of less leaves whose thickness varies from the center to the outer side

following a parabolic pattern. The mathematical equation between the thickness & the length of the spring is that of a parabola & hence it has been named as parabolic leaf spring. This results in less inter leaf friction, because of which the only contact point between the springs in vehicle is at the end and the center where the axle is connected. Spacers used in the new design prevent the other parts collisions. Besides being less in weight the main benefit of parabolic springs is their greater flexibility, which is translated as a high ride quality of the vehicle. It gives us the high ride quality which refers to the high degree of safety to the riders from the uneven road and gives high level of comfort.

Modified version of leaf springs is the parabolic leaf springs for automobiles and has better load bearing capacity with less weight. Other benefits include improved fuel economy, load carrying capacity & enhanced suspension.

In the present work parabolic leaf spring of a mini loader truck is considered for analysis. The modeling of the PLS has been carried out in CATIA V5 R20 and has the following dimensions:

1. Camber – 90.81mm
2. Distance between eyes(Eye Distance) : 1025mm
3. Thickness at the central part : 10.81mm

Note: The above dimensions have been taken with the help of an inextensible measuring tape and a vernier caliper and then the procedure of modeling the spring was initiated. The basic views of the considered parabolic leaf spring are shown in fig. 1.

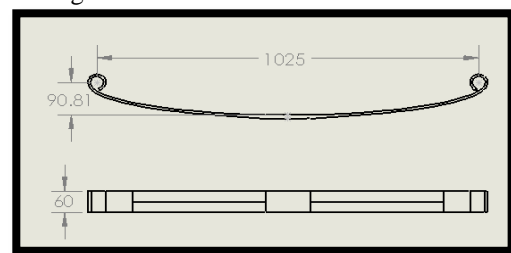


Fig.1 Front & Top view
Note : All dimensions are in mm

III. EXISTING MATERIAL

The material used for experimentation is EN45 and its mechanical properties has been mentioned in Table-1

Table--1

Material		Young's Modulus (E) Gpa	Poisson's Ratio (M)	Density (Kg/M ³)	Yield Strength (Mpa)
EN	IS(Old)				
EN45	55Si2 Mn90	200	0.3	7850	1500

IV. Result And Analysis Using Method Of Finite Elements

1.1 Meshing

Meshing is basically the process of breaking the CAD model into very small elements. It is also known as piecewise approximation. Meshing are of different types, it may be comprising of 1D, 2D or 3D elements. In present case selected is shown in Table-2

Table--2

Mesh			Element type	
S. N.	Entity	Size	Connectivity	Statistics
1	Nodes	12084	Connectivity	Statistics
2	Elements	5905	TE10(Tetrahedron element)	5905 (100.00 %)

1.2 Boundary Conditions

As shown in Fig. 2, one eye of the leaf spring will be fixed and the other eye will have certain degree of rotation to allow the leaf spring to deflect by some amount. It has been mathematically calculated that the maximum load which the spring will be subjected to 3800 N. This particular calculation has been done on the basis of GVW (Gross Vehicle Weight), which may be defined as the total weight of the loaded vehicle. This includes the vehicle itself and the cargo that is loaded within that vehicle.

In order to perform static structural analysis it is very essential to restraint the CAD model in the same manner as it is done physically. As far as parabolic leaf springs are concerned it has two eye ends, one of which is fixed with the upper body of the mini loader truck, while the other end is attached to a shackle which allows the spring to expand along its leaf span thereby causing some degree of rotation in the shackle.

Similarly we have applied constraints to our CAD model of parabolic leaf spring shown in Fig. 3 & 4.

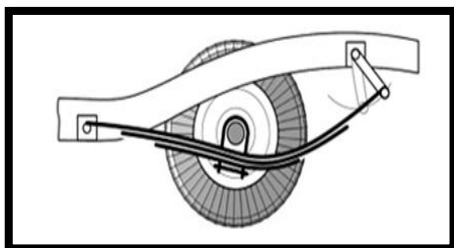


Fig.2 Suspension and Constraints

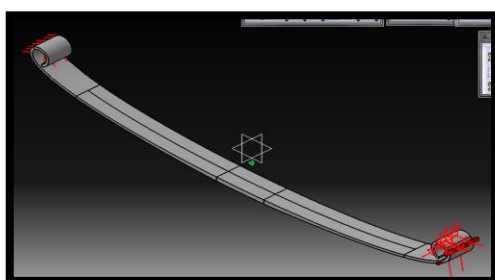


Fig.3 Applying Constraints.

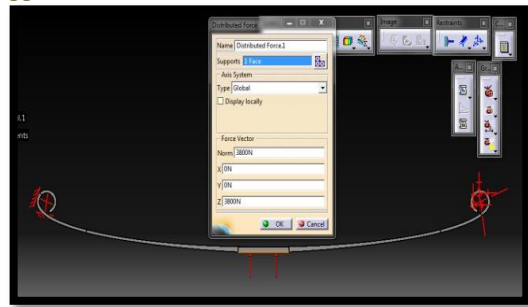


Fig.4 Applying Load

As shown in Fig. 4, the leaf spring is being treated as a simply supported beam which has a central load of 3800 N directed upwards.

4.3 Static Structural Analysis in CATIA V5 R20

After applying the boundary conditions the maximum von mises stress and maximum displacement is shown in Fig. 5 & 6.

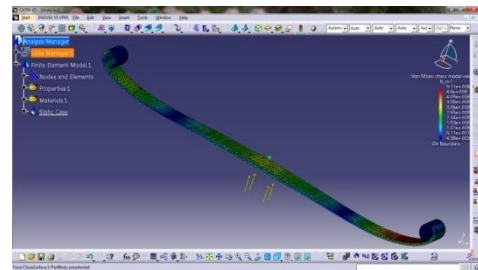


Fig.5 Von Mises Stress

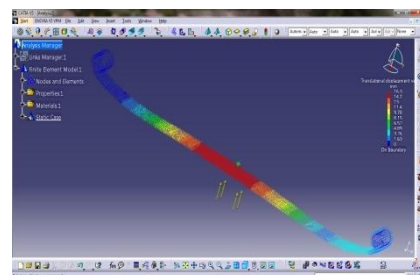


Fig.6 Displacement

Outputs on the basis of existing dimensions has been mentioned in Table-3 :

Table--3

S.N.	Output Parameter	Value
1	Maximum Displacement	16.3079mm
2	Maximum Von mises stress	5.11017e+008 N_m2
3	Energy	30.008 J
4	Mass	4.549kg

V. DESIGN OF EXPIREMENTS

The Design of experiments (DOE) is a tool for determining the significance of different factors affecting process quality and for calculating optimal settings for controllable factors. For example we may believe that operating temperature and wave height affects the number of defects from a wave solder machine. DOE provides a fast & efficient means for determining the values of these parameters that would produce the fewer number of defects. DOE Procedure:

- Select factors to be tested & a measure of process outcome.
- Select test setting for each factor.
- Select the appropriate orthogonal array.
- Run the tests.
- Analyze the results.
- Calculate optimum setting for each factor.
- Run confirmation test(s).

In this work camber and eye distance are selected as input parameters and max displacement, max von mises stress as output parameters. Design of experiments has been implemented by varying camber from 90 mm to 95 mm in steps of 10 and by varying eye distance from 1020 mm to 1030 mm in steps of 10. After running design of experiments the graphs between input and output parameters has been plotted which is shown in Fig.9, 10, 11 and 12.

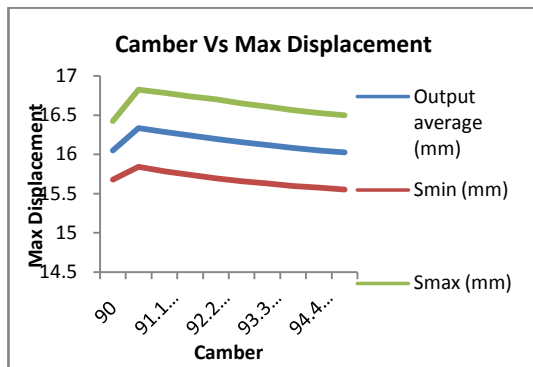


Fig.9 Effect of varying camber on Displacement

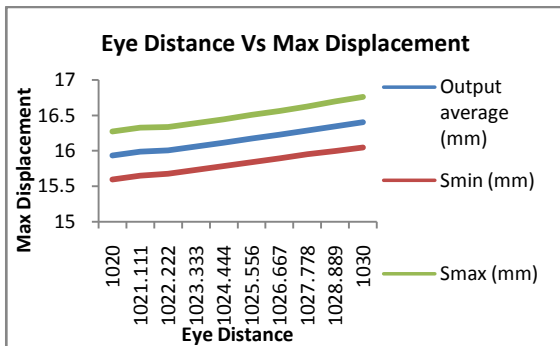


Fig.10 Effect of varying eye distance on displacement

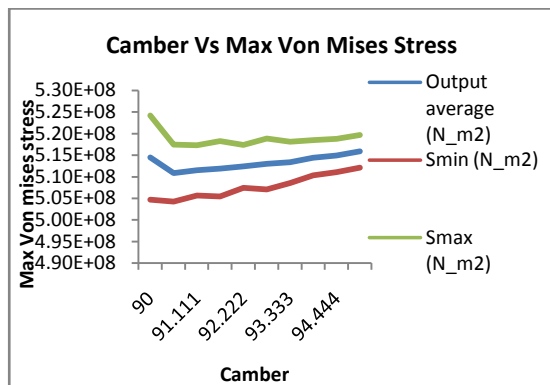


Fig.11 Effect of varying camber on von mises stress

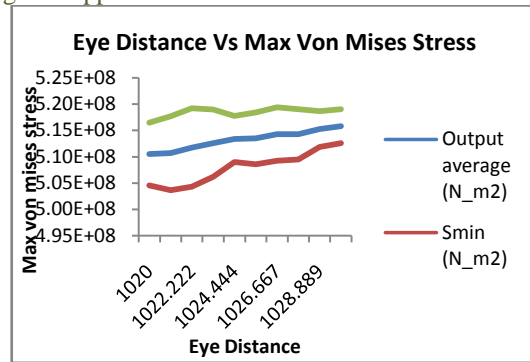


Fig.12 Effect of varying eye distance on Von mises stress

VI. CONCLUSION

After performing the design of experiments the following observations have been made:

- With reference to fig.9, as the camber is increased there is a decrease in the average amount of displacement.
- With reference to fig. 10, if the eye distance is increased there is an increase in the average amount of displacement.
- With reference to fig. 11, if the camber is increased there is an increase in the average amount of von mises stress.
- With reference to fig. 12, if the eye distance is increased there is an increase in the average amount on mises stress.

Hence it is conclude that the optimum setting of dimensions pertaining to parabolic leaf spring can be achieved by studying the various plots obtained from Design of Experiments.

References

- Doshi N.P., Ingole N.K., Gulhane U.D., Analysis and Modification of Leaf Spring of Tractor Trailer Using Analytical and Finite Element Method, *International Journal of Modern Engineering Research (IJMER)*, Vol.1, Issue.2, pp-719-722.
- Kumar K., Aggarwal M.L., A Finite Element Approach for Analysis of a Multi Leaf Spring using CAE Tools, *Research Journal of Recent Sciences*, Vol. 1(2), 92-96, Feb. (2012).
- Rajendran I., Vijayarangan S., Design and Analysis of a Composite Leaf Spring, *Journal of Institute of Engineers India* 82 2002: pp. 180 – 187.
- Jadhao K.K., Dalu R.S., Experimental Investigation & Numerical Analysis of Composite Leaf Spring, *International Journal of Engineering Science and Technology*, ISSN : 0975-5462 Vol. 3 No. 6 June 2011.
- Rajendran, I., Vijayarangan, S. Design and Analysis of a Composite Leaf Spring, *Journal of Institute of Engineers India* 82 2002: pp. 180 – 187.
- Rajendran, I., Vijayarangan, S. Optimal Design of a Composite Leaf Spring using Genetic Algorithms *Int. Jr.of Computer and Structures* 79 2001: pp. 1121 – 1129.
- R.S. Khurmi, J.K. Gupta. A text book of Machine Design, 2000.
- V.B. Bhandari, Design of Machine Elements, 2012.

Oofp: Mapping the Oose Models into Function Points: Rules, Tool and Case Study

¹Durga Gehlot, ²Prof. Meena Sharma

¹Department of Computer Engineering, Institute of Engineering and Technology, DAVV Indore, India

²HOD of Computer Engineering, Institute of Engineering and Technology, DAVV Indore, India

Abstract: Function point analysis is useful to measure size of software projects in terms of functionality requested by user. The main advantage of function point analysis is that it is independent of the technology used for implementation. When we apply function points to object-oriented software projects, the concepts of development method have to be mapped into abstract models that contain functional items of the application. This proposed idea implement a tool for mapping function points into use case driven OOSE (object-oriented software engineering) Jacobson approach. In this idea we only considers analysis phase of OOSE life cycle. OOFP tool measures function point from requirements models and analysis model.

Keyword: function points, size, requirements model, and analysis model, OOFP.

I. INTRODUCTION

Function Points Analysis (FPA) is one of the earliest models that are used to predict the size of software in the early stages. Albrecht proposed the FPA model in 1979 and it measures the size of software based on its functionalities [1]. The main advantages of the FPA model are that it is independent of the technology. Up to the present, various FPA versions based on the Albrecht's version have been proposed (e.g. IFPUG method, MarkII, COSMIC-FFP and they have been accepted as ISO/IEC standards. The current version of counting rules is recorded in the Counting Practices Manual [2]. This counting method is implicitly based on the high-level model of software applications. Though independent of implementation, counting rules are thus based on the implicit assumptions on the abstract model of software applications. The items in the abstract model that are then counted include transaction and file types. These items are typically identified from documents of traditional, structured design technique e.g. data flow diagrams, hierarchical process models or database structures. The proposed paper focus on object oriented models based on the OOSE Jacobson approach. The transaction and file type items are counted from models of analysis phase. The models of analysis phase of OOSE includes use case model, domain object model and analysis model but this research paper focuses on counting function points from analysis model and use case model.

1.1 Function Point Analysis with object – oriented design methods

The Function Point software measure does not require a particular development technique. However, the high level concepts of object-oriented development methods cannot be mapped directly to the concepts of Function Point Analysis. In order to apply this software measure early in the development process, the object-oriented concepts corresponding to transactional and data function types have to be determined.

Object-oriented methods differ, especially in their early development phases. The Object-Oriented method of Jacobson et al. is based on so-called use cases. The OO-Jacobson identifies the functionality of an application with requirements use case model. Data types are described with domain or analysis object model on the requirements level. The work proposes rules to map these models into function point counting procedures. With proposed rules, it is possible to count software developed with the OO-Jacobson method.

In this research paper, we focus on the approach of Jacobson et al [3]. This method is called Object-Oriented Software Engineering. The OOSE method defines a process to transform formalized requirements into a sequence of models. The steps include the requirements, analysis, design, implementation and testing models. The use case model is the basis on which all the models are developed. Together with the domain object model it forms requirements model as shown in Figure 1.

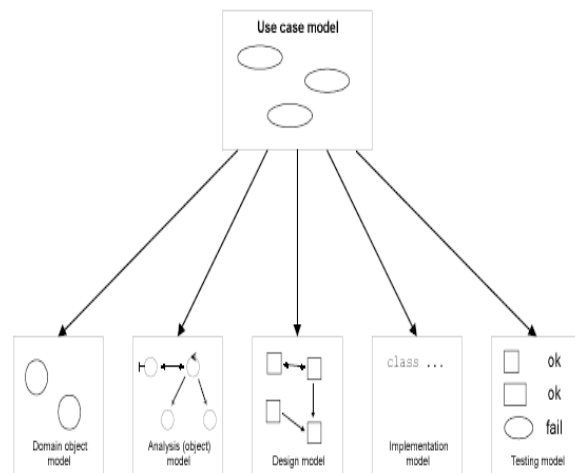


Figure 1: The use case model is the basis on which all other models of OOSE approach are developed.

The objectives of this research paper are:

1. The application of Function Point Analysis following the IFPUG standards.
2. To measure for software developed with OOSE method.
3. To count early in the life cycle, in the requirements analysis phase.

1.2 Related Work

Little work has been published on Function Point Analysis in the context of object-oriented software engineering techniques. But these approaches are based on a model that consists with objects together with their methods. In these approaches objects are treated as data files and methods as transactions which are the counting items in the Function Point Analysis. These approaches do not applicable to early OOSE documents. It is also questionable whether each individual method is to be counted as a transaction.

Whitmire[4] considers each class as an internal logical file and treats messages sent outside the system boundary as transactions.

The ASMA paper takes a similar approach. Services delivered by objects to the client are considered as transactions. The complexity of services is weighted based on accessed attributes and communications. Objects are treated as files, their attributes determining their complexity.

IFPUG [5] is working on a case study which illustrates the use of the counting practices for object-oriented analysis and design. This case study, which is currently in draft form, uses object models in which the methods of classes are identical with the services recorded in the requirements. Under this assumption, the methods can be counted as transactions.

Karner [6] proposes a new measure called Use Case Points for projects developed with the OOSE method. The structure of this measure is similar to Function Points, but it does not conform to the concepts of Function Points.

Thomas Fetcke[7] proposes rules for mapping the OO-Jacobson approach into Function Point Analysis. This paper is based on Thomas proposed rules. This research paper considers how to apply these rules to OOSE models to measure data and transaction functions. In this paper data files and transaction functions counting is done using models of analysis phase of the OOSE life cycle. Analysis phase model includes use case model and analysis model.

II. Brief Introduction To Oose

The OOSE method is divided into three major consecutive processes: analysis, constructive and testing. The analysis phase is further divided into two steps called requirements analysis and robustness analysis as shown in Figure 2. The first step derives the requirements model from the informal customer requirements. This model is expressed in terms of use case model, and may be augmented by a domain object model. The second step, robustness analysis, then structures the use case model into the analysis model by applying use case analysis. The succeeding process further transforms these models, as indicated in Figure 1.

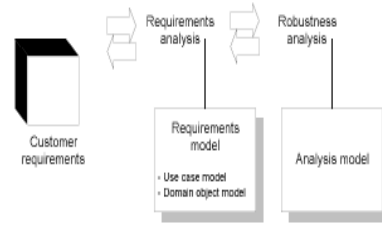


Figure 2: Analysis Phase of the OOSE life cycle.

At the focus of our work are the models developed in analysis phase as shown in Figure2. As Jacobson et al. state, the requirements model can be regarded as formulating the functional requirements specification based on the needs of the users. The goal of this research paper work is to count Function Points early in the life cycle, measuring the functionality requested by the user from these models. The overview of these three models discussed in [7].

III. Fuction Point Concepts

3.1 Function Point model

A high level model of the FPA mode is given in Figure 3 [7]. The function Point model specifies which component types of the software application will be measured and from which viewpoint this will be done. What is to be counted, and measured, are the internal files and external files of the application, together with the inputs, outputs and inquiries from and to the user. Software components or deliverables which are not visible from a user viewpoint are not considered part of the Function Point measurement model.

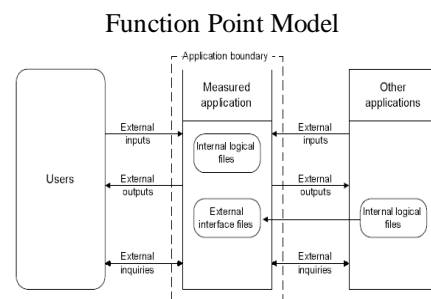


Figure 3: High-level view of the abstract Function Point model with users and links to other applications. The dotted line marks the application boundary.

3.2 Function Point Counting Process

In the IFPUG version, the counting procedure of function point consists of the following seven steps. The details of these seven steps are discussed in IFPUG [2].

1. Determine type of function point count.
2. Identify the application boundary (A boundary indicates the border between the application or project being measured and the external applications or the user domain. A boundary establishes which functions are included in the function point count).
3. Identify and rate transactional function types to determine their contribution to the unadjusted function point count.
4. Identify and rate data function types to determine their contribution to the unadjusted function point count.

5. Determine the Unadjusted function point counts.
 6. Determine the value adjustment factor (VAF) that takes so-called global system characteristics into account, e.g. data communication, performance or end user efficiency. This adjustment is external of and independent from the concepts of the abstract FPA model. The global system characteristics determine an adjustment factor that is multiplied with the unadjusted count.
 7. Calculate the adjusted function point count.
- The next section describes the proposed mapping of OOSE models to function points along these five steps.

IV. Mapping Concepts (Proposed Method)

The aim of this research paper is to calculate the Unadjusted Function Point. The paper work proposes the following five steps to apply IFPUG version to the OOSE requirements analysis models (use case model and analysis model).

- 4.1 **Step1**(Determine the type of function count): This paper handles only the application project function point.
- 4.2 **Step2**(Identify the application boundary): The counting boundary is determined by the type of actors appeared in use case model of OOSE requirement analysis phase.

Proposed mapping rules to identify the application boundary

1. Accept each human actor as a *user* of the system.
2. Accept each non-human actor, which is separate system not design to provide functionality solely to the system under consideration as an *external application*.
3. Reject each non-human actor, which is part of the underlying system, e.g. a rational database system or a printing device.

The result is a representation of the application boundary as a set of users and applications external to the one under consideration as shown in Figure 4.

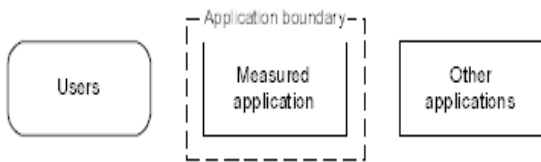


Figure 4: Step2- Identification of the counting boundary.

4.3 **Step3** (Identify and rate transactional function types to determine their contribution to the unadjusted Function point count.):

The transaction functions are automatically decided based on actors and use cases of the use case model. Use cases are the OOSE concept corresponding to transactions.

Proposed mapping rules to identify and rate transaction function types

4. Select every use case that has a direct relation to an actor accepted by rule 1 or 2. This use case will be a candidate for one or several transactions.

5. Select every use case that extends a use case selected by rule 4 as a candidate.
 6. No other use cases will be counted.
- Determining the types of transaction (external input (EI), external output (EO) and external inquiry (EQ) is based on a set of detailed rules in FPA [1]. The rules are recorded in the IFPUG Counting Practices Manual [2]. The relevant sections are:
 “External Input Counting Rules”,
 “External Output Counting Rules”, and
 “External Inquiry Counting Rules”.

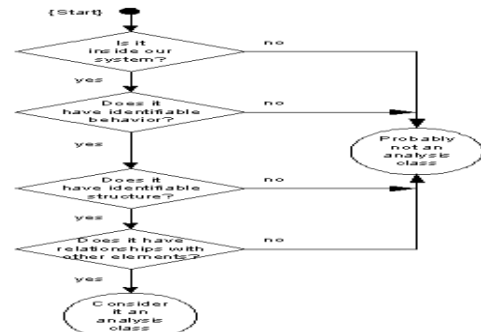
The rates of transactions are based on detailed rules in the counting practices Manual. The rules require the determination of data element types (DET) and file types that are referenced (FTR), illustrated in Figure 5

4.4 **Step4** (Identify and rate data function types to determine their contribution to the unadjusted function point count.):

Data files are automatically decided based on analysis classes of analysis model. In the analysis model, the objects are typed into three groups, namely entity, interface and control objects. The set of objects that have to be analyzed is limited to the entity objects and is thus set of objects typically smaller. Interface (boundary) and control objects are part of implementation.

4.4.1 Finding of Analysis Classes from Use Case Model

1. Is this candidate inside our system boundary?
 2. If not, it might be an actor of our system.
 Does this candidate have identifiable behavior for our problem domain? (i.e., can we name the services/functions that are needed in our problem domain and that this candidate would own and provide?)
3. Does this candidate have identifiable structure? (i.e., can we identify some set of data this candidate should own and manage?)
4. Does this candidate have relationships with any other candidates?



If you find a "no," then the candidate is probably not a class; move on to the next candidate. If the answer is "yes," keep asking the questions. If you get all "yes" answers, conclude the candidate is a class, and get the next candidate to evaluate.

Proposed mapping rules to identify and rate data function types

7. Select every object of entity type as a candidate for a logical file.
8. No other objects will be selected.

For aggregation relationships

9. An entity objects that is part of another object (is aggregated into another object) is not a candidate for a logical file, but it is a candidate for a record element type (RET) for the file related to the aggregating top-level object

For inheritance relationships

10. An abstract object is not a candidate for a logical file. It is a candidate for a RET for each object that inherits its properties.
11. Sub-objects of a concrete object are candidates for a logical file or for a RET of that object.
12. If use cases make implicit use of logical files that are not represented in the analysis object (class) model, these files have to be included in the set of files.

Determining the types of data files (internal logical files (ILF) and external interface files (EIF)) is based on a set of detailed rules in FPA [1]. The rules are recorded in the IFPUG Counting Practices Manual [2]. The relevant section is “ILF/EIF counting rules”.

The rates of data files are based on detailed rules in the counting practices Manual. The rules require the determination of data element types (DET) and record element types (RET), illustrated in Figure 5.

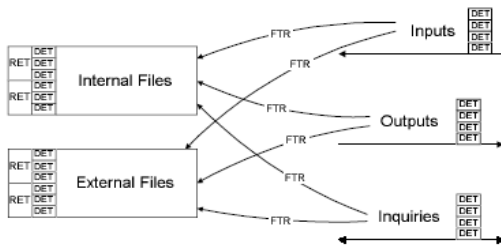


Figure 5: Step3 and Step4- Rating of data and transaction function types.

Proposed Mapping Rules for determining DET, RET and FTR

13. Attributes of objects are candidates for data element types (DET) for files and for the transactions by which it is read and maintained.
14. Candidates for record element types are determined by subgroups of files and by rules 9-11.
15. Each object maintained and /or read by a use case counts as a file type referenced (FTR) for the associated transaction(s), if and only if the object has been identified as a file in step 4.

After determining DETs, RETs, FTRs rate the data files and transaction functions according to rating matrix and then allot weighs according to weighting matrix in the Counting Practices Manual [2]. The total weight of data files types and transaction types are the required unadjusted function points count.

4.5 Step 5 (Determine the unadjusted function point counts)

As the result of Step3 and Step4, the counts for each function type are automatically classified according to complexity and then weighted. The total for all function types is the unadjusted function point count.

V. CASE STUDY

In this section the rules proposed in section 4 are applied to OOSE approach based project. The documentation provided included use case models and analysis object models together with the textual description these models.

5.1 Example of OOSE based analysis models

In OOSE life cycle, analysis phase is divided into two phases: requirement analysis and robustness analysis. Requirement analysis consists with two models, use case models and domain object models. Robustness analysis consists with a model known as analysis model. This research work focuses on use case models and analysis classes.

Case Study: A part of Course Registration System Use Case Model

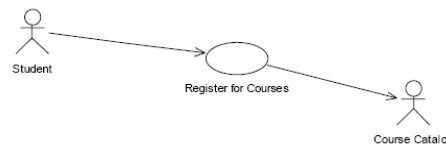


Figure6: Use Case: Register for Courses

This use case allows a Student to register for course offerings in the current semester. The Student can also update or delete course selections if changes are made within add/drop period at the beginning of the semester. The Course Catalog System provides a list of all the course offerings for the current semester.

5.2 Finding Analysis classes from use case model (Behavior)

Register for Courses Use Case-This use case starts when a Student wishes to register for course offerings, or to change his/her existing course schedule.

1. The system requests that the Student specify the function he/she would like to perform (Create a Schedule, Update a Schedule, or Delete a Schedule).
2. Once the Student provides the requested information, one of the sub flows is executed. If the Registrar selected “Create a Schedule”, the Create a Schedule sub flow is executed. If the Registrar selected “Update a Schedule”, the Update a Schedule sub flow is executed. If the Registrar selected “Delete a Schedule”, the Delete a Schedule sub flow is executed.

Candidates for entity (noun) and applying 4 conditions of section 4.4.1 to make them entity analysis classes as shown in Figure7.

1. **Student-**A person enrolled in classes at the university.
2. **Schedule-**The courses a student has selected for the current semester.

3. Course Offering-A specific delivery of the course for a specific semester – you could run the same course in parallel sessions in the semester. Includes the days of the week and times it is offered.

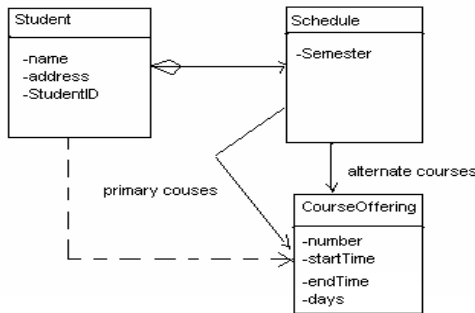


Figure7: Analysis class model consists with entity analysis classes

5.3 Now, applying proposed rules to Analysis Class Model and Use Case Model of above Case Study:

By rules 1, 2 and 3 application boundary includes-
 Human actors- student
 Non-human actors- Nil

By rules 4-12 and 13-15 candidates for transaction/data function types with ratings and weight are shown in Table1.

Transaction/ data function name	Transaction/ data function type	No. of DET	No. of RET/ FTR	Comple xity	Weight/ Value
Register for courses	EI	3	2FTRs (Student, Schedule)	low	3
Register for courses	EO	3	2FTRs (Student, Schedule)	low	3
Register for courses	EQ	4	1FTR (Course Offering)	low	4
Student	ILF	3	1RET(Schedule)	low	7
Course Offering	ILF	4	1RET(Schedule)	low	7
UAFP					24 FPs

Table1: Transaction/Data function types with ratings and weight.

In order to make it adjusted function point, we have to calculate and tabulate the GSC and come out with the VAF as shown in Table2.

GSC	Value (0-5)
Data communications	1
Distributed data processing	1
Performance	4
Heavily used configuration	0
Transaction rate	1
On-Line data entry	0
End-user efficiency	4
On-Line update	0
Complex processing	0
Reusability	3
Installation ease	4
Operational ease	4
Multiple sites	0
Facilitate change	0
Total	22

Table2: Global System Characteristics (GSC)

So using formulae:

$$VAF = 0.65 + ((\text{sum of all GSC factor})/100).$$

$$= 0.65 + (22/100) = 0.87$$

This factor affects the whole FP like anything, be very particular with this factor.

So now, calculating the Adjusted FP (AFP) = VAF * Total Unadjusted FP (UAFP)

$$= 0.87 * 24 = 20.88,$$

=Rounded to 21 FPs

Compared with the approaches proposed in the literature, these mapping rules have certain advantages.

1. The mapping rules are based on the standard FPA defined in the IFPUG Counting Practice Manual. This widely used measure independent of technology.
2. The count is based on requirements models, which are the first models available in the OOSE life cycle. For the purpose of effort estimation based on Function Points, this is an essential prerequisite.

This approach also has some limitations.

1. The main limitation is the focus on the Jacobson OOSE method. Mapping rules are based on the requirements models of this approach and cannot be applied to methods that do not develop these models. Also an advantage this focus on OOSE, that the models are unambiguously defined in the method.

VI. OOFP TOOL

The concept of mapping the object oriented software models into function Points lead to implement a tool called OOFP. This tool is implemented in java language. The inputs for the tool are use case model and analysis class (object) model and the output includes the values of function points, transactional functions, and data functions.

The OOFP tool is automated using XMI (xml metadata interchange) parser. The XMI parser takes .xmi or .xml files of use case and analysis class models as input then read and extracts the use cases, actors, entity classes from these files. Extracted candidates are then used for calculating function points.

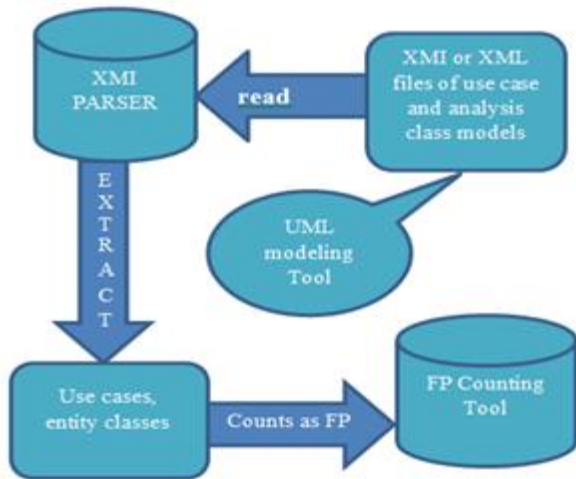


Figure: 8 Function Point Counting Tool (OOFP tool).

VII. SUMMARY

This work demonstrated the applicability of function points as a measure of functional software size to the object-oriented Jacobson approach, OOSE. This work supports that the function point measures independent of the technology used for implementation and that it can be used in the object-oriented paradigm.

Future work in the field has to deal with the mapping of OOSE design model into function points.

References

- [1] A. J. Albrecht. Measuring Application Development Productivity. IBM Applications Development Symposium, Monterey, CA, 1979
- [2] Function Point Counting Practices Manual, Release 4.0. Westerville, Ohio, International Function Point Users Group, 1994.
- [3] Jacobson, I, M. Christerson et al. Object-Oriented Software Engineering. A Use Case driven Approach. Addison-Wesely, 1992.
- [4] Whitmire, S.A. Applying function points to object-oriented software models, 1992. In Software engineering productivity handbook. J. Keyes, McGraw-Hill, pp.229-244.
- [5] Function Point Counting Practices: case Study3- Object-Oriented Analysis. Object-Oriented Analysis. Object-Oriented Design (Draft), International Function Point Users Group, 1995.
- [6] Karner, G. Resource Estimation for Objectory Projects, Objectory Systems, 1993.
- [7] ThomasFetcke, Alain Abran and THo- Hau Nguyen.Mapping the OO-Jacobson Approach into Function Point Analysis, 1997.Published in the Proceeding of TOOLS- 23'97.
- [8] "CostEstimatingWebSite", <http://cost.jsc.nasa.gov/COCOMO.html>
- [9] "Construx Estimate tool", www.construx.com
- [10] "CoStar tool", www.softstarsystems.com
- [11] "An introduction (tutorial) to Function Point Analysis", www.devdaily.com/FunctionPoints.

VIII. APPENDIX: Screenshots For OOFP Tool

The following screenshots show how function points are calculated using OOFP (Object oriented function point) tool.



Screen1: Function Point Calculation



Screen 2: Value Adjustment Factor



Screen 3: Function Point Report for a Project

Edge Coloring of a Complement Fuzzy Graph

Arindam Dey, Dhrubajyoti Ghosh, Anita Pal

*Departments of Mathematics, National Institute of Technology Durgapur,
Durgapur-713209, West Bengal, India*

ABSTRACT: Graph coloring is one of the most important problems of combinatorial optimization. Many problems of practical interest can be modeled as coloring problems. Two types of coloring namely vertex coloring and edge coloring are usually associated with any graph. Edge coloring is a function which assigns colors to the edges so that incident edges receive different colors. Let $G=(V,\mu,\sigma)$ be a simple connected undirected graph where V is a set of vertices and each vertices has a membership value μ and each edge has a membership value σ . Minimum number of color needed to color the graph is known as chromatic number of that graph. Graph coloring is a NP complete problem. In our paper, we introduce an algorithm to find the complement of any fuzzy graph with $O(n^2)$ time and also coloring this complement fuzzy graph using α cut.

Keywords: Complement fuzzy graph, edge color, α cut of fuzzy graph

I. INTRODUCTION

We know that graphs are simple model of relation. A graph is a convenient way of representing information involving relationship between objects. The object is represented by vertices and relations by edges. When there is vagueness in the description of the objects or in its relationships or in both we need to design fuzzy graph model. One of the most important properties of fuzzy graph model is fuzzy graph coloring which is used to solve problems of combinatorial optimization like traffic light control, exam-scheduling, register allocation etc. Two types of coloring namely vertex coloring and edge coloring are usually associated with any graph. The paper is organized in five sections. 1st section includes introduction of fuzzy graph model. Section two defines fuzzy graph and its properties. Section three, we find the complement of a fuzzy graph and define a coloring function which is based on α cut to color the complement fuzzy graph and finding the chromatic number for this fuzzy graph.

II. FUZZY GRAPH

A fuzzy graph is a pair of functions $G: (\sigma, \mu)$ where σ is a fuzzy subset X and μ is a symmetric relation on σ i.e. $\sigma: X \rightarrow [0, 1]$ and $\mu: X \times X \rightarrow [0, 1]$ such that $\mu(x, y) \leq \sigma(x) \wedge \sigma(y)$ for all x, y in X . we denote the crisp graph of $G: (\sigma, \mu)$ by $G^*: (\sigma^*, \mu^*)$ where σ^* is referred to as the nonempty set X of nodes and $\mu^* = E \in X \times X$. Now crisp graph (X, E) is a special case of a fuzzy graph with each vertex and edge of (X, E) having degree of membership value 1 where loops are not consider and μ is reflexive.

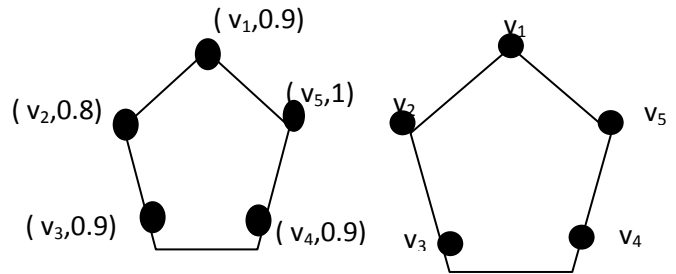


Fig 1 Fuzzy graph (G)

Fig 2 Crisp graph(G^*)

2.1 COMPLEMENT OF FUZZY GRAPH

Complement of a fuzzy graph has been defined by Moderson [1]. Complement of a fuzzy graph $G: (\sigma, \mu)$ as a fuzzy graph $G^c: (\sigma^c, \mu^c)$ where $\sigma^c = \sigma$ and $\mu^c(x, y) = 0$ if $\mu(x, y) > 0$ and $\mu^c(x, y) = \sigma(x) \wedge \sigma(y)$ otherwise. From the definition G^c is a fuzzy graph even if G is not and $(G^c)^c = G$ if and only if G is a strong fuzzy graph. Also, automorphism group of G and G^c are not identical. But there is some drawbacks in the definition of complement of a fuzzy graph mentioned above. In fig 5 $(G^c)^c \neq G$ and note that they are identical provided G is a strong fuzzy graph

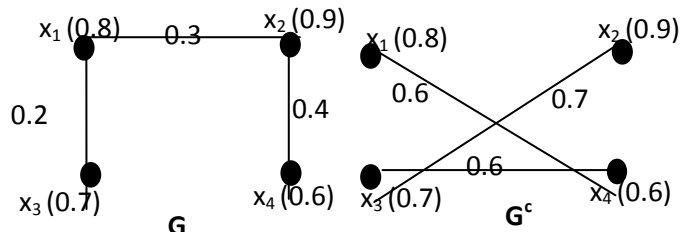


Fig 3 Fuzzy graph

Fig 4 Complement Fuzzy graph

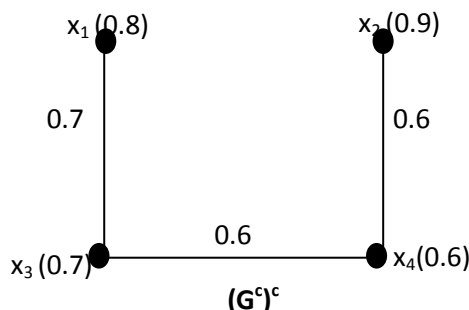


Fig .5 Complement of complement Fuzzy graph

Now the complement of a fuzzy graph $G: (\sigma, \mu)$ is the fuzzy graph $\bar{G}: (\bar{\sigma}, \bar{\mu})$ where $\bar{\sigma} \equiv \sigma$ and $\bar{\mu}(x, y) = \sigma(x) \wedge \sigma(y) - \mu(x, y) \forall x, y \in X$ (1)

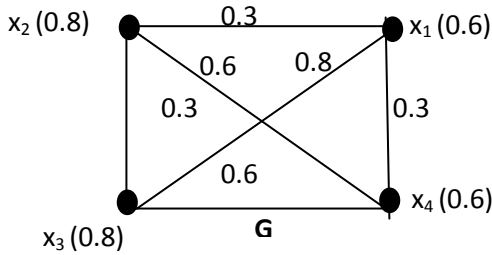


Fig. 6 Fuzzy graph

For solving this problem we have done the calculation into three cases. in 1st case we take a fuzzy graph (G) which have five vertices and five edges. All the vertices and edges have fuzzy membership value. In the second case we find the complement of this fuzzy graph (G₁). In third section we define the edge coloring function to color the complement fuzzy graph.

CASE 1:

We consider a fuzzy graph with have five vertices, v_1, v_2, v_3, v_4, v_5 and corresponding membership values 0.9, 0.75, 0.95, 0.95, 0.9. Graph consist of five edges e_1, e_2, e_3, e_4, e_5 with their corresponding membership value 0.75, 0.9, 0.85, 0.15, 0.6. Corresponding fuzzy graph is shown in fig. 9

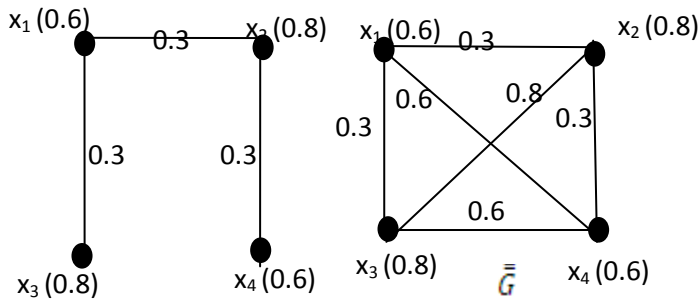


Fig. 7 Complement Fuzzy graph

Fig. 8 Complement of complement Fuzzy graph

$$\mu_1 = \begin{bmatrix} v_1 & v_2 & v_3 & v_4 & v_5 \\ v_1 & 0.0 & 0.75 & 0.0 & 0.0 & 0.9 \\ v_2 & 0.75 & 0.6 & 0.0 & 0.0 & 0.0 \\ v_3 & 0.0 & 0.6 & 0.0 & 0.15 & 0.0 \\ v_4 & 0.7 & 0.5 & 0.14 & 0.0 & 0.85 \\ v_5 & 0.5 & 0.6 & 0.85 & 0.5 & 0.9 \end{bmatrix}$$

Adjacent matrix 1

Now, $\bar{\bar{\sigma}} = \bar{\sigma} = \sigma$ and $\bar{\bar{\mu}}(x, y) = \bar{\sigma}(x) \wedge \bar{\sigma}(y) - \bar{\mu}(x, y) = \sigma(x) \wedge \sigma(y) - ((\sigma(x) \wedge \sigma(y) - \mu(x, y))) = \mu(x, y) \forall x, y$. Hence $\bar{\bar{G}} = G$

Fig. 8 shows the Complement of complement fuzzy graph is a fuzzy graph

2.2 α CUT OF A FUZZY GRAPH

α cut set of fuzzy set A is denoted as A_α is made up of members whose membership is not less than α . $A_\alpha = \{x \in X \mid \mu_A(x) \geq \alpha\}$. α cut set of fuzzy set is crisp set. In this paper, α cut set depend on vertex and edge membership value. The α cut of fuzzy graph defined as $G_\alpha = (V_\alpha, E_\alpha)$ where $V_\alpha = \{v \in V \mid \sigma \geq \alpha\}$ and $E_\alpha = \{e \in E \mid \mu \geq \alpha\}$

III. COLORING OF COMPLEMENT FUZZY GRAPH

In our previous paper [8] we have done a C program to find the complement a fuzzy graph using the condition (1). In this paper we find the complement of the fuzzy graph using the C program. We find all the different membership value of vertices and edges in the complement of a fuzzy graph. This membership value will work as a α cut of this complement fuzzy graph. Depend upon the values of α cut we find different types of fuzzy graphs for the same complement fuzzy graph. Then we color all the edges of the complement fuzzy graph so that no incident edges will not get the same color and find the minimum number of color will need to color the complement fuzzy graph is known as chromatic number.

$$E_1 = \begin{bmatrix} v_1 & v_2 & v_3 & v_4 & v_5 \\ v_1 & 0 & e_1 & 0 & 0 & e_5 \\ v_2 & e_1 & 0 & e_3 & 0 & 0 \\ v_3 & 0 & e_2 & 0 & e_4 & 0 \\ v_4 & 0 & 0 & e_3 & 0 & e_4 \\ v_5 & 0 & 0 & 0 & 0 & 0 \end{bmatrix}$$

Adjacent matrix 2

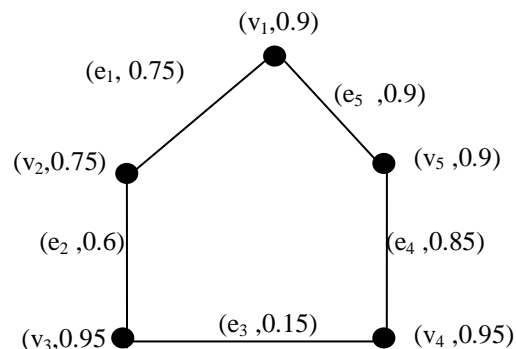


fig.9 G (fuzzy graph)

Adjacent matrix 1 represents the membership value of edges and adjacent matrix2 represents the existence of edges between the vertices

CASE 2:

We find the complement of a fuzzy graph using [8].

For $\alpha = 0.05$ Fuzzy graph $G = (V, \sigma, \mu)$ where $\sigma = \{0.9, 0.75, 0.95, 0.95, 0.9\}$ and

$$\mu_2 = \begin{matrix} & v_1 & v_2 & v_3 & v_4 & v_5 \\ \begin{matrix} v_1 \\ v_2 \\ v_3 \\ v_4 \\ v_5 \end{matrix} & \begin{bmatrix} 0.0 & 0.0 & 0.9 & 0.9 & 0.0 \\ 0.0 & 0.0 & 0.15 & 0.75 & 0.75 \\ 0.9 & 0.15 & 0.0 & 0.0 & 0.9 \\ 0.75 & 0.75 & 0.0 & 0.0 & 0.05 \\ 0.0 & 0.75 & 0.9 & 0.05 & 0.0 \end{bmatrix} \end{matrix}$$

Adjacent matrix 3

$\mu_3 =$

$$\begin{matrix} & v_1 & v_2 & v_3 & v_4 & v_5 \\ \begin{matrix} v_1 \\ v_2 \\ v_3 \\ v_4 \\ v_5 \end{matrix} & \begin{bmatrix} 0.0 & 0.0 & 0.9 & 0.9 & 0.0 \\ 0.0 & 0.0 & 0.15 & 0.75 & 0.75 \\ 0.9 & 0.15 & 0.0 & 0.0 & 0.9 \\ 0.75 & 0.75 & 0.0 & 0.0 & 0.05 \\ 0.0 & 0.75 & 0.9 & 0.05 & 0.0 \end{bmatrix} \end{matrix}$$

Adjacent matrix 5

$$E_2 = \begin{matrix} & v_1 & v_2 & v_3 & v_4 & v_5 \\ \begin{matrix} v_1 \\ v_2 \\ v_3 \\ v_4 \\ v_5 \end{matrix} & \begin{bmatrix} 0 & 0 & e_1 & e_2 & 0 \\ 0 & 0 & e_4 & e_6 & e_3 \\ e_1 & e_4 & 0 & 0 & e_5 \\ e_2 & e_6 & 0 & 0 & e_7 \\ 0 & e_3 & e_5 & e_7 & 0 \end{bmatrix} \end{matrix}$$

$$E_3 = \begin{matrix} & v_1 & v_2 & v_3 & v_4 & v_5 \\ \begin{matrix} v_1 \\ v_2 \\ v_3 \\ v_4 \\ v_5 \end{matrix} & \begin{bmatrix} 0 & 0 & e_1 & e_2 & 0 \\ 0 & 0 & e_4 & e_6 & e_3 \\ e_1 & e_4 & 0 & 0 & e_5 \\ e_2 & e_6 & 0 & 0 & e_7 \\ 0 & e_3 & e_5 & e_7 & 0 \end{bmatrix} \end{matrix}$$

Adjacent matrix 6

Adjacent matrix 4

Adjacent matrix 3 represents the membership value of edges and adjacent matrix 4 represents the existence of edges edge between the vertices

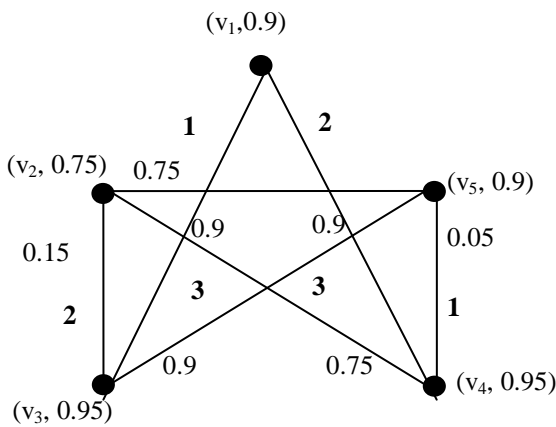


Fig.10 G_1 (complement fuzzy graph)

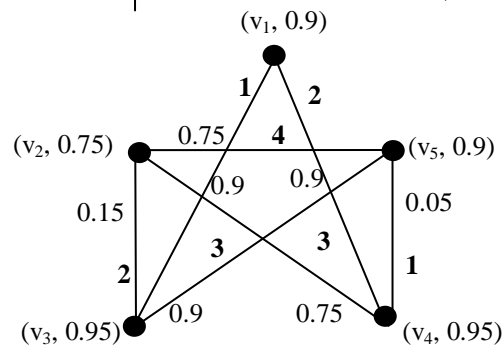


Fig.11 $\chi_{(0.05)} = 4$

For α cut value 0.05 we find the graph $G_{0.05}$ (Fig. 11). Then we proper color all the edges of this graph and find the chromatic number of this graph is 4.

For $\alpha = 0.15$ Fuzzy graph $G = (V, \sigma, \mu)$ where $\sigma = \{0.9, 0.75, 0.95, 0.95, 0.9\}$ and

CASE 3:

Given a fuzzy graph $G=(V_F, E_F)$, its edge chromatic number is fuzzy number $\chi(G)=\{x_\alpha, \alpha\}$ where x_α is the edge chromatic number of G_α and α values are the different membership value of vertex and edge of graph G .

In this fuzzy graph, there are six α cuts. They are $\{0.05, 0.15, 0.75, 0.9, 0.95\}$. For every value of α , we find graph G_α and find its fuzzy edge chromatic number.

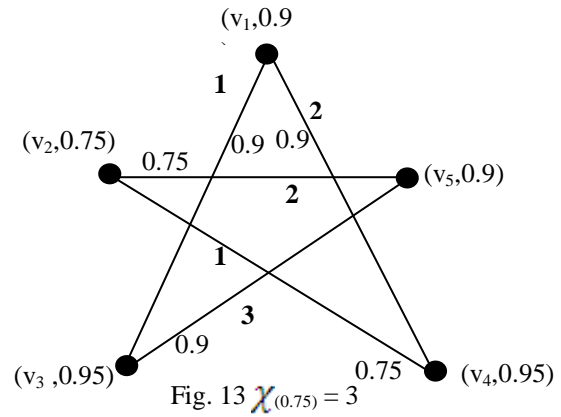
$$\mu_4 = \begin{matrix} & v_1 & v_2 & v_3 & v_4 & v_5 \\ \begin{matrix} v_1 \\ v_2 \\ v_3 \\ v_4 \\ v_5 \end{matrix} & \begin{bmatrix} 0.0 & 0.0 & 0.9 & 0.9 & 0.0 \\ 0.0 & 0.0 & 0.15 & 0.75 & 0.75 \\ 0.9 & 0.15 & 0.0 & 0.0 & 0.9 \\ 0.75 & 0.75 & 0.0 & 0.0 & 0.0 \\ 0.0 & 0.75 & 0.9 & 0.0 & 0.0 \end{bmatrix} \end{matrix}$$

Adjacent matrix 7

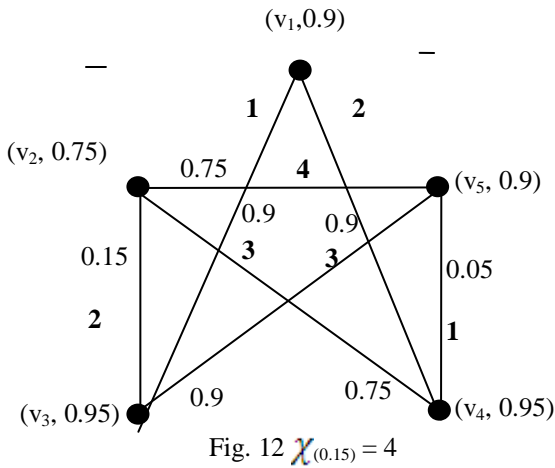
$v_1 \quad v_2 \quad v_3 \quad v_4 \quad v_5$

$$E_4 = \begin{bmatrix} v_1 & 0 & 0 & e_1 & e_2 & 0 \\ v_2 & 0 & 0 & e_4 & e_6 & e_3 \\ v_3 & e_1 & e_4 & 0 & 0 & e_5 \\ v_4 & e_2 & e_6 & 0 & 0 & 0 \\ v_5 & 0 & e_3 & e_5 & 0 & 0 \end{bmatrix}$$

Adjacent matrix 8



Now for α cut value 0.75 we find the graph $G_{0.75}$ (Fig. 13). Then we proper color all the edges of this graph and find the chromatic number of this graph is 3. For $\alpha = 0.9$ Fuzzy graph $G = (V, \sigma, \mu)$ where $\sigma = \{0.9, 0.95, 0.95, 0.9\}$ and



For α cut value 0.15 we find the graph $G_{0.15}$ (Fig. 12). Then we proper color all the edges of this graph and find the chromatic number of this graph is 4. For $\alpha = 0.75$ Fuzzy graph $G = (V, \sigma, \mu)$ where $\sigma = \{0.9, 0.75, 0.95, 0.95, 0.9\}$

$$\mu_6 = \begin{bmatrix} v_1 & v_2 & v_3 & v_4 & v_5 \\ v_1 & 0.0 & 0.0 & 0.9 & 0.9 & 0.0 \\ v_2 & 0.0 & 0.0 & 0.0 & 0.0 & 0.0 \\ v_3 & 0.9 & 0.0 & 0.0 & 0.0 & 0.9 \\ v_4 & 0.0 & 0.0 & 0.0 & 0.0 & 0.0 \\ v_5 & 0.0 & 0.0 & 0.9 & 0.0 & 0.0 \end{bmatrix}$$

Adjacent matrix 11

$$\mu_5 = \begin{bmatrix} v_1 & v_2 & v_3 & v_4 & v_5 \\ v_1 & 0.0 & 0.0 & 0.9 & 0.9 & 0.0 \\ v_2 & 0.0 & 0.0 & 0.0 & 0.75 & 0.75 \\ v_3 & 0.9 & 0.0 & 0.0 & 0.0 & 0.9 \\ v_4 & 0.75 & 0.75 & 0.0 & 0.0 & 0.0 \\ v_5 & 0.0 & 0.75 & 0.9 & 0.0 & 0.0 \end{bmatrix}$$

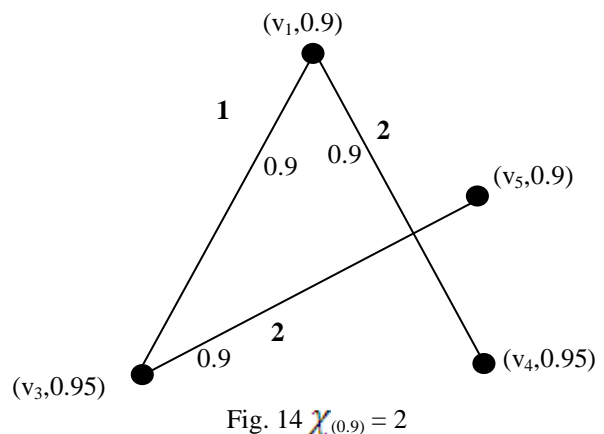
Adjacent matrix 9

$$E_6 = \begin{bmatrix} v_1 & v_2 & v_3 & v_4 & v_5 \\ v_1 & 0 & 0 & e_1 & e_2 & 0 \\ v_2 & 0 & 0 & 0 & 0 & 0 \\ v_3 & e_1 & 0 & 0 & 0 & e_5 \\ v_4 & 0 & 0 & 0 & 0 & 0 \\ v_5 & 0 & 0 & e_5 & 0 & 0 \end{bmatrix}$$

Adjacent matrix 12

$$E_5 = \begin{bmatrix} v_1 & v_2 & v_3 & v_4 & v_5 \\ v_1 & 0 & 0 & e_1 & e_2 & 0 \\ v_2 & 0 & 0 & 0 & e_6 & e_3 \\ v_3 & e_1 & 0 & 0 & 0 & e_5 \\ v_4 & e_2 & e_6 & 0 & 0 & 0 \\ v_5 & 0 & e_3 & e_5 & 0 & 0 \end{bmatrix}$$

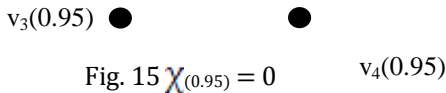
Adjacent matrix 10



For α cut value 0.9 we find the graph $G_{0.9}$ (Fig. 14). Then we proper color all the edges of this graph and find the chromatic number of this graph is 2.

For $\alpha= 0.95$ Fuzzy graph $G = (V, \sigma, \mu)$ where $\sigma = \{0.95\}$ and

$$\mu_{0.95} = \begin{matrix} & v_3 & v_4 \\ \begin{matrix} v_3 \\ v_4 \end{matrix} & \begin{bmatrix} 0.0 & 0.0 \\ 0.0 & 0.0 \end{bmatrix} \end{matrix}$$



For α cut value 0.95 we find the graph $G_{0.95}$ (Fig. 15). Then we proper color all the edges of this graph and find the chromatic number of this graph is 0.

In the above example, five crisp graph $G_\alpha = (V_\alpha, E_\alpha)$ are obtained by considering different values of α . Now for the edge chromatic number χ_α for any α , it can be shown that the chromatic number of fuzzy graph G is $\chi(G) = \{(4, 0.05), (4, 0.15), (3, 0.75), (2, 0.9), (0, 0.95)\}$

IV. CONCLUSION

In this paper we find the complement fuzzy graph and color all the edges of that complement fuzzy graph. Here edge chromatic number depends on α cut value. In our next paper, we shall try to design an algorithm on edge coloring function to any fuzzy graph.

REFERENCES

[1] Mordeson J.N., Peng C.S., Operations on fuzzy graphs, Information Sciences, 79 (1994), 159-170.

[2] Rosenfield A., Fuzzy graphs, In fuzzy sets and their Applications to cognitive and decision processes, Zadeh. L.A., Fu, K.S., Shimura, M., Eds; Academic Press, New York (1975) 77-95.

[3] Yeh R.T., Bang S. Y. Fuzzy relations, Fuzzy graphs and their applications to clustering analysis, In Fuzzy Sets and their Applications to Cognitive and Decision processes, Zadeh, L.A., Fu, K.S., Shimura, M., Eds; Academic Press, New York (1975) 125-149

[4] Bhattacharya P., Suraweera F, An algorithm to compute the max-min powers and property of fuzzy graphs, Pattern Recognition Lett. 12 (1991), 413 -420.

[5] Bhutani K.R., On automorphisms of fuzzy graphs, Pattern Recognition Lett. 9 (1989) 159- 162

[6] Mordeson J. N., Fuzzy line graphs, Pattern Recognition Lett. 4 (1993) 381-384.

[7] Sunitha M.S., Vijaya Kumar A., Complement of a Fuzzy graph, Indian J. pure appl. Math., 33(9): 1451-1464, September 2002.

[8] Dey Arindam, Ghosh Dhrubajyoti and Pal Anita, Operations on Complement of Fuzzy Graph, RAMES March, 2012, ISBN 978- 93 -5067-395-9.

[9] M.S. Sunitha, Studies on Fuzzy Graphs, Thesis of Doctor Of Philosophy, Cochin University of Sciences and Technology, Department of Mathematics.

A class of Harmonic Univalent Functions with Varying Arguments Defined by Generalized Derivative Operator

Y. P. Yadav, N. D. Sangle

¹(Research Scholar, Department of Mathematics, Singhania University, Pachari Bari,
Dist-Jhunjhunu, Rajasthan-333515)

²(Department of Mathematics, Annasaheb Dange College of Engineering,
Ashta, Sangali, (M.S) India 416 301)

Abstract: In this paper, we have introduced a new class of complex valued harmonic functions which are orientation preserving and univalent in the open unit disc and are related to uniformly convex functions. Coefficient bounds, neighborhood and extreme points for the functions belonging to this class are obtained.

2000 AMS subject classification: Primary 30C45, Secondary 30C50, 30C55.

Key Words: Harmonic, derivative operator, univalent, Neighborhoods, extreme points.

I. INTRODUCTION

A continuous complex-valued function $f(z) = u + iv$ is defined in a simply-connected complex domain D is said to be harmonic in D if both u and v are real harmonic in D . Such functions can be expressed as

$$f(z) = h(z) + \overline{g(z)} \quad (1.1)$$

where $h(z)$ and $g(z)$ are analytic in D . We call $h(z)$ the analytic part and $g(z)$ the co-analytic part of $f(z)$. A necessary and sufficient condition for $f(z)$ to be locally univalent and sense preserving in D is that $|\overline{h'(z)}| > |g'(z)|$ for all z in D , Clunie and Shell-Smail [2]. Let H be the class of functions of the form (1.1) that are harmonic univalent and sense-preserving in the unit disk $U = \{z : |z| < 1\}$ for which $f(0) = f_z(0) - 1 = 0$. Then for $f(z) = h(z) + \overline{g(z)} \in H$,

we may express the analytic functions $h(z)$ and $g(z)$ as

$$h(z) = z + \sum_{k=2}^{\infty} a_k z^k, \quad g(z) = \sum_{k=1}^{\infty} b_k z^k, \quad z \in U, \quad |b_1| < 1 \quad (1.2)$$

In 1984, Clunie and Sheil-Small [2] investigated the class S_H as well as its geometric subclasses and obtained some coefficient bounds. Since then, there have been several related papers on S_H and its subclasses. Now we will introduce a generalized derivative operator for $f(z) = h(z) + \overline{g(z)}$ given by (1.2). For fixed positive natural m and $\lambda_2 \geq \lambda_1 \geq 0$,

$$D_{\lambda_1, \lambda_2}^{m, k} f(z) = D_{\lambda_1, \lambda_2}^{m, k} h(z) + \overline{D_{\lambda_1, \lambda_2}^{m, k} g(z)}, \quad z \in U \quad (1.3)$$

where

$$D_{\lambda_1, \lambda_2}^{m, k} h(z) = z + \sum_{k=2}^{\infty} \left(\frac{1 + (\lambda_1 + \lambda_2)(k-1)}{1 + \lambda_2(k-1)} \right)^m a_k z^k$$

and

$$D_{\lambda_1, \lambda_2}^{m, k} g(z) = \sum_{k=1}^{\infty} \left(\frac{1 + (\lambda_1 + \lambda_2)(k-1)}{1 + \lambda_2(k-1)} \right)^m b_k z^k.$$

We note that by specializing the parameters, especially when $\lambda_1 = \lambda_2 = 0$, $D_{\lambda_1, \lambda_2}^{m, k}$ reduces to D_m which introduced by Salagean in [6].

Now we will introduce the following definition.

Definition 1.1. For $0 \leq l < 1$, let $G_H(l, m, k, \lambda_1, \lambda_2)$ denote the subfamily of starlike harmonic functions $f(z) \in H$ of the form (1.1) such that

$$\operatorname{Re} \left\{ \left(1 + e^{i\psi} \right) \frac{z \left(D_{\lambda_1, \lambda_2}^{m, k} f(z) \right)' }{z' \left(D_{\lambda_1, \lambda_2}^{m, k} f_t(z) \right)} - e^{i\psi} \right\} \geq l \quad \text{for } z \in U, \quad (1.4)$$

Where $f_t(z) = (1-t)z + t(h(z) + \overline{g(z)})$,

$$\left(D_{\lambda_1, \lambda_2}^{m, k} f(z) \right)' = \frac{d}{d\theta} \left(D_{\lambda_1, \lambda_2}^{m, k} f(re^{i\theta}) \right), \frac{d}{d\theta} (z = re^{i\theta}).$$

We also let $V_H(l, m, k, \lambda_1, \lambda_2) = G_H(l, m, k, \lambda_1, \lambda_2) \cap V_H$ where V_H is the class of harmonic functions with varying arguments introduced by Jahangiri and Silverman [3] consisting of functions $f(z)$ of the form (1.1) in H for which there exists a real number ϕ such that

$$\eta_k + (k-1)\phi = \pi \pmod{2\pi}, \quad \delta_k + (k-1)\phi = 0 \pmod{2\pi} \quad (k \geq 2), \quad (1.5)$$

where $\eta_k = \arg(a_k)$ and $\delta_k = \arg(b_k)$. The same class introduced in [4] with different differential operator.

In this paper, we obtain a sufficient coefficient condition for functions $f(z)$ given by (1.2) to be in the class $G_H(l, m, k, \lambda_1, \lambda_2)$. It is shown that this coefficient condition is necessary also for functions belonging to the class $V_H(l, m, k, \lambda_1, \lambda_2)$. Further, extreme points for functions in $V_H(l, m, k, \lambda_1, \lambda_2)$ are also obtained.

II. MAIN RESULT

We begin deriving a sufficient coefficient condition for the functions belonging to the class $G_H(l, m, k, \lambda_1, \lambda_2)$. This result is contained in the following.

Theorem 2.1. Let $f(z) = h(z) + \overline{g(z)}$ given by (1.2). Furthermore, let

$$\sum_{k=2}^{\infty} \left(\frac{2k-t-lt}{1-l} |a_k| + \frac{2k+t+lt}{1-l} |b_k| \right) \left(\frac{1+(\lambda_1+\lambda_2)(k-1)}{1+\lambda_2(k-1)} \right)^m \leq 1 - \frac{2+t+lt}{3-l} b_1 \quad (2.1)$$

where $0 \leq l < 1$, then $f \in G_H(l, m, k, \lambda_1, \lambda_2)$.

Proof: We first show that if the inequality (2.1) holds for the coefficients of $f(z) = h(z) + \overline{g(z)}$, then the required condition (1.4) is satisfied. Using (1.3) and (1.4), we can write

$$\operatorname{Re} \left\{ \left(1 + e^{i\psi} \right) \frac{z \left(D_{\lambda_1, \lambda_2}^{m, k} h(z) \right)' - z \left(D_{\lambda_1, \lambda_2}^{m, k} g(z) \right)'}{(1-t)z + t \left(D_{\lambda_1, \lambda_2}^{m, k} h(z) + \overline{D_{\lambda_1, \lambda_2}^{m, k} g(z)} \right)} - e^{i\psi} \right\} = \operatorname{Re} \left\{ \frac{A(z)}{B(z)} \right\} \quad (2.2)$$

where

$$A(z) = \left(1 + e^{i\psi} \right) \left[z \left(D_{\lambda_1, \lambda_2}^{m, k} h(z) \right)' - z \left(D_{\lambda_1, \lambda_2}^{m, k} g(z) \right)' \right] - e^{i\psi} \left[(1-t)z + t \left(D_{\lambda_1, \lambda_2}^{m, k} h(z) + \overline{D_{\lambda_1, \lambda_2}^{m, k} g(z)} \right) \right]$$

$$B(z) = (1-t)z + t \left(D_{\lambda_1, \lambda_2}^{m, k} h(z) + \overline{D_{\lambda_1, \lambda_2}^{m, k} g(z)} \right).$$

In view of the simple assertion that $\operatorname{Re}(w) \geq l$ if and only if $|1-l+w| \geq |1+l-w|$, it suffices to show that

$$|A(z) + (1-l)B(z)| - |A(z) - (1+l)B(z)| \geq 0. \quad (2.3)$$

Substituting for $A(z)$ and $B(z)$ the appropriate expressions in (2.3), we get

$$\begin{aligned} & |A(z) + (1-l)B(z)| - |A(z) - (1+l)B(z)| \\ & \geq 2(1-l)|z| - \sum_{k=2}^{\infty} (4k-2t-2lt) \left(\frac{1+(\lambda_1+\lambda_2)(k-1)}{1+\lambda_2(k-1)} \right)^m |a_k| |z|^k \end{aligned}$$

$$\begin{aligned}
 & -\sum_{k=2}^{\infty} (4k + 2t + 2lt) \left(\frac{1 + (\lambda_1 + \lambda_2)(k-1)}{1 + \lambda_2(k-1)} \right)^m |b_k| |z|^k - 4|b_1| - 2t|b_1| - 2lt|b_1| \\
 \geq & 2(1-l) \left\{ 1 - \frac{2+t+lt}{1-l} |b_1| - \sum_{k=2}^{\infty} \left(\frac{2k-t-lt}{1-l} \left(\frac{1 + (\lambda_1 + \lambda_2)(k-1)}{\lambda_2(k-1)} \right)^m |a_k| \right. \right. \\
 & \left. \left. + \frac{2k+t+lt}{1-l} \left(\frac{1 + (\lambda_1 + \lambda_2)(k-1)}{\lambda_2(k-1)} \right)^m |b_k| \right) \right\} \geq 0
 \end{aligned}$$

by virtue of the inequality (2.1). This implies that $f(z) \in G_H(l, m, k, \lambda_1, \lambda_2)$.

Now we obtain the necessary and sufficient condition for function $f(z) = h(z) + \overline{g(z)}$ be given with condition (1.5).

Theorem 2.2. Let $f(z) = h(z) + \overline{g(z)}$ be given by (2). Then $f(z) \in V_H(l, m, k, \lambda_1, \lambda_2)$ if and only if

$$\sum_{k=2}^{\infty} \left[\frac{2k-t-lt}{1-l} |a_k| + \frac{2k+t+lt}{1-l} |b_k| \right] \left[\left(\frac{1 + (\lambda_1 + \lambda_2)(k-1)}{\lambda_2(k-1)} \right)^m \right] \leq 1 - \frac{2+t+lt}{3-l} |b_1| \quad (2.4) \text{ where}$$

$0 \leq l < 1$.

Proof. Since $V_H(l, m, k, \lambda_1, \lambda_2) \subset G_H(l, m, k, \lambda_1, \lambda_2)$, we only need to prove the necessary part of the theorem. Assume that $f(z) \in V_H(l, m, k, \lambda_1, \lambda_2)$, then by virtue of (1.3) to (1.4), we obtain

$$\operatorname{Re} \left\{ \left(1 + e^{i\psi} \right) \frac{z \left(D_{\lambda_1, \lambda_2}^{m, k} h(z) \right)' - \overline{z \left(D_{\lambda_1, \lambda_2}^{m, k} g(z) \right)'}}{(1-t)z + t \left(D_{\lambda_1, \lambda_2}^{m, k} h(z) + \overline{D_{\lambda_1, \lambda_2}^{m, k} g(z)} \right)} - (e^{i\psi} + l) \right\} \geq 0. \quad (2.5)$$

The above inequality is equivalent to

$$\begin{aligned}
 & \operatorname{Re} \left\{ \left(1 + e^{i\psi} \right) \left[z \left(D_{\lambda_1, \lambda_2}^{m, k} h(z) \right)' - \overline{z \left(D_{\lambda_1, \lambda_2}^{m, k} g(z) \right)' } \right] - (e^{i\psi} + l) \left[(1-t)z + t \left(D_{\lambda_1, \lambda_2}^{m, k} h(z) + \overline{D_{\lambda_1, \lambda_2}^{m, k} g(z)} \right) \right] \right\} \\
 & \quad \times \left((1-t)z + t \left(D_{\lambda_1, \lambda_2}^{m, k} h(z) + \overline{D_{\lambda_1, \lambda_2}^{m, k} g(z)} \right) \right)^{-1} \\
 & = \operatorname{Re} \left\{ (1-l)z + \left(\sum_{k=2}^{\infty} \left[k(1 + e^{i\psi}) - e^{i\psi}t - lt \right] \left(\frac{1 + (\lambda_1 + \lambda_2)(k-1)}{1 + \lambda_2(k-1)} \right)^m a_k z^k \right. \right. \\
 & \quad \left. \left. - \sum_{k=1}^{\infty} \left[k(1 + e^{i\psi}) + e^{i\psi}t + lt \right] \left(\frac{1 + (\lambda_1 + \lambda_2)(k-1)}{1 + \lambda_2(k-1)} \right)^m b_k z^{-k} \right) \right. \\
 & \quad \left. \times \left(z + t \sum_{k=1}^{\infty} \left(\frac{1 + (\lambda_1 + \lambda_2)(k-1)}{1 + \lambda_2(k-1)} \right)^m a_k z^k + t \sum_{k=1}^{\infty} \left(\frac{1 + (\lambda_1 + \lambda_2)(k-1)}{1 + \lambda_2(k-1)} \right)^m b_k z^{-k} \right)^{-1} \right\} \\
 & = \operatorname{Re} \left\{ (1-l) + \left(\sum_{k=2}^{\infty} \left[k(1 + e^{i\psi}) - e^{i\psi}t - lt \right] \left(\frac{1 + (\lambda_1 + \lambda_2)(k-1)}{1 + \lambda_2(k-1)} \right)^m a_k z^{k-1} \right. \right.
 \end{aligned}$$

$$\left. -\frac{\bar{z}}{z} \sum_{k=1}^{\infty} \left[k(1+e^{i\psi}) + e^{i\psi}t + lt \right] \left(\frac{1+(\lambda_1+\lambda_2)(k-1)}{1+\lambda_2(k-1)} \right)^m b_k \bar{z}^{-k-1} \right) \\ \times \left(1+t \sum_{k=1}^{\infty} \left(\frac{1+(\lambda_1+\lambda_2)(k-1)}{1+\lambda_2(k-1)} \right)^m a_k z^{k-1} + t \frac{\bar{z}}{z} \sum_{k=1}^{\infty} \left(\frac{1+(\lambda_1+\lambda_2)(k-1)}{1+\lambda_2(k-1)} \right)^m b_k \bar{z}^{-k-1} \right)^{-1} \Bigg\} \geq 0.$$

This condition must hold for all values of z , such that $|z|=r < 1$. Upon choosing ϕ according to (1.5) and noting that $\operatorname{Re}(-e^{i\psi}) \geq -|e^{i\psi}| = -1$, the above inequality reduces to

$$(1-l) + (2+t+lt)b_1 - \left(\sum_{k=2}^{\infty} \left[k(1+e^{i\psi}) - e^{i\psi}t - lt \right] \left(\frac{1+(\lambda_1+\lambda_2)(k-1)}{1+\lambda_2(k-1)} \right)^m |a_k| r^{k-1} \right. \\ \left. + \left[k(1+e^{i\psi}) + e^{i\psi}t + lt \right] \left(\frac{1+(\lambda_1+\lambda_2)(k-1)}{1+\lambda_2(k-1)} \right)^m |b_k| r^{k-1} \right) \\ \times \left(1+t \sum_{k=1}^{\infty} \left(\frac{1+(\lambda_1+\lambda_2)(k-1)}{1+\lambda_2(k-1)} \right)^m |a_k| r^{k-1} + t \sum_{k=1}^{\infty} \left(\frac{1+(\lambda_1+\lambda_2)(k-1)}{1+\lambda_2(k-1)} \right)^m |b_k| r^{k-1} \right)^{-1} \Bigg\} \geq 0. \quad (2.6)$$

If (2.4) does not hold, then the numerator in (2.6) is negative for r sufficiently close to 1. Therefore, there exists a point $z_0 = r_0$ in $(0,1)$ for which the quotient in (2.6) is negative. This contradicts our assumption that $f(z) \in V_H(l, m, k, \lambda_1, \lambda_2)$. We thus conclude that it is both necessary and sufficient that the coefficient bound inequality (2.4) holds true when $f(z) \in V_H(l, m, k, \lambda_1, \lambda_2)$.

This completes the proof of Theorem 2.2.

Theorem 2.3. The closed convex hull of $f(z) \in V_H(l, m, k, \lambda_1, \lambda_2)$ (denoted by $clcoV_H(l, m, k, \lambda_1, \lambda_2)$) is

$$\left\{ f(z) = z + \sum_{k=2}^{\infty} |a_k| z^k + \overline{\sum_{k=1}^{\infty} |b_k| z^k} : \sum_{k=2}^{\infty} k[|a_k| + |b_k|] < 1 - b_1 \right\}$$

By setting

$$\lambda_k = \frac{1-l}{(2k-t-lt) \left(\frac{1+(\lambda_1+\lambda_2)(k-1)}{\lambda_2(k-1)} \right)^m} \text{ and } \mu_k = \frac{1+l}{(2k+t+lt) \left(\frac{1+(\lambda_1+\lambda_2)(k-1)}{\lambda_2(k-1)} \right)^m}, \text{ then}$$

for b_1 fixed, the extreme points for $clcoV_H(l, m, k, \lambda_1, \lambda_2)$ are

$$\{z + \lambda_k x z^k + \overline{b_1 z}\} \cup \{z + \overline{b_1 z} + \mu_k x z^k\} \quad (2.7)$$

where $k \geq 2$ and $|x| = 1 - |b_1|$.

Proof: Any function $f(z)$ in $clcoV_H(l, m, k, \lambda_1, \lambda_2)$ may be expressed as

$$f(z) = z + \sum_{k=2}^{\infty} |a_k| e^{i\eta k} z^k + \overline{b_1 z} + \sum_{k=1}^{\infty} |b_k| e^{i\delta k} z^k$$

where the coefficients satisfy the inequality (2.1). Set $h_1(z) = z$, $g_1(z) = b_1z$, $h_k(z) = z + \lambda_k e^{i\eta k} z^k$, $g_k(z) = b_1z + \mu_k e^{i\delta k} z^k$ for $k = 2, 3, 4, \dots$. Writing $\chi_k = \frac{|a_k|}{\lambda_k}$, $Y_k = \frac{|b_k|}{\mu_k}$, $k = 2, 3, 4, \dots$ and $\chi_1 = 1 - \sum_{k=2}^{\infty} \chi_k$;

$Y_1 = 1 - \sum_{k=2}^{\infty} Y_k$, we get

$$f(z) = \sum_{k=1}^{\infty} (\chi_k h_k(z) + Y_k g_k(z)).$$

In particular, setting $f_1(z) = z + \overline{b_1}z$ and $f_k(z) = z + \lambda_k xz^k + \overline{b_1}z + \overline{\mu_k y}z^k$, ($k \geq 2, |x| + |y| = 1 - |b_1|$),

we see that extreme points of $clco f(z) \in V_H(l, m, k, \lambda_1, \lambda_2) \subset \{f_k(z)\}$.

To see that $f_1(z)$ is not in extreme point, note that $f_1(z)$ may written as

$$f_1(z) = \frac{1}{2} \{f_1(z) + \lambda_2(1 - |b_1|)z^2\} + \frac{1}{2} \{f_1(z) - \lambda_2(1 - |b_1|)z^2\}$$

a convex linear combination of functions in $clcoV_H(l, m, k, \lambda_1, \lambda_2)$.

To see that f_m is not an extreme point if both $|x| \neq 0$ and $|y| \neq 0$, we will show that it can then also be expressed as a convex linear combinations of functions in $clcoV_H(l, m, k, \lambda_1, \lambda_2)$. Without loss of generality, assume $|x| \geq |y|$.

Choose $\epsilon > 0$ small enough so that $\epsilon > \left| \frac{x}{y} \right|$. Set $A = 1 + \epsilon$ and $B = 1 + \left| \frac{\epsilon x}{y} \right|$. We then see that both

$$t_1(z) = z + \lambda_k Axz^k + \overline{b_1}z + \overline{\mu_k y}Bz^k \text{ and}$$

$$t_2(z) = z + \lambda_k (2 - A)xz^k + \overline{b_1}z + \overline{\mu_k y}(2 - B)z^k \text{ are in } clcoV_H(l, m, k, \lambda_1, \lambda_2) \text{ and that}$$

$$f_k(z) = \frac{1}{2} \{t_1(z) + t_2(z)\}.$$

The extremal coefficient bounds show that functions of the form (12) are the extreme points for $clcoV_H(l, m, k, \lambda_1, \lambda_2)$, and so the proof is complete.

Following Avici and Zlotkiewicz [1] and Ruscheweyh [5], we refer to the δ -neighborhood of the functions $f(z)$ defined by (1.2) to be the set of functions F for which

$$N_\delta(f) = \left\{ F(z) = z + \sum_{k=2}^{\infty} A_k z^k + \sum_{k=1}^{\infty} \overline{B_k} z^k, \sum_{k=2}^{\infty} k (|a_k - A_k| + |b_k - B_k| + |b_1 - B_1|) \leq \delta \right\} \quad (2.8)$$

In our case, let us define the generalized δ -neighborhood of $f(z)$ to be the set

$$N_\delta(f) = \left\{ F(z) : \sum_{k=2}^{\infty} \left(\frac{1 + (\lambda_1 + \lambda_2)(k-1)}{\lambda_2(k-1)} \right)^m [(2k - t - lt)|a_k - A_k| + (2k + t + lt)|b_k - B_k|] + (1-l)|b_1 - B_1| \leq (1-l)\delta \right\}. \quad (2.9)$$

Theorem 2.4. Let $f(z)$ be given by (1.2). If $f(z)$ satisfies the conditions

$$\sum_{k=2}^{\infty} k(2k - t - lt)|a_k| \left(\frac{1 + (\lambda_1 + \lambda_2)(k-1)}{\lambda_2(k-1)} \right)^m$$

$$+\sum_{k=1}^{\infty} k(2k+t+lt)|b_k|\left(\frac{1+(\lambda_1+\lambda_2)(k-1)}{\lambda_2(k-1)}\right)^m \leq (1-l), \quad (2.10)$$

where $0 \leq l < 1$ and $\delta = \frac{1-l}{3-t-lt} \left(1 - \frac{2+t+lt}{1-l}|b_1|\right)$ (2.11)

then $N(f) \subset G_H(l, m, k, \lambda_1, \lambda_2)$.

Proof. Let $f(z)$ satisfy (15) and $F(z)$ be given by

$$F(z) = z + \overline{B_1}z + \sum_{k=2}^{\infty} (A_k z^k + \overline{B_k} z^k)$$

which belong to to $N(f)$. We obtain

$$\begin{aligned} & (2+t+lt)|B_1| + \sum_{k=2}^{\infty} ((2k-t-lt)|A_k| + (2k+t+lt)|B_k|) \left(\frac{1+(\lambda_1+\lambda_2)(k-1)}{\lambda_2(k-1)}\right)^m \\ & \leq (2+t+lt)|B_1 - b_1| + (2+t+lt)|b_1| \\ & \quad + \sum_{k=2}^{\infty} ((2k-t-lt)|A_k - a_k| + (2k+t+lt)|B_k - b_k|) \left(\frac{1+(\lambda_1+\lambda_2)(k-1)}{\lambda_2(k-1)}\right)^m \\ & \quad + \sum_{k=2}^{\infty} ((2k-t-lt)|a_k| + (2k+t+lt)|b_k|) \left(\frac{1+(\lambda_1+\lambda_2)(k-1)}{\lambda_2(k-1)}\right)^m \\ & \leq (1-l)\delta + (2+t+lt)|b_1| \\ & \quad + \frac{1}{3-l} \sum_{k=2}^{\infty} k((2k-t-lt)|a_k| + (2k+t+lt)|b_k|) \left(\frac{1+(\lambda_1+\lambda_2)(k-1)}{\lambda_2(k-1)}\right)^m \\ & \leq (1-l)\delta + (2+t+lt)|b_1| + \frac{1}{3-l} [(1-l) - (2+t+lt)|b_1|] \leq 1-l. \end{aligned}$$

Hence for $\delta = \frac{1-l}{3-l} \left(1 - \frac{2+t+lt}{1-l}|b_1|\right)$, we infer that $F(z) \in G_H(l, m, k, \lambda_1, \lambda_2)$ which concludes the proof Theorem 2.4.

REFERENCES

- [1] Y. Avici and E. Zlotkiewicz, On harmonic univalent mappings, *Ann. Univ. Mariae Curie-Sklodowska Sect. A* **44** (1990), 1-7.
- [2] J. Clunie and T. Shell-Smail, Harmonic univalent functions, *Ann. Acad. Sci. Fenn. Ser. A. I. Math.*, **9**:(1984), 3-25.
- [3] J. M. Jahangiri and H. Silverman, Harmonic univalent functions with varying arguments, *Int. J. Appl. Math.* **8**(3):(2002), 267-275.
- [4] G.Murugusundaramoorthy, K. Vijaya, and R. K. Raina, A subclass of harmonic functions with varying arguments defined by Dziok-Srivastava operator, *Archivum Mathematicum*. **45** (2009), 37-46.
- [5] S. Ruscheweyh. Neighborhoods of univalent functions, *Proc. Amer. Math. Soc.* **81** (1981), 521-528.
- [6] G. S. Salagean, Subclass of univalent functions, Lecture Notes in Math., *Springer-Verlag, Berlin, Heidelberg and New York.*, **1013**:(1983), 362-372.

Image Watermarking Algorithm in DWT Domain

Mr. Chaudhari M. A¹, Prof. Gunjal B. L²

¹ME Computer Engineering
Amrutvahini College of Engineering Sangamner(MS),422605
²Assit.Prof.Computer Department
Amrutvahini College of Engineering Sangamner(MS),422605

Abstract: To authenticate the given image is important task in the internet communication. For this the technique is proposed in this paper. The original image is first converted into the gray scale image. Then consider the Y component of the given image get divided into different block size i.e. (2x2, 4x4 or 8x8). The Y component is get divided into 2 level decomposition. With the help of the canny edge detector we can get features to generate the watermark. By using this we get the watermark which is used for embedding in the given image. The arnold transform is used to remove the space relativity in DWT. After extraction process with the help of key we authenticate the given image. There is no degradation to the original image. Experiments shows that system is useful to get authentication requirement.

Keywords: Discrete Wavelet Transform; contour authentication;

I. INTRODUCTION

As the electronic media is get popular for communication, the secure communication is the important task in electronic media. Now a days there are large techniques available with different technologies. among them authentication is the important task for secure communication. On the basis of authentication we can able to find out the authorized user, image or data.

There are number of existing technique which provides the authentication on which we can find the authorized data. The most important technique used for digital data authentication is encryption i.e. public key encryption which is also called traditional method of authentication. Another technique available is watermarking. Digital watermarking is a technique which hide some logo or data in the given image so that we prevent copyright, integrity and/or the authenticity of the original data [1-2]. Usually, a robust watermarking is used to protect the copyright while a fragile or semi-fragile watermarking is used to verify the authenticity [3-4]. Authentication of image data is a challenging task. Content modification or tampering is defined as an object appearance or disappearance, a modification to an object position, or changes to texture, color or edges. Image watermarking algorithm used to detect tampering has several essential properties. First is transparency. The embedding processing should not degrade the quality of the original digital media and should be perceptually invisible to maintain its protective secrecy and sensitivity. The embedded watermark is robust to resist normal image processing (such as JPEG compression) while it is fragile to malicious tampering to image content. The watermark is embedded in a secure way and it can't be removed illegally [5-10].

We propose the new technique of authentication in which we can use the watermark which is generated from the same cover image. Watermark is generated with the help of DWT method for the contour image and apply the arnold transform for the given image. The watermark which is generated is stored into LH or HL band so we get the standard result.

This paper is organized as follows: Section 1 introduces related works. Section 2 details the system diagram & workflow steps. Section 3 details the detailed steps. Experiments are presented in section 4. Finally, conclusions are drawn in section 5.

II. SYSTEM ARCHITECTURE

The design of given system is basically divided into the two steps. In this first is watermark embedding and second watermark extraction. As we are going in detailed we found some properties of image make the watermark embedding as easy task.

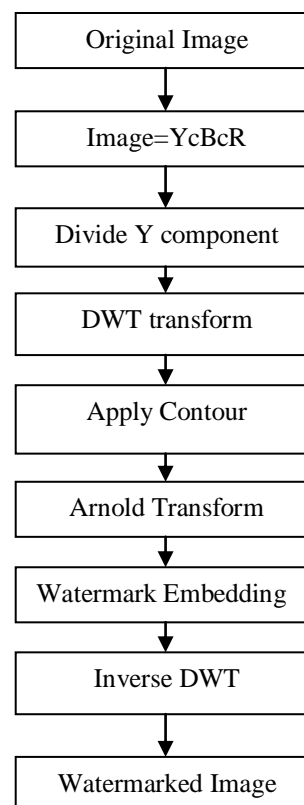


Figure 1: Watermark Embedding process

The above diagram for the watermark embedding and details of the diagram are given in the mathematical model.

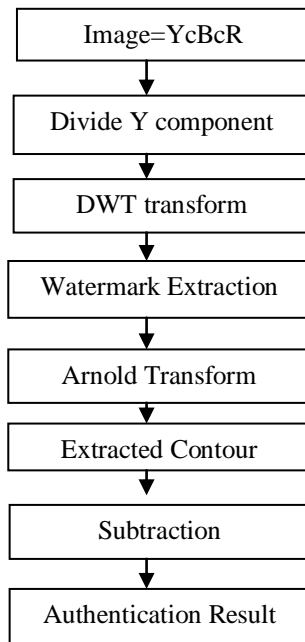


Figure 2: Watermark Extraction Process

As watermark is embedded we need to extract the watermark. Block diagram for the watermark extraction are shown above.

III. DETAILED DESIGN

1. Watermark Embedding Process

The watermark embedding process is shown with following steps:

- Step1. Original image is converted into YcBcR color space.
- Step2. The subdivision Y is divided into 4x4,2x2 and 8x8 image blocks. Then perform two-level DWT transform block by block.
- Step3. The image contour is calculated based on sub-band image LL2 using Canny edge detector and then filtered to get a binary image as a watermark.
- Step4. Watermark image is Arnold transformed to increases the security of watermarking algorithm greatly.
- Step5. The middle coefficients of first level DWT transform HL1 and LH1 are selected to embed watermark bits.
- Step6. Apply the inverse DWT transform to all the blocks to get the watermarked image.

After embedding the watermark PSNR is calculated for all these three blocks size.

2. Watermark Extraction Process

- Step1. Original image is executed two level DWT transforms to calculate the contour image W using Canny calculator just like the operations in watermark embedding.
- Step2. The watermark information is extracted from middle coefficients which are selected to embed watermark . Construct the watermark image by

the inverse displacing, and we get the extracted watermark image W*.

$$D(i,j)=|W(i,j)-W^*(i,j)|$$

where i,j denotes the rows and column number.

Step3. The calculated image and extracted image is subtracted, the result will be used to authenticate image content.

IV. EXPERIMENTAL RESULTS

The experiments in this paper are tested with MATLAB 7.0. The original image used to test is a 512x512 image.

1. PSNR

The PSNR rates for all three images are calculated. From the results we found that 8x8 block shows good authentication results. Also if we go for compression the PSNR rate is decreases.

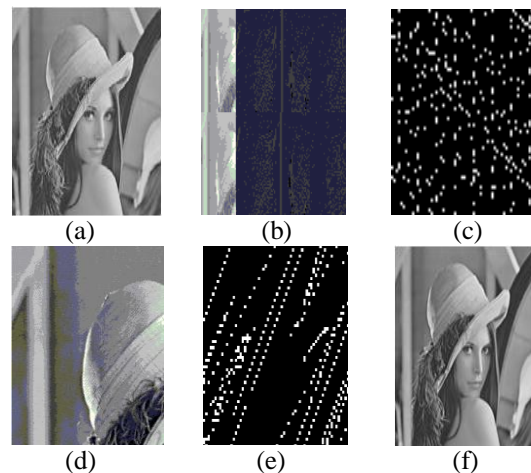


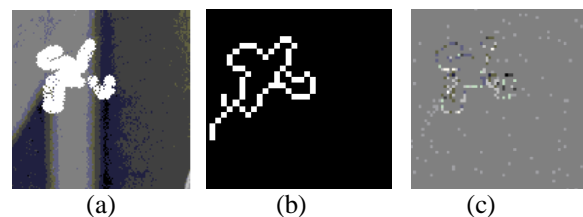
Figure 3: Perceptibility Test (a)Original Image (b) 2-level DWT (c) Contour Image (d) Selected area (e) Inverse DWT (f) Watermarked Image

TABLE1: COMPARISION OF PSNR

Block size	Watermark Region	PSNR
2x2	LH or HL	47.94
4x4	LH or HL	58.36
8x8	LH or HL	65.07

2. Operational Test:

In the different operational test we found the given algorithm is best for paste attacked image.



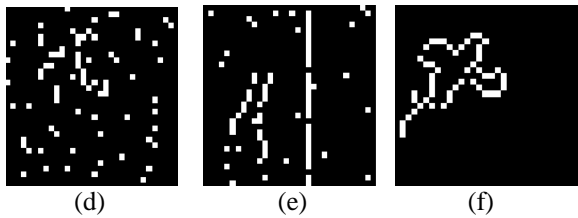


Figure 4: (a) Original Image (b) Canny Image (c) Gray scale Image (d) Arnold Transfer (e) Inverse DWT Authentication

From the above results we can say that our algorithm is sensitive for the authentication of watermarked image.

V. CONCLUSION

In this paper we used DWT transform method for watermark embedding. Also due to arnold transform space relativity is get reduced. From the above result we can say that algorithm which is proposed here is good as compared to previous one.

In this particular algorithm we can use any logo or another image as the watermark to embed in the given region. So it is easy to improve the result by such experiment.

REFERENCES

- [1] I. J. Cox, M. L. Miller and J. A. Bloom, Digital Watermarking, New York: Academic Press , 2002.
- [2] I. Cox, J. Kilian, F. T. Leighton and T. Shamoan, "Secure spread spectrum watermarking for ultimedia," IEEE Transactions on Image Processing, vol. 6, pp. 1673-1687, December 1997.
- [3] S. Walton, "Authentication for a slippery new age," Dr. Dobb's Journal, vol. 20, no. 4, pp. 18-26, April 1995.
- [4] C. Lu and H. Liao, "Multipurpose watermarking for image authentication and protection," IEEE Transactions on Image Processing, vol. 10, no. 10, pp. 1579- 1592, October 2001.
- [5] C. Y. Lin and S. F. Chang. "Semi-fragile watermarking for authenticating JPEG visual content," Proceedings of the SPIE International Conference on Security and Watermarking of Multimedia Contents II, San Jose, USA, vol.3971, pp.140-151, 2000.
- [6] S. Yang, Z. Lu and F. Zou. "A Novel Semi-fragile Watermarking Technique for Image Authentication," ICSP Proceedings, pp. 2282-2285, 2005.
- [7] J. Huang, Y. Shi and W. Cheng, "Image watermarking in DCT: An embedding strategy and algorithm," Acta Electronica Sinic, vol.28, no.4, pp.57-60, 2000. (in Chinese)
- [8] X. Li, "Blocked DCT and quantization based blind image watermark algorithm," Computer Engineering, vol.32, no.21, pp.139-144, 2006. (in Chinese)
- [9] J. Zhang and C. Zhang, "Semi-fragile watermarking for JPEG2000 image authentication," ACTA Electronica Sinica, vol.32, no.1, pp.157-160, 2004. (in Chinese)
- [10] X. Wang, L. Meng and H. Yang, "Geometrically invariant color image watermarking scheme using feature points," Sci China Ser F-Inf Sci, vol.52, no.9, pp.1605-1616, September.

Mathematical Model of ECG Signal for OFF Line Adaptive Signal Processing in MATLAB

Gade S. S., Shendage S. B., Uplane M. D.

¹(Bio-Medical Engg. department of Bharat-Ratna Indira Gandhi College of Engg., Solapur Maharashtra)

²(Computer Engg. department of PVP Institute of Technology, Budhgaon, Sangli)

³(Electronics department of Shivaji University, Kolhapur Maharashtra)

Abstract: this paper is outlined basic model based on Fourier series is capable of generating realistic synthetic electrocardiogram (ECG) signals. The operator can specify the heart rate, the variation, position and amplitude of pulses. The beat-to-beat variation and timing of the human ECG, including QT and R-peak amplitude are shown in result. An adaptive LMS filter is implemented to remove the noise of ECG signal. This model may be employed to consider biomedical signal processing techniques that are used to calculate clinical statistics from the ECG signal. Model is derived and successfully simulated in MATLAB.

Keywords: ECG signal, Heart rate variation, realistic model, PQRST pulse, QRS analysis, Adaptive filtering, LMS algorithm.

I. INTRODUCTION

ECG is vital in order to find out heart disease in early phase of its occurrence. The real time ECG signal is more multifaceted in nature and to represent ECG signal adequate mathematical analysis should prefer over the range and nature of signal. The various models have been proposed for clearing up ECG signal OFF line generation. A realistic synthetic ECG signal was modelling using dynamic model [1] and thus authors have taken the efforts to exact curve fitting of ECG signal. An intracellular potential based skin surface model [3] has been suggested and simulating for normal heart operation. In most of time percentage, root mean square difference [4] is used to reconstruct ECG signal. However, the voltage difference method [5] has recommended exact procedure of obtaining an ECG signal with enhanced features. The present paper discusses the natures of ECG signal and derivation of mathematical equation that describe resultant ECG pulse approximately close to realistic ECG signal. The ECG signal has modelled using Fourier series method [6].

ECG signal is influenced with many artefacts and thus noise can add into ECG signal. The de-noising of ECG signal is essential for detecting heart disease. An adaptive filter algorithm is used for de-nosing of ECG signal. The analog filter is implemented followed by adaptive filter for better performance. The de-noising is essential especially for power line noise and base line wonder and should separate from ECG signal. An attempt is made in this present work to remove out ECG noise using adaptive filtering technique.

The ECG signal is the resultant function of heart activity and intracellular potential developed due to action of heart. SA node, atrial muscle, AV node, common bundle fibres,

bundle Branches, Purkinje fibres, ventricular muscles are literal cause of resultant ECG signal, and hence any abnormality can be localised by observing ECG signal [7]. A normal form of ECG signal is presenting in figure 1.

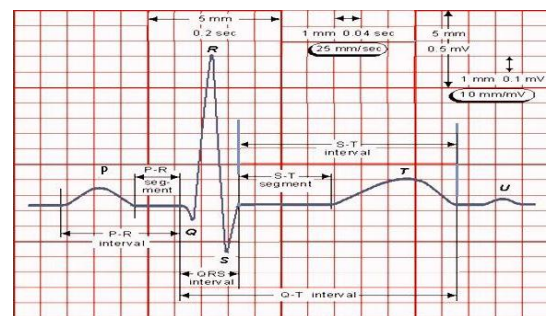


Figure 1: A normal form of ECG signal

II. MATHEMATICAL MODEL

An ECG signal is the combination of number of pulses resulting due to heart activity. if mathematical model of one pulse is derived then on similar basis other pulses can be represented. Consider $S(t)$ is the ECG signal in time domain. According to the geometry of one ECG pulse it is represented as

$$S(t) = A_0(1 - e^{-\frac{t}{\tau}}) - A_0 e^{-\frac{t}{\tau}}$$

$$S(t) = A_0(1 - 2e^{-\frac{t}{\tau}})$$

ECG is the resultant signal obtaining after addition of minimum three to maximum n number of pulses.

$$S(t) = A_0(1 - 2e^{-\frac{t}{\tau_0}}) + A_1(1 - 2e^{-\frac{t}{\tau_1}}) + \dots + A_n(1 - 2e^{-\frac{t}{\tau_n}})$$

The pulses are periodic and continuous pulses and represented by using Fourier series method. The one pulse is given by using Fourier series method.

$$S(t) = a_0 + \sum_n a_n \cos(2\pi n f_0 t) + \sum_n b_n \sin(2\pi n f_0 t)$$

Where,

$$a_0 = \frac{1}{T} \int_{t_0}^{t_0+T} S(t) dt$$

$$a_n = \frac{2}{T} \int_{t_0}^{t_0+T} S(t) \cos(2\pi n f_0 t) dt$$

$$b_n = \frac{2}{T} \int_{t_0}^{t_0+T} S(t) \sin(2\pi n f_0 t) dt$$

Consider general one pulse segment

$$S(t) = A(1 - 2e^{-\frac{t}{\tau}})$$

$$a_0 = \frac{1}{T} \int_0^T A(1 - 2e^{-\frac{t}{\tau}}) dt$$

$$a_n = \frac{2}{T} \int_0^T A(1 - 2e^{-\frac{t}{\tau}}) \cos(2\pi n f_0 t) dt$$

$$b_n = \frac{2}{T} \int_0^T A(1 - 2e^{-\frac{t}{\tau}}) \sin(2\pi n f_0 t) dt$$

The solution is

$$a_0 = A + \frac{2A\tau}{T} \left(e^{-\frac{T}{\tau}} - 1 \right)$$

$$a_n = \frac{4/T}{\left(\frac{1}{\tau}\right)^2 + (2\pi n f_0)^2} \left(e^{-\frac{T}{\tau}} - \frac{1}{\tau} \right)$$

$$b_n = \frac{-A}{\pi n} - \frac{(4/T)(2\pi n f_0)}{\left(\frac{1}{\tau}\right)^2 + (2\pi n f_0)^2} \left(1 - e^{-\frac{T}{\tau}} \right)$$

One pulse of ECG signal is represented by using Fourier series as

$$S(t) = A + \frac{2A\tau}{T} \left(e^{-\frac{T}{\tau}} - 1 \right) + \sum_{n=1,2,3} \left(\frac{4/T}{\left(\frac{1}{\tau}\right)^2 + (2\pi n f_0)^2} \left(e^{-\frac{T}{\tau}} - \frac{1}{\tau} \right) \right) \cos(2\pi n f_0 t) + \sum_{n=1,2,3} \left(\frac{-A}{\pi n} - \frac{(4/T)(2\pi n f_0)}{\left(\frac{1}{\tau}\right)^2 + (2\pi n f_0)^2} \left(1 - e^{-\frac{T}{\tau}} \right) \right) \sin(2\pi n f_0 t)$$

III. MATLAB MODEL

Mathematical model of ECG signal is discussed in previous section. The equation in terms of Fourier series is representing ECG signal. MATLAB model is constructed to implement the mathematical ECG signal. Figure 2 shows one pulse model of ECG signal. Thus one pulse is generated using MATLAB model. Minimum three pulses are needed to represent ECG signal. Seven pulses are sufficient to simulate complete ECG signal. Figure 3

shows a five pulse model of ECG signal and finally figure 4 is ECG toolbox created for OFF line ECG processing.

Removal of power line noise and base line wander is vital problem in ECG signal processing. The various types of filters are useful for removing of noise. Here, an attempt is made using adaptive List Mean Square (LMS) algorithm based filters to remove the ECG noise. Figure 5 shows the matlab model containing OFF line ECG generator, noise adder, equalised LMS filter, analog filter, and scope. Analog filter is used after the adaptive LMS filter, the figure 6 shoes the results.

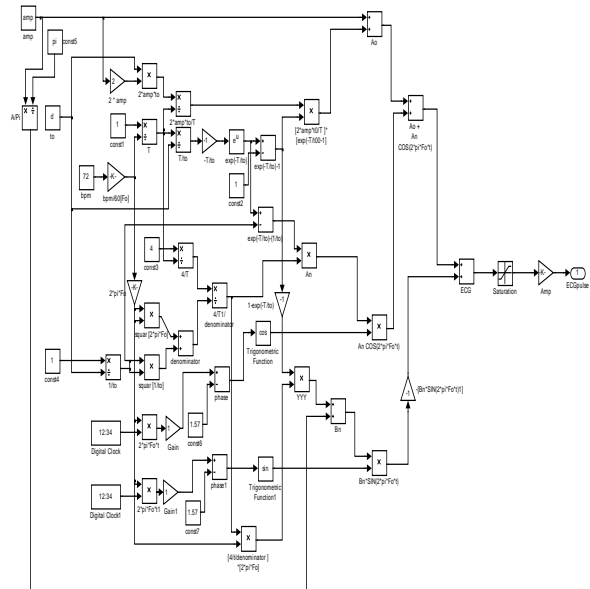


Figure 2 MATLAB equation model

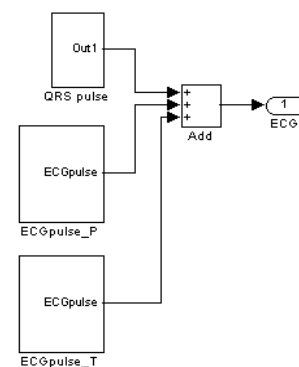


Figure 3 Five pulse ECG signal



Figure 4 ECG tool box

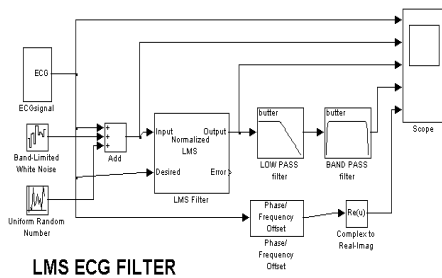


Figure 5 LMS filter

IV. RESULTS

Properties of ECG pulses are given in table 1.

Table 1 Properties of ECG pulses [1]

Index (i)	P	Q	R	S	T
Time (secs)	-0.2	-0.05	0	0.05	0.3
θ_i (radians)	$-\frac{1}{3}\pi$	$-\frac{1}{12}\pi$	0	$\frac{1}{12}\pi$	$\frac{1}{2}\pi$
a_i	1.2	-5.0	30.0	-7.5	0.75
b_i	0.25	0.1	0.1	0.1	0.4

Typical ECG is used to suggest suitable times, angles and values of the PQRST points. The times and angles are specified relative to the position of the R-peak as shown in Table I. Output result is shown in figure 6. The 1st wave is reference ECG signal generated using Fourier series method. The 2nd waveform is showing ECG signal with added noise. The 3rd waveform shows output of adaptive LMS filter. This output waveform contains high and mid band frequency noise. This noise may remain present due to adaptive iteration action. Finally analog low pass and band pass filter is used to remove out remaining noise present in ECG signal. The 4th wave form indicating final output after analog filtering.



Figure 6 Results

V. CONCLUSION

Mathematical model has been introduced which is capable of intrigues the significant features of the ECG signal. Realistic ECG has important relevance in medical signal processing techniques. As compared with noise ECG signal with adaptive filter output waveform, it is clear that LMS filtering technique removes most of the noise present in the ECG signal. When analog filter is followed by after adaptive filtering, it is clear from the waveform that noises have been removed completely. Hence, the combination of adaptive and analog filtering removes noises present in the signal.

VI. REFERENCE

- [1] Patrick E. McSharry, Gari D. Clifford, Lionel Tarassenko, and Leonard A. Smith, "A Dynamical Model for Generating Synthetic Electrocardiogram Signals", IEEE TRANSACTIONS ON BIOMEDICAL ENGINEERING, VOL. 50, NO. 3, MARCH 2003, pp 289-294.
- [2] Frederick M. Schultz, Winchester, Mass, assignor toRaytheon Company, Lexington, Mass., a corporation or Delaware, "Electronic Trigonometric Multiplier", United State patent office, filed May 28, 1964, Ser. No. 370,956 10 claims. (CI. 235-194)
- [3] WALTER T. MILLER, III, AND DAVID B. GESELOWITZ, "Simulation Studies of the Electrocardiogram", American Heart Association, 1978,ISSN: 0009-7330, pp 301-315
- [4] Mikhled Alfaouri, Khaled Daqrouq, Ibrahim N. Abu-Isbeih, Emad F. Khalaf, Abdel-Rahman Al-Qawasmi and Wael Al-Sawalmeh, "Quality Evaluation of Reconstructed Biological Signals", American Journal of Applied Sciences , 2009,6 (1): 187-193, 2009 ISSN 1546-9239
- [5] Berbari, E. J. "Principles of Electrocardiography." The Biomedical Engineering andbook: Second Edition. Ed. Joseph D. Bronzino Boca Raton: CRC Press LLC, 2000
- [6] Ronald L. Allen, Duncan W. Mills, "SIGNAL ANALYSIS TIME, FREQUENCY, SCALE, AND STRUCTURE", IEEE press A John Wiley & Sons, Inc., Publication, 2004, ISBN: 0-471-23441-9
- [7] Swagatika Priyadarshini, "ECG SIGNAL ANALYSIS: ENHANCEMENT AND R-PEAK DETECTION", National Institute of Technology, Rourkela, India 2010

Detection the Ratio of Bilirubin in Human Body Using Laser Technology

Mohammed F. Mohammed¹, Dina J. Matti², Rasha K. Mohammed³
Laser and Optoelectronics Engineering Department, Nahrain University/ Baghdad – Iraq

Abstract: In this work, an analytical study to detect the ratio of bilirubin in human body by determining the level of it in blood using a 532nm laser light transported through some samples of bilirubin has been presented. A second harmonic generation of Nd:YAG laser with measured maximum output power 52.5 mW was used to determine the concentration of total bilirubin in blood. Initially, the cuvette was filled with a sample of standard bilirubin level and then it is filled by a sample of blood containing unknown levels of bilirubin. The absorption factor was calculated for four samples of adults' blood and five samples of babies' blood, and the scattering factor was neglected for each sample. The unknown concentration of total bilirubin was determined and the transmitted power through these samples of blood was measured. In this work, a good matching was obtained between the results of the concentrations of bilirubin in blood using laser technique and the results of the classical medical procedure of measuring the bilirubin concentrations. Therefore, the jaundice in human was detected.

I. INTRODUCTION

Jaundice is a yellowish staining of the skin, sclera and mucous membranes by deposition of bilirubin (a yellow orange bile pigment) in these tissues. Jaundice was once called the "morbus regius" (the regal disease) in the belief that only the touch of king could cure it. Jaundice indicates excessive levels of conjugated or unconjugated bilirubin in the blood and it is clinically apparent when the bilirubin level exceeds 2mg/dl (34.2 $\mu\text{mol/L}$) [1].

In fair-skinned patients, jaundice is most noticeable on face, trunk, and sclerae; in dark-skinned patients, its noticeable on the hard palate, sclerae, and conjunctivae-pseudo jaundice may be found in black patients with pigmented sclera, from carotinemia, uremia (a sallow yellowish pallor), and quinacrine (a yellow-green color) [2]. Causes of jaundice can be classified into Pre-hepatic, hepatic or post hepatic [2]. Tissue deposition of bilirubin occurs only in the presence of serum hyperbilirubinemia and is a sign of either liver disease or, less often, hemolytic disorder. Another sensitive indicator of increased serum bilirubin is darkening of the urine, which is due to the renal excretion of conjugated bilirubin. Patients often describe their urine as tea or cola colored [3].

Jaundice can be classified into two groups; the first group is the physiological jaundice and the second group is the pathological jaundice of neonates. The causes of jaundice can be grouped into the following categories in Fig.1 [3]

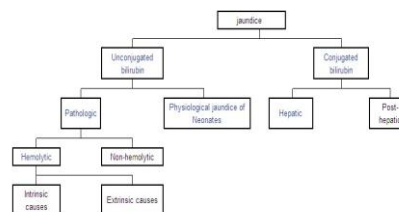


Fig.1 Causes of jaundice

II. BILIRUBIN

Bilirubin (formerly referred to as hematoidin) is the yellow breakdown product of normal heme catabolism. It is excreted in bile and urine, and elevated levels may indicate certain diseases. It is responsible for the yellow color of bruises, urine, and the yellow discoloration in jaundice [4].

Bilirubin consists of open chain of four pyrrole-like rings (tetrapyrrole). In heme, by contrast, these four rings are connected into a larger ring called a porphyrin ring as shown in Fig.2 and the molecular formula of bilirubin is $\text{C}_{33}\text{H}_{36}\text{N}_4\text{O}_6$ [4].

Bilirubin is created by the activity of biliverdin reductase on biliverdin, a green tetrapyrrolic bile pigment which is also a product of heme catabolism [5, 6].



Fig.2 The atomic structure of bilirubin

III. UNCONJUGATED BILIRUBIN

Erythrocytes (red blood cells) generated in the bone marrow are disposed of in the spleen when they get old or damaged. This released hemoglobin, which is broken down to heme as the globin parts. The heme is then turned into unconjugated bilirubin in the reticuloendothelial cells of the spleen, which is not soluble in water. It is then bound to albumin and sent to the liver [5,6].

IV. CONJUGATED BILIRUBIN

In the liver it's conjugated with glucuronic acid by the enzyme glucuronyltransferase, making it soluble in water. Much of it goes into the bile and thus out into the small intestine. Some of the conjugated bilirubin remains in the large intestine and is metabolized by colonic

bacteria to urobilinogen, which is further metabolized to stercobilinogen, and finally oxidized to stercobilin, which it gives feces its brown color [5, 6].

There are many methods for determination the concentration of bilirubin such as [6]:

A. Determination of the concentration of bilirubin in serum by:

- Rapid micro-method employing photoelectric colorimeter.
- Rapid micro-method employing color standards.

B. Determination of free bilirubin and its binding capacity by HAS using a microfluidic chip-capillary electrophoresis device with multi-segment circular-ferrofluid-driven micro mixing injection.

C. Measurements the concentration of bilirubin by using laser technology, this method depends on the laser beam attenuation and it's considered in this work.

V. ATTENUATION OF LIGHT

The beam attenuation coefficient $\alpha(\lambda)$ is used to characterize the optical transmission properties of matter, it's a measure of decay of the unscattered light and its given by the equation (1) [7]

$$P_1(\lambda) = P_o(\lambda)e^{-\alpha(\lambda)L} \quad \text{Eq.(1)}$$

Where $P_1(\lambda)$ is the measured beam radiant power,

$P_o(\lambda)$ is the initial beam radiant power, and

L is the optical path length.

The beam attenuation coefficient is the sum of the absorption coefficient $a(\lambda)$ and the scattering coefficient $s(\lambda)$ which is defined by [7]:

$$\alpha(\lambda) = a(\lambda) + s(\lambda) \quad \text{Eq.(2)}$$

The scattering phenomenon is negligible because of the dependence of scattering on wavelength. With a given size of particles, long waves would be expected to be less effectively scattered than short ones, because the particles present obstructions to the waves which are smaller compared with the wavelength for long waves than short ones [8]. Then

$$\alpha(\lambda) = a(\lambda) \quad \text{Eq.(3)}$$

When a beam of light is passed through matter in the solid, liquid or gaseous state, its propagation is affected in two important ways. In the first way, the intensity will always decrease to a greater or less extent as the light penetrates farther into the medium. In the second way, the velocity will be less in the medium than in free space. The loss of intensity is chiefly due to absorption. Then absorption is a way of interaction of the electromagnetic radiation with matter, energy absorbed and transformed to other type, the absorption coefficient ($\alpha(\lambda) \text{ cm}^{-1}$) is a property of matter [8].

The observed power is converted to a specific absorption coefficient by using the following formula [7]

$$\alpha = \frac{-\ln[(P/A)/(P_o/A_o)]}{L} \quad \text{Eq.(4)}$$

where P is the measured beam power after sample (mW),

P_o is the incident beam power before sample (mW),

A is the spot area of beam after sample,

A_o is the spot area of beam before sample, and

L is the length of the cuvette (cm).

Resulting from short distance between the container of sample (cuvette) and power meter, then $A = A_o$. Therefore,

$$\alpha = \frac{-\ln[P/P_o]}{L} \quad \text{Eq.(5)}$$

The transmitted beam is defined by [7]

$$T(\lambda) = \frac{P(\lambda)}{P_o(\lambda)} \quad \text{Eq.(6)}$$

and the absorption coefficient becomes as:

$$\alpha = \frac{1}{L} \ln \frac{1}{T(\lambda)} \quad \text{Eq.(7)}$$

VI. EXPERIMENTAL SET UP

The essential components in the setup includes: light source (green laser), a precision glass cuvette as the blood container, and a power meter as shown in Fig. 3

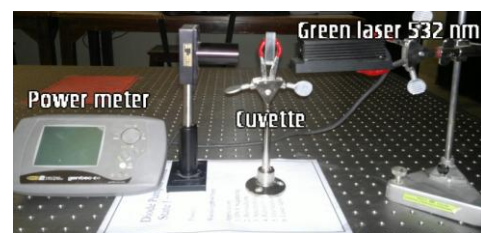


Fig.3 Experimental setup

An Nd: YAG laser (second harmonic generation) with a wavelength of $\approx 532 \text{ nm}$ and the measured output power was about $\approx 52.5 \text{ mW}$ as the light source. When a green laser light passed through some samples of blood container the concentration of bilirubin in blood was determined. Initially, the container was filled by a sample of blood containing a standard bilirubin level and then by sample of blood containing unknown levels of bilirubin. For each case, the output power would be measured and calculated by using equations (6) and (7). Its attenuation which was occurred where laser light passing through the sample of blood.

Spectrophotometer was used to measure the absorption coefficient of human blood as a function of wavelength when the cuvette is filled with a sample contains a standard bilirubin level and the result as shown in Fig 4.

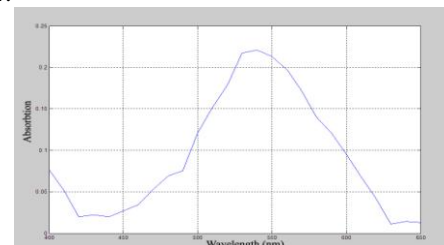


Fig.4 Absorption curve of human blood as a function of wavelength

From Fig.4 the maximum absorption coefficient occurs at range 530-540 nm which has value closely to absorption occur at 532 nm. Therefore a second harmonic generation Nd: YAG laser of 532nm was used.

The samples of blood are dissolved with reagent material because of the normal blood is heavy and the laser cannot be able to pass through it, these reagent material cause an amplification of bilirubin molecules

resulting in dominance of bilirubin molecules on other molecules substances involved in human blood.

The sample work solution by mix 20R1 (sulfanilic acid 30mmol/l, hydrochloric 150mmol/l, dimethylsulfoxide 7mmol/l) volume with 1R3 (sodium nitrite 20mmol/l) volume and R4 represent the standard concentration of bilirubin which its equal 83 μmol/l, then added to the sample. The color of the work solution change to the violet which represent the (test) and when the reagent R1 was added alone to the same sample then the solution color became yellow which represent the (blank). These results of work solution as shown in Fig.5

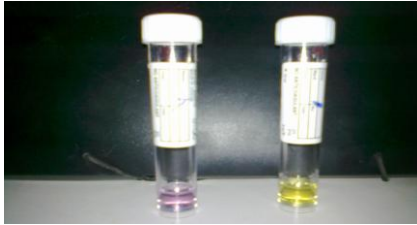


Fig.5 Preparation of sample for measurement

VII. Calculations And Measurements Results

In this work, the concentrations of bilirubin in human blood for all samples were measured by two methods; the first one is the medical laboratory measurements and the other one is the optical activity method using SHG Nd:YAG laser of measured power about 52.5mW.

The concentration of total bilirubin of human blood can be calculated using the below empirical equation:

$$Concentration = \frac{\alpha_{Sample}}{\alpha_{Standard}} \times C_{Standard} \quad Eq.(8)$$

Where

$\alpha_{Standard}$ is the measured absorption coefficient of standard sample = 0.434 cm⁻¹, C Standard is the standard concentration of total bilirubin of human blood = 83mg/dl.

The range of the total bilirubin concentrations of blood is about (0.2 -1) mg/dl. Four samples of adults and five samples of babies were taken in this work.

The experiment recording reading of power meter and the medical tested of the concentration of adults samples are shown in table I and figures 6a and 6b using equation (8).

TABLE I

ILLUSTRATE RECORDING POWER AS A FUNCTION OF THE CONCENTRATION OF BLOOD SAMPLES FOR ADULTS

Absorbed power (mw)	Transmitted Power (mw)	Concentration (mg/dl) of samples for adults		Error rate %
		Experimental measurement	Medical laboratory measurement	
14.15	38.35	3.533	3.589	1.5
19.75	32.75	5.308	5.384	1.4
28.02	24.48	8.132	8.256	1.5
3.98	48.52	0.886	0.9	1.5

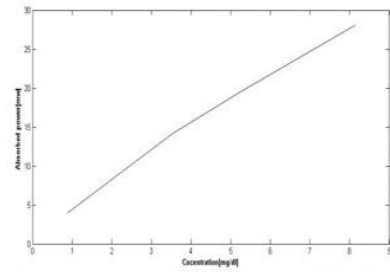


Fig.6a Absorbed power as a function of concentrations (for adults)

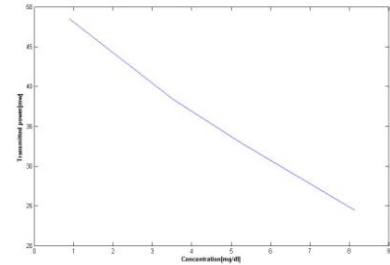


Fig.6b Transmitted power as a function of the concentration (for adult)

From table I, the error rate between experiment results and medical tested of blood samples was about 1.5% and it is acceptable value.

For sample of babies, the error rate was about 2% and the measurement results are shown in table 2 and figures 7a and 7b using equation (8).

TABLE II

ILLUSTRATE RECORDING POWER AS A FUNCTION OF THE CONCENTRATION OF BLOOD SAMPLES FOR BABIES.

Absorbed power (mw)	Transmitted Power (mw)	Concentration (mg/dl) of samples for Babies		Error rate %
		Experimental measurement	Medical laboratory measurement	
21.37	31.13	5.879	5.983	1.7
24.76	27.8	7.152	7.323	0.2
41.6	10.9	17.685	17.973	1.6
27.7	24.8	8.436	8.56	1.4
29.4	23.1	9.235	9.4	1.7

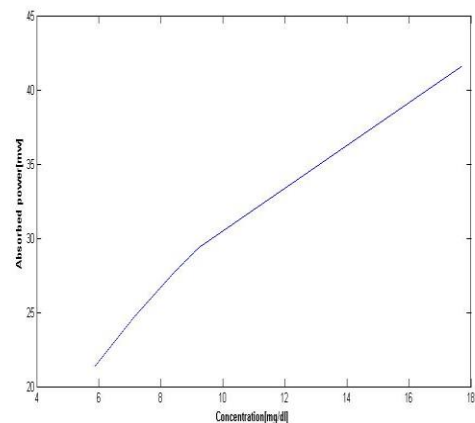


Fig. 7a Absorbed power as a function of the Concentration (for Babies)

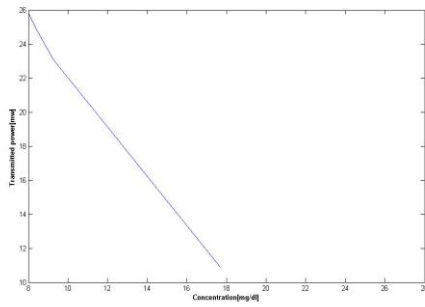


Fig.7b Transmitted power as a function of the Concentration (for Babies)

Figures (8 a, b) show a transmitted power for adults and babies samples as a function of the concentrations of bilirubin measured by two methods

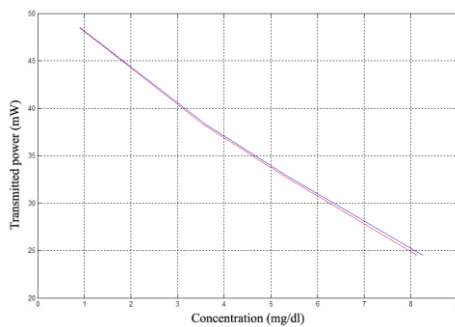


Fig.8a Variations of concentration of bilirubin measured by medical laboratory and concentration measured experimentally (for Adults)

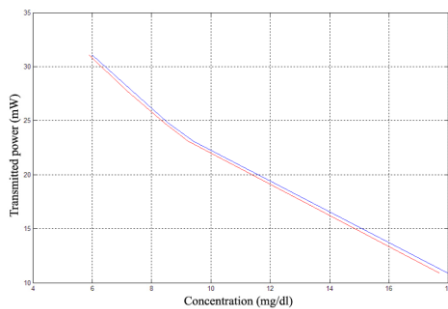


Fig. 8b Variations of concentration of bilirubin measured by medical laboratory and concentration measured experimentally (for Babies)

VIII. CONCLUSIONS

- 1- A good matching occurs between the experimental measurements and medical laboratory tested of a human blood samples contained bilirubin.
- 2- The results demonstrate the ability of the power meter to be accurately measure bilirubin concentrations in blood. This method represents an important step toward the development of a noninvasive bilirubin sensor that may eventually be capable of detecting bilirubin levels in the blood.
- 3- The error (2%) result from the existence of human blood several type of molecules substances, imperfect environment of experimental work, the variation of wavelength for laser used and the peak absorption wavelength and the very small variation of both spot area of laser beam before and after the cuvette which assumed to be equal.

REFERENCES

- [1] S. P. Roche and R. Kobos, "Jaundice in the adult patient", *American Family Physician* 69(2):299-304, 2004.
- [2] C. D. Briggs and M. Peterson, "Investigation and management of obstructive Jaundice", 2007, pp 74-80.
- [3] C. Lynn and C. Christy, "Mosby's pediatric clinical advisor: instant diagnosis and treatment", 2010, Elsevier Health Sciences. pp. 200-206.
- [4] C. Piron, H. Priestap and D. Lee, "The animal pigment bilirubin discovered in plants", *Journal of the American chemical society*, 131(8):2830,2009.
- [5] DE. Baranano, M. Rao, CD. Ferris, and SH. Snyder, "Biliverdin reductase: a major physiologic cytoprotectant", *Proc. Natl. Acad. Sci. U.S.A.* 99 (25), 2002.
- [6] Y. Liu, P. Li, J. Lu, W .Xiong, J. Oger, W. Tetzlaff, and M. Cynader, "Bilirubin possesses powerful immunomodulatory activity and suppresses experimental autoimmune encephalomyelitis". *J. Immunol.* 181 (3), 2008.
- [7] Peter W. Milionni and Joseph H. Eberly, "lasers", John Wiley, and Sons, Inc., 1988.
- [8] Jenkins and White, "Fundamentals of Optics", 3rd edition, McGraw-Hill Book Company, Inc., 1971.

Symmetric Key Cryptography on Images in AES Algorithm and Hiding Data Losslessly

T. Arumuga Maria Devi¹,

Assistant Professor, Dept. of CITE

Sabitha.S²

M.Tech Student, Dept. of CITE

Centre for Information Technology and Engineering,
Manonmaniam Sundaranar University, Tirunelveli

Abstract: Reversible (lossless) data embedding (hiding) has drawn lots of interest recently. Being reversible, the original cover content can be completely restored. This paper proposes a novel reversible data hiding scheme with a lower computational complexity and can be used in applications where both the image and the hidden information is highly confidential. It consists of three phases –AES image encryption, data embedding and data extraction/image-recovery phases. Here, the encrypted image is made highly secured by using an AES (Advanced Encryption standard) stream cipher. Although a data-hider does not know the original image content, he can embed additional data into the encrypted image using the data hiding key. A receiver may firstly decrypt the encrypted image using the encryption key. This decrypted image is similar to the original image. With the data-hiding key, the embedded data can be correctly extracted while the original image can be perfectly recovered.

Index Terms: AES encryption – Data Embedding – Image Recovery.

I. INTRODUCTION

Data hiding is a technique that is used to hide information in digital media such as images, audio, video etc. The information that is hidden depends upon the purpose of application. Owing to data hiding, some distortion may occur in the original cover medium and cannot be inverted back to the original medium. Such a data hiding is called lossy data hiding. But in applications such as medical image system, law enforcement, remote sensing, military imaging etc it is desired to recover the original image content with greater accuracy for legal considerations. The data hiding scheme that satisfies this requirement is called reversible or lossless data hiding. Reversible data hiding was first proposed for authentication and its important feature is reversibility. It hides the secret data in the digital image in such a way that only the authorized person could decode the secret information and restore the original image. Several data hiding methods have been proposed. The performance of a reversible data embedding algorithm is measured by its payload capacity, complexity, visual quality and security. Earlier methods have lower embedding capacity and poor image quality. As the embedding capacity and image quality improved, this method became a covert communication channel. Not only should the data hiding algorithm be given importance. The image on which the data is hidden should also be highly secured.

In this paper, both the cover image and the secret data are given equal importance. The visual quality after encryption as well as the PSNR is also improved. It consists of three phases – AES image encryption, data embedding and data extraction/image-recovery phases. In the first phase, the data of original image are entirely encrypted by an AES (Advanced Encryption standard) stream cipher. The data encryption standard (DES) is weak due to smaller key size, 56 bit. Whereas AES can use three different key sizes: 128, 192 and 256 bits. In the second phase, although a data-hider does not know the original image content, he can embed additional data into the encrypted image by modifying a part of encrypted data using the data hiding key. In the third phase, a receiver may firstly decrypt the encrypted image containing the embedded data using the encryption key. This decrypted image is similar to the original image. With the data-hiding key, the embedded data can be correctly extracted while the original image can be perfectly recovered.

II. EXISTING METHODS

In Difference Expansion method [1], the differences between two adjacent neighboring pixels are doubled to generate a new least significant bit where the new data is hidden providing large information package. In Generalized DE based method [2], Tian's pixel-pair difference expansion was extended using difference expansion of vectors. In Generalized LSB method [3], the cover image undergoes lossless compression to create a space where the new data is added. Thus the PSNR is reduced. In Histogram shift mechanism [4], the pixel values at the zero and the peak points of the histogram are modified to add the new data. In wavelet technique and sorting [5], Kamstra *et al.* improved the location map by sorting possible expandable locations. In integer-to-integer wavelet transform method [6], LSB substitution and bit shifting was done to add new data to the wavelet coefficients obtained from integer-to-integer wavelet transform. In [7], Wang *et al.* uses 2-D vector maps in the cover image. In [8], Thodi *et al.* made better use of redundancy of neighbouring pixels by using payload independent overflow location map. But the compressibility is undesirable in some image types. In [9], Hu *et al.* solved the problem in [8] by constructing an efficient payload dependent overflow location map which has good compressibility. In [10], Hong *et al.* proposes the method of orthogonal projection and modifies the prediction error values to add the secret data. In [11], the data is hidden by modifying a part of the encrypted

image. But the encrypted image is not highly secured and also the PSNR value is low.

III. PROPOSED SCHEME

Figure 1 shows the block diagram of the proposed scheme. There are three phases – AES image encryption, data embedding and data extraction / image-recovery phases.

AES Image Encryption

The original image is in uncompressed format. Firstly, if the image is a colour image, then encrypt each red, green and blue channels otherwise convert it into a gray scale image with each pixel value ranging in between [0-255] represented by 8 bits and then encrypt the image. The pixel bits are represented as $b_{i,j,0}, b_{i,j,1}, \dots, b_{i,j,7}$.

AES is a substitution-permutation network, which is a series of mathematical operations that uses substitutions and permutations such that each output bit depends upon every input bit. The AES algorithm consists of a set of processing steps repeated for a number of iterations called rounds. The number of rounds depends upon the key size. Each round is a cipher with four operations except the last round which is having only three operations. First, AddRoundKey step is performed where the incoming data and the key are added together. Then it performs the round operation. Figure 2 shows the operations in each round [12].

SubByte: each byte of the block is replaced by its substitute in the substitution box(S-box).

ShiftRow: bytes in last three rows are cyclically shifted

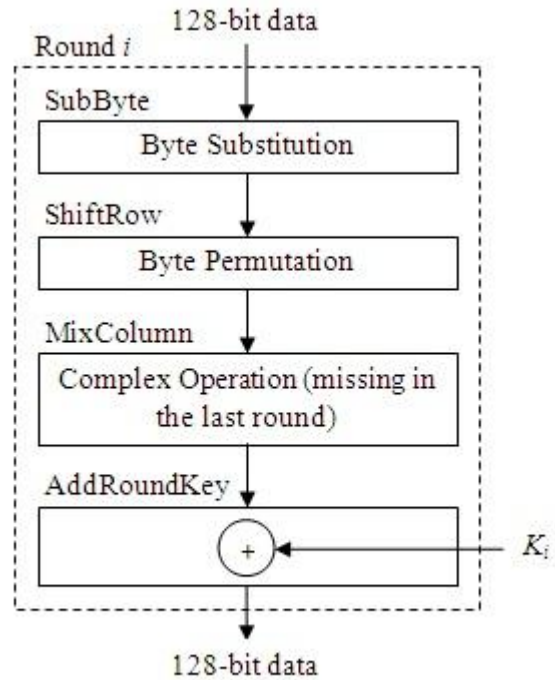


Figure 2. AES Encryption

Data Embedding

In this phase, even though a data hider doesn't know the original content of the image he can embed the secret data into the encrypted image by modifying a small part of the encrypted image.

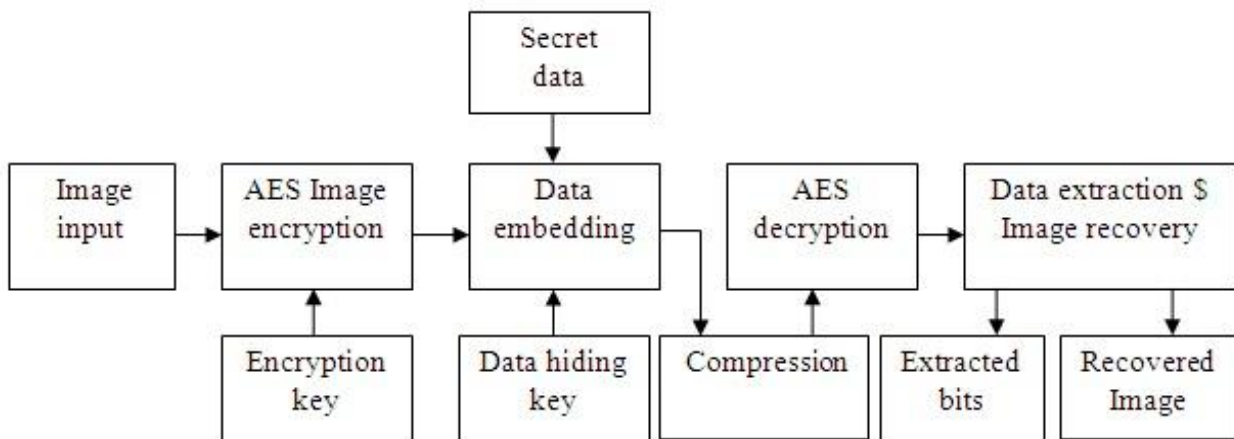


Figure 1. Block Diagram

left over different number of offsets.

MixColumn: Each column is multiplied with a known matrix. Multiplying by 1 means leaving unchanged, by 2 means shifting byte to the left and by 3 means shifting to the left and then performing XOR with the initial unshifted value.

AddRoundKey: XOR with the actual data and the subkey. In final round there is no MixColumn step. These steps are done for 10 rounds. Thus it becomes difficult for the attacker to obtain any information about the original content from the encrypted image.

Firstly, the encrypted image is divided into several segments of block size $s \times s$. Each block is then used to carry one bit. The sum total of the pixel values of each block is calculated. It is then compared with a threshold value which is set manually such as to obtain greater PSNR value. The data is then added to the block whose sum of the pixel value is greater than the threshold value by xor-ing the original pixel bits with the secret data. In order to receive the image properly at the receiver, the image is compressed using wavelet transform which is a lossless compression method.

Data Extraction and Image Recovery

In this phase, the image is decrypted using AES decryption. The steps are AddRoundkey, inverse subbyte using inverse S-box, inverse shiftrow where the bits are cyclically shifted towards right, inverse mixcolumn step using inverse P-box, and AddRoundkey.

The average energy of error between the original and decrypted pixel value is,

$$E_A = 1/8 \sum_{u=0}^7 [u - (7 - u)]^2 \quad [1]$$

u is the no. of bits.

PSNR of the decrypted image,

$$PSNR = 10 \log_{10} \frac{255^2}{E_A/2} = 55.11dB \quad [2]$$

The decrypted image is segmented into blocks. The sum total of pixel values of each block is found then. For each block, if this value is greater than the threshold value then the data is hidden in that block and is extracted by xor-ing the original bits with the decrypted bits. Finally combine the extracted bits to obtain the secret data and collect the recovered blocks to form the original image.

IV. EXPERIMENTAL SETUP

Figure 3(a) shows the original cover media used. 3(b) shows the encrypted image. 3(c) shows the decrypted image carrying the secret data and the value of PSNR caused by data embedding is 55.11dB. At last, the embedded data was successfully extracted and the cover image was recovered. Figure 4 shows the PSNR with respect to the data set values.

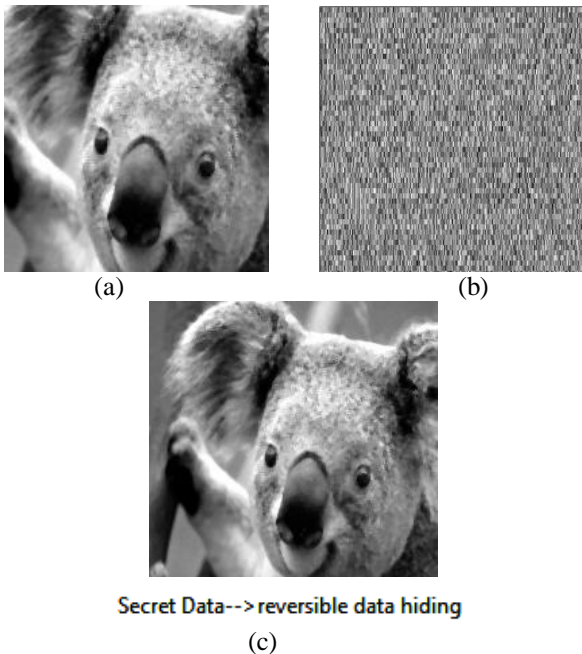


Figure 3. (a) Original image, (b) Encrypted image, (c) Decrypted image with the secret data

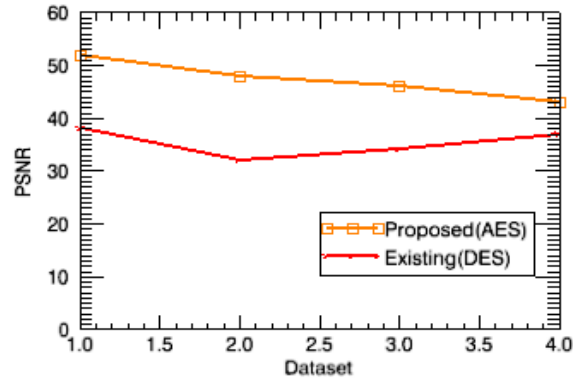


Figure 4. PSNR Vs Data set

V. CONCLUSION

In this work, the cover medium is highly secured for reversible data hiding with lower computational complexity. The data of the original image is completely encrypted by AES stream cipher which overcomes the disadvantages of DES stream cipher. Even though the data hider doesn't know the original content, he can hide the data by modifying a part of the encrypted image. The receiver decrypts the image using AES decryption. The PSNR value of the decrypted image is high. The hidden data is then extracted with the data hiding key and the original image is recovered. This work may be applicable where both the hidden data and the cover media are highly confidential.

VI. ACKNOWLEDGMENT

The authors would like to thank the members of the Dept. of CITE, M S University, Tirunelveli for various algorithms used in this research, and all the people who helped in preparing and carrying out the experiments and data collection.

REFERENCES

- [1] Jun Tian, "Reversible data embedding using a difference expansion," *IEEE Transactions on Circuits System and Video Technology*, vol. 13, no. 8, pp. 890-896, Aug. 2003.
- [2] A.M. Alattar, "Reversible watermark using the difference expansion of a generalized integer transform," *IEEE Trans. Image Process.*, vol. 13, no. 8, pp. 1147-1156, Aug. 2004.
- [3]. M.U.Celik, G.Sharma, A.M Tekalp, and E. Saber, "Loseless Generalized-LSB data embedding," *IEEE Trans. Image Process.*, vol. 14, no. 2, pp. 253-266, Feb. 2005.
- [4]. Z. Ni, Y.Q. Shi, N. Ansari, and W. Su, "Reversible data hiding," *IEEE Transactions on Circuits System and Video Technology*, vol. 16, no.3, pp. 354-362, Aug. 2006.
- [5]. L. Kamstra and H. J. A. M. Heijmans, "Reversible data embedding into images using wavelet

techniques and sorting.” *IEEE Trans. Image Process.*, vol. 14, no.12, pp. 2082-2090, Dec. 2005.

- [6]. S. Lee, C. D. Yoo, and T. Kalker, “Reversible image watermarking based on integer-to-integer wavelet transform,” *IEEE Trans. Inf. Forensics Security*, vol. 2, no. 3, pp. 321-330, Sep. 2007.
- [7]. X. T. Wang, C. Y. Shao, X. G. Xu and X. M. Niu “Reversible data hiding scheme for 2-D vector maps based on difference expansion,” *IEEE Trans. Inf. Forensics Security*, vol. 2, no. 3, pp. 311-320, Sep. 2007.
- [8]. D.M. Thodi and J.J. Rodriguez, “Expansion embedding techniques for reversible watermarking,” *IEEE Trans. Image Process.*, vol. 16, no. 3, pp. 721-730, Mar. 2007.
- [9]. Y. Hu, H.K. Lee, and J. Li, “DE based Reversible data hiding with improved overflow location map,” *IEEE Transactions on Circuits System and Video Technology*, vol. 19, no.3, pp. 250-260, Feb. 2009.
- [10]. W. Hong, T. S. Chen, Y. P Chang, C. W. Shiu, “A high capacity reversible data hiding scheme using orthogonal projection and prediction error modification,” *Signal Processing.*, vol. 90, no.12, pp. 2911-2922, May. 2010
- [11]. Xinpeng Zhang, “Reversible data hiding in encrypted image,” *IEEE Signal Processing.*, vol. 18, no.4, pp. 255-258, April. 2011

BOOKS

- [12]. Data Communications and Networking, Behrouz A. Forouzan, fourth edition.

AUTHORS



S. Sabitha received B.Tech. Degree in Electronics and Communication Engineering from Mount Zion College of Engg., Mahatma Gandhi University, Kerala in 2010. Currently, she is doing M.Tech in Computer and Information Technology in Manonmaniam Sundaranar University, Tirunelveli. Her research interests include Signal and Image Processing and Software Engineering.



T. Arumuga Maria Devi received B.E. Degree in Electronics and Communication Engineering from Manonmaniam Sundaranar University, Tirunelveli, India in 2003, M.Tech degree in Computer and Information Technology from Manonmaniam Sundaranar University, Tirunelveli, India in 2005 and worked as Lecturer in the Department of Electronics and Communication in Sardar Raja College of Engineering. Currently, she has submitted thesis for Ph.D in Information Technology-Computer Science Engineering and also is the Assistant Professor of Centre for Information Technology and Engineering of Manonmaniam Sundaranar University. Her research interests include Signal and Image Processing, Multimedia and Remote Communication.

EDXRF Analysis of Soil Samples to Study the Role of Trace Elements in Optimizing the Yield

Virendra Singh¹, H.M. Agrawal²

^{1,2}Department of Physics, G.B.Pant University, Pantnagar, 263145, India

Abstract : The crops always demand the best composition of soils for them to grow well and so the multielemental study of soil is essential for the betterment of crop production. The EDXRF technique has been used for multielemental analysis of the soil, under study. The soil samples investigated here were treated already with macro, micro and biofertilizers. The concentrations of eight trace elements namely V, Cr, Mn, Fe, Co, Ni, Cu and Zn have been determined in soil samples. The grain yields of wheat and rice crops were obtained and it has been found that the yields depend strongly on the given treatments and the concentrations of the trace elements in the soil. Some of the micronutrients like Zn, Cu, Fe and Mn have shown the major role in the productive yields.

The concentration equations of the eight trace elements as a function of atomic number were fitted using the cubic spline method. The equations may be useful for database purpose and the cross validation can be done in subsequent years to obtain more accurate empirical relation for the studied soil.

Keywords – Cubic Spline Method, EDXRF, Fertilizers, Yield

Introduction

The multi-elemental study of soils is much needed in order to study the role of different elements in plant growth. The data on the concentration of trace elements and metals in soil are valuable for predicting the availability of these elements to plants as well as any toxic effect that might have occur on crops and on their biological activities in soils. The concentrations of micronutrients, e.g. Mn, Cu and Zn in soil are minute in comparison to macro nutrients but they are essential, particularly for cereal crops [1], for proper plants growth and functioning. These micronutrients are also indispensable for humans and animals in minute amount and can be taken through the food chain.

The multielemental analysis of soil samples has been carried out with Energy Dispersive X-Ray Fluorescence (EDXRF) technique. The technique has many advantages over other techniques, like AAS, ICP-MS and chemical methods, that it is multielemental, non-destructive and has better sensitivity and precision. The total concentrations of eight trace elements (V, Cr, Mn, Fe, Co, Ni, Cu and Zn) have been determined in samples which were treated with various fertilizers. In EDXRF, the atoms in the sample material are excited by X-rays, emitted from an X-ray tube. All element specific X-ray fluorescence signals, the intensities of which is proportional to concentration of respective elements, emitted by the atoms after the photoelectric ionization are measured simultaneously by detector.

In case of soil analysis, EDXRF probe has been used in last decade by researchers and scientists for various purposes of study. Multielemental analysis of soil has been done to investigate the uptake mechanism in the herbal drugs [2]. Yu et al. [3] determined the multielemental profile of Hong Kong soils using energy dispersive X-ray fluorescence (EDXRF). The distribution of soil nutrients with depth was studied to understand the importance of plants in structuring the vertical distributions of the nutrients [4].

The empirical relations of elemental concentrations were obtained by fitting the curve using cubic spline method. The concentrations of elements, as a function of atomic number, were given by a set of equations governed by a single function. Every equation is in the form of cubic polynomial and having four parameters.

Experimental Procedures

2.1 Experimental Site & Soil Taxonomy

The soil samples have been collected from an agricultural field of G.B.Pant University of Agriculture and Technology, Pantnagar, lying in tarai region of Uttarakhand, India. The site is in the foothills of Shiwalik range of Himalayas at 29° N latitude, 79°3' E and an altitude of 283.8 m. It is an Agro ecological sub region - 14.1. Based on physico-chemical and morphological characteristics, the soils of this particular tarai region have been classified as Mollisols. The soil of experiment has subgroup-Aquic hapludoll, Family- Fine Loamy and series-Silty Clay Loam.

2.2 Treatments

Five treatments were being given to soil under study. The soil samples from control field were also investigated. The treatments code and details are given in TABLE 2.

Fertilizer doses (Kg ha⁻¹) used at optimal level (100 % NPK) were based on initial soil tests in terms of nutrients. Quantitatively the doses are given below:

TABLE 1.

Crop	N (kg ha ⁻¹)	P(kg ha ⁻¹)	K(kg ha ⁻¹)
Rice	120	26	37
Wheat	120	26	33

In the treatments, the nitrogen (N), phosphorus (P) and potassium (K) were given in the form of urea [(NH₂)₂CO], phosphorus pentaoxide (P₂O₅) and muriate of potass (KCl) respectively.

2.3 Sample Collection and Preparation

The soil samples have been collected from 0-25 cm depth. The samples were air dried, sieved and crushed homogeneously. A 200 mg sample is used to make the pellet by press pelletizer applying the pressure of 150 Kg/cm². A 13 mm die was used to make the pellets.

2.4 Soil Sample Analysis

Jordan Valley EX-3600 EDXRF spectrometer was used to carry out all the measurements under vacuum condition. All the samples were analyzed in three replicates for better results. The inbuilt ExWin software was used for the quantitative analysis.

2.5 Cubic Spline Method

The method was used to fit the curve drawn by data points of concentration vs. Atomic number (Z). The condition for a cubic spline fit is that a set of cubics is passed through the points, using a new cubic in each interval. Briefly the method is discussed here:

The cubic for *i*th interval, which lies between the points (x_i, y_i) and (x_{i+1}, y_{i+1}) would be

$$y = a_i(x - x_i)^3 + b_i(x - x_i)^2 + c_i(x - x_i) + d_i \quad (1)$$

Since it fits at the two end points of the interval, then:

$$y_i = a_i(x_i - x_i)^3 + b_i(x_i - x_i)^2 + c_i(x_i - x_i) + d_i = d_i \quad (2)$$

and

$$y_{i+1} = a_i(x_{i+1} - x_i)^3 + b_i(x_{i+1} - x_i)^2 + c_i(x_{i+1} - x_i) + d_i$$

$$= a_i h_i^3 + b_i h_i^2 + c_i h_i + d_i \quad (3)$$

Where $h_i = \Delta x_i$ is the *i*th interval

Let S_i represents the second derivative at the point (x_i, y_i). Differentiating (1) by two times and equating the slopes and curvature of joining polynomials, we get the values of parameters. Substituting the values of *a*, *b*, *c* and *d* in terms of *S* and *y*, finally we got the relation:

$$h_{i-1}S_{i-1} + (2h_{i-1} + 2h_i)S_i + h_iS_{i+1} = 6 \left(\frac{y_{i+1} - y_i}{h_i} - \frac{y_i - y_{i-1}}{h_{i-1}} \right) \quad (4)$$

(4) applies at each interval point from *i*=2 to *i*=*n*-1, *n* being the total number of points. So we get *n*-2 equations. Two more equations will be obtained by taking linear extrapolation of S₁ with S₂ and S₃, with analogous linearity of S_{*n*}, S_{*n*-1} and S_{*n*-2}:

$$\frac{S_2 - S_1}{h_1} = \frac{S_3 - S_2}{h_2}, \quad h_2S_1 - (h_1 + h_2)S_2 + h_1S_3 = 0 \quad (5)$$

and

$$\frac{S_n - S_{n-1}}{h_{n-1}} = \frac{S_{n-1} - S_{n-2}}{h_{n-2}}, \quad h_{n-1}S_{n-2} - (h_{n-2} + h_{n-1})S_{n-1} + h_{n-2}S_n = 0 \quad (6)$$

Finally, we have a set of data which are fitted throughout by a single cubic.

Results and Discussion

The concentrations of elements, determined by EDXRF technique, are presented in TABLE 3. Arithmetic mean and arithmetic standard deviation (ASD) of concentrations have been calculated also.

The Vanadium was found in bit high amount in the T1 and T2 samples, which were treated with NPK fertilizers. Both V and Cr are poorly soluble and the use of FYM seems to improve the uptake of both of the elements. The usefulness of Cr and V is limited for the plants but these elements were illustrated as essential for the humans [5]. A similar trend was observed for iron and manganese concentration values. Added weedicides and Zn increased the uptake of Fe and Mn as shown by the decreasing concentrations in T1, T2 and T3. This result was also supported by Singh and Nand Ram [6] who studied the uptake of Fe, Mn, Cu and Zn micronutrients for same soil samples and treatments, and observed the highest uptake for T4 treatment (i.e. 100 % NPK+FYM) with decreasing order as T4 > T3 > T2 > T1 > T5 > C. In all the soil samples, the Fe concentration was found to be high and this humid sub-tropical region was considered to be the Fe rich region. Despite the higher amount of iron in soil, no symptoms of iron toxicity have been monitored in the rice and wheat plants. The reason is that the iron toxicity occurs in soils high in active iron and potential acidity (mostly Ultisols, Oxisols, and acid sulfate soils) and not in Mollisols. Besides that, the application of nutrients such as P, K, and Zn reduce iron toxicity, improve growth, and increase rice yield [7]. A least amount of all trace elements and also the poor crop grain yields was observed in T5, i.e. soil treated with biofertilizers. Application of azolla biofertilizer has been found to improves the properties of soil but these improvements were considerable only for nitrogen, organic matter and other cations (Mg, Ca and Na) released into the soil [8]. Cobalt was in quite high amount in all the samples and that could be due to the high amount of Co in the ground water used for irrigation or/and pesticides used here.

The Ni and Cu concentrations were found in a low amount in all the soil samples; although the role of nickel is not clear in the growth of rice and wheat plants. Cu, Mn, Fe and Zn were considered the most essential trace elements for rice and wheat crop and proper fertilizer should be chosen to prevent the deficiency of these elements [9]. Cu concentration and Cu uptake both were highest for T4 sample; indicated that the Cu is highly associated with OM which is the main content of FYM [10]. The second most considerable results were obtained by the addition of Zn concerning the plants growth and yield. The highest and almost same concentration of Zn was obtained for T3 and T4 treatments. It may be concluded by results that along with Cu, significant amount of zinc is also contained with FYM.

The graphs of yields of rice and wheat grain vs. years have been plotted (Fig.1 to Fig.6). The best grain yield of Rice and Wheat is obtained for the treatment T4 (Fig. 4). Addition of FYM with 100% NPK have offered the superior crop production with a higher uptake of micronutrients. FYM is consist of 26.38 % Organic matter which is one of the main soil parameter governing the processes of sorption and desorption of trace elements [11]. The yield of rice and wheat has been increased also

in the subsequent years by the adding FYM. Addition of Zn has clearly enhanced the grain yields of both rice and wheat by substantial amount. A slightly better yield was obtained by adding biofertilizers in soil (Fig. 5) compared to control (Fig. 6). The use of biofertilizers with Zn or FYM could be a better option.

The empirical relations, for concentrations values as a function of atomic number, have been obtained.

If the concentration (in $\mu\text{g/g}$) is denoted by $C(Z)$, the equations of $C(Z)$ as a function of atomic numbers are:

$$\begin{aligned}
 C(Z) &= 0.7780709925 \times 10^8 - 0.1016150467 \times 10^8 + 442082.2227 Z^2 - 6406.988733 Z^3, \text{ for } Z = 23 \\
 &= -0.4591923012 \times 10^9 + 0.5696341861 \times 10^8 Z - 0.2354789657 \times 10^7 Z^2 + 32438.45405 Z^3, \text{ for } Z = 24 \\
 &= \\
 &0.1102960231 \times 10^{10} - 0.1304948853 \times 10^9 Z + 0.5143542504 \times 10^7 Z^2 - 67539.30812 Z^3, \text{ for } Z = 25 \\
 &= -0.1277355453 \times 10^{10} + 0.1441569241 \times 10^9 Z - 0.5419988627 \times 10^7 Z^2 + 67890.57818 Z^3, \text{ for } Z = 26 \\
 &= \\
 &0.7165788765 \times 10^9 - 0.7739133459 \times 10^8 Z + 0.2785502433 \times 10^7 Z^2 - 33411.78057 Z^3, \text{ for } Z = 27 \\
 &= \\
 &-0.2099348092 \times 10^9 + 0.2187798883 \times 10^8 Z - 759830.5453 Z^2 + 8794.564393 Z^3, \text{ for } Z = 28 \\
 &= \\
 &0.4761506567 \times 10^8 - 0.4765101657 \times 10^7 Z + 158896.7127 Z^2 - 1765.519030 Z^3, \text{ for } Z = 29 \text{ \& } Z = 30
 \end{aligned}$$

(7)

Generally it is not so easy to fit the data points which have large variations in the values and less in number, as the case here. To fit a smooth curve to such data points, the cubic spline method is a better approach. The method covers all data points and the fitted curve will be discontinuous on intermediate points.

The (7) were fitted well with the experimental values of concentrations of different elements (TABLE 4). More research in later years may be done to obtain the more accurate empirical relations. Moreover, after creating a database of subsequent years, the variation trends of elemental concentrations may also be studied.

Conclusion

Soil composition for trace elements depends strongly on the given fertilizers treatments and fertilizers concentration. EDXRF is competent technique for analyzing the soil like complex material. Application of farmyard manure (FYM) with 100% NPK has the highest effect on the yield of wheat and rice crops. It also improves the concentrations of some essential trace elements like Cu and Zn in the soil, as confirmed by EDXRF results. The study also pronounces that chemical fertilizers can not be substituted by biofertilizers, concerning plant growth of rice and wheat. Zn has proven to be the most important trace element for rice-wheat cropping system and has a significant role in obtaining higher yield. Except Co, the concentrations of all the trace elements, determined here, in the soil were found to be influenced by the treatments of different fertilizers. The empirical relations obtained by cubic spline method are useful for current and future research purposes.

References

- [1] S.K. Shukla, and A.S. Warsi, Effect of sulphur and micronutrients on growth, nutrient content and yield of wheat (*Triticum aestivum* L.), *Indian J. Agric. Res.*, 34, 2000, 203-205.
- [2] S. Razic, S. Dogo, and L. Slavkovic, Inorganic analysis of herbal drugs. Part II. Plant and soil analysis – diverse bioavailability and uptake of essential and toxic elements, *J. Serb. Chem. Soc.*, 71, 2006, 1095–1105.
- [3] K.N. Yu, Z.L.L. Yeung, L.Y.L. Lee, M.J. Stokesa, and R.C.W. Kwok, Determination of multi-element profiles of soil using energy dispersive X-ray fluorescence (EDXRF), *Appl. Radiat. Isot.*, 57, 2002, 279–284.
- [4] E.G. Jobbagay, and R.B. Jackson, The distribution of soil nutrients with depth: Global patterns and the imprint of plants. *Biogeochemistry*, 53, 2001, 51–77.
- [5] M.H. Nagoka, T. Yamazaki, and T. Maitani, Binding patterns of vanadium ions with different valence states to human serum transferring studied by HPLC/high resolution ICP-MS, *Biochem. Biophys Res. Commun.*, 296, 2002, 1207-1214.
- [6] V. Singh, and N. Ram, Effect of 25 years of continuous fertilizer use on response to applied nutrients on uptake of micronutrients by rice-wheat-cowpea system, *Cereal Res. Comm.*, 33, 2005, 589-594.
- [7] V.K. Nayyar, C.L. Arora, and P.K. Katak, Management of Soil Micronutrient Deficiencies in the Rice-Wheat Cropping System, in P.K Katak (Ed.), *The Rice-Wheat Cropping Systems of South Asia: Efficient Production Management* (New York: Food Products Press, 2001) 87-131.
- [8] M.A. Awodun, Effect of Azolla (*Azolla* Species) on physiological properties of the soil, *World J. of Agri. Sciences*, 4, 2008, 157-160.
- [9] A.R. Demikiran, Determination of Fe, Cu and Zn contents of wheat and corns grains from different growing site, *J. of Animal & Vet. Adv.*, 8, 2009, 1563-1567.
- [10] R.B. Herbert, Partitioning of heavy metals in podzol soils contaminated by mine drainage water, Dalarna, Sweden, *Water Air Soil Poll.*, 96, 1997, 39-59.
- [10] E. Merian, M. Anke, M. Ichnat, and M. Stoeppler, *Elements and their Compounds in the Environment-2nd Edition* (Weinheim, WILEY-VCH, 2004)

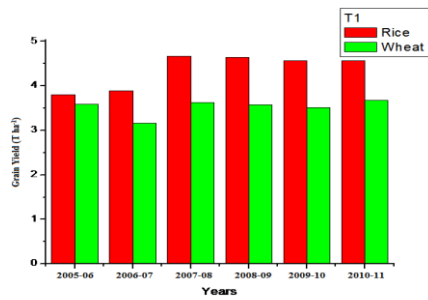


Fig. 1: Grain yield bar graph of rice and wheat crops for the consecutive years and for treatment T1

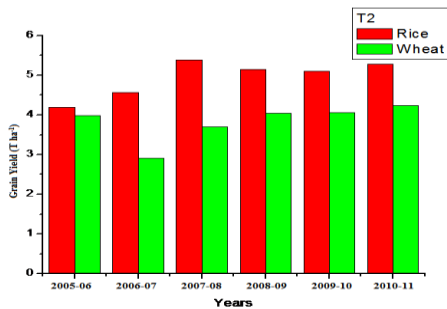


Fig. 2: Grain yield bar graph of rice and wheat crops for the consecutive years and for treatment T1. Addition of Zn alone has substantially enhanced the yields

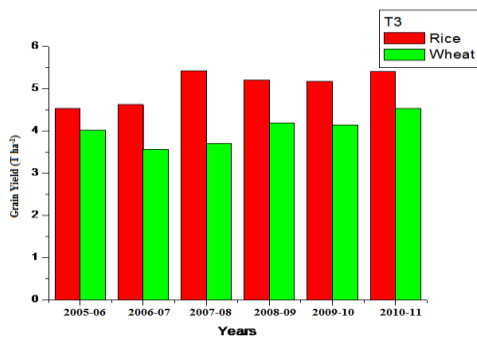


Fig. 3: Grain yield bar graph of rice and wheat crops for the consecutive years and for treatment T3. The grain yields were almost same as for T2.

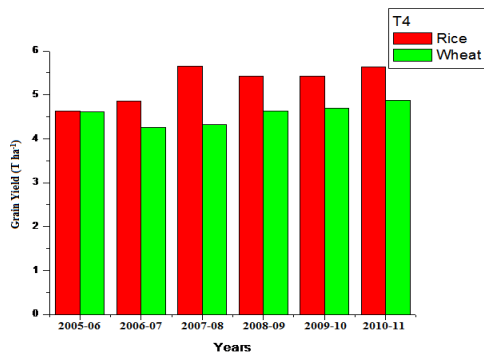


Fig. 4: The highest yield was obtained for the T4 (100% NPK+FYM). FYM has some essential trace elements associated with, for proper plants growth

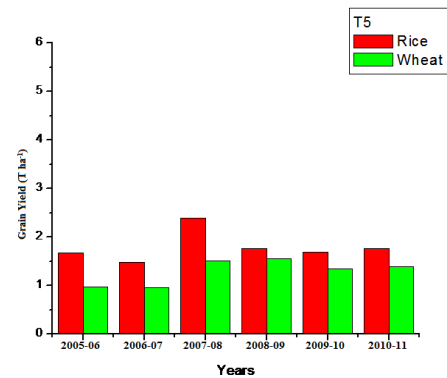


Fig. 5: A slightly greater yield than Control is obtained for T5. The addition of biofertilizers alone in soil is not sufficient for proper plants growth.

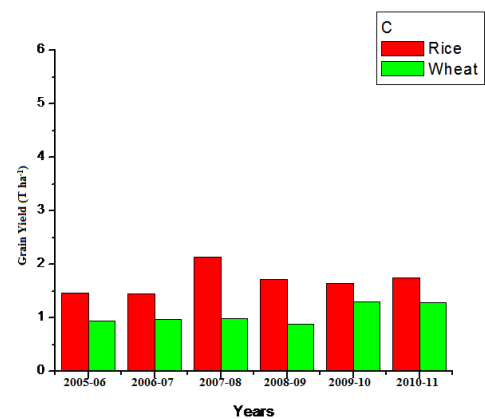


Fig. 6: The lowest yield was obtained for Control.

TABLE 2: The Treatments Given to Soil Prior to Sampling for EDXRF Analysis

Treatments	Treatment Code	Treatment Detail
Treatment 1	T 1	100 % NPK ^a of recommended dose
Treatment 2	T 2	100 % NPK+Hand Weeding+Zinc
Treatment 3	T 3	100 % NPK+ Zinc
Treatment 4	T 4	100 % NPK+ Farmacyd Manure (FYM)
Treatment 5	T 5	Biofertilizers
Control	C	Control

TABLE 3: Concentrations of Eight Trace Elements Determined by EDXRF Technique. The Concentrations were Given in the Form of 'Arithmetic Mean \pm Arithmetic Standard Deviation'.

Treatments	Concentration in $\mu\text{g/g}$							
	V	Cr	Mn	Fe	Co	Ni	Cu	Zn
T 1	117.48 ± 5.17	114.65 ± 3.7	497.78 ± 25.24	60429.58 ± 1620.7	39.09 ± 1.75	6.97 ± 0.45	8.49 ± 0.5	40.78 ± 2.81
T 2	128.27 ± 8.78	99.57 ± 19.14	483.39 ± 5.37	58542.35 ± 1437.31	35.95 ± 1.24	6.84 ± 0.72	8.31 ± 0.68	48.36 ± 4.55
T 3	111.95 ± 5.61	98.73 ± 12.17	470.05 ± 19.95	57760.67 ± 4910.49	39.42 ± 5.27	7.24 ± 0.09	8.23 ± 1.38	43.43 ± 6.04
T 4	114.3 ± 4.82	92.06 ± 8.96	473.25 ± 26.1	57063.91 ± 3688.6	39.12 ± 0.37	8.12 ± 0.94	9.34 ± 0.28	43.53 ± 2.43
T 5	106.22 ± 1.72	94.69 ± 14.78	436.69 ± 10.12	53385.35 ± 1898.35	37.69 ± 1.75	5.91 ± 1.09	9.03 ± 0.36	36.99 ± 2.01
C	118.5 ± 5.23	100.05 ± 16.41	472.89 ± 13.64	57765.63 ± 2252.19	36.71 ± 4.76	5.96 ± 0.71	8.76 ± 0.06	40.61 ± 0.97

TABLE 4: The Experimentally Obtained Concentration values and the Values Fitted by Cubic Spline Method

Element	Atomic Number (Z)	Experimental Values (in $\mu\text{g/g}$) (Arithmetic Mean)	Arithmetic Standard Deviation	Fitted Values
Vanadium (V)	23	114.3	4.82	114.33
Chromium (Cr)	24	92.06	8.96	91.8
Manganese (Mn)	25	473.25	26.1	474.12
Iron (Fe)	26	57063.91	3688.6	57063.84
Nickel (Ni)	27	39.12	0.37	39.27
Cobalt (Co)	28	8.12	0.94	8.08
Copper (Cu)	29	9.34	0.28	9.38
Zinc (Zn)	30	43.53	2.43	43.58

Protection of Privacy in Distributed Databases using Clustering

Ganesh P.¹, KamalRaj R², Dr. Karthik S.³

^{1,2,3}Department of Computer Science Engineering SNS College of Technology

Abstract: Clustering is the technique which discovers groups over huge amount of data, based on similarities, regardless of their structure (multi-dimensional or two dimensional). We applied an algorithm (DSOM) to cluster distributed datasets, based on self-organizing maps (SOM) and extends this approach presenting a strategy for efficient cluster analysis in distributed databases using SOM and K-means. The proposed strategy applies SOM algorithm separately in each distributed dataset, relative to database horizontal partitions, to obtain a representative subset of each local dataset. In the sequence, these representative subsets are sent to a central site, which performs a fusion of the partial results and applies SOM and K-means algorithms to obtain a final result.

I. Introduction

In the recent years, there has been an increasing of data volume in organizations, due to many factors such as the automation of the data acquisition and reduced storage costs. For that reason, there has been also a growing interest in computational algorithms that can be used to extracting relevant information from recorded data.

Data mining is the process of applying various methods and techniques to databases, with the objective of extract information hidden in large amounts of data. A frequently used method is cluster analysis, which can be defined as the process of partition data into a certain number of clusters (or groups) of similar objects, where each group consists of similar objects amongst themselves (internal homogeneity) and different from the objects of the other groups (external heterogeneity), i.e., patterns in the same cluster should be similar to each other, while patterns in different clusters should not [1].

More formally, given a set of N input patterns:

$X = \{x_1, \dots, x_N\}$, where each $x_j = (x_{j1}, \dots, x_{jp})$ represents a p -dimensional vector and each measure x_{ji} represents a attribute (or variable) from dataset, a clustering process attempts to seek a K partition of X , denoted by $C = \{C_1, \dots, C_K\}$, ($K \leq N$). Artificial neural networks are an important computational tool with strong inspiration neurobiological and widely used in the solution of complex problems, which cannot be handled with traditional algorithmic solutions [13]. Applications for RNA include pattern recognition, signal analysis and processing, analysis tasks, diagnosis and prognostic, data classification and clustering.

In some works, they presented a simple and efficient algorithm to cluster distributed datasets, based on multiples parallel SOM, denominated partSOM [5]. The algorithm is particularly interesting in situations where the data volume is very large or when data privacy and security policies forbid data consolidation into a single location.

This work extends this approach presenting a strategy for efficient cluster analysis in distributed databases using SOM and K-means. The strategy is to apply SOM algorithm separately in each distributed dataset, horizontal

partitions of data, to obtain a representative subset of each local dataset. In the sequence these representative subsets are sent to a central site, which performs a fusion of the results and applies SOM and K-means algorithms to obtain the final result.

The remainder of the article is organized as follows: section 2 presents a brief review about distributed data clustering algorithms and section 3 describes the main aspects of the SOM. The proposed algorithm is presented in section 4 describes the methodology. Finally, section 5 presents conclusions and future research directions.

II. Bibliography Review

Cluster analysis algorithms groups data based on the similarities between patterns. The complexity of cluster analysis process increases with data cardinality and dimensionality. Cardinality :- (N , the number of objects in a database) and dimensionality:- (p , the number of attributes). Clustering methods range from those that are Largely heuristic method to statistic method. Several algorithms have been developed based on different strategies, including hierarchical clustering, vector quantization, graph theory, fuzzy logic, neural networks and others. A recent survey of cluster analysis algorithms is presented in Xu and Wunsch [1].

Searching clusters in high-dimensional databases is a non trivial task. Some common algorithms, such as traditional agglomerative hierarchical methods, are improper to large datasets. The increase in the number of attributes of each entrance does not just influence negatively in the time of processing of the algorithm, as well as it hinders the process of identification of the clusters. An alternative approach is divide database into partitions and to perform data clustering each one separately.

Some current applications have so large databases that are not possible to maintain them integrally in the main memory, even using robust machines. Kantardzic[2] points three approaches to solve that problem:

- a) The data are stored in secondary memory and data subsets are clustered separately. A subsequent stage is needed to merge results;
- b) Usage of an incremental grouping algorithm. Each element is individually stored in the main memory and associated to one of the existent groups or allocated in a new group;
- c) Usage of a parallel implementation. Several algorithms work simultaneously on the stored data.

Two approaches are usually used to partition dataset: the first, and more usual, is to divide horizontally the database, creating homogeneous subsets of the data. Each algorithm operates on the same attributes. Another approach is to divide horizontally the database, creating heterogeneous

data subsets. In this case, each algorithm operates on the same registrations, but handle on different sets of attributes.

Some recent works about distributed data clustering include Forman and Zhang [3] that describes a technique to parallel several algorithms in order to obtain larger efficiency in data mining process of multiple distributed databases. Authors reinforce the concern need in relation to reducing communication

Several organizations maintain geographically distributed databases as a form of increasing the safety of their information. In that way, if safety policies fail, the invader has just access to a part of the existent information. Vaidya and Clifton [18] approaches vertically partitioned databases using a distributed K-means algorithm. Jagannathan et al. [11] present a variant of K-means algorithm to clustering horizontally partitioned databases. Oliveira and Zaiane [9] proposed a spatial data transformation method to protecting attributes values when sharing data for clustering, called RBT, that and is independent of any clustering algorithm.

In databases with a large number of attributes, another approach sometimes used is to accomplish the analysis considering only a subset of the attributes, instead of considering all of them. An obvious difficulty of this approach is to identify which attributes are more important in the process of clusters identification. Some papers related with this approach have frequently used statistical methods as Principal Components Analysis (PCA) and Factor Analysis to treat this problem. Kargupta et al. [10] presented a PCA-based technique denominated Collective Principal Component Analysis (CPCA) for cluster analysis of high-dimensional heterogeneous distributed databases. The authors demonstrated concern in reducing data transfers taxes among distributed sites.

Other works consider the possibility to partition attributes in subsets, but considering each one of them in data mining process. This is of particular interest for the maintenance of whole characteristics present in initial dataset. He et al. [12] analyzed the influence of data types in clustering process and presented a strategy that divided the attributes in two subsets, one with the numerical attributes and other with the categorical ones. Subsequently, they propose to cluster separately of each one of the subsets, using appropriate algorithms for each one of the types. The cluster results were combined in a new database, which was again submitted to a clustering algorithm for categorical data.

III. Self-Organizing Map

The self-organizing feature map (SOM) has been widely used as a tool for visualization of high-dimensional data. Important features include information compression while preserving topological and metric relationship of the primary data items [14]. SOM is composed of two layers of neurons, input and output layers. A neighbouring relation with neurons defines the topology of the map. Training is similar to neural competitive learning, but the best match unit (c or BMU) is updated as well as they neighbors. Each input is mapped to a BMU, which has weight vectors most similar to the presented data.

A number of methods for visualizing data relations in a trained SOM have been proposed [17], such as multiple views of component planes, mesh visualization using

projections and 2D and 3D surface plots of distance matrices. The U-matrix method [17] enables visualization of the topological relations of the neurons in an organized SOM. A gradient image (2D) or a surface plot is generated by computing distances between adjacent neurons. High values in the U-matrix encode dissimilarities between neurons and correspond to cluster borders. Strategies for cluster detection using U-matrix were proposed by Costa and Netto [16]. The algorithms were developed for automatic partitioning and labeling of a trained SOM network. The result is a segmented SOM output with regions of neurons describing the data clusters.

IV. Proposed Methodology

Distributed clustering algorithms usually work in two stages. Initially, the data are analyzed locally, in each unit that is part of the distributed database. In a second stage, a central instance gathers partial results and combines them into an overall result.

This section presents a strategy for clustering similar objects located in distributed databases, using parallel self-organizing maps and K-means algorithm. The process is divided in three stages.

- a) Traditional SOM algorithm is applied locally in each one of the distributed bases, in order to elect a representative subset from input data;
- b) Traditional SOM is applied again, this time to the representatives of each one of the distributed bases that are unified in a central unit;
- c) K-means algorithm is applied over trained self-organizing map, to create a definitive result.

The proposed algorithm, consisting of six steps: step 1 applies local clustering in each local dataset (horizontal parties from the database) using traditional SOM. Thus, the algorithm is applied to an attribute subset in each of the remote units, obtaining a reference vector from each data subset. This reference vector, known as the codebook, is the self-organizing map trained.

In step 2, a projection is made of the input data on the map in the previous stage, in each local unit. Each input is presented to the trained map and the index corresponding to the closest vector (BMU) present in the codebook is stored in an index vector. So, a data index is created based on representative objects instead of original objects. Despite the difference from the original dataset, representative objects in the index vector are very similar to the original data, since maintenance of data topology is an important characteristic of the SOM.

In step 3, each remote unit sends its index and reference vector to the central unit, which is responsible for unifying all partial results. An additional advantage of the proposed algorithm is that the amount of transferred data is considerably reduced, since index vectors have only one column (containing an integer value) and the codebook is usually much less than the original data. So, reducing data transfer and communication overload are considered by the proposed algorithm.

Step 4 is responsible for receiving the index vector and the codebook from each local unit and combining partial results to remount a database based on received data. To remount each dataset, index vector indexes are substituted by the equivalent value in the

codebook. Datasets are combined juxtaposing partial datasets; however, it is important to ensure that objects are in the same order as that of the original datasets. Note that the new database is slightly different from the original data, but data topology is maintained.

In step 5, the SOM algorithm is again applied over the complete database obtained in step 4. The expectation is that the results obtained in that stage can be generalized as being equivalent to the clustering process of the entire database. The data obtained after the step 4 and that will serve as input in stage 5 correspond to values close to the original, because vectors correspondents in codebook are representatives of input dataset.

In step 6, K-means algorithm is applied over the final trained map, in order to improve the quality of the visualization results.

V. Conclusion

Self-organizing map is neural network concept, unsupervised learning strategy, has been widely used in clustering applications. However, SOM approach is normally applied to single and local datasets. In one of the research work, they introduced partSOM, an efficient strategy SOM-based to perform distributed data clustering on geographically distributed databases.

However, SOM and partSOM approaches have some limitations for presenting results. In this work we join partSOM strategy with an alternative approach for cluster detection using K-means algorithm.

References

- [1] R. Xu and D. Wunsch II. "Survey of Clustering Algorithms", IEEE Trans. on Neural Networks, Vol.16, Iss.3, May 2005, pp. 645-678.
- [2] M. Kantardzic, Data Mining: Concepts, Models, Methods, and Algorithms, IEEE Press, 2003.
- [3] G. Forman and B. Zhang, "Distributed data clustering can be efficient and exact". SIGKDD Explor. Newsl. 2, Dec. 2000, pp 34-38.
- [4] Chak-Man Lam, Xiao-Feng Zhang and W. K. Cheung, "Mining Local Data Sources for Learning Global Cluster Models", Web Intelligence, Proceedings IEEE/WIC/ACM International Conference on WI 2004, Iss. 20-24, Sept. 2004, pp. 748-751.
- [5] F. L. Gorgônio and J. A. F. Costa, "Parallel Self-Organizing Maps with Applications in Clustering Distributed Data", International Joint Conference on Neural Networks (IJCNN'2008), (Accepted).
- [6] A. Asuncion and D.J. Newman. UCI Machine Learning Repository, available at <http://www.ics.uci.edu/~mlern/MLRepository.html>, Irvine, CA, 2007.
- [7] J. C. Silva and M. Klusch, "Inference in distributed data clustering", Engineering Applications of Artificial Intelligence, vol. 19, 2006, pp. 363-369.
- [8] P. Berkhin, "A Survey of Clustering Data Mining Techniques", In: J. Kogan et al., Grouping Multidimensional Data: Recent Advances in Clustering, New York: Springer- Verlag, 2006.
- [9] S. R. M. Oliveira and O. R. Zaiane, "Privacy Preservation When Sharing Data For Clustering", In: Proceedings of the International Workshop on Secure Data Management in a Connected World, 2004.
- [10] H. Kargupta, W. Huang, K. Sivakumar and E. Johnson, "Distributed Clustering Using Collective Principal Component Analysis", Knowledge and Information Systems Journal, Vol. 3, Num. 4, May 2001, pp. 422-448.
- [11] G. Jagannathan, K. Pillaipakkamatt and R. N. Wright, "A

- New Privacy-Preserving Distributed k-Clustering Algorithm", In: Proceedings of the 2006 SIAM International Conference on Data Mining (SDM), 2006.
- [12] Z. He, X. Xu and S. Deng, "Clustering Mixed Numeric and Categorical Data: A Cluster Ensemble Approach", Technical Report, <http://aps.arxiv.org/ftp/cs/papers/0509/0509011.pdf>, 2005.
- [13] S. Haykin, "Neural networks: A comprehensive foundation", 2nd ed., N. York: Macmillan College Publishing Company, 1999.
- [14] T. Kohonen, Self-Organizing Maps, 3rd ed., New York: Springer-Verlag, 2001.
- [15] J. Vesanto, "Using SOM in Data Mining", Licentiate's Thesis, Department of Computer Science and Engineering, Helsinki University of Technology, Espoo, Finland, 2000
- [16] J. A. F. Costa and M. L. de Andrade Netto, "Clustering of complex shaped data sets via Kohonen maps and mathematical morphology". In: Proceedings of the SPIE, Data Mining and Knowledge Discovery. B. Dasarathy (Ed.), Vol. 4384, 2001, pp. 16-27.
- [17] A. Ultsch, "Self-Organizing Neural Networks for Visualization and Classification", In: O. Opitz et al. (Eds). Information and Classification, Springer Berlin, 1993, pp.301-306.
- [18] J. Vaidya and C. Clifton, "Privacy-preserving k-means clustering over vertically partitioned data". In: Proc. of the Ninth ACM SIGKDD Intl. Conf. on Knowledge Discovery and Data Mining, New York, 2003, pp.206-215.

Effect Of TO & CFO on OFDM and SIR Analysis and Interference Cancellation in MIMO-OFDM

N. Sreekanth¹, Dr. M. N. Giri Prasad²

¹Asso Prof., Department of ECE, K.S.R.M.College of Engineering, Kadapa, A.P., India

²Professor , Department of ECE, J.N.T U.A ,Anantapur ,A.P, India

Abstract: OFDM is a multicarrier modulation technique in which a high rate bit stream is split into N parallel bit-streams of lower rate and each of these are modulated using one of N orthogonal sub-carriers. In a basic communication system, the data is modulated onto a single carrier frequency. OFDM is a promising candidate for achieving high data rates in mobile environment because of its multicarrier modulation technique. The available bandwidth is then totally occupied by each symbol. The variations in Time Offset (TO) can lead to inter-symbol-interference (ISI) in case of frequency selective channel. A well known problem of OFDM is its sensitivity to frequency offset between the transmitted and received signals, which may be caused by Doppler shift in the channel, or by the difference between the transmitter and receiver local oscillator frequencies. This carrier frequency offset(CFO) causes loss of orthogonality between sub-carriers and the signals transmitted on each carrier are not independent of each other, which results in inter-carrier interference (ICI).The undesired ICI degrades the performance of the system. ICI mitigation techniques are essential in improving the performance of an OFDM system in an environment which induces frequency offset error in the transmitted signal. In this paper , the focus is on the problem of ICI. We proposed ICI reduction using self cancellation scheme and compared with standard OFDM system. . The simulation of OFDM was done with different digital modulation schemes such as BPSK and QPSK modulation techniques . the performance of the designed OFDM system by finding their bit error rate (BER) for different values of signal to noise ratio (SNR). Later we proposed MIMO diversity technique such as STBC OFDM to enhance the performance of the system by reducing the BER for different values of signal to noise ratio (SNR). BER Analysis for BPSK in Rayleigh channel With two transmit and one receive antenna as well as two transmit and two receive antennas for Alamouti STBC case shows higher performance, which effectively alleviates the effects of ISI and ICI.

Keywords: TO, CFO, ISI, ICI, Doppler shift, Self cancellation, CIR, STBC, BER etc.

1. INTRODUCTION

Orthogonal Frequency Division Multiplexing (OFDM) is a technique in which the total transmission bandwidth is split into a number of orthogonal subcarriers so that a wideband signal is transformed in a parallel arrangement

of narrowband 'orthogonal' signals. In this way, a high data rate stream that would otherwise require a channel bandwidth far beyond the actual coherence bandwidth can be divided into a number of lower rate streams. Increasing the number of subcarriers increases the symbol period so that, ideally, a frequency selective fading channel is turned into a flat fading one. In other words, OFDM handles frequency selective fading resulting from time dispersion of multipath channels by expanding the symbol duration [1]. Very high data rates are consequently possible and for this reason it has been chosen as the transmission method for many standards from cable-based Asymmetric Digital Subscriber Line (ADSL), to wireless systems such as the IEEE 802.11a/g local area network, the IEEE 802.16 for broadband metropolitan area network and digital video and audio broadcasting. The fact that the

OFDM symbol period is longer than in single carrier modulation, assures a greater robustness against Inter-Symbol Interference (ISI) caused by delay spread. On the other hand, this makes the system more sensitive to time variations that may cause the loss of orthogonality among subcarriers thus introducing cross interference among subcarriers. Other possible causes of this loss may be due to frequency or sampling offsets emerging at the local oscillator, phase noise and synchronization errors: the combination of all these factors forms the frequency domain OFDM channel response that can be summarized in an ICI matrix. Estimation of this channel matrix is crucial to maximize performance, but in real world OFDM systems this task can be very tough, since the size of the ICI matrix depends on the number of OFDM subcarriers which can be in the order of hundreds or thousands. Several channel estimation algorithms and methods to obtain ICI cancellation have been reported in the literature in both frequency and time domain: although blind techniques are possible without reduction of Spectrum efficiency, commercial systems include pilot patterns to improve the estimation process. These are exploited for example in [2] where a pilot-symbol-aided estimation in the time domain is proposed. Other approaches tend to exploit some other redundancy in the signal structure. In [3][4], training symbols are used to estimate the frequency offset, in [5] the authors propose to use the cyclic-prefix and then Independent Component Analysis (ICA) is applied to the received subcarriers. In [6] frequency offset estimation is obtained by repeated information symbols. The paper is organized as follows. In Section 2 the OFDM system model and formulation of the OFDM channel in frequency domain is introduced together with the ICI matrix approximation. In

Section 3 the problem due to inter carrier interference is analyzed. In Section 4 the proposed method is described. Section 5 the simulations results are analyzed. Section 6 the MIMO STBC model is introduced and in Section 7 the BER analysis of proposed STBC method is derived and simulated. Finally conclusions and some perspectives are given.

2. SYSTEM MODEL

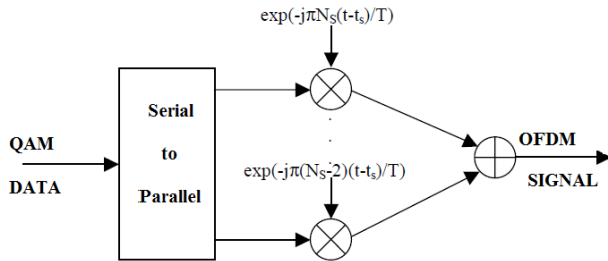


Fig 2.1 OFDM system model

In an OFDM system, the input bit stream is multiplexed into N symbol streams, each with symbol period T, and each symbol stream is used to modulate parallel, synchronous sub-carriers [1]. The sub-carriers are spaced by 1 in frequency, thus they are orthogonal over the interval (0, T).

A typical discrete-time baseband OFDM transceiver system is shown in Figure 2.1. First, a serial-to-parallel (S/P) converter groups the stream of input bits from the source encoder into groups of log₂ M bits, where M is the alphabet of size of the digital modulation scheme employed on each sub-carrier. A total of N such symbols, X_m, are created. Then, the N symbols are mapped to bins of an inverse fast Fourier transform (IFFT). These IFFT bins correspond to the orthogonal sub-carriers in the OFDM symbol. Therefore, the OFDM symbol can be expressed as

$$X(n) = \frac{1}{N} \sum_{m=0}^{N-1} X(m) \exp\left(\frac{j2\pi nm}{N}\right) \text{-----(2.1)}$$

where the X(m)'s are the baseband symbols on each sub-carrier. The digital-to-analog (D/A) converter then creates an analog time-domain signal which is transmitted through the channel.

At the receiver, the signal is converted back to a discrete N point sequence y(n), corresponding to each sub-carrier. This discrete signal is demodulated using an N-point fast Fourier transform (FFT) operation at the receiver. The demodulated symbol stream is given by:

$$Y(m) = \sum_{n=0}^{N-1} y(n) \exp\left(\frac{-j2\pi nm}{N}\right) + W(m) \text{---(2.2)}$$

where, W(m) corresponds to the FFT of the samples of w(n), which is the Additive White Gaussian Noise (AWGN) introduced in the channel.

The high speed data rates for OFDM are accomplished by the simultaneous transmission of data at a lower rate on each of the orthogonal sub-carriers. Because of the low data rate transmission, distortion in the received signal induced by

multi-path delay in the channel is not as significant as compared to single-carrier high-data rate systems. For example, a narrowband signal sent at a high data rate through a multipath channel will experience greater negative effects of the multipath delay spread, because the symbols are much closer together [3]. Multipath distortion can also cause inter-symbol interference (ISI) where adjacent symbols overlap with each other. This is prevented in OFDM by the insertion of a cyclic prefix between successive OFDM symbols. This cyclic prefix is discarded at the receiver to cancel out ISI. It is due to the robustness of OFDM to ISI and multipath distortion that it has been considered for various wireless applications and standards[3].

2.1 DERIVATIONS OF ICI COEFFICIENTS:

say Y_k is the Discrete Fourier Transform of y(n). Then we get,

$$\begin{aligned} Y(k) &= \sum_{n=0}^{N-1} x(n) \exp\left(\frac{j2\pi n\epsilon}{N}\right) \exp\left(\frac{-j2\pi nk}{N}\right) \\ &= \sum_{n=0}^{N-1} \frac{1}{N} \left(\sum_{m=0}^{N-1} X(m) \exp\left(\frac{j2\pi nm}{N}\right) \exp\left(\frac{j2\pi n(\epsilon-k)}{N}\right)\right) \\ &= \frac{1}{N} \sum_{m=0}^{N-1} X(m) \sum_{n=0}^{N-1} \exp\left(\frac{j2\pi n(m+\epsilon-k)}{N}\right) = \frac{1}{N} \\ &\sum_{m=0}^{N-1} X(m) \sum_{n=0}^{N-1} \exp\left(\frac{j2\pi n(m+\epsilon-k)}{N}\right) \text{ (B.1)} \end{aligned}$$

We can expand $\frac{1}{N} \sum_{n=0}^{N-1} \exp\left(\frac{j2\pi n(m+\epsilon-k)}{N}\right)$ using the geometric series as,

$$\begin{aligned} \frac{1}{N} \sum_{n=0}^{N-1} \exp\left(\frac{j2\pi n(m+\epsilon-k)}{N}\right) &= \frac{1}{N} \frac{1 - \exp\left(\frac{j2\pi N(m+\epsilon-k)}{N}\right)}{1 - \exp\left(\frac{j2\pi(m+\epsilon-k)}{N}\right)} \\ &= \left(\frac{1}{N}\right) \frac{\exp\left(\frac{j2\pi(m+\epsilon-k)}{2}\right) \left(\exp\left(-\frac{j2\pi(m+\epsilon-k)}{2}\right) - \exp\left(\frac{j2\pi(m+\epsilon-k)}{2}\right)\right)}{\exp\left(\frac{j2\pi(m+\epsilon-k)}{2N}\right) \left(\exp\left(-\frac{j2\pi(m+\epsilon-k)}{2N}\right) - \exp\left(\frac{j2\pi(m+\epsilon-k)}{2N}\right)\right)} \\ \text{(B.2)} &= \frac{1}{N} \exp\left(j2\pi(m+\epsilon-k)\right) \left(1 - \frac{1}{N}\right) \frac{\text{SIN}\left(\pi(m+\epsilon-k)\right)}{\text{SIN}\left(\frac{\pi(m+\epsilon-k)}{N}\right)} \end{aligned}$$

Substituting (B.2) in (B.1), we get,

$$\begin{aligned} Y(k) &= \sum_{m=0}^{N-1} X(m) S(m-k) \text{ Where ,} \\ S(m-k) &= \exp\left(j2\pi(m+\epsilon-k)\right) \left(1 - \frac{1}{N}\right) \frac{\text{SIN}\left(\pi(m+\epsilon-k)\right)}{\text{SIN}\left(\frac{\pi(m+\epsilon-k)}{N}\right)} \end{aligned}$$

Which are the required ICI coefficients.

3. ANALYSIS OF INTER CARRIER INTERFERENCE

The main disadvantage of OFDM, however, is its susceptibility to small differences in frequency at the transmitter and receiver, normally referred to as frequency offset. This frequency offset can be caused by Doppler shift due to relative motion between the transmitter and receiver, or by differences between the frequencies of the local oscillators at the transmitter and receiver. In this project, the frequency offset is modeled as a multiplicative factor introduced in the channel[10].

The received signal is given by

$$Y(n) = x(n) \exp\left(\frac{j2\pi n\epsilon}{N}\right) + W(n) \text{---(3.1)}$$

where ε is the normalized frequency offset, and is given by ΔfNT . Δf is the frequency difference between the transmitted

and received carrier frequencies and T_s is the subcarrier symbol period. $w(n)$ is the AWGN introduced in the channel.

The effect of this frequency offset on the received symbol stream can be understood by considering the received

$$Y(k) = x(k)S(0) + \sum_{l=0, l \neq k}^{N-1} X(l)S(l-k) + n_k \quad (3.2)$$

where N is the total number of subcarriers, $X(k)$ is the transmitted symbol (M-ary phase-shift keying (M-PSK), for example) for the k subcarrier, is the FFT of $w(n)$, and $S(l-k)$ are the complex coefficients for the ICI components in the received signal. The ICI components are the interfering signals transmitted on sub-carriers other than the k sub-carrier. The complex coefficients are given by

$$S(l-k) = \frac{\sin(\pi(l+\epsilon-k))}{N \sin(\frac{\pi(l+\epsilon-k)}{N})} \exp(j\pi(1-1/N)(l+\epsilon-k)) \quad (3.3)$$

The carrier-to-interference ratio (CIR) is the ratio of the signal power to the power in the interference components. It serves as a good indication of signal quality. It has been derived from (3.2) in [7] and is given below. The derivation assumes that the standard transmitted data has zero mean and the symbols transmitted on the different sub-carriers are statistically independent.

$$CIR = \frac{|s(k)|^2}{\sum_{l=0, l \neq k}^{N-1} |s(l-k)|^2} = \frac{|s(0)|^2}{\sum_{l=0}^{N-1} |s(l)|^2} \quad (3.4)$$

4. ICI SELF-CANCELLATION SCHEME

ICI self-cancellation is a scheme that was introduced by Yuping Zhao and Sven-Gustav Häggman in 2001 in [8] to combat and suppress ICI in OFDM. Succinctly, the main idea is to modulate the input data symbol onto a group of subcarriers with predefined coefficients such that the generated ICI signals within that group cancel each other, hence the name self-cancellation [6].

4.1 ICI Canceling Modulation

The ICI self-cancellation scheme shown in Fig 4.1.1 requires that the transmitted signals be constrained such that $X(1) = -X(0)$, $X(3) = -X(2)$, ..., $X(N-1) = -X(N-2)$. Using (3.3), this assignment of transmitted symbols allows the received signal on subcarriers k and $k+1$ to be written as

$$Y(K) = \sum_{l=0, l \text{ even}}^{N-2} x(l)[S(l-k) - S(l+1-k)] + n_k$$

$$Y(K+1) = \sum_{l=0, l \text{ even}}^{N-2} x(l)[S(l-k-1) - S(l-k)] + n_{k+1} \quad (4.1)$$

and the ICI coefficient $S'(l-k)$ is denoted as

$$S'(l-k) = S(l-k) - S(l+1-k) \quad (4.2)$$

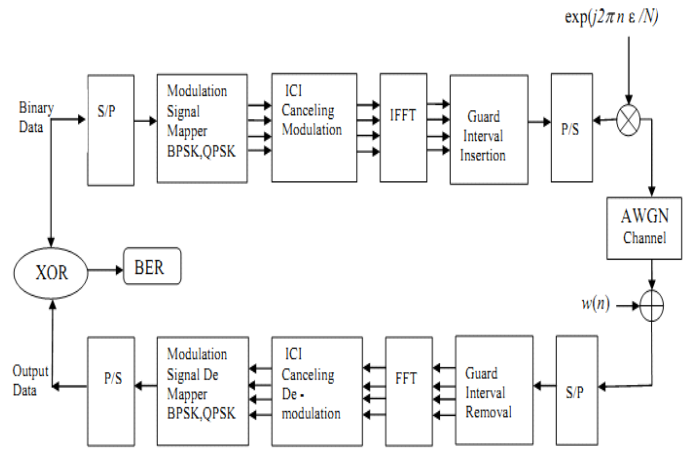


Fig.4.1.1 – OFDM Model with Self cancellation

ICI coefficients $S(l-k)$ Vs subcarrier k is plotted in figure 4.1.2

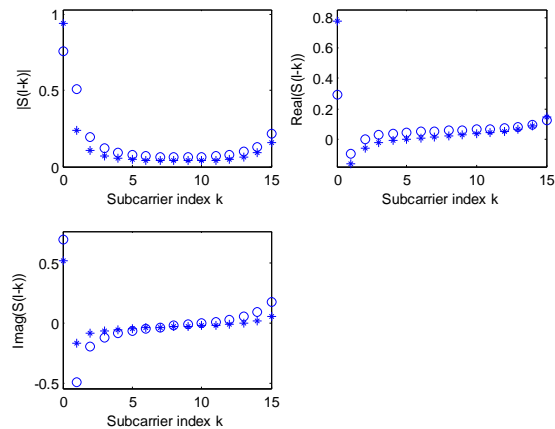


Fig 4.1.2 ICI coefficients $S(l-k)$ Vs subcarrier k

Fig.4.1.3 shows a comparison between $|S'(l-k)|$ and $|S(l-k)|$ on a logarithmic scale. It is seen that $|S'(l-k)| \ll |S(l-k)|$ for most of the $l-k$ values. Hence, the ICI components are much smaller in (4.2) than they are in (3.3). Also, the total number of interference signals is halved in (4.2) as opposed to (3.3) since only the even subcarriers are involved in the summation.

comparison of $|S(l-k)|$, $|S'(l-k)|$, and $|S''(l-k)|$ for $\epsilon = 0.2$ and $N=64$

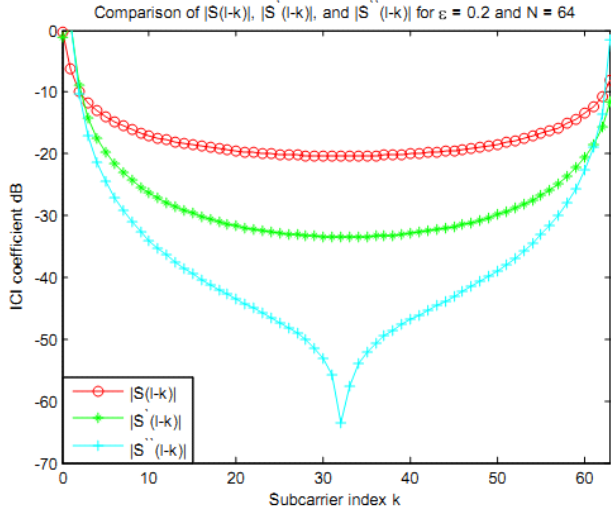


Fig.4.1.3. comparison of S (l-k), S' (l-k) and S''(l-k) Vs subcarrier k

4.2 ICI Canceling Demodulation

ICI modulation introduces redundancy in the received signal since each pair of subcarriers transmit only one data symbol. This redundancy can be exploited to improve the system power performance, while it surely decreases the bandwidth efficiency. To take advantage of this redundancy, the received signal at the (k + 1) subcarrier, where k is even, is subtracted

$$\begin{aligned}
 Y''(k) &= Y'(k) - Y'(k+1) \\
 &= \sum_{l=0, l=even}^{N-2} x(l)[-S(l-k-1)+2S(l-k)-S(l-k+1)] \\
 &\quad + n_k - n_{k+1}
 \end{aligned}$$

Subsequently, the ICI coefficients for this received signal becomes

$$S''(l-k) = -S(l-k-1) + 2S(l-k) - S(l-k+1) \quad \text{---(4.4)}$$

When compared to the two previous ICI coefficients |S(l-k)| for the standard OFDM system and |S'(l-k)| for the ICI canceling modulation, |S''(l-k)| has the smallest ICI coefficients, for the majority of l-k values, followed by |S'(l-k)| and |S(l-k)|. This is shown in Figure 4.1.3 for N = 64 and ε = 0.2. The combined modulation and demodulation method is called the ICI self-cancellation scheme. The reduction of the ICI signal levels in the ICI self-cancellation scheme leads to a higher CIR.

From (4.4), the theoretical CIR can be derived as

$$CIR = \frac{|-s(-1)+2s(0)-s(1)|^2}{\sum_{l=2,4,6}^{N-1} |-s(l-1)+2s(l)-s(l+1)|^2} \quad \text{---(4.5)}$$

Fig. (4.2.1) shows the comparison of the theoretical CIR curve of the ICI self-cancellation scheme, calculated by (4.5), and the CIR of a standard OFDM system calculated by (3.3). As expected, the CIR is greatly improved using the ICI self-cancellation scheme[9]. The improvement can be greater than 15 dB for 0 < ε < 0.5.

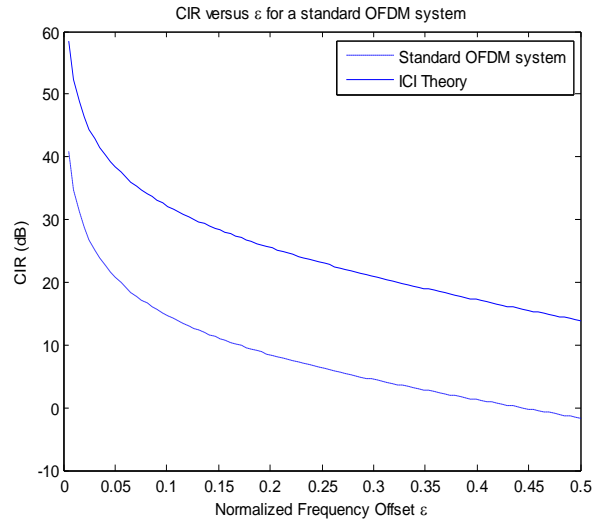


Fig. 4.2.1. CIR Vs Normalized frequency offset

As mentioned above, the redundancy in this scheme reduces the bandwidth efficiency by half. This could be compensated by transmitting signals of larger alphabet size. Using the theoretical results for the improvement of the CIR should increase the power efficiency in the system and gives better results for the BER shown in Fig. 4.2.2.

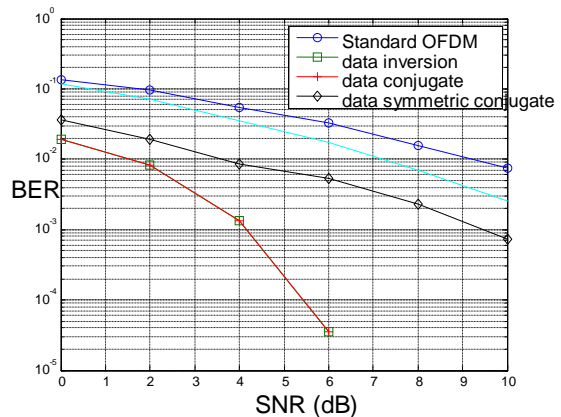


Fig. 4.2.2. BER Vs SNR for an OFDM system

Hence, there is a tradeoff between bandwidth and power tradeoff in the ICI self-cancellation scheme.

5. SIMULATION RESULTS and DISCUSSION

Fig.4.1.1 shows the Fast Fourier transform (FFT) based N-subcarrier OFDM system model used for simulation [1]. The simulation parameters used for the model shown in Figure 4.1 is as given below.

Parameter	Specifications
IFFT Size	64
Number of Carriers in one OFDM Symbol	52
channel	AWGN
Frequency Offset	0,0.15,0.3
Guard Interval	12
Modulation	BPSK,QPSK
OFDM Symbols for one loop	1000

Table 5.1- Simulation Parameters

5.1 BER performance of BPSK OFDM system:

(a) BER performance of a BPSK OFDM system with & without self cancellation :

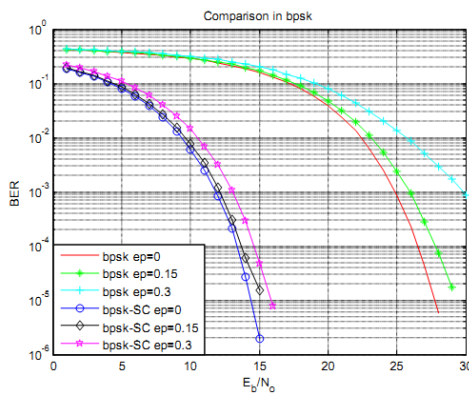


Fig 5.1.1 BER performance of a BPSK OFDM system with & without Self Cancellation

BER performance of a BPSK OFDM system with & without Self Cancellation shown in Fig. 5.1.1. This is the plot which shows the comparison between standard OFDM and OFDM with self cancellation technique for different values of frequency offset for the modulation BPSK. From the figure we observe that as the value of carrier frequency offset ϵ increases, the BER increases. We can infer that self cancellation technique in OFDM has less BER compared to without self cancellation.

5.2 BER performance of QPSK OFDM system

(a) BER performance of a QPSK OFDM system with & without Self Cancellation:

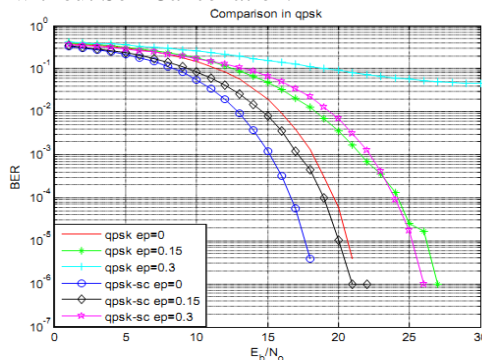


Fig.5.2.1 BER performance of a QPSK OFDM system with & without Self Cancellation

From the Fig. 5.2.1 we observe that as the value of carrier frequency offset ϵ increases, the BER increases. As SNR increases QPSK BER curve leans downward which indicates reduction in bit error rate. This is the plot which shows the comparison between standard OFDM and OFDM with self cancellation technique for different values of frequency offset for the modulation QPSK.

We can infer that self cancellation technique in OFDM has low BER compared to standard OFDM.

(b) BER performances of QPSK, BPSK OFDM systems with constant frequency offsets is simulated in Fig.(5.2.2).

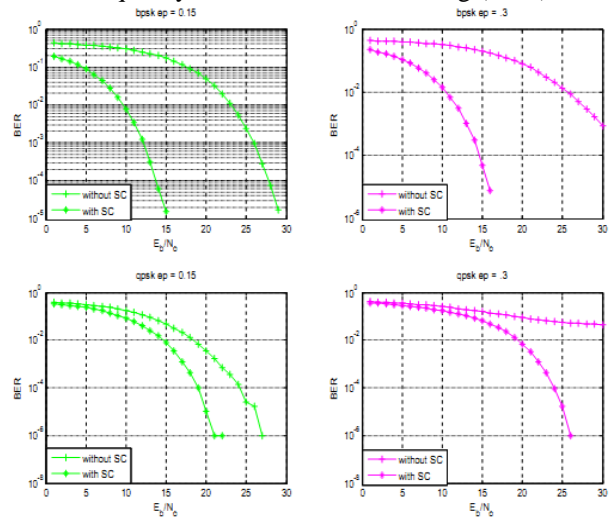


Fig 5.2.2 BER performances of QPSK, BPSK OFDM systems with constant frequency offsets

5.3 Comparison of BER performances of BPSK, QPSK OFDM systems

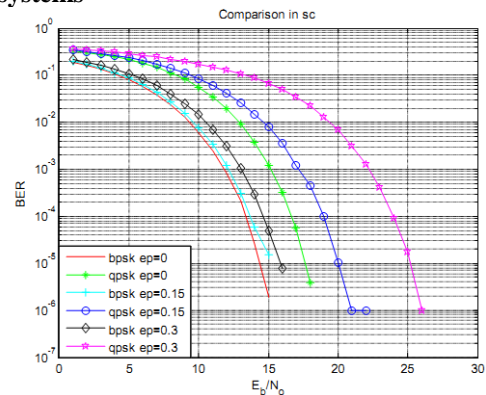


Fig 5.3.1 BER performance of a BPSK, QPSK OFDM systems with Self Cancellation.

This plot shown in Fig.5.3.1. is the comparison between two modulation techniques for different values of frequency offset. Here only self cancellation technique is considered. We notice that as the value of carrier frequency offset ϵ increases, the BER increases. For low frequency offset value BER is less. For constant ϵ value, BER of BPSK is less than BER of QPSK.

6. ALTAMONTE STBC

6.1 Transmitter with Alamouti STBC

Three receive diversity schemes – Selection combining, Equal Gain Combining and Maximal Ratio Combining. All the three approaches used the antenna array at the receiver to improve the demodulation performance, albeit with different levels of complexity. Time to move on to a **transmit diversity**[11] scheme where the information is spread across multiple antennas at the transmitter. Lets discuss a popular transmit diversity scheme called **Alamouti Space Time Block Coding (STBC)**[13]. For the discussion, we will assume that the channel is a flat fading Rayleigh multipath channel and the modulation is BPSK.

A simple Space Time Code, suggested by Mr. Siavash M Alamouti in his landmark October 1998 paper – A Simple Transmit Diversity Technique for Wireless Communication[13], offers a simple method for achieving spatial diversity with two transmit antennas. The scheme is as follows:

1. Consider that we have a transmission sequence, For example $\{x_1, x_2, x_3, \dots, x_n\}$
2. In normal transmission, we will be sending x_1 in the first time slot, x_2 in the second time slot, x_3 and so on.
3. However, Alamouti suggested that we group the symbols into groups of two. In the first time slot, send x_1 and x_2 from the first and second antenna. In second time slot send $-x_2^*$ and x_1^* from the first and second antenna. In the third time slot send x_3 and x_4 from the first and second antenna. In fourth time slot, send $-x_4^*$ and x_3^* from the first and second antenna and so on.
4. Notice that though we are grouping two symbols, we still need two time slots to send two symbols. Hence, there is no change in the data rate.
5. This forms the simple explanation of the transmission scheme with Alamouti Space Time Block coding shown in Fig.6.1.1.

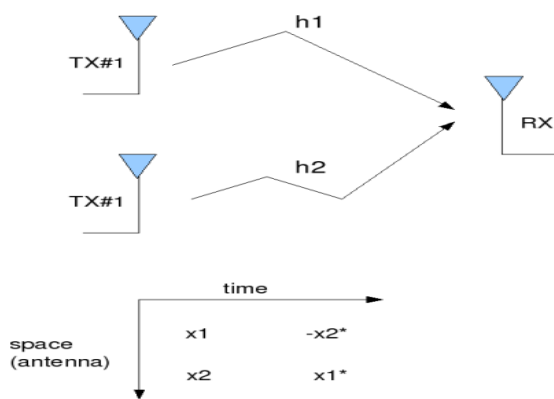


Fig. 6.1.1. Alamouti's 2Tx and 1Rx STBC Scheme

Other Assumptions

1. The channel is flat fading – In simple terms, it means that the multipath channel has only one tap. So, the convolution operation reduces to a simple multiplication.

2. The channel experience by each transmit antenna is independent from the channel experienced by other transmit antennas.

3. For the i^{th} transmit antenna, each transmitted symbol gets multiplied by a randomly varying complex number h_i . As the channel under consideration is a Rayleigh channel, the real and imaginary parts of h_i are Gaussian distributed having mean $\mu_{h_i} = 0$ and variance $\sigma_{h_i}^2 = \frac{1}{2}$.

4. The channel experienced between each transmit to the receive antenna is randomly varying in time. However, the channel is **assumed to remain constant over two time slots**.

5. On the receive antenna, the noise n has the Gaussian probability density function with

$$p(n) = \frac{1}{\sqrt{2\pi\sigma^2}} e^{-\frac{(n-\mu)^2}{2\sigma^2}} \quad \text{with} \quad \mu = 0 \text{ and } \sigma^2 = \frac{N_0}{2}$$

6. The channel h_i is known at the receiver.

6.2 Receiver with Alamouti STBC

In the first time slot, the received signal is,

$$y_1 = h_1 x_1 + h_2 x_2 + n_1 = [h_1 \ h_2] \begin{bmatrix} x_1 \\ x_2 \end{bmatrix} + n_1$$

In the second time slot, the received signal is,

$$y_2 = -h_1 x_2^* + h_2 x_1^* + n_2 = [h_1 \ h_2] \begin{bmatrix} -x_2^* \\ x_1^* \end{bmatrix} + n_2$$

Where

y_1, y_2 is the received symbol on the first and second time slot respectively,

h_1 is the channel from 1st transmit antenna to receive antenna,

h_2 is the channel from 2nd transmit antenna to receive antenna,

x_1, x_2 are the transmitted symbols and n_1, n_2 is the noise on 1st, 2nd time slots.

Since the two noise terms are independent and identically distributed,

$$E \left\{ \begin{bmatrix} n_1 \\ n_2^* \end{bmatrix} \begin{bmatrix} n_1^* & n_2 \end{bmatrix} \right\} = \begin{bmatrix} |n_1|^2 & 0 \\ 0 & |n_2|^2 \end{bmatrix}$$

For convenience, the above equation can be represented in matrix notation as follows:

$$\begin{bmatrix} y_1 \\ y_2^* \end{bmatrix} = \underbrace{\begin{bmatrix} h_1 & h_2 \\ h_2^* & -h_1^* \end{bmatrix}}_{\mathbf{H}} \begin{bmatrix} x_1 \\ x_2 \end{bmatrix} + \begin{bmatrix} n_1 \\ n_2^* \end{bmatrix}$$

$$\mathbf{H} = \begin{bmatrix} h_1 & h_2 \\ h_2^* & -h_1^* \end{bmatrix}$$

Let us define

$\begin{bmatrix} x_1 \\ x_2 \end{bmatrix}$, we know that we need to find the inverse of \mathbf{H}

. We know, for a general $m \times n$ matrix, the pseudo inverse is defined as,

$$\mathbf{H}^+ = (\mathbf{H}^H \mathbf{H})^{-1} \mathbf{H}^H$$

The term,

$$(\mathbf{H}^H \mathbf{H}) = \begin{bmatrix} h_1^* & h_2 \\ h_2^* & -h_1 \end{bmatrix} \begin{bmatrix} h_1 & h_2 \\ h_2^* & -h_1^* \end{bmatrix} = \begin{bmatrix} |h_1|^2 + |h_2|^2 & 0 \\ 0 & |h_1|^2 + |h_2|^2 \end{bmatrix}$$

. Since this is a diagonal matrix, the inverse is just the inverse of the diagonal elements, i.e

$$(\mathbf{H}^H \mathbf{H})^{-1} = \begin{bmatrix} \frac{1}{|h_1|^2 + |h_2|^2} & 0 \\ 0 & \frac{1}{|h_1|^2 + |h_2|^2} \end{bmatrix}$$

The estimate of the transmitted symbol is,

$$\begin{aligned} \begin{bmatrix} \hat{x}_1 \\ \hat{x}_2 \end{bmatrix} &= (\mathbf{H}^H \mathbf{H})^{-1} \mathbf{H}^H \begin{bmatrix} y_1 \\ y_2^* \end{bmatrix} \\ &= (\mathbf{H}^H \mathbf{H})^{-1} \mathbf{H}^H \left(\mathbf{H} \begin{bmatrix} x_1 \\ x_2 \end{bmatrix} + \begin{bmatrix} n_1 \\ n_2^* \end{bmatrix} \right) \\ &= \begin{bmatrix} x_1 \\ x_2 \end{bmatrix} + (\mathbf{H}^H \mathbf{H})^{-1} \mathbf{H}^H \begin{bmatrix} n_1 \\ n_2^* \end{bmatrix} \end{aligned}$$

By compare the above equation with the estimated symbol following equalization in Maximal Ratio Combining, we can see that the equations are identical.

6.3 Alamouti STBC with two receive antenna

The principle of space time block coding with 2 transmit antenna . With two receive antenna's the system can be modeled as shown in the Fig.6.3.1. below.

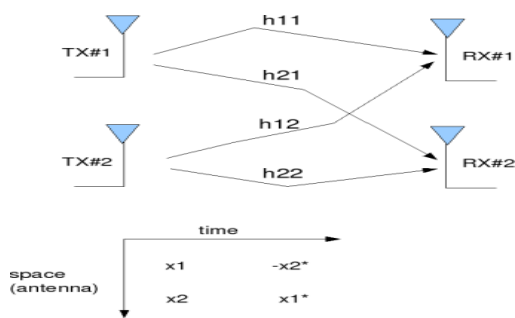


Fig.6.3.1. Transmit 2 Receive Alamouti STBC

The received signal in the first time slot is,

$$\begin{bmatrix} y_1^1 \\ y_2^1 \end{bmatrix} = \begin{bmatrix} h_{11} & h_{12} \\ h_{21} & h_{22} \end{bmatrix} \begin{bmatrix} x_1 \\ x_2 \end{bmatrix} + \begin{bmatrix} n_1^1 \\ n_2^1 \end{bmatrix}$$

Assuming that the channel remains constant for the second time slot, the received signal is in the second time slot is,

$$\begin{bmatrix} y_1^2 \\ y_2^2 \end{bmatrix} = \begin{bmatrix} h_{11} & h_{12} \\ h_{21} & h_{22} \end{bmatrix} \begin{bmatrix} -x_2^* \\ x_1^* \end{bmatrix} + \begin{bmatrix} n_1^2 \\ n_2^2 \end{bmatrix}$$

where

$\begin{bmatrix} y_1^1 \\ y_2^1 \end{bmatrix}$ are the received information at time slot 1 on receive antenna 1, 2 respectively,

$\begin{bmatrix} y_1^2 \\ y_2^2 \end{bmatrix}$ are the received information at time slot 2 on receive antenna 1, 2 respectively, h_{ij} is the channel from i^{th} receive antenna to j^{th} transmit antenna,

x_1, x_2 are the transmitted symbols,

$\begin{bmatrix} n_1^1 \\ n_2^1 \end{bmatrix}$ are the noise at time slot 1 on receive antenna 1, 2 respectively and

$\begin{bmatrix} n_1^2 \\ n_2^2 \end{bmatrix}$ are the noise at time slot 2 on receive antenna 1, 2 respectively. Combining the equations at time slot 1 and 2,

$$\begin{bmatrix} y_1^1 \\ y_2^1 \\ y_2^{2*} \\ y_1^{2*} \end{bmatrix} = \begin{bmatrix} h_{11} & h_{12} \\ h_{21} & h_{22} \\ h_{12}^* & -h_{11}^* \\ h_{22}^* & -h_{21}^* \end{bmatrix} \begin{bmatrix} x_1 \\ x_2 \end{bmatrix} + \begin{bmatrix} n_1^1 \\ n_2^1 \\ n_2^{2*} \\ n_1^{2*} \end{bmatrix}$$

Let us define

$\mathbf{H} = \begin{bmatrix} h_{11} & h_{12} \\ h_{21} & h_{22} \\ h_{12}^* & -h_{11}^* \\ h_{22}^* & -h_{21}^* \end{bmatrix}$, To solve for $\begin{bmatrix} x_1 \\ x_2 \end{bmatrix}$, we know that we need to find the inverse of \mathbf{H} .
 $\mathbf{H}^+ = (\mathbf{H}^H \mathbf{H})^{-1} \mathbf{H}^H$. The term,

$$(H^H H) = \begin{bmatrix} |h_{11}|^2 + |h_{21}|^2 + |h_{12}|^2 + |h_{22}|^2 & 0 \\ 0 & |h_{11}|^2 + |h_{21}|^2 + |h_{12}|^2 + |h_{22}|^2 \end{bmatrix}$$

Since this is a diagonal matrix, the inverse is just the inverse of the diagonal elements, i.e

$$(H^H H)^{-1} = \begin{bmatrix} \frac{1}{|h_{11}|^2 + |h_{21}|^2 + |h_{12}|^2 + |h_{22}|^2} & 0 \\ 0 & \frac{1}{|h_{11}|^2 + |h_{21}|^2 + |h_{12}|^2 + |h_{22}|^2} \end{bmatrix}$$

The estimate of the transmitted symbol is,

$$\begin{bmatrix} \hat{x}_1 \\ \hat{x}_2^* \end{bmatrix} = (H^H H)^{-1} H^H \begin{bmatrix} y_1 \\ y_2 \\ y_2^* \\ y_1^* \end{bmatrix}$$

7. BER analysis with Alamouti STBC

Since the estimate of the transmitted symbol with the Alamouti STBC scheme is identical to that obtained from MRC, the BER with above described Alamouti scheme should be same as that for MRC. However, there is a small catch.

With Alamouti STBC, we are transmitting from two antennas. Hence the total transmits power in the Alamouti scheme is twice that of that used in MRC. To make the comparison fair, we need to make the total transmit power from two antennas in STBC case to be equal to that of power transmitted from a single antenna in the MRC case[14]. With this scaling, we can see that **BER performance of 2Tx, 1Rx Alamouti STBC case has a roughly 3dB poorer performance that 1Tx, 2Rx MRC case.**

From the Maximal Ratio Combining, the bit error rate for BPSK modulation in Rayleigh channel [17]with 1 transmit, 2 receive case is,

$$P_{e,MRC} = p_{MRC}^2 \left[1 + 2(1 - p_{MRC}) \right]$$

$$p_{MRC} = \frac{1}{2} - \frac{1}{2} \left(1 + \frac{1}{E_b/N_0} \right)^{-1/2}$$

where

With **Alamouti 2 transmit antenna, 1 receive antenna STBC case,**

$$p_{STBC} = \frac{1}{2} - \frac{1}{2} \left(1 + \frac{2}{E_b/N_0} \right)^{-1/2} \quad \text{and}$$

Bit Error Rate is

$$P_{e,STBC} = p_{STBC}^2 \left[1 + 2(1 - p_{STBC}) \right]$$

1. There is no cross talk between x_1, x_2 after the equalizer.

2. The noise term is still white.

$$E \left\{ H^H \begin{bmatrix} n_1 \\ n_2^* \end{bmatrix} \begin{bmatrix} n_1^* \\ n_2 \end{bmatrix} H \right\} = H^H \begin{bmatrix} |n_1|^2 & 0 \\ 0 & |n_2|^2 \end{bmatrix} H = \begin{bmatrix} |n_1|^2 & 0 \\ 0 & |n_2|^2 \end{bmatrix} \begin{bmatrix} |h_{11}|^2 + |h_{21}|^2 & 0 \\ 0 & |h_{11}|^2 + |h_{21}|^2 \end{bmatrix}$$

Simulation Model for BPSK in Rayleigh channel With two transmit and one receive antenna:

The Matlab simulation performs the following

- (a) Generate random binary sequence of +1's and -1's.
- (b) Group them into pair of two symbols
- (c) Code it per the Alamouti Space Time code, multiply the symbols with the channel and then add white Gaussian noise.
- (d) Equalize the received symbols
- (e) Perform hard decision decoding and count the bit errors
- (f) Repeat for multiple values of E_b/N_0 and plot the simulation and theoretical results.

The simulation results are as shown in the plot below Fig.7.1.1..

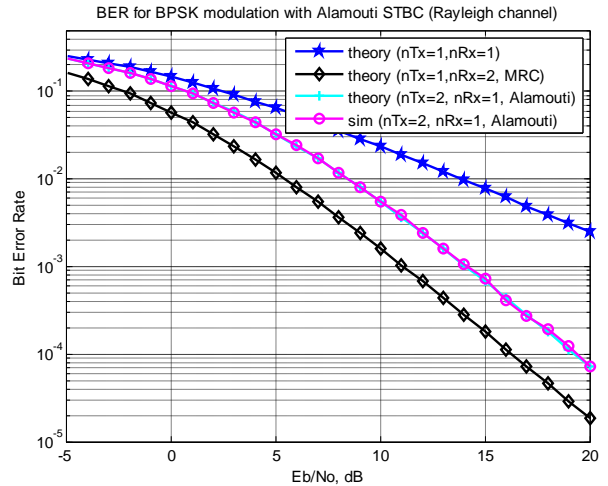


Fig.7.1.1. BER plot for BPSK in Rayleigh channel With two transmit and one receive antenna

Simulation Model for BPSK in Rayleigh channel With two transmit and two receive antenna:

The Matlab simulation performs the following

- (a) Generate random binary sequence of +1's and -1's.
- (b) Group them into pair of two symbols
- (c) Code it per the Alamouti Space Time code, multiply the symbols with the channel and then add white Gaussian noise.
- (d) Equalize the received symbols
- (e) Perform hard decision decoding and count the bit errors
- (f) Repeat for multiple values of E_b/N_0 and plot the simulation and theoretical results.

The simulation results are as shown in the plot below Fig.7.1.2.

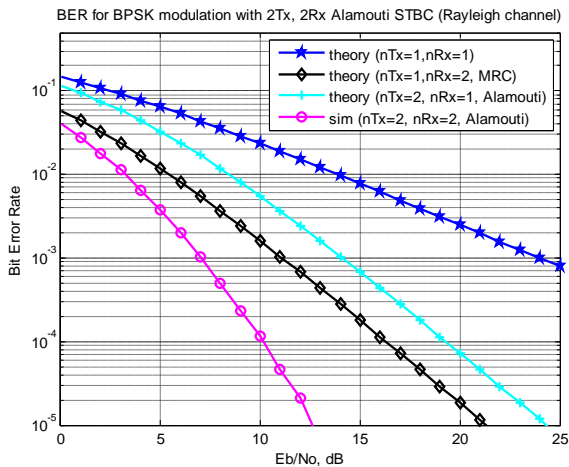


**Fig.7.1.2. BER plot for BPSK in Rayleigh channel
With two transmit and two receive antenna**

6. CONCLUSION

In this paper, the performance of OFDM systems in the presence of frequency offset between the transmitter and the receiver has been studied in terms of the Carrier-to-Interference ratio(CIR). Inter-carrier interference (ICI) which results from the frequency offset degrades the performance of the OFDM system. The variations in Time Offset(TO) can lead to inter-symbol-interference (ISI) in case of frequency selective channel can be reduced by using cyclic prefix as well as diversity in receiver design. One of the main disadvantages of OFDM is its sensitivity against carrier frequency offset which causes attenuation and rotation of subcarriers, and inter carrier interference (ICI). Orthogonality of the sub-carriers in OFDM helps to extract the symbols at the receiver without interference with each other. This work investigates an ICI self-cancellation scheme for combating the impact of ICI on OFDM systems for different frequency offset values. Different modulation techniques are considered for ICI reduction and compared with each other for their performances. It is also suitable for multipath fading channels. It is less complex and effective. The proposed scheme provides significant CIR improvement, which has been studied theoretically and by simulations. Under the condition of the same bandwidth efficiency and larger frequency offsets, the proposed OFDM system using the ICI self-cancellation scheme performs much better than standard OFDM systems. In addition, In this work we develop a generally applicable equalization technique for space-time block coded (STBC) MIMO orthogonal frequency division multiplexing (OFDM) communication systems. We can observe that the BER performance is much better than 1 transmit 2 receive MRC case. This is because the effective channel concatenating the information from 2 receive antennas over two symbols results in a diversity order of 4. In general, with m receive antennas, the diversity order for 2 transmit antenna Alamouti STBC is $2m$. BER plots for BPSK in Rayleigh channel With two transmit and one receive antenna as well as two transmit and two receive antennas for

Alamouti case are derived and simulated.

7. SCOPE OF FUTURE WORK:

Following are the areas of future study which can be considered for further research work.

1. Coding associated with frequency (among carriers) and time interleaving make the system very robust in frequency selective fading. Hence Channel coding is very important in OFDM systems. COFDM (Coded OFDM) Systems can be used for ICI reduction using self cancellation technique.
2. This self cancellation technique can also be applied under different multipath propagation mobile conditions such as Rayleigh fading channel, urban, rural area channels etc.
3. This self cancellation scheme can be extended to Multiple input and Multiple output (MIMO) OFDM systems for more number of transmitters and receivers..

References

1. Cimini, "Analysis and simulation of a digital mobile channel using orthogonal frequency division multiplexing", *IEEE Transactions on Communications*, vol. COMM-33, pp. 665-675, July 1985.
2. P. H. Moose, "A Technique for Orthogonal Frequency Division Multiplexing Frequency Offset Correction," *IEEE Transactions on Communications*, vol. 42, no. 10, pp. 2908-2914, Oct. 1994
3. T. M. Schmidl and D. C. Cox, "Robust Frequency and Timing Synchronization for OFDM," *IEEE Transactions on Communications*, pp.1613-1621, vol. 45, no. 12, Dec. 1997.
4. C. A. Montemayor, P. K. Flikkema, "Near-Optimum Iterative Estimation of Dispersive Multipath Channels," *IEEE Vehicular Technology Conference*, vol. 3, pp. 2246-2250, 1998.
5. M. Morelli and U. Mengali, "An Improved Frequency Offset Estimator for OFDM Applications," *IEEE Communications Letters*, pp. 75-77, vol.3, no. 3, Mar. 1999.
6. Z. Yuping and S.-G. Haggman, "Intercarrier interference self-cancellation scheme for OFDM mobile communication systems," *IEEE Trans. On Commun.*, vol. 49, no. 7, pp. 1185-1191, 2001
7. J.-D. Kim, Y.-S. Byun, "A New Inter-Carrier Interference Cancellation Using CP-ICA Scheme in OFDM Systems," *IEEE 65th Vehicular Technology Conference, 2007. VTC2007-Spring, Dublin (Ir)*, 22-25 April 2007, pp. 2369 - 2373.
8. Sharifah Kamilah Syed Yusof and Anis Izzati Ahmad Zamani "Intercarrier Interference Self-Cancellation for Space-Time-Frequency MIMO OFDM System " 2008 *IEEE international rf and microwave conference proceedings december 2-4, 2008, kuala lumpur, malaysia* .
9. K. Raghunath and A. Chockalingam, *Senior Member, IEEE* "SIR Analysis and Interference Cancellation in

- Uplink OFDMA with Large Carrier Frequency/Timing Offsets” *IEEE Transactions on Wireless Communications*, vol. 8, no. 5, May 2009.
10. Bahai A.S. and Saltzberg B. R., “ Multi-Carrier Digital Communications Theory and Applications of OFDM”, Kluwer Academic Publishers, 2002.
 11. Vahid Tarokh, Nambi Seshadri, and A. R. Calderbank, "Space-Time Codes for High Data Rate Wireless Communication: Performance Criterion and Code Construction" , *IEEE Transactions on Information Theory*, March, 1998, 44(2).
 12. Vahid Tarokh, Hamid Jafarkhani, and A. Robert Calderbank, "Space-Time Block Coding for Wireless Communications: Performance Results", *IEEE Journal on Selected Areas in Communications*, March 1999, 17(3).
 13. Siavash M. Alamouti, "A Simple Transmit Diversity Technique for Wireless Communications", *IEEE Journal On Select Areas in Communications*, 1998, 16(8).
 14. Hoojin LEE, "Low Peak-to-Minimum Power Ratio Transmission Scheme for Coordinate Interleaved Orthogonal Design with Two Transmit Antennas over Time-Selective Fading Channels", *IEICE Trans. Commun.*, 2007, E90-B(8), 2172-2174.
 15. Mohammad Azizul Hasan, "Performance Evaluation of WiMAX/IEEE 802.16 OFDM Physical Layer", Thesis submitted in partial fulfillment of the requirements for the degree of Master of Science in Technology, Espoo, June 2007, Helsinki University of Technology.
 16. Mehdi Naderi, Ali Pourmina M., " Space-Frequency Block Codes in Improved MB-OFDM Systems", *European Journal of Scientific Research*, 2010, 42(2), 242-252.
 17. Ding-Bing Lin, Ping-Hung Chiang, and Hsueh-Jyh Li, "Performance Analysis of Two-Branch Transmit Diversity Block-Coded OFDM Systems in Time-Varying Multipath Rayleigh-Fading Channels", *IEEE Transactions on Vehicular Technology*, January 2005, 54(1).
 18. Sreekanth, N. and Dr M. N. GiriPrasad. "Reduction of ICI Using ICI Self Cancellation Scheme in OFDM Systems". *IJECCE* 3.3 (2012): 356-361



N. Sreekanth is native of Kadapa town of Kadapa District of Andhra Pradesh, India. He received A.M.I.E.(ECE) degree from I.E.I.(INDIA) India in 2001, M.Tech degree from SriKrishnadevaraya University, Anantapur, Andhra Pradesh, India in 2005. Currently he is pursuing

PhD from J.N.T.U., Anantapur, A.P under the esteemed guidance of Dr.M.N.GiriPrasad. And his area of interest is Digital and wireless communications. He is a member of ISTE, IEI.



Dr. M. N. Giri Prasad is native of Hindupur town of Anantapur District of Andhra Pradesh, India. He received B.Tech degree from J.N.T University College of Engineering, Anantapur, Andhra Pradesh, India in 1982, M.Tech degree from SriVenkateshwara University, Tirupati, Andhra Pradesh,

India in 1994 and He has been honored with PhD in 2003 from J.N.T.U. Hyderabad., Andhra Pradesh, India. Presently he is working as Professor in department of Electronics and Communication at J.N.T.U.A., Anantapur, Andhra Pradesh, India. His research areas are Wireless Communications and Biomedical Instrumentation. He is a member of ISTE, IE & NAFE.

Implementation and Performance Analysis of MIMO Digital Video Broadcasting-T2

A. Ramya¹, Prof. Mrs. B. Devi²

*II- ME (Communication Systems), Assistant HOD/ECE
SNS College of Technology, Coimbatore (dt), Tamilnadu, India*

Abstract: The Digital Video Broadcasting second generation (DVB – T2) system transmitter and receiver are to be implemented and simulated using MATLAB. The existing system uses the Multiple Input Single Output processing unit (MISO) technology as a means of transmission. The proposing system is the implementation of the DVB – T2 system with the support of multiple antenna transmission and multiple antenna reception. Multiple Input Multiple Output–Orthogonal Frequency Division Multiplexing (MIMO-OFDM) is implemented in order to support the multiple antenna transmission and reception. Here MISO processing unit has been replaced by the MIMO processing unit. In DVB-T2 system transmitter section, reduce the peak to average power ratio to make transmission cheaper. DVBT2 also supports service specific robustness levels so that both fixed and portable devices will be used. MIMO systems can deliver both higher data throughput and greater robustness by taking advantage of the additional signal paths between a transmitter and a receiver.

Keywords: DVB, Constellation, Alamouti scheme, MIMO, OFDM.

I. Introduction

Digital Video Broadcasting Terrestrial (DVB – T) is the most popular and successful standard for Digital Terrestrial Television (DTT). For TV broadcasting most of the governments at present are moving to analog switch off. Even though the digital broadcast standards have been available for many years for both terrestrial as well as over satellite and cable, there has not been much benefits in migration for the users. On the other hand the demand for High Definition TV (HDTV) has been increased with the recent changes in television formats. These services are at present already used for delivery over Digital Video Broadcasting-Satellite (DVBS) and over cable. But to achieve it over DVB-T is difficult. The governments and the industries can get attractive possibilities with the usage of new HDTV services and migration from analog to digital. In order to increase the performance of DVB-T services, new opportunities have been provided by the DVB-T2 along with changes in channel coding and encoding compression. Hence without increasing the radio bandwidth HDTV services can be provided. There has been a wide interest all around the world for HDTV services and before now the services have been planned and implemented. The migration of encoding of video streams, the change of multiplexing techniques and the implementation of the new mechanisms in the radio layer is essential in order to make

the services to succeed and also to deliver more digital bandwidth and better forward error recovery. The Digital Video Broadcasting –Terrestrial second generation (DVB-T2) uses the Orthogonal Frequency Division Multiplexing(OFDM) modulation which is similar to the DVB-T system. A toolkit is provided with different numbers of carrier such as 1k, 2k, 4k, 8k, 16k, 32k, 16k and 32k extended modulation constellations such as Quadrature Phase Shift Keying (QPSK), 16-QAM (Quadrature Amplitude Modulation), 64-QAM, and 256-QAM. Bose-Chaudhuri-Hocquengham (BCH) and Low density parity check (LDPC) coding are used by DVB-T2 for the case of error protection. Under certain conditions in order to provide additional robustness a new technique has been introduced called as the Rotated Constellations. DVB-T2 system has proposed with Multiple Input Single Output (MISO) transmission technology which has multiple transmitting antenna and single receiving antenna. Increasing number of users uses the High Definition (HD) television its need better transmission technology that can satisfied the user demands. MIMO (Multiple Input Multiple Output) is one of the technologies which can satisfy. In this MIMO transmission multiple antennas can be used for both transmitting and receiving.

The aim of this project are implementing and simulating the transmitter of DVB – T2 system with integration of MIMO – OFDM and also to reduce the Peak to Average Power Ratio. The MATLAB simulator is going to be used for implementation and simulation of DVB – T2 system with MIMO – OFDM.

II. Dvb-T2 System Architecture

The diagram shown below represents the generic model of the T2 system. The input given to the Pre-processor indicated by TS or GS stands for one or more MPEG-2 Transport streams and one or more Generic streams. From the diagram we can say that the Input Pre-processor is not a part of the T2 system but it contains the Service splitter or the demultiplexer for separating the services of the transport streams into system inputs for the T2. These are then passed on to the individual PLPs (Physical Layer Pipes). The total input data capacity of one T2 frame over its duration should not exceed the total available T2 data capacity.

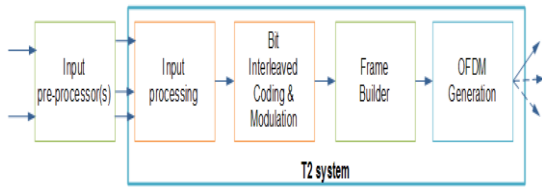


Fig 1: DVB-T2 Architecture block diagram

A.MIMO PROCESSING

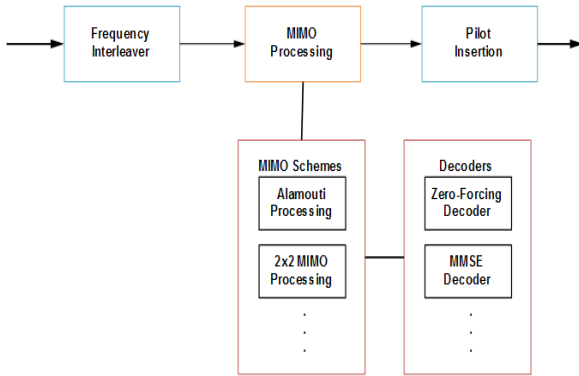


Fig 2: Block of MIMO Processing Unit

The main function of the Alamouti sub block here is to encode the signal along with the Alamouti space time block code. This will work on the OFDM cells. Since the block sends the output to two antennas, we can say that the output data will be twice the size of the input. In the first time slot, transmitter 0 (TX0) sends out s_0 and transmitter 1 (TX1) sends out s_1 . In the second time slot, TX0 sends out $-s_1^*$ and TX1 s_0^* . Here, * denotes the complex conjugate. The Alamouti scheme is a full rate transmission scheme as one unique symbol is transmitted in each time slot.

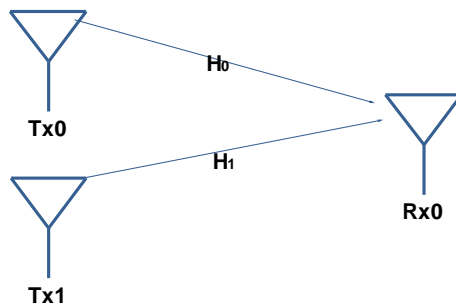


Fig 3: Illustration of Alamouti scheme.

The signals travel through two channels, h_0 and h_1 , to the receiver. The two signals must have a correlation of less than 0.7 and roughly equal transmit powers in order for the scheme to provide diversity gain.

B. PEAK TO AVERAGE POWER RATIO (PAPR) REDUCTION

In order to decrease the PAPR, two modifications are allowed for the transmitted OFDM symbol. The two techniques which are used are the Active Constellation Extension Technique and the Tone Reservation Technique. Both can be used simultaneously. These techniques are used on the active portion of the OFDM symbol excluding P1, and after this the guard intervals are inserted. When

both the techniques are being used simultaneously, the Active Constellation Extension Technique will be used in the first place to the signal. But this cannot be used on the Pilot carriers or the reserved tones or even when the rotated constellations are being used.

III. DVB-T2 RECEIVER

The main function of an MIMO receiver separates the signals received from the transmitter using signatures of the spatial signal. The receiver antenna always receives the combined form the sent signals and the signal should be de-correlated in order to get the original signal. Here we are about to see the different types of receiver architectures and their characteristics. They are the zero forcing receiver, V-BLAST receiver and the maximum likelihood receiver.

A..Zero Forcing Receiver

This is also known as the linear de-correlator. Here the architecture of the receiver is very simple and it gains knowledge from the channel matrix. With this it estimates the sent signal. The estimated signal is calculated from the equation given below.

$$\hat{s} = H^T r$$

Where H value is given by

$$H^T = (H^* H)^{-1} H^*$$

Where H^* is the complex conjugate, it is transpose of the H and r is denoted by the receive signal. One of the main advantages of the zero forcing receivers is that it separates the signals perfectly from the transmitter. But it is only suitable in case where the SNR value is high because it will enhance the noise at low SNR[6].

B.Minimum Mean-Square Error Receiver

Another method called the minimum mean square error also helps in the separating of the co channel signals. It does this by minimising the impact created by co-channel interference and noise present in the received signal. The following equation helps in calculating the the signal estimation,[2]

$$\hat{s} = (H^* H + \alpha^2 I)^{-1} H^* r$$

This receiver is less sensitive to noise and on the other hand does not produce a high separation quality. For high SNR conditions $\alpha^2 \approx 0$ [6].

C.V.Blast Receiver

V-BLAST is abbreviated as the Vertical Bell Labs Space Time Architecture. It works by increasing the computational capability of the receiver comparatively to the minimum mean square receiver and zero forcing receivers. But at the same time it provides a thorough signal separation and the capability of tolerance towards noise. It operates by separating the signals iteratively by order of strength and finally when all the signals have been detected and separated it reconstructs the signals[2].

D. Maximum Likelihood Receiver

This receiver has a better error rate performance than the remaining receivers, but it is as equally complex in its architecture.

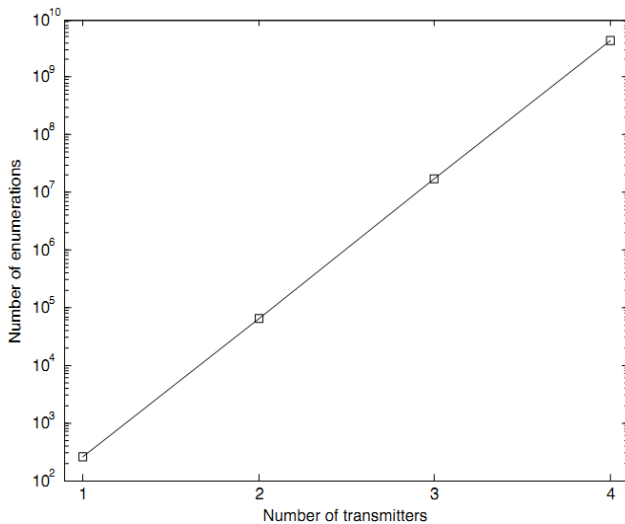


Fig. 4. Maximum Likelihood receiver using 256-QAM modulation showing computational complexity.

The above figure shows the increase in growing of computational complexity by using highest order modulation in the DVB-T2 system which uses 256QAM. The following equation helps in the calculation of the maximum likelihood estimation.

$$\hat{s} = \underset{s}{\operatorname{argmin}} \|r - Hs\|^2$$

It calculates the minimum over all possible code word vector s , and this in turn leads to the computational complexity as with the increasing number of complex antennas.

D. RECEIVER BLOCK DIAGRAM

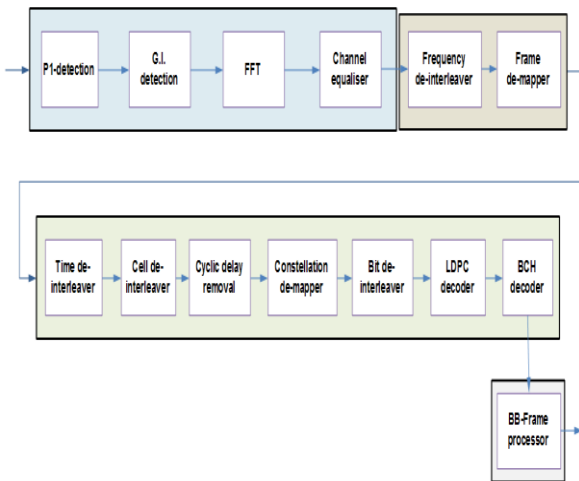


Fig. 5. DVB-T2 Demodulator

It is about the consumer receivers whose main function is to decode and produce an output which combines the Transport stream carried by one PLP and its common PLP interface. Certain parts belonging to the receiver corresponds directly to any of the blocks or features in the modulator and other part such as synchronization does not play any counterpart with the receiver [2].

IV. RESULTS AND ANALYSIS

MATLAB code has been written for each block and link all the blocks. Input Bit stream has generated given to

the BCH encoder .Bit stream length is 43040 for LDPC cord identifier 2/3. The DVB-T2 transmission system transmitter and receiver has been implemented with Multiple Input Single Output technique which already with the system. Because more time consumed for developing the DVB-T2 standard system the MIMO technology could not implemented in the MATLAB. But most part of the DVB-T2 system has been implemented and simulated using MATLAB.

From the implemented blocks, the input to the BCH encoder and output from the BCH decoder has been compared and bit error rate calculated for the SNR value of 1:15. Output from the QAM and Rotated QAM has been plotted. Finally Bit error probability graph plotted between SNR vs. BER.

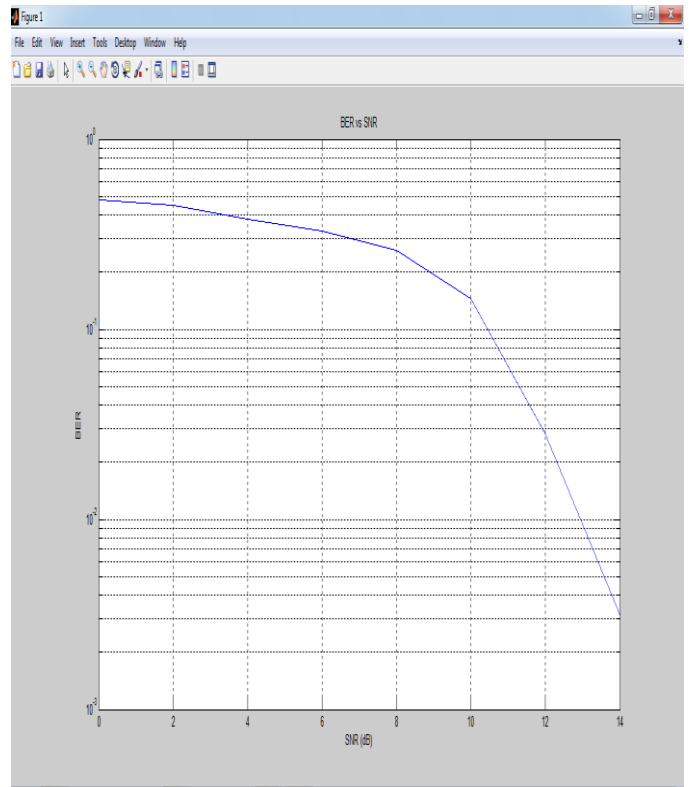


Figure 6. Plotted graph between SNR vs. BER

BER is the measure of error rate compare between transmitted and received bits. With the help of BER transmission accuracy can be measure easily. The above fig obtained is used to calculate how error free transmission has been achieved. The graph is exponentially decaying as the amount of noise level is decreased gradually. We can see that the E_b/N_0 value at about 14 dbhas very less BER.

V. CONCLUSIONS

Before starting the development process, lot of primary as well as secondary research has been made. During this research period I have learned a much about the DVB-T2 system and MIMO-OFDM technology. After making the necessary background required to do the development, I have explored the MATLAB and learned different coding techniques, logics and working principle of MATLAB. During the development of the DVB2 simulator, I learned how the wireless communication

simulation can be achieved using MATLAB before implementing in the real world. Since the OFDM is very flexible as it supports different modulation techniques. During this implementation the transmission of random binary stream using the 16-QAM the constellation received from the transmitter is accurate which proves that the transmission method is going on the right way. It is concluded that the MIMO technology will provide a better solution for a large number of users using HDTV. The obtained BER vs. SNR graph shows the accuracy of the system after the execution.

REFERENCES

- [1] Jong-Soo Seo (2011), 'Improved CIR Based Receiver Design for DVB-T2 System in Large Delay Spread Channels: Synchronization and Equalization' Vol. 57, No. 1
- [2] Hala M. Mahmoud, Allam S. Mousa, Rashid Saleem (2010), 'Channel Estimation Based in Comb-Type Pilots Arrangement for OFDM System over Time Varying Channel' Journal of Networks, Vol. 5, No. 7
- [3] Jokela, T., Tupala, M., Paavola, J. (2010), 'Analysis of Physical Layer Signaling in DVB-T2 Systems' IEEE Transactions on Broadcasting, Vol. 56, Issue. 3
- [4] Lukasz Kondrad, Vinod Kumar, Imed Bouazizi, Miika Tupala, and Moncef Gabbouj (2010) 'Cross-Layer Optimization of DVB-T2 System for Mobile Services' International Journal of Digital Multimedia Broadcasting, Volume 2010, Article ID 435405
- [5] Robert J. Barsanti, James Larue, Ph.D. (2011), 'Peak to Average Power Ratio Reduction For Digital Video Broadcast T2', IEEE Conference paper.
- [6] A. J. Paulraj and H. Bolcskei, Multiple-Input Multiple-Output (MIMO) Wireless Systems, The Communications Handbook, CRC Press, second edition, 2002.

Pressure Sensor based Event Data Recorder

Dinesh¹, Sree Rajendra²

^{1,2}(Department of Mechanical Engineering, Malnad College of Engineering, Hassan, India)

Abstract : Airbag Control Module (ACM) is designed to detect the vehicle crash, measure the severity and to deploy airbags if necessary. ACM's another function is to record the crash related data from vehicles internal accelerometers and sensors from different modules. The system is also known as Event Data Recorder (EDR). This paper describes the operations of an EDR, which detects the crash based on pressure, applied on to the vehicle during a collision, sensed by a pressure sensor. This paper also describes the operations and characteristics of vehicle speed and ultrasonic sensor during the time of crash.

Keywords: Airbags, Airbag Control Module (ACM), Event Data Recorder (EDR), Pre-Crash Data, Vehicle Crash Analysis

I. INTRODUCTION

Most vehicles are equipped with airbags. The purpose of the airbag is to help protect the occupant in a collision. Airbags are only effective and therefore only deploy in collisions of certain severity and direction. In order for the airbag system to know when and how to deploy the airbag, it must know what is going on and predict what is going to happen. The system accomplishes this by measuring specific data, such as vehicle speed and acceleration, collision direction, occupant seatbelt use, and other criteria [1].

Event data recorders (EDR) have been installed in vehicles for over 30 years, with General Motors (GM) being at the forefront of the use of this technology by introducing it in select vehicle models starting in 1974. The EDR's in these vehicles were primarily used to control and record airbag deployments [2].

Airbag equipped vehicles use a crash sensing algorithm to decide when to deploy the airbags. It is a predictive algorithm, typically making deployment decisions within 15-50 Millie sec after impact [3].

EDR's have been used for many years to record the crash related metrics, including deceleration characteristics of the vehicle, be it airplane, train, ship, or highway vehicle. Aviation has long been the proving ground for on-board recording devices. Crash protected flight data recorders have been around since the early 1950's, while the cockpit voice recorders were introduced in late 1960's. Significant improvements in safety have been realized in aviation as a result of flight data and cockpit voice recorders [4].

GM introduced the first regular production driver/passenger airbag systems as an option in selected 1974 production vehicles. In 1990, a more complex Diagnostic and Energy Reserve Module (DERM) was introduced with the added capability to record closure times for both arming and discriminating sensors as well as any fault codes present at the time of deployment. In 1992, GM installed sophisticated crash-data recorders on 70 Indy race cars. While impractical for high volume production, these recorders provided new information on human body tolerance to impact that can help improve both passenger

vehicle occupant and race car driver safety. For the 1994 model year, the multiple electromechanical switches previously used for crash sensing were replaced by the combination of a single solid state analog accelerometer and a computer algorithm integrated in a Sensing & Diagnostic Module (SDM) [5].

Depending upon the year and model of vehicle, the SDM module may contain all or some of the following information [6]:

- Brake status and Throttle position up to 5 seconds before impact
- Vehicle forward speed and Engine speed up to 5 seconds before impact
- Air bag warning lamp, driver's seat belt buckle and right front passenger air bag suppression switch status
- Number of ignition cycles at the time of the incident and at the time of the investigation
- Other relevant times and longitudinal speed changes in relation to near deployment or deployment

Pre-crash sensing may well have the most impact in reducing injuries from night time accidents involving impaired drivers. However, the advanced safety features enabled by pre-crash sensing will provide a significant benefit in all cases of poor lighting, bad weather, or driver distraction [7].

Today's airbag and seatbelt systems will be more effective if advanced occupant sensors are added to pre-crash sensors, creating occupant protections with advanced restraints that adapt to whoever happens to be sitting in the vehicle and to the demands of a variety of crash scenarios [8].

II. PRINCIPLE OF OPERATION

In this section we discuss about the principle behind the operation of the proposed pressure sensor based pre-crash data recording system with respect to its flexibility, robustness, performance and complexity of the airbag deployment function.

During a crash, the system does not deploy the airbags unnecessarily. The system measures the severity of the crash against a set of pre-defined deployment criteria. The system deploys the airbags in real-time when the applied pressure crosses its threshold within the specified time. The Fig.1 shows the principle of operation behind the airbag deployment.

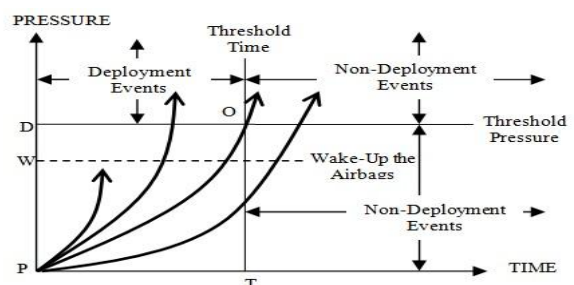


Fig.1. Airbag deployment operational characteristics

From the Fig.1, consider a vehicle moving at a constant speed collides with an obstacle at a point P. Due to the impact of collision, the pressure on the vehicle body increases quickly with time. The rising curves in the Fig.1 shows the rise in the pressure. The line originating from the point 'W' indicates the airbag wake up time and the line originating from the point 'D' represents the threshold pressure. The line originating from point 'T' represents the threshold time. The system measures the rising pressure to calculate the crash severity. The system measures the crash severity to decide the event as a deployment or as a non-deployment event.

When the pressure building on the vehicle reaches the threshold pressure within the threshold time, then the system considers the event as a severe crash and deployment criteria's are fulfilled. Then the system deploys the airbag. This is shown in the Fig.1 as when the pressure line crosses the threshold pressure line 'D' within the threshold time line 'T'. The point 'O' is an optimum point for the deployment. When the pressure on the vehicle does not reach the threshold pressure or when the pressure reach the threshold pressure after the threshold time, the system considers the event is of less severity and does not deploy the airbags.

When the pressure reaches the line originating from the point 'W', i.e., wake-up the airbags line, the system initializes the airbags. This is due to avoid the delay in opening of the airbags in a severe crash. In the Fig.1, the area above the line DO represents the deployment events.

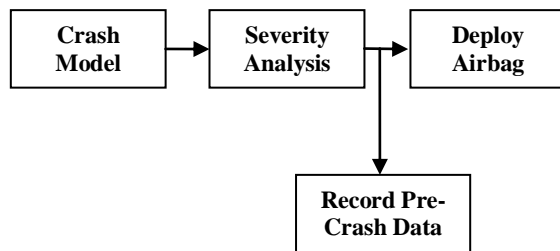


Fig.2. Functional Block Diagram

Fig.2 shows the functional block diagram of the system. Consider the Fig.2; the crash model consists of the required hardware and the software units. When the vehicle is collided with an obstacle, this unit detects the crash and crash sends the signals to the severity analysis unit continuously for which time the pressure on the vehicle body increases. The severity analysis unit measures these signals comparing with the predefined set of truth tables and algorithms to decide the event as a deployment event, near deployment event or as a non-deployment event. If the crash signals meet the deployment criteria, then the system deploys the airbags and simultaneously records the system status at the time of collision from different sensors of different modules and their trend at the time of crash for some time. If the crash criteria's does not meet the deployment criteria, then the system does not deploy the airbags and record the event as a near deployment event and records the pre-crash data.

III. MODEL DEVELOPMENT

3.1. Hardware Organization

The Fig.3 shows the hardware organization of the system. Different sensors and simulators are connected to the Central Processing Unit (CPU) or a microcontroller

using a suitable circuits, buses and protocols. The hardware details and their applications and utilization in the system are as follows.

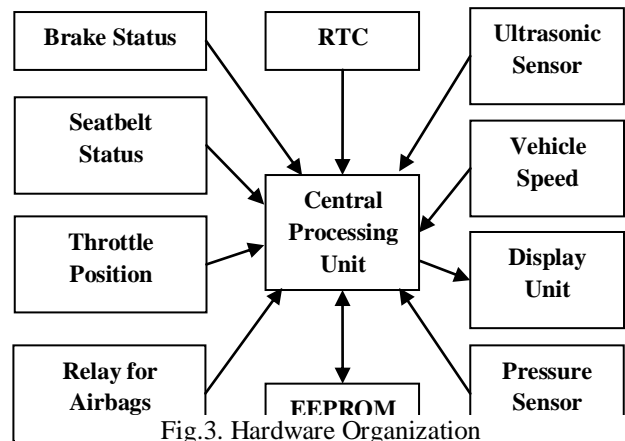


Fig.3. Hardware Organization

- **Pressure Sensor:** Pressure sensor is the main component in the system. When the vehicle collides with an obstacle it senses the increasing pressure on the vehicle body. It immediately generates an interrupt signal and sends it to the CPU. The CPU halts the current execution and waits for the further signals from the pressure sensor. The pressure sensor measures the impact and sends the signals to the CPU continuously. The CPU takes further action to measure the crash severity and to decide the event as a deployment event or as a non-deployment event.
- **Central Processing Unit (CPU):** The CPU or a microcontroller is the heart of the system. It controls and coordinates the entire system. The CPU executes the software instructions as required. The required software and the algorithms for the crash sensing and severity analysis are stored in the memory unit of the CPU. The CPU loads these instructions at the time of vehicle start or the system initialization and executes them. When the crash is detected by the pressure sensor, it receives the interrupt and halts the execution of the system and wait for further signals from pressure sensor. The CPU calculates the crash severity based on the pressure applied on the vehicle for a fixed period of time. If the pressure built reaches the threshold pressure within the threshold time, the system immediately deploys airbags. Simultaneously it writes the crash data from internal modules and sensors into the EEPROM. If the crash does not meet the deployment criteria's then the system does not deploy the airbags and writes the crash data into the EEPROM.
- **Vehicle Speed:** The vehicle speed is simulated using a rotary potentiometer. The vehicle speed is an important parameter in the crash analysis. The vehicle speed is measured to determine the speed of the vehicle at the time of crash and its trend before and after the crash.
- **Ultrasonic Sensor:** Ultrasonic sensor measures the distance between the obstacle in front of the vehicle. The distance between the vehicle and the obstacle has many applications in crash analysis. During driving, this sensor measures distance between the obstacle coming ahead to the vehicle and give information to the occupant.

- Relays for Airbags: Airbags are the balloon like structures, which are hidden in front and sides of the passenger seats. During a crash, if the crash parameters reach the deployment criteria, then they get ejected. The airbags should be ejected at correct time so that the occupant must be utilized optimally. Relay is a switch, which is activated by a CPU when the deployment criteria's reached, which turns ON the airbags.
- Display Unit: Display unit comprises of a Liquid Crystal Display (LCD) screen, which displays the actions that are going in the system continuously. It displays the speed of the vehicle, distance between the forward obstacle and the vehicle and other parameters such as temperature, engine speed. The CPU fetches the data from the vehicle modules and transfers the strings to LCD to display.
- Throttle Position: Throttle measures the amount of fuel flowing into the engine. The accelerator pedal controls the throttle. The throttle position is closely associated with the vehicle speed. The amount of throttle opened is equal to the amount of accelerator pedal is pressed. In the experimental environment, consider as a vehicle is moving on a smooth road at its topmost gear. The amount of vehicle speed simulating potentiometer rotated indicates the amount of throttle opened or the accelerator pedal pressed.
- Brake status: Brakes are used to stop the vehicle while moving. At the time of vehicle start, the system checks for the proper functioning of the brakes and displays the information. At the time of collision, the system records the braking variations for a fixed period of time.
- Seatbelt Status: Seatbelts are used to place the occupant on the seat during collision and helps the occupant to utilize the airbags so as to minimize the injuries. At the time of vehicle start, the system checks for the seatbelt status whether they are fastened or not. If they are not fastened, the system displays a warning string on the LCD.
- EEPROM: Electrically Erasable Programmable Read Only Memory (EEPROM) is a fast memory unit, which is used to store the pre-crash, crash and post-crash data. When the airbags are deployed, the CPU immediately writes the pre-crash data into EEPROM. The data include sensor and simulators status at the time of collision and their trends at the time of crash for a fixed period.
- RTC: Real Time Clock (RTC) is a clock that causes occurrences of regular interval interrupts on its each tick (timeout). In the system, RTC provides the current time. It gives the exact time of crash. It is associated with a battery, so it never stops.

3.2. Functional Modules Used

The software required to the system are divided into suitable modules and stored in the memory which can be accessible by the CPU. The functional modules and their functions are as follows.

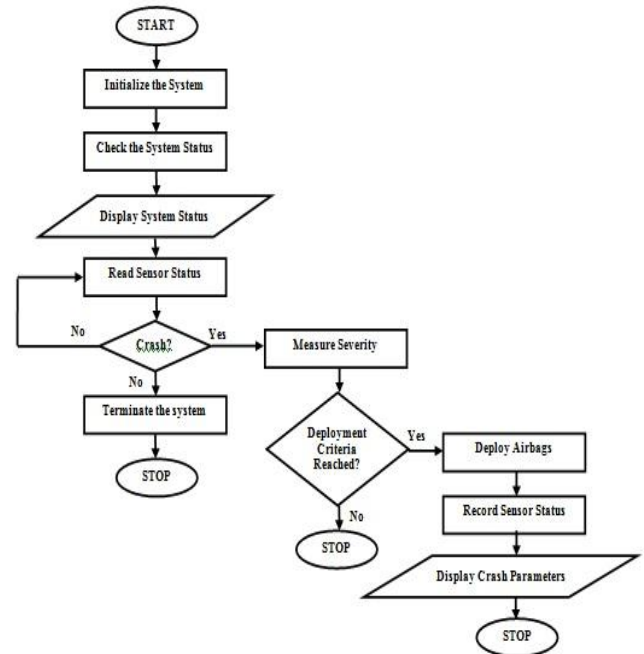


Fig. 4. Functional Flow Chart

- Analog-to-digital Conversion (ADC): This module manipulates the analog sensors such as potentiometers, ultrasonic sensors, pressure sensors and temperature sensors. This module assigns ADC channels of the CPU to different sensors and converts their analog values into digital values. These values are returned when they are called.
- Universal Asynchronous Receiver and Transmitter (UART): This module is used to retrieve the crash data using a Personnel Computer. This is also used to check the operations that are taking place in the system.
- Controller Area Network (CAN): This module is designed to test brakes and seatbelt at the start. This module also monitors and gives the result of how much braking is done at the time of crash. Before analyzing brakes and seatbelts, this module tests CAN for network malfunctions and breakages.
- Inter-Integrated-Circuit (I2C): This is a serial bus protocol used to connect different devices within the board. This used to write the crash data to the EEPROM.
- Interrupt: This module is activated whenever a crash is reported. When the crash happens, the pressure sensor sends an interrupt signal to the CPU which halts the current execution and calls the Interrupt Service Routine (ISR). The ISR actually measure the crash severity and returns its status to CPU to decide the event as a deployment event or as a non-deployment event.

Fig.4 shows the sequence of operations that take place in the proposed EDR.

3.3. Parameters being recorded

- Vehicle Speed: The speed of the vehicle at the time of crash and its trend for the period of 5 seconds before the crash.
- Distance between the obstacle and the vehicle: Using the ultrasonic sensor, distance between the obstacle and the vehicle is measured for a period of 5 seconds before the crash.
- Brake status: The amount of brake applied at the time of crash is measured for a period of 5 seconds.
- Seatbelt status: Seatbelt status, whether it is fastened or not at the time of crash.
- Throttle position: The amount of throttle opened at the time of crash and its trend before the crash for a period of 5 seconds.

IV. EXPERIMENTAL RESULTS

4.1. Vehicle Speed

The proposed system continuously read the speed of the vehicle since its initialization to its termination. The sample variation in the speed of the vehicle because of acceleration and deceleration in a sample period of one minute is shown in the Fig.5. Fig.6 illustrates the speed characteristics at the time of crash. The curve shows the decrease in speed due to the possible application of brakes or releasing the accelerator pedal at the moment of crash.

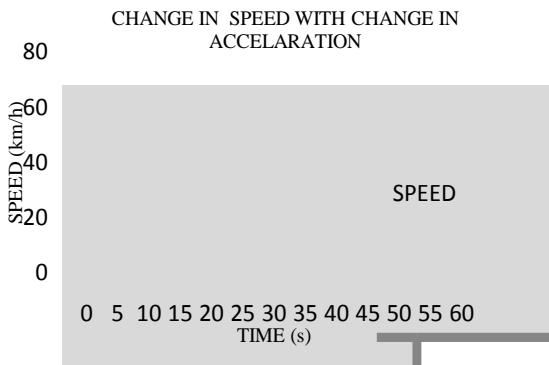


Fig.4. Speed variations during a normal drive

4.2. Throttle Position and Braking

The throttle position indicates amount of fuel flowing into the engine. This also shows the operators acceleration inputs and its trend while driving. In the experiment, consider a vehicle moving on a smooth road at its topmost gear. In normal driving the amount of braking can be ignored because braking will be at a moderate rate. The Fig.7 shows the sample variation of the percentage throttle during vehicle driving taken over a period of one minute.

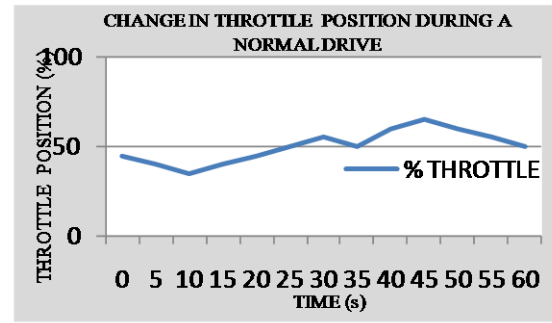
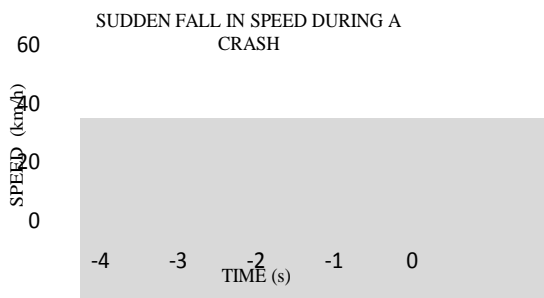


Fig.5. Sudden deceleration during a crash
Fig.7. Throttle position during a normal drive

During a crash event the operator's input to the accelerator pedal is most unpredictable. He can either press the pedal more or release his foot from the pedal and tries to put it on break. The characteristic of the throttle and braking during a crash is shown in Fig.8.

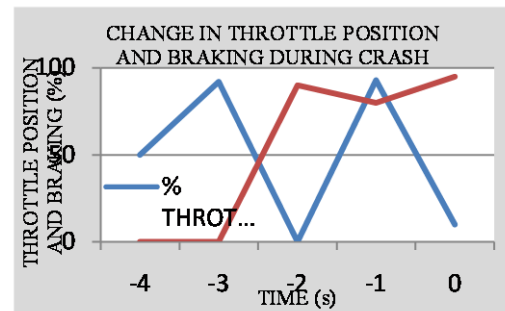


Fig.8. Change of throttle position and braking during a crash

4.3. Ultrasonic Sensor

Ultrasonic sensor measures distance between the vehicle and the obstacle in the line of the vehicle. The Fig.9 shows the sample variation of distance between the obstacle vehicle moving along the same line of the occupant vehicle which is incorporated with the proposed EDR, considering the vehicle moving at a constant speed. The simulation distance was taken in inches measured over a period of one minute.

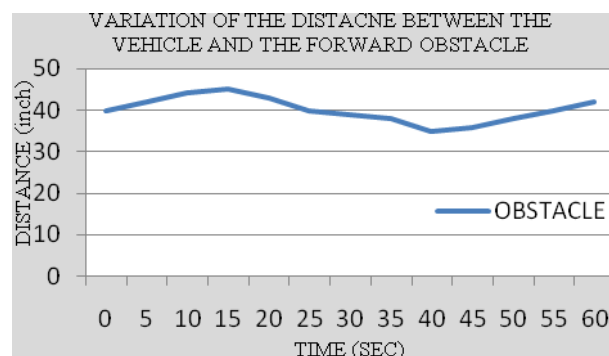


Fig.9. Variation of distance during a normal drive

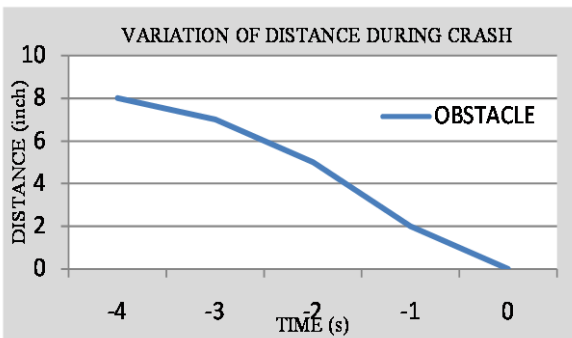
REFERENCES

Fig.10. Variation of distance during crash

The Fig.10 depicts the characteristic curve of the ultrasonic sensor during a crash event. During crash event the distance between the vehicle and the colliding object becomes zero in a short period of time. The graph shows, the time taken to reach a distance of 8 inch to 0 inch is 5 seconds in the prototype by simulation.

V. ADVANTAGES

5.1 Pressure Sensor

The system detects the crash based on the pressure rather than the sudden deceleration as in traditional methods. By detecting the collision by sensing pressure has advantage over the collision detection by quick deceleration. The system can detect the collision even when the occupant vehicle is at rest and hit by an obstacle. The system can detect the frontal crash; rear crash, side crash, and roll over crash more accurately than the traditional deceleration technique. The system deploys the airbags only in the events of severe crash and at correct time. This avoids unnecessary opening of airbags and unwanted losses.

5.2 Ultrasonic Sensor

Ultrasonic sensor measures the distance between the forward obstacle and the vehicle. This sensor predicts the crash based on the sudden decrease in the distance and helps in waking up the airbags. If the measured distance become very less than the threshold, it gives a warning message to the occupant about its crash prediction. The ultrasonic sensor can also be used in the application of Adaptive Cruise Control (ACC) for the better comfort driving.

VI. SUMMARY

This paper describes the operations and functions of the pre-crash data recording system or an Event Data recorder (EDR) which detects the crash based on the pressure applied on the vehicle body by a colliding obstacle. The system is accurate, robust and flexible. The system predicts the crash using the readings from the ultrasonic sensor. The system wakes up the airbags at the time of collision to avoid the unwanted delay in deployment. The system checks for the brake and seatbelt status at the time of the vehicle start and give warnings to the occupant if there any malfunctions. The recorded pre-crash data is accurate and this data can be used by the governing authorities to improve the safety in vehicles and also can be used in legal issues.

- [1] Chris Valcourt, P. Eng., "Event Data Recorders, or "Black Boxes"", Western Forensic Engineering Ltd., Feb. 2006.
- [2] National Highway Traffic Safety Administration, Analysis of Event Data Recorder Data for Vehicle Safety Improvement, DOT HS 810 935, April 2008.
- [3] Don Gilman, "Automotive Black Box Data Recovery Systems", Sept. 5, 2003.
- [4] Augustus "Chip" B. Chidester, John Hinch, Thomas A. Rostan, "Real World Experience with Event Data Recorders", National Highway Traffic Safety Administration, United States of America, Paper Number 247, DOT HS 809 220, June 2001.
- [5] Augustus Chidester, John Hinch, Thomas C. Mercer, Keith S. Schultz, "Recording Automotive Crash Event Data, International Symposium on Transportation Recorders, Arlington, Virginia, May 1999.
- [6] Sam Kods, B. Eng., P.Eng., "CRASH DATA RETRIEVAL", 2006.
- [7] Charles Birdsong, Peter Schuster, John Carlin, Daniel Kawano, William Thompson, "Test Methods and Results for Sensors in a Pre-Crash Detection System", California Polytechnic State University, San Luis Obispo, California, Paper Number 06AE-19, Copyright © SAE International, 2005.
- [8] Ana Maria Eigen, Wassim G. Najm, "Detailed Analysis of Target Crashes For Pre-Crash Sensing Applications", 21st International Technical Conference On the Enhanced Safety of Vehicles, Stuttgart, Germany, 2009.

Von Neumann Entropy in Quantum Computation and Sine qua non Relativistic Parameters- a Gesellschaft-Gemeinschaft Model

¹Dr. K. N. Prasanna Kumar, ²Prof. B. S. Kiranagi, ³Prof. C. S. Bagewadi

¹Post doctoral researcher, Dr KNP Kumar has three PhD's, one each in Mathematics, Economics and Political science and a D.Litt. in Political Science, Department of studies in Mathematics, Kuvempu University, Shimoga, Karnataka, India
²UGC Emeritus Professor (Department of studies in Mathematics), Manasagangotri, University of Mysore, Karnataka, India
³Chairman, Department of studies in Mathematics and Computer science, Jnanasahyadri Kuvempu university, Shankarghatta, Shimoga district, Karnataka, India

ABSTRACT: Von Neumann Entropy and computational complexity theory is a branch of the theory of computation in theoretical computer science and mathematics that focuses on classifying computational problems according to their inherent difficulty, and relating those classes to each other. In this context, a computational problem is understood to be a task that is in principle amenable to being solved by a computer (which basically means that the problem can be stated by a set of mathematical instructions). Informally, a computational problem consists of problem instances and solutions to these problem instances. For example, primality testing is the problem of determining whether a given number is prime or not. The instances of this problem are natural numbers, and the solution to an instance is yes or no based on whether the number is prime or not. A problem is regarded as inherently difficult if its solution requires significant resources, whatever the algorithm used. The theory formalizes this intuition, by introducing mathematical models of computation to study these problems and quantifying the amount of resources needed to solve them, such as time and storage. Other complexity measures are also used, such as the amount of communication (used in communication complexity), the number of gates in a circuit (used in circuit complexity) and the number of processors (used in parallel computing). One of the roles of computational complexity theory is to determine the practical limits on what computers can and cannot do. Closely related fields in theoretical computer science are analysis of algorithms and computability theory. A key distinction between analysis of algorithms and computational complexity theory is that the former is devoted to analyzing the amount of resources needed by a particular algorithm to solve a problem, whereas the latter asks a more general question about all possible algorithms that could be used to solve the same problem. More precisely, it tries to classify problems that can or cannot be solved with appropriately restricted resources. In turn, imposing restrictions on the available resources is what distinguishes computational complexity from computability theory: the latter theory asks what kind of problems can, in principle, be solved algorithmically. Low-energy excitations of one-dimensional spin-orbital models which consist of spin waves, orbital waves, and joint spin-orbital excitations. Among the latter we identify strongly entangled spin-orbital bound states which appear as peaks in the von Neumann entropy (vNE) spectral function introduced in this work. The strong entanglement of bound states is manifested by a universal logarithmic scaling of the vNE with system size, while the vNE of other spin-orbital excitations saturates. We suggest that spin-orbital entanglement can be experimentally explored by the measurement of the dynamical spin-orbital correlations using resonant inelastic x-ray scattering, where strong spin-orbit coupling associated with the core hole plays a role. Distinguish ability of States and von Neumann Entropy have been studied by Richard Jozsa, Juergen Schlienz. Consider an ensemble of pure quantum states $|\psi_j\rangle$, $j=1,\dots,n$ taken with prior probabilities p_j respectively. It has been shown that it is possible to increase all of the pair wise overlaps $|\langle\psi_i|\psi_j\rangle|$ i.e. make each constituent pair of the states more parallel (while keeping the prior probabilities the same), in such a way that the von Neumann entropy S is increased, and dually, make all pairs more orthogonal while decreasing S . This phenomenon cannot occur for ensembles in two dimensions but that it is a feature of almost all ensembles of three states in three dimensions. It is known that the von Neumann entropy characterizes the classical and quantum information capacities of the ensemble and we argue that information capacity in turn, is a manifestation of the distinguish ability of the signal states. Hence our result shows that the notion of distinguish ability within an ensemble is a global property that cannot be reduced to considering distinguish ability of each constituent pair of states.

Key words: Von Neumann entropy, Quantum computation, Governing equations

Introduction

Von Neumann entropy

In quantum statistical mechanics, von Neumann entropy, named after John von Neumann, is the extension of classical entropy concepts to the field of quantum mechanics. John von Neumann rigorously established the mathematical framework for quantum mechanics in his work *Mathematische Grundlagen der Quantenmechanik*. In it, he provided a theory of measurement, where the usual notion of wave-function collapse is described as an irreversible process (the so-called von Neumann or projective measurement).

The density matrix was introduced, with different motivations, by von Neumann and by Lev Landau. The motivation that inspired Landau was the impossibility of describing a subsystem of a composite quantum system by a state vector. On the

other hand, von Neumann introduced the density matrix in order to develop both quantum statistical mechanics and a theory of quantum measurements. The density matrix formalism was developed to extend the tools of classical statistical mechanics to the quantum domain. In the classical framework, we compute the partition function of the system in order to evaluate all possible thermodynamic quantities. Von Neumann introduced the density matrix in the context of states and operators in a Hilbert space. The knowledge of the statistical density matrix operator would allow us to compute all average quantities in a conceptually similar, but mathematically different way. Let us suppose we have a set of wave functions $|\Psi\rangle$ which depend parametrically on a set of quantum numbers n_1, n_2, \dots, n_N . The natural variable which we have is the amplitude with which a particular wavefunction of the basic set participates in the actual wavefunction of the system. Let us denote the square of this amplitude by $p(n_1, n_2, \dots, n_N)$. The goal is to turn this quantity p into the classical density function in phase space. We have to verify that p goes over into the density function in the classical limit, and that it has ergodic properties. After checking that $p(n_1, n_2, \dots, n_N)$ is a constant of motion, an ergodic assumption for the probabilities $p(n_1, n_2, \dots, n_N)$ makes p a function of the energy only.

After this procedure, one finally arrives at the density matrix formalism when seeking a form where $p(n_1, n_2, \dots, n_N)$ is invariant with respect to the representation used. In the form it is written, it will only yield the correct expectation values for quantities which are diagonal with respect to the quantum numbers n_1, n_2, \dots, n_N . Expectation values of operators which are not diagonal involve the phases of the quantum amplitudes. Suppose we encode the quantum numbers n_1, n_2, \dots, n_N into the single index i or j . Then our wave function has the form

$$|\Psi\rangle = \sum_i a_i |\psi_i\rangle.$$

The expectation value of an operator B which is not diagonal in these wave functions, so

$$\langle B \rangle = \sum_{i,j} a_i^* a_j \langle i|B|j\rangle.$$

The role, which was originally reserved for the quantities, $|a_i|^2$ is thus taken over by the density matrix of the system S .

$$\langle j|\rho|i\rangle = a_j a_i^*.$$

Therefore $\langle B \rangle$ reads as $\langle B \rangle = \text{Tr}(\rho B)$.

The invariance of the above term is described by matrix theory. A mathematical framework was described where the expectation value of quantum operators, as described by matrices, is obtained by taking the trace of the product of the density operator $\hat{\rho}$ and an operator \hat{B} (Hilbert scalar product between operators). The matrix formalism here is in the statistical mechanics framework, although it applies as well for finite quantum systems, which is usually the case, where the state of the system cannot be described by a pure state, but as a statistical operator $\hat{\rho}$ of the above form. Mathematically, $\hat{\rho}$ is a positive, semi definite Hermitian matrix with unit trace

Given the density matrix ρ , von Neumann defined the entropy as $S(\rho) = -\text{Tr}(\rho \ln \rho)$,

Which is a proper extension of the Gibbs entropy (up to a factor k_B) and the Shannon entropy to the quantum case. To compute $S(\rho)$ it is convenient (see logarithm of a matrix) to compute the Eigen decomposition of $\rho = \sum_j n_j |j\rangle \langle j|$. The von Neumann entropy is then given by

$$S(\rho) = -\sum_j n_j \ln n_j.$$

Since, for a pure state, the density matrix is idempotent, $\rho^2 = \rho$, the entropy $S(\rho)$ for it vanishes. Thus, if the system is finite (finite dimensional matrix representation), the entropy (ρ) quantifies the departure of the system from a pure state. In other words, it codifies the degree of mixing of the state describing a given finite system. Measurement decohere a quantum system into something noninterfering and ostensibly classical; so, e.g., the vanishing entropy of a pure state $|\Psi\rangle = (|0\rangle + |1\rangle)/\sqrt{2}$, corresponding to a density matrix

$$\rho = \frac{1}{2} \begin{pmatrix} 1 & 1 \\ 1 & 1 \end{pmatrix} \text{ increases to } S = \ln 2 = 0.69 \text{ for the measurement outcome mixture}$$

$$\rho = \frac{1}{2} \begin{pmatrix} 1 & 0 \\ 0 & 1 \end{pmatrix} \text{ As the quantum interference information is erased.}$$

Properties

Some properties of the von Neumann entropy:

$S(\rho)$ is only zero for pure states.

$S(\rho)$ is maximal and equal to $\ln N$ for a maximally mixed state, N being the dimension of the Hilbert space.

$S(\rho)$ is invariant under changes in the basis of ρ , that is, $S(\rho) = S(U\rho U^\dagger)$, with U a unitary transformation.

$S(\rho)$ is concave, that is, given a collection of positive numbers λ_i which sum to unity ($\sum_i \lambda_i = 1$) and density operators ρ_i , we have

$$S\left(\sum_{i=1}^k \lambda_i \rho_i\right) \geq \sum_{i=1}^k \lambda_i S(\rho_i).$$

$S(\rho)$ is additive for independent systems. Given two density matrices ρ_A, ρ_B describing independent systems A and B, we have $S(\rho_A \otimes \rho_B) = S(\rho_A) + S(\rho_B)$.

$S(\rho)$ strongly sub additive for any three systems A, B, and C:
 $S(\rho_{ABC}) + S(\rho_B) \leq S(\rho_{AB}) + S(\rho_{BC})$.

This automatically means that $S(\rho)$ is sub additive:

$$S(\rho_{AC}) + S(\rho_B) \leq S(\rho_A) + S(\rho_C).$$

Below, the concept of subadditivity is discussed, followed by its generalization to strong Subadditivity.

Subadditivity

If ρ_A, ρ_B are the reduced density matrices of the general state ρ_{AB} , then

$$|S(\rho_A) - S(\rho_B)| \leq S(\rho_{AB}) \leq S(\rho_A) + S(\rho_B).$$

This right hand inequality is known as subadditivity. The two inequalities together are sometimes known as the triangle inequality. They were proved in 1970 by Huzihiro Araki and Elliott H. Lieb While in Shannon's theory the entropy of a composite system can never be lower than the entropy of any of its parts, in quantum theory this is not the case, i.e., it is possible that $S(\rho_{AB}) = 0$ while $S(\rho_A) > 0$ and $S(\rho_B) > 0$.

Intuitively, this can be understood as follows: In quantum mechanics, the entropy of the joint system can be less than the sum of the entropy of its components because the components may be entangled. For instance, the Bell state of two spin-1/2's, $|\psi\rangle = |\uparrow\downarrow\rangle + |\downarrow\uparrow\rangle$, is a pure state with zero entropy, but each spin has maximum entropy when considered individually. The entropy in one spin can be "cancelled" by being correlated with the entropy of the other. The left-hand inequality can be roughly interpreted as saying that entropy can only be canceled by an equal amount of entropy.

If system A and system B have different amounts of entropy, the lesser can only partially cancel the greater, and some entropy must be left over. Likewise, the right-hand inequality can be interpreted as saying that the entropy of a composite system is maximized when its components are uncorrelated, in which case the total entropy is just a sum of the sub-entropies. This may be more intuitive in the phase space, instead of Hilbert space, representation, where the Von Neumann entropy amounts to minus the expected value of the *-logarithm of the Wigner function up to an offset shift.

Strong Subadditivity

The von Neumann entropy is also strongly sub additive. Given three Hilbert spaces, A, B, C,

$$S(\rho_{ABC}) + S(\rho_B) \leq S(\rho_{AB}) + S(\rho_{BC}).$$

This is a more difficult theorem and was proved in 1973 by Elliott H. Lieb and Mary Beth Ruskai using a matrix inequality of Elliott H. Lieb proved in 1973. By using the proof technique that establishes the left side of the triangle inequality above, one can show that the strong subadditivity inequality is equivalent to the following inequality.

$$S(\rho_A) + S(\rho_C) \leq S(\rho_{AB}) + S(\rho_{BC})$$

When ρ_{AB} , etc. are the reduced density matrices of a density matrix ρ_{ABC} . If we apply ordinary subadditivity to the left side of this inequality, and consider all permutations of A, B, C, we obtain the triangle inequality for ρ_{ABC} : Each of the three numbers $S(\rho_{AB}), S(\rho_{BC}), S(\rho_{AC})$ is less than or equal to the sum of the other two.

Uses

The von Neumann entropy is being extensively used in different forms (conditional entropies, relative entropies, etc.) in the framework of quantum information theory. Entanglement measures are based upon some quantity directly related to the von Neumann entropy. However, there have appeared in the literature several papers dealing with the possible inadequacy of the Shannon information measure, and consequently of the von Neumann entropy as an appropriate quantum generalization of Shannon entropy. The main argument is that in classical measurement the Shannon information measure is a natural measure of our ignorance about the properties of a system, whose existence is independent of measurement.

Conversely, quantum measurement cannot be claimed to reveal the properties of a system that existed before the measurement was made. This controversy has encouraged some authors to introduce the non-additivity property of Tsallis entropy (a generalization of the standard Boltzmann–Gibbs entropy) as the main reason for recovering a true quantal information measure in the quantum context, claiming that non-local correlations ought to be described because of the particularity of Tsallis entropy.

THE SYSTEM IN QUESTION IS:

1. Von Neumann Entropy And Quantum Entanglement
2. Velocity Field Of The Particle And Wave Function
3. Matter Presence In Abundance And Break Down Of Parity Conservation
4. Dissipation In Quantum Computation And Efficiency Of Quantum Algorithms
5. Decoherence And Computational Complexity
6. Coherent Superposition Of Outputs And Different Possible Inputs In The Form Of Qubits

VON NEUMANN ENTROPY AND QUANTUM ENTANGLEMENT: MODULE ONE

NOTATION :

- G_{13} : Category One Of Quantum Entanglement
- G_{14} : Category Two Of Quantum Entanglement
- G_{15} : Category Three Of Quantum Entanglement
- T_{13} : Category One Of Von Neumann Entropy
- T_{14} : Category Two Of Von Neumann Entropy
- T_{15} : Category Three Of Von Neumann Entropy

WAVE FUNCTIONS AND VELOCITY FIELD OF THE PARTICLES: MODULE TWO

- G_{16} : Category One Of Velocity Field Of The Particles
- G_{17} : Category Two Of The Velocity Field Of The Particles
- G_{18} : Category Three Of The Velocity Field Of The Particles
- T_{16} : Category One Of Wave Functions Concomitant To The Velocity Fields
- T_{17} : Category Two Of Wave Functions Corresponding To Category Two Of Velocity Field
- T_{18} : Category Three Of Wave Functions-

BREAK DOWN OF PARITY CONSERVATION AND ABUNDANCE OF MATTER PRESCENCE: MODULE THREE:

- G_{20} : Category One Of Systems Where There Is Break Down Of Parity Conservation
- G_{21} : Category Two Of Systems Where There Is Break Down In Parity Conservation
- G_{22} : Category Three Of Systems Where There Is Break Down Of Parity Conservation
- T_{20} : Category Three Of Systems Where There Is Break Down Of Parity Conservation
- T_{21} : Category One Of Systems Where There Is Abundance Of Matter
- T_{22} : Category Two Of Systems Where There Is Abundance Of Matter
- G_{24} : Category Three Of Systems Where There Is Abundance Of Matter

EFFICIENCY OF QUANTUM ALGORITHMS AND DISSIPATION IN QUANTUM COMPUTATION MODULE NUMBERED FOUR:

- G_{25} : Category Two Of Efficiency Of Quantum Algorithms
- G_{26} : Category Three Of efficiency Of Quantum Algorithms
- G_{24} : Category One Of Efficiency Of Quantum Algorithms
- T_{24} : Category Three Of Dissipation In Quantum Computation
- T_{25} : Category One Of Systems With Efficiency In Quantum Algorithm
- T_{26} : Category Two Of Systems With Quantum Algorithm Of Efficiency (Different From Category One)

COMPUTATIONAL COMPLEXITY AND DECOHERENCE MODULE NUMBERED FIVE

- G_{28} : Category One Of Computational Complexity
- G_{29} : Category Two Of Computational Complexity
- G_{30} : Category Three Of Computational Complexity
- T_{28} : Category One Of Decoherence
- T_{29} : Category Two Of Decoherence
- T_{30} : Category Three Of Decoherence

DIFFERENT POSSIBLE INPUTS (QUBITS) AND QUANTUM SUPERPOSITION OF OUTPUTS MODULE NUMBERED SIX

- G_{32} : Category One Of Different Possible Qubits Inputs
- G_{33} : Category Two Of Different Possible Qubits Inputs
- G_{34} : Category Three Of Different Possible Qubits Inputs
- T_{32} : Category One Of Coherent Superposition Of Outputs
- T_{33} : Category Two Of Coherent Superposition Of Outputs
- T_{34} : Category Three Of Coherent Superposition Of Outputs

ACCENTUATION COEFFICIENTS OF THE HOLISTIC SYSTEM

- Von Neumann Entropy And Quantum Entanglement
- Velocity Field Of The Particle And Wave Function
- Matter Presence In Abundance And Break Down Of Parity Conservation
- Dissipation In Quantum Computation And Efficiency Of Quantum Algorithms
- Decoherence And Computational Complexity
- Coherent Superposition Of Outputs And Different Possible Inputs In The Form Of Qubits

$$(a_{13})^{(1)}, (a_{14})^{(1)}, (a_{15})^{(1)}, (b_{13})^{(1)}, (b_{14})^{(1)}, (b_{15})^{(1)}, (a_{16})^{(2)}, (a_{17})^{(2)}, (a_{18})^{(2)}, (b_{16})^{(2)}, (b_{17})^{(2)}, (b_{18})^{(2)}, (a_{20})^{(3)}, (a_{21})^{(3)}, (a_{22})^{(3)}, (b_{20})^{(3)}, (b_{21})^{(3)}, (b_{22})^{(3)}, (a_{24})^{(4)}, (a_{25})^{(4)}, (a_{26})^{(4)}, (b_{24})^{(4)}, (b_{25})^{(4)}, (b_{26})^{(4)}, (b_{28})^{(5)}, (b_{29})^{(5)}, (b_{30})^{(5)}, (a_{28})^{(5)}, (a_{29})^{(5)}, (a_{30})^{(5)}, (a_{32})^{(6)}, (a_{33})^{(6)}, (a_{34})^{(6)}, (b_{32})^{(6)}, (b_{33})^{(6)}, (b_{34})^{(6)}$$

DISSIPATION COEFFICIENTS:

$$(a'_{13})^{(1)}, (a'_{14})^{(1)}, (a'_{15})^{(1)}, (b'_{13})^{(1)}, (b'_{14})^{(1)}, (b'_{15})^{(1)}, (a'_{16})^{(2)}, (a'_{17})^{(2)}, (a'_{18})^{(2)}, (b'_{16})^{(2)}, (b'_{17})^{(2)}, (b'_{18})^{(2)}, (a''_{20})^{(3)}, (a''_{21})^{(3)}, (a''_{22})^{(3)}, (b''_{20})^{(3)}, (b''_{21})^{(3)}, (b''_{22})^{(3)}, (a'_{24})^{(4)}, (a'_{25})^{(4)}, (a'_{26})^{(4)}, (b'_{24})^{(4)}, (b'_{25})^{(4)}, (b'_{26})^{(4)}, (b'_{28})^{(5)}, (b'_{29})^{(5)}, (b'_{30})^{(5)}, (a'_{28})^{(5)}, (a'_{29})^{(5)}, (a'_{30})^{(5)}, (a''_{32})^{(6)}, (a''_{33})^{(6)}, (a''_{34})^{(6)}, (b''_{32})^{(6)}, (b''_{33})^{(6)}, (b''_{34})^{(6)}$$

GOVERNING EQUATIONS: OF THE SYSTEM VONNEUMANN ENTROPY AND QUANTUM ENTANGLEMENT

The differential system of this model is now -

$$\begin{aligned} \frac{dG_{13}}{dt} &= (a_{13})^{(1)}G_{14} - [(a'_{13})^{(1)} + (a''_{13})^{(1)}(T_{14}, t)]G_{13} - \\ \frac{dG_{14}}{dt} &= (a_{14})^{(1)}G_{13} - [(a'_{14})^{(1)} + (a''_{14})^{(1)}(T_{14}, t)]G_{14} - \\ \frac{dG_{15}}{dt} &= (a_{15})^{(1)}G_{14} - [(a'_{15})^{(1)} + (a''_{15})^{(1)}(T_{14}, t)]G_{15} - \\ \frac{dT_{13}}{dt} &= (b_{13})^{(1)}T_{14} - [(b'_{13})^{(1)} - (b''_{13})^{(1)}(G, t)]T_{13} - \\ \frac{dT_{14}}{dt} &= (b_{14})^{(1)}T_{13} - [(b'_{14})^{(1)} - (b''_{14})^{(1)}(G, t)]T_{14} - \\ \frac{dT_{15}}{dt} &= (b_{15})^{(1)}T_{14} - [(b'_{15})^{(1)} - (b''_{15})^{(1)}(G, t)]T_{15} - \\ &+ (a''_{13})^{(1)}(T_{14}, t) = \text{First augmentation factor} - \\ &- (b''_{13})^{(1)}(G, t) = \text{First detritions factor} - \end{aligned}$$

GOVERNING EQUATIONS OF THE SYSTEM VELOCITY FIELD OF THE PARTICLE AND WAVE FUNCTION:

The differential system of this model is now -

$$\begin{aligned} \frac{dG_{16}}{dt} &= (a_{16})^{(2)}G_{17} - [(a'_{16})^{(2)} + (a''_{16})^{(2)}(T_{17}, t)]G_{16} - \\ \frac{dG_{17}}{dt} &= (a_{17})^{(2)}G_{16} - [(a'_{17})^{(2)} + (a''_{17})^{(2)}(T_{17}, t)]G_{17} - \\ \frac{dG_{18}}{dt} &= (a_{18})^{(2)}G_{17} - [(a'_{18})^{(2)} + (a''_{18})^{(2)}(T_{17}, t)]G_{18} - \\ \frac{dT_{16}}{dt} &= (b_{16})^{(2)}T_{17} - [(b'_{16})^{(2)} - (b''_{16})^{(2)}((G_{19}), t)]T_{16} - \\ \frac{dT_{17}}{dt} &= (b_{17})^{(2)}T_{16} - [(b'_{17})^{(2)} - (b''_{17})^{(2)}((G_{19}), t)]T_{17} - \\ \frac{dT_{18}}{dt} &= (b_{18})^{(2)}T_{17} - [(b'_{18})^{(2)} - (b''_{18})^{(2)}((G_{19}), t)]T_{18} - \\ &+ (a''_{16})^{(2)}(T_{17}, t) = \text{First augmentation factor} - \\ &- (b''_{16})^{(2)}((G_{19}), t) = \text{First detritions factor} - \end{aligned}$$

GOVERNING EQUATIONS: OF BREAK DOWN OF PARITY CONSERVATION AND MATTER ABUNDANCE:

The differential system of this model is now -

$$\begin{aligned} \frac{dG_{20}}{dt} &= (a_{20})^{(3)}G_{21} - [(a'_{20})^{(3)} + (a''_{20})^{(3)}(T_{21}, t)]G_{20} - \\ \frac{dG_{21}}{dt} &= (a_{21})^{(3)}G_{20} - [(a'_{21})^{(3)} + (a''_{21})^{(3)}(T_{21}, t)]G_{21} - \\ \frac{dG_{22}}{dt} &= (a_{22})^{(3)}G_{21} - [(a'_{22})^{(3)} + (a''_{22})^{(3)}(T_{21}, t)]G_{22} - \\ \frac{dT_{20}}{dt} &= (b_{20})^{(3)}T_{21} - [(b'_{20})^{(3)} - (b''_{20})^{(3)}(G_{23}, t)]T_{20} - \\ \frac{dT_{21}}{dt} &= (b_{21})^{(3)}T_{20} - [(b'_{21})^{(3)} - (b''_{21})^{(3)}(G_{23}, t)]T_{21} - \\ \frac{dT_{22}}{dt} &= (b_{22})^{(3)}T_{21} - [(b'_{22})^{(3)} - (b''_{22})^{(3)}(G_{23}, t)]T_{22} - \\ &+ (a''_{20})^{(3)}(T_{21}, t) = \text{First augmentation factor} - \\ &- (b''_{20})^{(3)}(G_{23}, t) = \text{First detritions factor} - \end{aligned}$$

GOVERNING EQUATIONS: OF DISSIPATION IN QUANTUM COMPUTATION AND EFFICIENCY OF QUANTUM ALGORITHMS:

The differential system of this model is now -

$$\frac{dG_{24}}{dt} = (a_{24})^{(4)}G_{25} - [(a'_{24})^{(4)} + (a''_{24})^{(4)}(T_{25}, t)]G_{24} -$$

$$\begin{aligned} \frac{dG_{25}}{dt} &= (a_{25})^{(4)} G_{24} - [(a'_{25})^{(4)} + (a''_{25})^{(4)}(T_{25}, t)] G_{25} - \\ \frac{dG_{26}}{dt} &= (a_{26})^{(4)} G_{25} - [(a'_{26})^{(4)} + (a''_{26})^{(4)}(T_{25}, t)] G_{26} - \\ \frac{dT_{24}}{dt} &= (b_{24})^{(4)} T_{25} - [(b'_{24})^{(4)} - (b''_{24})^{(4)}((G_{27}), t)] T_{24} - \\ \frac{dT_{25}}{dt} &= (b_{25})^{(4)} T_{24} - [(b'_{25})^{(4)} - (b''_{25})^{(4)}((G_{27}), t)] T_{25} - \\ \frac{dT_{26}}{dt} &= (b_{26})^{(4)} T_{25} - [(b'_{26})^{(4)} - (b''_{26})^{(4)}((G_{27}), t)] T_{26} - \\ &+ (a''_{24})^{(4)}(T_{25}, t) = \text{First augmentation factor} - \\ &- (b''_{24})^{(4)}((G_{27}), t) = \text{First detritions factor} - \end{aligned}$$

GOVERNING EQUATIONS:OF THE SYSTEM DECOHERENCE AND COMPUTATIONAL COMPLEXITY:

The differential system of this model is now -

$$\begin{aligned} \frac{dG_{28}}{dt} &= (a_{28})^{(5)} G_{29} - [(a'_{28})^{(5)} + (a''_{28})^{(5)}(T_{29}, t)] G_{28} - \\ \frac{dG_{29}}{dt} &= (a_{29})^{(5)} G_{28} - [(a'_{29})^{(5)} + (a''_{29})^{(5)}(T_{29}, t)] G_{29} - \\ \frac{dG_{30}}{dt} &= (a_{30})^{(5)} G_{29} - [(a'_{30})^{(5)} + (a''_{30})^{(5)}(T_{29}, t)] G_{30} - \\ \frac{dT_{28}}{dt} &= (b_{28})^{(5)} T_{29} - [(b'_{28})^{(5)} - (b''_{28})^{(5)}((G_{31}), t)] T_{28} - \\ \frac{dT_{29}}{dt} &= (b_{29})^{(5)} T_{28} - [(b'_{29})^{(5)} - (b''_{29})^{(5)}((G_{31}), t)] T_{29} - \\ \frac{dT_{30}}{dt} &= (b_{30})^{(5)} T_{29} - [(b'_{30})^{(5)} - (b''_{30})^{(5)}((G_{31}), t)] T_{30} - \\ &+ (a''_{28})^{(5)}(T_{29}, t) = \text{First augmentation factor} - \\ &- (b''_{28})^{(5)}((G_{31}), t) = \text{First detritions factor} - \end{aligned}$$

GOVERNING EQUATIONS:COHERENT SUPERPOSITION OF OUTPUTS AND DIFFERENT POSSIBILITIES OF QUBIT INPUTS

The differential system of this model is now -

$$\begin{aligned} \frac{dG_{32}}{dt} &= (a_{32})^{(6)} G_{33} - [(a'_{32})^{(6)} + (a''_{32})^{(6)}(T_{33}, t)] G_{32} - \\ \frac{dG_{33}}{dt} &= (a_{33})^{(6)} G_{32} - [(a'_{33})^{(6)} + (a''_{33})^{(6)}(T_{33}, t)] G_{33} - \\ \frac{dG_{34}}{dt} &= (a_{34})^{(6)} G_{33} - [(a'_{34})^{(6)} + (a''_{34})^{(6)}(T_{33}, t)] G_{34} - \\ \frac{dT_{32}}{dt} &= (b_{32})^{(6)} T_{33} - [(b'_{32})^{(6)} - (b''_{32})^{(6)}((G_{35}), t)] T_{32} - \\ \frac{dT_{33}}{dt} &= (b_{33})^{(6)} T_{32} - [(b'_{33})^{(6)} - (b''_{33})^{(6)}((G_{35}), t)] T_{33} - \\ \frac{dT_{34}}{dt} &= (b_{34})^{(6)} T_{33} - [(b'_{34})^{(6)} - (b''_{34})^{(6)}((G_{35}), t)] T_{34} - \\ &+ (a''_{32})^{(6)}(T_{33}, t) = \text{First augmentation factor} - \\ &- (b''_{32})^{(6)}((G_{35}), t) = \text{First detritions factor} - \end{aligned}$$

CONCATENATED GOVERNING SYSTEMS OF THE HOLISTIC GLOBAL SYSTEM:

- (1) Von Neumann Entropy And Quantum Entanglement
- (2) Velocity Field Of The Particle And Wave Function
- (3) Matter Presence In Abundance And Break Down Of Parity Conservation
- (4) Dissipation In Quantum Computation And Efficiency Of Quantum Algorithms
- (5) Decoherence And Computational Complexity

Coherent Superposition Of Outputs And Different Possible Inputs In The Form Of Qubits-

$$\begin{aligned} \frac{dG_{13}}{dt} &= (a_{13})^{(1)} G_{14} - \left[\begin{array}{|c|c|c|c|} \hline (a'_{13})^{(1)} & + (a''_{13})^{(1)}(T_{14}, t) & + (a''_{16})^{(2,2)}(T_{17}, t) & + (a''_{20})^{(3,3)}(T_{21}, t) \\ \hline + (a''_{24})^{(4,4,4,4)}(T_{25}, t) & + (a''_{28})^{(5,5,5,5)}(T_{29}, t) & + (a''_{32})^{(6,6,6,6)}(T_{33}, t) & \\ \hline \end{array} \right] G_{13} - \\ \frac{dG_{14}}{dt} &= (a_{14})^{(1)} G_{13} - \left[\begin{array}{|c|c|c|c|} \hline (a'_{14})^{(1)} & + (a''_{14})^{(1)}(T_{14}, t) & + (a''_{17})^{(2,2)}(T_{17}, t) & + (a''_{21})^{(3,3)}(T_{21}, t) \\ \hline + (a''_{25})^{(4,4,4,4)}(T_{25}, t) & + (a''_{29})^{(5,5,5,5)}(T_{29}, t) & + (a''_{33})^{(6,6,6,6)}(T_{33}, t) & \\ \hline \end{array} \right] G_{14} - \\ \frac{dG_{15}}{dt} &= (a_{15})^{(1)} G_{14} - \left[\begin{array}{|c|c|c|c|} \hline (a'_{15})^{(1)} & + (a''_{15})^{(1)}(T_{14}, t) & + (a''_{18})^{(2,2)}(T_{17}, t) & + (a''_{22})^{(3,3)}(T_{21}, t) \\ \hline + (a''_{26})^{(4,4,4,4)}(T_{25}, t) & + (a''_{30})^{(5,5,5,5)}(T_{29}, t) & + (a''_{34})^{(6,6,6,6)}(T_{33}, t) & \\ \hline \end{array} \right] G_{15} - \end{aligned}$$

Where $(a''_{13})^{(1)}(T_{14}, t)$, $(a''_{14})^{(1)}(T_{14}, t)$, $(a''_{15})^{(1)}(T_{14}, t)$ are first augmentation coefficients for category 1, 2 and 3
 $+ (a''_{16})^{(2,2)}(T_{17}, t)$, $+ (a''_{17})^{(2,2)}(T_{17}, t)$, $+ (a''_{18})^{(2,2)}(T_{17}, t)$ are second augmentation coefficient for category 1, 2 and 3

$\boxed{+(a''_{20})^{(3,3,3)}(T_{21}, t)}$, $\boxed{+(a''_{21})^{(3,3,3)}(T_{21}, t)}$, $\boxed{+(a''_{22})^{(3,3,3)}(T_{21}, t)}$ are third augmentation coefficient for category 1, 2 and 3
 $\boxed{+(a''_{24})^{(4,4,4,4)}(T_{25}, t)}$, $\boxed{+(a''_{25})^{(4,4,4,4)}(T_{25}, t)}$, $\boxed{+(a''_{26})^{(4,4,4,4)}(T_{25}, t)}$ are fourth augmentation coefficient for category 1, 2 and 3
 $\boxed{+(a''_{28})^{(5,5,5,5)}(T_{29}, t)}$, $\boxed{+(a''_{29})^{(5,5,5,5)}(T_{29}, t)}$, $\boxed{+(a''_{30})^{(5,5,5,5)}(T_{29}, t)}$ are fifth augmentation coefficient for category 1, 2 and 3
 $\boxed{+(a''_{32})^{(6,6,6,6)}(T_{33}, t)}$, $\boxed{+(a''_{33})^{(6,6,6,6)}(T_{33}, t)}$, $\boxed{+(a''_{34})^{(6,6,6,6)}(T_{33}, t)}$ are sixth augmentation coefficient for category 1, 2 and 3-

$$\frac{dT_{13}}{dt} = (b_{13})^{(1)}T_{14} - \left[\begin{array}{ccc} \boxed{(b'_{13})^{(1)} - \boxed{-(b''_{13})^{(1)}(G, t)} - \boxed{-(b''_{16})^{(2,2)}(G_{19}, t)} - \boxed{-(b''_{20})^{(3,3)}(G_{23}, t)} \\ \boxed{-(b''_{24})^{(4,4,4,4)}(G_{27}, t)} - \boxed{-(b''_{28})^{(5,5,5,5)}(G_{31}, t)} - \boxed{-(b''_{32})^{(6,6,6,6)}(G_{35}, t)} \end{array} \right] T_{13} -$$

$$\frac{dT_{14}}{dt} = (b_{14})^{(1)}T_{13} - \left[\begin{array}{ccc} \boxed{(b'_{14})^{(1)} - \boxed{-(b''_{14})^{(1)}(G, t)} - \boxed{-(b''_{17})^{(2,2)}(G_{19}, t)} - \boxed{-(b''_{21})^{(3,3)}(G_{23}, t)} \\ \boxed{-(b''_{25})^{(4,4,4,4)}(G_{27}, t)} - \boxed{-(b''_{29})^{(5,5,5,5)}(G_{31}, t)} - \boxed{-(b''_{33})^{(6,6,6,6)}(G_{35}, t)} \end{array} \right] T_{14} -$$

$$\frac{dT_{15}}{dt} = (b_{15})^{(1)}T_{14} - \left[\begin{array}{ccc} \boxed{(b'_{15})^{(1)} - \boxed{-(b''_{15})^{(1)}(G, t)} - \boxed{-(b''_{18})^{(2,2)}(G_{19}, t)} - \boxed{-(b''_{22})^{(3,3)}(G_{23}, t)} \\ \boxed{-(b''_{26})^{(4,4,4,4)}(G_{27}, t)} - \boxed{-(b''_{30})^{(5,5,5,5)}(G_{31}, t)} - \boxed{-(b''_{34})^{(6,6,6,6)}(G_{35}, t)} \end{array} \right] T_{15} -$$

Where $\boxed{-(b''_{13})^{(1)}(G, t)}$, $\boxed{-(b''_{14})^{(1)}(G, t)}$, $\boxed{-(b''_{15})^{(1)}(G, t)}$ are first detrition coefficients for category 1, 2 and 3
 $\boxed{-(b''_{16})^{(2,2)}(G_{19}, t)}$, $\boxed{-(b''_{17})^{(2,2)}(G_{19}, t)}$, $\boxed{-(b''_{18})^{(2,2)}(G_{19}, t)}$ are second detrition coefficients for category 1, 2 and 3
 $\boxed{-(b''_{20})^{(3,3)}(G_{23}, t)}$, $\boxed{-(b''_{21})^{(3,3)}(G_{23}, t)}$, $\boxed{-(b''_{22})^{(3,3)}(G_{23}, t)}$ are third detrition coefficients for category 1, 2 and 3
 $\boxed{-(b''_{24})^{(4,4,4,4)}(G_{27}, t)}$, $\boxed{-(b''_{25})^{(4,4,4,4)}(G_{27}, t)}$, $\boxed{-(b''_{26})^{(4,4,4,4)}(G_{27}, t)}$ are fourth detrition coefficients for category 1, 2 and 3
 $\boxed{-(b''_{28})^{(5,5,5,5)}(G_{31}, t)}$, $\boxed{-(b''_{29})^{(5,5,5,5)}(G_{31}, t)}$, $\boxed{-(b''_{30})^{(5,5,5,5)}(G_{31}, t)}$ are fifth detrition coefficients for category 1, 2 and 3
 $\boxed{-(b''_{32})^{(6,6,6,6)}(G_{35}, t)}$, $\boxed{-(b''_{33})^{(6,6,6,6)}(G_{35}, t)}$, $\boxed{-(b''_{34})^{(6,6,6,6)}(G_{35}, t)}$ are sixth detrition coefficients for category 1, 2 and 3

$$3 \frac{dG_{16}}{dt} = (a_{16})^{(2)}G_{17} - \left[\begin{array}{ccc} \boxed{(a'_{16})^{(2)} + \boxed{+(a''_{16})^{(2)}(T_{17}, t)} + \boxed{+(a''_{13})^{(1,1)}(T_{14}, t)} + \boxed{+(a''_{20})^{(3,3,3)}(T_{21}, t)} \\ \boxed{+(a''_{24})^{(4,4,4,4,4)}(T_{25}, t)} + \boxed{+(a''_{28})^{(5,5,5,5,5)}(T_{29}, t)} + \boxed{+(a''_{32})^{(6,6,6,6,6)}(T_{33}, t)} \end{array} \right] G_{16} -$$

$$\frac{dG_{17}}{dt} = (a_{17})^{(2)}G_{16} - \left[\begin{array}{ccc} \boxed{(a'_{17})^{(2)} + \boxed{+(a''_{17})^{(2)}(T_{17}, t)} + \boxed{+(a''_{14})^{(1,1)}(T_{14}, t)} + \boxed{+(a''_{21})^{(3,3,3)}(T_{21}, t)} \\ \boxed{+(a''_{25})^{(4,4,4,4,4)}(T_{25}, t)} + \boxed{+(a''_{29})^{(5,5,5,5,5)}(T_{29}, t)} + \boxed{+(a''_{33})^{(6,6,6,6,6)}(T_{33}, t)} \end{array} \right] G_{17} -$$

$$\frac{dG_{18}}{dt} = (a_{18})^{(2)}G_{17} - \left[\begin{array}{ccc} \boxed{(a'_{18})^{(2)} + \boxed{+(a''_{18})^{(2)}(T_{17}, t)} + \boxed{+(a''_{15})^{(1,1)}(T_{14}, t)} + \boxed{+(a''_{22})^{(3,3,3)}(T_{21}, t)} \\ \boxed{+(a''_{26})^{(4,4,4,4,4)}(T_{25}, t)} + \boxed{+(a''_{30})^{(5,5,5,5,5)}(T_{29}, t)} + \boxed{+(a''_{34})^{(6,6,6,6,6)}(T_{33}, t)} \end{array} \right] G_{18} -$$

Where $\boxed{+(a''_{16})^{(2)}(T_{17}, t)}$, $\boxed{+(a''_{17})^{(2)}(T_{17}, t)}$, $\boxed{+(a''_{18})^{(2)}(T_{17}, t)}$ are first augmentation coefficients for category 1, 2 and 3
 $\boxed{+(a''_{13})^{(1,1)}(T_{14}, t)}$, $\boxed{+(a''_{14})^{(1,1)}(T_{14}, t)}$, $\boxed{+(a''_{15})^{(1,1)}(T_{14}, t)}$ are second augmentation coefficient for category 1, 2 and 3
 $\boxed{+(a''_{20})^{(3,3,3)}(T_{21}, t)}$, $\boxed{+(a''_{21})^{(3,3,3)}(T_{21}, t)}$, $\boxed{+(a''_{22})^{(3,3,3)}(T_{21}, t)}$ are third augmentation coefficient for category 1, 2 and 3
 $\boxed{+(a''_{24})^{(4,4,4,4,4)}(T_{25}, t)}$, $\boxed{+(a''_{25})^{(4,4,4,4,4)}(T_{25}, t)}$, $\boxed{+(a''_{26})^{(4,4,4,4,4)}(T_{25}, t)}$ are fourth augmentation coefficient for category 1, 2 and 3
 $\boxed{+(a''_{28})^{(5,5,5,5,5)}(T_{29}, t)}$, $\boxed{+(a''_{29})^{(5,5,5,5,5)}(T_{29}, t)}$, $\boxed{+(a''_{30})^{(5,5,5,5,5)}(T_{29}, t)}$ are fifth augmentation coefficient for category 1, 2 and 3
 $\boxed{+(a''_{32})^{(6,6,6,6,6)}(T_{33}, t)}$, $\boxed{+(a''_{33})^{(6,6,6,6,6)}(T_{33}, t)}$, $\boxed{+(a''_{34})^{(6,6,6,6,6)}(T_{33}, t)}$ are sixth augmentation coefficient for category 1, 2 and 3 -

$$\frac{dT_{16}}{dt} = (b_{16})^{(2)}T_{17} - \left[\begin{array}{ccc} \boxed{(b'_{16})^{(2)} - \boxed{-(b''_{16})^{(2)}(G_{19}, t)} - \boxed{-(b''_{13})^{(1,1)}(G, t)} - \boxed{-(b''_{20})^{(3,3,3)}(G_{23}, t)} \\ \boxed{-(b''_{24})^{(4,4,4,4,4)}(G_{27}, t)} - \boxed{-(b''_{28})^{(5,5,5,5,5)}(G_{31}, t)} - \boxed{-(b''_{32})^{(6,6,6,6,6)}(G_{35}, t)} \end{array} \right] T_{16} -$$

$$\frac{dT_{17}}{dt} = (b_{17})^{(2)}T_{16} - \left[\begin{array}{ccc} \boxed{(b'_{17})^{(2)} - \boxed{-(b''_{17})^{(2)}(G_{19}, t)} - \boxed{-(b''_{14})^{(1,1)}(G, t)} - \boxed{-(b''_{21})^{(3,3,3)}(G_{23}, t)} \\ \boxed{-(b''_{25})^{(4,4,4,4,4)}(G_{27}, t)} - \boxed{-(b''_{29})^{(5,5,5,5,5)}(G_{31}, t)} - \boxed{-(b''_{33})^{(6,6,6,6,6)}(G_{35}, t)} \end{array} \right] T_{17} -$$

$$\frac{dT_{18}}{dt} = (b_{18})^{(2)}T_{17} - \left[\begin{array}{ccc} (b'_{18})^{(2)} \boxed{-(b''_{18})^{(2)}(G_{19}, t)} & \boxed{-(b''_{15})^{(1,1)}(G, t)} & \boxed{-(b''_{22})^{(3,3,3)}(G_{23}, t)} \\ \boxed{-(b''_{26})^{(4,4,4,4,4)}(G_{27}, t)} & \boxed{-(b''_{30})^{(5,5,5,5,5)}(G_{31}, t)} & \boxed{-(b''_{34})^{(6,6,6,6,6)}(G_{35}, t)} \end{array} \right] T_{18} -$$

where $\boxed{-(b''_{16})^{(2)}(G_{19}, t)}$, $\boxed{-(b''_{17})^{(2)}(G_{19}, t)}$, $\boxed{-(b''_{18})^{(2)}(G_{19}, t)}$ are first detrition coefficients for category 1, 2 and 3

$\boxed{-(b''_{13})^{(1,1)}(G, t)}$, $\boxed{-(b''_{14})^{(1,1)}(G, t)}$, $\boxed{-(b''_{15})^{(1,1)}(G, t)}$ are second detrition coefficients for category 1,2 and 3

$\boxed{-(b''_{20})^{(3,3,3)}(G_{23}, t)}$, $\boxed{-(b''_{21})^{(3,3,3)}(G_{23}, t)}$, $\boxed{-(b''_{22})^{(3,3,3)}(G_{23}, t)}$ are third detrition coefficients for category 1,2 and 3

$\boxed{-(b''_{24})^{(4,4,4,4,4)}(G_{27}, t)}$, $\boxed{-(b''_{25})^{(4,4,4,4,4)}(G_{27}, t)}$, $\boxed{-(b''_{26})^{(4,4,4,4,4)}(G_{27}, t)}$ are fourth detrition coefficients for category 1,2 and 3

$\boxed{-(b''_{28})^{(5,5,5,5,5)}(G_{31}, t)}$, $\boxed{-(b''_{29})^{(5,5,5,5,5)}(G_{31}, t)}$, $\boxed{-(b''_{30})^{(5,5,5,5,5)}(G_{31}, t)}$ are fifth detrition coefficients for category 1,2 and 3

$\boxed{-(b''_{32})^{(6,6,6,6,6)}(G_{35}, t)}$, $\boxed{-(b''_{33})^{(6,6,6,6,6)}(G_{35}, t)}$, $\boxed{-(b''_{34})^{(6,6,6,6,6)}(G_{35}, t)}$ are sixth detrition coefficients for category 1,2 and 3 -

$$\frac{dG_{20}}{dt} = (a_{20})^{(3)}G_{21} - \left[\begin{array}{ccc} (a'_{20})^{(3)} \boxed{+(a''_{20})^{(3)}(T_{21}, t)} & \boxed{+(a''_{16})^{(2,2,2)}(T_{17}, t)} & \boxed{+(a''_{13})^{(1,1,1)}(T_{14}, t)} \\ \boxed{+(a''_{24})^{(4,4,4,4,4)}(T_{25}, t)} & \boxed{+(a''_{28})^{(5,5,5,5,5)}(T_{29}, t)} & \boxed{+(a''_{32})^{(6,6,6,6,6)}(T_{33}, t)} \end{array} \right] G_{20} -$$

$$\frac{dG_{21}}{dt} = (a_{21})^{(3)}G_{20} - \left[\begin{array}{ccc} (a'_{21})^{(3)} \boxed{+(a''_{21})^{(3)}(T_{21}, t)} & \boxed{+(a''_{17})^{(2,2,2)}(T_{17}, t)} & \boxed{+(a''_{14})^{(1,1,1)}(T_{14}, t)} \\ \boxed{+(a''_{25})^{(4,4,4,4,4)}(T_{25}, t)} & \boxed{+(a''_{29})^{(5,5,5,5,5)}(T_{29}, t)} & \boxed{+(a''_{33})^{(6,6,6,6,6)}(T_{33}, t)} \end{array} \right] G_{21} -$$

$$\frac{dG_{22}}{dt} = (a_{22})^{(3)}G_{21} - \left[\begin{array}{ccc} (a'_{22})^{(3)} \boxed{+(a''_{22})^{(3)}(T_{21}, t)} & \boxed{+(a''_{18})^{(2,2,2)}(T_{17}, t)} & \boxed{+(a''_{15})^{(1,1,1)}(T_{14}, t)} \\ \boxed{+(a''_{26})^{(4,4,4,4,4)}(T_{25}, t)} & \boxed{+(a''_{30})^{(5,5,5,5,5)}(T_{29}, t)} & \boxed{+(a''_{34})^{(6,6,6,6,6)}(T_{33}, t)} \end{array} \right] G_{22} -$$

$\boxed{+(a''_{20})^{(3)}(T_{21}, t)}$, $\boxed{+(a''_{21})^{(3)}(T_{21}, t)}$, $\boxed{+(a''_{22})^{(3)}(T_{21}, t)}$ are first augmentation coefficients for category 1, 2 and 3

$\boxed{+(a''_{16})^{(2,2,2)}(T_{17}, t)}$, $\boxed{+(a''_{17})^{(2,2,2)}(T_{17}, t)}$, $\boxed{+(a''_{18})^{(2,2,2)}(T_{17}, t)}$ are second augmentation coefficients for category 1, 2 and 3

$\boxed{+(a''_{13})^{(1,1,1)}(T_{14}, t)}$, $\boxed{+(a''_{14})^{(1,1,1)}(T_{14}, t)}$, $\boxed{+(a''_{15})^{(1,1,1)}(T_{14}, t)}$ are third augmentation coefficients for category 1, 2 and 3

$\boxed{+(a''_{24})^{(4,4,4,4,4)}(T_{25}, t)}$, $\boxed{+(a''_{25})^{(4,4,4,4,4)}(T_{25}, t)}$, $\boxed{+(a''_{26})^{(4,4,4,4,4)}(T_{25}, t)}$ are fourth augmentation coefficients for category 1, 2 and 3

$\boxed{+(a''_{28})^{(5,5,5,5,5)}(T_{29}, t)}$, $\boxed{+(a''_{29})^{(5,5,5,5,5)}(T_{29}, t)}$, $\boxed{+(a''_{30})^{(5,5,5,5,5)}(T_{29}, t)}$ are fifth augmentation coefficients for category 1, 2 and 3

$\boxed{+(a''_{32})^{(6,6,6,6,6)}(T_{33}, t)}$, $\boxed{+(a''_{33})^{(6,6,6,6,6)}(T_{33}, t)}$, $\boxed{+(a''_{34})^{(6,6,6,6,6)}(T_{33}, t)}$ are sixth augmentation coefficients for category 1, 2 and 3 -

$$\frac{dT_{20}}{dt} = (b_{20})^{(3)}T_{21} - \left[\begin{array}{ccc} (b'_{20})^{(3)} \boxed{-(b''_{20})^{(3)}(G_{23}, t)} & \boxed{-(b''_{16})^{(2,2,2)}(G_{19}, t)} & \boxed{-(b''_{13})^{(1,1,1)}(G, t)} \\ \boxed{-(b''_{24})^{(4,4,4,4,4)}(G_{27}, t)} & \boxed{-(b''_{28})^{(5,5,5,5,5)}(G_{31}, t)} & \boxed{-(b''_{32})^{(6,6,6,6,6)}(G_{35}, t)} \end{array} \right] T_{20} -$$

$$\frac{dT_{21}}{dt} = (b_{21})^{(3)}T_{20} - \left[\begin{array}{ccc} (b'_{21})^{(3)} \boxed{-(b''_{21})^{(3)}(G_{23}, t)} & \boxed{-(b''_{17})^{(2,2,2)}(G_{19}, t)} & \boxed{-(b''_{14})^{(1,1,1)}(G, t)} \\ \boxed{-(b''_{25})^{(4,4,4,4,4)}(G_{27}, t)} & \boxed{-(b''_{29})^{(5,5,5,5,5)}(G_{31}, t)} & \boxed{-(b''_{33})^{(6,6,6,6,6)}(G_{35}, t)} \end{array} \right] T_{21} -$$

$$\frac{dT_{22}}{dt} = (b_{22})^{(3)}T_{21} - \left[\begin{array}{ccc} (b'_{22})^{(3)} \boxed{-(b''_{22})^{(3)}(G_{23}, t)} & \boxed{-(b''_{18})^{(2,2,2)}(G_{19}, t)} & \boxed{-(b''_{15})^{(1,1,1)}(G, t)} \\ \boxed{-(b''_{26})^{(4,4,4,4,4)}(G_{27}, t)} & \boxed{-(b''_{30})^{(5,5,5,5,5)}(G_{31}, t)} & \boxed{-(b''_{34})^{(6,6,6,6,6)}(G_{35}, t)} \end{array} \right] T_{22} -$$

$\boxed{-(b''_{20})^{(3)}(G_{23}, t)}$, $\boxed{-(b''_{21})^{(3)}(G_{23}, t)}$, $\boxed{-(b''_{22})^{(3)}(G_{23}, t)}$ are first detrition coefficients for category 1, 2 and 3

$\boxed{-(b''_{16})^{(2,2,2)}(G_{19}, t)}$, $\boxed{-(b''_{17})^{(2,2,2)}(G_{19}, t)}$, $\boxed{-(b''_{18})^{(2,2,2)}(G_{19}, t)}$ are second detrition coefficients for category 1, 2 and 3

$\boxed{-(b''_{13})^{(1,1,1)}(G, t)}$, $\boxed{-(b''_{14})^{(1,1,1)}(G, t)}$, $\boxed{-(b''_{15})^{(1,1,1)}(G, t)}$ are third detrition coefficients for category 1,2 and 3

$\boxed{-(b''_{24})^{(4,4,4,4,4)}(G_{27}, t)}$, $\boxed{-(b''_{25})^{(4,4,4,4,4)}(G_{27}, t)}$, $\boxed{-(b''_{26})^{(4,4,4,4,4)}(G_{27}, t)}$ are fourth detrition coefficients for category 1, 2 and 3

$\boxed{-(b''_{28})^{(5,5,5,5,5)}(G_{31}, t)}$, $\boxed{-(b''_{29})^{(5,5,5,5,5)}(G_{31}, t)}$, $\boxed{-(b''_{30})^{(5,5,5,5,5)}(G_{31}, t)}$ are fifth detrition coefficients for category 1, 2 and 3

$-(b''_{32})^{(6,6,6,6,6,6)}(G_{35}, t)$, $-(b''_{33})^{(6,6,6,6,6,6)}(G_{35}, t)$, $-(b''_{34})^{(6,6,6,6,6,6)}(G_{35}, t)$ are sixth detrition coefficients for category 1, 2 and 3 -

$$\begin{aligned} \frac{dG_{24}}{dt} &= (a_{24})^{(4)}G_{25} - \left[\begin{array}{c} (a'_{24})^{(4)} + (a''_{24})^{(4)}(T_{25}, t) + (a''_{28})^{(5,5)}(T_{29}, t) + (a''_{32})^{(6,6)}(T_{33}, t) \\ + (a''_{13})^{(1,1,1,1)}(T_{14}, t) + (a''_{16})^{(2,2,2,2)}(T_{17}, t) + (a''_{20})^{(3,3,3,3)}(T_{21}, t) \end{array} \right] G_{24} - \\ \frac{dG_{25}}{dt} &= (a_{25})^{(4)}G_{24} - \left[\begin{array}{c} (a'_{25})^{(4)} + (a''_{25})^{(4)}(T_{25}, t) + (a''_{29})^{(5,5)}(T_{29}, t) + (a''_{33})^{(6,6)}(T_{33}, t) \\ + (a''_{14})^{(1,1,1,1)}(T_{14}, t) + (a''_{17})^{(2,2,2,2)}(T_{17}, t) + (a''_{21})^{(3,3,3,3)}(T_{21}, t) \end{array} \right] G_{25} - \\ \frac{dG_{26}}{dt} &= (a_{26})^{(4)}G_{25} - \left[\begin{array}{c} (a'_{26})^{(4)} + (a''_{26})^{(4)}(T_{25}, t) + (a''_{30})^{(5,5)}(T_{29}, t) + (a''_{34})^{(6,6)}(T_{33}, t) \\ + (a''_{15})^{(1,1,1,1)}(T_{14}, t) + (a''_{18})^{(2,2,2,2)}(T_{17}, t) + (a''_{22})^{(3,3,3,3)}(T_{21}, t) \end{array} \right] G_{26} - \end{aligned}$$

Where $(a''_{24})^{(4)}(T_{25}, t)$, $(a''_{25})^{(4)}(T_{25}, t)$, $(a''_{26})^{(4)}(T_{25}, t)$ are first augmentation coefficients for category 1, 2 and 3
 $(a''_{28})^{(5,5)}(T_{29}, t)$, $(a''_{29})^{(5,5)}(T_{29}, t)$, $(a''_{30})^{(5,5)}(T_{29}, t)$ are second augmentation coefficient for category 1, 2 and 3
 $(a''_{32})^{(6,6)}(T_{33}, t)$, $(a''_{33})^{(6,6)}(T_{33}, t)$, $(a''_{34})^{(6,6)}(T_{33}, t)$ are third augmentation coefficient for category 1, 2 and 3
 $(a''_{13})^{(1,1,1,1)}(T_{14}, t)$, $(a''_{14})^{(1,1,1,1)}(T_{14}, t)$, $(a''_{15})^{(1,1,1,1)}(T_{14}, t)$ are fourth augmentation coefficients for category 1, 2, and 3
 $(a''_{16})^{(2,2,2,2)}(T_{17}, t)$, $(a''_{17})^{(2,2,2,2)}(T_{17}, t)$, $(a''_{18})^{(2,2,2,2)}(T_{17}, t)$ are fifth augmentation coefficients for category 1, 2, and 3
 $(a''_{20})^{(3,3,3,3)}(T_{21}, t)$, $(a''_{21})^{(3,3,3,3)}(T_{21}, t)$, $(a''_{22})^{(3,3,3,3)}(T_{21}, t)$ are sixth augmentation coefficients for category 1, 2, and 3 -

$$\begin{aligned} \frac{dT_{24}}{dt} &= (b_{24})^{(4)}T_{25} - \left[\begin{array}{c} (b'_{24})^{(4)} - (b''_{24})^{(4)}(G_{27}, t) - (b''_{28})^{(5,5)}(G_{31}, t) - (b''_{32})^{(6,6)}(G_{35}, t) \\ - (b''_{13})^{(1,1,1,1)}(G, t) - (b''_{16})^{(2,2,2,2)}(G_{19}, t) - (b''_{20})^{(3,3,3,3)}(G_{23}, t) \end{array} \right] T_{24} - \\ \frac{dT_{25}}{dt} &= (b_{25})^{(4)}T_{24} - \left[\begin{array}{c} (b'_{25})^{(4)} - (b''_{25})^{(4)}(G_{27}, t) - (b''_{29})^{(5,5)}(G_{31}, t) - (b''_{33})^{(6,6)}(G_{35}, t) \\ - (b''_{14})^{(1,1,1,1)}(G, t) - (b''_{17})^{(2,2,2,2)}(G_{19}, t) - (b''_{21})^{(3,3,3,3)}(G_{23}, t) \end{array} \right] T_{25} - \\ \frac{dT_{26}}{dt} &= (b_{26})^{(4)}T_{25} - \left[\begin{array}{c} (b'_{26})^{(4)} - (b''_{26})^{(4)}(G_{27}, t) - (b''_{30})^{(5,5)}(G_{31}, t) - (b''_{34})^{(6,6)}(G_{35}, t) \\ - (b''_{15})^{(1,1,1,1)}(G, t) - (b''_{18})^{(2,2,2,2)}(G_{19}, t) - (b''_{22})^{(3,3,3,3)}(G_{23}, t) \end{array} \right] T_{26} - \end{aligned}$$

Where $-(b''_{24})^{(4)}(G_{27}, t)$, $-(b''_{25})^{(4)}(G_{27}, t)$, $-(b''_{26})^{(4)}(G_{27}, t)$ are first detrition coefficients for category 1, 2 and 3
 $-(b''_{28})^{(5,5)}(G_{31}, t)$, $-(b''_{29})^{(5,5)}(G_{31}, t)$, $-(b''_{30})^{(5,5)}(G_{31}, t)$ are second detrition coefficients for category 1, 2 and 3
 $-(b''_{32})^{(6,6)}(G_{35}, t)$, $-(b''_{33})^{(6,6)}(G_{35}, t)$, $-(b''_{34})^{(6,6)}(G_{35}, t)$ are third detrition coefficients for category 1, 2 and 3
 $-(b''_{13})^{(1,1,1,1)}(G, t)$, $-(b''_{14})^{(1,1,1,1)}(G, t)$, $-(b''_{15})^{(1,1,1,1)}(G, t)$ are fourth detrition coefficients for category 1, 2 and 3
 $-(b''_{16})^{(2,2,2,2)}(G_{19}, t)$, $-(b''_{17})^{(2,2,2,2)}(G_{19}, t)$, $-(b''_{18})^{(2,2,2,2)}(G_{19}, t)$ are fifth detrition coefficients for category 1, 2 and 3
 $-(b''_{20})^{(3,3,3,3)}(G_{23}, t)$, $-(b''_{21})^{(3,3,3,3)}(G_{23}, t)$, $-(b''_{22})^{(3,3,3,3)}(G_{23}, t)$ are sixth detrition coefficients for category 1, 2 and 3 -

$$\begin{aligned} \frac{dG_{28}}{dt} &= (a_{28})^{(5)}G_{29} - \left[\begin{array}{c} (a'_{28})^{(5)} + (a''_{28})^{(5)}(T_{29}, t) + (a''_{24})^{(4,4)}(T_{25}, t) + (a''_{32})^{(6,6,6)}(T_{33}, t) \\ + (a''_{13})^{(1,1,1,1,1)}(T_{14}, t) + (a''_{16})^{(2,2,2,2,2)}(T_{17}, t) + (a''_{20})^{(3,3,3,3,3)}(T_{21}, t) \end{array} \right] G_{28} - \\ \frac{dG_{29}}{dt} &= (a_{29})^{(5)}G_{28} - \left[\begin{array}{c} (a'_{29})^{(5)} + (a''_{29})^{(5)}(T_{29}, t) + (a''_{25})^{(4,4)}(T_{25}, t) + (a''_{33})^{(6,6,6)}(T_{33}, t) \\ + (a''_{14})^{(1,1,1,1,1)}(T_{14}, t) + (a''_{17})^{(2,2,2,2,2)}(T_{17}, t) + (a''_{21})^{(3,3,3,3,3)}(T_{21}, t) \end{array} \right] G_{29} - \\ \frac{dG_{30}}{dt} &= (a_{30})^{(5)}G_{29} - \left[\begin{array}{c} (a'_{30})^{(5)} + (a''_{30})^{(5)}(T_{29}, t) + (a''_{26})^{(4,4)}(T_{25}, t) + (a''_{34})^{(6,6,6)}(T_{33}, t) \\ + (a''_{15})^{(1,1,1,1,1)}(T_{14}, t) + (a''_{18})^{(2,2,2,2,2)}(T_{17}, t) + (a''_{22})^{(3,3,3,3,3)}(T_{21}, t) \end{array} \right] G_{30} - \end{aligned}$$

Where $(a''_{28})^{(5)}(T_{29}, t)$, $(a''_{29})^{(5)}(T_{29}, t)$, $(a''_{30})^{(5)}(T_{29}, t)$ are first augmentation coefficients for category 1, 2 and 3

And $\boxed{+(a''_{24})^{(4,4)}(T_{25}, t)}$, $\boxed{+(a''_{25})^{(4,4)}(T_{25}, t)}$, $\boxed{+(a''_{26})^{(4,4)}(T_{25}, t)}$ are second augmentation coefficient for category 1, 2 and 3
 $\boxed{+(a''_{32})^{(6,6,6)}(T_{33}, t)}$, $\boxed{+(a''_{33})^{(6,6,6)}(T_{33}, t)}$, $\boxed{+(a''_{34})^{(6,6,6)}(T_{33}, t)}$ are third augmentation coefficient for category 1, 2 and 3
 $\boxed{+(a''_{13})^{(1,1,1,1,1)}(T_{14}, t)}$, $\boxed{+(a''_{14})^{(1,1,1,1,1)}(T_{14}, t)}$, $\boxed{+(a''_{15})^{(1,1,1,1,1)}(T_{14}, t)}$ are fourth augmentation coefficients for category 1, 2, and 3
 $\boxed{+(a''_{16})^{(2,2,2,2,2)}(T_{17}, t)}$, $\boxed{+(a''_{17})^{(2,2,2,2,2)}(T_{17}, t)}$, $\boxed{+(a''_{18})^{(2,2,2,2,2)}(T_{17}, t)}$ are fifth augmentation coefficients for category 1, 2, and 3
 $\boxed{+(a''_{20})^{(3,3,3,3,3)}(T_{21}, t)}$, $\boxed{+(a''_{21})^{(3,3,3,3,3)}(T_{21}, t)}$, $\boxed{+(a''_{22})^{(3,3,3,3,3)}(T_{21}, t)}$ are sixth augmentation coefficients for category 1, 2, 3 -

$$\begin{aligned} \frac{dT_{28}}{dt} &= (b_{28})^{(5)}T_{29} - \left[\begin{array}{ccc} \boxed{(b'_{28})^{(5)} - \boxed{(b''_{28})^{(5)}(G_{31}, t)} - \boxed{(b''_{24})^{(4,4)}(G_{27}, t)} - \boxed{(b''_{32})^{(6,6,6)}(G_{35}, t)} \\ \boxed{-(b''_{13})^{(1,1,1,1,1)}(G, t)} - \boxed{-(b''_{16})^{(2,2,2,2,2)}(G_{19}, t)} - \boxed{-(b''_{20})^{(3,3,3,3,3)}(G_{23}, t)} \end{array} \right] T_{28} - \\ \frac{dT_{29}}{dt} &= (b_{29})^{(5)}T_{28} - \left[\begin{array}{ccc} \boxed{(b'_{29})^{(5)} - \boxed{(b''_{29})^{(5)}(G_{31}, t)} - \boxed{(b''_{25})^{(4,4)}(G_{27}, t)} - \boxed{(b''_{33})^{(6,6,6)}(G_{35}, t)} \\ \boxed{-(b''_{14})^{(1,1,1,1,1)}(G, t)} - \boxed{-(b''_{17})^{(2,2,2,2,2)}(G_{19}, t)} - \boxed{-(b''_{21})^{(3,3,3,3,3)}(G_{23}, t)} \end{array} \right] T_{29} - \\ \frac{dT_{30}}{dt} &= (b_{30})^{(5)}T_{29} - \left[\begin{array}{ccc} \boxed{(b'_{30})^{(5)} - \boxed{(b''_{30})^{(5)}(G_{31}, t)} - \boxed{(b''_{26})^{(4,4)}(G_{27}, t)} - \boxed{(b''_{34})^{(6,6,6)}(G_{35}, t)} \\ \boxed{-(b''_{15})^{(1,1,1,1,1)}(G, t)} - \boxed{-(b''_{18})^{(2,2,2,2,2)}(G_{19}, t)} - \boxed{-(b''_{22})^{(3,3,3,3,3)}(G_{23}, t)} \end{array} \right] T_{30} - \end{aligned}$$

where $\boxed{-(b''_{28})^{(5)}(G_{31}, t)}$, $\boxed{-(b''_{29})^{(5)}(G_{31}, t)}$, $\boxed{-(b''_{30})^{(5)}(G_{31}, t)}$ are first detrition coefficients for category 1, 2 and 3
 $\boxed{-(b''_{24})^{(4,4)}(G_{27}, t)}$, $\boxed{-(b''_{25})^{(4,4)}(G_{27}, t)}$, $\boxed{-(b''_{26})^{(4,4)}(G_{27}, t)}$ are second detrition coefficients for category 1, 2 and 3
 $\boxed{-(b''_{32})^{(6,6,6)}(G_{35}, t)}$, $\boxed{-(b''_{33})^{(6,6,6)}(G_{35}, t)}$, $\boxed{-(b''_{34})^{(6,6,6)}(G_{35}, t)}$ are third detrition coefficients for category 1, 2 and 3
 $\boxed{-(b''_{13})^{(1,1,1,1,1)}(G, t)}$, $\boxed{-(b''_{14})^{(1,1,1,1,1)}(G, t)}$, $\boxed{-(b''_{15})^{(1,1,1,1,1)}(G, t)}$ are fourth detrition coefficients for category 1, 2, and 3
 $\boxed{-(b''_{16})^{(2,2,2,2,2)}(G_{19}, t)}$, $\boxed{-(b''_{17})^{(2,2,2,2,2)}(G_{19}, t)}$, $\boxed{-(b''_{18})^{(2,2,2,2,2)}(G_{19}, t)}$ are fifth detrition coefficients for category 1, 2, and 3
 $\boxed{-(b''_{20})^{(3,3,3,3,3)}(G_{23}, t)}$, $\boxed{-(b''_{21})^{(3,3,3,3,3)}(G_{23}, t)}$, $\boxed{-(b''_{22})^{(3,3,3,3,3)}(G_{23}, t)}$ are sixth detrition coefficients for category 1, 2, and 3-

$$\begin{aligned} \frac{dG_{32}}{dt} &= (a_{32})^{(6)}G_{33} - \left[\begin{array}{ccc} \boxed{(a'_{32})^{(6)} + \boxed{(a''_{32})^{(6)}(T_{33}, t)} + \boxed{(a''_{28})^{(5,5,5)}(T_{29}, t)} + \boxed{(a''_{24})^{(4,4,4)}(T_{25}, t)} \\ \boxed{+(a''_{13})^{(1,1,1,1,1)}(T_{14}, t)} + \boxed{+(a''_{16})^{(2,2,2,2,2)}(T_{17}, t)} + \boxed{+(a''_{20})^{(3,3,3,3,3)}(T_{21}, t)} \end{array} \right] G_{32} - \\ \frac{dG_{33}}{dt} &= (a_{33})^{(6)}G_{32} - \left[\begin{array}{ccc} \boxed{(a'_{33})^{(6)} + \boxed{(a''_{33})^{(6)}(T_{33}, t)} + \boxed{(a''_{29})^{(5,5,5)}(T_{29}, t)} + \boxed{(a''_{25})^{(4,4,4)}(T_{25}, t)} \\ \boxed{+(a''_{14})^{(1,1,1,1,1)}(T_{14}, t)} + \boxed{+(a''_{17})^{(2,2,2,2,2)}(T_{17}, t)} + \boxed{+(a''_{21})^{(3,3,3,3,3)}(T_{21}, t)} \end{array} \right] G_{33} - \\ \frac{dG_{34}}{dt} &= (a_{34})^{(6)}G_{33} - \left[\begin{array}{ccc} \boxed{(a'_{34})^{(6)} + \boxed{(a''_{34})^{(6)}(T_{33}, t)} + \boxed{(a''_{30})^{(5,5,5)}(T_{29}, t)} + \boxed{(a''_{26})^{(4,4,4)}(T_{25}, t)} \\ \boxed{+(a''_{15})^{(1,1,1,1,1)}(T_{14}, t)} + \boxed{+(a''_{18})^{(2,2,2,2,2)}(T_{17}, t)} + \boxed{+(a''_{22})^{(3,3,3,3,3)}(T_{21}, t)} \end{array} \right] G_{34} - \end{aligned}$$

$\boxed{+(a''_{32})^{(6)}(T_{33}, t)}$, $\boxed{+(a''_{33})^{(6)}(T_{33}, t)}$, $\boxed{+(a''_{34})^{(6)}(T_{33}, t)}$ are first augmentation coefficients for category 1, 2 and 3
 $\boxed{+(a''_{28})^{(5,5,5)}(T_{29}, t)}$, $\boxed{+(a''_{29})^{(5,5,5)}(T_{29}, t)}$, $\boxed{+(a''_{30})^{(5,5,5)}(T_{29}, t)}$ are second augmentation coefficients for category 1, 2 and 3
 $\boxed{+(a''_{24})^{(4,4,4)}(T_{25}, t)}$, $\boxed{+(a''_{25})^{(4,4,4)}(T_{25}, t)}$, $\boxed{+(a''_{26})^{(4,4,4)}(T_{25}, t)}$ are third augmentation coefficients for category 1, 2 and 3
 $\boxed{+(a''_{13})^{(1,1,1,1,1)}(T_{14}, t)}$, $\boxed{+(a''_{14})^{(1,1,1,1,1)}(T_{14}, t)}$, $\boxed{+(a''_{15})^{(1,1,1,1,1)}(T_{14}, t)}$ - are fourth augmentation coefficients
 $\boxed{+(a''_{16})^{(2,2,2,2,2)}(T_{17}, t)}$, $\boxed{+(a''_{17})^{(2,2,2,2,2)}(T_{17}, t)}$, $\boxed{+(a''_{18})^{(2,2,2,2,2)}(T_{17}, t)}$ - fifth augmentation coefficients
 $\boxed{+(a''_{20})^{(3,3,3,3,3)}(T_{21}, t)}$, $\boxed{+(a''_{21})^{(3,3,3,3,3)}(T_{21}, t)}$, $\boxed{+(a''_{22})^{(3,3,3,3,3)}(T_{21}, t)}$ sixth augmentation coefficients -

$$\frac{dT_{32}}{dt} = (b_{32})^{(6)}T_{33} - \left[\begin{array}{ccc} \boxed{(b'_{32})^{(6)} - \boxed{(b''_{32})^{(6)}(G_{35}, t)} - \boxed{(b''_{28})^{(5,5,5)}(G_{31}, t)} - \boxed{(b''_{24})^{(4,4,4)}(G_{27}, t)} \\ \boxed{-(b''_{13})^{(1,1,1,1,1)}(G, t)} - \boxed{-(b''_{16})^{(2,2,2,2,2)}(G_{19}, t)} - \boxed{-(b''_{20})^{(3,3,3,3,3)}(G_{23}, t)} \end{array} \right] T_{32} -$$

$$\frac{dT_{33}}{dt} = (b_{33})^{(6)}T_{32} - \left[\begin{array}{c} (b_{33}^{(6)})^{(6)} \boxed{-(b_{33}^{(6)})^{(6)}(G_{35}, t)} \quad \boxed{-(b_{29}^{(5,5,5)})^{(5,5,5)}(G_{31}, t)} \quad \boxed{-(b_{25}^{(4,4,4)})^{(4,4,4)}(G_{27}, t)} \\ \boxed{-(b_{14}^{(1,1,1,1,1,1)})^{(1,1,1,1,1,1)}(G, t)} \quad \boxed{-(b_{17}^{(2,2,2,2,2,2)})^{(2,2,2,2,2,2)}(G_{19}, t)} \quad \boxed{-(b_{21}^{(3,3,3,3,3,3)})^{(3,3,3,3,3,3)}(G_{23}, t)} \end{array} \right] T_{33} -$$

$$\frac{dT_{34}}{dt} = (b_{34})^{(6)}T_{33} - \left[\begin{array}{c} (b_{34}^{(6)})^{(6)} \boxed{-(b_{34}^{(6)})^{(6)}(G_{35}, t)} \quad \boxed{-(b_{30}^{(5,5,5)})^{(5,5,5)}(G_{31}, t)} \quad \boxed{-(b_{26}^{(4,4,4)})^{(4,4,4)}(G_{27}, t)} \\ \boxed{-(b_{15}^{(1,1,1,1,1,1)})^{(1,1,1,1,1,1)}(G, t)} \quad \boxed{-(b_{18}^{(2,2,2,2,2,2)})^{(2,2,2,2,2,2)}(G_{19}, t)} \quad \boxed{-(b_{22}^{(3,3,3,3,3,3)})^{(3,3,3,3,3,3)}(G_{23}, t)} \end{array} \right] T_{34} -$$

$\boxed{-(b_{32}^{(6)})^{(6)}(G_{35}, t)}$, $\boxed{-(b_{33}^{(6)})^{(6)}(G_{35}, t)}$, $\boxed{-(b_{34}^{(6)})^{(6)}(G_{35}, t)}$ are first detrition coefficients for category 1, 2 and 3
 $\boxed{-(b_{28}^{(5,5,5)})^{(5,5,5)}(G_{31}, t)}$, $\boxed{-(b_{29}^{(5,5,5)})^{(5,5,5)}(G_{31}, t)}$, $\boxed{-(b_{30}^{(5,5,5)})^{(5,5,5)}(G_{31}, t)}$ are second detrition coefficients for category 1, 2 and 3
 $\boxed{-(b_{24}^{(4,4,4)})^{(4,4,4)}(G_{27}, t)}$, $\boxed{-(b_{25}^{(4,4,4)})^{(4,4,4)}(G_{27}, t)}$, $\boxed{-(b_{26}^{(4,4,4)})^{(4,4,4)}(G_{27}, t)}$ are third detrition coefficients for category 1, 2 and 3
 $\boxed{-(b_{13}^{(1,1,1,1,1,1)})^{(1,1,1,1,1,1)}(G, t)}$, $\boxed{-(b_{14}^{(1,1,1,1,1,1)})^{(1,1,1,1,1,1)}(G, t)}$, $\boxed{-(b_{15}^{(1,1,1,1,1,1)})^{(1,1,1,1,1,1)}(G, t)}$ are fourth detrition coefficients for category 1, 2, and 3
 $\boxed{-(b_{16}^{(2,2,2,2,2,2)})^{(2,2,2,2,2,2)}(G_{19}, t)}$, $\boxed{-(b_{17}^{(2,2,2,2,2,2)})^{(2,2,2,2,2,2)}(G_{19}, t)}$, $\boxed{-(b_{18}^{(2,2,2,2,2,2)})^{(2,2,2,2,2,2)}(G_{19}, t)}$ are fifth detrition coefficients for category 1, 2, and 3
 $\boxed{-(b_{20}^{(3,3,3,3,3,3)})^{(3,3,3,3,3,3)}(G_{23}, t)}$, $\boxed{-(b_{21}^{(3,3,3,3,3,3)})^{(3,3,3,3,3,3)}(G_{23}, t)}$, $\boxed{-(b_{22}^{(3,3,3,3,3,3)})^{(3,3,3,3,3,3)}(G_{23}, t)}$ are sixth detrition coefficients for category 1, 2, and 3-

Where we suppose-

- (A) $(a_i)^{(1)}, (a_i'')^{(1)}, (a_i''')^{(1)}, (b_i)^{(1)}, (b_i')^{(1)}, (b_i'')^{(1)} > 0$,
 $i, j = 13, 14, 15$
 (B) The functions $(a_i'')^{(1)}, (b_i'')^{(1)}$ are positive continuous increasing and bounded.

Definition of $(p_i)^{(1)}, (r_i)^{(1)}$:

$$(a_i'')^{(1)}(T_{14}, t) \leq (p_i)^{(1)} \leq (\hat{A}_{13})^{(1)}$$

$$(b_i'')^{(1)}(G, t) \leq (r_i)^{(1)} \leq (b_i')^{(1)} \leq (\hat{B}_{13})^{(1)}.$$

- (C) $\lim_{T_2 \rightarrow \infty} (a_i'')^{(1)}(T_{14}, t) = (p_i)^{(1)}$
 $\lim_{G \rightarrow \infty} (b_i'')^{(1)}(G, t) = (r_i)^{(1)}$

Definition of $(\hat{A}_{13})^{(1)}, (\hat{B}_{13})^{(1)}$:

Where $\boxed{(\hat{A}_{13})^{(1)}, (\hat{B}_{13})^{(1)}, (p_i)^{(1)}, (r_i)^{(1)}}$ are positive constants and $\boxed{i = 13, 14, 15}$ -

They satisfy Lipschitz condition:

$$|(a_i'')^{(1)}(T'_{14}, t) - (a_i'')^{(1)}(T_{14}, t)| \leq (\hat{k}_{13})^{(1)} |T'_{14} - T_{14}| e^{-(\hat{M}_{13})^{(1)}t}$$

$$|(b_i'')^{(1)}(G', t) - (b_i'')^{(1)}(G, t)| < (\hat{k}_{13})^{(1)} \|G - G'\| e^{-(\hat{M}_{13})^{(1)}t}.$$

With the Lipschitz condition, we place a restriction on the behavior of functions

$(a_i'')^{(1)}(T'_{14}, t)$ and $(a_i'')^{(1)}(T_{14}, t)$. (T'_{14}, t) and (T_{14}, t) are points belonging to the interval $[(\hat{k}_{13})^{(1)}, (\hat{M}_{13})^{(1)}]$. It is to be noted that $(a_i'')^{(1)}(T_{14}, t)$ is uniformly continuous. In the eventuality of the fact, that if $(\hat{M}_{13})^{(1)} = 1$ then the function $(a_i'')^{(1)}(T_{14}, t)$, the first augmentation coefficient would be absolutely continuous. -

Definition of $(\hat{M}_{13})^{(1)}, (\hat{k}_{13})^{(1)}$:

- (D) $(\hat{M}_{13})^{(1)}, (\hat{k}_{13})^{(1)}$, are positive constants

$$\frac{(a_i)^{(1)}}{(\hat{M}_{13})^{(1)}}, \frac{(b_i)^{(1)}}{(\hat{M}_{13})^{(1)}} < 1 -$$

Definition of $(\hat{P}_{13})^{(1)}, (\hat{Q}_{13})^{(1)}$:

- (E) There exists two constants $(\hat{P}_{13})^{(1)}$ and $(\hat{Q}_{13})^{(1)}$ which together with $(\hat{M}_{13})^{(1)}, (\hat{k}_{13})^{(1)}, (\hat{A}_{13})^{(1)}$ and $(\hat{B}_{13})^{(1)}$ and the constants $(a_i)^{(1)}, (a_i')^{(1)}, (b_i)^{(1)}, (b_i')^{(1)}, (p_i)^{(1)}, (r_i)^{(1)}, i = 13, 14, 15$, satisfy the inequalities

$$\frac{1}{(\hat{M}_{13})^{(1)}} [(a_i)^{(1)} + (a_i')^{(1)} + (\hat{A}_{13})^{(1)} + (\hat{P}_{13})^{(1)} (\hat{k}_{13})^{(1)}] < 1$$

$$\frac{1}{(\hat{M}_{13})^{(1)}} [(b_i)^{(1)} + (b_i')^{(1)} + (\hat{B}_{13})^{(1)} + (\hat{Q}_{13})^{(1)} (\hat{k}_{13})^{(1)}] < 1 -$$

Where we suppose-

$$(a_i)^{(2)}, (a_i')^{(2)}, (a_i'')^{(2)}, (b_i)^{(2)}, (b_i')^{(2)}, (b_i'')^{(2)} > 0, \quad i, j = 16, 17, 18 -$$

The functions $(a_i'')^{(2)}, (b_i'')^{(2)}$ are positive continuous increasing and bounded. -

Definition of $(p_i)^{(2)}, (r_i)^{(2)}$:-

$$(a_i'')^{(2)}(T_{17}, t) \leq (p_i)^{(2)} \leq (\hat{A}_{16})^{(2)} -$$

$$(b_i'')^{(2)}(G_{19}, t) \leq (r_i)^{(2)} \leq (b_i')^{(2)} \leq (\hat{B}_{16})^{(2)} -$$

$$\lim_{T_2 \rightarrow \infty} (a_i'')^{(2)}(T_{17}, t) = (p_i)^{(2)} -$$

$$\lim_{G \rightarrow \infty} (b_i'')^{(2)}(G_{19}, t) = (r_i)^{(2)} -$$

Definition of $(\hat{A}_{16})^{(2)}, (\hat{B}_{16})^{(2)}$:

Where $(\hat{A}_{16})^{(2)}, (\hat{B}_{16})^{(2)}, (p_i)^{(2)}, (r_i)^{(2)}$ are positive constants and $i = 16, 17, 18$ -

They satisfy Lipschitz condition:-

$$|(a_i'')^{(2)}(T_{17}, t) - (a_i'')^{(2)}(T_{17}, t)| \leq (\hat{k}_{16})^{(2)} |T_{17} - T_{17}'| e^{-(M_{16})^{(2)}t} -$$

$$|(b_i'')^{(2)}(G_{19}, t) - (b_i'')^{(2)}(G_{19}, t)| < (\hat{k}_{16})^{(2)} |(G_{19}) - (G_{19})'| e^{-(M_{16})^{(2)}t} -$$

With the Lipschitz condition, we place a restriction on the behavior of functions $(a_i'')^{(2)}(T_{17}, t)$ and $(a_i'')^{(2)}(T_{17}, t) \cdot (T_{17}', t)$ and (T_{17}, t) are points belonging to the interval $[(\hat{k}_{16})^{(2)}, (\hat{M}_{16})^{(2)}]$. It is to be noted that $(a_i'')^{(2)}(T_{17}, t)$ is uniformly continuous. In the eventuality of the fact, that if $(\hat{M}_{16})^{(2)} = 1$ then the function $(a_i'')^{(2)}(T_{17}, t)$, the SECOND augmentation coefficient would be absolutely continuous. -

Definition of $(\hat{M}_{16})^{(2)}, (\hat{k}_{16})^{(2)}$:-

(F) $(\hat{M}_{16})^{(2)}, (\hat{k}_{16})^{(2)}$, are positive constants

$$\frac{(a_i)^{(2)}}{(\hat{M}_{16})^{(2)}}, \frac{(b_i)^{(2)}}{(\hat{M}_{16})^{(2)}} < 1 -$$

Definition of $(\hat{P}_{16})^{(2)}, (\hat{Q}_{16})^{(2)}$:

There exists two constants $(\hat{P}_{16})^{(2)}$ and $(\hat{Q}_{16})^{(2)}$ which together with $(\hat{M}_{16})^{(2)}, (\hat{k}_{16})^{(2)}, (\hat{A}_{16})^{(2)}$ and $(\hat{B}_{16})^{(2)}$ and the constants $(a_i)^{(2)}, (a_i')^{(2)}, (b_i)^{(2)}, (b_i')^{(2)}, (p_i)^{(2)}, (r_i)^{(2)}, i = 16, 17, 18$, satisfy the inequalities -

$$\frac{1}{(\hat{M}_{16})^{(2)}} [(a_i)^{(2)} + (a_i')^{(2)} + (\hat{A}_{16})^{(2)} + (\hat{P}_{16})^{(2)} (\hat{k}_{16})^{(2)}] < 1 -$$

$$\frac{1}{(\hat{M}_{16})^{(2)}} [(b_i)^{(2)} + (b_i')^{(2)} + (\hat{B}_{16})^{(2)} + (\hat{Q}_{16})^{(2)} (\hat{k}_{16})^{(2)}] < 1 -$$

Where we suppose-

(G) $(a_i)^{(3)}, (a_i')^{(3)}, (a_i'')^{(3)}, (b_i)^{(3)}, (b_i')^{(3)}, (b_i'')^{(3)} > 0, i, j = 20, 21, 22$

The functions $(a_i'')^{(3)}, (b_i'')^{(3)}$ are positive continuous increasing and bounded.

Definition of $(p_i)^{(3)}, (r_i)^{(3)}$:

$$(a_i'')^{(3)}(T_{21}, t) \leq (p_i)^{(3)} \leq (\hat{A}_{20})^{(3)}$$

$$(b_i'')^{(3)}(G_{23}, t) \leq (r_i)^{(3)} \leq (b_i')^{(3)} \leq (\hat{B}_{20})^{(3)} -$$

$$\lim_{T_2 \rightarrow \infty} (a_i'')^{(3)}(T_{21}, t) = (p_i)^{(3)}$$

$$\lim_{G \rightarrow \infty} (b_i'')^{(3)}(G_{23}, t) = (r_i)^{(3)}$$

Definition of $(\hat{A}_{20})^{(3)}, (\hat{B}_{20})^{(3)}$:

Where $(\hat{A}_{20})^{(3)}, (\hat{B}_{20})^{(3)}, (p_i)^{(3)}, (r_i)^{(3)}$ are positive constants and $i = 20, 21, 22$ -

They satisfy Lipschitz condition:

$$|(a_i'')^{(3)}(T_{21}, t) - (a_i'')^{(3)}(T_{21}, t)| \leq (\hat{k}_{20})^{(3)} |T_{21} - T_{21}'| e^{-(M_{20})^{(3)}t} -$$

$$|(b_i'')^{(3)}(G_{23}, t) - (b_i'')^{(3)}(G_{23}, t)| < (\hat{k}_{20})^{(3)} |(G_{23}) - (G_{23})'| e^{-(M_{20})^{(3)}t} -$$

With the Lipschitz condition, we place a restriction on the behavior of functions $(a_i'')^{(3)}(T_{21}, t)$ and $(a_i'')^{(3)}(T_{21}, t) \cdot (T_{21}', t)$ and (T_{21}, t) are points belonging to the interval $[(\hat{k}_{20})^{(3)}, (\hat{M}_{20})^{(3)}]$. It is to be noted that $(a_i'')^{(3)}(T_{21}, t)$ is uniformly continuous. In the eventuality of the fact, that if $(\hat{M}_{20})^{(3)} = 1$ then the function $(a_i'')^{(3)}(T_{21}, t)$, the THIRD first augmentation coefficient would be absolutely continuous. -

Definition of $(\hat{M}_{20})^{(3)}, (\hat{k}_{20})^{(3)}$:

(H) $(\hat{M}_{20})^{(3)}, (\hat{k}_{20})^{(3)}$, are positive constants

$$\frac{(a_i)^{(3)}}{(\hat{M}_{20})^{(3)}}, \frac{(b_i)^{(3)}}{(\hat{M}_{20})^{(3)}} < 1 -$$

There exists two constants There exists two constants $(\hat{P}_{20})^{(3)}$ and $(\hat{Q}_{20})^{(3)}$ which together with $(\hat{M}_{20})^{(3)}, (\hat{k}_{20})^{(3)}, (\hat{A}_{20})^{(3)}$ and $(\hat{B}_{20})^{(3)}$ and the constants $(a_i)^{(3)}, (a_i')^{(3)}, (b_i)^{(3)}, (b_i')^{(3)}, (p_i)^{(3)}, (r_i)^{(3)}, i = 20, 21, 22$, satisfy the inequalities

$$\frac{1}{(\hat{M}_{20})^{(3)}} [(a_i)^{(3)} + (a_i')^{(3)} + (\hat{A}_{20})^{(3)} + (\hat{P}_{20})^{(3)} (\hat{k}_{20})^{(3)}] < 1 -$$

$$\frac{1}{(\hat{M}_{20})^{(3)}} [(b_i)^{(3)} + (b_i')^{(3)} + (\hat{B}_{20})^{(3)} + (\hat{Q}_{20})^{(3)} (\hat{k}_{20})^{(3)}] < 1 -$$

Where we suppose-

- (I) $(a_i)^{(4)}, (a_i')^{(4)}, (a_i'')^{(4)}, (b_i)^{(4)}, (b_i')^{(4)}, (b_i'')^{(4)} > 0, \quad i, j = 24, 25, 26$
 (J) The functions $(a_i'')^{(4)}, (b_i'')^{(4)}$ are positive continuous increasing and bounded.

Definition of $(p_i)^{(4)}, (r_i)^{(4)}$:

$$(a_i'')^{(4)}(T_{25}, t) \leq (p_i)^{(4)} \leq (\hat{A}_{24})^{(4)}$$

$$(b_i'')^{(4)}((G_{27}), t) \leq (r_i)^{(4)} \leq (b_i')^{(4)} \leq (\hat{B}_{24})^{(4)}.$$

(K) $\lim_{T_2 \rightarrow \infty} (a_i'')^{(4)}(T_{25}, t) = (p_i)^{(4)}$

$\lim_{G \rightarrow \infty} (b_i'')^{(4)}((G_{27}), t) = (r_i)^{(4)}$

Definition of $(\hat{A}_{24})^{(4)}, (\hat{B}_{24})^{(4)}$:

Where $(\hat{A}_{24})^{(4)}, (\hat{B}_{24})^{(4)}, (p_i)^{(4)}, (r_i)^{(4)}$ are positive constants and $i = 24, 25, 26$.

They satisfy Lipschitz condition:

$$|(a_i'')^{(4)}(T'_{25}, t) - (a_i'')^{(4)}(T_{25}, t)| \leq (\hat{k}_{24})^{(4)} |T'_{25} - T_{25}| e^{-(\hat{M}_{24})^{(4)}t}$$

$$|(b_i'')^{(4)}((G_{27})', t) - (b_i'')^{(4)}((G_{27}), t)| < (\hat{k}_{24})^{(4)} |(G_{27})' - (G_{27})| e^{-(\hat{M}_{24})^{(4)}t}.$$

With the Lipschitz condition, we place a restriction on the behavior of functions $(a_i'')^{(4)}(T'_{25}, t)$ and $(a_i'')^{(4)}(T_{25}, t) \cdot (T'_{25}, t)$ and (T_{25}, t) are points belonging to the interval $[(\hat{k}_{24})^{(4)}, (\hat{M}_{24})^{(4)}]$. It is to be noted that $(a_i'')^{(4)}(T_{25}, t)$ is uniformly continuous. In the eventuality of the fact, that if $(\hat{M}_{24})^{(4)} = 4$ then the function $(a_i'')^{(4)}(T_{25}, t)$, the **FOURTH augmentation coefficient** would be absolutely continuous. -

Definition of $(\hat{M}_{24})^{(4)}, (\hat{k}_{24})^{(4)}$:

(L) $(\hat{M}_{24})^{(4)}, (\hat{k}_{24})^{(4)}$, are positive constants

$$\frac{(a_i)^{(4)}}{(\hat{M}_{24})^{(4)}} + \frac{(b_i)^{(4)}}{(\hat{M}_{24})^{(4)}} < 1 -$$

Definition of $(\hat{P}_{24})^{(4)}, (\hat{Q}_{24})^{(4)}$:

(M) There exists two constants $(\hat{P}_{24})^{(4)}$ and $(\hat{Q}_{24})^{(4)}$ which together with $(\hat{M}_{24})^{(4)}, (\hat{k}_{24})^{(4)}, (\hat{A}_{24})^{(4)}$ and $(\hat{B}_{24})^{(4)}$ and the constants $(a_i)^{(4)}, (a_i')^{(4)}, (b_i)^{(4)}, (b_i')^{(4)}, (p_i)^{(4)}, (r_i)^{(4)}, i = 24, 25, 26$, satisfy the inequalities

$$\frac{1}{(\hat{M}_{24})^{(4)}} [(a_i)^{(4)} + (a_i')^{(4)} + (\hat{A}_{24})^{(4)} + (\hat{P}_{24})^{(4)} (\hat{k}_{24})^{(4)}] < 1$$

$$\frac{1}{(\hat{M}_{24})^{(4)}} [(b_i)^{(4)} + (b_i')^{(4)} + (\hat{B}_{24})^{(4)} + (\hat{Q}_{24})^{(4)} (\hat{k}_{24})^{(4)}] < 1 -$$

Where we suppose-

- (N) $(a_i)^{(5)}, (a_i')^{(5)}, (a_i'')^{(5)}, (b_i)^{(5)}, (b_i')^{(5)}, (b_i'')^{(5)} > 0, \quad i, j = 28, 29, 30$
 (O) The functions $(a_i'')^{(5)}, (b_i'')^{(5)}$ are positive continuous increasing and bounded.

Definition of $(p_i)^{(5)}, (r_i)^{(5)}$:

$$(a_i'')^{(5)}(T_{29}, t) \leq (p_i)^{(5)} \leq (\hat{A}_{28})^{(5)}$$

$$(b_i'')^{(5)}((G_{31}), t) \leq (r_i)^{(5)} \leq (b_i')^{(5)} \leq (\hat{B}_{28})^{(5)}.$$

(P) $\lim_{T_2 \rightarrow \infty} (a_i'')^{(5)}(T_{29}, t) = (p_i)^{(5)}$

$\lim_{G \rightarrow \infty} (b_i'')^{(5)}(G_{31}, t) = (r_i)^{(5)}$

Definition of $(\hat{A}_{28})^{(5)}, (\hat{B}_{28})^{(5)}$:

Where $(\hat{A}_{28})^{(5)}, (\hat{B}_{28})^{(5)}, (p_i)^{(5)}, (r_i)^{(5)}$ are positive constants and $i = 28, 29, 30$.

They satisfy Lipschitz condition:

$$|(a_i'')^{(5)}(T'_{29}, t) - (a_i'')^{(5)}(T_{29}, t)| \leq (\hat{k}_{28})^{(5)} |T'_{29} - T_{29}| e^{-(\hat{M}_{28})^{(5)}t}$$

$$|(b_i'')^{(5)}((G_{31})', t) - (b_i'')^{(5)}((G_{31}), t)| < (\hat{k}_{28})^{(5)} |(G_{31})' - (G_{31})| e^{-(\hat{M}_{28})^{(5)}t}.$$

With the Lipschitz condition, we place a restriction on the behavior of functions $(a_i'')^{(5)}(T'_{29}, t)$ and $(a_i'')^{(5)}(T_{29}, t) \cdot (T'_{29}, t)$ and (T_{29}, t) are points belonging to the interval $[(\hat{k}_{28})^{(5)}, (\hat{M}_{28})^{(5)}]$. It is to be noted that $(a_i'')^{(5)}(T_{29}, t)$ is uniformly continuous. In the eventuality of the fact, that if $(\hat{M}_{28})^{(5)} = 5$ then the function $(a_i'')^{(5)}(T_{29}, t)$, the **FIFTH augmentation coefficient** would be absolutely continuous. -

Definition of $(\hat{M}_{28})^{(5)}, (\hat{k}_{28})^{(5)}$:

(Q) $(\hat{M}_{28})^{(5)}, (\hat{k}_{28})^{(5)}$, are positive constants

$$\frac{(a_i)^{(5)}}{(\hat{M}_{28})^{(5)}} + \frac{(b_i)^{(5)}}{(\hat{M}_{28})^{(5)}} < 1 -$$

Definition of $(\hat{P}_{28})^{(5)}, (\hat{Q}_{28})^{(5)}$:

(R) There exists two constants $(\hat{P}_{28})^{(5)}$ and $(\hat{Q}_{28})^{(5)}$ which together with $(\hat{M}_{28})^{(5)}, (\hat{k}_{28})^{(5)}, (\hat{A}_{28})^{(5)}$ and $(\hat{B}_{28})^{(5)}$ and the constants $(a_i)^{(5)}, (a_i')^{(5)}, (b_i)^{(5)}, (b_i')^{(5)}, (p_i)^{(5)}, (r_i)^{(5)}, i = 28, 29, 30$, satisfy the inequalities

$$\frac{1}{(\hat{M}_{28})^{(5)}} [(a_i)^{(5)} + (a_i')^{(5)} + (\hat{A}_{28})^{(5)} + (\hat{P}_{28})^{(5)} (\hat{k}_{28})^{(5)}] < 1$$

$$\frac{1}{(\hat{M}_{28})^{(5)}} [(b_i)^{(5)} + (b_i')^{(5)} + (\hat{B}_{28})^{(5)} + (\hat{Q}_{28})^{(5)} (\hat{k}_{28})^{(5)}] < 1 -$$

Where we suppose-

$$(a_i)^{(6)}, (a_i')^{(6)}, (a_i'')^{(6)}, (b_i)^{(6)}, (b_i')^{(6)}, (b_i'')^{(6)} > 0, \quad i, j = 32, 33, 34$$

(S) The functions $(a_i'')^{(6)}, (b_i'')^{(6)}$ are positive continuous increasing and bounded.

Definition of $(p_i)^{(6)}, (r_i)^{(6)}$:

$$(a_i'')^{(6)}(T_{33}, t) \leq (p_i)^{(6)} \leq (\hat{A}_{32})^{(6)}$$

$$(b_i'')^{(6)}((G_{35}), t) \leq (r_i)^{(6)} \leq (b_i')^{(6)} \leq (\hat{B}_{32})^{(6)}.$$

$$(T) \quad \lim_{T_2 \rightarrow \infty} (a_i'')^{(6)}(T_{33}, t) = (p_i)^{(6)}$$

$$\lim_{G \rightarrow \infty} (b_i'')^{(6)}((G_{35}), t) = (r_i)^{(6)}$$

Definition of $(\hat{A}_{32})^{(6)}, (\hat{B}_{32})^{(6)}$:

Where $(\hat{A}_{32})^{(6)}, (\hat{B}_{32})^{(6)}, (p_i)^{(6)}, (r_i)^{(6)}$ are positive constants and $i = 32, 33, 34$.

They satisfy Lipschitz condition:

$$|(a_i'')^{(6)}(T_{33}, t) - (a_i'')^{(6)}(T_{33}, t)| \leq (\hat{k}_{32})^{(6)} |T_{33} - T_{33}'| e^{-(\hat{M}_{32})^{(6)}t}$$

$$|(b_i'')^{(6)}((G_{35}), t) - (b_i'')^{(6)}((G_{35}), t)| < (\hat{k}_{32})^{(6)} \|(G_{35}) - (G_{35}')\| e^{-(\hat{M}_{32})^{(6)}t} -$$

With the Lipschitz condition, we place a restriction on the behavior of functions $(a_i'')^{(6)}(T_{33}, t)$ and $(a_i'')^{(6)}(T_{33}, t)$. (T_{33}', t) and (T_{33}, t) are points belonging to the interval $[(\hat{k}_{32})^{(6)}, (\hat{M}_{32})^{(6)}]$. It is to be noted that $(a_i'')^{(6)}(T_{33}, t)$ is uniformly continuous. In the eventuality of the fact, that if $(\hat{M}_{32})^{(6)} = 6$ then the function $(a_i'')^{(6)}(T_{33}, t)$, the **SIXTH augmentation coefficient** would be absolutely continuous. -

Definition of $(\hat{M}_{32})^{(6)}, (\hat{k}_{32})^{(6)}$:

$(\hat{M}_{32})^{(6)}, (\hat{k}_{32})^{(6)}$, are positive constants

$$\frac{(a_i)^{(6)}}{(\hat{M}_{32})^{(6)}} + \frac{(b_i)^{(6)}}{(\hat{M}_{32})^{(6)}} < 1 -$$

Definition of $(\hat{P}_{32})^{(6)}, (\hat{Q}_{32})^{(6)}$:

There exists two constants $(\hat{P}_{32})^{(6)}$ and $(\hat{Q}_{32})^{(6)}$ which together with $(\hat{M}_{32})^{(6)}, (\hat{k}_{32})^{(6)}, (\hat{A}_{32})^{(6)}$ and $(\hat{B}_{32})^{(6)}$ and the constants $(a_i)^{(6)}, (a_i')^{(6)}, (b_i)^{(6)}, (b_i')^{(6)}, (p_i)^{(6)}, (r_i)^{(6)}, i = 32, 33, 34$, satisfy the inequalities

$$\frac{1}{(\hat{M}_{32})^{(6)}} [(a_i)^{(6)} + (a_i')^{(6)} + (\hat{A}_{32})^{(6)} + (\hat{P}_{32})^{(6)} (\hat{k}_{32})^{(6)}] < 1$$

$$\frac{1}{(\hat{M}_{32})^{(6)}} [(b_i)^{(6)} + (b_i')^{(6)} + (\hat{B}_{32})^{(6)} + (\hat{Q}_{32})^{(6)} (\hat{k}_{32})^{(6)}] < 1 -$$

Theorem 1: if the conditions above are fulfilled, there exists a solution satisfying the conditions

Definition of $G_i(0), T_i(0)$:

$$G_i(t) \leq (\hat{P}_{13})^{(1)} e^{(\hat{M}_{13})^{(1)}t}, \quad G_i(0) = G_i^0 > 0$$

$$T_i(t) \leq (\hat{Q}_{13})^{(1)} e^{(\hat{M}_{13})^{(1)}t}, \quad T_i(0) = T_i^0 > 0 -$$

if the conditions above are fulfilled, there exists a solution satisfying the conditions

Definition of $G_i(0), T_i(0)$

$$G_i(t) \leq (\hat{P}_{16})^{(2)} e^{(\hat{M}_{16})^{(2)}t}, \quad G_i(0) = G_i^0 > 0$$

$$T_i(t) \leq (\hat{Q}_{16})^{(2)} e^{(\hat{M}_{16})^{(2)}t}, \quad T_i(0) = T_i^0 > 0 -$$

if the conditions above are fulfilled, there exists a solution satisfying the conditions

$$G_i(t) \leq (\hat{P}_{20})^{(3)} e^{(\hat{M}_{20})^{(3)}t}, \quad G_i(0) = G_i^0 > 0$$

$$T_i(t) \leq (\hat{Q}_{20})^{(3)} e^{(\hat{M}_{20})^{(3)}t}, \quad T_i(0) = T_i^0 > 0 -$$

if the conditions above are fulfilled, there exists a solution satisfying the conditions

Definition of $G_i(0), T_i(0)$:

$$G_i(t) \leq (\hat{P}_{24})^{(4)} e^{(\hat{M}_{24})^{(4)}t}, \quad G_i(0) = G_i^0 > 0$$

$$T_i(t) \leq (\hat{Q}_{24})^{(4)} e^{(\hat{M}_{24})^{(4)}t}, \quad T_i(0) = T_i^0 > 0 -$$

if the conditions above are fulfilled, there exists a solution satisfying the conditions

Definition of $G_i(0), T_i(0)$:

$$G_i(t) \leq (\hat{P}_{28})^{(5)} e^{(\hat{M}_{28})^{(5)}t}, \quad G_i(0) = G_i^0 > 0$$

$$T_i(t) \leq (\hat{Q}_{28})^{(5)} e^{(\hat{M}_{28})^{(5)}t}, \quad T_i(0) = T_i^0 > 0 -$$

if the conditions above are fulfilled, there exists a solution satisfying the conditions

Definition of $G_i(0), T_i(0)$:

$$G_i(t) \leq (\hat{P}_{32})^{(6)} e^{(\hat{M}_{32})^{(6)}t}, \quad G_i(0) = G_i^0 > 0$$

$$T_i(t) \leq (\hat{Q}_{32})^{(6)} e^{(M_{32})^{(6)}t}, \quad \boxed{T_i(0) = T_i^0 > 0}.$$

Proof: Consider operator $\mathcal{A}^{(1)}$ defined on the space of sextuples of continuous functions $G_i, T_i: \mathbb{R}_+ \rightarrow \mathbb{R}_+$ which satisfy

$$\begin{aligned} G_i(0) &= G_i^0, T_i(0) = T_i^0, G_i^0 \leq (\hat{P}_{13})^{(1)}, T_i^0 \leq (\hat{Q}_{13})^{(1)}, - \\ 0 &\leq G_i(t) - G_i^0 \leq (\hat{P}_{13})^{(1)} e^{(M_{13})^{(1)}t} - \\ 0 &\leq T_i(t) - T_i^0 \leq (\hat{Q}_{13})^{(1)} e^{(M_{13})^{(1)}t} - \end{aligned}$$

By

$$\begin{aligned} \bar{G}_{13}(t) &= G_{13}^0 + \int_0^t \left[(a_{13})^{(1)} G_{14}(s_{(13)}) - \left((a'_{13})^{(1)} + a''_{13}(s_{(13)}) \right) G_{13}(s_{(13)}) \right] ds_{(13)} - \\ \bar{G}_{14}(t) &= G_{14}^0 + \int_0^t \left[(a_{14})^{(1)} G_{13}(s_{(13)}) - \left((a'_{14})^{(1)} + a''_{14}(s_{(13)}) \right) G_{14}(s_{(13)}) \right] ds_{(13)} - \\ \bar{G}_{15}(t) &= G_{15}^0 + \int_0^t \left[(a_{15})^{(1)} G_{14}(s_{(13)}) - \left((a'_{15})^{(1)} + a''_{15}(s_{(13)}) \right) G_{15}(s_{(13)}) \right] ds_{(13)} - \\ \bar{T}_{13}(t) &= T_{13}^0 + \int_0^t \left[(b_{13})^{(1)} T_{14}(s_{(13)}) - \left((b'_{13})^{(1)} - (b''_{13})^{(1)}(G(s_{(13)}), s_{(13)})) \right) T_{13}(s_{(13)}) \right] ds_{(13)} - \\ \bar{T}_{14}(t) &= T_{14}^0 + \int_0^t \left[(b_{14})^{(1)} T_{13}(s_{(13)}) - \left((b'_{14})^{(1)} - (b''_{14})^{(1)}(G(s_{(13)}), s_{(13)})) \right) T_{14}(s_{(13)}) \right] ds_{(13)} - \\ \bar{T}_{15}(t) &= T_{15}^0 + \int_0^t \left[(b_{15})^{(1)} T_{14}(s_{(13)}) - \left((b'_{15})^{(1)} - (b''_{15})^{(1)}(G(s_{(13)}), s_{(13)})) \right) T_{15}(s_{(13)}) \right] ds_{(13)} \end{aligned}$$

Where $s_{(13)}$ is the integrand that is integrated over an interval $(0, t)$ -

Consider operator $\mathcal{A}^{(2)}$ defined on the space of sextuples of continuous functions $G_i, T_i: \mathbb{R}_+ \rightarrow \mathbb{R}_+$ which satisfy

$$\begin{aligned} G_i(0) &= G_i^0, T_i(0) = T_i^0, G_i^0 \leq (\hat{P}_{16})^{(2)}, T_i^0 \leq (\hat{Q}_{16})^{(2)}, - \\ 0 &\leq G_i(t) - G_i^0 \leq (\hat{P}_{16})^{(2)} e^{(M_{16})^{(2)}t} - \\ 0 &\leq T_i(t) - T_i^0 \leq (\hat{Q}_{16})^{(2)} e^{(M_{16})^{(2)}t} - \end{aligned}$$

By

$$\begin{aligned} \bar{G}_{16}(t) &= G_{16}^0 + \int_0^t \left[(a_{16})^{(2)} G_{17}(s_{(16)}) - \left((a'_{16})^{(2)} + a''_{16}(s_{(16)}) \right) G_{16}(s_{(16)}) \right] ds_{(16)} - \\ \bar{G}_{17}(t) &= G_{17}^0 + \int_0^t \left[(a_{17})^{(2)} G_{16}(s_{(16)}) - \left((a'_{17})^{(2)} + a''_{17}(s_{(16)}) \right) G_{17}(s_{(16)}) \right] ds_{(16)} - \\ \bar{G}_{18}(t) &= G_{18}^0 + \int_0^t \left[(a_{18})^{(2)} G_{17}(s_{(16)}) - \left((a'_{18})^{(2)} + a''_{18}(s_{(16)}) \right) G_{18}(s_{(16)}) \right] ds_{(16)} - \\ \bar{T}_{16}(t) &= T_{16}^0 + \int_0^t \left[(b_{16})^{(2)} T_{17}(s_{(16)}) - \left((b'_{16})^{(2)} - (b''_{16})^{(2)}(G(s_{(16)}), s_{(16)})) \right) T_{16}(s_{(16)}) \right] ds_{(16)} - \\ \bar{T}_{17}(t) &= T_{17}^0 + \int_0^t \left[(b_{17})^{(2)} T_{16}(s_{(16)}) - \left((b'_{17})^{(2)} - (b''_{17})^{(2)}(G(s_{(16)}), s_{(16)})) \right) T_{17}(s_{(16)}) \right] ds_{(16)} - \\ \bar{T}_{18}(t) &= T_{18}^0 + \int_0^t \left[(b_{18})^{(2)} T_{17}(s_{(16)}) - \left((b'_{18})^{(2)} - (b''_{18})^{(2)}(G(s_{(16)}), s_{(16)})) \right) T_{18}(s_{(16)}) \right] ds_{(16)} \end{aligned}$$

Where $s_{(16)}$ is the integrand that is integrated over an interval $(0, t)$ -

Consider operator $\mathcal{A}^{(3)}$ defined on the space of sextuples of continuous functions $G_i, T_i: \mathbb{R}_+ \rightarrow \mathbb{R}_+$ which satisfy

$$\begin{aligned} G_i(0) &= G_i^0, T_i(0) = T_i^0, G_i^0 \leq (\hat{P}_{20})^{(3)}, T_i^0 \leq (\hat{Q}_{20})^{(3)}, - \\ 0 &\leq G_i(t) - G_i^0 \leq (\hat{P}_{20})^{(3)} e^{(M_{20})^{(3)}t} - \\ 0 &\leq T_i(t) - T_i^0 \leq (\hat{Q}_{20})^{(3)} e^{(M_{20})^{(3)}t} - \end{aligned}$$

By

$$\begin{aligned} \bar{G}_{20}(t) &= G_{20}^0 + \int_0^t \left[(a_{20})^{(3)} G_{21}(s_{(20)}) - \left((a'_{20})^{(3)} + a''_{20}(s_{(20)}) \right) G_{20}(s_{(20)}) \right] ds_{(20)} - \\ \bar{G}_{21}(t) &= G_{21}^0 + \int_0^t \left[(a_{21})^{(3)} G_{20}(s_{(20)}) - \left((a'_{21})^{(3)} + a''_{21}(s_{(20)}) \right) G_{21}(s_{(20)}) \right] ds_{(20)} - \\ \bar{G}_{22}(t) &= G_{22}^0 + \int_0^t \left[(a_{22})^{(3)} G_{21}(s_{(20)}) - \left((a'_{22})^{(3)} + a''_{22}(s_{(20)}) \right) G_{22}(s_{(20)}) \right] ds_{(20)} - \\ \bar{T}_{20}(t) &= T_{20}^0 + \int_0^t \left[(b_{20})^{(3)} T_{21}(s_{(20)}) - \left((b'_{20})^{(3)} - (b''_{20})^{(3)}(G(s_{(20)}), s_{(20)})) \right) T_{20}(s_{(20)}) \right] ds_{(20)} - \\ \bar{T}_{21}(t) &= T_{21}^0 + \int_0^t \left[(b_{21})^{(3)} T_{20}(s_{(20)}) - \left((b'_{21})^{(3)} - (b''_{21})^{(3)}(G(s_{(20)}), s_{(20)})) \right) T_{21}(s_{(20)}) \right] ds_{(20)} - \\ \bar{T}_{22}(t) &= T_{22}^0 + \int_0^t \left[(b_{22})^{(3)} T_{21}(s_{(20)}) - \left((b'_{22})^{(3)} - (b''_{22})^{(3)}(G(s_{(20)}), s_{(20)})) \right) T_{22}(s_{(20)}) \right] ds_{(20)} \end{aligned}$$

Where $s_{(20)}$ is the integrand that is integrated over an interval $(0, t)$ -

Consider operator $\mathcal{A}^{(4)}$ defined on the space of sextuples of continuous functions $G_i, T_i: \mathbb{R}_+ \rightarrow \mathbb{R}_+$ which satisfy

$$\begin{aligned} G_i(0) &= G_i^0, T_i(0) = T_i^0, G_i^0 \leq (\hat{P}_{24})^{(4)}, T_i^0 \leq (\hat{Q}_{24})^{(4)}, - \\ 0 &\leq G_i(t) - G_i^0 \leq (\hat{P}_{24})^{(4)} e^{(M_{24})^{(4)}t} - \\ 0 &\leq T_i(t) - T_i^0 \leq (\hat{Q}_{24})^{(4)} e^{(M_{24})^{(4)}t} - \end{aligned}$$

By

$$\begin{aligned} \bar{G}_{24}(t) &= G_{24}^0 + \int_0^t \left[(a_{24})^{(4)} G_{25}(s_{(24)}) - \left((a'_{24})^{(4)} + a''_{24}(s_{(24)}) \right) G_{24}(s_{(24)}) \right] ds_{(24)} - \\ \bar{G}_{25}(t) &= G_{25}^0 + \int_0^t \left[(a_{25})^{(4)} G_{24}(s_{(24)}) - \left((a'_{25})^{(4)} + a''_{25}(s_{(24)}) \right) G_{25}(s_{(24)}) \right] ds_{(24)} - \\ \bar{G}_{26}(t) &= G_{26}^0 + \int_0^t \left[(a_{26})^{(4)} G_{25}(s_{(24)}) - \left((a'_{26})^{(4)} + a''_{26}(s_{(24)}) \right) G_{26}(s_{(24)}) \right] ds_{(24)} - \end{aligned}$$

$$\begin{aligned} \bar{T}_{24}(t) &= T_{24}^0 + \int_0^t \left[(b_{24})^{(4)} T_{25}(s_{(24)}) - \left((b'_{24})^{(4)} - (b''_{24})^{(4)} (G(s_{(24)}), s_{(24)}) \right) T_{24}(s_{(24)}) \right] ds_{(24)} - \\ \bar{T}_{25}(t) &= T_{25}^0 + \int_0^t \left[(b_{25})^{(4)} T_{24}(s_{(24)}) - \left((b'_{25})^{(4)} - (b''_{25})^{(4)} (G(s_{(24)}), s_{(24)}) \right) T_{25}(s_{(24)}) \right] ds_{(24)} - \\ \bar{T}_{26}(t) &= T_{26}^0 + \int_0^t \left[(b_{26})^{(4)} T_{25}(s_{(24)}) - \left((b'_{26})^{(4)} - (b''_{26})^{(4)} (G(s_{(24)}), s_{(24)}) \right) T_{26}(s_{(24)}) \right] ds_{(24)} \end{aligned}$$

Where $s_{(24)}$ is the integrand that is integrated over an interval $(0, t)$ -

Consider operator $\mathcal{A}^{(5)}$ defined on the space of sextuples of continuous functions $G_i, T_i: \mathbb{R}_+ \rightarrow \mathbb{R}_+$ which satisfy

$$\begin{aligned} G_i(0) &= G_i^0, T_i(0) = T_i^0, G_i^0 \leq (\hat{P}_{28})^{(5)}, T_i^0 \leq (\hat{Q}_{28})^{(5)}, - \\ 0 &\leq G_i(t) - G_i^0 \leq (\hat{P}_{28})^{(5)} e^{(\hat{M}_{28})^{(5)}t} - \\ 0 &\leq T_i(t) - T_i^0 \leq (\hat{Q}_{28})^{(5)} e^{(\hat{M}_{28})^{(5)}t} - \end{aligned}$$

By

$$\begin{aligned} \bar{G}_{28}(t) &= G_{28}^0 + \int_0^t \left[(a_{28})^{(5)} G_{29}(s_{(28)}) - \left((a'_{28})^{(5)} + (a''_{28})^{(5)} (T_{29}(s_{(28)}), s_{(28)}) \right) G_{28}(s_{(28)}) \right] ds_{(28)} - \\ \bar{G}_{29}(t) &= G_{29}^0 + \int_0^t \left[(a_{29})^{(5)} G_{28}(s_{(28)}) - \left((a'_{29})^{(5)} + (a''_{29})^{(5)} (T_{29}(s_{(28)}), s_{(28)}) \right) G_{29}(s_{(28)}) \right] ds_{(28)} - \\ \bar{G}_{30}(t) &= G_{30}^0 + \int_0^t \left[(a_{30})^{(5)} G_{29}(s_{(28)}) - \left((a'_{30})^{(5)} + (a''_{30})^{(5)} (T_{29}(s_{(28)}), s_{(28)}) \right) G_{30}(s_{(28)}) \right] ds_{(28)} - \\ \bar{T}_{28}(t) &= T_{28}^0 + \int_0^t \left[(b_{28})^{(5)} T_{29}(s_{(28)}) - \left((b'_{28})^{(5)} - (b''_{28})^{(5)} (G(s_{(28)}), s_{(28)}) \right) T_{28}(s_{(28)}) \right] ds_{(28)} - \\ \bar{T}_{29}(t) &= T_{29}^0 + \int_0^t \left[(b_{29})^{(5)} T_{28}(s_{(28)}) - \left((b'_{29})^{(5)} - (b''_{29})^{(5)} (G(s_{(28)}), s_{(28)}) \right) T_{29}(s_{(28)}) \right] ds_{(28)} - \\ \bar{T}_{30}(t) &= T_{30}^0 + \int_0^t \left[(b_{30})^{(5)} T_{29}(s_{(28)}) - \left((b'_{30})^{(5)} - (b''_{30})^{(5)} (G(s_{(28)}), s_{(28)}) \right) T_{30}(s_{(28)}) \right] ds_{(28)} \end{aligned}$$

Where $s_{(28)}$ is the integrand that is integrated over an interval $(0, t)$ -

Consider operator $\mathcal{A}^{(6)}$ defined on the space of sextuples of continuous functions $G_i, T_i: \mathbb{R}_+ \rightarrow \mathbb{R}_+$ which satisfy

$$\begin{aligned} G_i(0) &= G_i^0, T_i(0) = T_i^0, G_i^0 \leq (\hat{P}_{32})^{(6)}, T_i^0 \leq (\hat{Q}_{32})^{(6)}, - \\ 0 &\leq G_i(t) - G_i^0 \leq (\hat{P}_{32})^{(6)} e^{(\hat{M}_{32})^{(6)}t} - \\ 0 &\leq T_i(t) - T_i^0 \leq (\hat{Q}_{32})^{(6)} e^{(\hat{M}_{32})^{(6)}t} - \end{aligned}$$

By

$$\begin{aligned} \bar{G}_{32}(t) &= G_{32}^0 + \int_0^t \left[(a_{32})^{(6)} G_{33}(s_{(32)}) - \left((a'_{32})^{(6)} + (a''_{32})^{(6)} (T_{33}(s_{(32)}), s_{(32)}) \right) G_{32}(s_{(32)}) \right] ds_{(32)} - \\ \bar{G}_{33}(t) &= G_{33}^0 + \int_0^t \left[(a_{33})^{(6)} G_{32}(s_{(32)}) - \left((a'_{33})^{(6)} + (a''_{33})^{(6)} (T_{33}(s_{(32)}), s_{(32)}) \right) G_{33}(s_{(32)}) \right] ds_{(32)} - \\ \bar{G}_{34}(t) &= G_{34}^0 + \int_0^t \left[(a_{34})^{(6)} G_{33}(s_{(32)}) - \left((a'_{34})^{(6)} + (a''_{34})^{(6)} (T_{33}(s_{(32)}), s_{(32)}) \right) G_{34}(s_{(32)}) \right] ds_{(32)} - \\ \bar{T}_{32}(t) &= T_{32}^0 + \int_0^t \left[(b_{32})^{(6)} T_{33}(s_{(32)}) - \left((b'_{32})^{(6)} - (b''_{32})^{(6)} (G(s_{(32)}), s_{(32)}) \right) T_{32}(s_{(32)}) \right] ds_{(32)} - \\ \bar{T}_{33}(t) &= T_{33}^0 + \int_0^t \left[(b_{33})^{(6)} T_{32}(s_{(32)}) - \left((b'_{33})^{(6)} - (b''_{33})^{(6)} (G(s_{(32)}), s_{(32)}) \right) T_{33}(s_{(32)}) \right] ds_{(32)} - \\ \bar{T}_{34}(t) &= T_{34}^0 + \int_0^t \left[(b_{34})^{(6)} T_{33}(s_{(32)}) - \left((b'_{34})^{(6)} - (b''_{34})^{(6)} (G(s_{(32)}), s_{(32)}) \right) T_{34}(s_{(32)}) \right] ds_{(32)} \end{aligned}$$

Where $s_{(32)}$ is the integrand that is integrated over an interval $(0, t)$ -

(a) The operator $\mathcal{A}^{(1)}$ maps the space of functions satisfying GLOBAL EQUATIONS into itself .Indeed it is obvious that

$$\begin{aligned} G_{13}(t) &\leq G_{13}^0 + \int_0^t \left[(a_{13})^{(1)} \left(G_{14}^0 + (\hat{P}_{13})^{(1)} e^{(\hat{M}_{13})^{(1)}s_{(13)}} \right) \right] ds_{(13)} = \\ &= \left(1 + (a_{13})^{(1)}t \right) G_{14}^0 + \frac{(a_{13})^{(1)}(\hat{P}_{13})^{(1)}}{(\hat{M}_{13})^{(1)}} \left(e^{(\hat{M}_{13})^{(1)}t} - 1 \right) - \end{aligned}$$

From which it follows that

$$(G_{13}(t) - G_{13}^0) e^{-(\hat{M}_{13})^{(1)}t} \leq \frac{(a_{13})^{(1)}}{(\hat{M}_{13})^{(1)}} \left[\left((\hat{P}_{13})^{(1)} + G_{14}^0 \right) e^{-\frac{(\hat{P}_{13})^{(1)} + G_{14}^0}{G_{14}^0}} + (\hat{P}_{13})^{(1)} \right]$$

(G_i^0) is as defined in the statement of theorem 1-

Analogous inequalities hold also for $G_{14}, G_{15}, T_{13}, T_{14}, T_{15}$ -

The operator $\mathcal{A}^{(2)}$ maps the space of functions satisfying GLOBAL EQUATIONS into itself .Indeed it is obvious that-

$$G_{16}(t) \leq G_{16}^0 + \int_0^t \left[(a_{16})^{(2)} \left(G_{17}^0 + (\hat{P}_{16})^{(2)} e^{(\hat{M}_{16})^{(2)}s_{(16)}} \right) \right] ds_{(16)} = \left(1 + (a_{16})^{(2)}t \right) G_{17}^0 + \frac{(a_{16})^{(2)}(\hat{P}_{16})^{(2)}}{(\hat{M}_{16})^{(2)}} \left(e^{(\hat{M}_{16})^{(2)}t} - 1 \right)$$

From which it follows that

$$(G_{16}(t) - G_{16}^0) e^{-(\hat{M}_{16})^{(2)}t} \leq \frac{(a_{16})^{(2)}}{(\hat{M}_{16})^{(2)}} \left[\left((\hat{P}_{16})^{(2)} + G_{17}^0 \right) e^{-\frac{(\hat{P}_{16})^{(2)} + G_{17}^0}{G_{17}^0}} + (\hat{P}_{16})^{(2)} \right] -$$

Analogous inequalities hold also for $G_{17}, G_{18}, T_{16}, T_{17}, T_{18}$ -

(a) The operator $\mathcal{A}^{(3)}$ maps the space of functions satisfying GLOBAL EQUATIONS into itself .Indeed it is obvious that

$$G_{20}(t) \leq G_{20}^0 + \int_0^t \left[(a_{20})^{(3)} \left(G_{21}^0 + (\hat{P}_{20})^{(3)} e^{(\hat{M}_{20})^{(3)}s_{(20)}} \right) \right] ds_{(20)} =$$

$$(1 + (a_{20})^{(3)}t)G_{21}^0 + \frac{(a_{20})^{(3)}(P_{20})^{(3)}}{(\bar{M}_{20})^{(3)}}(e^{(\bar{M}_{20})^{(3)}t} - 1) -$$

From which it follows that

$$(G_{20}(t) - G_{20}^0)e^{-(\bar{M}_{20})^{(3)}t} \leq \frac{(a_{20})^{(3)}}{(\bar{M}_{20})^{(3)}} \left[((\hat{P}_{20})^{(3)} + G_{21}^0)e^{-\frac{((\hat{P}_{20})^{(3)} + G_{21}^0)}{G_{21}^0}} + (\hat{P}_{20})^{(3)} \right] -$$

Analogous inequalities hold also for $G_{21}, G_{22}, T_{20}, T_{21}, T_{22}$ -

(b) The operator $\mathcal{A}^{(4)}$ maps the space of functions satisfying GLOBAL EQUATIONS into itself. Indeed it is obvious that

$$G_{24}(t) \leq G_{24}^0 + \int_0^t [(a_{24})^{(4)} (G_{25}^0 + (\hat{P}_{24})^{(4)} e^{(\bar{M}_{24})^{(4)}s(24)})] ds_{(24)} =$$

$$(1 + (a_{24})^{(4)}t)G_{25}^0 + \frac{(a_{24})^{(4)}(P_{24})^{(4)}}{(\bar{M}_{24})^{(4)}}(e^{(\bar{M}_{24})^{(4)}t} - 1) -$$

From which it follows that

$$(G_{24}(t) - G_{24}^0)e^{-(\bar{M}_{24})^{(4)}t} \leq \frac{(a_{24})^{(4)}}{(\bar{M}_{24})^{(4)}} \left[((\hat{P}_{24})^{(4)} + G_{25}^0)e^{-\frac{((\hat{P}_{24})^{(4)} + G_{25}^0)}{G_{25}^0}} + (\hat{P}_{24})^{(4)} \right]$$

(G_i^0) is as defined in the statement of theorem -

(c) The operator $\mathcal{A}^{(5)}$ maps the space of functions satisfying GLOBAL EQUATIONS into itself. Indeed it is obvious that

$$G_{28}(t) \leq G_{28}^0 + \int_0^t [(a_{28})^{(5)} (G_{29}^0 + (\hat{P}_{28})^{(5)} e^{(\bar{M}_{28})^{(5)}s(28)})] ds_{(28)} =$$

$$(1 + (a_{28})^{(5)}t)G_{29}^0 + \frac{(a_{28})^{(5)}(P_{28})^{(5)}}{(\bar{M}_{28})^{(5)}}(e^{(\bar{M}_{28})^{(5)}t} - 1) -$$

From which it follows that

$$(G_{28}(t) - G_{28}^0)e^{-(\bar{M}_{28})^{(5)}t} \leq \frac{(a_{28})^{(5)}}{(\bar{M}_{28})^{(5)}} \left[((\hat{P}_{28})^{(5)} + G_{29}^0)e^{-\frac{((\hat{P}_{28})^{(5)} + G_{29}^0)}{G_{29}^0}} + (\hat{P}_{28})^{(5)} \right]$$

(G_i^0) is as defined in the statement of theorem -

(d) The operator $\mathcal{A}^{(6)}$ maps the space of functions satisfying GLOBAL EQUATIONS into itself. Indeed it is obvious that

$$G_{32}(t) \leq G_{32}^0 + \int_0^t [(a_{32})^{(6)} (G_{33}^0 + (\hat{P}_{32})^{(6)} e^{(\bar{M}_{32})^{(6)}s(32)})] ds_{(32)} =$$

$$(1 + (a_{32})^{(6)}t)G_{33}^0 + \frac{(a_{32})^{(6)}(P_{32})^{(6)}}{(\bar{M}_{32})^{(6)}}(e^{(\bar{M}_{32})^{(6)}t} - 1) -$$

From which it follows that

$$(G_{32}(t) - G_{32}^0)e^{-(\bar{M}_{32})^{(6)}t} \leq \frac{(a_{32})^{(6)}}{(\bar{M}_{32})^{(6)}} \left[((\hat{P}_{32})^{(6)} + G_{33}^0)e^{-\frac{((\hat{P}_{32})^{(6)} + G_{33}^0)}{G_{33}^0}} + (\hat{P}_{32})^{(6)} \right]$$

(G_i^0) is as defined in the statement of theorem 1

Analogous inequalities hold also for $G_{25}, G_{26}, T_{24}, T_{25}, T_{26}$ -

It is now sufficient to take $\frac{(a_i)^{(1)}}{(\bar{M}_{13})^{(1)}}, \frac{(b_i)^{(1)}}{(\bar{M}_{13})^{(1)}} < 1$ and to choose

$(\hat{P}_{13})^{(1)}$ and $(\hat{Q}_{13})^{(1)}$ large to have-

$$\frac{(a_i)^{(1)}}{(\bar{M}_{13})^{(1)}} \left[((\hat{P}_{13})^{(1)} + ((\hat{P}_{13})^{(1)} + G_j^0)e^{-\frac{((\hat{P}_{13})^{(1)} + G_j^0)}{G_j^0}}) \right] \leq (\hat{P}_{13})^{(1)} -$$

$$\frac{(b_i)^{(1)}}{(\bar{M}_{13})^{(1)}} \left[((\hat{Q}_{13})^{(1)} + T_j^0)e^{-\frac{((\hat{Q}_{13})^{(1)} + T_j^0)}{T_j^0}} + (\hat{Q}_{13})^{(1)} \right] \leq (\hat{Q}_{13})^{(1)} -$$

In order that the operator $\mathcal{A}^{(1)}$ transforms the space of sextuples of functions G_i, T_i satisfying GLOBAL EQUATIONS into itself-

The operator $\mathcal{A}^{(1)}$ is a contraction with respect to the metric

$$d((G^{(1)}, T^{(1)}), (G^{(2)}, T^{(2)})) =$$

$$\sup_i \{ \max_{t \in \mathbb{R}_+} |G_i^{(1)}(t) - G_i^{(2)}(t)| e^{-(\bar{M}_{13})^{(1)}t}, \max_{t \in \mathbb{R}_+} |T_i^{(1)}(t) - T_i^{(2)}(t)| e^{-(\bar{M}_{13})^{(1)}t} \} -$$

Indeed if we denote

$$\text{Definition of } \tilde{G}, \tilde{T} : (\tilde{G}, \tilde{T}) = \mathcal{A}^{(1)}(G, T)$$

It results

$$|\tilde{G}_{13}^{(1)} - \tilde{G}_{13}^{(2)}| \leq \int_0^t (a_{13})^{(1)} |G_{14}^{(1)} - G_{14}^{(2)}| e^{-(\bar{M}_{13})^{(1)}s(13)} e^{(\bar{M}_{13})^{(1)}s(13)} ds_{(13)} +$$

$$\int_0^t \{ (a'_{13})^{(1)} |G_{13}^{(1)} - G_{13}^{(2)}| e^{-(\bar{M}_{13})^{(1)}s(13)} e^{-(\bar{M}_{13})^{(1)}s(13)} +$$

$$(a''_{13})^{(1)} (T_{14}^{(1)}, s(13)) |G_{13}^{(1)} - G_{13}^{(2)}| e^{-(\bar{M}_{13})^{(1)}s(13)} e^{(\bar{M}_{13})^{(1)}s(13)} +$$

$$G_{13}^{(2)} |(a_{13}^{(1)})^{(1)}(T_{14}^{(1)}, s_{(13)}) - (a_{13}^{(2)})^{(1)}(T_{14}^{(2)}, s_{(13)})| e^{-(\bar{M}_{13})^{(1)}s_{(13)}} e^{(\bar{M}_{13})^{(1)}s_{(13)}} ds_{(13)}$$

Where $s_{(13)}$ represents integrand that is integrated over the interval $[0, t]$

From the hypotheses it follows-

$$|G^{(1)} - G^{(2)}| e^{-(\bar{M}_{13})^{(1)}t} \leq \frac{1}{(\bar{M}_{13})^{(1)}} ((a_{13})^{(1)} + (a'_{13})^{(1)} + (\bar{A}_{13})^{(1)} + (\bar{P}_{13})^{(1)}(\bar{k}_{13})^{(1)}) d((G^{(1)}, T^{(1)}; G^{(2)}, T^{(2)}))$$

And analogous inequalities for G_i and T_i . Taking into account the hypothesis the result follows-

Remark 1: The fact that we supposed $(a_{13}^{(1)})^{(1)}$ and $(b_{13}^{(1)})^{(1)}$ depending also on t can be considered as not conformal with the reality, however we have put this hypothesis, in order that we can postulate condition necessary to prove the uniqueness of the solution bounded by $(\bar{P}_{13})^{(1)} e^{(\bar{M}_{13})^{(1)}t}$ and $(\bar{Q}_{13})^{(1)} e^{(\bar{M}_{13})^{(1)}t}$ respectively of \mathbb{R}_+ .

If instead of proving the existence of the solution on \mathbb{R}_+ , we have to prove it only on a compact then it suffices to consider that $(a_i^{(1)})^{(1)}$ and $(b_i^{(1)})^{(1)}$, $i = 13, 14, 15$ depend only on T_{14} and respectively on G (and not on t) and hypothesis can be replaced by a usual Lipschitz condition.

Remark 2: There does not exist any t where $G_i(t) = 0$ and $T_i(t) = 0$

From 19 to 24 it results

$$G_i(t) \geq G_i^0 e^{-\int_0^t \{(a_i^{(1)})^{(1)} - (a_i^{(2)})^{(1)}\}(T_{14}(s_{(13)}), s_{(13)}) ds_{(13)}} \geq 0$$

$$T_i(t) \geq T_i^0 e^{-(b_i^{(1)})^{(1)}t} > 0 \text{ for } t > 0$$

Definition of $((\bar{M}_{13})^{(1)})_1, ((\bar{M}_{13})^{(1)})_2$ and $((\bar{M}_{13})^{(1)})_3$:

Remark 3: if G_{13} is bounded, the same property have also G_{14} and G_{15} . indeed if

$$G_{13} < (\bar{M}_{13})^{(1)} \text{ it follows } \frac{dG_{14}}{dt} \leq ((\bar{M}_{13})^{(1)})_1 - (a'_{14})^{(1)}G_{14} \text{ and by integrating}$$

$$G_{14} \leq ((\bar{M}_{13})^{(1)})_2 = G_{14}^0 + 2(a_{14})^{(1)}((\bar{M}_{13})^{(1)})_1 / (a'_{14})^{(1)}$$

In the same way, one can obtain

$$G_{15} \leq ((\bar{M}_{13})^{(1)})_3 = G_{15}^0 + 2(a_{15})^{(1)}((\bar{M}_{13})^{(1)})_2 / (a'_{15})^{(1)}$$

If G_{14} or G_{15} is bounded, the same property follows for G_{13} , G_{15} and G_{13} , G_{14} respectively.

Remark 4: If G_{13} is bounded, from below, the same property holds for G_{14} and G_{15} . The proof is analogous with the preceding one. An analogous property is true if G_{14} is bounded from below.

Remark 5: If T_{13} is bounded from below and $\lim_{t \rightarrow \infty} ((b_i^{(1)})^{(1)}(G(t), t)) = (b'_{14})^{(1)}$ then $T_{14} \rightarrow \infty$.

Definition of $(m)^{(1)}$ and ε_1 :

Indeed let t_1 be so that for $t > t_1$

$$(b_{14})^{(1)} - (b_i^{(1)})^{(1)}(G(t), t) < \varepsilon_1, T_{13}(t) > (m)^{(1)}$$

Then $\frac{dT_{14}}{dt} \geq (a_{14})^{(1)}(m)^{(1)} - \varepsilon_1 T_{14}$ which leads to

$$T_{14} \geq \left(\frac{(a_{14})^{(1)}(m)^{(1)}}{\varepsilon_1} \right) (1 - e^{-\varepsilon_1 t}) + T_{14}^0 e^{-\varepsilon_1 t} \text{ If we take } t \text{ such that } e^{-\varepsilon_1 t} = \frac{1}{2} \text{ it results}$$

$$T_{14} \geq \left(\frac{(a_{14})^{(1)}(m)^{(1)}}{2} \right), t = \log \frac{2}{\varepsilon_1} \text{ By taking now } \varepsilon_1 \text{ sufficiently small one sees that } T_{14} \text{ is unbounded. The same property}$$

holds for T_{15} if $\lim_{t \rightarrow \infty} ((b_{15}^{(1)})^{(1)}(G(t), t)) = (b'_{15})^{(1)}$

We now state a more precise theorem about the behaviors at infinity of the solutions -

It is now sufficient to take $\frac{(a_i)^{(2)}}{(\bar{M}_{16})^{(2)}}, \frac{(b_i)^{(2)}}{(\bar{M}_{16})^{(2)}} < 1$ and to choose

$(\bar{P}_{16})^{(2)}$ and $(\bar{Q}_{16})^{(2)}$ large to have-

$$\frac{(a_i)^{(2)}}{(\bar{M}_{16})^{(2)}} \left[(\bar{P}_{16})^{(2)} + ((\bar{P}_{16})^{(2)} + G_j^0) e^{-\left(\frac{(\bar{P}_{16})^{(2)} + G_j^0}{G_j^0} \right)} \right] \leq (\bar{P}_{16})^{(2)}$$

$$\frac{(b_i)^{(2)}}{(\bar{M}_{16})^{(2)}} \left[((\bar{Q}_{16})^{(2)} + T_j^0) e^{-\left(\frac{(\bar{Q}_{16})^{(2)} + T_j^0}{T_j^0} \right)} + (\bar{Q}_{16})^{(2)} \right] \leq (\bar{Q}_{16})^{(2)}$$

In order that the operator $\mathcal{A}^{(2)}$ transforms the space of sextuples of functions G_i, T_i satisfying GLOBAL EQUATIONS into itself-

The operator $\mathcal{A}^{(2)}$ is a contraction with respect to the metric

$$d(((G_{19})^{(1)}, (T_{19})^{(1)}), ((G_{19})^{(2)}, (T_{19})^{(2)})) =$$

$$\sup_i \{ \max_{t \in \mathbb{R}_+} |G_i^{(1)}(t) - G_i^{(2)}(t)| e^{-(\bar{M}_{16})^{(2)}t}, \max_{t \in \mathbb{R}_+} |T_i^{(1)}(t) - T_i^{(2)}(t)| e^{-(\bar{M}_{16})^{(2)}t} \}$$

Indeed if we denote

Definition of $\widetilde{G}_{19}, \widetilde{T}_{19}$: $(\widetilde{G}_{19}, \widetilde{T}_{19}) = \mathcal{A}^{(2)}(G_{19}, T_{19})$

It results

$$|\widetilde{G}_{16}^{(1)} - \widetilde{G}_{16}^{(2)}| \leq \int_0^t (a_{16})^{(2)} |G_{17}^{(1)} - G_{17}^{(2)}| e^{-(\bar{M}_{16})^{(2)}s_{(16)}} e^{(\bar{M}_{16})^{(2)}s_{(16)}} ds_{(16)} + \int_0^t \{(a'_{16})^{(2)} |G_{16}^{(1)} - G_{16}^{(2)}| e^{-(\bar{M}_{16})^{(2)}s_{(16)}} e^{-(\bar{M}_{16})^{(2)}s_{(16)}} +$$

$$(a''_{16})^{(2)}(T_{17}^{(1)}, s_{(16)}) |G_{16}^{(1)} - G_{16}^{(2)}| e^{-(\bar{M}_{16})^{(2)}s_{(16)}} e^{(\bar{M}_{16})^{(2)}s_{(16)}} + G_{16}^{(2)} |(a''_{16})^{(2)}(T_{17}^{(1)}, s_{(16)}) - (a''_{16})^{(2)}(T_{17}^{(2)}, s_{(16)})| e^{-(\bar{M}_{16})^{(2)}s_{(16)}} e^{(\bar{M}_{16})^{(2)}s_{(16)}} ds_{(16)} -$$

Where $s_{(16)}$ represents integrand that is integrated over the interval $[0, t]$

From the hypotheses it follows-

$$|(G_{19})^{(1)} - (G_{19})^{(2)}| e^{-(\bar{M}_{16})^{(2)}t} \leq \frac{1}{(\bar{M}_{16})^{(2)}} ((a_{16})^{(2)} + (a'_{16})^{(2)} + (\hat{A}_{16})^{(2)} + (\hat{P}_{16})^{(2)}(\hat{k}_{16})^{(2)}) d((G_{19})^{(1)}, (T_{19})^{(1)}; (G_{19})^{(2)}, (T_{19})^{(2)}) -$$

And analogous inequalities for G_i and T_i . Taking into account the hypothesis the result follows-

Remark 1: The fact that we supposed $(a''_{16})^{(2)}$ and $(b''_{16})^{(2)}$ depending also on t can be considered as not conformal with the reality, however we have put this hypothesis, in order that we can postulate condition necessary to prove the uniqueness of the solution bounded by $(\hat{P}_{16})^{(2)}e^{(\bar{M}_{16})^{(2)}t}$ and $(\hat{Q}_{16})^{(2)}e^{(\bar{M}_{16})^{(2)}t}$ respectively of \mathbb{R}_+ .

If instead of proving the existence of the solution on \mathbb{R}_+ , we have to prove it only on a compact then it suffices to consider that $(a''_i)^{(2)}$ and $(b''_i)^{(2)}$, $i = 16, 17, 18$ depend only on T_{17} and respectively on (G_{19}) (and not on t) and hypothesis can be replaced by a usual Lipschitz condition.

Remark 2: There does not exist any t where $G_i(t) = 0$ and $T_i(t) = 0$

From CONCATENATED SYTEM OF GLOBAL EQUATIONS it results

$$G_i(t) \geq G_i^0 e^{-\int_0^t \{(a'_i)^{(2)} - (a''_i)^{(2)}(T_{17}(s_{(16)}), s_{(16)})\} ds_{(16)}} \geq 0$$

$$T_i(t) \geq T_i^0 e^{-(b'_i)^{(2)}t} > 0 \text{ for } t > 0 -$$

Definition of $(\bar{M}_{16})^{(2)}_1, (\bar{M}_{16})^{(2)}_2$ and $(\bar{M}_{16})^{(2)}_3$:

Remark 3: if G_{16} is bounded, the same property have also G_{17} and G_{18} . indeed if

$$G_{16} < (\bar{M}_{16})^{(2)} \text{ it follows } \frac{dG_{17}}{dt} \leq ((\bar{M}_{16})^{(2)})_1 - (a'_{17})^{(2)}G_{17} \text{ and by integrating}$$

$$G_{17} \leq ((\bar{M}_{16})^{(2)})_2 = G_{17}^0 + 2(a_{17})^{(2)}((\bar{M}_{16})^{(2)})_1 / (a'_{17})^{(2)}$$

In the same way, one can obtain

$$G_{18} \leq ((\bar{M}_{16})^{(2)})_3 = G_{18}^0 + 2(a_{18})^{(2)}((\bar{M}_{16})^{(2)})_2 / (a'_{18})^{(2)}$$

If G_{17} or G_{18} is bounded, the same property follows for G_{16} , G_{18} and G_{16} , G_{17} respectively.

Remark 4: If G_{16} is bounded, from below, the same property holds for G_{17} and G_{18} . The proof is analogous with the preceding one. An analogous property is true if G_{17} is bounded from below.

Remark 5: If T_{16} is bounded from below and $\lim_{t \rightarrow \infty} ((b''_i)^{(2)}((G_{19})(t), t)) = (b'_{17})^{(2)}$ then $T_{17} \rightarrow \infty$.

Definition of $(m)^{(2)}$ and ε_2 :

Indeed let t_2 be so that for $t > t_2$

$$(b_{17})^{(2)} - (b''_i)^{(2)}((G_{19})(t), t) < \varepsilon_2, T_{16}(t) > (m)^{(2)} -$$

Then $\frac{dT_{17}}{dt} \geq (a_{17})^{(2)}(m)^{(2)} - \varepsilon_2 T_{17}$ which leads to

$$T_{17} \geq \left(\frac{(a_{17})^{(2)}(m)^{(2)}}{\varepsilon_2} \right) (1 - e^{-\varepsilon_2 t}) + T_{17}^0 e^{-\varepsilon_2 t} \text{ If we take } t \text{ such that } e^{-\varepsilon_2 t} = \frac{1}{2} \text{ it results -}$$

$$T_{17} \geq \left(\frac{(a_{17})^{(2)}(m)^{(2)}}{2} \right), t = \log \frac{2}{\varepsilon_2} \text{ By taking now } \varepsilon_2 \text{ sufficiently small one sees that } T_{17} \text{ is unbounded. The same property}$$

holds for T_{18} if $\lim_{t \rightarrow \infty} (b''_{18})^{(2)}((G_{19})(t), t) = (b'_{18})^{(2)}$

We now state a more precise theorem about the behaviors at infinity of the solutions -

It is now sufficient to take $\frac{(a_i)^{(3)}}{(M_{20})^{(3)}}, \frac{(b_i)^{(3)}}{(M_{20})^{(3)}} < 1$ and to choose

$(\hat{P}_{20})^{(3)}$ and $(\hat{Q}_{20})^{(3)}$ large to have-

$$\frac{(a_i)^{(3)}}{(M_{20})^{(3)}} \left[(\hat{P}_{20})^{(3)} + ((\hat{P}_{20})^{(3)} + G_j^0) e^{-\left(\frac{(\hat{P}_{20})^{(3)} + G_j^0}{G_j^0} \right)} \right] \leq (\hat{P}_{20})^{(3)} -$$

$$\frac{(b_i)^{(3)}}{(M_{20})^{(3)}} \left[((\hat{Q}_{20})^{(3)} + T_j^0) e^{-\left(\frac{(\hat{Q}_{20})^{(3)} + T_j^0}{T_j^0} \right)} + (\hat{Q}_{20})^{(3)} \right] \leq (\hat{Q}_{20})^{(3)} -$$

In order that the operator $\mathcal{A}^{(3)}$ transforms the space of sextuples of functions G_i, T_i satisfying GLOBAL EQUATIONS into itself-

The operator $\mathcal{A}^{(3)}$ is a contraction with respect to the metric

$$d(((G_{23})^{(1)}, (T_{23})^{(1)}), ((G_{23})^{(2)}, (T_{23})^{(2)})) =$$

$$\sup_i \{ \max_{t \in \mathbb{R}_+} |G_i^{(1)}(t) - G_i^{(2)}(t)| e^{-(M_{20})^{(3)}t}, \max_{t \in \mathbb{R}_+} |T_i^{(1)}(t) - T_i^{(2)}(t)| e^{-(M_{20})^{(3)}t} \} -$$

Indeed if we denote

$$\text{Definition of } \bar{G}_{23}, \bar{T}_{23} : ((\bar{G}_{23}), (\bar{T}_{23})) = \mathcal{A}^{(3)}((G_{23}), (T_{23})) -$$

It results

$$|\bar{G}_{20}^{(1)} - \bar{G}_i^{(2)}| \leq \int_0^t (a_{20})^{(3)} |G_{21}^{(1)} - G_{21}^{(2)}| e^{-(\bar{M}_{20})^{(3)}s_{(20)}} e^{(\bar{M}_{20})^{(3)}s_{(20)}} ds_{(20)} + \int_0^t \{ (a'_{20})^{(3)} |G_{20}^{(1)} - G_{20}^{(2)}| e^{-(\bar{M}_{20})^{(3)}s_{(20)}} e^{-(\bar{M}_{20})^{(3)}s_{(20)}} + (a''_{20})^{(3)} (T_{21}^{(1)}, s_{(20)}) |G_{20}^{(1)} - G_{20}^{(2)}| e^{-(\bar{M}_{20})^{(3)}s_{(20)}} e^{(\bar{M}_{20})^{(3)}s_{(20)}} + G_{20}^{(2)} | (a''_{20})^{(3)} (T_{21}^{(1)}, s_{(20)}) - (a''_{20})^{(3)} (T_{21}^{(2)}, s_{(20)}) | e^{-(\bar{M}_{20})^{(3)}s_{(20)}} e^{(\bar{M}_{20})^{(3)}s_{(20)}} \} ds_{(20)}$$

Where $s_{(20)}$ represents integrand that is integrated over the interval $[0, t]$

From the hypotheses it follows-

$$|G^{(1)} - G^{(2)}| e^{-(\bar{M}_{20})^{(3)}t} \leq \frac{1}{(\bar{M}_{20})^{(3)}} ((a_{20})^{(3)} + (a'_{20})^{(3)} + (\bar{A}_{20})^{(3)} + (\bar{P}_{20})^{(3)} (\hat{k}_{20})^{(3)}) d((G_{23})^{(1)}, (T_{23})^{(1)}; (G_{23})^{(2)}, (T_{23})^{(2)})$$

And analogous inequalities for G_i and T_i . Taking into account the hypothesis (34,35,36) the result follows-

Remark 1: The fact that we supposed $(a''_{20})^{(3)}$ and $(b''_{20})^{(3)}$ depending also on t can be considered as not conformal with the reality, however we have put this hypothesis, in order that we can postulate condition necessary to prove the uniqueness of the solution bounded by $(\bar{P}_{20})^{(3)} e^{(\bar{M}_{20})^{(3)}t}$ and $(\bar{Q}_{20})^{(3)} e^{(\bar{M}_{20})^{(3)}t}$ respectively of \mathbb{R}_+ .

If instead of proving the existence of the solution on \mathbb{R}_+ , we have to prove it only on a compact then it suffices to consider that $(a''_i)^{(3)}$ and $(b''_i)^{(3)}$, $i = 20, 21, 22$ depend only on T_{21} and respectively on (G_{23}) (and not on t) and hypothesis can be replaced by a usual Lipschitz condition.

Remark 2: There does not exist any t where $G_i(t) = 0$ and $T_i(t) = 0$

From 19 to 24 it results

$$G_i(t) \geq G_i^0 e^{-\int_0^t \{ (a'_i)^{(3)} - (a''_i)^{(3)} (T_{21}(s_{(20)}), s_{(20)}) \} ds_{(20)}} \geq 0$$

$$T_i(t) \geq T_i^0 e^{-(b'_i)^{(3)}t} > 0 \text{ for } t > 0$$

Definition of $(\bar{M}_{20})^{(3)}_1, (\bar{M}_{20})^{(3)}_2$ and $(\bar{M}_{20})^{(3)}_3$:

Remark 3: if G_{20} is bounded, the same property have also G_{21} and G_{22} . indeed if

$$G_{20} < (\bar{M}_{20})^{(3)} \text{ it follows } \frac{dG_{21}}{dt} \leq ((\bar{M}_{20})^{(3)}_1 - (a'_{21})^{(3)}) G_{21} \text{ and by integrating}$$

$$G_{21} \leq ((\bar{M}_{20})^{(3)}_2) = G_{21}^0 + 2(a_{21})^{(3)} ((\bar{M}_{20})^{(3)}_1) / (a'_{21})^{(3)}$$

In the same way, one can obtain

$$G_{22} \leq ((\bar{M}_{20})^{(3)}_3) = G_{22}^0 + 2(a_{22})^{(3)} ((\bar{M}_{20})^{(3)}_2) / (a'_{22})^{(3)}$$

If G_{21} or G_{22} is bounded, the same property follows for G_{20} , G_{22} and G_{20} , G_{21} respectively.

Remark 4: If G_{20} is bounded, from below, the same property holds for G_{21} and G_{22} . The proof is analogous with the preceding one. An analogous property is true if G_{21} is bounded from below.

Remark 5: If T_{20} is bounded from below and $\lim_{t \rightarrow \infty} ((b'_i)^{(3)} ((G_{23})(t), t)) = (b'_{21})^{(3)}$ then $T_{21} \rightarrow \infty$.

Definition of $(m)^{(3)}$ and ε_3 :

Indeed let t_3 be so that for $t > t_3$

$$(b_{21})^{(3)} - (b''_i)^{(3)} ((G_{23})(t), t) < \varepsilon_3, T_{20}(t) > (m)^{(3)}$$

Then $\frac{dT_{21}}{dt} \geq (a_{21})^{(3)} (m)^{(3)} - \varepsilon_3 T_{21}$ which leads to

$$T_{21} \geq \left(\frac{(a_{21})^{(3)} (m)^{(3)}}{\varepsilon_3} \right) (1 - e^{-\varepsilon_3 t}) + T_{21}^0 e^{-\varepsilon_3 t} \text{ If we take } t \text{ such that } e^{-\varepsilon_3 t} = \frac{1}{2} \text{ it results}$$

$$T_{21} \geq \left(\frac{(a_{21})^{(3)} (m)^{(3)}}{2} \right), t = \log \frac{2}{\varepsilon_3} \text{ By taking now } \varepsilon_3 \text{ sufficiently small one sees that } T_{21} \text{ is unbounded. The same property}$$

holds for T_{22} if $\lim_{t \rightarrow \infty} (b''_{22})^{(3)} ((G_{23})(t), t) = (b'_{22})^{(3)}$

We now state a more precise theorem about the behaviors at infinity of the solutions-

It is now sufficient to take $\frac{(a_i)^{(4)}}{(\bar{M}_{24})^{(4)}}, \frac{(b_i)^{(4)}}{(\bar{M}_{24})^{(4)}} < 1$ and to choose

$(\bar{P}_{24})^{(4)}$ and $(\bar{Q}_{24})^{(4)}$ large to have-

$$\frac{(a_i)^{(4)}}{(\bar{M}_{24})^{(4)}} \left[(\bar{P}_{24})^{(4)} + ((\bar{P}_{24})^{(4)} + G_j^0) e^{-\left(\frac{(\bar{P}_{24})^{(4)} + G_j^0}{G_j^0} \right)} \right] \leq (\bar{P}_{24})^{(4)}$$

$$\frac{(b_i)^{(4)}}{(\bar{M}_{24})^{(4)}} \left[((\bar{Q}_{24})^{(4)} + T_j^0) e^{-\left(\frac{(\bar{Q}_{24})^{(4)} + T_j^0}{T_j^0} \right)} + (\bar{Q}_{24})^{(4)} \right] \leq (\bar{Q}_{24})^{(4)}$$

In order that the operator $\mathcal{A}^{(4)}$ transforms the space of sextuples of functions G_i, T_i satisfying GLOBAL EQUATIONS into itself-

The operator $\mathcal{A}^{(4)}$ is a contraction with respect to the metric

$$d(((G_{27})^{(1)}, (T_{27})^{(1)}), ((G_{27})^{(2)}, (T_{27})^{(2)})) =$$

$$\sup_i \{ \max_{t \in \mathbb{R}_+} |G_i^{(1)}(t) - G_i^{(2)}(t)| e^{-(\bar{M}_{24})^{(4)}t}, \max_{t \in \mathbb{R}_+} |T_i^{(1)}(t) - T_i^{(2)}(t)| e^{-(\bar{M}_{24})^{(4)}t} \}$$

Indeed if we denote

Definition of $(\overline{G_{27}}, \overline{T_{27}}) : ((\overline{G_{27}}, \overline{T_{27}})) = \mathcal{A}^{(4)}((G_{27}), (T_{27}))$

It results

$$|\overline{G_{24}}^{(1)} - \overline{G_{24}}^{(2)}| \leq \int_0^t (a_{24})^{(4)} |G_{25}^{(1)} - G_{25}^{(2)}| e^{-(\overline{M_{24}})^{(4)} s_{(24)}} e^{(\overline{M_{24}})^{(4)} s_{(24)}} ds_{(24)} + \int_0^t \{ (a'_{24})^{(4)} |G_{24}^{(1)} - G_{24}^{(2)}| e^{-(\overline{M_{24}})^{(4)} s_{(24)}} e^{-(\overline{M_{24}})^{(4)} s_{(24)}} + (a''_{24})^{(4)} (T_{25}^{(1)}, s_{(24)}) |G_{24}^{(1)} - G_{24}^{(2)}| e^{-(\overline{M_{24}})^{(4)} s_{(24)}} e^{(\overline{M_{24}})^{(4)} s_{(24)}} + G_{24}^{(2)} | (a''_{24})^{(4)} (T_{25}^{(1)}, s_{(24)}) - (a''_{24})^{(4)} (T_{25}^{(2)}, s_{(24)}) | e^{-(\overline{M_{24}})^{(4)} s_{(24)}} e^{(\overline{M_{24}})^{(4)} s_{(24)}} \} ds_{(24)}$$

Where $s_{(24)}$ represents integrand that is integrated over the interval $[0, t]$

From the hypotheses it follows-

$$|(G_{27})^{(1)} - (G_{27})^{(2)}| e^{-(\overline{M_{24}})^{(4)} t} \leq \frac{1}{(\overline{M_{24}})^{(4)}} ((a_{24})^{(4)} + (a'_{24})^{(4)} + (\overline{A_{24}})^{(4)} + (\overline{P_{24}})^{(4)} (\overline{k_{24}})^{(4)}) d(((G_{27})^{(1)}, (T_{27})^{(1)}); (G_{27})^{(2)}, (T_{27})^{(2)})$$

And analogous inequalities for G_i and T_i . Taking into account the hypothesis the result follows-

Remark 1: The fact that we supposed $(a''_{24})^{(4)}$ and $(b''_{24})^{(4)}$ depending also on t can be considered as not conformal with the reality, however we have put this hypothesis, in order that we can postulate condition necessary to prove the uniqueness of the solution bounded by $(\overline{P_{24}})^{(4)} e^{(\overline{M_{24}})^{(4)} t}$ and $(\overline{Q_{24}})^{(4)} e^{(\overline{M_{24}})^{(4)} t}$ respectively of \mathbb{R}_+ .

If instead of proving the existence of the solution on \mathbb{R}_+ , we have to prove it only on a compact then it suffices to consider that $(a''_i)^{(4)}$ and $(b''_i)^{(4)}$, $i = 24, 25, 26$ depend only on T_{25} and respectively on (G_{27}) (and not on t) and hypothesis can be replaced by a usual Lipschitz condition.

Remark 2: There does not exist any t where $G_i(t) = 0$ and $T_i(t) = 0$

From THE CONCATENATED SYTEM OF GLOBAL EQUATIONS it results

$$G_i(t) \geq G_i^0 e^{-\int_0^t \{ (a'_i)^{(4)} - (a''_i)^{(4)} (T_{25}(s_{(24)}), s_{(24)}) \} ds_{(24)}} \geq 0$$

$$T_i(t) \geq T_i^0 e^{-(b'_i)^{(4)} t} > 0 \text{ for } t > 0$$

Definition of $((\overline{M_{24}})^{(4)})_1, ((\overline{M_{24}})^{(4)})_2$ and $((\overline{M_{24}})^{(4)})_3$:

Remark 3: if G_{24} is bounded, the same property have also G_{25} and G_{26} . indeed if

$$G_{24} < (\overline{M_{24}})^{(4)} \text{ it follows } \frac{dG_{25}}{dt} \leq ((\overline{M_{24}})^{(4)})_1 - (a'_{25})^{(4)} G_{25} \text{ and by integrating}$$

$$G_{25} \leq ((\overline{M_{24}})^{(4)})_2 = G_{25}^0 + 2(a_{25})^{(4)} ((\overline{M_{24}})^{(4)})_1 / (a'_{25})^{(4)}$$

In the same way, one can obtain

$$G_{26} \leq ((\overline{M_{24}})^{(4)})_3 = G_{26}^0 + 2(a_{26})^{(4)} ((\overline{M_{24}})^{(4)})_2 / (a'_{26})^{(4)}$$

If G_{25} or G_{26} is bounded, the same property follows for G_{24} , G_{26} and G_{24} , G_{25} respectively.

Remark 4: If G_{24} is bounded, from below, the same property holds for G_{25} and G_{26} . The proof is analogous with the preceding one. An analogous property is true if G_{25} is bounded from below.

Remark 5: If T_{24} is bounded from below and $\lim_{t \rightarrow \infty} ((b'_i)^{(4)} ((G_{27})(t), t)) = (b'_{25})^{(4)}$ then $T_{25} \rightarrow \infty$.

Definition of $(m)^{(4)}$ and ε_4 :

Indeed let t_4 be so that for $t > t_4$

$$(b_{25})^{(4)} - (b'_i)^{(4)} ((G_{27})(t), t) < \varepsilon_4, T_{24}(t) > (m)^{(4)} :$$

Then $\frac{dT_{25}}{dt} \geq (a_{25})^{(4)} (m)^{(4)} - \varepsilon_4 T_{25}$ which leads to

$$T_{25} \geq \left(\frac{(a_{25})^{(4)} (m)^{(4)}}{\varepsilon_4} \right) (1 - e^{-\varepsilon_4 t}) + T_{25}^0 e^{-\varepsilon_4 t} \text{ If we take } t \text{ such that } e^{-\varepsilon_4 t} = \frac{1}{2} \text{ it results}$$

$$T_{25} \geq \left(\frac{(a_{25})^{(4)} (m)^{(4)}}{2} \right), t = \log \frac{2}{\varepsilon_4} \text{ By taking now } \varepsilon_4 \text{ sufficiently small one sees that } T_{25} \text{ is unbounded. The same property}$$

holds for T_{26} if $\lim_{t \rightarrow \infty} (b'_{26})^{(4)} ((G_{27})(t), t) = (b'_{26})^{(4)}$

We now state a more precise theorem about the behaviors at infinity of the solutions ANALOGOUS inequalities hold also for $G_{29}, G_{30}, T_{28}, T_{29}, T_{30}$:

It is now sufficient to take $\frac{(a_i)^{(5)}}{(\overline{M_{28}})^{(5)}} , \frac{(b_i)^{(5)}}{(\overline{M_{28}})^{(5)}} < 1$ and to choose

$(\overline{P_{28}})^{(5)}$ and $(\overline{Q_{28}})^{(5)}$ large to have-

$$\frac{(a_i)^{(5)}}{(\overline{M_{28}})^{(5)}} \left[(\overline{P_{28}})^{(5)} + ((\overline{P_{28}})^{(5)} + G_j^0) e^{-\left(\frac{(\overline{P_{28}})^{(5)} + G_j^0}{G_j^0} \right)} \right] \leq (\overline{P_{28}})^{(5)} -$$

$$\frac{(b_i)^{(5)}}{(\overline{M_{28}})^{(5)}} \left[((\overline{Q_{28}})^{(5)} + T_j^0) e^{-\left(\frac{(\overline{Q_{28}})^{(5)} + T_j^0}{T_j^0} \right)} + (\overline{Q_{28}})^{(5)} \right] \leq (\overline{Q_{28}})^{(5)} -$$

In order that the operator $\mathcal{A}^{(5)}$ transforms the space of sextuples of functions G_i, T_i satisfying GLOBAL EQUATIONS into itself-

The operator $\mathcal{A}^{(5)}$ is a contraction with respect to the metric

$$d(((G_{31})^{(1)}, (T_{31})^{(1)}), ((G_{31})^{(2)}, (T_{31})^{(2)})) =$$

$$\sup_i \{ \max_{t \in \mathbb{R}_+} |G_i^{(1)}(t) - G_i^{(2)}(t)| e^{-(\widehat{M}_{28})^{(5)}t}, \max_{t \in \mathbb{R}_+} |T_i^{(1)}(t) - T_i^{(2)}(t)| e^{-(\widehat{M}_{28})^{(5)}t} \}$$

Indeed if we denote

Definition of $(\widehat{G}_{31}), (\widehat{T}_{31}) : ((\widehat{G}_{31}), (\widehat{T}_{31})) = \mathcal{A}^{(5)}((G_{31}), (T_{31}))$

It results

$$|\widehat{G}_{28}^{(1)} - \widehat{G}_i^{(2)}| \leq \int_0^t (a_{28})^{(5)} |G_{29}^{(1)} - G_{29}^{(2)}| e^{-(\widehat{M}_{28})^{(5)}s} e^{(\widehat{M}_{28})^{(5)}s} ds + \int_0^t \{ (a'_{28})^{(5)} |G_{28}^{(1)} - G_{28}^{(2)}| e^{-(\widehat{M}_{28})^{(5)}s} e^{-(\widehat{M}_{28})^{(5)}s} + (a''_{28})^{(5)} (T_{29}^{(1)}, s_{(28)}) |G_{28}^{(1)} - G_{28}^{(2)}| e^{-(\widehat{M}_{28})^{(5)}s} e^{(\widehat{M}_{28})^{(5)}s} + G_{28}^{(2)} | (a''_{28})^{(5)} (T_{29}^{(1)}, s_{(28)}) - (a''_{28})^{(5)} (T_{29}^{(2)}, s_{(28)}) | e^{-(\widehat{M}_{28})^{(5)}s} e^{(\widehat{M}_{28})^{(5)}s} \} ds$$

Where $s_{(28)}$ represents integrand that is integrated over the interval $[0, t]$

From the hypotheses it follows-

$$|(G_{31})^{(1)} - (G_{31})^{(2)}| e^{-(\widehat{M}_{28})^{(5)}t} \leq \frac{1}{(\widehat{M}_{28})^{(5)}} ((a_{28})^{(5)} + (a'_{28})^{(5)} + (\widehat{A}_{28})^{(5)} + (\widehat{P}_{28})^{(5)} (\widehat{k}_{28})^{(5)}) d((G_{31})^{(1)}, (T_{31})^{(1)}; (G_{31})^{(2)}, (T_{31})^{(2)})$$

And analogous inequalities for G_i and T_i . Taking into account the hypothesis (35,35,36) the result follows-

Remark 1: The fact that we supposed $(a''_{28})^{(5)}$ and $(b''_{28})^{(5)}$ depending also on t can be considered as not conformal with the reality, however we have put this hypothesis in order that we can postulate condition necessary to prove the uniqueness of the solution bounded by $(\widehat{P}_{28})^{(5)} e^{(\widehat{M}_{28})^{(5)}t}$ and $(\widehat{Q}_{28})^{(5)} e^{(\widehat{M}_{28})^{(5)}t}$ respectively of \mathbb{R}_+ .

If instead of proving the existence of the solution on \mathbb{R}_+ , we have to prove it only on a compact then it suffices to consider that $(a''_i)^{(5)}$ and $(b''_i)^{(5)}, i = 28, 29, 30$ depend only on T_{29} and respectively on (G_{31}) (and not on t) and hypothesis can be replaced by a usual Lipschitz condition.-

Remark 2: There does not exist any t where $G_i(t) = 0$ and $T_i(t) = 0$

From 19 to 28 it results

$$G_i(t) \geq G_i^0 e^{-\int_0^t \{ (a'_i)^{(5)} - (a''_i)^{(5)} (T_{29}(s_{(28)}), s_{(28)}) \} ds} \geq 0$$

$$T_i(t) \geq T_i^0 e^{-(b'_i)^{(5)}t} > 0 \text{ for } t > 0$$

Definition of $(\widehat{M}_{28})^{(5)}_1, (\widehat{M}_{28})^{(5)}_2$ and $(\widehat{M}_{28})^{(5)}_3 :$

Remark 3: if G_{28} is bounded, the same property have also G_{29} and G_{30} . indeed if

$$G_{28} < (\widehat{M}_{28})^{(5)} \text{ it follows } \frac{dG_{29}}{dt} \leq ((\widehat{M}_{28})^{(5)})_1 - (a'_{29})^{(5)} G_{29} \text{ and by integrating}$$

$$G_{29} \leq ((\widehat{M}_{28})^{(5)})_2 = G_{29}^0 + 2(a_{29})^{(5)} ((\widehat{M}_{28})^{(5)})_1 / (a'_{29})^{(5)}$$

In the same way, one can obtain

$$G_{30} \leq ((\widehat{M}_{28})^{(5)})_3 = G_{30}^0 + 2(a_{30})^{(5)} ((\widehat{M}_{28})^{(5)})_2 / (a'_{30})^{(5)}$$

If G_{29} or G_{30} is bounded, the same property follows for G_{28}, G_{30} and G_{28}, G_{29} respectively.-

Remark 4: If G_{28} is bounded, from below, the same property holds for G_{29} and G_{30} . The proof is analogous with the preceding one. An analogous property is true if G_{29} is bounded from below.-

Remark 5: If T_{28} is bounded from below and $\lim_{t \rightarrow \infty} ((b'_i)^{(5)} ((G_{31})(t), t)) = (b'_{29})^{(5)}$ then $T_{29} \rightarrow \infty$.

Definition of $(m)^{(5)}$ and $\varepsilon_5 :$

Indeed let t_5 be so that for $t > t_5$

$$(b_{29})^{(5)} - (b''_i)^{(5)} ((G_{31})(t), t) < \varepsilon_5, T_{28}(t) > (m)^{(5)}$$

Then $\frac{dT_{29}}{dt} \geq (a_{29})^{(5)} (m)^{(5)} - \varepsilon_5 T_{29}$ which leads to

$$T_{29} \geq \left(\frac{(a_{29})^{(5)} (m)^{(5)}}{\varepsilon_5} \right) (1 - e^{-\varepsilon_5 t}) + T_{29}^0 e^{-\varepsilon_5 t} \text{ If we take } t \text{ such that } e^{-\varepsilon_5 t} = \frac{1}{2} \text{ it results}$$

$$T_{29} \geq \left(\frac{(a_{29})^{(5)} (m)^{(5)}}{2} \right), t = \log \frac{2}{\varepsilon_5} \text{ By taking now } \varepsilon_5 \text{ sufficiently small one sees that } T_{29} \text{ is unbounded. The same property}$$

holds for T_{30} if $\lim_{t \rightarrow \infty} (b''_{30})^{(5)} ((G_{31})(t), t) = (b'_{30})^{(5)}$

We now state a more precise theorem about the behaviors at infinity of the solutions

Analogous inequalities hold also for $G_{33}, G_{34}, T_{32}, T_{33}, T_{34}$

It is now sufficient to take $\frac{(a_i)^{(6)}}{(\widehat{M}_{32})^{(6)}}, \frac{(b_i)^{(6)}}{(\widehat{M}_{32})^{(6)}} < 1$ and to choose

$(\widehat{P}_{32})^{(6)}$ and $(\widehat{Q}_{32})^{(6)}$ large to have-

$$\frac{(a_i)^{(6)}}{(\widehat{M}_{32})^{(6)}} \left[(\widehat{P}_{32})^{(6)} + ((\widehat{P}_{32})^{(6)} + G_j^0) e^{-\left(\frac{(\widehat{P}_{32})^{(6)} + G_j^0}{G_j^0} \right)} \right] \leq (\widehat{P}_{32})^{(6)}$$

$$\frac{(b_i)^{(6)}}{(\widehat{M}_{32})^{(6)}} \left[((\widehat{Q}_{32})^{(6)} + T_j^0) e^{-\left(\frac{(\widehat{Q}_{32})^{(6)} + T_j^0}{T_j^0} \right)} + (\widehat{Q}_{32})^{(6)} \right] \leq (\widehat{Q}_{32})^{(6)}$$

In order that the operator $\mathcal{A}^{(6)}$ transforms the space of sextuples of functions G_i, T_i satisfying GLOBAL EQUATIONS into itself-

The operator $\mathcal{A}^{(6)}$ is a contraction with respect to the metric

$$d\left(\left((G_{35})^{(1)}, (T_{35})^{(1)}\right), \left((G_{35})^{(2)}, (T_{35})^{(2)}\right)\right) = \sup_i \left\{ \max_{t \in \mathbb{R}_+} |G_i^{(1)}(t) - G_i^{(2)}(t)| e^{-(M_{32})^{(6)}t}, \max_{t \in \mathbb{R}_+} |T_i^{(1)}(t) - T_i^{(2)}(t)| e^{-(M_{32})^{(6)}t} \right\}$$

Indeed if we denote

$$\widehat{(G_{35})}, \widehat{(T_{35})} : \left(\widehat{(G_{35})}, \widehat{(T_{35})} \right) = \mathcal{A}^{(6)}\left((G_{35}), (T_{35})\right)$$

It results

$$\begin{aligned} |\widehat{G}_{32}^{(1)} - \widehat{G}_i^{(2)}| &\leq \int_0^t (a_{32})^{(6)} |G_{33}^{(1)} - G_{33}^{(2)}| e^{-(M_{32})^{(6)}s_{(32)}} e^{(M_{32})^{(6)}s_{(32)}} ds_{(32)} + \\ &\int_0^t \{ (a'_{32})^{(6)} |G_{32}^{(1)} - G_{32}^{(2)}| e^{-(M_{32})^{(6)}s_{(32)}} e^{-(M_{32})^{(6)}s_{(32)}} + \\ &(a''_{32})^{(6)} (T_{33}^{(1)}, s_{(32)}) |G_{32}^{(1)} - G_{32}^{(2)}| e^{-(M_{32})^{(6)}s_{(32)}} e^{(M_{32})^{(6)}s_{(32)}} + \\ &G_{32}^{(2)} | (a''_{32})^{(6)} (T_{33}^{(1)}, s_{(32)}) - (a''_{32})^{(6)} (T_{33}^{(2)}, s_{(32)}) | e^{-(M_{32})^{(6)}s_{(32)}} e^{(M_{32})^{(6)}s_{(32)}} \} ds_{(32)} \end{aligned}$$

Where $s_{(32)}$ represents integrand that is integrated over the interval $[0, t]$

From the hypotheses it follows-

$$\begin{aligned} |(G_{35})^{(1)} - (G_{35})^{(2)}| e^{-(M_{32})^{(6)}t} &\leq \\ \frac{1}{(M_{32})^{(6)}} \left((a_{32})^{(6)} + (a'_{32})^{(6)} + (\widehat{A}_{32})^{(6)} + (\widehat{P}_{32})^{(6)} (\widehat{K}_{32})^{(6)} \right) &d\left(\left((G_{35})^{(1)}, (T_{35})^{(1)}\right); \left((G_{35})^{(2)}, (T_{35})^{(2)}\right)\right) \end{aligned}$$

And analogous inequalities for G_i and T_i . Taking into account the hypothesis the result follows-

Remark 1: The fact that we supposed $(a'_{32})^{(6)}$ and $(b'_{32})^{(6)}$ depending also on t can be considered as not conformal with the reality, however we have put this hypothesis in order that we can postulate condition necessary to prove the uniqueness of the solution bounded by $(\widehat{P}_{32})^{(6)} e^{(M_{32})^{(6)}t}$ and $(\widehat{Q}_{32})^{(6)} e^{(M_{32})^{(6)}t}$ respectively of \mathbb{R}_+ .

If instead of proving the existence of the solution on \mathbb{R}_+ , we have to prove it only on a compact then it suffices to consider that $(a''_i)^{(6)}$ and $(b''_i)^{(6)}$, $i = 32, 33, 34$ depend only on T_{33} and respectively on (G_{35}) (and not on t) and hypothesis can be replaced by a usual Lipschitz condition.-

Remark 2: There does not exist any t where $G_i(t) = 0$ and $T_i(t) = 0$

From 69 to 32 it results

$$G_i(t) \geq G_i^0 e^{-\int_0^t \{ (a'_i)^{(6)} - (a''_i)^{(6)} (T_{33}(s_{(32)}), s_{(32)}) \} ds_{(32)}} \geq 0$$

$$T_i(t) \geq T_i^0 e^{-(b'_i)^{(6)}t} > 0 \text{ for } t > 0-$$

Definition of $((\widehat{M}_{32})^{(6)})_1, ((\widehat{M}_{32})^{(6)})_2$ and $((\widehat{M}_{32})^{(6)})_3$:

Remark 3: if G_{32} is bounded, the same property have also G_{33} and G_{34} . indeed if

$$G_{32} < (\widehat{M}_{32})^{(6)} \text{ it follows } \frac{dG_{33}}{dt} \leq ((\widehat{M}_{32})^{(6)})_1 - (a'_{33})^{(6)} G_{33} \text{ and by integrating}$$

$$G_{33} \leq ((\widehat{M}_{32})^{(6)})_2 = G_{33}^0 + 2(a_{33})^{(6)} ((\widehat{M}_{32})^{(6)})_1 / (a'_{33})^{(6)}$$

In the same way, one can obtain

$$G_{34} \leq ((\widehat{M}_{32})^{(6)})_3 = G_{34}^0 + 2(a_{34})^{(6)} ((\widehat{M}_{32})^{(6)})_2 / (a'_{34})^{(6)}$$

If G_{33} or G_{34} is bounded, the same property follows for G_{32} , G_{34} and G_{32} , G_{33} respectively.-

Remark 4: If G_{32} is bounded, from below, the same property holds for G_{33} and G_{34} . The proof is analogous with the preceding one. An analogous property is true if G_{33} is bounded from below.-

Remark 5: If T_{32} is bounded from below and $\lim_{t \rightarrow \infty} ((b'_i)^{(6)} ((G_{35})(t), t)) = (b'_{33})^{(6)}$ then $T_{33} \rightarrow \infty$.

Definition of $(m)^{(6)}$ and ε_6 :

Indeed let t_6 be so that for $t > t_6$

$$(b_{33})^{(6)} - (b'_i)^{(6)} ((G_{35})(t), t) < \varepsilon_6, T_{32}(t) > (m)^{(6)}_-$$

Then $\frac{dT_{33}}{dt} \geq (a_{33})^{(6)} (m)^{(6)} - \varepsilon_6 T_{33}$ which leads to

$$T_{33} \geq \left(\frac{(a_{33})^{(6)} (m)^{(6)}}{\varepsilon_6} \right) (1 - e^{-\varepsilon_6 t}) + T_{33}^0 e^{-\varepsilon_6 t} \text{ If we take } t \text{ such that } e^{-\varepsilon_6 t} = \frac{1}{2} \text{ it results}$$

$$T_{33} \geq \left(\frac{(a_{33})^{(6)} (m)^{(6)}}{2} \right), t = \log \frac{2}{\varepsilon_6} \text{ By taking now } \varepsilon_6 \text{ sufficiently small one sees that } T_{33} \text{ is unbounded. The same property}$$

holds for T_{34} if $\lim_{t \rightarrow \infty} (b'_{34})^{(6)} ((G_{35})(t), t) = (b'_{34})^{(6)}$

We now state a more precise theorem about the behaviors at infinity of the solutions of the system-

Behavior of the solutions

Theorem 2: If we denote and define

$$\text{Definition of } (\sigma_1)^{(1)}, (\sigma_2)^{(1)}, (\tau_1)^{(1)}, (\tau_2)^{(1)} :$$

(a) $(\sigma_1)^{(1)}, (\sigma_2)^{(1)}, (\tau_1)^{(1)}, (\tau_2)^{(1)}$ four constants satisfying

$$-(\sigma_2)^{(1)} \leq -(a'_{13})^{(1)} + (a'_{14})^{(1)} - (a''_{13})^{(1)} (T_{14}, t) + (a''_{14})^{(1)} (T_{14}, t) \leq -(\sigma_1)^{(1)}$$

$$-(\tau_2)^{(1)} \leq -(b'_{13})^{(1)} + (b'_{14})^{(1)} - (b''_{13})^{(1)} (G, t) - (b''_{14})^{(1)} (G, t) \leq -(\tau_1)^{(1)} -$$

Definition of $(v_1)^{(1)}, (v_2)^{(1)}, (u_1)^{(1)}, (u_2)^{(1)}, v^{(1)}, u^{(1)} :$

By $(v_1)^{(1)} > 0, (v_2)^{(1)} < 0$ and respectively $(u_1)^{(1)} > 0, (u_2)^{(1)} < 0$ the roots of the equations $(a_{14})^{(1)}(v^{(1)})^2 + (\sigma_1)^{(1)}v^{(1)} - (a_{13})^{(1)} = 0$ and $(b_{14})^{(1)}(u^{(1)})^2 + (\tau_1)^{(1)}u^{(1)} - (b_{13})^{(1)} = 0$:

Definition of $(\bar{v}_1)^{(1)}, (\bar{v}_2)^{(1)}, (\bar{u}_1)^{(1)}, (\bar{u}_2)^{(1)}$:

By $(\bar{v}_1)^{(1)} > 0, (\bar{v}_2)^{(1)} < 0$ and respectively $(\bar{u}_1)^{(1)} > 0, (\bar{u}_2)^{(1)} < 0$ the roots of the equations $(a_{14})^{(1)}(v^{(1)})^2 + (\sigma_2)^{(1)}v^{(1)} - (a_{13})^{(1)} = 0$ and $(b_{14})^{(1)}(u^{(1)})^2 + (\tau_2)^{(1)}u^{(1)} - (b_{13})^{(1)} = 0$ -

Definition of $(m_1)^{(1)}, (m_2)^{(1)}, (\mu_1)^{(1)}, (\mu_2)^{(1)}, (v_0)^{(1)}$:-

(b) If we define $(m_1)^{(1)}, (m_2)^{(1)}, (\mu_1)^{(1)}, (\mu_2)^{(1)}$ by
 $(m_2)^{(1)} = (v_0)^{(1)}, (m_1)^{(1)} = (v_1)^{(1)}$, if $(v_0)^{(1)} < (v_1)^{(1)}$
 $(m_2)^{(1)} = (v_1)^{(1)}, (m_1)^{(1)} = (\bar{v}_1)^{(1)}$, if $(v_1)^{(1)} < (v_0)^{(1)} < (\bar{v}_1)^{(1)}$,

and $(v_0)^{(1)} = \frac{G_{13}^0}{G_{14}^0}$

$(m_2)^{(1)} = (v_1)^{(1)}, (m_1)^{(1)} = (v_0)^{(1)}$, if $(\bar{v}_1)^{(1)} < (v_0)^{(1)}$:

and analogously

$(\mu_2)^{(1)} = (u_0)^{(1)}, (\mu_1)^{(1)} = (u_1)^{(1)}$, if $(u_0)^{(1)} < (u_1)^{(1)}$

$(\mu_2)^{(1)} = (u_1)^{(1)}, (\mu_1)^{(1)} = (\bar{u}_1)^{(1)}$, if $(u_1)^{(1)} < (u_0)^{(1)} < (\bar{u}_1)^{(1)}$,

and $(u_0)^{(1)} = \frac{T_{13}^0}{T_{14}^0}$

$(\mu_2)^{(1)} = (u_1)^{(1)}, (\mu_1)^{(1)} = (u_0)^{(1)}$, if $(\bar{u}_1)^{(1)} < (u_0)^{(1)}$ where $(u_1)^{(1)}, (\bar{u}_1)^{(1)}$

are defined respectively:

Then the solution of CONCATENATED GLOBAL EQUATIONS satisfies the inequalities

$$G_{13}^0 e^{((S_1)^{(1)} - (p_{13})^{(1)})t} \leq G_{13}(t) \leq G_{13}^0 e^{(S_1)^{(1)}t}$$

where $(p_i)^{(1)}$ is defined by equation 25

$$\frac{1}{(m_1)^{(1)}} G_{13}^0 e^{((S_1)^{(1)} - (p_{13})^{(1)})t} \leq G_{14}(t) \leq \frac{1}{(m_2)^{(1)}} G_{13}^0 e^{(S_1)^{(1)}t} -$$

$$\left(\frac{(a_{15})^{(1)} G_{13}^0}{(m_1)^{(1)} ((S_1)^{(1)} - (p_{13})^{(1)} - (S_2)^{(1)})} \left[e^{((S_1)^{(1)} - (p_{13})^{(1)})t} - e^{-(S_2)^{(1)}t} \right] + G_{15}^0 e^{-(S_2)^{(1)}t} \leq G_{15}(t) \leq \frac{(a_{15})^{(1)} G_{13}^0}{(m_2)^{(1)} ((S_1)^{(1)} - (a_{15})^{(1)})} \left[e^{(S_1)^{(1)}t} - e^{-(a_{15})^{(1)}t} \right] + G_{15}^0 e^{-(a_{15})^{(1)}t} \right) -$$

$$\left(\frac{T_{13}^0 e^{(R_1)^{(1)}t} \leq T_{13}(t) \leq T_{13}^0 e^{((R_1)^{(1)} + (r_{13})^{(1)})t} \right) -$$

$$\frac{1}{(\mu_1)^{(1)}} T_{13}^0 e^{(R_1)^{(1)}t} \leq T_{13}(t) \leq \frac{1}{(\mu_2)^{(1)}} T_{13}^0 e^{((R_1)^{(1)} + (r_{13})^{(1)})t} -$$

$$\frac{(b_{15})^{(1)} T_{13}^0}{(\mu_1)^{(1)} ((R_1)^{(1)} - (b_{15})^{(1)})} \left[e^{(R_1)^{(1)}t} - e^{-(b_{15})^{(1)}t} \right] + T_{15}^0 e^{-(b_{15})^{(1)}t} \leq T_{15}(t) \leq$$

$$\frac{(a_{15})^{(1)} T_{13}^0}{(\mu_2)^{(1)} ((R_1)^{(1)} + (r_{13})^{(1)} + (R_2)^{(1)})} \left[e^{((R_1)^{(1)} + (r_{13})^{(1)})t} - e^{-(R_2)^{(1)}t} \right] + T_{15}^0 e^{-(R_2)^{(1)}t} -$$

Definition of $(S_1)^{(1)}, (S_2)^{(1)}, (R_1)^{(1)}, (R_2)^{(1)}$:-

Where $(S_1)^{(1)} = (a_{13})^{(1)}(m_2)^{(1)} - (a_{13})^{(1)}$

$(S_2)^{(1)} = (a_{15})^{(1)} - (p_{15})^{(1)}$

$(R_1)^{(1)} = (b_{13})^{(1)}(\mu_2)^{(1)} - (b_{13})^{(1)}$

$(R_2)^{(1)} = (b_{15})^{(1)} - (r_{15})^{(1)}$ -

Behavior of the solutions

If we denote and define-

Definition of $(\sigma_1)^{(2)}, (\sigma_2)^{(2)}, (\tau_1)^{(2)}, (\tau_2)^{(2)}$:

$(\sigma_1)^{(2)}, (\sigma_2)^{(2)}, (\tau_1)^{(2)}, (\tau_2)^{(2)}$ four constants satisfying-

$$-(\sigma_2)^{(2)} \leq -(a'_{16})^{(2)} + (a'_{17})^{(2)} - (a''_{16})^{(2)}(T_{17}, t) + (a''_{17})^{(2)}(T_{17}, t) \leq -(\sigma_1)^{(2)} -$$

$$-(\tau_2)^{(2)} \leq -(b'_{16})^{(2)} + (b'_{17})^{(2)} - (b''_{16})^{(2)}(G_{19}, t) - (b''_{17})^{(2)}(G_{19}, t) \leq -(\tau_1)^{(2)} -$$

Definition of $(v_1)^{(2)}, (v_2)^{(2)}, (u_1)^{(2)}, (u_2)^{(2)}$:-

By $(v_1)^{(2)} > 0, (v_2)^{(2)} < 0$ and respectively $(u_1)^{(2)} > 0, (u_2)^{(2)} < 0$ the roots-

of the equations $(a_{17})^{(2)}(v^{(2)})^2 + (\sigma_1)^{(2)}v^{(2)} - (a_{16})^{(2)} = 0$ -

and $(b_{14})^{(2)}(u^{(2)})^2 + (\tau_1)^{(2)}u^{(2)} - (b_{16})^{(2)} = 0$ and-

Definition of $(\bar{v}_1)^{(2)}, (\bar{v}_2)^{(2)}, (\bar{u}_1)^{(2)}, (\bar{u}_2)^{(2)}$:-

By $(\bar{v}_1)^{(2)} > 0, (\bar{v}_2)^{(2)} < 0$ and respectively $(\bar{u}_1)^{(2)} > 0, (\bar{u}_2)^{(2)} < 0$ the-

roots of the equations $(a_{17})^{(2)}(v^{(2)})^2 + (\sigma_2)^{(2)}v^{(2)} - (a_{16})^{(2)} = 0$ -

and $(b_{17})^{(2)}(u^{(2)})^2 + (\tau_2)^{(2)}u^{(2)} - (b_{16})^{(2)} = 0$ -

Definition of $(m_1)^{(2)}, (m_2)^{(2)}, (\mu_1)^{(2)}, (\mu_2)^{(2)}$:-

If we define $(m_1)^{(2)}, (m_2)^{(2)}, (\mu_1)^{(2)}, (\mu_2)^{(2)}$ by-

$(m_2)^{(2)} = (v_0)^{(2)}, (m_1)^{(2)} = (v_1)^{(2)}$, if $(v_0)^{(2)} < (v_1)^{(2)}$ -

$(m_2)^{(2)} = (v_1)^{(2)}, (m_1)^{(2)} = (\bar{v}_1)^{(2)}$, if $(v_1)^{(2)} < (v_0)^{(2)} < (\bar{v}_1)^{(2)}$,

and
$$(v_0)^{(2)} = \frac{G_{16}^0}{G_{17}^0} -$$

$(m_2)^{(2)} = (v_1)^{(2)}, (m_1)^{(2)} = (v_0)^{(2)}, \text{ if } (\bar{v}_1)^{(2)} < (v_0)^{(2)} -$

and analogously

$(\mu_2)^{(2)} = (u_0)^{(2)}, (\mu_1)^{(2)} = (u_1)^{(2)}, \text{ if } (u_0)^{(2)} < (u_1)^{(2)}$
 $(\mu_2)^{(2)} = (u_1)^{(2)}, (\mu_1)^{(2)} = (\bar{u}_1)^{(2)}, \text{ if } (u_1)^{(2)} < (u_0)^{(2)} < (\bar{u}_1)^{(2)},$

and
$$(u_0)^{(2)} = \frac{T_{16}^0}{T_{17}^0} -$$

$(\mu_2)^{(2)} = (u_1)^{(2)}, (\mu_1)^{(2)} = (u_0)^{(2)}, \text{ if } (\bar{u}_1)^{(2)} < (u_0)^{(2)} -$

Then the solution of CONCATENATED GLOBAL EQUATIONS satisfies the inequalities

$G_{16}^0 e^{(S_1)^{(2)} - (p_{16})^{(2)} t} \leq G_{16}(t) \leq G_{16}^0 e^{(S_1)^{(2)} t} -$

$(p_i)^{(2)}$ is defined -

$$\frac{1}{(m_1)^{(2)}} G_{16}^0 e^{((S_1)^{(2)} - (p_{16})^{(2)}) t} \leq G_{17}(t) \leq \frac{1}{(m_2)^{(2)}} G_{16}^0 e^{(S_1)^{(2)} t} -$$

$$\left(\frac{(a_{18})^{(2)} G_{16}^0}{(m_1)^{(2)} ((S_1)^{(2)} - (p_{16})^{(2)} - (S_2)^{(2)})} \left[e^{((S_1)^{(2)} - (p_{16})^{(2)}) t} - e^{-(S_2)^{(2)} t} \right] + G_{18}^0 e^{-(S_2)^{(2)} t} \leq G_{18}(t) \leq \frac{(a_{18})^{(2)} G_{16}^0}{(m_2)^{(2)} ((S_1)^{(2)} - (a_{18})^{(2)})} \left[e^{(S_1)^{(2)} t} - e^{-(a_{18})^{(2)} t} \right] + G_{18}^0 e^{-(a_{18})^{(2)} t} -$$

$$\frac{T_{16}^0 e^{(R_1)^{(2)} t} \leq T_{16}(t) \leq T_{16}^0 e^{((R_1)^{(2)} + (r_{16})^{(2)}) t} -$$

$$\frac{1}{(\mu_1)^{(2)}} T_{16}^0 e^{(R_1)^{(2)} t} \leq T_{16}(t) \leq \frac{1}{(\mu_2)^{(2)}} T_{16}^0 e^{((R_1)^{(2)} + (r_{16})^{(2)}) t} -$$

$$\frac{(b_{18})^{(2)} T_{16}^0}{(\mu_1)^{(2)} ((R_1)^{(2)} - (b_{18})^{(2)})} \left[e^{(R_1)^{(2)} t} - e^{-(b_{18})^{(2)} t} \right] + T_{18}^0 e^{-(b_{18})^{(2)} t} \leq T_{18}(t) \leq$$

$$\frac{(a_{18})^{(2)} T_{16}^0}{(\mu_2)^{(2)} ((R_1)^{(2)} + (r_{16})^{(2)} + (R_2)^{(2)})} \left[e^{((R_1)^{(2)} + (r_{16})^{(2)}) t} - e^{-(R_2)^{(2)} t} \right] + T_{18}^0 e^{-(R_2)^{(2)} t} -$$

Definition of $(S_1)^{(2)}, (S_2)^{(2)}, (R_1)^{(2)}, (R_2)^{(2)}$:-

Where $(S_1)^{(2)} = (a_{16})^{(2)} (m_2)^{(2)} - (a_{16})^{(2)}$

$(S_2)^{(2)} = (a_{18})^{(2)} - (p_{18})^{(2)} -$

$(R_1)^{(2)} = (b_{16})^{(2)} (\mu_2)^{(1)} - (b'_{16})^{(2)}$

$(R_2)^{(2)} = (b'_{18})^{(2)} - (r_{18})^{(2)} -$

Behavior of the solutions

If we denote and define

Definition of $(\sigma_1)^{(3)}, (\sigma_2)^{(3)}, (\tau_1)^{(3)}, (\tau_2)^{(3)}$:

(a) $\sigma_1^{(3)}, \sigma_2^{(3)}, \tau_1^{(3)}, \tau_2^{(3)}$ four constants satisfying

$-(\sigma_2)^{(3)} \leq -(a'_{20})^{(3)} + (a''_{21})^{(3)} - (a''_{20})^{(3)} (T_{21}, t) + (a_{21})^{(3)} (T_{21}, t) \leq -(\sigma_1)^{(3)}$

$-(\tau_2)^{(3)} \leq -(b'_{20})^{(3)} + (b''_{21})^{(3)} - (b''_{20})^{(3)} (G, t) - (b_{21})^{(3)} ((G_{23}), t) \leq -(\tau_1)^{(3)} -$

Definition of $(v_1)^{(3)}, (v_2)^{(3)}, (u_1)^{(3)}, (u_2)^{(3)}$:

(b) By $(v_1)^{(3)} > 0, (v_2)^{(3)} < 0$ and respectively $(u_1)^{(3)} > 0, (u_2)^{(3)} < 0$ the roots of the equations

$(a_{21})^{(3)} (v^{(3)})^2 + (\sigma_1)^{(3)} v^{(3)} - (a_{20})^{(3)} = 0$

and $(b_{21})^{(3)} (u^{(3)})^2 + (\tau_1)^{(3)} u^{(3)} - (b_{20})^{(3)} = 0$ and

By $(\bar{v}_1)^{(3)} > 0, (\bar{v}_2)^{(3)} < 0$ and respectively $(\bar{u}_1)^{(3)} > 0, (\bar{u}_2)^{(3)} < 0$ the

roots of the equations $(a_{21})^{(3)} (v^{(3)})^2 + (\sigma_2)^{(3)} v^{(3)} - (a_{20})^{(3)} = 0$

and $(b_{21})^{(3)} (u^{(3)})^2 + (\tau_2)^{(3)} u^{(3)} - (b_{20})^{(3)} = 0$:-

Definition of $(m_1)^{(3)}, (m_2)^{(3)}, (\mu_1)^{(3)}, (\mu_2)^{(3)}$:-

(c) If we define $(m_1)^{(3)}, (m_2)^{(3)}, (\mu_1)^{(3)}, (\mu_2)^{(3)}$ by

$(m_2)^{(3)} = (v_0)^{(3)}, (m_1)^{(3)} = (v_1)^{(3)}, \text{ if } (v_0)^{(3)} < (v_1)^{(3)}$

$(m_2)^{(3)} = (v_1)^{(3)}, (m_1)^{(3)} = (\bar{v}_1)^{(3)}, \text{ if } (v_1)^{(3)} < (v_0)^{(3)} < (\bar{v}_1)^{(3)},$

and
$$(v_0)^{(3)} = \frac{G_{20}^0}{G_{21}^0} -$$

$(m_2)^{(3)} = (v_1)^{(3)}, (m_1)^{(3)} = (v_0)^{(3)}, \text{ if } (\bar{v}_1)^{(3)} < (v_0)^{(3)} -$

and analogously

$(\mu_2)^{(3)} = (u_0)^{(3)}, (\mu_1)^{(3)} = (u_1)^{(3)}, \text{ if } (u_0)^{(3)} < (u_1)^{(3)}$

$(\mu_2)^{(3)} = (u_1)^{(3)}, (\mu_1)^{(3)} = (\bar{u}_1)^{(3)}, \text{ if } (u_1)^{(3)} < (u_0)^{(3)} < (\bar{u}_1)^{(3)}, \text{ and } (u_0)^{(3)} = \frac{T_{20}^0}{T_{21}^0}$

$(\mu_2)^{(3)} = (u_1)^{(3)}, (\mu_1)^{(3)} = (u_0)^{(3)}, \text{ if } (\bar{u}_1)^{(3)} < (u_0)^{(3)}$

Then the solution satisfies the inequalities

$G_{20}^0 e^{(S_1)^{(3)} - (p_{20})^{(3)} t} \leq G_{20}(t) \leq G_{20}^0 e^{(S_1)^{(3)} t}$

$(p_i)^{(3)}$ is defined-

$$\frac{1}{(m_1)^{(3)}} G_{20}^0 e^{((S_1)^{(3)} - (p_{20})^{(3)})t} \leq G_{21}(t) \leq \frac{1}{(m_2)^{(3)}} G_{20}^0 e^{(S_1)^{(3)}t} -$$

$$\left(\frac{(a_{22})^{(3)} G_{20}^0}{(m_1)^{(3)}((S_1)^{(3)} - (p_{20})^{(3)} - (S_2)^{(3)})} \left[e^{((S_1)^{(3)} - (p_{20})^{(3)})t} - e^{-(S_2)^{(3)}t} \right] + G_{22}^0 e^{-(S_2)^{(3)}t} \leq G_{22}(t) \leq \frac{(a_{22})^{(3)} G_{20}^0}{(m_2)^{(3)}((S_1)^{(3)} - (a_{22})^{(3)})} \left[e^{(S_1)^{(3)}t} - e^{-(a_{22})^{(3)}t} \right] + G_{22}^0 e^{-(a_{22})^{(3)}t} -$$

$$\boxed{T_{20}^0 e^{(R_1)^{(3)}t} \leq T_{20}(t) \leq T_{20}^0 e^{((R_1)^{(3)} + (r_{20})^{(3)})t} - \frac{1}{(\mu_1)^{(3)}} T_{20}^0 e^{(R_1)^{(3)}t} \leq T_{20}(t) \leq \frac{1}{(\mu_2)^{(3)}} T_{20}^0 e^{((R_1)^{(3)} + (r_{20})^{(3)})t} -$$

$$\frac{(b_{22})^{(3)} T_{20}^0}{(\mu_1)^{(3)}((R_1)^{(3)} - (b_{22})^{(3)})} \left[e^{(R_1)^{(3)}t} - e^{-(b_{22})^{(3)}t} \right] + T_{22}^0 e^{-(b_{22})^{(3)}t} \leq T_{22}(t) \leq$$

$$\frac{(a_{22})^{(3)} T_{20}^0}{(\mu_2)^{(3)}((R_1)^{(3)} + (r_{20})^{(3)} + (R_2)^{(3)})} \left[e^{((R_1)^{(3)} + (r_{20})^{(3)})t} - e^{-(R_2)^{(3)}t} \right] + T_{22}^0 e^{-(R_2)^{(3)}t} -$$

Definition of $(S_1)^{(3)}, (S_2)^{(3)}, (R_1)^{(3)}, (R_2)^{(3)}$:-

Where $(S_1)^{(3)} = (a_{20})^{(3)}(m_2)^{(3)} - (a'_{20})^{(3)}$

$$(S_2)^{(3)} = (a_{22})^{(3)} - (p_{22})^{(3)}$$

$$(R_1)^{(3)} = (b_{20})^{(3)}(\mu_2)^{(3)} - (b'_{20})^{(3)}$$

$$(R_2)^{(3)} = (b_{22})^{(3)} - (r_{22})^{(3)}$$

Behavior of the solutions

If we denote and define

Definition of $(\sigma_1)^{(4)}, (\sigma_2)^{(4)}, (\tau_1)^{(4)}, (\tau_2)^{(4)}$:

(d) $(\sigma_1)^{(4)}, (\sigma_2)^{(4)}, (\tau_1)^{(4)}, (\tau_2)^{(4)}$ four constants satisfying

$$-(\sigma_2)^{(4)} \leq -(a'_{24})^{(4)} + (a'_{25})^{(4)} - (a''_{24})^{(4)}(T_{25}, t) + (a''_{25})^{(4)}(T_{25}, t) \leq -(\sigma_1)^{(4)}$$

$$-(\tau_2)^{(4)} \leq -(b'_{24})^{(4)} + (b'_{25})^{(4)} - (b''_{24})^{(4)}(G_{27}, t) - (b''_{25})^{(4)}(G_{27}, t) \leq -(\tau_1)^{(4)}$$

Definition of $(v_1)^{(4)}, (v_2)^{(4)}, (u_1)^{(4)}, (u_2)^{(4)}, v^{(4)}, u^{(4)}$:

(e) By $(v_1)^{(4)} > 0, (v_2)^{(4)} < 0$ and respectively $(u_1)^{(4)} > 0, (u_2)^{(4)} < 0$ the roots of the equations

$$(a_{25})^{(4)}(v^{(4)})^2 + (\sigma_1)^{(4)}v^{(4)} - (a_{24})^{(4)} = 0$$

$$\text{and } (b_{25})^{(4)}(u^{(4)})^2 + (\tau_1)^{(4)}u^{(4)} - (b_{24})^{(4)} = 0 \text{ and}$$

Definition of $(\bar{v}_1)^{(4)}, (\bar{v}_2)^{(4)}, (\bar{u}_1)^{(4)}, (\bar{u}_2)^{(4)}$:

By $(\bar{v}_1)^{(4)} > 0, (\bar{v}_2)^{(4)} < 0$ and respectively $(\bar{u}_1)^{(4)} > 0, (\bar{u}_2)^{(4)} < 0$ the

roots of the equations $(a_{25})^{(4)}(v^{(4)})^2 + (\sigma_2)^{(4)}v^{(4)} - (a_{24})^{(4)} = 0$

$$\text{and } (b_{25})^{(4)}(u^{(4)})^2 + (\tau_2)^{(4)}u^{(4)} - (b_{24})^{(4)} = 0$$

Definition of $(m_1)^{(4)}, (m_2)^{(4)}, (\mu_1)^{(4)}, (\mu_2)^{(4)}, (v_0)^{(4)}$:-

(f) If we define $(m_1)^{(4)}, (m_2)^{(4)}, (\mu_1)^{(4)}, (\mu_2)^{(4)}$ by

$$(m_2)^{(4)} = (v_0)^{(4)}, (m_1)^{(4)} = (v_1)^{(4)}, \text{ if } (v_0)^{(4)} < (v_1)^{(4)}$$

$$(m_2)^{(4)} = (v_1)^{(4)}, (m_1)^{(4)} = (\bar{v}_1)^{(4)}, \text{ if } (v_1)^{(4)} < (v_0)^{(4)} < (\bar{v}_1)^{(4)}, \text{ and } \boxed{(v_0)^{(4)} = \frac{G_{24}^0}{G_{25}^0}}$$

$$(m_2)^{(4)} = (v_4)^{(4)}, (m_1)^{(4)} = (v_0)^{(4)}, \text{ if } (\bar{v}_4)^{(4)} < (v_0)^{(4)}$$

and analogously

$$(\mu_2)^{(4)} = (u_0)^{(4)}, (\mu_1)^{(4)} = (u_1)^{(4)}, \text{ if } (u_0)^{(4)} < (u_1)^{(4)}$$

$$(\mu_2)^{(4)} = (u_1)^{(4)}, (\mu_1)^{(4)} = (\bar{u}_1)^{(4)}, \text{ if } (u_1)^{(4)} < (u_0)^{(4)} < (\bar{u}_1)^{(4)}, \text{ and } \boxed{(u_0)^{(4)} = \frac{T_{24}^0}{T_{25}^0}}$$

$$(\mu_2)^{(4)} = (u_1)^{(4)}, (\mu_1)^{(4)} = (u_0)^{(4)}, \text{ if } (\bar{u}_1)^{(4)} < (u_0)^{(4)} \text{ where } (u_1)^{(4)}, (\bar{u}_1)^{(4)} \text{ are defined}$$

Then the solution of CONCATENATED GLOBAL EQUATIONS satisfies the inequalities

$$G_{24}^0 e^{((S_1)^{(4)} - (p_{24})^{(4)})t} \leq G_{24}(t) \leq G_{24}^0 e^{(S_1)^{(4)}t}$$

where $(p_i)^{(4)}$ is defined

$$\frac{1}{(m_1)^{(4)}} G_{24}^0 e^{((S_1)^{(4)} - (p_{24})^{(4)})t} \leq G_{25}(t) \leq \frac{1}{(m_2)^{(4)}} G_{24}^0 e^{(S_1)^{(4)}t}$$

$$\left(\frac{(a_{26})^{(4)} G_{24}^0}{(m_1)^{(4)}((S_1)^{(4)} - (p_{24})^{(4)} - (S_2)^{(4)})} \left[e^{((S_1)^{(4)} - (p_{24})^{(4)})t} - e^{-(S_2)^{(4)}t} \right] + G_{26}^0 e^{-(S_2)^{(4)}t} \leq G_{26}(t) \leq \right. \\ \left. (a_{26})^{(4)} G_{24}^0 (m_2)^{(4)} (S_1)^{(4)} - (a_{26}')^{(4)} e^{(S_1)^{(4)}t} - e^{-(a_{26}')^{(4)}t} + G_{26}^0 e^{-(a_{26}')^{(4)}t} \right]$$

$$\boxed{T_{24}^0 e^{(R_1)^{(4)}t} \leq T_{24}(t) \leq T_{24}^0 e^{((R_1)^{(4)} + (r_{24})^{(4)})t}$$

$$\frac{1}{(\mu_1)^{(4)}} T_{24}^0 e^{(R_1)^{(4)}t} \leq T_{24}(t) \leq \frac{1}{(\mu_2)^{(4)}} T_{24}^0 e^{((R_1)^{(4)} + (r_{24})^{(4)})t}$$

$$\frac{(b_{26})^{(4)} T_{24}^0}{(\mu_1)^{(4)}((R_1)^{(4)} - (b_{26})^{(4)})} \left[e^{(R_1)^{(4)}t} - e^{-(b_{26})^{(4)}t} \right] + T_{26}^0 e^{-(b_{26})^{(4)}t} \leq T_{26}(t) \leq$$

$$\frac{(a_{26})^{(4)} T_{24}^0}{(\mu_2)^{(4)}((R_1)^{(4)} + (r_{24})^{(4)} + (R_2)^{(4)})} \left[e^{((R_1)^{(4)} + (r_{24})^{(4)})t} - e^{-(R_2)^{(4)}t} \right] + T_{26}^0 e^{-(R_2)^{(4)}t}$$

Definition of $(S_1)^{(4)}, (S_2)^{(4)}, (R_1)^{(4)}, (R_2)^{(4)}$:-

$$(S_1)^{(4)} = (a_{24})^{(4)}(m_2)^{(4)} - (a'_{24})^{(4)}$$

$$(S_2)^{(4)} = (a_{26})^{(4)} - (p_{26})^{(4)}$$

$$(R_1)^{(4)} = (b_{24})^{(4)}(\mu_2)^{(4)} - (b'_{24})^{(4)} \text{ and } (R_2)^{(4)} = (b'_{26})^{(4)} - (r_{26})^{(4)}$$

Behavior of the solutions

Theorem 2: If we denote and define

Definition of $(\sigma_1)^{(5)}, (\sigma_2)^{(5)}, (\tau_1)^{(5)}, (\tau_2)^{(5)}$:

(g) $(\sigma_1)^{(5)}, (\sigma_2)^{(5)}, (\tau_1)^{(5)}, (\tau_2)^{(5)}$ four constants satisfying

$$-(\sigma_2)^{(5)} \leq -(a'_{28})^{(5)} + (a'_{29})^{(5)} - (a''_{28})^{(5)}(T_{29}, t) + (a''_{29})^{(5)}(T_{29}, t) \leq -(\sigma_1)^{(5)}$$

$$-(\tau_2)^{(5)} \leq -(b'_{28})^{(5)} + (b'_{29})^{(5)} - (b''_{28})^{(5)}(G_{31}, t) - (b''_{29})^{(5)}(G_{31}, t) \leq -(\tau_1)^{(5)}$$

Definition of $(v_1)^{(5)}, (v_2)^{(5)}, (u_1)^{(5)}, (u_2)^{(5)}, v^{(5)}, u^{(5)}$:

(h) By $(v_1)^{(5)} > 0, (v_2)^{(5)} < 0$ and respectively $(u_1)^{(5)} > 0, (u_2)^{(5)} < 0$ the roots of the equations

$$(a_{29})^{(5)}(v^{(5)})^2 + (\sigma_1)^{(5)}v^{(5)} - (a_{28})^{(5)} = 0$$

$$\text{and } (b_{29})^{(5)}(u^{(5)})^2 + (\tau_1)^{(5)}u^{(5)} - (b_{28})^{(5)} = 0 \text{ and}$$

Definition of $(\bar{v}_1)^{(5)}, (\bar{v}_2)^{(5)}, (\bar{u}_1)^{(5)}, (\bar{u}_2)^{(5)}$:

By $(\bar{v}_1)^{(5)} > 0, (\bar{v}_2)^{(5)} < 0$ and respectively $(\bar{u}_1)^{(5)} > 0, (\bar{u}_2)^{(5)} < 0$ the

$$\text{roots of the equations } (a_{29})^{(5)}(v^{(5)})^2 + (\sigma_2)^{(5)}v^{(5)} - (a_{28})^{(5)} = 0$$

$$\text{and } (b_{29})^{(5)}(u^{(5)})^2 + (\tau_2)^{(5)}u^{(5)} - (b_{28})^{(5)} = 0$$

Definition of $(m_1)^{(5)}, (m_2)^{(5)}, (\mu_1)^{(5)}, (\mu_2)^{(5)}, (v_0)^{(5)}$:-

(i) If we define $(m_1)^{(5)}, (m_2)^{(5)}, (\mu_1)^{(5)}, (\mu_2)^{(5)}$ by

$$(m_2)^{(5)} = (v_0)^{(5)}, (m_1)^{(5)} = (v_1)^{(5)}, \text{ if } (v_0)^{(5)} < (v_1)^{(5)}$$

$$(m_2)^{(5)} = (v_1)^{(5)}, (m_1)^{(5)} = (\bar{v}_1)^{(5)}, \text{ if } (v_1)^{(5)} < (v_0)^{(5)} < (\bar{v}_1)^{(5)}, \text{ and } (v_0)^{(5)} = \frac{G_{28}^0}{G_{29}^0}$$

$$(m_2)^{(5)} = (v_1)^{(5)}, (m_1)^{(5)} = (v_0)^{(5)}, \text{ if } (\bar{v}_1)^{(5)} < (v_0)^{(5)}$$

and analogously

$$(\mu_2)^{(5)} = (u_0)^{(5)}, (\mu_1)^{(5)} = (u_1)^{(5)}, \text{ if } (u_0)^{(5)} < (u_1)^{(5)}$$

$$(\mu_2)^{(5)} = (u_1)^{(5)}, (\mu_1)^{(5)} = (\bar{u}_1)^{(5)}, \text{ if } (u_1)^{(5)} < (u_0)^{(5)} < (\bar{u}_1)^{(5)}, \text{ and } (u_0)^{(5)} = \frac{T_{28}^0}{T_{29}^0}$$

$$(\mu_2)^{(5)} = (u_1)^{(5)}, (\mu_1)^{(5)} = (u_0)^{(5)}, \text{ if } (\bar{u}_1)^{(5)} < (u_0)^{(5)} \text{ where } (u_1)^{(5)}, (\bar{u}_1)^{(5)} \text{ are defined}$$

Then the solution of CONCATENATED SYSTEM OF GLOBAL EQUATIONS satisfies the inequalities

$$G_{28}^0 e^{((S_1)^{(5)} - (p_{28})^{(5)})t} \leq G_{28}(t) \leq G_{28}^0 e^{(S_1)^{(5)}t}$$

where $(p_i)^{(5)}$ is defined

$$\frac{1}{(m_5)^{(5)}} G_{28}^0 e^{((S_1)^{(5)} - (p_{28})^{(5)})t} \leq G_{29}(t) \leq \frac{1}{(m_2)^{(5)}} G_{28}^0 e^{(S_1)^{(5)}t}$$

$$\left(\frac{(a_{30})^{(5)} G_{28}^0}{(m_1)^{(5)}((S_1)^{(5)} - (p_{28})^{(5)}) - (S_2)^{(5)}} \right) \left[e^{((S_1)^{(5)} - (p_{28})^{(5)})t} - e^{-(S_2)^{(5)}t} \right] + G_{30}^0 e^{-(S_2)^{(5)}t} \leq G_{30}(t) \leq$$

$$(a_{30})^{(5)} G_{28}^0 (m_2)^{(5)} (S_1)^{(5)} - (a_{30}')^{(5)} 5e^{(S_1)^{(5)}t} - e^{-(a_{30}')^{(5)}t} + G_{30}^0 e^{-(a_{30}')^{(5)}t}$$

$$\frac{T_{28}^0 e^{(R_1)^{(5)}t} \leq T_{28}(t) \leq T_{28}^0 e^{((R_1)^{(5)} + (r_{28})^{(5)})t}$$

$$\frac{1}{(\mu_1)^{(5)}} T_{28}^0 e^{(R_1)^{(5)}t} \leq T_{28}(t) \leq \frac{1}{(\mu_2)^{(5)}} T_{28}^0 e^{((R_1)^{(5)} + (r_{28})^{(5)})t}$$

$$\frac{(b_{30})^{(5)} T_{28}^0}{(\mu_1)^{(5)}((R_1)^{(5)} - (b_{30})^{(5)})} \left[e^{(R_1)^{(5)}t} - e^{-(b_{30})^{(5)}t} \right] + T_{30}^0 e^{-(b_{30})^{(5)}t} \leq T_{30}(t) \leq$$

$$\frac{(a_{30})^{(5)} T_{28}^0}{(\mu_2)^{(5)}((R_1)^{(5)} + (r_{28})^{(5)} + (R_2)^{(5)})} \left[e^{((R_1)^{(5)} + (r_{28})^{(5)})t} - e^{-(R_2)^{(5)}t} \right] + T_{30}^0 e^{-(R_2)^{(5)}t}$$

Definition of $(S_1)^{(5)}, (S_2)^{(5)}, (R_1)^{(5)}, (R_2)^{(5)}$:-

Where $(S_1)^{(5)} = (a_{28})^{(5)}(m_2)^{(5)} - (a'_{28})^{(5)}$

$$(S_2)^{(5)} = (a_{30})^{(5)} - (p_{30})^{(5)}$$

$$(R_1)^{(5)} = (b_{28})^{(5)}(\mu_2)^{(5)} - (b'_{28})^{(5)}$$

$$(R_2)^{(5)} = (b'_{30})^{(5)} - (r_{30})^{(5)}$$

Behavior of the solutions

Theorem 2: If we denote and define

Definition of $(\sigma_1)^{(6)}, (\sigma_2)^{(6)}, (\tau_1)^{(6)}, (\tau_2)^{(6)}$:

(j) $(\sigma_1)^{(6)}, (\sigma_2)^{(6)}, (\tau_1)^{(6)}, (\tau_2)^{(6)}$ four constants satisfying

$$-(\sigma_2)^{(6)} \leq -(a'_{32})^{(6)} + (a'_{33})^{(6)} - (a''_{32})^{(6)}(T_{33}, t) + (a''_{33})^{(6)}(T_{33}, t) \leq -(\sigma_1)^{(6)}$$

$$-(\tau_2)^{(6)} \leq -(b'_{32})^{(6)} + (b'_{33})^{(6)} - (b''_{32})^{(6)}(G_{35}, t) - (b''_{33})^{(6)}(G_{35}, t) \leq -(\tau_1)^{(6)}$$

Definition of $(v_1)^{(6)}, (v_2)^{(6)}, (u_1)^{(6)}, (u_2)^{(6)}, v^{(6)}, u^{(6)}$:

(k) By $(v_1)^{(6)} > 0, (v_2)^{(6)} < 0$ and respectively $(u_1)^{(6)} > 0, (u_2)^{(6)} < 0$ the roots of the equations

$$(a_{33})^{(6)}(v^{(6)})^2 + (\sigma_1)^{(6)}v^{(6)} - (a_{32})^{(6)} = 0$$

and $(b_{33})^{(6)}(u^{(6)})^2 + (\tau_1)^{(6)}u^{(6)} - (b_{32})^{(6)} = 0$ and

Definition of $(\bar{v}_1)^{(6)}, (\bar{v}_2)^{(6)}, (\bar{u}_1)^{(6)}, (\bar{u}_2)^{(6)}$:

By $(\bar{v}_1)^{(6)} > 0, (\bar{v}_2)^{(6)} < 0$ and respectively $(\bar{u}_1)^{(6)} > 0, (\bar{u}_2)^{(6)} < 0$ the roots of the equations $(a_{33})^{(6)}(v^{(6)})^2 + (\sigma_2)^{(6)}v^{(6)} - (a_{32})^{(6)} = 0$

$$\text{and } (b_{33})^{(6)}(u^{(6)})^2 + (\tau_2)^{(6)}u^{(6)} - (b_{32})^{(6)} = 0$$

Definition of $(m_1)^{(6)}, (m_2)^{(6)}, (\mu_1)^{(6)}, (\mu_2)^{(6)}, (v_0)^{(6)}$:-

(1) If we define $(m_1)^{(6)}, (m_2)^{(6)}, (\mu_1)^{(6)}, (\mu_2)^{(6)}$ by $(m_2)^{(6)} = (v_0)^{(6)}, (m_1)^{(6)} = (v_1)^{(6)}$, **if** $(v_0)^{(6)} < (v_1)^{(6)}$

$$(m_2)^{(6)} = (v_1)^{(6)}, (m_1)^{(6)} = (\bar{v}_6)^{(6)}, \text{ if } (v_1)^{(6)} < (v_0)^{(6)} < (\bar{v}_1)^{(6)}, \text{ and } (v_0)^{(6)} = \frac{G_{32}^0}{G_{33}^0}$$

$$(m_2)^{(6)} = (v_1)^{(6)}, (m_1)^{(6)} = (v_0)^{(6)}, \text{ if } (\bar{v}_1)^{(6)} < (v_0)^{(6)}$$

and analogously

$$(\mu_2)^{(6)} = (u_0)^{(6)}, (\mu_1)^{(6)} = (u_1)^{(6)}, \text{ if } (u_0)^{(6)} < (u_1)^{(6)}$$

$$(\mu_2)^{(6)} = (u_1)^{(6)}, (\mu_1)^{(6)} = (\bar{u}_1)^{(6)}, \text{ if } (u_1)^{(6)} < (u_0)^{(6)} < (\bar{u}_1)^{(6)}, \text{ and } (u_0)^{(6)} = \frac{T_{32}^0}{T_{33}^0}$$

$(\mu_2)^{(6)} = (u_1)^{(6)}, (\mu_1)^{(6)} = (u_0)^{(6)}$, **if** $(\bar{u}_1)^{(6)} < (u_0)^{(6)}$ where $(u_1)^{(6)}, (\bar{u}_1)^{(6)}$ are defined respectively

Then the solution of CONCATENATED SYSTEM OF GLOBAL EQUATIONS satisfies the inequalities

$$G_{32}^0 e^{((S_1)^{(6)} - (p_{32})^{(6)})t} \leq G_{32}(t) \leq G_{32}^0 e^{(S_1)^{(6)}t}$$

where $(p_i)^{(6)}$ is defined

$$\frac{1}{(m_1)^{(6)}} G_{32}^0 e^{((S_1)^{(6)} - (p_{32})^{(6)})t} \leq G_{32}(t) \leq \frac{1}{(m_2)^{(6)}} G_{32}^0 e^{(S_1)^{(6)}t}$$

$$\left(\frac{(a_{34})^{(6)} G_{32}^0}{(m_1)^{(6)} ((S_1)^{(6)} - (p_{32})^{(6)} - (S_2)^{(6)})} \left[e^{((S_1)^{(6)} - (p_{32})^{(6)})t} - e^{-(S_2)^{(6)}t} \right] + G_{34}^0 e^{-(S_2)^{(6)}t} \right) \leq G_{34}(t) \leq (a_{34})^{(6)} G_{32}^0 (m_2)^{(6)} (S_1)^{(6)} - (a_{34})^{(6)} G_{32}^0 (S_1)^{(6)} t - e^{-(a_{34})^{(6)} t} + G_{34}^0 e^{-(a_{34})^{(6)} t}$$

$$T_{32}^0 e^{(R_1)^{(6)}t} \leq T_{32}(t) \leq T_{32}^0 e^{((R_1)^{(6)} + (r_{32})^{(6)})t}$$

$$\frac{1}{(\mu_1)^{(6)}} T_{32}^0 e^{(R_1)^{(6)}t} \leq T_{32}(t) \leq \frac{1}{(\mu_2)^{(6)}} T_{32}^0 e^{((R_1)^{(6)} + (r_{32})^{(6)})t}$$

$$\frac{(b_{34})^{(6)} T_{32}^0}{(\mu_1)^{(6)} ((R_1)^{(6)} - (b_{34})^{(6)})} \left[e^{(R_1)^{(6)}t} - e^{-(b_{34})^{(6)}t} \right] + T_{34}^0 e^{-(b_{34})^{(6)}t} \leq T_{34}(t) \leq$$

$$\frac{(a_{34})^{(6)} T_{32}^0}{(\mu_2)^{(6)} ((R_1)^{(6)} + (r_{32})^{(6)} + (R_2)^{(6)})} \left[e^{((R_1)^{(6)} + (r_{32})^{(6)})t} - e^{-(R_2)^{(6)}t} \right] + T_{34}^0 e^{-(R_2)^{(6)}t}$$

Definition of $(S_1)^{(6)}, (S_2)^{(6)}, (R_1)^{(6)}, (R_2)^{(6)}$:-

Where $(S_1)^{(6)} = (a_{32})^{(6)}(m_2)^{(6)} - (a'_{32})^{(6)}$

$$(S_2)^{(6)} = (a_{34})^{(6)} - (p_{34})^{(6)}$$

$$(R_1)^{(6)} = (b_{32})^{(6)}(\mu_2)^{(6)} - (b'_{32})^{(6)}$$

$$(R_2)^{(6)} = (b_{34})^{(6)} - (r_{34})^{(6)}$$

Proof : From GLOBAL EQUATIONS we obtain

$$\frac{dv^{(1)}}{dt} = (a_{13})^{(1)} - \left((a'_{13})^{(1)} - (a'_{14})^{(1)} + (a''_{13})^{(1)}(T_{14}, t) \right) - (a''_{14})^{(1)}(T_{14}, t)v^{(1)} - (a_{14})^{(1)}v^{(1)}$$

Definition of $v^{(1)}$:- $v^{(1)} = \frac{G_{13}}{G_{14}}$

It follows

$$- \left((a_{14})^{(1)}(v^{(1)})^2 + (\sigma_2)^{(1)}v^{(1)} - (a_{13})^{(1)} \right) \leq \frac{dv^{(1)}}{dt} \leq - \left((a_{14})^{(1)}(v^{(1)})^2 + (\sigma_1)^{(1)}v^{(1)} - (a_{13})^{(1)} \right)$$

From which one obtains

Definition of $(\bar{v}_1)^{(1)}, (v_0)^{(1)}$:-

(a) For $0 < (v_0)^{(1)} = \frac{G_{13}^0}{G_{14}^0} < (v_1)^{(1)} < (\bar{v}_1)^{(1)}$

$$v^{(1)}(t) \geq \frac{(v_1)^{(1)} + (C)^{(1)}(v_2)^{(1)} e^{[-(a_{14})^{(1)}(v_1)^{(1)} - (v_0)^{(1)}]t}}{1 + (C)^{(1)} e^{[-(a_{14})^{(1)}(v_1)^{(1)} - (v_0)^{(1)}]t}}, \quad (C)^{(1)} = \frac{(v_1)^{(1)} - (v_0)^{(1)}}{(v_0)^{(1)} - (v_2)^{(1)}}$$

it follows $(v_0)^{(1)} \leq v^{(1)}(t) \leq (v_1)^{(1)}$

In the same manner, we get

$$v^{(1)}(t) \leq \frac{(\bar{v}_1)^{(1)} + (\bar{C})^{(1)}(\bar{v}_2)^{(1)} e^{[-(a_{14})^{(1)}(\bar{v}_1)^{(1)} - (\bar{v}_2)^{(1)}]t}}{1 + (\bar{C})^{(1)} e^{[-(a_{14})^{(1)}(\bar{v}_1)^{(1)} - (\bar{v}_2)^{(1)}]t}}, \quad (\bar{C})^{(1)} = \frac{(\bar{v}_1)^{(1)} - (v_0)^{(1)}}{(v_0)^{(1)} - (\bar{v}_2)^{(1)}}$$

From which we deduce $(v_0)^{(1)} \leq v^{(1)}(t) \leq (\bar{v}_1)^{(1)}$

(b) If $0 < (v_1)^{(1)} < (v_0)^{(1)} = \frac{G_{13}^0}{G_{14}^0} < (\bar{v}_1)^{(1)}$ we find like in the previous case,

$$(v_1)^{(1)} \leq \frac{(v_1)^{(1)} + (C)^{(1)}(v_2)^{(1)} e^{[-(a_{14})^{(1)}(v_1)^{(1)} - (v_2)^{(1)}]t}}{1 + (C)^{(1)} e^{[-(a_{14})^{(1)}(v_1)^{(1)} - (v_2)^{(1)}]t}} \leq v^{(1)}(t) \leq \frac{(\bar{v}_1)^{(1)} + (C)^{(1)}(\bar{v}_2)^{(1)} e^{[-(a_{14})^{(1)}(\bar{v}_1)^{(1)} - (\bar{v}_2)^{(1)}]t}}{1 + (C)^{(1)} e^{[-(a_{14})^{(1)}(\bar{v}_1)^{(1)} - (\bar{v}_2)^{(1)}]t}} \leq (\bar{v}_1)^{(1)}$$

(c) If $0 < (v_1)^{(1)} \leq (\bar{v}_1)^{(1)} \leq (v_0)^{(1)} = \frac{G_{13}^0}{G_{14}^0}$, we obtain

$$(v_1)^{(1)} \leq v^{(1)}(t) \leq \frac{(\bar{v}_1)^{(1)} + (C)^{(1)}(\bar{v}_2)^{(1)} e^{[-(a_{14})^{(1)}(\bar{v}_1)^{(1)} - (\bar{v}_2)^{(1)}]t}}{1 + (C)^{(1)} e^{[-(a_{14})^{(1)}(\bar{v}_1)^{(1)} - (\bar{v}_2)^{(1)}]t}} \leq (v_0)^{(1)}$$

And so with the notation of the first part of condition (c), we have

Definition of $v^{(1)}(t)$:-

$$(m_2)^{(1)} \leq v^{(1)}(t) \leq (m_1)^{(1)}, \quad v^{(1)}(t) = \frac{G_{13}(t)}{G_{14}(t)}$$

In a completely analogous way, we obtain

Definition of $u^{(1)}(t)$:-

$$(\mu_2)^{(1)} \leq u^{(1)}(t) \leq (\mu_1)^{(1)}, \quad u^{(1)}(t) = \frac{T_{13}(t)}{T_{14}(t)}$$

Now, using this result and replacing it in CONCATENATED GLOBAL EQUATIONS we get easily the result stated in the theorem.

Particular case :

If $(a_{13}^{(1)}) = (a_{14}^{(1)})$, then $(\sigma_1)^{(1)} = (\sigma_2)^{(1)}$ and in this case $(v_1)^{(1)} = (\bar{v}_1)^{(1)}$ if in addition $(v_0)^{(1)} = (v_1)^{(1)}$ then $v^{(1)}(t) = (v_0)^{(1)}$ and as a consequence $G_{13}(t) = (v_0)^{(1)}G_{14}(t)$ this also defines $(v_0)^{(1)}$ for the special case

Analogously if $(b_{13}^{(1)}) = (b_{14}^{(1)})$, then $(\tau_1)^{(1)} = (\tau_2)^{(1)}$ and then

$(u_1)^{(1)} = (\bar{u}_1)^{(1)}$ if in addition $(u_0)^{(1)} = (u_1)^{(1)}$ then $T_{13}(t) = (u_0)^{(1)}T_{14}(t)$ This is an important consequence of the relation between $(v_1)^{(1)}$ and $(\bar{v}_1)^{(1)}$, and definition of $(u_0)^{(1)}$.

From CONCATENATED SYSTEM OF GLOBAL EQUATIONS we obtain

$$\frac{dv^{(2)}}{dt} = (a_{16})^{(2)} - \left((a'_{16})^{(2)} - (a'_{17})^{(2)} + (a''_{16})^{(2)}(T_{17}, t) \right) - (a''_{17})^{(2)}(T_{17}, t)v^{(2)} - (a_{17})^{(2)}v^{(2)}$$

Definition of $v^{(2)}$:-

$$v^{(2)} = \frac{G_{16}}{G_{17}}$$

It follows

$$- \left((a_{17})^{(2)}(v^{(2)})^2 + (\sigma_2)^{(2)}v^{(2)} - (a_{16})^{(2)} \right) \leq \frac{dv^{(2)}}{dt} \leq - \left((a_{17})^{(2)}(v^{(2)})^2 + (\sigma_1)^{(2)}v^{(2)} - (a_{16})^{(2)} \right)$$

From which one obtains

Definition of $(\bar{v}_1)^{(2)}, (v_0)^{(2)}$:-

(d) For $0 < (v_0)^{(2)} = \frac{G_{16}^0}{G_{17}^0} < (v_1)^{(2)} < (\bar{v}_1)^{(2)}$

$$v^{(2)}(t) \geq \frac{(v_1)^{(2)} + (C)^{(2)}(v_2)^{(2)} e^{[-(a_{17})^{(2)}(v_1)^{(2)} - (v_0)^{(2)}]t}}{1 + (C)^{(2)} e^{[-(a_{17})^{(2)}(v_1)^{(2)} - (v_0)^{(2)}]t}}, \quad (C)^{(2)} = \frac{(v_1)^{(2)} - (v_0)^{(2)}}{(v_0)^{(2)} - (v_2)^{(2)}}$$

it follows $(v_0)^{(2)} \leq v^{(2)}(t) \leq (v_1)^{(2)}$

In the same manner, we get

$$v^{(2)}(t) \leq \frac{(\bar{v}_1)^{(2)} + (\bar{C})^{(2)}(\bar{v}_2)^{(2)} e^{[-(a_{17})^{(2)}(\bar{v}_1)^{(2)} - (\bar{v}_2)^{(2)}]t}}{1 + (\bar{C})^{(2)} e^{[-(a_{17})^{(2)}(\bar{v}_1)^{(2)} - (\bar{v}_2)^{(2)}]t}}, \quad (\bar{C})^{(2)} = \frac{(\bar{v}_1)^{(2)} - (v_0)^{(2)}}{(v_0)^{(2)} - (\bar{v}_2)^{(2)}}$$

From which we deduce $(v_0)^{(2)} \leq v^{(2)}(t) \leq (\bar{v}_1)^{(2)}$

(e) If $0 < (v_1)^{(2)} < (v_0)^{(2)} = \frac{G_{16}^0}{G_{17}^0} < (\bar{v}_1)^{(2)}$ we find like in the previous case,

$$(v_1)^{(2)} \leq \frac{(v_1)^{(2)} + (C)^{(2)}(v_2)^{(2)} e^{[-(a_{17})^{(2)}(v_1)^{(2)} - (v_2)^{(2)}]t}}{1 + (C)^{(2)} e^{[-(a_{17})^{(2)}(v_1)^{(2)} - (v_2)^{(2)}]t}} \leq v^{(2)}(t) \leq \frac{(\bar{v}_1)^{(2)} + (\bar{C})^{(2)}(\bar{v}_2)^{(2)} e^{[-(a_{17})^{(2)}(\bar{v}_1)^{(2)} - (\bar{v}_2)^{(2)}]t}}{1 + (\bar{C})^{(2)} e^{[-(a_{17})^{(2)}(\bar{v}_1)^{(2)} - (\bar{v}_2)^{(2)}]t}} \leq (\bar{v}_1)^{(2)}$$

(f) If $0 < (v_1)^{(2)} \leq (\bar{v}_1)^{(2)} \leq (v_0)^{(2)} = \frac{G_{16}^0}{G_{17}^0}$, we obtain

$$(v_1)^{(2)} \leq v^{(2)}(t) \leq \frac{(\bar{v}_1)^{(2)} + (\bar{C})^{(2)}(\bar{v}_2)^{(2)} e^{[-(a_{17})^{(2)}(\bar{v}_1)^{(2)} - (\bar{v}_2)^{(2)}]t}}{1 + (\bar{C})^{(2)} e^{[-(a_{17})^{(2)}(\bar{v}_1)^{(2)} - (\bar{v}_2)^{(2)}]t}} \leq (v_0)^{(2)}$$

And so with the notation of the first part of condition (c), we have

Definition of $v^{(2)}(t)$:-

$$(m_2)^{(2)} \leq v^{(2)}(t) \leq (m_1)^{(2)}, \quad v^{(2)}(t) = \frac{G_{16}(t)}{G_{17}(t)}$$

In a completely analogous way, we obtain

Definition of $u^{(2)}(t)$:-

$$(\mu_2)^{(2)} \leq u^{(2)}(t) \leq (\mu_1)^{(2)}, \quad u^{(2)}(t) = \frac{T_{16}(t)}{T_{17}(t)}$$

Now, using this result and replacing it in CONCATENATED SYSTEM OF GLOBAL EQUATIONS we get easily the result stated in the theorem.

Particular case :

If $(a''_{16})^{(2)} = (a''_{17})^{(2)}$, then $(\sigma_1)^{(2)} = (\sigma_2)^{(2)}$ and in this case $(v_1)^{(2)} = (\bar{v}_1)^{(2)}$ if in addition $(v_0)^{(2)} = (v_1)^{(2)}$ then $v^{(2)}(t) = (v_0)^{(2)}$ and as a consequence $G_{16}(t) = (v_0)^{(2)}G_{17}(t)$

Analogously if $(b''_{16})^{(2)} = (b''_{17})^{(2)}$, then $(\tau_1)^{(2)} = (\tau_2)^{(2)}$ and then

$(u_1)^{(2)} = (\bar{u}_1)^{(2)}$ if in addition $(u_0)^{(2)} = (u_1)^{(2)}$ then $T_{16}(t) = (u_0)^{(2)}T_{17}(t)$ This is an important consequence of the relation between $(v_1)^{(2)}$ and $(\bar{v}_1)^{(2)}$

: From CONCATENATED GLOBAL EQUATIONS we obtain

$$\frac{dv^{(3)}}{dt} = (a_{20})^{(3)} - \left((a'_{20})^{(3)} - (a'_{21})^{(3)} + (a''_{20})^{(3)}(T_{21}, t) \right) - (a''_{21})^{(3)}(T_{21}, t)v^{(3)} - (a_{21})^{(3)}v^{(3)}$$

Definition of $v^{(3)}$:-

$$v^{(3)} = \frac{G_{20}}{G_{21}}$$

It follows

$$- \left((a_{21})^{(3)}(v^{(3)})^2 + (\sigma_2)^{(3)}v^{(3)} - (a_{20})^{(3)} \right) \leq \frac{dv^{(3)}}{dt} \leq - \left((a_{21})^{(3)}(v^{(3)})^2 + (\sigma_1)^{(3)}v^{(3)} - (a_{20})^{(3)} \right)$$

From which one obtains

(a) For $0 < (v_0)^{(3)} = \frac{G_{20}^0}{G_{21}^0} < (v_1)^{(3)} < (\bar{v}_1)^{(3)}$

$$v^{(3)}(t) \geq \frac{(v_1)^{(3)} + (C)^{(3)}(v_2)^{(3)} e^{[-(a_{21})^{(3)}((v_1)^{(3)} - (v_0)^{(3)})t]}}{1 + (C)^{(3)} e^{[-(a_{21})^{(3)}((v_1)^{(3)} - (v_0)^{(3)})t]}} , \quad (C)^{(3)} = \frac{(v_1)^{(3)} - (v_0)^{(3)}}{(v_0)^{(3)} - (v_2)^{(3)}}$$

it follows $(v_0)^{(3)} \leq v^{(3)}(t) \leq (v_1)^{(3)}$

In the same manner, we get

$$v^{(3)}(t) \leq \frac{(\bar{v}_1)^{(3)} + (\bar{C})^{(3)}(\bar{v}_2)^{(3)} e^{[-(a_{21})^{(3)}((\bar{v}_1)^{(3)} - (\bar{v}_2)^{(3)})t]}}{1 + (\bar{C})^{(3)} e^{[-(a_{21})^{(3)}((\bar{v}_1)^{(3)} - (\bar{v}_2)^{(3)})t]}} , \quad (\bar{C})^{(3)} = \frac{(\bar{v}_1)^{(3)} - (v_0)^{(3)}}{(v_0)^{(3)} - (\bar{v}_2)^{(3)}}$$

Definition of $(\bar{v}_1)^{(3)}$:-

From which we deduce $(v_0)^{(3)} \leq v^{(3)}(t) \leq (\bar{v}_1)^{(3)}$

(b) If $0 < (v_1)^{(3)} < (v_0)^{(3)} = \frac{G_{20}^0}{G_{21}^0} < (\bar{v}_1)^{(3)}$ we find like in the previous case,

$$(v_1)^{(3)} \leq \frac{(v_1)^{(3)} + (C)^{(3)}(v_2)^{(3)} e^{[-(a_{21})^{(3)}((v_1)^{(3)} - (v_2)^{(3)})t]}}{1 + (C)^{(3)} e^{[-(a_{21})^{(3)}((v_1)^{(3)} - (v_2)^{(3)})t]}} \leq v^{(3)}(t) \leq$$

$$\frac{(\bar{v}_1)^{(3)} + (\bar{C})^{(3)}(\bar{v}_2)^{(3)} e^{[-(a_{21})^{(3)}((\bar{v}_1)^{(3)} - (\bar{v}_2)^{(3)})t]}}{1 + (\bar{C})^{(3)} e^{[-(a_{21})^{(3)}((\bar{v}_1)^{(3)} - (\bar{v}_2)^{(3)})t]}} \leq (\bar{v}_1)^{(3)}$$

(c) If $0 < (v_1)^{(3)} \leq (\bar{v}_1)^{(3)} \leq (v_0)^{(3)} = \frac{G_{20}^0}{G_{21}^0}$, we obtain

$$(v_1)^{(3)} \leq v^{(3)}(t) \leq \frac{(\bar{v}_1)^{(3)} + (\bar{C})^{(3)}(\bar{v}_2)^{(3)} e^{[-(a_{21})^{(3)}((\bar{v}_1)^{(3)} - (\bar{v}_2)^{(3)})t]}}{1 + (\bar{C})^{(3)} e^{[-(a_{21})^{(3)}((\bar{v}_1)^{(3)} - (\bar{v}_2)^{(3)})t]}} \leq (v_0)^{(3)}$$

And so with the notation of the first part of condition (c), we have

Definition of $v^{(3)}(t)$:-

$$(m_2)^{(3)} \leq v^{(3)}(t) \leq (m_1)^{(3)}, \quad v^{(3)}(t) = \frac{G_{20}(t)}{G_{21}(t)}$$

In a completely analogous way, we obtain

Definition of $u^{(3)}(t)$:-

$$(\mu_2)^{(3)} \leq u^{(3)}(t) \leq (\mu_1)^{(3)}, \quad u^{(3)}(t) = \frac{T_{20}(t)}{T_{21}(t)}$$

Now, using this result and replacing it in GLOBAL EQUATIONS we get easily the result stated in the theorem.

Particular case :

If $(a''_{20})^{(3)} = (a''_{21})^{(3)}$, then $(\sigma_1)^{(3)} = (\sigma_2)^{(3)}$ and in this case $(v_1)^{(3)} = (\bar{v}_1)^{(3)}$ if in addition $(v_0)^{(3)} = (v_1)^{(3)}$ then $v^{(3)}(t) = (v_0)^{(3)}$ and as a consequence $G_{20}(t) = (v_0)^{(3)}G_{21}(t)$

Analogously if $(b''_{20})^{(3)} = (b''_{21})^{(3)}$, then $(\tau_1)^{(3)} = (\tau_2)^{(3)}$ and then

$(u_1)^{(3)} = (\bar{u}_1)^{(3)}$ if in addition $(u_0)^{(3)} = (u_1)^{(3)}$ then $T_{20}(t) = (u_0)^{(3)}T_{21}(t)$ This is an important consequence of the relation between $(v_1)^{(3)}$ and $(\bar{v}_1)^{(3)}$

: From GLOBAL EQUATIONS we obtain

$$\frac{dv^{(4)}}{dt} = (a_{24})^{(4)} - \left((a'_{24})^{(4)} - (a'_{25})^{(4)} + (a''_{24})^{(4)}(T_{25}, t) \right) - (a''_{25})^{(4)}(T_{25}, t)v^{(4)} - (a_{25})^{(4)}v^{(4)}$$

Definition of $v^{(4)}$:-
$$v^{(4)} = \frac{G_{24}}{G_{25}}$$

It follows

$$-\left((a_{25})^{(4)}(v^{(4)})^2 + (\sigma_2)^{(4)}v^{(4)} - (a_{24})^{(4)}\right) \leq \frac{dv^{(4)}}{dt} \leq -\left((a_{25})^{(4)}(v^{(4)})^2 + (\sigma_4)^{(4)}v^{(4)} - (a_{24})^{(4)}\right)$$

From which one obtains

Definition of $(\bar{v}_1)^{(4)}, (v_0)^{(4)}$:-

(d) For $0 < \frac{G_{24}^0}{G_{25}^0} < (v_1)^{(4)} < (\bar{v}_1)^{(4)}$

$$v^{(4)}(t) \geq \frac{(v_1)^{(4)} + (C)^{(4)}(v_2)^{(4)}e^{[-(a_{25})^{(4)}(v_1)^{(4)} - (v_0)^{(4)}]t}}{4 + (C)^{(4)}e^{[-(a_{25})^{(4)}(v_1)^{(4)} - (v_0)^{(4)}]t}}, \quad (C)^{(4)} = \frac{(v_1)^{(4)} - (v_0)^{(4)}}{(v_0)^{(4)} - (v_2)^{(4)}}$$

it follows $(v_0)^{(4)} \leq v^{(4)}(t) \leq (v_1)^{(4)}$

In the same manner, we get

$$v^{(4)}(t) \leq \frac{(\bar{v}_1)^{(4)} + (\bar{C})^{(4)}(\bar{v}_2)^{(4)}e^{[-(a_{25})^{(4)}(\bar{v}_1)^{(4)} - (\bar{v}_2)^{(4)}]t}}{4 + (\bar{C})^{(4)}e^{[-(a_{25})^{(4)}(\bar{v}_1)^{(4)} - (\bar{v}_2)^{(4)}]t}}, \quad (\bar{C})^{(4)} = \frac{(\bar{v}_1)^{(4)} - (v_0)^{(4)}}{(v_0)^{(4)} - (\bar{v}_2)^{(4)}}$$

From which we deduce $(v_0)^{(4)} \leq v^{(4)}(t) \leq (\bar{v}_1)^{(4)}$

(e) If $0 < (v_1)^{(4)} < (v_0)^{(4)} = \frac{G_{24}^0}{G_{25}^0} < (\bar{v}_1)^{(4)}$ we find like in the previous case,

$$(v_1)^{(4)} \leq \frac{(v_1)^{(4)} + (C)^{(4)}(v_2)^{(4)}e^{[-(a_{25})^{(4)}(v_1)^{(4)} - (v_2)^{(4)}]t}}{1 + (C)^{(4)}e^{[-(a_{25})^{(4)}(v_1)^{(4)} - (v_2)^{(4)}]t}} \leq v^{(4)}(t) \leq \frac{(\bar{v}_1)^{(4)} + (\bar{C})^{(4)}(\bar{v}_2)^{(4)}e^{[-(a_{25})^{(4)}(\bar{v}_1)^{(4)} - (\bar{v}_2)^{(4)}]t}}{1 + (\bar{C})^{(4)}e^{[-(a_{25})^{(4)}(\bar{v}_1)^{(4)} - (\bar{v}_2)^{(4)}]t}} \leq (\bar{v}_1)^{(4)}$$

(f) If $0 < (v_1)^{(4)} \leq (\bar{v}_1)^{(4)} \leq \frac{G_{24}^0}{G_{25}^0}$, we obtain

$$(v_1)^{(4)} \leq v^{(4)}(t) \leq \frac{(\bar{v}_1)^{(4)} + (\bar{C})^{(4)}(\bar{v}_2)^{(4)}e^{[-(a_{25})^{(4)}(\bar{v}_1)^{(4)} - (\bar{v}_2)^{(4)}]t}}{1 + (\bar{C})^{(4)}e^{[-(a_{25})^{(4)}(\bar{v}_1)^{(4)} - (\bar{v}_2)^{(4)}]t}} \leq (v_0)^{(4)}$$

And so with the notation of the first part of condition (c), we have

Definition of $v^{(4)}(t)$:-

$$(m_2)^{(4)} \leq v^{(4)}(t) \leq (m_1)^{(4)}, \quad v^{(4)}(t) = \frac{G_{24}(t)}{G_{25}(t)}$$

In a completely analogous way, we obtain

Definition of $u^{(4)}(t)$:-

$$(\mu_2)^{(4)} \leq u^{(4)}(t) \leq (\mu_1)^{(4)}, \quad u^{(4)}(t) = \frac{T_{24}(t)}{T_{25}(t)}$$

Now, using this result and replacing it in GLOBAL EQUATIONS we get easily the result stated in the theorem.

Particular case :

If $(a_{24}^{(4)})'' = (a_{25}^{(4)})''$, then $(\sigma_1)^{(4)} = (\sigma_2)^{(4)}$ and in this case $(v_1)^{(4)} = (\bar{v}_1)^{(4)}$ if in addition $(v_0)^{(4)} = (v_1)^{(4)}$ then $v^{(4)}(t) = (v_0)^{(4)}$ and as a consequence $G_{24}(t) = (v_0)^{(4)}G_{25}(t)$ **this also defines $(v_0)^{(4)}$ for the special case.**

Analogously if $(b_{24}^{(4)})'' = (b_{25}^{(4)})''$, then $(\tau_1)^{(4)} = (\tau_2)^{(4)}$ and then

$(u_1)^{(4)} = (\bar{u}_4)^{(4)}$ if in addition $(u_0)^{(4)} = (u_1)^{(4)}$ then $T_{24}(t) = (u_0)^{(4)}T_{25}(t)$ This is an important consequence of the relation between $(v_1)^{(4)}$ and $(\bar{v}_1)^{(4)}$, **and definition of $(u_0)^{(4)}$.**

From GLOBAL EQUATIONS we obtain

$$\frac{dv^{(5)}}{dt} = (a_{28})^{(5)} - \left((a'_{28})^{(5)} - (a'_{29})^{(5)} + (a''_{28})^{(5)}(T_{29}, t) \right) - (a''_{29})^{(5)}(T_{29}, t)v^{(5)} - (a_{29})^{(5)}v^{(5)}$$

Definition of $v^{(5)}$:-
$$v^{(5)} = \frac{G_{28}}{G_{29}}$$

It follows

$$-\left((a_{29})^{(5)}(v^{(5)})^2 + (\sigma_2)^{(5)}v^{(5)} - (a_{28})^{(5)}\right) \leq \frac{dv^{(5)}}{dt} \leq -\left((a_{29})^{(5)}(v^{(5)})^2 + (\sigma_1)^{(5)}v^{(5)} - (a_{28})^{(5)}\right)$$

From which one obtains

Definition of $(\bar{v}_1)^{(5)}, (v_0)^{(5)}$:-

(g) For $0 < \frac{G_{28}^0}{G_{29}^0} < (v_1)^{(5)} < (\bar{v}_1)^{(5)}$

$$v^{(5)}(t) \geq \frac{(v_1)^{(5)} + (C)^{(5)}(v_2)^{(5)}e^{[-(a_{29})^{(5)}(v_1)^{(5)} - (v_0)^{(5)}]t}}{5 + (C)^{(5)}e^{[-(a_{29})^{(5)}(v_1)^{(5)} - (v_0)^{(5)}]t}}, \quad (C)^{(5)} = \frac{(v_1)^{(5)} - (v_0)^{(5)}}{(v_0)^{(5)} - (v_2)^{(5)}}$$

it follows $(v_0)^{(5)} \leq v^{(5)}(t) \leq (v_1)^{(5)}$

In the same manner, we get

$$v^{(5)}(t) \leq \frac{(\bar{v}_1)^{(5)} + (\bar{C})^{(5)}(\bar{v}_2)^{(5)}e^{[-(a_{29})^{(5)}(\bar{v}_1)^{(5)} - (\bar{v}_2)^{(5)}]t}}{5 + (\bar{C})^{(5)}e^{[-(a_{29})^{(5)}(\bar{v}_1)^{(5)} - (\bar{v}_2)^{(5)}]t}}, \quad (\bar{C})^{(5)} = \frac{(\bar{v}_1)^{(5)} - (v_0)^{(5)}}{(v_0)^{(5)} - (\bar{v}_2)^{(5)}}$$

From which we deduce $(v_0)^{(5)} \leq v^{(5)}(t) \leq (\bar{v}_1)^{(5)}$

(h) If $0 < (v_1)^{(5)} < (v_0)^{(5)} = \frac{G_{28}^0}{G_{29}^0} < (\bar{v}_1)^{(5)}$ we find like in the previous case,

$$(v_1)^{(5)} \leq \frac{(v_1)^{(5)} + (C)^{(5)}(v_2)^{(5)} e^{[-(a_{29})^{(5)}(v_1)^{(5)} - (v_2)^{(5)}]t}}{1 + (C)^{(5)} e^{[-(a_{29})^{(5)}(v_1)^{(5)} - (v_2)^{(5)}]t}} \leq v^{(5)}(t) \leq \frac{(\bar{v}_1)^{(5)} + (C)^{(5)}(\bar{v}_2)^{(5)} e^{[-(a_{29})^{(5)}(\bar{v}_1)^{(5)} - (\bar{v}_2)^{(5)}]t}}{1 + (C)^{(5)} e^{[-(a_{29})^{(5)}(\bar{v}_1)^{(5)} - (\bar{v}_2)^{(5)}]t}} \leq (\bar{v}_1)^{(5)}$$

(i) If $0 < (v_1)^{(5)} \leq (\bar{v}_1)^{(5)} \leq (v_0)^{(5)} = \frac{G_{28}^0}{G_{29}^0}$, we obtain

$$(v_1)^{(5)} \leq v^{(5)}(t) \leq \frac{(\bar{v}_1)^{(5)} + (C)^{(5)}(\bar{v}_2)^{(5)} e^{[-(a_{29})^{(5)}(\bar{v}_1)^{(5)} - (\bar{v}_2)^{(5)}]t}}{1 + (C)^{(5)} e^{[-(a_{29})^{(5)}(\bar{v}_1)^{(5)} - (\bar{v}_2)^{(5)}]t}} \leq (v_0)^{(5)}$$

And so with the notation of the first part of condition (c), we have

Definition of $v^{(5)}(t)$:-

$$(m_2)^{(5)} \leq v^{(5)}(t) \leq (m_1)^{(5)}, \quad v^{(5)}(t) = \frac{G_{28}(t)}{G_{29}(t)}$$

In a completely analogous way, we obtain

Definition of $u^{(5)}(t)$:-

$$(\mu_2)^{(5)} \leq u^{(5)}(t) \leq (\mu_1)^{(5)}, \quad u^{(5)}(t) = \frac{T_{28}(t)}{T_{29}(t)}$$

Now, using this result and replacing it in CONCATENATED GOVERNING EQUATIONS OF THE GLOBAL SYSTEM we get easily the result stated in the theorem.

Particular case :

If $(a_{28}^{''})^{(5)} = (a_{29}^{''})^{(5)}$, then $(\sigma_1)^{(5)} = (\sigma_2)^{(5)}$ and in this case $(v_1)^{(5)} = (\bar{v}_1)^{(5)}$ if in addition $(v_0)^{(5)} = (v_5)^{(5)}$ then $v^{(5)}(t) = (v_0)^{(5)}$ and as a consequence $G_{28}(t) = (v_0)^{(5)}G_{29}(t)$ **this also defines $(v_0)^{(5)}$ for the special case .**

Analogously if $(b_{28}^{''})^{(5)} = (b_{29}^{''})^{(5)}$, then $(\tau_1)^{(5)} = (\tau_2)^{(5)}$ and then

$(u_1)^{(5)} = (\bar{u}_1)^{(5)}$ if in addition $(u_0)^{(5)} = (u_1)^{(5)}$ then $T_{28}(t) = (u_0)^{(5)}T_{29}(t)$ This is an important consequence of the relation between $(v_1)^{(5)}$ and $(\bar{v}_1)^{(5)}$, **and definition of $(u_0)^{(5)}$.**

From GLOBAL EQUATIONS we obtain

$$\frac{dv^{(6)}}{dt} = (a_{32})^{(6)} - \left((a_{32}')^{(6)} - (a_{33}')^{(6)} + (a_{32}'')^{(6)}(T_{33}, t) \right) - (a_{33}'')^{(6)}(T_{33}, t)v^{(6)} - (a_{33})^{(6)}v^{(6)}$$

Definition of $v^{(6)}$:- $v^{(6)} = \frac{G_{32}}{G_{33}}$

It follows

$$- \left((a_{33})^{(6)}(v^{(6)})^2 + (\sigma_2)^{(6)}v^{(6)} - (a_{32})^{(6)} \right) \leq \frac{dv^{(6)}}{dt} \leq - \left((a_{33})^{(6)}(v^{(6)})^2 + (\sigma_1)^{(6)}v^{(6)} - (a_{32})^{(6)} \right)$$

From which one obtains

Definition of $(\bar{v}_1)^{(6)}, (v_0)^{(6)}$:-

(j) For $0 < (v_0)^{(6)} = \frac{G_{32}^0}{G_{33}^0} < (v_1)^{(6)} < (\bar{v}_1)^{(6)}$

$$v^{(6)}(t) \geq \frac{(v_1)^{(6)} + (C)^{(6)}(v_2)^{(6)} e^{[-(a_{33})^{(6)}(v_1)^{(6)} - (v_0)^{(6)}]t}}{1 + (C)^{(6)} e^{[-(a_{33})^{(6)}(v_1)^{(6)} - (v_0)^{(6)}]t}}, \quad (C)^{(6)} = \frac{(v_1)^{(6)} - (v_0)^{(6)}}{(v_0)^{(6)} - (v_2)^{(6)}}$$

it follows $(v_0)^{(6)} \leq v^{(6)}(t) \leq (v_1)^{(6)}$

In the same manner, we get

$$v^{(6)}(t) \leq \frac{(\bar{v}_1)^{(6)} + (\bar{C})^{(6)}(\bar{v}_2)^{(6)} e^{[-(a_{33})^{(6)}(\bar{v}_1)^{(6)} - (\bar{v}_2)^{(6)}]t}}{1 + (\bar{C})^{(6)} e^{[-(a_{33})^{(6)}(\bar{v}_1)^{(6)} - (\bar{v}_2)^{(6)}]t}}, \quad (\bar{C})^{(6)} = \frac{(\bar{v}_1)^{(6)} - (v_0)^{(6)}}{(v_0)^{(6)} - (\bar{v}_2)^{(6)}}$$

From which we deduce $(v_0)^{(6)} \leq v^{(6)}(t) \leq (\bar{v}_1)^{(6)}$

(k) If $0 < (v_1)^{(6)} < (v_0)^{(6)} = \frac{G_{32}^0}{G_{33}^0} < (\bar{v}_1)^{(6)}$ we find like in the previous case,

$$(v_1)^{(6)} \leq \frac{(v_1)^{(6)} + (C)^{(6)}(v_2)^{(6)} e^{[-(a_{33})^{(6)}(v_1)^{(6)} - (v_2)^{(6)}]t}}{1 + (C)^{(6)} e^{[-(a_{33})^{(6)}(v_1)^{(6)} - (v_2)^{(6)}]t}} \leq v^{(6)}(t) \leq \frac{(\bar{v}_1)^{(6)} + (C)^{(6)}(\bar{v}_2)^{(6)} e^{[-(a_{33})^{(6)}(\bar{v}_1)^{(6)} - (\bar{v}_2)^{(6)}]t}}{1 + (C)^{(6)} e^{[-(a_{33})^{(6)}(\bar{v}_1)^{(6)} - (\bar{v}_2)^{(6)}]t}} \leq (\bar{v}_1)^{(6)}$$

(l) If $0 < (v_1)^{(6)} \leq (\bar{v}_1)^{(6)} \leq (v_0)^{(6)} = \frac{G_{32}^0}{G_{33}^0}$, we obtain

$$(v_1)^{(6)} \leq v^{(6)}(t) \leq \frac{(\bar{v}_1)^{(6)} + (\bar{C})^{(6)}(\bar{v}_2)^{(6)} e^{[-(a_{33})^{(6)}(\bar{v}_1)^{(6)} - (\bar{v}_2)^{(6)}]t}}{1 + (\bar{C})^{(6)} e^{[-(a_{33})^{(6)}(\bar{v}_1)^{(6)} - (\bar{v}_2)^{(6)}]t}} \leq (v_0)^{(6)}$$

And so with the notation of the first part of condition (c), we have

Definition of $v^{(6)}(t)$:-

$$(m_2)^{(6)} \leq v^{(6)}(t) \leq (m_1)^{(6)}, \quad v^{(6)}(t) = \frac{G_{32}(t)}{G_{33}(t)}$$

In a completely analogous way, we obtain

Definition of $u^{(6)}(t)$:-

$$(\mu_2)^{(6)} \leq u^{(6)}(t) \leq (\mu_1)^{(6)}, \quad u^{(6)}(t) = \frac{T_{32}(t)}{T_{33}(t)}$$

Now, using this result and replacing it in GLOBAL EQUATIONS we get easily the result stated in the theorem.

Particular case :

If $(a''_{32})^{(6)} = (a''_{33})^{(6)}$, then $(\sigma_1)^{(6)} = (\sigma_2)^{(6)}$ and in this case $(v_1)^{(6)} = (\bar{v}_1)^{(6)}$ if in addition $(v_0)^{(6)} = (v_1)^{(6)}$ then $v^{(6)}(t) = (v_0)^{(6)}$ and as a consequence $G_{32}(t) = (v_0)^{(6)}G_{33}(t)$ **this also defines $(v_0)^{(6)}$ for the special case .**

Analogously if $(b''_{32})^{(6)} = (b''_{33})^{(6)}$, then $(\tau_1)^{(6)} = (\tau_2)^{(6)}$ and then

$(u_1)^{(6)} = (\bar{u}_1)^{(6)}$ if in addition $(u_0)^{(6)} = (u_1)^{(6)}$ then $T_{32}(t) = (u_0)^{(6)}T_{33}(t)$ This is an important consequence of the relation between $(v_1)^{(6)}$ and $(\bar{v}_1)^{(6)}$, **and definition of $(u_0)^{(6)}$.**

We can prove the following

Theorem 3: If $(a'_i)^{(1)}$ and $(b'_i)^{(1)}$ are independent on t , and the conditions (with the notations 25,26,27,28)

$$(a'_{13})^{(1)}(a'_{14})^{(1)} - (a_{13})^{(1)}(a_{14})^{(1)} < 0$$

$$(a'_{13})^{(1)}(a'_{14})^{(1)} - (a_{13})^{(1)}(a_{14})^{(1)} + (a_{13})^{(1)}(p_{13})^{(1)} + (a'_{14})^{(1)}(p_{14})^{(1)} + (p_{13})^{(1)}(p_{14})^{(1)} > 0$$

$$(b'_{13})^{(1)}(b'_{14})^{(1)} - (b_{13})^{(1)}(b_{14})^{(1)} > 0,$$

$$(b'_{13})^{(1)}(b'_{14})^{(1)} - (b_{13})^{(1)}(b_{14})^{(1)} - (b'_{13})^{(1)}(r_{14})^{(1)} - (b'_{14})^{(1)}(r_{14})^{(1)} + (r_{13})^{(1)}(r_{14})^{(1)} < 0$$

with $(p_{13})^{(1)}, (r_{14})^{(1)}$ as defined are satisfied, then the system

If $(a''_i)^{(2)}$ and $(b''_i)^{(2)}$ are independent on t , and the conditions

$$(a'_{16})^{(2)}(a'_{17})^{(2)} - (a_{16})^{(2)}(a_{17})^{(2)} < 0$$

$$(a'_{16})^{(2)}(a'_{17})^{(2)} - (a_{16})^{(2)}(a_{17})^{(2)} + (a_{16})^{(2)}(p_{16})^{(2)} + (a'_{17})^{(2)}(p_{17})^{(2)} + (p_{16})^{(2)}(p_{17})^{(2)} > 0$$

$$(b'_{16})^{(2)}(b'_{17})^{(2)} - (b_{16})^{(2)}(b_{17})^{(2)} > 0,$$

$$(b'_{16})^{(2)}(b'_{17})^{(2)} - (b_{16})^{(2)}(b_{17})^{(2)} - (b'_{16})^{(2)}(r_{17})^{(2)} - (b'_{17})^{(2)}(r_{17})^{(2)} + (r_{16})^{(2)}(r_{17})^{(2)} < 0$$

with $(p_{16})^{(2)}, (r_{17})^{(2)}$ as defined are satisfied, then the system

If $(a''_i)^{(3)}$ and $(b''_i)^{(3)}$ are independent on t , and the conditions

$$(a'_{20})^{(3)}(a'_{21})^{(3)} - (a_{20})^{(3)}(a_{21})^{(3)} < 0$$

$$(a'_{20})^{(3)}(a'_{21})^{(3)} - (a_{20})^{(3)}(a_{21})^{(3)} + (a_{20})^{(3)}(p_{20})^{(3)} + (a'_{21})^{(3)}(p_{21})^{(3)} + (p_{20})^{(3)}(p_{21})^{(3)} > 0$$

$$(b'_{20})^{(3)}(b'_{21})^{(3)} - (b_{20})^{(3)}(b_{21})^{(3)} > 0,$$

$$(b'_{20})^{(3)}(b'_{21})^{(3)} - (b_{20})^{(3)}(b_{21})^{(3)} - (b'_{20})^{(3)}(r_{21})^{(3)} - (b'_{21})^{(3)}(r_{21})^{(3)} + (r_{20})^{(3)}(r_{21})^{(3)} < 0$$

with $(p_{20})^{(3)}, (r_{21})^{(3)}$ as defined by equation 25 are satisfied, then the system

If $(a''_i)^{(4)}$ and $(b''_i)^{(4)}$ are independent on t , and the conditions WE CAN UNMISTAKABLY PROVE THAT:

$$(a'_{24})^{(4)}(a'_{25})^{(4)} - (a_{24})^{(4)}(a_{25})^{(4)} < 0$$

$$(a'_{24})^{(4)}(a'_{25})^{(4)} - (a_{24})^{(4)}(a_{25})^{(4)} + (a_{24})^{(4)}(p_{24})^{(4)} + (a'_{25})^{(4)}(p_{25})^{(4)} + (p_{24})^{(4)}(p_{25})^{(4)} > 0$$

$$(b'_{24})^{(4)}(b'_{25})^{(4)} - (b_{24})^{(4)}(b_{25})^{(4)} > 0,$$

$$(b'_{24})^{(4)}(b'_{25})^{(4)} - (b_{24})^{(4)}(b_{25})^{(4)} - (b'_{24})^{(4)}(r_{25})^{(4)} - (b'_{25})^{(4)}(r_{25})^{(4)} + (r_{24})^{(4)}(r_{25})^{(4)} < 0$$

with $(p_{24})^{(4)}, (r_{25})^{(4)}$ as defined are satisfied, then the system

If $(a''_i)^{(5)}$ and $(b''_i)^{(5)}$ are independent on t , and the conditions

$$(a'_{28})^{(5)}(a'_{29})^{(5)} - (a_{28})^{(5)}(a_{29})^{(5)} < 0$$

$$(a'_{28})^{(5)}(a'_{29})^{(5)} - (a_{28})^{(5)}(a_{29})^{(5)} + (a_{28})^{(5)}(p_{28})^{(5)} + (a'_{29})^{(5)}(p_{29})^{(5)} + (p_{28})^{(5)}(p_{29})^{(5)} > 0$$

$$(b'_{28})^{(5)}(b'_{29})^{(5)} - (b_{28})^{(5)}(b_{29})^{(5)} > 0,$$

$$(b'_{28})^{(5)}(b'_{29})^{(5)} - (b_{28})^{(5)}(b_{29})^{(5)} - (b'_{28})^{(5)}(r_{29})^{(5)} - (b'_{29})^{(5)}(r_{29})^{(5)} + (r_{28})^{(5)}(r_{29})^{(5)} < 0$$

with $(p_{28})^{(5)}, (r_{29})^{(5)}$ as defined are satisfied, then the system

If $(a''_i)^{(6)}$ and $(b''_i)^{(6)}$ are independent on t , and the conditions

$$(a'_{32})^{(6)}(a'_{33})^{(6)} - (a_{32})^{(6)}(a_{33})^{(6)} < 0$$

$$(a'_{32})^{(6)}(a'_{33})^{(6)} - (a_{32})^{(6)}(a_{33})^{(6)} + (a_{32})^{(6)}(p_{32})^{(6)} + (a'_{33})^{(6)}(p_{33})^{(6)} + (p_{32})^{(6)}(p_{33})^{(6)} > 0$$

$$(b'_{32})^{(6)}(b'_{33})^{(6)} - (b_{32})^{(6)}(b_{33})^{(6)} > 0,$$

$$(b'_{32})^{(6)}(b'_{33})^{(6)} - (b_{32})^{(6)}(b_{33})^{(6)} - (b'_{32})^{(6)}(r_{33})^{(6)} - (b'_{33})^{(6)}(r_{33})^{(6)} + (r_{32})^{(6)}(r_{33})^{(6)} < 0$$

with $(p_{32})^{(6)}, (r_{33})^{(6)}$ as defined are satisfied, then the system

$$(a_{13})^{(1)}G_{14} - [(a'_{13})^{(1)} + (a''_{13})^{(1)}(T_{14})]G_{13} = 0$$

$$(a_{14})^{(1)}G_{13} - [(a'_{14})^{(1)} + (a''_{14})^{(1)}(T_{14})]G_{14} = 0$$

$$(a_{15})^{(1)}G_{14} - [(a'_{15})^{(1)} + (a''_{15})^{(1)}(T_{14})]G_{15} = 0$$

$$(b_{13})^{(1)}T_{14} - [(b'_{13})^{(1)} - (b''_{13})^{(1)}(G)]T_{13} = 0$$

$$(b_{14})^{(1)}T_{13} - [(b'_{14})^{(1)} - (b''_{14})^{(1)}(G)]T_{14} = 0$$

$$(b_{15})^{(1)}T_{14} - [(b'_{15})^{(1)} - (b''_{15})^{(1)}(G)]T_{15} = 0$$

has a unique positive solution, which is an equilibrium solution

$$(a_{16})^{(2)}G_{17} - [(a'_{16})^{(2)} + (a''_{16})^{(2)}(T_{17})]G_{16} = 0$$

$$(a_{17})^{(2)}G_{16} - [(a'_{17})^{(2)} + (a''_{17})^{(2)}(T_{17})]G_{17} = 0$$

$$(a_{18})^{(2)}G_{17} - [(a'_{18})^{(2)} + (a''_{18})^{(2)}(T_{17})]G_{18} = 0$$

$$(b_{16})^{(2)}T_{17} - [(b'_{16})^{(2)} - (b''_{16})^{(2)}(G_{19})]T_{16} = 0$$

$$(b_{17})^{(2)}T_{16} - [(b'_{17})^{(2)} - (b''_{17})^{(2)}(G_{19})]T_{17} = 0$$

$$(b_{18})^{(2)}T_{17} - [(b'_{18})^{(2)} - (b''_{18})^{(2)}(G_{19})]T_{18} = 0$$

has a unique positive solution , which is an equilibrium solution for THE SYSTEM

$$(a_{20})^{(3)}G_{21} - [(a'_{20})^{(3)} + (a''_{20})^{(3)}(T_{21})]G_{20} = 0$$

$$(a_{21})^{(3)}G_{20} - [(a'_{21})^{(3)} + (a''_{21})^{(3)}(T_{21})]G_{21} = 0$$

$$(a_{22})^{(3)}G_{21} - [(a'_{22})^{(3)} + (a''_{22})^{(3)}(T_{21})]G_{22} = 0$$

$$(b_{20})^{(3)}T_{21} - [(b'_{20})^{(3)} - (b''_{20})^{(3)}(G_{23})]T_{20} = 0$$

$$(b_{21})^{(3)}T_{20} - [(b'_{21})^{(3)} - (b''_{21})^{(3)}(G_{23})]T_{21} = 0$$

$$(b_{22})^{(3)}T_{21} - [(b'_{22})^{(3)} - (b''_{22})^{(3)}(G_{23})]T_{22} = 0$$

has a unique positive solution , which is an equilibrium solution for THE HOLISTIC SYSTEM

$$(a_{24})^{(4)}G_{25} - [(a'_{24})^{(4)} + (a''_{24})^{(4)}(T_{25})]G_{24} = 0$$

$$(a_{25})^{(4)}G_{24} - [(a'_{25})^{(4)} + (a''_{25})^{(4)}(T_{25})]G_{25} = 0$$

$$(a_{26})^{(4)}G_{25} - [(a'_{26})^{(4)} + (a''_{26})^{(4)}(T_{25})]G_{26} = 0$$

$$(b_{24})^{(4)}T_{25} - [(b'_{24})^{(4)} - (b''_{24})^{(4)}(G_{27})]T_{24} = 0$$

$$(b_{25})^{(4)}T_{24} - [(b'_{25})^{(4)} - (b''_{25})^{(4)}(G_{27})]T_{25} = 0$$

$$(b_{26})^{(4)}T_{25} - [(b'_{26})^{(4)} - (b''_{26})^{(4)}(G_{27})]T_{26} = 0$$

has a unique positive solution , which is an equilibrium solution for the system HOLISTIC SYSTEM

$$(a_{28})^{(5)}G_{29} - [(a'_{28})^{(5)} + (a''_{28})^{(5)}(T_{29})]G_{28} = 0$$

$$(a_{29})^{(5)}G_{28} - [(a'_{29})^{(5)} + (a''_{29})^{(5)}(T_{29})]G_{29} = 0$$

$$(a_{30})^{(5)}G_{29} - [(a'_{30})^{(5)} + (a''_{30})^{(5)}(T_{29})]G_{30} = 0$$

$$(b_{28})^{(5)}T_{29} - [(b'_{28})^{(5)} - (b''_{28})^{(5)}(G_{31})]T_{28} = 0$$

$$(b_{29})^{(5)}T_{28} - [(b'_{29})^{(5)} - (b''_{29})^{(5)}(G_{31})]T_{29} = 0$$

$$(b_{30})^{(5)}T_{29} - [(b'_{30})^{(5)} - (b''_{30})^{(5)}(G_{31})]T_{30} = 0$$

has a unique positive solution , which is an equilibrium solution for the system (HOLISTIC SYSTEM)

$$(a_{32})^{(6)}G_{33} - [(a'_{32})^{(6)} + (a''_{32})^{(6)}(T_{33})]G_{32} = 0$$

$$(a_{33})^{(6)}G_{32} - [(a'_{33})^{(6)} + (a''_{33})^{(6)}(T_{33})]G_{33} = 0$$

$$(a_{34})^{(6)}G_{33} - [(a'_{34})^{(6)} + (a''_{34})^{(6)}(T_{33})]G_{34} = 0$$

$$(b_{32})^{(6)}T_{33} - [(b'_{32})^{(6)} - (b''_{32})^{(6)}(G_{35})]T_{32} = 0$$

$$(b_{33})^{(6)}T_{32} - [(b'_{33})^{(6)} - (b''_{33})^{(6)}(G_{35})]T_{33} = 0$$

$$(b_{34})^{(6)}T_{33} - [(b'_{34})^{(6)} - (b''_{34})^{(6)}(G_{35})]T_{34} = 0$$

has a unique positive solution , which is an equilibrium solution for the system (GLOBAL)

Proof:

(a) Indeed the first two equations have a nontrivial solution G_{13}, G_{14} if

$$F(T) =$$

$$(a'_{13})^{(1)}(a'_{14})^{(1)} - (a_{13})^{(1)}(a_{14})^{(1)} + (a'_{13})^{(1)}(a''_{14})^{(1)}(T_{14}) + (a'_{14})^{(1)}(a''_{13})^{(1)}(T_{14}) + (a''_{13})^{(1)}(T_{14})(a''_{14})^{(1)}(T_{14}) = 0$$

(a) Indeed the first two equations have a nontrivial solution G_{16}, G_{17} if

$$F(T_{19}) =$$

$$(a'_{16})^{(2)}(a'_{17})^{(2)} - (a_{16})^{(2)}(a_{17})^{(2)} + (a'_{16})^{(2)}(a''_{17})^{(2)}(T_{17}) + (a'_{17})^{(2)}(a''_{16})^{(2)}(T_{17}) + (a''_{16})^{(2)}(T_{17})(a''_{17})^{(2)}(T_{17}) = 0$$

(a) Indeed the first two equations have a nontrivial solution G_{20}, G_{21} if

$$F(T_{23}) =$$

$$(a'_{20})^{(3)}(a'_{21})^{(3)} - (a_{20})^{(3)}(a_{21})^{(3)} + (a'_{20})^{(3)}(a''_{21})^{(3)}(T_{21}) + (a'_{21})^{(3)}(a''_{20})^{(3)}(T_{21}) + (a''_{20})^{(3)}(T_{21})(a''_{21})^{(3)}(T_{21}) = 0$$

(a) Indeed the first two equations have a nontrivial solution G_{24}, G_{25} if

$F(T_{27}) = (a'_{24})^{(4)}(a'_{25})^{(4)} - (a_{24})^{(4)}(a_{25})^{(4)} + (a'_{24})^{(4)}(a''_{25})^{(4)}(T_{25}) + (a'_{25})^{(4)}(a''_{24})^{(4)}(T_{25}) + (a''_{24})^{(4)}(T_{25})(a''_{25})^{(4)}(T_{25}) = 0$
 (a) Indeed the first two equations have a nontrivial solution G_{28}, G_{29} if

$F(T_{31}) = (a'_{28})^{(5)}(a'_{29})^{(5)} - (a_{28})^{(5)}(a_{29})^{(5)} + (a'_{28})^{(5)}(a''_{29})^{(5)}(T_{29}) + (a'_{29})^{(5)}(a''_{28})^{(5)}(T_{29}) + (a''_{28})^{(5)}(T_{29})(a''_{29})^{(5)}(T_{29}) = 0$
 (a) Indeed the first two equations have a nontrivial solution G_{32}, G_{33} if

$F(T_{35}) = (a'_{32})^{(6)}(a'_{33})^{(6)} - (a_{32})^{(6)}(a_{33})^{(6)} + (a'_{32})^{(6)}(a''_{33})^{(6)}(T_{33}) + (a'_{33})^{(6)}(a''_{32})^{(6)}(T_{33}) + (a''_{32})^{(6)}(T_{33})(a''_{33})^{(6)}(T_{33}) = 0$

Definition and uniqueness of T_{14}^* :-

After hypothesis $f(0) < 0, f(\infty) > 0$ and the functions $(a''_i)^{(1)}(T_{14})$ being increasing, it follows that there exists a unique T_{14}^* for which $f(T_{14}^*) = 0$. With this value, we obtain from the three first equations

$$G_{13} = \frac{(a_{13})^{(1)}G_{14}}{[(a'_{13})^{(1)} + (a''_{13})^{(1)}(T_{14}^*)]} , \quad G_{15} = \frac{(a_{15})^{(1)}G_{14}}{[(a'_{15})^{(1)} + (a''_{15})^{(1)}(T_{14}^*)]}$$

Definition and uniqueness of T_{17}^* :-

After hypothesis $f(0) < 0, f(\infty) > 0$ and the functions $(a''_i)^{(2)}(T_{17})$ being increasing, it follows that there exists a unique T_{17}^* for which $f(T_{17}^*) = 0$. With this value, we obtain from the three first equations

$$G_{16} = \frac{(a_{16})^{(2)}G_{17}}{[(a'_{16})^{(2)} + (a''_{16})^{(2)}(T_{17}^*)]} , \quad G_{18} = \frac{(a_{18})^{(2)}G_{17}}{[(a'_{18})^{(2)} + (a''_{18})^{(2)}(T_{17}^*)]}$$

Definition and uniqueness of T_{21}^* :-

After hypothesis $f(0) < 0, f(\infty) > 0$ and the functions $(a''_i)^{(1)}(T_{21})$ being increasing, it follows that there exists a unique T_{21}^* for which $f(T_{21}^*) = 0$. With this value, we obtain from the three first equations

$$G_{20} = \frac{(a_{20})^{(3)}G_{21}}{[(a'_{20})^{(3)} + (a''_{20})^{(3)}(T_{21}^*)]} , \quad G_{22} = \frac{(a_{22})^{(3)}G_{21}}{[(a'_{22})^{(3)} + (a''_{22})^{(3)}(T_{21}^*)]}$$

Definition and uniqueness of T_{25}^* :-

After hypothesis $f(0) < 0, f(\infty) > 0$ and the functions $(a''_i)^{(4)}(T_{25})$ being increasing, it follows that there exists a unique T_{25}^* for which $f(T_{25}^*) = 0$. With this value, we obtain from the three first equations

$$G_{24} = \frac{(a_{24})^{(4)}G_{25}}{[(a'_{24})^{(4)} + (a''_{24})^{(4)}(T_{25}^*)]} , \quad G_{26} = \frac{(a_{26})^{(4)}G_{25}}{[(a'_{26})^{(4)} + (a''_{26})^{(4)}(T_{25}^*)]}$$

Definition and uniqueness of T_{29}^* :-

After hypothesis $f(0) < 0, f(\infty) > 0$ and the functions $(a''_i)^{(5)}(T_{29})$ being increasing, it follows that there exists a unique T_{29}^* for which $f(T_{29}^*) = 0$. With this value, we obtain from the three first equations

$$G_{28} = \frac{(a_{28})^{(5)}G_{29}}{[(a'_{28})^{(5)} + (a''_{28})^{(5)}(T_{29}^*)]} , \quad G_{30} = \frac{(a_{30})^{(5)}G_{29}}{[(a'_{30})^{(5)} + (a''_{30})^{(5)}(T_{29}^*)]}$$

Definition and uniqueness of T_{33}^* :-

After hypothesis $f(0) < 0, f(\infty) > 0$ and the functions $(a''_i)^{(6)}(T_{33})$ being increasing, it follows that there exists a unique T_{33}^* for which $f(T_{33}^*) = 0$. With this value, we obtain from the three first equations

$$G_{32} = \frac{(a_{32})^{(6)}G_{33}}{[(a'_{32})^{(6)} + (a''_{32})^{(6)}(T_{33}^*)]} , \quad G_{34} = \frac{(a_{34})^{(6)}G_{33}}{[(a'_{34})^{(6)} + (a''_{34})^{(6)}(T_{33}^*)]}$$

(e) By the same argument, the equations (SOLUTIONALOF THE GLOBAL EQUATIONS) admit solutions G_{13}, G_{14} if

$$\varphi(G) = (b'_{13})^{(1)}(b'_{14})^{(1)} - (b_{13})^{(1)}(b_{14})^{(1)} - [(b'_{13})^{(1)}(b'_{14})^{(1)}(G) + (b'_{14})^{(1)}(b''_{13})^{(1)}(G)] + (b''_{13})^{(1)}(G)(b''_{14})^{(1)}(G) = 0$$

Where in $G(G_{13}, G_{14}, G_{15}), G_{13}, G_{15}$ must be replaced by their values. It is easy to see that φ is a decreasing function in G_{14} taking into account the hypothesis $\varphi(0) > 0, \varphi(\infty) < 0$ it follows that there exists a unique G_{14}^* such that $\varphi(G^*) = 0$

(f) By the same argument, the equations 92,93 admit solutions G_{16}, G_{17} if

$$\varphi(G_{19}) = (b'_{16})^{(2)}(b'_{17})^{(2)} - (b_{16})^{(2)}(b_{17})^{(2)} - [(b'_{16})^{(2)}(b'_{17})^{(2)}(G_{19}) + (b'_{17})^{(2)}(b''_{16})^{(2)}(G_{19})] + (b''_{16})^{(2)}(G_{19})(b''_{17})^{(2)}(G_{19}) = 0$$

Where in $(G_{19})(G_{16}, G_{17}, G_{18}), G_{16}, G_{18}$ must be replaced by their values from 96. It is easy to see that φ is a decreasing function in G_{17} taking into account the hypothesis $\varphi(0) > 0, \varphi(\infty) < 0$ it follows that there exists a unique G_{14}^* such that $\varphi((G_{19})^*) = 0$

(g) By the same argument, the equations 92,93 admit solutions G_{20}, G_{21} if

$$\varphi(G_{23}) = (b'_{20})^{(3)}(b'_{21})^{(3)} - (b_{20})^{(3)}(b_{21})^{(3)} - [(b'_{20})^{(3)}(b'_{21})^{(3)}(G_{23}) + (b'_{21})^{(3)}(b''_{20})^{(3)}(G_{23})] + (b''_{20})^{(3)}(G_{23})(b''_{21})^{(3)}(G_{23}) = 0$$

Where in $G_{23}(G_{20}, G_{21}, G_{22}), G_{20}, G_{22}$ must be replaced by their values from 96. It is easy to see that φ is a decreasing function in G_{21} taking into account the hypothesis $\varphi(0) > 0, \varphi(\infty) < 0$ it follows that there exists a unique G_{21}^* such that $\varphi((G_{23})^*) = 0$

(h) By the same argument, the equations SOLUTIONAL SYSTEM OF THE GLOBAL EQUATIONS admit solutions G_{24}, G_{25} if

$$\varphi(G_{27}) = (b'_{24})^{(4)}(b'_{25})^{(4)} - (b_{24})^{(4)}(b_{25})^{(4)} - [(b'_{24})^{(4)}(b'_{25})^{(4)}(G_{27}) + (b'_{25})^{(4)}(b''_{24})^{(4)}(G_{27})] + (b''_{24})^{(4)}(G_{27})(b''_{25})^{(4)}(G_{27}) = 0$$

Where in $(G_{27})(G_{24}, G_{25}, G_{26}), G_{24}, G_{26}$ must be replaced by their values from 96. It is easy to see that φ is a decreasing function in G_{25} taking into account the hypothesis $\varphi(0) > 0, \varphi(\infty) < 0$ it follows that there exists a unique G_{25}^* such that $\varphi((G_{27})^*) = 0$

(i) By the same argument, the equations SOLUTIONAL SYSTEM OF THE GLOBAL EQUATIONS admit solutions G_{28}, G_{29} if

$$\varphi(G_{31}) = (b'_{28})^{(5)}(b'_{29})^{(5)} - (b_{28})^{(5)}(b_{29})^{(5)} - [(b'_{28})^{(5)}(b''_{29})^{(5)}(G_{31}) + (b'_{29})^{(5)}(b''_{28})^{(5)}(G_{31})] + (b''_{28})^{(5)}(G_{31})(b''_{29})^{(5)}(G_{31}) = 0$$

Where in $(G_{31})(G_{28}, G_{29}, G_{30}), G_{28}, G_{30}$ must be replaced by their values from 96. It is easy to see that φ is a decreasing function in G_{29} taking into account the hypothesis $\varphi(0) > 0, \varphi(\infty) < 0$ it follows that there exists a unique G_{29}^* such that $\varphi((G_{31})^*) = 0$

(j) By the same argument, the equations SOLUTIONAL SYSTEM OF THE GLOBAL EQUATIONS admit solutions G_{32}, G_{33} if

$$\varphi(G_{35}) = (b'_{32})^{(6)}(b'_{33})^{(6)} - (b_{32})^{(6)}(b_{33})^{(6)} - [(b'_{32})^{(6)}(b''_{33})^{(6)}(G_{35}) + (b'_{33})^{(6)}(b''_{32})^{(6)}(G_{35})] + (b''_{32})^{(6)}(G_{35})(b''_{33})^{(6)}(G_{35}) = 0$$

Where in $(G_{35})(G_{32}, G_{33}, G_{34}), G_{32}, G_{34}$ must be replaced by their values It is easy to see that φ is a decreasing function in G_{33} taking into account the hypothesis $\varphi(0) > 0, \varphi(\infty) < 0$ it follows that there exists a unique G_{33}^* such that $\varphi(G^*) = 0$

Finally we obtain the unique solution of THE HOLISTIC SYSTEM

G_{14}^* given by $\varphi(G^*) = 0, T_{14}^*$ given by $f(T_{14}^*) = 0$ and

$$G_{13}^* = \frac{(a_{13})^{(1)}G_{14}^*}{[(a'_{13})^{(1)} + (a''_{13})^{(1)}(T_{14}^*)]}, \quad G_{15}^* = \frac{(a_{15})^{(1)}G_{14}^*}{[(a'_{15})^{(1)} + (a''_{15})^{(1)}(T_{14}^*)]}$$

$$T_{13}^* = \frac{(b_{13})^{(1)}T_{14}^*}{[(b'_{13})^{(1)} - (b''_{13})^{(1)}(G^*)]}, \quad T_{15}^* = \frac{(b_{15})^{(1)}T_{14}^*}{[(b'_{15})^{(1)} - (b''_{15})^{(1)}(G^*)]}$$

Obviously, these values represent an equilibrium solution of THE GLOBAL SYSTEM OF GOVERNING EQUATIONS

Finally we obtain the unique solution of THE HOLISTIC SYSTEM

G_{17}^* given by $\varphi((G_{19})^*) = 0, T_{17}^*$ given by $f(T_{17}^*) = 0$ and

$$G_{16}^* = \frac{(a_{16})^{(2)}G_{17}^*}{[(a'_{16})^{(2)} + (a''_{16})^{(2)}(T_{17}^*)]}, \quad G_{18}^* = \frac{(a_{18})^{(2)}G_{17}^*}{[(a'_{18})^{(2)} + (a''_{18})^{(2)}(T_{17}^*)]}$$

$$T_{16}^* = \frac{(b_{16})^{(2)}T_{17}^*}{[(b'_{16})^{(2)} - (b''_{16})^{(2)}((G_{19})^*)]}, \quad T_{18}^* = \frac{(b_{18})^{(2)}T_{17}^*}{[(b'_{18})^{(2)} - (b''_{18})^{(2)}((G_{19})^*)]}$$

Obviously, these values represent an equilibrium solution of THE HOLISTIC SYSTEM

Finally we obtain the unique solution of SOLUTIONAL EQUATIONS OF THE GLOBAL SYSTEM

G_{21}^* given by $\varphi((G_{23})^*) = 0, T_{21}^*$ given by $f(T_{21}^*) = 0$ and

$$G_{20}^* = \frac{(a_{20})^{(3)}G_{21}^*}{[(a'_{20})^{(3)} + (a''_{20})^{(3)}(T_{21}^*)]}, \quad G_{22}^* = \frac{(a_{22})^{(3)}G_{21}^*}{[(a'_{22})^{(3)} + (a''_{22})^{(3)}(T_{21}^*)]}$$

$$T_{20}^* = \frac{(b_{20})^{(3)}T_{21}^*}{[(b'_{20})^{(3)} - (b''_{20})^{(3)}(G_{23}^*)]}, \quad T_{22}^* = \frac{(b_{22})^{(3)}T_{21}^*}{[(b'_{22})^{(3)} - (b''_{22})^{(3)}(G_{23}^*)]}$$

Obviously, these values represent an equilibrium solution of THE GLOBAL GOVERNING EQUATIONS

Finally we obtain the unique solution of SOLUTIONS FOR THE GLOBAL GOVERNING EQUATIONS

G_{25}^* given by $\varphi(G_{27}) = 0, T_{25}^*$ given by $f(T_{25}^*) = 0$ and

$$G_{24}^* = \frac{(a_{24})^{(4)}G_{25}^*}{[(a'_{24})^{(4)} + (a''_{24})^{(4)}(T_{25}^*)]}, \quad G_{26}^* = \frac{(a_{26})^{(4)}G_{25}^*}{[(a'_{26})^{(4)} + (a''_{26})^{(4)}(T_{25}^*)]}$$

$$T_{24}^* = \frac{(b_{24})^{(4)}T_{25}^*}{[(b'_{24})^{(4)} - (b''_{24})^{(4)}((G_{27})^*)]}, \quad T_{26}^* = \frac{(b_{26})^{(4)}T_{25}^*}{[(b'_{26})^{(4)} - (b''_{26})^{(4)}((G_{27})^*)]}$$

Obviously, these values represent an equilibrium solution of GLOBAL GOVERNING EQUATIONS

Finally we obtain the unique solution of THE HOLISTIC SYSTEM

G_{29}^* given by $\varphi((G_{31})^*) = 0, T_{29}^*$ given by $f(T_{29}^*) = 0$ and

$$G_{28}^* = \frac{(a_{28})^{(5)}G_{29}^*}{[(a'_{28})^{(5)} + (a''_{28})^{(5)}(T_{29}^*)]}, \quad G_{30}^* = \frac{(a_{30})^{(5)}G_{29}^*}{[(a'_{30})^{(5)} + (a''_{30})^{(5)}(T_{29}^*)]}$$

$$T_{28}^* = \frac{(b_{28})^{(5)}T_{29}^*}{[(b'_{28})^{(5)} - (b''_{28})^{(5)}((G_{31})^*)]}, \quad T_{30}^* = \frac{(b_{30})^{(5)}T_{29}^*}{[(b'_{30})^{(5)} - (b''_{30})^{(5)}((G_{31})^*)]}$$

Obviously, these values represent an equilibrium solution of THE HOLISTIC SYSTEM

Finally we obtain the unique solution of SOLUTIONAL EQUATIONS OF THE CONCATENATED EQUATIONS

G_{33}^* given by $\varphi((G_{35})^*) = 0, T_{33}^*$ given by $f(T_{33}^*) = 0$ and

$$G_{32}^* = \frac{(a_{32})^{(6)}G_{33}^*}{[(a'_{32})^{(6)} + (a''_{32})^{(6)}(T_{33}^*)]}, \quad G_{34}^* = \frac{(a_{34})^{(6)}G_{33}^*}{[(a'_{34})^{(6)} + (a''_{34})^{(6)}(T_{33}^*)]}$$

$$T_{32}^* = \frac{(b_{32})^{(6)}T_{33}^*}{[(b'_{32})^{(6)} - (b''_{32})^{(6)}((G_{35})^*)]}, \quad T_{34}^* = \frac{(b_{34})^{(6)}T_{33}^*}{[(b'_{34})^{(6)} - (b''_{34})^{(6)}((G_{35})^*)]}$$

Obviously, these values represent an equilibrium solution of THE GLOBAL SYSTEM

ASYMPTOTIC STABILITY ANALYSIS

Theorem 4: If the conditions of the previous theorem are satisfied and if the functions $(a_i'')^{(1)}$ and $(b_i'')^{(1)}$ belong to $C^1(\mathbb{R}_+)$ then the above equilibrium point is asymptotically stable.

Proof: Denote

Definition of G_i, T_i :-

$$G_i = G_i^* + \mathbb{G}_i, T_i = T_i^* + \mathbb{T}_i$$

$$\frac{\partial(a_{14}'')^{(1)}}{\partial T_{14}}(T_{14}^*) = (q_{14})^{(1)}, \frac{\partial(b_i'')^{(1)}}{\partial G_j}(G^*) = s_{ij}$$

Then taking into account equations OF SOLUTIONALEQUATIONS OF THE GLOBAL SYSTEM and neglecting the terms of power 2, we obtain

$$\frac{dG_{13}}{dt} = -((a'_{13})^{(1)} + (p_{13})^{(1)})G_{13} + (a_{13})^{(1)}G_{14} - (q_{13})^{(1)}G_{13}^*T_{14}$$

$$\frac{dG_{14}}{dt} = -((a'_{14})^{(1)} + (p_{14})^{(1)})G_{14} + (a_{14})^{(1)}G_{13} - (q_{14})^{(1)}G_{14}^*T_{14}$$

$$\frac{dG_{15}}{dt} = -((a'_{15})^{(1)} + (p_{15})^{(1)})G_{15} + (a_{15})^{(1)}G_{14} - (q_{15})^{(1)}G_{15}^*T_{14}$$

$$\frac{dT_{13}}{dt} = -((b'_{13})^{(1)} - (r_{13})^{(1)})T_{13} + (b_{13})^{(1)}T_{14} + \sum_{j=13}^{15} (s_{(13)(j)})T_{13}^*G_j$$

$$\frac{dT_{14}}{dt} = -((b'_{14})^{(1)} - (r_{14})^{(1)})T_{14} + (b_{14})^{(1)}T_{13} + \sum_{j=13}^{15} (s_{(14)(j)})T_{14}^*G_j$$

$$\frac{dT_{15}}{dt} = -((b'_{15})^{(1)} - (r_{15})^{(1)})T_{15} + (b_{15})^{(1)}T_{14} + \sum_{j=13}^{15} (s_{(15)(j)})T_{15}^*G_j$$

If the conditions of the previous theorem are satisfied and if the functions $(a_i'')^{(2)}$ and $(b_i'')^{(2)}$ Belong to $C^{(2)}(\mathbb{R}_+)$ then the above equilibrium point is asymptotically stable

Denote

Definition of G_i, T_i :-

$$G_i = G_i^* + \mathbb{G}_i, T_i = T_i^* + \mathbb{T}_i$$

$$\frac{\partial(a_{17}'')^{(2)}}{\partial T_{17}}(T_{17}^*) = (q_{17})^{(2)}, \frac{\partial(b_i'')^{(2)}}{\partial G_j}((G_{19})^*) = s_{ij}$$

$$\frac{dG_{16}}{dt} = -((a'_{16})^{(2)} + (p_{16})^{(2)})G_{16} + (a_{16})^{(2)}G_{17} - (q_{16})^{(2)}G_{16}^*T_{17}$$

$$\frac{dG_{17}}{dt} = -((a'_{17})^{(2)} + (p_{17})^{(2)})G_{17} + (a_{17})^{(2)}G_{16} - (q_{17})^{(2)}G_{17}^*T_{17}$$

$$\frac{dG_{18}}{dt} = -((a'_{18})^{(2)} + (p_{18})^{(2)})G_{18} + (a_{18})^{(2)}G_{17} - (q_{18})^{(2)}G_{18}^*T_{17}$$

$$\frac{dT_{16}}{dt} = -((b'_{16})^{(2)} - (r_{16})^{(2)})T_{16} + (b_{16})^{(2)}T_{17} + \sum_{j=16}^{18} (s_{(16)(j)})T_{16}^*G_j$$

$$\frac{dT_{17}}{dt} = -((b'_{17})^{(2)} - (r_{17})^{(2)})T_{17} + (b_{17})^{(2)}T_{16} + \sum_{j=16}^{18} (s_{(17)(j)})T_{17}^*G_j$$

$$\frac{dT_{18}}{dt} = -((b'_{18})^{(2)} - (r_{18})^{(2)})T_{18} + (b_{18})^{(2)}T_{17} + \sum_{j=16}^{18} (s_{(18)(j)})T_{18}^*G_j$$

If the conditions of the previous theorem are satisfied and if the functions $(a_i'')^{(3)}$ and $(b_i'')^{(3)}$ Belong to $C^{(3)}(\mathbb{R}_+)$ then the above equilibrium point is asymptotically stable

Denote

Definition of G_i, T_i :-

$$G_i = G_i^* + \mathbb{G}_i, T_i = T_i^* + \mathbb{T}_i$$

$$\frac{\partial(a_{21}'')^{(3)}}{\partial T_{21}}(T_{21}^*) = (q_{21})^{(3)}, \frac{\partial(b_i'')^{(3)}}{\partial G_j}((G_{23})^*) = s_{ij}$$

$$\frac{dG_{20}}{dt} = -((a'_{20})^{(3)} + (p_{20})^{(3)})G_{20} + (a_{20})^{(3)}G_{21} - (q_{20})^{(3)}G_{20}^*T_{21}$$

$$\frac{dG_{21}}{dt} = -((a'_{21})^{(3)} + (p_{21})^{(3)})G_{21} + (a_{21})^{(3)}G_{20} - (q_{21})^{(3)}G_{21}^*T_{21}$$

$$\frac{dG_{22}}{dt} = -((a'_{22})^{(3)} + (p_{22})^{(3)})G_{22} + (a_{22})^{(3)}G_{21} - (q_{22})^{(3)}G_{22}^*T_{21}$$

$$\frac{dT_{20}}{dt} = -((b'_{20})^{(3)} - (r_{20})^{(3)})T_{20} + (b_{20})^{(3)}T_{21} + \sum_{j=20}^{22} (s_{(20)(j)})T_{20}^*G_j$$

$$\frac{dT_{21}}{dt} = -((b'_{21})^{(3)} - (r_{21})^{(3)})T_{21} + (b_{21})^{(3)}T_{20} + \sum_{j=20}^{22} (s_{(21)(j)})T_{21}^*G_j$$

$$\frac{dT_{22}}{dt} = -((b'_{22})^{(3)} - (r_{22})^{(3)})T_{22} + (b_{22})^{(3)}T_{21} + \sum_{j=20}^{22} (s_{(22)(j)})T_{22}^*G_j$$

If the conditions of the previous theorem are satisfied and if the functions $(a_i'')^{(4)}$ and $(b_i'')^{(4)}$ Belong to $C^{(4)}(\mathbb{R}_+)$ then the above equilibrium point is asymptotically stable

Denote

Definition of G_i, T_i :-

$$G_i = G_i^* + \mathbb{G}_i, T_i = T_i^* + \mathbb{T}_i$$

$$\frac{\partial(a_{25}'')^{(4)}}{\partial T_{25}}(T_{25}^*) = (q_{25})^{(4)}, \frac{\partial(b_i'')^{(4)}}{\partial G_j}((G_{27})^*) = s_{ij}$$

$$\frac{dG_{24}}{dt} = -((a'_{24})^{(4)} + (p_{24})^{(4)})G_{24} + (a_{24})^{(4)}G_{25} - (q_{24})^{(4)}G_{24}^*T_{25}$$

$$\frac{dG_{25}}{dt} = -((a'_{25})^{(4)} + (p_{25})^{(4)})G_{25} + (a_{25})^{(4)}G_{24} - (q_{25})^{(4)}G_{25}^*T_{25}$$

$$\frac{dG_{26}}{dt} = -((a'_{26})^{(4)} + (p_{26})^{(4)})G_{26} + (a_{26})^{(4)}G_{25} - (q_{26})^{(4)}G_{26}^*T_{25}$$

$$\frac{dT_{24}}{dt} = -((b'_{24})^{(4)} - (r_{24})^{(4)})T_{24} + (b_{24})^{(4)}T_{25} + \sum_{j=24}^{26} (s_{(24)(j)})T_{24}^*G_j$$

$$\frac{dT_{25}}{dt} = -((b'_{25})^{(4)} - (r_{25})^{(4)})T_{25} + (b_{25})^{(4)}T_{24} + \sum_{j=24}^{26} (s_{(25)(j)})T_{25}^*G_j$$

$$\frac{dT_{26}}{dt} = -((b'_{26})^{(4)} - (r_{26})^{(4)})T_{26} + (b_{26})^{(4)}T_{25} + \sum_{j=24}^{26} (s_{(26)(j)})T_{26}^*G_j$$

If the conditions of the previous theorem are satisfied and if the functions $(a''_i)^{(5)}$ and $(b''_i)^{(5)}$ belong to $C^{(5)}(\mathbb{R}_+)$ then the above equilibrium point is asymptotically stable

Denote

Definition of G_i, T_i :-

$$G_i = G_i^* + G_i, T_i = T_i^* + T_i$$

$$\frac{\partial (a_{29})^{(5)}}{\partial T_{29}} (T_{29}^*) = (q_{29})^{(5)}, \frac{\partial (b''_i)^{(5)}}{\partial G_j} ((G_{31})^*) = s_{ij}$$

$$\frac{dG_{28}}{dt} = -((a'_{28})^{(5)} + (p_{28})^{(5)})G_{28} + (a_{28})^{(5)}G_{29} - (q_{28})^{(5)}G_{28}^*T_{29}$$

$$\frac{dG_{29}}{dt} = -((a'_{29})^{(5)} + (p_{29})^{(5)})G_{29} + (a_{29})^{(5)}G_{28} - (q_{29})^{(5)}G_{29}^*T_{29}$$

$$\frac{dG_{30}}{dt} = -((a'_{30})^{(5)} + (p_{30})^{(5)})G_{30} + (a_{30})^{(5)}G_{29} - (q_{30})^{(5)}G_{30}^*T_{29}$$

$$\frac{dT_{28}}{dt} = -((b'_{28})^{(5)} - (r_{28})^{(5)})T_{28} + (b_{28})^{(5)}T_{29} + \sum_{j=28}^{30} (s_{(28)(j)})T_{28}^*G_j$$

$$\frac{dT_{29}}{dt} = -((b'_{29})^{(5)} - (r_{29})^{(5)})T_{29} + (b_{29})^{(5)}T_{28} + \sum_{j=28}^{30} (s_{(29)(j)})T_{29}^*G_j$$

$$\frac{dT_{30}}{dt} = -((b'_{30})^{(5)} - (r_{30})^{(5)})T_{30} + (b_{30})^{(5)}T_{29} + \sum_{j=28}^{30} (s_{(30)(j)})T_{30}^*G_j$$

If the conditions of the previous theorem are satisfied and if the functions $(a''_i)^{(6)}$ and $(b''_i)^{(6)}$ belong to $C^{(6)}(\mathbb{R}_+)$ then the above equilibrium point is asymptotically stable

Denote

Definition of G_i, T_i :-

$$G_i = G_i^* + G_i, T_i = T_i^* + T_i$$

$$\frac{\partial (a_{33})^{(6)}}{\partial T_{33}} (T_{33}^*) = (q_{33})^{(6)}, \frac{\partial (b''_i)^{(6)}}{\partial G_j} ((G_{35})^*) = s_{ij}$$

$$\frac{dG_{32}}{dt} = -((a'_{32})^{(6)} + (p_{32})^{(6)})G_{32} + (a_{32})^{(6)}G_{33} - (q_{32})^{(6)}G_{32}^*T_{33}$$

$$\frac{dG_{33}}{dt} = -((a'_{33})^{(6)} + (p_{33})^{(6)})G_{33} + (a_{33})^{(6)}G_{32} - (q_{33})^{(6)}G_{33}^*T_{33}$$

$$\frac{dG_{34}}{dt} = -((a'_{34})^{(6)} + (p_{34})^{(6)})G_{34} + (a_{34})^{(6)}G_{33} - (q_{34})^{(6)}G_{34}^*T_{33}$$

$$\frac{dT_{32}}{dt} = -((b'_{32})^{(6)} - (r_{32})^{(6)})T_{32} + (b_{32})^{(6)}T_{33} + \sum_{j=32}^{34} (s_{(32)(j)})T_{32}^*G_j$$

$$\frac{dT_{33}}{dt} = -((b'_{33})^{(6)} - (r_{33})^{(6)})T_{33} + (b_{33})^{(6)}T_{32} + \sum_{j=32}^{34} (s_{(33)(j)})T_{33}^*G_j$$

$$\frac{dT_{34}}{dt} = -((b'_{34})^{(6)} - (r_{34})^{(6)})T_{34} + (b_{34})^{(6)}T_{33} + \sum_{j=32}^{34} (s_{(34)(j)})T_{34}^*G_j$$

The characteristic equation of this system is

$$((\lambda)^{(1)} + (b'_{15})^{(1)} - (r_{15})^{(1)})\{((\lambda)^{(1)} + (a'_{15})^{(1)} + (p_{15})^{(1)})$$

$$\left[((\lambda)^{(1)} + (a'_{13})^{(1)} + (p_{13})^{(1)})(q_{14})^{(1)}G_{14}^* + (a_{14})^{(1)}(q_{13})^{(1)}G_{13}^* \right]$$

$$\left(((\lambda)^{(1)} + (b'_{13})^{(1)} - (r_{13})^{(1)})s_{(14),(14)}T_{14}^* + (b_{14})^{(1)}s_{(13),(14)}T_{14}^* \right)$$

$$+ \left(((\lambda)^{(1)} + (a'_{14})^{(1)} + (p_{14})^{(1)})(q_{13})^{(1)}G_{13}^* + (a_{13})^{(1)}(q_{14})^{(1)}G_{14}^* \right)$$

$$\left(((\lambda)^{(1)} + (b'_{13})^{(1)} - (r_{13})^{(1)})s_{(14),(13)}T_{14}^* + (b_{14})^{(1)}s_{(13),(13)}T_{13}^* \right)$$

$$\left(((\lambda)^{(1)})^2 + ((a'_{13})^{(1)} + (a'_{14})^{(1)} + (p_{13})^{(1)} + (p_{14})^{(1)}) (\lambda)^{(1)} \right)$$

$$\left(((\lambda)^{(1)})^2 + ((b'_{13})^{(1)} + (b'_{14})^{(1)} - (r_{13})^{(1)} + (r_{14})^{(1)}) (\lambda)^{(1)} \right)$$

$$+ \left(((\lambda)^{(1)})^2 + ((a'_{13})^{(1)} + (a'_{14})^{(1)} + (p_{13})^{(1)} + (p_{14})^{(1)}) (\lambda)^{(1)} \right) (q_{15})^{(1)}G_{15}$$

$$+ ((\lambda)^{(1)} + (a'_{13})^{(1)} + (p_{13})^{(1)}) \left((a_{15})^{(1)}(q_{14})^{(1)}G_{14}^* + (a_{14})^{(1)}(a_{15})^{(1)}(q_{13})^{(1)}G_{13}^* \right)$$

$$\left(((\lambda)^{(1)} + (b'_{13})^{(1)} - (r_{13})^{(1)})s_{(14),(15)}T_{14}^* + (b_{14})^{(1)}s_{(13),(15)}T_{13}^* \right)\} = 0$$

$$+$$

$$((\lambda)^{(2)} + (b'_{18})^{(2)} - (r_{18})^{(2)})\{((\lambda)^{(2)} + (a'_{18})^{(2)} + (p_{18})^{(2)})$$

$$\left[((\lambda)^{(2)} + (a'_{16})^{(2)} + (p_{16})^{(2)})(q_{17})^{(2)}G_{17}^* + (a_{17})^{(2)}(q_{16})^{(2)}G_{16}^* \right]$$

$$\left(((\lambda)^{(2)} + (b'_{16})^{(2)} - (r_{16})^{(2)})s_{(17),(17)}T_{17}^* + (b_{17})^{(2)}s_{(16),(17)}T_{17}^* \right)$$

$$+ \left(((\lambda)^{(2)} + (a'_{17})^{(2)} + (p_{17})^{(2)})(q_{16})^{(2)}G_{16}^* + (a_{16})^{(2)}(q_{17})^{(2)}G_{17}^* \right)$$

$$\left(((\lambda)^{(2)} + (b'_{16})^{(2)} - (r_{16})^{(2)})s_{(17),(16)}T_{17}^* + (b_{17})^{(2)}s_{(16),(16)}T_{16}^* \right)$$

$$\left(((\lambda)^{(2)})^2 + ((a'_{16})^{(2)} + (a'_{17})^{(2)} + (p_{16})^{(2)} + (p_{17})^{(2)}) (\lambda)^{(2)} \right)$$

$$\left(((\lambda)^{(2)})^2 + ((b'_{16})^{(2)} + (b'_{17})^{(2)} - (r_{16})^{(2)} + (r_{17})^{(2)}) (\lambda)^{(2)} \right)$$

$$+ \left(((\lambda)^{(2)})^2 + ((a'_{16})^{(2)} + (a'_{17})^{(2)} + (p_{16})^{(2)} + (p_{17})^{(2)}) (\lambda)^{(2)} \right) (q_{18})^{(2)}G_{18}$$

$$\begin{aligned}
& + ((\lambda)^{(2)} + (a'_{16})^{(2)} + (p_{16})^{(2)}) ((a_{18})^{(2)}(q_{17})^{(2)}G_{17}^* + (a_{17})^{(2)}(a_{18})^{(2)}(q_{16})^{(2)}G_{16}^*) \\
& \left(((\lambda)^{(2)} + (b'_{16})^{(2)} - (r_{16})^{(2)})s_{(17),(18)}T_{17}^* + (b_{17})^{(2)}s_{(16),(18)}T_{16}^* \right) \} = 0 \\
& + \\
& ((\lambda)^{(3)} + (b'_{22})^{(3)} - (r_{22})^{(3)}) \{ ((\lambda)^{(3)} + (a'_{22})^{(3)} + (p_{22})^{(3)}) \\
& \left[((\lambda)^{(3)} + (a'_{20})^{(3)} + (p_{20})^{(3)})(q_{21})^{(3)}G_{21}^* + (a_{21})^{(3)}(q_{20})^{(3)}G_{20}^* \right] \\
& \left(((\lambda)^{(3)} + (b'_{20})^{(3)} - (r_{20})^{(3)})s_{(21),(21)}T_{21}^* + (b_{21})^{(3)}s_{(20),(21)}T_{21}^* \right) \\
& + \left(((\lambda)^{(3)} + (a'_{21})^{(3)} + (p_{21})^{(3)})(q_{20})^{(3)}G_{20}^* + (a_{20})^{(3)}(q_{21})^{(1)}G_{21}^* \right) \\
& \left(((\lambda)^{(3)} + (b'_{20})^{(3)} - (r_{20})^{(3)})s_{(21),(20)}T_{21}^* + (b_{21})^{(3)}s_{(20),(20)}T_{20}^* \right) \\
& \left(((\lambda)^{(3)})^2 + ((a'_{20})^{(3)} + (a'_{21})^{(3)} + (p_{20})^{(3)} + (p_{21})^{(3)}) (\lambda)^{(3)} \right) \\
& \left(((\lambda)^{(3)})^2 + ((b'_{20})^{(3)} + (b'_{21})^{(3)} - (r_{20})^{(3)} + (r_{21})^{(3)}) (\lambda)^{(3)} \right) \\
& + \left(((\lambda)^{(3)})^2 + ((a'_{20})^{(3)} + (a'_{21})^{(3)} + (p_{20})^{(3)} + (p_{21})^{(3)}) (\lambda)^{(3)} \right) (q_{22})^{(3)}G_{22} \\
& + ((\lambda)^{(3)} + (a'_{20})^{(3)} + (p_{20})^{(3)}) ((a_{22})^{(3)}(q_{21})^{(3)}G_{21}^* + (a_{21})^{(3)}(a_{22})^{(3)}(q_{20})^{(3)}G_{20}^*) \\
& \left(((\lambda)^{(3)} + (b'_{20})^{(3)} - (r_{20})^{(3)})s_{(21),(22)}T_{21}^* + (b_{21})^{(3)}s_{(20),(22)}T_{20}^* \right) \} = 0 \\
& + \\
& ((\lambda)^{(4)} + (b'_{26})^{(4)} - (r_{26})^{(4)}) \{ ((\lambda)^{(4)} + (a'_{26})^{(4)} + (p_{26})^{(4)}) \\
& \left[((\lambda)^{(4)} + (a'_{24})^{(4)} + (p_{24})^{(4)})(q_{25})^{(4)}G_{25}^* + (a_{25})^{(4)}(q_{24})^{(4)}G_{24}^* \right] \\
& \left(((\lambda)^{(4)} + (b'_{24})^{(4)} - (r_{24})^{(4)})s_{(25),(25)}T_{25}^* + (b_{25})^{(4)}s_{(24),(25)}T_{25}^* \right) \\
& + \left(((\lambda)^{(4)} + (a'_{25})^{(4)} + (p_{25})^{(4)})(q_{24})^{(4)}G_{24}^* + (a_{24})^{(4)}(q_{25})^{(4)}G_{25}^* \right) \\
& \left(((\lambda)^{(4)} + (b'_{24})^{(4)} - (r_{24})^{(4)})s_{(25),(24)}T_{25}^* + (b_{25})^{(4)}s_{(24),(24)}T_{24}^* \right) \\
& \left(((\lambda)^{(4)})^2 + ((a'_{24})^{(4)} + (a'_{25})^{(4)} + (p_{24})^{(4)} + (p_{25})^{(4)}) (\lambda)^{(4)} \right) \\
& \left(((\lambda)^{(4)})^2 + ((b'_{24})^{(4)} + (b'_{25})^{(4)} - (r_{24})^{(4)} + (r_{25})^{(4)}) (\lambda)^{(4)} \right) \\
& + \left(((\lambda)^{(4)})^2 + ((a'_{24})^{(4)} + (a'_{25})^{(4)} + (p_{24})^{(4)} + (p_{25})^{(4)}) (\lambda)^{(4)} \right) (q_{26})^{(4)}G_{26} \\
& + ((\lambda)^{(4)} + (a'_{24})^{(4)} + (p_{24})^{(4)}) ((a_{26})^{(4)}(q_{25})^{(4)}G_{25}^* + (a_{25})^{(4)}(a_{26})^{(4)}(q_{24})^{(4)}G_{24}^*) \\
& \left(((\lambda)^{(4)} + (b'_{24})^{(4)} - (r_{24})^{(4)})s_{(25),(26)}T_{25}^* + (b_{25})^{(4)}s_{(24),(26)}T_{24}^* \right) \} = 0 \\
& + \\
& ((\lambda)^{(5)} + (b'_{30})^{(5)} - (r_{30})^{(5)}) \{ ((\lambda)^{(5)} + (a'_{30})^{(5)} + (p_{30})^{(5)}) \\
& \left[((\lambda)^{(5)} + (a'_{28})^{(5)} + (p_{28})^{(5)})(q_{29})^{(5)}G_{29}^* + (a_{29})^{(5)}(q_{28})^{(5)}G_{28}^* \right] \\
& \left(((\lambda)^{(5)} + (b'_{28})^{(5)} - (r_{28})^{(5)})s_{(29),(29)}T_{29}^* + (b_{29})^{(5)}s_{(28),(29)}T_{29}^* \right) \\
& + \left(((\lambda)^{(5)} + (a'_{29})^{(5)} + (p_{29})^{(5)})(q_{28})^{(5)}G_{28}^* + (a_{28})^{(5)}(q_{29})^{(5)}G_{29}^* \right) \\
& \left(((\lambda)^{(5)} + (b'_{28})^{(5)} - (r_{28})^{(5)})s_{(29),(28)}T_{29}^* + (b_{29})^{(5)}s_{(28),(28)}T_{28}^* \right) \\
& \left(((\lambda)^{(5)})^2 + ((a'_{28})^{(5)} + (a'_{29})^{(5)} + (p_{28})^{(5)} + (p_{29})^{(5)}) (\lambda)^{(5)} \right) \\
& \left(((\lambda)^{(5)})^2 + ((b'_{28})^{(5)} + (b'_{29})^{(5)} - (r_{28})^{(5)} + (r_{29})^{(5)}) (\lambda)^{(5)} \right) \\
& + \left(((\lambda)^{(5)})^2 + ((a'_{28})^{(5)} + (a'_{29})^{(5)} + (p_{28})^{(5)} + (p_{29})^{(5)}) (\lambda)^{(5)} \right) (q_{30})^{(5)}G_{30} \\
& + ((\lambda)^{(5)} + (a'_{28})^{(5)} + (p_{28})^{(5)}) ((a_{30})^{(5)}(q_{29})^{(5)}G_{29}^* + (a_{29})^{(5)}(a_{30})^{(5)}(q_{28})^{(5)}G_{28}^*) \\
& \left(((\lambda)^{(5)} + (b'_{28})^{(5)} - (r_{28})^{(5)})s_{(29),(30)}T_{29}^* + (b_{29})^{(5)}s_{(28),(30)}T_{28}^* \right) \} = 0 \\
& + \\
& ((\lambda)^{(6)} + (b'_{34})^{(6)} - (r_{34})^{(6)}) \{ ((\lambda)^{(6)} + (a'_{34})^{(6)} + (p_{34})^{(6)}) \\
& \left[((\lambda)^{(6)} + (a'_{32})^{(6)} + (p_{32})^{(6)})(q_{33})^{(6)}G_{33}^* + (a_{33})^{(6)}(q_{32})^{(6)}G_{32}^* \right] \\
& \left(((\lambda)^{(6)} + (b'_{32})^{(6)} - (r_{32})^{(6)})s_{(33),(33)}T_{33}^* + (b_{33})^{(6)}s_{(32),(33)}T_{33}^* \right) \\
& + \left(((\lambda)^{(6)} + (a'_{33})^{(6)} + (p_{33})^{(6)})(q_{32})^{(6)}G_{32}^* + (a_{32})^{(6)}(q_{33})^{(6)}G_{33}^* \right) \\
& \left(((\lambda)^{(6)} + (b'_{32})^{(6)} - (r_{32})^{(6)})s_{(33),(32)}T_{33}^* + (b_{33})^{(6)}s_{(32),(32)}T_{32}^* \right) \\
& \left(((\lambda)^{(6)})^2 + ((a'_{32})^{(6)} + (a'_{33})^{(6)} + (p_{32})^{(6)} + (p_{33})^{(6)}) (\lambda)^{(6)} \right) \\
& \left(((\lambda)^{(6)})^2 + ((b'_{32})^{(6)} + (b'_{33})^{(6)} - (r_{32})^{(6)} + (r_{33})^{(6)}) (\lambda)^{(6)} \right)
\end{aligned}$$

$$\begin{aligned}
 &+ \left(((\lambda)^{(6)})^2 + ((a'_{32})^{(6)} + (a'_{33})^{(6)} + (p_{32})^{(6)} + (p_{33})^{(6)}) (\lambda)^{(6)} \right) (q_{34})^{(6)} G_{34} \\
 &+ \left((\lambda)^{(6)} + (a'_{32})^{(6)} + (p_{32})^{(6)} \right) \left((a_{34})^{(6)} (q_{33})^{(6)} G_{33}^* + (a_{33})^{(6)} (a_{34})^{(6)} (q_{32})^{(6)} G_{32}^* \right) \\
 &\left(((\lambda)^{(6)} + (b'_{32})^{(6)} - (r_{32})^{(6)}) s_{(33),(34)} T_{33}^* + (b_{33})^{(6)} s_{(32),(34)} T_{32}^* \right) \} = 0
 \end{aligned}$$

And as one sees, all the coefficients are positive. It follows that all the roots have negative real part, and this proves the theorem.

Acknowledgments

The introduction is a collection of information from various articles, Books, News Paper reports, Home Pages Of authors, Journal Reviews, the internet including Wikipedia. We acknowledge all authors who have contributed to the same. In the eventuality of the fact that there has been any act of omission on the part of the authors, We regret with great deal of compunction, contrition, and remorse. As Newton said, it is only because erudite and eminent people allowed one to piggy ride on their backs; probably an attempt has been made to look slightly further. Once again, it is stated that the references are only illustrative and not comprehensive

References

- [1] A Haimovici: "On the growth of a two species ecological system divided on age groups". Tensor, Vol 37 (1982), Commemoration volume dedicated to Professor Akitsugu Kawaguchi on his 80th birthday
- [2] Fritjof Capra: "The web of life" Flamingo, Harper Collins See "Dissipative structures" pages 172-188
- [3] Heylighen F. (2001): "The Science of Self-organization and Adaptivity", in L. D. Kiel, (ed) . Knowledge Management, Organizational Intelligence and Learning, and Complexity, in: The Encyclopedia of Life Support Systems ((EOLSS), (Eolss Publishers, Oxford) [http://www.eolss.net
- [4] Matsui, T, H. Masunaga, S. M. Kreidenweis, R. A. Pielke Sr., W.-K. Tao, M. Chin, and Y. J Kaufman (2006), "Satellite-based assessment of marine low cloud variability associated with aerosol, atmospheric stability, and the diurnal cycle", J. Geophys. Res., 111, D17204, doi:10.1029/2005JD006097
- [5] Stevens, B, G. Feingold, W.R. Cotton and R.L. Walko, "Elements of the microphysical structure of numerically simulated nonprecipitating stratocumulus" J. Atmos. Sci., 53, 980-1006
- [6] Feingold, G, Koren, I; Wang, HL; Xue, HW; Brewer, WA (2010), "Precipitation-generated oscillations in open cellular cloud fields" *Nature*, 466 (7308) 849-852, doi: 10.1038/nature09314, Published 12-Aug 2010
- [7] R Wood "The rate of loss of cloud droplets by coalescence in warm clouds" J.Geophys. Res., 111, doi: 10.1029/2006JD007553, 2006
- [8] H. Rund, "The Differential Geometry of Finsler Spaces", Grund. Math. Wiss. Springer-Verlag, Berlin, 1959
- [9] A. Dold, "Lectures on Algebraic Topology", 1972, Springer-Verlag
- [10] S Levin "Some Mathematical questions in Biology vii ,Lectures on Mathematics in life sciences, vol 8" The American Mathematical society, Providence , Rhode island 1976

First Author: ¹**Mr. K. N.Prasanna Kumar** has three doctorates one each in Mathematics, Economics, Political Science. Thesis was based on Mathematical Modeling. He was recently awarded D.litt., for his work on 'Mathematical Models in Political Science'--- Department of studies in Mathematics, Kuvempu University, Shimoga, Karnataka, India

Second Author: ²**Prof. B.S Kiranagi** is the Former Chairman of the Department of Studies in Mathematics, Manasa Gangotri and present Professor Emeritus of UGC in the Department. Professor Kiranagi has guided over 25 students and he has received many encomiums and laurels for his contribution to Co homology Groups and Mathematical Sciences. Known for his prolific writing, and one of the senior most Professors of the country, he has over 150 publications to his credit. A prolific writer and a prodigious thinker, he has to his credit several books on Lie Groups, Co Homology Groups, and other mathematical application topics, and excellent publication history.-- UGC Emeritus Professor (Department of studies in Mathematics), Manasagangotri, University of Mysore, Karnataka, India

Third Author: ³**Prof. C.S. Bagewadi** is the present Chairman of Department of Mathematics and Department of Studies in Computer Science and has guided over 25 students. He has published articles in both national and international journals. Professor Bagewadi specializes in Differential Geometry and its wide-ranging ramifications. He has to his credit more than 159 research papers. Several Books on Differential Geometry, Differential Equations are coauthored by him--- Chairman, Department of studies in Mathematics and Computer science, Jnanasahyadri Kuvempu University, Shankarghatta, Shimoga district, Karnataka, India

Wireless Sensor Networks for Paddy Field Crop Monitoring Application in Kuttanad

Santhosh Simon¹, K Paulose Jacob²

(Department of Computer Science, Cochin University of Science and Technology, Kerala, India)

Abstract : The evolution of wireless sensor network technology has enabled us to develop advanced systems for real time monitoring. In the present scenario wireless sensor networks are increasingly being used for precision agriculture. The advantages of using wireless sensor networks in agriculture are distributed data collection and monitoring, monitor and control of climate, irrigation and nutrient supply. Hence decreasing the cost of production and increasing the efficiency of production. This paper describes the application of wireless sensor network for crop monitoring in the paddy fields of kuttanad, a region of Kerala, the southern state of India.

Keywords—Crop monitoring, Precision agriculture, Wireless sensor networks, Zigbee.

Kuttanad, the rice bowl of Kerala, is unique among the rice ecologies of the world; the biggest wetlands of the country, located 0.5 – 2.5 metres below mean sea level (msl). Rice is grown by construction of bunds and dewatering the so formed polders mainly during the pucha (rabi) season from Oct. – Nov. to Jan. – Feb. The soils of Kuttanad are low to medium in fertility. Soil is enriched by annual silt deposition during the monsoon floods. The soils are alluvial with silty clay texture and are acid sulphate in nature with excessive iron content. The major problems faced by Kuttanad rice are flood and lack of drainage, intrusion of saline water and soil acidity. In spite of the sharp decline in area under rice; Kuttanad rice bowl (53600 ha.) accounts for 18 per cent of the rice growing area and 25 per cent of total production of the State. The major occupation in Kuttanad is farming. Rice is the important agricultural product, giving Kuttanad the moniker of “The Rice Bowl of Kerala”. Three crops are grown every year now instead of the traditional two per year. Large farming areas near Vembanad Lake were actually reclaimed from the lake.

I. THE KUTTANAD REGION

Rice is the one of the most widely grown crops in the world and is one of the major food crops grown extensively in India. The most important rice producing states of India are West Bengal, Andhra Pradesh, Bihar, Tamil Nadu, Assam and Kerala. In Kerala, Palghat, Trichur and Kuttanad are the main rice producing regions. Kuttanad popularly known as the rice bowl of Kerala, located in central Kerala, is a large wetland habitat comprising of paddy fields, marshes, lakes and rivers. Kuttanad consists of 54 revenue villages spread over 10 taluks in the districts of Alleppey, Kottayam and Pathanamthitta. It is separated from the Arabian sea by a narrow strip of land and is deltaic formation of four river systems, namely Meenachil, Pampa,

Manimala and Achenkovil, together with the lying areas (marshes) in and around the Vembanad lake. Most of the vast expanse in this region is lying 1 – 1.5 m below mean sea level, water-logged throughout the year, subjected to continued flood submergence during monsoon and saline water ingress during the summer month.



The vast area of paddy fields in Kuttanad extends from 9° 17' N to 9° 40' N and 76° 19' E to 76° 33' E. These are divided into “padasekharams” literally meaning groups or blocks of paddy fields and are separated by canals, bunds and water-logged masses. The pucha lands of Kuttanad are classified under three categories based on elevation, geographical formation and soil characteristics, into Karappadoms, Kayal lands and Kari lands. The Karappadoms are generally situated along with the waterways and constitute the lower reached of the eastern and southern periphery of Kuttanad, usually 1-2 m below mean sea level. Vembanad Lake for agricultural purpose and the elevation ranges from 1.5 to 2.5 m below the mean sea level. The Kari lands situated in Ambalappuzha, and Vaikomtaluks is peaty and marshy in nature and are overgrown in many areas with wild weeds and grass and most of the Kari lands lie at or below mean sea level.

‘Puncha’ is the main paddy crop in Kuttanad sown in November or December and harvested by the end of March. The ‘virippu’ is the additional crop grown from May to the end of June and harvested in September or October. High yielding varieties of rice are sown in all the areas of Kuttanad. The gap between demand and local production of rice in Kerala is widening primarily because of the continuous pace at which rice are giving way to urbanization.

II. AUTOMATED WATER LEVEL REGULATION

The soil of the paddy fields of Kuttanad is salty and is extremely acidic. The acidity is due to the production of sulphuric acid by microbiological oxidation of sulphur compound present in the soil. High amount of iron, manganese, aluminum and sulphides are present in the soil. This acidity of the soil is a major constraint which retards the production of rice in the Kuttanad area. Regular rinsing of the soil by water can reduce the acidity and increase the production. Rice is a crop which needs high amount of water

for its growth. The main factor to be considered here is that the water should not be too much or too low. Periodic monitoring and controlling water level is essential for the healthy growth of the rice plant.

Due to the socio-economic states prevailing in the state of Kerala the labor community is getting narrower. The paddy field owners are not able to recruit sufficient labors for these processes. The initial activities like plowing, seeding etc and the final activities like harvesting are done as a group and hence can be easily coordinated. The periodic monitoring of needs, controlling the pests and water level monitoring is a tedious process. Majority of the paddy field farmers are employed in some other activities or are considering this activation as a secondary business. Hence their insolvent on a daily basis should be greatly reduced.

Since the pumping of water to and from the field is the major activity from plowing to harvesting, automating the process can greatly reduce the load on farmers. Automated systems may monitor the water level and regulate the levels by sophisticated systems and can send messages to the farmers.

III. SENSORS FOR MONITORING WATER LEVEL

Paddy field is a large area and is nearly flat in nature. Normally the water level in a field will be uniform throughout the field. Water wells can be made as per the need and the water level in each well can be monitored. Water level sensors can be used for sensing the levels. These sensors can monitor the level according to the user needs. Normally there can be three levels, normal, high and low. These sensors are electro-mechanical devices. Even though electronic sensors are available due to the environmental conditions electro-mechanical devices are more applicable. The mechanical part in the devices will float on water and the electrical part will produce the signals based on the portion of the floating device.

These values or signals generated by the sensor needs to be transmitted to the farmers. Transmitting the electrical signal from the device in the field to the farmer through copper wire is not practical, since it is so long and we many wells and sensors at different locations in the field. A farmer may have hectors of area as paddy field and need hundred of sensors for monitoring. Hence wired devices are not practical. Use of commonly used wireless communication technology is also not advisable due to complexity of the communication system and the high power needs of such systems. Proving power supply or having a solar panel is also not economical. High battery power may be needed by such devices and regular charging or replacement of the batteries is highly costly. Alternative solution is to provide power from a solar panel. The solar panels are of high cost and hence are after prove to theft. The paddy fields are of large area and ensuring security to each solar panel is also not possible. Low cost communication devices which needs low power and less maintenance, which can operate on a wireless architecture is the solution. The new generation wireless sensor networks can be considered for the situation.

IV. WIRELESS SENSOR NETWORKS FOR COMMUNICATION

Wireless sensor Network (WSN) is a major technology used for real time monitoring of environmental assets. WSN has the advantages of large scale deployment, low maintenance, scalability, adaptability, less power needs etc. with the disadvantages of low memory, low power, low bandwidth etc. They can be employed in hostile environments and the features like use of low power and low maintenance makes them the most suited technology for real-time environmental monitoring. They can be highly useful in monitoring the water level in the paddy fields.

ZigBee is the most commonly used network standard today and it is a low-cost, low-power consumption, low data-rate, two-way wireless networking standard that is aimed at remote control and sensor applications which is suitable for operation in harsh radio environments and in isolated locations. It builds on the IEEE standard 802.15.4-2003 which defines the physical layer and medium access control sub layer. Above this, ZigBee defines the application and security layer specifications enabling interoperability between products from different manufacturers. There are several different network topologies that a wireless sensor network can form: star, tree, bus, ring, and mesh. All these topologies have their own individual benefits but the mesh network topology is best suited in our case. A ZigBee WSN is shown in Fig 1. It consists of three types of nodes: a ZigBee Coordinator, ZigBee Routers, and ZigBee End-Devices.

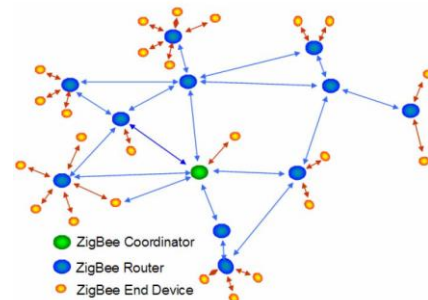


Figure 1-Typical ZigBee WSN – Mesh Architecture

V. WSN SYSTEM ARCHITECTURE

In our project the water wells are constructed at suitable location in the field and sensor columns are attached. The electro-mechanical sensors will measure the water level and the valves can be transmitted through the WSN for this the entire paddy field can be divided into a number of clusters and these clusters can have number of water wells or sensor wells. Each cluster will have a cluster head and all sensor nodes in that cluster will communicate the data to the cluster heads. The water level sensed by the sensor can be low, normal or high. These valves are sent to the cluster head then the cluster head aggregates these valves and compare them. If all the valves are normal then it need not send any data to the user. If any valve is high or low then it needs to be communicated to the user. For this the cluster head transmits the data to the sink node. The sink node is the node which is connected to all the cluster heads or in other words the cluster heads can communicate to the sink node in one hop.

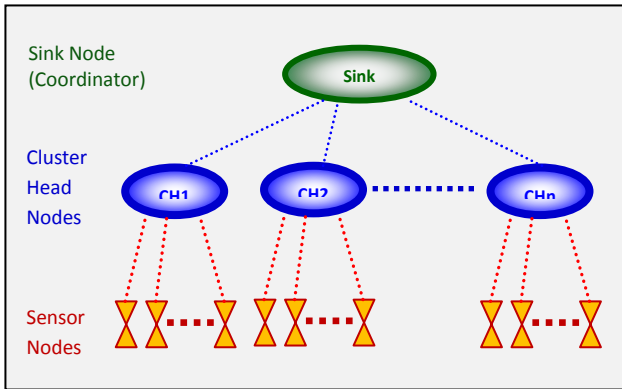


Figure 2 – WSN Architecture

Different topologies can be adopted in the WSN. In our project we are using a mesh topology. The WSN architecture used for the project is shown in fig 2. The sensor nodes in on region will form a mesh structure and each of these mesh structure will be a cluster. These nodes will together have a head node called the cluster head. For example in a wireless sensor network with hundred nodes, the nodes can be divided region wire ten to twelve nodes can form a cluster which operate in a mesh topology. Each of these meshes will have a head node called the cluster head node. Similarly another ten to twelve nodes form another mesh cluster. Totally we may have eight to ten clusters and their cluster heads. Then cluster heads are operating in the mesh topology so we have a mesh with two levels. These cluster heads communicating to the sink node which is on top of the network architecture.

Sudden increase in the water level or decline in the water level is not often occurred hence real-time monitoring or a full time monitor is not necessary. The monitoring can be done on a six hour basis, that is four times a day and its remedial measures can be taken. The remedial measure in the sense, pumping in water if water level is low and pumping out water if water level is high. As stated earlier in the introduction, Kuttanad area is lying below the mean sea level. The water level in the surrounding water bodies of the paddy field are higher than that of the paddy fields so pumping in water is easy by just opening the inlet valves located at the outer boundaries of the paddy fields. At situation where water level is high the excess water needs to be pumped out for this to happen there are electrical pump stations at different locations. The paddy fields are connected each other through water canals and these canals will have the pumping station. These pumps can be operated and the water can be pumped out.

Normally the low level sensor nodes will be in the sleep state and will be active only on the sixth hourly basis. When active they sense the water level and send it to the cluster head. After sensing and transmitting it goes to the sleep state for power usage optimization and will be active in the next sixth hour slot or otherwise instructed by the cluster head.

VI. DATA AGGREGATION

Initially when the network gets booted up each low level sensor node will measure the water level through the electro mechanical sensors and this valve will be sent to the cluster head. The cluster head upon receiving the data

packet from all its subordinate nodes will start analyzing the data. It compares the valves of water level with the predetermined values. These predetermined values are fed to the system by the farmer. These values will be different according to different seasons and processes initiated by the farmer, for example, the field needs to be dry for some days after de-weeding and more water needs to be present for applying fertilizer.

On analysis if the cluster head is finding the value to be higher or lower than the predetermined value, it enters into a state from *normal* to *alert state*. Otherwise it continues to be in the *normal state*. On *alert state* the cluster head sends the data packets to the sink node and the remaining processes will be done by the sink node. It also instructs the subordinate sensor nodes to *sniff state*. The sensor nodes are having two states, *sniff state* and *sleep state*.

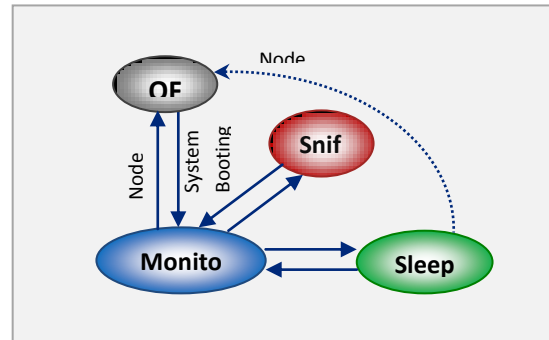


Figure 3 – Sensor Node State Transition

State	Description
OFF	Initial State of the system, Once booted up the node reaches this state when the node is shutdown or fails
Monitor	Normal operation - sensing and transmission at longer intervals
Sniff	Sensing and transmission at shorter intervals
Sleep	No sensing and transmission, a state of low power usage.

During *sniff state*, the sensors will be measuring the water levels at a high rate i.e. at short intervals of time T_{sniff} . It measures the valves and sends these valves to the cluster head. During *sleep state* the sensor nodes will be idle most of the time. Here the sensing intervals will be longer with a larger valve for time, T_{sleep} . The sensor node will initiate a counter for T_{sleep} and goes into *sleep state*, until the counter valve is reached. It wakes up after T_{sleep} and repeats the process by sensing and transmitting data to cluster head.

The state transition from *sleep* to *sniff* and reverse of the sensor nodes is instructed by the cluster head. The cluster head does this after receiving an *alert* value from any of its sensor nodes. Then the cluster head enters into *alert state* and instruct the nodes to enter into *sniff state*. Along with this the data will be reported to the sink node by the cluster head. The sink node will not perform any analysis of the data. It just forwards the matter to the Field Control

Centre (FCC). The Field Control Centre is a program which is running on the user computer. The FCC will receive the data from all the cluster heads through the sink node. The FCC will process these data and decides the remedial actions. It accesses the regions which are affected and then issue commands to the pumping stations of that region to either pump in or pump out the water.

Once the situation of the water level changes it will be reflected on the values received by the cluster heads from the sensor nodes. But it continues to be in the *alert state* until all the sensor nodes are sending values within predefined limit. When this situation is arrived it sends the message to the sink node and instructs all the sensor nodes to go to sleep state and enters into normal state. This state continues for a period of T_{sleep} and the above processes are repeated. Once the situation of the field is under control the full network will be in a sleep state for a period of T_{sleep} .

VII. CONCLUSION AND FUTURE WORK

India is developing at a faster rate but due to urbanization crop fields are getting converted to new forms of the urban world. Also farming community is becoming narrower day by day due to better opportunities. The gap between need and production is increasing at a rapid rate. These problems get elevated when production is decreased. This paper discussed the environmental and socio economical back ground of Kuttanad, the problems faced in agriculture and proposed use of wireless sensor networks for overcoming some difficulties. In the future this proposed system will be fabricated, deployed and tested.

REFERENCES

- [1] I. F. Akyildiz and E. P. Stuntebeck, "Wireless underground sensor networks: research challenges," *Ad Hoc Networks*, vol.4, no. 6, pp. 669–686, 2006.
- [2] H. R. Bogena, J. A. Huisman, H. Meier, U. Rosenbaum, and A. Weuthen, "Hybrid wireless underground sensor networks: quantification of signal attenuation in soil," *Vadose Zone Journal*, vol. 8, no. 3, pp. 755–761, 2009.
- [3] J. Tiusanen, "Wireless soil scout prototype radio signal reception compared to the attenuation model," *Precision Agriculture*, vol. 10, no. 5, pp. 372–381, 2009.
- [4] A. R. Silva and M. C. Vuran, "Empirical evaluation of wireless underground-to-underground communication in wireless underground sensor networks," in *Proceedings of the 5th IEEE International Conference on Distributed Computing in Sensor Systems (DCOSS '09)*, vol. 5516 of *Lecture Notes in Computer Science*, pp. 231–244, Marina del Rey, Calif, USA, June 2009.
- [5] Jacques Panchar "Wireless Sensor Networks for marginal Farming in India" IngenieurDiplom'e en Syst`emes de Communication (M.Sc.), EcoleolytechniqueF'ed' erale de Lausanne, Suisse A. Arora, R. Ramnath, and.Ertin.Exscal: *Elements of an extreme scale wireless sensor network*, 2005.
- [6] I.F. Akyildiz, W. Su, Y. Sankarasubramaniam, and E. Cayirci. A Survey on Sensor Networks. *IEEE Communications Magazine*, Vol. 40, No. 8, 2002. J. Burrell, T. Brooke, and R. Beckwith.
- [7] J. Burrell, T. Brooke, and R. Beckwith. "Vineyard computing: sensor networks in agricultural production". *IEEE Pervasive Computing*, 3(1):38–45, Jan-Mar 2004.
- [8] E K Mathew, Madhusudan Nair, T D Raju, U Jaikumaran, "Drainage Digest" – A report based on two
- [9] Anurag D, Siuli Roy and SomprakashBandyopadhyay "Agro-Sense : Precision Agriculture using sensor bases wireless mesh networks" *Indian Institute of Management Kolkatta*
- [10] J. Burrell et al. Vineyard computing: sensor networks in agricultural production. *IEEE Pervasive Computing*, 3(1):38–45, Jan-Mar 2004.
- [11] D.D.Chaudhary, S.P.Nayse, .Waghmare "Application of wireless sensor networks for greenhouse parameter control in precision agriculture" *International Journal of Wireless & Mobile Networks (IJWMN) Vol. 3, No. 1, February 2011*
- [12] Kavi K. Khedo, Rajiv Perseedoss and AvinashMungur "A wireless sensor network air pollution monitoring system" *International Journal of wireless and mobile networks (IJWMN) Vol.2, No.2, May 2010.*
- [13] AndrzejPawlowski, Jose L. Guzman, Francisco Rodriguez, Manuel Berenguel, Jose Sanchezand Sebastian Dormido, 2009. Simulation of greenhouse climate monitoring and control with wireless sensor network and event-based control. *Sensors*, 9(1): 232-252. DOI:10.3390/s90100232.
- [14] Carlos Serodio, J. Boaventura Cunha, Raul Morais, Carlos Couto, Joao Monteiro, 2001. A networked platform for agricultural management systems. *Computers and Electronics in Agriculture*, 31 (1): 75-90. DOI: 10.1016/S0168-1699(00)00175-7.
- [15] Hui Liu, ZhijunMeng, Maohua Wang, 2009. A Wireless Sensor Network for Cropland Environmental Monitoring. *International Conference on Networks Security, Wireless Communications and Trusted Computing*, 2009. *NSWCTC '09, Volume 1: 65 - 68. DOI:10.1109/NSWCTC.2009.306*
- [16] Hui Liu, ZhijunMeng, Shuanghu Cui, 2007. A wireless sensor network prototype forenvironmental monitoring in greenhouses. *Proceedings of the International Conference on Wireless Communications, Networking and Mobile Computing*, 2007 (WiCom 2007), 21-25 Sept. 2007, pp: 2344 - 2347.
- [17] Hyun-joongKang ,Meong-hun Lee and Hyun Yoe, 2008. Effect of Sensor Specific Crop Location on Wireless Sensor Network Performance. *Studies in Computational Intelligence, Volume 131/2008: 219-229. DOI: 10.1007/978-3-540-79187-4.*

Stiffness Metrics for Design of 3-RRR Flexible Manipulator

K. V. Varalakshmi¹, Dr. J. Srinivas²

Department of Mechanical Engineering, NIT Rourkela-769 008, India

Abstract : This paper presents the kinematics and stiffness analysis of flexible parallel manipulators. As a primary step, the forward kinematic solutions are obtained using soft computing approaches based on Genetic Algorithms (GAs) and Neural networks (NN) and workspace configuration is arrived. The Jacobian and platform stiffness matrices are evaluated within the defined workspace. The flexible link configuration with compliant joints is analyzed using a pseudo rigid-body model. The revolute joint compliance is considered with narrow rectangular flexure hinges which are idealized as equivalent torsional springs in pseudo rigid-body model. Having the defined link dimensions and joint cross-sections at any configuration, the model is discretized with frame and plate elements and the assembled system is analyzed statically and dynamically. The methodology is illustrated with 3-RRR flexible parallel manipulator and the results are compared with commercial software solution.

Keywords: Kinematics, Workspace, Flexible links, Forward kinematics, Pseudo rigid body model.

I. Introduction

Nowadays parallel manipulators have become an attractive topic of interest in several applications, such as machine tools, motion simulators, micro robots, medical devices and physical sensors, due to their intrinsic advantages in the factors of payload, stiffness, accuracy, operational velocity and acceleration. Parallel manipulators which are closed kinematic structures composed of two platforms interconnected by few links. The top platform (referred to as end-effector) is the mobile one controlled with respect to the base platform through variable link lengths to obtain the final position and orientation of the end-effector. The inverse kinematics of such manipulators, which maps the task space to the joint space, is a straight-forward problem; while the direct kinematics is often complex involving multiple solutions in Cartesian space. Direct kinematics is concerned with the determination of the end-effector pose from the given set of link lengths or joint angles. It has no closed form solution since it involves solving a series of simultaneous nonlinear algebraic equations and non-unique multiple set of solutions referred to the assembly modes, are obtained from one set of data.

Several approaches have been proposed for the forward kinematics of such manipulators. The analytical approach formulates a system of nonlinear equations and then converts it to a high degree univariate polynomial which can be solved by numerical techniques. It has been shown that for the most general parallel manipulators, this approach leads to

a polynomial of degree 40, resulting in 40 distinct solutions [1-2]. However, the challenging problem is not to find all the solutions, but to directly determine a unique solution among all possible solutions. Two approaches achieve this requirement, namely the iterative approach and the use of additional sensors [3-5]. These approaches have their own disadvantages in terms of complexity and cost. The Jacobian matrix of the system [6] is also of importance in static analysis and velocity kinematics, which in turn required in trajectory control tasks.

In practice, the functionality of linkage would be drastically affected by treating the closed-loop assembly as a compliant mechanism. Monolithic skeleton joining all the links with narrow cross sectional segments forms such compliant mechanism. There are several advantages of these compliant mechanisms and many studies [7-8] revealed the analysis of such compliant parallel linkages. The workspace characteristics, including total (or reachable) and primary (or dexterous) spaces and the singularity characteristics are also important factors in design as well as control coordination of parallel manipulators. The total workspace is the region over which the end-effector can reach with at least one orientation, whereas the primary workspace is that the end-effector can reach with all orientations [9]. Many researchers have addressed the workspace analysis of parallel manipulators and the predominant approach used as seen in the literature in general, has been a geometric mapping. For example, the boundary of the dexterous workspace for a 3-degree of freedom (DOF) planar parallel manipulator was determined by using screw theory [10] and geometric reasoning [11-12]. For a broader class of parallel manipulators, a study to classify the various shapes of workspace due to changes in link lengths was reported in [13] and a formulation of an architecture-independent method based on kinematic mapping can be found in [14]. The manipulator sometimes loses degrees of freedom at some inverse kinematic singularities within the workspace. It is shown that at these instants stiffness of manipulator reaches a maximum value. Several recent works focused on such studies to improve the effectiveness of the manipulation.

In this line, the present work deals with forward and inverse kinematics, workspace and stiffness analysis of parallel manipulators. The forward kinematics solutions are obtained numerically by minimizing the squared-error defined in terms of Cartesian pose vector and the solutions are validated with radial-basis function neural network outputs. Jacobian matrix at a particular platform pose is then obtained and platform stiffness matrix is determined. For the analysis of the link-flexibility and joint compliance effects, a finite element model is proposed with frame and plate elements

along with equivalent torsional stiffness at the joints. This facilitates in evaluation of changes in platform stiffness matrix of manipulator. The stiffness indices are validated with commercial finite element code. The paper is organized as follows: Section-2 deals with the mathematical modelling of illustrated 3-RRR planar parallel manipulator and various indices to represent the kinematic characteristics along with an introduction to the proposed FE model. Section-3 describes the results and discussion.

II. Mathematical Modelling

The 3-RRR is a three degree-of-freedom planar parallel manipulator. It has a mobile platform and three R-R-R serial chains that join it to a fixed base. Each chain is composed by three rotational revolute (R) joints. As shown in Fig.1, the point P(x,y) is the end-effector position in the global reference frame and ϕ be its orientation. The point O is the origin of the fixed reference frame and the points A_i, B_i, C_i , with $i=1,2,3$, define the rotational articulations of each limb. Points A_i are actuated, so that the actuators are fixed to the base. Thus, the three fixed pivots A_1, A_2 and A_3 define the geometry of a fixed base and the three moving pivots C_1, C_2 and C_3 define the geometry of a moving platform. Together, the mechanism consists of eight links and nine revolute joints. In the programming of a robot manipulator, typically a set of desired positions and orientation, and perhaps the time derivatives of the positions and orientations of the end-effector are specified in space. The problem is to find all possible sets of actuated joint variables and their corresponding time derivatives which will bring the end-effector to the set of desired positions and orientations with the desired motion characteristics. This process is known as inverse kinematics. On the other hand, sometimes the actuated joint variables and possibly their time derivatives are obtained from reading of sensors installed at the joints, from which all possible sets of end-effector positions and orientations and their corresponding time derivatives are obtained. This procedure is called direct or forward kinematics. The closure loop equations are extremely important in order to analyze and solve these kinematics problems of parallel robots, as they implicitly include the constraints of the mechanism. For direct kinematics of a 3-RRR manipulator, Gosselin [15] showed that a maximum of six solutions are possible. However, due to the trajectory tracking procedure, only one of the solutions is deemed to be correct. Kinematics problems can be solved by various methods such as geometric vector analysis, matrix algebra, direct search and screw-theory.

2.1 Inverse Kinematics

Inverse kinematics of 3-RRR is a straight-forward problem, which is an essential step for the velocity kinematics [16-17]. The base coordinate frame $O-X_0-Y_0$ shown in Fig. 1 is fixed at joint A_1 and a moving or mobile coordinate frame $P-X-Y$ is attached at the center of the moving platform. Let a and h denote the width of the base and moving platforms respectively. It is also assumed that the length of each link in the limb as l .

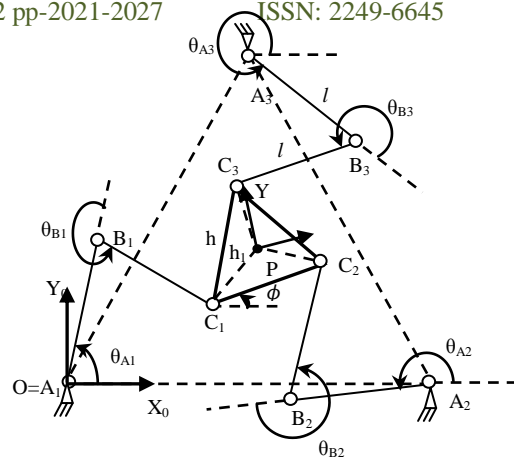


Fig.1 Schematic of 3-RRR Planar Parallel Manipulator

The position vector of point B_i ($i=1,2,3$) in the base coordinate frame can be expressed as

$$r_{Bi} = r_{Ai} + l \begin{bmatrix} \cos \theta_{Ai} \\ \sin \theta_{Ai} \end{bmatrix}, \quad i = 1,2,3. \tag{1}$$

where r_{Ai} and r_{Bi} are the position vectors of joint points A_i and B_i . Also, θ_{Ai} are rotation angles of links A_iB_i . The position vector of C_i can be written as

$$r_{Ci} = r_p + [R]r_{Ci}^p \tag{2}$$

Here again, r_p is the position vector of P with respect to base coordinate frame $O-X_0-Y_0$ and r_{Ci}^p is the position vector of C_i in the mobile frame $P-X-Y$, $[R] = \begin{bmatrix} \cos \phi & -\sin \phi \\ \sin \phi & \cos \phi \end{bmatrix}$ is the rotation matrix for transforming the coordinate system $P-X-Y$ to $O-X_0-Y_0$ and θ_{Bi} is the rotation angle of links B_iC_i . The constraint equation associated with the i^{th} kinematic chain can be expressed as a second-order norm given by:

$$\|r_{Ci} - r_{Bi}\| = l, \quad i=1, 2, 3 \tag{3}$$

These are three equations in-terms of actuation degree of freedom θ_{Ai} for given set of coordinates of P and they correspond to workspace space circles. The above equation (3) can be written as

$$e_{1i} \sin \theta_{Ai} + e_{2i} \cos \theta_{Ai} + e_{3i} = 0 \tag{4}$$

Based on equation above equation, the inverse kinematics solution for 3-RRR mechanism can be expressed as

$$\theta_{Ai} = 2 \tan^{-1} \frac{-e_{3i} \pm \sqrt{e_{1i}^2 + e_{2i}^2 - e_{3i}^2}}{e_{3i} - e_{2i}}, \quad i = 1,2,3. \tag{5}$$

where

$$e_{1i} = -2l \left(y - \frac{h \sin \phi}{2} - \frac{\sqrt{3} h \cos \phi}{6} \right) \tag{6}$$

$$e_{21} = -2l \left(x - \frac{h \cos \phi}{2} + \frac{\sqrt{3} h \sin \phi}{6} \right) \quad (7)$$

$$e_{31} = \left(x - \frac{h \cos \phi}{2} + \frac{\sqrt{3} h \sin \phi}{6} \right)^2 + \left(y - \frac{h \sin \phi}{2} - \frac{\sqrt{3} h \cos \phi}{6} \right)^2 \quad (8)$$

$$e_{12} = -2l \left(y + \frac{h \sin \phi}{2} - \frac{\sqrt{3} h \cos \phi}{6} \right) \quad (9)$$

$$e_{22} = -2l \left(x + \frac{h \cos \phi}{2} + \frac{\sqrt{3} h \sin \phi}{6} - a \right) \quad (10)$$

$$e_{32} = \left(x + \frac{h \cos \phi}{2} + \frac{\sqrt{3} h \sin \phi}{6} - a \right)^2 + \left(y + \frac{h \sin \phi}{2} - \frac{\sqrt{3} h \cos \phi}{6} \right)^2 \quad (11)$$

$$e_{13} = -2l \left(y + \frac{\sqrt{3} h \cos \phi}{3} - \frac{\sqrt{3}}{2} a \right) \quad (12)$$

$$e_{23} = -2l \left(x - \frac{\sqrt{3} h \sin \phi}{3} - \frac{1}{2} a \right) \quad (13)$$

$$e_{33} = \left(x - \frac{\sqrt{3} h \sin \phi}{3} - \frac{1}{2} a \right)^2 + \left(y + \frac{\sqrt{3} h \cos \phi}{3} - \frac{\sqrt{3}}{2} a \right)^2 \quad (14)$$

Taking the time derivative of the Eq. (3) leads to:

$$\begin{bmatrix} D_{11} & 0 & 0 \\ 0 & D_{22} & 0 \\ 0 & 0 & D_{33} \end{bmatrix} \begin{Bmatrix} \dot{\theta}_{A1} \\ \dot{\theta}_{A2} \\ \dot{\theta}_{A3} \end{Bmatrix} = \begin{bmatrix} Q_{11} & Q_{12} & Q_{13} \\ Q_{21} & Q_{22} & Q_{23} \\ Q_{31} & Q_{32} & Q_{33} \end{bmatrix} \begin{Bmatrix} \dot{X} \\ \dot{Y} \\ \dot{\phi} \end{Bmatrix} \quad (15)$$

Where

$$Q_{i1} = 2l \cos \theta_{Ai} + e_{2i}/l \quad (16)$$

$$Q_{i2} = 2l \sin \theta_{Ai} + e_{1i}/l \quad (17)$$

$$D_{ii} = e_{1i} \cos \theta_{Ai} - e_{2i} \sin \theta_{Ai} \quad (18)$$

$$Q_{13} = \left(\frac{h \sin \phi}{2} + \frac{\sqrt{3} h \cos \phi}{6} \right) Q_{11} - \left(\frac{h \cos \phi}{2} - \frac{\sqrt{3} h \sin \phi}{6} \right) Q_{12} \quad (19)$$

$$Q_{23} = \left(\frac{h \cos \phi}{2} + \frac{\sqrt{3} h \sin \phi}{6} \right) Q_{22} + \left(-\frac{h \sin \phi}{2} + \frac{\sqrt{3} h \cos \phi}{6} \right) Q_{21} \quad (20)$$

$$Q_{33} = -\frac{\sqrt{3} h \sin \phi}{3} Q_{32} - \frac{\sqrt{3} h \cos \phi}{3} Q_{31} \quad (21)$$

Equation (15) can be written as: $[J_q]\{\dot{q}\}=[J_x]\{\dot{X}\}$ with $[J_q]$ and $[J_x]$ as two Jacobian matrices; one giving the condition for direct singularity problem and other gives that of the inverse singularity states.

2.2 Forward Kinematics Solutions

The investigation of forward kinematics issue is important and practical for the manipulation and control of the pose of the parallel manipulator. In present paper, two soft computing tools are proposed based on (i) minimization of positional error of platform joints and (ii) integrating a neural network with inverse kinematics model. Referring to Fig.2, if the six input angles and all the link-lengths are specified, the positions of points C_i are calculated from the following equation [18]:

$$C_i = [A_i + l \cos(\theta_{Ai}) + l \cos(\theta_{Ai} + \theta_{Bi}),$$

$$l \sin(\theta_{Ai}) + l \sin(\theta_{Ai} + \theta_{Bi})], \quad i=1, 2, 3 \quad (22)$$

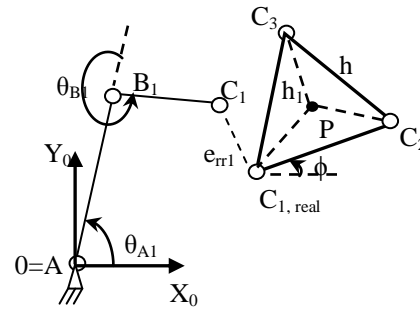


Fig.2 Connectivity of point C_1 in one limb

On the other hand, the real coordinates $C_{i,real}$, are obtained from a set of Cartesian pose vector $(x, y$ and $\phi)$ of the table centre according to the following inverse relations:

$$C_{1,real} = [x - h_1 \cos\left(\frac{\pi}{6} + \phi\right), y - h_1 \sin\left(\frac{\pi}{6} + \phi\right)] \quad (23)$$

$$C_{2,real} = [x + h_1 \cos\left(\frac{\pi}{6} - \phi\right), y - h_1 \sin\left(\frac{\pi}{6} - \phi\right)] \quad (24)$$

$$C_{3,real} = [x - h_1 \sin(\phi), y + h_1 \cos(\phi)] \quad (25)$$

The connectivity error $f = \sum_{i=1}^3 e_{rr_i} = \sum_{i=1}^3 \|C_{i,real} - C_i\|$, between the two sets of points $C_{i,real}$ and C_i constitutes the objective function to be minimized. When this error is close to zero, the manipulator achieves a desired position and orientation of the mobile platform. In present work, binary coded genetic algorithms (GA) approach is used to obtain the optimum solution. GA [19-20] is computational method meant to solve complex and nonlinear optimization problems. They are inspired by the genetic processes of living organisms. In nature, individuals of a population compete for basic resources. Those individuals achieving better surviving rates have higher probabilities to attract possible partners and to generate descendants. As a consequence, best adapted individuals' have higher chances to be passed on to the next generations. GA, in order to emulate this behavior, works with a population of individuals. Each individual represents the possible solution of a problem (for example the best set of features to identify disruptions). The quality of each individual in evolutionary terms is evaluated on the basis of a fitness function. A higher probability to have descendants is assigned to those individuals with better fitness functions. The most promising areas of the searching space are explored by favoring the crossing between the better adapted individuals.

Neural networks are noted for the ability of complex functions learning and relationship building, which led to their extensive applications including pattern classification, function approximation and optimization. They can be utilized to address the forward kinematics problem of parallel manipulators. As the solution of inverse kinematics problem for parallel manipulators is simpler than forward kinematics problem, neural network addresses the forward kinematics model through the use of inverse kinematics solution. Training set for neural network is selected out of the set of

inverse kinematics solutions. Discrete points of each actuated joint are taken as inputs and corresponding poses about the motion of platform center are considered as outputs. The neural network is trained using the above off-line training set and gives the solution of the forward kinematics model. In present work, conventional radial basis function network [21] with a nonlinear hidden layer and a linear output layer is employed. Each of the units in hidden layer applies a fixed-feature detector which uses a specified kernel function (Gaussian) to detect and respond to localized portions of the input vector space. The network output is a weighted linear summation of the output of the hidden neurons. This network is a universal function approximates that demonstrates more robustness and flexibility than traditional regression approaches such as polynomial fits. Fig.3 shows the proposed methodology of solving forward kinematics.

2.3 Workspace of the linkage

An important characteristic of a parallel manipulator is its workspace. Several types of workspaces have been proposed, such as the constant orientation workspace, the maximal workspace, the inclusive maximal workspace, and the dexterous workspace. The constant orientation workspace of a planar parallel mechanism can be found as the intersection of annular regions corresponding to the reachable workspaces of its kinematics chains.

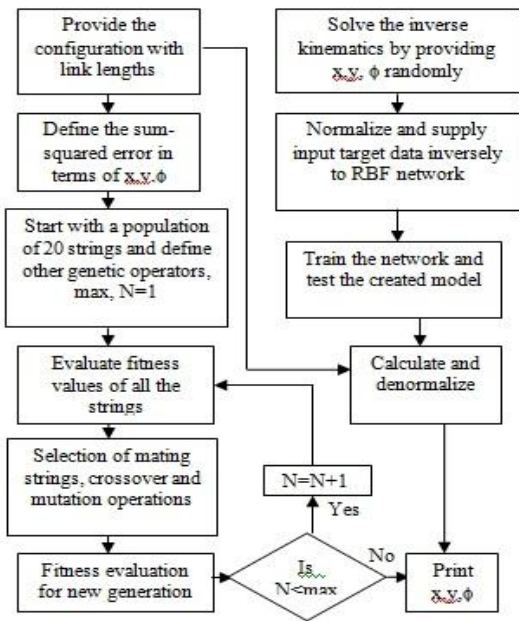


Fig.3 Flowchart for the forward kinematics methodology

The equations of workspace circles can be expressed as [16]:

$$(x+C_{ix}'\cos \phi - C_{iy}'\sin \phi - A_{ix})^2 + (y + C_{ix}'\sin \phi + C_{iy}'\cos \phi - A_{iy})^2 = (l_1 \pm l_2)^2 \quad (26)$$

Here l_1 and l_2 are the lengths of links A_iB_i and B_iC_i respectively. The prime ' indicates that coordinate measurement is with respect to mobile frame of reference. Thus, workspace essentially depends on x,y and ϕ . If $l_1 \neq l_2$,

there are two concentric circles correspond to every center. In practice, the link lengths are taken identical in most of the cases.

2.4 Jacobian analysis

Let the actuated joint variables and the location of the moving platform be denoted by the vectors q and x , respectively. Then the kinematic relations can be written in the general form as $f(x,q)=0$ where f is the function of $x=(x, y, \phi)^T$ and $q=(\theta_{A1}, \theta_{A2}, \theta_{A3})^T$ and 0 is an n -dimensional zero vector. The variables x, y and ϕ are the coordinates of the end-effector point P with respect to the base and orientation of the platform, respectively. Moreover, θ_{A1}, θ_{A2} and θ_{A3} denote actuated joints. Differentiating the f with respect to the time, $[J_x]\{\dot{x}\} + [J_q]\{\dot{q}\}=0$ is obtained. Here \dot{x} and \dot{q} are the time derivatives of x and q , respectively. Here $[J_q]$ and $[J_x]$ are two separate Jacobian matrices. The overall Jacobian matrix for a parallel manipulator can be obtained as $[J] = [J_q]^{-1}[J_x]$ and also corresponding stiffness

2.5 Stiffness Analysis & Dexterity index

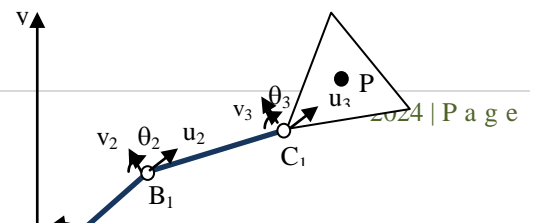
The value of stiffness evolves according to the geometry, topology of the structure and position and orientation of the platform within the workspace. The stiffness of a parallel robot at a given point of its workspace can be characterized by its stiffness matrix. This matrix combines the forces and moments applied to the platform. For rigid body model, the stiffness matrix is defined as follows [22]:

$$[S]=k[J]^T[J]^{-1}=k([J][J]^T)^{-1} \quad (27)$$

where k is the stiffness of actuated joint which is assumed to be same for all the joints. The condition number is quite often used as an index to describe the accuracy/dexterity of a robot and the closeness of a pose to a singularity. Condition number of a matrix is used in numerical analysis to estimate the error generated in the solution of a linear system of equations by the error on the data. When applied to the Jacobian matrix, the condition number will give a measure of the accuracy of the Cartesian velocity of the end-effector and the static load acting on the end-effector. The dexterity of a manipulator can be denoted as the condition number of its Jacobian matrix. Dexterity has recently emerged has a measure for manipulator kinematic performance.

2.6 Finite element model

Links are considered as flexible members undergoing flexural and axial deformations. For analysis of flexibility effects, each limb ($i=1,2,3$) of the manipulator is discretized with frame elements and therefore the stiffness matrix for each of the three limbs is calculated as an assemblage of individual link stiffness matrices. In present case, there are three degrees of freedom at each node namely axial deformation (u) and bending deflection (v) and slope (θ) as shown in Fig.4.



(mm)	0	0	0	900	450	779
Mobile joints (mm)	C ₁		C ₂		C ₃	
	x	y	x	y	x	y
	414	230	493	244	441	305

Fig.4 Finite element model

The unknown displacements at the joints are calculated from the applied joint torques and the elemental forces and corresponding stresses are obtained. Joint compliance is considered as a torsional spring in our pseudo-rigid body model. Here the joint is approximated as a narrow rectangular cross-sectioned element, whose spring constant is given as [23] $(E_n I_n)/l_n$, where E_n is the elastic modulus, I_n is the moment of inertia of narrow cross-section which is equal to $\frac{1}{12}bt^3$, for rectangle. Here, b, t, l_n are respectively width, thickness and length of the section.

III. Results and Discussion

The parameters of the manipulator considered in the present analysis are depicted in Table-1. The material chosen is steel with density $\rho=7800\text{kg/m}^3$ and elastic modulus $E=2.1 \times 10^5 \text{N/mm}^2$. This data is needed during the finite element modelling.

Table-1. Dimensional Parameters of Manipulator[24]:

Parameter	Dimension (mm)
Length of each link	400
Thickness of each link	6
Width of each link	23
Side length of the moving platform	80
Side length of the fixed platform	900
Thickness of the moving & fixed platform	25
Length of the narrow cross-section	40
Thickness of the narrow cross-section	1.5
Width of the narrow cross-section	23

Table-2 shows the input configuration of the manipulator in terms of the base and mobile platform coordinates.

Table-2. The 3-RRR planar parallel manipulator configuration

Base Joints	A ₁		A ₂		A ₃	
	x	y	x	y	x	y

First, the genetic algorithm with uniform crossover and mutation used in finding forward kinematic solution has a crossover rate of 0.999 and mutation rate of 0.001. The high crossover rate ensures that maximum global search. The population size is taken as 40, and the outputs are tested by varying the number of generations. The variable ranges considered in the present task are shown in Table-3.

Table-3. The upper and lower bounds of the design variables.

Design variables	Variable limits
Cartesian coordinate moving platform (x)	[0 – 600 mm]
Cartesian coordinate moving platform (y)	[0 – 600 mm]
Angle of the moving platform (ϕ)	[-360° - 360°]

During neural network analysis, initially an inverse kinematics problem is solved by geometric method for a range of Cartesian coordinates of the end-effector X, Y and ϕ chosen according to $X=[445,450 \text{ mm}]$, $Y=[255,262 \text{ mm}]$ and $\phi=[-10^\circ \ 10^\circ]$. Now RBF neural network model is trained with the output of the above inverse kinematics solution as input data, while the corresponding Cartesian coordinates are treated as target data. The number of training patterns taken here are 1008 and the spread constant employed is 1.0. Table-4 shows the comparison forward kinematic solution with genetic algorithms and neural networks.

Table-4. Forward kinematic solution using Genetic Algorithms and Neural networks

Method	No. of Iterations	X (mm)	Y (mm)	ϕ (deg)
GA	5000	449.85	260.41	9.50
	6000	451.61	259.82	9.50
Neural networks	1008	448.94	257.64	10.18
	1008	451.81	259.34	9.78

It is observed that the results obtained from genetic algorithms and neural networks are very close to each other. Fig.5 shows the fitness variation with number of iterations in genetic algorithms.

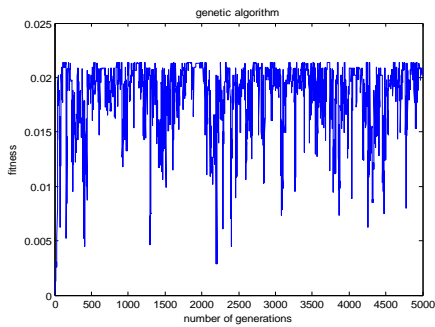


Fig.5 Fitness Vs number of generations
The performance curve for neural network is shown in Fig.6.

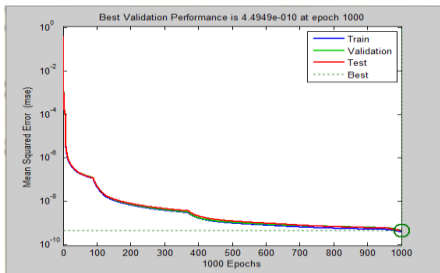
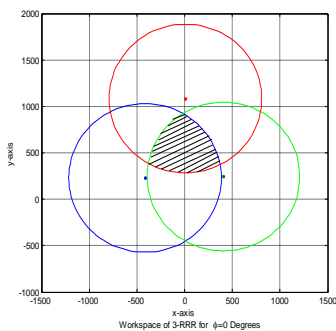
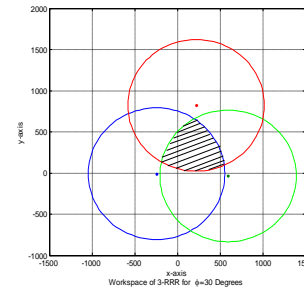


Fig.6 Graph of Training Performance in neural network

The constant orientated workspace is plotted for different angles of the moving platform as shown in Fig.7 and it is observed that the area of the workspace decreases when ϕ varies from 0° to 30° . The dexterity of a mechanism can be considered as its ability to perform small displacements of its end effector at a specified pose of its workspace. It is based on the condition number of the homogeneous Jacobian matrix here the inverse condition number is mapped on a constant orientation workspace to determine the dexterity of the manipulator as shown in Fig.8. It is well known that as inverse condition number is equal to 1 represents a perfect isotropic dexterity and 0 represents singular configuration. Here in Fig.8 all the values around the boundary of the workspace are close to zero, indicating the singularity regions. In order to verify and examine the static performance, a finite element model is prepared. The analysis is carried out using the ANSYS (V13) software.



(a) $\phi=0^\circ$



(b) $\phi=30^\circ$

Fig.7 Constant orientation work spaces at X=450mm, and Y=259.81mm

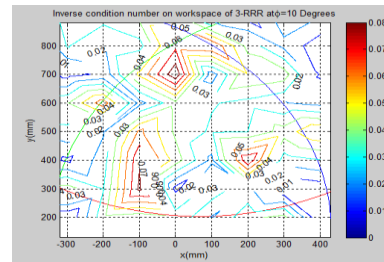


Fig.8 Inverse condition number mapping on constant orientation workspace

The distributions for the scaled minimum stiffness are illustrated in Fig.9. It can be observed that, the distribution of stiffness in a x-y plane the lowest value of minimum stiffness occurs around the boundary of the workspace, where the manipulator approaches direct singularities.

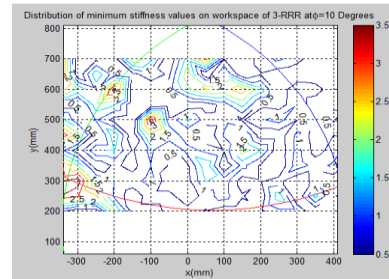


Fig.9 Distribution of minimum stiffness on constant orientation workspace

The finite element model is built based on the original geometrical prototype dimensions, as shown in Fig.10,

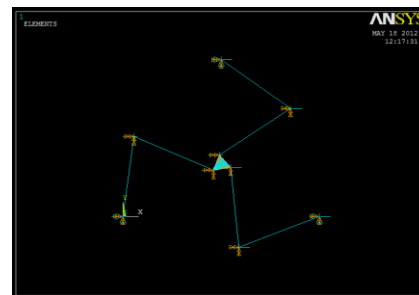


Fig.10 ANSYS image of the model

2-D BEAM188 elements with realistic parameters for limbs and four-node SHELL181 element for moving platform and at each joint combination 14 (spring constant) are

adopted to mesh the model. Forces are applied on the actuated joints so as to get a deformation on the moving platform. The displacements of the model at each node are carefully examined. The analysis results are close to the theoretical outputs as shown in Table-5.

Table-5. Displacement of the end-effector at each node

S.No	Displacements at the end-effector (mm)	
	Theoretical	ANSYS
1	0.0010	0.0022
2	0.0014	0.0023
3	0.0000	0.0021

And also the stiffness at one platform pose (i.e., $x=450\text{mm}$, $y=259.81\text{mm}$, $\phi=10^\circ$) of the moving platform is presented. Here, it is observed that the trace of the Jacobian matrix of the rigid body model as -0.123 . The manipulator stiffness is estimated from the nodal displacements and corresponding reaction forces in the finite element model. Using ANSYS software, it is found to be $0.1007 \times 10^9 \text{ N/mm}$, which is quite larger than $0.816 \times 10^5 \text{ N/mm}$ as obtained from conventional rigid body model with Jacobian matrix. The discrepancy of stiffness may be due to mismatch of the degrees of freedom in the elements under consideration for meshing.

IV. Conclusions

This paper has presented forward kinematic solutions for rigid body model using genetic algorithms and neural networks and also a constant orientation workspace is calculated. Within this workspace, Jacobian and stiffness analysis are conducted and to know the performance of the manipulator the inverse condition number and minimum stiffness values are plotted. Finally at one particular platform pose, finite element model is developed in ANSYS and displacements of the end-effector and stiffness index values are estimated.

REFERENCES

- [1] M. L. Husty, An algorithm for solving the direct kinematics of general Stewart-Gough platforms, *Journal of Mech. Mach. Theory*, 31(4), 1996, 365-380.
- [2] M. Raghavan, The Stewart platform of general geometry has 40 configurations, *ASME Journal of Mech. Design*, 115, 1993, 277-282.
- [3] Y. Wang, A direct numerical solution to forward kinematics of general Stewart-Gough platforms, *Journal of Robotica*, 25(1), 2007, 121-128.
- [4] J-P. Merlet, Closed-form resolution of the direct kinematics of parallel manipulators using extra sensors, *Proc. IEEE Int. Con. Robotics and Automation*, 1993, 200-204.
- [5] I. A. Bonev, J. Ryu, S-G. Kim and S-K. Lee, A closed-form solution to the direct kinematics of nearly general parallel manipulators with optimally located three linear extra sensors, *IEEE Trans. Robot. And Automation*, 17(2), 2001, 148-156.
- [6] Gosselin C, Dexterity Indices for Planar and Spatial Robotic Manipulators, *IEEE International Conference on Robotics and Automation, Cincinnati, OH, USA*, 1990, 650-655.
- [7] Alba, O. G., Pamanes, J. A. Wenger, P., Trajectory planning of a redundant parallel manipulator changing of working mode, *proc.12th IFToMM World Congress*. 2007, 18-21.
- [8] A. Ghafoor, J.S. Dai and J. Duffy, Stiffness Modelling of the Soft Finger Grasp in Robotic Applications, *Submitted to ASME Journal of Mechanical Design*, 2001.
- [9] M. Griffis and J. Duffy, Global stiffness modelling of a class of simple compliant coupling, *Journal of Mech. Mach. Theory*, 28(2), 1993, 207-224.
- [10] Ming Z. Huang, Jean-Lue Thebert, A study of workspace and singularity characteristics for design of 3-DOF planar parallel robots", *Int.J.Adv Mannuf Technol.*, 51, 2010, 789-797.
- [11] Pennock GR, Kassner DJ, The workspace of a general geometry planar three-degree-of-freedom platform-type manipulator, *ASME Journal of Mech. Design* 115, 1993, 269-276.
- [12] Merlet J-P, Gosselin C, Mouly N, Workspace of planar parallel manipulators, *Journal of Mech. Mach. Theory*, 33, 1998, 7-20.
- [13] Gao F, Liu X-J, Chen X, The relationships between the shapes of the workspaces and the link lengths of 3-DOF symmetrical planar parallel manipulators, *Journal of Mech. Mach. Theory, Mech. Mach. Theory*, 36, 2001, 205-220.
- [14] Hayes MJD, Architecture independent workspace analysis of planar three-legged manipulators, *In: Proceedings of the workshop on fundamental issues and future research directions for parallel mechanisms and manipulators*, Quebec City, Quebec, Canada, 2002.
- [15] C. Gosselin, J. Angeles, *Kinematics of Parallel Manipulators*, PhD Thesis, McGill University Montreal, Quebec, Canada, 1989.
- [16] M.Arsenault and R.Boudreau, The synthesis of three degree of freedom planar parallel mechanism with revolute joints (3-RRR) for an optimal singularity-free workspace, *Journal of Robotic Systems*, 21, 2004, 259-274.
- [17] Jun Wu, Jinsong Wang, Zheng You, A comparison study on the dynamics of planar 3-DOF 4-RRR, 3-RRR and 2-RRR parallel manipulators, *Journal of Robotics and Computer-Integrated Manufacturing*, 27, 2011, 150-156.
- [18] Lucas Weihmann, Daniel Martins ans Leandro dos Santos Coelho, Modified differential evolution approach for optimization of planar manipulators force capabilities, *Journal of Expert systems with Applications*, 39, 2012, 6150-6156.
- [19] L. Rolland, Synthesis on the forward kinematics problem algebraic modelling for the planar parallel manipulator, *Journal of Adv. Robotics*, 20, 2006, 1035-1065.
- [20] Rohitash Chandra a, Luc Rolland, On solving the forward kinematics of 3RPR planar parallel manipulator using hybrid metaheuristics, *Journal of Applied Mathematics and Computation*, 217, 2011, 8997-9008.
- [21] Dan Zhang and ZhenGao, Forward kinematics, performance analysis, and multi-objective optimization of a bio-inspired parallel manipulator, *Journal of Robotics and Computer-Integrated Manufacturing*, 28, 2012, 484-492.
- [22] Ridha Kelaiaia, Olivier Company and Abdelouhab Zaatri, Multi objective optimization of a linear Delta parallel robot, *Mechanism and Machine Theory*, 50, 2012, 159-178.
- [23] Engin Tanik, Transmission angle in compliant slider-crank mechanism, *Journal of Mechanism and Machine Theory*, 46(11), 2011, 1623-1632.
- [24] Yue-Qing Yu, Zhao-Cai Du, Jian-Xin Yang, and Yuan Li, An Experimental Study on the Dynamics of a 3-RRR Flexible Parallel Robot, *IEEE Transactions on Robotics*, 27(5), 2011, 992-997.

Turing Machine Operation-A Checks and Balances Model

¹Dr. K. N. Prasanna Kumar, ²Prof. B. S. Kiranagi, ³ Prof C S Bagewadi

ABSTRACT: A state register that stores the state of the Turing machine, one of finitely many. There is one special start state with which the state register is initialized. These states, writes Turing, replace the "state of mind" a person performing computations would ordinarily be in. It is like bank ledger, which has Debits and Credits. Note that in double entry computation, both debits and credits are entered in to the systems, namely the Bank Ledger and balance is posted. Individual Debits are equivalent to individual credits. On a generalizational and globalist scale, a "General Ledger" is written which records in all its wide ranging manifestation the Debits and Credits. This is also conservative. In other words Assets is equivalent to Liabilities. True, Profit is distributed among overheads and charges, and there shall be another account in the General ledger that is the account of Profit. This account is credited with the amount earned as commission, exchange, or discount of bills. Now when we write the "General Ledger" of Turing machine, the *Prima Donna* and *terra firma* of the model, we are writing the General Theory of all the variables that are incorporated in the model. So for every variable, we have an anti variable. This is the dissipation factor. Conservation laws do hold well in computers. They do not break the conservation laws. Thus energy is not dissipated in to the atmosphere when computation is being performed. To repeat we are suggesting a General Theory Of working of a simple Computer and in further papers, we want to extend this theory to both nanotechnology and Quantum Computation. Turing's work is the proponent, precursor, primogeniture, progenitor and promethaleon for the development of Quantum Computers. Computers follow conservation laws. This work is one which formed the primordial concept of diurnal dynamics and hypostasized dynamism of Quantum computers which is the locus of essence, sense and expression of the present day to day musings and mundane drooling. Verily Turing and Churchill stand out like connoisseurs, rancouteurs, and cognescenti of eminent persons, who strode like colossus the screen of collective consciousness of people. We dedicate this paper on the eve of one hundred years of Turing innovation. Model is based on Hill and Peterson diagram.

INTRODUCTION

Turing machine –A beckoning begorra (Extensive excerpts from Wikipedia AND PAGES OF Turing, Churchill, and other noted personalities-Emphasis is mine)

A Turing machine is a device that manipulates symbols on a strip of tape according to a table of rules. Despite its simplicity, a Turing machine can be adapted to simulate the logic of any computer algorithm, and is particularly useful in explaining the functions of a CPU inside a computer.

The "Turing" machine was described by Alan Turing in 1936 who called it an "a (automatic)-machine". The Turing machine is not intended as a practical computing technology, but rather as a hypothetical device representing a computing machine. Turing machines help computer scientists understand the limits of mechanical computation.

Turing gave a succinct and candid definition of the experiment in his 1948 essay, "Intelligent Machinery". Referring to his 1936 publication, Turing wrote that the Turing machine, here called a Logical Computing Machine, consisted of:

...an infinite memory capacity obtained in the form of an infinite tape marked out into squares, on each of which a symbol could be printed. At any moment there is one symbol in the machine; it is called the scanned symbol. The machine can alter the scanned symbol and its behavior is in part determined by that symbol, but the symbols on the tape elsewhere do not affect the behaviour of the machine. However, the tape can be moved back and forth through the machine, this being one of the elementary operations of the machine. Any symbol on the tape may therefore eventually have an innings. (Turing 1948, p. 61)

A Turing machine that is able to simulate any other Turing machine is called a universal Turing machine (UTM, or simply a universal machine). A more mathematically oriented definition with a similar "universal" nature was introduced by Alonzo Church, whose work on calculus intertwined with Turing's in a formal theory of computation known as the Church–Turing thesis. The thesis states that Turing machines indeed capture the informal notion of effective method in logic and mathematics, and provide a precise definition of an algorithm or 'mechanical procedure'.

In computability theory, the Church–Turing thesis (also known as the Church–Turing conjecture, Church's thesis, Church's conjecture, and Turing's thesis) is a combined hypothesis ("thesis") about the nature of functions whose values are effectively calculable; or, in more modern terms, functions whose values are algorithmically computable. In simple terms, the Church–Turing thesis states that "everything algorithmically computable is computable by a Turing machine."

American mathematician Alonzo Church created a method for defining functions called the λ -calculus,

Church, along with mathematician Stephen Kleene and logician J.B. Rosser created a formal definition of a class of functions whose values could be calculated by recursion.

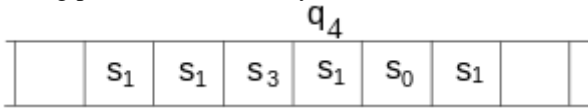
All three computational processes (recursion, the λ -calculus, and the Turing machine) were shown to be equivalent—all three approaches define the same class of functions this has led mathematicians and computer scientists to believe that the concept of computability is accurately characterized by these three equivalent processes. Informally the Church–Turing thesis states that if some method (algorithm) exists to carry out a calculation, then the same calculation can also be carried out by a Turing machine (as well as by a recursively definable function, and by a λ -function).

The Church–Turing thesis is a statement that characterizes the nature of computation and cannot be formally proven. Even though the three processes mentioned above proved to be equivalent, the fundamental premise behind the thesis—the

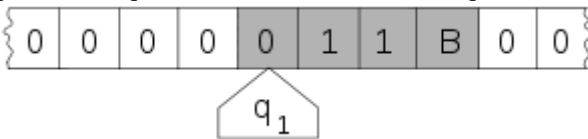
notion of what it means for a function to be "effectively calculable" (computable)—is "a somewhat vague intuitive one" Thus, the "thesis" remains a hypothesis.

Desultory Bureaucratic burdock or a Driving dromedary?

The Turing machine mathematically models a machine that **mechanically operates on** a tape. On this tape are symbols which the machine can read and write, one at a time, using a tape head. Operation is **fully determined** by a finite set of elementary instructions such as "in state q_2 , if the symbol seen is 0, write a 1; if the symbol seen is 1, change into state q_1 ; in state q_1 , if the symbol seen is 0, write a 1 and change to state q_0 ;" etc. In the original article, Turing imagines not a mechanism, but a person whom he calls the "computer", who **executes these** deterministic mechanical rules slavishly (or as Turing puts it, "in a desultory manner").



The head is always over a particular square of the tape; only a finite stretch of squares is shown. The instruction to be performed (q_4) is shown over the scanned square. (Drawing after Kleene (1952) p.375.)



Here, the internal state (q_1) is shown inside the head, and the illustration describes the tape as being infinite and pre-filled with "0", the symbol serving as blank. The system's full state (its configuration) **consists** of the internal state, the contents of the shaded squares including the blank scanned by the head ("11B"), and the position of the head. (Drawing after Minsky (1967) p. 121).

Sequestration dispensation:

A tape which **is divided** into cells, one next to the other. Each cell **contains a** symbol from some finite alphabet. The alphabet **contains a** special blank symbol (here written as 'B') and one or more other symbols. The tape is assumed to be arbitrarily **extendable** to the left and to the right, i.e., the Turing machine is always **supplied with** as much tape as it needs for its computation. Cells that have not been written to before are assumed to be filled with the blank symbol. In some models the tape has a left end marked with a **special symbol; the tape extends or is indefinitely extensible to the right.** A head that can read and write symbols on the tape and move the tape left and right one (and only one) cell at a time. In some models the head **moves and the tape is stationary.**

A state register **that stores** the state of the Turing machine, one of finitely many. There is one special start state with which the state register is initialized. These states, writes Turing, **replace the** "state of mind" a person performing computations would ordinarily be in. It is like bank ledger, which has Debits and Credits. Note that in double entry computation, both debits and credits are entered in to the systems, namely the Bank Ledger and balance is posted. Individual Debits are equivalent to individual Credits. On a generalizational and globalist scale, a "General Ledger" is written which records in all its wide ranging manifestation the Debits and Credits. This is also conservative. In other words Assets is equivalent to Liabilities. True, Profit is distributed among overheads and charges, and there shall be another account in the General ledger that is the account of Profit. This account is credited with the amount earned as commission, exchange, or discount of bills. Now when we write the "General Ledger" of Turing machine, the Primma Donna and terra firma of the model, we are writing the General Theory of all the variables that are incorporated in the model. So for every variable, we have an anti variable. This is the dissipation factor. Conservation laws do hold well in computers. They do not break the conservation laws. Thus energy is not dissipated in to the atmosphere when computation is being performed. To repeat we are suggesting a General Theory Of working of a simple Computer and in further papers, we want to extend this theory to both nanotechnology and Quantum Computation.

A finite table (occasionally called **an action table or transition function**) of instructions (usually quintuples [5-tuples]: $q_i a_j \rightarrow q_l a_k d_k$, but sometimes 4-tuples) that, given the state (q_i) the machine is currently in and the symbol (a_j) it is reading on the tape (symbol currently under the head) tells the machine to do the following in sequence (for the 5-tuple models):

Either **erase or write** a symbol (replacing a_j with a_k), and then

Move the head (which is described by d_k and can have values: 'L' for one step left or 'R' for one step right or 'N' for staying in the same place), and then

Assume the same or a new state as prescribed (go to state q_l).

In the 4-tuple models, erasing or writing a symbol (a_k) and moving the head left or right (d_k) are specified as separate instructions. Specifically, the table tells the machine to (ia) erase or write a symbol or (ib) move the head **left or right**, and then (ii) assume the **same or a new state** as prescribed, **but not both actions** (ia) and (ib) in the same instruction. In some models, if there is no entry in the table for the current combination of symbol and state then the machine will halt; other models require all entries to be filled.

Note that every part of the machine—its state and symbol-collections—and its actions—printing, erasing and tape motion—is finite, discrete and distinguishable; **Only a virus can act as a predator to it.** It is the potentially unlimited amount of tape **that gives it an** unbounded amount of storage space.

Quantum mechanical Hamiltonian models of Turing machines are constructed here on a finite lattice of spin- $\frac{1}{2}$ systems. The **models do not** dissipate any energy and they operate at the quantum limit in that the system (energy uncertainty) / (computation speed) is close to the limit given by the time-energy uncertainty principle.

Regarding finite state machines as Markov chains **facilitates the** application of probabilistic methods to very large logic synthesis and formal verification problems. Variational concepts and exegetic evanescence of the subject matter is done by Hachtel, G.D. Macii, E. ; Pardo, A. ; Somenzi, F. with symbolic algorithms to compute the steady-state probabilities for very large finite state machines (up to 1027 states). These algorithms, **based on** Algebraic Decision Diagrams (ADD's) **-an extension of** BDD's **that allows** arbitrary values **to be associated** with the terminal nodes of the diagrams **-determine the** steady-state probabilities by regarding finite state machines as homogeneous, discrete-parameter Markov chains with finite state spaces, and by solving the corresponding Chapman-Kolmogorov equations. Finite state machines with state graphs **composed of a** single terminal strongly connected component systems authors **have used** two solution techniques: One is based on the Gauss-Jacobi iteration, the other one is based on simple matrix multiplication. Extension of the treatment is done to the most general case of systems which can be modeled as finite state machines with arbitrary **transition** structures; until a certain temporal point, having no relevant options **and effects for** the decision maker beyond that point. Structural morphology and easy decomposition is resorted to towards the consummation of results. Conservation Laws powerhouse performance and no breakage is done with heterogeneous synthesis of conditionalities. Accumulation. Formulation and experimentation are by word and watch word.

Logistics of misnomerliness and anathema:

In any scientific discipline there are many reasons **to use** terms that have precise definitions. Understanding the terminology of a discipline is **essential to** learning a subject and precise **terminology enables us to** communicate ideas clearly with other people. In computer science the problem is even more acute: we **need to construct** software and hardware components that must smoothly **interoperate** across interfaces with clients and other components in distributed systems. The definitions of these interfaces need to be precisely specified for interoperability and good systems performance.

Using the term "computation" without qualification often **generates a** lot of confusion. Part of the problem is that the nature of systems **exhibiting** computational behavior is varied and the term computation means different things to different people depending on the kinds of computational systems they are studying and the kinds of problems they are investigating. Since computation refers to a process that **is defined** in terms of some underlying model of computation, we would achieve clearer communication if we made clear what the underlying model is.

Rather than talking about a vague notion of "computation," suggestion is to use the term in conjunction with a well-defined model of computation whose semantics is clear and which matches the problem being investigated. Computer science already has a number of useful clearly defined models of computation whose behaviors and capabilities are well understood. We should use such models as part of any definition of the term computation. However, for new domains of investigation where there are no appropriate models it may be necessary to invent new formalisms to represent the systems under study.

Courage of conviction and will for vindication:

We consider computational thinking to be the thought processes involved in formulating problems so their solutions can be represented as computational steps and algorithms. An important part of this process is finding appropriate models of computation with which to formulate the problem and derive its solutions. A familiar example would be the use of finite automata to solve string pattern matching problems. A less familiar example might be the quantum circuits and order finding formulation that Peter Schor used to devise an integer-factoring algorithm that runs in polynomial time on a quantum computer. Associated with the basic models of computation in computer science is a wealth of well-known algorithm-design and problem-solving techniques that can be used to solve common problems arising in computing.

However, as the computer systems we wish to build become more complex and as we apply computer science abstractions to new problem domains, we discover that we do not always have the appropriate models to devise solutions. In these cases, computational thinking becomes a research activity that includes inventing appropriate new models of computation.

Corrado Priami and his colleagues at the Centre for Computational and Systems Biology in Trento, Italy have been using process calculi as a model of computation to create programming languages to simulate biological processes. Priami states "the basic feature of computational thinking is abstraction of reality in such a way that the neglected details in the model make it executable by a machine." [Priami, 2007]

As we shall see, finding or devising appropriate models of computation to formulate problems is a central and often nontrivial part of computational thinking.

Hero or Zero?

In the last half century, what we think of as a computational system has expanded dramatically. In the earliest days of computing, a computer was an isolated machine with limited memory to which programs were submitted one at a time to be compiled and run. Today, in the Internet era, we have networks consisting of millions **of interconnected** computers and as we move into cloud computing, many foresee a global computing environment with billions of clients having universal on-demand access to computing services and **data hosted** in gigantic data centers located around the planet. Anything from a PC or a phone or a TV or a sensor can be a client and a data center may consist of hundreds of thousands of servers.

Needless to say, the models for studying such a universally accessible, complex, highly concurrent distributed system are very different from the ones for a single isolated computer. In fact, our aim is to build the model for infinite number of interconnectedness of computers.

Another force at play is that **because of** heat dissipation considerations the architecture of computers **is changing**. An ordinary PC today has many different computing elements such as multicore chips and graphics processing units, and an exascale supercomputer by the end of this decade is expected to be a giant parallel machine with up to a million nodes each with possibly a thousand processors. Our understanding of how to write efficient programs for these machines **is limited**. Good models of parallel computation and parallel algorithm design techniques are a vital open research area for effective parallel computing.

In addition, there is increasing interest in applying computation to studying virtually all areas of human endeavor. One fascinating example **is simulating the** highly parallel biological processes found in human cells and organs for the purposes of understanding disease and drug design. Good computational models for biological processes are still in their infancy. And it is not clear we will ever be able to find a computational model for the human brain that would account for emergent phenomena such **as consciousness or intelligence**.

Queen or show piece:

The theory of computation has been and still is one of the core areas of computer science. It explores the fundamental capabilities and limitations of models of computation. A model of computation is a mathematical **abstraction of a** computing system. The most important model of sequential computation studied in computer science is the Turing machine, first proposed by Alan Turing in 1936.

We can think of a Turing machine as a **finite-state control** attached to a tape head that can read and write symbols on the squares of a semi-infinite tape. Initially, a finite string of length n representing the input is in the leftmost n squares of the tape. An infinite sequence of blanks follows the input string. The tape head is reading the symbol in the leftmost square and the finite control is in a predefined initial state.

The Turing machine then makes a sequence of moves. In a move it reads the symbol on the tape under the tape head and **consults a** transition table in the finite-state control which specifies a symbol to be overprinted on the square under the tape head, a direction the tape head is to move (one square to the left or right), and a state **to enter** next. If the Turing machine **enters an** accepting halting state (one with no next move), the string of nonblank symbols remaining on the input tape at that point in time is its output.

Mathematically, a Turing machine **consists of seven components**: a finite set of states; a finite input alphabet (not containing the blank); a finite tape alphabet (which includes the input alphabet and the blank); a transition function that maps a state and a tape symbol into a state, tape symbol, and direction (left or right); a start state; **an accept state** from which there are no further moves; and a **reject state** from which there are no further moves.

We can characterize the **configuration of** a Turing machine at a given moment in time by three quantities:

1. the state of the finite-state control,
2. the string of nonblank symbols on the tape, and
3. the location of the input head on the tape.

A computation of a Turing machine **on an input w** is a sequence of configurations the machine can go through starting from the initial configuration with w on the tape and terminating (if the computation terminates) in a halting configuration. We say a function f from strings to strings is computable if there is some Turing machine M that given any input string w **always halts in** the accepting state with just $f(w)$ on its tape. We say that M computes f .

The Turing machine provides a precise **definition for** the term algorithm: an algorithm for a function f is just a Turing machine that computes f .

There are scores of models of computation that are equivalent to Turing machines in the sense that these models compute exactly the same set of functions that Turing machines can compute. Among these Turing-complete models of computation are **multitape Turing machines, lambda-calculus, random access machines, production systems, cellular automata, and all general-purpose programming languages**.

The reason there are so many different models of computation equivalent to Turing machines is that we rarely want to implement an algorithm as a Turing machine program; we would like to use a computational notation such as a programming language that is easy to write and easy to understand. But no matter what notation we choose, the famous **Church-Turing thesis** hypothesizes that **any function that can be computed can be computed by a Turing machine**.

Note that if there is one algorithm to compute a function f , then there is an infinite number. Much of computer science is devoted to finding efficient algorithms to compute a given function.

For clarity, we should point out that we have defined a computation as a sequence of configurations a Turing machine can go through on a given input. This sequence could be infinite if the machine does not halt or one of a number of possible sequences in case the machine is nondeterministic.

The reason we went through this explanation is to point out how much detail is involved in precisely defining the term computation for the Turing machine, one of the simplest models of computation. It is not surprising, then, as we move to more complex models, the amount of effort needed to precisely formulate computation in terms of those models grows substantially.

Sublime synthesis not dismal anchorage:

Many real-world computational systems compute more than just a single function—the world has moved to **interactive computing** [Goldin, Smolka, Wegner, 2006]. The term reactive system **is used to** describe a system that maintains an ongoing interaction with its environment. Examples of reactive systems include **operating systems and embedded systems**.

A distributed system is one that consists of autonomous computing systems that communicate with one another through some kind **of network using** message passing. Examples of distributed systems **include** telecommunications systems, the Internet, air-traffic control systems, and parallel computers. **Many distributed systems are also reactive systems**.

Perhaps the most intriguing examples of **reactive** distributed computing systems are biological systems such as cells and organisms. We could even consider the human brain to be **a biological computing** system. Formulation of appropriate models of computation for understanding biological processes is a formidable scientific challenge in the intersection of biology and computer science.

Distributed systems can **exhibit** behaviors such as deadlock, live lock, race conditions, and the like that cannot be usefully studied **using a** sequential model of computation. Moreover, solving problems such as determining the throughput, latency, and performance of a distributed system cannot be productively formulated with a single-thread model of computation. For these reasons, computer scientists **have developed a number** of models of concurrent computation which can **be used** to study these phenomena and to architect tools and components for building distributed systems. Many authors have studied these aspects in wider detail (See for example Alfred V. Aho),

There are many theoretical models for concurrent computation. One is **the message-passing Actor model**, consisting of computational entities called actors [Hewitt, Bishop, Steiger, 1973].

An actor can send and receive messages, make local decisions, create more actors, and fix the behavior to be used for the next message it receives. These actions may be executed in parallel and in no fixed order. The Actor model was devised to study the behavioral properties of parallel computing machines consisting of large numbers of independent processors **communicating by** passing messages through a network. Other well-studied models of concurrent computation include **Petri nets and the process calculi such as pi-calculus and mu-calculus**.

Many variants of computational models for distributed systems are being devised to study and understand the behaviors of biological systems. For example, Dematte, Priami, and Romanel [2008] describe a language called BlenX that is based on a process calculus called Beta-binders for modeling and simulating biological systems.

We do not have the space to describe these concurrent models in any detail. However, it is still an open research area to find practically useful concurrent models of computation that combine control and data for many areas of distributed computing.

Comprehensive envelope of expression not an identarian instance of semantic jugglery:

In addition to aiding education and understanding, there are many practical benefits to having appropriate models of computation for the systems we are trying to build. In cloud computing, for example, there are still a host of poorly understood concerns for systems of this scale. We need to better understand the architectural tradeoffs needed to achieve the desired levels of reliability, performance, scalability and adaptivity in the services these systems are expected to provide. We do not have appropriate abstractions to describe these properties in such a way that they can be automatically mapped from a model of computation into an implementation (or the other way around).

In cloud computing, there are a host of research challenges for system developers and tool builders. As examples, we need programming languages, compilers, verification tools, defect detection tools, and service management tools that can scale to the huge number of clients and servers involved in the networks and data centers of the future. Cloud computing is one important area that can benefit from innovative computational thinking.

The Finale:

Mathematical abstractions called models of computation are at the heart of computation and computational thinking. Computation is a process that is defined in terms of an underlying model of computation and computational thinking is the thought processes involved in formulating problems so their solutions can be represented as computational steps and algorithms. Useful models of computation for solving problems arising in sequential computation can range from simple finite-state machines to Turing-complete models such as random access machines. Useful models of concurrent computation for solving problems arising in the design and analysis of complex distributed systems are still a subject of current research.

The P versus NP problem is to determine whether every language accepted by some nondeterministic algorithm in polynomial time is also accepted by some (deterministic) algorithm in polynomial time. To define the problem precisely it is necessary to give a formal model of a computer. The standard computer model in computability theory is the Turing machine, introduced by Alan Turing in 1936 [Tur36]. Although the model was introduced before physical computers were built, it nevertheless continues to be accepted as the proper computer model for the purpose of defining the notion of computable function.

Examples of Turing machines

3-state busy beaver

Formal definition

Hopcroft and Ullman (1979, p. 148) formally define a (one-tape) Turing machine as a 7-

tuple $M = \langle Q, \Gamma, b, \Sigma, \delta, q_0, F \rangle$ where

Q Is a finite, non-empty set of states

Γ Is a finite, non-empty set of the tape alphabet/symbols

$b \in \Gamma$ is the blank symbol (the only symbol allowed to occur on the tape infinitely often at any step during the computation)

$\Sigma \subseteq \Gamma \setminus \{b\}$ is the set of input symbols

$q_0 \in Q$ is the initial state

$F \subseteq Q$ is the set of final or accepting states.

$\delta : Q \setminus F \times \Gamma \rightarrow Q \times \Gamma \times \{L, R\}$ is a partial function called the transition function, where L is left shift, R is right shift. (A relatively uncommon variant allows "no shift", say N, as a third element of the latter set.)

Anything that operates according to these specifications is a Turing machine.

The 7-tuple for the 3-state busy beaver looks like this (see more about this busy beaver at Turing machine examples):

$Q = \{A, B, C, \text{HALT}\}$

$\Gamma = \{0, 1\}$

$b = 0$ ("Blank")

$\Sigma = \{1\}$

$q_0 = A$ (the initial state)

$F = \{\text{HALT}\}$

$\delta =$ see state-table below

Initially all tape cells are marked with 0.

State table for 3 state, 2 symbol busy beaver

Tape symbol-Current state A-Current state B-Current state C

-Write symbol-Move tape-Next state-Write symbol-Move tape-Next state-Write symbol-Move tape-Next state

0-1-R-B-1-L-A-1-L-B

1-1-L-C-1-R-B-1-R-HALT

In the words of van Emde Boas (1990), p. 6: "The set-theoretical object his formal seven-tuple description similar to the above] provides only partial information on how the machine will behave and what its computations will look like."

For instance,

There will need to be some decision on what the symbols actually look like, and a failproof way of reading and writing symbols indefinitely.

The shift left and shift right operations may shift the tape head across the tape, but when **actually building a** Turing machine it is more practical to make the tape slide back and forth under the head instead.

The tape can be finite, and **automatically extended** with blanks as needed (which is closest to the mathematical definition), but it is more common to think of it as stretching infinitely at both ends and being pre-filled with blanks except on the explicitly given finite fragment the tape head is on. (This is, of course, not implementable in practice.) The tape cannot be fixed in length, since that would not correspond to the given definition and would seriously limit the range of computations the machine can perform to those of a linear bounded automaton.

Contradictions and complementarities:

Definitions in literature sometimes differ slightly, to make arguments or proofs easier or clearer, but this is always done in such a way that the resulting machine has the same computational power. For example, changing the set $\{L, R\}$

to $\{L, R, N\}$, where N ("None" or "No-operation") would allow the machine to stay on the same tape cell instead of moving left or right, does not increase the machine's computational power.

The most common convention represents each "Turing instruction" in a "Turing table" by one of nine 5-tuples, per the convention of Turing/Davis (Turing (1936) in Undecidable, p. 126-127 and Davis (2000) p. 152):

(Definition 1): ($q_i, S_j, S_k/E/N, L/R/N, q_m$)

(Current state q_i , symbol scanned S_j , print symbol S_k /erase E/none N, move_tape_one_square left L/right R/none N, new state q_m)

Other authors (Minsky (1967) p. 119, Hopcroft and Ullman (1979) p. 158, Stone (1972) p. 9) adopt a different convention, with new state q_m listed immediately after the scanned symbol S_j :

(Definition 2): ($q_i, S_j, q_m, S_k/E/N, L/R/N$)

(Current state q_i , symbol scanned S_j , new state q_m , print symbol S_k /erase E/none N, move_tape_one_square left L/right R/none N)

For the remainder of this article "definition 1" (the Turing/Davis convention) will be used.

Example: state table for the 3-state 2-symbol busy beaver reduced to 5-tuples

Current state-Scanned symbol--Print symbol-Move tape-Final (i.e. next) state-5-tuples

A-0--1-R-B-(A, 0, 1, R, B)

A-1--1-L-C-(A, 1, 1, L, C)

B-0--1-L-A-(B, 0, 1, L, A)

B-1--1-R-B-(B, 1, 1, R, B)

C-0--1-L-B-(C, 0, 1, L, B)

C-1--1-N-H-(C, 1, 1, N, H)

In the following table, Turing's original model allowed only the first three lines that he called N1, N2, N3 (cf Turing in Undecidable, p. 126). He allowed for erasure of the "scanned square" by naming a 0th symbol S_0 = "erase" or "blank", etc. However, he did not allow for non-printing, so every instruction-line includes "print symbol S_k " or "erase" (cf footnote 12 in Post (1947), Undecidable p. 300). The abbreviations are Turing's (Undecidable p. 119). Subsequent to Turing's original paper in 1936–1937, machine-models have allowed all nine possible types of five-tuples:

-Current m-configuration (Turing state)-Tape symbol-Print-operation-Tape-motion-Final m-configuration (Turing state)-5-tuple-5-tuple comments-4-tuple

N1-qi-Sj-Print(S_k)-Left L-qm-(qi, Sj, S_k , L, qm)-"blank" = S_0 , 1= S_1 , etc.-

N2-qi-Sj-Print(S_k)-Right R-qm-(qi, Sj, S_k , R, qm)-"blank" = S_0 , 1= S_1 , etc.-

N3-qi-Sj-Print(S_k)-None N-qm-(qi, Sj, S_k , N, qm)-"blank" = S_0 , 1= S_1 , etc.-(qi, Sj, S_k , qm)

4-qi-Sj-None N-Left L-qm-(qi, Sj, N, L, qm)--(qi, Sj, L, qm)

5-qi-Sj-None N-Right R-qm-(qi, Sj, N, R, qm)--(qi, Sj, R, qm)

6-qi-Sj-None N-None N-qm-(qi, Sj, N, N, qm)-Direct "jump"-(qi, Sj, N, qm)

7-qi-Sj-Erase-Left L-qm-(qi, Sj, E, L, qm)--

8-qi-Sj-Erase-Right R-qm-(qi, Sj, E, R, qm)--

9-qi-Sj-Erase-None N-qm-(qi, Sj, E, N, qm)--(qi, Sj, E, qm)

Any Turing table (list of instructions) can be constructed from the above nine 5-tuples. For technical reasons, the three non-printing or "N" instructions (4, 5, 6) can usually be dispensed with. For examples see Turing machine examples.

Less frequently the use of 4-tuples is encountered: these represent a further atomization of the Turing instructions (cf Post (1947), Boolos & Jeffrey (1974, 1999), Davis-Sigal-Weyuker (1994)); also see more at Post–Turing machine.

The "state"

The word "state" used in context of Turing machines can be a source of confusion, as it can mean two things. Most commentators after Turing have used "state" to mean the name/designator of the current instruction to be performed—i.e. the contents of the state register. But Turing (1936) made a strong distinction between a record of what he called the machine's "m-configuration", (its internal state) and the machine's (or person's) "state of progress" through the computation - the current state of the total system. What Turing called "the state formula" includes both the current instruction and all the symbols on the tape:

Thus the state of progress of the computation at any stage is completely determined by the note of instructions and the symbols on the tape. That is, the state of the system may be described by a single expression (sequence of symbols) consisting of the symbols on the tape followed by Δ (which we suppose not to appear elsewhere) and then by the note of instructions. This expression is called the 'state formula'.

—Undecidable, p.139–140, emphasis added

Earlier in his paper Turing carried this even further: he gives an example where he places a symbol of the current "m-configuration"—the instruction's label—beneath the scanned square, together with all the symbols on the tape (Undecidable, p. 121); this he calls "the complete configuration" (Undecidable, p. 118). To print the "complete configuration" on one line he places the state-label/m-configuration to the left of the scanned symbol.

A variant of this is seen in Kleene (1952) where Kleene shows how to write the Gödel number of a machine's "situation": he places the "m-configuration" symbol q_4 over the scanned square in roughly the center of the 6 non-blank squares on the tape (see the Turing-tape figure in this article) and puts it to the right of the scanned square. But Kleene refers to " q_4 " itself as "the machine state" (Kleene, p. 374-375). Hopcroft and Ullman call this composite the "instantaneous description" and follow the Turing convention of putting the "current state" (instruction-label, m-configuration) to the left of the scanned symbol (p. 149).

Example: total state of 3-state 2-symbol busy beaver after 3 "moves" (taken from example "run" in the figure below):

1A1

This means: after three moves the tape has ... 000110000 ... on it, the head is scanning the right-most 1, and the state is A. Blanks (in this case represented by "0"s) can be part of the total state as shown here: B01 ; the tape has a single 1 on it, but the head is scanning the 0 ("blank") to its left and the state is B.

"State" in the context of Turing machines should be clarified as to which is being described: (i) the current instruction, or (ii) the list of symbols on the tape together with the current instruction, or (iii) the list of symbols on the tape together with the current instruction placed to the left of the scanned symbol or to the right of the scanned symbol.

Turing's biographer Andrew Hodges (1983: 107) has noted and discussed this confusion.

Turing machine "state" diagrams

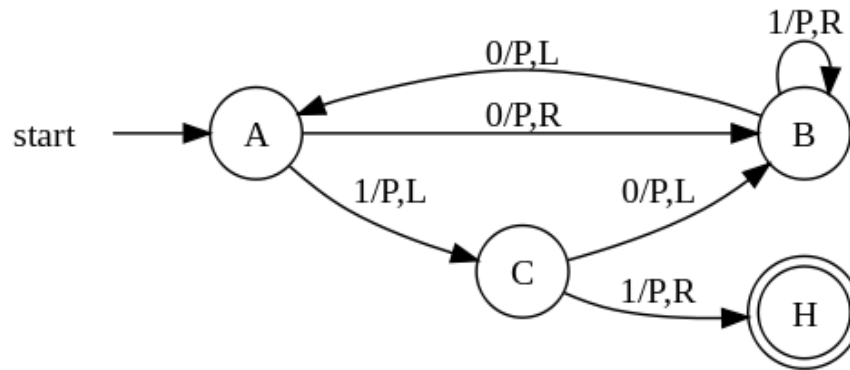
The table for the 3-state busy beaver ("P" = print/write a "1")

Tape symbol-Current state A-Current state B-Current state C

-Write symbol-Move tape-Next state-Write symbol-Move tape-Next state-Write symbol-Move tape-Next state

0-P-R-B-P-L-A-P-L-B

1-P-L-C-P-R-B-P-R-HALT

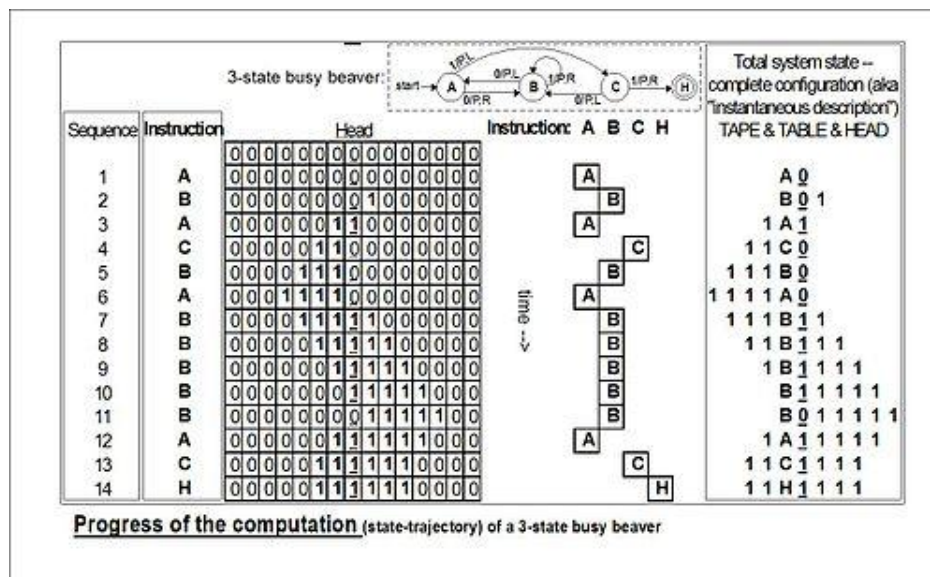


The "3-state busy beaver" Turing machine in a finite state representation. Each circle represents a "state" of the TABLE—an "m-configuration" or "instruction". "Direction" of a state transition is shown by an arrow. The label (e.g. 0/P, R) near the outgoing state (at the "tail" of the arrow) specifies the scanned symbol that causes a particular transition (e.g. 0) followed by a slash /, followed by the subsequent "behaviors" of the machine, e.g. "P Print" then move tape "R Right". No general accepted format exists. The convention shown is after McClusky (1965), Booth (1967), Hill and Peterson (1974).

To the right: the above TABLE as expressed as a "state transition" diagram.

Usually large TABLES are better left as tables (Booth, p. 74). They are more readily simulated by computer in tabular form (Booth, p. 74). However, certain concepts—e.g. machines with "reset" states and machines with repeating patterns (cf Hill and Peterson p. 244ff)—can be more readily seen when viewed as a drawing.

Whether a drawing represents an improvement on its TABLE must be decided by the reader for the particular context. See Finite state machine for more.



The evolution of the busy-beaver's computation starts at the top and proceeds to the bottom.

The reader should again be cautioned that such diagrams represent a snapshot of their TABLE frozen in time, not the course ("trajectory") of a computation through time and/or space. While every time the busy beaver machine "runs" it will always follow the same state-trajectory, this is not true for the "copy" machine that can be provided with variable input "parameters".

The diagram "Progress of the computation" shows the 3-state busy beaver's "state" (instruction) progress through its computation from start to finish. On the far right is the Turing "complete configuration" (Kleene "situation", Hopcroft-Ullman "instantaneous description") at each step. If the machine were to be stopped and cleared to blank both the "state register" and entire tape, these "configurations" could be used to rekindle a computation anywhere in its progress (cf Turing (1936) Undecidable pp. 139-140).

Register machine,

Machines that might be thought to have more computational capability than a simple universal Turing machine can be shown to have no more power (Hopcroft and Ullman p. 159, cf Minsky (1967)). They might compute faster, perhaps, or use less memory, or their instruction set might be smaller, but they cannot compute more powerfully (i.e. more mathematical functions). (Recall that the Church-Turing thesis hypothesizes this to be true for any kind of machine: that anything that can be "computed" can be computed by some Turing machine.)

A Turing machine is equivalent to a pushdown automaton that has been made more flexible and concise by relaxing the last-in-first-out requirement of its stack.

At the other extreme, some very simple models turn out to be Turing-equivalent, i.e. to have the same computational power as the Turing machine model.

Common equivalent models are the multi-tape Turing machine, multi-track Turing machine, machines with input and output, and the non-deterministic Turing machine (NDTM) as opposed to the deterministic Turing machine (DTM) for which the action table has at most one entry for each combination of symbol and state.

Read-only, right-moving Turing machines are equivalent to NDFAs (as well as DFAs by conversion using the NDFA to DFA conversion algorithm).

For practical and didactical intentions the equivalent register machine can be used as a usual assembly programming language.

Choice c-machines, Oracle o-machines

Early in his paper (1936) Turing makes a distinction between an "automatic machine"—its "motion ... completely determined by the configuration" and a "choice machine":

...whose motion is only partially determined by the configuration ... When such a machine reaches one of these ambiguous configurations; it cannot go on until some arbitrary choice has been made by an external operator. This would be the case if we were using machines to deal with axiomatic systems.

—Undecidable, p. 118

Turing (1936) does not elaborate further except in a footnote in which he describes how to use an a-machine to "find all the provable formulae of the [Hilbert] calculus" rather than use a choice machine. He "supposes[s] that the choices are always between two possibilities 0 and 1. Each proof will then be determined by a sequence of choices i_1, i_2, \dots , in ($i_1 = 0$ or $1, i_2 = 0$ or $1, \dots, i_n = 0$ or 1), and hence the number $2^{i_1}2^{n-1} + 2^{i_2}2^{n-2} + \dots + i_n$ completely determines the proof. The automatic machine carries out successively proof 1, proof 2, proof 3, ..." (Footnote ‡, Undecidable, p. 138)

This is indeed the technique by which a deterministic (i.e. a-) Turing machine can be used to mimic the action of a nondeterministic Turing machine; Turing solved the matter in a footnote and appears to dismiss it from further consideration.

An oracle machine or o-machine is a Turing a-machine that pauses its computation at state "o" while, to complete its calculation, it "awaits the decision" of "the oracle"—an unspecified entity "apart from saying that it cannot be a machine" (Turing (1939), Undecidable p. 166–168). The concept is now actively used by mathematicians.

Universal Turing machines

As Turing wrote in Undecidable, p. 128 (italics added):

It is possible to invent a single machine which can be used to compute any computable sequence. If this machine U is supplied with the tape on the beginning of which is written the string of quintuples separated by semicolons of some computing machine M, then U will compute the same sequence as M.

This finding is now taken for granted, but at the time (1936) it was considered astonishing. The model of computation that Turing called his "universal machine"—"U" for short—is considered by some (cf Davis (2000)) to have been the fundamental theoretical breakthrough that led to the notion of the Stored-program computer.

Turing's paper ... contains, in essence, the invention of the modern computer and some of the programming techniques that accompanied it.

—Minsky (1967), p. 104

In terms of computational complexity, a multi-tape universal Turing machine need only be slower by logarithmic factor compared to the machines it simulates. This result was obtained in 1966 by F. C. Hennie and R. E. Stearns. (Arora and Barak, 2009, theorem 1.9)

Comparison with real machines

It is often said that Turing machines, unlike simpler automata, are as powerful as real machines, and are able to execute any operation that a real program can. What is missed in this statement is that, because a real machine can only be in finitely many configurations, in fact this "real machine" is nothing but a linear bounded automaton. On the other hand, Turing machines **are equivalent to** machines that have an unlimited amount of storage space for their computations. In fact, Turing machines are not intended to model computers, but rather they are intended to model computation itself; historically, computers, which compute only on their (fixed) internal storage, were developed only later.

There are a number of ways to explain why Turing machines are useful models of real computers:

Anything a real computer can compute, a Turing machine can also compute. For example: "A Turing machine can simulate any type of subroutine found in programming languages, including recursive procedures and any of the known parameter-passing mechanisms" (Hopcroft and Ullman p. 157). A large enough FSA can also model any real computer, disregarding IO. Thus, a statement about the limitations of Turing machines will also apply to real computers.

The difference lies only with the ability of a Turing machine to manipulate an unbounded amount of data. However, given a finite amount of time, a Turing machine (like a real machine) can only manipulate a finite amount of data.

Like a Turing machine, a real machine can have its storage space enlarged as needed, by acquiring more disks or other storage media. If the supply of these runs short, the Turing machine may become less useful as a model. But the fact is that

neither Turing machines nor real machines need astronomical amounts of storage space in order to perform useful computation. The processing time required is usually much more of a problem.

Descriptions of real machine programs using simpler abstract models are often much more complex than descriptions using Turing machines. For example, a Turing machine describing an algorithm may have a few hundred states, while the equivalent deterministic finite automaton on a given real machine has quadrillions. This makes the DFA representation infeasible to analyze.

Turing machines describe algorithms independent of how much memory they use. There is a limit to the memory possessed by any current machine, but this limit can rise arbitrarily in time. Turing machines allow us to make statements about algorithms which will (theoretically) hold forever, regardless of advances in conventional computing machine architecture.

Turing machines simplify the statement of algorithms. Algorithms running on Turing-equivalent abstract machines are usually more general than their counterparts running on real machines, because they have arbitrary-precision data types available and never have to deal with unexpected conditions (including, but not limited to, running out of memory).

One way in which Turing machines are a poor model for programs is that many real programs, such as operating systems and word processors, are written to receive unbounded input over time, and therefore do not halt. Turing machines do not model such ongoing computation well (but can still model portions of it, such as individual procedures).

Computational complexity theory

A limitation of Turing machines is that they do not model the strengths of a particular arrangement well. For instance, modern stored-program computers are actually instances of a more specific form of abstract machine known as the random access stored program machine or RASP machine model. Like the Universal Turing machine the RASP stores its "program" in "memory" external to its finite-state machine's "instructions". Unlike the universal Turing machine, the RASP has an infinite number of distinguishable, numbered but unbounded "registers"—memory "cells" that can contain any integer (cf. Elgot and Robinson (1964), Hartmanis (1971), and in particular Cook-Rechow (1973); references at random access machine). The RASP's finite-state machine is equipped with the capability for indirect addressing (e.g. the contents of one register can be used as an address to specify another register); thus the RASP's "program" can address any register in the register-sequence. The upshot of this distinction is that there are computational optimizations that can be performed based on the memory indices, which are not possible in a general Turing machine; thus when Turing machines are used as the basis for bounding running times, a 'false lower bound' can be proven on certain algorithms' running times (due to the false simplifying assumption of a Turing machine). An example of this is binary search, an algorithm that can be shown to perform more quickly when using the RASP model of computation rather than the Turing machine model.

Concurrency

Another limitation of Turing machines is that they do not model concurrency well. For example, there is a bound on the size of integer that can be computed by an always-halting nondeterministic Turing machine starting on a blank tape. (See article on unbounded nondeterminism.) By contrast, there are always-halting concurrent systems with no inputs that can compute an integer of unbounded size. (A process can be created with local storage that is initialized with a count of 0 that concurrently sends itself both a stop and a go message. When it receives a go message, it increments its count by 1 and sends itself a go message. When it receives a stop message, it stops with an unbounded number in its local storage.)

**“A” AND “B”(SEE FIGURE REPRESENTS AN “M CONFIGURATION” OR “INSTRUCTIONS) OR STATE:
THE CONVENTION SHOWN IS AFTER MCCLUSKY,BOOTH,HILL AND PETERSON.**

MODULE NUMBERED ONE

NOTATION :

G_{13} : CATEGORY ONE OF "A"

G_{14} : CATEGORY TWO OF "A"

G_{15} : CATEGORY THREE OF 'A'

T_{13} : CATEGORY ONE OF 'B'

T_{14} : CATEGORY TWO OF 'B'

T_{15} :CATEGORY THREE OF 'B'

**“B” AND “A”(SEE FIGURE REPRESENTS AN “M CONFIGURATION” OR “INSTRUCTIONS) OR STATE:
THE CONVENTION SHOWN IS AFTER MCCLUSKY,BOOTH,HILL AND PETERSON.**

MODULE NUMBERED TWO

**NOTE: THE ACCENTUATION COEFFICIENT AND DISSIPATION COEFFICIENT NEED NOT BE THE SAME
IT MAY BE ZERO, OR MIGHT BE SAME,I ALL THE THREE CASES THE MODEL COULD BE CHANGED
EASILY BY REPLACING THE COEFFICIENTS BY EQUALITY SIGN OR GIVING IT THE POSITION OF
ZERO.**

G_{16} : CATEGORY ONE OF 'B' (NOTE THAT THEY REPRESENT CONFIGURATIONS,INSTRUCTIONS OR STATES)

G_{17} : CATEGORY TWO OF 'B'

G_{18} : CATEGORY THREE OF 'B'
 T_{16} :CATEGORY ONE OF 'A'
 T_{17} : CATEGORY TWO OF 'A'
 T_{18} : CATEGORY THREE OF 'A'

**"A" AND "C"(SEE FIGURE REPRESENTS AN "M CONFIGURATION" OR "INSTRUCTIONS) OR STATE:
THE CONVENTION SHOWN IS AFTER MCCLUSKY,BOOTH,HILL AND PETERSON.
MODULE NUMBERED THREE**

G_{20} : CATEGORY ONE OF 'A'
 G_{21} :CATEGORY TWO OF 'A'
 G_{22} : CATEGORY THREE OF 'A'
 T_{20} : CATEGORY ONE OF 'C'
 T_{21} :CATEGORY TWO OF 'C'
 T_{22} : CATEGORY THREE OF 'C'

**"C" AND "B"(SEE FIGURE REPRESENTS AN "M CONFIGURATION" OR "INSTRUCTIONS) OR STATE:
THE CONVENTION SHOWN IS AFTER MCCLUSKY,BOOTH,HILL AND PETERSON.
MODULE NUMBERED FOUR**

**NOTE: THE ACCENTUATION COEFFICIENT AND DISSIPATION COEFFICIENT NEED NOT BE THE SAME
.IT MAY BE ZERO, OR MIGHT BE SAME,I ALL THE THREE CASES THE MODEL COULD BE CHANGED
EAILY BY REPLACING THE COEFFICIENTS BY EQUALITY SIGN OR GIVING IT THE POSITION OF
ZERO**

G_{24} : CATEGORY ONE OF "C"(EVALUATIVE PARAMETRICIZATION OF SITUATIONAL ORIENTATIONS AND
ESSENTIAL COGNITIVE ORIENTATION AND CHOICE VARIABLES OF THE SYSTEM TO WHICH
CONFIGURATION IS APPLICABLE)
 G_{25} : CATEGORY TWO OF "C"
 G_{26} : CATEGORY THREE OF "C"
 T_{24} :CATEGORY ONE OF "B"
 T_{25} :CATEGORY TWO OF "B"(SYSTEMIC INSTRUMENTAL CHARACTERISATIONS AND ACTION
ORIENTATIONS AND FUNCTIONAL IMPERATIVES OF CHANGE MANIFESTED THEREIN)
 T_{26} : CATEGORY THREE OF "B"

**"C" AND "H"(SEE FIGURE REPRESENTS AN "M CONFIGURATION" OR "INSTRUCTIONS) OR STATE:
THE CONVENTION SHOWN IS AFTER MCCLUSKY,BOOTH,HILL AND PETERSON.
MODULE NUMBERED FIVE**

**NOTE: THE ACCENTUATION COEFFICIENT AND DISSIPATION COEFFICIENT NEED NOT BE THE SAME
.IT MAY BE ZERO, OR MIGHT BE SAME,I ALL THE THREE CASES THE MODEL COULD BE CHANGED
EAILY BY REPLACING THE COEFFICIENTS BY EQUALITY SIGN OR GIVING IT THE POSITION OF
ZERO:**

G_{28} : CATEGORY ONE OF "C"
 G_{29} : CATEGORY TWO OF "C"
 G_{30} :CATEGORY THREE OF "C"
 T_{28} :CATEGORY ONE OF "H"
 T_{29} :CATEGORY TWO OF "H"
 T_{30} :CATEGORY THREE OF "H"

**"B" AND "B"(SEE FIGURE REPRESENTS AN "M CONFIGURATION" OR "INSTRUCTIONS) OR STATE:
THE CONVENTION SHOWN IS AFTER MCCLUSKY,BOOTH,HILL AND PETERSON.
THE SYSTEM HERE IS ONE OF SELF TRANSFORMATIONAL,SYSTEM CHANGING,STRUCTURALLY
MUTATIONAL,SYLOGISTICALLY CHANGEABLE AND CONFIGURATIONALLY ALTERABLE(VERY
VERY IMPORTANT SYSTEM IN ALMOST ALL SUBJECTS BE IT IN QUANTUM SYSTEMS OR
DISSIPATIVE STRUCTURES
MODULE NUMBERED SIX**

**NOTE: THE ACCENTUATION COEFFICIENT AND DISSIPATION COEFFICIENT NEED NOT BE THE SAME
.IT MAY BE ZERO, OR MIGHT BE SAME,I ALL THE THREE CASES THE MODEL COULD BE CHANGED**

EAILY BY REPLACING THE COEFFICIENTS BY EQUALITY SIGN OR GIVING IT THE POSITION OF ZERO:

G_{32} : CATEGORY ONE OF "B"
 G_{33} : CATEGORY TWO OF "B"
 G_{34} : CATEGORY THREE OF "B"

INTERACTS WITH:ITSELF:

T_{32} : CATEGORY ONE OF "B"
 T_{33} : CATEGORY TWO OF "B"
 T_{34} : CATEGORY THREE OF "B"

"INPUT" AND "A"(SEE FIGURE REPRESENTS AN "M CONFIGURATION" OR "INSTRUCTIONS) OR STATE: THE CONVENTION SHOWN IS AFTER MCCLUSKY,BOOTH,HILL AND PETERSON. MODULE NUMBERED SEVEN

NOTE: THE ACCENTUATION COEFFICIENT AND DISSIPATION COEFFICIENT NEED NOT BE THE SAME ,IT MAY BE ZERO, OR MIGHT BE SAME,I ALL THE THREE CASES THE MODEL COULD BE CHANGED EAILY BY REPLACING THE COEFFICIENTS BY EQUALITY SIGN OR GIVING IT THE POSITION OF ZERO:

G_{36} : CATEGORY ONE OF "INPUT"
 G_{37} : CATEGORY TWO OF "INPUT"
 G_{38} : CATEGORY THREE OF "INPUT" (INPUT FEEDING AND CONCOMITANT GENERATION OF ENERGY DIFFERENTIAL-TIME LAG OR INSTANTANEOUSNESSMIGHT EXISTS WHEREBY ACCENTUATION AND ATTRITIONS MODEL MAY ASSUME ZERO POSITIONS)
 T_{36} : CATEGORY ONE OF "A"
 T_{37} : CATEGORY TWO OF "A"
 T_{38} : CATEGORY THREE OF "A"

$(a_{13})^{(1)}, (a_{14})^{(1)}, (a_{15})^{(1)}, (b_{13})^{(1)}, (b_{14})^{(1)}, (b_{15})^{(1)}, (a_{16})^{(2)}, (a_{17})^{(2)}, (a_{18})^{(2)}, (b_{16})^{(2)}, (b_{17})^{(2)}, (b_{18})^{(2)}$;
 $(a_{20})^{(3)}, (a_{21})^{(3)}, (a_{22})^{(3)}, (b_{20})^{(3)}, (b_{21})^{(3)}, (b_{22})^{(3)}$
 $(a_{24})^{(4)}, (a_{25})^{(4)}, (a_{26})^{(4)}, (b_{24})^{(4)}, (b_{25})^{(4)}, (b_{26})^{(4)}, (b_{28})^{(5)}, (b_{29})^{(5)}, (b_{30})^{(5)}, (a_{28})^{(5)}, (a_{29})^{(5)}, (a_{30})^{(5)}$;
 $(a_{32})^{(6)}, (a_{33})^{(6)}, (a_{34})^{(6)}, (b_{32})^{(6)}, (b_{33})^{(6)}, (b_{34})^{(6)}$
 are Accentuation coefficients

$(a'_{13})^{(1)}, (a'_{14})^{(1)}, (a'_{15})^{(1)}, (b'_{13})^{(1)}, (b'_{14})^{(1)}, (b'_{15})^{(1)}, (a'_{16})^{(2)}, (a'_{17})^{(2)}, (a'_{18})^{(2)}, (b'_{16})^{(2)}, (b'_{17})^{(2)}, (b'_{18})^{(2)}$
 $, (a'_{20})^{(3)}, (a'_{21})^{(3)}, (a'_{22})^{(3)}, (b'_{20})^{(3)}, (b'_{21})^{(3)}, (b'_{22})^{(3)}$
 $(a'_{24})^{(4)}, (a'_{25})^{(4)}, (a'_{26})^{(4)}, (b'_{24})^{(4)}, (b'_{25})^{(4)}, (b'_{26})^{(4)}, (b'_{28})^{(5)}, (b'_{29})^{(5)}, (b'_{30})^{(5)}, (a'_{28})^{(5)}, (a'_{29})^{(5)}, (a'_{30})^{(5)}$;
 $(a'_{32})^{(6)}, (a'_{33})^{(6)}, (a'_{34})^{(6)}, (b'_{32})^{(6)}, (b'_{33})^{(6)}, (b'_{34})^{(6)}$
 are Dissipation coefficients-

"A" AND "B"(SEE FIGURE REPRESENTS AN "M CONFIGURATION" OR "INSTRUCTIONS) OR STATE: THE CONVENTION SHOWN IS AFTER MCCLUSKY,BOOTH,HILL AND PETERSON.

MODULE NUMBERED ONE

The differential system of this model is now (Module Numbered one)-1

$$\begin{aligned} \frac{dG_{13}}{dt} &= (a_{13})^{(1)}G_{14} - [(a'_{13})^{(1)} + (a''_{13})^{(1)}(T_{14}, t)]G_{13} -2 \\ \frac{dG_{14}}{dt} &= (a_{14})^{(1)}G_{13} - [(a'_{14})^{(1)} + (a''_{14})^{(1)}(T_{14}, t)]G_{14} -3 \\ \frac{dG_{15}}{dt} &= (a_{15})^{(1)}G_{14} - [(a'_{15})^{(1)} + (a''_{15})^{(1)}(T_{14}, t)]G_{15} -4 \\ \frac{dT_{13}}{dt} &= (b_{13})^{(1)}T_{14} - [(b'_{13})^{(1)} - (b''_{13})^{(1)}(G, t)]T_{13} -5 \\ \frac{dT_{14}}{dt} &= (b_{14})^{(1)}T_{13} - [(b'_{14})^{(1)} - (b''_{14})^{(1)}(G, t)]T_{14} -6 \\ \frac{dT_{15}}{dt} &= (b_{15})^{(1)}T_{14} - [(b'_{15})^{(1)} - (b''_{15})^{(1)}(G, t)]T_{15} -7 \\ + (a''_{13})^{(1)}(T_{14}, t) &= \text{First augmentation factor} -8 \\ - (b''_{13})^{(1)}(G, t) &= \text{First detritions factor} - \end{aligned}$$

“B” AND “A”(SEE FIGURE REPRESENTS AN “M CONFIGURATION” OR “INSTRUCTIONS) OR STATE: THE CONVENTION SHOWN IS AFTER MCCLUSKY,BOOTH,HILL AND PETERSON.

MODULE NUMBERED TWO

NOTE: THE ACCENTUATION COEFFICIENT AND DISSIPATION COEFFICIENT NEED NOT BE THE SAME IT MAY BE ZERO, OR MIGHT BE SAME,I ALL THE THREE CASES THE MODEL COULD BE CHANGED EAILY BY REPLACING THE COEFFICIENTS BY EQUALITY SIGN OR GIVING IT THE POSITION OF ZERO.

The differential system of this model is now (Module numbered two)-9

$$\frac{dG_{16}}{dt} = (a_{16})^{(2)}G_{17} - [(a'_{16})^{(2)} + (a''_{16})^{(2)}(T_{17}, t)]G_{16} -10$$

$$\frac{dG_{17}}{dt} = (a_{17})^{(2)}G_{16} - [(a'_{17})^{(2)} + (a''_{17})^{(2)}(T_{17}, t)]G_{17} -11$$

$$\frac{dG_{18}}{dt} = (a_{18})^{(2)}G_{17} - [(a'_{18})^{(2)} + (a''_{18})^{(2)}(T_{17}, t)]G_{18} -12$$

$$\frac{dT_{16}}{dt} = (b_{16})^{(2)}T_{17} - [(b'_{16})^{(2)} - (b''_{16})^{(2)}((G_{19}, t))]T_{16} -13$$

$$\frac{dT_{17}}{dt} = (b_{17})^{(2)}T_{16} - [(b'_{17})^{(2)} - (b''_{17})^{(2)}((G_{19}, t))]T_{17} -14$$

$$\frac{dT_{18}}{dt} = (b_{18})^{(2)}T_{17} - [(b'_{18})^{(2)} - (b''_{18})^{(2)}((G_{19}, t))]T_{18} -15$$

$$+(a''_{16})^{(2)}(T_{17}, t) = \text{First augmentation factor} -16$$

$$-(b''_{16})^{(2)}((G_{19}, t)) = \text{First detritions factor} -17$$

:

A” AND

“C”(SEE FIGURE REPRESENTS AN “M CONFIGURATION” OR “INSTRUCTIONS) OR STATE: THE CONVENTION SHOWN IS AFTER MCCLUSKY,BOOTH,HILL AND PETERSON.

MODULE NUMBERED THREE

The differential system of this model is now (Module numbered three)-18

$$\frac{dG_{20}}{dt} = (a_{20})^{(3)}G_{21} - [(a'_{20})^{(3)} + (a''_{20})^{(3)}(T_{21}, t)]G_{20} -19$$

$$\frac{dG_{21}}{dt} = (a_{21})^{(3)}G_{20} - [(a'_{21})^{(3)} + (a''_{21})^{(3)}(T_{21}, t)]G_{21} -20$$

$$\frac{dG_{22}}{dt} = (a_{22})^{(3)}G_{21} - [(a'_{22})^{(3)} + (a''_{22})^{(3)}(T_{21}, t)]G_{22} -21$$

$$\frac{dT_{20}}{dt} = (b_{20})^{(3)}T_{21} - [(b'_{20})^{(3)} - (b''_{20})^{(3)}(G_{23}, t)]T_{20} -22$$

$$\frac{dT_{21}}{dt} = (b_{21})^{(3)}T_{20} - [(b'_{21})^{(3)} - (b''_{21})^{(3)}(G_{23}, t)]T_{21} -23$$

$$\frac{dT_{22}}{dt} = (b_{22})^{(3)}T_{21} - [(b'_{22})^{(3)} - (b''_{22})^{(3)}(G_{23}, t)]T_{22} -24$$

$$+(a''_{20})^{(3)}(T_{21}, t) = \text{First augmentation factor}-$$

$$-(b''_{20})^{(3)}(G_{23}, t) = \text{First detritions factor} -25$$

“C” AND “B”(SEE FIGURE REPRESENTS AN “M CONFIGURATION” OR “INSTRUCTIONS) OR STATE: THE CONVENTION SHOWN IS AFTER MCCLUSKY,BOOTH,HILL AND PETERSON.

MODULE NUMBERED FOUR

NOTE: THE ACCENTUATION COEFFICIENT AND DISSIPATION COEFFICIENT NEED NOT BE THE SAME IT MAY BE ZERO, OR MIGHT BE SAME,I ALL THE THREE CASES THE MODEL COULD BE CHANGED EAILY BY REPLACING THE COEFFICIENTS BY EQUALITY SIGN OR GIVING IT THE POSITION OF ZERO.

The differential system of this model is now (Module numbered Four)-26

$$\frac{dG_{24}}{dt} = (a_{24})^{(4)}G_{25} - [(a'_{24})^{(4)} + (a''_{24})^{(4)}(T_{25}, t)]G_{24} -27$$

$$\frac{dG_{25}}{dt} = (a_{25})^{(4)}G_{24} - [(a'_{25})^{(4)} + (a''_{25})^{(4)}(T_{25}, t)]G_{25} -28$$

$$\frac{dG_{26}}{dt} = (a_{26})^{(4)}G_{25} - [(a'_{26})^{(4)} + (a''_{26})^{(4)}(T_{25}, t)]G_{26} -29$$

$$\frac{dT_{24}}{dt} = (b_{24})^{(4)}T_{25} - [(b'_{24})^{(4)} - (b''_{24})^{(4)}((G_{27}, t))]T_{24} -30$$

$$\frac{dT_{25}}{dt} = (b_{25})^{(4)}T_{24} - [(b'_{25})^{(4)} - (b''_{25})^{(4)}((G_{27}, t))]T_{25} -31$$

$$\frac{dT_{26}}{dt} = (b_{26})^{(4)}T_{25} - [(b'_{26})^{(4)} - (b''_{26})^{(4)}((G_{27}, t))]T_{26} -32$$

$$+(a''_{24})^{(4)}(T_{25}, t) = \text{First augmentation factor}-33$$

$$-(b''_{24})^{(4)}((G_{27}, t)) = \text{First detritions factor} -34$$

**“C” AND “H”(SEE FIGURE REPRESENTS AN “M CONFIGURATION” OR “INSTRUCTIONS) OR STATE:
 THE CONVENTION SHOWN IS AFTER MCCLUSKY,BOOTH,HILL AND PETERSON.**

MODULE NUMBERED FIVE

**NOTE: THE ACCENTUATION COEFFICIENT AND DISSIPATION COEFFICIENT NEED NOT BE THE SAME
 IT MAY BE ZERO, OR MIGHT BE SAME,I ALL THE THREE CASES THE MODEL COULD BE CHANGED
 EAILY BY REPLACING THE COEFFICIENTS BY EQUALITY SIGN OR GIVING IT THE POSITION OF
 ZERO**

The differential system of this model is now (Module number five)-35

$$\frac{dG_{28}}{dt} = (a_{28})^{(5)} G_{29} - [(a'_{28})^{(5)} + (a''_{28})^{(5)}(T_{29}, t)] G_{28} -36$$

$$\frac{dG_{29}}{dt} = (a_{29})^{(5)} G_{28} - [(a'_{29})^{(5)} + (a''_{29})^{(5)}(T_{29}, t)] G_{29} -37$$

$$\frac{dG_{30}}{dt} = (a_{30})^{(5)} G_{29} - [(a'_{30})^{(5)} + (a''_{30})^{(5)}(T_{29}, t)] G_{30} -38$$

$$\frac{dT_{28}}{dt} = (b_{28})^{(5)} T_{29} - [(b'_{28})^{(5)} - (b''_{28})^{(5)}((G_{31}, t))] T_{28} -39$$

$$\frac{dT_{29}}{dt} = (b_{29})^{(5)} T_{28} - [(b'_{29})^{(5)} - (b''_{29})^{(5)}((G_{31}, t))] T_{29} -40$$

$$\frac{dT_{30}}{dt} = (b_{30})^{(5)} T_{29} - [(b'_{30})^{(5)} - (b''_{30})^{(5)}((G_{31}, t))] T_{30} -41$$

$$+(a''_{28})^{(5)}(T_{29}, t) = \text{First augmentation factor} -42$$

$$-(b''_{28})^{(5)}((G_{31}, t)) = \text{First detritions factor} -43$$

**B” AND “B”(SEE FIGURE REPRESENTS AN “M CONFIGURATION” OR “INSTRUCTIONS) OR STATE:
 THE CONVENTION SHOWN IS AFTER MCCLUSKY,BOOTH,HILL AND PETERSON.**

**THE SYSTEM HERE IS ONE OF SELF TRANSFORMATIONAL,SYSTEM CHANGING,STRUCTURALLY
 MUTATIONAL,SYLOGISTICALLY CHANGEABLE AND CONFIGURATIONALLY ALTERABLE(VERY
 VERY IMPORTANT SYSTEM IN ALMOST ALL SUBJECTS BE IT IN QUANTUM SYSTEMS OR**

DISSIPATIVE STRUCTURES

MODULE NUMBERED SIX

**NOTE: THE ACCENTUATION COEFFICIENT AND DISSIPATION COEFFICIENT NEED NOT BE THE SAME
 IT MAY BE ZERO, OR MIGHT BE SAME,I ALL THE THREE CASES THE MODEL COULD BE CHANGED
 EAILY BY REPLACING THE COEFFICIENTS BY EQUALITY SIGN OR GIVING IT THE POSITION OF
 ZERO**

:

The differential system of this model is now (Module numbered Six)-44

45

$$\frac{dG_{32}}{dt} = (a_{32})^{(6)} G_{33} - [(a'_{32})^{(6)} + (a''_{32})^{(6)}(T_{33}, t)] G_{32} -46$$

$$\frac{dG_{33}}{dt} = (a_{33})^{(6)} G_{32} - [(a'_{33})^{(6)} + (a''_{33})^{(6)}(T_{33}, t)] G_{33} -47$$

$$\frac{dG_{34}}{dt} = (a_{34})^{(6)} G_{33} - [(a'_{34})^{(6)} + (a''_{34})^{(6)}(T_{33}, t)] G_{34} -48$$

$$\frac{dT_{32}}{dt} = (b_{32})^{(6)} T_{33} - [(b'_{32})^{(6)} - (b''_{32})^{(6)}((G_{35}, t))] T_{32} -49$$

$$\frac{dT_{33}}{dt} = (b_{33})^{(6)} T_{32} - [(b'_{33})^{(6)} - (b''_{33})^{(6)}((G_{35}, t))] T_{33} -50$$

$$\frac{dT_{34}}{dt} = (b_{34})^{(6)} T_{33} - [(b'_{34})^{(6)} - (b''_{34})^{(6)}((G_{35}, t))] T_{34} -51$$

$$+(a''_{32})^{(6)}(T_{33}, t) = \text{First augmentation factor}-52$$

**“INPUT” AND “A”(SEE FIGURE REPRESENTS AN “M CONFIGURATION” OR “INSTRUCTIONS) OR
 STATE: THE CONVENTION SHOWN IS AFTER MCCLUSKY,BOOTH,HILL AND PETERSON.**

MODULE NUMBERED SEVEN

**NOTE: THE ACCENTUATION COEFFICIENT AND DISSIPATION COEFFICIENT NEED NOT BE THE SAME
 IT MAY BE ZERO, OR MIGHT BE SAME,I ALL THE THREE CASES THE MODEL COULD BE CHANGED
 EAILY BY REPLACING THE COEFFICIENTS BY EQUALITY SIGN OR GIVING IT THE POSITION OF
 ZERO**

:

The differential system of this model is now (SEVENTH MODULE)

-53

$$\frac{dG_{36}}{dt} = (a_{36})^{(7)} G_{37} - [(a'_{36})^{(7)} + (a''_{36})^{(7)}(T_{37}, t)] G_{36} -54$$

$$\frac{dG_{37}}{dt} = (a_{37})^{(7)} G_{36} - [(a'_{37})^{(7)} + (a''_{37})^{(7)}(T_{37}, t)] G_{37} -55$$

$$\frac{dG_{38}}{dt} = (a_{38})^{(7)}G_{37} - [(a'_{38})^{(7)} + (a''_{38})^{(7)}(T_{37}, t)]G_{38} - 56$$

$$\frac{dT_{36}}{dt} = (b_{36})^{(7)}T_{37} - [(b'_{36})^{(7)} - (b''_{36})^{(7)}((G_{39}), t)]T_{36} - 57$$

$$\frac{dT_{37}}{dt} = (b_{37})^{(7)}T_{36} - [(b'_{37})^{(7)} - (b''_{37})^{(7)}((G_{39}), t)]T_{37} - 58$$

59

$$\frac{dT_{38}}{dt} = (b_{38})^{(7)}T_{37} - [(b'_{38})^{(7)} - (b''_{38})^{(7)}((G_{39}), t)]T_{38} - 60$$

$$+(a''_{36})^{(7)}(T_{37}, t) = \text{First augmentation factor} - 61$$

$$-(b''_{36})^{(7)}((G_{39}), t) = \text{First detritions factor}$$

FIRST MODULE CONCATENATION:

$$\frac{dG_{13}}{dt} = (a_{13})^{(1)}G_{14} - \left[\begin{array}{c} (a'_{13})^{(1)} \boxed{+(a''_{13})^{(1)}(T_{14}, t)} \boxed{+(a''_{16})^{(2,2)}(T_{17}, t)} \boxed{+(a''_{20})^{(3,3)}(T_{21}, t)} \\ \boxed{+(a''_{24})^{(4,4,4,4)}(T_{25}, t)} \boxed{+(a''_{28})^{(5,5,5,5)}(T_{29}, t)} \boxed{+(a''_{32})^{(6,6,6,6)}(T_{33}, t)} \\ \boxed{+(a''_{36})^{(7)}(T_{37}, t)} \end{array} \right] G_{13}$$

$$\frac{dG_{14}}{dt} = (a_{14})^{(1)}G_{13} - \left[\begin{array}{c} (a'_{14})^{(1)} \boxed{+(a''_{14})^{(1)}(T_{14}, t)} \boxed{+(a''_{17})^{(2,2)}(T_{17}, t)} \boxed{+(a''_{21})^{(3,3)}(T_{21}, t)} \\ \boxed{+(a''_{25})^{(4,4,4,4)}(T_{25}, t)} \boxed{+(a''_{29})^{(5,5,5,5)}(T_{29}, t)} \boxed{+(a''_{33})^{(6,6,6,6)}(T_{33}, t)} \\ \boxed{+(a''_{37})^{(7)}(T_{37}, t)} \end{array} \right] G_{14}$$

$$\frac{dG_{15}}{dt} = (a_{15})^{(1)}G_{14} - \left[\begin{array}{c} (a'_{15})^{(1)} \boxed{+(a''_{15})^{(1)}(T_{14}, t)} \boxed{+(a''_{18})^{(2,2)}(T_{17}, t)} \boxed{+(a''_{22})^{(3,3)}(T_{21}, t)} \\ \boxed{+(a''_{26})^{(4,4,4,4)}(T_{25}, t)} \boxed{+(a''_{30})^{(5,5,5,5)}(T_{29}, t)} \boxed{+(a''_{34})^{(6,6,6,6)}(T_{33}, t)} \\ \boxed{+(a''_{38})^{(7)}(T_{37}, t)} \end{array} \right] G_{15}$$

Where $\boxed{+(a''_{13})^{(1)}(T_{14}, t)}$, $\boxed{+(a''_{14})^{(1)}(T_{14}, t)}$, $\boxed{+(a''_{15})^{(1)}(T_{14}, t)}$ are first augmentation coefficients for category 1, 2 and 3
 $\boxed{+(a''_{16})^{(2,2)}(T_{17}, t)}$, $\boxed{+(a''_{17})^{(2,2)}(T_{17}, t)}$, $\boxed{+(a''_{18})^{(2,2)}(T_{17}, t)}$ are second augmentation coefficient for category 1, 2 and 3
 $\boxed{+(a''_{20})^{(3,3)}(T_{21}, t)}$, $\boxed{+(a''_{21})^{(3,3)}(T_{21}, t)}$, $\boxed{+(a''_{22})^{(3,3)}(T_{21}, t)}$ are third augmentation coefficient for category 1, 2 and 3
 $\boxed{+(a''_{24})^{(4,4,4,4)}(T_{25}, t)}$, $\boxed{+(a''_{25})^{(4,4,4,4)}(T_{25}, t)}$, $\boxed{+(a''_{26})^{(4,4,4,4)}(T_{25}, t)}$ are fourth augmentation coefficient for category 1, 2 and 3
 $\boxed{+(a''_{28})^{(5,5,5,5)}(T_{29}, t)}$, $\boxed{+(a''_{29})^{(5,5,5,5)}(T_{29}, t)}$, $\boxed{+(a''_{30})^{(5,5,5,5)}(T_{29}, t)}$ are fifth augmentation coefficient for category 1, 2 and 3
 $\boxed{+(a''_{32})^{(6,6,6,6)}(T_{33}, t)}$, $\boxed{+(a''_{33})^{(6,6,6,6)}(T_{33}, t)}$, $\boxed{+(a''_{34})^{(6,6,6,6)}(T_{33}, t)}$ are sixth augmentation coefficient for category 1, 2 and 3

ARE SEVENTH AUGMENTATION COEFFICIENTS

$$\frac{dT_{13}}{dt} = (b_{13})^{(1)}T_{14} - \left[\begin{array}{c} (b'_{13})^{(1)} \boxed{-(b''_{16})^{(1)}(G, t)} \boxed{-(b''_{36})^{(7)}(G_{39}, t)} \boxed{-(b''_{20})^{(3,3)}(G_{23}, t)} \\ \boxed{-(b''_{24})^{(4,4,4,4)}(G_{27}, t)} \boxed{-(b''_{28})^{(5,5,5,5)}(G_{31}, t)} \boxed{-(b''_{32})^{(6,6,6,6)}(G_{35}, t)} \\ \boxed{-(b''_{36})^{(7)}(G_{39}, t)} \end{array} \right] T_{13}$$

$$\frac{dT_{14}}{dt} = (b_{14})^{(1)}T_{13} - \left[\begin{array}{c} (b'_{14})^{(1)} \boxed{-(b''_{14})^{(1)}(G, t)} \boxed{-(b''_{17})^{(2,2)}(G_{19}, t)} \boxed{-(b''_{21})^{(3,3)}(G_{23}, t)} \\ \boxed{-(b''_{25})^{(4,4,4,4)}(G_{27}, t)} \boxed{-(b''_{29})^{(5,5,5,5)}(G_{31}, t)} \boxed{-(b''_{33})^{(6,6,6,6)}(G_{35}, t)} \\ \boxed{-(b''_{37})^{(7)}(G_{39}, t)} \end{array} \right] T_{14}$$

$$\frac{dT_{15}}{dt} = (b_{15})^{(1)}T_{14} - \left[\begin{array}{c} (b'_{15})^{(1)} \boxed{-(b''_{15})^{(1)}(G, t)} \boxed{-(b''_{18})^{(2,2)}(G_{19}, t)} \boxed{-(b''_{22})^{(3,3)}(G_{23}, t)} \\ \boxed{-(b''_{26})^{(4,4,4,4)}(G_{27}, t)} \boxed{-(b''_{30})^{(5,5,5,5)}(G_{31}, t)} \boxed{-(b''_{34})^{(6,6,6,6)}(G_{35}, t)} \\ \boxed{-(b''_{38})^{(7)}(G_{39}, t)} \end{array} \right] T_{15}$$

Where $\boxed{-(b''_{13})^{(1)}(G, t)}$, $\boxed{-(b''_{14})^{(1)}(G, t)}$, $\boxed{-(b''_{15})^{(1)}(G, t)}$ are first detritions coefficients for category 1, 2 and 3
 $\boxed{-(b''_{16})^{(2,2)}(G_{19}, t)}$, $\boxed{-(b''_{17})^{(2,2)}(G_{19}, t)}$, $\boxed{-(b''_{18})^{(2,2)}(G_{19}, t)}$ are second detritions coefficients for category 1, 2 and 3

$-(b''_{20})^{(3,3,3)}(G_{23}, t)$, $-(b''_{21})^{(3,3,3)}(G_{23}, t)$, $-(b''_{22})^{(3,3,3)}(G_{23}, t)$ are third detritions coefficients for category 1, 2 and 3
 $-(b''_{24})^{(4,4,4,4)}(G_{27}, t)$, $-(b''_{25})^{(4,4,4,4)}(G_{27}, t)$, $-(b''_{26})^{(4,4,4,4)}(G_{27}, t)$ are fourth detritions coefficients for category 1, 2 and 3
 $-(b''_{28})^{(5,5,5,5)}(G_{31}, t)$, $-(b''_{29})^{(5,5,5,5)}(G_{31}, t)$, $-(b''_{30})^{(5,5,5,5)}(G_{31}, t)$ are fifth detritions coefficients for category 1, 2 and 3
 $-(b''_{32})^{(6,6,6,6)}(G_{35}, t)$, $-(b''_{33})^{(6,6,6,6)}(G_{35}, t)$, $-(b''_{34})^{(6,6,6,6)}(G_{35}, t)$ are sixth detritions coefficients for category 1, 2 and 3
 $-(b''_{36})^{(7)}(G_{39}, t)$, $-(b''_{36})^{(7)}(G_{39}, t)$, $-(b''_{36})^{(7)}(G_{39}, t)$ ARE SEVENTH DETRITION COEFFICIENTS

-62

$$\frac{dT_{15}}{dt} = (b_{15})^{(1)}T_{14} - \left[\begin{array}{l} (b'_{15})^{(1)} \left[\begin{array}{l} -(b''_{15})^{(1)}(G, t) \quad -(b''_{18})^{(2,2)}(G_{19}, t) \quad -(b''_{22})^{(3,3,3)}(G_{23}, t) \\ -(b''_{26})^{(4,4,4,4)}(G_{27}, t) \quad -(b''_{30})^{(5,5,5,5)}(G_{31}, t) \quad -(b''_{34})^{(6,6,6,6)}(G_{35}, t) \end{array} \right] \end{array} \right] T_{15} \quad -63$$

Where $-(b''_{13})^{(1)}(G, t)$, $-(b''_{14})^{(1)}(G, t)$, $-(b''_{15})^{(1)}(G, t)$ are first detrition coefficients for category 1, 2 and 3
 $-(b''_{16})^{(2,2)}(G_{19}, t)$, $-(b''_{17})^{(2,2)}(G_{19}, t)$, $-(b''_{18})^{(2,2)}(G_{19}, t)$ are second detritions coefficients for category 1, 2 and 3
 $-(b''_{20})^{(3,3,3)}(G_{23}, t)$, $-(b''_{21})^{(3,3,3)}(G_{23}, t)$, $-(b''_{22})^{(3,3,3)}(G_{23}, t)$ are third detritions coefficients for category 1, 2 and 3
 $-(b''_{24})^{(4,4,4,4)}(G_{27}, t)$, $-(b''_{25})^{(4,4,4,4)}(G_{27}, t)$, $-(b''_{26})^{(4,4,4,4)}(G_{27}, t)$ are fourth detritions coefficients for category 1, 2 and 3
 $-(b''_{28})^{(5,5,5,5)}(G_{31}, t)$, $-(b''_{29})^{(5,5,5,5)}(G_{31}, t)$, $-(b''_{30})^{(5,5,5,5)}(G_{31}, t)$ are fifth detritions coefficients for category 1, 2 and 3
 $-(b''_{32})^{(6,6,6,6)}(G_{35}, t)$, $-(b''_{33})^{(6,6,6,6)}(G_{35}, t)$, $-(b''_{34})^{(6,6,6,6)}(G_{35}, t)$ are sixth detritions coefficients for category 1, 2 and 3 -64

SECOND MODULE CONCATENATION:-

$$65 \frac{dG_{16}}{dt} = (a_{16})^{(2)}G_{17} - \left[\begin{array}{l} (a'_{16})^{(2)} \left[\begin{array}{l} +(a''_{16})^{(2)}(T_{17}, t) \quad +(a''_{13})^{(1,1)}(T_{14}, t) \quad +(a''_{20})^{(3,3,3)}(T_{21}, t) \\ +(a''_{24})^{(4,4,4,4)}(T_{25}, t) \quad +(a''_{28})^{(5,5,5,5)}(T_{29}, t) \quad +(a''_{32})^{(6,6,6,6)}(T_{33}, t) \end{array} \right] \\ +(a''_{36})^{(7,7)}(T_{37}, t) \end{array} \right] G_{16} \quad -66$$

$$\frac{dG_{17}}{dt} = (a_{17})^{(2)}G_{16} - \left[\begin{array}{l} (a'_{17})^{(2)} \left[\begin{array}{l} +(a''_{17})^{(2)}(T_{17}, t) \quad +(a''_{14})^{(1,1)}(T_{14}, t) \quad +(a''_{21})^{(3,3,3)}(T_{21}, t) \\ +(a''_{25})^{(4,4,4,4)}(T_{25}, t) \quad +(a''_{29})^{(5,5,5,5)}(T_{29}, t) \quad +(a''_{33})^{(6,6,6,6)}(T_{33}, t) \end{array} \right] \\ +(a''_{37})^{(7,7)}(T_{37}, t) \end{array} \right] G_{17} \quad -67$$

$$\frac{dG_{18}}{dt} = (a_{18})^{(2)}G_{17} - \left[\begin{array}{l} (a'_{18})^{(2)} \left[\begin{array}{l} +(a''_{18})^{(2)}(T_{17}, t) \quad +(a''_{15})^{(1,1)}(T_{14}, t) \quad +(a''_{22})^{(3,3,3)}(T_{21}, t) \\ +(a''_{26})^{(4,4,4,4)}(T_{25}, t) \quad +(a''_{30})^{(5,5,5,5)}(T_{29}, t) \quad +(a''_{34})^{(6,6,6,6)}(T_{33}, t) \end{array} \right] \\ +(a''_{38})^{(7,7)}(T_{37}, t) \end{array} \right] G_{18} \quad -68$$

Where $+(a''_{16})^{(2)}(T_{17}, t)$, $+(a''_{17})^{(2)}(T_{17}, t)$, $+(a''_{18})^{(2)}(T_{17}, t)$ are first augmentation coefficients for category 1, 2 and 3
 $+(a''_{13})^{(1,1)}(T_{14}, t)$, $+(a''_{14})^{(1,1)}(T_{14}, t)$, $+(a''_{15})^{(1,1)}(T_{14}, t)$ are second augmentation coefficient for category 1, 2 and 3
 $+(a''_{20})^{(3,3,3)}(T_{21}, t)$, $+(a''_{21})^{(3,3,3)}(T_{21}, t)$, $+(a''_{22})^{(3,3,3)}(T_{21}, t)$ are third augmentation coefficient for category 1, 2 and 3
 $+(a''_{24})^{(4,4,4,4)}(T_{25}, t)$, $+(a''_{25})^{(4,4,4,4)}(T_{25}, t)$, $+(a''_{26})^{(4,4,4,4)}(T_{25}, t)$ are fourth augmentation coefficient for category 1, 2 and 3
 $+(a''_{28})^{(5,5,5,5)}(T_{29}, t)$, $+(a''_{29})^{(5,5,5,5)}(T_{29}, t)$, $+(a''_{30})^{(5,5,5,5)}(T_{29}, t)$ are fifth augmentation coefficient for category 1, 2 and 3
 $+(a''_{32})^{(6,6,6,6)}(T_{33}, t)$, $+(a''_{33})^{(6,6,6,6)}(T_{33}, t)$, $+(a''_{34})^{(6,6,6,6)}(T_{33}, t)$ are sixth augmentation coefficient for category 1, 2 and 3 -69

$+(a''_{36})^{(7,7)}(T_{37}, t) + (a''_{37})^{(7,7)}(T_{37}, t) + (a''_{38})^{(7,7)}(T_{37}, t)$ ARE SEVENTH DETRITION COEFFICIENTS-71

$$\frac{dT_{16}}{dt} = (b_{16})^{(2)}T_{17} - \left[\begin{array}{l} (b'_{16})^{(2)} \boxed{-(b''_{16})^{(2)}(G_{19}, t)} \quad \boxed{-(b''_{13})^{(1,1)}(G, t)} \quad \boxed{-(b''_{20})^{(3,3,3)}(G_{23}, t)} \\ \boxed{-(b''_{24})^{(4,4,4,4,4)}(G_{27}, t)} \quad \boxed{-(b''_{28})^{(5,5,5,5,5)}(G_{31}, t)} \quad \boxed{-(b''_{32})^{(6,6,6,6,6)}(G_{35}, t)} \\ \boxed{-(b''_{36})^{(7,7)}(G_{39}, t)} \end{array} \right] T_{16} -72$$

$$\frac{dT_{17}}{dt} = (b_{17})^{(2)}T_{16} - \left[\begin{array}{l} (b'_{17})^{(2)} \boxed{-(b''_{17})^{(2)}(G_{19}, t)} \quad \boxed{-(b''_{14})^{(1,1)}(G, t)} \quad \boxed{-(b''_{21})^{(3,3,3)}(G_{23}, t)} \\ \boxed{-(b''_{25})^{(4,4,4,4,4)}(G_{27}, t)} \quad \boxed{-(b''_{29})^{(5,5,5,5,5)}(G_{31}, t)} \quad \boxed{-(b''_{33})^{(6,6,6,6,6)}(G_{35}, t)} \\ \boxed{-(b''_{37})^{(7,7)}(G_{39}, t)} \end{array} \right] T_{17} -73$$

$$\frac{dT_{18}}{dt} = (b_{18})^{(2)}T_{17} - \left[\begin{array}{l} (b'_{18})^{(2)} \boxed{-(b''_{18})^{(2)}(G_{19}, t)} \quad \boxed{-(b''_{15})^{(1,1)}(G, t)} \quad \boxed{-(b''_{22})^{(3,3,3)}(G_{23}, t)} \\ \boxed{-(b''_{26})^{(4,4,4,4,4)}(G_{27}, t)} \quad \boxed{-(b''_{30})^{(5,5,5,5,5)}(G_{31}, t)} \quad \boxed{-(b''_{34})^{(6,6,6,6,6)}(G_{35}, t)} \\ \boxed{-(b''_{38})^{(7,7)}(G_{39}, t)} \end{array} \right] T_{18} -74$$

where $\boxed{-(b''_{16})^{(2)}(G_{19}, t)}$, $\boxed{-(b''_{17})^{(2)}(G_{19}, t)}$, $\boxed{-(b''_{18})^{(2)}(G_{19}, t)}$ are first detrition coefficients for category 1, 2 and 3

$\boxed{-(b''_{13})^{(1,1)}(G, t)}$, $\boxed{-(b''_{14})^{(1,1)}(G, t)}$, $\boxed{-(b''_{15})^{(1,1)}(G, t)}$ are second detrition coefficients for category 1,2 and 3

$\boxed{-(b''_{20})^{(3,3,3)}(G_{23}, t)}$, $\boxed{-(b''_{21})^{(3,3,3)}(G_{23}, t)}$, $\boxed{-(b''_{22})^{(3,3,3)}(G_{23}, t)}$ are third detrition coefficients for category 1,2 and 3

$\boxed{-(b''_{24})^{(4,4,4,4,4)}(G_{27}, t)}$, $\boxed{-(b''_{25})^{(4,4,4,4,4)}(G_{27}, t)}$, $\boxed{-(b''_{26})^{(4,4,4,4,4)}(G_{27}, t)}$ are fourth detritions coefficients for category 1,2 and 3

$\boxed{-(b''_{28})^{(5,5,5,5,5)}(G_{31}, t)}$, $\boxed{-(b''_{29})^{(5,5,5,5,5)}(G_{31}, t)}$, $\boxed{-(b''_{30})^{(5,5,5,5,5)}(G_{31}, t)}$ are fifth detritions coefficients for category 1,2 and 3

$\boxed{-(b''_{32})^{(6,6,6,6,6)}(G_{35}, t)}$, $\boxed{-(b''_{33})^{(6,6,6,6,6)}(G_{35}, t)}$, $\boxed{-(b''_{34})^{(6,6,6,6,6)}(G_{35}, t)}$ are sixth detritions coefficients for category 1,2 and 3

$\boxed{-(b''_{36})^{(7,7)}(G_{39}, t)}$, $\boxed{-(b''_{37})^{(7,7)}(G_{39}, t)}$, $\boxed{-(b''_{38})^{(7,7)}(G_{39}, t)}$ are seventh detrition coefficients

THIRD MODULE CONCATENATION:-75

$$\frac{dG_{20}}{dt} = (a_{20})^{(3)}G_{21} - \left[\begin{array}{l} (a'_{20})^{(3)} \boxed{+(a''_{20})^{(3)}(T_{21}, t)} \quad \boxed{+(a''_{16})^{(2,2,2)}(T_{17}, t)} \quad \boxed{+(a''_{13})^{(1,1,1)}(T_{14}, t)} \\ \boxed{+(a''_{24})^{(4,4,4,4,4)}(T_{25}, t)} \quad \boxed{+(a''_{28})^{(5,5,5,5,5)}(T_{29}, t)} \quad \boxed{+(a''_{32})^{(6,6,6,6,6)}(T_{33}, t)} \\ \boxed{+(a''_{36})^{(7,7,7)}(T_{37}, t)} \end{array} \right] G_{20} -76$$

$$\frac{dG_{21}}{dt} = (a_{21})^{(3)}G_{20} - \left[\begin{array}{l} (a'_{21})^{(3)} \boxed{+(a''_{21})^{(3)}(T_{21}, t)} \quad \boxed{+(a''_{17})^{(2,2,2)}(T_{17}, t)} \quad \boxed{+(a''_{14})^{(1,1,1)}(T_{14}, t)} \\ \boxed{+(a''_{25})^{(4,4,4,4,4)}(T_{25}, t)} \quad \boxed{+(a''_{29})^{(5,5,5,5,5)}(T_{29}, t)} \quad \boxed{+(a''_{33})^{(6,6,6,6,6)}(T_{33}, t)} \\ \boxed{+(a''_{37})^{(7,7,7)}(T_{37}, t)} \end{array} \right] G_{21} -77$$

$$\frac{dG_{22}}{dt} = (a_{22})^{(3)}G_{21} - \left[\begin{array}{l} (a'_{22})^{(3)} \boxed{+(a''_{22})^{(3)}(T_{21}, t)} \quad \boxed{+(a''_{18})^{(2,2,2)}(T_{17}, t)} \quad \boxed{+(a''_{15})^{(1,1,1)}(T_{14}, t)} \\ \boxed{+(a''_{26})^{(4,4,4,4,4)}(T_{25}, t)} \quad \boxed{+(a''_{30})^{(5,5,5,5,5)}(T_{29}, t)} \quad \boxed{+(a''_{34})^{(6,6,6,6,6)}(T_{33}, t)} \\ \boxed{+(a''_{38})^{(7,7,7)}(T_{37}, t)} \end{array} \right] G_{22} -78$$

$\boxed{+(a''_{20})^{(3)}(T_{21}, t)}$, $\boxed{+(a''_{21})^{(3)}(T_{21}, t)}$, $\boxed{+(a''_{22})^{(3)}(T_{21}, t)}$ are first augmentation coefficients for category 1, 2 and 3

$\boxed{+(a''_{16})^{(2,2,2)}(T_{17}, t)}$, $\boxed{+(a''_{17})^{(2,2,2)}(T_{17}, t)}$, $\boxed{+(a''_{18})^{(2,2,2)}(T_{17}, t)}$ are second augmentation coefficients for category 1, 2 and 3

$\boxed{+(a''_{13})^{(1,1,1)}(T_{14}, t)}$, $\boxed{+(a''_{14})^{(1,1,1)}(T_{14}, t)}$, $\boxed{+(a''_{15})^{(1,1,1)}(T_{14}, t)}$ are third augmentation coefficients for category 1, 2 and 3

$\boxed{+(a''_{24})^{(4,4,4,4,4)}(T_{25}, t)}$, $\boxed{+(a''_{25})^{(4,4,4,4,4)}(T_{25}, t)}$, $\boxed{+(a''_{26})^{(4,4,4,4,4)}(T_{25}, t)}$ are fourth augmentation coefficients for category 1, 2 and 3

$\boxed{+(a''_{28})^{(5,5,5,5,5)}(T_{29}, t)}$, $\boxed{+(a''_{29})^{(5,5,5,5,5)}(T_{29}, t)}$, $\boxed{+(a''_{30})^{(5,5,5,5,5)}(T_{29}, t)}$ are fifth augmentation coefficients for category 1, 2 and 3

$\boxed{+(a''_{32})^{(6,6,6,6,6)}(T_{33}, t)}$, $\boxed{+(a''_{33})^{(6,6,6,6,6)}(T_{33}, t)}$, $\boxed{+(a''_{34})^{(6,6,6,6,6)}(T_{33}, t)}$ are sixth augmentation coefficients for category 1, 2 and 3 -79

80

$\boxed{+(a''_{36})^{(7,7,7)}(T_{37}, t)}$, $\boxed{+(a''_{37})^{(7,7,7)}(T_{37}, t)}$, $\boxed{+(a''_{38})^{(7,7,7)}(T_{37}, t)}$ are seventh augmentation coefficient-81

$$\left. \begin{aligned} \frac{dT_{20}}{dt} &= (b_{20})^{(3)}T_{21} - \left[\begin{array}{l} \boxed{(b'_{20})^{(3)} - \boxed{(b''_{20})^{(3)}(G_{23}, t)} - \boxed{(b''_{36})^{(7,7,7)}(G_{19}, t)} - \boxed{(b''_{13})^{(1,1,1)}(G, t)} \\ \boxed{-(b''_{24})^{(4,4,4,4,4)}(G_{27}, t)} - \boxed{(b''_{28})^{(5,5,5,5,5)}(G_{31}, t)} - \boxed{(b''_{32})^{(6,6,6,6,6)}(G_{35}, t)} \\ \boxed{-(b''_{36})^{(7,7,7)}(G_{39}, t)} \end{array} \right] T_{20} \quad -82 \\ \frac{dT_{21}}{dt} &= (b_{21})^{(3)}T_{20} - \left[\begin{array}{l} \boxed{(b'_{21})^{(3)} - \boxed{(b''_{21})^{(3)}(G_{23}, t)} - \boxed{(b''_{17})^{(2,2,2)}(G_{19}, t)} - \boxed{(b''_{14})^{(1,1,1)}(G, t)} \\ \boxed{-(b''_{25})^{(4,4,4,4,4)}(G_{27}, t)} - \boxed{(b''_{29})^{(5,5,5,5,5)}(G_{31}, t)} - \boxed{(b''_{33})^{(6,6,6,6,6)}(G_{35}, t)} \\ \boxed{-(b''_{37})^{(7,7,7)}(G_{39}, t)} \end{array} \right] T_{21} \quad -83 \\ \frac{dT_{22}}{dt} &= (b_{22})^{(3)}T_{21} - \left[\begin{array}{l} \boxed{(b'_{22})^{(3)} - \boxed{(b''_{22})^{(3)}(G_{23}, t)} - \boxed{(b''_{18})^{(2,2,2)}(G_{19}, t)} - \boxed{(b''_{15})^{(1,1,1)}(G, t)} \\ \boxed{-(b''_{26})^{(4,4,4,4,4)}(G_{27}, t)} - \boxed{(b''_{30})^{(5,5,5,5,5)}(G_{31}, t)} - \boxed{(b''_{34})^{(6,6,6,6,6)}(G_{35}, t)} \\ \boxed{-(b''_{38})^{(7,7,7)}(G_{39}, t)} \end{array} \right] T_{22} \quad -84 \end{aligned} \right.$$

$\boxed{-(b''_{20})^{(3)}(G_{23}, t)}$, $\boxed{-(b''_{21})^{(3)}(G_{23}, t)}$, $\boxed{-(b''_{22})^{(3)}(G_{23}, t)}$ are first detritions coefficients for category 1, 2 and 3

$\boxed{-(b''_{16})^{(2,2,2)}(G_{19}, t)}$, $\boxed{-(b''_{17})^{(2,2,2)}(G_{19}, t)}$, $\boxed{-(b''_{18})^{(2,2,2)}(G_{19}, t)}$ are second detritions coefficients for category 1, 2 and 3

$\boxed{-(b''_{13})^{(1,1,1)}(G, t)}$, $\boxed{-(b''_{14})^{(1,1,1)}(G, t)}$, $\boxed{-(b''_{15})^{(1,1,1)}(G, t)}$ are third detrition coefficients for category 1,2 and 3

$\boxed{-(b''_{24})^{(4,4,4,4,4)}(G_{27}, t)}$, $\boxed{-(b''_{25})^{(4,4,4,4,4)}(G_{27}, t)}$, $\boxed{-(b''_{26})^{(4,4,4,4,4)}(G_{27}, t)}$ are fourth detritions coefficients for category 1, 2 and 3

$\boxed{-(b''_{28})^{(5,5,5,5,5)}(G_{31}, t)}$, $\boxed{-(b''_{29})^{(5,5,5,5,5)}(G_{31}, t)}$, $\boxed{-(b''_{30})^{(5,5,5,5,5)}(G_{31}, t)}$ are fifth detritions coefficients for category 1, 2 and 3

$\boxed{-(b''_{32})^{(6,6,6,6,6)}(G_{35}, t)}$, $\boxed{-(b''_{33})^{(6,6,6,6,6)}(G_{35}, t)}$, $\boxed{-(b''_{34})^{(6,6,6,6,6)}(G_{35}, t)}$ are sixth detritions coefficients for category 1, 2 and 3 -85

$\boxed{-(b''_{36})^{(7,7,7)}(G_{39}, t)}$, $\boxed{-(b''_{37})^{(7,7,7)}(G_{39}, t)}$, $\boxed{-(b''_{38})^{(7,7,7)}(G_{39}, t)}$ are seventh detritions coefficients

FOURTH MODULE CONCATENATION:-86

$$\left. \begin{aligned} \frac{dG_{24}}{dt} &= (a_{24})^{(4)}G_{25} - \left[\begin{array}{l} \boxed{(a'_{24})^{(4)} + \boxed{(a''_{24})^{(4)}(T_{25}, t)} + \boxed{(a''_{28})^{(5,5)}(T_{29}, t)} + \boxed{(a''_{32})^{(6,6)}(T_{33}, t)} \\ \boxed{+(a''_{13})^{(1,1,1,1)}(T_{14}, t)} + \boxed{(a''_{16})^{(2,2,2,2)}(T_{17}, t)} + \boxed{(a''_{20})^{(3,3,3,3)}(T_{21}, t)} \\ \boxed{+(a''_{36})^{(7,7,7,7)}(T_{37}, t)} \end{array} \right] G_{24} \quad -87 \\ \frac{dG_{25}}{dt} &= (a_{25})^{(4)}G_{24} - \left[\begin{array}{l} \boxed{(a'_{25})^{(4)} + \boxed{(a''_{25})^{(4)}(T_{25}, t)} + \boxed{(a''_{29})^{(5,5)}(T_{29}, t)} + \boxed{(a''_{33})^{(6,6)}(T_{33}, t)} \\ \boxed{+(a''_{14})^{(1,1,1,1)}(T_{14}, t)} + \boxed{(a''_{17})^{(2,2,2,2)}(T_{17}, t)} + \boxed{(a''_{21})^{(3,3,3,3)}(T_{21}, t)} \\ \boxed{+(a''_{37})^{(7,7,7,7)}(T_{37}, t)} \end{array} \right] G_{25} \quad -88 \\ \frac{dG_{26}}{dt} &= (a_{26})^{(4)}G_{25} - \left[\begin{array}{l} \boxed{(a'_{26})^{(4)} + \boxed{(a''_{26})^{(4)}(T_{25}, t)} + \boxed{(a''_{30})^{(5,5)}(T_{29}, t)} + \boxed{(a''_{34})^{(6,6)}(T_{33}, t)} \\ \boxed{+(a''_{15})^{(1,1,1,1)}(T_{14}, t)} + \boxed{(a''_{18})^{(2,2,2,2)}(T_{17}, t)} + \boxed{(a''_{22})^{(3,3,3,3)}(T_{21}, t)} \\ \boxed{+(a''_{38})^{(7,7,7,7)}(T_{37}, t)} \end{array} \right] G_{26} \quad -89 \end{aligned} \right.$$

Where $\boxed{(a''_{24})^{(4)}(T_{25}, t)}$, $\boxed{(a''_{25})^{(4)}(T_{25}, t)}$, $\boxed{(a''_{26})^{(4)}(T_{25}, t)}$ are first augmentation coefficients for category 1, 2 and 3

$\boxed{+(a''_{28})^{(5,5)}(T_{29}, t)}$, $\boxed{+(a''_{29})^{(5,5)}(T_{29}, t)}$, $\boxed{+(a''_{30})^{(5,5)}(T_{29}, t)}$ are second augmentation coefficient for category 1, 2 and 3

$\boxed{+(a''_{32})^{(6,6)}(T_{33}, t)}$, $\boxed{+(a''_{33})^{(6,6)}(T_{33}, t)}$, $\boxed{+(a''_{34})^{(6,6)}(T_{33}, t)}$ are third augmentation coefficient for category 1, 2 and 3
 $\boxed{+(a''_{13})^{(1,1,1,1)}(T_{14}, t)}$, $\boxed{+(a''_{14})^{(1,1,1,1)}(T_{14}, t)}$, $\boxed{+(a''_{15})^{(1,1,1,1)}(T_{14}, t)}$ are fourth augmentation coefficients for category 1, 2, and 3
 $\boxed{+(a''_{16})^{(2,2,2,2)}(T_{17}, t)}$, $\boxed{+(a''_{17})^{(2,2,2,2)}(T_{17}, t)}$, $\boxed{+(a''_{18})^{(2,2,2,2)}(T_{17}, t)}$ are fifth augmentation coefficients for category 1, 2, and 3
 $\boxed{+(a''_{20})^{(3,3,3,3)}(T_{21}, t)}$, $\boxed{+(a''_{21})^{(3,3,3,3)}(T_{21}, t)}$, $\boxed{+(a''_{22})^{(3,3,3,3)}(T_{21}, t)}$ are sixth augmentation coefficients for category 1, 2, and 3
 $\boxed{+(a''_{36})^{(7,7,7,7)}(T_{37}, t)}$, $\boxed{+(a''_{36})^{(7,7,7,7)}(T_{37}, t)}$, $\boxed{+(a''_{36})^{(7,7,7,7)}(T_{37}, t)}$ ARE SEVENTH augmentation coefficients-90

91
-92

$$\frac{dT_{24}}{dt} = (b_{24})^{(4)}T_{25} - \left[\begin{array}{l} \boxed{(b'_{24})^{(4)} - (b''_{24})^{(4)}(G_{27}, t)} \quad \boxed{-(b''_{28})^{(5,5)}(G_{31}, t)} \quad \boxed{-(b''_{32})^{(6,6)}(G_{35}, t)} \\ \boxed{-(b''_{13})^{(1,1,1,1)}(G, t)} \quad \boxed{-(b''_{16})^{(2,2,2,2)}(G_{19}, t)} \quad \boxed{-(b''_{20})^{(3,3,3,3)}(G_{23}, t)} \\ \boxed{-(b''_{36})^{(7,7,7,7)}(G_{39}, t)} \end{array} \right] T_{24} -93$$

$$\frac{dT_{25}}{dt} = (b_{25})^{(4)}T_{24} - \left[\begin{array}{l} \boxed{(b'_{25})^{(4)} - (b''_{25})^{(4)}(G_{27}, t)} \quad \boxed{-(b''_{29})^{(5,5)}(G_{31}, t)} \quad \boxed{-(b''_{33})^{(6,6)}(G_{35}, t)} \\ \boxed{-(b''_{14})^{(1,1,1,1)}(G, t)} \quad \boxed{-(b''_{17})^{(2,2,2,2)}(G_{19}, t)} \quad \boxed{-(b''_{21})^{(3,3,3,3)}(G_{23}, t)} \\ \boxed{-(b''_{37})^{(7,7,7,7)}(G_{39}, t)} \end{array} \right] T_{25} -94$$

$$\frac{dT_{26}}{dt} = (b_{26})^{(4)}T_{25} - \left[\begin{array}{l} \boxed{(b'_{26})^{(4)} - (b''_{26})^{(4)}(G_{27}, t)} \quad \boxed{-(b''_{30})^{(5,5)}(G_{31}, t)} \quad \boxed{-(b''_{34})^{(6,6)}(G_{35}, t)} \\ \boxed{-(b''_{15})^{(1,1,1,1)}(G, t)} \quad \boxed{-(b''_{18})^{(2,2,2,2)}(G_{19}, t)} \quad \boxed{-(b''_{22})^{(3,3,3,3)}(G_{23}, t)} \\ \boxed{-(b''_{38})^{(7,7,7,7)}(G_{39}, t)} \end{array} \right] T_{26} -95$$

Where $\boxed{-(b''_{24})^{(4)}(G_{27}, t)}$, $\boxed{-(b''_{25})^{(4)}(G_{27}, t)}$, $\boxed{-(b''_{26})^{(4)}(G_{27}, t)}$ are first detrition coefficients for category 1, 2 and 3
 $\boxed{-(b''_{28})^{(5,5)}(G_{31}, t)}$, $\boxed{-(b''_{29})^{(5,5)}(G_{31}, t)}$, $\boxed{-(b''_{30})^{(5,5)}(G_{31}, t)}$ are second detrition coefficients for category 1, 2 and 3
 $\boxed{-(b''_{32})^{(6,6)}(G_{35}, t)}$, $\boxed{-(b''_{33})^{(6,6)}(G_{35}, t)}$, $\boxed{-(b''_{34})^{(6,6)}(G_{35}, t)}$ are third detrition coefficients for category 1, 2 and 3
 $\boxed{-(b''_{13})^{(1,1,1,1)}(G, t)}$, $\boxed{-(b''_{14})^{(1,1,1,1)}(G, t)}$, $\boxed{-(b''_{15})^{(1,1,1,1)}(G, t)}$ are fourth detrition coefficients for category 1, 2 and 3
 $\boxed{-(b''_{16})^{(2,2,2,2)}(G_{19}, t)}$, $\boxed{-(b''_{17})^{(2,2,2,2)}(G_{19}, t)}$, $\boxed{-(b''_{18})^{(2,2,2,2)}(G_{19}, t)}$ are fifth detrition coefficients for category 1, 2 and 3
 $\boxed{-(b''_{20})^{(3,3,3,3)}(G_{23}, t)}$, $\boxed{-(b''_{21})^{(3,3,3,3)}(G_{23}, t)}$, $\boxed{-(b''_{22})^{(3,3,3,3)}(G_{23}, t)}$ are sixth detrition coefficients for category 1, 2 and 3
 $\boxed{-(b''_{36})^{(7,7,7,7)}(G_{39}, t)}$, $\boxed{-(b''_{37})^{(7,7,7,7)}(G_{39}, t)}$, $\boxed{-(b''_{38})^{(7,7,7,7)}(G_{39}, t)}$ ARE SEVENTH DETRITION COEFFICIENTS-96

-97

FIFTH MODULE CONCATENATION:-

$$98 \frac{dG_{28}}{dt} = (a_{28})^{(5)}G_{29} - \left[\begin{array}{l} \boxed{(a'_{28})^{(5)} + (a''_{28})^{(5)}(T_{29}, t)} \quad \boxed{+(a''_{24})^{(4,4)}(T_{25}, t)} \quad \boxed{+(a''_{32})^{(6,6,6)}(T_{33}, t)} \\ \boxed{+(a''_{13})^{(1,1,1,1,1)}(T_{14}, t)} \quad \boxed{+(a''_{16})^{(2,2,2,2,2)}(T_{17}, t)} \quad \boxed{+(a''_{20})^{(3,3,3,3,3)}(T_{21}, t)} \\ \boxed{+(a''_{36})^{(7,7,7,7,7)}(T_{37}, t)} \end{array} \right] G_{28} -99$$

$$\frac{dG_{29}}{dt} = (a_{29})^{(5)}G_{28} - \left[\begin{array}{l} \boxed{(a'_{29})^{(5)} + (a''_{29})^{(5)}(T_{29}, t)} \quad \boxed{+(a''_{25})^{(4,4)}(T_{25}, t)} \quad \boxed{+(a''_{33})^{(6,6,6)}(T_{33}, t)} \\ \boxed{+(a''_{14})^{(1,1,1,1,1)}(T_{14}, t)} \quad \boxed{+(a''_{17})^{(2,2,2,2,2)}(T_{17}, t)} \quad \boxed{+(a''_{21})^{(3,3,3,3,3)}(T_{21}, t)} \\ \boxed{+(a''_{37})^{(7,7,7,7,7)}(T_{37}, t)} \end{array} \right] G_{29} -100$$

$$\frac{dG_{30}}{dt} = (a_{30})^{(5)}G_{29} - \left[\begin{array}{l} \boxed{(a'_{30})^{(5)} + (a''_{30})^{(5)}(T_{29}, t)} \quad \boxed{+(a''_{26})^{(4,4)}(T_{25}, t)} \quad \boxed{+(a''_{34})^{(6,6,6)}(T_{33}, t)} \\ \boxed{+(a''_{15})^{(1,1,1,1,1)}(T_{14}, t)} \quad \boxed{+(a''_{18})^{(2,2,2,2,2)}(T_{17}, t)} \quad \boxed{+(a''_{22})^{(3,3,3,3,3)}(T_{21}, t)} \\ \boxed{+(a''_{38})^{(7,7,7,7,7)}(T_{37}, t)} \end{array} \right] G_{30} -101$$

Where $\boxed{+(a''_{28})^{(5)}(T_{29}, t)}$, $\boxed{+(a''_{29})^{(5)}(T_{29}, t)}$, $\boxed{+(a''_{30})^{(5)}(T_{29}, t)}$ are first augmentation coefficients for category 1, 2 and 3
 And $\boxed{+(a''_{24})^{(4,4)}(T_{25}, t)}$, $\boxed{+(a''_{25})^{(4,4)}(T_{25}, t)}$, $\boxed{+(a''_{26})^{(4,4)}(T_{25}, t)}$ are second augmentation coefficient for category 1, 2 and 3
 $\boxed{+(a''_{32})^{(6,6,6)}(T_{33}, t)}$, $\boxed{+(a''_{33})^{(6,6,6)}(T_{33}, t)}$, $\boxed{+(a''_{34})^{(6,6,6)}(T_{33}, t)}$ are third augmentation coefficient for category 1, 2 and 3
 $\boxed{+(a''_{13})^{(1,1,1,1,1)}(T_{14}, t)}$, $\boxed{+(a''_{14})^{(1,1,1,1,1)}(T_{14}, t)}$, $\boxed{+(a''_{15})^{(1,1,1,1,1)}(T_{14}, t)}$ are fourth augmentation coefficients for category 1, 2, and 3
 $\boxed{+(a''_{16})^{(2,2,2,2,2)}(T_{17}, t)}$, $\boxed{+(a''_{17})^{(2,2,2,2,2)}(T_{17}, t)}$, $\boxed{+(a''_{18})^{(2,2,2,2,2)}(T_{17}, t)}$ are fifth augmentation coefficients for category 1, 2, and 3
 $\boxed{+(a''_{20})^{(3,3,3,3,3)}(T_{21}, t)}$, $\boxed{+(a''_{21})^{(3,3,3,3,3)}(T_{21}, t)}$, $\boxed{+(a''_{22})^{(3,3,3,3,3)}(T_{21}, t)}$ are sixth augmentation coefficients for category 1, 2, 3 -102
 -103

$$\frac{dT_{28}}{dt} = (b_{28})^{(5)}T_{29} - \left[\begin{array}{l} \boxed{(b'_{28})^{(5)} \boxed{-(b''_{28})^{(5)}(G_{31}, t)} \boxed{-(b''_{24})^{(4,4)}(G_{23}, t)} \boxed{-(b''_{32})^{(6,6,6)}(G_{35}, t)}} \\ \boxed{-(b''_{13})^{(1,1,1,1,1)}(G, t)} \boxed{-(b''_{16})^{(2,2,2,2,2)}(G_{19}, t)} \boxed{-(b''_{20})^{(3,3,3,3,3)}(G_{23}, t)} \\ \boxed{-(b''_{36})^{(7,7,7,7,7)}(G_{38}, t)} \end{array} \right] T_{28} -104$$

$$\frac{dT_{29}}{dt} = (b_{29})^{(5)}T_{28} - \left[\begin{array}{l} \boxed{(b'_{29})^{(5)} \boxed{-(b''_{29})^{(5)}(G_{31}, t)} \boxed{-(b''_{25})^{(4,4)}(G_{27}, t)} \boxed{-(b''_{33})^{(6,6,6)}(G_{35}, t)}} \\ \boxed{-(b''_{14})^{(1,1,1,1,1)}(G, t)} \boxed{-(b''_{17})^{(2,2,2,2,2)}(G_{19}, t)} \boxed{-(b''_{21})^{(3,3,3,3,3)}(G_{23}, t)} \\ \boxed{-(b''_{37})^{(7,7,7,7,7)}(G_{38}, t)} \end{array} \right] T_{29} -105$$

$$\frac{dT_{30}}{dt} = (b_{30})^{(5)}T_{29} - \left[\begin{array}{l} \boxed{(b'_{30})^{(5)} \boxed{-(b''_{30})^{(5)}(G_{31}, t)} \boxed{-(b''_{26})^{(4,4)}(G_{27}, t)} \boxed{-(b''_{34})^{(6,6,6)}(G_{35}, t)}} \\ \boxed{-(b''_{15})^{(1,1,1,1,1)}(G, t)} \boxed{-(b''_{18})^{(2,2,2,2,2)}(G_{19}, t)} \boxed{-(b''_{22})^{(3,3,3,3,3)}(G_{23}, t)} \\ \boxed{-(b''_{38})^{(7,7,7,7,7)}(G_{38}, t)} \end{array} \right] T_{30} -106$$

where $\boxed{-(b''_{28})^{(5)}(G_{31}, t)}$, $\boxed{-(b''_{29})^{(5)}(G_{31}, t)}$, $\boxed{-(b''_{30})^{(5)}(G_{31}, t)}$ are first detrition coefficients for category 1, 2 and 3
 $\boxed{-(b''_{24})^{(4,4)}(G_{27}, t)}$, $\boxed{-(b''_{25})^{(4,4)}(G_{27}, t)}$, $\boxed{-(b''_{26})^{(4,4)}(G_{27}, t)}$ are second detrition coefficients for category 1, 2 and 3
 $\boxed{-(b''_{32})^{(6,6,6)}(G_{35}, t)}$, $\boxed{-(b''_{33})^{(6,6,6)}(G_{35}, t)}$, $\boxed{-(b''_{34})^{(6,6,6)}(G_{35}, t)}$ are third detrition coefficients for category 1, 2 and 3
 $\boxed{-(b''_{13})^{(1,1,1,1,1)}(G, t)}$, $\boxed{-(b''_{14})^{(1,1,1,1,1)}(G, t)}$, $\boxed{-(b''_{15})^{(1,1,1,1,1)}(G, t)}$ are fourth detrition coefficients for category 1, 2, and 3
 $\boxed{-(b''_{16})^{(2,2,2,2,2)}(G_{19}, t)}$, $\boxed{-(b''_{17})^{(2,2,2,2,2)}(G_{19}, t)}$, $\boxed{-(b''_{18})^{(2,2,2,2,2)}(G_{19}, t)}$ are fifth detrition coefficients for category 1, 2, and 3
 $\boxed{-(b''_{20})^{(3,3,3,3,3)}(G_{23}, t)}$, $\boxed{-(b''_{21})^{(3,3,3,3,3)}(G_{23}, t)}$, $\boxed{-(b''_{22})^{(3,3,3,3,3)}(G_{23}, t)}$ are sixth detrition coefficients for category 1, 2, and 3-107

SIXTH MODULE CONCATENATION-108

$$\frac{dG_{32}}{dt} = (a_{32})^{(6)}G_{33} - \left[\begin{array}{l} \boxed{(a'_{32})^{(6)} \boxed{+(a''_{32})^{(6)}(T_{33}, t)} \boxed{+(a''_{28})^{(5,5,5)}(T_{29}, t)} \boxed{+(a''_{24})^{(4,4,4)}(T_{25}, t)}} \\ \boxed{+(a''_{13})^{(1,1,1,1,1)}(T_{14}, t)} \boxed{+(a''_{16})^{(2,2,2,2,2)}(T_{17}, t)} \boxed{+(a''_{20})^{(3,3,3,3,3)}(T_{21}, t)} \\ \boxed{+(a''_{36})^{(7,7,7,7,7)}(T_{37}, t)} \end{array} \right] G_{32} -109$$

$$\frac{dG_{33}}{dt} = (a_{33})^{(6)}G_{32} - \left[\begin{array}{l} \boxed{(a'_{33})^{(6)} \boxed{+(a''_{33})^{(6)}(T_{33}, t)} \boxed{+(a''_{29})^{(5,5,5)}(T_{29}, t)} \boxed{+(a''_{25})^{(4,4,4)}(T_{25}, t)}} \\ \boxed{+(a''_{14})^{(1,1,1,1,1)}(T_{14}, t)} \boxed{+(a''_{17})^{(2,2,2,2,2)}(T_{17}, t)} \boxed{+(a''_{21})^{(3,3,3,3,3)}(T_{21}, t)} \\ \boxed{+(a''_{37})^{(7,7,7,7,7)}(T_{37}, t)} \end{array} \right] G_{33} -110$$

$$\frac{dG_{34}}{dt} = (a_{34})^{(6)}G_{33} - \left[\begin{array}{l} \boxed{(a'_{34})^{(6)} \boxed{+(a''_{34})^{(6)}(T_{33}, t)} \boxed{+(a''_{30})^{(5,5,5)}(T_{29}, t)} \boxed{+(a''_{26})^{(4,4,4)}(T_{25}, t)}} \\ \boxed{+(a''_{15})^{(1,1,1,1,1)}(T_{14}, t)} \boxed{+(a''_{18})^{(2,2,2,2,2)}(T_{17}, t)} \boxed{+(a''_{22})^{(3,3,3,3,3)}(T_{21}, t)} \\ \boxed{+(a''_{38})^{(7,7,7,7,7)}(T_{37}, t)} \end{array} \right] G_{34} -111$$

$\boxed{+(a''_{32})^{(6)}(T_{33}, t)}$, $\boxed{+(a''_{33})^{(6)}(T_{33}, t)}$, $\boxed{+(a''_{34})^{(6)}(T_{33}, t)}$ are first augmentation coefficients for category 1, 2 and 3
 $\boxed{+(a''_{28})^{(5,5,5)}(T_{29}, t)}$, $\boxed{+(a''_{29})^{(5,5,5)}(T_{29}, t)}$, $\boxed{+(a''_{30})^{(5,5,5)}(T_{29}, t)}$ are second augmentation coefficients for category 1, 2 and 3

$\boxed{+(a''_{24})^{(4,4,4,4)}(T_{25}, t)}$, $\boxed{+(a''_{25})^{(4,4,4,4)}(T_{25}, t)}$, $\boxed{+(a''_{26})^{(4,4,4,4)}(T_{25}, t)}$ are third augmentation coefficients for category 1, 2 and 3

$\boxed{+(a''_{13})^{(1,1,1,1,1,1)}(T_{14}, t)}$, $\boxed{+(a''_{14})^{(1,1,1,1,1,1)}(T_{14}, t)}$, $\boxed{+(a''_{15})^{(1,1,1,1,1,1)}(T_{14}, t)}$ - are fourth augmentation coefficients

$\boxed{+(a''_{16})^{(2,2,2,2,2,2)}(T_{17}, t)}$, $\boxed{+(a''_{17})^{(2,2,2,2,2,2)}(T_{17}, t)}$, $\boxed{+(a''_{18})^{(2,2,2,2,2,2)}(T_{17}, t)}$ - fifth augmentation coefficients

$\boxed{+(a''_{20})^{(3,3,3,3,3,3)}(T_{21}, t)}$, $\boxed{+(a''_{21})^{(3,3,3,3,3,3)}(T_{21}, t)}$, $\boxed{+(a''_{22})^{(3,3,3,3,3,3)}(T_{21}, t)}$ sixth augmentation coefficients

$\boxed{+(a''_{36})^{(7,7,7,7,7,7)}(T_{37}, t)}$, $\boxed{+(a''_{36})^{(7,7,7,7,7,7)}(T_{37}, t)}$, $\boxed{+(a''_{36})^{(7,7,7,7,7,7)}(T_{37}, t)}$ ARE SEVENTH AUGMENTATION

COEFFICIENTS-112

-113

$$\frac{dT_{32}}{dt} = (b_{32})^{(6)} T_{33} - \left[\begin{array}{l} \boxed{(b'_{32})^{(6)}} \boxed{-(b''_{32})^{(6)}(G_{35}, t)} \boxed{-(b''_{28})^{(5,5,5)}(G_{31}, t)} \boxed{-(b''_{24})^{(4,4,4)}(G_{27}, t)} \\ \boxed{-(b''_{13})^{(1,1,1,1,1,1)}(G, t)} \boxed{-(b''_{16})^{(2,2,2,2,2,2)}(G_{19}, t)} \boxed{-(b''_{20})^{(3,3,3,3,3,3)}(G_{23}, t)} \\ \boxed{-(b''_{36})^{(7,7,7,7,7,7)}(G_{39}, t)} \end{array} \right] T_{32} \quad -114$$

$$\frac{dT_{33}}{dt} = (b_{33})^{(6)} T_{32} - \left[\begin{array}{l} \boxed{(b'_{33})^{(6)}} \boxed{-(b''_{33})^{(6)}(G_{35}, t)} \boxed{-(b''_{29})^{(5,5,5)}(G_{31}, t)} \boxed{-(b''_{25})^{(4,4,4)}(G_{27}, t)} \\ \boxed{-(b''_{14})^{(1,1,1,1,1,1)}(G, t)} \boxed{-(b''_{17})^{(2,2,2,2,2,2)}(G_{19}, t)} \boxed{-(b''_{21})^{(3,3,3,3,3,3)}(G_{23}, t)} \\ \boxed{-(b''_{37})^{(7,7,7,7,7,7)}(G_{39}, t)} \end{array} \right] T_{33} \quad -115$$

$$\frac{dT_{34}}{dt} = (b_{34})^{(6)} T_{33} - \left[\begin{array}{l} \boxed{(b'_{34})^{(6)}} \boxed{-(b''_{34})^{(6)}(G_{35}, t)} \boxed{-(b''_{30})^{(5,5,5)}(G_{31}, t)} \boxed{-(b''_{26})^{(4,4,4)}(G_{27}, t)} \\ \boxed{-(b''_{15})^{(1,1,1,1,1,1)}(G, t)} \boxed{-(b''_{18})^{(2,2,2,2,2,2)}(G_{19}, t)} \boxed{-(b''_{22})^{(3,3,3,3,3,3)}(G_{23}, t)} \\ \boxed{-(b''_{38})^{(7,7,7,7,7,7)}(G_{39}, t)} \end{array} \right] T_{34} \quad -116$$

$\boxed{-(b''_{32})^{(6)}(G_{35}, t)}$, $\boxed{-(b''_{33})^{(6)}(G_{35}, t)}$, $\boxed{-(b''_{34})^{(6)}(G_{35}, t)}$ are first detrition coefficients for category 1, 2, and 3

$\boxed{-(b''_{28})^{(5,5,5)}(G_{31}, t)}$, $\boxed{-(b''_{29})^{(5,5,5)}(G_{31}, t)}$, $\boxed{-(b''_{30})^{(5,5,5)}(G_{31}, t)}$ are second detrition coefficients for category 1, 2, and 3

$\boxed{-(b''_{24})^{(4,4,4)}(G_{27}, t)}$, $\boxed{-(b''_{25})^{(4,4,4)}(G_{27}, t)}$, $\boxed{-(b''_{26})^{(4,4,4)}(G_{27}, t)}$ are third detrition coefficients for category 1, 2, and 3

$\boxed{-(b''_{13})^{(1,1,1,1,1,1)}(G, t)}$, $\boxed{-(b''_{14})^{(1,1,1,1,1,1)}(G, t)}$, $\boxed{-(b''_{15})^{(1,1,1,1,1,1)}(G, t)}$ are fourth detrition coefficients for category 1, 2, and 3

$\boxed{-(b''_{16})^{(2,2,2,2,2,2)}(G_{19}, t)}$, $\boxed{-(b''_{17})^{(2,2,2,2,2,2)}(G_{19}, t)}$, $\boxed{-(b''_{18})^{(2,2,2,2,2,2)}(G_{19}, t)}$ are fifth detrition coefficients for category 1, 2, and 3

$\boxed{-(b''_{20})^{(3,3,3,3,3,3)}(G_{23}, t)}$, $\boxed{-(b''_{21})^{(3,3,3,3,3,3)}(G_{23}, t)}$, $\boxed{-(b''_{22})^{(3,3,3,3,3,3)}(G_{23}, t)}$ are sixth detrition coefficients for category 1, 2, and 3

$\boxed{-(b''_{36})^{(7,7,7,7,7,7)}(G_{39}, t)}$, $\boxed{-(b''_{36})^{(7,7,7,7,7,7)}(G_{39}, t)}$, $\boxed{-(b''_{36})^{(7,7,7,7,7,7)}(G_{39}, t)}$ ARE SEVENTH DETRITION

COEFFICIENTS-117

-118

SEVENTH MODULE CONCATENATION:-119

$$\frac{dG_{36}}{dt} = (a_{36})^{(7)} G_{37} - \left[(a'_{36})^{(7)} \boxed{+(a''_{36})^{(7)}(T_{37}, t)} + \boxed{(a''_{16})^{(7)}(T_{17}, t)} + \boxed{(a''_{20})^{(7)}(T_{21}, t)} + \boxed{(a''_{24})^{(7)}(T_{23}, t)} G_{36} \right] + \square 28''7 \square 29, \square + \square 32''7 \square 33, \square + \square 13''7 \square 14, \square \square 36-120$$

121

$$\frac{dG_{37}}{dt} = (a_{37})^{(7)} G_{36} - \left[(a'_{37})^{(7)} + \boxed{(a''_{37})^{(7)}(T_{37}, t)} \right] + \boxed{(a''_{14})^{(7)}(T_{14}, t)} + \boxed{(a''_{21})^{(7)}(T_{21}, t)} + \boxed{(a''_{17})^{(7)}(T_{17}, t)} + \square 25''7 \square 25, \square + \square 33''7 \square 33, \square + \square 29''7 \square 29, \square \square 37$$

-122

$$\frac{dG_{38}}{dt} = (a_{38})^{(7)} G_{37} - \left[(a'_{38})^{(7)} + \boxed{(a''_{38})^{(7)}(T_{37}, t)} + \boxed{(a''_{15})^{(7)}(T_{14}, t)} + \boxed{(a''_{22})^{(7)}(T_{21}, t)} + \boxed{(a''_{18})^{(7)}(T_{17}, t)} \right] +$$

□26''7□25, □ + □34''7□33, □ + □30''7□29, □ □38

-123
124

$$\frac{dT_{36}}{dt} = (b_{36})^{(7)} T_{37} - \left[(b'_{36})^{(7)} - \boxed{(b''_{36})^{(7)}(G_{39}, t)} - \boxed{(b''_{16})^{(7)}(G_{19}, t)} - \boxed{(b''_{13})^{(7)}(G_{14}, t)} \right] -$$

□20''7□231, □ - □24''7□27, □ - □28''7□31, □ - □32''7□35, □ □36

-126

$$\frac{dT_{37}}{dt} = (b_{37})^{(7)} T_{36} - \left[(b'_{36})^{(7)} - \boxed{(b''_{37})^{(7)}(G_{39}, t)} - \boxed{(b''_{17})^{(7)}(G_{19}, t)} - \boxed{(b''_{19})^{(7)}(G_{14}, t)} \right] -$$

□21''7□231, □ - □25''7□27, □ - □29''7□31, □ - □33''7□35, □ □37

-127
Where we suppose

- (A) $(a_i)^{(1)}, (a'_i)^{(1)}, (a''_i)^{(1)}, (b_i)^{(1)}, (b'_i)^{(1)}, (b''_i)^{(1)} > 0,$
 $i, j = 13, 14, 15$
- (B) The functions $(a''_i)^{(1)}, (b''_i)^{(1)}$ are positive continuous increasing and bounded.
Definition of $(p_i)^{(1)}, (r_i)^{(1)}$:

$$(a''_i)^{(1)}(T_{14}, t) \leq (p_i)^{(1)} \leq (\hat{A}_{13})^{(1)}$$

$$(b''_i)^{(1)}(G, t) \leq (r_i)^{(1)} \leq (b'_i)^{(1)} \leq (\hat{B}_{13})^{(1)}$$

- (C) $\lim_{T_2 \rightarrow \infty} (a''_i)^{(1)}(T_{14}, t) = (p_i)^{(1)}$
 $\lim_{G \rightarrow \infty} (b''_i)^{(1)}(G, t) = (r_i)^{(1)}$

Definition of $(\hat{A}_{13})^{(1)}, (\hat{B}_{13})^{(1)}$:

Where $\boxed{(\hat{A}_{13})^{(1)}, (\hat{B}_{13})^{(1)}, (p_i)^{(1)}, (r_i)^{(1)}}$ are positive constants
 and $\boxed{i = 13, 14, 15}$

They satisfy Lipschitz condition:

$$|(a''_i)^{(1)}(T'_{14}, t) - (a''_i)^{(1)}(T_{14}, t)| \leq (\hat{k}_{13})^{(1)} |T'_{14} - T_{14}| e^{-(\hat{M}_{13})^{(1)}t}$$

$$|(b''_i)^{(1)}(G', t) - (b''_i)^{(1)}(G, t)| < (\hat{k}_{13})^{(1)} \|G' - G\| e^{-(\hat{M}_{13})^{(1)}t}$$

With the Lipschitz condition, we place a restriction on the behavior of functions $(a''_i)^{(1)}(T'_{14}, t)$ and $(a''_i)^{(1)}(T_{14}, t)$. (T'_{14}, t) and (T_{14}, t) are points belonging to the interval $[(\hat{k}_{13})^{(1)}, (\hat{M}_{13})^{(1)}]$. It is to be noted that $(a''_i)^{(1)}(T_{14}, t)$ is uniformly continuous. In the eventuality of the fact, that if $(\hat{M}_{13})^{(1)} = 1$ then the function $(a''_i)^{(1)}(T_{14}, t)$, the **first augmentation coefficient** attributable to terrestrial organisms, would be absolutely continuous.

Definition of $(\hat{M}_{13})^{(1)}, (\hat{k}_{13})^{(1)}$:

- (D) $(\hat{M}_{13})^{(1)}, (\hat{k}_{13})^{(1)}$, are positive constants

$$\frac{(a_i)^{(1)}}{(\hat{M}_{13})^{(1)}} , \frac{(b_i)^{(1)}}{(\hat{M}_{13})^{(1)}} < 1$$

Definition of $(\hat{P}_{13})^{(1)}, (\hat{Q}_{13})^{(1)}$:

(E) There exists two constants $(\hat{P}_{13})^{(1)}$ and $(\hat{Q}_{13})^{(1)}$ which together with $(\hat{M}_{13})^{(1)}, (\hat{k}_{13})^{(1)}, (\hat{A}_{13})^{(1)}$ and $(\hat{B}_{13})^{(1)}$ and the constants $(a_i)^{(1)}, (a'_i)^{(1)}, (b_i)^{(1)}, (b'_i)^{(1)}, (p_i)^{(1)}, (r_i)^{(1)}, i = 13,14,15$, satisfy the inequalities

$$\frac{1}{(\hat{M}_{13})^{(1)}} [(a_i)^{(1)} + (a'_i)^{(1)} + (\hat{A}_{13})^{(1)} + (\hat{P}_{13})^{(1)} (\hat{k}_{13})^{(1)}] < 1$$

$$\frac{1}{(\hat{M}_{13})^{(1)}} [(b_i)^{(1)} + (b'_i)^{(1)} + (\hat{B}_{13})^{(1)} + (\hat{Q}_{13})^{(1)} (\hat{k}_{13})^{(1)}] < 1$$

$$\frac{dT_{38}}{dt} = (b_{38})^{(7)}T_{37} - \left[(b'_{38})^{(7)} - \boxed{(b''_{38})^{(7)}((G_{39}), t)} - \boxed{(b''_{18})^{(7)}((G_{19}), t)} - \boxed{(b''_{20})^{(7)}((G_{14}), t)} \right] - \quad 128$$

$$b_{22}'' 7G_{23}, t - b_{26}'' 7G_{27}, t - b_{30}'' 7G_{31}, t - b_{34}'' 7G_{35}, t \quad 129$$

$$T_{38} \quad 130$$

$$\quad 131$$

$$\quad 132$$

$$\quad 133$$

$$\quad 134$$

$$+(a''_{36})^{(7)}(T_{37}, t) = \text{First augmentation factor} \quad 135$$

$$(1)(a_i)^{(2)}, (a'_i)^{(2)}, (a''_i)^{(2)}, (b_i)^{(2)}, (b'_i)^{(2)}, (b''_i)^{(2)} > 0, \quad i, j = 16,17,18 \quad 136$$

$$(F) \quad (2) \text{ The functions } (a''_i)^{(2)}, (b''_i)^{(2)} \text{ are positive continuous increasing and bounded.} \quad 137$$

$$\quad 138$$

$$\quad 139$$

$$\quad 140$$

$$\quad 141$$

$$\quad 142$$

$$\quad 143$$

$$\quad 144$$

$$\quad 145$$

$$\quad 146$$

$$\quad 147$$

$$\quad 148$$

$$\quad 149$$

$$\quad 150$$

$$\quad 151$$

$$\quad 152$$

$$\quad 153$$

$$\quad 154$$

$$\quad 155$$

$$\quad 156$$

$$\quad 157$$

$$\quad 158$$

$$\quad 159$$

$$\quad 160$$

$$\quad 161$$

$$\quad 162$$

$$\quad 163$$

$$\quad 164$$

$$\quad 165$$

$$\quad 166$$

$$\quad 167$$

$$\quad 168$$

Definition of $(\hat{A}_{16})^{(2)}, (\hat{B}_{16})^{(2)}$:

Where $\boxed{(\hat{A}_{16})^{(2)}, (\hat{B}_{16})^{(2)}, (p_i)^{(2)}, (r_i)^{(2)}}$ are positive constants and $\boxed{i = 16,17,18}$

They satisfy Lipschitz condition:

$$|(a''_i)^{(2)}(T'_{17}, t) - (a''_i)^{(2)}(T_{17}, t)| \leq (\hat{k}_{16})^{(2)} |T'_{17} - T_{17}| e^{-(\hat{M}_{16})^{(2)}t} \quad 144$$

$$|(b''_i)^{(2)}((G_{19})', t) - (b''_i)^{(2)}((G_{19}), t)| < (\hat{k}_{16})^{(2)} |(G_{19}) - (G_{19})'| e^{-(\hat{M}_{16})^{(2)}t} \quad 145$$

With the Lipschitz condition, we place a restriction on the behavior of functions $(a''_i)^{(2)}(T'_{17}, t)$ and $(a''_i)^{(2)}(T_{17}, t)$. (T'_{17}, t) and (T_{17}, t) are points belonging to the interval $[(\hat{k}_{16})^{(2)}, (\hat{M}_{16})^{(2)}]$. It is to be noted that $(a''_i)^{(2)}(T_{17}, t)$ is uniformly continuous. In the eventuality of the fact, that if $(\hat{M}_{16})^{(2)} = 1$ then the function $(a''_i)^{(2)}(T_{17}, t)$, the SECOND augmentation coefficient would be absolutely continuous.

Definition of $(\hat{M}_{16})^{(2)}, (\hat{k}_{16})^{(2)}$:

(H) (4) $(\hat{M}_{16})^{(2)}, (\hat{k}_{16})^{(2)}$, are positive constants 148

$$\frac{(a_i)^{(2)}}{(M_{16})^{(2)}}, \frac{(b_i)^{(2)}}{(M_{16})^{(2)}} < 1$$

Definition of $(\hat{P}_{13})^{(2)}, (\hat{Q}_{13})^{(2)}$: 149

There exists two constants $(\hat{P}_{16})^{(2)}$ and $(\hat{Q}_{16})^{(2)}$ which together with $(\hat{M}_{16})^{(2)}, (\hat{k}_{16})^{(2)}, (\hat{A}_{16})^{(2)}$ and $(\hat{B}_{16})^{(2)}$ and the constants $(a_i)^{(2)}, (a'_i)^{(2)}, (b_i)^{(2)}, (b'_i)^{(2)}, (p_i)^{(2)}, (r_i)^{(2)}, i = 16,17,18,$

satisfy the inequalities

$$\frac{1}{(\hat{M}_{16})^{(2)}} [(a_i)^{(2)} + (a'_i)^{(2)} + (\hat{A}_{16})^{(2)} + (\hat{P}_{16})^{(2)} (\hat{k}_{16})^{(2)}] < 1 \quad 150$$

$$\frac{1}{(\hat{M}_{16})^{(2)}} [(b_i)^{(2)} + (b'_i)^{(2)} + (\hat{B}_{16})^{(2)} + (\hat{Q}_{16})^{(2)} (\hat{k}_{16})^{(2)}] < 1 \quad 151$$

Where we suppose 152

$$(I) \quad (5) \quad (a_i)^{(3)}, (a'_i)^{(3)}, (a''_i)^{(3)}, (b_i)^{(3)}, (b'_i)^{(3)}, (b''_i)^{(3)} > 0, \quad i, j = 20,21,22 \quad 153$$

The functions $(a''_i)^{(3)}, (b''_i)^{(3)}$ are positive continuous increasing and bounded.

Definition of $(p_i)^{(3)}, (r_i)^{(3)}$:

$$(a''_i)^{(3)}(T_{21}, t) \leq (p_i)^{(3)} \leq (\hat{A}_{20})^{(3)}$$

$$(b''_i)^{(3)}(G_{23}, t) \leq (r_i)^{(3)} \leq (b'_i)^{(3)} \leq (\hat{B}_{20})^{(3)}$$

$$\lim_{T_2 \rightarrow \infty} (a''_i)^{(3)}(T_{21}, t) = (p_i)^{(3)} \quad 154$$

$$\lim_{G \rightarrow \infty} (b''_i)^{(3)}(G_{23}, t) = (r_i)^{(3)} \quad 155$$

Definition of $(\hat{A}_{20})^{(3)}, (\hat{B}_{20})^{(3)}$: 156

Where $(\hat{A}_{20})^{(3)}, (\hat{B}_{20})^{(3)}, (p_i)^{(3)}, (r_i)^{(3)}$ are positive constants and $i = 20,21,22$

They satisfy Lipschitz condition: 157

$$|(a''_i)^{(3)}(T'_{21}, t) - (a''_i)^{(3)}(T_{21}, t)| \leq (\hat{k}_{20})^{(3)} |T'_{21} - T_{21}| e^{-(M_{20})^{(3)}t} \quad 158$$

$$|(b''_i)^{(3)}(G'_{23}, t) - (b''_i)^{(3)}(G_{23}, t)| < (\hat{k}_{20})^{(3)} ||G_{23} - G'_{23}|| e^{-(M_{20})^{(3)}t} \quad 159$$

With the Lipschitz condition, we place a restriction on the behavior of functions $(a''_i)^{(3)}(T'_{21}, t)$ and $(a''_i)^{(3)}(T_{21}, t) \cdot (T'_{21}, t)$ and (T_{21}, t) are points belonging to the interval $[(\hat{k}_{20})^{(3)}, (\hat{M}_{20})^{(3)}]$. It is to be noted that $(a''_i)^{(3)}(T_{21}, t)$ is uniformly continuous. In the eventuality of the fact, that if $(\hat{M}_{20})^{(3)} = 1$ then the function $(a''_i)^{(3)}(T_{21}, t)$, the THIRD augmentation coefficient, would be absolutely continuous. 160

Definition of $(\hat{M}_{20})^{(3)}, (\hat{k}_{20})^{(3)}$: 161

(J) $(6) \quad (\hat{M}_{20})^{(3)}, (\hat{k}_{20})^{(3)}$, are positive constants

$$\frac{(a_i)^{(3)}}{(M_{20})^{(3)}}, \frac{(b_i)^{(3)}}{(M_{20})^{(3)}} < 1$$

There exists two constants $(\hat{P}_{20})^{(3)}$ and $(\hat{Q}_{20})^{(3)}$ which together with $(\hat{M}_{20})^{(3)}, (\hat{k}_{20})^{(3)}, (\hat{A}_{20})^{(3)}$ and $(\hat{B}_{20})^{(3)}$ and the constants $(a_i)^{(3)}, (a'_i)^{(3)}, (b_i)^{(3)}, (b'_i)^{(3)}, (p_i)^{(3)}, (r_i)^{(3)}, i = 20,21,22,$ 162

satisfy the inequalities 163

$$\frac{1}{(\hat{M}_{20})^{(3)}} [(a_i)^{(3)} + (a'_i)^{(3)} + (\hat{A}_{20})^{(3)} + (\hat{P}_{20})^{(3)} (\hat{k}_{20})^{(3)}] < 1 \quad 164$$

$$\frac{1}{(\hat{M}_{20})^{(3)}} [(b_i)^{(3)} + (b'_i)^{(3)} + (\hat{B}_{20})^{(3)} + (\hat{Q}_{20})^{(3)} (\hat{k}_{20})^{(3)}] < 1 \quad 165$$

$$\frac{1}{(\hat{M}_{20})^{(3)}} [(b_i)^{(3)} + (b_i')^{(3)} + (\hat{B}_{20})^{(3)} + (\hat{Q}_{20})^{(3)} (\hat{k}_{20})^{(3)}] < 1 \quad 166$$

167

Where we suppose

168

$$(a_i)^{(4)}, (a_i')^{(4)}, (a_i'')^{(4)}, (b_i)^{(4)}, (b_i')^{(4)}, (b_i'')^{(4)} > 0, \quad i, j = 24, 25, 26 \quad 169$$

(L) (7) The functions $(a_i'')^{(4)}, (b_i'')^{(4)}$ are positive continuous increasing and bounded.

Definition of $(p_i)^{(4)}, (r_i)^{(4)}$:

$$(a_i'')^{(4)}(T_{25}, t) \leq (p_i)^{(4)} \leq (\hat{A}_{24})^{(4)}$$

$$(b_i'')^{(4)}((G_{27}), t) \leq (r_i)^{(4)} \leq (b_i')^{(4)} \leq (\hat{B}_{24})^{(4)}$$

170

$$(M) \quad (8) \quad \lim_{T_2 \rightarrow \infty} (a_i'')^{(4)}(T_{25}, t) = (p_i)^{(4)} \\ \lim_{G \rightarrow \infty} (b_i'')^{(4)}((G_{27}), t) = (r_i)^{(4)}$$

Definition of $(\hat{A}_{24})^{(4)}, (\hat{B}_{24})^{(4)}$:

Where $(\hat{A}_{24})^{(4)}, (\hat{B}_{24})^{(4)}, (p_i)^{(4)}, (r_i)^{(4)}$ are positive constants and $i = 24, 25, 26$

They satisfy Lipschitz condition:

171

$$|(a_i'')^{(4)}(T_{25}', t) - (a_i'')^{(4)}(T_{25}, t)| \leq (\hat{k}_{24})^{(4)} |T_{25}' - T_{25}| e^{-(\hat{M}_{24})^{(4)}t}$$

$$|(b_i'')^{(4)}((G_{27})', t) - (b_i'')^{(4)}((G_{27}), t)| < (\hat{k}_{24})^{(4)} |(G_{27})' - (G_{27})| e^{-(\hat{M}_{24})^{(4)}t}$$

With the Lipschitz condition, we place a restriction on the behavior of functions $(a_i'')^{(4)}(T_{25}', t)$ and $(a_i'')^{(4)}(T_{25}, t) \cdot (T_{25}', t)$ and (T_{25}, t) are points belonging to the interval $[(\hat{k}_{24})^{(4)}, (\hat{M}_{24})^{(4)}]$. It is to be noted that $(a_i'')^{(4)}(T_{25}, t)$ is uniformly continuous. In the eventuality of the fact, that if $(\hat{M}_{24})^{(4)} = 4$ then the function $(a_i'')^{(4)}(T_{25}, t)$, the **FOURTH augmentation coefficient WOULD** be absolutely continuous.

172

173

Definition of $(\hat{M}_{24})^{(4)}, (\hat{k}_{24})^{(4)}$:

174

$(\hat{M}_{24})^{(4)}, (\hat{k}_{24})^{(4)}$, are positive constants

$$\frac{(a_i)^{(4)}}{(\hat{M}_{24})^{(4)}}, \frac{(b_i)^{(4)}}{(\hat{M}_{24})^{(4)}} < 1$$

Definition of $(\hat{P}_{24})^{(4)}, (\hat{Q}_{24})^{(4)}$:

175

(P) (9) There exists two constants $(\hat{P}_{24})^{(4)}$ and $(\hat{Q}_{24})^{(4)}$ which together with $(\hat{M}_{24})^{(4)}, (\hat{k}_{24})^{(4)}, (\hat{A}_{24})^{(4)}$ and $(\hat{B}_{24})^{(4)}$ and the constants $(a_i)^{(4)}, (a_i')^{(4)}, (b_i)^{(4)}, (b_i')^{(4)}, (p_i)^{(4)}, (r_i)^{(4)}, i = 24, 25, 26$, satisfy the inequalities

$$\frac{1}{(\hat{M}_{24})^{(4)}} [(a_i)^{(4)} + (a_i')^{(4)} + (\hat{A}_{24})^{(4)} + (\hat{P}_{24})^{(4)} (\hat{k}_{24})^{(4)}] < 1$$

$$\frac{1}{(\hat{M}_{24})^{(4)}} [(b_i)^{(4)} + (b_i')^{(4)} + (\hat{B}_{24})^{(4)} + (\hat{Q}_{24})^{(4)} (\hat{k}_{24})^{(4)}] < 1$$

Where we suppose 176

$$(a_i)^{(5)}, (a_i')^{(5)}, (a_i'')^{(5)}, (b_i)^{(5)}, (b_i')^{(5)}, (b_i'')^{(5)} > 0, \quad i, j = 28, 29, 30 \quad 177$$

(R) (10) The functions $(a_i'')^{(5)}, (b_i'')^{(5)}$ are positive continuous increasing and bounded.

Definition of $(p_i)^{(5)}, (r_i)^{(5)}$:

$$(a_i'')^{(5)}(T_{29}, t) \leq (p_i)^{(5)} \leq (\hat{A}_{28})^{(5)}$$

$$(b_i'')^{(5)}(G_{31}, t) \leq (r_i)^{(5)} \leq (b_i')^{(5)} \leq (\hat{B}_{28})^{(5)}$$

178

$$(S) \quad (11) \quad \lim_{T_2 \rightarrow \infty} (a_i'')^{(5)}(T_{29}, t) = (p_i)^{(5)} \\ \lim_{G \rightarrow \infty} (b_i'')^{(5)}(G_{31}, t) = (r_i)^{(5)}$$

Definition of $(\hat{A}_{28})^{(5)}, (\hat{B}_{28})^{(5)}$:

Where $(\hat{A}_{28})^{(5)}, (\hat{B}_{28})^{(5)}, (p_i)^{(5)}, (r_i)^{(5)}$ are positive constants and $i = 28, 29, 30$

They satisfy Lipschitz condition: 179

$$|(a_i'')^{(5)}(T'_{29}, t) - (a_i'')^{(5)}(T_{29}, t)| \leq (\hat{k}_{28})^{(5)} |T_{29} - T'_{29}| e^{-(\hat{M}_{28})^{(5)}t}$$

$$|(b_i'')^{(5)}(G'_{31}, t) - (b_i'')^{(5)}(G_{31}, t)| < (\hat{k}_{28})^{(5)} |(G_{31}) - (G'_{31})| e^{-(\hat{M}_{28})^{(5)}t}$$

With the Lipschitz condition, we place a restriction on the behavior of functions $(a_i'')^{(5)}(T'_{29}, t)$ and $(a_i'')^{(5)}(T_{29}, t)$. (T'_{29}, t) and (T_{29}, t) are points belonging to the interval $[(\hat{k}_{28})^{(5)}, (\hat{M}_{28})^{(5)}]$. It is to be noted that $(a_i'')^{(5)}(T_{29}, t)$ is uniformly continuous. In the eventuality of the fact, that if $(\hat{M}_{28})^{(5)} = 5$ then the function $(a_i'')^{(5)}(T_{29}, t)$, the FIFTH **augmentation coefficient** attributable would be absolutely continuous. 180

Definition of $(\hat{M}_{28})^{(5)}, (\hat{k}_{28})^{(5)}$: 181

$(\hat{M}_{28})^{(5)}, (\hat{k}_{28})^{(5)}$, are positive constants

$$\frac{(a_i)^{(5)}}{(\hat{M}_{28})^{(5)}}, \frac{(b_i)^{(5)}}{(\hat{M}_{28})^{(5)}} < 1$$

Definition of $(\hat{P}_{28})^{(5)}, (\hat{Q}_{28})^{(5)}$: 182

There exists two constants $(\hat{P}_{28})^{(5)}$ and $(\hat{Q}_{28})^{(5)}$ which together with $(\hat{M}_{28})^{(5)}, (\hat{k}_{28})^{(5)}, (\hat{A}_{28})^{(5)}$ and $(\hat{B}_{28})^{(5)}$ and the constants $(a_i)^{(5)}, (a_i')^{(5)}, (b_i)^{(5)}, (b_i')^{(5)}, (p_i)^{(5)}, (r_i)^{(5)}, i = 28, 29, 30$, satisfy the inequalities

$$\frac{1}{(\hat{M}_{28})^{(5)}} [(a_i)^{(5)} + (a_i')^{(5)} + (\hat{A}_{28})^{(5)} + (\hat{P}_{28})^{(5)} (\hat{k}_{28})^{(5)}] < 1$$

$$\frac{1}{(\hat{M}_{28})^{(5)}} [(b_i)^{(5)} + (b_i')^{(5)} + (\hat{B}_{28})^{(5)} + (\hat{Q}_{28})^{(5)} (\hat{k}_{28})^{(5)}] < 1$$

Where we suppose 183

$$(a_i)^{(6)}, (a_i')^{(6)}, (a_i'')^{(6)}, (b_i)^{(6)}, (b_i')^{(6)}, (b_i'')^{(6)} > 0, \quad i, j = 32, 33, 34 \quad 184$$

(12) The functions $(a_i'')^{(6)}, (b_i'')^{(6)}$ are positive continuous increasing and bounded.

Definition of $(p_i)^{(6)}, (r_i)^{(6)}$:

$$(a_i'')^{(6)}(T_{33}, t) \leq (p_i)^{(6)} \leq (\hat{A}_{32})^{(6)}$$

$$(b_i'')^{(6)}(G_{35}, t) \leq (r_i)^{(6)} \leq (b_i')^{(6)} \leq (\hat{B}_{32})^{(6)}$$

$$(13) \lim_{T_2 \rightarrow \infty} (a_i'')^{(6)}(T_{33}, t) = (p_i)^{(6)}$$

$$\lim_{G \rightarrow \infty} (b_i'')^{(6)}(G_{35}, t) = (r_i)^{(6)}$$

Definition of $(\hat{A}_{32})^{(6)}, (\hat{B}_{32})^{(6)}$:

Where $(\hat{A}_{32})^{(6)}, (\hat{B}_{32})^{(6)}, (p_i)^{(6)}, (r_i)^{(6)}$ are positive constants and $i = 32, 33, 34$

They satisfy Lipschitz condition:

186

$$|(a_i'')^{(6)}(T_{33}', t) - (a_i'')^{(6)}(T_{33}, t)| \leq (\hat{k}_{32})^{(6)} |T_{33}' - T_{33}| e^{-(M_{32})^{(6)}t}$$

$$|(b_i'')^{(6)}(G_{35}', t) - (b_i'')^{(6)}(G_{35}, t)| < (\hat{k}_{32})^{(6)} |(G_{35}') - (G_{35})| e^{-(M_{32})^{(6)}t}$$

With the Lipschitz condition, we place a restriction on the behavior of functions $(a_i'')^{(6)}(T_{33}', t)$ and $(a_i'')^{(6)}(T_{33}, t)$. (T_{33}', t) and (T_{33}, t) are points belonging to the interval $[(\hat{k}_{32})^{(6)}, (\hat{M}_{32})^{(6)}]$. It is to be noted that $(a_i'')^{(6)}(T_{33}, t)$ is uniformly continuous. In the eventuality of the fact, that if $(\hat{M}_{32})^{(6)} = 6$ then the function $(a_i'')^{(6)}(T_{33}, t)$, the SIXTH **augmentation coefficient** would be absolutely continuous.

187

Definition of $(\hat{M}_{32})^{(6)}, (\hat{k}_{32})^{(6)}$:

188

$(\hat{M}_{32})^{(6)}, (\hat{k}_{32})^{(6)}$ are positive constants

$$\frac{(a_i)^{(6)}}{(M_{32})^{(6)}}, \frac{(b_i)^{(6)}}{(M_{32})^{(6)}} < 1$$

Definition of $(\hat{P}_{32})^{(6)}, (\hat{Q}_{32})^{(6)}$:

189

There exists two constants $(\hat{P}_{32})^{(6)}$ and $(\hat{Q}_{32})^{(6)}$ which together with $(\hat{M}_{32})^{(6)}, (\hat{k}_{32})^{(6)}, (\hat{A}_{32})^{(6)}$ and $(\hat{B}_{32})^{(6)}$ and the constants $(a_i)^{(6)}, (a_i')^{(6)}, (b_i)^{(6)}, (b_i')^{(6)}, (p_i)^{(6)}, (r_i)^{(6)}, i = 32, 33, 34$, satisfy the inequalities

$$\frac{1}{(M_{32})^{(6)}} [(a_i)^{(6)} + (a_i')^{(6)} + (\hat{A}_{32})^{(6)} + (\hat{P}_{32})^{(6)} (\hat{k}_{32})^{(6)}] < 1$$

$$\frac{1}{(M_{32})^{(6)}} [(b_i)^{(6)} + (b_i')^{(6)} + (\hat{B}_{32})^{(6)} + (\hat{Q}_{32})^{(6)} (\hat{k}_{32})^{(6)}] < 1$$

Where we suppose

190

$$(V) \quad (a_i)^{(7)}, (a_i')^{(7)}, (a_i'')^{(7)}, (b_i)^{(7)}, (b_i')^{(7)}, (b_i'')^{(7)} > 0,$$

$$i, j = 36, 37, 38$$

191

(W) The functions $(a_i'')^{(7)}, (b_i'')^{(7)}$ are positive continuous increasing and bounded.

Definition of $(p_i)^{(7)}, (r_i)^{(7)}$:

$$(a_i'')^{(7)}(T_{37}, t) \leq (p_i)^{(7)} \leq (\hat{A}_{36})^{(7)}$$

$$(b_i'')^{(7)}(G, t) \leq (r_i)^{(7)} \leq (b_i')^{(7)} \leq (\hat{B}_{36})^{(7)}$$

$$\lim_{T_2 \rightarrow \infty} (a_i'')^{(7)}(T_{37}, t) = (p_i)^{(7)}$$

192

$$\lim_{G \rightarrow \infty} (b_i'')^{(7)}(G_{39}, t) = (r_i)^{(7)}$$

Definition of $(\hat{A}_{36})^{(7)}, (\hat{B}_{36})^{(7)}$:

Where $(\hat{A}_{36})^{(7)}, (\hat{B}_{36})^{(7)}, (p_i)^{(7)}, (r_i)^{(7)}$ are positive constants
 and $i = 36, 37, 38$

They satisfy Lipschitz condition:

193

$$|(a_i'')^{(7)}(T_{37}, t) - (a_i'')^{(7)}(T_{37}, t)| \leq (\hat{k}_{36})^{(7)} |T_{37} - T_{37}'| e^{-(\hat{M}_{36})^{(7)}t}$$

$$|(b_i'')^{(7)}((G_{39})', t) - (b_i'')^{(7)}((G_{39}), (T_{39}))| < (\hat{k}_{36})^{(7)} |(G_{39}) - (G_{39})'| e^{-(\hat{M}_{36})^{(7)}t}$$

With the Lipschitz condition, we place a restriction on the behavior of functions $(a_i'')^{(7)}(T_{37}, t)$ and $(a_i'')^{(7)}(T_{37}, t) \cdot (T_{37}, t)$ and (T_{37}, t) are points belonging to the interval $[(\hat{k}_{36})^{(7)}, (\hat{M}_{36})^{(7)}]$. It is to be noted that $(a_i'')^{(7)}(T_{37}, t)$ is uniformly continuous. In the eventuality of the fact, that if $(\hat{M}_{36})^{(7)} = 7$ then the function $(a_i'')^{(7)}(T_{37}, t)$, the **first augmentation coefficient** attributable to terrestrial organisms, would be absolutely continuous.

194

Definition of $(\hat{M}_{36})^{(7)}, (\hat{k}_{36})^{(7)}$:

195

(X) $(\hat{M}_{36})^{(7)}, (\hat{k}_{36})^{(7)}$, are positive constants
 $\frac{(a_i)^{(7)}}{(\hat{M}_{36})^{(7)}}, \frac{(b_i)^{(7)}}{(\hat{M}_{36})^{(7)}} < 1$

Definition of $(\hat{P}_{36})^{(7)}, (\hat{Q}_{36})^{(7)}$:

196

(Y) There exists two constants $(\hat{P}_{36})^{(7)}$ and $(\hat{Q}_{36})^{(7)}$ which together with $(\hat{M}_{36})^{(7)}, (\hat{k}_{36})^{(7)}, (\hat{A}_{36})^{(7)}$ and $(\hat{B}_{36})^{(7)}$ and the constants $(a_i)^{(7)}, (a_i')^{(7)}, (b_i)^{(7)}, (b_i')^{(7)}, (p_i)^{(7)}, (r_i)^{(7)}, i = 36, 37, 38$, satisfy the inequalities

$$\frac{1}{(\hat{M}_{36})^{(7)}} [(a_i)^{(7)} + (a_i')^{(7)} + (\hat{A}_{36})^{(7)} + (\hat{P}_{36})^{(7)} (\hat{k}_{36})^{(7)}] < 1$$

$$\frac{1}{(\hat{M}_{36})^{(7)}} [(b_i)^{(7)} + (b_i')^{(7)} + (\hat{B}_{36})^{(7)} + (\hat{Q}_{36})^{(7)} (\hat{k}_{36})^{(7)}] < 1$$

Definition of $G_i(0), T_i(0)$:

197

$$G_i(t) \leq (\hat{P}_{28})^{(5)} e^{(\hat{M}_{28})^{(5)}t}, \quad G_i(0) = G_i^0 > 0$$

$$T_i(t) \leq (\hat{Q}_{28})^{(5)} e^{(\hat{M}_{28})^{(5)}t}, \quad T_i(0) = T_i^0 > 0$$

198

Definition of $G_i(0), T_i(0)$:

199

$$G_i(t) \leq (\hat{P}_{32})^{(6)} e^{(\hat{M}_{32})^{(6)}t}, \quad G_i(0) = G_i^0 > 0$$

$$T_i(t) \leq (\hat{Q}_{32})^{(6)} e^{(\hat{M}_{32})^{(6)}t}, \quad T_i(0) = T_i^0 > 0$$

Definition of $G_i(0), T_i(0)$:

$$G_i(t) \leq (\hat{P}_{36})^{(7)} e^{(\hat{M}_{36})^{(7)}t}, \quad G_i(0) = G_i^0 > 0$$

$$T_i(t) \leq (\hat{Q}_{36})^{(7)} e^{(M_{36})^{(7)}t} , \quad \boxed{T_i(0) = T_i^0 > 0}$$

Proof: Consider operator $\mathcal{A}^{(1)}$ defined on the space of sextuples of continuous functions $G_i, T_i: \mathbb{R}_+ \rightarrow \mathbb{R}_+$ which satisfy 200

$$G_i(0) = G_i^0, T_i(0) = T_i^0, G_i^0 \leq (\hat{P}_{13})^{(1)}, T_i^0 \leq (\hat{Q}_{13})^{(1)}, \quad 201$$

$$0 \leq G_i(t) - G_i^0 \leq (\hat{P}_{13})^{(1)} e^{(M_{13})^{(1)}t} \quad 202$$

$$0 \leq T_i(t) - T_i^0 \leq (\hat{Q}_{13})^{(1)} e^{(M_{13})^{(1)}t} \quad 203$$

By 204

$$\bar{G}_{13}(t) = G_{13}^0 + \int_0^t \left[(a_{13})^{(1)} G_{14}(s_{(13)}) - \left((a'_{13})^{(1)} + a''_{13}(s_{(13)}, s_{(13)}) \right) G_{13}(s_{(13)}) \right] ds_{(13)}$$

$$\bar{G}_{14}(t) = G_{14}^0 + \int_0^t \left[(a_{14})^{(1)} G_{13}(s_{(13)}) - \left((a'_{14})^{(1)} + a''_{14}(s_{(13)}, s_{(13)}) \right) G_{14}(s_{(13)}) \right] ds_{(13)} \quad 205$$

$$\bar{G}_{15}(t) = G_{15}^0 + \int_0^t \left[(a_{15})^{(1)} G_{14}(s_{(13)}) - \left((a'_{15})^{(1)} + a''_{15}(s_{(13)}, s_{(13)}) \right) G_{15}(s_{(13)}) \right] ds_{(13)} \quad 206$$

$$\bar{T}_{13}(t) = T_{13}^0 + \int_0^t \left[(b_{13})^{(1)} T_{14}(s_{(13)}) - \left((b'_{13})^{(1)} - b''_{13}(s_{(13)}, s_{(13)}) \right) T_{13}(s_{(13)}) \right] ds_{(13)} \quad 207$$

$$\bar{T}_{14}(t) = T_{14}^0 + \int_0^t \left[(b_{14})^{(1)} T_{13}(s_{(13)}) - \left((b'_{14})^{(1)} - b''_{14}(s_{(13)}, s_{(13)}) \right) T_{14}(s_{(13)}) \right] ds_{(13)} \quad 208$$

$$\bar{T}_{15}(t) = T_{15}^0 + \int_0^t \left[(b_{15})^{(1)} T_{14}(s_{(13)}) - \left((b'_{15})^{(1)} - b''_{15}(s_{(13)}, s_{(13)}) \right) T_{15}(s_{(13)}) \right] ds_{(13)} \quad 209$$

Where $s_{(13)}$ is the integrand that is integrated over an interval $(0, t)$

210

if the conditions IN THE FOREGOING above are fulfilled, there exists a solution satisfying the conditions

Definition of $G_i(0), T_i(0)$:

$$G_i(t) \leq (\hat{P}_{36})^{(7)} e^{(M_{36})^{(7)}t} , \quad \boxed{G_i(0) = G_i^0 > 0}$$

$$T_i(t) \leq (\hat{Q}_{36})^{(7)} e^{(M_{36})^{(7)}t} , \quad \boxed{T_i(0) = T_i^0 > 0}$$

Consider operator $\mathcal{A}^{(7)}$ defined on the space of sextuples of continuous functions $G_i, T_i: \mathbb{R}_+ \rightarrow \mathbb{R}_+$ which satisfy

$$G_i(0) = G_i^0, T_i(0) = T_i^0, G_i^0 \leq (\hat{P}_{36})^{(7)}, T_i^0 \leq (\hat{Q}_{36})^{(7)},$$

$$0 \leq G_i(t) - G_i^0 \leq (\hat{P}_{36})^{(7)} e^{(M_{36})^{(7)}t}$$

$$0 \leq T_i(t) - T_i^0 \leq (\hat{Q}_{36})^{(7)} e^{(M_{36})^{(7)}t}$$

By

$$\bar{G}_{36}(t) = G_{36}^0 + \int_0^t \left[(a_{36})^{(7)} G_{37}(s_{(36)}) - \left((a'_{36})^{(7)} + a''_{36}(s_{(36)}, s_{(36)}) \right) G_{36}(s_{(36)}) \right] ds_{(36)}$$

$$\bar{G}_{37}(t) = G_{37}^0 + \int_0^t \left[(a_{37})^{(7)} G_{36}(s_{(36)}) - \left((a'_{37})^{(7)} + a''_{37}(s_{(36)}, s_{(36)}) \right) G_{37}(s_{(36)}) \right] ds_{(36)}$$

$$\bar{G}_{38}(t) = G_{38}^0 + \int_0^t \left[(a_{38})^{(7)} G_{37}(s_{(36)}) - \left((a'_{38})^{(7)} + (a''_{38})^{(7)} (T_{37}(s_{(36)}), s_{(36)}) \right) G_{38}(s_{(36)}) \right] ds_{(36)}$$

$$\bar{T}_{36}(t) = T_{36}^0 + \int_0^t \left[(b_{36})^{(7)} T_{37}(s_{(36)}) - \left((b'_{36})^{(7)} - (b''_{36})^{(7)} (G(s_{(36)}), s_{(36)}) \right) T_{36}(s_{(36)}) \right] ds_{(36)}$$

$$\bar{T}_{37}(t) = T_{37}^0 + \int_0^t \left[(b_{37})^{(7)} T_{36}(s_{(36)}) - \left((b'_{37})^{(7)} - (b''_{37})^{(7)} (G(s_{(36)}), s_{(36)}) \right) T_{37}(s_{(36)}) \right] ds_{(36)}$$

$$\bar{T}_{38}(t) = T_{38}^0 + \int_0^t \left[(b_{38})^{(7)} T_{37}(s_{(36)}) - \left((b'_{38})^{(7)} - (b''_{38})^{(7)} (G(s_{(36)}), s_{(36)}) \right) T_{38}(s_{(36)}) \right] ds_{(36)}$$

Where $s_{(36)}$ is the integrand that is integrated over an interval $(0, t)$

Consider operator $\mathcal{A}^{(2)}$ defined on the space of sextuples of continuous functions $G_i, T_i: \mathbb{R}_+ \rightarrow \mathbb{R}_+$ which satisfy 211

$$G_i(0) = G_i^0, T_i(0) = T_i^0, G_i^0 \leq (\hat{P}_{16})^{(2)}, T_i^0 \leq (\hat{Q}_{16})^{(2)}, \tag{212}$$

$$0 \leq G_i(t) - G_i^0 \leq (\hat{P}_{16})^{(2)} e^{(\bar{M}_{16})^{(2)}t} \tag{213}$$

$$0 \leq T_i(t) - T_i^0 \leq (\hat{Q}_{16})^{(2)} e^{(\bar{M}_{16})^{(2)}t} \tag{214}$$

By 215

$$\bar{G}_{16}(t) = G_{16}^0 + \int_0^t \left[(a_{16})^{(2)} G_{17}(s_{(16)}) - \left((a'_{16})^{(2)} + a''_{16}^{(2)} (T_{17}(s_{(16)}), s_{(16)}) \right) G_{16}(s_{(16)}) \right] ds_{(16)}$$

$$\bar{G}_{17}(t) = G_{17}^0 + \int_0^t \left[(a_{17})^{(2)} G_{16}(s_{(16)}) - \left((a'_{17})^{(2)} + (a''_{17})^{(2)} (T_{17}(s_{(16)}), s_{(17)}) \right) G_{17}(s_{(16)}) \right] ds_{(16)} \tag{216}$$

$$\bar{G}_{18}(t) = G_{18}^0 + \int_0^t \left[(a_{18})^{(2)} G_{17}(s_{(16)}) - \left((a'_{18})^{(2)} + (a''_{18})^{(2)} (T_{17}(s_{(16)}), s_{(16)}) \right) G_{18}(s_{(16)}) \right] ds_{(16)} \tag{217}$$

$$\bar{T}_{16}(t) = T_{16}^0 + \int_0^t \left[(b_{16})^{(2)} T_{17}(s_{(16)}) - \left((b'_{16})^{(2)} - (b''_{16})^{(2)} (G(s_{(16)}), s_{(16)}) \right) T_{16}(s_{(16)}) \right] ds_{(16)} \tag{218}$$

$$\bar{T}_{17}(t) = T_{17}^0 + \int_0^t \left[(b_{17})^{(2)} T_{16}(s_{(16)}) - \left((b'_{17})^{(2)} - (b''_{17})^{(2)} (G(s_{(16)}), s_{(16)}) \right) T_{17}(s_{(16)}) \right] ds_{(16)} \tag{219}$$

$$\bar{T}_{18}(t) = T_{18}^0 + \int_0^t \left[(b_{18})^{(2)} T_{17}(s_{(16)}) - \left((b'_{18})^{(2)} - (b''_{18})^{(2)} (G(s_{(16)}), s_{(16)}) \right) T_{18}(s_{(16)}) \right] ds_{(16)} \tag{220}$$

Where $s_{(16)}$ is the integrand that is integrated over an interval $(0, t)$

Consider operator $\mathcal{A}^{(3)}$ defined on the space of sextuples of continuous functions $G_i, T_i: \mathbb{R}_+ \rightarrow \mathbb{R}_+$ which satisfy 221

$$G_i(0) = G_i^0, T_i(0) = T_i^0, G_i^0 \leq (\hat{P}_{20})^{(3)}, T_i^0 \leq (\hat{Q}_{20})^{(3)}, \tag{222}$$

$$0 \leq G_i(t) - G_i^0 \leq (\hat{P}_{20})^{(3)} e^{(\bar{M}_{20})^{(3)}t} \tag{223}$$

$$0 \leq T_i(t) - T_i^0 \leq (\hat{Q}_{20})^{(3)} e^{(\bar{M}_{20})^{(3)}t} \tag{224}$$

By 225

$$\bar{G}_{20}(t) = G_{20}^0 + \int_0^t \left[(a_{20})^{(3)} G_{21}(s_{(20)}) - \left((a'_{20})^{(3)} + a''_{20}(s_{(20)}) \right) T_{21}(s_{(20)}, s_{(20)}) \right] G_{20}(s_{(20)}) ds_{(20)} \quad 226$$

$$\bar{G}_{21}(t) = G_{21}^0 + \int_0^t \left[(a_{21})^{(3)} G_{20}(s_{(20)}) - \left((a'_{21})^{(3)} + a''_{21}(s_{(20)}) \right) T_{21}(s_{(20)}, s_{(20)}) \right] G_{21}(s_{(20)}) ds_{(20)} \quad 227$$

$$\bar{G}_{22}(t) = G_{22}^0 + \int_0^t \left[(a_{22})^{(3)} G_{21}(s_{(20)}) - \left((a'_{22})^{(3)} + a''_{22}(s_{(20)}) \right) T_{21}(s_{(20)}, s_{(20)}) \right] G_{22}(s_{(20)}) ds_{(20)} \quad 228$$

$$\bar{T}_{20}(t) = T_{20}^0 + \int_0^t \left[(b_{20})^{(3)} T_{21}(s_{(20)}) - \left((b'_{20})^{(3)} - (b''_{20})^{(3)}(G(s_{(20)}, s_{(20)})) \right) T_{20}(s_{(20)}) \right] ds_{(20)} \quad 229$$

$$\bar{T}_{21}(t) = T_{21}^0 + \int_0^t \left[(b_{21})^{(3)} T_{20}(s_{(20)}) - \left((b'_{21})^{(3)} - (b''_{21})^{(3)}(G(s_{(20)}, s_{(20)})) \right) T_{21}(s_{(20)}) \right] ds_{(20)} \quad 230$$

$$\bar{T}_{22}(t) = T_{22}^0 + \int_0^t \left[(b_{22})^{(3)} T_{21}(s_{(20)}) - \left((b'_{22})^{(3)} - (b''_{22})^{(3)}(G(s_{(20)}, s_{(20)})) \right) T_{22}(s_{(20)}) \right] ds_{(20)} \quad 231$$

Where $s_{(20)}$ is the integrand that is integrated over an interval $(0, t)$

Consider operator $\mathcal{A}^{(4)}$ defined on the space of sextuples of continuous functions $G_i, T_i: \mathbb{R}_+ \rightarrow \mathbb{R}_+$ which satisfy 231

$$G_i(0) = G_i^0, T_i(0) = T_i^0, G_i^0 \leq (\hat{P}_{24})^{(4)}, T_i^0 \leq (\hat{Q}_{24})^{(4)}, \quad 232$$

$$0 \leq G_i(t) - G_i^0 \leq (\hat{P}_{24})^{(4)} e^{(M_{24})^{(4)}t} \quad 233$$

$$0 \leq T_i(t) - T_i^0 \leq (\hat{Q}_{24})^{(4)} e^{(M_{24})^{(4)}t} \quad 234$$

By 235

$$\bar{G}_{24}(t) = G_{24}^0 + \int_0^t \left[(a_{24})^{(4)} G_{25}(s_{(24)}) - \left((a'_{24})^{(4)} + a''_{24}(s_{(24)}) \right) T_{25}(s_{(24)}, s_{(24)}) \right] G_{24}(s_{(24)}) ds_{(24)}$$

$$\bar{G}_{25}(t) = G_{25}^0 + \int_0^t \left[(a_{25})^{(4)} G_{24}(s_{(24)}) - \left((a'_{25})^{(4)} + a''_{25}(s_{(24)}) \right) T_{25}(s_{(24)}, s_{(24)}) \right] G_{25}(s_{(24)}) ds_{(24)} \quad 236$$

$$\bar{G}_{26}(t) = G_{26}^0 + \int_0^t \left[(a_{26})^{(4)} G_{25}(s_{(24)}) - \left((a'_{26})^{(4)} + a''_{26}(s_{(24)}) \right) T_{25}(s_{(24)}, s_{(24)}) \right] G_{26}(s_{(24)}) ds_{(24)} \quad 237$$

$$\bar{T}_{24}(t) = T_{24}^0 + \int_0^t \left[(b_{24})^{(4)} T_{25}(s_{(24)}) - \left((b'_{24})^{(4)} - (b''_{24})^{(4)}(G(s_{(24)}, s_{(24)})) \right) T_{24}(s_{(24)}) \right] ds_{(24)} \quad 238$$

$$\bar{T}_{25}(t) = T_{25}^0 + \int_0^t \left[(b_{25})^{(4)} T_{24}(s_{(24)}) - \left((b'_{25})^{(4)} - (b''_{25})^{(4)}(G(s_{(24)}, s_{(24)})) \right) T_{25}(s_{(24)}) \right] ds_{(24)} \quad 239$$

$$\bar{T}_{26}(t) = T_{26}^0 + \int_0^t \left[(b_{26})^{(4)} T_{25}(s_{(24)}) - \left((b'_{26})^{(4)} - (b''_{26})^{(4)}(G(s_{(24)}, s_{(24)})) \right) T_{26}(s_{(24)}) \right] ds_{(24)} \quad 240$$

Where $s_{(24)}$ is the integrand that is integrated over an interval $(0, t)$

Consider operator $\mathcal{A}^{(5)}$ defined on the space of sextuples of continuous functions $G_i, T_i: \mathbb{R}_+ \rightarrow \mathbb{R}_+$ which satisfy 241

$$G_i(0) = G_i^0, T_i(0) = T_i^0, G_i^0 \leq (\hat{P}_{28})^{(5)}, T_i^0 \leq (\hat{Q}_{28})^{(5)}, \quad 242$$

$$0 \leq G_i(t) - G_i^0 \leq (\hat{P}_{28})^{(5)} e^{(M_{28})^{(5)}t} \quad 243$$

$$0 \leq T_i(t) - T_i^0 \leq (\hat{Q}_{28})^{(5)} e^{(M_{28})^{(5)}t} \quad 244$$

By 245

$$\bar{G}_{28}(t) = G_{28}^0 + \int_0^t \left[(a_{28})^{(5)} G_{29}(s_{(28)}) - \left((a'_{28})^{(5)} + a''_{28}(s_{(28)}) \right) T_{29}(s_{(28)}, s_{(28)}) \right] G_{28}(s_{(28)}) ds_{(28)} \quad 246$$

$$\bar{G}_{29}(t) = G_{29}^0 + \int_0^t \left[(a_{29})^{(5)} G_{28}(s_{(28)}) - \left((a'_{29})^{(5)} + (a''_{29})^{(5)} (T_{29}(s_{(28)}), s_{(28)}) \right) G_{29}(s_{(28)}) \right] ds_{(28)} \quad 247$$

$$\bar{G}_{30}(t) = G_{30}^0 + \int_0^t \left[(a_{30})^{(5)} G_{29}(s_{(28)}) - \left((a'_{30})^{(5)} + (a''_{30})^{(5)} (T_{29}(s_{(28)}), s_{(28)}) \right) G_{30}(s_{(28)}) \right] ds_{(28)} \quad 248$$

$$\bar{T}_{28}(t) = T_{28}^0 + \int_0^t \left[(b_{28})^{(5)} T_{29}(s_{(28)}) - \left((b'_{28})^{(5)} - (b''_{28})^{(5)} (G(s_{(28)}), s_{(28)}) \right) T_{28}(s_{(28)}) \right] ds_{(28)} \quad 249$$

$$\bar{T}_{29}(t) = T_{29}^0 + \int_0^t \left[(b_{29})^{(5)} T_{28}(s_{(28)}) - \left((b'_{29})^{(5)} - (b''_{29})^{(5)} (G(s_{(28)}), s_{(28)}) \right) T_{29}(s_{(28)}) \right] ds_{(28)} \quad 250$$

$$\bar{T}_{30}(t) = T_{30}^0 + \int_0^t \left[(b_{30})^{(5)} T_{29}(s_{(28)}) - \left((b'_{30})^{(5)} - (b''_{30})^{(5)} (G(s_{(28)}), s_{(28)}) \right) T_{30}(s_{(28)}) \right] ds_{(28)} \quad 251$$

Where $s_{(28)}$ is the integrand that is integrated over an interval $(0, t)$

Consider operator $\mathcal{A}^{(6)}$ defined on the space of sextuples of continuous functions $G_i, T_i: \mathbb{R}_+ \rightarrow \mathbb{R}_+$ which satisfy 252

$$G_i(0) = G_i^0, T_i(0) = T_i^0, G_i^0 \leq (\hat{P}_{32})^{(6)}, T_i^0 \leq (\hat{Q}_{32})^{(6)}, \quad 253$$

$$0 \leq G_i(t) - G_i^0 \leq (\hat{P}_{32})^{(6)} e^{(M_{32})^{(6)}t} \quad 254$$

$$0 \leq T_i(t) - T_i^0 \leq (\hat{Q}_{32})^{(6)} e^{(M_{32})^{(6)}t} \quad 255$$

By 256

$$\bar{G}_{32}(t) = G_{32}^0 + \int_0^t \left[(a_{32})^{(6)} G_{33}(s_{(32)}) - \left((a'_{32})^{(6)} + (a''_{32})^{(6)} (T_{33}(s_{(32)}), s_{(32)}) \right) G_{32}(s_{(32)}) \right] ds_{(32)}$$

$$\bar{G}_{33}(t) = G_{33}^0 + \int_0^t \left[(a_{33})^{(6)} G_{32}(s_{(32)}) - \left((a'_{33})^{(6)} + (a''_{33})^{(6)} (T_{33}(s_{(32)}), s_{(32)}) \right) G_{33}(s_{(32)}) \right] ds_{(32)} \quad 257$$

$$\bar{G}_{34}(t) = G_{34}^0 + \int_0^t \left[(a_{34})^{(6)} G_{33}(s_{(32)}) - \left((a'_{34})^{(6)} + (a''_{34})^{(6)} (T_{33}(s_{(32)}), s_{(32)}) \right) G_{34}(s_{(32)}) \right] ds_{(32)} \quad 258$$

$$\bar{T}_{32}(t) = T_{32}^0 + \int_0^t \left[(b_{32})^{(6)} T_{33}(s_{(32)}) - \left((b'_{32})^{(6)} - (b''_{32})^{(6)} (G(s_{(32)}), s_{(32)}) \right) T_{32}(s_{(32)}) \right] ds_{(32)} \quad 259$$

$$\bar{T}_{33}(t) = T_{33}^0 + \int_0^t \left[(b_{33})^{(6)} T_{32}(s_{(32)}) - \left((b'_{33})^{(6)} - (b''_{33})^{(6)} (G(s_{(32)}), s_{(32)}) \right) T_{33}(s_{(32)}) \right] ds_{(32)} \quad 260$$

$$\bar{T}_{34}(t) = T_{34}^0 + \int_0^t \left[(b_{34})^{(6)} T_{33}(s_{(32)}) - \left((b'_{34})^{(6)} - (b''_{34})^{(6)} (G(s_{(32)}), s_{(32)}) \right) T_{34}(s_{(32)}) \right] ds_{(32)} \quad 261$$

Where $s_{(32)}$ is the integrand that is integrated over an interval $(0, t)$

: if the conditions IN THE FOREGOING are fulfilled, there exists a solution satisfying the conditions 262

Definition of $G_i(0), T_i(0)$:

$$G_i(t) \leq (\hat{P}_{36})^{(7)} e^{(M_{36})^{(7)}t}, \quad \boxed{G_i(0) = G_i^0 > 0}$$

$$T_i(t) \leq (\hat{Q}_{36})^{(7)} e^{(M_{36})^{(7)}t}, \quad \boxed{T_i(0) = T_i^0 > 0}$$

Proof:

Consider operator $\mathcal{A}^{(7)}$ defined on the space of sextuples of continuous functions $G_i, T_i: \mathbb{R}_+ \rightarrow \mathbb{R}_+$ which satisfy

$$G_i(0) = G_i^0, T_i(0) = T_i^0, G_i^0 \leq (\hat{P}_{36})^{(7)}, T_i^0 \leq (\hat{Q}_{36})^{(7)}, \quad 263$$

$$0 \leq G_i(t) - G_i^0 \leq (\hat{P}_{36})^{(7)} e^{(M_{36})^{(7)}t} \quad 264$$

$$0 \leq T_i(t) - T_i^0 \leq (\hat{Q}_{36})^{(7)} e^{(M_{36})^{(7)}t} \quad 265$$

By 266

$$\bar{G}_{36}(t) = G_{36}^0 + \int_0^t \left[(a_{36})^{(7)} G_{37}(s_{(36)}) - \left((a'_{36})^{(7)} + a''_{36})^{(7)} (T_{37}(s_{(36)}), s_{(36)}) \right) G_{36}(s_{(36)}) \right] ds_{(36)} \quad 267$$

$$\bar{G}_{37}(t) = G_{37}^0 + \int_0^t \left[(a_{37})^{(7)} G_{36}(s_{(36)}) - \left((a'_{37})^{(7)} + (a''_{37})^{(7)} (T_{37}(s_{(36)}), s_{(36)}) \right) G_{37}(s_{(36)}) \right] ds_{(36)}$$

$$\bar{G}_{38}(t) = G_{38}^0 + \int_0^t \left[(a_{38})^{(7)} G_{37}(s_{(36)}) - \left((a'_{38})^{(7)} + (a''_{38})^{(7)} (T_{37}(s_{(36)}), s_{(36)}) \right) G_{38}(s_{(36)}) \right] ds_{(36)} \quad 268$$

$$\bar{T}_{36}(t) = T_{36}^0 + \int_0^t \left[(b_{36})^{(7)} T_{37}(s_{(36)}) - \left((b'_{36})^{(7)} - (b''_{36})^{(7)} (G(s_{(36)}), s_{(36)}) \right) T_{36}(s_{(36)}) \right] ds_{(36)} \quad 269$$

$$\bar{T}_{37}(t) = T_{37}^0 + \int_0^t \left[(b_{37})^{(7)} T_{36}(s_{(36)}) - \left((b'_{37})^{(7)} - (b''_{37})^{(7)} (G(s_{(36)}), s_{(36)}) \right) T_{37}(s_{(36)}) \right] ds_{(36)} \quad 270$$

$$\bar{T}_{38}(t) = T_{38}^0 + \int_0^t \left[(b_{38})^{(7)} T_{37}(s_{(36)}) - \left((b'_{38})^{(7)} - (b''_{38})^{(7)} (G(s_{(36)}), s_{(36)}) \right) T_{38}(s_{(36)}) \right] ds_{(36)} \quad 271$$

Where $s_{(36)}$ is the integrand that is integrated over an interval $(0, t)$

Analogous inequalities hold also for $G_{21}, G_{22}, T_{20}, T_{21}, T_{22}$ 272

(a) The operator $\mathcal{A}^{(4)}$ maps the space of functions satisfying GLOBAL EQUATIONS into itself. Indeed it is obvious that 273

$$G_{24}(t) \leq G_{24}^0 + \int_0^t \left[(a_{24})^{(4)} \left(G_{25}^0 + (\hat{P}_{24})^{(4)} e^{(\bar{M}_{24})^{(4)} s_{(24)}} \right) \right] ds_{(24)} =$$

$$(1 + (a_{24})^{(4)} t) G_{25}^0 + \frac{(a_{24})^{(4)} (\hat{P}_{24})^{(4)}}{(\bar{M}_{24})^{(4)}} \left(e^{(\bar{M}_{24})^{(4)} t} - 1 \right)$$

From which it follows that 274

$$(G_{24}(t) - G_{24}^0) e^{-(\bar{M}_{24})^{(4)} t} \leq \frac{(a_{24})^{(4)}}{(\bar{M}_{24})^{(4)}} \left[\left((\hat{P}_{24})^{(4)} + G_{25}^0 \right) e^{\left(-\frac{(\hat{P}_{24})^{(4)} + G_{25}^0}{G_{25}^0} \right)} + (\hat{P}_{24})^{(4)} \right]$$

(G_i^0) is as defined in the statement of theorem 1

(b) The operator $\mathcal{A}^{(5)}$ maps the space of functions satisfying GLOBAL EQUATIONS into itself .Indeed it is obvious that 275

$$G_{28}(t) \leq G_{28}^0 + \int_0^t \left[(a_{28})^{(5)} \left(G_{29}^0 + (\hat{P}_{28})^{(5)} e^{(\bar{M}_{28})^{(5)} s_{(28)}} \right) \right] ds_{(28)} =$$

$$(1 + (a_{28})^{(5)} t) G_{29}^0 + \frac{(a_{28})^{(5)} (\hat{P}_{28})^{(5)}}{(\bar{M}_{28})^{(5)}} \left(e^{(\bar{M}_{28})^{(5)} t} - 1 \right)$$

From which it follows that 276

$$(G_{28}(t) - G_{28}^0) e^{-(\bar{M}_{28})^{(5)} t} \leq \frac{(a_{28})^{(5)}}{(\bar{M}_{28})^{(5)}} \left[\left((\hat{P}_{28})^{(5)} + G_{29}^0 \right) e^{\left(-\frac{(\hat{P}_{28})^{(5)} + G_{29}^0}{G_{29}^0} \right)} + (\hat{P}_{28})^{(5)} \right]$$

(G_i^0) is as defined in the statement of theorem 1

(c) The operator $\mathcal{A}^{(6)}$ maps the space of functions satisfying GLOBAL EQUATIONS into itself .Indeed it is obvious that 277

$$G_{32}(t) \leq G_{32}^0 + \int_0^t \left[(a_{32})^{(6)} \left(G_{33}^0 + (\hat{P}_{32})^{(6)} e^{(\bar{M}_{32})^{(6)} s_{(32)}} \right) \right] ds_{(32)} =$$

$$(1 + (a_{32})^{(6)} t) G_{33}^0 + \frac{(a_{32})^{(6)} (\hat{P}_{32})^{(6)}}{(\bar{M}_{32})^{(6)}} \left(e^{(\bar{M}_{32})^{(6)} t} - 1 \right)$$

From which it follows that 278

$$(G_{32}(t) - G_{32}^0) e^{-(\bar{M}_{32})^{(6)} t} \leq \frac{(a_{32})^{(6)}}{(\bar{M}_{32})^{(6)}} \left[\left((\hat{P}_{32})^{(6)} + G_{33}^0 \right) e^{\left(-\frac{(\hat{P}_{32})^{(6)} + G_{33}^0}{G_{33}^0} \right)} + (\hat{P}_{32})^{(6)} \right]$$

(G_i^0) is as defined in the statement of theorem1

Analogous inequalities hold also for $G_{25}, G_{26}, T_{24}, T_{25}, T_{26}$

(d) The operator $\mathcal{A}^{(7)}$ maps the space of functions satisfying 37,35,36 into itself .Indeed it is obvious that 279

$$G_{36}(t) \leq G_{36}^0 + \int_0^t \left[(a_{36})^{(7)} \left(G_{37}^0 + (\hat{P}_{36})^{(7)} e^{(\bar{M}_{36})^{(7)} s_{(36)}} \right) \right] ds_{(36)} =$$

$$(1 + (a_{36})^{(7)} t) G_{37}^0 + \frac{(a_{36})^{(7)} (\hat{P}_{36})^{(7)}}{(\bar{M}_{36})^{(7)}} \left(e^{(\bar{M}_{36})^{(7)} t} - 1 \right)$$

280

From which it follows that

$$(G_{36}(t) - G_{36}^0)e^{-(M_{36})^{(7)}t} \leq \frac{(a_{36})^{(7)}}{(M_{36})^{(7)}} \left[((\hat{P}_{36})^{(7)} + G_{37}^0)e^{-\frac{(\hat{P}_{36})^{(7)} + G_{37}^0}{G_{37}^0}} + (\hat{P}_{36})^{(7)} \right]$$

(G_i^0) is as defined in the statement of theorem 7

It is now sufficient to take $\frac{(a_i)^{(1)}}{(M_{13})^{(1)}}, \frac{(b_i)^{(1)}}{(M_{13})^{(1)}} < 1$ and to choose 281

$(\hat{P}_{13})^{(1)}$ and $(\hat{Q}_{13})^{(1)}$ large to have 282

$$\frac{(a_i)^{(1)}}{(M_{13})^{(1)}} \left[(\hat{P}_{13})^{(1)} + ((\hat{P}_{13})^{(1)} + G_j^0)e^{-\frac{(\hat{P}_{13})^{(1)} + G_j^0}{G_j^0}} \right] \leq (\hat{P}_{13})^{(1)} \quad 283$$

$$\frac{(b_i)^{(1)}}{(M_{13})^{(1)}} \left[((\hat{Q}_{13})^{(1)} + T_j^0)e^{-\frac{(\hat{Q}_{13})^{(1)} + T_j^0}{T_j^0}} + (\hat{Q}_{13})^{(1)} \right] \leq (\hat{Q}_{13})^{(1)} \quad 284$$

In order that the operator $\mathcal{A}^{(1)}$ transforms the space of sextuples of functions G_i, T_i satisfying GLOBAL EQUATIONS into itself 285

The operator $\mathcal{A}^{(1)}$ is a contraction with respect to the metric 286

$$d((G^{(1)}, T^{(1)}), (G^{(2)}, T^{(2)})) = \sup_i \{ \max_{t \in \mathbb{R}_+} |G_i^{(1)}(t) - G_i^{(2)}(t)| e^{-(M_{13})^{(1)}t}, \max_{t \in \mathbb{R}_+} |T_i^{(1)}(t) - T_i^{(2)}(t)| e^{-(M_{13})^{(1)}t} \}$$

Indeed if we denote 287

Definition of \tilde{G}, \tilde{T} :

$$(\tilde{G}, \tilde{T}) = \mathcal{A}^{(1)}(G, T)$$

It results

$$|\tilde{G}_{13}^{(1)} - \tilde{G}_{13}^{(2)}| \leq \int_0^t (a_{13})^{(1)} |G_{14}^{(1)} - G_{14}^{(2)}| e^{-(M_{13})^{(1)}s_{(13)}} e^{(M_{13})^{(1)}s_{(13)}} ds_{(13)} + \int_0^t \{ (a'_{13})^{(1)} |G_{13}^{(1)} - G_{13}^{(2)}| e^{-(M_{13})^{(1)}s_{(13)}} e^{-(M_{13})^{(1)}s_{(13)}} + (a''_{13})^{(1)} (T_{14}^{(1)}, s_{(13)}) |G_{13}^{(1)} - G_{13}^{(2)}| e^{-(M_{13})^{(1)}s_{(13)}} e^{(M_{13})^{(1)}s_{(13)}} + G_{13}^{(2)} | (a'_{13})^{(1)} (T_{14}^{(1)}, s_{(13)}) - (a'_{13})^{(1)} (T_{14}^{(2)}, s_{(13)}) | e^{-(M_{13})^{(1)}s_{(13)}} e^{(M_{13})^{(1)}s_{(13)}} \} ds_{(13)}$$

Where $s_{(13)}$ represents integrand that is integrated over the interval $[0, t]$

From the hypotheses it follows

$$|G^{(1)} - G^{(2)}| e^{-(M_{13})^{(1)}t} \leq \frac{1}{(M_{13})^{(1)}} ((a_{13})^{(1)} + (a'_{13})^{(1)} + (\hat{A}_{13})^{(1)} + (\hat{P}_{13})^{(1)} (\hat{k}_{13})^{(1)}) d((G^{(1)}, T^{(1)}), (G^{(2)}, T^{(2)})) \quad 288$$

And analogous inequalities for G_i and T_i . Taking into account the hypothesis the result follows

Remark 1: The fact that we supposed $(a'_{13})^{(1)}$ and $(b'_{13})^{(1)}$ depending also on t can be considered as not 289

conformal with the reality, however we have put this hypothesis in order that we can postulate condition necessary to prove the uniqueness of the solution bounded by $(\widehat{P}_{13})^{(1)} e^{(\widehat{M}_{13})^{(1)}t}$ and $(\widehat{Q}_{13})^{(1)} e^{(\widehat{M}_{13})^{(1)}t}$ respectively of \mathbb{R}_+ .

If instead of proving the existence of the solution on \mathbb{R}_+ , we have to prove it only on a compact then it suffices to consider that $(a_i'')^{(1)}$ and $(b_i'')^{(1)}$, $i = 13,14,15$ depend only on T_{14} and respectively on G (and not on t) and hypothesis can be replaced by a usual Lipschitz condition.

Remark 2: There does not exist any t where $G_i(t) = 0$ and $T_i(t) = 0$ 290

From 19 to 24 it results

$$G_i(t) \geq G_i^0 e^{-\int_0^t \{(a_i')^{(1)} - (a_i'')^{(1)}(T_{14}(s_{(13)}), s_{(13)})\} ds_{(13)}} \geq 0 \quad 291$$

$$T_i(t) \geq T_i^0 e^{-(b_i')^{(1)}t} > 0 \quad \text{for } t > 0$$

Definition of $((\widehat{M}_{13})^{(1)})_1$, and $((\widehat{M}_{13})^{(1)})_3$: 292

Remark 3: if G_{13} is bounded, the same property have also G_{14} and G_{15} . indeed if

$$G_{13} < ((\widehat{M}_{13})^{(1)}) \text{ it follows } \frac{dG_{14}}{dt} \leq ((\widehat{M}_{13})^{(1)})_1 - (a'_{14})^{(1)}G_{14} \text{ and by integrating}$$

$$G_{14} \leq ((\widehat{M}_{13})^{(1)})_2 = G_{14}^0 + 2(a_{14})^{(1)}((\widehat{M}_{13})^{(1)})_1 / (a'_{14})^{(1)}$$

In the same way, one can obtain

$$G_{15} \leq ((\widehat{M}_{13})^{(1)})_3 = G_{15}^0 + 2(a_{15})^{(1)}((\widehat{M}_{13})^{(1)})_2 / (a'_{15})^{(1)}$$

If G_{14} or G_{15} is bounded, the same property follows for G_{13} , G_{15} and G_{13} , G_{14} respectively.

Remark 4: If G_{13} is bounded, from below, the same property holds for G_{14} and G_{15} . The proof is analogous with the preceding one. An analogous property is true if G_{14} is bounded from below. 293

Remark 5: If T_{13} is bounded from below and $\lim_{t \rightarrow \infty} ((b_i'')^{(1)}(G(t), t)) = (b'_{14})^{(1)}$ then $T_{14} \rightarrow \infty$. 294

Definition of $(m)^{(1)}$ and ε_1 :

Indeed let t_1 be so that for $t > t_1$

$$(b_{14})^{(1)} - (b_i'')^{(1)}(G(t), t) < \varepsilon_1, T_{13}(t) > (m)^{(1)}$$

Then $\frac{dT_{14}}{dt} \geq (a_{14})^{(1)}(m)^{(1)} - \varepsilon_1 T_{14}$ which leads to 295

$$T_{14} \geq \left(\frac{(a_{14})^{(1)}(m)^{(1)}}{\varepsilon_1} \right) (1 - e^{-\varepsilon_1 t}) + T_{14}^0 e^{-\varepsilon_1 t} \text{ If we take } t \text{ such that } e^{-\varepsilon_1 t} = \frac{1}{2} \text{ it results}$$

$T_{14} \geq \left(\frac{(a_{14})^{(1)}(m)^{(1)}}{2} \right)$, $t = \log \frac{2}{\varepsilon_1}$ By taking now ε_1 sufficiently small one sees that T_{14} is unbounded. The same property holds for T_{15} if $\lim_{t \rightarrow \infty} (b_{15}'')^{(1)}(G(t), t) = (b'_{15})^{(1)}$

We now state a more precise theorem about the behaviors at infinity of the solutions

296

It is now sufficient to take $\frac{(a_i)^{(2)}}{(\widehat{M}_{16})^{(2)}} , \frac{(b_i)^{(2)}}{(\widehat{M}_{16})^{(2)}} < 1$ and to choose

297

$(\widehat{P}_{16})^{(2)}$ and $(\widehat{Q}_{16})^{(2)}$ large to have

$$\frac{(a_i)^{(2)}}{(\bar{M}_{16})^{(2)}} \left[((\hat{P}_{16})^{(2)}) + ((\hat{P}_{16})^{(2)} + G_j^0) e^{-\left(\frac{(\hat{P}_{16})^{(2)} + G_j^0}{G_j^0}\right)} \right] \leq (\hat{P}_{16})^{(2)} \quad 298$$

$$\frac{(b_i)^{(2)}}{(\bar{M}_{16})^{(2)}} \left[((\hat{Q}_{16})^{(2)} + T_j^0) e^{-\left(\frac{(\hat{Q}_{16})^{(2)} + T_j^0}{T_j^0}\right)} + (\hat{Q}_{16})^{(2)} \right] \leq (\hat{Q}_{16})^{(2)} \quad 299$$

In order that the operator $\mathcal{A}^{(2)}$ transforms the space of sextuples of functions G_i, T_i satisfying 300

The operator $\mathcal{A}^{(2)}$ is a contraction with respect to the metric 301

$$d\left((G_{19})^{(1)}, (T_{19})^{(1)}, (G_{19})^{(2)}, (T_{19})^{(2)} \right) = \sup_i \left\{ \max_{t \in \mathbb{R}_+} |G_i^{(1)}(t) - G_i^{(2)}(t)| e^{-(\bar{M}_{16})^{(2)}t}, \max_{t \in \mathbb{R}_+} |T_i^{(1)}(t) - T_i^{(2)}(t)| e^{-(\bar{M}_{16})^{(2)}t} \right\}$$

Indeed if we denote 302

Definition of $\tilde{G}_{19}, \tilde{T}_{19} : (\tilde{G}_{19}, \tilde{T}_{19}) = \mathcal{A}^{(2)}(G_{19}, T_{19})$

It results 303

$$\begin{aligned} |\tilde{G}_{16}^{(1)} - \tilde{G}_{16}^{(2)}| &\leq \int_0^t (a_{16})^{(2)} |G_{17}^{(1)} - G_{17}^{(2)}| e^{-(\bar{M}_{16})^{(2)}s_{(16)}} e^{(\bar{M}_{16})^{(2)}s_{(16)}} ds_{(16)} + \\ &\int_0^t \{ (a'_{16})^{(2)} |G_{16}^{(1)} - G_{16}^{(2)}| e^{-(\bar{M}_{16})^{(2)}s_{(16)}} e^{-(\bar{M}_{16})^{(2)}s_{(16)}} + \\ &(a''_{16})^{(2)} (T_{17}^{(1)}, s_{(16)}) |G_{16}^{(1)} - G_{16}^{(2)}| e^{-(\bar{M}_{16})^{(2)}s_{(16)}} e^{(\bar{M}_{16})^{(2)}s_{(16)}} + \\ &G_{16}^{(2)} | (a'_{16})^{(2)} (T_{17}^{(1)}, s_{(16)}) - (a''_{16})^{(2)} (T_{17}^{(2)}, s_{(16)}) | e^{-(\bar{M}_{16})^{(2)}s_{(16)}} e^{(\bar{M}_{16})^{(2)}s_{(16)}} \} ds_{(16)} \end{aligned}$$

Where $s_{(16)}$ represents integrand that is integrated over the interval $[0, t]$ 304

From the hypotheses it follows

$$\begin{aligned} |(G_{19})^{(1)} - (G_{19})^{(2)}| e^{-(\bar{M}_{16})^{(2)}t} &\leq \\ \frac{1}{(\bar{M}_{16})^{(2)}} \left((a_{16})^{(2)} + (a'_{16})^{(2)} + (\hat{A}_{16})^{(2)} + (\hat{P}_{16})^{(2)} (\hat{\kappa}_{16})^{(2)} \right) &d\left((G_{19})^{(1)}, (T_{19})^{(1)}, (G_{19})^{(2)}, (T_{19})^{(2)} \right) \end{aligned} \quad 305$$

And analogous inequalities for G_i and T_i . Taking into account the hypothesis the result follows 306

Remark 1: The fact that we supposed $(a''_{16})^{(2)}$ and $(b''_{16})^{(2)}$ depending also on t can be considered as not conformal with the reality, however we have put this hypothesis in order that we can postulate condition necessary to prove the uniqueness of the solution bounded by $(\hat{P}_{16})^{(2)} e^{(\bar{M}_{16})^{(2)}t}$ and $(\hat{Q}_{16})^{(2)} e^{(\bar{M}_{16})^{(2)}t}$ respectively of \mathbb{R}_+ . 307

If instead of proving the existence of the solution on \mathbb{R}_+ , we have to prove it only on a compact then it suffices to consider that $(a''_i)^{(2)}$ and $(b''_i)^{(2)}$, $i = 16, 17, 18$ depend only on T_{17} and respectively on (G_{19}) (and not on t) and hypothesis can be replaced by a usual Lipschitz condition.

Remark 2: There does not exist any t where $G_i(t) = 0$ and $T_i(t) = 0$ 308

From 19 to 24 it results

$$G_i(t) \geq G_i^0 e^{-\int_0^t \{ (a'_i)^{(2)} - (a''_i)^{(2)} (T_{17}(s_{(16)}), s_{(16)}) \} ds_{(16)}} \geq 0$$

$$T_i(t) \geq T_i^0 e^{-(b'_i)^{(2)}t} > 0 \quad \text{for } t > 0$$

Definition of $((\widehat{M}_{16})^{(2)})_1$, $((\widehat{M}_{16})^{(2)})_2$ and $((\widehat{M}_{16})^{(2)})_3$: 309

Remark 3: if G_{16} is bounded, the same property have also G_{17} and G_{18} . indeed if

$G_{16} < ((\widehat{M}_{16})^{(2)})$ it follows $\frac{dG_{17}}{dt} \leq ((\widehat{M}_{16})^{(2)})_1 - (a'_{17})^{(2)}G_{17}$ and by integrating

$$G_{17} \leq ((\widehat{M}_{16})^{(2)})_2 = G_{17}^0 + 2(a_{17})^{(2)}((\widehat{M}_{16})^{(2)})_1 / (a'_{17})^{(2)}$$

In the same way , one can obtain

$$G_{18} \leq ((\widehat{M}_{16})^{(2)})_3 = G_{18}^0 + 2(a_{18})^{(2)}((\widehat{M}_{16})^{(2)})_2 / (a'_{18})^{(2)} \tag{310}$$

If G_{17} or G_{18} is bounded, the same property follows for G_{16} , G_{18} and G_{16} , G_{17} respectively.

Remark 4: If G_{16} is bounded, from below, the same property holds for G_{17} and G_{18} . The proof is analogous with the preceding one. An analogous property is true if G_{17} is bounded from below. 311

Remark 5: If T_{16} is bounded from below and $\lim_{t \rightarrow \infty} ((b''_i)^{(2)}((G_{19})(t), t)) = (b'_{17})^{(2)}$ then $T_{17} \rightarrow \infty$. 312

Definition of $(m)^{(2)}$ and ε_2 :

Indeed let t_2 be so that for $t > t_2$

$$(b_{17})^{(2)} - (b''_i)^{(2)}((G_{19})(t), t) < \varepsilon_2, T_{16}(t) > (m)^{(2)}$$

Then $\frac{dT_{17}}{dt} \geq (a_{17})^{(2)}(m)^{(2)} - \varepsilon_2 T_{17}$ which leads to 313

$$T_{17} \geq \left(\frac{(a_{17})^{(2)}(m)^{(2)}}{\varepsilon_2} \right) (1 - e^{-\varepsilon_2 t}) + T_{17}^0 e^{-\varepsilon_2 t} \text{ If we take } t \text{ such that } e^{-\varepsilon_2 t} = \frac{1}{2} \text{ it results}$$

$$T_{17} \geq \left(\frac{(a_{17})^{(2)}(m)^{(2)}}{2} \right), \quad t = \log \frac{2}{\varepsilon_2} \text{ By taking now } \varepsilon_2 \text{ sufficiently small one sees that } T_{17} \text{ is unbounded. The same property holds for } T_{18} \text{ if } \lim_{t \rightarrow \infty} (b''_{18})^{(2)}((G_{19})(t), t) = (b'_{18})^{(2)} \tag{314}$$

We now state a more precise theorem about the behaviors at infinity of the solutions

315

It is now sufficient to take $\frac{(a_i)^{(3)}}{(M_{20})^{(3)}} , \frac{(b_i)^{(3)}}{(M_{20})^{(3)}} < 1$ and to choose 316

$(\widehat{P}_{20})^{(3)}$ and $(\widehat{Q}_{20})^{(3)}$ large to have

$$\frac{(a_i)^{(3)}}{(M_{20})^{(3)}} \left[(\widehat{P}_{20})^{(3)} + ((\widehat{P}_{20})^{(3)} + G_j^0) e^{-\left(\frac{(\widehat{P}_{20})^{(3)} + G_j^0}{G_j^0} \right)} \right] \leq (\widehat{P}_{20})^{(3)} \tag{317}$$

$$\frac{(b_i)^{(3)}}{(M_{20})^{(3)}} \left[((\widehat{Q}_{20})^{(3)} + T_j^0) e^{-\left(\frac{(\widehat{Q}_{20})^{(3)} + T_j^0}{T_j^0} \right)} + (\widehat{Q}_{20})^{(3)} \right] \leq (\widehat{Q}_{20})^{(3)} \tag{318}$$

In order that the operator $\mathcal{A}^{(3)}$ transforms the space of sextuples of functions G_i, T_i into itself 319

The operator $\mathcal{A}^{(3)}$ is a contraction with respect to the metric 320

$$d \left(((G_{23})^{(1)}, (T_{23})^{(1)}), ((G_{23})^{(2)}, (T_{23})^{(2)}) \right) =$$

$$\sup_i \{ \max_{t \in \mathbb{R}_+} |G_i^{(1)}(t) - G_i^{(2)}(t)| e^{-(M_{20})^{(3)}t}, \max_{t \in \mathbb{R}_+} |T_i^{(1)}(t) - T_i^{(2)}(t)| e^{-(M_{20})^{(3)}t} \}$$

Indeed if we denote 321

Definition of $\widetilde{G}_{23}, \widetilde{T}_{23} : ((\widetilde{G}_{23}), (\widetilde{T}_{23})) = \mathcal{A}^{(3)}((G_{23}), (T_{23}))$

It results 322

$$\begin{aligned}
 |\widetilde{G}_{20}^{(1)} - \widetilde{G}_i^{(2)}| &\leq \int_0^t (a_{20})^{(3)} |G_{21}^{(1)} - G_{21}^{(2)}| e^{-(\overline{M}_{20})^{(3)}s_{(20)}} e^{(\overline{M}_{20})^{(3)}s_{(20)}} ds_{(20)} + \\
 &\int_0^t \{(a'_{20})^{(3)} |G_{20}^{(1)} - G_{20}^{(2)}| e^{-(\overline{M}_{20})^{(3)}s_{(20)}} e^{-(\overline{M}_{20})^{(3)}s_{(20)}} + \\
 &(a''_{20})^{(3)} (T_{21}^{(1)}, s_{(20)}) |G_{20}^{(1)} - G_{20}^{(2)}| e^{-(\overline{M}_{20})^{(3)}s_{(20)}} e^{(\overline{M}_{20})^{(3)}s_{(20)}} + \\
 &G_{20}^{(2)} |(a''_{20})^{(3)} (T_{21}^{(1)}, s_{(20)}) - (a''_{20})^{(3)} (T_{21}^{(2)}, s_{(20)})| e^{-(\overline{M}_{20})^{(3)}s_{(20)}} e^{(\overline{M}_{20})^{(3)}s_{(20)}}\} ds_{(20)}
 \end{aligned}$$
323

Where $s_{(20)}$ represents integrand that is integrated over the interval $[0, t]$

From the hypotheses it follows

$$\begin{aligned}
 |G^{(1)} - G^{(2)}| e^{-(\overline{M}_{20})^{(3)}t} &\leq \\
 \frac{1}{(\overline{M}_{20})^{(3)}} &((a_{20})^{(3)} + (a'_{20})^{(3)} + (\widehat{A}_{20})^{(3)} + (\widehat{P}_{20})^{(3)} (\widehat{k}_{20})^{(3)}) d\left(((G_{23})^{(1)}, (T_{23})^{(1)}); (G_{23})^{(2)}, (T_{23})^{(2)} \right)
 \end{aligned}$$
324

And analogous inequalities for G_i and T_i . Taking into account the hypothesis the result follows

Remark 1: The fact that we supposed $(a''_{20})^{(3)}$ and $(b''_{20})^{(3)}$ depending also on t can be considered as not conformal with the reality, however we have put this hypothesis in order that we can postulate condition necessary to prove the uniqueness of the solution bounded by $(\widehat{P}_{20})^{(3)} e^{(\overline{M}_{20})^{(3)}t}$ and $(\widehat{Q}_{20})^{(3)} e^{(\overline{M}_{20})^{(3)}t}$ respectively of \mathbb{R}_+ . 325

If instead of proving the existence of the solution on \mathbb{R}_+ , we have to prove it only on a compact then it suffices to consider that $(a''_i)^{(3)}$ and $(b''_i)^{(3)}$, $i = 20, 21, 22$ depend only on T_{21} and respectively on (G_{23}) (and not on t) and hypothesis can be replaced by a usual Lipschitz condition.

Remark 2: There does not exist any t where $G_i(t) = 0$ and $T_i(t) = 0$ 326

From 19 to 24 it results

$$G_i(t) \geq G_i^0 e^{[-\int_0^t \{(a'_i)^{(3)} - (a''_i)^{(3)}\} (T_{21}(s_{(20)}), s_{(20)})\} ds_{(20)}]} \geq 0$$

$$T_i(t) \geq T_i^0 e^{-(b'_i)^{(3)}t} > 0 \text{ for } t > 0$$

Definition of $((\widehat{M}_{20})^{(3)})_1, ((\widehat{M}_{20})^{(3)})_2$ and $((\widehat{M}_{20})^{(3)})_3$: 327

Remark 3: if G_{20} is bounded, the same property have also G_{21} and G_{22} . indeed if

$$G_{20} < (\widehat{M}_{20})^{(3)} \text{ it follows } \frac{dG_{21}}{dt} \leq ((\widehat{M}_{20})^{(3)})_1 - (a'_{21})^{(3)} G_{21} \text{ and by integrating}$$

$$G_{21} \leq ((\widehat{M}_{20})^{(3)})_2 = G_{21}^0 + 2(a_{21})^{(3)} ((\widehat{M}_{20})^{(3)})_1 / (a'_{21})^{(3)}$$

In the same way, one can obtain

$$G_{22} \leq ((\widehat{M}_{20})^{(3)})_3 = G_{22}^0 + 2(a_{22})^{(3)} ((\widehat{M}_{20})^{(3)})_2 / (a'_{22})^{(3)}$$

If G_{21} or G_{22} is bounded, the same property follows for G_{20} , G_{22} and G_{20} , G_{21} respectively.

Remark 4: If G_{20} is bounded, from below, the same property holds for G_{21} and G_{22} . The proof is analogous with the preceding one. An analogous property is true if G_{21} is bounded from below. 328

Remark 5: If T_{20} is bounded from below and $\lim_{t \rightarrow \infty} ((b''_i)^{(3)} ((G_{23})(t), t)) = (b'_{21})^{(3)}$ then $T_{21} \rightarrow \infty$. 329

Definition of $(m)^{(3)}$ and ε_3 :

Indeed let t_3 be so that for $t > t_3$ 330

$$(b_{21})^{(3)} - (b_i'')^{(3)}((G_{23})(t), t) < \varepsilon_3, T_{20}(t) > (m)^{(3)}$$

Then $\frac{dT_{21}}{dt} \geq (a_{21})^{(3)}(m)^{(3)} - \varepsilon_3 T_{21}$ which leads to 331

$$T_{21} \geq \left(\frac{(a_{21})^{(3)}(m)^{(3)}}{\varepsilon_3} \right) (1 - e^{-\varepsilon_3 t}) + T_{21}^0 e^{-\varepsilon_3 t} \text{ If we take } t \text{ such that } e^{-\varepsilon_3 t} = \frac{1}{2} \text{ it results}$$

$T_{21} \geq \left(\frac{(a_{21})^{(3)}(m)^{(3)}}{2} \right)$, $t = \log \frac{2}{\varepsilon_3}$ By taking now ε_3 sufficiently small one sees that T_{21} is unbounded. The same property holds for T_{22} if $\lim_{t \rightarrow \infty} (b_{22}'')^{(3)}((G_{23})(t), t) = (b_{22}')^{(3)}$

We now state a more precise theorem about the behaviors at infinity of the solutions

332

It is now sufficient to take $\frac{(a_i)^{(4)}}{(\bar{M}_{24})^{(4)}}, \frac{(b_i)^{(4)}}{(\bar{M}_{24})^{(4)}} < 1$ and to choose 333

$(\hat{P}_{24})^{(4)}$ and $(\hat{Q}_{24})^{(4)}$ large to have

$$\frac{(a_i)^{(4)}}{(\bar{M}_{24})^{(4)}} \left[(\hat{P}_{24})^{(4)} + ((\hat{P}_{24})^{(4)} + G_j^0) e^{-\left(\frac{(\hat{P}_{24})^{(4)} + G_j^0}{G_j^0} \right)} \right] \leq (\hat{P}_{24})^{(4)} \quad 334$$

$$\frac{(b_i)^{(4)}}{(\bar{M}_{24})^{(4)}} \left[((\hat{Q}_{24})^{(4)} + T_j^0) e^{-\left(\frac{(\hat{Q}_{24})^{(4)} + T_j^0}{T_j^0} \right)} + (\hat{Q}_{24})^{(4)} \right] \leq (\hat{Q}_{24})^{(4)} \quad 335$$

In order that the operator $\mathcal{A}^{(4)}$ transforms the space of sextuples of functions G_i, T_i satisfying IN to itself 336

The operator $\mathcal{A}^{(4)}$ is a contraction with respect to the metric 337

$$d \left(((G_{27})^{(1)}, (T_{27})^{(1)}), ((G_{27})^{(2)}, (T_{27})^{(2)}) \right) =$$

$$\sup_i \left\{ \max_{t \in \mathbb{R}_+} |G_i^{(1)}(t) - G_i^{(2)}(t)| e^{-(\bar{M}_{24})^{(4)}t}, \max_{t \in \mathbb{R}_+} |T_i^{(1)}(t) - T_i^{(2)}(t)| e^{-(\bar{M}_{24})^{(4)}t} \right\}$$

Indeed if we denote

$$\text{Definition of } (\widetilde{G_{27}}, \widetilde{T_{27}}) : (\widetilde{G_{27}}, \widetilde{T_{27}}) = \mathcal{A}^{(4)}((G_{27}), (T_{27}))$$

It results

$$\begin{aligned} |\tilde{G}_{24}^{(1)} - \tilde{G}_i^{(2)}| &\leq \int_0^t (a_{24})^{(4)} |G_{25}^{(1)} - G_{25}^{(2)}| e^{-(\bar{M}_{24})^{(4)}s_{(24)}} e^{(\bar{M}_{24})^{(4)}s_{(24)}} ds_{(24)} + \\ &\int_0^t \{ (a_{24}')^{(4)} |G_{24}^{(1)} - G_{24}^{(2)}| e^{-(\bar{M}_{24})^{(4)}s_{(24)}} e^{-(\bar{M}_{24})^{(4)}s_{(24)}} + \\ &(a_{24}'')^{(4)}(T_{25}^{(1)}, s_{(24)}) |G_{24}^{(1)} - G_{24}^{(2)}| e^{-(\bar{M}_{24})^{(4)}s_{(24)}} e^{(\bar{M}_{24})^{(4)}s_{(24)}} + \\ &G_{24}^{(2)} |(a_{24}'')^{(4)}(T_{25}^{(1)}, s_{(24)}) - (a_{24}'')^{(4)}(T_{25}^{(2)}, s_{(24)})| e^{-(\bar{M}_{24})^{(4)}s_{(24)}} e^{(\bar{M}_{24})^{(4)}s_{(24)}} \} ds_{(24)} \end{aligned}$$

Where $s_{(24)}$ represents integrand that is integrated over the interval $[0, t]$

From the hypotheses it follows

$$|(G_{27})^{(1)} - (G_{27})^{(2)}| e^{-(\widehat{M}_{24})^{(4)}t} \leq \frac{1}{(\widehat{M}_{24})^{(4)}} ((a_{24})^{(4)} + (a'_{24})^{(4)} + (\widehat{A}_{24})^{(4)} + (\widehat{P}_{24})^{(4)}(\widehat{K}_{24})^{(4)}) d \left(((G_{27})^{(1)}, (T_{27})^{(1)}); (G_{27})^{(2)}, (T_{27})^{(2)} \right) \tag{339}$$

And analogous inequalities for G_i and T_i . Taking into account the hypothesis the result follows

Remark 1: The fact that we supposed $(a''_{24})^{(4)}$ and $(b''_{24})^{(4)}$ depending also on t can be considered as not conformal with the reality, however we have put this hypothesis, in order that we can postulate condition necessary to prove the uniqueness of the solution bounded by $(\widehat{P}_{24})^{(4)} e^{(\widehat{M}_{24})^{(4)}t}$ and $(\widehat{Q}_{24})^{(4)} e^{(\widehat{M}_{24})^{(4)}t}$ respectively of \mathbb{R}_+ . 340

If instead of proving the existence of the solution on \mathbb{R}_+ , we have to prove it only on a compact then it suffices to consider that $(a''_i)^{(4)}$ and $(b''_i)^{(4)}, i = 24, 25, 26$ depend only on T_{25} and respectively on (G_{27}) (and not on t) and hypothesis can be replaced by a usual Lipschitz condition.

Remark 2: There does not exist any t where $G_i(t) = 0$ and $T_i(t) = 0$ 341

From GLOBAL EQUATIONS it results

$$G_i(t) \geq G_i^0 e^{-\int_0^t \{(a'_i)^{(4)} - (a''_i)^{(4)}(T_{25}(s_{(24)}), s_{(24)})\} ds_{(24)}} \geq 0$$

$$T_i(t) \geq T_i^0 e^{-(b'_i)^{(4)}t} > 0 \text{ for } t > 0$$

Definition of $((\widehat{M}_{24})^{(4)})_1, ((\widehat{M}_{24})^{(4)})_2$ and $((\widehat{M}_{24})^{(4)})_3$: 342

Remark 3: if G_{24} is bounded, the same property have also G_{25} and G_{26} . indeed if

$$G_{24} < ((\widehat{M}_{24})^{(4)})_1 \text{ it follows } \frac{dG_{25}}{dt} \leq ((\widehat{M}_{24})^{(4)})_1 - (a'_{25})^{(4)}G_{25} \text{ and by integrating}$$

$$G_{25} \leq ((\widehat{M}_{24})^{(4)})_2 = G_{25}^0 + 2(a_{25})^{(4)}((\widehat{M}_{24})^{(4)})_1 / (a'_{25})^{(4)}$$

In the same way, one can obtain

$$G_{26} \leq ((\widehat{M}_{24})^{(4)})_3 = G_{26}^0 + 2(a_{26})^{(4)}((\widehat{M}_{24})^{(4)})_2 / (a'_{26})^{(4)}$$

If G_{25} or G_{26} is bounded, the same property follows for G_{24} , G_{26} and G_{24} , G_{25} respectively.

Remark 4: If G_{24} is bounded, from below, the same property holds for G_{25} and G_{26} . The proof is analogous with the preceding one. An analogous property is true if G_{25} is bounded from below. 343

Remark 5: If T_{24} is bounded from below and $\lim_{t \rightarrow \infty} ((b''_i)^{(4)}((G_{27})(t), t)) = (b'_{25})^{(4)}$ then $T_{25} \rightarrow \infty$. 344

Definition of $(m)^{(4)}$ and ε_4 :

Indeed let t_4 be so that for $t > t_4$

$$(b_{25})^{(4)} - (b''_i)^{(4)}((G_{27})(t), t) < \varepsilon_4, T_{24}(t) > (m)^{(4)}$$

Then $\frac{dT_{25}}{dt} \geq (a_{25})^{(4)}(m)^{(4)} - \varepsilon_4 T_{25}$ which leads to 345

$$T_{25} \geq \left(\frac{(a_{25})^{(4)}(m)^{(4)}}{\varepsilon_4} \right) (1 - e^{-\varepsilon_4 t}) + T_{25}^0 e^{-\varepsilon_4 t} \text{ If we take } t \text{ such that } e^{-\varepsilon_4 t} = \frac{1}{2} \text{ it results}$$

$$T_{25} \geq \left(\frac{(a_{25})^{(4)}(m)^{(4)}}{2} \right), \quad t = \log \frac{2}{\varepsilon_4} \text{ By taking now } \varepsilon_4 \text{ sufficiently small one sees that } T_{25} \text{ is unbounded. The}$$

same property holds for T_{26} if $\lim_{t \rightarrow \infty} (b''_{26})^{(4)}((G_{27})(t), t) = (b'_{26})^{(4)}$

We now state a more precise theorem about the behaviors at infinity of the solutions ANALOGOUS inequalities hold also for $G_{29}, G_{30}, T_{28}, T_{29}, T_{30}$

346

It is now sufficient to take $\frac{(a_i)^{(5)}}{(\bar{M}_{28})^{(5)}}, \frac{(b_i)^{(5)}}{(\bar{M}_{28})^{(5)}} < 1$ and to choose

347

$(\hat{P}_{28})^{(5)}$ and $(\hat{Q}_{28})^{(5)}$ large to have

$$\frac{(a_i)^{(5)}}{(\bar{M}_{28})^{(5)}} \left[(\hat{P}_{28})^{(5)} + ((\hat{P}_{28})^{(5)} + G_j^0) e^{-\left(\frac{(\hat{P}_{28})^{(5)} + G_j^0}{G_j^0}\right)} \right] \leq (\hat{P}_{28})^{(5)}$$

348

$$\frac{(b_i)^{(5)}}{(\bar{M}_{28})^{(5)}} \left[((\hat{Q}_{28})^{(5)} + T_j^0) e^{-\left(\frac{(\hat{Q}_{28})^{(5)} + T_j^0}{T_j^0}\right)} + (\hat{Q}_{28})^{(5)} \right] \leq (\hat{Q}_{28})^{(5)}$$

349

In order that the operator $\mathcal{A}^{(5)}$ transforms the space of sextuples of functions G_i, T_i into itself

350

The operator $\mathcal{A}^{(5)}$ is a contraction with respect to the metric

351

$$d\left((G_{31})^{(1)}, (T_{31})^{(1)}, (G_{31})^{(2)}, (T_{31})^{(2)} \right) =$$

$$\sup_i \left\{ \max_{t \in \mathbb{R}_+} |G_i^{(1)}(t) - G_i^{(2)}(t)| e^{-(\bar{M}_{28})^{(5)}t}, \max_{t \in \mathbb{R}_+} |T_i^{(1)}(t) - T_i^{(2)}(t)| e^{-(\bar{M}_{28})^{(5)}t} \right\}$$

Indeed if we denote

Definition of $(\widetilde{G_{31}}, \widetilde{T_{31}})$: $(\widetilde{G_{31}}, \widetilde{T_{31}}) = \mathcal{A}^{(5)}((G_{31}), (T_{31}))$

It results

$$\begin{aligned} |\tilde{G}_{28}^{(1)} - \tilde{G}_i^{(2)}| &\leq \int_0^t (a_{28})^{(5)} |G_{29}^{(1)} - G_{29}^{(2)}| e^{-(\bar{M}_{28})^{(5)}s_{(28)}} e^{(\bar{M}_{28})^{(5)}s_{(28)}} ds_{(28)} + \\ &\int_0^t \{ (a'_{28})^{(5)} |G_{28}^{(1)} - G_{28}^{(2)}| e^{-(\bar{M}_{28})^{(5)}s_{(28)}} e^{-(\bar{M}_{28})^{(5)}s_{(28)}} + \\ &(a''_{28})^{(5)} (T_{29}^{(1)}, s_{(28)}) |G_{28}^{(1)} - G_{28}^{(2)}| e^{-(\bar{M}_{28})^{(5)}s_{(28)}} e^{(\bar{M}_{28})^{(5)}s_{(28)}} + \\ &G_{28}^{(2)} | (a''_{28})^{(5)} (T_{29}^{(1)}, s_{(28)}) - (a''_{28})^{(5)} (T_{29}^{(2)}, s_{(28)}) | e^{-(\bar{M}_{28})^{(5)}s_{(28)}} e^{(\bar{M}_{28})^{(5)}s_{(28)}} \} ds_{(28)} \end{aligned}$$

Where $s_{(28)}$ represents integrand that is integrated over the interval $[0, t]$

From the hypotheses it follows

352

$$\begin{aligned} |(G_{31})^{(1)} - (G_{31})^{(2)}| e^{-(\bar{M}_{28})^{(5)}t} &\leq \\ \frac{1}{(\bar{M}_{28})^{(5)}} &\left((a_{28})^{(5)} + (a'_{28})^{(5)} + (\hat{A}_{28})^{(5)} + (\hat{P}_{28})^{(5)} (\hat{k}_{28})^{(5)} \right) d\left(((G_{31})^{(1)}, (T_{31})^{(1)}); (G_{31})^{(2)}, (T_{31})^{(2)} \right) \end{aligned}$$

353

And analogous inequalities for G_i and T_i . Taking into account the hypothesis (35,35,36) the result follows

Remark 1: The fact that we supposed $(a''_{28})^{(5)}$ and $(b''_{28})^{(5)}$ depending also on t can be considered as not conformal with the reality, however we have put this hypothesis, in order that we can postulate condition necessary to prove the uniqueness of the solution bounded by $(\widehat{P}_{28})^{(5)} e^{(\widehat{M}_{28})^{(5)}t}$ and $(\widehat{Q}_{28})^{(5)} e^{(\widehat{M}_{28})^{(5)}t}$ respectively of \mathbb{R}_+ . 354

If instead of proving the existence of the solution on \mathbb{R}_+ , we have to prove it only on a compact then it suffices to consider that $(a''_i)^{(5)}$ and $(b''_i)^{(5)}, i = 28, 29, 30$ depend only on T_{29} and respectively on (G_{31}) (and not on t) and hypothesis can be replaced by a usual Lipschitz condition.

Remark 2: There does not exist any t where $G_i(t) = 0$ and $T_i(t) = 0$ 355

From GLOBAL EQUATIONS it results

$$G_i(t) \geq G_i^0 e^{-\int_0^t \{(a'_i)^{(5)} - (a''_i)^{(5)}(T_{29}(s_{(28)}), s_{(28)})\} ds_{(28)}} \geq 0$$

$$T_i(t) \geq T_i^0 e^{-(b'_i)^{(5)}t} > 0 \text{ for } t > 0$$

Definition of $((\widehat{M}_{28})^{(5)})_1, ((\widehat{M}_{28})^{(5)})_2$ and $((\widehat{M}_{28})^{(5)})_3$: 356

Remark 3: if G_{28} is bounded, the same property have also G_{29} and G_{30} . indeed if

$$G_{28} < (\widehat{M}_{28})^{(5)} \text{ it follows } \frac{dG_{29}}{dt} \leq ((\widehat{M}_{28})^{(5)})_1 - (a'_{29})^{(5)}G_{29} \text{ and by integrating}$$

$$G_{29} \leq ((\widehat{M}_{28})^{(5)})_2 = G_{29}^0 + 2(a_{29})^{(5)}((\widehat{M}_{28})^{(5)})_1 / (a'_{29})^{(5)}$$

In the same way, one can obtain

$$G_{30} \leq ((\widehat{M}_{28})^{(5)})_3 = G_{30}^0 + 2(a_{30})^{(5)}((\widehat{M}_{28})^{(5)})_2 / (a'_{30})^{(5)}$$

If G_{29} or G_{30} is bounded, the same property follows for G_{28} , G_{30} and G_{28} , G_{29} respectively.

Remark 4: If G_{28} is bounded, from below, the same property holds for G_{29} and G_{30} . The proof is analogous with the preceding one. An analogous property is true if G_{29} is bounded from below. 357

Remark 5: If T_{28} is bounded from below and $\lim_{t \rightarrow \infty} ((b'_i)^{(5)}((G_{31})(t), t)) = (b'_{29})^{(5)}$ then $T_{29} \rightarrow \infty$. 358

Definition of $(m)^{(5)}$ and ε_5 :

Indeed let t_5 be so that for $t > t_5$

$$(b_{29})^{(5)} - (b''_i)^{(5)}((G_{31})(t), t) < \varepsilon_5, T_{28}(t) > (m)^{(5)}$$

359

Then $\frac{dT_{29}}{dt} \geq (a_{29})^{(5)}(m)^{(5)} - \varepsilon_5 T_{29}$ which leads to 360

$$T_{29} \geq \left(\frac{(a_{29})^{(5)}(m)^{(5)}}{\varepsilon_5} \right) (1 - e^{-\varepsilon_5 t}) + T_{29}^0 e^{-\varepsilon_5 t} \text{ If we take } t \text{ such that } e^{-\varepsilon_5 t} = \frac{1}{2} \text{ it results}$$

$T_{29} \geq \left(\frac{(a_{29})^{(5)}(m)^{(5)}}{2} \right), t = \log \frac{2}{\varepsilon_5}$ By taking now ε_5 sufficiently small one sees that T_{29} is unbounded. The same property holds for T_{30} if $\lim_{t \rightarrow \infty} (b''_{30})^{(5)}((G_{31})(t), t) = (b'_{30})^{(5)}$

We now state a more precise theorem about the behaviors at infinity of the solutions

Analogous inequalities hold also for $G_{33}, G_{34}, T_{32}, T_{33}, T_{34}$

361

It is now sufficient to take $\frac{(a_i)^{(6)}}{(M_{32})^{(6)}}, \frac{(b_i)^{(6)}}{(M_{32})^{(6)}} < 1$ and to choose

362

$(\hat{P}_{32})^{(6)}$ and $(\hat{Q}_{32})^{(6)}$ large to have

$$\frac{(a_i)^{(6)}}{(M_{32})^{(6)}} \left[(\hat{P}_{32})^{(6)} + ((\hat{P}_{32})^{(6)} + G_j^0) e^{-\left(\frac{(\hat{P}_{32})^{(6)} + G_j^0}{G_j^0}\right)} \right] \leq (\hat{P}_{32})^{(6)} \tag{363}$$

$$\frac{(b_i)^{(6)}}{(M_{32})^{(6)}} \left[((\hat{Q}_{32})^{(6)} + T_j^0) e^{-\left(\frac{(\hat{Q}_{32})^{(6)} + T_j^0}{T_j^0}\right)} + (\hat{Q}_{32})^{(6)} \right] \leq (\hat{Q}_{32})^{(6)} \tag{364}$$

In order that the operator $\mathcal{A}^{(6)}$ transforms the space of sextuples of functions G_i, T_i into itself 365

The operator $\mathcal{A}^{(6)}$ is a contraction with respect to the metric 366

$$d\left((G_{35})^{(1)}, (T_{35})^{(1)}, (G_{35})^{(2)}, (T_{35})^{(2)} \right) =$$

$$\sup_i \left\{ \max_{t \in \mathbb{R}_+} |G_i^{(1)}(t) - G_i^{(2)}(t)| e^{-(M_{32})^{(6)}t}, \max_{t \in \mathbb{R}_+} |T_i^{(1)}(t) - T_i^{(2)}(t)| e^{-(M_{32})^{(6)}t} \right\}$$

Indeed if we denote

Definition of $(\widehat{G_{35}}, \widehat{T_{35}})$: $(\widehat{G_{35}}, \widehat{T_{35}}) = \mathcal{A}^{(6)}((G_{35}), (T_{35}))$

It results

$$\begin{aligned} |\widehat{G}_{32}^{(1)} - \widehat{G}_{32}^{(2)}| &\leq \int_0^t (a_{32})^{(6)} |G_{33}^{(1)} - G_{33}^{(2)}| e^{-(M_{32})^{(6)}s_{(32)}} e^{(M_{32})^{(6)}s_{(32)}} ds_{(32)} + \\ &\int_0^t \{ (a'_{32})^{(6)} |G_{32}^{(1)} - G_{32}^{(2)}| e^{-(M_{32})^{(6)}s_{(32)}} e^{-(M_{32})^{(6)}s_{(32)}} + \\ &(a''_{32})^{(6)}(T_{33}^{(1)}, s_{(32)}) |G_{32}^{(1)} - G_{32}^{(2)}| e^{-(M_{32})^{(6)}s_{(32)}} e^{(M_{32})^{(6)}s_{(32)}} + \\ &G_{32}^{(2)} | (a''_{32})^{(6)}(T_{33}^{(1)}, s_{(32)}) - (a''_{32})^{(6)}(T_{33}^{(2)}, s_{(32)}) | e^{-(M_{32})^{(6)}s_{(32)}} e^{(M_{32})^{(6)}s_{(32)}} \} ds_{(32)} \end{aligned}$$

Where $s_{(32)}$ represents integrand that is integrated over the interval $[0, t]$ 367

From the hypotheses it follows

$$(1) \quad (a'_i)^{(1)}, (a''_i)^{(1)}, (b_i)^{(1)}, (b'_i)^{(1)}, (b''_i)^{(1)} > 0, \\ i, j = 13, 14, 15$$

(2) The functions $(a''_i)^{(1)}, (b''_i)^{(1)}$ are positive continuous increasing and bounded.

Definition of $(p_i)^{(1)}, (r_i)^{(1)}$:

$$(a''_i)^{(1)}(T_{14}, t) \leq (p_i)^{(1)} \leq (\hat{A}_{13})^{(1)}$$

$$(b''_i)^{(1)}(G, t) \leq (r_i)^{(1)} \leq (b'_i)^{(1)} \leq (\hat{B}_{13})^{(1)}$$

$$(3) \quad \lim_{T_2 \rightarrow \infty} (a''_i)^{(1)}(T_{14}, t) = (p_i)^{(1)} \\ \lim_{G \rightarrow \infty} (b''_i)^{(1)}(G, t) = (r_i)^{(1)}$$

Definition of $(\hat{A}_{13})^{(1)}, (\hat{B}_{13})^{(1)}$:

Where $(\hat{A}_{13})^{(1)}, (\hat{B}_{13})^{(1)}, (p_i)^{(1)}, (r_i)^{(1)}$ are positive constants
 and $i = 13, 14, 15$

They satisfy Lipschitz condition:

$$|(a_i'')^{(1)}(T'_{14}, t) - (a_i'')^{(1)}(T_{14}, t)| \leq (\hat{k}_{13})^{(1)} |T'_{14} - T_{14}| e^{-(\hat{M}_{13})^{(1)}t}$$

$$|(b_i'')^{(1)}(G', t) - (b_i'')^{(1)}(G, T)| < (\hat{k}_{13})^{(1)} ||G - G'| e^{-(\hat{M}_{13})^{(1)}t}$$

With the Lipschitz condition, we place a restriction on the behavior of functions $(a_i'')^{(1)}(T'_{14}, t)$ and $(a_i'')^{(1)}(T_{14}, t)$. (T'_{14}, t) and (T_{14}, t) are points belonging to the interval $[(\hat{k}_{13})^{(1)}, (\hat{M}_{13})^{(1)}]$. It is to be noted that $(a_i'')^{(1)}(T_{14}, t)$ is uniformly continuous. In the eventuality of the fact, that if $(\hat{M}_{13})^{(1)} = 1$ then the function $(a_i'')^{(1)}(T_{14}, t)$, the **first augmentation coefficient** attributable to terrestrial organisms, would be absolutely continuous.

Definition of $(\hat{M}_{13})^{(1)}, (\hat{k}_{13})^{(1)}$:

(Z) $(\hat{M}_{13})^{(1)}, (\hat{k}_{13})^{(1)}$, are positive constants

$$\frac{(a_i)^{(1)}}{(\hat{M}_{13})^{(1)}} , \frac{(b_i)^{(1)}}{(\hat{M}_{13})^{(1)}} < 1$$

Definition of $(\hat{P}_{13})^{(1)}, (\hat{Q}_{13})^{(1)}$:

(AA) There exists two constants $(\hat{P}_{13})^{(1)}$ and $(\hat{Q}_{13})^{(1)}$ which together with $(\hat{M}_{13})^{(1)}, (\hat{k}_{13})^{(1)}, (\hat{A}_{13})^{(1)}$ and $(\hat{B}_{13})^{(1)}$ and the constants $(a_i)^{(1)}, (a_i')^{(1)}, (b_i)^{(1)}, (b_i')^{(1)}, (p_i)^{(1)}, (r_i)^{(1)}, i = 13, 14, 15$, satisfy the inequalities

$$\frac{1}{(\hat{M}_{13})^{(1)}} [(a_i)^{(1)} + (a_i')^{(1)} + (\hat{A}_{13})^{(1)} + (\hat{P}_{13})^{(1)} (\hat{k}_{13})^{(1)}] < 1$$

$$\frac{1}{(\hat{M}_{13})^{(1)}} [(b_i)^{(1)} + (b_i')^{(1)} + (\hat{B}_{13})^{(1)} + (\hat{Q}_{13})^{(1)} (\hat{k}_{13})^{(1)}] < 1$$

Analogous inequalities hold also for $G_{37}, G_{38}, T_{36}, T_{37}, T_{38}$

368

It is now sufficient to take $\frac{(a_i)^{(7)}}{(\hat{M}_{36})^{(7)}}, \frac{(b_i)^{(7)}}{(\hat{M}_{36})^{(7)}} < 7$ and to choose

$(\hat{P}_{36})^{(7)}$ and $(\hat{Q}_{36})^{(7)}$ large to have

$$\frac{(a_i)^{(7)}}{(\hat{M}_{36})^{(7)}} \left[(\hat{P}_{36})^{(7)} + ((\hat{P}_{36})^{(7)} + G_j^0) e^{-\left(\frac{(\hat{P}_{36})^{(7)} + G_j^0}{G_j^0}\right)} \right] \leq (\hat{P}_{36})^{(7)}$$

369

$$\frac{(b_i)^{(7)}}{(\hat{M}_{36})^{(7)}} \left[((\hat{Q}_{36})^{(7)} + T_j^0) e^{-\left(\frac{(\hat{Q}_{36})^{(7)} + T_j^0}{T_j^0}\right)} + (\hat{Q}_{36})^{(7)} \right] \leq (\hat{Q}_{36})^{(7)}$$

370

371

The operator $\mathcal{A}^{(7)}$ is a contraction with respect to the metric

372

$$d\left(\left((G_{39})^{(1)}, (T_{39})^{(1)}\right), \left((G_{39})^{(2)}, (T_{39})^{(2)}\right)\right) = \sup_i \left\{ \max_{t \in \mathbb{R}_+} |G_i^{(1)}(t) - G_i^{(2)}(t)| e^{-(M_{36})^{(7)}t}, \max_{t \in \mathbb{R}_+} |T_i^{(1)}(t) - T_i^{(2)}(t)| e^{-(M_{36})^{(7)}t} \right\}$$

Indeed if we denote

Definition of $(\widehat{G_{39}}), (\widehat{T_{39}})$:

$$((\widehat{G_{39}}), (\widehat{T_{39}})) = \mathcal{A}^{(7)}((G_{39}), (T_{39}))$$

It results

$$\begin{aligned} |\widehat{G}_{36}^{(1)} - \widehat{G}_{36}^{(2)}| &\leq \int_0^t (a_{36})^{(7)} |G_{37}^{(1)} - G_{37}^{(2)}| e^{-(M_{36})^{(7)}s_{(36)}} e^{(M_{36})^{(7)}s_{(36)}} ds_{(36)} + \\ &\int_0^t \{(a'_{36})^{(7)} |G_{36}^{(1)} - G_{36}^{(2)}| e^{-(M_{36})^{(7)}s_{(36)}} e^{-(M_{36})^{(7)}s_{(36)}} + \\ &(a''_{36})^{(7)} (T_{37}^{(1)}, s_{(36)}) |G_{36}^{(1)} - G_{36}^{(2)}| e^{-(M_{36})^{(7)}s_{(36)}} e^{(M_{36})^{(7)}s_{(36)}} + \\ &G_{36}^{(2)} |(a''_{36})^{(7)} (T_{37}^{(1)}, s_{(36)}) - (a''_{36})^{(7)} (T_{37}^{(2)}, s_{(36)})| e^{-(M_{36})^{(7)}s_{(36)}} e^{(M_{36})^{(7)}s_{(36)}}\} ds_{(36)} \end{aligned}$$

Where $s_{(36)}$ represents integrand that is integrated over the interval $[0, t]$

From the hypotheses it follows

373

$$\begin{aligned} |(G_{39})^{(1)} - (G_{39})^{(2)}| e^{-(M_{36})^{(7)}t} &\leq \\ \frac{1}{(M_{36})^{(7)}} &\left((a_{36})^{(7)} + (a'_{36})^{(7)} + (\widehat{A}_{36})^{(7)} + (\widehat{P}_{36})^{(7)} (\widehat{K}_{36})^{(7)} \right) d\left(\left((G_{39})^{(1)}, (T_{39})^{(1)}\right); \left((G_{39})^{(2)}, (T_{39})^{(2)}\right)\right) \end{aligned}$$

And analogous inequalities for G_i and T_i . Taking into account the hypothesis (37,35,36) the result follows

374

Remark 1: The fact that we supposed $(a''_{36})^{(7)}$ and $(b''_{36})^{(7)}$ depending also on t can be considered as not conformal with the reality, however we have put this hypothesis, in order that we can postulate condition necessary to prove the uniqueness of the solution bounded by $(\widehat{P}_{36})^{(7)} e^{(M_{36})^{(7)}t}$ and $(\widehat{Q}_{36})^{(7)} e^{(M_{36})^{(7)}t}$ respectively of \mathbb{R}_+ .

375

If instead of proving the existence of the solution on \mathbb{R}_+ , we have to prove it only on a compact then it suffices to consider that $(a''_i)^{(7)}$ and $(b''_i)^{(7)}$, $i = 36, 37, 38$ depend only on T_{37} and respectively on (G_{39}) (and not on t) and hypothesis can be replaced by a usual Lipschitz condition.

Remark 2: There does not exist any t where $G_i(t) = 0$ and $T_i(t) = 0$

376

From 79 to 36 it results

$$\begin{aligned} G_i(t) &\geq G_i^0 e^{-\int_0^t \{(a'_i)^{(7)} - (a''_i)^{(7)}(T_{37}(s_{(36)}), s_{(36)})\} ds_{(36)}} \geq 0 \\ T_i(t) &\geq T_i^0 e^{-(b'_i)^{(7)}t} > 0 \quad \text{for } t > 0 \end{aligned}$$

Definition of $((\widehat{M}_{36})^{(7)})_1, ((\widehat{M}_{36})^{(7)})_2$ and $((\widehat{M}_{36})^{(7)})_3$:

377

Remark 3: if G_{36} is bounded, the same property have also G_{37} and G_{38} . indeed if

$G_{36} < (\widehat{M}_{36})^{(7)}$ it follows $\frac{dG_{37}}{dt} \leq ((\widehat{M}_{36})^{(7)})_1 - (a'_{37})^{(7)} G_{37}$ and by integrating

$$G_{37} \leq ((\widehat{M}_{36})^{(7)})_2 = G_{37}^0 + 2(a_{37})^{(7)} ((\widehat{M}_{36})^{(7)})_1 / (a'_{37})^{(7)}$$

In the same way, one can obtain

$$G_{38} \leq ((\overline{M}_{36})^{(7)})_3 = G_{38}^0 + 2(a_{38})^{(7)}((\overline{M}_{36})^{(7)})_2 / (a'_{38})^{(7)}$$

If G_{37} or G_{38} is bounded, the same property follows for G_{36} , G_{38} and G_{36} , G_{37} respectively.

Remark 7: If G_{36} is bounded, from below, the same property holds for G_{37} and G_{38} . The proof is analogous with the preceding one. An analogous property is true if G_{37} is bounded from below. 378

Remark 5: If T_{36} is bounded from below and $\lim_{t \rightarrow \infty} ((b''_i)^{(7)}((G_{39})(t), t)) = (b'_{37})^{(7)}$ then $T_{37} \rightarrow \infty$. 379

Definition of $(m)^{(7)}$ and ε_7 :

Indeed let t_7 be so that for $t > t_7$

$$(b_{37})^{(7)} - (b''_i)^{(7)}((G_{39})(t), t) < \varepsilon_7, T_{36}(t) > (m)^{(7)}$$

Then $\frac{dT_{37}}{dt} \geq (a_{37})^{(7)}(m)^{(7)} - \varepsilon_7 T_{37}$ which leads to 380

$$T_{37} \geq \left(\frac{(a_{37})^{(7)}(m)^{(7)}}{\varepsilon_7} \right) (1 - e^{-\varepsilon_7 t}) + T_{37}^0 e^{-\varepsilon_7 t} \text{ If we take } t \text{ such that } e^{-\varepsilon_7 t} = \frac{1}{2} \text{ it results}$$

$T_{37} \geq \left(\frac{(a_{37})^{(7)}(m)^{(7)}}{2} \right)$, $t = \log \frac{2}{\varepsilon_7}$ By taking now ε_7 sufficiently small one sees that T_{37} is unbounded. The same property holds for T_{38} if $\lim_{t \rightarrow \infty} (b''_{38})^{(7)}((G_{39})(t), t) = (b'_{38})^{(7)}$

We now state a more precise theorem about the behaviors at infinity of the solutions of equations 37 to 72

In order that the operator $\mathcal{A}^{(7)}$ transforms the space of sextuples of functions G_i, T_i satisfying GLOBAL EQUATIONS AND ITS CONCOMITANT CONDITIONALITIES into itself 381

The operator $\mathcal{A}^{(7)}$ is a contraction with respect to the metric 383

$$d \left(((G_{39})^{(1)}, (T_{39})^{(1)}), ((G_{39})^{(2)}, (T_{39})^{(2)}) \right) = \sup_i \{ \max_{t \in \mathbb{R}_+} |G_i^{(1)}(t) - G_i^{(2)}(t)| e^{-(\overline{M}_{36})^{(7)}t}, \max_{t \in \mathbb{R}_+} |T_i^{(1)}(t) - T_i^{(2)}(t)| e^{-(\overline{M}_{36})^{(7)}t} \}$$

Indeed if we denote

Definition of $(\overline{G}_{39}), (\overline{T}_{39})$:

$$((\overline{G}_{39}), (\overline{T}_{39})) = \mathcal{A}^{(7)}((G_{39}), (T_{39}))$$

It results

$$\begin{aligned} |\overline{G}_{36}^{(1)} - \overline{G}_i^{(2)}| &\leq \int_0^t (a_{36})^{(7)} |G_{37}^{(1)} - G_{37}^{(2)}| e^{-(\overline{M}_{36})^{(7)}s_{(36)}} e^{(\overline{M}_{36})^{(7)}s_{(36)}} ds_{(36)} + \\ &\int_0^t \{ (a'_{36})^{(7)} |G_{36}^{(1)} - G_{36}^{(2)}| e^{-(\overline{M}_{36})^{(7)}s_{(36)}} e^{-(\overline{M}_{36})^{(7)}s_{(36)}} + \\ &(a''_{36})^{(7)} (T_{37}^{(1)}, s_{(36)}) |G_{36}^{(1)} - G_{36}^{(2)}| e^{-(\overline{M}_{36})^{(7)}s_{(36)}} e^{(\overline{M}_{36})^{(7)}s_{(36)}} + \\ &G_{36}^{(2)} |(a''_{36})^{(7)} (T_{37}^{(1)}, s_{(36)}) - (a''_{36})^{(7)} (T_{37}^{(2)}, s_{(36)})| e^{-(\overline{M}_{36})^{(7)}s_{(36)}} e^{(\overline{M}_{36})^{(7)}s_{(36)}} \} ds_{(36)} \end{aligned}$$

Where $s_{(36)}$ represents integrand that is integrated over the interval $[0, t]$

From the hypotheses it follows

$$\left| (G_{39})^{(1)} - (G_{39})^{(2)} \right| e^{-(\widehat{M}_{36})^{(7)}t} \leq \frac{1}{(\widehat{M}_{36})^{(7)}} \left((a_{36})^{(7)} + (a'_{36})^{(7)} + (\widehat{A}_{36})^{(7)} + (\widehat{P}_{36})^{(7)} (\widehat{k}_{36})^{(7)} \right) d \left(((G_{39})^{(1)}, (T_{39})^{(1)}); (G_{39})^{(2)}, (T_{39})^{(2)} \right)$$

And analogous inequalities for G_i and T_i . Taking into account the hypothesis the result follows

Remark 1: The fact that we supposed $(a''_{36})^{(7)}$ and $(b''_{36})^{(7)}$ depending also on t can be considered as not conformal with the reality, however we have put this hypothesis, in order that we can postulate condition necessary to prove the uniqueness of the solution bounded by $(\widehat{P}_{36})^{(7)} e^{(\widehat{M}_{36})^{(7)}t}$ and $(\widehat{Q}_{36})^{(7)} e^{(\widehat{M}_{36})^{(7)}t}$ respectively of \mathbb{R}_+ . 385

If instead of proving the existence of the solution on \mathbb{R}_+ , we have to prove it only on a compact then it suffices to consider that $(a''_i)^{(7)}$ and $(b''_i)^{(7)}, i = 36, 37, 38$ depend only on T_{37} and respectively on (G_{39}) (and not on t) and hypothesis can be replaced by a usual Lipschitz condition.

Remark 2: There does not exist any t where $G_i(t) = 0$ and $T_i(t) = 0$ 386

From CONCATENATED GLOBAL EQUATIONS it results

$$G_i(t) \geq G_i^0 e^{-\int_0^t \{(a'_i)^{(7)} - (a''_i)^{(7)}\} (T_{37}(s_{(36)}), s_{(36)}) ds_{(36)}} \geq 0$$

$$T_i(t) \geq T_i^0 e^{-(b'_i)^{(7)}t} > 0 \text{ for } t > 0$$

Definition of $((\widehat{M}_{36})^{(7)})_1, ((\widehat{M}_{36})^{(7)})_2$ and $((\widehat{M}_{36})^{(7)})_3$: 387

Remark 3: if G_{36} is bounded, the same property have also G_{37} and G_{38} . indeed if

$$G_{36} < (\widehat{M}_{36})^{(7)} \text{ it follows } \frac{dG_{37}}{dt} \leq ((\widehat{M}_{36})^{(7)})_1 - (a'_{37})^{(7)} G_{37} \text{ and by integrating}$$

$$G_{37} \leq ((\widehat{M}_{36})^{(7)})_2 = G_{37}^0 + 2(a_{37})^{(7)} ((\widehat{M}_{36})^{(7)})_1 / (a'_{37})^{(7)}$$

In the same way, one can obtain

$$G_{38} \leq ((\widehat{M}_{36})^{(7)})_3 = G_{38}^0 + 2(a_{38})^{(7)} ((\widehat{M}_{36})^{(7)})_2 / (a'_{38})^{(7)}$$

If G_{37} or G_{38} is bounded, the same property follows for G_{36}, G_{38} and G_{36}, G_{37} respectively.

Remark 7: If G_{36} is bounded, from below, the same property holds for G_{37} and G_{38} . The proof is analogous with the preceding one. An analogous property is true if G_{37} is bounded from below. 388

Remark 5: If T_{36} is bounded from below and $\lim_{t \rightarrow \infty} ((b''_i)^{(7)} ((G_{39})(t), t)) = (b'_{37})^{(7)}$ then $T_{37} \rightarrow \infty$. 389

Definition of $(m)^{(7)}$ and ε_7 :

Indeed let t_7 be so that for $t > t_7$

$$(b_{37})^{(7)} - (b''_i)^{(7)} ((G_{39})(t), t) < \varepsilon_7, T_{36}(t) > (m)^{(7)}$$

Then $\frac{dT_{37}}{dt} \geq (a_{37})^{(7)} (m)^{(7)} - \varepsilon_7 T_{37}$ which leads to 390

$$T_{37} \geq \left(\frac{(a_{37})^{(7)} (m)^{(7)}}{\varepsilon_7} \right) (1 - e^{-\varepsilon_7 t}) + T_{37}^0 e^{-\varepsilon_7 t} \text{ If we take } t \text{ such that } e^{-\varepsilon_7 t} = \frac{1}{2} \text{ it results}$$

$$T_{37} \geq \left(\frac{(a_{37})^{(7)} (m)^{(7)}}{2} \right), \quad t = \log \frac{2}{\varepsilon_7} \text{ By taking now } \varepsilon_7 \text{ sufficiently small one sees that } T_{37} \text{ is unbounded. The}$$

same property holds for T_{38} if $\lim_{t \rightarrow \infty} (b_{38}'')^{(7)}((G_{39})(t), t) = (b_{38}')^{(7)}$

We now state a more precise theorem about the behaviors at infinity of the solutions

$$-(\sigma_2)^{(2)} \leq -(a_{16}')^{(2)} + (a_{17}')^{(2)} - (a_{16}'')^{(2)}(T_{17}, t) + (a_{17}'')^{(2)}(T_{17}, t) \leq -(\sigma_1)^{(2)} \quad 391$$

$$-(\tau_2)^{(2)} \leq -(b_{16}')^{(2)} + (b_{17}')^{(2)} - (b_{16}'')^{(2)}((G_{19}), t) - (b_{17}'')^{(2)}((G_{19}), t) \leq -(\tau_1)^{(2)} \quad 392$$

Definition of $(v_1)^{(2)}, (v_2)^{(2)}, (u_1)^{(2)}, (u_2)^{(2)}$: 393

By $(v_1)^{(2)} > 0, (v_2)^{(2)} < 0$ and respectively $(u_1)^{(2)} > 0, (u_2)^{(2)} < 0$ the roots 394

(a) of the equations $(a_{17})^{(2)}(v^{(2)})^2 + (\sigma_1)^{(2)}v^{(2)} - (a_{16})^{(2)} = 0$ 395

and $(b_{14})^{(2)}(u^{(2)})^2 + (\tau_1)^{(2)}u^{(2)} - (b_{16})^{(2)} = 0$ and 396

Definition of $(\bar{v}_1)^{(2)}, (\bar{v}_2)^{(2)}, (\bar{u}_1)^{(2)}, (\bar{u}_2)^{(2)}$: 397

By $(\bar{v}_1)^{(2)} > 0, (\bar{v}_2)^{(2)} < 0$ and respectively $(\bar{u}_1)^{(2)} > 0, (\bar{u}_2)^{(2)} < 0$ the 398

roots of the equations $(a_{17})^{(2)}(v^{(2)})^2 + (\sigma_2)^{(2)}v^{(2)} - (a_{16})^{(2)} = 0$ 399

and $(b_{17})^{(2)}(u^{(2)})^2 + (\tau_2)^{(2)}u^{(2)} - (b_{16})^{(2)} = 0$ 400

Definition of $(m_1)^{(2)}, (m_2)^{(2)}, (\mu_1)^{(2)}, (\mu_2)^{(2)}$:- 401

(b) If we define $(m_1)^{(2)}, (m_2)^{(2)}, (\mu_1)^{(2)}, (\mu_2)^{(2)}$ by 402

$$(m_2)^{(2)} = (v_0)^{(2)}, (m_1)^{(2)} = (v_1)^{(2)}, \text{ if } (v_0)^{(2)} < (v_1)^{(2)} \quad 403$$

$$(m_2)^{(2)} = (v_1)^{(2)}, (m_1)^{(2)} = (\bar{v}_1)^{(2)}, \text{ if } (v_1)^{(2)} < (v_0)^{(2)} < (\bar{v}_1)^{(2)}, \quad 404$$

and
$$(v_0)^{(2)} = \frac{G_{16}^0}{G_{17}^0}$$

$$(m_2)^{(2)} = (v_1)^{(2)}, (m_1)^{(2)} = (v_0)^{(2)}, \text{ if } (\bar{v}_1)^{(2)} < (v_0)^{(2)} \quad 405$$

and analogously 406

$$(\mu_2)^{(2)} = (u_0)^{(2)}, (\mu_1)^{(2)} = (u_1)^{(2)}, \text{ if } (u_0)^{(2)} < (u_1)^{(2)}$$

$$(\mu_2)^{(2)} = (u_1)^{(2)}, (\mu_1)^{(2)} = (\bar{u}_1)^{(2)}, \text{ if } (u_1)^{(2)} < (u_0)^{(2)} < (\bar{u}_1)^{(2)},$$

and
$$(u_0)^{(2)} = \frac{T_{16}^0}{T_{17}^0}$$

$$(\mu_2)^{(2)} = (u_1)^{(2)}, (\mu_1)^{(2)} = (u_0)^{(2)}, \text{ if } (\bar{u}_1)^{(2)} < (u_0)^{(2)} \quad 407$$

Then the solution satisfies the inequalities 408

$$G_{16}^0 e^{((S_1)^{(2)} - (p_{16})^{(2)})t} \leq G_{16}(t) \leq G_{16}^0 e^{(S_1)^{(2)}t}$$

$(p_i)^{(2)}$ is defined 409

$$\frac{1}{(m_1)^{(2)}} G_{16}^0 e^{((S_1)^{(2)} - (p_{16})^{(2)})t} \leq G_{17}(t) \leq \frac{1}{(m_2)^{(2)}} G_{16}^0 e^{(S_1)^{(2)}t} \quad 410$$

$$\left(\frac{(a_{18})^{(2)} G_{16}^0}{(m_1)^{(2)} ((S_1)^{(2)} - (p_{16})^{(2)} - (S_2)^{(2)})} \right) \left[e^{((S_1)^{(2)} - (p_{16})^{(2)})t} - e^{-(S_2)^{(2)}t} \right] + G_{18}^0 e^{-(S_2)^{(2)}t} \leq G_{18}(t) \leq \quad 411$$

$$\frac{(a_{18})^{(2)}G_{16}^0}{(m_2)^{(2)}((S_1)^{(2)}-(a'_{18})^{(2)})} [e^{(S_1)^{(2)}t} - e^{-(a'_{18})^{(2)}t}] + G_{18}^0 e^{-(a'_{18})^{(2)}t}$$

$$\boxed{T_{16}^0 e^{(R_1)^{(2)}t} \leq T_{16}(t) \leq T_{16}^0 e^{((R_1)^{(2)}+(r_{16})^{(2)})t}} \quad 412$$

$$\frac{1}{(\mu_1)^{(2)}} T_{16}^0 e^{(R_1)^{(2)}t} \leq T_{16}(t) \leq \frac{1}{(\mu_2)^{(2)}} T_{16}^0 e^{((R_1)^{(2)}+(r_{16})^{(2)})t} \quad 413$$

$$\frac{(b_{18})^{(2)}T_{16}^0}{(\mu_1)^{(2)}((R_1)^{(2)}-(b'_{18})^{(2)})} [e^{(R_1)^{(2)}t} - e^{-(b'_{18})^{(2)}t}] + T_{18}^0 e^{-(b'_{18})^{(2)}t} \leq T_{18}(t) \leq \quad 414$$

$$\frac{(a_{18})^{(2)}T_{16}^0}{(\mu_2)^{(2)}((R_1)^{(2)}+(r_{16})^{(2)}+(R_2)^{(2)})} [e^{((R_1)^{(2)}+(r_{16})^{(2)})t} - e^{-(R_2)^{(2)}t}] + T_{18}^0 e^{-(R_2)^{(2)}t}$$

Definition of $(S_1)^{(2)}, (S_2)^{(2)}, (R_1)^{(2)}, (R_2)^{(2)}$:- 415

Where $(S_1)^{(2)} = (a_{16})^{(2)}(m_2)^{(2)} - (a'_{16})^{(2)}$ 416

$$(S_2)^{(2)} = (a_{18})^{(2)} - (p_{18})^{(2)}$$

$$(R_1)^{(2)} = (b_{16})^{(2)}(\mu_2)^{(1)} - (b'_{16})^{(2)} \quad 417$$

$$(R_2)^{(2)} = (b'_{18})^{(2)} - (r_{18})^{(2)}$$

418

Behavior of the solutions 419

If we denote and define

Definition of $(\sigma_1)^{(3)}, (\sigma_2)^{(3)}, (\tau_1)^{(3)}, (\tau_2)^{(3)}$:

(a) $(\sigma_1)^{(3)}, (\sigma_2)^{(3)}, (\tau_1)^{(3)}, (\tau_2)^{(3)}$ four constants satisfying

$$-(\sigma_2)^{(3)} \leq -(a'_{20})^{(3)} + (a'_{21})^{(3)} - (a''_{20})^{(3)}(T_{21}, t) + (a''_{21})^{(3)}(T_{21}, t) \leq -(\sigma_1)^{(3)}$$

$$-(\tau_2)^{(3)} \leq -(b'_{20})^{(3)} + (b'_{21})^{(3)} - (b''_{20})^{(3)}(G, t) - (b''_{21})^{(3)}((G_{23}), t) \leq -(\tau_1)^{(3)}$$

Definition of $(v_1)^{(3)}, (v_2)^{(3)}, (u_1)^{(3)}, (u_2)^{(3)}$: 420

(b) By $(v_1)^{(3)} > 0, (v_2)^{(3)} < 0$ and respectively $(u_1)^{(3)} > 0, (u_2)^{(3)} < 0$ the roots of the equations
 $(a_{21})^{(3)}(v^{(3)})^2 + (\sigma_1)^{(3)}v^{(3)} - (a_{20})^{(3)} = 0$

and $(b_{21})^{(3)}(u^{(3)})^2 + (\tau_1)^{(3)}u^{(3)} - (b_{20})^{(3)} = 0$ and

By $(\bar{v}_1)^{(3)} > 0, (\bar{v}_2)^{(3)} < 0$ and respectively $(\bar{u}_1)^{(3)} > 0, (\bar{u}_2)^{(3)} < 0$ the

roots of the equations $(a_{21})^{(3)}(v^{(3)})^2 + (\sigma_2)^{(3)}v^{(3)} - (a_{20})^{(3)} = 0$

and $(b_{21})^{(3)}(u^{(3)})^2 + (\tau_2)^{(3)}u^{(3)} - (b_{20})^{(3)} = 0$

Definition of $(m_1)^{(3)}, (m_2)^{(3)}, (\mu_1)^{(3)}, (\mu_2)^{(3)}$:- 421

(c) If we define $(m_1)^{(3)}, (m_2)^{(3)}, (\mu_1)^{(3)}, (\mu_2)^{(3)}$ by

$$(m_2)^{(3)} = (v_0)^{(3)}, (m_1)^{(3)} = (v_1)^{(3)}, \text{ if } (v_0)^{(3)} < (v_1)^{(3)}$$

$$(m_2)^{(3)} = (v_1)^{(3)}, (m_1)^{(3)} = (\bar{v}_1)^{(3)}, \text{ if } (v_1)^{(3)} < (v_0)^{(3)} < (\bar{v}_1)^{(3)},$$

and $\boxed{(v_0)^{(3)} = \frac{G_{20}^0}{G_{21}^0}}$

$$(m_2)^{(3)} = (v_1)^{(3)}, (m_1)^{(3)} = (v_0)^{(3)}, \text{ if } (\bar{v}_1)^{(3)} < (v_0)^{(3)}$$

and analogously

422

$$(\mu_2)^{(3)} = (u_0)^{(3)}, (\mu_1)^{(3)} = (u_1)^{(3)}, \text{ if } (u_0)^{(3)} < (u_1)^{(3)}$$

$$(\mu_2)^{(3)} = (u_1)^{(3)}, (\mu_1)^{(3)} = (\bar{u}_1)^{(3)}, \text{ if } (u_1)^{(3)} < (u_0)^{(3)} < (\bar{u}_1)^{(3)}, \text{ and } (u_0)^{(3)} = \frac{T_{20}^0}{T_{21}^0}$$

$$(\mu_2)^{(3)} = (u_1)^{(3)}, (\mu_1)^{(3)} = (u_0)^{(3)}, \text{ if } (\bar{u}_1)^{(3)} < (u_0)^{(3)}$$

Then the solution satisfies the inequalities

$$G_{20}^0 e^{((S_1)^{(3)} - (p_{20})^{(3)})t} \leq G_{20}(t) \leq G_{20}^0 e^{(S_1)^{(3)}t}$$

$(p_i)^{(3)}$ is defined

423

$$\frac{1}{(m_1)^{(3)}} G_{20}^0 e^{((S_1)^{(3)} - (p_{20})^{(3)})t} \leq G_{21}(t) \leq \frac{1}{(m_2)^{(3)}} G_{20}^0 e^{(S_1)^{(3)}t}$$

424

$$\left(\frac{(a_{22})^{(3)} G_{20}^0}{(m_1)^{(3)} ((S_1)^{(3)} - (p_{20})^{(3)} - (S_2)^{(3)})} \left[e^{((S_1)^{(3)} - (p_{20})^{(3)})t} - e^{-(S_2)^{(3)}t} \right] + G_{22}^0 e^{-(S_2)^{(3)}t} \right) \leq G_{22}(t) \leq \frac{(a_{22})^{(3)} G_{20}^0}{(m_2)^{(3)} ((S_1)^{(3)} - (a_{22})^{(3)})} \left[e^{(S_1)^{(3)}t} - e^{-(a_{22}')^{(3)}t} \right] + G_{22}^0 e^{-(a_{22}')^{(3)}t}$$

425

$$\boxed{T_{20}^0 e^{(R_1)^{(3)}t} \leq T_{20}(t) \leq T_{20}^0 e^{((R_1)^{(3)} + (r_{20})^{(3)})t}}$$

426

$$\frac{1}{(\mu_1)^{(3)}} T_{20}^0 e^{(R_1)^{(3)}t} \leq T_{20}(t) \leq \frac{1}{(\mu_2)^{(3)}} T_{20}^0 e^{((R_1)^{(3)} + (r_{20})^{(3)})t}$$

427

$$\frac{(b_{22})^{(3)} T_{20}^0}{(\mu_1)^{(3)} ((R_1)^{(3)} - (b_{22})^{(3)})} \left[e^{(R_1)^{(3)}t} - e^{-(b_{22}')^{(3)}t} \right] + T_{22}^0 e^{-(b_{22}')^{(3)}t} \leq T_{22}(t) \leq$$

428

$$\frac{(a_{22})^{(3)} T_{20}^0}{(\mu_2)^{(3)} ((R_1)^{(3)} + (r_{20})^{(3)} + (R_2)^{(3)})} \left[e^{((R_1)^{(3)} + (r_{20})^{(3)})t} - e^{-(R_2)^{(3)}t} \right] + T_{22}^0 e^{-(R_2)^{(3)}t}$$

Definition of $(S_1)^{(3)}, (S_2)^{(3)}, (R_1)^{(3)}, (R_2)^{(3)}$:-

429

$$\text{Where } (S_1)^{(3)} = (a_{20})^{(3)} (m_2)^{(3)} - (a_{20}')^{(3)}$$

$$(S_2)^{(3)} = (a_{22})^{(3)} - (p_{22})^{(3)}$$

$$(R_1)^{(3)} = (b_{20})^{(3)} (\mu_2)^{(3)} - (b_{20}')^{(3)}$$

$$(R_2)^{(3)} = (b_{22}')^{(3)} - (r_{22})^{(3)}$$

430

431

432

If we denote and define

Definition of $(\sigma_1)^{(4)}, (\sigma_2)^{(4)}, (\tau_1)^{(4)}, (\tau_2)^{(4)}$:

(d) $(\sigma_1)^{(4)}, (\sigma_2)^{(4)}, (\tau_1)^{(4)}, (\tau_2)^{(4)}$ four constants satisfying

$$-(\sigma_2)^{(4)} \leq -(a_{24}')^{(4)} + (a_{25}')^{(4)} - (a_{24}'')^{(4)}(T_{25}, t) + (a_{25}'')^{(4)}(T_{25}, t) \leq -(\sigma_1)^{(4)}$$

$$-(\tau_2)^{(4)} \leq -(b_{24}')^{(4)} + (b_{25}')^{(4)} - (b_{24}'')^{(4)}((G_{27}), t) - (b_{25}'')^{(4)}((G_{27}), t) \leq -(\tau_1)^{(4)}$$

Definition of $(v_1)^{(4)}, (v_2)^{(4)}, (u_1)^{(4)}, (u_2)^{(4)}, v^{(4)}, u^{(4)}$:

433

(e) By $(v_1)^{(4)} > 0, (v_2)^{(4)} < 0$ and respectively $(u_1)^{(4)} > 0, (u_2)^{(4)} < 0$ the roots of the equations

$$(a_{25})^{(4)}(v^{(4)})^2 + (\sigma_1)^{(4)}v^{(4)} - (a_{24})^{(4)} = 0$$

and $(b_{25})^{(4)}(u^{(4)})^2 + (\tau_1)^{(4)}u^{(4)} - (b_{24})^{(4)} = 0$ and

Definition of $(\bar{v}_1)^{(4)}, (\bar{v}_2)^{(4)}, (\bar{u}_1)^{(4)}, (\bar{u}_2)^{(4)}$: 434
435

By $(\bar{v}_1)^{(4)} > 0, (\bar{v}_2)^{(4)} < 0$ and respectively $(\bar{u}_1)^{(4)} > 0, (\bar{u}_2)^{(4)} < 0$ the roots of the equations $(a_{25})^{(4)}(v^{(4)})^2 + (\sigma_2)^{(4)}v^{(4)} - (a_{24})^{(4)} = 0$ and $(b_{25})^{(4)}(u^{(4)})^2 + (\tau_2)^{(4)}u^{(4)} - (b_{24})^{(4)} = 0$

Definition of $(m_1)^{(4)}, (m_2)^{(4)}, (\mu_1)^{(4)}, (\mu_2)^{(4)}, (v_0)^{(4)}$:- 436

(f) If we define $(m_1)^{(4)}, (m_2)^{(4)}, (\mu_1)^{(4)}, (\mu_2)^{(4)}$ by

$$(m_2)^{(4)} = (v_0)^{(4)}, (m_1)^{(4)} = (v_1)^{(4)}, \text{ if } (v_0)^{(4)} < (v_1)^{(4)}$$

$$(m_2)^{(4)} = (v_1)^{(4)}, (m_1)^{(4)} = (\bar{v}_1)^{(4)}, \text{ if } (v_4)^{(4)} < (v_0)^{(4)} < (\bar{v}_1)^{(4)},$$

$$\text{and } (v_0)^{(4)} = \frac{G_{24}^0}{G_{25}^0}$$

$$(m_2)^{(4)} = (v_4)^{(4)}, (m_1)^{(4)} = (v_0)^{(4)}, \text{ if } (\bar{v}_4)^{(4)} < (v_0)^{(4)}$$

and analogously 437

$$(\mu_2)^{(4)} = (u_0)^{(4)}, (\mu_1)^{(4)} = (u_1)^{(4)}, \text{ if } (u_0)^{(4)} < (u_1)^{(4)}$$

$$(\mu_2)^{(4)} = (u_1)^{(4)}, (\mu_1)^{(4)} = (\bar{u}_1)^{(4)}, \text{ if } (u_1)^{(4)} < (u_0)^{(4)} < (\bar{u}_1)^{(4)},$$

$$\text{and } (u_0)^{(4)} = \frac{T_{24}^0}{T_{25}^0}$$

$(\mu_2)^{(4)} = (u_1)^{(4)}, (\mu_1)^{(4)} = (u_0)^{(4)}, \text{ if } (\bar{u}_1)^{(4)} < (u_0)^{(4)}$ where $(u_1)^{(4)}, (\bar{u}_1)^{(4)}$ are defined respectively

Then the solution satisfies the inequalities 439

$$G_{24}^0 e^{((S_1)^{(4)} - (p_{24})^{(4)})t} \leq G_{24}(t) \leq G_{24}^0 e^{(S_1)^{(4)}t}$$

where $(p_i)^{(4)}$ is defined 440
441
442
443
444
445

$$\frac{1}{(m_1)^{(4)}} G_{24}^0 e^{((S_1)^{(4)} - (p_{24})^{(4)})t} \leq G_{25}(t) \leq \frac{1}{(m_2)^{(4)}} G_{24}^0 e^{(S_1)^{(4)}t}$$

$$\left(\frac{(a_{26})^{(4)} G_{24}^0}{(m_1)^{(4)} ((S_1)^{(4)} - (p_{24})^{(4)}) - (S_2)^{(4)}} \right) \left[e^{((S_1)^{(4)} - (p_{24})^{(4)})t} - e^{-(S_2)^{(4)}t} \right] + G_{26}^0 e^{-(S_2)^{(4)}t} \leq G_{26}(t) \leq (a_{26})^{(4)} G_{24}^0 (m_2)^{(4)} (S_1)^{(4)} - (a_{26}')^{(4)} e^{(S_1)^{(4)}t} + G_{26}^0 e^{-(a_{26}')^{(4)}t}$$

$$T_{24}^0 e^{(R_1)^{(4)}t} \leq T_{24}(t) \leq T_{24}^0 e^{((R_1)^{(4)} + (r_{24})^{(4)})t}$$

$$\frac{1}{(\mu_1)^{(4)}} T_{24}^0 e^{(R_1)^{(4)}t} \leq T_{24}(t) \leq \frac{1}{(\mu_2)^{(4)}} T_{24}^0 e^{((R_1)^{(4)} + (r_{24})^{(4)})t}$$

$$\frac{(b_{26})^{(4)} T_{24}^0}{(\mu_1)^{(4)} ((R_1)^{(4)} - (b_{26}')^{(4)})} \left[e^{(R_1)^{(4)}t} - e^{-(b_{26}')^{(4)}t} \right] + T_{26}^0 e^{-(b_{26}')^{(4)}t} \leq T_{26}(t) \leq$$

$$\frac{(a_{26})^{(4)} T_{24}^0}{(\mu_2)^{(4)} ((R_1)^{(4)} + (r_{24})^{(4)} + (R_2)^{(4)})} \left[e^{((R_1)^{(4)} + (r_{24})^{(4)})t} - e^{-(R_2)^{(4)}t} \right] + T_{26}^0 e^{-(R_2)^{(4)}t}$$

Definition of $(S_1)^{(4)}, (S_2)^{(4)}, (R_1)^{(4)}, (R_2)^{(4)}$:- 452

$$\text{Where } (S_1)^{(4)} = (a_{24})^{(4)}(m_2)^{(4)} - (a'_{24})^{(4)}$$

$$(S_2)^{(4)} = (a_{26})^{(4)} - (p_{26})^{(4)}$$

$$(R_1)^{(4)} = (b_{24})^{(4)}(\mu_2)^{(4)} - (b'_{24})^{(4)}$$

$$(R_2)^{(4)} = (b'_{26})^{(4)} - (r_{26})^{(4)} \quad 453$$

Behavior of the solutions 454

If we denote and define

Definition of $(\sigma_1)^{(5)}, (\sigma_2)^{(5)}, (\tau_1)^{(5)}, (\tau_2)^{(5)}$:

(g) $(\sigma_1)^{(5)}, (\sigma_2)^{(5)}, (\tau_1)^{(5)}, (\tau_2)^{(5)}$ four constants satisfying

$$-(\sigma_2)^{(5)} \leq -(a'_{28})^{(5)} + (a'_{29})^{(5)} - (a''_{28})^{(5)}(T_{29}, t) + (a''_{29})^{(5)}(T_{29}, t) \leq -(\sigma_1)^{(5)}$$

$$-(\tau_2)^{(5)} \leq -(b'_{28})^{(5)} + (b'_{29})^{(5)} - (b''_{28})^{(5)}((G_{31}), t) - (b''_{29})^{(5)}((G_{31}), t) \leq -(\tau_1)^{(5)}$$

Definition of $(v_1)^{(5)}, (v_2)^{(5)}, (u_1)^{(5)}, (u_2)^{(5)}, v^{(5)}, u^{(5)}$: 455

(h) By $(v_1)^{(5)} > 0, (v_2)^{(5)} < 0$ and respectively $(u_1)^{(5)} > 0, (u_2)^{(5)} < 0$ the roots of the equations

$$(a_{29})^{(5)}(v^{(5)})^2 + (\sigma_1)^{(5)}v^{(5)} - (a_{28})^{(5)} = 0$$

$$\text{and } (b_{29})^{(5)}(u^{(5)})^2 + (\tau_1)^{(5)}u^{(5)} - (b_{28})^{(5)} = 0 \text{ and}$$

Definition of $(\bar{v}_1)^{(5)}, (\bar{v}_2)^{(5)}, (\bar{u}_1)^{(5)}, (\bar{u}_2)^{(5)}$: 456

By $(\bar{v}_1)^{(5)} > 0, (\bar{v}_2)^{(5)} < 0$ and respectively $(\bar{u}_1)^{(5)} > 0, (\bar{u}_2)^{(5)} < 0$ the

roots of the equations $(a_{29})^{(5)}(v^{(5)})^2 + (\sigma_2)^{(5)}v^{(5)} - (a_{28})^{(5)} = 0$

and $(b_{29})^{(5)}(u^{(5)})^2 + (\tau_2)^{(5)}u^{(5)} - (b_{28})^{(5)} = 0$

Definition of $(m_1)^{(5)}, (m_2)^{(5)}, (\mu_1)^{(5)}, (\mu_2)^{(5)}, (v_0)^{(5)}$:-

(i) If we define $(m_1)^{(5)}, (m_2)^{(5)}, (\mu_1)^{(5)}, (\mu_2)^{(5)}$ by

$$(m_2)^{(5)} = (v_0)^{(5)}, (m_1)^{(5)} = (v_1)^{(5)}, \text{ if } (v_0)^{(5)} < (v_1)^{(5)}$$

$$(m_2)^{(5)} = (v_1)^{(5)}, (m_1)^{(5)} = (\bar{v}_1)^{(5)}, \text{ if } (v_1)^{(5)} < (v_0)^{(5)} < (\bar{v}_1)^{(5)},$$

$$\text{and } (v_0)^{(5)} = \frac{a_{28}^0}{a_{29}^0}$$

$$(m_2)^{(5)} = (v_1)^{(5)}, (m_1)^{(5)} = (v_0)^{(5)}, \text{ if } (\bar{v}_1)^{(5)} < (v_0)^{(5)}$$

and analogously 457

$$(\mu_2)^{(5)} = (u_0)^{(5)}, (\mu_1)^{(5)} = (u_1)^{(5)}, \text{ if } (u_0)^{(5)} < (u_1)^{(5)}$$

$$(\mu_2)^{(5)} = (u_1)^{(5)}, (\mu_1)^{(5)} = (\bar{u}_1)^{(5)}, \text{ if } (u_1)^{(5)} < (u_0)^{(5)} < (\bar{u}_1)^{(5)},$$

$$\text{and } (u_0)^{(5)} = \frac{T_{28}^0}{T_{29}^0}$$

$(\mu_2)^{(5)} = (u_1)^{(5)}, (\mu_1)^{(5)} = (u_0)^{(5)}, \text{ if } (\bar{u}_1)^{(5)} < (u_0)^{(5)}$ where $(u_1)^{(5)}, (\bar{u}_1)^{(5)}$ are defined respectively

Then the solution satisfies the inequalities 458

$$G_{28}^0 e^{((S_1)^{(5)} - (p_{28})^{(5)})t} \leq G_{28}(t) \leq G_{28}^0 e^{(S_1)^{(5)}t}$$

where $(p_i)^{(5)}$ is defined

$$\frac{1}{(m_5)^{(5)}} G_{28}^0 e^{((S_1)^{(5)} - (p_{28})^{(5)})t} \leq G_{29}(t) \leq \frac{1}{(m_2)^{(5)}} G_{28}^0 e^{(S_1)^{(5)}t} \quad 459$$

$$\left(\frac{(a_{30})^{(5)} G_{28}^0}{(m_1)^{(5)} ((S_1)^{(5)} - (p_{28})^{(5)} - (S_2)^{(5)})} \left[e^{((S_1)^{(5)} - (p_{28})^{(5)})t} - e^{-(S_2)^{(5)}t} \right] + G_{30}^0 e^{-(S_2)^{(5)}t} \leq G_{30}(t) \leq (a_{30})^{(5)} G_{28}^0 (m_2)^{(5)} (S_1)^{(5)} - (a_{30})^{(5)} e^{(S_1)^{(5)}t} + G_{30}^0 e^{-(a_{30})^{(5)}t} \right. \quad 460$$

$$\left. (a_{30})^{(5)} G_{28}^0 (m_2)^{(5)} (S_1)^{(5)} - (a_{30})^{(5)} e^{(S_1)^{(5)}t} + G_{30}^0 e^{-(a_{30})^{(5)}t} \right] \quad 461$$

$$\boxed{T_{28}^0 e^{(R_1)^{(5)}t} \leq T_{28}(t) \leq T_{28}^0 e^{((R_1)^{(5)} + (r_{28})^{(5)})t}} \quad 462$$

$$\frac{1}{(\mu_1)^{(5)}} T_{28}^0 e^{(R_1)^{(5)}t} \leq T_{28}(t) \leq \frac{1}{(\mu_2)^{(5)}} T_{28}^0 e^{((R_1)^{(5)} + (r_{28})^{(5)})t} \quad 463$$

$$\frac{(b_{30})^{(5)} T_{28}^0}{(\mu_1)^{(5)} ((R_1)^{(5)} - (b_{30})^{(5)})} \left[e^{(R_1)^{(5)}t} - e^{-(b_{30})^{(5)}t} \right] + T_{30}^0 e^{-(b_{30})^{(5)}t} \leq T_{30}(t) \leq \quad 464$$

$$\frac{(a_{30})^{(5)} T_{28}^0}{(\mu_2)^{(5)} ((R_1)^{(5)} + (r_{28})^{(5)} + (R_2)^{(5)})} \left[e^{((R_1)^{(5)} + (r_{28})^{(5)})t} - e^{-(R_2)^{(5)}t} \right] + T_{30}^0 e^{-(R_2)^{(5)}t}$$

Definition of $(S_1)^{(5)}, (S_2)^{(5)}, (R_1)^{(5)}, (R_2)^{(5)}$:- 465

$$\text{Where } (S_1)^{(5)} = (a_{28})^{(5)} (m_2)^{(5)} - (a'_{28})^{(5)}$$

$$(S_2)^{(5)} = (a_{30})^{(5)} - (p_{30})^{(5)}$$

$$(R_1)^{(5)} = (b_{28})^{(5)} (\mu_2)^{(5)} - (b'_{28})^{(5)}$$

$$(R_2)^{(5)} = (b'_{30})^{(5)} - (r_{30})^{(5)}$$

Behavior of the solutions 466

If we denote and define

Definition of $(\sigma_1)^{(6)}, (\sigma_2)^{(6)}, (\tau_1)^{(6)}, (\tau_2)^{(6)}$:

(j) $(\sigma_1)^{(6)}, (\sigma_2)^{(6)}, (\tau_1)^{(6)}, (\tau_2)^{(6)}$ four constants satisfying

$$-(\sigma_2)^{(6)} \leq -(a'_{32})^{(6)} + (a'_{33})^{(6)} - (a''_{32})^{(6)}(T_{33}, t) + (a''_{33})^{(6)}(T_{33}, t) \leq -(\sigma_1)^{(6)}$$

$$-(\tau_2)^{(6)} \leq -(b'_{32})^{(6)} + (b'_{33})^{(6)} - (b''_{32})^{(6)}((G_{35}), t) - (b''_{33})^{(6)}((G_{35}), t) \leq -(\tau_1)^{(6)}$$

Definition of $(v_1)^{(6)}, (v_2)^{(6)}, (u_1)^{(6)}, (u_2)^{(6)}, v^{(6)}, u^{(6)}$: 467

(k) By $(v_1)^{(6)} > 0, (v_2)^{(6)} < 0$ and respectively $(u_1)^{(6)} > 0, (u_2)^{(6)} < 0$ the roots of the equations

$$(a_{33})^{(6)} (v^{(6)})^2 + (\sigma_1)^{(6)} v^{(6)} - (a_{32})^{(6)} = 0$$

$$\text{and } (b_{33})^{(6)} (u^{(6)})^2 + (\tau_1)^{(6)} u^{(6)} - (b_{32})^{(6)} = 0 \text{ and}$$

Definition of $(\bar{v}_1)^{(6)}, (\bar{v}_2)^{(6)}, (\bar{u}_1)^{(6)}, (\bar{u}_2)^{(6)}$: 468

By $(\bar{v}_1)^{(6)} > 0, (\bar{v}_2)^{(6)} < 0$ and respectively $(\bar{u}_1)^{(6)} > 0, (\bar{u}_2)^{(6)} < 0$ the

$$\text{roots of the equations } (a_{33})^{(6)} (v^{(6)})^2 + (\sigma_2)^{(6)} v^{(6)} - (a_{32})^{(6)} = 0$$

$$\text{and } (b_{33})^{(6)} (u^{(6)})^2 + (\tau_2)^{(6)} u^{(6)} - (b_{32})^{(6)} = 0$$

Definition of $(m_1)^{(6)}, (m_2)^{(6)}, (\mu_1)^{(6)}, (\mu_2)^{(6)}, (v_0)^{(6)}$:-

(l) If we define $(m_1)^{(6)}, (m_2)^{(6)}, (\mu_1)^{(6)}, (\mu_2)^{(6)}$ by

$$(m_2)^{(6)} = (v_0)^{(6)}, (m_1)^{(6)} = (v_1)^{(6)}, \text{ if } (v_0)^{(6)} < (v_1)^{(6)}$$

$$(m_2)^{(6)} = (v_1)^{(6)}, (m_1)^{(6)} = (\bar{v}_6)^{(6)}, \text{ if } (v_1)^{(6)} < (v_0)^{(6)} < (\bar{v}_1)^{(6)},$$

470

$$\text{and } (v_0)^{(6)} = \frac{a_{32}^0}{a_{33}^0}$$

$$(m_2)^{(6)} = (v_1)^{(6)}, (m_1)^{(6)} = (v_0)^{(6)}, \text{ if } (\bar{v}_1)^{(6)} < (v_0)^{(6)}$$

and analogously 471

$$(\mu_2)^{(6)} = (u_0)^{(6)}, (\mu_1)^{(6)} = (u_1)^{(6)}, \text{ if } (u_0)^{(6)} < (u_1)^{(6)}$$

$$(\mu_2)^{(6)} = (u_1)^{(6)}, (\mu_1)^{(6)} = (\bar{u}_1)^{(6)}, \text{ if } (u_1)^{(6)} < (u_0)^{(6)} < (\bar{u}_1)^{(6)},$$

$$\text{and } (u_0)^{(6)} = \frac{T_{32}^0}{T_{33}^0}$$

$(\mu_2)^{(6)} = (u_1)^{(6)}, (\mu_1)^{(6)} = (u_0)^{(6)}, \text{ if } (\bar{u}_1)^{(6)} < (u_0)^{(6)}$ where $(u_1)^{(6)}, (\bar{u}_1)^{(6)}$ are defined respectively

Then the solution satisfies the inequalities 472

$$G_{32}^0 e^{((S_1)^{(6)} - (p_{32})^{(6)})t} \leq G_{32}(t) \leq G_{32}^0 e^{(S_1)^{(6)}t}$$

where $(p_i)^{(6)}$ is defined

$$\frac{1}{(m_1)^{(6)}} G_{32}^0 e^{((S_1)^{(6)} - (p_{32})^{(6)})t} \leq G_{33}(t) \leq \frac{1}{(m_2)^{(6)}} G_{32}^0 e^{(S_1)^{(6)}t}$$

473

$$\left(\frac{(a_{34})^{(6)} G_{32}^0}{(m_1)^{(6)} ((S_1)^{(6)} - (p_{32})^{(6)} - (S_2)^{(6)})} \left[e^{((S_1)^{(6)} - (p_{32})^{(6)})t} - e^{-(S_2)^{(6)}t} \right] + G_{34}^0 e^{-(S_2)^{(6)}t} \right) \leq G_{34}(t) \leq (a_{34})^{(6)} G_{32}^0 (m_2)^{(6)} (S_1)^{(6)} - (a_{34}')^{(6)} e^{(S_1)^{(6)}t} - e^{-(a_{34}')^{(6)}t} + G_{34}^0 e^{-(a_{34}')^{(6)}t}$$

474

$$T_{32}^0 e^{(R_1)^{(6)}t} \leq T_{32}(t) \leq T_{32}^0 e^{((R_1)^{(6)} + (r_{32})^{(6)})t}$$

475

$$\frac{1}{(\mu_1)^{(6)}} T_{32}^0 e^{(R_1)^{(6)}t} \leq T_{32}(t) \leq \frac{1}{(\mu_2)^{(6)}} T_{32}^0 e^{((R_1)^{(6)} + (r_{32})^{(6)})t}$$

476

$$\frac{(b_{34})^{(6)} T_{32}^0}{(\mu_1)^{(6)} ((R_1)^{(6)} - (b_{34}')^{(6)})} \left[e^{(R_1)^{(6)}t} - e^{-(b_{34}')^{(6)}t} \right] + T_{34}^0 e^{-(b_{34}')^{(6)}t} \leq T_{34}(t) \leq$$

477

$$\frac{(a_{34})^{(6)} T_{32}^0}{(\mu_2)^{(6)} ((R_1)^{(6)} + (r_{32})^{(6)} + (R_2)^{(6)})} \left[e^{((R_1)^{(6)} + (r_{32})^{(6)})t} - e^{-(R_2)^{(6)}t} \right] + T_{34}^0 e^{-(R_2)^{(6)}t}$$

Definition of $(S_1)^{(6)}, (S_2)^{(6)}, (R_1)^{(6)}, (R_2)^{(6)}$:- 478

$$\text{Where } (S_1)^{(6)} = (a_{32})^{(6)} (m_2)^{(6)} - (a_{32}')^{(6)}$$

$$(S_2)^{(6)} = (a_{34})^{(6)} - (p_{34})^{(6)}$$

$$(R_1)^{(6)} = (b_{32})^{(6)} (\mu_2)^{(6)} - (b_{32}')^{(6)}$$

$$(R_2)^{(6)} = (b_{34}')^{(6)} - (r_{34})^{(6)}$$

479

If we denote and define

Definition of $(\sigma_1)^{(7)}, (\sigma_2)^{(7)}, (\tau_1)^{(7)}, (\tau_2)^{(7)}$:

(m) $(\sigma_1)^{(7)}, (\sigma_2)^{(7)}, (\tau_1)^{(7)}, (\tau_2)^{(7)}$ four constants satisfying

$$-(\sigma_2)^{(7)} \leq -(a'_{36})^{(7)} + (a'_{37})^{(7)} - (a''_{36})^{(7)}(T_{37}, t) + (a''_{37})^{(7)}(T_{37}, t) \leq -(\sigma_1)^{(7)}$$

$$-(\tau_2)^{(7)} \leq -(b'_{36})^{(7)} + (b'_{37})^{(7)} - (b''_{36})^{(7)}((G_{39}), t) - (b''_{37})^{(7)}((G_{39}), t) \leq -(\tau_1)^{(7)}$$

Definition of $(v_1)^{(7)}, (v_2)^{(7)}, (u_1)^{(7)}, (u_2)^{(7)}, v^{(7)}, u^{(7)}$: 480

(n) By $(v_1)^{(7)} > 0, (v_2)^{(7)} < 0$ and respectively $(u_1)^{(7)} > 0, (u_2)^{(7)} < 0$ the roots of the equations

$$(a_{37})^{(7)}(v^{(7)})^2 + (\sigma_1)^{(7)}v^{(7)} - (a_{36})^{(7)} = 0 \quad 481$$

$$\text{and } (b_{37})^{(7)}(u^{(7)})^2 + (\tau_1)^{(7)}u^{(7)} - (b_{36})^{(7)} = 0 \text{ and}$$

Definition of $(\bar{v}_1)^{(7)}, (\bar{v}_2)^{(7)}, (\bar{u}_1)^{(7)}, (\bar{u}_2)^{(7)}$: 482

By $(\bar{v}_1)^{(7)} > 0, (\bar{v}_2)^{(7)} < 0$ and respectively $(\bar{u}_1)^{(7)} > 0, (\bar{u}_2)^{(7)} < 0$ the

$$\text{roots of the equations } (a_{37})^{(7)}(v^{(7)})^2 + (\sigma_2)^{(7)}v^{(7)} - (a_{36})^{(7)} = 0$$

$$\text{and } (b_{37})^{(7)}(u^{(7)})^2 + (\tau_2)^{(7)}u^{(7)} - (b_{36})^{(7)} = 0$$

Definition of $(m_1)^{(7)}, (m_2)^{(7)}, (\mu_1)^{(7)}, (\mu_2)^{(7)}, (v_0)^{(7)}$:-

(o) If we define $(m_1)^{(7)}, (m_2)^{(7)}, (\mu_1)^{(7)}, (\mu_2)^{(7)}$ by

$$(m_2)^{(7)} = (v_0)^{(7)}, (m_1)^{(7)} = (v_1)^{(7)}, \text{ if } (v_0)^{(7)} < (v_1)^{(7)}$$

$$(m_2)^{(7)} = (v_1)^{(7)}, (m_1)^{(7)} = (\bar{v}_1)^{(7)}, \text{ if } (v_1)^{(7)} < (v_0)^{(7)} < (\bar{v}_1)^{(7)},$$

$$\text{and } \boxed{(v_0)^{(7)} = \frac{G_{36}^0}{G_{37}^0}}$$

$$(m_2)^{(7)} = (v_1)^{(7)}, (m_1)^{(7)} = (v_0)^{(7)}, \text{ if } (\bar{v}_1)^{(7)} < (v_0)^{(7)}$$

and analogously 483

$$(\mu_2)^{(7)} = (u_0)^{(7)}, (\mu_1)^{(7)} = (u_1)^{(7)}, \text{ if } (u_0)^{(7)} < (u_1)^{(7)}$$

$$(\mu_2)^{(7)} = (u_1)^{(7)}, (\mu_1)^{(7)} = (\bar{u}_1)^{(7)}, \text{ if } (u_1)^{(7)} < (u_0)^{(7)} < (\bar{u}_1)^{(7)},$$

$$\text{and } \boxed{(u_0)^{(7)} = \frac{T_{36}^0}{T_{37}^0}}$$

$$(\mu_2)^{(7)} = (u_1)^{(7)}, (\mu_1)^{(7)} = (u_0)^{(7)}, \text{ if } (\bar{u}_1)^{(7)} < (u_0)^{(7)} \text{ where } (u_1)^{(7)}, (\bar{u}_1)^{(7)}$$

are defined respectively

Then the solution satisfies the inequalities 484

$$G_{36}^0 e^{((s_1)^{(7)} - (p_{36})^{(7)})t} \leq G_{36}(t) \leq G_{36}^0 e^{(s_1)^{(7)}t}$$

where $(p_i)^{(7)}$ is defined

$$\frac{1}{(m_7)^{(7)}} G_{36}^0 e^{((S_1)^{(7)} - (p_{36})^{(7)})t} \leq G_{37}(t) \leq \frac{1}{(m_2)^{(7)}} G_{36}^0 e^{(S_1)^{(7)}t}$$

(487

$$\frac{(a_{38})^{(7)} G_{36}^0}{(m_1)^{(7)}((S_1)^{(7)} - (p_{36})^{(7)} - (S_2)^{(7)})} \left[e^{((S_1)^{(7)} - (p_{36})^{(7)})t} - e^{-(S_2)^{(7)}t} \right] + G_{38}^0 e^{-(S_2)^{(7)}t} \leq G_{38}(t) \leq$$

$$\frac{(a_{38})^{(7)} G_{36}^0}{(m_2)^{(7)}((S_1)^{(7)} - (a'_{38})^{(7)})} \left[e^{(S_1)^{(7)}t} - e^{-(a'_{38})^{(7)}t} \right] + G_{38}^0 e^{-(a'_{38})^{(7)}t}$$

$$\boxed{T_{36}^0 e^{(R_1)^{(7)}t} \leq T_{36}(t) \leq T_{36}^0 e^{((R_1)^{(7)} + (r_{36})^{(7)})t}$$

$$\frac{1}{(\mu_1)^{(7)}} T_{36}^0 e^{(R_1)^{(7)}t} \leq T_{36}(t) \leq \frac{1}{(\mu_2)^{(7)}} T_{36}^0 e^{((R_1)^{(7)} + (r_{36})^{(7)})t}$$

$$\frac{(b_{38})^{(7)} T_{36}^0}{(\mu_1)^{(7)}((R_1)^{(7)} - (b_{38})^{(7)})} \left[e^{(R_1)^{(7)}t} - e^{-(b'_{38})^{(7)}t} \right] + T_{38}^0 e^{-(b'_{38})^{(7)}t} \leq T_{38}(t) \leq$$

$$\frac{(a_{38})^{(7)} T_{36}^0}{(\mu_2)^{(7)}((R_1)^{(7)} + (r_{36})^{(7)} + (R_2)^{(7)})} \left[e^{((R_1)^{(7)} + (r_{36})^{(7)})t} - e^{-(R_2)^{(7)}t} \right] + T_{38}^0 e^{-(R_2)^{(7)}t}$$

Definition of $(S_1)^{(7)}, (S_2)^{(7)}, (R_1)^{(7)}, (R_2)^{(7)}$:- 491

Where $(S_1)^{(7)} = (a_{36})^{(7)}(m_2)^{(7)} - (a'_{36})^{(7)}$
 $(S_2)^{(7)} = (a_{38})^{(7)} - (p_{38})^{(7)}$
 $(R_1)^{(7)} = (b_{36})^{(7)}(\mu_2)^{(7)} - (b'_{36})^{(7)}$
 $(R_2)^{(7)} = (b'_{38})^{(7)} - (r_{38})^{(7)}$

From GLOBAL EQUATIONS we obtain 492

$$\frac{dv^{(7)}}{dt} = (a_{36})^{(7)} - \left((a'_{36})^{(7)} - (a'_{37})^{(7)} + (a''_{36})^{(7)}(T_{37}, t) \right) -$$

$$(a''_{37})^{(7)}(T_{37}, t)v^{(7)} - (a_{37})^{(7)}v^{(7)}$$

Definition of $v^{(7)}$:- $\boxed{v^{(7)} = \frac{G_{36}}{G_{37}}}$

It follows

$$- \left((a_{37})^{(7)}(v^{(7)})^2 + (\sigma_2)^{(7)}v^{(7)} - (a_{36})^{(7)} \right) \leq \frac{dv^{(7)}}{dt} \leq$$

$$- \left((a_{37})^{(7)}(v^{(7)})^2 + (\sigma_1)^{(7)}v^{(7)} - (a_{36})^{(7)} \right)$$

From which one obtains

Definition of $(\bar{v}_1)^{(7)}, (v_0)^{(7)}$:-

(a) For $0 < \boxed{(v_0)^{(7)} = \frac{G_{36}^0}{G_{37}^0}} < (v_1)^{(7)} < (\bar{v}_1)^{(7)}$

$$v^{(7)}(t) \geq \frac{(v_1)^{(7)} + (C)^{(7)}(v_2)^{(7)} e^{-(a_{37})^{(7)}((v_1)^{(7)} - (v_0)^{(7)})t}}{1 + (C)^{(7)} e^{-(a_{37})^{(7)}((v_1)^{(7)} - (v_0)^{(7)})t}}, \quad \boxed{(C)^{(7)} = \frac{(v_1)^{(7)} - (v_0)^{(7)}}{(v_0)^{(7)} - (v_2)^{(7)}}$$

it follows $(v_0)^{(7)} \leq v^{(7)}(t) \leq (v_1)^{(7)}$

In the same manner, we get 493

$$v^{(7)}(t) \leq \frac{(\bar{v}_1)^{(7)} + (\bar{C})^{(7)}(\bar{v}_2)^{(7)} e^{-(a_{37})^{(7)}((\bar{v}_1)^{(7)} - (\bar{v}_2)^{(7)})t}}{1 + (\bar{C})^{(7)} e^{-(a_{37})^{(7)}((\bar{v}_1)^{(7)} - (\bar{v}_2)^{(7)})t}}, \quad \boxed{(\bar{C})^{(7)} = \frac{(\bar{v}_1)^{(7)} - (v_0)^{(7)}}{(v_0)^{(7)} - (\bar{v}_2)^{(7)}}$$

From which we deduce $(v_0)^{(7)} \leq v^{(7)}(t) \leq (\bar{v}_1)^{(7)}$

(b) If $0 < (v_1)^{(7)} < (v_0)^{(7)} = \frac{G_{36}^0}{G_{37}^0} < (\bar{v}_1)^{(7)}$ we find like in the previous case, 494

$$(v_1)^{(7)} \leq \frac{(v_1)^{(7)} + (c)^{(7)}(v_2)^{(7)} e^{[-(a_{37})^{(7)}(v_1)^{(7)} - (v_2)^{(7)}]t}}{1 + (c)^{(7)} e^{[-(a_{37})^{(7)}(v_1)^{(7)} - (v_2)^{(7)}]t}} \leq v^{(7)}(t) \leq$$

$$\frac{(\bar{v}_1)^{(7)} + (c)^{(7)}(\bar{v}_2)^{(7)} e^{[-(a_{37})^{(7)}(\bar{v}_1)^{(7)} - (\bar{v}_2)^{(7)}]t}}{1 + (c)^{(7)} e^{[-(a_{37})^{(7)}(\bar{v}_1)^{(7)} - (\bar{v}_2)^{(7)}]t}} \leq (\bar{v}_1)^{(7)}$$

(c) If $0 < (v_1)^{(7)} \leq (\bar{v}_1)^{(7)} \leq \boxed{(v_0)^{(7)} = \frac{G_{36}^0}{G_{37}^0}}$, we obtain

495

$$(v_1)^{(7)} \leq v^{(7)}(t) \leq \frac{(\bar{v}_1)^{(7)} + (c)^{(7)}(\bar{v}_2)^{(7)} e^{[-(a_{37})^{(7)}(\bar{v}_1)^{(7)} - (\bar{v}_2)^{(7)}]t}}{1 + (c)^{(7)} e^{[-(a_{37})^{(7)}(\bar{v}_1)^{(7)} - (\bar{v}_2)^{(7)}]t}} \leq (v_0)^{(7)}$$

And so with the notation of the first part of condition (c), we have

Definition of $v^{(7)}(t)$:-

$$(m_2)^{(7)} \leq v^{(7)}(t) \leq (m_1)^{(7)}, \quad \boxed{v^{(7)}(t) = \frac{G_{36}(t)}{G_{37}(t)}}$$

In a completely analogous way, we obtain

Definition of $u^{(7)}(t)$:-

$$(\mu_2)^{(7)} \leq u^{(7)}(t) \leq (\mu_1)^{(7)}, \quad \boxed{u^{(7)}(t) = \frac{T_{36}(t)}{T_{37}(t)}}$$

Now, using this result and replacing it in GLOBAL EQUATIONS we get easily the result stated in the theorem.

Particular case :

If $(a''_{36})^{(7)} = (a''_{37})^{(7)}$, then $(\sigma_1)^{(7)} = (\sigma_2)^{(7)}$ and in this case $(v_1)^{(7)} = (\bar{v}_1)^{(7)}$ if in addition $(v_0)^{(7)} = (v_1)^{(7)}$ then $v^{(7)}(t) = (v_0)^{(7)}$ and as a consequence $G_{36}(t) = (v_0)^{(7)}G_{37}(t)$ **this also defines $(v_0)^{(7)}$ for the special case .**

Analogously if $(b''_{36})^{(7)} = (b''_{37})^{(7)}$, then $(\tau_1)^{(7)} = (\tau_2)^{(7)}$ and then

$(u_1)^{(7)} = (\bar{u}_1)^{(7)}$ if in addition $(u_0)^{(7)} = (u_1)^{(7)}$ then $T_{36}(t) = (u_0)^{(7)}T_{37}(t)$ This is an important consequence of the relation between $(v_1)^{(7)}$ and $(\bar{v}_1)^{(7)}$, **and definition of $(u_0)^{(7)}$.**

We can prove the following

If $(a''_i)^{(7)}$ and $(b''_i)^{(7)}$ are independent on t , and the conditions

$$(a'_{36})^{(7)}(a'_{37})^{(7)} - (a_{36})^{(7)}(a_{37})^{(7)} < 0$$

$$(a_{36})^{(7)}(a'_{37})^{(7)} - (a_{36})^{(7)}(a_{37})^{(7)} + (a_{36})^{(7)}(p_{36})^{(7)} + (a'_{37})^{(7)}(p_{37})^{(7)} + (p_{36})^{(7)}(p_{37})^{(7)} > 0$$

$$(b'_{36})^{(7)}(b'_{37})^{(7)} - (b_{36})^{(7)}(b_{37})^{(7)} > 0,$$

$$(b'_{36})^{(7)}(b'_{37})^{(7)} - (b_{36})^{(7)}(b_{37})^{(7)} - (b'_{36})^{(7)}(r_{37})^{(7)} - (b'_{37})^{(7)}(r_{37})^{(7)} + (r_{36})^{(7)}(r_{37})^{(7)} < 0$$

with $(p_{36})^{(7)}, (r_{37})^{(7)}$ as defined are satisfied, then the system WITH THE SATISFACTION OF THE FOLLOWING PROPERTIES HAS A SOLUTION AS DERIVED BELOW.

Particular case :

If $(a''_{16})^{(2)} = (a''_{17})^{(2)}$, then $(\sigma_1)^{(2)} = (\sigma_2)^{(2)}$ and in this case $(v_1)^{(2)} = (\bar{v}_1)^{(2)}$ if in addition $(v_0)^{(2)} = (v_1)^{(2)}$ then $v^{(2)}(t) = (v_0)^{(2)}$ and as a consequence $G_{16}(t) = (v_0)^{(2)}G_{17}(t)$

Analogously if $(b''_{16})^{(2)} = (b''_{17})^{(2)}$, then $(\tau_1)^{(2)} = (\tau_2)^{(2)}$ and then

$(u_1)^{(2)} = (\bar{u}_1)^{(2)}$ if in addition $(u_0)^{(2)} = (u_1)^{(2)}$ then $T_{16}(t) = (u_0)^{(2)}T_{17}(t)$ This is an important consequence of the relation between $(v_1)^{(2)}$ and $(\bar{v}_1)^{(2)}$

From GLOBAL EQUATIONS we obtain

496
496A
496B
496C
497C
497D
497E
497F
497G

498

499

500

$$\frac{dv^{(3)}}{dt} = (a_{20})^{(3)} - \left((a'_{20})^{(3)} - (a'_{21})^{(3)} + (a''_{20})^{(3)}(T_{21}, t) \right) - (a''_{21})^{(3)}(T_{21}, t)v^{(3)} - (a_{21})^{(3)}v^{(3)}$$

Definition of $v^{(3)}$:- $v^{(3)} = \frac{G_{20}}{G_{21}}$ 501

It follows

$$- \left((a_{21})^{(3)}(v^{(3)})^2 + (\sigma_2)^{(3)}v^{(3)} - (a_{20})^{(3)} \right) \leq \frac{dv^{(3)}}{dt} \leq - \left((a_{21})^{(3)}(v^{(3)})^2 + (\sigma_1)^{(3)}v^{(3)} - (a_{20})^{(3)} \right)$$
502

From which one obtains

(a) For $0 < (v_0)^{(3)} = \frac{G_{20}^0}{G_{21}^0} < (v_1)^{(3)} < (\bar{v}_1)^{(3)}$

$$v^{(3)}(t) \geq \frac{(v_1)^{(3)} + (C)^{(3)}(v_2)^{(3)}e^{[-(a_{21})^{(3)}((v_1)^{(3)} - (v_0)^{(3)})t]}}{1 + (C)^{(3)}e^{[-(a_{21})^{(3)}((v_1)^{(3)} - (v_0)^{(3)})t]}}$$
 $(C)^{(3)} = \frac{(v_1)^{(3)} - (v_0)^{(3)}}{(v_0)^{(3)} - (v_2)^{(3)}}$

it follows $(v_0)^{(3)} \leq v^{(3)}(t) \leq (v_1)^{(3)}$

In the same manner, we get

$$v^{(3)}(t) \leq \frac{(\bar{v}_1)^{(3)} + (\bar{C})^{(3)}(\bar{v}_2)^{(3)}e^{[-(a_{21})^{(3)}((\bar{v}_1)^{(3)} - (\bar{v}_2)^{(3)})t]}}{1 + (\bar{C})^{(3)}e^{[-(a_{21})^{(3)}((\bar{v}_1)^{(3)} - (\bar{v}_2)^{(3)})t]}}$$
 $(\bar{C})^{(3)} = \frac{(\bar{v}_1)^{(3)} - (v_0)^{(3)}}{(v_0)^{(3)} - (\bar{v}_2)^{(3)}}$
503

Definition of $(\bar{v}_1)^{(3)}$:-

From which we deduce $(v_0)^{(3)} \leq v^{(3)}(t) \leq (\bar{v}_1)^{(3)}$

(b) If $0 < (v_1)^{(3)} < (v_0)^{(3)} = \frac{G_{20}^0}{G_{21}^0} < (\bar{v}_1)^{(3)}$ we find like in the previous case, 504

$$(v_1)^{(3)} \leq \frac{(v_1)^{(3)} + (C)^{(3)}(v_2)^{(3)}e^{[-(a_{21})^{(3)}((v_1)^{(3)} - (v_2)^{(3)})t]}}{1 + (C)^{(3)}e^{[-(a_{21})^{(3)}((v_1)^{(3)} - (v_2)^{(3)})t]}} \leq v^{(3)}(t) \leq \frac{(\bar{v}_1)^{(3)} + (\bar{C})^{(3)}(\bar{v}_2)^{(3)}e^{[-(a_{21})^{(3)}((\bar{v}_1)^{(3)} - (\bar{v}_2)^{(3)})t]}}{1 + (\bar{C})^{(3)}e^{[-(a_{21})^{(3)}((\bar{v}_1)^{(3)} - (\bar{v}_2)^{(3)})t]}} \leq (\bar{v}_1)^{(3)}$$

(c) If $0 < (v_1)^{(3)} \leq (\bar{v}_1)^{(3)} \leq (v_0)^{(3)} = \frac{G_{20}^0}{G_{21}^0}$, we obtain 505

$$(v_1)^{(3)} \leq v^{(3)}(t) \leq \frac{(\bar{v}_1)^{(3)} + (\bar{C})^{(3)}(\bar{v}_2)^{(3)}e^{[-(a_{21})^{(3)}((\bar{v}_1)^{(3)} - (\bar{v}_2)^{(3)})t]}}{1 + (\bar{C})^{(3)}e^{[-(a_{21})^{(3)}((\bar{v}_1)^{(3)} - (\bar{v}_2)^{(3)})t]}} \leq (v_0)^{(3)}$$

And so with the notation of the first part of condition (c), we have

Definition of $v^{(3)}(t)$:-

$$(m_2)^{(3)} \leq v^{(3)}(t) \leq (m_1)^{(3)}, \quad v^{(3)}(t) = \frac{G_{20}(t)}{G_{21}(t)}$$

In a completely analogous way, we obtain

Definition of $u^{(3)}(t)$:-

$$(\mu_2)^{(3)} \leq u^{(3)}(t) \leq (\mu_1)^{(3)}, \quad u^{(3)}(t) = \frac{T_{20}(t)}{T_{21}(t)}$$

Now, using this result and replacing it in GLOBAL EQUATIONS we get easily the result stated in the theorem.

Particular case :

If $(a''_{20})^{(3)} = (a''_{21})^{(3)}$, then $(\sigma_1)^{(3)} = (\sigma_2)^{(3)}$ and in this case $(v_1)^{(3)} = (\bar{v}_1)^{(3)}$ if in addition $(v_0)^{(3)} = (v_1)^{(3)}$ then $v^{(3)}(t) = (v_0)^{(3)}$ and as a consequence $G_{20}(t) = (v_0)^{(3)}G_{21}(t)$

Analogously if $(b''_{20})^{(3)} = (b''_{21})^{(3)}$, then $(\tau_1)^{(3)} = (\tau_2)^{(3)}$ and then

$(u_1)^{(3)} = (\bar{u}_1)^{(3)}$ if in addition $(u_0)^{(3)} = (u_1)^{(3)}$ then $T_{20}(t) = (u_0)^{(3)}T_{21}(t)$ This is an important consequence of the relation between $(v_1)^{(3)}$ and $(\bar{v}_1)^{(3)}$

: From GLOBAL EQUATIONS we obtain

$$\frac{dv^{(4)}}{dt} = (a_{24})^{(4)} - \left((a'_{24})^{(4)} - (a'_{25})^{(4)} + (a''_{24})^{(4)}(T_{25}, t) \right) - (a''_{25})^{(4)}(T_{25}, t)v^{(4)} - (a_{25})^{(4)}v^{(4)}$$

Definition of $v^{(4)}$:- $v^{(4)} = \frac{G_{24}}{G_{25}}$ 508

It follows

$$- \left((a_{25})^{(4)}(v^{(4)})^2 + (\sigma_2)^{(4)}v^{(4)} - (a_{24})^{(4)} \right) \leq \frac{dv^{(4)}}{dt} \leq - \left((a_{25})^{(4)}(v^{(4)})^2 + (\sigma_4)^{(4)}v^{(4)} - (a_{24})^{(4)} \right)$$

From which one obtains

Definition of $(\bar{v}_1)^{(4)}, (v_0)^{(4)}$:-

(d) For $0 < \boxed{(v_0)^{(4)} = \frac{G_{24}^0}{G_{25}^0}} < (v_1)^{(4)} < (\bar{v}_1)^{(4)}$

$$v^{(4)}(t) \geq \frac{(v_1)^{(4)} + (C)^{(4)}(v_2)^{(4)} e^{[-(a_{25})^{(4)}((v_1)^{(4)} - (v_0)^{(4)})t]}}{4 + (C)^{(4)} e^{[-(a_{25})^{(4)}((v_1)^{(4)} - (v_0)^{(4)})t]}} , \quad \boxed{(C)^{(4)} = \frac{(v_1)^{(4)} - (v_0)^{(4)}}{(v_0)^{(4)} - (v_2)^{(4)}}$$

it follows $(v_0)^{(4)} \leq v^{(4)}(t) \leq (v_1)^{(4)}$

In the same manner , we get

509

$$v^{(4)}(t) \leq \frac{(\bar{v}_1)^{(4)} + (\bar{C})^{(4)}(\bar{v}_2)^{(4)} e^{[-(a_{25})^{(4)}((\bar{v}_1)^{(4)} - (\bar{v}_2)^{(4)})t]}}{4 + (\bar{C})^{(4)} e^{[-(a_{25})^{(4)}((\bar{v}_1)^{(4)} - (\bar{v}_2)^{(4)})t]}} , \quad \boxed{(\bar{C})^{(4)} = \frac{(\bar{v}_1)^{(4)} - (v_0)^{(4)}}{(v_0)^{(4)} - (\bar{v}_2)^{(4)}}$$

From which we deduce $(v_0)^{(4)} \leq v^{(4)}(t) \leq (\bar{v}_1)^{(4)}$

(e) If $0 < (v_1)^{(4)} < (v_0)^{(4)} = \frac{G_{24}^0}{G_{25}^0} < (\bar{v}_1)^{(4)}$ we find like in the previous case,

510

$$(v_1)^{(4)} \leq \frac{(v_1)^{(4)} + (C)^{(4)}(v_2)^{(4)} e^{[-(a_{25})^{(4)}((v_1)^{(4)} - (v_2)^{(4)})t]}}{1 + (C)^{(4)} e^{[-(a_{25})^{(4)}((v_1)^{(4)} - (v_2)^{(4)})t]}} \leq v^{(4)}(t) \leq$$

$$\frac{(\bar{v}_1)^{(4)} + (\bar{C})^{(4)}(\bar{v}_2)^{(4)} e^{[-(a_{25})^{(4)}((\bar{v}_1)^{(4)} - (\bar{v}_2)^{(4)})t]}}{1 + (\bar{C})^{(4)} e^{[-(a_{25})^{(4)}((\bar{v}_1)^{(4)} - (\bar{v}_2)^{(4)})t]}} \leq (\bar{v}_1)^{(4)}$$

511

(f) If $0 < (v_1)^{(4)} \leq (\bar{v}_1)^{(4)} \leq \boxed{(v_0)^{(4)} = \frac{G_{24}^0}{G_{25}^0}}$, we obtain

512

$$(v_1)^{(4)} \leq v^{(4)}(t) \leq \frac{(\bar{v}_1)^{(4)} + (\bar{C})^{(4)}(\bar{v}_2)^{(4)} e^{[-(a_{25})^{(4)}((\bar{v}_1)^{(4)} - (\bar{v}_2)^{(4)})t]}}{1 + (\bar{C})^{(4)} e^{[-(a_{25})^{(4)}((\bar{v}_1)^{(4)} - (\bar{v}_2)^{(4)})t]}} \leq (v_0)^{(4)}$$

And so with the notation of the first part of condition (c) , we have

Definition of $v^{(4)}(t)$:-

$$(m_2)^{(4)} \leq v^{(4)}(t) \leq (m_1)^{(4)} , \quad \boxed{v^{(4)}(t) = \frac{G_{24}(t)}{G_{25}(t)}}$$

In a completely analogous way, we obtain

Definition of $u^{(4)}(t)$:-

$$(\mu_2)^{(4)} \leq u^{(4)}(t) \leq (\mu_1)^{(4)} , \quad \boxed{u^{(4)}(t) = \frac{T_{24}(t)}{T_{25}(t)}}$$

Now, using this result and replacing it in GLOBAL EQUATIONS we get easily the result stated in the theorem.

Particular case :

If $(a_{24}'')^{(4)} = (a_{25}'')^{(4)}$, then $(\sigma_1)^{(4)} = (\sigma_2)^{(4)}$ and in this case $(v_1)^{(4)} = (\bar{v}_1)^{(4)}$ if in addition $(v_0)^{(4)} = (v_1)^{(4)}$ then $v^{(4)}(t) = (v_0)^{(4)}$ and as a consequence $G_{24}(t) = (v_0)^{(4)}G_{25}(t)$ **this also defines $(v_0)^{(4)}$ for the special case .**

513

Analogously if $(b_{24}'')^{(4)} = (b_{25}'')^{(4)}$, then $(\tau_1)^{(4)} = (\tau_2)^{(4)}$ and then $(u_1)^{(4)} = (\bar{u}_1)^{(4)}$ if in addition $(u_0)^{(4)} = (u_1)^{(4)}$ then $T_{24}(t) = (u_0)^{(4)}T_{25}(t)$ This is an important consequence of the relation between $(v_1)^{(4)}$ and $(\bar{v}_1)^{(4)}$, **and definition of $(u_0)^{(4)}$.**

514

From GLOBAL EQUATIONS we obtain

515

$$\frac{dv^{(5)}}{dt} = (a_{28})^{(5)} - \left((a'_{28})^{(5)} - (a'_{29})^{(5)} + (a''_{28})^{(5)}(T_{29}, t) \right) - (a''_{29})^{(5)}(T_{29}, t)v^{(5)} - (a_{29})^{(5)}v^{(5)}$$

Definition of $v^{(5)}$:-
$$v^{(5)} = \frac{G_{28}}{G_{29}}$$

It follows

$$- \left((a_{29})^{(5)}(v^{(5)})^2 + (\sigma_2)^{(5)}v^{(5)} - (a_{28})^{(5)} \right) \leq \frac{dv^{(5)}}{dt} \leq - \left((a_{29})^{(5)}(v^{(5)})^2 + (\sigma_1)^{(5)}v^{(5)} - (a_{28})^{(5)} \right)$$

From which one obtains

Definition of $(\bar{v}_1)^{(5)}, (v_0)^{(5)}$:-

(g) For $0 < \boxed{(v_0)^{(5)} = \frac{G_{28}^0}{G_{29}^0}} < (v_1)^{(5)} < (\bar{v}_1)^{(5)}$

$$v^{(5)}(t) \geq \frac{(v_1)^{(5)} + (C)^{(5)}(v_2)^{(5)} e^{[-(a_{29})^{(5)}(v_1)^{(5)} - (v_0)^{(5)}]t}}{5 + (C)^{(5)} e^{[-(a_{29})^{(5)}(v_1)^{(5)} - (v_0)^{(5)}]t}}, \quad \boxed{(C)^{(5)} = \frac{(v_1)^{(5)} - (v_0)^{(5)}}{(v_0)^{(5)} - (v_2)^{(5)}}$$

it follows $(v_0)^{(5)} \leq v^{(5)}(t) \leq (v_1)^{(5)}$

In the same manner , we get

516

$$v^{(5)}(t) \leq \frac{(\bar{v}_1)^{(5)} + (\bar{C})^{(5)}(\bar{v}_2)^{(5)} e^{[-(a_{29})^{(5)}(\bar{v}_1)^{(5)} - (\bar{v}_2)^{(5)}]t}}{5 + (\bar{C})^{(5)} e^{[-(a_{29})^{(5)}(\bar{v}_1)^{(5)} - (\bar{v}_2)^{(5)}]t}}, \quad \boxed{(\bar{C})^{(5)} = \frac{(\bar{v}_1)^{(5)} - (v_0)^{(5)}}{(v_0)^{(5)} - (\bar{v}_2)^{(5)}}$$

From which we deduce $(v_0)^{(5)} \leq v^{(5)}(t) \leq (\bar{v}_5)^{(5)}$

(h) If $0 < (v_1)^{(5)} < (v_0)^{(5)} = \frac{G_{28}^0}{G_{29}^0} < (\bar{v}_1)^{(5)}$ we find like in the previous case,

517

$$(v_1)^{(5)} \leq \frac{(v_1)^{(5)} + (C)^{(5)}(v_2)^{(5)} e^{[-(a_{29})^{(5)}(v_1)^{(5)} - (v_2)^{(5)}]t}}{1 + (C)^{(5)} e^{[-(a_{29})^{(5)}(v_1)^{(5)} - (v_2)^{(5)}]t}} \leq v^{(5)}(t) \leq$$

$$\frac{(\bar{v}_1)^{(5)} + (\bar{C})^{(5)}(\bar{v}_2)^{(5)} e^{[-(a_{29})^{(5)}(\bar{v}_1)^{(5)} - (\bar{v}_2)^{(5)}]t}}{1 + (\bar{C})^{(5)} e^{[-(a_{29})^{(5)}(\bar{v}_1)^{(5)} - (\bar{v}_2)^{(5)}]t}} \leq (\bar{v}_1)^{(5)}$$

(i) If $0 < (v_1)^{(5)} \leq (\bar{v}_1)^{(5)} \leq \boxed{(v_0)^{(5)} = \frac{G_{28}^0}{G_{29}^0}}$, we obtain

518

$$(v_1)^{(5)} \leq v^{(5)}(t) \leq \frac{(\bar{v}_1)^{(5)} + (\bar{C})^{(5)}(\bar{v}_2)^{(5)} e^{[-(a_{29})^{(5)}(\bar{v}_1)^{(5)} - (\bar{v}_2)^{(5)}]t}}{1 + (\bar{C})^{(5)} e^{[-(a_{29})^{(5)}(\bar{v}_1)^{(5)} - (\bar{v}_2)^{(5)}]t}} \leq (v_0)^{(5)}$$

519

And so with the notation of the first part of condition (c) , we have

Definition of $v^{(5)}(t)$:-

$$(m_2)^{(5)} \leq v^{(5)}(t) \leq (m_1)^{(5)}, \quad \boxed{v^{(5)}(t) = \frac{G_{28}(t)}{G_{29}(t)}}$$

In a completely analogous way, we obtain

Definition of $u^{(5)}(t)$:-

$$(\mu_2)^{(5)} \leq u^{(5)}(t) \leq (\mu_1)^{(5)}, \quad \boxed{u^{(5)}(t) = \frac{T_{28}(t)}{T_{29}(t)}}$$

Now, using this result and replacing it in GLOBAL EQUATIONS we get easily the result stated in the theorem.

Particular case :

If $(a''_{28})^{(5)} = (a''_{29})^{(5)}$, then $(\sigma_1)^{(5)} = (\sigma_2)^{(5)}$ and in this case $(v_1)^{(5)} = (\bar{v}_1)^{(5)}$ if in addition $(v_0)^{(5)} = (v_5)^{(5)}$ then $v^{(5)}(t) = (v_0)^{(5)}$ and as a consequence $G_{28}(t) = (v_0)^{(5)}G_{29}(t)$ **this also defines $(v_0)^{(5)}$ for the special case .**

Analogously if $(b''_{28})^{(5)} = (b''_{29})^{(5)}$, then $(\tau_1)^{(5)} = (\tau_2)^{(5)}$ and then $(u_1)^{(5)} = (\bar{u}_1)^{(5)}$ if in addition $(u_0)^{(5)} = (u_1)^{(5)}$ then $T_{28}(t) = (u_0)^{(5)}T_{29}(t)$ This is an important consequence of the relation between $(v_1)^{(5)}$ and $(\bar{v}_1)^{(5)}$, **and definition of $(u_0)^{(5)}$.**

we obtain

520
521

$$\frac{dv^{(6)}}{dt} = (a_{32})^{(6)} - \left((a'_{32})^{(6)} - (a'_{33})^{(6)} + (a''_{32})^{(6)}(T_{33}, t) \right) - (a''_{33})^{(6)}(T_{33}, t)v^{(6)} - (a_{33})^{(6)}v^{(6)}$$

Definition of $v^{(6)}$:- $v^{(6)} = \frac{G_{32}}{G_{33}}$

It follows

$$- \left((a_{33})^{(6)}(v^{(6)})^2 + (\sigma_2)^{(6)}v^{(6)} - (a_{32})^{(6)} \right) \leq \frac{dv^{(6)}}{dt} \leq - \left((a_{33})^{(6)}(v^{(6)})^2 + (\sigma_1)^{(6)}v^{(6)} - (a_{32})^{(6)} \right)$$

From which one obtains

Definition of $(\bar{v}_1)^{(6)}, (v_0)^{(6)}$:-

(j) For $0 < \boxed{(v_0)^{(6)} = \frac{G_{32}^0}{G_{33}^0}} < (v_1)^{(6)} < (\bar{v}_1)^{(6)}$

$$v^{(6)}(t) \geq \frac{(v_1)^{(6)} + (C)^{(6)}(v_2)^{(6)} e^{[-(a_{33})^{(6)}((v_1)^{(6)} - (v_0)^{(6)})t]}}{1 + (C)^{(6)} e^{[-(a_{33})^{(6)}((v_1)^{(6)} - (v_0)^{(6)})t]}} , \quad \boxed{(C)^{(6)} = \frac{(v_1)^{(6)} - (v_0)^{(6)}}{(v_0)^{(6)} - (v_2)^{(6)}}$$

it follows $(v_0)^{(6)} \leq v^{(6)}(t) \leq (v_1)^{(6)}$

In the same manner , we get

522

$$v^{(6)}(t) \leq \frac{(\bar{v}_1)^{(6)} + (\bar{C})^{(6)}(\bar{v}_2)^{(6)} e^{[-(a_{33})^{(6)}((\bar{v}_1)^{(6)} - (\bar{v}_2)^{(6)})t]}}{1 + (\bar{C})^{(6)} e^{[-(a_{33})^{(6)}((\bar{v}_1)^{(6)} - (\bar{v}_2)^{(6)})t]}} , \quad \boxed{(\bar{C})^{(6)} = \frac{(\bar{v}_1)^{(6)} - (v_0)^{(6)}}{(v_0)^{(6)} - (\bar{v}_2)^{(6)}}$$

523

From which we deduce $(v_0)^{(6)} \leq v^{(6)}(t) \leq (\bar{v}_1)^{(6)}$

(k) If $0 < (v_1)^{(6)} < (v_0)^{(6)} = \frac{G_{32}^0}{G_{33}^0} < (\bar{v}_1)^{(6)}$ we find like in the previous case,

524

$$(v_1)^{(6)} \leq \frac{(v_1)^{(6)} + (C)^{(6)}(v_2)^{(6)} e^{[-(a_{33})^{(6)}((v_1)^{(6)} - (v_2)^{(6)})t]}}{1 + (C)^{(6)} e^{[-(a_{33})^{(6)}((v_1)^{(6)} - (v_2)^{(6)})t]}} \leq v^{(6)}(t) \leq$$

$$\frac{(\bar{v}_1)^{(6)} + (\bar{C})^{(6)}(\bar{v}_2)^{(6)} e^{[-(a_{33})^{(6)}((\bar{v}_1)^{(6)} - (\bar{v}_2)^{(6)})t]}}{1 + (\bar{C})^{(6)} e^{[-(a_{33})^{(6)}((\bar{v}_1)^{(6)} - (\bar{v}_2)^{(6)})t]}} \leq (\bar{v}_1)^{(6)}$$

(l) If $0 < (v_1)^{(6)} \leq (\bar{v}_1)^{(6)} \leq \boxed{(v_0)^{(6)} = \frac{G_{32}^0}{G_{33}^0}}$, we obtain

525

$$(v_1)^{(6)} \leq v^{(6)}(t) \leq \frac{(\bar{v}_1)^{(6)} + (\bar{c})^{(6)} (\bar{v}_2)^{(6)} e^{[-(a_{33})^{(6)} ((\bar{v}_1)^{(6)} - (\bar{v}_2)^{(6)}) t]}}{1 + (\bar{c})^{(6)} e^{[-(a_{33})^{(6)} ((\bar{v}_1)^{(6)} - (\bar{v}_2)^{(6)}) t]}} \leq (v_0)^{(6)}$$

And so with the notation of the first part of condition (c) , we have

Definition of $v^{(6)}(t)$:-

$$(m_2)^{(6)} \leq v^{(6)}(t) \leq (m_1)^{(6)}, \quad \boxed{v^{(6)}(t) = \frac{G_{32}(t)}{G_{33}(t)}}$$

In a completely analogous way, we obtain

Definition of $u^{(6)}(t)$:-

$$(\mu_2)^{(6)} \leq u^{(6)}(t) \leq (\mu_1)^{(6)}, \quad \boxed{u^{(6)}(t) = \frac{T_{32}(t)}{T_{33}(t)}}$$

Now, using this result and replacing it in GLOBAL EQUATIONS we get easily the result stated in the theorem.

Particular case :

If $(a''_{32})^{(6)} = (a''_{33})^{(6)}$, then $(\sigma_1)^{(6)} = (\sigma_2)^{(6)}$ and in this case $(v_1)^{(6)} = (\bar{v}_1)^{(6)}$ if in addition $(v_0)^{(6)} = (v_1)^{(6)}$ then $v^{(6)}(t) = (v_0)^{(6)}$ and as a consequence $G_{32}(t) = (v_0)^{(6)} G_{33}(t)$ **this also defines $(v_0)^{(6)}$ for the special case .**

Analogously if $(b''_{32})^{(6)} = (b''_{33})^{(6)}$, then $(\tau_1)^{(6)} = (\tau_2)^{(6)}$ and then $(u_1)^{(6)} = (\bar{u}_1)^{(6)}$ if in addition $(u_0)^{(6)} = (u_1)^{(6)}$ then $T_{32}(t) = (u_0)^{(6)} T_{33}(t)$ This is an important consequence of the relation between $(v_1)^{(6)}$ and $(\bar{v}_1)^{(6)}$, **and definition of $(u_0)^{(6)}$.**

526
527

Behavior of the solutions

If we denote and define

Definition of $(\sigma_1)^{(7)}, (\sigma_2)^{(7)}, (\tau_1)^{(7)}, (\tau_2)^{(7)}$:

(p) $(\sigma_1)^{(7)}, (\sigma_2)^{(7)}, (\tau_1)^{(7)}, (\tau_2)^{(7)}$ four constants satisfying

$$-(\sigma_2)^{(7)} \leq -(a'_{36})^{(7)} + (a'_{37})^{(7)} - (a''_{36})^{(7)}(T_{37}, t) + (a''_{37})^{(7)}(T_{37}, t) \leq -(\sigma_1)^{(7)}$$

$$-(\tau_2)^{(7)} \leq -(b'_{36})^{(7)} + (b'_{37})^{(7)} - (b''_{36})^{(7)}((G_{39}), t) - (b''_{37})^{(7)}((G_{39}), t) \leq -(\tau_1)^{(7)}$$

Definition of $(v_1)^{(7)}, (v_2)^{(7)}, (u_1)^{(7)}, (u_2)^{(7)}, v^{(7)}, u^{(7)}$:

(q) By $(v_1)^{(7)} > 0, (v_2)^{(7)} < 0$ and respectively $(u_1)^{(7)} > 0, (u_2)^{(7)} < 0$ the roots of the equations

$$(a_{37})^{(7)}(v^{(7)})^2 + (\sigma_1)^{(7)}v^{(7)} - (a_{36})^{(7)} = 0$$

$$\text{and } (b_{37})^{(7)}(u^{(7)})^2 + (\tau_1)^{(7)}u^{(7)} - (b_{36})^{(7)} = 0 \text{ and}$$

Definition of $(\bar{v}_1)^{(7)}, (\bar{v}_2)^{(7)}, (\bar{u}_1)^{(7)}, (\bar{u}_2)^{(7)}$:

By $(\bar{v}_1)^{(7)} > 0, (\bar{v}_2)^{(7)} < 0$ and respectively $(\bar{u}_1)^{(7)} > 0, (\bar{u}_2)^{(7)} < 0$ the

$$\text{roots of the equations } (a_{37})^{(7)}(v^{(7)})^2 + (\sigma_2)^{(7)}v^{(7)} - (a_{36})^{(7)} = 0$$

$$\text{and } (b_{37})^{(7)}(u^{(7)})^2 + (\tau_2)^{(7)}u^{(7)} - (b_{36})^{(7)} = 0$$

Definition of $(m_1)^{(7)}, (m_2)^{(7)}, (\mu_1)^{(7)}, (\mu_2)^{(7)}, (v_0)^{(7)}$:-

(r) If we define $(m_1)^{(7)}, (m_2)^{(7)}, (\mu_1)^{(7)}, (\mu_2)^{(7)}$ by

528

529

530.

$$(m_2)^{(7)} = (v_0)^{(7)}, (m_1)^{(7)} = (v_1)^{(7)}, \text{ if } (v_0)^{(7)} < (v_1)^{(7)}$$

$$(m_2)^{(7)} = (v_1)^{(7)}, (m_1)^{(7)} = (\bar{v}_1)^{(7)}, \text{ if } (v_1)^{(7)} < (v_0)^{(7)} < (\bar{v}_1)^{(7)},$$

and
$$(v_0)^{(7)} = \frac{G_{36}^0}{G_{37}^0}$$

$$(m_2)^{(7)} = (v_1)^{(7)}, (m_1)^{(7)} = (v_0)^{(7)}, \text{ if } (\bar{v}_1)^{(7)} < (v_0)^{(7)}$$

and analogously

531

$$(\mu_2)^{(7)} = (u_0)^{(7)}, (\mu_1)^{(7)} = (u_1)^{(7)}, \text{ if } (u_0)^{(7)} < (u_1)^{(7)}$$

$$(\mu_2)^{(7)} = (u_1)^{(7)}, (\mu_1)^{(7)} = (\bar{u}_1)^{(7)}, \text{ if } (u_1)^{(7)} < (u_0)^{(7)} < (\bar{u}_1)^{(7)},$$

and
$$(u_0)^{(7)} = \frac{T_{36}^0}{T_{37}^0}$$

$(\mu_2)^{(7)} = (u_1)^{(7)}, (\mu_1)^{(7)} = (u_0)^{(7)}, \text{ if } (\bar{u}_1)^{(7)} < (u_0)^{(7)}$ where $(u_1)^{(7)}, (\bar{u}_1)^{(7)}$ are defined by 59 and 67 respectively

Then the solution of GLOBAL EQUATIONS satisfies the inequalities

532

$$G_{36}^0 e^{((S_1)^{(7)} - (p_{36})^{(7)})t} \leq G_{36}(t) \leq G_{36}^0 e^{(S_1)^{(7)}t}$$

where $(p_i)^{(7)}$ is defined

$$\frac{1}{(m_7)^{(7)}} G_{36}^0 e^{((S_1)^{(7)} - (p_{36})^{(7)})t} \leq G_{37}(t) \leq \frac{1}{(m_2)^{(7)}} G_{36}^0 e^{(S_1)^{(7)}t}$$

533

$$\left(\frac{(a_{38})^{(7)} G_{36}^0}{(m_1)^{(7)} ((S_1)^{(7)} - (p_{36})^{(7)} - (S_2)^{(7)})} \left[e^{((S_1)^{(7)} - (p_{36})^{(7)})t} - e^{-(S_2)^{(7)}t} \right] + G_{38}^0 e^{-(S_2)^{(7)}t} \leq G_{38}(t) \leq \frac{(a_{38})^{(7)} G_{36}^0}{(m_2)^{(7)} ((S_1)^{(7)} - (a_{38})^{(7)})} \left[e^{(S_1)^{(7)}t} - e^{-(a_{38})^{(7)}t} \right] + G_{38}^0 e^{-(a_{38})^{(7)}t} \right)$$

534

$$\boxed{T_{36}^0 e^{(R_1)^{(7)}t} \leq T_{36}(t) \leq T_{36}^0 e^{((R_1)^{(7)} + (r_{36})^{(7)})t}$$

535

$$\frac{1}{(\mu_1)^{(7)}} T_{36}^0 e^{(R_1)^{(7)}t} \leq T_{36}(t) \leq \frac{1}{(\mu_2)^{(7)}} T_{36}^0 e^{((R_1)^{(7)} + (r_{36})^{(7)})t}$$

536

$$\frac{(b_{38})^{(7)} T_{36}^0}{(\mu_1)^{(7)} ((R_1)^{(7)} - (b_{38})^{(7)})} \left[e^{(R_1)^{(7)}t} - e^{-(b_{38})^{(7)}t} \right] + T_{38}^0 e^{-(b_{38})^{(7)}t} \leq T_{38}(t) \leq \frac{(a_{38})^{(7)} T_{36}^0}{(\mu_2)^{(7)} ((R_1)^{(7)} + (r_{36})^{(7)} + (R_2)^{(7)})} \left[e^{((R_1)^{(7)} + (r_{36})^{(7)})t} - e^{-(R_2)^{(7)}t} \right] + T_{38}^0 e^{-(R_2)^{(7)}t}$$

537

Definition of $(S_1)^{(7)}, (S_2)^{(7)}, (R_1)^{(7)}, (R_2)^{(7)}$:-

538

Where $(S_1)^{(7)} = (a_{36})^{(7)}(m_2)^{(7)} - (a_{36})^{(7)}$

$$(S_2)^{(7)} = (a_{38})^{(7)} - (p_{38})^{(7)}$$

$$(R_1)^{(7)} = (b_{36})^{(7)}(\mu_2)^{(7)} - (b_{36})^{(7)}$$

$$(R_2)^{(7)} = (b_{38})^{(7)} - (r_{38})^{(7)}$$

539

From CONCATENATED GLOBAL EQUATIONS we obtain

540

$$\frac{dv^{(7)}}{dt} = (a_{36})^{(7)} - \left((a_{36}')^{(7)} - (a_{37}')^{(7)} + (a_{36}'')^{(7)}(T_{37}, t) \right) - (a_{37}'')^{(7)}(T_{37}, t)v^{(7)} - (a_{37})^{(7)}v^{(7)}$$

Definition of $v^{(7)}$:-
$$v^{(7)} = \frac{G_{36}}{G_{37}}$$

It follows

$$-\left((a_{37})^{(7)}(v^{(7)})^2 + (\sigma_2)^{(7)}v^{(7)} - (a_{36})^{(7)}\right) \leq \frac{dv^{(7)}}{dt} \leq -\left((a_{37})^{(7)}(v^{(7)})^2 + (\sigma_1)^{(7)}v^{(7)} - (a_{36})^{(7)}\right)$$

From which one obtains

Definition of $(\bar{v}_1)^{(7)}, (v_0)^{(7)}$:-

(m) For $0 < (v_0)^{(7)} = \frac{G_{36}^0}{G_{37}^0} < (v_1)^{(7)} < (\bar{v}_1)^{(7)}$

$$v^{(7)}(t) \geq \frac{(v_1)^{(7)} + (C)^{(7)}(v_2)^{(7)} e^{[-(a_{37})^{(7)}(v_1)^{(7)} - (v_0)^{(7)}]t}}{1 + (C)^{(7)} e^{[-(a_{37})^{(7)}(v_1)^{(7)} - (v_0)^{(7)}]t}}, \quad (C)^{(7)} = \frac{(v_1)^{(7)} - (v_0)^{(7)}}{(v_0)^{(7)} - (v_2)^{(7)}}$$

it follows $(v_0)^{(7)} \leq v^{(7)}(t) \leq (v_1)^{(7)}$

In the same manner , we get

$$v^{(7)}(t) \leq \frac{(\bar{v}_1)^{(7)} + (\bar{C})^{(7)}(\bar{v}_2)^{(7)} e^{[-(a_{37})^{(7)}(\bar{v}_1)^{(7)} - (\bar{v}_2)^{(7)}]t}}{1 + (\bar{C})^{(7)} e^{[-(a_{37})^{(7)}(\bar{v}_1)^{(7)} - (\bar{v}_2)^{(7)}]t}}, \quad (\bar{C})^{(7)} = \frac{(\bar{v}_1)^{(7)} - (v_0)^{(7)}}{(v_0)^{(7)} - (\bar{v}_2)^{(7)}}$$

541

From which we deduce $(v_0)^{(7)} \leq v^{(7)}(t) \leq (\bar{v}_1)^{(7)}$

(n) If $0 < (v_1)^{(7)} < (v_0)^{(7)} = \frac{G_{36}^0}{G_{37}^0} < (\bar{v}_1)^{(7)}$ we find like in the previous case,

542

$$(v_1)^{(7)} \leq \frac{(v_1)^{(7)} + (C)^{(7)}(v_2)^{(7)} e^{[-(a_{37})^{(7)}(v_1)^{(7)} - (v_2)^{(7)}]t}}{1 + (C)^{(7)} e^{[-(a_{37})^{(7)}(v_1)^{(7)} - (v_2)^{(7)}]t}} \leq v^{(7)}(t) \leq \frac{(\bar{v}_1)^{(7)} + (\bar{C})^{(7)}(\bar{v}_2)^{(7)} e^{[-(a_{37})^{(7)}(\bar{v}_1)^{(7)} - (\bar{v}_2)^{(7)}]t}}{1 + (\bar{C})^{(7)} e^{[-(a_{37})^{(7)}(\bar{v}_1)^{(7)} - (\bar{v}_2)^{(7)}]t}} \leq (\bar{v}_1)^{(7)}$$

(o) If $0 < (v_1)^{(7)} \leq (\bar{v}_1)^{(7)} \leq (v_0)^{(7)} = \frac{G_{36}^0}{G_{37}^0}$, we obtain

543

$$(v_1)^{(7)} \leq v^{(7)}(t) \leq \frac{(\bar{v}_1)^{(7)} + (\bar{C})^{(7)}(\bar{v}_2)^{(7)} e^{[-(a_{37})^{(7)}(\bar{v}_1)^{(7)} - (\bar{v}_2)^{(7)}]t}}{1 + (\bar{C})^{(7)} e^{[-(a_{37})^{(7)}(\bar{v}_1)^{(7)} - (\bar{v}_2)^{(7)}]t}} \leq (v_0)^{(7)}$$

And so with the notation of the first part of condition (c) , we have

Definition of $v^{(7)}(t)$:-

$$(m_2)^{(7)} \leq v^{(7)}(t) \leq (m_1)^{(7)}, \quad v^{(7)}(t) = \frac{G_{36}(t)}{G_{37}(t)}$$

In a completely analogous way, we obtain

Definition of $u^{(7)}(t)$:-

$$(\mu_2)^{(7)} \leq u^{(7)}(t) \leq (\mu_1)^{(7)}, \quad u^{(7)}(t) = \frac{T_{36}(t)}{T_{37}(t)}$$

Now, using this result and replacing it in CONCATENATED GLOBAL EQUATIONS we get easily the result

stated in the theorem.

Particular case :

If $(a_{36}''^{(7)} = (a_{37}''^{(7)})$, then $(\sigma_1)^{(7)} = (\sigma_2)^{(7)}$ and in this case $(v_1)^{(7)} = (\bar{v}_1)^{(7)}$ if in addition $(v_0)^{(7)} = (v_1)^{(7)}$ then $v^{(7)}(t) = (v_0)^{(7)}$ and as a consequence $G_{36}(t) = (v_0)^{(7)}G_{37}(t)$ **this also defines $(v_0)^{(7)}$ for the special case .**

Analogously if $(b_{36}''^{(7)} = (b_{37}''^{(7)})$, then $(\tau_1)^{(7)} = (\tau_2)^{(7)}$ and then $(u_1)^{(7)} = (\bar{u}_1)^{(7)}$ if in addition $(u_0)^{(7)} = (u_1)^{(7)}$ then $T_{36}(t) = (u_0)^{(7)}T_{37}(t)$ This is an important consequence of the relation between $(v_1)^{(7)}$ and $(\bar{v}_1)^{(7)}$, **and definition of $(u_0)^{(7)}$.**

$$(b_{14})^{(1)}T_{13} - [(b'_{14})^{(1)} - (b''_{14})^{(1)}(G)]T_{14} = 0 \tag{544}$$

$$(b_{15})^{(1)}T_{14} - [(b'_{15})^{(1)} - (b''_{15})^{(1)}(G)]T_{15} = 0 \tag{545}$$

has a unique positive solution , which is an equilibrium solution for the system 546

$$(a_{16})^{(2)}G_{17} - [(a'_{16})^{(2)} + (a''_{16})^{(2)}(T_{17})]G_{16} = 0 \tag{547}$$

$$(a_{17})^{(2)}G_{16} - [(a'_{17})^{(2)} + (a''_{17})^{(2)}(T_{17})]G_{17} = 0 \tag{548}$$

$$(a_{18})^{(2)}G_{17} - [(a'_{18})^{(2)} + (a''_{18})^{(2)}(T_{17})]G_{18} = 0 \tag{549}$$

$$(b_{16})^{(2)}T_{17} - [(b'_{16})^{(2)} - (b''_{16})^{(2)}(G_{19})]T_{16} = 0 \tag{550}$$

$$(b_{17})^{(2)}T_{16} - [(b'_{17})^{(2)} - (b''_{17})^{(2)}(G_{19})]T_{17} = 0 \tag{551}$$

$$(b_{18})^{(2)}T_{17} - [(b'_{18})^{(2)} - (b''_{18})^{(2)}(G_{19})]T_{18} = 0 \tag{552}$$

has a unique positive solution , which is an equilibrium solution for 553

$$(a_{20})^{(3)}G_{21} - [(a'_{20})^{(3)} + (a''_{20})^{(3)}(T_{21})]G_{20} = 0 \tag{554}$$

$$(a_{21})^{(3)}G_{20} - [(a'_{21})^{(3)} + (a''_{21})^{(3)}(T_{21})]G_{21} = 0 \tag{555}$$

$$(a_{22})^{(3)}G_{21} - [(a'_{22})^{(3)} + (a''_{22})^{(3)}(T_{21})]G_{22} = 0 \tag{556}$$

$$(b_{20})^{(3)}T_{21} - [(b'_{20})^{(3)} - (b''_{20})^{(3)}(G_{23})]T_{20} = 0 \tag{557}$$

$$(b_{21})^{(3)}T_{20} - [(b'_{21})^{(3)} - (b''_{21})^{(3)}(G_{23})]T_{21} = 0 \tag{558}$$

$$(b_{22})^{(3)}T_{21} - [(b'_{22})^{(3)} - (b''_{22})^{(3)}(G_{23})]T_{22} = 0 \tag{559}$$

has a unique positive solution , which is an equilibrium solution 560

$$(a_{24})^{(4)}G_{25} - [(a'_{24})^{(4)} + (a''_{24})^{(4)}(T_{25})]G_{24} = 0 \tag{561}$$

$$(a_{25})^{(4)}G_{24} - [(a'_{25})^{(4)} + (a''_{25})^{(4)}(T_{25})]G_{25} = 0 \tag{563}$$

$$(a_{26})^{(4)}G_{25} - [(a'_{26})^{(4)} + (a''_{26})^{(4)}(T_{25})]G_{26} = 0 \tag{564}$$

$$(b_{24})^{(4)}T_{25} - [(b'_{24})^{(4)} - (b''_{24})^{(4)}((G_{27}))]T_{24} = 0 \tag{565}$$

$$(b_{25})^{(4)}T_{24} - [(b'_{25})^{(4)} - (b''_{25})^{(4)}((G_{27}))]T_{25} = 0 \tag{566}$$

$$(b_{26})^{(4)}T_{25} - [(b'_{26})^{(4)} - (b''_{26})^{(4)}((G_{27}))]T_{26} = 0 \tag{567}$$

has a unique positive solution , which is an equilibrium solution for the system 568

$$(a_{28})^{(5)}G_{29} - [(a'_{28})^{(5)} + (a''_{28})^{(5)}(T_{29})]G_{28} = 0 \tag{569}$$

$$(a_{29})^{(5)}G_{28} - [(a'_{29})^{(5)} + (a''_{29})^{(5)}(T_{29})]G_{29} = 0 \tag{570}$$

$$(a_{30})^{(5)}G_{29} - [(a'_{30})^{(5)} + (a''_{30})^{(5)}(T_{29})]G_{30} = 0 \tag{571}$$

$$(b_{28})^{(5)}T_{29} - [(b'_{28})^{(5)} - (b''_{28})^{(5)}(G_{31})]T_{28} = 0 \tag{572}$$

$$(b_{29})^{(5)}T_{28} - [(b'_{29})^{(5)} - (b''_{29})^{(5)}(G_{31})]T_{29} = 0 \tag{573}$$

$$(b_{30})^{(5)}T_{29} - [(b'_{30})^{(5)} - (b''_{30})^{(5)}(G_{31})]T_{30} = 0 \quad 574$$

has a unique positive solution , which is an equilibrium solution for the system 575

$$(a_{32})^{(6)}G_{33} - [(a'_{32})^{(6)} + (a''_{32})^{(6)}(T_{33})]G_{32} = 0 \quad 576$$

$$(a_{33})^{(6)}G_{32} - [(a'_{33})^{(6)} + (a''_{33})^{(6)}(T_{33})]G_{33} = 0 \quad 577$$

$$(a_{34})^{(6)}G_{33} - [(a'_{34})^{(6)} + (a''_{34})^{(6)}(T_{33})]G_{34} = 0 \quad 578$$

$$(b_{32})^{(6)}T_{33} - [(b'_{32})^{(6)} - (b''_{32})^{(6)}(G_{35})]T_{32} = 0 \quad 579$$

$$(b_{33})^{(6)}T_{32} - [(b'_{33})^{(6)} - (b''_{33})^{(6)}(G_{35})]T_{33} = 0 \quad 580$$

$$(b_{34})^{(6)}T_{33} - [(b'_{34})^{(6)} - (b''_{34})^{(6)}(G_{35})]T_{34} = 0 \quad 584$$

has a unique positive solution , which is an equilibrium solution for the system 582

$$(a_{36})^{(7)}G_{37} - [(a'_{36})^{(7)} + (a''_{36})^{(7)}(T_{37})]G_{36} = 0 \quad 583$$

$$(a_{37})^{(7)}G_{36} - [(a'_{37})^{(7)} + (a''_{37})^{(7)}(T_{37})]G_{37} = 0 \quad 584$$

$$(a_{38})^{(7)}G_{37} - [(a'_{38})^{(7)} + (a''_{38})^{(7)}(T_{37})]G_{38} = 0 \quad 585$$

586

$$(b_{36})^{(7)}T_{37} - [(b'_{36})^{(7)} - (b''_{36})^{(7)}(G_{39})]T_{36} = 0 \quad 587$$

$$(b_{37})^{(7)}T_{36} - [(b'_{37})^{(7)} - (b''_{37})^{(7)}(G_{39})]T_{37} = 0 \quad 588$$

$$(b_{38})^{(7)}T_{37} - [(b'_{38})^{(7)} - (b''_{38})^{(7)}(G_{39})]T_{38} = 0 \quad 589$$

has a unique positive solution , which is an equilibrium solution for the system 560

(a) Indeed the first two equations have a nontrivial solution G_{36}, G_{37} if

$$F(T_{39}) = (a'_{36})^{(7)}(a'_{37})^{(7)} - (a_{36})^{(7)}(a_{37})^{(7)} + (a'_{36})^{(7)}(a''_{37})^{(7)}(T_{37}) + (a'_{37})^{(7)}(a''_{36})^{(7)}(T_{37}) + (a''_{36})^{(7)}(T_{37})(a''_{37})^{(7)}(T_{37}) = 0$$

Definition and uniqueness of T_{37}^* :- 561

After hypothesis $f(0) < 0, f(\infty) > 0$ and the functions $(a''_i)^{(7)}(T_{37})$ being increasing, it follows that there exists a unique T_{37}^* for which $f(T_{37}^*) = 0$. With this value , we obtain from the three first equations

$$G_{36} = \frac{(a_{36})^{(7)}G_{37}}{[(a'_{36})^{(7)} + (a''_{36})^{(7)}(T_{37}^*)]} \quad , \quad G_{38} = \frac{(a_{38})^{(7)}G_{37}}{[(a'_{38})^{(7)} + (a''_{38})^{(7)}(T_{37}^*)]}$$

(e) By the same argument, the equations(SOLUTIONAL) admit solutions G_{36}, G_{37} if

$$\varphi(G_{39}) = (b'_{36})^{(7)}(b'_{37})^{(7)} - (b_{36})^{(7)}(b_{37})^{(7)} - [(b'_{36})^{(7)}(b''_{37})^{(7)}(G_{39}) + (b'_{37})^{(7)}(b''_{36})^{(7)}(G_{39})] + (b''_{36})^{(7)}(G_{39})(b''_{37})^{(7)}(G_{39}) = 0$$

Where in $(G_{39})(G_{36}, G_{37}, G_{38}), G_{36}, G_{38}$ must be replaced by their values from 96. It is easy to see that φ is a decreasing function in G_{37} taking into account the hypothesis $\varphi(0) > 0, \varphi(\infty) < 0$ it follows that there exists a unique G_{37}^* such that $\varphi(G^*) = 0$ 562

Finally we obtain the unique solution OF THE SYSTEM

G_{37}^* given by $\varphi((G_{39})^*) = 0, T_{37}^*$ given by $f(T_{37}^*) = 0$ and

$$G_{36}^* = \frac{(a_{36})^{(7)} G_{37}^*}{[(a'_{36})^{(7)} + (a''_{36})^{(7)}(T_{37}^*)]} \quad , \quad G_{38}^* = \frac{(a_{38})^{(7)} G_{37}^*}{[(a'_{38})^{(7)} + (a''_{38})^{(7)}(T_{37}^*)]}$$

$$T_{36}^* = \frac{(b_{36})^{(7)} T_{37}^*}{[(b'_{36})^{(7)} - (b''_{36})^{(7)}((G_{39})^*)]} \quad , \quad T_{38}^* = \frac{(b_{38})^{(7)} T_{37}^*}{[(b'_{38})^{(7)} - (b''_{38})^{(7)}((G_{39})^*)]} \quad \text{563}$$

Definition and uniqueness of T_{21}^* :- 564

After hypothesis $f(0) < 0, f(\infty) > 0$ and the functions $(a_i'')^{(1)}(T_{21})$ being increasing, it follows that there exists a unique T_{21}^* for which $f(T_{21}^*) = 0$. With this value, we obtain from the three first equations

$$G_{20} = \frac{(a_{20})^{(3)} G_{21}}{[(a'_{20})^{(3)} + (a''_{20})^{(3)}(T_{21}^*)]} \quad , \quad G_{22} = \frac{(a_{22})^{(3)} G_{21}}{[(a'_{22})^{(3)} + (a''_{22})^{(3)}(T_{21}^*)]} \quad \text{565}$$

Definition and uniqueness of T_{25}^* :- 566

After hypothesis $f(0) < 0, f(\infty) > 0$ and the functions $(a_i'')^{(4)}(T_{25})$ being increasing, it follows that there exists a unique T_{25}^* for which $f(T_{25}^*) = 0$. With this value, we obtain from the three first equations

$$G_{24} = \frac{(a_{24})^{(4)} G_{25}}{[(a'_{24})^{(4)} + (a''_{24})^{(4)}(T_{25}^*)]} \quad , \quad G_{26} = \frac{(a_{26})^{(4)} G_{25}}{[(a'_{26})^{(4)} + (a''_{26})^{(4)}(T_{25}^*)]}$$

Definition and uniqueness of T_{29}^* :- 567

After hypothesis $f(0) < 0, f(\infty) > 0$ and the functions $(a_i'')^{(5)}(T_{29})$ being increasing, it follows that there exists a unique T_{29}^* for which $f(T_{29}^*) = 0$. With this value, we obtain from the three first equations

$$G_{28} = \frac{(a_{28})^{(5)} G_{29}}{[(a'_{28})^{(5)} + (a''_{28})^{(5)}(T_{29}^*)]} \quad , \quad G_{30} = \frac{(a_{30})^{(5)} G_{29}}{[(a'_{30})^{(5)} + (a''_{30})^{(5)}(T_{29}^*)]}$$

Definition and uniqueness of T_{33}^* :- 568

After hypothesis $f(0) < 0, f(\infty) > 0$ and the functions $(a_i'')^{(6)}(T_{33})$ being increasing, it follows that there exists a unique T_{33}^* for which $f(T_{33}^*) = 0$. With this value, we obtain from the three first equations

$$G_{32} = \frac{(a_{32})^{(6)} G_{33}}{[(a'_{32})^{(6)} + (a''_{32})^{(6)}(T_{33}^*)]} \quad , \quad G_{34} = \frac{(a_{34})^{(6)} G_{33}}{[(a'_{34})^{(6)} + (a''_{34})^{(6)}(T_{33}^*)]}$$

(f) By the same argument, the equations 92,93 admit solutions G_{13}, G_{14} if 569

$$\varphi(G) = (b'_{13})^{(1)}(b'_{14})^{(1)} - (b_{13})^{(1)}(b_{14})^{(1)} -$$

$$[(b'_{13})^{(1)}(b''_{14})^{(1)}(G) + (b'_{14})^{(1)}(b''_{13})^{(1)}(G)] + (b''_{13})^{(1)}(G)(b''_{14})^{(1)}(G) = 0$$

Where in $G(G_{13}, G_{14}, G_{15}), G_{13}, G_{15}$ must be replaced by their values from 96. It is easy to see that φ is a decreasing function in G_{14} taking into account the hypothesis $\varphi(0) > 0, \varphi(\infty) < 0$ it follows that there exists a unique G_{14}^* such that $\varphi(G^*) = 0$

(g) By the same argument, the equations 92,93 admit solutions G_{16}, G_{17} if 570

$$\varphi(G_{19}) = (b'_{16})^{(2)}(b'_{17})^{(2)} - (b_{16})^{(2)}(b_{17})^{(2)} -$$

$$[(b'_{16})^{(2)}(b''_{17})^{(2)}(G_{19}) + (b'_{17})^{(2)}(b''_{16})^{(2)}(G_{19})] + (b''_{16})^{(2)}(G_{19})(b''_{17})^{(2)}(G_{19}) = 0$$

Where in $(G_{19})(G_{16}, G_{17}, G_{18}), G_{16}, G_{18}$ must be replaced by their values from 96. It is easy to see that φ is a decreasing function in G_{17} taking into account the hypothesis $\varphi(0) > 0, \varphi(\infty) < 0$ it follows that there exists a unique G_{14}^* such that $\varphi((G_{19})^*) = 0$ 571

(a) By the same argument, the concatenated equations admit solutions G_{20}, G_{21} if 572

$$\varphi(G_{23}) = (b'_{20})^{(3)}(b'_{21})^{(3)} - (b_{20})^{(3)}(b_{21})^{(3)} -$$

$$[(b'_{20})^{(3)}(b''_{21})^{(3)}(G_{23}) + (b'_{21})^{(3)}(b''_{20})^{(3)}(G_{23})] + (b''_{20})^{(3)}(G_{23})(b''_{21})^{(3)}(G_{23}) = 0$$

Where in $G_{23}(G_{20}, G_{21}, G_{22}), G_{20}, G_{22}$ must be replaced by their values from 96. It is easy to see that φ is a decreasing function in G_{21} taking into account the hypothesis $\varphi(0) > 0, \varphi(\infty) < 0$ it follows that there exists a unique G_{21}^* such that $\varphi((G_{23})^*) = 0$ 573

(b) By the same argument, the equations of modules admit solutions G_{24}, G_{25} if 574

$$\varphi(G_{27}) = (b'_{24})^{(4)}(b'_{25})^{(4)} - (b_{24})^{(4)}(b_{25})^{(4)} -$$

$$[(b'_{24})^{(4)}(b''_{25})^{(4)}(G_{27}) + (b'_{25})^{(4)}(b''_{24})^{(4)}(G_{27})] + (b''_{24})^{(4)}(G_{27})(b''_{25})^{(4)}(G_{27}) = 0$$

Where in $(G_{27})(G_{24}, G_{25}, G_{26}), G_{24}, G_{26}$ must be replaced by their values from 96. It is easy to see that φ is a decreasing function in G_{25} taking into account the hypothesis $\varphi(0) > 0, \varphi(\infty) < 0$ it follows that there exists a unique G_{25}^* such that $\varphi((G_{27})^*) = 0$

(c) By the same argument, the equations (modules) admit solutions G_{28}, G_{29} if 575

$$\varphi(G_{31}) = (b'_{28})^{(5)}(b'_{29})^{(5)} - (b_{28})^{(5)}(b_{29})^{(5)} -$$

$$[(b'_{28})^{(5)}(b''_{29})^{(5)}(G_{31}) + (b'_{29})^{(5)}(b''_{28})^{(5)}(G_{31})] + (b''_{28})^{(5)}(G_{31})(b''_{29})^{(5)}(G_{31}) = 0$$

Where in $(G_{31})(G_{28}, G_{29}, G_{30}), G_{28}, G_{30}$ must be replaced by their values from 96. It is easy to see that φ is a decreasing function in G_{29} taking into account the hypothesis $\varphi(0) > 0, \varphi(\infty) < 0$ it follows that there exists a unique G_{29}^* such that $\varphi((G_{31})^*) = 0$

(d) By the same argument, the equations (modules) admit solutions G_{32}, G_{33} if 578

$$\varphi(G_{35}) = (b'_{32})^{(6)}(b'_{33})^{(6)} - (b_{32})^{(6)}(b_{33})^{(6)} -$$

$$[(b'_{32})^{(6)}(b''_{33})^{(6)}(G_{35}) + (b'_{33})^{(6)}(b''_{32})^{(6)}(G_{35})] + (b''_{32})^{(6)}(G_{35})(b''_{33})^{(6)}(G_{35}) = 0$$

Where in $(G_{35})(G_{32}, G_{33}, G_{34}), G_{32}, G_{34}$ must be replaced by their values It is easy to see that φ is a decreasing function in G_{33} taking into account the hypothesis $\varphi(0) > 0, \varphi(\infty) < 0$ it follows that there exists a unique G_{33}^* such that $\varphi(G^*) = 0$ 581

Finally we obtain the unique solution of 89 to 94 582

G_{14}^* given by $\varphi(G^*) = 0, T_{14}^*$ given by $f(T_{14}^*) = 0$ and

$$G_{13}^* = \frac{(a_{13})^{(1)}G_{14}^*}{[(a'_{13})^{(1)} + (a''_{13})^{(1)}(T_{14}^*)]} , G_{15}^* = \frac{(a_{15})^{(1)}G_{14}^*}{[(a'_{15})^{(1)} + (a''_{15})^{(1)}(T_{14}^*)]}$$

$$T_{13}^* = \frac{(b_{13})^{(1)}T_{14}^*}{[(b'_{13})^{(1)} - (b''_{13})^{(1)}(G^*)]} , T_{15}^* = \frac{(b_{15})^{(1)}T_{14}^*}{[(b'_{15})^{(1)} - (b''_{15})^{(1)}(G^*)]}$$

Obviously, these values represent an equilibrium solution

Finally we obtain the unique solution

G_{17}^* given by $\varphi((G_{19})^*) = 0$, T_{17}^* given by $f(T_{17}^*) = 0$ and

$$G_{16}^* = \frac{(a_{16})^{(2)}G_{17}^*}{[(a'_{16})^{(2)}+(a''_{16})^{(2)}(T_{17}^*)]} , G_{18}^* = \frac{(a_{18})^{(2)}G_{17}^*}{[(a'_{18})^{(2)}+(a''_{18})^{(2)}(T_{17}^*)]}$$

$$T_{16}^* = \frac{(b_{16})^{(2)}T_{17}^*}{[(b'_{16})^{(2)}-(b''_{16})^{(2)}((G_{19})^*)]} , T_{18}^* = \frac{(b_{18})^{(2)}T_{17}^*}{[(b'_{18})^{(2)}-(b''_{18})^{(2)}((G_{19})^*)]}$$

Obviously, these values represent an equilibrium solution

Finally we obtain the unique solution

G_{21}^* given by $\varphi((G_{23})^*) = 0$, T_{21}^* given by $f(T_{21}^*) = 0$ and

$$G_{20}^* = \frac{(a_{20})^{(3)}G_{21}^*}{[(a'_{20})^{(3)}+(a''_{20})^{(3)}(T_{21}^*)]} , G_{22}^* = \frac{(a_{22})^{(3)}G_{21}^*}{[(a'_{22})^{(3)}+(a''_{22})^{(3)}(T_{21}^*)]}$$

$$T_{20}^* = \frac{(b_{20})^{(3)}T_{21}^*}{[(b'_{20})^{(3)}-(b''_{20})^{(3)}(G_{23}^*)]} , T_{22}^* = \frac{(b_{22})^{(3)}T_{21}^*}{[(b'_{22})^{(3)}-(b''_{22})^{(3)}(G_{23}^*)]}$$

Obviously, these values represent an equilibrium solution

Finally we obtain the unique solution

G_{25}^* given by $\varphi(G_{27}) = 0$, T_{25}^* given by $f(T_{25}^*) = 0$ and

$$G_{24}^* = \frac{(a_{24})^{(4)}G_{25}^*}{[(a'_{24})^{(4)}+(a''_{24})^{(4)}(T_{25}^*)]} , G_{26}^* = \frac{(a_{26})^{(4)}G_{25}^*}{[(a'_{26})^{(4)}+(a''_{26})^{(4)}(T_{25}^*)]}$$

$$T_{24}^* = \frac{(b_{24})^{(4)}T_{25}^*}{[(b'_{24})^{(4)}-(b''_{24})^{(4)}((G_{27})^*)]} , T_{26}^* = \frac{(b_{26})^{(4)}T_{25}^*}{[(b'_{26})^{(4)}-(b''_{26})^{(4)}((G_{27})^*)]}$$

Obviously, these values represent an equilibrium solution

Finally we obtain the unique solution

G_{29}^* given by $\varphi((G_{31})^*) = 0$, T_{29}^* given by $f(T_{29}^*) = 0$ and

$$G_{28}^* = \frac{(a_{28})^{(5)}G_{29}^*}{[(a'_{28})^{(5)}+(a''_{28})^{(5)}(T_{29}^*)]} , G_{30}^* = \frac{(a_{30})^{(5)}G_{29}^*}{[(a'_{30})^{(5)}+(a''_{30})^{(5)}(T_{29}^*)]}$$

$$T_{28}^* = \frac{(b_{28})^{(5)}T_{29}^*}{[(b'_{28})^{(5)}-(b''_{28})^{(5)}((G_{31})^*)]} , T_{30}^* = \frac{(b_{30})^{(5)}T_{29}^*}{[(b'_{30})^{(5)}-(b''_{30})^{(5)}((G_{31})^*)]}$$

Obviously, these values represent an equilibrium solution

Finally we obtain the unique solution

G_{33}^* given by $\varphi((G_{35})^*) = 0$, T_{33}^* given by $f(T_{33}^*) = 0$ and

$$G_{32}^* = \frac{(a_{32})^{(6)}G_{33}^*}{[(a'_{32})^{(6)}+(a''_{32})^{(6)}(T_{33}^*)]} , G_{34}^* = \frac{(a_{34})^{(6)}G_{33}^*}{[(a'_{34})^{(6)}+(a''_{34})^{(6)}(T_{33}^*)]}$$

$$T_{32}^* = \frac{(b_{32})^{(6)}T_{33}^*}{[(b'_{32})^{(6)}-(b''_{32})^{(6)}((G_{35})^*)]} , T_{34}^* = \frac{(b_{34})^{(6)}T_{33}^*}{[(b'_{34})^{(6)}-(b''_{34})^{(6)}((G_{35})^*)]}$$

Obviously, these values represent an equilibrium solution

ASYMPTOTIC STABILITY ANALYSIS

595

Theorem 4: If the conditions of the previous theorem are satisfied and if the functions $(a_i'')^{(1)}$ and $(b_i'')^{(1)}$ Belong to $C^{(1)}(\mathbb{R}_+)$ then the above equilibrium point is asymptotically stable.

Proof: Denote

Definition of G_i, T_i :-

$$G_i = G_i^* + G_i \quad , \quad T_i = T_i^* + T_i \tag{596}$$

$$\frac{\partial (a_{14}'')^{(1)}}{\partial T_{14}}(T_{14}^*) = (q_{14})^{(1)} \quad , \quad \frac{\partial (b_i'')^{(1)}}{\partial G_j}(G^*) = s_{ij}$$

Then taking into account equations (global) and neglecting the terms of power 2, we obtain 597

$$\frac{dG_{13}}{dt} = -((a'_{13})^{(1)} + (p_{13})^{(1)})G_{13} + (a_{13})^{(1)}G_{14} - (q_{13})^{(1)}G_{13}^*T_{14} \tag{598}$$

$$\frac{dG_{14}}{dt} = -((a'_{14})^{(1)} + (p_{14})^{(1)})G_{14} + (a_{14})^{(1)}G_{13} - (q_{14})^{(1)}G_{14}^*T_{14} \tag{599}$$

$$\frac{dG_{15}}{dt} = -((a'_{15})^{(1)} + (p_{15})^{(1)})G_{15} + (a_{15})^{(1)}G_{14} - (q_{15})^{(1)}G_{15}^*T_{14} \tag{600}$$

$$\frac{dT_{13}}{dt} = -((b'_{13})^{(1)} - (r_{13})^{(1)})T_{13} + (b_{13})^{(1)}T_{14} + \sum_{j=13}^{15} (s_{(13)(j)})T_{13}^*G_j \tag{601}$$

$$\frac{dT_{14}}{dt} = -((b'_{14})^{(1)} - (r_{14})^{(1)})T_{14} + (b_{14})^{(1)}T_{13} + \sum_{j=13}^{15} (s_{(14)(j)})T_{14}^*G_j \tag{602}$$

$$\frac{dT_{15}}{dt} = -((b'_{15})^{(1)} - (r_{15})^{(1)})T_{15} + (b_{15})^{(1)}T_{14} + \sum_{j=13}^{15} (s_{(15)(j)})T_{15}^*G_j \tag{603}$$

If the conditions of the previous theorem are satisfied and if the functions $(a_i'')^{(2)}$ and $(b_i'')^{(2)}$ Belong to $C^{(2)}(\mathbb{R}_+)$ then the above equilibrium point is asymptotically stable 604

Denote 605

Definition of G_i, T_i :-

$$G_i = G_i^* + G_i \quad , \quad T_i = T_i^* + T_i \tag{606}$$

$$\frac{\partial (a_{17}'')^{(2)}}{\partial T_{17}}(T_{17}^*) = (q_{17})^{(2)} \quad , \quad \frac{\partial (b_i'')^{(2)}}{\partial G_j}(G_{19}^*) = s_{ij} \tag{607}$$

taking into account equations (global)and neglecting the terms of power 2, we obtain 608

$$\frac{dG_{16}}{dt} = -((a'_{16})^{(2)} + (p_{16})^{(2)})G_{16} + (a_{16})^{(2)}G_{17} - (q_{16})^{(2)}G_{16}^*T_{17} \tag{609}$$

$$\frac{dG_{17}}{dt} = -((a'_{17})^{(2)} + (p_{17})^{(2)})G_{17} + (a_{17})^{(2)}G_{16} - (q_{17})^{(2)}G_{17}^*T_{17} \tag{610}$$

$$\frac{dG_{18}}{dt} = -((a'_{18})^{(2)} + (p_{18})^{(2)})G_{18} + (a_{18})^{(2)}G_{17} - (q_{18})^{(2)}G_{18}^*T_{17} \tag{611}$$

$$\frac{dT_{16}}{dt} = -((b'_{16})^{(2)} - (r_{16})^{(2)})T_{16} + (b_{16})^{(2)}T_{17} + \sum_{j=16}^{18} (s_{(16)(j)})T_{16}^*G_j \tag{612}$$

$$\frac{dT_{17}}{dt} = -((b'_{17})^{(2)} - (r_{17})^{(2)})T_{17} + (b_{17})^{(2)}T_{16} + \sum_{j=16}^{18} (s_{(17)(j)})T_{17}^*G_j \tag{613}$$

$$\frac{dT_{18}}{dt} = -((b'_{18})^{(2)} - (r_{18})^{(2)})T_{18} + (b_{18})^{(2)}T_{17} + \sum_{j=16}^{18} (s_{(18)(j)})T_{18}^*G_j \tag{614}$$

If the conditions of the previous theorem are satisfied and if the functions $(a_i'')^{(3)}$ and $(b_i'')^{(3)}$ Belong to $C^{(3)}(\mathbb{R}_+)$ then the above equilibrium point is asymptotically stable 615

Denote

616

Definition of G_i, T_i :-

$$G_i = G_i^* + G_i \quad , T_i = T_i^* + T_i$$

$$\frac{\partial (a_{21}'')^{(3)}}{\partial T_{21}} (T_{21}^*) = (q_{21})^{(3)} \quad , \quad \frac{\partial (b_i'')^{(3)}}{\partial G_j} ((G_{23})^*) = s_{ij}$$

Then taking into account equations (global) and neglecting the terms of power 2, we obtain

617

$$\frac{dG_{20}}{dt} = -((a'_{20})^{(3)} + (p_{20})^{(3)})G_{20} + (a_{20})^{(3)}G_{21} - (q_{20})^{(3)}G_{20}^* T_{21}$$

618

$$\frac{dG_{21}}{dt} = -((a'_{21})^{(3)} + (p_{21})^{(3)})G_{21} + (a_{21})^{(3)}G_{20} - (q_{21})^{(3)}G_{21}^* T_{21}$$

619

$$\frac{dG_{22}}{dt} = -((a'_{22})^{(3)} + (p_{22})^{(3)})G_{22} + (a_{22})^{(3)}G_{21} - (q_{22})^{(3)}G_{22}^* T_{21}$$

6120

$$\frac{dT_{20}}{dt} = -((b'_{20})^{(3)} - (r_{20})^{(3)})T_{20} + (b_{20})^{(3)}T_{21} + \sum_{j=20}^{22} (s_{(20)(j)}) T_{20}^* G_j$$

621

$$\frac{dT_{21}}{dt} = -((b'_{21})^{(3)} - (r_{21})^{(3)})T_{21} + (b_{21})^{(3)}T_{20} + \sum_{j=20}^{22} (s_{(21)(j)}) T_{21}^* G_j$$

622

$$\frac{dT_{22}}{dt} = -((b'_{22})^{(3)} - (r_{22})^{(3)})T_{22} + (b_{22})^{(3)}T_{21} + \sum_{j=20}^{22} (s_{(22)(j)}) T_{22}^* G_j$$

623

If the conditions of the previous theorem are satisfied and if the functions $(a_i'')^{(4)}$ and $(b_i'')^{(4)}$ belong to $C^{(4)}(\mathbb{R}_+)$ then the above equilibrium point is asymptotically stable

624

Denote

Definition of G_i, T_i :-

625

$$G_i = G_i^* + G_i \quad , T_i = T_i^* + T_i$$

$$\frac{\partial (a_{25}'')^{(4)}}{\partial T_{25}} (T_{25}^*) = (q_{25})^{(4)} \quad , \quad \frac{\partial (b_i'')^{(4)}}{\partial G_j} ((G_{27})^*) = s_{ij}$$

Then taking into account equations (global) and neglecting the terms of power 2, we obtain

626

$$\frac{dG_{24}}{dt} = -((a'_{24})^{(4)} + (p_{24})^{(4)})G_{24} + (a_{24})^{(4)}G_{25} - (q_{24})^{(4)}G_{24}^* T_{25}$$

627

$$\frac{dG_{25}}{dt} = -((a'_{25})^{(4)} + (p_{25})^{(4)})G_{25} + (a_{25})^{(4)}G_{24} - (q_{25})^{(4)}G_{25}^* T_{25}$$

628

$$\frac{dG_{26}}{dt} = -((a'_{26})^{(4)} + (p_{26})^{(4)})G_{26} + (a_{26})^{(4)}G_{25} - (q_{26})^{(4)}G_{26}^* T_{25}$$

629

$$\frac{dT_{24}}{dt} = -((b'_{24})^{(4)} - (r_{24})^{(4)})T_{24} + (b_{24})^{(4)}T_{25} + \sum_{j=24}^{26} (s_{(24)(j)}) T_{24}^* G_j$$

630

$$\frac{dT_{25}}{dt} = -((b'_{25})^{(4)} - (r_{25})^{(4)})T_{25} + (b_{25})^{(4)}T_{24} + \sum_{j=24}^{26} (s_{(25)(j)}) T_{25}^* G_j$$

631

$$\frac{dT_{26}}{dt} = -((b'_{26})^{(4)} - (r_{26})^{(4)})T_{26} + (b_{26})^{(4)}T_{25} + \sum_{j=24}^{26} (s_{(26)(j)}) T_{26}^* G_j$$

632

633

If the conditions of the previous theorem are satisfied and if the functions $(a_i'')^{(5)}$ and $(b_i'')^{(5)}$ belong to $C^{(5)}(\mathbb{R}_+)$ then the above equilibrium point is asymptotically stable

Denote

Definition of $\mathbb{G}_i, \mathbb{T}_i$:- 634

$$G_i = G_i^* + \mathbb{G}_i \quad , \quad T_i = T_i^* + \mathbb{T}_i$$

$$\frac{\partial (a_{29}^{(5)})}{\partial T_{29}} (T_{29}^*) = (q_{29})^{(5)} \quad , \quad \frac{\partial (b_i^{(5)})}{\partial G_j} ((G_{31})^*) = s_{ij}$$

Then taking into account equations (global) and neglecting the terms of power 2, we obtain 635

$$\frac{d\mathbb{G}_{28}}{dt} = -((a'_{28})^{(5)} + (p_{28})^{(5)})\mathbb{G}_{28} + (a_{28})^{(5)}\mathbb{G}_{29} - (q_{28})^{(5)}G_{28}^* \mathbb{T}_{29} \quad 636$$

$$\frac{d\mathbb{G}_{29}}{dt} = -((a'_{29})^{(5)} + (p_{29})^{(5)})\mathbb{G}_{29} + (a_{29})^{(5)}\mathbb{G}_{28} - (q_{29})^{(5)}G_{29}^* \mathbb{T}_{29} \quad 637$$

$$\frac{d\mathbb{G}_{30}}{dt} = -((a'_{30})^{(5)} + (p_{30})^{(5)})\mathbb{G}_{30} + (a_{30})^{(5)}\mathbb{G}_{29} - (q_{30})^{(5)}G_{30}^* \mathbb{T}_{29} \quad 638$$

$$\frac{d\mathbb{T}_{28}}{dt} = -((b'_{28})^{(5)} - (r_{28})^{(5)})\mathbb{T}_{28} + (b_{28})^{(5)}\mathbb{T}_{29} + \sum_{j=28}^{30} (s_{(28)(j)}) T_{28}^* \mathbb{G}_j \quad 639$$

$$\frac{d\mathbb{T}_{29}}{dt} = -((b'_{29})^{(5)} - (r_{29})^{(5)})\mathbb{T}_{29} + (b_{29})^{(5)}\mathbb{T}_{28} + \sum_{j=28}^{30} (s_{(29)(j)}) T_{29}^* \mathbb{G}_j \quad 640$$

$$\frac{d\mathbb{T}_{30}}{dt} = -((b'_{30})^{(5)} - (r_{30})^{(5)})\mathbb{T}_{30} + (b_{30})^{(5)}\mathbb{T}_{29} + \sum_{j=28}^{30} (s_{(30)(j)}) T_{30}^* \mathbb{G}_j \quad 641$$

If the conditions of the previous theorem are satisfied and if the functions $(a_i^{(6)})$ and $(b_i^{(6)})$ belong to $C^{(6)}(\mathbb{R}_+)$ then the above equilibrium point is asymptotically stable 642

Denote

Definition of $\mathbb{G}_i, \mathbb{T}_i$:- 643

$$G_i = G_i^* + \mathbb{G}_i \quad , \quad T_i = T_i^* + \mathbb{T}_i$$

$$\frac{\partial (a_{33}^{(6)})}{\partial T_{33}} (T_{33}^*) = (q_{33})^{(6)} \quad , \quad \frac{\partial (b_i^{(6)})}{\partial G_j} ((G_{35})^*) = s_{ij}$$

Then taking into account equations(global) and neglecting the terms of power 2, we obtain 644

$$\frac{d\mathbb{G}_{32}}{dt} = -((a'_{32})^{(6)} + (p_{32})^{(6)})\mathbb{G}_{32} + (a_{32})^{(6)}\mathbb{G}_{33} - (q_{32})^{(6)}G_{32}^* \mathbb{T}_{33} \quad 645$$

$$\frac{d\mathbb{G}_{33}}{dt} = -((a'_{33})^{(6)} + (p_{33})^{(6)})\mathbb{G}_{33} + (a_{33})^{(6)}\mathbb{G}_{32} - (q_{33})^{(6)}G_{33}^* \mathbb{T}_{33} \quad 646$$

$$\frac{d\mathbb{G}_{34}}{dt} = -((a'_{34})^{(6)} + (p_{34})^{(6)})\mathbb{G}_{34} + (a_{34})^{(6)}\mathbb{G}_{33} - (q_{34})^{(6)}G_{34}^* \mathbb{T}_{33} \quad 647$$

$$\frac{d\mathbb{T}_{32}}{dt} = -((b'_{32})^{(6)} - (r_{32})^{(6)})\mathbb{T}_{32} + (b_{32})^{(6)}\mathbb{T}_{33} + \sum_{j=32}^{34} (s_{(32)(j)}) T_{32}^* \mathbb{G}_j \quad 648$$

$$\frac{d\mathbb{T}_{33}}{dt} = -((b'_{33})^{(6)} - (r_{33})^{(6)})\mathbb{T}_{33} + (b_{33})^{(6)}\mathbb{T}_{32} + \sum_{j=32}^{34} (s_{(33)(j)}) T_{33}^* \mathbb{G}_j \quad 649$$

$$\frac{d\mathbb{T}_{34}}{dt} = -((b'_{34})^{(6)} - (r_{34})^{(6)})\mathbb{T}_{34} + (b_{34})^{(6)}\mathbb{T}_{33} + \sum_{j=32}^{34} (s_{(34)(j)}) T_{34}^* \mathbb{G}_j \quad 650$$

Obviously, these values represent an equilibrium solution of 79,20,36,22,23, 651

If the conditions of the previous theorem are satisfied and if the functions $(a_i^{(7)})$ and $(b_i^{(7)})$ belong to $C^{(7)}(\mathbb{R}_+)$ then the above equilibrium point is asymptotically stable.

Proof: Denote

Definition of $\mathbb{G}_i, \mathbb{T}_i$:-

652
653

$$G_i = G_i^* + \mathbb{G}_i, T_i = T_i^* + \mathbb{T}_i$$

$$\frac{\partial (a_{37}^{(7)})}{\partial T_{37}} (T_{37}^*) = (q_{37})^{(7)}, \frac{\partial (b_i^{(7)})}{\partial G_j} ((G_{39})^{**}) = s_{ij}$$

Then taking into account equations(SOLUTIONAL) and neglecting the terms of power 2, we obtain

654

$$\frac{d\mathbb{G}_{36}}{dt} = -((a'_{36})^{(7)} + (p_{36})^{(7)})\mathbb{G}_{36} + (a_{36})^{(7)}\mathbb{G}_{37} - (q_{36})^{(7)}G_{36}^* \mathbb{T}_{37}$$

655
656

$$\frac{d\mathbb{G}_{37}}{dt} = -((a'_{37})^{(7)} + (p_{37})^{(7)})\mathbb{G}_{37} + (a_{37})^{(7)}\mathbb{G}_{36} - (q_{37})^{(7)}G_{37}^* \mathbb{T}_{37}$$

657

$$\frac{d\mathbb{G}_{38}}{dt} = -((a'_{38})^{(7)} + (p_{38})^{(7)})\mathbb{G}_{38} + (a_{38})^{(7)}\mathbb{G}_{37} - (q_{38})^{(7)}G_{38}^* \mathbb{T}_{37}$$

658

$$\frac{d\mathbb{T}_{36}}{dt} = -((b'_{36})^{(7)} - (r_{36})^{(7)})\mathbb{T}_{36} + (b_{36})^{(7)}\mathbb{T}_{37} + \sum_{j=36}^{38} (s_{(36)(j)})T_{36}^* \mathbb{G}_j$$

659

$$\frac{d\mathbb{T}_{37}}{dt} = -((b'_{37})^{(7)} - (r_{37})^{(7)})\mathbb{T}_{37} + (b_{37})^{(7)}\mathbb{T}_{36} + \sum_{j=36}^{38} (s_{(37)(j)})T_{37}^* \mathbb{G}_j$$

660

$$\frac{d\mathbb{T}_{38}}{dt} = -((b'_{38})^{(7)} - (r_{38})^{(7)})\mathbb{T}_{38} + (b_{38})^{(7)}\mathbb{T}_{37} + \sum_{j=36}^{38} (s_{(38)(j)})T_{38}^* \mathbb{G}_j$$

661

2.

The characteristic equation of this system is

$$\left((\lambda)^{(1)} + (b'_{15})^{(1)} - (r_{15})^{(1)} \right) \left\{ \left((\lambda)^{(1)} + (a'_{15})^{(1)} + (p_{15})^{(1)} \right) \right. \\ \left. \left[\left((\lambda)^{(1)} + (a'_{13})^{(1)} + (p_{13})^{(1)} \right) (q_{14})^{(1)} G_{14}^* + (a_{14})^{(1)} (q_{13})^{(1)} G_{13}^* \right] \right\} \\ \left(\left((\lambda)^{(1)} + (b'_{13})^{(1)} - (r_{13})^{(1)} \right) s_{(14),(14)} T_{14}^* + (b_{14})^{(1)} s_{(13),(14)} T_{14}^* \right) \\ + \left(\left((\lambda)^{(1)} + (a'_{14})^{(1)} + (p_{14})^{(1)} \right) (q_{13})^{(1)} G_{13}^* + (a_{13})^{(1)} (q_{14})^{(1)} G_{14}^* \right) \\ \left(\left((\lambda)^{(1)} + (b'_{13})^{(1)} - (r_{13})^{(1)} \right) s_{(14),(13)} T_{14}^* + (b_{14})^{(1)} s_{(13),(13)} T_{13}^* \right) \\ \left(\left((\lambda)^{(1)} \right)^2 + \left((a'_{13})^{(1)} + (a'_{14})^{(1)} + (p_{13})^{(1)} + (p_{14})^{(1)} \right) (\lambda)^{(1)} \right) \\ \left(\left((\lambda)^{(1)} \right)^2 + \left((b'_{13})^{(1)} + (b'_{14})^{(1)} - (r_{13})^{(1)} + (r_{14})^{(1)} \right) (\lambda)^{(1)} \right) \\ + \left(\left((\lambda)^{(1)} \right)^2 + \left((a'_{13})^{(1)} + (a'_{14})^{(1)} + (p_{13})^{(1)} + (p_{14})^{(1)} \right) (\lambda)^{(1)} \right) (q_{15})^{(1)} G_{15} \\ + \left((\lambda)^{(1)} + (a'_{13})^{(1)} + (p_{13})^{(1)} \right) \left((a_{15})^{(1)} (q_{14})^{(1)} G_{14}^* + (a_{14})^{(1)} (a_{15})^{(1)} (q_{13})^{(1)} G_{13}^* \right) \\ \left(\left((\lambda)^{(1)} + (b'_{13})^{(1)} - (r_{13})^{(1)} \right) s_{(14),(15)} T_{14}^* + (b_{14})^{(1)} s_{(13),(15)} T_{13}^* \right) \} = 0$$

+

$$\left((\lambda)^{(2)} + (b'_{18})^{(2)} - (r_{18})^{(2)} \right) \left\{ \left((\lambda)^{(2)} + (a'_{18})^{(2)} + (p_{18})^{(2)} \right) \right. \\ \left. \left[\left((\lambda)^{(2)} + (a'_{16})^{(2)} + (p_{16})^{(2)} \right) (q_{17})^{(2)} G_{17}^* + (a_{17})^{(2)} (q_{16})^{(2)} G_{16}^* \right] \right\} \\ \left(\left((\lambda)^{(2)} + (b'_{16})^{(2)} - (r_{16})^{(2)} \right) s_{(17),(17)} T_{17}^* + (b_{17})^{(2)} s_{(16),(17)} T_{17}^* \right) \\ + \left(\left((\lambda)^{(2)} + (a'_{17})^{(2)} + (p_{17})^{(2)} \right) (q_{16})^{(2)} G_{16}^* + (a_{16})^{(2)} (q_{17})^{(2)} G_{17}^* \right) \\ \left(\left((\lambda)^{(2)} + (b'_{16})^{(2)} - (r_{16})^{(2)} \right) s_{(17),(16)} T_{17}^* + (b_{17})^{(2)} s_{(16),(16)} T_{16}^* \right) \\ \left(\left((\lambda)^{(2)} \right)^2 + \left((a'_{16})^{(2)} + (a'_{17})^{(2)} + (p_{16})^{(2)} + (p_{17})^{(2)} \right) (\lambda)^{(2)} \right)$$

$$\begin{aligned} & \left(((\lambda)^{(2)})^2 + (b'_{16})^{(2)} + (b'_{17})^{(2)} - (r_{16})^{(2)} + (r_{17})^{(2)} \right) (\lambda)^{(2)} \\ & + \left(((\lambda)^{(2)})^2 + (a'_{16})^{(2)} + (a'_{17})^{(2)} + (p_{16})^{(2)} + (p_{17})^{(2)} \right) (\lambda)^{(2)} (q_{18})^{(2)} G_{18} \\ & + ((\lambda)^{(2)} + (a'_{16})^{(2)} + (p_{16})^{(2)}) ((a_{18})^{(2)} (q_{17})^{(2)} G_{17}^* + (a_{17})^{(2)} (a_{18})^{(2)} (q_{16})^{(2)} G_{16}^*) \\ & \left(((\lambda)^{(2)} + (b'_{16})^{(2)} - (r_{16})^{(2)}) s_{(17),(18)} T_{17}^* + (b_{17})^{(2)} s_{(16),(18)} T_{16}^* \right) \} = 0 \end{aligned}$$

$$\begin{aligned} & + \\ & \left((\lambda)^{(3)} + (b'_{22})^{(3)} - (r_{22})^{(3)} \right) \{ (\lambda)^{(3)} + (a'_{22})^{(3)} + (p_{22})^{(3)} \} \\ & \left[\left((\lambda)^{(3)} + (a'_{20})^{(3)} + (p_{20})^{(3)} \right) (q_{21})^{(3)} G_{21}^* + (a_{21})^{(3)} (q_{20})^{(3)} G_{20}^* \right] \\ & \left((\lambda)^{(3)} + (b'_{20})^{(3)} - (r_{20})^{(3)} \right) s_{(21),(21)} T_{21}^* + (b_{21})^{(3)} s_{(20),(21)} T_{21}^* \\ & + \left((\lambda)^{(3)} + (a'_{21})^{(3)} + (p_{21})^{(3)} \right) (q_{20})^{(3)} G_{20}^* + (a_{20})^{(3)} (q_{21})^{(1)} G_{21}^* \\ & \left((\lambda)^{(3)} + (b'_{20})^{(3)} - (r_{20})^{(3)} \right) s_{(21),(20)} T_{21}^* + (b_{21})^{(3)} s_{(20),(20)} T_{20}^* \\ & \left(((\lambda)^{(3)})^2 + (a'_{20})^{(3)} + (a'_{21})^{(3)} + (p_{20})^{(3)} + (p_{21})^{(3)} \right) (\lambda)^{(3)} \\ & \left(((\lambda)^{(3)})^2 + (b'_{20})^{(3)} + (b'_{21})^{(3)} - (r_{20})^{(3)} + (r_{21})^{(3)} \right) (\lambda)^{(3)} \\ & + \left(((\lambda)^{(3)})^2 + (a'_{20})^{(3)} + (a'_{21})^{(3)} + (p_{20})^{(3)} + (p_{21})^{(3)} \right) (\lambda)^{(3)} (q_{22})^{(3)} G_{22} \\ & + ((\lambda)^{(3)} + (a'_{20})^{(3)} + (p_{20})^{(3)}) ((a_{22})^{(3)} (q_{21})^{(3)} G_{21}^* + (a_{21})^{(3)} (a_{22})^{(3)} (q_{20})^{(3)} G_{20}^*) \\ & \left((\lambda)^{(3)} + (b'_{20})^{(3)} - (r_{20})^{(3)} \right) s_{(21),(22)} T_{21}^* + (b_{21})^{(3)} s_{(20),(22)} T_{20}^* \} = 0 \end{aligned}$$

$$\begin{aligned} & + \\ & \left((\lambda)^{(4)} + (b'_{26})^{(4)} - (r_{26})^{(4)} \right) \{ (\lambda)^{(4)} + (a'_{26})^{(4)} + (p_{26})^{(4)} \} \\ & \left[\left((\lambda)^{(4)} + (a'_{24})^{(4)} + (p_{24})^{(4)} \right) (q_{25})^{(4)} G_{25}^* + (a_{25})^{(4)} (q_{24})^{(4)} G_{24}^* \right] \\ & \left((\lambda)^{(4)} + (b'_{24})^{(4)} - (r_{24})^{(4)} \right) s_{(25),(25)} T_{25}^* + (b_{25})^{(4)} s_{(24),(25)} T_{25}^* \\ & + \left((\lambda)^{(4)} + (a'_{25})^{(4)} + (p_{25})^{(4)} \right) (q_{24})^{(4)} G_{24}^* + (a_{24})^{(4)} (q_{25})^{(4)} G_{25}^* \\ & \left((\lambda)^{(4)} + (b'_{24})^{(4)} - (r_{24})^{(4)} \right) s_{(25),(24)} T_{25}^* + (b_{25})^{(4)} s_{(24),(24)} T_{24}^* \\ & \left(((\lambda)^{(4)})^2 + (a'_{24})^{(4)} + (a'_{25})^{(4)} + (p_{24})^{(4)} + (p_{25})^{(4)} \right) (\lambda)^{(4)} \\ & \left(((\lambda)^{(4)})^2 + (b'_{24})^{(4)} + (b'_{25})^{(4)} - (r_{24})^{(4)} + (r_{25})^{(4)} \right) (\lambda)^{(4)} \\ & + \left(((\lambda)^{(4)})^2 + (a'_{24})^{(4)} + (a'_{25})^{(4)} + (p_{24})^{(4)} + (p_{25})^{(4)} \right) (\lambda)^{(4)} (q_{26})^{(4)} G_{26} \\ & + ((\lambda)^{(4)} + (a'_{24})^{(4)} + (p_{24})^{(4)}) ((a_{26})^{(4)} (q_{25})^{(4)} G_{25}^* + (a_{25})^{(4)} (a_{26})^{(4)} (q_{24})^{(4)} G_{24}^*) \\ & \left((\lambda)^{(4)} + (b'_{24})^{(4)} - (r_{24})^{(4)} \right) s_{(25),(26)} T_{25}^* + (b_{25})^{(4)} s_{(24),(26)} T_{24}^* \} = 0 \end{aligned}$$

$$\begin{aligned} & + \\ & \left((\lambda)^{(5)} + (b'_{30})^{(5)} - (r_{30})^{(5)} \right) \{ (\lambda)^{(5)} + (a'_{30})^{(5)} + (p_{30})^{(5)} \} \\ & \left[\left((\lambda)^{(5)} + (a'_{28})^{(5)} + (p_{28})^{(5)} \right) (q_{29})^{(5)} G_{29}^* + (a_{29})^{(5)} (q_{28})^{(5)} G_{28}^* \right] \end{aligned}$$

$$\left(\left((\lambda)^{(5)} + (b'_{28})^{(5)} - (r_{28})^{(5)} \right) s_{(29),(29)} T_{29}^* + (b_{29})^{(5)} s_{(28),(29)} T_{29}^* \right) + \left(((\lambda)^{(5)} + (a'_{29})^{(5)} + (p_{29})^{(5)}) (q_{28})^{(5)} G_{28}^* + (a_{28})^{(5)} (q_{29})^{(5)} G_{29}^* \right) \left(\left((\lambda)^{(5)} + (b'_{28})^{(5)} - (r_{28})^{(5)} \right) s_{(29),(28)} T_{29}^* + (b_{29})^{(5)} s_{(28),(28)} T_{28}^* \right) \left(((\lambda)^{(5)})^2 + \left((a'_{28})^{(5)} + (a'_{29})^{(5)} + (p_{28})^{(5)} + (p_{29})^{(5)} \right) (\lambda)^{(5)} \right) \left(((\lambda)^{(5)})^2 + \left((b'_{28})^{(5)} + (b'_{29})^{(5)} - (r_{28})^{(5)} + (r_{29})^{(5)} \right) (\lambda)^{(5)} \right) + \left(((\lambda)^{(5)})^2 + \left((a'_{28})^{(5)} + (a'_{29})^{(5)} + (p_{28})^{(5)} + (p_{29})^{(5)} \right) (\lambda)^{(5)} \right) (q_{30})^{(5)} G_{30} + \left((\lambda)^{(5)} + (a'_{28})^{(5)} + (p_{28})^{(5)} \right) \left((a_{30})^{(5)} (q_{29})^{(5)} G_{29}^* + (a_{29})^{(5)} (a_{30})^{(5)} (q_{28})^{(5)} G_{28}^* \right) \left(\left((\lambda)^{(5)} + (b'_{28})^{(5)} - (r_{28})^{(5)} \right) s_{(29),(30)} T_{29}^* + (b_{29})^{(5)} s_{(28),(30)} T_{28}^* \right) \} = 0$$

+

$$\left((\lambda)^{(6)} + (b'_{34})^{(6)} - (r_{34})^{(6)} \right) \left\{ \left((\lambda)^{(6)} + (a'_{34})^{(6)} + (p_{34})^{(6)} \right) \left[\left(\left((\lambda)^{(6)} + (a'_{32})^{(6)} + (p_{32})^{(6)} \right) (q_{33})^{(6)} G_{33}^* + (a_{33})^{(6)} (q_{32})^{(6)} G_{32}^* \right) \right] \right. \\ \left. \left(\left((\lambda)^{(6)} + (b'_{32})^{(6)} - (r_{32})^{(6)} \right) s_{(33),(33)} T_{33}^* + (b_{33})^{(6)} s_{(32),(33)} T_{33}^* \right) + \left(((\lambda)^{(6)} + (a'_{33})^{(6)} + (p_{33})^{(6)}) (q_{32})^{(6)} G_{32}^* + (a_{32})^{(6)} (q_{33})^{(6)} G_{33}^* \right) \right. \\ \left. \left(\left((\lambda)^{(6)} + (b'_{32})^{(6)} - (r_{32})^{(6)} \right) s_{(33),(32)} T_{33}^* + (b_{33})^{(6)} s_{(32),(32)} T_{32}^* \right) \right) \left(((\lambda)^{(6)})^2 + \left((a'_{32})^{(6)} + (a'_{33})^{(6)} + (p_{32})^{(6)} + (p_{33})^{(6)} \right) (\lambda)^{(6)} \right) \\ \left(((\lambda)^{(6)})^2 + \left((b'_{32})^{(6)} + (b'_{33})^{(6)} - (r_{32})^{(6)} + (r_{33})^{(6)} \right) (\lambda)^{(6)} \right) + \left(((\lambda)^{(6)})^2 + \left((a'_{32})^{(6)} + (a'_{33})^{(6)} + (p_{32})^{(6)} + (p_{33})^{(6)} \right) (\lambda)^{(6)} \right) (q_{34})^{(6)} G_{34} \\ + \left((\lambda)^{(6)} + (a'_{32})^{(6)} + (p_{32})^{(6)} \right) \left((a_{34})^{(6)} (q_{33})^{(6)} G_{33}^* + (a_{33})^{(6)} (a_{34})^{(6)} (q_{32})^{(6)} G_{32}^* \right) \\ \left. \left(\left((\lambda)^{(6)} + (b'_{32})^{(6)} - (r_{32})^{(6)} \right) s_{(33),(34)} T_{33}^* + (b_{33})^{(6)} s_{(32),(34)} T_{32}^* \right) \right\} = 0$$

+

$$\left((\lambda)^{(7)} + (b'_{38})^{(7)} - (r_{38})^{(7)} \right) \left\{ \left((\lambda)^{(7)} + (a'_{38})^{(7)} + (p_{38})^{(7)} \right) \left[\left(\left((\lambda)^{(7)} + (a'_{36})^{(7)} + (p_{36})^{(7)} \right) (q_{37})^{(7)} G_{37}^* + (a_{37})^{(7)} (q_{36})^{(7)} G_{36}^* \right) \right] \right. \\ \left. \left(\left((\lambda)^{(7)} + (b'_{36})^{(7)} - (r_{36})^{(7)} \right) s_{(37),(37)} T_{37}^* + (b_{37})^{(7)} s_{(36),(37)} T_{37}^* \right) + \left(((\lambda)^{(7)} + (a'_{37})^{(7)} + (p_{37})^{(7)}) (q_{36})^{(7)} G_{36}^* + (a_{36})^{(7)} (q_{37})^{(7)} G_{37}^* \right) \right. \\ \left. \left(\left((\lambda)^{(7)} + (b'_{36})^{(7)} - (r_{36})^{(7)} \right) s_{(37),(36)} T_{37}^* + (b_{37})^{(7)} s_{(36),(36)} T_{36}^* \right) \right) \left(((\lambda)^{(7)})^2 + \left((a'_{36})^{(7)} + (a'_{37})^{(7)} + (p_{36})^{(7)} + (p_{37})^{(7)} \right) (\lambda)^{(7)} \right) \\ \left(((\lambda)^{(7)})^2 + \left((b'_{36})^{(7)} + (b'_{37})^{(7)} - (r_{36})^{(7)} + (r_{37})^{(7)} \right) (\lambda)^{(7)} \right) + \left(((\lambda)^{(7)})^2 + \left((a'_{36})^{(7)} + (a'_{37})^{(7)} + (p_{36})^{(7)} + (p_{37})^{(7)} \right) (\lambda)^{(7)} \right) (q_{38})^{(7)} G_{38} \\ + \left((\lambda)^{(7)} + (a'_{36})^{(7)} + (p_{36})^{(7)} \right) \left((a_{38})^{(7)} (q_{37})^{(7)} G_{37}^* + (a_{37})^{(7)} (a_{38})^{(7)} (q_{36})^{(7)} G_{36}^* \right) \\ \left. \left(\left((\lambda)^{(7)} + (b'_{36})^{(7)} - (r_{36})^{(7)} \right) s_{(37),(38)} T_{37}^* + (b_{37})^{(7)} s_{(36),(38)} T_{36}^* \right) \right\} = 0$$

REFERENCES

- =====
- (1) A HAIMOVICI: "On the growth of a two species ecological system divided on age groups". Tensor, Vol 37 (1982), Commemoration volume dedicated to Professor Akitsugu Kawaguchi on his 80th birthday
 - (2) FRTJOF CAPRA: "The web of life" Flamingo, Harper Collins See "Dissipative structures" pages 172-188
 - (3) HEYLIGHEN F. (2001): "The Science of Self-organization and Adaptivity", in L. D. Kiel, (ed) . Knowledge Management, Organizational Intelligence and Learning, and Complexity, in: The Encyclopedia of Life Support Systems ((EOLSS), (Eolss Publishers, Oxford) [<http://www.eolss.net>]
 - (4) MATSUI, T, H. Masunaga, S. M. Kreidenweis, R. A. Pielke Sr., W.-K. Tao, M. Chin, and Y. J Kaufman (2006), "Satellite-based assessment of marine low cloud variability associated with aerosol, atmospheric stability, and the diurnal cycle", J. Geophys. Res., 111, D17204, doi:10.1029/2005JD006097
 - (5) STEVENS, B, G. Feingold, W.R. Cotton and R.L. Walko, "Elements of the microphysical structure of numerically simulated nonprecipitating stratocumulus" J. Atmos. Sci., 53, 980-1006
 - (6) FEINGOLD, G, Koren, I; Wang, HL; Xue, HW; Brewer, WA (2010), "Precipitation-generated oscillations in open cellular cloud fields" *Nature*, 466 (7308) 849-852, doi: [10.1038/nature09314](https://doi.org/10.1038/nature09314), Published 12-Aug 2010
 - (7) HEYLIGHEN F. (2001): "The Science of Self-organization and Adaptivity", in L. D. Kiel, (ed) . Knowledge Management, Organizational Intelligence and Learning, and Complexity, in: The Encyclopedia of Life Support Systems ((EOLSS), (Eolss Publishers, Oxford) [<http://www.eolss.net>]
 - (8) MATSUI, T, H. Masunaga, S. M. Kreidenweis, R. A. Pielke Sr., W.-K. Tao, M. Chin, and Y. J Kaufman (2006), "Satellite-based assessment of marine low cloud variability associated with aerosol, atmospheric stability, and the diurnal cycle", J. Geophys. Res., 111, D17204, doi:10.1029/2005JD006097
 - (8A) STEVENS, B, G. Feingold, W.R. Cotton and R.L. Walko, "Elements of the microphysical structure of numerically simulated nonprecipitating stratocumulus" J. Atmos. Sci., 53, 980-1006
 - (8B) FEINGOLD, G, Koren, I; Wang, HL; Xue, HW; Brewer, WA (2010), "Precipitation-generated oscillations in open cellular cloud fields" *Nature*, 466 (7308) 849-852, doi: [10.1038/nature09314](https://doi.org/10.1038/nature09314), Published 12-Aug 2010

- 9)^ a b c Einstein, A. (1905), "Ist die Trägheit eines Körpers von seinem Energieinhalt abhängig?", Annalen der Physik 18: 639 Bibcode 1905AnP...323..639E, DOI:10.1002/andp.19053231314. See also the English translation.
- 10)^ a b Paul Allen Tipler, Ralph A. Llewellyn (2003-01), Modern Physics, W. H. Freeman and Company, pp. 87–88, ISBN 0-7167-4345-0
- 11)^ a b Rainville, S. et al. World Year of Physics: A direct test of $E=mc^2$. Nature 438, 1096-1097 (22 December 2005) | doi: 10.1038/4381096a; Published online 21 December 2005.
- 12)^ In F. Fernflores. The Equivalence of Mass and Energy. Stanford Encyclopedia of Philosophy
- 13)^ Note that the relativistic mass, in contrast to the rest mass m_0 , is not a relativistic invariant, and that the velocity is not a Minkowski four-vector, in contrast to the quantity dx^μ , where dx^μ is the differential of the proper time. However, the energy-momentum four-vector is a genuine Minkowski four-vector, and the intrinsic origin of the square-root in the definition of the relativistic mass is the distinction between $d\tau$ and dt .
- 14)^ Relativity DeMystified, D. McMahon, Mc Graw Hill (USA), 2006, ISBN 0-07-145545-0
- 15)^ Dynamics and Relativity, J.R. Forshaw, A.G. Smith, Wiley, 2009, ISBN 978-0-470-01460-8
- 16)^ Hans, H. S.; Puri, S. P. (2003). Mechanics (2 ed.). Tata McGraw-Hill. p. 433. ISBN 0-07-047360-9., Chapter 12 page 433
- 17)^ E. F. Taylor and J. A. Wheeler, Spacetime Physics, W.H. Freeman and Co., NY. 1992. ISBN 0-7167-2327-1, see pp. 248-9 for discussion of mass remaining constant after detonation of nuclear bombs, until heat is allowed to escape.
- 18)^ Mould, Richard A. (2002). Basic relativity (2 ed.). Springer. p. 126. ISBN 0-387-95210-1., Chapter 5 page 126
- 19)^ Chow, Tail L. (2006). Introduction to electromagnetic theory: a modern perspective. Jones & Bartlett Learning. p. 392. ISBN 0-7637-3827-1., Chapter 10 page 392
- 20)^ [2] Cockcroft-Walton experiment
- 21)^ a b c Conversions used: 1956 International (Steam) Table (IT) values where one calorie \equiv 4.1868 J and one BTU \equiv 1055.05585262 J. Weapons designers' conversion value of one gram TNT \equiv 1000 calories used.
- 22)^ Assuming the dam is generating at its peak capacity of 6,809 MW.
- 23)^ Assuming a 90/10 alloy of Pt/Ir by weight, a Cp of 25.9 for Pt and 25.1 for Ir, a Pt-dominated average Cp of 25.8, 5.134 moles of metal, and 132 J.K⁻¹ for the prototype. A variation of ± 1.5 picograms is of course, much smaller than the actual uncertainty in the mass of the international prototype, which are ± 2 micrograms.
- 24)^ [3] Article on Earth rotation energy. Divided by c^2 .
- 25)^ a b Earth's gravitational self-energy is 4.6×10^{-10} that of Earth's total mass, or 2.7 trillion metric tons. Citation: The Apache Point Observatory Lunar Laser-Ranging Operation (APOLLO), T.

W. Murphy, Jr. et al. University of Washington, Dept. of Physics (132 kB PDF, [here.](#)).

- 26)^ There is usually more than one possible way to define a field energy, because any field can be made to couple to gravity in many different ways. By general scaling arguments, the correct answer at everyday distances, which are long compared to the quantum gravity scale, should be minimal coupling, which means that no powers of the curvature tensor appear. Any non-minimal couplings, along with other higher order terms, are presumably only determined by a theory of quantum gravity, and within string theory, they only start to contribute to experiments at the string scale.
- 27)^ G. 't Hooft, "Computation of the quantum effects due to a four-dimensional pseudoparticle", *Physical Review D* 14:3432–3450 (1976).
- 28)^ A. Belavin, A. M. Polyakov, A. Schwarz, Yu. Tyupkin, "Pseudoparticle Solutions to Yang Mills Equations", *Physics Letters* 59B:85 (1975).
- 29)^ F. Klinkhammer, N. Manton, "A Saddle Point Solution in the Weinberg Salam Theory", *Physical Review D* 30:2212.
- 30)^ Rubakov V. A. "Monopole Catalysis of Proton Decay", *Reports on Progress in Physics* 51:189–241 (1988).
- 31)^ S.W. Hawking "Black Holes Explosions?" *Nature* 248:30 (1974).
- 32)^ Einstein, A. (1905), "Zur Elektrodynamik bewegter Körper." (PDF), *Annalen der Physik* 17: 891–921, Bibcode 1905AnP...322...891E, DOI:10.1002/andp.19053221004. English translation.
- 33)^ See e.g. Lev B.Okun, The concept of Mass, *Physics Today* 42 (6), June 1969, p. 31–36, http://www.physicstoday.org/vol-42/iss-6/vol42no6p31_36.pdf
- 34)^ Max Jammer (1999), *Concepts of mass in contemporary physics and philosophy*, Princeton University Press, p. 51, ISBN 0-691-01017-X
- 35)^ Eriksen, Erik; Vøyenli, Kjell (1976), "The classical and relativistic concepts of mass", *Foundations of Physics* (Springer) 6: 115–124, Bibcode 1976FoPh....6..115E, DOI:10.1007/BF00708670
- 36)^ a b Jannsen, M., Mecklenburg, M. (2007), *From classical to relativistic mechanics: Electromagnetic models of the electron.*, in V. F. Hendricks, et al., , *Interactions: Mathematics, Physics and Philosophy* (Dordrecht: Springer): 65–134
- 37)^ a b Whittaker, E.T. (1951–1953), 2. Edition: *A History of the theories of aether and electricity*, vol. 1: The classical theories / vol. 2: The modern theories 1900–1926, London: Nelson
- 38)^ Miller, Arthur I. (1981), *Albert Einstein's special theory of relativity. Emergence (1905) and early interpretation (1905–1911)*, Reading: Addison–Wesley, ISBN 0-201-04679-2
- 39)^ a b Darrigol, O. (2005), "The Genesis of the theory of relativity." (PDF), *Séminaire Poincaré* 1: 1–22
- 40)^ Philip Ball (Aug 23, 2011). "Did Einstein discover $E = mc^2$?" *Physics World*.
- 41)^ Ives, Herbert E. (1952), "Derivation of the mass-energy relation", *Journal of the Optical Society of America* 42 (8): 540–543, DOI:10.1364/JOSA.42.000540

- 42)^ Jammer, Max (1961/1997). *Concepts of Mass in Classical and Modern Physics*. New York: Dover. ISBN 0-486-29998-8.
- 43)^ Stachel, John; Torretti, Roberto (1982), "Einstein's first derivation of mass-energy equivalence", *American Journal of Physics* 50 (8): 760–763, Bibcode1982AmJPh..50..760S, DOI:10.1119/1.12764
- 44)^ Ohanian, Hans (2008), "Did Einstein prove $E=mc^2$?", *Studies In History and Philosophy of Science Part B* 40 (2): 167–173, arXiv:0805.1400, DOI:10.1016/j.shpsb.2009.03.002
- 45)^ Hecht, Eugene (2011), "How Einstein confirmed $E_0=mc^2$ ", *American Journal of Physics* 79 (6): 591–600, Bibcode 2011AmJPh..79..591H, DOI:10.1119/1.3549223
- 46)^ Rohrlich, Fritz (1990), "An elementary derivation of $E=mc^2$ ", *American Journal of Physics* 58 (4): 348–349, Bibcode 1990AmJPh..58..348R, DOI:10.1119/1.16168
- 47) (1996). *Lise Meitner: A Life in Physics*. California Studies in the History of Science. 13. Berkeley: University of California Press. pp. 236–237. ISBN 0-520-20860-
-
- (48)^ UIBK.ac.at
- (49)^ J. J. L. Morton; *et al.* (2008). "Solid-state quantum memory using the ^{31}P nuclear spin". *Nature* 455 (7216): 1085–1088. Bibcode 2008Natur.455.1085M. DOI:10.1038/nature07295.
- (50)^ S. Weisner (1983). "Conjugate coding". *Association of Computing Machinery, Special Interest Group in Algorithms and Computation Theory* 15: 78–88.
- (51)^ A. Zeilinger, *Dance of the Photons: From Einstein to Quantum Teleportation*, Farrar, Straus & Giroux, New York, 2010, pp. 189, 192, ISBN 0374239665
- (52)^ B. Schumacher (1995). "Quantum coding". *Physical Review A* 51 (4): 2738–2747. Bibcode 1995PhRvA..51.2738S. DOI:10.1103/PhysRevA.51.2738.
- (53) Delamotte, Bertrand; *A hint of renormalization*, *American Journal of Physics* 72 (2004) pp. 170–184.
Beautiful elementary introduction to the ideas, no prior knowledge of field theory being necessary. Full text available at: hep-th/0212049
- (54) Baez, John; *Renormalization Made Easy*, (2005). A qualitative introduction to the subject.
- (55) Blechman, Andrew E. ; *Renormalization: Our Greatly Misunderstood Friend*, (2002). Summary of a lecture; has more information about specific regularization and divergence-subtraction schemes.
- (56) Cao, Tian Yu & Schweber, Silvan S. ; *The Conceptual Foundations and the Philosophical Aspects of Renormalization Theory*, *Synthese*, 97(1) (1993), 33–108.

- (57) Shirkov, Dmitry; *Fifty Years of the Renormalization Group*, C.E.R.N. Courier 41(7) (2001). Full text available at: *I.O.P Magazines*.
- (58) E. Elizalde; *Zeta regularization techniques with Applications*.
- (59) N. N. Bogoliubov, D. V. Shirkov (1959): *The Theory of Quantized Fields*. New York, Interscience. The first text-book on the renormalization group theory.
- (60) Ryder, Lewis H. ; *Quantum Field Theory* (Cambridge University Press, 1985), ISBN 0-521-33859-X Highly readable textbook, certainly the best introduction to relativistic Q.F.T. for particle physics.
- (61) Zee, Anthony; *Quantum Field Theory in a Nutshell*, Princeton University Press (2003) ISBN 0-691-01019-6. Another excellent textbook on Q.F.T.
- (62) Weinberg, Steven; *The Quantum Theory of Fields* (3 volumes) Cambridge University Press (1995). A monumental treatise on Q.F.T. written by a leading expert, *Nobel laureate 1979*.
- (63) Pokorski, Stefan; *Gauge Field Theories*, Cambridge University Press (1987) ISBN 0-521-47816-2.
- (64) 't Hooft, Gerard; *The Glorious Days of Physics – Renormalization of Gauge theories*, lecture given at Erice (August/September 1998) by the *Nobel laureate 1999* . Full text available at: *hep-th/9812203*.
- (65) Rivasseau, Vincent; *An introduction to renormalization*, Poincaré Seminar (Paris, Oct. 12, 2002), published in: Duplantier, Bertrand; Rivasseau, Vincent (Eds.) ; *Poincaré Seminar 2002*, Progress in Mathematical Physics 30, Birkhäuser (2003) ISBN 3-7643-0579-7. Full text available in *PostScript*.
- (66) Rivasseau, Vincent; *From perturbative to constructive renormalization*, Princeton University Press (1991) ISBN 0-691-08530-7. Full text available in *PostScript*.
- (67) Iagolnitzer, Daniel & Magnen, J. ; *Renormalization group analysis*, Encyclopaedia of Mathematics, Kluwer Academic Publisher (1996). Full text available in *PostScript* and *pdfhere*.
- (68) Scharf, Günter; *Finite quantum electrodynamics: The casual approach*, Springer Verlag Berlin Heidelberg New York (1995) ISBN 3-540-60142-2.
- (69) A. S. Švarc (Albert Schwarz), *Математические основы квантовой теории поля*, (Mathematical aspects of quantum field theory), Atomizdat, Moscow, 1975. 368 pp.
- (70) A. N. Vasil'ev *The Field Theoretic Renormalization Group in Critical Behavior Theory and Stochastic Dynamics* (Routledge Chapman & Hall 2004); ISBN 978-0-415-31002-4
- (71) Nigel Goldenfeld ; *Lectures on Phase Transitions and the Renormalization Group*, Frontiers in Physics 85, West view Press (June, 1992) ISBN 0-201-55409-7. Covering the elementary aspects of the physics of phase's transitions and the renormalization group, this popular book emphasizes understanding and clarity rather than technical manipulations.
- (72) Zinn-Justin, Jean; *Quantum Field Theory and Critical Phenomena*, Oxford University Press (4th edition – 2002) ISBN 0-19-850923-5. A masterpiece on applications of renormalization methods to the calculation of critical exponents in statistical mechanics, following Wilson's ideas (Kenneth Wilson was *Nobel laureate 1982*).

- (73) Dematte, L., Priami, C., and Romanel, A. The BlenX language, a tutorial. In M. Bernardo, P. Degano, and G. Zavattaro (Eds.): SFM 2008, LNCS 5016, pp. 313-365, Springer, 2008.
- Denning, P. J. Beyond computational thinking. Comm. ACM, pp. 28-30, June 2009.
- (74) Goldin, D., Smolka, S., and Wegner, P. Interactive Computation: The New Paradigm, Springer, 2006.
- (75) Hewitt, C., Bishop, P., and Steiger, R. A universal modular ACTOR formalism for artificial intelligence. In Proc. of the 3rd IJCAI, pp. 235-245, Stanford, USA, 1973.
- (76) Priami, C. Computational thinking in biology, Trans. on Comput. Syst. Biol. VIII, LNBI 4780, pp. 63-76, Springer, 2007.
- (77) Schor, P. Algorithms for quantum computation: discrete logarithms and factoring. In Proc. 35th Annual Symposium on Foundations of Computer Science, IEEE Press, Los Almitos, CA, 1994.
- (78) Turing, A. On computable numbers with an application to the Entscheidungsproblem. In Proc. London Mathematical Society 42, pp. 230-265, 1936.
- (79) Wing, J. Computational thinking. Comm. ACM, pp. 33-35, March 2006

===== Acknowled

gments:

The introduction is a collection of information from various articles, Books, News Paper reports, Home Pages Of authors, Journal Reviews, Nature 's Letters, Article Abstracts, Research papers, Abstracts Of Research Papers, Stanford Encyclopedia, Web Pages, Ask a Physicist Column, Deliberations with Professors, the internet including Wikipedia. We acknowledge all authors who have contributed to the same. In the eventuality of the fact that there has been any act of omission on the part of the authors, we regret with great deal of compunction, contrition, regret, trepidation and remorse. As Newton said, it is only because erudite and eminent people allowed one to piggy ride on their backs; probably an attempt has been made to look slightly further. Once again, it is stated that the references are only illustrative and not comprehensive

First Author: ¹Mr. K. N.Prasanna Kumar has three doctorates one each in Mathematics, Economics, Political Science. Thesis was based on Mathematical Modeling. He was recently awarded D.litt. for his work on 'Mathematical Models in Political Science'--- Department of studies in Mathematics, Kuvempu University, Shimoga, Karnataka, India Corresponding **Author:drknpkumar@gmail.com**

Second Author: ²Prof. B.S Kiranagi is the Former Chairman of the Department of Studies in Mathematics, Manasa Gangotri and present Professor Emeritus of UGC in the Department. Professor Kiranagi has guided over 25 students and he has received many encomiums and laurels for his contribution to Co homology Groups and Mathematical Sciences. Known for his prolific writing, and one of the senior most Professors of the country, he has over 150 publications to his credit. A prolific writer and a prodigious thinker, he has to his credit several books on Lie Groups, Co Homology Groups, and other mathematical application topics, and excellent publication history.-- UGC Emeritus Professor (Department of studies in Mathematics), Manasagangotri, University of Mysore, Karnataka, India

Third Author: ³Prof. C.S. Bagewadi is the present Chairman of Department of Mathematics and Department of Studies in Computer Science and has guided over 25 students. He has published articles in both national and international journals. Professor Bagewadi specializes in Differential Geometry and its wide-ranging ramifications. He has to his credit more than 159 research papers. Several Books on Differential Geometry, Differential Equations are coauthored by him--- Chairman, Department of studies in Mathematics and Computer science, Jnanasahyadri Kuvempu University, Shankarghatta, Shimoga district, Karnataka, India

Shell Matrices and Fermion Vertices-Predicational Anteriority and Character Constitution Thereof

¹Dr. K. N. Prasanna Kumar, ²Prof. B. S. Kiranagi, ³Prof. C. S. Bagewadi

Abstract: In quantum physics, in order to quantize a gauge theory, like for example Yang-Mills theory, Chern-Simons or BF model, one method is to perform a gauge fixing. This is done in the BRST and Batalin-Vilkovisky formulation. Another is to factor out the symmetry by dispensing with vector potentials altogether (they're not physically observable anyway) and work directly with Wilson loops, Wilson lines contracted with other charged fields at its endpoints and spin networks Presently renormalization prescriptions of the Cabibbo-Kobayashi-Maskawa (CKM) quark mixing matrix have been investigated by many authors like Yong Zhou. Based on one prescription which is formulated by comparing with the fictitious case of no mixing of quark generations, they have proposed the substantive limits, singular pauses, general rests, logical attributes and real relations therefore a new prescription intermodal manifestation which can make the physical amplitude involving quark's mixing gauge independent and ultraviolet finite. Compared with the previous prescriptions this prescription is very simple and suitable for actual calculations. Through analytical calculations we also give a strong Proof for the important hypothesis that in order to keep the CKM matrix gauge independent the unitarity of the CKM matrix must be preserved. Mass-shell renormalization of fermion mixing matrices have also been delineated and investigated upon by K.-P.O Diener, B.A Kniehl wherein they consider favorable extensions of the standard model (SM) where the lepton sector contains Majorana neutrinos with vanishing left-handed mass terms, thus allowing for the see-saw mechanism to operate, and propose physical on-mass-shell (OS) renormalization conditions for the lepton mixing matrices that comply with ultraviolet finiteness, gauge-parameter independence, and (pseudo)unitarity This is an important result that motivated us to draw up the consolidation of some of the most important variables in Fermion and graviton vertices.. A crucial feature is that the texture zero in the neutrino mass matrix is preserved by renormalization, which is not automatically the case for possible generalizations of existing renormalization prescriptions for the Cabibbo-Kobayashi-Maskawa (CKM) quark mixing matrix in the SM. Our renormalization prescription also applies to the special case of the SM and leads to a physical OS definition of the renormalized CKM matrix. A consummate and link model is built for the variables like gravity, matter field, virtual photons and other important variables. Nevertheless the stormy petrel Neutrino seems to rule the roost with its own disnormative prescriptions for itself. Rich IN ITS twists and turns, the Model seems to offer a parade of variables bent on aggrandizement agenda.

I. Introduction:

Ward-Takahashi identity

In quantum field theory, a Ward-Takahashi identity is an identity between correlation functions that follows from the global or gauged symmetries of the theory, and which remains valid after renormalization.

The Ward-Takahashi identity of quantum electrodynamics was originally used by John Clive Ward and Yasushi Takahashi to relate the wave function renormalization of the electron to its vertex renormalization factor $F_1(0)$, guaranteeing the cancellation of the ultraviolet divergence to all orders of perturbation theory. Later uses include the extension of the proof of Goldstone's theorem to all orders of perturbation theory.

The Ward-Takahashi identity is a quantum version of the classical Noether's theorem, and any symmetry in a quantum field theory can lead to an equation of motion for correlation functions..

The Ward-Takahashi identity applies to correlation functions in momentum space, which do not necessarily have all their external momenta on-shell. Let

$$\mathcal{M}(k; p_1 \cdots p_n; q_1 \cdots q_n) = \epsilon_\mu(k) \mathcal{M}^\mu(k; p_1 \cdots p_n; q_1 \cdots q_n)$$

be a QED correlation function involving an external photon with momentum k (where $\epsilon_\mu(k)$ is the polarization vector of the photon), n initial-state electrons with momenta $p_1 \cdots p_n$, and n final-state electrons with momenta $q_1 \cdots q_n$.

Also define \mathcal{M}_0 to be the simpler amplitude that is **obtained by removing** the photon with momentum k from original amplitude. Then the Ward-Takahashi identity reads

$$k_\mu \mathcal{M}^\mu(k; p_1 \cdots p_n; q_1 \cdots q_n) = -e \sum_i [\mathcal{M}_0(p_1 \cdots p_n; q_1 \cdots (q_i - k) \cdots q_n) - \mathcal{M}_0(p_1 \cdots (p_i + k) \cdots p_n; q_1 \cdots q_n)]$$

where $-e$ is the charge of the electron. Note that if \mathcal{M} has its external electrons on-shell, then the amplitudes on the right-hand side of this identity each had one external particle off-shell, and therefore they do not contribute to S-matrix elements.

The Ward identity

The Ward identity is a specialization of the Ward-Takahashi identity to S-matrix elements, which describe physically possible scattering processes and thus have all their external particles on-shell. Again let $\mathcal{M}(k) = \epsilon_\mu(k) \mathcal{M}^\mu(k)$

be the amplitude for some QED process involving an external photon with momentum k , where $\epsilon_\mu(k)$ is the polarization vector of the photon. Then the Ward identity reads:

$$k_\mu \mathcal{M}^\mu(k) = 0$$

Physically, what this identity means is the longitudinal polarization of the photon which arises in the ξ gauge is unphysical and disappears from the S-matrix.

II. Some Reviews:

Flavor Changing Fermion-Graviton Vertices (SEE FOR DETAILS G. Degrassi, E. Gabrielli, L. Trentadue-emphasis mine) Authors study the flavor-changing quark-graviton vertex that is induced at the one-loop level when gravitational interactions are coupled to the standard model. Because of the conservation of the energy-momentum tensor the corresponding form factors turn out to be finite and gauge-invariant. Analytical expressions of the form factors are provided at leading order in the external masses. Authors show that flavor-changing interactions in gravity are local if the graviton is strictly massless while if the graviton has a small mass long-range interactions inducing a flavor-changing contribution in the Newton potential appear. Flavor-changing processes with massive spin-2 particles are also briefly discussed in the paper. . These results can be generalized to the case of the lepton-graviton coupling.

Examples of its use include constraining the tensor structure of the vacuum polarization and of the electron vertex function in QED. Gauge dependence of the on-shell renormalized mixing matrices WAS STUDIED BY Youichi Yamada It was recently pointed out that the on-shell renormalization of the CabibboKobayashi-Maskawa (CKM) matrix in the method by Denner and Sack causes a gauge parameter dependence of the amplitudes. Authors analyze the gauge dependence of the on-shell renormalization of the mixing matrices both for fermions and scalars in general cases, at the one-loop level. It is also shown that this gauge dependence can be avoided by fixing the counterterm for the mixing matrices in terms of the off-diagonal wave function corrections for fermions and scalars after a rearrangement, in a similar manner to the pinch technique for gauge bosons. Particles in the same representation under unbroken symmetries can mix with each other. The neutral gauge bosons, quarks, and massive neutrinos in the Standard Model (SM) are well-known examples. New particles in extensions of the Standard Model also show the mixings. For example, in the minimal supersymmetric (SUSY) standard model (MSSM), a very promising extension, super partners of most SM particles show the mixing .The mixing of particles is expressed in terms of the mixing matrix, which represents the relations between the gauge eigenstates and the mass eigenstates of the particles. The mixing matrices always appear at the couplings of these particles in the mass eigenbasis. Because of the fact that mass eigenstates at the tree-level mix with each other by radiative corrections, (it calls for) the mixing matrices have to be renormalized to obtain ultraviolet (UV) finite amplitudes. Denner and Sack have proposed a simple scheme to renormalize the mixing matrix of Dirac fermions at the one-loop level, which is usually called the on-shell renormalization scheme. They have required the counterterm for the renormalized mixing matrix to completely absorb the anti-Hermitian part of the wave function correction δZ_{ij} for the external on-shell fields*

III. GRAVITY AND MATTER FIELDS:

MODULE NUMBERED ONE NOTATION :

- G_{13} : CATEGORY ONE OF GRAVITY
- G_{14} : CATEGORY TWO OF GRAVITY
- G_{15} : CATEGORY THREE OF GRAVITY
- T_{13} : CATEGORY ONE OF MATTER FIELDS
- T_{14} : CATEGORY TWO OF MATTER FIELDS
- T_{15} : CATEGORY THREE OF MATTER FIELDS

GRAVITON FIELD AND CONSERVED MATTER ENERGY MOMENTUM TENSOR(LIKE IN A BANK THE RULE THAT ASSETS AND LIABILITIES ARE EQUIVALENT IS APPLIED TO THE INDIVIDUAL SYSTEMS, THE CONSERVATION OF ENERGY MOMENTUM TENSOR IS APPLICABLE TO VARIOUS SYSTEMS AND THE CLASSIFICATION IS BASED ON THE CHARACTERISTICS OF THE SYSTEMS TO WHICH THE CONSERVATION PRINCIPLE IS APPLIED):

MODULE NUMBERED TWO:

- G_{16} : CATEGORY ONE OF GRAVITON FIELD
- G_{17} : CATEGORY TWO OF GRAVITON FIELD
- G_{18} : CATEGORY THREE OF GRAVITON FIELD
- T_{16} : CATEGORY ONE OF CONSERVED MATTER-ENERGY-MOMENTUM TENSOR(WE ARE HERE SPEAKING OF SYSTEMS TO WHICH IT IS APPLICABLE. PLEASE THE BANK EXAMPLE GIVEN ABOVE)
- T_{17} : CATEGORY TWO OF CONSERVED MATTER-ENERGY-MOMENTUM TENSOR
- T_{18} : CATEGORY THREE OF CONSERVED MATTER-ENERGY-MOMENTUM TENSOR

VIRTUAL PHOTONS AND GRAVITON PHOTON VERTEX:

MODULE NUMBERED THREE:

G_{20} : CATEGORY ONE OF VIRTUAL PHOTONS(WE HERE SPEAK OF THE CHARACTERISED SYSTEMS FOR WHICH QUANTUM GAUGE THEORY IS APPLICABLE)

G_{21} :CATEGORY TWO OF VIRTUAL PHOTONS

G_{22} : CATEGORY THREE OF VIRTUAL PHOTONS

T_{20} : CATEGORY ONE OF GRAVITON ELECTRON VERTEX

T_{21} :CATEGORY TWO OF GRAVITON ELECTRON VERTEX

T_{22} : CATEGORY THREE OF GRAVITON ELECTRON VERTEX

QUANTUM FIELD THEORY(AGAIN,PARAMETRICIZED SYSTEMS TO WHICH QFT COULD BE APPLIED IS TAKEN IN TO CONSIDERATION AND RENORMALIZATION THEORY(BASED ON CERTAIN VARIABLES OF THE SYSTEM WHICH CONSEQUENTIALLY CLSSIFIABLE ON PARAMETERS)
: MODULE NUMBERED FOUR:

G_{24} : CATEGORY ONE OF QUANTUM FIELD THEORY(EVALUATIVE PARAMETRICIZATION OF SITUATIONAL ORIENTATIONS AND ESSENTIAL COGNITIVE ORIENTATION AND CHOICE VARIABLES OF THE SYSTEM TO WHICH QFT IS APPLICABLE)

G_{25} : CATEGORY TWO OF QUANTUM FIELD THEORY

G_{26} : CATEGORY THREE OF QUANTUM FIELD THEORY

T_{24} :CATEGORY ONE OF RENORMALIZATION THEORY

T_{25} :CATEGORY TWO OF RENORMALIZATION THEORY(SYSTEMIC INSTRUMENTAL CHARACTERISATIONS AND ACTION ORIENTATIONS AND FUYNCTIONAL IMPERATIVES OF CHANGE MANIFESTED THEREIN)

T_{26} : CATEGORY THREE OF QUANTUM FIELD THEORY

VIRTUAL ELECTRONS AND GRAVITON PHOTON VERTEX
MODULE NUMBERED FIVE:

G_{28} : CATEGORY ONE OF VIRTUAL ELECTRONS

G_{29} : CATEGORY TWO OF VIRTUAL ELECTRONS

G_{30} :CATEGORY THREE OF VIRTUAL ELECTRONS

T_{28} :CATEGORY ONE OF GRAVITON PHOTON VERTEX

T_{29} :CATEGORY TWO OF GRAVITON PHOTON VERTEX

T_{30} :CATEGORY THREE OF GRAVITON PHOTON VERTEX

QUANTUM CORRECTIONS TO ON SHELL MATRIX (VIRTUAKL GRAVITONS ARE NOT INCLUDED IN THE LOOPS) AND WARD IDENTITIES FROM MATTER ENERGY MOMENTUM CONSERVATION(LOT OF SYSTEMS CONSERVE THE MASS ENERGY AND THE CLASSIFICATION IS BASED ON THE PARAMETRICIZATION OF THE SYSTEMS)

MODULE NUMBERED SIX:

G_{32} : CATEGORY ONE OF QUANTUM CORRECTION TO SHELL MATRIX

G_{33} : CATEGORY TWO OF QUANTUM CORRECTIONS TO SHELL MATRIX

G_{34} : CATEGORY THREE OF QUANTUM CORRECTIONS TO SHELL MATRIX

T_{32} : CATEGORY ONE OF WARD IDENTITIES FROM MASS-ENERGY-MOMENTUM CONSERVATION(AGAIN WE RECAPITUALTE THE BANK EXAMPLES THERE ARE MILLIONS OF SYSTEMS FOR WHICH THE CONSERVATION HOLDS AND WE ARE CLASSIFYING THE SYSTEMS AND WARD IDENTITIES THEREOF)

T_{33} : CATEGORY TWO OF WARD IDENTITIES

T_{34} : CATEGORY THREE OF WARD IDENTITIES

CHARGED WEAK CURRENTS AND ONE LOOP FLAVOUR CHANGING NEUTRAL CURRENTS(FCNC) IN THE FERMION PORTFOLIO:

MODULE NUMBERED SEVEN

G_{36} : CATEGORY ONE OF CHARGED WEAK CURRENTS

G_{37} : CATEGORY TWO OF CHARGED WEAK CURRENTS

G_{38} : CATEGORY THREE OF CHARGED WEAK CURRENTS (ENERGY EXCITATION OF THE VACUUM AND CONCOMITANT GENERATION OF ENERGY DIFFERENTIAL-TIME LAG OR INSTANTANEOUSNESSMIGHT EXISTS WHEREBY ACCENTUATION AND ATTRITIONS MODEL MAY ASSUME ZERO POSITIONS IS AN EXAMPLE)

T_{36} : CATEGORY ONE OF FCNC IN THE FERMIONS SECTOR

T_{37} : CATEGORY TWO OF FCNC IN THE FERMIONS SECTOR

T_{38} : CATEGORY THREE OF FCNC IN THE FERMIONS SECTOR

$$(a_{13})^{(1)}, (a_{14})^{(1)}, (a_{15})^{(1)}, (b_{13})^{(1)}, (b_{14})^{(1)}, (b_{15})^{(1)} \quad (a_{16})^{(2)}, (a_{17})^{(2)}, (a_{18})^{(2)} \quad (b_{16})^{(2)}, (b_{17})^{(2)}, (b_{18})^{(2)}:$$

$$(a_{20})^{(3)}, (a_{21})^{(3)}, (a_{22})^{(3)}, (b_{20})^{(3)}, (b_{21})^{(3)}, (b_{22})^{(3)}$$

$$(a_{24})^{(4)}, (a_{25})^{(4)}, (a_{26})^{(4)}, (b_{24})^{(4)}, (b_{25})^{(4)}, (b_{26})^{(4)}, (b_{28})^{(5)}, (b_{29})^{(5)}, (b_{30})^{(5)}, (a_{28})^{(5)}, (a_{29})^{(5)}, (a_{30})^{(5)},$$

$$(a_{32})^{(6)}, (a_{33})^{(6)}, (a_{34})^{(6)}, (b_{32})^{(6)}, (b_{33})^{(6)}, (b_{34})^{(6)}$$

are Accentuation coefficients

$$(a'_{13})^{(1)}, (a'_{14})^{(1)}, (a'_{15})^{(1)}, (b'_{13})^{(1)}, (b'_{14})^{(1)}, (b'_{15})^{(1)}, (a'_{16})^{(2)}, (a'_{17})^{(2)}, (a'_{18})^{(2)}, (b'_{16})^{(2)}, (b'_{17})^{(2)}, (b'_{18})^{(2)}$$

$$, (a'_{20})^{(3)}, (a'_{21})^{(3)}, (a'_{22})^{(3)}, (b'_{20})^{(3)}, (b'_{21})^{(3)}, (b'_{22})^{(3)}$$

$$(a'_{24})^{(4)}, (a'_{25})^{(4)}, (a'_{26})^{(4)}, (b'_{24})^{(4)}, (b'_{25})^{(4)}, (b'_{26})^{(4)}, (b'_{28})^{(5)}, (b'_{29})^{(5)}, (b'_{30})^{(5)} \quad (a'_{28})^{(5)}, (a'_{29})^{(5)}, (a'_{30})^{(5)}$$

$$(a'_{32})^{(6)}, (a'_{33})^{(6)}, (a'_{34})^{(6)}, (b'_{32})^{(6)}, (b'_{33})^{(6)}, (b'_{34})^{(6)}$$

are Dissipation coefficients*

GRAVITY AND MATTER FIELDS:
MODULE NUMBERED ONE

The differential system of this model is now (Module Numbered one)*1

$$\frac{dG_{13}}{dt} = (a_{13})^{(1)}G_{14} - [(a'_{13})^{(1)} + (a''_{13})^{(1)}(T_{14}, t)]G_{13} \quad *2$$

$$\frac{dG_{14}}{dt} = (a_{14})^{(1)}G_{13} - [(a'_{14})^{(1)} + (a''_{14})^{(1)}(T_{14}, t)]G_{14} \quad *3$$

$$\frac{dG_{15}}{dt} = (a_{15})^{(1)}G_{14} - [(a'_{15})^{(1)} + (a''_{15})^{(1)}(T_{14}, t)]G_{15} \quad *4$$

$$\frac{dT_{13}}{dt} = (b_{13})^{(1)}T_{14} - [(b'_{13})^{(1)} - (b''_{13})^{(1)}(G, t)]T_{13} \quad *5$$

$$\frac{dT_{14}}{dt} = (b_{14})^{(1)}T_{13} - [(b'_{14})^{(1)} - (b''_{14})^{(1)}(G, t)]T_{14} \quad *6$$

$$\frac{dT_{15}}{dt} = (b_{15})^{(1)}T_{14} - [(b'_{15})^{(1)} - (b''_{15})^{(1)}(G, t)]T_{15} \quad *7$$

$$+(a''_{13})^{(1)}(T_{14}, t) = \text{First augmentation factor} \quad *8$$

$$-(b''_{13})^{(1)}(G, t) = \text{First detritions factor} \quad *$$

GRAVITON FIELD AND CONSERVED MATTER ENERGY MOMENTUM TENSOR(LIKE IN A BANK THE RULE THAT ASSETS AND LIABILITIES ARE EQUIVALENT IS APPLIED TO THE INDIVIDUAL SYSTEMS, THE CONSERVATION OF ENERGY MOMENTUM TENSOR IS APPLICABLE TO VARIOUS SYSTEMS AND THE CLASSIFICATION IS BASED ON THE CHARACTERISTICS OF THE SYSTEMS TO WHICH THE CONSERVATION PRINCIPLE IS APPLIED):

MODULE NUMBERED TWO:

∴

The differential system of this model is now (Module numbered two)*9

$$\frac{dG_{16}}{dt} = (a_{16})^{(2)}G_{17} - [(a'_{16})^{(2)} + (a''_{16})^{(2)}(T_{17}, t)]G_{16} \quad *10$$

$$\frac{dG_{17}}{dt} = (a_{17})^{(2)}G_{16} - [(a'_{17})^{(2)} + (a''_{17})^{(2)}(T_{17}, t)]G_{17} \quad *11$$

$$\frac{dG_{18}}{dt} = (a_{18})^{(2)}G_{17} - [(a'_{18})^{(2)} + (a''_{18})^{(2)}(T_{17}, t)]G_{18} \quad *12$$

$$\frac{dT_{16}}{dt} = (b_{16})^{(2)}T_{17} - [(b'_{16})^{(2)} - (b''_{16})^{(2)}((G_{19}), t)]T_{16} \quad *13$$

$$\frac{dT_{17}}{dt} = (b_{17})^{(2)}T_{16} - [(b'_{17})^{(2)} - (b''_{17})^{(2)}((G_{19}), t)]T_{17} \quad *14$$

$$\frac{dT_{18}}{dt} = (b_{18})^{(2)}T_{17} - [(b'_{18})^{(2)} - (b''_{18})^{(2)}((G_{19}), t)]T_{18} \quad *15$$

$$+(a''_{16})^{(2)}(T_{17}, t) = \text{First augmentation factor} \quad *16$$

$$-(b''_{16})^{(2)}((G_{19}), t) = \text{First detritions factor} \quad *17$$

VIRTUAL PHOTONS AND GRAVITON PHOTON VERTEX:
MODULE NUMBERED THREE

The differential system of this model is now (Module numbered three)*18

$$\frac{dG_{20}}{dt} = (a_{20})^{(3)}G_{21} - [(a'_{20})^{(3)} + (a''_{20})^{(3)}(T_{21}, t)]G_{20} \quad *19$$

$$\frac{dG_{21}}{dt} = (a_{21})^{(3)}G_{20} - [(a'_{21})^{(3)} + (a''_{21})^{(3)}(T_{21}, t)]G_{21} \quad *20$$

$$\frac{dG_{22}}{dt} = (a_{22})^{(3)}G_{21} - [(a'_{22})^{(3)} + (a''_{22})^{(3)}(T_{21}, t)]G_{22} \quad *21$$

$$\frac{dT_{20}}{dt} = (b_{20})^{(3)}T_{21} - [(b'_{20})^{(3)} - (b''_{20})^{(3)}(G_{23}, t)]T_{20} \quad *22$$

$$\frac{dT_{21}}{dt} = (b_{21})^{(3)}T_{20} - [(b'_{21})^{(3)} - (b''_{21})^{(3)}(G_{23}, t)]T_{21} \quad *23$$

$$\frac{dT_{22}}{dt} = (b_{22})^{(3)}T_{21} - [(b'_{22})^{(3)} - (b''_{22})^{(3)}(G_{23}, t)]T_{22} \quad *24$$

$$+(a''_{20})^{(3)}(T_{21}, t) = \text{First augmentation factor}^*$$

$$-(b''_{20})^{(3)}(G_{23}, t) = \text{First detritions factor} *25$$

QUANTUM FIELD THEORY (AGAIN, PARAMETRIZED SYSTEMS TO WHICH QFT COULD BE APPLIED IS TAKEN IN TO CONSIDERATION AND RENORMALIZATION THEORY (BASED ON CERTAIN VARIABLES OF THE SYSTEM WHICH CONSEQUENTIALLY CLASSIFIABLE ON PARAMETERS)

: MODULE NUMBERED FOUR

The differential system of this model is now (Module numbered Four)*26

$$\frac{dG_{24}}{dt} = (a_{24})^{(4)}G_{25} - [(a'_{24})^{(4)} + (a''_{24})^{(4)}(T_{25}, t)]G_{24} *27$$

$$\frac{dG_{25}}{dt} = (a_{25})^{(4)}G_{24} - [(a'_{25})^{(4)} + (a''_{25})^{(4)}(T_{25}, t)]G_{25} *28$$

$$\frac{dG_{26}}{dt} = (a_{26})^{(4)}G_{25} - [(a'_{26})^{(4)} + (a''_{26})^{(4)}(T_{25}, t)]G_{26} *29$$

$$\frac{dT_{24}}{dt} = (b_{24})^{(4)}T_{25} - [(b'_{24})^{(4)} - (b''_{24})^{(4)}((G_{27}, t))]T_{24} *30$$

$$\frac{dT_{25}}{dt} = (b_{25})^{(4)}T_{24} - [(b'_{25})^{(4)} - (b''_{25})^{(4)}((G_{27}, t))]T_{25} *31$$

$$\frac{dT_{26}}{dt} = (b_{26})^{(4)}T_{25} - [(b'_{26})^{(4)} - (b''_{26})^{(4)}((G_{27}, t))]T_{26} *32$$

$$+(a''_{24})^{(4)}(T_{25}, t) = \text{First augmentation factor} *33$$

$$-(b''_{24})^{(4)}((G_{27}, t)) = \text{First detritions factor} *34$$

VIRTUAL ELECTRONS AND GRAVITON PHOTON VERTEX

MODULE NUMBERED FIVE

The differential system of this model is now (Module number five)*35

$$\frac{dG_{28}}{dt} = (a_{28})^{(5)}G_{29} - [(a'_{28})^{(5)} + (a''_{28})^{(5)}(T_{29}, t)]G_{28} *36$$

$$\frac{dG_{29}}{dt} = (a_{29})^{(5)}G_{28} - [(a'_{29})^{(5)} + (a''_{29})^{(5)}(T_{29}, t)]G_{29} *37$$

$$\frac{dG_{30}}{dt} = (a_{30})^{(5)}G_{29} - [(a'_{30})^{(5)} + (a''_{30})^{(5)}(T_{29}, t)]G_{30} *38$$

$$\frac{dT_{28}}{dt} = (b_{28})^{(5)}T_{29} - [(b'_{28})^{(5)} - (b''_{28})^{(5)}((G_{31}, t))]T_{28} *39$$

$$\frac{dT_{29}}{dt} = (b_{29})^{(5)}T_{28} - [(b'_{29})^{(5)} - (b''_{29})^{(5)}((G_{31}, t))]T_{29} *40$$

$$\frac{dT_{30}}{dt} = (b_{30})^{(5)}T_{29} - [(b'_{30})^{(5)} - (b''_{30})^{(5)}((G_{31}, t))]T_{30} *41$$

$$+(a''_{28})^{(5)}(T_{29}, t) = \text{First augmentation factor} *42$$

$$-(b''_{28})^{(5)}((G_{31}, t)) = \text{First detritions factor} *43$$

QUANTUM CORRECTIONS TO ON SHELL MATRIX (VIRTUAKL GRAVITONS ARE NOT INCLUDED IN THE LOOPS) AND WARD IDENTITIES FROM MATTER ENERGY MOMENTUM CONSERVATION (LOT OF SYSTEMS CONSERVE THE MASS ENERGY AND THE CLASSIFICATION IS BASED ON THE PARAMETRIZATION OF THE SYSTEMS)

MODULE NUMBERED SIX:

The differential system of this model is now (Module numbered Six)*44

45

$$\frac{dG_{32}}{dt} = (a_{32})^{(6)}G_{33} - [(a'_{32})^{(6)} + (a''_{32})^{(6)}(T_{33}, t)]G_{32} *46$$

$$\frac{dG_{33}}{dt} = (a_{33})^{(6)}G_{32} - [(a'_{33})^{(6)} + (a''_{33})^{(6)}(T_{33}, t)]G_{33} *47$$

$$\frac{dG_{34}}{dt} = (a_{34})^{(6)}G_{33} - [(a'_{34})^{(6)} + (a''_{34})^{(6)}(T_{33}, t)]G_{34} *48$$

$$\frac{dT_{32}}{dt} = (b_{32})^{(6)}T_{33} - [(b'_{32})^{(6)} - (b''_{32})^{(6)}((G_{35}, t))]T_{32} *49$$

$$\frac{dT_{33}}{dt} = (b_{33})^{(6)}T_{32} - [(b'_{33})^{(6)} - (b''_{33})^{(6)}((G_{35}, t))]T_{33} *50$$

$$\frac{dT_{34}}{dt} = (b_{34})^{(6)}T_{33} - [(b'_{34})^{(6)} - (b''_{34})^{(6)}((G_{35}, t))]T_{34} *51$$

$$+(a''_{32})^{(6)}(T_{33}, t) = \text{First augmentation factor} *52$$

CHARGED WEAK CURRENTS AND ONE LOOP FLAVOUR CHANGING NEUTRAL CURRENTS (FCNC) IN THE FERMION PORTFOLIO:

MODULE NUMBERED SEVEN

The differential system of this model is now (SEVENTH MODULE)*53

$$\frac{dG_{36}}{dt} = (a_{36})^{(7)}G_{37} - [(a'_{36})^{(7)} + (a''_{36})^{(7)}(T_{37}, t)]G_{36} *54$$

$$\frac{dG_{37}}{dt} = (a_{37})^{(7)}G_{36} - [(a'_{37})^{(7)} + (a''_{37})^{(7)}(T_{37}, t)]G_{37} *55$$

$$\frac{dG_{38}}{dt} = (a_{38})^{(7)}G_{37} - [(a'_{38})^{(7)} + (a''_{38})^{(7)}(T_{37}, t)]G_{38} *56$$

$$\frac{dT_{36}}{dt} = (b_{36})^{(7)}T_{37} - [(b'_{36})^{(7)} - (b''_{36})^{(7)}((G_{39}), t)]T_{36} \quad *57$$

$$\frac{dT_{37}}{dt} = (b_{37})^{(7)}T_{36} - [(b'_{37})^{(7)} - (b''_{37})^{(7)}((G_{39}), t)]T_{37} \quad *58$$

59

$$\frac{dT_{38}}{dt} = (b_{38})^{(7)}T_{37} - [(b'_{38})^{(7)} - (b''_{38})^{(7)}((G_{39}), t)]T_{38} \quad *60$$

$$+(a''_{36})^{(7)}(T_{37}, t) = \text{First augmentation factor} \quad *61$$

$$-(b''_{36})^{(7)}((G_{39}), t) = \text{First detritions factor}$$

FIRST MODULE CONCATENATION:

$$\frac{dG_{13}}{dt} = (a_{13})^{(1)}G_{14} - \left[\begin{array}{c} (a'_{13})^{(1)} \boxed{+(a''_{13})^{(1)}(T_{14}, t)} \boxed{+(a''_{16})^{(2,2)}(T_{17}, t)} \boxed{+(a''_{20})^{(3,3)}(T_{21}, t)} \\ \boxed{+(a''_{24})^{(4,4,4,4)}(T_{25}, t)} \boxed{+(a''_{28})^{(5,5,5,5)}(T_{29}, t)} \boxed{+(a''_{32})^{(6,6,6,6)}(T_{33}, t)} \\ \boxed{+(a''_{36})^{(7)}(T_{37}, t)} \end{array} \right] G_{13}$$

$$\frac{dG_{14}}{dt} = (a_{14})^{(1)}G_{13} - \left[\begin{array}{c} (a'_{14})^{(1)} \boxed{+(a''_{14})^{(1)}(T_{14}, t)} \boxed{+(a''_{17})^{(2,2)}(T_{17}, t)} \boxed{+(a''_{21})^{(3,3)}(T_{21}, t)} \\ \boxed{+(a''_{25})^{(4,4,4,4)}(T_{25}, t)} \boxed{+(a''_{29})^{(5,5,5,5)}(T_{29}, t)} \boxed{+(a''_{33})^{(6,6,6,6)}(T_{33}, t)} \\ \boxed{+(a''_{37})^{(7)}(T_{37}, t)} \end{array} \right] G_{14}$$

$$\frac{dG_{15}}{dt} = (a_{15})^{(1)}G_{14} - \left[\begin{array}{c} (a'_{15})^{(1)} \boxed{+(a''_{15})^{(1)}(T_{14}, t)} \boxed{+(a''_{18})^{(2,2)}(T_{17}, t)} \boxed{+(a''_{22})^{(3,3)}(T_{21}, t)} \\ \boxed{+(a''_{26})^{(4,4,4,4)}(T_{25}, t)} \boxed{+(a''_{30})^{(5,5,5,5)}(T_{29}, t)} \boxed{+(a''_{34})^{(6,6,6,6)}(T_{33}, t)} \\ \boxed{+(a''_{38})^{(7)}(T_{37}, t)} \end{array} \right] G_{15}$$

Where $\boxed{(a''_{13})^{(1)}(T_{14}, t)}$, $\boxed{(a''_{14})^{(1)}(T_{14}, t)}$, $\boxed{(a''_{15})^{(1)}(T_{14}, t)}$ are first augmentation coefficients for category 1, 2 and 3
 $\boxed{+(a''_{16})^{(2,2)}(T_{17}, t)}$, $\boxed{+(a''_{17})^{(2,2)}(T_{17}, t)}$, $\boxed{+(a''_{18})^{(2,2)}(T_{17}, t)}$ are second augmentation coefficient for category 1, 2 and 3
 $\boxed{+(a''_{20})^{(3,3)}(T_{21}, t)}$, $\boxed{+(a''_{21})^{(3,3)}(T_{21}, t)}$, $\boxed{+(a''_{22})^{(3,3)}(T_{21}, t)}$ are third augmentation coefficient for category 1, 2 and 3
 $\boxed{+(a''_{24})^{(4,4,4,4)}(T_{25}, t)}$, $\boxed{+(a''_{25})^{(4,4,4,4)}(T_{25}, t)}$, $\boxed{+(a''_{26})^{(4,4,4,4)}(T_{25}, t)}$ are fourth augmentation coefficient for category 1, 2 and 3
 $\boxed{+(a''_{28})^{(5,5,5,5)}(T_{29}, t)}$, $\boxed{+(a''_{29})^{(5,5,5,5)}(T_{29}, t)}$, $\boxed{+(a''_{30})^{(5,5,5,5)}(T_{29}, t)}$ are fifth augmentation coefficient for category 1, 2 and 3
 $\boxed{+(a''_{32})^{(6,6,6,6)}(T_{33}, t)}$, $\boxed{+(a''_{33})^{(6,6,6,6)}(T_{33}, t)}$, $\boxed{+(a''_{34})^{(6,6,6,6)}(T_{33}, t)}$ are sixth augmentation coefficient for category 1, 2 and 3
 $\boxed{+(a''_{36})^{(7)}(T_{37}, t)}$, $\boxed{+(a''_{37})^{(7)}(T_{37}, t)}$, $\boxed{+(a''_{38})^{(7)}(T_{37}, t)}$ ARE SEVENTH AUGMENTATION COEFFICIENTS

$$\frac{dT_{13}}{dt} = (b_{13})^{(1)}T_{14} - \left[\begin{array}{c} (b'_{13})^{(1)} \boxed{-(b''_{16})^{(1)}(G, t)} \boxed{-(b''_{36})^{(7)}(G_{39}, t)} \boxed{-(b''_{20})^{(3,3)}(G_{23}, t)} \\ \boxed{-(b''_{24})^{(4,4,4,4)}(G_{27}, t)} \boxed{-(b''_{28})^{(5,5,5,5)}(G_{31}, t)} \boxed{-(b''_{32})^{(6,6,6,6)}(G_{35}, t)} \\ \boxed{-(b''_{36})^{(7)}(G_{39}, t)} \end{array} \right] T_{13}$$

$$\frac{dT_{14}}{dt} = (b_{14})^{(1)}T_{13} - \left[\begin{array}{c} (b'_{14})^{(1)} \boxed{-(b''_{14})^{(1)}(G, t)} \boxed{-(b''_{17})^{(2,2)}(G_{19}, t)} \boxed{-(b''_{21})^{(3,3)}(G_{23}, t)} \\ \boxed{-(b''_{25})^{(4,4,4,4)}(G_{27}, t)} \boxed{-(b''_{29})^{(5,5,5,5)}(G_{31}, t)} \boxed{-(b''_{33})^{(6,6,6,6)}(G_{35}, t)} \\ \boxed{-(b''_{37})^{(7)}(G_{39}, t)} \end{array} \right] T_{14}$$

$$\frac{dT_{15}}{dt} = (b_{15})^{(1)}T_{14} - \left[\begin{array}{c} (b'_{15})^{(1)} \boxed{-(b''_{15})^{(1)}(G, t)} \boxed{-(b''_{18})^{(2,2)}(G_{19}, t)} \boxed{-(b''_{22})^{(3,3)}(G_{23}, t)} \\ \boxed{-(b''_{26})^{(4,4,4,4)}(G_{27}, t)} \boxed{-(b''_{30})^{(5,5,5,5)}(G_{31}, t)} \boxed{-(b''_{34})^{(6,6,6,6)}(G_{35}, t)} \\ \boxed{-(b''_{38})^{(7)}(G_{39}, t)} \end{array} \right] T_{15}$$

Where $\boxed{-(b''_{13})^{(1)}(G, t)}$, $\boxed{-(b''_{14})^{(1)}(G, t)}$, $\boxed{-(b''_{15})^{(1)}(G, t)}$ are first detritions coefficients for category 1, 2 and 3
 $\boxed{-(b''_{16})^{(2,2)}(G_{19}, t)}$, $\boxed{-(b''_{17})^{(2,2)}(G_{19}, t)}$, $\boxed{-(b''_{18})^{(2,2)}(G_{19}, t)}$ are second detritions coefficients for category 1, 2 and 3
 $\boxed{-(b''_{20})^{(3,3)}(G_{23}, t)}$, $\boxed{-(b''_{21})^{(3,3)}(G_{23}, t)}$, $\boxed{-(b''_{22})^{(3,3)}(G_{23}, t)}$ are third detritions coefficients for category 1, 2 and 3
 $\boxed{-(b''_{24})^{(4,4,4,4)}(G_{27}, t)}$, $\boxed{-(b''_{25})^{(4,4,4,4)}(G_{27}, t)}$, $\boxed{-(b''_{26})^{(4,4,4,4)}(G_{27}, t)}$ are fourth detritions coefficients for category 1, 2 and 3

$-(b''_{28})^{(5,5,5,5)}(G_{31}, t)$, $-(b''_{29})^{(5,5,5,5)}(G_{31}, t)$, $-(b''_{30})^{(5,5,5,5)}(G_{31}, t)$ are fifth detritions coefficients for category 1, 2 and 3

$-(b''_{32})^{(6,6,6,6)}(G_{35}, t)$, $-(b''_{33})^{(6,6,6,6)}(G_{35}, t)$, $-(b''_{34})^{(6,6,6,6)}(G_{35}, t)$ are sixth detritions coefficients for category 1, 2 and 3

$-(b''_{36})^{(7,7)}(G_{39}, t)$, $-(b''_{36})^{(7,7)}(G_{39}, t)$, $-(b''_{36})^{(7,7)}(G_{39}, t)$ ARE SEVENTH DETRITION COEFFICIENTS

*62

$$\frac{dT_{15}}{dt} = (b_{15})^{(1)}T_{14} - \left[\begin{array}{ccc} (b'_{15})^{(1)} \left[\begin{array}{ccc} -(b''_{15})^{(1)}(G, t) & -(b''_{18})^{(2,2)}(G_{19}, t) & -(b''_{22})^{(3,3)}(G_{23}, t) \end{array} \right] \\ - (b''_{26})^{(4,4,4,4)}(G_{27}, t) & - (b''_{30})^{(5,5,5,5)}(G_{31}, t) & - (b''_{34})^{(6,6,6,6)}(G_{35}, t) \end{array} \right] T_{15} \quad *63$$

Where $-(b''_{13})^{(1)}(G, t)$, $-(b''_{14})^{(1)}(G, t)$, $-(b''_{15})^{(1)}(G, t)$ are first detrition coefficients for category 1, 2 and 3

$-(b''_{16})^{(2,2)}(G_{19}, t)$, $-(b''_{17})^{(2,2)}(G_{19}, t)$, $-(b''_{18})^{(2,2)}(G_{19}, t)$ are second detritions coefficients for category 1, 2 and 3

$-(b''_{20})^{(3,3)}(G_{23}, t)$, $-(b''_{21})^{(3,3)}(G_{23}, t)$, $-(b''_{22})^{(3,3)}(G_{23}, t)$ are third detritions coefficients for category 1, 2 and 3

$-(b''_{24})^{(4,4,4,4)}(G_{27}, t)$, $-(b''_{25})^{(4,4,4,4)}(G_{27}, t)$, $-(b''_{26})^{(4,4,4,4)}(G_{27}, t)$ are fourth detritions coefficients for category 1, 2 and 3

$-(b''_{28})^{(5,5,5,5)}(G_{31}, t)$, $-(b''_{29})^{(5,5,5,5)}(G_{31}, t)$, $-(b''_{30})^{(5,5,5,5)}(G_{31}, t)$ are fifth detritions coefficients for category 1, 2 and 3

$-(b''_{32})^{(6,6,6,6)}(G_{35}, t)$, $-(b''_{33})^{(6,6,6,6)}(G_{35}, t)$, $-(b''_{34})^{(6,6,6,6)}(G_{35}, t)$ are sixth detritions coefficients for category 1, 2 and 3 *64

SECOND MODULE CONCATENATION: *65

$$\frac{dG_{16}}{dt} = (a_{16})^{(2)}G_{17} - \left[\begin{array}{ccc} (a'_{16})^{(2)} \left[\begin{array}{ccc} +(a''_{16})^{(2)}(T_{17}, t) & +(a''_{13})^{(1,1)}(T_{14}, t) & +(a''_{20})^{(3,3,3)}(T_{21}, t) \end{array} \right] \\ +(a''_{24})^{(4,4,4,4,4)}(T_{25}, t) & +(a''_{28})^{(5,5,5,5,5)}(T_{29}, t) & +(a''_{32})^{(6,6,6,6,6)}(T_{33}, t) \\ +(a''_{36})^{(7,7,7)}(T_{37}, t) \end{array} \right] G_{16} \quad *66$$

$$\frac{dG_{17}}{dt} = (a_{17})^{(2)}G_{16} - \left[\begin{array}{ccc} (a'_{17})^{(2)} \left[\begin{array}{ccc} +(a''_{17})^{(2)}(T_{17}, t) & +(a''_{14})^{(1,1)}(T_{14}, t) & +(a''_{21})^{(3,3,3)}(T_{21}, t) \end{array} \right] \\ +(a''_{25})^{(4,4,4,4,4)}(T_{25}, t) & +(a''_{29})^{(5,5,5,5,5)}(T_{29}, t) & +(a''_{33})^{(6,6,6,6,6)}(T_{33}, t) \\ +(a''_{37})^{(7,7,7)}(T_{37}, t) \end{array} \right] G_{17} \quad *67$$

$$\frac{dG_{18}}{dt} = (a_{18})^{(2)}G_{17} - \left[\begin{array}{ccc} (a'_{18})^{(2)} \left[\begin{array}{ccc} +(a''_{18})^{(2)}(T_{17}, t) & +(a''_{15})^{(1,1)}(T_{14}, t) & +(a''_{22})^{(3,3,3)}(T_{21}, t) \end{array} \right] \\ +(a''_{26})^{(4,4,4,4,4)}(T_{25}, t) & +(a''_{30})^{(5,5,5,5,5)}(T_{29}, t) & +(a''_{34})^{(6,6,6,6,6)}(T_{33}, t) \\ +(a''_{38})^{(7,7,7)}(T_{37}, t) \end{array} \right] G_{18} \quad *68$$

Where $+(a''_{16})^{(2)}(T_{17}, t)$, $+(a''_{17})^{(2)}(T_{17}, t)$, $+(a''_{18})^{(2)}(T_{17}, t)$ are first augmentation coefficients for category 1, 2 and 3

$+(a''_{13})^{(1,1)}(T_{14}, t)$, $+(a''_{14})^{(1,1)}(T_{14}, t)$, $+(a''_{15})^{(1,1)}(T_{14}, t)$ are second augmentation coefficient for category 1, 2 and 3

$+(a''_{20})^{(3,3,3)}(T_{21}, t)$, $+(a''_{21})^{(3,3,3)}(T_{21}, t)$, $+(a''_{22})^{(3,3,3)}(T_{21}, t)$ are third augmentation coefficient for category 1, 2 and 3

$+(a''_{24})^{(4,4,4,4,4)}(T_{25}, t)$, $+(a''_{25})^{(4,4,4,4,4)}(T_{25}, t)$, $+(a''_{26})^{(4,4,4,4,4)}(T_{25}, t)$ are fourth augmentation coefficient for category 1, 2 and 3

$+(a''_{28})^{(5,5,5,5,5)}(T_{29}, t)$, $+(a''_{29})^{(5,5,5,5,5)}(T_{29}, t)$, $+(a''_{30})^{(5,5,5,5,5)}(T_{29}, t)$ are fifth augmentation coefficient for category 1, 2 and 3

$+(a''_{32})^{(6,6,6,6,6)}(T_{33}, t)$, $+(a''_{33})^{(6,6,6,6,6)}(T_{33}, t)$, $+(a''_{34})^{(6,6,6,6,6)}(T_{33}, t)$ are sixth augmentation coefficient for category 1, 2 and 3 *69

70

$+(a''_{36})^{(7,7,7)}(T_{37}, t)$, $+(a''_{37})^{(7,7,7)}(T_{37}, t)$, $+(a''_{38})^{(7,7,7)}(T_{37}, t)$ ARE SEVENTH DETRITION COEFFICIENTS *71

$$\frac{dT_{16}}{dt} = (b_{16})^{(2)}T_{17} - \left[\begin{array}{ccc} (b'_{16})^{(2)} \left[\begin{array}{ccc} -(b''_{16})^{(2)}(G_{19}, t) & -(b''_{13})^{(1,1)}(G, t) & -(b''_{20})^{(3,3,3)}(G_{23}, t) \end{array} \right] \\ -(b''_{24})^{(4,4,4,4,4)}(G_{27}, t) & -(b''_{28})^{(5,5,5,5,5)}(G_{31}, t) & -(b''_{32})^{(6,6,6,6,6)}(G_{35}, t) \\ -(b''_{36})^{(7,7,7)}(G_{39}, t) \end{array} \right] T_{16} \quad *72$$

$$\frac{dT_{17}}{dt} = (b_{17})^{(2)}T_{16} - \left[\begin{array}{l} (b'_{17})^{(2)} \boxed{-(b''_{17})^{(2)}(G_{19}, t)} \boxed{-(b''_{14})^{(1,1)}(G, t)} \boxed{-(b''_{21})^{(3,3,3)}(G_{23}, t)} \\ \boxed{-(b''_{25})^{(4,4,4,4,4)}(G_{27}, t)} \boxed{-(b''_{29})^{(5,5,5,5,5)}(G_{31}, t)} \boxed{-(b''_{33})^{(6,6,6,6,6)}(G_{35}, t)} \\ \boxed{-(b''_{37})^{(7,7)}(G_{39}, t)} \end{array} \right] T_{17} *73$$

$$\frac{dT_{18}}{dt} = (b_{18})^{(2)}T_{17} - \left[\begin{array}{l} (b'_{18})^{(2)} \boxed{-(b''_{18})^{(2)}(G_{19}, t)} \boxed{-(b''_{15})^{(1,1)}(G, t)} \boxed{-(b''_{22})^{(3,3,3)}(G_{23}, t)} \\ \boxed{-(b''_{26})^{(4,4,4,4,4)}(G_{27}, t)} \boxed{-(b''_{30})^{(5,5,5,5,5)}(G_{31}, t)} \boxed{-(b''_{34})^{(6,6,6,6,6)}(G_{35}, t)} \\ \boxed{-(b''_{38})^{(7,7)}(G_{39}, t)} \end{array} \right] T_{18} *74$$

where $\boxed{-(b''_{16})^{(2)}(G_{19}, t)}$, $\boxed{-(b''_{17})^{(2)}(G_{19}, t)}$, $\boxed{-(b''_{18})^{(2)}(G_{19}, t)}$ are first detrition coefficients for category 1, 2 and 3
 $\boxed{-(b''_{13})^{(1,1)}(G, t)}$, $\boxed{-(b''_{14})^{(1,1)}(G, t)}$, $\boxed{-(b''_{15})^{(1,1)}(G, t)}$ are second detrition coefficients for category 1,2 and 3
 $\boxed{-(b''_{20})^{(3,3,3)}(G_{23}, t)}$, $\boxed{-(b''_{21})^{(3,3,3)}(G_{23}, t)}$, $\boxed{-(b''_{22})^{(3,3,3)}(G_{23}, t)}$ are third detrition coefficients for category 1,2 and 3
 $\boxed{-(b''_{24})^{(4,4,4,4,4)}(G_{27}, t)}$, $\boxed{-(b''_{25})^{(4,4,4,4,4)}(G_{27}, t)}$, $\boxed{-(b''_{26})^{(4,4,4,4,4)}(G_{27}, t)}$ are fourth detritions coefficients for category 1,2 and 3
 $\boxed{-(b''_{28})^{(5,5,5,5,5)}(G_{31}, t)}$, $\boxed{-(b''_{29})^{(5,5,5,5,5)}(G_{31}, t)}$, $\boxed{-(b''_{30})^{(5,5,5,5,5)}(G_{31}, t)}$ are fifth detritions coefficients for category 1,2 and 3
 $\boxed{-(b''_{32})^{(6,6,6,6,6)}(G_{35}, t)}$, $\boxed{-(b''_{33})^{(6,6,6,6,6)}(G_{35}, t)}$, $\boxed{-(b''_{34})^{(6,6,6,6,6)}(G_{35}, t)}$ are sixth detritions coefficients for category 1,2 and 3
 $\boxed{-(b''_{36})^{(7,7)}(G_{39}, t)}$, $\boxed{-(b''_{36})^{(7,7)}(G_{39}, t)}$, $\boxed{-(b''_{36})^{(7,7)}(G_{39}, t)}$ are seventh detrition coefficients

THIRD MODULE CONCATENATION: *75

$$\frac{dG_{20}}{dt} = (a_{20})^{(3)}G_{21} - \left[\begin{array}{l} (a'_{20})^{(3)} \boxed{+(a''_{20})^{(3)}(T_{21}, t)} \boxed{+(a''_{16})^{(2,2,2)}(T_{17}, t)} \boxed{+(a''_{13})^{(1,1,1)}(T_{14}, t)} \\ \boxed{+(a''_{24})^{(4,4,4,4,4)}(T_{25}, t)} \boxed{+(a''_{28})^{(5,5,5,5,5)}(T_{29}, t)} \boxed{+(a''_{32})^{(6,6,6,6,6)}(T_{33}, t)} \\ \boxed{+(a''_{36})^{(7,7,7)}(T_{37}, t)} \end{array} \right] G_{20} *76$$

$$\frac{dG_{21}}{dt} = (a_{21})^{(3)}G_{20} - \left[\begin{array}{l} (a'_{21})^{(3)} \boxed{+(a''_{21})^{(3)}(T_{21}, t)} \boxed{+(a''_{17})^{(2,2,2)}(T_{17}, t)} \boxed{+(a''_{14})^{(1,1,1)}(T_{14}, t)} \\ \boxed{+(a''_{25})^{(4,4,4,4,4)}(T_{25}, t)} \boxed{+(a''_{29})^{(5,5,5,5,5)}(T_{29}, t)} \boxed{+(a''_{33})^{(6,6,6,6,6)}(T_{33}, t)} \\ \boxed{+(a''_{37})^{(7,7,7)}(T_{37}, t)} \end{array} \right] G_{21} *77$$

$$\frac{dG_{22}}{dt} = (a_{22})^{(3)}G_{21} - \left[\begin{array}{l} (a'_{22})^{(3)} \boxed{+(a''_{22})^{(3)}(T_{21}, t)} \boxed{+(a''_{18})^{(2,2,2)}(T_{17}, t)} \boxed{+(a''_{15})^{(1,1,1)}(T_{14}, t)} \\ \boxed{+(a''_{26})^{(4,4,4,4,4)}(T_{25}, t)} \boxed{+(a''_{30})^{(5,5,5,5,5)}(T_{29}, t)} \boxed{+(a''_{34})^{(6,6,6,6,6)}(T_{33}, t)} \\ \boxed{+(a''_{38})^{(7,7,7)}(T_{37}, t)} \end{array} \right] G_{22} *78$$

$\boxed{+(a''_{20})^{(3)}(T_{21}, t)}$, $\boxed{+(a''_{21})^{(3)}(T_{21}, t)}$, $\boxed{+(a''_{22})^{(3)}(T_{21}, t)}$ are first augmentation coefficients for category 1, 2 and 3
 $\boxed{+(a''_{16})^{(2,2,2)}(T_{17}, t)}$, $\boxed{+(a''_{17})^{(2,2,2)}(T_{17}, t)}$, $\boxed{+(a''_{18})^{(2,2,2)}(T_{17}, t)}$ are second augmentation coefficients for category 1, 2 and 3
 $\boxed{+(a''_{13})^{(1,1,1)}(T_{14}, t)}$, $\boxed{+(a''_{14})^{(1,1,1)}(T_{14}, t)}$, $\boxed{+(a''_{15})^{(1,1,1)}(T_{14}, t)}$ are third augmentation coefficients for category 1, 2 and 3
 $\boxed{+(a''_{24})^{(4,4,4,4,4)}(T_{25}, t)}$, $\boxed{+(a''_{25})^{(4,4,4,4,4)}(T_{25}, t)}$, $\boxed{+(a''_{26})^{(4,4,4,4,4)}(T_{25}, t)}$ are fourth augmentation coefficients for category 1, 2 and 3
 $\boxed{+(a''_{28})^{(5,5,5,5,5)}(T_{29}, t)}$, $\boxed{+(a''_{29})^{(5,5,5,5,5)}(T_{29}, t)}$, $\boxed{+(a''_{30})^{(5,5,5,5,5)}(T_{29}, t)}$ are fifth augmentation coefficients for category 1, 2 and 3
 $\boxed{+(a''_{32})^{(6,6,6,6,6)}(T_{33}, t)}$, $\boxed{+(a''_{33})^{(6,6,6,6,6)}(T_{33}, t)}$, $\boxed{+(a''_{34})^{(6,6,6,6,6)}(T_{33}, t)}$ are sixth augmentation coefficients for category 1, 2 and 3 *79

80

$\boxed{+(a''_{36})^{(7,7,7)}(T_{37}, t)}$, $\boxed{+(a''_{37})^{(7,7,7)}(T_{37}, t)}$, $\boxed{+(a''_{38})^{(7,7,7)}(T_{37}, t)}$ are seventh augmentation coefficient *81

$$\frac{dT_{20}}{dt} = (b_{20})^{(3)}T_{21} - \left[\begin{array}{l} (b'_{20})^{(3)} \boxed{-(b''_{20})^{(3)}(G_{23}, t)} \boxed{-(b''_{36})^{(7,7,7)}(G_{19}, t)} \boxed{-(b''_{13})^{(1,1,1)}(G, t)} \\ \boxed{-(b''_{24})^{(4,4,4,4,4)}(G_{27}, t)} \boxed{-(b''_{28})^{(5,5,5,5,5)}(G_{31}, t)} \boxed{-(b''_{32})^{(6,6,6,6,6)}(G_{35}, t)} \\ \boxed{-(b''_{36})^{(7,7,7)}(G_{39}, t)} \end{array} \right] T_{20} \quad *82$$

$$\frac{dT_{21}}{dt} = (b_{21})^{(3)}T_{20} - \left[\begin{array}{l} (b'_{21})^{(3)} \boxed{-(b''_{21})^{(3)}(G_{23}, t)} \boxed{-(b''_{17})^{(2,2,2)}(G_{19}, t)} \boxed{-(b''_{14})^{(1,1,1)}(G, t)} \\ \boxed{-(b''_{25})^{(4,4,4,4,4)}(G_{27}, t)} \boxed{-(b''_{29})^{(5,5,5,5,5)}(G_{31}, t)} \boxed{-(b''_{33})^{(6,6,6,6,6)}(G_{35}, t)} \\ \boxed{-(b''_{37})^{(7,7,7)}(G_{39}, t)} \end{array} \right] T_{21} \quad *83$$

$$\frac{dT_{22}}{dt} = (b_{22})^{(3)}T_{21} - \left[\begin{array}{l} (b'_{22})^{(3)} \boxed{-(b''_{22})^{(3)}(G_{23}, t)} \boxed{-(b''_{18})^{(2,2,2)}(G_{19}, t)} \boxed{-(b''_{15})^{(1,1,1)}(G, t)} \\ \boxed{-(b''_{26})^{(4,4,4,4,4)}(G_{27}, t)} \boxed{-(b''_{30})^{(5,5,5,5,5)}(G_{31}, t)} \boxed{-(b''_{34})^{(6,6,6,6,6)}(G_{35}, t)} \\ \boxed{-(b''_{38})^{(7,7,7)}(G_{39}, t)} \end{array} \right] T_{22} \quad *84$$

$\boxed{-(b''_{20})^{(3)}(G_{23}, t)}$, $\boxed{-(b''_{21})^{(3)}(G_{23}, t)}$, $\boxed{-(b''_{22})^{(3)}(G_{23}, t)}$ are first detritions coefficients for category 1, 2 and 3
 $\boxed{-(b''_{16})^{(2,2,2)}(G_{19}, t)}$, $\boxed{-(b''_{17})^{(2,2,2)}(G_{19}, t)}$, $\boxed{-(b''_{18})^{(2,2,2)}(G_{19}, t)}$ are second detritions coefficients for category 1, 2 and 3
 $\boxed{-(b''_{13})^{(1,1,1)}(G, t)}$, $\boxed{-(b''_{14})^{(1,1,1)}(G, t)}$, $\boxed{-(b''_{15})^{(1,1,1)}(G, t)}$ are third detrition coefficients for category 1,2 and 3
 $\boxed{-(b''_{24})^{(4,4,4,4,4)}(G_{27}, t)}$, $\boxed{-(b''_{25})^{(4,4,4,4,4)}(G_{27}, t)}$, $\boxed{-(b''_{26})^{(4,4,4,4,4)}(G_{27}, t)}$ are fourth detritions coefficients for category 1, 2 and 3
 $\boxed{-(b''_{28})^{(5,5,5,5,5)}(G_{31}, t)}$, $\boxed{-(b''_{29})^{(5,5,5,5,5)}(G_{31}, t)}$, $\boxed{-(b''_{30})^{(5,5,5,5,5)}(G_{31}, t)}$ are fifth detritions coefficients for category 1, 2 and 3
 $\boxed{-(b''_{32})^{(6,6,6,6,6)}(G_{35}, t)}$, $\boxed{-(b''_{33})^{(6,6,6,6,6)}(G_{35}, t)}$, $\boxed{-(b''_{34})^{(6,6,6,6,6)}(G_{35}, t)}$ are sixth detritions coefficients for category 1, 2 and 3 *85
 $\boxed{-(b''_{36})^{(7,7,7)}(G_{39}, t)}$, $\boxed{-(b''_{37})^{(7,7,7)}(G_{39}, t)}$, $\boxed{-(b''_{38})^{(7,7,7)}(G_{39}, t)}$ are seventh detritions coefficients

FOURTH MODULE CONCATENATION: *86

$$\frac{dG_{24}}{dt} = (a_{24})^{(4)}G_{25} - \left[\begin{array}{l} (a'_{24})^{(4)} \boxed{+(a''_{24})^{(4)}(T_{25}, t)} \boxed{+(a''_{28})^{(5,5)}(T_{29}, t)} \boxed{+(a''_{32})^{(6,6)}(T_{33}, t)} \\ \boxed{+(a''_{13})^{(1,1,1,1)}(T_{14}, t)} \boxed{+(a''_{16})^{(2,2,2,2)}(T_{17}, t)} \boxed{+(a''_{20})^{(3,3,3,3)}(T_{21}, t)} \\ \boxed{+(a''_{36})^{(7,7,7,7)}(T_{37}, t)} \end{array} \right] G_{24} \quad *87$$

$$\frac{dG_{25}}{dt} = (a_{25})^{(4)}G_{24} - \left[\begin{array}{l} (a'_{25})^{(4)} \boxed{+(a''_{25})^{(4)}(T_{25}, t)} \boxed{+(a''_{29})^{(5,5)}(T_{29}, t)} \boxed{+(a''_{33})^{(6,6)}(T_{33}, t)} \\ \boxed{+(a''_{14})^{(1,1,1,1)}(T_{14}, t)} \boxed{+(a''_{17})^{(2,2,2,2)}(T_{17}, t)} \boxed{+(a''_{21})^{(3,3,3,3)}(T_{21}, t)} \\ \boxed{+(a''_{37})^{(7,7,7,7)}(T_{37}, t)} \end{array} \right] G_{25} \quad *88$$

$$\frac{dG_{26}}{dt} = (a_{26})^{(4)}G_{25} - \left[\begin{array}{l} (a'_{26})^{(4)} \boxed{+(a''_{26})^{(4)}(T_{25}, t)} \boxed{+(a''_{30})^{(5,5)}(T_{29}, t)} \boxed{+(a''_{34})^{(6,6)}(T_{33}, t)} \\ \boxed{+(a''_{15})^{(1,1,1,1)}(T_{14}, t)} \boxed{+(a''_{18})^{(2,2,2,2)}(T_{17}, t)} \boxed{+(a''_{22})^{(3,3,3,3)}(T_{21}, t)} \\ \boxed{+(a''_{38})^{(7,7,7,7)}(T_{37}, t)} \end{array} \right] G_{26} \quad *89$$

Where $\boxed{(a''_{24})^{(4)}(T_{25}, t)}$, $\boxed{(a''_{25})^{(4)}(T_{25}, t)}$, $\boxed{(a''_{26})^{(4)}(T_{25}, t)}$ are first augmentation coefficients for category 1, 2 and 3
 $\boxed{+(a''_{28})^{(5,5)}(T_{29}, t)}$, $\boxed{+(a''_{29})^{(5,5)}(T_{29}, t)}$, $\boxed{+(a''_{30})^{(5,5)}(T_{29}, t)}$ are second augmentation coefficient for category 1, 2 and 3
 $\boxed{+(a''_{32})^{(6,6)}(T_{33}, t)}$, $\boxed{+(a''_{33})^{(6,6)}(T_{33}, t)}$, $\boxed{+(a''_{34})^{(6,6)}(T_{33}, t)}$ are third augmentation coefficient for category 1, 2 and 3
 $\boxed{+(a''_{13})^{(1,1,1,1)}(T_{14}, t)}$, $\boxed{+(a''_{14})^{(1,1,1,1)}(T_{14}, t)}$, $\boxed{+(a''_{15})^{(1,1,1,1)}(T_{14}, t)}$ are fourth augmentation coefficients for category 1, 2, and 3
 $\boxed{+(a''_{16})^{(2,2,2,2)}(T_{17}, t)}$, $\boxed{+(a''_{17})^{(2,2,2,2)}(T_{17}, t)}$, $\boxed{+(a''_{18})^{(2,2,2,2)}(T_{17}, t)}$ are fifth augmentation coefficients for category 1, 2, and 3
 $\boxed{+(a''_{20})^{(3,3,3,3)}(T_{21}, t)}$, $\boxed{+(a''_{21})^{(3,3,3,3)}(T_{21}, t)}$, $\boxed{+(a''_{22})^{(3,3,3,3)}(T_{21}, t)}$ are sixth augmentation coefficients for category 1, 2, and 3
 $\boxed{+(a''_{36})^{(7,7,7,7)}(T_{37}, t)}$, $\boxed{+(a''_{37})^{(7,7,7,7)}(T_{37}, t)}$, $\boxed{+(a''_{38})^{(7,7,7,7)}(T_{37}, t)}$ ARE SEVENTH augmentation coefficients *90

91

*92

$$\frac{dT_{24}}{dt} = (b_{24})^{(4)}T_{25} - \left[\begin{array}{c} (b'_{24})^{(4)} - (b''_{24})^{(4)}(G_{27}, t) \quad - (b''_{28})^{(5,5)}(G_{31}, t) \quad - (b''_{32})^{(6,6)}(G_{35}, t) \\ - (b''_{13})^{(1,1,1,1)}(G, t) \quad - (b''_{16})^{(2,2,2,2)}(G_{19}, t) \quad - (b''_{20})^{(3,3,3,3)}(G_{23}, t) \\ - (b''_{36})^{(7,7,7,7,,)}(G_{39}, t) \end{array} \right] T_{24} \quad *93$$

$$\frac{dT_{25}}{dt} = (b_{25})^{(4)}T_{24} - \left[\begin{array}{c} (b'_{25})^{(4)} - (b''_{25})^{(4)}(G_{27}, t) \quad - (b''_{29})^{(5,5)}(G_{31}, t) \quad - (b''_{33})^{(6,6)}(G_{35}, t) \\ - (b''_{14})^{(1,1,1,1)}(G, t) \quad - (b''_{17})^{(2,2,2,2)}(G_{19}, t) \quad - (b''_{21})^{(3,3,3,3)}(G_{23}, t) \\ - (b''_{37})^{(7,7,7,7,,)}(G_{39}, t) \end{array} \right] T_{25} \quad *94$$

$$\frac{dT_{26}}{dt} = (b_{26})^{(4)}T_{25} - \left[\begin{array}{c} (b'_{26})^{(4)} - (b''_{26})^{(4)}(G_{27}, t) \quad - (b''_{30})^{(5,5)}(G_{31}, t) \quad - (b''_{34})^{(6,6)}(G_{35}, t) \\ - (b''_{15})^{(1,1,1,1)}(G, t) \quad - (b''_{18})^{(2,2,2,2)}(G_{19}, t) \quad - (b''_{22})^{(3,3,3,3)}(G_{23}, t) \\ - (b''_{38})^{(7,7,7,7,,)}(G_{39}, t) \end{array} \right] T_{26} \quad *95$$

Where $-(b''_{24})^{(4)}(G_{27}, t)$, $-(b''_{25})^{(4)}(G_{27}, t)$, $-(b''_{26})^{(4)}(G_{27}, t)$ are first detrition coefficients for category 1, 2 and 3
 $-(b''_{28})^{(5,5)}(G_{31}, t)$, $-(b''_{29})^{(5,5)}(G_{31}, t)$, $-(b''_{30})^{(5,5)}(G_{31}, t)$ are second detrition coefficients for category 1, 2 and 3
 $-(b''_{32})^{(6,6)}(G_{35}, t)$, $-(b''_{33})^{(6,6)}(G_{35}, t)$, $-(b''_{34})^{(6,6)}(G_{35}, t)$ are third detrition coefficients for category 1, 2 and 3
 $-(b''_{13})^{(1,1,1,1)}(G, t)$, $-(b''_{14})^{(1,1,1,1)}(G, t)$, $-(b''_{15})^{(1,1,1,1)}(G, t)$ are fourth detrition coefficients for category 1, 2 and 3
 $-(b''_{16})^{(2,2,2,2)}(G_{19}, t)$, $-(b''_{17})^{(2,2,2,2)}(G_{19}, t)$, $-(b''_{18})^{(2,2,2,2)}(G_{19}, t)$ are fifth detrition coefficients for category 1, 2 and 3
 $-(b''_{20})^{(3,3,3,3)}(G_{23}, t)$, $-(b''_{21})^{(3,3,3,3)}(G_{23}, t)$, $-(b''_{22})^{(3,3,3,3)}(G_{23}, t)$ are sixth detrition coefficients for category 1, 2 and 3
 $-(b''_{36})^{(7,7,7,7,,)}(G_{39}, t)$, $-(b''_{37})^{(7,7,7,7,,)}(G_{39}, t)$, $-(b''_{38})^{(7,7,7,7,,)}(G_{39}, t)$ ARE SEVENTH DETRITION COEFFICIENTS*96

*97

FIFTH MODULE CONCATENATION:*98

$$\frac{dG_{28}}{dt} = (a_{28})^{(5)}G_{29} - \left[\begin{array}{c} (a'_{28})^{(5)} + (a''_{28})^{(5)}(T_{29}, t) \quad + (a''_{24})^{(4,4)}(T_{25}, t) \quad + (a''_{32})^{(6,6,6)}(T_{33}, t) \\ + (a''_{13})^{(1,1,1,1,1)}(T_{14}, t) \quad + (a''_{16})^{(2,2,2,2,2)}(T_{17}, t) \quad + (a''_{20})^{(3,3,3,3,3)}(T_{21}, t) \\ + (a''_{36})^{(7,7,,7,,7,7)}(T_{37}, t) \end{array} \right] G_{28} \quad *99$$

$$\frac{dG_{29}}{dt} = (a_{29})^{(5)}G_{28} - \left[\begin{array}{c} (a'_{29})^{(5)} + (a''_{29})^{(5)}(T_{29}, t) \quad + (a''_{25})^{(4,4)}(T_{25}, t) \quad + (a''_{33})^{(6,6,6)}(T_{33}, t) \\ + (a''_{14})^{(1,1,1,1,1)}(T_{14}, t) \quad + (a''_{17})^{(2,2,2,2,2)}(T_{17}, t) \quad + (a''_{21})^{(3,3,3,3,3)}(T_{21}, t) \\ + (a''_{37})^{(7,7,,7,,7,7)}(T_{37}, t) \end{array} \right] G_{29} \quad *100$$

$$\frac{dG_{30}}{dt} = (a_{30})^{(5)}G_{29} - \left[\begin{array}{c} (a'_{30})^{(5)} + (a''_{30})^{(5)}(T_{29}, t) \quad + (a''_{26})^{(4,4)}(T_{25}, t) \quad + (a''_{34})^{(6,6,6)}(T_{33}, t) \\ + (a''_{15})^{(1,1,1,1,1)}(T_{14}, t) \quad + (a''_{18})^{(2,2,2,2,2)}(T_{17}, t) \quad + (a''_{22})^{(3,3,3,3,3)}(T_{21}, t) \\ + (a''_{38})^{(7,7,,7,,7,7)}(T_{37}, t) \end{array} \right] G_{30} \quad *101$$

Where $+(a''_{28})^{(5)}(T_{29}, t)$, $+(a''_{29})^{(5)}(T_{29}, t)$, $+(a''_{30})^{(5)}(T_{29}, t)$ are first augmentation coefficients for category 1, 2 and 3
 And $+(a''_{24})^{(4,4)}(T_{25}, t)$, $+(a''_{25})^{(4,4)}(T_{25}, t)$, $+(a''_{26})^{(4,4)}(T_{25}, t)$ are second augmentation coefficient for category 1, 2 and 3
 $+(a''_{32})^{(6,6,6)}(T_{33}, t)$, $+(a''_{33})^{(6,6,6)}(T_{33}, t)$, $+(a''_{34})^{(6,6,6)}(T_{33}, t)$ are third augmentation coefficient for category 1, 2 and 3
 $+(a''_{13})^{(1,1,1,1,1)}(T_{14}, t)$, $+(a''_{14})^{(1,1,1,1,1)}(T_{14}, t)$, $+(a''_{15})^{(1,1,1,1,1)}(T_{14}, t)$ are fourth augmentation coefficients for category 1, 2, and 3
 $+(a''_{16})^{(2,2,2,2,2)}(T_{17}, t)$, $+(a''_{17})^{(2,2,2,2,2)}(T_{17}, t)$, $+(a''_{18})^{(2,2,2,2,2)}(T_{17}, t)$ are fifth augmentation coefficients for category 1, 2, and 3
 $+(a''_{20})^{(3,3,3,3,3)}(T_{21}, t)$, $+(a''_{21})^{(3,3,3,3,3)}(T_{21}, t)$, $+(a''_{22})^{(3,3,3,3,3)}(T_{21}, t)$ are sixth augmentation coefficients for category 1, 2, 3 *102

*103

$$\frac{dT_{28}}{dt} = (b_{28})^{(5)}T_{29} - \left[\begin{array}{l} (b'_{28})^{(5)} \boxed{-(b''_{28})^{(5)}(G_{31}, t)} \quad \boxed{-(b''_{24})^{(4,4)}(G_{23}, t)} \quad \boxed{-(b''_{32})^{(6,6,6)}(G_{35}, t)} \\ \boxed{-(b''_{13})^{(1,1,1,1,1)}(G, t)} \quad \boxed{-(b''_{16})^{(2,2,2,2,2)}(G_{19}, t)} \quad \boxed{-(b''_{20})^{(3,3,3,3,3)}(G_{23}, t)} \\ \boxed{-(b''_{36})^{(7,7,7,7,7)}(G_{38}, t)} \end{array} \right] T_{28} *104$$

$$\frac{dT_{29}}{dt} = (b_{29})^{(5)}T_{28} - \left[\begin{array}{l} (b'_{29})^{(5)} \boxed{-(b''_{29})^{(5)}(G_{31}, t)} \quad \boxed{-(b''_{25})^{(4,4)}(G_{27}, t)} \quad \boxed{-(b''_{33})^{(6,6,6)}(G_{35}, t)} \\ \boxed{-(b''_{14})^{(1,1,1,1,1)}(G, t)} \quad \boxed{-(b''_{17})^{(2,2,2,2,2)}(G_{19}, t)} \quad \boxed{-(b''_{21})^{(3,3,3,3,3)}(G_{23}, t)} \\ \boxed{-(b''_{37})^{(7,7,7,7,7)}(G_{38}, t)} \end{array} \right] T_{29} *105$$

$$\frac{dT_{30}}{dt} = (b_{30})^{(5)}T_{29} - \left[\begin{array}{l} (b'_{30})^{(5)} \boxed{-(b''_{30})^{(5)}(G_{31}, t)} \quad \boxed{-(b''_{26})^{(4,4)}(G_{27}, t)} \quad \boxed{-(b''_{34})^{(6,6,6)}(G_{35}, t)} \\ \boxed{-(b''_{15})^{(1,1,1,1,1)}(G, t)} \quad \boxed{-(b''_{18})^{(2,2,2,2,2)}(G_{19}, t)} \quad \boxed{-(b''_{22})^{(3,3,3,3,3)}(G_{23}, t)} \\ \boxed{-(b''_{38})^{(7,7,7,7,7)}(G_{38}, t)} \end{array} \right] T_{30} *106$$

where $\boxed{-(b''_{28})^{(5)}(G_{31}, t)}$, $\boxed{-(b''_{29})^{(5)}(G_{31}, t)}$, $\boxed{-(b''_{30})^{(5)}(G_{31}, t)}$ are first detrition coefficients for category 1, 2 and 3

$\boxed{-(b''_{24})^{(4,4)}(G_{27}, t)}$, $\boxed{-(b''_{25})^{(4,4)}(G_{27}, t)}$, $\boxed{-(b''_{26})^{(4,4)}(G_{27}, t)}$ are second detrition coefficients for category 1,2 and 3

$\boxed{-(b''_{32})^{(6,6,6)}(G_{35}, t)}$, $\boxed{-(b''_{33})^{(6,6,6)}(G_{35}, t)}$, $\boxed{-(b''_{34})^{(6,6,6)}(G_{35}, t)}$ are third detrition coefficients for category 1,2 and 3

$\boxed{-(b''_{13})^{(1,1,1,1,1)}(G, t)}$, $\boxed{-(b''_{14})^{(1,1,1,1,1)}(G, t)}$, $\boxed{-(b''_{15})^{(1,1,1,1,1)}(G, t)}$ are fourth detrition coefficients for category 1,2, and 3

$\boxed{-(b''_{16})^{(2,2,2,2,2)}(G_{19}, t)}$, $\boxed{-(b''_{17})^{(2,2,2,2,2)}(G_{19}, t)}$, $\boxed{-(b''_{18})^{(2,2,2,2,2)}(G_{19}, t)}$ are fifth detrition coefficients for category 1,2, and 3

$\boxed{-(b''_{20})^{(3,3,3,3,3)}(G_{23}, t)}$, $\boxed{-(b''_{21})^{(3,3,3,3,3)}(G_{23}, t)}$, $\boxed{-(b''_{22})^{(3,3,3,3,3)}(G_{23}, t)}$ are sixth detrition coefficients for category 1,2, and 3*107

SIXTH MODULE CONCATENATION*108

$$\frac{dG_{32}}{dt} = (a_{32})^{(6)}G_{33} - \left[\begin{array}{l} (a'_{32})^{(6)} \boxed{+(a''_{32})^{(6)}(T_{33}, t)} \quad \boxed{+(a''_{28})^{(5,5,5)}(T_{29}, t)} \quad \boxed{+(a''_{24})^{(4,4,4)}(T_{25}, t)} \\ \boxed{+(a''_{13})^{(1,1,1,1,1)}(T_{14}, t)} \quad \boxed{+(a''_{16})^{(2,2,2,2,2)}(T_{17}, t)} \quad \boxed{+(a''_{20})^{(3,3,3,3,3)}(T_{21}, t)} \\ \boxed{+(a''_{36})^{(7,7,7,7,7)}(T_{37}, t)} \end{array} \right] G_{32} *109$$

$$\frac{dG_{33}}{dt} = (a_{33})^{(6)}G_{32} - \left[\begin{array}{l} (a'_{33})^{(6)} \boxed{+(a''_{33})^{(6)}(T_{33}, t)} \quad \boxed{+(a''_{29})^{(5,5,5)}(T_{29}, t)} \quad \boxed{+(a''_{25})^{(4,4,4)}(T_{25}, t)} \\ \boxed{+(a''_{14})^{(1,1,1,1,1)}(T_{14}, t)} \quad \boxed{+(a''_{17})^{(2,2,2,2,2)}(T_{17}, t)} \quad \boxed{+(a''_{21})^{(3,3,3,3,3)}(T_{21}, t)} \\ \boxed{+(a''_{37})^{(7,7,7,7,7)}(T_{37}, t)} \end{array} \right] G_{33} *110$$

$$\frac{dG_{34}}{dt} = (a_{34})^{(6)}G_{33} - \left[\begin{array}{l} (a'_{34})^{(6)} \boxed{+(a''_{34})^{(6)}(T_{33}, t)} \quad \boxed{+(a''_{30})^{(5,5,5)}(T_{29}, t)} \quad \boxed{+(a''_{26})^{(4,4,4)}(T_{25}, t)} \\ \boxed{+(a''_{15})^{(1,1,1,1,1)}(T_{14}, t)} \quad \boxed{+(a''_{18})^{(2,2,2,2,2)}(T_{17}, t)} \quad \boxed{+(a''_{22})^{(3,3,3,3,3)}(T_{21}, t)} \\ \boxed{+(a''_{38})^{(7,7,7,7,7)}(T_{37}, t)} \end{array} \right] G_{34} *111$$

$\boxed{+(a''_{32})^{(6)}(T_{33}, t)}$, $\boxed{+(a''_{33})^{(6)}(T_{33}, t)}$, $\boxed{+(a''_{34})^{(6)}(T_{33}, t)}$ are first augmentation coefficients for category 1, 2 and 3

$\boxed{+(a''_{28})^{(5,5,5)}(T_{29}, t)}$, $\boxed{+(a''_{29})^{(5,5,5)}(T_{29}, t)}$, $\boxed{+(a''_{30})^{(5,5,5)}(T_{29}, t)}$ are second augmentation coefficients for category 1,2 and 3

$\boxed{+(a''_{24})^{(4,4,4)}(T_{25}, t)}$, $\boxed{+(a''_{25})^{(4,4,4)}(T_{25}, t)}$, $\boxed{+(a''_{26})^{(4,4,4)}(T_{25}, t)}$ are third augmentation coefficients for category 1, 2 and 3

$\boxed{+(a''_{13})^{(1,1,1,1,1)}(T_{14}, t)}$, $\boxed{+(a''_{14})^{(1,1,1,1,1)}(T_{14}, t)}$, $\boxed{+(a''_{15})^{(1,1,1,1,1)}(T_{14}, t)}$ - are fourth augmentation coefficients

$\boxed{+(a''_{16})^{(2,2,2,2,2)}(T_{17}, t)}$, $\boxed{+(a''_{17})^{(2,2,2,2,2)}(T_{17}, t)}$, $\boxed{+(a''_{18})^{(2,2,2,2,2)}(T_{17}, t)}$ - fifth augmentation coefficients

$\boxed{+(a''_{20})^{(3,3,3,3,3)}(T_{21}, t)}$, $\boxed{+(a''_{21})^{(3,3,3,3,3)}(T_{21}, t)}$, $\boxed{+(a''_{22})^{(3,3,3,3,3)}(T_{21}, t)}$ sixth augmentation coefficients

$\boxed{+(a''_{36})^{(7,7,7,7,7)}(T_{37}, t)}$, $\boxed{+(a''_{36})^{(7,7,7,7,7)}(T_{37}, t)}$, $\boxed{+(a''_{36})^{(7,7,7,7,7)}(T_{37}, t)}$ ARE SVENTH AUGMENTATION COEFFICIENTS*112

*113

$$\frac{dT_{32}}{dt} = (b_{32})^{(6)}T_{33} - \left[\begin{array}{l} (b'_{32})^{(6)} \boxed{-(b''_{32})^{(6)}(G_{35}, t)} \quad \boxed{-(b''_{28})^{(5,5,5)}(G_{31}, t)} \quad \boxed{-(b''_{24})^{(4,4,4)}(G_{27}, t)} \\ \boxed{-(b''_{13})^{(1,1,1,1,1)}(G, t)} \quad \boxed{-(b''_{16})^{(2,2,2,2,2)}(G_{19}, t)} \quad \boxed{-(b''_{20})^{(3,3,3,3,3)}(G_{23}, t)} \\ \boxed{-(b''_{36})^{(7,7,7,7,7)}(G_{39}, t)} \end{array} \right] T_{32} *114$$

$$\frac{dT_{33}}{dt} = (b_{33})^{(6)}T_{32} - \left[\begin{array}{l} (b'_{33})^{(6)} - (b''_{33})^{(6)}(G_{35}, t) - (b''_{29})^{(5,5,5)}(G_{31}, t) - (b''_{25})^{(4,4,4)}(G_{27}, t) \\ - (b''_{14})^{(1,1,1,1,1,1)}(G, t) - (b''_{17})^{(2,2,2,2,2,2)}(G_{19}, t) - (b''_{21})^{(3,3,3,3,3,3)}(G_{23}, t) \\ - (b''_{37})^{(7,7,7,7,7,7)}(G_{39}, t) \end{array} \right] T_{33} \quad *115$$

$$\frac{dT_{34}}{dt} = (b_{34})^{(6)}T_{33} - \left[\begin{array}{l} (b'_{34})^{(6)} - (b''_{34})^{(6)}(G_{35}, t) - (b''_{30})^{(5,5,5)}(G_{31}, t) - (b''_{26})^{(4,4,4)}(G_{27}, t) \\ - (b''_{15})^{(1,1,1,1,1,1)}(G, t) - (b''_{18})^{(2,2,2,2,2,2)}(G_{19}, t) - (b''_{22})^{(3,3,3,3,3,3)}(G_{23}, t) \\ - (b''_{38})^{(7,7,7,7,7,7)}(G_{39}, t) \end{array} \right] T_{34} \quad *116$$

$-(b''_{32})^{(6)}(G_{35}, t)$, $-(b''_{33})^{(6)}(G_{35}, t)$, $-(b''_{34})^{(6)}(G_{35}, t)$ are first detrition coefficients for category 1, 2 and 3
 $-(b''_{28})^{(5,5,5)}(G_{31}, t)$, $-(b''_{29})^{(5,5,5)}(G_{31}, t)$, $-(b''_{30})^{(5,5,5)}(G_{31}, t)$ are second detrition coefficients for category 1, 2 and 3
 $-(b''_{24})^{(4,4,4)}(G_{27}, t)$, $-(b''_{25})^{(4,4,4)}(G_{27}, t)$, $-(b''_{26})^{(4,4,4)}(G_{27}, t)$ are third detrition coefficients for category 1, 2 and 3
 $-(b''_{13})^{(1,1,1,1,1,1)}(G, t)$, $-(b''_{14})^{(1,1,1,1,1,1)}(G, t)$, $-(b''_{15})^{(1,1,1,1,1,1)}(G, t)$ are fourth detrition coefficients for category 1, 2, and 3
 $-(b''_{16})^{(2,2,2,2,2,2)}(G_{19}, t)$, $-(b''_{17})^{(2,2,2,2,2,2)}(G_{19}, t)$, $-(b''_{18})^{(2,2,2,2,2,2)}(G_{19}, t)$ are fifth detrition coefficients for category 1, 2, and 3
 $-(b''_{20})^{(3,3,3,3,3,3)}(G_{23}, t)$, $-(b''_{21})^{(3,3,3,3,3,3)}(G_{23}, t)$, $-(b''_{22})^{(3,3,3,3,3,3)}(G_{23}, t)$ are sixth detrition coefficients for category 1, 2, and 3
 $-(b''_{36})^{(7,7,7,7,7,7)}(G_{39}, t)$, $-(b''_{36})^{(7,7,7,7,7,7)}(G_{39}, t)$, $-(b''_{36})^{(7,7,7,7,7,7)}(G_{39}, t)$ ARE SEVENTH DETRITION COEFFICIENTS*117

*118
 SEVENTH MODULE CONCATENATION: *119

$$\frac{dG_{36}}{dt} = (a_{36})^{(7)}G_{37} - \left[(a'_{36})^{(7)} + (a''_{36})^{(7)}(T_{37}, t) \right] + (a''_{16})^{(7)}(T_{17}, t) + (a''_{20})^{(7)}(T_{21}, t) + (a''_{24})^{(7)}(T_{23}, t)G_{36} + a_{28}''7T_{29,t} + a_{32}''7T_{33,t} + a_{13}''7T_{14,t}G_{36} \quad *120$$

121

$$\frac{dG_{37}}{dt} = (a_{37})^{(7)}G_{36} - \left[(a'_{37})^{(7)} + (a''_{37})^{(7)}(T_{37}, t) \right] + (a''_{14})^{(7)}(T_{14}, t) + (a''_{21})^{(7)}(T_{21}, t) + (a''_{17})^{(7)}(T_{17}, t) + a_{25}''7T_{25,t} + a_{33}''7T_{33,t} + a_{29}''7T_{29,t} \quad G_{37}$$

*122

$$\frac{dG_{38}}{dt} = (a_{38})^{(7)}G_{37} - \left[(a'_{38})^{(7)} + (a''_{38})^{(7)}(T_{37}, t) \right] + (a''_{15})^{(7)}(T_{14}, t) + (a''_{22})^{(7)}(T_{21}, t) + (a''_{18})^{(7)}(T_{17}, t) + a_{26}''7T_{25,t} + a_{34}''7T_{33,t} + a_{30}''7T_{29,t} \quad G_{38}$$

*123

124
125

$$\frac{dT_{36}}{dt} = (b_{36})^{(7)}T_{37} - \left[(b'_{36})^{(7)} - (b''_{36})^{(7)}(G_{39}, t) - (b''_{16})^{(7)}(G_{19}, t) - (b''_{13})^{(7)}(G_{14}, t) - (b''_{20})^{(7)}(G_{231}, t) \right] - b_{24}''7G_{27,t} - b_{28}''7G_{31,t} - b_{32}''7G_{35,t} \quad T_{36}$$

*126

$$\frac{dT_{37}}{dt} = (b_{37})^{(7)}T_{36} - \left[(b'_{36})^{(7)} - (b''_{37})^{(7)}(G_{39}, t) - (b''_{17})^{(7)}(G_{19}, t) - (b''_{19})^{(7)}(G_{14}, t) - (b''_{21})^{(7)}(G_{231}, t) - (b''_{25})^{(7)}(G_{27}, t) - (b''_{29})^{(7)}(G_{31}, t) - (b''_{33})^{(7)}(G_{35}, t) \right] T_{37}$$

*127

Where we suppose

(A) $(a_i)^{(1)}, (a'_i)^{(1)}, (a''_i)^{(1)}, (b_i)^{(1)}, (b'_i)^{(1)}, (b''_i)^{(1)} > 0,$

$i, j = 13, 14, 15$

(B) The functions $(a_i'')^{(1)}, (b_i'')^{(1)}$ are positive continuous increasing and bounded.

Definition of $(p_i)^{(1)}, (r_i)^{(1)}$:

$$(a_i'')^{(1)}(T_{14}, t) \leq (p_i)^{(1)} \leq (\hat{A}_{13})^{(1)}$$

$$(b_i'')^{(1)}(G, t) \leq (r_i)^{(1)} \leq (b_i')^{(1)} \leq (\hat{B}_{13})^{(1)}$$

(C) $\lim_{T_2 \rightarrow \infty} (a_i'')^{(1)}(T_{14}, t) = (p_i)^{(1)}$

$$\lim_{G \rightarrow \infty} (b_i'')^{(1)}(G, t) = (r_i)^{(1)}$$

Definition of $(\hat{A}_{13})^{(1)}, (\hat{B}_{13})^{(1)}$:

Where $(\hat{A}_{13})^{(1)}, (\hat{B}_{13})^{(1)}, (p_i)^{(1)}, (r_i)^{(1)}$ are positive constants and $i = 13, 14, 15$

They satisfy Lipschitz condition:

$$|(a_i'')^{(1)}(T_{14}', t) - (a_i'')^{(1)}(T_{14}, t)| \leq (\hat{k}_{13})^{(1)} |T_{14}' - T_{14}| e^{-(M_{13})^{(1)}t}$$

$$|(b_i'')^{(1)}(G', t) - (b_i'')^{(1)}(G, T)| < (\hat{k}_{13})^{(1)} \|G - G'\| e^{-(M_{13})^{(1)}t}$$

With the Lipschitz condition, we place a restriction on the behavior of functions $(a_i'')^{(1)}(T_{14}', t)$ and $(a_i'')^{(1)}(T_{14}, t)$. (T_{14}', t) and (T_{14}, t) are points belonging to the interval $[(\hat{k}_{13})^{(1)}, (\hat{M}_{13})^{(1)}]$. It is to be noted that $(a_i'')^{(1)}(T_{14}, t)$ is uniformly continuous. In the eventuality of the fact, that if $(\hat{M}_{13})^{(1)} = 1$ then the function $(a_i'')^{(1)}(T_{14}, t)$, the **first augmentation coefficient** attributable to terrestrial organisms, would be absolutely continuous.

Definition of $(\hat{M}_{13})^{(1)}, (\hat{k}_{13})^{(1)}$:

(D) $(\hat{M}_{13})^{(1)}, (\hat{k}_{13})^{(1)}$, are positive constants

$$\frac{(a_i)^{(1)}}{(M_{13})^{(1)}}, \frac{(b_i)^{(1)}}{(M_{13})^{(1)}} < 1$$

Definition of $(\hat{P}_{13})^{(1)}, (\hat{Q}_{13})^{(1)}$:

(E) There exists two constants $(\hat{P}_{13})^{(1)}$ and $(\hat{Q}_{13})^{(1)}$ which together with $(\hat{M}_{13})^{(1)}, (\hat{k}_{13})^{(1)}, (\hat{A}_{13})^{(1)}$ and $(\hat{B}_{13})^{(1)}$ and the constants $(a_i)^{(1)}, (a_i')^{(1)}, (b_i)^{(1)}, (b_i')^{(1)}, (p_i)^{(1)}, (r_i)^{(1)}, i = 13, 14, 15$, satisfy the inequalities

$$\frac{1}{(\hat{M}_{13})^{(1)}} [(a_i)^{(1)} + (a_i')^{(1)} + (\hat{A}_{13})^{(1)} + (\hat{P}_{13})^{(1)} (\hat{k}_{13})^{(1)}] < 1$$

$$\frac{1}{(\hat{M}_{13})^{(1)}} [(b_i)^{(1)} + (b_i')^{(1)} + (\hat{B}_{13})^{(1)} + (\hat{Q}_{13})^{(1)} (\hat{k}_{13})^{(1)}] < 1$$

$$\frac{dT_{38}}{dt} = (b_{38})^{(7)}T_{37} - \left[(b_{38})^{(7)} - \frac{(b_{38})^{(7)}((G_{39}), t)}{b26''7G27,t} - \frac{(b_{18})^{(7)}((G_{19}), t)}{-b30''7G31,t} - \frac{(b_{20})^{(7)}((G_{14}), t)}{-b34''7G35,t} \right] - \quad \begin{matrix} 128 \\ 129 \\ 130 \\ 131 \\ 132 \end{matrix}$$

$$+ (a_{36})^{(7)}(T_{37}, t) = \text{First augmentation factor} \quad 134$$

$$(1)(a_i)^{(2)}, (a_i')^{(2)}, (a_i'')^{(2)}, (b_i)^{(2)}, (b_i')^{(2)}, (b_i'')^{(2)} > 0, \quad i, j = 16, 17, 18 \quad 135$$

(F) (2) The functions $(a_i'')^{(2)}, (b_i'')^{(2)}$ are positive continuous increasing and bounded. 136

Definition of $(p_i)^{(2)}, (r_i)^{(2)}$: 137

$$(a_i'')^{(2)}(T_{17}, t) \leq (p_i)^{(2)} \leq (\hat{A}_{16})^{(2)} \quad 138$$

$$(b_i'')^{(2)}(G_{19}, t) \leq (r_i)^{(2)} \leq (b_i')^{(2)} \leq (\hat{B}_{16})^{(2)} \quad 139$$

(G) (3) $\lim_{T_2 \rightarrow \infty} (a_i'')^{(2)}(T_{17}, t) = (p_i)^{(2)}$ 140

$$\lim_{G \rightarrow \infty} (b_i'')^{(2)}((G_{19}), t) = (r_i)^{(2)} \tag{141}$$

Definition of $(\hat{A}_{16})^{(2)}, (\hat{B}_{16})^{(2)}$: 142

Where $(\hat{A}_{16})^{(2)}, (\hat{B}_{16})^{(2)}, (p_i)^{(2)}, (r_i)^{(2)}$ are positive constants and $i = 16, 17, 18$

They satisfy Lipschitz condition: 143

$$|(a_i'')^{(2)}(T_{17}', t) - (a_i'')^{(2)}(T_{17}, t)| \leq (\hat{k}_{16})^{(2)} |T_{17}' - T_{17}| e^{-(M_{16})^{(2)}t} \tag{144}$$

$$|(b_i'')^{(2)}((G_{19})', t) - (b_i'')^{(2)}((G_{19}), t)| < (\hat{k}_{16})^{(2)} |(G_{19})' - (G_{19})| e^{-(M_{16})^{(2)}t} \tag{145}$$

With the Lipschitz condition, we place a restriction on the behavior of functions $(a_i'')^{(2)}(T_{17}', t)$ and $(a_i'')^{(2)}(T_{17}, t)$ 146

(T_{17}', t) and (T_{17}, t) are points belonging to the interval $[(\hat{k}_{16})^{(2)}, (\hat{M}_{16})^{(2)}]$. It is to be noted that $(a_i'')^{(2)}(T_{17}, t)$

is uniformly continuous. In the eventuality of the fact, that if $(\hat{M}_{16})^{(2)} = 1$ then the function $(a_i'')^{(2)}(T_{17}, t)$, the SECOND augmentation coefficient would be absolutely continuous.

Definition of $(\hat{M}_{16})^{(2)}, (\hat{k}_{16})^{(2)}$: 147

(H) (4) $(\hat{M}_{16})^{(2)}, (\hat{k}_{16})^{(2)}$, are positive constants 148

$$\frac{(a_i)^{(2)}}{(\hat{M}_{16})^{(2)}}, \frac{(b_i)^{(2)}}{(\hat{M}_{16})^{(2)}} < 1$$

Definition of $(\hat{P}_{13})^{(2)}, (\hat{Q}_{13})^{(2)}$: 149

There exists two constants $(\hat{P}_{16})^{(2)}$ and $(\hat{Q}_{16})^{(2)}$ which together with $(\hat{M}_{16})^{(2)}, (\hat{k}_{16})^{(2)}, (\hat{A}_{16})^{(2)}$ and $(\hat{B}_{16})^{(2)}$

and the constants $(a_i)^{(2)}, (a_i')^{(2)}, (b_i)^{(2)}, (b_i')^{(2)}, (p_i)^{(2)}, (r_i)^{(2)}, i = 16, 17, 18$,

satisfy the inequalities

$$\frac{1}{(\hat{M}_{16})^{(2)}} [(a_i)^{(2)} + (a_i')^{(2)} + (\hat{A}_{16})^{(2)} + (\hat{P}_{16})^{(2)} (\hat{k}_{16})^{(2)}] < 1 \tag{150}$$

$$\frac{1}{(\hat{M}_{16})^{(2)}} [(b_i)^{(2)} + (b_i')^{(2)} + (\hat{B}_{16})^{(2)} + (\hat{Q}_{16})^{(2)} (\hat{k}_{16})^{(2)}] < 1 \tag{151}$$

Where we suppose 152

(I) (5) $(a_i)^{(3)}, (a_i')^{(3)}, (a_i'')^{(3)}, (b_i)^{(3)}, (b_i')^{(3)}, (b_i'')^{(3)} > 0, i, j = 20, 21, 22$ 153

The functions $(a_i'')^{(3)}, (b_i'')^{(3)}$ are positive continuous increasing and bounded.

Definition of $(p_i)^{(3)}, (r_i)^{(3)}$:

$$(a_i'')^{(3)}(T_{21}, t) \leq (p_i)^{(3)} \leq (\hat{A}_{20})^{(3)}$$

$$(b_i'')^{(3)}(G_{23}, t) \leq (r_i)^{(3)} \leq (b_i')^{(3)} \leq (\hat{B}_{20})^{(3)}$$

$$\lim_{T_2 \rightarrow \infty} (a_i'')^{(3)}(T_{21}, t) = (p_i)^{(3)} \tag{154}$$

$$\lim_{G \rightarrow \infty} (b_i'')^{(3)}(G_{23}, t) = (r_i)^{(3)} \tag{155}$$

Definition of $(\hat{A}_{20})^{(3)}, (\hat{B}_{20})^{(3)}$: 156

Where $(\hat{A}_{20})^{(3)}, (\hat{B}_{20})^{(3)}, (p_i)^{(3)}, (r_i)^{(3)}$ are positive constants and $i = 20, 21, 22$

They satisfy Lipschitz condition: 157

$$|(a_i'')^{(3)}(T_{21}', t) - (a_i'')^{(3)}(T_{21}, t)| \leq (\hat{k}_{20})^{(3)} |T_{21}' - T_{21}| e^{-(M_{20})^{(3)}t} \tag{158}$$

$$|(b_i'')^{(3)}(G_{23}', t) - (b_i'')^{(3)}(G_{23}, t)| < (\hat{k}_{20})^{(3)} |G_{23}' - G_{23}| e^{-(M_{20})^{(3)}t} \tag{159}$$

With the Lipschitz condition, we place a restriction on the behavior of functions $(a_i'')^{(3)}(T_{21}', t)$ and $(a_i'')^{(3)}(T_{21}, t)$ 160

(T_{21}', t) and (T_{21}, t) are points belonging to the interval $[(\hat{k}_{20})^{(3)}, (\hat{M}_{20})^{(3)}]$. It is to be noted that

$(a_i'')^{(3)}(T_{21}, t)$ is uniformly continuous. In the eventuality of the fact, that if $(\hat{M}_{20})^{(3)} = 1$ then the function

$(a_i'')^{(3)}(T_{21}, t)$, the THIRD augmentation coefficient, would be absolutely continuous.

Definition of $(\hat{M}_{20})^{(3)}, (\hat{k}_{20})^{(3)}$: 161

(J) (6) $(\hat{M}_{20})^{(3)}, (\hat{k}_{20})^{(3)}$, are positive constants

$$\frac{(a_i)^{(3)}}{(\hat{M}_{20})^{(3)}}, \frac{(b_i)^{(3)}}{(\hat{M}_{20})^{(3)}} < 1$$

There exists two constants There exists two constants $(\hat{P}_{20})^{(3)}$ and $(\hat{Q}_{20})^{(3)}$ which together with 162

$(\hat{M}_{20})^{(3)}, (\hat{k}_{20})^{(3)}, (\hat{A}_{20})^{(3)}$ and $(\hat{B}_{20})^{(3)}$ and the constants $(a_i)^{(3)}, (a_i')^{(3)}, (b_i)^{(3)}, (b_i')^{(3)}, (p_i)^{(3)}, (r_i)^{(3)}, i =$ 163

20, 21, 22, 164

satisfy the inequalities 165

$$\frac{1}{(\hat{M}_{20})^{(3)}} [(a_i)^{(3)} + (a_i')^{(3)} + (\hat{A}_{20})^{(3)} + (\hat{P}_{20})^{(3)} (\hat{k}_{20})^{(3)}] < 1 \tag{166}$$

$$\frac{1}{(\hat{M}_{20})^{(3)}} [(b_i)^{(3)} + (b_i')^{(3)} + (\hat{B}_{20})^{(3)} + (\hat{Q}_{20})^{(3)} (\hat{k}_{20})^{(3)}] < 1 \tag{167}$$

Where we suppose 168

(K) (7) $(a_i)^{(4)}, (a_i')^{(4)}, (a_i'')^{(4)}, (b_i)^{(4)}, (b_i')^{(4)}, (b_i'')^{(4)} > 0, i, j = 24, 25, 26$ 169

(L) (7) The functions $(a_i'')^{(4)}, (b_i'')^{(4)}$ are positive continuous increasing and bounded.

Definition of $(p_i)^{(4)}, (r_i)^{(4)}$:

$$(a_i'')^{(4)}(T_{25}, t) \leq (p_i)^{(4)} \leq (\hat{A}_{24})^{(4)}$$

$$(b_i'')^{(4)}(G_{27}, t) \leq (r_i)^{(4)} \leq (b_i')^{(4)} \leq (\hat{B}_{24})^{(4)}$$

$$(M) \quad (8) \quad \lim_{T_2 \rightarrow \infty} (a_i'')^{(4)}(T_{25}, t) = (p_i)^{(4)}$$

$$\lim_{G \rightarrow \infty} (b_i'')^{(4)}((G_{27}), t) = (r_i)^{(4)}$$

Definition of $(\hat{A}_{24})^{(4)}, (\hat{B}_{24})^{(4)}$:

Where $(\hat{A}_{24})^{(4)}, (\hat{B}_{24})^{(4)}, (p_i)^{(4)}, (r_i)^{(4)}$ are positive constants and $i = 24, 25, 26$

171

They satisfy Lipschitz condition:

$$|(a_i'')^{(4)}(T_{25}', t) - (a_i'')^{(4)}(T_{25}, t)| \leq (\hat{k}_{24})^{(4)} |T_{25}' - T_{25}| e^{-(\hat{M}_{24})^{(4)}t}$$

$$|(b_i'')^{(4)}((G_{27})', t) - (b_i'')^{(4)}((G_{27}), t)| \leq (\hat{k}_{24})^{(4)} |(G_{27})' - (G_{27})| e^{-(\hat{M}_{24})^{(4)}t}$$

With the Lipschitz condition, we place a restriction on the behavior of functions $(a_i'')^{(4)}(T_{25}', t)$ and $(a_i'')^{(4)}(T_{25}, t)$. (T_{25}', t) and (T_{25}, t) are points belonging to the interval $[(\hat{k}_{24})^{(4)}, (\hat{M}_{24})^{(4)}]$. It is to be noted that $(a_i'')^{(4)}(T_{25}, t)$ is uniformly continuous. In the eventuality of the fact, that if $(\hat{M}_{24})^{(4)} = 4$ then the function $(a_i'')^{(4)}(T_{25}, t)$, the **FOURTH augmentation coefficient WOULD** be absolutely continuous.

172

173

Definition of $(\hat{M}_{24})^{(4)}, (\hat{k}_{24})^{(4)}$:

174

$(\hat{M}_{24})^{(4)}, (\hat{k}_{24})^{(4)}$, are positive constants

$$\frac{(a_i)^{(4)}}{(\hat{M}_{24})^{(4)}} , \frac{(b_i)^{(4)}}{(\hat{M}_{24})^{(4)}} < 1$$

Definition of $(\hat{P}_{24})^{(4)}, (\hat{Q}_{24})^{(4)}$:

175

(P) (9) There exists two constants $(\hat{P}_{24})^{(4)}$ and $(\hat{Q}_{24})^{(4)}$ which together with $(\hat{M}_{24})^{(4)}, (\hat{k}_{24})^{(4)}, (\hat{A}_{24})^{(4)}$ and $(\hat{B}_{24})^{(4)}$ and the constants $(a_i)^{(4)}, (a_i')^{(4)}, (b_i)^{(4)}, (b_i')^{(4)}, (p_i)^{(4)}, (r_i)^{(4)}, i = 24, 25, 26$, satisfy the inequalities

$$\frac{1}{(\hat{M}_{24})^{(4)}} [(a_i)^{(4)} + (a_i')^{(4)} + (\hat{A}_{24})^{(4)} + (\hat{P}_{24})^{(4)} (\hat{k}_{24})^{(4)}] < 1$$

$$\frac{1}{(\hat{M}_{24})^{(4)}} [(b_i)^{(4)} + (b_i')^{(4)} + (\hat{B}_{24})^{(4)} + (\hat{Q}_{24})^{(4)} (\hat{k}_{24})^{(4)}] < 1$$

Where we suppose

176

$$(a_i)^{(5)}, (a_i')^{(5)}, (a_i'')^{(5)}, (b_i)^{(5)}, (b_i')^{(5)}, (b_i'')^{(5)} > 0, \quad i, j = 28, 29, 30$$

177

(R) (10) The functions $(a_i'')^{(5)}, (b_i'')^{(5)}$ are positive continuous increasing and bounded.

Definition of $(p_i)^{(5)}, (r_i)^{(5)}$:

$$(a_i'')^{(5)}(T_{29}, t) \leq (p_i)^{(5)} \leq (\hat{A}_{28})^{(5)}$$

$$(b_i'')^{(5)}((G_{31}), t) \leq (r_i)^{(5)} \leq (\hat{B}_{28})^{(5)}$$

178

$$(S) \quad (11) \quad \lim_{T_2 \rightarrow \infty} (a_i'')^{(5)}(T_{29}, t) = (p_i)^{(5)}$$

$$\lim_{G \rightarrow \infty} (b_i'')^{(5)}(G_{31}, t) = (r_i)^{(5)}$$

Definition of $(\hat{A}_{28})^{(5)}, (\hat{B}_{28})^{(5)}$:

Where $(\hat{A}_{28})^{(5)}, (\hat{B}_{28})^{(5)}, (p_i)^{(5)}, (r_i)^{(5)}$ are positive constants and $i = 28, 29, 30$

They satisfy Lipschitz condition:

179

$$|(a_i'')^{(5)}(T_{29}', t) - (a_i'')^{(5)}(T_{29}, t)| \leq (\hat{k}_{28})^{(5)} |T_{29}' - T_{29}| e^{-(\hat{M}_{28})^{(5)}t}$$

$$|(b_i'')^{(5)}((G_{31})', t) - (b_i'')^{(5)}((G_{31}), t)| \leq (\hat{k}_{28})^{(5)} |(G_{31})' - (G_{31})| e^{-(\hat{M}_{28})^{(5)}t}$$

With the Lipschitz condition, we place a restriction on the behavior of functions $(a_i'')^{(5)}(T_{29}', t)$ and $(a_i'')^{(5)}(T_{29}, t)$. (T_{29}', t) and (T_{29}, t) are points belonging to the interval $[(\hat{k}_{28})^{(5)}, (\hat{M}_{28})^{(5)}]$. It is to be noted that $(a_i'')^{(5)}(T_{29}, t)$ is uniformly continuous. In the eventuality of the fact, that if $(\hat{M}_{28})^{(5)} = 5$ then the function $(a_i'')^{(5)}(T_{29}, t)$, the **FIFTH augmentation coefficient** attributable would be absolutely continuous.

180

181

Definition of $(\hat{M}_{28})^{(5)}, (\hat{k}_{28})^{(5)}$:

$(\hat{M}_{28})^{(5)}, (\hat{k}_{28})^{(5)}$, are positive constants

$$\frac{(a_i)^{(5)}}{(\hat{M}_{28})^{(5)}} , \frac{(b_i)^{(5)}}{(\hat{M}_{28})^{(5)}} < 1$$

Definition of $(\hat{P}_{28})^{(5)}, (\hat{Q}_{28})^{(5)}$:

182

There exists two constants $(\hat{P}_{28})^{(5)}$ and $(\hat{Q}_{28})^{(5)}$ which together with $(\hat{M}_{28})^{(5)}, (\hat{k}_{28})^{(5)}, (\hat{A}_{28})^{(5)}$ and $(\hat{B}_{28})^{(5)}$ and the constants $(a_i)^{(5)}, (a_i')^{(5)}, (b_i)^{(5)}, (b_i')^{(5)}, (p_i)^{(5)}, (r_i)^{(5)}, i = 28, 29, 30$, satisfy the inequalities

$$\frac{1}{(\hat{M}_{28})^{(5)}} [(a_i)^{(5)} + (a_i')^{(5)} + (\hat{A}_{28})^{(5)} + (\hat{P}_{28})^{(5)} (\hat{k}_{28})^{(5)}] < 1$$

$$\frac{1}{(\hat{M}_{28})^{(5)}} [(b_i)^{(5)} + (b_i')^{(5)} + (\hat{B}_{28})^{(5)} + (\hat{Q}_{28})^{(5)} (\hat{k}_{28})^{(5)}] < 1$$

Where we suppose

183

$$(a_i)^{(6)}, (a_i')^{(6)}, (a_i'')^{(6)}, (b_i)^{(6)}, (b_i')^{(6)}, (b_i'')^{(6)} > 0, \quad i, j = 32, 33, 34$$

184

(12) The functions $(a_i'')^{(6)}, (b_i'')^{(6)}$ are positive continuous increasing and bounded.

Definition of $(p_i)^{(6)}, (r_i)^{(6)}$:
 $(a_i'')^{(6)}(T_{33}, t) \leq (p_i)^{(6)} \leq (\hat{A}_{32})^{(6)}$
 $(b_i'')^{(6)}((G_{35}), t) \leq (r_i)^{(6)} \leq (b_i')^{(6)} \leq (\hat{B}_{32})^{(6)}$

185

(13) $\lim_{T_2 \rightarrow \infty} (a_i'')^{(6)}(T_{33}, t) = (p_i)^{(6)}$
 $\lim_{G \rightarrow \infty} (b_i'')^{(6)}((G_{35}), t) = (r_i)^{(6)}$

Definition of $(\hat{A}_{32})^{(6)}, (\hat{B}_{32})^{(6)}$:

Where $(\hat{A}_{32})^{(6)}, (\hat{B}_{32})^{(6)}, (p_i)^{(6)}, (r_i)^{(6)}$ are positive constants and $i = 32, 33, 34$

They satisfy Lipschitz condition:

186

$$|(a_i'')^{(6)}(T'_{33}, t) - (a_i'')^{(6)}(T_{33}, t)| \leq (\hat{k}_{32})^{(6)} |T'_{33} - T_{33}| e^{-(M_{32})^{(6)}t}$$

$$|(b_i'')^{(6)}((G_{35})', t) - (b_i'')^{(6)}((G_{35}), t)| < (\hat{k}_{32})^{(6)} ||G_{35} - (G_{35})'| e^{-(M_{32})^{(6)}t}$$

With the Lipschitz condition, we place a restriction on the behavior of functions $(a_i'')^{(6)}(T'_{33}, t)$ and $(a_i'')^{(6)}(T_{33}, t)$. (T'_{33}, t) and (T_{33}, t) are points belonging to the interval $[(\hat{k}_{32})^{(6)}, (\hat{M}_{32})^{(6)}]$. It is to be noted that $(a_i'')^{(6)}(T_{33}, t)$ is uniformly continuous. In the eventuality of the fact, that if $(\hat{M}_{32})^{(6)} = 6$ then the function $(a_i'')^{(6)}(T_{33}, t)$, the **SIXTH augmentation coefficient** would be absolutely continuous.

187

Definition of $(\hat{M}_{32})^{(6)}, (\hat{k}_{32})^{(6)}$:

188

$(\hat{M}_{32})^{(6)}, (\hat{k}_{32})^{(6)}$, are positive constants

$$\frac{(a_i)^{(6)}}{(\hat{M}_{32})^{(6)}}, \frac{(b_i)^{(6)}}{(\hat{M}_{32})^{(6)}} < 1$$

Definition of $(\hat{P}_{32})^{(6)}, (\hat{Q}_{32})^{(6)}$:

189

There exists two constants $(\hat{P}_{32})^{(6)}$ and $(\hat{Q}_{32})^{(6)}$ which together with $(\hat{M}_{32})^{(6)}, (\hat{k}_{32})^{(6)}, (\hat{A}_{32})^{(6)}$ and $(\hat{B}_{32})^{(6)}$ and the constants $(a_i)^{(6)}, (a_i')^{(6)}, (b_i)^{(6)}, (b_i')^{(6)}, (p_i)^{(6)}, (r_i)^{(6)}, i = 32, 33, 34$, satisfy the inequalities

$$\frac{1}{(\hat{M}_{32})^{(6)}} [(a_i)^{(6)} + (a_i')^{(6)} + (\hat{A}_{32})^{(6)} + (\hat{P}_{32})^{(6)} (\hat{k}_{32})^{(6)}] < 1$$

$$\frac{1}{(\hat{M}_{32})^{(6)}} [(b_i)^{(6)} + (b_i')^{(6)} + (\hat{B}_{32})^{(6)} + (\hat{Q}_{32})^{(6)} (\hat{k}_{32})^{(6)}] < 1$$

Where we suppose

190

(V) $(a_i)^{(7)}, (a_i')^{(7)}, (a_i'')^{(7)}, (b_i)^{(7)}, (b_i')^{(7)}, (b_i'')^{(7)} > 0$,
 $i, j = 36, 37, 38$

191

(W) The functions $(a_i'')^{(7)}, (b_i'')^{(7)}$ are positive continuous increasing and bounded.

Definition of $(p_i)^{(7)}, (r_i)^{(7)}$:

$$(a_i'')^{(7)}(T_{37}, t) \leq (p_i)^{(7)} \leq (\hat{A}_{36})^{(7)}$$

$$(b_i'')^{(7)}(G, t) \leq (r_i)^{(7)} \leq (b_i')^{(7)} \leq (\hat{B}_{36})^{(7)}$$

192

(X) $\lim_{T_2 \rightarrow \infty} (a_i'')^{(7)}(T_{37}, t) = (p_i)^{(7)}$
 $\lim_{G \rightarrow \infty} (b_i'')^{(7)}((G_{39}), t) = (r_i)^{(7)}$

Definition of $(\hat{A}_{36})^{(7)}, (\hat{B}_{36})^{(7)}$:

Where $(\hat{A}_{36})^{(7)}, (\hat{B}_{36})^{(7)}, (p_i)^{(7)}, (r_i)^{(7)}$ are positive constants and $i = 36, 37, 38$

They satisfy Lipschitz condition:

193

$$|(a_i'')^{(7)}(T'_{37}, t) - (a_i'')^{(7)}(T_{37}, t)| \leq (\hat{k}_{36})^{(7)} |T'_{37} - T_{37}| e^{-(M_{36})^{(7)}t}$$

$$|(b_i'')^{(7)}((G_{39})', t) - (b_i'')^{(7)}((G_{39}), (T_{39}))| < (\hat{k}_{36})^{(7)} ||G_{39} - (G_{39})'| e^{-(M_{36})^{(7)}t}$$

With the Lipschitz condition, we place a restriction on the behavior of functions $(a_i'')^{(7)}(T'_{37}, t)$ and $(a_i'')^{(7)}(T_{37}, t)$. (T'_{37}, t) and (T_{37}, t) are points belonging to the interval $[(\hat{k}_{36})^{(7)}, (\hat{M}_{36})^{(7)}]$. It is to be noted that $(a_i'')^{(7)}(T_{37}, t)$ is uniformly continuous. In the eventuality of the fact, that if $(\hat{M}_{36})^{(7)} = 7$ then the function $(a_i'')^{(7)}(T_{37}, t)$, the **first augmentation coefficient** attributable to terrestrial organisms, would be absolutely continuous.

194

Definition of $(\hat{M}_{36})^{(7)}, (\hat{k}_{36})^{(7)}$:

195

(Y) $(\hat{M}_{36})^{(7)}, (\hat{k}_{36})^{(7)}$, are positive constants

$$\frac{(a_i)^{(7)}}{(\hat{M}_{36})^{(7)}}, \frac{(b_i)^{(7)}}{(\hat{M}_{36})^{(7)}} < 1$$

Definition of $(\hat{P}_{36})^{(7)}, (\hat{Q}_{36})^{(7)}$:

196

(Z) There exists two constants $(\hat{P}_{36})^{(7)}$ and $(\hat{Q}_{36})^{(7)}$ which together with $(\hat{M}_{36})^{(7)}, (\hat{k}_{36})^{(7)}, (\hat{A}_{36})^{(7)}$ and $(\hat{B}_{36})^{(7)}$ and the constants $(a_i)^{(7)}, (a'_i)^{(7)}, (b_i)^{(7)}, (b'_i)^{(7)}, (p_i)^{(7)}, (r_i)^{(7)}, i = 36, 37, 38$, satisfy the inequalities

$$\frac{1}{(\hat{M}_{36})^{(7)}} [(a_i)^{(7)} + (a'_i)^{(7)} + (\hat{A}_{36})^{(7)} + (\hat{P}_{36})^{(7)} (\hat{k}_{36})^{(7)}] < 1$$

$$\frac{1}{(\hat{M}_{36})^{(7)}} [(b_i)^{(7)} + (b'_i)^{(7)} + (\hat{B}_{36})^{(7)} + (\hat{Q}_{36})^{(7)} (\hat{k}_{36})^{(7)}] < 1$$

197

Definition of $G_i(0), T_i(0)$:

$$G_i(t) \leq (\hat{P}_{28})^{(5)} e^{(M_{28})^{(5)}t}, \quad \boxed{G_i(0) = G_i^0 > 0}$$

$$T_i(t) \leq (\hat{Q}_{28})^{(5)} e^{(M_{28})^{(5)}t}, \quad \boxed{T_i(0) = T_i^0 > 0}$$

198

Definition of $G_i(0), T_i(0)$:

$$G_i(t) \leq (\hat{P}_{32})^{(6)} e^{(M_{32})^{(6)}t}, \quad \boxed{G_i(0) = G_i^0 > 0}$$

$$T_i(t) \leq (\hat{Q}_{32})^{(6)} e^{(M_{32})^{(6)}t}, \quad \boxed{T_i(0) = T_i^0 > 0}$$

199

Definition of $G_i(0), T_i(0)$:

$$G_i(t) \leq (\hat{P}_{36})^{(7)} e^{(M_{36})^{(7)}t}, \quad \boxed{G_i(0) = G_i^0 > 0}$$

$$T_i(t) \leq (\hat{Q}_{36})^{(7)} e^{(M_{36})^{(7)}t}, \quad \boxed{T_i(0) = T_i^0 > 0}$$

Proof: Consider operator $\mathcal{A}^{(1)}$ defined on the space of sextuples of continuous functions $G_i, T_i: \mathbb{R}_+ \rightarrow \mathbb{R}_+$ which satisfy 200

$$G_i(0) = G_i^0, T_i(0) = T_i^0, G_i^0 \leq (\hat{P}_{13})^{(1)}, T_i^0 \leq (\hat{Q}_{13})^{(1)}, \quad 201$$

$$0 \leq G_i(t) - G_i^0 \leq (\hat{P}_{13})^{(1)} e^{(M_{13})^{(1)}t} \quad 202$$

$$0 \leq T_i(t) - T_i^0 \leq (\hat{Q}_{13})^{(1)} e^{(M_{13})^{(1)}t} \quad 203$$

By 204

$$\bar{G}_{13}(t) = G_{13}^0 + \int_0^t [(a_{13})^{(1)} G_{14}(s_{(13)}) - ((a'_{13})^{(1)} + a''_{13})^{(1)} (T_{14}(s_{(13)}), s_{(13)}) G_{13}(s_{(13)})] ds_{(13)}$$

$$\bar{G}_{14}(t) = G_{14}^0 + \int_0^t [(a_{14})^{(1)} G_{13}(s_{(13)}) - ((a'_{14})^{(1)} + (a''_{14})^{(1)} (T_{14}(s_{(13)}), s_{(13)})) G_{14}(s_{(13)})] ds_{(13)} \quad 205$$

$$\bar{G}_{15}(t) = G_{15}^0 + \int_0^t [(a_{15})^{(1)} G_{14}(s_{(13)}) - ((a'_{15})^{(1)} + (a''_{15})^{(1)} (T_{14}(s_{(13)}), s_{(13)})) G_{15}(s_{(13)})] ds_{(13)} \quad 206$$

$$\bar{T}_{13}(t) = T_{13}^0 + \int_0^t [(b_{13})^{(1)} T_{14}(s_{(13)}) - ((b'_{13})^{(1)} - (b''_{13})^{(1)} (G(s_{(13)}), s_{(13)})) T_{13}(s_{(13)})] ds_{(13)} \quad 207$$

$$\bar{T}_{14}(t) = T_{14}^0 + \int_0^t [(b_{14})^{(1)} T_{13}(s_{(13)}) - ((b'_{14})^{(1)} - (b''_{14})^{(1)} (G(s_{(13)}), s_{(13)})) T_{14}(s_{(13)})] ds_{(13)} \quad 208$$

$$\bar{T}_{15}(t) = T_{15}^0 + \int_0^t [(b_{15})^{(1)} T_{14}(s_{(13)}) - ((b'_{15})^{(1)} - (b''_{15})^{(1)} (G(s_{(13)}), s_{(13)})) T_{15}(s_{(13)})] ds_{(13)} \quad 209$$

Where $s_{(13)}$ is the integrand that is integrated over an interval $(0, t)$

210

if the conditions IN THE FOREGOING above are fulfilled, there exists a solution satisfying the conditions

Definition of $G_i(0), T_i(0)$:

$$G_i(t) \leq (\hat{P}_{36})^{(7)} e^{(M_{36})^{(7)}t}, \quad \boxed{G_i(0) = G_i^0 > 0}$$

$$T_i(t) \leq (\hat{Q}_{36})^{(7)} e^{(M_{36})^{(7)}t}, \quad \boxed{T_i(0) = T_i^0 > 0}$$

Consider operator $\mathcal{A}^{(7)}$ defined on the space of sextuples of continuous functions $G_i, T_i: \mathbb{R}_+ \rightarrow \mathbb{R}_+$ which satisfy

$$G_i(0) = G_i^0, T_i(0) = T_i^0, G_i^0 \leq (\hat{P}_{36})^{(7)}, T_i^0 \leq (\hat{Q}_{36})^{(7)},$$

$$0 \leq G_i(t) - G_i^0 \leq (\hat{P}_{36})^{(7)} e^{(M_{36})^{(7)}t}$$

$$0 \leq T_i(t) - T_i^0 \leq (\hat{Q}_{36})^{(7)} e^{(M_{36})^{(7)}t}$$

By

$$\bar{G}_{36}(t) = G_{36}^0 + \int_0^t \left[(a_{36})^{(7)} G_{37}(s_{(36)}) - \left((a'_{36})^{(7)} + a''_{36}(s_{(36)}) \right) G_{36}(s_{(36)}) \right] ds_{(36)}$$

$$\bar{G}_{37}(t) = G_{37}^0 + \int_0^t \left[(a_{37})^{(7)} G_{36}(s_{(36)}) - \left((a'_{37})^{(7)} + a''_{37}(s_{(36)}) \right) G_{37}(s_{(36)}) \right] ds_{(36)}$$

$$\bar{G}_{38}(t) = G_{38}^0 + \int_0^t \left[(a_{38})^{(7)} G_{37}(s_{(36)}) - \left((a'_{38})^{(7)} + a''_{38}(s_{(36)}) \right) G_{38}(s_{(36)}) \right] ds_{(36)}$$

$$\bar{T}_{36}(t) = T_{36}^0 + \int_0^t \left[(b_{36})^{(7)} T_{37}(s_{(36)}) - \left((b'_{36})^{(7)} - (b''_{36})^{(7)}(G(s_{(36)}), s_{(36)}) \right) T_{36}(s_{(36)}) \right] ds_{(36)}$$

$$\bar{T}_{37}(t) = T_{37}^0 + \int_0^t \left[(b_{37})^{(7)} T_{36}(s_{(36)}) - \left((b'_{37})^{(7)} - (b''_{37})^{(7)}(G(s_{(36)}), s_{(36)}) \right) T_{37}(s_{(36)}) \right] ds_{(36)}$$

$$\bar{T}_{38}(t) = T_{38}^0 + \int_0^t \left[(b_{38})^{(7)} T_{37}(s_{(36)}) - \left((b'_{38})^{(7)} - (b''_{38})^{(7)}(G(s_{(36)}), s_{(36)}) \right) T_{38}(s_{(36)}) \right] ds_{(36)}$$

Where $s_{(36)}$ is the integrand that is integrated over an interval $(0, t)$

Consider operator $\mathcal{A}^{(2)}$ defined on the space of sextuples of continuous functions $G_i, T_i: \mathbb{R}_+ \rightarrow \mathbb{R}_+$ which satisfy 211

$$G_i(0) = G_i^0, T_i(0) = T_i^0, G_i^0 \leq (\hat{P}_{16})^{(2)}, T_i^0 \leq (\hat{Q}_{16})^{(2)}, \quad 212$$

$$0 \leq G_i(t) - G_i^0 \leq (\hat{P}_{16})^{(2)} e^{(M_{16})^{(2)}t} \quad 213$$

$$0 \leq T_i(t) - T_i^0 \leq (\hat{Q}_{16})^{(2)} e^{(M_{16})^{(2)}t} \quad 214$$

By 215

$$\bar{G}_{16}(t) = G_{16}^0 + \int_0^t \left[(a_{16})^{(2)} G_{17}(s_{(16)}) - \left((a'_{16})^{(2)} + a''_{16}(s_{(16)}) \right) G_{16}(s_{(16)}) \right] ds_{(16)}$$

$$\bar{G}_{17}(t) = G_{17}^0 + \int_0^t \left[(a_{17})^{(2)} G_{16}(s_{(16)}) - \left((a'_{17})^{(2)} + a''_{17}(s_{(16)}) \right) G_{17}(s_{(16)}) \right] ds_{(16)} \quad 216$$

$$\bar{G}_{18}(t) = G_{18}^0 + \int_0^t \left[(a_{18})^{(2)} G_{17}(s_{(16)}) - \left((a'_{18})^{(2)} + a''_{18}(s_{(16)}) \right) G_{18}(s_{(16)}) \right] ds_{(16)} \quad 217$$

$$\bar{T}_{16}(t) = T_{16}^0 + \int_0^t \left[(b_{16})^{(2)} T_{17}(s_{(16)}) - \left((b'_{16})^{(2)} - (b''_{16})^{(2)}(G(s_{(16)}), s_{(16)}) \right) T_{16}(s_{(16)}) \right] ds_{(16)} \quad 218$$

$$\bar{T}_{17}(t) = T_{17}^0 + \int_0^t \left[(b_{17})^{(2)} T_{16}(s_{(16)}) - \left((b'_{17})^{(2)} - (b''_{17})^{(2)}(G(s_{(16)}), s_{(16)}) \right) T_{17}(s_{(16)}) \right] ds_{(16)} \quad 219$$

$$\bar{T}_{18}(t) = T_{18}^0 + \int_0^t \left[(b_{18})^{(2)} T_{17}(s_{(16)}) - \left((b'_{18})^{(2)} - (b''_{18})^{(2)} (G(s_{(16)}), s_{(16)}) \right) T_{18}(s_{(16)}) \right] ds_{(16)} \quad 220$$

Where $s_{(16)}$ is the integrand that is integrated over an interval $(0, t)$

221

Consider operator $\mathcal{A}^{(3)}$ defined on the space of sextuples of continuous functions $G_i, T_i: \mathbb{R}_+ \rightarrow \mathbb{R}_+$ which satisfy

$$G_i(0) = G_i^0, T_i(0) = T_i^0, G_i^0 \leq (\hat{P}_{20})^{(3)}, T_i^0 \leq (\hat{Q}_{20})^{(3)}, \quad 222$$

$$0 \leq G_i(t) - G_i^0 \leq (\hat{P}_{20})^{(3)} e^{(M_{20})^{(3)}t} \quad 223$$

$$0 \leq T_i(t) - T_i^0 \leq (\hat{Q}_{20})^{(3)} e^{(M_{20})^{(3)}t} \quad 224$$

By 225

$$\bar{G}_{20}(t) = G_{20}^0 + \int_0^t \left[(a_{20})^{(3)} G_{21}(s_{(20)}) - \left((a'_{20})^{(3)} + a''_{20}{}^{(3)} (T_{21}(s_{(20)}), s_{(20)}) \right) G_{20}(s_{(20)}) \right] ds_{(20)} \quad 226$$

$$\bar{G}_{21}(t) = G_{21}^0 + \int_0^t \left[(a_{21})^{(3)} G_{20}(s_{(20)}) - \left((a'_{21})^{(3)} + (a''_{21})^{(3)} (T_{21}(s_{(20)}), s_{(20)}) \right) G_{21}(s_{(20)}) \right] ds_{(20)} \quad 227$$

$$\bar{G}_{22}(t) = G_{22}^0 + \int_0^t \left[(a_{22})^{(3)} G_{21}(s_{(20)}) - \left((a'_{22})^{(3)} + (a''_{22})^{(3)} (T_{21}(s_{(20)}), s_{(20)}) \right) G_{22}(s_{(20)}) \right] ds_{(20)} \quad 228$$

$$\bar{T}_{20}(t) = T_{20}^0 + \int_0^t \left[(b_{20})^{(3)} T_{21}(s_{(20)}) - \left((b'_{20})^{(3)} - (b''_{20})^{(3)} (G(s_{(20)}), s_{(20)}) \right) T_{20}(s_{(20)}) \right] ds_{(20)} \quad 229$$

$$\bar{T}_{21}(t) = T_{21}^0 + \int_0^t \left[(b_{21})^{(3)} T_{20}(s_{(20)}) - \left((b'_{21})^{(3)} - (b''_{21})^{(3)} (G(s_{(20)}), s_{(20)}) \right) T_{21}(s_{(20)}) \right] ds_{(20)} \quad 230$$

$$\bar{T}_{22}(t) = T_{22}^0 + \int_0^t \left[(b_{22})^{(3)} T_{21}(s_{(20)}) - \left((b'_{22})^{(3)} - (b''_{22})^{(3)} (G(s_{(20)}), s_{(20)}) \right) T_{22}(s_{(20)}) \right] ds_{(20)} \quad 230$$

Where $s_{(20)}$ is the integrand that is integrated over an interval $(0, t)$

Consider operator $\mathcal{A}^{(4)}$ defined on the space of sextuples of continuous functions $G_i, T_i: \mathbb{R}_+ \rightarrow \mathbb{R}_+$ which satisfy 231

$$G_i(0) = G_i^0, T_i(0) = T_i^0, G_i^0 \leq (\hat{P}_{24})^{(4)}, T_i^0 \leq (\hat{Q}_{24})^{(4)}, \quad 232$$

$$0 \leq G_i(t) - G_i^0 \leq (\hat{P}_{24})^{(4)} e^{(M_{24})^{(4)}t} \quad 233$$

$$0 \leq T_i(t) - T_i^0 \leq (\hat{Q}_{24})^{(4)} e^{(M_{24})^{(4)}t} \quad 234$$

By 235

$$\bar{G}_{24}(t) = G_{24}^0 + \int_0^t \left[(a_{24})^{(4)} G_{25}(s_{(24)}) - \left((a'_{24})^{(4)} + a''_{24}{}^{(4)} (T_{25}(s_{(24)}), s_{(24)}) \right) G_{24}(s_{(24)}) \right] ds_{(24)} \quad 236$$

$$\bar{G}_{25}(t) = G_{25}^0 + \int_0^t \left[(a_{25})^{(4)} G_{24}(s_{(24)}) - \left((a'_{25})^{(4)} + (a''_{25})^{(4)} (T_{25}(s_{(24)}), s_{(24)}) \right) G_{25}(s_{(24)}) \right] ds_{(24)} \quad 237$$

$$\bar{G}_{26}(t) = G_{26}^0 + \int_0^t \left[(a_{26})^{(4)} G_{25}(s_{(24)}) - \left((a'_{26})^{(4)} + (a''_{26})^{(4)} (T_{25}(s_{(24)}), s_{(24)}) \right) G_{26}(s_{(24)}) \right] ds_{(24)} \quad 238$$

$$\bar{T}_{24}(t) = T_{24}^0 + \int_0^t \left[(b_{24})^{(4)} T_{25}(s_{(24)}) - \left((b'_{24})^{(4)} - (b''_{24})^{(4)} (G(s_{(24)}), s_{(24)}) \right) T_{24}(s_{(24)}) \right] ds_{(24)} \quad 239$$

$$\bar{T}_{25}(t) = T_{25}^0 + \int_0^t \left[(b_{25})^{(4)} T_{24}(s_{(24)}) - \left((b'_{25})^{(4)} - (b''_{25})^{(4)} (G(s_{(24)}), s_{(24)}) \right) T_{25}(s_{(24)}) \right] ds_{(24)} \quad 240$$

$$\bar{T}_{26}(t) = T_{26}^0 + \int_0^t \left[(b_{26})^{(4)} T_{25}(s_{(24)}) - \left((b'_{26})^{(4)} - (b''_{26})^{(4)} (G(s_{(24)}), s_{(24)}) \right) T_{26}(s_{(24)}) \right] ds_{(24)} \quad 240$$

Where $s_{(24)}$ is the integrand that is integrated over an interval $(0, t)$

Consider operator $\mathcal{A}^{(5)}$ defined on the space of sextuples of continuous functions $G_i, T_i: \mathbb{R}_+ \rightarrow \mathbb{R}_+$ which satisfy 241

$$G_i(0) = G_i^0, T_i(0) = T_i^0, G_i^0 \leq (\hat{P}_{28})^{(5)}, T_i^0 \leq (\hat{Q}_{28})^{(5)}, \quad 242$$

$$0 \leq G_i(t) - G_i^0 \leq (\hat{P}_{28})^{(5)} e^{(M_{28})^{(5)}t} \quad 243$$

$$0 \leq T_i(t) - T_i^0 \leq (\hat{Q}_{28})^{(5)} e^{(M_{28})^{(5)}t} \quad 244$$

By 245

$$\bar{G}_{28}(t) = G_{28}^0 + \int_0^t \left[(a_{28})^{(5)} G_{29}(s_{(28)}) - \left((a'_{28})^{(5)} + a''_{28}{}^{(5)} (T_{29}(s_{(28)}), s_{(28)}) \right) G_{28}(s_{(28)}) \right] ds_{(28)} \quad 246$$

$$\bar{G}_{29}(t) = G_{29}^0 + \int_0^t \left[(a_{29})^{(5)} G_{28}(s_{(28)}) - \left((a'_{29})^{(5)} + (a''_{29})^{(5)} (T_{29}(s_{(28)}), s_{(28)}) \right) G_{29}(s_{(28)}) \right] ds_{(28)} \quad 247$$

$$\bar{G}_{30}(t) = G_{30}^0 + \int_0^t \left[(a_{30})^{(5)} G_{29}(s_{(28)}) - \left((a'_{30})^{(5)} + (a''_{30})^{(5)} (T_{29}(s_{(28)}), s_{(28)}) \right) G_{30}(s_{(28)}) \right] ds_{(28)} \quad 248$$

$$\bar{T}_{28}(t) = T_{28}^0 + \int_0^t \left[(b_{28})^{(5)} T_{29}(s_{(28)}) - \left((b'_{28})^{(5)} - (b''_{28})^{(5)} (G(s_{(28)}), s_{(28)}) \right) T_{28}(s_{(28)}) \right] ds_{(28)} \quad 249$$

$$\bar{T}_{29}(t) = T_{29}^0 + \int_0^t \left[(b_{29})^{(5)} T_{28}(s_{(28)}) - \left((b'_{29})^{(5)} - (b''_{29})^{(5)} (G(s_{(28)}), s_{(28)}) \right) T_{29}(s_{(28)}) \right] ds_{(28)} \quad 250$$

$$\bar{T}_{30}(t) = T_{30}^0 + \int_0^t \left[(b_{30})^{(5)} T_{29}(s_{(28)}) - \left((b'_{30})^{(5)} - (b''_{30})^{(5)} (G(s_{(28)}), s_{(28)}) \right) T_{30}(s_{(28)}) \right] ds_{(28)} \quad 251$$

Where $s_{(28)}$ is the integrand that is integrated over an interval $(0, t)$

252

Consider operator $\mathcal{A}^{(6)}$ defined on the space of sextuples of continuous functions $G_i, T_i: \mathbb{R}_+ \rightarrow \mathbb{R}_+$ which satisfy

$$G_i(0) = G_i^0, T_i(0) = T_i^0, G_i^0 \leq (\hat{P}_{32})^{(6)}, T_i^0 \leq (\hat{Q}_{32})^{(6)}, \quad 253$$

$$0 \leq G_i(t) - G_i^0 \leq (\hat{P}_{32})^{(6)} e^{(M_{32})^{(6)}t} \quad 254$$

$$0 \leq T_i(t) - T_i^0 \leq (\hat{Q}_{32})^{(6)} e^{(M_{32})^{(6)}t} \quad 255$$

By 256

$$\bar{G}_{32}(t) = G_{32}^0 + \int_0^t \left[(a_{32})^{(6)} G_{33}(s_{(32)}) - \left((a'_{32})^{(6)} + a''_{32}(s_{(32)}) \right) T_{33}(s_{(32)}) \right] G_{32}(s_{(32)}) ds_{(32)} \quad 257$$

$$\bar{G}_{33}(t) = G_{33}^0 + \int_0^t \left[(a_{33})^{(6)} G_{32}(s_{(32)}) - \left((a'_{33})^{(6)} + a''_{33}(s_{(32)}) \right) T_{33}(s_{(32)}) \right] G_{33}(s_{(32)}) ds_{(32)} \quad 258$$

$$\bar{G}_{34}(t) = G_{34}^0 + \int_0^t \left[(a_{34})^{(6)} G_{33}(s_{(32)}) - \left((a'_{34})^{(6)} + a''_{34}(s_{(32)}) \right) T_{33}(s_{(32)}) \right] G_{34}(s_{(32)}) ds_{(32)} \quad 259$$

$$\bar{T}_{32}(t) = T_{32}^0 + \int_0^t \left[(b_{32})^{(6)} T_{33}(s_{(32)}) - \left((b'_{32})^{(6)} - (b''_{32})^{(6)}(G(s_{(32)}), s_{(32)})) \right) T_{32}(s_{(32)}) \right] ds_{(32)} \quad 260$$

$$\bar{T}_{33}(t) = T_{33}^0 + \int_0^t \left[(b_{33})^{(6)} T_{32}(s_{(32)}) - \left((b'_{33})^{(6)} - (b''_{33})^{(6)}(G(s_{(32)}), s_{(32)})) \right) T_{33}(s_{(32)}) \right] ds_{(32)} \quad 261$$

$$\bar{T}_{34}(t) = T_{34}^0 + \int_0^t \left[(b_{34})^{(6)} T_{33}(s_{(32)}) - \left((b'_{34})^{(6)} - (b''_{34})^{(6)}(G(s_{(32)}), s_{(32)})) \right) T_{34}(s_{(32)}) \right] ds_{(32)} \quad 262$$

Where $s_{(32)}$ is the integrand that is integrated over an interval $(0, t)$

: if the conditions IN THE FOREGOING are fulfilled, there exists a solution satisfying the conditions

Definition of $G_i(0), T_i(0)$:

$$G_i(t) \leq (\hat{P}_{36})^{(7)} e^{(M_{36})^{(7)}t}, \quad \boxed{G_i(0) = G_i^0 > 0}$$

$$T_i(t) \leq (\hat{Q}_{36})^{(7)} e^{(M_{36})^{(7)}t}, \quad \boxed{T_i(0) = T_i^0 > 0}$$

Proof:

Consider operator $\mathcal{A}^{(7)}$ defined on the space of sextuples of continuous functions $G_i, T_i: \mathbb{R}_+ \rightarrow \mathbb{R}_+$ which satisfy

$$G_i(0) = G_i^0, T_i(0) = T_i^0, G_i^0 \leq (\hat{P}_{36})^{(7)}, T_i^0 \leq (\hat{Q}_{36})^{(7)}, \quad 263$$

$$0 \leq G_i(t) - G_i^0 \leq (\hat{P}_{36})^{(7)} e^{(M_{36})^{(7)}t} \quad 264$$

$$0 \leq T_i(t) - T_i^0 \leq (\hat{Q}_{36})^{(7)} e^{(M_{36})^{(7)}t} \quad 265$$

By 266

$$\bar{G}_{36}(t) = G_{36}^0 + \int_0^t \left[(a_{36})^{(7)} G_{37}(s_{(36)}) - \left((a'_{36})^{(7)} + a''_{36}(s_{(36)}) \right) T_{37}(s_{(36)}) \right] G_{36}(s_{(36)}) ds_{(36)} \quad 267$$

$$\bar{G}_{37}(t) = G_{37}^0 + \int_0^t \left[(a_{37})^{(7)} G_{36}(s_{(36)}) - \left((a'_{37})^{(7)} + a''_{37}(s_{(36)}) \right) T_{37}(s_{(36)}) \right] G_{37}(s_{(36)}) ds_{(36)}$$

$$\bar{G}_{38}(t) = G_{38}^0 + \int_0^t \left[(a_{38})^{(7)} G_{37}(s_{(36)}) - \left((a'_{38})^{(7)} + a''_{38}(s_{(36)}) \right) T_{37}(s_{(36)}) \right] G_{38}(s_{(36)}) ds_{(36)} \quad 268$$

$$\bar{T}_{36}(t) = T_{36}^0 + \int_0^t \left[(b_{36})^{(7)} T_{37}(s_{(36)}) - \left((b'_{36})^{(7)} - (b''_{36})^{(7)}(G(s_{(36)}), s_{(36)})) \right) T_{36}(s_{(36)}) \right] ds_{(36)} \quad 269$$

$$\bar{T}_{37}(t) = T_{37}^0 + \int_0^t \left[(b_{37})^{(7)} T_{36}(s_{(36)}) - \left((b'_{37})^{(7)} - (b''_{37})^{(7)}(G(s_{(36)}), s_{(36)})) \right) T_{37}(s_{(36)}) \right] ds_{(36)} \quad 270$$

$$\bar{T}_{38}(t) = T_{38}^0 + \int_0^t \left[(b_{38})^{(7)} T_{37}(s_{(36)}) - \left((b'_{38})^{(7)} - (b''_{38})^{(7)}(G(s_{(36)}), s_{(36)})) \right) T_{38}(s_{(36)}) \right] ds_{(36)} \quad 271$$

Where $s_{(36)}$ is the integrand that is integrated over an interval $(0, t)$

Analogous inequalities hold also for $G_{21}, G_{22}, T_{20}, T_{21}, T_{22}$ 272

(a) The operator $\mathcal{A}^{(4)}$ maps the space of functions satisfying GLOBAL EQUATIONS into itself. Indeed it is obvious that 273

$$G_{24}(t) \leq G_{24}^0 + \int_0^t \left[(a_{24})^{(4)} \left(G_{25}^0 + (\hat{P}_{24})^{(4)} e^{(M_{24})^{(4)}s_{(24)}} \right) \right] ds_{(24)} =$$

$$(1 + (a_{24})^{(4)}t)G_{25}^0 + \frac{(a_{24})^{(4)}(P_{24})^{(4)}}{(M_{24})^{(4)}}(e^{(M_{24})^{(4)}t} - 1)$$

From which it follows that

274

$$(G_{24}(t) - G_{24}^0)e^{-(M_{24})^{(4)}t} \leq \frac{(a_{24})^{(4)}}{(M_{24})^{(4)}} \left[((\hat{P}_{24})^{(4)} + G_{25}^0)e^{-\frac{((\hat{P}_{24})^{(4)} + G_{25}^0)}{G_{25}^0}} + (\hat{P}_{24})^{(4)} \right]$$

(G_i^0) is as defined in the statement of theorem 1

(b) The operator $\mathcal{A}^{(5)}$ maps the space of functions satisfying GLOBAL EQUATIONS into itself .Indeed it is obvious that

275

$$G_{28}(t) \leq G_{28}^0 + \int_0^t [(a_{28})^{(5)}(G_{29}^0 + (\hat{P}_{28})^{(5)}e^{(M_{28})^{(5)}s(28)})] ds_{(28)} = (1 + (a_{28})^{(5)}t)G_{29}^0 + \frac{(a_{28})^{(5)}(P_{28})^{(5)}}{(M_{28})^{(5)}}(e^{(M_{28})^{(5)}t} - 1)$$

From which it follows that

276

$$(G_{28}(t) - G_{28}^0)e^{-(M_{28})^{(5)}t} \leq \frac{(a_{28})^{(5)}}{(M_{28})^{(5)}} \left[((\hat{P}_{28})^{(5)} + G_{29}^0)e^{-\frac{((\hat{P}_{28})^{(5)} + G_{29}^0)}{G_{29}^0}} + (\hat{P}_{28})^{(5)} \right]$$

(G_i^0) is as defined in the statement of theorem 1

(c) The operator $\mathcal{A}^{(6)}$ maps the space of functions satisfying GLOBAL EQUATIONS into itself .Indeed it is obvious that

277

$$G_{32}(t) \leq G_{32}^0 + \int_0^t [(a_{32})^{(6)}(G_{33}^0 + (\hat{P}_{32})^{(6)}e^{(M_{32})^{(6)}s(32)})] ds_{(32)} = (1 + (a_{32})^{(6)}t)G_{33}^0 + \frac{(a_{32})^{(6)}(P_{32})^{(6)}}{(M_{32})^{(6)}}(e^{(M_{32})^{(6)}t} - 1)$$

From which it follows that

278

$$(G_{32}(t) - G_{32}^0)e^{-(M_{32})^{(6)}t} \leq \frac{(a_{32})^{(6)}}{(M_{32})^{(6)}} \left[((\hat{P}_{32})^{(6)} + G_{33}^0)e^{-\frac{((\hat{P}_{32})^{(6)} + G_{33}^0)}{G_{33}^0}} + (\hat{P}_{32})^{(6)} \right]$$

(G_i^0) is as defined in the statement of theorem 1

Analogous inequalities hold also for $G_{25}, G_{26}, T_{24}, T_{25}, T_{26}$

(d) The operator $\mathcal{A}^{(7)}$ maps the space of functions satisfying 37,35,36 into itself .Indeed it is obvious that

279

$$G_{36}(t) \leq G_{36}^0 + \int_0^t [(a_{36})^{(7)}(G_{37}^0 + (\hat{P}_{36})^{(7)}e^{(M_{36})^{(7)}s(36)})] ds_{(36)} = (1 + (a_{36})^{(7)}t)G_{37}^0 + \frac{(a_{36})^{(7)}(P_{36})^{(7)}}{(M_{36})^{(7)}}(e^{(M_{36})^{(7)}t} - 1)$$

From which it follows that

280

$$(G_{36}(t) - G_{36}^0)e^{-(M_{36})^{(7)}t} \leq \frac{(a_{36})^{(7)}}{(M_{36})^{(7)}} \left[((\hat{P}_{36})^{(7)} + G_{37}^0)e^{-\frac{((\hat{P}_{36})^{(7)} + G_{37}^0)}{G_{37}^0}} + (\hat{P}_{36})^{(7)} \right]$$

(G_i^0) is as defined in the statement of theorem 7

It is now sufficient to take $\frac{(a_i)^{(1)}}{(M_{13})^{(1)}}, \frac{(b_i)^{(1)}}{(M_{13})^{(1)}} < 1$ and to choose

281

$(\hat{P}_{13})^{(1)}$ and $(\hat{Q}_{13})^{(1)}$ large to have

282

$$\frac{(a_i)^{(1)}}{(M_{13})^{(1)}} \left[(\hat{P}_{13})^{(1)} + ((\hat{P}_{13})^{(1)} + G_j^0)e^{-\frac{((\hat{P}_{13})^{(1)} + G_j^0)}{G_j^0}} \right] \leq (\hat{P}_{13})^{(1)}$$

283

$$\frac{(b_i)^{(1)}}{(M_{13})^{(1)}} \left[((\hat{Q}_{13})^{(1)} + T_j^0)e^{-\frac{((\hat{Q}_{13})^{(1)} + T_j^0)}{T_j^0}} + (\hat{Q}_{13})^{(1)} \right] \leq (\hat{Q}_{13})^{(1)}$$

284

In order that the operator $\mathcal{A}^{(1)}$ transforms the space of sextuples of functions G_i, T_i satisfying GLOBAL EQUATIONS into itself

285

The operator $\mathcal{A}^{(1)}$ is a contraction with respect to the metric

286

$$d((G^{(1)}, T^{(1)}), (G^{(2)}, T^{(2)})) =$$

$$\sup_i \{ \max_{t \in \mathbb{R}_+} |G_i^{(1)}(t) - G_i^{(2)}(t)|e^{-(M_{13})^{(1)}t}, \max_{t \in \mathbb{R}_+} |T_i^{(1)}(t) - T_i^{(2)}(t)|e^{-(M_{13})^{(1)}t} \}$$

Indeed if we denote

287

Definition of \tilde{G}, \tilde{T} :

$$(\tilde{G}, \tilde{T}) = \mathcal{A}^{(1)}(G, T)$$

It results

$$|\tilde{G}_{13}^{(1)} - \tilde{G}_i^{(2)}| \leq \int_0^t (a_{13})^{(1)} |G_{14}^{(1)} - G_{14}^{(2)}| e^{-(\bar{M}_{13})^{(1)}s_{(13)}} e^{(\bar{M}_{13})^{(1)}s_{(13)}} ds_{(13)} + \int_0^t \{(a'_{13})^{(1)} |G_{13}^{(1)} - G_{13}^{(2)}| e^{-(\bar{M}_{13})^{(1)}s_{(13)}} e^{-(\bar{M}_{13})^{(1)}s_{(13)}} + (a''_{13})^{(1)} (T_{14}^{(1)}, s_{(13)}) |G_{13}^{(1)} - G_{13}^{(2)}| e^{-(\bar{M}_{13})^{(1)}s_{(13)}} e^{(\bar{M}_{13})^{(1)}s_{(13)}} + G_{13}^{(2)} |(a'_{13})^{(1)} (T_{14}^{(1)}, s_{(13)}) - (a''_{13})^{(1)} (T_{14}^{(2)}, s_{(13)})| e^{-(\bar{M}_{13})^{(1)}s_{(13)}} e^{(\bar{M}_{13})^{(1)}s_{(13)}}\} ds_{(13)}$$

Where $s_{(13)}$ represents integrand that is integrated over the interval $[0, t]$

From the hypotheses it follows

$$|G^{(1)} - G^{(2)}| e^{-(\bar{M}_{13})^{(1)}t} \leq \frac{1}{(\bar{M}_{13})^{(1)}} ((a_{13})^{(1)} + (a'_{13})^{(1)} + (\hat{A}_{13})^{(1)} + (\hat{P}_{13})^{(1)} (\hat{k}_{13})^{(1)}) d((G^{(1)}, T^{(1)}; G^{(2)}, T^{(2)})) \tag{288}$$

And analogous inequalities for G_i and T_i . Taking into account the hypothesis the result follows

Remark 1: The fact that we supposed $(a''_{13})^{(1)}$ and $(b''_{13})^{(1)}$ depending also on t can be considered as not conformal with the reality, however we have put this hypothesis, in order that we can postulate condition necessary to prove the uniqueness of the solution bounded by $(\hat{P}_{13})^{(1)} e^{(\bar{M}_{13})^{(1)}t}$ and $(\hat{Q}_{13})^{(1)} e^{(\bar{M}_{13})^{(1)}t}$ respectively of \mathbb{R}_+ . 289

If instead of proving the existence of the solution on \mathbb{R}_+ , we have to prove it only on a compact then it suffices to consider that $(a_i'')^{(1)}$ and $(b_i'')^{(1)}$, $i = 13, 14, 15$ depend only on T_{14} and respectively on G (and not on t) and hypothesis can be replaced by a usual Lipschitz condition.

Remark 2: There does not exist any t where $G_i(t) = 0$ and $T_i(t) = 0$ 290

From 19 to 24 it results

$$G_i(t) \geq G_i^0 e^{-\int_0^t \{(a'_i)^{(1)} - (a''_i)^{(1)}(T_{14}(s_{(13)}), s_{(13)})\} ds_{(13)}} \geq 0 \tag{291}$$

$$T_i(t) \geq T_i^0 e^{-(b'_i)^{(1)}t} > 0 \text{ for } t > 0$$

Definition of $((\bar{M}_{13})^{(1)})_1$, and $((\bar{M}_{13})^{(1)})_3$: 292

Remark 3: if G_{13} is bounded, the same property have also G_{14} and G_{15} . indeed if

$G_{13} < (\bar{M}_{13})^{(1)}$ it follows $\frac{dG_{14}}{dt} \leq ((\bar{M}_{13})^{(1)})_1 - (a'_{14})^{(1)} G_{14}$ and by integrating

$$G_{14} \leq ((\bar{M}_{13})^{(1)})_2 = G_{14}^0 + 2(a_{14})^{(1)} ((\bar{M}_{13})^{(1)})_1 / (a'_{14})^{(1)}$$

In the same way, one can obtain

$$G_{15} \leq ((\bar{M}_{13})^{(1)})_3 = G_{15}^0 + 2(a_{15})^{(1)} ((\bar{M}_{13})^{(1)})_2 / (a'_{15})^{(1)}$$

If G_{14} or G_{15} is bounded, the same property follows for G_{13} , G_{15} and G_{13} , G_{14} respectively.

Remark 4: If G_{13} is bounded, from below, the same property holds for G_{14} and G_{15} . The proof is analogous with the preceding one. An analogous property is true if G_{14} is bounded from below. 293

Remark 5: If T_{13} is bounded from below and $\lim_{t \rightarrow \infty} ((b''_i)^{(1)}(G(t), t)) = (b'_{14})^{(1)}$ then $T_{14} \rightarrow \infty$. 294

Definition of $(m)^{(1)}$ and ε_1 :

Indeed let t_1 be so that for $t > t_1$

$$(b_{14})^{(1)} - (b''_i)^{(1)}(G(t), t) < \varepsilon_1, T_{13}(t) > (m)^{(1)}$$

Then $\frac{dT_{14}}{dt} \geq (a_{14})^{(1)}(m)^{(1)} - \varepsilon_1 T_{14}$ which leads to 295

$$T_{14} \geq \left(\frac{(a_{14})^{(1)}(m)^{(1)}}{\varepsilon_1} \right) (1 - e^{-\varepsilon_1 t}) + T_{14}^0 e^{-\varepsilon_1 t} \text{ If we take } t \text{ such that } e^{-\varepsilon_1 t} = \frac{1}{2} \text{ it results}$$

$$T_{14} \geq \left(\frac{(a_{14})^{(1)}(m)^{(1)}}{2} \right), t = \log \frac{2}{\varepsilon_1} \text{ By taking now } \varepsilon_1 \text{ sufficiently small one sees that } T_{14} \text{ is unbounded. The}$$

same property holds for T_{15} if $\lim_{t \rightarrow \infty} ((b''_{15})^{(1)}(G(t), t)) = (b'_{15})^{(1)}$

We now state a more precise theorem about the behaviors at infinity of the solutions 296

It is now sufficient to take $\frac{(a_i)^{(2)}}{(\bar{M}_{16})^{(2)}}, \frac{(b_i)^{(2)}}{(\bar{M}_{16})^{(2)}} < 1$ and to choose 297

$(\hat{P}_{16})^{(2)}$ and $(\hat{Q}_{16})^{(2)}$ large to have

$$\frac{(a_i)^{(2)}}{(\bar{M}_{16})^{(2)}} \left[(\hat{P}_{16})^{(2)} + ((\hat{P}_{16})^{(2)} + G_j^0) e^{-\left(\frac{(\hat{P}_{16})^{(2)} + G_j^0}{G_j^0} \right)} \right] \leq (\hat{P}_{16})^{(2)} \tag{298}$$

$$\frac{(b_i)^{(2)}}{(\bar{M}_{16})^{(2)}} \left[((\hat{Q}_{16})^{(2)} + T_j^0) e^{-\left(\frac{(\hat{Q}_{16})^{(2)} + T_j^0}{T_j^0} \right)} + (\hat{Q}_{16})^{(2)} \right] \leq (\hat{Q}_{16})^{(2)} \tag{299}$$

In order that the operator $\mathcal{A}^{(2)}$ transforms the space of sextuples of functions G_i, T_i satisfying 300

The operator $\mathcal{A}^{(2)}$ is a contraction with respect to the metric 301

$$d(((G_{19})^{(1)}, (T_{19})^{(1)}), ((G_{19})^{(2)}, (T_{19})^{(2)})) =$$

$$\sup_i \{ \max_{t \in \mathbb{R}_+} |G_i^{(1)}(t) - G_i^{(2)}(t)| e^{-(\bar{M}_{16})^{(2)}t}, \max_{t \in \mathbb{R}_+} |T_i^{(1)}(t) - T_i^{(2)}(t)| e^{-(\bar{M}_{16})^{(2)}t} \}$$

Indeed if we denote

$$\underline{\text{Definition of}} \widetilde{G}_{19}, \widetilde{T}_{19} : (\widetilde{G}_{19}, \widetilde{T}_{19}) = \mathcal{A}^{(2)}(G_{19}, T_{19})$$

It results

$$\begin{aligned} |\widetilde{G}_{16}^{(1)} - \widetilde{G}_i^{(2)}| &\leq \int_0^t (a_{16})^{(2)} |G_{17}^{(1)} - G_{17}^{(2)}| e^{-(\bar{M}_{16})^{(2)}s_{(16)}} e^{(\bar{M}_{16})^{(2)}s_{(16)}} ds_{(16)} + \\ &\int_0^t \{ (a'_{16})^{(2)} |G_{16}^{(1)} - G_{16}^{(2)}| e^{-(\bar{M}_{16})^{(2)}s_{(16)}} e^{-(\bar{M}_{16})^{(2)}s_{(16)}} + \\ &(a''_{16})^{(2)} (T_{17}^{(1)}, s_{(16)}) |G_{16}^{(1)} - G_{16}^{(2)}| e^{-(\bar{M}_{16})^{(2)}s_{(16)}} e^{(\bar{M}_{16})^{(2)}s_{(16)}} + \\ &G_{16}^{(2)} | (a''_{16})^{(2)} (T_{17}^{(1)}, s_{(16)}) - (a''_{16})^{(2)} (T_{17}^{(2)}, s_{(16)}) | e^{-(\bar{M}_{16})^{(2)}s_{(16)}} e^{(\bar{M}_{16})^{(2)}s_{(16)}} \} ds_{(16)} \end{aligned}$$

Where $s_{(16)}$ represents integrand that is integrated over the interval $[0, t]$

From the hypotheses it follows

$$\begin{aligned} |(G_{19})^{(1)} - (G_{19})^{(2)}| e^{-(\bar{M}_{16})^{(2)}t} &\leq \\ \frac{1}{(\bar{M}_{16})^{(2)}} &((a_{16})^{(2)} + (a'_{16})^{(2)} + (\widehat{A}_{16})^{(2)} + (\widehat{P}_{16})^{(2)} (\widehat{k}_{16})^{(2)}) d((G_{19})^{(1)}, (T_{19})^{(1)}; (G_{19})^{(2)}, (T_{19})^{(2)}) \end{aligned}$$

And analogous inequalities for G_i and T_i . Taking into account the hypothesis the result follows

Remark 1: The fact that we supposed $(a''_{16})^{(2)}$ and $(b''_{16})^{(2)}$ depending also on t can be considered as not conformal with the reality, however we have put this hypothesis in order that we can postulate condition necessary to prove the uniqueness of the solution bounded by $(\widehat{P}_{16})^{(2)} e^{(\bar{M}_{16})^{(2)}t}$ and $(\widehat{Q}_{16})^{(2)} e^{(\bar{M}_{16})^{(2)}t}$ respectively of \mathbb{R}_+ .

If instead of proving the existence of the solution on \mathbb{R}_+ , we have to prove it only on a compact then it suffices to consider that $(a''_i)^{(2)}$ and $(b''_i)^{(2)}$, $i = 16, 17, 18$ depend only on T_{17} and respectively on (G_{19}) (and not on t) and hypothesis can be replaced by a usual Lipschitz condition.

Remark 2: There does not exist any t where $G_i(t) = 0$ and $T_i(t) = 0$

From 19 to 24 it results

$$G_i(t) \geq G_i^0 e^{-\int_0^t \{ (a'_i)^{(2)} - (a''_i)^{(2)} (T_{17}(s_{(16)}), s_{(16)}) \} ds_{(16)}} \geq 0$$

$$T_i(t) \geq T_i^0 e^{-(b'_i)^{(2)}t} > 0 \quad \text{for } t > 0$$

Definition of $((\bar{M}_{16})^{(2)})_1, ((\bar{M}_{16})^{(2)})_2$ and $((\bar{M}_{16})^{(2)})_3$:

Remark 3: if G_{16} is bounded, the same property have also G_{17} and G_{18} . indeed if

$$G_{16} < ((\bar{M}_{16})^{(2)}) \text{ it follows } \frac{dG_{17}}{dt} \leq ((\bar{M}_{16})^{(2)})_1 - (a'_{17})^{(2)} G_{17} \text{ and by integrating}$$

$$G_{17} \leq ((\bar{M}_{16})^{(2)})_2 = G_{17}^0 + 2(a_{17})^{(2)} ((\bar{M}_{16})^{(2)})_1 / (a'_{17})^{(2)}$$

In the same way, one can obtain

$$G_{18} \leq ((\bar{M}_{16})^{(2)})_3 = G_{18}^0 + 2(a_{18})^{(2)} ((\bar{M}_{16})^{(2)})_2 / (a'_{18})^{(2)}$$

If G_{17} or G_{18} is bounded, the same property follows for G_{16} , G_{18} and G_{16} , G_{17} respectively.

Remark 4: If G_{16} is bounded, from below, the same property holds for G_{17} and G_{18} . The proof is analogous with the preceding one. An analogous property is true if G_{17} is bounded from below.

Remark 5: If T_{16} is bounded from below and $\lim_{t \rightarrow \infty} ((b'_i)^{(2)} ((G_{19})(t), t)) = (b'_{17})^{(2)}$ then $T_{17} \rightarrow \infty$.

Definition of $(m)^{(2)}$ and ε_2 :

Indeed let t_2 be so that for $t > t_2$

$$(b_{17})^{(2)} - (b''_i)^{(2)} ((G_{19})(t), t) < \varepsilon_2, T_{16}(t) > (m)^{(2)}$$

Then $\frac{dT_{17}}{dt} \geq (a_{17})^{(2)} (m)^{(2)} - \varepsilon_2 T_{17}$ which leads to

$$T_{17} \geq \left(\frac{(a_{17})^{(2)} (m)^{(2)}}{\varepsilon_2} \right) (1 - e^{-\varepsilon_2 t}) + T_{17}^0 e^{-\varepsilon_2 t} \text{ If we take } t \text{ such that } e^{-\varepsilon_2 t} = \frac{1}{2} \text{ it results}$$

$$T_{17} \geq \left(\frac{(a_{17})^{(2)} (m)^{(2)}}{2} \right), \quad t = \log \frac{2}{\varepsilon_2} \text{ By taking now } \varepsilon_2 \text{ sufficiently small one sees that } T_{17} \text{ is unbounded. The}$$

same property holds for T_{18} if $\lim_{t \rightarrow \infty} (b''_{18})^{(2)} ((G_{19})(t), t) = (b'_{18})^{(2)}$

We now state a more precise theorem about the behaviors at infinity of the solutions

It is now sufficient to take $\frac{(a_i)^{(3)}}{(M_{20})^{(3)}}, \frac{(b_i)^{(3)}}{(M_{20})^{(3)}} < 1$ and to choose

$(\widehat{P}_{20})^{(3)}$ and $(\widehat{Q}_{20})^{(3)}$ large to have

$$\frac{(a_i)^{(3)}}{(M_{20})^{(3)}} \left[(\widehat{P}_{20})^{(3)} + ((\widehat{P}_{20})^{(3)} + G_j^0) e^{-\left(\frac{(\widehat{P}_{20})^{(3)} + G_j^0}{G_j^0} \right)} \right] \leq (\widehat{P}_{20})^{(3)}$$

$$\frac{(b_i)^{(3)}}{(M_{20})^{(3)}} \left[((\widehat{Q}_{20})^{(3)} + T_j^0) e^{-\left(\frac{(\widehat{Q}_{20})^{(3)} + T_j^0}{T_j^0} \right)} + (\widehat{Q}_{20})^{(3)} \right] \leq (\widehat{Q}_{20})^{(3)}$$

In order that the operator $\mathcal{A}^{(3)}$ transforms the space of sextuples of functions G_i, T_i into itself

The operator $\mathcal{A}^{(3)}$ is a contraction with respect to the metric

$$d\left(\left((G_{23})^{(1)}, (T_{23})^{(1)}\right), \left((G_{23})^{(2)}, (T_{23})^{(2)}\right)\right) = \sup_{t \in \mathbb{R}_+} \left\{ \max_{i \in \mathbb{R}_+} |G_i^{(1)}(t) - G_i^{(2)}(t)| e^{-(\bar{M}_{20})^{(3)}t}, \max_{i \in \mathbb{R}_+} |T_i^{(1)}(t) - T_i^{(2)}(t)| e^{-(\bar{M}_{20})^{(3)}t} \right\}$$

320

Indeed if we denote

$$\underline{\text{Definition of}} \widetilde{G}_{23}, \widetilde{T}_{23} : \left((\widetilde{G}_{23}), (\widetilde{T}_{23}) \right) = \mathcal{A}^{(3)}\left((G_{23}), (T_{23}) \right)$$

321

It results

$$\begin{aligned} |\widetilde{G}_{20}^{(1)} - \widetilde{G}_i^{(2)}| &\leq \int_0^t (a_{20})^{(3)} |G_{21}^{(1)} - G_{21}^{(2)}| e^{-(\bar{M}_{20})^{(3)}s_{(20)}} e^{(\bar{M}_{20})^{(3)}s_{(20)}} ds_{(20)} + \\ &\int_0^t \left\{ (a'_{20})^{(3)} |G_{20}^{(1)} - G_{20}^{(2)}| e^{-(\bar{M}_{20})^{(3)}s_{(20)}} e^{-(\bar{M}_{20})^{(3)}s_{(20)}} + \right. \\ &(a''_{20})^{(3)} (T_{21}^{(1)}, s_{(20)}) |G_{20}^{(1)} - G_{20}^{(2)}| e^{-(\bar{M}_{20})^{(3)}s_{(20)}} e^{(\bar{M}_{20})^{(3)}s_{(20)}} + \\ &\left. G_{20}^{(2)} |(a'_{20})^{(3)} (T_{21}^{(1)}, s_{(20)}) - (a'_{20})^{(3)} (T_{21}^{(2)}, s_{(20)})| e^{-(\bar{M}_{20})^{(3)}s_{(20)}} e^{(\bar{M}_{20})^{(3)}s_{(20)}} \right\} ds_{(20)} \end{aligned}$$

322

323

Where $s_{(20)}$ represents integrand that is integrated over the interval $[0, t]$

From the hypotheses it follows

$$|G^{(1)} - G^{(2)}| e^{-(\bar{M}_{20})^{(3)}t} \leq$$

324

$$\frac{1}{(\bar{M}_{20})^{(3)}} \left((a_{20})^{(3)} + (a'_{20})^{(3)} + (\bar{A}_{20})^{(3)} + (\bar{P}_{20})^{(3)} (\bar{k}_{20})^{(3)} \right) d\left(\left((\widetilde{G}_{23})^{(1)}, (T_{23})^{(1)}\right); (G_{23})^{(2)}, (T_{23})^{(2)}\right)$$

And analogous inequalities for G_i and T_i . Taking into account the hypothesis the result follows

Remark 1: The fact that we supposed $(a''_{20})^{(3)}$ and $(b''_{20})^{(3)}$ depending also on t can be considered as not conformal with the reality, however we have put this hypothesis, in order that we can postulate condition necessary to prove the uniqueness of the solution bounded by $(\bar{P}_{20})^{(3)} e^{(\bar{M}_{20})^{(3)}t}$ and $(\bar{Q}_{20})^{(3)} e^{(\bar{M}_{20})^{(3)}t}$ respectively of \mathbb{R}_+ .

325

If instead of proving the existence of the solution on \mathbb{R}_+ , we have to prove it only on a compact then it suffices to consider that $(a''_i)^{(3)}$ and $(b''_i)^{(3)}$, $i = 20, 21, 22$ depend only on T_{21} and respectively on (G_{23}) (and not on t) and hypothesis can be replaced by a usual Lipschitz condition.

Remark 2: There does not exist any t where $G_i(t) = 0$ and $T_i(t) = 0$

326

From 19 to 24 it results

$$G_i(t) \geq G_i^0 e^{-\int_0^t \left\{ (a'_i)^{(3)} - (a''_i)^{(3)} (T_{21}(s_{(20)}), s_{(20)}) \right\} ds_{(20)}} \geq 0$$

$$T_i(t) \geq T_i^0 e^{-(b'_i)^{(3)}t} > 0 \text{ for } t > 0$$

Definition of $((\bar{M}_{20})^{(3)})_1$, $((\bar{M}_{20})^{(3)})_2$ and $((\bar{M}_{20})^{(3)})_3$:

327

Remark 3: if G_{20} is bounded, the same property have also G_{21} and G_{22} . indeed if

$$G_{20} < (\bar{M}_{20})^{(3)} \text{ it follows } \frac{dG_{21}}{dt} \leq ((\bar{M}_{20})^{(3)})_1 - (a'_{21})^{(3)} G_{21} \text{ and by integrating}$$

$$G_{21} \leq ((\bar{M}_{20})^{(3)})_2 = G_{21}^0 + 2(a_{21})^{(3)} ((\bar{M}_{20})^{(3)})_1 / (a'_{21})^{(3)}$$

In the same way, one can obtain

$$G_{22} \leq ((\bar{M}_{20})^{(3)})_3 = G_{22}^0 + 2(a_{22})^{(3)} ((\bar{M}_{20})^{(3)})_2 / (a'_{22})^{(3)}$$

If G_{21} or G_{22} is bounded, the same property follows for G_{20} , G_{22} and G_{20} , G_{21} respectively.

Remark 4: If G_{20} is bounded, from below, the same property holds for G_{21} and G_{22} . The proof is analogous with the preceding one. An analogous property is true if G_{21} is bounded from below.

328

Remark 5: If T_{20} is bounded from below and $\lim_{t \rightarrow \infty} ((b'_i)^{(3)}((G_{23})(t), t)) = (b'_{21})^{(3)}$ then $T_{21} \rightarrow \infty$.

329

Definition of $(m)^{(3)}$ and ε_3 :

Indeed let t_3 be so that for $t > t_3$

$$(b_{21})^{(3)} - (b'_i)^{(3)}((G_{23})(t), t) < \varepsilon_3, T_{20}(t) > (m)^{(3)}$$

330

Then $\frac{dT_{21}}{dt} \geq (a_{21})^{(3)}(m)^{(3)} - \varepsilon_3 T_{21}$ which leads to

331

$$T_{21} \geq \left(\frac{(a_{21})^{(3)}(m)^{(3)}}{\varepsilon_3} \right) (1 - e^{-\varepsilon_3 t}) + T_{21}^0 e^{-\varepsilon_3 t} \text{ If we take } t \text{ such that } e^{-\varepsilon_3 t} = \frac{1}{2} \text{ it results}$$

$$T_{21} \geq \left(\frac{(a_{21})^{(3)}(m)^{(3)}}{2} \right), t = \log \frac{2}{\varepsilon_3} \text{ By taking now } \varepsilon_3 \text{ sufficiently small one sees that } T_{21} \text{ is unbounded. The}$$

same property holds for T_{22} if $\lim_{t \rightarrow \infty} (b''_{22})^{(3)}((G_{23})(t), t) = (b'_{22})^{(3)}$

We now state a more precise theorem about the behaviors at infinity of the solutions

332

It is now sufficient to take $\frac{(a_i)^{(4)}}{(\bar{M}_{24})^{(4)}} , \frac{(b_i)^{(4)}}{(\bar{M}_{24})^{(4)}} < 1$ and to choose

333

$(\bar{P}_{24})^{(4)}$ and $(\bar{Q}_{24})^{(4)}$ large to have

$$\frac{(a_i)^{(4)}}{(\widehat{M}_{24})^{(4)}} \left[(\widehat{P}_{24})^{(4)} + ((\widehat{P}_{24})^{(4)} + G_j^0) e^{-\left(\frac{(\widehat{P}_{24})^{(4)} + G_j^0}{G_j^0}\right)} \right] \leq (\widehat{P}_{24})^{(4)} \quad 334$$

$$\frac{(b_i)^{(4)}}{(\widehat{M}_{24})^{(4)}} \left[((\widehat{Q}_{24})^{(4)} + T_j^0) e^{-\left(\frac{(\widehat{Q}_{24})^{(4)} + T_j^0}{T_j^0}\right)} + (\widehat{Q}_{24})^{(4)} \right] \leq (\widehat{Q}_{24})^{(4)} \quad 335$$

In order that the operator $\mathcal{A}^{(4)}$ transforms the space of sextuples of functions G_i, T_i satisfying IN to itself 336

The operator $\mathcal{A}^{(4)}$ is a contraction with respect to the metric 337

$$d \left(((G_{27})^{(1)}, (T_{27})^{(1)}), ((G_{27})^{(2)}, (T_{27})^{(2)}) \right) = \sup_i \left\{ \max_{t \in \mathbb{R}_+} |G_i^{(1)}(t) - G_i^{(2)}(t)| e^{-(\widehat{M}_{24})^{(4)}t}, \max_{t \in \mathbb{R}_+} |T_i^{(1)}(t) - T_i^{(2)}(t)| e^{-(\widehat{M}_{24})^{(4)}t} \right\}$$

Indeed if we denote

Definition of $(\widehat{G}_{27}), (\widehat{T}_{27}) : ((\widehat{G}_{27}), (\widehat{T}_{27})) = \mathcal{A}^{(4)}((G_{27}), (T_{27}))$

It results

$$\begin{aligned} |\widehat{G}_{24}^{(1)} - \widehat{G}_{24}^{(2)}| &\leq \int_0^t (a_{24})^{(4)} |G_{25}^{(1)} - G_{25}^{(2)}| e^{-(\widehat{M}_{24})^{(4)}s(24)} e^{(\widehat{M}_{24})^{(4)}s(24)} ds(24) + \\ &\int_0^t \{ (a_{24}')^{(4)} |G_{24}^{(1)} - G_{24}^{(2)}| e^{-(\widehat{M}_{24})^{(4)}s(24)} e^{-(\widehat{M}_{24})^{(4)}s(24)} + \\ &(a_{24}'')^{(4)} (T_{25}^{(1)}, s(24)) |G_{24}^{(1)} - G_{24}^{(2)}| e^{-(\widehat{M}_{24})^{(4)}s(24)} e^{(\widehat{M}_{24})^{(4)}s(24)} + \\ &G_{24}^{(2)} |(a_{24}'')^{(4)} (T_{25}^{(1)}, s(24)) - (a_{24}'')^{(4)} (T_{25}^{(2)}, s(24))| e^{-(\widehat{M}_{24})^{(4)}s(24)} e^{(\widehat{M}_{24})^{(4)}s(24)} \} ds(24) \end{aligned}$$

Where $s(24)$ represents integrand that is integrated over the interval $[0, t]$

From the hypotheses it follows 338

$$|(G_{27})^{(1)} - (G_{27})^{(2)}| e^{-(\widehat{M}_{24})^{(4)}t} \leq \frac{1}{(\widehat{M}_{24})^{(4)}} \left((a_{24})^{(4)} + (a_{24}')^{(4)} + (\widehat{A}_{24})^{(4)} + (\widehat{P}_{24})^{(4)} (\widehat{K}_{24})^{(4)} \right) d \left(((G_{27})^{(1)}, (T_{27})^{(1)}); (G_{27})^{(2)}, (T_{27})^{(2)} \right) \quad 339$$

And analogous inequalities for G_i and T_i . Taking into account the hypothesis the result follows

Remark 1: The fact that we supposed $(a_{24}'')^{(4)}$ and $(b_{24}'')^{(4)}$ depending also on t can be considered as not conformal with the reality, however we have put this hypothesis, in order that we can postulate condition necessary to prove the uniqueness of the solution bounded by $(\widehat{P}_{24})^{(4)} e^{(\widehat{M}_{24})^{(4)}t}$ and $(\widehat{Q}_{24})^{(4)} e^{(\widehat{M}_{24})^{(4)}t}$ respectively of \mathbb{R}_+ . 340

If instead of proving the existence of the solution on \mathbb{R}_+ , we have to prove it only on a compact then it suffices to consider that $(a_i'')^{(4)}$ and $(b_i'')^{(4)}$, $i = 24, 25, 26$ depend only on T_{25} and respectively on (G_{27}) (and not on t) and hypothesis can be replaced by a usual Lipschitz condition.

Remark 2: There does not exist any t where $G_i(t) = 0$ and $T_i(t) = 0$ 341

From GLOBAL EQUATIONS it results

$$G_i(t) \geq G_i^0 e^{-\int_0^t \{ (a_i')^{(4)} - (a_i'')^{(4)} (T_{25}(s(24)), s(24)) \} ds(24)} \geq 0$$

$$T_i(t) \geq T_i^0 e^{-(b_i')^{(4)}t} > 0 \text{ for } t > 0$$

Definition of $((\widehat{M}_{24})^{(4)})_1, ((\widehat{M}_{24})^{(4)})_2$ and $((\widehat{M}_{24})^{(4)})_3$: 342

Remark 3: if G_{24} is bounded, the same property have also G_{25} and G_{26} . indeed if

$$G_{24} < (\widehat{M}_{24})^{(4)} \text{ it follows } \frac{dG_{25}}{dt} \leq ((\widehat{M}_{24})^{(4)})_1 - (a_{25}')^{(4)} G_{25} \text{ and by integrating}$$

$$G_{25} \leq ((\widehat{M}_{24})^{(4)})_2 = G_{25}^0 + 2(a_{25})^{(4)} ((\widehat{M}_{24})^{(4)})_1 / (a_{25}')^{(4)}$$

In the same way, one can obtain

$$G_{26} \leq ((\widehat{M}_{24})^{(4)})_3 = G_{26}^0 + 2(a_{26})^{(4)} ((\widehat{M}_{24})^{(4)})_2 / (a_{26}')^{(4)}$$

If G_{25} or G_{26} is bounded, the same property follows for G_{24}, G_{26} and G_{24}, G_{25} respectively.

Remark 4: If G_{24} is bounded, from below, the same property holds for G_{25} and G_{26} . The proof is analogous with the preceding one. An analogous property is true if G_{25} is bounded from below. 343

Remark 5: If T_{24} is bounded from below and $\lim_{t \rightarrow \infty} ((b_i'')^{(4)}((G_{27})(t), t)) = (b_{25}')^{(4)}$ then $T_{25} \rightarrow \infty$. 344

Definition of $(m)^{(4)}$ and ε_4 :

Indeed let t_4 be so that for $t > t_4$

$$(b_{25})^{(4)} - (b_i'')^{(4)}((G_{27})(t), t) < \varepsilon_4, T_{24}(t) > (m)^{(4)}$$

Then $\frac{dT_{25}}{dt} \geq (a_{25})^{(4)}(m)^{(4)} - \varepsilon_4 T_{25}$ which leads to 345

$$T_{25} \geq \left(\frac{(a_{25})^{(4)}(m)^{(4)}}{\varepsilon_4} \right) (1 - e^{-\varepsilon_4 t}) + T_{25}^0 e^{-\varepsilon_4 t} \text{ If we take } t \text{ such that } e^{-\varepsilon_4 t} = \frac{1}{2} \text{ it results}$$

$T_{25} \geq \left(\frac{(a_{25})^{(4)}(m)^{(4)}}{2} \right), t = \log \frac{2}{\varepsilon_4}$ By taking now ε_4 sufficiently small one sees that T_{25} is unbounded. The same property holds for T_{26} if $\lim_{t \rightarrow \infty} (b_{26}'')^{(4)}((G_{27})(t), t) = (b_{26}')^{(4)}$

We now state a more precise theorem about the behaviors at infinity of the solutions ANALOGOUS inequalities

hold also for $G_{29}, G_{30}, T_{28}, T_{29}, T_{30}$

346

It is now sufficient to take $\frac{(a_i)^{(5)}}{(\widehat{M}_{28})^{(5)}}, \frac{(b_i)^{(5)}}{(\widehat{M}_{28})^{(5)}} < 1$ and to choose $(\widehat{P}_{28})^{(5)}$ and $(\widehat{Q}_{28})^{(5)}$ large to have

347

$$\frac{(a_i)^{(5)}}{(\widehat{M}_{28})^{(5)}} \left[(\widehat{P}_{28})^{(5)} + ((\widehat{P}_{28})^{(5)} + G_j^0) e^{-\left(\frac{(\widehat{P}_{28})^{(5)} + G_j^0}{G_j^0}\right)} \right] \leq (\widehat{P}_{28})^{(5)}$$

348

$$\frac{(b_i)^{(5)}}{(\widehat{M}_{28})^{(5)}} \left[((\widehat{Q}_{28})^{(5)} + T_j^0) e^{-\left(\frac{(\widehat{Q}_{28})^{(5)} + T_j^0}{T_j^0}\right)} + (\widehat{Q}_{28})^{(5)} \right] \leq (\widehat{Q}_{28})^{(5)}$$

349

In order that the operator $\mathcal{A}^{(5)}$ transforms the space of sextuples of functions G_i, T_i into itself

350

The operator $\mathcal{A}^{(5)}$ is a contraction with respect to the metric

351

$$d\left(\left((G_{31})^{(1)}, (T_{31})^{(1)}\right), \left((G_{31})^{(2)}, (T_{31})^{(2)}\right)\right) = \sup_i \left\{ \max_{t \in \mathbb{R}_+} |G_i^{(1)}(t) - G_i^{(2)}(t)| e^{-(\widehat{M}_{28})^{(5)}t}, \max_{t \in \mathbb{R}_+} |T_i^{(1)}(t) - T_i^{(2)}(t)| e^{-(\widehat{M}_{28})^{(5)}t} \right\}$$

352

Indeed if we denote

$$\text{Definition of } (\widehat{G}_{31}), (\widehat{T}_{31}) : \left((\widehat{G}_{31}), (\widehat{T}_{31}) \right) = \mathcal{A}^{(5)}\left((G_{31}), (T_{31}) \right)$$

It results

$$\begin{aligned} |\widehat{G}_{28}^{(1)} - \widehat{G}_{28}^{(2)}| &\leq \int_0^t (a_{28})^{(5)} |G_{29}^{(1)} - G_{29}^{(2)}| e^{-(\widehat{M}_{28})^{(5)}s_{(28)}} e^{(\widehat{M}_{28})^{(5)}s_{(28)}} ds_{(28)} + \\ &\int_0^t \left\{ (a'_{28})^{(5)} |G_{28}^{(1)} - G_{28}^{(2)}| e^{-(\widehat{M}_{28})^{(5)}s_{(28)}} e^{-(\widehat{M}_{28})^{(5)}s_{(28)}} + \right. \\ &(a''_{28})^{(5)} (T_{29}^{(1)}, s_{(28)}) |G_{28}^{(1)} - G_{28}^{(2)}| e^{-(\widehat{M}_{28})^{(5)}s_{(28)}} e^{(\widehat{M}_{28})^{(5)}s_{(28)}} + \\ &\left. G_{28}^{(2)} |(a''_{28})^{(5)} (T_{29}^{(1)}, s_{(28)}) - (a''_{28})^{(5)} (T_{29}^{(2)}, s_{(28)})| e^{-(\widehat{M}_{28})^{(5)}s_{(28)}} e^{(\widehat{M}_{28})^{(5)}s_{(28)}} \right\} ds_{(28)} \end{aligned}$$

Where $s_{(28)}$ represents integrand that is integrated over the interval $[0, t]$

From the hypotheses it follows

$$\begin{aligned} |(G_{31})^{(1)} - (G_{31})^{(2)}| e^{-(\widehat{M}_{28})^{(5)}t} &\leq \\ \frac{1}{(\widehat{M}_{28})^{(5)}} \left((a_{28})^{(5)} + (a'_{28})^{(5)} + (\widehat{A}_{28})^{(5)} + (\widehat{P}_{28})^{(5)} (\widehat{k}_{28})^{(5)} \right) &d\left(\left((G_{31})^{(1)}, (T_{31})^{(1)}\right); (G_{31})^{(2)}, (T_{31})^{(2)}\right) \end{aligned}$$

353

And analogous inequalities for G_i and T_i . Taking into account the hypothesis (35,35,36) the result follows

Remark 1: The fact that we supposed $(a''_{28})^{(5)}$ and $(b''_{28})^{(5)}$ depending also on t can be considered as not conformal with the reality, however we have put this hypothesis, in order that we can postulate condition necessary to prove the uniqueness of the solution bounded by $(\widehat{P}_{28})^{(5)} e^{(\widehat{M}_{28})^{(5)}t}$ and $(\widehat{Q}_{28})^{(5)} e^{(\widehat{M}_{28})^{(5)}t}$ respectively of \mathbb{R}_+ .

354

If instead of proving the existence of the solution on \mathbb{R}_+ , we have to prove it only on a compact then it suffices to consider that $(a''_i)^{(5)}$ and $(b''_i)^{(5)}, i = 28, 29, 30$ depend only on T_{29} and respectively on (G_{31}) (and not on t) and hypothesis can be replaced by a usual Lipschitz condition.

Remark 2: There does not exist any t where $G_i(t) = 0$ and $T_i(t) = 0$

355

From GLOBAL EQUATIONS it results

$$G_i(t) \geq G_i^0 e^{-\int_0^t \{(a'_i)^{(5)} - (a''_i)^{(5)}(T_{29}(s_{(28)}), s_{(28)})\} ds_{(28)}} \geq 0$$

$$T_i(t) \geq T_i^0 e^{-(b'_i)^{(5)}t} > 0 \text{ for } t > 0$$

$$\text{Definition of } ((\widehat{M}_{28})^{(5)})_1, ((\widehat{M}_{28})^{(5)})_2 \text{ and } ((\widehat{M}_{28})^{(5)})_3 :$$

356

Remark 3: if G_{28} is bounded, the same property have also G_{29} and G_{30} . indeed if

$$G_{28} < (\widehat{M}_{28})^{(5)} \text{ it follows } \frac{dG_{29}}{dt} \leq ((\widehat{M}_{28})^{(5)})_1 - (a'_{29})^{(5)} G_{29} \text{ and by integrating}$$

$$G_{29} \leq ((\widehat{M}_{28})^{(5)})_2 = G_{29}^0 + 2(a_{29})^{(5)} ((\widehat{M}_{28})^{(5)})_1 / (a'_{29})^{(5)}$$

In the same way, one can obtain

$$G_{30} \leq ((\widehat{M}_{28})^{(5)})_3 = G_{30}^0 + 2(a_{30})^{(5)} ((\widehat{M}_{28})^{(5)})_2 / (a'_{30})^{(5)}$$

If G_{29} or G_{30} is bounded, the same property follows for G_{28}, G_{30} and G_{28}, G_{29} respectively.

Remark 4: If G_{28} is bounded, from below, the same property holds for G_{29} and G_{30} . The proof is analogous with the preceding one. An analogous property is true if G_{29} is bounded from below.

357

Remark 5: If T_{28} is bounded from below and $\lim_{t \rightarrow \infty} ((b''_i)^{(5)}((G_{31})(t), t)) = (b'_{29})^{(5)}$ then $T_{29} \rightarrow \infty$.

358

Definition of $(m)^{(5)}$ and ε_5 :

Indeed let t_5 be so that for $t > t_5$

$$(b_{29})^{(5)} - (b''_i)^{(5)}((G_{31})(t), t) < \varepsilon_5, T_{28}(t) > (m)^{(5)}$$

Then $\frac{dT_{29}}{dt} \geq (a_{29})^{(5)}(m)^{(5)} - \varepsilon_5 T_{29}$ which leads to

360

$$T_{29} \geq \left(\frac{(a_{29})^{(5)}(m)^{(5)}}{\varepsilon_5} \right) (1 - e^{-\varepsilon_5 t}) + T_{29}^0 e^{-\varepsilon_5 t}$$

If we take t such that $e^{-\varepsilon_5 t} = \frac{1}{2}$ it results

$$T_{29} \geq \left(\frac{(a_{29})^{(5)}(m)^{(5)}}{2} \right), \quad t = \log \frac{2}{\varepsilon_5}$$

By taking now ε_5 sufficiently small one sees that T_{29} is unbounded. The

same property holds for T_{30} if $\lim_{t \rightarrow \infty} (b_{30}'')^{(5)}((G_{31})(t), t) = (b_{30}')^{(5)}$

We now state a more precise theorem about the behaviors at infinity of the solutions

Analogous inequalities hold also for $G_{33}, G_{34}, T_{32}, T_{33}, T_{34}$

361

It is now sufficient to take $\frac{(a_i)^{(6)}}{(M_{32})^{(6)}}, \frac{(b_i)^{(6)}}{(M_{32})^{(6)}} < 1$ and to choose

362

$(\hat{P}_{32})^{(6)}$ and $(\hat{Q}_{32})^{(6)}$ large to have

$$\frac{(a_i)^{(6)}}{(M_{32})^{(6)}} \left[(\hat{P}_{32})^{(6)} + ((\hat{P}_{32})^{(6)} + G_j^0) e^{-\left(\frac{(\hat{P}_{32})^{(6)} + G_j^0}{G_j^0}\right)} \right] \leq (\hat{P}_{32})^{(6)}$$

363

$$\frac{(b_i)^{(6)}}{(M_{32})^{(6)}} \left[((\hat{Q}_{32})^{(6)} + T_j^0) e^{-\left(\frac{(\hat{Q}_{32})^{(6)} + T_j^0}{T_j^0}\right)} + (\hat{Q}_{32})^{(6)} \right] \leq (\hat{Q}_{32})^{(6)}$$

364

In order that the operator $\mathcal{A}^{(6)}$ transforms the space of sextuples of functions G_i, T_i into itself

365

The operator $\mathcal{A}^{(6)}$ is a contraction with respect to the metric

366

$$d\left(((G_{35})^{(1)}, (T_{35})^{(1)}), ((G_{35})^{(2)}, (T_{35})^{(2)}) \right) =$$

$$\sup_i \left\{ \max_{t \in \mathbb{R}_+} |G_i^{(1)}(t) - G_i^{(2)}(t)| e^{-(M_{32})^{(6)}t}, \max_{t \in \mathbb{R}_+} |T_i^{(1)}(t) - T_i^{(2)}(t)| e^{-(M_{32})^{(6)}t} \right\}$$

Indeed if we denote

$$\underline{\text{Definition of}} (\widehat{G_{35}}, \widehat{T_{35}}) : (\widehat{G_{35}}, \widehat{T_{35}}) = \mathcal{A}^{(6)}((G_{35}), (T_{35}))$$

It results

$$\begin{aligned} |\widehat{G}_{32}^{(1)} - \widehat{G}_{32}^{(2)}| &\leq \int_0^t (a_{32})^{(6)} |G_{33}^{(1)} - G_{33}^{(2)}| e^{-(M_{32})^{(6)}s} e^{(M_{32})^{(6)}s} ds + \\ &\int_0^t \{ (a_{32}')^{(6)} |G_{32}^{(1)} - G_{32}^{(2)}| e^{-(M_{32})^{(6)}s} e^{-(M_{32})^{(6)}s} + \\ &(a_{32}'')^{(6)} (T_{33}^{(1)}, s) |G_{32}^{(1)} - G_{32}^{(2)}| e^{-(M_{32})^{(6)}s} e^{(M_{32})^{(6)}s} + \\ &G_{32}^{(2)} | (a_{32}'')^{(6)} (T_{33}^{(1)}, s) - (a_{32}'')^{(6)} (T_{33}^{(2)}, s) | e^{-(M_{32})^{(6)}s} e^{(M_{32})^{(6)}s} \} ds \end{aligned}$$

367

Where $s_{(32)}$ represents integrand that is integrated over the interval $[0, t]$

From the hypotheses it follows

$$(1) \quad (a_i')^{(1)}, (a_i'')^{(1)}, (b_i)^{(1)}, (b_i')^{(1)}, (b_i'')^{(1)} > 0, \\ i, j = 13, 14, 15$$

(2) The functions $(a_i'')^{(1)}, (b_i'')^{(1)}$ are positive continuous increasing and bounded.

Definition of $(p_i)^{(1)}, (r_i)^{(1)}$:

$$(a_i'')^{(1)}(T_{14}, t) \leq (p_i)^{(1)} \leq (\hat{A}_{13})^{(1)}$$

$$(b_i'')^{(1)}(G, t) \leq (r_i)^{(1)} \leq (b_i')^{(1)} \leq (\hat{B}_{13})^{(1)}$$

$$(3) \quad \lim_{T_2 \rightarrow \infty} (a_i'')^{(1)}(T_{14}, t) = (p_i)^{(1)}$$

$$\lim_{G \rightarrow \infty} (b_i'')^{(1)}(G, t) = (r_i)^{(1)}$$

Definition of $(\hat{A}_{13})^{(1)}, (\hat{B}_{13})^{(1)}$:

Where $(\hat{A}_{13})^{(1)}, (\hat{B}_{13})^{(1)}, (p_i)^{(1)}, (r_i)^{(1)}$ are positive constants
 and $i = 13, 14, 15$

They satisfy Lipschitz condition:

$$|(a_i'')^{(1)}(T_{14}, t) - (a_i'')^{(1)}(T_{14}, t)| \leq (\hat{k}_{13})^{(1)} |T_{14} - T_{14}'| e^{-(M_{13})^{(1)}t}$$

$$|(b_i'')^{(1)}(G', t) - (b_i'')^{(1)}(G, T)| < (\hat{k}_{13})^{(1)} \|G - G'\| e^{-(M_{13})^{(1)}t}$$

With the Lipschitz condition, we place a restriction on the behavior of functions $(a_i'')^{(1)}(T_{14}, t)$ and $(a_i'')^{(1)}(T_{14}, t)$. (T_{14}, t) and (T_{14}, t) are points belonging to the interval $[(\hat{k}_{13})^{(1)}, (\hat{M}_{13})^{(1)}]$. It is to be noted that $(a_i'')^{(1)}(T_{14}, t)$ is uniformly continuous. In the eventuality of the fact, that if $(\hat{M}_{13})^{(1)} = 1$ then the function $(a_i'')^{(1)}(T_{14}, t)$, the **first augmentation coefficient** attributable to terrestrial organisms, would be absolutely continuous.

Definition of $(\hat{M}_{13})^{(1)}, (\hat{k}_{13})^{(1)}$:

(AA) $(\hat{M}_{13})^{(1)}, (\hat{k}_{13})^{(1)}$, are positive constants

$$\frac{(a_i)^{(1)}}{(\hat{M}_{13})^{(1)}}, \frac{(b_i)^{(1)}}{(\hat{M}_{13})^{(1)}} < 1$$

Definition of $(\hat{P}_{13})^{(1)}, (\hat{Q}_{13})^{(1)}$:

(BB) There exists two constants $(\hat{P}_{13})^{(1)}$ and $(\hat{Q}_{13})^{(1)}$ which together with $(\hat{M}_{13})^{(1)}, (\hat{k}_{13})^{(1)}, (\hat{A}_{13})^{(1)}$ and $(\hat{B}_{13})^{(1)}$ and the constants $(a_i)^{(1)}, (a_i')^{(1)}, (b_i)^{(1)}, (b_i')^{(1)}, (p_i)^{(1)}, (r_i)^{(1)}, i = 13, 14, 15$, satisfy the inequalities

$$\frac{1}{(\hat{M}_{13})^{(1)}} [(a_i)^{(1)} + (a_i')^{(1)} + (\hat{A}_{13})^{(1)} + (\hat{P}_{13})^{(1)} (\hat{k}_{13})^{(1)}] < 1$$

$$\frac{1}{(\hat{M}_{13})^{(1)}} [(b_i)^{(1)} + (b_i')^{(1)} + (\hat{B}_{13})^{(1)} + (\hat{Q}_{13})^{(1)} (\hat{k}_{13})^{(1)}] < 1$$

Analogous inequalities hold also for $G_{37}, G_{38}, T_{36}, T_{37}, T_{38}$

368

It is now sufficient to take $\frac{(a_i)^{(7)}}{(\hat{M}_{36})^{(7)}}, \frac{(b_i)^{(7)}}{(\hat{M}_{36})^{(7)}} < 7$ and to choose $(\hat{P}_{36})^{(7)}$ and $(\hat{Q}_{36})^{(7)}$ large to have

$$\frac{(a_i)^{(7)}}{(\hat{M}_{36})^{(7)}} \left[(\hat{P}_{36})^{(7)} + ((\hat{P}_{36})^{(7)} + G_j^0) e^{-\left(\frac{(\hat{P}_{36})^{(7)} + G_j^0}{G_j^0}\right)} \right] \leq (\hat{P}_{36})^{(7)}$$

369

$$\frac{(b_i)^{(7)}}{(\hat{M}_{36})^{(7)}} \left[((\hat{Q}_{36})^{(7)} + T_j^0) e^{-\left(\frac{(\hat{Q}_{36})^{(7)} + T_j^0}{T_j^0}\right)} + (\hat{Q}_{36})^{(7)} \right] \leq (\hat{Q}_{36})^{(7)}$$

370

In order that the operator $\mathcal{A}^{(7)}$ transforms the space of sextuples of functions G_i, T_i satisfying 37,35,36 into itself

371

The operator $\mathcal{A}^{(7)}$ is a contraction with respect to the metric

372

$$d\left((G_{39})^{(1)}, (T_{39})^{(1)}, (G_{39})^{(2)}, (T_{39})^{(2)}\right) = \sup_i \left\{ \max_{t \in \mathbb{R}_+} |G_i^{(1)}(t) - G_i^{(2)}(t)| e^{-(\hat{M}_{36})^{(7)}t}, \max_{t \in \mathbb{R}_+} |T_i^{(1)}(t) - T_i^{(2)}(t)| e^{-(\hat{M}_{36})^{(7)}t} \right\}$$

Indeed if we denote

Definition of $(\widehat{G}_{39}), (\widehat{T}_{39})$:

$$((\widehat{G}_{39}), (\widehat{T}_{39})) = \mathcal{A}^{(7)}((G_{39}), (T_{39}))$$

It results

$$\begin{aligned} |\widehat{G}_{36}^{(1)} - \widehat{G}_{36}^{(2)}| &\leq \int_0^t (a_{36})^{(7)} |G_{37}^{(1)} - G_{37}^{(2)}| e^{-(\hat{M}_{36})^{(7)}s} e^{(\hat{M}_{36})^{(7)}s} ds + \\ &\int_0^t \{(a_{36}')^{(7)} |G_{36}^{(1)} - G_{36}^{(2)}| e^{-(\hat{M}_{36})^{(7)}s} e^{-(\hat{M}_{36})^{(7)}s} + \\ &(a_{36}'')^{(7)} (T_{37}^{(1)}, s) |G_{36}^{(1)} - G_{36}^{(2)}| e^{-(\hat{M}_{36})^{(7)}s} e^{(\hat{M}_{36})^{(7)}s} + \end{aligned}$$

Where $s_{(36)}$ represents integrand that is integrated over the interval $[0, t]$

From the hypotheses it follows

373

$$\begin{aligned} & |(G_{39})^{(1)} - (G_{39})^{(2)}| e^{-(\widehat{M}_{36})^{(7)}t} \leq \\ & \frac{1}{(\widehat{M}_{36})^{(7)}} ((a_{36})^{(7)} + (a_{36}')^{(7)} + (\widehat{A}_{36})^{(7)} + (\widehat{P}_{36})^{(7)}(\widehat{k}_{36})^{(7)}) d((G_{39})^{(1)}, (T_{39})^{(1)}; (G_{39})^{(2)}, (T_{39})^{(2)}) \end{aligned}$$

And analogous inequalities for G_i and T_i . Taking into account the hypothesis (37,35,36) the result follows 374

Remark 1: The fact that we supposed $(a_{36}''^{(7)})$ and $(b_{36}''^{(7)})$ depending also on t can be considered as not conformal with the reality, however we have put this hypothesis, in order that we can postulate condition necessary to prove the uniqueness of the solution bounded by $(\widehat{P}_{36})^{(7)} e^{(\widehat{M}_{36})^{(7)}t}$ and $(\widehat{Q}_{36})^{(7)} e^{(\widehat{M}_{36})^{(7)}t}$ respectively of \mathbb{R}_+ . 375

If instead of proving the existence of the solution on \mathbb{R}_+ , we have to prove it only on a compact then it suffices to consider that $(a_i''^{(7)})$ and $(b_i''^{(7)})$, $i = 36, 37, 38$ depend only on T_{37} and respectively on (G_{39}) (and not on t) and hypothesis can be replaced by a usual Lipschitz condition.

376

Remark 2: There does not exist any t where $G_i(t) = 0$ and $T_i(t) = 0$

From 79 to 36 it results

$$\begin{aligned} G_i(t) & \geq G_i^0 e^{-\int_0^t \{(a_i')^{(7)} - (a_i'')^{(7)}(T_{37}(s_{(36)}), s_{(36)})\} ds_{(36)}} \geq 0 \\ T_i(t) & \geq T_i^0 e^{-(b_i')^{(7)}t} > 0 \quad \text{for } t > 0 \end{aligned}$$

Definition of $((\widehat{M}_{36})^{(7)})_1, ((\widehat{M}_{36})^{(7)})_2$ and $((\widehat{M}_{36})^{(7)})_3$: 377

Remark 3: if G_{36} is bounded, the same property have also G_{37} and G_{38} . indeed if

$G_{36} < (\widehat{M}_{36})^{(7)}$ it follows $\frac{dG_{37}}{dt} \leq ((\widehat{M}_{36})^{(7)})_1 - (a_{37}')^{(7)}G_{37}$ and by integrating

$$G_{37} \leq ((\widehat{M}_{36})^{(7)})_2 = G_{37}^0 + 2(a_{37})^{(7)}((\widehat{M}_{36})^{(7)})_1 / (a_{37}')^{(7)}$$

In the same way, one can obtain

$$G_{38} \leq ((\widehat{M}_{36})^{(7)})_3 = G_{38}^0 + 2(a_{38})^{(7)}((\widehat{M}_{36})^{(7)})_2 / (a_{38}')^{(7)}$$

If G_{37} or G_{38} is bounded, the same property follows for G_{36} , G_{38} and G_{36} , G_{37} respectively.

Remark 7: If G_{36} is bounded, from below, the same property holds for G_{37} and G_{38} . The proof is analogous with the preceding one. An analogous property is true if G_{37} is bounded from below. 378

Remark 5: If T_{36} is bounded from below and $\lim_{t \rightarrow \infty} ((b_i'')^{(7)}((G_{39})(t), t)) = (b_{37}')^{(7)}$ then $T_{37} \rightarrow \infty$. 379

Definition of $(m)^{(7)}$ and ε_7 :

Indeed let t_7 be so that for $t > t_7$

$$(b_{37})^{(7)} - (b_i'')^{(7)}((G_{39})(t), t) < \varepsilon_7, T_{36}(t) > (m)^{(7)}$$

Then $\frac{dT_{37}}{dt} \geq (a_{37})^{(7)}(m)^{(7)} - \varepsilon_7 T_{37}$ which leads to 380

$$T_{37} \geq \left(\frac{(a_{37})^{(7)}(m)^{(7)}}{\varepsilon_7} \right) (1 - e^{-\varepsilon_7 t}) + T_{37}^0 e^{-\varepsilon_7 t} \text{ If we take } t \text{ such that } e^{-\varepsilon_7 t} = \frac{1}{2} \text{ it results}$$

$$T_{37} \geq \left(\frac{(a_{37})^{(7)}(m)^{(7)}}{2} \right), \quad t = \log \frac{2}{\varepsilon_7} \text{ By taking now } \varepsilon_7 \text{ sufficiently small one sees that } T_{37} \text{ is unbounded. The same property holds for } T_{38} \text{ if } \lim_{t \rightarrow \infty} (b_{38}'')^{(7)} ((G_{39})(t), t) = (b_{38}')^{(7)}$$

We now state a more precise theorem about the behaviors at infinity of the solutions of equations 37 to 72

In order that the operator $\mathcal{A}^{(7)}$ transforms the space of sextuples of functions G_i, T_i satisfying GLOBAL EQUATIONS AND ITS CONCOMITANT CONDITIONALITIES into itself 381

The operator $\mathcal{A}^{(7)}$ is a contraction with respect to the metric 382
383

$$d \left(((G_{39})^{(1)}, (T_{39})^{(1)}), ((G_{39})^{(2)}, (T_{39})^{(2)}) \right) = \sup_i \{ \max_{t \in \mathbb{R}_+} |G_i^{(1)}(t) - G_i^{(2)}(t)| e^{-(M_{36})^{(7)}t}, \max_{t \in \mathbb{R}_+} |T_i^{(1)}(t) - T_i^{(2)}(t)| e^{-(M_{36})^{(7)}t} \}$$

Indeed if we denote

Definition of $(\widehat{G_{39}}), (\widehat{T_{39}})$:

$$((\widehat{G_{39}}), (\widehat{T_{39}})) = \mathcal{A}^{(7)}((G_{39}), (T_{39}))$$

It results

$$\begin{aligned} |\widehat{G}_{36}^{(1)} - \widehat{G}_{36}^{(2)}| &\leq \int_0^t (a_{36})^{(7)} |G_{37}^{(1)} - G_{37}^{(2)}| e^{-(M_{36})^{(7)}s_{(36)}} e^{(M_{36})^{(7)}s_{(36)}} ds_{(36)} + \\ &\int_0^t \{ (a_{36}')^{(7)} |G_{36}^{(1)} - G_{36}^{(2)}| e^{-(M_{36})^{(7)}s_{(36)}} e^{-(M_{36})^{(7)}s_{(36)}} + \\ &(a_{36}'')^{(7)} (T_{37}^{(1)}, s_{(36)}) |G_{36}^{(1)} - G_{36}^{(2)}| e^{-(M_{36})^{(7)}s_{(36)}} e^{(M_{36})^{(7)}s_{(36)}} + \\ &G_{36}^{(2)} |(a_{36}'')^{(7)} (T_{37}^{(1)}, s_{(36)}) - (a_{36}'')^{(7)} (T_{37}^{(2)}, s_{(36)})| e^{-(M_{36})^{(7)}s_{(36)}} e^{(M_{36})^{(7)}s_{(36)}} \} ds_{(36)} \end{aligned}$$

Where $s_{(36)}$ represents integrand that is integrated over the interval $[0, t]$

From the hypotheses it follows 384

$$\begin{aligned} |(G_{39})^{(1)} - (G_{39})^{(2)}| e^{-(M_{36})^{(7)}t} &\leq \\ \frac{1}{(M_{36})^{(7)}} &((a_{36})^{(7)} + (a_{36}')^{(7)} + (\widehat{A}_{36})^{(7)} + (\widehat{P}_{36})^{(7)} (\widehat{k}_{36})^{(7)}) d \left(((G_{39})^{(1)}, (T_{39})^{(1)}; (G_{39})^{(2)}, (T_{39})^{(2)}) \right) \end{aligned}$$

And analogous inequalities for G_i and T_i . Taking into account the hypothesis the result follows

Remark 1: The fact that we supposed $(a_{36}'')^{(7)}$ and $(b_{36}'')^{(7)}$ depending also on t can be considered as not conformal with the reality, however we have put this hypothesis in order that we can postulate condition necessary to prove the uniqueness of the solution bounded by $(\widehat{P}_{36})^{(7)} e^{(M_{36})^{(7)}t}$ and $(\widehat{Q}_{36})^{(7)} e^{(M_{36})^{(7)}t}$ respectively of \mathbb{R}_+ . 385

If instead of proving the existence of the solution on \mathbb{R}_+ , we have to prove it only on a compact then it suffices to consider that $(a_i'')^{(7)}$ and $(b_i'')^{(7)}, i = 36, 37, 38$ depend only on T_{37} and respectively on (G_{39}) (and not on t) and hypothesis can be replaced by a usual Lipschitz condition.

Remark 2: There does not exist any t where $G_i(t) = 0$ and $T_i(t) = 0$ 386

From CONCATENATED GLOBAL EQUATIONS it results

$$\begin{aligned} G_i(t) &\geq G_i^0 e^{-\int_0^t \{ (a_i')^{(7)} - (a_i'')^{(7)} (T_{37}(s_{(36)}), s_{(36)}) \} ds_{(36)}} \geq 0 \\ T_i(t) &\geq T_i^0 e^{-(b_i')^{(7)}t} > 0 \text{ for } t > 0 \end{aligned}$$

Definition of $((\widehat{M}_{36})^{(7)})_1, ((\widehat{M}_{36})^{(7)})_2$ and $((\widehat{M}_{36})^{(7)})_3$: 387

Remark 3: if G_{36} is bounded, the same property have also G_{37} and G_{38} . indeed if

$$G_{36} < (\widehat{M}_{36})^{(7)} \text{ it follows } \frac{dG_{37}}{dt} \leq ((\widehat{M}_{36})^{(7)})_1 - (a_{37}')^{(7)} G_{37} \text{ and by integrating}$$

$$G_{37} \leq ((\widehat{M}_{36})^{(7)})_2 = G_{37}^0 + 2(a_{37})^{(7)} ((\widehat{M}_{36})^{(7)})_1 / (a_{37}')^{(7)}$$

In the same way, one can obtain

$$G_{38} \leq ((\widehat{M}_{36})^{(7)})_3 = G_{38}^0 + 2(a_{38})^{(7)} ((\widehat{M}_{36})^{(7)})_2 / (a_{38}')^{(7)}$$

If G_{37} or G_{38} is bounded, the same property follows for G_{36} , G_{38} and G_{36} , G_{37} respectively.

Remark 7: If G_{36} is bounded, from below, the same property holds for G_{37} and G_{38} . The proof is analogous with the preceding one. An analogous property is true if G_{37} is bounded from below. 388

Remark 5: If T_{36} is bounded from below and $\lim_{t \rightarrow \infty} ((b_i'')^{(7)}((G_{39})(t), t)) = (b_{37}')^{(7)}$ then $T_{37} \rightarrow \infty$. 389

Definition of $(m)^{(7)}$ and ε_7 :

Indeed let t_7 be so that for $t > t_7$

$$(b_{37})^{(7)} - (b_i'')^{(7)}((G_{39})(t), t) < \varepsilon_7, T_{36}(t) > (m)^{(7)}$$

Then $\frac{dT_{37}}{dt} \geq (a_{37})^{(7)}(m)^{(7)} - \varepsilon_7 T_{37}$ which leads to 390

$$T_{37} \geq \left(\frac{(a_{37})^{(7)}(m)^{(7)}}{\varepsilon_7} \right) (1 - e^{-\varepsilon_7 t}) + T_{37}^0 e^{-\varepsilon_7 t} \text{ If we take } t \text{ such that } e^{-\varepsilon_7 t} = \frac{1}{2} \text{ it results}$$

$T_{37} \geq \left(\frac{(a_{37})^{(7)}(m)^{(7)}}{2} \right)$, $t = \log \frac{2}{\varepsilon_7}$ By taking now ε_7 sufficiently small one sees that T_{37} is unbounded. The

same property holds for T_{38} if $\lim_{t \rightarrow \infty} (b_{38}'')^{(7)}((G_{39})(t), t) = (b_{38}')^{(7)}$

We now state a more precise theorem about the behaviors at infinity of the solutions

$$-(\sigma_2)^{(2)} \leq -(a'_{16})^{(2)} + (a'_{17})^{(2)} - (a''_{16})^{(2)}(T_{17}, t) + (a''_{17})^{(2)}(T_{17}, t) \leq -(\sigma_1)^{(2)} \quad 391$$

$$-(\tau_2)^{(2)} \leq -(b'_{16})^{(2)} + (b'_{17})^{(2)} - (b''_{16})^{(2)}((G_{19}), t) - (b''_{17})^{(2)}((G_{19}), t) \leq -(\tau_1)^{(2)} \quad 392$$

Definition of $(v_1)^{(2)}, (v_2)^{(2)}, (u_1)^{(2)}, (u_2)^{(2)}$: 393

By $(v_1)^{(2)} > 0, (v_2)^{(2)} < 0$ and respectively $(u_1)^{(2)} > 0, (u_2)^{(2)} < 0$ the roots 394

(a) of the equations $(a_{17})^{(2)}(v^{(2)})^2 + (\sigma_1)^{(2)}v^{(2)} - (a_{16})^{(2)} = 0$ 395

and $(b_{14})^{(2)}(u^{(2)})^2 + (\tau_1)^{(2)}u^{(2)} - (b_{16})^{(2)} = 0$ and 396

Definition of $(\bar{v}_1)^{(2)}, (\bar{v}_2)^{(2)}, (\bar{u}_1)^{(2)}, (\bar{u}_2)^{(2)}$: 397

By $(\bar{v}_1)^{(2)} > 0, (\bar{v}_2)^{(2)} < 0$ and respectively $(\bar{u}_1)^{(2)} > 0, (\bar{u}_2)^{(2)} < 0$ the 398

roots of the equations $(a_{17})^{(2)}(v^{(2)})^2 + (\sigma_2)^{(2)}v^{(2)} - (a_{16})^{(2)} = 0$ 399

and $(b_{17})^{(2)}(u^{(2)})^2 + (\tau_2)^{(2)}u^{(2)} - (b_{16})^{(2)} = 0$ 400

Definition of $(m_1)^{(2)}, (m_2)^{(2)}, (\mu_1)^{(2)}, (\mu_2)^{(2)}$:- 401

(b) If we define $(m_1)^{(2)}, (m_2)^{(2)}, (\mu_1)^{(2)}, (\mu_2)^{(2)}$ by 402

$$(m_2)^{(2)} = (v_0)^{(2)}, (m_1)^{(2)} = (v_1)^{(2)}, \text{ if } (v_0)^{(2)} < (v_1)^{(2)} \quad 403$$

$$(m_2)^{(2)} = (v_1)^{(2)}, (m_1)^{(2)} = (\bar{v}_1)^{(2)}, \text{ if } (v_1)^{(2)} < (v_0)^{(2)} < (\bar{v}_1)^{(2)}, \quad 404$$

and $(v_0)^{(2)} = \frac{G_{16}^0}{G_{17}^0}$

$$(m_2)^{(2)} = (v_1)^{(2)}, (m_1)^{(2)} = (v_0)^{(2)}, \text{ if } (\bar{v}_1)^{(2)} < (v_0)^{(2)} \quad 405$$

and analogously 406

$$(\mu_2)^{(2)} = (u_0)^{(2)}, (\mu_1)^{(2)} = (u_1)^{(2)}, \text{ if } (u_0)^{(2)} < (u_1)^{(2)}$$

$$(\mu_2)^{(2)} = (u_1)^{(2)}, (\mu_1)^{(2)} = (\bar{u}_1)^{(2)}, \text{ if } (u_1)^{(2)} < (u_0)^{(2)} < (\bar{u}_1)^{(2)},$$

and $(u_0)^{(2)} = \frac{T_{16}^0}{T_{17}^0}$

$$(\mu_2)^{(2)} = (u_1)^{(2)}, (\mu_1)^{(2)} = (u_0)^{(2)}, \text{ if } (\bar{u}_1)^{(2)} < (u_0)^{(2)} \quad 407$$

Then the solution satisfies the inequalities 408

$$G_{16}^0 e^{(S_1)^{(2)} - (p_{16})^{(2)} t} \leq G_{16}(t) \leq G_{16}^0 e^{(S_1)^{(2)} t}$$

$(p_i)^{(2)}$ is defined 409

$$\frac{1}{(m_1)^{(2)}} G_{16}^0 e^{(S_1)^{(2)} - (p_{16})^{(2)} t} \leq G_{17}(t) \leq \frac{1}{(m_2)^{(2)}} G_{16}^0 e^{(S_1)^{(2)} t} \quad 410$$

$$\left(\frac{(a_{18})^{(2)} G_{16}^0}{(m_1)^{(2)} ((S_1)^{(2)} - (p_{16})^{(2)} - (S_2)^{(2)})} \left[e^{((S_1)^{(2)} - (p_{16})^{(2)}) t} - e^{-(S_2)^{(2)} t} \right] + G_{18}^0 e^{-(S_2)^{(2)} t} \right) \leq G_{18}(t) \leq \quad 411$$

$$\frac{(a_{18})^{(2)} G_{16}^0}{(m_2)^{(2)} ((S_1)^{(2)} - (a_{18})^{(2)})} \left[e^{(S_1)^{(2)} t} - e^{-(a_{18})^{(2)} t} \right] + G_{18}^0 e^{-(a_{18})^{(2)} t}$$

$$\boxed{T_{16}^0 e^{(R_1)^{(2)} t} \leq T_{16}(t) \leq T_{16}^0 e^{((R_1)^{(2)} + (r_{16})^{(2)}) t} \quad 412$$

$$\frac{1}{(\mu_1)^{(2)}} T_{16}^0 e^{(R_1)^{(2)} t} \leq T_{16}(t) \leq \frac{1}{(\mu_2)^{(2)}} T_{16}^0 e^{((R_1)^{(2)} + (r_{16})^{(2)}) t} \quad 413$$

$$\frac{(b_{18})^{(2)} T_{16}^0}{(\mu_1)^{(2)} ((R_1)^{(2)} - (b_{18})^{(2)})} \left[e^{(R_1)^{(2)} t} - e^{-(b_{18})^{(2)} t} \right] + T_{18}^0 e^{-(b_{18})^{(2)} t} \leq T_{18}(t) \leq \quad 414$$

$$\frac{(a_{18})^{(2)} T_{16}^0}{(\mu_2)^{(2)} ((R_1)^{(2)} + (r_{16})^{(2)} + (R_2)^{(2)})} \left[e^{((R_1)^{(2)} + (r_{16})^{(2)}) t} - e^{-(R_2)^{(2)} t} \right] + T_{18}^0 e^{-(R_2)^{(2)} t}$$

Definition of $(S_1)^{(2)}, (S_2)^{(2)}, (R_1)^{(2)}, (R_2)^{(2)}$:- 415

Where $(S_1)^{(2)} = (a_{16})^{(2)}(m_2)^{(2)} - (a'_{16})^{(2)}$ 416

$$(S_2)^{(2)} = (a_{18})^{(2)} - (p_{18})^{(2)}$$

$$(R_1)^{(2)} = (b_{16})^{(2)}(\mu_2)^{(1)} - (b'_{16})^{(2)} \quad 417$$

$$(R_2)^{(2)} = (b'_{18})^{(2)} - (r_{18})^{(2)}$$

418
419

Behavior of the solutions

If we denote and define

Definition of $(\sigma_1)^{(3)}, (\sigma_2)^{(3)}, (\tau_1)^{(3)}, (\tau_2)^{(3)}$:

- (a) $(\sigma_1)^{(3)}, (\sigma_2)^{(3)}, (\tau_1)^{(3)}, (\tau_2)^{(3)}$ four constants satisfying
 $-(\sigma_2)^{(3)} \leq -(a'_{20})^{(3)} + (a'_{21})^{(3)} - (a''_{20})^{(3)}(T_{21}, t) + (a''_{21})^{(3)}(T_{21}, t) \leq -(\sigma_1)^{(3)}$
 $-(\tau_2)^{(3)} \leq -(b'_{20})^{(3)} + (b'_{21})^{(3)} - (b''_{20})^{(3)}(G, t) - (b''_{21})^{(3)}((G_{23}), t) \leq -(\tau_1)^{(3)}$

Definition of $(v_1)^{(3)}, (v_2)^{(3)}, (u_1)^{(3)}, (u_2)^{(3)}$:

- (b) By $(v_1)^{(3)} > 0, (v_2)^{(3)} < 0$ and respectively $(u_1)^{(3)} > 0, (u_2)^{(3)} < 0$ the roots of the equations

$$(a_{21})^{(3)}(v^{(3)})^2 + (\sigma_1)^{(3)}v^{(3)} - (a_{20})^{(3)} = 0$$

$$\text{and } (b_{21})^{(3)}(u^{(3)})^2 + (\tau_1)^{(3)}u^{(3)} - (b_{20})^{(3)} = 0 \text{ and}$$

By $(\bar{v}_1)^{(3)} > 0, (\bar{v}_2)^{(3)} < 0$ and respectively $(\bar{u}_1)^{(3)} > 0, (\bar{u}_2)^{(3)} < 0$ the roots of the equations $(a_{21})^{(3)}(v^{(3)})^2 + (\sigma_2)^{(3)}v^{(3)} - (a_{20})^{(3)} = 0$

$$\text{and } (b_{21})^{(3)}(u^{(3)})^2 + (\tau_2)^{(3)}u^{(3)} - (b_{20})^{(3)} = 0$$

Definition of $(m_1)^{(3)}, (m_2)^{(3)}, (\mu_1)^{(3)}, (\mu_2)^{(3)}$:-

- (c) If we define $(m_1)^{(3)}, (m_2)^{(3)}, (\mu_1)^{(3)}, (\mu_2)^{(3)}$ by
 $(m_2)^{(3)} = (v_0)^{(3)}, (m_1)^{(3)} = (v_1)^{(3)}$, **if** $(v_0)^{(3)} < (v_1)^{(3)}$
 $(m_2)^{(3)} = (v_1)^{(3)}, (m_1)^{(3)} = (\bar{v}_1)^{(3)}$, **if** $(v_1)^{(3)} < (v_0)^{(3)} < (\bar{v}_1)^{(3)}$,

$$\text{and } (v_0)^{(3)} = \frac{G_{20}^0}{G_{21}^0}$$

$(m_2)^{(3)} = (v_1)^{(3)}, (m_1)^{(3)} = (v_0)^{(3)}$, **if** $(\bar{v}_1)^{(3)} < (v_0)^{(3)}$

and analogously

$$(u_2)^{(3)} = (u_0)^{(3)}, (\mu_1)^{(3)} = (u_1)^{(3)}$$
, **if** $(u_0)^{(3)} < (u_1)^{(3)}$

$$(u_2)^{(3)} = (u_1)^{(3)}, (\mu_1)^{(3)} = (\bar{u}_1)^{(3)}$$
, **if** $(u_1)^{(3)} < (u_0)^{(3)} < (\bar{u}_1)^{(3)}$, and $(u_0)^{(3)} = \frac{T_{20}^0}{T_{21}^0}$

$(\mu_2)^{(3)} = (u_1)^{(3)}, (\mu_1)^{(3)} = (u_0)^{(3)}$, **if** $(\bar{u}_1)^{(3)} < (u_0)^{(3)}$

Then the solution satisfies the inequalities

$$G_{20}^0 e^{((S_1)^{(3)} - (p_{20})^{(3)})t} \leq G_{20}(t) \leq G_{20}^0 e^{(S_1)^{(3)}t}$$

$(p_i)^{(3)}$ is defined

$$\frac{1}{(m_1)^{(3)}} G_{20}^0 e^{((S_1)^{(3)} - (p_{20})^{(3)})t} \leq G_{21}(t) \leq \frac{1}{(m_2)^{(3)}} G_{20}^0 e^{(S_1)^{(3)}t}$$

$$\left(\frac{(a_{22})^{(3)} G_{20}^0}{(m_1)^{(3)}((S_1)^{(3)} - (p_{20})^{(3)} - (S_2)^{(3)})} \left[e^{((S_1)^{(3)} - (p_{20})^{(3)})t} - e^{-(S_2)^{(3)}t} \right] + G_{22}^0 e^{-(S_2)^{(3)}t} \right) \leq G_{22}(t) \leq$$

$$\frac{(a_{22})^{(3)} G_{20}^0}{(m_2)^{(3)}((S_1)^{(3)} - (a_{22})^{(3)})} \left[e^{(S_1)^{(3)}t} - e^{-(a_{22})^{(3)}t} \right] + G_{22}^0 e^{-(a_{22})^{(3)}t}$$

$$\boxed{T_{20}^0 e^{(R_1)^{(3)}t} \leq T_{20}(t) \leq T_{20}^0 e^{((R_1)^{(3)} + (r_{20})^{(3)})t}}$$

$$\frac{1}{(\mu_1)^{(3)}} T_{20}^0 e^{(R_1)^{(3)}t} \leq T_{20}(t) \leq \frac{1}{(\mu_2)^{(3)}} T_{20}^0 e^{((R_1)^{(3)} + (r_{20})^{(3)})t}$$

$$\frac{(b_{22})^{(3)} T_{20}^0}{(\mu_1)^{(3)}((R_1)^{(3)} - (b_{22})^{(3)})} \left[e^{(R_1)^{(3)}t} - e^{-(b_{22})^{(3)}t} \right] + T_{22}^0 e^{-(b_{22})^{(3)}t} \leq T_{22}(t) \leq$$

$$\frac{(a_{22})^{(3)} T_{20}^0}{(\mu_2)^{(3)}((R_1)^{(3)} + (r_{20})^{(3)} + (R_2)^{(3)})} \left[e^{((R_1)^{(3)} + (r_{20})^{(3)})t} - e^{-(R_2)^{(3)}t} \right] + T_{22}^0 e^{-(R_2)^{(3)}t}$$

Definition of $(S_1)^{(3)}, (S_2)^{(3)}, (R_1)^{(3)}, (R_2)^{(3)}$:-

$$\text{Where } (S_1)^{(3)} = (a_{20})^{(3)}(m_2)^{(3)} - (a'_{20})^{(3)}$$

$$(S_2)^{(3)} = (a_{22})^{(3)} - (p_{22})^{(3)}$$

$$(R_1)^{(3)} = (b_{20})^{(3)}(\mu_2)^{(3)} - (b'_{20})^{(3)}$$

$$(R_2)^{(3)} = (b_{22})^{(3)} - (r_{22})^{(3)}$$

430
431
432

If we denote and define

Definition of $(\sigma_1)^{(4)}, (\sigma_2)^{(4)}, (\tau_1)^{(4)}, (\tau_2)^{(4)}$:

- (d) $(\sigma_1)^{(4)}, (\sigma_2)^{(4)}, (\tau_1)^{(4)}, (\tau_2)^{(4)}$ four constants satisfying

$$-(\sigma_2)^{(4)} \leq -(a'_{24})^{(4)} + (a'_{25})^{(4)} - (a''_{24})^{(4)}(T_{25}, t) + (a''_{25})^{(4)}(T_{25}, t) \leq -(\sigma_1)^{(4)}$$

$$-(\tau_2)^{(4)} \leq -(b_{24}')^{(4)} + (b_{25}')^{(4)} - (b_{24}'')^{(4)}((G_{27}), t) - (b_{25}'')^{(4)}((G_{27}), t) \leq -(\tau_1)^{(4)}$$

Definition of $(v_1)^{(4)}, (v_2)^{(4)}, (u_1)^{(4)}, (u_2)^{(4)}, v^{(4)}, u^{(4)}$: 433

(e) By $(v_1)^{(4)} > 0, (v_2)^{(4)} < 0$ and respectively $(u_1)^{(4)} > 0, (u_2)^{(4)} < 0$ the roots of the equations
 $(a_{25})^{(4)}(v^{(4)})^2 + (\sigma_1)^{(4)}v^{(4)} - (a_{24})^{(4)} = 0$
 and $(b_{25})^{(4)}(u^{(4)})^2 + (\tau_1)^{(4)}u^{(4)} - (b_{24})^{(4)} = 0$ and

Definition of $(\bar{v}_1)^{(4)}, (\bar{v}_2)^{(4)}, (\bar{u}_1)^{(4)}, (\bar{u}_2)^{(4)}$: 434
435

By $(\bar{v}_1)^{(4)} > 0, (\bar{v}_2)^{(4)} < 0$ and respectively $(\bar{u}_1)^{(4)} > 0, (\bar{u}_2)^{(4)} < 0$ the roots of the equations $(a_{25})^{(4)}(v^{(4)})^2 + (\sigma_2)^{(4)}v^{(4)} - (a_{24})^{(4)} = 0$
 and $(b_{25})^{(4)}(u^{(4)})^2 + (\tau_2)^{(4)}u^{(4)} - (b_{24})^{(4)} = 0$

Definition of $(m_1)^{(4)}, (m_2)^{(4)}, (\mu_1)^{(4)}, (\mu_2)^{(4)}, (v_0)^{(4)}$:- 436

(f) If we define $(m_1)^{(4)}, (m_2)^{(4)}, (\mu_1)^{(4)}, (\mu_2)^{(4)}$ by

$$(m_2)^{(4)} = (v_0)^{(4)}, (m_1)^{(4)} = (v_1)^{(4)}, \text{ if } (v_0)^{(4)} < (v_1)^{(4)}$$

$$(m_2)^{(4)} = (v_1)^{(4)}, (m_1)^{(4)} = (\bar{v}_1)^{(4)}, \text{ if } (v_4)^{(4)} < (v_0)^{(4)} < (\bar{v}_1)^{(4)},$$

and $(v_0)^{(4)} = \frac{G_{24}^0}{G_{25}^0}$

$$(m_2)^{(4)} = (v_4)^{(4)}, (m_1)^{(4)} = (v_0)^{(4)}, \text{ if } (\bar{v}_4)^{(4)} < (v_0)^{(4)}$$

and analogously 437
438

$$(\mu_2)^{(4)} = (u_0)^{(4)}, (\mu_1)^{(4)} = (u_1)^{(4)}, \text{ if } (u_0)^{(4)} < (u_1)^{(4)}$$

$$(\mu_2)^{(4)} = (u_1)^{(4)}, (\mu_1)^{(4)} = (\bar{u}_1)^{(4)}, \text{ if } (u_1)^{(4)} < (u_0)^{(4)} < (\bar{u}_1)^{(4)},$$

and $(u_0)^{(4)} = \frac{T_{24}^0}{T_{25}^0}$

$(\mu_2)^{(4)} = (u_1)^{(4)}, (\mu_1)^{(4)} = (u_0)^{(4)}, \text{ if } (\bar{u}_1)^{(4)} < (u_0)^{(4)}$ where $(u_1)^{(4)}, (\bar{u}_1)^{(4)}$ are defined respectively

Then the solution satisfies the inequalities 439

$$G_{24}^0 e^{((S_1)^{(4)} - (p_{24})^{(4)})t} \leq G_{24}(t) \leq G_{24}^0 e^{(S_1)^{(4)}t}$$

where $(p_i)^{(4)}$ is defined

$$\frac{1}{(m_1)^{(4)}} G_{24}^0 e^{((S_1)^{(4)} - (p_{24})^{(4)})t} \leq G_{25}(t) \leq \frac{1}{(m_2)^{(4)}} G_{24}^0 e^{(S_1)^{(4)}t}$$

$$\left(\frac{(a_{26})^{(4)} G_{24}^0}{(m_1)^{(4)} ((S_1)^{(4)} - (p_{24})^{(4)} - (S_2)^{(4)})} \right) \left[e^{((S_1)^{(4)} - (p_{24})^{(4)})t} - e^{-(S_2)^{(4)}t} \right] + G_{26}^0 e^{-(S_2)^{(4)}t} \leq G_{26}(t) \leq (a_{26})^{(4)} G_{24}^0 (m_2)^{(4)} (S_1)^{(4)} - (a_{26}')^{(4)} e^{(S_1)^{(4)}t} + G_{26}^0 e^{-(a_{26}')^{(4)}t}$$

$$\boxed{T_{24}^0 e^{(R_1)^{(4)}t} \leq T_{24}(t) \leq T_{24}^0 e^{((R_1)^{(4)} + (r_{24})^{(4)})t}}$$

$$\frac{1}{(\mu_1)^{(4)}} T_{24}^0 e^{(R_1)^{(4)}t} \leq T_{24}(t) \leq \frac{1}{(\mu_2)^{(4)}} T_{24}^0 e^{((R_1)^{(4)} + (r_{24})^{(4)})t}$$

$$\frac{(b_{26})^{(4)} T_{24}^0}{(\mu_1)^{(4)} ((R_1)^{(4)} - (b_{26}')^{(4)})} \left[e^{(R_1)^{(4)}t} - e^{-(b_{26}')^{(4)}t} \right] + T_{26}^0 e^{-(b_{26}')^{(4)}t} \leq T_{26}(t) \leq$$

$$\frac{(a_{26})^{(4)}T_{24}^0}{(\mu_2)^{(4)}((R_1)^{(4)}+(r_{24})^{(4)}+(R_2)^{(4)})} \left[e^{((R_1)^{(4)}+(r_{24})^{(4)})t} - e^{-(R_2)^{(4)}t} \right] + T_{26}^0 e^{-(R_2)^{(4)}t}$$

Definition of $(S_1)^{(4)}, (S_2)^{(4)}, (R_1)^{(4)}, (R_2)^{(4)}$:- 452

Where $(S_1)^{(4)} = (a_{24})^{(4)}(m_2)^{(4)} - (a'_{24})^{(4)}$

$$(S_2)^{(4)} = (a_{26})^{(4)} - (p_{26})^{(4)}$$

$$(R_1)^{(4)} = (b_{24})^{(4)}(\mu_2)^{(4)} - (b'_{24})^{(4)}$$

$$(R_2)^{(4)} = (b'_{26})^{(4)} - (r_{26})^{(4)} \span style="float: right;">453$$

Behavior of the solutions 454

If we denote and define

Definition of $(\sigma_1)^{(5)}, (\sigma_2)^{(5)}, (\tau_1)^{(5)}, (\tau_2)^{(5)}$:

(g) $(\sigma_1)^{(5)}, (\sigma_2)^{(5)}, (\tau_1)^{(5)}, (\tau_2)^{(5)}$ four constants satisfying

$$-(\sigma_2)^{(5)} \leq -(a'_{28})^{(5)} + (a'_{29})^{(5)} - (a''_{28})^{(5)}(T_{29}, t) + (a''_{29})^{(5)}(T_{29}, t) \leq -(\sigma_1)^{(5)}$$

$$-(\tau_2)^{(5)} \leq -(b'_{28})^{(5)} + (b'_{29})^{(5)} - (b''_{28})^{(5)}((G_{31}), t) - (b''_{29})^{(5)}((G_{31}), t) \leq -(\tau_1)^{(5)}$$

Definition of $(v_1)^{(5)}, (v_2)^{(5)}, (u_1)^{(5)}, (u_2)^{(5)}, v^{(5)}, u^{(5)}$: 455

(h) By $(v_1)^{(5)} > 0, (v_2)^{(5)} < 0$ and respectively $(u_1)^{(5)} > 0, (u_2)^{(5)} < 0$ the roots of the equations

$$(a_{29})^{(5)}(v^{(5)})^2 + (\sigma_1)^{(5)}v^{(5)} - (a_{28})^{(5)} = 0$$

$$\text{and } (b_{29})^{(5)}(u^{(5)})^2 + (\tau_1)^{(5)}u^{(5)} - (b_{28})^{(5)} = 0 \text{ and}$$

Definition of $(\bar{v}_1)^{(5)}, (\bar{v}_2)^{(5)}, (\bar{u}_1)^{(5)}, (\bar{u}_2)^{(5)}$: 456

By $(\bar{v}_1)^{(5)} > 0, (\bar{v}_2)^{(5)} < 0$ and respectively $(\bar{u}_1)^{(5)} > 0, (\bar{u}_2)^{(5)} < 0$ the

roots of the equations $(a_{29})^{(5)}(v^{(5)})^2 + (\sigma_2)^{(5)}v^{(5)} - (a_{28})^{(5)} = 0$

and $(b_{29})^{(5)}(u^{(5)})^2 + (\tau_2)^{(5)}u^{(5)} - (b_{28})^{(5)} = 0$

Definition of $(m_1)^{(5)}, (m_2)^{(5)}, (\mu_1)^{(5)}, (\mu_2)^{(5)}, (v_0)^{(5)}$:-

(i) If we define $(m_1)^{(5)}, (m_2)^{(5)}, (\mu_1)^{(5)}, (\mu_2)^{(5)}$ by

$$(m_2)^{(5)} = (v_0)^{(5)}, (m_1)^{(5)} = (v_1)^{(5)}, \text{ if } (v_0)^{(5)} < (v_1)^{(5)}$$

$$(m_2)^{(5)} = (v_1)^{(5)}, (m_1)^{(5)} = (\bar{v}_1)^{(5)}, \text{ if } (v_1)^{(5)} < (v_0)^{(5)} < (\bar{v}_1)^{(5)},$$

$$\text{and } (v_0)^{(5)} = \frac{a_{28}^0}{a_{29}^0}$$

$$(m_2)^{(5)} = (v_1)^{(5)}, (m_1)^{(5)} = (v_0)^{(5)}, \text{ if } (\bar{v}_1)^{(5)} < (v_0)^{(5)}$$

and analogously 457

$$(\mu_2)^{(5)} = (u_0)^{(5)}, (\mu_1)^{(5)} = (u_1)^{(5)}, \text{ if } (u_0)^{(5)} < (u_1)^{(5)}$$

$$(\mu_2)^{(5)} = (u_1)^{(5)}, (\mu_1)^{(5)} = (\bar{u}_1)^{(5)}, \text{ if } (u_1)^{(5)} < (u_0)^{(5)} < (\bar{u}_1)^{(5)},$$

$$\text{and } (u_0)^{(5)} = \frac{T_{28}^0}{T_{29}^0}$$

$(\mu_2)^{(5)} = (u_1)^{(5)}, (\mu_1)^{(5)} = (u_0)^{(5)}, \text{ if } (\bar{u}_1)^{(5)} < (u_0)^{(5)}$ where $(u_1)^{(5)}, (\bar{u}_1)^{(5)}$ are defined respectively

Then the solution satisfies the inequalities 458

$$G_{28}^0 e^{((S_1)^{(5)} - (p_{28})^{(5)})t} \leq G_{28}(t) \leq G_{28}^0 e^{(S_1)^{(5)}t}$$

where $(p_i)^{(5)}$ is defined

$$\frac{1}{(m_5)^{(5)}} G_{28}^0 e^{((S_1)^{(5)} - (p_{28})^{(5)})t} \leq G_{29}(t) \leq \frac{1}{(m_2)^{(5)}} G_{28}^0 e^{(S_1)^{(5)}t} \quad 459$$

$$\left(\frac{(a_{30})^{(5)} G_{28}^0}{(m_1)^{(5)} ((S_1)^{(5)} - (p_{28})^{(5)} - (S_2)^{(5)})} \left[e^{((S_1)^{(5)} - (p_{28})^{(5)})t} - e^{-(S_2)^{(5)}t} \right] + G_{30}^0 e^{-(S_2)^{(5)}t} \right) \leq G_{30}(t) \leq \quad 460$$

$$(a_{30})^{(5)} G_{28}^0 (m_2)^{(5)} (S_1)^{(5)} - (a_{30})^{(5)} e^{(S_1)^{(5)}t} - e^{-(a_{30})^{(5)}t} + G_{30}^0 e^{-(a_{30})^{(5)}t} \quad 461$$

$$\boxed{T_{28}^0 e^{(R_1)^{(5)}t} \leq T_{28}(t) \leq T_{28}^0 e^{((R_1)^{(5)} + (r_{28})^{(5)})t}} \quad 462$$

$$\frac{1}{(\mu_1)^{(5)}} T_{28}^0 e^{(R_1)^{(5)}t} \leq T_{28}(t) \leq \frac{1}{(\mu_2)^{(5)}} T_{28}^0 e^{((R_1)^{(5)} + (r_{28})^{(5)})t} \quad 463$$

$$\frac{(b_{30})^{(5)} T_{28}^0}{(\mu_1)^{(5)} ((R_1)^{(5)} - (b_{30})^{(5)})} \left[e^{(R_1)^{(5)}t} - e^{-(b_{30})^{(5)}t} \right] + T_{30}^0 e^{-(b_{30})^{(5)}t} \leq T_{30}(t) \leq \quad 464$$

$$\frac{(a_{30})^{(5)} T_{28}^0}{(\mu_2)^{(5)} ((R_1)^{(5)} + (r_{28})^{(5)} + (R_2)^{(5)})} \left[e^{((R_1)^{(5)} + (r_{28})^{(5)})t} - e^{-(R_2)^{(5)}t} \right] + T_{30}^0 e^{-(R_2)^{(5)}t} \quad 465$$

Definition of $(S_1)^{(5)}, (S_2)^{(5)}, (R_1)^{(5)}, (R_2)^{(5)}$:- 465

$$\text{Where } (S_1)^{(5)} = (a_{28})^{(5)} (m_2)^{(5)} - (a'_{28})^{(5)}$$

$$(S_2)^{(5)} = (a_{30})^{(5)} - (p_{30})^{(5)}$$

$$(R_1)^{(5)} = (b_{28})^{(5)} (\mu_2)^{(5)} - (b'_{28})^{(5)}$$

$$(R_2)^{(5)} = (b'_{30})^{(5)} - (r_{30})^{(5)}$$

Behavior of the solutions 466

If we denote and define

Definition of $(\sigma_1)^{(6)}, (\sigma_2)^{(6)}, (\tau_1)^{(6)}, (\tau_2)^{(6)}$:

(j) $(\sigma_1)^{(6)}, (\sigma_2)^{(6)}, (\tau_1)^{(6)}, (\tau_2)^{(6)}$ four constants satisfying

$$-(\sigma_2)^{(6)} \leq -(a'_{32})^{(6)} + (a'_{33})^{(6)} - (a''_{32})^{(6)}(T_{33}, t) + (a''_{33})^{(6)}(T_{33}, t) \leq -(\sigma_1)^{(6)}$$

$$-(\tau_2)^{(6)} \leq -(b'_{32})^{(6)} + (b'_{33})^{(6)} - (b''_{32})^{(6)}((G_{35}), t) - (b''_{33})^{(6)}((G_{35}), t) \leq -(\tau_1)^{(6)}$$

Definition of $(v_1)^{(6)}, (v_2)^{(6)}, (u_1)^{(6)}, (u_2)^{(6)}, v^{(6)}, u^{(6)}$: 467

(k) By $(v_1)^{(6)} > 0, (v_2)^{(6)} < 0$ and respectively $(u_1)^{(6)} > 0, (u_2)^{(6)} < 0$ the roots of the equations

$$(a_{33})^{(6)} (v^{(6)})^2 + (\sigma_1)^{(6)} v^{(6)} - (a_{32})^{(6)} = 0$$

$$\text{and } (b_{33})^{(6)} (u^{(6)})^2 + (\tau_1)^{(6)} u^{(6)} - (b_{32})^{(6)} = 0 \text{ and}$$

Definition of $(\bar{v}_1)^{(6)}, (\bar{v}_2)^{(6)}, (\bar{u}_1)^{(6)}, (\bar{u}_2)^{(6)}$: 468

By $(\bar{v}_1)^{(6)} > 0, (\bar{v}_2)^{(6)} < 0$ and respectively $(\bar{u}_1)^{(6)} > 0, (\bar{u}_2)^{(6)} < 0$ the roots of the equations $(a_{33})^{(6)} (v^{(6)})^2 + (\sigma_2)^{(6)} v^{(6)} - (a_{32})^{(6)} = 0$

$$\text{and } (b_{33})^{(6)} (u^{(6)})^2 + (\tau_2)^{(6)} u^{(6)} - (b_{32})^{(6)} = 0$$

Definition of $(m_1)^{(6)}, (m_2)^{(6)}, (\mu_1)^{(6)}, (\mu_2)^{(6)}, (v_0)^{(6)}$:-

(l) If we define $(m_1)^{(6)}, (m_2)^{(6)}, (\mu_1)^{(6)}, (\mu_2)^{(6)}$ by

$$(m_2)^{(6)} = (v_0)^{(6)}, (m_1)^{(6)} = (v_1)^{(6)}, \text{ if } (v_0)^{(6)} < (v_1)^{(6)}$$

$$(m_2)^{(6)} = (v_1)^{(6)}, (m_1)^{(6)} = (\bar{v}_6)^{(6)}, \text{ if } (v_1)^{(6)} < (v_0)^{(6)} < (\bar{v}_1)^{(6)},$$

$$\text{and } (v_0)^{(6)} = \frac{G_{32}^0}{G_{33}^0}$$

$$(m_2)^{(6)} = (v_1)^{(6)}, (m_1)^{(6)} = (v_0)^{(6)}, \text{ if } (\bar{v}_1)^{(6)} < (v_0)^{(6)}$$

and analogously

471

$$(\mu_2)^{(6)} = (u_0)^{(6)}, (\mu_1)^{(6)} = (u_1)^{(6)}, \text{ if } (u_0)^{(6)} < (u_1)^{(6)}$$

$$(\mu_2)^{(6)} = (u_1)^{(6)}, (\mu_1)^{(6)} = (\bar{u}_1)^{(6)}, \text{ if } (u_1)^{(6)} < (u_0)^{(6)} < (\bar{u}_1)^{(6)},$$

$$\text{and } (u_0)^{(6)} = \frac{T_{32}^0}{T_{33}^0}$$

$(\mu_2)^{(6)} = (u_1)^{(6)}, (\mu_1)^{(6)} = (u_0)^{(6)}, \text{ if } (\bar{u}_1)^{(6)} < (u_0)^{(6)}$ where $(u_1)^{(6)}, (\bar{u}_1)^{(6)}$ are defined respectively

Then the solution satisfies the inequalities

472

$$G_{32}^0 e^{((S_1)^{(6)} - (p_{32})^{(6)})t} \leq G_{32}(t) \leq G_{32}^0 e^{(S_1)^{(6)}t}$$

where $(p_i)^{(6)}$ is defined

$$\frac{1}{(m_1)^{(6)}} G_{32}^0 e^{((S_1)^{(6)} - (p_{32})^{(6)})t} \leq G_{33}(t) \leq \frac{1}{(m_2)^{(6)}} G_{32}^0 e^{(S_1)^{(6)}t}$$

473

$$\left(\frac{(a_{34})^{(6)} G_{32}^0}{(m_1)^{(6)} ((S_1)^{(6)} - (p_{32})^{(6)} - (S_2)^{(6)})} \right) \left[e^{((S_1)^{(6)} - (p_{32})^{(6)})t} - e^{-(S_2)^{(6)}t} \right] + G_{34}^0 e^{-(S_2)^{(6)}t} \leq G_{34}(t) \leq (a_{34})^{(6)} G_{32}^0 (m_2)^{(6)} (S_1)^{(6)} - (a_{34}')^{(6)} e^{(S_1)^{(6)}t} + G_{34}^0 e^{-(a_{34}')^{(6)}t}$$

474

$$T_{32}^0 e^{(R_1)^{(6)}t} \leq T_{32}(t) \leq T_{32}^0 e^{((R_1)^{(6)} + (r_{32})^{(6)})t}$$

475

$$\frac{1}{(\mu_1)^{(6)}} T_{32}^0 e^{(R_1)^{(6)}t} \leq T_{32}(t) \leq \frac{1}{(\mu_2)^{(6)}} T_{32}^0 e^{((R_1)^{(6)} + (r_{32})^{(6)})t}$$

476

$$\frac{(b_{34})^{(6)} T_{32}^0}{(\mu_1)^{(6)} ((R_1)^{(6)} - (b_{34}')^{(6)})} \left[e^{(R_1)^{(6)}t} - e^{-(b_{34}')^{(6)}t} \right] + T_{34}^0 e^{-(b_{34}')^{(6)}t} \leq T_{34}(t) \leq$$

477

$$\frac{(a_{34})^{(6)} T_{32}^0}{(\mu_2)^{(6)} ((R_1)^{(6)} + (r_{32})^{(6)} + (R_2)^{(6)})} \left[e^{((R_1)^{(6)} + (r_{32})^{(6)})t} - e^{-(R_2)^{(6)}t} \right] + T_{34}^0 e^{-(R_2)^{(6)}t}$$

Definition of $(S_1)^{(6)}, (S_2)^{(6)}, (R_1)^{(6)}, (R_2)^{(6)}$:-

478

$$\text{Where } (S_1)^{(6)} = (a_{32})^{(6)} (m_2)^{(6)} - (a_{32}')^{(6)}$$

$$(S_2)^{(6)} = (a_{34})^{(6)} - (p_{34})^{(6)}$$

$$(R_1)^{(6)} = (b_{32})^{(6)} (\mu_2)^{(6)} - (b_{32}')^{(6)}$$

$$(R_2)^{(6)} = (b_{34}')^{(6)} - (r_{34})^{(6)}$$

479

If we denote and define

Definition of $(\sigma_1)^{(7)}, (\sigma_2)^{(7)}, (\tau_1)^{(7)}, (\tau_2)^{(7)}$:

(m) $(\sigma_1)^{(7)}, (\sigma_2)^{(7)}, (\tau_1)^{(7)}, (\tau_2)^{(7)}$ four constants satisfying

$$-(\sigma_2)^{(7)} \leq -(a_{36}')^{(7)} + (a_{37}')^{(7)} - (a_{36}'')^{(7)} (T_{37}, t) + (a_{37}'')^{(7)} (T_{37}, t) \leq -(\sigma_1)^{(7)}$$

$$-(\tau_2)^{(7)} \leq -(b_{36}')^{(7)} + (b_{37}')^{(7)} - (b_{36}'')^{(7)} ((G_{39}), t) - (b_{37}'')^{(7)} ((G_{39}), t) \leq -(\tau_1)^{(7)}$$

Definition of $(v_1)^{(7)}, (v_2)^{(7)}, (u_1)^{(7)}, (u_2)^{(7)}, v^{(7)}, u^{(7)}$:

480

(n) By $(v_1)^{(7)} > 0, (v_2)^{(7)} < 0$ and respectively $(u_1)^{(7)} > 0, (u_2)^{(7)} < 0$ the roots of the equations

$$(a_{37})^{(7)} (v^{(7)})^2 + (\sigma_1)^{(7)} v^{(7)} - (a_{36})^{(7)} = 0$$

481

$$\text{and } (b_{37})^{(7)} (u^{(7)})^2 + (\tau_1)^{(7)} u^{(7)} - (b_{36})^{(7)} = 0 \text{ and}$$

Definition of $(\bar{v}_1)^{(7)}, (\bar{v}_2)^{(7)}, (\bar{u}_1)^{(7)}, (\bar{u}_2)^{(7)}$:

By $(\bar{v}_1)^{(7)} > 0, (\bar{v}_2)^{(7)} < 0$ and respectively $(\bar{u}_1)^{(7)} > 0, (\bar{u}_2)^{(7)} < 0$ the

roots of the equations $(a_{37})^{(7)}(v^{(7)})^2 + (\sigma_2)^{(7)}v^{(7)} - (a_{36})^{(7)} = 0$

and $(b_{37})^{(7)}(u^{(7)})^2 + (\tau_2)^{(7)}u^{(7)} - (b_{36})^{(7)} = 0$

Definition of $(m_1)^{(7)}, (m_2)^{(7)}, (\mu_1)^{(7)}, (\mu_2)^{(7)}, (v_0)^{(7)}$:-

(o) If we define $(m_1)^{(7)}, (m_2)^{(7)}, (\mu_1)^{(7)}, (\mu_2)^{(7)}$ by

$$(m_2)^{(7)} = (v_0)^{(7)}, (m_1)^{(7)} = (v_1)^{(7)}, \text{ if } (v_0)^{(7)} < (v_1)^{(7)}$$

$$(m_2)^{(7)} = (v_1)^{(7)}, (m_1)^{(7)} = (\bar{v}_1)^{(7)}, \text{ if } (v_1)^{(7)} < (v_0)^{(7)} < (\bar{v}_1)^{(7)},$$

$$\text{and } (v_0)^{(7)} = \frac{G_{36}^0}{G_{37}^0}$$

$$(m_2)^{(7)} = (v_1)^{(7)}, (m_1)^{(7)} = (v_0)^{(7)}, \text{ if } (\bar{v}_1)^{(7)} < (v_0)^{(7)}$$

and analogously

$$(\mu_2)^{(7)} = (u_0)^{(7)}, (\mu_1)^{(7)} = (u_1)^{(7)}, \text{ if } (u_0)^{(7)} < (u_1)^{(7)}$$

$$(\mu_2)^{(7)} = (u_1)^{(7)}, (\mu_1)^{(7)} = (\bar{u}_1)^{(7)}, \text{ if } (u_1)^{(7)} < (u_0)^{(7)} < (\bar{u}_1)^{(7)},$$

$$\text{and } (u_0)^{(7)} = \frac{T_{36}^0}{T_{37}^0}$$

$$(\mu_2)^{(7)} = (u_1)^{(7)}, (\mu_1)^{(7)} = (u_0)^{(7)}, \text{ if } (\bar{u}_1)^{(7)} < (u_0)^{(7)} \text{ where } (u_1)^{(7)}, (\bar{u}_1)^{(7)}$$

are defined respectively

Then the solution satisfies the inequalities

$$G_{36}^0 e^{((S_1)^{(7)} - (p_{36})^{(7)})t} \leq G_{36}(t) \leq G_{36}^0 e^{(S_1)^{(7)}t}$$

where $(p_i)^{(7)}$ is defined

$$\frac{1}{(m_7)^{(7)}} G_{36}^0 e^{((S_1)^{(7)} - (p_{36})^{(7)})t} \leq G_{37}(t) \leq \frac{1}{(m_2)^{(7)}} G_{36}^0 e^{(S_1)^{(7)}t}$$

(

$$\frac{(a_{38})^{(7)} G_{36}^0}{(m_1)^{(7)}((S_1)^{(7)} - (p_{36})^{(7)} - (S_2)^{(7)})} \left[e^{((S_1)^{(7)} - (p_{36})^{(7)})t} - e^{-(S_2)^{(7)}t} \right] + G_{38}^0 e^{-(S_2)^{(7)}t} \leq G_{38}(t) \leq$$

$$\frac{(a_{38})^{(7)} G_{36}^0}{(m_2)^{(7)}((S_1)^{(7)} - (a_{38})^{(7)})} \left[e^{(S_1)^{(7)}t} - e^{-(a_{38})^{(7)}t} \right] + G_{38}^0 e^{-(a_{38})^{(7)}t}$$

$$\frac{T_{36}^0 e^{(R_1)^{(7)}t} \leq T_{36}(t) \leq T_{36}^0 e^{((R_1)^{(7)} + (r_{36})^{(7)})t}$$

$$\frac{1}{(\mu_1)^{(7)}} T_{36}^0 e^{(R_1)^{(7)}t} \leq T_{36}(t) \leq \frac{1}{(\mu_2)^{(7)}} T_{36}^0 e^{((R_1)^{(7)} + (r_{36})^{(7)})t}$$

$$\frac{(b_{38})^{(7)} T_{36}^0}{(\mu_1)^{(7)}((R_1)^{(7)} - (b_{38})^{(7)})} \left[e^{(R_1)^{(7)}t} - e^{-(b_{38})^{(7)}t} \right] + T_{38}^0 e^{-(b_{38})^{(7)}t} \leq T_{38}(t) \leq$$

$$\frac{(a_{38})^{(7)} T_{36}^0}{(\mu_2)^{(7)}((R_1)^{(7)} + (r_{36})^{(7)} + (R_2)^{(7)})} \left[e^{((R_1)^{(7)} + (r_{36})^{(7)})t} - e^{-(R_2)^{(7)}t} \right] + T_{38}^0 e^{-(R_2)^{(7)}t}$$

Definition of $(S_1)^{(7)}, (S_2)^{(7)}, (R_1)^{(7)}, (R_2)^{(7)}$:-

$$\text{Where } (S_1)^{(7)} = (a_{36})^{(7)}(m_2)^{(7)} - (a'_{36})^{(7)}$$

$$(S_2)^{(7)} = (a_{38})^{(7)} - (p_{38})^{(7)}$$

$$(R_1)^{(7)} = (b_{36})^{(7)}(\mu_2)^{(7)} - (b'_{36})^{(7)}$$

$$(R_2)^{(7)} = (b_{38})^{(7)} - (r_{38})^{(7)}$$

From GLOBAL EQUATIONS we obtain

$$\frac{dv^{(7)}}{dt} = (a_{36})^{(7)} - \left((a'_{36})^{(7)} - (a'_{37})^{(7)} + (a''_{36})^{(7)}(T_{37}, t) \right) -$$

Definition of $v^{(7)}$:-
$$v^{(7)} = \frac{G_{36}}{G_{37}}$$

It follows

$$- \left((a_{37})^{(7)}(v^{(7)})^2 + (\sigma_2)^{(7)}v^{(7)} - (a_{36})^{(7)} \right) \leq \frac{dv^{(7)}}{dt} \leq - \left((a_{37})^{(7)}(v^{(7)})^2 + (\sigma_1)^{(7)}v^{(7)} - (a_{36})^{(7)} \right)$$

From which one obtains

Definition of $(\bar{v}_1)^{(7)}, (v_0)^{(7)}$:-

(a) For $0 < \left(v_0 \right)^{(7)} = \frac{G_{36}^0}{G_{37}^0} < (v_1)^{(7)} < (\bar{v}_1)^{(7)}$

$$v^{(7)}(t) \geq \frac{(v_1)^{(7)} + (C)^{(7)}(v_2)^{(7)} e^{[-(a_{37})^{(7)}(v_1)^{(7)} - (v_0)^{(7)}]t}}{1 + (C)^{(7)} e^{[-(a_{37})^{(7)}(v_1)^{(7)} - (v_0)^{(7)}]t}}, \quad (C)^{(7)} = \frac{(v_1)^{(7)} - (v_0)^{(7)}}{(v_0)^{(7)} - (v_2)^{(7)}}$$

it follows $(v_0)^{(7)} \leq v^{(7)}(t) \leq (v_1)^{(7)}$

In the same manner , we get

493

$$v^{(7)}(t) \leq \frac{(\bar{v}_1)^{(7)} + (\bar{C})^{(7)}(\bar{v}_2)^{(7)} e^{[-(a_{37})^{(7)}(\bar{v}_1)^{(7)} - (\bar{v}_2)^{(7)}]t}}{1 + (\bar{C})^{(7)} e^{[-(a_{37})^{(7)}(\bar{v}_1)^{(7)} - (\bar{v}_2)^{(7)}]t}}, \quad (\bar{C})^{(7)} = \frac{(\bar{v}_1)^{(7)} - (v_0)^{(7)}}{(v_0)^{(7)} - (\bar{v}_2)^{(7)}}$$

From which we deduce $(v_0)^{(7)} \leq v^{(7)}(t) \leq (\bar{v}_1)^{(7)}$

(b) If $0 < (v_1)^{(7)} < (v_0)^{(7)} = \frac{G_{36}^0}{G_{37}^0} < (\bar{v}_1)^{(7)}$ we find like in the previous case,

494

$$(v_1)^{(7)} \leq \frac{(v_1)^{(7)} + (C)^{(7)}(v_2)^{(7)} e^{[-(a_{37})^{(7)}(v_1)^{(7)} - (v_2)^{(7)}]t}}{1 + (C)^{(7)} e^{[-(a_{37})^{(7)}(v_1)^{(7)} - (v_2)^{(7)}]t}} \leq v^{(7)}(t) \leq \frac{(\bar{v}_1)^{(7)} + (\bar{C})^{(7)}(\bar{v}_2)^{(7)} e^{[-(a_{37})^{(7)}(\bar{v}_1)^{(7)} - (\bar{v}_2)^{(7)}]t}}{1 + (\bar{C})^{(7)} e^{[-(a_{37})^{(7)}(\bar{v}_1)^{(7)} - (\bar{v}_2)^{(7)}]t}} \leq (\bar{v}_1)^{(7)}$$

(c) If $0 < (v_1)^{(7)} \leq (\bar{v}_1)^{(7)} \leq \left(v_0 \right)^{(7)} = \frac{G_{36}^0}{G_{37}^0}$, we obtain

495

$$(v_1)^{(7)} \leq v^{(7)}(t) \leq \frac{(\bar{v}_1)^{(7)} + (\bar{C})^{(7)}(\bar{v}_2)^{(7)} e^{[-(a_{37})^{(7)}(\bar{v}_1)^{(7)} - (\bar{v}_2)^{(7)}]t}}{1 + (\bar{C})^{(7)} e^{[-(a_{37})^{(7)}(\bar{v}_1)^{(7)} - (\bar{v}_2)^{(7)}]t}} \leq (v_0)^{(7)}$$

And so with the notation of the first part of condition (c) , we have

Definition of $v^{(7)}(t)$:-

$$(m_2)^{(7)} \leq v^{(7)}(t) \leq (m_1)^{(7)}, \quad v^{(7)}(t) = \frac{G_{36}(t)}{G_{37}(t)}$$

In a completely analogous way, we obtain

Definition of $u^{(7)}(t)$:-

$$(\mu_2)^{(7)} \leq u^{(7)}(t) \leq (\mu_1)^{(7)}, \quad u^{(7)}(t) = \frac{T_{36}(t)}{T_{37}(t)}$$

Now, using this result and replacing it in GLOBAL EQUATIONS we get easily the result stated in the theorem.

Particular case :

If $(a_{36}'')^{(7)} = (a_{37}'')^{(7)}$, then $(\sigma_1)^{(7)} = (\sigma_2)^{(7)}$ and in this case $(v_1)^{(7)} = (\bar{v}_1)^{(7)}$ if in addition $(v_0)^{(7)} = (v_1)^{(7)}$ then $v^{(7)}(t) = (v_0)^{(7)}$ and as a consequence $G_{36}(t) = (v_0)^{(7)}G_{37}(t)$ **this also defines $(v_0)^{(7)}$ for the special case .**

Analogously if $(b_{36}'')^{(7)} = (b_{37}'')^{(7)}$, then $(\tau_1)^{(7)} = (\tau_2)^{(7)}$ and then

$(u_1)^{(7)} = (\bar{u}_1)^{(7)}$ if in addition $(u_0)^{(7)} = (u_1)^{(7)}$ then $T_{36}(t) = (u_0)^{(7)}T_{37}(t)$ This is an important consequence of the relation between $(v_1)^{(7)}$ and $(\bar{v}_1)^{(7)}$, **and definition of $(u_0)^{(7)}$.**

We can prove the following

If $(a_i'')^{(7)}$ and $(b_i'')^{(7)}$ are independent on t , and the conditions

$$(a'_{36})^{(7)}(a'_{37})^{(7)} - (a_{36})^{(7)}(a_{37})^{(7)} < 0$$

$$(a'_{36})^{(7)}(a'_{37})^{(7)} - (a_{36})^{(7)}(a_{37})^{(7)} + (a_{36})^{(7)}(p_{36})^{(7)} + (a'_{37})^{(7)}(p_{37})^{(7)} + (p_{36})^{(7)}(p_{37})^{(7)} > 0$$

$$(b'_{36})^{(7)}(b'_{37})^{(7)} - (b_{36})^{(7)}(b_{37})^{(7)} > 0,$$

$$(b'_{36})^{(7)}(b'_{37})^{(7)} - (b_{36})^{(7)}(b_{37})^{(7)} - (b'_{36})^{(7)}(r_{37})^{(7)} - (b'_{37})^{(7)}(r_{37})^{(7)} + (r_{36})^{(7)}(r_{37})^{(7)} < 0$$

with $(p_{36})^{(7)}, (r_{37})^{(7)}$ as defined are satisfied, then the system WITH THE SATISFACTION OF THE FOLLOWING PROPERTIES HAS A SOLUTION AS DERIVED BELOW.

Particular case :

If $(a''_{16})^{(2)} = (a''_{17})^{(2)}$, then $(\sigma_1)^{(2)} = (\sigma_2)^{(2)}$ and in this case $(v_1)^{(2)} = (\bar{v}_1)^{(2)}$ if in addition $(v_0)^{(2)} = (v_1)^{(2)}$ then $v^{(2)}(t) = (v_0)^{(2)}$ and as a consequence $G_{16}(t) = (v_0)^{(2)}G_{17}(t)$

Analogously if $(b''_{16})^{(2)} = (b''_{17})^{(2)}$, then $(\tau_1)^{(2)} = (\tau_2)^{(2)}$ and then

$(u_1)^{(2)} = (\bar{u}_1)^{(2)}$ if in addition $(u_0)^{(2)} = (u_1)^{(2)}$ then $T_{16}(t) = (u_0)^{(2)}T_{17}(t)$ This is an important consequence of the relation between $(v_1)^{(2)}$ and $(\bar{v}_1)^{(2)}$

From GLOBAL EQUATIONS we obtain

$$\frac{dv^{(3)}}{dt} = (a_{20})^{(3)} - \left((a'_{20})^{(3)} - (a'_{21})^{(3)} + (a''_{20})^{(3)}(T_{21}, t) \right) - (a''_{21})^{(3)}(T_{21}, t)v^{(3)} - (a_{21})^{(3)}v^{(3)}$$

Definition of $v^{(3)}$:-

$$v^{(3)} = \frac{G_{20}}{G_{21}}$$

It follows

$$- \left((a_{21})^{(3)}(v^{(3)})^2 + (\sigma_2)^{(3)}v^{(3)} - (a_{20})^{(3)} \right) \leq \frac{dv^{(3)}}{dt} \leq - \left((a_{21})^{(3)}(v^{(3)})^2 + (\sigma_1)^{(3)}v^{(3)} - (a_{20})^{(3)} \right)$$

From which one obtains

(a) For $0 < (v_0)^{(3)} = \frac{G_{20}^0}{G_{21}^0} < (v_1)^{(3)} < (\bar{v}_1)^{(3)}$

$$v^{(3)}(t) \geq \frac{(v_1)^{(3)} + (C)^{(3)}(v_2)^{(3)} e^{[-(a_{21})^{(3)}((v_1)^{(3)} - (v_0)^{(3)})t]}}{1 + (C)^{(3)} e^{[-(a_{21})^{(3)}((v_1)^{(3)} - (v_0)^{(3)})t]}} , \quad (C)^{(3)} = \frac{(v_1)^{(3)} - (v_0)^{(3)}}{(v_0)^{(3)} - (v_2)^{(3)}}$$

it follows $(v_0)^{(3)} \leq v^{(3)}(t) \leq (v_1)^{(3)}$

In the same manner, we get

$$v^{(3)}(t) \leq \frac{(\bar{v}_1)^{(3)} + (\bar{C})^{(3)}(\bar{v}_2)^{(3)} e^{[-(a_{21})^{(3)}((\bar{v}_1)^{(3)} - (\bar{v}_2)^{(3)})t]}}{1 + (\bar{C})^{(3)} e^{[-(a_{21})^{(3)}((\bar{v}_1)^{(3)} - (\bar{v}_2)^{(3)})t]}} , \quad (\bar{C})^{(3)} = \frac{(\bar{v}_1)^{(3)} - (v_0)^{(3)}}{(v_0)^{(3)} - (\bar{v}_2)^{(3)}}$$

Definition of $(\bar{v}_1)^{(3)}$:-

From which we deduce $(v_0)^{(3)} \leq v^{(3)}(t) \leq (\bar{v}_1)^{(3)}$

(b) If $0 < (v_1)^{(3)} < (v_0)^{(3)} = \frac{G_{20}^0}{G_{21}^0} < (\bar{v}_1)^{(3)}$ we find like in the previous case,

$$(v_1)^{(3)} \leq \frac{(v_1)^{(3)} + (C)^{(3)}(v_2)^{(3)} e^{[-(a_{21})^{(3)}((v_1)^{(3)} - (v_2)^{(3)})t]}}{1 + (C)^{(3)} e^{[-(a_{21})^{(3)}((v_1)^{(3)} - (v_2)^{(3)})t]}} \leq v^{(3)}(t) \leq \frac{(\bar{v}_1)^{(3)} + (\bar{C})^{(3)}(\bar{v}_2)^{(3)} e^{[-(a_{21})^{(3)}((\bar{v}_1)^{(3)} - (\bar{v}_2)^{(3)})t]}}{1 + (\bar{C})^{(3)} e^{[-(a_{21})^{(3)}((\bar{v}_1)^{(3)} - (\bar{v}_2)^{(3)})t]}} \leq (\bar{v}_1)^{(3)}$$

(c) If $0 < (v_1)^{(3)} \leq (\bar{v}_1)^{(3)} \leq (v_0)^{(3)} = \frac{G_{20}^0}{G_{21}^0}$, we obtain

$$(v_1)^{(3)} \leq v^{(3)}(t) \leq \frac{(\bar{v}_1)^{(3)} + (\bar{C})^{(3)}(\bar{v}_2)^{(3)} e^{[-(a_{21})^{(3)}((\bar{v}_1)^{(3)} - (\bar{v}_2)^{(3)})t]}}{1 + (\bar{C})^{(3)} e^{[-(a_{21})^{(3)}((\bar{v}_1)^{(3)} - (\bar{v}_2)^{(3)})t]}} \leq (v_0)^{(3)}$$

And so with the notation of the first part of condition (c), we have

Definition of $v^{(3)}(t)$:-

$$(m_2)^{(3)} \leq v^{(3)}(t) \leq (m_1)^{(3)}, \quad v^{(3)}(t) = \frac{G_{20}(t)}{G_{21}(t)}$$

In a completely analogous way, we obtain

Definition of $u^{(3)}(t)$:-

$$(\mu_2)^{(3)} \leq u^{(3)}(t) \leq (\mu_1)^{(3)}, \quad \boxed{u^{(3)}(t) = \frac{T_{20}(t)}{T_{21}(t)}}$$

Now, using this result and replacing it in GLOBAL EQUATIONS we get easily the result stated in the theorem.

Particular case :

If $(a''_{20})^{(3)} = (a''_{21})^{(3)}$, then $(\sigma_1)^{(3)} = (\sigma_2)^{(3)}$ and in this case $(v_1)^{(3)} = (\bar{v}_1)^{(3)}$ if in addition $(v_0)^{(3)} = (v_1)^{(3)}$ then $v^{(3)}(t) = (v_0)^{(3)}$ and as a consequence $G_{20}(t) = (v_0)^{(3)}G_{21}(t)$

Analogously if $(b''_{20})^{(3)} = (b''_{21})^{(3)}$, then $(\tau_1)^{(3)} = (\tau_2)^{(3)}$ and then

$(u_1)^{(3)} = (\bar{u}_1)^{(3)}$ if in addition $(u_0)^{(3)} = (u_1)^{(3)}$ then $T_{20}(t) = (u_0)^{(3)}T_{21}(t)$ This is an important consequence of the relation between $(v_1)^{(3)}$ and $(\bar{v}_1)^{(3)}$

506

: From GLOBAL EQUATIONS we obtain

507

$$\frac{dv^{(4)}}{dt} = (a_{24})^{(4)} - \left((a'_{24})^{(4)} - (a'_{25})^{(4)} + (a''_{24})^{(4)}(T_{25}, t) \right) - (a''_{25})^{(4)}(T_{25}, t)v^{(4)} - (a_{25})^{(4)}v^{(4)}$$

Definition of $v^{(4)}$:-

$$\boxed{v^{(4)} = \frac{G_{24}}{G_{25}}}$$

508

It follows

$$- \left((a_{25})^{(4)}(v^{(4)})^2 + (\sigma_2)^{(4)}v^{(4)} - (a_{24})^{(4)} \right) \leq \frac{dv^{(4)}}{dt} \leq - \left((a_{25})^{(4)}(v^{(4)})^2 + (\sigma_4)^{(4)}v^{(4)} - (a_{24})^{(4)} \right)$$

From which one obtains

Definition of $(\bar{v}_1)^{(4)}, (v_0)^{(4)}$:-

(d) For $0 < \boxed{(v_0)^{(4)} = \frac{G_{24}^0}{G_{25}^0}} < (v_1)^{(4)} < (\bar{v}_1)^{(4)}$

$$v^{(4)}(t) \geq \frac{(v_1)^{(4)} + (C)^{(4)}(v_2)^{(4)} e^{[-(a_{25})^{(4)}((v_1)^{(4)} - (v_0)^{(4)})t]}}{4 + (C)^{(4)} e^{[-(a_{25})^{(4)}((v_1)^{(4)} - (v_0)^{(4)})t]}} , \quad \boxed{(C)^{(4)} = \frac{(v_1)^{(4)} - (v_0)^{(4)}}{(v_0)^{(4)} - (v_2)^{(4)}}$$

it follows $(v_0)^{(4)} \leq v^{(4)}(t) \leq (v_1)^{(4)}$

In the same manner , we get

509

$$v^{(4)}(t) \leq \frac{(\bar{v}_1)^{(4)} + (\bar{C})^{(4)}(\bar{v}_2)^{(4)} e^{[-(a_{25})^{(4)}((\bar{v}_1)^{(4)} - (\bar{v}_2)^{(4)})t]}}{4 + (\bar{C})^{(4)} e^{[-(a_{25})^{(4)}((\bar{v}_1)^{(4)} - (\bar{v}_2)^{(4)})t]}} , \quad \boxed{(\bar{C})^{(4)} = \frac{(\bar{v}_1)^{(4)} - (v_0)^{(4)}}{(v_0)^{(4)} - (\bar{v}_2)^{(4)}}$$

From which we deduce $(v_0)^{(4)} \leq v^{(4)}(t) \leq (\bar{v}_1)^{(4)}$

(e) If $0 < (v_1)^{(4)} < (v_0)^{(4)} = \frac{G_{24}^0}{G_{25}^0} < (\bar{v}_1)^{(4)}$ we find like in the previous case,

510

$$(v_1)^{(4)} \leq \frac{(v_1)^{(4)} + (C)^{(4)}(v_2)^{(4)} e^{[-(a_{25})^{(4)}((v_1)^{(4)} - (v_2)^{(4)})t]}}{1 + (C)^{(4)} e^{[-(a_{25})^{(4)}((v_1)^{(4)} - (v_2)^{(4)})t]}} \leq v^{(4)}(t) \leq$$

$$\frac{(\bar{v}_1)^{(4)} + (\bar{C})^{(4)}(\bar{v}_2)^{(4)} e^{[-(a_{25})^{(4)}((\bar{v}_1)^{(4)} - (\bar{v}_2)^{(4)})t]}}{1 + (\bar{C})^{(4)} e^{[-(a_{25})^{(4)}((\bar{v}_1)^{(4)} - (\bar{v}_2)^{(4)})t]}} \leq (\bar{v}_1)^{(4)}$$

511

512

(f) If $0 < (v_1)^{(4)} \leq (\bar{v}_1)^{(4)} \leq \boxed{(v_0)^{(4)} = \frac{G_{24}^0}{G_{25}^0}}$, we obtain

$$(v_1)^{(4)} \leq v^{(4)}(t) \leq \frac{(\bar{v}_1)^{(4)} + (\bar{C})^{(4)}(\bar{v}_2)^{(4)} e^{[-(a_{25})^{(4)}((\bar{v}_1)^{(4)} - (\bar{v}_2)^{(4)})t]}}{1 + (\bar{C})^{(4)} e^{[-(a_{25})^{(4)}((\bar{v}_1)^{(4)} - (\bar{v}_2)^{(4)})t]}} \leq (v_0)^{(4)}$$

And so with the notation of the first part of condition (c) , we have

Definition of $v^{(4)}(t)$:-

$$(m_2)^{(4)} \leq v^{(4)}(t) \leq (m_1)^{(4)}, \quad \boxed{v^{(4)}(t) = \frac{G_{24}(t)}{G_{25}(t)}}$$

In a completely analogous way, we obtain

Definition of $u^{(4)}(t)$:-

$$(\mu_2)^{(4)} \leq u^{(4)}(t) \leq (\mu_1)^{(4)}, \quad \boxed{u^{(4)}(t) = \frac{T_{24}(t)}{T_{25}(t)}}$$

Now, using this result and replacing it in GLOBAL EQUATIONS we get easily the result stated in the theorem.

Particular case :

If $(a''_{24})^{(4)} = (a''_{25})^{(4)}$, then $(\sigma_1)^{(4)} = (\sigma_2)^{(4)}$ and in this case $(v_1)^{(4)} = (\bar{v}_1)^{(4)}$ if in addition $(v_0)^{(4)} = (v_1)^{(4)}$ then $v^{(4)}(t) = (v_0)^{(4)}$ and as a consequence $G_{24}(t) = (v_0)^{(4)}G_{25}(t)$ **this also defines $(v_0)^{(4)}$ for the special case .** 513

Analogously if $(b''_{24})^{(4)} = (b''_{25})^{(4)}$, then $(\tau_1)^{(4)} = (\tau_2)^{(4)}$ and then $(u_1)^{(4)} = (\bar{u}_1)^{(4)}$ if in addition $(u_0)^{(4)} = (u_1)^{(4)}$ then $T_{24}(t) = (u_0)^{(4)}T_{25}(t)$ This is an important consequence of the relation between $(v_1)^{(4)}$ and $(\bar{v}_1)^{(4)}$, **and definition of $(u_0)^{(4)}$.**

From GLOBAL EQUATIONS we obtain

514
515

$$\frac{dv^{(5)}}{dt} = (a_{28})^{(5)} - \left((a'_{28})^{(5)} - (a'_{29})^{(5)} + (a''_{28})^{(5)}(T_{29}, t) \right) - (a''_{29})^{(5)}(T_{29}, t)v^{(5)} - (a_{29})^{(5)}v^{(5)}$$

Definition of $v^{(5)}$:- $\boxed{v^{(5)} = \frac{G_{28}}{G_{29}}}$

It follows

$$- \left((a_{29})^{(5)}(v^{(5)})^2 + (\sigma_2)^{(5)}v^{(5)} - (a_{28})^{(5)} \right) \leq \frac{dv^{(5)}}{dt} \leq - \left((a_{29})^{(5)}(v^{(5)})^2 + (\sigma_1)^{(5)}v^{(5)} - (a_{28})^{(5)} \right)$$

From which one obtains

Definition of $(\bar{v}_1)^{(5)}, (v_0)^{(5)}$:-

(g) For $0 < \boxed{(v_0)^{(5)} = \frac{G_{28}^0}{G_{29}^0}} < (v_1)^{(5)} < (\bar{v}_1)^{(5)}$

$$v^{(5)}(t) \geq \frac{(v_1)^{(5)} + (C)^{(5)}(v_2)^{(5)} e^{[-(a_{29})^{(5)}(v_1)^{(5)} - (v_0)^{(5)}]t}}{5 + (C)^{(5)} e^{[-(a_{29})^{(5)}(v_1)^{(5)} - (v_0)^{(5)}]t}}, \quad \boxed{(C)^{(5)} = \frac{(v_1)^{(5)} - (v_0)^{(5)}}{(v_0)^{(5)} - (v_2)^{(5)}}$$

it follows $(v_0)^{(5)} \leq v^{(5)}(t) \leq (v_1)^{(5)}$

In the same manner , we get

516

$$v^{(5)}(t) \leq \frac{(\bar{v}_1)^{(5)} + (\bar{C})^{(5)}(\bar{v}_2)^{(5)} e^{[-(a_{29})^{(5)}(\bar{v}_1)^{(5)} - (\bar{v}_2)^{(5)}]t}}{5 + (\bar{C})^{(5)} e^{[-(a_{29})^{(5)}(\bar{v}_1)^{(5)} - (\bar{v}_2)^{(5)}]t}}, \quad \boxed{(\bar{C})^{(5)} = \frac{(\bar{v}_1)^{(5)} - (v_0)^{(5)}}{(v_0)^{(5)} - (\bar{v}_2)^{(5)}}$$

From which we deduce $(v_0)^{(5)} \leq v^{(5)}(t) \leq (\bar{v}_5)^{(5)}$

(h) If $0 < (v_1)^{(5)} < (v_0)^{(5)} = \frac{G_{28}^0}{G_{29}^0} < (\bar{v}_1)^{(5)}$ we find like in the previous case,

517

$$(v_1)^{(5)} \leq \frac{(v_1)^{(5)} + (C)^{(5)}(v_2)^{(5)} e^{[-(a_{29})^{(5)}(v_1)^{(5)} - (v_2)^{(5)}]t}}{1 + (C)^{(5)} e^{[-(a_{29})^{(5)}(v_1)^{(5)} - (v_2)^{(5)}]t}} \leq v^{(5)}(t) \leq$$

$$\frac{(\bar{v}_1)^{(5)} + (C)^{(5)}(\bar{v}_2)^{(5)} e^{[-(a_{29})^{(5)}(\bar{v}_1)^{(5)} - (\bar{v}_2)^{(5)}]t}}{1 + (C)^{(5)} e^{[-(a_{29})^{(5)}(\bar{v}_1)^{(5)} - (\bar{v}_2)^{(5)}]t}} \leq (\bar{v}_1)^{(5)}$$

(i) If $0 < (v_1)^{(5)} \leq (\bar{v}_1)^{(5)} \leq \boxed{(v_0)^{(5)} = \frac{G_{28}^0}{G_{29}^0}}$, we obtain

518

$$(v_1)^{(5)} \leq v^{(5)}(t) \leq \frac{(\bar{v}_1)^{(5)} + (C)^{(5)}(\bar{v}_2)^{(5)} e^{[-(a_{29})^{(5)}(\bar{v}_1)^{(5)} - (\bar{v}_2)^{(5)}]t}}{1 + (C)^{(5)} e^{[-(a_{29})^{(5)}(\bar{v}_1)^{(5)} - (\bar{v}_2)^{(5)}]t}} \leq (v_0)^{(5)}$$

519

And so with the notation of the first part of condition (c), we have

Definition of $v^{(5)}(t)$:-

$$(m_2)^{(5)} \leq v^{(5)}(t) \leq (m_1)^{(5)}, \quad \boxed{v^{(5)}(t) = \frac{G_{28}(t)}{G_{29}(t)}}$$

In a completely analogous way, we obtain

Definition of $u^{(5)}(t)$:-

$$(\mu_2)^{(5)} \leq u^{(5)}(t) \leq (\mu_1)^{(5)}, \quad \boxed{u^{(5)}(t) = \frac{T_{28}(t)}{T_{29}(t)}}$$

Now, using this result and replacing it in GLOBAL EQUATIONS we get easily the result stated in the theorem.

Particular case :

If $(a''_{28})^{(5)} = (a''_{29})^{(5)}$, then $(\sigma_1)^{(5)} = (\sigma_2)^{(5)}$ and in this case $(v_1)^{(5)} = (\bar{v}_1)^{(5)}$ if in addition $(v_0)^{(5)} = (v_5)^{(5)}$ then $v^{(5)}(t) = (v_0)^{(5)}$ and as a consequence $G_{28}(t) = (v_0)^{(5)}G_{29}(t)$ **this also defines $(v_0)^{(5)}$ for the special case**.

Analogously if $(b''_{28})^{(5)} = (b''_{29})^{(5)}$, then $(\tau_1)^{(5)} = (\tau_2)^{(5)}$ and then $(u_1)^{(5)} = (\bar{u}_1)^{(5)}$ if in addition $(u_0)^{(5)} = (u_1)^{(5)}$ then $T_{28}(t) = (u_0)^{(5)}T_{29}(t)$ This is an important consequence of the relation between $(v_1)^{(5)}$ and $(\bar{v}_1)^{(5)}$, **and definition of $(u_0)^{(5)}$** .

520

we obtain

521

$$\frac{dv^{(6)}}{dt} = (a_{32})^{(6)} - \left((a'_{32})^{(6)} - (a'_{33})^{(6)} + (a''_{32})^{(6)}(T_{33}, t) \right) - (a''_{33})^{(6)}(T_{33}, t)v^{(6)} - (a_{33})^{(6)}v^{(6)}$$

Definition of $v^{(6)}$:- $\boxed{v^{(6)} = \frac{G_{32}}{G_{33}}}$

It follows

$$- \left((a_{33})^{(6)}(v^{(6)})^2 + (\sigma_2)^{(6)}v^{(6)} - (a_{32})^{(6)} \right) \leq \frac{dv^{(6)}}{dt} \leq - \left((a_{33})^{(6)}(v^{(6)})^2 + (\sigma_1)^{(6)}v^{(6)} - (a_{32})^{(6)} \right)$$

From which one obtains

Definition of $(\bar{v}_1)^{(6)}, (v_0)^{(6)}$:-

(j) For $0 < \boxed{(v_0)^{(6)} = \frac{G_{32}^0}{G_{33}^0}} < (v_1)^{(6)} < (\bar{v}_1)^{(6)}$

$$v^{(6)}(t) \geq \frac{(v_1)^{(6)} + (C)^{(6)}(v_2)^{(6)} e^{[-(a_{33})^{(6)}(v_1)^{(6)} - (v_0)^{(6)}]t}}{1 + (C)^{(6)} e^{[-(a_{33})^{(6)}(v_1)^{(6)} - (v_0)^{(6)}]t}}, \quad \boxed{(C)^{(6)} = \frac{(v_1)^{(6)} - (v_0)^{(6)}}{(v_0)^{(6)} - (v_2)^{(6)}}$$

it follows $(v_0)^{(6)} \leq v^{(6)}(t) \leq (v_1)^{(6)}$

In the same manner, we get

522

523

$$v^{(6)}(t) \leq \frac{(\bar{v}_1)^{(6)} + (\bar{C})^{(6)} (\bar{v}_2)^{(6)} e^{[-(a_{33})^{(6)} (\bar{v}_1)^{(6)} - (\bar{v}_2)^{(6)}] t}}{1 + (\bar{C})^{(6)} e^{[-(a_{33})^{(6)} (\bar{v}_1)^{(6)} - (\bar{v}_2)^{(6)}] t}}, \quad \boxed{(\bar{C})^{(6)} = \frac{(\bar{v}_1)^{(6)} - (v_0)^{(6)}}{(v_0)^{(6)} - (\bar{v}_2)^{(6)}}$$

From which we deduce $(v_0)^{(6)} \leq v^{(6)}(t) \leq (\bar{v}_1)^{(6)}$

(k) If $0 < (v_1)^{(6)} < (v_0)^{(6)} = \frac{G_{32}^0}{G_{33}^0} < (\bar{v}_1)^{(6)}$ we find like in the previous case, 524

$$(v_1)^{(6)} \leq \frac{(v_1)^{(6)} + (\bar{C})^{(6)} (v_2)^{(6)} e^{[-(a_{33})^{(6)} (v_1)^{(6)} - (v_2)^{(6)}] t}}{1 + (\bar{C})^{(6)} e^{[-(a_{33})^{(6)} (v_1)^{(6)} - (v_2)^{(6)}] t}} \leq v^{(6)}(t) \leq$$

$$\frac{(\bar{v}_1)^{(6)} + (\bar{C})^{(6)} (\bar{v}_2)^{(6)} e^{[-(a_{33})^{(6)} (\bar{v}_1)^{(6)} - (\bar{v}_2)^{(6)}] t}}{1 + (\bar{C})^{(6)} e^{[-(a_{33})^{(6)} (\bar{v}_1)^{(6)} - (\bar{v}_2)^{(6)}] t}} \leq (\bar{v}_1)^{(6)}$$

(l) If $0 < (v_1)^{(6)} \leq (\bar{v}_1)^{(6)} \leq (v_0)^{(6)} = \frac{G_{32}^0}{G_{33}^0}$, we obtain 525

$$(v_1)^{(6)} \leq v^{(6)}(t) \leq \frac{(\bar{v}_1)^{(6)} + (\bar{C})^{(6)} (\bar{v}_2)^{(6)} e^{[-(a_{33})^{(6)} (\bar{v}_1)^{(6)} - (\bar{v}_2)^{(6)}] t}}{1 + (\bar{C})^{(6)} e^{[-(a_{33})^{(6)} (\bar{v}_1)^{(6)} - (\bar{v}_2)^{(6)}] t}} \leq (v_0)^{(6)}$$

And so with the notation of the first part of condition (c), we have

Definition of $v^{(6)}(t)$:-

$$(m_2)^{(6)} \leq v^{(6)}(t) \leq (m_1)^{(6)}, \quad \boxed{v^{(6)}(t) = \frac{G_{32}(t)}{G_{33}(t)}}$$

In a completely analogous way, we obtain

Definition of $u^{(6)}(t)$:-

$$(\mu_2)^{(6)} \leq u^{(6)}(t) \leq (\mu_1)^{(6)}, \quad \boxed{u^{(6)}(t) = \frac{T_{32}(t)}{T_{33}(t)}}$$

Now, using this result and replacing it in GLOBAL EQUATIONS we get easily the result stated in the theorem.

Particular case :

If $(a_{32})^{(6)} = (a_{33})^{(6)}$, then $(\sigma_1)^{(6)} = (\sigma_2)^{(6)}$ and in this case $(v_1)^{(6)} = (\bar{v}_1)^{(6)}$ if in addition $(v_0)^{(6)} = (v_1)^{(6)}$ then $v^{(6)}(t) = (v_0)^{(6)}$ and as a consequence $G_{32}(t) = (v_0)^{(6)} G_{33}(t)$ **this also defines $(v_0)^{(6)}$ for the special case .**

Analogously if $(b_{32})^{(6)} = (b_{33})^{(6)}$, then $(\tau_1)^{(6)} = (\tau_2)^{(6)}$ and then $(u_1)^{(6)} = (\bar{u}_1)^{(6)}$ if in addition $(u_0)^{(6)} = (u_1)^{(6)}$ then $T_{32}(t) = (u_0)^{(6)} T_{33}(t)$ This is an important consequence of the relation between $(v_1)^{(6)}$ and $(\bar{v}_1)^{(6)}$, **and definition of $(u_0)^{(6)}$.**

526

Behavior of the solutions

527

If we denote and define

Definition of $(\sigma_1)^{(7)}, (\sigma_2)^{(7)}, (\tau_1)^{(7)}, (\tau_2)^{(7)}$:

(p) $(\sigma_1)^{(7)}, (\sigma_2)^{(7)}, (\tau_1)^{(7)}, (\tau_2)^{(7)}$ four constants satisfying

$$-(\sigma_2)^{(7)} \leq -(a'_{36})^{(7)} + (a'_{37})^{(7)} - (a''_{36})^{(7)}(T_{37}, t) + (a''_{37})^{(7)}(T_{37}, t) \leq -(\sigma_1)^{(7)}$$

$$-(\tau_2)^{(7)} \leq -(b'_{36})^{(7)} + (b'_{37})^{(7)} - (b''_{36})^{(7)}((G_{39}), t) - (b''_{37})^{(7)}((G_{39}), t) \leq -(\tau_1)^{(7)}$$

Definition of $(v_1)^{(7)}, (v_2)^{(7)}, (u_1)^{(7)}, (u_2)^{(7)}, v^{(7)}, u^{(7)}$: 528

(q) By $(v_1)^{(7)} > 0, (v_2)^{(7)} < 0$ and respectively $(u_1)^{(7)} > 0, (u_2)^{(7)} < 0$ the roots of the equations

$$(a_{37})^{(7)}(v^{(7)})^2 + (\sigma_1)^{(7)}v^{(7)} - (a_{36})^{(7)} = 0$$

$$\text{and } (b_{37})^{(7)}(u^{(7)})^2 + (\tau_1)^{(7)}u^{(7)} - (b_{36})^{(7)} = 0 \text{ and}$$

529

Definition of $(\bar{v}_1)^{(7)}, (\bar{v}_2)^{(7)}, (\bar{u}_1)^{(7)}, (\bar{u}_2)^{(7)}$:

530.

By $(\bar{v}_1)^{(7)} > 0, (\bar{v}_2)^{(7)} < 0$ and respectively $(\bar{u}_1)^{(7)} > 0, (\bar{u}_2)^{(7)} < 0$ the

roots of the equations $(a_{37})^{(7)}(v^{(7)})^2 + (\sigma_2)^{(7)}v^{(7)} - (a_{36})^{(7)} = 0$

and $(b_{37})^{(7)}(u^{(7)})^2 + (\tau_2)^{(7)}u^{(7)} - (b_{36})^{(7)} = 0$

Definition of $(m_1)^{(7)}, (m_2)^{(7)}, (\mu_1)^{(7)}, (\mu_2)^{(7)}, (v_0)^{(7)}$:-

(r) If we define $(m_1)^{(7)}, (m_2)^{(7)}, (\mu_1)^{(7)}, (\mu_2)^{(7)}$ by

$$(m_2)^{(7)} = (v_0)^{(7)}, (m_1)^{(7)} = (v_1)^{(7)}, \text{ if } (v_0)^{(7)} < (v_1)^{(7)}$$

$$(m_2)^{(7)} = (v_1)^{(7)}, (m_1)^{(7)} = (\bar{v}_1)^{(7)}, \text{ if } (v_1)^{(7)} < (v_0)^{(7)} < (\bar{v}_1)^{(7)},$$

$$\text{and } (v_0)^{(7)} = \frac{G_{36}^0}{G_{37}^0}$$

$$(m_2)^{(7)} = (v_1)^{(7)}, (m_1)^{(7)} = (v_0)^{(7)}, \text{ if } (\bar{v}_1)^{(7)} < (v_0)^{(7)}$$

and analogously

$$(\mu_2)^{(7)} = (u_0)^{(7)}, (\mu_1)^{(7)} = (u_1)^{(7)}, \text{ if } (u_0)^{(7)} < (u_1)^{(7)}$$

$$(\mu_2)^{(7)} = (u_1)^{(7)}, (\mu_1)^{(7)} = (\bar{u}_1)^{(7)}, \text{ if } (u_1)^{(7)} < (u_0)^{(7)} < (\bar{u}_1)^{(7)},$$

$$\text{and } (u_0)^{(7)} = \frac{T_{36}^0}{T_{37}^0}$$

$(\mu_2)^{(7)} = (u_1)^{(7)}, (\mu_1)^{(7)} = (u_0)^{(7)}$, if $(\bar{u}_1)^{(7)} < (u_0)^{(7)}$ where $(u_1)^{(7)}, (\bar{u}_1)^{(7)}$ are defined by 59 and 67 respectively

Then the solution of GLOBAL EQUATIONS satisfies the inequalities

$$G_{36}^0 e^{((S_1)^{(7)} - (p_{36})^{(7)})t} \leq G_{36}(t) \leq G_{36}^0 e^{(S_1)^{(7)}t}$$

where $(p_i)^{(7)}$ is defined

$$\frac{1}{(m_7)^{(7)}} G_{36}^0 e^{((S_1)^{(7)} - (p_{36})^{(7)})t} \leq G_{37}(t) \leq \frac{1}{(m_2)^{(7)}} G_{36}^0 e^{(S_1)^{(7)}t}$$

$$\left(\frac{(a_{38})^{(7)} G_{36}^0}{(m_1)^{(7)}((S_1)^{(7)} - (p_{36})^{(7)} - (S_2)^{(7)})} \left[e^{((S_1)^{(7)} - (p_{36})^{(7)})t} - e^{-(S_2)^{(7)}t} \right] + G_{38}^0 e^{-(S_2)^{(7)}t} \leq G_{38}(t) \leq \frac{(a_{38})^{(7)} G_{36}^0}{(m_2)^{(7)}((S_1)^{(7)} - (a'_{38})^{(7)})} \left[e^{(S_1)^{(7)}t} - e^{-(a'_{38})^{(7)}t} \right] + G_{38}^0 e^{-(a'_{38})^{(7)}t} \right)$$

$$\boxed{T_{36}^0 e^{(R_1)^{(7)}t} \leq T_{36}(t) \leq T_{36}^0 e^{((R_1)^{(7)} + (r_{36})^{(7)})t}$$

$$\frac{1}{(\mu_1)^{(7)}} T_{36}^0 e^{(R_1)^{(7)}t} \leq T_{36}(t) \leq \frac{1}{(\mu_2)^{(7)}} T_{36}^0 e^{((R_1)^{(7)} + (r_{36})^{(7)})t}$$

$$\frac{(b_{38})^{(7)} T_{36}^0}{(\mu_1)^{(7)}((R_1)^{(7)} - (b_{38})^{(7)})} \left[e^{(R_1)^{(7)}t} - e^{-(b'_{38})^{(7)}t} \right] + T_{38}^0 e^{-(b'_{38})^{(7)}t} \leq T_{38}(t) \leq$$

$$\frac{(a_{38})^{(7)} T_{36}^0}{(\mu_2)^{(7)}((R_1)^{(7)} + (r_{36})^{(7)} + (R_2)^{(7)})} \left[e^{((R_1)^{(7)} + (r_{36})^{(7)})t} - e^{-(R_2)^{(7)}t} \right] + T_{38}^0 e^{-(R_2)^{(7)}t}$$

Definition of $(S_1)^{(7)}, (S_2)^{(7)}, (R_1)^{(7)}, (R_2)^{(7)}$:-

Where $(S_1)^{(7)} = (a_{36})^{(7)}(m_2)^{(7)} - (a'_{36})^{(7)}$

$$\begin{aligned} (S_2)^{(7)} &= (a_{38})^{(7)} - (p_{38})^{(7)} \\ (R_1)^{(7)} &= (b_{36})^{(7)}(\mu_2)^{(7)} - (b'_{36})^{(7)} \\ (R_2)^{(7)} &= (b_{38})^{(7)} - (r_{38})^{(7)} \end{aligned}$$

From CONCATENATED GLOBAL EQUATIONS we obtain

$$\frac{dv^{(7)}}{dt} = (a_{36})^{(7)} - \left((a'_{36})^{(7)} - (a'_{37})^{(7)} + (a''_{36})^{(7)}(T_{37}, t) \right) - (a''_{37})^{(7)}(T_{37}, t)v^{(7)} - (a_{37})^{(7)}v^{(7)}$$

Definition of $v^{(7)}$:-
$$v^{(7)} = \frac{G_{36}}{G_{37}}$$

It follows

$$-\left((a_{37})^{(7)}(v^{(7)})^2 + (\sigma_2)^{(7)}v^{(7)} - (a_{36})^{(7)}\right) \leq \frac{dv^{(7)}}{dt} \leq -\left((a_{37})^{(7)}(v^{(7)})^2 + (\sigma_1)^{(7)}v^{(7)} - (a_{36})^{(7)}\right)$$

From which one obtains

Definition of $(\bar{v}_1)^{(7)}, (v_0)^{(7)}$:-

(m) For $0 < \frac{G_{36}^0}{G_{37}^0} < (v_1)^{(7)} < (\bar{v}_1)^{(7)}$

$$v^{(7)}(t) \geq \frac{(v_1)^{(7)} + (C)^{(7)}(v_2)^{(7)} e^{[-(a_{37})^{(7)}(v_1)^{(7)} - (v_0)^{(7)}]t}}{1 + (C)^{(7)} e^{[-(a_{37})^{(7)}(v_1)^{(7)} - (v_0)^{(7)}]t}}, \quad (C)^{(7)} = \frac{(v_1)^{(7)} - (v_0)^{(7)}}{(v_0)^{(7)} - (v_2)^{(7)}}$$

it follows $(v_0)^{(7)} \leq v^{(7)}(t) \leq (v_1)^{(7)}$

In the same manner, we get

$$v^{(7)}(t) \leq \frac{(\bar{v}_1)^{(7)} + (\bar{C})^{(7)}(\bar{v}_2)^{(7)} e^{[-(a_{37})^{(7)}(\bar{v}_1)^{(7)} - (\bar{v}_2)^{(7)}]t}}{1 + (\bar{C})^{(7)} e^{[-(a_{37})^{(7)}(\bar{v}_1)^{(7)} - (\bar{v}_2)^{(7)}]t}}, \quad (\bar{C})^{(7)} = \frac{(\bar{v}_1)^{(7)} - (v_0)^{(7)}}{(v_0)^{(7)} - (\bar{v}_2)^{(7)}}$$

541

From which we deduce $(v_0)^{(7)} \leq v^{(7)}(t) \leq (\bar{v}_1)^{(7)}$

(n) If $0 < (v_1)^{(7)} < (v_0)^{(7)} = \frac{G_{36}^0}{G_{37}^0} < (\bar{v}_1)^{(7)}$ we find like in the previous case,

542

$$(v_1)^{(7)} \leq \frac{(v_1)^{(7)} + (C)^{(7)}(v_2)^{(7)} e^{[-(a_{37})^{(7)}(v_1)^{(7)} - (v_2)^{(7)}]t}}{1 + (C)^{(7)} e^{[-(a_{37})^{(7)}(v_1)^{(7)} - (v_2)^{(7)}]t}} \leq v^{(7)}(t) \leq \frac{(\bar{v}_1)^{(7)} + (\bar{C})^{(7)}(\bar{v}_2)^{(7)} e^{[-(a_{37})^{(7)}(\bar{v}_1)^{(7)} - (\bar{v}_2)^{(7)}]t}}{1 + (\bar{C})^{(7)} e^{[-(a_{37})^{(7)}(\bar{v}_1)^{(7)} - (\bar{v}_2)^{(7)}]t}} \leq (\bar{v}_1)^{(7)}$$

(o) If $0 < (v_1)^{(7)} \leq (\bar{v}_1)^{(7)} \leq \frac{G_{36}^0}{G_{37}^0}$, we obtain

543

$$(v_1)^{(7)} \leq v^{(7)}(t) \leq \frac{(\bar{v}_1)^{(7)} + (\bar{C})^{(7)}(\bar{v}_2)^{(7)} e^{[-(a_{37})^{(7)}(\bar{v}_1)^{(7)} - (\bar{v}_2)^{(7)}]t}}{1 + (\bar{C})^{(7)} e^{[-(a_{37})^{(7)}(\bar{v}_1)^{(7)} - (\bar{v}_2)^{(7)}]t}} \leq (v_0)^{(7)}$$

And so with the notation of the first part of condition (c), we have

Definition of $v^{(7)}(t)$:-

$$(m_2)^{(7)} \leq v^{(7)}(t) \leq (m_1)^{(7)}, \quad v^{(7)}(t) = \frac{G_{36}(t)}{G_{37}(t)}$$

In a completely analogous way, we obtain

Definition of $u^{(7)}(t)$:-

$$(\mu_2)^{(7)} \leq u^{(7)}(t) \leq (\mu_1)^{(7)}, \quad u^{(7)}(t) = \frac{T_{36}(t)}{T_{37}(t)}$$

Now, using this result and replacing it in CONCATENATED GLOBAL EQUATIONS we get easily the result stated in the theorem.

Particular case :

If $(a_{36})^{(7)} = (a_{37})^{(7)}$, then $(\sigma_1)^{(7)} = (\sigma_2)^{(7)}$ and in this case $(v_1)^{(7)} = (\bar{v}_1)^{(7)}$ if in addition $(v_0)^{(7)} = (v_1)^{(7)}$ then $v^{(7)}(t) = (v_0)^{(7)}$ and as a consequence $G_{36}(t) = (v_0)^{(7)}G_{37}(t)$ **this also defines $(v_0)^{(7)}$ for the special case.**

Analogously if $(b_{36})^{(7)} = (b_{37})^{(7)}$, then $(\tau_1)^{(7)} = (\tau_2)^{(7)}$ and then

$(u_1)^{(7)} = (\bar{u}_1)^{(7)}$ if in addition $(u_0)^{(7)} = (u_1)^{(7)}$ then $T_{36}(t) = (u_0)^{(7)}T_{37}(t)$ This is an important consequence of the relation between $(v_1)^{(7)}$ and $(\bar{v}_1)^{(7)}$, **and definition of $(u_0)^{(7)}$.**

$$(b_{14})^{(1)}T_{13} - [(b'_{14})^{(1)} - (b''_{14})^{(1)}(G)]T_{14} = 0$$

544

$$(b_{15})^{(1)}T_{14} - [(b'_{15})^{(1)} - (b''_{15})^{(1)}(G)]T_{15} = 0$$

545

has a unique positive solution, which is an equilibrium solution for the system

546

$(a_{16})^{(2)}G_{17} - [(a'_{16})^{(2)} + (a''_{16})^{(2)}(T_{17})]G_{16} = 0$	547
$(a_{17})^{(2)}G_{16} - [(a'_{17})^{(2)} + (a''_{17})^{(2)}(T_{17})]G_{17} = 0$	548
$(a_{18})^{(2)}G_{17} - [(a'_{18})^{(2)} + (a''_{18})^{(2)}(T_{17})]G_{18} = 0$	549
$(b_{16})^{(2)}T_{17} - [(b'_{16})^{(2)} - (b''_{16})^{(2)}(G_{19})]T_{16} = 0$	550
$(b_{17})^{(2)}T_{16} - [(b'_{17})^{(2)} - (b''_{17})^{(2)}(G_{19})]T_{17} = 0$	551
$(b_{18})^{(2)}T_{17} - [(b'_{18})^{(2)} - (b''_{18})^{(2)}(G_{19})]T_{18} = 0$	552
has a unique positive solution , which is an equilibrium solution for	553
$(a_{20})^{(3)}G_{21} - [(a'_{20})^{(3)} + (a''_{20})^{(3)}(T_{21})]G_{20} = 0$	554
$(a_{21})^{(3)}G_{20} - [(a'_{21})^{(3)} + (a''_{21})^{(3)}(T_{21})]G_{21} = 0$	555
$(a_{22})^{(3)}G_{21} - [(a'_{22})^{(3)} + (a''_{22})^{(3)}(T_{21})]G_{22} = 0$	556
$(b_{20})^{(3)}T_{21} - [(b'_{20})^{(3)} - (b''_{20})^{(3)}(G_{23})]T_{20} = 0$	557
$(b_{21})^{(3)}T_{20} - [(b'_{21})^{(3)} - (b''_{21})^{(3)}(G_{23})]T_{21} = 0$	558
$(b_{22})^{(3)}T_{21} - [(b'_{22})^{(3)} - (b''_{22})^{(3)}(G_{23})]T_{22} = 0$	559
has a unique positive solution , which is an equilibrium solution	560
$(a_{24})^{(4)}G_{25} - [(a'_{24})^{(4)} + (a''_{24})^{(4)}(T_{25})]G_{24} = 0$	561
$(a_{25})^{(4)}G_{24} - [(a'_{25})^{(4)} + (a''_{25})^{(4)}(T_{25})]G_{25} = 0$	563
$(a_{26})^{(4)}G_{25} - [(a'_{26})^{(4)} + (a''_{26})^{(4)}(T_{25})]G_{26} = 0$	564
$(b_{24})^{(4)}T_{25} - [(b'_{24})^{(4)} - (b''_{24})^{(4)}((G_{27}))]T_{24} = 0$	565
$(b_{25})^{(4)}T_{24} - [(b'_{25})^{(4)} - (b''_{25})^{(4)}((G_{27}))]T_{25} = 0$	566
$(b_{26})^{(4)}T_{25} - [(b'_{26})^{(4)} - (b''_{26})^{(4)}((G_{27}))]T_{26} = 0$	567
has a unique positive solution , which is an equilibrium solution for the system	568
$(a_{28})^{(5)}G_{29} - [(a'_{28})^{(5)} + (a''_{28})^{(5)}(T_{29})]G_{28} = 0$	569
$(a_{29})^{(5)}G_{28} - [(a'_{29})^{(5)} + (a''_{29})^{(5)}(T_{29})]G_{29} = 0$	570
$(a_{30})^{(5)}G_{29} - [(a'_{30})^{(5)} + (a''_{30})^{(5)}(T_{29})]G_{30} = 0$	571
$(b_{28})^{(5)}T_{29} - [(b'_{28})^{(5)} - (b''_{28})^{(5)}(G_{31})]T_{28} = 0$	572
$(b_{29})^{(5)}T_{28} - [(b'_{29})^{(5)} - (b''_{29})^{(5)}(G_{31})]T_{29} = 0$	573
$(b_{30})^{(5)}T_{29} - [(b'_{30})^{(5)} - (b''_{30})^{(5)}(G_{31})]T_{30} = 0$	574
has a unique positive solution , which is an equilibrium solution for the system	575
$(a_{32})^{(6)}G_{33} - [(a'_{32})^{(6)} + (a''_{32})^{(6)}(T_{33})]G_{32} = 0$	576
$(a_{33})^{(6)}G_{32} - [(a'_{33})^{(6)} + (a''_{33})^{(6)}(T_{33})]G_{33} = 0$	577
$(a_{34})^{(6)}G_{33} - [(a'_{34})^{(6)} + (a''_{34})^{(6)}(T_{33})]G_{34} = 0$	578
$(b_{32})^{(6)}T_{33} - [(b'_{32})^{(6)} - (b''_{32})^{(6)}(G_{35})]T_{32} = 0$	579
$(b_{33})^{(6)}T_{32} - [(b'_{33})^{(6)} - (b''_{33})^{(6)}(G_{35})]T_{33} = 0$	580

$$(b_{34})^{(6)}T_{33} - [(b'_{34})^{(6)} - (b''_{34})^{(6)}(G_{35})]T_{34} = 0 \quad 584$$

has a unique positive solution , which is an equilibrium solution for the system 582

$$(a_{36})^{(7)}G_{37} - [(a'_{36})^{(7)} + (a''_{36})^{(7)}(T_{37})]G_{36} = 0 \quad 583$$

$$(a_{37})^{(7)}G_{36} - [(a'_{37})^{(7)} + (a''_{37})^{(7)}(T_{37})]G_{37} = 0 \quad 584$$

$$(a_{38})^{(7)}G_{37} - [(a'_{38})^{(7)} + (a''_{38})^{(7)}(T_{37})]G_{38} = 0 \quad 585$$

$$(b_{36})^{(7)}T_{37} - [(b'_{36})^{(7)} - (b''_{36})^{(7)}(G_{39})]T_{36} = 0 \quad 586$$

$$(b_{37})^{(7)}T_{36} - [(b'_{37})^{(7)} - (b''_{37})^{(7)}(G_{39})]T_{37} = 0 \quad 588$$

$$(b_{38})^{(7)}T_{37} - [(b'_{38})^{(7)} - (b''_{38})^{(7)}(G_{39})]T_{38} = 0 \quad 589$$

has a unique positive solution , which is an equilibrium solution for the system 560

(a) Indeed the first two equations have a nontrivial solution G_{36}, G_{37} if

$$F(T_{39}) = (a'_{36})^{(7)}(a'_{37})^{(7)} - (a_{36})^{(7)}(a_{37})^{(7)} + (a'_{36})^{(7)}(a''_{37})^{(7)}(T_{37}) + (a'_{37})^{(7)}(a''_{36})^{(7)}(T_{37}) + (a_{36})^{(7)}(T_{37})(a''_{37})^{(7)}(T_{37}) = 0$$

Definition and uniqueness of T_{37}^* :- 561

After hypothesis $f(0) < 0, f(\infty) > 0$ and the functions $(a_i'')^{(7)}(T_{37})$ being increasing, it follows that there exists a unique T_{37}^* for which $f(T_{37}^*) = 0$. With this value , we obtain from the three first equations

$$G_{36} = \frac{(a_{36})^{(7)}G_{37}}{[(a'_{36})^{(7)} + (a_{36})^{(7)}(T_{37}^*)]} , \quad G_{38} = \frac{(a_{38})^{(7)}G_{37}}{[(a'_{38})^{(7)} + (a_{38})^{(7)}(T_{37}^*)]}$$

(e) By the same argument, the equations(SOLUTIONAL) admit solutions G_{36}, G_{37} if

$$\varphi(G_{39}) = (b'_{36})^{(7)}(b'_{37})^{(7)} - (b_{36})^{(7)}(b_{37})^{(7)} - [(b'_{36})^{(7)}(b''_{37})^{(7)}(G_{39}) + (b'_{37})^{(7)}(b''_{36})^{(7)}(G_{39})] + (b''_{36})^{(7)}(G_{39})(b''_{37})^{(7)}(G_{39}) = 0$$

Where in $(G_{39})(G_{36}, G_{37}, G_{38}), G_{36}, G_{38}$ must be replaced by their values from 96. It is easy to see that φ is a decreasing function in G_{37} taking into account the hypothesis $\varphi(0) > 0, \varphi(\infty) < 0$ it follows that there exists a unique G_{37}^* such that $\varphi(G^*) = 0$ 562

Finally we obtain the unique solution OF THE SYSTEM

G_{37}^* given by $\varphi((G_{39})^*) = 0, T_{37}^*$ given by $f(T_{37}^*) = 0$ and

$$G_{36}^* = \frac{(a_{36})^{(7)}G_{37}^*}{[(a'_{36})^{(7)} + (a_{36})^{(7)}(T_{37}^*)]} , \quad G_{38}^* = \frac{(a_{38})^{(7)}G_{37}^*}{[(a'_{38})^{(7)} + (a_{38})^{(7)}(T_{37}^*)]}$$

$$T_{36}^* = \frac{(b_{36})^{(7)}T_{37}^*}{[(b'_{36})^{(7)} - (b_{36})^{(7)}((G_{39})^*)]} , \quad T_{38}^* = \frac{(b_{38})^{(7)}T_{37}^*}{[(b'_{38})^{(7)} - (b_{38})^{(7)}((G_{39})^*)]} \quad 563$$

Definition and uniqueness of T_{21}^* :- 564

After hypothesis $f(0) < 0, f(\infty) > 0$ and the functions $(a_i'')^{(1)}(T_{21})$ being increasing, it follows that there exists a unique T_{21}^* for which $f(T_{21}^*) = 0$. With this value , we obtain from the three first equations

$$G_{20} = \frac{(a_{20})^{(3)}G_{21}}{[(a'_{20})^{(3)} + (a_{20})^{(3)}(T_{21}^*)]} , \quad G_{22} = \frac{(a_{22})^{(3)}G_{21}}{[(a'_{22})^{(3)} + (a_{22})^{(3)}(T_{21}^*)]}$$

Definition and uniqueness of T_{25}^* :- 566

After hypothesis $f(0) < 0, f(\infty) > 0$ and the functions $(a_i'')^{(4)}(T_{25})$ being increasing, it follows that there exists a unique T_{25}^* for which $f(T_{25}^*) = 0$. With this value , we obtain from the three first equations

$$G_{24} = \frac{(a_{24})^{(4)}G_{25}}{[(a'_{24})^{(4)} + (a_{24})^{(4)}(T_{25}^*)]} , \quad G_{26} = \frac{(a_{26})^{(4)}G_{25}}{[(a'_{26})^{(4)} + (a_{26})^{(4)}(T_{25}^*)]}$$

Definition and uniqueness of T_{29}^* :- 567

After hypothesis $f(0) < 0, f(\infty) > 0$ and the functions $(a_i'')^{(5)}(T_{29})$ being increasing, it follows that there exists a unique T_{29}^* for which $f(T_{29}^*) = 0$. With this value , we obtain from the three first equations

$$G_{28} = \frac{(a_{28})^{(5)}G_{29}}{[(a'_{28})^{(5)} + (a_{28})^{(5)}(T_{29}^*)]} , \quad G_{30} = \frac{(a_{30})^{(5)}G_{29}}{[(a'_{30})^{(5)} + (a_{30})^{(5)}(T_{29}^*)]}$$

Definition and uniqueness of T_{33}^* :- 568

After hypothesis $f(0) < 0, f(\infty) > 0$ and the functions $(a_i'')^{(6)}(T_{33})$ being increasing, it follows that there exists a unique T_{33}^* for which $f(T_{33}^*) = 0$. With this value , we obtain from the three first equations

$$G_{32} = \frac{(a_{32})^{(6)}G_{33}}{[(a'_{32})^{(6)}+(a''_{32})^{(6)}(T_{33}^*)]} , \quad G_{34} = \frac{(a_{34})^{(6)}G_{33}}{[(a'_{34})^{(6)}+(a''_{34})^{(6)}(T_{33}^*)]}$$

(f) By the same argument, the equations 92,93 admit solutions G_{13}, G_{14} if 569

$$\varphi(G) = (b'_{13})^{(1)}(b'_{14})^{(1)} - (b''_{13})^{(1)}(b''_{14})^{(1)} - [(b'_{13})^{(1)}(b''_{14})^{(1)}(G) + (b'_{14})^{(1)}(b''_{13})^{(1)}(G)] + (b''_{13})^{(1)}(G)(b''_{14})^{(1)}(G) = 0$$

Where in $G(G_{13}, G_{14}, G_{15}), G_{13}, G_{15}$ must be replaced by their values from 96. It is easy to see that φ is a decreasing function in G_{14} taking into account the hypothesis $\varphi(0) > 0, \varphi(\infty) < 0$ it follows that there exists a unique G_{14}^* such that $\varphi(G^*) = 0$

(g) By the same argument, the equations 92,93 admit solutions G_{16}, G_{17} if 570

$$\varphi(G_{19}) = (b'_{16})^{(2)}(b'_{17})^{(2)} - (b''_{16})^{(2)}(b''_{17})^{(2)} - [(b'_{16})^{(2)}(b''_{17})^{(2)}(G_{19}) + (b'_{17})^{(2)}(b''_{16})^{(2)}(G_{19})] + (b''_{16})^{(2)}(G_{19})(b''_{17})^{(2)}(G_{19}) = 0$$

Where in $(G_{19})(G_{16}, G_{17}, G_{18}), G_{16}, G_{18}$ must be replaced by their values from 96. It is easy to see that φ is a decreasing function in G_{17} taking into account the hypothesis $\varphi(0) > 0, \varphi(\infty) < 0$ it follows that there exists a unique G_{17}^* such that $\varphi((G_{19})^*) = 0$ 571

(a) By the same argument, the concatenated equations admit solutions G_{20}, G_{21} if 572

$$\varphi(G_{23}) = (b'_{20})^{(3)}(b'_{21})^{(3)} - (b''_{20})^{(3)}(b''_{21})^{(3)} - [(b'_{20})^{(3)}(b''_{21})^{(3)}(G_{23}) + (b'_{21})^{(3)}(b''_{20})^{(3)}(G_{23})] + (b''_{20})^{(3)}(G_{23})(b''_{21})^{(3)}(G_{23}) = 0$$

Where in $G_{23}(G_{20}, G_{21}, G_{22}), G_{20}, G_{22}$ must be replaced by their values from 96. It is easy to see that φ is a decreasing function in G_{21} taking into account the hypothesis $\varphi(0) > 0, \varphi(\infty) < 0$ it follows that there exists a unique G_{21}^* such that $\varphi((G_{23})^*) = 0$ 573

(b) By the same argument, the equations of modules admit solutions G_{24}, G_{25} if 574

$$\varphi(G_{27}) = (b'_{24})^{(4)}(b'_{25})^{(4)} - (b''_{24})^{(4)}(b''_{25})^{(4)} - [(b'_{24})^{(4)}(b''_{25})^{(4)}(G_{27}) + (b'_{25})^{(4)}(b''_{24})^{(4)}(G_{27})] + (b''_{24})^{(4)}(G_{27})(b''_{25})^{(4)}(G_{27}) = 0$$

Where in $(G_{27})(G_{24}, G_{25}, G_{26}), G_{24}, G_{26}$ must be replaced by their values from 96. It is easy to see that φ is a decreasing function in G_{25} taking into account the hypothesis $\varphi(0) > 0, \varphi(\infty) < 0$ it follows that there exists a unique G_{25}^* such that $\varphi((G_{27})^*) = 0$

(c) By the same argument, the equations (modules) admit solutions G_{28}, G_{29} if 575

$$\varphi(G_{31}) = (b'_{28})^{(5)}(b'_{29})^{(5)} - (b''_{28})^{(5)}(b''_{29})^{(5)} - [(b'_{28})^{(5)}(b''_{29})^{(5)}(G_{31}) + (b'_{29})^{(5)}(b''_{28})^{(5)}(G_{31})] + (b''_{28})^{(5)}(G_{31})(b''_{29})^{(5)}(G_{31}) = 0$$

Where in $(G_{31})(G_{28}, G_{29}, G_{30}), G_{28}, G_{30}$ must be replaced by their values from 96. It is easy to see that φ is a decreasing function in G_{29} taking into account the hypothesis $\varphi(0) > 0, \varphi(\infty) < 0$ it follows that there exists a unique G_{29}^* such that $\varphi((G_{31})^*) = 0$

(d) By the same argument, the equations (modules) admit solutions G_{32}, G_{33} if 578

$$\varphi(G_{35}) = (b'_{32})^{(6)}(b'_{33})^{(6)} - (b''_{32})^{(6)}(b''_{33})^{(6)} - [(b'_{32})^{(6)}(b''_{33})^{(6)}(G_{35}) + (b'_{33})^{(6)}(b''_{32})^{(6)}(G_{35})] + (b''_{32})^{(6)}(G_{35})(b''_{33})^{(6)}(G_{35}) = 0$$

Where in $(G_{35})(G_{32}, G_{33}, G_{34}), G_{32}, G_{34}$ must be replaced by their values It is easy to see that φ is a decreasing function in G_{33} taking into account the hypothesis $\varphi(0) > 0, \varphi(\infty) < 0$ it follows that there exists a unique G_{33}^* such that $\varphi(G^*) = 0$ 580
581

Finally we obtain the unique solution of 89 to 94 582

G_{14}^* given by $\varphi(G^*) = 0, T_{14}^*$ given by $f(T_{14}^*) = 0$ and

$$G_{13}^* = \frac{(a_{13})^{(1)}G_{14}^*}{[(a'_{13})^{(1)}+(a''_{13})^{(1)}(T_{14}^*)]} , \quad G_{15}^* = \frac{(a_{15})^{(1)}G_{14}^*}{[(a'_{15})^{(1)}+(a''_{15})^{(1)}(T_{14}^*)]}$$

$$T_{13}^* = \frac{(b_{13})^{(1)}T_{14}^*}{[(b'_{13})^{(1)}-(b''_{13})^{(1)}(G^*)]} , \quad T_{15}^* = \frac{(b_{15})^{(1)}T_{14}^*}{[(b'_{15})^{(1)}-(b''_{15})^{(1)}(G^*)]}$$

Obviously, these values represent an equilibrium solution

Finally we obtain the unique solution 583

G_{17}^* given by $\varphi((G_{19})^*) = 0, T_{17}^*$ given by $f(T_{17}^*) = 0$ and 584

$$G_{16}^* = \frac{(a_{16})^{(2)}G_{17}^*}{[(a'_{16})^{(2)}+(a''_{16})^{(2)}(T_{17}^*)]} , \quad G_{18}^* = \frac{(a_{18})^{(2)}G_{17}^*}{[(a'_{18})^{(2)}+(a''_{18})^{(2)}(T_{17}^*)]}$$

$$T_{16}^* = \frac{(b_{16})^{(2)}T_{17}^*}{[(b'_{16})^{(2)}-(b''_{16})^{(2)}((G_{19})^*)]} , \quad T_{18}^* = \frac{(b_{18})^{(2)}T_{17}^*}{[(b'_{18})^{(2)}-(b''_{18})^{(2)}((G_{19})^*)]}$$

Obviously, these values represent an equilibrium solution 587

Finally we obtain the unique solution 588

G_{21}^* given by $\varphi((G_{23})^*) = 0, T_{21}^*$ given by $f(T_{21}^*) = 0$ and

$$G_{20}^* = \frac{(a_{20})^{(3)}G_{21}^*}{[(a'_{20})^{(3)}+(a''_{20})^{(3)}(T_{21}^*)]} , \quad G_{22}^* = \frac{(a_{22})^{(3)}G_{21}^*}{[(a'_{22})^{(3)}+(a''_{22})^{(3)}(T_{21}^*)]}$$

$$T_{20}^* = \frac{(b_{20})^{(3)}T_{21}^*}{[(b_{20})^{(3)} - (b_{20}'')^{(3)}(G_{23}^*)]} , T_{22}^* = \frac{(b_{22})^{(3)}T_{21}^*}{[(b_{22})^{(3)} - (b_{22}'')^{(3)}(G_{23}^*)]}$$

Obviously, these values represent an equilibrium solution

Finally we obtain the unique solution

G_{25}^* given by $\varphi(G_{27}) = 0$, T_{25}^* given by $f(T_{25}^*) = 0$ and

$$G_{24}^* = \frac{(a_{24})^{(4)}G_{25}^*}{[(a_{24})^{(4)} + (a_{24}'')^{(4)}(T_{25}^*)]} , G_{26}^* = \frac{(a_{26})^{(4)}G_{25}^*}{[(a_{26})^{(4)} + (a_{26}'')^{(4)}(T_{25}^*)]}$$

$$T_{24}^* = \frac{(b_{24})^{(4)}T_{25}^*}{[(b_{24})^{(4)} - (b_{24}'')^{(4)}((G_{27})^*)]} , T_{26}^* = \frac{(b_{26})^{(4)}T_{25}^*}{[(b_{26})^{(4)} - (b_{26}'')^{(4)}((G_{27})^*)]}$$

Obviously, these values represent an equilibrium solution

Finally we obtain the unique solution

G_{29}^* given by $\varphi((G_{31})^*) = 0$, T_{29}^* given by $f(T_{29}^*) = 0$ and

$$G_{28}^* = \frac{(a_{28})^{(5)}G_{29}^*}{[(a_{28})^{(5)} + (a_{28}'')^{(5)}(T_{29}^*)]} , G_{30}^* = \frac{(a_{30})^{(5)}G_{29}^*}{[(a_{30})^{(5)} + (a_{30}'')^{(5)}(T_{29}^*)]}$$

$$T_{28}^* = \frac{(b_{28})^{(5)}T_{29}^*}{[(b_{28})^{(5)} - (b_{28}'')^{(5)}((G_{31})^*)]} , T_{30}^* = \frac{(b_{30})^{(5)}T_{29}^*}{[(b_{30})^{(5)} - (b_{30}'')^{(5)}((G_{31})^*)]}$$

Obviously, these values represent an equilibrium solution

Finally we obtain the unique solution

G_{33}^* given by $\varphi((G_{35})^*) = 0$, T_{33}^* given by $f(T_{33}^*) = 0$ and

$$G_{32}^* = \frac{(a_{32})^{(6)}G_{33}^*}{[(a_{32})^{(6)} + (a_{32}'')^{(6)}(T_{33}^*)]} , G_{34}^* = \frac{(a_{34})^{(6)}G_{33}^*}{[(a_{34})^{(6)} + (a_{34}'')^{(6)}(T_{33}^*)]}$$

$$T_{32}^* = \frac{(b_{32})^{(6)}T_{33}^*}{[(b_{32})^{(6)} - (b_{32}'')^{(6)}((G_{35})^*)]} , T_{34}^* = \frac{(b_{34})^{(6)}T_{33}^*}{[(b_{34})^{(6)} - (b_{34}'')^{(6)}((G_{35})^*)]}$$

Obviously, these values represent an equilibrium solution

ASYMPTOTIC STABILITY ANALYSIS

Theorem 4: If the conditions of the previous theorem are satisfied and if the functions $(a_i'')^{(1)}$ and $(b_i'')^{(1)}$ Belong to $C^{(1)}(\mathbb{R}_+)$ then the above equilibrium point is asymptotically stable.

Proof: Denote

Definition of G_i, T_i :-

$$G_i = G_i^* + G_i , T_i = T_i^* + T_i$$

$$\frac{\partial (a_{14}'')^{(1)}}{\partial T_{14}}(T_{14}^*) = (q_{14})^{(1)} , \frac{\partial (b_i'')^{(1)}}{\partial G_j}(G^*) = s_{ij}$$

Then taking into account equations (global) and neglecting the terms of power 2, we obtain

$$\frac{dG_{13}}{dt} = -((a_{13}')^{(1)} + (p_{13})^{(1)})G_{13} + (a_{13})^{(1)}G_{14} - (q_{13})^{(1)}G_{13}^*T_{14}$$

$$\frac{dG_{14}}{dt} = -((a_{14}')^{(1)} + (p_{14})^{(1)})G_{14} + (a_{14})^{(1)}G_{13} - (q_{14})^{(1)}G_{14}^*T_{14}$$

$$\frac{dG_{15}}{dt} = -((a_{15}')^{(1)} + (p_{15})^{(1)})G_{15} + (a_{15})^{(1)}G_{14} - (q_{15})^{(1)}G_{15}^*T_{14}$$

$$\frac{dT_{13}}{dt} = -((b_{13}')^{(1)} - (r_{13})^{(1)})T_{13} + (b_{13})^{(1)}T_{14} + \sum_{j=13}^{15} (s_{(13)(j)})T_{13}^*G_j$$

$$\frac{dT_{14}}{dt} = -((b_{14}')^{(1)} - (r_{14})^{(1)})T_{14} + (b_{14})^{(1)}T_{13} + \sum_{j=13}^{15} (s_{(14)(j)})T_{14}^*G_j$$

$$\frac{dT_{15}}{dt} = -((b_{15}')^{(1)} - (r_{15})^{(1)})T_{15} + (b_{15})^{(1)}T_{14} + \sum_{j=13}^{15} (s_{(15)(j)})T_{15}^*G_j$$

If the conditions of the previous theorem are satisfied and if the functions $(a_i'')^{(2)}$ and $(b_i'')^{(2)}$ Belong to $C^{(2)}(\mathbb{R}_+)$ then the above equilibrium point is asymptotically stable

Denote

Definition of G_i, T_i :-

$$G_i = G_i^* + G_i , T_i = T_i^* + T_i$$

$$\frac{\partial (a_{17}'')^{(2)}}{\partial T_{17}}(T_{17}^*) = (q_{17})^{(2)} , \frac{\partial (b_i'')^{(2)}}{\partial G_j}((G_{19})^*) = s_{ij}$$

taking into account equations (global) and neglecting the terms of power 2, we obtain

$$\frac{dG_{16}}{dt} = -((a_{16}')^{(2)} + (p_{16})^{(2)})G_{16} + (a_{16})^{(2)}G_{17} - (q_{16})^{(2)}G_{16}^*T_{17}$$

$$\frac{dG_{17}}{dt} = -((a_{17}')^{(2)} + (p_{17})^{(2)})G_{17} + (a_{17})^{(2)}G_{16} - (q_{17})^{(2)}G_{17}^*T_{17}$$

$$\frac{dG_{18}}{dt} = -((a_{18}')^{(2)} + (p_{18})^{(2)})G_{18} + (a_{18})^{(2)}G_{17} - (q_{18})^{(2)}G_{18}^*T_{17}$$

$$\frac{dT_{16}}{dt} = -((b_{16}')^{(2)} - (r_{16})^{(2)})T_{16} + (b_{16})^{(2)}T_{17} + \sum_{j=16}^{18} (s_{(16)(j)})T_{16}^*G_j$$

$$\frac{dT_{17}}{dt} = -((b_{17}')^{(2)} - (r_{17})^{(2)})T_{17} + (b_{17})^{(2)}T_{16} + \sum_{j=16}^{18} (s_{(17)(j)})T_{17}^*G_j$$

$$\frac{dT_{18}}{dt} = -((b_{18}')^{(2)} - (r_{18})^{(2)})T_{18} + (b_{18})^{(2)}T_{17} + \sum_{j=16}^{18} (s_{(18)(j)})T_{18}^*G_j$$

If the conditions of the previous theorem are satisfied and if the functions $(a_i'')^{(3)}$ and $(b_i'')^{(3)}$ Belong to $C^{(3)}(\mathbb{R}_+)$ then the above equilibrium point is asymptotically stable

Denote

Definition of G_i, T_i :-

$$G_i = G_i^* + \mathbb{G}_i, T_i = T_i^* + \mathbb{T}_i$$

$$\frac{\partial (a_{21}''^{(3)})}{\partial T_{21}} (T_{21}^*) = (q_{21})^{(3)}, \frac{\partial (b_i''^{(3)})}{\partial G_j} ((G_{23})^*) = s_{ij}$$

Then taking into account equations (global) and neglecting the terms of power 2, we obtain

$$\frac{d\mathbb{G}_{20}}{dt} = -((a'_{20})^{(3)} + (p_{20})^{(3)})\mathbb{G}_{20} + (a_{20})^{(3)}\mathbb{G}_{21} - (q_{20})^{(3)}G_{20}^* \mathbb{T}_{21} \tag{616}$$

$$\frac{d\mathbb{G}_{21}}{dt} = -((a'_{21})^{(3)} + (p_{21})^{(3)})\mathbb{G}_{21} + (a_{21})^{(3)}\mathbb{G}_{20} - (q_{21})^{(3)}G_{21}^* \mathbb{T}_{21} \tag{617}$$

$$\frac{d\mathbb{G}_{22}}{dt} = -((a'_{22})^{(3)} + (p_{22})^{(3)})\mathbb{G}_{22} + (a_{22})^{(3)}\mathbb{G}_{21} - (q_{22})^{(3)}G_{22}^* \mathbb{T}_{21} \tag{618}$$

$$\frac{d\mathbb{T}_{20}}{dt} = -((b'_{20})^{(3)} - (r_{20})^{(3)})\mathbb{T}_{20} + (b_{20})^{(3)}\mathbb{T}_{21} + \sum_{j=20}^{22} (s_{(20)(j)})T_{20}^* \mathbb{G}_j \tag{619}$$

$$\frac{d\mathbb{T}_{21}}{dt} = -((b'_{21})^{(3)} - (r_{21})^{(3)})\mathbb{T}_{21} + (b_{21})^{(3)}\mathbb{T}_{20} + \sum_{j=20}^{22} (s_{(21)(j)})T_{21}^* \mathbb{G}_j \tag{620}$$

$$\frac{d\mathbb{T}_{22}}{dt} = -((b'_{22})^{(3)} - (r_{22})^{(3)})\mathbb{T}_{22} + (b_{22})^{(3)}\mathbb{T}_{21} + \sum_{j=20}^{22} (s_{(22)(j)})T_{22}^* \mathbb{G}_j \tag{621}$$

If the conditions of the previous theorem are satisfied and if the functions $(a_i'')^{(4)}$ and $(b_i'')^{(4)}$ belong to $C^{(4)}(\mathbb{R}_+)$ then the above equilibrium point is asymptotically stable

Denote

Definition of $\mathbb{G}_i, \mathbb{T}_i$:-

$$G_i = G_i^* + \mathbb{G}_i, T_i = T_i^* + \mathbb{T}_i$$

$$\frac{\partial (a_{25}''^{(4)})}{\partial T_{25}} (T_{25}^*) = (q_{25})^{(4)}, \frac{\partial (b_i''^{(4)})}{\partial G_j} ((G_{27})^*) = s_{ij}$$

Then taking into account equations (global) and neglecting the terms of power 2, we obtain

$$\frac{d\mathbb{G}_{24}}{dt} = -((a'_{24})^{(4)} + (p_{24})^{(4)})\mathbb{G}_{24} + (a_{24})^{(4)}\mathbb{G}_{25} - (q_{24})^{(4)}G_{24}^* \mathbb{T}_{25} \tag{622}$$

$$\frac{d\mathbb{G}_{25}}{dt} = -((a'_{25})^{(4)} + (p_{25})^{(4)})\mathbb{G}_{25} + (a_{25})^{(4)}\mathbb{G}_{24} - (q_{25})^{(4)}G_{25}^* \mathbb{T}_{25} \tag{623}$$

$$\frac{d\mathbb{G}_{26}}{dt} = -((a'_{26})^{(4)} + (p_{26})^{(4)})\mathbb{G}_{26} + (a_{26})^{(4)}\mathbb{G}_{25} - (q_{26})^{(4)}G_{26}^* \mathbb{T}_{25} \tag{624}$$

$$\frac{d\mathbb{T}_{24}}{dt} = -((b'_{24})^{(4)} - (r_{24})^{(4)})\mathbb{T}_{24} + (b_{24})^{(4)}\mathbb{T}_{25} + \sum_{j=24}^{26} (s_{(24)(j)})T_{24}^* \mathbb{G}_j \tag{625}$$

$$\frac{d\mathbb{T}_{25}}{dt} = -((b'_{25})^{(4)} - (r_{25})^{(4)})\mathbb{T}_{25} + (b_{25})^{(4)}\mathbb{T}_{24} + \sum_{j=24}^{26} (s_{(25)(j)})T_{25}^* \mathbb{G}_j \tag{626}$$

$$\frac{d\mathbb{T}_{26}}{dt} = -((b'_{26})^{(4)} - (r_{26})^{(4)})\mathbb{T}_{26} + (b_{26})^{(4)}\mathbb{T}_{25} + \sum_{j=24}^{26} (s_{(26)(j)})T_{26}^* \mathbb{G}_j \tag{627}$$

If the conditions of the previous theorem are satisfied and if the functions $(a_i'')^{(5)}$ and $(b_i'')^{(5)}$ belong to $C^{(5)}(\mathbb{R}_+)$ then the above equilibrium point is asymptotically stable

Denote

Definition of $\mathbb{G}_i, \mathbb{T}_i$:-

$$G_i = G_i^* + \mathbb{G}_i, T_i = T_i^* + \mathbb{T}_i$$

$$\frac{\partial (a_{29}''^{(5)})}{\partial T_{29}} (T_{29}^*) = (q_{29})^{(5)}, \frac{\partial (b_i''^{(5)})}{\partial G_j} ((G_{31})^*) = s_{ij}$$

Then taking into account equations (global) and neglecting the terms of power 2, we obtain

$$\frac{d\mathbb{G}_{28}}{dt} = -((a'_{28})^{(5)} + (p_{28})^{(5)})\mathbb{G}_{28} + (a_{28})^{(5)}\mathbb{G}_{29} - (q_{28})^{(5)}G_{28}^* \mathbb{T}_{29} \tag{628}$$

$$\frac{d\mathbb{G}_{29}}{dt} = -((a'_{29})^{(5)} + (p_{29})^{(5)})\mathbb{G}_{29} + (a_{29})^{(5)}\mathbb{G}_{28} - (q_{29})^{(5)}G_{29}^* \mathbb{T}_{29} \tag{629}$$

$$\frac{d\mathbb{G}_{30}}{dt} = -((a'_{30})^{(5)} + (p_{30})^{(5)})\mathbb{G}_{30} + (a_{30})^{(5)}\mathbb{G}_{29} - (q_{30})^{(5)}G_{30}^* \mathbb{T}_{29} \tag{630}$$

$$\frac{d\mathbb{T}_{28}}{dt} = -((b'_{28})^{(5)} - (r_{28})^{(5)})\mathbb{T}_{28} + (b_{28})^{(5)}\mathbb{T}_{29} + \sum_{j=28}^{30} (s_{(28)(j)})T_{28}^* \mathbb{G}_j \tag{631}$$

$$\frac{d\mathbb{T}_{29}}{dt} = -((b'_{29})^{(5)} - (r_{29})^{(5)})\mathbb{T}_{29} + (b_{29})^{(5)}\mathbb{T}_{28} + \sum_{j=28}^{30} (s_{(29)(j)})T_{29}^* \mathbb{G}_j \tag{632}$$

$$\frac{d\mathbb{T}_{30}}{dt} = -((b'_{30})^{(5)} - (r_{30})^{(5)})\mathbb{T}_{30} + (b_{30})^{(5)}\mathbb{T}_{29} + \sum_{j=28}^{30} (s_{(30)(j)})T_{30}^* \mathbb{G}_j \tag{633}$$

If the conditions of the previous theorem are satisfied and if the functions $(a_i'')^{(6)}$ and $(b_i'')^{(6)}$ belong to $C^{(6)}(\mathbb{R}_+)$ then the above equilibrium point is asymptotically stable

Denote

Definition of $\mathbb{G}_i, \mathbb{T}_i$:-

$$G_i = G_i^* + \mathbb{G}_i, T_i = T_i^* + \mathbb{T}_i$$

$$\frac{\partial (a_{33}''^{(6)})}{\partial T_{33}} (T_{33}^*) = (q_{33})^{(6)}, \frac{\partial (b_i''^{(6)})}{\partial G_j} ((G_{35})^*) = s_{ij}$$

Then taking into account equations(global) and neglecting the terms of power 2, we obtain

$$\frac{d\mathbb{G}_{32}}{dt} = -((a'_{32})^{(6)} + (p_{32})^{(6)})\mathbb{G}_{32} + (a_{32})^{(6)}\mathbb{G}_{33} - (q_{32})^{(6)}G_{32}^* \mathbb{T}_{33} \tag{634}$$

$$\frac{d\mathbb{G}_{33}}{dt} = -((a'_{33})^{(6)} + (p_{33})^{(6)})\mathbb{G}_{33} + (a_{33})^{(6)}\mathbb{G}_{32} - (q_{33})^{(6)}G_{33}^* \mathbb{T}_{33} \tag{635}$$

$$\frac{d\mathbb{G}_{34}}{dt} = -((a'_{34})^{(6)} + (p_{34})^{(6)})\mathbb{G}_{34} + (a_{34})^{(6)}\mathbb{G}_{33} - (q_{34})^{(6)}G_{34}^* \mathbb{T}_{33} \tag{636}$$

$$\frac{d\mathbb{T}_{32}}{dt} = -((b'_{32})^{(6)} - (r_{32})^{(6)})\mathbb{T}_{32} + (b_{32})^{(6)}\mathbb{T}_{33} + \sum_{j=32}^{34} (s_{(32)(j)})T_{32}^* \mathbb{G}_j \tag{637}$$

$$\frac{dT_{33}}{dt} = -((b'_{33})^{(6)} - (r_{33})^{(6)})T_{33} + (b_{33})^{(6)}T_{32} + \sum_{j=32}^{34} (s_{(33)(j)})T_{33}^* G_j \quad 649$$

$$\frac{dT_{34}}{dt} = -((b'_{34})^{(6)} - (r_{34})^{(6)})T_{34} + (b_{34})^{(6)}T_{33} + \sum_{j=32}^{34} (s_{(34)(j)})T_{34}^* G_j \quad 650$$

Obviously, these values represent an equilibrium solution of 79,20,36,22,23, 651

If the conditions of the previous theorem are satisfied and if the functions $(a_i'')^{(7)}$ and $(b_i'')^{(7)}$ belong to $C^{(7)}(\mathbb{R}_+)$ then the above equilibrium point is asymptotically stable.

Proof: Denote

Definition of G_i, T_i :- 652

$$G_i = G_i^* + G_i \quad , \quad T_i = T_i^* + T_i \quad 653$$

$$\frac{\partial (a_{37}'')^{(7)}}{\partial T_{37}}(T_{37}^*) = (q_{37})^{(7)} \quad , \quad \frac{\partial (b_i'')^{(7)}}{\partial G_j}((G_{39})^{**}) = s_{ij}$$

Then taking into account equations(SOLUTIONAL) and neglecting the terms of power 2, we obtain 654

$$\frac{dG_{36}}{dt} = -((a'_{36})^{(7)} + (p_{36})^{(7)})G_{36} + (a_{36})^{(7)}G_{37} - (q_{36})^{(7)}G_{36}^* T_{37} \quad 655$$

$$\frac{dG_{37}}{dt} = -((a'_{37})^{(7)} + (p_{37})^{(7)})G_{37} + (a_{37})^{(7)}G_{36} - (q_{37})^{(7)}G_{37}^* T_{37} \quad 657$$

$$\frac{dG_{38}}{dt} = -((a'_{38})^{(7)} + (p_{38})^{(7)})G_{38} + (a_{38})^{(7)}G_{37} - (q_{38})^{(7)}G_{38}^* T_{37} \quad 658$$

$$\frac{dT_{36}}{dt} = -((b'_{36})^{(7)} - (r_{36})^{(7)})T_{36} + (b_{36})^{(7)}T_{37} + \sum_{j=36}^{38} (s_{(36)(j)})T_{36}^* G_j \quad 659$$

$$\frac{dT_{37}}{dt} = -((b'_{37})^{(7)} - (r_{37})^{(7)})T_{37} + (b_{37})^{(7)}T_{36} + \sum_{j=36}^{38} (s_{(37)(j)})T_{37}^* G_j \quad 660$$

$$\frac{dT_{38}}{dt} = -((b'_{38})^{(7)} - (r_{38})^{(7)})T_{38} + (b_{38})^{(7)}T_{37} + \sum_{j=36}^{38} (s_{(38)(j)})T_{38}^* G_j \quad 661$$

2. 662

The characteristic equation of this system is

$$\begin{aligned} & ((\lambda)^{(1)} + (b'_{15})^{(1)} - (r_{15})^{(1)})\{((\lambda)^{(1)} + (a'_{15})^{(1)} + (p_{15})^{(1)}) \\ & \left[((\lambda)^{(1)} + (a'_{13})^{(1)} + (p_{13})^{(1)})(q_{14})^{(1)}G_{14}^* + (a_{14})^{(1)}(q_{13})^{(1)}G_{13}^* \right] \\ & \left(((\lambda)^{(1)} + (b'_{13})^{(1)} - (r_{13})^{(1)})s_{(14),(14)}T_{14}^* + (b_{14})^{(1)}s_{(13),(14)}T_{14}^* \right) \\ & + \left(((\lambda)^{(1)} + (a'_{14})^{(1)} + (p_{14})^{(1)})(q_{13})^{(1)}G_{13}^* + (a_{13})^{(1)}(q_{14})^{(1)}G_{14}^* \right) \\ & \left(((\lambda)^{(1)} + (b'_{13})^{(1)} - (r_{13})^{(1)})s_{(14),(13)}T_{14}^* + (b_{14})^{(1)}s_{(13),(13)}T_{13}^* \right) \\ & \left(((\lambda)^{(1)})^2 + ((a'_{13})^{(1)} + (a'_{14})^{(1)} + (p_{13})^{(1)} + (p_{14})^{(1)}) (\lambda)^{(1)} \right) \\ & \left(((\lambda)^{(1)})^2 + ((b'_{13})^{(1)} + (b'_{14})^{(1)} - (r_{13})^{(1)} + (r_{14})^{(1)}) (\lambda)^{(1)} \right) \\ & + \left(((\lambda)^{(1)})^2 + ((a'_{13})^{(1)} + (a'_{14})^{(1)} + (p_{13})^{(1)} + (p_{14})^{(1)}) (\lambda)^{(1)} \right) (q_{15})^{(1)}G_{15} \\ & + ((\lambda)^{(1)} + (a'_{13})^{(1)} + (p_{13})^{(1)}) ((a_{15})^{(1)}(q_{14})^{(1)}G_{14}^* + (a_{14})^{(1)}(a_{15})^{(1)}(q_{13})^{(1)}G_{13}^*) \\ & \left(((\lambda)^{(1)} + (b'_{13})^{(1)} - (r_{13})^{(1)})s_{(14),(15)}T_{14}^* + (b_{14})^{(1)}s_{(13),(15)}T_{13}^* \right)\} = 0 \\ & + \\ & ((\lambda)^{(2)} + (b'_{18})^{(2)} - (r_{18})^{(2)})\{((\lambda)^{(2)} + (a'_{18})^{(2)} + (p_{18})^{(2)}) \\ & \left[((\lambda)^{(2)} + (a'_{16})^{(2)} + (p_{16})^{(2)})(q_{17})^{(2)}G_{17}^* + (a_{17})^{(2)}(q_{16})^{(2)}G_{16}^* \right] \\ & \left(((\lambda)^{(2)} + (b'_{16})^{(2)} - (r_{16})^{(2)})s_{(17),(17)}T_{17}^* + (b_{17})^{(2)}s_{(16),(17)}T_{17}^* \right) \\ & + \left(((\lambda)^{(2)} + (a'_{17})^{(2)} + (p_{17})^{(2)})(q_{16})^{(2)}G_{16}^* + (a_{16})^{(2)}(q_{17})^{(2)}G_{17}^* \right) \\ & \left(((\lambda)^{(2)} + (b'_{16})^{(2)} - (r_{16})^{(2)})s_{(17),(16)}T_{17}^* + (b_{17})^{(2)}s_{(16),(16)}T_{16}^* \right) \\ & \left(((\lambda)^{(2)})^2 + ((a'_{16})^{(2)} + (a'_{17})^{(2)} + (p_{16})^{(2)} + (p_{17})^{(2)}) (\lambda)^{(2)} \right) \\ & \left(((\lambda)^{(2)})^2 + ((b'_{16})^{(2)} + (b'_{17})^{(2)} - (r_{16})^{(2)} + (r_{17})^{(2)}) (\lambda)^{(2)} \right) \\ & + \left(((\lambda)^{(2)})^2 + ((a'_{16})^{(2)} + (a'_{17})^{(2)} + (p_{16})^{(2)} + (p_{17})^{(2)}) (\lambda)^{(2)} \right) (q_{18})^{(2)}G_{18} \\ & + ((\lambda)^{(2)} + (a'_{16})^{(2)} + (p_{16})^{(2)}) ((a_{18})^{(2)}(q_{17})^{(2)}G_{17}^* + (a_{17})^{(2)}(a_{18})^{(2)}(q_{16})^{(2)}G_{16}^*) \end{aligned}$$

$$\begin{aligned}
& \left(((\lambda)^{(2)} + (b'_{16})^{(2)} - (r_{16})^{(2)})s_{(17),(18)}T_{17}^* + (b_{17})^{(2)}s_{(16),(18)}T_{16}^* \right) \} = 0 \\
& + \\
& \left((\lambda)^{(3)} + (b'_{22})^{(3)} - (r_{22})^{(3)} \right) \{ (\lambda)^{(3)} + (a'_{22})^{(3)} + (p_{22})^{(3)} \\
& \left[((\lambda)^{(3)} + (a'_{20})^{(3)} + (p_{20})^{(3)})(q_{21})^{(3)}G_{21}^* + (a_{21})^{(3)}(q_{20})^{(3)}G_{20}^* \right] \\
& \left(((\lambda)^{(3)} + (b'_{20})^{(3)} - (r_{20})^{(3)})s_{(21),(21)}T_{21}^* + (b_{21})^{(3)}s_{(20),(21)}T_{21}^* \right) \\
& + \left(((\lambda)^{(3)} + (a'_{21})^{(3)} + (p_{21})^{(3)})(q_{20})^{(3)}G_{20}^* + (a_{20})^{(3)}(q_{21})^{(1)}G_{21}^* \right) \\
& \left(((\lambda)^{(3)} + (b'_{20})^{(3)} - (r_{20})^{(3)})s_{(21),(20)}T_{21}^* + (b_{21})^{(3)}s_{(20),(20)}T_{20}^* \right) \\
& \left(((\lambda)^{(3)})^2 + ((a'_{20})^{(3)} + (a'_{21})^{(3)} + (p_{20})^{(3)} + (p_{21})^{(3)}) (\lambda)^{(3)} \right) \\
& \left(((\lambda)^{(3)})^2 + ((b'_{20})^{(3)} + (b'_{21})^{(3)} - (r_{20})^{(3)} + (r_{21})^{(3)}) (\lambda)^{(3)} \right) \\
& + \left(((\lambda)^{(3)})^2 + ((a'_{20})^{(3)} + (a'_{21})^{(3)} + (p_{20})^{(3)} + (p_{21})^{(3)}) (\lambda)^{(3)} \right) (q_{22})^{(3)}G_{22} \\
& + ((\lambda)^{(3)} + (a'_{20})^{(3)} + (p_{20})^{(3)}) ((a_{22})^{(3)}(q_{21})^{(3)}G_{21}^* + (a_{21})^{(3)}(a_{22})^{(3)}(q_{20})^{(3)}G_{20}^*) \\
& \left(((\lambda)^{(3)} + (b'_{20})^{(3)} - (r_{20})^{(3)})s_{(21),(22)}T_{21}^* + (b_{21})^{(3)}s_{(20),(22)}T_{20}^* \right) \} = 0 \\
& + \\
& \left((\lambda)^{(4)} + (b'_{26})^{(4)} - (r_{26})^{(4)} \right) \{ (\lambda)^{(4)} + (a'_{26})^{(4)} + (p_{26})^{(4)} \\
& \left[((\lambda)^{(4)} + (a'_{24})^{(4)} + (p_{24})^{(4)})(q_{25})^{(4)}G_{25}^* + (a_{25})^{(4)}(q_{24})^{(4)}G_{24}^* \right] \\
& \left(((\lambda)^{(4)} + (b'_{24})^{(4)} - (r_{24})^{(4)})s_{(25),(25)}T_{25}^* + (b_{25})^{(4)}s_{(24),(25)}T_{25}^* \right) \\
& + \left(((\lambda)^{(4)} + (a'_{25})^{(4)} + (p_{25})^{(4)})(q_{24})^{(4)}G_{24}^* + (a_{24})^{(4)}(q_{25})^{(4)}G_{25}^* \right) \\
& \left(((\lambda)^{(4)} + (b'_{24})^{(4)} - (r_{24})^{(4)})s_{(25),(24)}T_{25}^* + (b_{25})^{(4)}s_{(24),(24)}T_{24}^* \right) \\
& \left(((\lambda)^{(4)})^2 + ((a'_{24})^{(4)} + (a'_{25})^{(4)} + (p_{24})^{(4)} + (p_{25})^{(4)}) (\lambda)^{(4)} \right) \\
& \left(((\lambda)^{(4)})^2 + ((b'_{24})^{(4)} + (b'_{25})^{(4)} - (r_{24})^{(4)} + (r_{25})^{(4)}) (\lambda)^{(4)} \right) \\
& + \left(((\lambda)^{(4)})^2 + ((a'_{24})^{(4)} + (a'_{25})^{(4)} + (p_{24})^{(4)} + (p_{25})^{(4)}) (\lambda)^{(4)} \right) (q_{26})^{(4)}G_{26} \\
& + ((\lambda)^{(4)} + (a'_{24})^{(4)} + (p_{24})^{(4)}) ((a_{26})^{(4)}(q_{25})^{(4)}G_{25}^* + (a_{25})^{(4)}(a_{26})^{(4)}(q_{24})^{(4)}G_{24}^*) \\
& \left(((\lambda)^{(4)} + (b'_{24})^{(4)} - (r_{24})^{(4)})s_{(25),(26)}T_{25}^* + (b_{25})^{(4)}s_{(24),(26)}T_{24}^* \right) \} = 0 \\
& + \\
& \left((\lambda)^{(5)} + (b'_{30})^{(5)} - (r_{30})^{(5)} \right) \{ (\lambda)^{(5)} + (a'_{30})^{(5)} + (p_{30})^{(5)} \\
& \left[((\lambda)^{(5)} + (a'_{28})^{(5)} + (p_{28})^{(5)})(q_{29})^{(5)}G_{29}^* + (a_{29})^{(5)}(q_{28})^{(5)}G_{28}^* \right] \\
& \left(((\lambda)^{(5)} + (b'_{28})^{(5)} - (r_{28})^{(5)})s_{(29),(29)}T_{29}^* + (b_{29})^{(5)}s_{(28),(29)}T_{29}^* \right) \\
& + \left(((\lambda)^{(5)} + (a'_{29})^{(5)} + (p_{29})^{(5)})(q_{28})^{(5)}G_{28}^* + (a_{28})^{(5)}(q_{29})^{(5)}G_{29}^* \right) \\
& \left(((\lambda)^{(5)} + (b'_{28})^{(5)} - (r_{28})^{(5)})s_{(29),(28)}T_{29}^* + (b_{29})^{(5)}s_{(28),(28)}T_{28}^* \right) \\
& \left(((\lambda)^{(5)})^2 + ((a'_{28})^{(5)} + (a'_{29})^{(5)} + (p_{28})^{(5)} + (p_{29})^{(5)}) (\lambda)^{(5)} \right) \\
& \left(((\lambda)^{(5)})^2 + ((b'_{28})^{(5)} + (b'_{29})^{(5)} - (r_{28})^{(5)} + (r_{29})^{(5)}) (\lambda)^{(5)} \right) \\
& + \left(((\lambda)^{(5)})^2 + ((a'_{28})^{(5)} + (a'_{29})^{(5)} + (p_{28})^{(5)} + (p_{29})^{(5)}) (\lambda)^{(5)} \right) (q_{30})^{(5)}G_{30} \\
& + ((\lambda)^{(5)} + (a'_{28})^{(5)} + (p_{28})^{(5)}) ((a_{30})^{(5)}(q_{29})^{(5)}G_{29}^* + (a_{29})^{(5)}(a_{30})^{(5)}(q_{28})^{(5)}G_{28}^*) \\
& \left(((\lambda)^{(5)} + (b'_{28})^{(5)} - (r_{28})^{(5)})s_{(29),(30)}T_{29}^* + (b_{29})^{(5)}s_{(28),(30)}T_{28}^* \right) \} = 0 \\
& + \\
& \left((\lambda)^{(6)} + (b'_{34})^{(6)} - (r_{34})^{(6)} \right) \{ (\lambda)^{(6)} + (a'_{34})^{(6)} + (p_{34})^{(6)} \\
& \left[((\lambda)^{(6)} + (a'_{32})^{(6)} + (p_{32})^{(6)})(q_{33})^{(6)}G_{33}^* + (a_{33})^{(6)}(q_{32})^{(6)}G_{32}^* \right] \\
& \left(((\lambda)^{(6)} + (b'_{32})^{(6)} - (r_{32})^{(6)})s_{(33),(33)}T_{33}^* + (b_{33})^{(6)}s_{(32),(33)}T_{33}^* \right) \\
& + \left(((\lambda)^{(6)} + (a'_{33})^{(6)} + (p_{33})^{(6)})(q_{32})^{(6)}G_{32}^* + (a_{32})^{(6)}(q_{33})^{(6)}G_{33}^* \right) \\
& \left(((\lambda)^{(6)} + (b'_{32})^{(6)} - (r_{32})^{(6)})s_{(33),(32)}T_{33}^* + (b_{33})^{(6)}s_{(32),(32)}T_{32}^* \right) \\
& \left(((\lambda)^{(6)})^2 + ((a'_{32})^{(6)} + (a'_{33})^{(6)} + (p_{32})^{(6)} + (p_{33})^{(6)}) (\lambda)^{(6)} \right) \\
& \left(((\lambda)^{(6)})^2 + ((b'_{32})^{(6)} + (b'_{33})^{(6)} - (r_{32})^{(6)} + (r_{33})^{(6)}) (\lambda)^{(6)} \right) \\
& + \left(((\lambda)^{(6)})^2 + ((a'_{32})^{(6)} + (a'_{33})^{(6)} + (p_{32})^{(6)} + (p_{33})^{(6)}) (\lambda)^{(6)} \right) (q_{34})^{(6)}G_{34} \\
& + ((\lambda)^{(6)} + (a'_{32})^{(6)} + (p_{32})^{(6)}) ((a_{34})^{(6)}(q_{33})^{(6)}G_{33}^* + (a_{33})^{(6)}(a_{34})^{(6)}(q_{32})^{(6)}G_{32}^*)
\end{aligned}$$

$$\left\{ \left((\lambda)^{(6)} + (b'_{32})^{(6)} - (r_{32})^{(6)} \right) s_{(33),(34)} T_{33}^* + (b_{33})^{(6)} s_{(32),(34)} T_{32}^* \right\} = 0$$

+

$$\begin{aligned} & \left((\lambda)^{(7)} + (b'_{38})^{(7)} - (r_{38})^{(7)} \right) \left\{ \left((\lambda)^{(7)} + (a'_{38})^{(7)} + (p_{38})^{(7)} \right) \right. \\ & \left. \left[\left((\lambda)^{(7)} + (a'_{36})^{(7)} + (p_{36})^{(7)} \right) (q_{37})^{(7)} G_{37}^* + (a_{37})^{(7)} (q_{36})^{(7)} G_{36}^* \right] \right\} \\ & \left((\lambda)^{(7)} + (b'_{36})^{(7)} - (r_{36})^{(7)} \right) s_{(37),(37)} T_{37}^* + (b_{37})^{(7)} s_{(36),(37)} T_{37}^* \\ & + \left((\lambda)^{(7)} + (a'_{37})^{(7)} + (p_{37})^{(7)} \right) (q_{36})^{(7)} G_{36}^* + (a_{36})^{(7)} (q_{37})^{(7)} G_{37}^* \\ & \left((\lambda)^{(7)} + (b'_{36})^{(7)} - (r_{36})^{(7)} \right) s_{(37),(36)} T_{37}^* + (b_{37})^{(7)} s_{(36),(36)} T_{36}^* \\ & \left((\lambda)^{(7)} \right)^2 + \left((a'_{36})^{(7)} + (a'_{37})^{(7)} + (p_{36})^{(7)} + (p_{37})^{(7)} \right) (\lambda)^{(7)} \\ & \left((\lambda)^{(7)} \right)^2 + \left((b'_{36})^{(7)} + (b'_{37})^{(7)} - (r_{36})^{(7)} + (r_{37})^{(7)} \right) (\lambda)^{(7)} \\ & + \left((\lambda)^{(7)} \right)^2 + \left((a'_{36})^{(7)} + (a'_{37})^{(7)} + (p_{36})^{(7)} + (p_{37})^{(7)} \right) (\lambda)^{(7)} (q_{38})^{(7)} G_{38} \\ & + \left((\lambda)^{(7)} + (a'_{36})^{(7)} + (p_{36})^{(7)} \right) \left((a_{38})^{(7)} (q_{37})^{(7)} G_{37}^* + (a_{37})^{(7)} (a_{38})^{(7)} (q_{36})^{(7)} G_{36}^* \right) \\ & \left. \left((\lambda)^{(7)} + (b'_{36})^{(7)} - (r_{36})^{(7)} \right) s_{(37),(38)} T_{37}^* + (b_{37})^{(7)} s_{(36),(38)} T_{36}^* \right\} = 0 \end{aligned}$$

REFERENCES

=====

- (1) A HAIMOVICI: "On the growth of a two species ecological system divided on age groups". Tensor, Vol 37 (1982), Commemoration volume dedicated to Professor Akitsugu Kawaguchi on his 80th birthday
- (2) FRTJOF CAPRA: "The web of life" Flamingo, Harper Collins See "Dissipative structures" pages 172-188
- (3) HEYLIGHEN F. (2001): "The Science of Self-organization and Adaptivity", in L. D. Kiel, (ed) . Knowledge Management, Organizational Intelligence and Learning, and Complexity, in: The Encyclopedia of Life Support Systems (EOLSS), (Eolss Publishers, Oxford) [<http://www.eolss.net>]
- (4) MATSUI, T, H. Masunaga, S. M. Kreidenweis, R. A. Pielke Sr., W.-K. Tao, M. Chin, and Y. J Kaufman (2006), "Satellite-based assessment of marine low cloud variability associated with aerosol, atmospheric stability, and the diurnal cycle", J. Geophys. Res., 111, D17204, doi:10.1029/2005JD006097
- (5) STEVENS, B, G. Feingold, W.R. Cotton and R.L. Walko, "Elements of the microphysical structure of numerically simulated nonprecipitating stratocumulus" J. Atmos. Sci., 53, 980-1006
- (6) FEINGOLD, G, Koren, I; Wang, HL; Xue, HW; Brewer, WA (2010), "Precipitation-generated oscillations in open cellular cloud fields" *Nature*, 466 (7308) 849-852, doi: 10.1038/nature09314, Published 12-Aug 2010
- (7) HEYLIGHEN F. (2001): "The Science of Self-organization and Adaptivity", in L. D. Kiel, (ed) . Knowledge Management, Organizational Intelligence and Learning, and Complexity, in: The Encyclopedia of Life Support Systems (EOLSS), (Eolss Publishers, Oxford) [<http://www.eolss.net>]
- (8) MATSUI, T, H. Masunaga, S. M. Kreidenweis, R. A. Pielke Sr., W.-K. Tao, M. Chin, and Y. J Kaufman (2006), "Satellite-based assessment of marine low cloud variability associated with aerosol, atmospheric stability, and the diurnal cycle", J. Geophys. Res., 111, D17204, doi:10.1029/2005JD006097
- (8A) STEVENS, B, G. Feingold, W.R. Cotton and R.L. Walko, "Elements of the microphysical structure of numerically simulated nonprecipitating stratocumulus" J. Atmos. Sci., 53, 980-1006
- (8B) FEINGOLD, G, Koren, I; Wang, HL; Xue, HW; Brewer, WA (2010), "Precipitation-generated oscillations in open cellular cloud fields" *Nature*, 466 (7308) 849-852, doi: 10.1038/nature09314, Published 12-Aug 2010

(9)^{a b c} Einstein, A. (1905), "Ist die Trägheit eines Körpers von seinem Energieinhalt abhängig?", *Annalen der Physik* **18**: 639 Bibcode 1905AnP...323..639E, DOI:10.1002/andp.19053231314. See also the English translation.

(10)^{a b} Paul Allen Tipler, Ralph A. Llewellyn (2003-01), *Modern Physics*, W. H. Freeman and Company, pp. 87–88, ISBN 0-7167-4345-0

(11)^{a b} Rainville, S. et al. World Year of Physics: A direct test of $E=mc^2$. *Nature* 438, 1096-1097 (22 December 2005) | doi: 10.1038/4381096a; Published online 21 December 2005.

(12)[^] In F. Fernflores. The Equivalence of Mass and Energy. Stanford Encyclopedia of Philosophy

(13)[^] Note that the relativistic mass, in contrast to the rest mass m_0 , is not a relativistic invariant, and that the velocity is not a Minkowski four-vector, in contrast to the quantity dx^μ , where dx^μ is the differential of the proper time. However, the energy-momentum four-vector is a genuine Minkowski four-vector, and the intrinsic origin of the square-root in the definition of the relativistic mass is the distinction between $d\tau$ and dt .

(14)[^] Relativity DeMystified, D. McMahon, Mc Graw Hill (USA), 2006, ISBN 0-07-145545-0

(15)[^] Dynamics and Relativity, J.R. Forshaw, A.G. Smith, Wiley, 2009, ISBN 978-0-470-01460-8

(16)[^] Hans, H. S.; Puri, S. P. (2003). *Mechanics* (2 ed.). Tata McGraw-Hill. p. 433. ISBN 0-07-047360-9., Chapter 12 page 433

(17)[^] E. F. Taylor and J. A. Wheeler, **Spacetime Physics**, W.H. Freeman and Co., NY. 1992. ISBN 0-7167-2327-1, see pp. 248-9 for discussion of mass remaining constant after detonation of nuclear bombs, until heat is allowed to escape.

(18)[^] Mould, Richard A. (2002). *Basic relativity* (2 ed.). Springer. p. 126. ISBN 0-387-95210-1., Chapter 5 page 126

(19)[^] Chow, Tail L. (2006). *Introduction to electromagnetic theory: a modern perspective*. Jones & Bartlett Learning. p. 392. ISBN 0-7637-3827-1., Chapter 10 page 392

(20)[^] [2] Cockcroft-Walton experiment

(21)^{a b c} Conversions used: 1956 International (Steam) Table (IT) values where one calorie \equiv 4.1868 J and one BTU \equiv 1055.05585262 J. Weapons designers' conversion value of one gram TNT \equiv 1000 calories used.

(22)[^] Assuming the dam is generating at its peak capacity of 6,809 MW.

(23)[^] Assuming a 90/10 alloy of Pt/Ir by weight, a C_p of 25.9 for Pt and 25.1 for Ir, a Pt-dominated average C_p of 25.8, 5.134 moles of metal, and 132 J.K⁻¹ for the prototype. A variation of ± 1.5 picograms is of course, much smaller than the actual uncertainty in the mass of the international prototype, which are ± 2 micrograms.

(24)[^] [3] Article on Earth rotation energy. Divided by c^2 .

(25)^{a b} Earth's gravitational self-energy is 4.6×10^{10} that of Earth's total mass, or 2.7 trillion metric tons. Citation: *The Apache Point Observatory Lunar Laser-Ranging Operation (APOLLO)*, T. W. Murphy, Jr. et al. University of Washington, Dept. of Physics (132 kB PDF, here.).

(26)[^] There is usually more than one possible way to define a field energy, because any field can be made to couple to gravity in many different ways. By general scaling arguments, the correct answer at everyday distances, which are long compared to the quantum gravity scale, should be *minimal coupling*, which means that no powers of the curvature tensor appear. Any non-minimal couplings, along with other higher order terms, are presumably only determined by a theory of quantum gravity, and within string theory, they only start to contribute to experiments at the string scale.

- (27)[△] G. 't Hooft, "Computation of the quantum effects due to a four-dimensional pseudoparticle", *Physical Review D* 14:3432–3450 (1976).
- (28)[△] A. Belavin, A. M. Polyakov, A. Schwarz, Yu. Tyupkin, "Pseudoparticle Solutions to Yang Mills Equations", *Physics Letters* 59B:85 (1975).
- (29)[△] F. Klinkhammer, N. Manton, "A Saddle Point Solution in the Weinberg Salam Theory", *Physical Review D* 30:2212.
- (30)[△] Rubakov V. A. "Monopole Catalysis of Proton Decay", *Reports on Progress in Physics* 51:189–241 (1988).
- (31)[△] S.W. Hawking "Black Holes Explosions?" *Nature* 248:30 (1974).
- (32)[△] Einstein, A. (1905), "Zur Elektrodynamik bewegter Körper." (PDF), *Annalen der Physik* 17: 891–921, Bibcode 1905AnP...322...891E, DOI:10.1002/andp.19053221004. English translation.
- (33)[△] See e.g. Lev B.Okun, *The concept of Mass*, *Physics Today* 42 (6), June 1969, p. 31–36, http://www.physicstoday.org/vol-42/iss-6/vol42no6p31_36.pdf
- (34)[△] Max Jammer (1999), *Concepts of mass in contemporary physics and philosophy*, Princeton University Press, p. 51, ISBN 0-691-01017-X
- (35)[△] Eriksen, Erik; Vøyenli, Kjell (1976), "The classical and relativistic concepts of mass", *Foundations of Physics* (Springer) 6: 115–124, Bibcode 1976FoPh....6..115E, DOI:10.1007/BF00708670
- (36)^{△ a b} Janssen, M., Mecklenburg, M. (2007), *From classical to relativistic mechanics: Electromagnetic models of the electron.*, in V. F. Hendricks, et al., *Interactions: Mathematics, Physics and Philosophy* (Dordrecht: Springer): 65–134
- (37)^{△ a b} Whittaker, E.T. (1951–1953), 2. Edition: *A History of the theories of aether and electricity, vol. 1: The classical theories / vol. 2: The modern theories 1900–1926*, London: Nelson
- (38)[△] Miller, Arthur I. (1981), *Albert Einstein's special theory of relativity. Emergence (1905) and early interpretation (1905–1911)*, Reading: Addison–Wesley, ISBN 0-201-04679-2
- (39)^{△ a b} Darrigol, O. (2005), "The Genesis of the theory of relativity." (PDF), *Séminaire Poincaré* 1: 1–22
- (40)[△] Philip Ball (Aug 23, 2011). "Did Einstein discover $E = mc^2$?" *Physics World*.
- (41)[△] Ives, Herbert E. (1952), "Derivation of the mass-energy relation", *Journal of the Optical Society of America* 42 (8): 540–543, DOI:10.1364/JOSA.42.000540
- (42)[△] Jammer, Max (1961/1997). *Concepts of Mass in Classical and Modern Physics*. New York: Dover. ISBN 0-486-29998-8.
- (43)[△] Stachel, John; Torretti, Roberto (1982), "Einstein's first derivation of mass-energy equivalence", *American Journal of Physics* 50 (8): 760–763, Bibcode1982AmJPh..50..760S, DOI:10.1119/1.12764
- (44)[△] Ohanian, Hans (2008), "Did Einstein prove $E=mc^2$?", *Studies In History and Philosophy of Science Part B* 40 (2): 167–173, arXiv:0805.1400, DOI:10.1016/j.shpsb.2009.03.002
- (45)[△] Hecht, Eugene (2011), "How Einstein confirmed $E_0=mc^2$ ", *American Journal of Physics* 79 (6): 591–600, Bibcode 2011AmJPh..79..591H, DOI:10.1119/1.3549223
- (46)[△] Rohrlich, Fritz (1990), "An elementary derivation of $E=mc^2$ ", *American Journal of Physics* 58 (4): 348–

(47) (1996). *Lise Meitner: A Life in Physics*. California Studies in the History of Science. **13**. Berkeley: University of California Press. pp. 236–237. ISBN 0-520-20860-

(48)^ UIBK.ac.at

(49)^ J. J. L. Morton; *et al.* (2008). "Solid-state quantum memory using the ^{31}P nuclear spin". *Nature* **455** (7216): 1085–1088. Bibcode 2008Natur.455.1085M.DOI:10.1038/nature07295.

(50)^ S. Weisner (1983). "Conjugate coding". *Association of Computing Machinery, Special Interest Group in Algorithms and Computation Theory* **15**: 78–88.

(51)^ A. Zeilinger, *Dance of the Photons: From Einstein to Quantum Teleportation*, Farrar, Straus & Giroux, New York, 2010, pp. 189, 192, ISBN 0374239665

(52)^ B. Schumacher (1995). "Quantum coding". *Physical Review A* **51** (4): 2738–2747. Bibcode 1995PhRvA..51.2738S. DOI:10.1103/PhysRevA.51.2738.

(53)Delamotte, Bertrand; *A hint of renormalization*, American Journal of Physics 72 (2004) pp. 170–184. Beautiful elementary introduction to the ideas, no prior knowledge of field theory being necessary. Full text available at: hep-th/0212049

(54)Baez, John; *Renormalization Made Easy*, (2005). A qualitative introduction to the subject.

(55)Blechman, Andrew E. ; *Renormalization: Our Greatly Misunderstood Friend*, (2002). Summary of a lecture; has more information about specific regularization and divergence-subtraction schemes.

(56)Cao, Tian Yu & Schweber, Silvian S. ; *The Conceptual Foundations and the Philosophical Aspects of Renormalization Theory*, Synthese, 97(1) (1993), 33–108.

(57)Shirkov, Dmitry; *Fifty Years of the Renormalization Group*, C.E.R.N. Courier 41(7) (2001). Full text available at: *I.O.P Magazines*.

(58)E. Elizalde; *Zeta regularization techniques with Applications*.

(59)N. N. Bogoliubov, D. V. Shirkov (1959): *The Theory of Quantized Fields*. New York, Interscience. The first text-book on the renormalization group theory.

(60)Ryder, Lewis H. ; *Quantum Field Theory* (Cambridge University Press, 1985), ISBN 0-521-33859-X Highly readable textbook, certainly the best introduction to relativistic Q.F.T. for particle physics.

(61)Zee, Anthony; *Quantum Field Theory in a Nutshell*, Princeton University Press (2003) ISBN 0-691-01019-6. Another excellent textbook on Q.F.T.

(62)Weinberg, Steven; *The Quantum Theory of Fields* (3 volumes) Cambridge University Press (1995). A monumental treatise on Q.F.T. written by a leading expert, *Nobel laureate 1979*.

(63)Pokorski, Stefan; *Gauge Field Theories*, Cambridge University Press (1987) ISBN 0-521-47816-2.

(64)'t Hooft, Gerard; *The Glorious Days of Physics – Renormalization of Gauge theories*, lecture given at Erice (August/September 1998) by the *Nobel laureate 1999* . Full text available at: hep-th/9812203.

(65)Rivasseau, Vincent; *An introduction to renormalization*, Poincaré Seminar (Paris, Oct. 12, 2002), published in: Duplantier, Bertrand; Rivasseau, Vincent (Eds.) ; *Poincaré Seminar 2002*, Progress in Mathematical Physics

- (66) Rivasseau, Vincent; *From perturbative to constructive renormalization*, Princeton University Press (1991) ISBN 0-691-08530-7. Full text available in *PostScript*.
- (67) H.P. Nilles, Phys. Rep. 110, 1 (1984);
- (68) H.E. Haber and G.L. Kane, Phys. Rep. 117, 75 (1985);
- (69) R. Barbieri, Riv. Nuov. Cim. 11, 1 (1988).
- (70) J.F. Gunion and H.E. Haber, Nucl. Phys. B272, 1 (1986); B402, 567(E) (1993).
- (71) A. Sirlin, Nucl. Phys. B71, 29 (1974); Rev. Mod. Phys. 50, 573 (1978);
- (72) W.J. Marciano and A. Sirlin, Nucl. Phys. B93, 303 (1975).
- (73) A. Denner and T. Sack, Nucl. Phys. B347, 203 (1990).
- (74) B.A. Kniehl and A. Pilaftsis, Nucl. Phys. B474, 286 (1996).
- (75) J. Guasch, J. Sol`a, and W. Hollik, Phys. Lett. B 437, 88 (1998);
- (76) H. Eberl, S. Kraml, and W. Majerotto, JHEP 9905, 016 (1999);
- (77) J. Guasch, W. Hollik, and J. Sol`a, Phys. Lett. B 510, 211 (2001).
- [78] P. Gambino, P.A. Grassi, and F. Madricardo, Phys. Lett. B 454, 98 (1999).
- (79) B.A. Kniehl, F. Madricardo, and M. Steinhauser, Phys. Rev. D 62, 073010 (2000).
- (80) A. Barroso, L. Br`ucher, and R. Santos, Phys. Rev. D 62, 096003 (2000).
- (81) N. Cabibbo, Phys. Rev. Lett. 19, 531 (1963);
- (82) M. Kobayashi and M. Maskawa, Prog. Theor. Phys. 49, 652 (1973).
- (83) J.M. Cornwall, in Proceedings of the French-American Seminar on Theoretical Aspects of Quantum Chromodynamics, Marseille, France, 1981, edited by J.W. Dash (Centre de Physique Th´eorique, Marseille, 1982);
- (84) J.M. Cornwall, Phys. Rev. D 26, 1453 (1982);
- (85) J.M. Cornwall and J. Papavassiliou, Phys. Rev. D 40, 3474 (1989).

Acknowledgments:

The introduction is a collection of information from various articles, Books, News Paper reports, Home Pages Of authors, Journal Reviews, Nature 's Letters, Article Abstracts, Research papers, Abstracts Of Research Papers, Stanford Encyclopedia, Web Pages, Ask a Physicist Column, Deliberations with Professors, the internet including Wikipedia. We acknowledge all authors who have contributed to the same. In the eventuality of the fact that there has been any act of omission on the part of the authors, we regret with great deal of compunction, contrition, regret, trepidation and remorse. As Newton said, it is only because erudite and eminent people allowed one to piggy ride on their backs; probably an attempt has been made to look slightly further. Once again, it is stated that the references are only illustrative and not comprehensive

First Author: ¹Mr. K. N.Prasanna Kumar has three doctorates one each in Mathematics, Economics, Political Science. Thesis was based on Mathematical Modeling. He was recently awarded D.litt. for his work on 'Mathematical Models in Political Science'--- Department of studies in Mathematics, Kuvempu University, Shimoga, Karnataka, India Corresponding **Author:drknpkumar@gmail.com**

Second Author: ²Prof. B.S Kiranagi is the Former Chairman of the Department of Studies in Mathematics, Manasa Gangotri and present Professor Emeritus of UGC in the Department. Professor Kiranagi has guided over 25 students and he has received many encomiums and laurels for his contribution to Co homology Groups and Mathematical Sciences. Known for his prolific writing, and one of the senior most Professors of the country, he has over 150 publications to his credit. A prolific writer and a prodigious thinker, he has to his credit several books on Lie Groups, Co Homology Groups, and other mathematical application topics, and excellent publication history.-- UGC Emeritus Professor (Department of studies in Mathematics), Manasagangotri, University of Mysore, Karnataka, India

Third Author: ³Prof. C.S. Bagewadi is the present Chairman of Department of Mathematics and Department of Studies in Computer Science and has guided over 25 students. He has published articles in both national and international journals. Professor Bagewadi specializes in Differential Geometry and its wide-ranging ramifications. He has to his credit more than 159 research papers. Several Books on Differential Geometry, Differential Equations are coauthored by him--- Chairman, Department of studies in Mathematics and Computer science, Jnanasahyadri Kuvempu University, Shankarghatta, Shimoga district, Karnataka, India

Conventional Fuel Generated from Polypropylene (PP) Waste Plastic like Kerosene/Jet/ Aviation Grade with Activated Carbon

Moinuddin Sarker^{1*}, Mohammad Mamunor Rashid¹ and Muhammad Sadikur Rahman¹

¹Natural State Research, Inc. Department of Research and Development, 37 Brown House Road (2nd Floor)
Stamford, CT - 06902, USA,

ABSTRACT: The thermal degradation and fractional distillation process applied with polypropylene (PP) of waste plastic using stainless steel reactor without using any kind of catalyst. The polymer has been selected for the experiment 100% by weight and 1% activated carbon was used. The experimental temperature was used for thermal degradation liquefaction process at 100-400 °C and fractional distillation for third fraction fuel or aviation/kerosene/jet category fuel collection temperature was 180-210 °C and overall experiment run time was 6-6.30 hours. The obtained products density is 0.75 g/ml and production yield percentage are third fraction liquid fuel or aviation/kerosene/jet category fuel yield is 30.40%, other fraction fuel percentage was 62.60% light gas 3% and black carbon residue 4%. Various techniques (Gas Chromatography and Mass Spectrometer, FT-IR and DSC) were used for produced third fraction fuel or aviation/kerosene/jet category fractional fuel analysis purpose. GC/MS result is showing that hydrocarbon compound ranges in this fuel are C₈-C₁₉ and light gas are present hydrocarbon range C₁-C₄. Third fractional fuel or kerosene / jet / aviation category fuel analysis results is showing different carbon range and produced third fractional fuel present short chain to long chain hydrocarbon like alkane and alkene group. Produce fuel can be use for internal combustion engine or electricity generation or feed stock refinery process.

Keywords: PP, waste plastic, kerosene, fuel, activated carbon, GC/MS, polypropylene

I. INTRODUCTION

Solving the problem of waste materials such as used plastics, waste tires, and waste oils is undoubtedly a major challenge being faced in all the countries of the world to maintain the sustainable and environmentally compatible economic growth. One of the major problems caused in the recycling of waste plastics is the in homogeneity of the polymers in the waste. Actually, different types of polymers (polyethylene (PE), polypropylene (PP), polystyrene (PS), polyethylene terephthalate (PET), polyvinyl chloride (PVC), acrylonitrile-butadiene-styrene (ABS) and etc.) can be present in waste plastic mixture. Especially, co-processing of co-mingled waste plastics with waste motor oils through a tertiary recycling technique [1-4] can achieve the purpose of waste recycling into commercially viable chemicals or fuel oils. The growing amount of plastic waste is generating more and more environmental problems worldwide. The present rate of economic growth is unimaginable without saving of fossil energy like crude oil, natural gas or coal. Suitable waste management is another important aspect of sustainable

development. Plastic wastes represent a considerable part of municipal wastes; furthermore huge amounts of plastic waste arise as a by-product or faulty product in industry and agriculture. According to estimates, plastic wastes represent 15-25% of municipal waste. The amount of plastic materials was 25 Mt in Europe and it will reach 35 Mt by 2010 [5, 6].

Nowadays there are three ways to utilize plastic waste: landfilling, incineration with or without energy recovery and recycling. The largest amount of plastic wastes is disposed of by landfilling (65-70%), and incineration (20-25%), Recycling is only about 10%. At the present time, it is thought that efficient co-processing processes which are feasible in technical and economical aspects should be developed. In parallel with this, an overall national network system [7-10] such as waste plastics collection, pretreatment and regulatory considerations should be provided for successful recycling of waste materials. Korea produces 2.6 million tonnes per annum of thermoplastic wastes of which less than 10% is recycled for the material recovery (primary recycling). In addition, almost 120 million gallons of waste motor oils are generated each year posing severe environmental problems as a result of its metal compounds and high sulfur content (ca. 4000- 6000 ppm wt.) resulting from such additives as dispersants (Copolymer sulfonate), oxidation inhibitors (organic sulfur compounds, aminophenol), corrosion inhibitors (organic amines) and extreme pressure additives and from existing sulfur naturally in lube base stock. In this study, co-processing of waste plastics (HDPE, LDPE, PS, PP, PET and ABS) with waste oil by statistical rotatable pentagonal design experiments in a micro-reactor system (40 ml capacity) were explored to extract the optimum pyrolysis conditions for conversion of each plastic/ waste oil blend into oils [11].

II. MATERIALS & METHOD

PP waste plastic was collected from local city coffee shop and local restaurant. Coffee cup PP waste plastic color was transparent, food container and food container cover was white and black color. PP plastic comes with food particle and left over coffee because we collected PP waste plastic from store. After collection PP waste plastic wash with water and none foaming detergent by using electrical plastic washing machine. After finished wash PP waste plastic make it dry with using same machine at 22 °C temperature. During washing PP waste plastic also generating some waste water that waste water we did not discharge into drainage system because our main goal is waste plastic problem solve from land fill not to create another waste problem. Produced waste water treatment for reuse of waster again waste plastic washing purpose.

This type process is one kind of cyclic process not to generate waste water. Waste water was treated by using chemical and chemical is not harm fuel for human body because we are using only Sodium Hydroxide and Potash Alum. PP waste plastic after dried cut into small pieces manually by using scissor then transfer into grinder machine of grinding and size about 2-3mm. Small pieces grounded PP waste plastic transfer into steel reactor chamber for liquefaction process. Experimental process setup was shown into figure 1. PP waste plastic to kerosene/aviation/jet category fuel production process diagram describe fig.1 and describe figure 1 all number such as 1 = polypropylene waste plastic, 2= Steel reactor, 3 = Fractional distillation column, 4= 1st fraction temperature, 5= 2nd fraction temperature, 6=3rd fraction temperature, 7= 4th fraction temperature, 8= 5th fraction temperature, 9= light gas cleaning system, 10= 1st fraction fuel collection tank, 11=2nd fraction fuel collection tank, 12=3rd fraction fuel collection tank, 13=4th fraction fuel collection tank, 14 = 5th fraction fuel collection tank, 15 = small pump, 16 = Teflon bag for light gas storage. Fuel production process diagram was shown number 12 is aviation/ kerosene/jet fuel collection system. PP waste plastic to fuel production process grounded waste plastic put into reactor chamber and covered by reactor cover and screw tighten properly because we do not want to escape any gas during fuel production period. Condensation with fractional distillation column setup top of reactor with grading temperature wise with electrical coil and temperature was monitor by using watlow company provided watlow meter. For experimental purpose feed was use only 500 gm by weight and activated carbon was use only 1% by weight. In this experiment PP waste plastic to liquefaction temperature used 100 to 400 °C and collection aviation /kerosene/jet category fuel fractional temperature was 180-210 °C. Collection device end part was collected light gas

cleaning device and this device was fill up with alkali solution for removing light gas contamination and water portion which was generated from production. In this experiment did not apply vacuum system and did not apply any kind of catalyst. After finished all set up experimental procedure we start reactor electrical power for heated up PP waste plastic. PP waste plastic start to melt due to heat applies then turns into liquid slurry, liquid slurry turns into gas vapor this gas vapor pass through fractional column based on boiling point temperature at the end collected 3rd fractional or aviation/kerosene/jet grade fuel. In this experiment main goal was aviation/kerosene/jet category fuel collection. Activated carbon help to reduce fuel dye level because when heated up PP waste plastic with activated carbon, activated carbon absorbed plastic additives color and produce fuel made cleaner. PP waste plastic to 3rd fractional fuel or aviation/ kerosene/jet category fuel production period also generate some light gas its call natural gas and this gas hydrocarbon range C₁-C₄. These gases pass through alkali chamber and remove contamination transfer Teflon bag by using small pump for future use. Collected 3rd fractional fuel purified by RCI purification device and removed fuel sediment. Total experiment run time was 6-6.30 hours and input electricity was 6.12 kWh. From this experiment in mass balance calculation indicate that 3rd fractional fuel or aviation/kerosene/jet category fuel conversion 152 gm from 500 gm of initial feed. Light gas converted feed sample 15 gm, solid black residue leftover 20 gm from total feed and rest of other grade fuel generated 313 gm sample during in this experiment. In percentage ratio third fraction liquid fuel or aviation/kerosene/jet category fuel yield percentage is 30.40%, other fraction fuel percentage was 62.60% light gas 3% and black carbon residue 4%.

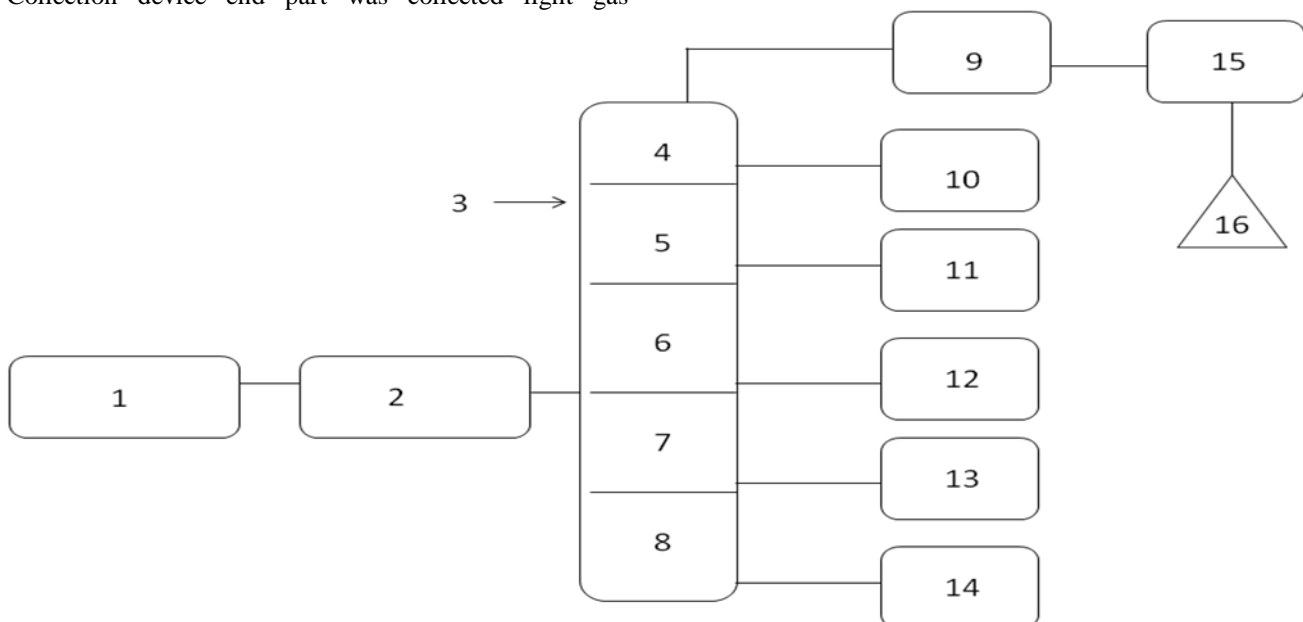


Fig.1: Polypropylene (PP) waste plastic to Kerosene/Jet/ Aviation grade fuel production process

III. RESULTS & DISCUSSION

From GC-MS analysis of PP waste plastic to 3rd fractional fuel or kerosene/jet/aviation (fig. 2 and table 1) in accordance with the various retention times and trace masses different types of hydrocarbon compounds are appeared in the analysis result index. Many compounds are emerged on the analysis carbon range C₈ to C₁₅ among them and few of compounds are discussed. Based on the retention time and trace mass following hydrocarbon compounds as follows such as at the initial phase of the analysis at retention time 4.59 and trace mass 41, compound is 1-Heptene, 4-methyl- (C₈H₁₆), retention time 4.74 and trace mass 71, compound is Heptane, 4-methyl- (C₈H₁₈), retention time 5.05 and trace mass 56, compound is 1-Heptene, 2-methyl- (C₈H₁₆), retention time 5.22 and trace mass 95, compound is 2,4-Hexadiene, 2,5-dimethyl-, (C₈H₁₄), retention time 5.93 and trace mass 111, compound is Cyclohexane, 1,3,5-trimethyl-, (1 α ,3 α ,5 α)-(C₉H₁₈), retention time 6.02 and trace

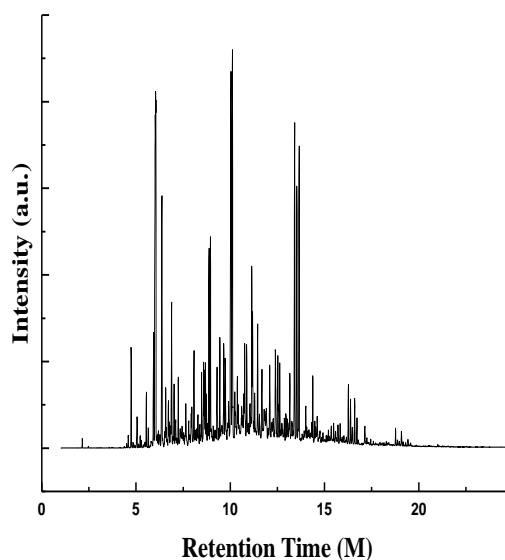


Fig. 2: GC/MS chromatogram of PP waste plastic to kerosene/aviation/ jet category fuel

mass 57, compound is 2,4-Dimethyl-1-heptene (C₉H₁₈), retention time 6.38 and trace mass 42, compound is Cyclohexane, 1,2,4-trimethyl-, (1 α ,2 β ,4 β)-(C₉H₁₈), retention time 6.58 and trace mass 109, compound is Cyclohexane, 1,2,4-trimethyl-, (1 α ,2 β ,4 β)-(C₉H₁₆), retention time 6.89 and trace mass 69, compound is 3-Octene, 2,2-dimethyl- (C₁₀H₂₀), retention time 7.02 and trace mass 43, compound is Hexane,2,4-Dimethyl-(C₈H₁₈), retention time 7.10 and trace mass 83, compound is 1,6-Octadiene, 5,7-dimethyl-, (R)-(C₁₀H₁₈), retention time 7.64 and trace mass 43, compound is 2-Undecanethiol, 2-methyl- (C₁₂H₂₆O), retention time 7.34 and trace mass 95, compound is Cyclohexene, 3-methyl-6-(1-methylethyl)-(C₁₀H₁₈), retention time 7.44 and trace mass 41, compound is compound is 1-Dodecyne (C₁₂H₂₂), retention time 7.96 and trace mass 41, compound is cis-3-Decene (C₁₀H₂₀), retention time 8.29 and trace mass 41, compound is trans-7-Methyl-3-octene (C₁₀H₁₈),

retention time 8.48 and trace mass 56, compound is 2-Methyl-1-Nonene (C₁₀H₂₂), retention time 8.59 and trace mass 41, compound is 3-Undecene,(Z),(C₁₁H₂₂), retention time 8.95 and trace mass 42 compound is Octane, 2,6-dimethyl- (C₁₀H₂₂), retention time 9.45 and trace mass 56, compound name is 3-Undecene, (Z)- (C₁₁H₂₂), retention time 10.87 and trace mass 43, compound is 2-Undecanethiol, 2-methyl- (C₁₂H₂₆S), retention time 11.68 and trace mass 69, compound is Cyclohexane, 1,1,4,4-tetramethyl- (C₁₀H₂₂), retention time 12.39 and trace mass 43, compound is Decane, 2,3,5,8-tetramethyl- (C₁₄H₃₀), retention time 13.65 and trace mass 55, compound is E-14-Hexadecenal (C₁₆H₃₀O), retention time 14.38 and trace mass 55, compound is E-2-Octadecadecen-1-ol (C₁₈H₃₆O), retention time 15.48 and trace mass 43, compound is Decane, 2,3,5,8-tetramethyl- (C₁₄H₃₀), retention time 16.27 and trace mass 43, compound is 2-Hexyl-1-octanol (C₁₄H₃₀O), retention time 17.14 and trace mass 55, compound is E-2-Octadecadecen-1-ol (C₁₈H₃₆O). Ultimately also at retention time 18.77 and trace mass 43, compound is 1-Heptadecene (C₁₇H₃₄) and ultimately retention time 19.57 and trace mass 69, compound is 11-Dodecen-1-ol, 2,4,6-trimethyl-, (R,R,R)- (C₁₅H₃₀O) respectively.

From FT-IR analysis of PP waste plastic to 3rd fractional fuel or jet/kerosene/aviation fuel (fig. 3 and table 2) according to their wave number and spectrum band following types of functional groups are appeared in the analysis. In the spectrum field we noticed that higher wave number are emerged in the initial phase and middle index of the spectrum and in higher wave number small and bulky both functional groups are available and in low wave number double bond and single bond functional groups are available such as methane group, cis and trans alkene etc. Hereafter wave number wave number 2927.06 cm⁻¹ and 2727.53 cm⁻¹ functional group is C-CH₃, wave number 1781.50 cm⁻¹ and 1648.95 cm⁻¹ functional group is Non-Conjugated, wave number 1470.16 cm⁻¹ functional group is CH₃, wave number 993.43 cm⁻¹ functional group is -CH=CH₂, wave number 964.95 cm⁻¹, functional group is -CH=CH-(trans) and ultimately wave number 887.95 cm⁻¹ functional group is C=CH₂ respectively. Energy values are calculated, using formula is E=hv, Where h=Planks Constant, h =6.626x10⁻³⁴ J, v= Frequency in Hertz (sec⁻¹), Where v=c/ λ , c=Speed of light, where, c=3x10¹⁰ m/s, W=1/ λ , where λ is wave length and W is wave number in cm⁻¹. Therefore the equation E=hv, can substitute by the following equation, E=hcW. According to their wave number such as for 2927.06 (cm⁻¹) calculated energy, E=5.81x10⁻²⁰ J, wave number 2727.53 (cm⁻¹) calculated energy, E=5.41x10⁻²⁰ J. Similarly, wave number 1781.50 (cm⁻¹) energy, E =3.53x10⁻²⁰ J, wave number 1648.95(cm⁻¹) calculated energy, E=3.27x10⁻²⁰ J, wave number 1470.16 (cm⁻¹) calculated energy, E = 2.92x10⁻²⁰ J, wave number 993.43 (cm⁻¹), calculated energy, E=1.97x10⁻²⁰ J, wave number 964.95 (cm⁻¹) calculated energy, E=1.91x10⁻²⁰ J and eventually wave number 894.22 (cm⁻¹) calculated energy, E =1.78x10⁻²⁰ J respectively.

Table1: GC/MS chromatogram of PP waste plastic to 3rd fractional or kerosene/jet/aviation fuel compound list

Peak Number	Retention Time (M)	Trace Mass (m/z)	Compound Name	Compound Formula	Molecular Weight	Probability %
1	4.59	41	1-Heptene, 4-methyl-	C ₈ H ₁₆	112	30.7
2	4.74	71	Heptane, 4-methyl-	C ₈ H ₁₈	114	54.6
3	5.05	56	1-Heptene, 2-methyl-	C ₈ H ₁₆	112	48.4
4	5.22	95	2,4-Hexadiene, 2,5-dimethyl-	C ₈ H ₁₄	110	13.9
5	5.55	69	Cyclopentane, 1,1,3,4-tetramethyl-, cis-	C ₉ H ₁₈	126	15.8
6	5.65	43	Hexane, 3-ethyl-	C ₈ H ₁₈	114	19.4
7	5.93	111	Cyclohexane, 1,3,5-trimethyl-, (1 α ,3 α ,5 α)-	C ₉ H ₁₈	126	31.1
8	6.02	57	2,4-Dimethyl-1-heptene	C ₉ H ₁₈	126	17.7
9	6.03	56	Cyclohexane, 1,1,2-trimethyl-	C ₉ H ₁₈	126	7.04
10	6.38	42	Cyclohexane, 1,2,4-trimethyl-, (1 α ,2 β ,4 β)-	C ₉ H ₁₈	126	19.4
11	6.58	109	Cyclohexene, 3,3,5-trimethyl-	C ₉ H ₁₆	124	41.5
12	6.76	56	trans-7-Methyl-3-octene	C ₉ H ₁₈	126	33.4
13	6.89	69	3-Octene, 2,2-dimethyl-	C ₁₀ H ₂₀	140	6.58
14	7.02	43	Hexane, 2,4-dimethyl-	C ₈ H ₁₈	114	9.82
15	7.10	83	1,6-Octadiene, 5,7-dimethyl-, (R)-	C ₁₀ H ₁₈	138	13.8
16	7.24	67	1,6-Octadiene, 2,6-dimethyl-, (Z)-	C ₁₀ H ₁₈	138	9.53
17	7.34	95	Cyclohexene, 3-methyl-6-(1-methylethyl)-	C ₁₀ H ₁₈	138	16.0
18	7.44	41	1-Dodecyne	C ₁₂ H ₂₂	166	7.63
19	7.64	43	2-Undecanethiol, 2-methyl-	C ₁₂ H ₂₆ S	202	6.50
20	7.80	41	1-Octene, 2,6-dimethyl-	C ₁₀ H ₂₀	140	9.54
21	7.92	41	1-Octyn-3-ol, 4-ethyl-	C ₁₀ H ₁₈ O	154	9.35
22	7.96	41	cis-3-Decene	C ₁₀ H ₂₀	140	16.1
23	8.08	43	Octane, 2,3-dimethyl-	C ₁₀ H ₂₂	142	17.7
24	8.29	41	Dihydromyrcene	C ₁₀ H ₁₈	138	12.5
25	8.48	56	2-Methyl-1-nonene	C ₁₀ H ₂₀	140	22.8
26	8.59	41	3-Undecene, (Z)-	C ₁₁ H ₂₂	154	6.97
27	8.87	43	Decane, 4-methyl-	C ₁₁ H ₂₄	156	13.8
28	8.95	42	Octane, 2,6-dimethyl-	C ₁₀ H ₂₂	142	10.2
29	9.29	41	2-Nonenal, (E)-	C ₉ H ₁₆ O	140	6.03
30	9.45	56	3-Undecene, (Z)-	C ₁₁ H ₂₂	154	7.76
31	10.04	69	1-Methyl-2-(4-methylpentyl)cyclopentane	C ₁₂ H ₂₄	168	2.96
32	10.12	69	1-Dodecene	C ₁₂ H ₂₄	168	4.61
33	10.38	43	Undecane	C ₁₁ H ₂₄	156	23.5
34	10.61	41	E-2-Octadecadecen-1-ol	C ₁₈ H ₃₆ O	268	3.55
35	10.72	69	1-Isopropyl-1,4,5-trimethylcyclohexane	C ₁₂ H ₂₄	168	30.3
36	10.76	43	1-Dodecanol, 3,7,11-trimethyl-	C ₁₅ H ₃₂ O	228	4.19
37	10.87	43	2-Undecanethiol, 2-methyl-	C ₁₂ H ₂₆ S	202	6.55
38	11.04	41	3-Dodecene, (E)-	C ₁₂ H ₂₄	168	7.31
39	11.14	69	7-Octadecyne, 2-methyl-	C ₁₉ H ₃₆	264	4.52
40	11.18	55	3-Tridecene	C ₁₃ H ₂₄	180	4.24

41	11.30	43	2,3-Dimethyldecane	C ₁₂ H ₂₆	170	11.3
42	11.45	69	1-Isopropyl-1,4,5-trimethylcyclohexane	C ₁₂ H ₂₄	168	22.9
43	11.68	69	Cyclohexane, 1,1,4,4-tetramethyl-	C ₁₀ H ₂₀	140	10.9
44	12.09	69	1-Isopropyl-1,4,5-trimethylcyclohexane	C ₁₂ H ₂₄	168	20.8
45	12.39	43	Decane, 2,3,5,8-tetramethyl-	C ₁₄ H ₃₀	198	7.56
46	13.16	43	3-Tetradecene, (E)-	C ₁₄ H ₂₈	196	4.21
47	13.53	69	9-Eicosene, (E)-	C ₂₀ H ₄₀	280	3.82
48	13.65	55	E-14-Hexadecenal	C ₁₆ H ₃₀ O	238	3.61
49	14.01	43	1-Dodecanol, 3,7,11-trimethyl-	C ₁₅ H ₃₂ O	228	3.29
50	14.38	55	E-2-Octadecadecen-1-ol	C ₁₈ H ₃₆ O	268	4.61
51	15.20	69	2-Piperidinone, N-[4-bromo-n-butyl]-	C ₉ H ₁₆ BrNO	233	7.25
52	15.48	43	Decane, 2,3,5,8-tetramethyl-	C ₁₄ H ₃₀	198	11.0
53	16.17	83	1-Nonadecanol	C ₁₉ H ₄₀ O	284	2.89
54	16.27	43	2-Hexyl-1-octanol	C ₁₄ H ₃₀ O	214	3.57
55	17.14	55	E-2-Octadecadecen-1-ol	C ₁₈ H ₃₆ O	268	4.68
56	18.77	43	1-Heptadecene	C ₁₇ H ₃₄	238	3.92
57	19.57	69	11-Dodecen-1-ol, 2,4,6-trimethyl-, (R,R,R)-	C ₁₅ H ₃₀ O	226	5.52

Table 2: FT-IR spectrum's PP waste plastic to 3rd fractional or jet/kerosene/aviation fuel functional group name

Number of Wave	Wave Number (cm ⁻¹)	Functional Group Name	Number of Wave	Wave Number (cm ⁻¹)	Functional Group Name
1	2927.06	C-CH ₃	5	1470.16	CH ₃
2	2727.53	C-CH ₃	6	993.43	-CH=CH ₂
3	1781.50	Non-Conjugated	7	964.95	-CH=CH-(trans)
4	1648.95	Non-Conjugated	8	894.22	C=CH ₂

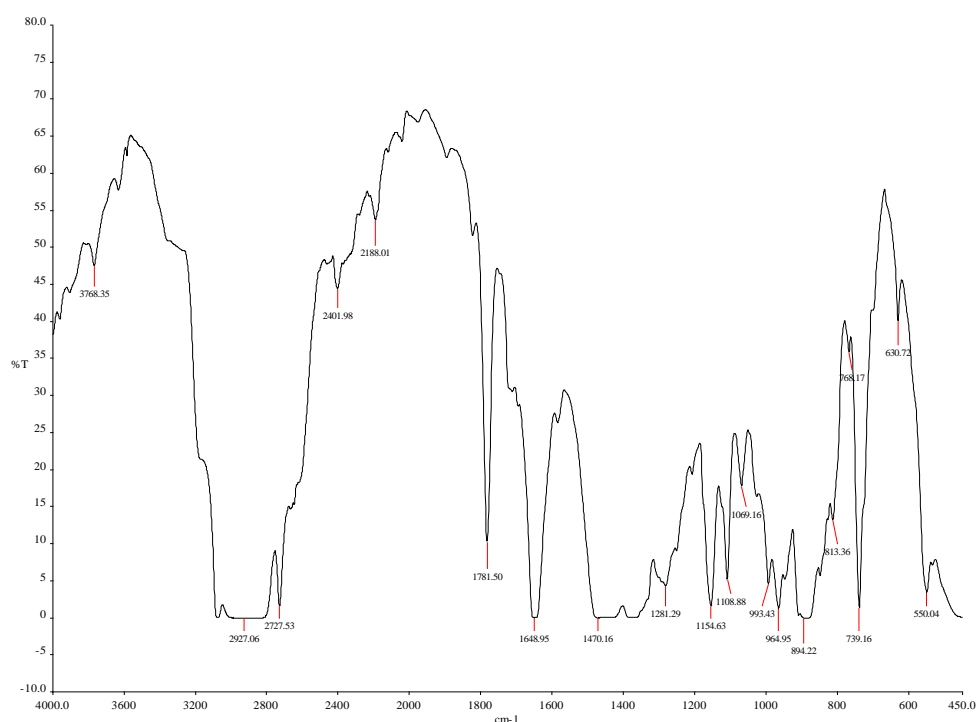


Fig. 3: FT-IR spectrum of PP waste plastic to 3rd fractional fuel or jet/kerosene/aviation fuel

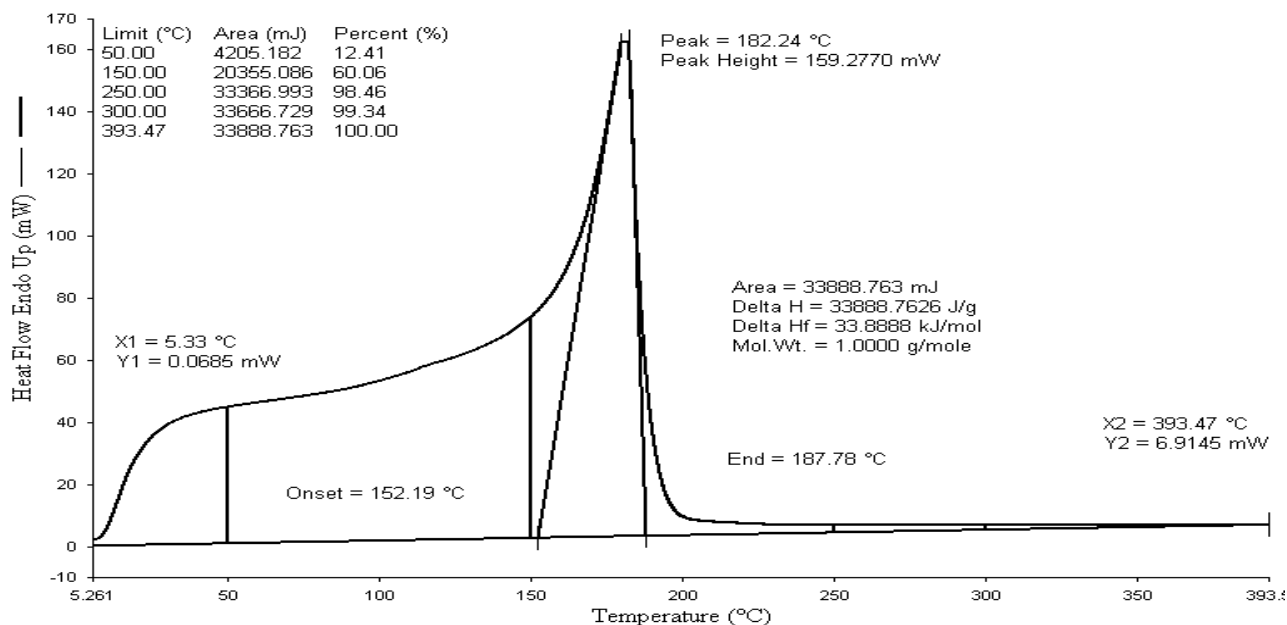


Fig.4: DSC graph of PP waste plastic to 3rd fractional or jet/kerosene/aviation fuel

Third (3rd) fractional fuel or kerosene/aviation/jet category fuel (seen fig. 4) collected from PP waste plastic by using fractional distillation column process at temperature range was 180-210 °C. This fuel category is similar to jet/kerosene/aviation fuel. This fuel looks like heavier fuel and 3rd fractional fuel was analyzed by using DSC for boiling point and enthalpy value measuring. After analyzed fraction fuel by DSC, we noticed that fuel graph showed fuel boil start 5.33 °C and 0.0685 mW, fuel graph onset temperature 152.19 °C and fuel boiling point peak temperature is 182.24 °C, peak height 159.2770 mW. 3rd fraction fuel or kerosene/aviation/ jet fuel heat enthalpy value delta H is 33888.7626 J/g and graph area 33888.763 mJ. Analysis fuel graph showing end temperature is 187.78 °C. Fuel boiling percentage shown at 50°C temperature was 12.41%, 150 °C temperature was 60.06% and finally 100 % fuel boil finished at temperature was 393.47 °C.

IV. CONCLUSION

PP waste plastic to 3rd fractional or kerosene/aviation/ jet category fuel production purposed was use 2 type temperatures profile one for liquefaction temperature and another one was fractional distillation temperature. PP waste plastic produced fuel percentage is 30.40% and in this experiment collected also other grade fuels. Produced fuel density is 0.75 g/ml. Different types of equipment were used for analysis 3rd fractional or aviation/kerosene/jet category fuel such as GC/MS, FTIR and DSC. GC-MS (Gas Chromatography and Mass Spectrometer) analysis result is indicates that in aviation/kerosene/jet category fuel contains extensive number of carbon chain compounds that are derived out by numerous retention time and trace masses of distinct compound. FT-IR analysis derived out available hydrocarbon functional groups are in the aviation/kerosene/jet category fuel and determined that the wide number of hydrocarbon functional group including alkane, alkene and alkyne (Saturated and unsaturated hydrocarbon) compounds are also present in

the fuel. Differential Scanning Calorimeter (DSC) giving the onset temperature of the fuel which represents the boiling point of the aviation/kerosene/jet category fuel. Fuel analysis of GC/MS results indicate that produce fuel hydrocarbon range C₈ to C₁₉. Produced fuel could be use as feed stock refinery for further modification or commercial use. By using this technology could be solve PP waste plastic problem and also reduce the land fill problem that is the cause of infertility of agriculture land.

ACKNOWLEDGEMENT

The author acknowledges the support of Dr. Karin Kaufman, the founder and sole owner of Natural State Research, Inc. The authors also acknowledge the valuable contributions NSR laboratory team members during the preparation of this manuscript.

REFERENCES

- [1] Leidner J. Plastics waste. Recovery of economic value. New York and Basel: Dekker (Marcel), (1981) pp. 218–275.
- [2] Paszun D, Spychaj T. Ind Enf Chem Rers 36, (1997), 1373.
- [3] Moliner R, Lazaro M, Suelves I. Energy and Fuels 11, (1997), 1165.
- [4] Anderson AE, Berger DJ. Symposium on coal and oil/resin coprocessing, presented before the div. of petroleum chem. Inc. 205th national meeting, ACS, Denver, CO, March 28–April 2, (1993), p. 305.
- [5] Aguado J, Serrano DP. In: Clark JH, editor. Feedstock recycling of plastic wastes. Cambridge: RSC; (1999).
- [6] Sartorius I. Development of Plastics Manufacturing Industry in Europe, ICS-UNIDO Conference, Italy, (2002).
- [7] Packaging Recycling Worldwide, Dual System Deutschland GmbH, (1996).
- [8] Recycling Data-Techniques and Trends, Dual System Deutschland GmbH, March (1996).
- [9] Changes and Developments – Plastic Recycling Today, Dual System Deutschland GmbH, (1995).
- [10] Taguchi T. Energy in Japan, 139, (1996), 22.
- [11] Wang L, Yoon, Jong S, Park, Heon Jung, Ho T. Lee, Deuk K. Lee, Optimization of pyrolytic co-processing of waste plastics and waste motor oil into fuel oils using statistical pentagonal experimental design. Fuel 78 (1999) 809–813

Design and Analysis of P&O and IP&O MPPT Techniques for Photovoltaic System

J. Surya Kumari¹ Dr. Ch. Sai Babu², A. Kamalakar Babu³

¹Asst. Professor, Dept of Electrical and Electronics Engg, RGM College of Engg & Tech, Nandyal, India.

²Professor, Dept of Electrical and Electronics Engg, JNT University, Kakinada, India.

³PG-Student, Dept of Electrical and Electronics Engg, RGM College of Engg & Tech, Nandyal, India

Abstract: Photovoltaic (PV) energy is the most important energy resource since it is clean, pollution free, and inexhaustible. Due to rapid growth in the semiconductor and power electronics techniques, it is important to operate PV energy conversion systems near the maximum power point to increase the output efficiency of PV arrays. The output power of PV arrays is always changing with weather conditions, which mean solar irradiation and atmospheric temperature. Some MPPT techniques are available in that perturbation and observation (P&O) and improved perturbation and observation (IP&O). A P&O method is the most simple, which moves the operating point toward the maximum power point periodically increasing or decreasing the PV array voltage. It was proved that the P&O method control system sometimes deviates from the maximum operating point. When the MPP is reached, the P&O method will oscillate around it in case of constant or slowly varying atmospheric conditions. This problem can be solved to decrease the perturbation step; however, the tracking response will be slower. In case of rapidly changing atmospheric conditions, the P&O method can occasionally make the system operation point far from the MPP. Perturbation and observation (P&O) is that the operating point oscillates around the maximum power point (MPP). The improved P&O method is introduced, based on hysteresis band and auto-tuning perturbation step. There is trade-off between dynamic response and steady state due to the selection of "dv". The Improved perturbation and observation (IP&O) has the tracking response will be higher. IP&O method has rapidly changing atmospheric conditions then the unpredictable performance with oscillations around maximum power point (MPP). In IP&O has high reliability and it is very complexity. A Mat lab-Simulink based simulation study of PV cell/PV module/PV array is carried out and presented.

Keywords: Photovoltaic system, Modeling of PV arrays, Boost converter, perturbation and observation, improved perturbation and observation and Simulation Results.

I. Introduction:

A photovoltaic system converts sunlight into electricity. The basic device of a photovoltaic system is the photovoltaic cell. Cells may be grouped to form panels or modules. Panels can be grouped to form large photovoltaic arrays. The term array is usually employed to describe a photovoltaic panel (with several cells connected in series and/or parallel) or a group of panels. The term array used henceforth means any photovoltaic device composed of several basic cells. The use of new efficient photovoltaic solar cells (PVSCs) has emerged as an alternative measure of

renewable green power, energy conservation and demand-side management. The performance of a PV array system depends on the operating conditions as well as the solar cell and array design quality. The output voltage, current and power of PV array vary as functions of solar irradiation level, temperature and load current. Therefore the effects of these three quantities must be considered in the design of PV arrays so that any change in temperature and solar irradiation levels should not adversely affect the PV array output to the load/utility, which is either a power company utility grid or any stand alone electrical type load.

Perturbation and Observation (P&O) can track the Maximum Power Point (MPP) all the time, irrespective of the atmospheric conditions, type of PV panel, and even aging, by processing actual values of PV voltage and current. Since the cost of the required circuitry for implementing on-line MPPTs is higher, they are usually employed for larger PV arrays. P&O method is widely used in PV systems because of its simplicity and easy of implementation. However, it presents drawbacks such as slow response speed, oscillation around the MPP in steady state, and even tracking in wrong way under rapidly changing atmospheric conditions. To overcome the above drawbacks of P&O method, provided that the computation is carried out at very fast rates. They are usually based on the comparison of average values of 'i_{p_v}' and 'v_{p_v}' obtained from low-pass filters, which introduce delays, and on the control of the average value of either 'i_{p_v}' or 'v_{p_v}' resulting in slow speeds of response. The proposes a new implementation of a P&O algorithm that mitigates the main drawbacks commonly related to the P&O Method.

An improved perturbation and observation method (IP&O) based on fixed algorithm is proposed, which is automatically adjusts the reference step size and hysteresis bandwidth for power comparison. The IP&O increases the total PV output power by 0.5% at an unsettled weather condition compare to traditional perturbation and observation method (P&O). The Improved perturbation and observation (IP&O) has the tracking response will be higher. When IP&O method has rapidly changing atmospheric conditions then the unpredictable performance with oscillations around maximum power point (MPP). In IP&O has high reliability and it is very complexity The improved P&O method is introduced, based on hysteresis band and auto-tuning perturbation step. There is trade-off between dynamic response and steady state due to the selection of 'dv'.

Organization of the paper is photovoltaic modelling, Equivalent electric circuit of Photovoltaic cell, Boost converter and Maximum power point tracking (MPPT) Techniques are Perturbation and Observation (P&O) in that

P&O with fixed Perturb, Improved Perturbation and Observation (IP&O) in that Improved P&O with fixed perturb, Simulation results, Comparison of P&O and IP&O curves and analytical comparison of P&O and IP&O curves.

II. Photovoltaic modeling

Equivalent Electric Circuit of Photovoltaic Cell:

A mathematical description of current voltage terminal characteristics for PV cells. The single exponential equation which models a PV cell is derived from the physics of the PN junction and is generally accepted as reflecting the characteristic behavior of the cell. A double exponential equation may be used for the polycrystalline silicon cells.

$$I = I_{ph} - I_s \left(\frac{\exp(q(V + IR_s))}{N.K.T} - 1 \right) - \frac{(V + IR_s)}{R_{sh}} \quad (1)$$

A solar cell, which is basically a *p-n* semiconductor junction directly, converts light energy into electricity. PV cells are grouped in larger units called PV modules, which are further interconnected in a parallel-series configuration to form PV arrays or generators. The photovoltaic cell considered can be modeled mathematically using the following procedure:

Voltage output of a PV cell:

$$V_{pv} = \left[\frac{N_s AKT}{q} \right] \ln \left[\frac{N_p \times I_{ph} - I_{pv} + N_p \times I_o}{I_o} \right] - I_{pv} R_s \quad (2)$$

Current output of a PV cell:

$$I_{pv} = N_p \times I_{ph} - N_p \times I_o \left[\exp \left\{ \frac{q \times (V_{pv} + I_{pv} R_s)}{N_s AKT} \right\} - 1 \right] \quad (3)$$

$$I_{ph} = [I_{scr} + K_t (T - 298)] \times \frac{\lambda}{100} \quad (4)$$

$$I_o = I_{or} \left[\frac{T}{T_r} \right]^3 \exp \left[\frac{q \times E_{go}}{BK} \left\{ \frac{1}{T_r} - \frac{1}{T} \right\} \right] \quad (5)$$

The PV array power P can be calculated using the following equation:

$$P_{pv} = I_{PV} \times V_{PV}$$

$$P_{pv} = V_{pv} \times N_p \times I_{ph} - V_{pv} \times N_p \times I_o \left[\exp \left\{ \frac{q \times (V_{pv} + I_{pv} R_s)}{N_s AKT} \right\} - 1 \right] \quad (6)$$

Where,

V_{pv} Is output voltage of a PV cell (V)

I_{pv} Is output current of a PV cell (A)

N_s Is the number of modules connected in series

N_p Is the number of modules connected in parallel

I_{ph} is the light generated current in a PV cell (A)

I_o is the PV cell saturation current (A)

R_s is the series resistance of a PV cell

$A=B$ is an ideality factor=1.6

K is Boltzmann constant=1.3805e-23Nm/K

T is the cell temperature in Kelvin=298K

Q is electron charge=1.6e-19Coulombs

T_r =The reference temperature=301.18k

I_{scr} =PV cell short-circuit current at 25°C and 100Mw/cm²=3.27A

N = number of cells

K_t =The short-circuit current temperature co-efficient at

I_{scr} =0.0017A/°C

R_{sh} = shunt resistance of a PV cell

I_s = saturation current

λ =is the PV cell illumination (MW/cm²)=100Mw/cm²

I_{or} =Saturation current at T_r =2.0793e^{-6A}

E_{go} = is the band gap for silicon=1.1eV

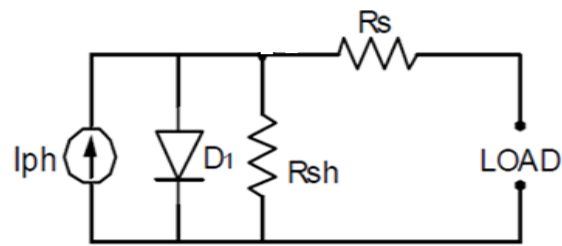


Figure1: PV Cell Circuit Model

The complete behavior of PV cells are described by five model parameters (I_{ph} , N , I_s , R_s , R_{sh}) which is representative of the physical behavior of PV cell/module. These five parameters of PV cell/module are in fact related to two environmental conditions of solar isolation & temperature. The determination of these model parameters is not straightforward owing to non-linear nature of equation.

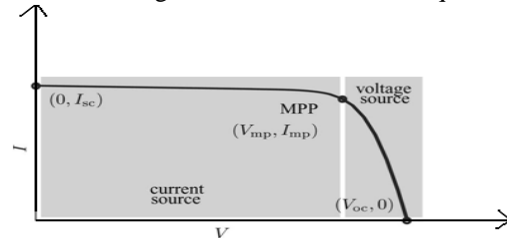


Figure 2: Maximum Power Point (V_{mp} , I_{mp})

Characteristic $I-V$ curve of a practical PV device and the three remarkable points: short circuit ($0, I_{sc}$), MPP (V_{mp}, I_{mp}), and open circuit ($V_{oc}, 0$).

III. MPPT Techniques

A. Perturbation and Observation:

P&O algorithms are widely used in MPPT because of their simple structure and the few measured parameters which are required. They operate by periodically perturbing (i.e. incrementing or decrementing) the array termed voltage and comparing the PV output power with that of the previous perturbation cycle. If the power is increasing, the perturbation will continue in the same direction in the next cycle, otherwise the perturbation direction will be reversed. This means the array terminal voltage is perturbed every

MPPT cycle, therefore when the P&O is reached, the P&O algorithm will oscillate around it resulting in a loss of PV power, especially in cases of constant or slowly varying atmospheric conditions. This problem can be solved by improving the logic of the P&O algorithm to compare the parameters of two preceding cycles in order to check when the P&O is reached, and bypass the perturbation stage. Another way to reduce the power loss around the P&O is to decrease the perturbation step, however, the algorithm will be slow in following the P&O when the atmospheric conditions start to vary and more power will be lost.

The implementation of P&O type MPPTs with increased refresh rates of current (I)-requires two things. First, the P&O algorithm should operate with high sampling rates and the sample values of voltage and current should reflect the tendency of the output power when increasing or decreasing the reference signal for the MPPT power converter. Second, the response time of the MPPT power converter should be very fast while keeping the switching losses (frequency) low. This can be done by comparing instantaneous, instead of average, values of V_{pv} and peak current control that presents one-cycle speed of response for small variations in the reference current, to further improve the performance of the system. The proposed MPPT system employs peak current control. The switch is turned on by a clock signal and turned off when the actual current reaches the reference current. Therefore, the reference current can be perturbed (increased or decreased) in every switching cycle, meaning that the perturbation cycle or refresh rate is equal to the switching cycle.

A.1 P&O With Fixed Perturb:

In this method, a fixed perturb value is utilized to generate a reference signal for the outer control loop. The Perturb signal is either the array reference voltage or current. The fixed perturb step is determined according to the system designer as a result of previous experience. Therefore, the solution provided by this method is not generic and system dependent. For small perturb steps, the tracking is slow but the power/voltage oscillations are minimal. In the case of large perturb step, faster tracking is achieved with increased oscillations. Hence, P&O techniques with fixed perturb suffer an inherent tracking-oscillations trade off problem. A PI/hysteresis Controller following the MPPT is utilized to control the power converter.

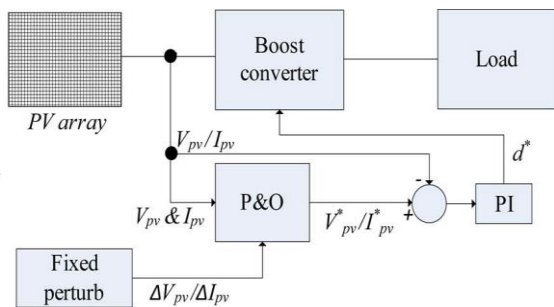


Fig.4 Fixed perturb with Perturbation and Observation

The size of the perturbation has to be chosen according to the inductor size and the switching (clock) frequency so that the switch always turns off before the next turn on signal. The perturbation and observation method (P&O), which moves the operation point of array toward the maximum power point (MPP) by periodically of any output voltage, is often used in many PV systems. It works well when the Irradiance changed very slowly, but the P&O method fails to track the MPP when irradiance changed suddenly by having slow dynamic response.

B. Improved Perturbation and Observation:

The improved perturbation and observation method (IP&O) is proposed. The IP&O method is implemented in a software program with fixed algorithm, which automatically adjusts the reference voltage step size and hysteresis band to achieve dynamic response and search exactly MPP under rapidly changing condition. The improved P&O method is introduced, based on hysteresis band and auto-tuning perturbation step. There is trade-off between dynamic response and steady state due to the selection of 'dv' the perturbation step. The system response of the IP&O method has faster dynamic response and higher induced-power than the Perturbation and Observation (P&O) method has. The overall Maximum Power Point (MPP) tracking efficiencies of Improved Perturbation and Observation (IP&O) method are also higher as around 0.5% in the unsettled weather condition than those of P&O method.

The number of samples per switching cycle, type (synchronized/ unsynchronized) and ideal instant for sampling (maximum and minimum current) are investigated in order to obtain fast calculation of the direction of the next perturbation. The Improved perturbation and observation was used to implement the proposed MPPT control system, which controls the dc/dc boost converter in the 3kW grid-connected PV power systems. The IP&O results shows that the increases total PV output power by 0.5% at an unsettled weather condition compare to traditional perturbation and observation.

The limitation of P&O methods is that they tend to mistrack the MPP under rapidly changing atmospheric conditions. During a transient it moves the operating point away from the MPP instead of towards it. This phenomenon shows how a faster IP&O implementation can reduce this problem. IP&O MPPT algorithms are based on the assumption of constant atmospheric conditions and that the variations in the output power are due to the injected perturbations. It compares values of p_{pv} and i_{pv} at are supposed to lie on the same curve. Problems arise when the two points are not on the same curve due to a sudden variation on the solar irradiation. Let's assume that the solar irradiation level is initially and then increases. Depending on the sampling frequency, the present values for P and I will be obtained from curves (high sampling rate). The IP&O algorithm would be decrease I, driving the operating point towards the new MPP. However, for low sampling rates, would then be increased by the IP&O algorithm driving the operating point away from the new MPP. Therefore, operation with high sampling rates (small perturbation

cycles) reduces the odds of wrong tracking the MPP during sudden solar irradiation variations.

B.1 Improved P&O With Fixed Perturb:

In this technique, instead of utilizing the array voltage or current as the perturbed signal, the converter duty ratio is used. This eases the control process as it eliminates the PI/hysteresis controller after the MPPT block, enabling direct control of the converter’s duty cycle. The perturb step is fixed and designer dependent. Hence, the previously mentioned trade off problem still persists. In order to improve the performance of P&O techniques, the modified calculation of the perturb value is utilized instead of the fixed values. The Improved P&O techniques review are discussed in the following sections.

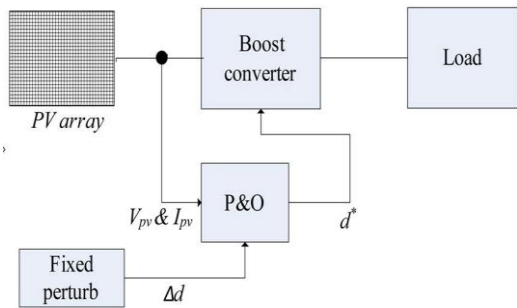


Fig5. Improved with fixed Perturbation and Observation

IV. Simulation Results

PV array Curves

The PV cell temperature is maintained constant at 25°C and the solar intensity is varied in steps up to the rated value of 100mWcm⁻². It is seen from the figure .6 that for a constant solar intensity the current remains constant with increasing voltage up to 100Volts after which it decreases. It is further observed that the current increase with increasing intensity thereby increasing the power output of the solar cell.

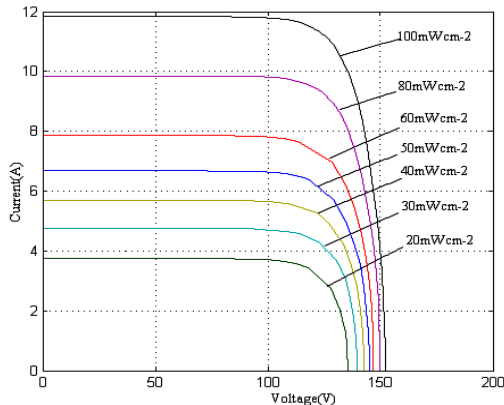


Figure6: V-I Curve with different irradiation

The PV cell temperature is maintained constant at 25°C and the solar intensity is varied in steps up to the rated value of 100mWcm⁻². It is seen from the figure .7 that for a

constant solar intensity the power remains constant with increasing voltage up to 100Volts after which it decreases.

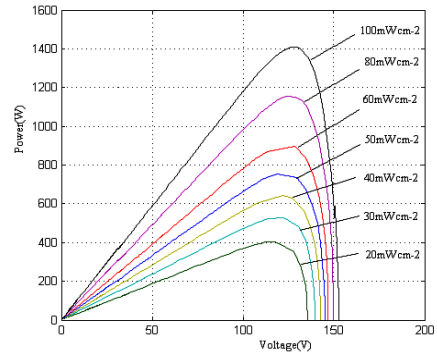


Figure7: P-V Curve with different irradianations

The effect of temperature variations on the V-I characteristics of the PV cell is shown in figure.8. A marginal variation in current is observed for a temperature variation from 25°C to 65°C for a voltage up to 65Volts. Above this value the current decreases in a sharp manner for small variation in voltage. It is further seen that the voltage of which the cell current becomes zero increases with decreasing temperature.

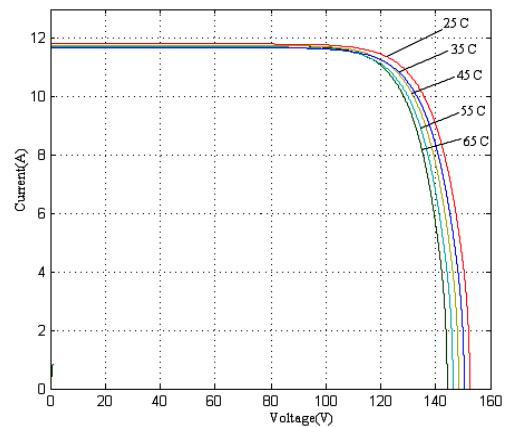


Figure8: V-I Curve with different temperature

The effect of temperature variations on the P-V characteristics of the PV cell is shown in figure 9. power variation is observed for a temperature variation from 25°C to 65°C for a voltage up to 65volts.the power decreases in a sharp manner for small variation in voltage.

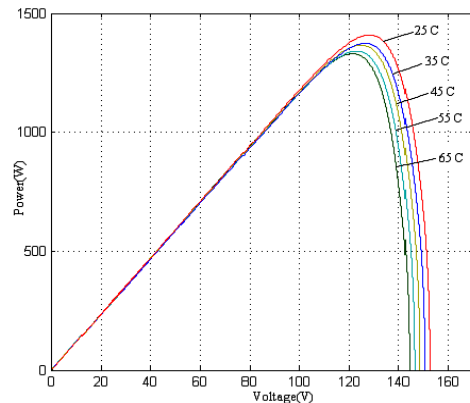


Figure9: P-V Curve with different Temperatures

Perturbation and Observation curves:

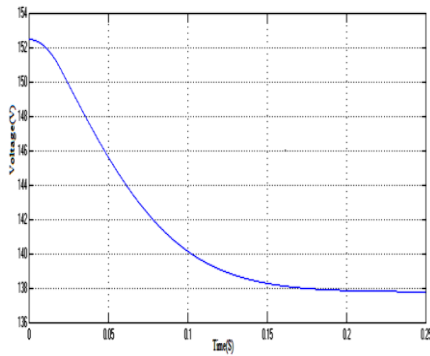


Fig 10(a): PV array output Voltage for P&O MPPT Technique

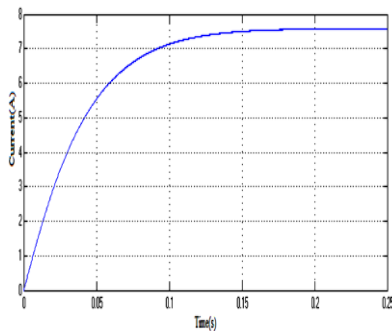


Fig 10(b): PV array output current for P&O MPPT Technique

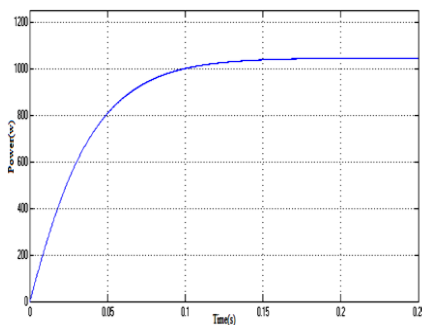


Fig 10(c): PV array output power for P&O MPPT Technique
 From Fig10. The response with perturbation and observation (P&O) MPPT Technique waveforms are (a) PV array output voltage (b) PV array output current (c) PV array output power at temperature=25°C and solar irradiation =100mWcm⁻².

Improved Perturbation and Observation curves:

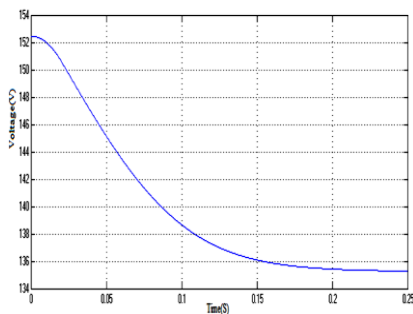


Fig 11(a): PV array output voltage for Improved P&O MPPT Technique

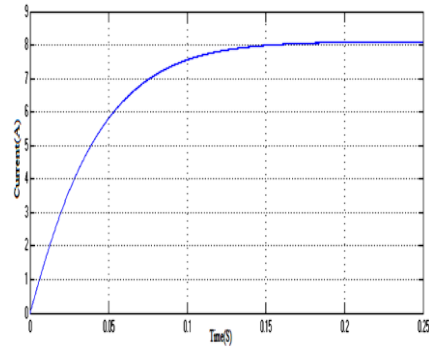


Fig 11(b): PV array output current for Improved P&O MPPT Technique

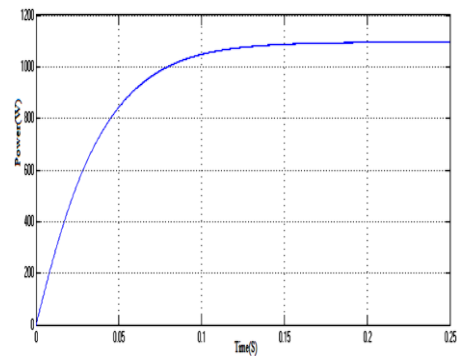


Fig 11(c): PV array output power for Improved P&O MPPT Technique

From Fig11. The response with Improved perturbation and observation (P&O) MPPT Technique waveforms are (a) PV array output voltage (b) PV array output current (c) PV array output power at temperature=25°C and solar irradiation =100mWcm⁻².

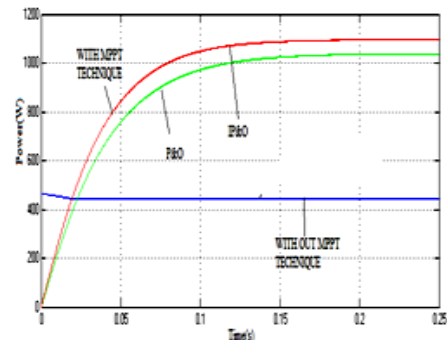


Fig12: Comparison of P&O and Improved P&O MPPT Technique power

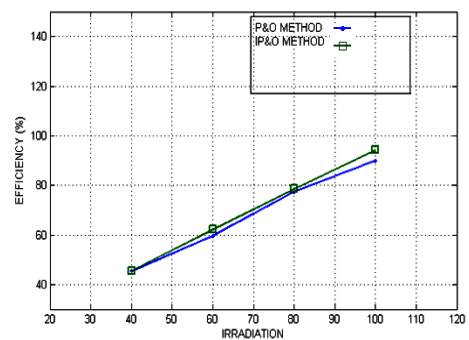


Fig13: Temperature constant and Irradiation vs. efficiency

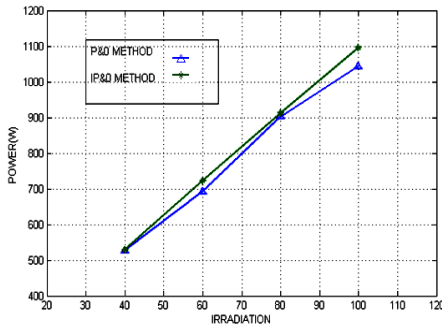


Fig14: Temperature constant and Irradiation vs. Power

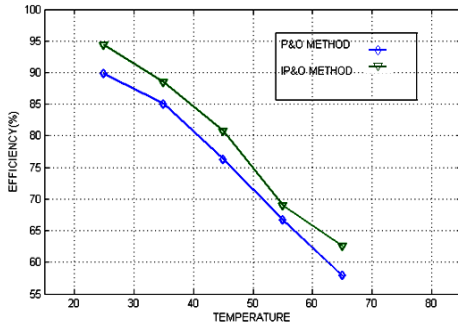


Fig15: Irradiation constant and Temperature vs. efficiency

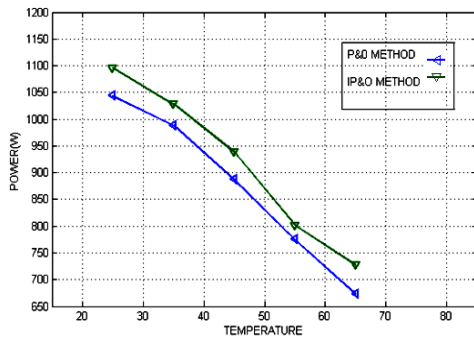


Fig16: Irradiation constant and Temperature vs. power

Table 1. Comparison of P&O and Improved P&O MPPT Techniques:

S.NO	MPPT TECHNIQUES	VOLTAGE (V)	CURRENT (A)	POWER (W)	EFFICIENCY (%)
1	PERTURBATION AND OBSERVATION	137.8	7.577	1044	90%
2	IMPROVED PERTURBATION AND OBSERVATION	135.2	8.104	1096	94.38%

Table2. Comparison of two MPPT methods:

Specifications	Perturbation and Observation	Improved Perturbation and Observation
Cost	Relatively lower	Moderately lower
Reliability	Accurate but oscillates around the MPP	Precise but oscillates around the MPP
Complexity	Easy but complex when site conditions vary	High
Realization	Easy to implement as few measured parameters	Difficult to implement as few measured parameters
Efficiency	High about 90%	High about 98%
Rapidly Changing Atmospheric conditions	Unpredictable performance with oscillations around MPP. slower response	Efficient performance with oscillations around MPP. Higher response

V. Conclusion

This paper proposes design of photo voltaic system, simple boost converter, perturbation and observation (P&O), improved perturbation and observation (IP&O). The PV cell output voltage varies with atmospheric parameters such as temperature and irradiation. By increasing series and parallel cells, voltage will be drop. The PV Array output voltage gradually decrease and then steady state conditions. PV array Cascaded with Boost converter is used to step up output voltage. Perturbation and observation (P&O) method is widely used in photovoltaic (PV) systems because of its simplicity and easily of implementation. A P&O method is the most simple, which moves the operating point towards the maximum power point. P&O method control system sometimes deviates from the maximum operating point. This paper proposes design of photo voltaic system, simple boost converter IP&O based on modified fixed algorithm is automatically adjusts the reference step size and hysteresis bandwidth for power conversion. The improved P&O method is based on auto-tuning perturbation. The Improved perturbation and observation (IP&O) has the tracking response will be higher. When IP&O method has rapidly changing atmospheric conditions then the unpredictable performance with oscillations around maximum power point (MPP). In IP&O has high reliability and it is very complexity. The advantage of improved perturbation and observation (IP&O). It finds the real MPP under any working conditions. No oscillation during tracking and steady state operations. Low computational burden required. Hence, fast tracking using low cost controller is achievable. Applications of Improved perturbation and observation (IP&O) are Impedance matching and Micro grid technology. In future, Advanced MPPT techniques are used like adaptive

perturbation (AP&O), fuzzy logic controller and neural networks.

Acknowledgement:

We express our sincere thanks to RGM CET for providing us good lab facilities. A heart full and sincere gratitude to my guide Mrs. J.Suryakumari for their tremendous motivation and moral support.

References:

- [1] N. Femia, G. Petrone, G. Spagnuolo, and M. Vitelli, "A technique for improving P&O MPPT performances of double-stage grid-connected photovoltaic systems," *IEEE Trans. Ind. Electron.*, vol. 56, no. 11, pp. 4473–4482, Nov. 2009.
- [2] S. Yuvarajan, J. Shoeb, "A fast and accurate maximum power point tracker for PV systems," *Applied Power Electronics Conference and Exposition, APEC 2008*, pp.167–172. 2970.
- [3] Nguyen, D y Lehman, B.:A Reconfigurable Solar Photovoltaic Array Under Shadow Conditions, *Applied Power Electronics Conference and Exposition*, pp. 980-986, 2008.
- [4] Sergio Daher, Jurgen Schmid and Fernando L.M Antunes, "Multilevel Inverter Topologies for Stand-Alone PV Systems" *IEEE Transactions on Industrial Electronics*. Vol.55, No.7, July 2008.
- [5] Jae-Sub Ko, Byung-Jin Jung, Ki-Tae Park, et al, "Maximum Power Point Tracking Control of PV System for DC Motors Drive with Neural Network," *Smart Manufacturing Application*, 2008. ICSMA 2008. International Conference on 9-11 April 2008, pp.:514–519.
- [6] N. Mutoh, M. Ohno, and T. Inoue, "A Control Method to Charge Series- Connected Ultra electric Double-Layer Capacitors Suitable for Photovoltaic Generate Systems Combining MPPT Control Method," *IEEE Transactions on Industrial Electronics*, 2007, vol. 54, no.1, pp.374-383.
- [7] B. Kavidha, K. Rajambal: Transformer less Cascaded Inverter Topology for Photovoltaic Applications, *Proceedings of India International Conference on Power Electronics 2006*.
- [8] N. S. D'Souza, L. A. C. Lopes, and X. Liu, "An intelligent maximum power point tracker using peak current control," in *Proc. IEEE 36th Power Electron. Spec. Conf.*, Jun. 16–16, 2005, pp. 172–177.
- [9] N. Femia, G. Petrone, G. Spagnuolo, and M. Vitelli, "Optimization of perturb and observe maximum power point tracking method," *IEEE Trans. Power Electron.*, vol. 20, no. 4, pp. 963–973, Jul. 2005.
- [10] C. Dorofte, U. Borup, F. Blaabjerg, "A combined two-method MPPT control scheme for grid-connected photovoltaic systems," *Power Electronics and Applications, European Conference*, Sept. 2005, pp.1-10.
- [11] Y. Jung, J. So, G. Yu, et al., "Improved perturbation and observation method (IP&O) of MPPT control for photovoltaic power systems," *Photovoltaic Specialists Conference*, 2005. 3-7 Jan. 2005, pp. 1788–1791.
- [12] P. J. Wolfs and L. Tang, "A single cell maximum power point tracking converter without a current sensor for high performance vehicle solar arrays," in *Proc. IEEE 36th Power Electron. Spec. Conf.*, Jun. 16–16, 2005, pp. 165–171.
- [13] S. Jain and V. Agarwal, "A new algorithm for rapid tracking of approximate maximum power point in photovoltaic systems," *IEEE Power Electron. Lett.* vol. 2, no. 1, pp. 16–19, Mar. 2004.
- [14] W. Xiaa and W.G. Dunford, 'A modified adaptive hill climbing method for photovoltaic power systems'. In *Proc. IEEE 35th PESC*. vol. 3, pp. 1957-1 963, June 2004
- [15] K.H. Hussein, I. Muta, T. Hoshino and M. Osakada, "Maximum photovoltaic power tracking : an algorithm for rapidly changing atmospheric conditions", *IEE Pm.Generation, Transmission and Distribution*, vol. 142, pp. 59-63, Jan. 1995 vol. 8, pp. 1359-1361, 2003.
- [16] Y. Jung, G. Yu, J. So, J. Choi and J. Choi, "A Study of MPPT Algorithm for PV PCS", *Proceeding of KIEE SAC*,
- [17] C. Hua, J. Lin and C. Shen, "Implementation of a DSP Controlled Photovoltaic. System with Peak Power Tracking", *IEEE Trans. Industrial Electronics*, vol. 45, pp. 99-107, Feb. 1998.
- [18] P. Midya P. T. krein, I. J. Turnbull, R. Reppa J. Kimball, " Dynamic Maximum Power Point Tracker for Photovoltaic Applications", *Proc. PESC, Baveno, Italy*, 21-27June 1996, pp.1710-1716.
- [19] K. H. Hussein, I. Muta, T. Hoshino, and M. Osakada "Maximum photovoltaic power tacking: An algorithm for rapidly changing atmospheric conditions", *Proc. IEE - Generation. Transmission. Distribution*, vol. 142.1\10. 1, Jan 1995, pp. 59-61.
- [20] M. Buresch: *Photovoltaic Energy Systems Design and Installation*, McGraw-Hill, New York, 1983.

A Hybrid Model to Identify Flaws in Textile

Kamaldeep Kaur¹, Deepak Goyal², Neeru³

^{#1,3} Deptt. Of ECE, B.B.S.B.E.C, Fatehgarh Sahib, Punjab
^{#2} C-DAC, Mohali, Punjab

ABSTRACT: The objective of fabric inspection is to ascertain whether the fabric received is of expected Quality standard or not. The main objective is detection of fabric defects as early as possible so that time and money are not wasted in the manufacturing, process. The ultimate goal of any quality control activity in clothing' industry is to satisfy the customers. Most defects in cloth occur while it is woven on the loom. Some of these fabric defects are visible, while others are not. Again some fabric defects may be rectified during weaving and after weaving while others are not. Often inspectors are given the responsibility of inspecting finished garments manually without adequate training in fabric defects and their causes. Detection of defects was generally carried out by time-consuming and tedious human inspection. Such manual inspection procedures are commonly agreed upon to be inefficient with detection efficiency suffering from deterioration due to boredom and lack of vigilance. The problem is accentuated by the presence of several types of defects those may occur in woven fabric at random. As we know that fabric are the main and costly raw materials of a garment. So it is very important to use fabric efficiently and control wastage of fabric. On the other hand fabric defects are the maximum defects of garments, for which many-unexpected problem may occur in a clothing industry. Such as- short shipment, discount, low price etc.

Keywords: Fabric inspection, Hybrid model, YCBCR technique, Wavelet transform (WT), Image distance difference algorithm.

I. INTRODUCTION

The production of quality fabric is the foremost goal of the modern textile industry. Typical textile mills employ humans to inspect and grade the fabric in the production facility. The job is monotonous, as it requires the employee to sit at an inspection frame and watch as fabric that is 5-9ft wide passes over the board at speeds ranging from 8-20 yards a minute, all the while visually scanning that wide area of fabric for possible defects as shown in Fig.1 Traditional fabric inspection. The average human inspection department is only able to find 60%-75% of existing defects, which translates into a substantial amount of second quality shipped or returned. This alone leads to a considerable reduction in production efficiency, as most customers will only accept a certain percentage of second quality fabric in their order, meaning that the production facility must spend time producing re-work to be able to meet the customer demands. In an effort to improve the efficiency of inspection departments and subsequently reduce the costs of production, textile manufacturers have begun turning to automate inspection

systems. An automated inspection system usually consists of a computer based vision system. Because they are computer based, these systems do not suffer the drawbacks of human visual inspection, such as fatigue, boredom, or inattentiveness. Automated systems are able to inspect fabric in a continuous manner without pause.



Fig.1 Traditional fabric inspections.

In this paper, a new fabric defect detection algorithm based on YCBCR technique is proposed. This technique is used to have more accurate results.

II. FABRIC DEFECTS

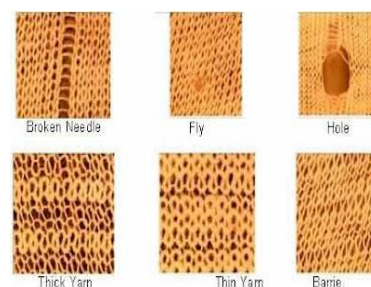
In fabric field there are different types of faults such as scratch, hole, dirty spots, color bleeding etc. If these faults are not detected properly it will affect the production system massively.

Major and Minor Defects

The following definitions are central to fabric inspection:

Major Defect: A defect that, if conspicuous on the finished product, would cause the item to be a second. (A "second" is a garment with a conspicuous defect that affects the salability or serviceability of the item.

Minor Defects: A defect that would not cause the product to be termed a second either because of severity or location. When inspecting piece goods prior to cutting, it is necessary to rate questionable defects as major, since the inspector will not know where the defect may occur on the item.



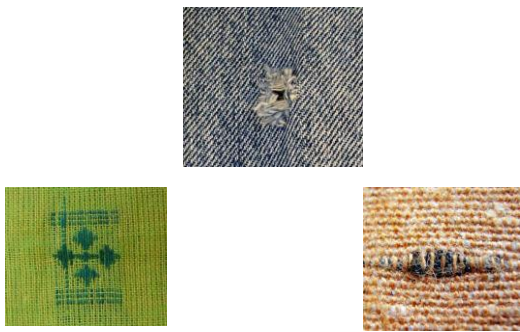


Fig.2 Defects in fabric

III. YCbCr TECHNIQUE

One of two primary color spaces used to represent digital component video (the other is RGB). **YCbCr**, **Y'CbCr**, or **Y Pb/Cb Pr/Cr**, also written as $Y C_B C_R$ or $Y' C_B C_R$, is a family of color spaces used as a part of the color image pipeline in video and digital photography systems. The difference between YCbCr and RGB is that YCbCr represents color as brightness and two color difference signals, while RGB represents color as red, green and blue. In YCbCr, the Y is the brightness (luma), Cb is blue minus luma (B-Y) and Cr is red minus luma (R-Y). **YCBCR = rgb2ycbcr(RGB)** converts the truecolor image RGB to the equivalent image in the YCbCr color space.

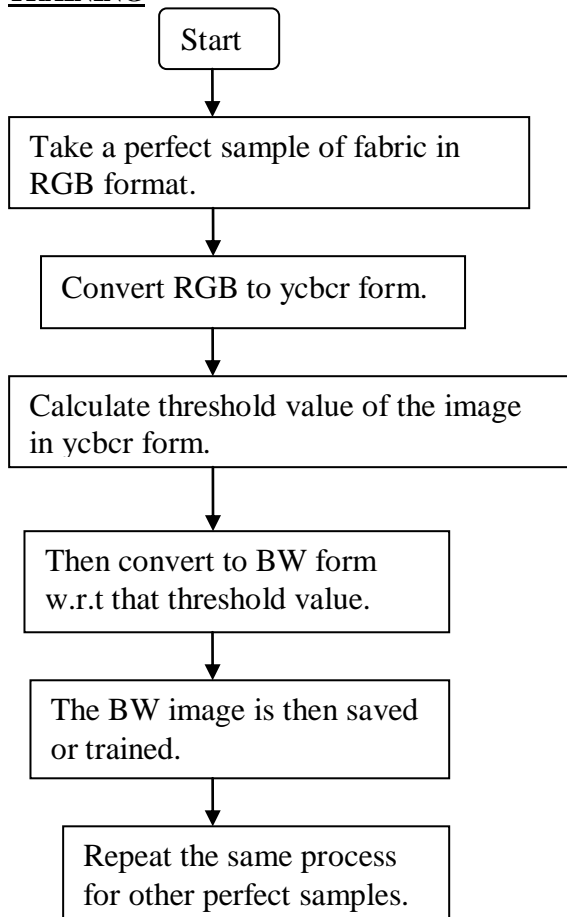
If the input is uint8, YCBCR is uint8, where Y is in the range [16 235], and Cb and Cr are in the range [16 240]. If the input is a double, Y is in the range [16/255 235/255] and Cb and Cr are in the range [16/255 240/255]. If the input is uint16, Y is in the range [4112 60395] and Cb and Cr are in the range [4112 61680]. YCbCr and Y'CbCr are a practical approximation to color processing and perceptual uniformity, where the primary colors corresponding roughly to red, green and blue are processed into perceptually meaningful information. By doing this, subsequent image/video processing, transmission and storage can do operations and introduce errors in perceptually meaningful ways. Y'CbCr is used to separate out a luma signal (Y') that can be stored with high resolution or transmitted at high bandwidth, and two chroma components (C_B and C_R) that can be bandwidth-reduced, subsampled, compressed, or otherwise treated separately for improved system efficiency.

IV. METHODOLOGY OF PAPER

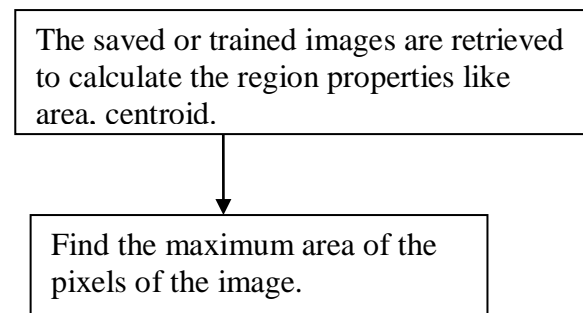
Our defect detection system consists mainly of three parts: **Training, feature extraction and testing (detection)**.

- The training and feature extraction part uses wavelet transform (WT) technique in decomposition of image into wavelets.
- The testing (detection) part utilizes image distance difference algorithm to find the absolute difference between the trained and tested image.

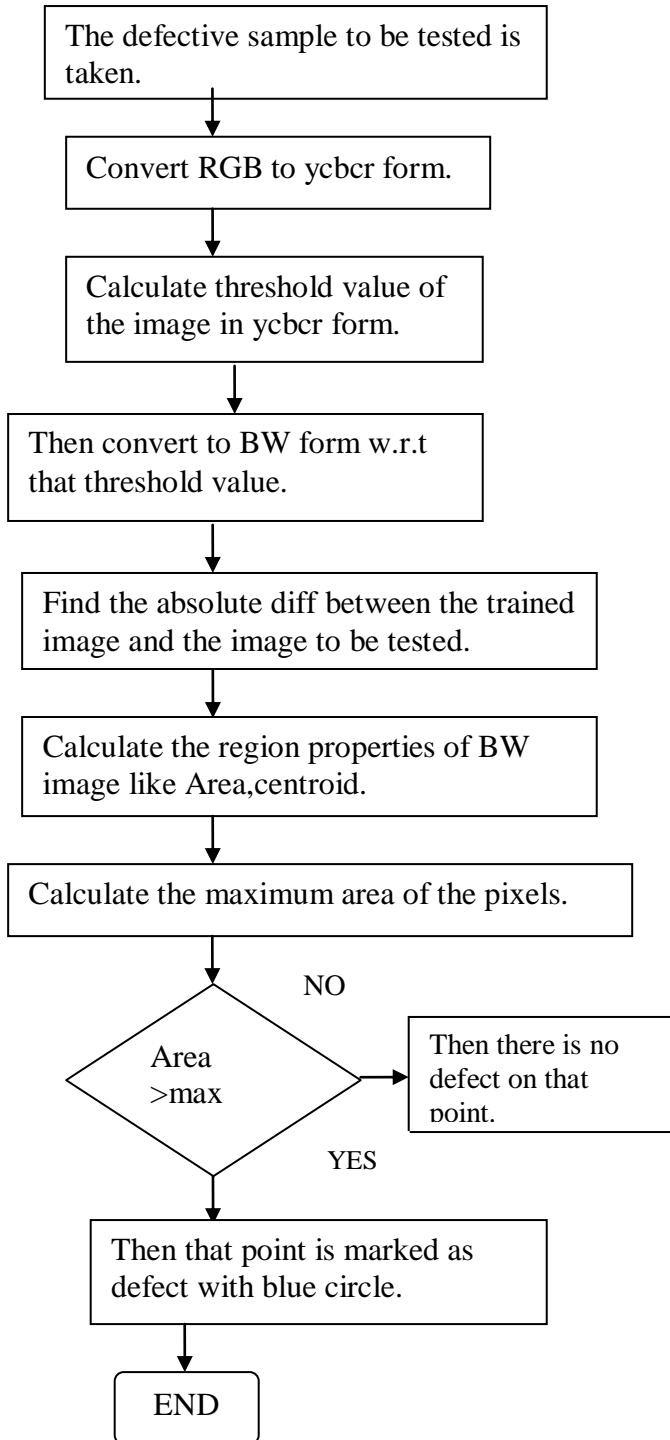
TRAINING



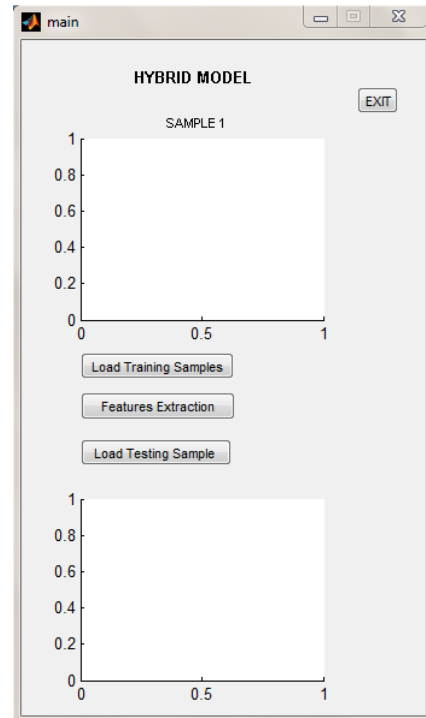
FEATURE EXTRACTION



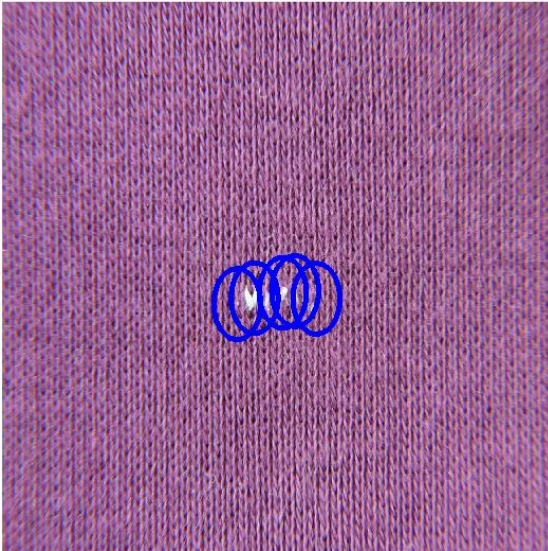
TESTING



SIMULATION RESULTS



Resulted Image



- [7] Xianying Feng, Chengliang Zhang, Bingsheng Yang and Lei Li, "*Foreign fibre recognition and detection algorithm based on RGB color space*," Journal of Shandong University (Engineering Science), Vol39, pp. 68-72, 2009.

V. CONCLUSION

The conclusions from this paper suggest that the combination of Wavelet Transform and image distance difference algorithm approaches can give better results than any single approach, and is suggested for further research. Experiments show that using YCbCr color space technique has improved the detection performance of the defective fabric.

As it is simple and efficient, it is also appropriate to real-time defect detection.

REFERENCES

- [1] Pooja Mehta and Naresh Kumar, **Detection Of Foreign Fibers And Cotton Contaminants By using Intensity And Hue Properties**, proceedings of the International Journal of Advances in electronics Engineering (IJAE).
- [2] Lu Yun, Zhang Jingmiao, "**Fabric Defect Detection Method Based on Image Distance Difference**", Micro-computer Information, No 23, 2007.
- [3] Jingmiao Zhang and Linru Li, "**A new algorithm for Fabric Defect Detection Based on Image Distance Difference**", *IEEE Trans.* 2009 Third International Symposium on Intelligent Information Technology Application.
- [4] Seyyed Meysam Hosseini, Hadi Sadoghi Yazdi and Saber Amjadi, "**A Novel Color Space Creating Method Applied to Skin Color Detection**", ICDIP '09 Proceedings of the International Conference on Digital Image Processing Pages 17-21.
- [5] Che-Seung Cho, Byeong-Mook Chung, "**Development of Real Time Vision-Based Fabric Inspection System**", *IEEE Transactions on industrial electronics*, Vol. 52, No. 4, AUGUST 2005.
- [6] X in and Huai "**A Fast Feature Extraction Algorithm for Detection of Foreign Fibre in Lint Cotton within a Complex Background**" vol. 36, No 6 June, 2010.

Theory of Alfa Ray Production, Quantum Tunneling, Redundancy, Entropy, Event, Cause, Space, Time, Storage Ability and Entanglement-A Tarantula-Guillemot Model

¹Dr. K. N. Prasanna Kumar, ²Prof. B. S. Kiranagi, ³Prof. C. S. Bagewadi

ABSTRACT: We propose a Theory of Alpha ray production(Radioactive decay), Quantum Tunneling, Redundancy, Entropy, Event, Cause, Space, Time, Storage ability, Quantum entanglement, Noise, Errors, by a Model that concatenates and consummates these important variables and provide predictive capacity, Stability analysis, and Solutional behaviour of the system,

I. INTRODUCTION

What is an event? Or for that matter an ideal event? An event is a singularity or rather a set of singularities or set of singular points characterizing a mathematical curve, a physical state of affairs, a psychological person or a moral person. Singularities are turning points and points of inflection: they are bottle necks, foyers and centers; they are points of fusion; condensation and boiling; points of tears and joy; sickness and health; hope and anxiety; they are so to say "sensitive" points; such singularities should not be confused or confounded, aggravated or exacerbated with personality of a system expressing itself; or the individuality and idiosyncrasies of a system which is designated with a proposition. They should also not be fused with the generalizational concept or universalistic axiomatic predications and postulation alcovishness, or the dipsomaniac flageolet dirge of a concept. Possible a concept could be signified by a figurative representation or a schematic configuration. "Singularity is essentially, pre individual, and has no personalized bias in it, or for that matter a prejudice or pre circumspection of a conceptual scheme. It is in this sense we can define a "singularity" as being neither affirmative nor non affirmative. it can be positive or negative; it can create or destroy. On the other hand it must be noted that singularity is different both in its thematic discursive from the run of the mill day to day musings and mundane drooling. There are in that sense "extra-ordinary".

Each singularity is a source and resource, the origin, reason and raison d'être of a mathematical series, it could be any series any type, and that is interpolated or extrapolated to the structural location of the destination of another singularity. This according to this standpoint, there are different, multifarious, myriad, series in a structure. In the eventuality of the fact that we conduct an unbiased and prudent examination of the series belonging to different "singularities" we can come to indubitable conclusion that the "singularity" of one system is different from the "other system" in the subterranean realm and ceratoid dualism of comparison and contrast

EPR experiment derived that there exists a communications between two particles. We go a further step to say that there exists a channel of communication however slovenly, inept, clumpy, between the two singularities. It is also possible the communication exchange could be one of belligerence, cantankerousness, tempestuousness, astutely truculent, with ensorcelled frenzy. That does not matter. All we are telling is that singularities communicate with each other.

Now, how do find the reaction of systems to these singularities. You do the same thing a boss does for you. "Problematize" the events and see how you behave. I will resort to "pressure tactics". "intimidation of deriding report", or "cut in the increment" to make you undergo trials, travails and tribulations. i am happy to see if you improve your work; but may or may not be sad if you succumb to it and hang yourself! We do the same thing with systems. systems show conducive response, felicitous reciprocation or behave erratically with inner roil, eponymous radicalism without and with blitz conviction say like a solipsist nature of bellicose and blustering particles, or for that matter coruscation, trepidational motion in fluid flows, or seemingly perfidious incendiaries in gormandizing fellow elementary particles, abnormal ebullitions, surcharges calumniation and unwarranted (you think so but the system does not!) unrighteous fulminations.

So the point that is made here is " like we problematize the "events" to understand the human behaviour we have to "problematize" the events of systems to understand their behaviour.

This statement is made in connection to the fact that there shall be creation or destruction of particles or complete obliteration of the systems (blackhole evaporation) or obfuscation of results. Some systems are like "inside traders" they will not put signature at all! How do you find they did it! Anyway, there are possibilities of a CIA/CBI finding out as they recently did! So we can do the same thing with systems to. This is accentuation, corroboration, fortification, .commendatory note to explain the various coefficients we have used in the model as also the dissipations called for In the bank example we have clarified that various systems are individually conservative, and their conservativeness extends holistically too.that one law is universal does not mean there is complete adjudication of nonexistence of totality or global or holistic figure. Total always exists and "individual" systems always exist, if we do not bring Kant in to picture! For the time being let us not! Equations would become more eneuretic and frenzied..

We TAKE In to consideration the following parameter:

- (1) Alpha ray production(Radioactive decay)
- (2) Quantum Tunneling
- (3) Redundancy
- (4) Entropy
- (5) Event
- (6) Cause
- (7) Space
- (8) Time
- (9) Storage ability
- (10) Quantum entanglement
- (11) Noise Errors.

QUANTUM TUNNELING AND ALPHA RAY PRODUCTION(RADIOACTIVE DECAY)

MODULE NUMBERED ONE.

NOTATION:

- G_{13} : CATEGORY ONE OF QUANTUM TUNNELING
 G_{14} : CATEGORY TWO OF QUANTUM TUNNELING
 G_{15} : CATEGORY THREE OF QUANTUM TUNNELING
 T_{13} : CATEGORY ONE OF ALPHA RAY PRODUCTION(RADIOACTIVE DECAY)
 T_{14} : CATEGORY TWO OF ALPHA RAY PRODUCTION (RADIOACTIVE DECAY)
 T_{15} :CATEGORY THREE OF ALPHA RAY PRODUCTION(RADIOACTIVE DECAY)
-

ENTROPY AND REDUNDANCY
MODULE NUMBERED TWO:

- G_{16} : CATEGORY ONE OF ENTROPY
 G_{17} : CATEGORY TWO OF ENTROPY
 G_{18} : CATEGORY THREE OF ENTROPY
 T_{16} :CATEGORY ONE OF REDUNDANCY
 T_{17} : CATEGORY TWO OF REDUNDANCY
 T_{18} : CATEGORY THREE OF REDUNDANCY
-

NOISE AND ERROR IN QUANTUM COMPUTATION:
MODULE NUMBERED THREE:

- G_{20} : CATEGORY ONE OF ERRORS
 G_{21} :CATEGORY TWO OF ERRORS
 G_{22} : CATEGORY THREE OF ERRORS
 T_{20} : CATEGORY ONE OF NOISE
 T_{21} :CATEGORY TWO OF NOISE
 T_{22} : CATEGORY THREE OF NOISE
-

CAUSE AND EVENT:
MODULE NUMBERED FOUR:

- G_{24} : CATEGORY ONE OF CAUSE
 G_{25} : CATEGORY TWO OF CAUSE
 G_{26} : CATEGORY THREE OF CAUSE
 T_{24} :CATEGORY ONE OF EVENT
 T_{25} :CATEGORY TWO OF EVENT
 T_{26} : CATEGORY THREE OF EVENT
-

SPACE AND TIME:
MODULE NUMBERED FIVE:

- G_{28} : CATEGORY ONE OF TIME
 G_{29} : CATEGORY TWO OF TIME
 G_{30} :CATEGORY THREE OF TIME
 T_{28} :CATEGORY ONE OF SPACE
 T_{29} :CATEGORY TWO OF SPACE
 T_{30} :CATEGORY THREE OF SPACE
-

STORAGE ABILITY AND ENTANGLEMENT :
MODULE NUMBERED SIX:

=====
 G_{32} : CATEGORY ONE OF ENTANGLEMENT
 G_{33} : CATEGORY TWO OF ENTANGLEMENT
 G_{34} : CATEGORY THREE OF ENTANGLEMENT
 T_{32} : CATEGORY ONE OF STORAGE ABILITY
 T_{33} : CATEGORY TWO OF STORAGE ABILITY
 T_{34} : CATEGORY THREE OF STORAGE ABILITY
 =====

$(a_{13})^{(1)}, (a_{14})^{(1)}, (a_{15})^{(1)}, (b_{13})^{(1)}, (b_{14})^{(1)}, (b_{15})^{(1)}, (a_{16})^{(2)}, (a_{17})^{(2)}, (a_{18})^{(2)}, (b_{16})^{(2)}, (b_{17})^{(2)}, (b_{18})^{(2)}$:
 $(a_{20})^{(3)}, (a_{21})^{(3)}, (a_{22})^{(3)}, (b_{20})^{(3)}, (b_{21})^{(3)}, (b_{22})^{(3)}$
 $(a_{24})^{(4)}, (a_{25})^{(4)}, (a_{26})^{(4)}, (b_{24})^{(4)}, (b_{25})^{(4)}, (b_{26})^{(4)}, (b_{28})^{(5)}, (b_{29})^{(5)}, (b_{30})^{(5)}, (a_{28})^{(5)}, (a_{29})^{(5)}, (a_{30})^{(5)}$,
 $(a_{32})^{(6)}, (a_{33})^{(6)}, (a_{34})^{(6)}, (b_{32})^{(6)}, (b_{33})^{(6)}, (b_{34})^{(6)}$

are Accentuation coefficients

$(a'_{13})^{(1)}, (a'_{14})^{(1)}, (a'_{15})^{(1)}, (b'_{13})^{(1)}, (b'_{14})^{(1)}, (b'_{15})^{(1)}, (a'_{16})^{(2)}, (a'_{17})^{(2)}, (a'_{18})^{(2)}, (b'_{16})^{(2)}, (b'_{17})^{(2)}, (b'_{18})^{(2)}$
 $, (a'_{20})^{(3)}, (a'_{21})^{(3)}, (a'_{22})^{(3)}, (b'_{20})^{(3)}, (b'_{21})^{(3)}, (b'_{22})^{(3)}$
 $(a'_{24})^{(4)}, (a'_{25})^{(4)}, (a'_{26})^{(4)}, (b'_{24})^{(4)}, (b'_{25})^{(4)}, (b'_{26})^{(4)}, (b'_{28})^{(5)}, (b'_{29})^{(5)}, (b'_{30})^{(5)}, (a'_{28})^{(5)}, (a'_{29})^{(5)}, (a'_{30})^{(5)}$,
 $(a'_{32})^{(6)}, (a'_{33})^{(6)}, (a'_{34})^{(6)}, (b'_{32})^{(6)}, (b'_{33})^{(6)}, (b'_{34})^{(6)}$

are Dissipation coefficients.

QUANTUM TUNNELING AND ALPHA RAY PRODUCTION(RADIOACTIVE DECAY)
MODULE NUMBERED ONE

The differential system of this model is now (Module Numbered one).

$$\begin{aligned} \frac{dG_{13}}{dt} &= (a_{13})^{(1)}G_{14} - [(a'_{13})^{(1)} + (a''_{13})^{(1)}(T_{14}, t)]G_{13} . \\ \frac{dG_{14}}{dt} &= (a_{14})^{(1)}G_{13} - [(a'_{14})^{(1)} + (a''_{14})^{(1)}(T_{14}, t)]G_{14} . \\ \frac{dG_{15}}{dt} &= (a_{15})^{(1)}G_{14} - [(a'_{15})^{(1)} + (a''_{15})^{(1)}(T_{14}, t)]G_{15} . \\ \frac{dT_{13}}{dt} &= (b_{13})^{(1)}T_{14} - [(b'_{13})^{(1)} - (b''_{13})^{(1)}(G, t)]T_{13} . \\ \frac{dT_{14}}{dt} &= (b_{14})^{(1)}T_{13} - [(b'_{14})^{(1)} - (b''_{14})^{(1)}(G, t)]T_{14} . \\ \frac{dT_{15}}{dt} &= (b_{15})^{(1)}T_{14} - [(b'_{15})^{(1)} - (b''_{15})^{(1)}(G, t)]T_{15} . \\ &+ (a''_{13})^{(1)}(T_{14}, t) = \text{First augmentation factor} . \\ &- (b''_{13})^{(1)}(G, t) = \text{First detritions factor} . \end{aligned}$$

ENTROPY AND REDUNDANCY
MODULE NUMBERED TWO

The differential system of this model is now (Module numbered two).

$$\begin{aligned} \frac{dG_{16}}{dt} &= (a_{16})^{(2)}G_{17} - [(a'_{16})^{(2)} + (a''_{16})^{(2)}(T_{17}, t)]G_{16} . \\ \frac{dG_{17}}{dt} &= (a_{17})^{(2)}G_{16} - [(a'_{17})^{(2)} + (a''_{17})^{(2)}(T_{17}, t)]G_{17} . \\ \frac{dG_{18}}{dt} &= (a_{18})^{(2)}G_{17} - [(a'_{18})^{(2)} + (a''_{18})^{(2)}(T_{17}, t)]G_{18} . \\ \frac{dT_{16}}{dt} &= (b_{16})^{(2)}T_{17} - [(b'_{16})^{(2)} - (b''_{16})^{(2)}((G_{19}), t)]T_{16} . \\ \frac{dT_{17}}{dt} &= (b_{17})^{(2)}T_{16} - [(b'_{17})^{(2)} - (b''_{17})^{(2)}((G_{19}), t)]T_{17} . \\ \frac{dT_{18}}{dt} &= (b_{18})^{(2)}T_{17} - [(b'_{18})^{(2)} - (b''_{18})^{(2)}((G_{19}), t)]T_{18} . \\ &+ (a''_{16})^{(2)}(T_{17}, t) = \text{First augmentation factor} . \\ &- (b''_{16})^{(2)}((G_{19}), t) = \text{First detritions factor} . \end{aligned}$$

NOISE AND ERROR IN QUANTUM COMPUTATION:
MODULE NUMBERED THREE

The differential system of this model is now (Module numbered three).

$$\begin{aligned} \frac{dG_{20}}{dt} &= (a_{20})^{(3)}G_{21} - [(a'_{20})^{(3)} + (a''_{20})^{(3)}(T_{21}, t)]G_{20} . \\ \frac{dG_{21}}{dt} &= (a_{21})^{(3)}G_{20} - [(a'_{21})^{(3)} + (a''_{21})^{(3)}(T_{21}, t)]G_{21} . \\ \frac{dG_{22}}{dt} &= (a_{22})^{(3)}G_{21} - [(a'_{22})^{(3)} + (a''_{22})^{(3)}(T_{21}, t)]G_{22} . \end{aligned}$$

$$\begin{aligned} \frac{dT_{20}}{dt} &= (b_{20})^{(3)}T_{21} - [(b'_{20})^{(3)} - (b''_{20})^{(3)}(G_{23}, t)]T_{20} . \\ \frac{dT_{21}}{dt} &= (b_{21})^{(3)}T_{20} - [(b'_{21})^{(3)} - (b''_{21})^{(3)}(G_{23}, t)]T_{21} . \\ \frac{dT_{22}}{dt} &= (b_{22})^{(3)}T_{21} - [(b'_{22})^{(3)} - (b''_{22})^{(3)}(G_{23}, t)]T_{22} . \\ + (a''_{20})^{(3)}(T_{21}, t) &= \text{First augmentation factor.} \\ - (b_{20})^{(3)}(G_{23}, t) &= \text{First detritions factor .} \end{aligned}$$

CAUSE AND EVENT:

MODULE NUMBERED FOUR:

The differential system of this model is now (Module numbered Four).

$$\begin{aligned} \frac{dG_{24}}{dt} &= (a_{24})^{(4)}G_{25} - [(a'_{24})^{(4)} + (a''_{24})^{(4)}(T_{25}, t)]G_{24} . \\ \frac{dG_{25}}{dt} &= (a_{25})^{(4)}G_{24} - [(a'_{25})^{(4)} + (a''_{25})^{(4)}(T_{25}, t)]G_{25} . \\ \frac{dG_{26}}{dt} &= (a_{26})^{(4)}G_{25} - [(a'_{26})^{(4)} + (a''_{26})^{(4)}(T_{25}, t)]G_{26} . \\ \frac{dT_{24}}{dt} &= (b_{24})^{(4)}T_{25} - [(b'_{24})^{(4)} - (b''_{24})^{(4)}((G_{27}), t)]T_{24} . \\ \frac{dT_{25}}{dt} &= (b_{25})^{(4)}T_{24} - [(b'_{25})^{(4)} - (b''_{25})^{(4)}((G_{27}), t)]T_{25} . \\ \frac{dT_{26}}{dt} &= (b_{26})^{(4)}T_{25} - [(b'_{26})^{(4)} - (b''_{26})^{(4)}((G_{27}), t)]T_{26} . \\ + (a''_{24})^{(4)}(T_{25}, t) &= \text{First augmentation factor.} \\ - (b''_{24})^{(4)}((G_{27}), t) &= \text{First detritions factor .} \end{aligned}$$

SPACE AND TIME:

MODULE NUMBERED FIVE

The differential system of this model is now (Module number five).

$$\begin{aligned} \frac{dG_{28}}{dt} &= (a_{28})^{(5)}G_{29} - [(a'_{28})^{(5)} + (a''_{28})^{(5)}(T_{29}, t)]G_{28} . \\ \frac{dG_{29}}{dt} &= (a_{29})^{(5)}G_{28} - [(a'_{29})^{(5)} + (a''_{29})^{(5)}(T_{29}, t)]G_{29} . \\ \frac{dG_{30}}{dt} &= (a_{30})^{(5)}G_{29} - [(a'_{30})^{(5)} + (a''_{30})^{(5)}(T_{29}, t)]G_{30} . \\ \frac{dT_{28}}{dt} &= (b_{28})^{(5)}T_{29} - [(b'_{28})^{(5)} - (b''_{28})^{(5)}((G_{31}), t)]T_{28} . \\ \frac{dT_{29}}{dt} &= (b_{29})^{(5)}T_{28} - [(b'_{29})^{(5)} - (b''_{29})^{(5)}((G_{31}), t)]T_{29} . \\ \frac{dT_{30}}{dt} &= (b_{30})^{(5)}T_{29} - [(b'_{30})^{(5)} - (b''_{30})^{(5)}((G_{31}), t)]T_{30} . \\ + (a''_{28})^{(5)}(T_{29}, t) &= \text{First augmentation factor .} \\ - (b''_{28})^{(5)}((G_{31}), t) &= \text{First detritions factor .} \end{aligned}$$

STORAGE ABILITY AND ENTANGLEMENT :
MODULE NUMBERED SIX

The differential system of this model is now (Module numbered Six).

$$\begin{aligned} \frac{dG_{32}}{dt} &= (a_{32})^{(6)}G_{33} - [(a'_{32})^{(6)} + (a''_{32})^{(6)}(T_{33}, t)]G_{32} . \\ \frac{dG_{33}}{dt} &= (a_{33})^{(6)}G_{32} - [(a'_{33})^{(6)} + (a''_{33})^{(6)}(T_{33}, t)]G_{33} . \\ \frac{dG_{34}}{dt} &= (a_{34})^{(6)}G_{33} - [(a'_{34})^{(6)} + (a''_{34})^{(6)}(T_{33}, t)]G_{34} . \\ \frac{dT_{32}}{dt} &= (b_{32})^{(6)}T_{33} - [(b'_{32})^{(6)} - (b''_{32})^{(6)}((G_{35}), t)]T_{32} . \\ \frac{dT_{33}}{dt} &= (b_{33})^{(6)}T_{32} - [(b'_{33})^{(6)} - (b''_{33})^{(6)}((G_{35}), t)]T_{33} . \\ \frac{dT_{34}}{dt} &= (b_{34})^{(6)}T_{33} - [(b'_{34})^{(6)} - (b''_{34})^{(6)}((G_{35}), t)]T_{34} . \\ + (a''_{32})^{(6)}(T_{33}, t) &= \text{First augmentation factor.} \\ - (b''_{32})^{(6)}((G_{35}), t) &= \text{First detritions factor .} \end{aligned}$$

HOLISTIC CONCATENATE SYTEMAL EQUATIONS HENCEFORTH REFERRED TO AS “GLOBAL EQUATIONS”

- (1) Alpha ray production(Radioactive decay)
- (2) Quantum Tunneling
- (3) Redundancy
- (4) Entropy
- (5) Event
- (6) Cause
- (7) Space
- (8) Time
- (9) Storage ability
- (10) Quantum entanglement
- (11) Noise
- (12) Errors

$$\begin{aligned} \frac{dG_{13}}{dt} &= (a_{13})^{(1)}G_{14} - \left[\begin{array}{|c|c|c|} \hline (a'_{13})^{(1)} & +(a''_{13})^{(1)}(T_{14}, t) & +(a''_{16})^{(2,2)}(T_{17}, t) & +(a''_{20})^{(3,3)}(T_{21}, t) \\ \hline \end{array} \right] G_{13} \cdot \\ & \left[\begin{array}{|c|c|c|} \hline +(a''_{24})^{(4,4,4,4)}(T_{25}, t) & +(a''_{28})^{(5,5,5,5)}(T_{29}, t) & +(a''_{32})^{(6,6,6,6)}(T_{33}, t) \\ \hline \end{array} \right] \\ \frac{dG_{14}}{dt} &= (a_{14})^{(1)}G_{13} - \left[\begin{array}{|c|c|c|} \hline (a'_{14})^{(1)} & +(a''_{14})^{(1)}(T_{14}, t) & +(a''_{17})^{(2,2)}(T_{17}, t) & +(a''_{21})^{(3,3)}(T_{21}, t) \\ \hline \end{array} \right] G_{14} \cdot \\ & \left[\begin{array}{|c|c|c|} \hline +(a''_{25})^{(4,4,4,4)}(T_{25}, t) & +(a''_{29})^{(5,5,5,5)}(T_{29}, t) & +(a''_{33})^{(6,6,6,6)}(T_{33}, t) \\ \hline \end{array} \right] \\ \frac{dG_{15}}{dt} &= (a_{15})^{(1)}G_{14} - \left[\begin{array}{|c|c|c|} \hline (a'_{15})^{(1)} & +(a''_{15})^{(1)}(T_{14}, t) & +(a''_{18})^{(2,2)}(T_{17}, t) & +(a''_{22})^{(3,3)}(T_{21}, t) \\ \hline \end{array} \right] G_{15} \cdot \\ & \left[\begin{array}{|c|c|c|} \hline +(a''_{26})^{(4,4,4,4)}(T_{25}, t) & +(a''_{30})^{(5,5,5,5)}(T_{29}, t) & +(a''_{34})^{(6,6,6,6)}(T_{33}, t) \\ \hline \end{array} \right] \end{aligned}$$

Where $(a'_{13})^{(1)}(T_{14}, t)$, $(a'_{14})^{(1)}(T_{14}, t)$, $(a'_{15})^{(1)}(T_{14}, t)$ are first augmentation coefficients for category 1, 2 and 3
 $+(a''_{16})^{(2,2)}(T_{17}, t)$, $+(a''_{17})^{(2,2)}(T_{17}, t)$, $+(a''_{18})^{(2,2)}(T_{17}, t)$ are second augmentation coefficient for category 1, 2 and 3
 $+(a''_{20})^{(3,3)}(T_{21}, t)$, $+(a''_{21})^{(3,3)}(T_{21}, t)$, $+(a''_{22})^{(3,3)}(T_{21}, t)$ are third augmentation coefficient for category 1, 2 and 3
 $+(a''_{24})^{(4,4,4,4)}(T_{25}, t)$, $+(a''_{25})^{(4,4,4,4)}(T_{25}, t)$, $+(a''_{26})^{(4,4,4,4)}(T_{25}, t)$ are fourth augmentation coefficient for category 1, 2 and 3
 $+(a''_{28})^{(5,5,5,5)}(T_{29}, t)$, $+(a''_{29})^{(5,5,5,5)}(T_{29}, t)$, $+(a''_{30})^{(5,5,5,5)}(T_{29}, t)$ are fifth augmentation coefficient for category 1, 2 and 3
 $+(a''_{32})^{(6,6,6,6)}(T_{33}, t)$, $+(a''_{33})^{(6,6,6,6)}(T_{33}, t)$, $+(a''_{34})^{(6,6,6,6)}(T_{33}, t)$ are sixth augmentation coefficient for category 1, 2 and 3.

$$\begin{aligned} \frac{dT_{13}}{dt} &= (b_{13})^{(1)}T_{14} - \left[\begin{array}{|c|c|c|} \hline (b'_{13})^{(1)} & -(b''_{13})^{(1)}(G, t) & -(b''_{16})^{(2,2)}(G_{19}, t) & -(b''_{20})^{(3,3)}(G_{23}, t) \\ \hline \end{array} \right] T_{13} \cdot \\ & \left[\begin{array}{|c|c|c|} \hline -(b''_{24})^{(4,4,4,4)}(G_{27}, t) & -(b''_{28})^{(5,5,5,5)}(G_{31}, t) & -(b''_{32})^{(6,6,6,6)}(G_{35}, t) \\ \hline \end{array} \right] \\ \frac{dT_{14}}{dt} &= (b_{14})^{(1)}T_{13} - \left[\begin{array}{|c|c|c|} \hline (b'_{14})^{(1)} & -(b''_{14})^{(1)}(G, t) & -(b''_{17})^{(2,2)}(G_{19}, t) & -(b''_{21})^{(3,3)}(G_{23}, t) \\ \hline \end{array} \right] T_{14} \cdot \\ & \left[\begin{array}{|c|c|c|} \hline -(b''_{25})^{(4,4,4,4)}(G_{27}, t) & -(b''_{29})^{(5,5,5,5)}(G_{31}, t) & -(b''_{33})^{(6,6,6,6)}(G_{35}, t) \\ \hline \end{array} \right] \\ \frac{dT_{15}}{dt} &= (b_{15})^{(1)}T_{14} - \left[\begin{array}{|c|c|c|} \hline (b'_{15})^{(1)} & -(b''_{15})^{(1)}(G, t) & -(b''_{18})^{(2,2)}(G_{19}, t) & -(b''_{22})^{(3,3)}(G_{23}, t) \\ \hline \end{array} \right] T_{15} \cdot \\ & \left[\begin{array}{|c|c|c|} \hline -(b''_{26})^{(4,4,4,4)}(G_{27}, t) & -(b''_{30})^{(5,5,5,5)}(G_{31}, t) & -(b''_{34})^{(6,6,6,6)}(G_{35}, t) \\ \hline \end{array} \right] \end{aligned}$$

Where $-(b''_{13})^{(1)}(G, t)$, $-(b''_{14})^{(1)}(G, t)$, $-(b''_{15})^{(1)}(G, t)$ are first detrition coefficients for category 1, 2 and 3
 $-(b''_{16})^{(2,2)}(G_{19}, t)$, $-(b''_{17})^{(2,2)}(G_{19}, t)$, $-(b''_{18})^{(2,2)}(G_{19}, t)$ are second detrition coefficients for category 1, 2 and 3
 $-(b''_{20})^{(3,3)}(G_{23}, t)$, $-(b''_{21})^{(3,3)}(G_{23}, t)$, $-(b''_{22})^{(3,3)}(G_{23}, t)$ are third detrition coefficients for category 1, 2 and 3
 $-(b''_{24})^{(4,4,4,4)}(G_{27}, t)$, $-(b''_{25})^{(4,4,4,4)}(G_{27}, t)$, $-(b''_{26})^{(4,4,4,4)}(G_{27}, t)$ are fourth detrition coefficients for category 1, 2 and 3
 $-(b''_{28})^{(5,5,5,5)}(G_{31}, t)$, $-(b''_{29})^{(5,5,5,5)}(G_{31}, t)$, $-(b''_{30})^{(5,5,5,5)}(G_{31}, t)$ are fifth detrition coefficients for category 1, 2 and 3

$-(b''_{32})^{(6,6,6,6,6)}(G_{35}, t)$, $-(b''_{33})^{(6,6,6,6,6)}(G_{35}, t)$, $-(b''_{34})^{(6,6,6,6,6)}(G_{35}, t)$ are sixth detrition coefficients for category 1, 2 and 3

$$\begin{aligned} \frac{dG_{16}}{dt} &= (a_{16})^{(2)}G_{17} - \left[\begin{array}{ccc} (a'_{16})^{(2)} + (a''_{16})^{(2)}(T_{17}, t) & + (a'_{13})^{(1,1)}(T_{14}, t) & + (a'_{20})^{(3,3,3)}(T_{21}, t) \\ + (a''_{24})^{(4,4,4,4,4)}(T_{25}, t) & + (a''_{28})^{(5,5,5,5,5)}(T_{29}, t) & + (a''_{32})^{(6,6,6,6,6)}(T_{33}, t) \end{array} \right] G_{16} \cdot \\ \frac{dG_{17}}{dt} &= (a_{17})^{(2)}G_{16} - \left[\begin{array}{ccc} (a'_{17})^{(2)} + (a''_{17})^{(2)}(T_{17}, t) & + (a'_{14})^{(1,1)}(T_{14}, t) & + (a'_{21})^{(3,3,3)}(T_{21}, t) \\ + (a''_{25})^{(4,4,4,4,4)}(T_{25}, t) & + (a''_{29})^{(5,5,5,5,5)}(T_{29}, t) & + (a''_{33})^{(6,6,6,6,6)}(T_{33}, t) \end{array} \right] G_{17} \cdot \\ \frac{dG_{18}}{dt} &= (a_{18})^{(2)}G_{17} - \left[\begin{array}{ccc} (a'_{18})^{(2)} + (a''_{18})^{(2)}(T_{17}, t) & + (a'_{15})^{(1,1)}(T_{14}, t) & + (a'_{22})^{(3,3,3)}(T_{21}, t) \\ + (a''_{26})^{(4,4,4,4,4)}(T_{25}, t) & + (a''_{30})^{(5,5,5,5,5)}(T_{29}, t) & + (a''_{34})^{(6,6,6,6,6)}(T_{33}, t) \end{array} \right] G_{18} \cdot \end{aligned}$$

Where $+(a''_{16})^{(2)}(T_{17}, t)$, $+(a''_{17})^{(2)}(T_{17}, t)$, $+(a''_{18})^{(2)}(T_{17}, t)$ are first augmentation coefficients for category 1, 2 and 3
 $+(a''_{13})^{(1,1)}(T_{14}, t)$, $+(a''_{14})^{(1,1)}(T_{14}, t)$, $+(a''_{15})^{(1,1)}(T_{14}, t)$ are second augmentation coefficient for category 1, 2 and 3
 $+(a''_{20})^{(3,3,3)}(T_{21}, t)$, $+(a''_{21})^{(3,3,3)}(T_{21}, t)$, $+(a''_{22})^{(3,3,3)}(T_{21}, t)$ are third augmentation coefficient for category 1, 2 and 3

$+(a''_{24})^{(4,4,4,4,4)}(T_{25}, t)$, $+(a''_{25})^{(4,4,4,4,4)}(T_{25}, t)$, $+(a''_{26})^{(4,4,4,4,4)}(T_{25}, t)$ are fourth augmentation coefficient for category 1, 2 and 3

$+(a''_{28})^{(5,5,5,5,5)}(T_{29}, t)$, $+(a''_{29})^{(5,5,5,5,5)}(T_{29}, t)$, $+(a''_{30})^{(5,5,5,5,5)}(T_{29}, t)$ are fifth augmentation coefficient for category 1, 2 and 3

$+(a''_{32})^{(6,6,6,6,6)}(T_{33}, t)$, $+(a''_{33})^{(6,6,6,6,6)}(T_{33}, t)$, $+(a''_{34})^{(6,6,6,6,6)}(T_{33}, t)$ are sixth augmentation coefficient for category 1, 2 and 3 .

$$\begin{aligned} \frac{dT_{16}}{dt} &= (b_{16})^{(2)}T_{17} - \left[\begin{array}{ccc} (b'_{16})^{(2)} - (b''_{16})^{(2)}(G_{19}, t) & - (b'_{13})^{(1,1)}(G, t) & - (b'_{20})^{(3,3,3)}(G_{23}, t) \\ - (b''_{24})^{(4,4,4,4,4)}(G_{27}, t) & - (b''_{28})^{(5,5,5,5,5)}(G_{31}, t) & - (b''_{32})^{(6,6,6,6,6)}(G_{35}, t) \end{array} \right] T_{16} \cdot \\ \frac{dT_{17}}{dt} &= (b_{17})^{(2)}T_{16} - \left[\begin{array}{ccc} (b'_{17})^{(2)} - (b''_{17})^{(2)}(G_{19}, t) & - (b'_{14})^{(1,1)}(G, t) & - (b'_{21})^{(3,3,3)}(G_{23}, t) \\ - (b''_{25})^{(4,4,4,4,4)}(G_{27}, t) & - (b''_{29})^{(5,5,5,5,5)}(G_{31}, t) & - (b''_{33})^{(6,6,6,6,6)}(G_{35}, t) \end{array} \right] T_{17} \cdot \\ \frac{dT_{18}}{dt} &= (b_{18})^{(2)}T_{17} - \left[\begin{array}{ccc} (b'_{18})^{(2)} - (b''_{18})^{(2)}(G_{19}, t) & - (b'_{15})^{(1,1)}(G, t) & - (b'_{22})^{(3,3,3)}(G_{23}, t) \\ - (b''_{26})^{(4,4,4,4,4)}(G_{27}, t) & - (b''_{30})^{(5,5,5,5,5)}(G_{31}, t) & - (b''_{34})^{(6,6,6,6,6)}(G_{35}, t) \end{array} \right] T_{18} \cdot \end{aligned}$$

where $-(b''_{16})^{(2)}(G_{19}, t)$, $-(b''_{17})^{(2)}(G_{19}, t)$, $-(b''_{18})^{(2)}(G_{19}, t)$ are first detrition coefficients for category 1, 2 and 3

$-(b''_{13})^{(1,1)}(G, t)$, $-(b''_{14})^{(1,1)}(G, t)$, $-(b''_{15})^{(1,1)}(G, t)$ are second detrition coefficients for category 1,2 and 3

$-(b'_{20})^{(3,3,3)}(G_{23}, t)$, $-(b'_{21})^{(3,3,3)}(G_{23}, t)$, $-(b'_{22})^{(3,3,3)}(G_{23}, t)$ are third detrition coefficients for category 1,2 and 3

$-(b''_{24})^{(4,4,4,4,4)}(G_{27}, t)$, $-(b''_{25})^{(4,4,4,4,4)}(G_{27}, t)$, $-(b''_{26})^{(4,4,4,4,4)}(G_{27}, t)$ are fourth detrition coefficients for category 1,2 and 3

$-(b''_{28})^{(5,5,5,5,5)}(G_{31}, t)$, $-(b''_{29})^{(5,5,5,5,5)}(G_{31}, t)$, $-(b''_{30})^{(5,5,5,5,5)}(G_{31}, t)$ are fifth detrition coefficients for category 1,2 and 3

$-(b''_{32})^{(6,6,6,6,6)}(G_{35}, t)$, $-(b''_{33})^{(6,6,6,6,6)}(G_{35}, t)$, $-(b''_{34})^{(6,6,6,6,6)}(G_{35}, t)$ are sixth detrition coefficients for category 1,2 and 3

$$\begin{aligned} \frac{dG_{20}}{dt} &= (a_{20})^{(3)}G_{21} - \left[\begin{array}{ccc} (a'_{20})^{(3)} + (a''_{20})^{(3)}(T_{21}, t) & + (a'_{16})^{(2,2,2)}(T_{17}, t) & + (a'_{13})^{(1,1,1)}(T_{14}, t) \\ + (a''_{24})^{(4,4,4,4,4)}(T_{25}, t) & + (a''_{28})^{(5,5,5,5,5)}(T_{29}, t) & + (a''_{32})^{(6,6,6,6,6)}(T_{33}, t) \end{array} \right] G_{20} \cdot \\ \frac{dG_{21}}{dt} &= (a_{21})^{(3)}G_{20} - \left[\begin{array}{ccc} (a'_{21})^{(3)} + (a''_{21})^{(3)}(T_{21}, t) & + (a'_{17})^{(2,2,2)}(T_{17}, t) & + (a'_{14})^{(1,1,1)}(T_{14}, t) \\ + (a''_{25})^{(4,4,4,4,4)}(T_{25}, t) & + (a''_{29})^{(5,5,5,5,5)}(T_{29}, t) & + (a''_{33})^{(6,6,6,6,6)}(T_{33}, t) \end{array} \right] G_{21} \cdot \\ \frac{dG_{22}}{dt} &= (a_{22})^{(3)}G_{21} - \left[\begin{array}{ccc} (a'_{22})^{(3)} + (a''_{22})^{(3)}(T_{21}, t) & + (a'_{18})^{(2,2,2)}(T_{17}, t) & + (a'_{15})^{(1,1,1)}(T_{14}, t) \\ + (a''_{26})^{(4,4,4,4,4)}(T_{25}, t) & + (a''_{30})^{(5,5,5,5,5)}(T_{29}, t) & + (a''_{34})^{(6,6,6,6,6)}(T_{33}, t) \end{array} \right] G_{22} \cdot \end{aligned}$$

$\boxed{+(a''_{20})^{(3)}(T_{21}, t)}$, $\boxed{+(a''_{21})^{(3)}(T_{21}, t)}$, $\boxed{+(a''_{22})^{(3)}(T_{21}, t)}$ are first augmentation coefficients for category 1, 2 and 3
 $\boxed{+(a''_{16})^{(2,2,2)}(T_{17}, t)}$, $\boxed{+(a''_{17})^{(2,2,2)}(T_{17}, t)}$, $\boxed{+(a''_{18})^{(2,2,2)}(T_{17}, t)}$ are second augmentation coefficients for category 1, 2 and 3

$\boxed{+(a''_{13})^{(1,1,1)}(T_{14}, t)}$, $\boxed{+(a''_{14})^{(1,1,1)}(T_{14}, t)}$, $\boxed{+(a''_{15})^{(1,1,1)}(T_{14}, t)}$ are third augmentation coefficients for category 1, 2 and 3

$\boxed{+(a''_{24})^{(4,4,4,4,4)}(T_{25}, t)}$, $\boxed{+(a''_{25})^{(4,4,4,4,4)}(T_{25}, t)}$, $\boxed{+(a''_{26})^{(4,4,4,4,4)}(T_{25}, t)}$ are fourth augmentation coefficients for category 1, 2 and 3

$\boxed{+(a''_{28})^{(5,5,5,5,5)}(T_{29}, t)}$, $\boxed{+(a''_{29})^{(5,5,5,5,5)}(T_{29}, t)}$, $\boxed{+(a''_{30})^{(5,5,5,5,5)}(T_{29}, t)}$ are fifth augmentation coefficients for category 1, 2 and 3

$\boxed{+(a''_{32})^{(6,6,6,6,6)}(T_{33}, t)}$, $\boxed{+(a''_{33})^{(6,6,6,6,6)}(T_{33}, t)}$, $\boxed{+(a''_{34})^{(6,6,6,6,6)}(T_{33}, t)}$ are sixth augmentation coefficients for category 1, 2 and 3

$$\begin{aligned} \frac{dT_{20}}{dt} &= (b_{20})^{(3)}T_{21} - \left[\begin{array}{ccc} \boxed{(b'_{20})^{(3)}} \boxed{-(b''_{20})^{(3)}(G_{23}, t)} \boxed{-(b''_{16})^{(2,2,2)}(G_{19}, t)} \boxed{-(b''_{13})^{(1,1,1)}(G, t)} \\ \boxed{-(b''_{24})^{(4,4,4,4,4)}(G_{27}, t)} \boxed{-(b''_{28})^{(5,5,5,5,5)}(G_{31}, t)} \boxed{-(b''_{32})^{(6,6,6,6,6)}(G_{35}, t)} \end{array} \right] T_{20} \cdot \\ \frac{dT_{21}}{dt} &= (b_{21})^{(3)}T_{20} - \left[\begin{array}{ccc} \boxed{(b'_{21})^{(3)}} \boxed{-(b''_{21})^{(3)}(G_{23}, t)} \boxed{-(b''_{17})^{(2,2,2)}(G_{19}, t)} \boxed{-(b''_{14})^{(1,1,1)}(G, t)} \\ \boxed{-(b''_{25})^{(4,4,4,4,4)}(G_{27}, t)} \boxed{-(b''_{29})^{(5,5,5,5,5)}(G_{31}, t)} \boxed{-(b''_{33})^{(6,6,6,6,6)}(G_{35}, t)} \end{array} \right] T_{21} \cdot \\ \frac{dT_{22}}{dt} &= (b_{22})^{(3)}T_{21} - \left[\begin{array}{ccc} \boxed{(b'_{22})^{(3)}} \boxed{-(b''_{22})^{(3)}(G_{23}, t)} \boxed{-(b''_{18})^{(2,2,2)}(G_{19}, t)} \boxed{-(b''_{15})^{(1,1,1)}(G, t)} \\ \boxed{-(b''_{26})^{(4,4,4,4,4)}(G_{27}, t)} \boxed{-(b''_{30})^{(5,5,5,5,5)}(G_{31}, t)} \boxed{-(b''_{34})^{(6,6,6,6,6)}(G_{35}, t)} \end{array} \right] T_{22} \cdot \end{aligned}$$

$\boxed{-(b''_{20})^{(3)}(G_{23}, t)}$, $\boxed{-(b''_{21})^{(3)}(G_{23}, t)}$, $\boxed{-(b''_{22})^{(3)}(G_{23}, t)}$ are first detrition coefficients for category 1, 2 and 3

$\boxed{-(b''_{16})^{(2,2,2)}(G_{19}, t)}$, $\boxed{-(b''_{17})^{(2,2,2)}(G_{19}, t)}$, $\boxed{-(b''_{18})^{(2,2,2)}(G_{19}, t)}$ are second detrition coefficients for category 1, 2 and 3

$\boxed{-(b''_{13})^{(1,1,1)}(G, t)}$, $\boxed{-(b''_{14})^{(1,1,1)}(G, t)}$, $\boxed{-(b''_{15})^{(1,1,1)}(G, t)}$ are third detrition coefficients for category 1, 2 and 3

$\boxed{-(b''_{24})^{(4,4,4,4,4)}(G_{27}, t)}$, $\boxed{-(b''_{25})^{(4,4,4,4,4)}(G_{27}, t)}$, $\boxed{-(b''_{26})^{(4,4,4,4,4)}(G_{27}, t)}$ are fourth detrition coefficients for category 1, 2 and 3

$\boxed{-(b''_{28})^{(5,5,5,5,5)}(G_{31}, t)}$, $\boxed{-(b''_{29})^{(5,5,5,5,5)}(G_{31}, t)}$, $\boxed{-(b''_{30})^{(5,5,5,5,5)}(G_{31}, t)}$ are fifth detrition coefficients for category 1, 2 and 3

$\boxed{-(b''_{32})^{(6,6,6,6,6)}(G_{35}, t)}$, $\boxed{-(b''_{33})^{(6,6,6,6,6)}(G_{35}, t)}$, $\boxed{-(b''_{34})^{(6,6,6,6,6)}(G_{35}, t)}$ are sixth detrition coefficients for category 1, 2 and 3

$$\begin{aligned} \frac{dG_{24}}{dt} &= (a_{24})^{(4)}G_{25} - \left[\begin{array}{ccc} \boxed{(a'_{24})^{(4)}} \boxed{+(a''_{24})^{(4)}(T_{25}, t)} \boxed{+(a''_{28})^{(5,5)}(T_{29}, t)} \boxed{+(a''_{32})^{(6,6)}(T_{33}, t)} \\ \boxed{+(a''_{13})^{(1,1,1,1)}(T_{14}, t)} \boxed{+(a''_{16})^{(2,2,2,2)}(T_{17}, t)} \boxed{+(a''_{20})^{(3,3,3,3)}(T_{21}, t)} \end{array} \right] G_{24} \cdot \\ \frac{dG_{25}}{dt} &= (a_{25})^{(4)}G_{24} - \left[\begin{array}{ccc} \boxed{(a'_{25})^{(4)}} \boxed{+(a''_{25})^{(4)}(T_{25}, t)} \boxed{+(a''_{29})^{(5,5)}(T_{29}, t)} \boxed{+(a''_{33})^{(6,6)}(T_{33}, t)} \\ \boxed{+(a''_{14})^{(1,1,1,1)}(T_{14}, t)} \boxed{+(a''_{17})^{(2,2,2,2)}(T_{17}, t)} \boxed{+(a''_{21})^{(3,3,3,3)}(T_{21}, t)} \end{array} \right] G_{25} \cdot \\ \frac{dG_{26}}{dt} &= (a_{26})^{(4)}G_{25} - \left[\begin{array}{ccc} \boxed{(a'_{26})^{(4)}} \boxed{+(a''_{26})^{(4)}(T_{25}, t)} \boxed{+(a''_{30})^{(5,5)}(T_{29}, t)} \boxed{+(a''_{34})^{(6,6)}(T_{33}, t)} \\ \boxed{+(a''_{15})^{(1,1,1,1)}(T_{14}, t)} \boxed{+(a''_{18})^{(2,2,2,2)}(T_{17}, t)} \boxed{+(a''_{22})^{(3,3,3,3)}(T_{21}, t)} \end{array} \right] G_{26} \cdot \end{aligned}$$

Where $\boxed{(a''_{24})^{(4)}(T_{25}, t)}$, $\boxed{(a''_{25})^{(4)}(T_{25}, t)}$, $\boxed{(a''_{26})^{(4)}(T_{25}, t)}$ are first augmentation coefficients for category 1, 2 and 3

$\boxed{+(a''_{28})^{(5,5)}(T_{29}, t)}$, $\boxed{+(a''_{29})^{(5,5)}(T_{29}, t)}$, $\boxed{+(a''_{30})^{(5,5)}(T_{29}, t)}$ are second augmentation coefficient for category 1, 2 and 3

$\boxed{+(a''_{32})^{(6,6)}(T_{33}, t)}$, $\boxed{+(a''_{33})^{(6,6)}(T_{33}, t)}$, $\boxed{+(a''_{34})^{(6,6)}(T_{33}, t)}$ are third augmentation coefficient for category 1, 2 and 3

$\boxed{+(a''_{13})^{(1,1,1,1)}(T_{14}, t)}$, $\boxed{+(a''_{14})^{(1,1,1,1)}(T_{14}, t)}$, $\boxed{+(a''_{15})^{(1,1,1,1)}(T_{14}, t)}$ are fourth augmentation coefficients for category 1, 2, and 3

$\boxed{+(a''_{16})^{(2,2,2,2)}(T_{17}, t)}$, $\boxed{+(a''_{17})^{(2,2,2,2)}(T_{17}, t)}$, $\boxed{+(a''_{18})^{(2,2,2,2)}(T_{17}, t)}$ are fifth augmentation coefficients for category 1, 2, and 3

$\boxed{+(a''_{20})^{(3,3,3,3)}(T_{21}, t)}$, $\boxed{+(a''_{21})^{(3,3,3,3)}(T_{21}, t)}$, $\boxed{+(a''_{22})^{(3,3,3,3)}(T_{21}, t)}$ are sixth augmentation coefficients for category 1, 2, and 3.

$$\begin{aligned} \frac{dT_{24}}{dt} &= (b_{24})^{(4)}T_{25} - \left[\begin{array}{ccc} (b'_{24})^{(4)} \boxed{-(b''_{24})^{(4)}(G_{27}, t)} & \boxed{-(b''_{28})^{(5,5)}(G_{31}, t)} & \boxed{-(b''_{32})^{(6,6)}(G_{35}, t)} \\ \boxed{-(b''_{13})^{(1,1,1,1)}(G, t)} & \boxed{-(b''_{16})^{(2,2,2,2)}(G_{19}, t)} & \boxed{-(b''_{20})^{(3,3,3,3)}(G_{23}, t)} \end{array} \right] T_{24} \cdot \\ \frac{dT_{25}}{dt} &= (b_{25})^{(4)}T_{24} - \left[\begin{array}{ccc} (b'_{25})^{(4)} \boxed{-(b''_{25})^{(4)}(G_{27}, t)} & \boxed{-(b''_{29})^{(5,5)}(G_{31}, t)} & \boxed{-(b''_{33})^{(6,6)}(G_{35}, t)} \\ \boxed{-(b''_{14})^{(1,1,1,1)}(G, t)} & \boxed{-(b''_{17})^{(2,2,2,2)}(G_{19}, t)} & \boxed{-(b''_{21})^{(3,3,3,3)}(G_{23}, t)} \end{array} \right] T_{25} \cdot \\ \frac{dT_{26}}{dt} &= (b_{26})^{(4)}T_{25} - \left[\begin{array}{ccc} (b'_{26})^{(4)} \boxed{-(b''_{26})^{(4)}(G_{27}, t)} & \boxed{-(b''_{30})^{(5,5)}(G_{31}, t)} & \boxed{-(b''_{34})^{(6,6)}(G_{35}, t)} \\ \boxed{-(b''_{15})^{(1,1,1,1)}(G, t)} & \boxed{-(b''_{18})^{(2,2,2,2)}(G_{19}, t)} & \boxed{-(b''_{22})^{(3,3,3,3)}(G_{23}, t)} \end{array} \right] T_{26} \cdot \end{aligned}$$

Where $\boxed{-(b''_{24})^{(4)}(G_{27}, t)}$, $\boxed{-(b''_{25})^{(4)}(G_{27}, t)}$, $\boxed{-(b''_{26})^{(4)}(G_{27}, t)}$ are first detrition coefficients for category 1, 2 and 3
 $\boxed{-(b''_{28})^{(5,5)}(G_{31}, t)}$, $\boxed{-(b''_{29})^{(5,5)}(G_{31}, t)}$, $\boxed{-(b''_{30})^{(5,5)}(G_{31}, t)}$ are second detrition coefficients for category 1, 2 and 3
 $\boxed{-(b''_{32})^{(6,6)}(G_{35}, t)}$, $\boxed{-(b''_{33})^{(6,6)}(G_{35}, t)}$, $\boxed{-(b''_{34})^{(6,6)}(G_{35}, t)}$ are third detrition coefficients for category 1, 2 and 3
 $\boxed{-(b''_{13})^{(1,1,1,1)}(G, t)}$, $\boxed{-(b''_{14})^{(1,1,1,1)}(G, t)}$, $\boxed{-(b''_{15})^{(1,1,1,1)}(G, t)}$
 are fourth detrition coefficients for category 1, 2 and 3
 $\boxed{-(b''_{16})^{(2,2,2,2)}(G_{19}, t)}$, $\boxed{-(b''_{17})^{(2,2,2,2)}(G_{19}, t)}$, $\boxed{-(b''_{18})^{(2,2,2,2)}(G_{19}, t)}$
 are fifth detrition coefficients for category 1, 2 and 3
 $\boxed{-(b''_{20})^{(3,3,3,3)}(G_{23}, t)}$, $\boxed{-(b''_{21})^{(3,3,3,3)}(G_{23}, t)}$, $\boxed{-(b''_{22})^{(3,3,3,3)}(G_{23}, t)}$
 are sixth detrition coefficients for category 1, 2 and 3 .

$$\begin{aligned} \frac{dG_{28}}{dt} &= (a_{28})^{(5)}G_{29} - \left[\begin{array}{ccc} (a'_{28})^{(5)} \boxed{+(a''_{28})^{(5)}(T_{29}, t)} & \boxed{+(a''_{24})^{(4,4)}(T_{25}, t)} & \boxed{+(a''_{32})^{(6,6,6)}(T_{33}, t)} \\ \boxed{+(a''_{13})^{(1,1,1,1,1)}(T_{14}, t)} & \boxed{+(a''_{16})^{(2,2,2,2,2)}(T_{17}, t)} & \boxed{+(a''_{20})^{(3,3,3,3,3)}(T_{21}, t)} \end{array} \right] G_{28} \cdot \\ \frac{dG_{29}}{dt} &= (a_{29})^{(5)}G_{28} - \left[\begin{array}{ccc} (a'_{29})^{(5)} \boxed{+(a''_{29})^{(5)}(T_{29}, t)} & \boxed{+(a''_{25})^{(4,4)}(T_{25}, t)} & \boxed{+(a''_{33})^{(6,6,6)}(T_{33}, t)} \\ \boxed{+(a''_{14})^{(1,1,1,1,1)}(T_{14}, t)} & \boxed{+(a''_{17})^{(2,2,2,2,2)}(T_{17}, t)} & \boxed{+(a''_{21})^{(3,3,3,3,3)}(T_{21}, t)} \end{array} \right] G_{29} \cdot \\ \frac{dG_{30}}{dt} &= (a_{30})^{(5)}G_{29} - \left[\begin{array}{ccc} (a'_{30})^{(5)} \boxed{+(a''_{30})^{(5)}(T_{29}, t)} & \boxed{+(a''_{26})^{(4,4)}(T_{25}, t)} & \boxed{+(a''_{34})^{(6,6,6)}(T_{33}, t)} \\ \boxed{+(a''_{15})^{(1,1,1,1,1)}(T_{14}, t)} & \boxed{+(a''_{18})^{(2,2,2,2,2)}(T_{17}, t)} & \boxed{+(a''_{22})^{(3,3,3,3,3)}(T_{21}, t)} \end{array} \right] G_{30} \cdot \end{aligned}$$

Where $\boxed{+(a''_{28})^{(5)}(T_{29}, t)}$, $\boxed{+(a''_{29})^{(5)}(T_{29}, t)}$, $\boxed{+(a''_{30})^{(5)}(T_{29}, t)}$ are first augmentation coefficients for category 1, 2 and 3
 And $\boxed{+(a''_{24})^{(4,4)}(T_{25}, t)}$, $\boxed{+(a''_{25})^{(4,4)}(T_{25}, t)}$, $\boxed{+(a''_{26})^{(4,4)}(T_{25}, t)}$ are second augmentation coefficient for category 1, 2 and 3
 $\boxed{+(a''_{32})^{(6,6,6)}(T_{33}, t)}$, $\boxed{+(a''_{33})^{(6,6,6)}(T_{33}, t)}$, $\boxed{+(a''_{34})^{(6,6,6)}(T_{33}, t)}$ are third augmentation coefficient for category 1, 2 and 3
 $\boxed{+(a''_{13})^{(1,1,1,1,1)}(T_{14}, t)}$, $\boxed{+(a''_{14})^{(1,1,1,1,1)}(T_{14}, t)}$, $\boxed{+(a''_{15})^{(1,1,1,1,1)}(T_{14}, t)}$ are fourth augmentation coefficients for category 1, 2, and 3
 $\boxed{+(a''_{16})^{(2,2,2,2,2)}(T_{17}, t)}$, $\boxed{+(a''_{17})^{(2,2,2,2,2)}(T_{17}, t)}$, $\boxed{+(a''_{18})^{(2,2,2,2,2)}(T_{17}, t)}$ are fifth augmentation coefficients for category 1, 2, and 3
 $\boxed{+(a''_{20})^{(3,3,3,3,3)}(T_{21}, t)}$, $\boxed{+(a''_{21})^{(3,3,3,3,3)}(T_{21}, t)}$, $\boxed{+(a''_{22})^{(3,3,3,3,3)}(T_{21}, t)}$ are sixth augmentation coefficients for category 1, 2, 3 .

$$\begin{aligned} \frac{dT_{28}}{dt} &= (b_{28})^{(5)}T_{29} - \left[\begin{array}{ccc} (b'_{28})^{(5)} \boxed{-(b''_{28})^{(5)}(G_{31}, t)} & \boxed{-(b''_{24})^{(4,4)}(G_{27}, t)} & \boxed{-(b''_{32})^{(6,6,6)}(G_{35}, t)} \\ \boxed{-(b''_{13})^{(1,1,1,1,1)}(G, t)} & \boxed{-(b''_{16})^{(2,2,2,2,2)}(G_{19}, t)} & \boxed{-(b''_{20})^{(3,3,3,3,3)}(G_{23}, t)} \end{array} \right] T_{28} \cdot \\ \frac{dT_{29}}{dt} &= (b_{29})^{(5)}T_{28} - \left[\begin{array}{ccc} (b'_{29})^{(5)} \boxed{-(b''_{29})^{(5)}(G_{31}, t)} & \boxed{-(b''_{25})^{(4,4)}(G_{27}, t)} & \boxed{-(b''_{33})^{(6,6,6)}(G_{35}, t)} \\ \boxed{-(b''_{14})^{(1,1,1,1,1)}(G, t)} & \boxed{-(b''_{17})^{(2,2,2,2,2)}(G_{19}, t)} & \boxed{-(b''_{21})^{(3,3,3,3,3)}(G_{23}, t)} \end{array} \right] T_{29} \cdot \\ \frac{dT_{30}}{dt} &= (b_{30})^{(5)}T_{29} - \left[\begin{array}{ccc} (b'_{30})^{(5)} \boxed{-(b''_{30})^{(5)}(G_{31}, t)} & \boxed{-(b''_{26})^{(4,4)}(G_{27}, t)} & \boxed{-(b''_{34})^{(6,6,6)}(G_{35}, t)} \\ \boxed{-(b''_{15})^{(1,1,1,1,1)}(G, t)} & \boxed{-(b''_{18})^{(2,2,2,2,2)}(G_{19}, t)} & \boxed{-(b''_{22})^{(3,3,3,3,3)}(G_{23}, t)} \end{array} \right] T_{30} \cdot \end{aligned}$$

where $\boxed{-(b''_{28})^{(5)}(G_{31}, t)}$, $\boxed{-(b''_{29})^{(5)}(G_{31}, t)}$, $\boxed{-(b''_{30})^{(5)}(G_{31}, t)}$ are first detrition coefficients for category 1, 2 and 3
 $\boxed{-(b''_{24})^{(4,4)}(G_{27}, t)}$, $\boxed{-(b''_{25})^{(4,4)}(G_{27}, t)}$, $\boxed{-(b''_{26})^{(4,4)}(G_{27}, t)}$ are second detrition coefficients for category 1, 2 and 3

$-(b''_{32})^{(6,6,6)}(G_{35}, t)$, $-(b''_{33})^{(6,6,6)}(G_{35}, t)$, $-(b''_{34})^{(6,6,6)}(G_{35}, t)$ are third detrition coefficients for category 1,2 and 3
 $-(b''_{13})^{(1,1,1,1,1)}(G, t)$, $-(b''_{14})^{(1,1,1,1,1)}(G, t)$, $-(b''_{15})^{(1,1,1,1,1)}(G, t)$ are fourth detrition coefficients for category 1,2, and 3
 $-(b''_{16})^{(2,2,2,2,2)}(G_{19}, t)$, $-(b''_{17})^{(2,2,2,2,2)}(G_{19}, t)$, $-(b''_{18})^{(2,2,2,2,2)}(G_{19}, t)$ are fifth detrition coefficients for category 1,2, and 3
 $-(b''_{20})^{(3,3,3,3,3)}(G_{23}, t)$, $-(b''_{21})^{(3,3,3,3,3)}(G_{23}, t)$, $-(b''_{22})^{(3,3,3,3,3)}(G_{23}, t)$ are sixth detrition coefficients for category 1,2, and 3.

$$\frac{dG_{32}}{dt} = (a_{32})^{(6)}G_{33} - \left[\begin{array}{ccc} (a''_{32})^{(6)} & + (a''_{32})^{(6)}(T_{33}, t) & + (a''_{28})^{(5,5,5)}(T_{29}, t) & + (a''_{24})^{(4,4,4)}(T_{25}, t) \\ + (a''_{13})^{(1,1,1,1,1)}(T_{14}, t) & + (a''_{16})^{(2,2,2,2,2)}(T_{17}, t) & + (a''_{20})^{(3,3,3,3,3)}(T_{21}, t) & \end{array} \right] G_{32} .$$

$$\frac{dG_{33}}{dt} = (a_{33})^{(6)}G_{32} - \left[\begin{array}{ccc} (a''_{33})^{(6)} & + (a''_{33})^{(6)}(T_{33}, t) & + (a''_{29})^{(5,5,5)}(T_{29}, t) & + (a''_{25})^{(4,4,4)}(T_{25}, t) \\ + (a''_{14})^{(1,1,1,1,1)}(T_{14}, t) & + (a''_{17})^{(2,2,2,2,2)}(T_{17}, t) & + (a''_{21})^{(3,3,3,3,3)}(T_{21}, t) & \end{array} \right] G_{33} .$$

$$\frac{dG_{34}}{dt} = (a_{34})^{(6)}G_{33} - \left[\begin{array}{ccc} (a''_{34})^{(6)} & + (a''_{34})^{(6)}(T_{33}, t) & + (a''_{30})^{(5,5,5)}(T_{29}, t) & + (a''_{26})^{(4,4,4)}(T_{25}, t) \\ + (a''_{15})^{(1,1,1,1,1)}(T_{14}, t) & + (a''_{18})^{(2,2,2,2,2)}(T_{17}, t) & + (a''_{22})^{(3,3,3,3,3)}(T_{21}, t) & \end{array} \right] G_{34} .$$

$+(a''_{32})^{(6)}(T_{33}, t)$, $+(a''_{33})^{(6)}(T_{33}, t)$, $+(a''_{34})^{(6)}(T_{33}, t)$ are first augmentation coefficients for category 1,2 and 3
 $+(a''_{28})^{(5,5,5)}(T_{29}, t)$, $+(a''_{29})^{(5,5,5)}(T_{29}, t)$, $+(a''_{30})^{(5,5,5)}(T_{29}, t)$ are second augmentation coefficients for category 1,2 and 3
 $+(a''_{24})^{(4,4,4)}(T_{25}, t)$, $+(a''_{25})^{(4,4,4)}(T_{25}, t)$, $+(a''_{26})^{(4,4,4)}(T_{25}, t)$ are third augmentation coefficients for category 1,2 and 3
 $+(a''_{13})^{(1,1,1,1,1)}(T_{14}, t)$, $+(a''_{14})^{(1,1,1,1,1)}(T_{14}, t)$, $+(a''_{15})^{(1,1,1,1,1)}(T_{14}, t)$ - are fourth augmentation coefficients
 $+(a''_{16})^{(2,2,2,2,2)}(T_{17}, t)$, $+(a''_{17})^{(2,2,2,2,2)}(T_{17}, t)$, $+(a''_{18})^{(2,2,2,2,2)}(T_{17}, t)$ - fifth augmentation coefficients
 $+(a''_{20})^{(3,3,3,3,3)}(T_{21}, t)$, $+(a''_{21})^{(3,3,3,3,3)}(T_{21}, t)$, $+(a''_{22})^{(3,3,3,3,3)}(T_{21}, t)$ sixth augmentation coefficients .

$$\frac{dT_{32}}{dt} = (b_{32})^{(6)}T_{33} - \left[\begin{array}{ccc} (b'_{32})^{(6)} & - (b''_{32})^{(6)}(G_{35}, t) & - (b''_{28})^{(5,5,5)}(G_{31}, t) & - (b''_{24})^{(4,4,4)}(G_{27}, t) \\ - (b''_{13})^{(1,1,1,1,1)}(G, t) & - (b''_{16})^{(2,2,2,2,2)}(G_{19}, t) & - (b''_{20})^{(3,3,3,3,3)}(G_{23}, t) & \end{array} \right] T_{32} .$$

$$\frac{dT_{33}}{dt} = (b_{33})^{(6)}T_{32} - \left[\begin{array}{ccc} (b'_{33})^{(6)} & - (b''_{33})^{(6)}(G_{35}, t) & - (b''_{29})^{(5,5,5)}(G_{31}, t) & - (b''_{25})^{(4,4,4)}(G_{27}, t) \\ - (b''_{14})^{(1,1,1,1,1)}(G, t) & - (b''_{17})^{(2,2,2,2,2)}(G_{19}, t) & - (b''_{21})^{(3,3,3,3,3)}(G_{23}, t) & \end{array} \right] T_{33} .$$

$$\frac{dT_{34}}{dt} = (b_{34})^{(6)}T_{33} - \left[\begin{array}{ccc} (b'_{34})^{(6)} & - (b''_{34})^{(6)}(G_{35}, t) & - (b''_{30})^{(5,5,5)}(G_{31}, t) & - (b''_{26})^{(4,4,4)}(G_{27}, t) \\ - (b''_{15})^{(1,1,1,1,1)}(G, t) & - (b''_{18})^{(2,2,2,2,2)}(G_{19}, t) & - (b''_{22})^{(3,3,3,3,3)}(G_{23}, t) & \end{array} \right] T_{34} .$$

$-(b''_{32})^{(6)}(G_{35}, t)$, $-(b''_{33})^{(6)}(G_{35}, t)$, $-(b''_{34})^{(6)}(G_{35}, t)$ are first detrition coefficients for category 1,2 and 3
 $-(b''_{28})^{(5,5,5)}(G_{31}, t)$, $-(b''_{29})^{(5,5,5)}(G_{31}, t)$, $-(b''_{30})^{(5,5,5)}(G_{31}, t)$ are second detrition coefficients for category 1,2 and 3
 $-(b''_{24})^{(4,4,4)}(G_{27}, t)$, $-(b''_{25})^{(4,4,4)}(G_{27}, t)$, $-(b''_{26})^{(4,4,4)}(G_{27}, t)$ are third detrition coefficients for category 1,2 and 3
 $-(b''_{13})^{(1,1,1,1,1)}(G, t)$, $-(b''_{14})^{(1,1,1,1,1)}(G, t)$, $-(b''_{15})^{(1,1,1,1,1)}(G, t)$ are fourth detrition coefficients for category 1, 2, and 3
 $-(b''_{16})^{(2,2,2,2,2)}(G_{19}, t)$, $-(b''_{17})^{(2,2,2,2,2)}(G_{19}, t)$, $-(b''_{18})^{(2,2,2,2,2)}(G_{19}, t)$ are fifth detrition coefficients for category 1, 2, and 3
 $-(b''_{20})^{(3,3,3,3,3)}(G_{23}, t)$, $-(b''_{21})^{(3,3,3,3,3)}(G_{23}, t)$, $-(b''_{22})^{(3,3,3,3,3)}(G_{23}, t)$ are sixth detrition coefficients for category 1, 2, and 3

Where we suppose.

- (A) $(a_i)^{(1)}, (a_i)^{(1)}, (a_i)^{(1)}, (b_i)^{(1)}, (b_i)^{(1)}, (b_i)^{(1)} > 0$,
 $i, j = 13, 14, 15$
 (B) The functions $(a_i)^{(1)}, (b_i)^{(1)}$ are positive continuous increasing and bounded.

Definition of $(p_i)^{(1)}, (\tau_i)^{(1)}$:

$$(a_i)^{(1)}(T_{14}, t) \leq (p_i)^{(1)} \leq (\hat{A}_{13})^{(1)}$$

$$(b_i'')^{(1)}(G, t) \leq (r_i)^{(1)} \leq (b_i')^{(1)} \leq (\hat{B}_{13})^{(1)}.$$

$$(C) \quad \lim_{T_2 \rightarrow \infty} (a_i'')^{(1)}(T_{14}, t) = (p_i)^{(1)}$$

$$\lim_{G \rightarrow \infty} (b_i'')^{(1)}(G, t) = (r_i)^{(1)}$$

Definition of $(\hat{A}_{13})^{(1)}, (\hat{B}_{13})^{(1)}$:

Where $(\hat{A}_{13})^{(1)}, (\hat{B}_{13})^{(1)}, (p_i)^{(1)}, (r_i)^{(1)}$ are positive constants and $i = 13, 14, 15$.

They satisfy Lipschitz condition:

$$|(a_i'')^{(1)}(T'_{14}, t) - (a_i'')^{(1)}(T_{14}, t)| \leq (\hat{k}_{13})^{(1)} |T'_{14} - T_{14}| e^{-(M_{13})^{(1)}t}$$

$$|(b_i'')^{(1)}(G', t) - (b_i'')^{(1)}(G, t)| < (\hat{k}_{13})^{(1)} \|G - G'\| e^{-(M_{13})^{(1)}t}.$$

With the Lipschitz condition, we place a restriction on the behavior of functions

$(a_i'')^{(1)}(T'_{14}, t)$ and $(a_i'')^{(1)}(T_{14}, t)$. (T'_{14}, t) and (T_{14}, t) are points belonging to the interval $[(\hat{k}_{13})^{(1)}, (\hat{M}_{13})^{(1)}]$. It is to be noted that $(a_i'')^{(1)}(T_{14}, t)$ is uniformly continuous. In the eventuality of the fact, that if $(\hat{M}_{13})^{(1)} = 1$ then the function $(a_i'')^{(1)}(T_{14}, t)$, the first augmentation coefficient WOULD be absolutely continuous. .

Definition of $(\hat{M}_{13})^{(1)}, (\hat{k}_{13})^{(1)}$:

(D) $(\hat{M}_{13})^{(1)}, (\hat{k}_{13})^{(1)}$, are positive constants

$$\frac{(a_i)^{(1)}}{(\hat{M}_{13})^{(1)}}, \frac{(b_i)^{(1)}}{(\hat{M}_{13})^{(1)}} < 1.$$

Definition of $(\hat{P}_{13})^{(1)}, (\hat{Q}_{13})^{(1)}$:

(E) There exists two constants $(\hat{P}_{13})^{(1)}$ and $(\hat{Q}_{13})^{(1)}$ which together with $(\hat{M}_{13})^{(1)}, (\hat{k}_{13})^{(1)}, (\hat{A}_{13})^{(1)}$ and $(\hat{B}_{13})^{(1)}$ and the constants $(a_i)^{(1)}, (a_i')^{(1)}, (b_i)^{(1)}, (b_i')^{(1)}, (p_i)^{(1)}, (r_i)^{(1)}, i = 13, 14, 15$, satisfy the inequalities

$$\frac{1}{(\hat{M}_{13})^{(1)}} [(a_i)^{(1)} + (a_i')^{(1)} + (\hat{A}_{13})^{(1)} + (\hat{P}_{13})^{(1)} (\hat{k}_{13})^{(1)}] < 1$$

$$\frac{1}{(\hat{M}_{13})^{(1)}} [(b_i)^{(1)} + (b_i')^{(1)} + (\hat{B}_{13})^{(1)} + (\hat{Q}_{13})^{(1)} (\hat{k}_{13})^{(1)}] < 1.$$

Where we suppose.

$$(a_i)^{(2)}, (a_i')^{(2)}, (a_i'')^{(2)}, (b_i)^{(2)}, (b_i')^{(2)}, (b_i'')^{(2)} > 0, \quad i, j = 16, 17, 18.$$

The functions $(a_i'')^{(2)}, (b_i'')^{(2)}$ are positive continuous increasing and bounded..

Definition of $(p_i)^{(2)}, (r_i)^{(2)}$:

$$(a_i'')^{(2)}(T'_{17}, t) \leq (p_i)^{(2)} \leq (\hat{A}_{16})^{(2)}.$$

$$(b_i'')^{(2)}(G_{19}, t) \leq (r_i)^{(2)} \leq (b_i')^{(2)} \leq (\hat{B}_{16})^{(2)}.$$

$$\lim_{T_2 \rightarrow \infty} (a_i'')^{(2)}(T_{17}, t) = (p_i)^{(2)}.$$

$$\lim_{G \rightarrow \infty} (b_i'')^{(2)}(G_{19}, t) = (r_i)^{(2)}.$$

Definition of $(\hat{A}_{16})^{(2)}, (\hat{B}_{16})^{(2)}$:

Where $(\hat{A}_{16})^{(2)}, (\hat{B}_{16})^{(2)}, (p_i)^{(2)}, (r_i)^{(2)}$ are positive constants and $i = 16, 17, 18$.

They satisfy Lipschitz condition:.

$$|(a_i'')^{(2)}(T'_{17}, t) - (a_i'')^{(2)}(T_{17}, t)| \leq (\hat{k}_{16})^{(2)} |T'_{17} - T_{17}| e^{-(M_{16})^{(2)}t}$$

$$|(b_i'')^{(2)}(G'_{19}, t) - (b_i'')^{(2)}(G_{19}, t)| < (\hat{k}_{16})^{(2)} \|G_{19} - G'_{19}\| e^{-(M_{16})^{(2)}t}.$$

With the Lipschitz condition, we place a restriction on the behavior of functions $(a_i'')^{(2)}(T'_{17}, t)$ and $(a_i'')^{(2)}(T_{17}, t)$. (T'_{17}, t) and (T_{17}, t) are points belonging to the interval $[(\hat{k}_{16})^{(2)}, (\hat{M}_{16})^{(2)}]$. It is to be noted that $(a_i'')^{(2)}(T_{17}, t)$ is uniformly continuous. In the eventuality of the fact, that if $(\hat{M}_{16})^{(2)} = 1$ then the function $(a_i'')^{(2)}(T_{17}, t)$, the SECOND augmentation coefficient would be absolutely continuous. .

Definition of $(\hat{M}_{16})^{(2)}, (\hat{k}_{16})^{(2)}$:

(F) $(\hat{M}_{16})^{(2)}, (\hat{k}_{16})^{(2)}$, are positive constants

$$\frac{(a_i)^{(2)}}{(\hat{M}_{16})^{(2)}}, \frac{(b_i)^{(2)}}{(\hat{M}_{16})^{(2)}} < 1.$$

Definition of $(\hat{P}_{16})^{(2)}, (\hat{Q}_{16})^{(2)}$:

There exists two constants $(\hat{P}_{16})^{(2)}$ and $(\hat{Q}_{16})^{(2)}$ which together with $(\hat{M}_{16})^{(2)}, (\hat{k}_{16})^{(2)}, (\hat{A}_{16})^{(2)}$ and $(\hat{B}_{16})^{(2)}$ and the constants $(a_i)^{(2)}, (a_i')^{(2)}, (b_i)^{(2)}, (b_i')^{(2)}, (p_i)^{(2)}, (r_i)^{(2)}, i = 16, 17, 18$, satisfy the inequalities .

$$\frac{1}{(\hat{M}_{16})^{(2)}} [(a_i)^{(2)} + (a_i')^{(2)} + (\hat{A}_{16})^{(2)} + (\hat{P}_{16})^{(2)} (\hat{k}_{16})^{(2)}] < 1.$$

$$\frac{1}{(\hat{M}_{16})^{(2)}} [(b_i)^{(2)} + (b_i')^{(2)} + (\hat{B}_{16})^{(2)} + (\hat{Q}_{16})^{(2)} (\hat{k}_{16})^{(2)}] < 1.$$

Where we suppose.

(G) $(a_i)^{(3)}, (a'_i)^{(3)}, (a''_i)^{(3)}, (b_i)^{(3)}, (b'_i)^{(3)}, (b''_i)^{(3)} > 0, \quad i, j = 20, 21, 22$

The functions $(a''_i)^{(3)}, (b''_i)^{(3)}$ are positive continuous increasing and bounded.

Definition of $(p_i)^{(3)}, (r_i)^{(3)}$:

$$(a''_i)^{(3)}(T_{21}, t) \leq (p_i)^{(3)} \leq (\hat{A}_{20})^{(3)}$$

$$(b''_i)^{(3)}(G_{23}, t) \leq (r_i)^{(3)} \leq (b'_i)^{(3)} \leq (\hat{B}_{20})^{(3)}.$$

$$\lim_{T_2 \rightarrow \infty} (a''_i)^{(3)}(T_{21}, t) = (p_i)^{(3)}$$

$$\lim_{G \rightarrow \infty} (b''_i)^{(3)}(G_{23}, t) = (r_i)^{(3)}$$

Definition of $(\hat{A}_{20})^{(3)}, (\hat{B}_{20})^{(3)}$:

Where $(\hat{A}_{20})^{(3)}, (\hat{B}_{20})^{(3)}, (p_i)^{(3)}, (r_i)^{(3)}$ are positive constants and $i = 20, 21, 22$.

They satisfy Lipschitz condition:

$$|(a''_i)^{(3)}(T'_{21}, t) - (a''_i)^{(3)}(T_{21}, t)| \leq (\hat{k}_{20})^{(3)} |T_{21} - T'_{21}| e^{-(M_{20})^{(3)}t}$$

$$|(b''_i)^{(3)}(G'_{23}, t) - (b''_i)^{(3)}(G_{23}, t)| < (\hat{k}_{20})^{(3)} ||G_{23} - G'_{23}'|| e^{-(M_{20})^{(3)}t}.$$

With the Lipschitz condition, we place a restriction on the behavior of functions $(a''_i)^{(3)}(T'_{21}, t)$ and $(a''_i)^{(3)}(T_{21}, t)$. (T'_{21}, t) and (T_{21}, t) are points belonging to the interval $[(\hat{k}_{20})^{(3)}, (\hat{M}_{20})^{(3)}]$. It is to be noted that $(a''_i)^{(3)}(T_{21}, t)$ is uniformly continuous. In the eventuality of the fact, that if $(\hat{M}_{20})^{(3)} = 1$ then the function $(a''_i)^{(3)}(T_{21}, t)$, the THIRD augmentation coefficient, would be absolutely continuous.

Definition of $(\hat{M}_{20})^{(3)}, (\hat{k}_{20})^{(3)}$:

(H) $(\hat{M}_{20})^{(3)}, (\hat{k}_{20})^{(3)}$, are positive constants

$$\frac{(a_i)^{(3)}}{(\hat{M}_{20})^{(3)}}, \frac{(b_i)^{(3)}}{(\hat{M}_{20})^{(3)}} < 1.$$

There exists two constants There exists two constants $(\hat{P}_{20})^{(3)}$ and $(\hat{Q}_{20})^{(3)}$ which together with $(\hat{M}_{20})^{(3)}, (\hat{k}_{20})^{(3)}, (\hat{A}_{20})^{(3)}$ and $(\hat{B}_{20})^{(3)}$ and the constants $(a_i)^{(3)}, (a'_i)^{(3)}, (b_i)^{(3)}, (b'_i)^{(3)}, (p_i)^{(3)}, (r_i)^{(3)}, i = 20, 21, 22$, satisfy the inequalities

$$\frac{1}{(\hat{M}_{20})^{(3)}} [(a_i)^{(3)} + (a'_i)^{(3)} + (\hat{A}_{20})^{(3)} + (\hat{P}_{20})^{(3)} (\hat{k}_{20})^{(3)}] < 1$$

$$\frac{1}{(\hat{M}_{20})^{(3)}} [(b_i)^{(3)} + (b'_i)^{(3)} + (\hat{B}_{20})^{(3)} + (\hat{Q}_{20})^{(3)} (\hat{k}_{20})^{(3)}] < 1.$$

Where we suppose.

(I) $(a_i)^{(4)}, (a'_i)^{(4)}, (a''_i)^{(4)}, (b_i)^{(4)}, (b'_i)^{(4)}, (b''_i)^{(4)} > 0, \quad i, j = 24, 25, 26$

(J) The functions $(a''_i)^{(4)}, (b''_i)^{(4)}$ are positive continuous increasing and bounded.

Definition of $(p_i)^{(4)}, (r_i)^{(4)}$:

$$(a''_i)^{(4)}(T_{25}, t) \leq (p_i)^{(4)} \leq (\hat{A}_{24})^{(4)}$$

$$(b''_i)^{(4)}((G_{27}), t) \leq (r_i)^{(4)} \leq (b'_i)^{(4)} \leq (\hat{B}_{24})^{(4)}.$$

$$(K) \quad \lim_{T_2 \rightarrow \infty} (a''_i)^{(4)}(T_{25}, t) = (p_i)^{(4)}$$

$$\lim_{G \rightarrow \infty} (b''_i)^{(4)}((G_{27}), t) = (r_i)^{(4)}$$

Definition of $(\hat{A}_{24})^{(4)}, (\hat{B}_{24})^{(4)}$:

Where $(\hat{A}_{24})^{(4)}, (\hat{B}_{24})^{(4)}, (p_i)^{(4)}, (r_i)^{(4)}$ are positive constants and $i = 24, 25, 26$.

They satisfy Lipschitz condition:

$$|(a''_i)^{(4)}(T'_{25}, t) - (a''_i)^{(4)}(T_{25}, t)| \leq (\hat{k}_{24})^{(4)} |T_{25} - T'_{25}| e^{-(M_{24})^{(4)}t}$$

$$|(b''_i)^{(4)}((G'_{27}), t) - (b''_i)^{(4)}((G_{27}), t)| < (\hat{k}_{24})^{(4)} ||G_{27} - (G'_{27})'|| e^{-(M_{24})^{(4)}t}.$$

With the Lipschitz condition, we place a restriction on the behavior of functions $(a''_i)^{(4)}(T'_{25}, t)$ and $(a''_i)^{(4)}(T_{25}, t)$. (T'_{25}, t) and (T_{25}, t) are points belonging to the interval $[(\hat{k}_{24})^{(4)}, (\hat{M}_{24})^{(4)}]$. It is to be noted that $(a''_i)^{(4)}(T_{25}, t)$ is uniformly continuous. In the eventuality of the fact, that if $(\hat{M}_{24})^{(4)} = 4$ then the function $(a''_i)^{(4)}(T_{25}, t)$, the FOURTH augmentation coefficient WOULD be absolutely continuous.

Definition of $(\hat{M}_{24})^{(4)}, (\hat{k}_{24})^{(4)}$:

(L) $(\hat{M}_{24})^{(4)}, (\hat{k}_{24})^{(4)}$, are positive constants

(M)
$$\frac{(a_i)^{(4)}}{(\hat{M}_{24})^{(4)}}, \frac{(b_i)^{(4)}}{(\hat{M}_{24})^{(4)}} < 1.$$

Definition of $(\hat{P}_{24})^{(4)}, (\hat{Q}_{24})^{(4)}$:

(N) There exists two constants $(\hat{P}_{24})^{(4)}$ and $(\hat{Q}_{24})^{(4)}$ which together with $(\hat{M}_{24})^{(4)}$, $(\hat{k}_{24})^{(4)}$, $(\hat{A}_{24})^{(4)}$ and $(\hat{B}_{24})^{(4)}$ and the constants $(a_i)^{(4)}$, $(a'_i)^{(4)}$, $(b_i)^{(4)}$, $(b'_i)^{(4)}$, $(p_i)^{(4)}$, $(r_i)^{(4)}$, $i = 24, 25, 26$, satisfy the inequalities

$$\frac{1}{(\hat{M}_{24})^{(4)}} [(a_i)^{(4)} + (a'_i)^{(4)} + (\hat{A}_{24})^{(4)} + (\hat{P}_{24})^{(4)} (\hat{k}_{24})^{(4)}] < 1$$

$$\frac{1}{(\hat{M}_{24})^{(4)}} [(b_i)^{(4)} + (b'_i)^{(4)} + (\hat{B}_{24})^{(4)} + (\hat{Q}_{24})^{(4)} (\hat{k}_{24})^{(4)}] < 1.$$

Where we suppose,

(O) $(a_i)^{(5)}$, $(a'_i)^{(5)}$, $(a''_i)^{(5)}$, $(b_i)^{(5)}$, $(b'_i)^{(5)}$, $(b''_i)^{(5)} > 0$, $i, j = 28, 29, 30$

(P) The functions $(a''_i)^{(5)}$, $(b''_i)^{(5)}$ are positive continuous increasing and bounded.

Definition of $(p_i)^{(5)}$, $(r_i)^{(5)}$:

$$(a''_i)^{(5)}(T_{29}, t) \leq (p_i)^{(5)} \leq (\hat{A}_{28})^{(5)}$$

$$(b''_i)^{(5)}(G_{31}, t) \leq (r_i)^{(5)} \leq (b'_i)^{(5)} \leq (\hat{B}_{28})^{(5)}.$$

$$(Q) \lim_{T_2 \rightarrow \infty} (a''_i)^{(5)}(T_{29}, t) = (p_i)^{(5)}$$

$$\lim_{G \rightarrow \infty} (b''_i)^{(5)}(G_{31}, t) = (r_i)^{(5)}$$

Definition of $(\hat{A}_{28})^{(5)}$, $(\hat{B}_{28})^{(5)}$:

Where $(\hat{A}_{28})^{(5)}$, $(\hat{B}_{28})^{(5)}$, $(p_i)^{(5)}$, $(r_i)^{(5)}$ are positive constants and $i = 28, 29, 30$.

They satisfy Lipschitz condition:

$$|(a''_i)^{(5)}(T'_{29}, t) - (a''_i)^{(5)}(T_{29}, t)| \leq (\hat{k}_{28})^{(5)} |T'_{29} - T_{29}| e^{-(\hat{M}_{28})^{(5)}t}$$

$$|(b''_i)^{(5)}(G'_{31}, t) - (b''_i)^{(5)}(G_{31}, t)| < (\hat{k}_{28})^{(5)} |(G'_{31}) - (G_{31})| e^{-(\hat{M}_{28})^{(5)}t}.$$

With the Lipschitz condition, we place a restriction on the behavior of functions $(a''_i)^{(5)}(T'_{29}, t)$ and $(a''_i)^{(5)}(T_{29}, t)$. (T'_{29}, t) and (T_{29}, t) are points belonging to the interval $[(\hat{k}_{28})^{(5)}, (\hat{M}_{28})^{(5)}]$. It is to be noted that $(a''_i)^{(5)}(T_{29}, t)$ is uniformly continuous. In the eventuality of the fact, that if $(\hat{M}_{28})^{(5)} = 5$ then the function $(a''_i)^{(5)}(T_{29}, t)$, the **FIFTH augmentation coefficient** attributable would be absolutely continuous. .

Definition of $(\hat{M}_{28})^{(5)}$, $(\hat{k}_{28})^{(5)}$:

(R) $(\hat{M}_{28})^{(5)}$, $(\hat{k}_{28})^{(5)}$, are positive constants

$$\frac{(a_i)^{(5)}}{(\hat{M}_{28})^{(5)}} , \frac{(b_i)^{(5)}}{(\hat{M}_{28})^{(5)}} < 1.$$

Definition of $(\hat{P}_{28})^{(5)}$, $(\hat{Q}_{28})^{(5)}$:

(S) There exists two constants $(\hat{P}_{28})^{(5)}$ and $(\hat{Q}_{28})^{(5)}$ which together with $(\hat{M}_{28})^{(5)}$, $(\hat{k}_{28})^{(5)}$, $(\hat{A}_{28})^{(5)}$ and $(\hat{B}_{28})^{(5)}$ and the constants $(a_i)^{(5)}$, $(a'_i)^{(5)}$, $(b_i)^{(5)}$, $(b'_i)^{(5)}$, $(p_i)^{(5)}$, $(r_i)^{(5)}$, $i = 28, 29, 30$, satisfy the inequalities

$$\frac{1}{(\hat{M}_{28})^{(5)}} [(a_i)^{(5)} + (a'_i)^{(5)} + (\hat{A}_{28})^{(5)} + (\hat{P}_{28})^{(5)} (\hat{k}_{28})^{(5)}] < 1$$

$$\frac{1}{(\hat{M}_{28})^{(5)}} [(b_i)^{(5)} + (b'_i)^{(5)} + (\hat{B}_{28})^{(5)} + (\hat{Q}_{28})^{(5)} (\hat{k}_{28})^{(5)}] < 1.$$

Where we suppose.

$(a_i)^{(6)}$, $(a'_i)^{(6)}$, $(a''_i)^{(6)}$, $(b_i)^{(6)}$, $(b'_i)^{(6)}$, $(b''_i)^{(6)} > 0$, $i, j = 32, 33, 34$

(T) The functions $(a''_i)^{(6)}$, $(b''_i)^{(6)}$ are positive continuous increasing and bounded.

Definition of $(p_i)^{(6)}$, $(r_i)^{(6)}$:

$$(a''_i)^{(6)}(T_{33}, t) \leq (p_i)^{(6)} \leq (\hat{A}_{32})^{(6)}$$

$$(b''_i)^{(6)}(G_{35}, t) \leq (r_i)^{(6)} \leq (b'_i)^{(6)} \leq (\hat{B}_{32})^{(6)}.$$

$$(U) \lim_{T_2 \rightarrow \infty} (a''_i)^{(6)}(T_{33}, t) = (p_i)^{(6)}$$

$$\lim_{G \rightarrow \infty} (b''_i)^{(6)}(G_{35}, t) = (r_i)^{(6)}$$

Definition of $(\hat{A}_{32})^{(6)}$, $(\hat{B}_{32})^{(6)}$:

Where $(\hat{A}_{32})^{(6)}$, $(\hat{B}_{32})^{(6)}$, $(p_i)^{(6)}$, $(r_i)^{(6)}$ are positive constants and $i = 32, 33, 34$.

They satisfy Lipschitz condition:

$$|(a''_i)^{(6)}(T'_{33}, t) - (a''_i)^{(6)}(T_{33}, t)| \leq (\hat{k}_{32})^{(6)} |T'_{33} - T_{33}| e^{-(\hat{M}_{32})^{(6)}t}$$

$$|(b''_i)^{(6)}(G'_{35}, t) - (b''_i)^{(6)}(G_{35}, t)| < (\hat{k}_{32})^{(6)} |(G'_{35}) - (G_{35})| e^{-(\hat{M}_{32})^{(6)}t}.$$

With the Lipschitz condition, we place a restriction on the behavior of functions $(a''_i)^{(6)}(T'_{33}, t)$ and $(a''_i)^{(6)}(T_{33}, t)$. (T'_{33}, t) and (T_{33}, t) are points belonging to the interval $[(\hat{k}_{32})^{(6)}, (\hat{M}_{32})^{(6)}]$. It is to be noted that $(a''_i)^{(6)}(T_{33}, t)$ is uniformly continuous. In the eventuality of the fact, that if $(\hat{M}_{32})^{(6)} = 6$ then the function $(a''_i)^{(6)}(T_{33}, t)$, the **SIXTH augmentation coefficient** would be absolutely continuous. .

Definition of $(\hat{M}_{32})^{(6)}$, $(\hat{k}_{32})^{(6)}$:

$(\hat{M}_{32})^{(6)}$, $(\hat{k}_{32})^{(6)}$, are positive constants

$$\frac{(a_i)^{(6)}}{(\hat{M}_{32})^{(6)}} , \frac{(b_i)^{(6)}}{(\hat{M}_{32})^{(6)}} < 1.$$

Definition of $(\hat{P}_{32})^{(6)}, (\hat{Q}_{32})^{(6)}$:

There exists two constants $(\hat{P}_{32})^{(6)}$ and $(\hat{Q}_{32})^{(6)}$ which together with $(\hat{M}_{32})^{(6)}, (\hat{k}_{32})^{(6)}, (\hat{A}_{32})^{(6)}$ and $(\hat{B}_{32})^{(6)}$ and the constants $(a_i)^{(6)}, (a'_i)^{(6)}, (b_i)^{(6)}, (b'_i)^{(6)}, (p_i)^{(6)}, (r_i)^{(6)}, i = 32, 33, 34$, satisfy the inequalities

$$\frac{1}{(\hat{M}_{32})^{(6)}} [(a_i)^{(6)} + (a'_i)^{(6)} + (\hat{A}_{32})^{(6)} + (\hat{P}_{32})^{(6)} (\hat{k}_{32})^{(6)}] < 1$$

$$\frac{1}{(\hat{M}_{32})^{(6)}} [(b_i)^{(6)} + (b'_i)^{(6)} + (\hat{B}_{32})^{(6)} + (\hat{Q}_{32})^{(6)} (\hat{k}_{32})^{(6)}] < 1 .$$

Theorem 1: if the conditions IN THE FOREGOING above are fulfilled, there exists a solution satisfying the conditions

Definition of $G_i(0), T_i(0)$:

$$G_i(t) \leq (\hat{P}_{13})^{(1)} e^{(\hat{M}_{13})^{(1)}t} , \quad \boxed{G_i(0) = G_i^0 > 0}$$

$$T_i(t) \leq (\hat{Q}_{13})^{(1)} e^{(\hat{M}_{13})^{(1)}t} , \quad \boxed{T_i(0) = T_i^0 > 0} .$$

Definition of $G_i(0), T_i(0)$

$$G_i(t) \leq (\hat{P}_{16})^{(2)} e^{(\hat{M}_{16})^{(2)}t} , \quad G_i(0) = G_i^0 > 0$$

$$T_i(t) \leq (\hat{Q}_{16})^{(2)} e^{(\hat{M}_{16})^{(2)}t} , \quad T_i(0) = T_i^0 > 0 .$$

$$G_i(t) \leq (\hat{P}_{20})^{(3)} e^{(\hat{M}_{20})^{(3)}t} , \quad G_i(0) = G_i^0 > 0$$

$$T_i(t) \leq (\hat{Q}_{20})^{(3)} e^{(\hat{M}_{20})^{(3)}t} , \quad T_i(0) = T_i^0 > 0 .$$

Definition of $G_i(0), T_i(0)$:

$$G_i(t) \leq (\hat{P}_{24})^{(4)} e^{(\hat{M}_{24})^{(4)}t} , \quad \boxed{G_i(0) = G_i^0 > 0}$$

$$T_i(t) \leq (\hat{Q}_{24})^{(4)} e^{(\hat{M}_{24})^{(4)}t} , \quad \boxed{T_i(0) = T_i^0 > 0}$$

Definition of $G_i(0), T_i(0)$:

$$G_i(t) \leq (\hat{P}_{28})^{(5)} e^{(\hat{M}_{28})^{(5)}t} , \quad \boxed{G_i(0) = G_i^0 > 0}$$

$$T_i(t) \leq (\hat{Q}_{28})^{(5)} e^{(\hat{M}_{28})^{(5)}t} , \quad \boxed{T_i(0) = T_i^0 > 0} .$$

Definition of $G_i(0), T_i(0)$:

$$G_i(t) \leq (\hat{P}_{32})^{(6)} e^{(\hat{M}_{32})^{(6)}t} , \quad \boxed{G_i(0) = G_i^0 > 0}$$

$$T_i(t) \leq (\hat{Q}_{32})^{(6)} e^{(\hat{M}_{32})^{(6)}t} , \quad \boxed{T_i(0) = T_i^0 > 0} .$$

Proof: Consider operator $\mathcal{A}^{(1)}$ defined on the space of sextuples of continuous functions $G_i, T_i: \mathbb{R}_+ \rightarrow \mathbb{R}_+$ which satisfy

$$G_i(0) = G_i^0, T_i(0) = T_i^0, G_i^0 \leq (\hat{P}_{13})^{(1)}, T_i^0 \leq (\hat{Q}_{13})^{(1)}, .$$

$$0 \leq G_i(t) - G_i^0 \leq (\hat{P}_{13})^{(1)} e^{(\hat{M}_{13})^{(1)}t} .$$

$$0 \leq T_i(t) - T_i^0 \leq (\hat{Q}_{13})^{(1)} e^{(\hat{M}_{13})^{(1)}t} .$$

By

$$\bar{G}_{13}(t) = G_{13}^0 + \int_0^t [(a_{13})^{(1)} G_{14}(s_{13}) - ((a'_{13})^{(1)} + a''_{13})^{(1)}(T_{14}(s_{13}), s_{13})) G_{13}(s_{13})] ds_{13} .$$

$$\bar{G}_{14}(t) = G_{14}^0 + \int_0^t [(a_{14})^{(1)} G_{13}(s_{13}) - ((a'_{14})^{(1)} + (a''_{14})^{(1)}(T_{14}(s_{13}), s_{13})) G_{14}(s_{13})] ds_{13} .$$

$$\bar{G}_{15}(t) = G_{15}^0 + \int_0^t [(a_{15})^{(1)} G_{14}(s_{13}) - ((a'_{15})^{(1)} + (a''_{15})^{(1)}(T_{14}(s_{13}), s_{13})) G_{15}(s_{13})] ds_{13} .$$

$$\bar{T}_{13}(t) = T_{13}^0 + \int_0^t [(b_{13})^{(1)} T_{14}(s_{13}) - ((b'_{13})^{(1)} - (b''_{13})^{(1)}(G(s_{13}), s_{13})) T_{13}(s_{13})] ds_{13} .$$

$$\bar{T}_{14}(t) = T_{14}^0 + \int_0^t [(b_{14})^{(1)} T_{13}(s_{13}) - ((b'_{14})^{(1)} - (b''_{14})^{(1)}(G(s_{13}), s_{13})) T_{14}(s_{13})] ds_{13} .$$

$$\bar{T}_{15}(t) = T_{15}^0 + \int_0^t [(b_{15})^{(1)} T_{14}(s_{13}) - ((b'_{15})^{(1)} - (b''_{15})^{(1)}(G(s_{13}), s_{13})) T_{15}(s_{13})] ds_{13}$$

Where s_{13} is the integrand that is integrated over an interval $(0, t)$.

Proof:

Consider operator $\mathcal{A}^{(2)}$ defined on the space of sextuples of continuous functions $G_i, T_i: \mathbb{R}_+ \rightarrow \mathbb{R}_+$ which satisfy

$$G_i(0) = G_i^0, T_i(0) = T_i^0, G_i^0 \leq (\hat{P}_{16})^{(2)}, T_i^0 \leq (\hat{Q}_{16})^{(2)}, .$$

$$0 \leq G_i(t) - G_i^0 \leq (\hat{P}_{16})^{(2)} e^{(\hat{M}_{16})^{(2)}t} .$$

$$0 \leq T_i(t) - T_i^0 \leq (\hat{Q}_{16})^{(2)} e^{(\hat{M}_{16})^{(2)}t} .$$

By

$$\bar{G}_{16}(t) = G_{16}^0 + \int_0^t [(a_{16})^{(2)} G_{17}(s_{16}) - ((a'_{16})^{(2)} + a''_{16})^{(2)}(T_{17}(s_{16}), s_{16})) G_{16}(s_{16})] ds_{16} .$$

$$\bar{G}_{17}(t) = G_{17}^0 + \int_0^t [(a_{17})^{(2)} G_{16}(s_{16}) - ((a'_{17})^{(2)} + (a''_{17})^{(2)}(T_{17}(s_{16}), s_{17})) G_{17}(s_{16})] ds_{16} .$$

$$\begin{aligned} \bar{G}_{18}(t) &= G_{18}^0 + \int_0^t \left[(a_{18})^{(2)} G_{17}(s_{(16)}) - \left((a'_{18})^{(2)} + (a''_{18})^{(2)} (T_{17}(s_{(16)}), s_{(16)}) \right) G_{18}(s_{(16)}) \right] ds_{(16)} \cdot \\ \bar{T}_{16}(t) &= T_{16}^0 + \int_0^t \left[(b_{16})^{(2)} T_{17}(s_{(16)}) - \left((b'_{16})^{(2)} - (b''_{16})^{(2)} (G(s_{(16)}), s_{(16)}) \right) T_{16}(s_{(16)}) \right] ds_{(16)} \cdot \\ \bar{T}_{17}(t) &= T_{17}^0 + \int_0^t \left[(b_{17})^{(2)} T_{16}(s_{(16)}) - \left((b'_{17})^{(2)} - (b''_{17})^{(2)} (G(s_{(16)}), s_{(16)}) \right) T_{17}(s_{(16)}) \right] ds_{(16)} \cdot \\ \bar{T}_{18}(t) &= T_{18}^0 + \int_0^t \left[(b_{18})^{(2)} T_{17}(s_{(16)}) - \left((b'_{18})^{(2)} - (b''_{18})^{(2)} (G(s_{(16)}), s_{(16)}) \right) T_{18}(s_{(16)}) \right] ds_{(16)} \end{aligned}$$

Where $s_{(16)}$ is the integrand that is integrated over an interval $(0, t)$.

Proof:

Consider operator $\mathcal{A}^{(3)}$ defined on the space of sextuples of continuous functions $G_i, T_i: \mathbb{R}_+ \rightarrow \mathbb{R}_+$ which satisfy

$$G_i(0) = G_i^0, T_i(0) = T_i^0, G_i^0 \leq (\hat{P}_{20})^{(3)}, T_i^0 \leq (\hat{Q}_{20})^{(3)},$$

$$0 \leq G_i(t) - G_i^0 \leq (\hat{P}_{20})^{(3)} e^{(M_{20})^{(3)}t}$$

$$0 \leq T_i(t) - T_i^0 \leq (\hat{Q}_{20})^{(3)} e^{(M_{20})^{(3)}t}$$

By

$$\begin{aligned} \bar{G}_{20}(t) &= G_{20}^0 + \int_0^t \left[(a_{20})^{(3)} G_{21}(s_{(20)}) - \left((a'_{20})^{(3)} + (a''_{20})^{(3)} (T_{21}(s_{(20)}), s_{(20)}) \right) G_{20}(s_{(20)}) \right] ds_{(20)} \cdot \\ \bar{G}_{21}(t) &= G_{21}^0 + \int_0^t \left[(a_{21})^{(3)} G_{20}(s_{(20)}) - \left((a'_{21})^{(3)} + (a''_{21})^{(3)} (T_{21}(s_{(20)}), s_{(20)}) \right) G_{21}(s_{(20)}) \right] ds_{(20)} \cdot \\ \bar{G}_{22}(t) &= G_{22}^0 + \int_0^t \left[(a_{22})^{(3)} G_{21}(s_{(20)}) - \left((a'_{22})^{(3)} + (a''_{22})^{(3)} (T_{21}(s_{(20)}), s_{(20)}) \right) G_{22}(s_{(20)}) \right] ds_{(20)} \cdot \\ \bar{T}_{20}(t) &= T_{20}^0 + \int_0^t \left[(b_{20})^{(3)} T_{21}(s_{(20)}) - \left((b'_{20})^{(3)} - (b''_{20})^{(3)} (G(s_{(20)}), s_{(20)}) \right) T_{20}(s_{(20)}) \right] ds_{(20)} \cdot \\ \bar{T}_{21}(t) &= T_{21}^0 + \int_0^t \left[(b_{21})^{(3)} T_{20}(s_{(20)}) - \left((b'_{21})^{(3)} - (b''_{21})^{(3)} (G(s_{(20)}), s_{(20)}) \right) T_{21}(s_{(20)}) \right] ds_{(20)} \cdot \\ \bar{T}_{22}(t) &= T_{22}^0 + \int_0^t \left[(b_{22})^{(3)} T_{21}(s_{(20)}) - \left((b'_{22})^{(3)} - (b''_{22})^{(3)} (G(s_{(20)}), s_{(20)}) \right) T_{22}(s_{(20)}) \right] ds_{(20)} \end{aligned}$$

Where $s_{(20)}$ is the integrand that is integrated over an interval $(0, t)$.

Consider operator $\mathcal{A}^{(4)}$ defined on the space of sextuples of continuous functions $G_i, T_i: \mathbb{R}_+ \rightarrow \mathbb{R}_+$ which satisfy

$$G_i(0) = G_i^0, T_i(0) = T_i^0, G_i^0 \leq (\hat{P}_{24})^{(4)}, T_i^0 \leq (\hat{Q}_{24})^{(4)},$$

$$0 \leq G_i(t) - G_i^0 \leq (\hat{P}_{24})^{(4)} e^{(M_{24})^{(4)}t}$$

$$0 \leq T_i(t) - T_i^0 \leq (\hat{Q}_{24})^{(4)} e^{(M_{24})^{(4)}t}$$

By

$$\begin{aligned} \bar{G}_{24}(t) &= G_{24}^0 + \int_0^t \left[(a_{24})^{(4)} G_{25}(s_{(24)}) - \left((a'_{24})^{(4)} + (a''_{24})^{(4)} (T_{25}(s_{(24)}), s_{(24)}) \right) G_{24}(s_{(24)}) \right] ds_{(24)} \cdot \\ \bar{G}_{25}(t) &= G_{25}^0 + \int_0^t \left[(a_{25})^{(4)} G_{24}(s_{(24)}) - \left((a'_{25})^{(4)} + (a''_{25})^{(4)} (T_{25}(s_{(24)}), s_{(24)}) \right) G_{25}(s_{(24)}) \right] ds_{(24)} \cdot \\ \bar{G}_{26}(t) &= G_{26}^0 + \int_0^t \left[(a_{26})^{(4)} G_{25}(s_{(24)}) - \left((a'_{26})^{(4)} + (a''_{26})^{(4)} (T_{25}(s_{(24)}), s_{(24)}) \right) G_{26}(s_{(24)}) \right] ds_{(24)} \cdot \\ \bar{T}_{24}(t) &= T_{24}^0 + \int_0^t \left[(b_{24})^{(4)} T_{25}(s_{(24)}) - \left((b'_{24})^{(4)} - (b''_{24})^{(4)} (G(s_{(24)}), s_{(24)}) \right) T_{24}(s_{(24)}) \right] ds_{(24)} \cdot \\ \bar{T}_{25}(t) &= T_{25}^0 + \int_0^t \left[(b_{25})^{(4)} T_{24}(s_{(24)}) - \left((b'_{25})^{(4)} - (b''_{25})^{(4)} (G(s_{(24)}), s_{(24)}) \right) T_{25}(s_{(24)}) \right] ds_{(24)} \cdot \\ \bar{T}_{26}(t) &= T_{26}^0 + \int_0^t \left[(b_{26})^{(4)} T_{25}(s_{(24)}) - \left((b'_{26})^{(4)} - (b''_{26})^{(4)} (G(s_{(24)}), s_{(24)}) \right) T_{26}(s_{(24)}) \right] ds_{(24)} \end{aligned}$$

Where $s_{(24)}$ is the integrand that is integrated over an interval $(0, t)$.

Consider operator $\mathcal{A}^{(5)}$ defined on the space of sextuples of continuous functions $G_i, T_i: \mathbb{R}_+ \rightarrow \mathbb{R}_+$ which satisfy

$$G_i(0) = G_i^0, T_i(0) = T_i^0, G_i^0 \leq (\hat{P}_{28})^{(5)}, T_i^0 \leq (\hat{Q}_{28})^{(5)},$$

$$0 \leq G_i(t) - G_i^0 \leq (\hat{P}_{28})^{(5)} e^{(M_{28})^{(5)}t}$$

$$0 \leq T_i(t) - T_i^0 \leq (\hat{Q}_{28})^{(5)} e^{(M_{28})^{(5)}t}$$

By

$$\begin{aligned} \bar{G}_{28}(t) &= G_{28}^0 + \int_0^t \left[(a_{28})^{(5)} G_{29}(s_{(28)}) - \left((a'_{28})^{(5)} + (a''_{28})^{(5)} (T_{29}(s_{(28)}), s_{(28)}) \right) G_{28}(s_{(28)}) \right] ds_{(28)} \cdot \\ \bar{G}_{29}(t) &= G_{29}^0 + \int_0^t \left[(a_{29})^{(5)} G_{28}(s_{(28)}) - \left((a'_{29})^{(5)} + (a''_{29})^{(5)} (T_{29}(s_{(28)}), s_{(28)}) \right) G_{29}(s_{(28)}) \right] ds_{(28)} \cdot \\ \bar{G}_{30}(t) &= G_{30}^0 + \int_0^t \left[(a_{30})^{(5)} G_{29}(s_{(28)}) - \left((a'_{30})^{(5)} + (a''_{30})^{(5)} (T_{29}(s_{(28)}), s_{(28)}) \right) G_{30}(s_{(28)}) \right] ds_{(28)} \cdot \\ \bar{T}_{28}(t) &= T_{28}^0 + \int_0^t \left[(b_{28})^{(5)} T_{29}(s_{(28)}) - \left((b'_{28})^{(5)} - (b''_{28})^{(5)} (G(s_{(28)}), s_{(28)}) \right) T_{28}(s_{(28)}) \right] ds_{(28)} \cdot \\ \bar{T}_{29}(t) &= T_{29}^0 + \int_0^t \left[(b_{29})^{(5)} T_{28}(s_{(28)}) - \left((b'_{29})^{(5)} - (b''_{29})^{(5)} (G(s_{(28)}), s_{(28)}) \right) T_{29}(s_{(28)}) \right] ds_{(28)} \cdot \\ \bar{T}_{30}(t) &= T_{30}^0 + \int_0^t \left[(b_{30})^{(5)} T_{29}(s_{(28)}) - \left((b'_{30})^{(5)} - (b''_{30})^{(5)} (G(s_{(28)}), s_{(28)}) \right) T_{30}(s_{(28)}) \right] ds_{(28)} \end{aligned}$$

Where $s_{(28)}$ is the integrand that is integrated over an interval $(0, t)$.

Consider operator $\mathcal{A}^{(6)}$ defined on the space of sextuples of continuous functions $G_i, T_i: \mathbb{R}_+ \rightarrow \mathbb{R}_+$ which satisfy

$$G_i(0) = G_i^0, T_i(0) = T_i^0, G_i^0 \leq (\hat{P}_{32})^{(6)}, T_i^0 \leq (\hat{Q}_{32})^{(6)},$$

$$0 \leq G_i(t) - G_i^0 \leq (\hat{P}_{32})^{(6)} e^{(\hat{M}_{32})^{(6)}t} .$$

$$0 \leq T_i(t) - T_i^0 \leq (\hat{Q}_{32})^{(6)} e^{(\hat{M}_{32})^{(6)}t} .$$

By

$$\bar{G}_{32}(t) = G_{32}^0 + \int_0^t \left[(a_{32})^{(6)} G_{33}(s_{(32)}) - \left((a'_{32})^{(6)} + a''_{32} \right)^{(6)} (T_{33}(s_{(32)}), s_{(32)}) G_{32}(s_{(32)}) \right] ds_{(32)} .$$

$$\bar{G}_{33}(t) = G_{33}^0 + \int_0^t \left[(a_{33})^{(6)} G_{32}(s_{(32)}) - \left((a'_{33})^{(6)} + (a''_{33})^{(6)} (T_{33}(s_{(32)}), s_{(32)}) \right) G_{33}(s_{(32)}) \right] ds_{(32)} .$$

$$\bar{G}_{34}(t) = G_{34}^0 + \int_0^t \left[(a_{34})^{(6)} G_{33}(s_{(32)}) - \left((a'_{34})^{(6)} + (a''_{34})^{(6)} (T_{33}(s_{(32)}), s_{(32)}) \right) G_{34}(s_{(32)}) \right] ds_{(32)} .$$

$$\bar{T}_{32}(t) = T_{32}^0 + \int_0^t \left[(b_{32})^{(6)} T_{33}(s_{(32)}) - \left((b'_{32})^{(6)} - (b''_{32})^{(6)} (G(s_{(32)}), s_{(32)}) \right) T_{32}(s_{(32)}) \right] ds_{(32)} .$$

$$\bar{T}_{33}(t) = T_{33}^0 + \int_0^t \left[(b_{33})^{(6)} T_{32}(s_{(32)}) - \left((b'_{33})^{(6)} - (b''_{33})^{(6)} (G(s_{(32)}), s_{(32)}) \right) T_{33}(s_{(32)}) \right] ds_{(32)} .$$

$$\bar{T}_{34}(t) = T_{34}^0 + \int_0^t \left[(b_{34})^{(6)} T_{33}(s_{(32)}) - \left((b'_{34})^{(6)} - (b''_{34})^{(6)} (G(s_{(32)}), s_{(32)}) \right) T_{34}(s_{(32)}) \right] ds_{(32)} .$$

Where $s_{(32)}$ is the integrand that is integrated over an interval $(0, t)$..

(a) The operator $\mathcal{A}^{(1)}$ maps the space of functions satisfying GLOBAL EQUATIONS into itself .Indeed it is obvious that

$$G_{13}(t) \leq G_{13}^0 + \int_0^t \left[(a_{13})^{(1)} \left(G_{14}^0 + (\hat{P}_{13})^{(1)} e^{(\hat{M}_{13})^{(1)}s_{(13)}} \right) \right] ds_{(13)} =$$

$$\left(1 + (a_{13})^{(1)}t \right) G_{14}^0 + \frac{(a_{13})^{(1)}(\hat{P}_{13})^{(1)}}{(\hat{M}_{13})^{(1)}} \left(e^{(\hat{M}_{13})^{(1)}t} - 1 \right) .$$

From which it follows that

$$(G_{13}(t) - G_{13}^0) e^{-(\hat{M}_{13})^{(1)}t} \leq \frac{(a_{13})^{(1)}}{(\hat{M}_{13})^{(1)}} \left[\left((\hat{P}_{13})^{(1)} + G_{14}^0 \right) e^{-\frac{(\hat{P}_{13})^{(1)} + G_{14}^0}{G_{14}^0}} + (\hat{P}_{13})^{(1)} \right]$$

(G_i^0) is as defined in the statement of theorem 1.

Analogous inequalities hold also for $G_{14}, G_{15}, T_{13}, T_{14}, T_{15}$.

The operator $\mathcal{A}^{(2)}$ maps the space of functions satisfying GLOBAL EQUATIONS into itself .Indeed it is obvious that.

$$G_{16}(t) \leq G_{16}^0 + \int_0^t \left[(a_{16})^{(2)} \left(G_{17}^0 + (\hat{P}_{16})^{(2)} e^{(\hat{M}_{16})^{(2)}s_{(16)}} \right) \right] ds_{(16)} = \left(1 + (a_{16})^{(2)}t \right) G_{17}^0 + \frac{(a_{16})^{(2)}(\hat{P}_{16})^{(2)}}{(\hat{M}_{16})^{(2)}} \left(e^{(\hat{M}_{16})^{(2)}t} - 1 \right) .$$

From which it follows that

$$(G_{16}(t) - G_{16}^0) e^{-(\hat{M}_{16})^{(2)}t} \leq \frac{(a_{16})^{(2)}}{(\hat{M}_{16})^{(2)}} \left[\left((\hat{P}_{16})^{(2)} + G_{17}^0 \right) e^{-\frac{(\hat{P}_{16})^{(2)} + G_{17}^0}{G_{17}^0}} + (\hat{P}_{16})^{(2)} \right]$$

Analogous inequalities hold also for $G_{17}, G_{18}, T_{16}, T_{17}, T_{18}$.

(a) The operator $\mathcal{A}^{(3)}$ maps the space of functions satisfying GLOBAL EQUATIONS into itself .Indeed it is obvious that

$$G_{20}(t) \leq G_{20}^0 + \int_0^t \left[(a_{20})^{(3)} \left(G_{21}^0 + (\hat{P}_{20})^{(3)} e^{(\hat{M}_{20})^{(3)}s_{(20)}} \right) \right] ds_{(20)} =$$

$$\left(1 + (a_{20})^{(3)}t \right) G_{21}^0 + \frac{(a_{20})^{(3)}(\hat{P}_{20})^{(3)}}{(\hat{M}_{20})^{(3)}} \left(e^{(\hat{M}_{20})^{(3)}t} - 1 \right) .$$

From which it follows that

$$(G_{20}(t) - G_{20}^0) e^{-(\hat{M}_{20})^{(3)}t} \leq \frac{(a_{20})^{(3)}}{(\hat{M}_{20})^{(3)}} \left[\left((\hat{P}_{20})^{(3)} + G_{21}^0 \right) e^{-\frac{(\hat{P}_{20})^{(3)} + G_{21}^0}{G_{21}^0}} + (\hat{P}_{20})^{(3)} \right]$$

Analogous inequalities hold also for $G_{21}, G_{22}, T_{20}, T_{21}, T_{22}$.

(b) The operator $\mathcal{A}^{(4)}$ maps the space of functions satisfying GLOBAL EQUATIONS into itself .Indeed it is obvious that

$$G_{24}(t) \leq G_{24}^0 + \int_0^t \left[(a_{24})^{(4)} \left(G_{25}^0 + (\hat{P}_{24})^{(4)} e^{(\hat{M}_{24})^{(4)}s_{(24)}} \right) \right] ds_{(24)} =$$

$$\left(1 + (a_{24})^{(4)}t \right) G_{25}^0 + \frac{(a_{24})^{(4)}(\hat{P}_{24})^{(4)}}{(\hat{M}_{24})^{(4)}} \left(e^{(\hat{M}_{24})^{(4)}t} - 1 \right) .$$

From which it follows that

$$(G_{24}(t) - G_{24}^0) e^{-(\hat{M}_{24})^{(4)}t} \leq \frac{(a_{24})^{(4)}}{(\hat{M}_{24})^{(4)}} \left[\left((\hat{P}_{24})^{(4)} + G_{25}^0 \right) e^{-\frac{(\hat{P}_{24})^{(4)} + G_{25}^0}{G_{25}^0}} + (\hat{P}_{24})^{(4)} \right]$$

(G_i^0) is as defined in the statement of theorem 1.

(c) The operator $\mathcal{A}^{(5)}$ maps the space of functions satisfying GLOBAL EQUATIONS into itself .Indeed it is obvious that

$$G_{28}(t) \leq G_{28}^0 + \int_0^t \left[(a_{28})^{(5)} \left(G_{29}^0 + (\hat{P}_{28})^{(5)} e^{(\hat{M}_{28})^{(5)}s_{(28)}} \right) \right] ds_{(28)} =$$

$$\left(1 + (a_{28})^{(5)}t \right) G_{29}^0 + \frac{(a_{28})^{(5)}(\hat{P}_{28})^{(5)}}{(\hat{M}_{28})^{(5)}} \left(e^{(\hat{M}_{28})^{(5)}t} - 1 \right) .$$

From which it follows that

$$(G_{28}(t) - G_{28}^0) e^{-(\hat{M}_{28})^{(5)}t} \leq \frac{(a_{28})^{(5)}}{(\hat{M}_{28})^{(5)}} \left[\left((\hat{P}_{28})^{(5)} + G_{29}^0 \right) e^{-\frac{(\hat{P}_{28})^{(5)} + G_{29}^0}{G_{29}^0}} + (\hat{P}_{28})^{(5)} \right]$$

(G_i^0) is as defined in the statement of theorem 1.

(d) The operator $\mathcal{A}^{(6)}$ maps the space of functions satisfying GLOBAL EQUATIONS into itself .Indeed it is obvious that

$$G_{32}(t) \leq G_{32}^0 + \int_0^t \left[(a_{32})^{(6)} \left(G_{33}^0 + (\hat{P}_{32})^{(6)} e^{(\mathcal{M}_{32})^{(6)} s_{(32)}} \right) \right] ds_{(32)} =$$

$$\left(1 + (a_{32})^{(6)} t \right) G_{33}^0 + \frac{(a_{32})^{(6)} (\hat{P}_{32})^{(6)}}{(\mathcal{M}_{32})^{(6)}} \left(e^{(\mathcal{M}_{32})^{(6)} t} - 1 \right).$$

From which it follows that

$$(G_{32}(t) - G_{32}^0) e^{-(\mathcal{M}_{32})^{(6)} t} \leq \frac{(a_{32})^{(6)}}{(\mathcal{M}_{32})^{(6)}} \left[\left((\hat{P}_{32})^{(6)} + G_{33}^0 \right) e^{-\frac{(\hat{P}_{32})^{(6)} + G_{33}^0}{G_{33}^0}} + (\hat{P}_{32})^{(6)} \right]$$

(G_i^0) is as defined in the statement of theorem 6

Analogous inequalities hold also for $G_{25}, G_{26}, T_{24}, T_{25}, T_{26}$.

It is now sufficient to take $\frac{(a_i)^{(1)}}{(\mathcal{M}_{13})^{(1)}}, \frac{(b_i)^{(1)}}{(\mathcal{M}_{13})^{(1)}} < 1$ and to choose

$(\hat{P}_{13})^{(1)}$ and $(\hat{Q}_{13})^{(1)}$ large to have.

$$\frac{(a_i)^{(1)}}{(\mathcal{M}_{13})^{(1)}} \left[(\hat{P}_{13})^{(1)} + \left((\hat{P}_{13})^{(1)} + G_j^0 \right) e^{-\frac{(\hat{P}_{13})^{(1)} + G_j^0}{G_j^0}} \right] \leq (\hat{P}_{13})^{(1)}.$$

$$\frac{(b_i)^{(1)}}{(\mathcal{M}_{13})^{(1)}} \left[\left((\hat{Q}_{13})^{(1)} + T_j^0 \right) e^{-\frac{(\hat{Q}_{13})^{(1)} + T_j^0}{T_j^0}} + (\hat{Q}_{13})^{(1)} \right] \leq (\hat{Q}_{13})^{(1)}.$$

In order that the operator $\mathcal{A}^{(1)}$ transforms the space of sextuples of functions G_i, T_i satisfying GLOBAL EQUATIONS into itself.

The operator $\mathcal{A}^{(1)}$ is a contraction with respect to the metric

$$d \left((G^{(1)}, T^{(1)}), (G^{(2)}, T^{(2)}) \right) =$$

$$\sup_i \left\{ \max_{t \in \mathbb{R}_+} |G_i^{(1)}(t) - G_i^{(2)}(t)| e^{-(\mathcal{M}_{13})^{(1)} t}, \max_{t \in \mathbb{R}_+} |T_i^{(1)}(t) - T_i^{(2)}(t)| e^{-(\mathcal{M}_{13})^{(1)} t} \right\}.$$

Indeed if we denote

Definition of \tilde{G}, \tilde{T} :

$$(\tilde{G}, \tilde{T}) = \mathcal{A}^{(1)}(G, T)$$

It results

$$|\tilde{G}_{13}^{(1)} - \tilde{G}_i^{(2)}| \leq \int_0^t (a_{13})^{(1)} |G_{14}^{(1)} - G_{14}^{(2)}| e^{-(\mathcal{M}_{13})^{(1)} s_{(13)}} e^{(\mathcal{M}_{13})^{(1)} s_{(13)}} ds_{(13)} +$$

$$\int_0^t \left\{ (a'_{13})^{(1)} |G_{13}^{(1)} - G_{13}^{(2)}| e^{-(\mathcal{M}_{13})^{(1)} s_{(13)}} e^{-(\mathcal{M}_{13})^{(1)} s_{(13)}} + \right.$$

$$(a''_{13})^{(1)} (T_{14}^{(1)}, s_{(13)}) |G_{13}^{(1)} - G_{13}^{(2)}| e^{-(\mathcal{M}_{13})^{(1)} s_{(13)}} e^{(\mathcal{M}_{13})^{(1)} s_{(13)}} +$$

$$\left. G_{13}^{(2)} |(a'_{13})^{(1)} (T_{14}^{(1)}, s_{(13)}) - (a'_{13})^{(1)} (T_{14}^{(2)}, s_{(13)})| e^{-(\mathcal{M}_{13})^{(1)} s_{(13)}} e^{(\mathcal{M}_{13})^{(1)} s_{(13)}} \right\} ds_{(13)}$$

Where $s_{(13)}$ represents integrand that is integrated over the interval $[0, t]$

From the hypotheses it follows.

$$|G^{(1)} - G^{(2)}| e^{-(\mathcal{M}_{13})^{(1)} t} \leq \frac{1}{(\mathcal{M}_{13})^{(1)}} \left((a_{13})^{(1)} + (a'_{13})^{(1)} + (\hat{A}_{13})^{(1)} + (\hat{P}_{13})^{(1)} (\hat{k}_{13})^{(1)} \right) d \left((G^{(1)}, T^{(1)}); (G^{(2)}, T^{(2)}) \right)$$

And analogous inequalities for G_i and T_i . Taking into account the hypothesis the result follows.

Remark 1: The fact that we supposed $(a'_{13})^{(1)}$ and $(b'_{13})^{(1)}$ depending also on t can be considered as not conformal with the reality, however we have put this hypothesis in order that we can postulate condition necessary to prove the uniqueness of the solution bounded by $(\hat{P}_{13})^{(1)} e^{(\mathcal{M}_{13})^{(1)} t}$ and $(\hat{Q}_{13})^{(1)} e^{(\mathcal{M}_{13})^{(1)} t}$ respectively of \mathbb{R}_+ .

If instead of proving the existence of the solution on \mathbb{R}_+ , we have to prove it only on a compact then it suffices to consider that $(a''_i)^{(1)}$ and $(b''_i)^{(1)}, i = 13, 14, 15$ depend only on T_{14} and respectively on G (and not on t) and hypothesis can be replaced by a usual Lipschitz condition..

Remark 2: There does not exist any t where $G_i(t) = 0$ and $T_i(t) = 0$

From 19 to 24 it results

$$G_i(t) \geq G_i^0 e^{-\int_0^t \left\{ (a'_i)^{(1)} - (a''_i)^{(1)} (T_{14}(s_{(13)}), s_{(13)}) \right\} ds_{(13)}} \geq 0$$

$$T_i(t) \geq T_i^0 e^{-(b'_i)^{(1)} t} > 0 \text{ for } t > 0.$$

Definition of $(\widehat{\mathcal{M}}_{13})^{(1)}_1, (\widehat{\mathcal{M}}_{13})^{(1)}_2$ and $(\widehat{\mathcal{M}}_{13})^{(1)}_3$:

Remark 3: if G_{13} is bounded, the same property have also G_{14} and G_{15} . indeed if

$$G_{13} < (\widehat{\mathcal{M}}_{13})^{(1)} \text{ it follows } \frac{dG_{14}}{dt} \leq ((\widehat{\mathcal{M}}_{13})^{(1)})_1 - (a'_{14})^{(1)} G_{14} \text{ and by integrating}$$

$$G_{14} \leq ((\widehat{\mathcal{M}}_{13})^{(1)})_2 = G_{14}^0 + 2(a_{14})^{(1)} ((\widehat{\mathcal{M}}_{13})^{(1)})_1 / (a'_{14})^{(1)}$$

In the same way, one can obtain

$$G_{15} \leq ((\widehat{\mathcal{M}}_{13})^{(1)})_3 = G_{15}^0 + 2(a_{15})^{(1)} ((\widehat{\mathcal{M}}_{13})^{(1)})_2 / (a'_{15})^{(1)}$$

If G_{14} or G_{15} is bounded, the same property follows for G_{13}, G_{15} and G_{13}, G_{14} respectively..

Remark 4: If G_{13} is bounded, from below, the same property holds for G_{14} and G_{15} . The proof is analogous with the preceding one. An analogous property is true if G_{14} is bounded from below..

Remark 5: If T_{13} is bounded from below and $\lim_{t \rightarrow \infty} ((b_i'')^{(1)}(G(t), t)) = (b_{14}')^{(1)}$ then $T_{14} \rightarrow \infty$.

Definition of $(m)^{(1)}$ and ε_1 :

Indeed let t_1 be so that for $t > t_1$

$$(b_{14})^{(1)} - (b_i'')^{(1)}(G(t), t) < \varepsilon_1, T_{13}(t) > (m)^{(1)}.$$

Then $\frac{dT_{14}}{dt} \geq (a_{14})^{(1)}(m)^{(1)} - \varepsilon_1 T_{14}$ which leads to

$$T_{14} \geq \left(\frac{(a_{14})^{(1)}(m)^{(1)}}{\varepsilon_1} \right) (1 - e^{-\varepsilon_1 t}) + T_{14}^0 e^{-\varepsilon_1 t} \text{ If we take } t \text{ such that } e^{-\varepsilon_1 t} = \frac{1}{2} \text{ it results}$$

$$T_{14} \geq \left(\frac{(a_{14})^{(1)}(m)^{(1)}}{2} \right), \quad t = \log \frac{2}{\varepsilon_1} \text{ By taking now } \varepsilon_1 \text{ sufficiently small one sees that } T_{14} \text{ is unbounded. The same property}$$

holds for T_{15} if $\lim_{t \rightarrow \infty} (b_{15}'')^{(1)}(G(t), t) = (b_{15}')^{(1)}$

We now state a more precise theorem about the behaviors at infinity of the solutions .

It is now sufficient to take $\frac{(a_i)^{(2)}}{(\bar{M}_{16})^{(2)}}, \frac{(b_i)^{(2)}}{(\bar{M}_{16})^{(2)}} < 1$ and to choose

$(\hat{P}_{16})^{(2)}$ and $(\hat{Q}_{16})^{(2)}$ large to have.

$$\frac{(a_i)^{(2)}}{(\bar{M}_{16})^{(2)}} \left[(\hat{P}_{16})^{(2)} + ((\hat{P}_{16})^{(2)} + G_j^0) e^{-\left(\frac{(\hat{P}_{16})^{(2)} + G_j^0}{G_j^0} \right)} \right] \leq (\hat{P}_{16})^{(2)}.$$

$$\frac{(b_i)^{(2)}}{(\bar{M}_{16})^{(2)}} \left[((\hat{Q}_{16})^{(2)} + T_j^0) e^{-\left(\frac{(\hat{Q}_{16})^{(2)} + T_j^0}{T_j^0} \right)} + (\hat{Q}_{16})^{(2)} \right] \leq (\hat{Q}_{16})^{(2)}.$$

In order that the operator $\mathcal{A}^{(2)}$ transforms the space of sextuples of functions G_i, T_i satisfying .

The operator $\mathcal{A}^{(2)}$ is a contraction with respect to the metric

$$d \left(((G_{19})^{(1)}, (T_{19})^{(1)}), ((G_{19})^{(2)}, (T_{19})^{(2)}) \right) =$$

$$\sup_i \left\{ \max_{t \in \mathbb{R}_+} |G_i^{(1)}(t) - G_i^{(2)}(t)| e^{-(\bar{M}_{16})^{(2)}t}, \max_{t \in \mathbb{R}_+} |T_i^{(1)}(t) - T_i^{(2)}(t)| e^{-(\bar{M}_{16})^{(2)}t} \right\}.$$

Indeed if we denote

$$\text{Definition of } \widehat{G}_{19}, \widehat{T}_{19} : (\widehat{G}_{19}, \widehat{T}_{19}) = \mathcal{A}^{(2)}(G_{19}, T_{19}).$$

It results

$$\begin{aligned} |\widehat{G}_{16}^{(1)} - \widehat{G}_{16}^{(2)}| &\leq \int_0^t (a_{16})^{(2)} |G_{17}^{(1)} - G_{17}^{(2)}| e^{-(\bar{M}_{16})^{(2)}s_{(16)}} e^{(\bar{M}_{16})^{(2)}s_{(16)}} ds_{(16)} + \\ &\int_0^t \{ (a'_{16})^{(2)} |G_{16}^{(1)} - G_{16}^{(2)}| e^{-(\bar{M}_{16})^{(2)}s_{(16)}} e^{-(\bar{M}_{16})^{(2)}s_{(16)}} + \\ &(a''_{16})^{(2)}(T_{17}^{(1)}, s_{(16)}) |G_{16}^{(1)} - G_{16}^{(2)}| e^{-(\bar{M}_{16})^{(2)}s_{(16)}} e^{(\bar{M}_{16})^{(2)}s_{(16)}} + \\ &G_{16}^{(2)} | (a''_{16})^{(2)}(T_{17}^{(1)}, s_{(16)}) - (a''_{16})^{(2)}(T_{17}^{(2)}, s_{(16)}) | e^{-(\bar{M}_{16})^{(2)}s_{(16)}} e^{(\bar{M}_{16})^{(2)}s_{(16)}} \} ds_{(16)}. \end{aligned}$$

Where $s_{(16)}$ represents integrand that is integrated over the interval $[0, t]$

From the hypotheses it follows.

$$|(G_{19})^{(1)} - (G_{19})^{(2)}| e^{-(\bar{M}_{16})^{(2)}t} \leq$$

$$\frac{1}{(\bar{M}_{16})^{(2)}} \left((a_{16})^{(2)} + (a'_{16})^{(2)} + (\widehat{A}_{16})^{(2)} + (\widehat{P}_{16})^{(2)} (\widehat{K}_{16})^{(2)} \right) d \left(((G_{19})^{(1)}, (T_{19})^{(1)}), ((G_{19})^{(2)}, (T_{19})^{(2)}) \right).$$

And analogous inequalities for G_i and T_i . Taking into account the hypothesis the result follows.

Remark 1: The fact that we supposed $(a'_{16})^{(2)}$ and $(b''_{16})^{(2)}$ depending also on t can be considered as not conformal with the reality, however we have put this hypothesis ,in order that we can postulate condition necessary to prove the uniqueness of the solution bounded by $(\widehat{P}_{16})^{(2)} e^{(\bar{M}_{16})^{(2)}t}$ and $(\widehat{Q}_{16})^{(2)} e^{(\bar{M}_{16})^{(2)}t}$ respectively of \mathbb{R}_+ .

If instead of proving the existence of the solution on \mathbb{R}_+ , we have to prove it only on a compact then it suffices to consider that $(a''_i)^{(2)}$ and $(b''_i)^{(2)}, i = 16, 17, 18$ depend only on T_{17} and respectively on (G_{19}) (and not on t) and hypothesis can be replaced by a usual Lipschitz condition..

Remark 2: There does not exist any t where $G_i(t) = 0$ and $T_i(t) = 0$

From 19 to 24 it results

$$G_i(t) \geq G_i^0 e^{-\int_0^t \{ (a'_i)^{(2)} - (a''_i)^{(2)}(T_{17}(s_{(16)}), s_{(16)}) \} ds_{(16)}} \geq 0$$

$$T_i(t) \geq T_i^0 e^{-(b'_i)^{(2)}t} > 0 \text{ for } t > 0.$$

Definition of $(\widehat{M}_{16})^{(2)}_1, (\widehat{M}_{16})^{(2)}_2$ and $(\widehat{M}_{16})^{(2)}_3$:

Remark 3: if G_{16} is bounded, the same property have also G_{17} and G_{18} . indeed if

$$G_{16} < (\widehat{M}_{16})^{(2)} \text{ it follows } \frac{dG_{17}}{dt} \leq ((\widehat{M}_{16})^{(2)})_1 - (a'_{17})^{(2)} G_{17} \text{ and by integrating}$$

$$G_{17} \leq ((\widehat{M}_{16})^{(2)})_2 = G_{17}^0 + 2(a_{17})^{(2)} ((\widehat{M}_{16})^{(2)})_1 / (a'_{17})^{(2)}$$

In the same way , one can obtain

$$G_{18} \leq ((\widehat{M}_{16})^{(2)})_3 = G_{18}^0 + 2(a_{18})^{(2)} ((\widehat{M}_{16})^{(2)})_2 / (a'_{18})^{(2)}$$

If G_{17} or G_{18} is bounded, the same property follows for G_{16} , G_{18} and G_{16} , G_{17} respectively..

Remark 4: If G_{16} is bounded, from below, the same property holds for G_{17} and G_{18} . The proof is analogous with the preceding one. An analogous property is true if G_{17} is bounded from below..

Remark 5: If T_{16} is bounded from below and $\lim_{t \rightarrow \infty} ((b_i'')^{(2)}((G_{19})(t), t)) = (b_{17}')^{(2)}$ then $T_{17} \rightarrow \infty$.

Definition of $(m)^{(2)}$ and ε_2 :

Indeed let t_2 be so that for $t > t_2$

$$(b_{17})^{(2)} - (b_i'')^{(2)}((G_{19})(t), t) < \varepsilon_2, T_{16}(t) > (m)^{(2)}.$$

Then $\frac{dT_{17}}{dt} \geq (a_{17})^{(2)}(m)^{(2)} - \varepsilon_2 T_{17}$ which leads to

$$T_{17} \geq \left(\frac{(a_{17})^{(2)}(m)^{(2)}}{\varepsilon_2} \right) (1 - e^{-\varepsilon_2 t}) + T_{17}^0 e^{-\varepsilon_2 t} \text{ If we take } t \text{ such that } e^{-\varepsilon_2 t} = \frac{1}{2} \text{ it results .}$$

$$T_{17} \geq \left(\frac{(a_{17})^{(2)}(m)^{(2)}}{2} \right), \quad t = \log \frac{2}{\varepsilon_2} \text{ By taking now } \varepsilon_2 \text{ sufficiently small one sees that } T_{17} \text{ is unbounded. The same property}$$

holds for T_{18} if $\lim_{t \rightarrow \infty} ((b_{18}'')^{(2)}((G_{19})(t), t)) = (b_{18}')^{(2)}$

We now state a more precise theorem about the behaviors at infinity of the solutions .

It is now sufficient to take $\frac{(a_i)^{(3)}}{(M_{20})^{(3)}}, \frac{(b_i)^{(3)}}{(M_{20})^{(3)}} < 1$ and to choose

$(\hat{P}_{20})^{(3)}$ and $(\hat{Q}_{20})^{(3)}$ large to have.

$$\frac{(a_i)^{(3)}}{(M_{20})^{(3)}} \left[(\hat{P}_{20})^{(3)} + ((\hat{P}_{20})^{(3)} + G_j^0) e^{-\left(\frac{(\hat{P}_{20})^{(3)} + G_j^0}{G_j^0} \right)} \right] \leq (\hat{P}_{20})^{(3)}.$$

$$\frac{(b_i)^{(3)}}{(M_{20})^{(3)}} \left[((\hat{Q}_{20})^{(3)} + T_j^0) e^{-\left(\frac{(\hat{Q}_{20})^{(3)} + T_j^0}{T_j^0} \right)} + (\hat{Q}_{20})^{(3)} \right] \leq (\hat{Q}_{20})^{(3)}.$$

In order that the operator $\mathcal{A}^{(3)}$ transforms the space of sextuples of functions G_i, T_i into itself.

The operator $\mathcal{A}^{(3)}$ is a contraction with respect to the metric

$$d \left(((G_{23})^{(1)}, (T_{23})^{(1)}), ((G_{23})^{(2)}, (T_{23})^{(2)}) \right) =$$

$$\sup_i \{ \max_{t \in \mathbb{R}_+} |G_i^{(1)}(t) - G_i^{(2)}(t)| e^{-(M_{20})^{(3)}t}, \max_{t \in \mathbb{R}_+} |T_i^{(1)}(t) - T_i^{(2)}(t)| e^{-(M_{20})^{(3)}t} \}.$$

Indeed if we denote

$$\text{Definition of } \widehat{G}_{23}, \widehat{T}_{23} : ((\widehat{G}_{23}), (\widehat{T}_{23})) = \mathcal{A}^{(3)}((G_{23}), (T_{23})).$$

It results

$$\begin{aligned} |\widehat{G}_{20}^{(1)} - \widehat{G}_i^{(2)}| &\leq \int_0^t (a_{20})^{(3)} |G_{21}^{(1)} - G_{21}^{(2)}| e^{-(M_{20})^{(3)}s_{(20)}} e^{(M_{20})^{(3)}s_{(20)}} ds_{(20)} + \\ &\int_0^t \{ (a_{20}')^{(3)} |G_{20}^{(1)} - G_{20}^{(2)}| e^{-(M_{20})^{(3)}s_{(20)}} e^{-(M_{20})^{(3)}s_{(20)}} + \\ &(a_{20}'')^{(3)} (T_{21}^{(1)}, s_{(20)}) |G_{20}^{(1)} - G_{20}^{(2)}| e^{-(M_{20})^{(3)}s_{(20)}} e^{(M_{20})^{(3)}s_{(20)}} + \\ &G_{20}^{(2)} | (a_{20}'')^{(3)} (T_{21}^{(1)}, s_{(20)}) - (a_{20}'')^{(3)} (T_{21}^{(2)}, s_{(20)}) | e^{-(M_{20})^{(3)}s_{(20)}} e^{(M_{20})^{(3)}s_{(20)}} \} ds_{(20)} \end{aligned}$$

Where $s_{(20)}$ represents integrand that is integrated over the interval $[0, t]$

From the hypotheses it follows.

$$|G^{(1)} - G^{(2)}| e^{-(M_{20})^{(3)}t} \leq$$

$$\frac{1}{(M_{20})^{(3)}} ((a_{20})^{(3)} + (a_{20}')^{(3)} + (\widehat{A}_{20})^{(3)} + (\widehat{P}_{20})^{(3)} (\widehat{k}_{20})^{(3)}) d \left(((G_{23})^{(1)}, (T_{23})^{(1)}); (G_{23})^{(2)}, (T_{23})^{(2)}) \right)$$

And analogous inequalities for G_i and T_i . Taking into account the hypothesis the result follows.

Remark 1: The fact that we supposed $(a_{20}'')^{(3)}$ and $(b_{20}'')^{(3)}$ depending also on t can be considered as not conformal with the reality, however we have put this hypothesis ,in order that we can postulate condition necessary to prove the uniqueness of the solution bounded by $(\widehat{P}_{20})^{(3)} e^{(M_{20})^{(3)}t}$ and $(\widehat{Q}_{20})^{(3)} e^{(M_{20})^{(3)}t}$ respectively of \mathbb{R}_+ .

If instead of proving the existence of the solution on \mathbb{R}_+ , we have to prove it only on a compact then it suffices to consider that $(a_i'')^{(3)}$ and $(b_i'')^{(3)}, i = 20, 21, 22$ depend only on T_{21} and respectively on (G_{23}) (and not on t) and hypothesis can be replaced by a usual Lipschitz condition..

Remark 2: There does not exist any t where $G_i(t) = 0$ and $T_i(t) = 0$

From 19 to 24 it results

$$G_i(t) \geq G_i^0 e^{-\int_0^t \{ (a_i')^{(3)} - (a_i'')^{(3)} (T_{21}(s_{(20)}), s_{(20)}) \} ds_{(20)}} \geq 0$$

$$T_i(t) \geq T_i^0 e^{-(b_i')^{(3)}t} > 0 \text{ for } t > 0.$$

Definition of $((\widehat{M}_{20})^{(3)})_1, ((\widehat{M}_{20})^{(3)})_2$ and $((\widehat{M}_{20})^{(3)})_3$:

Remark 3: if G_{20} is bounded, the same property have also G_{21} and G_{22} . indeed if

$$G_{20} < (\widehat{M}_{20})^{(3)} \text{ it follows } \frac{dG_{21}}{dt} \leq ((\widehat{M}_{20})^{(3)})_1 - (a_{21}')^{(3)} G_{21} \text{ and by integrating}$$

$$G_{21} \leq ((\widehat{M}_{20})^{(3)})_2 = G_{21}^0 + 2(a_{21})^{(3)} ((\widehat{M}_{20})^{(3)})_1 / (a_{21}')^{(3)}$$

In the same way , one can obtain

$$G_{22} \leq ((\widehat{M}_{20})^{(3)})_3 = G_{22}^0 + 2(a_{22})^{(3)}((\widehat{M}_{20})^{(3)})_2 / (a'_{22})^{(3)}$$

If G_{21} or G_{22} is bounded, the same property follows for G_{20} , G_{22} and G_{20} , G_{21} respectively..

Remark 4: If G_{20} is bounded, from below, the same property holds for G_{21} and G_{22} . The proof is analogous with the preceding one. An analogous property is true if G_{21} is bounded from below..

Remark 5: If T_{20} is bounded from below and $\lim_{t \rightarrow \infty} ((b''_i)^{(3)}((G_{23})(t), t)) = (b'_{21})^{(3)}$ then $T_{21} \rightarrow \infty$.

Definition of $(m)^{(3)}$ and ε_3 :

Indeed let t_3 be so that for $t > t_3$

$$(b_{21})^{(3)} - (b''_i)^{(3)}((G_{23})(t), t) < \varepsilon_3, T_{20}(t) > (m)^{(3)}.$$

Then $\frac{dT_{21}}{dt} \geq (a_{21})^{(3)}(m)^{(3)} - \varepsilon_3 T_{21}$ which leads to

$$T_{21} \geq \left(\frac{(a_{21})^{(3)}(m)^{(3)}}{\varepsilon_3} \right) (1 - e^{-\varepsilon_3 t}) + T_{21}^0 e^{-\varepsilon_3 t} \text{ If we take } t \text{ such that } e^{-\varepsilon_3 t} = \frac{1}{2} \text{ it results}$$

$$T_{21} \geq \left(\frac{(a_{21})^{(3)}(m)^{(3)}}{2} \right), t = \log \frac{2}{\varepsilon_3} \text{ By taking now } \varepsilon_3 \text{ sufficiently small one sees that } T_{21} \text{ is unbounded. The same property}$$

holds for T_{22} if $\lim_{t \rightarrow \infty} (b''_{22})^{(3)}((G_{23})(t), t) = (b'_{22})^{(3)}$

We now state a more precise theorem about the behaviors at infinity of the solutions .

It is now sufficient to take $\frac{(a_i)^{(4)}}{(\widehat{M}_{24})^{(4)}} , \frac{(b_i)^{(4)}}{(\widehat{M}_{24})^{(4)}} < 1$ and to choose

$(\widehat{P}_{24})^{(4)}$ and $(\widehat{Q}_{24})^{(4)}$ large to have.

$$\frac{(a_i)^{(4)}}{(\widehat{M}_{24})^{(4)}} \left[(\widehat{P}_{24})^{(4)} + ((\widehat{P}_{24})^{(4)} + G_j^0) e^{-\left(\frac{(\widehat{P}_{24})^{(4)} + G_j^0}{G_j^0} \right)} \right] \leq (\widehat{P}_{24})^{(4)}.$$

$$\frac{(b_i)^{(4)}}{(\widehat{M}_{24})^{(4)}} \left[((\widehat{Q}_{24})^{(4)} + T_j^0) e^{-\left(\frac{(\widehat{Q}_{24})^{(4)} + T_j^0}{T_j^0} \right)} + (\widehat{Q}_{24})^{(4)} \right] \leq (\widehat{Q}_{24})^{(4)}.$$

In order that the operator $\mathcal{A}^{(4)}$ transforms the space of sextuples of functions G_i, T_i satisfying IN to itself.

The operator $\mathcal{A}^{(4)}$ is a contraction with respect to the metric

$$d((G_{27})^{(1)}, (T_{27})^{(1)}, (G_{27})^{(2)}, (T_{27})^{(2)}) =$$

$$\sup_i \{ \max_{t \in \mathbb{R}_+} |G_i^{(1)}(t) - G_i^{(2)}(t)| e^{-(\widehat{M}_{24})^{(4)}t}, \max_{t \in \mathbb{R}_+} |T_i^{(1)}(t) - T_i^{(2)}(t)| e^{-(\widehat{M}_{24})^{(4)}t} \}$$

Indeed if we denote

$$\text{Definition of } (\widehat{G}_{27}), (\widehat{T}_{27}) : ((\widehat{G}_{27}), (\widehat{T}_{27})) = \mathcal{A}^{(4)}((G_{27}), (T_{27}))$$

It results

$$\begin{aligned} |\widehat{G}_{24}^{(1)} - \widehat{G}_i^{(2)}| &\leq \int_0^t (a_{24})^{(4)} |G_{25}^{(1)} - G_{25}^{(2)}| e^{-(\widehat{M}_{24})^{(4)}s_{(24)}} e^{(\widehat{M}_{24})^{(4)}s_{(24)}} ds_{(24)} + \\ &\int_0^t \{ (a'_{24})^{(4)} |G_{24}^{(1)} - G_{24}^{(2)}| e^{-(\widehat{M}_{24})^{(4)}s_{(24)}} e^{-(\widehat{M}_{24})^{(4)}s_{(24)}} + \\ &(a''_{24})^{(4)} (T_{25}^{(1)}, s_{(24)}) |G_{24}^{(1)} - G_{24}^{(2)}| e^{-(\widehat{M}_{24})^{(4)}s_{(24)}} e^{(\widehat{M}_{24})^{(4)}s_{(24)}} + \\ &G_{24}^{(2)} |(a''_{24})^{(4)} (T_{25}^{(1)}, s_{(24)}) - (a''_{24})^{(4)} (T_{25}^{(2)}, s_{(24)})| e^{-(\widehat{M}_{24})^{(4)}s_{(24)}} e^{(\widehat{M}_{24})^{(4)}s_{(24)}} \} ds_{(24)} \end{aligned}$$

Where $s_{(24)}$ represents integrand that is integrated over the interval $[0, t]$

From the hypotheses it follows.

$$|(G_{27})^{(1)} - (G_{27})^{(2)}| e^{-(\widehat{M}_{24})^{(4)}t} \leq$$

$$\frac{1}{(\widehat{M}_{24})^{(4)}} ((a_{24})^{(4)} + (a'_{24})^{(4)} + (\widehat{A}_{24})^{(4)} + (\widehat{P}_{24})^{(4)} (\widehat{k}_{24})^{(4)}) d(((G_{27})^{(1)}, (T_{27})^{(1)}); (G_{27})^{(2)}, (T_{27})^{(2)})$$

And analogous inequalities for G_i and T_i . Taking into account the hypothesis the result follows.

Remark 1: The fact that we supposed $(a''_{24})^{(4)}$ and $(b''_{24})^{(4)}$ depending also on t can be considered as not conformal with the reality, however we have put this hypothesis ,in order that we can postulate condition necessary to prove the uniqueness of the solution bounded by $(\widehat{P}_{24})^{(4)} e^{(\widehat{M}_{24})^{(4)}t}$ and $(\widehat{Q}_{24})^{(4)} e^{(\widehat{M}_{24})^{(4)}t}$ respectively of \mathbb{R}_+ .

If instead of proving the existence of the solution on \mathbb{R}_+ , we have to prove it only on a compact then it suffices to consider that $(a''_i)^{(4)}$ and $(b''_i)^{(4)}$, $i = 24, 25, 26$ depend only on T_{25} and respectively on (G_{27}) (and not on t) and hypothesis can be replaced by a usual Lipschitz condition..

Remark 2: There does not exist any t where $G_i(t) = 0$ and $T_i(t) = 0$

From 19 to 24 it results

$$G_i(t) \geq G_i^0 e^{-\int_0^t \{ (a'_i)^{(4)} - (a''_i)^{(4)} (T_{25}(s_{(24)}), s_{(24)}) \} ds_{(24)}} \geq 0$$

$$T_i(t) \geq T_i^0 e^{-(b'_i)^{(4)}t} > 0 \text{ for } t > 0.$$

Definition of $((\widehat{M}_{24})^{(4)})_1, ((\widehat{M}_{24})^{(4)})_2$ and $((\widehat{M}_{24})^{(4)})_3$:

Remark 3: if G_{24} is bounded, the same property have also G_{25} and G_{26} . indeed if

$G_{24} < (\widehat{M}_{24})^{(4)}$ it follows $\frac{dG_{25}}{dt} \leq ((\widehat{M}_{24})^{(4)})_1 - (a'_{25})^{(4)}G_{25}$ and by integrating
 $G_{25} \leq ((\widehat{M}_{24})^{(4)})_2 = G_{25}^0 + 2(a_{25})^{(4)}((\widehat{M}_{24})^{(4)})_1 / (a'_{25})^{(4)}$

In the same way, one can obtain

$$G_{26} \leq ((\widehat{M}_{24})^{(4)})_3 = G_{26}^0 + 2(a_{26})^{(4)}((\widehat{M}_{24})^{(4)})_2 / (a'_{26})^{(4)}$$

If G_{25} or G_{26} is bounded, the same property follows for G_{24} , G_{26} and G_{24} , G_{25} respectively..

Remark 4: If G_{24} is bounded, from below, the same property holds for G_{25} and G_{26} . The proof is analogous with the preceding one. An analogous property is true if G_{25} is bounded from below..

Remark 5: If T_{24} is bounded from below and $\lim_{t \rightarrow \infty} ((b''_i)^{(4)}((G_{27})(t), t)) = (b'_{25})^{(4)}$ then $T_{25} \rightarrow \infty$.

Definition of $(m)^{(4)}$ and ε_4 :

Indeed let t_4 be so that for $t > t_4$

$$(b_{25})^{(4)} - (b''_i)^{(4)}((G_{27})(t), t) < \varepsilon_4, T_{24}(t) > (m)^{(4)} :$$

Then $\frac{dT_{25}}{dt} \geq (a_{25})^{(4)}(m)^{(4)} - \varepsilon_4 T_{25}$ which leads to

$$T_{25} \geq \left(\frac{(a_{25})^{(4)}(m)^{(4)}}{\varepsilon_4} \right) (1 - e^{-\varepsilon_4 t}) + T_{25}^0 e^{-\varepsilon_4 t} \text{ If we take } t \text{ such that } e^{-\varepsilon_4 t} = \frac{1}{2} \text{ it results}$$

$T_{25} \geq \left(\frac{(a_{25})^{(4)}(m)^{(4)}}{2} \right)$, $t = \log \frac{2}{\varepsilon_4}$ By taking now ε_4 sufficiently small one sees that T_{25} is unbounded. The same property holds for T_{26} if $\lim_{t \rightarrow \infty} (b''_{26})^{(4)}((G_{27})(t), t) = (b'_{26})^{(4)}$

We now state a more precise theorem about the behaviors at infinity of the solutions ANALOGOUS inequalities hold also for $G_{29}, G_{30}, T_{28}, T_{29}, T_{30}$:

It is now sufficient to take $\frac{(a_i)^{(5)}}{(\widehat{M}_{28})^{(5)}}, \frac{(b_i)^{(5)}}{(\widehat{M}_{28})^{(5)}} < 1$ and to choose $(\widehat{P}_{28})^{(5)}$ and $(\widehat{Q}_{28})^{(5)}$ large to have

$$\frac{(a_i)^{(5)}}{(\widehat{M}_{28})^{(5)}} \left[(\widehat{P}_{28})^{(5)} + ((\widehat{P}_{28})^{(5)} + G_j^0) e^{-\left(\frac{(\widehat{P}_{28})^{(5)} + G_j^0}{G_j^0} \right)} \right] \leq (\widehat{P}_{28})^{(5)} .$$

$$\frac{(b_i)^{(5)}}{(\widehat{M}_{28})^{(5)}} \left[((\widehat{Q}_{28})^{(5)} + T_j^0) e^{-\left(\frac{(\widehat{Q}_{28})^{(5)} + T_j^0}{T_j^0} \right)} + (\widehat{Q}_{28})^{(5)} \right] \leq (\widehat{Q}_{28})^{(5)} .$$

In order that the operator $\mathcal{A}^{(5)}$ transforms the space of sextuples of functions G_i, T_i into itself.

The operator $\mathcal{A}^{(5)}$ is a contraction with respect to the metric

$$d \left(((G_{31})^{(1)}, (T_{31})^{(1)}), ((G_{31})^{(2)}, (T_{31})^{(2)}) \right) = \sup_i \left\{ \max_{t \in \mathbb{R}_+} |G_i^{(1)}(t) - G_i^{(2)}(t)| e^{-(\widehat{M}_{28})^{(5)}t}, \max_{t \in \mathbb{R}_+} |T_i^{(1)}(t) - T_i^{(2)}(t)| e^{-(\widehat{M}_{28})^{(5)}t} \right\}$$

Indeed if we denote

$$\text{Definition of } (\widehat{G}_{31}), (\widehat{T}_{31}) : ((\widehat{G}_{31}), (\widehat{T}_{31})) = \mathcal{A}^{(5)}((G_{31}), (T_{31}))$$

It results

$$\begin{aligned} |\widehat{G}_{28}^{(1)} - \widehat{G}_i^{(2)}| &\leq \int_0^t (a_{28})^{(5)} |G_{29}^{(1)} - G_{29}^{(2)}| e^{-(\widehat{M}_{28})^{(5)}s_{(28)}} e^{(\widehat{M}_{28})^{(5)}s_{(28)}} ds_{(28)} + \\ &\int_0^t \{ (a'_{28})^{(5)} |G_{28}^{(1)} - G_{28}^{(2)}| e^{-(\widehat{M}_{28})^{(5)}s_{(28)}} e^{-(\widehat{M}_{28})^{(5)}s_{(28)}} + \\ &(a''_{28})^{(5)} (T_{29}^{(1)}, s_{(28)}) |G_{28}^{(1)} - G_{28}^{(2)}| e^{-(\widehat{M}_{28})^{(5)}s_{(28)}} e^{(\widehat{M}_{28})^{(5)}s_{(28)}} + \\ &G_{28}^{(2)} | (a''_{28})^{(5)} (T_{29}^{(1)}, s_{(28)}) - (a''_{28})^{(5)} (T_{29}^{(2)}, s_{(28)}) | e^{-(\widehat{M}_{28})^{(5)}s_{(28)}} e^{(\widehat{M}_{28})^{(5)}s_{(28)}} \} ds_{(28)} \end{aligned}$$

Where $s_{(28)}$ represents integrand that is integrated over the interval $[0, t]$

From the hypotheses it follows.

$$\begin{aligned} |(G_{31})^{(1)} - (G_{31})^{(2)}| e^{-(\widehat{M}_{28})^{(5)}t} &\leq \\ \frac{1}{(\widehat{M}_{28})^{(5)}} & \left((a_{28})^{(5)} + (a'_{28})^{(5)} + (\widehat{A}_{28})^{(5)} + (\widehat{P}_{28})^{(5)} (\widehat{k}_{28})^{(5)} \right) d \left(((G_{31})^{(1)}, (T_{31})^{(1)}); (G_{31})^{(2)}, (T_{31})^{(2)} \right) \end{aligned}$$

And analogous inequalities for G_i and T_i . Taking into account the hypothesis (35,35,36) the result follows.

Remark 1: The fact that we supposed $(a''_{28})^{(5)}$ and $(b''_{28})^{(5)}$ depending also on t can be considered as not conformal with the reality, however we have put this hypothesis, in order that we can postulate condition necessary to prove the uniqueness of the solution bounded by $(\widehat{P}_{28})^{(5)} e^{(\widehat{M}_{28})^{(5)}t}$ and $(\widehat{Q}_{28})^{(5)} e^{(\widehat{M}_{28})^{(5)}t}$ respectively of \mathbb{R}_+ .

If instead of proving the existence of the solution on \mathbb{R}_+ , we have to prove it only on a compact then it suffices to consider that $(a''_i)^{(5)}$ and $(b''_i)^{(5)}$, $i = 28, 29, 30$ depend only on T_{29} and respectively on (G_{31}) (and not on t) and hypothesis can be replaced by a usual Lipschitz condition..

Remark 2: There does not exist any t where $G_i(t) = 0$ and $T_i(t) = 0$

From GLOBAL EQUATIONS it results

$$G_i(t) \geq G_i^0 e^{-\int_0^t \{(a_i')^{(5)} - (a_i'')^{(5)}\} (T_{29}(s_{(28)}), s_{(28)}) ds_{(28)}} \geq 0$$

$$T_i(t) \geq T_i^0 e^{-(b_i')^{(5)}t} > 0 \quad \text{for } t > 0.$$

Definition of $((\widehat{M}_{28})^{(5)})_1, ((\widehat{M}_{28})^{(5)})_2$ and $((\widehat{M}_{28})^{(5)})_3$:

Remark 3: if G_{28} is bounded, the same property have also G_{29} and G_{30} . indeed if

$G_{28} < ((\widehat{M}_{28})^{(5)})$ it follows $\frac{dG_{29}}{dt} \leq ((\widehat{M}_{28})^{(5)})_1 - (a_{29}')^{(5)}G_{29}$ and by integrating

$$G_{29} \leq ((\widehat{M}_{28})^{(5)})_2 = G_{29}^0 + 2(a_{29}')^{(5)}((\widehat{M}_{28})^{(5)})_1 / (a_{29}')^{(5)}$$

In the same way , one can obtain

$$G_{30} \leq ((\widehat{M}_{28})^{(5)})_3 = G_{30}^0 + 2(a_{30}')^{(5)}((\widehat{M}_{28})^{(5)})_2 / (a_{30}')^{(5)}$$

If G_{29} or G_{30} is bounded, the same property follows for G_{28} , G_{30} and G_{28} , G_{29} respectively..

Remark 4: If G_{28} is bounded, from below, the same property holds for G_{29} and G_{30} . The proof is analogous with the preceding one. An analogous property is true if G_{29} is bounded from below..

Remark 5: If T_{28} is bounded from below and $\lim_{t \rightarrow \infty} ((b_i'')^{(5)}((G_{31})(t), t)) = (b_{29}')^{(5)}$ then $T_{29} \rightarrow \infty$.

Definition of $(m)^{(5)}$ and ε_5 :

Indeed let t_5 be so that for $t > t_5$

$$(b_{29}')^{(5)} - (b_i'')^{(5)}((G_{31})(t), t) < \varepsilon_5, T_{28}(t) > (m)^{(5)}:$$

Then $\frac{dT_{29}}{dt} \geq (a_{29}')^{(5)}(m)^{(5)} - \varepsilon_5 T_{29}$ which leads to

$$T_{29} \geq \left(\frac{(a_{29}')^{(5)}(m)^{(5)}}{\varepsilon_5} \right) (1 - e^{-\varepsilon_5 t}) + T_{29}^0 e^{-\varepsilon_5 t} \quad \text{If we take } t \text{ such that } e^{-\varepsilon_5 t} = \frac{1}{2} \text{ it results}$$

$$T_{29} \geq \left(\frac{(a_{29}')^{(5)}(m)^{(5)}}{2} \right), \quad t = \log \frac{2}{\varepsilon_5} \quad \text{By taking now } \varepsilon_5 \text{ sufficiently small one sees that } T_{29} \text{ is unbounded. The same property}$$

holds for T_{30} if $\lim_{t \rightarrow \infty} (b_{30}'')^{(5)}((G_{31})(t), t) = (b_{30}')^{(5)}$

We now state a more precise theorem about the behaviors at infinity of the solutions

Analogous inequalities hold also for $G_{33}, G_{34}, T_{32}, T_{33}, T_{34}$:

It is now sufficient to take $\frac{(a_i)^{(6)}}{(\widehat{M}_{32})^{(6)}}, \frac{(b_i)^{(6)}}{(\widehat{M}_{32})^{(6)}} < 1$ and to choose

$(\widehat{P}_{32})^{(6)}$ and $(\widehat{Q}_{32})^{(6)}$ large to have.

$$\frac{(a_i)^{(6)}}{(\widehat{M}_{32})^{(6)}} \left[(\widehat{P}_{32})^{(6)} + ((\widehat{P}_{32})^{(6)} + G_j^0) e^{-\left(\frac{(\widehat{P}_{32})^{(6)} + G_j^0}{G_j^0} \right)} \right] \leq (\widehat{P}_{32})^{(6)} .$$

$$\frac{(b_i)^{(6)}}{(\widehat{M}_{32})^{(6)}} \left[((\widehat{Q}_{32})^{(6)} + T_j^0) e^{-\left(\frac{(\widehat{Q}_{32})^{(6)} + T_j^0}{T_j^0} \right)} + (\widehat{Q}_{32})^{(6)} \right] \leq (\widehat{Q}_{32})^{(6)} .$$

In order that the operator $\mathcal{A}^{(6)}$ transforms the space of sextuples of functions G_i, T_i into itself.

The operator $\mathcal{A}^{(6)}$ is a contraction with respect to the metric

$$d \left(((G_{35})^{(1)}, (T_{35})^{(1)}), ((G_{35})^{(2)}, (T_{35})^{(2)}) \right) =$$

$$\sup_i \left\{ \max_{t \in \mathbb{R}_+} |G_i^{(1)}(t) - G_i^{(2)}(t)| e^{-(\widehat{M}_{32})^{(6)}t}, \max_{t \in \mathbb{R}_+} |T_i^{(1)}(t) - T_i^{(2)}(t)| e^{-(\widehat{M}_{32})^{(6)}t} \right\}$$

Indeed if we denote

$$\text{Definition of } (\widehat{G}_{35}), (\widehat{T}_{35}) : ((\widehat{G}_{35}), (\widehat{T}_{35})) = \mathcal{A}^{(6)}((G_{35}), (T_{35}))$$

It results

$$\begin{aligned} |\widehat{G}_{32}^{(1)} - \widehat{G}_{32}^{(2)}| &\leq \int_0^t (a_{32})^{(6)} |G_{33}^{(1)} - G_{33}^{(2)}| e^{-(\widehat{M}_{32})^{(6)}s_{(32)}} e^{(\widehat{M}_{32})^{(6)}s_{(32)}} ds_{(32)} + \\ &\int_0^t \{(a_{32}')^{(6)} |G_{32}^{(1)} - G_{32}^{(2)}| e^{-(\widehat{M}_{32})^{(6)}s_{(32)}} e^{-(\widehat{M}_{32})^{(6)}s_{(32)}} + \\ &(a_{32}'')^{(6)}(T_{33}^{(1)}, s_{(32)}) |G_{32}^{(1)} - G_{32}^{(2)}| e^{-(\widehat{M}_{32})^{(6)}s_{(32)}} e^{(\widehat{M}_{32})^{(6)}s_{(32)}} + \\ &G_{32}^{(2)} |(a_{32}')^{(6)}(T_{33}^{(1)}, s_{(32)}) - (a_{32}')^{(6)}(T_{33}^{(2)}, s_{(32)})| e^{-(\widehat{M}_{32})^{(6)}s_{(32)}} e^{(\widehat{M}_{32})^{(6)}s_{(32)}}\} ds_{(32)} \end{aligned}$$

Where $s_{(32)}$ represents integrand that is integrated over the interval $[0, t]$

From the hypotheses it follows.

$$|(G_{35})^{(1)} - (G_{35})^{(2)}| e^{-(\widehat{M}_{32})^{(6)}t} \leq$$

$$\frac{1}{(\widehat{M}_{32})^{(6)}} ((a_{32})^{(6)} + (a_{32}')^{(6)} + (\widehat{A}_{32})^{(6)} + (\widehat{P}_{32})^{(6)} (\widehat{k}_{32})^{(6)}) d \left(((G_{35})^{(1)}, (T_{35})^{(1)}); (G_{35})^{(2)}, (T_{35})^{(2)} \right)$$

And analogous inequalities for G_i and T_i . Taking into account the hypothesis the result follows.

Remark 1: The fact that we supposed $(a_{32}'')^{(6)}$ and $(b_{32}'')^{(6)}$ depending also on t can be considered as not conformal with the reality, however we have put this hypothesis ,in order that we can postulate condition necessary to prove the uniqueness of the solution bounded by $(\widehat{P}_{32})^{(6)} e^{(\widehat{M}_{32})^{(6)}t}$ and $(\widehat{Q}_{32})^{(6)} e^{(\widehat{M}_{32})^{(6)}t}$ respectively of \mathbb{R}_+ .

If instead of proving the existence of the solution on \mathbb{R}_+ , we have to prove it only on a compact then it suffices to consider that $(a_i'')^{(6)}$ and $(b_i'')^{(6)}$, $i = 32, 33, 34$ depend only on T_{33} and respectively on $(G_{35})(t, t)$ (and not on t) and hypothesis can be replaced by a usual Lipschitz condition..

Remark 2: There does not exist any t where $G_i(t) = 0$ and $T_i(t) = 0$

From 69 to 32 it results

$$G_i(t) \geq G_i^0 e^{-\int_0^t \{(a_i')^{(6)} - (a_i'')^{(6)}(T_{33}(s_{(32)}), s_{(32)})\} ds_{(32)}} \geq 0$$

$$T_i(t) \geq T_i^0 e^{-(b_i')^{(6)}t} > 0 \text{ for } t > 0.$$

Definition of $((\widehat{M}_{32})^{(6)})_1, ((\widehat{M}_{32})^{(6)})_2$ and $((\widehat{M}_{32})^{(6)})_3$:

Remark 3: if G_{32} is bounded, the same property have also G_{33} and G_{34} . indeed if

$G_{32} < (\widehat{M}_{32})^{(6)}$ it follows $\frac{dG_{33}}{dt} \leq ((\widehat{M}_{32})^{(6)})_1 - (a_{33}')^{(6)}G_{33}$ and by integrating

$$G_{33} \leq ((\widehat{M}_{32})^{(6)})_2 = G_{33}^0 + 2(a_{33}')^{(6)}((\widehat{M}_{32})^{(6)})_1 / (a_{33}')^{(6)}$$

In the same way, one can obtain

$$G_{34} \leq ((\widehat{M}_{32})^{(6)})_3 = G_{34}^0 + 2(a_{34}')^{(6)}((\widehat{M}_{32})^{(6)})_2 / (a_{34}')^{(6)}$$

If G_{33} or G_{34} is bounded, the same property follows for G_{32} , G_{34} and G_{32} , G_{33} respectively..

Remark 4: If G_{32} is bounded, from below, the same property holds for G_{33} and G_{34} . The proof is analogous with the preceding one. An analogous property is true if G_{33} is bounded from below..

Remark 5: If T_{32} is bounded from below and $\lim_{t \rightarrow \infty} ((b_i'')^{(6)}((G_{35})(t), t)) = (b_{33}')^{(6)}$ then $T_{33} \rightarrow \infty$.

Definition of $(m)^{(6)}$ and ε_6 :

Indeed let t_6 be so that for $t > t_6$

$$(b_{33}')^{(6)} - (b_i'')^{(6)}((G_{35})(t), t) < \varepsilon_6, T_{32}(t) > (m)^{(6)} :$$

Then $\frac{dT_{33}}{dt} \geq (a_{33}')^{(6)}(m)^{(6)} - \varepsilon_6 T_{33}$ which leads to

$$T_{33} \geq \left(\frac{(a_{33}')^{(6)}(m)^{(6)}}{\varepsilon_6} \right) (1 - e^{-\varepsilon_6 t}) + T_{33}^0 e^{-\varepsilon_6 t} \text{ If we take } t \text{ such that } e^{-\varepsilon_6 t} = \frac{1}{2} \text{ it results}$$

$$T_{33} \geq \left(\frac{(a_{33}')^{(6)}(m)^{(6)}}{2} \right), t = \log \frac{2}{\varepsilon_6} \text{ By taking now } \varepsilon_6 \text{ sufficiently small one sees that } T_{33} \text{ is unbounded. The same property}$$

holds for T_{34} if $\lim_{t \rightarrow \infty} (b_{34}')^{(6)}((G_{35})(t), t(t), t) = (b_{34}')^{(6)}$

We now state a more precise theorem about the behaviors at infinity of the solutions.

Behavior of the solutions

If we denote and define

Definition of $(\sigma_1)^{(1)}, (\sigma_2)^{(1)}, (\tau_1)^{(1)}, (\tau_2)^{(1)}$:

- (a) $(\sigma_1)^{(1)}, (\sigma_2)^{(1)}, (\tau_1)^{(1)}, (\tau_2)^{(1)}$ four constants satisfying
 $-(\sigma_2)^{(1)} \leq -(a_{13}')^{(1)} + (a_{14}')^{(1)} - (a_{13}'')^{(1)}(T_{14}, t) + (a_{14}'')^{(1)}(T_{14}, t) \leq -(\sigma_1)^{(1)}$
 $-(\tau_2)^{(1)} \leq -(b_{13}')^{(1)} + (b_{14}')^{(1)} - (b_{13}'')^{(1)}(G, t) - (b_{14}'')^{(1)}(G, t) \leq -(\tau_1)^{(1)}$.

Definition of $(v_1)^{(1)}, (v_2)^{(1)}, (u_1)^{(1)}, (u_2)^{(1)}, v^{(1)}, u^{(1)}$:

By $(v_1)^{(1)} > 0, (v_2)^{(1)} < 0$ and respectively $(u_1)^{(1)} > 0, (u_2)^{(1)} < 0$ the roots of the equations $(a_{14})^{(1)}(v^{(1)})^2 + (\sigma_1)^{(1)}v^{(1)} - (a_{13})^{(1)} = 0$ and $(b_{14})^{(1)}(u^{(1)})^2 + (\tau_1)^{(1)}u^{(1)} - (b_{13})^{(1)} = 0$:

Definition of $(\bar{v}_1)^{(1)}, (\bar{v}_2)^{(1)}, (\bar{u}_1)^{(1)}, (\bar{u}_2)^{(1)}$:

By $(\bar{v}_1)^{(1)} > 0, (\bar{v}_2)^{(1)} < 0$ and respectively $(\bar{u}_1)^{(1)} > 0, (\bar{u}_2)^{(1)} < 0$ the roots of the equations $(a_{14})^{(1)}(v^{(1)})^2 + (\sigma_2)^{(1)}v^{(1)} - (a_{13})^{(1)} = 0$ and $(b_{14})^{(1)}(u^{(1)})^2 + (\tau_2)^{(1)}u^{(1)} - (b_{13})^{(1)} = 0$.

Definition of $(m_1)^{(1)}, (m_2)^{(1)}, (\mu_1)^{(1)}, (\mu_2)^{(1)}, (v_0)^{(1)}$:-

- (b) If we define $(m_1)^{(1)}, (m_2)^{(1)}, (\mu_1)^{(1)}, (\mu_2)^{(1)}$ by
 $(m_2)^{(1)} = (v_0)^{(1)}, (m_1)^{(1)} = (v_1)^{(1)}$, if $(v_0)^{(1)} < (v_1)^{(1)}$
 $(m_2)^{(1)} = (v_1)^{(1)}, (m_1)^{(1)} = (\bar{v}_1)^{(1)}$, if $(v_1)^{(1)} < (v_0)^{(1)} < (\bar{v}_1)^{(1)}$,

$$\text{and } (v_0)^{(1)} = \frac{G_{13}^0}{G_{14}^0}$$

$$(m_2)^{(1)} = (v_1)^{(1)}, (m_1)^{(1)} = (v_0)^{(1)}, \text{ if } (\bar{v}_1)^{(1)} < (v_0)^{(1)} :$$

and analogously

$$(\mu_2)^{(1)} = (u_0)^{(1)}, (\mu_1)^{(1)} = (u_1)^{(1)}, \text{ if } (u_0)^{(1)} < (u_1)^{(1)}$$

$$(\mu_2)^{(1)} = (u_1)^{(1)}, (\mu_1)^{(1)} = (\bar{u}_1)^{(1)}, \text{ if } (u_1)^{(1)} < (u_0)^{(1)} < (\bar{u}_1)^{(1)},$$

$$\text{and } (u_0)^{(1)} = \frac{T_{13}^0}{T_{14}^0}$$

$$(\mu_2)^{(1)} = (u_1)^{(1)}, (\mu_1)^{(1)} = (u_0)^{(1)}, \text{ if } (\bar{u}_1)^{(1)} < (u_0)^{(1)} \text{ where } (u_1)^{(1)}, (\bar{u}_1)^{(1)}$$

are defined respectively.

Then the solution satisfies the inequalities

$$G_{13}^0 e^{((s_1)^{(1)} - (p_{13})^{(1)})t} \leq G_{13}(t) \leq G_{13}^0 e^{(s_1)^{(1)}t}$$

where $(p_i)^{(1)}$ is defined

$$\frac{1}{(m_1)^{(1)}} G_{13}^0 e^{((S_1)^{(1)} - (p_{13})^{(1)})t} \leq G_{14}(t) \leq \frac{1}{(m_2)^{(1)}} G_{13}^0 e^{(S_1)^{(1)}t} .$$

$$\left(\frac{(a_{15})^{(1)} G_{13}^0}{(m_1)^{(1)}((S_1)^{(1)} - (p_{13})^{(1)} - (S_2)^{(1)})} \left[e^{((S_1)^{(1)} - (p_{13})^{(1)})t} - e^{-(S_2)^{(1)}t} \right] + G_{15}^0 e^{-(S_2)^{(1)}t} \leq G_{15}(t) \leq \frac{(a_{15})^{(1)} G_{13}^0}{(m_2)^{(1)}((S_1)^{(1)} - (a'_{15})^{(1)})} \left[e^{(S_1)^{(1)}t} - e^{-(a'_{15})^{(1)}t} \right] + G_{15}^0 e^{-(a'_{15})^{(1)}t} \right) .$$

$$\boxed{T_{13}^0 e^{(R_1)^{(1)}t} \leq T_{13}(t) \leq T_{13}^0 e^{((R_1)^{(1)} + (r_{13})^{(1)})t} .}$$

$$\frac{1}{(\mu_1)^{(1)}} T_{13}^0 e^{(R_1)^{(1)}t} \leq T_{13}(t) \leq \frac{1}{(\mu_2)^{(1)}} T_{13}^0 e^{((R_1)^{(1)} + (r_{13})^{(1)})t} .$$

$$\frac{(b_{15})^{(1)} T_{13}^0}{(\mu_1)^{(1)}((R_1)^{(1)} - (b'_{15})^{(1)})} \left[e^{(R_1)^{(1)}t} - e^{-(b'_{15})^{(1)}t} \right] + T_{15}^0 e^{-(b'_{15})^{(1)}t} \leq T_{15}(t) \leq \frac{(a_{15})^{(1)} T_{13}^0}{(\mu_2)^{(1)}((R_1)^{(1)} + (r_{13})^{(1)} + (R_2)^{(1)})} \left[e^{((R_1)^{(1)} + (r_{13})^{(1)})t} - e^{-(R_2)^{(1)}t} \right] + T_{15}^0 e^{-(R_2)^{(1)}t} .$$

Definition of $(S_1)^{(1)}, (S_2)^{(1)}, (R_1)^{(1)}, (R_2)^{(1)}$:-

Where $(S_1)^{(1)} = (a_{13})^{(1)}(m_2)^{(1)} - (a'_{13})^{(1)}$
 $(S_2)^{(1)} = (a_{15})^{(1)} - (p_{15})^{(1)}$
 $(R_1)^{(1)} = (b_{13})^{(1)}(\mu_2)^{(1)} - (b'_{13})^{(1)}$
 $(R_2)^{(1)} = (b'_{15})^{(1)} - (r_{15})^{(1)} .$

Behavior of the solutions

If we denote and define.

Definition of $(\sigma_1)^{(2)}, (\sigma_2)^{(2)}, (\tau_1)^{(2)}, (\tau_2)^{(2)}$:

$\sigma_1^{(2)}, (\sigma_2)^{(2)}, (\tau_1)^{(2)}, (\tau_2)^{(2)}$ four constants satisfying.
 $-(\sigma_2)^{(2)} \leq -(a'_{16})^{(2)} + (a'_{17})^{(2)} - (a''_{16})^{(2)}(T_{17}, t) + (a''_{17})^{(2)}(T_{17}, t) \leq -(\sigma_1)^{(2)} .$
 $-(\tau_2)^{(2)} \leq -(b'_{16})^{(2)} + (b'_{17})^{(2)} - (b''_{16})^{(2)}((G_{19}), t) - (b''_{17})^{(2)}((G_{19}), t) \leq -(\tau_1)^{(2)} .$

Definition of $(v_1)^{(2)}, (v_2)^{(2)}, (u_1)^{(2)}, (u_2)^{(2)}$:-

By $(v_1)^{(2)} > 0, (v_2)^{(2)} < 0$ and respectively $(u_1)^{(2)} > 0, (u_2)^{(2)} < 0$ the roots.

of the equations $(a_{17})^{(2)}(v^{(2)})^2 + (\sigma_1)^{(2)}v^{(2)} - (a_{16})^{(2)} = 0 .$

and $(b_{14})^{(2)}(u^{(2)})^2 + (\tau_1)^{(2)}u^{(2)} - (b_{16})^{(2)} = 0$ and.

Definition of $(\bar{v}_1)^{(2)}, (\bar{v}_2)^{(2)}, (\bar{u}_1)^{(2)}, (\bar{u}_2)^{(2)}$:-

By $(\bar{v}_1)^{(2)} > 0, (\bar{v}_2)^{(2)} < 0$ and respectively $(\bar{u}_1)^{(2)} > 0, (\bar{u}_2)^{(2)} < 0$ the

roots of the equations $(a_{17})^{(2)}(v^{(2)})^2 + (\sigma_2)^{(2)}v^{(2)} - (a_{16})^{(2)} = 0 .$

and $(b_{17})^{(2)}(u^{(2)})^2 + (\tau_2)^{(2)}u^{(2)} - (b_{16})^{(2)} = 0 .$

Definition of $(m_1)^{(2)}, (m_2)^{(2)}, (\mu_1)^{(2)}, (\mu_2)^{(2)}$:-

If we define $(m_1)^{(2)}, (m_2)^{(2)}, (\mu_1)^{(2)}, (\mu_2)^{(2)}$ by.

$(m_2)^{(2)} = (v_0)^{(2)}, (m_1)^{(2)} = (v_1)^{(2)}, \text{ if } (v_0)^{(2)} < (v_1)^{(2)} .$
 $(m_2)^{(2)} = (v_1)^{(2)}, (m_1)^{(2)} = (\bar{v}_1)^{(2)}, \text{ if } (v_1)^{(2)} < (v_0)^{(2)} < (\bar{v}_1)^{(2)},$

and $\boxed{(v_0)^{(2)} = \frac{G_{16}^0}{G_{17}^0}} .$

$(m_2)^{(2)} = (v_1)^{(2)}, (m_1)^{(2)} = (v_0)^{(2)}, \text{ if } (\bar{v}_1)^{(2)} < (v_0)^{(2)} .$

and analogously

$(\mu_2)^{(2)} = (u_0)^{(2)}, (\mu_1)^{(2)} = (u_1)^{(2)}, \text{ if } (u_0)^{(2)} < (u_1)^{(2)}$
 $(\mu_2)^{(2)} = (u_1)^{(2)}, (\mu_1)^{(2)} = (\bar{u}_1)^{(2)}, \text{ if } (u_1)^{(2)} < (u_0)^{(2)} < (\bar{u}_1)^{(2)},$

and $\boxed{(u_0)^{(2)} = \frac{T_{16}^0}{T_{17}^0}} .$

$(\mu_2)^{(2)} = (u_1)^{(2)}, (\mu_1)^{(2)} = (u_0)^{(2)}, \text{ if } (\bar{u}_1)^{(2)} < (u_0)^{(2)} .$

Then the solution satisfies the inequalities

$G_{16}^0 e^{(S_1)^{(2)} - (p_{16})^{(2)}t} \leq G_{16}(t) \leq G_{16}^0 e^{(S_1)^{(2)}t} .$

$(p_i)^{(2)}$ is defined.

$$\frac{1}{(m_1)^{(2)}} G_{16}^0 e^{((S_1)^{(2)} - (p_{16})^{(2)})t} \leq G_{17}(t) \leq \frac{1}{(m_2)^{(2)}} G_{16}^0 e^{(S_1)^{(2)}t} .$$

$$\left(\frac{(a_{18})^{(2)} G_{16}^0}{(m_1)^{(2)}((S_1)^{(2)} - (p_{16})^{(2)} - (S_2)^{(2)})} \left[e^{((S_1)^{(2)} - (p_{16})^{(2)})t} - e^{-(S_2)^{(2)}t} \right] + G_{18}^0 e^{-(S_2)^{(2)}t} \leq G_{18}(t) \leq \frac{(a_{18})^{(2)} G_{16}^0}{(m_2)^{(2)}((S_1)^{(2)} - (a'_{18})^{(2)})} \left[e^{(S_1)^{(2)}t} - e^{-(a'_{18})^{(2)}t} \right] + G_{18}^0 e^{-(a'_{18})^{(2)}t} \right) .$$

$$\boxed{T_{16}^0 e^{(R_1)^{(2)}t} \leq T_{16}(t) \leq T_{16}^0 e^{((R_1)^{(2)} + (r_{16})^{(2)})t} .}$$

$$\frac{1}{(\mu_1)^{(2)}} T_{16}^0 e^{(R_1)^{(2)}t} \leq T_{16}(t) \leq \frac{1}{(\mu_2)^{(2)}} T_{16}^0 e^{((R_1)^{(2)} + (r_{16})^{(2)})t} .$$

$$\frac{(b_{18})^{(2)}T_{16}^0}{(\mu_1)^{(2)}((R_1)^{(2)}-(b'_{18})^{(2)})} \left[e^{(R_1)^{(2)}t} - e^{-(b'_{18})^{(2)}t} \right] + T_{18}^0 e^{-(b'_{18})^{(2)}t} \leq T_{18}(t) \leq \frac{(a_{18})^{(2)}T_{16}^0}{(\mu_2)^{(2)}((R_1)^{(2)}+(r_{16})^{(2)}+(R_2)^{(2)})} \left[e^{((R_1)^{(2)}+(r_{16})^{(2)})t} - e^{-(R_2)^{(2)}t} \right] + T_{18}^0 e^{-(R_2)^{(2)}t} .$$

Definition of $(S_1)^{(2)}, (S_2)^{(2)}, (R_1)^{(2)}, (R_2)^{(2)}$:-

Where $(S_1)^{(2)} = (a_{16})^{(2)}(m_2)^{(2)} - (a'_{16})^{(2)}$
 $(S_2)^{(2)} = (a_{18})^{(2)} - (p_{18})^{(2)}$
 $(R_1)^{(2)} = (b_{16})^{(2)}(\mu_2)^{(1)} - (b'_{16})^{(2)}$
 $(R_2)^{(2)} = (b'_{18})^{(2)} - (r_{18})^{(2)}$.

Behavior of the solutions

If we denote and define

Definition of $(\sigma_1)^{(3)}, (\sigma_2)^{(3)}, (\tau_1)^{(3)}, (\tau_2)^{(3)}$:

(a) $(\sigma_1)^{(3)}, (\sigma_2)^{(3)}, (\tau_1)^{(3)}, (\tau_2)^{(3)}$ four constants satisfying
 $-(\sigma_2)^{(3)} \leq -(a'_{20})^{(3)} + (a'_{21})^{(3)} - (a''_{20})^{(3)}(T_{21}, t) + (a''_{21})^{(3)}(T_{21}, t) \leq -(\sigma_1)^{(3)}$
 $-(\tau_2)^{(3)} \leq -(b_{20})^{(3)} + (b_{21})^{(3)} - (b''_{20})^{(3)}(G, t) - (b''_{21})^{(3)}(G, t) \leq -(\tau_1)^{(3)}$.

Definition of $(v_1)^{(3)}, (v_2)^{(3)}, (u_1)^{(3)}, (u_2)^{(3)}$:

(b) By $(v_1)^{(3)} > 0, (v_2)^{(3)} < 0$ and respectively $(u_1)^{(3)} > 0, (u_2)^{(3)} < 0$ the roots of the equations $(a_{21})^{(3)}(v^{(3)})^2 + (\sigma_1)^{(3)}v^{(3)} - (a_{20})^{(3)} = 0$
 and $(b_{21})^{(3)}(u^{(3)})^2 + (\tau_1)^{(3)}u^{(3)} - (b_{20})^{(3)} = 0$ and
 By $(\bar{v}_1)^{(3)} > 0, (\bar{v}_2)^{(3)} < 0$ and respectively $(\bar{u}_1)^{(3)} > 0, (\bar{u}_2)^{(3)} < 0$ the roots of the equations $(a_{21})^{(3)}(v^{(3)})^2 + (\sigma_2)^{(3)}v^{(3)} - (a_{20})^{(3)} = 0$
 and $(b_{21})^{(3)}(u^{(3)})^2 + (\tau_2)^{(3)}u^{(3)} - (b_{20})^{(3)} = 0$:

Definition of $(m_1)^{(3)}, (m_2)^{(3)}, (\mu_1)^{(3)}, (\mu_2)^{(3)}$:-

(c) If we define $(m_1)^{(3)}, (m_2)^{(3)}, (\mu_1)^{(3)}, (\mu_2)^{(3)}$ by
 $(m_2)^{(3)} = (v_0)^{(3)}, (m_1)^{(3)} = (v_1)^{(3)}$, **if** $(v_0)^{(3)} < (v_1)^{(3)}$
 $(m_2)^{(3)} = (v_1)^{(3)}, (m_1)^{(3)} = (\bar{v}_1)^{(3)}$, **if** $(v_1)^{(3)} < (v_0)^{(3)} < (\bar{v}_1)^{(3)}$,
 and $(v_0)^{(3)} = \frac{a_{20}^0}{a_{21}^0}$

$(m_2)^{(3)} = (v_1)^{(3)}, (m_1)^{(3)} = (v_0)^{(3)}$, **if** $(\bar{v}_1)^{(3)} < (v_0)^{(3)}$;
 and analogously

$(\mu_2)^{(3)} = (u_0)^{(3)}, (\mu_1)^{(3)} = (u_1)^{(3)}$, **if** $(u_0)^{(3)} < (u_1)^{(3)}$
 $(\mu_2)^{(3)} = (u_1)^{(3)}, (\mu_1)^{(3)} = (\bar{u}_1)^{(3)}$, **if** $(u_1)^{(3)} < (u_0)^{(3)} < (\bar{u}_1)^{(3)}$, and $(u_0)^{(3)} = \frac{T_{20}^0}{T_{21}^0}$

$(\mu_2)^{(3)} = (u_1)^{(3)}, (\mu_1)^{(3)} = (u_0)^{(3)}$, **if** $(\bar{u}_1)^{(3)} < (u_0)^{(3)}$

Then the solution satisfies the inequalities

$G_{20}^0 e^{((S_1)^{(3)}-(p_{20})^{(3)})t} \leq G_{20}(t) \leq G_{20}^0 e^{(S_1)^{(3)}t}$

$(p_i)^{(3)}$ is defined .

$\frac{1}{(m_1)^{(3)}} G_{20}^0 e^{((S_1)^{(3)}-(p_{20})^{(3)})t} \leq G_{21}(t) \leq \frac{1}{(m_2)^{(3)}} G_{20}^0 e^{(S_1)^{(3)}t}$.

$\frac{(a_{22})^{(3)}G_{20}^0}{(m_1)^{(3)}((S_1)^{(3)}-(p_{20})^{(3)}-(S_2)^{(3)})} \left[e^{((S_1)^{(3)}-(p_{20})^{(3)})t} - e^{-(S_2)^{(3)}t} \right] + G_{22}^0 e^{-(S_2)^{(3)}t} \leq G_{22}(t) \leq \frac{(a_{22})^{(3)}G_{20}^0}{(m_2)^{(3)}((S_1)^{(3)}-(a_{22})^{(3)})} \left[e^{(S_1)^{(3)}t} - e^{-(a_{22})^{(3)}t} \right] + G_{22}^0 e^{-(a_{22})^{(3)}t}$.

$T_{20}^0 e^{(R_1)^{(3)}t} \leq T_{20}(t) \leq T_{20}^0 e^{((R_1)^{(3)}+(r_{20})^{(3)})t}$.

$\frac{1}{(\mu_1)^{(3)}} T_{20}^0 e^{(R_1)^{(3)}t} \leq T_{20}(t) \leq \frac{1}{(\mu_2)^{(3)}} T_{20}^0 e^{((R_1)^{(3)}+(r_{20})^{(3)})t}$.

$\frac{(b_{22})^{(3)}T_{20}^0}{(\mu_1)^{(3)}((R_1)^{(3)}-(b'_{22})^{(3)})} \left[e^{(R_1)^{(3)}t} - e^{-(b'_{22})^{(3)}t} \right] + T_{22}^0 e^{-(b'_{22})^{(3)}t} \leq T_{22}(t) \leq$

$\frac{(a_{22})^{(3)}T_{20}^0}{(\mu_2)^{(3)}((R_1)^{(3)}+(r_{20})^{(3)}+(R_2)^{(3)})} \left[e^{((R_1)^{(3)}+(r_{20})^{(3)})t} - e^{-(R_2)^{(3)}t} \right] + T_{22}^0 e^{-(R_2)^{(3)}t}$.

Definition of $(S_1)^{(3)}, (S_2)^{(3)}, (R_1)^{(3)}, (R_2)^{(3)}$:-

Where $(S_1)^{(3)} = (a_{20})^{(3)}(m_2)^{(3)} - (a'_{20})^{(3)}$
 $(S_2)^{(3)} = (a_{22})^{(3)} - (p_{22})^{(3)}$
 $(R_1)^{(3)} = (b_{20})^{(3)}(\mu_2)^{(3)} - (b'_{20})^{(3)}$
 $(R_2)^{(3)} = (b'_{22})^{(3)} - (r_{22})^{(3)}$.

Behavior of the solutions

If we denote and define

Definition of $(\sigma_1)^{(4)}, (\sigma_2)^{(4)}, (\tau_1)^{(4)}, (\tau_2)^{(4)}$:

(d) $(\sigma_1)^{(4)}, (\sigma_2)^{(4)}, (\tau_1)^{(4)}, (\tau_2)^{(4)}$ four constants satisfying

$$-(\sigma_2)^{(4)} \leq -(a'_{24})^{(4)} + (a'_{25})^{(4)} - (a''_{24})^{(4)}(T_{25}, t) + (a''_{25})^{(4)}(T_{25}, t) \leq -(\sigma_1)^{(4)}$$

$$-(\tau_2)^{(4)} \leq -(b'_{24})^{(4)} + (b'_{25})^{(4)} - (b''_{24})^{(4)}((G_{27}), t) - (b''_{25})^{(4)}((G_{27}), t) \leq -(\tau_1)^{(4)}$$

Definition of $(v_1)^{(4)}, (v_2)^{(4)}, (u_1)^{(4)}, (u_2)^{(4)}, v^{(4)}, u^{(4)}$:

(e) By $(v_1)^{(4)} > 0, (v_2)^{(4)} < 0$ and respectively $(u_1)^{(4)} > 0, (u_2)^{(4)} < 0$ the roots of the equations $(a_{25})^{(4)}(v^{(4)})^2 + (\sigma_1)^{(4)}v^{(4)} - (a_{24})^{(4)} = 0$

$$\text{and } (b_{25})^{(4)}(u^{(4)})^2 + (\tau_1)^{(4)}u^{(4)} - (b_{24})^{(4)} = 0 \text{ and}$$

Definition of $(\bar{v}_1)^{(4)}, (\bar{v}_2)^{(4)}, (\bar{u}_1)^{(4)}, (\bar{u}_2)^{(4)}$:

By $(\bar{v}_1)^{(4)} > 0, (\bar{v}_2)^{(4)} < 0$ and respectively $(\bar{u}_1)^{(4)} > 0, (\bar{u}_2)^{(4)} < 0$ the

$$\text{roots of the equations } (a_{25})^{(4)}(v^{(4)})^2 + (\sigma_2)^{(4)}v^{(4)} - (a_{24})^{(4)} = 0$$

$$\text{and } (b_{25})^{(4)}(u^{(4)})^2 + (\tau_2)^{(4)}u^{(4)} - (b_{24})^{(4)} = 0$$

Definition of $(m_1)^{(4)}, (m_2)^{(4)}, (\mu_1)^{(4)}, (\mu_2)^{(4)}, (v_0)^{(4)}$:-

(f) If we define $(m_1)^{(4)}, (m_2)^{(4)}, (\mu_1)^{(4)}, (\mu_2)^{(4)}$ by

$$(m_2)^{(4)} = (v_0)^{(4)}, (m_1)^{(4)} = (v_1)^{(4)}, \text{ if } (v_0)^{(4)} < (v_1)^{(4)}$$

$$(m_2)^{(4)} = (v_1)^{(4)}, (m_1)^{(4)} = (\bar{v}_1)^{(4)}, \text{ if } (v_4)^{(4)} < (v_0)^{(4)} < (\bar{v}_1)^{(4)},$$

$$\text{and } \boxed{(v_0)^{(4)} = \frac{\sigma_{24}^0}{\sigma_{25}^0}}$$

$$(m_2)^{(4)} = (v_4)^{(4)}, (m_1)^{(4)} = (v_0)^{(4)}, \text{ if } (\bar{v}_4)^{(4)} < (v_0)^{(4)}$$

and analogously

$$(\mu_2)^{(4)} = (u_0)^{(4)}, (\mu_1)^{(4)} = (u_1)^{(4)}, \text{ if } (u_0)^{(4)} < (u_1)^{(4)}$$

$$(\mu_2)^{(4)} = (u_1)^{(4)}, (\mu_1)^{(4)} = (\bar{u}_1)^{(4)}, \text{ if } (u_1)^{(4)} < (u_0)^{(4)} < (\bar{u}_1)^{(4)},$$

$$\text{and } \boxed{(u_0)^{(4)} = \frac{T_{24}^0}{T_{25}^0}}$$

$$(\mu_2)^{(4)} = (u_1)^{(4)}, (\mu_1)^{(4)} = (u_0)^{(4)}, \text{ if } (\bar{u}_1)^{(4)} < (u_0)^{(4)} \text{ where } (u_1)^{(4)}, (\bar{u}_1)^{(4)}$$

are defined by 59 and 64 respectively

Then the solution satisfies the inequalities

$$G_{24}^0 e^{((S_1)^{(4)} - (p_{24})^{(4)})t} \leq G_{24}(t) \leq G_{24}^0 e^{(S_1)^{(4)}t}$$

where $(p_i)^{(4)}$ is defined .

$$\frac{1}{(m_1)^{(4)}} G_{24}^0 e^{((S_1)^{(4)} - (p_{24})^{(4)})t} \leq G_{25}(t) \leq \frac{1}{(m_2)^{(4)}} G_{24}^0 e^{(S_1)^{(4)}t}$$

$$\left(\frac{(a_{26})^{(4)} G_{24}^0}{(m_1)^{(4)} ((S_1)^{(4)} - (p_{24})^{(4)} - (S_2)^{(4)})} \left[e^{((S_1)^{(4)} - (p_{24})^{(4)})t} - e^{-(S_2)^{(4)}t} \right] + G_{26}^0 e^{-(S_2)^{(4)}t} \right) \leq G_{26}(t) \leq \frac{(a_{26})^{(4)} G_{24}^0}{(m_2)^{(4)} ((S_1)^{(4)} - (a_{26})^{(4)})} \left[e^{(S_1)^{(4)}t} - e^{-(a_{26}')^{(4)}t} + G_{26}^0 e^{-(a_{26}')^{(4)}t} \right]$$

$$\boxed{T_{24}^0 e^{(R_1)^{(4)}t} \leq T_{24}(t) \leq T_{24}^0 e^{((R_1)^{(4)} + (r_{24})^{(4)})t}$$

$$\frac{1}{(\mu_1)^{(4)}} T_{24}^0 e^{(R_1)^{(4)}t} \leq T_{24}(t) \leq \frac{1}{(\mu_2)^{(4)}} T_{24}^0 e^{((R_1)^{(4)} + (r_{24})^{(4)})t}$$

$$\frac{(b_{26})^{(4)} T_{24}^0}{(\mu_1)^{(4)} ((R_1)^{(4)} - (b_{26})^{(4)})} \left[e^{(R_1)^{(4)}t} - e^{-(b_{26}')^{(4)}t} \right] + T_{26}^0 e^{-(b_{26}')^{(4)}t} \leq T_{26}(t) \leq$$

$$\frac{(a_{26})^{(4)} T_{24}^0}{(\mu_2)^{(4)} ((R_1)^{(4)} + (r_{24})^{(4)} + (R_2)^{(4)})} \left[e^{((R_1)^{(4)} + (r_{24})^{(4)})t} - e^{-(R_2)^{(4)}t} \right] + T_{26}^0 e^{-(R_2)^{(4)}t}$$

Definition of $(S_1)^{(4)}, (S_2)^{(4)}, (R_1)^{(4)}, (R_2)^{(4)}$:-

$$\text{Where } (S_1)^{(4)} = (a_{24})^{(4)}(m_2)^{(4)} - (a_{24}')^{(4)}$$

$$(S_2)^{(4)} = (a_{26})^{(4)} - (p_{26})^{(4)}$$

$$(R_1)^{(4)} = (b_{24})^{(4)}(\mu_2)^{(4)} - (b_{24}')^{(4)}$$

$$(R_2)^{(4)} = (b_{26}')^{(4)} - (r_{26})^{(4)}$$

Behavior of the solutions

If we denote and define

Definition of $(\sigma_1)^{(5)}, (\sigma_2)^{(5)}, (\tau_1)^{(5)}, (\tau_2)^{(5)}$:

(g) $(\sigma_1)^{(5)}, (\sigma_2)^{(5)}, (\tau_1)^{(5)}, (\tau_2)^{(5)}$ four constants satisfying

$$-(\sigma_2)^{(5)} \leq -(a_{28}')^{(5)} + (a_{29}')^{(5)} - (a_{28}'')^{(5)}(T_{29}, t) + (a_{29}'')^{(5)}(T_{29}, t) \leq -(\sigma_1)^{(5)}$$

$$-(\tau_2)^{(5)} \leq -(b_{28}')^{(5)} + (b_{29}')^{(5)} - (b_{28}'')^{(5)}((G_{31}), t) - (b_{29}'')^{(5)}((G_{31}), t) \leq -(\tau_1)^{(5)}$$

Definition of $(v_1)^{(5)}, (v_2)^{(5)}, (u_1)^{(5)}, (u_2)^{(5)}, v^{(5)}, u^{(5)}$:

(h) By $(v_1)^{(5)} > 0, (v_2)^{(5)} < 0$ and respectively $(u_1)^{(5)} > 0, (u_2)^{(5)} < 0$ the roots of the equations $(a_{29})^{(5)}(v^{(5)})^2 + (\sigma_1)^{(5)}v^{(5)} - (a_{28})^{(5)} = 0$

$$\text{and } (b_{29})^{(5)}(u^{(5)})^2 + (\tau_1)^{(5)}u^{(5)} - (b_{28})^{(5)} = 0 \text{ and}$$

Definition of $(\bar{v}_1)^{(5)}, (\bar{v}_2)^{(5)}, (\bar{u}_1)^{(5)}, (\bar{u}_2)^{(5)}$:

By $(\bar{v}_1)^{(5)} > 0, (\bar{v}_2)^{(5)} < 0$ and respectively $(\bar{u}_1)^{(5)} > 0, (\bar{u}_2)^{(5)} < 0$ the

$$\text{roots of the equations } (a_{29})^{(5)}(v^{(5)})^2 + (\sigma_2)^{(5)}v^{(5)} - (a_{28})^{(5)} = 0$$

$$\text{and } (b_{29})^{(5)}(u^{(5)})^2 + (\tau_2)^{(5)}u^{(5)} - (b_{28})^{(5)} = 0$$

Definition of $(m_1)^{(5)}, (m_2)^{(5)}, (\mu_1)^{(5)}, (\mu_2)^{(5)}, (v_0)^{(5)}$:-

(i) If we define $(m_1)^{(5)}, (m_2)^{(5)}, (\mu_1)^{(5)}, (\mu_2)^{(5)}$ by

$$(m_2)^{(5)} = (v_0)^{(5)}, (m_1)^{(5)} = (v_1)^{(5)}, \text{ if } (v_0)^{(5)} < (v_1)^{(5)}$$

$$(m_2)^{(5)} = (v_1)^{(5)}, (m_1)^{(5)} = (\bar{v}_1)^{(5)}, \text{ if } (v_1)^{(5)} < (v_0)^{(5)} < (\bar{v}_1)^{(5)},$$

$$\text{and } \boxed{(v_0)^{(5)} = \frac{G_{28}^0}{G_{29}^0}}$$

$$(m_2)^{(5)} = (v_1)^{(5)}, (m_1)^{(5)} = (v_0)^{(5)}, \text{ if } (\bar{v}_1)^{(5)} < (v_0)^{(5)}$$

and analogously

$$(\mu_2)^{(5)} = (u_0)^{(5)}, (\mu_1)^{(5)} = (u_1)^{(5)}, \text{ if } (u_0)^{(5)} < (u_1)^{(5)}$$

$$(\mu_2)^{(5)} = (u_1)^{(5)}, (\mu_1)^{(5)} = (\bar{u}_1)^{(5)}, \text{ if } (u_1)^{(5)} < (u_0)^{(5)} < (\bar{u}_1)^{(5)},$$

$$\text{and } \boxed{(u_0)^{(5)} = \frac{T_{28}^0}{T_{29}^0}}$$

$$(\mu_2)^{(5)} = (u_1)^{(5)}, (\mu_1)^{(5)} = (u_0)^{(5)}, \text{ if } (\bar{u}_1)^{(5)} < (u_0)^{(5)} \text{ where } (u_1)^{(5)}, (\bar{u}_1)^{(5)}$$

are defined respectively

Then the solution satisfies the inequalities

$$G_{28}^0 e^{((S_1)^{(5)} - (p_{28})^{(5)})t} \leq G_{28}(t) \leq G_{28}^0 e^{(S_1)^{(5)}t}$$

where $(p_i)^{(5)}$ is defined .

$$\frac{1}{(m_5)^{(5)}} G_{28}^0 e^{((S_1)^{(5)} - (p_{28})^{(5)})t} \leq G_{29}(t) \leq \frac{1}{(m_2)^{(5)}} G_{28}^0 e^{(S_1)^{(5)}t}$$

$$\left(\frac{(a_{30})^{(5)} G_{28}^0}{(m_1)^{(5)} ((S_1)^{(5)} - (p_{28})^{(5)} - (S_2)^{(5)})} \left[e^{((S_1)^{(5)} - (p_{28})^{(5)})t} - e^{-(S_2)^{(5)}t} \right] + G_{30}^0 e^{-(S_2)^{(5)}t} \right) \leq G_{30}(t) \leq \frac{(a_{30})^{(5)} G_{28}^0}{(m_2)^{(5)} ((S_1)^{(5)} - (a_{30})^{(5)})} \left[e^{(S_1)^{(5)}t} - e^{-(a_{30})^{(5)}t} + G_{30} e^{-(a_{30})^{(5)}t} \right]$$

$$\boxed{T_{28}^0 e^{(R_1)^{(5)}t} \leq T_{28}(t) \leq T_{28}^0 e^{((R_1)^{(5)} + (r_{28})^{(5)})t}}$$

$$\frac{1}{(\mu_1)^{(5)}} T_{28}^0 e^{(R_1)^{(5)}t} \leq T_{28}(t) \leq \frac{1}{(\mu_2)^{(5)}} T_{28}^0 e^{((R_1)^{(5)} + (r_{28})^{(5)})t}$$

$$\frac{(b_{30})^{(5)} T_{28}^0}{(\mu_1)^{(5)} ((R_1)^{(5)} - (b_{30})^{(5)})} \left[e^{(R_1)^{(5)}t} - e^{-(b_{30})^{(5)}t} \right] + T_{30}^0 e^{-(b_{30})^{(5)}t} \leq T_{30}(t) \leq$$

$$\frac{(a_{30})^{(5)} T_{28}^0}{(\mu_2)^{(5)} ((R_1)^{(5)} + (r_{28})^{(5)} + (R_2)^{(5)})} \left[e^{((R_1)^{(5)} + (r_{28})^{(5)})t} - e^{-(R_2)^{(5)}t} \right] + T_{30}^0 e^{-(R_2)^{(5)}t}$$

Definition of $(S_1)^{(5)}, (S_2)^{(5)}, (R_1)^{(5)}, (R_2)^{(5)}$:-

$$\text{Where } (S_1)^{(5)} = (a_{28})^{(5)} (m_2)^{(5)} - (a'_{28})^{(5)}$$

$$(S_2)^{(5)} = (a_{30})^{(5)} - (p_{30})^{(5)}$$

$$(R_1)^{(5)} = (b_{28})^{(5)}(\mu_2)^{(5)} - (b'_{28})^{(5)}$$

$$(R_2)^{(5)} = (b'_{30})^{(5)} - (r_{30})^{(5)}$$

Behavior of the solutions

If we denote and define

Definition of $(\sigma_1)^{(6)}, (\sigma_2)^{(6)}, (\tau_1)^{(6)}, (\tau_2)^{(6)}$:

(j) $(\sigma_1)^{(6)}, (\sigma_2)^{(6)}, (\tau_1)^{(6)}, (\tau_2)^{(6)}$ four constants satisfying

$$-(\sigma_2)^{(6)} \leq -(a'_{32})^{(6)} + (a'_{33})^{(6)} - (a''_{32})^{(6)}(T_{33}, t) + (a''_{33})^{(6)}(T_{33}, t) \leq -(\sigma_1)^{(6)}$$

$$-(\tau_2)^{(6)} \leq -(b'_{32})^{(6)} + (b'_{33})^{(6)} - (b''_{32})^{(6)}((G_{35}), t) - (b''_{33})^{(6)}((G_{35}), t) \leq -(\tau_1)^{(6)}$$

Definition of $(v_1)^{(6)}, (v_2)^{(6)}, (u_1)^{(6)}, (u_2)^{(6)}, v^{(6)}, u^{(6)}$:

(k) By $(v_1)^{(6)} > 0, (v_2)^{(6)} < 0$ and respectively $(u_1)^{(6)} > 0, (u_2)^{(6)} < 0$ the roots of the equations $(a_{33})^{(6)}(v^{(6)})^2 + (\sigma_1)^{(6)}v^{(6)} - (a_{32})^{(6)} = 0$

$$\text{and } (b_{33})^{(6)}(u^{(6)})^2 + (\tau_1)^{(6)}u^{(6)} - (b_{32})^{(6)} = 0 \text{ and}$$

Definition of $(\bar{v}_1)^{(6)}, (\bar{v}_2)^{(6)}, (\bar{u}_1)^{(6)}, (\bar{u}_2)^{(6)}$:

By $(\bar{v}_1)^{(6)} > 0, (\bar{v}_2)^{(6)} < 0$ and respectively $(\bar{u}_1)^{(6)} > 0, (\bar{u}_2)^{(6)} < 0$ the

$$\text{roots of the equations } (a_{33})^{(6)}(v^{(6)})^2 + (\sigma_2)^{(6)}v^{(6)} - (a_{32})^{(6)} = 0$$

$$\text{and } (b_{33})^{(6)}(u^{(6)})^2 + (\tau_2)^{(6)}u^{(6)} - (b_{32})^{(6)} = 0$$

Definition of $(m_1)^{(6)}, (m_2)^{(6)}, (\mu_1)^{(6)}, (\mu_2)^{(6)}, (v_0)^{(6)}$:-

(l) If we define $(m_1)^{(6)}, (m_2)^{(6)}, (\mu_1)^{(6)}, (\mu_2)^{(6)}$ by

$$(m_2)^{(6)} = (v_0)^{(6)}, (m_1)^{(6)} = (v_1)^{(6)}, \text{ if } (v_0)^{(6)} < (v_1)^{(6)}$$

$$(m_2)^{(6)} = (v_1)^{(6)}, (m_1)^{(6)} = (\bar{v}_6)^{(6)}, \text{ if } (v_1)^{(6)} < (v_0)^{(6)} < (\bar{v}_1)^{(6)},$$

$$\text{and } \boxed{(v_0)^{(6)} = \frac{a_{32}^0}{a_{33}^0}}$$

$$(m_2)^{(6)} = (v_1)^{(6)}, (m_1)^{(6)} = (v_0)^{(6)}, \text{ if } (\bar{v}_1)^{(6)} < (v_0)^{(6)}$$

and analogously

$$(\mu_2)^{(6)} = (u_0)^{(6)}, (\mu_1)^{(6)} = (u_1)^{(6)}, \text{ if } (u_0)^{(6)} < (u_1)^{(6)}$$

$$(\mu_2)^{(6)} = (u_1)^{(6)}, (\mu_1)^{(6)} = (\bar{u}_1)^{(6)}, \text{ if } (u_1)^{(6)} < (u_0)^{(6)} < (\bar{u}_1)^{(6)},$$

$$\text{and } \boxed{(u_0)^{(6)} = \frac{T_{32}^0}{T_{33}^0}}$$

$$(\mu_2)^{(6)} = (u_1)^{(6)}, (\mu_1)^{(6)} = (u_0)^{(6)}, \text{ if } (\bar{u}_1)^{(6)} < (u_0)^{(6)} \text{ where } (u_1)^{(6)}, (\bar{u}_1)^{(6)}$$

are defined respectively

Then the solution satisfies the inequalities

$$G_{32}^0 e^{((S_1)^{(6)} - (p_{32})^{(6)})t} \leq G_{32}(t) \leq G_{32}^0 e^{(S_1)^{(6)}t}$$

where $(p_i)^{(6)}$ is defined.

$$\frac{1}{(m_1)^{(6)}} G_{32}^0 e^{((S_1)^{(6)} - (p_{32})^{(6)})t} \leq G_{33}(t) \leq \frac{1}{(m_2)^{(6)}} G_{32}^0 e^{(S_1)^{(6)}t}$$

$$\left(\frac{(a_{34})^{(6)} G_{32}^0}{(m_1)^{(6)} ((S_1)^{(6)} - (p_{32})^{(6)} - (S_2)^{(6)})} \left[e^{((S_1)^{(6)} - (p_{32})^{(6)})t} - e^{-(S_2)^{(6)}t} \right] + G_{34}^0 e^{-(S_2)^{(6)}t} \right) \leq G_{34}(t) \leq \frac{(a_{34})^{(6)} G_{32}^0}{(m_2)^{(6)} ((S_1)^{(6)} - (a_{34}')^{(6)})} \left[e^{(S_1)^{(6)}t} - e^{-(a_{34}')^{(6)}t} + G_{340} e^{-(a_{34}')^{(6)}t} \right]$$

$$\boxed{T_{32}^0 e^{(R_1)^{(6)}t} \leq T_{32}(t) \leq T_{32}^0 e^{((R_1)^{(6)} + (r_{32})^{(6)})t}$$

$$\frac{1}{(\mu_1)^{(6)}} T_{32}^0 e^{(R_1)^{(6)}t} \leq T_{32}(t) \leq \frac{1}{(\mu_2)^{(6)}} T_{32}^0 e^{((R_1)^{(6)} + (r_{32})^{(6)})t}$$

$$\frac{(b_{34})^{(6)} T_{32}^0}{(\mu_1)^{(6)} ((R_1)^{(6)} - (b_{34})^{(6)})} \left[e^{(R_1)^{(6)}t} - e^{-(b_{34}')^{(6)}t} \right] + T_{34}^0 e^{-(b_{34}')^{(6)}t} \leq T_{34}(t) \leq$$

$$\frac{(a_{34})^{(6)} T_{32}^0}{(\mu_2)^{(6)} ((R_1)^{(6)} + (r_{32})^{(6)} + (R_2)^{(6)})} \left[e^{((R_1)^{(6)} + (r_{32})^{(6)})t} - e^{-(R_2)^{(6)}t} \right] + T_{34}^0 e^{-(R_2)^{(6)}t}$$

Definition of $(S_1)^{(6)}, (S_2)^{(6)}, (R_1)^{(6)}, (R_2)^{(6)}$:-

$$\text{Where } (S_1)^{(6)} = (a_{32})^{(6)}(m_2)^{(6)} - (a_{32}')^{(6)}$$

$$(S_2)^{(6)} = (a_{34})^{(6)} - (p_{34})^{(6)}$$

$$(R_1)^{(6)} = (b_{32})^{(6)}(\mu_2)^{(6)} - (b_{32}')^{(6)}$$

$$(R_2)^{(6)} = (b_{34}')^{(6)} - (r_{34})^{(6)}.$$

Proof : From GLOBAL EQUATIONS we obtain

$$\frac{dv^{(1)}}{dt} = (a_{13})^{(1)} - \left((a_{13}')^{(1)} - (a_{14}')^{(1)} + (a_{13}'')^{(1)}(T_{14}, t) \right) - (a_{14}'')^{(1)}(T_{14}, t)v^{(1)} - (a_{14})^{(1)}v^{(1)}$$

Definition of $v^{(1)}$:- $\boxed{v^{(1)} = \frac{G_{13}}{G_{14}}}$

It follows

$$- \left((a_{14})^{(1)}(v^{(1)})^2 + (\sigma_2)^{(1)}v^{(1)} - (a_{13})^{(1)} \right) \leq \frac{dv^{(1)}}{dt} \leq - \left((a_{14})^{(1)}(v^{(1)})^2 + (\sigma_1)^{(1)}v^{(1)} - (a_{13})^{(1)} \right)$$

From which one obtains

Definition of $(\bar{v}_1)^{(1)}, (v_0)^{(1)}$:-

(a) For $0 < \boxed{(v_0)^{(1)} = \frac{G_{13}^0}{G_{14}^0}} < (v_1)^{(1)} < (\bar{v}_1)^{(1)}$

$$v^{(1)}(t) \geq \frac{(v_1)^{(1)} + (C)^{(1)}(v_2)^{(1)} e^{-(a_{14})^{(1)}(v_1)^{(1)} - (v_0)^{(1)}t}}{1 + (C)^{(1)} e^{-(a_{14})^{(1)}(v_1)^{(1)} - (v_0)^{(1)}t}}, \quad \boxed{(C)^{(1)} = \frac{(v_1)^{(1)} - (v_0)^{(1)}}{(v_0)^{(1)} - (v_2)^{(1)}}$$

it follows $(v_0)^{(1)} \leq v^{(1)}(t) \leq (v_1)^{(1)}$.

In the same manner , we get

$$v^{(1)}(t) \leq \frac{(\bar{v}_1)^{(1)} + (\bar{C})^{(1)} (\bar{v}_2)^{(1)} e^{[-(a_{14})^{(1)} (\bar{v}_1)^{(1)} - (\bar{v}_2)^{(1)}] t}}{1 + (\bar{C})^{(1)} e^{[-(a_{14})^{(1)} (\bar{v}_1)^{(1)} - (\bar{v}_2)^{(1)}] t}} \quad , \quad \boxed{(\bar{C})^{(1)} = \frac{(\bar{v}_1)^{(1)} - (v_0)^{(1)}}{(v_0)^{(1)} - (\bar{v}_2)^{(1)}}$$

From which we deduce $(v_0)^{(1)} \leq v^{(1)}(t) \leq (\bar{v}_1)^{(1)}$

(b) If $0 < (v_1)^{(1)} < (v_0)^{(1)} = \frac{G_{13}^0}{G_{14}^0} < (\bar{v}_1)^{(1)}$ we find like in the previous case,

$$(v_1)^{(1)} \leq \frac{(v_1)^{(1)} + (\bar{C})^{(1)} (v_2)^{(1)} e^{[-(a_{14})^{(1)} ((v_1)^{(1)} - (v_2)^{(1)}) t]}}{1 + (\bar{C})^{(1)} e^{[-(a_{14})^{(1)} ((v_1)^{(1)} - (v_2)^{(1)}) t]}} \leq v^{(1)}(t) \leq \frac{(\bar{v}_1)^{(1)} + (\bar{C})^{(1)} (\bar{v}_2)^{(1)} e^{[-(a_{14})^{(1)} (\bar{v}_1)^{(1)} - (\bar{v}_2)^{(1)}] t}}{1 + (\bar{C})^{(1)} e^{[-(a_{14})^{(1)} (\bar{v}_1)^{(1)} - (\bar{v}_2)^{(1)}] t}} \leq (\bar{v}_1)^{(1)} .$$

(c) If $0 < (v_1)^{(1)} \leq (\bar{v}_1)^{(1)} \leq \boxed{(v_0)^{(1)} = \frac{G_{13}^0}{G_{14}^0}}$, we obtain

$$(v_1)^{(1)} \leq v^{(1)}(t) \leq \frac{(\bar{v}_1)^{(1)} + (\bar{C})^{(1)} (\bar{v}_2)^{(1)} e^{[-(a_{14})^{(1)} (\bar{v}_1)^{(1)} - (\bar{v}_2)^{(1)}] t}}{1 + (\bar{C})^{(1)} e^{[-(a_{14})^{(1)} (\bar{v}_1)^{(1)} - (\bar{v}_2)^{(1)}] t}} \leq (v_0)^{(1)}$$

And so with the notation of the first part of condition (c), we have

Definition of $v^{(1)}(t)$:-

$$(m_2)^{(1)} \leq v^{(1)}(t) \leq (m_1)^{(1)}, \quad \boxed{v^{(1)}(t) = \frac{G_{13}(t)}{G_{14}(t)}}$$

In a completely analogous way, we obtain

Definition of $u^{(1)}(t)$:-

$$(\mu_2)^{(1)} \leq u^{(1)}(t) \leq (\mu_1)^{(1)}, \quad \boxed{u^{(1)}(t) = \frac{T_{13}(t)}{T_{14}(t)}}$$

Now, using this result and replacing it in GLOBAL EQUATIONS we get easily the result stated in the theorem.

Particular case :

If $(a_{13}'')^{(1)} = (a_{14}'')^{(1)}$, then $(\sigma_1)^{(1)} = (\sigma_2)^{(1)}$ and in this case $(v_1)^{(1)} = (\bar{v}_1)^{(1)}$ if in addition $(v_0)^{(1)} = (v_1)^{(1)}$ then $v^{(1)}(t) = (v_0)^{(1)}$ and as a consequence $G_{13}(t) = (v_0)^{(1)} G_{14}(t)$ this also defines $(v_0)^{(1)}$ for the special case

Analogously if $(b_{13}'')^{(1)} = (b_{14}'')^{(1)}$, then $(\tau_1)^{(1)} = (\tau_2)^{(1)}$ and then

$(u_1)^{(1)} = (\bar{u}_1)^{(1)}$ if in addition $(u_0)^{(1)} = (u_1)^{(1)}$ then $T_{13}(t) = (u_0)^{(1)} T_{14}(t)$ This is an important consequence of the relation between $(v_1)^{(1)}$ and $(\bar{v}_1)^{(1)}$, and definition of $(u_0)^{(1)}$.

we obtain

$$\frac{dv^{(2)}}{dt} = (a_{16})^{(2)} - \left((a'_{16})^{(2)} - (a'_{17})^{(2)} + (a''_{16})^{(2)} (T_{17}, t) \right) - (a''_{17})^{(2)} (T_{17}, t) v^{(2)} - (a_{17})^{(2)} v^{(2)} .$$

Definition of $v^{(2)}$:- $\boxed{v^{(2)} = \frac{G_{16}}{G_{17}}}$

It follows

$$- \left((a_{17})^{(2)} (v^{(2)})^2 + (\sigma_2)^{(2)} v^{(2)} - (a_{16})^{(2)} \right) \leq \frac{dv^{(2)}}{dt} \leq - \left((a_{17})^{(2)} (v^{(2)})^2 + (\sigma_1)^{(2)} v^{(2)} - (a_{16})^{(2)} \right) .$$

From which one obtains

Definition of $(\bar{v}_1)^{(2)}, (v_0)^{(2)}$:-

(d) For $0 < (v_0)^{(2)} = \frac{G_{16}^0}{G_{17}^0} < (v_1)^{(2)} < (\bar{v}_1)^{(2)}$

$$v^{(2)}(t) \geq \frac{(v_1)^{(2)} + (C)^{(2)}(v_2)^{(2)} e^{[-(a_{17})^{(2)}((v_1)^{(2)} - (v_0)^{(2)})t]}}{1 + (C)^{(2)} e^{[-(a_{17})^{(2)}((v_1)^{(2)} - (v_0)^{(2)})t]}} , \quad \boxed{(C)^{(2)} = \frac{(v_1)^{(2)} - (v_0)^{(2)}}{(v_0)^{(2)} - (v_2)^{(2)}}$$

it follows $(v_0)^{(2)} \leq v^{(2)}(t) \leq (v_1)^{(2)}$.

In the same manner , we get

$$v^{(2)}(t) \leq \frac{(\bar{v}_1)^{(2)} + (\bar{C})^{(2)}(\bar{v}_2)^{(2)} e^{[-(a_{17})^{(2)}((\bar{v}_1)^{(2)} - (\bar{v}_2)^{(2)})t]}}{1 + (\bar{C})^{(2)} e^{[-(a_{17})^{(2)}((\bar{v}_1)^{(2)} - (\bar{v}_2)^{(2)})t]}} , \quad \boxed{(\bar{C})^{(2)} = \frac{(\bar{v}_1)^{(2)} - (v_0)^{(2)}}{(v_0)^{(2)} - (\bar{v}_2)^{(2)}}$$

From which we deduce $(v_0)^{(2)} \leq v^{(2)}(t) \leq (\bar{v}_1)^{(2)}$.

(e) If $0 < (v_1)^{(2)} < (v_0)^{(2)} = \frac{G_{16}^0}{G_{17}^0} < (\bar{v}_1)^{(2)}$ we find like in the previous case,

$$(v_1)^{(2)} \leq \frac{(v_1)^{(2)} + (C)^{(2)}(v_2)^{(2)} e^{[-(a_{17})^{(2)}((v_1)^{(2)} - (v_2)^{(2)})t]}}{1 + (C)^{(2)} e^{[-(a_{17})^{(2)}((v_1)^{(2)} - (v_2)^{(2)})t]}} \leq v^{(2)}(t) \leq$$

$$\frac{(\bar{v}_1)^{(2)} + (\bar{C})^{(2)}(\bar{v}_2)^{(2)} e^{[-(a_{17})^{(2)}((\bar{v}_1)^{(2)} - (\bar{v}_2)^{(2)})t]}}{1 + (\bar{C})^{(2)} e^{[-(a_{17})^{(2)}((\bar{v}_1)^{(2)} - (\bar{v}_2)^{(2)})t]}} \leq (\bar{v}_1)^{(2)} .$$

(f) If $0 < (v_1)^{(2)} \leq (\bar{v}_1)^{(2)} \leq (v_0)^{(2)} = \frac{G_{16}^0}{G_{17}^0}$, we obtain

$$(v_1)^{(2)} \leq v^{(2)}(t) \leq \frac{(\bar{v}_1)^{(2)} + (\bar{C})^{(2)}(\bar{v}_2)^{(2)} e^{[-(a_{17})^{(2)}((\bar{v}_1)^{(2)} - (\bar{v}_2)^{(2)})t]}}{1 + (\bar{C})^{(2)} e^{[-(a_{17})^{(2)}((\bar{v}_1)^{(2)} - (\bar{v}_2)^{(2)})t]}} \leq (v_0)^{(2)}$$

And so with the notation of the first part of condition (c) , we have .

Definition of $v^{(2)}(t)$:-

$$(m_2)^{(2)} \leq v^{(2)}(t) \leq (m_1)^{(2)} , \quad \boxed{v^{(2)}(t) = \frac{G_{16}(t)}{G_{17}(t)}} .$$

In a completely analogous way, we obtain

Definition of $u^{(2)}(t)$:-

$$(\mu_2)^{(2)} \leq u^{(2)}(t) \leq (\mu_1)^{(2)} , \quad \boxed{u^{(2)}(t) = \frac{T_{16}(t)}{T_{17}(t)}} .$$

Particular case :

If $(a_{16}'')^{(2)} = (a_{17}'')^{(2)}$, then $(\sigma_1)^{(2)} = (\sigma_2)^{(2)}$ and in this case $(v_1)^{(2)} = (\bar{v}_1)^{(2)}$ if in addition $(v_0)^{(2)} = (v_1)^{(2)}$ then $v^{(2)}(t) = (v_0)^{(2)}$ and as a consequence $G_{16}(t) = (v_0)^{(2)} G_{17}(t)$

Analogously if $(b_{16}'')^{(2)} = (b_{17}'')^{(2)}$, then $(\tau_1)^{(2)} = (\tau_2)^{(2)}$ and then

$(u_1)^{(2)} = (\bar{u}_1)^{(2)}$ if in addition $(u_0)^{(2)} = (u_1)^{(2)}$ then $T_{16}(t) = (u_0)^{(2)} T_{17}(t)$ This is an important consequence of the relation between $(v_1)^{(2)}$ and $(\bar{v}_1)^{(2)}$.

From GLOBAL EQUATIONS we obtain

$$\frac{dv^{(3)}}{dt} = (a_{20})^{(3)} - \left((a_{20}')^{(3)} - (a_{21}')^{(3)} + (a_{20}'')^{(3)}(T_{21}, t) \right) - (a_{21}'')^{(3)}(T_{21}, t)v^{(3)} - (a_{21})^{(3)}v^{(3)} .$$

Definition of $v^{(3)}$:- $\boxed{v^{(3)} = \frac{G_{20}}{G_{21}}}$

It follows

$$-\left((a_{21})^{(3)}(v^{(3)})^2 + (\sigma_2)^{(3)}v^{(3)} - (a_{20})^{(3)}\right) \leq \frac{dv^{(3)}}{dt} \leq -\left((a_{21})^{(3)}(v^{(3)})^2 + (\sigma_1)^{(3)}v^{(3)} - (a_{20})^{(3)}\right).$$

From which one obtains

(a) For $0 < (v_0)^{(3)} = \frac{G_{20}^0}{G_{21}^0} < (v_1)^{(3)} < (\bar{v}_1)^{(3)}$

$$v^{(3)}(t) \geq \frac{(v_1)^{(3)} + (C)^{(3)}(v_2)^{(3)} e^{[-(a_{21})^{(3)}((v_1)^{(3)} - (v_0)^{(3)})t]}}{1 + (C)^{(3)} e^{[-(a_{21})^{(3)}((v_1)^{(3)} - (v_0)^{(3)})t]}} , \quad \boxed{(C)^{(3)} = \frac{(v_1)^{(3)} - (v_0)^{(3)}}{(v_0)^{(3)} - (v_2)^{(3)}}}$$

it follows $(v_0)^{(3)} \leq v^{(3)}(t) \leq (v_1)^{(3)}$.

In the same manner, we get

$$v^{(3)}(t) \leq \frac{(\bar{v}_1)^{(3)} + (\bar{C})^{(3)}(\bar{v}_2)^{(3)} e^{[-(a_{21})^{(3)}((\bar{v}_1)^{(3)} - (\bar{v}_2)^{(3)})t]}}{1 + (\bar{C})^{(3)} e^{[-(a_{21})^{(3)}((\bar{v}_1)^{(3)} - (\bar{v}_2)^{(3)})t]}} , \quad \boxed{(\bar{C})^{(3)} = \frac{(\bar{v}_1)^{(3)} - (v_0)^{(3)}}{(v_0)^{(3)} - (\bar{v}_2)^{(3)}}$$

Definition of $(\bar{v}_1)^{(3)}$:-

From which we deduce $(v_0)^{(3)} \leq v^{(3)}(t) \leq (\bar{v}_1)^{(3)}$.

(b) If $0 < (v_1)^{(3)} < (v_0)^{(3)} = \frac{G_{20}^0}{G_{21}^0} < (\bar{v}_1)^{(3)}$ we find like in the previous case,

$$(v_1)^{(3)} \leq \frac{(v_1)^{(3)} + (C)^{(3)}(v_2)^{(3)} e^{[-(a_{21})^{(3)}((v_1)^{(3)} - (v_2)^{(3)})t]}}{1 + (C)^{(3)} e^{[-(a_{21})^{(3)}((v_1)^{(3)} - (v_2)^{(3)})t]}} \leq v^{(3)}(t) \leq$$

$$\frac{(\bar{v}_1)^{(3)} + (\bar{C})^{(3)}(\bar{v}_2)^{(3)} e^{[-(a_{21})^{(3)}((\bar{v}_1)^{(3)} - (\bar{v}_2)^{(3)})t]}}{1 + (\bar{C})^{(3)} e^{[-(a_{21})^{(3)}((\bar{v}_1)^{(3)} - (\bar{v}_2)^{(3)})t]}} \leq (\bar{v}_1)^{(3)}$$

(c) If $0 < (v_1)^{(3)} \leq (\bar{v}_1)^{(3)} \leq (v_0)^{(3)} = \frac{G_{20}^0}{G_{21}^0}$, we obtain

$$(v_1)^{(3)} \leq v^{(3)}(t) \leq \frac{(\bar{v}_1)^{(3)} + (\bar{C})^{(3)}(\bar{v}_2)^{(3)} e^{[-(a_{21})^{(3)}((\bar{v}_1)^{(3)} - (\bar{v}_2)^{(3)})t]}}{1 + (\bar{C})^{(3)} e^{[-(a_{21})^{(3)}((\bar{v}_1)^{(3)} - (\bar{v}_2)^{(3)})t]}} \leq (v_0)^{(3)}$$

And so with the notation of the first part of condition (c), we have

Definition of $v^{(3)}(t)$:-

$$(m_2)^{(3)} \leq v^{(3)}(t) \leq (m_1)^{(3)}, \quad \boxed{v^{(3)}(t) = \frac{G_{20}(t)}{G_{21}(t)}}$$

In a completely analogous way, we obtain

Definition of $u^{(3)}(t)$:-

$$(\mu_2)^{(3)} \leq u^{(3)}(t) \leq (\mu_1)^{(3)}, \quad \boxed{u^{(3)}(t) = \frac{T_{20}(t)}{T_{21}(t)}}$$

Now, using this result and replacing it in GLOBAL EQUATIONS we get easily the result stated in the theorem.

Particular case :

If $(a_{20})^{(3)} = (a_{21})^{(3)}$, then $(\sigma_1)^{(3)} = (\sigma_2)^{(3)}$ and in this case $(v_1)^{(3)} = (\bar{v}_1)^{(3)}$ if in addition $(v_0)^{(3)} = (v_1)^{(3)}$ then $v^{(3)}(t) = (v_0)^{(3)}$ and as a consequence $G_{20}(t) = (v_0)^{(3)}G_{21}(t)$

Analogously if $(b_{20})^{(3)} = (b_{21})^{(3)}$, then $(\tau_1)^{(3)} = (\tau_2)^{(3)}$ and then

$(u_1)^{(3)} = (\bar{u}_1)^{(3)}$ if in addition $(u_0)^{(3)} = (u_1)^{(3)}$ then $T_{20}(t) = (u_0)^{(3)}T_{21}(t)$ This is an important consequence of the relation between $(v_1)^{(3)}$ and $(\bar{v}_1)^{(3)}$.

From GLOBAL EQUATIONS we obtain

$$\frac{dv^{(4)}}{dt} = (a_{24})^{(4)} - \left((a'_{24})^{(4)} - (a'_{25})^{(4)} + (a''_{24})^{(4)}(T_{25}, t) \right) - (a''_{25})^{(4)}(T_{25}, t)v^{(4)} - (a_{25})^{(4)}v^{(4)}$$

Definition of $v^{(4)}$:- $v^{(4)} = \frac{G_{24}}{G_{25}}$

It follows

$$- \left((a_{25})^{(4)}(v^{(4)})^2 + (\sigma_2)^{(4)}v^{(4)} - (a_{24})^{(4)} \right) \leq \frac{dv^{(4)}}{dt} \leq - \left((a_{25})^{(4)}(v^{(4)})^2 + (\sigma_4)^{(4)}v^{(4)} - (a_{24})^{(4)} \right)$$

From which one obtains

Definition of $(v_1)^{(4)}, (v_0)^{(4)}$:-

(d) For $0 < \left[(v_0)^{(4)} = \frac{G_{24}^0}{G_{25}^0} \right] < (v_1)^{(4)} < (\bar{v}_1)^{(4)}$

$$v^{(4)}(t) \geq \frac{(v_1)^{(4)} + (C)^{(4)}(v_2)^{(4)} e^{[-(a_{25})^{(4)}((v_1)^{(4)} - (v_0)^{(4)})t]}}{4 + (C)^{(4)} e^{[-(a_{25})^{(4)}((v_1)^{(4)} - (v_0)^{(4)})t]}} , \quad \left[(C)^{(4)} = \frac{(v_1)^{(4)} - (v_0)^{(4)}}{(v_0)^{(4)} - (v_2)^{(4)}} \right]$$

it follows $(v_0)^{(4)} \leq v^{(4)}(t) \leq (v_1)^{(4)}$

In the same manner , we get

$$v^{(4)}(t) \leq \frac{(\bar{v}_1)^{(4)} + (\bar{C})^{(4)}(\bar{v}_2)^{(4)} e^{[-(a_{25})^{(4)}((\bar{v}_1)^{(4)} - (\bar{v}_2)^{(4)})t]}}{4 + (\bar{C})^{(4)} e^{[-(a_{25})^{(4)}((\bar{v}_1)^{(4)} - (\bar{v}_2)^{(4)})t]}} , \quad \left[(\bar{C})^{(4)} = \frac{(\bar{v}_1)^{(4)} - (v_0)^{(4)}}{(v_0)^{(4)} - (\bar{v}_2)^{(4)}} \right]$$

From which we deduce $(v_0)^{(4)} \leq v^{(4)}(t) \leq (\bar{v}_1)^{(4)}$

(e) If $0 < (v_1)^{(4)} < (v_0)^{(4)} = \frac{G_{24}^0}{G_{25}^0} < (\bar{v}_1)^{(4)}$ we find like in the previous case,

$$(v_1)^{(4)} \leq \frac{(v_1)^{(4)} + (C)^{(4)}(v_2)^{(4)} e^{[-(a_{25})^{(4)}((v_1)^{(4)} - (v_2)^{(4)})t]}}{1 + (C)^{(4)} e^{[-(a_{25})^{(4)}((v_1)^{(4)} - (v_2)^{(4)})t]}} \leq v^{(4)}(t) \leq \frac{(\bar{v}_1)^{(4)} + (\bar{C})^{(4)}(\bar{v}_2)^{(4)} e^{[-(a_{25})^{(4)}((\bar{v}_1)^{(4)} - (\bar{v}_2)^{(4)})t]}}{1 + (\bar{C})^{(4)} e^{[-(a_{25})^{(4)}((\bar{v}_1)^{(4)} - (\bar{v}_2)^{(4)})t]}} \leq (\bar{v}_1)^{(4)} .$$

(f) If $0 < (v_1)^{(4)} \leq (\bar{v}_1)^{(4)} \leq \left[(v_0)^{(4)} = \frac{G_{24}^0}{G_{25}^0} \right]$, we obtain

$$(v_1)^{(4)} \leq v^{(4)}(t) \leq \frac{(\bar{v}_1)^{(4)} + (\bar{C})^{(4)}(\bar{v}_2)^{(4)} e^{[-(a_{25})^{(4)}((\bar{v}_1)^{(4)} - (\bar{v}_2)^{(4)})t]}}{1 + (\bar{C})^{(4)} e^{[-(a_{25})^{(4)}((\bar{v}_1)^{(4)} - (\bar{v}_2)^{(4)})t]}} \leq (v_0)^{(4)}$$

And so with the notation of the first part of condition (c) , we have

Definition of $v^{(4)}(t)$:-

$$(m_2)^{(4)} \leq v^{(4)}(t) \leq (m_1)^{(4)} , \quad \left[v^{(4)}(t) = \frac{G_{24}(t)}{G_{25}(t)} \right]$$

In a completely analogous way, we obtain

Definition of $u^{(4)}(t) :-$

$$(\mu_2)^{(4)} \leq u^{(4)}(t) \leq (\mu_1)^{(4)}, \quad \boxed{u^{(4)}(t) = \frac{T_{24}(t)}{T_{25}(t)}}$$

Now, using this result and replacing it in GLOBAL EQUATIONS we get easily the result stated in the theorem.

Particular case :

If $(a''_{24})^{(4)} = (a''_{25})^{(4)}$, then $(\sigma_1)^{(4)} = (\sigma_2)^{(4)}$ and in this case $(v_1)^{(4)} = (\bar{v}_1)^{(4)}$ if in addition $(v_0)^{(4)} = (v_1)^{(4)}$ then $v^{(4)}(t) = (v_0)^{(4)}$ and as a consequence $G_{24}(t) = (v_0)^{(4)}G_{25}(t)$ **this also defines $(v_0)^{(4)}$ for the special case .**

Analogously if $(b''_{24})^{(4)} = (b''_{25})^{(4)}$, then $(\tau_1)^{(4)} = (\tau_2)^{(4)}$ and then

$(u_1)^{(4)} = (\bar{u}_4)^{(4)}$ if in addition $(u_0)^{(4)} = (u_1)^{(4)}$ then $T_{24}(t) = (u_0)^{(4)}T_{25}(t)$ This is an important consequence of the relation between $(v_1)^{(4)}$ and $(\bar{v}_1)^{(4)}$, **and definition of $(u_0)^{(4)}$.**

From GLOBAL EQUATIONS we obtain

$$\frac{dv^{(5)}}{dt} = (a_{28})^{(5)} - \left((a'_{28})^{(5)} - (a'_{29})^{(5)} + (a''_{28})^{(5)}(T_{29}, t) \right) - (a''_{29})^{(5)}(T_{29}, t)v^{(5)} - (a_{29})^{(5)}v^{(5)}$$

Definition of $v^{(5)} :-$ $\boxed{v^{(5)} = \frac{G_{28}}{G_{29}}}$

It follows

$$- \left((a_{29})^{(5)}(v^{(5)})^2 + (\sigma_2)^{(5)}v^{(5)} - (a_{28})^{(5)} \right) \leq \frac{dv^{(5)}}{dt} \leq - \left((a_{29})^{(5)}(v^{(5)})^2 + (\sigma_1)^{(5)}v^{(5)} - (a_{28})^{(5)} \right)$$

From which one obtains

Definition of $(\bar{v}_1)^{(5)}, (v_0)^{(5)} :-$

(g) For $0 < \boxed{(v_0)^{(5)} = \frac{G_{28}^0}{G_{29}^0}} < (v_1)^{(5)} < (\bar{v}_1)^{(5)}$

$$v^{(5)}(t) \geq \frac{(v_1)^{(5)} + (C)^{(5)}(v_2)^{(5)} e^{[-(a_{29})^{(5)}(v_1)^{(5)} - (v_0)^{(5)}]t}}{5 + (C)^{(5)} e^{[-(a_{29})^{(5)}(v_1)^{(5)} - (v_0)^{(5)}]t}}, \quad \boxed{(C)^{(5)} = \frac{(v_1)^{(5)} - (v_0)^{(5)}}{(v_0)^{(5)} - (v_2)^{(5)}}$$

it follows $(v_0)^{(5)} \leq v^{(5)}(t) \leq (v_1)^{(5)}$

In the same manner , we get

$$v^{(5)}(t) \leq \frac{(\bar{v}_1)^{(5)} + (\bar{C})^{(5)}(\bar{v}_2)^{(5)} e^{[-(a_{29})^{(5)}(\bar{v}_1)^{(5)} - (\bar{v}_2)^{(5)}]t}}{5 + (\bar{C})^{(5)} e^{[-(a_{29})^{(5)}(\bar{v}_1)^{(5)} - (\bar{v}_2)^{(5)}]t}}, \quad \boxed{(\bar{C})^{(5)} = \frac{(\bar{v}_1)^{(5)} - (v_0)^{(5)}}{(v_0)^{(5)} - (\bar{v}_2)^{(5)}}$$

From which we deduce $(v_0)^{(5)} \leq v^{(5)}(t) \leq (\bar{v}_5)^{(5)}$

(h) If $0 < (v_1)^{(5)} < (v_0)^{(5)} = \frac{G_{28}^0}{G_{29}^0} < (\bar{v}_1)^{(5)}$ we find like in the previous case,

$$(v_1)^{(5)} \leq \frac{(v_1)^{(5)} + (C)^{(5)}(v_2)^{(5)} e^{[-(a_{29})^{(5)}(v_1)^{(5)} - (v_2)^{(5)}]t}}{1 + (C)^{(5)} e^{[-(a_{29})^{(5)}(v_1)^{(5)} - (v_2)^{(5)}]t}} \leq v^{(5)}(t) \leq$$

$$\frac{(\bar{v}_1)^{(5)} + (\bar{C})^{(5)}(\bar{v}_2)^{(5)} e^{[-(a_{29})^{(5)}(\bar{v}_1)^{(5)} - (\bar{v}_2)^{(5)}]t}}{1 + (\bar{C})^{(5)} e^{[-(a_{29})^{(5)}(\bar{v}_1)^{(5)} - (\bar{v}_2)^{(5)}]t}} \leq (\bar{v}_1)^{(5)} .$$

(i) If $0 < (v_1)^{(5)} \leq (\bar{v}_1)^{(5)} \leq \boxed{(v_0)^{(5)} = \frac{G_{28}^0}{G_{29}^0}}$, we obtain

$$(v_1)^{(5)} \leq v^{(5)}(t) \leq \frac{(\bar{v}_1)^{(5)} + (C)^{(5)}(\bar{v}_2)^{(5)} e^{[-(a_{29})^{(5)}((\bar{v}_1)^{(5)} - (\bar{v}_2)^{(5)})t]}}{1 + (C)^{(5)} e^{[-(a_{29})^{(5)}((\bar{v}_1)^{(5)} - (\bar{v}_2)^{(5)})t]}} \leq (v_0)^{(5)}$$

And so with the notation of the first part of condition (c), we have

Definition of $v^{(5)}(t)$:-

$$(m_2)^{(5)} \leq v^{(5)}(t) \leq (m_1)^{(5)}, \quad \boxed{v^{(5)}(t) = \frac{G_{28}(t)}{G_{29}(t)}}$$

In a completely analogous way, we obtain

Definition of $u^{(5)}(t)$:-

$$(\mu_2)^{(5)} \leq u^{(5)}(t) \leq (\mu_1)^{(5)}, \quad \boxed{u^{(5)}(t) = \frac{T_{28}(t)}{T_{29}(t)}}$$

Now, using this result and replacing it in GLOBAL EQUATIONS we get easily the result stated in the theorem.

Particular case :

If $(a''_{28})^{(5)} = (a''_{29})^{(5)}$, then $(\sigma_1)^{(5)} = (\sigma_2)^{(5)}$ and in this case $(v_1)^{(5)} = (\bar{v}_1)^{(5)}$ if in addition $(v_0)^{(5)} = (v_5)^{(5)}$ then $v^{(5)}(t) = (v_0)^{(5)}$ and as a consequence $G_{28}(t) = (v_0)^{(5)}G_{29}(t)$ **this also defines $(v_0)^{(5)}$ for the special case .**

Analogously if $(b''_{28})^{(5)} = (b''_{29})^{(5)}$, then $(\tau_1)^{(5)} = (\tau_2)^{(5)}$ and then

$(u_1)^{(5)} = (\bar{u}_1)^{(5)}$ if in addition $(u_0)^{(5)} = (u_1)^{(5)}$ then $T_{28}(t) = (u_0)^{(5)}T_{29}(t)$ This is an important consequence of the relation between $(v_1)^{(5)}$ and $(\bar{v}_1)^{(5)}$, **and definition of $(u_0)^{(5)}$.**

we obtain

$$\frac{dv^{(6)}}{dt} = (a_{32})^{(6)} - \left((a'_{32})^{(6)} - (a'_{33})^{(6)} + (a''_{32})^{(6)}(T_{33}, t) \right) - (a''_{33})^{(6)}(T_{33}, t)v^{(6)} - (a_{33})^{(6)}v^{(6)}$$

Definition of $v^{(6)}$:- $\boxed{v^{(6)} = \frac{G_{32}}{G_{33}}}$

It follows

$$- \left((a_{33})^{(6)}(v^{(6)})^2 + (\sigma_2)^{(6)}v^{(6)} - (a_{32})^{(6)} \right) \leq \frac{dv^{(6)}}{dt} \leq - \left((a_{33})^{(6)}(v^{(6)})^2 + (\sigma_1)^{(6)}v^{(6)} - (a_{32})^{(6)} \right)$$

From which one obtains

Definition of $(\bar{v}_1)^{(6)}, (v_0)^{(6)}$:-

(j) For $0 < \boxed{(v_0)^{(6)} = \frac{G_{32}^0}{G_{33}^0}} < (v_1)^{(6)} < (\bar{v}_1)^{(6)}$

$$v^{(6)}(t) \geq \frac{(v_1)^{(6)} + (C)^{(6)}(v_2)^{(6)} e^{[-(a_{33})^{(6)}((v_1)^{(6)} - (v_0)^{(6)})t]}}{1 + (C)^{(6)} e^{[-(a_{33})^{(6)}((v_1)^{(6)} - (v_0)^{(6)})t]}} , \quad \boxed{(C)^{(6)} = \frac{(v_1)^{(6)} - (v_0)^{(6)}}{(v_0)^{(6)} - (v_2)^{(6)}}$$

it follows $(v_0)^{(6)} \leq v^{(6)}(t) \leq (v_1)^{(6)}$

In the same manner , we get

$$v^{(6)}(t) \leq \frac{(\bar{v}_1)^{(6)} + (\bar{C})^{(6)}(\bar{v}_2)^{(6)} e^{[-(a_{33})^{(6)}(\bar{v}_1)^{(6)} - (\bar{v}_2)^{(6)}]t}}{1 + (\bar{C})^{(6)} e^{[-(a_{33})^{(6)}(\bar{v}_1)^{(6)} - (\bar{v}_2)^{(6)}]t}} , \quad \boxed{(\bar{C})^{(6)} = \frac{(\bar{v}_1)^{(6)} - (v_0)^{(6)}}{(v_0)^{(6)} - (\bar{v}_2)^{(6)}}$$

From which we deduce $(v_0)^{(6)} \leq v^{(6)}(t) \leq (\bar{v}_1)^{(6)}$

(k) If $0 < (v_1)^{(6)} < (v_0)^{(6)} = \frac{G_{32}^0}{G_{33}^0} < (\bar{v}_1)^{(6)}$ we find like in the previous case,

$$(v_1)^{(6)} \leq \frac{(v_1)^{(6)} + (C)^{(6)}(v_2)^{(6)} e^{[-(a_{33})^{(6)}(v_1)^{(6)} - (v_2)^{(6)}]t}}{1 + (C)^{(6)} e^{[-(a_{33})^{(6)}(v_1)^{(6)} - (v_2)^{(6)}]t}} \leq v^{(6)}(t) \leq \frac{(\bar{v}_1)^{(6)} + (\bar{C})^{(6)}(\bar{v}_2)^{(6)} e^{[-(a_{33})^{(6)}(\bar{v}_1)^{(6)} - (\bar{v}_2)^{(6)}]t}}{1 + (\bar{C})^{(6)} e^{[-(a_{33})^{(6)}(\bar{v}_1)^{(6)} - (\bar{v}_2)^{(6)}]t}} \leq (\bar{v}_1)^{(6)} .$$

(l) If $0 < (v_1)^{(6)} \leq (\bar{v}_1)^{(6)} \leq \boxed{(v_0)^{(6)} = \frac{G_{32}^0}{G_{33}^0}}$, we obtain

$$(v_1)^{(6)} \leq v^{(6)}(t) \leq \frac{(\bar{v}_1)^{(6)} + (\bar{C})^{(6)}(\bar{v}_2)^{(6)} e^{[-(a_{33})^{(6)}(\bar{v}_1)^{(6)} - (\bar{v}_2)^{(6)}]t}}{1 + (\bar{C})^{(6)} e^{[-(a_{33})^{(6)}(\bar{v}_1)^{(6)} - (\bar{v}_2)^{(6)}]t}} \leq (v_0)^{(6)}$$

And so with the notation of the first part of condition (c) , we have

Definition of $v^{(6)}(t)$:-

$$(m_2)^{(6)} \leq v^{(6)}(t) \leq (m_1)^{(6)} , \quad \boxed{v^{(6)}(t) = \frac{G_{32}(t)}{G_{33}(t)}}$$

In a completely analogous way, we obtain

Definition of $u^{(6)}(t)$:-

$$(\mu_2)^{(6)} \leq u^{(6)}(t) \leq (\mu_1)^{(6)} , \quad \boxed{u^{(6)}(t) = \frac{T_{32}(t)}{T_{33}(t)}}$$

Now, using this result and replacing it in GLOBAL EQUATIONS we get easily the result stated in the theorem.

Particular case :

If $(a_{32}'')^{(6)} = (a_{33}'')^{(6)}$, then $(\sigma_1)^{(6)} = (\sigma_2)^{(6)}$ and in this case $(v_1)^{(6)} = (\bar{v}_1)^{(6)}$ if in addition $(v_0)^{(6)} = (v_1)^{(6)}$ then $v^{(6)}(t) = (v_0)^{(6)}$ and as a consequence $G_{32}(t) = (v_0)^{(6)}G_{33}(t)$ **this also defines $(v_0)^{(6)}$ for the special case .**

Analogously if $(b_{32}'')^{(6)} = (b_{33}'')^{(6)}$, then $(\tau_1)^{(6)} = (\tau_2)^{(6)}$ and then

$(u_1)^{(6)} = (\bar{u}_1)^{(6)}$ if in addition $(u_0)^{(6)} = (u_1)^{(6)}$ then $T_{32}(t) = (u_0)^{(6)}T_{33}(t)$ This is an important consequence of the relation between $(v_1)^{(6)}$ and $(\bar{v}_1)^{(6)}$, **and definition of $(u_0)^{(6)}$.**

We can prove the following

Theorem 3: If $(a_i'')^{(1)}$ and $(b_i'')^{(1)}$ are independent on t , and the conditions

$$(a'_{13})^{(1)}(a'_{14})^{(1)} - (a_{13})^{(1)}(a_{14})^{(1)} < 0$$

$$(a'_{13})^{(1)}(a'_{14})^{(1)} - (a_{13})^{(1)}(a_{14})^{(1)} + (a_{13})^{(1)}(p_{13})^{(1)} + (a'_{14})^{(1)}(p_{14})^{(1)} + (p_{13})^{(1)}(p_{14})^{(1)} > 0$$

$$(b'_{13})^{(1)}(b'_{14})^{(1)} - (b_{13})^{(1)}(b_{14})^{(1)} > 0 ,$$

$$(b'_{13})^{(1)}(b'_{14})^{(1)} - (b_{13})^{(1)}(b_{14})^{(1)} - (b'_{13})^{(1)}(r_{14})^{(1)} - (b'_{14})^{(1)}(r_{14})^{(1)} + (r_{13})^{(1)}(r_{14})^{(1)} < 0$$

with $(p_{13})^{(1)}, (r_{14})^{(1)}$ as defined, then the system.

If $(a_i'')^{(2)}$ and $(b_i'')^{(2)}$ are independent on t , and the conditions .

$$(a'_{16})^{(2)}(a'_{17})^{(2)} - (a_{16})^{(2)}(a_{17})^{(2)} < 0 .$$

$$(a'_{16})^{(2)}(a'_{17})^{(2)} - (a_{16})^{(2)}(a_{17})^{(2)} + (a_{16})^{(2)}(p_{16})^{(2)} + (a'_{17})^{(2)}(p_{17})^{(2)} + (p_{16})^{(2)}(p_{17})^{(2)} > 0 .$$

$$(b'_{16})^{(2)}(b'_{17})^{(2)} - (b_{16})^{(2)}(b_{17})^{(2)} > 0 , .$$

$$(b'_{16})^{(2)}(b'_{17})^{(2)} - (b_{16})^{(2)}(b_{17})^{(2)} - (b'_{16})^{(2)}(r_{17})^{(2)} - (b'_{17})^{(2)}(r_{17})^{(2)} + (r_{16})^{(2)}(r_{17})^{(2)} < 0$$

with $(p_{16})^{(2)}, (r_{17})^{(2)}$ as defined are satisfied , then the system.

If $(a_i'')^{(3)}$ and $(b_i'')^{(3)}$ are independent on t , and the conditions

$$(a'_{20})^{(3)}(a'_{21})^{(3)} - (a_{20})^{(3)}(a_{21})^{(3)} < 0$$

$$(a'_{20})^{(3)}(a'_{21})^{(3)} - (a_{20})^{(3)}(a_{21})^{(3)} + (a_{20})^{(3)}(p_{20})^{(3)} + (a'_{21})^{(3)}(p_{21})^{(3)} + (p_{20})^{(3)}(p_{21})^{(3)} > 0$$

$$(b'_{20})^{(3)}(b'_{21})^{(3)} - (b_{20})^{(3)}(b_{21})^{(3)} > 0 ,$$

$$(b'_{20})^{(3)}(b'_{21})^{(3)} - (b_{20})^{(3)}(b_{21})^{(3)} - (b'_{20})^{(3)}(r_{21})^{(3)} - (b'_{21})^{(3)}(r_{21})^{(3)} + (r_{20})^{(3)}(r_{21})^{(3)} < 0$$

with $(p_{20})^{(3)}, (r_{21})^{(3)}$ as defined are satisfied , then the system.

If $(a_i'')^{(4)}$ and $(b_i'')^{(4)}$ are independent on t , and the conditions

$$(a'_{24})^{(4)}(a'_{25})^{(4)} - (a_{24})^{(4)}(a_{25})^{(4)} < 0$$

$$(a'_{24})^{(4)}(a'_{25})^{(4)} - (a_{24})^{(4)}(a_{25})^{(4)} + (a_{24})^{(4)}(p_{24})^{(4)} + (a'_{25})^{(4)}(p_{25})^{(4)} + (p_{24})^{(4)}(p_{25})^{(4)} > 0$$

$$(b'_{24})^{(4)}(b'_{25})^{(4)} - (b_{24})^{(4)}(b_{25})^{(4)} > 0 ,$$

$$(b'_{24})^{(4)}(b'_{25})^{(4)} - (b_{24})^{(4)}(b_{25})^{(4)} - (b'_{24})^{(4)}(r_{25})^{(4)} - (b'_{25})^{(4)}(r_{25})^{(4)} + (r_{24})^{(4)}(r_{25})^{(4)} < 0$$

with $(p_{24})^{(4)}, (r_{25})^{(4)}$ as defined are satisfied , then the system.

If $(a_i'')^{(5)}$ and $(b_i'')^{(5)}$ are independent on t , and the conditions

$$(a'_{28})^{(5)}(a'_{29})^{(5)} - (a_{28})^{(5)}(a_{29})^{(5)} < 0$$

$$(a'_{28})^{(5)}(a'_{29})^{(5)} - (a_{28})^{(5)}(a_{29})^{(5)} + (a_{28})^{(5)}(p_{28})^{(5)} + (a'_{29})^{(5)}(p_{29})^{(5)} + (p_{28})^{(5)}(p_{29})^{(5)} > 0$$

$$(b'_{28})^{(5)}(b'_{29})^{(5)} - (b_{28})^{(5)}(b_{29})^{(5)} > 0 ,$$

$$(b'_{28})^{(5)}(b'_{29})^{(5)} - (b_{28})^{(5)}(b_{29})^{(5)} - (b'_{28})^{(5)}(r_{29})^{(5)} - (b'_{29})^{(5)}(r_{29})^{(5)} + (r_{28})^{(5)}(r_{29})^{(5)} < 0$$

with $(p_{28})^{(5)}, (r_{29})^{(5)}$ as defined satisfied , then the system.

If $(a_i'')^{(6)}$ and $(b_i'')^{(6)}$ are independent on t , and the conditions

$$(a'_{32})^{(6)}(a'_{33})^{(6)} - (a_{32})^{(6)}(a_{33})^{(6)} < 0$$

$$(a'_{32})^{(6)}(a'_{33})^{(6)} - (a_{32})^{(6)}(a_{33})^{(6)} + (a_{32})^{(6)}(p_{32})^{(6)} + (a'_{33})^{(6)}(p_{33})^{(6)} + (p_{32})^{(6)}(p_{33})^{(6)} > 0$$

$$(b'_{32})^{(6)}(b'_{33})^{(6)} - (b_{32})^{(6)}(b_{33})^{(6)} > 0 ,$$

$$(b'_{32})^{(6)}(b'_{33})^{(6)} - (b_{32})^{(6)}(b_{33})^{(6)} - (b'_{32})^{(6)}(r_{33})^{(6)} - (b'_{33})^{(6)}(r_{33})^{(6)} + (r_{32})^{(6)}(r_{33})^{(6)} < 0$$

with $(p_{32})^{(6)}, (r_{33})^{(6)}$ as defined are satisfied , then the system.

$$(a_{13})^{(1)}G_{14} - [(a'_{13})^{(1)} + (a''_{13})^{(1)}(T_{14})]G_{13} = 0 .$$

$$(a_{14})^{(1)}G_{13} - [(a'_{14})^{(1)} + (a''_{14})^{(1)}(T_{14})]G_{14} = 0 .$$

$$(a_{15})^{(1)}G_{14} - [(a'_{15})^{(1)} + (a''_{15})^{(1)}(T_{14})]G_{15} = 0 .$$

$$(b_{13})^{(1)}T_{14} - [(b'_{13})^{(1)} - (b''_{13})^{(1)}(G)]T_{13} = 0 .$$

$$(b_{14})^{(1)}T_{13} - [(b'_{14})^{(1)} - (b''_{14})^{(1)}(G)]T_{14} = 0 .$$

$$(b_{15})^{(1)}T_{14} - [(b'_{15})^{(1)} - (b''_{15})^{(1)}(G)]T_{15} = 0 .$$

has a unique positive solution , which is an equilibrium solution for the system.

$$(a_{16})^{(2)}G_{17} - [(a'_{16})^{(2)} + (a''_{16})^{(2)}(T_{17})]G_{16} = 0 .$$

$$(a_{17})^{(2)}G_{16} - [(a'_{17})^{(2)} + (a''_{17})^{(2)}(T_{17})]G_{17} = 0 .$$

$$(a_{18})^{(2)}G_{17} - [(a'_{18})^{(2)} + (a''_{18})^{(2)}(T_{17})]G_{18} = 0 .$$

$$(b_{16})^{(2)}T_{17} - [(b'_{16})^{(2)} - (b''_{16})^{(2)}(G_{19})]T_{16} = 0 .$$

$$(b_{17})^{(2)}T_{16} - [(b'_{17})^{(2)} - (b''_{17})^{(2)}(G_{19})]T_{17} = 0 .$$

$$(b_{18})^{(2)}T_{17} - [(b'_{18})^{(2)} - (b''_{18})^{(2)}(G_{19})]T_{18} = 0 .$$

has a unique positive solution , which is an equilibrium solution for .

$$(a_{20})^{(3)}G_{21} - [(a'_{20})^{(3)} + (a''_{20})^{(3)}(T_{21})]G_{20} = 0 .$$

$$(a_{21})^{(3)}G_{20} - [(a'_{21})^{(3)} + (a''_{21})^{(3)}(T_{21})]G_{21} = 0 .$$

$$(a_{22})^{(3)}G_{21} - [(a'_{22})^{(3)} + (a''_{22})^{(3)}(T_{21})]G_{22} = 0 .$$

$$(b_{20})^{(3)}T_{21} - [(b'_{20})^{(3)} - (b''_{20})^{(3)}(G_{23})]T_{20} = 0 .$$

$$(b_{21})^{(3)}T_{20} - [(b'_{21})^{(3)} - (b''_{21})^{(3)}(G_{23})]T_{21} = 0 .$$

$$(b_{22})^{(3)}T_{21} - [(b'_{22})^{(3)} - (b''_{22})^{(3)}(G_{23})]T_{22} = 0 .$$

has a unique positive solution , which is an equilibrium solution.

$$(a_{24})^{(4)}G_{25} - [(a'_{24})^{(4)} + (a''_{24})^{(4)}(T_{25})]G_{24} = 0$$

$$(a_{25})^{(4)}G_{24} - [(a'_{25})^{(4)} + (a''_{25})^{(4)}(T_{25})]G_{25} = 0$$

$$(a_{26})^{(4)}G_{25} - [(a'_{26})^{(4)} + (a''_{26})^{(4)}(T_{25})]G_{26} = 0$$

$$(b_{24})^{(4)}T_{25} - [(b'_{24})^{(4)} - (b''_{24})^{(4)}((G_{27}))]T_{24} = 0$$

$$(b_{25})^{(4)}T_{24} - [(b'_{25})^{(4)} - (b''_{25})^{(4)}((G_{27}))]T_{25} = 0$$

$$(b_{26})^{(4)}T_{25} - [(b'_{26})^{(4)} - (b''_{26})^{(4)}((G_{27}))]T_{26} = 0$$

has a unique positive solution , which is an equilibrium solution for the system

$$(a_{28})^{(5)}G_{29} - [(a'_{28})^{(5)} + (a''_{28})^{(5)}(T_{29})]G_{28} = 0$$

$$(a_{29})^{(5)}G_{28} - [(a'_{29})^{(5)} + (a''_{29})^{(5)}(T_{29})]G_{29} = 0$$

$$(a_{30})^{(5)}G_{29} - [(a'_{30})^{(5)} + (a''_{30})^{(5)}(T_{29})]G_{30} = 0$$

$$(b_{28})^{(5)}T_{29} - [(b'_{28})^{(5)} - (b''_{28})^{(5)}(G_{31})]T_{28} = 0$$

$$(b_{29})^{(5)}T_{28} - [(b'_{29})^{(5)} - (b''_{29})^{(5)}(G_{31})]T_{29} = 0$$

$$(b_{30})^{(5)}T_{29} - [(b'_{30})^{(5)} - (b''_{30})^{(5)}(G_{31})]T_{30} = 0$$

has a unique positive solution , which is an equilibrium solution for the system

$$(a_{32})^{(6)}G_{33} - [(a'_{32})^{(6)} + (a''_{32})^{(6)}(T_{33})]G_{32} = 0$$

$$(a_{33})^{(6)}G_{32} - [(a'_{33})^{(6)} + (a''_{33})^{(6)}(T_{33})]G_{33} = 0$$

$$(a_{34})^{(6)}G_{33} - [(a'_{34})^{(6)} + (a''_{34})^{(6)}(T_{33})]G_{34} = 0$$

$$(b_{32})^{(6)}T_{33} - [(b'_{32})^{(6)} - (b''_{32})^{(6)}(G_{35})]T_{32} = 0$$

$$(b_{33})^{(6)}T_{32} - [(b'_{33})^{(6)} - (b''_{33})^{(6)}(G_{35})]T_{33} = 0$$

$$(b_{34})^{(6)}T_{33} - [(b'_{34})^{(6)} - (b''_{34})^{(6)}(G_{35})]T_{34} = 0$$

has a unique positive solution , which is an equilibrium solution for the system

(a) Indeed the first two equations have a nontrivial solution G_{13}, G_{14} if

$$F(T) = (a'_{13})^{(1)}(a'_{14})^{(1)} - (a_{13})^{(1)}(a_{14})^{(1)} + (a'_{13})^{(1)}(a''_{14})^{(1)}(T_{14}) + (a'_{14})^{(1)}(a''_{13})^{(1)}(T_{14}) + (a''_{13})^{(1)}(T_{14})(a''_{14})^{(1)}(T_{14}) = 0 .$$

(a) Indeed the first two equations have a nontrivial solution G_{16}, G_{17} if

$$F(T_{19}) = (a'_{16})^{(2)}(a'_{17})^{(2)} - (a_{16})^{(2)}(a_{17})^{(2)} + (a'_{16})^{(2)}(a''_{17})^{(2)}(T_{17}) + (a'_{17})^{(2)}(a''_{16})^{(2)}(T_{17}) + (a''_{16})^{(2)}(T_{17})(a''_{17})^{(2)}(T_{17}) = 0 .$$

(a) Indeed the first two equations have a nontrivial solution G_{20}, G_{21} if

$$F(T_{23}) = (a'_{20})^{(3)}(a'_{21})^{(3)} - (a_{20})^{(3)}(a_{21})^{(3)} + (a'_{20})^{(3)}(a''_{21})^{(3)}(T_{21}) + (a'_{21})^{(3)}(a''_{20})^{(3)}(T_{21}) + (a''_{20})^{(3)}(T_{21})(a''_{21})^{(3)}(T_{21}) = 0 .$$

(a) Indeed the first two equations have a nontrivial solution G_{24}, G_{25} if

$$F(T_{27}) = (a'_{24})^{(4)}(a'_{25})^{(4)} - (a_{24})^{(4)}(a_{25})^{(4)} + (a'_{24})^{(4)}(a''_{25})^{(4)}(T_{25}) + (a'_{25})^{(4)}(a''_{24})^{(4)}(T_{25}) + (a''_{24})^{(4)}(T_{25})(a''_{25})^{(4)}(T_{25}) = 0 .$$

(a) Indeed the first two equations have a nontrivial solution G_{28}, G_{29} if

$$F(T_{31}) = (a'_{28})^{(5)}(a'_{29})^{(5)} - (a_{28})^{(5)}(a_{29})^{(5)} + (a'_{28})^{(5)}(a''_{29})^{(5)}(T_{29}) + (a'_{29})^{(5)}(a''_{28})^{(5)}(T_{29}) + (a''_{28})^{(5)}(T_{29})(a''_{29})^{(5)}(T_{29}) = 0 .$$

(a) Indeed the first two equations have a nontrivial solution G_{32}, G_{33} if

$$F(T_{35}) = (a'_{32})^{(6)}(a'_{33})^{(6)} - (a_{32})^{(6)}(a_{33})^{(6)} + (a'_{32})^{(6)}(a''_{33})^{(6)}(T_{33}) + (a'_{33})^{(6)}(a''_{32})^{(6)}(T_{33}) + (a''_{32})^{(6)}(T_{33})(a''_{33})^{(6)}(T_{33}) = 0 .$$

Definition and uniqueness of T_{14}^* :-

After hypothesis $f(0) < 0, f(\infty) > 0$ and the functions $(a_i'')^{(1)}(T_{14})$ being increasing, it follows that there exists a unique T_{14}^* for which $f(T_{14}^*) = 0$. With this value, we obtain from the three first equations

$$G_{13} = \frac{(a_{13})^{(1)}G_{14}}{[(a'_{13})^{(1)}+(a''_{13})^{(1)}(T_{14}^*)]} \quad , \quad G_{15} = \frac{(a_{15})^{(1)}G_{14}}{[(a'_{15})^{(1)}+(a''_{15})^{(1)}(T_{14}^*)]}$$

Definition and uniqueness of T_{17}^* :-

After hypothesis $f(0) < 0, f(\infty) > 0$ and the functions $(a_i'')^{(2)}(T_{17})$ being increasing, it follows that there exists a unique T_{17}^* for which $f(T_{17}^*) = 0$. With this value, we obtain from the three first equations .

$$G_{16} = \frac{(a_{16})^{(2)}G_{17}}{[(a'_{16})^{(2)}+(a''_{16})^{(2)}(T_{17}^*)]} \quad , \quad G_{18} = \frac{(a_{18})^{(2)}G_{17}}{[(a'_{18})^{(2)}+(a''_{18})^{(2)}(T_{17}^*)]}$$

Definition and uniqueness of T_{21}^* :-

After hypothesis $f(0) < 0, f(\infty) > 0$ and the functions $(a_i'')^{(3)}(T_{21})$ being increasing, it follows that there exists a unique T_{21}^* for which $f(T_{21}^*) = 0$. With this value, we obtain from the three first equations

$$G_{20} = \frac{(a_{20})^{(3)}G_{21}}{[(a'_{20})^{(3)}+(a''_{20})^{(3)}(T_{21}^*)]} \quad , \quad G_{22} = \frac{(a_{22})^{(3)}G_{21}}{[(a'_{22})^{(3)}+(a''_{22})^{(3)}(T_{21}^*)]}$$

Definition and uniqueness of T_{25}^* :-

After hypothesis $f(0) < 0, f(\infty) > 0$ and the functions $(a_i'')^{(4)}(T_{25})$ being increasing, it follows that there exists a unique T_{25}^* for which $f(T_{25}^*) = 0$. With this value, we obtain from the three first equations

$$G_{24} = \frac{(a_{24})^{(4)}G_{25}}{[(a'_{24})^{(4)}+(a''_{24})^{(4)}(T_{25}^*)]} \quad , \quad G_{26} = \frac{(a_{26})^{(4)}G_{25}}{[(a'_{26})^{(4)}+(a''_{26})^{(4)}(T_{25}^*)]}$$

Definition and uniqueness of T_{29}^* :-

After hypothesis $f(0) < 0, f(\infty) > 0$ and the functions $(a_i'')^{(5)}(T_{29})$ being increasing, it follows that there exists a unique T_{29}^* for which $f(T_{29}^*) = 0$. With this value, we obtain from the three first equations

$$G_{28} = \frac{(a_{28})^{(5)}G_{29}}{[(a'_{28})^{(5)}+(a''_{28})^{(5)}(T_{29}^*)]} \quad , \quad G_{30} = \frac{(a_{30})^{(5)}G_{29}}{[(a'_{30})^{(5)}+(a''_{30})^{(5)}(T_{29}^*)]}$$

Definition and uniqueness of T_{33}^* :-

After hypothesis $f(0) < 0, f(\infty) > 0$ and the functions $(a_i'')^{(6)}(T_{33})$ being increasing, it follows that there exists a unique T_{33}^* for which $f(T_{33}^*) = 0$. With this value, we obtain from the three first equations

$$G_{32} = \frac{(a_{32})^{(6)}G_{33}}{[(a'_{32})^{(6)}+(a''_{32})^{(6)}(T_{33}^*)]} \quad , \quad G_{34} = \frac{(a_{34})^{(6)}G_{33}}{[(a'_{34})^{(6)}+(a''_{34})^{(6)}(T_{33}^*)]}$$

(e) By the same argument, the equations 92,93 admit solutions G_{13}, G_{14} if

$$\varphi(G) = (b'_{13})^{(1)}(b'_{14})^{(1)} - (b_{13})^{(1)}(b_{14})^{(1)} - [(b'_{13})^{(1)}(b''_{14})^{(1)}(G) + (b'_{14})^{(1)}(b''_{13})^{(1)}(G)] + (b''_{13})^{(1)}(G)(b''_{14})^{(1)}(G) = 0$$

Where in $G(G_{13}, G_{14}, G_{15}), G_{13}, G_{15}$ must be replaced by their values from 96. It is easy to see that φ is a decreasing function in G_{14} taking into account the hypothesis $\varphi(0) > 0, \varphi(\infty) < 0$ it follows that there exists a unique G_{14}^* such that $\varphi(G^*) = 0$.

(f) By the same argument, the equations 92,93 admit solutions G_{16}, G_{17} if

$$\varphi(G_{19}) = (b'_{16})^{(2)}(b'_{17})^{(2)} - (b_{16})^{(2)}(b_{17})^{(2)} - [(b'_{16})^{(2)}(b''_{17})^{(2)}(G_{19}) + (b'_{17})^{(2)}(b''_{16})^{(2)}(G_{19})] + (b''_{16})^{(2)}(G_{19})(b''_{17})^{(2)}(G_{19}) = 0 .$$

Where in $(G_{19})(G_{16}, G_{17}, G_{18}), G_{16}, G_{18}$ must be replaced by their values from 96. It is easy to see that φ is a decreasing function in G_{17} taking into account the hypothesis $\varphi(0) > 0, \varphi(\infty) < 0$ it follows that there exists a unique G_{14}^* such that $\varphi((G_{19})^*) = 0$.

(g) By the same argument, the concatenated equations admit solutions G_{20}, G_{21} if

$$\varphi(G_{23}) = (b'_{20})^{(3)}(b'_{21})^{(3)} - (b_{20})^{(3)}(b_{21})^{(3)} -$$

$$[(b'_{20})^{(3)}(b''_{21})^{(3)}(G_{23}) + (b'_{21})^{(3)}(b''_{20})^{(3)}(G_{23})] + (b''_{20})^{(3)}(G_{23})(b''_{21})^{(3)}(G_{23}) = 0$$

Where in $G_{23}(G_{20}, G_{21}, G_{22}), G_{20}, G_{22}$ must be replaced by their values from 96. It is easy to see that φ is a decreasing function in G_{21} taking into account the hypothesis $\varphi(0) > 0, \varphi(\infty) < 0$ it follows that there exists a unique G_{21}^* such that $\varphi((G_{23})^*) = 0$.

(h) By the same argument, the equations of modules admit solutions G_{24}, G_{25} if

$$\varphi(G_{27}) = (b'_{24})^{(4)}(b'_{25})^{(4)} - (b_{24})^{(4)}(b_{25})^{(4)} -$$

$$[(b'_{24})^{(4)}(b''_{25})^{(4)}(G_{27}) + (b'_{25})^{(4)}(b''_{24})^{(4)}(G_{27})] + (b''_{24})^{(4)}(G_{27})(b''_{25})^{(4)}(G_{27}) = 0$$

Where in $(G_{27})(G_{24}, G_{25}, G_{26}), G_{24}, G_{26}$ must be replaced by their values from 96. It is easy to see that φ is a decreasing function in G_{25} taking into account the hypothesis $\varphi(0) > 0, \varphi(\infty) < 0$ it follows that there exists a unique G_{25}^* such that $\varphi((G_{27})^*) = 0$.

(i) By the same argument, the equations (modules) admit solutions G_{28}, G_{29} if

$$\varphi(G_{31}) = (b'_{28})^{(5)}(b'_{29})^{(5)} - (b_{28})^{(5)}(b_{29})^{(5)} -$$

$$[(b'_{28})^{(5)}(b''_{29})^{(5)}(G_{31}) + (b'_{29})^{(5)}(b''_{28})^{(5)}(G_{31})] + (b''_{28})^{(5)}(G_{31})(b''_{29})^{(5)}(G_{31}) = 0$$

Where in $(G_{31})(G_{28}, G_{29}, G_{30}), G_{28}, G_{30}$ must be replaced by their values from 96. It is easy to see that φ is a decreasing function in G_{29} taking into account the hypothesis $\varphi(0) > 0, \varphi(\infty) < 0$ it follows that there exists a unique G_{29}^* such that $\varphi((G_{31})^*) = 0$.

(j) By the same argument, the equations (modules) admit solutions G_{32}, G_{33} if

$$\varphi(G_{35}) = (b'_{32})^{(6)}(b'_{33})^{(6)} - (b_{32})^{(6)}(b_{33})^{(6)} -$$

$$[(b'_{32})^{(6)}(b''_{33})^{(6)}(G_{35}) + (b'_{33})^{(6)}(b''_{32})^{(6)}(G_{35})] + (b''_{32})^{(6)}(G_{35})(b''_{33})^{(6)}(G_{35}) = 0$$

Where in $(G_{35})(G_{32}, G_{33}, G_{34}), G_{32}, G_{34}$ must be replaced by their values It is easy to see that φ is a decreasing function in G_{33} taking into account the hypothesis $\varphi(0) > 0, \varphi(\infty) < 0$ it follows that there exists a unique G_{33}^* such that $\varphi(G^*) = 0$.

Finally we obtain the unique solution of 89 to 94

G_{14}^* given by $\varphi(G^*) = 0, T_{14}^*$ given by $f(T_{14}^*) = 0$ and

$$G_{13}^* = \frac{(a_{13})^{(1)}G_{14}^*}{[(a'_{13})^{(1)} + (a''_{13})^{(1)}(T_{14}^*)]} \quad , \quad G_{15}^* = \frac{(a_{15})^{(1)}G_{14}^*}{[(a'_{15})^{(1)} + (a''_{15})^{(1)}(T_{14}^*)]}$$

$$T_{13}^* = \frac{(b_{13})^{(1)}T_{14}^*}{[(b'_{13})^{(1)} - (b''_{13})^{(1)}(G^*)]} \quad , \quad T_{15}^* = \frac{(b_{15})^{(1)}T_{14}^*}{[(b'_{15})^{(1)} - (b''_{15})^{(1)}(G^*)]}$$

Obviously, these values represent an equilibrium solution .

Finally we obtain the unique solution .

G_{17}^* given by $\varphi((G_{19})^*) = 0$, T_{17}^* given by $f(T_{17}^*) = 0$ and.

$$G_{16}^* = \frac{(a_{16})^{(2)}G_{17}^*}{[(a'_{16})^{(2)}+(a''_{16})^{(2)}(T_{17}^*)]} , G_{18}^* = \frac{(a_{18})^{(2)}G_{17}^*}{[(a'_{18})^{(2)}+(a''_{18})^{(2)}(T_{17}^*)]} .$$

$$T_{16}^* = \frac{(b_{16})^{(2)}T_{17}^*}{[(b'_{16})^{(2)}-(b''_{16})^{(2)}((G_{19})^*)]} , T_{18}^* = \frac{(b_{18})^{(2)}T_{17}^*}{[(b'_{18})^{(2)}-(b''_{18})^{(2)}((G_{19})^*)]} .$$

Obviously, these values represent an equilibrium solution.

Finally we obtain the unique solution

G_{21}^* given by $\varphi((G_{23})^*) = 0$, T_{21}^* given by $f(T_{21}^*) = 0$ and

$$G_{20}^* = \frac{(a_{20})^{(3)}G_{21}^*}{[(a'_{20})^{(3)}+(a''_{20})^{(3)}(T_{21}^*)]} , G_{22}^* = \frac{(a_{22})^{(3)}G_{21}^*}{[(a'_{22})^{(3)}+(a''_{22})^{(3)}(T_{21}^*)]}$$

$$T_{20}^* = \frac{(b_{20})^{(3)}T_{21}^*}{[(b'_{20})^{(3)}-(b''_{20})^{(3)}(G_{23}^*)]} , T_{22}^* = \frac{(b_{22})^{(3)}T_{21}^*}{[(b'_{22})^{(3)}-(b''_{22})^{(3)}(G_{23}^*)]}$$

Obviously, these values represent an equilibrium solution .

Finally we obtain the unique solution

G_{25}^* given by $\varphi(G_{27}) = 0$, T_{25}^* given by $f(T_{25}^*) = 0$ and

$$G_{24}^* = \frac{(a_{24})^{(4)}G_{25}^*}{[(a'_{24})^{(4)}+(a''_{24})^{(4)}(T_{25}^*)]} , G_{26}^* = \frac{(a_{26})^{(4)}G_{25}^*}{[(a'_{26})^{(4)}+(a''_{26})^{(4)}(T_{25}^*)]} .$$

$$T_{24}^* = \frac{(b_{24})^{(4)}T_{25}^*}{[(b'_{24})^{(4)}-(b''_{24})^{(4)}((G_{27})^*)]} , T_{26}^* = \frac{(b_{26})^{(4)}T_{25}^*}{[(b'_{26})^{(4)}-(b''_{26})^{(4)}((G_{27})^*)]}$$

Obviously, these values represent an equilibrium solution .

Finally we obtain the unique solution

G_{29}^* given by $\varphi((G_{31})^*) = 0$, T_{29}^* given by $f(T_{29}^*) = 0$ and

$$G_{28}^* = \frac{(a_{28})^{(5)}G_{29}^*}{[(a'_{28})^{(5)}+(a''_{28})^{(5)}(T_{29}^*)]} , G_{30}^* = \frac{(a_{30})^{(5)}G_{29}^*}{[(a'_{30})^{(5)}+(a''_{30})^{(5)}(T_{29}^*)]}$$

$$T_{28}^* = \frac{(b_{28})^{(5)}T_{29}^*}{[(b'_{28})^{(5)}-(b''_{28})^{(5)}((G_{31})^*)]} , T_{30}^* = \frac{(b_{30})^{(5)}T_{29}^*}{[(b'_{30})^{(5)}-(b''_{30})^{(5)}((G_{31})^*)]}$$

Obviously, these values represent an equilibrium solution.

Finally we obtain the unique solution

G_{33}^* given by $\varphi((G_{35})^*) = 0$, T_{33}^* given by $f(T_{33}^*) = 0$ and

$$G_{32}^* = \frac{(a_{32})^{(6)}G_{33}^*}{[(a'_{32})^{(6)}+(a''_{32})^{(6)}(T_{33}^*)]} , G_{34}^* = \frac{(a_{34})^{(6)}G_{33}^*}{[(a'_{34})^{(6)}+(a''_{34})^{(6)}(T_{33}^*)]} .$$

$$T_{32}^* = \frac{(b_{32})^{(6)}T_{33}^*}{[(b'_{32})^{(6)}-(b''_{32})^{(6)}((G_{35})^*)]} , T_{34}^* = \frac{(b_{34})^{(6)}T_{33}^*}{[(b'_{34})^{(6)}-(b''_{34})^{(6)}((G_{35})^*)]}$$

Obviously, these values represent an equilibrium solution .

ASYMPTOTIC STABILITY ANALYSIS

Theorem 4: If the conditions of the previous theorem are satisfied and if the functions $(a_i'')^{(1)}$ and $(b_i'')^{(1)}$ Belong to $C^{(1)}(\mathbb{R}_+)$ then the above equilibrium point is asymptotically stable.

Proof: Denote

Definition of $\mathbb{G}_i, \mathbb{T}_i$:-

$$G_i = G_i^* + \mathbb{G}_i \quad , \quad T_i = T_i^* + \mathbb{T}_i$$

$$\frac{\partial (a_{14}'')^{(1)}}{\partial T_{14}} (T_{14}^*) = (q_{14})^{(1)} \quad , \quad \frac{\partial (b_i'')^{(1)}}{\partial G_j} (G^*) = s_{ij} .$$

Then taking into account equations (global) and neglecting the terms of power 2, we obtain .

$$\frac{d\mathbb{G}_{13}}{dt} = -((a'_{13})^{(1)} + (p_{13})^{(1)})\mathbb{G}_{13} + (a_{13})^{(1)}\mathbb{G}_{14} - (q_{13})^{(1)}G_{13}^*\mathbb{T}_{14} .$$

$$\frac{d\mathbb{G}_{14}}{dt} = -((a'_{14})^{(1)} + (p_{14})^{(1)})\mathbb{G}_{14} + (a_{14})^{(1)}\mathbb{G}_{13} - (q_{14})^{(1)}G_{14}^*\mathbb{T}_{14} .$$

$$\frac{d\mathbb{G}_{15}}{dt} = -((a'_{15})^{(1)} + (p_{15})^{(1)})\mathbb{G}_{15} + (a_{15})^{(1)}\mathbb{G}_{14} - (q_{15})^{(1)}G_{15}^*\mathbb{T}_{14} .$$

$$\frac{d\mathbb{T}_{13}}{dt} = -((b'_{13})^{(1)} - (r_{13})^{(1)})\mathbb{T}_{13} + (b_{13})^{(1)}\mathbb{T}_{14} + \sum_{j=13}^{15} (s_{(13)(j)})T_{13}^*\mathbb{G}_j .$$

$$\frac{d\mathbb{T}_{14}}{dt} = -((b'_{14})^{(1)} - (r_{14})^{(1)})\mathbb{T}_{14} + (b_{14})^{(1)}\mathbb{T}_{13} + \sum_{j=13}^{15} (s_{(14)(j)})T_{14}^*\mathbb{G}_j .$$

$$\frac{d\mathbb{T}_{15}}{dt} = -((b'_{15})^{(1)} - (r_{15})^{(1)})\mathbb{T}_{15} + (b_{15})^{(1)}\mathbb{T}_{14} + \sum_{j=13}^{15} (s_{(15)(j)})T_{15}^*\mathbb{G}_j .$$

If the conditions of the previous theorem are satisfied and if the functions $(a_i'')^{(2)}$ and $(b_i'')^{(2)}$ Belong to $C^{(2)}(\mathbb{R}_+)$ then the above equilibrium point is asymptotically stable.

Denote

Definition of $\mathbb{G}_i, \mathbb{T}_i$:-

$$G_i = G_i^* + \mathbb{G}_i \quad , \quad T_i = T_i^* + \mathbb{T}_i .$$

$$\frac{\partial (a_{17}'')^{(2)}}{\partial T_{17}} (T_{17}^*) = (q_{17})^{(2)} \quad , \quad \frac{\partial (b_i'')^{(2)}}{\partial G_j} ((G_{19})^*) = s_{ij} .$$

taking into account equations (global)and neglecting the terms of power 2, we obtain .

$$\frac{d\mathbb{G}_{16}}{dt} = -((a'_{16})^{(2)} + (p_{16})^{(2)})\mathbb{G}_{16} + (a_{16})^{(2)}\mathbb{G}_{17} - (q_{16})^{(2)}G_{16}^*\mathbb{T}_{17} .$$

$$\frac{d\mathbb{G}_{17}}{dt} = -((a'_{17})^{(2)} + (p_{17})^{(2)})\mathbb{G}_{17} + (a_{17})^{(2)}\mathbb{G}_{16} - (q_{17})^{(2)}G_{17}^*\mathbb{T}_{17} .$$

$$\frac{d\mathbb{G}_{18}}{dt} = -((a'_{18})^{(2)} + (p_{18})^{(2)})\mathbb{G}_{18} + (a_{18})^{(2)}\mathbb{G}_{17} - (q_{18})^{(2)}G_{18}^*\mathbb{T}_{17} .$$

$$\frac{d\mathbb{T}_{16}}{dt} = -((b'_{16})^{(2)} - (r_{16})^{(2)})\mathbb{T}_{16} + (b_{16})^{(2)}\mathbb{T}_{17} + \sum_{j=16}^{18} (s_{(16)(j)})T_{16}^*\mathbb{G}_j .$$

$$\frac{d\mathbb{T}_{17}}{dt} = -((b'_{17})^{(2)} - (r_{17})^{(2)})\mathbb{T}_{17} + (b_{17})^{(2)}\mathbb{T}_{16} + \sum_{j=16}^{18} (s_{(17)(j)})T_{17}^*\mathbb{G}_j .$$

$$\frac{d\mathbb{T}_{18}}{dt} = -((b'_{18})^{(2)} - (r_{18})^{(2)})\mathbb{T}_{18} + (b_{18})^{(2)}\mathbb{T}_{17} + \sum_{j=16}^{18} (s_{(18)(j)})T_{18}^*\mathbb{G}_j .$$

If the conditions of the previous theorem are satisfied and if the functions $(a_i'')^{(3)}$ and $(b_i'')^{(3)}$ Belong to $C^{(3)}(\mathbb{R}_+)$ then the above equilibrium point is asymptotically stabl

Denote

Definition of $\mathbb{G}_i, \mathbb{T}_i$:-

$$G_i = G_i^* + \mathbb{G}_i \quad , \quad T_i = T_i^* + \mathbb{T}_i$$

$$\frac{\partial (a_{21}'')^{(3)}}{\partial T_{21}} (T_{21}^*) = (q_{21})^{(3)} \quad , \quad \frac{\partial (b_i'')^{(3)}}{\partial G_j} ((G_{23})^*) = s_{ij} .$$

Then taking into account equations (global) and neglecting the terms of power 2, we obtain .

$$\frac{dG_{20}}{dt} = -((a'_{20})^{(3)} + (p_{20})^{(3)})G_{20} + (a_{20})^{(3)}G_{21} - (q_{20})^{(3)}G_{20}^* T_{21} .$$

$$\frac{dG_{21}}{dt} = -((a'_{21})^{(3)} + (p_{21})^{(3)})G_{21} + (a_{21})^{(3)}G_{20} - (q_{21})^{(3)}G_{21}^* T_{21} .$$

$$\frac{dG_{22}}{dt} = -((a'_{22})^{(3)} + (p_{22})^{(3)})G_{22} + (a_{22})^{(3)}G_{21} - (q_{22})^{(3)}G_{22}^* T_{21} .$$

$$\frac{dT_{20}}{dt} = -((b'_{20})^{(3)} - (r_{20})^{(3)})T_{20} + (b_{20})^{(3)}T_{21} + \sum_{j=20}^{22} (s_{(20)(j)})T_{20}^* G_j .$$

$$\frac{dT_{21}}{dt} = -((b'_{21})^{(3)} - (r_{21})^{(3)})T_{21} + (b_{21})^{(3)}T_{20} + \sum_{j=20}^{22} (s_{(21)(j)})T_{21}^* G_j .$$

$$\frac{dT_{22}}{dt} = -((b'_{22})^{(3)} - (r_{22})^{(3)})T_{22} + (b_{22})^{(3)}T_{21} + \sum_{j=20}^{22} (s_{(22)(j)})T_{22}^* G_j .$$

If the conditions of the previous theorem are satisfied and if the functions $(a''_i)^{(4)}$ and $(b''_i)^{(4)}$ belong to $C^{(4)}(\mathbb{R}_+)$ then the above equilibrium point is asymptotically stable

Denote.

Definition of G_i, T_i :-

$$G_i = G_i^* + G_i \quad , \quad T_i = T_i^* + T_i$$

$$\frac{\partial (a_{25})''^{(4)}}{\partial T_{25}} (T_{25}^*) = (q_{25})^{(4)} \quad , \quad \frac{\partial (b_i)''^{(4)}}{\partial G_j} ((G_{27})^*) = s_{ij} .$$

Then taking into account equations (global) and neglecting the terms of power 2, we obtain.

$$\frac{dG_{24}}{dt} = -((a'_{24})^{(4)} + (p_{24})^{(4)})G_{24} + (a_{24})^{(4)}G_{25} - (q_{24})^{(4)}G_{24}^* T_{25} .$$

$$\frac{dG_{25}}{dt} = -((a'_{25})^{(4)} + (p_{25})^{(4)})G_{25} + (a_{25})^{(4)}G_{24} - (q_{25})^{(4)}G_{25}^* T_{25} .$$

$$\frac{dG_{26}}{dt} = -((a'_{26})^{(4)} + (p_{26})^{(4)})G_{26} + (a_{26})^{(4)}G_{25} - (q_{26})^{(4)}G_{26}^* T_{25} .$$

$$\frac{dT_{24}}{dt} = -((b'_{24})^{(4)} - (r_{24})^{(4)})T_{24} + (b_{24})^{(4)}T_{25} + \sum_{j=24}^{26} (s_{(24)(j)})T_{24}^* G_j .$$

$$\frac{dT_{25}}{dt} = -((b'_{25})^{(4)} - (r_{25})^{(4)})T_{25} + (b_{25})^{(4)}T_{24} + \sum_{j=24}^{26} (s_{(25)(j)})T_{25}^* G_j .$$

$$\frac{dT_{26}}{dt} = -((b'_{26})^{(4)} - (r_{26})^{(4)})T_{26} + (b_{26})^{(4)}T_{25} + \sum_{j=24}^{26} (s_{(26)(j)})T_{26}^* G_j .$$

If the conditions of the previous theorem are satisfied and if the functions $(a''_i)^{(5)}$ and $(b''_i)^{(5)}$ belong to $C^{(5)}(\mathbb{R}_+)$ then the above equilibrium point is asymptotically stable

Denote.

Definition of G_i, T_i :-

$$G_i = G_i^* + G_i \quad , \quad T_i = T_i^* + T_i$$

$$\frac{\partial (a_{29})''^{(5)}}{\partial T_{29}} (T_{29}^*) = (q_{29})^{(5)} \quad , \quad \frac{\partial (b_i)''^{(5)}}{\partial G_j} ((G_{31})^*) = s_{ij} .$$

Then taking into account equations (global) and neglecting the terms of power 2, we obtain.

$$\frac{dG_{28}}{dt} = -((a'_{28})^{(5)} + (p_{28})^{(5)})G_{28} + (a_{28})^{(5)}G_{29} - (q_{28})^{(5)}G_{28}^* T_{29} .$$

$$\frac{dG_{29}}{dt} = -((a'_{29})^{(5)} + (p_{29})^{(5)})G_{29} + (a_{29})^{(5)}G_{28} - (q_{29})^{(5)}G_{29}^* T_{29} .$$

$$\frac{dG_{30}}{dt} = -((a'_{30})^{(5)} + (p_{30})^{(5)})G_{30} + (a_{30})^{(5)}G_{29} - (q_{30})^{(5)}G_{30}^* T_{29} .$$

$$\frac{dT_{28}}{dt} = -((b'_{28})^{(5)} - (r_{28})^{(5)})T_{28} + (b_{28})^{(5)}T_{29} + \sum_{j=28}^{30} (s_{(28)(j)}) T_{28}^* G_j .$$

$$\frac{dT_{29}}{dt} = -((b'_{29})^{(5)} - (r_{29})^{(5)})T_{29} + (b_{29})^{(5)}T_{28} + \sum_{j=28}^{30} (s_{(29)(j)}) T_{29}^* G_j .$$

$$\frac{dT_{30}}{dt} = -((b'_{30})^{(5)} - (r_{30})^{(5)})T_{30} + (b_{30})^{(5)}T_{29} + \sum_{j=28}^{30} (s_{(30)(j)}) T_{30}^* G_j .$$

If the conditions of the previous theorem are satisfied and if the functions $(a_i'')^{(6)}$ and $(b_i'')^{(6)}$ belong to $C^{(6)}(\mathbb{R}_+)$ then the above equilibrium point is asymptotically stable

Denote.

Definition of G_i, T_i :-

$$G_i = G_i^* + G_i \quad , \quad T_i = T_i^* + T_i$$

$$\frac{\partial (a_{33}'')^{(6)}}{\partial T_{33}} (T_{33}^*) = (q_{33})^{(6)} \quad , \quad \frac{\partial (b_i'')^{(6)}}{\partial G_j} ((G_{35})^*) = s_{ij} .$$

Then taking into account equations(global) and neglecting the terms of power 2, we obtain.

$$\frac{dG_{32}}{dt} = -((a'_{32})^{(6)} + (p_{32})^{(6)})G_{32} + (a_{32})^{(6)}G_{33} - (q_{32})^{(6)}G_{32}^* T_{33} .$$

$$\frac{dG_{33}}{dt} = -((a'_{33})^{(6)} + (p_{33})^{(6)})G_{33} + (a_{33})^{(6)}G_{32} - (q_{33})^{(6)}G_{33}^* T_{33} .$$

$$\frac{dG_{34}}{dt} = -((a'_{34})^{(6)} + (p_{34})^{(6)})G_{34} + (a_{34})^{(6)}G_{33} - (q_{34})^{(6)}G_{34}^* T_{33} .$$

$$\frac{dT_{32}}{dt} = -((b'_{32})^{(6)} - (r_{32})^{(6)})T_{32} + (b_{32})^{(6)}T_{33} + \sum_{j=32}^{34} (s_{(32)(j)}) T_{32}^* G_j .$$

$$\frac{dT_{33}}{dt} = -((b'_{33})^{(6)} - (r_{33})^{(6)})T_{33} + (b_{33})^{(6)}T_{32} + \sum_{j=32}^{34} (s_{(33)(j)}) T_{33}^* G_j .$$

$$\frac{dT_{34}}{dt} = -((b'_{34})^{(6)} - (r_{34})^{(6)})T_{34} + (b_{34})^{(6)}T_{33} + \sum_{j=32}^{34} (s_{(34)(j)}) T_{34}^* G_j .$$

The characteristic equation of this system is

$$\begin{aligned} & ((\lambda)^{(1)} + (b'_{15})^{(1)} - (r_{15})^{(1)}) \{ ((\lambda)^{(1)} + (a'_{15})^{(1)} + (p_{15})^{(1)}) \\ & \left[((\lambda)^{(1)} + (a'_{13})^{(1)} + (p_{13})^{(1)}) (q_{14})^{(1)} G_{14}^* + (a_{14})^{(1)} (q_{13})^{(1)} G_{13}^* \right] \\ & \left(((\lambda)^{(1)} + (b'_{13})^{(1)} - (r_{13})^{(1)}) s_{(14),(14)} T_{14}^* + (b_{14})^{(1)} s_{(13),(14)} T_{14}^* \right) \\ & + \left(((\lambda)^{(1)} + (a'_{14})^{(1)} + (p_{14})^{(1)}) (q_{13})^{(1)} G_{13}^* + (a_{13})^{(1)} (q_{14})^{(1)} G_{14}^* \right) \\ & \left(((\lambda)^{(1)} + (b'_{13})^{(1)} - (r_{13})^{(1)}) s_{(14),(13)} T_{14}^* + (b_{14})^{(1)} s_{(13),(13)} T_{13}^* \right) \\ & \left(((\lambda)^{(1)})^2 + ((a'_{13})^{(1)} + (a'_{14})^{(1)} + (p_{13})^{(1)} + (p_{14})^{(1)}) (\lambda)^{(1)} \right) \\ & \left(((\lambda)^{(1)})^2 + ((b'_{13})^{(1)} + (b'_{14})^{(1)} - (r_{13})^{(1)} + (r_{14})^{(1)}) (\lambda)^{(1)} \right) \\ & + \left(((\lambda)^{(1)})^2 + ((a'_{13})^{(1)} + (a'_{14})^{(1)} + (p_{13})^{(1)} + (p_{14})^{(1)}) (\lambda)^{(1)} \right) (q_{15})^{(1)} G_{15} \\ & + ((\lambda)^{(1)} + (a'_{13})^{(1)} + (p_{13})^{(1)}) \left((a_{15})^{(1)} (q_{14})^{(1)} G_{14}^* + (a_{14})^{(1)} (a_{15})^{(1)} (q_{13})^{(1)} G_{13}^* \right) \\ & \left. \left(((\lambda)^{(1)} + (b'_{13})^{(1)} - (r_{13})^{(1)}) s_{(14),(15)} T_{14}^* + (b_{14})^{(1)} s_{(13),(15)} T_{13}^* \right) \right\} = 0 \end{aligned}$$

+

$$\begin{aligned}
 & ((\lambda)^{(2)} + (b'_{18})^{(2)} - (r_{18})^{(2)})\{((\lambda)^{(2)} + (a'_{18})^{(2)} + (p_{18})^{(2)}) \\
 & [((\lambda)^{(2)} + (a'_{16})^{(2)} + (p_{16})^{(2)})(q_{17})^{(2)}G_{17}^* + (a_{17})^{(2)}(q_{16})^{(2)}G_{16}^*]\} \\
 & ((\lambda)^{(2)} + (b'_{16})^{(2)} - (r_{16})^{(2)})s_{(17),(17)}T_{17}^* + (b_{17})^{(2)}s_{(16),(17)}T_{17}^* \\
 & + ((\lambda)^{(2)} + (a'_{17})^{(2)} + (p_{17})^{(2)})(q_{16})^{(2)}G_{16}^* + (a_{16})^{(2)}(q_{17})^{(2)}G_{17}^* \\
 & ((\lambda)^{(2)} + (b'_{16})^{(2)} - (r_{16})^{(2)})s_{(17),(16)}T_{17}^* + (b_{17})^{(2)}s_{(16),(16)}T_{16}^* \\
 & ((\lambda)^{(2)})^2 + ((a'_{16})^{(2)} + (a'_{17})^{(2)} + (p_{16})^{(2)} + (p_{17})^{(2)}) (\lambda)^{(2)} \\
 & ((\lambda)^{(2)})^2 + ((b'_{16})^{(2)} + (b'_{17})^{(2)} - (r_{16})^{(2)} + (r_{17})^{(2)}) (\lambda)^{(2)} \\
 & + ((\lambda)^{(2)})^2 + ((a'_{16})^{(2)} + (a'_{17})^{(2)} + (p_{16})^{(2)} + (p_{17})^{(2)}) (\lambda)^{(2)} (q_{18})^{(2)}G_{18} \\
 & + ((\lambda)^{(2)} + (a'_{16})^{(2)} + (p_{16})^{(2)}) ((a_{18})^{(2)}(q_{17})^{(2)}G_{17}^* + (a_{17})^{(2)}(a_{18})^{(2)}(q_{16})^{(2)}G_{16}^*) \\
 & ((\lambda)^{(2)} + (b'_{16})^{(2)} - (r_{16})^{(2)})s_{(17),(18)}T_{17}^* + (b_{17})^{(2)}s_{(16),(18)}T_{16}^* \} = 0
 \end{aligned}$$

+

$$\begin{aligned}
 & ((\lambda)^{(3)} + (b'_{22})^{(3)} - (r_{22})^{(3)})\{((\lambda)^{(3)} + (a'_{22})^{(3)} + (p_{22})^{(3)}) \\
 & [((\lambda)^{(3)} + (a'_{20})^{(3)} + (p_{20})^{(3)})(q_{21})^{(3)}G_{21}^* + (a_{21})^{(3)}(q_{20})^{(3)}G_{20}^*]\} \\
 & ((\lambda)^{(3)} + (b'_{20})^{(3)} - (r_{20})^{(3)})s_{(21),(21)}T_{21}^* + (b_{21})^{(3)}s_{(20),(21)}T_{21}^* \\
 & + ((\lambda)^{(3)} + (a'_{21})^{(3)} + (p_{21})^{(3)})(q_{20})^{(3)}G_{20}^* + (a_{20})^{(3)}(q_{21})^{(1)}G_{21}^* \\
 & ((\lambda)^{(3)} + (b'_{20})^{(3)} - (r_{20})^{(3)})s_{(21),(20)}T_{21}^* + (b_{21})^{(3)}s_{(20),(20)}T_{20}^* \\
 & ((\lambda)^{(3)})^2 + ((a'_{20})^{(3)} + (a'_{21})^{(3)} + (p_{20})^{(3)} + (p_{21})^{(3)}) (\lambda)^{(3)} \\
 & ((\lambda)^{(3)})^2 + ((b'_{20})^{(3)} + (b'_{21})^{(3)} - (r_{20})^{(3)} + (r_{21})^{(3)}) (\lambda)^{(3)} \\
 & + ((\lambda)^{(3)})^2 + ((a'_{20})^{(3)} + (a'_{21})^{(3)} + (p_{20})^{(3)} + (p_{21})^{(3)}) (\lambda)^{(3)} (q_{22})^{(3)}G_{22} \\
 & + ((\lambda)^{(3)} + (a'_{20})^{(3)} + (p_{20})^{(3)}) ((a_{22})^{(3)}(q_{21})^{(3)}G_{21}^* + (a_{21})^{(3)}(a_{22})^{(3)}(q_{20})^{(3)}G_{20}^*) \\
 & ((\lambda)^{(3)} + (b'_{20})^{(3)} - (r_{20})^{(3)})s_{(21),(22)}T_{21}^* + (b_{21})^{(3)}s_{(20),(22)}T_{20}^* \} = 0
 \end{aligned}$$

+

$$((\lambda)^{(4)} + (b'_{26})^{(4)} - (r_{26})^{(4)})\{((\lambda)^{(4)} + (a'_{26})^{(4)} + (p_{26})^{(4)})$$

$$\begin{aligned}
 & \left[\left((\lambda)^{(4)} + (a'_{24})^{(4)} + (p_{24})^{(4)} \right) (q_{25})^{(4)} G_{25}^* + (a_{25})^{(4)} (q_{24})^{(4)} G_{24}^* \right] \\
 & \left((\lambda)^{(4)} + (b'_{24})^{(4)} - (r_{24})^{(4)} \right) s_{(25),(25)} T_{25}^* + (b_{25})^{(4)} s_{(24),(25)} T_{25}^* \\
 & + \left((\lambda)^{(4)} + (a'_{25})^{(4)} + (p_{25})^{(4)} \right) (q_{24})^{(4)} G_{24}^* + (a_{24})^{(4)} (q_{25})^{(4)} G_{25}^* \\
 & \left((\lambda)^{(4)} + (b'_{24})^{(4)} - (r_{24})^{(4)} \right) s_{(25),(24)} T_{25}^* + (b_{25})^{(4)} s_{(24),(24)} T_{24}^* \\
 & \left((\lambda)^{(4)} \right)^2 + \left((a'_{24})^{(4)} + (a'_{25})^{(4)} + (p_{24})^{(4)} + (p_{25})^{(4)} \right) (\lambda)^{(4)} \\
 & \left((\lambda)^{(4)} \right)^2 + \left((b'_{24})^{(4)} + (b'_{25})^{(4)} - (r_{24})^{(4)} + (r_{25})^{(4)} \right) (\lambda)^{(4)} \\
 & + \left((\lambda)^{(4)} \right)^2 + \left((a'_{24})^{(4)} + (a'_{25})^{(4)} + (p_{24})^{(4)} + (p_{25})^{(4)} \right) (\lambda)^{(4)} (q_{26})^{(4)} G_{26} \\
 & + \left((\lambda)^{(4)} + (a'_{24})^{(4)} + (p_{24})^{(4)} \right) \left((a_{26})^{(4)} (q_{25})^{(4)} G_{25}^* + (a_{25})^{(4)} (a_{26})^{(4)} (q_{24})^{(4)} G_{24}^* \right) \\
 & \left. \left((\lambda)^{(4)} + (b'_{24})^{(4)} - (r_{24})^{(4)} \right) s_{(25),(26)} T_{25}^* + (b_{25})^{(4)} s_{(24),(26)} T_{24}^* \right\} = 0
 \end{aligned}$$

+

$$\begin{aligned}
 & \left((\lambda)^{(5)} + (b'_{30})^{(5)} - (r_{30})^{(5)} \right) \left\{ (\lambda)^{(5)} + (a'_{30})^{(5)} + (p_{30})^{(5)} \right\} \\
 & \left[\left((\lambda)^{(5)} + (a'_{28})^{(5)} + (p_{28})^{(5)} \right) (q_{29})^{(5)} G_{29}^* + (a_{29})^{(5)} (q_{28})^{(5)} G_{28}^* \right] \\
 & \left((\lambda)^{(5)} + (b'_{28})^{(5)} - (r_{28})^{(5)} \right) s_{(29),(29)} T_{29}^* + (b_{29})^{(5)} s_{(28),(29)} T_{29}^* \\
 & + \left((\lambda)^{(5)} + (a'_{29})^{(5)} + (p_{29})^{(5)} \right) (q_{28})^{(5)} G_{28}^* + (a_{28})^{(5)} (q_{29})^{(5)} G_{29}^* \\
 & \left((\lambda)^{(5)} + (b'_{28})^{(5)} - (r_{28})^{(5)} \right) s_{(29),(28)} T_{29}^* + (b_{29})^{(5)} s_{(28),(28)} T_{28}^* \\
 & \left((\lambda)^{(5)} \right)^2 + \left((a'_{28})^{(5)} + (a'_{29})^{(5)} + (p_{28})^{(5)} + (p_{29})^{(5)} \right) (\lambda)^{(5)} \\
 & \left((\lambda)^{(5)} \right)^2 + \left((b'_{28})^{(5)} + (b'_{29})^{(5)} - (r_{28})^{(5)} + (r_{29})^{(5)} \right) (\lambda)^{(5)} \\
 & + \left((\lambda)^{(5)} \right)^2 + \left((a'_{28})^{(5)} + (a'_{29})^{(5)} + (p_{28})^{(5)} + (p_{29})^{(5)} \right) (\lambda)^{(5)} (q_{30})^{(5)} G_{30} \\
 & + \left((\lambda)^{(5)} + (a'_{28})^{(5)} + (p_{28})^{(5)} \right) \left((a_{30})^{(5)} (q_{29})^{(5)} G_{29}^* + (a_{29})^{(5)} (a_{30})^{(5)} (q_{28})^{(5)} G_{28}^* \right) \\
 & \left. \left((\lambda)^{(5)} + (b'_{28})^{(5)} - (r_{28})^{(5)} \right) s_{(29),(30)} T_{29}^* + (b_{29})^{(5)} s_{(28),(30)} T_{28}^* \right\} = 0
 \end{aligned}$$

+

$$\begin{aligned}
 & \left((\lambda)^{(6)} + (b'_{34})^{(6)} - (r_{34})^{(6)} \right) \left\{ (\lambda)^{(6)} + (a'_{34})^{(6)} + (p_{34})^{(6)} \right\} \\
 & \left[\left((\lambda)^{(6)} + (a'_{32})^{(6)} + (p_{32})^{(6)} \right) (q_{33})^{(6)} G_{33}^* + (a_{33})^{(6)} (q_{32})^{(6)} G_{32}^* \right] \\
 & \left((\lambda)^{(6)} + (b'_{32})^{(6)} - (r_{32})^{(6)} \right) s_{(33),(33)} T_{33}^* + (b_{33})^{(6)} s_{(32),(33)} T_{33}^*
 \end{aligned}$$

$$\begin{aligned}
 &+ \left((\lambda)^{(6)} + (a'_{33})^{(6)} + (p_{33})^{(6)} \right) (q_{32})^{(6)} G_{32}^* + (a_{32})^{(6)} (q_{33})^{(6)} G_{33}^* \\
 &\quad \left((\lambda)^{(6)} + (b'_{32})^{(6)} - (r_{32})^{(6)} \right) s_{(33),(32)} T_{33}^* + (b_{33})^{(6)} s_{(32),(32)} T_{32}^* \\
 &\left((\lambda)^{(6)} \right)^2 + \left((a'_{32})^{(6)} + (a'_{33})^{(6)} + (p_{32})^{(6)} + (p_{33})^{(6)} \right) (\lambda)^{(6)} \\
 &\quad \left((\lambda)^{(6)} \right)^2 + \left((b'_{32})^{(6)} + (b'_{33})^{(6)} - (r_{32})^{(6)} + (r_{33})^{(6)} \right) (\lambda)^{(6)} \\
 &+ \left((\lambda)^{(6)} \right)^2 + \left((a'_{32})^{(6)} + (a'_{33})^{(6)} + (p_{32})^{(6)} + (p_{33})^{(6)} \right) (\lambda)^{(6)} (q_{34})^{(6)} G_{34} \\
 &+ \left((\lambda)^{(6)} + (a'_{32})^{(6)} + (p_{32})^{(6)} \right) \left((a_{34})^{(6)} (q_{33})^{(6)} G_{33}^* + (a_{33})^{(6)} (a_{34})^{(6)} (q_{32})^{(6)} G_{32}^* \right) \\
 &\left. \left((\lambda)^{(6)} + (b'_{32})^{(6)} - (r_{32})^{(6)} \right) s_{(33),(34)} T_{33}^* + (b_{33})^{(6)} s_{(32),(34)} T_{32}^* \right\} = 0
 \end{aligned}$$

And as one sees, all the coefficients are positive. It follows that all the roots have negative real part, and this proves the theorem.

Acknowledgments:

The introduction is a collection of information from various articles, Books, News Paper reports, Home Pages Of authors, Journal Reviews, Nature 's L:etters,Article Abstracts, Research papers, Abstracts Of Research Papers, Stanford Encyclopedia, Web Pages, Ask a Physicist Column, Deliberations with Professors, the internet including Wikipedia. We acknowledge all authors who have contributed to the same. In the eventuality of the fact that there has been any act of omission on the part of the authors, we regret with great deal of compunction, contrition, regret, trepidiation and remorse. As Newton said, it is only because erudite and eminent people allowed one to piggy ride on their backs; probably an attempt has been made to look slightly further. Once again, it is stated that the references are only illustrative and not comprehensive

REFERENCES

- [1] Dr K N Prasanna Kumar, Prof B S Kiranagi, Prof C S Bagewadi - MEASUREMENT DISTURBS EXPLANATION OF QUANTUM MECHANICAL STATES-A HIDDEN VARIABLE THEORY - published at: "International Journal of Scientific and Research Publications, Volume 2, Issue 5, May 2012 Edition".
- [2] DR K N PRASANNA KUMAR, PROF B S KIRANAGI and PROF C S BAGEWADI -CLASSIC 2 FLAVOUR COLOR SUPERCONDUCTIVITY AND ORDINARY NUCLEAR MATTER-A NEW PARADIGM STATEMENT - published at: "International Journal of Scientific and Research Publications, Volume 2, Issue 5, May 2012 Edition".
- [3] A HAIMOVICI: "On the growth of a two species ecological system divided on age groups". Tensor, Vol 37 (1982),Commemoration volume dedicated to Professor Akitsugu Kawaguchi on his 80th birthday.
- [4] FRTJOF CAPRA: "The web of life" Flamingo, Harper Collins See "Dissipative structures" pages 172-188 .
- [5] HEYLIGHEN F. (2001): "The Science of Self-organization and Adaptivity", in L. D. Kiel, (ed) . Knowledge Management, Organizational Intelligence and Learning, and Complexity, in: The Encyclopedia of Life Support Systems ((EOLSS), (Eolss Publishers, Oxford) [http://www.eolss.net.
- [6] MATSUI, T, H. Masunaga, S. M. Kreidenweis, R. A. Pielke Sr., W.-K. Tao, M. Chin, and Y. J Kaufman (2006), "Satellite-based assessment of marine low cloud variability associated with aerosol, atmospheric stability, and the diurnal cycle", J. Geophys. Res., 111, D17204, doi:10.1029/2005JD006097.
- [7] STEVENS, B, G. Feingold, W.R. Cotton and R.L. Walko, "Elements of the microphysical structure of numerically simulated nonprecipitating stratocumulus" J. Atmos. Sci., 53, 980-1006.
- [8] FEINGOLD, G, Koren, I; Wang, HL; Xue, HW; Brewer, WA (2010), "Precipitation-generated oscillations in open cellular cloud fields" Nature, 466 (7308) 849-852, doi: 10.1038/nature09314, Published 12-Aug 2010.

[9] A b c Einstein, A. (1905), "Ist die Trägheit eines Körpers von seinem Energieinhalt abhängig?", Annalen der Physik 18: 639 Bibcode 1905AnP...323..639E,DOI:10.1002/andp.19053231314. See also the English translation.

- [10] a b Paul Allen Tipler, Ralph A. Llewellyn (2003-01), Modern Physics, W. H. Freeman and Company, pp. 87–88, ISBN 0-7167-4345-0
- [11] a b Rainville, S. et al. World Year of Physics: A direct test of $E=mc^2$. Nature 438, 1096-1097 (22 December 2005) | doi: 10.1038/4381096a; Published online 21 December 2005.
- [12] In F. Fernflores. The Equivalence of Mass and Energy. Stanford Encyclopedia of Philosophy
- [13] Note that the relativistic mass, in contrast to the rest mass m_0 , is not a relativistic invariant, and that the velocity is not a Minkowski four-vector, in contrast to the quantity dx^μ , where dx^μ is the differential of the proper time. However, the energy-momentum four-vector is a genuine Minkowski four-vector, and the intrinsic origin of the square-root in the definition of the relativistic mass is the distinction between dt and $d\tau$.
- [14] Relativity DeMystified, D. McMahon, Mc Graw Hill (USA), 2006, ISBN 0-07-145545-0
- [15] Dynamics and Relativity, J.R. Forshaw, A.G. Smith, Wiley, 2009, ISBN 978-0-470-01460-8
- [16] Hans, H. S.; Puri, S. P. (2003). Mechanics (2 ed.). Tata McGraw-Hill. p. 433. ISBN 0-07-047360-9., Chapter 12 page 433
- [17] E. F. Taylor and J. A. Wheeler, Spacetime Physics, W.H. Freeman and Co., NY. 1992. ISBN 0-7167-2327-1, see pp. 248-9 for discussion of mass remaining constant after detonation of nuclear bombs, until heat is allowed to escape.
- [18] Mould, Richard A. (2002). Basic relativity (2 ed.). Springer. p. 126. ISBN 0-387-95210-1., Chapter 5 page 126
- [19] Chow, Tail L. (2006). Introduction to electromagnetic theory: a modern perspective. Jones & Bartlett Learning. p. 392. ISBN 0-7637-3827-1., Chapter 10 page 392
- [20] [2] Cockcroft-Walton experiment
- [21] a b c Conversions used: 1956 International (Steam) Table (IT).
- [22] Assuming the dam is generating at its peak capacity of 6,809 MW.
- [23] Assuming a 90/10 alloy of Pt/Ir by weight, a C_p of 25.9 for Pt and 25.1 for Ir, a Pt-dominated average C_p of 25.8, 5.134 moles of metal, and 132 J.K⁻¹ for the prototype. A variation of ± 1.5 picograms is of course, much smaller than the actual uncertainty in the mass of the international prototype, which are ± 2 micrograms.
- [24] [3] Article on Earth rotation energy. Divided by c^2 .
- [25] a b Earth's gravitational self-energy is 4.6×10^{-10} that of Earth's total mass, or 2.7 trillion metric tons. Citation: The Apache Point Observatory Lunar Laser-Ranging Operation (APOLLO), T. W. Murphy, Jr. et al. University of Washington, Dept. of Physics (132 kB PDF, here.).
- [26] There is usually more than one possible way to define a field energy, because any field can be made to couple to gravity in many different ways. By general scaling arguments, the correct answer at everyday distances, which are long compared to the quantum gravity scale, should be minimal coupling, which means that no powers of the curvature tensor appear. Any non-minimal couplings, along with other higher order terms, are presumably only determined by a theory of quantum gravity, and within string theory, they only start to contribute to experiments at the string scale.
- [27] G. 't Hooft, "Computation of the quantum effects due to a four-dimensional pseudoparticle", Physical Review D14:3432–3450 (1976).
- [28] A. Belavin, A. M. Polyakov, A. Schwarz, Yu. Tyupkin, "Pseudoparticle Solutions to Yang Mills Equations", Physics Letters 59B:85 (1975).
- [29] F. Klinkhammer, N. Manton, "A Saddle Point Solution in the Weinberg Salam Theory", Physical Review D 30:2212.
- [30] Rubakov V. A. "Monopole Catalysis of Proton Decay", Reports on Progress in Physics 51:189–241 (1988).
- [31] S.W. Hawking "Black Holes Explosions?" Nature 248:30 (1974).
- [32] Einstein, A. (1905), "Zur Elektrodynamik bewegter Körper." (PDF), Annalen der Physik 17: 891–921, Bibcode 1905AnP...322...891E, DOI:10.1002/andp.19053221004. English translation.
- [33] See e.g. Lev B. Okun, The concept of Mass, Physics Today 42 (6), June 1969, p. 31–36, http://www.physicstoday.org/vol-42/iss-6/vol42no6p31_36.pdf
- [34] Max Jammer (1999), Concepts of mass in contemporary physics and philosophy, Princeton University Press, p. 51, ISBN 0-691-01017-X
- [35] Eriksen, Erik; Vøyenli, Kjell (1976), "The classical and relativistic concepts of mass", Foundations of Physics (Springer) 6: 115–124, Bibcode 1976FoPh....6..115E, DOI:10.1007/BF00708670
- [36] a b Janssen, M., Mecklenburg, M. (2007), From classical to relativistic mechanics: Electromagnetic models of the electron., in V. F. Hendricks, et al., , Interactions: Mathematics, Physics and Philosophy (Dordrecht: Springer): 65–134
- [37] a b Whittaker, E.T. (1951–1953), 2. Edition: A History of the theories of aether and electricity, vol. 1: The classical theories / vol. 2: The modern theories 1900–1926, London: Nelson
- [38] Miller, Arthur I. (1981), Albert Einstein's special theory of relativity. Emergence (1905) and early interpretation (1905–1911), Reading: Addison–Wesley, ISBN 0-201-04679-2
- [39] a b Darrigol, O. (2005), "The Genesis of the theory of relativity." (PDF), Séminaire Poincaré 1: 1–22

- [40] Philip Ball (Aug 23, 2011). "Did Einstein discover $E = mc^2$?" Physics World.
- [41] Ives, Herbert E. (1952), "Derivation of the mass-energy relation", Journal of the Optical Society of America 42 (8): 540–543, DOI:10.1364/JOSA.42.000540
- [42] Jammer, Max (1961/1997). Concepts of Mass in Classical and Modern Physics. New York: Dover. ISBN 0-486-29998-8.
- [43] Stachel, John; Torretti, Roberto (1982), "Einstein's first derivation of mass-energy equivalence", American Journal of Physics 50 (8): 760–763, Bibcode1982AmJPh..50..760S, DOI:10.1119/1.12764
- [44] Ohanian, Hans (2008), "Did Einstein prove $E=mc^2$ ", Studies In History and Philosophy of Science Part B 40 (2): 167–173, arXiv:0805.1400, DOI:10.1016/j.shpsb.2009.03.002
- [45] Hecht, Eugene (2011), "How Einstein confirmed $E=mc^2$ ", American Journal of Physics 79 (6): 591–600, Bibcode 2011AmJPh..79..591H, DOI:10.1119/1.3549223
- [46] Rohrlich, Fritz (1990), "An elementary derivation of $E=mc^2$ ", American Journal of Physics 58 (4): 348–349, Bibcode 1990AmJPh..58..348R, DOI:10.1119/1.16168
- [47] (1996). Lise Meitner: A Life in Physics. California Studies in the History of Science. 13. Berkeley: University of California Press. pp. 236–237. ISBN 0-520-20860-
- [48] R.C. Archibald (1914) Time as a fourth dimension Bulletin of the American Mathematical Society 20:409.
- [49] Gallier, Jean H. (2001). Geometric methods and applications: for computer science and engineering. Springer. p. 249. ISBN 0-387-95044-3., Chapter 8, page 249
- [50] Hermann Minkowski, "Raum und Zeit", 80. Versammlung Deutscher Naturforscher (Köln, 1908). Published in Physikalische Zeitschrift 10 104–111 (1909) and Jahresbericht der Deutschen Mathematiker-Vereinigung 18 75–88 (1909). For an English translation, see Lorentz et al. (1952).
- [51] Einstein, Albert, 1926, "Space-Time," Encyclopædia Britannica, 13th ed.
- [52] Matolcsi, Tamás (1994). Spacetime Without Reference Frames. Budapest: Akadémiai Kiadó
- [53] Ellis, G. F. R.; Williams, Ruth M. (2000). Flat and curved space-times (2nd ed.). Oxford University Press. p. 9. ISBN 0-19-850657-0.
- [54] Petkov, Vesselin (2010). Minkowski Spacetime: A Hundred Years Later. Springer. p. 70. ISBN 90-481-3474-9., Section 3.4, p. 70
- [55] See "Quantum Spacetime and the Problem of Time in Quantum Gravity" by Leszek M. Sokolowski, where on this page he writes "Each of these hyper surfaces is spacelike, in the sense that every curve, which entirely lies on one of such hyper surfaces, is a spacelike curve." More commonly a space-like hyper surface is defined technically as a surface such that the normal vector at every point is time-like, but the definition above may be somewhat more intuitive.
- [56] Ehrenfest, Paul (1920). "How do the fundamental laws of physics make manifest that Space has 3 dimensions?" Annalen der Physik 61 (5): 440. Bibcode1920AnP...366...440E. DOI:10.1002/andp.19203660503. Also see Ehrenfest, P. (1917) "In what way does it become manifest in the fundamental laws of physics that space has three dimensions?" Proceedings of the Amsterdam Academy 20: 200.
- [57] Weyl, H. (1922) Space, time, and matter. Dover reprint: 284.
- [58] Tangherlini, F. R. (1963). "Atoms in Higher Dimensions". Nuovo Cimento 14 (27): 636.
- [59] Tegmark, Max (April 1997). "On the dimensionality of spacetime". Classical and Quantum Gravity 14 (4): L69–L75. arXiv:gr-c/9702052. Bibcode1997CQGra..14L..69T. DOI:10.1088/0264-9381/14/4/002. Retrieved 2006-12-16.
- [60] Dorling, J. (1970). "The Dimensionality of Time". American Journal of Physics 38(4): 539–40. Bibcode 1970AmJPh..38...539D. DOI:10.1119/1.1976386.
- [61] Barrow, J. D. (2002). The Constants of Nature. Pantheon Books. ISBN 0-375-42221-8.
- [62] Whitrow, G. J. (1955) "The Structure and Evolution of the Universe." British Journal of the Philosophy of Science 6: 13. Also see his (1959) The Structure and Evolution of the Universe. London: Hutchinson.
- [63] Jan Ambjørn, Jerzy Jurkiewicz, and Renate Loll - "The Self-Organizing Quantum Universe", Scientific American, July 2008
- [64] First Author: 1Mr. K. N.Prasanna Kumar has three doctorates one each in Mathematics, Economics, Political Science. Thesis was based on Mathematical Modeling. He was recently awarded D.litt. for his work on 'Mathematical Models in Political Science'--- Department of studies in Mathematics, Kuvempu University, Shimoga, Karnataka, India Corresponding Author:drknpkumar@gmail.com
- [65] Second Author: 2Prof. B.S Kiranagi is the Former Chairman of the Department of Studies in Mathematics, Manasa Gangotri and present Professor Emeritus of UGC in the Department. Professor Kiranagi has guided over 25 students and he has received many encomiums and laurels for his contribution to Co homology Groups and Mathematical Sciences. Known for his prolific writing, and one of the senior most Professors of the country, he has over 150

publications to his credit. A prolific writer and a prodigious thinker, he has to his credit several books on Lie Groups, Co Homology Groups, and other mathematical application topics, and excellent publication history.-- UGC Emeritus Professor (Department of studies in Mathematics), Manasagangotri, University of Mysore, Karnataka, India

- [66] Third Author: 3Prof. C.S. Bagewadi is the present Chairman of Department of Mathematics and Department of Studies in Computer Science and has guided over 25 students. He has published articles in both national and international journals. Professor Bagewadi specializes in Differential Geometry and its wide-ranging ramifications. He has to his credit more than 159 research papers. Several Books on Differential Geometry, Differential Equations are coauthored by him--- Chairman, Department of studies in Mathematics and Computer science, Jnanasahyadri Kuvempu University, Shankarghatta, Shimoga district, Karnataka, India

Performance Evolution and Comparison of Geographical Location Aided Routing and AODV Routing In MANET

V. Kalpana¹, S. Kannan², Dr. S. Karthik³

¹Final ME CSE, SNS College of Technology, Coimbatore - 35, India

²Assistant Professor, SNS College of technology Coimbatore-35, India

³Head of the Department, Computer Science and Engineering, SNS College of Technology, Coimbatore, India

Abstract: A mobile ad-hoc network (MANET) consists of mobile computing entities such as laptop and palmtop computers which communicate with each other through wireless links and without relying on a static infrastructure such as a base station or access point. Without centralized administration, a MANET is highly unpredictable due to its unstable links and resource-poor as most of the nodes have limited battery power. Due to these physical limitations, we propose a geo graphically location aided routing; in this proposed method nodes are require the cooperation of other nodes to successfully send a message to a destination. Figure 1.1 shows the mobile Ad hoc network. We follow with a simulation study to evaluate the performance in large networks. In this paper, we specifically address the issues and comparison of AODV and with the proposed geographically location aided routing (Terminode Routing) using ns2 to illustrate that routing overhead is low and packet delivery ratio is high compared to AODV.

I. Introduction

1.1 MANET

A mobile ad hoc network is one where in all nodes work independent of any common centralized admin. Each one of them performs the tasks of a router. They should be self-adapting in that if their connection topology changes, their routing tables should reflect the change. There are numerous scenarios that do not have an available network infrastructure and could benefit from the creation of an ad hoc network:

- o Rescue/Emergency operations: Rapid installation of a communication infrastructure during a natural/environmental disaster (or a disaster due to terrorism) that demolished the previous communication infrastructure.
- o Law enforcement activities: Rapid installation of a communication infrastructure during special operations.
- o Tactical missions: Rapid installation of a communication infrastructure in a hostile and/or unknown territory.
- o Commercial projects: Simple installation of a communication infrastructure for commercial gatherings such as conferences, exhibitions, workshops and meetings.
- o Educational classrooms: Simple installation of a communication infrastructure to create an interactive classroom on demand.

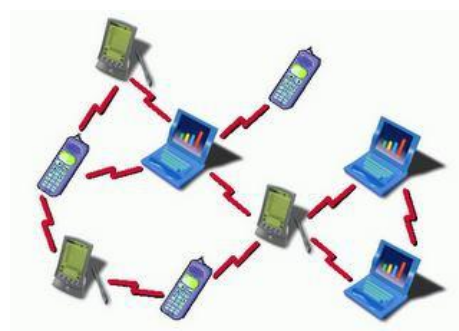


Fig:1.1 Mobile Ad Hoc Network

1.2 Main Characteristics of Ad-Hoc Networks

Dynamic topology: Hosts are mobile and can be connected dynamically in any arbitrary manner. Links of the network vary and are based on the proximity of one host to another one.

Variable capacity links: Wireless links have significantly lower capacity than their hardwired counterparts. Moreover, the realized throughput of wireless communications is often much less than a radio's maximum transmission rate.

Autonomous: No centralized administration entity is required to manage the operation of the different mobile hosts.

Bandwidth constrained: Wireless links have a significantly lower capacity than the wired ones; they are affected by several error sources that result in degradation of the received signal.

Energy constrained: Mobile hosts rely on battery power, which is a scarce resource the most important system design criterion for optimization may be energy conservation.

Limited security: Mobility implies higher security risks than static operations because portable devices may be stolen or their traffic may cross insecure wireless links.

1.3 Classification of Ad-hoc Protocols

Routing protocols can be classified into different categories depending on their properties:

- ▶ Centralized vs. Distributed
- ▶ Static vs. Adaptive
- ▶ Reactive vs. Proactive

In centralized algorithms, all route choices are made at central node, while in distributed algorithms, the computation of routers is shared among the network nodes.

1.4 Routing And Types Of Routing Protocols In Manet

In order to enable communication within a MANET, a routing protocol is required to establish routes between participating nodes. Because of limited transmission range, multiple network hops may be needed to enable data communication between two nodes in the network. Since MANET is an infrastructure less network, each mobile node operates not only as a host but also as a router, forwarding packets for other mobile nodes in the network. Mobile Ad hoc ETworks (MANET), are characterized by wireless nodes, which are free to move arbitrarily, but cooperate to forward packets for each other in a totally wireless environment.

The routing requirement of a mobile ad hoc network is achieved in distributed fashion among the nodes. Conventional routing protocols based on distance vector or link state algorithms cannot be applied here, since the amount of routing related traffic would waste a large portion of the wireless bandwidth, and such discovered routes would soon become obsolete due to mobility of Nodes. In MANETs mobile nodes share the same frequency channel thereby limiting the network capacity. Thus one of the highly desirable properties of a routing protocol for MANETs is that it should be bandwidth efficient. The routing protocols are categorized into two broad categories: namely, on-demand protocols and table driven protocols. They are also known as reactive and proactive protocols respectively.

1.4.1 Proactive or Table-driven protocols

It maintains one or more routing tables in every node in order to store routing information about other nodes in the MANET. These routing protocols attempt to update the routing table information either periodically or in response to change in network topology in order to maintain consistent and up-to-date routing information. The advantage of these protocols is that a source node does not need route-discovery procedures to find a route to a destination node. The drawback of these protocols is that maintaining a consistent and up-to-date routing table requires substantial messaging overhead, which consumes bandwidth and power usage, and decreases throughput, especially in the case of a large number of high-mobility mobile nodes. The different types of Table driven protocols are: Destination Sequenced Distance Vector routing (DSDV), Wireless routing protocol (WRP), Fish eye State Routing protocol (FSR), Optimized Link State Routing protocol (OLSR), Cluster Gateway switch routing protocol (CGSR), Topology Dissemination Based on Reverse path forwarding (TBRPF).

1.4.2 Reactive or On-demand routing protocols

Another in the family of routing protocols for mobile ad-hoc network is on-demand routing protocols. It initiates a route discovery mechanism by the source node to discover the route to the destination node when the source node has data packets to send to the destination node. After discovering the route, the route maintenance is initiated to main this route until the routes no longer required or the destination is not reachable. The main advantage of these protocols is that overhead messaging is less. One of the drawbacks of these protocols is the delay of discovering a new route. The different types of Reactive routing protocols are: Dynamic Source Routing (DSR), Ad hoc On-Demand Distance Vector routing (AODV), Location-Aided Routing (LAR), Temporally Ordered Routing Algorithm (TORA) and Dynamic MANET On-demand (DYMO).

1.5 Major MANET Issue Categories

In this section the MANET research issues are presented and classified. Hundreds of research aspects have been developed and discussed in this field. To analyze various research issues, this article covers most of the major investigation problems. Various fundamental and frequently discussed aspects of MANETs are identified and grouped into fifteen categories. These issues have the potential to significantly increase MANET survivability:

Routing: Routing is an essential one, because change in network topology occurs frequently. An efficient routing protocol is required to cope with highly fluid network conditions.

Multicasting/ Broadcasting: Multicast service supports users communicating with other members in a multicast group. Broadcast service supports users communicating with all members on a network.

Location Service: Location information uses the Global Positioning System (GPS) or the network-based geo-location technique to obtain the physical position of a destination.

Mobility Management: In the ad-hoc network environment, mobile hosts can move unrestricted from place to place. Mobility management handles the storage, maintenance and retrieval of the mobile node position information.

Multiple Accesses: A major issue is to develop efficient medium access protocols that optimize spectral reuse, and hence, maximize aggregate channel utilization in MANETs.

Bandwidth Management: Bandwidth management in MANETs is a typical characterization. Because the bandwidth is usually limited, effectively managing and using it is a very important issue.

Power Management: A power management approach would help reducing power consumption and hence prolonging the battery life of mobile nodes. Because most devices operate on batteries, power management becomes an important issue.

Security: The mobile nodes in MANETs are highly susceptible to malicious damage. Security issues are important in MANETs to prevent potential attacks, threats and system vulnerabilities.

Fault Tolerance: This issue involves detecting and correcting faults when network failures occur. Fault-tolerance techniques are brought in for maintenance when a failure occurs during node movement, joining, or leaving the network.

QoS/ Multimedia: Quality of Service (QoS) and Multimedia require high bandwidth, low delay, and high reliability.

Standards/ Products: The standards and products issues that allow the development of small scale is emerging for this field. For instance, Bluetooth is a low-cost technology for short-range communications techniques.

II. Geographical Map Path Discovery (GMPD)

The basic idea behind GMPD is that, mapping information of the network density is known to all nodes in the network. Areas with high node density are called “towns”. The Source node determines the town area in which it is actually situated; also determines the town area of the destination node. The Source node refers the network map in order to find anchor path from source to destination. The shortest path between source and destination is chosen for routing the packets. For GMPD each town, a map gives the location of its center and the size of the square area. A map of the network can be presented as a graph with nodes corresponding to towns and edges corresponding to highways. Macroscopically, the graph of towns does not change frequently.

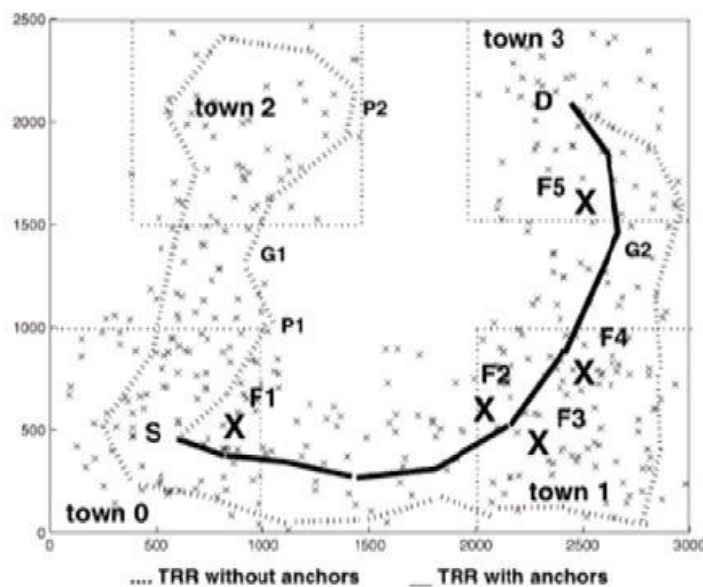


Fig: 2.1 GMPD with a given map of towns works as follows

For Figure 2.1 Source S determines from its own location LDAS the town area ST (Source town) in which S is situated (or, the nearest town to LDAS if it is not in the town area). In addition, since S knows the location of destination D (LDAD), it can determine from the LDAD the town area DT (Destination town), where D is situated (or, the nearest town to LDAD if it is not in the town area). Then, S accesses the network map in order to find the anchored path from S to D. An anchored path is the list of the geographical points: The points correspond to centers of the towns that the packet has to visit from ST in order to reach DT.

III. Location Based Routing

In ad hoc network location information to help routing is often routing (Terminode remote Routing, TRR), used when the destination is far, and link state routing (Terminode Local Routing (TLR), proposed as a means to achieve scalability in large mobile ad hoc networks. In order to enhance the life time of the network a location based routing protocol which uses anchored paths a list of geographic points is used as loose source routing information. It is a high probability that there are nodes to ensure connectivity from one town to another source and destination of the location have sufficient of its centre and size of the square area.

3.1 Terminode Routing

First, it combines a location-based routing method with a link state-based mechanism. Second, it uses a special form of restricted search mode (Restricted Local Flooding, RLF). These first two ingredients solve problems due to the inaccuracy of location information, in particular for control packets. Third, it introduces the concept of anchors, which are geographical points imagined by sources for routing to specific destinations. This helps efficiently route around connectivity holes. In order for the comparison to be fair to MANET protocols, we implemented an ad hoc location management scheme. In smaller ad hoc networks we compared Terminode routing to some existing MANET like routing protocols (AODV and LAR1) and found similar performance.

In larger mobile ad hoc networks of 500 nodes, MANET-like routing protocols do not perform well (except when mobility is small), while our routing protocol still performs well. In networks that are regularly populated with nodes, Terminode routing performs comparable to GPSR when the location management accuracy is high; however, terminode routing performs better when the location information accuracy is low. We also consider irregular networks with holes in node distribution. Here, too, we find that terminode routing outperforms GPSR. An existing MANET and location-based routing protocols we compared it to. Non uniform topologies are likely to appear in metropolitan .

IV. Performance Evaluation OF Terminode Routing

4.1. Performance Evaluation

In the NS 2 settings, The IEEE 802.11 Medium Access Control (MAC) protocol is used. And the radio range is 250 meters. The channel capacity is 2Mb/s. The propagation model is two-ray. It uses free space path loss for near sight and plane earth path loss for far sight.

4.2 Protocol Constants

We used the following configuration for the Helloing protocol. The HELLO timer is 1 second. Each entry in the routing table expires after two seconds, if it is not updated. All nodes promiscuously listen to all HELLO messages within their radio range. Nodes that have data or control packets to send should defer sending HELLO messages (up to the timer value) and piggyback the HELLO message to the data or control packet.

V. Network Simulator 2

The simulator used and the experimental results are explained in this chapter.

5.1 NS-2

The NS network simulator(www.isi.edu/nsnam/ns), from U.C. Berkeley/LBNL, is a object oriented discrete event simulator targeted at networking research and available as public domain. Its first version (NS-1) began in 1989 as a variant of the REAL network simulator and was developed by the Network Research Group at the Lawrence Berkeley National Laboratory (LBNL), USA. Its development was then part of the VINT project (www.isi.edu/nsnam/vint/index.html), supported by DARPA, at LBNL, Xerox PARC, and UCB, under which NS version 2.0 (NS-2) was released, evolving substantially from the first version. NS-2 is widely used in the networking research community and has found large acceptance as a tool to experiment new ideas, protocols and distributed algorithms.

Currently NS-2 development is still supported through DARPA. NS has always included substantial contributions from other researchers, including wireless code for both mobile ad hoc networks and wireless LANs from the UCB Daedalus and CMU Monarch projects and Sun Microsystems. At the time being, NS-2 is well suited for packets switched networks and wireless networks (ad hoc, local and satellite), and is used mostly for small scale simulations of queuing and routing algorithms, transport protocols, congestion control, and some multicast related work. It provides substantial support for simulation of TCP, routing, and multicast protocols over wired and wireless networks. NS-2 is suitable not only for simulation but also for emulation, that is, it is possible to introduce the simulator into a live network. Special objects within the simulator are capable of introducing live traffic into the simulator and injecting traffic from the simulator into the live network.

NS-2 plays an important role in the research community of mobile ad hoc networks, being a sort of reference simulator. NS-2 is the most used simulator for studies on mobile ad hoc networks, and it comes with a rich suite of algorithms and models. Unfortunately, its software architecture is such that adding new components and/or modifying existing ones is not a straightforward process. That is, in terms of ease to implement/test new algorithms or scenarios, NS-2 scores poorly with respect to other candidates. Moreover, NS-2 does not scale well in terms of number of nodes and it is

reported to be in general quite slow from a computational point of view. Implementation and simulation under NS-2 consists of 4 steps.

1. Implementing the protocol by adding a combination of c++ and Otcl code to NS-2 source base.
2. Describing the simulation in an Otcl script
3. Running the simulation
4. Analyzing the generated trace files.

VI. Simulation Results

6.1 Simulation Environment

An event driven simulator ns-2 was used for simulations. The simulation setup 10 nodes and Radio range of each node is assumed to be 250m. Reliable connections are established at random in the network and the connections with constant bit rate. Two ray ground propagation models were used. The size of the data payload was 512 bytes

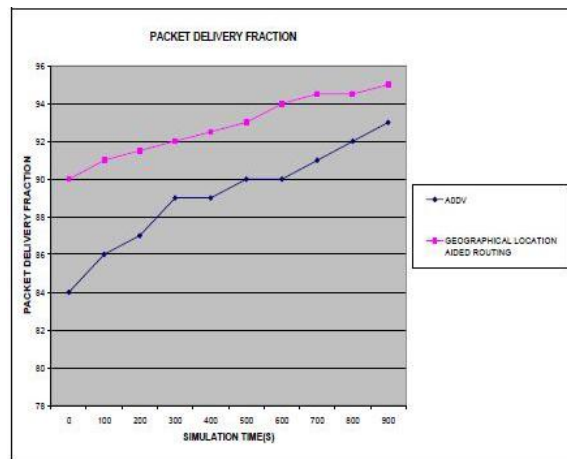


Fig:6.1 Cumulative sum of Numbers of Received Packets vs receive event time(s)

6.1.1 Cumulative sum of Numbers of Received Packets

In Figure 6.1 shows the Cumulative sum of Numbers of Received Packets vs received event time (s) of Geographical location aided routing

6.1.2 Packet Delivery Ratio

It is the ratio between the numbers of data packets delivered to that of the number of packets supposed to be received by it. This metric gives a measure about the packet loss. A high packet delivery ratio implies an efficient protocol. The figure 6a shows the packet delivery fraction vs simulation time of AODV and Geographical location aided routing. Packet Delivery Ratio (in%) = Actual packets received divided by Packets supposed to be received x 100. On an average, the packet delivery ratio improved by 5.08% than AODV.

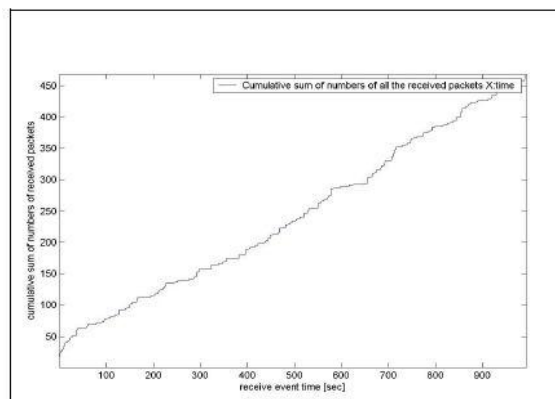


Fig:6.2 Packet Delivery fraction vs Simulation time(s)

6.1.3 Throughput

Throughput are mainly of network parameters in figure 6.5 and 6.6 shows the throughput receiving packets vs simulation time in that manner slightly increase in simulation of throughput receiving packets in simulation time of 300 sec. It is observed that throughput is better than AODV by 37.5%

VII. Conclusion

Terminode routing aims to support Geographical map path discovery (GMPD) location-based routing on irregular topologies with mobile nodes. It achieves its goal by combining a location-based routing method with a link state-based mechanism. Further, it introduces the concept of anchors, which are geographical points imagined by sources for routing to specific destinations, and proposes low overhead methods for computing anchors. Last, a special form of restricted search mode (Restricted Local Flooding, RLF), solves problems due to the inaccuracy of location information, in particular for control packets. The performance analysis shows that, in large mobile ad hoc networks, terminode routing performs better than existing location-based routing protocols. It does so by maintaining its routing overhead low and by efficiently solving location inaccuracies GMPD(Geographical Map Path Discovery) It is a high probability and packet received information's are good that there are nodes to ensure connectivity from one town to another source and destination of the location have sufficient of its centre and size of the square area.

VIII. Future Work

In this implementation, the communication is established between single sender and receiver in future versions, this can be extended to multiple senders and receivers and the performance levels and using Global positioning system still can be improved.

IX. Acknowledgement

The authors would like to thank the Director cum Secretary, Correspondent, Principal, SNS College of Technology, and Coimbatore for their motivation and constant encouragement. The authors would like to thank the Faculty Members of Department of Computer Science and Engineering for critical review of this manuscript and for his valuable input and fruitful discussions. Also, he takes privilege in extending gratitude to his family members and friends who rendered their support throughout this research work.

References

- [1] Karthik. S., V. P. Arunachalam. And T. Ravichandran, 2008, A comparative study of various IP trace back Strategies and simulation of IP trace back. Asian J.inform. Technol., 7: 454-458. http://www.medwelljournals.com/fulltext/ajit/2008/4_54-458.pdf.
- [2] Maheswari. C, Kowshika. A, and Karthik. S, "A Packet Forwarding Mechanism for MANET using MODRP in Dynamic Source Routing (DSR), Proc. of International Conference on Advances in Recent Technologies in Communication and Computing, 978-0-7695-4201-0/10 IEEE, October - 2010.
- [3] Maheswari. C, Kowshika. A, and Karthik. S, "An Efficient Packet Forwarding in MANET with AODV using Random Way Point Mobility Model," Journal of Mathematics and Technology, ISSN: 2078-0257, No.3, August, 2010.
- [4] Maheswari. C, Kowshika. A, and Karthik. S, "An Efficient Packet Forwarding in MANET with AODV using Random Way Point Mobility Model," Research Journal of Applied Science 5(2): 151-156. 2010, ISSN: 1815-932X.
- [5] <http://ica1www.epfl.ch/TNRouting>, 2004, Simulation Source Code of Terminode Routing (NS-2).
- [6] S. Basagni, I. Chlamtac, V. Syrotiuk, and B. Woodward, 1998, "A Distance Routing Effect Algorithm or Mobility (DREAM)," Proc. Fourth Ann. ACM/IEEE Int'l Conf. Mobile Computing and networking (MobiCom '98)
- [7] L. Blazevic, S. Giordano, and J.-Y. Le Boudec, 2002, "Anchored Path Discovery in Terminode Routing," Proc. Second IFIP-TC6 Networking Conf. (Networking 2005).
- [8] A. McDonal and T. Znabi, "A path availability model for wireless ad hoc networks", IEEE Wireless Communications and Networking Conference. New Orlean, USA: IEEE, 1999, pp.35-40
- [9] J. Broch, D. A. Maltz, D. B. Johnson, Y. C. Hu and J. Jetcheva: "A Performance comparison of Multi-hop Wireless Ad Hoc Network Routing Protocols", Proceedings of the 4th ACM Annual International Conference on Mobile Computing and Networking, pp.85 - 97 (1998).
- [10] Yuhong Luo, Jianxin Wang, Songqiao Chen "An Energy-efficient DSR Routing Protocol Based on Mobility Prediction", Proceedings of the 2006 International Symposium on a World of Wireless, Mobile and Multimedia Networks (WoWMoM'06)
- [11] L.M. Feeney, "An Energy Consumption Model for Performance Analysis of Routing Protocols for Mobile Ad Hoc Networks," Mobile Networks and Applications, vol. 6, no. 3, 239-249, 2001.

Some Contributions to Yang Mills Theory Fortification – Dissipation Models

¹Dr. K. N. Prasanna Kumar, ²Prof. B. S. Kiranagi, ³Prof. C. S. Bagewadi

ABSTRACT: We provide a series of Models for the problems that arise in Yang Mills Theory. No claim is made that the problem is solved. We do factorize the Yang Mills Theory and give a Model for the values of LHS and RHS of the yang Mills theory. We hope these forms the stepping stone for further factorizations and solutions to the subatomic denominations at Planck’s scale. Work also throws light on some important factors like mass acquisition by symmetry breaking, relation between strong interaction and weak interaction, Lagrangian Invariance despite transformations, Gauge field, Noncommutative symmetry group of Gauge Theory and Yang Mills Theory itself..

We take in to consideration the following parameters, processes and concepts:

- (1) Acquisition of mass
- (2) Symmetry Breaking
- (3) Strong interaction
- (4) Unified Electroweak interaction
- (5) Continuous group of local transformations
- (6) Lagrangian Variance
- (7) Group generator in Gauge Theory
- (8) Vector field or Gauge field
- (9) Non commutative symmetry group in Gauge Theory
- (10) Yang Mills Theory (We repeat the same Bank’s example. Individual debits and Credits are conservative so also the holistic one. Generalized theories are applied to various systems which are parameterized. And we live in ‘measurement world’. Classification is done on the parameters of various systems to which the Theory is applied.).
- (11) First Term of the Lagrangian of the Yang Mills Theory(LHS)

$$\mathcal{L}_{gf} = -\frac{1}{4} \text{Tr}(F^2) = -\frac{1}{4} F^{\mu\nu a} F_{\mu\nu}^a$$

(12) RHS of the Yang Mills Theory

$$\mathcal{L}_{gf} = -\frac{1}{4} \text{Tr}(F^2) = -\frac{1}{4} F^{\mu\nu a} F_{\mu\nu}^a$$

SYMMETRY BREAKING AND ACQUISITION OF MASS:

MODULE NUMBERED ONE

NOTATION:

- G_{13} : CATEGORY ONE OF SYMMETRY BREAKING
- G_{14} : CATEGORY TWO OF SYMMETRY BREAKING
- G_{15} : CATEGORY THREE OF SYMMETRY BREAKING
- T_{13} : CATEGORY ONE OF ACQUISITION OF MASS
- T_{14} : CATEGORY TWO OF ACQUISITION OF MASS
- T_{15} :CATEGORY THREE OF ACQUISITION OF MASS

UNIFIED ELECTROWEAK INTERACTION AND STRONG INTERACTION:

MODULE NUMBERED TWO:

- G_{16} : CATEGORY ONE OF UNIFIED ELECTROWEAK INTERACTION
- G_{17} : CATEGORY TWO OF UNIFIED ELECTROWEAK INTERACTION
- G_{18} : CATEGORY THREE OF UNIFIED ELECTROWEAK INTERACTION
- T_{16} :CATEGORY ONE OF STRONG INTERACTION
- T_{17} : CATEGORY TWO OF STRONG INTERACTION
- T_{18} : CATEGORY THREE OF STRONG INTERACTION

LAGRANGIAN INVARIANCE AND CONTINUOUS GROUP OF LOCAL TRANSFORMATIONS:

MODULE NUMBERED THREE:

- G_{20} : CATEGORY ONE OF CONTINUOUS GROUP OF LOCAL TRANSFORMATIONS

- G_{21} : CATEGORY TWO OF CONTINUOUS GROUP OF LOCAL TRANSFORMATIONS
 G_{22} : CATEGORY THREE OF CONTINUOUS GROUP OF LOCAL TRANSFORMATION
 T_{20} : CATEGORY ONE OF LAGRANGIAN INVARIANCE
 T_{21} : CATEGORY TWO OF LAGRANGIAN INVARIANCE
 T_{22} : CATEGORY THREE OF LAGRANGIAN INVARIANCE

GROUP GENERATOR OF GAUGE THEORY AND VECTOR FIELD(GAUGE FIELD):
: MODULE NUMBERED FOUR:

- G_{24} : CATEGORY ONE OF GROUP GENERATOR OF GAUGE THEORY
 G_{25} : CATEGORY TWO OF GROUP GENERATOR OF GAUGE THEORY
 G_{26} : CATEGORY THREE OF GROUP GENERATOR OF GAUGE THEORY
 T_{24} : CATEGORY ONE OF VECTOR FIELD NAMELY GAUGE FIELD
 T_{25} : CATEGORY TWO OF GAUGE FIELD
 T_{26} : CATEGORY THREE OF GAUGE FIELD

YANG MILLS THEORY AND NON COMMUTATIVE SYMMETRY GROUP IN GAUGE THEORY:
MODULE NUMBERED FIVE:

- G_{28} : CATEGORY ONE OF NON COMMUTATIVE SYMMETRY GROUP OF GAUGE THEORY
 G_{29} : CATEGORY TWO OF NON COMMUTATIVE SYMMETRY GROUP OF GAUGE THEORY
 G_{30} : CATEGORY THREE OF NON COMMUTATIVE SYMMETRY GROUP OF GAUGE THEORY
 T_{28} : CATEGORY ONE OF YANG MILLS THEORY (Theory is applied to various subatomic particle systems and the classification is done based on the parametrization of these systems. There is not a single system known which is not characterized by some properties)
 T_{29} : CATEGORY TWO OF YANG MILLS THEORY
 T_{30} : CATEGORY THREE OF YANG MILLS THEORY

LHS OF THE YANG MILLS THEORY AND RHS OF THE YANG MILLS THEORY. TAKEN TO THE OTHER
SIDE THE LHS WOULD DISSIPATE THE RHS WITH OR WITHOUT TIME LAG :

MODULE NUMBERED SIX:

$$\mathcal{L}_{gf} = -\frac{1}{4} \text{Tr}(F^2) = -\frac{1}{4} F^{\mu\nu a} F_{\mu\nu}^a$$

- G_{32} : CATEGORY ONE OF LHS OF YANG MILLS THEORY
 G_{33} : CATEGORY TWO OF LHS OF YANG MILLS THEORY
 G_{34} : CATEGORY THREE OF LHS OF YANG MILLS THEORY
 T_{32} : CATEGORY ONE OF RHS OF YANG MILLS THEORY
 T_{33} : CATEGORY TWO OF RHS OF YANG MILLS THEORY
 T_{34} : CATEGORY THREE OF RHS OF YANG MILLS THEORY (Theory applied to various characterized systems and the systemic characterizations form the basis for the formulation of the classification).

$(a_{13})^{(1)}, (a_{14})^{(1)}, (a_{15})^{(1)}, (b_{13})^{(1)}, (b_{14})^{(1)}, (b_{15})^{(1)}, (a_{16})^{(2)}, (a_{17})^{(2)}, (a_{18})^{(2)}, (b_{16})^{(2)}, (b_{17})^{(2)}, (b_{18})^{(2)}$
 $(a_{20})^{(3)}, (a_{21})^{(3)}, (a_{22})^{(3)}, (b_{20})^{(3)}, (b_{21})^{(3)}, (b_{22})^{(3)}$
 $(a_{24})^{(4)}, (a_{25})^{(4)}, (a_{26})^{(4)}, (b_{24})^{(4)}, (b_{25})^{(4)}, (b_{26})^{(4)}, (b_{28})^{(5)}, (b_{29})^{(5)}, (b_{30})^{(5)}, (a_{28})^{(5)}, (a_{29})^{(5)}, (a_{30})^{(5)}$
 $(a_{32})^{(6)}, (a_{33})^{(6)}, (a_{34})^{(6)}, (b_{32})^{(6)}, (b_{33})^{(6)}, (b_{34})^{(6)}$

are Accentuation coefficients

$(a'_{13})^{(1)}, (a'_{14})^{(1)}, (a'_{15})^{(1)}, (b'_{13})^{(1)}, (b'_{14})^{(1)}, (b'_{15})^{(1)}, (a'_{16})^{(2)}, (a'_{17})^{(2)}, (a'_{18})^{(2)}, (b'_{16})^{(2)}, (b'_{17})^{(2)}, (b'_{18})^{(2)}$
 $(a'_{20})^{(3)}, (a'_{21})^{(3)}, (a'_{22})^{(3)}, (b'_{20})^{(3)}, (b'_{21})^{(3)}, (b'_{22})^{(3)}$
 $(a'_{24})^{(4)}, (a'_{25})^{(4)}, (a'_{26})^{(4)}, (b'_{24})^{(4)}, (b'_{25})^{(4)}, (b'_{26})^{(4)}, (b'_{28})^{(5)}, (b'_{29})^{(5)}, (b'_{30})^{(5)}, (a'_{28})^{(5)}, (a'_{29})^{(5)}, (a'_{30})^{(5)}$
 $(a'_{32})^{(6)}, (a'_{33})^{(6)}, (a'_{34})^{(6)}, (b'_{32})^{(6)}, (b'_{33})^{(6)}, (b'_{34})^{(6)}$

are Dissipation coefficients.

SYMMETRY BREAKING AND ACQUISITION OF MASS:
MODULE NUMBERED ONE

The differential system of this model is now (Module Numbered one).I

$$\frac{dG_{13}}{dt} = (a_{13})^{(1)} G_{14} - [(a'_{13})^{(1)} + (a''_{13})^{(1)}(T_{14}, t)] G_{13} \quad .2$$

$$\frac{dG_{14}}{dt} = (a_{14})^{(1)} G_{13} - [(a'_{14})^{(1)} + (a''_{14})^{(1)}(T_{14}, t)] G_{14} \quad .3$$

$$\frac{dG_{15}}{dt} = (a_{15})^{(1)}G_{14} - [(a'_{15})^{(1)} + (a''_{15})^{(1)}(T_{14}, t)]G_{15} .4$$

$$\frac{dT_{13}}{dt} = (b_{13})^{(1)}T_{14} - [(b'_{13})^{(1)} - (b''_{13})^{(1)}(G, t)]T_{13} .5$$

$$\frac{dT_{14}}{dt} = (b_{14})^{(1)}T_{13} - [(b'_{14})^{(1)} - (b''_{14})^{(1)}(G, t)]T_{14} .6$$

$$\frac{dT_{15}}{dt} = (b_{15})^{(1)}T_{14} - [(b'_{15})^{(1)} - (b''_{15})^{(1)}(G, t)]T_{15} .7$$

$$+(a''_{13})^{(1)}(T_{14}, t) = \text{First augmentation factor} .8$$

$$-(b''_{13})^{(1)}(G, t) = \text{First detritions factor}.$$

**UNIFIED ELECTROWEAK INTERACTION AND STRONG INTERACTION:
MODULE NUMBERED TWO**

The differential system of this model is now (Module numbered two).9

$$\frac{dG_{16}}{dt} = (a_{16})^{(2)}G_{17} - [(a'_{16})^{(2)} + (a''_{16})^{(2)}(T_{17}, t)]G_{16} .10$$

$$\frac{dG_{17}}{dt} = (a_{17})^{(2)}G_{16} - [(a'_{17})^{(2)} + (a''_{17})^{(2)}(T_{17}, t)]G_{17} .11$$

$$\frac{dG_{18}}{dt} = (a_{18})^{(2)}G_{17} - [(a'_{18})^{(2)} + (a''_{18})^{(2)}(T_{17}, t)]G_{18} .12$$

$$\frac{dT_{16}}{dt} = (b_{16})^{(2)}T_{17} - [(b'_{16})^{(2)} - (b''_{16})^{(2)}((G_{19}), t)]T_{16} .13$$

$$\frac{dT_{17}}{dt} = (b_{17})^{(2)}T_{16} - [(b'_{17})^{(2)} - (b''_{17})^{(2)}((G_{19}), t)]T_{17} .14$$

$$\frac{dT_{18}}{dt} = (b_{18})^{(2)}T_{17} - [(b'_{18})^{(2)} - (b''_{18})^{(2)}((G_{19}), t)]T_{18} .15$$

$$+(a''_{16})^{(2)}(T_{17}, t) = \text{First augmentation factor} .16$$

$$-(b''_{16})^{(2)}((G_{19}), t) = \text{First detritions factor} .17$$

**LAGRANGIAN INVARIANCE AND CONTINOUS GROUP OF LOCAL TRANSFORMATIONS:
MODULE NUMBERED THREE**

The differential system of this model is now (Module numbered three).18

$$\frac{dG_{20}}{dt} = (a_{20})^{(3)}G_{21} - [(a'_{20})^{(3)} + (a''_{20})^{(3)}(T_{21}, t)]G_{20} .19$$

$$\frac{dG_{21}}{dt} = (a_{21})^{(3)}G_{20} - [(a'_{21})^{(3)} + (a''_{21})^{(3)}(T_{21}, t)]G_{21} .20$$

$$\frac{dG_{22}}{dt} = (a_{22})^{(3)}G_{21} - [(a'_{22})^{(3)} + (a''_{22})^{(3)}(T_{21}, t)]G_{22} .21$$

$$\frac{dT_{20}}{dt} = (b_{20})^{(3)}T_{21} - [(b'_{20})^{(3)} - (b''_{20})^{(3)}(G_{23}, t)]T_{20} .22$$

$$\frac{dT_{21}}{dt} = (b_{21})^{(3)}T_{20} - [(b'_{21})^{(3)} - (b''_{21})^{(3)}(G_{23}, t)]T_{21} .23$$

$$\frac{dT_{22}}{dt} = (b_{22})^{(3)}T_{21} - [(b'_{22})^{(3)} - (b''_{22})^{(3)}(G_{23}, t)]T_{22} .24$$

$$+(a''_{20})^{(3)}(T_{21}, t) = \text{First augmentation factor}.$$

$$-(b''_{20})^{(3)}(G_{23}, t) = \text{First detritions factor} .25$$

**GROUP GENERATOR OF GAUGE THEORY AND VECTOR FIELD(GAUGE FIELD):
: MODULE NUMBERED FOUR:**

=====

The differential system of this model is now (Module numbered Four).26

$$\frac{dG_{24}}{dt} = (a_{24})^{(4)}G_{25} - [(a'_{24})^{(4)} + (a''_{24})^{(4)}(T_{25}, t)]G_{24} .27$$

$$\frac{dG_{25}}{dt} = (a_{25})^{(4)}G_{24} - [(a'_{25})^{(4)} + (a''_{25})^{(4)}(T_{25}, t)]G_{25} .28$$

$$\frac{dG_{26}}{dt} = (a_{26})^{(4)}G_{25} - [(a'_{26})^{(4)} + (a''_{26})^{(4)}(T_{25}, t)]G_{26} .29$$

$$\frac{dT_{24}}{dt} = (b_{24})^{(4)}T_{25} - [(b'_{24})^{(4)} - (b''_{24})^{(4)}((G_{27}), t)]T_{24} .30$$

$$\frac{dT_{25}}{dt} = (b_{25})^{(4)}T_{24} - [(b'_{25})^{(4)} - (b''_{25})^{(4)}((G_{27}), t)]T_{25} .31$$

$$\frac{dT_{26}}{dt} = (b_{26})^{(4)}T_{25} - [(b'_{26})^{(4)} - (b''_{26})^{(4)}((G_{27}), t)]T_{26} .32$$

$$+(a''_{24})^{(4)}(T_{25}, t) = \text{First augmentation factor} .33$$

$$-(b''_{24})^{(4)}((G_{27}), t) = \text{First detritions factor} .34$$

**YANG MILLS THEORY AND NON COMMUTATIVE SYMMETRY GROUP IN GAUGE THEORY:
MODULE NUMBERED FIVE**

The differential system of this model is now (Module number five).35

$$\frac{dG_{28}}{dt} = (a_{28})^{(5)}G_{29} - [(a'_{28})^{(5)} + (a''_{28})^{(5)}(T_{29}, t)]G_{28} .36$$

$$\frac{dG_{29}}{dt} = (a_{29})^{(5)}G_{28} - [(a'_{29})^{(5)} + (a''_{29})^{(5)}(T_{29}, t)]G_{29} .37$$

$$\begin{aligned} \frac{dG_{30}}{dt} &= (a_{30})^{(5)}G_{29} - [(a'_{30})^{(5)} + (a''_{30})^{(5)}(T_{29}, t)]G_{30} \quad .38 \\ \frac{dT_{28}}{dt} &= (b_{28})^{(5)}T_{29} - [(b'_{28})^{(5)} - (b''_{28})^{(5)}((G_{31}), t)]T_{28} \quad .39 \\ \frac{dT_{29}}{dt} &= (b_{29})^{(5)}T_{28} - [(b'_{29})^{(5)} - (b''_{29})^{(5)}((G_{31}), t)]T_{29} \quad .40 \\ \frac{dT_{30}}{dt} &= (b_{30})^{(5)}T_{29} - [(b'_{30})^{(5)} - (b''_{30})^{(5)}((G_{31}), t)]T_{30} \quad .41 \\ &+ (a''_{28})^{(5)}(T_{29}, t) = \text{First augmentation factor} \quad .42 \\ &- (b''_{28})^{(5)}((G_{31}), t) = \text{First detritions factor} \quad .43 \end{aligned}$$

LHS OF THE YANG MILLS THEORY AND RHS OF THE YANG MILLS THEORY.TAKEN TO THE OTHER SIDE THE LHS WOULD DISSIPATE THE RHS WITH OR WITHOUT TIME LAG :

MODULE NUMBERED SIX

The differential system of this model is now (Module numbered Six).44

$$\begin{aligned} \frac{dG_{32}}{dt} &= (a_{32})^{(6)}G_{33} - [(a'_{32})^{(6)} + (a''_{32})^{(6)}(T_{33}, t)]G_{32} \quad .46 \\ \frac{dG_{33}}{dt} &= (a_{33})^{(6)}G_{32} - [(a'_{33})^{(6)} + (a''_{33})^{(6)}(T_{33}, t)]G_{33} \quad .47 \\ \frac{dG_{34}}{dt} &= (a_{34})^{(6)}G_{33} - [(a'_{34})^{(6)} + (a''_{34})^{(6)}(T_{33}, t)]G_{34} \quad .48 \\ \frac{dT_{32}}{dt} &= (b_{32})^{(6)}T_{33} - [(b'_{32})^{(6)} - (b''_{32})^{(6)}((G_{35}), t)]T_{32} \quad .49 \\ \frac{dT_{33}}{dt} &= (b_{33})^{(6)}T_{32} - [(b'_{33})^{(6)} - (b''_{33})^{(6)}((G_{35}), t)]T_{33} \quad .50 \\ \frac{dT_{34}}{dt} &= (b_{34})^{(6)}T_{33} - [(b'_{34})^{(6)} - (b''_{34})^{(6)}((G_{35}), t)]T_{34} \quad .51 \\ &+ (a''_{32})^{(6)}(T_{33}, t) = \text{First augmentation factor} \quad .52 \\ &- (b''_{32})^{(6)}((G_{35}), t) = \text{First detritions factor} \quad .53 \end{aligned}$$

HOLISTIC CONCATENATE SYTEMAL EQUATIONS HENCEFORTH REFERRED TO AS “GLOBAL EQUATIONS”

We take in to consideration the following parameters, processes and concepts:

- (1) Acquisition of mass
- (2) Symmetry Breaking
- (3) Strong interaction
- (4) Unified Electroweak interaction
- (5) Continuous group of local transformations
- (6) Lagrangian Variance
- (7) Group generator in Gauge Theory
- (8) Vector field or Gauge field
- (9) Non commutative symmetry group in Gauge Theory
- (10) Yang Mills Theory (We repeat the same Bank’s example. Individual debits and Credits are conservative so also the holistic one. Generalized theories are applied to various systems which are parameterized. And we live in ‘measurement world’. Classification is done on the parameters of various systems to which the Theory is applied.).
- (11) First Term of the Lagrangian of the Yang Mills Theory(LHS)

$$\mathcal{L}_{gf} = -\frac{1}{4} \text{Tr}(F^2) = -\frac{1}{4} F^{\mu\nu a} F_{\mu\nu}^a$$

(12) RHS of the Yang Mills Theory

$$\mathcal{L}_{gf} = -\frac{1}{4} \text{Tr}(F^2) = -\frac{1}{4} F^{\mu\nu a} F_{\mu\nu}^a \quad .54$$

$$\frac{dG_{13}}{dt} = (a_{13})^{(1)}G_{14} - \left[\begin{array}{|c|c|c|} \hline (a'_{13})^{(1)} & + (a''_{13})^{(1)}(T_{14}, t) & + (a''_{16})^{(2,2)}(T_{17}, t) & + (a''_{20})^{(3,3)}(T_{21}, t) \\ \hline + (a''_{24})^{(4,4,4,4)}(T_{25}, t) & + (a''_{28})^{(5,5,5,5)}(T_{29}, t) & + (a''_{32})^{(6,6,6,6)}(T_{33}, t) & \\ \hline \end{array} \right] G_{13} \quad .55$$

$$\frac{dG_{14}}{dt} = (a_{14})^{(1)}G_{13} - \left[\begin{array}{|c|c|c|} \hline (a'_{14})^{(1)} & + (a''_{14})^{(1)}(T_{14}, t) & + (a''_{17})^{(2,2)}(T_{17}, t) & + (a''_{21})^{(3,3)}(T_{21}, t) \\ \hline + (a''_{25})^{(4,4,4,4)}(T_{25}, t) & + (a''_{29})^{(5,5,5,5)}(T_{29}, t) & + (a''_{33})^{(6,6,6,6)}(T_{33}, t) & \\ \hline \end{array} \right] G_{14} \quad .56$$

$$\frac{dG_{15}}{dt} = (a_{15})^{(1)}G_{14} - \left[\begin{array}{|c|c|c|} \hline (a'_{15})^{(1)} & + (a''_{15})^{(1)}(T_{14}, t) & + (a''_{18})^{(2,2)}(T_{17}, t) & + (a''_{22})^{(3,3)}(T_{21}, t) \\ \hline + (a''_{26})^{(4,4,4,4)}(T_{25}, t) & + (a''_{30})^{(5,5,5,5)}(T_{29}, t) & + (a''_{34})^{(6,6,6,6)}(T_{33}, t) & \\ \hline \end{array} \right] G_{15} \quad .57$$

Where $(a''_{13})^{(1)}(T_{14}, t)$, $(a''_{14})^{(1)}(T_{14}, t)$, $(a''_{15})^{(1)}(T_{14}, t)$ are first augmentation coefficients for category 1, 2 and 3
 $(a''_{16})^{(2,2)}(T_{17}, t)$, $(a''_{17})^{(2,2)}(T_{17}, t)$, $(a''_{18})^{(2,2)}(T_{17}, t)$ are second augmentation coefficient for category 1, 2 and 3
 $(a''_{20})^{(3,3)}(T_{21}, t)$, $(a''_{21})^{(3,3)}(T_{21}, t)$, $(a''_{22})^{(3,3)}(T_{21}, t)$ are third augmentation coefficient for category 1, 2 and 3
 $(a''_{24})^{(4,4,4,4)}(T_{25}, t)$, $(a''_{25})^{(4,4,4,4)}(T_{25}, t)$, $(a''_{26})^{(4,4,4,4)}(T_{25}, t)$ are fourth augmentation coefficient for category 1, 2 and 3
 $(a''_{28})^{(5,5,5,5)}(T_{29}, t)$, $(a''_{29})^{(5,5,5,5)}(T_{29}, t)$, $(a''_{30})^{(5,5,5,5)}(T_{29}, t)$ are fifth augmentation coefficient for category 1, 2 and 3
 $(a''_{32})^{(6,6,6,6)}(T_{33}, t)$, $(a''_{33})^{(6,6,6,6)}(T_{33}, t)$, $(a''_{34})^{(6,6,6,6)}(T_{33}, t)$ are sixth augmentation coefficient for category 1, 2 and 3.58 59

.60

$$\frac{dT_{13}}{dt} = (b_{13})^{(1)}T_{14} - \left[\begin{array}{ccc} (b'_{13})^{(1)} - (b''_{13})^{(1)}(G, t) & - (b''_{16})^{(2,2)}(G_{19}, t) & - (b''_{20})^{(3,3)}(G_{23}, t) \\ - (b''_{24})^{(4,4,4,4)}(G_{27}, t) & - (b''_{28})^{(5,5,5,5)}(G_{31}, t) & - (b''_{32})^{(6,6,6,6)}(G_{35}, t) \end{array} \right] T_{13} \quad .61$$

$$\frac{dT_{14}}{dt} = (b_{14})^{(1)}T_{13} - \left[\begin{array}{ccc} (b'_{14})^{(1)} - (b''_{14})^{(1)}(G, t) & - (b''_{17})^{(2,2)}(G_{19}, t) & - (b''_{21})^{(3,3)}(G_{23}, t) \\ - (b''_{25})^{(4,4,4,4)}(G_{27}, t) & - (b''_{29})^{(5,5,5,5)}(G_{31}, t) & - (b''_{33})^{(6,6,6,6)}(G_{35}, t) \end{array} \right] T_{14} \quad .62$$

$$\frac{dT_{15}}{dt} = (b_{15})^{(1)}T_{14} - \left[\begin{array}{ccc} (b'_{15})^{(1)} - (b''_{15})^{(1)}(G, t) & - (b''_{18})^{(2,2)}(G_{19}, t) & - (b''_{22})^{(3,3)}(G_{23}, t) \\ - (b''_{26})^{(4,4,4,4)}(G_{27}, t) & - (b''_{30})^{(5,5,5,5)}(G_{31}, t) & - (b''_{34})^{(6,6,6,6)}(G_{35}, t) \end{array} \right] T_{15} \quad .63$$

Where $-(b''_{13})^{(1)}(G, t)$, $-(b''_{14})^{(1)}(G, t)$, $-(b''_{15})^{(1)}(G, t)$ are first detrition coefficients for category 1, 2 and 3
 $-(b''_{16})^{(2,2)}(G_{19}, t)$, $-(b''_{17})^{(2,2)}(G_{19}, t)$, $-(b''_{18})^{(2,2)}(G_{19}, t)$ are second detritions coefficients for category 1, 2 and 3
 $-(b''_{20})^{(3,3)}(G_{23}, t)$, $-(b''_{21})^{(3,3)}(G_{23}, t)$, $-(b''_{22})^{(3,3)}(G_{23}, t)$ are third detritions coefficients for category 1, 2 and 3
 $-(b''_{24})^{(4,4,4,4)}(G_{27}, t)$, $-(b''_{25})^{(4,4,4,4)}(G_{27}, t)$, $-(b''_{26})^{(4,4,4,4)}(G_{27}, t)$ are fourth detritions coefficients for category 1, 2 and 3
 $-(b''_{28})^{(5,5,5,5)}(G_{31}, t)$, $-(b''_{29})^{(5,5,5,5)}(G_{31}, t)$, $-(b''_{30})^{(5,5,5,5)}(G_{31}, t)$ are fifth detritions coefficients for category 1, 2 and 3
 $-(b''_{32})^{(6,6,6,6)}(G_{35}, t)$, $-(b''_{33})^{(6,6,6,6)}(G_{35}, t)$, $-(b''_{34})^{(6,6,6,6)}(G_{35}, t)$ are sixth detritions coefficients for category 1, 2 and 3 .64.65

$$\frac{dG_{16}}{dt} = (a_{16})^{(2)}G_{17} - \left[\begin{array}{ccc} (a'_{16})^{(2)} + (a''_{16})^{(2)}(T_{17}, t) & + (a''_{13})^{(1,1)}(T_{14}, t) & + (a''_{20})^{(3,3,3)}(T_{21}, t) \\ + (a''_{24})^{(4,4,4,4,4)}(T_{25}, t) & + (a''_{28})^{(5,5,5,5,5)}(T_{29}, t) & + (a''_{32})^{(6,6,6,6,6)}(T_{33}, t) \end{array} \right] G_{16} \quad .66$$

$$\frac{dG_{17}}{dt} = (a_{17})^{(2)}G_{16} - \left[\begin{array}{ccc} (a'_{17})^{(2)} + (a''_{17})^{(2)}(T_{17}, t) & + (a''_{14})^{(1,1)}(T_{14}, t) & + (a''_{21})^{(3,3,3)}(T_{21}, t) \\ + (a''_{25})^{(4,4,4,4,4)}(T_{25}, t) & + (a''_{29})^{(5,5,5,5,5)}(T_{29}, t) & + (a''_{33})^{(6,6,6,6,6)}(T_{33}, t) \end{array} \right] G_{17} \quad .67$$

$$\frac{dG_{18}}{dt} = (a_{18})^{(2)}G_{17} - \left[\begin{array}{ccc} (a'_{18})^{(2)} + (a''_{18})^{(2)}(T_{17}, t) & + (a''_{15})^{(1,1)}(T_{14}, t) & + (a''_{22})^{(3,3,3)}(T_{21}, t) \\ + (a''_{26})^{(4,4,4,4,4)}(T_{25}, t) & + (a''_{30})^{(5,5,5,5,5)}(T_{29}, t) & + (a''_{34})^{(6,6,6,6,6)}(T_{33}, t) \end{array} \right] G_{18} \quad .68$$

Where $(a''_{16})^{(2)}(T_{17}, t)$, $(a''_{17})^{(2)}(T_{17}, t)$, $(a''_{18})^{(2)}(T_{17}, t)$ are first augmentation coefficients for category 1, 2 and 3
 $(a''_{13})^{(1,1)}(T_{14}, t)$, $(a''_{14})^{(1,1)}(T_{14}, t)$, $(a''_{15})^{(1,1)}(T_{14}, t)$ are second augmentation coefficient for category 1, 2 and 3
 $(a''_{20})^{(3,3,3)}(T_{21}, t)$, $(a''_{21})^{(3,3,3)}(T_{21}, t)$, $(a''_{22})^{(3,3,3)}(T_{21}, t)$ are third augmentation coefficient for category 1, 2 and 3
 $(a''_{24})^{(4,4,4,4,4)}(T_{25}, t)$, $(a''_{25})^{(4,4,4,4,4)}(T_{25}, t)$, $(a''_{26})^{(4,4,4,4,4)}(T_{25}, t)$ are fourth augmentation coefficient for category 1, 2 and 3
 $(a''_{28})^{(5,5,5,5,5)}(T_{29}, t)$, $(a''_{29})^{(5,5,5,5,5)}(T_{29}, t)$, $(a''_{30})^{(5,5,5,5,5)}(T_{29}, t)$ are fifth augmentation coefficient for category 1, 2 and 3
 $(a''_{32})^{(6,6,6,6,6)}(T_{33}, t)$, $(a''_{33})^{(6,6,6,6,6)}(T_{33}, t)$, $(a''_{34})^{(6,6,6,6,6)}(T_{33}, t)$ are sixth augmentation coefficient for category 1, 2 and 3 .69 70.71

$-(b''_{20})^{(3)}(G_{23}, t)$, $-(b''_{21})^{(3)}(G_{23}, t)$, $-(b''_{22})^{(3)}(G_{23}, t)$ are first detritions coefficients for category 1, 2 and 3
 $-(b''_{16})^{(2,2,2)}(G_{19}, t)$, $-(b''_{17})^{(2,2,2)}(G_{19}, t)$, $-(b''_{18})^{(2,2,2)}(G_{19}, t)$ are second detritions coefficients for category 1, 2 and 3
 $-(b''_{13})^{(1,1,1)}(G, t)$, $-(b''_{14})^{(1,1,1)}(G, t)$, $-(b''_{15})^{(1,1,1)}(G, t)$ are third detrition coefficients for category 1,2 and 3
 $-(b''_{24})^{(4,4,4,4,4)}(G_{27}, t)$, $-(b''_{25})^{(4,4,4,4,4)}(G_{27}, t)$, $-(b''_{26})^{(4,4,4,4,4)}(G_{27}, t)$ are fourth detritions coefficients for category 1, 2 and 3
 $-(b''_{28})^{(5,5,5,5,5)}(G_{31}, t)$, $-(b''_{29})^{(5,5,5,5,5)}(G_{31}, t)$, $-(b''_{30})^{(5,5,5,5,5)}(G_{31}, t)$ are fifth detritions coefficients for category 1, 2 and 3
 $-(b''_{32})^{(6,6,6,6,6)}(G_{35}, t)$, $-(b''_{33})^{(6,6,6,6,6)}(G_{35}, t)$, $-(b''_{34})^{(6,6,6,6,6)}(G_{35}, t)$ are sixth detritions coefficients for category 1, 2 and 3 .85
 .86

$$\frac{dG_{24}}{dt} = (a_{24})^{(4)}G_{25} - \left[\begin{array}{ccc} (a''_{24})^{(4)} + (a''_{24})^{(4)}(T_{25}, t) & + (a''_{28})^{(5,5)}(T_{29}, t) & + (a''_{32})^{(6,6)}(T_{33}, t) \\ + (a''_{13})^{(1,1,1,1)}(T_{14}, t) & + (a''_{16})^{(2,2,2,2)}(T_{17}, t) & + (a''_{20})^{(3,3,3,3)}(T_{21}, t) \end{array} \right] G_{24} \quad .87$$

$$\frac{dG_{25}}{dt} = (a_{25})^{(4)}G_{24} - \left[\begin{array}{ccc} (a''_{25})^{(4)} + (a''_{25})^{(4)}(T_{25}, t) & + (a''_{29})^{(5,5)}(T_{29}, t) & + (a''_{33})^{(6,6)}(T_{33}, t) \\ + (a''_{14})^{(1,1,1,1)}(T_{14}, t) & + (a''_{17})^{(2,2,2,2)}(T_{17}, t) & + (a''_{21})^{(3,3,3,3)}(T_{21}, t) \end{array} \right] G_{25} \quad .88$$

$$\frac{dG_{26}}{dt} = (a_{26})^{(4)}G_{25} - \left[\begin{array}{ccc} (a''_{26})^{(4)} + (a''_{26})^{(4)}(T_{25}, t) & + (a''_{30})^{(5,5)}(T_{29}, t) & + (a''_{34})^{(6,6)}(T_{33}, t) \\ + (a''_{15})^{(1,1,1,1)}(T_{14}, t) & + (a''_{18})^{(2,2,2,2)}(T_{17}, t) & + (a''_{22})^{(3,3,3,3)}(T_{21}, t) \end{array} \right] G_{26} \quad .89$$

Where $(a''_{24})^{(4)}(T_{25}, t)$, $(a''_{25})^{(4)}(T_{25}, t)$, $(a''_{26})^{(4)}(T_{25}, t)$ are first augmentation coefficients for category 1, 2 and 3
 $+(a''_{28})^{(5,5)}(T_{29}, t)$, $+(a''_{29})^{(5,5)}(T_{29}, t)$, $+(a''_{30})^{(5,5)}(T_{29}, t)$ are second augmentation coefficient for category 1, 2 and 3
 $+(a''_{32})^{(6,6)}(T_{33}, t)$, $+(a''_{33})^{(6,6)}(T_{33}, t)$, $+(a''_{34})^{(6,6)}(T_{33}, t)$ are third augmentation coefficient for category 1, 2 and 3
 $+(a''_{13})^{(1,1,1,1)}(T_{14}, t)$, $+(a''_{14})^{(1,1,1,1)}(T_{14}, t)$, $+(a''_{15})^{(1,1,1,1)}(T_{14}, t)$ are fourth augmentation coefficients for category 1, 2, and 3
 $+(a''_{16})^{(2,2,2,2)}(T_{17}, t)$, $+(a''_{17})^{(2,2,2,2)}(T_{17}, t)$, $+(a''_{18})^{(2,2,2,2)}(T_{17}, t)$ are fifth augmentation coefficients for category 1, 2, and 3
 $+(a''_{20})^{(3,3,3,3)}(T_{21}, t)$, $+(a''_{21})^{(3,3,3,3)}(T_{21}, t)$, $+(a''_{22})^{(3,3,3,3)}(T_{21}, t)$ are sixth augmentation coefficients for category 1, 2, and 3 .90 91
 .92

$$\frac{dT_{24}}{dt} = (b_{24})^{(4)}T_{25} - \left[\begin{array}{ccc} (b'_{24})^{(4)} - (b''_{24})^{(4)}(G_{27}, t) & - (b''_{28})^{(5,5)}(G_{31}, t) & - (b''_{32})^{(6,6)}(G_{35}, t) \\ - (b''_{13})^{(1,1,1,1)}(G, t) & - (b''_{16})^{(2,2,2,2)}(G_{19}, t) & - (b''_{20})^{(3,3,3,3)}(G_{23}, t) \end{array} \right] T_{24} \quad .93$$

$$\frac{dT_{25}}{dt} = (b_{25})^{(4)}T_{24} - \left[\begin{array}{ccc} (b'_{25})^{(4)} - (b''_{25})^{(4)}(G_{27}, t) & - (b''_{29})^{(5,5)}(G_{31}, t) & - (b''_{33})^{(6,6)}(G_{35}, t) \\ - (b''_{14})^{(1,1,1,1)}(G, t) & - (b''_{17})^{(2,2,2,2)}(G_{19}, t) & - (b''_{21})^{(3,3,3,3)}(G_{23}, t) \end{array} \right] T_{25} \quad .94$$

$$\frac{dT_{26}}{dt} = (b_{26})^{(4)}T_{25} - \left[\begin{array}{ccc} (b'_{26})^{(4)} - (b''_{26})^{(4)}(G_{27}, t) & - (b''_{30})^{(5,5)}(G_{31}, t) & - (b''_{34})^{(6,6)}(G_{35}, t) \\ - (b''_{15})^{(1,1,1,1)}(G, t) & - (b''_{18})^{(2,2,2,2)}(G_{19}, t) & - (b''_{22})^{(3,3,3,3)}(G_{23}, t) \end{array} \right] T_{26} \quad .95$$

Where $-(b''_{24})^{(4)}(G_{27}, t)$, $-(b''_{25})^{(4)}(G_{27}, t)$, $-(b''_{26})^{(4)}(G_{27}, t)$ are first detrition coefficients for category 1, 2 and 3
 $-(b''_{28})^{(5,5)}(G_{31}, t)$, $-(b''_{29})^{(5,5)}(G_{31}, t)$, $-(b''_{30})^{(5,5)}(G_{31}, t)$ are second detrition coefficients for category 1, 2 and 3
 $-(b''_{32})^{(6,6)}(G_{35}, t)$, $-(b''_{33})^{(6,6)}(G_{35}, t)$, $-(b''_{34})^{(6,6)}(G_{35}, t)$ are third detrition coefficients for category 1, 2 and 3
 $-(b''_{13})^{(1,1,1,1)}(G, t)$, $-(b''_{14})^{(1,1,1,1)}(G, t)$, $-(b''_{15})^{(1,1,1,1)}(G, t)$ are fourth detrition coefficients for category 1, 2 and 3
 $-(b''_{16})^{(2,2,2,2)}(G_{19}, t)$, $-(b''_{17})^{(2,2,2,2)}(G_{19}, t)$, $-(b''_{18})^{(2,2,2,2)}(G_{19}, t)$ are fifth detrition coefficients for category 1, 2 and 3
 $-(b''_{20})^{(3,3,3,3)}(G_{23}, t)$, $-(b''_{21})^{(3,3,3,3)}(G_{23}, t)$, $-(b''_{22})^{(3,3,3,3)}(G_{23}, t)$ are sixth detrition coefficients for category 1, 2 and 3 .96, 9798

$$\frac{dG_{28}}{dt} = (a_{28})^{(5)}G_{29} - \left[\begin{array}{|c|c|c|c|} \hline (a'_{28})^{(5)} & +(a''_{28})^{(5)}(T_{29}, t) & +(a''_{24})^{(4,4)}(T_{25}, t) & +(a''_{32})^{(6,6,6)}(T_{33}, t) \\ \hline \end{array} \right] G_{28} \quad .99$$

$$\frac{dG_{29}}{dt} = (a_{29})^{(5)}G_{28} - \left[\begin{array}{|c|c|c|c|} \hline (a'_{29})^{(5)} & +(a''_{29})^{(5)}(T_{29}, t) & +(a''_{25})^{(4,4)}(T_{25}, t) & +(a''_{33})^{(6,6,6)}(T_{33}, t) \\ \hline \end{array} \right] G_{29} \quad .100$$

$$\frac{dG_{30}}{dt} = (a_{30})^{(5)}G_{29} - \left[\begin{array}{|c|c|c|c|} \hline (a'_{30})^{(5)} & +(a''_{30})^{(5)}(T_{29}, t) & +(a''_{26})^{(4,4)}(T_{25}, t) & +(a''_{34})^{(6,6,6)}(T_{33}, t) \\ \hline \end{array} \right] G_{30} \quad .101$$

Where $+(a''_{28})^{(5)}(T_{29}, t)$, $+(a''_{29})^{(5)}(T_{29}, t)$, $+(a''_{30})^{(5)}(T_{29}, t)$ are first augmentation coefficients for category 1, 2 and 3
 And $+(a''_{24})^{(4,4)}(T_{25}, t)$, $+(a''_{25})^{(4,4)}(T_{25}, t)$, $+(a''_{26})^{(4,4)}(T_{25}, t)$ are second augmentation coefficient for category 1, 2 and 3
 $+(a''_{32})^{(6,6,6)}(T_{33}, t)$, $+(a''_{33})^{(6,6,6)}(T_{33}, t)$, $+(a''_{34})^{(6,6,6)}(T_{33}, t)$ are third augmentation coefficient for category 1, 2 and 3
 $+(a''_{13})^{(1,1,1,1,1)}(T_{14}, t)$, $+(a''_{14})^{(1,1,1,1,1)}(T_{14}, t)$, $+(a''_{15})^{(1,1,1,1,1)}(T_{14}, t)$ are fourth augmentation coefficients for category 1, 2, and 3
 $+(a''_{16})^{(2,2,2,2,2)}(T_{17}, t)$, $+(a''_{17})^{(2,2,2,2,2)}(T_{17}, t)$, $+(a''_{18})^{(2,2,2,2,2)}(T_{17}, t)$ are fifth augmentation coefficients for category 1, 2, and 3
 $+(a''_{20})^{(3,3,3,3,3)}(T_{21}, t)$, $+(a''_{21})^{(3,3,3,3,3)}(T_{21}, t)$, $+(a''_{22})^{(3,3,3,3,3)}(T_{21}, t)$ are sixth augmentation coefficients for category 1, 2, 3 .102
 .103

$$\frac{dT_{28}}{dt} = (b_{28})^{(5)}T_{29} - \left[\begin{array}{|c|c|c|} \hline (b'_{28})^{(5)} & -(b''_{28})^{(5)}(G_{31}, t) & -(b''_{24})^{(4,4)}(G_{27}, t) & -(b''_{32})^{(6,6,6)}(G_{35}, t) \\ \hline \end{array} \right] T_{28} \quad .104$$

$$\frac{dT_{29}}{dt} = (b_{29})^{(5)}T_{28} - \left[\begin{array}{|c|c|c|} \hline (b'_{29})^{(5)} & -(b''_{29})^{(5)}(G_{31}, t) & -(b''_{25})^{(4,4)}(G_{27}, t) & -(b''_{33})^{(6,6,6)}(G_{35}, t) \\ \hline \end{array} \right] T_{29} \quad .105$$

$$\frac{dT_{30}}{dt} = (b_{30})^{(5)}T_{29} - \left[\begin{array}{|c|c|c|} \hline (b'_{30})^{(5)} & -(b''_{30})^{(5)}(G_{31}, t) & -(b''_{26})^{(4,4)}(G_{27}, t) & -(b''_{34})^{(6,6,6)}(G_{35}, t) \\ \hline \end{array} \right] T_{30} \quad .106$$

where $-(b''_{28})^{(5)}(G_{31}, t)$, $-(b''_{29})^{(5)}(G_{31}, t)$, $-(b''_{30})^{(5)}(G_{31}, t)$ are first detrition coefficients for category 1, 2 and 3
 $-(b''_{24})^{(4,4)}(G_{27}, t)$, $-(b''_{25})^{(4,4)}(G_{27}, t)$, $-(b''_{26})^{(4,4)}(G_{27}, t)$ are second detrition coefficients for category 1, 2 and 3
 $-(b''_{32})^{(6,6,6)}(G_{35}, t)$, $-(b''_{33})^{(6,6,6)}(G_{35}, t)$, $-(b''_{34})^{(6,6,6)}(G_{35}, t)$ are third detrition coefficients for category 1, 2 and 3
 $-(b''_{13})^{(1,1,1,1,1)}(G, t)$, $-(b''_{14})^{(1,1,1,1,1)}(G, t)$, $-(b''_{15})^{(1,1,1,1,1)}(G, t)$ are fourth detrition coefficients for category 1, 2, and 3
 $-(b''_{16})^{(2,2,2,2,2)}(G_{19}, t)$, $-(b''_{17})^{(2,2,2,2,2)}(G_{19}, t)$, $-(b''_{18})^{(2,2,2,2,2)}(G_{19}, t)$ are fifth detrition coefficients for category 1, 2, and 3
 $-(b''_{20})^{(3,3,3,3,3)}(G_{23}, t)$, $-(b''_{21})^{(3,3,3,3,3)}(G_{23}, t)$, $-(b''_{22})^{(3,3,3,3,3)}(G_{23}, t)$ are sixth detrition coefficients for category 1, 2, and 3.107
 .108

$$\frac{dG_{32}}{dt} = (a_{32})^{(6)}G_{33} - \left[\begin{array}{|c|c|c|c|} \hline (a'_{32})^{(6)} & +(a''_{32})^{(6)}(T_{33}, t) & +(a''_{28})^{(5,5,5)}(T_{29}, t) & +(a''_{24})^{(4,4,4)}(T_{25}, t) \\ \hline \end{array} \right] G_{32} \quad .109$$

$$\frac{dG_{33}}{dt} = (a_{33})^{(6)}G_{32} - \left[\begin{array}{|c|c|c|c|} \hline (a'_{33})^{(6)} & +(a''_{33})^{(6)}(T_{33}, t) & +(a''_{29})^{(5,5,5)}(T_{29}, t) & +(a''_{25})^{(4,4,4)}(T_{25}, t) \\ \hline \end{array} \right] G_{33} \quad .110$$

$$\frac{dG_{34}}{dt} = (a_{34})^{(6)}G_{33} - \left[\begin{array}{|c|c|c|c|} \hline (a'_{34})^{(6)} & +(a''_{34})^{(6)}(T_{33}, t) & +(a''_{30})^{(5,5,5)}(T_{29}, t) & +(a''_{26})^{(4,4,4)}(T_{25}, t) \\ \hline \end{array} \right] G_{34} \quad .111$$

$+(a''_{32})^{(6)}(T_{33}, t)$, $+(a''_{33})^{(6)}(T_{33}, t)$, $+(a''_{34})^{(6)}(T_{33}, t)$ are first augmentation coefficients for category 1, 2 and 3
 $+(a''_{28})^{(5,5,5)}(T_{29}, t)$, $+(a''_{29})^{(5,5,5)}(T_{29}, t)$, $+(a''_{30})^{(5,5,5)}(T_{29}, t)$ are second augmentation coefficients for category 1, 2 and 3

$+(a''_{24})^{(4,4,4)}(T_{25}, t)$, $+(a''_{25})^{(4,4,4)}(T_{25}, t)$, $+(a''_{26})^{(4,4,4)}(T_{25}, t)$ are third augmentation coefficients for category 1, 2 and 3

$+(a''_{13})^{(1,1,1,1,1,1)}(T_{14}, t)$, $+(a''_{14})^{(1,1,1,1,1,1)}(T_{14}, t)$, $+(a''_{15})^{(1,1,1,1,1,1)}(T_{14}, t)$ - are fourth augmentation coefficients

$+(a''_{16})^{(2,2,2,2,2,2)}(T_{17}, t)$, $+(a''_{17})^{(2,2,2,2,2,2)}(T_{17}, t)$, $+(a''_{18})^{(2,2,2,2,2,2)}(T_{17}, t)$ - fifth augmentation coefficients

$+(a''_{20})^{(3,3,3,3,3,3)}(T_{21}, t)$, $+(a''_{21})^{(3,3,3,3,3,3)}(T_{21}, t)$, $+(a''_{22})^{(3,3,3,3,3,3)}(T_{21}, t)$ sixth augmentation coefficients .112

.113

$$\frac{dT_{32}}{dt} = (b_{32})^{(6)}T_{33} - \left[\begin{array}{ccc} (b'_{32})^{(6)} - (b''_{32})^{(6)}(G_{35}, t) & - (b''_{28})^{(5,5,5)}(G_{31}, t) & - (b''_{24})^{(4,4,4)}(G_{27}, t) \\ - (b''_{13})^{(1,1,1,1,1,1)}(G, t) & - (b''_{16})^{(2,2,2,2,2,2)}(G_{19}, t) & - (b''_{20})^{(3,3,3,3,3,3)}(G_{23}, t) \end{array} \right] T_{32} .114$$

$$\frac{dT_{33}}{dt} = (b_{33})^{(6)}T_{32} - \left[\begin{array}{ccc} (b'_{33})^{(6)} - (b''_{33})^{(6)}(G_{35}, t) & - (b''_{29})^{(5,5,5)}(G_{31}, t) & - (b''_{25})^{(4,4,4)}(G_{27}, t) \\ - (b''_{14})^{(1,1,1,1,1,1)}(G, t) & - (b''_{17})^{(2,2,2,2,2,2)}(G_{19}, t) & - (b''_{21})^{(3,3,3,3,3,3)}(G_{23}, t) \end{array} \right] T_{33} .115$$

$$\frac{dT_{34}}{dt} = (b_{34})^{(6)}T_{33} - \left[\begin{array}{ccc} (b'_{34})^{(6)} - (b''_{34})^{(6)}(G_{35}, t) & - (b''_{30})^{(5,5,5)}(G_{31}, t) & - (b''_{26})^{(4,4,4)}(G_{27}, t) \\ - (b''_{15})^{(1,1,1,1,1,1)}(G, t) & - (b''_{18})^{(2,2,2,2,2,2)}(G_{19}, t) & - (b''_{22})^{(3,3,3,3,3,3)}(G_{23}, t) \end{array} \right] T_{34} .116$$

$-(b''_{32})^{(6)}(G_{35}, t)$, $-(b''_{33})^{(6)}(G_{35}, t)$, $-(b''_{34})^{(6)}(G_{35}, t)$ are first detrition coefficients for category 1, 2 and 3

$-(b''_{28})^{(5,5,5)}(G_{31}, t)$, $-(b''_{29})^{(5,5,5)}(G_{31}, t)$, $-(b''_{30})^{(5,5,5)}(G_{31}, t)$ are second detrition coefficients for category 1, 2 and 3

$-(b''_{24})^{(4,4,4)}(G_{27}, t)$, $-(b''_{25})^{(4,4,4)}(G_{27}, t)$, $-(b''_{26})^{(4,4,4)}(G_{27}, t)$ are third detrition coefficients for category 1, 2 and 3

$-(b''_{13})^{(1,1,1,1,1,1)}(G, t)$, $-(b''_{14})^{(1,1,1,1,1,1)}(G, t)$, $-(b''_{15})^{(1,1,1,1,1,1)}(G, t)$ are fourth detrition coefficients for category 1, 2, and 3

$-(b''_{16})^{(2,2,2,2,2,2)}(G_{19}, t)$, $-(b''_{17})^{(2,2,2,2,2,2)}(G_{19}, t)$, $-(b''_{18})^{(2,2,2,2,2,2)}(G_{19}, t)$ are fifth detrition coefficients for category 1, 2, and 3

$-(b''_{20})^{(3,3,3,3,3,3)}(G_{23}, t)$, $-(b''_{21})^{(3,3,3,3,3,3)}(G_{23}, t)$, $-(b''_{22})^{(3,3,3,3,3,3)}(G_{23}, t)$ are sixth detrition coefficients for category 1, 2, and 3

.117

.118

Where we suppose .119

(A) $(a_i)^{(1)}, (a'_i)^{(1)}, (a''_i)^{(1)}, (b_i)^{(1)}, (b'_i)^{(1)}, (b''_i)^{(1)} > 0$,
 $i, j = 13, 14, 15$

(B) The functions $(a''_i)^{(1)}, (b''_i)^{(1)}$ are positive continuous increasing and bounded.

Definition of $(p_i)^{(1)}, (r_i)^{(1)}$:

$$(a''_i)^{(1)}(T_{14}, t) \leq (p_i)^{(1)} \leq (\hat{A}_{13})^{(1)}$$

$$(b''_i)^{(1)}(G, t) \leq (r_i)^{(1)} \leq (b'_i)^{(1)} \leq (\hat{B}_{13})^{(1)}.120$$

.121

$$(C) \lim_{T_2 \rightarrow \infty} (a''_i)^{(1)}(T_{14}, t) = (p_i)^{(1)}$$

$$\lim_{G \rightarrow \infty} (b''_i)^{(1)}(G, t) = (r_i)^{(1)}$$

Definition of $(\hat{A}_{13})^{(1)}, (\hat{B}_{13})^{(1)}$:

Where $(\hat{A}_{13})^{(1)}, (\hat{B}_{13})^{(1)}, (p_i)^{(1)}, (r_i)^{(1)}$ are positive constants and $i = 13, 14, 15$.122

They satisfy Lipschitz condition:

$$|(a''_i)^{(1)}(T'_{14}, t) - (a''_i)^{(1)}(T_{14}, t)| \leq (\hat{k}_{13})^{(1)}|T'_{14} - T_{14}|e^{-(\hat{M}_{13})^{(1)}t}$$

$$|(b''_i)^{(1)}(G', t) - (b''_i)^{(1)}(G, t)| < (\hat{k}_{13})^{(1)}||G - G'||e^{-(\hat{M}_{13})^{(1)}t} .123$$

.125

With the Lipschitz condition, we place a restriction on the behavior of functions

$(a''_i)^{(1)}(T'_{14}, t)$ and $(a''_i)^{(1)}(T_{14}, t)$. (T'_{14}, t) and (T_{14}, t) are points belonging to the interval $[(\hat{k}_{13})^{(1)}, (\hat{M}_{13})^{(1)}]$. It is to be noted that $(a''_i)^{(1)}(T_{14}, t)$ is uniformly continuous. In the eventuality of the fact, that if $(\hat{M}_{13})^{(1)} = 1$ then the function $(a''_i)^{(1)}(T_{14}, t)$, the first augmentation coefficient WOULD be absolutely continuous. .126

Definition of $(\hat{M}_{13})^{(1)}, (\hat{k}_{13})^{(1)}$:

(D) $(\hat{M}_{13})^{(1)}, (\hat{k}_{13})^{(1)}$, are positive constants

$$\frac{(a_i)^{(1)}}{(\hat{M}_{13})^{(1)}}, \frac{(b_i)^{(1)}}{(\hat{M}_{13})^{(1)}} < 1.127$$

Definition of $(\hat{P}_{13})^{(1)}, (\hat{Q}_{13})^{(1)}$:

(E) There exists two constants $(\hat{P}_{13})^{(1)}$ and $(\hat{Q}_{13})^{(1)}$ which together with $(\hat{M}_{13})^{(1)}, (\hat{k}_{13})^{(1)}, (\hat{A}_{13})^{(1)}$ and $(\hat{B}_{13})^{(1)}$ and the constants $(a_i)^{(1)}, (a_i')^{(1)}, (b_i)^{(1)}, (b_i')^{(1)}, (p_i)^{(1)}, (r_i)^{(1)}, i = 13,14,15$, satisfy the inequalities

$$\frac{1}{(\hat{M}_{13})^{(1)}} [(a_i)^{(1)} + (a_i')^{(1)} + (\hat{A}_{13})^{(1)} + (\hat{P}_{13})^{(1)} (\hat{k}_{13})^{(1)}] < 1$$

$$\frac{1}{(\hat{M}_{13})^{(1)}} [(b_i)^{(1)} + (b_i')^{(1)} + (\hat{B}_{13})^{(1)} + (\hat{Q}_{13})^{(1)} (\hat{k}_{13})^{(1)}] < 1 .128$$

129
130
131

132

Where we suppose.134

$(a_i)^{(2)}, (a_i')^{(2)}, (a_i'')^{(2)}, (b_i)^{(2)}, (b_i')^{(2)}, (b_i'')^{(2)} > 0, i, j = 16,17,18.135$

The functions $(a_i'')^{(2)}, (b_i'')^{(2)}$ are positive continuous increasing and bounded..136

Definition of $(p_i)^{(2)}, (r_i)^{(2)}$:.137

$(a_i'')^{(2)}(T_{17}, t) \leq (p_i)^{(2)} \leq (\hat{A}_{16})^{(2)} .138$

$(b_i'')^{(2)}(G_{19}, t) \leq (r_i)^{(2)} \leq (b_i')^{(2)} \leq (\hat{B}_{16})^{(2)} .139$

$\lim_{T_2 \rightarrow \infty} (a_i'')^{(2)}(T_{17}, t) = (p_i)^{(2)} .140$

$\lim_{G \rightarrow \infty} (b_i'')^{(2)}(G_{19}, t) = (r_i)^{(2)} .141$

Definition of $(\hat{A}_{16})^{(2)}, (\hat{B}_{16})^{(2)}$:

Where $(\hat{A}_{16})^{(2)}, (\hat{B}_{16})^{(2)}, (p_i)^{(2)}, (r_i)^{(2)}$ are positive constants and $i = 16,17,18.142$

They satisfy Lipschitz condition:.143

$|(a_i'')^{(2)}(T_{17}, t) - (a_i'')^{(2)}(T_{17}, t)| \leq (\hat{k}_{16})^{(2)} |T_{17} - T_{17}'| e^{-(\hat{M}_{16})^{(2)}t} .144$

$|(b_i'')^{(2)}(G_{19}, t) - (b_i'')^{(2)}(G_{19}, t)| \leq (\hat{k}_{16})^{(2)} |(G_{19}) - (G_{19})'| e^{-(\hat{M}_{16})^{(2)}t} .145$

With the Lipschitz condition, we place a restriction on the behavior of functions $(a_i'')^{(2)}(T_{17}, t)$ and $(a_i'')^{(2)}(T_{17}, t) \cdot (T_{17}', t)$

And (T_{17}, t) are points belonging to the interval $[(\hat{k}_{16})^{(2)}, (\hat{M}_{16})^{(2)}]$. It is to be noted that $(a_i'')^{(2)}(T_{17}, t)$ is uniformly

continuous. In the eventuality of the fact, that if $(\hat{M}_{16})^{(2)} = 1$ then the function $(a_i'')^{(2)}(T_{17}, t)$, the SECOND augmentation coefficient would be absolutely continuous. .146

Definition of $(\hat{M}_{16})^{(2)}, (\hat{k}_{16})^{(2)}$:.147

(F) $(\hat{M}_{16})^{(2)}, (\hat{k}_{16})^{(2)}$, are positive constants

$$\frac{(a_i)^{(2)}}{(\hat{M}_{16})^{(2)}}, \frac{(b_i)^{(2)}}{(\hat{M}_{16})^{(2)}} < 1.148$$

Definition of $(\hat{P}_{16})^{(2)}, (\hat{Q}_{16})^{(2)}$:

There exists two constants $(\hat{P}_{16})^{(2)}$ and $(\hat{Q}_{16})^{(2)}$ which together with $(\hat{M}_{16})^{(2)}, (\hat{k}_{16})^{(2)}, (\hat{A}_{16})^{(2)}$ and $(\hat{B}_{16})^{(2)}$ and the constants $(a_i)^{(2)}, (a_i')^{(2)}, (b_i)^{(2)}, (b_i')^{(2)}, (p_i)^{(2)}, (r_i)^{(2)}, i = 16,17,18$,

satisfy the inequalities .149

$$\frac{1}{(\hat{M}_{16})^{(2)}} [(a_i)^{(2)} + (a_i')^{(2)} + (\hat{A}_{16})^{(2)} + (\hat{P}_{16})^{(2)} (\hat{k}_{16})^{(2)}] < 1 .150$$

$$\frac{1}{(\hat{M}_{16})^{(2)}} [(b_i)^{(2)} + (b_i')^{(2)} + (\hat{B}_{16})^{(2)} + (\hat{Q}_{16})^{(2)} (\hat{k}_{16})^{(2)}] < 1 .151$$

Where we suppose.152

(G) $(a_i)^{(3)}, (a_i')^{(3)}, (a_i'')^{(3)}, (b_i)^{(3)}, (b_i')^{(3)}, (b_i'')^{(3)} > 0, i, j = 20,21,22$

The functions $(a_i'')^{(3)}, (b_i'')^{(3)}$ are positive continuous increasing and bounded.

Definition of $(p_i)^{(3)}, (r_i)^{(3)}$:

$(a_i'')^{(3)}(T_{21}, t) \leq (p_i)^{(3)} \leq (\hat{A}_{20})^{(3)}$

$(b_i'')^{(3)}(G_{23}, t) \leq (r_i)^{(3)} \leq (b_i')^{(3)} \leq (\hat{B}_{20})^{(3)} .153$

$\lim_{T_2 \rightarrow \infty} (a_i'')^{(3)}(T_{21}, t) = (p_i)^{(3)}$

$\lim_{G \rightarrow \infty} (b_i'')^{(3)}(G_{23}, t) = (r_i)^{(3)}$

Definition of $(\hat{A}_{20})^{(3)}, (\hat{B}_{20})^{(3)}$:

Where $(\hat{A}_{20})^{(3)}, (\hat{B}_{20})^{(3)}, (p_i)^{(3)}, (r_i)^{(3)}$ are positive constants and $i = 20,21,22.154$

155

156

They satisfy Lipschitz condition:

$|(a_i'')^{(3)}(T_{21}, t) - (a_i'')^{(3)}(T_{21}, t)| \leq (\hat{k}_{20})^{(3)} |T_{21} - T_{21}'| e^{-(\hat{M}_{20})^{(3)}t}$

$|(b_i'')^{(3)}(G_{23}, t) - (b_i'')^{(3)}(G_{23}, t)| \leq (\hat{k}_{20})^{(3)} |(G_{23}) - G_{23}'| e^{-(\hat{M}_{20})^{(3)}t} .157$

158

159

With the Lipschitz condition, we place a restriction on the behavior of functions $(a_i'')^{(3)}(T_{21}, t)$ and $(a_i'')^{(3)}(T_{21}, t)$. (T_{21}, t) and (T_{21}, t) are points belonging to the interval $[(\hat{k}_{20})^{(3)}, (\bar{M}_{20})^{(3)}]$. It is to be noted that $(a_i'')^{(3)}(T_{21}, t)$ is uniformly continuous. In the eventuality of the fact, that if $(\bar{M}_{20})^{(3)} = 1$ then the function $(a_i'')^{(3)}(T_{21}, t)$, the THIRD augmentation coefficient, would be absolutely continuous. .160

Definition of $(\bar{M}_{20})^{(3)}, (\hat{k}_{20})^{(3)}$:

(H) $(\bar{M}_{20})^{(3)}, (\hat{k}_{20})^{(3)}$, are positive constants

$$\frac{(a_i)^{(3)}}{(\bar{M}_{20})^{(3)}} , \frac{(b_i)^{(3)}}{(\bar{M}_{20})^{(3)}} < 1.161$$

There exists two constants $(\hat{P}_{20})^{(3)}$ and $(\hat{Q}_{20})^{(3)}$ which together with $(\bar{M}_{20})^{(3)}, (\hat{k}_{20})^{(3)}, (\hat{A}_{20})^{(3)}$ and $(\hat{B}_{20})^{(3)}$ and the constants $(a_i)^{(3)}, (a_i')^{(3)}, (b_i)^{(3)}, (b_i')^{(3)}, (p_i)^{(3)}, (r_i)^{(3)}, i = 20, 21, 22$, satisfy the inequalities

$$\frac{1}{(\bar{M}_{20})^{(3)}} [(a_i)^{(3)} + (a_i')^{(3)} + (\hat{A}_{20})^{(3)} + (\hat{P}_{20})^{(3)} (\hat{k}_{20})^{(3)}] < 1$$

$$\frac{1}{(\bar{M}_{20})^{(3)}} [(b_i)^{(3)} + (b_i')^{(3)} + (\hat{B}_{20})^{(3)} + (\hat{Q}_{20})^{(3)} (\hat{k}_{20})^{(3)}] < 1 .162$$

163

164

165

166

167

Where we suppose.168

(I) $(a_i)^{(4)}, (a_i')^{(4)}, (a_i'')^{(4)}, (b_i)^{(4)}, (b_i')^{(4)}, (b_i'')^{(4)} > 0, i, j = 24, 25, 26$

(J) The functions $(a_i'')^{(4)}, (b_i'')^{(4)}$ are positive continuous increasing and bounded.

Definition of $(p_i)^{(4)}, (r_i)^{(4)}$:

$$(a_i'')^{(4)}(T_{25}, t) \leq (p_i)^{(4)} \leq (\hat{A}_{24})^{(4)}$$

$$(b_i'')^{(4)}((G_{27}), t) \leq (r_i)^{(4)} \leq (b_i')^{(4)} \leq (\hat{B}_{24})^{(4)}.169$$

(K) $\lim_{T_2 \rightarrow \infty} (a_i'')^{(4)}(T_{25}, t) = (p_i)^{(4)}$
 $\lim_{G \rightarrow \infty} (b_i'')^{(4)}((G_{27}), t) = (r_i)^{(4)}$

Definition of $(\hat{A}_{24})^{(4)}, (\hat{B}_{24})^{(4)}$:

Where $(\hat{A}_{24})^{(4)}, (\hat{B}_{24})^{(4)}, (p_i)^{(4)}, (r_i)^{(4)}$ are positive constants and $i = 24, 25, 26$.170

They satisfy Lipschitz condition:

$$|(a_i'')^{(4)}(T_{25}, t) - (a_i'')^{(4)}(T_{25}, t)| \leq (\hat{k}_{24})^{(4)} |T_{25} - T_{25}'| e^{-(M_{24})^{(4)}t}$$

$$|(b_i'')^{(4)}((G_{27}), t) - (b_i'')^{(4)}((G_{27}), t)| \leq (\hat{k}_{24})^{(4)} |(G_{27}) - (G_{27})'| e^{-(M_{24})^{(4)}t} .171$$

With the Lipschitz condition, we place a restriction on the behavior of functions $(a_i'')^{(4)}(T_{25}, t)$ and $(a_i'')^{(4)}(T_{25}, t)$. (T_{25}, t) and (T_{25}, t) are points belonging to the interval $[(\hat{k}_{24})^{(4)}, (\bar{M}_{24})^{(4)}]$. It is to be noted that $(a_i'')^{(4)}(T_{25}, t)$ is uniformly continuous. In the eventuality of the fact, that if $(\bar{M}_{24})^{(4)} = 4$ then the function $(a_i'')^{(4)}(T_{25}, t)$, the FOURTH augmentation coefficient WOULD be absolutely continuous. .172

173

Defi174nition of $(\bar{M}_{24})^{(4)}, (\hat{k}_{24})^{(4)}$:

(L) $(\bar{M}_{24})^{(4)}, (\hat{k}_{24})^{(4)}$, are positive constants

(M)

$$\frac{(a_i)^{(4)}}{(\bar{M}_{24})^{(4)}} , \frac{(b_i)^{(4)}}{(\bar{M}_{24})^{(4)}} < 1 .174$$

Definition of $(\hat{P}_{24})^{(4)}, (\hat{Q}_{24})^{(4)}$:

(N) There exists two constants $(\hat{P}_{24})^{(4)}$ and $(\hat{Q}_{24})^{(4)}$ which together with $(\bar{M}_{24})^{(4)}, (\hat{k}_{24})^{(4)}, (\hat{A}_{24})^{(4)}$ and $(\hat{B}_{24})^{(4)}$ and the constants $(a_i)^{(4)}, (a_i')^{(4)}, (b_i)^{(4)}, (b_i')^{(4)}, (p_i)^{(4)}, (r_i)^{(4)}, i = 24, 25, 26$, satisfy the inequalities

$$\frac{1}{(\bar{M}_{24})^{(4)}} [(a_i)^{(4)} + (a_i')^{(4)} + (\hat{A}_{24})^{(4)} + (\hat{P}_{24})^{(4)} (\hat{k}_{24})^{(4)}] < 1$$

$$\frac{1}{(\bar{M}_{24})^{(4)}} [(b_i)^{(4)} + (b_i')^{(4)} + (\hat{B}_{24})^{(4)} + (\hat{Q}_{24})^{(4)} (\hat{k}_{24})^{(4)}] < 1 .175$$

Where we suppose.176

(O) $(a_i)^{(5)}, (a_i')^{(5)}, (a_i'')^{(5)}, (b_i)^{(5)}, (b_i')^{(5)}, (b_i'')^{(5)} > 0, i, j = 28, 29, 30$

(P) The functions $(a_i'')^{(5)}, (b_i'')^{(5)}$ are positive continuous increasing and bounded.

Definition of $(p_i)^{(5)}, (r_i)^{(5)}$:

$$(a_i'')^{(5)}(T_{29}, t) \leq (p_i)^{(5)} \leq (\hat{A}_{28})^{(5)}$$

$$(b''_i)^{(5)}((G_{31}), t) \leq (r_i)^{(5)} \leq (b'_i)^{(5)} \leq (\hat{B}_{28})^{(5)}.177$$

$$(Q) \quad \lim_{T_2 \rightarrow \infty} (a''_i)^{(5)}(T_{29}, t) = (p_i)^{(5)} \\ \lim_{G \rightarrow \infty} (b''_i)^{(5)}((G_{31}), t) = (r_i)^{(5)}$$

Definition of $(\hat{A}_{28})^{(5)}, (\hat{B}_{28})^{(5)}$:

Where $(\hat{A}_{28})^{(5)}, (\hat{B}_{28})^{(5)}, (p_i)^{(5)}, (r_i)^{(5)}$ are positive constants and $i = 28, 29, 30$.178

They satisfy Lipschitz condition:

$$|(a''_i)^{(5)}(T'_{29}, t) - (a''_i)^{(5)}(T_{29}, t)| \leq (\hat{k}_{28})^{(5)} |T'_{29} - T_{29}| e^{-(M_{28})^{(5)}t} \\ |(b''_i)^{(5)}((G_{31})', t) - (b''_i)^{(5)}((G_{31}), t)| < (\hat{k}_{28})^{(5)} \|(G_{31})' - (G_{31})\| e^{-(M_{28})^{(5)}t}.179$$

With the Lipschitz condition, we place a restriction on the behavior of functions $(a''_i)^{(5)}(T'_{29}, t)$ and $(a''_i)^{(5)}(T_{29}, t) \cdot (T'_{29}, t)$ and (T_{29}, t) are points belonging to the interval $[(\hat{k}_{28})^{(5)}, (\hat{M}_{28})^{(5)}]$. It is to be noted that $(a''_i)^{(5)}(T_{29}, t)$ is uniformly continuous. In the eventuality of the fact, that if $(\hat{M}_{28})^{(5)} = 5$ then the function $(a''_i)^{(5)}(T_{29}, t)$, the **FIFTH augmentation coefficient** attributable would be absolutely continuous. .180

Definition of $(\hat{M}_{28})^{(5)}, (\hat{k}_{28})^{(5)}$:

(R) $(\hat{M}_{28})^{(5)}, (\hat{k}_{28})^{(5)}$, are positive constants

$$\frac{(a_i)^{(5)}}{(\hat{M}_{28})^{(5)}}, \frac{(b_i)^{(5)}}{(\hat{M}_{28})^{(5)}} < 1.181$$

Definition of $(\hat{P}_{28})^{(5)}, (\hat{Q}_{28})^{(5)}$:

(S) There exists two constants $(\hat{P}_{28})^{(5)}$ and $(\hat{Q}_{28})^{(5)}$ which together with $(\hat{M}_{28})^{(5)}, (\hat{k}_{28})^{(5)}, (\hat{A}_{28})^{(5)}$ and $(\hat{B}_{28})^{(5)}$ and the constants $(a_i)^{(5)}, (a'_i)^{(5)}, (b_i)^{(5)}, (b'_i)^{(5)}, (p_i)^{(5)}, (r_i)^{(5)}, i = 28, 29, 30$, satisfy the inequalities

$$\frac{1}{(\hat{M}_{28})^{(5)}} [(a_i)^{(5)} + (a'_i)^{(5)} + (\hat{A}_{28})^{(5)} + (\hat{P}_{28})^{(5)} (\hat{k}_{28})^{(5)}] < 1 \\ \frac{1}{(\hat{M}_{28})^{(5)}} [(b_i)^{(5)} + (b'_i)^{(5)} + (\hat{B}_{28})^{(5)} + (\hat{Q}_{28})^{(5)} (\hat{k}_{28})^{(5)}] < 1.182$$

Where we suppose.183

$$(a_i)^{(6)}, (a'_i)^{(6)}, (a''_i)^{(6)}, (b_i)^{(6)}, (b'_i)^{(6)}, (b''_i)^{(6)} > 0, \quad i, j = 32, 33, 34$$

(T) The functions $(a''_i)^{(6)}, (b''_i)^{(6)}$ are positive continuous increasing and bounded.

Definition of $(p_i)^{(6)}, (r_i)^{(6)}$:

$$(a''_i)^{(6)}(T_{33}, t) \leq (p_i)^{(6)} \leq (\hat{A}_{32})^{(6)} \\ (b''_i)^{(6)}((G_{35}), t) \leq (r_i)^{(6)} \leq (b'_i)^{(6)} \leq (\hat{B}_{32})^{(6)}.184$$

$$(U) \quad \lim_{T_2 \rightarrow \infty} (a''_i)^{(6)}(T_{33}, t) = (p_i)^{(6)} \\ \lim_{G \rightarrow \infty} (b''_i)^{(6)}((G_{35}), t) = (r_i)^{(6)}$$

Definition of $(\hat{A}_{32})^{(6)}, (\hat{B}_{32})^{(6)}$:

Where $(\hat{A}_{32})^{(6)}, (\hat{B}_{32})^{(6)}, (p_i)^{(6)}, (r_i)^{(6)}$ are positive constants and $i = 32, 33, 34$.185

They satisfy Lipschitz condition:

$$|(a''_i)^{(6)}(T'_{33}, t) - (a''_i)^{(6)}(T_{33}, t)| \leq (\hat{k}_{32})^{(6)} |T'_{33} - T_{33}| e^{-(M_{32})^{(6)}t} \\ |(b''_i)^{(6)}((G_{35})', t) - (b''_i)^{(6)}((G_{35}), t)| < (\hat{k}_{32})^{(6)} \|(G_{35})' - (G_{35})\| e^{-(M_{32})^{(6)}t}.186$$

With the Lipschitz condition, we place a restriction on the behavior of functions $(a''_i)^{(6)}(T'_{33}, t)$ and $(a''_i)^{(6)}(T_{33}, t) \cdot (T'_{33}, t)$ and (T_{33}, t) are points belonging to the interval $[(\hat{k}_{32})^{(6)}, (\hat{M}_{32})^{(6)}]$. It is to be noted that $(a''_i)^{(6)}(T_{33}, t)$ is uniformly continuous. In the eventuality of the fact, that if $(\hat{M}_{32})^{(6)} = 6$ then the function $(a''_i)^{(6)}(T_{33}, t)$, the **SIXTH augmentation coefficient** would be absolutely continuous. .187

Definition of $(\hat{M}_{32})^{(6)}, (\hat{k}_{32})^{(6)}$:

$(\hat{M}_{32})^{(6)}, (\hat{k}_{32})^{(6)}$, are positive constants

$$\frac{(a_i)^{(6)}}{(\hat{M}_{32})^{(6)}}, \frac{(b_i)^{(6)}}{(\hat{M}_{32})^{(6)}} < 1.188$$

Definition of $(\hat{P}_{32})^{(6)}, (\hat{Q}_{32})^{(6)}$:

There exists two constants $(\hat{P}_{32})^{(6)}$ and $(\hat{Q}_{32})^{(6)}$ which together with $(\hat{M}_{32})^{(6)}, (\hat{k}_{32})^{(6)}, (\hat{A}_{32})^{(6)}$ and $(\hat{B}_{32})^{(6)}$ and the constants $(a_i)^{(6)}, (a'_i)^{(6)}, (b_i)^{(6)}, (b'_i)^{(6)}, (p_i)^{(6)}, (r_i)^{(6)}, i = 32, 33, 34$, satisfy the inequalities

$$\frac{1}{(\hat{M}_{32})^{(6)}} [(a_i)^{(6)} + (a'_i)^{(6)} + (\hat{A}_{32})^{(6)} + (\hat{P}_{32})^{(6)} (\hat{k}_{32})^{(6)}] < 1 \\ \frac{1}{(\hat{M}_{32})^{(6)}} [(b_i)^{(6)} + (b'_i)^{(6)} + (\hat{B}_{32})^{(6)} + (\hat{Q}_{32})^{(6)} (\hat{k}_{32})^{(6)}] < 1.189$$

.190

Theorem 1: if the conditions IN THE FOREGOING above are fulfilled, there exists a solution satisfying the conditions

Definition of $G_i(0), T_i(0)$:

$$G_i(t) \leq (\hat{P}_{13})^{(1)} e^{(\hat{M}_{13})^{(1)}t} , \quad \boxed{G_i(0) = G_i^0 > 0}$$

$$T_i(t) \leq (\hat{Q}_{13})^{(1)} e^{(\hat{M}_{13})^{(1)}t} , \quad \boxed{T_i(0) = T_i^0 > 0} .191$$

.192

Definition of $G_i(0), T_i(0)$

$$G_i(t) \leq (\hat{P}_{16})^{(2)} e^{(\hat{M}_{16})^{(2)}t} , \quad G_i(0) = G_i^0 > 0$$

$$T_i(t) \leq (\hat{Q}_{16})^{(2)} e^{(\hat{M}_{16})^{(2)}t} , \quad T_i(0) = T_i^0 > 0 .193$$

.194

$$G_i(t) \leq (\hat{P}_{20})^{(3)} e^{(\hat{M}_{20})^{(3)}t} , \quad G_i(0) = G_i^0 > 0$$

$$T_i(t) \leq (\hat{Q}_{20})^{(3)} e^{(\hat{M}_{20})^{(3)}t} , \quad T_i(0) = T_i^0 > 0 .195$$

Definition of $G_i(0), T_i(0)$:

$$G_i(t) \leq (\hat{P}_{24})^{(4)} e^{(\hat{M}_{24})^{(4)}t} , \quad \boxed{G_i(0) = G_i^0 > 0}$$

$$T_i(t) \leq (\hat{Q}_{24})^{(4)} e^{(\hat{M}_{24})^{(4)}t} , \quad \boxed{T_i(0) = T_i^0 > 0} .196$$

Definition of $G_i(0), T_i(0)$:

$$G_i(t) \leq (\hat{P}_{28})^{(5)} e^{(\hat{M}_{28})^{(5)}t} , \quad \boxed{G_i(0) = G_i^0 > 0}$$

$$T_i(t) \leq (\hat{Q}_{28})^{(5)} e^{(\hat{M}_{28})^{(5)}t} , \quad \boxed{T_i(0) = T_i^0 > 0} .197$$

.198

Definition of $G_i(0), T_i(0)$:

$$G_i(t) \leq (\hat{P}_{32})^{(6)} e^{(\hat{M}_{32})^{(6)}t} , \quad \boxed{G_i(0) = G_i^0 > 0}$$

$$T_i(t) \leq (\hat{Q}_{32})^{(6)} e^{(\hat{M}_{32})^{(6)}t} , \quad \boxed{T_i(0) = T_i^0 > 0} .199$$

Proof: Consider operator $\mathcal{A}^{(1)}$ defined on the space of sextuples of continuous functions $G_i, T_i: \mathbb{R}_+ \rightarrow \mathbb{R}_+$ which satisfy

$$G_i(0) = G_i^0, T_i(0) = T_i^0, G_i^0 \leq (\hat{P}_{13})^{(1)}, T_i^0 \leq (\hat{Q}_{13})^{(1)}, .201$$

$$0 \leq G_i(t) - G_i^0 \leq (\hat{P}_{13})^{(1)} e^{(\hat{M}_{13})^{(1)}t} .202$$

$$0 \leq T_i(t) - T_i^0 \leq (\hat{Q}_{13})^{(1)} e^{(\hat{M}_{13})^{(1)}t} .203$$

By

$$\bar{G}_{13}(t) = G_{13}^0 + \int_0^t \left[(a_{13})^{(1)} G_{14}(s_{(13)}) - \left((a'_{13})^{(1)} + a''_{13}(s_{(13)}, s_{(13)}) \right) G_{13}(s_{(13)}) \right] ds_{(13)} .204$$

$$\bar{G}_{14}(t) = G_{14}^0 + \int_0^t \left[(a_{14})^{(1)} G_{13}(s_{(13)}) - \left((a'_{14})^{(1)} + a''_{14}(s_{(13)}, s_{(13)}) \right) G_{14}(s_{(13)}) \right] ds_{(13)} .205$$

$$\bar{G}_{15}(t) = G_{15}^0 + \int_0^t \left[(a_{15})^{(1)} G_{14}(s_{(13)}) - \left((a'_{15})^{(1)} + a''_{15}(s_{(13)}, s_{(13)}) \right) G_{15}(s_{(13)}) \right] ds_{(13)} .206$$

$$\bar{T}_{13}(t) = T_{13}^0 + \int_0^t \left[(b_{13})^{(1)} T_{14}(s_{(13)}) - \left((b'_{13})^{(1)} - b''_{13}(s_{(13)}, s_{(13)}) \right) T_{13}(s_{(13)}) \right] ds_{(13)} .207$$

$$\bar{T}_{14}(t) = T_{14}^0 + \int_0^t \left[(b_{14})^{(1)} T_{13}(s_{(13)}) - \left((b'_{14})^{(1)} - b''_{14}(s_{(13)}, s_{(13)}) \right) T_{14}(s_{(13)}) \right] ds_{(13)} .208$$

$$\bar{T}_{15}(t) = T_{15}^0 + \int_0^t \left[(b_{15})^{(1)} T_{14}(s_{(13)}) - \left((b'_{15})^{(1)} - b''_{15}(s_{(13)}, s_{(13)}) \right) T_{15}(s_{(13)}) \right] ds_{(13)}$$

Where $s_{(13)}$ is the integrand that is integrated over an interval $(0, t)$.209

.210

Proof:

Consider operator $\mathcal{A}^{(2)}$ defined on the space of sextuples of continuous functions $G_i, T_i: \mathbb{R}_+ \rightarrow \mathbb{R}_+$ which satisfy

.211

$$G_i(0) = G_i^0, T_i(0) = T_i^0, G_i^0 \leq (\hat{P}_{16})^{(2)}, T_i^0 \leq (\hat{Q}_{16})^{(2)}, .212$$

$$0 \leq G_i(t) - G_i^0 \leq (\hat{P}_{16})^{(2)} e^{(\hat{M}_{16})^{(2)}t} .213$$

$$0 \leq T_i(t) - T_i^0 \leq (\hat{Q}_{16})^{(2)} e^{(\hat{M}_{16})^{(2)}t} .214$$

By

$$\bar{G}_{16}(t) = G_{16}^0 + \int_0^t \left[(a_{16})^{(2)} G_{17}(s_{(16)}) - \left((a'_{16})^{(2)} + a''_{16}(s_{(16)}, s_{(16)}) \right) G_{16}(s_{(16)}) \right] ds_{(16)} .215$$

$$\bar{G}_{17}(t) = G_{17}^0 + \int_0^t \left[(a_{17})^{(2)} G_{16}(s_{(16)}) - \left((a'_{17})^{(2)} + a''_{17}(s_{(16)}, s_{(17)}) \right) G_{17}(s_{(16)}) \right] ds_{(16)} .216$$

$$\bar{G}_{18}(t) = G_{18}^0 + \int_0^t \left[(a_{18})^{(2)} G_{17}(s_{(16)}) - \left((a'_{18})^{(2)} + a''_{18}(s_{(16)}, s_{(16)}) \right) G_{18}(s_{(16)}) \right] ds_{(16)} .217$$

$$\bar{T}_{16}(t) = T_{16}^0 + \int_0^t \left[(b_{16})^{(2)} T_{17}(s_{(16)}) - \left((b'_{16})^{(2)} - b''_{16}(s_{(16)}, s_{(16)}) \right) T_{16}(s_{(16)}) \right] ds_{(16)} .218$$

$$\bar{T}_{17}(t) = T_{17}^0 + \int_0^t \left[(b_{17})^{(2)} T_{16}(s_{(16)}) - \left((b'_{17})^{(2)} - (b''_{17})^{(2)} (G(s_{(16)}), s_{(16)}) \right) T_{17}(s_{(16)}) \right] ds_{(16)} \quad .219$$

$$\bar{T}_{18}(t) = T_{18}^0 + \int_0^t \left[(b_{18})^{(2)} T_{17}(s_{(16)}) - \left((b'_{18})^{(2)} - (b''_{18})^{(2)} (G(s_{(16)}), s_{(16)}) \right) T_{18}(s_{(16)}) \right] ds_{(16)}$$

Where $s_{(16)}$ is the integrand that is integrated over an interval $(0, t)$.220

Proof:

Consider operator $\mathcal{A}^{(3)}$ defined on the space of sextuples of continuous functions $G_i, T_i: \mathbb{R}_+ \rightarrow \mathbb{R}_+$ which satisfy .221

$$G_i(0) = G_i^0, T_i(0) = T_i^0, G_i^0 \leq (\hat{P}_{20})^{(3)}, T_i^0 \leq (\hat{Q}_{20})^{(3)}, \quad .222$$

$$0 \leq G_i(t) - G_i^0 \leq (\hat{P}_{20})^{(3)} e^{(M_{20})^{(3)}t} \quad .223$$

$$0 \leq T_i(t) - T_i^0 \leq (\hat{Q}_{20})^{(3)} e^{(M_{20})^{(3)}t} \quad .224$$

By

$$\bar{G}_{20}(t) = G_{20}^0 + \int_0^t \left[(a_{20})^{(3)} G_{21}(s_{(20)}) - \left((a'_{20})^{(3)} + a''_{20}^{(3)} (T_{21}(s_{(20)}), s_{(20)}) \right) G_{20}(s_{(20)}) \right] ds_{(20)} \quad .225$$

$$\bar{G}_{21}(t) = G_{21}^0 + \int_0^t \left[(a_{21})^{(3)} G_{20}(s_{(20)}) - \left((a'_{21})^{(3)} + (a''_{21})^{(3)} (T_{21}(s_{(20)}), s_{(20)}) \right) G_{21}(s_{(20)}) \right] ds_{(20)} \quad .226$$

$$\bar{G}_{22}(t) = G_{22}^0 + \int_0^t \left[(a_{22})^{(3)} G_{21}(s_{(20)}) - \left((a'_{22})^{(3)} + (a''_{22})^{(3)} (T_{21}(s_{(20)}), s_{(20)}) \right) G_{22}(s_{(20)}) \right] ds_{(20)} \quad .227$$

$$\bar{T}_{20}(t) = T_{20}^0 + \int_0^t \left[(b_{20})^{(3)} T_{21}(s_{(20)}) - \left((b'_{20})^{(3)} - (b''_{20})^{(3)} (G(s_{(20)}), s_{(20)}) \right) T_{20}(s_{(20)}) \right] ds_{(20)} \quad .228$$

$$\bar{T}_{21}(t) = T_{21}^0 + \int_0^t \left[(b_{21})^{(3)} T_{20}(s_{(20)}) - \left((b'_{21})^{(3)} - (b''_{21})^{(3)} (G(s_{(20)}), s_{(20)}) \right) T_{21}(s_{(20)}) \right] ds_{(20)} \quad .229$$

$$\bar{T}_{22}(t) = T_{22}^0 + \int_0^t \left[(b_{22})^{(3)} T_{21}(s_{(20)}) - \left((b'_{22})^{(3)} - (b''_{22})^{(3)} (G(s_{(20)}), s_{(20)}) \right) T_{22}(s_{(20)}) \right] ds_{(20)}$$

Where $s_{(20)}$ is the integrand that is integrated over an interval $(0, t)$.230

Consider operator $\mathcal{A}^{(4)}$ defined on the space of sextuples of continuous functions $G_i, T_i: \mathbb{R}_+ \rightarrow \mathbb{R}_+$ which satisfy

.231

$$G_i(0) = G_i^0, T_i(0) = T_i^0, G_i^0 \leq (\hat{P}_{24})^{(4)}, T_i^0 \leq (\hat{Q}_{24})^{(4)}, \quad .232$$

$$0 \leq G_i(t) - G_i^0 \leq (\hat{P}_{24})^{(4)} e^{(M_{24})^{(4)}t} \quad .233$$

$$0 \leq T_i(t) - T_i^0 \leq (\hat{Q}_{24})^{(4)} e^{(M_{24})^{(4)}t} \quad .234$$

By

$$\bar{G}_{24}(t) = G_{24}^0 + \int_0^t \left[(a_{24})^{(4)} G_{25}(s_{(24)}) - \left((a'_{24})^{(4)} + a''_{24}^{(4)} (T_{25}(s_{(24)}), s_{(24)}) \right) G_{24}(s_{(24)}) \right] ds_{(24)} \quad .235$$

$$\bar{G}_{25}(t) = G_{25}^0 + \int_0^t \left[(a_{25})^{(4)} G_{24}(s_{(24)}) - \left((a'_{25})^{(4)} + (a''_{25})^{(4)} (T_{25}(s_{(24)}), s_{(24)}) \right) G_{25}(s_{(24)}) \right] ds_{(24)} \quad .236$$

$$\bar{G}_{26}(t) = G_{26}^0 + \int_0^t \left[(a_{26})^{(4)} G_{25}(s_{(24)}) - \left((a'_{26})^{(4)} + (a''_{26})^{(4)} (T_{25}(s_{(24)}), s_{(24)}) \right) G_{26}(s_{(24)}) \right] ds_{(24)} \quad .237$$

$$\bar{T}_{24}(t) = T_{24}^0 + \int_0^t \left[(b_{24})^{(4)} T_{25}(s_{(24)}) - \left((b'_{24})^{(4)} - (b''_{24})^{(4)} (G(s_{(24)}), s_{(24)}) \right) T_{24}(s_{(24)}) \right] ds_{(24)} \quad .238$$

$$\bar{T}_{25}(t) = T_{25}^0 + \int_0^t \left[(b_{25})^{(4)} T_{24}(s_{(24)}) - \left((b'_{25})^{(4)} - (b''_{25})^{(4)} (G(s_{(24)}), s_{(24)}) \right) T_{25}(s_{(24)}) \right] ds_{(24)} \quad .239$$

$$\bar{T}_{26}(t) = T_{26}^0 + \int_0^t \left[(b_{26})^{(4)} T_{25}(s_{(24)}) - \left((b'_{26})^{(4)} - (b''_{26})^{(4)} (G(s_{(24)}), s_{(24)}) \right) T_{26}(s_{(24)}) \right] ds_{(24)}$$

Where $s_{(24)}$ is the integrand that is integrated over an interval $(0, t)$.240

Consider operator $\mathcal{A}^{(5)}$ defined on the space of sextuples of continuous functions $G_i, T_i: \mathbb{R}_+ \rightarrow \mathbb{R}_+$ which satisfy

.241

242

$$G_i(0) = G_i^0, T_i(0) = T_i^0, G_i^0 \leq (\hat{P}_{28})^{(5)}, T_i^0 \leq (\hat{Q}_{28})^{(5)}, \quad .243$$

$$0 \leq G_i(t) - G_i^0 \leq (\hat{P}_{28})^{(5)} e^{(M_{28})^{(5)}t} \quad .244$$

$$0 \leq T_i(t) - T_i^0 \leq (\hat{Q}_{28})^{(5)} e^{(M_{28})^{(5)}t} \quad .245$$

By

$$\bar{G}_{28}(t) = G_{28}^0 + \int_0^t \left[(a_{28})^{(5)} G_{29}(s_{(28)}) - \left((a'_{28})^{(5)} + a''_{28}^{(5)} (T_{29}(s_{(28)}), s_{(28)}) \right) G_{28}(s_{(28)}) \right] ds_{(28)} \quad .246$$

$$\bar{G}_{29}(t) = G_{29}^0 + \int_0^t \left[(a_{29})^{(5)} G_{28}(s_{(28)}) - \left((a'_{29})^{(5)} + (a''_{29})^{(5)} (T_{29}(s_{(28)}), s_{(28)}) \right) G_{29}(s_{(28)}) \right] ds_{(28)} \quad .247$$

$$\bar{G}_{30}(t) = G_{30}^0 + \int_0^t \left[(a_{30})^{(5)} G_{29}(s_{(28)}) - \left((a'_{30})^{(5)} + (a''_{30})^{(5)} (T_{29}(s_{(28)}), s_{(28)}) \right) G_{30}(s_{(28)}) \right] ds_{(28)} \quad .248$$

$$\bar{T}_{28}(t) = T_{28}^0 + \int_0^t \left[(b_{28})^{(5)} T_{29}(s_{(28)}) - \left((b'_{28})^{(5)} - (b''_{28})^{(5)} (G(s_{(28)}), s_{(28)}) \right) T_{28}(s_{(28)}) \right] ds_{(28)} \quad .249$$

$$\bar{T}_{29}(t) = T_{29}^0 + \int_0^t \left[(b_{29})^{(5)} T_{28}(s_{(28)}) - \left((b'_{29})^{(5)} - (b''_{29})^{(5)} (G(s_{(28)}), s_{(28)}) \right) T_{29}(s_{(28)}) \right] ds_{(28)} \quad .250$$

$$\bar{T}_{30}(t) = T_{30}^0 + \int_0^t \left[(b_{30})^{(5)} T_{29}(s_{(28)}) - \left((b'_{30})^{(5)} - (b''_{30})^{(5)} (G(s_{(28)}), s_{(28)}) \right) T_{30}(s_{(28)}) \right] ds_{(28)}$$

Where $s_{(28)}$ is the integrand that is integrated over an interval $(0, t)$.251

Consider operator $\mathcal{A}^{(6)}$ defined on the space of sextuples of continuous functions $G_i, T_i: \mathbb{R}_+ \rightarrow \mathbb{R}_+$ which satisfy .252

$$G_i(0) = G_i^0, T_i(0) = T_i^0, G_i^0 \leq (\hat{P}_{32})^{(6)}, T_i^0 \leq (\hat{Q}_{32})^{(6)}, \quad .253$$

$$0 \leq G_i(t) - G_i^0 \leq (\hat{P}_{32})^{(6)} e^{(M_{32})^{(6)}t} \quad .254$$

$$0 \leq T_i(t) - T_i^0 \leq (\hat{Q}_{32})^{(6)} e^{(M_{32})^{(6)}t} \quad .255$$

By

$$\bar{G}_{32}(t) = G_{32}^0 + \int_0^t \left[(a_{32})^{(6)} G_{33}(s_{(32)}) - \left((a'_{32})^{(6)} + a''_{32} \right)^{(6)} (T_{33}(s_{(32)}, s_{(32)})) G_{32}(s_{(32)}) \right] ds_{(32)} \quad .256$$

$$\bar{G}_{33}(t) = G_{33}^0 + \int_0^t \left[(a_{33})^{(6)} G_{32}(s_{(32)}) - \left((a'_{33})^{(6)} + (a''_{33})^{(6)} (T_{33}(s_{(32)}, s_{(32)})) \right) G_{33}(s_{(32)}) \right] ds_{(32)} \quad .257$$

$$\bar{G}_{34}(t) = G_{34}^0 + \int_0^t \left[(a_{34})^{(6)} G_{33}(s_{(32)}) - \left((a'_{34})^{(6)} + (a''_{34})^{(6)} (T_{33}(s_{(32)}, s_{(32)})) \right) G_{34}(s_{(32)}) \right] ds_{(32)} \quad .258$$

$$\bar{T}_{32}(t) = T_{32}^0 + \int_0^t \left[(b_{32})^{(6)} T_{33}(s_{(32)}) - \left((b'_{32})^{(6)} - (b''_{32})^{(6)} (G(s_{(32)}, s_{(32)})) \right) T_{32}(s_{(32)}) \right] ds_{(32)} \quad .259$$

$$\bar{T}_{33}(t) = T_{33}^0 + \int_0^t \left[(b_{33})^{(6)} T_{32}(s_{(32)}) - \left((b'_{33})^{(6)} - (b''_{33})^{(6)} (G(s_{(32)}, s_{(32)})) \right) T_{33}(s_{(32)}) \right] ds_{(32)} \quad .260$$

$$\bar{T}_{34}(t) = T_{34}^0 + \int_0^t \left[(b_{34})^{(6)} T_{33}(s_{(32)}) - \left((b'_{34})^{(6)} - (b''_{34})^{(6)} (G(s_{(32)}, s_{(32)})) \right) T_{34}(s_{(32)}) \right] ds_{(32)}$$

Where $s_{(32)}$ is the integrand that is integrated over an interval $(0, t)$.261

262

(a) The operator $\mathcal{A}^{(1)}$ maps the space of functions satisfying GLOBAL EQUATIONS into itself .Indeed it is obvious that

$$G_{13}(t) \leq G_{13}^0 + \int_0^t \left[(a_{13})^{(1)} \left(G_{14}^0 + (\hat{P}_{13})^{(1)} e^{(\hat{M}_{13})^{(1)} s_{(13)}} \right) \right] ds_{(13)} =$$

$$\left(1 + (a_{13})^{(1)} t \right) G_{14}^0 + \frac{(a_{13})^{(1)} (\hat{P}_{13})^{(1)}}{(\hat{M}_{13})^{(1)}} \left(e^{(\hat{M}_{13})^{(1)} t} - 1 \right) \quad .263$$

From which it follows that

$$(G_{13}(t) - G_{13}^0) e^{-(\hat{M}_{13})^{(1)} t} \leq \frac{(a_{13})^{(1)}}{(\hat{M}_{13})^{(1)}} \left[\left((\hat{P}_{13})^{(1)} + G_{14}^0 \right) e^{-\frac{(\hat{P}_{13})^{(1)} + G_{14}^0}{G_{14}^0}} + (\hat{P}_{13})^{(1)} \right]$$

(G_i^0) is as defined in the statement of theorem 1.264

Analogous inequalities hold also for $G_{14}, G_{15}, T_{13}, T_{14}, T_{15}$.265

The operator $\mathcal{A}^{(2)}$ maps the space of functions satisfying GLOBAL EQUATIONS into itself .Indeed it is obvious that.266

$$G_{16}(t) \leq G_{16}^0 + \int_0^t \left[(a_{16})^{(2)} \left(G_{17}^0 + (\hat{P}_{16})^{(2)} e^{(\hat{M}_{16})^{(2)} s_{(16)}} \right) \right] ds_{(16)} = \left(1 + (a_{16})^{(2)} t \right) G_{17}^0 + \frac{(a_{16})^{(2)} (\hat{P}_{16})^{(2)}}{(\hat{M}_{16})^{(2)}} \left(e^{(\hat{M}_{16})^{(2)} t} - 1 \right)$$

.267

From which it follows that

$$(G_{16}(t) - G_{16}^0) e^{-(\hat{M}_{16})^{(2)} t} \leq \frac{(a_{16})^{(2)}}{(\hat{M}_{16})^{(2)}} \left[\left((\hat{P}_{16})^{(2)} + G_{17}^0 \right) e^{-\frac{(\hat{P}_{16})^{(2)} + G_{17}^0}{G_{17}^0}} + (\hat{P}_{16})^{(2)} \right] \quad .268$$

Analogous inequalities hold also for $G_{17}, G_{18}, T_{16}, T_{17}, T_{18}$.269

(a) The operator $\mathcal{A}^{(3)}$ maps the space of functions satisfying GLOBAL EQUATIONS into itself .Indeed it is obvious that

$$G_{20}(t) \leq G_{20}^0 + \int_0^t \left[(a_{20})^{(3)} \left(G_{21}^0 + (\hat{P}_{20})^{(3)} e^{(\hat{M}_{20})^{(3)} s_{(20)}} \right) \right] ds_{(20)} =$$

$$\left(1 + (a_{20})^{(3)} t \right) G_{21}^0 + \frac{(a_{20})^{(3)} (\hat{P}_{20})^{(3)}}{(\hat{M}_{20})^{(3)}} \left(e^{(\hat{M}_{20})^{(3)} t} - 1 \right) \quad .270$$

From which it follows that

$$(G_{20}(t) - G_{20}^0) e^{-(\hat{M}_{20})^{(3)} t} \leq \frac{(a_{20})^{(3)}}{(\hat{M}_{20})^{(3)}} \left[\left((\hat{P}_{20})^{(3)} + G_{21}^0 \right) e^{-\frac{(\hat{P}_{20})^{(3)} + G_{21}^0}{G_{21}^0}} + (\hat{P}_{20})^{(3)} \right] \quad .271$$

Analogous inequalities hold also for $G_{21}, G_{22}, T_{20}, T_{21}, T_{22}$.272

(b) The operator $\mathcal{A}^{(4)}$ maps the space of functions satisfying GLOBAL EQUATIONS into itself .Indeed it is obvious that

$$G_{24}(t) \leq G_{24}^0 + \int_0^t \left[(a_{24})^{(4)} \left(G_{25}^0 + (\hat{P}_{24})^{(4)} e^{(\hat{M}_{24})^{(4)} s_{(24)}} \right) \right] ds_{(24)} =$$

$$\left(1 + (a_{24})^{(4)} t \right) G_{25}^0 + \frac{(a_{24})^{(4)} (\hat{P}_{24})^{(4)}}{(\hat{M}_{24})^{(4)}} \left(e^{(\hat{M}_{24})^{(4)} t} - 1 \right) \quad .273$$

From which it follows that

$$(G_{24}(t) - G_{24}^0) e^{-(\hat{M}_{24})^{(4)} t} \leq \frac{(a_{24})^{(4)}}{(\hat{M}_{24})^{(4)}} \left[\left((\hat{P}_{24})^{(4)} + G_{25}^0 \right) e^{-\frac{(\hat{P}_{24})^{(4)} + G_{25}^0}{G_{25}^0}} + (\hat{P}_{24})^{(4)} \right]$$

(G_i^0) is as defined in the statement of theorem 1.274

(c) The operator $\mathcal{A}^{(5)}$ maps the space of functions satisfying GLOBAL EQUATIONS into itself .Indeed it is obvious that

$$G_{28}(t) \leq G_{28}^0 + \int_0^t \left[(a_{28})^{(5)} \left(G_{29}^0 + (\hat{P}_{28})^{(5)} e^{(\hat{M}_{28})^{(5)} s_{(28)}} \right) \right] ds_{(28)} =$$

$$\left(1 + (a_{28})^{(5)} t \right) G_{29}^0 + \frac{(a_{28})^{(5)} (\hat{P}_{28})^{(5)}}{(\hat{M}_{28})^{(5)}} \left(e^{(\hat{M}_{28})^{(5)} t} - 1 \right) \quad .275$$

From which it follows that

$$(G_{28}(t) - G_{28}^0) e^{-(\hat{M}_{28})^{(5)} t} \leq \frac{(a_{28})^{(5)}}{(\hat{M}_{28})^{(5)}} \left[\left((\hat{P}_{28})^{(5)} + G_{29}^0 \right) e^{-\frac{(\hat{P}_{28})^{(5)} + G_{29}^0}{G_{29}^0}} + (\hat{P}_{28})^{(5)} \right]$$

(G_i^0) is as defined in the statement of theorem 1.276

(d) The operator $\mathcal{A}^{(6)}$ maps the space of functions satisfying GLOBAL EQUATIONS into itself .Indeed it is obvious that

$$G_{32}(t) \leq G_{32}^0 + \int_0^t \left[(a_{32})^{(6)} \left(G_{33}^0 + (\hat{P}_{32})^{(6)} e^{(\bar{M}_{32})^{(6)} s_{(32)}} \right) \right] ds_{(32)} =$$

$$(1 + (a_{32})^{(6)} t) G_{33}^0 + \frac{(a_{32})^{(6)} (\hat{P}_{32})^{(6)}}{(\bar{M}_{32})^{(6)}} \left(e^{(\bar{M}_{32})^{(6)} t} - 1 \right) .277$$

From which it follows that

$$(G_{32}(t) - G_{32}^0) e^{-(\bar{M}_{32})^{(6)} t} \leq \frac{(a_{32})^{(6)}}{(\bar{M}_{32})^{(6)}} \left[\left((\hat{P}_{32})^{(6)} + G_{33}^0 \right) e^{-\left(\frac{(\hat{P}_{32})^{(6)} + G_{33}^0}{G_{33}^0} \right)} + (\hat{P}_{32})^{(6)} \right]$$

(G_i^0) is as defined in the statement of theorem 6

Analogous inequalities hold also for $G_{25}, G_{26}, T_{24}, T_{25}, T_{26}$.278

279

.280

It is now sufficient to take $\frac{(a_i)^{(1)}}{(\bar{M}_{13})^{(1)}}, \frac{(b_i)^{(1)}}{(\bar{M}_{13})^{(1)}} < 1$ and to choose $(\hat{P}_{13})^{(1)}$ and $(\hat{Q}_{13})^{(1)}$ large to have.281

282

$$\frac{(a_i)^{(1)}}{(\bar{M}_{13})^{(1)}} \left[(\hat{P}_{13})^{(1)} + \left((\hat{P}_{13})^{(1)} + G_j^0 \right) e^{-\left(\frac{(\hat{P}_{13})^{(1)} + G_j^0}{G_j^0} \right)} \right] \leq (\hat{P}_{13})^{(1)} .283$$

$$\frac{(b_i)^{(1)}}{(\bar{M}_{13})^{(1)}} \left[\left((\hat{Q}_{13})^{(1)} + T_j^0 \right) e^{-\left(\frac{(\hat{Q}_{13})^{(1)} + T_j^0}{T_j^0} \right)} + (\hat{Q}_{13})^{(1)} \right] \leq (\hat{Q}_{13})^{(1)} .284$$

In order that the operator $\mathcal{A}^{(1)}$ transforms the space of sextuples of functions G_i, T_i satisfying GLOBAL EQUATIONS into itself.285

The operator $\mathcal{A}^{(1)}$ is a contraction with respect to the metric

$$d \left((G^{(1)}, T^{(1)}), (G^{(2)}, T^{(2)}) \right) =$$

$$\sup_i \left\{ \max_{t \in \mathbb{R}_+} |G_i^{(1)}(t) - G_i^{(2)}(t)| e^{-(\bar{M}_{13})^{(1)} t}, \max_{t \in \mathbb{R}_+} |T_i^{(1)}(t) - T_i^{(2)}(t)| e^{-(\bar{M}_{13})^{(1)} t} \right\} .286$$

Indeed if we denote

Definition of \tilde{G}, \tilde{T} :

$$(\tilde{G}, \tilde{T}) = \mathcal{A}^{(1)}(G, T)$$

It results

$$|\tilde{G}_{13}^{(1)} - \tilde{G}_{13}^{(2)}| \leq \int_0^t (a_{13})^{(1)} |G_{14}^{(1)} - G_{14}^{(2)}| e^{-(\bar{M}_{13})^{(1)} s_{(13)}} e^{(\bar{M}_{13})^{(1)} s_{(13)}} ds_{(13)} +$$

$$\int_0^t \{ (a'_{13})^{(1)} |G_{13}^{(1)} - G_{13}^{(2)}| e^{-(\bar{M}_{13})^{(1)} s_{(13)}} e^{-(\bar{M}_{13})^{(1)} s_{(13)}} +$$

$$(a''_{13})^{(1)} (T_{14}^{(1)}, s_{(13)}) |G_{13}^{(1)} - G_{13}^{(2)}| e^{-(\bar{M}_{13})^{(1)} s_{(13)}} e^{(\bar{M}_{13})^{(1)} s_{(13)}} +$$

$$G_{13}^{(2)} | (a'_{13})^{(1)} (T_{14}^{(1)}, s_{(13)}) - (a'_{13})^{(1)} (T_{14}^{(2)}, s_{(13)}) | e^{-(\bar{M}_{13})^{(1)} s_{(13)}} e^{(\bar{M}_{13})^{(1)} s_{(13)}} \} ds_{(13)}$$

Where $s_{(13)}$ represents integrand that is integrated over the interval $[0, t]$

From the hypotheses it follows.287

$$|G^{(1)} - G^{(2)}| e^{-(\bar{M}_{13})^{(1)} t} \leq \frac{1}{(\bar{M}_{13})^{(1)}} \left((a_{13})^{(1)} + (a'_{13})^{(1)} + (\bar{A}_{13})^{(1)} + (\hat{P}_{13})^{(1)} (\hat{k}_{13})^{(1)} \right) d \left((G^{(1)}, T^{(1)}); (G^{(2)}, T^{(2)}) \right)$$

And analogous inequalities for G_i and T_i . Taking into account the hypothesis the result follows.288

Remark 1: The fact that we supposed $(a'_{13})^{(1)}$ and $(b'_{13})^{(1)}$ depending also on t can be considered as not conformal with the reality, however we have put this hypothesis ,in order that we can postulate condition necessary to prove the uniqueness of the solution bounded by $(\hat{P}_{13})^{(1)} e^{(\bar{M}_{13})^{(1)} t}$ and $(\hat{Q}_{13})^{(1)} e^{(\bar{M}_{13})^{(1)} t}$ respectively of \mathbb{R}_+ .

If instead of proving the existence of the solution on \mathbb{R}_+ , we have to prove it only on a compact then it suffices to consider that $(a_i)^{(1)}$ and $(b_i)^{(1)}, i = 13,14,15$ depend only on T_{14} and respectively on G (and not on t) and hypothesis can be replaced by a usual Lipschitz condition..289

Remark 2: There does not exist any t where $G_i(t) = 0$ and $T_i(t) = 0$

From 19 to 24 it results

$$G_i(t) \geq G_i^0 e^{-\int_0^t \{ (a'_i)^{(1)} - (a''_i)^{(1)} (T_{14}(s_{(13)}), s_{(13)}) \} ds_{(13)}} \geq 0$$

$$T_i(t) \geq T_i^0 e^{-(b'_i)^{(1)} t} > 0 \text{ for } t > 0.290$$

291

Definition of $(\bar{M}_{13})^{(1)}_1$, and $(\bar{M}_{13})^{(1)}_3$:

Remark 3: if G_{13} is bounded, the same property have also G_{14} and G_{15} . indeed if $G_{13} < (\bar{M}_{13})^{(1)}$ it follows $\frac{dG_{14}}{dt} \leq ((\bar{M}_{13})^{(1)})_1 - (a'_{14})^{(1)} G_{14}$ and by integrating

$$G_{14} \leq ((\widehat{M}_{13})^{(1)})_2 = G_{14}^0 + 2(a_{14})^{(1)}((\widehat{M}_{13})^{(1)})_1 / (a'_{14})^{(1)}$$

In the same way, one can obtain

$$G_{15} \leq ((\widehat{M}_{13})^{(1)})_3 = G_{15}^0 + 2(a_{15})^{(1)}((\widehat{M}_{13})^{(1)})_2 / (a'_{15})^{(1)}$$

If G_{14} or G_{15} is bounded, the same property follows for G_{13} , G_{15} and G_{13} , G_{14} respectively..292

Remark 4: If G_{13} is bounded, from below, the same property holds for G_{14} and G_{15} . The proof is analogous with the preceding one. An analogous property is true if G_{14} is bounded from below..293

Remark 5: If T_{13} is bounded from below and $\lim_{t \rightarrow \infty} ((b''_i)^{(1)}(G(t), t)) = (b'_{14})^{(1)}$ then $T_{14} \rightarrow \infty$.

Definition of $(m)^{(1)}$ and ε_1 :

Indeed let t_1 be so that for $t > t_1$

$$(b_{14})^{(1)} - (b''_i)^{(1)}(G(t), t) < \varepsilon_1, T_{13}(t) > (m)^{(1)} .294$$

Then $\frac{dT_{14}}{dt} \geq (a_{14})^{(1)}(m)^{(1)} - \varepsilon_1 T_{14}$ which leads to

$$T_{14} \geq \left(\frac{(a_{14})^{(1)}(m)^{(1)}}{\varepsilon_1} \right) (1 - e^{-\varepsilon_1 t}) + T_{14}^0 e^{-\varepsilon_1 t} \text{ If we take } t \text{ such that } e^{-\varepsilon_1 t} = \frac{1}{2} \text{ it results}$$

$T_{14} \geq \left(\frac{(a_{14})^{(1)}(m)^{(1)}}{2} \right), t = \log \frac{2}{\varepsilon_1}$ By taking now ε_1 sufficiently small one sees that T_{14} is unbounded. The same property holds for T_{15} if $\lim_{t \rightarrow \infty} ((b''_i)^{(1)}(G(t), t)) = (b'_{15})^{(1)}$

We now state a more precise theorem about the behaviors at infinity of the solutions .295
 .296

It is now sufficient to take $\frac{(a_i)^{(2)}}{(\widehat{M}_{16})^{(2)}}, \frac{(b_i)^{(2)}}{(\widehat{M}_{16})^{(2)}} < 1$ and to choose

$(\widehat{P}_{16})^{(2)}$ and $(\widehat{Q}_{16})^{(2)}$ large to have.297

$$\frac{(a_i)^{(2)}}{(\widehat{M}_{16})^{(2)}} \left[(\widehat{P}_{16})^{(2)} + ((\widehat{P}_{16})^{(2)} + G_j^0) e^{-\left(\frac{(\widehat{P}_{16})^{(2)} + G_j^0}{G_j^0} \right)} \right] \leq (\widehat{P}_{16})^{(2)} .298$$

$$\frac{(b_i)^{(2)}}{(\widehat{M}_{16})^{(2)}} \left[((\widehat{Q}_{16})^{(2)} + T_j^0) e^{-\left(\frac{(\widehat{Q}_{16})^{(2)} + T_j^0}{T_j^0} \right)} + (\widehat{Q}_{16})^{(2)} \right] \leq (\widehat{Q}_{16})^{(2)} .299$$

In order that the operator $\mathcal{A}^{(2)}$ transforms the space of sextuples of functions G_i, T_i satisfying .300

The operator $\mathcal{A}^{(2)}$ is a contraction with respect to the metric

$$d \left(((G_{19})^{(1)}, (T_{19})^{(1)}), ((G_{19})^{(2)}, (T_{19})^{(2)}) \right) =$$

$$\sup_i \left\{ \max_{t \in \mathbb{R}_+} |G_i^{(1)}(t) - G_i^{(2)}(t)| e^{-(\widehat{M}_{16})^{(2)}t}, \max_{t \in \mathbb{R}_+} |T_i^{(1)}(t) - T_i^{(2)}(t)| e^{-(\widehat{M}_{16})^{(2)}t} \right\} .301$$

Indeed if we denote

$$\underline{\text{Definition of}} \widehat{G}_{19}, \widehat{T}_{19} : (\widehat{G}_{19}, \widehat{T}_{19}) = \mathcal{A}^{(2)}(G_{19}, T_{19}).302$$

It results

$$\begin{aligned} & |\widehat{G}_{16}^{(1)} - \widehat{G}_{16}^{(2)}| \leq \int_0^t (a_{16})^{(2)} |G_{17}^{(1)} - G_{17}^{(2)}| e^{-(\widehat{M}_{16})^{(2)}s_{(16)}} e^{(\widehat{M}_{16})^{(2)}s_{(16)}} ds_{(16)} + \\ & \int_0^t \{ (a_{16}')^{(2)} |G_{16}^{(1)} - G_{16}^{(2)}| e^{-(\widehat{M}_{16})^{(2)}s_{(16)}} e^{-(\widehat{M}_{16})^{(2)}s_{(16)}} + \\ & (a_{16}'')^{(2)}(T_{17}^{(1)}, s_{(16)}) |G_{16}^{(1)} - G_{16}^{(2)}| e^{-(\widehat{M}_{16})^{(2)}s_{(16)}} e^{(\widehat{M}_{16})^{(2)}s_{(16)}} + \\ & G_{16}^{(2)} | (a_{16}'')^{(2)}(T_{17}^{(1)}, s_{(16)}) - (a_{16}'')^{(2)}(T_{17}^{(2)}, s_{(16)}) | e^{-(\widehat{M}_{16})^{(2)}s_{(16)}} e^{(\widehat{M}_{16})^{(2)}s_{(16)}} \} ds_{(16)} .303 \end{aligned}$$

Where $s_{(16)}$ represents integrand that is integrated over the interval $[0, t]$

From the hypotheses it follows.304

$$\begin{aligned} & |(G_{19})^{(1)} - (G_{19})^{(2)}| e^{-(\widehat{M}_{16})^{(2)}t} \leq \\ & \frac{1}{(\widehat{M}_{16})^{(2)}} \left((a_{16})^{(2)} + (a'_{16})^{(2)} + (\widehat{A}_{16})^{(2)} + (\widehat{P}_{16})^{(2)} (\widehat{k}_{16})^{(2)} \right) d \left(((G_{19})^{(1)}, (T_{19})^{(1)}); (G_{19})^{(2)}, (T_{19})^{(2)} \right) .305 \end{aligned}$$

And analogous inequalities for G_i and T_i . Taking into account the hypothesis the result follows.306

Remark 1: The fact that we supposed $(a''_{16})^{(2)}$ and $(b''_{16})^{(2)}$ depending also on t can be considered as not conformal with the reality, however we have put this hypothesis, in order that we can postulate condition necessary to prove the uniqueness of the solution bounded by $(\widehat{P}_{16})^{(2)} e^{(\widehat{M}_{16})^{(2)}t}$ and $(\widehat{Q}_{16})^{(2)} e^{(\widehat{M}_{16})^{(2)}t}$ respectively of \mathbb{R}_+ .

If instead of proving the existence of the solution on \mathbb{R}_+ , we have to prove it only on a compact then it suffices to consider that $(a''_i)^{(2)}$ and $(b''_i)^{(2)}$, $i = 16, 17, 18$ depend only on T_{17} and respectively on (G_{19}) (and not on t) and hypothesis can be replaced by a usual Lipschitz condition..307

Remark 2: There does not exist any t where $G_i(t) = 0$ and $T_i(t) = 0$

From 19 to 24 it results

$$G_i(t) \geq G_i^0 e^{-\int_0^t \{ (a'_i)^{(2)} - (a''_i)^{(2)}(T_{17}(s_{(16)}), s_{(16)}) \} ds_{(16)}} \geq 0$$

$$T_i(t) \geq T_i^0 e^{-(b'_i)^{(2)}t} > 0 \text{ for } t > 0.308$$

Definition of $((\widehat{M}_{16})^{(2)})_1, ((\widehat{M}_{16})^{(2)})_2$ and $((\widehat{M}_{16})^{(2)})_3$:

Remark 3: if G_{16} is bounded, the same property have also G_{17} and G_{18} . indeed if

$G_{16} < ((\widehat{M}_{16})^{(2)})$ it follows $\frac{dG_{17}}{dt} \leq ((\widehat{M}_{16})^{(2)})_1 - (a'_{17})^{(2)}G_{17}$ and by integrating

$$G_{17} \leq ((\widehat{M}_{16})^{(2)})_2 = G_{17}^0 + 2(a_{17})^{(2)}((\widehat{M}_{16})^{(2)})_1 / (a'_{17})^{(2)}$$

In the same way , one can obtain

$$G_{18} \leq ((\widehat{M}_{16})^{(2)})_3 = G_{18}^0 + 2(a_{18})^{(2)}((\widehat{M}_{16})^{(2)})_2 / (a'_{18})^{(2)}$$

If G_{17} or G_{18} is bounded, the same property follows for G_{16} , G_{18} and G_{16} , G_{17} respectively..309

310

Remark 4: If G_{16} is bounded, from below, the same property holds for G_{17} and G_{18} . The proof is analogous with the preceding one. An analogous property is true if G_{17} is bounded from below..311

Remark 5: If T_{16} is bounded from below and $\lim_{t \rightarrow \infty} ((b''_i)^{(2)}((G_{19})(t), t)) = (b'_{17})^{(2)}$ then $T_{17} \rightarrow \infty$.

Definition of $(m)^{(2)}$ and ε_2 :

Indeed let t_2 be so that for $t > t_2$

$$(b_{17})^{(2)} - (b''_i)^{(2)}((G_{19})(t), t) < \varepsilon_2, T_{16}(t) > (m)^{(2)} .312$$

Then $\frac{dT_{17}}{dt} \geq (a_{17})^{(2)}(m)^{(2)} - \varepsilon_2 T_{17}$ which leads to

$$T_{17} \geq \left(\frac{(a_{17})^{(2)}(m)^{(2)}}{\varepsilon_2} \right) (1 - e^{-\varepsilon_2 t}) + T_{17}^0 e^{-\varepsilon_2 t} \text{ If we take } t \text{ such that } e^{-\varepsilon_2 t} = \frac{1}{2} \text{ it results .313}$$

$T_{17} \geq \left(\frac{(a_{17})^{(2)}(m)^{(2)}}{2} \right), t = \log \frac{2}{\varepsilon_2}$ By taking now ε_2 sufficiently small one sees that T_{17} is unbounded. The same property

holds for T_{18} if $\lim_{t \rightarrow \infty} (b''_{18})^{(2)}((G_{19})(t), t) = (b'_{18})^{(2)}$

We now state a more precise theorem about the behaviors at infinity of the solutions .314

.315

It is now sufficient to take $\frac{(a_i)^{(3)}}{(M_{20})^{(3)}}, \frac{(b_i)^{(3)}}{(M_{20})^{(3)}} < 1$ and to choose

$(\widehat{P}_{20})^{(3)}$ and $(\widehat{Q}_{20})^{(3)}$ large to have.316

$$\frac{(a_i)^{(3)}}{(M_{20})^{(3)}} \left[(\widehat{P}_{20})^{(3)} + ((\widehat{P}_{20})^{(3)} + G_j^0) e^{-\left(\frac{(\widehat{P}_{20})^{(3)} + G_j^0}{G_j^0} \right)} \right] \leq (\widehat{P}_{20})^{(3)} .317$$

$$\frac{(b_i)^{(3)}}{(M_{20})^{(3)}} \left[((\widehat{Q}_{20})^{(3)} + T_j^0) e^{-\left(\frac{(\widehat{Q}_{20})^{(3)} + T_j^0}{T_j^0} \right)} + (\widehat{Q}_{20})^{(3)} \right] \leq (\widehat{Q}_{20})^{(3)} .318$$

In order that the operator $\mathcal{A}^{(3)}$ transforms the space of sextuples of functions G_i, T_i into itself.319

The operator $\mathcal{A}^{(3)}$ is a contraction with respect to the metric

$$d \left(((G_{23})^{(1)}, (T_{23})^{(1)}), ((G_{23})^{(2)}, (T_{23})^{(2)}) \right) =$$

$$\sup_i \left\{ \max_{t \in \mathbb{R}_+} |G_i^{(1)}(t) - G_i^{(2)}(t)| e^{-(M_{20})^{(3)}t}, \max_{t \in \mathbb{R}_+} |T_i^{(1)}(t) - T_i^{(2)}(t)| e^{-(M_{20})^{(3)}t} \right\} .320$$

Indeed if we denote

$$\widetilde{G}_{23}, \widetilde{T}_{23} : ((\widetilde{G}_{23}), (\widetilde{T}_{23})) = \mathcal{A}^{(3)}((G_{23}), (T_{23})) .321$$

It results

$$\begin{aligned} |\widetilde{G}_{20}^{(1)} - \widetilde{G}_{20}^{(2)}| &\leq \int_0^t (a_{20})^{(3)} |G_{21}^{(1)} - G_{21}^{(2)}| e^{-(M_{20})^{(3)}s_{(20)}} e^{(M_{20})^{(3)}s_{(20)}} ds_{(20)} + \\ &\int_0^t \{ (a'_{20})^{(3)} |G_{20}^{(1)} - G_{20}^{(2)}| e^{-(M_{20})^{(3)}s_{(20)}} e^{-(M_{20})^{(3)}s_{(20)}} + \\ &(a''_{20})^{(3)} (T_{21}^{(1)}, s_{(20)}) |G_{20}^{(1)} - G_{20}^{(2)}| e^{-(M_{20})^{(3)}s_{(20)}} e^{(M_{20})^{(3)}s_{(20)}} + \\ &G_{20}^{(2)} | (a''_{20})^{(3)} (T_{21}^{(1)}, s_{(20)}) - (a''_{20})^{(3)} (T_{21}^{(2)}, s_{(20)}) | e^{-(M_{20})^{(3)}s_{(20)}} e^{(M_{20})^{(3)}s_{(20)}} \} ds_{(20)} \end{aligned}$$

Where $s_{(20)}$ represents integrand that is integrated over the interval $[0, t]$

From the hypotheses it follows.322

323

$$|G^{(1)} - G^{(2)}| e^{-(M_{20})^{(3)}t} \leq$$

$$\frac{1}{(M_{20})^{(3)}} ((a_{20})^{(3)} + (a'_{20})^{(3)} + (\widehat{A}_{20})^{(3)} + (\widehat{P}_{20})^{(3)} (\widehat{k}_{20})^{(3)}) d \left(((G_{23})^{(1)}, (T_{23})^{(1)}); (G_{23})^{(2)}, (T_{23})^{(2)} \right)$$

And analogous inequalities for G_i and T_i . Taking into account the hypothesis the result follows.324

Remark 1: The fact that we supposed $(a''_{20})^{(3)}$ and $(b''_{20})^{(3)}$ depending also on t can be considered as not conformal with the reality, however we have put this hypothesis ,in order that we can postulate condition necessary to prove the uniqueness of the solution bounded by $(\widehat{P}_{20})^{(3)} e^{(M_{20})^{(3)}t}$ and $(\widehat{Q}_{20})^{(3)} e^{(M_{20})^{(3)}t}$ respectively of \mathbb{R}_+ .

If instead of proving the existence of the solution on \mathbb{R}_+ , we have to prove it only on a compact then it suffices to consider that $(a_i'')^{(3)}$ and $(b_i'')^{(3)}$, $i = 20, 21, 22$ depend only on T_{21} and respectively on (G_{23}) (and not on t) and hypothesis can be replaced by a usual Lipschitz condition..325

Remark 2: There does not exist any t where $G_i(t) = 0$ and $T_i(t) = 0$

From 19 to 24 it results

$$G_i(t) \geq G_i^0 e^{-\int_0^t \{(a_i')^{(3)} - (a_i'')^{(3)}\} (T_{21}(s_{(20)}), s_{(20)}) ds_{(20)}} \geq 0$$

$$T_i(t) \geq T_i^0 e^{-(b_i')^{(3)}t} > 0 \text{ for } t > 0.326$$

Definition of $((\widehat{M}_{20})^{(3)})_1, ((\widehat{M}_{20})^{(3)})_2$ and $((\widehat{M}_{20})^{(3)})_3$:

Remark 3: if G_{20} is bounded, the same property have also G_{21} and G_{22} . indeed if

$G_{20} < ((\widehat{M}_{20})^{(3)})$ it follows $\frac{dG_{21}}{dt} \leq ((\widehat{M}_{20})^{(3)})_1 - (a_{21}')^{(3)}G_{21}$ and by integrating

$$G_{21} \leq ((\widehat{M}_{20})^{(3)})_2 = G_{21}^0 + 2(a_{21}')^{(3)}((\widehat{M}_{20})^{(3)})_1 / (a_{21}')^{(3)}$$

In the same way , one can obtain

$$G_{22} \leq ((\widehat{M}_{20})^{(3)})_3 = G_{22}^0 + 2(a_{22}')^{(3)}((\widehat{M}_{20})^{(3)})_2 / (a_{22}')^{(3)}$$

If G_{21} or G_{22} is bounded, the same property follows for G_{20} , G_{22} and G_{20} , G_{21} respectively..327

Remark 4: If G_{20} is bounded, from below, the same property holds for G_{21} and G_{22} . The proof is analogous with the preceding one. An analogous property is true if G_{21} is bounded from below..328

Remark 5: If T_{20} is bounded from below and $\lim_{t \rightarrow \infty} ((b_i'')^{(3)})((G_{23})(t), t) = (b_{21}')^{(3)}$ then $T_{21} \rightarrow \infty$.

Definition of $(m)^{(3)}$ and ε_3 :

Indeed let t_3 be so that for $t > t_3$

$$(b_{21}')^{(3)} - (b_i'')^{(3)}((G_{23})(t), t) < \varepsilon_3, T_{20}(t) > (m)^{(3)} .329$$

330

Then $\frac{dT_{21}}{dt} \geq (a_{21}')^{(3)}(m)^{(3)} - \varepsilon_3 T_{21}$ which leads to

$$T_{21} \geq \left(\frac{(a_{21}')^{(3)}(m)^{(3)}}{\varepsilon_3} \right) (1 - e^{-\varepsilon_3 t}) + T_{21}^0 e^{-\varepsilon_3 t} \text{ If we take } t \text{ such that } e^{-\varepsilon_3 t} = \frac{1}{2} \text{ it results}$$

$$T_{21} \geq \left(\frac{(a_{21}')^{(3)}(m)^{(3)}}{2} \right), t = \log \frac{2}{\varepsilon_3} \text{ By taking now } \varepsilon_3 \text{ sufficiently small one sees that } T_{21} \text{ is unbounded. The same property}$$

holds for T_{22} if $\lim_{t \rightarrow \infty} ((b_{22}')^{(3)})((G_{23})(t), t) = (b_{22}')^{(3)}$

We now state a more precise theorem about the behaviors at infinity of the solutions .331

.332

It is now sufficient to take $\frac{(a_i)^{(4)}}{(\widehat{M}_{24})^{(4)}}, \frac{(b_i)^{(4)}}{(\widehat{M}_{24})^{(4)}} < 1$ and to choose

$(\widehat{P}_{24})^{(4)}$ and $(\widehat{Q}_{24})^{(4)}$ large to have.333

$$\frac{(a_i)^{(4)}}{(\widehat{M}_{24})^{(4)}} \left[(\widehat{P}_{24})^{(4)} + ((\widehat{P}_{24})^{(4)} + G_j^0) e^{-\left(\frac{(\widehat{P}_{24})^{(4)} + G_j^0}{G_j^0} \right)} \right] \leq (\widehat{P}_{24})^{(4)} .334$$

$$\frac{(b_i)^{(4)}}{(\widehat{M}_{24})^{(4)}} \left[((\widehat{Q}_{24})^{(4)} + T_j^0) e^{-\left(\frac{(\widehat{Q}_{24})^{(4)} + T_j^0}{T_j^0} \right)} + (\widehat{Q}_{24})^{(4)} \right] \leq (\widehat{Q}_{24})^{(4)} .335$$

In order that the operator $\mathcal{A}^{(4)}$ transforms the space of sextuples of functions G_i, T_i satisfying IN to itself.336

The operator $\mathcal{A}^{(4)}$ is a contraction with respect to the metric

$$d \left(((G_{27})^{(1)}, (T_{27})^{(1)}), ((G_{27})^{(2)}, (T_{27})^{(2)}) \right) =$$

$$\sup_i \left\{ \max_{t \in \mathbb{R}_+} |G_i^{(1)}(t) - G_i^{(2)}(t)| e^{-(\widehat{M}_{24})^{(4)}t}, \max_{t \in \mathbb{R}_+} |T_i^{(1)}(t) - T_i^{(2)}(t)| e^{-(\widehat{M}_{24})^{(4)}t} \right\}$$

Indeed if we denote

Definition of $(\widetilde{G}_{27}), (\widetilde{T}_{27})$: $((\widetilde{G}_{27}), (\widetilde{T}_{27})) = \mathcal{A}^{(4)}((G_{27}), (T_{27}))$

It results

$$\begin{aligned} |\widetilde{G}_{24}^{(1)} - \widetilde{G}_{24}^{(2)}| &\leq \int_0^t (a_{24})^{(4)} |G_{25}^{(1)} - G_{25}^{(2)}| e^{-(\widehat{M}_{24})^{(4)}s_{(24)}} e^{(\widehat{M}_{24})^{(4)}s_{(24)}} ds_{(24)} + \\ &\int_0^t \{(a_{24}')^{(4)} |G_{24}^{(1)} - G_{24}^{(2)}| e^{-(\widehat{M}_{24})^{(4)}s_{(24)}} e^{-(\widehat{M}_{24})^{(4)}s_{(24)}} + \\ &(a_{24}'')^{(4)}(T_{25}^{(1)}, s_{(24)}) |G_{24}^{(1)} - G_{24}^{(2)}| e^{-(\widehat{M}_{24})^{(4)}s_{(24)}} e^{(\widehat{M}_{24})^{(4)}s_{(24)}} + \\ &G_{24}^{(2)} |(a_{24}')^{(4)}(T_{25}^{(1)}, s_{(24)}) - (a_{24}')^{(4)}(T_{25}^{(2)}, s_{(24)})| e^{-(\widehat{M}_{24})^{(4)}s_{(24)}} e^{(\widehat{M}_{24})^{(4)}s_{(24)}}\} ds_{(24)} \end{aligned}$$

Where $s_{(24)}$ represents integrand that is integrated over the interval $[0, t]$

From the hypotheses it follows.337

338

$$\left| (G_{27})^{(1)} - (G_{27})^{(2)} \right| e^{-(\widehat{M}_{24})^{(4)}t} \leq \frac{1}{(\widehat{M}_{24})^{(4)}} \left((a_{24})^{(4)} + (a'_{24})^{(4)} + (\widehat{A}_{24})^{(4)} + (\widehat{P}_{24})^{(4)} (\widehat{k}_{24})^{(4)} \right) d \left(((G_{27})^{(1)}, (T_{27})^{(1)}; (G_{27})^{(2)}, (T_{27})^{(2)}) \right)$$

And analogous inequalities for G_i and T_i . Taking into account the hypothesis the result follows.339

Remark 1: The fact that we supposed $(a''_{24})^{(4)}$ and $(b''_{24})^{(4)}$ depending also on t can be considered as not conformal with the reality, however we have put this hypothesis, in order that we can postulate condition necessary to prove the uniqueness of the solution bounded by $(\widehat{P}_{24})^{(4)} e^{(\widehat{M}_{24})^{(4)}t}$ and $(\widehat{Q}_{24})^{(4)} e^{(\widehat{M}_{24})^{(4)}t}$ respectively of \mathbb{R}_+ .

If instead of proving the existence of the solution on \mathbb{R}_+ , we have to prove it only on a compact then it suffices to consider that $(a''_i)^{(4)}$ and $(b''_i)^{(4)}$, $i = 24, 25, 26$ depend only on T_{25} and respectively on (G_{27}) (and not on t) and hypothesis can be replaced by a usual Lipschitz condition..340

Remark 2: There does not exist any t where $G_i(t) = 0$ and $T_i(t) = 0$

From 19 to 24 it results

$$G_i(t) \geq G_i^0 e^{-\int_0^t \{(a'_i)^{(4)} - (a''_i)^{(4)}\} (T_{25}(s_{(24)}), s_{(24)}) ds_{(24)}} \geq 0$$

$$T_i(t) \geq T_i^0 e^{-(b'_i)^{(4)}t} > 0 \text{ for } t > 0.341$$

Definition of $(\widehat{M}_{24})^{(4)}_1, (\widehat{M}_{24})^{(4)}_2$ and $(\widehat{M}_{24})^{(4)}_3$:

Remark 3: if G_{24} is bounded, the same property have also G_{25} and G_{26} . indeed if

$G_{24} < (\widehat{M}_{24})^{(4)}$ it follows $\frac{dG_{25}}{dt} \leq ((\widehat{M}_{24})^{(4)})_1 - (a'_{25})^{(4)} G_{25}$ and by integrating

$$G_{25} \leq ((\widehat{M}_{24})^{(4)})_2 = G_{25}^0 + 2(a_{25})^{(4)} ((\widehat{M}_{24})^{(4)})_1 / (a'_{25})^{(4)}$$

In the same way, one can obtain

$$G_{26} \leq ((\widehat{M}_{24})^{(4)})_3 = G_{26}^0 + 2(a_{26})^{(4)} ((\widehat{M}_{24})^{(4)})_2 / (a'_{26})^{(4)}$$

If G_{25} or G_{26} is bounded, the same property follows for G_{24} , G_{26} and G_{24} , G_{25} respectively..342

Remark 4: If G_{24} is bounded, from below, the same property holds for G_{25} and G_{26} . The proof is analogous with the preceding one. An analogous property is true if G_{25} is bounded from below..343

Remark 5: If T_{24} is bounded from below and $\lim_{t \rightarrow \infty} ((b''_i)^{(4)}((G_{27})(t), t)) = (b'_{25})^{(4)}$ then $T_{25} \rightarrow \infty$.

Definition of $(m)^{(4)}$ and ε_4 :

Indeed let t_4 be so that for $t > t_4$

$$(b_{25})^{(4)} - (b''_i)^{(4)}((G_{27})(t), t) < \varepsilon_4, T_{24}(t) > (m)^{(4)} \quad .344$$

Then $\frac{dT_{25}}{dt} \geq (a_{25})^{(4)}(m)^{(4)} - \varepsilon_4 T_{25}$ which leads to

$$T_{25} \geq \left(\frac{(a_{25})^{(4)}(m)^{(4)}}{\varepsilon_4} \right) (1 - e^{-\varepsilon_4 t}) + T_{25}^0 e^{-\varepsilon_4 t} \text{ If we take } t \text{ such that } e^{-\varepsilon_4 t} = \frac{1}{2} \text{ it results}$$

$$T_{25} \geq \left(\frac{(a_{25})^{(4)}(m)^{(4)}}{2} \right), \quad t = \log \frac{2}{\varepsilon_4} \text{ By taking now } \varepsilon_4 \text{ sufficiently small one sees that } T_{25} \text{ is unbounded. The same property}$$

holds for T_{26} if $\lim_{t \rightarrow \infty} (b''_{26})^{(4)}((G_{27})(t), t) = (b'_{26})^{(4)}$

We now state a more precise theorem about the behaviors at infinity of the solutions ANALOGOUS inequalities hold also for $G_{29}, G_{30}, T_{28}, T_{29}, T_{30}$.345

.346

It is now sufficient to take $\frac{(a_i)^{(5)}}{(\widehat{M}_{28})^{(5)}}, \frac{(b_i)^{(5)}}{(\widehat{M}_{28})^{(5)}} < 1$ and to choose

$(\widehat{P}_{28})^{(5)}$ and $(\widehat{Q}_{28})^{(5)}$ large to have

.347

$$\frac{(a_i)^{(5)}}{(\widehat{M}_{28})^{(5)}} \left[(\widehat{P}_{28})^{(5)} + ((\widehat{P}_{28})^{(5)} + G_j^0) e^{-\left(\frac{(\widehat{P}_{28})^{(5)} + G_j^0}{G_j^0} \right)} \right] \leq (\widehat{P}_{28})^{(5)} \quad .348$$

$$\frac{(b_i)^{(5)}}{(\widehat{M}_{28})^{(5)}} \left[((\widehat{Q}_{28})^{(5)} + T_j^0) e^{-\left(\frac{(\widehat{Q}_{28})^{(5)} + T_j^0}{T_j^0} \right)} + (\widehat{Q}_{28})^{(5)} \right] \leq (\widehat{Q}_{28})^{(5)} \quad .349$$

In order that the operator $\mathcal{A}^{(5)}$ transforms the space of sextuples of functions G_i, T_i into itself.350

The operator $\mathcal{A}^{(5)}$ is a contraction with respect to the metric

$$d \left(((G_{31})^{(1)}, (T_{31})^{(1)}), ((G_{31})^{(2)}, (T_{31})^{(2)}) \right) =$$

$$\sup_i \left\{ \max_{t \in \mathbb{R}_+} |G_i^{(1)}(t) - G_i^{(2)}(t)| e^{-(\widehat{M}_{28})^{(5)}t}, \max_{t \in \mathbb{R}_+} |T_i^{(1)}(t) - T_i^{(2)}(t)| e^{-(\widehat{M}_{28})^{(5)}t} \right\}$$

Indeed if we denote

Definition of $(\widehat{G}_{31}), (\widehat{T}_{31})$: $(\widehat{G}_{31}), (\widehat{T}_{31}) = \mathcal{A}^{(5)}((G_{31}), (T_{31}))$

It results

$$|\widehat{G}_{28}^{(1)} - \widehat{G}_i^{(2)}| \leq \int_0^t (a_{28})^{(5)} |G_{29}^{(1)} - G_{29}^{(2)}| e^{-(\widehat{M}_{28})^{(5)}s_{(28)}} e^{(\widehat{M}_{28})^{(5)}s_{(28)}} ds_{(28)} +$$

$$\int_0^t \{ (a'_{28})^{(5)} |G_{28}^{(1)} - G_{28}^{(2)}| e^{-(\bar{M}_{28})^{(5)} s_{(28)}} e^{-(\bar{M}_{28})^{(5)} s_{(28)}} + (a''_{28})^{(5)} (T_{29}^{(1)}, s_{(28)}) |G_{28}^{(1)} - G_{28}^{(2)}| e^{-(\bar{M}_{28})^{(5)} s_{(28)}} e^{(\bar{M}_{28})^{(5)} s_{(28)}} + G_{28}^{(2)} | (a''_{28})^{(5)} (T_{29}^{(1)}, s_{(28)}) - (a''_{28})^{(5)} (T_{29}^{(2)}, s_{(28)}) | e^{-(\bar{M}_{28})^{(5)} s_{(28)}} e^{(\bar{M}_{28})^{(5)} s_{(28)}} \} ds_{(28)}$$

Where $s_{(28)}$ represents integrand that is integrated over the interval $[0, t]$
 From the hypotheses it follows.351

352

$$|(G_{31})^{(1)} - (G_{31})^{(2)}| e^{-(\bar{M}_{28})^{(5)} t} \leq \frac{1}{(\bar{M}_{28})^{(5)}} ((a_{28})^{(5)} + (a'_{28})^{(5)} + (\bar{A}_{28})^{(5)} + (\bar{P}_{28})^{(5)} (\bar{k}_{28})^{(5)}) d((G_{31})^{(1)}, (T_{31})^{(1)}; (G_{31})^{(2)}, (T_{31})^{(2)})$$

And analogous inequalities for G_i and T_i . Taking into account the hypothesis (35,35,36) the result follows.353

Remark 1: The fact that we supposed $(a''_{28})^{(5)}$ and $(b''_{28})^{(5)}$ depending also on t can be considered as not conformal with the reality, however we have put this hypothesis, in order that we can postulate condition necessary to prove the uniqueness of the solution bounded by $(\bar{P}_{28})^{(5)} e^{(\bar{M}_{28})^{(5)} t}$ and $(\bar{Q}_{28})^{(5)} e^{(\bar{M}_{28})^{(5)} t}$ respectively of \mathbb{R}_+ .

If instead of proving the existence of the solution on \mathbb{R}_+ , we have to prove it only on a compact then it suffices to consider that $(a''_i)^{(5)}$ and $(b''_i)^{(5)}$, $i = 28, 29, 30$ depend only on T_{29} and respectively on (G_{31}) (and not on t) and hypothesis can be replaced by a usual Lipschitz condition..354

Remark 2: There does not exist any t where $G_i(t) = 0$ and $T_i(t) = 0$

From GLOBAL EQUATIONS it results

$$G_i(t) \geq G_i^0 e^{-\int_0^t \{ (a'_i)^{(5)} - (a''_i)^{(5)} (T_{29}(s_{(28)}), s_{(28)}) \} ds_{(28)}} \geq 0$$

$$T_i(t) \geq T_i^0 e^{-(b'_i)^{(5)} t} > 0 \text{ for } t > 0.355$$

Definition of $((\bar{M}_{28})^{(5)})_1, ((\bar{M}_{28})^{(5)})_2$ and $((\bar{M}_{28})^{(5)})_3$:

Remark 3: if G_{28} is bounded, the same property have also G_{29} and G_{30} . indeed if

$$G_{28} < (\bar{M}_{28})^{(5)} \text{ it follows } \frac{dG_{29}}{dt} \leq ((\bar{M}_{28})^{(5)})_1 - (a'_{29})^{(5)} G_{29} \text{ and by integrating}$$

$$G_{29} \leq ((\bar{M}_{28})^{(5)})_2 = G_{29}^0 + 2(a_{29})^{(5)} ((\bar{M}_{28})^{(5)})_1 / (a'_{29})^{(5)}$$

In the same way, one can obtain

$$G_{30} \leq ((\bar{M}_{28})^{(5)})_3 = G_{30}^0 + 2(a_{30})^{(5)} ((\bar{M}_{28})^{(5)})_2 / (a'_{30})^{(5)}$$

If G_{29} or G_{30} is bounded, the same property follows for G_{28} , G_{30} and G_{28} , G_{29} respectively..356

Remark 4: If G_{28} is bounded, from below, the same property holds for G_{29} and G_{30} . The proof is analogous with the preceding one. An analogous property is true if G_{29} is bounded from below..357

Remark 5: If T_{28} is bounded from below and $\lim_{t \rightarrow \infty} ((b''_i)^{(5)} ((G_{31})(t), t)) = (b'_{29})^{(5)}$ then $T_{29} \rightarrow \infty$.

Definition of $(m)^{(5)}$ and ε_5 :

Indeed let t_5 be so that for $t > t_5$

$$(b_{29})^{(5)} - (b''_i)^{(5)} ((G_{31})(t), t) < \varepsilon_5, T_{28}(t) > (m)^{(5)}.358$$

359

Then $\frac{dT_{29}}{dt} \geq (a_{29})^{(5)} (m)^{(5)} - \varepsilon_5 T_{29}$ which leads to

$$T_{29} \geq \left(\frac{(a_{29})^{(5)} (m)^{(5)}}{\varepsilon_5} \right) (1 - e^{-\varepsilon_5 t}) + T_{29}^0 e^{-\varepsilon_5 t} \text{ If we take } t \text{ such that } e^{-\varepsilon_5 t} = \frac{1}{2} \text{ it results}$$

$$T_{29} \geq \left(\frac{(a_{29})^{(5)} (m)^{(5)}}{2} \right), t = \log \frac{2}{\varepsilon_5} \text{ By taking now } \varepsilon_5 \text{ sufficiently small one sees that } T_{29} \text{ is unbounded. The same property}$$

holds for T_{30} if $\lim_{t \rightarrow \infty} (b''_{30})^{(5)} ((G_{31})(t), t) = (b'_{30})^{(5)}$

We now state a more precise theorem about the behaviors at infinity of the solutions

Analogous inequalities hold also for $G_{33}, G_{34}, T_{32}, T_{33}, T_{34}$.360

.361

It is now sufficient to take $\frac{(a_i)^{(6)}}{(M_{32})^{(6)}}, \frac{(b_i)^{(6)}}{(M_{32})^{(6)}} < 1$ and to choose

$(\bar{P}_{32})^{(6)}$ and $(\bar{Q}_{32})^{(6)}$ large to have.362

$$\frac{(a_i)^{(6)}}{(M_{32})^{(6)}} \left[(\bar{P}_{32})^{(6)} + ((\bar{P}_{32})^{(6)} + G_j^0) e^{-\left(\frac{(\bar{P}_{32})^{(6)} + G_j^0}{G_j^0} \right)} \right] \leq (\bar{P}_{32})^{(6)}.363$$

$$\frac{(b_i)^{(6)}}{(M_{32})^{(6)}} \left[((\bar{Q}_{32})^{(6)} + T_j^0) e^{-\left(\frac{(\bar{Q}_{32})^{(6)} + T_j^0}{T_j^0} \right)} + (\bar{Q}_{32})^{(6)} \right] \leq (\bar{Q}_{32})^{(6)}.364$$

In order that the operator $\mathcal{A}^{(6)}$ transforms the space of sextuples of functions G_i, T_i into itself.365

The operator $\mathcal{A}^{(6)}$ is a contraction with respect to the metric

$$d\left(\left((G_{35})^{(1)}, (T_{35})^{(1)}\right), \left((G_{35})^{(2)}, (T_{35})^{(2)}\right)\right) = \sup_i \left\{ \max_{t \in \mathbb{R}_+} |G_i^{(1)}(t) - G_i^{(2)}(t)| e^{-(M_{32})^{(6)}t}, \max_{t \in \mathbb{R}_+} |T_i^{(1)}(t) - T_i^{(2)}(t)| e^{-(M_{32})^{(6)}t} \right\}$$

Indeed if we denote

Definition of $(\widehat{G_{35}}, \widehat{T_{35}}) : (\widehat{G_{35}}, \widehat{T_{35}}) = \mathcal{A}^{(6)}((G_{35}), (T_{35}))$

It results

$$|\widehat{G_{32}}^{(1)} - \widehat{G_i}^{(2)}| \leq \int_0^t (a_{32})^{(6)} |G_{33}^{(1)} - G_{33}^{(2)}| e^{-(M_{32})^{(6)}s_{(32)}} e^{(M_{32})^{(6)}s_{(32)}} ds_{(32)} + \int_0^t \{(a'_{32})^{(6)} |G_{32}^{(1)} - G_{32}^{(2)}| e^{-(M_{32})^{(6)}s_{(32)}} e^{-(M_{32})^{(6)}s_{(32)}} + (a''_{32})^{(6)} (T_{33}^{(1)}, s_{(32)}) |G_{32}^{(1)} - G_{32}^{(2)}| e^{-(M_{32})^{(6)}s_{(32)}} e^{(M_{32})^{(6)}s_{(32)}} + G_{32}^{(2)} | (a''_{32})^{(6)} (T_{33}^{(1)}, s_{(32)}) - (a''_{32})^{(6)} (T_{33}^{(2)}, s_{(32)}) | e^{-(M_{32})^{(6)}s_{(32)}} e^{(M_{32})^{(6)}s_{(32)}}\} ds_{(32)}$$

Where $s_{(32)}$ represents integrand that is integrated over the interval $[0, t]$

From the hypotheses it follows.366

367

$$|(G_{35})^{(1)} - (G_{35})^{(2)}| e^{-(M_{32})^{(6)}t} \leq \frac{1}{(M_{32})^{(6)}} \left((a_{32})^{(6)} + (a'_{32})^{(6)} + (\widehat{A}_{32})^{(6)} + (\widehat{P}_{32})^{(6)} (\widehat{k}_{32})^{(6)} \right) d\left(\left((G_{35})^{(1)}, (T_{35})^{(1)}\right); \left((G_{35})^{(2)}, (T_{35})^{(2)}\right)\right)$$

And analogous inequalities for G_i and T_i . Taking into account the hypothesis the result follows.368

Remark 1: The fact that we supposed $(a''_{32})^{(6)}$ and $(b''_{32})^{(6)}$ depending also on t can be considered as not conformal with the reality, however we have put this hypothesis ,in order that we can postulate condition necessary to prove the uniqueness of the solution bounded by $(\widehat{P}_{32})^{(6)} e^{(M_{32})^{(6)}t}$ and $(\widehat{Q}_{32})^{(6)} e^{(M_{32})^{(6)}t}$ respectively of \mathbb{R}_+ .

If instead of proving the existence of the solution on \mathbb{R}_+ , we have to prove it only on a compact then it suffices to consider that $(a''_i)^{(6)}$ and $(b''_i)^{(6)}$, $i = 32, 33, 34$ depend only on T_{33} and respectively on (G_{35}) (and not on t) and hypothesis can be replaced by a usual Lipschitz condition..369

Remark 2: There does not exist any t where $G_i(t) = 0$ and $T_i(t) = 0$

From 69 to 32 it results

$$G_i(t) \geq G_i^0 e^{-\int_0^t \{(a'_i)^{(6)} - (a''_i)^{(6)}\} (T_{33}(s_{(32)}), s_{(32)}) ds_{(32)}} \geq 0$$

$$T_i(t) \geq T_i^0 e^{-(b'_i)^{(6)}t} > 0 \text{ for } t > 0.370$$

Definition of $((\widehat{M}_{32})^{(6)})_1, ((\widehat{M}_{32})^{(6)})_2$ and $((\widehat{M}_{32})^{(6)})_3 :$

Remark 3: if G_{32} is bounded, the same property have also G_{33} and G_{34} . indeed if

$$G_{32} < (\widehat{M}_{32})^{(6)} \text{ it follows } \frac{dG_{33}}{dt} \leq ((\widehat{M}_{32})^{(6)})_1 - (a'_{33})^{(6)} G_{33} \text{ and by integrating}$$

$$G_{33} \leq ((\widehat{M}_{32})^{(6)})_2 = G_{33}^0 + 2(a_{33})^{(6)} ((\widehat{M}_{32})^{(6)})_1 / (a'_{33})^{(6)}$$

In the same way , one can obtain

$$G_{34} \leq ((\widehat{M}_{32})^{(6)})_3 = G_{34}^0 + 2(a_{34})^{(6)} ((\widehat{M}_{32})^{(6)})_2 / (a'_{34})^{(6)}$$

If G_{33} or G_{34} is bounded, the same property follows for G_{32} , G_{34} and G_{32} , G_{33} respectively..371

Remark 4: If G_{32} is bounded, from below, the same property holds for G_{33} and G_{34} . The proof is analogous with the preceding one. An analogous property is true if G_{33} is bounded from below..372

Remark 5: If T_{32} is bounded from below and $\lim_{t \rightarrow \infty} ((b''_i)^{(6)} ((G_{35})(t), t)) = (b'_{33})^{(6)}$ then $T_{33} \rightarrow \infty$.

Definition of $(m)^{(6)}$ and $\varepsilon_6 :$

Indeed let t_6 be so that for $t > t_6$

$$(b_{33})^{(6)} - (b''_i)^{(6)} ((G_{35})(t), t) < \varepsilon_6, T_{32}(t) > (m)^{(6)} \underline{.373}$$

374

Then $\frac{dT_{33}}{dt} \geq (a_{33})^{(6)} (m)^{(6)} - \varepsilon_6 T_{33}$ which leads to

$$T_{33} \geq \left(\frac{(a_{33})^{(6)} (m)^{(6)}}{\varepsilon_6} \right) (1 - e^{-\varepsilon_6 t}) + T_{33}^0 e^{-\varepsilon_6 t} \text{ If we take } t \text{ such that } e^{-\varepsilon_6 t} = \frac{1}{2} \text{ it results}$$

$$T_{33} \geq \left(\frac{(a_{33})^{(6)} (m)^{(6)}}{2} \right), \quad t = \log \frac{2}{\varepsilon_6} \text{ By taking now } \varepsilon_6 \text{ sufficiently small one sees that } T_{33} \text{ is unbounded. The same property}$$

holds for T_{34} if $\lim_{t \rightarrow \infty} (b''_{34})^{(6)} ((G_{35})(t), t) = (b'_{34})^{(6)}$

We now state a more precise theorem about the behaviors at infinity of the solutions .375

376

Behavior of the solutions

If we denote and define

Definition of $(\sigma_1)^{(1)}, (\sigma_2)^{(1)}, (\tau_1)^{(1)}, (\tau_2)^{(1)} :$

(a) $(\sigma_1)^{(1)}, (\sigma_2)^{(1)}, (\tau_1)^{(1)}, (\tau_2)^{(1)}$ four constants satisfying

$$-(\sigma_2)^{(1)} \leq -(a'_{13})^{(1)} + (a'_{14})^{(1)} - (a''_{13})^{(1)}(T_{14}, t) + (a''_{14})^{(1)}(T_{14}, t) \leq -(\sigma_1)^{(1)}$$

$$-(\tau_2)^{(1)} \leq -(b'_{13})^{(1)} + (b'_{14})^{(1)} - (b''_{13})^{(1)}(G, t) - (b''_{14})^{(1)}(G, t) \leq -(\tau_1)^{(1)} \quad .377$$

Definition of $(v_1)^{(1)}, (v_2)^{(1)}, (u_1)^{(1)}, (u_2)^{(1)}, v^{(1)}, u^{(1)}$:

By $(v_1)^{(1)} > 0, (v_2)^{(1)} < 0$ and respectively $(u_1)^{(1)} > 0, (u_2)^{(1)} < 0$ the roots of the equations $(a_{14})^{(1)}(v^{(1)})^2 + (\sigma_1)^{(1)}v^{(1)} - (a_{13})^{(1)} = 0$ and $(b_{14})^{(1)}(u^{(1)})^2 + (\tau_1)^{(1)}u^{(1)} - (b_{13})^{(1)} = 0$.378

Definition of $(\bar{v}_1)^{(1)}, (\bar{v}_2)^{(1)}, (\bar{u}_1)^{(1)}, (\bar{u}_2)^{(1)}$:

By $(\bar{v}_1)^{(1)} > 0, (\bar{v}_2)^{(1)} < 0$ and respectively $(\bar{u}_1)^{(1)} > 0, (\bar{u}_2)^{(1)} < 0$ the roots of the equations $(a_{14})^{(1)}(v^{(1)})^2 + (\sigma_2)^{(1)}v^{(1)} - (a_{13})^{(1)} = 0$ and $(b_{14})^{(1)}(u^{(1)})^2 + (\tau_2)^{(1)}u^{(1)} - (b_{13})^{(1)} = 0$.379

Definition of $(m_1)^{(1)}, (m_2)^{(1)}, (\mu_1)^{(1)}, (\mu_2)^{(1)}, (v_0)^{(1)}$:-

(b) If we define $(m_1)^{(1)}, (m_2)^{(1)}, (\mu_1)^{(1)}, (\mu_2)^{(1)}$ by
 $(m_2)^{(1)} = (v_0)^{(1)}, (m_1)^{(1)} = (v_1)^{(1)}$, if $(v_0)^{(1)} < (v_1)^{(1)}$
 $(m_2)^{(1)} = (v_1)^{(1)}, (m_1)^{(1)} = (\bar{v}_1)^{(1)}$, if $(v_1)^{(1)} < (v_0)^{(1)} < (\bar{v}_1)^{(1)}$,

$$\text{and } (v_0)^{(1)} = \frac{G_{13}^0}{G_{14}^0}$$

$(m_2)^{(1)} = (v_1)^{(1)}, (m_1)^{(1)} = (v_0)^{(1)}$, if $(\bar{v}_1)^{(1)} < (v_0)^{(1)}$.380

and analogously

$(\mu_2)^{(1)} = (u_0)^{(1)}, (\mu_1)^{(1)} = (u_1)^{(1)}$, if $(u_0)^{(1)} < (u_1)^{(1)}$
 $(\mu_2)^{(1)} = (u_1)^{(1)}, (\mu_1)^{(1)} = (\bar{u}_1)^{(1)}$, if $(u_1)^{(1)} < (u_0)^{(1)} < (\bar{u}_1)^{(1)}$,

$$\text{and } (u_0)^{(1)} = \frac{T_{13}^0}{T_{14}^0}$$

$(\mu_2)^{(1)} = (u_1)^{(1)}, (\mu_1)^{(1)} = (u_0)^{(1)}$, if $(\bar{u}_1)^{(1)} < (u_0)^{(1)}$ where $(u_1)^{(1)}, (\bar{u}_1)^{(1)}$ are defined respectively.381

382

Then the solution satisfies the inequalities

$$G_{13}^0 e^{((S_1)^{(1)} - (p_{13})^{(1)})t} \leq G_{13}(t) \leq G_{13}^0 e^{(S_1)^{(1)}t}$$

where $(p_i)^{(1)}$ is defined

$$\frac{1}{(m_1)^{(1)}} G_{13}^0 e^{((S_1)^{(1)} - (p_{13})^{(1)})t} \leq G_{14}(t) \leq \frac{1}{(m_2)^{(1)}} G_{13}^0 e^{(S_1)^{(1)}t} \quad .383$$

$$\left(\frac{(a_{15})^{(1)} G_{13}^0}{(m_1)^{(1)}((S_1)^{(1)} - (p_{13})^{(1)} - (S_2)^{(1)})} \left[e^{((S_1)^{(1)} - (p_{13})^{(1)})t} - e^{-(S_2)^{(1)}t} \right] + G_{15}^0 e^{-(S_2)^{(1)}t} \leq G_{15}(t) \leq \frac{(a_{15})^{(1)} G_{13}^0}{(m_2)^{(1)}((S_1)^{(1)} - (a_{15})^{(1)})} \left[e^{(S_1)^{(1)}t} - e^{-(a_{15})^{(1)}t} \right] + G_{15}^0 e^{-(a_{15})^{(1)}t} \right) \quad .384$$

$$T_{13}^0 e^{(R_1)^{(1)}t} \leq T_{13}(t) \leq T_{13}^0 e^{((R_1)^{(1)} + (r_{13})^{(1)})t} \quad .385$$

$$\frac{1}{(\mu_1)^{(1)}} T_{13}^0 e^{(R_1)^{(1)}t} \leq T_{13}(t) \leq \frac{1}{(\mu_2)^{(1)}} T_{13}^0 e^{((R_1)^{(1)} + (r_{13})^{(1)})t} \quad .386$$

$$\frac{(b_{15})^{(1)} T_{13}^0}{(\mu_1)^{(1)}((R_1)^{(1)} - (b'_{15})^{(1)})} \left[e^{(R_1)^{(1)}t} - e^{-(b'_{15})^{(1)}t} \right] + T_{15}^0 e^{-(b'_{15})^{(1)}t} \leq T_{15}(t) \leq$$

$$\frac{(a_{15})^{(1)} T_{13}^0}{(\mu_2)^{(1)}((R_1)^{(1)} + (r_{13})^{(1)} + (R_2)^{(1)})} \left[e^{((R_1)^{(1)} + (r_{13})^{(1)})t} - e^{-(R_2)^{(1)}t} \right] + T_{15}^0 e^{-(R_2)^{(1)}t}$$

.387

Definition of $(S_1)^{(1)}, (S_2)^{(1)}, (R_1)^{(1)}, (R_2)^{(1)}$:-

Where $(S_1)^{(1)} = (a_{13})^{(1)}(m_2)^{(1)} - (a'_{13})^{(1)}$

$(S_2)^{(1)} = (a_{15})^{(1)} - (p_{15})^{(1)}$

$(R_1)^{(1)} = (b_{13})^{(1)}(\mu_2)^{(1)} - (b'_{13})^{(1)}$

$(R_2)^{(1)} = (b'_{15})^{(1)} - (r_{15})^{(1)}$.388

Behavior of the solutions

If we denote and define.389

Definition of $(\sigma_1)^{(2)}, (\sigma_2)^{(2)}, (\tau_1)^{(2)}, (\tau_2)^{(2)}$:

$\sigma_1^{(2)}, (\sigma_2)^{(2)}, (\tau_1)^{(2)}, (\tau_2)^{(2)}$ four constants satisfying.390

$$-(\sigma_2)^{(2)} \leq -(a'_{16})^{(2)} + (a'_{17})^{(2)} - (a''_{16})^{(2)}(T_{17}, t) + (a''_{17})^{(2)}(T_{17}, t) \leq -(\sigma_1)^{(2)} \quad .391$$

$$-(\tau_2)^{(2)} \leq -(b'_{16})^{(2)} + (b'_{17})^{(2)} - (b''_{16})^{(2)}((G_{19}), t) - (b''_{17})^{(2)}((G_{19}), t) \leq -(\tau_1)^{(2)} \quad .392$$

Definition of $(v_1)^{(2)}, (v_2)^{(2)}, (u_1)^{(2)}, (u_2)^{(2)}$:.393

By $(v_1)^{(2)} > 0, (v_2)^{(2)} < 0$ and respectively $(u_1)^{(2)} > 0, (u_2)^{(2)} < 0$ the roots.394

of the equations $(a_{17})^{(2)}(v^{(2)})^2 + (\sigma_1)^{(2)}v^{(2)} - (a_{16})^{(2)} = 0$.395

and $(b_{14})^{(2)}(u^{(2)})^2 + (\tau_1)^{(2)}u^{(2)} - (b_{16})^{(2)} = 0$ and.396

Definition of $(\bar{v}_1)^{(2)}, (\bar{v}_2)^{(2)}, (\bar{u}_1)^{(2)}, (\bar{u}_2)^{(2)}$:.397

By $(\bar{v}_1)^{(2)} > 0, (\bar{v}_2)^{(2)} < 0$ and respectively $(\bar{u}_1)^{(2)} > 0, (\bar{u}_2)^{(2)} < 0$ the.398

roots of the equations $(a_{17})^{(2)}(v^{(2)})^2 + (\sigma_2)^{(2)}v^{(2)} - (a_{16})^{(2)} = 0$.399

and $(b_{17})^{(2)}(u^{(2)})^2 + (\tau_2)^{(2)}u^{(2)} - (b_{16})^{(2)} = 0$.400

Definition of $(m_1)^{(2)}, (m_2)^{(2)}, (\mu_1)^{(2)}, (\mu_2)^{(2)}$:- .401

If we define $(m_1)^{(2)}, (m_2)^{(2)}, (\mu_1)^{(2)}, (\mu_2)^{(2)}$ by .402

$(m_2)^{(2)} = (v_0)^{(2)}, (m_1)^{(2)} = (v_1)^{(2)}$, **if** $(v_0)^{(2)} < (v_1)^{(2)}$.403

$(m_2)^{(2)} = (v_1)^{(2)}, (m_1)^{(2)} = (\bar{v}_1)^{(2)}$, **if** $(v_1)^{(2)} < (v_0)^{(2)} < (\bar{v}_1)^{(2)}$,

and $(v_0)^{(2)} = \frac{G_{16}^0}{G_{17}^0}$.404

$(m_2)^{(2)} = (v_1)^{(2)}, (m_1)^{(2)} = (v_0)^{(2)}$, **if** $(\bar{v}_1)^{(2)} < (v_0)^{(2)}$.405

and analogously

$(\mu_2)^{(2)} = (u_0)^{(2)}, (\mu_1)^{(2)} = (u_1)^{(2)}$, **if** $(u_0)^{(2)} < (u_1)^{(2)}$

$(\mu_2)^{(2)} = (u_1)^{(2)}, (\mu_1)^{(2)} = (\bar{u}_1)^{(2)}$, **if** $(u_1)^{(2)} < (u_0)^{(2)} < (\bar{u}_1)^{(2)}$,

and $(u_0)^{(2)} = \frac{T_{16}^0}{T_{17}^0}$.406

$(\mu_2)^{(2)} = (u_1)^{(2)}, (\mu_1)^{(2)} = (u_0)^{(2)}$, **if** $(\bar{u}_1)^{(2)} < (u_0)^{(2)}$.407

Then the solution satisfies the inequalities

$$G_{16}^0 e^{(S_1)^{(2)} - (p_{16})^{(2)}t} \leq G_{16}(t) \leq G_{16}^0 e^{(S_1)^{(2)}t} .408$$

$(p_i)^{(2)}$ is defined .409

$$\frac{1}{(m_1)^{(2)}} G_{16}^0 e^{((S_1)^{(2)} - (p_{16})^{(2)})t} \leq G_{17}(t) \leq \frac{1}{(m_2)^{(2)}} G_{16}^0 e^{(S_1)^{(2)}t} .410$$

$$\left(\frac{(a_{18})^{(2)} G_{16}^0}{(m_1)^{(2)}((S_1)^{(2)} - (p_{16})^{(2)} - (S_2)^{(2)})} \left[e^{((S_1)^{(2)} - (p_{16})^{(2)})t} - e^{-(S_2)^{(2)}t} \right] + G_{18}^0 e^{-(S_2)^{(2)}t} \leq G_{18}(t) \leq \frac{(a_{18})^{(2)} G_{16}^0}{(m_2)^{(2)}((S_1)^{(2)} - (a_{18})^{(2)})} \left[e^{(S_1)^{(2)}t} - e^{-(a_{18})^{(2)}t} \right] + G_{18}^0 e^{-(a_{18})^{(2)}t} \right) .411$$

$$T_{16}^0 e^{(R_1)^{(2)}t} \leq T_{16}(t) \leq T_{16}^0 e^{((R_1)^{(2)} + (r_{16})^{(2)})t} .412$$

$$\frac{1}{(\mu_1)^{(2)}} T_{16}^0 e^{(R_1)^{(2)}t} \leq T_{17}(t) \leq \frac{1}{(\mu_2)^{(2)}} T_{16}^0 e^{((R_1)^{(2)} + (r_{16})^{(2)})t} .413$$

$$\frac{(b_{18})^{(2)} T_{16}^0}{(\mu_1)^{(2)}((R_1)^{(2)} - (b_{18})^{(2)})} \left[e^{(R_1)^{(2)}t} - e^{-(b_{18})^{(2)}t} \right] + T_{18}^0 e^{-(b_{18})^{(2)}t} \leq T_{18}(t) \leq$$

$$\frac{(a_{18})^{(2)} T_{16}^0}{(\mu_2)^{(2)}((R_1)^{(2)} + (r_{16})^{(2)} + (R_2)^{(2)})} \left[e^{((R_1)^{(2)} + (r_{16})^{(2)})t} - e^{-(R_2)^{(2)}t} \right] + T_{18}^0 e^{-(R_2)^{(2)}t} .414$$

Definition of $(S_1)^{(2)}, (S_2)^{(2)}, (R_1)^{(2)}, (R_2)^{(2)}$:- .415

Where $(S_1)^{(2)} = (a_{16})^{(2)}(m_2)^{(2)} - (a'_{16})^{(2)}$

$(S_2)^{(2)} = (a_{18})^{(2)} - (p_{18})^{(2)}$.416

$(R_1)^{(2)} = (b_{16})^{(2)}(\mu_2)^{(1)} - (b'_{16})^{(2)}$

$(R_2)^{(2)} = (b_{18})^{(2)} - (r_{18})^{(2)}$.417

.418

Behavior of the solutions

If we denote and define

Definition of $(\sigma_1)^{(3)}, (\sigma_2)^{(3)}, (\tau_1)^{(3)}, (\tau_2)^{(3)}$:

(a) $\sigma_1^{(3)}, \sigma_2^{(3)}, \tau_1^{(3)}, \tau_2^{(3)}$ four constants satisfying

$$-(\sigma_2)^{(3)} \leq -(a'_{20})^{(3)} + (a'_{21})^{(3)} - (a''_{20})^{(3)}(T_{21}, t) + (a''_{21})^{(3)}(T_{21}, t) \leq -(\sigma_1)^{(3)}$$

$$-(\tau_2)^{(3)} \leq -(b'_{20})^{(3)} + (b'_{21})^{(3)} - (b''_{20})^{(3)}(G, t) - (b''_{21})^{(3)}((G_{23}), t) \leq -(\tau_1)^{(3)} .419$$

Definition of $(v_1)^{(3)}, (v_2)^{(3)}, (u_1)^{(3)}, (u_2)^{(3)}$:

(b) By $(v_1)^{(3)} > 0, (v_2)^{(3)} < 0$ and respectively $(u_1)^{(3)} > 0, (u_2)^{(3)} < 0$ the roots of the equations $(a_{21})^{(3)}(v^{(3)})^2 + (\sigma_1)^{(3)}v^{(3)} - (a_{20})^{(3)} = 0$

and $(b_{21})^{(3)}(u^{(3)})^2 + (\tau_1)^{(3)}u^{(3)} - (b_{20})^{(3)} = 0$ and

By $(\bar{v}_1)^{(3)} > 0, (\bar{v}_2)^{(3)} < 0$ and respectively $(\bar{u}_1)^{(3)} > 0, (\bar{u}_2)^{(3)} < 0$ the

roots of the equations $(a_{21})^{(3)}(v^{(3)})^2 + (\sigma_2)^{(3)}v^{(3)} - (a_{20})^{(3)} = 0$

and $(b_{21})^{(3)}(u^{(3)})^2 + (\tau_2)^{(3)}u^{(3)} - (b_{20})^{(3)} = 0$.420

Definition of $(m_1)^{(3)}, (m_2)^{(3)}, (\mu_1)^{(3)}, (\mu_2)^{(3)}$:-

(c) If we define $(m_1)^{(3)}, (m_2)^{(3)}, (\mu_1)^{(3)}, (\mu_2)^{(3)}$ by

$(m_2)^{(3)} = (v_0)^{(3)}, (m_1)^{(3)} = (v_1)^{(3)}$, **if** $(v_0)^{(3)} < (v_1)^{(3)}$

$(m_2)^{(3)} = (v_1)^{(3)}, (m_1)^{(3)} = (\bar{v}_1)^{(3)}$, **if** $(v_1)^{(3)} < (v_0)^{(3)} < (\bar{v}_1)^{(3)}$,

and $(v_0)^{(3)} = \frac{G_{20}^0}{G_{21}^0}$

$(m_2)^{(3)} = (v_1)^{(3)}, (m_1)^{(3)} = (v_0)^{(3)}$, **if** $(\bar{v}_1)^{(3)} < (v_0)^{(3)}$.421

and analogously

$(\mu_2)^{(3)} = (u_0)^{(3)}, (\mu_1)^{(3)} = (u_1)^{(3)}$, **if** $(u_0)^{(3)} < (u_1)^{(3)}$

$$(\mu_2)^{(3)} = (u_1)^{(3)}, (\mu_1)^{(3)} = (\bar{u}_1)^{(3)}, \text{ if } (u_1)^{(3)} < (u_0)^{(3)} < (\bar{u}_1)^{(3)}, \text{ and } (u_0)^{(3)} = \frac{T_{20}^0}{T_{21}^0}$$

$$(\mu_2)^{(3)} = (u_1)^{(3)}, (\mu_1)^{(3)} = (u_0)^{(3)}, \text{ if } (\bar{u}_1)^{(3)} < (u_0)^{(3)}$$

Then the solution satisfies the inequalities

$$G_{20}^0 e^{((S_1)^{(3)} - (p_{20})^{(3)})t} \leq G_{20}(t) \leq G_{20}^0 e^{(S_1)^{(3)}t} \quad (p_i)^{(3)} \text{ is defined .422}$$

.423

$$\frac{1}{(m_1)^{(3)}} G_{20}^0 e^{((S_1)^{(3)} - (p_{20})^{(3)})t} \leq G_{21}(t) \leq \frac{1}{(m_2)^{(3)}} G_{20}^0 e^{(S_1)^{(3)}t} \quad .424$$

$$\left(\frac{(a_{22})^{(3)} G_{20}^0}{(m_1)^{(3)} ((S_1)^{(3)} - (p_{20})^{(3)} - (S_2)^{(3)})} \left[e^{((S_1)^{(3)} - (p_{20})^{(3)})t} - e^{-(S_2)^{(3)}t} \right] + G_{22}^0 e^{-(S_2)^{(3)}t} \leq G_{22}(t) \leq \frac{(a_{22})^{(3)} G_{20}^0}{(m_2)^{(3)} ((S_1)^{(3)} - (a'_{22})^{(3)})} \left[e^{(S_1)^{(3)}t} - e^{-(a'_{22})^{(3)}t} \right] + G_{22}^0 e^{-(a'_{22})^{(3)}t} \right) \quad .425$$

$$\boxed{T_{20}^0 e^{(R_1)^{(3)}t} \leq T_{20}(t) \leq T_{20}^0 e^{((R_1)^{(3)} + (r_{20})^{(3)})t}} \quad .426$$

$$\frac{1}{(\mu_1)^{(3)}} T_{20}^0 e^{(R_1)^{(3)}t} \leq T_{20}(t) \leq \frac{1}{(\mu_2)^{(3)}} T_{20}^0 e^{((R_1)^{(3)} + (r_{20})^{(3)})t} \quad .427$$

$$\frac{(b_{22})^{(3)} T_{20}^0}{(\mu_1)^{(3)} ((R_1)^{(3)} - (b'_{22})^{(3)})} \left[e^{(R_1)^{(3)}t} - e^{-(b'_{22})^{(3)}t} \right] + T_{22}^0 e^{-(b'_{22})^{(3)}t} \leq T_{22}(t) \leq$$

$$\frac{(a_{22})^{(3)} T_{20}^0}{(\mu_2)^{(3)} ((R_1)^{(3)} + (r_{20})^{(3)} + (R_2)^{(3)})} \left[e^{((R_1)^{(3)} + (r_{20})^{(3)})t} - e^{-(R_2)^{(3)}t} \right] + T_{22}^0 e^{-(R_2)^{(3)}t} \quad .428$$

Definition of $(S_1)^{(3)}, (S_2)^{(3)}, (R_1)^{(3)}, (R_2)^{(3)}$:-

$$\text{Where } (S_1)^{(3)} = (a_{20})^{(3)} (m_2)^{(3)} - (a'_{20})^{(3)}$$

$$(S_2)^{(3)} = (a_{22})^{(3)} - (p_{22})^{(3)}$$

$$(R_1)^{(3)} = (b_{20})^{(3)} (\mu_2)^{(3)} - (b'_{20})^{(3)}$$

$$(R_2)^{(3)} = (b_{22})^{(3)} - (r_{22})^{(3)} \quad .429$$

.430

.431

Behavior of the solutions

432

If we denote and define

Definition of $(\sigma_1)^{(4)}, (\sigma_2)^{(4)}, (\tau_1)^{(4)}, (\tau_2)^{(4)}$:

(d) $(\sigma_1)^{(4)}, (\sigma_2)^{(4)}, (\tau_1)^{(4)}, (\tau_2)^{(4)}$ four constants satisfying

$$-(\sigma_2)^{(4)} \leq -(a'_{24})^{(4)} + (a'_{25})^{(4)} - (a''_{24})^{(4)}(T_{25}, t) + (a''_{25})^{(4)}(T_{25}, t) \leq -(\sigma_1)^{(4)}$$

$$-(\tau_2)^{(4)} \leq -(b'_{24})^{(4)} + (b'_{25})^{(4)} - (b''_{24})^{(4)}((G_{27}), t) - (b''_{25})^{(4)}((G_{27}), t) \leq -(\tau_1)^{(4)}$$

Definition of $(v_1)^{(4)}, (v_2)^{(4)}, (u_1)^{(4)}, (u_2)^{(4)}, v^{(4)}, u^{(4)}$:

433

(e) By $(v_1)^{(4)} > 0, (v_2)^{(4)} < 0$ and respectively $(u_1)^{(4)} > 0, (u_2)^{(4)} < 0$ the roots of the equations

$$(a_{25})^{(4)} (v^{(4)})^2 + (\sigma_1)^{(4)} v^{(4)} - (a_{24})^{(4)} = 0$$

$$\text{and } (b_{25})^{(4)} (u^{(4)})^2 + (\tau_1)^{(4)} u^{(4)} - (b_{24})^{(4)} = 0 \text{ and}$$

Definition of $(\bar{v}_1)^{(4)}, (\bar{v}_2)^{(4)}, (\bar{u}_1)^{(4)}, (\bar{u}_2)^{(4)}$:

434

435

By $(\bar{v}_1)^{(4)} > 0, (\bar{v}_2)^{(4)} < 0$ and respectively $(\bar{u}_1)^{(4)} > 0, (\bar{u}_2)^{(4)} < 0$ the

roots of the equations $(a_{25})^{(4)} (v^{(4)})^2 + (\sigma_2)^{(4)} v^{(4)} - (a_{24})^{(4)} = 0$

and $(b_{25})^{(4)} (u^{(4)})^2 + (\tau_2)^{(4)} u^{(4)} - (b_{24})^{(4)} = 0$

436

Definition of $(m_1)^{(4)}, (m_2)^{(4)}, (\mu_1)^{(4)}, (\mu_2)^{(4)}, (v_0)^{(4)}$:-

(f) If we define $(m_1)^{(4)}, (m_2)^{(4)}, (\mu_1)^{(4)}, (\mu_2)^{(4)}$ by

$$(m_2)^{(4)} = (v_0)^{(4)}, (m_1)^{(4)} = (v_1)^{(4)}, \text{ if } (v_0)^{(4)} < (v_1)^{(4)}$$

$$(m_2)^{(4)} = (v_1)^{(4)}, (m_1)^{(4)} = (\bar{v}_1)^{(4)}, \text{ if } (v_4)^{(4)} < (v_0)^{(4)} < (\bar{v}_1)^{(4)},$$

$$\text{and } (v_0)^{(4)} = \frac{G_{24}^0}{G_{25}^0}$$

$$(m_2)^{(4)} = (v_4)^{(4)}, (m_1)^{(4)} = (v_0)^{(4)}, \text{ if } (\bar{v}_4)^{(4)} < (v_0)^{(4)}$$

and analogously

437
438

$$(\mu_2)^{(4)} = (u_0)^{(4)}, (\mu_1)^{(4)} = (u_1)^{(4)}, \text{ if } (u_0)^{(4)} < (u_1)^{(4)}$$

$$(\mu_2)^{(4)} = (u_1)^{(4)}, (\mu_1)^{(4)} = (\bar{u}_1)^{(4)}, \text{ if } (u_1)^{(4)} < (u_0)^{(4)} < (\bar{u}_1)^{(4)},$$

$$\text{and } (u_0)^{(4)} = \frac{T_{24}^0}{T_{25}^0}$$

$(\mu_2)^{(4)} = (u_1)^{(4)}, (\mu_1)^{(4)} = (u_0)^{(4)}, \text{ if } (\bar{u}_1)^{(4)} < (u_0)^{(4)}$ where $(u_1)^{(4)}, (\bar{u}_1)^{(4)}$ are defined by 59 and 64 respectively

Then the solution satisfies the inequalities

439
440
441
442
443
444
445

$$G_{24}^0 e^{((S_1)^{(4)} - (p_{24})^{(4)})t} \leq G_{24}(t) \leq G_{24}^0 e^{(S_1)^{(4)}t}$$

where $(p_i)^{(4)}$ is defined

$$\frac{1}{(m_1)^{(4)}} G_{24}^0 e^{((S_1)^{(4)} - (p_{24})^{(4)})t} \leq G_{25}(t) \leq \frac{1}{(m_2)^{(4)}} G_{24}^0 e^{(S_1)^{(4)}t}$$

446
447

$$\left(\frac{(a_{26})^{(4)} G_{24}^0}{(m_1)^{(4)} ((S_1)^{(4)} - (p_{24})^{(4)}) - (S_2)^{(4)}} \right) \left[e^{((S_1)^{(4)} - (p_{24})^{(4)})t} - e^{-(S_2)^{(4)}t} \right] + G_{26}^0 e^{-(S_2)^{(4)}t} \leq G_{26}(t) \leq (a_{26})^{(4)} G_{24}^0 (m_2)^{(4)} (S_1)^{(4)} - (a_{26}')^{(4)} 4e^{(S_1)^{(4)}t} - e^{-(a_{26}')^{(4)}t} + G_{26}^0 e^{-(a_{26}')^{(4)}t}$$

448

$$T_{24}^0 e^{(R_1)^{(4)}t} \leq T_{24}(t) \leq T_{24}^0 e^{((R_1)^{(4)} + (r_{24})^{(4)})t}$$

449

$$\frac{1}{(\mu_1)^{(4)}} T_{24}^0 e^{(R_1)^{(4)}t} \leq T_{24}(t) \leq \frac{1}{(\mu_2)^{(4)}} T_{24}^0 e^{((R_1)^{(4)} + (r_{24})^{(4)})t}$$

450

$$\frac{(b_{26})^{(4)} T_{24}^0}{(\mu_1)^{(4)} ((R_1)^{(4)} - (b_{26}')^{(4)})} \left[e^{(R_1)^{(4)}t} - e^{-(b_{26}')^{(4)}t} \right] + T_{26}^0 e^{-(b_{26}')^{(4)}t} \leq T_{26}(t) \leq$$

451

$$\frac{(a_{26})^{(4)} T_{24}^0}{(\mu_2)^{(4)} ((R_1)^{(4)} + (r_{24})^{(4)} + (R_2)^{(4)})} \left[e^{((R_1)^{(4)} + (r_{24})^{(4)})t} - e^{-(R_2)^{(4)}t} \right] + T_{26}^0 e^{-(R_2)^{(4)}t}$$

Definition of $(S_1)^{(4)}, (S_2)^{(4)}, (R_1)^{(4)}, (R_2)^{(4)}$:-

452

$$\text{Where } (S_1)^{(4)} = (a_{24})^{(4)} (m_2)^{(4)} - (a_{24}')^{(4)}$$

$$(S_2)^{(4)} = (a_{26})^{(4)} - (p_{26})^{(4)}$$

$$(R_1)^{(4)} = (b_{24})^{(4)} (\mu_2)^{(4)} - (b_{24}')^{(4)}$$

$$(R_2)^{(4)} = (b_{26}')^{(4)} - (r_{26})^{(4)}$$

453

Behavior of the solutions

454

If we denote and define

Definition of $(\sigma_1)^{(5)}, (\sigma_2)^{(5)}, (\tau_1)^{(5)}, (\tau_2)^{(5)}$:

(g) $(\sigma_1)^{(5)}, (\sigma_2)^{(5)}, (\tau_1)^{(5)}, (\tau_2)^{(5)}$ four constants satisfying

$$-(\sigma_2)^{(5)} \leq -(a_{28}')^{(5)} + (a_{29}')^{(5)} - (a_{28}'')^{(5)} (T_{29}, t) + (a_{29}'')^{(5)} (T_{29}, t) \leq -(\sigma_1)^{(5)}$$

$$-(\tau_2)^{(5)} \leq -(b_{28}')^{(5)} + (b_{29}')^{(5)} - (b_{28}'')^{(5)} ((G_{31}), t) - (b_{29}'')^{(5)} ((G_{31}), t) \leq -(\tau_1)^{(5)}$$

Definition of $(v_1)^{(5)}, (v_2)^{(5)}, (u_1)^{(5)}, (u_2)^{(5)}, v^{(5)}, u^{(5)}$:

455

(h) By $(v_1)^{(5)} > 0, (v_2)^{(5)} < 0$ and respectively $(u_1)^{(5)} > 0, (u_2)^{(5)} < 0$ the roots of the equations
 $(a_{29})^{(5)}(v^{(5)})^2 + (\sigma_1)^{(5)}v^{(5)} - (a_{28})^{(5)} = 0$
 and $(b_{29})^{(5)}(u^{(5)})^2 + (\tau_1)^{(5)}u^{(5)} - (b_{28})^{(5)} = 0$ and

Definition of $(\bar{v}_1)^{(5)}, (\bar{v}_2)^{(5)}, (\bar{u}_1)^{(5)}, (\bar{u}_2)^{(5)}$: 456

By $(\bar{v}_1)^{(5)} > 0, (\bar{v}_2)^{(5)} < 0$ and respectively $(\bar{u}_1)^{(5)} > 0, (\bar{u}_2)^{(5)} < 0$ the roots of the equations $(a_{29})^{(5)}(v^{(5)})^2 + (\sigma_2)^{(5)}v^{(5)} - (a_{28})^{(5)} = 0$
 and $(b_{29})^{(5)}(u^{(5)})^2 + (\tau_2)^{(5)}u^{(5)} - (b_{28})^{(5)} = 0$

Definition of $(m_1)^{(5)}, (m_2)^{(5)}, (\mu_1)^{(5)}, (\mu_2)^{(5)}, (v_0)^{(5)}$:-

(i) If we define $(m_1)^{(5)}, (m_2)^{(5)}, (\mu_1)^{(5)}, (\mu_2)^{(5)}$ by

$$(m_2)^{(5)} = (v_0)^{(5)}, (m_1)^{(5)} = (v_1)^{(5)}, \text{ if } (v_0)^{(5)} < (v_1)^{(5)}$$

$$(m_2)^{(5)} = (v_1)^{(5)}, (m_1)^{(5)} = (\bar{v}_1)^{(5)}, \text{ if } (v_1)^{(5)} < (v_0)^{(5)} < (\bar{v}_1)^{(5)},$$

and $\boxed{(v_0)^{(5)} = \frac{G_{28}^0}{G_{29}^0}}$

$$(m_2)^{(5)} = (v_1)^{(5)}, (m_1)^{(5)} = (v_0)^{(5)}, \text{ if } (\bar{v}_1)^{(5)} < (v_0)^{(5)}$$

and analogously 457

$$(\mu_2)^{(5)} = (u_0)^{(5)}, (\mu_1)^{(5)} = (u_1)^{(5)}, \text{ if } (u_0)^{(5)} < (u_1)^{(5)}$$

$$(\mu_2)^{(5)} = (u_1)^{(5)}, (\mu_1)^{(5)} = (\bar{u}_1)^{(5)}, \text{ if } (u_1)^{(5)} < (u_0)^{(5)} < (\bar{u}_1)^{(5)},$$

and $\boxed{(u_0)^{(5)} = \frac{T_{28}^0}{T_{29}^0}}$

$(\mu_2)^{(5)} = (u_1)^{(5)}, (\mu_1)^{(5)} = (u_0)^{(5)}, \text{ if } (\bar{u}_1)^{(5)} < (u_0)^{(5)}$ where $(u_1)^{(5)}, (\bar{u}_1)^{(5)}$ are defined respectively

Then the solution satisfies the inequalities 458

$$G_{28}^0 e^{((s_1)^{(5)} - (p_{28})^{(5)})t} \leq G_{28}(t) \leq G_{28}^0 e^{(s_1)^{(5)}t}$$

where $(p_i)^{(5)}$ is defined

$$\frac{1}{(m_5)^{(5)}} G_{28}^0 e^{((s_1)^{(5)} - (p_{28})^{(5)})t} \leq G_{29}(t) \leq \frac{1}{(m_2)^{(5)}} G_{28}^0 e^{(s_1)^{(5)}t} \quad 459$$

$$\left(\frac{(a_{30})^{(5)} G_{28}^0}{(m_1)^{(5)} ((s_1)^{(5)} - (p_{28})^{(5)} - (s_2)^{(5)})} \left[e^{((s_1)^{(5)} - (p_{28})^{(5)})t} - e^{-(s_2)^{(5)}t} \right] + G_{30}^0 e^{-(s_2)^{(5)}t} \right) \leq G_{30}(t) \leq \quad 460$$

$$(a_{30})^{(5)} G_{28}^0 (m_2)^{(5)} (s_1)^{(5)} - (a_{30})^{(5)} 5e^{(s_1)^{(5)}t} - e^{-(a_{30})^{(5)}t} + G_{30}^0 e^{-(a_{30})^{(5)}t} \quad 461$$

$$\boxed{T_{28}^0 e^{(R_1)^{(5)}t} \leq T_{28}(t) \leq T_{28}^0 e^{((R_1)^{(5)} + (r_{28})^{(5)})t}} \quad 462$$

$$\frac{1}{(\mu_1)^{(5)}} T_{28}^0 e^{(R_1)^{(5)}t} \leq T_{28}(t) \leq \frac{1}{(\mu_2)^{(5)}} T_{28}^0 e^{((R_1)^{(5)} + (r_{28})^{(5)})t} \quad 463$$

$$\frac{(b_{30})^{(5)} T_{28}^0}{(\mu_1)^{(5)} ((R_1)^{(5)} - (b_{30})^{(5)})} \left[e^{(R_1)^{(5)}t} - e^{-(b_{30})^{(5)}t} \right] + T_{30}^0 e^{-(b_{30})^{(5)}t} \leq T_{30}(t) \leq \quad 464$$

$$\frac{(a_{30})^{(5)} T_{28}^0}{(\mu_2)^{(5)} ((R_1)^{(5)} + (r_{28})^{(5)} + (R_2)^{(5)})} \left[e^{((R_1)^{(5)} + (r_{28})^{(5)})t} - e^{-(R_2)^{(5)}t} \right] + T_{30}^0 e^{-(R_2)^{(5)}t}$$

Definition of $(S_1)^{(5)}, (S_2)^{(5)}, (R_1)^{(5)}, (R_2)^{(5)}$:- 465

Where $(S_1)^{(5)} = (a_{28})^{(5)}(m_2)^{(5)} - (a'_{28})^{(5)}$

$$(S_2)^{(5)} = (a_{30})^{(5)} - (p_{30})^{(5)}$$

$$(R_1)^{(5)} = (b_{28})^{(5)}(\mu_2)^{(5)} - (b'_{28})^{(5)}$$

$$(R_2)^{(5)} = (b'_{30})^{(5)} - (r_{30})^{(5)}$$

Behavior of the solutions

466

If we denote and define

Definition of $(\sigma_1)^{(6)}, (\sigma_2)^{(6)}, (\tau_1)^{(6)}, (\tau_2)^{(6)}$:

- (j) $(\sigma_1)^{(6)}, (\sigma_2)^{(6)}, (\tau_1)^{(6)}, (\tau_2)^{(6)}$ four constants satisfying
- $$-(\sigma_2)^{(6)} \leq -(a'_{32})^{(6)} + (a'_{33})^{(6)} - (a''_{32})^{(6)}(T_{33}, t) + (a''_{33})^{(6)}(T_{33}, t) \leq -(\sigma_1)^{(6)}$$
- $$-(\tau_2)^{(6)} \leq -(b'_{32})^{(6)} + (b'_{33})^{(6)} - (b''_{32})^{(6)}((G_{35}), t) - (b''_{33})^{(6)}((G_{35}), t) \leq -(\tau_1)^{(6)}$$

Definition of $(v_1)^{(6)}, (v_2)^{(6)}, (u_1)^{(6)}, (u_2)^{(6)}, v^{(6)}, u^{(6)}$:

467

- (k) By $(v_1)^{(6)} > 0, (v_2)^{(6)} < 0$ and respectively $(u_1)^{(6)} > 0, (u_2)^{(6)} < 0$ the roots of the equations
- $$(a_{33})^{(6)}(v^{(6)})^2 + (\sigma_1)^{(6)}v^{(6)} - (a_{32})^{(6)} = 0$$
- and $(b_{33})^{(6)}(u^{(6)})^2 + (\tau_1)^{(6)}u^{(6)} - (b_{32})^{(6)} = 0$ and

Definition of $(\bar{v}_1)^{(6)}, (\bar{v}_2)^{(6)}, (\bar{u}_1)^{(6)}, (\bar{u}_2)^{(6)}$:

468

By $(\bar{v}_1)^{(6)} > 0, (\bar{v}_2)^{(6)} < 0$ and respectively $(\bar{u}_1)^{(6)} > 0, (\bar{u}_2)^{(6)} < 0$ the roots of the equations $(a_{33})^{(6)}(v^{(6)})^2 + (\sigma_2)^{(6)}v^{(6)} - (a_{32})^{(6)} = 0$ and $(b_{33})^{(6)}(u^{(6)})^2 + (\tau_2)^{(6)}u^{(6)} - (b_{32})^{(6)} = 0$

Definition of $(m_1)^{(6)}, (m_2)^{(6)}, (\mu_1)^{(6)}, (\mu_2)^{(6)}, (v_0)^{(6)}$:-

- (l) If we define $(m_1)^{(6)}, (m_2)^{(6)}, (\mu_1)^{(6)}, (\mu_2)^{(6)}$ by

$$(m_2)^{(6)} = (v_0)^{(6)}, (m_1)^{(6)} = (v_1)^{(6)}, \text{ if } (v_0)^{(6)} < (v_1)^{(6)}$$

470

$$(m_2)^{(6)} = (v_1)^{(6)}, (m_1)^{(6)} = (\bar{v}_6)^{(6)}, \text{ if } (v_1)^{(6)} < (v_0)^{(6)} < (\bar{v}_1)^{(6)},$$

$$\text{and } \boxed{(v_0)^{(6)} = \frac{G_{32}^0}{G_{33}^0}}$$

$$(m_2)^{(6)} = (v_1)^{(6)}, (m_1)^{(6)} = (v_0)^{(6)}, \text{ if } (\bar{v}_1)^{(6)} < (v_0)^{(6)}$$

and analogously

471

$$(\mu_2)^{(6)} = (u_0)^{(6)}, (\mu_1)^{(6)} = (u_1)^{(6)}, \text{ if } (u_0)^{(6)} < (u_1)^{(6)}$$

$$(\mu_2)^{(6)} = (u_1)^{(6)}, (\mu_1)^{(6)} = (\bar{u}_1)^{(6)}, \text{ if } (u_1)^{(6)} < (u_0)^{(6)} < (\bar{u}_1)^{(6)},$$

$$\text{and } \boxed{(u_0)^{(6)} = \frac{T_{32}^0}{T_{33}^0}}$$

$(\mu_2)^{(6)} = (u_1)^{(6)}, (\mu_1)^{(6)} = (u_0)^{(6)}, \text{ if } (\bar{u}_1)^{(6)} < (u_0)^{(6)}$ where $(u_1)^{(6)}, (\bar{u}_1)^{(6)}$ are defined respectively

Then the solution satisfies the inequalities

472

$$G_{32}^0 e^{((S_1)^{(6)} - (p_{32})^{(6)})t} \leq G_{32}(t) \leq G_{32}^0 e^{(S_1)^{(6)}t}$$

where $(p_i)^{(6)}$ is defined

$$\frac{1}{(m_1)^{(6)}} G_{32}^0 e^{((S_1)^{(6)} - (p_{32})^{(6)})t} \leq G_{33}(t) \leq \frac{1}{(m_2)^{(6)}} G_{32}^0 e^{(S_1)^{(6)}t}$$

473

$$\left(\frac{(a_{34})^{(6)} G_{32}^0}{(m_1)^{(6)}((S_1)^{(6)} - (p_{32})^{(6)} - (S_2)^{(6)})} \left[e^{((S_1)^{(6)} - (p_{32})^{(6)})t} - e^{-(S_2)^{(6)}t} \right] + G_{34}^0 e^{-(S_2)^{(6)}t} \leq G_{34}(t) \leq \right. \\ \left. (a_{34})^{(6)} G_{32}^0 (m_2)^{(6)} (S_1)^{(6)} - (a_{34}')^{(6)} e^{(S_1)^{(6)}t} - e^{-(a_{34}')^{(6)}t} + G_{34}^0 e^{-(a_{34}')^{(6)}t} \right] \leq G_{34}(t) \leq$$

$$\boxed{T_{32}^0 e^{(R_1)^{(6)}t} \leq T_{32}(t) \leq T_{32}^0 e^{((R_1)^{(6)} + (r_{32})^{(6)})t} \quad 475}$$

$$\frac{1}{(\mu_1)^{(6)}} T_{32}^0 e^{(R_1)^{(6)}t} \leq T_{32}(t) \leq \frac{1}{(\mu_2)^{(6)}} T_{32}^0 e^{((R_1)^{(6)} + (r_{32})^{(6)})t} \quad 476}$$

$$\frac{(b_{34})^{(6)} T_{32}^0}{(\mu_1)^{(6)}((R_1)^{(6)} - (b_{34})^{(6)})} \left[e^{(R_1)^{(6)}t} - e^{-(b_{34}')^{(6)}t} \right] + T_{34}^0 e^{-(b_{34}')^{(6)}t} \leq T_{34}(t) \leq \quad 477}$$

$$\frac{(a_{34})^{(6)} T_{32}^0}{(\mu_2)^{(6)}((R_1)^{(6)} + (r_{32})^{(6)} + (R_2)^{(6)})} \left[e^{((R_1)^{(6)} + (r_{32})^{(6)})t} - e^{-(R_2)^{(6)}t} \right] + T_{34}^0 e^{-(R_2)^{(6)}t}$$

Definition of $(S_1)^{(6)}, (S_2)^{(6)}, (R_1)^{(6)}, (R_2)^{(6)}$:- 478

Where $(S_1)^{(6)} = (a_{32})^{(6)}(m_2)^{(6)} - (a_{32}')^{(6)}$

$$(S_2)^{(6)} = (a_{34})^{(6)} - (p_{34})^{(6)}$$

$$(R_1)^{(6)} = (b_{32})^{(6)}(\mu_2)^{(6)} - (b_{32}')^{(6)}$$

$$(R_2)^{(6)} = (b_{34}')^{(6)} - (r_{34})^{(6)}$$

Proof : From GLOBAL EQUATIONS we obtain 479

$$\frac{dv^{(1)}}{dt} = (a_{13})^{(1)} - \left((a_{13}')^{(1)} - (a_{14}')^{(1)} + (a_{13}'')^{(1)}(T_{14}, t) \right) - (a_{14}'')^{(1)}(T_{14}, t)v^{(1)} - (a_{14})^{(1)}v^{(1)} \quad 480$$

Definition of $v^{(1)}$:- $\boxed{v^{(1)} = \frac{G_{13}}{G_{14}}}$ 481

It follows

$$- \left((a_{14})^{(1)}(v^{(1)})^2 + (\sigma_2)^{(1)}v^{(1)} - (a_{13})^{(1)} \right) \leq \frac{dv^{(1)}}{dt} \leq - \left((a_{14})^{(1)}(v^{(1)})^2 + (\sigma_1)^{(1)}v^{(1)} - (a_{13})^{(1)} \right)$$

From which one obtains

Definition of $(\bar{v}_1)^{(1)}, (v_0)^{(1)}$:-

(a) For $0 < \boxed{(v_0)^{(1)} = \frac{G_{13}^0}{G_{14}^0}} < (v_1)^{(1)} < (\bar{v}_1)^{(1)}$

$$v^{(1)}(t) \geq \frac{(v_1)^{(1)} + (C)^{(1)}(v_2)^{(1)} e^{-(a_{14})^{(1)}(v_1)^{(1)} - (v_0)^{(1)}t}}{1 + (C)^{(1)} e^{-(a_{14})^{(1)}(v_1)^{(1)} - (v_0)^{(1)}t}}, \quad \boxed{(C)^{(1)} = \frac{(v_1)^{(1)} - (v_0)^{(1)}}{(v_0)^{(1)} - (v_2)^{(1)}}$$

it follows $(v_0)^{(1)} \leq v^{(1)}(t) \leq (v_1)^{(1)}$

In the same manner , we get 482

$$v^{(1)}(t) \leq \frac{(\bar{v}_1)^{(1)} + (\bar{C})^{(1)}(\bar{v}_2)^{(1)} e^{-(a_{14})^{(1)}((\bar{v}_1)^{(1)} - (\bar{v}_2)^{(1)})t}}{1 + (\bar{C})^{(1)} e^{-(a_{14})^{(1)}((\bar{v}_1)^{(1)} - (\bar{v}_2)^{(1)})t}}, \quad \boxed{(\bar{C})^{(1)} = \frac{(\bar{v}_1)^{(1)} - (v_0)^{(1)}}{(v_0)^{(1)} - (\bar{v}_2)^{(1)}}$$

From which we deduce $(v_0)^{(1)} \leq v^{(1)}(t) \leq (\bar{v}_1)^{(1)}$

(b) If $0 < (v_1)^{(1)} < (v_0)^{(1)} = \frac{G_{13}^0}{G_{14}^0} < (\bar{v}_1)^{(1)}$ we find like in the previous case, 483

$$(v_1)^{(1)} \leq \frac{(v_1)^{(1)} + (C)^{(1)}(v_2)^{(1)} e^{-(a_{14})^{(1)}(v_1)^{(1)} - (v_2)^{(1)}t}}{1 + (C)^{(1)} e^{-(a_{14})^{(1)}(v_1)^{(1)} - (v_2)^{(1)}t}} \leq v^{(1)}(t) \leq \\ \frac{(\bar{v}_1)^{(1)} + (\bar{C})^{(1)}(\bar{v}_2)^{(1)} e^{-(a_{14})^{(1)}((\bar{v}_1)^{(1)} - (\bar{v}_2)^{(1)})t}}{1 + (\bar{C})^{(1)} e^{-(a_{14})^{(1)}((\bar{v}_1)^{(1)} - (\bar{v}_2)^{(1)})t}} \leq (\bar{v}_1)^{(1)}$$

(c) If $0 < (v_1)^{(1)} \leq (\bar{v}_1)^{(1)} \leq \boxed{(v_0)^{(1)} = \frac{G_{13}^0}{G_{14}^0}}$, we obtain 484

$$(v_1)^{(1)} \leq v^{(1)}(t) \leq \frac{(\bar{v}_1)^{(1)} + (\bar{C})^{(1)}(\bar{v}_2)^{(1)} e^{-(a_{14})^{(1)}((\bar{v}_1)^{(1)} - (\bar{v}_2)^{(1)})t}}{1 + (\bar{C})^{(1)} e^{-(a_{14})^{(1)}((\bar{v}_1)^{(1)} - (\bar{v}_2)^{(1)})t}} \leq (v_0)^{(1)}$$

And so with the notation of the first part of condition (c) , we have

Definition of $v^{(1)}(t)$:-

$$(m_2)^{(1)} \leq v^{(1)}(t) \leq (m_1)^{(1)}, \quad v^{(1)}(t) = \frac{G_{13}(t)}{G_{14}(t)}$$

In a completely analogous way, we obtain

Definition of $u^{(1)}(t)$:-

$$(\mu_2)^{(1)} \leq u^{(1)}(t) \leq (\mu_1)^{(1)}, \quad u^{(1)}(t) = \frac{T_{13}(t)}{T_{14}(t)}$$

485

Now, using this result and replacing it in GLOBAL E486QUATIONS we get easily the result stated in the theorem.

Particular case :

If $(a''_{13})^{(1)} = (a''_{14})^{(1)}$, then $(\sigma_1)^{(1)} = (\sigma_2)^{(1)}$ and in this case $(v_1)^{(1)} = (\bar{v}_1)^{(1)}$ if in addition $(v_0)^{(1)} = (v_1)^{(1)}$ then $v^{(1)}(t) = (v_0)^{(1)}$ and as a consequence $G_{13}(t) = (v_0)^{(1)}G_{14}(t)$ this also defines $(v_0)^{(1)}$ for the special case

Analogously if $(b''_{13})^{(1)} = (b''_{14})^{(1)}$, then $(\tau_1)^{(1)} = (\tau_2)^{(1)}$ and then

$(u_1)^{(1)} = (\bar{u}_1)^{(1)}$ if in addition $(u_0)^{(1)} = (u_1)^{(1)}$ then $T_{13}(t) = (u_0)^{(1)}T_{14}(t)$ This is an important consequence of the relation between $(v_1)^{(1)}$ and $(\bar{v}_1)^{(1)}$, and definition of $(u_0)^{(1)}$.

486

we obtain

487

$$\frac{dv^{(2)}}{dt} = (a_{16})^{(2)} - \left((a'_{16})^{(2)} - (a'_{17})^{(2)} + (a''_{16})^{(2)}(T_{17}, t) \right) - (a''_{17})^{(2)}(T_{17}, t)v^{(2)} - (a_{17})^{(2)}v^{(2)}$$

Definition of $v^{(2)}$:-

$$v^{(2)} = \frac{G_{16}}{G_{17}}$$

488

It follows

489

$$- \left((a_{17})^{(2)}(v^{(2)})^2 + (\sigma_2)^{(2)}v^{(2)} - (a_{16})^{(2)} \right) \leq \frac{dv^{(2)}}{dt} \leq - \left((a_{17})^{(2)}(v^{(2)})^2 + (\sigma_1)^{(2)}v^{(2)} - (a_{16})^{(2)} \right)$$

From which one obtains

490

Definition of $(\bar{v}_1)^{(2)}, (v_0)^{(2)}$:-

$$(d) \text{ For } 0 < (v_0)^{(2)} = \frac{G_{16}^0}{G_{17}^0} < (v_1)^{(2)} < (\bar{v}_1)^{(2)}$$

$$v^{(2)}(t) \geq \frac{(v_1)^{(2)} + (C)^{(2)}(v_2)^{(2)} e^{-(a_{17})^{(2)}(v_1)^{(2)} - (v_0)^{(2)}t}}{1 + (C)^{(2)} e^{-(a_{17})^{(2)}(v_1)^{(2)} - (v_0)^{(2)}t}}, \quad (C)^{(2)} = \frac{(v_1)^{(2)} - (v_0)^{(2)}}{(v_0)^{(2)} - (v_2)^{(2)}}$$

it follows $(v_0)^{(2)} \leq v^{(2)}(t) \leq (v_1)^{(2)}$

In the same manner , we get

491

$$v^{(2)}(t) \leq \frac{(\bar{v}_1)^{(2)} + (\bar{C})^{(2)}(\bar{v}_2)^{(2)} e^{-(a_{17})^{(2)}(\bar{v}_1)^{(2)} - (\bar{v}_2)^{(2)}t}}{1 + (\bar{C})^{(2)} e^{-(a_{17})^{(2)}(\bar{v}_1)^{(2)} - (\bar{v}_2)^{(2)}t}}, \quad (\bar{C})^{(2)} = \frac{(\bar{v}_1)^{(2)} - (v_0)^{(2)}}{(v_0)^{(2)} - (\bar{v}_2)^{(2)}}$$

From which we deduce $(v_0)^{(2)} \leq v^{(2)}(t) \leq (\bar{v}_1)^{(2)}$

492

(e) If $0 < (v_1)^{(2)} < (v_0)^{(2)} = \frac{G_{16}^0}{G_{17}^0} < (\bar{v}_1)^{(2)}$ we find like in the previous case,

493

$$(v_1)^{(2)} \leq \frac{(v_1)^{(2)} + (C)^{(2)}(v_2)^{(2)} e^{-(a_{17})^{(2)}(v_1)^{(2)} - (v_2)^{(2)}t}}{1 + (C)^{(2)} e^{-(a_{17})^{(2)}(v_1)^{(2)} - (v_2)^{(2)}t}} \leq v^{(2)}(t) \leq \frac{(\bar{v}_1)^{(2)} + (\bar{C})^{(2)}(\bar{v}_2)^{(2)} e^{-(a_{17})^{(2)}(\bar{v}_1)^{(2)} - (\bar{v}_2)^{(2)}t}}{1 + (\bar{C})^{(2)} e^{-(a_{17})^{(2)}(\bar{v}_1)^{(2)} - (\bar{v}_2)^{(2)}t}} \leq (\bar{v}_1)^{(2)}$$

(f) If $0 < (v_1)^{(2)} \leq (\bar{v}_1)^{(2)} \leq (v_0)^{(2)} = \frac{G_{16}^0}{G_{17}^0}$, we obtain

494

$$(v_1)^{(2)} \leq v^{(2)}(t) \leq \frac{(\bar{v}_1)^{(2)} + (\bar{C})^{(2)}(\bar{v}_2)^{(2)} e^{-(a_{17})^{(2)}(\bar{v}_1)^{(2)} - (\bar{v}_2)^{(2)}t}}{1 + (\bar{C})^{(2)} e^{-(a_{17})^{(2)}(\bar{v}_1)^{(2)} - (\bar{v}_2)^{(2)}t}} \leq (v_0)^{(2)}$$

And so with the notation of the first part of condition (c) , we have

Definition of $v^{(2)}(t)$:-

495

$$(m_2)^{(2)} \leq v^{(2)}(t) \leq (m_1)^{(2)}, \quad v^{(2)}(t) = \frac{G_{16}(t)}{G_{17}(t)}$$

In a completely analogous way, we obtain

496

Definition of $u^{(2)}(t)$:-

$$(\mu_2)^{(2)} \leq u^{(2)}(t) \leq (\mu_1)^{(2)}, \quad u^{(2)}(t) = \frac{T_{16}(t)}{T_{17}(t)}$$

497

Particular case :

498

If $(a''_{16})^{(2)} = (a''_{17})^{(2)}$, then $(\sigma_1)^{(2)} = (\sigma_2)^{(2)}$ and in this case $(v_1)^{(2)} = (\bar{v}_1)^{(2)}$ if in addition $(v_0)^{(2)} = (v_1)^{(2)}$ then $v^{(2)}(t) = (v_0)^{(2)}$ and as a consequence $G_{16}(t) = (v_0)^{(2)}G_{17}(t)$

Analogously if $(b''_{16})^{(2)} = (b''_{17})^{(2)}$, then $(\tau_1)^{(2)} = (\tau_2)^{(2)}$ and then $(u_1)^{(2)} = (\bar{u}_1)^{(2)}$ if in addition $(u_0)^{(2)} = (u_1)^{(2)}$ then $T_{16}(t) = (u_0)^{(2)}T_{17}(t)$ This is an important consequence of the relation between $(v_1)^{(2)}$ and $(\bar{v}_1)^{(2)}$

499

From GLOBAL EQUATIONS we obtain

500

$$\frac{dv^{(3)}}{dt} = (a_{20})^{(3)} - \left((a'_{20})^{(3)} - (a'_{21})^{(3)} + (a''_{20})^{(3)}(T_{21}, t) \right) - (a''_{21})^{(3)}(T_{21}, t)v^{(3)} - (a_{21})^{(3)}v^{(3)}$$

Definition of $v^{(3)}$:-

$$v^{(3)} = \frac{G_{20}}{G_{21}}$$

501

It follows

$$- \left((a_{21})^{(3)}(v^{(3)})^2 + (\sigma_2)^{(3)}v^{(3)} - (a_{20})^{(3)} \right) \leq \frac{dv^{(3)}}{dt} \leq - \left((a_{21})^{(3)}(v^{(3)})^2 + (\sigma_1)^{(3)}v^{(3)} - (a_{20})^{(3)} \right)$$

502

From which one obtains

(a) For $0 < (v_0)^{(3)} = \frac{G_{20}^0}{G_{21}^0} < (v_1)^{(3)} < (\bar{v}_1)^{(3)}$

$$v^{(3)}(t) \geq \frac{(v_1)^{(3)} + (C)^{(3)}(v_2)^{(3)} e^{[-(a_{21})^{(3)}(v_1)^{(3)} - (v_0)^{(3)}]t}}{1 + (C)^{(3)} e^{[-(a_{21})^{(3)}(v_1)^{(3)} - (v_0)^{(3)}]t}}, \quad (C)^{(3)} = \frac{(v_1)^{(3)} - (v_0)^{(3)}}{(v_0)^{(3)} - (v_2)^{(3)}}$$

it follows $(v_0)^{(3)} \leq v^{(3)}(t) \leq (v_1)^{(3)}$

In the same manner, we get

503

$$v^{(3)}(t) \leq \frac{(\bar{v}_1)^{(3)} + (\bar{C})^{(3)}(\bar{v}_2)^{(3)} e^{[-(a_{21})^{(3)}(\bar{v}_1)^{(3)} - (\bar{v}_2)^{(3)}]t}}{1 + (\bar{C})^{(3)} e^{[-(a_{21})^{(3)}(\bar{v}_1)^{(3)} - (\bar{v}_2)^{(3)}]t}}, \quad (\bar{C})^{(3)} = \frac{(\bar{v}_1)^{(3)} - (v_0)^{(3)}}{(v_0)^{(3)} - (\bar{v}_2)^{(3)}}$$

Definition of $(\bar{v}_1)^{(3)}$:-

From which we deduce $(v_0)^{(3)} \leq v^{(3)}(t) \leq (\bar{v}_1)^{(3)}$

(b) If $0 < (v_1)^{(3)} < (v_0)^{(3)} = \frac{G_{20}^0}{G_{21}^0} < (\bar{v}_1)^{(3)}$ we find like in the previous case,

504

$$(v_1)^{(3)} \leq \frac{(v_1)^{(3)} + (C)^{(3)}(v_2)^{(3)} e^{[-(a_{21})^{(3)}(v_1)^{(3)} - (v_2)^{(3)}]t}}{1 + (C)^{(3)} e^{[-(a_{21})^{(3)}(v_1)^{(3)} - (v_2)^{(3)}]t}} \leq v^{(3)}(t) \leq \frac{(\bar{v}_1)^{(3)} + (\bar{C})^{(3)}(\bar{v}_2)^{(3)} e^{[-(a_{21})^{(3)}(\bar{v}_1)^{(3)} - (\bar{v}_2)^{(3)}]t}}{1 + (\bar{C})^{(3)} e^{[-(a_{21})^{(3)}(\bar{v}_1)^{(3)} - (\bar{v}_2)^{(3)}]t}} \leq (\bar{v}_1)^{(3)}$$

(c) If $0 < (v_1)^{(3)} \leq (\bar{v}_1)^{(3)} \leq (v_0)^{(3)} = \frac{G_{20}^0}{G_{21}^0}$, we obtain

505

$$(v_1)^{(3)} \leq v^{(3)}(t) \leq \frac{(\bar{v}_1)^{(3)} + (\bar{C})^{(3)}(\bar{v}_2)^{(3)} e^{[-(a_{21})^{(3)}(\bar{v}_1)^{(3)} - (\bar{v}_2)^{(3)}]t}}{1 + (\bar{C})^{(3)} e^{[-(a_{21})^{(3)}(\bar{v}_1)^{(3)} - (\bar{v}_2)^{(3)}]t}} \leq (v_0)^{(3)}$$

And so with the notation of the first part of condition (c), we have

Definition of $v^{(3)}(t)$:-

$$(m_2)^{(3)} \leq v^{(3)}(t) \leq (m_1)^{(3)}, \quad v^{(3)}(t) = \frac{G_{20}(t)}{G_{21}(t)}$$

In a completely analogous way, we obtain

Definition of $u^{(3)}(t)$:-

$$(\mu_2)^{(3)} \leq u^{(3)}(t) \leq (\mu_1)^{(3)}, \quad u^{(3)}(t) = \frac{T_{20}(t)}{T_{21}(t)}$$

Now, using this result and replacing it in GLOBAL EQUATIONS we get easily the result stated in the theorem.

Particular case :

If $(a''_{20})^{(3)} = (a''_{21})^{(3)}$, then $(\sigma_1)^{(3)} = (\sigma_2)^{(3)}$ and in this case $(v_1)^{(3)} = (\bar{v}_1)^{(3)}$ if in addition $(v_0)^{(3)} = (v_1)^{(3)}$ then $v^{(3)}(t) = (v_0)^{(3)}$ and as a consequence $G_{20}(t) = (v_0)^{(3)}G_{21}(t)$

Analogously if $(b''_{20})^{(3)} = (b''_{21})^{(3)}$, then $(\tau_1)^{(3)} = (\tau_2)^{(3)}$ and then

$(u_1)^{(3)} = (\bar{u}_1)^{(3)}$ if in addition $(u_0)^{(3)} = (u_1)^{(3)}$ then $T_{20}(t) = (u_0)^{(3)}T_{21}(t)$ This is an important consequence of the relation between $(v_1)^{(3)}$ and $(\bar{v}_1)^{(3)}$

506

: From GLOBAL EQUATIONS we obtain

507

$$\frac{dv^{(4)}}{dt} = (a_{24})^{(4)} - \left((a'_{24})^{(4)} - (a'_{25})^{(4)} + (a''_{24})^{(4)}(T_{25}, t) \right) - (a''_{25})^{(4)}(T_{25}, t)v^{(4)} - (a_{25})^{(4)}v^{(4)}$$

508

Definition of $v^{(4)}$:- $v^{(4)} = \frac{G_{24}}{G_{25}}$

It follows

$$-\left((a_{25})^{(4)}(v^{(4)})^2 + (\sigma_2)^{(4)}v^{(4)} - (a_{24})^{(4)}\right) \leq \frac{dv^{(4)}}{dt} \leq -\left((a_{25})^{(4)}(v^{(4)})^2 + (\sigma_4)^{(4)}v^{(4)} - (a_{24})^{(4)}\right)$$

From which one obtains

Definition of $(\bar{v}_1)^{(4)}, (v_0)^{(4)}$:-

(d) For $0 < \left[(v_0)^{(4)} = \frac{G_{24}^0}{G_{25}^0} \right] < (v_1)^{(4)} < (\bar{v}_1)^{(4)}$

$$v^{(4)}(t) \geq \frac{(v_1)^{(4)} + (C)^{(4)}(v_2)^{(4)} e^{[-(a_{25})^{(4)}(v_1)^{(4)} - (v_0)^{(4)}]t}}{4 + (C)^{(4)} e^{[-(a_{25})^{(4)}(v_1)^{(4)} - (v_0)^{(4)}]t}}, \quad \left[(C)^{(4)} = \frac{(v_1)^{(4)} - (v_0)^{(4)}}{(v_0)^{(4)} - (v_2)^{(4)}} \right]$$

it follows $(v_0)^{(4)} \leq v^{(4)}(t) \leq (v_1)^{(4)}$

In the same manner , we get

509

$$v^{(4)}(t) \leq \frac{(\bar{v}_1)^{(4)} + (\bar{C})^{(4)}(\bar{v}_2)^{(4)} e^{[-(a_{25})^{(4)}(\bar{v}_1)^{(4)} - (\bar{v}_2)^{(4)}]t}}{4 + (\bar{C})^{(4)} e^{[-(a_{25})^{(4)}(\bar{v}_1)^{(4)} - (\bar{v}_2)^{(4)}]t}}, \quad \left[(\bar{C})^{(4)} = \frac{(\bar{v}_1)^{(4)} - (v_0)^{(4)}}{(v_0)^{(4)} - (\bar{v}_2)^{(4)}} \right]$$

From which we deduce $(v_0)^{(4)} \leq v^{(4)}(t) \leq (\bar{v}_1)^{(4)}$

(e) If $0 < (v_1)^{(4)} < (v_0)^{(4)} = \frac{G_{24}^0}{G_{25}^0} < (\bar{v}_1)^{(4)}$ we find like in the previous case,

510

$$(v_1)^{(4)} \leq \frac{(v_1)^{(4)} + (C)^{(4)}(v_2)^{(4)} e^{[-(a_{25})^{(4)}(v_1)^{(4)} - (v_2)^{(4)}]t}}{1 + (C)^{(4)} e^{[-(a_{25})^{(4)}(v_1)^{(4)} - (v_2)^{(4)}]t}} \leq v^{(4)}(t) \leq \frac{(\bar{v}_1)^{(4)} + (\bar{C})^{(4)}(\bar{v}_2)^{(4)} e^{[-(a_{25})^{(4)}(\bar{v}_1)^{(4)} - (\bar{v}_2)^{(4)}]t}}{1 + (\bar{C})^{(4)} e^{[-(a_{25})^{(4)}(\bar{v}_1)^{(4)} - (\bar{v}_2)^{(4)}]t}} \leq (\bar{v}_1)^{(4)}$$

511

512

(f) If $0 < (v_1)^{(4)} \leq (\bar{v}_1)^{(4)} \leq \left[(v_0)^{(4)} = \frac{G_{24}^0}{G_{25}^0} \right]$, we obtain

$$(v_1)^{(4)} \leq v^{(4)}(t) \leq \frac{(\bar{v}_1)^{(4)} + (\bar{C})^{(4)}(\bar{v}_2)^{(4)} e^{[-(a_{25})^{(4)}(\bar{v}_1)^{(4)} - (\bar{v}_2)^{(4)}]t}}{1 + (\bar{C})^{(4)} e^{[-(a_{25})^{(4)}(\bar{v}_1)^{(4)} - (\bar{v}_2)^{(4)}]t}} \leq (v_0)^{(4)}$$

And so with the notation of the first part of condition (c), we have

Definition of $v^{(4)}(t)$:-

$$(m_2)^{(4)} \leq v^{(4)}(t) \leq (m_1)^{(4)}, \quad \left[v^{(4)}(t) = \frac{G_{24}(t)}{G_{25}(t)} \right]$$

In a completely analogous way, we obtain

Definition of $u^{(4)}(t)$:-

$$(\mu_2)^{(4)} \leq u^{(4)}(t) \leq (\mu_1)^{(4)}, \quad \left[u^{(4)}(t) = \frac{T_{24}(t)}{T_{25}(t)} \right]$$

Now, using this result and replacing it in GLOBAL EQUATIONS we get easily the result stated in the theorem.

Particular case :

If $(a_{24}'')^{(4)} = (a_{25}'')^{(4)}$, then $(\sigma_1)^{(4)} = (\sigma_2)^{(4)}$ and in this case $(v_1)^{(4)} = (\bar{v}_1)^{(4)}$ if in addition $(v_0)^{(4)} = (v_1)^{(4)}$ then $v^{(4)}(t) = (v_0)^{(4)}$ and as a consequence $G_{24}(t) = (v_0)^{(4)}G_{25}(t)$ **this also defines $(v_0)^{(4)}$ for the special case .**

513

Analogously if $(b_{24}'')^{(4)} = (b_{25}'')^{(4)}$, then $(\tau_1)^{(4)} = (\tau_2)^{(4)}$ and then

$(u_1)^{(4)} = (\bar{u}_4)^{(4)}$ if in addition $(u_0)^{(4)} = (u_1)^{(4)}$ then $T_{24}(t) = (u_0)^{(4)}T_{25}(t)$ This is an important consequence of the relation between $(v_1)^{(4)}$ and $(\bar{v}_1)^{(4)}$, **and definition of $(u_0)^{(4)}$.**

514
515

From GLOBAL EQUATIONS we obtain

$$\frac{dv^{(5)}}{dt} = (a_{28})^{(5)} - \left((a'_{28})^{(5)} - (a'_{29})^{(5)} + (a''_{28})^{(5)}(T_{29}, t) \right) - (a''_{29})^{(5)}(T_{29}, t)v^{(5)} - (a_{29})^{(5)}v^{(5)}$$

Definition of $v^{(5)}$:- $v^{(5)} = \frac{G_{28}}{G_{29}}$

It follows

$$- \left((a_{29})^{(5)}(v^{(5)})^2 + (\sigma_2)^{(5)}v^{(5)} - (a_{28})^{(5)} \right) \leq \frac{dv^{(5)}}{dt} \leq - \left((a_{29})^{(5)}(v^{(5)})^2 + (\sigma_1)^{(5)}v^{(5)} - (a_{28})^{(5)} \right)$$

From which one obtains

Definition of $(\bar{v}_1)^{(5)}, (v_0)^{(5)}$:-

(g) For $0 < \left(v_0 \right)^{(5)} = \frac{G_{28}^0}{G_{29}^0} < (v_1)^{(5)} < (\bar{v}_1)^{(5)}$

$$v^{(5)}(t) \geq \frac{(v_1)^{(5)} + (C)^{(5)}(v_2)^{(5)} e^{[-(a_{29})^{(5)}(v_1)^{(5)} - (v_0)^{(5)}]t}}{5 + (C)^{(5)} e^{[-(a_{29})^{(5)}(v_1)^{(5)} - (v_0)^{(5)}]t}}, \quad \left(C \right)^{(5)} = \frac{(v_1)^{(5)} - (v_0)^{(5)}}{(v_0)^{(5)} - (v_2)^{(5)}}$$

it follows $(v_0)^{(5)} \leq v^{(5)}(t) \leq (v_1)^{(5)}$

In the same manner , we get

516

$$v^{(5)}(t) \leq \frac{(\bar{v}_1)^{(5)} + (\bar{C})^{(5)}(\bar{v}_2)^{(5)} e^{[-(a_{29})^{(5)}(\bar{v}_1)^{(5)} - (\bar{v}_2)^{(5)}]t}}{5 + (\bar{C})^{(5)} e^{[-(a_{29})^{(5)}(\bar{v}_1)^{(5)} - (\bar{v}_2)^{(5)}]t}}, \quad (\bar{C})^{(5)} = \frac{(\bar{v}_1)^{(5)} - (v_0)^{(5)}}{(v_0)^{(5)} - (\bar{v}_2)^{(5)}}$$

From which we deduce $(v_0)^{(5)} \leq v^{(5)}(t) \leq (\bar{v}_5)^{(5)}$

(h) If $0 < (v_1)^{(5)} < (v_0)^{(5)} = \frac{G_{28}^0}{G_{29}^0} < (\bar{v}_1)^{(5)}$ we find like in the previous case,

517

$$(v_1)^{(5)} \leq \frac{(v_1)^{(5)} + (C)^{(5)}(v_2)^{(5)} e^{[-(a_{29})^{(5)}(v_1)^{(5)} - (v_2)^{(5)}]t}}{1 + (C)^{(5)} e^{[-(a_{29})^{(5)}(v_1)^{(5)} - (v_2)^{(5)}]t}} \leq v^{(5)}(t) \leq$$

$$\frac{(\bar{v}_1)^{(5)} + (\bar{C})^{(5)}(\bar{v}_2)^{(5)} e^{[-(a_{29})^{(5)}(\bar{v}_1)^{(5)} - (\bar{v}_2)^{(5)}]t}}{1 + (\bar{C})^{(5)} e^{[-(a_{29})^{(5)}(\bar{v}_1)^{(5)} - (\bar{v}_2)^{(5)}]t}} \leq (\bar{v}_1)^{(5)}$$

(i) If $0 < (v_1)^{(5)} \leq (\bar{v}_1)^{(5)} \leq \left(v_0 \right)^{(5)} = \frac{G_{28}^0}{G_{29}^0}$, we obtain

518

$$(v_1)^{(5)} \leq v^{(5)}(t) \leq \frac{(\bar{v}_1)^{(5)} + (\bar{C})^{(5)}(\bar{v}_2)^{(5)} e^{[-(a_{29})^{(5)}(\bar{v}_1)^{(5)} - (\bar{v}_2)^{(5)}]t}}{1 + (\bar{C})^{(5)} e^{[-(a_{29})^{(5)}(\bar{v}_1)^{(5)} - (\bar{v}_2)^{(5)}]t}} \leq (v_0)^{(5)}$$

519

And so with the notation of the first part of condition (c) , we have

Definition of $v^{(5)}(t)$:-

$$(m_2)^{(5)} \leq v^{(5)}(t) \leq (m_1)^{(5)}, \quad \left(v \right)^{(5)}(t) = \frac{G_{28}(t)}{G_{29}(t)}$$

In a completely analogous way, we obtain

Definition of $u^{(5)}(t)$:-

$$(\mu_2)^{(5)} \leq u^{(5)}(t) \leq (\mu_1)^{(5)}, \quad \left(u \right)^{(5)}(t) = \frac{T_{28}(t)}{T_{29}(t)}$$

Now, using this result and replacing it in GLOBAL EQUATIONS we get easily the result stated in the theorem.

Particular case :

If $(a''_{28})^{(5)} = (a''_{29})^{(5)}$, then $(\sigma_1)^{(5)} = (\sigma_2)^{(5)}$ and in this case $(v_1)^{(5)} = (\bar{v}_1)^{(5)}$ if in addition $(v_0)^{(5)} = (v_5)^{(5)}$ then $v^{(5)}(t) = (v_0)^{(5)}$ and as a consequence $G_{28}(t) = (v_0)^{(5)}G_{29}(t)$ **this also defines $(v_0)^{(5)}$ for the special case .**

Analogously if $(b''_{28})^{(5)} = (b''_{29})^{(5)}$, then $(\tau_1)^{(5)} = (\tau_2)^{(5)}$ and then $(u_1)^{(5)} = (\bar{u}_1)^{(5)}$ if in addition $(u_0)^{(5)} = (u_1)^{(5)}$ then $T_{28}(t) = (u_0)^{(5)}T_{29}(t)$ This is an important consequence of the relation between $(v_1)^{(5)}$ and $(\bar{v}_1)^{(5)}$, **and definition of $(u_0)^{(5)}$.**

we obtain

520
521

$$\frac{dv^{(6)}}{dt} = (a_{32})^{(6)} - \left((a'_{32})^{(6)} - (a'_{33})^{(6)} + (a''_{32})^{(6)}(T_{33}, t) \right) - (a''_{33})^{(6)}(T_{33}, t)v^{(6)} - (a_{33})^{(6)}v^{(6)}$$

Definition of $v^{(6)}$:- $v^{(6)} = \frac{G_{32}}{G_{33}}$

It follows

$$- \left((a_{33})^{(6)}(v^{(6)})^2 + (\sigma_2)^{(6)}v^{(6)} - (a_{32})^{(6)} \right) \leq \frac{dv^{(6)}}{dt} \leq - \left((a_{33})^{(6)}(v^{(6)})^2 + (\sigma_1)^{(6)}v^{(6)} - (a_{32})^{(6)} \right)$$

From which one obtains

Definition of $(\bar{v}_1)^{(6)}, (v_0)^{(6)}$:-

(j) For $0 < \left[(v_0)^{(6)} = \frac{G_{32}^0}{G_{33}^0} \right] < (v_1)^{(6)} < (\bar{v}_1)^{(6)}$

$$v^{(6)}(t) \geq \frac{(v_1)^{(6)} + (C)^{(6)}(v_2)^{(6)} e^{[-(a_{33})^{(6)}(v_1)^{(6)} - (v_0)^{(6)}]t}}{1 + (C)^{(6)} e^{[-(a_{33})^{(6)}(v_1)^{(6)} - (v_0)^{(6)}]t}}, \quad \left[(C)^{(6)} = \frac{(v_1)^{(6)} - (v_0)^{(6)}}{(v_0)^{(6)} - (v_2)^{(6)}} \right]$$

it follows $(v_0)^{(6)} \leq v^{(6)}(t) \leq (v_1)^{(6)}$

In the same manner , we get

522

$$v^{(6)}(t) \leq \frac{(\bar{v}_1)^{(6)} + (\bar{C})^{(6)}(\bar{v}_2)^{(6)} e^{[-(a_{33})^{(6)}(\bar{v}_1)^{(6)} - (\bar{v}_2)^{(6)}]t}}{1 + (\bar{C})^{(6)} e^{[-(a_{33})^{(6)}(\bar{v}_1)^{(6)} - (\bar{v}_2)^{(6)}]t}}, \quad \left[(\bar{C})^{(6)} = \frac{(\bar{v}_1)^{(6)} - (v_0)^{(6)}}{(v_0)^{(6)} - (\bar{v}_2)^{(6)}} \right]$$

523

From which we deduce $(v_0)^{(6)} \leq v^{(6)}(t) \leq (\bar{v}_1)^{(6)}$

(k) If $0 < (v_1)^{(6)} < (v_0)^{(6)} = \frac{G_{32}^0}{G_{33}^0} < (\bar{v}_1)^{(6)}$ we find like in the previous case,

524

$$(v_1)^{(6)} \leq \frac{(v_1)^{(6)} + (C)^{(6)}(v_2)^{(6)} e^{[-(a_{33})^{(6)}(v_1)^{(6)} - (v_2)^{(6)}]t}}{1 + (C)^{(6)} e^{[-(a_{33})^{(6)}(v_1)^{(6)} - (v_2)^{(6)}]t}} \leq v^{(6)}(t) \leq$$

$$\frac{(\bar{v}_1)^{(6)} + (\bar{C})^{(6)}(\bar{v}_2)^{(6)} e^{[-(a_{33})^{(6)}(\bar{v}_1)^{(6)} - (\bar{v}_2)^{(6)}]t}}{1 + (\bar{C})^{(6)} e^{[-(a_{33})^{(6)}(\bar{v}_1)^{(6)} - (\bar{v}_2)^{(6)}]t}} \leq (\bar{v}_1)^{(6)}$$

(l) If $0 < (v_1)^{(6)} \leq (\bar{v}_1)^{(6)} \leq \left[(v_0)^{(6)} = \frac{G_{32}^0}{G_{33}^0} \right]$, we obtain

525

$$(v_1)^{(6)} \leq v^{(6)}(t) \leq \frac{(\bar{v}_1)^{(6)} + (\bar{C})^{(6)}(\bar{v}_2)^{(6)} e^{[-(a_{33})^{(6)}(\bar{v}_1)^{(6)} - (\bar{v}_2)^{(6)}]t}}{1 + (\bar{C})^{(6)} e^{[-(a_{33})^{(6)}(\bar{v}_1)^{(6)} - (\bar{v}_2)^{(6)}]t}} \leq (v_0)^{(6)}$$

And so with the notation of the first part of condition (c), we have

Definition of $v^{(6)}(t)$:-

$$(m_2)^{(6)} \leq v^{(6)}(t) \leq (m_1)^{(6)}, \quad v^{(6)}(t) = \frac{G_{32}(t)}{G_{33}(t)}$$

In a completely analogous way, we obtain

Definition of $u^{(6)}(t)$:-

$$(\mu_2)^{(6)} \leq u^{(6)}(t) \leq (\mu_1)^{(6)}, \quad u^{(6)}(t) = \frac{T_{32}(t)}{T_{33}(t)}$$

Now, using this result and replacing it in GLOBAL EQUATIONS we get easily the result stated in the theorem.

Particular case :

If $(a''_{32})^{(6)} = (a''_{33})^{(6)}$, then $(\sigma_1)^{(6)} = (\sigma_2)^{(6)}$ and in this case $(v_1)^{(6)} = (\bar{v}_1)^{(6)}$ if in addition $(v_0)^{(6)} = (v_1)^{(6)}$ then $v^{(6)}(t) = (v_0)^{(6)}$ and as a consequence $G_{32}(t) = (v_0)^{(6)}G_{33}(t)$ **this also defines $(v_0)^{(6)}$ for the special case.**

Analogously if $(b''_{32})^{(6)} = (b''_{33})^{(6)}$, then $(\tau_1)^{(6)} = (\tau_2)^{(6)}$ and then $(u_1)^{(6)} = (\bar{u}_1)^{(6)}$ if in addition $(u_0)^{(6)} = (u_1)^{(6)}$ then $T_{32}(t) = (u_0)^{(6)}T_{33}(t)$ This is an important consequence of the relation between $(v_1)^{(6)}$ and $(\bar{v}_1)^{(6)}$, **and definition of $(u_0)^{(6)}$.**

526
527
528

527

We can prove the following

Theorem 3: If $(a_i'')^{(1)}$ and $(b_i'')^{(1)}$ are independent on t , and the conditions

$$\begin{aligned} &(a'_{13})^{(1)}(a'_{14})^{(1)} - (a_{13})^{(1)}(a_{14})^{(1)} < 0 \\ &(a'_{13})^{(1)}(a'_{14})^{(1)} - (a_{13})^{(1)}(a_{14})^{(1)} + (a_{13})^{(1)}(p_{13})^{(1)} + (a'_{14})^{(1)}(p_{14})^{(1)} + (p_{13})^{(1)}(p_{14})^{(1)} > 0 \\ &(b'_{13})^{(1)}(b'_{14})^{(1)} - (b_{13})^{(1)}(b_{14})^{(1)} > 0, \\ &(b'_{13})^{(1)}(b'_{14})^{(1)} - (b_{13})^{(1)}(b_{14})^{(1)} - (b'_{13})^{(1)}(r_{14})^{(1)} - (b'_{14})^{(1)}(r_{14})^{(1)} + (r_{13})^{(1)}(r_{14})^{(1)} < 0 \end{aligned}$$

with $(p_{13})^{(1)}, (r_{14})^{(1)}$ as defined, then the system

529

If $(a_i'')^{(2)}$ and $(b_i'')^{(2)}$ are independent on t , and the conditions

$$\begin{aligned} &(a'_{16})^{(2)}(a'_{17})^{(2)} - (a_{16})^{(2)}(a_{17})^{(2)} < 0 \\ &(a'_{16})^{(2)}(a'_{17})^{(2)} - (a_{16})^{(2)}(a_{17})^{(2)} + (a_{16})^{(2)}(p_{16})^{(2)} + (a'_{17})^{(2)}(p_{17})^{(2)} + (p_{16})^{(2)}(p_{17})^{(2)} > 0 \\ &(b'_{16})^{(2)}(b'_{17})^{(2)} - (b_{16})^{(2)}(b_{17})^{(2)} > 0, \\ &(b'_{16})^{(2)}(b'_{17})^{(2)} - (b_{16})^{(2)}(b_{17})^{(2)} - (b'_{16})^{(2)}(r_{17})^{(2)} - (b'_{17})^{(2)}(r_{17})^{(2)} + (r_{16})^{(2)}(r_{17})^{(2)} < 0 \end{aligned}$$

with $(p_{16})^{(2)}, (r_{17})^{(2)}$ as defined are satisfied, then the system

530.

531

532

533

534

If $(a_i'')^{(3)}$ and $(b_i'')^{(3)}$ are independent on t , and the conditions

$$\begin{aligned} &(a'_{20})^{(3)}(a'_{21})^{(3)} - (a_{20})^{(3)}(a_{21})^{(3)} < 0 \\ &(a'_{20})^{(3)}(a'_{21})^{(3)} - (a_{20})^{(3)}(a_{21})^{(3)} + (a_{20})^{(3)}(p_{20})^{(3)} + (a'_{21})^{(3)}(p_{21})^{(3)} + (p_{20})^{(3)}(p_{21})^{(3)} > 0 \\ &(b'_{20})^{(3)}(b'_{21})^{(3)} - (b_{20})^{(3)}(b_{21})^{(3)} > 0, \\ &(b'_{20})^{(3)}(b'_{21})^{(3)} - (b_{20})^{(3)}(b_{21})^{(3)} - (b'_{20})^{(3)}(r_{21})^{(3)} - (b'_{21})^{(3)}(r_{21})^{(3)} + (r_{20})^{(3)}(r_{21})^{(3)} < 0 \end{aligned}$$

with $(p_{20})^{(3)}, (r_{21})^{(3)}$ as defined are satisfied, then the system

535

If $(a_i'')^{(4)}$ and $(b_i'')^{(4)}$ are independent on t , and the conditions

$$\begin{aligned} &(a'_{24})^{(4)}(a'_{25})^{(4)} - (a_{24})^{(4)}(a_{25})^{(4)} < 0 \\ &(a'_{24})^{(4)}(a'_{25})^{(4)} - (a_{24})^{(4)}(a_{25})^{(4)} + (a_{24})^{(4)}(p_{24})^{(4)} + (a'_{25})^{(4)}(p_{25})^{(4)} + (p_{24})^{(4)}(p_{25})^{(4)} > 0 \\ &(b'_{24})^{(4)}(b'_{25})^{(4)} - (b_{24})^{(4)}(b_{25})^{(4)} > 0, \\ &(b'_{24})^{(4)}(b'_{25})^{(4)} - (b_{24})^{(4)}(b_{25})^{(4)} - (b'_{24})^{(4)}(r_{25})^{(4)} - (b'_{25})^{(4)}(r_{25})^{(4)} + (r_{24})^{(4)}(r_{25})^{(4)} < 0 \end{aligned}$$

with $(p_{24})^{(4)}, (r_{25})^{(4)}$ as defined are satisfied, then the system

536

If $(a_i'')^{(5)}$ and $(b_i'')^{(5)}$ are independent on t , and the conditions

$$\begin{aligned} &(a'_{28})^{(5)}(a'_{29})^{(5)} - (a_{28})^{(5)}(a_{29})^{(5)} < 0 \\ &(a'_{28})^{(5)}(a'_{29})^{(5)} - (a_{28})^{(5)}(a_{29})^{(5)} + (a_{28})^{(5)}(p_{28})^{(5)} + (a'_{29})^{(5)}(p_{29})^{(5)} + (p_{28})^{(5)}(p_{29})^{(5)} > 0 \\ &(b'_{28})^{(5)}(b'_{29})^{(5)} - (b_{28})^{(5)}(b_{29})^{(5)} > 0, \\ &(b'_{28})^{(5)}(b'_{29})^{(5)} - (b_{28})^{(5)}(b_{29})^{(5)} - (b'_{28})^{(5)}(r_{29})^{(5)} - (b'_{29})^{(5)}(r_{29})^{(5)} + (r_{28})^{(5)}(r_{29})^{(5)} < 0 \end{aligned}$$

with $(p_{28})^{(5)}, (r_{29})^{(5)}$ as defined satisfied, then the system

537

If $(a_i'')^{(6)}$ and $(b_i'')^{(6)}$ are independent on t , and the conditions

$$\begin{aligned} &(a'_{32})^{(6)}(a'_{33})^{(6)} - (a_{32})^{(6)}(a_{33})^{(6)} < 0 \\ &(a'_{32})^{(6)}(a'_{33})^{(6)} - (a_{32})^{(6)}(a_{33})^{(6)} + (a_{32})^{(6)}(p_{32})^{(6)} + (a'_{33})^{(6)}(p_{33})^{(6)} + (p_{32})^{(6)}(p_{33})^{(6)} > 0 \end{aligned}$$

538

$(b'_{32})^{(6)}(b'_{33})^{(6)} - (b_{32})^{(6)}(b_{33})^{(6)} > 0$,	539
$(b'_{32})^{(6)}(b'_{33})^{(6)} - (b_{32})^{(6)}(b_{33})^{(6)} - (b'_{32})^{(6)}(r_{33})^{(6)} - (b'_{33})^{(6)}(r_{33})^{(6)} + (r_{32})^{(6)}(r_{33})^{(6)} < 0$	
with $(p_{32})^{(6)}, (r_{33})^{(6)}$ as defined are satisfied, then the system	
$(a_{13})^{(1)}G_{14} - [(a'_{13})^{(1)} + (a''_{13})^{(1)}(T_{14})]G_{13} = 0$	540
$(a_{14})^{(1)}G_{13} - [(a'_{14})^{(1)} + (a''_{14})^{(1)}(T_{14})]G_{14} = 0$	541
$(a_{15})^{(1)}G_{14} - [(a'_{15})^{(1)} + (a''_{15})^{(1)}(T_{14})]G_{15} = 0$	542
$(b_{13})^{(1)}T_{14} - [(b'_{13})^{(1)} - (b''_{13})^{(1)}(G)]T_{13} = 0$	543
$(b_{14})^{(1)}T_{13} - [(b'_{14})^{(1)} - (b''_{14})^{(1)}(G)]T_{14} = 0$	544
$(b_{15})^{(1)}T_{14} - [(b'_{15})^{(1)} - (b''_{15})^{(1)}(G)]T_{15} = 0$	545
has a unique positive solution, which is an equilibrium solution for the system	546
$(a_{16})^{(2)}G_{17} - [(a'_{16})^{(2)} + (a''_{16})^{(2)}(T_{17})]G_{16} = 0$	547
$(a_{17})^{(2)}G_{16} - [(a'_{17})^{(2)} + (a''_{17})^{(2)}(T_{17})]G_{17} = 0$	548
$(a_{18})^{(2)}G_{17} - [(a'_{18})^{(2)} + (a''_{18})^{(2)}(T_{17})]G_{18} = 0$	549
$(b_{16})^{(2)}T_{17} - [(b'_{16})^{(2)} - (b''_{16})^{(2)}(G_{19})]T_{16} = 0$	550
$(b_{17})^{(2)}T_{16} - [(b'_{17})^{(2)} - (b''_{17})^{(2)}(G_{19})]T_{17} = 0$	551
$(b_{18})^{(2)}T_{17} - [(b'_{18})^{(2)} - (b''_{18})^{(2)}(G_{19})]T_{18} = 0$	552
has a unique positive solution, which is an equilibrium solution for	553
$(a_{20})^{(3)}G_{21} - [(a'_{20})^{(3)} + (a''_{20})^{(3)}(T_{21})]G_{20} = 0$	554
$(a_{21})^{(3)}G_{20} - [(a'_{21})^{(3)} + (a''_{21})^{(3)}(T_{21})]G_{21} = 0$	555
$(a_{22})^{(3)}G_{21} - [(a'_{22})^{(3)} + (a''_{22})^{(3)}(T_{21})]G_{22} = 0$	556
$(b_{20})^{(3)}T_{21} - [(b'_{20})^{(3)} - (b''_{20})^{(3)}(G_{23})]T_{20} = 0$	557
$(b_{21})^{(3)}T_{20} - [(b'_{21})^{(3)} - (b''_{21})^{(3)}(G_{23})]T_{21} = 0$	558
$(b_{22})^{(3)}T_{21} - [(b'_{22})^{(3)} - (b''_{22})^{(3)}(G_{23})]T_{22} = 0$	559
has a unique positive solution, which is an equilibrium solution	560
$(a_{24})^{(4)}G_{25} - [(a'_{24})^{(4)} + (a''_{24})^{(4)}(T_{25})]G_{24} = 0$	561
$(a_{25})^{(4)}G_{24} - [(a'_{25})^{(4)} + (a''_{25})^{(4)}(T_{25})]G_{25} = 0$	563
$(a_{26})^{(4)}G_{25} - [(a'_{26})^{(4)} + (a''_{26})^{(4)}(T_{25})]G_{26} = 0$	564
$(b_{24})^{(4)}T_{25} - [(b'_{24})^{(4)} - (b''_{24})^{(4)}((G_{27}))]T_{24} = 0$	565
$(b_{25})^{(4)}T_{24} - [(b'_{25})^{(4)} - (b''_{25})^{(4)}((G_{27}))]T_{25} = 0$	566
$(b_{26})^{(4)}T_{25} - [(b'_{26})^{(4)} - (b''_{26})^{(4)}((G_{27}))]T_{26} = 0$	567
has a unique positive solution, which is an equilibrium solution for the system	568
$(a_{28})^{(5)}G_{29} - [(a'_{28})^{(5)} + (a''_{28})^{(5)}(T_{29})]G_{28} = 0$	569
$(a_{29})^{(5)}G_{28} - [(a'_{29})^{(5)} + (a''_{29})^{(5)}(T_{29})]G_{29} = 0$	570
$(a_{30})^{(5)}G_{29} - [(a'_{30})^{(5)} + (a''_{30})^{(5)}(T_{29})]G_{30} = 0$	571
$(b_{28})^{(5)}T_{29} - [(b'_{28})^{(5)} - (b''_{28})^{(5)}(G_{31})]T_{28} = 0$	572
$(b_{29})^{(5)}T_{28} - [(b'_{29})^{(5)} - (b''_{29})^{(5)}(G_{31})]T_{29} = 0$	573
$(b_{30})^{(5)}T_{29} - [(b'_{30})^{(5)} - (b''_{30})^{(5)}(G_{31})]T_{30} = 0$	574
has a unique positive solution, which is an equilibrium solution for the system	575

$$(a_{32})^{(6)}G_{33} - [(a'_{32})^{(6)} + (a''_{32})^{(6)}(T_{33})]G_{32} = 0 \quad 576$$

$$(a_{33})^{(6)}G_{32} - [(a'_{33})^{(6)} + (a''_{33})^{(6)}(T_{33})]G_{33} = 0 \quad 577$$

$$(a_{34})^{(6)}G_{33} - [(a'_{34})^{(6)} + (a''_{34})^{(6)}(T_{33})]G_{34} = 0 \quad 578$$

$$(b_{32})^{(6)}T_{33} - [(b'_{32})^{(6)} - (b''_{32})^{(6)}(G_{35})]T_{32} = 0 \quad 579$$

$$(b_{33})^{(6)}T_{32} - [(b'_{33})^{(6)} - (b''_{33})^{(6)}(G_{35})]T_{33} = 0 \quad 580$$

$$(b_{34})^{(6)}T_{33} - [(b'_{34})^{(6)} - (b''_{34})^{(6)}(G_{35})]T_{34} = 0 \quad 584$$

has a unique positive solution , which is an equilibrium solution for the system 582

(a) Indeed the first two equations have a nontrivial solution G_{13}, G_{14} if

$$F(T) =$$

$$(a'_{13})^{(1)}(a'_{14})^{(1)} - (a_{13})^{(1)}(a_{14})^{(1)} + (a'_{13})^{(1)}(a''_{14})^{(1)}(T_{14}) + (a'_{14})^{(1)}(a''_{13})^{(1)}(T_{14}) + (a''_{13})^{(1)}(T_{14})(a''_{14})^{(1)}(T_{14}) = 0$$

583
584

585

(a) Indeed the first two equations have a nontrivial solution G_{16}, G_{17} if

$$F(T_{19}) =$$

$$(a'_{16})^{(2)}(a'_{17})^{(2)} - (a_{16})^{(2)}(a_{17})^{(2)} + (a'_{16})^{(2)}(a''_{17})^{(2)}(T_{17}) + (a'_{17})^{(2)}(a''_{16})^{(2)}(T_{17}) + (a''_{16})^{(2)}(T_{17})(a''_{17})^{(2)}(T_{17}) = 0$$

586

(a) Indeed the first two equations have a nontrivial solution G_{20}, G_{21} if

$$F(T_{23}) =$$

$$(a'_{20})^{(3)}(a'_{21})^{(3)} - (a_{20})^{(3)}(a_{21})^{(3)} + (a'_{20})^{(3)}(a''_{21})^{(3)}(T_{21}) + (a'_{21})^{(3)}(a''_{20})^{(3)}(T_{21}) + (a''_{20})^{(3)}(T_{21})(a''_{21})^{(3)}(T_{21}) = 0$$

587

(a) Indeed the first two equations have a nontrivial solution G_{24}, G_{25} if

$$F(T_{27}) =$$

$$(a'_{24})^{(4)}(a'_{25})^{(4)} - (a_{24})^{(4)}(a_{25})^{(4)} + (a'_{24})^{(4)}(a''_{25})^{(4)}(T_{25}) + (a'_{25})^{(4)}(a''_{24})^{(4)}(T_{25}) + (a''_{24})^{(4)}(T_{25})(a''_{25})^{(4)}(T_{25}) = 0$$

588

(a) Indeed the first two equations have a nontrivial solution G_{28}, G_{29} if

$$F(T_{31}) =$$

$$(a'_{28})^{(5)}(a'_{29})^{(5)} - (a_{28})^{(5)}(a_{29})^{(5)} + (a'_{28})^{(5)}(a''_{29})^{(5)}(T_{29}) + (a'_{29})^{(5)}(a''_{28})^{(5)}(T_{29}) + (a''_{28})^{(5)}(T_{29})(a''_{29})^{(5)}(T_{29}) = 0$$

589

(a) Indeed the first two equations have a nontrivial solution G_{32}, G_{33} if

$$F(T_{35}) =$$

$$(a'_{32})^{(6)}(a'_{33})^{(6)} - (a_{32})^{(6)}(a_{33})^{(6)} + (a'_{32})^{(6)}(a''_{33})^{(6)}(T_{33}) + (a'_{33})^{(6)}(a''_{32})^{(6)}(T_{33}) + (a''_{32})^{(6)}(T_{33})(a''_{33})^{(6)}(T_{33}) = 0$$

560

Definition and uniqueness of T_{14}^* :-

After hypothesis $f(0) < 0, f(\infty) > 0$ and the functions $(a_i'')^{(1)}(T_{14})$ being increasing, it follows that there exists a unique T_{14}^* for which $f(T_{14}^*) = 0$. With this value , we obtain from the three first equations

$$G_{13} = \frac{(a_{13})^{(1)}G_{14}}{[(a'_{13})^{(1)} + (a''_{13})^{(1)}(T_{14}^*)]} \quad , \quad G_{15} = \frac{(a_{15})^{(1)}G_{14}}{[(a'_{15})^{(1)} + (a''_{15})^{(1)}(T_{14}^*)]}$$

561

Definition and uniqueness of T_{17}^* :-

After hypothesis $f(0) < 0, f(\infty) > 0$ and the functions $(a_i'')^{(2)}(T_{17})$ being increasing, it follows that there exists a unique T_{17}^* for which $f(T_{17}^*) = 0$. With this value , we obtain from the three first equations

$$G_{16} = \frac{(a_{16})^{(2)}G_{17}}{[(a'_{16})^{(2)} + (a''_{16})^{(2)}(T_{17}^*)]} \quad , \quad G_{18} = \frac{(a_{18})^{(2)}G_{17}}{[(a'_{18})^{(2)} + (a''_{18})^{(2)}(T_{17}^*)]}$$

562

Definition and uniqueness of T_{21}^* :-

563

564

After hypothesis $f(0) < 0, f(\infty) > 0$ and the functions $(a_i'')^{(1)}(T_{21})$ being increasing, it follows that there exists a unique T_{21}^* for which $f(T_{21}^*) = 0$. With this value, we obtain from the three first equations

$$G_{20} = \frac{(a_{20})^{(3)}G_{21}}{[(a_{20}')^{(3)}+(a_{20}'')^{(3)}(T_{21}^*)]} \quad , \quad G_{22} = \frac{(a_{22})^{(3)}G_{21}}{[(a_{22}')^{(3)}+(a_{22}'')^{(3)}(T_{21}^*)]}$$

565
566

Definition and uniqueness of T_{25}^* :-

After hypothesis $f(0) < 0, f(\infty) > 0$ and the functions $(a_i'')^{(4)}(T_{25})$ being increasing, it follows that there exists a unique T_{25}^* for which $f(T_{25}^*) = 0$. With this value, we obtain from the three first equations

$$G_{24} = \frac{(a_{24})^{(4)}G_{25}}{[(a_{24}')^{(4)}+(a_{24}'')^{(4)}(T_{25}^*)]} \quad , \quad G_{26} = \frac{(a_{26})^{(4)}G_{25}}{[(a_{26}')^{(4)}+(a_{26}'')^{(4)}(T_{25}^*)]}$$

567

Definition and uniqueness of T_{29}^* :-

After hypothesis $f(0) < 0, f(\infty) > 0$ and the functions $(a_i'')^{(5)}(T_{29})$ being increasing, it follows that there exists a unique T_{29}^* for which $f(T_{29}^*) = 0$. With this value, we obtain from the three first equations

$$G_{28} = \frac{(a_{28})^{(5)}G_{29}}{[(a_{28}')^{(5)}+(a_{28}'')^{(5)}(T_{29}^*)]} \quad , \quad G_{30} = \frac{(a_{30})^{(5)}G_{29}}{[(a_{30}')^{(5)}+(a_{30}'')^{(5)}(T_{29}^*)]}$$

568

Definition and uniqueness of T_{33}^* :-

After hypothesis $f(0) < 0, f(\infty) > 0$ and the functions $(a_i'')^{(6)}(T_{33})$ being increasing, it follows that there exists a unique T_{33}^* for which $f(T_{33}^*) = 0$. With this value, we obtain from the three first equations

$$G_{32} = \frac{(a_{32})^{(6)}G_{33}}{[(a_{32}')^{(6)}+(a_{32}'')^{(6)}(T_{33}^*)]} \quad , \quad G_{34} = \frac{(a_{34})^{(6)}G_{33}}{[(a_{34}')^{(6)}+(a_{34}'')^{(6)}(T_{33}^*)]}$$

569

(e) By the same argument, the equations 92,93 admit solutions G_{13}, G_{14} if

$$\varphi(G) = (b_{13}')^{(1)}(b_{14}')^{(1)} - (b_{13}'')^{(1)}(b_{14}'')^{(1)} - [(b_{13}')^{(1)}(b_{14}'')^{(1)}(G) + (b_{14}')^{(1)}(b_{13}'')^{(1)}(G)] + (b_{13}'')^{(1)}(G)(b_{14}'')^{(1)}(G) = 0$$

Where in $G(G_{13}, G_{14}, G_{15}), G_{13}, G_{15}$ must be replaced by their values from 96. It is easy to see that φ is a decreasing function in G_{14} taking into account the hypothesis $\varphi(0) > 0, \varphi(\infty) < 0$ it follows that there exists a unique G_{14}^* such that $\varphi(G^*) = 0$

570

(f) By the same argument, the equations 92,93 admit solutions G_{16}, G_{17} if

$$\varphi(G_{19}) = (b_{16}')^{(2)}(b_{17}')^{(2)} - (b_{16}'')^{(2)}(b_{17}'')^{(2)} - [(b_{16}')^{(2)}(b_{17}'')^{(2)}(G_{19}) + (b_{17}')^{(2)}(b_{16}'')^{(2)}(G_{19})] + (b_{16}'')^{(2)}(G_{19})(b_{17}'')^{(2)}(G_{19}) = 0$$

571

Where in $(G_{19})(G_{16}, G_{17}, G_{18}), G_{16}, G_{18}$ must be replaced by their values from 96. It is easy to see that φ is a decreasing function in G_{17} taking into account the hypothesis $\varphi(0) > 0, \varphi(\infty) < 0$ it follows that there exists a unique G_{17}^* such that $\varphi((G_{19})^*) = 0$

572

(g) By the same argument, the concatenated equations admit solutions G_{20}, G_{21} if

$$\varphi(G_{23}) = (b_{20}')^{(3)}(b_{21}')^{(3)} - (b_{20}'')^{(3)}(b_{21}'')^{(3)} - [(b_{20}')^{(3)}(b_{21}'')^{(3)}(G_{23}) + (b_{21}')^{(3)}(b_{20}'')^{(3)}(G_{23})] + (b_{20}'')^{(3)}(G_{23})(b_{21}'')^{(3)}(G_{23}) = 0$$

573

Where in $G_{23}(G_{20}, G_{21}, G_{22}), G_{20}, G_{22}$ must be replaced by their values from 96. It is easy to see that φ is a decreasing function in G_{21} taking into account the hypothesis $\varphi(0) > 0, \varphi(\infty) < 0$ it follows that there exists a unique G_{21}^* such that $\varphi((G_{23})^*) = 0$

574

(h) By the same argument, the equations of modules admit solutions G_{24}, G_{25} if

$$\varphi(G_{27}) = (b_{24}')^{(4)}(b_{25}')^{(4)} - (b_{24}'')^{(4)}(b_{25}'')^{(4)} - [(b_{24}')^{(4)}(b_{25}'')^{(4)}(G_{27}) + (b_{25}')^{(4)}(b_{24}'')^{(4)}(G_{27})] + (b_{24}'')^{(4)}(G_{27})(b_{25}'')^{(4)}(G_{27}) = 0$$

575

Where in $(G_{27})(G_{24}, G_{25}, G_{26}), G_{24}, G_{26}$ must be replaced by their values from 96. It is easy to see that φ is a decreasing function in G_{25} taking into account the hypothesis $\varphi(0) > 0, \varphi(\infty) < 0$ it follows that there exists a unique G_{25}^* such that $\varphi((G_{27})^*) = 0$

575

(i) By the same argument, the equations (modules) admit solutions G_{28}, G_{29} if

$$\varphi(G_{31}) = (b_{28}')^{(5)}(b_{29}')^{(5)} - (b_{28}'')^{(5)}(b_{29}'')^{(5)} - [(b_{28}')^{(5)}(b_{29}'')^{(5)}(G_{31}) + (b_{29}')^{(5)}(b_{28}'')^{(5)}(G_{31})] + (b_{28}'')^{(5)}(G_{31})(b_{29}'')^{(5)}(G_{31}) = 0$$

578

Where in $(G_{31})(G_{28}, G_{29}, G_{30}), G_{28}, G_{30}$ must be replaced by their values from 96. It is easy to see that φ is a decreasing function in G_{29} taking into account the hypothesis $\varphi(0) > 0, \varphi(\infty) < 0$ it follows that there exists a unique G_{29}^* such that $\varphi((G_{31})^*) = 0$

579

(j) By the same argument, the equations (modules) admit solutions G_{32}, G_{33} if

$$\varphi(G_{35}) = (b_{32}')^{(6)}(b_{33}')^{(6)} - (b_{32}'')^{(6)}(b_{33}'')^{(6)} - [(b_{32}')^{(6)}(b_{33}'')^{(6)}(G_{35}) + (b_{33}')^{(6)}(b_{32}'')^{(6)}(G_{35})] + (b_{32}'')^{(6)}(G_{35})(b_{33}'')^{(6)}(G_{35}) = 0$$

580

Where in $(G_{35})(G_{32}, G_{33}, G_{34}), G_{32}, G_{34}$ must be replaced by their values It is easy to see that φ is a decreasing function in G_{33} taking into account the hypothesis $\varphi(0) > 0, \varphi(\infty) < 0$ it follows that there exists a unique G_{33}^*

581

such that $\varphi(G^*) = 0$

Finally we obtain the unique solution of 89 to 94 582

G_{14}^* given by $\varphi(G^*) = 0$, T_{14}^* given by $f(T_{14}^*) = 0$ and

$$G_{13}^* = \frac{(a_{13})^{(1)}G_{14}^*}{[(a'_{13})^{(1)} + (a''_{13})^{(1)}(T_{14}^*)]} , G_{15}^* = \frac{(a_{15})^{(1)}G_{14}^*}{[(a'_{15})^{(1)} + (a''_{15})^{(1)}(T_{14}^*)]}$$

$$T_{13}^* = \frac{(b_{13})^{(1)}T_{14}^*}{[(b'_{13})^{(1)} - (b''_{13})^{(1)}(G^*)]} , T_{15}^* = \frac{(b_{15})^{(1)}T_{14}^*}{[(b'_{15})^{(1)} - (b''_{15})^{(1)}(G^*)]}$$

Obviously, these values represent an equilibrium solution

Finally we obtain the unique solution 583

G_{17}^* given by $\varphi((G_{19})^*) = 0$, T_{17}^* given by $f(T_{17}^*) = 0$ and 584

$$G_{16}^* = \frac{(a_{16})^{(2)}G_{17}^*}{[(a'_{16})^{(2)} + (a''_{16})^{(2)}(T_{17}^*)]} , G_{18}^* = \frac{(a_{18})^{(2)}G_{17}^*}{[(a'_{18})^{(2)} + (a''_{18})^{(2)}(T_{17}^*)]} \span style="float: right;">585$$

$$T_{16}^* = \frac{(b_{16})^{(2)}T_{17}^*}{[(b'_{16})^{(2)} - (b''_{16})^{(2)}((G_{19})^*)]} , T_{18}^* = \frac{(b_{18})^{(2)}T_{17}^*}{[(b'_{18})^{(2)} - (b''_{18})^{(2)}((G_{19})^*)]} \span style="float: right;">586$$

Obviously, these values represent an equilibrium solution 587

Finally we obtain the unique solution 588

G_{21}^* given by $\varphi((G_{23})^*) = 0$, T_{21}^* given by $f(T_{21}^*) = 0$ and

$$G_{20}^* = \frac{(a_{20})^{(3)}G_{21}^*}{[(a'_{20})^{(3)} + (a''_{20})^{(3)}(T_{21}^*)]} , G_{22}^* = \frac{(a_{22})^{(3)}G_{21}^*}{[(a'_{22})^{(3)} + (a''_{22})^{(3)}(T_{21}^*)]}$$

$$T_{20}^* = \frac{(b_{20})^{(3)}T_{21}^*}{[(b'_{20})^{(3)} - (b''_{20})^{(3)}(G_{23}^*)]} , T_{22}^* = \frac{(b_{22})^{(3)}T_{21}^*}{[(b'_{22})^{(3)} - (b''_{22})^{(3)}(G_{23}^*)]}$$

Obviously, these values represent an equilibrium solution

Finally we obtain the unique solution 589

G_{25}^* given by $\varphi(G_{27}) = 0$, T_{25}^* given by $f(T_{25}^*) = 0$ and

$$G_{24}^* = \frac{(a_{24})^{(4)}G_{25}^*}{[(a'_{24})^{(4)} + (a''_{24})^{(4)}(T_{25}^*)]} , G_{26}^* = \frac{(a_{26})^{(4)}G_{25}^*}{[(a'_{26})^{(4)} + (a''_{26})^{(4)}(T_{25}^*)]}$$

$$T_{24}^* = \frac{(b_{24})^{(4)}T_{25}^*}{[(b'_{24})^{(4)} - (b''_{24})^{(4)}((G_{27})^*)]} , T_{26}^* = \frac{(b_{26})^{(4)}T_{25}^*}{[(b'_{26})^{(4)} - (b''_{26})^{(4)}((G_{27})^*)]} \span style="float: right;">590$$

Obviously, these values represent an equilibrium solution

Finally we obtain the unique solution 591

G_{29}^* given by $\varphi((G_{31})^*) = 0$, T_{29}^* given by $f(T_{29}^*) = 0$ and

$$G_{28}^* = \frac{(a_{28})^{(5)}G_{29}^*}{[(a'_{28})^{(5)} + (a''_{28})^{(5)}(T_{29}^*)]} , G_{30}^* = \frac{(a_{30})^{(5)}G_{29}^*}{[(a'_{30})^{(5)} + (a''_{30})^{(5)}(T_{29}^*)]}$$

$$T_{28}^* = \frac{(b_{28})^{(5)}T_{29}^*}{[(b'_{28})^{(5)} - (b''_{28})^{(5)}((G_{31})^*)]} , T_{30}^* = \frac{(b_{30})^{(5)}T_{29}^*}{[(b'_{30})^{(5)} - (b''_{30})^{(5)}((G_{31})^*)]} \span style="float: right;">592$$

Obviously, these values represent an equilibrium solution

Finally we obtain the unique solution 593

G_{33}^* given by $\varphi((G_{35})^*) = 0$, T_{33}^* given by $f(T_{33}^*) = 0$ and

$$G_{32}^* = \frac{(a_{32})^{(6)}G_{33}^*}{[(a'_{32})^{(6)} + (a''_{32})^{(6)}(T_{33}^*)]} , G_{34}^* = \frac{(a_{34})^{(6)}G_{33}^*}{[(a'_{34})^{(6)} + (a''_{34})^{(6)}(T_{33}^*)]}$$

$$T_{32}^* = \frac{(b_{32})^{(6)}T_{33}^*}{[(b'_{32})^{(6)} - (b''_{32})^{(6)}((G_{35})^*)]} , T_{34}^* = \frac{(b_{34})^{(6)}T_{33}^*}{[(b'_{34})^{(6)} - (b''_{34})^{(6)}((G_{35})^*)]} \span style="float: right;">594$$

Obviously, these values represent an equilibrium solution

ASYMPTOTIC STABILITY ANALYSIS 595

Theorem 4: If the conditions of the previous theorem are satisfied and if the functions $(a_i'')^{(1)}$ and $(b_i'')^{(1)}$ Belong to $C^{(1)}(\mathbb{R}_+)$ then the above equilibrium point is asymptotically stable.

Proof: Denote

Definition of G_i, T_i :-

$$G_i = G_i^* + G_i , T_i = T_i^* + T_i$$

$$\frac{\partial (a_{14}'')^{(1)}}{\partial T_{14}}(T_{14}^*) = (q_{14})^{(1)} , \frac{\partial (b_i'')^{(1)}}{\partial G_j}(G^*) = s_{ij}$$
596

Then taking into account equations (global) and neglecting the terms of power 2, we obtain 597

$$\frac{dG_{13}}{dt} = -((a'_{13})^{(1)} + (p_{13})^{(1)})G_{13} + (a_{13})^{(1)}G_{14} - (q_{13})^{(1)}G_{13}^*T_{14} \span style="float: right;">598$$

$$\frac{dG_{14}}{dt} = -((a'_{14})^{(1)} + (p_{14})^{(1)})G_{14} + (a_{14})^{(1)}G_{13} - (q_{14})^{(1)}G_{14}^*T_{14} \span style="float: right;">599$$

$$\frac{dG_{15}}{dt} = -((a'_{15})^{(1)} + (p_{15})^{(1)})G_{15} + (a_{15})^{(1)}G_{14} - (q_{15})^{(1)}G_{15}^*T_{14} \span style="float: right;">600$$

$$\frac{dT_{13}}{dt} = -((b'_{13})^{(1)} - (r_{13})^{(1)})T_{13} + (b_{13})^{(1)}T_{14} + \sum_{j=13}^{15} (s_{(13)(j)})T_{13}^*G_j \span style="float: right;">601$$

$$\frac{dT_{14}}{dt} = -((b'_{14})^{(1)} - (r_{14})^{(1)})T_{14} + (b_{14})^{(1)}T_{13} + \sum_{j=13}^{15} (s_{(14)(j)})T_{14}^*G_j \span style="float: right;">602$$

$$\frac{dT_{15}}{dt} = -((b'_{15})^{(1)} - (r_{15})^{(1)})T_{15} + (b_{15})^{(1)}T_{14} + \sum_{j=13}^{15} (s_{(15)(j)})T_{15}^*G_j \span style="float: right;">603$$

If the conditions of the previous theorem are satisfied and if the functions $(a_i'')^{(2)}$ and $(b_i'')^{(2)}$ Belong to $C^{(2)}(\mathbb{R}_+)$ then the above equilibrium point is asymptotically stable 604

Denote 605

Definition of G_i, T_i :-

$$G_i = G_i^* + G_i, T_i = T_i^* + T_i \tag{606}$$

$$\frac{\partial (a_{17})^{(2)}}{\partial T_{17}} (T_{17}^*) = (q_{17})^{(2)}, \frac{\partial (b_i'')^{(2)}}{\partial G_j} ((G_{19})^*) = s_{ij} \tag{607}$$

taking into account equations (global) and neglecting the terms of power 2, we obtain 608

$$\frac{dG_{16}}{dt} = -((a'_{16})^{(2)} + (p_{16})^{(2)})G_{16} + (a_{16})^{(2)}G_{17} - (q_{16})^{(2)}G_{16}^*T_{17} \tag{609}$$

$$\frac{dG_{17}}{dt} = -((a'_{17})^{(2)} + (p_{17})^{(2)})G_{17} + (a_{17})^{(2)}G_{16} - (q_{17})^{(2)}G_{17}^*T_{17} \tag{610}$$

$$\frac{dG_{18}}{dt} = -((a'_{18})^{(2)} + (p_{18})^{(2)})G_{18} + (a_{18})^{(2)}G_{17} - (q_{18})^{(2)}G_{18}^*T_{17} \tag{611}$$

$$\frac{dT_{16}}{dt} = -((b'_{16})^{(2)} - (r_{16})^{(2)})T_{16} + (b_{16})^{(2)}T_{17} + \sum_{j=16}^{18} (s_{(16)(j)})T_{16}^*G_j \tag{612}$$

$$\frac{dT_{17}}{dt} = -((b'_{17})^{(2)} - (r_{17})^{(2)})T_{17} + (b_{17})^{(2)}T_{16} + \sum_{j=16}^{18} (s_{(17)(j)})T_{17}^*G_j \tag{613}$$

$$\frac{dT_{18}}{dt} = -((b'_{18})^{(2)} - (r_{18})^{(2)})T_{18} + (b_{18})^{(2)}T_{17} + \sum_{j=16}^{18} (s_{(18)(j)})T_{18}^*G_j \tag{614}$$

If the conditions of the previous theorem are satisfied and if the functions $(a_i'')^{(3)}$ and $(b_i'')^{(3)}$ belong to $C^{(3)}(\mathbb{R}_+)$ then the above equilibrium point is asymptotically stable 615

Denote

Definition of G_i, T_i :-

$$G_i = G_i^* + G_i, T_i = T_i^* + T_i$$

$$\frac{\partial (a_{21})^{(3)}}{\partial T_{21}} (T_{21}^*) = (q_{21})^{(3)}, \frac{\partial (b_i'')^{(3)}}{\partial G_j} ((G_{23})^*) = s_{ij} \tag{616}$$

Then taking into account equations (global) and neglecting the terms of power 2, we obtain 617

$$\frac{dG_{20}}{dt} = -((a'_{20})^{(3)} + (p_{20})^{(3)})G_{20} + (a_{20})^{(3)}G_{21} - (q_{20})^{(3)}G_{20}^*T_{21} \tag{618}$$

$$\frac{dG_{21}}{dt} = -((a'_{21})^{(3)} + (p_{21})^{(3)})G_{21} + (a_{21})^{(3)}G_{20} - (q_{21})^{(3)}G_{21}^*T_{21} \tag{619}$$

$$\frac{dG_{22}}{dt} = -((a'_{22})^{(3)} + (p_{22})^{(3)})G_{22} + (a_{22})^{(3)}G_{21} - (q_{22})^{(3)}G_{22}^*T_{21} \tag{6120}$$

$$\frac{dT_{20}}{dt} = -((b'_{20})^{(3)} - (r_{20})^{(3)})T_{20} + (b_{20})^{(3)}T_{21} + \sum_{j=20}^{22} (s_{(20)(j)})T_{20}^*G_j \tag{621}$$

$$\frac{dT_{21}}{dt} = -((b'_{21})^{(3)} - (r_{21})^{(3)})T_{21} + (b_{21})^{(3)}T_{20} + \sum_{j=20}^{22} (s_{(21)(j)})T_{21}^*G_j \tag{622}$$

$$\frac{dT_{22}}{dt} = -((b'_{22})^{(3)} - (r_{22})^{(3)})T_{22} + (b_{22})^{(3)}T_{21} + \sum_{j=20}^{22} (s_{(22)(j)})T_{22}^*G_j \tag{623}$$

If the conditions of the previous theorem are satisfied and if the functions $(a_i'')^{(4)}$ and $(b_i'')^{(4)}$ belong to $C^{(4)}(\mathbb{R}_+)$ then the above equilibrium point is asymptotically stable 624

Denote

Definition of G_i, T_i :-

$$G_i = G_i^* + G_i, T_i = T_i^* + T_i$$

$$\frac{\partial (a_{25})^{(4)}}{\partial T_{25}} (T_{25}^*) = (q_{25})^{(4)}, \frac{\partial (b_i'')^{(4)}}{\partial G_j} ((G_{27})^*) = s_{ij} \tag{625}$$

Then taking into account equations (global) and neglecting the terms of power 2, we obtain 626

$$\frac{dG_{24}}{dt} = -((a'_{24})^{(4)} + (p_{24})^{(4)})G_{24} + (a_{24})^{(4)}G_{25} - (q_{24})^{(4)}G_{24}^*T_{25} \tag{627}$$

$$\frac{dG_{25}}{dt} = -((a'_{25})^{(4)} + (p_{25})^{(4)})G_{25} + (a_{25})^{(4)}G_{24} - (q_{25})^{(4)}G_{25}^*T_{25} \tag{628}$$

$$\frac{dG_{26}}{dt} = -((a'_{26})^{(4)} + (p_{26})^{(4)})G_{26} + (a_{26})^{(4)}G_{25} - (q_{26})^{(4)}G_{26}^*T_{25} \tag{629}$$

$$\frac{dT_{24}}{dt} = -((b'_{24})^{(4)} - (r_{24})^{(4)})T_{24} + (b_{24})^{(4)}T_{25} + \sum_{j=24}^{26} (s_{(24)(j)})T_{24}^*G_j \tag{630}$$

$$\frac{dT_{25}}{dt} = -((b'_{25})^{(4)} - (r_{25})^{(4)})T_{25} + (b_{25})^{(4)}T_{24} + \sum_{j=24}^{26} (s_{(25)(j)})T_{25}^*G_j \tag{631}$$

$$\frac{dT_{26}}{dt} = -((b'_{26})^{(4)} - (r_{26})^{(4)})T_{26} + (b_{26})^{(4)}T_{25} + \sum_{j=24}^{26} (s_{(26)(j)})T_{26}^*G_j \tag{632}$$

If the conditions of the previous theorem are satisfied and if the functions $(a_i'')^{(5)}$ and $(b_i'')^{(5)}$ belong to $C^{(5)}(\mathbb{R}_+)$ then the above equilibrium point is asymptotically stable 633

Denote

Definition of G_i, T_i :-

$$G_i = G_i^* + G_i, T_i = T_i^* + T_i$$

$$\frac{\partial (a_{29})^{(5)}}{\partial T_{29}} (T_{29}^*) = (q_{29})^{(5)}, \frac{\partial (b_i'')^{(5)}}{\partial G_j} ((G_{31})^*) = s_{ij} \tag{634}$$

Then taking into account equations (global) and neglecting the terms of power 2, we obtain 635

$$\frac{dG_{28}}{dt} = -((a'_{28})^{(5)} + (p_{28})^{(5)})G_{28} + (a_{28})^{(5)}G_{29} - (q_{28})^{(5)}G_{28}^*T_{29} \tag{636}$$

$$\frac{dG_{29}}{dt} = -((a'_{29})^{(5)} + (p_{29})^{(5)})G_{29} + (a_{29})^{(5)}G_{28} - (q_{29})^{(5)}G_{29}^*T_{29} \tag{637}$$

$$\frac{dG_{30}}{dt} = -((a'_{30})^{(5)} + (p_{30})^{(5)})G_{30} + (a_{30})^{(5)}G_{29} - (q_{30})^{(5)}G_{30}^*T_{29} \tag{638}$$

$$\begin{aligned} \frac{dT_{28}}{dt} &= -((b'_{28})^{(5)} - (r_{28})^{(5)})T_{28} + (b_{28})^{(5)}T_{29} + \sum_{j=28}^{30} (s_{(28)(j)})T_{28}^*G_j & 639 \\ \frac{dT_{29}}{dt} &= -((b'_{29})^{(5)} - (r_{29})^{(5)})T_{29} + (b_{29})^{(5)}T_{28} + \sum_{j=28}^{30} (s_{(29)(j)})T_{29}^*G_j & 640 \\ \frac{dT_{30}}{dt} &= -((b'_{30})^{(5)} - (r_{30})^{(5)})T_{30} + (b_{30})^{(5)}T_{29} + \sum_{j=28}^{30} (s_{(30)(j)})T_{30}^*G_j & 641 \end{aligned}$$

If the conditions of the previous theorem are satisfied and if the functions $(a_i'')^{(6)}$ and $(b_i'')^{(6)}$ belong to $C^{(6)}(\mathbb{R}_+)$ then the above equilibrium point is asymptotically stable 642

Denote

Definition of G_i, T_i :- 643

$$\begin{aligned} G_i &= G_i^* + G_i, \quad T_i = T_i^* + T_i \\ \frac{\partial (a_{33}'')^{(6)}}{\partial T_{33}}(T_{33}^*) &= (q_{33})^{(6)}, \quad \frac{\partial (b_i'')^{(6)}}{\partial G_j}((G_{35})^*) = s_{ij} \end{aligned}$$

Then taking into account equations(global) and neglecting the terms of power 2, we obtain 644

$$\begin{aligned} \frac{dG_{32}}{dt} &= -((a_{32}')^{(6)} + (p_{32})^{(6)})G_{32} + (a_{32})^{(6)}G_{33} - (q_{32})^{(6)}G_{32}^*T_{33} & 645 \\ \frac{dG_{33}}{dt} &= -((a_{33}')^{(6)} + (p_{33})^{(6)})G_{33} + (a_{33})^{(6)}G_{32} - (q_{33})^{(6)}G_{33}^*T_{33} & 646 \\ \frac{dG_{34}}{dt} &= -((a_{34}')^{(6)} + (p_{34})^{(6)})G_{34} + (a_{34})^{(6)}G_{33} - (q_{34})^{(6)}G_{34}^*T_{33} & 647 \\ \frac{dT_{32}}{dt} &= -((b'_{32})^{(6)} - (r_{32})^{(6)})T_{32} + (b_{32})^{(6)}T_{33} + \sum_{j=32}^{34} (s_{(32)(j)})T_{32}^*G_j & 648 \\ \frac{dT_{33}}{dt} &= -((b'_{33})^{(6)} - (r_{33})^{(6)})T_{33} + (b_{33})^{(6)}T_{32} + \sum_{j=32}^{34} (s_{(33)(j)})T_{33}^*G_j & 649 \\ \frac{dT_{34}}{dt} &= -((b'_{34})^{(6)} - (r_{34})^{(6)})T_{34} + (b_{34})^{(6)}T_{33} + \sum_{j=32}^{34} (s_{(34)(j)})T_{34}^*G_j & 650 \end{aligned}$$

The characteristic equation of this system is 651

$$\begin{aligned} &((\lambda)^{(1)} + (b'_{15})^{(1)} - (r_{15})^{(1)})\{((\lambda)^{(1)} + (a'_{15})^{(1)} + (p_{15})^{(1)}) \\ & \left[((\lambda)^{(1)} + (a'_{13})^{(1)} + (p_{13})^{(1)})(q_{14})^{(1)}G_{14}^* + (a_{14})^{(1)}(q_{13})^{(1)}G_{13}^* \right] \\ & ((\lambda)^{(1)} + (b'_{13})^{(1)} - (r_{13})^{(1)})s_{(14),(14)}T_{14}^* + (b_{14})^{(1)}s_{(13),(14)}T_{14}^* \\ & + ((\lambda)^{(1)} + (a'_{14})^{(1)} + (p_{14})^{(1)})(q_{13})^{(1)}G_{13}^* + (a_{13})^{(1)}(q_{14})^{(1)}G_{14}^* \\ & ((\lambda)^{(1)} + (b'_{13})^{(1)} - (r_{13})^{(1)})s_{(14),(13)}T_{14}^* + (b_{14})^{(1)}s_{(13),(13)}T_{13}^* \\ & ((\lambda)^{(1)})^2 + ((a'_{13})^{(1)} + (a'_{14})^{(1)} + (p_{13})^{(1)} + (p_{14})^{(1)}) (\lambda)^{(1)} \\ & ((\lambda)^{(1)})^2 + ((b'_{13})^{(1)} + (b'_{14})^{(1)} - (r_{13})^{(1)} + (r_{14})^{(1)}) (\lambda)^{(1)} \\ & + ((\lambda)^{(1)})^2 + ((a'_{13})^{(1)} + (a'_{14})^{(1)} + (p_{13})^{(1)} + (p_{14})^{(1)}) (\lambda)^{(1)} (q_{15})^{(1)}G_{15} \\ & + ((\lambda)^{(1)} + (a'_{13})^{(1)} + (p_{13})^{(1)}) ((a_{15})^{(1)}(q_{14})^{(1)}G_{14}^* + (a_{14})^{(1)}(a_{15})^{(1)}(q_{13})^{(1)}G_{13}^*) \\ & ((\lambda)^{(1)} + (b'_{13})^{(1)} - (r_{13})^{(1)})s_{(14),(15)}T_{14}^* + (b_{14})^{(1)}s_{(13),(15)}T_{13}^* \} = 0 \\ & + \\ & ((\lambda)^{(2)} + (b'_{18})^{(2)} - (r_{18})^{(2)})\{((\lambda)^{(2)} + (a'_{18})^{(2)} + (p_{18})^{(2)}) \\ & \left[((\lambda)^{(2)} + (a'_{16})^{(2)} + (p_{16})^{(2)})(q_{17})^{(2)}G_{17}^* + (a_{17})^{(2)}(q_{16})^{(2)}G_{16}^* \right] \\ & ((\lambda)^{(2)} + (b'_{16})^{(2)} - (r_{16})^{(2)})s_{(17),(17)}T_{17}^* + (b_{17})^{(2)}s_{(16),(17)}T_{17}^* \\ & + ((\lambda)^{(2)} + (a'_{17})^{(2)} + (p_{17})^{(2)})(q_{16})^{(2)}G_{16}^* + (a_{16})^{(2)}(q_{17})^{(2)}G_{17}^* \\ & ((\lambda)^{(2)} + (b'_{16})^{(2)} - (r_{16})^{(2)})s_{(17),(16)}T_{17}^* + (b_{17})^{(2)}s_{(16),(16)}T_{16}^* \\ & ((\lambda)^{(2)})^2 + ((a'_{16})^{(2)} + (a'_{17})^{(2)} + (p_{16})^{(2)} + (p_{17})^{(2)}) (\lambda)^{(2)} \\ & ((\lambda)^{(2)})^2 + ((b'_{16})^{(2)} + (b'_{17})^{(2)} - (r_{16})^{(2)} + (r_{17})^{(2)}) (\lambda)^{(2)} \\ & + ((\lambda)^{(2)})^2 + ((a'_{16})^{(2)} + (a'_{17})^{(2)} + (p_{16})^{(2)} + (p_{17})^{(2)}) (\lambda)^{(2)} (q_{18})^{(2)}G_{18} \\ & + ((\lambda)^{(2)} + (a'_{16})^{(2)} + (p_{16})^{(2)}) ((a_{18})^{(2)}(q_{17})^{(2)}G_{17}^* + (a_{17})^{(2)}(a_{18})^{(2)}(q_{16})^{(2)}G_{16}^*) \\ & ((\lambda)^{(2)} + (b'_{16})^{(2)} - (r_{16})^{(2)})s_{(17),(18)}T_{17}^* + (b_{17})^{(2)}s_{(16),(18)}T_{16}^* \} = 0 \\ & + \\ & ((\lambda)^{(3)} + (b'_{22})^{(3)} - (r_{22})^{(3)})\{((\lambda)^{(3)} + (a'_{22})^{(3)} + (p_{22})^{(3)}) \\ & \left[((\lambda)^{(3)} + (a'_{20})^{(3)} + (p_{20})^{(3)})(q_{21})^{(3)}G_{21}^* + (a_{21})^{(3)}(q_{20})^{(3)}G_{20}^* \right] \\ & ((\lambda)^{(3)} + (b'_{20})^{(3)} - (r_{20})^{(3)})s_{(21),(21)}T_{21}^* + (b_{21})^{(3)}s_{(20),(21)}T_{21}^* \\ & + ((\lambda)^{(3)} + (a'_{21})^{(3)} + (p_{21})^{(3)})(q_{20})^{(3)}G_{20}^* + (a_{20})^{(3)}(q_{21})^{(3)}G_{21}^* \\ & ((\lambda)^{(3)} + (b'_{20})^{(3)} - (r_{20})^{(3)})s_{(21),(20)}T_{21}^* + (b_{21})^{(3)}s_{(20),(20)}T_{20}^* \} \end{aligned}$$

$$\begin{aligned}
 & \left((\lambda^{(3)})^2 + (a'_{20})^{(3)} + (a'_{21})^{(3)} + (p_{20})^{(3)} + (p_{21})^{(3)} \right) (\lambda^{(3)}) \\
 & \left((\lambda^{(3)})^2 + (b'_{20})^{(3)} + (b'_{21})^{(3)} - (r_{20})^{(3)} + (r_{21})^{(3)} \right) (\lambda^{(3)}) \\
 & + \left((\lambda^{(3)})^2 + (a'_{20})^{(3)} + (a'_{21})^{(3)} + (p_{20})^{(3)} + (p_{21})^{(3)} \right) (\lambda^{(3)}) (q_{22})^{(3)} G_{22} \\
 & + \left((\lambda^{(3)} + (a'_{20})^{(3)} + (p_{20})^{(3)}) (a_{22})^{(3)} (q_{21})^{(3)} G_{21}^* + (a_{21})^{(3)} (a_{22})^{(3)} (q_{20})^{(3)} G_{20}^* \right) \\
 & \left((\lambda^{(3)} + (b'_{20})^{(3)} - (r_{20})^{(3)}) s_{(21),(22)} T_{21}^* + (b_{21})^{(3)} s_{(20),(22)} T_{20}^* \right) \} = 0 \\
 & + \\
 & \left((\lambda^{(4)} + (b'_{26})^{(4)} - (r_{26})^{(4)}) \{ (\lambda^{(4)} + (a'_{26})^{(4)} + (p_{26})^{(4)}) \right. \\
 & \left. \left[\left((\lambda^{(4)} + (a'_{24})^{(4)} + (p_{24})^{(4)}) (q_{25})^{(4)} G_{25}^* + (a_{25})^{(4)} (q_{24})^{(4)} G_{24}^* \right) \right] \right. \\
 & \left((\lambda^{(4)} + (b'_{24})^{(4)} - (r_{24})^{(4)}) s_{(25),(25)} T_{25}^* + (b_{25})^{(4)} s_{(24),(25)} T_{25}^* \right) \\
 & + \left((\lambda^{(4)} + (a'_{25})^{(4)} + (p_{25})^{(4)}) (q_{24})^{(4)} G_{24}^* + (a_{24})^{(4)} (q_{25})^{(4)} G_{25}^* \right) \\
 & \left((\lambda^{(4)} + (b'_{24})^{(4)} - (r_{24})^{(4)}) s_{(25),(24)} T_{25}^* + (b_{25})^{(4)} s_{(24),(24)} T_{24}^* \right) \\
 & \left. \left((\lambda^{(4)})^2 + (a'_{24})^{(4)} + (a'_{25})^{(4)} + (p_{24})^{(4)} + (p_{25})^{(4)} \right) (\lambda^{(4)}) \right. \\
 & \left. \left((\lambda^{(4)})^2 + (b'_{24})^{(4)} + (b'_{25})^{(4)} - (r_{24})^{(4)} + (r_{25})^{(4)} \right) (\lambda^{(4)}) \right. \\
 & + \left((\lambda^{(4)})^2 + (a'_{24})^{(4)} + (a'_{25})^{(4)} + (p_{24})^{(4)} + (p_{25})^{(4)} \right) (\lambda^{(4)}) (q_{26})^{(4)} G_{26} \\
 & + \left((\lambda^{(4)} + (a'_{24})^{(4)} + (p_{24})^{(4)}) (a_{26})^{(4)} (q_{25})^{(4)} G_{25}^* + (a_{25})^{(4)} (a_{26})^{(4)} (q_{24})^{(4)} G_{24}^* \right) \\
 & \left. \left((\lambda^{(4)} + (b'_{24})^{(4)} - (r_{24})^{(4)}) s_{(25),(26)} T_{25}^* + (b_{25})^{(4)} s_{(24),(26)} T_{24}^* \right) \} = 0 \\
 & + \\
 & \left((\lambda^{(5)} + (b'_{30})^{(5)} - (r_{30})^{(5)}) \{ (\lambda^{(5)} + (a'_{30})^{(5)} + (p_{30})^{(5)}) \right. \\
 & \left. \left[\left((\lambda^{(5)} + (a'_{28})^{(5)} + (p_{28})^{(5)}) (q_{29})^{(5)} G_{29}^* + (a_{29})^{(5)} (q_{28})^{(5)} G_{28}^* \right) \right] \right. \\
 & \left((\lambda^{(5)} + (b'_{28})^{(5)} - (r_{28})^{(5)}) s_{(29),(29)} T_{29}^* + (b_{29})^{(5)} s_{(28),(29)} T_{29}^* \right) \\
 & + \left((\lambda^{(5)} + (a'_{29})^{(5)} + (p_{29})^{(5)}) (q_{28})^{(5)} G_{28}^* + (a_{28})^{(5)} (q_{29})^{(5)} G_{29}^* \right) \\
 & \left((\lambda^{(5)} + (b'_{28})^{(5)} - (r_{28})^{(5)}) s_{(29),(28)} T_{29}^* + (b_{29})^{(5)} s_{(28),(28)} T_{28}^* \right) \\
 & \left. \left((\lambda^{(5)})^2 + (a'_{28})^{(5)} + (a'_{29})^{(5)} + (p_{28})^{(5)} + (p_{29})^{(5)} \right) (\lambda^{(5)}) \right. \\
 & \left. \left((\lambda^{(5)})^2 + (b'_{28})^{(5)} + (b'_{29})^{(5)} - (r_{28})^{(5)} + (r_{29})^{(5)} \right) (\lambda^{(5)}) \right. \\
 & + \left((\lambda^{(5)})^2 + (a'_{28})^{(5)} + (a'_{29})^{(5)} + (p_{28})^{(5)} + (p_{29})^{(5)} \right) (\lambda^{(5)}) (q_{30})^{(5)} G_{30} \\
 & + \left((\lambda^{(5)} + (a'_{28})^{(5)} + (p_{28})^{(5)}) (a_{30})^{(5)} (q_{29})^{(5)} G_{29}^* + (a_{29})^{(5)} (a_{30})^{(5)} (q_{28})^{(5)} G_{28}^* \right) \\
 & \left. \left((\lambda^{(5)} + (b'_{28})^{(5)} - (r_{28})^{(5)}) s_{(29),(30)} T_{29}^* + (b_{29})^{(5)} s_{(28),(30)} T_{28}^* \right) \} = 0 \\
 & + \\
 & \left((\lambda^{(6)} + (b'_{34})^{(6)} - (r_{34})^{(6)}) \{ (\lambda^{(6)} + (a'_{34})^{(6)} + (p_{34})^{(6)}) \right. \\
 & \left. \left[\left((\lambda^{(6)} + (a'_{32})^{(6)} + (p_{32})^{(6)}) (q_{33})^{(6)} G_{33}^* + (a_{33})^{(6)} (q_{32})^{(6)} G_{32}^* \right) \right] \right. \\
 & \left((\lambda^{(6)} + (b'_{32})^{(6)} - (r_{32})^{(6)}) s_{(33),(33)} T_{33}^* + (b_{33})^{(6)} s_{(32),(33)} T_{33}^* \right) \\
 & + \left((\lambda^{(6)} + (a'_{33})^{(6)} + (p_{33})^{(6)}) (q_{32})^{(6)} G_{32}^* + (a_{32})^{(6)} (q_{33})^{(6)} G_{33}^* \right) \\
 & \left((\lambda^{(6)} + (b'_{32})^{(6)} - (r_{32})^{(6)}) s_{(33),(32)} T_{33}^* + (b_{33})^{(6)} s_{(32),(32)} T_{32}^* \right) \\
 & \left. \left((\lambda^{(6)})^2 + (a'_{32})^{(6)} + (a'_{33})^{(6)} + (p_{32})^{(6)} + (p_{33})^{(6)} \right) (\lambda^{(6)}) \right. \\
 & \left. \left((\lambda^{(6)})^2 + (b'_{32})^{(6)} + (b'_{33})^{(6)} - (r_{32})^{(6)} + (r_{33})^{(6)} \right) (\lambda^{(6)}) \right. \\
 & + \left((\lambda^{(6)})^2 + (a'_{32})^{(6)} + (a'_{33})^{(6)} + (p_{32})^{(6)} + (p_{33})^{(6)} \right) (\lambda^{(6)}) (q_{34})^{(6)} G_{34} \\
 & + \left((\lambda^{(6)} + (a'_{32})^{(6)} + (p_{32})^{(6)}) (a_{34})^{(6)} (q_{33})^{(6)} G_{33}^* + (a_{33})^{(6)} (a_{34})^{(6)} (q_{32})^{(6)} G_{32}^* \right) \\
 & \left. \left((\lambda^{(6)} + (b'_{32})^{(6)} - (r_{32})^{(6)}) s_{(33),(34)} T_{33}^* + (b_{33})^{(6)} s_{(32),(34)} T_{32}^* \right) \} = 0
 \end{aligned}$$

And as one sees, all the coefficients are positive. It follows that all the roots have negative real part, and this proves the theorem.

Acknowledgments:

The introduction is a collection of information from various articles, Books, News Paper reports, Home Pages Of authors, Journal Reviews, Nature 's Letters, Article Abstracts, Research papers, Abstracts Of Research Papers, Stanford Encyclopedia, Web Pages, Ask a Physicist Column, Deliberations with Professors, the internet including Wikipedia. We acknowledge all authors who have contributed to the

same. In the eventuality of the fact that there has been any act of omission on the part of the authors, we regret with great deal of compunction, contrition, regret, trepidation and remorse. As Newton said, it is only because erudite and eminent people allowed one to piggy ride on their backs; probably an attempt has been made to look slightly further. Once again, it is stated that the references are only illustrative and not comprehensive

REFERENCES

1. Dr K N Prasanna Kumar, Prof B S Kiranagi, Prof C S Bagewadi - MEASUREMENT DISTURBS EXPLANATION OF QUANTUM MECHANICAL STATES-A HIDDEN VARIABLE THEORY - published at: "International Journal of Scientific and Research Publications, Volume 2, Issue 5, May 2012 Edition".
2. DR K N PRASANNA KUMAR, PROF B S KIRANAGI and PROF C S BAGEWADI -CLASSIC 2 FLAVOUR COLOR SUPERCONDUCTIVITY AND ORDINARY NUCLEAR MATTER-A NEW PARADIGM STATEMENT - published at: "International Journal of Scientific and Research Publications, Volume 2, Issue 5, May 2012 Edition".
3. A HAIMOVICI: "On the growth of a two species ecological system divided on age groups". Tensor, Vol 37 (1982), Commemoration volume dedicated to Professor Akitsugu Kawaguchi on his 80th birthday.
4. FRTJOF CAPRA: "The web of life" Flamingo, Harper Collins See "Dissipative structures" pages 172-188 HEYLIGHEN F. (2001): "The Science of Self-organization and Adaptivity", in L. D. Kiel, (ed) . Knowledge Management, Organizational Intelligence and Learning, and Complexity, in: The Encyclopedia of Life Support Systems ((EOLSS), (Eolss Publishers, Oxford) [http://www.eolss.net.
5. MATSUI, T, H. Masunaga, S. M. Kreidenweis, R. A. Pielke Sr., W.-K. Tao, M. Chin, and Y. J Kaufman (2006), "Satellite-based assessment of marine low cloud variability associated with aerosol, atmospheric stability, and the diurnal cycle", J. Geophys. Res., 111, D17204, doi:10.1029/2005JD006097.
6. STEVENS, B, G. Feingold, W.R. Cotton and R.L. Walko, "Elements of the microphysical structure of numerically simulated nonprecipitating stratocumulus" J. Atmos. Sci., 53, 980-1006.
7. FEINGOLD, G, Koren, I; Wang, HL; Xue, HW; Brewer, WA (2010), "Precipitation-generated oscillations in open cellular cloud fields" Nature, 466 (7308) 849-852, doi: 10.1038/nature09314, Published 12-Aug 2010.
8. a b c Einstein, A. (1905), "Ist die Trägheit eines Körpers von seinem Energieinhalt abhängig?", Annalen der Physik 18: 639 Bibcode 1905AnP...323..639E,DOI:10.1002/andp.19053231314. See also the English translation.
9. a b Paul Allen Tipler, Ralph A. Llewellyn (2003-01), Modern Physics, W. H. Freeman and Company, pp. 87–88, ISBN 0-7167-4345-0
10. a b Rainville, S. et al. World Year of Physics: A direct test of $E=mc^2$. Nature 438, 1096-1097 (22 December 2005) | doi: 10.1038/4381096a; Published online 21 December 2005.
11. n F. Fernflores. The Equivalence of Mass and Energy. Stanford Encyclopedia of Philosophy
12. Note that the relativistic mass, in contrast to the rest mass m_0 , is not a relativistic invariant, and that the velocity is not a Minkowski four-vector, in contrast to the quantity dx^μ , where dx^μ is the differential of the proper time. However, the energy-momentum four-vector p^μ is a genuine Minkowski four-vector, and the intrinsic origin of the square-root in the definition of the relativistic mass is the distinction between $d\tau$ and dt .
13. Relativity DeMystified, D. McMahon, Mc Graw Hill (USA), 2006, ISBN 0-07-145545-0
14. Dynamics and Relativity, J.R. Forshaw, A.G. Smith, Wiley, 2009, ISBN 978-0-470-01460-8
15. Hans, H. S.; Puri, S. P. (2003). Mechanics (2 ed.). Tata McGraw-Hill. p. 433. ISBN 0-07-047360-9., Chapter 12 page 433
16. E. F. Taylor and J. A. Wheeler, Spacetime Physics, W.H. Freeman and Co., NY. 1992.ISBN 0-7167-2327-1, see pp. 248-9 for discussion of mass remaining constant after detonation of nuclear bombs, until heat is allowed to escape.
17. Mould, Richard A. (2002). Basic relativity (2 ed.). Springer. p. 126. ISBN 0-387-95210-1., Chapter 5 page 126
18. Chow, Tail L. (2006). Introduction to electromagnetic theory: a modern perspective. Jones & Bartlett Learning. p. 392. ISBN 0-7637-3827-1., Chapter 10 page 392
19. a b c Conversions used: 1956 International (Steam) Table (IT) values where one calorie \equiv 4.1868 J and one BTU \equiv 1055.05585262 J. Weapons designers' conversion value of one gram TNT \equiv 1000 calories used.
20. Assuming the dam is generating at its peak capacity of 6,809 MW.
21. Assuming a 90/10 alloy of Pt/Ir by weight, a C_p of 25.9 for Pt and 25.1 for Ir, a Pt-dominated average C_p of 25.8, 5.134 moles of metal, and 132 J.K-1 for the prototype. A variation of ± 1.5 picograms is of course, much smaller than the actual uncertainty in the mass of the international prototype, which are ± 2 micrograms.
22. [3] Article on Earth rotation energy. Divided by c^2 .
23. a b Earth's gravitational self-energy is 4.6×10^{-10} that of Earth's total mass, or 2.7 trillion metric tons. Citation: The Apache Point Observatory Lunar Laser-Ranging Operation (APOLLO), T. W. Murphy, Jr. et al. University of Washington, Dept. of Physics (132 kB PDF, here.).
24. There is usually more than one possible way to define a field energy, because any field can be made to couple to gravity in many different ways. By general scaling arguments, the correct answer at everyday distances, which are long compared to the quantum gravity scale, should be minimal coupling, which means that no powers of the curvature tensor appear. Any non-minimal couplings, along with other higher order terms, are presumably only

determined by a theory of quantum gravity, and within string theory, they only start to contribute to experiments at the string scale.

25. G. 't Hooft, "Computation of the quantum effects due to a four-dimensional pseudoparticle", *Physical Review D* 14:3432–3450 (1976).
26. A. Belavin, A. M. Polyakov, A. Schwarz, Yu. Tyupkin, "Pseudoparticle Solutions to Yang Mills Equations", *Physics Letters* 59B:85 (1975).
27. F. Klinkhammer, N. Manton, "A Saddle Point Solution in the Weinberg Salam Theory", *Physical Review D* 30:2212.
28. Rubakov V. A. "Monopole Catalysis of Proton Decay", *Reports on Progress in Physics* 51:189–241 (1988).
29. S.W. Hawking "Black Holes Explosions?" *Nature* 248:30 (1974).
30. Einstein, A. (1905), "Zur Elektrodynamik bewegter Körper." (PDF), *Annalen der Physik* 17: 891–921, Bibcode 1905AnP...322...891E, DOI:10.1002/andp.19053221004. English translation.
31. See e.g. Lev B. Okun, The concept of Mass, *Physics Today* 42 (6), June 1969, p. 31–36, http://www.physicstoday.org/vol-42/iss-6/vol42no6p31_36.pdf
32. Max Jammer (1999), *Concepts of mass in contemporary physics and philosophy*, Princeton University Press, p. 51, ISBN 0-691-01017-X
33. Eriksen, Erik; Vøyenli, Kjell (1976), "The classical and relativistic concepts of mass", *Foundations of Physics* (Springer) 6: 115–124, Bibcode 1976FoPh...6..115E, DOI:10.1007/BF00708670
34. a b Janssen, M., Mecklenburg, M. (2007), *From classical to relativistic mechanics: Electromagnetic models of the electron.*, in V. F. Hendricks, et al., *Interactions: Mathematics, Physics and Philosophy* (Dordrecht: Springer): 65–134
35. a b Whittaker, E.T. (1951–1953), 2. Edition: *A History of the theories of aether and electricity*, vol. 1: The classical theories / vol. 2: The modern theories 1900–1926, London: Nelson
36. Miller, Arthur I. (1981), *Albert Einstein's special theory of relativity. Emergence (1905) and early interpretation (1905–1911)*, Reading: Addison–Wesley, ISBN 0-201-04679-2
37. a b Darrigol, O. (2005), "The Genesis of the theory of relativity." (PDF), *Séminaire Poincaré* 1: 1–22
38. Philip Ball (Aug 23, 2011). "Did Einstein discover $E = mc^2$?" *Physics World*.
39. Ives, Herbert E. (1952), "Derivation of the mass-energy relation", *Journal of the Optical Society of America* 42 (8): 540–543, DOI:10.1364/JOSA.42.000540
40. Jammer, Max (1961/1997). *Concepts of Mass in Classical and Modern Physics*. New York: Dover. ISBN 0-486-29998-8.
41. Stachel, John; Torretti, Roberto (1982), "Einstein's first derivation of mass-energy equivalence", *American Journal of Physics* 50 (8): 760–763, Bibcode1982AmJPh..50..760S, DOI:10.1119/1.12764
42. Ohanian, Hans (2008), "Did Einstein prove $E=mc^2$?", *Studies In History and Philosophy of Science Part B* 40 (2): 167–173, arXiv:0805.1400, DOI:10.1016/j.shpsb.2009.03.002
43. Hecht, Eugene (2011), "How Einstein confirmed $E_0=mc^2$ ", *American Journal of Physics* 79 (6): 591–600, Bibcode 2011AmJPh..79..591H, DOI:10.1119/1.3549223
44. Röhrlich, Fritz (1990), "An elementary derivation of $E=mc^2$ ", *American Journal of Physics* 58 (4): 348–349, Bibcode 1990AmJPh..58..348R, DOI:10.1119/1.16168 (1996).
45. Lise Meitner: *A Life in Physics*. California Studies in the History of Science. 13. Berkeley: University of California Press. pp. 236–237. ISBN 0-520-20860-UIBK.ac.at
46. J. J. L. Morton; et al. (2008). "Solid-state quantum memory using the 31P nuclear spin". *Nature* 455 (7216): 1085–1088. Bibcode 2008Natur.455.1085M. DOI:10.1038/nature07295.
47. S. Weisner (1983). "Conjugate coding". *Association of Computing Machinery, Special Interest Group in Algorithms and Computation Theory* 15: 78–88.
48. A. Zehinger, *Dance of the Photons: From Einstein to Quantum Teleportation*, Farrar, Straus & Giroux, New York, 2010, pp. 189, 192, ISBN 0374239665
49. B. Schumacher (1995). "Quantum coding". *Physical Review A* 51 (4): 2738–2747. Bibcode 1995PhRvA..51.2738S. DOI:10.1103/PhysRevA.51.2738.
50. a b Straumann, N (2000). "On Pauli's invention of non-abelian Kaluza-Klein Theory in 1953". ArXiv: gr-qc/0012054 [gr-qc].
51. See Abraham Pais' account of this period as well as L. Susskind's "Superstrings, *Physics World* on the first non-abelian gauge theory" where Susskind wrote that Yang–Mills was "rediscovered" only because Pauli had chosen not to publish.
52. Reifler, N (2007). "Conditions for exact equivalence of Kaluza-Klein and Yang-Mills theories". ArXiv: gr-qc/0707.3790 [gr-qc].
53. Yang, C. N.; Mills, R. (1954). "Conservation of Isotopic Spin and Isotopic Gauge Invariance". *Physical Review* 96 (1): 191–195. Bibcode 1954PhRv...96...191Y. DOI:10.1103/PhysRev.96.191.
54. Caprini, I.; Colangelo, G.; Leutwyler, H. (2006). "Mass and width of the lowest resonance in QCD". *Physical Review Letters* 96 (13): 132001. ArXiv: hep-ph/0512364. Bibcode 2006PhRvL..96m2001C. DOI:10.1103/PhysRevLett.96.132001.
55. Yndurain, F. J.; Garcia-Martin, R.; Pelaez, J. R. (2007). "Experimental status of the $\pi\pi$ isoscalar S wave at low energy: f₀ (600) pole and scattering length". *Physical Review D* 76 (7): 074034. ArXiv: hep-ph/0701025. Bibcode 2007PhRvD..76g4034G. DOI:10.1103/PhysRevD.76.074034.

56. Novikov, V. A.; Shifman, M. A.; A. I. Vainshtein, A. I.; Zakharov, V. I. (1983). "Exact Gell-Mann-Low Function of Supersymmetric Yang-Mills Theories From Instanton Calculus". Nuclear 229 (2): 381–393. Bibcode 1983NuPhB.229..381N.DOI:10.1016/0550-3213(83)90338-3.
57. Rytov, T.; Sannino, F. (2008). "Super symmetry Inspired QCD Beta Function". Physical Review D 78 (6): 065001. Bibcode 2008PhRvD..78f5001R.DOI:10.1103/PhysRevD.78.065001
58. Bogolubsky, I. L.; Ilgenfritz, E.-M.; A. I. Müller-Preussker, M.; Sternbeck, A. (2009). "Lattice gluodynamics computation of Landau-gauge Green's functions in the deep infrared". Physics Letters B 676 (1-3): 69–73. Bibcode 2009PhLB..676...69B.DOI:10.1016/j.physletb.2009.04.076.

First Author: 1Mr. K. N.Prasanna Kumar has three doctorates one each in Mathematics, Economics, Political Science. Thesis was based on Mathematical Modeling. He was recently awarded D.litt. for his work on 'Mathematical Models in Political Science'--- Department of studies in Mathematics, Kuvempu University, Shimoga, Karnataka, India Corresponding

Second Author: ²**Prof. B.S Kiranagi** is the Former Chairman of the Department of Studies in Mathematics, Manasa Gangotri and present Professor Emeritus of UGC in the Department. Professor Kiranagi has guided over 25 students and he has received many encomiums and laurels for his contribution to Co homology Groups and Mathematical Sciences. Known for his prolific writing, and one of the senior most Professors of the country, he has over 150 publications to his credit. A prolific writer and a prodigious thinker, he has to his credit several books on Lie Groups, Co Homology Groups, and other mathematical application topics, and excellent publication history.-- UGC Emeritus Professor (Department of studies in Mathematics), Manasagangotri, University of Mysore, Karnataka, India

Third Author: ³**Prof. C.S. Bagewadi** is the present Chairman of Department of Mathematics and Department of Studies in Computer Science and has guided over 25 students. He has published articles in both national and international journals. Professor Bagewadi specializes in Differential Geometry and its wide-ranging ramifications. He has to his credit more than 159 research papers. Several Books on Differential Geometry, Differential Equations are coauthored by him--- Chairman, Department of studies in Mathematics and Computer science, Jnanasahyadri Kuvempu University, Shankarghatta, Shimoga district, Karnataka, India

=====

Privileged Cryptography

Abhishek Dhull*, Priti**

*(Department of Computer Science & Applications, M.D. University, India)

** (Asstt. Prof., Department of Computer Science & Applications, M.D. University, India)

ABSTRACT: Cryptography is the practice and study of techniques for secure communication in the presence of third parties (called adversaries). More generally, it is about constructing and analyzing protocols that overcome the influence of adversaries and which are related to various aspects in information security such as data confidentiality, data integrity, and authentication. This paper presents the way of protecting the information from:

- Intruders: those who capture the packet and alter the information.
- Cryptanalysts: those who decrypt cipher text into plain text without key.

Keywords: Cryptanalyst, Decryption, Encryption, Intruder, Private key, Public key.

I. INTRODUCTION

Modern cryptography is heavily based on mathematical theory and computer science practice. Cryptographic algorithms are designed around computational hardness assumptions, making such algorithms hard to break in practice by any adversary. It is theoretically possible to break such a system but it is infeasible to do so by any known practical means. These schemes are therefore termed computationally secure; theoretical advances (e.g., improvements in integer factorization algorithms) and faster computing technology require these solutions to be continually adapted. There exist information-theoretically secure schemes that provably cannot be broken even with unlimited computing power—an example is the one-time pad—but these schemes are more difficult to implement than the best theoretically breakable but computationally secure mechanisms. Until modern times cryptography referred almost exclusively to *encryption*, which is the process of converting ordinary information (called plaintext) into unintelligible gibberish (called cipher text). Decryption is the reverse, in other words, moving from the unintelligible cipher text back to plaintext. A *cipher* (or *cypher*) is a pair of algorithms that create the encryption and the reversing decryption. The detailed operation of a cipher is controlled both by the algorithm and in each instance by a "key" [6]. This is a secret parameter (ideally known only to the communicants) for a specific message exchange context. A "cryptosystem" is the ordered list of elements of finite possible plaintexts, finite possible cipher texts, finite possible keys, and the encryption and decryption algorithms which correspond to each key[2]. Keys are important, as ciphers without variable keys can be trivially broken with only the knowledge of the cipher used

and are therefore useless (or even counter-productive) for most purposes. Historically, ciphers were often used directly for encryption or decryption without additional procedures such as authentication or integrity checks.

In colloquial use, the term "code" is often used to mean any method of encryption or concealment of meaning. However, in cryptography, *code* has a more specific meaning. It means the replacement of a unit of plaintext (i.e., a meaningful word or phrase) with a code word (for example, wallaby replaces attack at dawn). Codes are no longer used in serious cryptography—except incidentally for such things as unit designations (e.g., Bronco Flight or Operation Overlord)—since properly chosen ciphers are both more practical and more secure than even the best codes and also are better adapted to computers.

Cryptanalysis is the term used for the study of methods for obtaining the meaning of encrypted information without access to the key normally required to do so; i.e., it is the study of how to crack encryption algorithms or their implementations.

II. EXISTING WAYS OF CRYPTOGRAPHY

Some use the terms *cryptography* and *cryptology* interchangeably in English, while others (including US military practice generally) use *cryptography* to refer specifically to the use and practice of cryptographic techniques and *cryptology* refer to the combined study of cryptography and cryptanalysis [3]. English is more flexible than several other languages in which *cryptology* (done by cryptologists) is always used in the second sense above.

2.1 Symmetric-key cryptography

Symmetric-key cryptography refers to encryption methods in which both the sender and receiver share the same key (or, less commonly, in which their keys are different, but related in an easily computable way). This was the only kind of encryption publicly known until June 1976 One round (out of 8.5) of the patented IDEA cipher, used in some versions of PGP for high-speed encryption of, for instance, e-mail Symmetric key ciphers are implemented as either block ciphers or stream ciphers. A block cipher enciphers input in blocks of plaintext as opposed to individual characters, the input form used by a stream cipher.

The Data Encryption Standard (DES) and the Advanced Encryption Standard (AES) are block cipher designs which have been designated cryptography standards by the US government (though DES's designation was finally withdrawn after the AES was adopted). Despite its

deprecation as an official standard, DES (especially its still-approved and much more secure triple-DES variant) remains quite popular; it is used across a wide range of applications, from ATM encryption to e-mail privacy and secure remote access. Many other block ciphers have been designed and released, with considerable variation in quality.

Stream ciphers, in contrast to the 'block' type, create an arbitrarily long stream of key material, which is combined with the plaintext bit-by-bit or character-by-character, somewhat like the one-time pad. In a stream cipher, the output stream is created based on a hidden internal state which changes as the cipher operates. That internal state is initially set up using the secret key material. RC4 is a widely used stream cipher. Block ciphers can be used as stream ciphers.

2.2 Symmetric-key algorithms

Symmetric-key algorithms are a class of algorithms for cryptography that use trivially related, often identical, cryptographic keys for both encryption of plaintext and decryption of cipher text. Symmetric algorithms, sometimes called Conventional algorithms, are algorithms where the encryption key can be calculated from the decryption key and vice versa [1, 4]. The encryption key is trivially related to the decryption key, in that they may be identical or there is a simple transformation to go between the two keys. The keys, in practice, represent a shared secret between two or more parties that can be used to maintain a private information link. Other terms for symmetric-key encryption are secret-key, single-key, shared-key, one-key, and private-key encryption. Use of the last and first terms can create ambiguity with similar terminology used in public-key cryptography. Symmetric-key cryptography is to be contrasted with asymmetric-key cryptography [8].

2.3 Types of symmetric-key algorithms:

Symmetric-key encryption can use either stream ciphers or block ciphers.

- Stream ciphers encrypt the bits of a message one at a time.
- Block ciphers take a number of bits and encrypt them as a single unit. Blocks of 64 bits have been commonly used. The Advanced Encryption Standard (AES) algorithm approved by NIST in December 2001 uses 128-bit blocks [7].

2.3.1 Basic algorithm and terminology

RSA encryption and decryption are essentially mathematical operations. They are what are termed *exponentiation, modulo* a particular number. Because of this, RSA keys actually consist of numbers involved in this calculation, as follows:

- the public key consists of the modulus and a public exponent; the private key consists of that same modulus plus a private exponent.

2.3.2 Security of Public Key Schemes

- like private key schemes brute force exhaustive search attack is always theoretically possible
- but keys used are too large (>512bits)
- The public-key algorithms are based on a known hard problem. The its just made too hard to do in practise
- RSA Problem: Given $n=pq$, with p and q primes. Find p and q .
- requires the use of very large numbers, hence is slow compared to private key schemes

2.3.3 Existing Cryptography

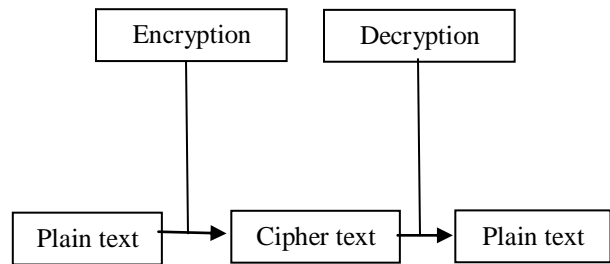


Fig. 1 Existing Cryptography

III. PROPOSED MODEL

3.1 Construction of Symmetric Ciphers

Many modern block ciphers are based on a construction proposed by Horst Feistel. Feistel's construction makes it possible to build invertible functions from other functions that are themselves not invertible.

3.2 Security of Symmetric Ciphers

Construction of the functions for each round can greatly reduce the chances of a successful attack.

3.3 Key Generation

When used with asymmetric ciphers for key transfer, pseudorandom key generators are nearly always used to generate the symmetric cipher session keys. However, lack of randomness in those generators or in their initialization vectors is disastrous and has led to cryptanalytic breaks in the past. Therefore, it is essential that an implementation uses a source of high entropy for its initialization. Symmetric ciphers have historically been susceptible to known-plaintext attacks, chosen plaintext attacks, differential cryptanalysis and linear cryptanalysis.

3.3.1 Detection of Intruder's Activity

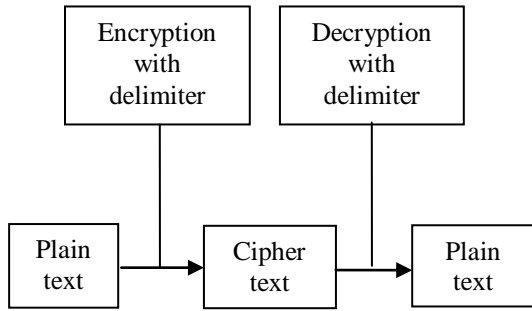


Fig.2 Encryption and Decryption with delimiter

Some time intruder make change in cipher text as a result it becomes difficult to know. Information becomes meaningless. A delimiter can be set with plain text during encryption so that at the time of decryption user could know whether cipher text was altered or not. If it is altered delimiter will not be visible at receiving end and packet will be retransmitted

3.3.2 Privileged Cryptography with IP Filtering

To protect information from cryptanalyst IP Filter would be attached in decryption module

Sometime cryptanalyst decrypt information without key, this problem can be solved using IP filtering

If there is decryption request from different IP then packets will be deleted.

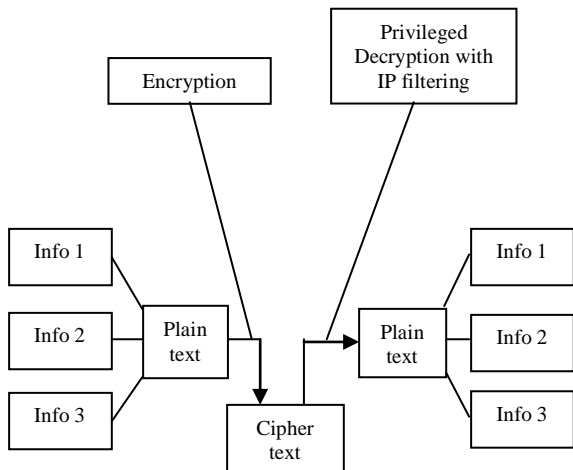


Fig. 3 Decryption with IP filtering

IV. CONCLUSION

It will improve the security of the text while sending it from sender to receiver. A delimiter can be set during encryption and decryption to know whether the data has been altered by an intruder or not. We can also protect our information from cryptanalyst, who can decrypt information without using key, by attaching IP filter during decryption. Hence our data becomes more secure when transmitted from sender to receiver.

REFERENCES

- [1] Bruce Schneier, *Applied Cryptography*, 2nd ed.
- [2] C.M. Adams, *Simple and Effective Key Scheduling for Symmetric Ciphers*, Workshop on Selected Areas in Cryptography-Workshop Record, Kingston, Ontario, May 1994, pp.129-133.
- [3] C.M.Adams and H.Meijer, *Security-Related Comments Regarding McEliece's Public-Key Cryptosystem*, Advances in Cryptology-CRYPTO'87 Proceedings, Sringer-Verlag, 1988, pp. 224-230.
- [4] B.S Adiga and P.Shankar, *Modified Lu-Lee Cryptosystem*, Electronics Letters, v.21, n.18, 29 Aug 1985, pp.794-795.
- [5] L.M. Adleman, *On Breaking Generalized Knapsack Public Key Cryptosystems*, Proceedings of the 15th ACM Symposium on Theory of Computing, 1983, pp.402-412.
- [6] Matt Blaze, *Cryptology and Physical Security: Rights Amplification in Master Keyed Mechanical Locks*, IEEE Security and Privacy, March 2003.
- [7] G.B. Agnew, R.C. Mullin, I.M. Onyszchuk, and S.A. Vanstone, *An Implementatin for a Fast Public-Key Cryptosystem*, Journal of Cryptology, v.3, n. 2, 1991, pp. 63-79.
- [8] G.B. Agnew, *Random Sources for Cryptographic Systems*, Advances in Cryptology- Eurocrypt'87 Proceedings, Springer-Verlag, 1988, pp. 77-81.

Shape Recognition based on Features matching using Morphological Operations

Shikha Garg¹, Gianetan Singh Sekhon²

¹(Student, M.Tech Department of Computer Engineering, YCOE, Punjabi University, Patiala, India)

²(Assistant Professor, M.Tech Department of Computer Engineering, YCOE, Punjabi University, Patiala, India)

ABSTRACT: This paper presents the implementation of method of shape recognition among different regular geometrical shapes using morphological operations. Many algorithms have been proposed for this problem but the major issue that has been enlightened in this paper is over segmentation dodging among different objects. After an introduction to shape recognition concept, we describe the process of extracting the boundaries of objects in order to avoid over segmentation. Then, a shape recognition approach is proposed. It is based on some mathematical formulae. Our new algorithm detects the shapes in the following cases when (i) There are distinct objects in the given image. (ii) The objects are touching in the given image. (iii) The objects are overlapping in the given image. (iv) One object is contained in the other in the given image. Then with the help of boundaries concentrate and shape properties, classification of the shapes is done.

Keywords: Edge detection, geometrical shapes, morphological operations, over segmentation, Shape recognition.

I. Introduction

In an image, shape plays a significant role. Shape of an image is one of the key information when an eye recognizes an object. Shape of an image does not change when colour of image is changed. Shape recognition finds its applications in robotics, fingerprint analysis, handwriting mapping, face recognition, remote sensors etc [6]. In pattern recognition shape is one of the significant research areas. Main focus of the pattern recognition is the classification between objects.

In a computer system, shape of an object can be interpreted as a region encircled by an outline of the object. The important job in shape recognition is to find and represent the exact shape information. Many algorithms for shape representation have been proposed so far.

Many methods for 2D shape representation and recognition have been reported. Curvature scale space (CSS), dynamic programming, shape context, Fourier descriptor, and wavelet descriptor are as the example of these approaches [8]. There are two methods for shape recognition, area based and boundary based technique. In area based technique, all pixels within the region of image are taken into consideration to get shape representation. Common area based technique uses moment descriptors to depict the shape. Whereas boundary based technique focuses mainly on object boundary. Boundary based technique represents shape feature of object more clearly as compared to area based technique. It is fast in processing and needs less computation than area based

technique. Due to fast processing and easy computation it is widely used in real time and practical applications. In this paper we consider just the boundary based technique.

In the previous work of shape recognition, object detection approaches based on color/texture segmentation or image binarization and foreground extraction is proposed, which can be used in this case. Other shape detection solutions are based on edge-detection, sliding-windows or generalized Hough transforms. The identified image objects are then recognized by their shapes. The focus of this paper is shape recognition by edge detection using morphological operations. In this paper the problem of over segmentation among different objects has been taken into consideration for shape recognition. The different objects in the given image are processed one by one and then they are clustered together to form the output image. This process is executed in two stages: firstly, the image is read in from the user and objects which are touching one another are segmented. Then we will match the features of the current object with the preloaded features in the database or we can say training set for recognition.

II. Materials and methods

The computation of proposed method can be briefly summarised in 2 steps (1) Avoidance of over segmentation among different objects like circle, rectangle, square etc with the use of morphological operations (2) Labelling the objects after recognition of various objects within the image.

2.1 Over segmentation avoidance

The proposed method is trying to prevent the over segmentation and segment some overlapping areas to extract the boundaries of various objects within the image. For this, read the RGB image in from the user and convert the RGB (coloured) image to gray scale and then to binary image. Invert the binary image in order to speed up the time of processing. Then morphological operation is implemented so that all the objects are eroded from all the sides and then the boundaries of small radius are enhanced along the edges of the objects.

```
se = strel('disk', 1);  
dummy1=imerode(dummy,se);
```

SE = strel('disk', R,) creates a flat, disk-shaped structuring element, where R specifies the radius. R must be a nonnegative integer. Here the value of R is 1. Imerode performs binary erosion; otherwise it performs gray scale erosion. If SE is an array of structuring element objects,

imerode performs multiple erosions of the input image, using each structuring element in SE in succession.

2.2 Recognition and labelling of objects

In this algorithm when the objects are being segmented from each other, the final stage is to identify the shape of the objects. This is done by using filtering technique. Some properties like sensitivity factor and corners of the objects are needed to predict the shapes of varying objects. Then with these mathematical parameters, objects of input image are matched with the preloaded features of the objects in the database or we can say training set and thus we can recognize the shape of the objects.

CIRCLE > Number of corners = 0 > Absolute difference b/w length and breadth < 25 > Sensitivity Factor = 0.24	TRIANGLE > Number of corners = 3 > Sensitivity Factor = 0.24	SQUARE > Number of corners = 4 > Absolute difference b/w length and breadth < 10 > Sensitivity Factor = 0.24
RECTANGLE > Number of corners = 4 > Absolute difference b/w length and breadth > 10 > Sensitivity Factor = 0.24	POLYGON > Number of corners > 4 > Absolute difference b/w length and breadth > 10 > Sensitivity Factor = 0.2	

Fig.1 filters used to distinguish objects

III. Experiments

We have performed numerous experiments using the described shape recognition approach. The proposed technique has been tested on various image datasets and satisfactory results have been obtained. A high recognition rate, of approximately 95 %, is achieved by our method. It represents a better rate that those of many other object recognition approaches.

An indexed image consists of an array and a colormap matrix. The pixel values in the array are direct indices into a colormap. An indexed image uses direct mapping of pixel values to colormap values. The color of each image pixel is determined by using the corresponding value of X as an index. As RGB image is having an index value of 255 therefore we set this parameter to a scalar between 250 and 0 and in loop this scalar value go on decrementing with a value 5. As this scalar value matches with the index value of object, the particular object is identified. The image is then converted in the binary form, then the binary image is processed using some morphological operations, to eliminate the over segmented area and retain only the important image regions.

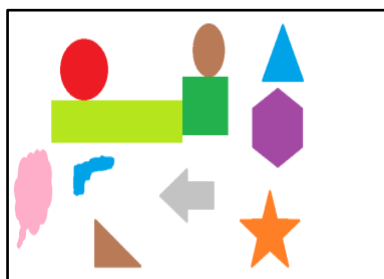


Fig.2 Image containing several objects

A shape recognition example is described in the next figures. Thus, in Fig.3 there is an displayed image containing objects which are segmented. Each object is marked with the *obj_i* value in the picture, $i = 2 \dots, 12$.

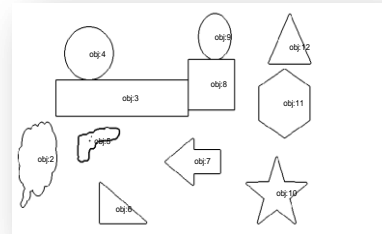


Fig.3 segmented objects

The connected components of the enhanced binary image are detected, thus the image foreground, containing the main objects, being extracted. The feature extraction process is then applied on the detected shapes. The obtained shapes are then classified using the presented shape recognition algorithm. The shape names corresponding to the image from Fig. 2 are represented in Fig. 4. As one can see in that figure, each object is labelled with the name matched with its features defined in Fig. 1. The final recognition result are, circle{obj4,obj6}, square{obj8}, rectangle{obj3}, triangle{obj5,obj12}, polygon{obj11}.

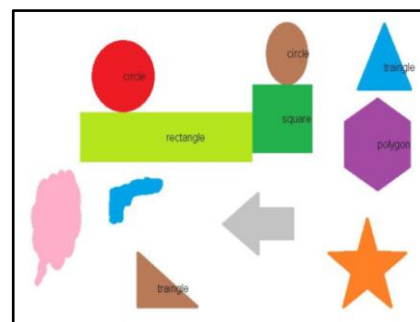


Fig.4 The resulted labelled objects

IV. Conclusion

In this study, a new method of shape recognition is proposed which takes into account the problem of over segmentation. By integrating the structural features like distance measure and centroid, the proposed method extracts the structural information of shapes. Based on those properties, various shapes can be recognized. The identification of the appropriate name of shape clusters automatizes the classification method, which represents a very important thing. That means our recognition technique can be used successfully for very large sets of images, containing a high number of shapes.

Experiments have shown that this method produces accurate and fast results with different images provided. The results of this provided recognition technique can be applied successfully in important domains, such as object recognition and segmentation.

[10] REN Honge, ZHONG Qiubo, KANG Junfen, Object Recognition Algorithm Research Based on Variable Illumination, *Proceedings of the IEEE International Conference on Automation and Logistics Shenyang*, 150040, China, 2009.

REFERENCES

- [1] S. W.Chen, S. T. Tung, and C. Y. Fang, Extended Attributed String Matching for Shape Recognition, *COMPUTER VISION AND IMAGE UNDERSTANDING*, Vol. 70, No. 1, April, pp. 36–50, 1998.
- [2] Sajjad Baloch, Object Recognition Through Topo-Geometric Shape Models Using Error-Tolerant Subgraph Isomorphism, *IEEE TRANSACTIONS ON IMAGE PROCESSING*, VOL. 19, NO. 5, 1191, 2010.
- [3] Rong Wang, Fanliang Bu, Hua Jin, Lihua Li, TOE SHAPE RECOGNITION ALGORITHM BASED ON FUZZY NEURAL NETWORKS, *Third International Conference on Natural Computation (ICNC 2007)*,0-7695-2875-9/07, © 2007.
- [4] Ruixia Song , Zhaoxia Zhao, Yanan Yanan Li, Qiaoxia Zhang, Xi Chen, The Method of Shape Recognition Based on V-system, *Fifth International Conference on Frontier of Computer Science and Technology*, China, 100144,2010.
- [5] S. Thilagamani, N.Shanthi, A Novel Recursive Clustering Algorithm for Image algorithm, *European Journal of Scientific Research*, ISSN 1450-216X, Vol.52, No.3, 2011.
- [6] Ehsan Moomivand, A Modified Structural Method for Shape Recognition, *IEEE Symposium on Industrial Electronics and Applications (ISIEA2011)*, September 25-28, Langkawi, Malaysia, 2011.
- [7] Jon Almaz´an, Alicia Forn´ Third es, Ernest Valveny, A Non-Rigid Feature Extraction Method for Shape Recognition, *International Conference on Document Analysis and Recognition*, Spain, 2011.
- [8] Kosorl Thourn and Yuttana Kitjaidure, Multi-View Shape Recognition Based on Principal Component Analysis, *International Conference on Advanced Computer Control Department of Electronics*, Bangkok, 10520, 2008.
- [9] Sen Wang, Yang Wang, Miao Jin, Xian feng David Gu, and Dimitris Samaras, Conformal Geometry and Its Applications on 3D Shape Matching, Recognition, and Stitching, *IEEE TRANSACTIONS ON PATTERN ANALYSIS AND MACHINE INTELLIGENCE*, VOL. 29, NO. 7, JULY 2007.

Performance of Symmetrical and Asymmetrical Multilevel Inverters

K. Lakshmi Ganesh, U. Chandra Rao

**(Department of Electrical and Electronics Engineering, Sri Vasavi Engineering College, India)*

*** (Department of Electrical and Electronics Engineering, Sri Vasavi Engineering College, India)*

ABSTRACT: *Distributed Energy Resources (DER) are systems that produce electrical power at the site where the power is needed. If only electrical power is used then the technology is called Distributed Generation (DG). The objective of this paper is to study a novel more than five level multistring inverter topology for DERs based DC/AC conversion system. The distributed energy resource based single-phase inverter is usually adopted in the microgrid system. In order to reduce the conversion losses, the key is to saving costs and size by removing any kind of transformer as well as reducing the power switches. In this study, a high step-up converter is introduced as a front-end stage to improve the conversion efficiency of conventional boost converters and to stabilize the output DC voltage of various DERs such as photovoltaic for use with the simplified multilevel inverter. In addition, two active switches are operated under line frequency. In this project a novel asymmetrical configuration is proposed. The proposed asymmetrical configuration uses less number of switches to get more levels. It will reduce the cost, reduce the number of sources, complexity, losses and improves reliability. The proposed converter is simulated by Matlab/Simulink software and simulation results are presented.*

Key words: *DC/AC power conversion, multilevel inverter, harmonic analysis and Total Harmonic Distortion (THD).*

I. INTRODUCTION

The continuous economic development of many countries and the environmental issues (gas emissions and the green house effect) observed in the last decades forced an intense research in renewable energy sources. Distributed energy resources are small, modular, energy generation and storage technologies that provide electric capacity or energy where you need it. Typically producing less than 10 megawatts (MW) of power, DER systems can usually be sized to meet your particular needs and installed on site.

DER technologies include wind turbines, photo voltaic (PV), fuel cells, micro turbines, reciprocating engines, Hydro, combustion turbines and energy storage systems are the most explored technologies due to their considerable advantages [1],[2], such as reliability, reasonable installation and energy

production costs, low environmental impact, capability to support micro grid [3].

The renewable energy resources consists of photovoltaic, fuel cells are generate the voltage are dc voltage. But I want the ac voltage because of mostly used the loads are ac loads. So we are convert the dc power to ac power processing interface is required and is Commercial, homes, factories and utility grid standards [4],[7].

Differing converter topographies have been acquired DERs establish effectual power flow control performance of DERs. DER systems may be either connected to the local electric power grid or isolated from the grid in stand-alone applications [7], [10].

The dc-dc converters are two types. They are without galvanic isolation and with galvanic isolation (high frequency transformer).The with galvanic isolation converter (high power applications) are used corresponding to size, weight, expense reduces. So low and medium power applications without galvanic isolation means make no use of transformers corresponding to reduces the size, weight expense [7], [8].

The next procedure the output voltage level increases of the inverter output then automatically harmonic component of the output voltage of inverter reduces and also corresponding to small size of filters are used simultaneously the cost reduces. The differing multilevel topographies are usually characterizing by strong reduction of switching power losses and electromagnetic interference (EMI) [6], [7], [8].

A new simplified single-phase multistring five-level multilevel inverter topography of dc/ac power conversion with auxiliary circuit proposed [8], [9]. This topography are used, the number of switching devices and output harmonics are reduced. The THD of the multistring five-level inverter is much less than the conventional multistring three-level inverter because of additional auxiliary circuit has high switching losses [9].

The objective of this paper is to study a newly constructed transformerless five level multistring inverter topology for DERS. In this letter aforesaid GZV-based inverter is reduced to a multistring multilevel inverter topography that require only 6 active switches instead of existing cascaded H-bridge multilevel inverter have eight switches[10].Multi string multilevel inverter have six active switches. They are middle two switches are operated

fundamental frequency and remaining four switches are operated switching frequency. A high efficiency dc-dc boost converter reduction of transformer and device voltage and current stresses with continuous input current leakage inductance energy recovery, and avoiding the use of electrolytic capacitor due to reduced ripple current[13]. Operation of the system configuration of operation is shown below. The performance of symmetrical and asymmetrical single phase multilevel inverter with respect to harmonics content and number of switches and input voltage source is DC is simulated by MATLAB/Simulink. A detailed harmonic analysis is done on the multilevel inverter by considering up to 23rd harmonics for 7 levels to 13 levels operation.

II. SYSTEM CONFIGURATION OF OPERATION PRINCIPLES

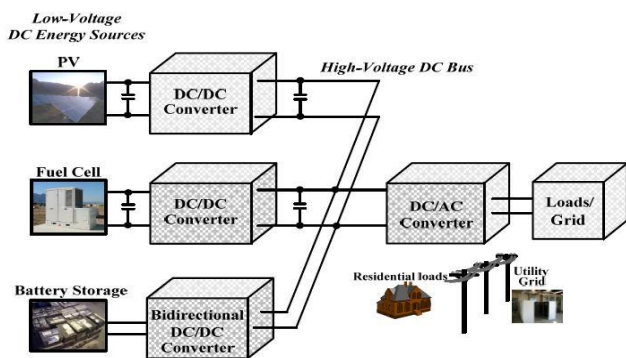


Fig.1 Different type of DERs are system configuration of Multistring Inverter

The above Fig.1 shows the DERs have photovoltaics or Fuel cell inverter are taken as [14]. The individual dc/dc boost converter are connected to the photovoltaic modules or Fuel cell. The bidirectional (buck-boost) dc/dc converter is connected to the only for battery storage. The individual dc/dc boost converter is connected to the multistring inverter. These common inverter for interface with all dc/dc converters of DERs [15]. The two modes of operation above Fig.1. They are standalone mode and grid connected mode. In grid connected mode, the battery storage energy is not connected to the grid. In standalone operation, the battery storage energy is connected to the load.

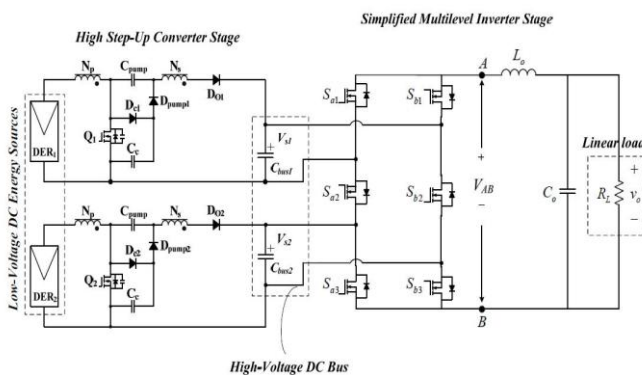


Fig.2 Single phase simplified multistring five-level inverter topography for high stepup converter from DERs

The above Fig.2 shows DER module-1 is connected to the high step up dc/dc converter and DER module-2 is connected to high step up dc/dc converter. These two converters are connected to their individual dc-bus capacitor and a simplified multilevel inverter. The resistive load is connected output of the simplified multilevel inverter from DER through high step up dc/dc converter. The input sources of DERs are photovoltaic or Fuel cells. The basic circuit have eight switches of cascaded H-bridge Multilevel inverter (CHB) with phase shift carrier pulse width modulation scheme are used. The simplified multilevel inverter have six switches then best merits of improved output waveforms, reduced the filter size, low EMI and THD [11],[12]. It should be noted that, by using independent voltage regulation control of the individual high step-up converter, voltage balance control for the two bus capacitors C_{bus1} , C_{bus2} can be achieved normally.

2.1. High Step-Up Converter Stage

In this study, High Efficiency Converter with Charge Pump and Coupled Inductor for Wide Input Photovoltaic AC Module Applications [13]. This simplified multilevel inverter combines the behavior of three different converter topologies: boost, flyback and charge pump. The flyback aspect of the topology allows the design to be optimized in terms of the transformer turns-ratio, allowing for much higher voltage gains than would be possible with a boost converter. However, flyback converters are notoriously inefficient and are very sensitive to leakage inductance, which can cause undue voltage-stress on switches and diodes. By using a clamp-circuit- identical to the output of a boost-converter- after the main switch, much of the efficiency issues can be resolved and the transformer design becomes less complicated. Finally, adding a charge-pump capacitor across the primary and secondary windings of the transformers gives higher converter voltage-gain and reduced peak current stress by allowing the current of the primary-windings to continuous.

The equivalent circuit of the proposed converter is shown in Fig.3. The coupled inductor is modeled as a magnetizing inductor L_m an ideal transformer with a turn's ratio of $N_s : N_p$ primary leakage inductor L_{Lk1} and secondary leakage inductor L_{Lk2} . C_c is the clamp capacitor, S is the Active switch, D_0 is the output diode C_{pump} is the charge pump capacitor.

According to voltage-seconds balance condition of the magnetizing inductor, the voltage of the primary winding can be derived as

$$V_{pri} = V_{in} \frac{D}{1-D} \tag{1}$$

Where V_m represents each the low-voltage dc energy input sources and voltage of the secondary winding is

$$V_{sec} = \frac{N_S}{N_P} \cdot V_{pri} = \frac{N_S}{N_P} \cdot V_{in} \frac{D}{1-D} \quad (2)$$

Similar to that of the boost converter, the voltage of the charge-pump capacitor C_{pump} and clamp capacitor C_c can be expressed as

$$V_{C_{pump}} = V_{C_c} = V_{in} \cdot \frac{1}{1-D} \quad (3)$$

Hence, the voltage conversion ratio of the high step-up converter, named input voltage to bus voltage ratio, can be derived as [13].

$$\frac{V_0}{V_{in}} = \frac{\left(2 + \frac{N_S}{N_P} \cdot D\right)}{1-D} \quad (4)$$

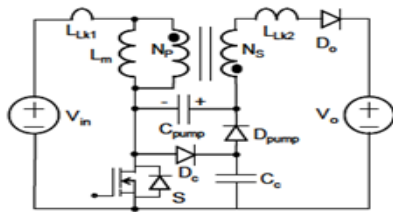


Fig.3. Equivalent circuit of the high step-up boost converter

2.2 Simplified Multilevel Inverter Stage

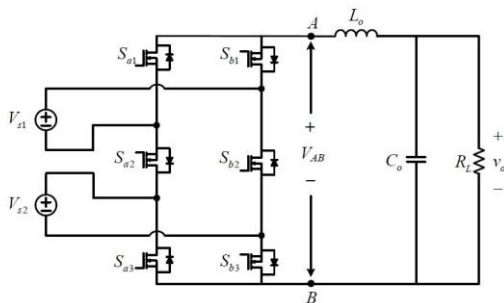


Fig.4 Basic Five-level inverter Circuitry of six switches

The simplified multilevel inverter is the conventional circuit of five level inverter Fig.4 shows above. A new single phase multistring topography, as a new basic circuitry in Fig.4. Referring to Fig.2, it is should assumed that, in this configuration, the two capacitors in the capacitive voltage divider are connected directly across the dc bus and all switching combinations are activated in an output cycle. The dynamic voltage balance between the two capacitors is automatically controlled by the preceding high step-up converter stage. Then, we can assume $V_{s1} = V_{s2} = V_s$.

This circuit has six power switches compare the basic circuit of cascaded H-bridge has eight power switches which drastically reduces the power circuit complexity and simplifies modulation circuit design and implementation. The phase disposition (PD) pulse width modulation (PWM) control scheme is introduced to generate switching signals

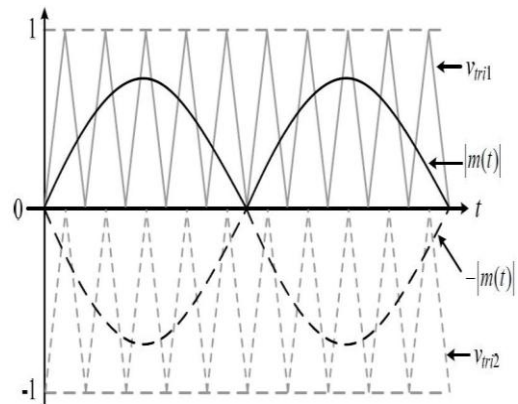
and to produce five output voltage levels: $0, V_s, 2V_s, -V_s$ and $2V_s$

This inverter topology uses two carrier signals and one reference signal to generate the PWM signals for the switches the modulation strategy and its implemented logic scheme in Fig.5 (a) and (b) area widely used alternative for Phase disposition modulation. With the exception of an offset value equivalent to the carrier signal amplitude. Two comparators are used in this scheme with identical carrier signals V_{tri1} and V_{tri2} to provide high-frequency switching signals

for S_{a1}, S_{b1}, S_{a3} and S_{b3} . Another comparator is used for zero-crossing detection to provide line-frequency switching signals for switches S_{a2} and S_{b2} .

For Fig.4 the switching function of the switch defined as follows.

- $S_{aj} = 1, S_{aj}$ ON
- $S_{aj} = 0, S_{aj}$ OFF for $j=1, 2, 3$
- $S_{bj} = 1, S_{bj}$ ON
- $S_{bj} = 0, S_{bj}$ OFF for $j=1, 2, 3$



(a)

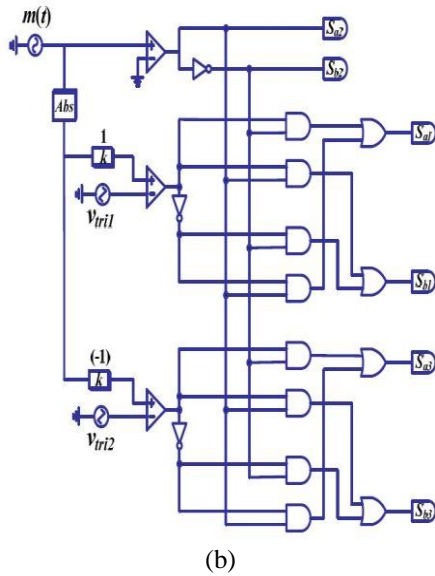


Fig.5. Modulation strategy a) Carrier/reference signals
 (b) modulation logic

Table-I

Simplified Five Level Inverter Switching Combination

S_{a1}	S_{a2}	S_{a3}	S_{b1}	S_{b2}	S_{b3}	V_{AB}
0	1	0	1	0	1	$2V_S$
0	1	1	1	0	0	V_S
1	1	0	0	0	1	V_S
1	1	1	0	0	0	0
0	0	0	1	1	1	0
1	0	0	0	1	1	$-V_S$
0	0	1	1	1	0	$-V_S$
1	0	1	0	1	0	$-2V_S$

Table-I lists switching combinations that generate the required five output levels. The corresponding operation modes of the simplified multilevel inverter stage are described clearly as follows.

1) Maximum positive output voltage ($2V_S$): Active switches S_{a2} , S_{b3} and S_{b1} are ON. The voltage applied to the LC output filter is $2V_S$.

2) Half level positive output voltage ($+V_S$): The two switching combinations are there. One switching combination is that active switches S_{a2} , S_{a3} and S_{b1} are ON, the other is active switches S_{a2} , S_{a1} and S_{b3} are ON. During this operating stage, the voltage applied to the LC output filter $+V_S$.

3) Zero Output, (0): This output condition either one of the leg are left or right all switches are ON. The load is short-circuited, and the voltage applied to the load terminals zero.

4) Half level negative output voltage ($-V_S$): the two switching combinations are there. One switching combination is such that active switches S_{a1} , S_{b2} and S_{b3} are ON, the other switching is active switches S_{b2} , S_{b1} and S_{a3} .

5) Maximum negative output ($-2V_S$): During this stage, active switches S_{a1} , S_{a3} and S_{b2} are ON, and the output voltage applied to the LC output filter $-2V_S$.

In these circuit operations, it can be observed that the open voltage stress of the active power switches S_{a1} , S_{b1} , S_{a3} and S_{b3} is equal to input voltage V_S and the main active switches S_{a2} and S_{b2} are operated at the line frequency. Hence, the switching losses are reduced in the new topology and the overall conversion efficiency is improved.

In Fig.5 control circuit diagram as shown, $m(t)$ is the sinusoidal modulation signal. Both V_{ri1} and V_{ri2} are two carrier signals. The magnitude value and frequency of the sinusoidal modulation signal are given as $m_{peak}=0.7$ and $f_m=60\text{Hz}$. The peak to peak value of the triangular modulation signals is equal to 1 and the switching frequency f_{ri1} and f_{ri2} are both given as 18.06 kHz.

The two input voltage sources feeding from the high step up converter is controlled at 100V that is $V_{s1} = V_{s2} = 100\text{V}$. The five level output of the phase voltage of the simulation waveform is shown in Fig.6.

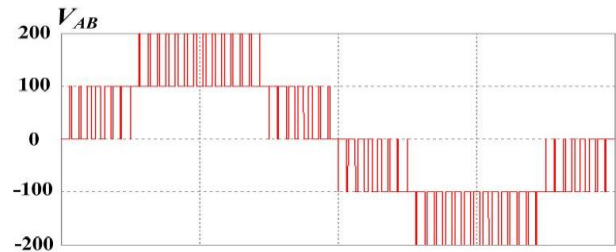


Fig.6 Simplified multilevel five level output phase voltage of simulation waveform V_{AB}

2.3 Basic circuit of Cascaded H-Bridge (CHB) Inverter

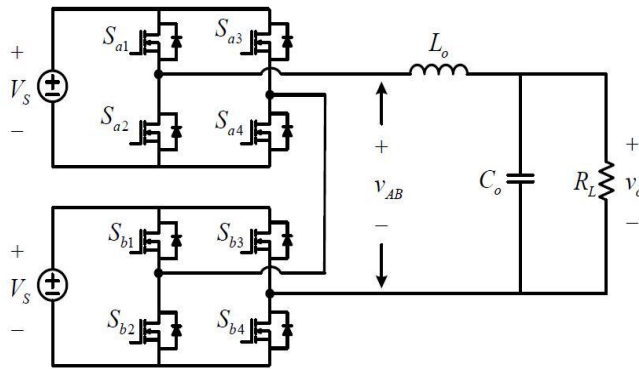


Fig.7 Basic circuit of five-level inverter topology of CHB inverter have eight switches

The above figure shows the Basic circuit of five level inverter CCHB inverter have eight switches. The carrier based sinusoidal phase shift carrier pulse width modulations are used in the basic circuit of CHB inverter. The eight switches are operated of the switching frequency. The CHB inverter are operate at the switching frequency is same as 18.06kHz the same modulation index $m_a=0.7$.

The simplified multilevel inverter and Cascaded H-bridge inverter are operated the same switching frequency and same modulation index m_a , the same input voltage $V_s=100V$ and output L-C filter, $L_o=20mH, C_o=200\mu F, R-load=100\Omega$. Table VII and Table VIII shows the harmonic component and THD Cascaded H-Bridge Inverter and Simplified multilevel inverter. The simplified multilevel inverter have the lesser THD compare to the Cascaded H-bridge inverter. So the low values of LC filter.

The symmetrical multilevel inverters are Cascaded H-bridge inverter and Simplified multilevel inverter. These are taken the equal voltage values. The symmetrical multilevel inverters above are operated with PWM method. The Proposing methods of asymmetrical multilevel inverters are repeating sequence is used for Seven, Nine, Eleven and Thirteen levels. The seven level have 6 switches and Nine, Eleven and Thirteen level have 8 switches. The Seven, Nine, Eleven and Thirteen levels are get by using 12,16,20,24 switches are necessity in symmetrical configuration of Cascaded H-bridge inverter. So the less number of switches are in asymmetrical configuration to get more number of voltage levels, lesser the THD, low cost, reducing the DC sources, reduce the complexity and driving circuits.

III. PROPOSED SYTEM

3.1 Seven Level Multi Level Inverter (MLI)

Table- II
Seven Level Multilevel Inverter (MLI)

S_{a1}	S_{a2}	S_{a3}	S_{b1}	S_{b2}	S_{b3}	V_0
----------	----------	----------	----------	----------	----------	-------

0	1	0	1	0	1	$3V_s$
1	1	0	0	0	1	$2V_s$
0	1	1	1	0	0	V_s
1	1	1	0	0	0	0
0	0	0	1	1	1	0
1	0	0	0	1	1	$-V_s$
0	0	1	1	1	0	$-2V_s$
1	0	1	0	1	0	$-3V_s$

The above Table II is shows the active switches operation of seven level, 1 means the switch is ON, the 0 means the switch is OFF. Then we will get the seven level output voltage from the six switches only.

3.2 Nine Level Multi Level Inverter (MLI)

Table- III
Nine level Multilevel (MLI)

S_1	S_2	S_3	S_4	S_5	S_6	S_7	S_8	V_0
0	1	0	1	1	0	1	0	$4V_s$
1	1	0	1	0	0	1	0	$3V_s$
0	0	0	1	1	1	1	0	$2V_s$
0	1	1	1	1	0	0	0	V_s
1	1	1	1	0	0	0	0	0
0	0	0	0	1	1	1	1	0
1	0	0	0	0	1	1	1	$-V_s$
1	1	1	0	0	0	0	1	$-2V_s$
0	0	1	0	1	1	0	1	$-3V_s$
1	0	1	0	0	1	0	1	$-4V_s$

The above Table III is shows the active switches operation of eight switches with nine level, 1 means the switch is ON, the 0 means the switch is OFF. Then we will get the nine level output voltage from the eight switches only.

3.3 Eleven Level Multilevel inverter (MLI)

Table- IV
Eleven level multilevel Inverter (MLI)

S_1	S_2	S_3	S_4	S_5	S_6	S_7	S_8	V_0
0	1	0	1	1	0	1	0	$5V_s$

1	1	0	1	0	0	1	0	$4V_s$
0	1	0	0	1	0	1	1	$3V_s$
1	1	0	0	0	0	1	1	$2V_s$
0	1	1	1	1	0	0	0	V_s
1	1	1	1	0	0	0	0	0
0	0	0	0	1	1	1	1	0
1	0	0	0	0	1	1	1	$-V_s$
0	0	1	1	1	1	0	0	$-2V_s$
1	0	1	1	0	1	0	0	$-3V_s$
0	0	1	0	1	1	0	1	$-4V_s$
1	0	1	0	0	1	0	1	$-5V_s$

3.5 Different voltages are taken as the source voltages of the asymmetrical multilevel inverters

TABLE VI
DIFFEERENT VOLTAGES

No of levels	No of Switches	V1	V2	V3	Output Voltage in V
7	6	V_s	$2V_s$	-	$3V_s$
9	8	V_s	V_s	$2V_s$	$4V_s$
11	8	V_s	$2V_s$	$2V_s$	$5V_s$
13	8	V_s	$2V_s$	$3V_s$	$6V_s$

The above Table VI is shows the active switches operation of eight switches with eleven level, 1 means the switch is ON, the 0 means the switch is OFF. Then we will get the eleven level output voltage from the eight switches only.

3.4 Thirteen Level multi Level inverter

Table-V
Thirteen level multi level inverter (MLI)

S_1	S_2	S_3	S_4	S_5	S_6	S_7	S_8	V_0
0	1	0	1	1	0	1	0	$6V_s$
0	1	0	0	1	0	1	1	$5V_s$
1	1	0	1	0	0	1	0	$4V_s$
1	1	0	0	0	0	1	1	$3V_s$
0	1	1	1	1	0	0	0	$2V_s$
0	0	0	1	1	1	1	0	V_s
1	1	1	1	0	0	0	0	0
0	0	0	0	1	1	1	1	0
1	1	1	0	0	0	0	1	$-V_s$
1	0	0	0	0	1	1	1	$-2V_s$
0	0	1	1	1	1	0	0	$-3V_s$
0	0	1	0	1	1	0	1	$-4V_s$
1	0	1	1	0	1	0	0	$-5V_s$
1	0	1	0	0	1	0	1	$-6V_s$

The above Table V is shows the active switches operation of eight switches with thirteen level, 1 means the switch is ON, the 0 means the switch is OFF. Then we will get the thirteen level output voltage from the eight switches only.

The seven level output voltage are get only from six switches only. The nine level, eleven level and thirteen level output voltage are get only from eight switches corresponding to respective voltage sources are taken.

The above table VI shows different voltages are taken for asymmetrical multilevel inverters. The asymmetrical multilevel inverters are simulated the output voltage are designed by using 200V. The seven level output voltage are get by using $V_1=66.66V$, $V_2=133.33V$. The nine level output voltage are get by using $V_1=50V$, $V_2=50V$, $V_3=100V$. The eleven level output voltage are get by using $V_1=40V$, $V_2=80V$, $V_3=80V$. The thirteen level output voltage are get by using $V_1=66.66V$, $V_2=99.99V$, $V_3=33.33V$. The asymmetrical multilevel inverters are simulate the above written voltage values.

IV. MATLAB/SIMULATION RESULTS

4.1 Basic circuit of Cascaded H-Bridge five level Inverter

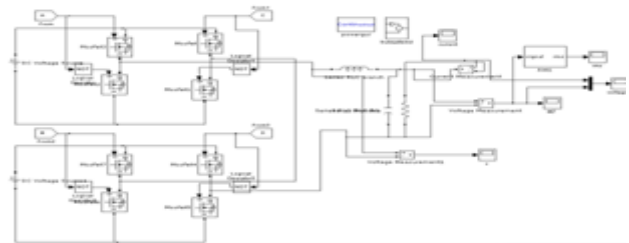


Fig.8 shows the five level inverter CHB simulink circuit

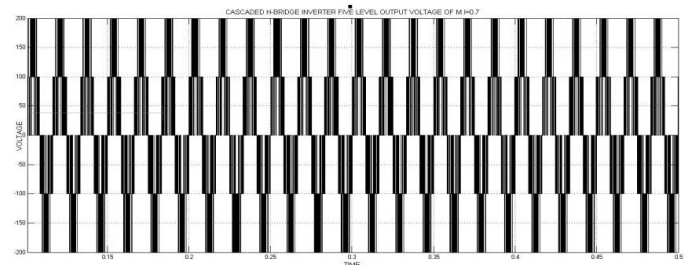


Fig.9 shows the five level output voltage CHB inverter without LC of M.I=0.7

Harmonics of CHB Inverter with and without LC

Harmonics	$m_a=0.7$	$m_a=0.8$
Fundamental 1	154.02	183.84
h3	2.40	3.31
h5	1.19	0.11
h7	0.24	0.07
h9	0.05	0.20
h11	0.02	0.09
%THD WITHOUT LC	0.146	0.114
%THD WITH LC	0.015	0.013

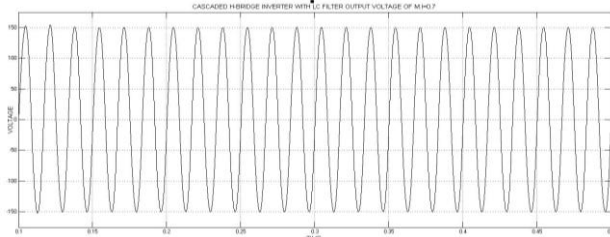


Fig.10 shows the output voltage with LC filter of CHB inverter of M.I=0.7

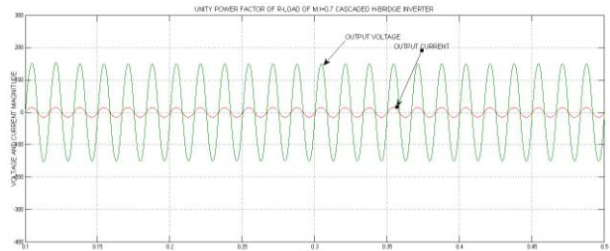


Fig.11 shows the unity power factor at the R-Load with LC filter of CHB inverter of M.I=0.7

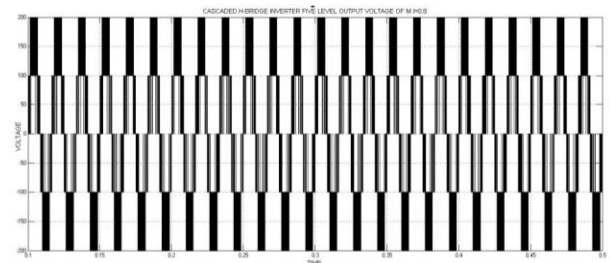


Fig.12 shows the five level output voltage CHB inverter without LC of M.I=0.8

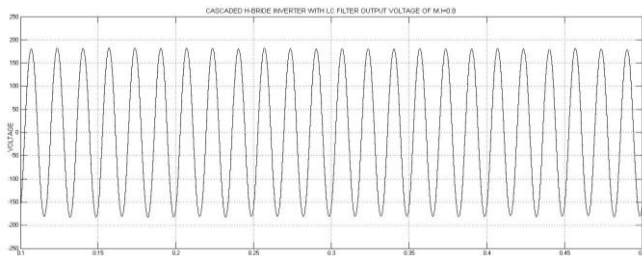


Fig.13 shows the output voltage with LC filter of CHB inverter of M.I=0.8

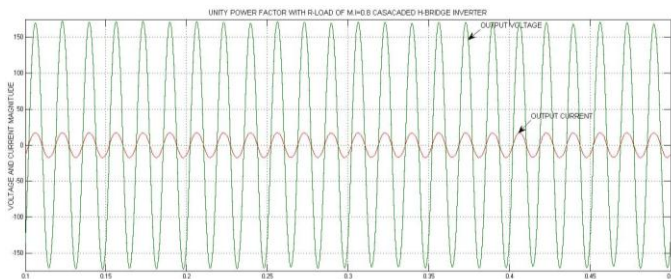


Fig.14 shows the unity power factor at the R-Load with LC filter of CHB inverter of M.I=0.8

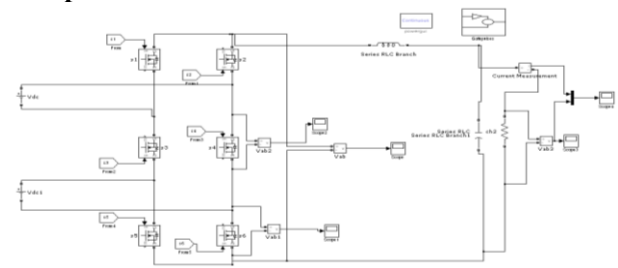


Fig.15. The simulink of simplified five level multilevel inverter

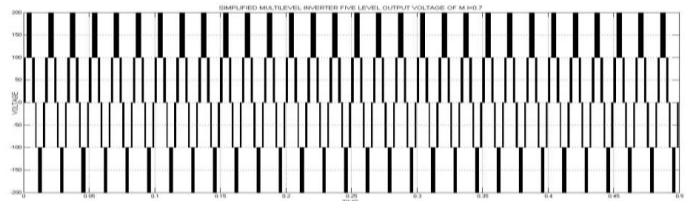


Fig.16 shows the five level output voltage of simplified five level inverter without LC of M.I=0.7

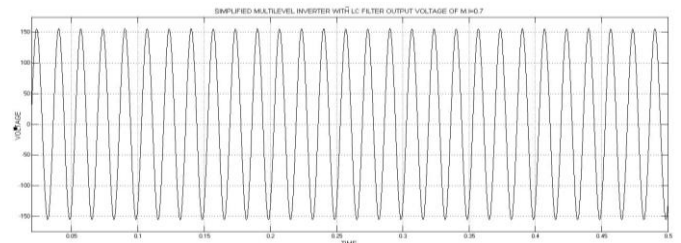


Fig.17 shows the output voltage with LC filter of simplified five level inverter of M.I=0.7

WITHOUT LC		
%THD	0.005	0.003
WITH LC		

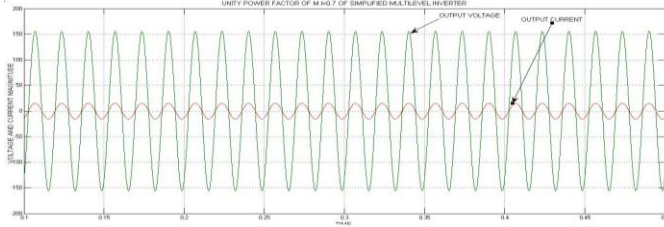


Fig.18 shows the unity power factor at the R-Load with LC filter of simplified five level inverter of M.I=0.7

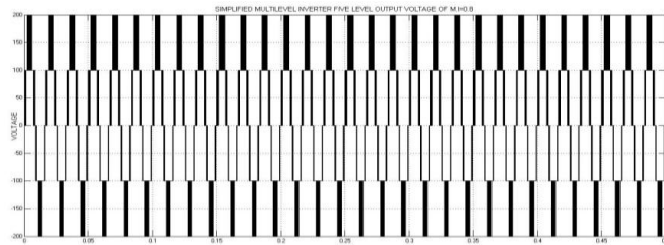


Fig.19 shows the five level output voltage simplified five level inverter without LC of M.I=0.8

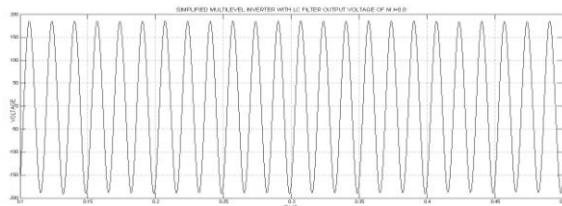


Fig.20 shows the output voltage with LC filter of simplified five level inverter of M.I=0.8

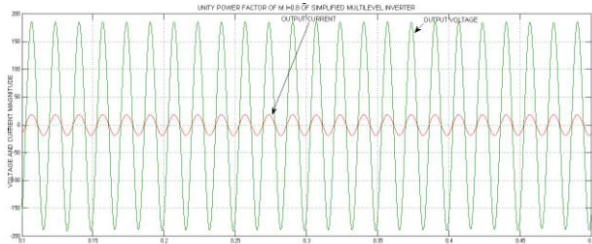


Fig.21 shows the unity power factor at the R-Load with LC filter simplified five level inverter of M.I=0.8

Table-VIII

Harmonics of Simplified Five Level Inverter with and without LC

Harmonics	$m_a=0.7$	$m_a=0.8$
Fundamental	157.77	185.66
1		
h3	0.81	1.98
h5	0.25	0.17
h7	0.17	0.32
h9	0.06	0.06
h11	0.07	0.05
%THD	0.0701	0.0684

The Table VIII shows the simplified five level inverter operating two modulation indexes. They are 0.7 and 0.8 without and with LC filter.

The modulating frequency (Switching frequency) is 18060Hz.

The CHB five level inverter operated with $m_a=0.7$ and $m_a=0.8$ with phase shift carrier pulse width modulation technique then I would get the fundamental component voltage increases and THD value decreases when modulation index $m_a=0.8$ compare to the $m_a=0.7$. The simplified five level inverter operated the same modulation index with phase disposition pulse width modulation technique then I would get the fundamental component voltage increases and THD value decreases compare to the CHB inverter. After clearly understand reduce the number of switches, improved output waveforms, smaller filter size and lower EMI of simplified multistring five level inverter compared to the CHB inverter.

4.3 Proposing system of Seven Level multilevel inverter

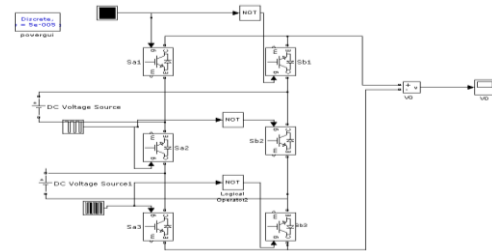


Fig.22 Simulink of the seven level multilevel inverter

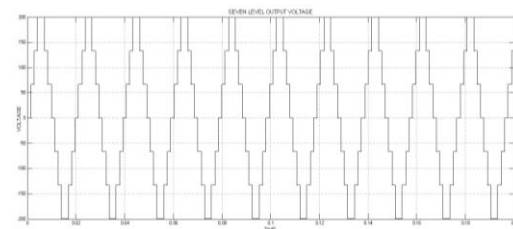


Fig.23 Seven level multivoltage inverter output voltage

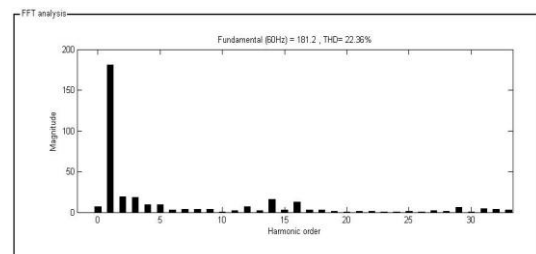


Fig.24 THD value of the Seven level multilevel inverter using FFT analysis

4.4 Proposing System of Nine Level multilevel inverter

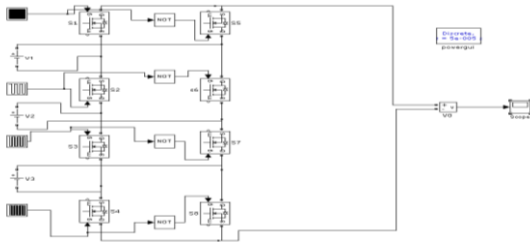


Fig.25 .Simulink of the nine, eleven and thirteen level multilevel inverter

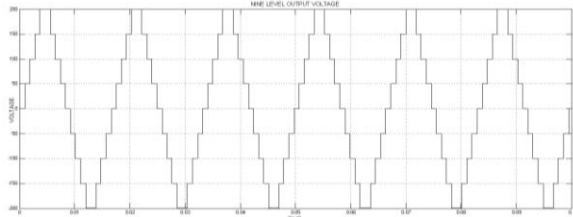


Fig.26 Nine level multilevel Inverter output voltage

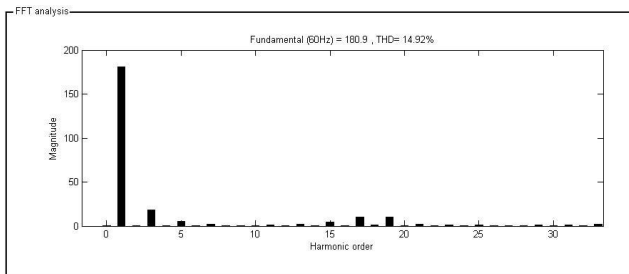


Fig.27 THD value of the nine level multilevel inverter using FFT analysis

4.4 Proposing System of Eleven Level multilevel inverter

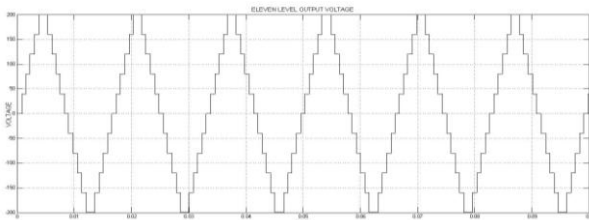


Fig.28 Eleven level multilevel Inverter output voltage

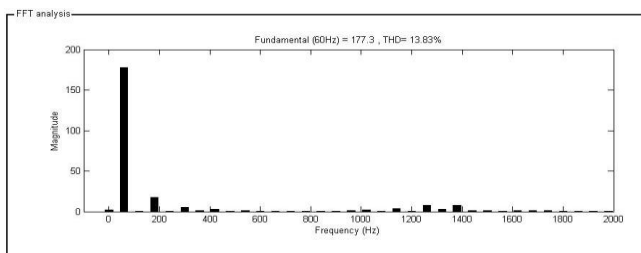


Fig. 29 THD value of the eleven level multilevel inverter using FFT analysis

4.5 Proposing System of Thirteen Level multilevel inverter

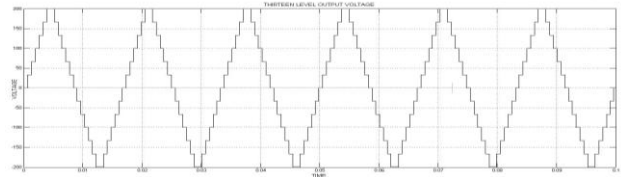


Fig.30 Thirteen level multilevel Inverter output voltage

Table-IX

Fundamental Component and THD value of the Multilevel inverter of Various Values

Magnitude of individual Harmonic content	No of Levels			
	7	9	11	13
Fundamental	181.25	180.90	177.34	175.34
h3	17.99	17.93	17.68	18.18
h5	9.11	5.21	5.43	5.79
h7	3.45	2.09	3.11	2.66
h9	3.71	0.05	1.23	1.21
h11	1.68	1.24	0.40	0.83
h13	2.32	2.19	0.79	0.07
h15	2.59	4.12	0.73	0.24
h17	2.81	10.16	2.08	0.79
h19	1.23	9.78	3.55	1.10
h21	0.86	2.17	7.70	1.69
h23	0.46	1.06	7.32	2.97
(%THD)	22.36 %	14.92%	13.83 %	13.33%

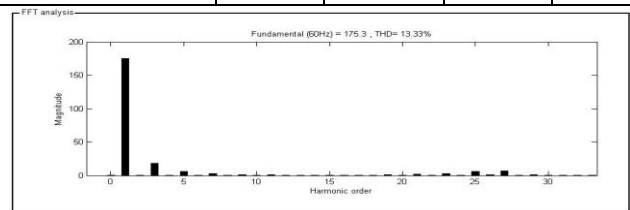


Fig.31 THD value of the thirteen level multilevel inverter using FFT analysis

Table-X

Dominant Harmonics in Various Multilevel inverters

Various Multilevel Inverter	Dominant Harmonics
Seven Level	3 rd , 5 th , 9 th , 7 th
Nine Level	3 rd , 17 th , 19 th , 5 th
Eleven Level	3 rd , 21 st , 23 rd , 5 th , 19 th
Thirteen Level	3 rd , 5 th

V. CONCLUSION

This work reports a Performance analysis of symmetrical and asymmetrical multilevel inverters, so reduce the number of switching devices, reduce the number of DC sources, driving circuits and cost reduces and also THD decreases.

Multistring multilevel inverters have low stress, high conversion efficiency and can also be easily interfaced with renewable energy sources (PV, Fuel cell). Asymmetrical multilevel inverter uses least number of devices to produce higher voltage level. As number of level increases, the THD content approaches to small value as expected. Thus it eliminates the need for filter. Though, THD decreases with increase in number of levels, some lower or higher harmonic contents remain dominant in each level. These will be more dangerous in induction drives.

Hence the future work may be focused to determine the pwm techniques of seven to thirteen level asymmetrical multilevel inverters.

REFERENCES

- [1] "Key world energy statistics-2009", International Energy Agency(IEA),2009. Available at:<http://www.iaea.org>.
- [2] F. Kininger, "Photovoltaic systems technology". Kassel, Germany: *Universitat Kassel, Institute for Rationelle Energiewandlung*, 2003. Available at:www.uni-Kassel.de/re.
- [3] M. Liserre. T.Sauter. J.Y. Hung, "Future energy systems: integrating renewable energy sources into the smart power grid through industrial electronics," *IEEE Industrial Electronics Magazine*, vol.4,no.1,pp.18-37,Mar.2010.
- [4] C. L. Chen, Y. Wang, J. S.Lai, Y.S. Lee and D. Martin, "Design of parallel inverters for smooth mode transfer microgrid applications," *IEEE Trans.Power Electronics*, Vol. 25, no.1, pp.6-16, Jan.2010
- [5] F. Blaabjerg, Z. Chen and S. B. Kjaer, "Power electronics as efficient interface in dispersed power generation systems," *IEEE Trans. Power Electronics*, vol. 19, no.5, pp.1184- 1194, Sep.2004.
- [6] D. G. Infield, P. Onions, A. D. Simmons and G. A. Smith, "Power quality from multiple grid-connected single-phase inverters," *IEEE Trans. Power Delivery*, vol. 19, no.4, PP. 1983- 1989, Oct. 2004.
- [7] T. Kerkes. R. Teoderescu and U. Borup. "Transformerless photovoltaic inverters connected to the grid," *IEEE Applied Power Electronics Conference. 2007* PP.1733-1737.
- [8] G.Ceglia V.Guzman, C.Sanchez, F.Ibanez, J. Walter, and M. I. Gimenez " A new simplified multilevel inverter topology for DC-AC conversion," *IEEE Trans. Power Electronics*, vol.21, n0.5, pp.1311-1319, Sep.2006.
- [9] N.A. Rahim and J. Selvaraj, "Multistring five-level inverter with novel PWM control scheme for PV application," *IEEE Trans. Power Electronics*, vol.57 no.6 pp. 2111-2123, Jun.2010.
- [10] S. Vazquez, J.I.Leon, J.M.Carrasco, L.G. Franquelo, E. Galvan, M. Reyes, J.A. Sanchez, and E. Dominguez, "Analysis of the power balance in the cells of multilevel Cascaded H-bridge converter," *IEEE Trans. Industrial Electronics*, vol.57, no.7, PP.2287-2296, Jul.2010.
- [11] S. Kouro, J. Rebolledo, and J.Rodriguez, "Reduced switching-frequency modulation algorithm for high-power multilevel inverter," *IEEE Trans. Industrial Electronics*, vol.54, no.5, PP.2894-2901, Oct.2007.
- [12] Y. Liu, H.Hong, and A. Q. Huang, "Real-time calculation of switching angles minimizing THD for multilevel inverters with step modulation," *IEEE Trans. Industrial Electronics*, vol. 56, no.2, pp.285-293, FEB.2009.
- [13] W.Yu. C. Hutchens, J.S.Lai, J. Zhang, G.Lisi, A. Djabbari, G.Smith, and T. Hegarty, "High Efficiency Converter with Charge Pump and Coupled Inductor for Wide Input Photovoltaic AC Module Applications," *IEEE Energy Conversion Congress and Exposition*, PP.3895-3900, 2009.
- [14] S. Daher, J.Schmid and F.L.M. Antunes, "Multilevel inverter topologies for Stand-alone PV systems," *IEEE Trans. Industrial Electronics*, Vol.55, no.7, PP.2703-2712, Jul.2008
- [15] M. Meinhardt and G.Cramer, "Past, present and future of grid-connected photovoltaic and hybrid-power systems," *IEEE-PES Summer Meeting*, PP.1283-1288,2000

Synthesis, Characterization ac conductivity of Ni²⁺ doped in magnesium ferrite

Pathan Amjadkhan Noorkhan¹ and Sangshetty Kalayne^{2*}

¹Department of Physics, Singhania University, Pachari- Bari, JhunJunnu, Rajasthan

^{2*}Department of Physics, Rural Engineering College, Bhalki, Bidar, Karnataka, India.

ABSTRACT: Magnesium nickel ferrites were synthesized by employing sol gel technique at 1473 K sintering temperature. A critical Rietveld analysis of XRD reveals that the presence of a very small amount of NiO phase along with the ferrite phase. It indicates that almost a stoichiometric (Mg,Ni)-ferrite phase has been obtained at 1473 K. SEM image shows that of (MgNi)-ferrite is regular in shape have granular in structure, compact and well connected grain to each others. The ac conductivity increases with increase in applied frequency. The magnesium nickel ferrite ($MgNiFe_2O_4$) shows σ_{ac} conductivity of 1.2×10^{-4} S/cm. This is may be attributed to the dipole polarization i.e., the rotation of dipoles between two equivalent equilibrium positions is involved. The high value of dielectric constant of the sample $MgNiFe_2O_4$ may be the structural changes associated with the magnesium nickel ferrite when the grain size is reduced. Therefore, this ferrites material is attracted to use in many science and technological applications.

Keywords: Ac conductivity, (MgNi) ferrite, dielectric constant, Impedance spectra, X-ray diffraction.

I. INTRODUCTION

Small ferrimagnetic oxides, technically known as ferrites have attracted considerable attention not only from a fundamental scientific interest but also from a practical point of view for growing applications in the magnetic, electronic and microwave fields [1-3]. Simultaneous presence of magnetic and dielectric nature of ferrites is vastly exploited in a variety of applications at different frequencies. The special feature of these materials is that the properties can be tailored over wide ranges by appropriate substitution of various ions in the chemical formula unit and control of processing procedures. Ferrites are extensively used in magnetic recording, information storage, colour imaging, bio-processing, magnetic refrigeration and in magneto optical devices [4, 5].

Ferrites also have great promise for atomic engineering of materials with functional magnetic properties. The formation of corrosion product on the out of core surfaces in pressurized heavy water reactors (PHWRs) are major problem. Ferrite having spinal structure such as magnetic and nickel etc play a major role to prevent such problem. Thus attempts are being made to study the various ferrites to evaluate the impact of substitution of the divalent metal ions to modify the properties of these oxides [6-8].

In the present study authors, report synthesis, characterization and dielectric studies of $MgNiFe_2O_4$. A critical Rietveld analysis of XRD reveals that the presence of a very small amount of NiO phase along with the ferrite

phase. It indicates that almost a stoichiometric (Mg,Ni)-ferrite phase has been obtained at 1473 K. SEM image shows that of (MgNi) ferrite is regular in shape have granular in structure, compact and well connected grain to each others. The ac conductivity increases with increase in applied frequency and dielectric constant decreases. Therefore, this ferrites material is attracted to use in many science and technological applications.

II. EXPERIMENTAL

All Chemicals used were analytical grade (AR). The magnesium chloride, nickel chloride (purity 99.99%) and dehydrated ferric chloride were procured and were used as received.

1.1 SYNTHESIS OF MAGNESIUM NICKEL FERRITE

The chloride salts of magnesium, nickel chloride and ferric chloride are mixed in calculated stoichiometric with oxalic acid in equimolar ratio so as to form nickel ferric oxalate precursor. The precursor is then filtered and dried at 323K to achieve constant weight. The precursor is mixed with polyethylene glycol (PEG) in the ratio 1:5 and is ignited. The combustion propagates throughout the precursor. After completion of combustion nickel ferrite ($MgNiFe_2O_4$) is formed. The $MgNi$ -ferrite is sonicated in acetone media for 20min and then calcinated at 1473 K to remove the impurities. Finally, fine graded nanosized nickel ferrite particles are formed [9, 10].

The pellets of 10 mm diameter are prepared with thickness varying up to 2 mm by applying pressure of 10 Tons in a UTM – 40 (40 Ton Universal testing machine). For temperature dependent conductivity and sensor studies, the pellets are coated with silver paste on either side of the surfaces to obtain better contacts.

1.2 CHARACTERIZATION

The X-ray diffraction (XRD) pattern of the $MgNiFe_2O_4$ was recorded at room temperature by employing an x-ray powder diffractometer (Rigaku Miniflex) with $CuK\alpha$ radiation ($\lambda=1.5405\text{\AA}$) in the 2θ (Bragg angles) range ($2^\circ \leq 2\theta \leq 10^\circ$) at a scan speed of $0.5^\circ \text{ minute}^{-1}$.

The percentage transmittances for the entire sample are measured from 300 to 4000 cm^{-1} . The SEM images of $MgNiFe_2O_4$ were recorded using Philips XL-30 (ESEM) scanning electron microscopy. The set up used for measuring ac conductivity is Hioki 3050 impedance analyzer, which is in turn interfaced to the computer.

III. RESULTS AND DISCUSSION

2.1 X-RAYS DIFFRACTION

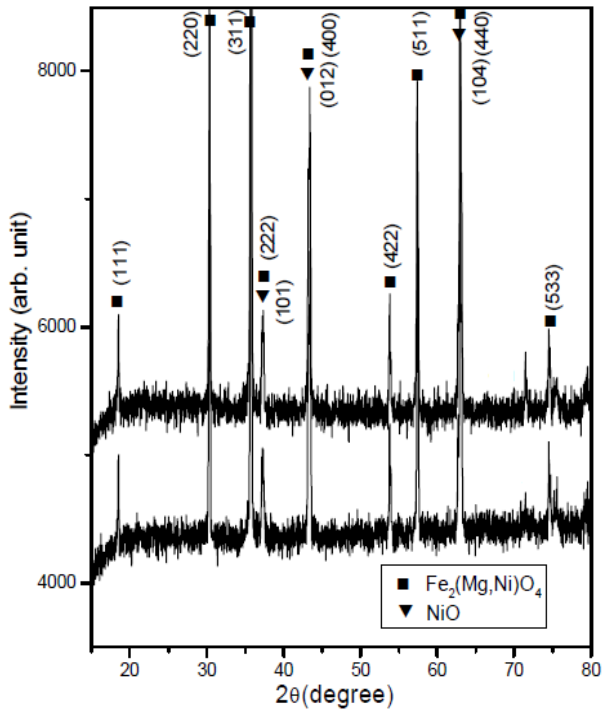


Figure 1 shows the XRD patterns of Mg,Ni)-ferrite annealed at temperature 1473 K.

It seems that the (Mg,Ni)-ferrite phase is formed completely after this heat-treatment. However, a critical rietveld analysis reveals the presence of a very small amount of NiO phase along with the ferrite phase. It indicates that almost a stoichiometric (Mg,Ni)-ferrite phase has been obtained at 1473 K. This indicates that the amount of ferrite phase formation is dependent of annealing time. By measuring particle size we actually measure the coherently diffracting zone of a grain. The particle or crystallites re separated from each other by grain boundaries and the grain boundaries are nothing but bulk crystal imperfections in a crystal [11]. The size of the crystallite in the nanometer range. As can be seen from the experiment, annealing the sample increases the size of the particles. Heat energy helps to annihilate the deformations in the crystals. As a result of grain boundaries started to vanish during annealing and the small crystallites agglomerate together to form larger particles due to intra-grain diffusion.

2.2 SCANNING ELECTRON MICROSCOPY

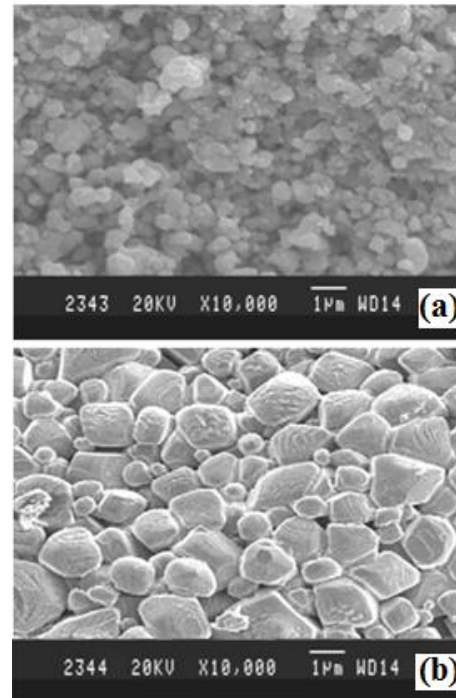


Figure 2 shows the SEM image of (a) NiO and (b) MgNi-ferrite at 1473 K.

Figure 2 (a) shows that SEM image of nickel oxide. It is clearly observed from the image they are agglomerated, highly branched and porous in nature. The average grain size was calculated by using line intercept formula and it is found to be 0.21µm.

Figure 2 (c) shows that SEM image of (MgNi) ferrite. It is found that the image is regular in shape have granular in structure, compact and well connected grain to each others. The average grain size was calculated by using line intercept formula and it is found to be 0.7µm.

2.3 AC CONDUCTIVITY

The variation of σ_{ac} of $MnNiFe_2O_4$ as a function of frequency as shown in figure 3. The conductivity of nickel ferrites is increases with increase in frequency. The magnesium nickel ferrite ($MnNiFe_2O_4$) shows σ_{ac} conductivity of 1.2×10^{-4} S/cm.

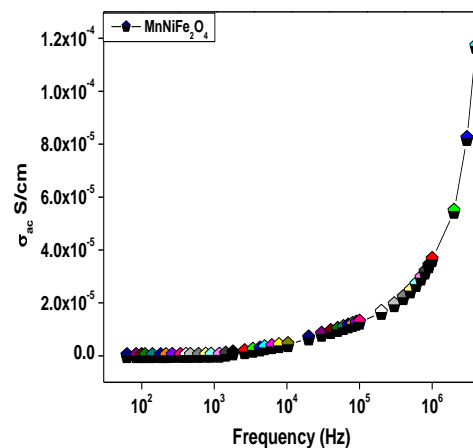


Figure 3 shows the variation of σ_{ac} of $MnNiFe_2O_4$ as a function of frequency.

This is may be attributed to the dipole polarization i.e., the rotation of dipoles between two equivalent equilibrium positions is involved. It is the spontaneous alignment of dipoles in one of the equilibrium positions that give rise to the nonlinear polarization behavior of this composition.

This behaviour of $MnNiFe_2O_4$ obeys the universal power law, $\sigma(\omega) = \sigma_0 \sigma_{dc} \sigma_{ac} \omega^{-n}$ (the solid line is the fit to the expression), where σ_0 is the dc conductivity (frequency independent plateau in the low frequency region), A is the pre-exponential factor, and n is the fractional exponent between 0 and 1 [12]. On crystallization, the conductivity spectrum remains similar as that of the nickel ferrite except dispersion in the low frequency region, where the deviation from σ_{dc} (plateau region) is more prominent. The deviation from σ_{dc} (plateau region) value in the conductivity spectrum (in the low frequency region) is due to the electrode polarization effect. The values of σ_0 , A , and n were obtained by fitting the $\sigma(\omega)$ to $\sigma(\omega) = \sigma_0 \sigma_{dc} \sigma_{ac} \omega^{-n}$. The overall behavior of σ_{ac} follows the universal dynamic response, which has widely been observed in disordered materials like ionically conducting glasses and also doped crystalline solids, and is generally believed to be reflected in the mechanism of charge transport behavior of charge carriers.

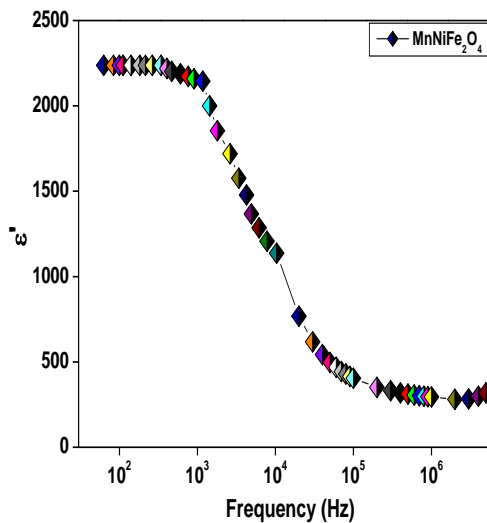


Figure 4 shows the variation real permittivity (ϵ') of nickel ferrite as a function of frequency.

Figure 4 shows the variation real permittivity (ϵ') of nickel ferrite of various composition as a function of logarithmic frequency. It is found that in all these nickel ferrite compositions, as frequency increases, dielectric constant decreases up to the frequency range of 10^5 Hz and after that it remains constant for further increasing in frequency [13]. The strong frequency dispersion of permittivity is observed in the low frequency region followed by a nearly frequency independent behaviour above 10^3 Hz. It is observed that Debye type relaxation mechanism is responsible for higher value of $MnNiFe_2O_4$.

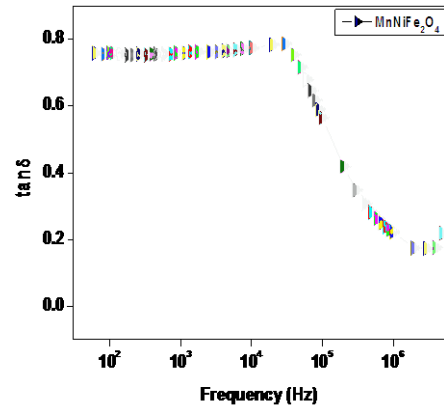


Figure 5 shows the variation of dielectric constant as a function of frequency of $MnNiFe_2O_4$

Figure 5 shows the variation of dielectric constant as a function of frequency for $MnNiFe_2O_4$. The high value of dielectric constant of the sample $MnNiFe_2O_4$ may be explained on the basis of the structural changes associated with the magnesium nickel ferrite when the grain size is reduced. Magnesium nickel ferrite crystallizes into a cubic close-packed arrangement of oxygen ions. It belongs to the class of ferrites with an inverse spinel structure having structural formula, $Fe^{3+}[Mg^{2+}Ni^{3+}]O_4$. The metal ions given in the square bracket are called octahedral (B site) ions and that outside the square bracket are called tetrahedral (A site) ions. The nickel ions (Ni^{2+}) together with half of the iron ions (Fe^{3+}) occupy the B site and the Mg^{2+} occupy the remaining half of the iron ions reside in A site. The presence of Mg^{2+} and Ni^{3+} ions gives rise to p-type carriers (holes) whereas Fe^{2+} and Fe^{3+} ions produce n-type carriers (electrons). Therefore, both electrons and holes that are present in the B sites are due to the presence of Mg and Ni ions. Since Mg ions are present in A sites, electrons are the carriers in A sites. The distance between the ions in A sites (0.357 nm) is larger than the distance between the ions in B site (0.292 nm) [14-16]. Also, the degree of covalency for the A site ions is higher than that of the B site ions. All the above factors result in a high activation energy for the A sites compared to the B sites. Hence, in ordinary magnesium nickel ferrite with an inverse spinel structure the electron movement in B sites dominates compared to that in A sites.

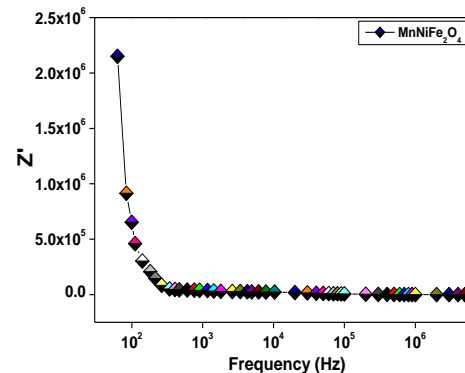


Figure 6 the variation of real part of impedance as a function of frequency

The variation of real part of impedance of MnNiFe₂O₄ is shown in figure 6 as a function of increasing frequency. It is observed that the real part of impedance decreases with increase in frequency. The initial decrease in impedance value due to the increase in conductivity at lower frequency region up to 10³ Hz and further increases in applied frequency, the impedance value remains constant. This indicates that after 10³ Hz the ferrite acts as lossless materials. Therefore, these ferrites can be used in many technological applications such as memory device, microwave, sensor, transducer, solar cell etc.

IV. CONCLUSION

Sol-gel technique was employed to prepare the magnesium nickel ferrites were at 1473 K sintering temperature. A critical Rietveld analysis of XRD reveals that the presence of a very small amount of NiO phase along with the ferrite phase. It indicates that almost a stoichiometric (Mg,Ni)-ferrite phase has been obtained at 1473 K. SEM image shows that of (MgNi) ferrite is regular in shape have granular in structure, compact and well connected grain to each others. The ac conductivity increases with increase in applied frequency. The magnesium nickel ferrite (MnNiFe₂O₄) shows σ_{ac} conductivity of 1.2×10^{-4} S/cm. This is may be attributed to the dipole polarization i.e., the rotation of dipoles between two equivalent equilibrium positions is involved. The high value of dielectric constant of the sample MnNiFe₂O₄ may be the structural changes associated with the magnesium nickel ferrite when the grain size is reduced. It is observed that the real part of impedance decreases with increase in frequency. The initial decrease in impedance value due to the increase in conductivity at lower frequency region up to 10³ Hz and further increases in applied frequency, the impedance value remains constant. Therefore, this ferrites material is attracted to use in many science and technological applications.

REFERENCE

- [1] I. Anton, I. D. Dabata and L. Vekas, "Application Orientated Researches on Magnetic Fluids," *Journal of Magnetism and Magnetic Materials*, 85 (1), 1990, 219-226.
- [2] R. D. McMickael, R. D. Shull, L. J. Swartzendruber, L. H. Bennett and R. E. Watson, "Magnetocaloric Effect in Superparamagnets," *Journal of Magnetism and Magnetic Materials*, 111(1), 1992, 29-33.
- [3] D. L. Leslie-Pelecky and R. D. Rieke, "Magnetic Properties of Nanostructures Materials," *Chemistry of Materials*, 8 (8), 1996, 1770-1783.
- [4] T. Hirai, J. Kobayashi and I. Koasawa, "Preparation of Acicular Ferrite Fine Particles Using an Emulsion Liquid Membrane System," *Langmuir*, 15 (19), 1999, 6291-6298.
- [5] R. H. Kodama, "Magnetic Nanoparticles," *Journal of Magnetism and Magnetic Materials*, 200 (1), 1999, 359-372.
- [6] K. V. P. M. Shafi, Y. Koltypin, A. Gedanken, R. Prozorov, J. Balogh, J. Lendvai and I. Felner, "Sonochemical Preparation of Nanosized Amorphous NiFe₂O₄ Particles," *The Journal of Physical Chemistry B*, 101 (33), 1996, 6409-6414.
- [7] D. Niznansky, M. Drillon and J. L. Renspinger, "Preparation of Magnetic Nanoparticles (γ -Fe₂O₃) in the Silica Matrix," *IEEE Transaction on Magnetics*, 30 (2), 1994, 821-823.
- [8] J. M. Yang, W. J. Tsuo and F. S. J. Yen, "Preparation of Ultrafine Nickel Ferrite Powder Using Ni and Fe Tartrates," *Journal of Solid State Chemistry*, 145(1), 1999, 50-57.
- [9] Y. Shi, J. Ding, X. Liu and J. Wang, "NiFe₂O₄ Ultrafine Particles Prepared by Co- Precipitation / Mechanical Alloying," *Journal of Magnetism and Magnetic Materials*, 205 (2), 1999, 249-254.
- [10] P. Druska, U. Steinike and V. Sepelak, "Surface Structure of Mechanically Activated and of Mechano-synthesized Zinc Ferrite," *Journal of Solid State Chemistry*, 146 (1), 1999, 13-21.
- [11] V. Sepelak, K. Tkacova, V. V. Boldyrev and U. Steinike, "Crystal Srtucture Refinement of the Mechanically Activated Spinel-Ferrite," *Materials Science Forum*, 228, 1996, 783-788.
- [12] V. Sepelak, A. Yu, U. Rogachev, D. Steinike, C. Uecker, S. Wibmann and K. D. Becker, "Structure of Nanocrystalline Spinel Ferrite Produced by High Energy Ballmilling Method," *Acta Crystallographica A*, 52, 1996, C367
- [13] V. Sepelak, U. Steinike, D. C. Uecker, S. Wibmann and K. D. Becker, "Structural Disorder in Mechano-synthesized by Zinc Ferrite," *Journal of Solid State Chemistry*, 135 (1), 1998, 52-58.
- [14] H. M. Rietveld, "Line Profile of Neutron Powder Diffraction Peaks for Structure Refinement," *Acta Crystallographica*, 22, 1967, 151-152.
- [15] H. M. Rietveld, "A Profile Refinement Method for Nuclear and Magnetic Structures," *Journal of Applied Crystallography*, 2, 1969, 65-71.
- [16] L. Lutterotti, P. Scardi and P. Maistrelli, "LSI-a Computer Program for Simultaneous Refinement of Material Structure and Microstructure," *Journal of Applied Crystallography*, 25 (3), 1992, 459-462.

The Effects of Different Temperatures and Temperature Cycling on Breakdown Voltages of Tantalum Capacitors

Johanna Virkki

Department of Electronics/Tampere University of Technology, Finland

ABSTRACT: *This study focuses on the effects of different temperatures and temperature cycling on breakdown voltages of tantalum capacitors. High and low temperature tests and temperature cycling tests were done. In all tests the used temperatures were inside component's operating temperature limits. After the tests, capacitors were tested for their breakdown voltage. According to results of this research, high or low temperature testing inside component's operating temperature limits does not have an effect on the breakdown voltage of tantalum capacitors. However, temperature cycling inside component's operating temperature limits can lower the breakdown voltage of tantalum capacitors.*

Keywords: *accelerated testing, reliability, tantalum capacitors, temperature, temperature cycling*

I. INTRODUCTION

In today's competitive market, it is important for a company to know the reliability of its products and to be able to control it for continued production at optimum reliability. Sometimes there is a need to examine the performance of a specific electronic component: it may be radically redesigned, or there may be an individual reliability specification for that component. That is why reliability testing of components has become a concern for electronics manufacturers. Also, in many cases, component-level reliability testing is undertaken to begin characterizing a product's reliability when full system-level test units are unavailable.

Electronic components are often stored and used at high or low temperatures, and sometimes temperature can change radically during component's lifetime. Temperature and temperature changes can have various, often unpredictable effects on components. Reliability tests seek to simulate the component's use environment in order to find the effects of environmental stresses. Because such testing is very time-consuming, accelerated testing becomes necessary. Accelerated testing is a procedure in which conditions are intensified to cut down the time required to obtain a weakening effect similar to one encountered in normal service conditions [1].

High Temperature Storage Life (HTSL), JESD22-A103C, and Low Temperature Storage Life (LTSL), JESD22-A119, tests "are applicable for evaluation, screening, monitoring, and/or qualification of all solid state devices and typically used to determine the effect of time and temperature, under storage conditions, for thermally activated failure mechanisms of solid state electronic

devices [2, 3].“ The standard HTSL test is run for 1000 hours (42 days) and the standard LTSL test for 168 hours (7 days) [2, 3]. During the tests, increased/reduced temperatures (test conditions) are used without electrical stress.

Temperature cycling, according to the standard JESD22-A104D, "is conducted to determine the ability of components and solder interconnects to withstand mechanical stresses induced by alternating high- and low-temperature extremes. Permanent changes in electrical and/or physical characteristics can result from these mechanical stresses [4]." This standard test includes numerous temperature cycling conditions. The test usually lasts 500 or 1000 cycles.

These standard accelerated tests are commonly used for testing reliability of electronics and were used in this research. The object of this research was to test the effects of low temperature, high temperature, and the effects of temperature cycling on tantalum capacitors.

II. TANTALUM CAPACITORS

Surface mount solid tantalum capacitors (henceforth referred to as "tantalum capacitors", shown in Fig. 1) of a maximum voltage of 50V, a capacitance of 10 μ F, and an operating and non-operating temperature of -55 $^{\circ}$ C to 125 $^{\circ}$ C were used in this research. The structure of these capacitors is presented more detailed in Fig 2.

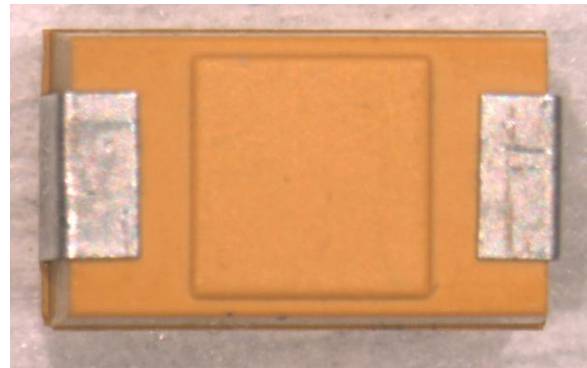


Figure 1. Bottom side of a surface mount tantalum capacitor used in this research.

A. Structure of tantalum capacitors

A tantalum capacitor (structure shown in Fig. 2) consists of three main elements: anode, cathode, and a dielectric layer of tantalum pentoxide that separates them. The capacitor contains an embedded tantalum pellet (anode), surrounded by a tantalum pentoxide, amorphous dielectric layer. The

cathode is a semiconductor, manganese dioxide. This pellet is coated with carbon and then with silver to provide the final connecting layer to the cathode terminal. The tantalum wire passes through these layers and connects the positive termination to the tantalum pellet. The negative termination of the capacitor is attached with a silver adhesive to the silver paint layer. Next sections focus on possible failure mechanisms caused by temperature and changes in it.

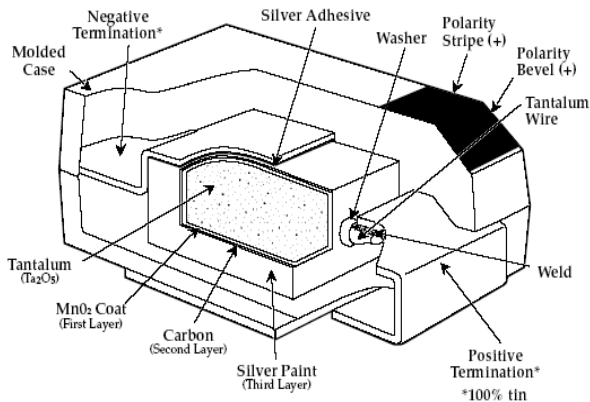


Figure 2. Structure of a tantalum capacitor [5].

B. Effects of temperature and temperature cycling on tantalum capacitors

Temperature, whether generated externally or internally, degrades the performance and reliability of tantalum capacitors. The use of tantalum capacitors at high temperatures has been studied, and manufacturing tantalum capacitors for high-temperature applications is found to be challenging [6, 7]. Mechanical stresses related to the temperature changes during reflow-manufacturing and use of surface mount tantalum capacitors at high temperatures affect their performance and reliability and can account for their breakdowns. Due to mismatch of the coefficients of thermal expansion between the constituent materials, significant mechanical stresses develop in the bulk of materials and at the interfaces. During heating, shear forces are exerted on the anode wire. The molded case pushes on the lead frame in one direction and the pellet in another, generating forces that pull the wire away from the anode structure. Once the device has passed through high temperatures and its elements are shrinking while cooling, they may not fit together as they did before the expansion. Compressive forces may appear on the pellet structure and produce fractures. In addition, these stresses may cause cracking in the tantalum pentoxide dielectric and/or delaminations at the interfaces, resulting in different failure modes of the components. A crack in the dielectric at a corner or edge, when exposed to high stress, may lead to failure [9-11]. The cracking increases leakage current, decreases breakdown voltage, and may cause short-circuits. On the other hand, delaminations can raise the effective series resistance and thus increase power dissipation and temperature of the capacitor, which can decrease its reliability. Severe delaminations may result in intermittent contacts and open-circuit failures of the components [11].

Temperature has also a specific effect inside a tantalum capacitor, known as crystal growth [12-14]. The tantalum pentoxide dielectric is considered an amorphous material. An amorphous state tends to order and crystallize to reduce its internal energy. Surface impurities can induce direct growth of tantalum pentoxide crystals and any imperfection in the dielectric structure is a potential site for crystals to grow. Once the dielectric crystallizes, conductivity and leakage current increase. The presence of impurities is not the only mechanism that may lead to a growth of crystals; Crystal growth can also be initiated in small areas of crystalline order in the dielectric. The conductivity of the crystallized structure has been reported to be higher than that of a dielectric in an amorphous state [14]. However, the latest findings suggest that the crystals themselves are good insulators with very limited conductivity [12, 13]. The exact conductivity mechanism related to the crystal phase is not yet fully understood. The increase in leakage current may still be caused by other mechanisms accelerated by the crystal growth. However, studies show that field crystallization may have only a limited impact on the end use of tantalum capacitors [12].

The temperature cycling of tantalum capacitors has been studied before [11, 15] with capacitors subjected to temperature cycling in a range from -40°C to 85°C [15], -65°C to 125°C , and -65°C to 150°C [11]. Results indicate that tantalum capacitors are capable of withstanding up to 500 cycles of temperature ranging from -65°C to 150°C . However, different lots show different robustness under cycling conditions, and though parts may not fail formally by exceeding specified limits, a significant degradation in the leakage current and breakdown voltages indicates an increased propensity of some lots to failure after temperature cycling. Cracking in the tantalum pentoxide dielectric, which develops during temperature cycling, results not only in increased leakage current, but also increases the probability of scintillation breakdowns [11]. The results suggested that a harmful temperature cycling effect can be achieved in a much shorter time than in 500 cycles [15].

III. RELIABILITY TESTING

Testing was divided into five tests, hereafter called Tests A, B, C, D, and E. Test A was a low temperature test in -40°C temperature and lasted for 168h. Tests B and C were high temperature tests, Test B was done in 85°C and Test C was done in 125°C . Both tests lasted for 1000h. Tests D and E were temperature cycling tests. Both tests lasted for 500 cycles and one cycle lasted for 0.5h. In test D, the temperature changed between -40°C and 85°C and in Test E, temperature changed between -40°C and 125°C . In all tests, 18 capacitors were tested. Because the capacitors were rated for an operating and non-operating temperature of -55°C to 125°C , they were tested here within their operating limits. This was done in order to get information on their usability in such field conditions and to compare the effects of different temperatures and temperature

voltages. More testing work needs be done in order to collect statistical data for conclusions. Such results would be useful in addition to these results, where conclusions are mostly done based on literature review.

REFERENCES

- [1] D. Kececioglu, *Reliability engineering handbook, vol. 1 and 2* (New Jersey, Prentice Hall, Inc., 1991)
- [2] JEDEC standard. High Temperature Storage Life, JESD22-A103. Published by JEDEC Solid State Technology Association, Arlington, 2004.
- [3] JEDEC standard. Low Temperature Storage Life, JESD22-A119. Published by JEDEC Solid State Technology Association, Arlington, 2004.
- [4] JEDEC standard. Temperature Cycling, JESD22-A104D (2009). Published by JEDEC Solid State Technology Association, Arlington, 2009.
- [5] Solid tantalum chip capacitors, T494 SERIES—Low ESR, Industrial grade. KEMET Electronics Corporation. Datasheet. 7p.
- [6] E. Reed, Tantalum chip capacitor reliability in high surge and ripple current applications, *Proc. Electronic Components and Technology Conference*, 1994, pp. 861-868.
- [7] Y. Freeman, R. Hahn, P. Lessner, and J. Prymak, Reliability and critical applications of tantalum capacitors, *Proc. Capacitor and Resistor Technology Europe Symposium*, 2007, 11p.
- [8] B. Long, M. Prevallet, and J.D. Prymak, Reliability effects with proofing of tantalum capacitors, *Proc. Capacitor and Resistor Technology Symposium*, 2005, pp. 167-172.
- [9] J. Marshall and J. Prymak, Surge step stress testing of tantalum capacitors, *Proc. Capacitor and Resistor Technology Symposium*, 2001, pp. 181-187.
- [10] D.M. Edson, and J.B. Fortin, Improving thermal shock resistance of surface mount tantalum capacitors, *Proc. Capacitor and Resistor Technology Symposium*, 1994, pp. 169-176.
- [11] A. Teverovsky, Effect of temperature cycling and exposure to extreme temperatures on reliability of solid tantalum capacitors, *NASA Electronic Parts and Packaging (NEPP) Program*, 2007, 70p.
- [12] T. Zednicek, J. Sikula, and H. Leibovitz, A study of field crystallization in tantalum capacitors and its effect on DCL and reliability, *Proc. Capacitor and Resistor Technology Symposium*, 2009, 16p.
- [13] E. Atanassova and A. Paskaleva, Breakdown fields and conduction mechanisms in thin Ta₂O₅ layers on Si for high density DRAMs, *Microelectronics Reliability*, 42(2), 2002, 157-173.
- [14] S. Ezhilvalavan and T.-Y. Tseng, Conduction mechanisms in amorphous and crystalline Ta₂O₅ thin films, *Journal of Applied Physics*, 83(9), 1998, 4797-4801.
- [15] J. Virkki and S. Tuukkanen, Testing the effects of temperature cycling on tantalum capacitors, *Microelectronics Reliability*, 50(8), 2010, 1121-112

An Algorithm for Image Compression Using 2D Wavelet Transform

Mr. B. H. Deokate¹, Dr. P. M. Patil²

Shri Jagdishprasad Jhabarmal Tibrewala University (JJTU)

Abstract: Wavelet Transform has been successfully applied in different fields, ranging from pure mathematics to applied sciences. Numerous studies carried out on Wavelet Transform have proven its advantages in image processing and data compression. Recent progress has made it the basic encoding technique in data compression standards. Pure software implementations of the Discrete Wavelet Transform, however, appear to be the performance bottleneck in real-time systems. Therefore, hardware acceleration of the Discrete Wavelet Transform has become a topic of interest. The goal of this paper is to investigate the feasibility of hardware acceleration of Discrete Wavelet Transform for image compression applications, and to compare the performance improvement against the software implementation. In this paper, a design for efficient hardware acceleration of the Discrete Wavelet Transform is proposed. The hardware is designed to be integrated as an extension to custom-computing platform and can be used to accelerate multimedia applications as JPEG2000.

Keywords: Wavelet transforms, Image compression, Haar wavelet.

I. INTRODUCTION

A majority of today's Internet bandwidth is estimated to be used for images and video [4]. Recent multimedia applications for handheld and portable devices place a limit on the available wireless bandwidth. The bandwidth is limited even with new connection standards. JPEG image compression that is in widespread use today took several years for it to be perfected. Wavelet based techniques such as JPEG2000 for image compression has a lot more to offer than conventional methods in terms of compression ratio. Currently wavelet implementations are still under development lifecycle and are being perfected. Flexible energy-efficient hardware implementations that can handle multimedia functions such as image processing, coding and decoding are critical, especially in hand-held portable multimedia wireless devices.

II. BACKGROUND

Computer data compression is, of course, a powerful, enabling technology that plays a vital role in the information age. Among the various types of data commonly transferred over networks, image and video data comprises the bulk of the bit traffic. For example, current estimates indicate that image data take up over 40% of the volume on the Internet. [4] The explosive growth in demand for image and video data, coupled with delivery bottlenecks has kept compression technology at a premium. Among the several 1 compression standards available, the JPEG image compression standard is in wide spread use today. JPEG

uses the Discrete Cosine Transform (DCT) as the transform, applied to 8-by-8 blocks of image data. The newer standard JPEG2000 is based on the Wavelet Transform (WT). Wavelet Transform offers multi-resolution image analysis, which appears to be well matched to the low level characteristic of human vision. The DCT is essentially unique but WT has many possible realizations. Wavelets provide us with a basis more suitable for representing images. This is because it can represent information at a variety of scales, with local contrast changes, as well as larger scale structures and thus is a better fit for image data. Field programmable gate arrays (FPGAs) provide a rapid prototyping platform. FPGAs are devices that can be reprogrammed to achieve different functionalities without incurring the non-recurring engineering costs typically associated with custom IC fabrication. In this work, DWT architecture is implemented on a reconfigurable FPGA hardware. The target platform is the Xilinx Virtex FPGA. The design is based on the multi-level decomposition implementation of the Discrete Wavelet Transform. The design utilizes various techniques and specific features of the Xilinx Virtex XSV FPGA to accelerate the computation of the transform. Performance analysis includes the investigation of the performance enhancement due to the hardware acceleration. It is expected that the proposed design can substantially accelerate the DWT and the inherent scalability can be exploited to reach a higher performance in the future. The implementation can be easily modified to act as a co-processing environment for wavelet compression/decompression or even as a part of the algorithms to be used in future mobile devices for image encoding/decoding using wavelets. One drawback of the FPGA, however, is that due to the rather coarse grained reconfigurable blocks, an implementation on an FPGA is often not as efficient, in terms of space and time, as on a custom IC.

III. WAVELET TRANSFORM BASED IMAGE COMPRESSION

III.1 Introduction

Image compression is different from binary data compression. When binary data compression techniques are applied to images, the results are not optimal. In lossless compression, the data (such as executables, documents, etc.) are compressed such that when decompressed, it gives an exact replica of the original data. They need to be exactly reproduced when decompressed. For example, the popular PC utilities like Winzip or and Adobe Acrobat perform lossless compression. On the other hand, images need not be reproduced exactly. A 'good' approximation of the original image is enough for most purposes, as long as the error between the original and the compressed image is

tolerable. Lossy compression techniques can be used in this application. This is because images have certain statistical properties, which can be exploited by encoders specifically designed for them. Also, some of the finer details in the image can be sacrificed for the sake of saving bandwidth or storage space. In digital images the neighboring pixels are correlated and therefore contain redundant information. Before the image is compressed, the pixels, which are correlated is to be found. The fundamental components of compression are redundancy and irrelevancy reduction. Redundancy means duplication and irrelevancy means the parts of signal that will not be noticed by the signal receiver, which is the Human Visual System (HVS). There are three types of redundancy that can be identified:

Spatial Redundancy is the correlation between neighboring pixel values.

Spectral Redundancy is the correlation between different color planes or spectral bands.

Temporal Redundancy is the correlation between adjacent frames in a sequence of images (in video applications). Image compression focuses on reducing the number of bits needed to represent an image by removing the spatial and spectral redundancies. Since our work focuses on still image compression, therefore temporal redundancy is not discussed.

III.2 Principles of Image Compression

A typical lossy image compression scheme is shown in Figure 3.2.1. The system consists of three main components, namely, the source encoder, the quantizer, and the entropy encoder. The input signal (image) has a lot of redundancies that needs to be removed to achieve compression. These redundancies are not obvious in the time domain. Therefore, some kind of transform such as discrete cosine, fourier, or wavelet transform is applied to the input signal to bring the signal to the spectral domain. The spectral domain output from the transformer is quantized using some quantizing scheme. The signal then undergoes entropy encoding to generate the compressed signal. The wavelet transform mainly applies on the source encoder component portion.

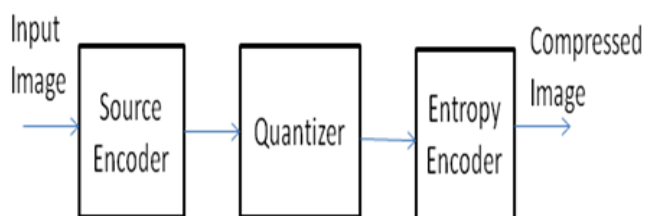


Figure 3.2.1 Image compression scheme

Source Encoder

An encoder is the first major component of image compression system. A variety of linear transforms are available such as Discrete Fourier Transform (DFT), Discrete Cosine Transform (DCT), and Discrete Wavelet Transform (DWT). The Discrete Wavelet Transform is main focus of my work.

Quantizer

A quantizer reduces the precision of the values generated from the encoder and therefore reduces the number of bits required to save the transform co-coefficients. This process is lossy and quantization can be performed on each individual coefficient. This is known as Scalar Quantization (SQ). If it is performed on a group of coefficients together then it is called Vector Quantization (VQ).

Entropy Encoder

An entropy encoder does further compression on the quantized values. This is done to achieve even better overall compression. The various commonly used entropy encoders are the Huffman encoder, arithmetic encoder, and simple run-length encoder. For improved performance with the compression technique, it's important to have the best of all the three components.

III.4 JPEG 2000

JPEG 2000 is a wavelet-based image compression standard created by the Joint Photographic Expert Group (JPEG) committee in 2000 with the aim of replacing the original discrete cosine transform-based JPEG. This part specifies the core and minimal functionality and is known as JPEG2000 codec.[5]

The main advantages of JPEG2000 against the classical JPEG are:

- Superior compression performance: specially at low bitrate (e.g. less than 0.25 bits/pixel).
- Multiple resolution representation.
- Progressive transmission: after a smaller part of the whole file has been received, the viewer can see a lower quality version of the final picture.
- Lossless and lossy compression.
- Random codestream access and processing: different grades of compression could be given to some Regions of Interest (ROI) of the image.
- Error resilience: small independent block avoid error propagation.

The JPEG2000 algorithm flow shown in Figure 3.4.1 reveals the first and simple stages: The whole raw image in divided in the three Red-Green-Blue (RGB) components. Each component is divided in equal smaller pieces called tiles, which are coded independently. The RGB components are transformed in YUV model that requires less memory. The last stages: Discrete Wavelet Transform (DWT) and T1 Entropy Encoding.

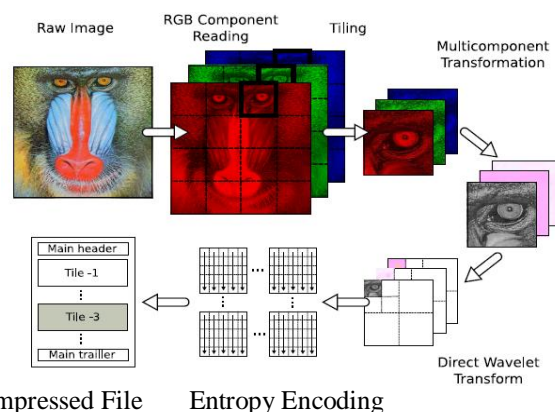


Figure 3.4.1 JPEG 2000 algorithm flow.

IV. WAVELET TRANSFORM AS THE SOURCE ENCODER

Just as in any other image compression schemes the wavelet method for image compression also follows the same procedure. The discrete wavelet transform constitutes the function of the source encoder. The theory behind wavelet transform is discussed below.

IV.1 Measuring Frequency Content by Wavelet Transform

Wavelet transform is capable of providing the time and frequency information simultaneously. Hence it gives a time-frequency representation of the signal. When we are interested in knowing what spectral component exists at any given instant of time, we want to know the particular spectral component at that instant. In these cases it may be very beneficial to know the time intervals these particular spectral components occur. Wavelets are functions defined over a finite interval and having an average value of zero. The basic idea of the wavelet transform is to represent any arbitrary function $f(t)$ as a superposition of a set of such wavelets or basis functions. These basis functions are obtained from a single wave, by dilations or contractions (scaling) and translations (shifts). The discrete wavelet transform of a finite length signal $x(n)$ having N components, for example, is expressed by an $N \times N$ matrix similar to the discrete cosine transform .

V. WAVELET-BASED COMPRESSION

Digital image is represented as a two-dimensional array of coefficients, each coefficient representing the brightness level in that point. We can differentiate between coefficients as more important ones, and lesser important ones. Most natural images have smooth color variations, with the fine details being represented as sharp edges in between the smooth variations. Technically, the smooth variations in color can be termed as low frequency variations, and the sharp variations as high frequency variations.

The low frequency components constitute the base of an image, and the high frequency components add upon them to refine the image, thereby giving a detailed image. Hence, the smooth variations are more important than the details. Separating the smooth variations and details of the image can be performed in many ways. One way is the decomposition of the image using the discrete wavelet transform. Digital image compression is based on the ideas of discrete wavelet transforms. Wavelets which refer to a set of basis functions are defined recursively from a set of scaling coefficients and scaling functions. The DWT is defined using these scaling functions and can be used to analyze digital images with superior performance than classical short-time Fourier-based techniques, such as the DCT. The basic difference between wavelet-based and Fourier-based techniques is that short-time Fourier-based techniques use a fixed analysis window, while wavelet-based techniques can be considered using a short window at high spatial frequency data and a long window at low spatial frequency data. This makes DWT more accurate in analyzing image signals at different spatial frequency, and thus can represent more precisely both smooth and dynamic regions in image. The compression system includes forward wavelet transform, a quantizer, and

a lossless entropy encoder. The corresponding decompressed image is formed by the lossless entropy decoder, a de-quantizer, and an inverse wavelet transform.

V.1 Wavelet Decomposition

There are several ways wavelet transforms can decompose a signal into various sub bands. These include uniform decomposition, octave-band decomposition, and adaptive or wavelet-packet decomposition. Out of these, octave-band decomposition is the most widely used.

The procedure is as follows: wavelet has two functions “wavelet” and “scaling function”. They are such that there are half the frequencies between them. They act like a low pass filter and a high pass filter. The decomposition of the signal into different frequency bands is simply obtained by successive high pass and low pass filtering of the time domain signal. This filter pair is called the analysis filter pair. First, the low pass filter is applied for each row of data, thereby getting the low frequency components of the row. But since the low pass filter is a half band filter, the output data contains frequencies only in the first half of the original frequency range. By Shannon's Sampling Theorem, they can be sub-sampled by two, so that the output data now contains only half the original number of samples. Now, the high pass filter is applied for the same row of data, and similarly the high pass components are separated.

This is a non-uniform band splitting method that decomposes the lower frequency part into narrower bands and the high-pass output at each level is left without any further decomposition. This procedure is done for all rows. Next, the filtering is done for each column of the intermediate data. The resulting two-dimensional array of coefficients contains four bands of data, each labeled as LL (low-low), HL (high-low), LH (low-high) and HH (high-high). The LL band can be decomposed once again in the same manner, thereby producing even more sub bands. This can be done up to any level, thereby resulting in a pyramidal decomposition as shown in figure 5.1.1

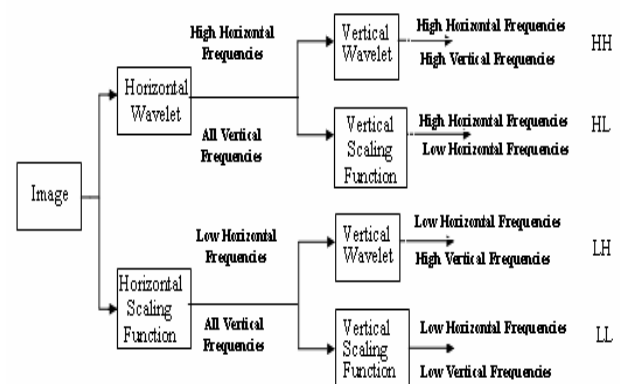


Figure 5.1.1 Pyramidal Decomposition of an image

V.2 Haar Wavelet Transform

The first DWT was invented by the Hungarian mathematician Alfréd Haar. For an input represented by a list of $2n$ numbers, the Haar wavelet transform may be considered to simply pair up input values, storing the difference and passing the sum. This process is repeated recursively, pairing up the sums to provide the next scale: finally resulting in $2n - 1$ differences and one final sum (The Haar scaling function) Let be defined by

$$\emptyset : R \rightarrow R$$

Define as

$$\emptyset(t) = \begin{cases} 1 & t \in [0,1) \\ 0 & t \in [1,2) \end{cases} \quad (1)$$

$$\emptyset_i^j : R \rightarrow R$$

$$\emptyset_i^j(t) = \sqrt{2^j} \emptyset(2^j t - i) \quad j=0,1,\dots \quad (2)$$

$i=0,1,\dots, 2^j - 1$

Defines the vector space

$$V^j = sp \{ \emptyset_i^j \} \quad i = 0, \dots, 2^j - 1$$

For encoding the transform image used various type. For example Huffman coding, EZW coding, Run length encoding, thresholding technique is also used for encoding. In this scheme i used soft & hard thresholding technique

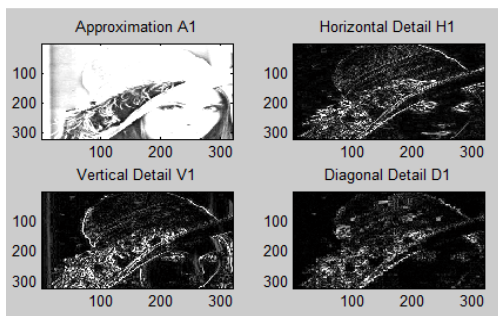
VI. EXPERIMENTAL RESULT

Original image of Lena of size 320 x 320 pixel which is compressed by using Harr wavelet & thresholding technique. By developing a code in Matlab for compression of image using wavelet transform results are shown in following figure.

Original still image of Lenna 320 x 320 pixel true colour image.



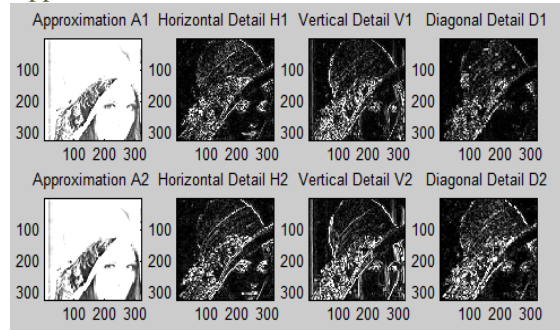
First Approximation component.



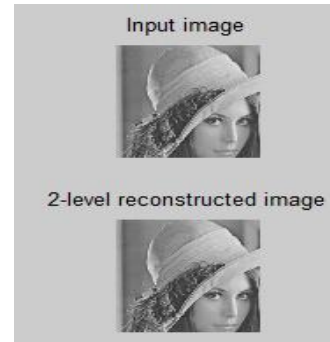
First level reconstruction image.



Second level Approximation component



Second level Reconstructed image.



Output image at 1 st level compression.



Output image at 2nd level compression.



The number of rows in input image are 320
 The number of columns in input image are 320 The decomposition level 2
 Decomposition vector of size 1*524288 .
 Coressponding book keeping matrix
 80 80
 80 80
 160 160
 320 320
 Level-dependent thresholds 0.5000
 The entropy used is threshold
 The type of thersholding is Hard Thresholding
 Approximation coefficients are 1
 Wavelet packet best tree decomposition of XD
 Wavelet Packet Object Structure

Size of initial data : [320 320]
 Order : 4
 Depth : 2
 Terminal nodes : [5 6 7 8 9 10 11 12 13 14 15
 16 17 18 19 20]

Wavelet Name : haar
 Low Decomposition filter : [0.7071 0.7071]
 High Decomposition filter: [-0.7071 0.7071]
 Low Reconstruction filter : [0.7071 0.7071]
 High Reconstruction filter : [0.7071 0.7071]

Entropy Name : threshold
 Entropy Parameter : 0.5

The compression scores in percentages 23.6035

VII. CONCLUSION

This paper introduced the basic wavelet theory used for wavelet transform based image compression. Wavelet based image compression is ideal for adaptive compression since it is inherently a multi-resolution scheme. Variable levels of compression can be easily achieved. The number of waveletting stages can be varied, resulting in different number of sub bands. Different filter banks with different characteristics can be used. Efficient fast algorithm for the computation of discrete wavelet coefficients makes a wavelet transform based encoder computationally efficient. BY using this method the compression ratio is 23.60% and this will be increase more using different entropy encoding technique.

REFERENCES

- [1] S. Mallat, "Multifrequency channel decompositions of images and wavelet models", IEEE Trans. Acoust., Speech, Signal Process., vol. 37, no. 12, pp. 2091- 2110, Dec. 1989.
- [2] "JPEG2000 Image Coding System", JPEG 2000 final committee draft version 1.0, March 2000 (available from <http://www.jpeg.org/public/fcd15444-1.pdf>)
- [3] Rohit Arora, Madan Lal Sharma," An Algorithm for Image Compression Using 2D Wavelet Trans -form" Rohit Arora et al. / International Journal of Engineering Science and Technology (IJEST)
- [4] Mulcahy, Colm Image Compression Using the Haar Wavelet Transform
- [5] Hongsong Li, DaLi" A New Image Coding Scheme Based Upon Image Pattern Recognition" IEEE 2010.
- [6] Julio C. Rolon, Antonio Ortega and Philippe Salembier" Modeling Of Contours In Wavelet Domain For Generalized Lifting image Compression" IEEE 2009.
- [7] D. U. Shah1, C. H. Vithlani," Efficient Implementations Of Discrete Wavelet Transforms Using Fpgas" International Journal of Advances in Engineering & Technology, Sept 2011.

[8] Sanjeev Chopra, Deeksha Gupta" Comparative Analysis of Wavelet Transform and Wavelet Packet Transform for Image Compression at Decomposition Level 2" 2011 International Conference on Information and Network Technology.

[9] Peggy Morton, Arne Petersen"Image compression using Haar wavelet transform "IEEE December 1997.



Deokate Balasaheb is currently an Assistant professor in the Department of Electronic & Telecommunication at Vidya Pratishthan's College of Engineering, Baramati, India. He received M.E. in E&Tc (Microwave) from Pune University in 2010 .His teaching experience is 7 years. He has 6 International conference papers. His research interest includes light wave systems and optical access networks based on WDM-PON, VLSI, and digital image processing.



Patil Pradeep M. is currently an Principal / Director of Technical Campus of RMD Sinhgad School of Engineering, Warje. He had received Ph. D. (Electronics and Computer). His teaching experience is 24 years. He has 26 international journals, 26 international conference, 06 national journals & 22 national conference papers.

The Terminal System Design based on hybrid RFID-GPS in Vehicular communications

A. Rajasekhar reddy¹, P.Anwar basha²

*(ECE, AITS/ JNTU anantapur, India)

** (Department of ECE, AITS/JNTU anantapur, India)

ABSTRACT: In this paper, vehicle terminal system is proposed to realize continuous monitoring and tracking the location of cargos or goods loaded on board for digital logistics. The embedded design of the terminal system is combines both the RFID with GPS technologies. The ultra-low power 16-bit RISC microcontroller is used as the central control unit considering both small size and high efficiency. The vehicle terminal system can give the automatic identification of cargos loaded, the real-time vehicle location, the data and voice communication, and continuous monitoring. The results specify that the combination of RFID and GPS can provide the reliability of the system, which further improve the accuracy and efficiency of digital logistics management.

Keywords: digital Logistics; vehicular communications; RFID; GPS; vehicle terminal system

I. INTRODUCTION

In recent years, the RFID (Radio Frequency Identification) technology is known for real-time identification and tracking. Because of its accurate and fast identification, RFID is used extensively to improve the logistics management, supply chain operation and asset tracking. The GPS (Global Positioning System) is the most popular technology to acquire the position information in outdoor environments. Always GPS is used for tracking of vehicles over a wide geographic area. With simultaneous data received from four satellites and ideal conditions and minimal Ionosphere, users can calculate an object's location including mainly latitude, longitude, and altitude. The powerful combination of information and intelligent technologies will advance the supply chain monitoring and management capabilities from the origin to final destination. There have been some related works that are focused on the integration of RFID and GPS in certain fields. A hybrid RFID-GPS system was explored and tested in, which allowed for the real-time location of human resources both indoors and outdoors. In, an embedded pedestrian navigation system comprising a self-contained sensor, the GPS and an active RFID tag system was presented, and a method of complementary compensation algorithm for the GPS/RFID localization was proposed. From we find a new integrated solution, which makes the cargos and container monitored and located through moving RFID and GPS equipment. Using both RFID and DGPS technique, solved the limitations of existing yield mapping systems for manual fresh fruit harvesting, which was also tested in the field. In a

stray prevention system that integrated RFID, GPS, GSM, and GIS technologies was constructed for elderly patients without interfering their activities of daily livings. In mobile supply chain management, it is also very necessary to propose an advanced, flexible, intelligent and ultra-low-power vehicle terminal system to ensure logistics goods and transport vehicles against damage, loss or theft. Cooperating with the remote monitoring centre, the mobile vehicles and cargos loaded can be localized quickly, which will improve management visibility and centralized control energetically. The main components of the terminal system are composed of the ultra-low power 16-bit MCU LPC 2148, the acquisition unit of RFID tags information, the receiver module of GPS information, the GSM wireless communication module, and the temperature sensor. The RFID-GPS-based tracking vehicle terminal system can provide identify, monitor, track, localize and manage key mobile supply chain assets, even though in the hard environmental conditions. Moreover, the system can perform real-time stock checks, locate missing stock soon, position drivers quickly and protect drivers from danger in case of emergency. Experimental results show that the vehicle terminal device can distinguish correctly RFID tags and receive accurately GPS information. The RFID tags information and the GPS data can be processed in time. The processing results can be transmitted to the logistics monitoring center via the GSM mobile networks. The performances indicate that the system can improve the real-time management of movable supply chains. The organization of this paper is as follows. Section II depicts an overall framework of the vehicle terminal system. In section III, the system architecture and prototype design are presented. Section IV describes the prototype system test and evaluation. Finally, conclusive remarks are made in Section V.

II. OVERVIEW OF THE SYSTEM FRAMEWORK

II.1 System Description

During logistics management, one of the constant challenges is to ensure the celerity, accuracy, security and safety of consignment. When cargos or goods are loaded in vehicles, Transport Company should know immediately a detailed product description, which will act as the identification information of different cargos or goods. During the transportation, the logistics management center need to know whether the products are security and safety, whether the

products are damaged or stolen, and what is the real-time geographic position of the vehicle. When the vehicle arrives at the destination, transport company should know how many and what kind of products should be unloaded. Thus the logistics management center has to monitor more closely the supply chain using the real-time automatic visibility afforded by expert and advanced technologies such as RFID and GPS. RFID technology is stable and evolving, and it cannot be easily replicated. Therefore, RFID is becoming increasingly available in variety of fields, including manufacture, transportation, warehousing, distribution, retail, healthcare, and security. RFID systems play a key role in managing updates of stocks, transportation and logistics of the product, which enables counterfeit identification, parcel tracking, shipment monitoring and tracing, access controlling, and so on. A typical RFID system consists of a reader, tags, antennas and a connection to database management system. The reader can receive the information (a unique ID) of tags in the available range of the reader. Using the merit of accurate and fast identification and tag reading from a greater distance, all kinds of related messages can be received by the RFID reader when the tagged products are loaded or unloaded. Hence RFID can improve movable asset management accuracy and efficiency. GPS technology has provided major breakthroughs in transportation fleet management (vehicle tracking, speed, waiting time, etc.). Through GPS, the object position coordinates and the time of the determination, which is related to a value referred to as clock bias, can be obtained by picking up signals from four satellites and measure the time. So GPS is used extensively to trace, locate and navigate. Considering the advantages of RFID and GPS, we proposed to design and develop a hybrid RFID/GPS vehicle terminal system for mobile supply chain assets tracking and monitoring.

II.2 Overall System Framework

To solve accurate consignment and realize real-time monitoring service in the transport management, the overall framework of the digital logistics management system can be proposed as figure 1. Working in coordination, the system can implement corresponding function to track goods and vehicle movement in real time. Once the position and the product ID information are captured through GPS and RFID, the vehicle terminal can send the messages to the logistics monitoring center through GSM/GPRS base stations.

The system operating procedures consist of three basic stages. Firstly, when the products leave the warehouse and are handed over to transport company, the product identification data can be found by the RFID reader. Meanwhile, the product's departure and arrival information can be automatically registered as well. The transporting information of goods is sent to transport company momentarily. Then, the GPS module achieves the message (latitude, longitude, and altitude) of vehicle position; RFID reader detects whether a product data is changed. Both the product information and the combined GPS position information are sent in real time. Once the information is

inconsistent with the present manifest, the vehicle terminal system raises the alarm to ask for help towards the logistics monitoring center. Finally, when the vehicle gets to the destination and the goods are unloaded, the information database is updated immediately.

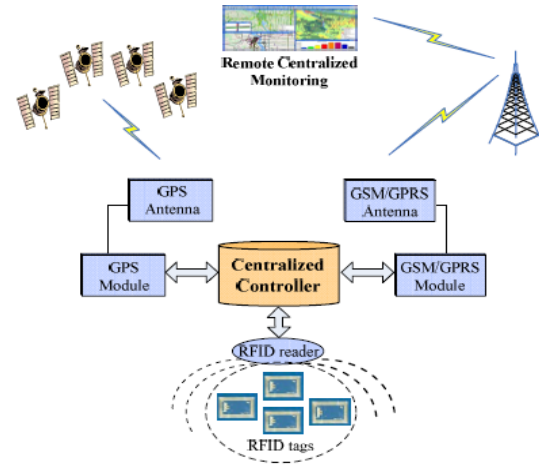


Figure 1. The overall system framework.

III. System Structure and Prototype Design

III.1 Analysis of hardware Structure

The hardware structure of the vehicle terminal system is depicted as Fig. 2. The main components are described as follows.

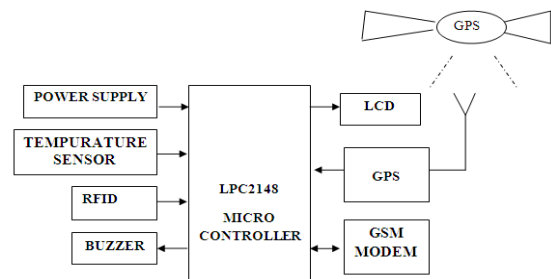


Figure 2. Block diagram of the vehicle terminal system.

III.1.1 Micro controller: The LPC2148 micro controller is based on a 32-bit/16-bit ARM7TDMI-S CPU with real-time emulation and embedded trace support, that combine microcontroller with embedded high speed flash memory ranging from 32 kB to 512 kB. A 128-bit wide memory interface and unique accelerator architecture enable 32-bit code execution at the maximum clock rate. For critical code size applications, the alternative 16-bit Thumb mode reduces code by more than 30% with minimal performance penalty. Due to their tiny size and low power consumption, LPC2146/48 are ideal for applications where miniaturization is a key requirement, such as access control and point-of-sale. Serial communications interfaces ranging from a USB 2.0 Full-speed device, multiple UARTs, SPI, SSP to I2C-bus and on-chip SRAM of 8 kB up to 40 kB, make these devices very well suited for communication gateways and protocol converters, soft modems, voice recognition and low end imaging, providing both large buffer size and high

processing power. Various 32-bit timers, single or dual 10-bit ADC(s), 10-bit DAC, PWM channels and 45 fast GPIO lines with up to nine edge or level sensitive external interrupt pins make these microcontrollers suitable for industrial control and medical systems.

III.1.2 RFID reader Module: This is used to automatically identify the products tagged within the communication range of the reader, which will be able to provide the accurate consignments and real-time automatically manifest, and improve movable asset management accuracy and efficiency.

III.1.3 GPS Module: It is used to provide satellite localization information to trace and locate the vehicle of transportation, such as WGS84 coordinates (latitude, longitude and altitude), time, speed, and direction.

III.1.4 GSM Module: It provides a communication channel to transmit product tag messages, geography location messages or emergency rescue messages, and receives commands from the transport company or the remote monitor center.

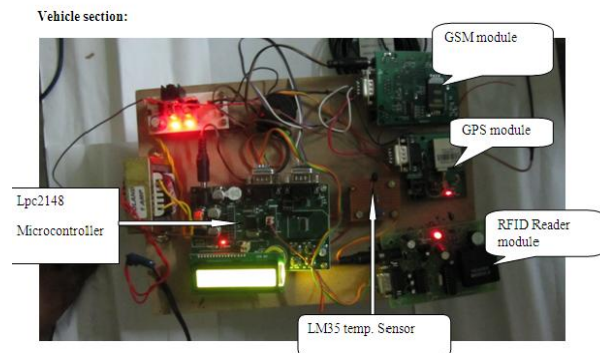


Figure 3. Prototype of the vehicle terminal system.

III.2 Building the Prototype System

As is depicted in Fig. 3, the vehicle terminal prototype system consists of a low-power microcontroller, a RFID reader, GPS module, a GSM module, power management, and other interface circuits. The LPC 2148 micro controller is chosen as the centralized control unit due to its ultra-low power.

The MCU power consumption of active mode is $280\mu\text{A}$ and only $1.6\mu\text{A}$ in standby mode. The RFID reader of the vehicle terminal is performed by a TI TRF7960 13.56MHz RFID reader, which supports the ISO 14443A/B, ISO 15693, ISO 18000-3 standards, and TI's Tag-It RFID protocol. The GPS and GSM functions of the vehicle terminals are performed by a FALCOM JP7-T GPS receiver module and a Siemens TC35-i GSM module. JP7-T is a standard receiver using the L1 band and C/A coding by stand alone positioning with 12 channels, 10m position accuracy, 0.1m/s velocity accuracy and its power consumption is 200mW in continues mode. Working in coordination, the vehicle terminal system provides the ability to capture and trace supply chain assets movement in real time. The system supports combined RFID

and GPS message reporting. We can also create custom rules associated with products or vehicles passing into or out of the zone that may trigger further actions or messages.

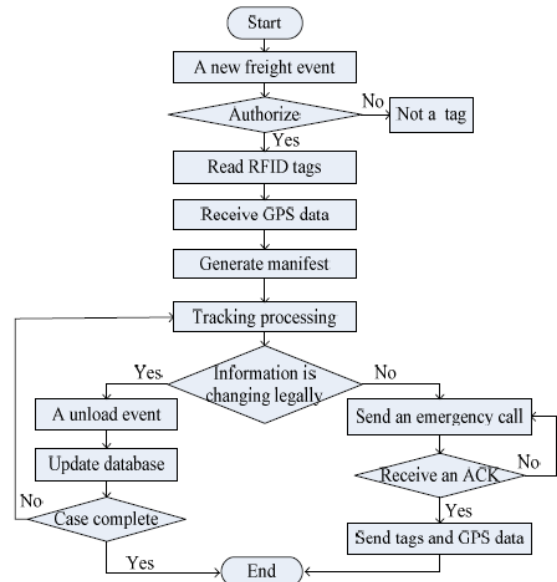


Figure 4. The operation flow of the vehicle terminal system.

III.3 System operation flow

The vehicle terminal system operation flow is depicted as Fig.4. Once a new freight event occurs, the RFID reader will continuously read RFID tags. Then the data combined with GPS position are sent to the remote monitor center for further processing through GSM communication module. Meanwhile a real-time automatic manifest is generated, including data from RFID tags with a unique ID which describes a tagged product's manufacturer, type, and serial number. When a legal unload event happens, related database will be updated. If a transportation case is completed, the system will enter standby mode and wait for a next freight event.

Whenever an abnormal situation happens, the vehicle Terminal system will immediately send out a message Containing the product's status and GPS information to the remote monitor center. After the monitor center receives the data packet, it will manage or convert the longitude and latitude coordinates, and combine this location with other basic information such as product characteristics, type, material, shape and size to generate the complete information needed for search and assistance tasks.

IV. EXPERIMENTS AND RELATED RESULTS

We have conducted related experiments and evaluations in a simulation transportation scene. The vehicle terminal system was mounted at an automobile carrier. Each product has a fixed RFID tag working at 13.56MHz band, which supports ISO15693 protocol and provides 9600bps communication link. When the products tagged enter the operational zone of the RFID reader, each of unique ID is acquired. Meanwhile,

the reader can get the detected time of the product tagged. One of the experiment results is shown in Fig. 5.

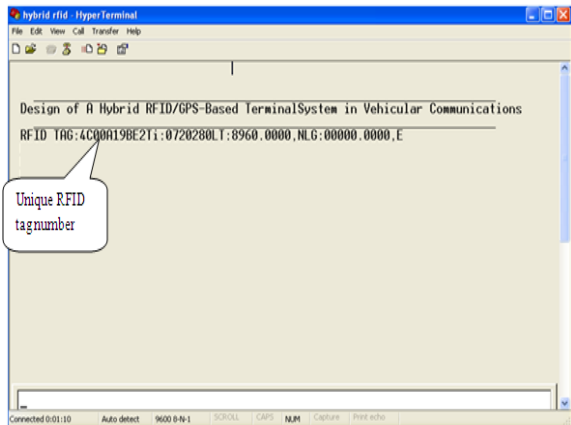


Figure 5. RFID Testing Experiment.

During the experiment run, the GPS module receives the longitude, latitude values which will give the real-time location message from different satellites shown in figure 6.

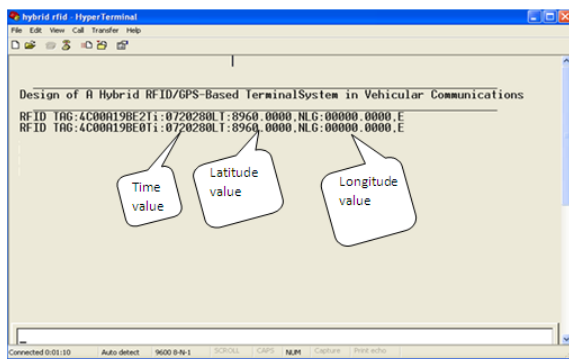


Figure 6. Locating the longitude & latitude values.

Fig.7 shows that when the temperature exceeds more than 50°C then the message “fire accident occurred” is sent to the control section.

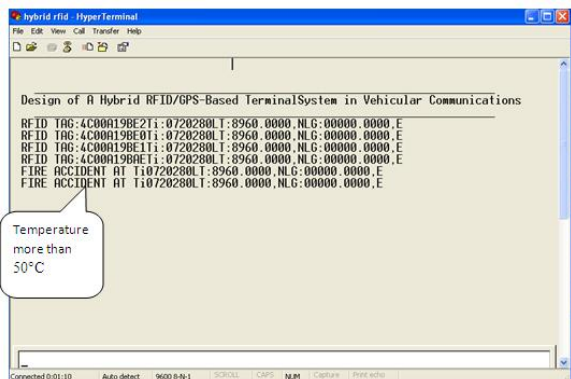


Figure 7. The message when temperature more than 50°C.

V. CONCLUSIONS

A new solution that integrates RFID identifying and GPS tracking is proposed and implemented, which can enhance automatic management, information security, real-time trace and location, and anti-theft in digital logistics management. Experimental results show that the vehicle terminal system can identify quickly mobile supply chain assets, trace and locate mobile equipment in real time, reduce loss and theft and enhance management control as well. Soon the system will be further improved through the integration with GIS technology, which will enhance the visibility of the supply chain. It is conceivable that this research will bring more efficient and intelligent logistic transportation.

REFERENCES

- [1] Asif, Z., "Integrating the Supply Chain with RFID: A Technical and Business Analysis," *Communications of the AITS*, pp 393-427, 2005.
- [2] Kumar, S., and K. B. Moore. "The Evolution of Global Positioning System (GPS)," *Journal of Science Education and Technology*, pp 59-80, 2002.
- [3] Manon G. Guillemette, Isabelle Fontaine, and Claude Caron, "A hybrid RFID-GPS real-time location system for human resources: development, impacts and perspectives," in *Proceedings of the 41th Hawaii International Conference on System Sciences*, Los Alamitos, 2008.
- [4] Masakatsu Kourogil, Nobuchika Sakata, Takashi Okuma1, and Takeshi Kurata, "Indoor/outdoor pedestrian navigation with an embedded GPS/RFID/Self-contained sensor system," *Springer-Verlag Berlin Heidelberg* pp.1310-1321, 2006.
- [5] Zhengwu Yuan, Dongli Huang, "A novel RFID-based shipping containers location and identification solution in multimodal transport," *IEEE CCECE/CCGEI, Niagara Falls, Canada*, 2008.
- [6] Y.G.Ampatzidis, S.G.Vougioukas, D.D.Bochtis, C.A.Tsatsarelis, "A yield mapping system for hand-harvested fruits based on RFID and GPS location technologies: field testing," *Springer Science Business Media*, 2008.
- [7] Chung-chih Lin, Ming-jang Chiu, Chun-Chieh Hsiao, Ren-Guey Lee, and Yuh-Show Tsai, "A wireless healthcare service system for elderly with dementia," *IEEE Transaction on Information Technology in Biomedicine*, 2006.

Implementation of Flux-Charge Control Model to Multifunctional Dynamic Voltage Restorer for Emergency Control in Distribution Systems

Nyamathulla.Shaik^{*}, Anupama.S^{**}, Sudheer babu.M^{***}

^{*}(Electrical and Electronics Engineering, AITS, JNTUA, India)

^{**}(Electrical and Electronics Engineering, AITS, JNTUA, India)

^{***}(Electrical and Electronics Engineering, AITS, JNTUA, India)

ABSTRACT: The dynamic voltage restorer (DVR) is one of the modern devices used in distribution systems to protect consumers against sudden changes in voltage amplitude. In this paper, emergency control in distribution systems is discussed by using the proposed multifunctional DVR control strategy. Also, the multi loop controller using the Posicast and P+Resonant controllers is proposed in order to improve the transient response and eliminate the steady-state error in DVR response, respectively. The proposed algorithm is applied to some disturbances in load voltage caused by induction motors starting, and a three-phase short circuit fault. Also, the capability of the proposed DVR has been tested to limit the downstream fault current. The current limitation will restore the point of common coupling (PCC) (the bus to which all feeders under study are connected) voltage and protect the DVR itself. The innovation here is that the DVR acts as virtual impedance with the main aim of protecting the PCC voltage during downstream fault without any problem in real power injection into the DVR. Simulation results show the capability of the DVR to control the emergency conditions of the distribution systems.

Keywords: Dynamic voltage restorer (DVR), emergency control, voltage sag, voltage swells.

I. INTRODUCTION

Voltage sag and voltage swell are two of the most important power-quality (PQ) problems that encompass almost 80% of the distribution system PQ problems. According to the IEEE 1959–1995 standard, voltage sag is the decrease of 0.1 to 0.9 p.u. in the rms voltage level at system frequency and with the duration of half a cycle to 1 min. Short circuits, starting large motors, sudden changes of load, and energization of transformers are the main causes of voltage sags [3]. According to the definition and nature of voltage sag, it can be found that this is a transient phenomenon whose causes are classified as low- or medium-frequency transient Events. In recent years, considering the use of sensitive devices in modern industries, different methods of compensation of voltage sags have been used. One of these methods is using the DVR to improve the PQ and compensate the load voltage. Previous works have been done on different aspects of DVR performance, and different control strategies have been found. These methods mostly depend on the purpose of using DVR. In some methods, the main purpose is to detect and compensate for the voltage sag with minimum DVR active power injection.

Also, the in-phase compensation method can be used for sag and swell mitigation. The multiline DVR can be used for eliminating the battery in the DVR structure and controlling more than one line. Moreover, research has been made on using the DVR in medium level voltage. Harmonic mitigation and control of DVR under frequency variations are also in the area of research. The closed-loop control with load voltage and current feedback is introduced as a simple method to control the DVR in Also, Posicast and P+Resonant controllers can be used to improve the transient response and eliminate the steady-state error in DVR. The Posicast controller is a kind of step function with two parts and is used to improve the damping of the transient oscillations initiated at the start instant from the voltage sag. The P+Resonant controller consists of a proportional function plus a resonant function and it eliminates the steady-state voltage tracking error. The state feed forward and feedback methods, symmetrical components estimation, robust control, and wavelet transform have also been proposed as different methods of controlling the DVR. In all of the aforementioned methods, the source of disturbance is assumed to be on the feeder which is parallel to the DVR feeder. In this paper, a multifunctional control system is proposed in which the DVR protects the load voltage using Posicast and P+Resonant controllers when the Source of disturbance is the parallel feeders. On the other hand, during a downstream fault, the equipment protects the PCC voltage, limits the fault current, and protects itself from large fault current. Although this latest condition has been described in using the flux control method, the DVR proposed there acts like a virtual inductance with a constant value so that it does not receive any active power during limiting the fault current. But in the proposed method when the fault current passes through the DVR, it acts like series variable impedance (unlike where the equivalent impedance was a constant).

The basis of the proposed control strategy in this paper is that when the fault current does not pass through the DVR, an outer feedback loop of the load voltage with an inner feedback loop of the filter capacitor current will be used. Also, a feed forward loop will be used to improve the dynamic response of the load voltage. Moreover, to improve the transient response, the Posicast controller and to eliminate the steady-state error, the P+Resonant controller are used. But in case the fault current passes

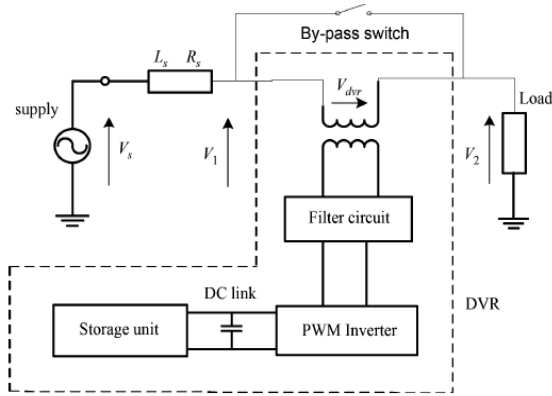


Fig. 1. Typical DVR-connected distribution system.

Through the DVR, using the flux control algorithm, the series voltage is injected in the opposite direction and, therefore, the DVR acts like series variable impedance. The remainder of this paper is organized as follows: The general operation of DVR and its state space description are provided in Section II. The closed-loop control using Posicast and P+Resonant controllers has been presented in Section III. In Section IV, the multifunctional DVR is introduced. The basis of the proposed control method is described in Section V. Finally, the simulation results are provided in Section VI which shows that the control capability of the proposed DVR system is satisfactory.

II. DVR COMPONENTS AND ITS BASIC OPERATIONAL PRINCIPLE

A. DVR Components

A typical DVR-connected distribution system is shown in Fig. 1, where the DVR consists of essentially a series-connected injection transformer, a voltage-source inverter, an inverter output filter, and an energy storage device that is connected to the dc link. Before injecting the inverter output to the system, it must be filtered so that harmonics due to switching function in the inverter are eliminated. It should be noted that when using the DVR in real situations, the injection transformer will be connected in parallel with a bypass switch (Fig. 1). When there is no disturbances in voltage, the injection transformer (hence, the DVR) will be short circuited by this switch to minimize losses and maximize cost effectiveness. Also, this switch can be in the form of two parallel thyristors, as they have high on and off speed. A financial assessment of voltage sag events and use of flexible ac transmission systems (FACTS) devices, such as DVR, to mitigate them is provided in. It is obvious that the flexibility of the DVR output depends on the switching accuracy of the pulse width modulation (PWM) scheme and the control method. The PWM generates sinusoidal signals by comparing a sinusoidal wave with a saw tooth wave and sending appropriate signals to the inverter switches.

B. Basic Operational Principle of DVR

The DVR system shown in Fig. 1, controls the load voltage by injecting an appropriate voltage phasor in series with the

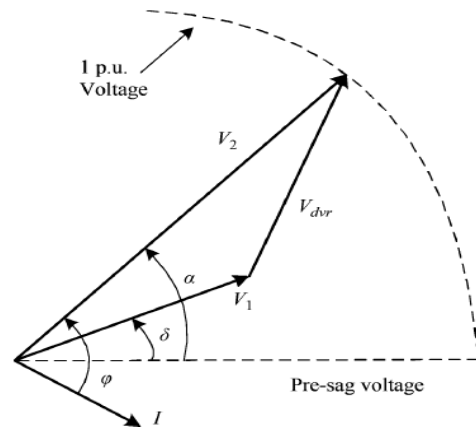


Fig. 2. Phasor diagram of the electrical conditions during voltage sag.

System using the injection series transformer. In most of the sag compensation techniques, it is necessary that during compensation, the DVR injects some active power to the system. Therefore, the capacity of the storage unit can be a limiting factor in compensation, especially during long-term voltage sags. The phasor diagram in Fig. 2 shows the electrical conditions during voltage sag, where, for clarity, only one phase is shown. Voltages V_1 , V_2 and V_{dvr} are the source-side voltage, the load side voltage, and the DVR injected voltage, respectively. Also, the operators I , ϕ , δ and α are the load current, the load power factor angle, the source phase voltage angle, and the voltage phase advance angle, respectively. It should be noted that in addition to the in-phase injection technique, another technique, namely “the phase advance voltage compensation technique” is also used. One of the advantages of this method over the in-phase method is that less active power should be transferred from the storage unit to the distribution system. This results in compensation for deeper sags or sags with longer durations. Due to the existence of semiconductor switches in the DVR inverter, this piece of equipment is nonlinear. However, the state equations can be linearized using linearization techniques.

The dynamic characteristic of the DVR is influenced by the filter and the load. Although the modeling of the filter (that usually is a simple LC circuit) is easy to do, the load modeling is not as simple because the load can vary from a linear time invariant one to a nonlinear time-variant one. In this paper, the simulations are performed with two types of loads: 1) a constant power load and 2) a motor load. As Fig. 3 shows, the load voltage is regulated by the DVR through injecting V_{dvr} . For simplicity, the bypass switch shown in Fig. 1 is not presented in this figure. Here, it is assumed that the load has a resistance R_L and an inductance L_L . The DVR harmonic filter has an inductance of L_f , a resistance of R_f , and a capacitance of C_f . Also, the DVR injection transformer has a combined winding resistance of R_t , a leakage inductance of L_t , and turns ratio of 1: n.

The Posicast controller is used in order to improve the transient response. Fig. 4 shows a typical control block diagram of the DVR. Note that because in real situations, we are dealing with multiple feeders connected to a common bus, namely “the Point of Common Coupling (PCC),” from now on, V_1 and V_2 will be replaced with V_{pcc}

and V_L , respectively, to make a generalized sense. As shown in the figure, in the open-loop control, the voltage on the source side of the DVR is compared with a load-side reference voltage (V_L^*) so that the necessary injection voltage (V_{inv}^*) is derived. A simple method to continue is to feed the error signal into the PWM inverter of the DVR. But the problem with this is that the transient oscillations initiated at the start instant from the voltage sag could not be damped sufficiently.

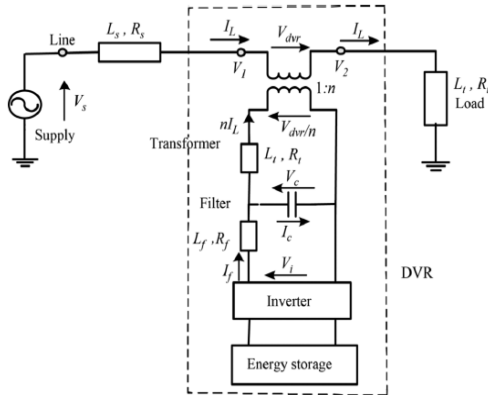


Fig. 3. Distribution system with the DVR

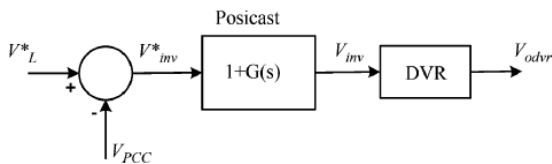


Fig. 4. Open-loop control using the Posicast controller.

To improve the damping, as shown in Fig. 4, the Posicast controller can be used just before transferring the signal to the PWM inverter of the DVR. The transfer function of the controller can be described as follows:

$$1 + G(s) = 1 + \frac{\delta}{1 + \delta} \left(e^{-sT_d/2} - 1 \right) \quad (1)$$

Where δ and T_d are the step response overshoot and the period of damped response signal, respectively. It should be noted that the Posicast controller has limited high-frequency gain; hence, low sensitivity to noise.

To find the appropriate values of δ and T_d and, first the DVR model will be derived according to Fig. 3, as follows:

$$\begin{aligned} V_i &= V_c + I_f R_f + L_f \frac{dI_f}{dt} \\ I_f &= I_c + n \cdot I_t \\ I_c &= C_f \frac{dV_c}{dt} \end{aligned}$$

$$V_{dvr} = n \left[V_c - n \left(R_t I_t + L_t \frac{dI_t}{dt} \right) \right]$$

$$V_2 = V_1 + V_{dvr}$$

Then, according to (2) and the definitions of damping and the delay time in the control literature, and are derived as follows:

$$\begin{aligned} T_d &= \frac{2\pi}{\omega_r} = \frac{\pi}{\sqrt{\frac{1}{L_f C_f} - \frac{R_f^2}{4L_f^2}}} \\ \delta &= e^{\xi\pi/\sqrt{1-\xi^2}} = e^{-R_f\pi\sqrt{C_f}/\sqrt{4L_f - R_f^2 C_f}} \end{aligned} \quad (3)$$

The Posicast controller works by pole elimination and proper regulation of its parameters is necessary. For this reason, it is sensitive to inaccurate information of the system damping resonance frequency. To decrease this sensitivity, as is shown in Fig. 5, the open-loop controller can be converted to a closed loop controller by adding a multi loop feedback path parallel to the existing feed forward path. Inclusion of a feed forward and a feedback path is commonly referred to as two-degrees-of freedom (2-DOF) control in the literature. As the name implies, 2-DOF control provides a DOF for ensuring fast dynamic tracking through the feed forward path and a second degree of freedom for the independent tuning of the system disturbance compensation through the feedback path. The feedback path consists of an outer voltage loop and a fast inner current loop. To eliminate the steady-state voltage tracking error, a computationally less intensive P+Resonant compensator is added to the outer voltage loop. The ideal P+Resonant compensator can be mathematically expressed as

$$G_R(s) = k_p + \frac{2k_I s}{s^2 + \omega_0^2} \quad (4)$$

Where k_p and k_I are gain constants and ω_0 is the controller resonant frequency. Theoretically, the resonant controller compensates by introducing an infinite gain at the resonant frequency of 50 Hz to force the steady-state voltage error to zero. The ideal resonant controller, however, acts like a network with an infinite quality factor, which is not realizable in practice. A more practical (non ideal) compensator is therefore used here, and is expressed as

$$G_R(s) = k_p + \frac{2k_I \omega_{cut} s}{s^2 + 2\omega_{cut} s + \omega_0^2} \quad (5)$$

Where ω_{cut} is the compensator cutoff frequency which is 1 rad/s

III. PROPOSED MULTIFUNCTIONAL DVR

In addition to the aforementioned capabilities of DVR, it can be used in the medium-voltage level (as in Fig. 6) to protect a group of consumers when the cause of disturbance is in the downstream of the DVR's feeder and the large fault current passes through the DVR itself. In this case, the equipment can limit the fault current and protect the loads in parallel feeders until the breaker works and disconnects the faulted feeder. The large fault current will cause the PCC voltage to drop and the loads on the other feeders connected to this bus will be affected. Furthermore, if not controlled properly, the DVR might also contribute to this PCC voltage sag in the process of compensating the missing voltage, hence further worsening the fault situation.

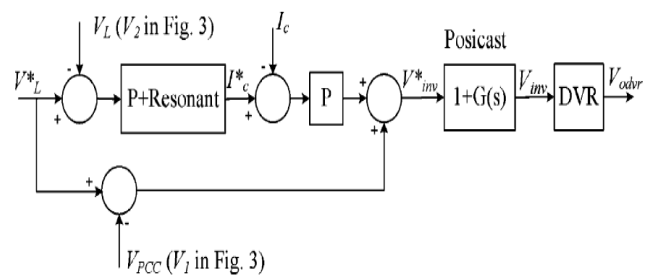


Fig. 5. Multiloop control using the Posicast and P+Resonant controllers.

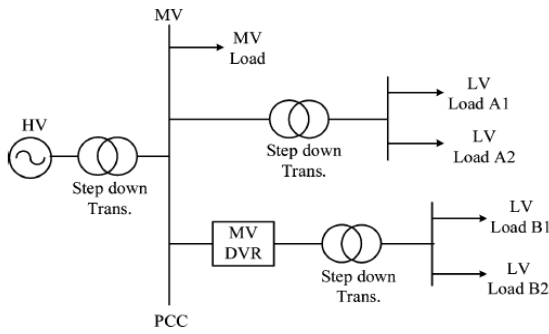


Fig. 6DVR connected in a medium-voltage level power system.

To limit the fault current, a flux-charge model has been proposed and used to make DVR act like a pure virtual inductance which does not take any real power from the external system and, therefore, protects the dc-link capacitor and battery as shown in Fig.1. But in this model, the value of the virtual inductance of DVR is a fixed one and the reference of the control loop is the flux of the injection transformer winding, and the PCC voltage is not mentioned in the control loop. In this paper, the PCC voltage is used as the main reference signal and the DVR acts like a variable impedance. For this reason, the absorption of real power is harmful for the battery and dc-link capacitor. To solve this problem, impedance including a resistance and an inductance will be connected in parallel with the dc-link capacitor. This capacitor will be separated from the circuit, and the battery will be connected in series with a diode just when the downstream fault occurs so that the power does not enter the battery and the dc-link capacitor. It should be noted here that the inductance is used mainly to prevent large oscillations in the current. The active power mentioned is, therefore, absorbed by the impedance.

IV. PROPOSED METHOD FOR USING THE FLUX-CHARGE MODEL

In this part, an algorithm is proposed for the DVR to restore the PCC voltage, limit the fault current, and, therefore, protect the DVR components. The flux-charge model here is used in a way so that the DVR acts as a virtual inductance with a variable value in Series with the distribution feeder. To do this, the DVR must be controlled in a way to inject a proper voltage having the opposite polarity with respect to usual cases. It should be noted that over current tripping is not possible in this case, unless additional Communication between the DVR and the downstream side over current circuit breaker (CB) is available. If it is necessary to operate the over current CB at PCC, communication between the DVR and the PCC breaker might have to be made and this can be easily done by sending a signal to the breaker when the DVR is in the fault-current limiting mode as the DVR is just located after PCC.

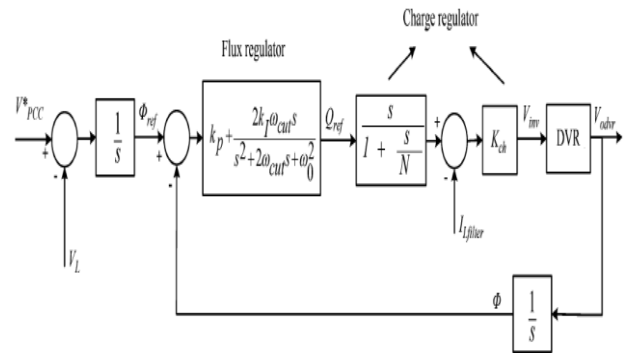


Fig. 7. Proposed method.

The proposed DVR control method is illustrated in Fig. 7. It should also be noted that the reference flux (ϕ_{ref}) is derived by integration of the subtraction of the PCC reference voltage (V_{pcc}^*) and the DVR load-side voltage. In this control strategy, the control variable used for the outer flux model is the inverter-filtered terminal flux defined as:

$$\Phi = \int V_{odvr} dt \tag{6}$$

Where is the filter capacitor voltage of the DVR (at the DVR power converter side of the injection transformer). The flux error is then fed to the flux regulator, which is a P+Resonant controller, with a transfer function given in (6). On the other hand, it can be shown that a single flux-model would not damp out the resonant peak of the LC filter connected to the output of the inverter.

To stabilize the system, an inner charge model is therefore considered. In this loop, the filter inductor charge, which is derived by integration of its current, tracks the reference charge Output Q_{ref} of the flux regulator. The calculated charge error is then fed to the charge regulator with the transfer function

$$G_{charge}(s) = k_{ch} \frac{S}{1 + \frac{S}{N}} \tag{7}$$

Which is actually a practical form of the derivative controller. In this transfer function, the regulator gain is limited to at high frequencies to prevent noise amplification. The derivative term in $S/(1+(S/N))$ neutralizes the effects of voltage and current integrations at the inputs of the flux-charge model, resulting in the proposed algorithm having the same regulation performance as the multiloop voltage-current feedback control, with the only difference being the presence of an additional low-pass filter in the flux control loop in the form of $1/(1+(S/N))$. The bandwidth of this low-pass filter is tuned (through varying) with consideration for measurement noise attenuation, DVR LC-filter transient resonance attenuation, and System stability margins.

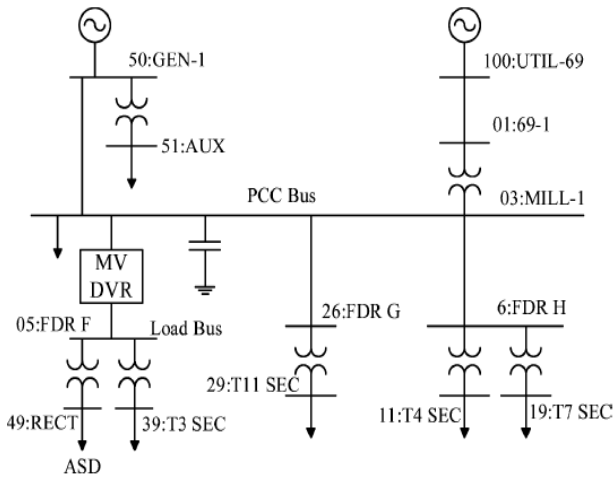


Fig. 8. Under Study test system.

V. SIMULATION RESULTS

In this part, the proposed DVR topology and control algorithm will be used for emergency control during the voltage sag. The three-phase short circuit and the start of a three-phase large induction motor will be considered as the cause of distortion in the simulations.

A. Under Study Test System

In this paper, the IEEE standard 13-bus balanced industrial system will be used as the test system. The one-line diagram of this system is shown in Fig. 9. The test system is modeled in MATLAB SIMULINK software. Control methods of Figs. 5 and 7 were applied to control the DVR, and the voltage, current, flux, and charge errors were included as the figures show. A 12-pulse inverter was used so that each phase could be controlled separately. Detailed specifications of the DVR components are provided in the Appendix.

The plant is fed from a utility supply at 69 kV and the Local plant distribution system operates at 13.8 kV. The local (in-plant) generator is represented as a simple Thevenin equivalent. The internal voltage, determined from the converged power-flow solution, is $13.8 \angle -1.52^\circ$ kV. The equivalent impedance is the subtransient impedance which is $0.036 + j1.3651 \Omega$. The plant power factor correction capacitors are rated at 6000 kvar. As is typically done, leakage and series resistance of the bank are neglected in this study. The detailed description of the system can be found in [1]. In the simulations, the DVR is placed between buses "03: MILL-1" and "05: FDR F."

B. Three-Phase Short Circuit

In this part, the three-phase short circuit is applied on bus "26: FDR G," and the capability of the DVR in protecting the voltage on bus "05: FDR F" will be studied. The DVR parameters and the control system specifications are provided in Appendices A and B. At $t=205$ ms, the fault is applied at $t=285$ ms, and the breaker works and separates the line between buses "03: MILL-1" and "26: FDR G" from the system. At $t=305$ ms, the fault will be recovered and, finally, at $t=310$ ms, the separated line will be rejoined to the system by the breaker. The simulation results are shown in Fig. 9. As can be seen in the figure, the rms voltage of PCC drops to about 0.25 p.u. during the fault.

The DVR will start the compensation just after the detection of sag.

C. Starting the Induction Motor

A large induction motor is started on bus "03: MILL-1." The motor specifications are provided in Appendix C. The large motor starting current will cause the PCC voltage (bus "03: MILL-1" voltage) to drop. The simulation results in the case of using the DVR are shown in Fig. 10. In this simulation, the motor is started at $t=405$ ms. As can be seen in Fig. 10, at this time, the PCC rms voltage drops to about 0.8 p.u. The motor speed reaches the nominal value in about 1 s. During this period, the PCC bus is under voltage sag. From $t=1.4$ s, as the speed approaches nominal, the voltage also approaches the normal condition.

D. Fault Current Limiting

The last simulation is run for a symmetrical downstream fault, and the capability of the DVR to reduce the fault current and restore the PCC voltage is tested. For this purpose, a three-phase short circuit is applied on bus "05: FDR F". In Fig. 11, the fault current, without the DVR compensation, is shown. For the simulation with DVR compensation, the three-phase fault is applied at $t=205$ ms and then removed after 0.1 s. Also, a breaker will remove the faulted bus from the entire system at $t=300$ ms. Fig. 12 shows the DVR operation during the fault. As can be seen, the rms load bus voltage reaches zero during the fault, and as the enlarged figure shows, in about half a cycle, the DVR has succeeded in restoring the PCC voltage wave shape to the normal condition.

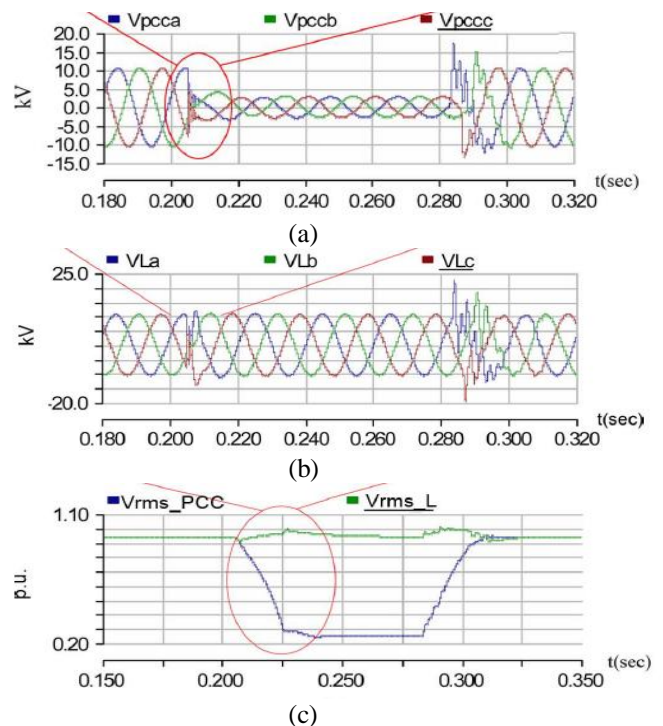


Fig. 9. Three-phase fault compensation by DVR. (a) Three-phase PCC voltages. (b) Three-phase load voltages. (c) RMS voltages of PCC and load.

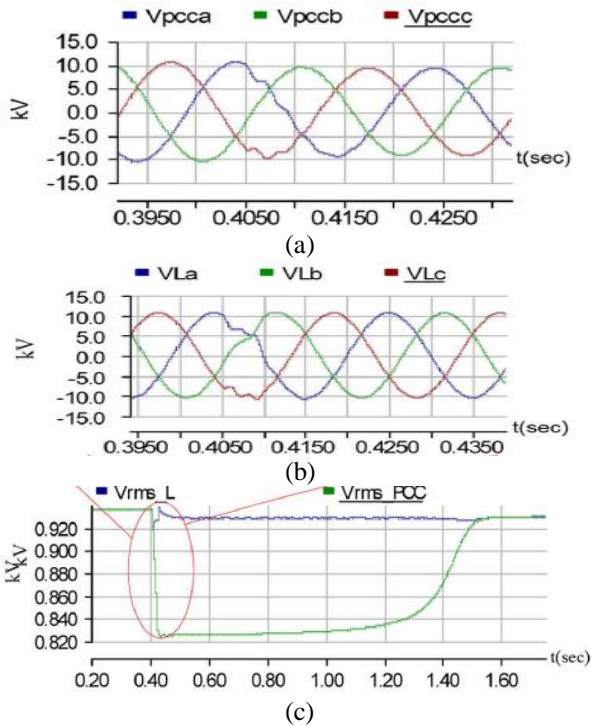


Fig. 10. Starting of an induction motor and the DVR compensation. (a) Three phase PCC voltages. (b) Three-phase load voltages. (c) RMS voltages of PCC and load.

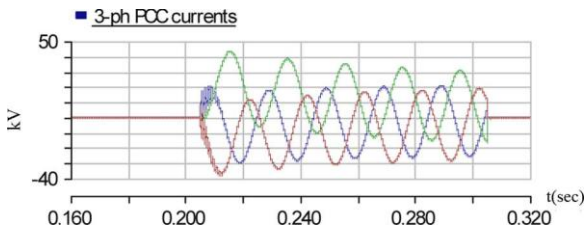


Fig. 11. Current wave shape due to the three-phase short-circuit fault without DVR compensation.

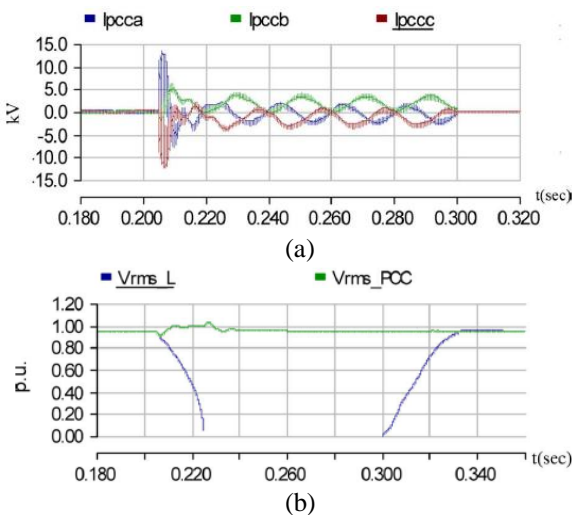


Fig. 12. Fault current limiting by DVR. (a) Three-phase currents. (b) RMS voltages of the PCC and load.

VI. CONCLUSION

In this paper, for improving the transient response and eliminating the steady-state error, the Posicast and P+Resonant controllers are used. As the second function of this DVR, using the flux-charge model, the equipment is controlled so that it limits the downstream fault currents and protects the PCC voltage during these faults by acting as variable impedance. The simulation results verify the effectiveness and capability of the proposed DVR in compensating for the voltage sags caused by short circuits and the large induction motor starting and limiting the downstream fault currents and protecting the PCC voltage.

APPENDIX

DVR Parameters:

Filter inductance (L_f) = 1mH
 Filter capacitance (C_f) = 700 μ F
 Inverter modulation ratio = 21
 Kind of DVR inverter: 12 Pulse
 DC-link capacitance: 26 mF
 Entered resistance for current limiting: 3 ohms
 Entered inductance for current limiting: 2 mH
 Supply battery: 12 kV.

Control System Parameters:

$\delta = 1$
 $T_d = 41.56$
 $K_p = 1$
 $K_i = 100$
 $\omega_0 = 314$ rad/s
 $\omega_{cut} = 1.0$ rad/s

Induction Motor Parameters:

Rated power: 2.4 MVA
 Rated voltage: 13.8 kV
 Moment of inertia: 3.7267 sec
 Number of rotor squirrel cages: 1
 Base frequency: 50 Hz
 Stator resistance: 0.0034 p.u.
 Rotor resistance: 0.298 p.u.
 Stator inductance: 0.0102 p.u.
 Rotor inductance: 0.05 p.u.
 Magnetizing inductance: 0.9 p.u.

REFERENCES

1. M. H. Rashid, *Power Electronics-Circuits, Devices and Applications*, 3rd ed. India: Prentice-Hall of India, Aug. 2006.
2. Understanding FACTS: concepts and technology of Flexible Ac transmission systems/Narain G.Hingorani, Laszlo Gyugyi
3. Facts Controllers In Power Transmission and Distribution by Padiyar, K.R. , ISBN: 978-81-224-2142-2: June, 2007.
4. Fitzer, M. Barnes, and P. Green, "Voltage sag detection technique for a dynamic voltage restore," *IEEE Trans. Ind. Appl.*, vol. 2, no. 1, pp. 203–212, Jan./Feb. 2004.
5. "Task force on harmonics modeling & simulation (co-author), test systems for harmonics modeling and simulation," *IEEE Trans. Power Del.*, vol. 14, no. 2, pp. 579–585, Apr. 1999.

A Review on Finite Element Simulations in Metal Forming

Dr. P. V. R. Ravindra Reddy¹, G. Chandra Mohan Reddy²,
P. Radhakrishna Prasad³

^{1,3}Associate Professors, Dept. of Mech. Engg., CBIT, Gandipet, Hyderabad-75;

²Principal, MGIT, Gandipet, Hyderabad-75

Abstract: *Finite element simulations are often required to reduce the experimental cost and time by reducing number of trials in the product development cycle. Metal forming is one of such area where a lot of trials are required to arrive at the die design to produce defect free parts. Hence in this paper the authors review the literature on finite element analysis in the area of metal forming*

Key Words: *Metal Forming, Finite Element Analysis, Simulations*

The term simulation is derived from the Latin word “simulare” what means “to pretend”. However, the technical meaning of simulation is the description and reproduction of physical and technical processes by use of mathematical and physical models. In comparison with practical tests, the simulation often is cheaper and not so dangerous. Combined with modern methods of computation, the simulation is a powerful tool which gains more and more importance for describing and developing new processing methods. Because of higher requirements on the quality of products and narrow tolerances of measures, optimizing, planning and simulating of forming processes becomes more and more important. As the computational power has increased during the last years, numerical methods play an outstanding roll. The most important numerical method is the method of finite elements (FEM). Numerous finite element programmes have been developed which are able to solve linear, non linear, static, dynamic, elastic, plastic, elastic – plastic, steady state, transient, isothermal as well as non isothermal problems [1].

The deep drawing process is applied with the intention of manufacturing a product with a desired shape and no failures. The final product shape after deep drawing is defined by the tools, the blank and the process parameters. An incorrect design of the tools and blank shape or an incorrect choice of material and process parameters can yield a product with a deviating shape or with failures. A deviating shape is caused by elastic springback after forming and retracting the tools. The most frequent types of failure are wrinkling, necking (and subsequently tearing), scratching and orange peel. Wrinkling may occur in areas with high compressive strains, necking may occur in areas with high tensile strains, scratching is caused by defects of the tool surface and orange peel may occur after excessive deformations, depending on the grain size of the material. The deformation patterns of the sheet material are influenced by the material properties and the processing and tooling variables. Generally, sheet material behaves anisotropically which means that the material shows a different deformation behavior in different directions because of the rolling process. An example of anisotropy is the development of ‘ears’ in cylindrical cup drawing. The friction conditions during forming depend on the lubricant, the presence of coatings on the blank, surface roughness of the tools and the blank, blank holder pressure and process velocity. Without extensive knowledge of the influences of all these variables on the deep drawing process, it is hardly possible to design the tools adequately and make a proper choice of blank material and lubricant to manufacture a product with the desired shape and performance. As a result, after the first design of the tools and choice of blank material and lubricant, an extensive and time consuming trial and error process is started to determine the proper tool design and all other variables, leading to the desired product. This trial and error process can yield an unnecessary number of deep drawing strokes, or may even require redesigning the expensive tools. To reduce this waste of time and cost, process modeling for computer simulation can be used to replace the experimental trial and error process by a virtual trial and error process. The prime objective of an analysis is to assist in the design of a product. To design or select the tools and the equipment, such design essentially consists of predicting the material flow, determining whether it is possible to form the part without surface or internal defects, predicting the forces necessary to execute the forming operation and stresses induced during the operation.

Analytical study of Metal forming processes was started in the mid of 20th century [2,3]. Later a number of analyzing methods have been developed and applied to various forming processes. Some of these methods are the slab method, the slip-line field method, the viscoplasticity method, upper and lower bound techniques and Hill’s general method. These methods have been useful in qualitatively predicting forming loads, overall geometry changes of the deformed blank and material flow and approximate optimum process conditions. Numerical procedures (finite difference method) were applied to analyze axisymmetric deep drawing process in 1960s[4] Although the work contributed to greatly to the development of theory of sheet metal forming analysis, that could not be applicable to the industrial components. However, a more accurate determination of the effects of various process parameters on the deep drawing process has become possible only, when the non linear finite element method was developed for these analyses [5-7]. Later, three dimensional auto body panel forming process was simulated using elasto-plastic finite element method by Arlinghaus [8] and Tang [9]. They simulated the drawing process of and left window outer and binder wrapping process of deck lid. But they were in the state of testing and evaluation. Because finite element analysis by that time is was still extremely time consuming and unreliable tool to the engineers in the press shop.

Rapid developments in computer hardware make the finite element analysis of complex deformation responses increasingly applicable. The finite element method is used worldwide to simulate the deep drawing process and has become a reliable numerical simulation technology. For an accurate simulation of a real-life deep drawing process an accurate numerical description of the tools is necessary, as well as an accurate description of material behavior, contact behavior and other process variables. The numerical description of the tools is provided by CAD packages which are generally used by tool designers. The description of material behavior, contact behavior and other process variables evolved from rather simple models in the earlier days to more and more sophisticated models nowadays. Developments have been made in the field of finite element types, mesh adaptivity, material laws, failure criteria, wrinkling and surface defects, springback, contact algorithms, friction, and simulation of new processes (optimization and process design). The conventional finite element codes are based on implicit time integration. This involves repeated solutions of large systems of equations. Furthermore, equilibrium must be fulfilled after each incremental step. As a result, implicit codes are computational time and memory consuming. Hence, a new class of finite element codes based on explicit time integration was developed, resulting in a drastic decrease of computational time. Honecker et.al [10] first demonstrated the deep drawing of an oil pan and a radiator part by explicit method, obtaining deeply drawn shapes including wrinkle on the flange. After this several dynamic explicit codes specialized to the sheet metal forming were developed and many automotive industries started to develop these codes. In an explicit code no system of equations needs to be solved and static equilibrium is not checked after each incremental step, as the algorithm assumes an inertia dominated process. The explicit procedure is conditionally stable with a critical time step, which is proportional to the smallest element in the mesh [11]. However, in most sheet metal forming processes inertia effects can be neglected. In order to apply the explicit algorithms in these processes, it is necessary to assume artificially high velocities and accelerations or artificially high mass density, which seems rather unrealistic [12]. On the other hand one step method proposed by Batoz et.al [13] was developed based on the idea of Chung and Lee [14] in which single time step was used, deforming the sheet inversely from final part configuration to initial blank configuration. A major advantage of this method is very short computation time. Mean while there were several activities to develop codes based on static implicit incremental approach [15-19]. But convergence is the basic problem of this approach. To avoid the convergence problem static explicit codes were developed [20,21].

In a nutshell all these codes may be classified into five categories based on the formulation and solution strategy used. These are dynamic explicit codes, static explicit codes, Static implicit incremental codes, Static implicit large step code and Static implicit one step code.

The dynamic explicit approach was originally developed for the problems in which dynamic effects are important, such as impact problems and crash simulation, and includes inertia in the equilibrium equations. The reasons for using a method like this in metal forming are two fold. The method is extremely robust and it is very efficient for large scale problems. In this approach the central difference explicit scheme is used to integrate the equations of motion. Lumped mass matrices are used, which implies that the mass matrix is diagonal, and no system equations has to be solved. A typical time step is of the order of a micro seconds and the number of time steps in typical sheet forming simulation are normally several tens of thousands. In spite of its success for industrial applications, it has also some intrinsic drawbacks i.e. in order to achieve significant computational advantage several numerical artifacts have to be introduced into the explicit solution procedure. In particular the parameters like mass density, punch velocity, loading history etc are to be modified. Since the maximum permissible time step, as defined by the current stability limit is directly proportional to the square root of the material density, this parameter is increased, usually by at least one order of magnitude. In order to reduce the total number of time steps necessary to model the sheet metal forming process, the punch velocity is increased, again by at least one order of magnitude. Since increase in both the material density and punch velocity results in increased inertia forces, the punch travel must be suitably controlled so as to minimize the inertia effects. Thus, the very nature of the dynamic explicit method, the simulation of forming defects requires a considerable experience on the user side for adequately designing the finite element mesh and choosing the scaling parameters of mass, velocity and damping. Other issues that must be given attention in the dynamic explicit analysis is the simulation of the spring back. One way of improving reliability of spring back is to combine the dynamic explicit analysis with quasi -static implicit simulation.

In the static explicit method, the system of equations representing the rate of equilibrium is integrated with a simple forward Euler scheme, involving no iterations. This implies that equilibrium equations are satisfied only in rate form and the obtained solution can gradually drift away from the true one. In order to reduce the error involved vary small incremental steps have to be taken. An ordinary simulations normally involves several thousand steps. The main advantage of this approach is the robustness, since there are no iterative processes.

The Static implicit incremental approach may seem ideally suited for metal forming problems, since the static equilibrium equations are solved iteratively, ensuring that the equilibrium conditions are full filled in every step. However, in practice complex nonlinear problems involving many contacts may results in slow or even lack of convergence. The method is also inefficient for solving large scale problems, since time taken for solving the system of equations increases approximately quadratically with the number of degrees of freedom.

Static implicit large step codes employ large incremental time step under special contact treatment, uncoupled bending and stretching solution algorithm, and adoptive mesh refinement of refinement levels. These features, specialized for the simulations of thin sheet metal forming renders code extremely efficient ,but unfortunately also make the results approximate in respects. For instance, the contact and discontact process are not accurately simulated and there fore wrinkling and buckling are poorly predicted.

In static implicit one step codes use a single time step, usually taking the deformation process from the final part configuration to the initial flat blank configuration, assuming a linear strain path and neglecting the history of contact.

Although, this method incorporates significantly drastic simplifications, its major advantage is a very short computation time and less input data. These features enable the use of these codes at the product design stage, in the absence of information of the stamping tools.

Currently, the accuracy and reliability of numerical simulations of sheet metal forming processes do not yet satisfy the industrial requirements. One of the limitations of numerical simulations is still the high computational time for complex deep drawing parts, despite the development of iterative solvers, fast contact algorithms and the ever ongoing progress in computer hardware. Another limitation is the lack of detailed knowledge of material physics such as material behavior at high deformations and contact behavior. Therefore extensive research in the field of sheet metal forming is and will be necessary to decrease the existing gap between the real-life deep drawing process and the predictions obtained from deep drawing simulations.

Deep drawing, even though is one of the most basic processes in sheet metal working, it involves very complicated deformation mechanics. The numerical difficulty in the finite element analysis of the deep drawing processes arises due to the existence of compressive stress in the sheet plane and the occurrence of unloading. The drawing load increases with the punch displacement. As the punch moves, the flange part of the sheet is drawn into the die cavity. The punch load decreases after a critical point because less resisting force to drawing is developed in the flange. In the range of decreasing punch load, unloading occurs at the wall of a drawn cup. Therefore, in analyzing the bending-dominant processes like deep drawing, the effect of unloading should be also considered. The state of stress at the wall and at the flange is basically tensile stress in axial or radial direction and compressive stress in the circumferential direction. As the sheet metal has relatively a small dimension in the thickness direction, the compressive stress may cause wrinkling in the actual process or numerical buckling in simulation [22]. The numerical buckling is the mesh buckling phenomenon occurring in the finite element analysis at the region of high compressive stress like actual buckling.

The modeling of the blank elements can be done by two alternative approaches [23] namely a structural based elasto-plastic / elasto-viscoplastic approach or rigid-plastic/ rigid-visco- plastic approach. Elastic-plastic analysis of sheet metal forming can be broadly classified into three categories according to the element types; membrane analysis, continuum analysis and shell analysis. Membrane analysis done by Wang [24] Arlinghaus [25], Mattiason [26], Massoni (27), Saran (28) and Batoz (29), has been widely applied to various sheet metal forming problems because of small computation time and small memory size. However, it provides insufficient information when treating the bending-dominant processes. Continuum analysis by Wifi (30), Anderson (31), Stalman (32), Makinouchi (33,34), Keck (35) has several merits; e.g. the bending effect can be considered and the formulation is much simpler than other methods of analysis using different element types. The continuum analysis, however, involves extremely large computation time and enormous memory size when three-dimensional problems are to be treated for any practical purposes. The shell analysis by Tatenami (36), Wang (37, 38), Gelin (39), Honnor (40), Batoz (29) and Honecker (41) may be regarded as a compromise between the continuum analysis and the membrane analysis. It is possible to consider the effect of bending with much less computation time and less memory size than the continuum analysis. However, most of the applications using shell elements are limited to the axisymmetric and plane strain problems because of the difficulty in treating kinematics of three-dimensional shells, computation time and memory size etc. Recently, the effect of bending has been studied through the comparison between the membrane analysis, the continuum analysis and the shell analysis. Wang and Tang (38) analyzed stretching and deep drawing with axisymmetric membrane elements and axisymmetric shell elements. In the analysis of stretching, both theories do not show any appreciable discrepancy, while the discrepancy between two theories becomes apparent in the analysis of deep drawing. Hambrecht et al. (42) studied the effect of bending in the plane strain punch stretching and axisymmetric stretching by the comparison of above-mentioned three kinds of approaches. Through the study, the continuum or shell theory is necessary in analyzing deep drawing and above three kinds of approaches do not give any difference in analyzing stretching. Yang et al. (22) analyzed stretching of a square plate as well as deep drawing of a cylindrical cup with the rigid-plastic finite element analyses using membrane and then they have investigated the effect of bending in the stretch dominant process and draw-dominant processes. Now, the effect of bending has become significant in the modelling of sheet metal forming process in order to obtain more accurate information for the die design of deep drawing. Shim and Yang [43] analysed deep drawing of cylindrical and square cups using membrane and shell elements. They found that both theories are in good agreement with each other in case of load-displacement curve. However in the neighborhood of punch round, the thinning appearing in the experiment can not be predicted by membrane analysis. In the shell analysis the thickness strain distribution is better predicted over whole range of sheet. It is due to the fact that bending of sheet effects considerably the thickness strain distribution and bending has no significant affect in load-displacement curve. So shell element is considered to be most suitable for the analysis in deep drawing process.

Finite Element models for rigid visco-plastic thin sheet problems was presented by Bellet et.al.[44]. A viscous shell formulation was introduced by Onate et.al [28] , who considered visco-plastic deformation of the work material as well as frictional affects of punch and die. Onate et.al [45]discussed viscous shell approach based on bending and membrane shell elements.

References

1. Otto Harrer "Finite element simulation in metal forming" *Acta Montanistica Slovaca Ročník* 8 (2003), p 176.
2. Swift H.W, 1948, "Plastic bending under tension", *Engineering* Vol 166,Pp 333-357.
3. Hill.R, 1950, A theory of plastic bulging of metal diaphragm by lateral pressure ' *Philosophical Mazine*, Vol 41 Pp 1133.
4. Woo.D.M, 1964, "Analysis of cup drawing process" *Journal of Mechanical Engineering Science*, Vol 6, Pp116.
5. Wang N.M, Budiansky B, 1978, "Analysis of sheet metal forming by finite element method" *Jorunal of Applied Mechanics* Vol.45, Pp73.
6. Kobayashi.S, Kim J.H, 1978, "Deformation analysis of axi-symmetric sheet metal forming processes by the rigid plastic finite element method" in *Mechanics os sheet metal forming* edited by Koinstinen D.P, Wang N.M (ed.) plenum press, Newyork ,Pp341.
7. Tang S.C, 1980, "Computer prediction of deformed shape of draw blank during the binder-wrap stage", *Jorunal of Applied Metal Working*, Vol 1, Pp22.
8. Alinghaus F.J., Frey W.H, Stoughton T.B, Murthy, B.K, 1985, *Finite Element Modelling of a stretch formed part* symposium on computer modeling of sheet metal forming, The Metallurgical Society Inc. Ann Arbor, Michigan, 1985, Pp51.
9. Tang S.C, "Verificaiton and Application of Binder-wrap Analysis" symposium on computer modeling of sheet metal forming, The Metallurgical Society Inc Ann Arbor, Michigan, 1985, Pp193.
10. Honecker A, Mattiasson K, " Finite Element Procedures for 3D Sheet Forming Simulation" *Numerical Methods in industrial forming processes NUMIFORM'89*, 1989, Pp 457.
11. Matiasson K., L. Bernspang, A. Honecker, E. Schedin, T. Hamman, A. Melander, 'On the use of explicit time integration in finite element simulation of industrial sheet metal forming processes', *Proceedings of the 1st International Conference on Numerical Simulations of 3-D Sheet Metal Forming Processes*, VDI-Berichte 894, VDI Verlag GmbH, Dusseldorf, p. 479-498, 1991
12. Carleer B.D., J. Huétink, 'Closing the gap between the workshop and numerical simulation in sheet metal forming', *Computational Methods in Applied Sciences: Eccomas '96*, J.-A. Désidéri et al. (eds.), p. 554-560, 1996
13. Batoz J.L, Guo Y.Q, Duroux P, Detraux J.M "An efficient alorithm to estimate the large strains in deep drawing", *NUMIFORM'9*, 1989, Pp 383
14. Chung K and Lee D, 1984, "Computer Aided Analysis of Sheet Metal Forming Processes", *Advanced Technology of Plasticity*, Vol 1, Pp 660.
15. Tang S.C, Chappuis L.B, Matke J, 1991, "A Quasistatic Analysis of Forming Processes for Automotive panels" *International Conference on FE-Simulation 3D Sheet Metal Forming Processes in Automotive Industry*, Zurich, Switzerland May 14-16 , Pp247.
16. Hillmann M, Kabisch A, Fuchs F, El Rifai Kasserm K, Mathik F, Sunkel R,1991, "A highly vectorised FE-program for sheet metal forming simulation for automotive industry" *International Conference on FE-Simulation 3D Sheet Metal Forming Processes in Automotive Industry*, Zurich, Switzerland May 14-16 , Pp549.
17. Anderheggen E, "on the design of new programe to simulate thin sheet forming processes" *International Conference on FE-Simulation 3D Sheet Metal Forming Processes in Automotive Industry*, Zurich, Switzerland May 14-16, 1991 , Pp231.
18. Kubli W,Anderheggen E,Ressner J, 1991, "Nonlinear solver with uncoupled bending and stretching deformation for simulating thin sheet metal forming" *International Conference on FE-Simulation 3D Sheet Metal Forming Processes in Automotive Industry*, Zurich, Switzerland May 14-16, 1991 , Pp549.
19. Kubli W, Reissner J, 1993 1993, "Optimisation of sheet metal forming processes unusing the special purpose programme, Autoform" *NUMISHEET'3*, 2nd interanational conference on simulation of 3-D sheet metal forming processes ,Isehera, Japan, 31st Aug- 2nd Sep. P 271.
20. Kawka M, Makinouchi A, 1993, "Shell element formulation in the static explicit FEM code for simulation of sheet stamping" , *NUMISHEET'3*, 2nd interanational conference on simulation of 3-D sheet metal forming processes ,Isehera, Japan, 31st Aug- 2nd Sep. Pp97
21. Santos A, Mekanouchi A, "Contact strategies to deal with different tool descriptions in static explicit FEM for 3-D sheet metal forming simulation", *NUMISHEET'3*, 2nd interanational conference on simulation of 3-D sheet metal forming processes ,Isehera, Japan, 31st Aug- 2nd Sep. P 261.
22. Yang, D. Y., Chung, W. J., and Shim, H. B., 1990, "Rigid-plastic Finite Element Analysis of Sheet Metal Forming Considering Contact With Initial Guess Generation," *Int. J. Mech. Sci.*, Vol. 32, pp. 687-708.
23. M.E.Honer and R.D.Wood "Finite element analysis of axi-symmetric deepdrawing using simple two noded Mindlin shell elements" *Numerical Methods for nonlinear problems*, Pinridge press, Pp 440-449.
24. Wang, N. M., and Budiansky, B., 1978, "Analysis of Sheet Metal Stamping by a Finite Element Method," *ASME Journal of Applied Mechanics*, Vol. 45, pp. 73-82.
25. Arlinghaus, F. J., Frey, W. H., and Stoughton, T. B., 1985, "Finite Element Modelling of a Stretch-Formed Part," *Computer Modelling of Sheet Metal Forming Process*, N. M. Wang and S. C. Tang, eds., AIME, pp. 51-64.
26. Mattiason, K., et al. 4, 1987, "Finite Element Simulation of Deep Drawing of Low and High Strength Steel," *Advanced Technology of Plasticity*, K. Lange, ed., Springer-Verlag, Heidelberg, pp. 657-663.

27. Massoni, E., et al. 1987, "A Finite Element Modelling for Deep Drawing of Thin Sheet in Automotive Industry," *Advanced Technology of Plasticity*, K.Lange, ed., Springer-Verlag, Heidelberg, pp. 719-725.
28. Saran, M., and Samuelsson, 1989, "An Elastoplastic Formulation for Numerical Simulation of Sheet Metal Forming Processes," *Proc. NUMIFORM '89 Conf*, A. A. Balkema, Rotterdam, pp. 45-54.
29. Batoz, J. L., et al. 1989, "A Membrane Bending Finite Element Model for Sheet Forming," *Proc. NUMIFORM '89 Conf*, A. A. Balkema, Rotterdam, pp. 389-394.
30. Wifi, A. S., 1976, "An Incremental Complete Solution of the Stretch Forming and Deep Drawing of a Circular Blank Using a Hemispherical Punch," *Int. J.Mech. Sci.*, Vol. 24, pp. 23-31.
31. Anderson, B. S., 1982, "A Numerical Study of the Deep Drawing Processes," *Numerical Methods in Industrial Forming Processes*, J. F. T. Pittman et al., eds., Pineridge Press, Swansea, pp. 709-721.
32. Stalman, A. P., 1986, "Numerical Simulation of Axisymmetric Deep Drawing Processes by the Finite Element Method," *Workshop Stuttgart*, Springer-Verlag, Heidelberg, pp. 261-278.
33. Makinouchi, A., 1987, "A Elastic-plastic Stress Analysis of U-bend Process of Sheet Metal," *Advanced Technology of Plasticity*, K. Lange, ed., Springer-Verlag, Heidelberg, pp. 672-677.
34. Makinouchi, A., 1989, "Finite Element Modelling of Draw Bending Process of Sheet Metal," *Proc. NUMIFORM '89 Conf*, A. A. Balkema, Rotterdam, pp. 327-332.
35. Keck, P., et al. 4, 1989, "Comparison of Different Finite Element Models for the Simulation of Sheet Metal Forming," *Proc. NUMIFORM '89 Conf*, A. A. Balkema, Rotterdam, pp. 481-488.
36. Tatemani, T. Y., Makamura, Y., and Sato, K., 1982, "An Analysis of Deep Drawing Process Combined With Bending," *Numerical Methods in Industrial Forming Processes*, J. F. T. Pittman et al., eds., Pineridge Press, Swansea, pp. 687-696.
37. Wang, N. M., and Tang, S. C , 1986, "Analysis of Bending Effects in Sheet Forming Operations," *Proc. NUMIFORM '86 Conf*, Gothenberg, Sweden, pp.71-76.
38. Wang, N. M., and Tang, S. C , 1988, "Analysis of Bending Effects in Sheet Forming Operations," *Int. J. for Num. Meth. in Engng.*, Vol. 25, pp. 253-267.
39. Gelin, J. C , and Daniel, J. L., 1989, "A Finite Element Simulation of Sheet Metal Forming Processes Using a General Non-flat Shell Element," *Proc. NUMIFORM'*
40. Honnor, M. E., and Wood, R. D., 1987, "Finite Element Analysis of Axisymmetric Deep Drawing Using a Simple Two-noded Mindlin Shell Element," *Numerical Methods for Nonlinear Problems*, C. Taylor et al., eds., Pineridge Press, Swansea, pp. 440-449.
41. Honecker, A., and Mattiason, K., 1989, "Finite Element Procedures for 3D Sheet Forming Simulation," *Proc. NUMIFORM'89 Conf*, A. A. Balkema, Rotterdam, pp. 457-464.
42. Hambrecht, J., et al. 3, 1989, "Numerical Study of Two-dimensional Sheet Forming Processes Using Bending, Membrane, and Solid Finite Element Models," *Proc. of the NUMIFORM '89 conference*, Balkema, Rotterdam, pp. 451-456.
43. Shim H.B, Yang D.Y, "Elastic-plastic Finite Element Analysis of Deep Drawing Processes by Membrane and Shell Elements", *Journal of Manufacturing Science and Engineering*, August'1997, Vol. 119, P.341-349.
44. M.Bellet, I.Massoni and J.I.chennot, "A rigid visco-plastic membrane formulation for three dimensional analysis of thin metal forming", *International Conference on computational Plasticity*, 1987, Barcelona.
45. E.Onate and C.Agelet-De Sarsibar "A viscous shell formulation for the analysis of thin sheet metal forming", *International Journal of Mechanical Science*, Vol 5, 1993 Pp 305-335.

Shift variance behavior for different sub-band coding systems, Biorthogonal, Orthogonal and Bspline wavelets

Gamal Fahmy

Electrical Engineering Dept., Majmaah University, KSA

Abstract: Sub-band coding has long been utilized and adopted in different compression, coding and reconstruction techniques in most signal processing applications. It has wide applications in communications, bit rate codec's, sampling, and compression for images, videos and speech. However sub-band coding systems in general suffer from a certain amount of shift variance of the output reconstructed signal, due to the frequency overlap between different sub-bands in the analysis stage. This overlap is known as non-ideal anti-aliasing.

In this paper we simplify the shift variance analysis of sub-band coding systems in general, and we present different metrics that have been reported in the literature to measure the bounds of shift variance for Perfect Reconstruction (PR) sub-band systems, we simplify its mathematical analysis and illustrate with graphs the reasons for these bounds and compare them. We apply these metrics on Biorthogonal, Orthogonal and Bspline wavelets and present the worst case scenario for different input signals in terms of shift variance for all these sub-band coding systems, both numerically and graphically. We finally compare the shift variance behavior for different sub-band PR systems for different types of input signals.

Keywords: Shift variance, Bspline, multirate system

1. Introduction

Multirate systems employ by definition sampling rate conversion which introduces an amount of linear periodical shift variance (LPSV) in the output reconstructed signal [1-3], in spite of the fact that the adopted sub-band filters are linear shift invariant (LSI). This LPSV can be noticed in different applications such as block transform, fractional sampling rate converters, multirate filter banks, sub-band quantization, and motion estimation. Several approaches in the literature tried to reduce or prevent LPSV has adopted Complex wavelets [4], cycle spinning [5], and circular shifted wavelets [6]. In [7-9] several effects of shift variance, and some of its consequences like cyclostationarities on re-sampled data and images, were presented.

In this paper we present a quantitative measure for shift variance in different sub-band coding systems. We derive the worst case scenario for the amount of shift introduced in the output reconstructed signal from different types of input signals (such as a narrow band input signal or a wide band one). We analyze different metrics for shift variance that has been reported in the literature [10] in a simplified form and we apply it on different PR sub-band coding systems that have different orthogonality characteristics (Biorthogonal, Orthogonal and Bspline wavelets). We selected Bspline wavelets to be included in our comparison as they are well known of being semi orthogonal, as they are orthogonal across different scales/channels, but not orthogonal within the same channel, in other words they are orthogonal across time shifts but not across time scale. We present an upper bound for shift variance for these systems mathematically and experimentally. Finally we discuss our results and provide a tradeoff analysis between different sub-band coding structures. We claim that our main contribution is presenting the shift variance metrics reported in [10-13] in a much simplified forms, as well as applying and comparing it on different sub-band systems.

Section 2 analyzes different shift variance bounds and metrics for multirate sub-band coding systems in general. Section 3 presents the bounds on shift variance for two channel (2-CH) PR sub-band coding systems for either orthogonal or biorthogonal systems. Section 4 presents our own developed shift variance bounds on Bspline PR sub-band coding systems. Finally a comparative result analysis of different bounds of shift variance on Biorthogonal, Orthogonal and Bspline wavelets is presented in section 5. Discussion and Conclusion in section 6 & 7, respectively

2. Shift variance for subband coding system

In this paper we will note the following, for a M band multirate filter bank, Fig. 1, if the input signal is $s[n]$, and the output of $s[n]$ is $y[n]$, then when the input signal is shifted by m samples so that the input is $s[n-m]$, the output is denoted by $x^m[n]$, while $y^m[n] = y[n-m]$. Hence for a system to be fully shift invariant $x^m[n]$ should be equal to $y^m[n]$. We denote $r^m[n] = x^m[n] - y^m[n]$. The residual energy for any band, which is the energy for the difference signal $r^m[n]$ for a given input $s[n]$, which is proportional to the amount of shift variance in the band, would be,

$$E_r[m] = \|r^m[z]\|_2^2 = \frac{1}{2\pi} \int_{-\pi}^{\pi} |R^m(e^{j\omega})|^2 d\omega = \frac{1}{2\pi} \int_{-\pi/M}^{\pi/M} \|r_M^m(e^{j\omega})\|_2^2 d\omega \quad (1)$$

Where $r_M^m[z]$, which is the modulation vector for the difference signal $r^m[n]$, is

$$r_M^m(z) = X_M^m(z) - Y_M^m(z) = \frac{z^{-m}}{M} [g_M(z)h_M^T(z)D^{-m} - D^{-m}g_M(z)h_M^T(z)]s_M(z) = T(m, z)s_M(z) \quad (2)$$

Where $D \in C^{M \times M}$ a diagonal matrix $\text{diag} [1, W, W^2, \dots, W^{M-1}]$, Hence, $D^{-m} = \text{diag} [1, W^{-m}, W^{-2m}, \dots, W^{-m(M-1)}]$

The norm of $r_M^m[z]$ would be

$$\|r_M^m(z)\|_2^2 = (r_M^m(z))^T \overline{r_M^m(z)} = s_M^*(z)T^*(m, z)T(m, z)s_M(z) = s_M^*(z)A(m, z)s_M(z) \quad (3)$$

Where the matrices $T(m, z), A(m, z) \in C^{M \times M}$. Thus the residual energy would be

$$E_r[m] = \frac{1}{2\pi} \int_{-\pi/M}^{\pi/M} s_M^*(z)A(m, z)s_M(z)d\omega \quad (4)$$

In any subband coding system for a filter bank K , if the output $x^m[n]$ which is because of the shifted input $s[n-m]$ can be expressed as $x^m = K \circ \tau_m(s)$, where K, \circ are the filter bank and the concatenation process, and τ_m is the shift operator.

Then, the shifted output signal $y^m[n]$ can be expressed as $y^m = \tau_m \circ K(s)$. Hence for a the filter bank K to be fully shift variant, $[K, \tau_m] = K \circ \tau_m - \tau_m \circ K$ should be zero for any input. This last term $[K, \tau_m]$ is known as a commutator [10-13], and

$$it\ should\ be\ proportional\ to\ the\ mean\ square\ error\ between\ x^m[n]\ and\ y^m[n].\ Thus,\ E_r[m] = \|[K, \tau_m](s)\|_2^2 \quad (5)$$

We note here that in any subband coding system channel, fig.2, even if the analysis and synthesis filters are fully shift invariant, the processing inside the band (decimators and interpolators) causes a certain amount of shift variance. Even though this analogy may seem strange, as for any band M the decimation and interpolation by factor M shouldn't lose any data and is completely reversible in a any PR system [3,14], but if we remember that there is an amount of overlap between different channels (overlap of frequency between High Pass and Low Pass filters in a 2-CH system) that causes this data alteration (shift variance), we justify why the PR system is shift variant.

Hence in an ideal scenario, where all analysis (or synthesis) filters are ideal with sharp transition and no overlap between the filters, there PR system would be fully shift invariant in spite of the processing in the band. This can be verified in the result section where we see that most amount of shift variance is at frequency overlap regions in the filter frequency response graph, fig. 3-10.

Since we are interested in finding the worst shift variance behavior for a PR system, the error energy $E_r[m]$ should be maximum, this will happen if the residual input signal is $\|s[n]\|_2 \leq 1$ for any input. Hence because of eq. 1-5, [10-13], the

max eigenvalue of the operator norm $\|r_M^m(z)\|_2^2$, would be the upper bound of $E_r[m]$, which is the worst case scenario for shift variance in a M band multirate filter bank channel. The upper bound of $E_r[m]$ is denoted $E[m]$, where $E[m] = \sup E_r[m]$ and sup stands for supremum which is the least upper bound.

$$Hence \quad E[m] = \|[K, \tau_m](s)\|_\infty^2 = \max \lambda_1(m, e^{j\omega}) \quad (6)$$

Example of shift variance in a subband PR system (2-CH)

For a single channel case of a 2-CH PR filter bank, D and T would be,

$$D^{-1} = \begin{bmatrix} 1 & 0 \\ 0 & -1 \end{bmatrix} \text{ and } T_i(z) = z^{-1} \begin{bmatrix} 0 & -G_i(z)H_i(-z) \\ G_i(-z)H_i(z) & 0 \end{bmatrix} \quad (7)$$

Resulting in

$$\lambda_{i1}(e^{j\omega}) = \max(|G_i(-e^{j\omega})H_i(e^{j\omega})|^2, |G_i(e^{j\omega})H_i(-e^{j\omega})|^2) \quad (8)$$

,which is the max eigenvalue for channel i . For a 2-CH multi-rate system, the PR property would imply

$$s_M(z) = \frac{1}{2}(g_{0M}(z)h_{0M}(z)^T + g_{1M}(z)h_{1M}(z))s_M(z) \quad (9)$$

$$\text{where } G(z) = \begin{bmatrix} G_0(z) & G_1(z) \\ G_0(-z) & G_1(-z) \end{bmatrix} \quad H(z) = \begin{bmatrix} H_0(z) & H_0(z) \\ H_1(z) & H_1(z) \end{bmatrix}. \text{ Hence, } G_0(z) = \frac{2H_1(-z)}{\det(H(z))} \text{ and } G_1(z) = \frac{2H_0(-z)}{\det(H(z))}$$

$$\text{So, } \lambda_{01}(e^{j\omega}) = \max\left(\frac{2H_1(e^{j\omega})H_0(e^{j\omega})}{|\det(H(-e^{j\omega}))|^2}, \frac{2H_1(-e^{j\omega})H_0(-e^{j\omega})}{|\det(H(e^{j\omega}))|^2}\right) \text{ and } \lambda_{01}(e^{j\omega}) = \lambda_{11}(e^{j\omega}) \quad (10)$$

In the last equation, the 2 eigenvalues of the norm of the 2-CH system were equal, as it is a perfect reconstruction system. This would lead to the following equation

$$\|[K_0, \tau_1]\|_\infty = \|[K_1, \tau_1]\|_\infty \quad (11)$$

Fig. 3-6 shows examples of the worst case scenario of shift variance in different 2-Ch PR systems, we also show the frequency response of the associated analysis filters. It can be easily noticed that the max amount of shift variance exists around the overlap area.

3. Bounds of Shift variance for 2-CH orthogonal and biorthogonal systems

As orthogonal subband PR system are more restrictive by definition and nature [1,3,14] and they also have less overlap between the Low Pass and High Pass regions, it is normal to expect that they introduce an amount of shift variance that is less than biorthogonal ones.

Since the max amount of shift variance for a 2-CH PR system, as in eq. 10, is

$$\lambda_{01}(e^{j\omega}) = \max\left(\frac{2H_1(e^{j\omega})H_0(e^{j\omega})}{|\det(H(-e^{j\omega}))|^2}, \frac{2H_1(-e^{j\omega})H_0(-e^{j\omega})}{|\det(H(e^{j\omega}))|^2}\right)$$

and since $\frac{2H_1(e^{j\omega})H_0(e^{j\omega})}{|\det(H(-e^{j\omega}))|^2}$ or $\frac{2H_1(-e^{j\omega})H_0(-e^{j\omega})}{|\det(H(e^{j\omega}))|^2}$ typically equals a value of 1 for orthogonal 2-CH PR systems

[3,14]. It can be easily proved that the max amount of shift variance for an orthogonal system would not exceed a value of 1 in a normalized frequency response graph, fig.3-6

For biorthogonal systems due to their more degrees of freedom nature, their maximum eigenvalue (commutator) would exceed the value of 1, fig.5-6. For bi-orthogonal 2-CH PR systems, the $\lambda_1(m, e^{j\omega})$ function has a maximum higher than that of unitary (orthogonal) filter banks and corresponds to worst case scenario for shift variance for this band. The areas under both curves $\lambda_1(m, e^{j\omega})$ and $\lambda_2(m, e^{j\omega})$ for the bi-orthogonal systems are equal, and their worst case shift variance frequency is not center at $\pi/2$, but around it. The higher the maximum value of the curve in fig.4, the more shift variance it has. Table 1, lists the $E_r[m]$ values for different 2-CH PR filter banks. It can be realized that the shift variance behavior for all orthogonal systems tends to be the same for different filter types, this also applies for biorthogonal filter banks. Hence we can conclude that the worst case scenario for shift variance is more dependent of the filter bank structure (orthogonal or bi-orthogonal) rather than the filter type. We can also see that the higher the order of the utilized filter, the less is the $\lambda_1(m, e^{j\omega})$ value for the same filter type, which means less shift variance, as the filter frequency response is more ideal with sharper transition (and less overlap).

Wide band Input signals

It can be seen in fig. 3-7, that the worst case scenario of shift variance or near maximizers, is a narrow band signal around the transition frequency. To complement this worst case shift variance behavior, and to capture more of the filter properties rather than properties of the filter banks structure, we can apply an additional bound for shift variance, under the assumption that the input signal for the subband PR system exhibit a given amplitude spectra. Similar to earlier work in [10-13], we will use a wide band model spectra as the input signal, like a signal with a flat spectrum

If we specify an amplitude spectrum $|S(e^{j\omega})| = \Phi(e^{j\omega})$ we would also be specifying absolute values of the entries of the

modulation vector $s_M(e^{j\omega})$. Hence, from the weight function $\omega(e^{j\omega}) = \sum_{m=0}^{M-1} |\Phi(W^m e^{j\omega})|^2$ formed from the modulated

versions $\Phi(e^{j\omega})$, we can define this wide band input signal additional measure of shift variance by

$$\tilde{E}_w[m] = \frac{1}{2\pi} \int_{-\pi/M}^{\pi/M} \lambda_1(m, e^{j\omega}) \omega(e^{j\omega}) d\omega \quad (12)$$

Hence, for these types of signals, the worst case scenario for shift variance corresponds to a weighted integration of the max eigenvalue of the commutator, $\sqrt{\lambda_1(m, e^{j\omega})}$, rather than its peak height as eq. 1-5. Similarly to eq.6 & 12, this additional

measure $\tilde{E}_w[m]$ is also is the same for both channels $\tilde{E}_w[m]$, as $\| [K, \tau_m](s) \|_2^2 = \tilde{E}_w[m]$

For a 2-CH PR filter bank, we would have: $\tilde{E}_w[1] = \| [K, \tau_1](s) \|_2^2$, for every signal s with $|S(e^{j\omega})| = \Phi(e^{j\omega})$. By choosing $\Phi(e^{j\omega})$ to be wide band, this would correspond to the additional measure of shift variance for wide band signals. This additional bound corresponds to the area under $\lambda_1(m, e^{j\omega})$ and would typically decrease with the increase of the filter length, which would imply less width of either of the 2 curves in fig.4-7.

Table 1 also lists the $\tilde{E}_w[m]$ values for the same orthogonal and biorthogonal PR system of the previous subsection. It can be seen that this additional shift variance measure is more dependent on the filter type, rather than the filter structure. It is also eliminated when there is no overlap in the frequency response between the analysis filters in different channels, as it represents the area of the overlap, while the previous narrow band shift variance measure $E_r[m]$ corresponds to the max

value in the overlap region. Hence, the wide band input shift variance measure $\tilde{E}_w[m]$ is a stronger measure than narrow band shift variance measure $E_r[m]$, as it assumes that the input signal has a wide band flat spectrum.

4. Shift variance bounds on Bspline PR sub-band coding systems

The m^{th} order Bspline function $B_m(t)$, has a finite support and equals zero at $t=0, m$, and is represented by a polynomial of order $m-1$ at the knots $1, 2, \dots, m$. It satisfies the recurrence relation:

$$B_m(t) = \frac{t}{m-1} B_{m-1}(t) + \frac{m-t}{m-1} B_{m-1}(t-1) \tag{13}$$

$$\frac{\partial B_m(t)}{\partial t} = B_{m-1}(t) - B_{m-1}(t-1)$$

The m^{th} order Bspline time domain equivalent function would imply

$$B_m(t) = B_1(t) * B_1(t) * \dots * B_1(t) \quad \leftarrow \text{---} \quad m \text{ times} \quad \text{---} \rightarrow \tag{14}$$

$$B_m(t) \text{ is also symmetric about } m/2; \text{ i.e. } B_m\left(\frac{m}{2} + t\right) = B_m\left(\frac{m}{2} - t\right) \tag{15}$$

In [15], a Bspline based PR multi-scale representation was introduced and for a 2-CH system, as in fig.2, it was shown that the analysis and synthesis filters are:

$$H_0 = \frac{B_m(\omega)}{B_m(\omega/2)} = \frac{1}{2^m} \sum_{k=0}^m \binom{m}{k} z^{-k} = \left(\frac{1+z^{-1}}{2}\right)^m, \quad z = e^{j\frac{\omega}{2}} \tag{16}$$

$$H_1 = -E(-z)\tilde{H}_0(-z), \quad E(z) = \sum_{k=1}^{2m-1} B_{2m}(k)z^{-(k-1)} \quad F_0 = z \frac{E(z)}{E(z^2)} \tilde{H}_0(z) \quad \text{and} \quad F_1 = z^{-1} \frac{\tilde{H}_0(-z^{-1})}{E(z^2)} \tag{17}$$

As shown before the shift variance for a Bspline PR sub-band coding system, could be assessed by a single channel case for either H_0 & G_0 or H_1 & G_1 , Fig.1.

Hence, the max eigenvalue for either channel in a Bspline based 2-CH PR system, would be:

$$\lambda_{11} = \frac{|H_0(z)H_1(-z)|^2}{|\det H(z)|^2} = \frac{\left(\frac{1+z^{-1}}{2}\right)^m \left(\frac{1+(-z)^{-1}}{2}\right)^m \sum_{k=1}^{2m-1} B_{2m}(k)z^{-k-1}}{|\det H(z)|^2} \tag{18}$$

Where m in this case represents the Bspline order used, rather than the PR channel index as in section 3. As shown in eq.18, the eigenvalue of the operator norm would depend on the Bspline order m . We note here that the area under the operator norm curve for either channel is the same for any Bspline order, as in the case of orthogonal and bi-orthogonal filters. We also note that the worst case behavior of shift variance for narrow band input signals would be represented in the peak of the operator norm and would be around $\pi/2$ as the biorthogonal one. The additional bound of shift variance which is for wide band input signals, would correspond to the area under the max eigenvalue curve.

5. Result Analysis

We carried out extensive simulation tests to measure both metrics $E_r[m]$ and $\tilde{E}_w[m]$ for different types of orthogonal, Bi-orthogonal and Bspline PR filters banks. Table 1, compares the numerical values of them for all utilized filters banks. Fig.3-9, shows the maximum Eigen value for both channels λ_0 and λ_1 for the whole frequency band for different orthogonal, bi-orthogonal and Bsplined based systems. As proven in sections 2, 3, and 4, the worst case scenario for shift variance for narrow band signals for a Bspline based PR system, would correspond to the peak point in the curves, while the worst case scenario for shift variance for wide band input signals would correspond to the range of frequencies inside the curve.

6. Discussion

It can be easily proven both experimentally and mathematically that the worst case scenario for narrow band input shift variance signal for orthogonal PR subband coding systems won't exceed the unity value for a normalized frequency response graph, fig. 3, as proven in eq.10. For bi-orthogonal systems this narrow band input shift variance signal gets higher than 1 due to the more overlap between the high and Low bands. For the additional shift variance bound of wide band input signal, orthogonal PR systems in general has a less area under the curve and less $\tilde{E}_w[m]$ value, which implies that their shift variance behavior is much less compared to biorthogonal PR systems.

For different Bspline orders, (sometimes) the higher the B-spline order, the higher is the pulse at the worst case scenario frequency (which would imply more shift variance). This is unexpected due to the increased filter length, which is supposed to imply less shift variance. However, the interpolating nature of Bsplines that is not suited for narrow band signals [16] can justify for us this behavior, also the wide band input signal behavior, which is the area under the operator norm

curve, λ_0 or λ_1 , can make this small increase eliminated. For higher B-spline orders, this width of the operator norm curve is smaller, (which would imply less shift variance). From analyzing fig 5-7, it can be realized that the amount of increase in the frequency peak at the worst case scenario for the error norm is negligible compared to the amount of reduction of the width of the curve, for different Bspline orders. Hence the higher the B-spline order for this 2-Ch PR multi-rate system, the more shift invariant it is. Bsplines are also more suitable for wideband spectrum input signals. We note here that the average number of taps for an analysis/synthesis filter was 14 for the cubic Bspline, 25 for the quadratic Bspline and 35 for the 5th order B-spline. Typically for an ideal shift invariant Bspline filter, $\tilde{E}_w[m]$ tends to go to zero, while $E_r[1]$ tends to be 1. This analogy has been verified experimentally as in fig 4-6; however it was not possible to prove mathematically, eq.18. The cubic B-spline (order 3) tends to outperform some of the well known orthogonal or bi-orthogonal filter banks in terms of $E_r[1]$ or $\tilde{E}_w[1]$ values. It is obvious from comparing fig.3-9, that Bspline decomposition filters exhibits much less shift variance for similar filters lengths of other structures. We note here that this improvement for shift variance behavior with a Bspline subband coding PR system in general, is mainly due to the nature of Bsplines that are semi orthogonal, as they are orthogonal across different scales/channels, but not within the same channel [17] (orthogonal across time shifts, but not across time scale). Hence the overlap between different channels is reduced than in similar bi-orthogonal filters bank systems. This justifies their shift variance behavior improvement, it can also be seen in the frequency response High Pass and Low Pass graphs, fig 8-10.

7. Conclusion and Acknowledgement

In this paper we presented some of the most popular metrics for shift variance, previously reported in [10-13] in a clear manner. Mathematical proof as well experimental simulations are illustrated to prove the achieved results and the shift variance worst bounds for different input scenarios on different decomposition structures (i.e. orthogonal and biorthogonal systems). We also applied the proposed shift variance bounds on a Bspline 2-CH multirate PR systems. Our analysis and testing implied that a higher order Bspline would correspond to less shift variance and would have a larger impact in reducing the shift variance behavior than higher corresponding orders for other PR systems such as orthogonal or biorthogonal systems. The author would like to acknowledge the help received from Prof. Til Aach, RWTH Aachen University, for the extensive help and simulation code. This work is funded from the Alexander von Humboldt foundation, Germany

Reference

1. R. E. Crochiere and L. R. Rabiner, Multirate Digital Signal Processing, Englewood Cliffs: Prentice-Hall, 1983.
2. C. M. Loeffler and C. S. Burrus, "Optimal design of periodically time-varying and multirate digital filters," IEEE Transactions on Acoustics, Speech, and Signal Processing, vol. 32, no. 5, pp. 991–997, 1984.
3. P. P. Vaidyanathan and S. K. Mitra, "Polyphase networks, block digital filtering, LPTV systems, and alias-free QMF banks: A unified approach based on pseudocirculants," IEEE Transactions on Acoustics, Speech, and Signal Processing, vol. 36, pp. 381–391, 1988.
4. I. W. Selesnick, R. G. Baraniuk, and N. G. Kingsbury, "The dual-tree complex wavelet transform," IEEE Signal Processing Magazine, vol. November, pp. 123–151, 2005
5. R. R. Coifman and D. L. Donoho, "Translation-invariant de-noising," in Wavelets and Statistics, A. Antoniadis and G. Oppenheim, Eds. New York: Springer, 1995, pp. 125–150.
6. R. Leonardi and A. Signoroni, "Cyclostationary error analysis and filter properties in a 3D wavelet coding framework," Signal Processing: Image Communication, vol. 21, pp. 653–675, 2006.
7. S. Akkarakaran and P. P. Vaidyanathan, "Bifrequency and bispectrum maps: A new look at multirate systems with stochastic inputs," IEEE Transactions on Signal Processing, vol. 48, no. 3, pp. 723–736, 2000.
8. V. P. Sathé and P. P. Vaidyanathan, "Effects of multirate systems on the statistical properties of random signals," IEEE Transactions on Signal Processing, vol. 41, no. 1, pp. 131–146, 1993.
9. A. K. Soman and P. P. Vaidyanathan, "Coding gain in paraunitary analysis/synthesis systems," IEEE Transactions on Signal Processing, vol. 41, no. 5, pp. 1824–1835, 1993.
10. T. Aach and H. Fuhr, "On Bounds of Shift Variance in Two-Channel Multirate Filter Banks", IEEE Transactions on Signal Processing, vol. 57, issue 11, pp. 4292-4303, 2009
11. T. Aach and D. Kunz, "A lapped directional transform for spectral image analysis and its application to restoration and enhancement," Signal Processing, vol. 80, no. 11, pp. 2347–2364, 2000.
12. T. Aach, "Comparative analysis of shift variance and cyclostationarity in multirate filterbanks," IEEE Transactions on Circuits and Systems–I: Regular Papers, vol. 54, no. 5, pp. 1077–1087, 2007.
13. T. Aach and H. Fuhr, "Shift variance, cyclostationarity and expected shift variance in multirate LPSV systems" IEEE Statistical Signal Processing Workshop (SSP), pp. 781 – 784, June 2011
14. Feng Fan, Ignace Bruyland, Weile Zhua, "Analysis/synthesis filter banks designed for subband video compression", Signal Processing Vol. 55 (1), Nov. 1996, Pages 117-122
15. M. F. Fahmy, G. Fahmy and O. F. Fahmy, "B-splines Wavelets for Signal Denoising and Image Compression", Journal of Signal, Image and Video Processing, Springer London Volume 5, Issue 2 (2011), Page 141.
16. M. Unser, A. Aldroubi and M. Eden, "B-Spline signal processing: Part I- Theory", IEEE Transactions on Signal Processing, vol. 41, No. 2, pp.821-833, February 1993.

17. G. Fahmy and T. Aach, "Enhanced Bspline based compression performance for images", IEEE International conference on Acoustics, Speech and Signal Processing, ICASSP, Dallas, March 2010.

Table 1 Uniform bound $E(1)$ and $\tilde{E}_w(1)$

Filter	$E(1)$	$\tilde{E}_w(1)$
B-spline order 3 (Cubic)	1.0053	0.1274
B-spline order 4 (Quad)	1.0624	0.0905
B-spline order 5	1.0314	0.0662
Johnston QMF 16	0.9902	0.1265
Johnston QMF 8	1.0047	0.2696
Smith Barnwell 16	1.0000	0.1207
Smith Barnwell 8	1.0000	0.2230
Multiplierless 4	1.0000	0.4136
Multiplierless 6	1.0018	0.3126
Multiplierless 8	1.0000	0.2813
Haar	1.0000	0.5000
Daubechies 10	1.0000	0.1609
Daubechies 30	1.0000	0.0928
Coiflet-5	1.0000	0.1544
Symmlet-8	1.0000	0.1799
Bi-orthogonal 5-3	1.158	0.3906
Bi-orthogonal 6-10	1.0841	0.2712
Bi-orthogonal 9-7	1.0301	0.2678

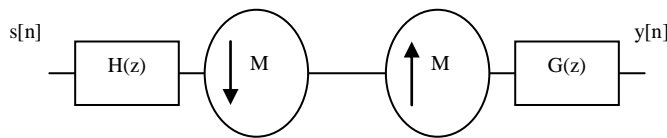


Fig. 1 Single Channel of a Multirate System

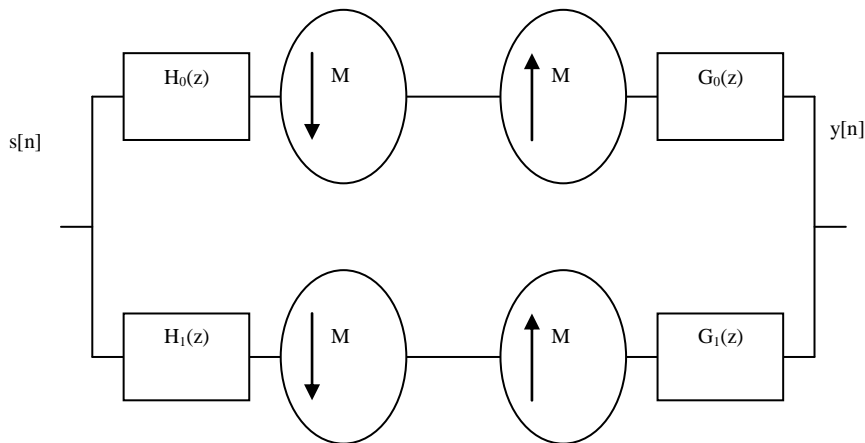


Fig. 2 2Ch PR Multirate System

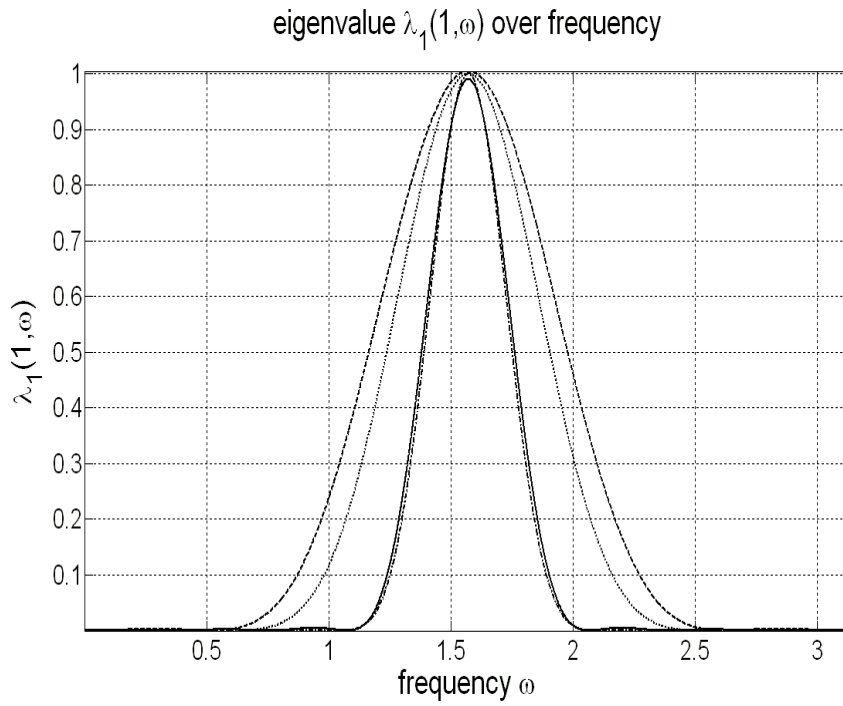


Fig. 3 max norm value (Eigen values) for different orthogonal filter banks, Johnston 16(solid), Johnston 8 (dashed line), Smith-Barnwell 16 & 8 (dotted-dotted dashed)

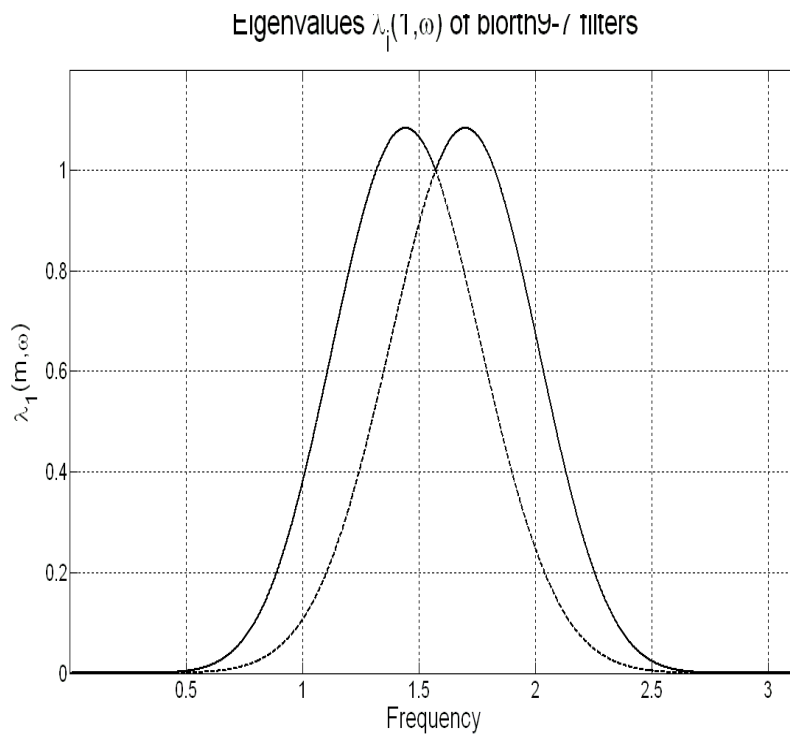


Fig. 4 max norm value (Eigen values) for Biorthogonal 9-7 Antonini filter banks

Eigenvalues $\lambda_1(1, \omega)$ of Cubic B-spline filters

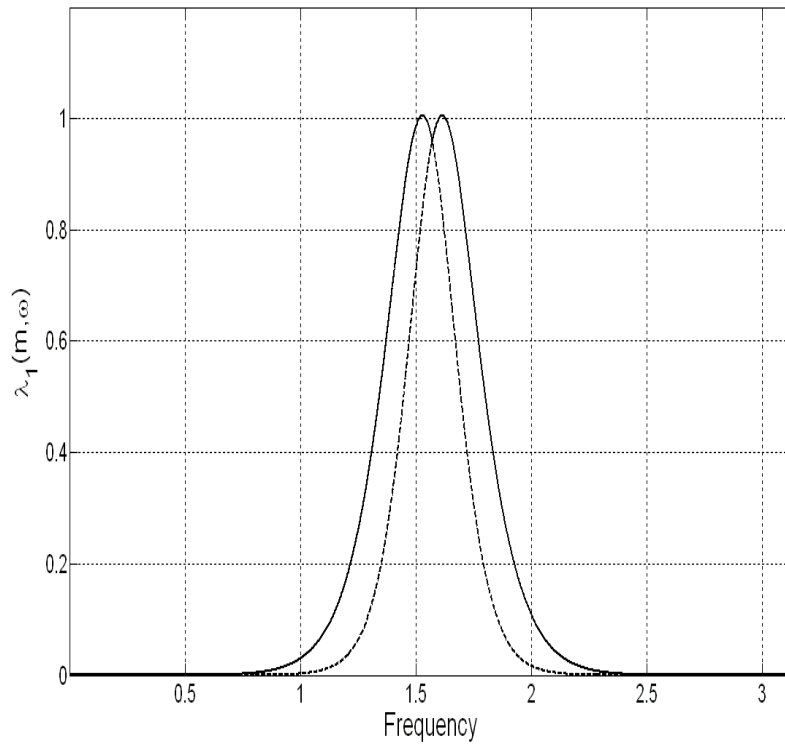


Fig. 5 max norm for Cubic B-spline filter banks

Eigenvalues $\lambda_1(1, \omega)$ of Quadratic B-spline filters

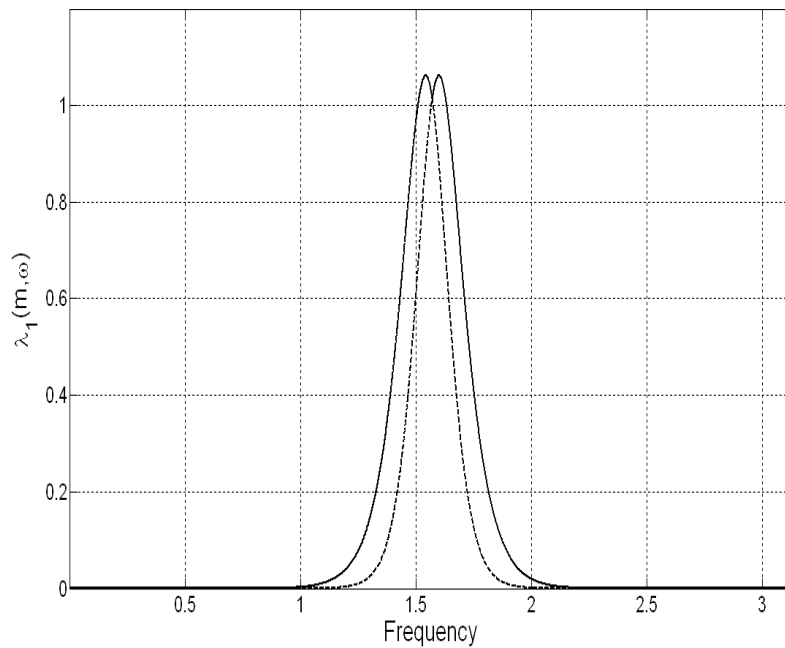


Fig. 6 max norm for Quadratic B-spline filter banks

Eigenvalues $\lambda_1(1, \omega)$ of 5th order Bspline filters

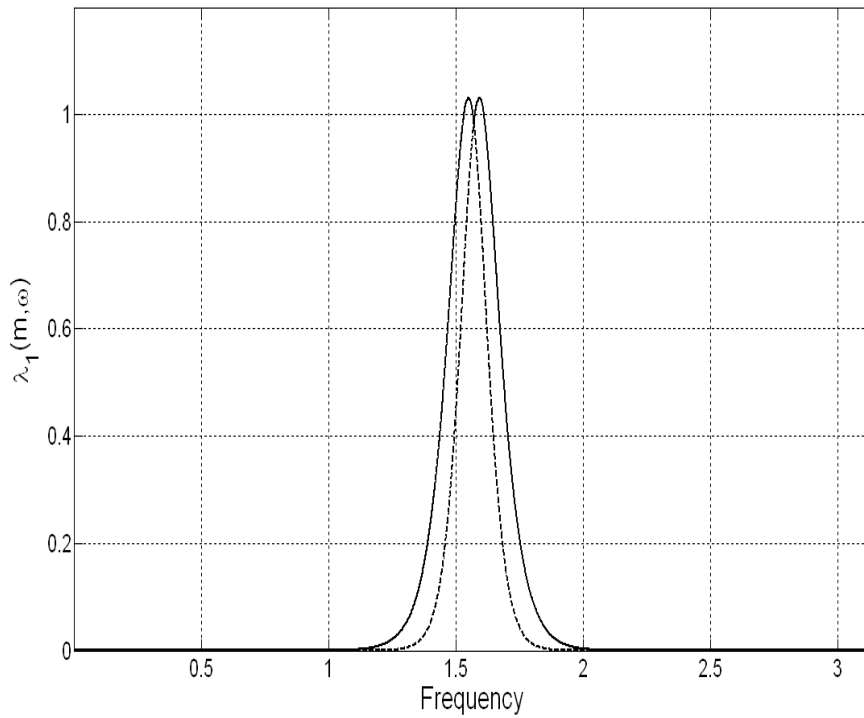


Fig. 7 max norm for 5th order Bspline filter banks

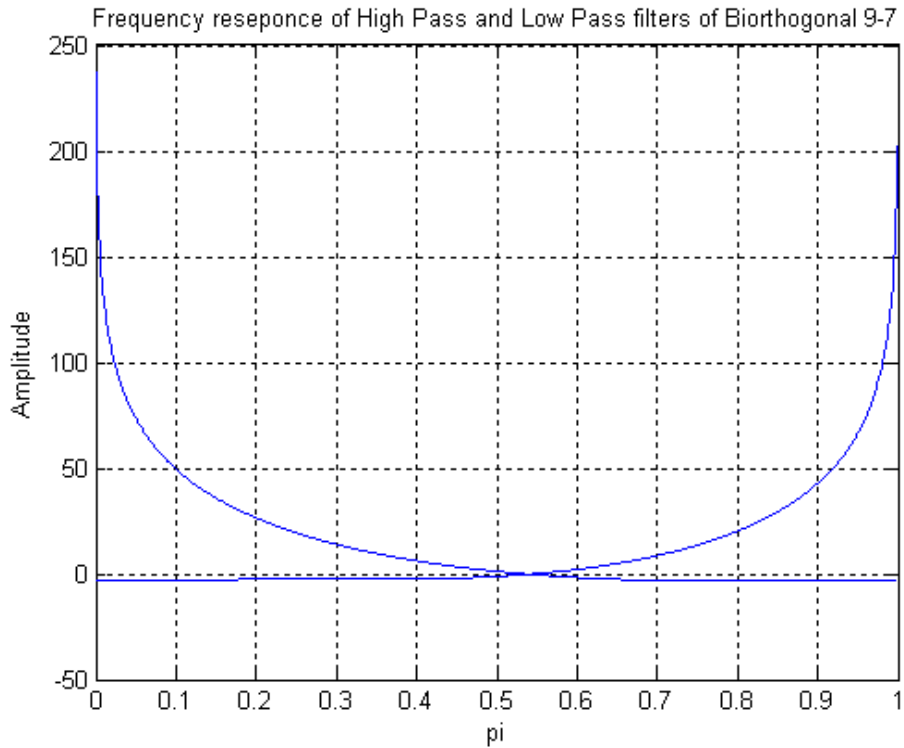


Fig. 8 frequency responses overlap for Biorthogonal PR systems

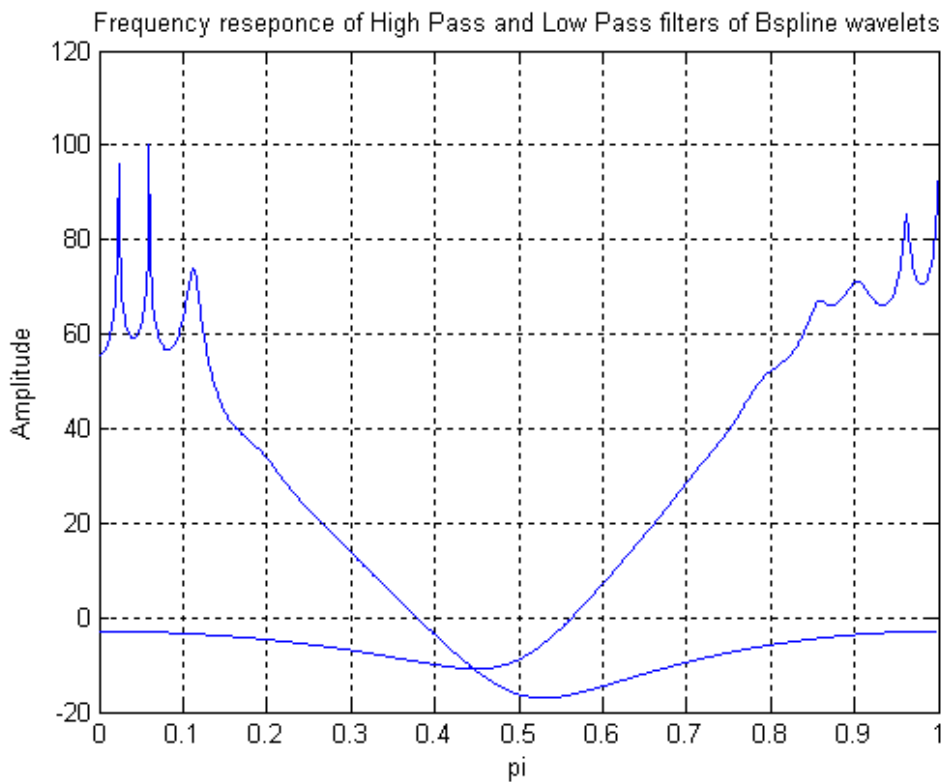


Fig. 9 frequency responses overlap for B-spline PR systems

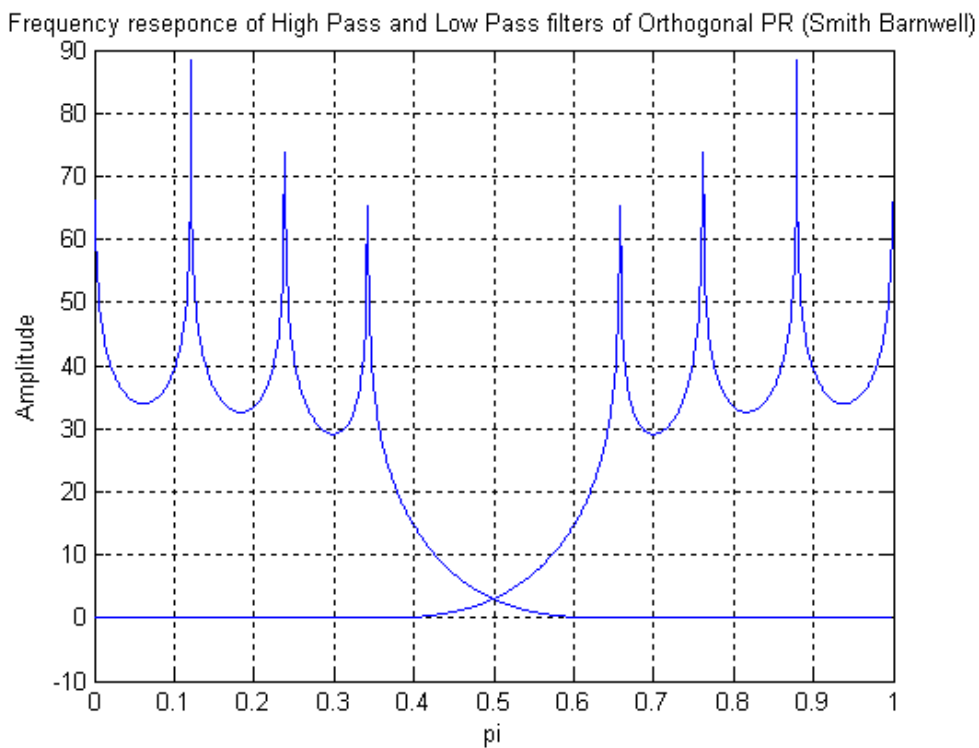


Fig. 10 frequency responses overlap for Orthogonal PR systems

Joint Watermarking and Compression for Images in Transform Domain

Gamal Fahmy

Electrical Engineering Dept., Majmaah University, KSA

Abstract: Image watermarking, authentication and encryption have gained an increased importance during the last decade. This is due to the widespread use of visual media over the Internet and in several digital media applications. Several watermarking techniques have been proposed, some in spatial domain, and more recently in the transform/frequency domain and have been reported to be robust against different attacks, namely compression. It is also well known the importance and effectiveness of compression techniques to store transmit and retrieve visual information. However, the creation or development of a joint watermarking and compression framework for images has yet to be explored, where watermarking and compression could be pursued jointly on a trade-off manner. In other words, watermarking embedding/extraction can be performed on compressed domain data, while compression parameters could be used as watermarking keys. The primary focus of this paper is to explore this novel/unique idea. We propose a joint watermarking and compression (JWC) technique in the transform domain. This transform domain is based on the Natural Preserve Transform and can be utilized to achieve a balance between watermarking and compression for visual information. Watermarking performance is evaluated blindly for different compressed domain data scenarios, while compression performance is analyzed for other watermarking cases. Extensive simulation results that demonstrate the efficiency of the proposed joint watermarking and compression technique are presented.

Keywords: Image Watermarking, Natural Preserve Transform, Image Compression; Hartley Transform

I. Introduction

The rapid growth of visual media based applications necessitates sophisticated compression techniques in order to store, transmit and retrieve audio-visual information. The recent MPEG 4 and JPEG 2000 standards address the need for content based coding and manipulation of visual media. With the widespread use of the Internet and the rapid and massive development of multimedia, there is an impending need for efficient and powerfully effective copyright protection techniques [1-3]. Digital watermarking schemes are typically classified into three categories. (1) Private watermarking which requires the prior knowledge of the original information and secret keys, at the receiver, (2) Semi-private or semi-blind watermarking where the watermark information and secret keys may be available at the receiver, and (3) public or blind watermarking where the receiver must only know the secret keys [4]. The robustness of private watermarking schemes is high to endure signal processing attacks. While private watermarking is suitable for high security applications such as financial or defense data, it is not feasible in real applications, such as DVD copy protection where the original information may not be available for watermark detection. On the other hand, semi-blind and blind watermarking schemes are more feasible in that situation [5], but they have lower robustness than the private watermarking schemes [6]. Hence, while private watermarking is mainly utilized for authentication and verification, blind or public watermarking is for copy protection applications. In general, the requirements of a watermarking system fall into three categories: robustness, visibility, and capacity [7]

A variety of image watermarking methods have been proposed mostly based on transform domain [7-9]. In spite of the successful performance of most watermarking techniques reported in the literature, they still suffer from being semi-fragile due to the energy concentration of their transform domains (DCT and Wavelets), which makes them discard much of the mid and high frequency watermarked data in compression [10-13].

Watermarking compressed domain data will obviate the need for it to be decompressed for watermark extraction, while compressing watermarks would store and transmit visual data efficiently. Hence, there is an impending need for sophisticated joint watermarking and compression techniques that could compress, protect and watermark data simultaneously. While compression aims at concentrating data in the least possible information, watermarking aims at distributing and hiding logos and parameters. Hence, compression and watermarking are inversely related and they have to be treated on a trade-off manner. The amount of extracted/retrieved watermarked data is affected by the compression degree of the host data, while the efficiency of compression is affected by the amount of data that needs to be embedded and extracted.

In this paper we propose a transform domain based technique for data watermarking that has been previously reported in [14], and [15]. This transform domain is based upon the Natural Preserve Transform (NPT) originally reported in [16]. We utilized this transform domain to present our main contribution in this paper, which is to develop a joint compression and watermarking system based on the NPT and wavelet domains for visual data. We try to achieve a framework/equation that includes both compression and watermarking jointly in our proposed system. The organization of this paper is as follows. Section 2 contains necessary mathematical background about the NPT based watermarking approach. Section 3 briefly explains the watermarking embedding and extraction process in the NPT domain. Section 4 shows the robustness of the watermarking technique against several attacks. Section 5 shows our proposed joint

watermarking and compression framework, analysis and results. Discussion is in section 6, followed by conclusions in section 7.

2. Mathematical Background for NPT based Watermarking

The NPT was first used as a new orthogonal transform that holds some unusual properties that can be used for encoding and reconstructing lost data from images. The NPT transform of an image S of size $N \times N$ is given by:

$$S_{tr} = \psi(\alpha) S \psi(\alpha) \quad (1)$$

As $\psi(\alpha)$ is the transformation kernel defined as in [17-18].

$$\psi(\alpha) = \alpha I_N + (1 - \alpha) H_N \quad (2)$$

I_N is N^{th} order identity matrix, $0 \leq \alpha \leq 1$, and H_N is any orthogonal transform, like Hadamard, DCT, Hartley, etc. Throughout this paper, we use the 2-D Hartley transform, defined by

$$H_N(k, j) = \frac{1}{\sqrt{N}} \left(\cos \left(\frac{2(k-1)\pi}{N} \right) + \sin \left(\frac{2(j-1)\pi}{N} \right) \right) \quad (3)$$

We note here that the Hartley transform was utilized due to its circular symmetry performance, as it evenly distributes the energy of the original image in the 4 corners of the orthogonally projected transform image, Fig. 1(a). Hence the Hartley transform achieves a trade-off point between the energy concentration feature (which is crucial for any transform domain for compression purposes) and the even distribution and spreading feature (which is crucial for watermarking and data hiding applications).

After the transformation kernel ψ is calculated in eq. 2, it is multiplied by the input image as a separable 2-D kernel, eq.1. The value of α in eq. 2, gives a balance between the original domain (that would be multiplied by the identity matrix) and the transform domain (that would be multiplied by the Hartley basis). Clearly, when $\alpha = 1$, the transformed image is the original image, whereas when $\alpha = 0$, it is its orthogonal projection (which is the Hartley transform as in this paper). Hence the NPT transform is capable of concentrating energy of the image while still preserving its original sample values on a trade-off basis. This makes the NPT transform domain image has both almost original pixel values (that can not be visually distinguished from the original image) and a capability feature of retrieving the logo watermark image from a small part of the transformed image (provided that this small part has enough energy concentration in it).

The original image can be retrieved from the transformed image S_{tr} , using

$$S = \psi^{-1}(\alpha) S_{tr} \psi^{-1}(\alpha) \quad (4)$$

If H is symmetric, as in Hartley matrices, the matrix $\psi^{-1}(\alpha)$ can be computed as follows:

$$\psi^{-1}(\alpha) \equiv \phi = \frac{1}{\alpha} \left[I - \frac{1-\alpha}{\alpha} H + \left(\frac{1-\alpha}{\alpha} H \right)^2 - \left(\frac{1-\alpha}{\alpha} H \right)^3 + \dots \right] \quad (5)$$

Fig. 1(b-c) shows the Lena image and its NPT transformed image. α is adjusted to a value of 0.994, which yields a nominal PSNR of around 45 dB. The high similarity between the original and transformed images, suggests that NPT is very convenient for watermarking and data hiding.

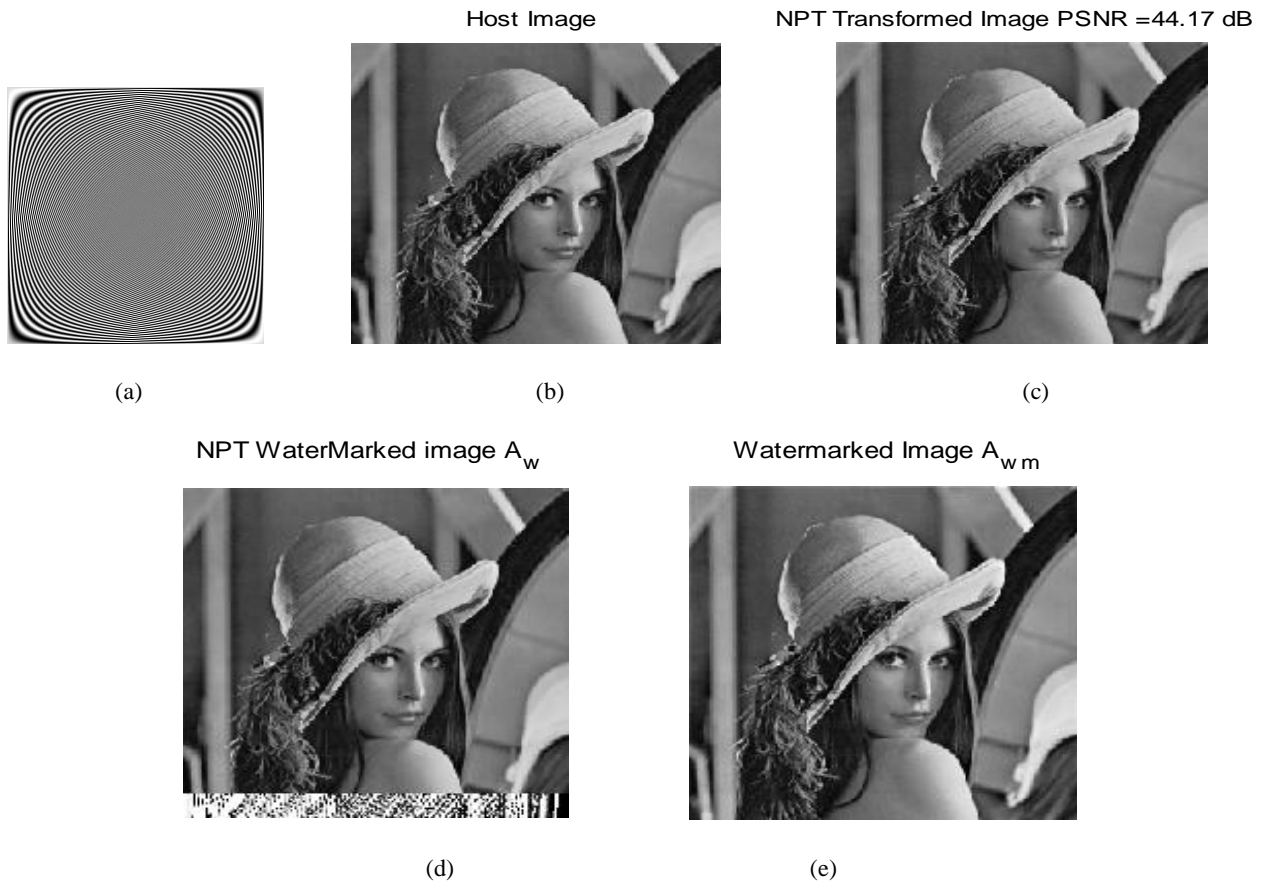


Fig. 1. (a) Transform basis of the Hartely. (b-c) Original image and its NPT image, computed with $\alpha = 0.994$. (d) NPT watermarked image with logo in last r rows. (e) NPT watermarked image with last r rows replace with last r rows of original image

3.1 Watermark Embedding

Let the host image S , (size $N \times N$) be watermarked by a watermarking logo (image) w , of size $(m \times n)$. In the bottom embedding technique [14-15], the logo is embedded to S as the last r bottom lines. Hence, the logo matrix is reshaped to be a matrix w_l (of size $r \times N$, $r = \frac{mn}{N}$). Then, the last r rows of S are replaced by the reshaped logo w_l , as in Fig. 1(d). This would

yield a watermarked image S_{wm} , $S_{wm} = \begin{bmatrix} S_1 \\ w_l \end{bmatrix}$, $S_1 = S(1 : N - r, :)$. Then the NPT of S_{wm} is obtained as:

$$A_w = \psi(\alpha) S_{wm} \psi(\alpha) \equiv \begin{bmatrix} A_{0w} \\ z \end{bmatrix} \begin{matrix} \updownarrow (N-r) \\ \updownarrow r \end{matrix} \begin{matrix} \leftarrow N \rightarrow \end{matrix} \quad (6)$$

This step in eq. 6, would register the watermark (distribute its energy) over the entire host image. In order to make the watermarking logo invisible, we replace the last r rows z of A_w with the last r of the original image S , Fig 1(e).

$$A_{wm} = \begin{bmatrix} A_{0w} \\ S(N-r+1 : N, :) \end{bmatrix} \quad (7)$$

3.2 Watermark Extraction

The watermarking extraction process is divided into a non-blind case, and a blind case. In the non blind case the original host image is known at the receiver side and we only try to extract the logo from the watermarked image. In the blind case the host image is not known at the receiver side, and we try to extract both the host and logo images from the watermark image, A_{wm} .

3.2.1 The Non Blind Case

Assuming that the original image S , the parameter α of eq. 1 and the type of the orthogonal transformation H_N , are known at the receiver, the extraction of the watermark from the received A_{wm} proceeds as follows:

1. Since the size of the watermark $m \times n$ is known at the receiver side, as well as the number of rows of w . Form

$$Y = A_{wm} \phi \equiv \begin{bmatrix} Y_1 \\ Y_2 \end{bmatrix} = \psi S_{wm} = \psi \begin{bmatrix} S_1 \\ w_1 \end{bmatrix}. \quad (8)$$

$$2. \text{ Partition } \psi = \begin{bmatrix} \psi_{11} & \psi_{12} \\ \psi_{21} & \psi_{22} \end{bmatrix} \begin{matrix} \Downarrow (N-r) \\ \Downarrow r \end{matrix}. \quad (9)$$

$$\leftarrow N \rightarrow \leftarrow r \rightarrow$$

Then, as long as $N-r \geq r$, the watermark w is the least squares solution of the system

$$Y_1 - \psi_{11} S_1 = \psi_{12} w_1 \quad (10)$$

The quality of extraction is judged by computing the normalized correlation $NCORR$ between the original and extracted

$$\text{logo, i.e. } NCORR = \frac{\sum_{i=1}^m \sum_{j=1}^n w_{ij} w_{exij}}{\|w\| \cdot \|w_{ex}\|} \quad (11)$$

w_{ex} is the extracted watermark. The non-blind extracted logo, in our experiments achieved a $NCORR = 1$ performance factor.

3.2.2 The Quasi Blind Case

When the prior knowledge of the host image S is not available, the following quasi blind technique is proposed for watermarking extraction of an NPT-based watermarked image. The proposed technique can be described as follows:

$$1. \text{ Partition } \psi = \begin{bmatrix} \psi_{11} & \psi_{12} \\ \psi_{21} & \psi_{22} \end{bmatrix} \begin{matrix} \Downarrow (N-r) \\ \Downarrow r \end{matrix} \quad (12)$$

$$\leftarrow N \rightarrow \leftarrow r \rightarrow$$

As $A_w \phi = \psi S_{wm}$ from eq. (6, 7, and 8), we can show that

$$\begin{bmatrix} A_{0w} \\ S(N-r+1:N,:) \end{bmatrix} \phi = \begin{bmatrix} \psi_{11} & \psi_{12} \\ \psi_{21} & \psi_{22} \end{bmatrix} \begin{bmatrix} S_1 \\ w_1 \end{bmatrix} \quad \text{i.e. } A_{0w} \phi = \psi_{11} S_1 + \psi_{12} w_1 \quad (13)$$

2. To cancel the effect of S_1 in eq. 13, construct an $(N-r)$ square matrix V such that $V^t \psi_{12} = 0$. This matrix can be easily constructed by expressing its k^{th} vector V_k as follows :

$$V_k = I_{N-r,k} - \sum_{j=1}^r \alpha_{jk} \psi_{12}(:, j), \quad \text{and } I_{N-r,k} \equiv I_{N-r}(:, k), \quad 1 \leq k \leq N-r \quad (14)$$

The α_{jk} are obtained by solving a set of r linear equations satisfying the following condition:

$$\text{Since } \psi_{12} \text{ is an } (N-r) \times r \text{ matrix, } V_k^t \psi_{12}(:, j) = 0 \quad 1 \leq j \leq r$$

then its maximum rank is r . Consequently, the rank of the matrix V is $(N-2r)$, [19].

$$3. \text{ Pre-multiply Equation (13) by } V^t \text{ to yield } V^t A_{0w} \phi = V^t \psi_{11} S_1 \quad (15)$$

As the rank of ψ_{11} is $(N-r)$, the rank of $V^t \psi_{11}$ is $(N-2r)$. So, to have a unique solution of eq.15, r arbitrary parameters of every column of S_1 have to be known at the receiver/extractor. This can be achieved if in the watermarked image A_w , we choose the matrix z (eq. 6), to be $S(N-2r+1:N-r,:)$ instead of $S(N-r+1:N,:)$. (it basically means replicating the r last rows of the image as in Fig. 2 (a)).

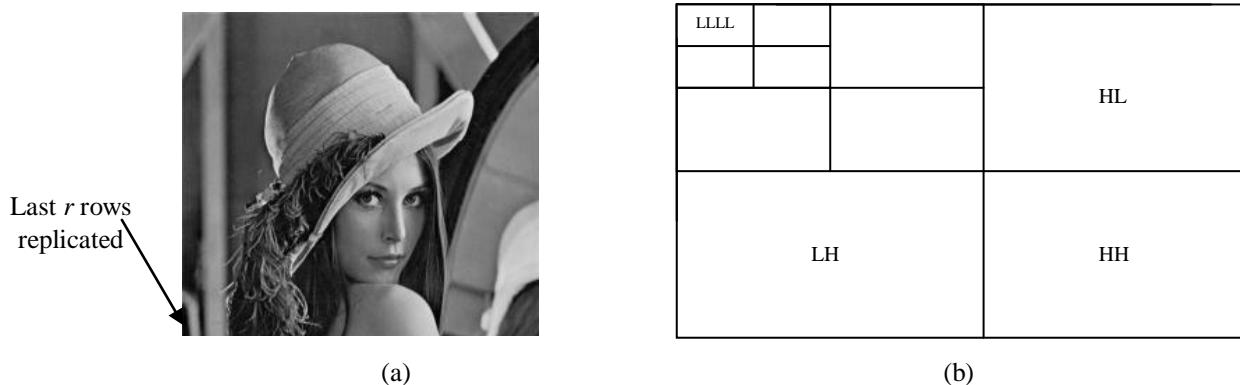


Fig.2. (a) Example of host images with last r rows replicated, $N=256$, $r=8$

(b) LLLL is the lowest band in a 2 layer wavelet decomposition

Having obtained S_j as the unique solution of eq.15, w_j (the logo) is extracted as in the non-blind case, and subsequently reshaped to regain the original watermark w . We used the terminology quasi blind, as a minor amount of information has to be known (r parameters of every column) at the receiver side. We note here that having r rows of the host image known at the receiver side as a mandatory condition for our blind technique is a slight draw back. However if we replicate the r rows of our host image, $S(N-2r+1:N-r,:)$, as the last r rows, our host image would be like fig.4(a) with negligible effect for this replication process, especially if the host image has a large size compared to r , as $N \gg r$.

4. Robustness against attacks (compression, noise and cropping)

The proposed watermarking techniques has been reported to be robust against compression (which is mainly shown in the next section), cropping and noise attacks [14-15]. Although this paper is primarily aimed at introducing a joint compression and watermarking system, we report here the performance against different attacks and compare it with other literature performances.

Regarding the cropping attack [14], if we crop the host watermarked image up to 50% of its original size, full extraction of the watermarked logo is shown to be possible, as in the non blind case, provided that the remaining watermarked size is at least the logo size. This ratio outperforms most of the other watermarking techniques against this kind of attack.

Regarding the noise attack, as reported in [15], we mixed the watermarked image with different amounts of noise such as the salt and pepper noise and the AWGN noise, so that the PSNR value of the original image went as low as 22-25 dB. The watermarking logo was correctly extracted with a correlation rate higher than 90%, which is very competitive with the recent literature [8].

We note here that studying the compression attack's impact on the proposed watermarking scheme is thoroughly examined in the next section, as it is part of the proposed joint compression and watermarking system, but we briefly state that the proposed watermarking approach can fully extract the hidden logo (more than 90% NCORR value) with up 1.0 bpp compression using the SPIHT compression approach.

5. NPT based joint watermarking and Compression

In our proposed system, we watermark our host image with a logo image to obtain a watermarked image. Then we compress the watermarked image through any transform based image compression standard. In our case we selected the SPIHT wavelet based image codec [20], to compress and then decompress (at the receiver side) the watermarked image, and then the extraction process takes place for the host and logo images. In our system we measure the compression performance by the PSNR quality of the reconstructed image (with respect to the original image) for a specific bit rate, while we measure the watermarking performance by the PSNR quality of the extracted image (host and logo) for a specific bit rate with a specific logo size. It can also be easily proven that the target compression bit rate would significantly affect the watermarking extraction quality, as shown next.

We also watermark compressed domain data, by watermarking the LL band image in the wavelet transform of any compression process, Fig. 2(b). It can also be shown that the amount of watermarked data (with its target extraction quality) would significantly affect the compression reconstruction performance; it is also dependent on which wavelet level (number of layers) its LL band is being watermarked as also shown in the next section. We note here that the higher the LL band (more layers) that is being watermarked, the less the quality of the reconstructed image from wavelet based compression theories. This is due to the fact that more data would be concentrated in LL band of the highest layer; therefore any manipulation to the band coefficients, as what happens by NPT, would more deteriorate the reconstructed image, also as a larger number of high band frequencies are dependent on it as in SPIHT or EBCOT [20-21]. We note here that if there is no watermark, zero number of embedded bottom lines, then increasing the number of wavelet layers would definitely enhance the PSNR of reconstructed image from enhanced resolution, but if there is a watermark, even if it is small (5 rows), it will affect (negatively) the reconstructed host image, and hence increasing the number of wavelet decomposition layers would further deteriorate the PSNR of the reconstructed host image. Increasing the number of wavelet layers would also

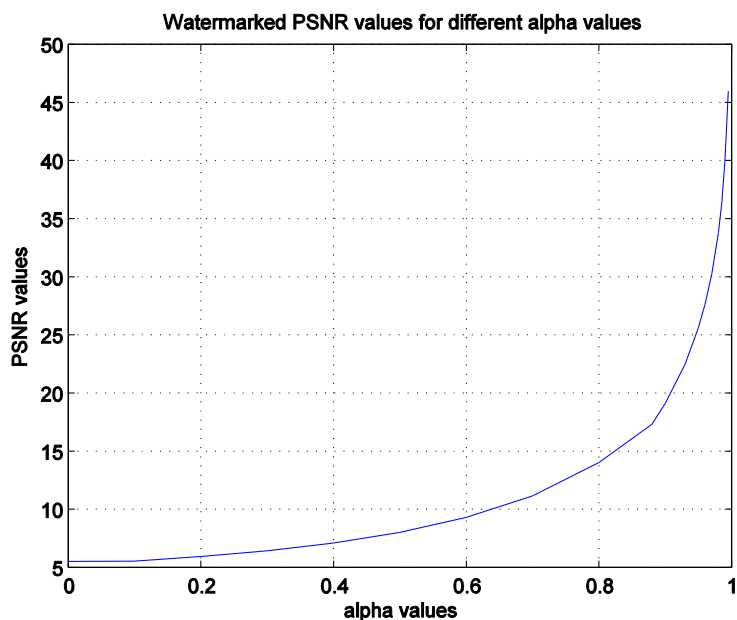
double the number of r rows in the bottom embedding process, as the logo (watermark) has a fixed size and the last LL band would be half the number of rows and columns of the previous case for every decomposition level. This would provide us with one more justification for the deteriorated PSNR reconstruction quality of the host image for increasing the number of wavelet layers from this joint watermarking and compression process.

For a watermarking system that is based on section 3, Fig.3 shows the PSNR values of the watermarked image for different values of alpha (α), along with the corresponding NCORR values of the extracted image, when the watermarked image is compressed using SPIHT with bpp (bits per pixel) =2.5, and no wavelet decomposition layers. It can be seen in the figure, that the smaller the value of alpha, the less contribution of the original image in eq.2, and the lower the PSNR, but the more contribution of the Hartley basis, which means more energy distribution, which will yield better extraction, better NCORR, and vice versa. A value of alpha in the range 0.985-0.99, is the optimal trade-off point between the 2 curves for this watermarking case, as in Fig. 3.

Fig. 4, shows a block diagram for our proposed joint watermarking and compression system. There are primarily three parameters that can significantly affect the performance of both watermarking and compression. The alpha parameter (α) as in eq.2, the number of wavelet layers and the target bit-rate in compression in the adopted SPIHT.

While it can be easily proven that the higher the bit-rate, the better is the PSNR of the extracted image (both host and logo) and the lower is the compression performance from basic rate-distortion theories [20-22]. The higher the value of α the more weight of the original image would be in eq.2, which would imply less contribution of the Hartley basis, which means lower amount of energy distribution, which means less watermarking performance.

On the other hand, more wavelet decomposition layers, which would imply more resolutions levels, and would lead to better compression performance as well known from successful wavelet based coders [20, 21]. Since in our system we watermark the LL band in the last wavelet layer, increasing the number of layers would deteriorate the compression reconstruction quality of watermarking extracted images, as higher band frequencies are added to it in reconstruction, as in Fig. 6. Therefore increasing the number of wavelet layers in our system would imply less PSNR for the reconstructed image (that has been watermarked and extracted). Hence, while increasing the bit rate would enhance the reconstruction quality of watermarking an extracted image, increasing the number of wavelet decomposition layers would deteriorate it in our joint watermarking and compression system, and the lower the value of alpha, the better the watermarking extraction as the NCORR curve in Fig. 3. Since the number of wavelet decomposition layers and the bit rate are two compression parameters and they have an inverse impact on the watermarking performance, they could be jointly combined in a single variable C , according to this relation, $C=K_1 * bpp + (1/K_2 * No. \text{ of wavelet layers})$



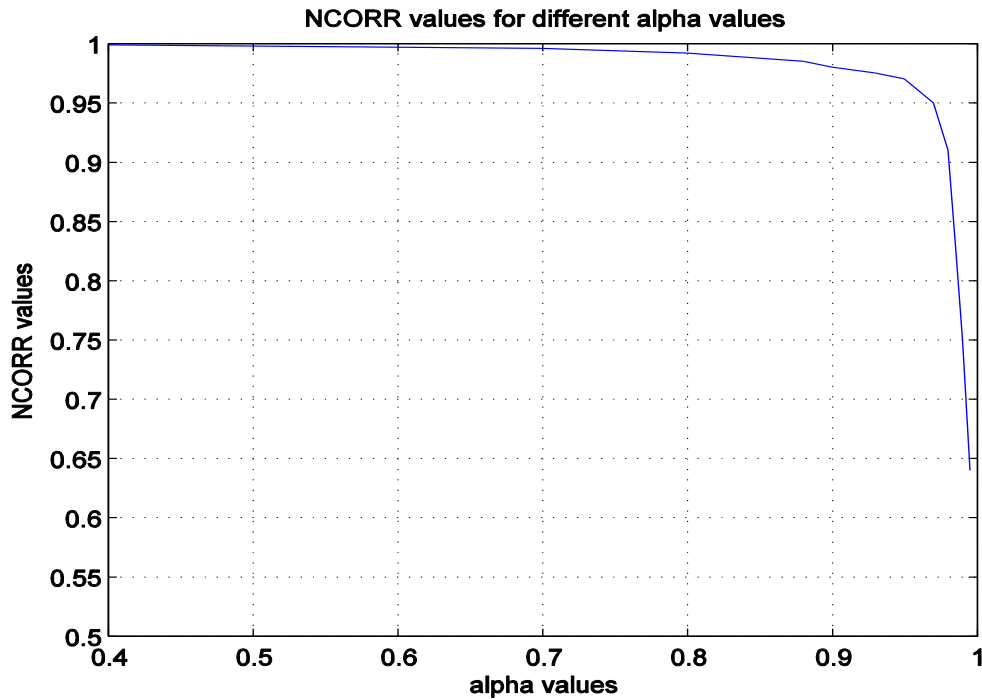


Fig. 3 PSNR and NCORR values for differential alpha values for different

From all above, we can identify the two variables of alpha and C as the parameters that affect the performance of our proposed joint watermarking and compression system. As shown above, each of them can significantly affect the performance of both watermarking and compression (JWC) on an inverse manner. Hence these two parameters can be combined into a single equation with a Lagrange multiplier as in eq. 16. The Lagrange multiplier can be adjusted to control both alpha (α) and C on a trade-off manner. JWC stand for performance of our joint system.

$$JWC = \alpha + \lambda * C \tag{16}$$

Fig.4 shows a block diagram of the proposed joint watermarking and compression system with a Lagrange multiplier as an adjustor that controls the trade-off between both. Fig. 5 shows the PSNR and the NCORR values for different alpha values on the same curve, it can be shown that an alpha value of 0.985 is optimal on that curve's trade-off.

Fig.6 shows the reconstructed PSNR quality of host images from watermarking the LL band for different number of layers, with an alpha (α) value of 0.985 and 2.5 target bpp. Fig. 7 shows the reconstructed PSNR quality of host images for different bit rates from one wavelet decomposition layer with an alpha value of 0.985.

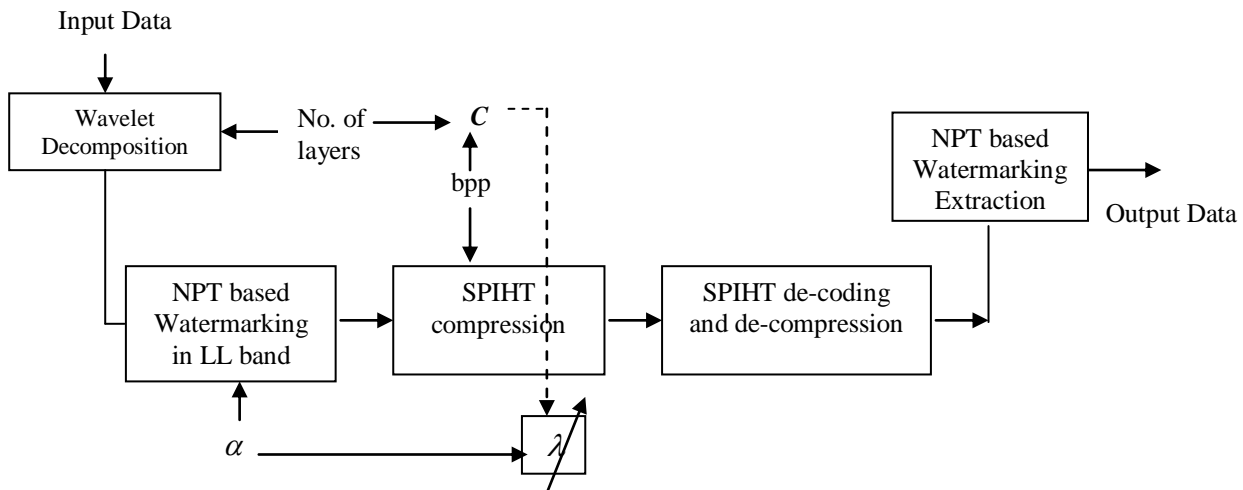


Fig. 4 Block diagram of a joint watermarking and compression system

We note here the variables of K_1 , K_2 and λ are image dependent, and can be adjusted according to the needed point on the compression and watermarking trade-off.

Fig. 8 shows the PSNR of the reconstructed and extracted host image with a bpp 2.5 with different numbers of bottom embedding rows, which imply different logo sizes. It is obvious that the increased number of bottom rows of the logo image, would deteriorate the PSNR of the reconstructed host image.

Fig. 9 shows the compression performance (PSNR reconstruction quality of watermarked host image) and the watermarking performance (NCORR correlation of the extracted logo), both against different alpha (α) values as well as different C values, a higher C value would imply high bit rate and less number of wavelet decomposition layers. It can be shown that the compression and watermarking performances are inversely affected by changing the value of either alpha or C ; hence they have to be treated on a trade-off manner.

5. Discussion

In this paper we presented a joint watermarking and compression system that can both compress and watermark a host image on a trade-off manner. We note here that our primary objective was to present the idea of joint compression and watermarking, rather than a regular single watermarking or compression technique like the recent literature, or our work in [14-15].

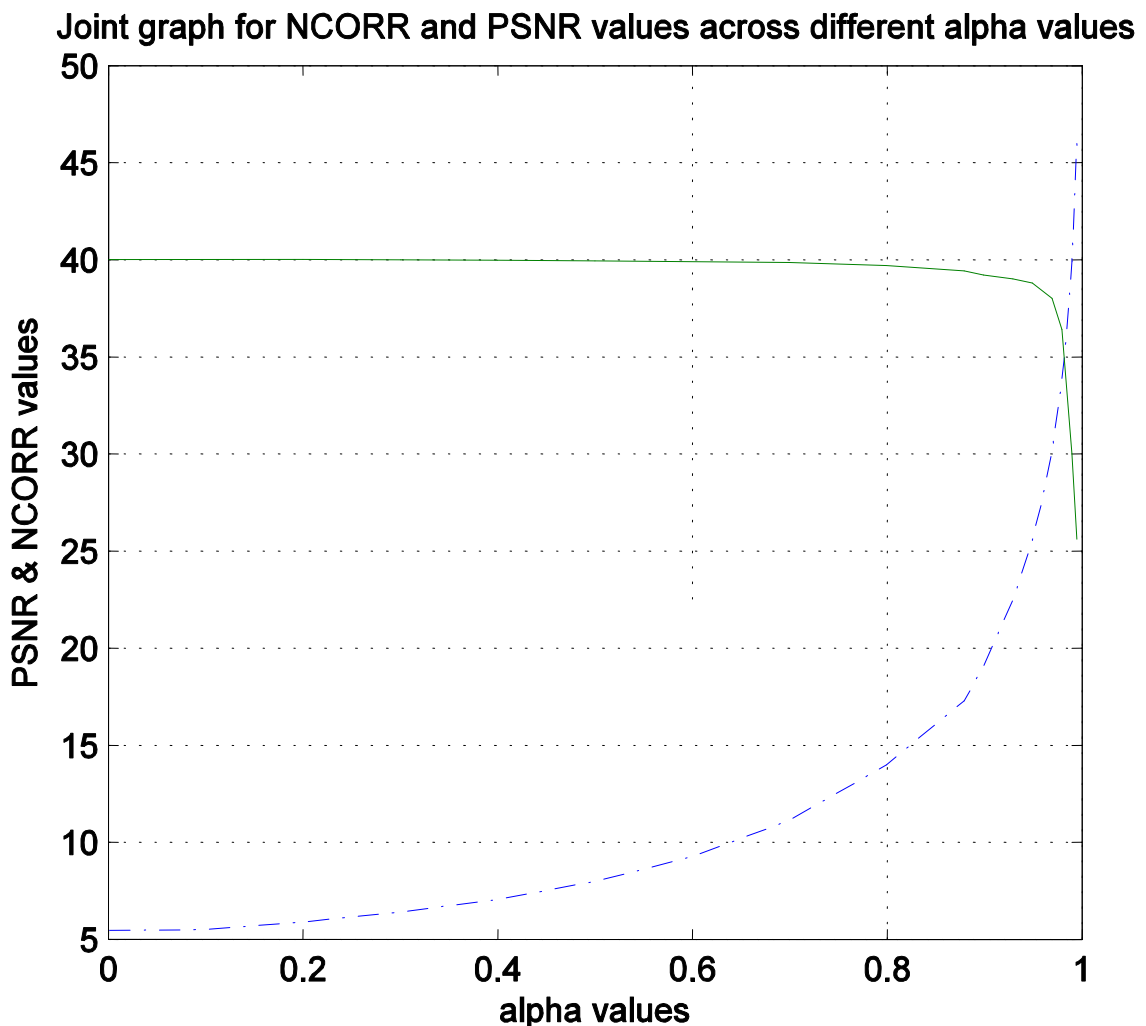


Fig. 5 Joint graph for PSNR and NCORR values for different alpha values

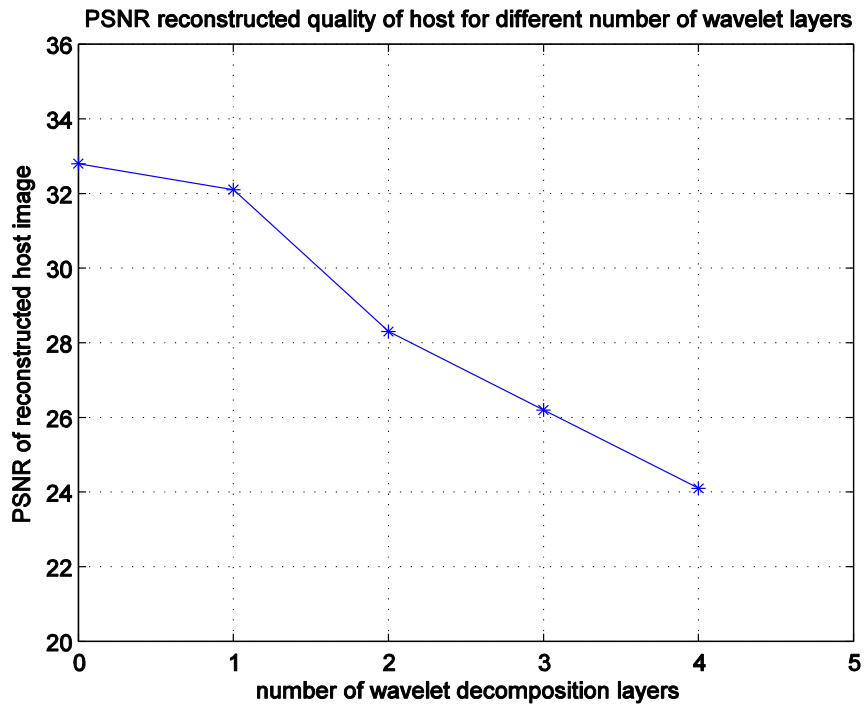


Fig. 6 PSNR reconstructed quality of host for different number of wavelet layers

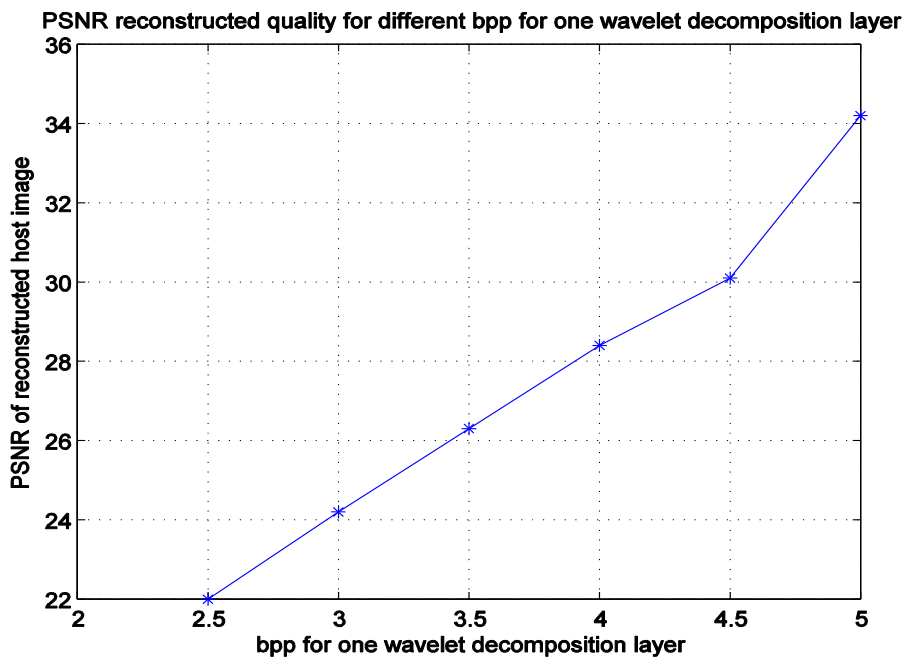


Fig. 7 PSNR reconstructed quality for different bpp for one wavelet decomposition layer

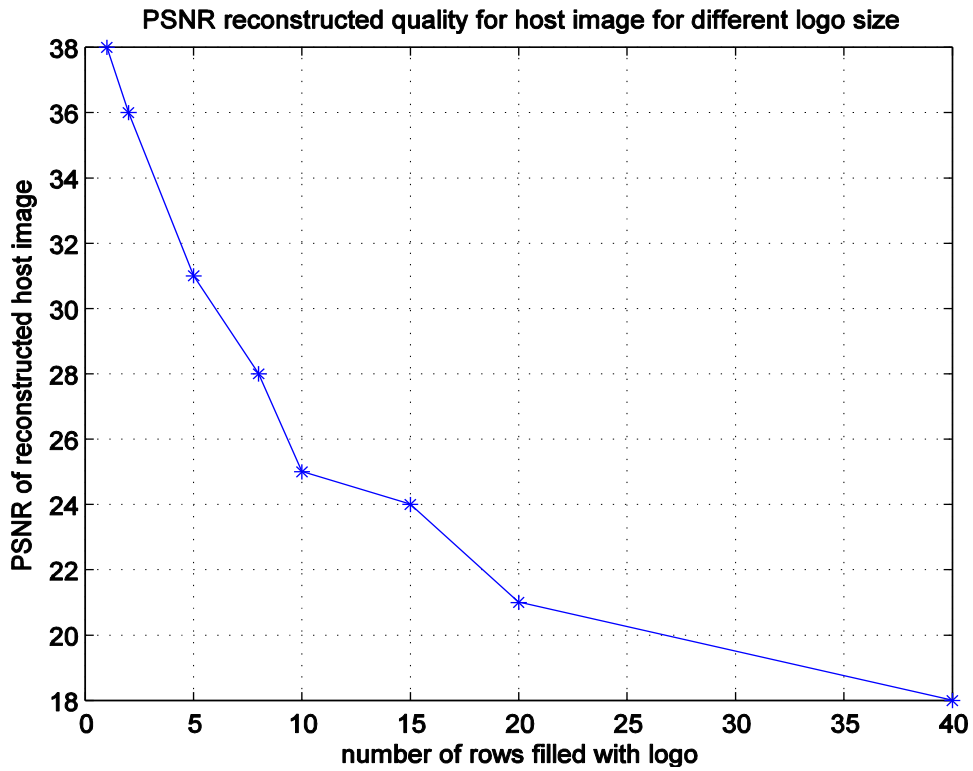


Fig. 8 PSNR reconstructed quality for host for different logo sizes

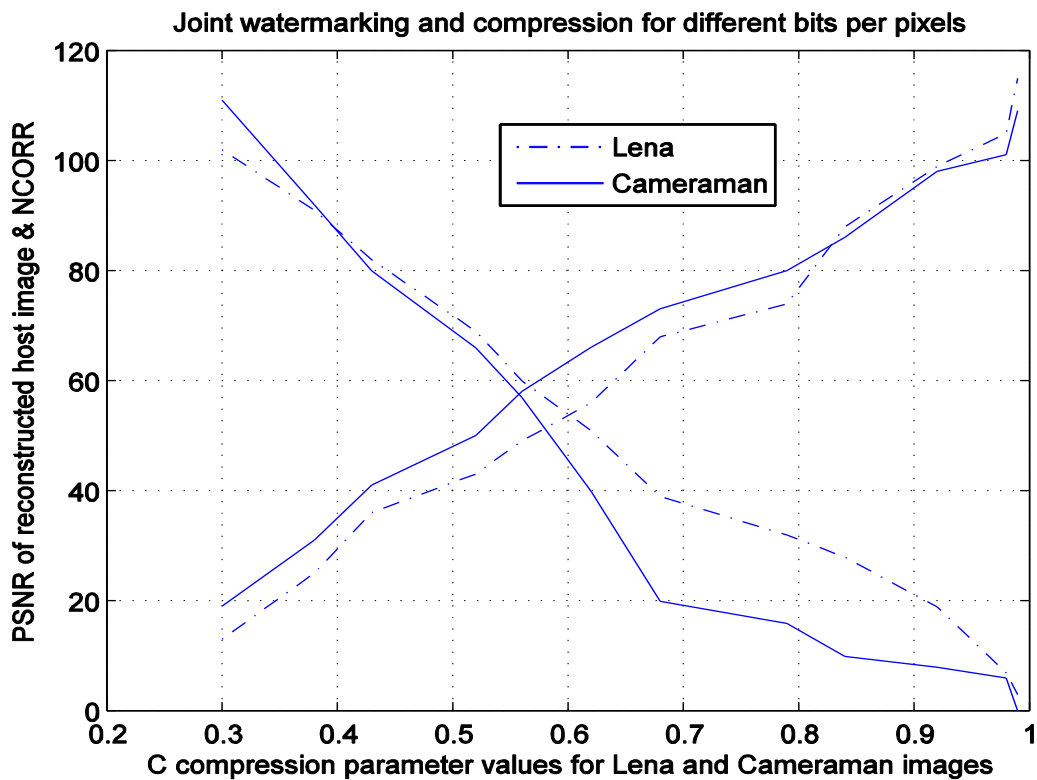


Fig. 9 Joint watermarking and Compression for different alpha values for Lena and Cameraman images

When treating compression and watermarking jointly, compression parameters can be treated as security keys, while watermarking data or keys can be considered as compression indices. Our proposed simulation results showed that there were three variables that could significantly affect the performance of both watermarking and compression. Bit rate, number of wavelet decomposition layers and the alpha value, which controls the balance between energy concentration (compression) and energy distribution (watermarking). The number of wavelet decomposition layers and the bit rate are two compression parameters that are typically defined in any wavelet-based compression process and they were combined in a single compression parameter C . Since both the alpha value and the C compression parameter had inverse impact on the performance of both compression and watermarking, a Lagrange multiplier equation was introduced that controls the balance between alpha and C on a trade-off manner. We note here the Lagrange multiplier value would depend on both the image class/type/content in addition to the desired point between compression and watermarking performances.

7. Conclusions

Our proposed system can be utilized in joint watermarking and compression applications that exploits compression parameters as watermarking variables, while compression indices could be used as watermarking actuators/adjustors. Our illustrated simulation results support our hypotheses and analogies in joint watermarking and compression, that they are inversely related and there is a trade-off relation between them, hence they should be treated jointly to achieve the optimal point of them. This work is funded by the ministry of Communication and Information Technology, Egypt, ITIDA. It has also been funded partly by the Alexander von Humboldt foundation, Germany.

References

1. C. Y. Lin and S. F. Chang, "A robust image authentication method distinguishing JPEG compression from malicious manipulation," *IEEE Trans. Circuits Syst. Video Technol.*, vol. 11, no. 2, pp. 153–168, Feb. 2001.
2. N. Nikolaidis and I. Pitas, Robust image watermarking in the spatial domain, Signal Processing, Elsevier, vol. 66, no. 3, pp. 385–403, 1998.
3. P. V. K. Borges and J. Mayer, "Text luminance modulation for hardcopy watermarking" Signal Processing, Elsevier, Vol. 87, Issue 7, July 2007.
4. Y. Hsien-Chu Wu and Chin-Chen Chang, "A novel digital image watermarking scheme based on the vector quantization technique", *Computers & Security*, Elsevier, Vol. 24, pp.460-471, 2005.
5. Y. Wang, A. Pearmain, Blind image data hiding based on self reference, *Pattern Recognition Letters* 25 (2004) 1681–1689.
6. P. H.W. Wong, Oscar C. Au, Y.M. Yeung, A novel blind multiple watermarking technique for images, *IEEE Transactions on Circuits and Systems for Video Technology* 13 (8) (2003) 813– 830.
7. J. R. Hernandez, M. Amado, and F. Perez-Gonzalez, DCT-domain watermarking techniques for still image: Detector performance analysis and a new structure, *IEEE Trans. Image Processing*, (9) (2000) 55–68.
8. H. Munawer Al-Otum, N. Abdul Samara A robust blind color image watermarking based on wavelet tree bit host difference selection, pp. 2498-2512 *Signal Processing (Elsevier) Volume 90, Issue 8, Aug. 2010*.
9. I.J. Cox, J. Kilian, F.T. Leighton, T. Shamoon, Secure spread spectrum watermarking for multimedia, *IEEE Transactions on Image Processing* 6 (12) (1997) 1673–1687.
10. J. Fridrich, "A hybrid watermark for tamper detection in digital images," in *Proc. Int. Symp. Signal Processing and Applications*, Aug. 1999, pp. 301–304.
11. C. Deng, X.-B. Gao, and et al. A Local Tchebichef Moments-Based Robust Image Watermarking. *Signal Processing (Elsevier)*, Vol.89, No.8, pp.1531-1539, August, 2009.
12. E. First, X. Qi, A Composite Approach for Blind Grayscale Logo Watermarking, *ICIP*, 2007, 265-268.
13. T. Duy Hien, I. Kei, H. Harak, Yen-Wei Chen, Y. Nagata, Z. Nakao, "Curvelet-Domain Image Watermarking Based on Edge-Embedding", *proc. of the 11th International Conference on Knowledge-Based Intelligent Information and Engineering Systems (KES 2007)*. (2007) 311-317.
14. M. F. Fahmy, O. M. Fahmy and G. Fahmy, " A Quasi Blind Watermark Extraction of Watermarked Natural Preserve Transform Images ", *IEEE International Conference on Image Processing, ICIP November 2009*.
15. G. Fahmy, M. F. Fahmy and U. S. Mohamed, "Non Blind and Quasi-Blind Natural Preserve Transform Watermarking and Data Hiding Technique", *EURASIP Journal of advances on Signal Processing, volume 2010, ID. 452548*.
16. R. Yarlagda, J. Hershey, Natural Preserving Transform for Image Coding and Reconstruction, *IEEE Trans. Acoustic, Speech and Signal Processing*, 4 (33) (1985)1005-1012
17. M. Ahmed, Digital Image Watermarking using Fuzzy Logic and Naturalness Preserving Transform, A Ph.D. Thesis, Kansas State University (2004).
18. D. D. Day and A.M. Ahmed, A Modified Natural Preserving Transform for data hiding and Image Watermarking, *Proc. JCIS 7th Joint Conf. of IASTED Int. Conf. on Signal and Image Processing*, 2003, 44-48.
19. J. W. Daniels, "Applied Linear Algebra " Prentice Hall International Inc., Engle wood Cliff, New Jersey, U.S.A., 1988.
20. A. Said and W. Pearlman, A new, fast and efficient image codec based on set partitioning in hierarchical trees," in *IEEE Trans. Circuits and Systems for Video Technology*. 6(3) (1996) 243-250.
21. D. Taubman, "High Performance Scalable Image Compression with EBCOT", *IEEE Transactions on Image Processing*, vol. 9, No. 7, July 2000

An Experimental Study on the Effect of Weld Parameters on Mechanical and Micro structural Properties of Dissimilar Aluminium Alloy FS Welds

R.Madhusudhan¹, M.M.M.Sarcar², N.Ramanaiah³, K.PrasadaRao⁴
^{1,2,3} Department of Mechanical Engineering, AU College of Engineering, Visakhapatnam, A.P.
India.

Abstract: Friction stir welding (FSW), a solid state joining technique is widely used for joining Aluminum alloys in marine, aerospace, automotive and many other applications of commercial importance. In the present study, dissimilar Aluminum alloy (AA 6262-T6 and AA 7075-T6) plates were FS welded by varying the weld parameters such as Tool rotational speed, weld speed and axial force with square tool pin profile. The mechanical properties (hardness and tensile strength) of the Dissimilar Friction Stir welded (DFS welded) specimens were tested and compared with the base materials. The observations have been elaborated in detail along with microstructures of parent and welded specimens through Optical Microscopy and it is observed that the weld parameters have a significant effect on mechanical and micro structural properties of the welds.

Keywords: Aluminum alloys, Friction stir welding, dissimilar welds, mechanical properties and microstructure.

INTRODUCTION

The marine and the aeronautic industries are definitely the most Wanted, interested and focused fields of research now-a-days predominantly on joining techniques. Actually, mechanical strength and performances, corrosion resistance, residual stress state, and weight reduction are some of the most significant issues which are painstaking in the assembly of aeronautical components and also in transport industry [1]. Heat treatable wrought aluminium-magnesium-silicon alloy conforming to AA6262 is of medium strength and possess good welding characteristics over the high strength aluminium alloys and also have similar chemistry to AA6061 except small addition of lead and bismuth to enhance machinability whereas aluminium-zinc-magnesium alloy namely AA7075[2] is of high strength and possess low welding characteristics. Both the materials AA6262 and AA7075 are extensively employed in marine fittings, couplings, hinge pins, camera parts, screw machine products, automobiles and aircraft applications [3,4,5].

In contrast to many of the fusion welding processes that are routinely used for joining structural alloys, FSW is an emerging solid state joining process in which the material that is being welded does not melt and recast. FSW was invented at The Welding Institute (TWI), UK in 1991 [6-13]. FSW is a continuous, hot shear, autogenous process involving a non-consumable rotating tool of harder material than the substrate material [14, 15]. Defect-free welds with good mechanical

properties have been made in a variety of aluminium alloys. When alloys are friction stir welded, phase transformations that occur during the cooling of the weld are of a solid-state type. Due to the absence of parent metal melting, the new FSW process is observed to offer several advantages over fusion welding. The material flow behavior is predominantly influenced by the FSW tool profiles, FSW tool dimensions and FSW process parameters namely tool rotational speed, weld speed and axial force [16-19].

In the present study, the dissimilar Aluminum alloys AA 6262-T6 and AA 7075-T6 of 6mm thick plates were joined by FSW considering welding parameters as tool rotational speed (1000rpm, 1200 rpm and 1400rpm), weld speed (0.4 mm/sec, 0.6 mm/sec and 0.8 mm/sec) and axial force (8kN, 9kN and 10kN) with a square tool pin profile made of H13 tool steel.

EXPERIMENTAL WORK

Plates of 6mm thick of 6262-T6 and 7075-T6 Al alloys were friction stir butt welded using a tool made of H13 tool steel having 18mm shoulder diameter and the swept diameter of the square pin measuring 6mm. AA 6262 was kept on the advancing side (AS) of the tool and AA 7075 was kept on retreating side (RS).

Chemical compositions in weight percentage and mechanical properties at room temperature of base metals (BMs) AA 6262 and AA 7075 are presented in Table 1 and Table 2 respectively. Square butt joint configuration was prepared to fabricate the FSW joints. The initial joint configuration was obtained by securing the plates in position using mechanical clamps. The direction of welding was normal to the rolling direction. Single pass welding procedure was adopted to fabricate the joints. An indigenously designed and developed FSW machine (15 HP; 3000 RPM; 25 kN) was used to fabricate the joints. The welding parameters considered and tool geometry are presented in Table 3.

Macro and micro structural analysis were carried out using a light optical microscope (Make: Union Opticals, Japan; Model: VERSAMET-3). The specimens for metallographic examinations were sectioned to the required dimension from the joint comprising stirred zone (SZ), thermo mechanically affected zone (TMAZ), and base metal (BM) regions and were polished using different grades of emery papers. Final polishing was done using the diamond paste on the disc polishing machine. Specimens were etched with Keller's reagent to reveal the macro and microstructures.

Hardness testing was carried out using Vickers pyramid hardness testing machine (Make: Leco and LV

700) with a load of 5 kg. Hardness survey along the transverse direction of the weld was conducted with hardness measurements at regular intervals of 2 mm from the centerline of the weld on both sides of the weld.

The tensile test specimens were prepared by Electro Discharge Machining and tested according to ASTM-E8 standards on 10tonne, computer controlled Universal Testing Machine at an initial strain rate of $6.7 \times 10^{-5} \text{ s}^{-1}$ at room temperature. The tensile properties of the joint were evaluated using three tensile specimens in each condition prepared from the same joint. All the specimens were mechanically polished before tests in order to eliminate the effect of possible surface irregularities [20, 21]. The specimen finally fails after necking and the load versus displacement was recorded. The Ultimate Tensile Strength (UTS), Yield Strength (YS), and percentage of Elongation (%E) were evaluated.

Table 1 Chemical composition (wt %) of BM's

Elements	Si	Cu	Mn	Mg	Zn	Al
AA6262	0.640	0.262	0.096	0.88	0.048	Bal
AA7075	0.104	1.560	0.063	2.32	5.950	Bal

Table 2 Mechanical properties of BM's

Material	UTS (MPa)	YS (MPa)	%E	Hardness (VHN)
AA6262-T6	346	319	22.8	108
AA7075-T6	589	471	20.8	195

Table 3 Welding Parameters and Tool geometry

S.no	Process Parameters	Values
1	Tool rotational Speed(rpm)	1000,1200, 1400
2	Weld Speed(mm/sec)	0.4,0.6, 0.8
3	Axial Force (kN)	8,9,10
4	Tool shoulder diameter (mm)	18
5	Tool Pin swept diameter (mm)	6
6	Pin Length (mm)	5.8

RESULTS AND DISCUSSIONS

3.1 Macro and Microstructural observations

The FSW joints were successfully produced. The obtained joints shown no porosity or other defects in both top and root weld surface in all the welding conditions. Fig.1 shows the macrograph of the produced weld after thoroughly etched with the Keller's reagent marked as "SZ", "TMAZ" and "BM". From the different etching response of each material the AA6262 Al alloy appeared darker colored than the AA7075 one. It is clear that the microstructure of the SZ is mainly composed of the AA6262 fixed on the AS than AA7075 fixed on RS.

The SZ is the region that experienced the highest strain and undergoes recrystallization. Its microstructure is due to the mechanical action of the tool probe that generates a continuous dynamic recrystallization process. The higher temperature and the severe plastic deformation during the welding in the SZ result in a new equiaxed fine grain structure.

Fig.2 shows the Optical microstructures of the BM's and that of the welds at SZ and TMAZ. The left-hand side micrograph of the BM region indicates that microstructure consists of Mg_2Si precipitates and that on right side indicates Al_2Zn precipitates. The SZ has equiaxed grains with both the precipitates. The appreciable variation in grain size and distribution of strengthening particles in TMAZ region was observed on both AS and RS compared to SZ, which is due to various reasons such as FSW parameters, tool geometry, work piece composition & temperature, vertical pressure and active cooling.

3.2 Hardness observations

Table 4 shows the micro hardness values in SZ, tensile test results of all the DFS welded specimens and also the position of tensile failure considering all the conditions. It is observed that out of all the

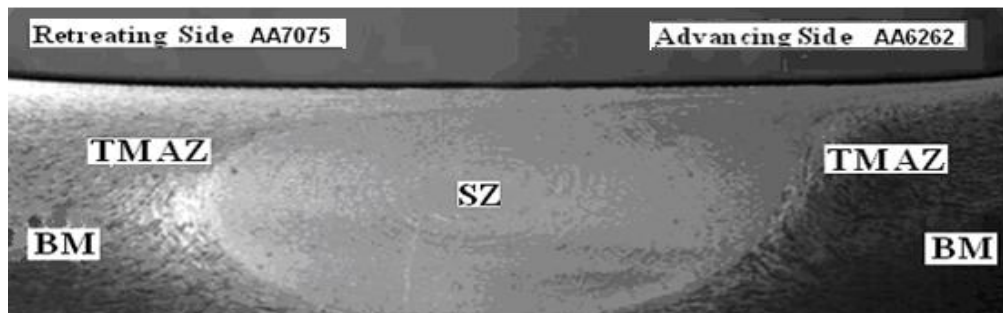


Fig.1 Typical macrograph showing various regions of the FS welded plates on AS, RS.

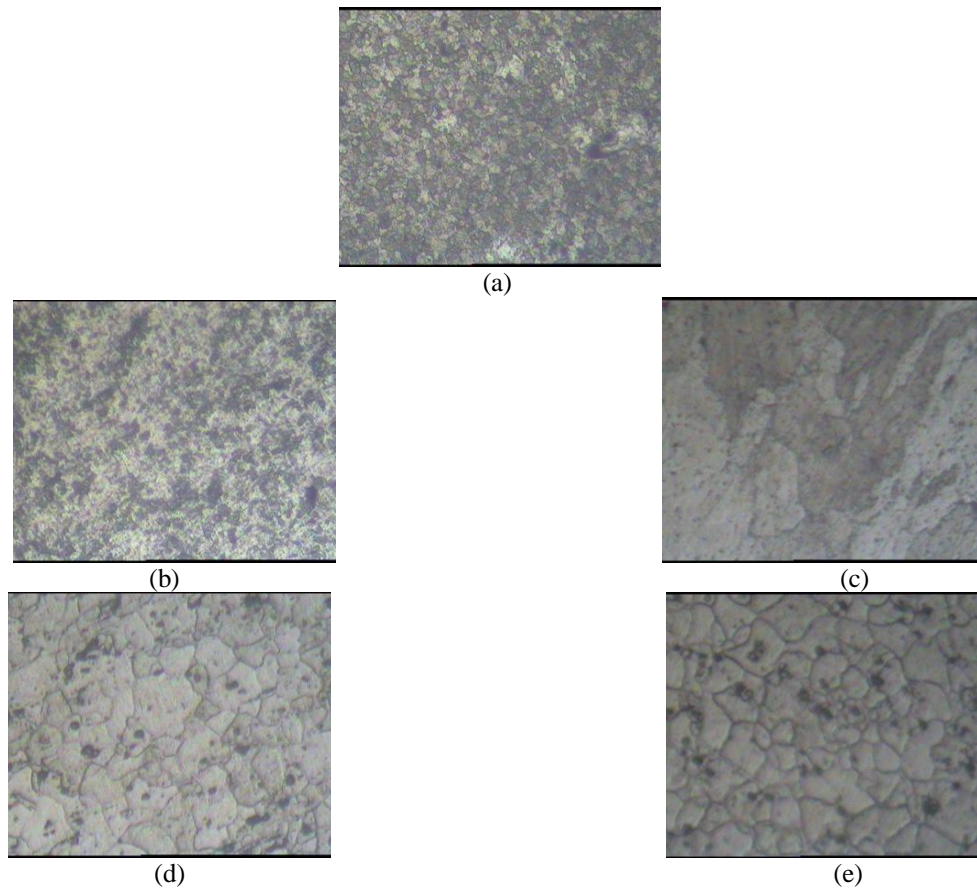


Fig. 2 Optical micrographs with main distinct regions of a dissimilar FS weld: (a) Stirred Zone (SZ) (b) TMAZ on AA6262 side (c) TMAZ on AA7075 side (d) Base metal AA6262 and (e) Base Metal AA7075.

DFS welded plates, the plate welded with 1200 rpm tool rotational speed, 0.6mm/sec weld speed and 9 kN axial force showed better micro hardness value at the SZ. Fig 3 shows the effect of tool rotational speed on the hardness variation across the weld line of the DFS welded plate with 0.6mm/sec weld speed and 9 kN axial force as it showed better hardness value. It is observed that the plates welded with 1200 rpm tool rotational speed shows better results

compared to the other two tool rotational speeds and also the hardness in the region of tool pin interaction with the plates is found to be higher than the hardness of AA6262 BM whereas lower than that of AA7075 BM. Hardness gradually decreases to the TMAZs on both the sides of SZ and then increases towards the ends (BMs) of the DFS welded plate.

Table 4. Mechanical properties (Tensile and Hardness) of Dissimilar Friction Stir Welded specimens

S.no	Tool rotational Speed rpm	Weld speed, mm/sec	Axial force, kN	UTS (MPa)	YS (MPa)	%E	Vicker's hardness	Failure position
1	1400	0.4	8	240.53	195.11	9.25	120.9	SZ
2	1400	0.4	9	248.43	207.87	12.06	128.16	HAZ of 6262
3	1400	0.4	10	247.04	201.25	10.14	125.16	HAZ of 6262
4	1400	0.6	8	243.87	203.85	9.37	123.83	SZ
5	1400	0.6	9	252.85	214.89	13.17	129.8	HAZ of 6262
6	1400	0.6	10	248.47	209.65	11.53	128.25	SZ
7	1400	0.8	8	239.05	194.53	7.84	118.86	SZ
8	1400	0.8	9	245.93	202.28	10.27	126.14	HAZ of 6262
9	1400	0.8	10	241.93	199.86	9.84	123.37	SZ

10	1200	0.4	8	244.39	198.69	9.61	122.92	HAZ of 6262
11	1200	0.4	9	251.89	212.09	12.47	132.1	HAZ of 6262
12	1200	0.4	10	249.47	206.32	10.52	128.73	HAZ of 6262
13	1200	0.6	8	249.79	207.58	9.53	126.58	HAZ of 6262
14	1200	0.6	9	256.73	218.22	13.38	134.4	HAZ of 6262
15	1200	0.6	10	252.31	213.69	11.82	131.8	HAZ of 6262
16	1200	0.8	8	240.51	199.97	8.02	119.98	SZ
17	1200	0.8	9	248.08	207.29	10.62	129.05	HAZ of 6262
18	1200	0.8	10	244.97	203.84	10.07	125.46	HAZ of 6262
19	1000	0.4	8	232.67	189.81	8.18	112.83	SZ
20	1000	0.4	9	239.78	195.66	11.53	119.61	SZ
21	1000	0.4	10	237.7	193.01	9.18	114.1	SZ
22	1000	0.6	8	237.43	197.93	8.11	115.26	SZ
23	1000	0.6	9	243.93	204.9	11.98	122.17	HAZ of 6262
24	1000	0.6	10	241.85	201.22	10.08	119.98	HAZ of 6262
25	1000	0.8	8	230.47	185.41	6.86	109.76	SZ
26	1000	0.8	9	237.63	196.52	9.14	116.85	SZ
27	1000	0.8	10	234.86	191.65	8.95	113.74	SZ

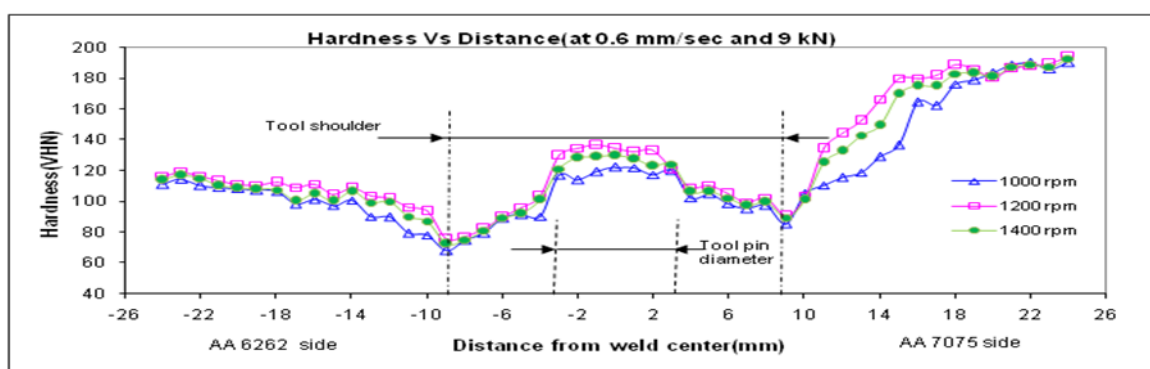


Fig.3 Hardness variation at 0.6mm/sec feed rate, 9kN axial force

3.3 Tensile Observations

Traverse tensile properties of DFS welded joints fabricated using square tool pin profile with all possible conditions were evaluated. Three specimens were tested for each condition and average of these is reported in Table 4. The results show that Tool rotational speed is having significant influence on tensile properties of the welded specimens and also it is observed that most of the

specimens failed in the HAZ region of retreating side i.e. AA6262 side and a few of them failed in SZ region. The joints fabricated with 1200 rpm tool rotational speed, 0.6 mm/sec weld speed and 9kN axial force showed highest tensile strength, where as joints fabricated using 1000 rpm tool rotational speed with 0.8 mm/sec weld speed and 8kN axial force showed lowest tensile strength.

CONCLUSIONS

- The Friction stir welding used successfully to join dissimilar aluminium alloys (AA6262 and AA7075).
- Better mechanical properties (hardness and tensile strength) were obtained with the FSW plate fabricated with 1200 rpm tool rotational speed, 0.6 mm/sec weld speed and 9kN axial force compared to all other conditions.
- The SZ region shows a new equiaxed fine grain structure compared to the base metals.

REFERENCES

- [1] F.Acerro, G.Buffa, Livan Fratini, G.Troiano, "On the FSW of Aa2024-T4 and AA 7075-T6 T-joints: an industrial case study", *Int J Adv Manuf Technology*, Springer-Verlag public, October' 2009.
- [2] C. Yeni, "The effect of welding parameters on the microstructure and mechanical properties of friction stir welded AA 7075", *Practical Metallurgy* 45/10 (2008) 479-494.
- [3] W.M. Thomas, *US Patent 5460317*, October 24 (1995).
- [4] A.K. Lakshminarayanan & V. Balasubramanian & K. Elangovan "Effect of welding processes on tensile properties of AA6061 aluminium alloy joints" *Int J Adv Manuf Technol* (2009) 40:286-296.
- [5] P.Cavaliere, E.Cerri, A.Squillace, "Mechanical response of 2024-7075 aluminium alloys joined by Friction Stir Welding", *J. of mat. Sc*, 40(2005) pp. 3669-3676.
- [6] Mishra RS, Ma ZY (2005) Friction stir welding and processing. *Mater Sci Eng R Rep* 50:1-78
- [7] W. M. Thomas, E. D. Nicholas, J. C. Needham, M. G. Murch, P. Temple-Smith, and C. J. Dawes, *International Patent Application No. PCT/GB92/02203*; *GB Patent Application No. 9125978.8*; *U.S Patent No. 5,460,317 (1991)*.

- [8] C.Dawes,W.Thomas,*TWI Bulletin 6, November/December 1995,p.124.*
- [9] Von Strombeck, A., Çam, G., Dos Santos,J. F., Ventzke, V., and Koçak, M. 2001. "A comparison between microstructure, properties,and toughness behavior of power beam and friction stir welds in Al-alloys". *Proc. of the TMS 2001 Annual Meeting Aluminum, Automotive &Joining. Eds:S. K. Das, J. G. Kaufman, and T. J. Lienert, pp. 249–264. TMS, Warrendale, Pa.*
- [10] Kallee, S. W., et al. 2001. *Proc. of 8th Int. Conf. on Joints in Aluminium, Munich, Germany, p. 16.*
- [11] Murr, L. E., Liu, G., and McClure, J. C. 1997. *J. Mater. Sci. 16: 1801.*
- [12] Murr, L. E., Liu, G., and McClure, J. C.1998. *J. Mater. Sci. 33: 1243.*
- [13] Mahoney, M. W., et al. 1998. *Metal. Mater.Trans. 29A: 1955.*
- [14] C. J. Dawes, *Weld. Met. Fab. 63, 13 (1995).*
- [15] S. Babu*, K. Elangovan, V. Balasubramanian, and M. Balasubramanian "Optimizing Friction Stir Welding Parameters to Maximize Tensile Strength of AA2219 Aluminum Alloy Joints " *Met. Mater. Int., Vol.15, No. 2(2009), pp. 321~330.*
- [16] P. Bahemmat, A. Rahbari, M. Haghpanahi, M. K. Besharati,2008 " Experimental study on the effect of rotational speed and tool pin profile on AA 2024 aluminium Friction Stir Welded butt joints"*Proceedings of ECTC 2008,October 3-4, 2008,Miami, Florida, USA.,p 1.1-1.7.*
- [17] Yingchun Chen, Huijie Liu,Feng Jicai,*Mater. Sci.Eng. A 420 (2006) 21-25.*
- [18] A. Oostercamp, L.Djapic Oostercamp,A.Nordeide, *Weld.J. 92004) 225s-231s.*
- [19] K.Elangovan, V. Balasubramanian, "Influences of pin profile and rotational speed of the tool on the formation of friction stir processing zone in AA 2219 aluminium alloy",*J. of Mater. Sci.Engg. A 459 (2007) pp 7 – 18.*
- [20] R.Priya, V.Subramanya Sarma and K. Prasad Rao "Effect of post weld heat treatment on the microstructure and tensile properties of dissimilar friction stir welded AA 2219 and AA 6061 alloys" : *Trans. IIM Vol. 62, Issue 1, Feb '2009.*
- [21] M.P. Miles, D.W. Melton, and T.W. Nelson, "Formability of Friction-Stir-Welded Dissimilar-Aluminum-Alloy Sheets" *Metallurgical and Materials Transactions A, volume 36A, Dec '2005-3335-3342.*

Implementation of ANN Based Controllers to Improve the Dynamic Performance of a Shunt Active Power Filter

D. Gowtami¹ S. Ravindra² S. Surya Kalavathi³

¹(M.Tech Student, St.Johns College of Engineering and Technology, Yemmiganoor, Andhra Pradesh)

²(EEE Department, St.Johns College of Engineering and Technology, Yemmiganoor, Andhra Pradesh)

³(EEE Dept, JNTUniversity, Hyderabad, Andhra Pradesh)

ABSTRACT: This paper attempts to enhance the dynamic performance of a shunt-type active power filter. The predictive and adaptive properties of artificial neural networks (ANNs) are used for fast estimation of the compensating current. The dynamics of the dc-link voltage is utilized in a predictive controller to generate the first estimate followed by convergence of the algorithm by an adaptive ANN (adaline) based network. Weights in adaline are tuned to minimize the total harmonic distortion of the source current. Extensive simulations and experimentations confirm the validity of the proposed scheme for all kinds of load (balanced and unbalanced) for a three-phase three-wire system.

Keywords: Adaline, current control, nonlinear load, shunt active power filter (APF), total harmonic distortion (THD), voltage source inverter.

I. INTRODUCTION

Harmonic compensations have become increasingly important in power systems due to the widespread use of adjustable-speed drives, arc furnace, switched-mode power supply, uninterruptible power supply, etc. Harmonics not only increase the losses but also produce unwanted disturbance to the communication network, more voltage and/or current stress, etc. Different mitigation solutions, e.g., passive filter, active power line conditioner, and also hybrid filter, have been proposed and used [1]–[8]. Recent technological advancement of switching devices and availability of cheaper controlling devices, e.g., DSP-/field-programmable-gate-array-based system, make active power line conditioner a natural choice to compensate for harmonics. Shunt-type active power filter (APF) is used to eliminate the current harmonics.

The dynamic performance of an APF is mainly dependent on how quickly and how accurately the harmonic components are extracted from the load current. Many harmonic extraction techniques are available, and their responses have been explored. Proposed techniques include traditional $d-q$ [2] and $p-q$ theory [3]–[5] based approaches and application of adaptive filters [6], wavelet [7], genetic algorithm (GA), artificial neural network (ANN), etc., for quick estimation of the compensating current [8]. A critical evaluation of such techniques is recently reported by the authors [8].

Recently, ANNs have attracted much attention in different applications, including the APF [9]–[20], [22]. Dash *et al.* [14] computed the Fourier coefficients of the signal by using *adaline*, and Chen and O'Connell [15] used an ANN that is trained with GA and back

propagation. Lai *et al.* [16] used a Hopfield neural network for real-time computation of frequency and harmonic content of the signal. Improved performance has been observed compared to discrete Fourier transform, fast Fourier transform, or Kalman- Tey *et al.* [17] reported a modified version of [10]. An additional PI controller is used to regulate the dc-link voltage. A full “neuromimetic” strategy involving several *adalines* has been reported by Abdeslam *et al.* [18]. The controller can adapt for unbalance and change in working conditions. Lin [19] proposed an intelligent neural-network-based harmonic detection, which is first trained with enough data (1400 patterns). The working model could compute the harmonic components with only onehalf of the distorted wave. An *adaline*-based harmonic compensation is reported by Singh *et al.* [20]. Weights are computed online by the LMS algorithm. Luo *et al.* [21] demonstrated a 200-kVA laboratory prototype for a combined system for harmonic suppression and reactive power compensation using an optimal nonlinear PI controller, whereas a two-stage recursive least square based *adaline* is reported by Chang *et al.* [22] for harmonic measurement.

Note that parallel developments on predictive control techniques are reported for power controllers. These are also applied to APF [23], [24]. The implementation of APF using power balance at the dc link is reported by Singh *et al.* [25]. The dc-link voltage has been used to find the peak magnitude of the supply current for self-supporting dc bus. However, no detail analysis of the dynamics of the dc-link voltage is available. This paper is an integration of predictive and adaptive control techniques for fast convergence and reduced computations. Two ANN-based controllers are used for such purpose. The predictive controller generates the first estimate of the compensating current quickly after the change in load is detected. The change in voltage across the capacitor is used for this purpose. This is followed by an *adaline*-based controller to fast converge to the steady value. This paper is organized in Eight sections. Section II deals with the Basic Block Diagram. Section III Estimation of Current Reference. Regulation of DC link Voltage in APF is covered in Section IV. Fast estimation of compensating current using ANN is presented in Section V. Section VI presents the Adaptive Current Detection Technique, Section VII presents the MATLAB Model and Simulation results. Section VIII concludes the work.

II. BASIC BLOCK DIAGRAM

A general block diagram of a APF with a non-linear load is shown below. Two ANN-based controllers are used for such purpose. The predictive controller generates the first

estimate of the compensating current quickly after the change in load is detected. The change in voltage across the capacitor is used for this purpose. This is followed by an *adaline*-based controller to fast converge to the steady value.

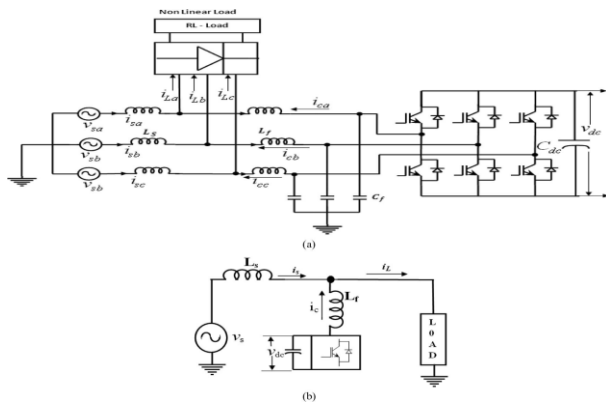


Fig. 1. (a) APF to compensate for a nonlinear load. (b) Single phase of shunt APF.

III. ESTIMATION OF CURRENT REFERENCE

Fig. 1(a) shows the APF compensating a nonlinear load. Fig. 1(b) shows the corresponding schematic diagram. A general expression for the load current [corresponding to Fig. 1(b)] is

$$iL(t) = i\alpha 1(t) + i\beta 1(t) + ih(t). \tag{1}$$

The in-phase and quadrature components of the phase current at fundamental frequency are $i\alpha 1$ and $i\beta 1$, respectively. All other harmonics are included in ih . The per-phase source voltage and the corresponding in-phase component of the load current may be expressed as

$$v_s(t) = V_m \cos \omega t \tag{2}$$

$$i\alpha 1(t) = I\alpha 1 \cos \omega t. \tag{3}$$

Assuming that the APF will compensate for harmonic and reactive power, the compensating current becomes

$$i_c(t) = iL(t) - i\alpha 1(t) = iL(t) - I\alpha 1 \cos \omega t \tag{4}$$

where $I\alpha 1$ is the peak magnitude of the in-phase current that the mains should supply and hence needs to be estimated. Once $I\alpha 1$ estimation is over, the reference current for the APF may easily be set as per (4)

IV. REGULATION OF DC-LINK VOLTAGE IN APF

The dynamics of the dc-link voltage is an indirect measure of the performance of the APF. Whenever there is a change in the load, the voltage across the dc-link capacitor also undergoes a corresponding change. A controller is used to keep the voltage regulated at a desired value. In this section, a simple analysis of the dynamics of the dc-link voltage is first carried out. Parameters that govern the dynamics are identified, following which an algorithm is developed to estimate the compensating current of the APF.

To maintain the dc-bus voltage to a desired magnitude, the capacitor draws in-phase (i.e., in phase with

the source voltage) current i_{sa} . This is in addition to the compensating current i_c . From the power balance equation

$$P_{dc} = C_{dc} v_{dc} \frac{dv_{dc}}{dt} \tag{5}$$

where p_{dc} is the power required to maintain the voltage v_{dc} across the dc link. From the power balance equation

$$\sum_{i=a,b,c} v_{si}(t) i_{sai}(t) - \sum_{i=a,b,c} R_f (i_{sai}^2(t) + i_{ci}^2(t)) - \frac{1}{2} \sum_{i=a,b,c} L_f \frac{d}{dt} (i_{sai}^2(t) + i_{ci}^2(t)) = i_{dc}(t) v_{dc}(t) = P_{dc}$$

where R_f and L_f are the resistance and inductance of the inductor that is connected in between the point of common coupling and the voltage source inverter. Note that i_{sa} supplies the system loss at the steady state and charges/discharges the capacitor during transient to maintain the dc-link voltage. Considering that “power” is a scalar quantity, (6) for a balanced three-phase system may be expressed as

$$3v_s(t) i_{sa}(t) - 3R_f (i_{sa}^2(t) + i_c^2(t)) - \frac{3}{2} L_f \frac{d}{dt} (i_{sa}^2(t) + i_c^2(t)) = i_{dc}(t) v_{dc}(t) = P_{dc} \tag{7}$$

Applying small perturbations in i_c , i_{sa} , v_{dc} , and v_s , around

an operating point, the following new set of variables may be obtained:

$$i_c(t) = I_c + \Delta i_c \tag{8}$$

$$i_{sa}(t) = I_{sa} + \Delta i_{sa} \tag{9}$$

$$v_{dc}(t) = V_{dc} + \Delta v_{dc} \tag{10}$$

$$v_s(t) = V_s + \Delta v_s \tag{11}$$

where I_c , I_{sa} , and V_s are rms and V_{dc} is the dc value of the corresponding quantities at the operating point. Again, in steady state

$$3V_s I_{sa} - 3R_f (I_{sa}^2 + I_c^2) = 0 \tag{12}$$

Substituting (8)–(12) in (7), the following equation is obtained:

$$3(\Delta v_s I_{sa} + V_s \Delta i_{sa}) - 6R_f (I_{sa} \Delta i_{sa} + I_c \Delta i_c) + 3L_f (I_{sa} \frac{d\Delta i_{sa}}{dt} + I_c \frac{d\Delta i_c}{dt}) = C_{dc} V_{dc} \frac{d\Delta v_{dc}}{dt} \tag{13}$$

Converting the variables to s -domain and after rearranging, (13) may be expressed as

$$\Delta V_{dc}(s) = \frac{K G_2(s) G_1(s) G_2(s)}{1 + K G_2(s) G_1(s) G_2(s)} \Delta V_{dc}^*(s) - \frac{G_2(s) G_3(s)}{1 + K G_2(s) G_1(s) G_2(s)}$$

$$\Delta I_c(s) + \frac{G_2(s) G_4(s)}{1 + K G_2(s) G_1(s) G_2(s)} \Delta V_s(s) \quad (14)$$

where K is the small-signal gain.

$$\Delta V_{dc}(s) = - \frac{G_2(s) G_3(s)}{1 + K G_2(s) G_1(s) G_2(s)} \Delta I_c(s) \quad (15)$$

This explores the possibility of extracting an estimate of the compensating current from the change in vdc.

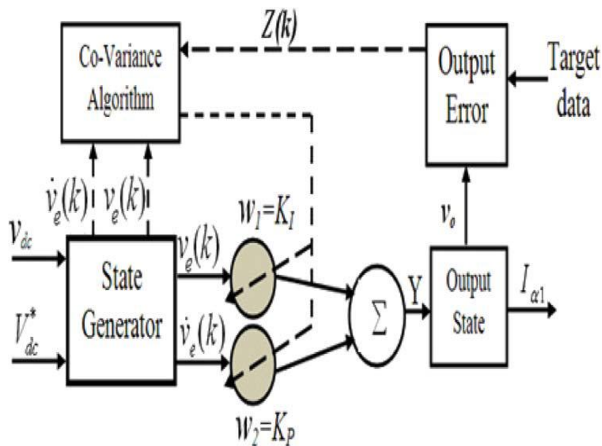


Fig 2. Block Diagram of ANN-Based Peak Value Predictor

$$I_s < \frac{C_{dc} V_{dc}^*}{3 K_P L_f} \quad (16)$$

$$I_s \leq \frac{K_P V_s}{2 R_f K_P + L_f K_i} \quad (17)$$

All the ac quantities in (16) and (17) are expressed as rms value. I_s , V_{dc}^* , and V_s are the source current, reference dc-link voltage, and source voltage, respectively. Equations (16) and (17) are used to generate an initial guess of K_P and K_I and also to set their limits.

V. FAST ESTIMATION OF COMPENSATING CURRENT USING ANN

An ANN-based PI controller plays a dual role. It ensures faster reference generation and is also accountable for better regulation of dc-bus voltage. The structure of the system (i.e., ANN-tuned adaptive PI controller) is shown in Fig. 2. To reduce computational burden, a single-layer ANN structure is used. The input vector as expressed in (18) is fed to the state exchanger. In our scheme, error voltage and its gradient are chosen as the state of the system to ensure faster corrective action

$$u = [V_{dc}^* \ v_{dc}]^T \quad (18)$$

The task of the state generator block is to generate states x_1 and x_2 as follows:

$$x_1 = v_e(k) \quad x_2 = \frac{\delta x_1}{\delta k} \quad (19)$$

where $v_e(k) = V_{dc}^* - v_{dc}(k)$. The output error $z(k)$ is represented as

$$z(k) = v_o(k) - v_o(k-1) \quad (20)$$

The output $v_o(k)$ is fed to output state to estimate I_{a1} . Neuron cell generates controlling signal through interrelated gathering [27], [28] as

$$u(k) = u(k-1) \sum_{i=1}^n w_i(k) x_i(k) \quad (21)$$

where w_i is the weight of the system

Here, a neuron is trained by Hebb's rule [27], [28]. Therefore, the change of weight of the neuron cell at k th instant may be represented as

$$w_i(k+1) = (1-c)w_i(k) + \eta r_i(k) \quad (22)$$

$$r_i(k) = z(k)u(k)x_i(k) \quad (23)$$

where r_i is the progressive signal, η is Hebb's studying ratio

(learning rate), and " c " is a constant. Substituting (22) and (23) in (21), the following equation may be obtained:

$$\Delta w_i(k) = w_i(k+1) - w_i(k) = -c[w_i(k) - \eta z(k)u(k)x_i(k)/c] \quad (24)$$

$\Delta w_i(k)$ is the change of weight at k th step. Weights of the neuron are tuned according to Hebb's assumption. Hebb's assumption is popularly known as the covariance algorithm.

$$\Delta w_i(k) = F_i(y_1(k), x_i(k)) \quad (25)$$

where $F_i(*)$ is a function of both postsynaptic and presynaptic signals and y_1 is the output of the individual neuron. If $F_i(*)$ is differentiable, then $\delta F_i / \delta w_i$ may be represented as

$$\frac{\delta F_i}{\delta w_i} = w_i(k) - \frac{\eta}{c} z(k)u(k)x_i(k) \quad (26)$$

From (26), the change of weight in k th sample may be expressed as

$$\Delta w_i(k) = -c \frac{\delta F_i(k)}{\delta w_i(k)} \quad (27)$$

Thus, by adjusting the values of $w_i(k)$, K_P and K_I are tuned.

The weights $w_i(k)$ are searched according to the negative slope of function $F_i(*)$. Equations (26) and (27) are used to tune the parameter used in (28) and (29). Finally, for the PI controller, the weights are represented by

$$w_1(k+1) = w_1(k) + \eta_1 z(k)x_1(k) \quad (28)$$

$$w_2(k+1) = w_2(k) + \eta_2 z(k)x_2(k) \quad (29)$$

Whenever the ANN is initiated, it starts with a set of controller gains to generate the first estimate of the compensating current. These initial values of controller parameters are set by offline training of the ANN. The controller parameters are then adjusted following (28) and (29) to regulate the dc-link voltage.

VI. ADAPTIVE CURRENT DETECTION TECHNIQUE

The ANN in Section IV provides an initial guess for any change in system dynamics. To generate more accurate reference for APF, load current samples are fed to the *adaline*-based network shown in Fig. 3. *Adaline* is designed to minimize the total harmonic distortion (THD) of source current. Uncompensated source current sample $s(k)$ may be represented as

$$s(k) = I_{\alpha 1} \cos(\omega k t_s) + I_{\beta 1} \sin(\omega k t_s) + \sum_{n=2}^R I_n \cos(n\omega k t_s + \phi_n) \tag{30}$$

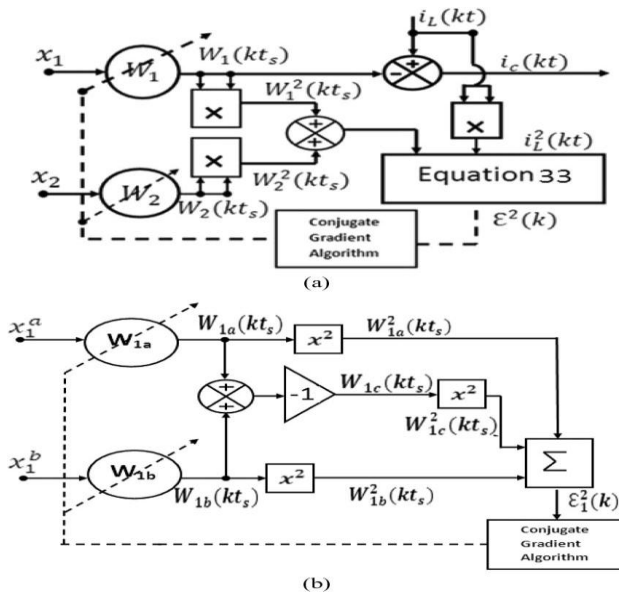


Fig 3: a) Adaline Based Harmonic Extraction for a Three Phase Balanced Network b) Adaline Based Harmonic Extraction for a Three Phase UnBalanced Network

The error terms for k th sample may be expressed as

$$\epsilon^2(k) = \left[\frac{(s^2(k) - 2s(k)\bar{a}(k))}{a^2(k)} + 1 \right] \tag{31}$$

Where

$$a^2(k) = I_{\alpha 1}^2(k) \cos^2(\omega k t_s) + I_{\beta 1}^2(k) \sin^2(\omega k t_s) \tag{32}$$

Equation (31) may also be represented as

$$\epsilon^2(k) = \left[\frac{(s^2(k) - 2s(k)\bar{a}(k))}{X^T(k)\bar{a}(k)\bar{a}^T(k)X(k)} + 1 \right] \tag{33}$$

where the vector

$$\bar{a}(k) = [I_{\alpha 1}(k), I_{\beta 1}(k)] \tag{34}$$

and the input vector

$$X(k) = [\cos \omega k t_s, \sin \omega k t_s]^T \tag{35}$$

Equation (33) is further modified to fit in terms of a quadratic equation as

$$A[\bar{a}^T(k)X(k)]^T[\bar{a}^T(k)X(k)] - B[\bar{a}^T(k)X(k)] + C = 0 \tag{36}$$

Equation (36) is minimized by *conjugate gradient* (CG) method [27]–[29].

Thus, the error function (i.e., THD) is minimized to calculate the in-phase component of the fundamental

load current. The compensating current is then calculated according to (4). Fig. 3(a) shows the details of current detection for a three phase balanced system, while Fig. 3(b) shows the same for an unbalanced (three-phase and three-wire) network. $W1a$, $W1b$, and $W1c$ are the corresponding in-phase components of the current for phase-a, phase-b and phase-c, respectively.

VII. MATLAB MODELLING

Block Diagram

A general block diagram of the ANN model Simulink is given in Fig.4. Simulations have been conducted for balanced and unbalanced loads using SIMULINK for different controller configurations. The whole system is built in SIMULINK where the ANN routine is called whenever necessary.

First, simulation study is made for the case with only predictive algorithm. A quick estimate helped, the waveform quality is poor due to the lack of any corrective mechanism in the system. The simulation results obtained. Next, the adaptive algorithm is tried. Simulation have done to check the performance of the system for a step change in load. Balance three-phase nonlinear load is considered similar to the case with predictive algorithm.

Now, to have the advantage of predictive and adaptive controllers, the system is run with both the algorithms. Fig4 show the situation with both the predictive and adaptive controllers in operation. The results have confirmed very satisfactory performance in terms of waveform quality and response time.

The controller is found to operate satisfactorily. The source current, load current, and compensating current are shown in top-to-bottom order. The controller took 51 s to converge, whereas the proposed controller with predictive and adaptive algorithm converged within less than one-quarter of a cycle with acceptable current quality.

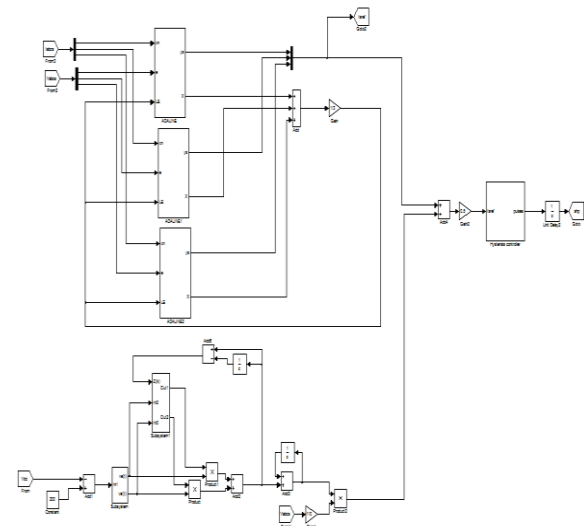


Fig 4: Operational functional block diagram of the ANN Model

VIII. RESULTS AND DISCUSSION

Simulations have been conducted for balanced and unbalanced loads. First simulation study is made for the case of only predictive algorithm Fig 5 gives simulation results with predictive ANN. Fig 6 gives simulation results of APF with adaline. Fig 7. Performance of the APF with predictive and adaptive controllers.

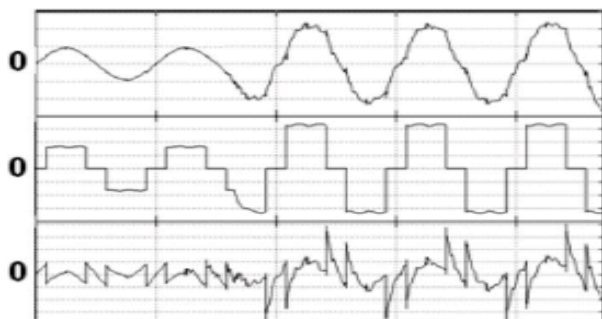


Fig. 5. Performance of the APF with predictive ANN (simulation results). Top waveform: Source current of phase A (scale: 5 A/div). Middle waveform: Load current of phase A (scale: 5 A/div). Bottom waveform: Compensating current of phase A (scale: 5 A/div). Time scale: 20 ms/div.

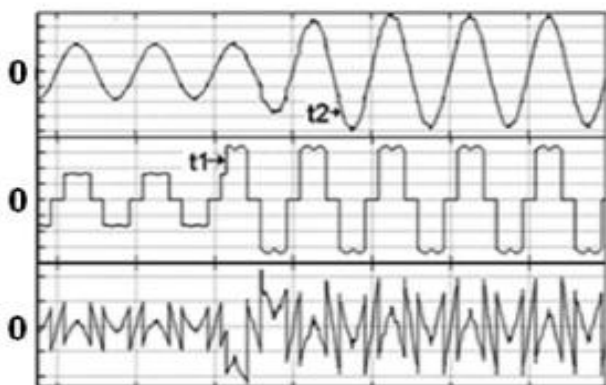


Fig. 6. Performance of the APF with *adaline* (simulation results). Top waveform: Source current of phase A (scale: 5 A/div). Middle waveform: Load current of phase A (scale: 5 A/div). Bottom waveform: Compensating current of phase A (scale: 5 A/div). Time Scale: 20 ms/div.)

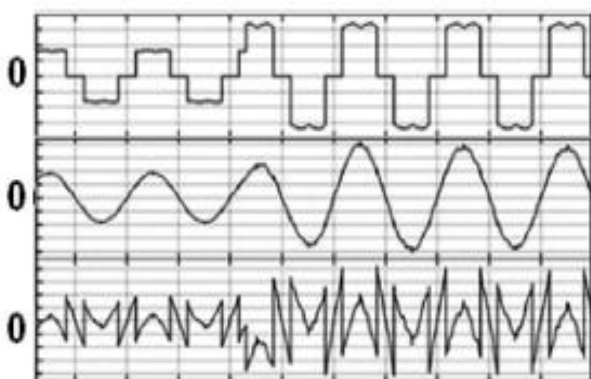


Fig. 7. Performance of the APF with predictive and adaptive controllers (simulation results). (a) Load current of phase A (scale: 5 A/div). (b) Source current of phase A

(scale: 20 A/div). (c) Compensating current of phase A (scale: 5 A/div). Time scale: 10 ms/div.

IX. CONCLUSION

An integration of predictive and adaptive ANN-based controller for a shunt-type APF has been presented in this paper to improve the convergence and reduce the computational requirement. The predictive algorithm is derived from an ANN based PI controller used to regulate the dc-link voltage in the APF. This is followed by an *adaline*-based THD minimization technique. *Adaline* is trained by CG method to minimize THD. Use of only two weights and two input vectors makes the convergence very fast. The system is extensively simulated in MATLAB/SIMULINK.

REFERENCES

- [1] B. Singh, K. Al-Haddad, and A. Chandra, "A review of active power filters for power quality improvements," *IEEE Trans. Ind. Electron.*, vol. 46, no. 5, pp. 960–971, Oct. 1999.
- [2] S. Bhattacharya, T. M. Frank, D. M. Divan, and B. Banerjee, "Active filter system implementation," *IEEE Ind. Appl. Mag.*, vol. 4, no. 5, pp. 47–63, Sep./Oct. 1998.
- [3] H. Akagi, Y. Kanazawa, and A. Nabae, "Instantaneous reactive power compensators comprising switching devices without energy storage components," *IEEE Trans. Ind. Appl.*, vol. IA-20, no. 3, pp. 625–630, May 1984.
- [4] F. Z. Peng, G.W. Ott, Jr., and D. J. Adams, "Harmonic and reactive power compensation based on the generalized instantaneous reactive power theory for three phase four wire system," *IEEE Trans. Power Electron.*, vol. 13, no. 6, pp. 1174–1181, Nov. 1998.
- [5] R. S. Herrera and P. Salmeron, "Instantaneous reactive power theory: A reference in the nonlinear loads compensation," *IEEE Trans. Ind. Electron.*, vol. 56, no. 6, pp. 2015–2022, Jun. 2009.
- [6] H. Karimi, M. Karimi-Ghartemani, and M. R. Irvani, "An adaptive filter for synchronous extraction of harmonics and distortions," *IEEE Trans. Power Del.*, vol. 18, no. 4, pp. 1350–1356, Oct. 2003.
- [7] M. Forghani and S. Afsharnia, "Online wavelet transform-based control strategy for UPQC control system," *IEEE Trans. Power Del.*, vol. 22, no. 1, pp. 481–491, Jan. 2007.
- [8] A. Bhattacharya, C. Chakraborty, and S. Bhattacharya, "Current compensation in shunt type active power filters," *IEEE Ind. Electron. Mag.*, vol. 3, no. 3, pp. 38–49, Sep. 2009.
- [9] A. Hamadi, S. Rahmani, and K. Al-Haddad, "A hybrid passive filter configuration for VAR control and harmonic compensation," *IEEE Trans. Ind. Electron.*, vol. 57, no. 7, pp. 2419–2434, Jul. 2010.
- [10] B. Widrow and M. A. Lehr, "30 years of adaptive neural networks: Perceptron, madaline and backpropagation," *Proc. IEEE*, vol. 78, no. 9, pp. 1415–1442, Sep. 1990.

- [11] C.-C. Tsai, H.-C. Huang, and S.-C. Lin, "Adaptive neural network control of a self-balancing two-wheeled scooter," *IEEE Trans. Ind. Electron.*, vol. 57, no. 4, pp. 1420–1428, Apr. 2010.
- [12] A. Dinu, M. N. Cirstea, and S. E. Cirstea, "Direct neural-network hardware-implementation algorithm," *IEEE Trans. Ind. Electron.*, vol. 57, no. 5, pp. 1845–1848, May 2010.
- [13] G. W. Chang, C.-I. Chen, and Y.-F. Teng, "Radial-basis-function-based neural network for harmonic detection," *IEEE Trans. Ind. Electron.*, vol. 57, no. 6, pp. 2171–2179, Jun. 2010.
- [14] P. K. Dash, D. P. Swain, A. C. Liew, and S. Rahman, "An adaptive linear combiner for on-line tracking of power system harmonics," *IEEE Trans Power Syst.*, vol. 11, no. 4, pp. 1730–1735, Nov. 1996.
- [15] Y. M. Chen and R. M. O'Connell, "Active power line conditioner with a neural network control," *IEEE Trans. Ind. Appl.*, vol. 33, no. 4, pp. 1131–1136, Jul./Aug. 1997.
- [16] L. L. Lai, C. T. Tse, W. L. Chan, and A. T. P. So, "Real time frequency and harmonic evaluation using artificial neural network," *IEEE Trans. Power Del.*, vol. 14, no. 1, pp. 52–59, Jan. 1999.
- [17] L. H. Tey, P. L. So, and Y. C. Chu, "Improvement of power quality using adaptive shunt filter," *IEEE Trans. Power Del.*, vol. 20, no. 2, pp. 1558–1568, Apr. 2005.
- [18] D. O. Abdeslam, P. Wira, J. Merckle, D. Flieller, and Y. A. Chapuis, "A unified artificial neural network architecture for active power filters," *IEEE Trans. Ind. Electron.*, vol. 54, no. 1, pp. 61–76, Feb. 2007.
- [19] H. C. Lin, "Intelligent neural network-based fast power system harmonic detection," *IEEE Trans. Ind. Electron.*, vol. 54, no. 1, pp. 43–52, Feb. 2007.
- [20] B. Singh, V. Verma, and J. Solanki, "Neural network-based selective compensation of current quality problems in distribution system," *IEEE Trans. Ind. Electron.*, vol. 54, no. 1, pp. 53–60, Feb. 2007.
- [21] A. Luo, Z. Shuai, W. Zhu, and Z. J. Shen, "Combined system for harmonic suppression and reactive power compensation," *IEEE Trans. Ind. Electron.*, vol. 56, no. 2, pp. 418–428, Feb. 2009.
- [22] G. W. Chang, C. I. Chen, and Q. W. Liang, "A two-stage adaline for harmonics and interharmonics measurement," *IEEE Trans. Ind. Electron.*, vol. 56, no. 6, pp. 2220–2228, Jun. 2009.
- [23] J. H. Marks and T. C. Green, "Predictive transient-following control of shunt and series active power filters," *IEEE Trans. Power Electron.* vol. 17, no. 4, pp. 574–584, Jul. 2002.
- [24] M. Routimo, M. Salo, and H. Tuusa, "A novel simple prediction based current reference generation method for an active power filter," in *Proc. IEEE APEC*, 2004, pp. 3215–3220.
- [25] B. N. Singh, B. Singh, A. Chandra, and K. Al-Haddad, "Design and digital implementation of active filter with power balance theory," *Proc. Inst. Elect. Eng.—Electr. Power Appl.*, vol. 152, no. 5, pp. 1149–1160, Sep. 2005.
- [26] M. H. Rashid, *Recent Development in Power Electronics: Selected Reading*. Piscataway, NJ: IEEE Press, 1996.
- [27] S. Kumar, *Neural Networks—A Class Room Approach*. New Delhi, India: Tata McGraw-Hill, 2004.
- [28] F. M. Ham and I. Kostanic, *Principles of Neurocomputing for Science & Engineering*. New Delhi, India: Tata McGraw-Hill, 2002.
- [29] J. Nocedal and S. J. Wright, *Numerical Optimization*. New York: Springer-Verlag, 1999.

BIOGRAPHIES



D. Gowtami is born in 1987 in India. She is graduated from JNTU Anantapur in 2008. Presently she is doing Post graduation in Power Electronics and Electrical Drives Specialization at J.N.T.U.A, Anantapur Her main areas of interest includes Electrical machines, Power Electronics & Converters, Power Electronic Drives & FACTS.



S. Ravindra, M. Tech, working as Asst. Professor in St. Johns College of Engineering and Technology, Affiliated to JNTUA, Approved by AICTE. New Delhi. He completed his M.Tech in 2010 from JNTU Hyderabad. He has five years teaching experience in Electrical Engineering. He has published four Conferences in electrical engineering.



Dr. M. Surya Kalavathi, Ph.D, working as professor in JNTU university. She has qualifications of B.Tech. (EEE) SVU, M.Tech. (PSOC) SVU, Ph.D (JNTU), Post Doc (CMU, USA). Got a vast teaching experience. Published many papers and presently guiding to 5 Ph.D scholars.

Analytical Study on Seismic Performance of Hybrid (DUAL) Structural System Subjected To Earthquake

Nabin Raj .C¹, S.Elavenil²

Department of civil engineering, Faculty of engineering and technology,
SRM UNIVERSITY, Kattankulathur- 603203, Chennai,

Abstract: Steel braced frame is one of the structural systems used to resist earthquake loads in multi-storeyed buildings. Many existing reinforced concrete (RC) buildings can be retrofitted to overcome deficiencies, to resist seismic loads at the same time steel bracings can be incorporated with RC frames which in combine can be called as dual system to resist lateral force in the new buildings. Steel bracing is economical, easy to erect, occupies less space and has flexibility to design for meeting the required strength and stiffness. In the present study, the seismic performance of reinforced concrete buildings using concentric steel bracing is investigated. The bracings are provided at peripheral columns. A six, twelve and eighteen storied buildings are analysed for seismic zone V as per IS 1893: 2002 using SAP 2000 software. Response spectrum analysis is performed for the buildings. For getting eigen values and eigen vectors the MathCAD Prime software is used. And hence storey shear and base shear are computed. The seismic performance of the building is evaluated in terms of storey drifts.

I. INTRODUCTION

This paper presents a study of three dimensional elastic behaviour of medium rise and high rise buildings having combination of rigid frame and vertical steel bracings which combine can be called as dual system. In present the parameters taken for analysis are displacements, reinforcement demands of frame members, moments, drift pattern for different types of bracing systems. As the height of the structure increases, effect of lateral load becomes more and more predominant and additional structure materials are required to resist it.

+ PG student, SRM University, Chennai.

++ Professor, SRM University, Chennai

Steel bracing of RC frames has received some attention in recent years both as retrofitting to increase shear capacity of the existing building and as a shear resisting element in seismic design of new buildings. The direct bracing of RC frames has received more attention since it is less costly, and can be used not for retrofitting but also as viable alternative to RC shear walls at pre-construction design level.

II. DUAL SYSTEM

In present contest many buildings are provided with more than one type of seismic resisting systems. Usually in these days structures are designed in such a way that it lateral force resistance is provided by frames and shear walls, frames and infill and frames and bracings. This combined system can be said as dual system.

Dual system may combine the advantages of the constituent elements. Ductile frames, interacting with steel bracings, can provide a significant amount of energy dissipation when required particularly in upper stories of the building. On other hand as result of large stiffness of frame, good story drift during earthquake can be achieved.

Despite the attractiveness and prevalence of dual system, it is only recently that research effort has been directed toward the developing relevant seismic design methodologies. This paper involves the analytical studies of proposed new apartment building, using dynamic analysis and the overall response of braced frame.

III. RC STRUCTURES WITH STEEL BRACINGS

Steel bracing is a highly efficient and economical method of resisting horizontal forces in a frame structure. Bracing has been used to stabilize laterally, the majority of the world's tallest building structures as well as one of the major retrofit measures. Bracing is efficient because the diagonals work in axial stress and therefore call for minimum member sizes in providing stiffness and strength against horizontal shear. A number of researchers have investigated various techniques such as infilling walls, adding walls to existing columns, encasing columns, and adding steel bracing to improve the strength and/or ductility of existing buildings and new buildings

Bracing system improves the seismic performance of the frame by increasing its lateral stiffness and capacity. Through the addition of the bracing system, load could be transferred out of the frame and into the braces, bypassing the weak columns. Steel braced frames are efficient structural systems for buildings subjected to seismic or wind lateral loadings. Therefore, the use of steel bracing systems for both retrofitting as well as in newly constructed reinforced concrete frames with adequate lateral resistance is attractive.

IV. TYPES OF BRACINGS

There are two types of bracing systems, Concentric Bracing System and Eccentric Bracing System.

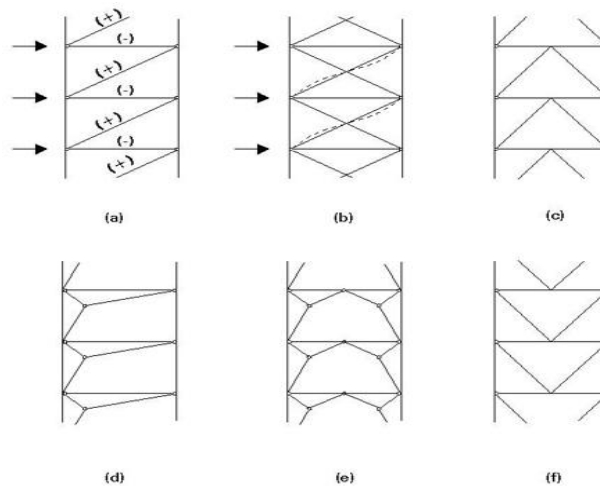


Fig. 1 Type of bracings

The steel braces are usually placed in vertically aligned spans. This system allows obtaining a great increase of stiffness with a minimal added weight, and so it is very effective for structure for which the poor lateral stiffness is the main problem. The concentric bracings increase the lateral stiffness of the frame, thus increasing the natural frequency and also usually decreasing the lateral drift. However, increase in the stiffness may attract a larger inertia force due to earthquake. Further, while the bracing decrease the bending moments and shear forces in columns, they increase the axial compression in the columns to which they are connected. Since reinforced concrete columns are strong in compression, it may not pose a problem in RC frame using concentric steel bracings.

Eccentric Bracings reduce the lateral stiffness of the system and improve the energy dissipation capacity. Due to eccentric connection of the braces to beams, the lateral stiffness of the system depends upon the flexural stiffness of the beams and columns, thus reducing the lateral stiffness of the frame. The vertical component of the bracing forces due to earthquake causes lateral concentrated load on the beams at the point of connection of the eccentric bracings.

V. MODELING

The SAP2000 software is utilized to create 3D model and carry out the analysis. The buildings are modelled as a series of load resisting elements. The dead load, live load and lateral loads to be applied on the buildings are based on the Indian standards. The study is performed for seismic zone V as per IS 1893:2002. The buildings adopted consist of reinforced concrete and brick masonry elements. The frames are assumed to be firmly fixed at the bottom and the soil–structure interaction is neglected.

The six, twelve, and eighteen storied buildings are analysed for zone V without bracing and with diagonal and X type bracings at peripheral columns only.

MODEL DATA OF BUILDING

Structure OMRF	
Plan dimension:	16.229m*11.275m
No. of stories	G + 5, G+11 and G+18
Storey height	3.148 m
Type of building use	Apartment

Material Properties

Young's modulus of M20 concrete, E	22.36 x 10 ⁶ KN/m ²
Grade of concrete	M20
Grade of steel	Fe 415
Density of reinforced concrete	25 KN/ m ³
Density of brick masonry	19.20 KN/ m ³

Member Properties

Thickness of slab	0.125 m.
Thickness of wall	0.23 m.
Dead Load Intensities	
Floor finishes	1.0 KN/ m ²
Live Load Intensities	
Floor	2.0 KN/ m ²

Roof	1.5 KN/ m ²
Floor 0.25 x 3.0	0.75kN/ m ²
Seismic Zone	V
Zone factor, Z	0.36
Importance factor, I	1.00
Response reduction factor, R	5.00

Table 1 Dimension of Beam and Column

Structure	Slab depth	Beam size (m)	Column size(m)
(G+5)	0.125	0.25*0.35	0.45*0.45
(G+11)	0.125	0.30*0.45	0.60*0.60
(G+17)	0.125	0.35*0.50	0.70*0.70

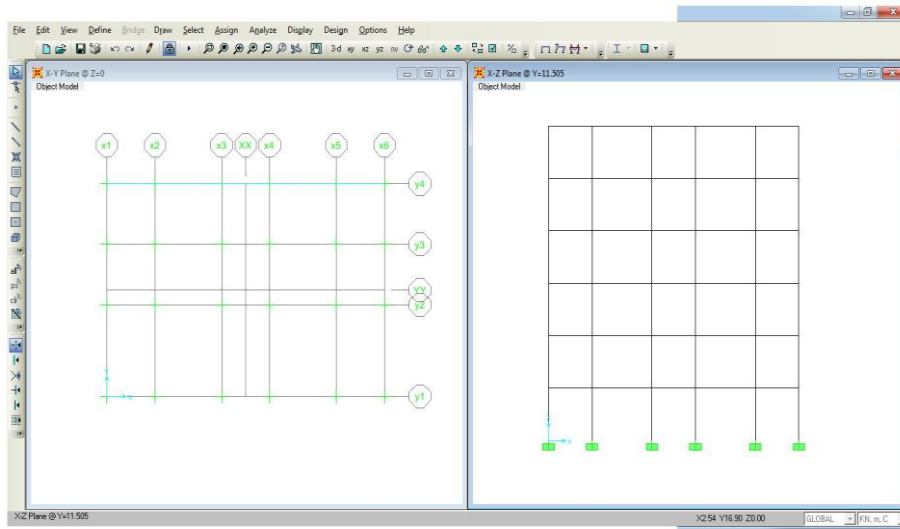


Fig. 2 Plan and elevation of six storey building

VI. RESULTS

Lateral displacements

The lateral displacements of non braced building for the cases of dead live and earthquake load for seismic analysis in all the three directions are presented in Table. The results are compared with that of buildings with various types of concentric bracings. It is observed that the maximum lateral displacements are reduced due to the presence of bracings. It is observed that the lateral displacements are reduced to the largest extent for X type of bracing systems then diagonal one.

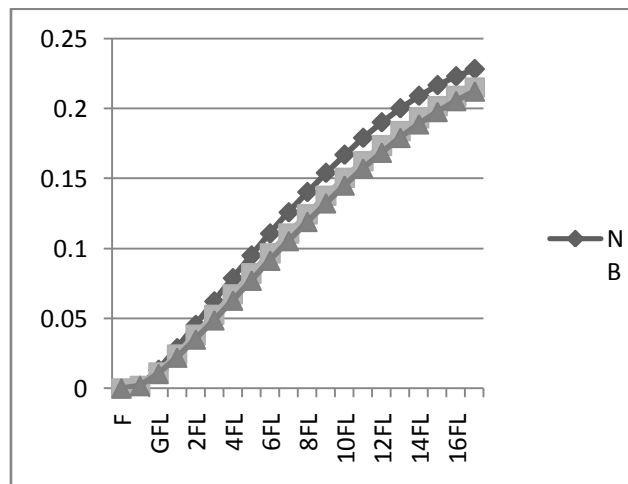


Fig. 3 Lateral deformation curves in X direction (18-Storey)

From the results obtained from building frame, it is observed that among concentric bracing system the X intersection type of bracing system is the most effective type of bracing system which can reduce the lateral displacements and moments in the structures. Therefore, the X type of bracing system can be used for seismic minimizing part of multi storied buildings. For all analysis of six twelve and eighteen storied building frames; X type of bracing system is considered. These buildings are analyzed for earthquake zone V. The lateral displacement is obtained for these structures, for the seismic load along with load combinations. The percentage reduction in lateral displacements is found out for increase in the number of stories. It is observed that the X bracing system reduces the displacements considerably than diagonal one.

Table 2 Maximum bending moment (KNm) for column for zone V

Floor level	Seismic Load			
	NODE	NB	DB	XB
GFL	1	699.24	472.68	396.27
1FL	2	440.20	326.87	273.35
2FL	3	347.93	218.77	180.11
3FL	4	302.25	184.85	150.63
4FL	5	272.38	155.40	123.46
5FL	6	248.79	134.11	104.11
6FL	7	228.86	133.78	89.78
7FL	8	211.04	125.34	79.61
8FL	9	194.45	117.48	72.59
9FL	10	178.17	110.55	67.38
10FL	11	160.99	104.58	62.80
11FL	12	142.01	72.62	58.57
12FL	13	120.38	64.99	54.50
13FL	14	95.81	57.80	50.97
14FL	16	152.29	81.31	64.37
15FL	17	127.90	66.83	51.87
16FL	18	107.93	68.16	60.99
17FL	19	91.20	118.60	109.48

Table 3. Inter storey drift (mm) for 18 storey building for zone V

X	Non Brace		D- Brace		X-Brace	
		Y	X	Y	X	Y
FDN	0.00	0.00	0.00	0.00	0.00	0.00
BASE	3.633	0.183	0.595	0.207	0.464	0.199
GFL	4.905	1.170	3.014	0.943	2.870	0.830
1FL	5.273	1.607	4.081	1.277	3.734	1.109
2FL	5.334	1.745	4.448	1.373	4.140	1.203
3FL	5.272	1.771	4.611	1.408	4.375	1.255
4FL	5.149	1.750	4.673	1.416	4.506	1.284
5FL	4.988	1.708	4.668	1.408	4.558	1.297
6FL	4.800	1.654	4.612	1.389	4.548	1.296
7FL	4.590	1.594	4.513	1.361	4.487	1.284
8FL	4.360	1.529	4.379	1.325	4.382	1.262
9FL	4.108	1.460	4.214	1.281	4.241	1.232
10FL	3.831	1.386	4.020	1.231	4.068	1.193
11FL	3.527	1.304	3.799	1.172	3.866	1.146
12FL	3.190	1.214	3.549	1.104	3.637	1.090
13FL	2.820	1.111	3.272	1.027	3.382	1.026
14FL	2.418	0.996	2.900	0.940	3.104	0.953
15FL	2.003	0.868	2.550	0.900	2.808	0.869
16FL	1.634	0.735	2.297	0.739	2.501	0.785
17FL	1.634	0.616	1.963	0.641	2.185	0.697

Table 4 Percent of reinforcement for 18 storeys

Column	Floor	Reinforcement (%)		
		NB	DB	XB
1	GF	3.99	2.59	2.18
2	1FL	3.03	1.79	1.52
3	2FL	2.46	1.46	1.34
4	3FL	1.87	1.19	1.13
5	4FL	1.41	0.96	0.90
6	5FL	0.91	0.80	0.80
7	6FL	0.80	0.80	0.80
8	7FL	0.80	0.80	0.80
9	8FL	0.80	0.80	0.80
10	9FL	0.80	0.80	0.80
11	10FL	0.80	0.80	0.80
12	11FL	0.80	0.80	0.80
13	12FL	0.80	0.80	0.80
14	13FL	0.80	0.80	0.80
15	14FL	0.80	0.80	0.80
16	15FL	0.80	0.80	0.80
17	16FL	0.80	0.80	0.80
18	17FL	0.80	0.80	0.80

VII. CONCLUSION

- Based on the observation made from analysis of the example buildings, various conclusions may be drawn.
- Stiffness: The bracings in bare frame increases the overall stiffness of the structure Hence performance of braced frame is much better than bare frame.
- Lateral displacement: The lateral displacement in bare frame is more in comparison to the frame with bracings .The bracings prevent the excessive damage in non structural elements. The percent reduced in lateral displacement between DB and XB is from 15% to 8%, similarly in 12 storey frame it reduces by 8% to 9% and so on in 18 storeys.
- Member forces: Significant reduction in moment in case of frame with bracings in comparison to bare frame .Moment reduced by
- 40% to 60% in 6 storey, 20 %to 30% in 12 storey and 35% to 45% in 18 storeys. So comparatively in XB the reduction of member force is higher.
- Reinforcement detailing: Significant reduction in reinforcement demand by the frame members other than the one associated with bracings. The bare frame steel demand is nearly 4% in 18 storey which is not practically possible so it is reduced to 2.58% with (DB) and 2.18% with (XB) similarly in 12 storeys and 6 storey it is reduced as shown in table above.
- Inter storey drift: The performance of frame with bracings is better and within the limit.
- The inter-storey drift is very important parameter in analysis and design of buildings. If the inter-storey drift values at each floor level reach their maximum allowable limits, then the roof displacement will reach undesirable values.
- Maximum ISD for frame without bracings is in storey just above the GF between 2nd and 3rd storey, it is because the frame structure deflects in shear configuration where the rate of change of deflection goes on reducing with height.
- For frame with bracings maximum ISD is found at height nearly to 30%-40% height of the building .Deflection pattern is of flexure shape at lower heights in which rate of deflection increase and follows the shear configuration in upper heights.
- This means the bracings governs flexural deflection, so it is desirable.

REFERENCES

1. Bush T. D., Jones E. A. and Jirsa J. O,(1991) "Behaviour of RC frame strengthened using structural steel bracing", Journal of Structural Engineering, Vol. 117, No.4.
2. Maheri M.R. and Sahebi A., (1997) "Use of steel bracings in reinforced concrete frames", Engineering Structures, Vol. 19, No.12.
3. Abou-Elfath H, Ghobarah A. (2000) "Behaviour of reinforced concrete frames rehabilitated with concentric steel bracing ", Canadian J Civil Eng; 27:433–44.
4. Mahmoud R. Maheri, (2005) "Recent advances in seismic retrofit of RC frames", Asian Journal of Civil Engineering (Building and Housing) Vol. 6, No. 5.
5. Ravikumar G. and Kalyanaraman V (2005) "Seismic design and retrofit of RC multistoried buildings with steel bracings", National Program on Earthquake Engineering Education.
6. Ghaffarzadeh H. and Maheri M.R.,(2006) "Cyclic tests on the internally braced RC frames", Dept. of Civil Engineering, Shiraz University, Shiraz, Iran.
7. Ferraioli, M., Avossa, A.M., Malangone P., (2006) "Performance based assessment of R.C. buildings strengthened with steel braces", Proceedings of the 2nd International Science Congress Naples,Italy .
8. Mahmoud R. Maheri,(2005) "Recent advances in seismic retrofit of RC frames", Asian Journal of Civil Engineering (Building and Housing) Vol. 6.
9. Viswanath K.G , Prakash K.B., Anant Desai(2010) "Seismic Analysis of Steel Braced Reinforced Concrete Frames", International journal of Civil and Structural Engineering ,Vol 1 No1.
10. Parvathaneni Subash, S.Elavenil (2011) "Time history analysis of multi storey building under earthquake ground motions", International journal of Civil, Structural, Environmental and Infrastructure Engineering Research and Development, Vol 1.Issue 2.

A Power Quality Enhancement in a Electric Grid Based Network Using MPFC with Fuzzy Controller

Y. Jhansi¹ K. Mahesh²

¹(M.Tech Student, S.K.T.R.M College of Engineering, Kondair-509125, Mahabubnagar, Andhra Pradesh)

²(EEE Department, S.K.T.R.M College of Engineering, Kondair-509125, Mahabubnagar, Andhra Pradesh)

Abstract: In this paper a novel modulated power filter compensator (MPFC) is used for power quality improvement on transmission side for the smart grid stabilization and efficient utilization. The MPFC is controlled by a novel tri-loop dynamic error driven inter coupled fuzzy controller. The Fuzzy logic controller based on fuzzy logic provides a means of converting a linguistic control strategy based on expert knowledge into automatic control strategy. This paper presents a Digital validation conducted for different cases of load, excursions and fault conditions using the Mat lab/Simulink/Sim-Power software environment without and with the modified power Filter Compensator scheme with fuzzy controller for effective voltage stabilization, power factor correction and transmission line loss reduction.

Keywords: FACTS, Dynamic Voltage stabilization, fuzzy controller, Smart Grid, Stabilization, Efficient, Utilization.

I. INTRODUCTION

The proliferation of microelectronics processors in a wide range of equipments, from home VCRs and digital clocks to automated industrial assembly lines and hospital diagnostics systems has increased the vulnerability of such equipment to power quality problems [1]. These problems include a variety of electrical disturbances, which may originate in several ways and have different effects on various kinds of sensitive loads. As a result of this vulnerability, increasing numbers of industrial and commercial facilities are trying to protect themselves by investing in more sophisticated equipment to improve power quality [2]. Harmonics, voltage sag/swell and persistent quasi steady state harmonics and dynamic switching excursions can result in electric equipment failure, malfunction, hot neutral, ground potential rise, fire and shock hazard in addition to poor power factor and inefficient utilization of electric energy manifested in increase reactive power supply to the hybrid load, poor power factor and severely distorted voltage and current waveforms. To improve the efficiency, capacitors are employed which also leads to the improvement of power factor of the mains [3]. Between the different technical options available to improve power quality, active power filters have proved to be an important alternative to compensate for current and voltage disturbances in power distribution systems [4], [5], [6]. Different active power filters topologies have been presented in the technical literature, [7] [8] and many of them are already available in the market [1], [2]. Modern active filters are superior in filtering performance smaller in physical size, and more flexible in application, compared to traditional passive filters [9], [10]. The shunt active filters are used for

providing compensation of harmonics, reactive power and/or neutral current in ac networks, regulation of terminal voltage, suppression of the voltage flicker, and to improve voltage balance in three-phase system [11], [12]. Hybrid filters effectively mitigate the problems of both passive filters and pure active filter and provide cost effective and practical harmonic compensation approach, particularly for high power nonlinear loads. The combination of low cost passive filters and control capability of small rating active filter effectively improve the compensation characteristics of passive filters and hence reduce the rating of the active filters, compared to pure shunt or series active filter solutions [13]-[15]. Many power filter compensation configurations are proposed in literature to enhance power quality and to improve power factor [16]-[18]. This paper explores design and analysis of a novel modulated power filter compensator along with fuzzy controller (Mamdani rule base) for efficient stabilization and utilization. Fuzzy inference systems have been successfully applied in fields such as automatic control, data classification, decision analysis, expert systems, and computer vision [19], [20]. Because of its multidisciplinary nature, fuzzy inference systems are associated with a number of names, such as fuzzy-rule-based systems, fuzzy expert systems, and fuzzy logic controllers [21]. The Mamdani rule base is a crisp model of a system, i.e. it takes crisp inputs and produces crisp outputs. It does this with the use of user-defined fuzzy rules on user-defined fuzzy variables. The idea behind using a Mamdani rule base to model crisp system behavior is that the rules for many Systems can be easily described by humans in terms of fuzzy variables. Thus we can effectively model a complex non-linear system, with common-sense rules on fuzzy variables [22], [23]. The proposed scheme proved success in improving the power quality, enhancing power factor, reduce transmission losses and limit transient over voltage and inrush current conditions. The paper is organized in seven sections. Section II deals with the Modified power filter compensator. Section III Tri loop error driven fuzzy controller with mat lab models. Ac study system is presented in Section IV. Section V presents the Digital simulation results when different loads are applied, Section VI concludes the work.

II. MODIFIED POWER FILTER COMPENSATOR

The low cost modulated dynamic series-shunt power filter and compensator is a switched type filter, used to provide measured filtering in addition to reactive Compensation. The modulated power filter and compensator is controlled by the on-off timing sequence of the Pulse Width Modulation (PWM)

switching pulses that are generated by the dynamic tri loop error driven fuzzy controller. The fuzzy controller is equipped with a error and error-sequenced compensation loop for fast effective dynamic response in addition to modified PID activation. This scheme of MPFC structure comprises a aeries fixed capacitor bank and two shunt fixed capacitor banks are connected to a

modulated PWM switched tuned arm filter through six pulse uncontrolled rectifier. The mat lab model of this scheme structure is shown in Fig. 1

III. T R I L O O P E R R O R D R I V E N F U Z Z Y C O N T R O L L E R

The tri-loop error-driven fuzzy controller is a novel dual action control used to modulate the power filter compensator [24], [25]. The global error signal is an input to the fuzzy controller to regulate the modulating control signal to the PWM switching block as shown in Figs. 2a & 2b. The fuzzy controller includes an error sequential activation supplementary loop to ensure fast dynamic response and affective damping of large excursion, in addition to modified PID structure.

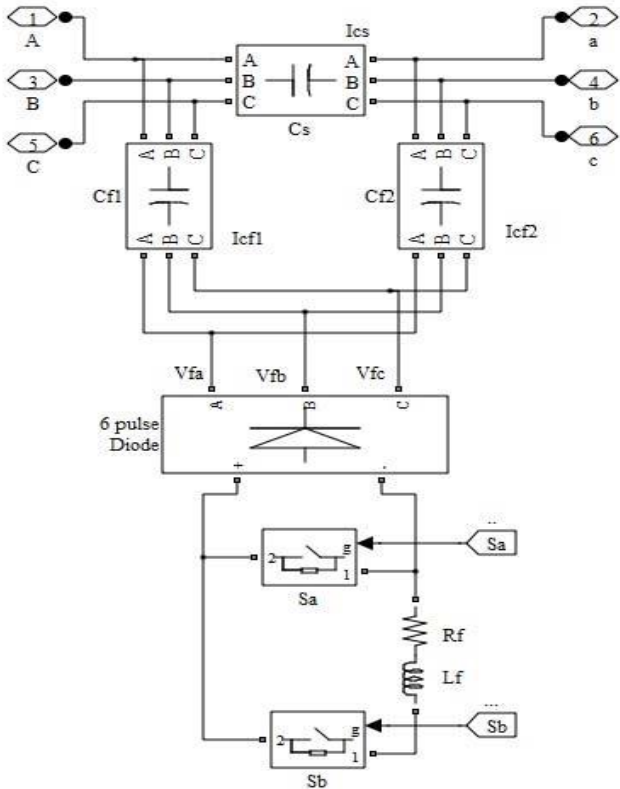


Fig. 1: Modified power filter compensator

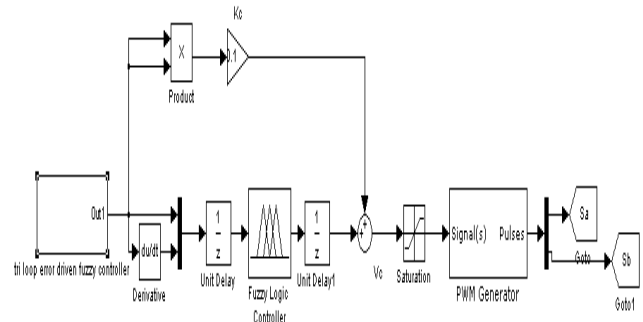


Fig. 2a Modified tri loop error driven fuzzy controller

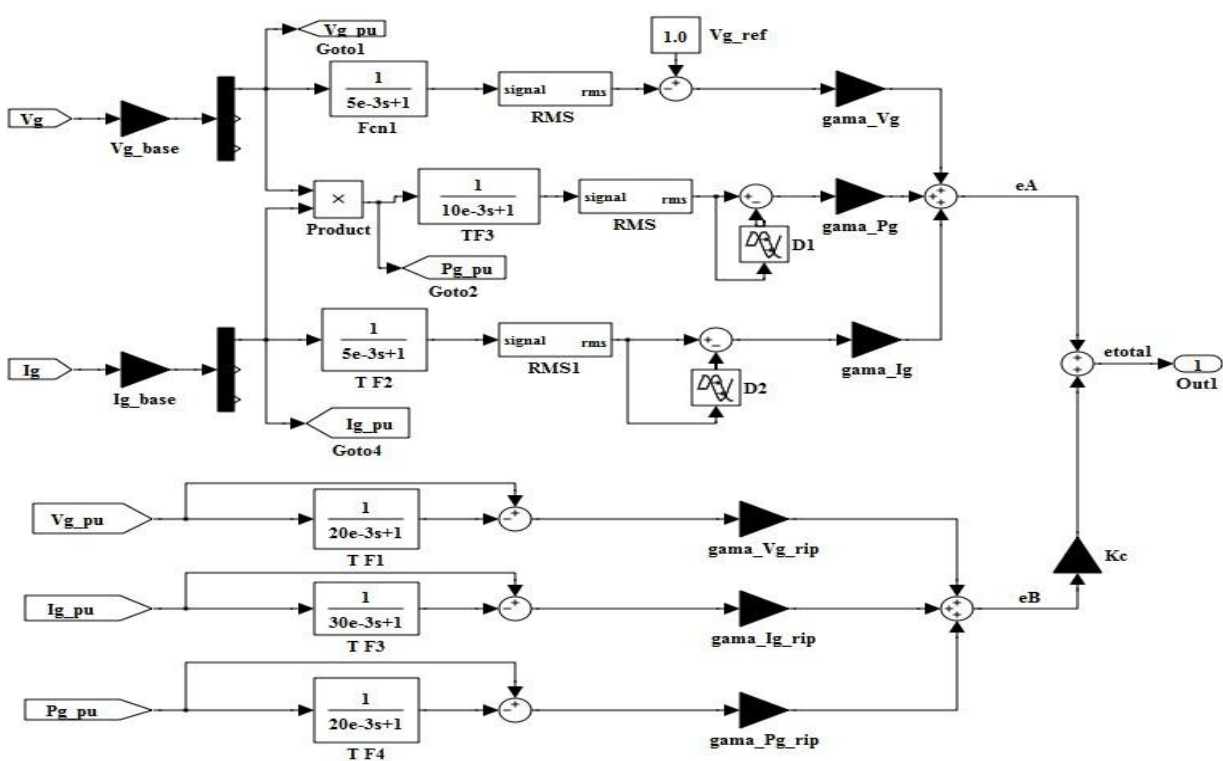


Fig. 2b Mat lab functional model of the Inter-coupled tri loop error driven fuzzy controller.

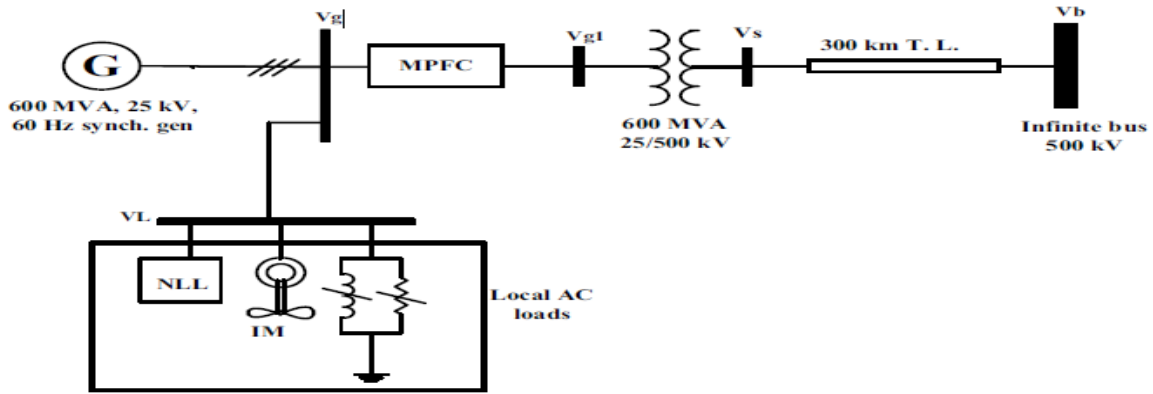


Fig. 3 The single line diagram of the unified EHV study AC system

IV. AC STUDY SYSTEM

The sample study AC grid network is shown in Fig. 3. It comprises a synchronous generator (driven by steam turbine) delivers the power to a local hybrid load (linear, non-linear and induction motor load) and is connected to an infinite bus through 300 km transmission line. The system, compensator parameters are given in the Appendix.

V. DIGITAL SIMULATION RESULTS

The Mat lab digital simulation results using MATLAB/SIMULINK/Sim-power Software Environment for proposed MPFC Scheme under three different study cases are:

A. Normal Loading Operating Case:

The dynamic responses of voltage, current, reactive power, power factor, $(THD)_V$, $(THD)_i$, $(FFT)_V$ and $(FFT)_i$ at generator bus (V_g), load bus (V_L) and infinite bus (V_b) under normal operation are shown Figs. 4-13. The RMS of voltage and current waveforms of the MPFC are shown in Fig. 14 and Fig. 15. The modulated tuned power filter switching signals that are generated by the dynamic tri loop error driven fuzzy controller are shown in Fig16. The stable voltage signal of synchronous generator power system stabilization (PSS) is depicted in Fig. 17. The Transmission line losses are shown in Table I.

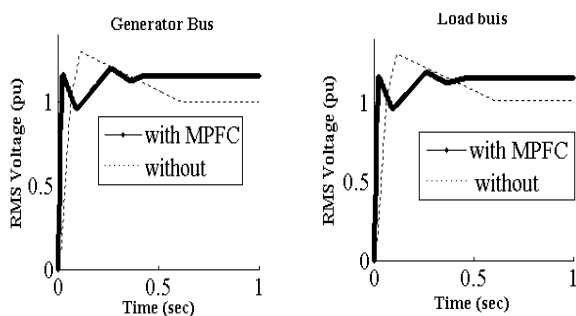


Fig. 4 The RMS voltage at AC buses under normal operation

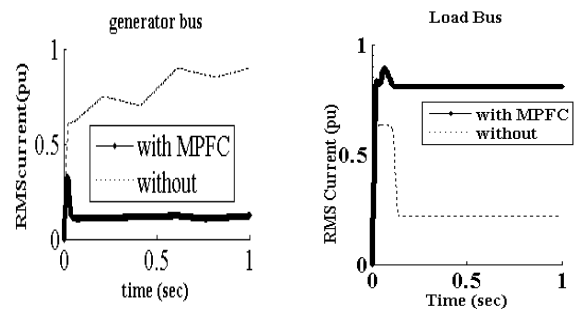


Fig. 5 The RMS current at AC buses under normal operation

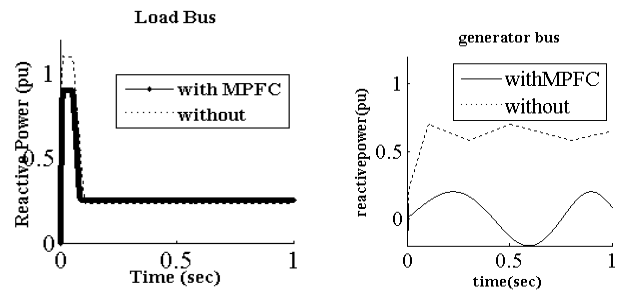


Fig. 6 The reactive power at AC buses under normal operation

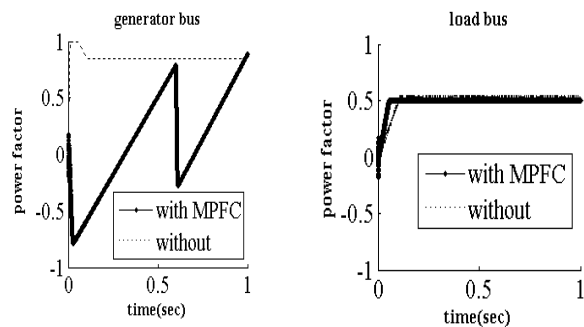


Fig. 7 The power factor at AC buses under normal operation

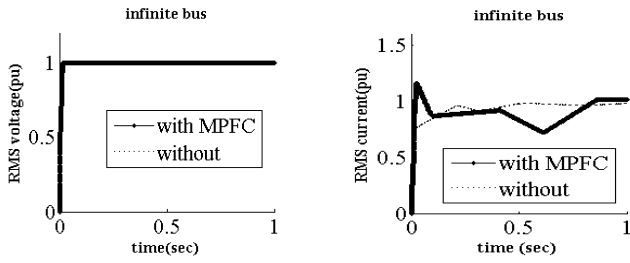


Fig. 8 The RMS voltage and current at the infinite bus under normal operation.

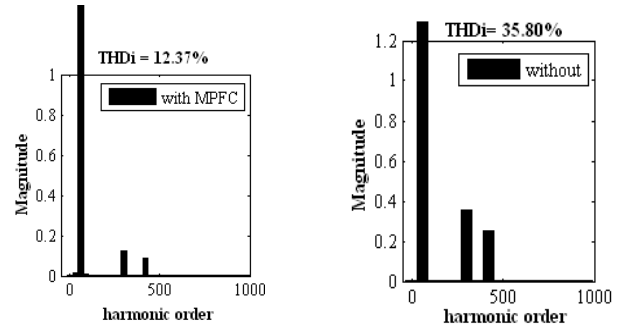


Fig. 13 THD and FFT of current waveforms at the infinite bus

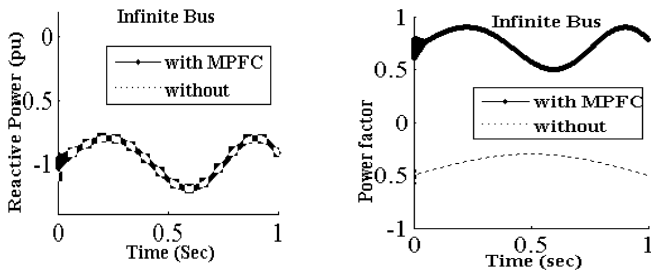


Fig. 9 The reactive power and power factor at the infinite bus under normal operation.

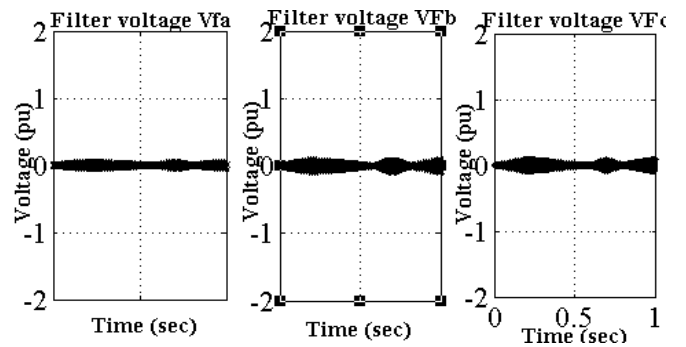


Fig. 14 The voltage waveforms of MPFC

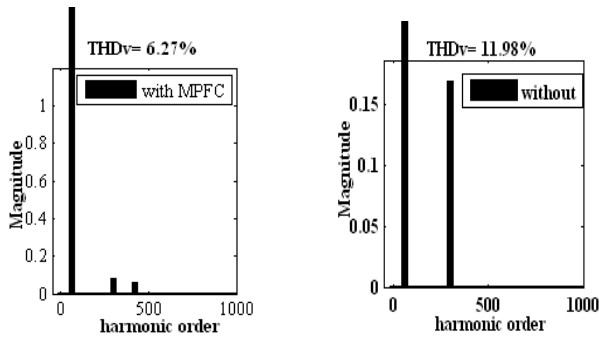


Fig. 10 THD and FFT of voltage waveforms at the load bus

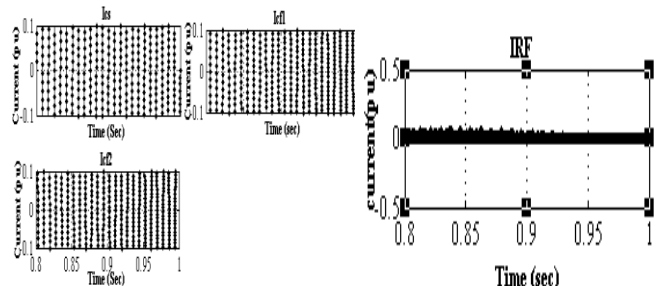


Fig. 15 The current waveforms of MPFC

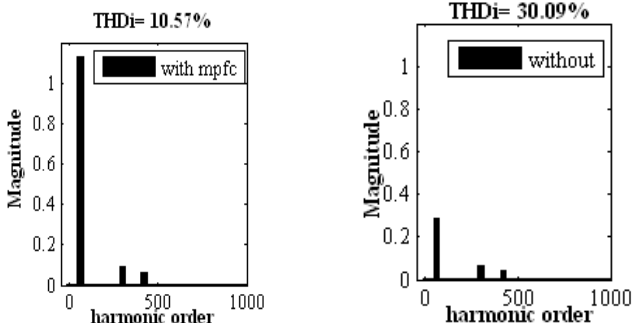


Fig. 11 THD and FFT of current waveforms at the load bus

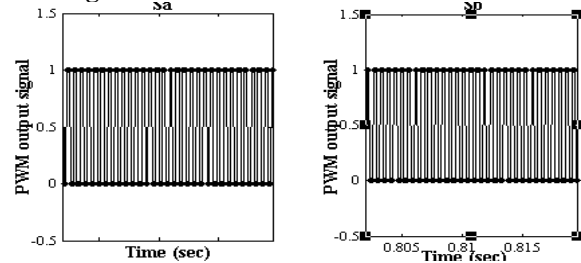


Fig. 16 Sa and Sb pulsing signals method

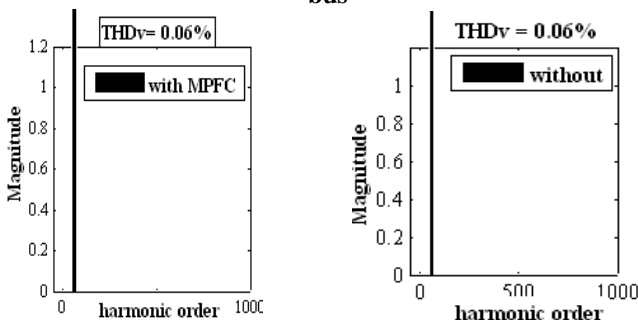


Fig. 12 THD and FFT of voltage waveforms at the infinite bus

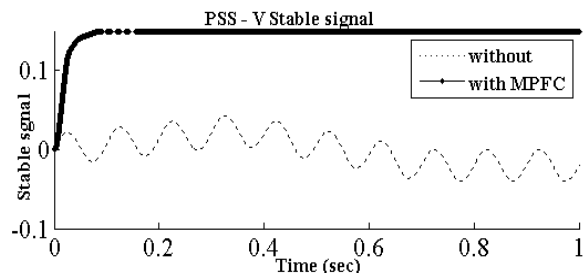


Fig. 17 PSS stable voltage signal

The previous figures confirm the compensation effectiveness as well as the harmonic filtering of the proposed MPFC.

B Short Circuit Fault Condition Case:

A three phase short circuit (SC) fault is occurred at bus V_s as shown in Fig. 3, for a duration of 0.1sec, from t=0.2 sec to t=0.3 sec. The RMS of voltage and current waveforms at generator and load buses are depicted in Figs. 18 & 19.

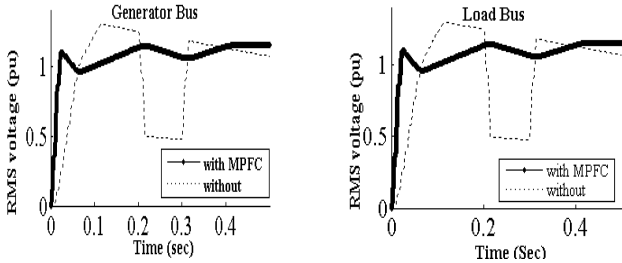


Fig. 18 The RMS Voltage at generator and load buses under short circuit (SC) fault condition at bus V_s

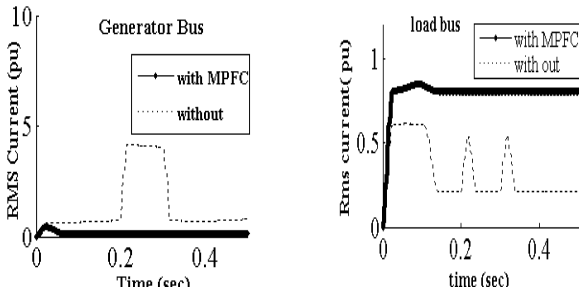


Fig. 19 The RMS current at generator and load buses under short circuit (SC) fault condition at bus V_s

As shown in figs.18&19, with using the proposed MPFC scheme, the remote short circuit fault has not any effect on the values of RMS voltage and RMS current of generator and load buses, so these schemes can be considered a good power quality mitigation method.

C Hybrid Local Load Excursions Case:

The real time dynamic responses of the system for a load excursion are obtained for the following time sequences

- At t = 0.1 sec, linear load is disconnected for a duration of 0.05 sec
- At t = 0.2 sec, nonlinear load is disconnected for a duration of 0.05 sec
- At t = 0.3 sec, the induction motor torque is decreased by 50% for a duration 0.05 sec.
- At t = 0.4 sec, the induction motor torque is Increased by 50% for duration 0.05 sec.

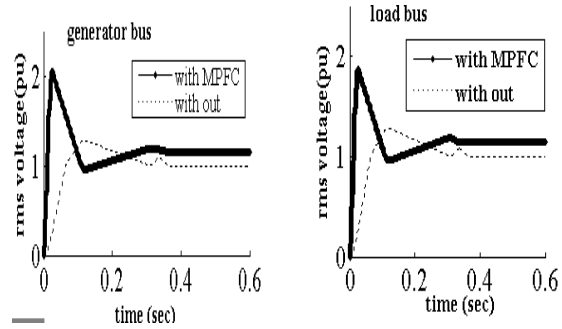


Fig. 20 The RMS voltage waveform at the generator and load buses under load excursions

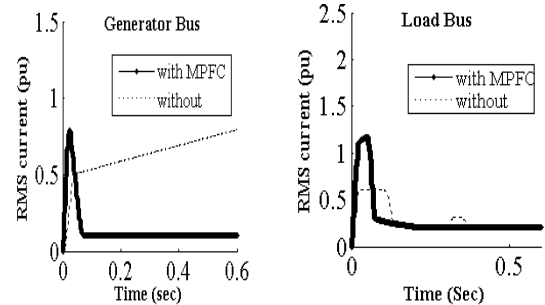


Fig. 21 The RMS current waveform at the generator and load buses Under load excursion

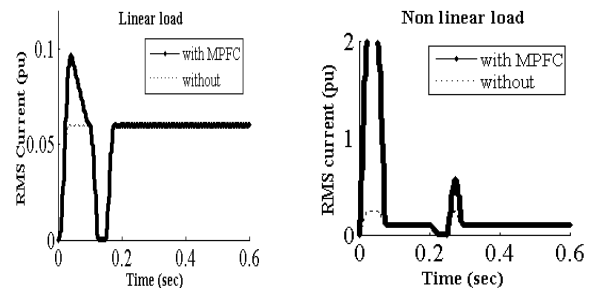


Fig. 22 The linear and nonlinear load RMS current waveforms

The RMS of voltage and current waveforms at generator and load buses under load excursions are depicted in Figs 20 & 21. The linear and nonlinear load RMS current waveforms are shown in Fig. 22 and the speed-torque relationship of induction motor (IM) is shown in Fig. 23.

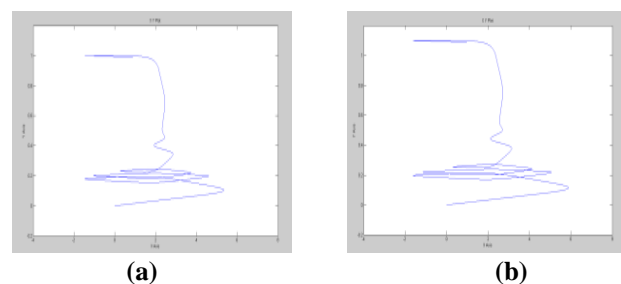


Fig. 23 The speed-torque relationship of the induction motor with (a) and without mpfc (b)

TABLE I THE TRANSMISSION LINE LOSSES

		PLoss	Qloss	Sloss
Case 1	without	0.0832	0.1542	0.1752
	with	0.008	0.005	0.005064
Case 2	without	0.1954	0.3467	0.398
	with	0.0008	0.005	0.005064
Case 3	without	0.1018	0.1869	0.2128
	with	0.0009	0.0045	0.004589

Comparing the dynamic response results without and with using the proposed MPFC under three study cases; normal operation, short circuit fault conditions and hybrid load excursion, it is quite apparent that the proposed MPFC enhanced the power quality, improved power factor voltage and reduced the transmission line losses.

VI. CONCLUSION

This paper presents a novel modulated switched power filter compensator (MPFC) scheme is controlled by a dynamic tri-loop dynamic error driven fuzzy controller. The proposed FACTS based scheme can be extended to other distributed/dispersed renewable energy interface and utilization systems and can be easily modified for other specific compensation requirements, voltage stabilization and efficient utilization. The proposed MPFC scheme has been validated for effective power quality improvement, voltage stabilization, and power factor correction and transmission line loss reduction when the system is extensively simulated in MATLAB/SIMULINK.

APPENDIX

1) Steam turbine

$P_{out} = 600$ MW, speed = 3600 rpm.

2) Synchronous generator

3 phase, 1 pair of poles, $V_g = 25$ kV (L-L), $S_g = 600$ MVA, $X_d = 1.79$, $X_d' = 0.169$, $X_d'' = 0.135$, $X_q = 1.71$, $X_q' = 0.228$, $X_q'' = 0.2$, $X_l = 0.13$.

3) Local Hybrid AC Load (90 MVA)

Linear load: 30 MVA, 0.85 lag pf.

Non-linear load: $P = 20$ kW, $Q = 22.4$ MVAR. Induction motor: 3phase, 30 MVA, no of poles=4, Stator resistance and leakage inductance (Pu)

$R_s = 0.01965$, $L_s = 0.0397$

Rotor resistance and leakage inductance (Pu)

$R_r = 0.01909$, $L_r = 0.0397$

Mutual inductance L_m (Pu) = 1.354

4) Transmission Line

$V_{L-L} = 500$ kV, 300 km length, $R/km = 0.01273$ Ω , $L/km = 0.9337$ mH

5) Infinte Bus: $V_{L-L} = 500$ kV

6) MPFC: $C_s = 30\mu F$, $C_{f1} = C_{f2} = 125\mu F$, $R_f = 0.25\Omega$, $L_f = 3mH$

REFERENCES

- [1] K. Eichert, T. Mangold, M. Weinhold, "Power Quality Issues and their Solution", in *VII Seminario de Electrónica de Potencia*, Valparaíso, Chile, Abril 1999.
- [2] M. Rahmani, A. Arora, R. Pfister, P. Huencho, "State of the Art Power Quality Devices and Innovative Concepts", in *VII Seminario de Electrónica de Potencia*, Valparaíso, Chile, Abril 1999.
- [3] A.M. Sharaf, Hong Huang, Liuchen Chang, "Power quality and nonlinear load voltage stabilization using error-driven switched passive power filter", *Proc of the IEEE Inter. Symp.on Industrial Electronics*, pp 616-621, 1995
- [4] G. Joos, L. Morán, "Principles of Active Power Filters", *Tutorial Course Note. of IEEE Ind. Appl. Society Annual Meeting*, Oct. 1998.
- [5] W. M. Grady, M.J. Samotyj, A. H. Noyola, "Survey of Active Power Line Conditioning Methodologies," in *IEEE Trans. on Power Delivery*, vol. 5, no 3, pp.1536-1542, July 1990.
- [6] H. Akagi, "New Trends in Active Filters for Power Conditioning," in *IEEE Trans. on Industry Applications*, vol. 32, no.6, pp1312-1322, Nov./Dec. 1996.
- [7] M. Aredes, K. Heuman and E. Watanabe, "An Universal Active Power Line Conditioner," in *IEEE Trans. on Power Delivery*, vol. 13, no 2, pp. 545-551, April 1998.
- [8] L. Morán, L. Fernández, J. Dixon, R. Wallace, "A Simple and Low Cost Control Strategy for Active Power Filters Connected in Cascade", in *IEEE Trans. on Industrial Electronics*, vol. 44, no. 5, pp.621-629, Oct. 1997.
- [9] A. Ametani, "Harmonic reduction in thyristor converters by harmonic current injection", *IEEE Trans. power Appl.syst.* 95 (2), 441-449 (1976)
- [10] L. Gyugi, and E.C.Strycula, "Active ac power filters", *IEEE-IAS Ann, Meeting*, 529-535 (1976)
- [11] H. Fujita and H. Akagi, "A practical approach to harmonic compensation in power system-series connection of passive, active filters," *IEEE Trans. Ind. Applicat.*, vol. 27, no. 6, pp.1020-1025, Nov./Dec. 1991.
- [12] A. M. Sharaf, Caixia Guo and Hong Huang, "Distribution/Utilization system voltage stabilization and power quality enhancement using intelligent smart filter", *UPEC'95*, England, UK, 1995.
- [13] M. Aredes, K. Heumann, and E. H. Watanabe, "An universal active power line conditioner," *IEEE Trans. Power Delivery*, vol. 13, no. 2, pp. 545-557, Apr. 1998.
- [14] M. Rastogi, N. Mohan, and A.-A. Edris, "Hybrid-active Filtering of harmonic currents in power systems," *IEEE Trans. Power Delivery*, vol. 10, no. 4, pp. 1994-2000, Oct. 1995.
- [15] H. Fujita and H. Akagi, "A hybrid active filter for damping of harmonic resonance in industrial power system," *IEEE Trans. Power Electron.*, vol. 15, no. 2, pp. 215-222, Mar. 2000.
- [16] A. M. Sharaf, and G. Wang, "Wind Energy System Voltage and Energy Enhancement using Low Cost Dynamic Capacitor Compensation Scheme."

Proceedings of the IEEE International Conference on Electrical, Electronic and Computer Engineering. pp. 804-807, 5-7 Sept. 2004.

- [17] A. M. Sharaf and Khaled Abo-Al-Ez, "A FACTS Based Dynamic Capacitor Scheme for Voltage Compensation and Power Quality Enhancement", *Proceedings of the IEEEISIE 2006 Conference*, Montreal, Quebec Canada, July 2006.
- [18] A. Sharaf, R. Chhetri, "A novel dynamic capacitor compensator/green plug scheme for 3-phase 4-wire utilization loads", *Proceeding IEEE-CCECE conference*, Ottawa, Ontario, Canada 2006.
- [19] L. A. Zadeh, "fuzzy sets," *Informat. control*. vol.8. pp. 338-353
- [20] Jang, J.-S. R. and C.-T. Sun, *Neuro-Fuzzy and Soft Computing: A Computational Approach to Learning and Machine Intelligence*, Prentice Hall, 1997.
- [21] Mamdani, E.H. and S. Assilian, "An experiment in linguistic synthesis with a fuzzy logic controller," *International Journal of Man-Machine Studies*, Vol. 7, No. 1, pp. 1-13, 1975.
- [22] Sugeno, M., *Industrial applications of fuzzy control*, Elsevier Science Pub. Co., 1985.
- [23] Zadeh, L.A., "Outline of a new approach to the analysis of complex systems and decision processes," *IEEE Transactions on Systems, Man, and Cybernetics*, Vol. 3, No. 1, pp. 28-44, Jan. 1973.
- [24] A. M. Sharaf, Hassan A.Mahasneh and Yevgen Biletskiy, "Energy Efficient Enhancement in AC Utilization Systems" *The 2007 IEEE Canadian Conference on Electrical and Computer Eng*
- [25] A. M. Sharaf, W. Wang, and I.H. Altas, "A Novel Modulated Power Filter Compensator for Distribution Networks with Distributed Wind Energy." *International Journal of Emerging Electric Power Systems*. Vol. 8, Issue 3, Article 6, Aug. 2007.

BIOGRAPHIES



Y. Jhansi is born in 1988 in India. She is graduated from JNTU Hyderabad in 2009. Presently she is doing Post graduation in Electrical Power Systems Specialization at J.N.T.U.H, Hyderabad. Her main areas of interest include Electrical machines, Power systems, Power Electronics & FACTS.



K. Mahesh. M.Tech, working as Associate Professor in S.K.T.R.M College of Engineering, Affiliated to JNTUH, Approved by AICTE. New Delhi. He completed his M.Tech in 2003 from JNTU. He has nine years teaching experience in Electrical Engineering. He has published three Conferences in electrical engineering.

MRI images de-noising based in Dual-Tree complex Wavelet and Bayesian MAP Estimator

R.Mavudila¹, Lh.Masmoudi², M.Cherkaoui³, N.Hassanain⁴

(physics department ,LETS Laboratory /Faculty of Science/, Mohammed V University/Morocco)

(physics department ,LETS Laboratory /Faculty of Science/, Mohammed V University/Morocco)

(Faculty of medicine and pharmacy/, SIDI Mohammed Ben Abdellah University/CHU CheikZaid/ Morocco)

(physics department ,LETS Laboratory /Faculty of Science/, Mohammed V University/Morocco)

ABSTRACT: MRI images are often subject to noise (artifacts). We evaluated the performance of DT-CWT combined to Bayesian MAP Estimator to restore those images.

We chose the images from two of four sequences commonly used in coronal and axial MRI with and without contrast agent. The image with contrast agent was used as a reference, and the image without where we added artificially noise was subjected to de-noising by forward Dual-Tree Wavelet Transform (DT-CWT) combined to Bayesian MAP estimator. A test was submitted to radiologists for an assessment of the de-noised images to compare the proposed algorithm to other effective techniques from the recent literature using MRI images. Our approach contributed effectively to the MRI images de-noising, with better results. In general, wavelets and Bayesian estimator contributed effectively to the de-noising process and to other image processing methods, but ranging from classic to complex wavelet transforms, the results gradually improved.

Keywords: Bayesian MAP, Complex Wavelet, Dual-Tree Wavelet transform, Image de-noising, MRI images.

I. INTRODUCTION

The digital representation of images has been controversial since the early days of computing. Because images are innately strong in semantic content, they quickly became a frequently used communication medium.

Images are also an essential tool in the fields of biomedicine and satellite and astronomical imaging, among others.

Medical imaging has revolutionized medicine by allowing doctors to retrieve potentially vital information from inside the human body in a noninvasive manner, as is the case for MRI that we focused on in our study. In Magnetic resonance, the practical limits of the acquisition time impose a trade-off between the SNR and the image resolution [1,2,3]

In this paper, we address the problem of MRI images de-noising.

In MRI, acquisition protocols lead to image quality loss, particularly with contrast, because of the presence of artifacts that make their interpretation difficult [4,6] and this noise in the MRI image magnitude is Rician [5], having a signal dependent mean.

Many challengers have been made to remove this noise using wavelet transform as described briefly.

WiemFourati and Mohammed Salim. B (2007) proposed a de-noising method based on the statistical dependency of wavelet coefficients and on the application of an adaptive Bivshrink type MAP filter (Maximum Posterior Estimator) [7].

From a method described by Donoho, Alendru in [9]. I and al. have proposed a de-noising scheme based on a wavelet transform named discrete wavelet transform with enriched diversity (TODDE), combining several families of wavelets and various estimators in Bishrink occurrence to eliminate the noise (speckle) in the images, which also applies to ultrasound images [8].

Previously proposed wavelet domain filtering techniques were based on different thresholding schemes where the coefficient selection was based on inter-scale correlations [5,11,12],

It was noted that due to the signal dependent mean of the Rician noise, both wavelet and scaling coefficients of a noisy MRI image are biased estimates of their noise-free counterparts [5].

In addition it was shown that one can efficiently overcome this problem by filtering the square of the MRI image in wavelet domain.

In the wavelet domain, the Discrete Wavelet Transform (DWT) has a limits and major disadvantages that undermines its application for some image processing as; lack of shift invariance, poor directional selectivity for diagonal features and other.. [10].

A comprehensive review of previous work shows the performance of these tools for image de-noising, although performance suffers from the classical wavelet limits of certain processing treatments, especially for the specificity of medical images.

The objective of this study was to use the DT-CWT and Bayesian approach that is based on a Symmetric Normal Inverse Gaussian (SNIG) [13] this model is useful for smoothing disease relative risk estimates.

The object is to de-noise images, in which the use of contrast agents could have affected the distinct visualization of healthy and pathological tissues.

The images with contrast agent were used as controls, and the images without contrast were used as images to restore, with the aim of obtaining images similar to the ones with contrast agent. In spite of existing mathematical methods, such as PSNR, correlation, and so forth, we used a human visual system (HSV), consisting of a blind test based on specific and precise criteria such as quality, sharpness, and the clinicians' ability to arrive at a correct diagnosis.

The paper is organized as follows: In the next section, we first described briefly the DT-CWT with has advantages in noise study, Section III provides some necessary preliminaries on Bayesian MAP Estimator, as Symmetric Normal Inverse Gaussian (SNIG) processes and presents results on the modeling that indicating their heavy-tailed nature. The design of a Bayesian estimator that exploits the signal. The proposed method and choice of MRI is described in section IV. Section V compares the performance of our proposed algorithm with the performance of current de-noising methods, and quantifies the achieved performance improvement. Finally we conclude.

II. DUAL-TREE COMPLEX WAVELET TRANSFORM (DT-CWT).

Remember that the classical discrete wavelet transform (DWT) provides a means of implementing a multiscale analysis, based on a critically sampled filter bank with perfect reconstruction [14] [15].

However, questions arise regarding the good qualities or properties of the wavelets and the results obtained using these tools, the standard DWT suffers from the following problems described as below:

Shift sensitivity: it has been observed that DWT is seriously disadvantaged by the shift sensitivity that arises from down samples in the DWT implementation [16,17].

Poor directionality: an m-dimension transform (m>1) suffers poor directionality when the transform coefficients reveal only a few feature in the spatial domain.

Absence of phase information: filtering the image with DWT increases its size and adds phase distortions; human visual system is sensitive to phase distortion [18]. Such DWT implementations cannot provide the local phase information.

In other applications, and for certain types of images, it is necessary to think of other, more complex wavelets, who gives a good way, because the complex wavelets filters which can be made to suppress negative frequency components. As we shall see the CWT has improved shift-invariance and directional selectivity [19].

The discrete complex dual tree wavelet transform (DT-CWT) was introduced by N. Kingsburg around in 1990.

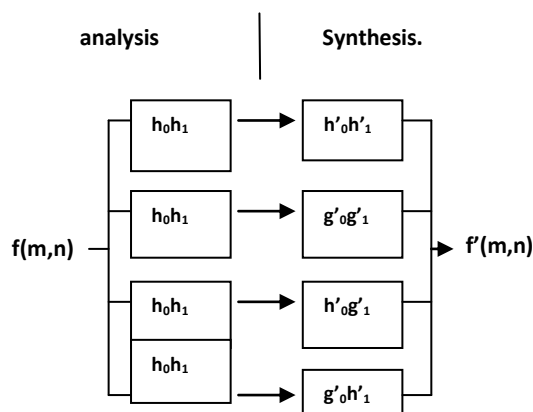
This implementation uses consists in analyzing the signal by two different DWT trees, with filters chosen so that at the end, the signal returns with the approximate decomposition by an analytical wavelet.

The dual-tree structure has an extension of conjugate filtering in 2-D case; this structure is shown in "Fig.1".

This structure needs four trees for analysis as well as for synthesis. The pairs of conjugate filters are applied to two dimensions (0 and 1), which can be expressed as:

$$(h_0 + jg_0)(h_1 + jg_1) = (h_0h_1 - g_0g_1) + j(h_0g_1 + g_0h_1) \tag{1}$$

The synthesis of filters suitable for this structure was performed by several people.



Imaginary trees

Figure.1. Filter bank structure for DT-DWT

The wavelet corresponding to the tree's "imaginary part" is very close to the Hilbert transform of the wavelet corresponding to the tree's "real part" [20].

For J level decomposition, the corresponding details subbands at leven η are denoted :HLη^{real},

$$HLη^{im}, LHη^{real}, LHη^{im}, HHη^{real} and HHη^{im}.$$

Where η = 1,2,...,J.

Because of the existence of two trees, it appears that the second noise coefficients moments from such decomposition can be precisely characterized.

The DT-CWT ensures filtering of the results without distortion and with a good ability for the localization function and the perfect reconstruction (PR) of signal.

In the noise study, as with any redundant frame analysis, when a stationary noise, even if white, is subject to a dual decomposition tree, statistical dependencies appear between coefficients [12,18,19], because of the existence of two trees, it appears that the second noise coefficients moments from such decomposition can be precisely characterized.

We observe a de-correlation between primal and dual coefficients located at the same spatial position and an inter-scale correlation, which allows us to choose between several estimators, taking this phenomenon into account.

If we consider an image degraded by a Gaussian n, white, and centered, additive Gaussian noise with a spectral density, the decomposition coefficients are also affected by that same noise as part of the linearity property [22, 20, and 28].

With this advantage we can choose an appropriate estimator for de-noising and the case of DT-DWT

The mathematical expression for a signal observed at point whose coordinates (x,y) in the image is modeled as follows:

$$g(x,y) = f(x,y) + \epsilon(x,y) \tag{2}$$

With g(x,y), f(x,y) and ε(x,y) are respectively the noise coefficient, the original coefficient, and the

Gaussian independent noise. Our goal is to estimate f from g . To do this, we will use an MPE (Maximum Posterior Estimator) filter [7].

In considering the linearity Property In the noise study, as with any redundant frame analysis, when a stationary noise, even if white, is subject to a dual decomposition tree, statistical dependencies appear between coefficients [26,27].

After applying the DT-CWT on (2), we obtain:

$$g_{\eta}(x, y) = f_{\eta}(x, y) + \varepsilon\eta(x, y) \quad (3),$$

Where, $g_{\eta}(x, y)$, $f_{\eta}(x, y)$ and $\varepsilon\eta(x, y)$ denote (x, y) -th wavelet coefficient at level of a particular detail subband of the DT-CWT of g , f , and ε , respectively and η ($\eta=1, 2, \dots, J$).

III. BAYESIAN MAP ESTIMATOR

It is recognized that parametric Bayesian processing presupposes proper modeling for the prior probability density function (PDF) of the signal.

Bayesian models use prior distributions for parameters, this prior can be multi-level and has distributions can control the model results

In this section we describe the Symmetric Normal Inverse Gaussian (SNIG) distribution and some it proprieties before presenting the model, we refer the reader to a recent work of M. I. H. Bhuiyan et al [13,23]. showed that distributions, a family of heavy-tailed densities, are sufficiently flexible and rich to appropriately mode wavelet coefficients of images in image de-noising applications with better models the prior statistics of the signal components, its probability density function reads as follows [23]:

$$P_f(f) = A \frac{K_1(\alpha\sqrt{\delta^2+f^2})}{\sqrt{\delta^2+f^2}} \quad (4)$$

Where $A = \frac{\alpha \delta \exp(\delta \alpha)}{\pi}$, K_1 denotes the modified Bessel function of second kind with index 1 [24], the parameter α control the shape of the distribution and δ is the a scale parameter. IN additional to illustrate the efficiency of the proposed prior, the generally Gaussian (GG) and SNIG PDFs are fitted to wavelet coefficients of the subbands $HH^{real}1$ for the medical image. Since in DT-CWT, we applied two real DWT, we assure the distribution of the noise coefficients in each DWT is a Gaussian with zero mean and standard deviation σ_{ε}^2 , and denote it by $P_{\varepsilon}(\varepsilon)$.

The Bayesian MAP estimator is given by [8] as follow:

$$\hat{x}(g) = \arg \max P_{\varepsilon}(g - f)P_f(f) \quad (5)$$

To obtain the MAP estimate, the derivative of the logarithm of the in (5) is the st to resulting in:

$$\frac{x-y}{\sigma^2} + p'(f) = 0 \quad (6)$$

Where $p(f) = \ln P_f(f)$ and $p'(f) = \frac{\partial}{\partial f} p(f)$. Using the approach proposed by Hyvarinen [25], an approximate solution of [7] is obtained as:

$$\hat{x}(g) \text{sign}(g) \max(|g| - \sigma_{\eta}^2 |B|, 0) \quad (7) \text{Where}$$

$$B = \frac{2g}{\delta^2+g^2} + \frac{\alpha g}{\sqrt{\delta^2+g^2}} \frac{K_0(\alpha\sqrt{\delta^2+g^2})}{K_1(\alpha\sqrt{\delta^2+g^2})} \quad (8)$$

In this step we need to estimate the parameters α , δ and σ_{η}^2 to obtain the MAP estimates. In order to take noise correction into account for each real DWT tree of the DT-CWT. The corresponding value of σ_{η} is obtained using the coefficients in the corresponding finestsubbands of diagonal orientation as:

$$C = C \frac{D_1+D_2}{2} \quad (9) \text{Where } D_1 = \text{MAD}(g(k,l)) / 0,6745, g(k,l) \in \text{HH1 and}$$

$D_2 = \text{MAD}(g(k,l)) / 0,6745, g(k,l) \in \text{HH2}$, C is a smoothing factor, (MAD is the Median absolute deviation).

To obtain the SNIG parameters for the (k, l) -th coefficient, the estimates of the second and fourth order signal moments denoted by $\widehat{m}_2(k, l)$ and $\widehat{m}_4(k, l)$, respectively, as obtained as:

$$\widehat{m}_2(k, l) = \max((m_2(k, l) - \sigma_{\eta}^2), 0) \quad (10)$$

$$\widehat{m}_4(k, l) = \max((m_4(k, l) - \sigma_{\eta}^2 m_2(k, l) - 3\sigma_{\eta}^4), 0)$$

The values of $m_2(k, l)$ are obtained using a DXD square window as

$$m_2(k, l) = \frac{1}{D^2} \sum_{i=-(M)/2}^{(M)/2} \sum_{j=-(M)/2}^{(M)/2} g(k-i, l-j)^2 \quad (11)$$

$$m_4(k, l) = \frac{1}{D^2} \sum_{i=-(M)/2}^{(M)/2} \sum_{j=-(M)/2}^{(M)/2} g(k-i, l-j)^4$$

Where $M = D-1$. Next, the corresponding second and fourth order cumulants, denoted by \widehat{K}_2 and \widehat{K}_4 respectively, are obtained as:

$$\widehat{K}_2 = \widehat{m}_2$$

$$\widehat{K}_4 = \max((\widehat{m}_4 - 3\widehat{m}_2^2), 0) \quad (12)$$

The parameters α and δ are estimated as

$$\alpha = \sqrt{\frac{3\widehat{K}_2}{\widehat{K}_4}} \delta = \alpha \widehat{K}_2 \quad (13)$$

IV. PROPOSED METHOD

The de-noising diagram involves the following steps shown in diagram "Fig. 2".

- (1) Take the MRI image without contrast agent
- (2) Add noisy into this image (to obtain a noisy MRI image)
- (3) Compute the DT-CWT (dual-tree complex wavelet) of the noisy MRI image,
- (4) Obtain the Bayesian MAP estimator using equation (5)
 - or Compute the threshold value for each pixel for Visu shrink in all sub band details wavelet coefficients [26]
 - or applying Bivariate MAP estimator, in all sub band details wavelet coefficients [27].

- (5) Compute the inverse dual-tree complex (IDT-CWT) using synthesis filter bank forobtained the de-noised image.

where \hat{I} and I denote the noise free and the noised images respectively and N^2 is the total pixels [29].

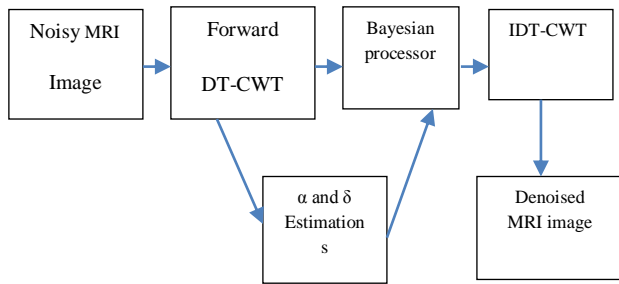


Fig 2. Diagram of proposed de-noising method

Choice of the images

MRI images are diverse and specific. Our study takes into account the behavior of different structures in comparison to contrast agents, because we are convinced that all structures do not react the same way to these agents. Our choice is geared to cranial images, in collaboration with the MRI department of the CHEIK ZHAID International University Hospital, based in Morocco. We selected brain MRI images of two of the four most commonly used sequences, axial and coronal ‘‘Fig. 3’’, for ethical reasons, we decline to identify the patient.

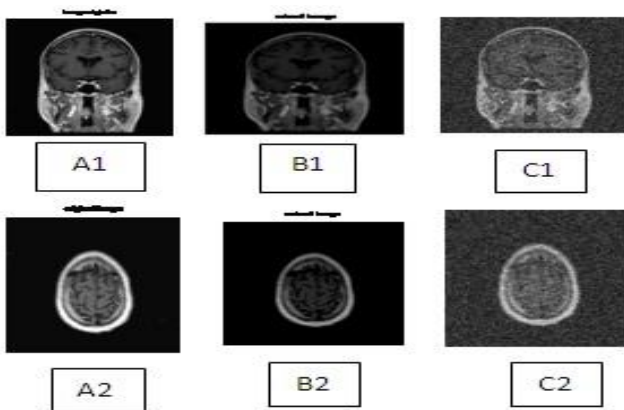


Figure 3.Reference images with contrast agent (A1 and A2.), the same images without contrast (B1 and B2) and noisy images (C1 and C2) respectively.

We compare our proposed algorithm to other effective techniques from the recent literature using MRI images.

From the first category of thresholding, we select the Vusu Shrinkage and Bivariate shrinkage[26], [27], in the second set we used only the adaptive Wiener filter implemented in CWT domain and considered window of size 7x7 within subband.

To quantify the noising performance of each algorithm, we employed the Peak-Signal to-Noise-Ratio (PSNR) defined as

$$PSNR = 20 \log_{10} \left(\frac{256}{\sqrt{\frac{1}{N^2} \sum (\hat{I} - I)^2}} \right) \tag{14}$$

V.Results and Discussion

In the simulations, complex zero mean white Gaussian noise with standard deviation $\sigma \epsilon = 20$, was added to the images without contrast agent (C1 and c2)

The noisy image is decomposed using only the dual tree wavelet transform (DT-CWT), for both the discrete (real DWT) and the complex parts (CWT), because the previous works have sufficiently proved the superiority of DT-CWT over DWT in image de-noising [15,28]

For each decomposition, the number of resolution levels is set in order to obtain equivalent size approximations (as much as possible) at the coarser resolution.

Table 1 give the results obtained the category of thresholding, has, Visu Shrinkage and Bivariate Shrinkage. In Table2, we show results obtained with adaptive Wiener adaptive filter

From the tables it can be seen that our approach achieves the best results in most situations, followed by Bivariate method.

Figure 4 and 5 illustrates the results with the first set of thresholding and Wiener adaptive filter respectively.

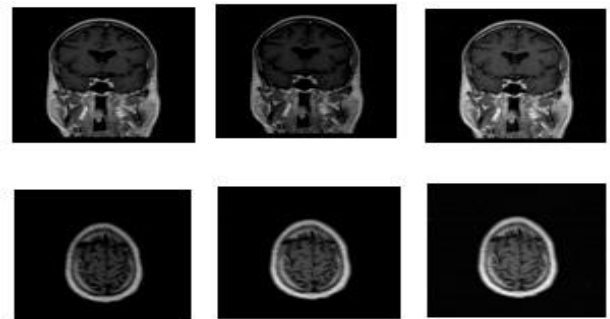


Figure 4. Coronal and Axial images de-noised with Visushrink (left), Bishrink (middle) and proposed method (right) with ($\sigma = 10$)

The PSNRs and Similarity between restored and original image as shown in table1 and2 for each case.

Table 1.PSNR VALUES (dB) OBTAINED BY THE TREE DE-NOISING METHODS

Image	Coronal MRI Image				Axial MRI Image			
	10	15	20	25	10	15	20	25
σ	10	15	20	25	10	15	20	25
Noisy	27.18	23.65	21.14	20.17	28.26	24.55	22.25	20.45
Visushrink	30.76	29.00	28.25	27.44	31.51	30.43	27.92	26.74
Bishrink	32.85	31.00	29.81	28.77	33.77	32.78	30.11	29.43
Proposed method.	33.26	31.22	30.00	29.09	34.75	33.03	31.87	30.01

TABLE 2. PSNR VALUES (dB) OBTAINED BY WIENER FILTER AND PROPOSED METHOD

σ	Axial MRI Image			Coronal MRI Image		
	Noisy	Wiener filter	Proposed Method	Noisy	Wiener filter	Proposed Method
10	28.26	32.51	33.61	27.18	32.34	32.85
15	24.55	30.43	31.63	23.65	30.87	31.90
20	22.55	28.92	30.19	21.14	29.17	30.17
25	20.45	27.74	29.21	20.17	28.10	29.85
30	18.62	26.73	28.51	18.62	26.13	28.87

We observed a decrease of PSNR between the reference images and those subject to de-noising. To assert the difference caused by the use of a contrast agent in the image, the correlation between the two images is lower, as it is to the naked eye. We clearly noticed that some details were quite visible, due to the contrast agent.

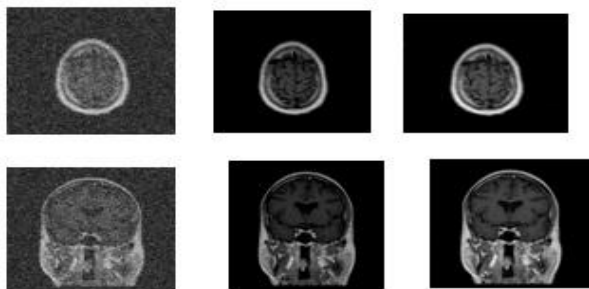


Figure 5. Axial and coronal images de-noised, where noisy images (left), Wiener filter (middle) and proposed method (right) with ($\sigma = 10$)

For the other images with Visu-shrinkage or Bivariate shrinkage (Bishrink), the proposed method shows an even better performance with the Bishrink estimator, where values have improved.

In all cases, the best results were obtained with the proposed method, followed by Bivariate shrinkage with Wiener filter and finally Visu shrinkage, figures and tables shows.

One can also note that the poorer performance was obtained for Visu shrinkage (increased the value of σ , which remains well below the Bivariate threshold as indicated in Table 1.

Here, we focused particularly on the ability of the our processor structure to de-noise MRI images. In comparison with several existing de-noised methods, the proposed approach out performs results in all cases, the obtained results are provided in Tables 1 and Table 2.

When considering the initial PSNR between original images and degraded images, it shown this approach providing a superior gain for each estimator. We then turned our attention to the test addressed to radiologists on the image quality, also obtaining, in their consideration and as a result of the simulations, a better performance for our processor, compared to other techniques.

The test methodology is detailed below:

Considering the brain images of four sequences commonly used in MRI, axial, coronal, presented to four experienced radiologists working in university hospitals and Sino-congolaise hospital.

In a first stage, the anonymous images were given to the radiologists and they were asked whether the image presented to them was original or restored and if it was acceptable for the diagnosis, to which they could answer yes or no.

Secondly, the restored images compared to the reference images were placed side by side and in this case the original was revealed to the observer, blinded to the type of transform used to restore the image to compare. The radiologists were asked to quantify on a scale of 1 to 9, as follows:

- 9 No visible difference
- 7 No loss of diagnostic information
- 5 In the limit of information loss, discrete anomalies may be omitted.
- 3 Important diagnostic information may be omitted, and the degradation affects the interpretation.
- 1 Unsatisfactory for diagnosis; indisputable loss of diagnostic information.

From this test, we obtained the following observations:

For two of four observers, axial sequence images de-noised with Visu shrink estimator ($\sigma > 20$) were considered non-diagnostic cases.

One observer rejected the coronal sequence images restored with Visushrink estimator ($\sigma > 20$).

Axial images were considered acceptable for diagnosis by all observers for all techniques without Visu shrink estimator ($\sigma > 20$)

In the case where the original or reference image is revealed, we obtained the following results:

Axial: 75% of the observers found no significant loss of diagnostic information for the proposed approach. One observer judged the images de-noised with the Visushrink estimator ($\sigma > 15$) estimator too degraded to be reliable.

Coronal: One observer has considered an image de-noised Visushrinkage at the limit of information loss and marked it as a 5.

Axial: All observers agreed on the absence of significant loss of diagnostic information for proposed method, images with the Bivariate estimator and Wiener filter.

Axial: Three observers classified the images in the 5-6 categories, within the diagnostic information loss limit, for Visu Shrinkage.

VI. CONCLUSION

Given the simulation results obtained with our approach, we can state, as described in the literature, this processor is more efficient than others. Its extension to the complex case has especially proved to be interesting and leads to better results than the discrete case. Moreover, the combination with DT-CWT and different MAP estimator offered encouraging results.

Far from the consideration of matching or competing with the use of contrast agents, our study is meant as a statement, indicating that it is possible, with computer processing and the appropriate estimators, to restore a noisy medical image and to highlight certain pathologies the distinction of healthy and pathological tissue.

This can result in a solution on the social level, taking into account the cost of an MRI exam with contrast agents. Finally, the results of the simulation carried out on selected MRI images has allowed us to ascertain that our approach is very favorably positioned compared to the existing medical image de-noising techniques.

ACKNOWLEDGEMENTS

WE WOULD LIKE TO THANK THE RADIOLOGIST RESPONDENTS IN UCH CHEIKZAID AND SINO-CONGOLAISE HOSPITAL FOR THEIR EXCELLENT SCIENTIFIC CONTRIBUTIONS.

REFERENCES

[1] W.A. Edelstein, G. Glover, C. Hardy, and R. Redington, "The intrinsic signal-to-noise ratio in NMR imaging," *Magn. Reson. Med.*, vol. 3, pp. 604–618, 1986.

[2] H. Gudbjartsson and S. Patz, "The Rician distribution of noisy MRI data," *Magn. Reson. Med.*, vol. 34, pp. 910–914, 1995.

[3] X. Li and M. Orchard, "Spatially adaptive denoising under overcomplete expansion," *Proc. IEEE Internat. Conf. on Image Proc., ICIP00*, Vancouver, Canada, Sep 2000.

[4] E.R. McVeigh, R.M. Henkelman, and M.J. Bronskill, "Noise and filtration in magnetic resonance imaging," *Med. Phys.*, vol. 3, pp.

[5] R.D. Nowak, "Wavelet-based Rician noise removal for magnetic resonance imaging," *IEEE Trans. Image Proc.*, vol. 8, pp. 1408–1419, Oct 1999.

[6] A. Macovski, "Noise in MRI," *Magn. Reson. Med.*, vol. 36, pp. 494–497, 1996.

[7] Wiem Fourati & Mohamed Salim Bouhlel, "Nouvelle méthode pour le débruitage d'images," *4th International Conference: Sciences of Electronic, Technologies of Information and Telecommunications* March 25-29, 2007 – TUNISIA.

[8] Achim, A., Bezerianos, A., and Tsakalides, P. (2001). Novel bayesian multiscale method for speckle removal in medical. *IEEE Transactions on Medical Imaging*, 20(8):772-783.

[9] Junmei Zhong and Ruola Ning, "Image Denoising based on wavelets and Multifractals for singularity detection," *IEEE transaction on image processing*, vol.14, n0.10, october 2005.

[10] Alexandru SAR, André QUINQUIS and al, "Débruitage des images SAR : Application de la TODDE (Transformée en Ondelettes Discrète à Diversité enrichie)" *IEEE Transactions*, 2003.

[11] J. Weaver, Y. Xu, D. Healy, and J. Driscoll, "Filtering MRI images in the wavelet transform domain," *Magn. Reson. Med.*, vol. 21, pp. 288–295, 1991.

[12] Y. Xu, J. B. Weaver, D. M. Healy, J. Lu, "Wavelet transform domain filters: a spatially selective noise filtration technique," *IEEE Trans. Image Proc.*, vol. 3, no. 6, pp. 747–758, Nov. 1994

[13] M.I.H Bhuiyan, M.Omain Ahmad and al, 'wavelet-based despeckling of medical ultrasound images with the Symmetric Normal Inverse Gaussian prior' 2007 *IEEE, ICASSP* 2007.

[14] Mallat, 'A wavelet tour of signal processing' San Diego, CA, USA : *Academic Press*, 1998

[15] RudraPratap Singh Chauhan, Sanjay Singh and al, 'Study and Performance Appraisal of CDWT for Image Quality Improvement and De-noising', *Pragyaan : Journal of Information Technology* Volume 9 : Issue 2, 'December 2011

[16] N.G Kinsbury. Image processing with complex wavelets'. *Phil. Trans. Royal Society* London, 1999.

[17] N.G Kinsbury. 'A dual-tree complex wavelet transform with improved orthogonality and symmetry proprieties'. In *Proceedings of the IEEE, Int. Conf. on Image Proc. (ICIP)*, 2000

[18] H.Guo, 'Theory and applications of shift-invariant, time-varying and undecimated wavelet transform' MS thesis, Rice University, 1995.

[19] N.G Kinsbury. 'Image processing with complex wavelets'. *Phil. Trans. Royal Society* London, 1999.

[20] I. Selesnick and K. Li. 'videodenoising using 2D and 3D dual-tree complex wavelet transforms: in wavelet applications in signal and image processing' *X (proc. SPIE 5207)* 2003.

[21] N.G Kinsbury. 'A dual-tree complex wavelet transform with improved orthogonality and symmetry proprieties'. In *Proceedings of the IEEE, Int. Conf. on Image Proc. (ICIP)*, 2000

[22] I. Selesnick, R.G. Baraniuk and N.G. Kingsbury, 'The dual-tree complex wavelet transform: *IEE Signal Processing magazine*, vol.22, n°6, pp.123-151, nov.2005.

[23] M.I.H Bhuiyan, M.Omain Ahmad and al, 'Spatially adaptive wavelet-based method using the Cauchy prior for de-noising the SAR images', *IEEE Trans. on Circuits, Systems and video Thecnology* (in press), 2007.

[24] A. Hanssen and T. A. Oigard, 'The normal inverse Gaussian distribution for heavy-tailed processes,' in *Proc. IEEE EUEASIP Workshop on Nonlinear Signal and Image processing*, 2001.

[25] A. Hyvarinen, 'Sparse code shrinkage: Denoising of nonGaussian data by maximum likelihood estimation,' *Neural Computation*, vol. 11, pp. 1739–1768, 1999.

[26] D L Donoho, 'Denoising by soft thresholding', *IEE Trans. Info, Theory*, 41(3), 613-627, 1995.

[27] L. Sendur and Ivan Selesnick 'Bivariate Shrinkage function for wavelet-based denoising exploiting interscale dependency', *IEEE Trans. On Signal proc.* 50(11): 2744-2756. (2002).

[28] RudraPratap Singh Chauhan, Sanjay Singh, Sanjeev Kumar, 'A Practical Approach of Complex Dual Tree DWT for Image Quality Improvement and De-noising' *International Journal of Modern Engineering Research (IJMER)* Vol. 1, Issue.2, pp-632-636

[29] APPEL W. 'Mathématiques pour la physique et pour les physiciens', *H&K, Paris*, 2002.

On the Estimation of the Software Process Maturity using COCOMO II's Effort Estimation based on CMMI

Yousef Alkouni Alghdr¹, M. Afshar Alam², Mugeem Ahmed³

Department of Computer Science, Jamia Hamdard Delhi India

Department of computer science Jamia Millia Islamia Delhi India

Abstract: Software resource estimation methods and models have had a major impact on successful software engineering practice. They provide milestone budgets and schedules that help projects determine when they are making satisfactory progress and when they need corrective action. The software capability maturity model is a most popular model to enhance software processes with the goal of developing best quality of the software which are under the control of budget and schedule. The last stage of updating of the software cost estimation model, constructive cost model has a different set of seventeen cost drivers and a set of five scale factors. The Process maturity is one of the important five scale factors whose ratings are based on the software capability maturity model. This paper is an attempt to determine the effect of process maturity on the software development effort by deriving a new set of constructive cost model II's process maturity rating values based on the most recent version of CMM, i.e., capability maturity model integration. The effect of the constructive cost model II's process maturity scale factor is determined by considering the ideal scale factor methodology. Precedentedness shows all prediction accuracies compared to the generic, constructive cost model II estimation.

I. Introduction

The Software is one the most important and yet one of the most economically challenging technologies of the current era. As a purely intellectual product, it is among the most labor intensive, complex, and error-prone technologies in human history [1]. The software industry is not untouched by the quality by the quality movement that dramatically affected the product of other industries. But constant demand from the industry for cheaper and better software, make this goal (quality of software) more challenging. Each and every company knows, to remain competitive, it must deliver quality product at time and within budget[2]. Consequently many software companies has turned to software process improvement as a way of enhancing the quality of their products ,reducing the cost and accelerating the development process. The delivery of the software on time, within the budget and with the expected functionalities and quality is a challenge for all software development organizations. Inaccurate estimations in software development industry is one of the most serious problems that cause the software failure[2].It is also well known that the quality of software products depends on the software development capabilities and the quality of the maintenance process to a great extent. Thus an organization have no possesses well-trained developers, it will be difficult to them to build the foundation which supports successful improvement of the software development

process. Therefore, the fundamental way of ensuring the software quality is to improve the software productivity of the enterprises. And the software productivity of the enterprises depends on their software development capability, especially the maturity of software development and production. Software cost estimation is the process of predicting the effort required to develop a software [3].These types of process becomes one of the major challenges which also the most expensive component in software development. While software cost estimation may be simple in concept, it is difficult and complex in reality [4]. The different estimation models have been developed; most of them have disappeared without any kind of rigorous evaluation. The main reason for that was that these types of models were not good and precise enough [5]. The other reason was that the people who are working in the software development prefer to use their own estimation techniques rather than improving and applying the work of the others. The most of the organizations have relied on experience and "Price-to-win" strategies for getting past competitors. Despite the emergence of concepts like because of the rapidly changing technologies, the Software Capability Maturity Model one can never rely completely on experience based estimation in the software industry which renders the experience-based estimates ineffective. The price-to-win strategy is not very favorable for most of the organization [6].Hence the requirement of effective cost model arises to account for the effort spent on the developing software systems. It is an important input to software cost estimation models. The Capability Maturity Model for software was enveloped by Software Engineering Institute to describe the principles and practices underlying software process maturity. Its aim is to help organizations improve their software process maturity through an evolutionary path and process predictability [7]. Despite the fact that the Software Engineering Institute has released the Capability Maturity Model Integration, which is the updated version of the original CMM, COCOMO II still relies on SW-CMM to assess its process maturity scale factor.

This paper is an attempt to describes the effect of process maturity on software development effort by deriving a new set of constructive cost model II's process maturity rating values based on the most recent version of CMMI capability maturity model integration.

II. Review of Literature

The Software development become an important part for many organizations; software estimation is gaining an ever increasing importance in effective software project management. Boehm was the first researcher who considered the software estimation from an economic point

of view, and came up with the cost estimation model, COCOMO in 1981, after investigating a large set of data in the 1970's (Boehm, A, and Chulani,2000). Putnam also developed an early model known as, the Software Lifecycle Management, (Putnam, 1978).The software estimation includes the effort/schedule estimation, quality estimation, risk analysis, etc. The most accurate software estimation can provide powerful assistance for software management decisions (Boehm, 2000). The most new computational techniques are used for cost estimation that are non-algorithmic in the 1990's. The researchers have turned their attention to different approaches which are based on soft computing methods that include artificial neural networks, fuzzy logic models and genetic algorithms. The Artificial neural network is able to generalize from trained data set. Over a known set of training data, a neural-network learning algorithm constructs rules that fit the data and predicts previously unseen data in a reasonable manner (Schofield, 1998). The most popular estimation methods are discussed in detail by Khatibiand J (2011). The COCOMO, SLIM and Albrect's function point methods that measures the amount of functionality in a system were all based on linear regression techniques by collecting data from historical project as the major input to their models. The different algorithmic methods are deliberated as the most popular methods and many researchers used the selected algorithmic methods (Musilek, et al. 2002; Yahiya, et al. 2008; Lavazza and Garavaglia 2009; Yinchuan et al. 2009; Sikka et al. 2010).The Software estimation techniques can support the planning and tracking of software development projects. The efficiently controlling the expensive investment of software development is of prime importance (Gray, MacDonell and Gray, 1997; Jingzhou and Guenther, 2008; Kastro and Bener, 2008; Strike et al., 2001). ImanAttarzadeh and Siew Hock Ow (2010) proposed amodels which is based on COCOMO II and fuzzy logic to the NASA dataset and found that the proposed model performed better than ordinary COCOMO II model and also achieved the results which were closer to the actual effort. The relative error for proposed model using two-side Gaussian membership functions is found to be lower than that of the error obtained using ordinary COCOMO II. A novel neuro-fuzzy Constructive Cost Model is used for software cost estimation and this model carried some of the desirable features of a neuro-fuzzy approach, such as learning ability and good interpretability, while maintaining the merits of the COCOMO model (XishiHuang et al., 2005).

III. Background

A. COCOMO II Model

The COCOMO was originated in 1981[8], and became one of most popular cost estimation models of the 1980s. But the COCOMO faced different difficulties in the 90s, and different complications in cost estimation of software that were developed to a new life cycle processes such as non-sequential and rapid development process models, reuse-driven approaches, and object-oriented approaches [9].Thus, COCOMO II was published initially in the annals of software engineering in 1995 with three sub models; an application-composition model, an early design model and a post-architecture model. The COCOMO II has, as an

input, a set of seventeen Effort Multipliers or cost drivers which are used to adjust the nominal effort to reflect the software product being developed. The seventeen COCOMO II factors are shown in Table 1 [10].

a. Effort Estimation

The equation a is formulated the COCOMO II effort estimation model. The effort estimates by both early design and post-architecture models. The inputs are the size of software development, a constant A , an exponent E , and the number of Effort Multipliers (EM). The number of effort multipliers depends on the model being used.

$$PM = A \times SIZE^E \times \prod_{i=1}^N EM_i \quad (a)$$

Where the constant $A=2.94$, and the exponent E will be described in the bellow.

b. Scale Factors

The study accomplished by [12] presents the conclusion that the most critical input to the COCOMO II model is size, so, a good size estimate is very important for any good model estimation. The Size in COCOMO II is consider as a special cost driver, so it has an exponential factor, E . The exponent E in equation 2 is an aggregation of five scale factors. All scale factors have rating levels. These rating levels are Very Low, Low, Nominal, High, Very High and Extra High. Each rating level has a weight W , which is a quantitative value used in the COCOMO II model. The five COCOMO II scale factors are shown in Table 1

$$E = B + 0.01 \times \sum_{j=1}^N SF_j \quad (b)$$

Where B is a constant = 0.91. A and B are constant values devised by the COCOMO team by calibrating to the actual effort values for the 161 projects currently in COCOMO II database.

Table 1. Scale factors of COCOMO II.

Scale Factor	Description
Precedentedness	Reflects the previous experience of the organization.
Development Flexibility	Reflects the degree of flexibility in the development process.
Risk Resolution (RESL)	Reflects the extent of risk analysis carried out.
Team Cohesion	Reflects how well the development team knows each other and work together.
Process Maturity	Reflects the process maturity of the organization.

Table 2. Cost drivers of COCOMO II.

Cost Driver	Description
RELY	Required Software Reliability
DATA	Data base size
RUSE	Developed for Reusability
DOCU	Documentation needs
CPLX	Product Complexity
TIME	Execution Time Constraints
STOR	Main storage Constraints
PVOL	Platform Volatility
ACAP	Analyst Capability
PCAP	Programmer Capability
APEX	Application Experience
PLEX	Platform Experience
LTEX	Language and Tool Experience
PCON	Personnel Continuity
TOOL	Use of Software Tools
SITE	Multisite Development
SCED	Required Development Schedule

The procedure for determining procedure maturity which is the factor of interest in this study- is organized around the SEI-CMM, Table 3

Table 3. The rating levels ,values, and Process Maturity Scale Factor.

Process maturity Description	CMM	CMM	CMM	CMM	CMM	CMM
	Level 1 (lower)	Level 1 (upper)	Level 2	Level 3	Level 4	Level 5
Rating	Very Low	Low	Nominal	High	Very High	Extra High
Values	7.80	6.24	4.68	3.12	1.56	0.00

The CMM level 1 is for organizations that don't focus on processes or documenting lessons learned. The CMM level 1 is for organizations that have implemented most of the requirements that would satisfy CMM level 2. In CMM's published definition, level 1 (lower half) and (Upper half) are grouped into level 1.

B. The CMM Based Process Maturity

The Software Engineering Institute at Carnegie-Mellon University published the CMM is used to rate an organization's process maturity [11]. It provides a number of requirements that all organizations can use in setting up the software processes used to control software product development. There are five levels of process maturity, level 1 (lowest half) to level 5 (highest). The CMM specifies "what" should be in the software process rather than "when" or "for how long". To be rated at a particular level, the organization should demonstrates capabilities in a set of Key Process Areas associated with a specific CMM level. The capabilities demonstrated in moving from

lower levels to higher levels are cumulative. For example, level 3 organizations should show compliance with all key process areas in levels 2 and 3. The CMM process maturity framework is presented in Table 4

Table 4. The Framework of CMM.

CMM Level	Key Process Area
Level 1	None
Level 2 Repeatable	Requirements Management
	Software Project Planning
	Software Project Tracking and Oversight
	Software Subcontract Management
	Software Quality Assurance
Level 3 Defined	Software Configuration Management
	Organization Process Focus
	Organization Process Definition
	Training Program
	Integrated Software Management
	Software Product Engineering
Level 4 Managed	Intergroup Coordination
	Peer Reviews
	Quantitative Process Management
	Software Quality Management
Level 5 Optimizing	Defect Prevention
	Technology Change Management
	Process Change Management

All the organizations are supposed to start at level 1. Which is known as Initial level? At this level, few processes are defined, and the success depends on individual effort which makes the software process unpredictable because it changes as work progresses. Project Schedules, budgets, functionality, and product quality are also unpredictable. Every key process area has a set of goals, capabilities, key practices, measurements and verification practices. The goals state the scope, boundaries, and intent of a key process area. A key practice describes "what" should happen in that key process area. There are a total of 52 goals and 150 key practices.

IV. Methodology

The methodology of our work is the primary data collection tool was a questionnaire that has been used to collect a data from individual projects, i.e., each and every questionnaire should be applied only on one of the project. The questionnaire is based on "COCOMO II cost estimation"

A. The Data Collection

The data collection procedures 55 questionnaires distributed to 20 software development organizations, 35 questionnaires were returned. Some of the questionnaires could not be verified by project managers or senior project

staff; therefore, 16 questionnaires were rejected and eliminated from this study. Therefore, 40 questionnaires were analyzed. The datasets were returned from different fields like banking, insurance, communication, simulation, web development, etc. The questionnaires were distributed to software organizations that have already achieved one of the CMMI levels, and spanned the range of its levels, from level 1) to level 4, i.e., 8 data points were collected from each level. For each project, there was a meeting with the project manager or team leader for each project, who would be filling out the forms, in order to clarify each question to ensure that it was well understood and each manager would answer consistently.

B. The Data Analysis

The questionnaires were checked for consistency and went through a data validation process, based on some constraints determined in [6]. There are four aspects that would be extracted and computed: for each questionnaire.

- The set of seventeen COCOMO II's cost drivers. To deal with these seventeen cost drivers, we computed their multiplication. A sample of the cost drivers is shown in Table 5.
- The set of five exponential scale factors. To deal with these five scale factors, we computed their summation. A sample of these scale factors is shown in Table 6 (excluding the last row).
- The Actual effort in Person Months, which extracted for the person hours, as shown in Table 7.
- We collected the project size as a thousand lines of code (KLOC), which is the baseline size in COCOMO II.

We applied equation 1 To predict the effort in person month, which is the basic COCOMO II's formula [6]. At last this analysis, we got the estimated effort for the generic COCOMO II as well as the actual effort for this project.

C. Ideal Scale Factor Analysis on Process Maturity

Boehm[7] has described normalization method out contaminating effects of individual cost driver attributes in order to get clear picture of that cost driver's contribution. Since we have relatively similar situation, i.e., we need to normalize out contaminating effects of a scale factor in process maturity rather than a cost driver. Therefore, for the given project P, compute the estimated development effort using the COCOMO II estimation procedure, with one exception: do not include the value for the Scale Factor Attribute being analyzed. Call this estimate PM (P, Scale Factor Attributes). Then the Ideal Scale Factor, for this project/scale-factor combination is defined as the value which, if used in COCOMO II, would make the estimated development effort for the project equal to its actual development effort PM (P, Actual). i.e.,
 Ideal scale factor(P, Process Maturity) =

$$\frac{PM(P, Actual)}{PM(P, Process Maturity)} \quad (c)$$

Where Ideal Scale Factor (P, Process Maturity): the ideal scale factor on Process Maturity for project P.

PM (P, Actual): the actual development effort for the project P.

PM (P, Process Maturity): COCOMO II estimate excluding the Process Maturity Scale Factor.

We performed the following steps to complete the Ideal scale factor-Process maturity analysis on our datasets:

1. The first step Compute the PM (P, Scale Factor Attribute), using the following formulas:

$$PM = A \times \sum_{i=1}^{17} SIZE_i \times IEM_i \quad (d)$$

where A is a model constant, EM is a set of seventeen effort multipliers as shown in Table 1, and

$$E = B + 0.01 \times \sum_{j=1}^4 SF_But_ProMat_j \quad (e)$$

Where B is a model constant, and scale factor_But the process maturity refers to scale factors except Process Maturity, including Precededenes REC, Flexibility, Resolution, and Team.

2. Compute the ideal scale factor (P, Scale Factor Attributes) using equation 6.
3. Group Ideal Scale Factor (P, Scale Factor Attributes) by the current CMM process maturity rating (i.e., VL, L, N, H, VH).
4. Compute the mean value for each group as ideal scale factor -Process maturity value for that rating.

This step involves the computation of the mean value of ideal scale factor-process maturity for each CMM rating level.

D. The Prediction Accuracy evaluation

The purpose of this paper is on the degree to which the model's estimated effort measured in Person-Month matches the actual effort. If the model is perfect then for any project, Process maturity =Person month matches. The most common criterion for the evaluation of the cost estimation models is the Relative Error or the Magnitude of Relative Error, which are shown below :

$$\text{Relative Error} = \frac{\text{Person month matches} - \text{process maturity}}{\text{process maturity}} \quad (f)$$

$$\text{Magnitude of relative Error} = \frac{|\text{Person month Matches} - \text{Process Maturity}|}{\text{Process Maturity}} \quad (g)$$

The Relative Error and Magnitude of Relative Error values are calculated for each project whose effort is predicted. Another criterion that is commonly used is the percentage of predictions that fall within P % of the actual, denoted as Predictions (P) [13],

$$\text{Prediction (P)} = K / N \quad (h)$$

K is the number of projects where magnitude of relative error is less than or equal to P, and N is the number of projects. According to the [10], a standard method for assessing the COCOMO performance is prediction. Therefore we used this criterion to assess the COCOMO II performance as compared to the proposed model. Table 5 through Table 10 shows samples of the calculated data, that represents one project from our forty datasets.

Table 5. COCOMO II Effort Multipliers with their Cost Drivers

Cost Driver	Value
RELY	1.1
DATA	1
RUSE	1
DOCU	1.21
TIME	1.26
STOR	1.01
PVOL	0.77
ACAP	0.61
PCAP	0.68
PCON	0.7
APEX	0.71
PLEX	0.75
LTEX	0.74
TOOL	0.68
SITE	0.76
SCED	1
CPLX	1.21

Table 6. Scale factors of COCOMO II and their values.

Scale Factor	Value
Precedentedness	2.62
Flexibility	1.01
Risk Resolution	1.83
Team Cohesion	1.19
Process Maturity	.59
New process maturity	.03

Table 7. The actual time, effort, size, estimated time, and the cost drivers multiplication.

Description	Value
Actual Time	165
Actual Effort	133.32
Size (KSLOC)	110
Estimated Time, T	173
II Cost Drivers, EM	0.344

Table 8. The generic COCOMO II Estimated effort.

Description	Value
Σ Scale Factors,	10.210
Estimated Effort,	158.04
Magnitude Relative Error	0.17

Table 9. Ideal Scale Factor and Estimated effort without process maturity value.

Description	Value
Σ Scale Factors-BUT- Process Maturity	9.75
Estimated Effort, but- Process Maturity	156.14
Ideal Scale Factor,	0.92

Table 10. Estimated effort with new process maturity values.

Description	Value
Σ scale factors with ISF-process maturity	10.78
Estimated Effort with ISF-process maturity	163.87
Magnitude Relative Error=	0.14

The new set of process maturity rating values under CMMI derived by applying our methodology to the datasets in Table 11.

Table 11. The New Process Maturity Rating values.

Process maturity Description	CM MI Level 1 lower	CM MI Level 1 Upper	CMMI Level2	CM MI Level 3	CM MI Level 4	CMMI Level5
Rating level	Very low	low	Nominal	High	Very high	Extra High
New Process Maturity Values	6.44	3.45	2.34	1.34	.98	0.0

In the Figure 1, X axis represents the projects used in CMMI level 4 organization in our study and the Y axis represents the effort. Each project has three columns: the left column represents the actual effort, the middle column represents the generic COCOMO II effort estimation, and the right column represents the effort estimation for the proposed COCOMO II model with new Ideal Scale Factor - Process Maturity Values.

The figure shows that how the proposed model give an estimated effort which is closer to the actual effort than generic COCOMO II estimations due to some data anomalies, especially for low levels companies that do not have good and precise documentations for their historical projects. This case is not absolute, i.e., in some little cases like in CMMI level 1 (lower and upper) and level 2 datasets, the estimated efforts by the generic COCOMO II were relatively closer to the actual effort than the proposed model's estimation.

The proposed model here is uniformly overestimated the effort for most of the 8 projects, so it could still be a consistent model.

The black line in Figure 2 shows the current process maturity scale factor values used in COCOMO II. It shows that an increase in process maturity level corresponds with a reduction in project effort. It shows the new process maturity values derived from the ideal scale factor-process maturity analysis.

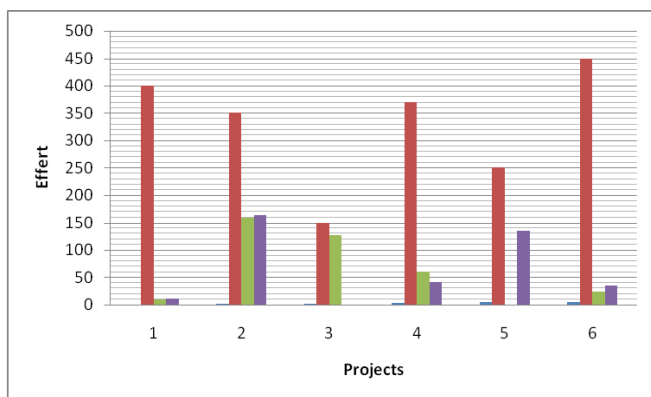


Figure 1. The Estimated and Actual effort in both generic COCOMO II and COCOMO II with Ideal Scale Factor-Process Maturity.

The few number of different Process Areas are assigned to this level, and success still depends on individual effort that is very low and low rating levels in COCOMO II's procedure maturity are categorized under CMMI level 1. Therefore, level 1 companies still need much effort to accomplish their projects, particularly for CMMI level 1 companies that rely on "heroes" to do the jobs and do not show any compliance that would satisfy subsequent levels.

The second observation is the nominal and high rating levels demonstrated a relatively obvious reduction in the procedure maturity values, which appears as a deviation first line in Figure 2. The underlying explanation behind this reduction might be due to the major additions and refinements that have occurred at CMMI maturity levels 2 and 3. As an example, going from seven key process areas in CMM level 3, to 14 process areas in CMMI level 3, and just two were dropped. These additions and refinements in maturity levels 2 and 3 reflect their significance and definitely will reduce the effort required to develop the software systems in CMMI maturity levels 2 and 3 organizations.

Ideal Scale Factor Process Maturity VS COCOMO II Process Maturity

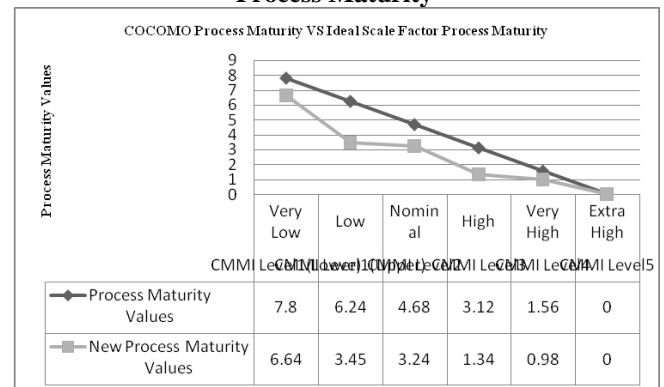


Figure 2. The Ideal scale factor -process maturity values. vs COCOMO II's process maturity values.

E. The Results of the Model Accuracy with ideal scale factor

The improvement in the model's accuracy has been realized which is shown in the below after applying the derived ideal scale factor-process maturity values back to our datasets, in the below Table 12.

Table 12. The Analysis of Accuracy Results

Level	Generic COCOMO II	COCOMO II with New Process Maturity Values	Improvement
Level 1 (Lower)	43%	55%	9%
Level 1 (Upper)	30%	43%	11%
Level 2	18%	55%	34%
Level 3	18%	58%	47%
Level 4	30%	77%	21%

The above Table shows the analysis of accuracy results that by applying the ideal scale factor procedure maturity values into our datasets which had been collected from CMMI organizations, the accuracy in all maturity levels increased by 9%, 11%, 34%, 47%, and 21% respectively as we have already mentioned and justified, that level 3 has the highest percentage of improvement, and the level 1 has lowest percentage of improvement.

V. Conclusions

The software development cost estimation is very important in all the aspects of project such as budgeting, planning and effective control of management. There are various software cost estimation models which have various inputs. The most important inputs to software cost estimation models is the process maturity. According to survey, the present values for the COCOMO II process maturity scale factor does not adequately reflect the impact of CMMI-based process maturity on development efforts. Therefore, by using the ideal scale factor method and with the aid of our datasets, we have identified the new process maturity values which better reflect the impact of CMMI based process maturity on software development effort. The new values provide an improvement in COCOMO II model accuracies 9% for CMMI level one, 11% for CMMI level one, 34% for CMMI level two, 47% for CMMI level three, and 21% for CMMI level four organizations. In future the amount of datasets allocated to each CMMI maturity level could be expanded to get a clearer picture of the impact of CMMI-based process maturity on software development effort and the locally calibrating the proposed model parameters to a particular organization, which requires collecting data from more projects belonging to the same Organization.

References

- [1] Miyazaki Y. and Mori K., "COCOMO Evaluation and Tailoring," in *Proceedings of ICSE 8, IEEE-ACM-BCS*, pp. 292-299, 1985.
- [2] Al-Sakran H., "Software Cost Estimation Model Based on Integration of Multi Agent and Case Based Reasoning," *Journal of Computer Science*, vol. 2, no. 3
- [3] OLGA F, LEONOR T, HELENA A." Software Effort Estimation with Multiple Linear Regression: review and practical application" *Journal of Information Science and Engineering* xx, xxx-xxx 2011
- [4] Jones C. "Software Cost Estimation in 2002," *Computer Journal of Defense Software Engineering*, vol. 15, no. 6, pp. 4-8, 2002.
- [5] Miyazaki Y. and Mori K. "COCOMO Evaluation and Tailoring," *Proceedings of ICSE 8, IEEE-ACM-BCS*, pp. 292-299, 1985.
- [6] Dillibabu R. and Krishnaiah K., "Cost Estimation of a Software Product Using COCOMO II.2000 Model a Case Study," *International Journal of Project Management*, vol. 23, no. 2, pp. 297-307, 2005.
- [7] Jianguo Li, Jinghui Li, and Hongbo Li," Research on Software Process Improvement Model Based on CMM" *World Academy of Science, Engineering and Technology* 39 2008
- [8] Boehm B., "Software Engineering Economics", Prentice Hall, 1981.
- [9] Boehm B., Clark B., Horowitz E., Westland C., Madachy R., and Selby R., "Cost Models for Future Software Life Cycle Processes: COCOMO 2.0," *Proceedings of Special Volume on Software Process and Product Measurement*, Amsterdam, pp. 45-60, 1995.
- [10] Boehm B., Horowitz E., Madachy R., Reifer D., Clark B., Steece B., Brown A., Chulani S., and Abts C., "Software Cost Estimation with COCOMO II", Prentice Hall, 2000.
- [11] Yang Y. and Clark B., "COCOMO II.2003 Calibration Status," http://sunset.usc.edu/events/2003/March_2003/COCOMO_II_2003_Recalibration.
- [12] Musilek P., Pedrycz W., Sun N., and Succi G., "On the Sensitivity of COCOMO II Software Cost Estimation Model," *Proceedings of the 8th IEEE Symposium on Software Metrics*, IEEE Computer Society, Washington, pp. 13, 2002.
- [13] Conte S., Dunsmore H., and Shen V., "Software Engineering Metrics and Models," Menlo Park, CA, Benjamin/Cummings, 1986.

Polyaniline Based Polymeric Nano composite Containing TiO₂ and SnO₂ for Environmental and Energy Applications

Rajeev Arora^{1*}, Anupam Srivastav², Utam Kumar Mandal³

1. Mechanical Engineering Department, Invertis University, Invertis Village, Bareilly.

2. Mechanical Engineering Department, I.F.T.M. University, Lodipur village, Delhi road, Moradabad.

3. School of Chemical Engineering, Guru Gobind Singh Indraprastha University, Delhi.

Abstract: With the addition of inorganic spherical nanoparticles to polymers allows the modification of the polymers physical properties in the polymer matrix. This review article covers considerations on special the aspects of TiO₂ nanoparticles composite materials in polyaniline during the polymerization. Classical nanocomposite properties, as thermo mechanical, dielectric, conductive, magnetic, as well as, mechanical properties will be summarized. Finally, typical existing and potential applications will be shown with the focus on new and innovative applications, like in energy solar systems and environment systems.

Keywords: Nanocomposites; polymer matrix; spherical nanoparticles; physical property tailoring, polymer-nanoparticles-interface

I. Introduction

The environment and energy are the biggest challenges of the 21st century. Nanomaterials, with attractive chemical and physical properties, are being explored for potential uses in energy and environmental applications. Considerable effort has been made to design, fabricate, and manipulate nanostructure materials by innovative approaches. The precise control of nanoscale structures will pave the way not only for elucidating unique size/shape dependent physicochemical properties but also for realizing new applications in science and technology. Nanotechnology offers unprecedented opportunities for improving our daily lives and the environment in which we live. The addition of inorganic spherical nanoparticles to polymers allows the modification of the polymers physical properties. The resulting thermal, mechanical, optical, magnetic or conducting properties of the nanocomposites are influenced by the filler properties as well as from the fillers surface properties. Specific interest is to develop the polymeric nanocomposite with good thermo mechanical properties, rheological characteristics and thermal stability for energy and environmental applications [1]. As global environmental and energy issues increasingly demand our attention, numerous challenges in materials science and technology will arise. Polyaniline is electro-conducting polymer containing a system of conjugated double bonds, and its properties combine semiconducting and metal physics with the molecular and solid-state chemistry. To make this polymer electrically conductive it is necessary to introduce mobile charge carriers. This can be done by oxidation or reduction reactions, commonly called "doping" and "dedoping", respectively, which can be performed by different chemical or electrochemical processing. Chemical doping-dedoping occurs when the polymer is exposed to an oxidizing or reducing agent; whereas electrochemical doping-dedoping can be obtained by anodic and cathodic polarization in suitable electrolytes [2-4]. The nanostructured metal oxides are promising new materials for blending with polymers for obtaining low weight nanocomposites with excellent mechanical, electrical, thermal, and multifunctional properties. The creation of nanocomposites based on electro-conductive polymers and

nanostructured metal oxides, i.e. incorporation of inorganic filler into polymer matrixes, can dramatically improve their processibility [5-7]. The main goal in this work is to enlarge the existing knowledge of the preparation of new advanced materials consisting of polymer matrix with nanoparticles.

II. Conductive Polymer

Conductivity or can be semiconductors. The biggest advantage of conductive polymers is their processibility, mainly by dispersion. Conductive polymers are generally not plastics, i.e. they are not thermoformable. But, like insulating polymers, they are organic materials. They can offer high electrical conductivity but do not show mechanical properties as other commercially used polymers do. The electrical properties can be fine tuned using the methods of organic synthesis (9) and by advanced dispersion techniques (10). The linear -backbone "polymer blacks" (Polyacetylene, Polypyrrole, and Polyaniline) and their copolymers are the main class of conductive polymers. Historically, these are known as melanins

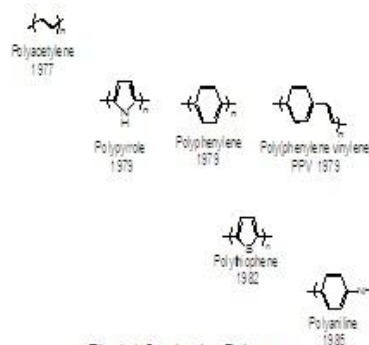


Fig. 1.1 Conducting Polymers

..Poly (p-phenylene) (PPV) and its soluble derivatives have emerged as the prototypical electroluminescent semiconducting polymers. Today, Poly (3-alkylthiophenes) is the archetypical materials for solar cells and transistors (9).

2.1 Polyaniline properties and structure:

2.1.1. Chemical properties

The name of polyaniline is a family of polymers which have the length of polymer chain, differ in oxidation state, redox properties and the value of conductivity. There are three oxidation states of polyaniline; Leucoemeraldine (LE), Emeraldine (E) and Pernigraniline (PNA).

The reduced states of polyaniline are LE and PNA in which all the nitrogen atoms are amine and the fully oxidized all the nitrogen atoms are imine forms respectively and in E the ratio amine / imine is 0.5. Standard electrochemical or chemical oxidation gives the electrically insulating LE, electrically conducting E, as for other conducting polymers [11].

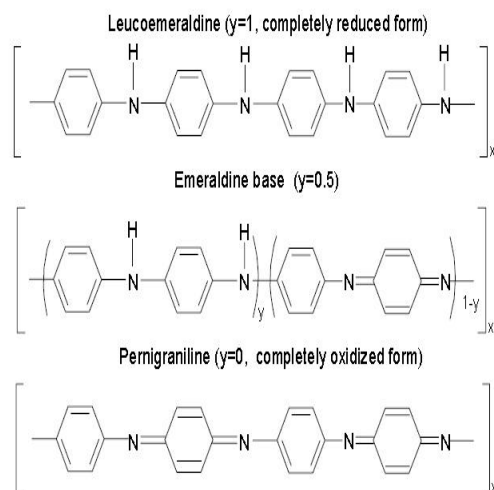


Fig 1.2 Non-conducting Polyaniline Structure

The second redox process by the oxidation gives an insulating material -PNA. Addition to this changing in behaviors of conductivity as decreases by order of ten in magnitude by the treatment of the conductivity E in neutral or alkaline medium. There is no change in the number of π electrons while protonation induces for the transition of insulator to conductor.

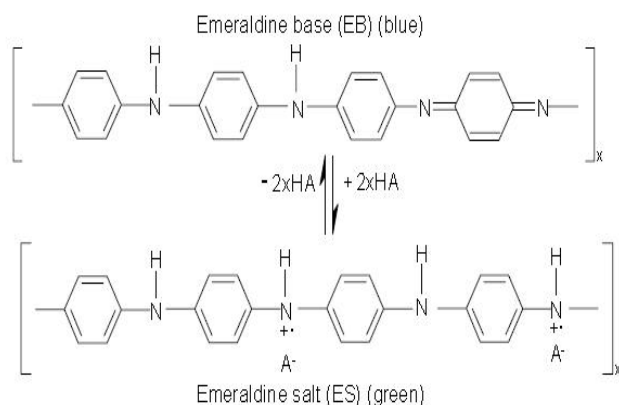


FIG 1.3 Protonated emeraldine form in transition phase from polyaniline base form. Arbitrary anion represented by A^-

Recently the structure of polyaniline was established as poly (P-phenyleneamine quinonedimine) as emeraldine base form [12]

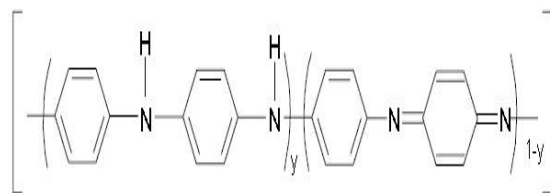


FIG 1.4 Poly (p-phenyleneamine quinonedimine) structure

The above structure of polyaniline was confirmed by the ^{13}C -NMR [13], IR and Raman spectroscopy experimental data [14, 15]. Accordance to the results, the bands C=N movement mode, C-N bending mode, for the movement of benzenoid and quinoid rings are observed. The chemical or electrochemical polyaniline oxidation gives the idea of quinoid diamine units and changing of the part of benzenoid diamine units, these results are verified by the analytical results [16] and FTIR spectroscopy [17]. The quantitative p-benzoquinone almost formed by the oxidation of Polyaniline [18]. The salts of PANI can be prepared by the protonic acids as the presence of basic amine and imine nitrogen atoms, 50% of nitrogen atoms can be protonated explained by the existence of strong effective pushing away between protons near to neighboring nitrogen atoms [18]. Aromatic amines, phenols, N, N-dimethylformamide phenols are some organic solvents and in aqueous solutions of acids, in cold 80% acetic acid, 60-88% formic acid in which polyaniline is partially soluble. The molecular weight of polyaniline base soluble in tetrahydrofuran, electrochemically obtained in aqueous solution gives the maximum value is 4300 [19] and maximum 50,000-55000, these value gives the idea of different synthesizing methods and method of treatments resulted in the molecular weight distribution shifts to the low molecular weight side [20]. The molecular weight of polyaniline effected by the temperature of synthesis, as temperature decreases of synthesis molecular weight increases [21].

2.1.2 Thermal, dielectric and mechanical properties of Polyaniline

2.1.2.1. Thermal properties

Thermal stability of Polyaniline in both conducting and insulating forms by thermo gravimetric analysis (TGA) and differential scanning calorimetry (DSC) have been studied by the researchers [22-25]. The thermogram of Polyaniline represents weight loss process in three steps.

- Due to evaporation of water or solvent molecules from the polymer between temperature ranges 65-125 °C [22].
- Loss of low molecular weight polymer and unbounded dopant ions from a Polyaniline chain between 125-350 °C [23].
- The degradation of the main polyaniline chain after the elimination of bounded dopant 350-520 °C between [24].

Thermal stability of doped polyaniline depends upon the counter anion as methane sulfonic acid (MSA) doped

polyaniline was stable up to 250 °C [26]. The first step occurring in the range of 65-125 °C is attributed to the evaporation of water or solvent molecules from the polymer [23]. The second-step weight loss occurs between 125-350 °C and is due to the loss of low molecular weight polymer and unbounded dopant ions from a PANI chain [24]. The third-step weight loss occurs between 350 and 520 °C and is due to the degradation of the main PANI chain after the elimination of bounded dopant [25]. But it should be mentioned that the thermal stability of doped PANI is dependent on the counter anion. For example, methane sulfonic acid (MSA) doped PANI was found to be stable up to 250 °C [26].

2.1.2.2. Dielectric properties

The electric field effects on polyaniline depend on the different factors temperature, electric field frequency, acid doping, and water content. The dielectric function $\epsilon(\omega)$ gives the information of transport mechanism in the system. The dielectric response is described by the complex permittivity

$$\epsilon(\omega) = \epsilon'(\omega) - i\epsilon''(\omega)$$

Where $\epsilon'(\omega)$ is storage energy in each cycle of applied electric field,

$\epsilon''(\omega)$ loss of energy in each cycle of applied electric field.

At high frequency the value of the value of $\epsilon'(\omega)$ is constant in comparisons to at low frequency and high temperature [27]. The increase of the dielectric permittivity with doping is a result of contributions from the backbone emeraldine base and the formed polaron and bipolarons to the polarization [27].

2.1.2.3. Mechanical properties

As it is known, the main disadvantages of PANI are its poor processibility and mechanical properties caused by its backbone stiffness. It was found that the mechanical property of PANI can be substantially enhanced when it was prepared from the gel and after the cross linking [28, 29]. The influence of the PANI oxidation state on the mechanical property was also established [28]. It was found that the tensile strength of EB film was improved by about 25% upon heating to 150 °C. This improvement was attributed to the interchain cross linking of PANI at high temperature and the formation of the PANI aggregates through interchain hydrogen bonding. The tensile strength of LE improved only upon its exposure to air at 200 °C, but, at the same time, the color of the film changed from yellow to blue [28]. The XPS results revealed the conversion of amine units to imines ones at this temperature [30]. Also, with the help of XPS analysis it was found that the mechanical property of the PANI film is closely related to the oxidation state of the polymer and the degree of cross linking [30]. The film orientation also was found to influence the mechanical properties. Monkman et al [30] showed that the tensile strength increases with elongation which indicates the alignment of polymer chains along the stretch direction. X-ray diffraction analysis suggested [29] a possible link of the mechanical behavior and changes in crystallinity with elongation.

2.1.3. Effect of acid-dopants on the polyaniline preparation and properties

The rate of polymerization as well as conductivity and others properties of PANI strongly depend on the used acid-dopant [31-32]. It is known that the electrical conductivity is influenced by the size and shape of the counter ion [33].

On one hand, higher the penetration of counter ions in the formed film is, the higher its conductivity is. But, on the other hand, the small molecular weight anions are more quickly removed from the polymer. That's why the choice of dopant might be a very important factor – if we need thermally stable conducting PANI we should use larger molecular weight acids, if the high value of conductivity is more important – it is better to use small protonic anions. The size of counter ion can also affect the interchain distance and, correspondingly, intermolecular interaction that can change the disorder in the polymer system [34]. Therefore, the choice of the dopant depends on the PANI application.

It should be mentioned that the rate of the aniline polymerization also changes depending on the acid in such sequence: HCl < HClO₄ < HBF₄ < HF < H₃PO₄ < H₂SO₄ [32, 35]. The acid nature at the same doping level determines also the PANI conductivity as one can see from the results in Table 1.1. Therefore, it is shown the same anion differently influences the rate of polymerization and the conductivity value of formed PANI.

In recent studies of PANI doped with various protonic acids [33, 36, 37] it was found that hydrochloric and sulphuric acids are the best dopants in terms of stability of conductivity. Kiattibutr et al [38] producing sensors for SO₂-N₂ mixtures found that at the same doping level specific conductivity of PANI-HCl is greater as compared with PANI-CSA because of two factors: a more closely packed crystalline mobility, and the ability to absorb more water molecules which induced ionic conductivity. But, in the other work [39] the opposite results can be found – the authors showed that poly (*o*-methoxyaniline) (POMA) doped with HCl is easily.

Table 1.1 Influence of the anion nature on the PANI conductivity [33]

Anion	Doping level	Conductivity, $\Omega^{-1} \cdot \text{cm}^{-1}$
CF ₃ COO ⁻	0.33	0.7
BF ₄ ⁻	0.34	0.8
ClO ₄ ⁻	0.31	2.0
Cl ⁻	0.36	1.4
NO ₃ ⁻	0.33	1.9
SO ₄ ²⁻	0.23	0.5

deprotonated in comparison to polymer doped by *p*-toluene sulphonic acid (TSA). The Cl⁻ anion is a weaker base than *p*-toluene sulphonate, thus, Cl⁻ ions are more easily removed [39]. Also, amic acids were found to be dopants for PANI [40]. PANI reacted with the selected amic acid by mixing the *N*-methyl pyrrolidone (NMP) solutions of the two materials in appropriate ratios. It was found that the conductivity in all the polymer matrices was limited by geometric limitations between the two polymers.

Phosphoric acid diesters with long alkyl substituents are also very good candidates for protonating agents which induce solution and melt processability of conducting PANI [41]. Due to their lower pH value, compared to the parent acid, they are sufficiently acidic to protonate emeraldine base. Their hydrophobic alkyl chains also induce solubility of PANI. Phosphoric acid esters are known as plasticizers for a variety of polymers. Thus, the esters can serve as plasticizers and protonating agents for PANI. Protonation of PANI was achieved by treatment with diester [bis-(2-ethylhexyl) hydrogen phosphate] (DiOHP) and diester [bis-(2-methylpropyl) hydrogen phosphate] (DiBHP) dissolved in an appropriate solvent (toluene, decaline, chlorinated hydrocarbons, *m*-cresol) or by mechanical mixing of PANI with neat diester. Phosphoric acid esters are also known to form strong intramolecular H-bonds [41].

The PANI-dopant interaction can be related to an increase in the polymer molecular weight, the polymer crystallinity and/or the molecular conformation of doped PANI that changes from a compact coil to an open coil-like structure. Not only conductivity, but also electrochromic properties depend strongly on the acid-dopant. Gazotti et al [39] established that POMA doped with TSA presents a higher optical contrast in the visible region than the same polymer doped by HCl.

Many researchers also reported that the dopant mixtures induced high conductivity and processibility [37, 42]. Dopant mixtures gave higher conductivity to PANI than a single dopant, because they could provide an effective conjugation length and a high protonated level. It should also be pointed out that not only dopant can influence the PANI properties, but also the used solvent. As it was shown, the conductivity of the PANI samples varies with dopants (TSA, CSA, and benzene sulphonic and naphthalene sulphonic (NSA) acids) in the same solvent [42]. However, using different solvents (*m*-cresol, chloroform, 2-hydroxybutanol (BeOH)) conductivity with the same dopant dramatically changes [42], which indicates that transport properties can be controlled by both dopants and solvents.

Taking into account a specificity of used systems, the observed divergences in obtained experimental results may be explained by using different polymerization methods and conditions. Significant fact may have been here also attributed to the different PANI-dopant interactions.

2.2 Synthetic methods of the polyaniline preparation

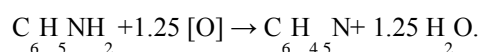
PANI is synthesized by the chemical or electrochemical oxidative polymerization of aniline [11]. There exists also a method of plasma polymerization [43], but this method is not very convenient and not easy in

application. So, we will speak only about two ways of the PANI obtaining – chemical and electrochemical polymerization.

It is possible to select such conditions under which PANI is the main reaction product. In this case the chemical and electrochemical ways of the PANI preparation produce polymers of the same composition since their electrochemical behavior is practically identical [44-46].

2.2.1. Chemical way of obtaining polyaniline

Suitable oxidants such as ammonium persulphate (APS) $(\text{NH}_4)_2\text{S}_2\text{O}_8$, sodium chlorate NaClO_3 , potassium dichromate $\text{K}_2\text{Cr}_2\text{O}_7$, Fenton reagent, hydrogen peroxide H_2O_2 , etc. [46-50] in solutions containing mineral or organic acids. As a result, dark green product is obtained, which because of its color received the name “Emeraldine”. The treatment of this product by alkaline or ammonium solution converts it into dark blue Emeraldine base (Fig. 1.2). Under these conditions Emeraldine can be received quantitatively: if oxidant is taken on the basis of 1.25 mol per one aniline molecule, so the yield reaches 97% [26]. Similar values have been found recently [31]: 1.15 ± 0.04 mol of APS per mol of aniline. These results are in good agreement with the Emeraldine formula proposed on the basis of elemental analysis and quantitative ratio [32] including quinoneimine units 1/4, brutto formula $\text{C}_6\text{H}_4.5\text{N}$



This formula is, certainly, approximate, but is close enough to reality. The aniline oxidation reaction is an exothermal reaction with an induction period [51]. It was established that the presence of PANI leads to the decrease of induction period time, i.e. the chemical oxidation as well as electrochemical one is an autocatalytic process. The properties of formed PANI are practically independent of the chosen oxidant, but only under conditions when the oxidant is not taken in excess. In the case of oxidant excess the decrease of the PANI yield is observed which is due to the PANI decomposition [31]. Moreover, the polymer formed is a little more oxidized and as a result the value of its conductivity is lower [31].

2.3 COMPOSITE MATERIAL

Ceramics and polymers, composites, especially polymer-matrix composites (PMC), allow for a physical property tailoring using different type of fillers [52, 53]. Depending on the particle size, particle shape, specific surface area and chemical nature, the following polymer matrix properties can be modified:

- Electrical and thermal conductivity
- Polymer phase behavior and thermal stability
- Mechanical properties like stiffness, Young's modulus, wear, fatigue, and others
- Flame retardancy [54]
- Density
- Physical properties such as magnetic, optic or dielectric properties.

In principle, the whole bandwidth of polymer processing technology can be used for shaping, molding or replication of the polymer-based composites enabling a low

cost fabrication of components and devices. On the one hand new potential applications can be realized using nanoparticles with small sizes, but on the other hand they complicate the realization of homogeneous and highly filled composites. Polymer matrix composites containing different kinds of nanosized fillers like clay, carbon nanotubes, and others, can be found in [54-55].

2.3.1. Features of Nanoparticles

2.3.1.1. Particle size dependent properties of inorganic nanoparticles

Ensembles of isolated nanoparticles with particle sizes below around 20 nm exhibit physical properties that may differ from their bulk counterparts. The effects are sometimes crucial, as they will strongly influence the desired or expected property of the nanocomposite. A significant influence of particle size is observed as well as on magnetic, dielectric, electronic, optical, thermodynamic, and thermo mechanical, and on structural properties. The following explanations rely on general features, found in metallic, ceramic and semiconducting nanoparticles. Size-dependent magnetic properties have been studied for around two decades. Tang *et al.* [56, 57] reported an increasing saturation magnetization in the particle size range from 7.5 nm to 25 nm. In this size regime, the authors also observed a decrease of the transition temperature. Han *et al.* described similar behavior for Co-containing ferrite nanoparticles [25]. The size dependence of saturation magnetization is depicted exemplarily in Figure 2 (left). These dependencies can be stated as general rules as nanoparticles are typically covered by a 0.5 to 1 nm thin, nonmagnetic surface layer. As the amount of surface increases with decreasing particle size, the ratio of nonmagnetic surface layer to magnetic material also increases.

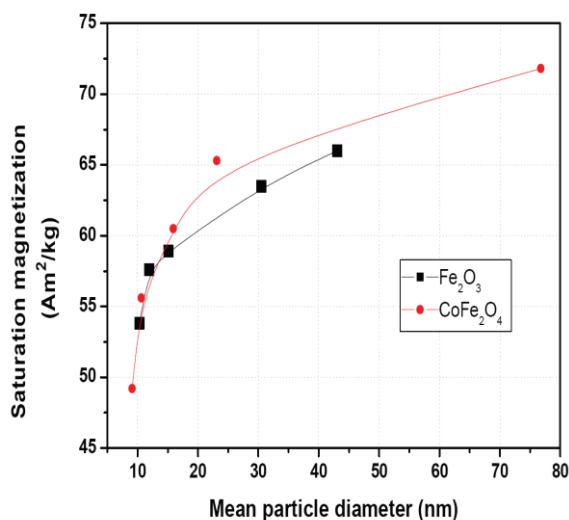


Figure 2.1 a. Examples for typical particle size-dependent physical properties. Left: Saturation magnetization as a function of particle size. Data taken from [58]. Right: Band gap energy for SnO₂ as a function of particle size. Data taken from [59]

Size-dependent refractive indices were reported for narrow band-gap semiconducting nanoparticles such as PbS by Kyprianidou-Leodidou *et al.* [60]. Above 25 nm particle

size the refractive index of PbS at different wavelengths was more or less independent of the particle size, and near the bulk values, respectively. For PbS particles with diameters below 25 nm the refractive indices decreased significantly with size. Similar observations were made from these authors featuring the absorption coefficient. In Si-nanoclusters a significant luminescence peak blue-shift was calculated for decreasing particle size. In parallel the

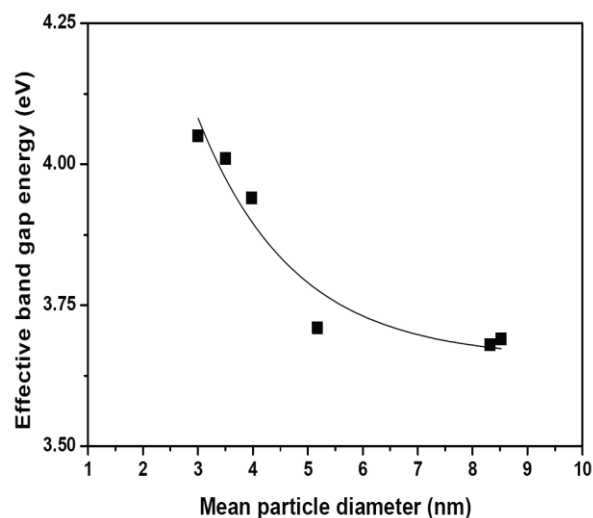


Figure 2.1 b Examples for typical particle size-dependent physical properties. Left: Saturation magnetization as a function of particle size. Data taken from [58]. Right: Band gap energy for SnO₂ as a function of particle size. Data taken from [59]

Spectra became broader with decreasing particle size. These effects were described in the size regime from 2 to 6 nm [61]. Theoretical considerations predicted size-dependent energy band gap and dielectric constants for semiconducting nanoparticles [62]. Lee *et al.* [59] studied the size dependence of band gap energies in SnO₂ quantum dots. Figure 2 (right) shows the significant increasing band gap energy with decreasing particle size. Nienhaus *et al.* [63] and Szabo *et al.* [64] observed a blue shift of the plasmon losses with decreasing particle size in SnO₂. Concerning thermodynamic properties such as phase transitions or phase stabilities, interesting observations were made for materials existing in several polymorphs. The physical properties such as optoelectronic, photochemical or catalytic properties may be influenced by phase as well as by size. This is the case for ZnO₂ and TiO₂, both existing in different phases, and very interesting as nanofillers in composites. Suresh *et al.* [65] described an inverse relationship between transformation temperature and particle size in ZnO₂, and deduced a grain size dependent phase diagram. Li *et al.* [66] made energetic considerations and calculated decreasing transition temperatures with decreasing particle sizes for nanoscaled ZnO₂. Zhang and Banfield [67] analyzed the phase stability of nanocrystalline TiO₂. They found anatase to be more stable than rutile when the particle size decreased below around 14 nm. Phase stabilities of TiO₂ and ZnO₂ were also investigated by Schlabach *et al.* [68, 69]. Both ceramics were found to occur in non-typical phases as nanoparticles compared to the bulk material and are subject to phase transformation and grain growth with increasing temperature. Coating the

nanoparticles with a different ceramic layer suppresses phase transformations and obstructs grain growth. The knowledge about which phase is stable under which conditions is in-so-far important, as TiO₂ is frequently used as filler to modify optical properties of polymers. The phases differ in their refractive indices: bulk anatase is characterized by a refractive index of 2.54 (at 550 nm) and a band gap of 3.20 eV, whereas rutile is characterized by a refractive index of 2.75 (at 550 nm) and a band gap of 3.03 eV for bulk, respectively. For amorphous thin TiO₂ films a refractive index of 2.51 (at 550 nm) and a band gap of 3.27 eV were reported [70]. Size effects regarding electrochemical properties and cycling stability were described for nanoscaled TiO₂ [71, 72]. With decreasing anatase particle size from 30 nm to 6 nm, an increase of capacity was observed, indicating an improved lithium storage capability [38]. Similar effects were observed for rutile [72]. Here the authors found a significant increase in capacity with decreasing size from 300 nm to 15 nm for rutile particles. As both phases were cycled under different conditions, the results cannot be compared directly. Deng *et al.* [73] comment that anatase - among all different TiO₂ phases - presents the most interesting potential regarding electrochemical properties.

2.3.1.2. Thermo mechanical Composite Properties

For many years, micron sized fillers have been used for the reinforcement of the polymers poor mechanical

properties. In a rough approximation, the resulting composite properties correlate with the filler volume content in the matrix. In contrast, the use of nanofillers with particle or agglomerate sizes below 100 nm and primary particles below 30 nm does not follow this simple approach in all cases, because due to size effects the following additional aspects have to be considered:

- Particle shape, agglomeration, and size distribution
- Particle specific surface area and related surface chemistry
- Particle-polymer matrix interface and interaction
- Compounding method and related shear forces.

Quite often the influence of nanoparticles on the polymer properties is not unique, but in general some trends can be observed. Jordan and coworkers collected in a very comprehensive overview the main trends of the nanofillers impact on the resulting composite mechanical behavior, considering attractive as well as repulsive interactions of the filler with an amorphous or crystalline polymer matrix [74]. Table 2.1 gives a selection of the influence trend of nanoparticles on the mechanical properties of amorphous polymers taken from [74]. Table 2.2 lists the related information for semi crystalline polymers, also taken from [74].

Table 2.1 Impact of nanoparticles on composite properties with amorphous polymer matrix.

Item	Polymer filler Interaction Impact	Item
Elastic modulus	Attractive/repulsive	Increase with volume fraction
	Attractive/repulsive	Increase with size decrease
Density/volume	Attractive	Increased volume as size decreases
	Repulsive	n.a.
Glass transition temperature	Attractive	Increase with size decrease
	Repulsive	Level until 0.5%, drops off level from 1–10%

Table 2.2 Impact of nanoparticles on composite properties with semi crystalline polymer matrix.

Item	Polymer filler Interaction	Impact Item
Elastic modulus	Attractive/repulsive	Increase with volume fraction
	Attractive/repulsive	Increase with size decrease
Density/volume	Attractive	Increased volume as size decreases
	Repulsive	n.a.
Glass transition temperature	Attractive	Decrease with addition of particles
	Repulsive	n.a.
Crystalline	Attractive/repulsive	No major effect

In the following, a few examples demonstrate the influence of nanoparticles on the phase behavior, elastic modulus, scratch resistance, hardness and elastic properties. A comprehensive review covering the impact of different nano particle types like clay, carbon nanotubes and spherical particles on the mechanical properties of polymer nanocomposites was published by Tjong in 2006 [75].

2.3.1.3 Glass transition temperature and coefficient of thermal expansion

The Rensselaer group of Siegel investigated the influence of coated and uncoated Al₂O₃ (average particle size around 39 nm) on the glass transition (TG) behavior of PMMA [76, 77]. They found, that uncoated Al₂O₃ caused, at concentrations greater than 0.5 wt %, a significant TG-drop of around 25 °C. The silanization of the Al₂O₃ enabled a constant TG even at higher Al₂O₃ load of 10 wt %. In contrast, the Hu group found that the addition of

hydrophobic nanosized SiO₂ (Aerosil®) to PMMA yielded a pronounced increase of the glass transition temperature up to 15 °C at a solid load of 4 wt % due to a strong attractive interaction of the non-polar nanoparticle with a huge specific surface area up to 200 m²/g and the non-polar polymer [78]. The decomposition temperatures of the composites were elevated remarkably even at low SiO₂ contents. Both groups used sonification in MMA as dispersing method prior to the polymerization to the final PMMA-based composite [76, 78]. The addition of two different nanosized Al₂O₃ (primary particle sizes 13 and 38 nm, solid load up to 10 wt %) to a methylmethacrylate based reactive resin caused after polymerization only a slight drop of TG [79]. The coefficient of thermal expansion (CTE) was more affected by the 13 nm Al₂O₃, which can be explained by the larger specific surface area of 107 m²/g than the 38 nm Al₂O₃ with only 34 m²/g enabling pronounced polymer chain immobility. Although a TG-increase could not be detected in PMMA/SiO₂ nanocomposites by thermal analysis (DSC), dielectric and IR-spectroscopy gave evidence for a strong attractive interaction of the nanoparticles with the polymer chains by means of reduced chain movement and longer relaxation times [80]. The direct chemical bonding of monodisperse nanosized SiO₂ to a polymer backbone, here polystyrene (PS), via grafting, caused a TG increase up to 6 °C at 2 wt %, while the simple physical mixing via sonification generated a slight TG decay [81]. Composites, consisting of nanosized Al₂O₃ and the semi crystalline high performance polymer polyetheretherketone (PEEK), fabricated by wet chemical methods followed by hot pressing, showed an elevated decomposition temperature in comparison to the neat polymer [82]. In contrast, the melting temperature was not affected by the addition of the nanosized Al₂O₃ even at very high load (30 wt %). The crystallization temperature increased slightly with load. Due to the increasing ceramic content the CTE was reduced [82]. Chen and coworkers [83] found, that small amounts (5 wt %) of the nanofiller induced a higher thermal stability, while larger Al₂O₃ concentrations (9 wt %) caused a pronounced weight loss even at low temperatures [83]. Same behavior could be found for TG. A TG increase up to Al₂O₃ filler concentrations of 5 wt % were reported by Omrani and coworkers as well [84]. Surface modified nanosized SiO₂ monospheres with an average diameter of 400 nm, dispersed in an epoxy matrix, caused an increase of TG as well as a reduction of the CTE with solid content [85]. A chemical bonding to the polymer amplified these effects. Summarizing the data the following statements can be made:

- The addition of ceramic fillers lowers the CTE.
- An increase of TG can be observed if an attractive interaction of the nanofillers with the polymer matrix by physic- or chemisorptions is given.
- A decrease of TG occurs if the nanoparticle has a repulsive interaction with the matrix.

2.3.1.4 Elastic modulus, tensile strength, flexural strength and impact performance

Hot compression molding of surface modified SiO₂ (primary particle size 12 nm) or Al₂O₃ (primary particle sizes 15 and 90 nm), mixed with micron sized PEEK powder, was used for the fabrication of test specimens for mechanical testing [86]. The authors investigated the influence of different mixing methods (direct mechanical mixing, liquid-solid mechanical dispersing, sonification, ball milling) and particle sizes on the composite properties. In agreement to results listed earlier the addition of the nanofillers to PEEK caused an increase of TG but no remarkable change of the melting behavior. The amount of crystalline domains in the polymer decreased. The authors found, that tensile and compressive strength increased with Al₂O₃ particle diameter while the flexural strength was not affected. Comparable trends could be detected for the Al₂O₃ and SiO₂ fillers load increase. Both materials showed an optimized concentration of 5 wt % for a raise of the tensile, compressive and impact strength; but a further filler concentration increase yielded a strength reduction. A nanofillers surface modification using different coupling agents did not result in a unique trend of mechanical property reinforcement or weakening. A clear influence of the dispersing method on the investigated mechanical properties was not found [86]. Surface modified nanosized Al₂O₃ (primary particle size 39 nm), dispersed in PMMA, caused an increase in strain-to-failure over 28% at a solid load of 5 wt % enabling a ductile flow in the glassy state [87]. Thin films, consisting of up to 22.8 wt % SiO₂ and polyamide 6, were investigated with respect to their mechanical properties [88]. A significant change of the viscoelastic properties (increase of storage and loss modulus) with increasing load as well as of the Young's modulus as function of solid load and temperature was reported. The mechanical properties of an *in situ* synthesized and surface modified nanosized TiO₂ using acrylates as reactive resin matrix were investigated after polymerization [89]. The sol-gel based nanoparticle synthesis and the *in situ* composite formation avoided particle agglomeration guaranteeing a homogenous particle distribution in the matrix. Increasing TiO₂ content caused an increase of hardness (from 0.030 GPa for the pure polymer and 0.198 GPa for a TiO₂ content of 10 wt %) and Young's modulus (from 2.83 GPa for the pure polymer and 4.98 GPa for a TiO₂ content of 10 wt %). The thermal stability was improved also, an increase of the refractive index in the visible range from 1.5 up to 1.8 (TiO₂ load 50 wt %) due to the high intrinsic refractive index value of TiO₂ accompanied with a good optical transmittance was measured [89]. The effect of the nanoparticle size and amount on resulting mechanical composite properties were measured by Cannillo *et al.* [90]. Fracture images showed a strong bond between the surface-modified SiO₂ and the polymer matrix. Tensile tests showed an improvement of the Young's modulus with solid load; in case of untreated, hydrophilic SiO₂ no reinforcement was observed. Hence, for a numerical description of the mechanical behavior using FEM-methods an interfacial layer between the filler and the matrix had to be assumed. Cho and coworkers found, that a pronounced dependence of the mechanical properties like Young's modulus and tensile strength is given [91]. Surface coated nanosized Fe₂O₃ with a nominal

particle size of 9 nm, dispersed in an epoxy matrix, induced an improved thermal stability of the resulting composite, a significant TG increase of 15 °C at a 10 wt % solid load as well as an improved pencil hardness [92]. The properties of nanosized SiO₂-latex composites are described by Oberdisse [93].

As a short resume the particle size, size distribution, specific surface area, particle load, degree of dispersion, and the particle morphology determine especially the composite's mechanical behavior [94]. The formation of disordered aggregates and agglomerates generating flexible micron sized clusters instead of isolated nanosized particles affect directly the mechanical properties. Hence a pronounced modulus enhancement in thermoplastic polymers is difficult.

2.3.1.5 Scratch resistance, wear and creep properties

Ng and coworkers [95] compared the influence of micron-sized and nanosized TiO₂ (10 wt %, average particle size 0.24 μm and 32 nm, respectively) on the scratch resistance of an epoxy. They found an improvement of the scratch resistance when using the nanosized in comparison to the micron-sized filled polymer and the neat polymer. Same trend was found for the strain to failure behavior; interestingly at other concentrations no impact relative to the pure polymer of the nanosized TiO₂ was found. The grafting of nanosized SiO₂ (average particle size 9 nm) with acrylamide and the dispersion in an epoxy matrix via stirring and sonification yielded composites with improved wear properties and reduced friction coefficient relative to the pure polymer and a composite with the untreated SiO₂ even at low nanofillers content (~2 vol %)[96]. A slight increase of the glass transition temperature due to an attractive filler-matrix interaction and the resulting reduced polymer chain mobility was observed also. Surprisingly no difference between the uncoated and grafted nanosilica was observed. Highly transparent composites, consisting of surface modified SiO₂ (Aerosil® 600, average primary particle size 40 nm) and Al₂O₃ (average primary particle size: 20 nm), dispersed in an acrylate-based polymer, with improved scratch resistance were synthesized by Bauer *et al.* [88, 89]. Melt mixing of polyethyleneterephthalate and nanosized Al₂O₃ yielded a composite with slightly increased friction coefficient and reduced wear rate at low filler contents up to 2 wt % [99]. In contrast, a further Al₂O₃ addition caused an increase of the wear rate to values significantly higher than the pristine polymer. This optimized filler concentration of 2 wt % correlates with a reduction of the polymers crystallinity [99]. Daseri and coworkers published quite recently a comprehensive overview covering all aspects of wear and scratch resistance in polymer-based nanocomposites [100]. Co-extrusion of nanosized TiO₂ (primary particle size 21 nm) with polyamide 6, 6 yielded composites, which were examined with respect to their creep resistance under ambient conditions and at elevated temperature (50 °C) [101]. Test specimens were fabricated by injection molding. Composites containing 1 vol % TiO₂ possesses a significant improvement of the creep resistance and a reduction of the creep strain in comparison to the unfilled polyamide.

2.4 Energy and Environment application

2.4.1 Intrinsic conductive polymer nanocomposites and organic solar cells

Organic solar cells are widely under investigation by O'Regan and Graetzel in 1991 dealing with the photocurrent generation after photon absorption by an organic dye and electron injection into the conduction band of a n-type semiconductor like TiO₂ [102]. Modern dye-sensitized organic solar cell uses polymer electrolytes quite similar to systems used in lithium-ion batteries [103]. Quite recently the positive influence of nanosized TiO₂ (13 nm, Degussa/Evonik), dispersed in PVDF, on the long term stability of the solar cell was demonstrated [104]. Intrinsic conductive polymers have gained more importance at the latest since the Noble prize for Alan J. Heeger in chemistry in 2000. These polymers, like polyaniline (PANI), polythiophene (PTP), PPy or PPV, are expected to be used in organic solar cells, display technology, photodiodes or batteries. In the last years the addition of nanosized ceramics like SiO₂, Al₂O₃, or TiO₂ for a chemical stabilization, an improvement of the physical properties as well as a better dispersibility in water or organic solvents has been investigated. Ballav and Biswas prepared composites consisting of PTP and nanosized alumina (particle size: 22–74 nm) [105]. They found a slight increase in the electrical conductivity and an improved thermal stability in contrast to the pure homopolymer. In contrast to the neat polymer, the composite showed the formation of stable suspensions in water and isopropanol. Yang and coworkers investigated the influence of nanosized SiO₂ (20 nm) and TiO₂ (20 nm) on the stability of the PPV-precursor molecule [106].

2.4.2 Sensors

Public awareness of environmental issues rises and governments make international commitments to reduce emissions, sensor arrays (electronic noses) can play a very important role in the protection of our environment [107]. Nanostructured TiO₂ films have been widely explored as sensor units for various gases. Grimes *et al.* reported that TiO₂ nanotubes prepared by anodization exhibited high sensitivity to hydrogen at temperatures as low as 180 °C [108]. It was reported by Birkefeld and co-workers that the conductivity of anatase TiO₂ varied in the presence of CO and H₂ at temperatures above 500 °C but Al-doped TiO₂ (10%) became selective to H₂ [109]. For ZnO, a variety of nanostructures such as nanowires, nanorods, nanotetrapods, and nanoparticles have been investigated for gas sensing [110-111].

III. Conclusion

The results and data discussed above allow us making a conclusion that the formation of composite materials based on PANI and common polymers opens new possibilities for production of the materials with desired conductivity, mechanical, thermal and other properties. Although a lot of such composite systems have been well known, their industrial applications are still very limited, and in the case of the important polyaniline TiO₂ / SnO₂ and polyvinyl alcohol composites are unknown. This fact can be explained by a lack of data on effects of the chemistry and physico-chemistry of the aniline polymerization process in

the presence of the matrix polymer on conductivity, thermo stability, mechanical, structural and other properties of the composite materials.

- To synthesis conductive (PANI) and polyaniline- TiO₂ / SnO₂ composite through in situ polymerization technique.s
- To make conductive films of PANI/other polymer like PVA and PANi-TiO₂/ SnO₂ other polymer like PVA by using solution casting method.
- To study the effect of TiO₂ / SnO₂ content on the conductivity behavior of the blends with varying TiO₂/aniline weight ratio.
- To study the heating effect on conductivity behavior.
- To study the effect of weight fractions of conductive components (PANI and PANI-TiO₂).

References

1. Hanemann Thomas, Szabo Vinga Dorothee, Polymer-Nanoparticle Composites: From Synthesis to Modern Applications; Materials 2010, 3, 3468-3517.
2. A. Gruger, A. El Khalki, Ph. Colomban, Protonation, sol formation and precipitation of poly- and oligoanilines, *J.Raman Spectrosc.*, **34**, 438-450 (2003).
3. A. Efremova, Lj. Arsov, Electrodeposition of aniline at irreversible redox processes *Bull. Chem. Technol. Macedonia*, **10**, 27-32 (1991).
4. A. Efremova, A. Regis, Lj. Arsov, Electrochemical formation and deposition of polyaniline on electrode surface; in-situ Raman spectroscopical study, *Electrochim. Acta*, **6**, 839-845 (1994).
5. Shi-Jian Su, N. Kuramoto, Processible polyaniline-titanium dioxide nanocomposites; effect of the titanium dioxide on the conductivity, *Synth. Met.*, **114**, 147-153 (2000).
6. A. Dey, S. De, A. De, S. K. De, Characterization and dielectric properties of polyaniline-TiO₂ nanocomposites, *Nanotechnology*, **15**, 1277-1283 (2004).
7. L. Zhang, M. Wan, Polyaniline/TiO₂ Composite Nanotubes, *J. Phys. Chem. B.*, **107** (28), 6748-6753 (2003).
8. Gyorgy Inzelt (2008). *Conducting Polymers A New Era in Electrochemistry. Springer. pp. 265-269.*
9. Herbert Naarmann "Polymers, Electrically Conducting" in Ullmann's Encyclopedia of Industrial Chemistry 2002 Wiley-VCH, Weinheim.
10. Handbook of Nanostructured Materials and Nanotechnology; Nalwa, H.S., Ed.; Academic Press: New York, NY, USA, 2000; Volume 5, pp. 501-575.
11. Kang E.T., Neoh K.G., Tan K.G., Tan K.L. Polyaniline: a polymer with interesting intrinsic redox states // *Prog. Polym. Sci.*-1998.-23-P.227-324.
12. Lu F.L., Wudi F., Nowak M., Heeger A.J. Phenyl-capped octaaniline (COA): An excellent model for polyaniline // *J. Am. Chem. Soc.*- 1986-Vol.108, No.26, P 8311-8313.
13. Glarum S.H., Marshall J.H. The in situ ESR and electrochemical behavior of poly (aniline) electrode films // *J. Electrochem. Soc.* - 1987.-Vol.134, No. 9.
14. Zeng X.-R., Ko T.-M. Structures and properties of chemically reduced polyanilines // *Polymer*-1998-Vol.39, No. 5 -P.1187-1195.
15. Ping Z., Nauuer G.E., Neugebauer H., Theiner J., Neckel A. In situ Fourier transform infrared attenuated total reflection (FTIR- ATR) spectroscopic investigations on the base acid transitions of leucoemeraldine // *electrochimica Acta.*- 1997.-Vol.42, No. 11- P 1693-1700.
16. Mohilner D.M., Adams R.N., Argersinger W.J. Investigation of the kinetics and mechanism of the anodic oxidation of aniline in aqueous sulfuric acid solution at a platinum electrode // *J. Am. Chem. Soc.* - 1962. - Vol. 84, № 19. - P. 3618 - 3622.
17. Erdem E., Karakisla M., Sacak M. The chemical synthesis of conductive polyaniline doped with dicarboxylic acids // *European Polymer Journal.* - 2004. - Vol. 40, № 4. - P. 785 - 791.
18. Reiss H. Theoretical analysis of protonic acid doping of the emeraldine form of polyaniline // *J. Phys. Chem.* - 1988. - 92. - P. 3657 - 3662.
19. Mohilner D.M., Adams R.N., Argersinger W.J. Investigation of the kinetics and mechanism of the anodic oxidation of aniline in aqueous sulfuric acid solution at a platinum electrode // *J. Am. Chem. Soc.* - 1962. - Vol. 84, № 19. - P. 3618 - 3622.
20. Watanabe A., Mori K., Iwasaki Y., Nakamura Y. Molecular weight of electropolymerized polyaniline // *J. Chem. Soc. Chem. Commun.* - 1987. - 1. - P. 3- 4.
21. Stejskal J., Riede A., Hlavata D., Prokes J., Helmstedt M., Holler P. The effect of polymerization temperature on molecular weight, crystallinity and electrical conductivity of polyaniline // *Synthetic Metals.* - 1998. - 96. - P. 55 - 61.
22. Chandrakanthi N., Careem M.A. Thermal stability of polyaniline // *Polymer Bulletin.* - 2000. - Vol. 44, № 1. - P. 101 - 108.
23. Chan H.S.O., Ho P.K.H., Khor E., Tan M.M., Tan K.L., Tan B.T.G., Lim Y.K. Preparation of polyaniline doped in mixed protonic acids: their characterization by X-ray photoelectron spectroscopy and thermogravimetry // *Synthetic Metals.* - 1989. - 31. - P. 95 - 108
24. Ding L., Wang X., Gregory R.V. Thermal properties of chemically synthesized polyaniline (EB) powder // *Synthetic Metals.* - 1999. - 104. - P. 73 - 78.
25. Lu X., Tan C.Y., Xu J., He C. Thermal degradation of electrical conductivity of polyacrylic acid doped polyaniline: effect of molecular weight of the dopants // *Synthetic Metals.* - 2003. - 138. - P. 429 - 440.
26. Morales G.M., Miras M.C., Barbero C. Anion effects on aniline polymerisation // *Synthetic Metals.* - 1996. - 101. - P. 686.
27. Pinto N.J., Sinha G.P., Aliev F.M. Frequency-dependent conductivity and dielectric permittivity of emeraldine base and weakly doped poly(*o*-toluidine) // *Synthetic Metals.* - 1998. - 94. - P. 199 - 203.
28. Li Z.F., Kang E.T., Neoh K.G., Tan K.L. Effect of thermal processing conditions on the intrinsic oxidation states and mechanical properties of

- polyaniline films // *Synthetic Metals*. – 1997. – 87. – P. 45 - 52.
29. Tzou K., Gregory R.V. Mechanically strong, flexible highly conducting polyaniline structures formed from polyaniline gels // *Synthetic Metals*. – 1993. – P. 555. – P. 983 – 988.
 30. Laughlin P.J., Monkman A.P. Mechanical properties of oriented emeraldine base polyaniline // *Synthetic Metals*. – 1997. – 84. – P. 765 – 766.
 31. Ayad M.M., Salahuddin N., Sheneshin M.A. Optimum reaction conditions for in situ polyaniline films // *Synthetic Metals*. – 2003. - Vol.132, № 2. – P. 185 - 190.
 32. Hussain A.M.P., Kumar A. Electrochemical synthesis and characterization of chloride doped polyaniline // *Bull. Mater. Sci.* – 2003. - Vol. 26, № 3. – P. 329 – 334.
 33. Morales G.M., Miras M.C., Barbero C. Anion effects on aniline polymerisation // *Synthetic Metals*. – 1996. – 101. – P. 686.
 34. Stafstrom S., Bredas J.L., Epstein A.J., Woo H.S., Tanner D.B., Huang W.S., MacDiarmid A.G. Polaron lattice in highly conducting polyaniline: theoretical and optical studies // *Phys. Rev. Lett.* – 1987. – 59. – P. 1464 - 1467.
 35. Norris I.D., Kane-Maguire L.A.P., Wallace G.G. Electrochemical synthesis and chiroptical properties of optically active poly(*o*-methoxyaniline) // *Macromolecules*. - 2000. - Vol. 33. - P. 3237 – 3243.
 36. Borole D.D., Kapadi U.R., Kumbhar P.P., Hundiwale D.G. Effect of inorganic dopants (in presence of electrolyte) on the conductivity of polyaniline, poly(*o*-toluidine) and their copolymer thin films // *Materials Letters*. – 2002. – 57. – P. 844 – 852.
 37. Kim S.H., Seong J.H., Oh K.W. Effect of dopant mixture on the conductivity and thermal stability of polyaniline/Nomex conductive fabric // *J. Appl. Pol. Sci.*. – 2002. - Vol. 83. – P. 2245 – 2254.
 38. Kiattibutr P., Tarachiwin L., Ruangchuay L., Sirivat A., Schwank J. Electrical conductivity responses of polyaniline films to SO₂-N₂ mixtures: effect of dopant type and doping level // *Reactive and functional polymers*. – 2002. – 53. – P. 29 – 37.
 39. Gazotti W.A.Jr., Jannini M.J.D.M., Cordoba de Torresi S.I., Paoli M.-A. de Influence of dopant, pH and potential on the spectral changes of poly(*o*-methoxyaniline): relationship with the redox processes // *J. Electroanal. Chem.* – 1997. – 440. – P. 193 - 199.
 40. Angelopoulos M., Patel N., Saraf R. Amic acid doping of polyaniline: Characterization and resulting blends // *Synthetic Metals*. – 1993. – Vol. 55, № 2-3. – P. 1552 – 1557.
 41. Pron A., Osterholm J.-E., Smith P., Heeger A.J., Laska J., Zagorska M. Processable conducting polyaniline // *Synthetic Metals*. – 1993. - Vol. 57, № 1. – P. 3520 – 3525.
 42. Joo J., Chung Y.C., Song H.G., Baeck J.S., Lee W.P., Epstein A.J., MacDiarmid A.G., Jeong S.K., Oh E.J. Charge transport studies of doped polyanilines with various dopants and their mixtures // *Synthetic Metals*. – 1997. – 84. – P. 739 – 740.
 43. Mathai C.J., Saravanan S., Jayalekshmi S., Venkitachalam S., Anantharaman M.R. Conduction mechanism in plasma polymerized aniline thin films // *Materials Letters*. – 2003. – 57. – P. 2253 - 2257.
 44. Karakisla M., Sacak M., Erdem E., Akbulut U. Synthesis and characterization of malonic acid-doped polyaniline // *J. Appl. Electrochem.* – 1997. – 27. – P. 309 – 316.
 45. Delvaux M., Duchet J., Stavaux P.-Y., Legras R., Demoustier-Champagne S. Chemical and electrochemical synthesis of polyaniline micro- and nano-tubules // *Synthetic Metals*. – 2000. – 113. – P. 275 - 280.
 46. Palaniappan S. Chemical and electrochemical polymerization of aniline using tartaric acid // *European Polymer Journal*. – 2001. – 37. - P. 975 - 981.
 47. Adams P.N., Monkman A.P. Characterization of high molecular weight polyaniline synthesized at –40 °C using a 0.25:1 mole ratio of persulfate oxidant to aniline // *Synthetic Metals*. – 1997. – 87. – P. 165 - 169.
 48. Sun Z., Geng Y., Li J., Jing X., Wang F. Chemical polymerization of aniline with hydrogen peroxide as oxidant // *Synthetic Metals*. – 1997. – 84. – P. 99 - 100.
 49. Zhu H., Mu S. Effect of Fenton reagent on the synthesis of polyaniline // *Synthetic Metals*. – 2001. – 123. – P. 293 - 297.
 50. Genies E.M., Lapkowski M., Tsintavis C. La polyaniline: preparations, properties et applications // *New J. Chem.* - 1988. - Vol. 12, № 4. - P. 181 - 196.
 51. Sapurina I., Riede A., Stejskal J. In-situ polymerized polyaniline films 3. Film formation // *Synthetic Metals*. – 2001. – 123. – P. 503 – 507.
 52. Talreja, R., Manson, J.A.E., Eds. *Polymer Matrix Composites*; Elsevier Science Ltd: Oxford,UK, 2002.
 53. Gerard, J.F., Ed. *Fillers and Filled Polymers*; Wiley-VCH: Weinheim, Germany, 2001; Volume 169. 9.
 - Mittal, V. Polymer layered silicate nanocomposites: a review. *Materials* **2009**, 2, 992-1057.
 54. Mittal, V. Polymer layered silicate nanocomposites: a review. *Materials* **2009**, 2, 992-1057.
 55. Ajayan, P.M.; Schadler, L.S.; Braun, P.V. *Nanocomposite Science and Technology*; Wiley-VCH:Weinheim, Germany, 2003.
 56. Tang, Z.X.; Sorensen, C.M.; Klabunde, K.J.; Hadjipanayis, G.C. Size-dependent magnetic properties of manganese ferrite fine particles. *J. Appl. Phys.* **1991**, 69, 5279-5281.
 57. Tang, Z.X.; Sorensen, C.M.; Klabunde, K.J.; Hadjipanayis, G.C. Size-dependent Curietemperature in nanoscaled MnFe₂O₄ particles. *Phys. Rev. Lett.* **1991**, 67, 3602-3605.
 58. Han, D.H.; Wang, J.P.; Luo, H.L. Crystallite Size Effect on Saturation Magnetization of Fine Ferrimagnetic Particles. *J. Magn. Magn. Mater.* **1994**, 136, 176-182.
 59. Davied S., Nicolau Y.F., Melis F., Revillon A. Molecular weight of polyaniline synthesized by oxidation of aniline // *Synthetic Metals*. – 1995. – 69. – P. 125 - 126.

60. Kyprianidou-Leodidou, T.; Caseri, W.; Suter, U.W. Size variation of PbS Particles in highrefractive-index nanocomposites. *J. Phys. Chem.* **1994**, *98*, 8992-8997.
61. Trwoga, P.F.; Kenyon, A.J.; Pitt, C.W. Modelling the contribution of quantum confinement to luminescence from silicon nanoclusters. *J. Appl. Phys.* **1998**, *83*, 3789-3794.
62. Sharma, A.C. Size-dependent energy band gap and dielectric constant within the generalized Penn model applied to a semiconductor nanocrystallite. *J. Appl. Phys.* **2006**, *100*, 084301:1-084301:8.
63. Nienhaus, H.; Kravets, V.; Koutouzov, S.; Meier, C.; Lorke, A.; Wiggers, H.; Kennedy, M.K.; Kruis, F E. Quantum size effect of valence band plasmon energies in Si and SnO_x nanoparticles. *J. Vac. Sci. Technol. B* **2006**, *24*, 1156-1161.
64. D.V.; Schlabach, S.; Ochs, R. Analytical TEM investigations of size effects in SnO₂ nanoparticles produced by microwave plasma synthesis. *Microsc. Microanal* **2007**, *13* (Suppl. 3),430-431.
65. Suresh, A.; Mayo, M.J.; Porter, W.D. Thermodynamics of the tetragonal-to-monoclinic phase transformation in fine and nanocrystalline yttria-stabilized zirconia powders. *J. Mater. Res.* **2003**, *18*, 2912-2921.
66. Li, S.; Zheng, W.T.; Jiang, Q. Size and pressure effects on solid transition temperatures of ZnO₂. *Scr. Mater.* **2006**, *54*, 2091-2094.
67. Zhang, H.; Banfield, J.F. Thermodynamic analysis of phase stability of nanocrystalline titania. *J. Mater. Chem.* **1998**, *8*, 2073-2076.
68. Schlabach, S.; Szabó, D.V.; Vollath, D.; de la Presa, P.; Forker, M. Structure and grain growth of TiO₂ nanoparticles investigated by electron and X-ray diffractions and Ta-181 perturbed angular correlations. *J. Appl. Phys.* **2006**, *100*, 024305:1-024305:9.
69. Schlabach, S.; Szabó, D.V.; Vollath, D.; de la Presa, P.; Forker, M. Zirconia and titania nanoparticles studied by electric hyperfine interactions, XRD and TEM. *J. Alloy. Compd.* **2007**, *434*, 590-593.
70. Zhang, M.; Lin, G.; Dong, C.; Wen, L. Amorphous TiO₂ films with high refractive index deposited by pulsed bias arc ion plating. *Surf. Coat. Tech.* **2007**, *201*, 7252-7258.
71. Jiang, C.; Wei, M.; Qi, Z.; Kudo, T.; Honma, I.; Zhou, H. Particle size dependence of the lithium storage capability and high rate performance of nanocrystalline anatase TiO₂ electrode. *J. Power Sources* **2007**, *166*, 239-243.
72. Jiang, C.H.; Honma, I.; Kudo, T.; Zhou, H.S. Nanocrystalline rutile TiO₂ electrode for highcapacity and high-rate lithium storage. *Electrochem. Solid-State Lett.* **2007**, *10*, A127-A129.
73. Deng, D.; Kim, M.G.; Lee, J.Y.; Cho, J. Green energy storage materials: Nanostructured TiO₂ and Sn-based anodes for lithium-ion batteries. *Energy Environ. Sci.* **2009**, *2*, 818-837.
74. Jordan, J.; Jacob, K.I.; Tannenbaum, R.; Sharaf, M.A.; Jasiuk, I. Experimental trends in polymer nanocomposites - a review. *Mater. Sci. Eng. A* **2005**, *393*, 1-11.
75. Tjong, S.C. Structural and mechanical properties of polymer nanocomposites. *Mater. Sci. Eng. R* **2006**, *53*, 73-197.
76. Ash, B.J.; Schadler, L.S.; Siegel, R.W. Glass transition behavior of alumina/polymethylmethacrylate nanocomposites. *Mater. Lett.* **2002**, *55*, 83-87.
77. Ash, B.J.; Schadler, L.S.; Siegel, R.W.; Glass transition behavior of alumina/polymethylmethacrylate (PMMA) nanocomposites. *Polym. Prepr.* **2003**, *44*, 2445-2446.
78. Hu, Y.H.; Chen, C.Y.; Wang, C.C. Viscoelastic properties and thermal degradation kinetics of silica/PMMA nanocomposites. *Polym. Degrad. Stab.* **2004**, *84*, 545-553.
79. Ritzhaupt-Kleissl, E.; Haußelt, J.; Hanemann, T. Thermo-mechanical properties of thermoplastic polymer-nanofiller composites. In *Proceedings of the 4M 2005 conference (Multi-Material- Micro-Manufacture)*; Menz, W., Dimov, S., Eds.; Elsevier Publisher: Oxford, UK, 2005; pp. 87-90.
80. Li, C.; Wu, J.; Zhao, J.; Zhao, D.; Fan, Q. Effect of inorganic phase on polymeric relaxation dynamics in PMMA/silica hybrids studied by dielectric analysis. *Eur. Polym. J.* **2004**, *40*, 1807-1814.
81. Bansal, A.; Li, C.; Yang, H.; Benicewicz, B.C.; Kumar, S.K.; Schadler, L.S. Glass transition behavior of polystyrene filled with surface modified silica nanoparticles. *PMSE Prepr.* **2005**, *92*, 260-261.
82. Goyal, R.K.; Tiwari, A.N.; Mulik, U.P.; Negi, Y.S. Novel high performance Al₂O₃/ poly(etherether ketone) nanocomposites for electronics applications. *Compos. Sci. Technol.* **2007**, *67*, 1802-1812.
83. Chen, C.H.; Jin, J.Y.; Yen, F.S. Preparation and characterization of epoxy/γ-aluminium oxide nanocomposites. *Compos. Pt. A-Appl. Sci. Manuf.* **2009**, *40*, 463-468.
84. Omrani, A.; Simon, L.C.; Rostami, A.A. The effects of alumina nanoparticle on the properties of an epoxy resin system. *Mater. Chem. Phys.* **2009**, *114*, 145-150.
85. Kang, S.; Hong, S.I.; Choe, C.R.; Park, M.; Rim, S.; Kim, J. Preparation and characterization of epoxy composites filled with functionalized nanosilica particles obtained via sol-gel process. *Polymer* **2001**, *42*, 879-887.
86. Pan, G.; Guo, Q.; Tian, A.; He, Z. Mechanical behaviors of Al₂O₃ nanoparticles reinforced polyetheretherketone. *Mater. Sci. Eng. A* **2008**, *492*, 383-391.
87. Siegel, R.W.; Chang, S.K.; Ash, B.J.; Stone, J. Ajayan, P.M.; Doremus, R.W.; Schadler, L.S. Mechanical behavior of polymer and ceramic matrix nanocomposites. *Scr. Mater.* **2001**, *44*, 2061-2064.
88. Garcia, M.; Garica-Turiel, J.; Norder, B.; Chavez, F.; Kooi, B.J.; van Zyl, W.E.; Verweij, H.; Blank, D.H.A. Polyamide-6/silica nanocomposites. *Adv. Eng. Mater.* **2004**, *6*, 724-729.
89. Xiong, M.; Zhou, S.; Wu, L.; Wang, B.; Yang, L. Sol-gel derived organic-inorganic hybrid from trialkoxysilane-capped acrylic resin and titania:

- effects of preparation conditions on the structure and properties. *Polymer* **2004**, *45*, 8127-8138.
90. Canillo, V.; Bondioli, F.; Lusvarghi, L.; Montorsi, M.; Avella, M.; Errico, M.E.; Malinconico, M. Modeling of ceramic particles filled polymer-matrix nanocomposites. *Compos. Sci. Technol.* **2006**, *66*, 1030-1037.
 91. Cho, J.; Joshi, M.S.; Sun, C.T. Effect of inclusion size on mechanical properties of polymeric composites with micro and nano particles. *Compos. Sci. Technol.* **2006**, *66*, 1941-1952. 82.120. Sangermann, M.; Priola, A.; Kortaberria, Jimeno, A.; Garcia, I.; Mondragon, I.; Rizza, G. Photopolymerization of epoxy coatings containing iron-oxide nanoparticles. *Macromol. Mater. Eng.* **2007**, *292*, 956-961.
 92. Oberdisse, J. Aggregation of colloidal nanoparticles in polymer matrices. *Soft Matter* **2006**, *2*, 29-36.
 93. Schaefer, D.W.; Justice, R.S. How nano are nanocomposites. *Macromolecules* **2007**, *40*, 8501-8517.
 94. Ng, C.B.; Schadler, L.S.; Siegel, R.W. Synthesis and mechanical properties of TiO₂-epoxy nanocomposites. *Nanostruct. Mater.* **1999**, *12*, 507-510.
 95. Zhang, M.Q.; Rong, M.Z.; Yu, S.L.; Wetzel, B.; Friedrich, K. Effect of particle surface treatment on the tribological performance of epoxy based nanocomposites. *Wear* **2002**, *253*, 1086-1093.
 96. Bauer, F.; Gläsel, H.J.; Decker, U.; Ernst, H.; Freyer, A.; Hartmann, E.; Sauerland, V.; Mehnert, R. Trialkoxysilane grafting onto nanoparticles for the preparation of clear coat polyacrylate system with excellent scratch performance. *Prog. Org. Coat.* **2003**, *47*, 147-153.
 97. Bauer, F.; Mehnert, R. UV curable acrylate nanocomposites: properties and applications. *J. Polym. Res.* **2005**, *12*, 483-491.
 98. Bhimaraj, P.; Burris, D.L.; Action, J.; Sawyer, W.G.; Toney, C.G.; Siegel, R.W.; Schadler, L.S. Effect of matrix morphology on the wear and friction behavior of alumina nanoparticle/poly(ethylene) terephthalate composites. *Wear* **2005**, *258*, 1437-1443.
 99. Daseri, A.; Yu, Z.Z.; Nai, Y.W. Fundamental aspects and recent progress on wear/scratch damage in polymer nanocomposites. *Mater. Sci. Eng. R* **2009**, *63*, 31-80, Zhang, Z.; Yang, J.L.; Friedrich, K. Creep resistant polymeric nanocomposites. *Polymer* **2004**, *45*, 3481-3485.
 100. O'Regan, B.; Graetzel, M. A low-cost, high efficiency solar cell based on dye-sensitized colloidal TiO₂ films. *Nature* **1991**, *353*, 737-740.
 101. Kim, M.R.; Jin, S.H.; Park, S.H.; Lee, H.J.; Kang, E.H.; Lee, J.K. Photovoltaic properties and preparations of dye-sensitized solar cells using solid-state polymer electrolytes. *Mol. Cryst. Liq. Cryst.* **2006**, *444*, 233-239.
 102. Anandan, S.; Sivakumar, R. Effect of loaded TiO₂ nanofiller on heropolyacid-impregnated PVDF polymer electrolyte for the performance of dye-sensitized solar cells. *Phys. Status Solidi a* **2009**, *206*, 343-350.
 103. Ballav, N.; Biswas, M. Preparation and evaluation of a nanocomposite of polythiophen with Al₂O₃. *Polym. Int.* **2003**, *52*, 179-184.
 104. Yang, B.D.; Yoon, K.H.; Chung, K.W. Effect of TiO₂ and SiO₂ nanoparticles on the stability of poly (p-phenylene vinylene) precursor. *Synth. Met.* **2004**, *143*, 25-29.
 105. Fryxell, G. E.; Cao, G., Environmental Applications of Nanomaterials: Sensors, Sorbents and Sensors; Imperial College Press: London, 2007.
 106. Varghese, O. K.; Gong, D. W.; Paulose, M.; Ong, K. G.; Grimes, C. A. Sens. Actuators, B 2003, *93*, 338.
 107. Birkefeld, L. D.; Azad, A. M.; Akbar, S. A. J. Am. Ceram. Soc. 1992, *75*, 2964.
 108. Wan, Q.; Li, Q. H.; Chen, Y. J.; Wang, T. H.; He, X. L.; Li, J. P.; Wang, J. X.; Sun, X. W.; Yang, Y.; Huang, H.; Lee, Y. C.; Tan, O. K.; Vayssieres, L. Nanotechnology 2006, *17*, 4995.
 109. Chu, X. F.; Jiang, D. L.; Djuricic, A. B.; Yu, H. L. Chem. Phys. Lett. 2005, *401*, 426.
 110. Tang, H. X.; Yan, M.; Ma, X. F.; Zhang, H.; Wang, M.; Yang, D. R. Sens. Actuators, B 2006, *113*, 324.

A COMPARATIVE STUDY ON EFFECTIVE SCHEMES FOR NETWORK SELECTION IN 4G COMMUNICATION SYSTEMS

Jeeva Susan Jacob¹, Preetha K. G.²

¹Department of Computer Science, Rajagiri School of Engineering and Technology, Rajagiri Valley, Cochin, India.

²Department of Information Technology, Rajagiri School of Engineering and Technology, Rajagiri Valley, Cochin, India.

Abstract: Wireless technologies have been adopted into the field of communication in the recent past. The fast pace in the growth of advanced wireless hardware and technologies have caused the evolution and generation of five wireless communication standards within this short span of time. The fourth generation (4G) communication standard, which is the most recent of these five, is a promising area for research. 4G systems aim at implementing a global communication network by integrating all existing telecommunication standards. It modifies the main goal of wireless communication from “AlwaysConnected” to “Always Best Connected”. Major issues which are delaying the commercial release of 4G devices include network selection, vertical handoff, billing issues, jamming and spoofing, location privacy and QoS support. The main expectation about 4G is the freedom for the users to choose and switch between services provided by various service providers integrated into the 4G network.. The main purpose of this paper is to explore the various network selection schemes which have been proposed by various researchers in the area. This paper discusses the method or technique of network selection, benefits and shortcomings of each of these selection schemes. And also the paper tries to accomplish a comparative study on their effectiveness in performance. A proposal is also made to improve the network selection scheme based on QoS technique to make it suitable for emergency situations by adding a preplanner module.

KEYWORDS: 4G SYSTEMS, NETWORK SELECTION, MOBILE COMPUTING, WIRELESS COMMUNICATION, COMPARATIVE STUDY.

I. INTRODUCTION

Communication Techniques are evolving at the fastest pace ever known to mankind, with the worldwide development of new and efficient technologies in every split second. By instigating 4G, an integrated network of all networks, everything from laptops to smart phones and communication facilities from LANs to portable internet packages, grows to be a part of a common global standard. With a data rate of 100 Mbps to 1Gbps, 4G is the technology of the future. Techniques like OFDMA (Orthogonal Frequency Division Multiple Access), SDR (Software Defined Radio), MIMO (Multiple Input and Multiple Output) and so on adds to the boons of 4G wireless communication standard. This results in making computing and communication a much easily accessible and simple activity. The comparative study on various communication standards evolved in the course of the telecommunication era, shown in the figure 1, reveals further benefits of 4G standard.

	0G	1G	2G	3G	4G
TECHNOLOGY	ANALOG	DIGITAL	DIGITAL	DIGITAL	DIGITAL
PERIOD	1970s	1980s	1995+	2006+	2010+
DATA RATE	-	14.4Kbps	144-200Kbps	250Kbps-14.4 Mbps	100Mbps-1Gbps
SWITCHING	-	CIRCUIT	PACKET	PACKET	BROAD-BAND
PROTOCOLS	PSTN	NMT,AMPS ,TACS	GSM,GPRS, EDGE	DECT,HSPA ,WiMAX	OFDMA, MIMO

Figure 1. The figure shows comparative study on various communication standards.

A prominent aspect of 4G systems is the network selection scheme by which the users can choose the best connected network available for each of the services required. Suppose a user needs high security for a call, he can select the most secure call service from the available service providers. Similarly in the case where he requires a messaging service with the cheapest rate for messages he can choose the one which is cheaper among the available lot. Selection can also be made based on the values of multiple parameters as well. Thus the system always promises the best services provided by the best service providers.

To choose the suitable technology for each service at a particular place and time, assessing services provided by each of the service providers can be a tedious and complicated task. Researches on numerous schemes are going on in different parts of the world to simplify and improve the process.

Researchers around the world have accepted network selection as an NP-hard problem. The primary reason for this is the heterogeneous nature of the 4G system. In a normal mobile communication system the network utilized depends only on the signal strength from the base station. Network Selection in 4G depends on multiple criteria like bandwidth, security, cost of service, performance in heterogeneous network, user preference and so forth. Thus analysing each of these parameter values for all the networks available at each unit time for every single service turns out to be a herculean task.

Vertical handoffs, billing frauds, service theft, privacy attacks and the like may also create nuisance in efficient selection of network and its utilization. We found scores of indispensable proposals for solutions on network selection from many researchers related to the area. In this paper we discuss a few of the renowned schemes for network selection in 4G communication systems. We also try to analyze the benefits and detriments of each in performing network selection.

The rest of this paper is organized as follows. Section II provides an overview on the basic architecture of 4G. Section III to X discusses the significant schemes as analyzed by us for network selection. The comparative study on the analysis of their performance based on certain parameters is described in section XI. Section XII explains the new proposal with the preplanner module. Section XIII expounds future enhancements and section XIV the conclusion.

II. 4G : BASIC ARCHITECTURE AND FUNCTIONING

Advanced devices with imminent technologies are required for implementing 4G with its entire functional package. Various appliances developed with the aim of accomplishing this failed in executing one fragment or the other of the 4G functional plan. Although fundamental properties and functionalities were devised much earlier, the lack of suitable equipments with adaptable architecture has delayed the introduction of 4G in the communication zone. However, numerous proposals have been made by inquisitive brains around the world for developing a basic architecture for 4G systems which promise a revolution in this field.

Long Term Evolution (LTE) developed by the Third Generation Partnership Project (3GPP) is a great improvement in the Telecommunications Systems. With the use of advanced techniques like OFDM and MIMO, LTE paves the way for the integration of ubiquity into the field of wireless communication and mobile computing. Here, users are assured with Quality of Service (QoS) with the help of Evolved Packet System (EPS). It supports both Frequency Division Duplexing (FDD) and Time Division Duplexing (TDD). It gives much better performance than Code Division Multiple Access (CDMA) with bandwidths ranging from 1.4MHz to 20MHz. The actual practical implementation process of 4G is proved to be accelerated by the development of LTE. The basic LTE system architecture configuration consists of logical components like :

- User Equipment (UE) such as a smartphone for individual users
- Evolved Universal Terrestrial Radio Access Node-Bs (e-UTRAN) which act like the Base stations
- Mobility Management Entity (MME) which manages the user's mobility
- Serving Gateway(S-GW) for tunnel management and switching of UE
- Packet Data Network Gateway (PDN-GW) which is the IP point of attachment for the UE
- Policy and Charging Resource Function (PCRF) which is responsible for Policy and Charging Control (PCC) for various service providers
- IP Multimedia Subsystem (IMS) to provide services using Session Initiation Protocol (SIP)
- Home Subscription Server (HSS) which is the data repository of the subscriber's profile

By implementing the perfect architecture 4G is expected to have high performance, good interoperability, perfect networking, high bandwidth, advanced technological functions, ubiquitous coverage, convergent connectivity, better device interfaces, good scalability, high quality service and a cheaper globally connected communication system. The potential applications which are expected to be developed or improved by the effective implementation of 4G systems include virtual presence, virtual navigation, tele-medicine, tele-geoprocessing, crisis management, education, mobile banking and other emergency services. The basic functioning of 4G is based on the provision of users to select the required network for performing particular services. The following sessions describe various solutions proposed by researchers around the world for effective network selection in 4G.

III. QOS BASED NETWORK SELECTION SCHEME

Quality of Service (QoS) is the key constraint for most of the technologies in all major fields of societal life. QoS based scheme ensures the best service for maximum user satisfaction and the best approach for resource utilization.

In this scheme [21], QoS is ensured by creating the ranklist based on certain parameters evaluated during performance. Miscellaneous performance parameters to ensure QoS for the users are taken into account. Cost of the service, available bandwidth, connectivity during handover and the like are encompassed in this set of parameters. The algorithm used includes calculating the distance function based on these parameters and creating ranklists for each network as the initial step. Weighted distance function is performed on the results thus obtained and network with the highest score is selected for providing the required service.

The greatest advantage is the user has a choice in the parameters to be considered for each service selection. Also, the number of parameters considered can vary according to the required service. When considering only a single parameter, weighted distance function calculation can be skipped and network can be chosen from the rank list for that particular parameter. There is still the drawback of overhead because of repeated calculations for each and every service. In spite of this slight shortcoming, this is so far the best method for network selection as per our analysis.

IV. QOE BASED NETWORK SELECTION SCHEME

V.

Since 4G is a network of numerous existing networks and service providers, the selection based on the parameter values of individual networks may not be accurate for its proper functioning. Thus, a new scheme was anticipated where the performance of each network, in the presence of other networks, is evaluated.

Quality of Experience (QoE) in this scenario means the performance of a particular service provider or network in a heterogeneous network of networks in providing proffered services. In this scheme [14] a number of packet-switched networks are compared based on certain parameters evaluated for each network in the presence of other heterogeneous networks and the one providing highest QoE standard is chosen. The techniques of Analytical Hierarchy Process (AHP) and Grey Relational Analysis (GRA) are combined in this method. Then the available networks are ranked to discover the apt one.

This method guarantees the best performing network in a miscellaneous set of networks. But it does not consider the performance of the networks individually, which deteriorates the performance by a fraction since the number available networks can diverge in the milieu.

VI. OPEN RESOURCES BASED NETWORK SELECTION SCHEME

Resources of a network comprises of aspects like area covered, services provided, expandability, files, memory, power, external devices and so forth. For each service requested by the user, the networks with the appropriate resources to perform it need only be considered. Thus the selection process thus prunes the list of available networks and confines the list of networks to the best suited ones with the required set of resources only. So this is basically a selection process based on elimination.

In this scheme request sent by user is processed and the resources required are gathered together. Then each of the networks available is explored to confirm whether any of them comply with the request. Thus the network with maximum suitability with the request is selected and designated to provide the service to the user. If more than one network qualifies for the actual selection process, additional weights are added as per user preference before selection. If none qualifies in its entirety, the one that has the maximum match score with the resources required is selected.

Better resource utilization for the users is the foremost benefit of this method. Since no complex calculations are involved, this scheme does not generate much overhead. On the contrary, efficiency in functioning is low in comparison with the other schemes discussed earlier.

VII. USER REQUISITES BASED NETWORK SELECTION SCHEME

This is the scheme [8] which assigns utmost importance to the choice and demands of users of the system. Network selection is done based on dynamic adaptation with respect to the user's preference. Here a user agent and a network agent, its client side image, are used.

The selection algorithm is integrated into a middleware layer which hides the complexity of the system from the users. Cost functions are executed to determine service cost, power conception, network availability, bandwidth degradation and network unreliability. Each cost parameter is dynamically mapped to a weight which is dynamically calculated as per user preferences.

The scheme provides a higher dynamicity to the whole selection process. Thus it achieves a more effective criterion for selecting the access network selection. Although it has much calculation overhead and complexity in the lower layers, this is the best and user affable scheme which suits the user's preference factors.

Game theory can be used for effective modeling and resource allocation for networks. This scheme [3] models network selection problem as a game in the 4G global network. The major components included in game theory are players, strategies, payoffs and resources.

All available networks become the players of the game. These networks compete with each other in a non-cooperating manner for several rounds. Thus their pay-off values are maximized, which means the performance parameters of the services received by users have high values. Strategies are the adaptations done by the networks to provide the best service for users. Resources are the features of each network like bandwidth, power usage, coverage, security and so on.

Since this is held between access networks, users do not get tangled in the complexities of the selection process. But user participation can be ensured by collecting their preference values for the participating networks. As in every other discipline, competition improves Quality of Service among the various service provider networks involved in the 4G communication systems. Conflicts tend to occur in this scheme due to the preference factors. Also, the initial stage tends to be much tedious.

IX. RANKING BASED NETWORK SELECTION SCHEME

This scheme [5] is a collaboration technique of methods of network selection based on user preferences and open resources. It removes abnormalities due to other selection schemes and also scores high on efficiency. The critical attributes used for selection are cost per byte, total bandwidth, available bandwidth, delay, jitter, packet loss, signal strength and utilization. Terminal power consumption is also considered at times.

Initially, a list of available networks which can provide the requested service is created. Then weight matrix along with user preferences is obtained by classifying the attributes into speed, cost and quality categories. Then a ranking algorithm is executed and rounding off is done on the ranks. The network with the best rank is chosen from the results obtained.

This is a much easier method when compared to earlier techniques. Although much hectic calculations are to be performed till the rank list is obtained, choices can be made easily based on the ranks. The consistency of the algorithm paves the way for a stable ranking system.

X. UTILITY THEORY BASED NETWORK SELECTION SCHEME

Utility, in this context, implies the efficacy of a network in gratifying the user's demands. Fundamental utility theory of Von Neumann mathematically defines a set $U(w,x)$, where x is the set of user's observation on product criteria and w is the set of user preferences, both rounded off to real numbers.

The aim of this scheme [16] is to provide "Always Best Connected" (ABC) service, replacing the existing intent of providing "Always Connected" (AC) service. A new multi-criteria utility theory function has been developed in the scheme to suit the network selection process in 4G, which is expected to be consisting of dissimilar networks with contradicting attribute values. It has been created after numerical analysis on existing utility theory functions and to overcome the shortcomings of them.

Strict and effective selection is possible through this method. Also the user's preferences limits the whole lot of available networks to a few which makes the selection process much easier. However, for simple services such amount of complex mathematics ruins the objective.

XI. AGENT ACUITY BASED NETWORK SELECTION SCHEME

Agent based learning systems dynamically adapts to the environment in which they function through continuous perception. An agent is required to be adaptable to the environment its acting on for any minute changes which may happen. Cognitive networks are a group of such networks which functions on constant perception and actions based on thus acquired data. This scheme [7] provides an improved technique for the network selection by individual cognitive terminals. It also aims at improving the adaptability of the system by enhancing the resource utilization of the system.

A Q-learning algorithm is a sort of classic reinforcement learning algorithm. Constant perception is performed and actions are taken from the knowledge acquired to adapt to the system. For each state the environment is in, a particular action is adopted. Trend of performing a particular action depends on the rewards obtained on previous adaptation of the action. To determine the optimum action to be adopted an objective function is executed.

Since the system is dynamically adaptable, continuous connectivity is guaranteed throughout the service performed. Constant perception may require high memory and much complex lower level functions. Also vertical handover issues may affect the adaptation process adversely.

XII. COMPARATIVE STUDY ON THE SCHEMES

The sections above discussed the renowned schemes in performing network selection in 4G communication systems. The method adopted for network selection, benefits and shortcomings were discussed earlier. Here we make a comparative analysis on each of these methods with each other. A comparative study on these schemes based on attributes like bandwidth, user preference, dynamic adaptability, security and the like is shown in figure 2.

Network Selection Schemes Based on	Bandwidth	User preference	Dynamic Adaptability	Connectivity Maintenance	Overhead	Security	Power Requirement	Cost of Service	Heterogeneity Adaptation	Memory Requirement	Best Service
QoS	✓	✓	X	✓	✓	✓	✓	✓	✓	X	✓
QoE	✓	X	X	✓	X	✓	✓	✓	✓	X	✓
Open Resources	✓	✓	X	X	X	✓	✓	✓	X	✓	X
User Requisites	✓	✓	✓	✓	✓	X	✓	✓	✓	X	X
Network Competition	✓	✓	X	X	✓	✓	✓	✓	X	X	✓
Ranking Algorithm	✓	✓	X	✓	✓	✓	✓	✓	X	✓	✓
Utility Theory	✓	✓	X	X	✓	X	X	✓	✓	X	✓
Cognitive networks	✓	X	✓	✓	✓	✓	X	✓	✓	✓	✓

Fig. 2. The figure shows comparative study on various network selection schemes.

As per the comparative study, all the schemes provide the necessary bandwidth and consider the cost of service on network selection. Dynamic adaptation to the environment's functional situation is possible in user requisites based method and Cognitive networks utilizing Agent Acuity. However vertical handoff issues destroy this scope on practical implementation.

The best method for network selection as per the study is the QoS based method. Overhead due to calculations, which affects its performance a bit, when compared to other techniques, is much lower. Since it takes into account almost all parameters to be considered it would be easy to implement and enhance.

XIII. A NEW PROPOSAL FOR EMERGENCY SERVICES

Selection of application as per the user preference based on QoS (Quality of Service) is one of the best solution for the issue. This user-centric system works on the basis to provide best services of the network to the users. Here, a selection algorithm has been proposed which provides a better way to implement user preferences as per the features of 4G by adding a memory portion to the QoS based scheme. The steps involved in this new proposal are described in figure 3 and 4.

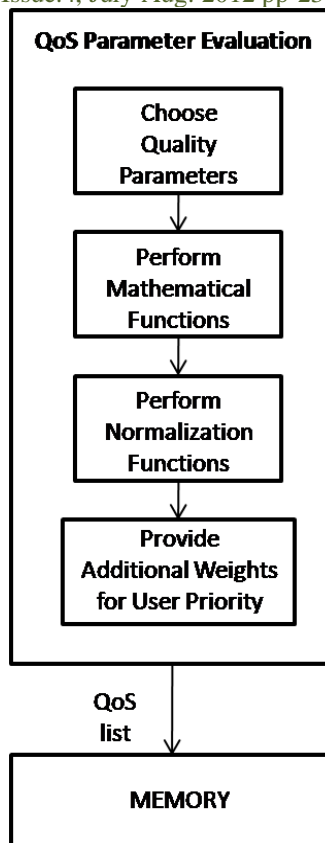


Fig. 3. The figure shows the creation of the QoS list to be stored in the memory

As in the QoS based scheme [21] for network selection, we first fix the parameters to be considered. It can be done based on the quality parameters usually considered and also with the user's demand for certain parameters if any. For example, for the deals between business empires the primary quality they prefer during communication will be secured connectivity rather than cost of communication.

Next, the values of these parameters are calculated using mathematical functions. Round off functions can be performed on the results to normalize and confine them to a scale from 0 to 10. Additional weights can be allotted to include user priorities. This list is stored in memory and is updated periodically as per the changes in each network's functionalities or policies.

The usual method based on QoS is repeated for each new service accessed by user since parameter values considered may vary in every fraction of time. This creates much overhead for emergency communication requirements. So, with the list stored in memory, a preplanner module is added to the method which enables user to plan in advance and select the networks suitable for different services so as to avoid overhead of calculations during emergencies. Plans are updated periodically to suit major changes in parameter values under consideration.

So the actual network selection process in this proposal is done as follows. Initially, the global 4G network is analyzed for available service providers in that particular area at that particular time. Then we determine the QoS score for each of the network from the QoS value list previously stored in memory.

User's requests for additional parameters are also taken care of and their values are also considered. Additional weights are added for user priorities. Again normalization is applied to obtain uniformly standardized values. Finally, the rank list is made from these scores. The best scoring network is selected for accomplishing the service.

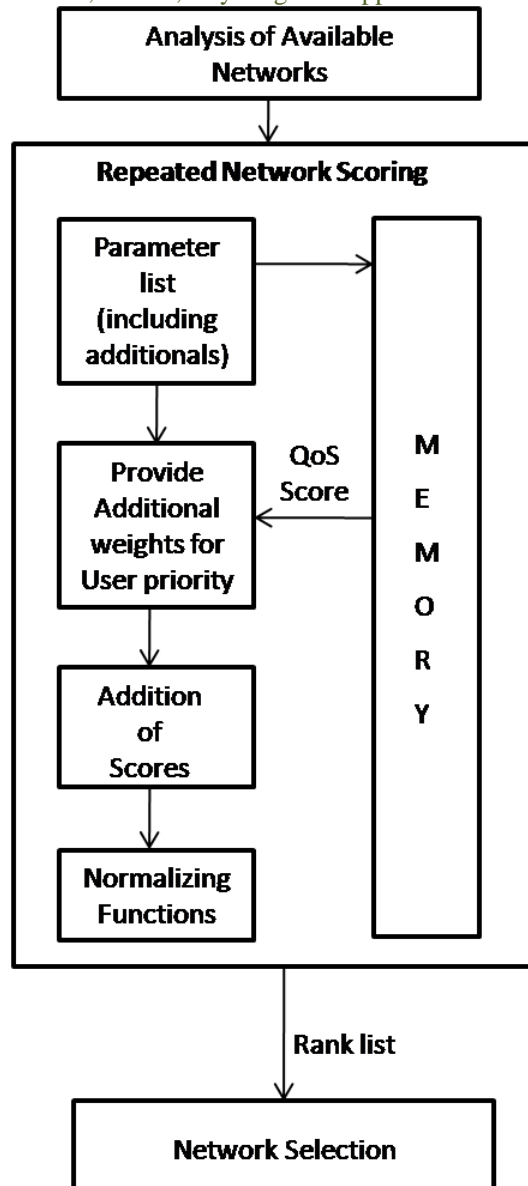


Fig. 3. The figure shows the creation of the QoS list to be stored in the memory

For emergency services, instead of repeating the whole process of calculations and selection, the network which is best from the preplanned list can be selected as suited for the required service. Thus the use of memory for storage of scores can reduce the overhead in selection in almost all normal scenarios.

For example, a user makes a call after selecting a network from the available networks.. After the call is ended he/she realizes he/she forgot to say something to the callee. When the user attempts to call again, in the normal QoS method the whole process needs to be repeated again. But with the new method, a suitable network can be selected from the preplanner module to perform the call. Of course, this is possible only if the second call is done within a particular period of time, say maximum one minute, from the first call.

XIV. FUTURE ENHANCEMENTS

Future work includes the comparison of these techniques on practical implementation factors. Of course that would take time as 4G system implementation has not yet been perfectly accomplished. Enhancing the QoS based method to reduce the overhead can make it the best method for network selection. In the case of the new solution proposed, overhead during the initial stages of the method, even though does not affect the network selection process directly, need to be reduced for effective implementation of network selection.

Emergency services require fast selection and handover processes even when services are going on. Also techniques for effectively resolving vertical handoff issues are yet to be researched on. There exists much scope on using genetic algorithmic methods for solving network selection problem in 4G.

XV. CONCLUSION

In this paper we discuss the network selection issue in 4G communication systems. A comparative study on the various technical schemes for resolving network selection issue is discussed here. Even though a bit of overhead exists in the scoring phases, the main process of network selection gets easier with lists to support the calculations involved. Numerous new proposals from many researchers are emerging day by day. 4G systems on implementation can pave the way for the ubiquitous standard of communication. This would enable “anytime anywhere” computing which is a huge leap forward in the field of global telecommunication system.

REFERENCES

- [1] Afaq H. Khan, Mohammed A. Qadeer, Juned A. Ansari, Sariya Waheed, “4G as a Next Generation Wireless Network”, pp: 334, International conference on Future Computer and Communication, ICFCC 2009.
- [2] Akan, A.; Edemen C., “Path to 4G wireless networks”, pp: 405, Personal, Indoor and Mobile Radio Communications Workshops, 2010 IEEE 21st International Symposium on 2010.
- [3] Antoniou, J.; Pitsillides, A.; “4G Converged Environment: Modeling Network Selection as a Game”, pp: 1, Mobile and Wireless Communications Summit, 2007. 16th IST, 2007.
- [4] Bill Krenik, “4G Wireless Technology: When will it happen? What does it offer?”, pp: 141, Solid-State Circuits Conference, 2008. A-SSCC '08. IEEE Asian, 2008.
- [5] Dhar, J.; Kiran S, R.; Reddy K, Y.; “Network Selection in Heterogeneous Wireless Environment: A Ranking Algorithm”, pp:41, Wireless Communication and Sensor Networks, 2007. WCSN '07. Third International Conference on, 2008.
- [6] Govil, J., “4G: Functionalities Development and an Analysis of Mobile Wireless Grid”, pp: 270, Emerging Trends in Engineering and Technology, 2008. ICETET '08. First International Conference on, 2008.
- [7] Haifeng Tan; Yizhe Li; Yami Chen; Li Tan; Qian Li; “A novel access network selection scheme using Q-learning algorithm for cognitive terminal”, pp : 1, Communications and Networking in China (CHINACOM), 2010, 5th International ICST Conference on, 2011.
- [8] Iera, A.; Molinaro, A.; Campolo, C.; Amadeo, M., “An Access Network Selection Algorithm Dynamically Adapted to User Needs and Preferences”, pp: 1, Personal, Indoor and Mobile Radio Communications, 2006 IEEE 17th International Symposium on, 2006.
- [9] Jamil, M.; Shaikh, S.P.; Shahzad, M.; Awaais, Q., “4G: The Future Mobile Technology”, pp: 1, 2008-2008 IEEE Region 10 Conference, 2009.
- [10] Jivesh Govil, Jivika Govil, “4G Mobile Communication Systems: Turns, Trends and Transition”, pp: 13, International Conference on Convergence Information Technology, 2007.
- [11] Kyung-Ho Kim; “Key technologies for the next generation wireless communications”, pp: 266, Hardware/Software Codesign and System Synthesis, 2006. CODES+ISSS '06. Proceedings of the 4th International Conference, 2007.
- [12] Li Zhen, Zhou Wenan, Song Junde, Hou Chunping, “Consideration and research issues for the future generation of mobile communication”, pp:1276, Electrical and Computer Engineering, 2002. IEEE CCECE 2002.
- [13] Makhecha, K.P.; Wandra, K.H.; “4G Wireless Networks: Opportunities and Challenges”, pp:1, Conference (INDICON), 2009 Annual IEEE, 2010.
- [14] Markaki, O.; Charilas, D.; Nikitopoulos, D.; “Enhancing Quality of Experience in Next Generation Networks Through Network Selection Mechanisms”, pp: 1, Personal, Indoor and Mobile Radio Communications, PIMRC 2007. IEEE 18th International Symposium on, 2007.
- [15] Nossenson, R., “Long-term evolution network architecture”, pp: 1, Microwaves, Communications, Antennas and Electronics Systems, 2009. IEEE International Conference on, 2010.
- [16] Quoc-Thinh Nguyen-Vuong; Ghamri-Doudane, Y.; Agoulmine, N., “On utility models for access network selection in wireless heterogeneous networks”, pp: 144, Network Operations and Management Symposium, 2008. NOMS 2008.
- [17] Rahman, M.; Mir, F.A.M.; “Fourth Generation (4G) Mobile Networks – Features, Technologies Issues”, 3G and Beyond, 2005 6th IEEE International Conference on 2007.
- [18] Rouffet, Denis; Sehier, Philippe; “Convergence and Competition on the Way Towards 4G”, pp: 277, Radio and Wireless Symposium, 2007 IEEE, 2007.
- [19] Santhi, K.R; Kumaran, G.S.; ”Migration to 4G: Mobile IP based Solutions”, pp: 76, Telecommunications, 2006. AICT-ICIW '06. International Conference on Internet and Web Applications and Services, 2006.
- [20] Santhi, K.R; Srivastava, V.K.; senthilKumaran, G.; Butare, A., “Goals of true broadband's wireless next wave (4G-5G)”, pp: 2317, Vehicular Technology Conference, 2003. VTC 2003-Fall. 2003 IEEE 58th,2004.
- [21] Sehgal, A.; Agrawal, R.; “QoS based network selection scheme for 4G systems”, pp:560, Consumer Electronics, IEEE Transactions on, 2010.
- [22] Suk Yu Hui ; Kai Hau Yeung; “Challenges in the migration to 4G mobile systems”, pp: 54, Communications Magazine, IEEE 2003.
- [23] J. Govil, “An Empirical Feasibility Study of 4G's Key Technology”, Electro Information Technologies, pages 267 – 270, 2008.

- [24] D. Charilas, O. Markaki, D. Nikitopoulos, M. Theologou, "Packet Switched Network Selection with Highest QoS in 4G Networks", Computer Networks: The International Journal of Computer and Telecommunications Networking, vol 52, issue 1, pages 248 – 258, 2008.
- [25] V. Gazis, N. Alonistioti, L. Merakos, Toward a Generic "Always Best Connected" Capability in Integrated WLAN/UMTS Cellular Mobile Networks (and Beyond), IEEE Wireless Communications, June 2005
- [26] Bellavista, M. Cinque, D. Cotroneo, and L. Foschini, "Integrated support for handoff management and context awareness in heterogeneous wireless networks", ACM International Conference Proceeding Series, vol. 115, pp. 1 - 8, 2005.
- [27] S. Ryu, S. Park, and D. Oh et al, "Research Activities on the Next Generation Mobile Communications and Services in Korea," IEEE Communications Magazine, Vol. 43, Issue 9, Sept. 2005, pp. 122-131

Authors

Ms. Jeeva Susan Jacob

Ms. Jeeva Susan Jacob completed her B.Tech Degree in Computer Science and Engineering from Mahatma Gandhi University, Kerala India in 2010. Currently she is pursuing her M.Tech degree in Computer Science and Engineering with specialization in Information Systems at Rajagiri School of Engineering and Technology, Cochin, India. Her research areas of interest include Mobile Computing, Pervasive Computing, Green Computing, Computer Networks and Wireless Communication.



Ms. Preetha K.G.

Ms. Preetha K G completed her B Tech and M Tech in Computer Science and Engineering from Calicut University and Dr. MGR University in the year 1999 and 2007 respectively. She is associated with Rajagiri School of Engineering & Technology, Cochin, India as an Assistant professor in Department of Information Technology. She has around 10 years of academic experience. Currently she is pursuing PhD at Cochin University of Science & Technology. Her research interest includes mobile computing, ad hoc networks, and Wireless Networks.



A Simulation Based Performance Analysis of AODV and DSDV Routing Protocols in MANETs

Biswaraj Sen¹, Sanku Sinha²

¹Department of Computer Sc & Engineering, Sikkim Manipal Institute of Technology, India

²Department of Computer Sc & Engineering, Sikkim Manipal Institute of Technology, India

ABSTRACT: A Mobile Ad hoc Network (MANET) is an infrastructure less, decentralized multi-hop network where the mobile nodes are free to move randomly, thus making the network topology dynamic. Various routing protocols have been designed which aims at establishment of correct and efficient routes between a pair of mobile nodes. In this work, an attempt has been made to understand the characteristics/behavior of Ad hoc On Demand Distance Vector (AODV) and Destination Sequence Distance Vector (DSDV) routing protocols when operating in more challenging environment such as frequent change in network topology and node density. The performance differentials are analyzed using throughput, average end-to-end delay and normalized routing load which shall provide an insight about the sensitivity of the protocols under consideration when exposed in more challenging environment. Simulation based analysis of the protocols have been done using NS-2.

Keywords: AODV, DSDV, MANET, NS-2.

1. Introduction

A mobile Ad hoc network is a collection of wireless mobile nodes forming a temporary network without any centralized administration or fixed infrastructure, which makes any node in the network as a potential router [1, 13]. Since the nodes are highly mobile in nature, the changes in network topology are very frequent and the nodes are dynamically connected in an arbitrary manner. Further, the limitation imposed on the transmission range of the nodes have lead to the development of routing policy where packets are allowed to traverse through multiple nodes thus making each node act as terminal as well as router. Since the topology of Ad hoc network is dynamic in nature, design of suitable routing protocol is essential to adapt the dynamic behavior of the network.

Further, it is worth mentioning that node density and pause time will have significant effect in the performance of the any routing policy due to the fact that an increase in node density will tend to increase the hop count thus changing the topology significantly. Pause time indicates the mobility of the nodes in the network. Therefore, it is imperative to state that high pause time implies a stable network topology while low pause time indicates that the topology changes frequently. This paper makes an attempt to analyze the performance of two most popular Ad hoc routing protocols, viz. AODV and DSDV where both the above discussed factors i.e. Pause Time and Node Density vary considerably. Though both protocols use sequence number to prevent routing loops and to ensure freshness of routing information, the main mechanism of routing differs drastically in AODV and DSDV in the fact

that they belong to two different routing families [3]. AODV is from reactive routing family where routes are only generated on demand, in order to reduce routing loads [5], while DSDV is from proactive routing family where routing tables are updated frequently regardless of need [2]. The rest of this paper is organized as follows: In the next section, brief overviews of both routing protocols have been discussed. Section 3 discusses the simulation environment in which both the protocols have been tested. Section 4 includes analysis of the performance of both the protocols under a varying node density environment and varying pause time with respect to performance metrics such as throughput, average end-to-end delay and packet delivery fraction. Section 5 provides conclusion, limitation and future work.

II. Overview of the Protocol

1.1 Ad hoc On Demand Distance Vector (AODV):

Ad hoc On Demand Distance Vector Routing Protocol (AODV) is a reactive routing protocol designed for Ad hoc wireless network and it is capable of both unicast as well as multicast routing [3]. The Route Discovery process in this protocol is performed using control messages RouteRequest (RREQ) and RouteReply (RREP) whenever a node wishes to send packet to destination. Traditional routing tables is used, one entry per destination [2]. During a route discovery process, the source node broadcasts a RouteRequest packet to its neighbors. This control packet includes the last known sequence number for that destination. If any of the neighbors has a route to the destination, it replies to the query with RouteReply packet; otherwise, the neighbors rebroadcast the RouteRequest packet. Finally, some of these query control packets reach the destination, or nodes that have a route to the destination. At this point, a reply packet is generated and transmitted tracing back the route traversed by the query control packet. In the event when a valid route is not found or the query or reply packets are lost, the source node rebroadcasts the query packet if no reply is received by the source after a time-out.

In order to maintain freshness node list, AODV normally requires that each node periodically transmit a HELLO message, with a default rate of one per second [9]. When a node fails to receive three consecutive HELLO messages from its neighbor, the node takes it as an indication that the link to its neighbor is down. If the destination with this neighbor as the next hop is believed not to be far away (from the invalid routing entry), local repair mechanism may be launched to rebuild the route towards the destination; otherwise, a RouteError (RERR) packet is sent to the neighbors in the precursor list

associated with the routing entry to inform them of the link failure [12].

1.2 Destination Sequenced Distance Vector (DSDV):

Destination-Sequenced Distance-Vector Routing (DSDV) [3] is a proactive routing protocol designed for Ad hoc mobile networks based on the Bellman-Ford algorithm [10]. The improvement made to the Bellman-Ford algorithm includes freedom from loops in routing tables by using sequence numbers. In mobile Ad hoc network, using of DSDV protocol assumes that each participating node as a router. Every node always maintains a routing table that consists of all the possible destinations. Each entry of the routing table contains the address identifier of a destination, the shortest known distance metric to that destination measured in hop counts and the address identifier of the node that is the first hop on the shortest path to the destination [11]. Each mobile node in the system maintains a routing table in which all the possible destinations and the number of hops to them in the network are recorded. Each route or path to the destination associated with a sequence number [4]. The route with the highest sequence number is always used and this sequence number helps to identify the stale routes from the new ones and thus it avoids the formation of loops. To minimize the traffic there are two types of packets in the system. One is known as "full dump" [5], which carries all the information about a change. However, when occasional movement occurs in the network, "incremental" [5] packet are used, which carries just the changes and this increases the overall efficiency of the system. DSDV requires a regular update of its routing tables, which uses up battery power and a small amount of bandwidth even when there is no change in the network topology. Whenever the topology of the network changes, a new sequence number is necessary before the network re-converges; thus, DSDV is not scalable in Ad hoc networks, which have limited bandwidth and whose topologies are highly dynamic [1].

III. Simulation Methodology

Simulation based study using Network Simulator NS-2 [6] has been used to compare two protocols viz. AODV and DSDV under varying node density and varying pause time, assuming that the size of network, maximum speed of nodes and transmission rate are fixed. Tables 1 and 2 summarize the parameters used in the communication and movement models for simulation.

III.2 Communication Model

The simulator assumes constant bit rate (CBR) traffic with a transmission rate of 8 packets per second. The number of nodes varies from 25 to 100 in the denomination of 25, 50, 75 and 100. given on the last line.

Table 1. Parameters of Communication Model

Parameter	Value
Traffic type	CBR
Number of nodes	25, 50, 75, 100
Transmission rate	8 packets/second

IV.2 Movement Model

In line with the realistic mobility pattern of the mobile nodes, the simulation assumes a Random Waypoint Model [7], where a node is allowed to move in any direction arbitrarily. The nodes select any random destination in the 500 X 500 space and moves to that destination at a speed distributed uniformly between 1 and nodes maximum speed (assumed to be 20 meter per second). Upon reaching the destination, the node pauses for fixed time, selects another destination, and proceeds there as discussed above. After testing all possible connection for a specific scenario, pause time changes to test the next scenario. This behavior repeats throughout the duration of the simulation (500 seconds). Meanwhile, number of nodes and pause time has been varied to compare the performance of the protocols for low as well as high density environment and for low mobility of the nodes to high mobility. Table 2 lists the movement parameters of the simulations.

Table 2. Parameters of movement model

Parameter	Value
Simulator	NS-2
Simulation time	500 seconds
Area of the network	500 m x 500 m
Number of nodes	25, 50, 100, 200
Pause time	10 seconds
Maximum speed of nodes	20 meters per second
Mobility Model	Random waypoint

V.2 Performance Metrics

Three performance metrics has been measured for the protocols:

3.3.1 Throughput: Throughput is the number of packet that is passing through the channel in a particular unit of time [8]. This performance metric shows the total number of packets that have been successfully delivered from source node to destination node. Factors that affect throughput include frequent topology changes, unreliable communication, limited bandwidth and limited energy.

$$Throughput = \frac{Received_Packet_Size}{Time_to_Send} \quad (1)$$

3.3.2 Average End-to-End Delay: A specific packet is transmitting from source to destination node and calculates the difference between send times and received times. This metric describes the packet delivery time. Delays due to route discovery, queuing, propagation and transfer time are included metric [9].

$$Avg_End_to_End_Delay = \frac{\sum_i^n (CBR_Sent_Time - CBR_Recv_Time)}{\sum_i^n CBR_Recv} \quad (2)$$

3.3.3 Normalized Routing Load: Normalized Routing Load is the ratio of total number of routing packet received and total number of data packets received [10].

$$Normalized_Routing_Load = \frac{Number_of_Routing_Pkts_Recvd}{Number_of_Data_Pkts_Recvd} \quad (3)$$

2. Simulation Result And Analysis

Figures 1, 2 and 3 represent the performance analysis in terms of throughput, average end-to-end delay and normalized routing load respectively. In all the cases the node density varies from 25 to 100 and pause time varies from 5 to 20 second.

4.1 Throughput:

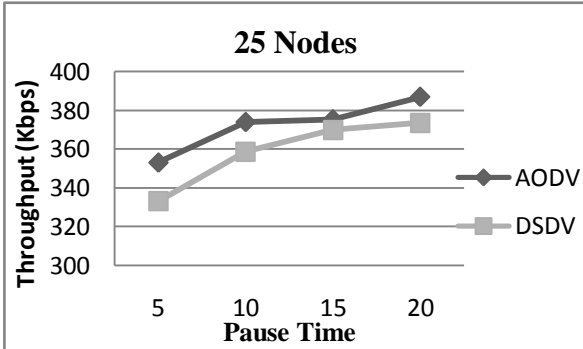


Figure 1 (a): Throughput for 25 nodes

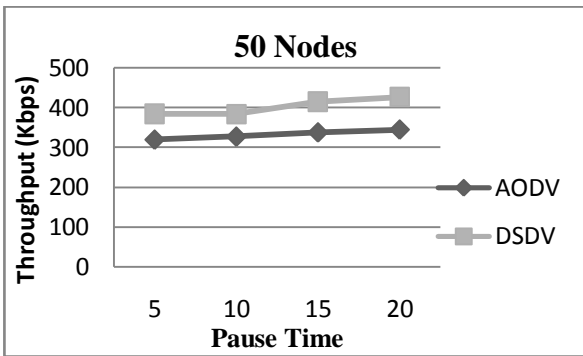


Figure 1 (b): Throughput for 50 nodes

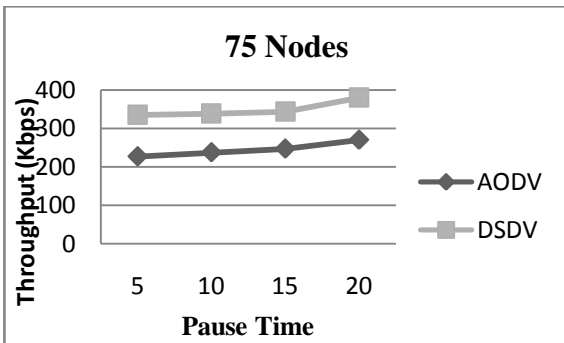


Figure 1 (c): Throughput for 75 nodes

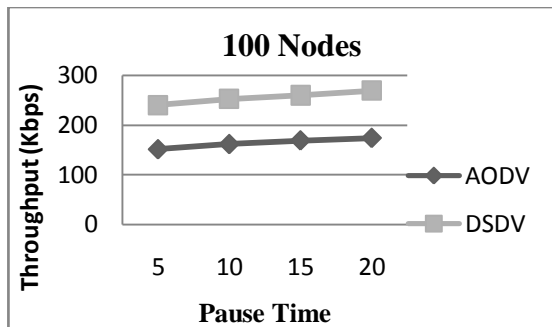


Figure 1 (d): Throughput for 100 nodes

Based on the result of simulation as indicated in Fig 1(a) it is evident that performance of AODV is better than DSDV in a low node density environment but with a rise in node density DSDV out performs AODV which is evident from Fig 1(b), 1(c) and 1(d). Another characteristic that has come to the notice is that pause time does not have significant bearing on the throughput whereas the performance is dictated only by the density of the network. The possible reason for the same is due to proactive nature of DSDV routing protocol, which causes less number of table update in a stable topology, thus producing better throughput.

4.2 Average End-to-End Delay:

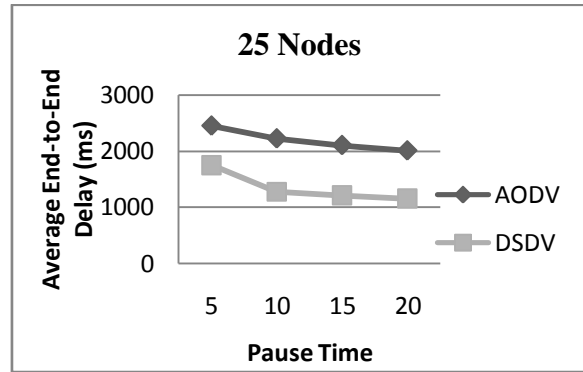


Figure 2 (a): Average End-to-End Delay for 25 nodes

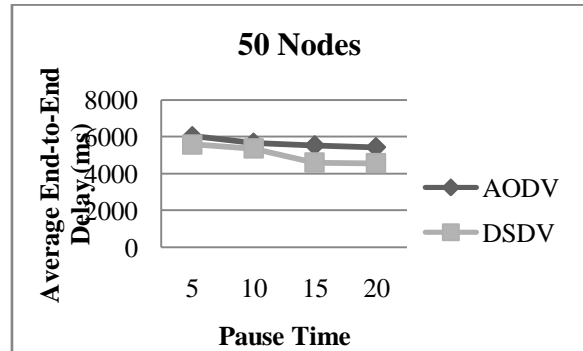


Figure 2 (b): Average End-to-End Delay for 50 nodes

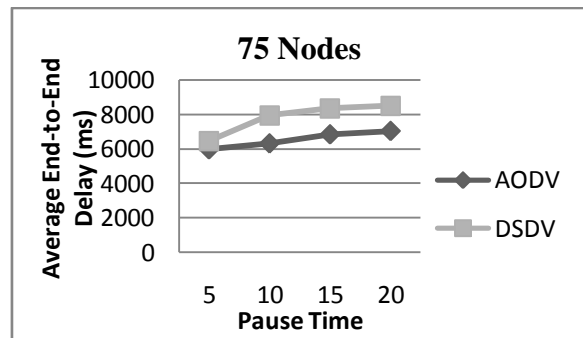


Figure 2 (c): Average End-to-End Delay for 75 nodes

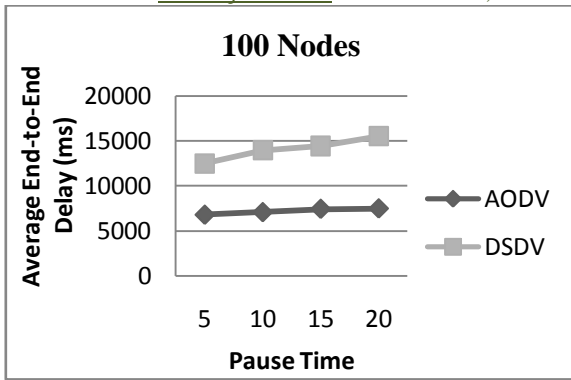


Figure 2(d): Average End-to-End Delay for 100 nodes

The simulation result as indicated in Fig 2(a) and 2 (b) shows that in case of low node density, the average end-to-end delay of AODV is higher than DSDV whereas Fig 2(c) and 2(d) indicates that with an increase in node density, AODV outperforms DSDV. It also has been observed that with an increase in pause time there is a decline in the average end-to-end for both the protocols under low node density environment (Fig 2a and 2b). However, this is not true when there is a rise in the network density. The possible reason for such behavior is the presence of more number of nodes between source and destination which effects in increase of hop count thus resulting in increased average end-to-end delay.

4.3 Normalized Routing Load:

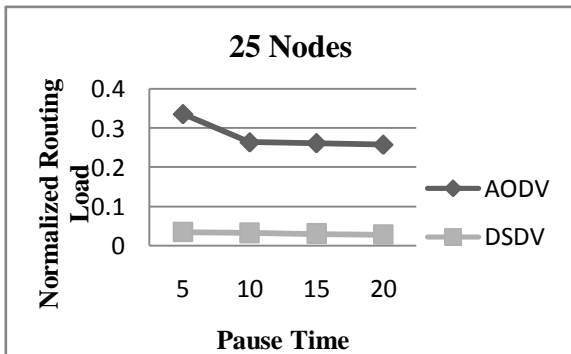


Figure 3(a): Normalized Routing Load for 25 nodes

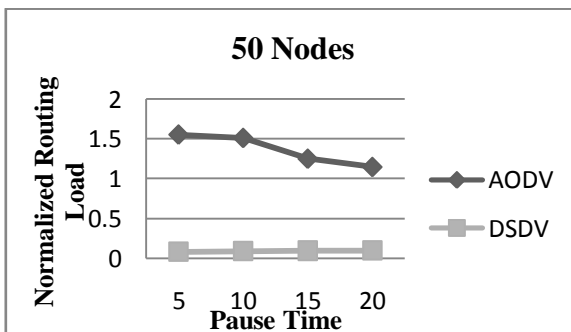


Figure 3(b): Normalized Routing Load for 50 nodes

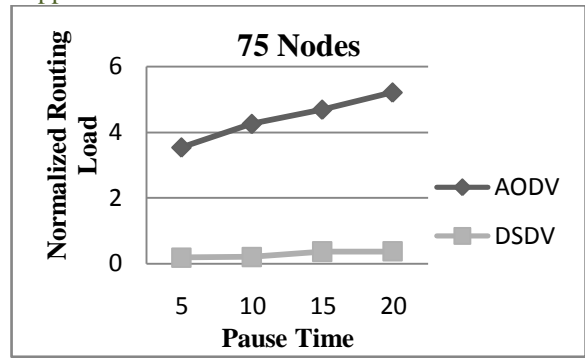


Figure 3 (c): Normalized Routing Load for 75 nodes

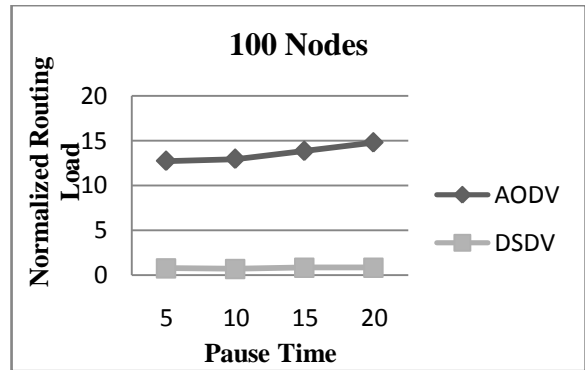


Figure 3 (d): Normalized Routing Load for 100 nodes

Fig 3(a), Fig 3(b), Fig 3(c) and Fig 3(d) indicates that normalized routing load of AODV is always higher than DSDV under any scenario. The performance of DSDV in terms of normalized routing load is not influenced in any way with respect to change in node density and pause time. The reactive nature of AODV routing protocol causes more number of control overhead than DSDV. Therefore, normalized routing load for AODV will always be higher than DSDV.

CONCLUSION

The performance evaluation of two routing protocols, AODV and DSDV, has been done with respect to metrics viz. throughput, average end-to-end delay and normalized routing load under varying node density and varying pause time. From the result analysis, it has been observed that in high node density the performance of both protocols decreases significantly. The increase of node density in the network causes more number of control packets in the network for route establishment between a pair of source and destination nodes. This is the main reason of performance degradation of the routing protocols in high node density [14]. On other hand, increase of pause time indicates more stable network. Thus the performance of both routing protocols increases with the increment of pause time. It has been observed that in low node density the performance of AODV is better than DSDV in terms of throughput, whereas the performance of DSDV is better in high node density (upto 100 nodes). Another observation has been found from the result that increment of pause time does not affect much in the performance of DSDV where the performance of AODV varies significantly with the pause time. In Current work, only three performance metrics have been considered to analyze the performance of AODV and DSDV. Inclusion of other performance metrics

will provide indepth comparison of these two protocols which may provide an insight on the realistic behavior of the protocols under more challenging environment. The current work has been limited with fixed simulation area (500x500m) with CBR traffic and node density is upto 100 nodes. From previous work [14], it has been observed that in higher node density (200 nodes) AODV performs better than DSDV. Varying simulation area and higher node density with different traffic will provide indepth performance analysis of these two protocols.

REFERENCES

- [1] C. Siva Ram Murthy and B.S. Manoj. *Ad Hoc Wireless Networks, Architecture and Protocols*, Pearson Education, 2004
- [2] Charles E. Perkins, Elizabeth M. Royer, Samir R. Das and Mahesh K. Marina, *Performance Comparison of Two On-Demand Routing Protocols for Ad Hoc Networks*, IEEE Personal Communications, February 2001
- [3] Charles E. Perkins. *Ad Hoc Networking*, Addison-Wesley, 2001
- [4] Charles E. Perkins & P. Bhagwat, *Highly Dynamic Destination-Sequenced Distance Vector Routing (DSDV) for Mobile Computers*, Proceedings of ACM SIGCOMM'94, London, UK, Sep. 1994
- [5] Mehran Abolhasan, Tadeusz Wysocki, Eryk Dutkiewicz. *A review of routing protocols for mobile ad hoc networks*, Telecommunication and Information Research Institute, University of Wollongong, Wollongong, NSW 2522, Australia, June 2003
- [6] Kevin Fall, Kannan Varadhan, *The ns Manual*, November 2011
- [7] Deepanshu Shukla and Prof. Sridhar Iyer, *Mobility models in Ad Hoc Networks*, KReSIT-IIT Bombay, November 2001
- [8] Sachin Kumar Gupta and R. K. Saket, *Performance Metric Comparison of AODV and DSDV Routing Protocols in MANETs Using NS-2*, IJRRAS, June 2011
- [9] S H Manjula, C N Abhilash, Shaila K, K R Venugopal, and L M Patnaik, *Performance of AODV Routing Protocol using Group and Entity Models in Wireless Sensor Networks*, IMECS, Hong Kong, March 2008
- [10] Comer and Douglas E., *Computer Networks and Internet*, Prentice Hall, 2008
- [11] V. Ramesh, Dr. P. Subbaiah, N. Koteswar Rao and M. Janardhana Raju, *Performance Comparison and Analysis of DSDV and AODV for MANET*, International Journal on Computer Science and Engineering, 2010
- [12] C. E. Perkins, E. M. Royer and S. Das, *Ad Hoc On Demand Distance Vector (AODV) Routing*, IETFInternet Draft, draft-ietf-manet-aodv-08.txt, March 2001
- [13] David B. Johnson. P, *Routing in Ad Hoc Networks of Mobile Hosts*, Proceedings of the IEEE Workshop on Mobile Computing Systems and Applications (WMCSA'94), December 1994.
- [14] Sanku Sinha and Biswaraj Sen. Performance Analysis of AODV And DSDV Routing Protocols in Mobile Ad Hoc Networks Under Varying Node Density, in the proceedings of international conference RTCMC-2012, OITM, Hissar, February 25-26, 2012 pp. 171-174

Transaction Processing In Replicated Data in the DDBMS

Ashish Srivastava¹, Udai Shankar², Sanjay Kumar Tiwari³

*(Department Deptt. of Computer Science & Engineering, Madan Mohan Malaviya Engineering College, Gorakhpur).

ABSTRACT: *The transactional Processing in Replicated Data for distributed system has been around for many years and it is considered a well-established and mature technology. The conventional transaction model, although suitable for predictable database applications such as banking and airline reservation systems, does not provide much flexibility and high performance when used for complex applications such as object oriented systems, long-lived transactions or distributed systems. In this paper we describe the transaction-processing model of distributed database includes data, Transaction, Data Manager, and Transaction Manager and their transaction process. We will study about concurrency problem of sequence of synchronization techniques for transaction with respect to distributed database. The spirit of discussion in a decomposition of the concurrency control problem into two major sub problems: read-write and write-write synchronization. We describe a sequence of synchronization techniques for solving each sub complexity.*

Keywords: *Real time system, Replication, Distributed Database, Distributed processing, Transaction, Transaction Manager, two-phase commit, Concurrency Control, Synchronization.*

I. Introduction

A real-time system is one that must process information and produce a response within a specified time, else risk severe consequences, including failure. That is, in a system with a real-time constraint it is no good to have the correct action or the correct answer after a certain deadline: it is either by the deadline or it is useless. Database replication based on group communication systems has been proposed as an efficient and flexible solution for data replication. Replicated is the key characteristic in improving the availability of data distributed systems. Replicated data is stored at multiple server sites so that it can be accessed by the user even when some of the copies are not available due to server/site failures.[1] A Major restriction to using replication is that replicated copies must behave like a single copy, i.e. mutual consistency as well internal consistency must be preserved, Synchronization techniques for replicated data in distributed database systems have been studied in order to increase the degree of consistency and to reduce the possibility of transaction rollback. [2]

In replicated database systems, copies of the data items can be stored at multiple sites. The potential of data replication for high data availability and improved read performance is crucial to RTDBS. In contrast, data replication introduces its own problems. Access to a data item is no longer control exclusively by a single site; instead, the access control is distributed across the sites each storing the copy of the data item. It is necessary to ensure that mutual consistency of the replicated data is provided

Distributed data base system is a technique that is used to solve a single problem in a heterogeneous computer network system. A major issue in building a distributed database system is the transactions atomicity. When a transaction runs across into two sites, it may happen that one site may commit and other one may fail due to an inconsistent state of transaction. Two-phase commit protocol is widely used to solve these problems. The choice of commit protocol is an important design decision for distributed database system. A commit protocol in a distributed database transaction should uniformly commit to ensure that all the participating sites agree to the final outcome and the result may be either a commit or an abort situation. Many real times database applications are distributed in nature [3] these include the aircraft control, stock trading, network management, factory automation etc.

II. DISTRIBUTED DATABASE SYSTEMS (DDBS)

A distributed database is a database that is under the control of a central database management system (DBMS) in which storage devices are not all attached to a common CPU. It may be stored in multiple computers located in the same physical location, or may be dispersed over a network of interconnected computers. Collections of data can be distributed across multiple physical locations. Distributed database system (DDBS) is system that has distributed data and replicated over several locations. Data may be replicated over a network using horizontal and vertical fragmentation similar to projection and selection operations in Structured Query Language (SQL). The database shares the problems of access control and transaction management, such as user concurrent access control and deadlock detection and resolution. On the other hand, however, DDBS must also cope with different problems. Accessing of data control and transaction management in DDBS needs different methods to monitor data access and update to distributed and replicated databases. Distributed database systems (DDBS) are systems that have their data distributed and replicated over several locations; unlike the centralized data base system (CDBS), where one copy of the data is stored. Data may be replicated over a network using horizontal and vertical fragmentation similar to projection and selection operations in Structured Query Language (SQL). Both types of database share the same problems of access control and transaction management, such as user concurrent access control and deadlock detection and resolution. On the other hand however, DDBS must also cope with different problems. Access control and transaction management in DDBS require different rules to monitor data retrieval and update to distributed and replicated databases [4, 5]. Oracle, as a leading Database Management Systems (DBMS) employs the two-phase commit technique to maintain a consistent state for the databases [6]. The objective of this paper is to

explain transaction management in DDBMS and how to implements this technique. To assist in understanding this process, an example is given in the last section. It is hoped that this understanding will encourage organizations to use and academics to discuss DDBS and to successfully capitalize on this feature of Database. The next section presents advantages, disadvantages, and failures in Distributed Database Systems. Subsequent sections provide discussions on the fundamentals of transaction management, two-phase commit, homogenous distributed database system implementation of the two-phase commit, and, finally, an example on how the two phases commit works.

2.1 Advantages of Distributed Database system (DDBS)

Since organizations tend to be geographically dispersed, a DDBS fits the organizational structure better than traditional centralized DBS. Improved Availability-A failure does not make the entire system inoperable and Improved Reliability-Data may be replicated Each location will have its local data as well as the ability to get needed data from other locations via a communication network. Moreover, the failure of one of the servers at one site won't render the distributed database system inaccessible. The affected site will be the only one directly involved with that failed server. In addition, if any data is required from a site exhibiting a failure, such data may be retrieved from other locations containing the replicated data [7]. The performance of the system will improve, since several machines take care of distributing the load of the CPU and the I/O. Also, the expansion of the distributed system is relatively easy, since adding a new location doesn't affect the existing ones.

2.2 Disadvantages of Distributed DBS

On the other hand, DDBS has several disadvantages. A distributed system usually exhibits more complexity and cost more than a centralized one. Security-network must be made secure Integrity Control More Difficult This is true because the hardware and software involved need to maintain a reliable and an efficient system. All the replication and data retrieval from all sites should be transparent to the user. The cost of maintaining the system is considerable since technicians and experts are required at every site. Another main disadvantage of distributed database systems is the issue of security. Handling security across several locations is more complicated. In addition, the communication between sites may be tapped to.

2.3 Issues in Distributed Database Design

We have to consider three key issues in distributed database design

- Data Allocation: where are data placed? Data should be stored at site with "optimal" distribution.
- Fragmentation: relation may be divided into a number of sub-relations (called fragments), which are stored in different sites.
- Replication: copy of fragment may be maintained at several sites.

III. FUNDAMENTALS OF TRANSACTION

Transaction deals with the problems of keeping the database in a consistent state even when concurrent accesses and failures occur.

3.1 What is a Transaction

A transaction consists of a series of operations performed on a database. The important issue in transaction management is that if a database was in a consistent state prior to the initiation of a transaction, then the database should return to a consistent state after the transaction is completed. This should be done irrespective of the fact that transactions were successfully executed simultaneously or there were failures during the execution,[8]. A transaction is a sequence of operations that takes the database from a consistent state to another consistent state. It represents a complete and correct computation. Two types of transactions are allowed in our environment: query transactions and update transactions. Query transactions consist only of read operations that access data objects and return their values to the user. Thus, query transactions do not modify the database state. Two transactions conflict if the read-set of one transaction intersects with the write-set of the other transaction. During the voting process, Update transactions consist of both read and write operations. Transactions have their time-stamps constructed by adding 1 to the greater of either the current time or the highest time-stamp of their base variables. Thus; a transaction is a unit of consistency and reliability. The properties of transactions will be discussed later in the properties section. Each transaction has to terminate. The outcome of the termination depends on the success or failure of the transaction. When a transaction starts executing, it may terminate with one of two possibilities:

1. The transaction aborts if a failure occurred during its execution
 2. The transaction commits if it was completed successfully.
- Example of a transaction that aborts during process 2 (P2). On the other hand, an example of a transaction that commits, since all of its processes are successfully completed [9, 10].

3.2 Properties of Transactions

A Transaction has four properties that lead to the consistency and reliability of a distributed data base. These are Atomicity, Consistency, Isolation, and Durability [6].

ACID property of transaction: The concept of a database transaction (or atomic transaction) has evolved in order to enable both a well-understood database system behavior in a faulty environment where crashes can happen any time, and recovery from a crash to a well understood database state. A database transaction is a unit of work, typically encapsulating a number of operations over a database (e.g., reading a database object, writing, acquiring lock, etc.), an abstraction supported in database and also other systems. Each transaction has well defined boundaries in terms of which program/code executions are included in that transaction (determined by the transaction's programmer via special transaction commands). Every database transaction obeys the following rules (by support in the database system; i.e., a database system is designed to guarantee them for the transactions it runs):

Atomicity: This refers to the fact that a transaction is treated as a unit of operation. Consequently, it dictates that either all the actions related to a transaction are completed or none of them is carried out. For example, in the case of a crash, the system should complete the remainder of the transaction, or it will undo all the actions pertaining to this transaction. The recovery of the transaction is split into two types corresponding to the two types of failures: Atomicity means

that users do not have to worry about the effect of incomplete transactions. Transactions can fail for several kinds of reasons:

1. Hardware failure: A disk drive fails, preventing some of the transaction's database changes from taking effect.
2. System failure: The user loses their connection to the application before providing all necessary information.
3. Database failure: E.g., the database runs out of room to hold additional data.
4. Application failure: The application attempts to post data that violates a rule that the database itself enforces such as attempting to insert a duplicate value in a column.

Consistency: Every transaction must leave the database in a consistent (correct) state, i.e., maintain the predetermined integrity rules of the database (constraints upon and among the database's objects). A transaction must transform a database from one consistent state to another consistent state (however, it is the responsibility of the transaction's programmer to make sure that the transaction itself is correct, i.e., performs correctly what it intends to perform (from the application's point of view) while the predefined integrity rules are enforced by the DBMS). Thus since a database can be normally changed only by transactions, all the database's states are consistent. An aborted transaction does not change the database state it has started from, as if it never existed (atomicity above).

Isolation: According to this property, each transaction should see a consistent database at all times. Consequently, no other transaction can read or modify data that is being modified by another transaction. If this property is not maintained, one of two things could happen to the data base.

- a. Lost Updates: this occurs when another transaction (T2) updates the same data being modified by the first transaction (T1) in such a manner that T2 reads the value prior to the writing of T1 thus creating the problem of losing this update.
- b. Cascading Aborts: this problem occurs when the first transaction (T1) aborts, then the transactions that had read or modified data that has been used by T1 will also abort.

Durability: Durability is the DBMS's guarantee that once the user has been notified of a transaction's success the transaction will not be lost, the transaction's data changes will survive system failure, and that all integrity constraints have been satisfied, so the DBMS won't need to reverse the transaction. Many DBMSs implement durability by writing transactions into a transaction log that can be reprocessed to recreate the system state right before any later failure. A transaction is deemed committed only after it is entered in the log. Durability does not imply a permanent state of the database. A subsequent transaction may modify data changed by a prior transaction without violating the durability principle. The concept of atomic transaction has been extended during the years to what has become a Business transaction, which actually implement types of Workflow and are not atomic. However also such enhanced transactions typically utilize atomic transactions as components [11, 12].

3.3 Type of distributed transaction

By structure, distributed transaction is dividing into two types. A flat transaction, FT, is an operation, performed on a database, which may consist of several simple actions. From

the client's point of view the operation must be executed indivisibly. Main disadvantage with FTs that if one action fails the whole transaction must abort. Issues related to distributed transaction: There are a number of issues or problems, which are peculiar to a distributed database and these, require novel solutions. These include the following:

3.3.1 Distributed query optimisation: In a distributed database the optimisation of queries by the DBMS itself is critical to the efficient performance of the overall system. Query optimisation must take into account the extra communication costs of moving data from site to site, but can use whatever replicated copies of data are closest, to execute a query. Thus it is a more complex operation than query optimisation in centralised databases.

3.3.2 Distributed update propagation: Update propagation in a distributed database is problematic because of the fact that there may be more than one copy of a piece of data because of replication, and data may be split up because of partitioning. Any updates to data performed by any user must be propagated to all copies throughout the database. The use of snapshots is one technique for implementing this.

3.3.3 Distributed catalog management: The distributed database catalog entries must specify site(s) at which data is being stored in addition to data in a system catalog in a centralised DBMS. Because of data partitioning and replication, this extra information is needed. There are a number of approaches to implementing a distributed database catalog. Centralized- Keep one master copy of the catalog, fully replicated. Partitioned -Partition and replicate the catalog as usage patterns demand, Centralised/partitioned- Combination of the above.

3.3.4 Distributed concurrency control: Concurrency Control in distributed databases can be done in several ways. Locking and timestamping are two techniques, which can be used, but timestamping is generally preferred. The problems of concurrency control in a distributed DBMS are more severe than in a centralised DBMS because of the fact that data may be replicated and partitioned. If a user wants unique access to a piece of data, for example to perform an update or a read, the DBMS must be able to guarantee unique access to that data, which is difficult if there are copies throughout the sites in the distributed database.

A number of problems arise while dealing with concurrency control and recovery issues in distributed databases. Some of the major problems are:

Site failure: There are situation when one or more sites in a DDBMS fail. In such situations, consistency and integrity of the database must be restored.

Network Problems: When communication network fails, causing one or more sites to be cut off from the rest of the sites in the DDBMS environment

Data Duplication: Multiple copies of the database must be monitor carefully for maintaining consistency.

Distributed Transaction: A problem arise when a transaction distributed across various sites. Some of the sites are successfully committing/rolling, while the others may not be successfully done.

Distributed Deadlocks: In DDBMS, a deadlock may occur in any one or many sites. So, careful handling is necessary.

3.3.5 Transaction Concurrency: If transactions are executed serially, i.e., sequentially with no overlap in time, no transaction concurrency⁴ exists. However, if concurrent transactions with interleaving operations are allowed in an uncontrolled manner, some unexpected, undesirable result may occur. Here

IV. Transaction Processing In Replicated Data in the DDBMS

A transaction is a logical unit of work constituted by one or more SQL statements executed by a single user. A transaction begins with the user's first executable SQL statement and ends when it is committed or rolled back by that user. A remote transaction contains only statements that access a single remote node. A distributed transaction contains statements that access more than one node. A distributed transaction is a transaction that includes one or more statements that, individually or as a group, update data on two or more distinct nodes of a distributed database. The term replication refers to the operation of copying and maintaining database objects in multiple databases belonging to a distributed system. The terms distributed database system and database replication are related, yet distinct. In a pure (that is, not replicated) distributed database, the system manages a single copy of all data and supporting database objects. Typically, distributed database applications use distributed transactions to access both local and remote data and modify the global database in real-time. While replication relies on distributed database technology, database replication offers applications benefits that are not possible within a pure distributed database environment. Most commonly, replication is used to improve local database performance and protect the availability of applications because alternate data access options exist.[13,14,16] For example, an application may normally access a local database rather than a remote server to minimize network traffic and achieve maximum performance. Furthermore, the application can continue to function if the local server experiences a failure, but other servers with replicated data remain accessible. A new component, which is a replication manager module, has been recently added to the system, in order to maintain replicated data.

4.1 Transaction-Processing Model:

A DDBMS contains four components: transactions (T), Transaction Manager (TMR), Data Manager (DMR), and data (D). Transactions communicate with TMRs, TMRs communicate with DMRs, and DMRs manage the D. TMRs supervise transactions. Each transaction executed in the DDBMS is supervised by a single TMR, meaning that the transaction issues all of its database operations to that TMR. Any distributed computation that is needed to execute the transaction is managed by the TMR. Four operations are defined at the transaction-TMR interface.

READ (A): returns the value of A (a logical data item) in the current logical database state.

WRITE (A, new-value): creates a new logical database state in which A has the specified new value.

BEGIN and **END** operations to bracket transaction executions.

DMRs manage the stored database, functioning as backend database processors. In response to commands from transactions, TMRs issue commands to DMRs specifying stored data items to be read or written.

In a centralized DBMS, private workspaces are part of the Transaction Manager (TMR) and data can freely move between a transaction and its workspace, and between a workspace and the Data Manager (DMR). Whereas in a DDBMS TMRs and DMRs may run at different sites and the movement of data between a TM and a DM can be expensive. To reduce this cost, many DDBMSs employ query optimization procedures which regulate the flow of data between sites. How a Transaction (T) reads and writes data in these workspaces is a query optimization problem and has no direct effect on concurrency control. Suppose T is updating x, y, z stored at DMR_x, DMR_y, DMR_z, and suppose T's TMR fails after issuing DMR-write(x), but before issuing the dm-writes for y and z. At this point the database is incorrect. However, in a DDBMS, other TMRs remain operational and can access the incorrect database. To avoid this problem, prewrite commands must be modified slightly. In addition to specifying data items to be copied onto secure storage, prewrites also specify which other DMRs are involved in the commitment activity. Then if the TMR fails during the second phase of two-phase commit, the DMRs whose dm-writes were not issued can recognize the situation and consult the other DMRs involved in the commitment. If any DMR received a dmr-write, the remaining ones act as if they had also received the command. In a DDBMS these are processed as follows.

BEGIN: The TMR creates a private work space for T.

READ (A): The TMR checks T's private workspace to see if a copy of A is present. If so, that copy's value is made available to T. Otherwise the TMR selects some stored copy of A, say x_i, and issues read(x_i) to the DMR at which x_i is stored. The DMR responds by retrieving the stored value of x_i from the database, placing it in the private workspace. The TMR returns this value to T.

WRITE (A, new-value): The value of A in T's private workspace is updated to newvalue, assuming the workspace contains a copy of A. Otherwise; a copy of A with the new value is created in the workspace.

END: Two-phase commit begins.

For each A updated by T, and for each stored copy x_i of A, the TMR issues a prewrite (x_i) to the DMR that stores x_i. The DMR responds by copying the value of A from T's private workspace onto secure storage internal to the DMR. After all prewrites are processed, the TMR issues dm-writes for all copies of all logical data items updated by T.

A DMR responds to dmr-write(x_i) by copying the value of x_i from secure storage into the stored database. After all dm-writes are installed, T's execution is finished.

4.2 SYNCHRONIZATION TECHNIQUES BASED ON TWO-PHASE LOCKING

Two-phase locking (2PL) synchronizes reads and writes by explicitly detecting and preventing conflicts between concurrent operations. Earlier than reading data item x, a transaction must "own" a read lock on x. Before writing into x, it must "own" a write lock on x. The ownership of locks is governed by two rules:

(1) Different transactions cannot simultaneously own conflicting locks

(2) Once a transaction surrenders ownership of a lock, it may never obtain additional locks.

The definition of conflicting lock depends on the type of synchronization being performed:

For 'rw' synchronization two locks conflict if

- (a) Both are locks on the same data item, and
- (b) One is a read lock and the other is a write lock;

for 'ww' synchronization two locks conflict if

- (a) Both are locks on the same data item, and
- (b) Both are write locks.

The second lock ownership rule causes every transaction to obtain locks in a two-phase manner. During the growing phase the transaction obtains locks without releasing any locks. By releasing a lock the transaction enters the shrinking phase. During this phase the transaction releases locks, and, by rule 2, is prohibited from obtaining additional locks. When the transaction terminates (or aborts), all remaining locks are automatically released. A common variation is to require that transactions obtain all locks before beginning their main execution. This variation is called predeclaration. Some systems also require that transactions hold all locks until termination.

4.2.1 Performance of 2PL

A performance of 2PL amounts to building a 2PL scheduler, a software module that receives lock requests and lock releases and processes them according to the 2PL specification. The basic way to implement 2PL in a distributed database is to distribute the schedulers along with the database, placing the scheduler for data item x at the DMR where x is stored. In this implementation read locks may be implicitly requested by dmr reads and write locks may be implicitly requested by prewrites. If the requested lock cannot be granted, the operation is placed on a waiting queue for the desired data item. Write locks are implicitly released by dmr-writes. However, to release readlocks, special lockrelease operations are required. When a lock is released, the operations on the waiting queue of that data item are processed first-in/first-out (FIFO) order. However, if a transaction updates A , then it must update all copies of A , and so must obtain write locks on all copies of A .

4.2.2 Primary Copy 2PL

Primary copy 2PL is a 2PL technique that pays attention to data redundancy. One copy of each logical data item is designated the primary copy; before accessing any copy of the logical data item, the appropriate lock must be obtained on the primary copy. For read locks this technique requires more communication than basic 2PL. Suppose x_1 is the primary copy of logical data item A , and suppose transaction T wishes to read some other copy, x_i , of A . To read x_i , T must communicate with two DMRs, the DMR where A is stored. But under basic 2PL, T would only communicate with x_i 's DMR. For write locks, however, primary copy 2PL does not incur extra communication.

4.2.3 Voting 2PL Method

Voting 2PL is another performance of 2PL that exploits data redundancy. Voting 2PL is derived from the majority consensus technique of Thomas and is only suitable for 'ww' synchronization. To understand voting, we must examine it in the context of two-phase commit. Suppose transaction T wants to write into A . Its TMR sends prewrites to each DMR

holding a copy of A . For the voting protocol, the DMR always responds immediately. It acknowledges receipt of the prewrite and says "lock set" or "lock blocked." After the TM receives acknowledgments from the DMRs, it counts the number of "lockset" responses: if the number constitutes a majority, then the TMR behaves as if all locks were set. Otherwise, it waits for "lockset" operations from DMRs that originally said "lock blocked." Deadlocks aside, it will eventually receive enough "lockset" operations to proceed. Since only one transaction can hold a majority of locks on A at a time, only one transaction writing into A can be in its second commit phase at any time [17, 18]. All copies of A thereby have the same sequence of writes applied to them. transaction's locked point occurs when it has obtained a majority of its write locks on each data item in its write set. When updating many data items, a transaction must obtain a majority of locks on every data item before it issues any dmr-writes. In principle, voting 2PL could be adapted for 'rw' synchronization. Before reading any copy of a transaction requests read locks on all copies of A ; when a majority of locks are set, the transaction may read any copy. This technique works but is overly strong: Correctness only requires that a single copy of A be locked—namely, the copy that is read—yet this technique requests locks on all copies. For this reason we deem voting 2PL to be inappropriate for rw synchronization.

V. Two-Phase Commit of transaction in Distributed database System

In transaction processing, databases, and computer networking, the two-phase commit protocol (2PC) is a type of atomic commitment protocol (ACP). It is a distributed algorithm that coordinates all the processes that participate in a distributed atomic transaction on whether to commit or abort (roll back) the transaction (it is a specialized type of consensus protocol). The protocol achieves its goal even in many cases of temporary system failure (involving process, network node, communication, etc. failures), and is thus widely utilized [17, 18]. However, it is not resilient to all possible failure configurations, and in rare cases user (e.g., a system's administrator) intervention is needed to remedy outcome. To accommodate recovery from failure (automatic in most cases) the protocol's participants use logging of the protocol's states. Log records, which are typically slow to generate but survive failures, are used by the protocol's recovery procedures. Many protocol variants exist that primarily differ in logging strategies and recovery mechanisms. Though usually intended to be used infrequently, recovery procedures comprise a substantial portion of the protocol, due to many possible failure scenarios to be considered and supported by the protocol. In a "normal execution" of any single distributed transaction, i.e., when no failure occurs, which is typically the most frequent situation, the protocol comprises two phases:

1. The commit-request phase (or voting phase), in which a coordinator process attempts to prepare all the transaction's participating processes (named participants, cohorts, or workers) to take the necessary steps for either committing or aborting the transaction and to vote, either "Yes": commit (if the transaction participant's local portion execution has ended properly), or "No": abort (if a problem has been detected with the local portion).

2. The commit phase, in which, based on voting of the cohorts, the coordinator decides whether to commit (only if all have voted “Yes”) or abort the transaction (otherwise), and notifies the result to all the cohorts. The cohorts then follow with the needed actions (commit or abort) with their local transactional resources (also called recoverable resources; e.g., database data) and their respective portions in the transaction’s other output (if applicable).

5.1 Commit request phase

1. The coordinator sends a query to commit message to all cohorts and waits until it has received a reply from all cohorts.
2. The cohorts execute the transaction up to the point where they will be asked to commit. They each write an entry to their undo log and an entry to their redo log.
3. Each cohort replies with an agreement message (cohort votes Yes to commit), if the cohort’s actions succeeded, or an abort message (cohort votes No, not to commit), if the cohort experiences a failure that will make it impossible to commit.

5.2 Commit phase

Success: If the coordinator received an agreement message from all cohorts during the commit-request phase:

1. The coordinator sends a commit message to all the cohorts.
2. Each cohort completes the operation, and releases all the locks and resources held during the transaction.
3. Each cohort sends an acknowledgement to the coordinator.
4. The coordinator undoes the transaction when all acknowledgements have been received

Failure:

If any cohort votes No during the commit-request phase (or the coordinator’s timeout expires):

1. The coordinator sends a rollback message to all the cohorts.
2. Each cohort undoes the transaction using the undo log, and releases the resources and locks held during the transaction.
3. Each cohort sends an acknowledgement to the coordinator.
4. The coordinator undoes the transaction when all acknowledgements have been received.

The protocol proceeds in two phases, namely the prepare and the commit phase, which explains the protocol’s name. The protocol is executed by a coordinator process, while the participating servers are called participants. When the transaction’s initiator issues a request to commit the transaction, the coordinator starts the first phase of the 2PC protocol by querying—via prepare messages—all participants whether to abort or to commit the transaction. The master initiates the first phase of the protocol by sending PREPARE (to commit) messages in parallel to all the cohorts. Each cohort that is ready to commit first force-writes a prepare log record to its local stable storage and then sends a YES vote to the master. At this stage, the cohort has entered a prepared state wherein it cannot unilaterally commit or abort the transaction but has to wait for the final decision from the master. On the other hand, each cohort that decides to abort force-writes an abort log record and sends a NO vote to the master. Since a NO vote acts like a veto, the cohort is permitted to unilaterally abort the transaction without waiting for a response from the master.

After the master receives the votes from all the cohorts, it initiates the second phase of the protocol. If all the votes are YES, it moves to a committing state by force writing a commit log record and sending COMMIT messages to all the cohorts. Each cohort after receiving a COMMIT message moves to the committing state, force-writes a commit log record, and sends an ACK message to the master. If the master receives even one NO vote, it moves to the aborting state by force-writing an abort log record and sends ABORT messages to those cohorts that are in the prepared state. These cohorts, after receiving the ABORT message, move to the aborting state, force write an abort log record and send an ACK message to the master. Finally, the master, after receiving acknowledgements from all the prepared cohorts, writes an end log record and then “forgets” the transaction. The 2PC may be carried out with one of the following methods: Centralized 2PC, Linear 2PC, and Distributed 2PC, [17, 18].

5.3 The Centralized Two-Phase Commit Protocol

In the Centralized 2PC communication is done through the coordinator’s process only, and thus no communication between subordinates is allowed. The coordinator is responsible for transmitting the PREPARE message to the subordinates, and, when the votes of all the subordinates are received and evaluated, the coordinator decides on the course of action: either abort or COMMIT. This method has two phases:

1. First Phase: In this phase, when a user wants to COMMIT a transaction, the coordinator issues a PREPARE message to all the subordinates, (Mohan et al., 1986). When a subordinate receives the PREPARE message, it writes a PREPARE log and, if that subordinate is willing to COMMIT, sends a YES VOTE, and enters the PREPARED state; or, it writes an abort record and, if that subordinate is not willing to COMMIT, sends a NO VOTE. A subordinate sending a NO VOTE doesn’t need to enter a PREPARED state since it knows that the coordinator will issue an abort. In this case, the NO VOTE acts like a veto in the sense that only one NO VOTE is needed to abort the transaction. The following two rules apply to the coordinator’s decision.

- a. If even one participant votes to abort the transaction, the coordinator has to reach a global abort decision.
- b. If all the participants vote to COMMIT, the coordinator has to reach a global COMMIT decision.

2. Second Phase: After the coordinator reaches a vote, it has to relay that vote to the subordinates. If the decision is COMMIT, then the coordinator moves into the committing state and sends a COMMIT message to all the subordinates informing them of the COMMIT. When the subordinates receive the COMMIT message, they, in turn, move to the committing state and send an acknowledge (ACK) message to the coordinator. When the coordinator receives the ACK messages, it ends the transaction. If, on the other hand, the coordinator reaches an ABORT decision, it sends an ABORT message to all the subordinates. Here, the coordinator doesn’t need to send an ABORT message to the subordinate(s) that gave a NO VOTE.

5.4 The Linear Two-Phase Commit Protocol

In the linear 2PC, subordinates can communicate with each other. The sites are labeled 1 to N, where the coordinator is numbered as site 1. Accordingly, the propagation of the PREPARE message is done serially. As such, the time

required to complete the transaction is longer than centralized or distributed methods. Finally, node N is the one that issues the Global COMMIT. The two phases are discussed below:

First Phase: The coordinator sends a PREPARE message to participant 2. If participant 2 is not willing to COMMIT, then it sends a VOTE ABORT (VA) to participant 3 and the transaction is aborted at this point. If participant 2, on the other hand, is willing to commit, it sends a VOTE COMMIT (VC) to participant 3 and enters a READY state. In turn, participant 3 sends its vote till node N is reached and issues its vote.

Second Phase: Node N issues either a GLOBAL ABORT (GA) or a GLOBAL COMMIT (GC) and sends it to node N-1. Subsequently, node N-1 will enter an ABORT or COMMIT state. In turn, node N-1 will send the GA or GC to node N-2, until the final vote to commit or abort reaches the coordinator, node

5.5 The Distributed Two-Phase Commit Protocol

In the distributed 2PC, all the nodes communicate with each other. According to this protocol, as Figure 5 shows, the second phase is not needed as in other 2PC methods. Moreover, each node must have a list of all the participating nodes in order to know that each node has sent in its vote. The distributed 2PC starts when the coordinator sends a PREPARE message to all the participating nodes. When each participant gets the PREPARE message, it sends its vote to all the other participants. As such, each node maintains a complete list of the participants in every transaction. Each participant has to wait and receive the vote from all other participants. When a node receives all the votes from all the participants, it can decide directly on COMMIT or abort. There is no need to start the second phase, since the coordinator does not have to consolidate all the votes in order to arrive at the final decision.

VI. DATABASE MANAGEMENT SYSTEM: THE TWO-PHASE COMMIT

A distributed database system is a network of two or more databases that reside on one or more machines. A distributed system that connects four databases. An application can simultaneously access or modify the data in several databases in a single distributed environment. For a client application, the location and platform of the databases are transparent. You can also create synonyms for remote objects in the distributed system so that users can access them with the same syntax as local objects. For example, if you are connected to database mfg but want to access data on database headquarters, creating a synonym on manufacturing for the remote dept table enables you to issue this query [18]. The database is a distributed database management system, which employs the two-phase commit to achieve and maintain data reliability. The DB2 database is a distributed database management system, which employs the two-phase commit to achieve and maintain data reliability. The following sections explain DB2's two-phase implementation procedures. How Session maintains between nodes in each transaction, DB2 constructs a session tree for the participating nodes. The session tree describes the relations between the nodes participating in any given transaction. Each node plays one or more of the following roles:

6.1 The Branch Tree

In each transaction, Oracle constructs a branch tree for the participating nodes. The session tree describes the relations between the nodes participating in any given transaction. Each node plays one or more of the following roles [10]:

6.1.1 Client(C): A client is a node that references data from another node.

6.1.2. Database Server (DS): A server is a node that is being referenced by another node because it has needed data. A database server is a server that supports a local database.

6.1.3. Global Coordinator (GC): The global coordinator is the node that initiated the transaction, and thus, is the root of the branch tree. The operations performed by the global coordinator are as follows:

- In its role as a global coordinator and the root of the branch tree, all the SQL statements, procedure calls, etc., are sent to the referenced nodes by the global coordinator. Instructs all the nodes, except the COMMIT point site, to PREPARE
- If all sites PREPARE successfully, then the global coordinator instructs the COMMIT point site to initiate the commit phase
- If one or more of the nodes send an abort message, then the global coordinator instructs all nodes to perform a rollback.

6.1.4. Local Coordinator: A local coordinator is a node that must reference data on another node in order to complete its part. The local coordinator carries out the following functions:

- Receiving and relaying status information among the local nodes
- Passing queries to those nodes
- Receiving queries from those nodes and passing them on to other nodes
- Returning the results of the queries to the nodes that initiated them.

6.1.5. Commit Point Site: Before a COMMIT point site can be designated, the COMMIT point strength of each node must be determined. The COMMIT point strength of each node of the distributed database system is defined when the initial connection is made between the nodes. The COMMIT point site has to be a reliable node because it has to take care of all the messages. When the global coordinator initiates a transaction, it checks the direct references to see which one is going to act as a COMMIT point site. The COMMIT point site cannot be a read-only site. If multiple nodes have the same COMMIT point strength, then the global coordinator selects one of them. In case of a rollback, the PREPARE and COMMIT phases are not needed and thus a COMMIT point site is not selected. A transaction is considered to be committed once the COMMIT point site commits locally.

6.2 Two-Phase Commit and the Database Implementation

The transaction manager of the homogenous Oracle8 database necessitates that the decision on what to do with a transaction to be unanimous by all nodes. This requires all concerned nodes to make one of two decisions: commit and complete the transaction, or abort and rollback the transaction. The Oracle engine automatically takes care of the commit

[19]. or rollback of all transactions, thus, maintaining the integrity of the database. The following will describe the two phases of the transaction manager.

6.2.1. PREPARE Phase (PP): The PP starts when a node, the initiator, asks all participants, except the commit point site, to PREPARE. In the PP, the requested nodes have to record enough information to enable them either to commit or abort the transaction. The node, after replying to the requestor that it has PREPARED, cannot unilaterally perform a COMMIT or abort. Moreover, the data that is tied with the COMMIT or abort is not available for other transactions.

Each node may reply with one of three responses to the initiator. These responses are defined below:

a. Prepared: the data has already been modified and that the node is ready to COMMIT. All resources affected by the transaction are locked.

b. Read-only: the data on the node has not been modified. With this reply, the node does not PREPARE and does not participate in the second phase.

c. Abort: the data on the node could not be modified and thus the node frees any locked resources for this transaction and sends an abort message to the node that referenced it.

6.2.2. COMMIT Phase (CP): Before the CP begins, all the referenced nodes need to have successfully PREPARED. The COMMIT phase begins by the global coordinator sending a message to all the nodes instructing them to COMMIT. Thus, the databases across all nodes are consistent.

VII. CONCLUSIONS

At the present time Transaction management is an fully grown thought in distributed data base management systems (DDBMS) for research area for research. In this paper, we have reviewed the basic concepts Transaction Processing In Replicated Data. Many associations do not implement distributed databases because of its difficulty. They simply resort to centralized databases. However, with global organizations and multi-tier network architectures, distributed implementation becomes a necessity. It is hoped that this paper to will assist organization in the implementation of distributed databases when installing homogenous DBMS, or give confidence organizations to journey from centralized to distributed DBMS. We talk about the basic concept of transaction in distributed database systems, and also discussed the advantage, property and operations transaction in distributed environments. It is really important for database to have the ACID properties to perform. We have presented the basics of distributed database technology as well as the techniques that help in distribution of database in transaction-processing model. Also, Discussion regarding the framework for the design and analysis of distributed database concurrency control algorithms. The framework has two main components are system model that provides common terminology and concepts for describing a variety of concurrency control algorithms, and a problem decomposition that decomposes concurrency control algorithms into readwrite and write-write synchronization subalgorithms. We have considered synchronization subalgorithms outside the context of specific concurrency control algorithms.

References

- [1] R. Abbott and H. Garcia-Molin a, "Scheduling 'Real-Time Transactions: a Performance Evaluation'", F&C of 14th VLDB Conj., August 1988.
- [2] Sang Hyuk Son, "Replicated Data Management in Distributed Database Systems", ACM Sigmod., Vol. 17, Issue 4, Dec 1998, Newyork,USA, pp-62-69.
- [3] Jayant. H, Carey M, Livney,1992, "Data Access Scheduling in Firm Real time Database Systems", Real Time systems Journal, 4
- [4] M, Valduriez P, 1991, Principles of Distributed Database Systems, Prentice-Hall.P. Bernstein, V. Hadzilacos and N. Goodman,
- [5] G. Coulouris, J. Dollimore, T. Kindberg: Disributed Systems, Concepts and Design, Addison-Wesley, 1994.
- [6] Oracle8 Server Distributed Database Systems, Oracle, 3-1 – 3-35.
- [7] Ozsu, Tamer M., and V.alduriez, Patrick [1991], Principles of Distributed Database Systems, Prentice
- [8] Mohan, C.; Lindsay, B.; and Obermarck, R. [1986], "Transaction Management in the R* Distributed Database Management System." ACM Transactions on Database Systems, Vol. 11, No. 4, December1986, 379-395.
- [9] S. Ceri, M.A.W. Houtsma, A.M. Keller, P. Samarati: A Classification of Update Methods for Replicated Databases, via Internet, May 5, 1994.
- [10] D. Agrawal, A.El. Abbadi: The Tree Quorum Protocol: An Efficient Approach for Managing Replicated Data. in Proc. of VLDB Conf. pp 243-254, 1990.
- [11] Distributed Transaction Processing on an Ordering Network By Rashmi Srinivasa, Craig Williams, Paul F. Reynolds (2002)
- [12] Ghazi Alkhatib, Transaction Management in Distributed Database: the Case of Oracle's Two-Phase Commit, Vol. 13(2)
- [13] E. Cooper, "Analysis of Distributed Commit Protocols", Proc. of ACM Sigmod Conj., June 1982.
- [14] Ramamritham, Son S. H, and DiPippo L, 2004, Real-Time Databases and Data Services, Real-Time Systems J., vol. 28, 179-216.
- [15] Jayanta Singh and S.C Mehrotra et all, 2010, "Management of missed transaction in a distributed system through simulation", Proc. Of IEEE.
- [16] Udai Shanker, "Some Performance Issues In Distributed Real Time Database System", PhD Thesis, December, 2005
- [17] D. Agrawal, A.J. Bernstein, P. Gupta, S. Sengupta, "Distributed Optimistic Concurrency Control with Reduced Rollback," Distributed Computing, vol. 2, no. 1, pp. 45-59, 1987.
- [18] R. Agrawal, M.J. Carey and L.W. McVoy, "The Performance of Alternative Strategies for Dealing with Deadlocks in Database Management Systems," IEEE Trans. Software Eng., vol. 13, no. 12, pp. 1,348-1,363, Dec. 1987.
- [19] Boutros B. S. and Desai B. C., "A Two-Phase Commit Protocol and its Performance," in Proceedings of the 7th International Workshop on Database and Expert Systems Applications, pp.100-105, 1996.

Chance Constrained Quadratic Bi-level Programming Problem

Surapati Pramanik¹, Durga Banerjee²

^{*1} (Department of Mathematics, Nandalal Ghosh B.T. College, Panpur, North 24 Parganas)

^{**2} (Ranaghat Yusuf Institution, Rathtala, Ranaghat, Nadia, India)

ABSTRACT: This paper deals with fuzzy goal programming approach to solve chance constrained quadratic bi-level programming problem. Chance constraints are converted into equivalent deterministic constraints by the prescribed distribution functions. In the model formulation, the quadratic membership functions are formulated by using the individual best solution of the quadratic objective functions subject to the equivalent deterministic constraints. Using first order Taylor's series, the quadratic membership functions are approximated to linear membership functions expanding about the individual best solution points. For avoiding decision deadlock, each level decision maker provides a relaxation of bounds on the decision variables controlled by him. We use two fuzzy goal programming models to reach the highest degree of membership goals by minimizing negative deviational variables. Euclidean distance function is used to identify the most compromise optimal solution. To demonstrate the proposed approach, two numerical examples are solved.

Keyword: Bi-level programming, chance constraints, fuzzy goal programming, quadratic programming problem, Taylor's series.

I. INTRODUCTION

In bi-level programming problem (BLPP), there are two types of decision makers (DMs). One is first level decision maker (FLDM) and another is second level decision maker (SLDM). The execution of decision is sequential from first level to second level and each level DM independently controls only a set of decision variables. The FLDM makes his decision first. But SLDM may not be satisfied with the decision of FLDM. Consequently, decision deadlock occurs frequently in the hierarchical decision making context.

Candler and Townsley [1] as well as Fortuny –Amart and McCarl [2] developed the formal bi-level programming problem (BLPP). In 1991, Edmund and Bard [3] studied non linear bi-level programming problems. Malhotra and Arora [4] discussed fractional bi-level programming problem using preemptive goal programming. Sakawa and Nishizaki [5, 6] studied linear fractional BLPP based on interactive fuzzy programming. Using analytical hierarchy process due to Saaty [7], Mishra [8] developed weighting method for linear fractional BLPP. Pramanik and Dey [9] presented linear fractional BLPP based on fuzzy goal programming (FGP) using first order Taylor polynomial series.

Anandalingam [10] discussed multi level programming problem (MLPP) as well as bi-level decentralized programming problem by using Stackelberg solution approach. The concept of fuzzy set theory in MLPP was first introduced by Lai [11]. Shih et al. [12] and Shih and Lee [13] extended Lai's ideas by introducing non-compensatory max min aggregation operator and compensatory fuzzy operator respectively. Fuzzy goal programming for MLPP was studied by Pramanik and Roy [14].

Quadratic bi-level programming problem (QBLPP) is a special type of non-linear bi-level programming problem. In this paper, we consider the objective function of each level DM is quadratic function and the constraints are linear functions. There are many research fields where QBLPP arise such as robust data fitting, traffic assignment problems, portfolio optimizations, transportations. In 1994, Faustino and Judice [15] developed the linear QBLPP. Vicente et al. [16] presented descent method for QBLPP. Optimality conditions and algorithm for solving QBLPP were developed by Wang et al. [17]. QBLPP for integer variables was presented by Thirwani and Arora [18]. They used linearization method and obtained integer solution for QBLPP by using Gomory cut and dual simplex method. Using Karush-Kuhn-Tucker conditions and duality theory, Calvete and Gale [19] discussed optimality conditions for the linear fractional / quadratic BLPP. Pal and Moitra [20] developed FGP approach for solving QBLPP in 2003. Recently, Pramanik and Dey [21] studied multi objective quadratic programming problem. They [22] also developed priority based FGP approach to multi objective quadratic programming problem. They [23] also extended their ideas for solving QBLPP based on FGP.

Uncertainties may occur in the decision making situations. Generally, uncertainties can be fuzzily or stochastically described. Using probability theory, Dantzig [24] introduced stochastic programming. There are two main approaches of stochastic programming, namely, chance constrained programming (CCP) and two-stage programming. Charnes and Cooper [25] developed the CCP.

In the present paper, we present QBLPP with chance constraints which is called chance constrained QBLPP. We first convert the chance constraints into equivalent deterministic constraints with prescribed distribution functions and confidence levels. We form quadratic membership function by using individual best solution. Using first order Taylor's series, the quadratic membership function are approximated into linear membership functions by expanding about the respective individual best solution

point. For avoiding decision deadlock, each decision maker prefers some bounds on the decision variables controlled by him. Two FGP models are formulated and Euclidean distance function is used to determine the most compromise solution. Two numerical examples are solved to demonstrate the efficiency of the proposed approach.

The rest of the paper is organized in the following way. In Section II, we formulate chance constrained QBLPP. In Section III, chance constraints are transformed into equivalent deterministic constraints. Quadratic membership functions are constructed in Section IV. In Section V, technique of linearization of quadratic membership function is discussed by using first order Taylor's series. In Section VI, preference bounds on the decision variables are defined. Section VII is devoted to develop two FGP models for solving chance constrained QBLPP for maximization type objective functions. Section VIII discusses FGP model formulation for solving chance constrained QBLPP for minimization type objective functions. The Euclidean distance function is described in the next Section IX. The step wise descriptions of the whole paper are summarized in the Section X. Section XI presents two numerical examples. Finally, Section XII concludes the paper with final conclusion and future work.

II. FORMULATION OF CHANCE CONSTRAINED QUADRATIC BI-LEVEL PROGRAMMING PROBLEM

The generic form of chance constrained QBLPP is

$$[FLDM] \text{Max}_{\bar{X}_1} Z_1(\bar{X}) = \bar{A}_1 \bar{X} + \frac{1}{2} \bar{X}^T \bar{B}_1 \bar{X} \tag{1}$$

$$[SLDM] \text{Max}_{\bar{X}_2} Z_2(\bar{X}) = \bar{A}_2 \bar{X} + \frac{1}{2} \bar{X}^T \bar{B}_2 \bar{X} \tag{2}$$

subject to

$$\bar{X} \in X =$$

$$\{\bar{X} \in \mathbb{R}^n : \Pr(\bar{C}\bar{X} \leq \bar{d}) > \bar{I} - \bar{m}, \bar{X} \geq \bar{0}\} \tag{3}$$

Here, the decision vector $\bar{X}_1 = (x_{11}, x_{12}, x_{13}, \dots, x_{1n_1})$ is controlled by FLDM and $\bar{X}_2 = (x_{21}, x_{22}, x_{23}, \dots, x_{2n_2})$ is controlled by SLDM. $\bar{X}_1 \cup \bar{X}_2 = \bar{X} \in \mathbb{R}^n$, $n_1 + n_2 = n$, 'T' means transposition of vector. $\bar{A}_1, \bar{B}_1, \bar{A}_2, \bar{B}_2, \bar{I}, \bar{m}$ are given vectors. The order of \bar{A}_1, \bar{A}_2 are $1 \times n$, the order of symmetric matrices \bar{B}_1, \bar{B}_2 are $n \times n$, $\bar{I}, \bar{d}, \bar{m}$ are vectors of order $p \times 1$, every elements of \bar{I} is unity. \bar{C} is the given matrix of order $p \times n$. The polyhedron X is assumed to be non-empty and bounded.

III. CONVERSION OF STOCHASTIC CONSTRAINTS INTO DETERMINISTIC CONSTRAINTS

First, we consider the chance constraints of the form:

$$\Pr(\sum_{j=1}^n c_{ij} x_j \leq d_i) \geq 1 - m_i, \quad i = 1, 2, \dots, p_1. \tag{4}$$

$$\Rightarrow \Pr\left(\frac{\sum_{j=1}^n c_{ij} x_j - E(d_i)}{\sqrt{\text{var}(d_i)}} \leq \frac{d_i - E(d_i)}{\sqrt{\text{var}(d_i)}}\right) \geq 1 - m_i, \quad i = 1, 2, \dots, p_1$$

$$\Rightarrow m_i \geq 1 - \Pr\left(\frac{\sum_{j=1}^n c_{ij} x_j - E(d_i)}{\sqrt{\text{var}(d_i)}} \leq \frac{d_i - E(d_i)}{\sqrt{\text{var}(d_i)}}\right)$$

$$\Rightarrow m_i \geq \Pr\left(\frac{\sum_{j=1}^n c_{ij} x_j - E(d_i)}{\sqrt{\text{var}(d_i)}} > \frac{d_i - E(d_i)}{\sqrt{\text{var}(d_i)}}\right)$$

$$\Rightarrow \Psi^{-1}(m_i) \geq \frac{\sum_{j=1}^n c_{ij} x_j - E(d_i)}{\sqrt{\text{var}(d_i)}}$$

$$\Rightarrow \Psi^{-1}(m_i) \sqrt{\text{var}(d_i)} \geq \sum_{j=1}^n c_{ij} x_j - E(d_i)$$

$$\Rightarrow \sum_{j=1}^n c_{ij} x_j \leq E(d_i) + \Psi^{-1}(m_i) \sqrt{\text{var}(d_i)},$$

$$i = 1, 2, \dots, p_1 \tag{5}$$

Here $\Psi(\cdot)$ and $\Psi^{-1}(\cdot)$ represent the distribution function and inverse of distribution function of standard normal variable respectively.

Considering the case when $\Pr(\sum_{j=1}^n c_{ij} x_j \geq d_i) \geq 1 - m_i$,

$$i = p_1 + 1, p_1 + 2, \dots, p. \tag{6}$$

The constraints can be rewritten as:

$$\Pr\left(\frac{\sum_{j=1}^n c_{ij} x_j - E(d_i)}{\sqrt{\text{var}(d_i)}} \geq \frac{d_i - E(d_i)}{\sqrt{\text{var}(d_i)}}\right) \geq 1 - m_i, \quad i = p_1 + 1, p_1 + 2, \dots, p.$$

$$\Rightarrow \Psi\left(\frac{\sum_{j=1}^n c_{ij} x_j - E(d_i)}{\sqrt{\text{var}(d_i)}}\right) \geq 1 - m_i$$

$$\Rightarrow 1 - \Psi\left(-\frac{\sum_{j=1}^n c_{ij} x_j - E(d_i)}{\sqrt{\text{var}(d_i)}}\right) \geq 1 - m_i$$

$$\Rightarrow \Psi^{-1}(m_i) \geq -\frac{\sum_{j=1}^n c_{ij} x_j - E(d_i)}{\sqrt{\text{var}(d_i)}}$$

$$\Rightarrow \sum_{j=1}^n c_{ij} x_j \geq E(d_i) - \Psi^{-1}(m_i) \sqrt{\text{var}(d_i)}, \tag{7}$$

$$i = p_1 + 1, p_1 + 2, \dots, p.$$

$$\bar{X} \geq \bar{0} \tag{8}$$

Let us denote the equivalent deterministic system constraints (5), (7) and (8) by X. Here, X^* and X are equivalent set of constraints.

IV. CONSTRUCTION OF MEMBERSHIP FUNCTION

In order to construct quadratic membership function subject to the equivalent deterministic system constraints, the quadratic objective functions are maximized separately.

Let $\bar{X}_i^B = (x_{i1}^B, x_{i2}^B, x_{i3}^B, \dots, x_{in_i}^B), i = 1, 2$ be the individual best solution for the objective function $Z_i(\bar{X})$.

$$\text{Let } \max_{\bar{X} \in X} Z_1(\bar{X}) = Z_1^B = Z_1(\bar{X}_1^B) \text{ and } \max_{\bar{X} \in X} Z_2(\bar{X}) = Z_2^B = Z_2(\bar{X}_2^B).$$

Considering the individual best solution as the aspiration level, the fuzzy goal appears as:

$$Z_i(\bar{X}) \underset{\sim}{\geq} Z_i^B, i = 1, 2 \tag{9}$$

We consider $\min_{\bar{X} \in X} Z_1(\bar{X}) = Z_1^W$ and $\min_{\bar{X} \in X} Z_2(\bar{X}) = Z_2^W$ as the lower tolerance limits of the fuzzy objective goals of FLDM and SLDM.

Now, the membership function for the objective function $Z_1(\bar{X})$ of FLDM can be written as:

$$\mu_1(\bar{X}) = \left\langle \begin{array}{ll} 1, & \text{if } Z_1(\bar{X}) \geq Z_1^B, \\ \frac{Z_1(\bar{X}) - Z_1^W}{Z_1^B - Z_1^W}, & \text{if } Z_1^W \leq Z_1(\bar{X}) \leq Z_1^B, \\ 0, & \text{if } Z_1(\bar{X}) \leq Z_1^W \end{array} \right\rangle \tag{10}$$

and the membership function for the objective function $Z_2(\bar{X})$ of SLDM can be formulated as:

$$\mu_2(\bar{X}) = \left\langle \begin{array}{ll} 1, & \text{if } Z_2(\bar{X}) \geq Z_2^B, \\ \frac{Z_2(\bar{X}) - Z_2^W}{Z_2^B - Z_2^W}, & \text{if } Z_2^W \leq Z_2(\bar{X}) \leq Z_2^B, \\ 0, & \text{if } Z_2(\bar{X}) \leq Z_2^W \end{array} \right\rangle \tag{11}$$

Now, the chance constrained QBLP reduces to

$$\begin{aligned} &\max \mu_1(\bar{X}), \\ &\max \mu_2(\bar{X}), \\ &\text{subject to} \\ &\bar{X} \in X. \end{aligned} \tag{12}$$

V. LINEARIZATION OF QUADRATIC MEMBERSHIP FUNCTIONS BY USING TAYLOR'S SERIES APPROXIMATION

Let $\bar{X}_i^* = (x_{i1}^*, x_{i2}^*, x_{i3}^*, \dots, x_{in_i}^*, x_{in_i+1}^*, \dots, x_{in_i}^*)$, $i = 1, 2$ be the individual best solution of $\mu_i(\bar{X})$ subject to the equivalent deterministic system constraints. Then we transform the quadratic membership function $\mu_i(\bar{X})$ into an equivalent linear membership function $\mu_i^*(\bar{X})$ at the point \bar{X}_i^* by using first order Taylor's series as follows:

$$\begin{aligned} \mu_1(\bar{X}) &\cong \mu_1(\bar{X}_1^*) + (x_1 - x_{11}^*) \frac{\partial}{\partial x_1} \mu_1(\bar{X}_1^*) + \\ &(x_2 - x_{12}^*) \frac{\partial}{\partial x_2} \mu_1(\bar{X}_1^*) + \dots + \\ &(x_{n_1} - x_{1n_1}^*) \frac{\partial}{\partial x_{n_1}} \mu_1(\bar{X}_1^*) + \\ &(x_{n_1+1} - x_{1n_1+1}^*) \frac{\partial}{\partial x_{n_1+1}} \mu_1(\bar{X}_1^*) + \dots \\ &+ (x_n - x_{1n}^*) \frac{\partial}{\partial x_n} \mu_1(\bar{X}_1^*) = \mu_1^*(\bar{X}) \end{aligned} \tag{13}$$

$$\begin{aligned} \mu_2(\bar{X}) &\cong \mu_2(\bar{X}_2^*) + (x_1 - x_{21}^*) \frac{\partial}{\partial x_1} \mu_2(\bar{X}_2^*) + (x_2 - x_{22}^*) \\ &\frac{\partial}{\partial x_2} \mu_2(\bar{X}_2^*) + \dots + (x_{n_2} - x_{2n_2}^*) \frac{\partial}{\partial x_{n_2}} \mu_2(\bar{X}_2^*) + \\ &(x_{n_2+1} - x_{2n_2+1}^*) \frac{\partial}{\partial x_{n_2+1}} \mu_2(\bar{X}_2^*) + \dots + (x_n - x_{2n}^*) \\ &\frac{\partial}{\partial x_n} \mu_2(\bar{X}_2^*) = \mu_2^*(\bar{X}) \end{aligned} \tag{14}$$

VI. CHARACTERIZATION OF PREFERENCE BOUNDS ON THE DECISION VARIABLES FOR BOTH LEVEL DECISION MAKERS

Since the objectives of level DMs are conflicting, cooperation between the level DMs is necessary in order to reach compromise optimal solution. Each DM tries to reach maximum profit with the consideration of benefit of other. Here, the relaxations on both decision variables are considered for overall benefit.

Let $(x_{1j}^* - r_{1j}^-)$ and $(x_{1j}^* + r_{1j}^+)$ ($j = 1, 2, \dots, n_1$) be the lower and upper bounds of decision variable x_{1j} ($j = 1, 2, \dots, n_1$) provided by the FLDM. Here, $\bar{X}_1^* = (x_{11}^*, x_{12}^*, \dots, x_{1n_1}^*, x_{1n_1+1}^*, \dots, x_{1n}^*)$ is the individual best solution of the quadratic membership function $\mu_1(\bar{x})$ of FDLM when calculated in isolation subject to the equivalent deterministic system constraints.

Similarly, $(x_{2j}^* - r_{2j}^-)$ and $(x_{2j}^* + r_{2j}^+)$ ($j = 1, 2, \dots, n_2$) be the lower and upper bounds of decision variables x_{2j} ($j = 1, 2, \dots, n_2$) provided by the SLDM. $\bar{X}_2^* = (x_{21}^*, x_{22}^*, \dots, x_{2n_2}^*, x_{2n_2+1}^*)$ is the individual best solution of the quadratic membership function $\mu_2(\bar{x})$ of SLDM when calculated in isolation subject to the equivalent deterministic system constraints. Therefore, preference bounds on the decision variable can presented as follows:

$$\begin{aligned} (x_{1j}^* - r_{1j}^-) &\leq x_{1j} \leq (x_{1j}^* + r_{1j}^+) \quad (j = 1, 2, \dots, n_1) \tag{15} \\ (x_{2j}^* - r_{2j}^-) &\leq x_{2j} \leq (x_{2j}^* + r_{2j}^+) \quad (j = 1, 2, \dots, n_2) \tag{16} \end{aligned}$$

Here, r_{1j}^- and r_{1j}^+ ($j = 1, 2, \dots, n_1$) and are the negative and positive tolerance values, which are not necessarily same. Similarly, r_{2j}^- and r_{2j}^+ ($j = 1, 2, \dots, n_2$) are negative and positive tolerance values that may be not be necessarily same.

VII. FORMULATION OF FUZZY GOAL PROGRAMMING MODEL OF CHANCE CONSTRAINED QUADRATIC BI-LEVEL PROGRAMMING PROBLEM

The chance constrained QBLPP reduces to the following problem

$$\text{Max } \mu_1^*(\bar{X}),$$

$$\text{Max } \mu_2^*(\bar{X})$$

subject to

$$(x_{1j}^* - r_{1j}^-) \leq x_{1j} \leq (x_{1j}^* + r_{1j}^+), (j = 1, 2, \dots, n_1)$$

$$(x_{2j}^* - r_{2j}^-) \leq x_{2j} \leq (x_{2j}^* + r_{2j}^+), (j = 1, 2, \dots, n_2)$$

$$\bar{X} \in X \tag{17}$$

According to Pramanik and Dey, it can be written [23] as:

$$\mu_i^* + d_i^- = 1, i = 1, 2. \tag{18}$$

d_1^-, d_2^- are the negative deviational variables. Now, two FGP models are formulated as follows:

Model-I

$$\text{min } \lambda \tag{19}$$

subject to

$$\mu_1^*(\bar{X}) + d_1^- = 1,$$

$$\mu_2^*(\bar{X}) + d_2^- = 1,$$

$$\lambda \geq d_1^-,$$

$$\lambda \geq d_2^-,$$

$$0 \leq d_1^- \leq 1,$$

$$0 \leq d_2^- \leq 1,$$

$$(x_{1j}^* - r_{1j}^-) \leq x_{1j} \leq (x_{1j}^* + r_{1j}^+), (j = 1, 2, \dots, n_1)$$

$$(x_{2j}^* - r_{2j}^-) \leq x_{2j} \leq (x_{2j}^* + r_{2j}^+), (j = 1, 2, \dots, n_2)$$

$$\bar{X} \in X \tag{20}$$

Model -II

$$\text{Min } \xi = \sum_{i=1}^2 d_i^-$$

subject to

$$\mu_1^*(\bar{X}) + d_1^- = 1,$$

$$\mu_2^*(\bar{X}) + d_2^- = 1,$$

$$0 \leq d_1^- \leq 1,$$

$$0 \leq d_2^- \leq 1,$$

$$(x_{1j}^* - r_{1j}^-) \leq x_{1j} \leq (x_{1j}^* + r_{1j}^+), j = 1, 2, \dots, n_1$$

$$(x_{2j}^* - r_{2j}^-) \leq x_{2j} \leq (x_{2j}^* + r_{2j}^+), j = 1, 2, \dots, n_2$$

$$\bar{X} \in X$$

VIII. MODEL FORMULATION FOR QUADRATIC BI-LEVEL PROGRAMMING PROBLEM WITH CHANCE CONSTRAINTS FOR MINIMIZATION TYPE OBJECTIVE FUNCTIONS

Let us consider the following problem of chance constrained QBLPP with minimization type objective functions.

$$[\text{FLDM}] \text{Min}_{\bar{X}} Z_1(\bar{X}) = \bar{A}_1 \bar{X} + \frac{1}{2} \bar{X}^T \bar{B}_1 \bar{X} \tag{21}$$

$$[\text{SLDM}] \text{Min}_{\bar{X}_2} Z_2(\bar{X}) = \bar{A}_2 \bar{X} + \frac{1}{2} \bar{X}^T \bar{B}_2 \bar{X} \tag{22}$$

subject to

$$\bar{X} \in X =$$

$$\{\bar{X} \in \mathbb{R}^n : \Pr\{\bar{C}\bar{X} \leq \bar{d}\} > \bar{I} - m, \bar{X} \geq \bar{0}\} \tag{23}$$

The descriptions of the coefficients, matrices, and vectors of the problem are already provided in section 2.

The chance constraints are converted into equivalent deterministic constraints as described in (5) and (7). Then, the objective functions are solved separately subject to equivalent deterministic constraints. Let \bar{X}_1^B, \bar{X}_2^B be the individual best solutions for the quadratic objective functions $Z_1(\bar{X}), Z_2(\bar{X})$ and $\min_{\bar{X} \in X} Z_1(\bar{X}) = Z_1^B = Z_1(\bar{X}_1^B)$ and $\min_{\bar{X} \in X} Z_2(\bar{X}) = Z_2^B = Z_2(\bar{X}_2^B)$.

Considering the individual best solution as the aspiration level, the fuzzy goal appears as:

$Z_i(\bar{X}) \leq Z_i^B, i = 1, 2$

$$Z_i(\bar{X}) \leq Z_i^B, i = 1, 2 \tag{24}$$

We consider $\max_{\bar{X} \in X} Z_1(\bar{X}) = Z_1^W$ and $\max_{\bar{X} \in X} Z_2(\bar{X}) = Z_2^W$ as the upper tolerance limits of the fuzzy objective goals of FLDM and SLDM.

Now, the quadratic membership functions are formulated as:

$$\mu_i(\bar{X}) = \begin{cases} 1, & \text{if } Z_i(\bar{X}) \leq Z_i^B, \\ \frac{Z_i^W - Z_i(\bar{X})}{Z_i^W - Z_i^B}, & \text{if } Z_i^W \geq Z_i(\bar{X}) \geq Z_i^B, \\ 0, & \text{if } Z_i(\bar{X}) \geq Z_i^W \end{cases} \tag{25}$$

$i = 1, 2.$

The theoretical development of chance constrained QBLPP with minimization type objective functions is remain the same as developed for chance constrained QBLPP with maximization type objective functions.

IX. DISTANCE FUNCTION FOR DETERMINATION OF COMPROMISE SOLUTION

For multi objective programming, the objectives are incommensurable and conflicting in nature. The aim of decision makers is to find out the compromise solution which is as near as possible to the ideal solution points in the decision making context. Here, we use the Euclidean distance function [26] of the type

$$S_2 = \left[\sum_{i=1}^2 (1 - \mu_i^*)^2 \right]^{1/2}$$

The solution with the minimum distance is considered as the best compromise optimal solution.

X. SUMMARIZATION OF THE PROCESS FOR SOLVING CHANCE CONSTRAINTS QUADRATIC BI-LEVEL PROGRAMMING PROBLEM

To solve chance constrained QBLPP we use the following steps.

S-1. Transform the chance constraints into equivalent deterministic constraints.

S-2. Calculate individual best solution for each quadratic objective function of the level DM subject to the equivalent deterministic constraints.

S-3. Lower and upper tolerance limits are determined for each quadratic objective function by minimizing and maximizing separately subject to the equivalent deterministic constraints.

S-4. Quadratic membership functions are formulated by using individual best solutions subject to the equivalent deterministic system constraints.

S-5. Find out the individual best solution for each of the quadratic membership functions subject to the equivalent deterministic constraints.

S-6. Using first order Taylor's series, the quadratic membership functions are approximated into linear functions at the individual best solution point.

S-7. Both level DMs express their choices for the upper and lower preference bounds on the decision variables controlled by them.

S-8. Two FGP models are formulated and solved.

S-9. Determine the Euclidean distance for two optimal compromise solutions obtained from two FGP Models.

S-10. Select the solution with the minimum Euclidean distance as the best compromise optimal solution.

XI. ILLUSTRATIVE EXAMPLES OF CHANCE CONSTRAINED QUADRATIC BI-LEVEL PROGRAMMING PROBLEM

11.1 Example 1.

To illustrate the proposed FGP approach, the following chance constrained QBLPP with maximization type objective function at each level is considered.

$$\max_{x_2} Z_1(\bar{X}) = x_1^2 - 5x_2^2 + 2x_1x_2 \tag{26}$$

$$\max_{x_1} Z_2(\bar{X}) = 3x_1 + 12x_2 - x_1x_2 + 45 \tag{27}$$

subject to

$$\Pr(x_1 + x_2 \leq d_1) \geq 1 - m_1 \tag{28}$$

$$\Pr(-2x_1 + 5x_2 \leq d_2) \geq 1 - m_2 \tag{29}$$

$$\Pr(3x_1 - 4x_2 \geq d_3) \geq 1 - m_3 \tag{30}$$

$$x_1 \geq 0, x_2 \geq 0 \tag{31}$$

The mean, variance and the confidence levels are prescribed as follows:

$$E(d_1) = 3, \text{ var}(d_1) = 2, m_1 = 0.03 \tag{32}$$

$$E(d_2) = 12, \text{ var}(d_2) = 8, m_2 = 0.01 \tag{33}$$

$$E(d_3) = 10, \text{ var}(d_3) = 18, m_3 = 0.05 \tag{34}$$

Using (5) and (7), the chance constraints defined in (28), (29) and (30) can be converted into equivalent deterministic constraints as:

$$x_1 + x_2 \leq 5.66579 \tag{35}$$

$$-2x_1 + 5x_2 \leq 18.57609 \tag{36}$$

$$3x_1 - 4x_2 \geq 3.020856 \tag{37}$$

The individual solution for each quadratic objective function of level DM subject to the equivalent deterministic constraints is obtained as $Z_1^B = 32.10118$, at $\bar{X}_1^B = (5.66579, 0)$, and $Z_2^B = 72.64119$, at $\bar{X}_2^B = (3.669145, 1.996645)$.

The fuzzy goals appear as:

$$Z_1(\bar{X}) \underset{\sim}{\geq} 32.10118, Z_2(\bar{X}) \underset{\sim}{\geq} 72.64119 \tag{38}$$

The lower tolerance limits are obtained as $Z_1^W = 1.013952$ and $Z_2^W = 48.02086$

Now, the quadratic membership function for FLDM and SLDM are constructed as follows:

$$\mu_1(\bar{X}) =$$

$$\left\langle \begin{array}{l} 1, \quad \text{if } Z_1(\bar{X}) \geq 32.10118 \\ \frac{Z_1(\bar{X}) - 1.013952}{32.10118 - 1.013952}, \text{ if } 1.013952 \leq Z_1(\bar{X}) \leq 32.10118 \\ 0, \quad \text{if } Z_1(\bar{X}) \leq 1.013952 \end{array} \right\rangle \quad (39)$$

$$\mu_2(\bar{X}) =$$

$$\left\langle \begin{array}{l} 1, \quad \text{if } Z_2(\bar{X}) \geq 72.64119, \\ \frac{Z_2(\bar{X}) - 48.02086}{72.64119 - 48.02086}, \text{ if } 48.02086 \leq Z_2(\bar{X}) \leq 72.64119, \\ 0, \quad \text{if } Z_2(\bar{X}) \leq 48.02086 \end{array} \right\rangle \quad (40)$$

The quadratic membership functions are linearized at their individual best solution point at $\bar{X}_1^B = (5.66579, 0)$, $\bar{X}_2^B = (3.669145, 1.996645)$ and we obtained equivalent linear membership functions as follows:

$$\mu_1^*(\bar{X}) = 1 + (x_1 - 5.66579) \times (2 \times 5.66579 / 31.087228) + (x_2 - 0) \times (2 \times 5.66579 / 31.087228), \quad (41)$$

$$\mu_2^*(\bar{X}) = 1 + (x_1 - 3.669145) \times ((3 - 1.996645) / 24.62033) + (x_2 - 1.996645) \times ((12 - 3.669145) / 24.62033) \quad (42)$$

Let $0 \leq x_2 \leq 2$ and $3 \leq x_1 \leq 6$ be the preference bounds provided by the level DMs.

Proposed two FGP models (see Table 1) in (19) and (20) offer the same solution at $x_1 = 3.669145$, $x_2 = 1.996645$, with $Z_1 = 8.181629$ and $Z_2 = 72.64119$.

TABLE1. COMPARISON OF DISTANCES FOR THE OPTIMAL SOLUTIONS OBTAINED FROM TWO FGP MODELS OF THE PROBLEM 11.1

MODEL NUMBER	MEMBERSHIP FUNCTION	DISTANCE FUNCTION
Model I,	$\mu_1^* = 0.2305666$	0.7694334
Model II	$\mu_2^* = 1$	

It is clear from the table that two FGP Models offer the same result.

1.2 Example 2.

To illustrate the proposed FGP approach, the following chance constrained QBLPP with minimization type objective function at each level is considered.

$$\min_{x_1} Z_1(\bar{X}) = 7x_1^2 + 6x_2^2 + 8x_1 + 11x_2 \quad (43)$$

$$\min_{x_2} Z_2(\bar{X}) = (x_1 - 1)^2 + (x_2 + 3)^2 + 7x_1x_2 + 21 \quad (44)$$

subject

$$\Pr(2x_1 + 5x_2 \geq d_1) \geq 1 - m_1 \quad (45)$$

$$\Pr(3x_1 + 6x_2 \leq d_2) \geq 1 - m_2 \quad (46)$$

The means, variances and the confidence levels are prescribed as follows:

$$E(d_1) = 6, \text{ var}(d_1) = 9, m_1 = 0.06 \quad (47)$$

$$E(d_2) = 4, \text{ var}(d_2) = 4, m_2 = 0.04 \quad (48)$$

Using (5), (7) the chance constraints defined in (45), (46) can be converted into equivalent deterministic constraints as:

$$2x_1 + 5x_2 \geq 1.335 \quad (49)$$

$$3x_1 + 6x_2 \leq 7.51 \quad (50)$$

The individual solution for each quadratic objective function subject to equivalent deterministic system constraints is obtained as: $Z_1^B = 3.364734$,

$$\text{at } \bar{X}_1^B = (0, 0.267), Z_2^B = 30, \text{ at } \bar{X}_2^B = (1, 0) \quad (51)$$

The upper tolerance limits are obtained as $Z_1^W = 63.89341$

and $Z_2^W = 40.77668$.

The fuzzy goals assume the form:

$$Z_1(\bar{X}) \leq 3.364734, Z_2(\bar{X}) \leq 30$$

Now, the quadratic membership functions for FLDM and SLDM are formulated as follows:

$$\mu_1(\bar{X}) =$$

$$\left\langle \begin{array}{l} 1, \quad \text{if } Z_1(\bar{X}) \leq 3.364734, \\ \frac{63.89341 - Z_1(\bar{X})}{63.89341 - 3.364734}, \text{ if } 3.364734 \leq Z_1(\bar{X}) \leq 63.89341, \\ 0 \quad \text{if } Z_1(\bar{X}) \geq 63.89341 \end{array} \right\rangle \quad (52)$$

$$\mu_2(\bar{X}) = \left\langle \begin{array}{l} 1, \quad \text{if } Z_2(\bar{X}) \leq 30, \\ \frac{40.77668 - Z_2(\bar{X})}{40.77668 - 30}, \text{ if } 30 \leq Z_2(\bar{X}) \leq 40.77668, \\ 0 \quad \text{if } Z_2(\bar{X}) \geq 40.77668 \end{array} \right\rangle \quad (53)$$

The quadratic membership functions are linearized at their individual best solution point at $\bar{X}_1^B = (0, 0.267)$, $\bar{X}_2^B = (1, 0)$ by using Taylor's series approximation method as follows:

$$\mu_1^*(\bar{X}) = 1 + (x_1 - 0) \times (-8 / 60.5287) + (x_2 - 0.267) \times (-12 \times 0.267 + 11) / 60.5287 \quad (54)$$

$$\mu_2^*(\bar{X}) = 1 + (x_2 - 0) \times (-13 / 10.7767) \quad (55)$$

Let $0 \leq x_1 \leq 1$, $0 \leq x_2 \leq 0.5$ be the preference bounds provided by the level DMs.

FGP model I (see Table 2) offers the optimal solution at $x_1 = 0.6184107$, $x_2 = 0.0196357$ with $Z_1 = 7.842614$ and $Z_2 = 30.34881$.

FGP Model II (See Table 2) offers the optimal solution at $x_1 = 0.6675$, $x_2 = 0$, with $Z_1 = 8.458894$ and $Z_2 = 30.11056$.

TABLE2. COMPARISON OF DISTANCES FOR THE OPTIMAL SOLUTIONS OBTAINED FROM TWO FGP MODELS OF THE PROBLEM 11.2.

MODEL NUMBER	MEMBERSHIP FUNCTION	EUCLIDEAN DISTANCE FUNCTION
Model I	$\mu_1^* = 0.92602$, $\mu_2^* = 0.96763$	0.08075066
Model II	$\mu_1^* = 0.91584$, $\mu_2^* = 0.98974$	0.08478454

It is clear from the Table 2 that the Euclidean distance is minimal for the FGP Model I which implies that Model I provides better compromise solution for this example.

Note 1. Lingo ver.11.0 is used for solution purpose.

XII. CONCLUSION

In this paper, we present chance constrained QBLPP by using FGP approach which is simple to understand and easy to apply. After transforming the chance constraints into equivalent deterministic constraints, we transform quadratic bi-level programming problem into linear bi-level programming problem by using the first order Taylor's series approximation. To avoid decision deadlock, each level DM provides preference bounds on the decision variables controlled by him. Two FGP models are proposed for solution purpose. The proposed approach can be used to deal with chance constrained multi-level quadratic programming problem. The proposed approach can further be used for solving chance constrained linear quadratic fractional programming problem.

For the future study in the hierarchical decision making context, we hope, the proposed approach can be used for chance constrained quadratic decentralized multi-level multi-objective programming problems. We hope further that the proposed approach will be useful for the real decision making problems that arise in industrial belt, supply chain, marketing, IT sector, management sciences.

References

- [1] W. Candler, and R. Townsley, A linear bilevel programming problem, *Computers and Operations Research*, 9, 1982, 59-76.
- [2] J. Fortuni-Amat, and B. McCarl, A representation and economic interpretation of a two-level programming problem, *Journal of Operational Research Society*, 32(9), 1981, 783-792.
- [3] T. Edmunds, and J. Bard, Algorithms for nonlinear bilevel mathematical problems, *IEEE Transactions Systems, Man and Cybernetics*, 21(1), 1991, 83-89.
- [4] N. Malhotra, and S. R. Arora, An algorithm to solve linear fractional bilevel programming problem via goal programming, *Journal of Operational Society of India (OPSEARCH)*, 37(1), 2000, 1-13.
- [5] M. Sakawa, I. Nishizaki, and Y. Uemura, Interactive fuzzy programming for two-level linear fractional programming problems with fuzzy parameters, *Fuzzy Sets and Systems*, 115(1), 2000, 93-103.
- [6] M. Sakawa, and I. Nishizaki, Interactive fuzzy programming for two-level fractional programming problem, *Fuzzy Sets and Systems*, 119(1), 2001, 31-40.
- [7] T. L. Saaty, *The analytical hierarchy process* (Plenum Press, New York, 1980).
- [8] S. Mishra, Weighting method for bi-level linear fractional programming problems, *European Journal of Operational Research*, 183(1), 2007, 296-302.
- [9] S. Pramanik, and P. P. Dey, Bi-level linear fractional programming problem based on fuzzy goal programming approach, *International Journal of Computer Applications*, 25 (11), 2011, 34-40.
- [10] G. Anandalingam, A mathematical programming model of decentralized multi-level systems, *Journal of the Operational Research Society*, 39(11), 1988, 1021-1033.
- [11] Y. J. Lai, Hierarchical optimization: a satisfactory solution, *Fuzzy Sets and Systems*, 77(13), 1996, 321-335.
- [12] H. S. Shih, Y. J. Lai, and E. S. Lee, Fuzzy approach for multi-level programming problems, *Computers and Operations Research*, 23(1), 1996, 73-91.
- [13] H. S. Shih, and E. S. Lee, Compensatory fuzzy multiple level decision making, *Fuzzy Sets and Systems*, 114(1), 2000, 71-87.
- [14] S. Pramanik, and T. K. Roy, Fuzzy goal programming approach for multilevel programming problem. *European Journal of Operational Research*, 176 (2), 2007, 1151-1166.
- [15] J. Judice, and A. M. Faustino, The linear-quadratic bilevel programming problem, *Infor*, 32(2), 1994, 87-98.
- [16] L. Vicente, G. Savard, and J. Judice, Descent approaches for quadratic bilevel programming, *Journal of Optimization Theory and Applications*, 81(2), 1994, 379-399.
- [17] S. Wang, Q. Wang, and S. Romano-Rodriguez, Optimality conditions and an algorithm for linear-quadratic bilevel programs, *Optimization*, 31(2), 1994, 127-139.
- [18] D. Thirwani, and S. R. Arora, An algorithm for quadratic bilevel programming problem, *International Journal of Management and System*, 14(2), 1998, 89-98.
- [19] H. I. Calvete and C. Gale, Optimality conditions for the linear fractional / quadratic bilevel problem, *Monografias del Seminario Garcia de Geldeano*, 31, 2004, 285-294.
- [20] B. B. Pal and B. N. Moitra, A fuzzy goal programming procedure for solving quadratic bilevel

programming problems, *International Journal of Intelligence Systems*, 18(5), 2003, 529-540.

- [21] S. Pramanik and P. P. Dey, Multi-objective quadratic programming problem based on fuzzy goal programming, *International Journal of Pure and Applied Sciences and Technology*, 6(1), 2011, 45-53.
- [22] S. Pramanik, and P. P. Dey, Multi-objective quadratic programming problem: a priority based fuzzy goal programming, *International Journal of Computer Applications*, 26(10), 2011, 30-35.
- [23] S. Pramanik, and P. P. Dey, Quadratic bi-level programming problem based on fuzzy goal programming approach, *International Journal of Software Engineering and Applications*, 2(4), 2011, 30-35.
- [24] G. B. Dantzig, Linear programming under uncertainty, *Management Science*, 1, 1955, 197-206.
- [25] Charnes, and W. W. Cooper, Chance-constrained programming, *Management Science*, 6, 1959, 73-79.
- [26] S. Pramanik, and T. K. Roy, Multiobjective transportation model with fuzzy parameters: based on priority based fuzzy goal programming approach, *Journal of Transportation Systems Engineering and Information Technology*, 8(3), 2008, 40-48.



Dr. Surapati Pramanik received his Ph. D. degree in Mathematics from Bengal Engineering and Science University, Shibpur. He is an Assistant Professor of Mathematics in Nandalal Ghosh B.T. College, Panpur, P.O-Narayanpur, West Bengal, India. His field of research interest includes fuzzy optimization, grey system theory, neutrosophic game theory, and mathematics education. He is the author of more than 30 international journal articles.



Ms. Durga Banerjee passed M.Sc. with Operation Research as special paper from Jadavpur University in 2005 and B.Ed. from Kalyani University in 2007. Presently, she is an assistant teacher of Mathematics at Ranaghat Yusuf Institution, Ranaghat, Nadia, West Bengal, India. Her interest of research includes fuzzy optimization, decision making in stochastic environments. Her research papers were published in four international journals. Her articles have been also published in International conference proceedings and book.

An Efficient Classification Algorithm for Real Estate domain

Geetali Banerji*, Kanak Saxena**

*(IT Department, Institute of Information Technology & Management, New Delhi, India)

** (Computer Applications Department, Samrat Ashok Technological Institute, Vidisha, India)

Abstract: Classification rule mining aims to discover a small set of rules in the database that forms an accurate classifier. In classification rule mining there is one and only one predetermined target. In this paper, we proposed an algorithm, which performs preprocessing and cleaning prior to traditional classification. Experimental results show that the classifier built this way is, in general, more accurate than that produced by the state-of-the-art classification system. In addition, this helps to solve a number of problems that exist in the current classification systems. This algorithm is especially fit to applications where it may assist domain experts in their decisions. We have taken Real estate field, which is a good example, where such applications may appear. In our dataset, there is a considerable amount of information associated with the customer (e.g. Income, personal, educational, demographic and professional details). We have applied statistical analysis and Association rules on real estate actual data and found that if we consider only customer demographic and professional details then relationship among various attributes are not that strong and it only predicts the customers who are in higher income group are willing to invest. After removing demographic details like caste, status, religion etc. we found that the relationship among remaining attributes become much stronger and it shows that customer in middle income group, house owners are also willing to invest. Further not only a person's professional details helps to identify a potential customer, in Indian context, his other responsibilities, expenditure heads also plays a crucial role. It is further proven that by taking into account the bank transaction details and buying interest of a customer, there is a drastic improvement in the results i.e. not only those customers, who are in high income group and potentially strong enough to invest but because of their other social responsibilities they are not able to do so and at the same time those who are following in middle or lower income group or having rented house with other investment are also likely to invest.

Keywords: Association Rules, Classification, DT (Decision Table), Statistical Measures, RepTree

I. INTRODUCTION

Data mining is a process, which involves the application of specific algorithms for extracting patterns (test models) from data. New knowledge may be obtained in the process while eliminating one of the largest costs, viz., data collection [2]. Real Estate data, for example, often exists in vast quantities in an unstructured format. Our proposed classification algorithm which applies statistical analysis and association rules prior to traditional classification is proved better than the traditional ones because it cleans the data and removes the noise. Experimental results show that the classifier built this way is, in general, more accurate than that produced by the state-of-the-art classification system. The traditional classifiers are faster but in many cases accuracy is not so high. Moreover many of the rules found by proposed classification algorithm cannot be discovered by traditional classification algorithm. In earlier paper [9], we have already proved that in case of statistical analysis regression is used to determine the relationship among various attributes. We have tested various regression algorithms such as linear Regression, Least Median Square Isotonic and Pace Regression. Pace regression outperforms among various regression techniques because in this method it generates a pattern which assigns weights prior to processing and it is suitable with respect to Indian context because in India, caste, religion, social status plays a prominent roles In general context, multilayer perceptron is best among various machine learning algorithms because it applies weights on different hidden layer on the basis of different input weightage during processing which is suitable for other countries where the status, caste, religion does not have any role in purchasing behavior of a customer [11].

The rest of the paper is organized as follows. The concept of Classifiers is being discussed in section II. In section III, Statistical Analysis and Association Rules are discussed, the proposed algorithm has been introduced in Section IV, Section V discusses about Empirical Evaluation and Section VI concludes the paper.

II. CLASSIFICATION

In data mining, classification is one of the most important tasks. It maps the data in to predefined targets. It is a supervised learning as targets are predefined. The aim of the classification is to build a classifier based on some cases with some attributes to describe the objects or one attribute to describe the group of the objects. Then, the classifier is used to predict the group attributes of new cases from the domain based on the values of other attributes. It is a two step process, in the first step; a classifier is built describing a predetermined set of data classes or concept. This is the learning step, (or training phase), where a classification algorithm builds the classifier by learning from a training set made up of database tuples and their associated class labels. In the second step, the test model is used for classification [3, 4].

Preparing the data for classification

The following preprocessing steps may be applied to the data to help improve the accuracy, efficiency, and scalability of the classification process [3].

Data Cleaning: This refers to reduce noise or handling missing values. This step help reduce confusion during learning.

Relevance Analysis: This refers to remove irrelevant or redundant attributes. Correlation analysis can be used to identify whether two given attributes are statistically related. For Example a strong correlation between attribute A1 and A2 would suggest that one of the two could be reduced for further analysis.

Data Transformation and Reduction: It refers to generalizing the data to higher-level concepts or normalizing the data. Normalization involves scaling all values for a given attribute so that they fall within a small specified range, such as -1.0 to 1.0.

The data mining consists of various classification methods. Different methods serve different purposes, each method offering its own advantages and disadvantages. In this paper, we are discussing Decision Table and RepTree.

Decision Table

Decision Table algorithm classifier summarizes the dataset with a 'decision table' which contains the same number of attributes as the original dataset. Then, a new data item is assigned a category by finding the line in the decision table that matches the non-class values of the data item [6, 7]. Decision Table employs the wrapper method to find a good subset of attributes for inclusion in the table. By eliminating attributes that contribute little or nothing to a test model of the dataset, the algorithm reduces the likelihood of over-fitting and creates a smaller and condensed decision table. We choose to explore decision tables because it is a simpler, less compute intensive algorithm. In this paper, we have used the Weka tools [8, 13, 14, 15], which determine which attribute or combination of attributes needs to be included for predicting the class best. The attribute space is searched greedily either top to bottom or bottom to top. A top-to-bottom search adds attributes at each stage; this is called *forward selection*. A bottom-to-top search starts with a full set of attributes and deletes attributes one at a time; this is *backward elimination*.

RepTree

Fast decision tree learner. Builds a decision/regression tree using information gain/variance and prunes it using reduced-error pruning (with back fitting). Only sorts values for numeric attributes once. Missing values are dealt with by splitting the corresponding instances into pieces (i.e. as in C4.5).

Classification rule mining and association rule mining are two important data mining techniques. They are similar except that classification involves prediction of one attribute, i.e., the class, while association rule discovery can predict any attribute in the data set [16, 17]. Classification rule mining aims to discover a small set of rules in the database to form an accurate classifier [18, 19]. Classification rule mining is indispensable to practical applications. Thus, great savings and conveniences to the user could result if the two mining techniques can somehow be integrated. [1]

III. STATISTICAL ANALYSIS AND ASSOCIATION RULES

Statistical analysis involves use of observational data together with domain knowledge to develop a model to study and understand the trend of the data for prediction and decision. The data analysis is used to refine the model or possibly to select a different model, to determine appropriate values for terms in the model, and to use the model to make inferences concerning the process. Many alternative views of the data can be examined. Many different models can be explored. Massive amount of simulated data can be used to study the model/data possibilities. Regression analysis is a statistical tool for the investigation of relationships between variables. Usually, the investigator seeks to ascertain the causal effect of one variable upon another—the effect of a price increase upon demand, for example, or the effect of changes in the money supply upon the inflation rate. To explore such issues, the investigator assembles data on the underlying variables of interest and employs regression to estimate the quantitative effect of the causal variables upon the variable that they influence. The investigator also typically assesses the “statistical significance” of the estimated relationships, that is, the degree of confidence that the true relationship is close to the estimated relationship. Regression analysis with a single explanatory variable is termed as *Simple Regression* and with multiple explanatory is termed as *Multiple Regression*. At the outset of any regression study, one formulates some hypothesis about the relationship between the variables of interest. Multiple regression allows additional factors to enter the analysis separately so that the effect of each can be estimated. It is valuable for quantifying the impact of various simultaneous influences upon a single dependent variable. Further, because of omitted variables bias with simple regression, multiple regression is often essential even when the investigator is only interested in the effects of one of the independent variables. [12]

In general, the association rule is an expression of the form $X \Rightarrow Y$, where X is antecedent and Y is consequent. Association rule shows how many times Y has occurred if X has already occurred depending on the *support* and *confidence* value.

Support: It is the probability of item or item sets in the given transactional data base:

$\text{Support}(X) = n(X)/n$ where n is the total number of transactions in the database and $n(X)$ is the number of transactions that contains the item set X .

Confidence: It is conditional probability, for an association rule $X \Rightarrow Y$ and defined as $\text{Confidence}(X \Rightarrow Y) = \text{support}(X \text{ and } Y) / \text{support}(X)$. All the traditional association rule mining algorithms were developed to find positive associations between items. Positive associations refer to associations between items existing in transactions. In addition to the positive associations, negative associations can provide valuable information. In practical there are many situations where negation of products plays a major role. For example, if I work full time in IITM then I do not work full time in any other institution. If I am a female then I am not a male.

Negative association rule is an implication of the form $X \Rightarrow \neg Y$ where X and Y are item sets and $X \cap Y = \emptyset$.

Mining association rules can be broken down into the following two sub-problems:

1. Generating all item sets that have support greater than, or equal to, the user specified minimal support. That is, generating all large item sets.
2. Generating all the rules that have minimum confidence.

We can generate the association rule with more than one number of consequent items is generated by the following method:

- I. Find the rule in which number of consequents = 1.
- II. For the given rules $p(x \rightarrow y)$ and $p(x \rightarrow z)$, the rule $p(x \rightarrow yz)$ is generated by the intersection of both the association rules and get a new rule $p(x \rightarrow yz) = p(xyz) / p(x)$.

IV. PROPOSED ALGORITHM

In this algorithm, we have tried to remove noise by applying statistical and data mining methods on actual data and cleaned the data after that the classification is done on different methods and best method is identified. The steps are as follows: [5]

1. *Preprocessing the data based on statistical measures.*
 - i. *Identify relevant attributes by applying statistical techniques on actual data with Bank Transactions of customer and in general customer purchase Interest data.*
 - ii. *Applying Association rules to identify rules on actual data with Bank Transactions of customer and in general customer purchase Interest data.*
2. *Cleaning the data*
 - i. *Removing irrelevant data from the actual data set.*
 - ii. *Applying rules to remove noise from attributes.*
3. *Application of Classification algorithm*

Classification methods are applied on cleaned dataset. In our case, we have chosen the following two methods:

 - i. *Decision Table*
 - ii. *Rep Tree*
4. *Application of Classification algorithm on three different test modes.*
 - i. *Complete dataset as a training set*
 - ii. *Cross validation with 10 fold*
 - iii. *Splitting 75% as Training data set, 25% as Test data set*
5. *Determining the best combination.*

This algorithm makes the following contributions:

➤ It proposes a new way to build accurate classifiers.

Our Experimental results show that classifiers built this way are, in general, more accurate than those produced by the state-of-the-art classification system. (Table 1, Table 2, Graph 1 & Graph 2)

➤ It helps to solve the following important problems with the existing classification systems

- Most of the traditional data mining techniques failed because of the sheer size of the data. In our algorithm this problem is solved. In case of complete data set, the number of tuples got reduced from 5821 to 3421 attributes from 43 to 41 after preprocessing & cleaning. Where as in case of selected data set tuples are reduced from 5821 to 1440 and attributes from 26 to 24. (Table 1, Table 2, Graph 1 & Graph 2)

- Most of the algorithms assume the data to be noise-free. As a result, the most time-consuming part of solving problems becomes data preprocessing. Data formatting and experiment/result management are frequently just as time-consuming and frustrating. The concept of noisy data can be understood by the example of mining logs. A real life scenario can be if one wants to mine information from web logs. A user may have gone to a web site by mistake - incorrect URL or incorrect button press. In such a case, this information is useless if we are trying to deduce a sequence in which the user accessed the web pages. The logs may contain many such data items. These data items constitute data noise. A database may constitute upto 30-40% such Noisy data and pre-processing this data may take up more time than the actual algorithm execution time. This problem is handled at the time of preprocessing.

V. EMPIRICAL EVALUATION

We have taken Real Estate data set containing 5821 tuples and 43 attributes. Firstly, we have applied statistical analysis to identify the attributes that are strongly correlated with each other, followed by applicability of Association rules to identify rules on actual data with customer Bank transactions and customer purchase Interest data. Those attributes were removed which doesn't have any relationship. In next step we applied classification algorithm on three test modes in two different environments. In first case, we have taken all the attributes (complete) and compared the patterns, results of both the methods. In second case, the same tests are performed, after discarding demographic details of customers (selected) and then compared the various results. It is found that if we are not considering demographic details of customers, we are getting very accurate results as well as the error rate is decreased. After considering the Bank Transaction details and Customer Purchase Interest, there is a drastic improvement in the results. The following paragraphs discuss the outcomes of various tests.

Comparative Analysis

Table 1 shows the results of Decision table on Actual Real Estate complete dataset and selected data sets (after removing demographic details). Each of the tests is done on three test modes. The results are generated using WEKA 3-6-2, open source software for regression analysis and data mining.

The following are the findings, as per Table 1:

- As per traditional classification, in case of complete dataset, Training test mode takes minimum time, maximum correlation, minimum error rate. In general, if we consider complete data set then training test mode is the best method. It also depicts that the customers who are in the higher income group are willing to invest.
- As per our algorithm, in case of complete dataset, minimum time is taken by splitting test mode(75% training set and 25% test set)and maximum correlation, minimum error rates are generated by training test mode. In this case, customer in higher as well as higher middle income groups are willing to invest.
- As per traditional classification, in case of selected dataset (after removing demographic details), training test mode takes minimum time, maximum correlation, minimum error rates. Here it predicts that the customers who are in higher, middle income group, House owner are willing to invest.
- As per our algorithm, in case of selected dataset(after removing demographic details), minimum time is taken by Cross validation and splitting test mode, maximum correlation, minimum error rates are generated by training test mode. In this case, the customers from higher, middle as well as lower income group with other saving, rented house are willing to invest.

From the above results it is proved that there is a drastic improvement in results after preprocessing and cleaning, the factors which are very crucial in case of Indian context are having impact on the results. It also proves that training set gives the best results. Merit of best set is also improved after preprocessing and cleaning.

Table 2 shows the results of Reptree on Actual Real Estate dataset and selected data sets (after removing demographic details). Each of the tests is done on three test modes.

The following are the findings, as per Table 2:

- As per traditional classification , in case of complete dataset, minimum time is taken by splitting test mode(75% training set and 25% test set), maximum correlation, minimum error rate is taken by Training test mode i.e. in general, if we go for complete data set then training test mode is the best test mode.
- As per our algorithm, in case of complete dataset, minimum time is taken by splitting test mode(75% training set and 25% test set)and maximum correlation, minimum error rates are generated by training test mode.
- As per traditional classification , in case of selected dataset , all the test modes takes same time maximum correlation, minimum error rates are generated by training test mode.
- As per our algorithm, in case of selected dataset (after removing demographic details), minimum time is taken by Cross validation test mode, maximum correlation, minimum error rates are generated by training test mode.

After analyzing results of both classification methods, it is very much clear that after preprocessing and cleaning the results are more efficient and accurate. It is also proved that training test mode is best among other modes because it treats each tuple equally. Decision table method is better than Reptree because it is a simple, less compute intensive algorithm that involves the manipulation of counts associated with each of the table's entries. The attribute space is searched by a best-first search because this strategy is less likely to get stuck in a local maximum. The attribute selection is evaluated using a leave-one-out cross validation.

VI. CONCLUSIONS

This paper discusses about the traditional classification algorithm, its limitations and suggests an efficient algorithm which does preprocessing using statistical techniques and association rules to remove the noise and clean the data. The effectiveness of this algorithm is that it not only considers the customer real estate data but also considers the customer's bank transactions as well as purchasing interest and gives more accurate results. The classification is done using Decision Table and RepTree. After analyzing results from both the classification methods, it is very much clear that our algorithm outperforms traditional classification algorithm. The results are more efficient, accurate and the error rates are reduced drastically. It is also proved that training test mode is best among other modes because it treats each tuple equally. Decision

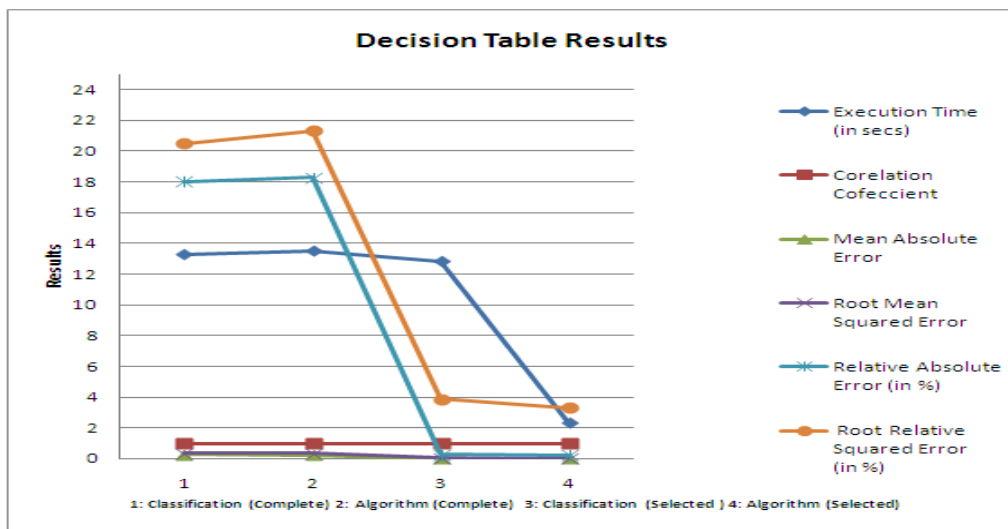
table method is better than Reptree because it is a simple, less compute intensive algorithm that involves the manipulation of counts associated with each of the table's entries. The attribute space is searched by a best-first search because this strategy is less likely to get stuck in a local maximum. The attribute selection is evaluated using a leave-one-out cross validation. It is proved that not only higher income group are willing to invest but also who in middle and higher middle group with other saving/investment with rented house or house owner are also willing to invest if, the bank transaction details and customer purchase interest are taken into account.

References

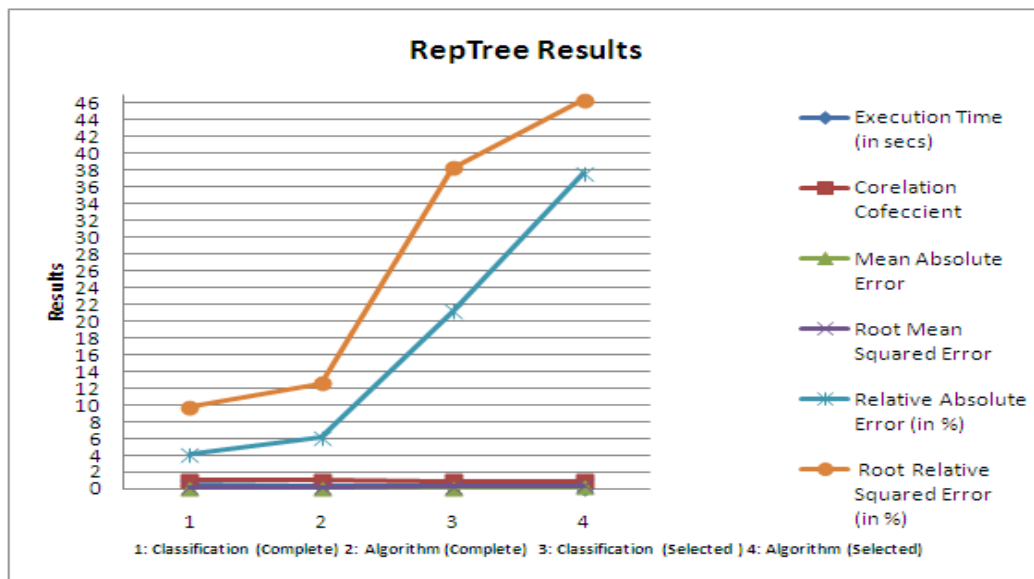
- [1] Bing Liu Wynne Hsu Yiming Ma, "Integrating Classification and Association Rule Mining", KDD-98 Proceedings. Copyright © 1998, AAAI (www.aaai.org).
- [2] Sunita Soni O.P.Vyas,"Using Associative Classifiers for Predictive Analysis in Health Care Data Mining", International Journal of Computer Applications (0975 – 8887) Volume 4 – No.5, July 2010
- [3] Han J. and Kamber M.,"Data Mining: Concepts and Techniques", 2nd ed., San Francisco, Morgan Kauffmann Publishers, 2001
- [4] Usama Fayyad, Gregory Piatetsky-Shapiro, and Padhraic Smyth, "From Data Mining to Knowledge Discovery in Databases", AI Magazine Volume 17 Number 3 (1996) (© AAAI)
- [5] Geetali Banerji, Kanak Saxena," An Algorithm for Rule based Classification", National Conference on Emerging Trends in Information Technology, March 2012, IITM New Delhi
- [6] Kathleen T. Durant Michael D. Smith , "Predicting UNIX commands using decision tables and decision trees", Research was supported in part by research grants from Compaq, IBM, Intel, Hewlett-Packard and Microsoft.
- [7] Ron Kohavi,"The Power of Decision table", 8th European Conference on Machine Learning, 174-189, 1995.
- [8] R. Bouckaert Remco, Eibe Frank et. al, "WEKA Manual for Version 3-6-2", January 11, 2010[8] R. Bouckaert Remco , Eibe Frank et. al, "WEKA Manual for Version 3-6-2",January 11, 2010
- [9] Geetali Banerji, Kanak Saxena, "Predictive Test model- A Boon for real estate" , International Journal for Wisdom Based Computing Volume(1) 2, April 2012
- [10] Geetali Banerji, Kanak Saxena," An Improved Apriori Based Algorithm with Single Scan of Database", National Conference on Converging Technologies Beyond 2020, April 2011, UIET, Kurukshetra University, India
- [11] Geetali Banerji, Kanak Saxena, "Analysis of Data Mining techniques on Real Estate", International Journal of Soft Computing and Engineering (IJSCE) ISSN:2231-2307 Volume-2, Issue-3, July 2012
- [12] <http://home.ubalt.edu/ntsbarsh/stat-data>
- [13] Witten I. frank, E. (2000),"Data Mining: *practical machine learning tools and techniques with Java implementations*, Morgan Kaufmann", San Francisco.
- [14] CBA. Data mining tool. Downloading page. http://www.comp.nus.edu.sg/~dm/p_download.html. Viewed on February 2010.
- [15] Weka. Data Mining software in Java. <http://www.cs.waikato.ac.nz/ml/weks>. Viewed on February 2010
- [16] Alaa AI Deen Mustafa Nofal and Sulieman Bani-Ahmad, "Classification Based on association Rule Mining Techniques: A general survey and Empirical Compative Evaluation".
- [17] B. Tunc and H. Dag, "Geneating Association Rules with Modified Apriori Algorithm", Proceedings of the 5th WSEAS Int. Conf. on Artificial Intelligence, Knowledge Engineering and Data Bases, Madrid, Spain, February 15-17, 2006
- [18] Breiman L., Friedman J.H., Olshen R.A., Stone C.J. (1984) Classification and Regression Trees, Wadsforth International Group.
- [19] Quinlan, J. R. 1992, "C4.5: Program for Machine Learning", Morgan Kaufmann.

Decision Tree*	Traditional Algorithm on Complete Data Set			Our Algorithm on Complete Data Set			Traditional Algorithm on Selected Data Set			Our Algorithm on Selected Data Set		
Attributes	43			41			26			24		
No of Instances	5821			3421			5821			1440		
Rules	55			160			1652			444		
Subsets	278			300			264			200		
MBS	0.365			0.396			0.288			0.363		
Feature set:	INH,INH,IPC			INH,INH,INMH,IPC			INH,INH,INMH,HO,INM,IPC			INH,INH,INMH,HO,INM,RH,OI,IPC		
Test Modes	i	ii	iii	i	ii	iii	i	ii	iii	i	ii	iii
Time (in secs)	13.3	21.25	22.97	13.52	13.59	8.31	12.84	13	13.33	2.34	2.16	2.16
CC	0.9788	0.977	0.976	0.977	0.9675	0.9703	0.999	0.928	0.907	0.999	0.852	0.847
MAE	0.2505	0.253	0.2649	0.2324	0.2747	0.2702	0.0019	0.0898	0.114	0.0012	0.1104	0.1202
RMSE	0.361	0.376	0.3841	0.345	0.409	0.4029	0.0306	0.296	0.336	0.024	0.383	0.399
RAE (in %)	18	18.17	18.78	18.29	21.62	20.77	0.284	13.59	17.13	0.248	23.624	24.347
RRSE (in %)	20.5	21.33	21.79	21.32	25.27	24.21	3.878	37.45	42.33	3.292	52.413	53.553

RepTree ⁺	Traditional Algorithm			Our Algorithm on			Traditional Algorithm on			Our Algorithm on Selected		
Attributes	43			41			26			24		
No of Instances	5821			3421			5821			1440		
Rules	305			219			425			121		
Test Modes	i	ii	iii	i	ii	iii	i	ii	iii	i	ii	iii
Time (in secs)	0.49	0.44	0.42	0.25	0.27	0.23	0.33	0.33	0.33	0.08	0.06	0.31
CC	0.9953	0.989	0.9873	0.9921	0.9846	0.9843	0.9239	0.8704	0.846	0.8862	0.7696	0.8205
MAE	0.057	0.097	0.1151	0.0779	0.1132	0.125	0.1399	0.1863	0.201	0.1754	0.255	0.2535
RMSE	0.171	0.257	0.28	0.203	0.283	0.295	0.3023	0.3904	0.427	0.3386	0.4695	0.4307
RAE (in %)	4.1	6.99	8.16	6.13	8.912	9.61	21.17	28.2	30.36	37.6	54.57	51.325
RRSE (in %)	9.73	14.56	15.88	12.57	17.51	17.71	38.27	49.41	53.85	46.34	64.22	57.852



Graph 1. Decision Table Results



Graph 2. Rep Tree Results

*CC: Coefficient of Correlation, MAE: Mean Absolute Error, RMSE: Root Mean Squared Error, RAE: Relative Absolute Error (%), RRSE: Root Relative Squared Error (%)

Real Estate

DATADICIONARY

NO.	Name	Description	NO.	Name	Description
1	CUSTYPE	Customer Subtype	21	SRS	Service
2	NOH	Number of houses	22	MGMT	Management
3	ASH	Avg size household	23	TL	Trained labor
4	AS	Avg age	24	UTL	Untrained labor
5	CMT	Customer main type	25	SCA	Social class A
6	NAT	Nationality	26	SCB1	Social class B1
7	CS	Caste	27	SCE2	Social class B2
8	SCS	Subcaste	28	SCC	Social class C
9	NR	No religion	29	SCD	1 Social class D
10	MRD	Married	30	RH	Rented house
11	LT	Living together	31	HO	Home owners
12	OR	Other relation	32	C1	1 car
13	SNG	Singles	33	C2	2 cars
14	HWTC	Household without children	34	NC	No car
15	HWTC	Household with children	35	PL	Policy Investment
16	HLE	High level education	36	OI	Other Investment
17	MLE	Medium level education	37	INL	Income < 20,000
18	LLL	Lower level education	38	INM	Income 20-55,000
19	HS	High status	39	INMH	Income 55-85,000
20	BUS	Business	40	INH	Income 85-125,000
41	INHH	Income >125,000	42	AI	Average income
43	IPC	Investment power class			

Bank Transaction Details

No.	Name	Description
1.	age	Age of the Customer
2.	sex	Sex of the Customer
3.	region	Region belongs
4.	income	Income Range
5.	save_act	Saving Account
6.	Curent_act	Current Account
7.	mortgage	Mortgage
8.	month_deposit	Monthly Deposit
9.	month_withdrawal	Monthly Withdrawal

Customer Purchase Interest

No.	Name	Description
1.	Location	Location of Flat/Plot
2.	Price	Total Price
3.	Bedrooms	No. of Bedrooms
4.	Bathrooms	No. of Bathrooms
5.	Size	Size of plot/Flat
6.	Price/SQ.Ft	Price per SQ. Feet

Moment Resisting Frame with Rubber Base Isolation for Development of Earthquake Resisting Structures

Evany Nithya S.¹, Dr. Rajesh Prasanna P.²

**(Civil engineering Department, Anna University of Technology, Tiruchirappalli, India)*

*** (Civil engineering Department, Anna University of Technology, Tiruchirappalli, India)*

ABSTRACT: Structural analysis for a base isolated four storied moment resisting frame with elastomeric seismic isolation bearing has been studied using SAP2000 software. Dynamic analysis was performed for the moment resisting frame with base isolation and the results were compared with the results obtained for moment resisting frame without base isolation. The isolating elastomer is a rubber and its total stiffness is calculated to be 3169 kN/m. The spectral displacement for the first mode suffered by the isolated building was calculated using the response spectrum curve, and found to be 0.121 m/sec². The thickness of required rubber material is calculated to be 0.121 m, assuming 100% maximum shear strain. The analysis showed that the displacement in the frame has decreased when the base isolator is added. This means that the force transferred to the building is reduced due to the presence of base isolator. The frame with base isolator produced a shear of 71.79kN – a significant shear reduction of around 88%. Thus, using rubber elastomer for base isolation, it is possible to avoid large plastic deformation of moment resisting frame and reduce shear resulting from large scale earthquake.

Keywords: Seismic Analysis, Seismic Base Shear, Base Isolation.

I. INTRODUCTION

Our intuition tells us “strengthen to resist damage”. But it is an illusion because when the foundation is rigidly fixed to the superstructure, the earthquake force will be directly transferred to the superstructure without any change in frequency resulting in heavy damage. In a base isolated structure the seismic protection is achieved by shifting its natural period away from the range of the frequencies for which the maximum amplification effect of ground motion is expected. In this way the input seismic energy introduction in to the structure is significantly reduced and consequently it is possible to avoid large plastic deformation and related damage phenomena due to non-linear response. In the base isolation strategy, at the same time it is possible to obtain a considerable reduction of large displacements attained at the base level as a consequence of the energy dissipation due to damping and hysteretic properties of isolation device. In simple words the basic concept in this approach is to uncouple a structure from the ground by interposing a flexible element/bearing between the structure and foundation. Many buildings have been constructed on some type of rubber bearings, and such structures have shown superior performance in earthquakes.

The system that has been adopted most widely in recent years is typified by the use of elastomeric bearings, the elastomer is made of either natural rubber or neoprene. In this approach, the building or structure is decoupled from the horizontal components of the earthquake ground motion by interposing a layer with low horizontal stiffness between the structure and the foundation. This layer gives the structure a fundamental frequency that is much lower than its fixed-base frequency and also much lower than the predominant frequencies of the ground motion. The first dynamic mode of the isolated structure involves deformation only in the isolation system, the structure above being to all intents and purposes rigid. The isolation system does not absorb the earthquake energy, but rather deflects it through the dynamics of the system.

II. DESIGN

The inclusion of base isolation means that a building is cushioned against the shocks of earthquakes. Instead of designing the building to resist high earthquake forces, the isolation system is designed to allow the building to stay more or less still while the ground moves underneath it in strong earthquakes. As a result the building need only be designed for much smaller forces. A seismic base isolator is a flexible support of a building, which should fulfill the following requirement:

- The material is stiff under low service loads like wind and small tremors.
- Period of vibration of the system is increased sufficiently so as to reduce the seismic force response.
- It should have the ability to with stand the large displacement and pulse-type base motions from near-fault earthquakes.
- It should have a parallel damping mechanism such that the relative deflection between the building and the ground is reduced.

To start with we have to calculate the load coming on the column. In this paper we have design the base isolation for the four storied moment resisting frame, when it is located in zone V. The frame taken for study was moment resisting frame with shear wall. Moment frames consist of beams and columns in which bending of these members provides the resistance to lateral forces. Moment-resisting frames are detailed to ensure ductile behavior of the beam-to-column joints and are normally used in zones of higher seismicity. It has 4 bay at a spacing of 5m in the X direction and 3 bay in the direction of Z at a spacing of 6m, 4.5m, 4.5, respectively. It has ground plus three stories. The height of the ground

floor is 4.5m and the heights of the rest of the three floors are 3.2m each as shown in Figure 1.

III. ELASTOMERIC RUBBER BEARING

III. I Calculation of horizontal stiffness of the rubber:

The total horizontal stiffness of the rubber isolators is computed using single degree of freedom system equation, Horizontal stiffness (K) was calculated using the below equation

$$K = 4 * \Pi * f^2 * \left[\frac{W}{g} \right]$$

From the above equation the total horizontal stiffness is calculated as 3169.01 kN/m

III. II Calculation of the thickness of the rubber:

The spectral displacement for the first mode suffered by the isolated building is calculated using the response spectrum curve for the given horizontal frequency and for the appropriate damping value and using the following expression.

Spectral displacement: S_d =Spectral displacement, S_a

$$S_d = \frac{S_a}{(2 * \Pi * f_n)^2}$$

S_a =displacement from response spectrum curve, f_n =horizontal frequency.

The Spectral displacement was found to be 0.121 m / sec². The thickness of the rubber material of the isolator is evaluated using the allowable maximum shear strain permitted for the isolator. The allowable maximum shear strain for the isolator is taken as 100%.

Thickness of rubber = S_d / γ , Where, γ =Allowable maximum shear strain. Thickness of rubber was calculated to be 0.121 m. Once the thickness and shear modulus of the rubber are know, the area of the rubber

$$K_i = \frac{G * A}{t_r}$$

material to produce the given amount of horizontal stiffness is calculated using the following expression.

Where K_i = Horizontal stiffness, G =Shear modulus of the rubber, A =Area of the rubber, t_r =Thickness of the rubber. From the above formula the area is calculated to be 0.0247 m².

From the area calculated above the diameter (180 mm) of the rubber is calculated. Thickness of individual layer of rubber are calculated as below,

$$S = D / 4 * t , \quad t = 5\text{mm.}$$

Total number of layers = total thickness / individual layer thickness = 25 numbers

The shim thickness is generally taken to be not less than 2.54mm and not greater than 3.16mm. Therefore, thickness of the shim =3mm.The end plates are usually between 19.1mm and 38.1 mm. Therefore, thickness of end plate =25mm.

IV. DISCUSSION

Dynamic analysis is performed for the moment resisting frame selected with the base isolation. The response of the structure when base isolation is added to the structure is compared with the response of the structure without base isolation. The analysis of the structure with base isolation is performed with the use of SAP2000 package. The results are compared as follows.

➤ Comparing the displacements:

The fig 3 and 4 clearly shows that there is a change in the displacement of the frame. The displacement in the frame has decreased when the base isolator is added. This decrease in the displacement show that the force transferred to the building is reduced due to the presence of base isolator. When this happens then there will be a reduction in the requirement of reinforcement in beams and columns. In this way the input seismic energy introduced in to the structure is significantly reduced and consequently it is possible to avoid large plastic deformation and will reduce the reinforcement requirement and prove to be economical and safe.

➤ Comparing the base shear:

Base shear can be put in simple words as the horizontal component of the seismic shaking. The horizontal components of shaking are the most damaging to buildings because structures are already designed to withstand the vertical force of gravity. From the analysis performed for the frame with base isolator and without base isolator in SAP2000 the base shear results are taken. The frame with fixed base has a base shear of 618kN. The frame with base isolation has a base shear of 71.79kN. There is a decrease of 88.38% in the base shear when the structure with base isolator is compared with the structure without base isolator.

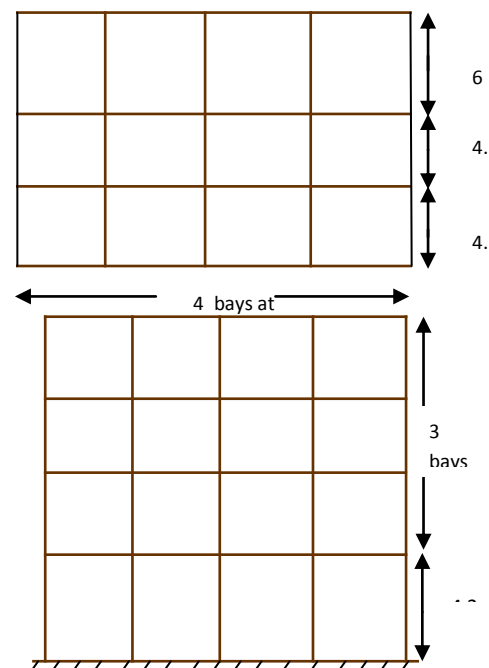


Fig .1 Plan and elevation of frame selected

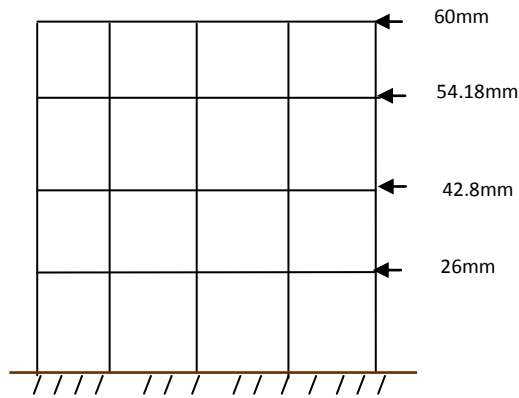


Fig. 2 Displacement of the frame without base isolation

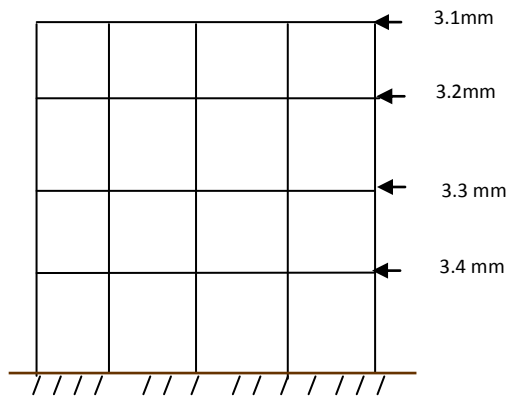


Fig. 3 Displacement of the frame with base isolation

V. CONCLUSION

Engineers realized the importance of keeping the superstructure stable while the foundation is being shaken by an earthquake. So there arises a need to design a system that puts this concept into practice. Along with many other engineers doing independent work in other countries, have produced a wealth of information about base isolators and have become common knowledge to structural engineers. By introducing base isolators the maximum expected lateral force that will occur due to seismic ground motion at the base of a structure is considerably reduced. This concept has created a breakthrough in structural design and as years go by will prove to be a life-saving innovation of historic proportions.

REFERENCES

- [1] Ahmed Ghobarah , Performance-based design in earthquake engineering: state of development, *Engineering structures*, 23(8), 2001, 878-884.
- [2] David J. Dowrick, *Earthquake Resistant Design For Engineers And Architects*, (John Wiley Heyden Publication)
- [3] Elghazouli A.Y., Castro J.M. and Izzuddin B.A., Seismic performance of composite moment-resisting frames, *Engineering Structures*, 30(7), 2008, 1802-1819.
- [4] James M. Kelly , "Earthquake Resistant Design With Rubber", Springer - verlag London Limited.
- [5] Javeed A., Munshi and Satyendra K. Ghosh, Analyses of seismic performance of a code designed

reinforced concrete building, *Engineering Structures*, 20(7), 1998, 608-616.

- [6] Mario Paz "International Handbook Of Earthquake Engineering Codes, Programs And Examples".
- [7] Sadjadi R., Kianoush M.R. and Talebi S., Seismic performance of reinforced concrete moment resisting frames, *Engineering Structures*, 29(9), 2007, 2365-2380.
- [8] Sean Wilkinson, Gordon Hurdman and Adrian Crowther, A moment resisting connection for earthquake resistant structures, *Journal of Constructional Steel Research*, 62(3), 2006, 295-302.
- [9] Smith K. G., Innovation in earthquake resistant concrete structure design philosophies; a century of progress since Hennebique's patent, *Engineering Structures*, 23(1), 2001, 72-81.
- [10] Wai-Fah Chen, Charles Scawthorn "Earthquake Engineering Handbook".
- [11] IS 1893 (part 1) : 2002 "Criteria For Earthquake Resistant Design Of Structures".
- [12] IS 4326:1993 "Earthquake Resistant Design And Construction Of Buildings-Code Of Practice"

Nigeria's Wind Energy Potentials: the Path to a Diversified Electricity Generation-Mix

Idris N.A.¹, Lamin, H.S.², Ladan, M.J.³ and Yusuf, B.H.⁴
Energy Commission of Nigeria

ABSTRACT: For many decades, conventional energy resources have continually remained major energy sources in Nigeria. This paper therefore looks at the enormous wind energy potentials in Nigeria. Available data on wind speed for some towns in Nigeria indicates very good prospects for wind energy development. This paper advocates the inclusion of wind energy in the nation's energy supply mix. This would diversify and reverse the current acute electricity deficit experienced in the country, as well as address environmental concerns and effect of climate change.

Keywords: Electricity, Energy, Nigeria, Potentials, Wind,

I. INTRODUCTION

Nigeria is a well endowed country with abundant wind energy resources which can be used to generate electricity. However, despite the abundance of these energy resources, there is persistent electricity supply deficit, which may be attributed to under utilization of these potentials. Other major barriers to the deployment of wind energy technology in the country include high initial cost of wind power generation, systemic issues governing reliable transmission and system integration, social acceptance of technology and energy market structure. The non-proper coordination of activities in the energy sector largely because of lack of concrete policy and energy plan is also worth mentioning.

Wind energy has been widely used in Nigeria to power water supply for many decades now. In recent times efforts are largely geared towards its use for electricity generation, for example, the Federal Government of Nigeria is currently constructing 10 MW Wind Farm at Katsina and work has reached advanced stage of completion, although there are some issues with grid integration. In Nigeria, typical wind pattern occurs mostly from the east for inland areas and from the west over the coastal areas. During the harmattan period (December – March) strong winds appear covering the country especially in the northern parts where the main wind direction shifts to west / south western directions. A study on the wind energy potentials for a number of Nigerian cities shows high wind speeds in the Sokoto region, Jos, Gembu and Kano / Funtua. The stations at Maiduguri, Lagos and Enugu also indicated relatively strong wind speeds, sufficient for energy generation by wind farms. Apart from these sites, other promising regions with usable wind potentials are located at the Nigeria's shoreline [1].

The proper utilization of these wind energy potentials will ensure promotion of socio-economic development as well as quality of life of the citizenry. Expanding the use of renewable resources such as wind will reduce carbon dioxide emissions which contribute to global warming and

lower long-term overdependence on fossil fuels. Further, wind energy like other power technologies based on renewable energy resources is fast evolving globally and widely available, thereby ensuring security of supply. Prior to construction of any wind farm, a detailed verification of the specific on-site wind conditions is necessary to come up with a suitable wind map in order to identify those areas which have favorable wind regimes and can therefore be selected for the development of wind energy projects.

This paper therefore attempts to give an overview of the nation's wind energy potentials, enumerating the numerous challenges hindering its development and identify some measures that will possibly lead to inclusion of wind in the energy supply mix to satisfy our growing energy demand, diversify our supply sources to guarantee energy security and align with the new global trend of green energy growth.

II. GLOBAL TRENDS IN WIND ENERGY DEVELOPMENT

Today wind energy is one of the fastest developing renewable energy technologies in the world and mainly onshore. Wind is among the cheapest renewable sources per unit of electricity produced. Analysis indicates that a network of land-based 2.5MW wind turbines could supply over 40 times current worldwide electricity consumption [2].

Wind energy generation market is continuously growing worldwide. In 2009, 82 countries used wind to generate energy, and 49 countries increased their installed capacity [3]. Middle East and Africa also recorded a total of 230MW of newly installed capacity with almost 90% growth rate in Morocco and 170% growth in Tunisia. Although these values are small compared with wind energy producing regions like North America, Europe and Asia, the presence of wind energy in remote locations of the world simply highlights the continued rapid growth in global demand for emissions-free wind power, which can be installed virtually everywhere around the globe.

Wind energy had over 238GW of installed capacity at the end of 2011[4] and is expected to play a crucial role in mitigating future greenhouse gas emissions. The Global Wind Energy Council forecasted that global wind market will grow by over 155% to reach 240GW of total installed capacity by the end of 2012. According to recent projections, wind energy is expected to contribute some 12% of global electricity by 2050, with 57% of this energy produced by non – OECD economies. However, USD3.2 trillion will have to be invested over the next 40 years to realize this improvement [5].

Currently, Europe is the leading market for global wind power, and will probably remain so for the next decade. It

is followed by the United States and then China as world leading wind power producers. China will probably overtake the United States and OECD Pacific countries as a major producer of wind energy by 2050, with projected figure of 1660 TWh. The rest of the world, including Africa and the Middle East, provide nearly one-fifth of wind electricity in 2050 [5].

III. NIGERIA'S WIND ENERGY POTENTIALS

Wind speed in Nigeria ranges from 1.4 - 3.0m/s in the southern areas and 4.0 - 5.12m/s in the extreme north. Wind speeds are generally weak in the southern part of the country except for the coastal regions and offshore location. Initial study has shown that total exploitable wind energy reserve at 10m height may vary from 8MWh/yr in Yola to 51MWh/yr in the mountainous areas of Jos Plateau and it is as high as 97MWh/yr in Sokoto [6].

Lahmeyer International's report [1] gives potential estimates for ten (10) selected sites in the country to be between 3.6 m/s to 5.4 m/s. These results when compared with the figures obtained from calculated wind speed using Climatic Model Mainz (KLIMM) gives difference of -4.3% to 4.1% which is within the acceptable limit of error. Table 1 presents the results for these ten (10) selected sites.

Table 1: Summary of measured data of annual Wind Speeds (Ten selected sites)

Site	Land-use Type	Altitude (m a.s.l.)	Height (m)	WIND SPEED (m/s)		Difference (%)
				Measured	KLIMM	
Enugu	Complex landscape	466	30	4.6	4.4	-4.3
Jos	Complex landscape	1,344	30	5.2	5.1	-1.9
Pankshin	Complex landscape	1,355	40	4.9	4.7	-4.1
Sokoto	Plain surface	352	30	5.4	5.2	-3.7
Kano	Plain surface	340	30	4.9	5.1	4.1
Gumel	Plain surface	393	30	4.1	4.2	2.4
Maiduguri	Plain surface	373	30	4.7	4.6	-3
Ibi	River valley	300	30	3.6	3.3	-8.3
Gembu	Highly complex landscape	1,800	40	5	5.2	1
Lagos	Coastal Area	2	30	4.7	4.9	4.3

Source: Wind Energy Resources Mapping and Related Work Project: (LI/FMST, Nigeria, 2005)

The estimated gross energy yield of the sites by wind turbine types is shown in Table 2.

Table 2: Gross Energy Yield for the Measure

Measurement Station	Gross Energy Yield Measurement (MWh)		
	FUHLÄNDER FL 100	FUHLÄNDER FL 250	VESTAS V52 850 52.0
	100/20	250/50	
Sok1	153.5	358.8	1,235.80
Jos01	129.6	299	1,025.80
Gem01	112.9	253.9	855.30
Pan01	117.1	272.1	936.60
Kan01	116.3	281.2	963.70
Mai01	102.7	262.2	906.10
Lag01	129.3	386.1	1,402.80
Enu01	92.9	217.9	734.20
Gum01	73.4	197.2	681.40
Ibi01	49.8	141.3	481.20

Source: Wind Energy Resources Mapping and Related Work Project (LI/FMST, Nigeria, 2005)

Table 3 [7] indicates high wind energy potentials for some selected states of the Federation. One percent of effective wind area of these 14 states has a potential to generate 50,046 MWh/y of electricity assuming 5MW/km² (a) and 30% capacity factor (b).

Table 3: Estimated Wind Energy Potentials for 14 Selected States

Selected State	Area (km ²)	Windy Area (%)	Effective Wind Area (km ²)	1% Area (km ²)	Potential capacity ^a (MW)	Potential Generation ^b (MWh/yr)
Adama wa	37,957	45%	17,080	170	854	2244
Bauchi	48,197	50%	24,098	240	1204	3166
Borno	72,767	100%	72,767	727	3638	9561
Gombe	17,428	100%	17,428	174	871	2290
Jigawa	23,415	100%	23,415	234	1170	3076
Kaduna	44,217	60%	26,530	265	1326	3486
Kano	20,389	90%	18,350	183	917	2411
Katsina	23,822	100%	23,822	238	1191	3130
Kebbi	36,320	25%	9,080	90	454	1193
Plateau	26,539	90%	23,885	238	1194	3138
Sokoto	32,146	90%	28,931	289	1446	3801
Taraba	59,180	40%	23,672	236	1183	3110
Yobe	44,880	100%	44,880	448	2244	5897
Zamfara	33,667	80%	26,933	269	1346	3539
Total				3,808	19,043	50,046

Source: Nigeria Climate Assessment, LCD Power Sector, preliminary report (WBG / Lumina Decision Systems, 2011)

Agbetuyi et al [8], estimates wind energy density at 25m height for some 22 selected sites across the country. Table 4 provides detailed potentials and wind energy densities of the sites.

Table 4: Wind Energy Density Estimates at 25m Height

S/N	Station	Mean wind speed at 25m level	Monthly mean wind Energy	Annual Wind Energy	Annual Wind Energy from a Wind Turbine (kWh)	
		m/s	kWh	kWh	10m Blade Diameter	25m Blade Diameter
1	Benin City	2.135	2.32	27.86	2,187.81	13,673.78
2	Calabar	1.702	1.12	13.42	1,053.69	6,587.53
3	Enugu	3.372	7.83	93.91	7,375.75	46,097.96
4	Ibadan	2.62	4.15	49.78	3,909.79	24,436.19
5	Ilorin	2.078	1.23	14.73	1,157.06	7,230.57
6	Jos	4.43	16.05	192.64	15,129.60	94,559.98
7	Kaduna	3.605	9.91	188.88	936.81	58,355.08
8	Kano	3.516	8.57	102.86	8,078.61	50,491.28
9	Lagos(Ikeja)	2.671	4.36	52.32	4,099.78	25,682.52
10	Lokoja	2.235	2.6	31.21	4,451.23	15,320.17
11	Maiduguri	3.486	8.42	101.01	7,933.61	49,583.17
12	Minna	1.589	1.05	12.6	989.60	6,185.01
13	Makurdi	2.689	4.44	53.27	4,183.51	26,148.85
14	Nguru	4.259	14.48	173.74	13,645.19	85,284.42
15	Oshogba	1.625	1.07	12.81	1,006.60	6,288.09
16	PH	2.64	4.17	49.98	3,925.48	24,533.88
17	Potiskum	3.636	9.44	113.25	8,894.35	55,591.46
18	Sokoto	4.476	16.47	197.68	15,525.75	97,035.94
19	Warri	2.027	2.02	24.2	1,900.66	11,879.15
20	Yelwa	3.36	7.76	93.13	7,314.88	45,714.59
21	Yola	1.824	1.45	17.34	1,361.88	8,511.75
22	Zaria	2.891	5.32	63.88	5,017.26	31,357.02
	Total		134.23	1680.5	120,078.90	790,548.39

Source: Wind energy Potential in Nigeria: (Agbetuyi et al, 2012)

IV. JUSTIFICATION FOR DEPLOYMENT

An analysis of the power generation capacity required to support the NV20:2020 economic vision shows that, Nigeria will need to generate electricity in the range of about 35,000 – 40,000MW by year 2020. To achieve this, there is need to aggressively pursue the harnessing of the nation’s wind and other renewable energy resources.

Thus, Sambo (2012) [9], gives some of Nigeria’s renewable energy resources as 14,750MW of hydro power potentials, 3.5 - 7.0 kWh/m²/day of solar radiation (485.1 million MWh/day using 0.1% Nigeria land area), (2-4) m/s at 10m height of wind speed, 72 million hectares of arable land for energy crops and agricultural production. Other conventional energy resources include 180.57 trillion SCF of natural gas, 2.734 billion tonnes of coal and lignite, 37.2 billion barrels of light crude oil, and yet to be quantified nuclear element. Despite all these renewable and non-renewable resources, Nigeria is generating electricity from only two sources (gas and hydro), which are both poorly harnessed and mismanaged.

As at 2009, the country’s total generation capacity was 8,876MW but only 3,653MW was available, which is less than 41% of the total installed capacity [10]. It is instructive for Nigeria to learn from experiences of other countries and diversify its energy supply mix to achieve energy security. Harnessing wind power offers environmental advantages in terms of reducing carbon dioxide emissions and other pollutants such as oxides of Sulphur and Nitrogen mostly

associated with burning of fossil fuels, thereby addressing global warming concerns.

V. WIND FOR ELECTRICITY GENERATION

For effective performance and maximum yield of wind power systems, project planning and siting as well as reliable prediction in terms of wind resource is a pre-requisite. Electricity is generated from wind through the use of wind turbines also known as wind energy converters (WEC). The main components of a WEC include rotor blade, generator, pitch, wind measurement system, brake, gear box, rotor hub, yaw mechanism, nacelle, transformer and tower.

The wind turbines convert the kinetic energy of wind into mechanical energy and then to electrical through the generator. The generator may be of fixed or variable speed. Due to changing wind speed and direction, the yaw mechanism is used to turn the blades of the wind turbines in line with wind direction to increase its output. The collection of wind turbines for purpose of electricity generation is called a wind farm and its planning involves series of processes.

Upon identification of the proposed site, wind data are collected for a period of at least 12 months on-site to ascertain general wind pattern for the whole year. Then, the data obtained is evaluated and analyzed with different wind turbines to determine the best for the site. The blade diameter, tower height and rated power all depends on wind data characteristics.

Other factors that need to be considered include accessibility and distance of the proposed site to the grid. Wind farm requires a considerable size of land area for its construction. In order to ensure efficiency, higher output and avoid wind theft, a minimum distance of 3D (3 times diameter of blade) between turbines and 5D to 7D in main wind direction is recommended [11].

Wind turbines are manufactured based on specification and are usually not off-shelf. Delivery may take up to a year and thus, setting up a wind farm from the scratch takes a period of at least 2 ½ years. WEC have maximum theoretical efficiency of 60% but only about 45% in practice.

Wind farms can be onshore or offshore. The offshore wind turbines need to have solid foundations and protection from corrosion. Hence, they are more expensive than onshore farms. The upside of offshore farms is the increase in yield. Load factor of onshore wind farms is usually 20-30% while that of offshore wind farms is 30-43% [5]. After about 20 years of operation wind turbines have to be decommissioned. Re-powering with a larger more efficient turbine is an economical choice.

VI. TARGET MARKETS AND COST ISSUES

Electricity from wind can be grid connected or off-grid with the latter being the most popular. Wind power is ideal for generating electricity at remote locations. Hence, clusters can be created with turbines generating electricity for remote villages or collection of thousands of households. With the low load factor of wind power plant, it can be used to boost the nation’s electricity by targeting intermediate to peak load demand taking its advantage of quick start and stop.

The cost of setting up wind farms is very high. Electricity transmission infrastructure typically accounts for around 10 – 20% of the capital costs of constructing an offshore wind farm. Wind turbines are subject to economies of scale. For example, a building-mounted turbine with 2.5kW capacity generation would cost around £10,000 and may not payback in the equipment lifetime. Whereas a large scale turbine (1MW – 2.5MW) would cost £2 – £3.3 million and the payback period could range from five years to less than one year respectively. Hence, large capacity wind farms are more economical.

The average cost of generating electricity from large scale onshore wind is now around 3 - 4 pence per kilowatt hour, competitive with new coal (2.5 – 4.5 pence) and cheaper than new nuclear (4 – 7 pence). As gas prices increase and wind turbine costs fall further as the market grows, wind energy is also likely to become competitive with gas fired power generation [12].

REFERENCES

- [1] Lahmeyer International and Federal Ministry of Science and Technology Nigeria, *Wind Energy Resources Mapping and Related Work Project*, (Abuja: 2004)
- [2] <http://www.pnas.org/content/106/27/10933>
- [3] World Wind Energy Report, *Global Installed Wind Power Capacity*, Brussels, 2009
- [4] <http://www.ewea.org/index.php?id=1639>
- [5] http://www.iea.org/papers/2009/wind_roadmap.pdf
- [6] Energy Commission of Nigeria, *Renewable Energy Masterplan*, (Kaduna: Shukrah Printers, 2005)
- [7] World Bank Group and Lumina Decisions System: *Presentation of the Nigeria Climate Assessment, Low Carbon Plan in the Power Sector Workshop*, Abuja, 2011.
- [8] Agbetuyi et al, Wind Energy Potential in Nigeria, *International Electrical Engineering Journal*, Vol. 3 No.1, pg. 59
- [9] A.S. Sambo, Energy Indicators for Sustainable Development: *Keynote Address at 2nd Summit of Energy and Sustainable Economic Growth*, Abuja, 2012.
- [10] Emovon et al, Power Generation in Nigeria: Problems and Solutions, *Proceedings of the 2012 conference of the Nigerian Association of Energy Economics (Green Energy and Energy Security Options for Africa)* pg. 313-321
- [11] <http://www.idea.gov.uk/idk/core/page.do?pageId=25287451>
- [12] RENAC, Session 02 & Exercise, *Onshore Wind Energy training course on Wind Farm Projects*, Berlin, 2009.

VII. CHALLENGES OF DEPLOYMENT

There are a series of challenges affecting wind energy deployment in the country. These include lack of financing and other fiscal incentives, lack of skilled manpower and lack of indigenous manufacturing capabilities. Others include, lack of policy and institutional framework to encourage investment and deployment of wind energy technology. Low load factor of wind farms makes it unsuitable for base load power plants.

VIII. CONCLUSION

The use of wind power to generate and supply electricity will expand Nigeria's energy base and reduced environmental pollution. Hence, sites identified with superb wind energy potentials should be adequately harnessed. Effort should be made to address issues of integration to the national grid.

All necessary policies and institutional framework should be put in place to eliminate barriers to deployment of wind energy technology in the country.

Electric Field Dependent Specific Heat of SrTiO₃, BaTiO₃ and KTaO₃ Ferroelectric Perovskites

Gaurav Kumar Aggarwal¹, Ashok Kumar², UC Naithani³

^{1, 2, 3}Department of Physics, H.N.B. Garhwal Central University, Pauri Campus,
Pauri (Garhwal), Uttarakhand., Pin – 246001, India.

Abstract: The field dependent specific heat of anharmonic ABO₃ type displacive ferroelectrics (SrTiO₃, BaTiO₃ & KTaO₃) is studied using double time Green's function technique along with Silverman-Joseph modified Hamiltonian which includes anharmonicity up to the fourth order due to the interaction of the soft mode. The soft mode contributions to specific heat are described by appropriate Einstein terms. The variation of specific heat with temperature and electric field is discussed. The specific heat in all three crystals increases non-linearly with temperature. The specific heat decreases with increase in external electric field. The effect of electric field on specific heat is more prominent in low temperature sides in all three crystals. The effect of temperature reduces in low field region and the change in specific heat arises mainly due to higher order anharmonic terms. The results are in agreement with previous experimental and theoretical results.

Keywords: anharmonicity, Cochran mode, Green's function, soft mode, Specific heat.

I. Introduction

Ferroelectricity is one of the most fascinating properties of dielectric solids. Ferroelectrics are the crystals that show spontaneous polarization which is reversible by stress or electric field. This phase transition is exhibited within the limited temperature range, called the Curie temperature T_c and is associated with a change in crystal structures and the anomalous behavior of some physical properties. All these materials are piezoelectric and have high electromechanical coupling coefficients. The ferroelectric materials have been grouped together because they have some common characteristics. There are more than a thousand ferroelectric compounds. The most commonly studied are the perovskites and the alkali dihydrogen phosphates. The perovskites have ABO₃ type structure, where A is a first, second, fourth or even fifth group ion of appropriate valency and B is a transitional metal ion such as Ti, Nb, Ta, Zr etc. For example NaTaO₃, KNbO₃, BaTiO₃, PbTiO₃, SrTiO₃, BiFeO₃ and KTaO₃ etc. are all ferroelectric perovskites.

Ferroelectrics have become a subject of considerable interest in the past few years, because of their wide potential applications in different fields. Their properties reveal many interesting applications in the ceramic industry, optoelectric devices for use in optical communication, memory display, coherent optical processing, modulators, beam reflectors, light valves and holographic storage media etc. As compared with similar magnetic devices, ferroelectric memory devices are very small in size and mass, consume less power and are not sensitive to external magnetic fields. Memory devices are constructed from ferroelectrics distinguished by a rectangular cycle of electric hysteresis, a short time needed for switching over (i.e. the time for changing the direction of spontaneous polarization).

It is now well known that several interesting temperature dependent properties of ferroelectric result from the temperature dependence of the low lying transverse optic mode of vibration [1]. One of the very interesting properties of these crystals is the electric field and temperature dependences of the low frequency transverse optic (TO) mode. The effect of electric field on the Cochran modes in SrTiO₃ and KTaO₃ was studied by Steigmeir [2], showing an upward shift in the TO-mode frequency which reduces the TO-LA interaction. All these studies reveal a remarkable effect of electric field on ferroelectric soft mode frequency. So the dynamic properties of ferroelectrics will be affected in the presence of electric field [3, 4] because of the effect of electric field on soft ferroelectric mode.

Low temperature specific heat of ferroelectric, superconducting and amorphous materials has been studied by several researchers [5,6]. These studies show that ferroelectric materials with field dependent low-lying modes will have associated field dependent specific heats at low temperatures [7]. The specific heat of all the three crystals (SrTiO₃, BaTiO₃ and KTaO₃) decreases with increase in applied electric field and this decrease is due to the hardening and splitting of the soft TO-mode frequency. There is also some published work on the specific heat of pure and mixed ferroelectric crystals [8-13]. A current review for perovskites type ferroelectric crystals is available in the literature [14-17].

The aim of the present work is to study theoretically the variation of specific heat with temperature and electric field both qualitatively and quantitatively using the method of double time temperature dependent Green's function in anharmonic ferroelectric crystals such as SrTiO₃, BaTiO₃ and KTaO₃ using a model Hamiltonian for ferroelectric crystal, augmented with anharmonicity up to fourth order. The expression for the specific heats of displacive type ferroelectric materials such as SrTiO₃, BaTiO₃ and KTaO₃ in paraelectric phase in presence of external electric field is obtained. We used double time Green's function technique to obtain thermally averaged correlation function and hence, the observable quantities with the help of Silverman-Joseph modified Hamiltonian which includes anharmonicity up to fourth order. The contribution of soft modes towards specific

heat has been taken into account. As in general, it is agreed that low temperature specific heat data can reveal the position(s) of low-lying vibrational levels in soft mode dielectric materials. The contributions from these levels are so large that specific heat data estimated from the acoustic spectrum (e.g. elastic constants) can be in error by as much as in order of magnitude. Also the soft mode contribution to the specific heat is described by appropriate Einstein terms. We make use of a unitary transformation which renders the most significant first order dipole-moment term to affect the specific heat via the applied electric field. The effect of an external electric field on the specific heat and soft mode frequency has been discussed in paraelectric phase for SrTiO₃, BaTiO₃ and KTaO₃ crystals. The properties of ferroelectric crystals are investigated both theoretically and experimentally by many workers. Calculated results have been compared with the results of other workers.

II. Theory

2.1 Green's function and the soft mode frequency

For the study of specific heat, we have used Silverman-Joseph modified Hamiltonian which includes anharmonicity up to fourth order in the potential energy similar to our previous study for zero defect case [4]. The interaction of the soft mode coordinates, resonant interactions, scattering and electric dipole moment terms are considered in the Hamiltonian.

To evaluate the expressions for various dynamic properties in presence of the electric field, we introduce the retarded double-time thermal Green's function for the optical phonon as:

$$G_0^0(t-t') = \ll A_0^0(t); A_0^0(t') \gg = -i\theta(t-t') \langle A_0^0(t); A_0^0(t') \rangle \quad \dots (1)$$

Where $\theta(t-t')$ is the usual Heaviside step function and the symbol $\langle \rangle$ denotes the statistical average. $A_0^0(t)$ and $A_0^0(t')$ are the annihilation and creation operators of the acoustic phonon of the wave vector k . While writing the equation of motion for the Green's function Eq. (1) with the help of the modified Hamiltonian, Fourier transforming and writing it in the Dyson's equation form, one obtains:

$$G_0^0(\omega + i\epsilon, E) = \frac{\omega_0^0}{\pi} [\omega^2 - \tilde{\nu}_0^0(\omega) - 2\omega_0^0 i \Gamma^0(\omega, E)] \quad \dots (2)$$

Where $\tilde{\nu}_0^{02} = \omega_0^{02} + 2\omega_0^0 \Delta^0(\omega, E)$... (3)

Here $\omega_0^{02} = \tilde{\omega}_0^{02} + \langle [F(t); A_0^0(t')] \rangle$... (4)

And $\tilde{\omega}_0^{02} = \omega_0^0 [\omega_0^0 + 2V + 12\Gamma'_1 gE + 24\Gamma'_2 g^2 E^2]$... (5)

Where the notations used are exactly similar and in the same sense as used in our previous calculations [12].

In Eqs (3) and (4), $\Delta^0(\omega, E)$ and $\Gamma^0(\omega, E)$ are the field dependent shift and width for the soft mode respectively, and are given by:

$$\begin{aligned} \Delta^0(\omega, E) = & 18\Gamma_1^2 N \left[\frac{2\Omega}{\{\omega^2 - (2\Omega)^2\}} \right] + 4\Gamma_2^2 (1 + N^2) \left[(1 + N^2) \frac{3\Omega}{\{\omega^2 - (3\Omega)^2\}} - (1 - N^2) \frac{\Omega}{\omega^2 - \Omega^2} \right] + \\ & 16 \sum |H|^2 \cdot \left[\frac{(N_k^a \pm N_k^0)(\Omega_k^a \pm \Omega_k^0)}{\omega^2 - (\Omega_k^a \pm \Omega_k^0)^2} \right] + \left[288\Gamma'_2 g^2 E^2 + 8NE^2 \times \sum |B^\lambda(k)|^2 \cdot \frac{2\Omega}{\{\omega^2 - (2\Omega)^2\}} \right] + \\ & \left[(-4|A|^2 \sum |F|^2 + 64g^2 E^2 \sum |H|^2) \frac{N\omega}{\omega^2 - \Omega^2} \right] \quad \dots (6) \end{aligned}$$

And $\Delta^0(T, E) = AT + BT^2 + CTE^2$... (7)

$$\begin{aligned} \Gamma^0(\omega, E) = & 9\pi\Gamma_1^2 N \{ \delta(\omega - 2\Omega) - \delta(\omega + 2\Omega) \} + 2\pi\Gamma_2^2 \{ (1 + 3N^2) \{ \delta(\omega - 3\Omega) + \delta(\omega + 3\Omega) \} - (1 - N^2) \{ \delta(\omega - \Omega) - \\ & \delta(\omega + \Omega) + 8\pi |H|^2 \times (Nk^a \pm Nk^0) \delta\omega - \Omega k^a - \Omega k^0 + \delta\omega + \Omega k^a + \Omega k^0 + \pi 144\Gamma'_2 g^2 E^2 + 4E^2 \times B\lambda k 2N \cdot \delta\omega - 2\Omega - \delta\omega + 2\Omega + \pi \{ [-2A2 \\ & |F|^2 + 64g^2 E^2 |H|^2] N \cdot \delta\omega - \Omega - \delta\omega + \Omega \} \} \quad \dots (8) \end{aligned}$$

And $\Gamma^0(T, E) = AT + BT^2 + CTE^2$... (9)

Where the notations used are exactly similar and in the same sense as used in our previous calculations [12].

Eqs. (7) and (9) show the temperature and field dependence of shift and width, respectively of optic phonons in frequency response.

The soft mode frequency for optic mode [Eqs (3-5)] may be written as:

$$\begin{aligned} \check{\omega}_0^{02} = & \omega_0^0 [\omega_0^0 + 2V + 12\Gamma_1' gE + 24\Gamma_2' g^2 E^2] + \langle [F(t); A_0^0(t')] \rangle > \\ & + \omega_0^0 [36\Gamma_1'^2 N \left[\frac{2\Omega}{\{\omega^2 - (2\Omega)^2\}} \right] + 8\Gamma_2'^2 \left[(1 + N^2) \frac{3\Omega}{\{\omega^2 - (3\Omega)^2\}} - (1 - N^2) \frac{\Omega}{\omega^2 - \Omega^2} \right] + 32 \sum |H|^2 \cdot \left[\frac{(N_k^0 \pm N_k^0)(\Omega_k^0 \pm \Omega_k^0)}{\omega^2 - (\Omega_k^0 \pm \Omega_k^0)^2} \right] + [576\Gamma_2' g^2 E^2 + \\ & 16NE^2 \times B\lambda k 2.2\Omega\omega^2 - 2\Omega^2 + (-8A2 |F|/2 + 128g^2 E^2 |H|/2) N\omega\omega^2 - \Omega^2 \end{aligned}$$

$$\text{Or } \check{\omega}_0^{02} = \omega_0^{02} + 2\omega_0^0 V + \gamma_1 + \gamma_2 T + \gamma_3 T^2 + \gamma_4 E + \gamma_5 E^2 \quad \dots (10)$$

Where γ_2 and γ_3 are the coefficients of T and T^2 , respectively and γ_4 and γ_5 are the coefficients of E and E^2 respectively. The square of the soft mode frequency varies as the square of the applied electric field which is in agreement with the experimental result [18]. The effect of the electric field on this mode also affects the interaction of soft mode with other modes, thus giving rise to electric field dependence of various dynamical properties.

2.2 General formulation for specific heat at constant volume (C_V)

The specific heat at constant volume (C_V) for the model of the pure crystals considered here can be obtained as follows:

$$C_V = K_B \sum_k E(Y_k) \quad \dots (11)$$

Here K_B is a Boltzmann constant and Y_k is defined as

$$Y_k = \hbar \Omega_k / (K_B T) \quad \dots (12)$$

Where Ω is the field dependent soft mode frequency of ferroelectric perovskites and $E(Y)$ is the Einstein function given by:

$$E(Y) = Y^2 \exp Y / (\exp Y - 1)^2 \quad \dots (13)$$

Substituting the value of the Einstein function $E(Y)$ for soft phonon mode ($k=0$) in Eq. (1) gives the specific heat at constant volume as

$$C_V = K_B Y^2 \exp Y / (\exp Y - 1)^2 \quad \dots (14)$$

Now substituting the value of Y (Y_k for $k=0$) from Eq. (2) into Eq. (4) it gives

$$C_V = K_B (\hbar \Omega / K_B T)^2 \exp(\hbar \Omega / K_B T) / [\exp(\hbar \Omega / K_B T) - 1]^2 \quad \dots (15)$$

For quantitative purposes, the authors consider that the Curie temperature changes with the electric field as suggested by Walter J. Merz [19], which is given by:

$$T'_c = T_c + \Delta T \text{ with } \Delta T = 1.9 \times 10^{-3} \times E$$

Where E is applied electric field in V/cm.

If the temperature is not too high, the temperature dependence of the soft mode frequency is given by:

$$\Omega_{k,T} \approx \{k(T - T_c)\}^{1/2} \quad \dots (16)$$

$$\Omega \approx \Omega_{k,E,T} \approx \Omega_{k,T} (E^2 + 1)^{1/2} (T - T'_c)^{1/2} / (T - T_c)^{1/2} \quad \dots (17)$$

Where T'_c is the changed Curie temperature in presence of electric field.

Thus the study of variation of soft mode frequency with temperature and applied electric field is necessary to study the variation of specific heat with temperature and applied electric field.

III. Results

Using Eqs (16) and (17), the soft mode frequency for all three crystals has been calculated for different temperatures in presence of external electric field. The variation of soft mode frequency with electric field at different temperatures for SrTiO₃, BaTiO₃, and KTaO₃ crystals is shown in Figs (1, 2 and 3) respectively. Soft mode frequency increases with increasing electric field and temperature. These results are in good agreement with the results of other researchers [8, 19, 20].

Specific heat at constant volume C_V of SrTiO₃, BaTiO₃ and KTaO₃ pure crystals has been calculated using Eq. (15) for different values of temperatures in presence of different electric fields. Curves of C_V against electric field for SrTiO₃, BaTiO₃ and KTaO₃ crystals at different temperatures are plotted in Figs (4, 5 and 6) respectively. It is observed from Figs (4, 5 and 6) that the specific heat increases with increase in temperature for all three crystals and for a constant temperature, the specific heat decreases with the increase in applied electric field for all three crystals.

IV. Discussion & Conclusions

Green's function technique and Dyson's equation treatment have been used to obtain an expression for the specific heat of SrTiO₃, BaTiO₃ and KTaO₃ perovskites in presence of an external electric field by using a model Hamiltonian in presence of higher order anharmonic and electric moment terms. The anharmonic coefficients and higher order electric moment terms give their contribution to various scattering processes.

It is observed from Eq (10) that the field dependence of specific heat is a clear consequence of the field dependence of the soft mode frequency. So in order to discuss the field dependence of specific heat of ferroelectric perovskite crystals, we shall first discuss the electric field dependence of the soft mode frequency. The soft modes, due to their large occupation number, should cause an appreciable scattering of other modes. It is the temperature-dependent soft mode and the process involving it, that give rise to effects peculiar to a ferroelectric material. The influence of electric field on this mode also affects the interaction

of soft modes with other modes, thus giving electric field dependence of various dynamic properties. The soft modes contribution to these properties is particularly important in the vicinity of T_C and is expected to give an anomalous behaviour. From eq. (10) it is clear that the soft mode frequency increases with the increase in applied electric field in conformity with the experimental results [18, 21]. Hence, this frequency is stabilized in the presence of electric field and anharmonicities. It is clear from Eqs (10), (11) and (12) that the presence of an applied electric field will increase the soft mode frequency and hence, will decrease the specific heat in conformity with the experimental results of Lawless [8]. Lawless [8] has described the field dependence of the soft mode using Lyddane-Sachs-Teller-Devonshire formalism [21], while we have described this electric field dependence by making use of a Hamiltonian proposed by Silverman and Joseph [22] and powerful thermal Green's function technique [12]. Also, the soft mode contribution to the specific heat is described by appropriate Einstein terms.

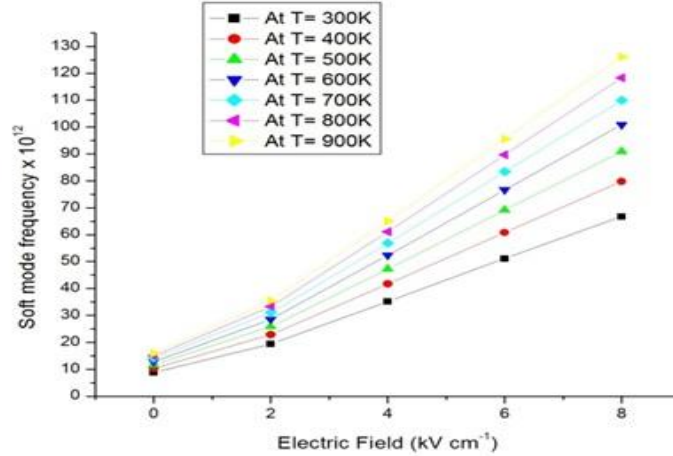


Fig. 1- Variation of soft mode frequency with electric field at different temperatures for SrTiO₃ crystal

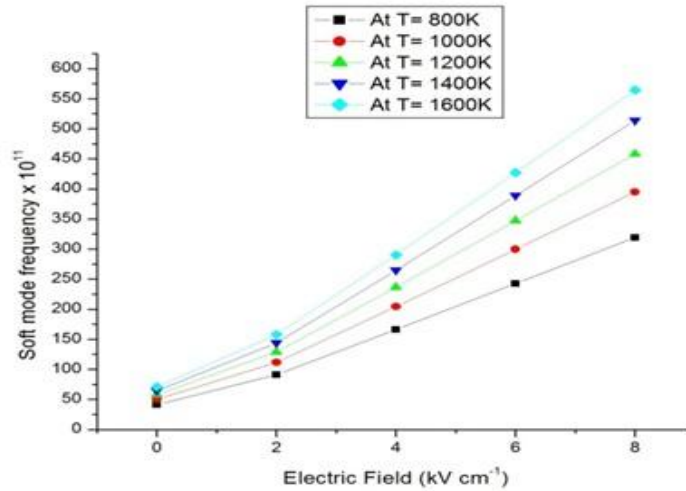


Fig. 2- Variation of soft mode frequency with electric field at different temperatures for BaTiO₃ crystal

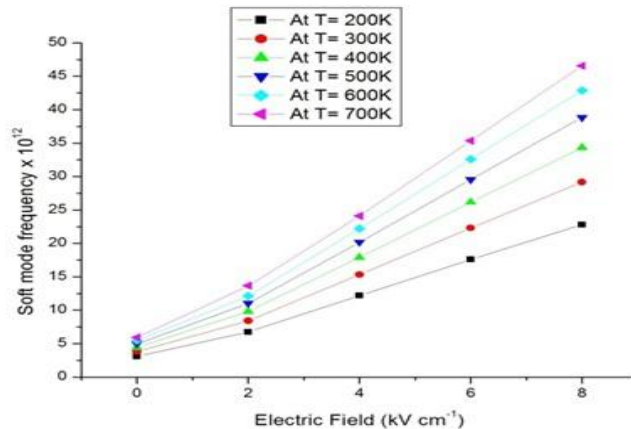


Fig. 3- Variation of soft mode frequency with electric field at different temperatures for KTaO₃ crystal

Figures (1, 2 and 3) show the variation of soft mode frequency with electric field at different temperatures for SrTiO₃, BaTiO₃ and KTaO₃ crystals respectively. The soft mode frequency increases with an increase in electric field. Taking any electric field as reference, the soft mode frequency increases with an increase in temperature. At low field's region, the temperature's effect is negligible for all the three crystals Fig. (1, 2 and 3).

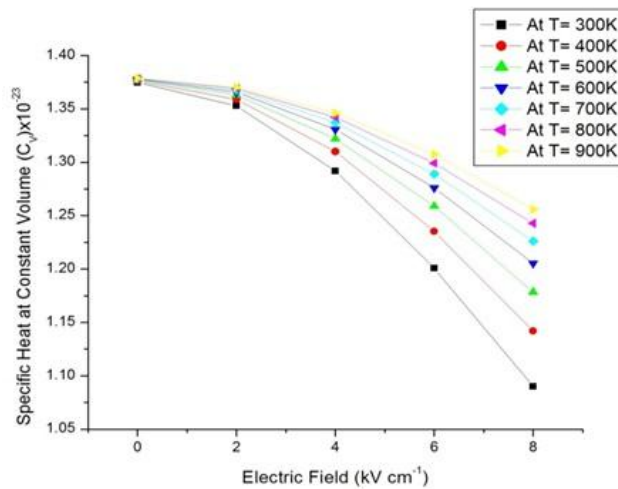


Fig. 4 – Specific heat at constant volume C_V versus electric field (in kV/cm) for SrTiO₃ at different temperatures

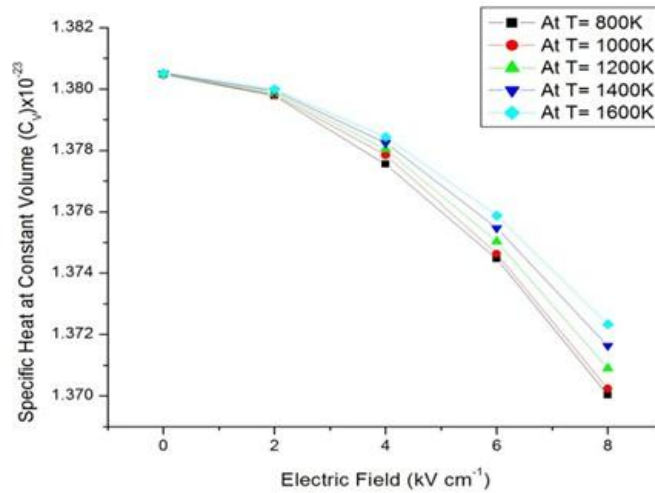


Fig. 5 – Specific heat at constant volume C_V versus electric field (in kV/cm) for BaTiO₃ at different temperatures

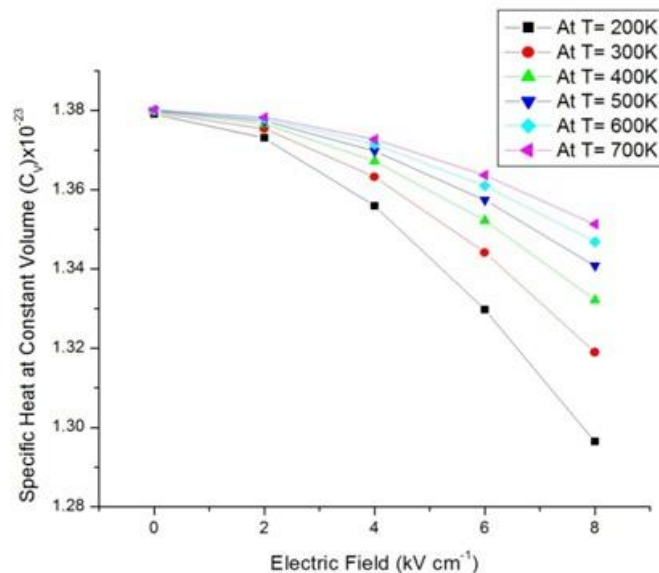


Fig. 6 - Specific heat at constant volume C_V versus electric field (in kV/cm) for KTaO₃ at different temperatures

Figures (4, 5 and 6) show the variation of specific heat with electric field at different temperatures for SrTiO₃, BaTiO₃ and KTaO₃ respectively. The specific heat at constant volume decreases with an increase in electric field. In low field region, the temperature's effect is negligible for all three crystals and the change in specific heat arises mainly due to higher anharmonic terms. Thus, our results are in good agreement with the experimental results obtained by Lawless [8] for ABO₃ type SrTiO₃ and KTaO₃ perovskites.

Strong phonon- phonon interactions due to vanishingly small frequency of the soft mode are held responsible for it. Anharmonicity is necessary in these crystals to observe these effects. Recently we have applied double time thermal Green's function technique in obtaining expression for electric field dependent inelastic scattering cross section of neutrons in BaTiO₃, SrTiO₃ and KTaO₃ displacive ferroelectric perovskites.[23]

REFERENCES

1. W. Cochran, Crystal Stability and the Theory of Ferroelectricity, *Physical Review Letters*, 3, 1959, 412-414.
2. E. F. Steigmeir, Field Effect on the Cochran Modes in SrTiO₃ and KTaO₃, *Physical Review*, 168(2), 1968, 523-530.
3. U C Naithani & B S Semwal, Electric field dependence of the Curie temperature and microwave absorption in displacive ferroelectrics with impurities, *Pramana- Journal of Physics*, 14(2), 1980, 149-158.
4. U C Naithani & B S Semwal, Sound attenuation in doped displacive ferroelectrics, *Pramana- Journal of Physics*, 11(2), 1978, 423-434.
5. W. N. Lawless, Specific heats of paraelectrics, ferroelectrics, and antiferroelectrics at low temperatures, *Physical Review B*, 14(1), 1976, 134-143.
6. P. Roedhammer, E. Gmelin and W. Weber, Influence of phonon anomalies on the specific heat of transition metal carbides, *Solid State Communications*, 16(10-11), 1975, 1205-1208.
7. I W Shepherd, Electrocaloric properties of OH⁻ molecules in KCl, *Journal of Physics and Chemistry of Solids*, 28(10), 1968, 2027-2036.
8. W. N. Lawless, Field-dependent specific heats and soft modes in KTaO₃ and SrTiO₃ at low temperatures, *Physical Review B*, 18(5), 1978, 2394-2396.
9. Masaharu Tokunaga, Rhodes- Wohlfarth ratio and anomalous specific heat in displacive type ferroelectrics, *Physica B: Condensed Matter*, 219, 1996, 587-589.
10. R Blinc & B Zesk, On the specific heat anomaly in ferroelectric Rochelle salt, *Physics Letters A*, 39(3), 1972, 167-168.
11. A. Kumar, U. C. Naithani & B. S. Semwal, Specific heat of Ba_xSr_{1-x}TiO₃ ferroelectric perovskites, *British Ceramic Transactions*, 103(4), 2004, 153-157.
12. U C Naithani and G N Baluni, Electric Field Dependence of Specific Heat of a Displacive Ferroelectric Crystal, *Indian Journal of Pure and Applied Physics*, 23, 1985, 261-266.
13. M B Salamon & P R Garnier, et al, Simultaneous measurement of the thermal diffusivity and specific heat near phase transitions, *Journal of Physics and Chemistry of Solids*, 35(7), 1974, 851-859.
14. Qing Pang, Jian Ming Zhang, Ke-Wei Xu and Vincent Ji, Structural, electronic properties and stability of the (1x1) PbTiO₃, *Applied Surface Science*, 255(18), 2009, 8145-8152.
15. George A Rossetti Jr and Nicola Maffei, Specific heat study and Landau analysis of the phase transition in PbTiO₃ single crystals, *Journal of Physics: Condensed Matter*, 17(25), 2005, 3953-3958.
16. L. W. Martin, Y. H Chu and R. Ramesh, Advances in the growth and characterization of magnetic, ferroele, *Material Science and Engineering: R: Reports*, 68(4), 2010, 89-133.
17. J. Tellier, B. Malic, B. Dkhil, D. Jenko, J. Cilensek and M. Kosec, Crystal structure and phase transitions of sodium potassium niob, *Solid State Sciences*, 11(2), 2009, 320-324.
18. J M Worlock & P A Fleury, Electric Field Dependence of Optical-Phonon Frequencies, *Physical Review Letters*, 19(20), 1967, 1176-1179.
19. Walter J. Merz, Double Hysteresis Loop of BaTiO₃ at the Curie Point, *Physical Review*, 91, 1953, 513-517.
20. R. F. Shaufele, M. J. Weber & B. D. Silverman, Electric field enhanced Raman scattering and frequency shift of the soft mode of SrTiO₃, *Physics Letters A*, 25(1), 1967, 47-48.
21. R. H. Lyddane, R. G. Sachs & E. Teller, On the Polar Vibrations of Alkali Halides, *Physical Review*, 59(8), 1941, 673-676.
22. B. D. Silverman and R. I. Joseph, Temperature Dependence of the Dielectric Constant of Paraelectric Materials, *Physical Review*, 129(5), 1963, 2062-2068.
23. Gaurav Kumar Aggarwal, Ashok Kumar and U.C. Naithani, Electric Field Dependent Inelastic Scattering Cross Section of Neutrons in BaTiO₃, SrTiO₃ and KTaO₃ Displacive Ferroelectric Perovskites, *International Journal of Physics and Applications*, 3 (2), 2011, 219-224.

Authors



Mr. Gaurav Kumar Aggarwal is pursuing D.Phil in Physics from H.N.B. Garhwal University, Srinagar, Uttarakhand, India. He received his M.Sc. degree in Physics from H.N.B. Garhwal University. His area of interest is Condensed Matter Physics and Electronics. He is actively involved in teaching and research. His field of research is ferroelectric materials particularly displacive ferroelectric perovskites.



Dr. Ashok Kumar obtained his PhD in Physics from H.N.B. Garhwal University, Srinagar, Uttarakhand, India. His area of interest is Condensed Matter Physics. He is actively involved in theoretical research in the field of ferroelectrics. He has published more than 30 research papers in reputed journals. His recent research is focused on designing and development of ferroelectric-perovskites.



Prof. U.C. Naithani presently holds the chair of Professor and Head, Deptt. of Physics, H.N.B. Garhwal University, Pauri Campus, Pauri, Uttarakhand, India. He did his PhD in Condensed Matter Physics. He is actively engaged in teaching and research since last 37 years. His major field of research is in the area of dielectric materials particularly ferroelectric perovskites. He has produced a dozen of PhD scholars and more than 70 research papers are to his credit in this field.

Cyclic Redundancy Check Generation Using Multiple Lookup Table Algorithms

Indu I¹, Manu T S²

*PG Scholar, Dept. of Electronics and Communication Engineering, TKM Institute of Technology, Kollam, affiliated to Cochin University of Science and Technology, Kerala, India.

**Asst. Professor, Dept. of Electronics and Communication Engineering, TKM Institute of Technology, Kollam, affiliated to Cochin University of Science and Technology, Kerala, India.

ABSTRACT: The primary goal of this paper is to generate cyclic redundancy check (CRC) using multiple lookup table algorithms. A compact architecture of CRC algorithm (Slicing-by-N algorithm) based on multiple lookup tables (LUT) approach is proposed. This algorithm can ideally read large amounts of data at a time, while optimizing their memory requirement to meet the constraints of specific computer architectures. The focus of this paper is the comparison of two algorithms. These two algorithms are Slicing by-N-algorithm and Sarwate algorithm, in which slicing by-N-algorithm can read arbitrarily 512 bits at a time, but Sarwate algorithm, which can read only 8 bits at a time. This paper proposes the generation of CRC using slicing by 8 algorithm. In this, message bits are chunked to 8 blocks. All are processed at a time. Proposed Slicing-by-8 algorithm can read 64 bits of input data at a time and it doubles the performance of existing implementations of Sarwate algorithm.

Keywords: CRC, LUT, Slicing-by-N.

I. Introduction

Cyclic Redundancy Check (CRC) is one of the methods of detecting the errors in the information during transmission. CRC is an error-checking code that is widely used in data communication systems and other serial data transmission systems [10]. CRC are used for detecting the corruption of digital content during its production, transmission, processing or storage. CRC algorithms treat each bit stream as a binary polynomial and calculate the remainder from the division of the stream with corresponding to the remainder is transmitted together with the bit stream. At the receiver side, CRC algorithms verify that the correct remainder is has been received. Long division is performed using modulo-2 arithmetic [3].

CRC is a polynomial-based block coding method for detecting errors in blocks or frames of data. A set of check digits is computed for each frame scheduled for transmission over a medium that may introduce error and is appended to its end. The computed check digits are known as the frame check sequence (FCS). A CRC value is calculated as a remainder of the modulo-2 division of the original transmitted data with a specific CRC generator polynomial. For example, Ethernet uses the 32-bit polynomial value,

$$G(x) = 1 + x + x^2 + x^4 + x^5 + x^7 + x^8 + x^{10} + x^{11} + x^{12} + x^{16} + x^{22} + x^{23} + x^{26} + x^{32} \quad (1)$$

To find the FCS, first a number of zeroes equal to the number of FCS digits to be generated are appended to the message $M(x)$. This is equivalent to multiplying $M(x)$ by 2^n , where "n" is the number of FCS digits. This value is then divided by the generator polynomial $G(x)$ (1), which contains one more digit than the FCS. The division uses modulo-2 arithmetic, where each digit is independent of its neighbour and numbers are not carried or borrowed, thus additions and subtractions are performed via an exclusive-OR (XOR) function. The remainder $R(x)$ is appended to the end of the message before transmission. At the receiver, the message plus the FCS is divided by the same polynomial. If the remainder is zero then it can be assumed that no error has occurred [2].

To accelerate the CRC generation process, a number of algorithms have been proposed. Among these algorithms the most commonly used today is the algorithm proposed by Sarwate. The Sarwate algorithm reads 8 bits at a time from stream and calculates the CRC value by performing lookups on a table of 256 32-bit entries [4]. Looking to overcome limitations of processing 8 bits of data at a time, new algorithm have been proposed [4] and they can read arbitrarily large amount of data at a time.

Recently time is the major concern. So in order to process large amount of data at a time, Multiple Lookup based approach is more efficient. Multiple Lookup based approach contains five CRC algorithms, called Slicing by-N algorithm ($N \in 4, 8, 16, 32, 64$), which is used to read up to 512 bits at a time. So performance of the system should be increased. Here proposing Slicing by-8 algorithm to read 64 bits at a time. Here proposed an efficient design of CRC generator using Slicing by-N algorithm ($N=8$). In this algorithm, input message stream is sliced into N slices and each slice has 8 bits. So using this Slicing by-8 algorithm, it can read 64 bits at a time and it triples the performance of existing implementation of Sarwate algorithm. In this algorithm, input data stream is sliced into 8 slices. Each slice has 8 bits and these total 64 bits are processed at a time. In this design 8 Look Up tables (LUT) are used, which contain the pre-computed CRC values. These CRC values are generated by using LFSR method and 256 combinations of CRC values corresponding to 8 bit input stream are generate. In this work CRC32 standard is used. Each slice returned CRC values from each LUT and all are XORed to get the final CRC value. This algorithm can reduce the memory usage and also number of operations significantly reduces compared to Sarwate algorithm.

II. System Architecture

Cyclic Redundancy Check is an error detecting codes that are widely used due to their capability to detect the alteration of data. Different algorithms are used for generating CRC. Existing algorithms are LFSR method and Sarwate algorithm. Here proposing an algorithm, this has five algorithms, called Slicing by-N algorithm which is used to generate CRC fastly. Every CRC algorithm treat input bit stream as a binary polynomial and calculate the remainder from the division of the stream with standard generator polynomial. In this work CRC32 standard is used as a generator polynomial. The binary words corresponding to the remainder are transmitted together with input stream. In this work slicing by-8 algorithm is used to generate CRC and it can read 64 bits at a time.

The main disadvantage of existing table-driven CRC generation algorithms is their memory space requirement when reading a large number of bits at a time. To solve this problem, a new algorithm that slices the CRC value produced in every iteration as well as the data bits read into small terms. These terms are used as indexes for performing lookups on different tables in parallel. For example, Slicing-by-4 algorithm can read 32 bits of input data at a time and it doubles the performance of existing implementations of Sarwate algorithm, while Slicing-by-8 triples the performance and reads 64 bits of input data at a time. In this way, here proposed algorithm is capable of reading 64 bits at a time, as opposed to 8, while keeping its memory space requirement to 8KB.

2.1 General Block Diagram of CRC Generation

The basic block diagram of CRC generator is shown in fig.1.

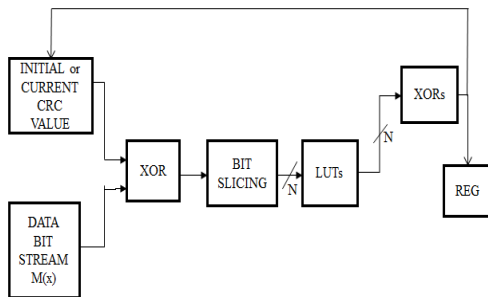


Fig.1 Block diagram of basic CRC Generator.

In this CRC generator, the data stream is firstly XORed with initial CRC value. In this work CRC32 standard is used as a generator polynomial. In the case of CRC32 standard, the initial CRC value is 0xFFFFFFFF [1] and other cases, that is, in other CRC standard initial CRC value is cleared. The output of the XOR block is then sliced into N slices and each slice has 8 bits. Each is given to each LUT for calculating the CRC value. Numbers of LUTs are same to N. Using this Slicing by-N algorithm up to 512 bits are processed at a time, that is, this Slicing by-N algorithm composed of five algorithms (N ∈ 4, 8, 16, 32, 64) in which fifth algorithm is used to read 512 bits at a time.

2.2 Block Diagram of CRC Generator Using Slicing By-8

Here proposing CRC generation using slicing by-8 algorithm which is used to read 64 bits at a time. The block diagram of Slicing by-8 algorithm is shown in fig.2 is

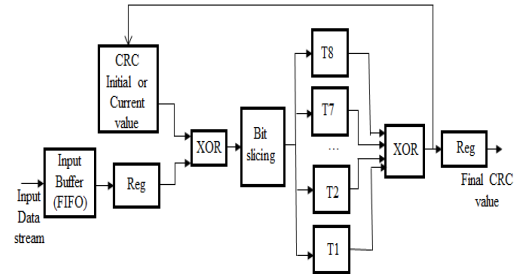


Fig.2 Block diagram of CRC Generator using Slicing by-8 Algorithm

In this, primarily the input data stream is stored in Buffer and buffer has size five and each location is 64 bit wide. Initially first 64 bit data is taken and it is XORed with initial CRC value. Here using CRC32 standard and its initial value is 0xFFFFFFFF. So the modified bit stream is got. This bit stream is sliced into 8 slices and each has 8 bit long. Each 8 bit data is given to each LUT. LUTs have the pre-computed CRC values. These LUTs have 256 entries with 32 bit wide, that is, 8 bit data has 28 (= 256) combinations of values, each has its own CRC value. The CRC value corresponding to each bit stream is getting from each LUT. Finally all CRC values are XORed to get the final CRC value.

2.2.1 Slicing-by-8 Algorithm Description

In this CRC generation process the pre computed value of CRC first stored in LUTs. The long division process is to pre-compute the current remainder that results from a group of bits and place the result in a table. Before the beginning of the long division process all possible remainders which result from groups of bits are pre-computed and placed into a Look up Table. In this way, several long division steps can be replaced by table lookup step. The benefit from slicing comes from the fact that modern processor architectures comprise large cache units. These cache units are capable of storing moderate size tables. If tables are stored in an external memory unit, the latency associated with accessing these tables may be significantly higher than when tables are stored in a cache unit. Slicing is also important because it reduces the number of operations performed for each byte of an input stream when compared to Sarwate. For each byte of an input stream the Sarwate algorithm performs the following: (i) an XOR operation between a byte read and the most significant byte of the current CRC value; (ii) a table lookup; (iii) a shift operation on the current CRC value; and (iv) an XOR operation between the shifted CRC value and the word read from the table. In contrast, for every byte of an input stream the Slicing by-8-algorithm performs only a table lookup and an XOR operation. This is the reason why the Slicing-by-8 algorithm is faster than the Sarwate algorithm.

Slicing by-N algorithm says that the current input stream is XORed with the current CRC and then the modified stream is produced. This modified stream is then sliced into N slices and each has one byte wide. Each slice

is given to the LUTs, which have the pre-computed CRC values. Output of these LUTs is then XORed to get the current CRC. Initially CRC value is 0xFFFFFFFF. Here slicing by-8 algorithm is explained. The steps of this algorithm as follows:

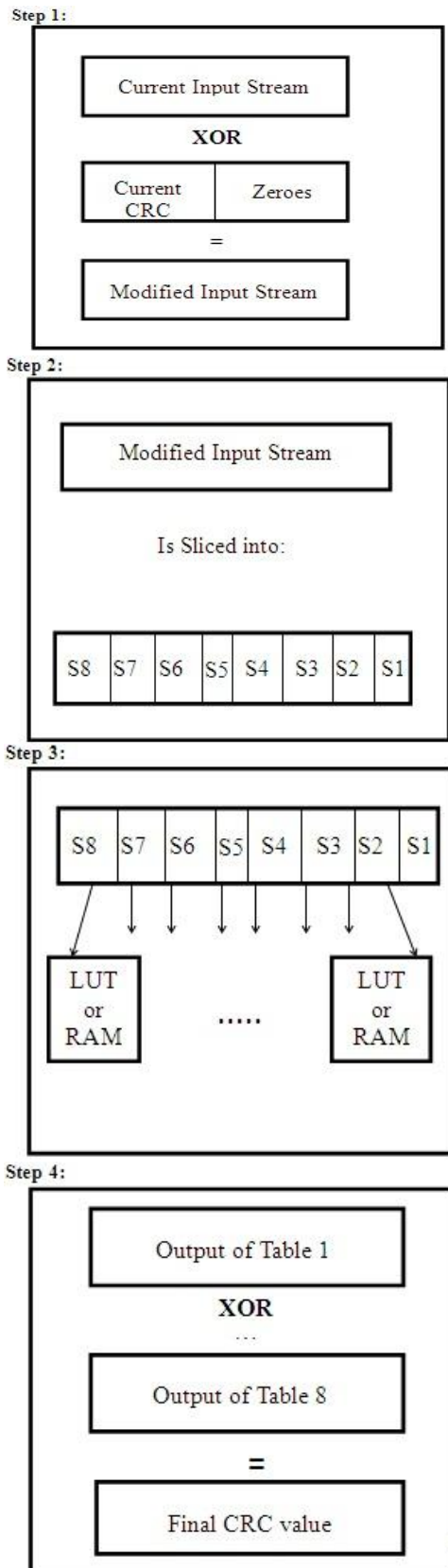


Fig.3 The Slicing by-8 Algorithm

These steps explain how this algorithm works in CRC generators. In the first step, the current input stream is XORed with the current CRC value. The input stream is 64 bit wide and CRC value is 32 bit wide. In order to perform XOR operation, 32 bit wide zeroes is appended to the current CRC value and is XORed with input stream. The modified bit is produced as output. In the second step this modified bit stream is sliced into eight slices. In the third step, each slice is given to LUTs as input and CRC value corresponding to input is produced from LUTs. In the fourth step, these outputs are XORed to get final CRC value.

2.3 Block Diagram of CRC Generator Using Sarwate Algorithm

Here explains the CRC generation using Sarwate algorithm which is used to process only 8 bit at a time. A more efficient approach to CRC computation in software was described by Sarwate [2]. This technique uses a table of pre computed effects on the shift register of 8-bit bytes, which allows the computation to run at one cycle per byte (instead of one cycle per bit) [4]. The long division process is a compute-intensive operation because it requires in the worst case one shift operation and one XOR logical operation for every bit of a bit stream. Most software-based CRC generation algorithms, however, perform the long division process quicker than the bit-by-bit marking technique. One commonly used technique for accelerating the long division process is to pre-compute the current remainder that results from a group of bits and place the result in a table. In this way, several long division steps can be replaced by a single table lookup step [3] [6].

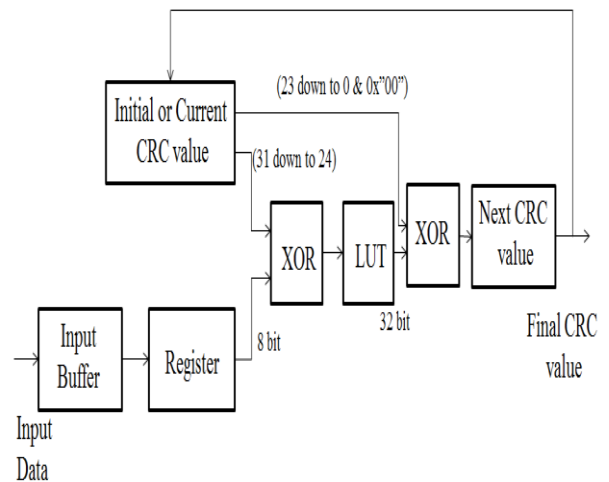


Fig.4 Block diagram of CRC Generator using Sarwate Algorithm

In both Sarwate algorithm and Slicing by 8 algorithms, Look Up Table is used for storing the 2^8 combinations of CRC values. These CRC values are computed using long division process. Long division steps are explained above. Initially the CRC value is set to 0xFFFFFFFF. The first 8 bit from the input stream is taken and is XORed with most significant 8 bits of the initial CRC value. This modified byte is given to the LUT, it produce the corresponding CRC value. It is finally XORed with the 24 least significant bits of the current CRC value, shifted by 8 bit positions to the left, which produce the next CRC value and this CRC value is used for next iteration.

2.3.1 Sarwate Algorithm Description

The most representative table-driven CRC generation algorithm used today is the algorithm proposed by Dilip.V.Sarwate. The length of the CRC value generated by the Sarwate algorithm is 32 bits. The Sarwate algorithm is more complicated than the straightforward lookup process because the amount of bits read at a time (8 bits) is smaller than the degree of the generator polynomial. Initially, the CRC value is set to a given number which depends on the standard implemented (e.g., this number is 0xFFFFFFFF for CRC32) [1]. For every byte of an input stream the algorithm performs the following steps:

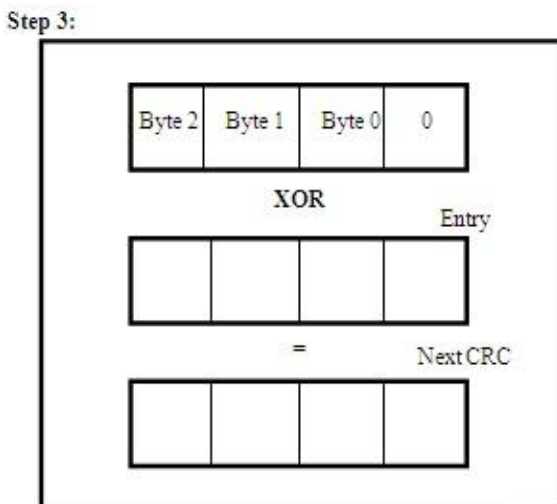
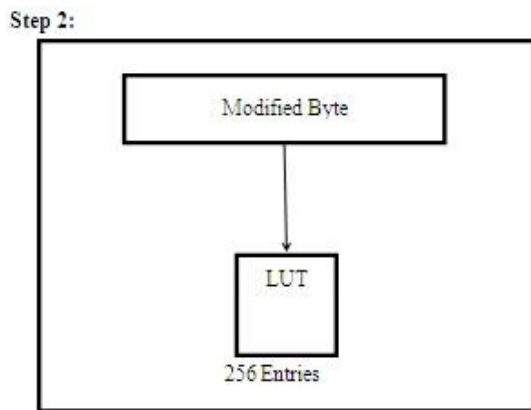
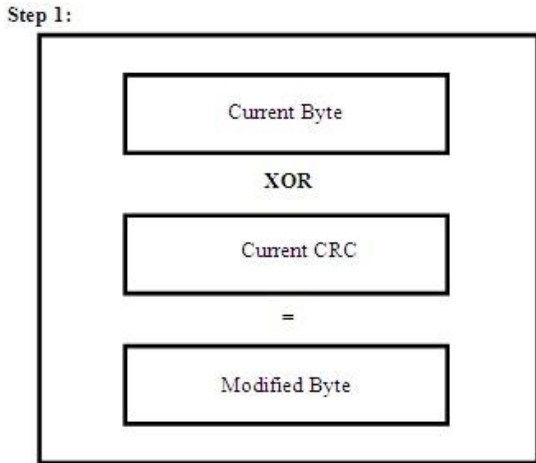


Fig.5 Sarwate Algorithm

In first step, the algorithm performs an XOR operation between the most significant byte of the current CRC value and the byte from the stream which is read. The 8-bit number which is produced by this XOR operation is used as an index for accessing a 256 entry table (Step 2). The lookup table used by the Sarwate algorithm stores the remainders from the division of all possible 8-bit numbers shifted by 32 bits to the left with the generator polynomial. The value returned from the table lookup is then XORed with the 24 least significant bits of the current CRC value, shifted by 8 bit positions to the left (Step 3). The result from this last XOR operation is the CRC value used in the next iteration of the algorithm's main loop. The iteration stops when all bits of the input stream have been taken into account.

Sarwate algorithm has been designed when computer architectures supported XOR operation with only eight bits. Today's processors support operations with 32 and 64 bits values, and if this algorithm is extended it would require lookup tables of $2^{32} = 4G$ entries for processing 32 bits of data at a time, and $2^{64} = 16G$ for 64 input data. These tables can't fit into a cache and would cause significant latency problem if in RAM.

III. 3. Simulation Results

The simulation was done using Modelsim PE 10.0c Simulator and the output waveforms is obtained as shown in fig. 6, 7,8,9,10. Slicing by-N algorithm is one of the CRC algorithms, which is used to read up to 512 bits at a time. It is Multiple Look Up based approach that is, in this N LUTs are used. In this paper, Slicing by-8 algorithm is used which it is used to read 64 at a time. Each 64 bits are sliced into 8 slices and each slice has 8 bits. In this algorithm 8 LUTs are used. Each slice is given to each LUT and these LUTs contain all 2^8 combinations of CRC values. Outputs of LUTs are CRC values corresponding to each slice and all outputs from LUTs are XORed to get final CRC value. Similarly Sarwate algorithm is used to read 8 bits at a time and in this, only one LUT is used for iteration.

3.1 Simulation waveforms

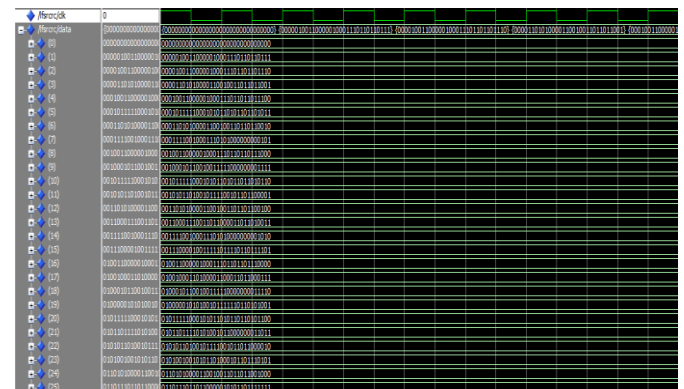


Fig.6 256 Combinations of CRC Using LFSR Method

Fig.6 shows the 256 combinations of CRC is generated using LFSR method in VHDL. In this, initially reset ('rst') is '1', all are cleared. After that, reset is '0', and calculating each CRC corresponding bits from "00000000" to "11111111". These are getting from the signal 'data'.

```

Editor - D:\mat-pgm\crc1.txt
1 [0 0 0 0 0 0 0 0 0 0 0 0 0 0 0 0 0 0 0 0 0 0 0 0 0 0 0 0 0 0 0 0]
2 [0 0 0 0 0 0 1 0 0 1 1 0 0 0 0 0 0 1 0 0 0 0 1 1 1 0 0 1 1 0 0 1 1 1]
3 [0 0 0 0 0 1 0 0 1 1 0 0 0 0 0 0 1 0 0 0 0 1 1 1 0 0 1 1 0 0 1 1 0 1]
4 [0 0 0 0 0 1 1 0 1 0 1 0 0 0 0 0 1 1 0 0 0 1 0 0 1 1 0 0 1 1 0 0 1 1]
5 [0 0 0 1 0 0 0 1 1 0 0 0 0 0 0 1 0 0 0 0 1 1 1 0 0 1 1 0 0 1 1 0 0 1]
6 [0 0 0 1 0 0 1 1 1 1 1 0 0 0 0 1 0 0 1 1 0 0 1 0 0 1 1 0 0 1 1 0 0 1]
7 [0 0 0 1 1 0 1 0 1 0 0 0 0 0 1 1 0 0 1 0 0 1 1 0 1 1 0 1 1 0 0 1 0]
8 [0 0 0 1 1 1 1 0 0 0 1 0 0 0 1 1 1 0 1 0 1 0 0 0 0 0 0 0 0 0 1 0 1]
9 [0 0 1 0 0 1 1 0 0 0 0 0 1 0 0 0 0 1 1 1 0 1 1 0 1 1 0 1 1 1 0 0 0]
10 [0 0 1 0 0 0 0 1 0 1 1 0 0 0 1 0 0 1 1 1 1 1 0 0 0 0 0 0 0 0 1 1 1]
11 [0 0 1 0 1 1 1 1 1 1 0 0 0 1 0 1 0 1 1 0 0 1 0 1 0 1 0 1 0 1 0 1 0]
12 [0 0 1 0 1 0 1 0 1 1 0 0 0 1 0 1 1 1 1 0 0 0 1 0 1 0 1 1 0 0 0 0 1]
13 [0 0 1 1 0 1 0 1 0 0 0 0 0 1 1 0 0 0 1 0 0 1 1 0 1 1 0 1 1 0 0 0 0]
14 [0 0 1 1 0 0 0 0 1 1 1 0 0 1 1 0 1 1 0 0 0 0 0 1 1 0 1 1 0 1 0 0 1]
15 [0 0 1 1 1 1 0 0 0 1 0 0 0 0 1 1 1 0 1 0 1 0 0 0 0 0 0 0 0 0 1 0 1]
16 [0 0 1 1 1 0 0 0 0 0 1 0 0 0 1 1 1 1 1 0 1 1 1 1 0 1 1 0 1 1 1 0 1]
17 [0 1 0 0 1 1 1 0 0 0 0 0 0 1 0 0 0 0 1 1 1 0 1 1 0 1 1 0 1 1 1 0 0 0]
    
```

Fig.7 256 Combinations of CRC values using MATLAB

Fig.7 shows 256 combinations of 32-bit CRC values can be generated by MATLAB. Using MATLAB, generated these CRCs by using the ‘Deconv’ function. This function is used for polynomial division. By dividing the input stream with the standard generator polynomial, which is 33-bits, getting the remainder which is 32 bit long. These generated CRC values are stored in a text file by generating a text file using ‘file generate’ and ‘file write’ functions.



Fig.8 Comparison output for CRC values

The comparison result of CRC generation using MATLAB and LFSR method got the same. Ie, generated CRC values using LFSR method is cross verified by MATLAB. This comparison gives the result that the CRC values produced by LFSR method are correct.

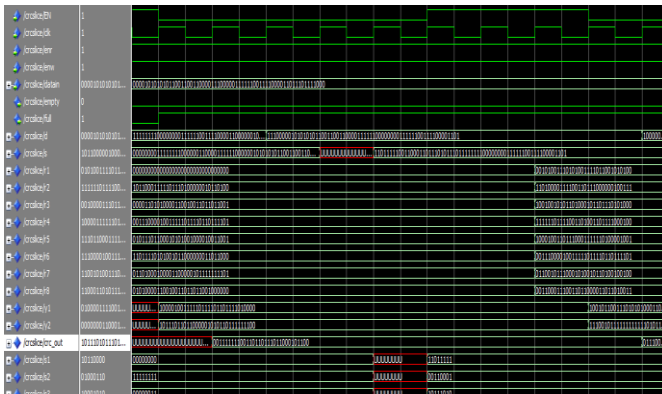


Fig.9 Output of CRC generation using Slicing by 8 Algorithm

Fig.9 shows the simulation result of CRC generation using Slicing by 8 algorithm. This result shows that the initial 64 bit from the input stream is taken and is modified with current CRC value by XORing. This output is given at the signal ‘s’. this output is slices into 8 slices, which is given at signal s1-s8. These output is given to each LUTs. This LUT produced corresponding CRC values of each byte(8 bytes), which is given at the signal ‘r1-r8’ and all are XORed to get next CRC value which is used for next iteration. This final CRC value is indicated by the signal ‘crc_out’.

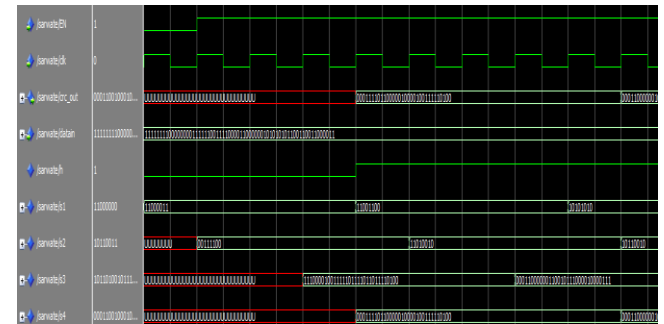


Fig.10 Output of CRC Generation Using Sarwate Algorithm

Fig.10 shows the simulation result of CRC generation using Sarwate algorithm. In this, the initial 8 bit data from the input message stream is taken (‘s1’) which is XORed with initial CRC value (0XFFFFFFF), ie, in this result if h is ‘low’ then the message bit is XORed with initial value and if h is ‘high’, then the input is XORed with MSB bit of current CRC value. This modified bit is indicated by the signal ‘s2’. This modified bit is given to LUT. In this, only one LUT is used for storing the pre computed CRC values. This LUT produce corresponding CRC value. This output is indicated by the signal ‘s3’. This output is XORed with 24 least significant bits of the current CRC value which is shifted by 8 bit positions to the left. This is the next CRC value. It is indicated by the signal ‘s4’. This CRC output is used for next iteration to get the modified bit and finally get the correct CRC value. This final CRC output is indicated by the signal ‘crc_out’.

IV. Synthesis Results

4.1 Comparison of Device Utilization

This comparison results explain how much amount of area are required for different algorithms.

4.1.1 Device Utilization Summary of Slicing by 8 and Sarwate Algorithm with 64 bit Input Stream

Device Utilization Summary (estimated values)			
Logic Utilization	Used	Available	Utilization
Number of Slices	183	4656	3%
Number of Slice Flip Flops	202	9312	2%
Number of 4 input LUTs	246	9312	2%
Number of bonded IOBs	98	232	42%
Number of BRAMs	1	20	5%
Number of GCLKs	1	24	4%

Fig.11 Device Utilization Summary of Sarwate Algorithm with 64 bit data

Device Utilization Summary (estimated values)			
Logic Utilization	Used	Available	Utilization
Number of Slices	238	4656	5%
Number of Slice Flip Flops	416	9312	4%
Number of 4 input LUTs	96	9312	1%
Number of bonded IOBs	98	232	42%
Number of BRAMs	4	20	20%
Number of GCLKs	1	24	4%

Fig.12 Device Utilization Summary of Slicing by 8 Algorithm with 64 bit data

These two summaries shows that number of slices used by Slicing by 8 algorithm is lightly greater compared to Sarwate algorithm, ie, 3% of slices are used in Sarwate algorithm and 5% of slices are used in Slicing by 8 algorithm. But the usage of 4-input LUTs are less in Slicing by 8 algorithm compared to Sarwate algorithm, ie, 2% of 4-input LUTs are used in Sarwate algorithm and 1% in Slicing by 8 algorithm. And IOB usage is same in Slicing by 8 algorithm and Sarwate algorithm, ie, 42% of IOBs are used.

4.1.2 Device Utilization Summary of Slicing by 8 and Sarwate Algorithm with 512 bit Input Stream

Device Utilization Summary (estimated values)			
Logic Utilization	Used	Available	Utilization
Number of Slices	253	4656	5%
Number of Slice Flip Flops	275	9312	2%
Number of 4 input LUTs	384	9312	4%
Number of bonded IOBs	102	232	43%
Number of BRAMs	1	20	5%
Number of GCLKs	1	24	4%

Fig.13 Device Utilization Summary of Sarwate Algorithm with 512 bit data

Device Utilization Summary (estimated values)			
Logic Utilization	Used	Available	Utilization
Number of Slices	310	4656	6%
Number of Slice Flip Flops	492	9312	5%
Number of 4 input LUTs	234	9312	2%
Number of bonded IOBs	102	232	43%
Number of BRAMs	4	20	20%
Number of GCLKs	1	24	4%

Fig.14 Device Utilization Summary of Slicing by 8 Algorithm with 512 bit data

These two summaries also gave the same comparison result with the input is 512 bits. Usage of 4-input LUTs are less and usage of slices are more in Slicing by 8 algorithm compared to Sarwate algorithm. 5% of slices are used in Sarwate algorithm and 6% in Slicing by 8 algorithm. 4% of 4-input LUTs are used in Sarwate algorithm and 2% in Slicing by 8 algorithm.

The above two comparisons, ie, for 64 bits and for 512 bits, the result shows that for 64 bits of data, number of slices used by Slicing by 8 is 2% greater compared to Sarwate algorithm and for 512 bits of data, number of slices used by slicing by 8 is only 1% greater compared to Sarwate algorithm. This result explains that by increasing the number of bits processed, number of slices used in Slicing by 8 algorithm is reduced compared to Sarwate algorithm. Also these two summaries explains that number of 4-input LUTs used by Sarwate algorithm is twice greater than Slicing by 8 algorithm.

4.2 comparison of time consumption

Fig.15 shows the comparison graph of time consumption. This graph clearly says that CRC generator with Slicing by 8 algorithm consume less time compared to Sarwate Algorithm and LFSR method. Slicing by 8 algorithm have minimum delay compared to other algorithms.

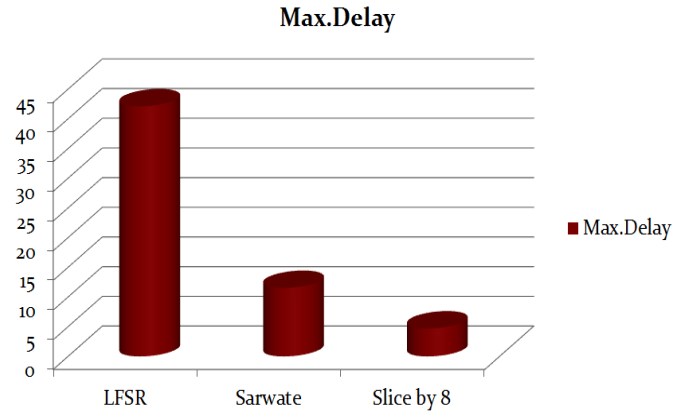


Fig.15 comparison of time delay

The below table clearly explains the comparison of different Algorithms for CRC generation purposes.

Algorithm\Data	Number of Slices	Number of 4-Input LUTs	Number of IOBs	Maximum delay
LFSR Method	1258	2301	43	42.142
Sarwate	253	384	102	11.56
Slice by 8	310	234	102	3.455

TABLE.1 Comparison of Device Utilization

4.3 Graphical Representation of Comparison Results

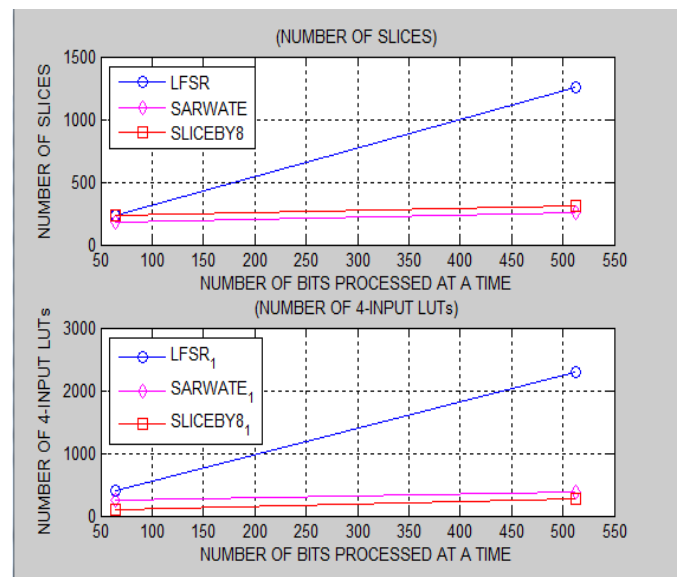


Fig.16 Graphical Representation of Comparison of Device Utilization using MATLAB

Fig.16 shows the graphical representation of comparison results of device utilization in different CRC generation methods. The first graph represents the number of slices used by LFSR, Sarwate, Slicing by 8 methods. This graph shows that slices used by LFSR are very much higher than Sarwate and Slicing by 8. The first graph represents the number of slices utilized by LFSR, Sarwate and Slicing by 8 for, 64 bits processed and also 512 bits processed. The second graph represent the number of 4-input LUTs. This graph also shows that LFSR method is high area consuming method. The second graph represents the number of 4-input LUTs are utilized by LFSR, Sarwate, Slicing by 8 in the case of both 64 bits processing and 512 bits processing.

V. Conclusion

The design of CRC generator using Multiple Look Up based approach is proposed. In this paper, slicing by-8 algorithm is designed, and compares this algorithm with the existing algorithms, that is, with Sarwate algorithm and LFSR method. In this work, first generated the CRC values using LFSR method and generated all 256 combinations of CRC using LFSR method. In this work, also generated these 256 combinations of CRC values using MATLAB. Outputs produced from MATLAB and LFSR method is cross verified. This clearly explains that these two CRC values are same. Designed Look Up Table (LUT) and stored all CRC values in the LUT. LUT contains 256 entries with 32 bit. The input stream is firstly stored in a buffer. In a buffer, five locations with each location has 64 bit wide. These 64 bit data is sliced into eight slices and each is given to each LUT. CRC values are generated from each LUTs corresponding to input stream and all are XORed and get the final CRC value. In this work CRC-32 is used for generating CRC values. So Slicing by-N algorithm can read arbitrarily large amount of data at a time that is used to reduce the time requirement. So this method is applied to CRC generator with Slicing by-N algorithm will be proposed in iSCSI (internet Small computer system interface).

Acknowledgement

We would like to thank the Principal, HOD and all the teaching and non-teaching staffs of TKM Institute of Technology for helping to complete the work as mentioned in the paper.

References

- [1] Amila Akagic, Hideharu Amano. "Performance Evaluation of Multiple Lookup Tables Algorithms for generating CRC on an FPGA", 1st International Symposium on Access Spaces (ISAS), IEEE-ISAS 2011.
- [2] C. Toal, K. McLaughlin, S. Sezer, and Xin Yang. "Design and Implementation of a Field Programmable CRC Circuit Architecture". *Very Large Integration (VLSI) Systems, IEEE Transactions on*, aug. 2009.
- [3] F. L. Berry M. E. Kounavis., "A Systematic Approach to Building High Performance Software-Based CRC Generators". In *ISCC '05: Proceedings of the 10th IEEE Symposium on Computers and Communications*, pages2, 2005.

- [4] Michael E. Kounavis, Frank L. Berry, "Novel Table Lookup-Based Algorithms for High-Performance CRC Generation", *IEEE transactions on Computers*, vol. 57, november 2008
- [5] S.M. Joshi, P.K. Dubey, and M.A. Kaplan. "A new parallel algorithm for CRC generation". In *Communications, IEEE International Conference*, pages 1764–1768 vol.3, 2000.
- [6] Abhijeet Joglekar, Michael E. Kounavis, and Frank L. Berry. "A scalable and high performance software iSCSI implementation". *Proceedings of the 4th conference on USENIX Conference*, page 20, 2005.
- [7] Yan Sun, Min Sik Kim. "A Pipelined CRC Calculation Using Lookup Tables", *IEEE Communications Society subject matter experts for publication in the IEEE CCNC 2010 proceedings*.
- [8] J. Bhasker. "AVHDL Primer", Prentice Hall, 2007.
- [9] Kennedy, Davis. "Electronic Communication Systems", Tata McGraw Hill, 1999.
- [10] C. Borrelli. *IEEE 802.3 Cyclic Redundancy Check*. http://www.xilinx.com/support/documentation/application_notes/xapp209.pdf.

ABOUT AUTHORS



Ms.Indu.I¹ has M.Tech in VLSI and Embedded systems from Cochin University of Science and Technology (CUSAT) and B.Tech in Electronics and Communication from CUSAT and now she is working as an Assistant professor of Electronics and Communication Department in Sree Buddha College of Engineering for Women, Ayathil, Pathanamthitta, which is an affiliated engineering college under Mahatma Gandhi University.



Mr.Manu.T.S² has M.Tech in Embedded systems and B.Tech in Electronics and Communication and he is working as an Assistant professor of Electronics and Communication Department in TKM Institute of Technology, Kollam, an affiliated engineering college under Cochin University of Science and Technology for last two years, Asst. Prof. Manu T.S has guided over 25 students for their academic project ,seminars and mini projects throughout his career and he undergone many training programs in VLSI and Embedded systems .He presented and Published Papers related to FPGA designs in National and International Conferences and Journals.

Zinc Oxide Nanorods: Synthesis and Its Applications in Solar Cell

Chittaranjan Bhakat¹, Prasoon Pal Singh²

* (School of Interdisciplinary Science and Technology, International Institute of Information Technology, India)

** (School of Interdisciplinary Science and Technology, International Institute of Information Technology, India)

ABSTRACT: *Nanosized materials have been an important subject in basic and applied sciences and these metal nanoparticles have been intensively studied within the past decade. Synthesis of hexagonal shape zinc oxide nanorods is achieved by thermal decomposition process. The sample was characterized by uv-vis spectrophotometer, X-ray diffraction Scanning electron microscope. Zinc Chloride (ZnCl₂) was used as precursor with sodium hydroxide (NaOH) in 1:2 molar ratios for the preparation of zinc oxide nanoparticles by the wet chemical method. Further its application in solar cell. The results indicate that the as-prepared ZnO Nano-rods are uniform with diameters of 100–200 nm and lengths of about 1 μm*

Keywords: *Nanostructures, Chemical Synthesis, UV spectroscopy, SEM, XRD, Solar cell*

I. INTRODUCTION

Nanotechnology is an emerging, highly interdisciplinary field; it has the ability to manipulate matter at an atomic scale. Nanotechnology can be useful in diagnostic techniques, drug delivery, sunscreens, antimicrobial bandages, disinfectant, and a friendly manufacturing process that reduce waste products. Nanorods and nanowires have recently attracted considerable attention towards scientific community because of their novel properties and potential technological applications; it is widely used in the field of catalyst [1], gas sensor [2], solar cell materials [3], antimicrobial materials [4], optoelectronics devices [5,6] etc. ZnO is as wide band gap (3.37eV) compound semiconductor materials with a large exciton binding energy of 60 meV, among several oxides semiconductor ZnO nanostructures is considered to be the best, it is clearly demonstrated in many studies that nanoparticles of ZnO have significantly higher antimicrobial effects than other metal oxide nanoparticles [7]. Currently, different nanostructure of ZnO have been reported such as nanorods, nanowires, nanocombs, nanorings, nanobridge, nanobelts, nanocages [8,9], etc and these nanostructures have potential applications in fabricating functional advanced Nano electronics devices. And a wide variety of techniques have been exploited to fabricate ZnO nanostructures. ZnO nanostructures can be grown either in solution or from gaseous phase, this includes the vapour transport process [10], the catalyst-assisted vapour-liquid-solid process [11], the metal-organic vapour phase epitaxial growth [12], spray pyrolysis [13], and hydrothermal methods [14, 15, 16] which are high temperature processing methods and require costly equipment.

In this paper, we are representing a simple, low cost and low temperature method with high yields of synthesizing ZnO nanostructures. Depending on the catalyst and reaction conditions, different shapes such as nanoparticles, nanoneedles, hexagonal nanoparticles (NPs), nanoflower like structures are obtained but in this case it is hexagonal nanoparticles of ZnO. These synthesized ZnO nanostructures were characterized using X-ray diffraction (XRD), Scanning electron microscope (SEM), UV-visible absorption spectrometer.

II. MATERIALS AND METHOD

Zinc acetate dihydrate, sodium hydroxide, potassium hydroxide and other reagents used were all analytical grade without further purification. Alcoholic media such as methanol, ethanol or propanol, is mostly used for the synthesis of ZnO nanostructures because in alcoholic media growth of oxide particles is slow and controllable [17], but in this study reaction is accomplished in both alcoholic and nonalcoholic media. In a typical synthesis, of ZnO nanorods is carried out by sol gel process, at 80-90°C. Solution of zinc acetate dihydrate [Zn (O₂CCH₃)₂(H₂O)₂] was prepared by dissolving 2.195 g of zinc acetate dihydrate in 100ml distilled water/ethanol, and stirred in ambient atmosphere. Potassium hydroxide KOH 1.122g is dissolved in 10ml distilled water and was added to the above solution drop wise under continuous stirring. After few minutes solution turn into jelly form and a milky white solution was obtained, the mixture was then further heated for 3 h at 80-90°C without stirring. The resulting suspension was centrifuged to retrieve the product, and the mixture was washed with distilled water in an ultrasonic bathwater and then the powder was dried at 70° C over night and determined in terms of their structural, morphology and optical properties.

The crystalline structures of the products were characterized by X-ray diffraction (XRD) analysis using a JEOL JDX-3535 diffractometer. The absorbance spectra were recorded on a vision light UV-vis spectrophotometer. Size and morphology of the products were observed by scanning electron microscopy (SEM) which was taken on a JEOL JEM-2010 electron microscopy using an accelerating voltage of 200 kV in bright field and electron diffraction (ED) modes. A small drop of the ZnO powder re-dispersed by ethanol was dropped on a carbon film-coated copper grid. The sizes of ZnO were measured and averaged by several SEM images ($n = 100$).

III. RESULTS AND DISCUSSIONS

UV-VIS absorption spectra of the ZnO nanorods are shown in Fig. 3, it is well known that the bulk ZnO has absorption at 375 nm in the UV-visible spectrum [18]. The general

morphologies of the synthesized ZnO nanorods were studied by scanning electron microscopy (SEM). A typical SEM image of the ZnO nanorods is shown in Fig. 1. The ZnO nanorods have an average diameter of 100 nm and show perfectly flat surfaces with hexagonal symmetry. The lengths of ZnO nanorods are about 1 μ m. Figure 1 also shows the morphology of the nanostructures obtained after the completion of the reaction with zinc acetate and potassium hydroxide/ sodium hydroxide at 90 $^{\circ}$ C by sol gel process. The image reveals short rod like ZnO nanostructures with an average diameter of 100 to 200 nm and length in micrometers. We have found variation in shape size and length in the nanorods; most of the nanorods are straight with a smooth surface having hexagonal structure at the end. And in some regions we have notice that bunch of nanorods are aligned together in different direction.

XRD pattern of synthesized ZnO nanostructures by sol gel reaction at 90 $^{\circ}$ C is shown in Fig. 2. All peaks of the obtained product are corresponding to the hexagonal wurtzite structure of Zn reported in many research works [19,20]. In Fig. 2, the detected peaks are at 2 θ values of 31.7 $^{\circ}$, 34.4 $^{\circ}$, 36.2 $^{\circ}$, 47.5 $^{\circ}$, 56.6 $^{\circ}$, 62.8 $^{\circ}$ corresponding to the following lattice planes: (100), (002), (101), (102), (110), (103), respectively. The growth process of ZnO NWs can be controlled through the chemical reactions. All of these reactions are in equilibrium and can be controlled by adjusting the reaction parameters, such as precursor concentration, growth temperature, and growth time, to push the reaction equilibrium forward or backward. The size of the nanostructure can be controlled by using stabilizing agents which prevent the growth of the nanostructure, the growth mechanism of the Nanotubes is explained in many research works, and it is found that crystal size grows with increasing in reaction time at an appropriate temperature. High quality of ZnO nanopowder was obtained after completion of the reaction. In most of the sol gel synthesis process, zinc acetate and urea is used in 1:7 molar ratio at higher temperature 500-800 $^{\circ}$ C for the growth of one dimensional nanostructure there is two well explained mechanism accepted for the growth of one dimensional nanostructures, viz. the vapour-liquid-solid (VLS) and vapour-solid (VS) mechanism. The VLS mechanism is a catalyst assisted process, in which the metal catalyst particles act as a liquid forming agent, while in this process no catalyst is used.

The results indicate that ZnO nanorods have been successfully prepared by chemical reaction at low temperature.

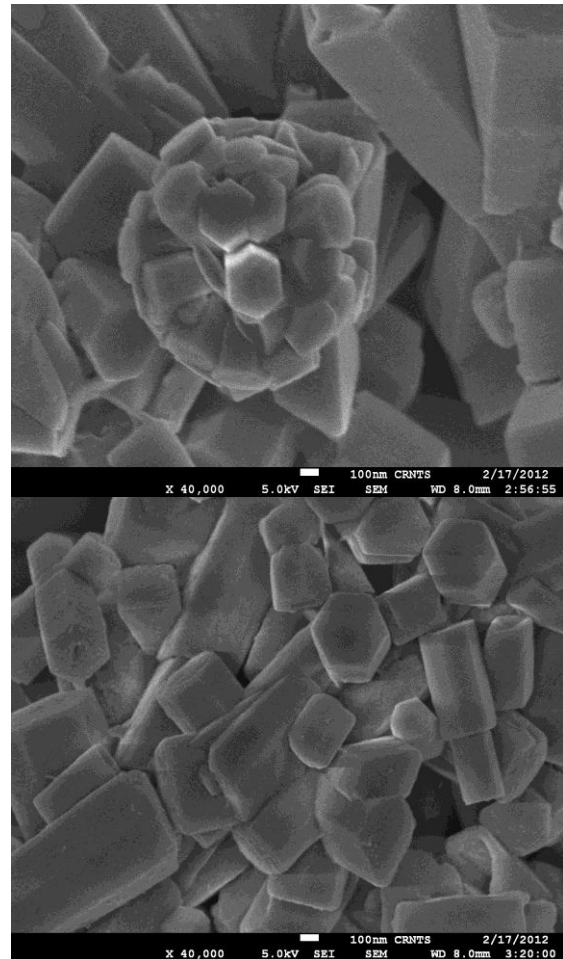


Figure 1. The SEM images of the ZnO nano-rods

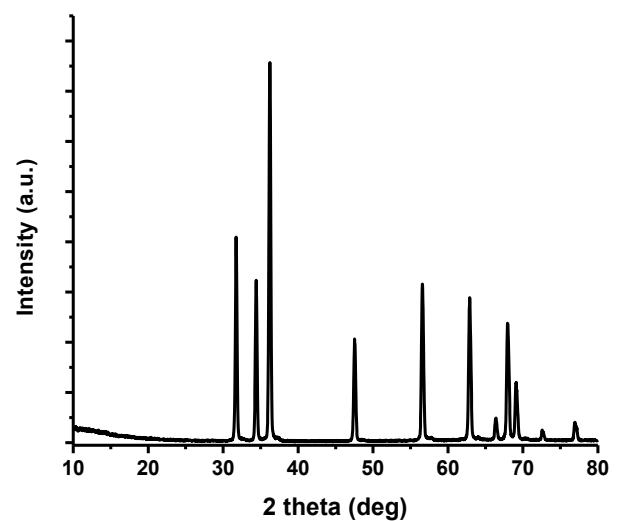


Figure 2. XRD pattern of ZnO nanorods

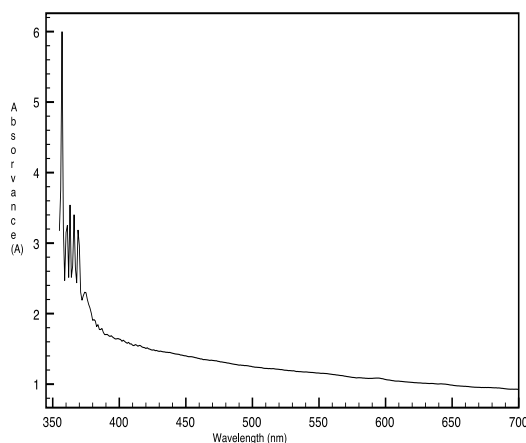


Figure 3. UV-Vis absorption spectra for ZnO nanoparticles

IV. CONCLUSION

Hexagonal ZnO nanorods were synthesized successfully without using any capping agent through sol gel process at 80-90°C. Zinc acetate dehydrate and zinc chloride was used as the zinc source. Absolute ethanol and water both are taken as a solvent, the synthesized ZnO nanorods prepared with deionized water have the diameter of 100-200nm.

ACKNOWLEDGEMENT:

We thank H.O.D School of interdisciplinary science and technology Prof. Rabinder Henry for the freedom to do experiments and we also would like to thank Prof. Manish Shinde for the encouragement, support, and guidance.

REFERENCES:

- [1] Lamia Saad* And Mary Riad, "Characterization of various zinc oxide catalysts and their activity in the dehydration-dehydrogenation of isobutanol", *J. Serb. Chem. Soc.* 73 (6) 997-1009 (2008).
- [2] Xudong Wang, Xudong Wang, Christopher J. Summers, and Zhong Lin Wang, "Large-Scale Hexagonal-Patterned Growth of Aligned ZnO Nanorods for Nano-optoelectronics and Nanosensor Arrays", *American Chemical Society, Nano Letters*, 2004, 4 (3), 423-426.
- [3] Thomas W. Hamann, Alex B. F. Martinson, Jeffrey W. Elam, Michael J. Pellin, and Joseph T. Hupp, "Aerogel Templated ZnO Dye-Sensitized Solar Cells", *Adv. Mater.* 20, 2008, 1560-1564.
- [4] Haritha Meruvu, Meena Vangalapati, Seema Chaitanya Chippada and Srinivasa Rao Bammidi, "Synthesis And Characterization Of Zinc Oxide Nanoparticles And Its Antimicrobial Activity Against Bacillus Subtilis And Escherichia Coli", *RASAYAN, J. Chem.* Vol.4, No.1 (2011), 217-222.
- [5] Xiang Liu, Xiaohua Wu, Hui Cao, and R. P. H. Chang, "Growth mechanism and properties of ZnO nanorods synthesized by plasma-enhanced chemical vapor deposition", *JOURNAL OF APPLIED PHYSICS*, Vol. 95, No. 6, 15 March 2004.
- [6] Oleg Lupan, Lee Chow, Guangyu Chai, Leonid Chernyak, Olena Lopatiuk-Tirpak, and Helge Heinrich, "Focused-ion-beam fabrication of ZnO nanorod-based UV photodetector using the in-situ lift-out technique", *phys. stat. sol. (a)* 205, No. 11, 2673-2678 (2008).

- [7] Nicole Jones, Binata Ray Koodali T. Ranjit & Adhar C. Manna, "Antibacterial activity of ZnO nanoparticle suspensions on a broad spectrum of microorganisms", *FEMS Microbiol Lett* 279 (2008) 71-76.
- [8] William L. Hughes and Zhong L. Wang, "Controlled synthesis and manipulation of ZnO nanorings and nanobows", *Appl. Phys. Lett.* 86, 043106 (2005).
- [9] Xue-Lian Yu • Hui-Ming Ji • Hong-Li Wang • Jing Sun • Xi-Wen Du, "Synthesis and Sensing Properties of ZnO/ZnS Nanocages", *Nanoscale Res Lett* (2010) 5:644-648.
- [10] Zhiyong Fan and Jia G. Lu, "Zinc Oxide Nanostructures: Synthesis and Properties", *Appl. Phys. Lett.* 81, 757 (2002).
- [11] C. N. R. Rao, Gautam Gundiah, F. L. Deepak, A. Govindaraj and A. K. Cheetham, "Carbon-assisted synthesis of inorganic nanowires", *J. Mater. Chem.*, 2004, 14, 440-450.
- [12] W.I. Park, G.-C. Yi, M. Kim, S.J. Pennycook, "ZnO Nanoneedles Grown Vertically on Si Substrates by Non-Catalytic Vapor-Phase Epitaxy", *Advanced Materials* Volume 14, Issue 24, pages 1841-1843, December, 2002.
- [13] O. Milošević, B. Jordovic, D. Uskoković, "Preparation of fine spherical ZnO powders by an ultrasonic spray pyrolysis method", *Materials Letters, Volume 19, Issues 3-4*, April 1994, Pages 165-170.
- [14] Pantelitsa Georgiou, Konstantinos Kolokotronis and Johannis Simitzis, "Synthesis of ZnO Nanostructures by Hydrothermal Method", *Journal of Nano Research* Vol. 6 (2009) pp 157-168.
- [15] Sunandan Baruah and Joydeep Dutta, "Hydrothermal growth of ZnO nanostructures", *Sci. Technol. Adv. Mater.* 10 (2009) 013001.
- [16] Hui Zhang, Deren Yang, Yujie Ji, Xiangyang Ma, Jinxu, and Duanlin Que, "Low Temperature Synthesis of Flowerlike ZnO Nanostructures by Cetyltrimethylammonium Bromide-Assisted Hydrothermal Process", *J. Phys. Chem. B*, 2004, 108 (13), pp 3955-3958
- [17] shriwas s ashtaputre, aparna deshpane, sonali marathe, me wankhede, jayashree chimanpure, renu pasricha, j urban, s k haram, s w gosavi and s k kulkarni, "Synthesis and analysis of ZnO and CdSe nanoparticles", *J. Phys.*, Vol. 65, No. 4, October 2005
- [18] M. A. Shah, "Formation of Zinc oxide Nanoparticles by the Reaction of Zinc Metal with Methanol at very low Temperature", *African Physics Review* (2008) 2:0011
- [19] Chira R Bhattacharjee1, Debraj Dhar Purkayastha1, Sumit Bhattacharjee1 and Abhijit Nath, "Homogeneous Chemical Precipitation Route to ZnO Nanosphericals", *Assam University Journal of Science & Technology, Physical Sciences and Technology* Vol. 7 Number II 122-127, 2011.
- [20] P. K. Giri, S. Bhattacharyya, B. Chetia, Satchi Kumari, Dilip K. Singh, and P. K. Iyer, "High-Yield Chemical Synthesis of Hexagonal ZnO Nanoparticles and Nanorods with Excellent Optical Properties", *Journal of Nanoscience and Nanotechnology* Vol. 11, 1-6, 2011

Performance Analysis of RS and CC Coding Methods in OFDM WiMAX System for BPSK and QPSK Modulation Techniques

Kavita Rani¹, Ankur Sood², Nitin Arora³

(Lecturer, Chhotu Ram Rural Institute of Technology, Kanjhawala, Delhi,)

(Assistant Professor, Ideal Institute of Technology, Ghaziabad, UP)

(Assistant Professor, Haryana Institute of Technology, Bahadurgarh)

ABSTRACT: Coding techniques is used for providing reliable information through the transmission channel to the user. In coding techniques the number of symbols in the source encoded message is increased in a controlled manner in order to facilitate two basic objectives at the receiver one is Error detection and other is Error correction. The amount of error detection and correction required and its effectiveness depends on the signal to noise ratio (SNR). In digital communication, coding techniques is a broadly used term mostly referring to the forward error correction code. The WiMAX technology based on air interface standard 802-16 wireless MAN is configured in the same way as a traditional cellular network with base stations using point to multipoint architecture to drive a service over a radius up to several kilometers. The range and the Non Line of Sight (NLOS) ability of WiMAX make the system very attractive for users, but there will be slightly higher BER at low SNR. In this paper, a comparison between the performance of WiMAX using convolution code and Convolution Product Code (CPC) is made. CPC enables to reduce BER at different SNR values compared to the convolution code.

Keywords: WiMAX, BER, CPC, IEEE 802.16

I. INTRODUCTION

WiMAX is introduced by the Institute of Electrical and Electronic Engineers (IEEE) which is designated by 802.16 to provide worldwide interoperability for microwave access. There are fixed (802.16d) and mobile (802.16e) WiMAX. This technology offers a high speed, secure, sophisticate, last mile broadband service, ensuring a flexible and cheap solution to certain rural access zones[1]-[7]. In a fixed wireless communication, WiMAX can replace the telephone company's copper wire networks, the cable TV's coaxial cable infrastructure.

In comparison with Wi-Fi and Cellular technology, Wi-Fi provides a high data rate, but only on a short range of distances and with a slow movement of the user. And Cellular offers larger ranges and vehicular mobility, but it provides lower data rates, and requires high investments for its deployment. WiMAX tries to balance this situation. WiMAX fills the gap between Wi-Fi and Cellular, thus providing vehicular mobility, and high service areas and data rates. WiMAX is a standards based technology for wireless MANs conforming to parameters which enable

interoperability[1][2]. WiMAX developments have been rapidly moving forward.

The main objective of this paper is to transmit the data in WiMAX with low bit error rate in the noisy environment for that we using Forward Error Correction method which is Convolution coding. This method is useful to reduce the bit error rate (BER) and increase the efficiency.

The paper is organized as follows: Section II introduces a description for the simulation model. Description of CC and CPC scheme is presented in Section III. Simulation results are given in Section IV, and finally conclusions are reflected in Section V.

II. CONVOLUTIONAL ENCODER

The channel coding scheme, IEEE 802-16, as shown in fig 1 is based on binary non-recursive Convolutional Coding (CC) [4]. The convolutional encoder uses a constituent encoder with constraint length 7, code rate 1/2 and generator polynomials (133,171) octal. In this stage, the CPC method will be applied for coding the message and this will be shown in the following section.

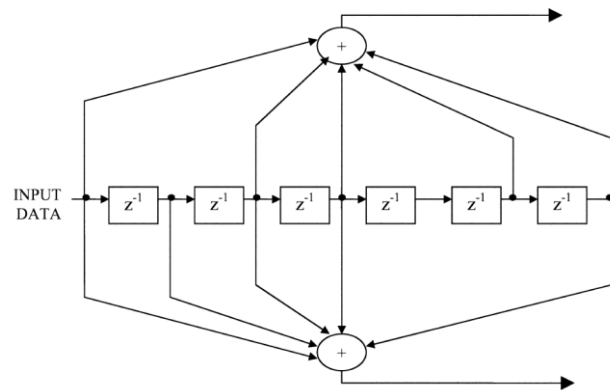


Fig: 1 Convolutional Encoder in IEEE 802.16e

A. CONVOLUTION PRODUCT CODE (CPC) METHOD

CPC is a new coding method [1], in which the information bits are placed into two dimensions (2D)

Matrix. The rows and the columns are encoded separately by using recursive systematic convolutional encoders. Each row of the matrix is encoded using a convolutional code the same recursive systematic convolutional code is used to encode each

row. Once all rows have been encoded, the matrix is sent, if desired, to an interleaver. Our original data matrix dimensions are (nxk), and the encoded data matrix dimensions will be (Znxk). The coded rows matrix is then recoded column by column using the same or different recursive systematic convolutional encoder. CPC uses a recursive systematic convolutional code with rate 1/2 and generator polynomials (1,5/7) octal to encode each row and column. Hence, the overall code rate is 1/4. The coding by CPC will be done in 2 stages. First each column will be independently coded, and then each row of the resulting matrix will be coded by the same generator polynomials.

III. REED SOLOMON CODING

The randomized data are arranged in block format before passing through the encoder [6] and a single 0X00 tail byte is appended to the end of each burst. The implemented RS encoder is derived from a systematic RS (N=255, K=239, T=8) code using GF (2⁸). The following polynomials are used for code generator and field generator.

$$G(x) = (x + \alpha^0)(x + \alpha^1) \dots (x + \alpha^{2^T-1}), \alpha = 02_{HEX}$$

$$p(x) = x^8 + x^4 + x^3 + x^2 + 1$$

IV. SIMULATION RESULTS

In this chapter the simulation results are shown and discussed.

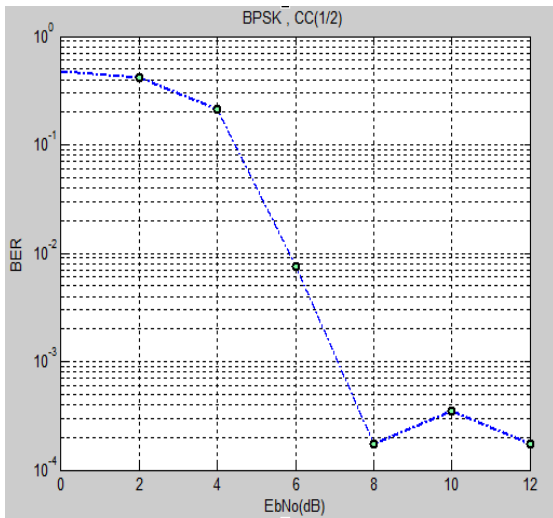


Fig: 2 BER vs EbNo for BPSK (1/2) with CC coding

We have presented various BER versus Eb/No plots for BPSK and QPSK according to the IEEE 802.16 standard. Fig: 2 and Fig: 5 BER versus Eb/No plots for BPSK and QPSK.

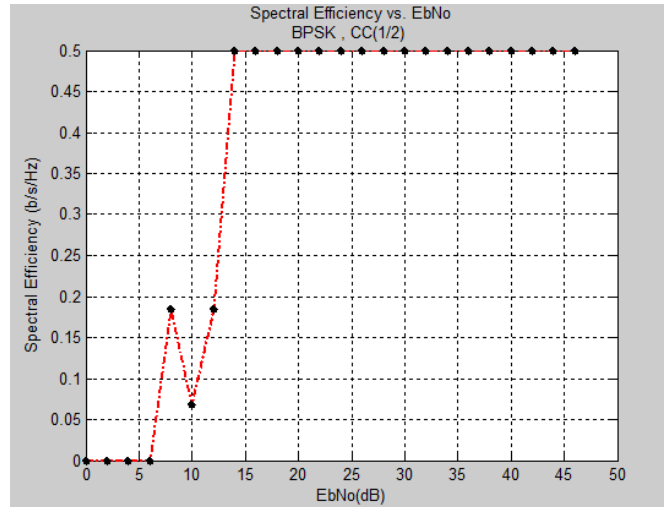


Fig: 3 Spectral Efficiency vs EbNo for BPSK (1/2) with CC coding

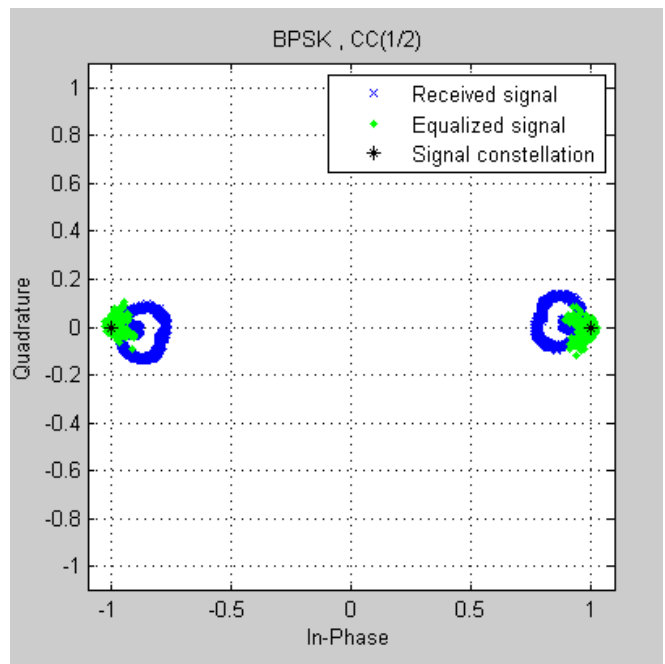


Fig: 4 Signal Constellation diagram for BPSK (1/2) with CC coding

We have presented various Spectral Efficiency versus Eb/No plots for BPSK and QPSK according to the IEEE 802.16 standard. Fig: 3 and Fig: 6 Spectral Efficiency versus Eb/No plots for BPSK and QPSK.

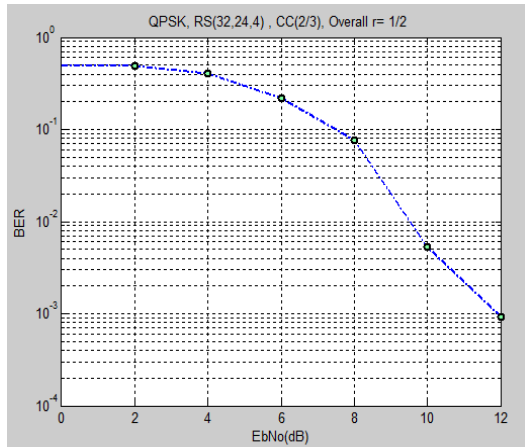


Fig: 5 BER vs EbNo for QPSK (1/2) with RS and CC coding

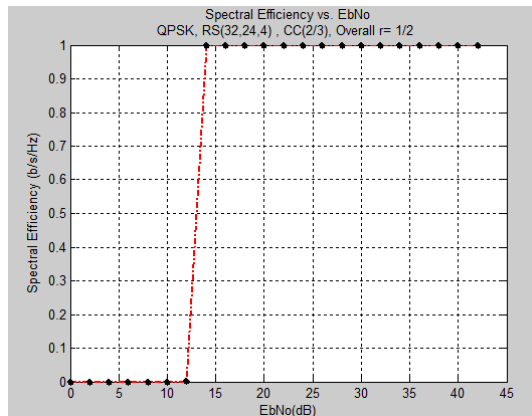


Fig: 6 Spectral Efficiency vs EbNo for QPSK (1/2) with RS and CC coding

We have presented various Signal Constellation diagram plots for BPSK and QPSK according to the IEEE 802.16 standard. Fig: 4 and Fig: 7 Signal Constellation diagram plots for BPSK and QPSK

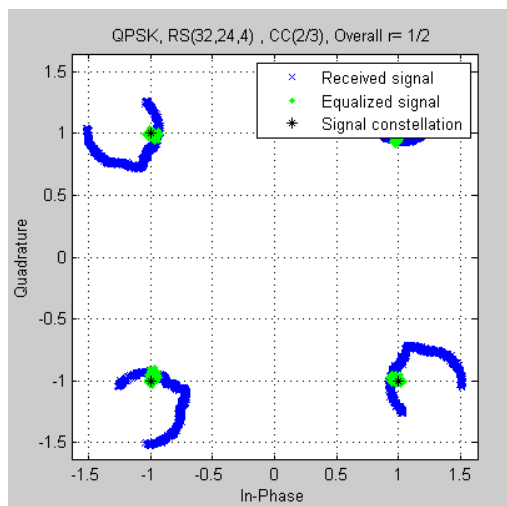


Fig: 7 Signal Constellation diagram for QPSK (1/2) with RS and CC coding

V. CONCLUSION

In this paper, performance of WIMAX systems is studied under using CC and CPC coding method using BPSK and QPSK modulation Techniques. This lead to the reduction of BER. We investigate the performance of the OFDM WiMAX system with BPSK and QPSK modulation scheme which lead to the improvement in the BER with QPSK scheme compare to the BPSK. Spectral efficiency of WiMAX system will also improve with QPSK modulation Scheme.

VI. FUTURE SCOPE

Further scope of this paper is that performance analysis of WiMAX MC-CDMA based system using CPC coding and convolution coding method. Which may gives better result as compare to WiMAX OFDMA based system using CPC coding and convolution coding method.

VII. REFERENCES

- [1] L. Nuaymi, "WiMAX: Technology for Broadband Wireless Access," John Wiley & Sons, 2007.
- [2] WiMAX Forum, "Mobile WiMAX - Part I: A Technical Overview and Performance Evaluation," White paper, August 2006.
- [3] IEEE 802.162004," IEEE Standard for Local and Metropolitan Area Networks Part 16: Air Interface for Fixed Broadband Wireless Access Systems", 1 October, 2004.
- [4] WiMAX Forum, "Mobile WiMAX - Part I: A Technical Overview and Performance Evaluation," white paper, August 2006.
- [5] Y. Xiao, "WiMAX-Mobile Fi: Advanced research and Technology," Auerbach publications, 2008.
- [6] Changlong Xu, "Soft Decoding Algorithm for RS-CC Concatenated Codes in Wimax System", Vehicular Technology Conference, 2007.
- [7] Jeffrey G Andrews, Arunabha Ghosh, and Rias Muhamed, "Fundamentals of WiMAX"

Global Block-Based Redundancy Architectures For Self-Repairing Of Embedded Memories

T. Govinda Rao¹, K. V. V. Satyannarayana², J. Sathish Kumar³

*(Department of ECE, Usha Rama College of Engg. & Tech., Telaprolu, India)

***(Department of ECE, Usha Rama College of Engg. & Tech., Telaprolu, India)

***(Department of ECE, Usha Rama College of Engg. & Tech., Telaprolu, India)

ABSTRACT: In this paper, global block-based redundancy architectures are proposed for self-repairing of embedded memories. The main memory and the redundant rows/columns are divided into row blocks/column blocks. The replacement of faulty memory cells can be performed at the row/column block level instead of the traditional row/column level. Note that the redundant row/column blocks are global, i.e., they can be used to replace faulty cells anywhere in the memory array. This global characteristic is helpful for repairing cluster faults. Since the redundancy can be designed independently. It can be easily integrated with the embedded memory cores. To perform redundancy analysis, the MESP algorithm suitable for built-in implementation is also proposed. According to experimental results, the area overhead for implementing the MESP algorithm is almost negligible. Due to the efficient usage of the redundancy, the manufacturing yield, repair rates, and reliabilities can be improved significantly

Keywords: Cluster fault, embedded memory, modified essential spare pivoting (MESP) algorithm, repair rate, yield.

I. INTRODUCTION

As we migrate to the nanometer technology era, we are seeing a rapid growing density of system-on-a-chip (SOC) designs. This trend makes the manufactured chips more susceptible to sophisticated defects. Moreover, according to the Semiconductor Industry Association (SIA) and Technology Roadmap for Semiconductors (ITRS) 2007, the relative silicon area occupied by embedded memories will approach 94% by 2014 [1]. Since embedded memories also have higher density than logic cores, the overall SOC yield is dominated by these memory cores. For example, the yield of a 24 M-bit embedded memory is about 20% [2]. In order to boost the manufacturing yield of embedded memories, one promising solution is the built-in self-repair (BISR) technique. To achieve the goals of BISR, three basic functions are usually required—memory built-in self-test (BIST), built-in redundancy analysis (BIRA), and address reconfiguration (remapping) (AR).

There are many BIRA/BISR techniques proposed in the past [3]–[12]. A comprehensive exhaustive search for built-in self analysis algorithm (CRESTA) has been proposed in [8]. Although this BISR scheme can achieve optimal repair rates, the hardware overhead for implementing the CRESTA scheme is very high. Wey and Lombardi in [9] propose a branch-and-bound technique with early screening in the repair process. A bipartite graph is applied to obtain the least required number of spare

allocation, i.e., the least number of spare rows/columns to repair the faulty rows/columns in the main memory array. In our previous work [10], hybrid redundancy architectures are proposed. We have also shown that the complexity of the redundancy allocation problem is nondeterministic-polynomial-time-complete (NP-complete). From the simulation results, the manufacturing yield, repair rate (the ratio of the repaired memories to the number of defective memories), and reliability can be improved significantly.

Divided word-line (DWL) and divided bit-line (DBL) techniques are proposed in [13] and [14] to reduce the power consumption and increase the access time. This divided characteristic can also be used for fault-tolerant applications, i.e., redundant rows and columns can be divided into row blocks and column blocks. The replacement can be performed at the block level instead of the traditional row/column level. However, if the redundant rows (columns) are used locally to replace faulty row (column) blocks in the same row (column) bank, there are still some drawbacks, which should be dealt with. First, if there are many faulty cells located within a row/column bank (to be defined later), there may not be sufficient spare blocks to re-place these faulty cells. The spare blocks allocated for other banks may not be used in this case. Therefore, for some defect distribution resulting in such condition, more redundant rows (columns) should be included for successful repair of the faulty memory. The usage of spares then is inefficient. Second, if *cluster faults* are considered, this dilemma becomes more severe. This is because cluster faults usually gather within a small memory area (though there are small-area, medium-area, and large-area clusters). The local characteristic of redundancy is not suitable (or efficient) to repair such faults. Third, the local spare row (column) blocks should be implemented together with the main memory array, but then it is difficult for SOC integration.

In this paper, the *global* block-based redundancy architectures is proposed. Redundant rows/columns are still divided into row/column blocks. However, the redundant row/column blocks can be used to replace faulty row (column) blocks anywhere in the memory array. This *global* characteristic is helpful for repairing cluster faults.

Based on the proposed global redundant architectures, a heuristic modified essential spare pivoting (MESP) algorithm suitable for BISR is proposed. The area overhead for implementing the MESP algorithm is very low for easier discussion of the proposed techniques.

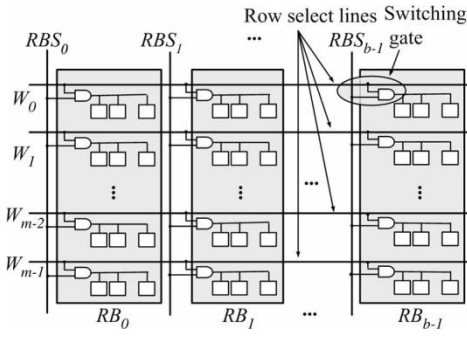


Fig. 1. DWL architecture.

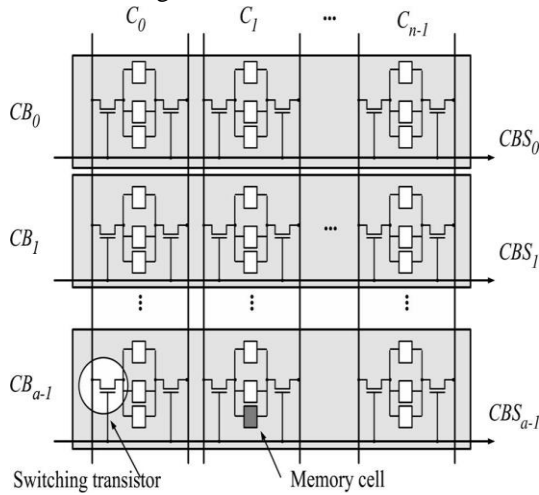


Fig. 2. DBL architecture.

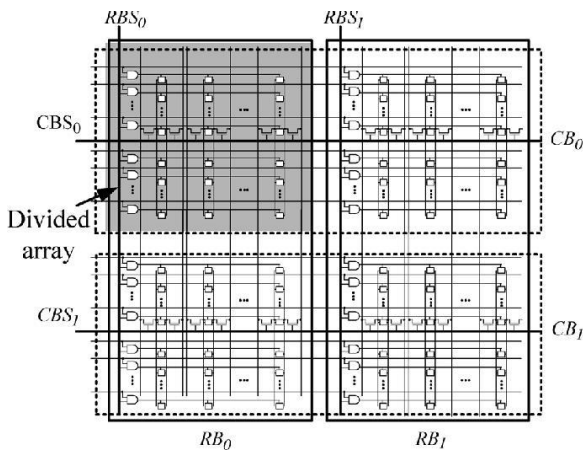


Fig. 3. DWL and DBL integration.

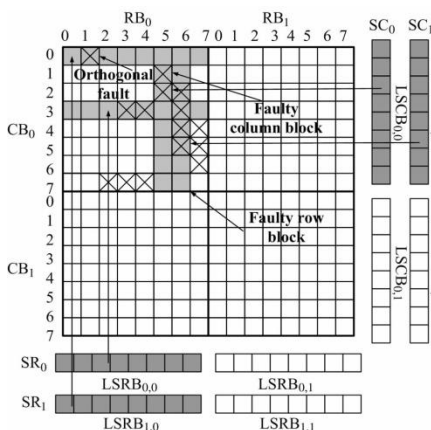


Fig. 4. Local block-level redundancy architecture.

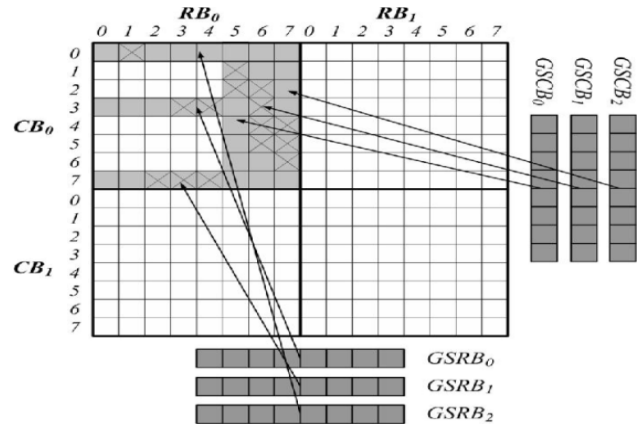


Fig. 5. Novel redundancy architecture (GBLRA).

The remainder of this paper is organized as follows. Section II reviews the DWL and DBL architectures. Section III introduces the proposed local and global block-based redundancy architecture. A heuristic built-in redundancy analysis algorithm named the MESP algorithm is described in Section IV. An example of the proposed MESP algorithm is delineated in Section V. Section VI describes the BISR circuits and the repair procedures. Experimental results are shown in Section VII. A practical 16 K × 32-bit memory chip with BISR is implemented and described in Section VIII. Finally, some conclusions are given in Section IX.

II. LOCAL AND GLOBAL BLOCK BASED REDUNDANCY ARCHITECTURES

As described above, the local block-based redundancy architectures have three major drawbacks. An example is shown in Fig. 4 where faulty memory cells are marked X's. From this figure, we can see that all faulty cells are contained in DA_{00} . Therefore, only the spare blocks in RB_0 and CB_0 can be used to replace faulty cells. An *orthogonal fault* (to be defined later) should be repaired by one spare row or column block. It is evident that the remaining faulty cells cannot be successfully repaired by using the remaining spare blocks.

The four used spare blocks are shaded, as shown in Fig. 4.

However, there are still two available spare row blocks ($LSRB_0$ and $LSRB_1$) and two spare column blocks ($LSCB_0$ and $LSCB_1$). These four spare blocks can also be used to replace the remaining faulty cells, it is evident that this faulty memory array can be repaired successfully. This scenario is more severe if cluster faults are considered. Therefore, in order to solve these drawbacks, the *global block-based redundancy architectures* are proposed in this paper. In Fig. 5, the faulty main memory array is the same as that shown in Fig. 4. However, three *global spare row blocks* (GSRBs) and three *global spare column blocks* (GSCBs) are added into the memory array. Based on this strategy, spare row blocks and column blocks are global, i.e., they can be used to replace the faulty cells anywhere in the memory array. Due to the global characteristic, we can reconfigure the memory more efficiently—the faulty memory array can be repaired successfully as indicated by the arrows shown in Fig. 5.

III. BUILT-IN REDUNDANCY ANALYSIS

The proposed MESP algorithm is based on the *essential spare pivoting (ESP) algorithm* [15]. However, we use the global block-based redundancies instead of the whole rows/columns. Before illustrating the proposed algorithm, we define some basic fault types (FTs) first.

1) Faulty row (column) block:

A row/column block that has more faulty cells than the threshold number (E_{th}) is called a *faulty row/column block*. We can use a *GSRB/GSCB* to replace the faulty row/column block. In this work, we assume that the threshold is 2.

2) **Orthogonal fault** [15]: For a faulty memory cell, if there is no other faulty cell located in the same row and column containing the faulty cell, then this faulty memory cell is

DA	LRA	LCA	FT
----	-----	-----	----

Fig. 6. Fields of the FCR.

said to have an *orthogonal fault*. For each orthogonal fault, a GSRB is required to replace it. To implement the proposed MESP algorithm, it is necessary to use the *fault collection registers (FCRs)* for fault collection. The FCRs contain $r+c$ entries, where r and c denote the numbers of GSRBs and GSCBs, respectively. During the BIST session, when a faulty cell is detected, fault information is stored into the FCR registers. There are four fields contained in each FCR, as shown in Fig. 6. The D'A field is used to store the index of the divided array containing the faulty cells. The local row (column) addresses of the faulty cells are stored in the LRA (LCA) field. The FT field identifies if the faulty memory cells are orthogonal faults (FT=0) or faulty row (FT=1)/column blocks (FT=2).

IV. BISR ARCHITECTURES AND PROCEDURES

Fig. 9 depicts the block diagram of the proposed BISR scheme that includes the BIST module, the BIRA module, and the redundant memory module containing the GSRBs and the GSCBs. The BIST module performs a specified March algorithm to detect functional faults in the redundant memory module and the main memory module. It can also locate the faulty addresses. The BIRA module performs the proposed MESP algorithm and includes two components named the *fault collection register (FCR)* and the *address remapping content-addressable memory (ARCAM)*. The FCR collects and analyzes the faulty cell information detected by the BIST module. The ARCAM is the address remapping mechanism when the memory operates in normal operation mode. After finishing the BIST session, the faulty information stored in the FCR will be shifted into the ARCAM. Fig. 10 shows the BISR procedures. In *test/repair* mode, the BIST circuit tests the spare elements first to identify fault-free spares. If a fault is detected from the spare memory, the signal is activated and the corresponding faulty flag in the ARCAM module will be set which means that the faulty spare element is unusable. After spare memory testing, the BIST circuitry

will test the main memory. If a fault is detected in the main memory, the signal will be activated. The BIST will be suspended, and the BISR performs built-in redundancy analysis (BIRA). When this procedure is completed and the memory test is not finished yet, the BIRA module will send the signal to the BIST module to resume the test procedure. After the BIST session is finished, the BIRA module shifts the *faulty information (FI)* stored in the FCRs to ARCAM. When all fault information is shifted, the ARCAM serves as an address remapping mechanism in the normal operation mode. Since the BIST controller will be suspended each time when a fault is detected. The only possible loss of fault detection capability is during the instant when the BIST controller is resumed (not at-speed testing). However, the impact of fault detection quality is very low since the number of faults existed in the memory array is usually very small.

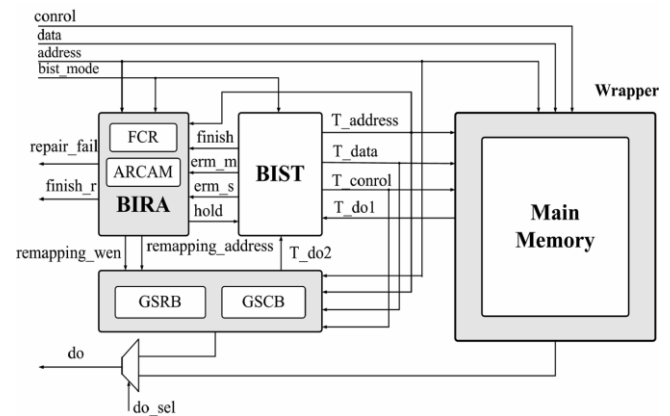


Figure 9: Block diagram of the proposed BISR scheme

The architectures of the FCR and ARCAM components are shown in Figs. 11 and 12, respectively. FCR component consists of the *FCR controller* and the *FCRs*. In *test/repair* mode, the reset signal is activated for one clock cycle to initialize all the internal registers. When a faulty cell in the spare elements is detected, the corresponding faulty flag in the ARCAM component will be set. After spare element testing, the ARCAM will send the signal to the FCRs to update the counters which count the numbers of available spare elements. If a faulty cell is detected in the main memory, this signal will force the FCR controller to send the hold signal to suspend the BIST circuit. Subsequently, the FCR controller will perform the MESP algorithm. The FCR controller is constructed with a finite-state machine with the state transition graph, as shown in Fig. 13. In this transition graph, if the BIST module does not detect faults or the fault has been repaired, it will remain in the state. Otherwise, it will enter the state. In the repair procedure state, if the detected fault is identified as a faulty row block and there are available GSRBs, the BIRA module will enter the state, which means that we can use GSRBs to repair the faulty cells. In the GSRB_repair state, the output signal will be activated. Similarly, if the incoming fault is identified as a faulty column block and there are still available GSCBs, the BIRA module will enter the state which means that we can use GSCBs to repair the faulty cells. In the GSCB_repair state, the output signal will be activated. If the incoming

fault is not identified as a faulty row block or a faulty column block and there are available GSRBs or GSCBs, the BIRA module will enter the state. The signal will be activated and the incoming faulty information will be stored into the FCRs. If the GSRBs and GSCBs are all used and there still exists some faulty cells, the *repair_fail* signal will be activated. When the BIST module finishes testing the spare memory and the main memory, the BISR procedure is finished. The signal will be activated.

V. EXPERIMENTAL RESULTS

In order to evaluate the proposed fault-tolerance techniques, the simulation model proposed in [18] is used to analyze our techniques. The number of such adjacent circuits is denoted as a . The parameter b denotes the cluster factor of the a th adjacent circuit. Similarly, the number of faults that have already occurred on the a th adjacent circuit is represented as b . Finally, the probabilities that a defect results in a faulty cell, a faulty column, a faulty row, and a cluster fault (a combination of several cell faults where the faulty cells are a cluster of any shape) are assumed to be 70%, 15%, 10%, and 5%, respectively. A simulator is implemented to simulate the proposed MESP algorithm. In our simulator, we set a as a constant. The values of b are set equal to a for simplification. The values of a and b are 0.65 and 1, respectively. We define *repair rate* as the probability of successful reconfigurations. In Fig. 14, we show the repair rates for the proposed MESP algorithm with different amounts of redundancy. The memory size is 1024 1024 bits. The average number of defects injected into a chip is assumed to be 15. From this figure we can see that if more redundancies are added, we get higher repair rates. Similarly, if the memory array is divided into more row and column banks, we will also obtain higher repair rates.

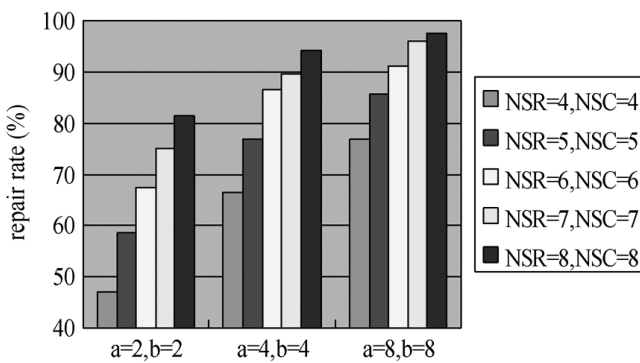


Fig. 14. Repair rates for different redundancy architectures based on the MESP algorithm.

We also compare the repair rates of the proposed MESP algorithm with those of the MESP (redundant row/column blocks are confined to their corresponding row/column banks) and ESP [15] (redundant rows/columns are not divided into row/column blocks) algorithms. The results are shown in Fig. 15. In this figure, the values of a and b are both set to 4. If the number of spare rows (columns) increases, the repair rates will also increase. From this figure we see that the MESP and MESP algorithms are much better than the ESP algorithm. It should be noted that if cluster faults are considered, the

MESP algorithm will have 10% improvement over the MESP algorithm on average. This improvement is very useful to further increase the manufacturing yield.

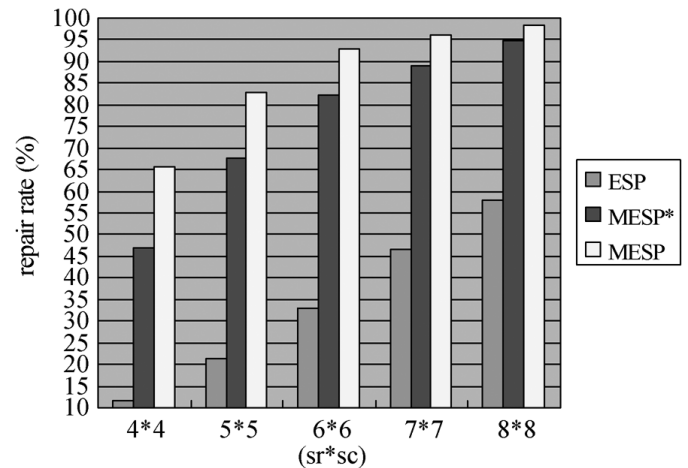


Fig. 15. Repair rates for the ESP, MESP and the MESP algorithms

If we change the values of a and b to 0.4 and 1.5, respectively, the results are, as shown in Fig. 16. The average number of defects injected into a chip is also the same. However, the injected faults are further clustered. Since the locations of defects are random and cluster faults may locate beyond the boundary of the chips or the divided arrays, the improvements of the MESP algorithm over the MESP algorithm are nearly the same as that shown in Fig. 15. From these figures, we can conclude that the proposed MESP algorithm is better than the other two algorithms. We have also tried to find the optimal solution by exhaustively searching the solution space. Therefore, massive simulations are conducted with different number of redundancies

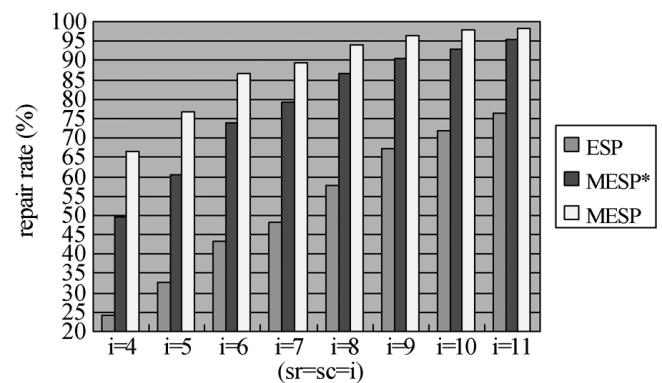


Fig. 16. Repair rates for the ESP, MESP, and the MESP algorithms

and compared the results with the optimal solution. According to our simulation results, the average repair rate is only 0.92% lower than the optimal repair rate. Therefore, by using the proposed MESP algorithm, near-optimal repair rate can be achieved.

VI. A PRACTICAL EXAMPLE

We have implemented a 16 K 32 word-oriented SRAM chip based on the TSMC 1P6M 0.18 m process. The specifications of this design are shown in Table II. The

memory blocks in this design are generated by a commercial memory compiler. We combine four 8 K 16-bit SRAMs into one 16 K 32-bit SRAM, and integrate all categories of the redundancy such as spare words, spare rows, and spare column group blocks into one 336 32-bit spare SRAM. The chip layout of the 16 K 32-bit SRAM with BISR is shown in Fig. 17. The number of I/O pins is 118. The *core size* and *chip size* is 5.0501 and 8.551 mm, respectively. According to the area of the physical layout shown in this figure, the hardware overhead of the spare elements and the BISR module is about 8.7%.

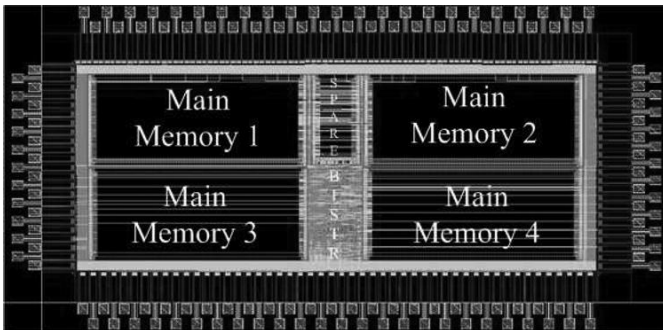


Fig. 17. Physical layout view of the 16 K x 32-bit SRAM with BISR.

VII. CONCLUSION

Instead of the traditional spare row/column redundancy architectures, *block-based* redundancy architectures are proposed in this paper. The redundant rows/columns are divided into row/column blocks. Therefore, the repair of faulty memory cells can be performed at the row/column-block level. Moreover, the redundant row/column blocks can be used to replace faulty cells anywhere in the memory array. This *global* characteristic is helpful for repairing cluster faults. The proposed redundancy architecture can be easily integrated with the embedded memory cores. Based on the proposed global redundancy architecture, a heuristic *modified essential spare pivoting (MESP)* algorithm suitable for built-in implementation is also proposed. According to experimental results, the area overhead for implementing the MESP algorithm is very low. Due to efficient usage of redundancy, the manufacturing yield, repair rate and reliability can be improved significantly.

REFERENCES

- [1] A. Allan, "2001 technology roadmap for semiconductors," *Computer*, vol. 35, no. 1, pp. 42–53, Jan. 2002.
- [2] Y. Zorian and S. Shoukourian, "Embedded-memory test and repair: Infrastructure IP for SOC yield," *IEEE Des. Test Comput.*, vol. 20, no.3, pp. 58–66, May 2003.
- [3] D. K. Bhavsar, "An algorithm for row-column self-repair of RAM's and its implementation in the Alpha 21264," in *Proc. Int. Test Conf.*, Sep. 1999, pp. 311–318.
- [4] I. Kim, Y. Zorian, G. Komoriya, H. Pham, F. P. Higgins, and J.L. Lewandowski, "Built-in self-repair for embedded high density SRAM," in *Proc. Int. Test Conf.*, 1998, pp. 1112–1119.
- [5] W. K. Huang, Y. H. Shen, and F. Lombardi, "New approaches for the repairs of memories with redundancy by row/column deletion for yield enhancement," *IEEE Trans. Comput.-Aided Des. Integr. Circuits Syst.*, vol. 9, no. 3, pp. 323–328, Mar. 1990.
- [6] P. Mazumder and Y. S. Jih, "A new built-in self-repair approach to VLSI memory yield enhancement by using neural-type circuits," *IEEE Trans. Comput.-Aided Des. Integr. Circuits Syst.*, vol. 12, no. 1, pp.24–36, Jan. 1993.
- [7] S. Y. Kuo and W. K. Fuchs, "Efficient spare allocation in reconfigurable arrays," *IEEE Des. Test Comput.*, vol. 4, no. 1, pp. 24–31, Jan.1987.
- [8] T. Kawagoe, J. Ohtani, M. Niuro, T. Ooishi, M. Hamada, and H.Hidaka, "A built-in self-repair analyzer (CRESTA) for embedded DRAMs," in *Proc. Int. Test Conf.*, Oct. 2000, pp. 567–574.
- [9] C. L.Wey and F. Lombardi, "On the repair of redundant RAM's," *IEEE Trans. Comput.-Aided Des. Integr. Circuits Syst.*, vol. CAD-6, no. 2, opp. 222–231, Mar. 1987.
- [10] S. K. Lu, C. H. Hsu, Y. C. Tsai, K. H.Wang, and C. W.Wu, "Efficient built-in redundancy analysis for embedded memories with 2-D redundancy," *IEEE Trans. Very Large Scale Integr. (VLSI) Syst.*, vol. 14, no. 1, pp. 31–42, Jan. 2006.
- [11] M. Nicolaidis, N. Achouri, and S. Boutobza, "Dynamic data-bit memory built-in self-repair," in *Proc. Int. Conf. Comput.-Aided Des.*, Nov. 2003, pp. 588–594.
- [12] M. Nicolaidis, N. Achouri, and L. Anghel, "Memory built-in self-repair for nanotechnologies," in *Proc. Int. On-Line Testing Symp.*, Jul. 2003, pp. 94–98.
- [13] M. Yoshimoto, K. Anami, H. Shinohara, T. Yoshihara, H. Takagi, S.Nagao, S. Kayano, and T. Nakano, "A divided word-line structure in the static RAM and its application to a 64 K full CMOS RAM," *IEEEJ. Solid-State Circuits*, vol. SC-18, no. 5, pp. 479–485, Oct. 1983.
- [14] A. Karandidar and K. K. Parhi, "Low power SRAM design using hierarchical divided bit-line approach," in *Proc. Int. Conf. Comput. Des.*, Oct. 1998, pp. 82–88.
- [15] C.-T. Huang, C.-F. Wu, J.-F. Li, and C.-W. Wu, "Built-in redundancy analysis for memory yield improvement," *IEEE Trans. Reliabil.*, vol. 52, no. 4, pp. 386–399, Dec. 2003.
- [16] R. F. Huang, J. F. Li, J. C. Yeh, and C. W. Wu, "A simulator for evaluating redundancy analysis

algorithms of repairable embedded memories,” in *Proc. IEEE Int. Workshop Mem. Technol., Des. Testing(MTDT)*, Jul. 2002, pp. 68–73.

- [17] S. K. Lu, C. L. Yang, and H. W. Lin, “Efficient BISR techniques for word-oriented embedded memories with hierarchical redundancy,” in *Proc. IEEE/ACIS Int. Conf. Comput. Inform. Sci.*, Jul. 2006, pp. 355–360.
- [18] C. H. Stapper, “Simulation of spatial fault distributions for integrated circuit yield estimations,” *IEEE Trans. Comput.-Aided Des.*, vol. 8, no.12, pp. 1314–1318, Dec. 1989.



J. Sathish Kumar received the M.Tech degree from Jawaharlal Nehru Technological University, Kakinada in 2011 in Electronics and Communication engineering. he is an Assistant Professor in the Department of Electronics and Communication engineering, Usha Rama College Of Engineering and Technology, Vijayawada.



T. GOVINDA RAO received the M.Tech (VLSISD) degree from Jawaharlal Nehru Technological University, Kakinada in 2011 in Electronics and Communication engineering. he is an Assistant Professor in the Department of Electronics and Communication engineering, Usha Rama College Of Engineering and Technology, Vijayawada. His current research interests include the areas of very large scale integration (VLSI) testing and fault-tolerant computing, video coding techniques, and Architectures design.



K. V. V. Satyanarayana received the M.Tech degree from Jawaharlal Nehru Technological University, Kakinada in 2008 in Electronics and Communication engineering. he is an Associate Professor in the Department of Electronics and Communication engineering, Usha Rama College Of Engineering and Technology, Vijayawada.

Formability of Magnesium Alloys

M. Sivanandini¹, Dr. S. S. Dhami², Dr. B. S. Pabla³

**(Mechanical Department, / National Institute of Technical Teachers Training and Research , India)*

*** (Department of Mechanical Engineering, NITTTR, India)*

ABSTRACT: *In recent decades, an interest in magnesium (Mg) alloys has progressively increased in numerous industrial fields. Magnesium alloys are characterized by favourable strength/weight ratio thus representing a valid alternative to aluminium alloys and High Strength Steels, largely adopted in those sectors where the production of lightweight parts is an important requirement (aerospace and automotive industries, electronics and sport). In order to produce Mg components with better mechanical properties, dimensional accuracy and finishing quality, sheet metal forming processes are the best manufacturing choice. Since the ductility of Mg alloys is quite poor at room temperature, the formed products of magnesium alloy is still limited. In order to find the forming method and conditions suitable for the sheet, the forming limit, i.e. the fracture initiation in sheet forming processes, has to be correctly predicted. Efforts were made to optimize process parameters by analyzing the causes of defects in order to improve the Limit Drawing Ratio of magnesium alloy work pieces. In recent years, quite a few efforts have been made to study the methods for improving the formability of wrought magnesium alloy. A great deal of research in literature confirms the effectiveness of the process parameter temperature in improving formability. A Brief overview in the field of forming operations at elevated temperatures has been reviewed to summarize the formability of magnesium alloy sheet. As, AZ31 can be more effectively formed to obtain complex geometries, which is usually measured evaluating the material formability as the locus of limit strains, more focus has been given to this alloy in the present review.*

Keywords: AZ31, Forming Limit, Limiting Drawing Ratio, Magnesium alloy, Sheet forming

I. INTRODUCTION

Magnesium alloy sheet was used in manufacturing, military, aircraft during and after the Second World War. They are used today in the automotive industry, mainly in sand and die castings; the development of light-weight vehicle is in great demand for enhancement of fuel efficiency and dynamic performance. The vehicle weight can be reduced effectively by using lightweight materials such as magnesium alloys. The low density of magnesium makes it ~35% lighter than aluminum and ~78% lighter than steel. Hence, successful implementation of magnesium in transportation industries would bring significant weight-saving benefits. Due to its lightweight and high specific strength, magnesium alloy have been considered as a promising alternative for high-strength steel and aluminum in some applications and has been widely used for structural components in the aerospace, electronics, and automobile industry to replace some existing materials[1,

2]. Because of lower density, better collision safety property and electromagnetic interference shielding capability, magnesium alloys are available for producing some structural parts such as the coverings of mobile telephones, notebook computers and portable mini-disks (MD). In the past, the demand for this alloy as a structural material was not high because of its less availability commercially as well as limited manufacturing methods. However, the use of magnesium alloys in sheet forming processes is still limited because of their low formability at room temperature and the lack of understanding of the forming process of magnesium alloys at elevated temperatures. The application of formed magnesium wrought alloys components, however, is restricted due to lack of knowledge for processing magnesium alloys, especially forming process, at elevated temperatures. However, since its alloy is a hexagonal close-packed metal and has poor formability, the formed products of magnesium alloy is still limited. In order to find the forming method and conditions suitable for the sheet, the forming limit, i.e. the fracture initiation in sheet forming processes, has to be correctly predicted. Therefore, previous studies [3–7] have been performed to summarize the formability of magnesium alloy sheet. Moreover, during the forming process, heat is generated by plastic deformation and the heat loss by conduction and by radiation and convection to the punch as well as to the environment can result in several property changes of the work piece. Therefore, this underscores the need for accurate methods to investigate a forming process of magnesium alloy not only deformation behavior but also heat transfer process, a task to which the finite element method is well suited. Finite element method (FEM) is a very effective method to simulate the forming processes with accurate prediction of the deformation behaviors. FEM can be used not only in the analysis but also in the design to estimate the optimum conditions of the forming processes. This can be done before carrying out the actual experiments for an economical and successful application of SPF to industrial components [8].

II. FORMABILITY OF MAGNESIUM ALLOYS

Magnesium possesses poor formability, difficult to be deformed at room temperature because of its hexagonal closed packed structure. It is necessary to enhance the forming temperature in order to improve formability of magnesium alloys effectively [9]. The research group has studied sheet metal forming processes of magnesium alloys in recent years [10–13] and found the mechanical properties of magnesium-alloy can be improved at elevated temperatures [14–18]. In this formability of magnesium alloy (more focus been given on AZ31 sheets) investigated by the experiment and FE analysis, various process like stamping, warm drawing, deep drawing, friction Stir

processing, Mg produced either by direct chill or twin roll continuous casting have been taken into account. Popular process used in assessment of formability of sheet metal is reviewed to determine the optimal processing parameters and explore novel forming technique [19, 20]. Fuh-Kuo Chen, Tyng-Bin Huang [21] conducted various experiments to study the formability of stamping magnesium-alloy AZ31 sheets of 1.2mm thickness at elevated temperatures. The mechanical properties of magnesium-alloy AZ31 rectangular specimens having the constant length of 140 mm, but with different widths ranging from 20 to 140mm in an increment of 20 mm, were tested at various temperatures ranging from room temperature to 400°C. A heating furnace was mounted on the MTS810 test machine and tensile tests at elevated temperatures were performed. Forming characteristics of AZ31 sheets, such as forming limit, conical cup value (CCV), spring back and minimum bending radius, were also examined by experiments. The stress-strain relations indicated that AZ31 sheets had higher yield stress and smaller elongation at room temperature, but the yield stress, the work-hardening coefficient n , dropped significantly when the sheet was heated to a temperature higher than 200°C. The experimental results showed that AZ31 sheets exhibited poor formability at room temperature, but the formability was improved significantly with greater possibility of local deformation, at elevated temperatures as in Fig.1 The sheets sustained more deformation before fracture at elevated forming temperatures. The V-bend tests revealed the spring back was reduced when AZ31 sheets were stamped at higher temperatures. In addition, the conical cup value (CCV) tests performed in the present study revealed that an optimum forming temperature, which was below 400 °C, existed, and a lower forming temperature has to be applied in the actual forming process.

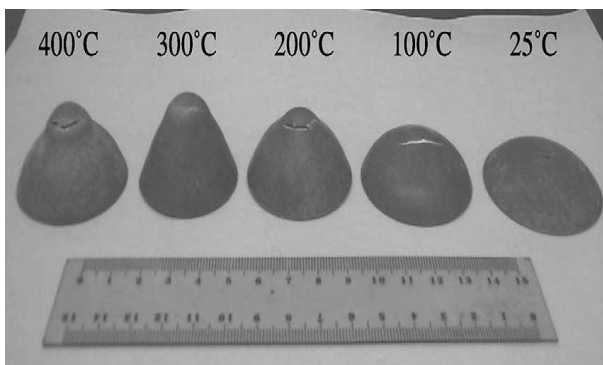


Fig.1.Fractured conical cups obtained from various temperatures.

In 2003, the square cup drawing of magnesium alloy AZ31 (aluminum 3%, zinc 1%) sheets was studied by experimental approach and the finite element analysis (The finite element software PAM STAMP). The mechanical properties of AZ31 sheets with 1.2 mm thickness according to the ASTM standards, at various forming temperatures were first obtained from the tensile tests and the forming limit tests. The test results in [22] indicated that AZ31 sheets exhibited poor formability at room temperature, but the formability could be improved significantly at elevated temperatures up to 200°C. The finite element simulations

investigated the effects of process parameters, such as punch and die corner radii, and forming temperature, on the formability of square cup drawing with AZ31 sheets. The other simulation parameters were: die clearance of 0.6 mm on each side, blank-holder force of 2.5kN, coefficient of friction of 0.1, and punch speed of 3 mm/s. In order to validate the finite element analysis, the deep drawing of square cups of AZ31 sheets at elevated temperatures was also performed. Both the tensile tests and the forming limit tests showed an inferior formability of AZ31 sheets if formed at room temperature. The formability dramatically improved when the AZ31 sheet was stamped at elevated temperatures. The punch radius (R_p) of 5 mm, die radius (R_d) of 6 mm, and corner radius (R_c) of 8 mm were the tooling dimensions used in both the finite element simulations and the experiments, both the finite element results and the experimental data revealed an optimum forming temperature of 200°C for the drawing of square cups, with 0.5 mm thick AZ31 sheets. This optimum temperature may vary with the sheet thickness and the part geometry to be formed. The finite element simulation results indicated that a larger punch radius allowed for a uniform material flow toward both of the two principal directions under the punch profile at corners delayed the occurrence of fracture and a smaller punch radius reduced the formability of square cup drawing. This strain-path pattern explained the reason why a larger punch radius leads to a better formability for the drawing of square cups. An optimum die corner radius for the drawing of square cups was also determined by both the finite element analysis and the experimental work. The investigation revealed that the formability improved as the die corner radius increased up to an optimum value, and became worse when the die corner radius was further increased. The strain path analysis indicated that the deformation of the sheet at the fracture location changed into the plane-strain mode from the stretch mode as the die corner radius was further increased from the optimum value, resulting in an early fracture since the plane-strain mode had a lower forming limit. The experimental data showed a good agreement with the simulation results, and the optimal forming temperature, punch radius and die corner radius were then determined for the square cup drawing of AZ31 sheets.

In this study [23], non-isothermal finite element (FE) simulation (DEFORM 2D and 3D, coupled thermo elastic-visco-plastic commercial FEM codes) has been conducted for forming round cups and rectangular pans from Mg alloy AZ31B sheet at elevated temperatures. The results were compared with experiments, conducted at the Technical University, Hanover. Load-stroke curve, thickness distribution and temperature distribution in the sheet obtained in experiments [24, 25] were compared with FE simulation results for various forming temperatures. The flow stress for the calculated strains, temperature and strain rate were logarithmically interpolated and extrapolated using the available input data. The friction coefficient, μ , used in the simulations was obtained from the strip draw test conducted by Droder [24] and Doege et al. [26] and it was assumed not to vary locally with interface temperature and pressure. The interface heat transfer coefficient was assumed to be uniform for the entire surface and the value was selected based on the results published in the literature [27]. The forming load predicted by simulation for round

cup and rectangular pan overestimated the experimental results. The trend predicted by simulation matched well with experiment. Higher punch force in the simulation could be due to the high frictional shear stress at interface. Coulomb friction coefficient of $\mu = 0.1$ was used in the simulation. Von Mises yield criteria was used in simulation to describe the yield surface of Mg alloy sheets. In the warm sheet forming of round cup and rectangular pan, the maximum thinning and tearing was observed at the cup wall in simulation and experiment. This was contrary to the observations in conventional stamping where the thinning occurred in the punch corner radius. This could be due to the fact that the cup walls in warm forming were at high temperature compared to punch corners, thus, the yield strength of material in cup wall was low compared to punch corner radius. A maximum thinning of 30% was observed in the simulation as compared to 10% in experiment. Excessive thinning observed in the simulation could be due to high process loads observed in simulation as compared to experiment. Simulation and experiments predicted increase in limiting draw ratio (LDR) with increase in temperature. Maximum LDR was obtained at the forming temperature of 200°C. LDR predicted by simulations for round cup for different forming temperatures were lower compared to the experimental results. Thermo-elastic-visco-plastic FEM code used in this study could successfully capture the deformation modes and the specific characteristics of the warm sheet forming process. At 300°C, the cup failed at the stroke of 32 mm. The maximum punch load obtained at all the simulated temperatures for LDR 2.3 was higher than the load obtained in experiment for corresponding temperatures. FE simulation results agreed well with experimental observations.

Tyng-Bin Huang et al. [28] studied the formability and non-isothermal deep drawing at elevated temperature of magnesium alloy AZ31B sheets by experiment and finite element analysis. The forming temperature, lubricant and sheet thickness was considered in this study. The peak punch force was increased as the diameter of blank increased. When the peak punch force was higher than the limit strength of the cup wall, the blank fractured, and the punch force decreased suddenly. The experimental results indicated that the highest limit drawing ratio (LDR) was at a forming temperature of 260°C for 0.58mm thick AZ31B sheet, and the highest LDR 2.63. The highest LDR was at a forming temperature of 200°C for 0.50mm thick AZ31B sheet, and the highest LDR 2.5 as shown in Fig.2 and Fig.3. The experimental data showed a good agreement with the simulation FEM code MSC Superform.

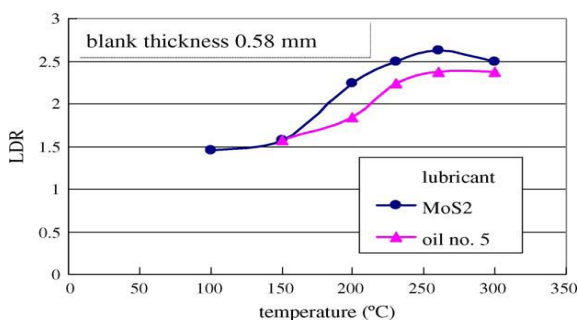


Fig.2. LDR from experiments at various forming temperature.

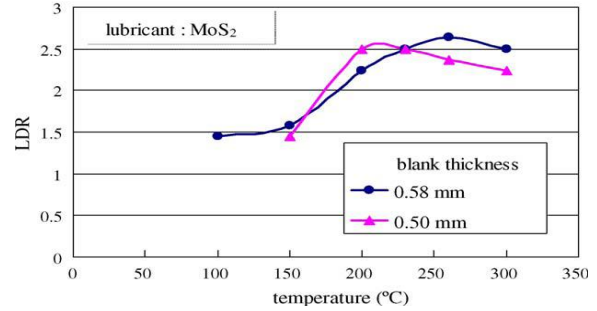


Fig.3. LDR of various sheet thickness from experiments.

In the research of [29], the forming limits on various forming process have been investigated using the experimental and FE analysis. Square cup drawing and stamping processes were used to investigate the formability of AZ31 sheet of 1.5mm thickness according to the ASTM standards. The mechanical properties of magnesium alloy AZ31 sheets at various temperatures ranging from room temperature to 400°C were obtained from experimental results and measured tensile properties were used to simulate the forming simulation by FEM commercial program, LSDyna™. The forming limit curve calculated based on the measured tensile properties could predict the fracture of formed part by FEM analysis. It showed some better formability at 400°C forming temperature. Fracture at 400°C forming temperature occurred by the diffuse necking due to the lower formability, because the work-hardening exponent was lower than that of 250 °C forming temperature. The best formability at 250 °C has been caused to the vital dynamic recrystallization as shown fig4. These experimental results well coincided with the FE analysis results predicted using the forming limit diagram (FLD) calculated by Keeler equation.

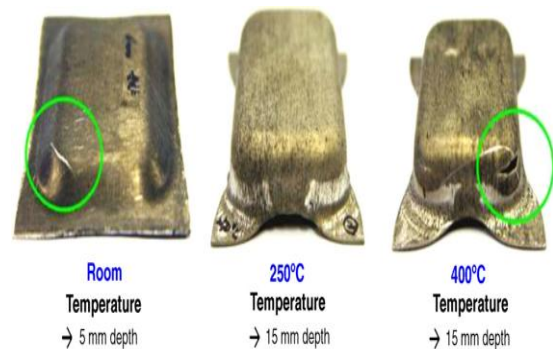


Fig.4. Square cups formed at each forming temperature.

A proper forming temperature range was determined in [30]. The effects of blank holding forces on the work piece quality were analyzed by warm deep drawing of cups from magnesium alloy sheets. Appropriate process parameters were selected to avoid forming defects effectively. In the paper, a rigid blank holder was used to adjust blank holding forces, using a 100 tonnes four-post multifunctional hydraulic press. A special liquid lubricant PTFE on the tool surfaces, punch diameter 65.6 mm/66.6 mm, punch shoulder radius 5 mm, die hole diameter 68mm and die shoulder radius 10 mm was used. The conditions of process defects, flange wrinkling and ruptures were analyzed. Experiments were carried out to verify the computer

simulation results. Efforts were made to optimize process parameters by analyzing the causes of defects in order to improve the Limit Drawing Ratio of magnesium alloy work pieces. Computer simulation with explicit finite element method was used to optimize the process parameters before carrying out the actual experiments. It was found that rolled magnesium alloy sheets had good deep drawing formability at a forming temperature range of 105–170°C with the limit drawing ratio up to 2.6. The cup of 0.4mm thickness had also been formed at this temperature. Some values greater than original thickness indicated the thickening on the flange. Formability would be reduced severely by excessive heating duration for a period of over 10 min in the preheated tools. Efforts were made to optimize process parameters by analyzing the causes of defects in order to improve the limit drawing ratio of magnesium alloy work pieces.

In the research work [31], an AZ31magnesium alloy sheet with excellent performances was fabricated by the cross-rolling and the uniform annealing treatments with annealing temperature 300°C and the holding time 1 h. The uniaxial tensile tests were conducted using a Gleeble 3500 thermal-mechanical simulator, and the mechanical properties of AZ31 magnesium alloy sheet were analyzed. Limiting drawing ratio (LDR) experiments were performed on double-acting hydraulic press. The uniaxial tensile tests showed that AZ31 magnesium alloy sheet was sensitive to the deforming temperatures and strain rates. The elongation increased from 18% to 50% with increasing temperatures from room temperatures to 200°C, and even reached 100% at 400°C. It was also found that the ductility of AZ31 magnesium alloy sheet increased sharply with the decrease of strain rates. The experiments showed that the LDR reached 2.0 at the forming temperature of 150°C and the drawing velocity of 15 mm/s. The AZ31 magnesium alloy sheet showed good formability at the temperature between 200 and 300 °C, LDR reached 3.0. The influences of drawing temperature and blank holder force on the formability are numerically investigated. A warm deep drawing process simulated by commercial explicit finite element code LS-Dyna demonstrated that variable blank holder force technology improved the LDR from 3.0 to 3.5, and decreased the wall thinning ratio from 15.21% to 12.35%.

ZE10 magnesium alloy sheets were prepared through ingot casting and the hot-rolling process. The mechanical properties, conical cup value (CCV), bore expanding performance, and limit drawing ratio (LDR) were investigated by [32] to examine the stamping formability of ZE10 alloy sheets, at temperatures ranging from 200 to 300 C. Tensile tests were carried out on SANSMT5105 testing machine. The results showed that the tensile strength decreased, whereas, plasticity, drawing-bulging performance, bore expanding properties, and deep drawing performance increased markedly at elevated temperatures. The CCV tests were performed on the universal testing machine according to the GB/T 15825.6-1995 standard. The CCV specimens could be drawn into the conical die's underside cylindrical hole from the conical cliff, without cracking, and could have the minimum CCV at 200 and 250°C. In the bore-expanding test, the bore (diameter 10mm) could be expanded to the dimension of the punch (dia. 25 mm) and the maximum bore-expanding

ratio could be achieved at above 150 C as in Fig.5. The limiting drawing ratio (LDR) of 2.85 was acquired during the deep drawing test at 230 °C as shown in Fig.6. with the punch temperature of 20 - 50 °C, the punch velocity of 50 mm * min⁻¹ and the mixture of graphite and cylinder grease as lubricant.

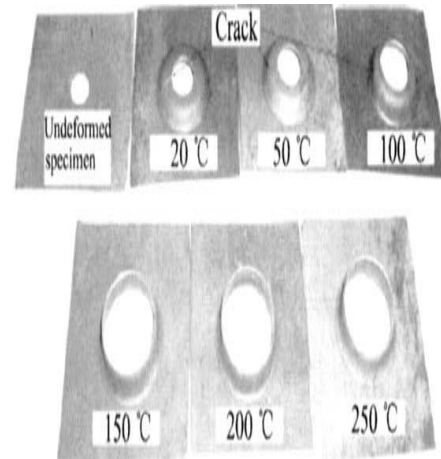


Fig.5 Specimens after bore-expanding tests at various temperatures

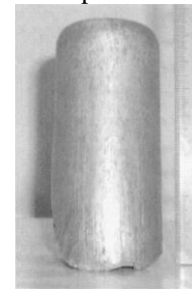


Fig. 6 LDR cup specimen at 230 C

Hai et.al [33] studied the deformation behavior of a cylindrical deep drawing of magnesium alloy sheets at elevated temperatures. Simulation was carried out by using a non-isothermal finite element based on DEFORM 3D commercial software. The experiments were conducted with a punch diameter of 40 mm, punch radius of 4 mm, die parameter of 42mm and die shoulder radius of 4 mm. The blank holder force was kept constant at 14 k N and the punch speed was 3mm/s. The tests were carried out at temperatures of tooling (die and blank holder) ranging from 423 to 523K while the temperature of punch was set at 298K. Teflon sheets were used as lubricant. In order to validate the finite element analysis, deep drawing test of cylindrical cup of AZ31 and AZ52 rolled sheets at given conditions was also performed. The LDRs of AZ31 and AZ52 increased with increasing in forming temperature and obtained the maximum values 3.2 and 2.8 at 498 K. the LDRs predicted by simulation were slightly lower compared to the experiment results. The punch force predicted by FE simulation overestimated the experiment results. This could be either due to high blank holder force and/or high shear stress caused by interface friction coefficient. The thermo-viscoplasticity FEM code, particularly Deform3D code could successfully capture the deformation behavior and specific characteristics of the warm sheet forming process. Maximum thinning of 32%

was observed in the simulation as compared to 27% in experiment. Thinning in the cup walls was greater than at the punch corner.

Forming limit diagrams were determined for a LZ61 alloy sheet with a thickness of 0.6mm by [34]. Uniaxial tension tests and press-forming tests were carried out at various temperatures. The influences of anisotropy and temperature on deformation characteristics were investigated. Formability parameters such as average plastic strain ratio, planar anisotropy, and work hardening exponent were determined by tensile test results. Tensile test results indicated that the normal anisotropy parameter value of LZ61 was not large enough to give good drawability at room temperature. The large negative value of the normal anisotropy parameter would result in serious ear formation during drawing process at room temperature. The forming limit diagrams have been experimentally evaluated at various temperatures. The LZ61 Mg alloy presented reasonable ductility at room temperature, but this alloy did not exhibit good stretchability and drawability. Anisotropic behaviors were observed in the mechanical properties at all test temperatures. The tensile properties and formability parameters were correlated with the forming limit diagrams. Some improvement of the stretchability of LZ61 alloy could be made by deforming the sheet at a higher temperature due to an increase in the normal anisotropy parameter value with temperature, though n value 0.159 dropped with increasing temperature. Increase in the normal anisotropy parameter value and decrease in the normal anisotropy parameter value with increasing temperature revealed that the drawability of LZ61 alloy could be improved by forming the sheet at elevated temperatures. Drawability improved for sheet deforming at 200°C, with the limiting fracture major strain about 25.22% and the limiting minor strain about 20.43% in tension–tension region, as shown in Fig. 7. In tension–compression region, the maximum major strain was about 43.35%, the minor strain around 24.75%.

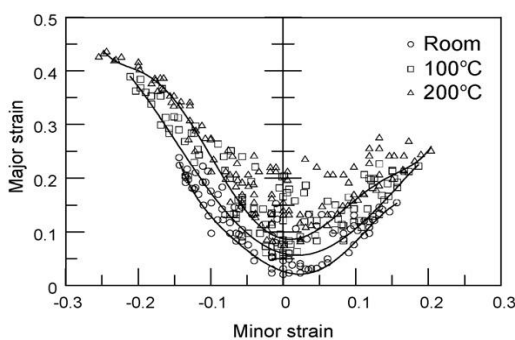


Fig. 7 Forming limit diagram of the LZ61 sheet at various temperatures.

In forming the Mg alloy AZ31-O, significant formability improvement was achieved at elevated temperatures compared to room temperature. Elevated temperature hydraulic bulge tests for Mg AZ31-O alloy sheets were conducted by [35] at the Institute for Production Engineering and Forming Machines (PtU), of Technische Universität Darmstadt using a submerged tool, designed to minimize the temperature variation in the sheet. Experiments were conducted between room temperature

and 225°C, at various approximate true strain rates. Strains upto 0.7 were obtained at 225°C and 0.025 s⁻¹. At higher temperatures and lower strain rates, thermal/work softening or stress dropped due to diffused necking. Bulge profiles at different bulge heights were measured using a CMM and the best radius values were calculated through least-square fit using several measured points. Residual plots were made to demonstrate the amount of deviation from a sphere with increasing bulge height. Twelve and 38mm bulge heights were obtained at room and elevated temperatures, respectively as shown in Fig.8. Measured and calculated bulge radius and thickness values were compared with the available analytical models and Amount of error that occurred in flow stress calculation by deploying the well-known membrane theory was investigated. Minimum thickness values were not always observed at the apex. Analytical models for thickness and radius calculations were found to be acceptable up to h_d/d_c ratios of 0.2 (h_d approx. 25 mm). At higher bulge heights ($h_d > 30$), comparisons between measured, calculated thickness and bulge radius values showed a difference of 8% and 6% from experiments, respectively.

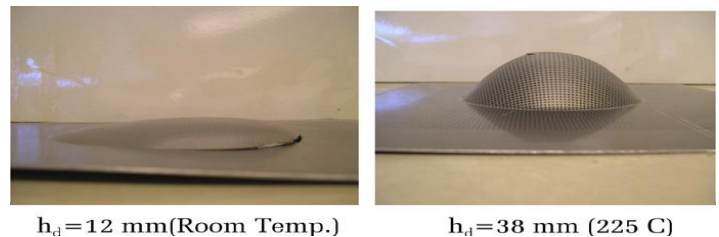


Fig.8. Variation in formability at room and elevated temperatures

In [36], warm formability of three sheet magnesium alloys AZ31, ZK10, and ZW41 was measured under isothermal conditions using the Ohio State University test (OSU) formability test adapted for testing at elevated temperatures ranging from 150 to 350°C and at a punch velocity of 1 mm/s. The punch and die were machined from D2 tool steel (ASTM A 681-08, 2007). The adapted test reliably enforced the plane strain tension over a significant fraction of the sample, thus providing an assessment of FLD(0), the minimum major strain value on a forming limit diagram. By mathematically modeling the strain as a function of punch displacement, a case was made that the punch displacement itself provided an expedient approach to ranking the relative formability of sheet metals. Combined with knowledge of the constitutive behavior of the material, the punch displacement strain relationship provided an explanation for the observed shape of the punch load versus displacement curves. Test results showed good formability at mildly elevated temperatures for the conventional magnesium alloys, AZ31 and ZK10, as well as superior formability of alloy ZW41, with an FLD(0) value of ~0.44 at 215°C (~37% improvement over the conventional). An anomalous formability decrease led to a formability minimum in all three alloys in the range of $T=250^\circ\text{C}$, due to the transition in failure mechanism from localized shear band-related plastic instability at low temperatures to more uniform necking at the highest temperatures. OSU formability test results showed that a new magnesium sheet alloy, yttrium-containing ZW41, was significantly more formable than

traditional magnesium alloys AZ31 and ZK10. The improvement was linked to a more random texture in the new alloy, which diminished the tendency for gross, catastrophic shear instability.

The authors in [37] proposed an experimental methodology based on the Marciniak stretch forming test to investigate sheet formability of the Mg alloy AZ31 in warm conditions (200°C), taking into account not only the temperature but also the strain rate effect. Specific tools to carry out such a formability test were designed and created: a flat punch of 92mm diameter (in line with Marciniak's test), embedded heating system was adopted in order to heat the central part of the specimen both rapidly and uniformly, where ruptures were forced due to the presence of a driving sheet between the specimen and the punch. A Digital Image Correlation system was also embedded in the formability equipment in order to acquire major and minor strains continuously and evaluated the moment and location of failures as in Fig.9. Finite Element simulations were run in order to define punch speed profiles (which differed according to the geometry of the specimen) that were able to keep a constant equivalent strain rate in the region where ruptures were forced. Experimental tests implementing the punch speed profiles were carried out in order to obtain temperature, load and strain data. FLCs at two different strain rate levels (0.02s⁻¹ and 0.002 s⁻¹) shifted upwards by about 35% at a temperature of 200°C. The proposed approach for FLC evaluation was effective for materials whose properties were strongly influenced by the strain rate. Such FLC data could be usefully implemented in numerical simulations of sheet metal forming processes: while tensile tests were used to determine variations in mechanical behaviour according to the strain rate, both the strain rate sensitivity index and the maximum elongation increased in line with the temperature. The punch speed profile seemed to be effective in keeping the strain rate constant for almost the whole test, reasonably near to the target strain rate value. The FLCs evaluated in this work allow us to determine the occurrence of strain path-dependent critical conditions according to the strain rate.

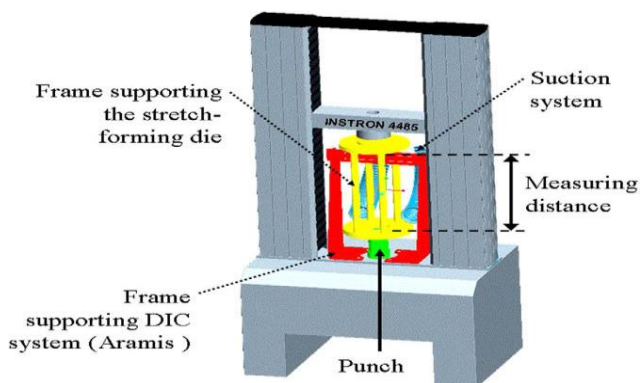


Fig. 9 Equipment for formability evaluation.

The sheet formability of AZ31 magnesium alloy has been widely investigated in [38] by means of uniaxial tensile and hemispherical punch tests, performed at different temperatures and strain rates, using samples with different fibre orientations on hydraulic testing machine by heating the samples, in the temperature range from 200 to 300°C, using a resistance furnace. Different samples keeping length

constant (100mm) and the width were varied from 12.5 to 100mm. The results of the uniaxial tensile tests were analysed in terms of flow curves, ductility and micro structural evolution. They showed that the flow stress decreased, strain rate reduced and ductility, strain rate sensitivity coefficient increased with increase in temperature whilst the strain hardening exponent increased with increasing strain rate and decreasing temperature and the ductility was independent of the fibre orientation, slightly affecting the flow stress values. The constitutive behaviour and strain rate analysed has been described using the well-known Backofen-type equation: $\sigma = A \epsilon^n \dot{\epsilon}^m$ where A, the strength coefficient, n the strain hardening exponent and m the strain rate sensitivity coefficient. Both m- and n-values were affected by the fibre orientation; The formability, described by the forming limit curves (FLCs), improved with increased temperature and decreasing strain rate with a more marked effect in the stretching side of the forming limit diagram; such behaviours were related to the micro structural evolution, that was strongly influenced by temperature and strain rate, due to the occurrence of grain boundary sliding, dynamic recrystallisation and grain growth. The formability along the rolling direction (RD) was higher than that along the transversal one (TD), even if the FLCs obtained along the TD had a larger extension in the drawing side than the ones along the RD. Such behaviours were related to the constitutive parameters and microstructure developed during deformation.

The authors in the study [39] focused on the improvement of formability of MgAZ31B alloy through friction stir processing. The friction stir processing was done on a vertical head milling machine, with the position of the tool fixed, relative to the surface of the sheet. A non-consumable taper threaded tool made of high carbon steel H13 with a shoulder diameter of 18 mm and a pin of diameter 6 mm and length 3 mm was used. Rectangular blanks of dimension 100 mm X 60 mm were used to conduct the LDH tests in plane-strain condition. Square specimens of size of 100 mm X 100 mm were blanked from the friction stir processed sheets for biaxial stretch forming. Specimens of size 140 mm long and 124 mm wide were used for Ohio State University test (OSU) test. All LDH tests were carried out in dry condition at a punch speed of 0.3 mm/s on a 50 ton hydraulic press. An optimum blank holding force in the range of 3–4 ton was applied. The processed samples were evaluated for elongation, strain hardening index, n, work hardening capacity, 1/YR and anisotropy, r. The formability of the processed samples was evaluated through two test methods namely the LDH test and Ohio State University test (OSU). The same trend of the formability behavior was found for all the samples tested irrespective of the different testing procedures followed. Further, it has been found that both rotational speed and traverse speed had significant effect on the formability. An inverse relationship existed between the yield strength and the LDH. It was found that, work hardening capacity, the inverse of yield ratio (YR), was an indicator of LDH value rather than the yield strength and uniform elongation. A statistical model has been developed to predict the formability characteristics. It was seen that, the friction stir processed material, has more FLD (0) values, and also higher than the base metal. FLD (0) was the lowest point in the FLD diagram. It was in the major

strain region and measured at plane-strain condition. The FLD of the base metal and processed metal are shown in Fig. 10. The developed model could replace the tedious formability testing procedures with a simple uniaxial tensile test, it was presumed that formability index, $FI = (e \times n \times 1/YR)/r$, FI was more for the samples with low r value, and thus, in the developed model, r was in the denominator. The results obtained from the developed model could be used as a basis for establishing the optimal friction stir process parameters, to develop the desired formability properties in Mg AZ31 alloy.

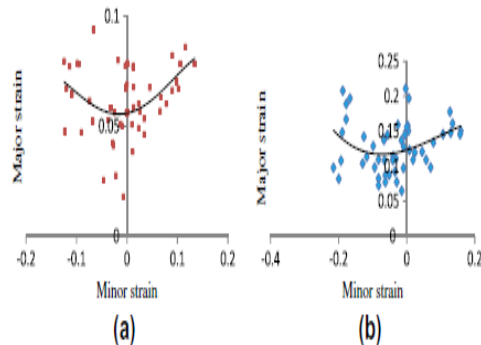


Fig.10 Forming Limits of (a) base sample (b) FSP sample

Formability of four magnesium AZ31B sheet materials, produced either by direct chill or twin roll continuous casting, was investigated by [40] at 400°C and $5 \times 10^{-3} \text{s}^{-1}$ using pneumatic stretching. Sheet specimens were deformed through a series of four elliptical die inserts, with aspect ratios ranging between 1.0 and 0.4, producing ellipsoidal domes with different biaxial strain combinations. Testing was carried out in two scenarios, i.e. with the major strains aligned either along or across the rolling direction of the material. Circle grid analysis was then used to map the planar strains of the deformed specimens; the latter were used to generate comprehensive material forming limits curves (FLCs) that bound the safe, marginal and failure deformation zones. For all four sheets, the 0° orientation showed greater formability limits than the 90° orientation. This was further confirmed through dome height measurements. Orientation effects were quantified by constructing a “composite FLD” for each of the four sheets; the diagrams collectively showed that greater formability limits were achieved along the material’s rolling direction, when the major strains accumulated along the rolling direction, and are larger than the minor strains. Detailed comparisons between the four sheets were carried out based on formability limits, deformation uniformity and maximum dome height prior to failure and fracture surface morphology and chemistry. By comparing the formability results obtained for the four sheets, it was found that the sheets produced by TRC casting outperformed the one produced by DC casting mainly due to the finer grain size of the former compared to the latter. Disparities in formability were linked to differences in grain structure and material inhomogeneities. Formability limits reduced and premature failure was due to internal material defects in the form of long oxide stringers. TRC cast sheets were more prone to this kind of defects.

III. CONCLUSION

The main objective of the present study is that of extending and improving research into the combined effect of strain rate and temperature on material formability. Formability test results showed that a new magnesium sheet alloy, yttrium-containing ZW41, was significantly more formable than traditional magnesium alloys AZ31 and ZK10. The improvement was linked to a more random texture in the new alloy, which diminished the tendency for gross, catastrophic shear instability. The formability of Magnesium alloys increased at elevated temperatures depending on the thickness and the forming process adopted. A brief review of formability of Magnesium alloys at elevated temperatures presented here would serve as platform for further development in light-weight metals and alloys and helpful in meeting the great demand for enhancement of fuel efficiency and dynamic performance of structural components in the aerospace, electronics, and automobile industry to replace some existing materials.

REFERENCES

- [1] M.B.L. Mordike, T. Ebert, Magnesium properties—application—potential, *Materials Science and Engineering A302* (2001) 37–45.
- [2] H. Furuya, N. Kogiso, S. Matunaga, K. Senda, Applications of magnesium-alloys for aerospace structure systems, *Materials Science Forum 350-351* (2000) 341–348.
- [3] F.-K. Chen, T.-B. Huang, Formability of stamping magnesium-alloy AZ31 sheets, *J. Mater. Process. Technol.* 142 (2003) 643–647.
- [4] F.-K. Chen, T.-B. Huang, C.-K. Chang, Deep drawing of square cups with magnesium alloy AZ31 sheets, *Int. J. Mach. Tools Manuf.* 43 (2003) 1553–1559.
- [5] E. Doege, K. Droeder, Sheet metal forming of magnesium wrought alloys—formability and process technology, *J. Mater. Process. Technol.* 115 (2001) 14–19.
- [6] H. Takuda, T. Yoshii, N. Hatta, Finite-element analysis of the formability of a magnesium-based alloy AZ31 sheet, *J. Mater. Process. Technol.* 89/90 (1999) 135–140.
- [7] H. Palaniswamy, G. Ngaile, T. Altan, Finite element simulation of magnesium alloy sheet forming at elevated temperatures, *J. Mater. Process. Technol.* 146 (2004) 52–60.
- [8] El-Morsy, K. Manabe, FE analysis on temperature and deformation of magnesium alloy sheet in warm deep-drawing process, in: *Proceedings of Numisheet'02*, 2002, pp. 171–176.
- [9] E.B. Konopleva, H.J. McQueen, *Scrip. Mater.* 37 (1997) 1789.
- [10] S.H. Zhang, Z.T. Wang, Y. Xu, W.L. Zhou, Plastic forming technology of magnesium alloy products, *Met. Form. Technol.* 20 (2002) 1–4 (in Chinese).
- [11] S.H. Zhang, Y. Xu, Z.T. Wang, W.L. Zhou, *Forming technology of Mg alloys*, in: *World SCI-TECH R&D*, vol. 23, 2001, pp. 18–21 (in Chinese).
- [12] K. Zhang, Z.T. Wang, S.H. Zhang, C.F. Yu, Research on magnesium alloy (AZ31B) sheets with thermal deep-drawing process, *Light Alloy Fabric. Technol.* 31 (2003) 14–17 (in Chinese).

- [13] S.H. Zhang, Q.L. Jin, Z.T. Wang, Development of plasticity processing of magnesium alloys, *Mater. Sci. Forum* 426–432 (2003) 545–550.
- [14] H. Watanabe, H. Tsutsui, T. Mukai, M. Kohzu, S. Tnabe, K. Higashi, Deformation mechanism in a coarse-grained Mg–Al–Zn alloy at elevated temperatures, *Int. J. Plast.* 17 (2001) 387–397.
- [15] K. Kitazono, E. Sato, K. Kuribayashi, *Internal stress superplasticity in polycrystalline AZ31 magnesium alloy Scripta Materialia* 44 (2001) 2695–2702.
- [16] J. Kaneko, M. Sugamata, M. Numa, Y. Nishikawa, H. Takada, Effect of texture on the mechanical properties and formability of magnesium wrought materials, *J. Jpn. Instit. Met.* 64 (2) (2000) 141–147.
- [17] A. Mwembela, E.B. Konopleva, H.J. McQueen, Microstructural development in Mg alloy AZ31 during hot working, *Scripta Materialia* 37 (11) (1997) 1789–1795.
- [18] H. Takuda, H. Fujimoto, N. Hatta, Modeling on flow stress of Mg–Al–Zn alloys at elevated temperatures, *J.Mater. Proc. Technol.* 80–81 (1998) 513–516.
- [19] Hariharasudhan Palaniswam, Gracious Ngaile, Taylan Altan, Finite element simulation of magnesium alloy sheet forming at elevated temperatures, *Journal of Materials Processing Technology* 146 (2004) 52–60.
- [20] H. Takuda, N. Hatta, Numerical analysis of formability of a commercially pure zirconium sheet in some sheet forming processes, *Material Science and Engineering A* 242 (1998) 15–21.
- [21] Fuh-Kuo Chen, Tyng-Bin Huang, Formability of stamping magnesium-alloy AZ31 sheets, *Journal of Materials Processing Technology* 142 (2003) 643–647.
- [22] Fuh-Kuo Chen, Tyng-Bin Huang, Chih-Kun Chang, Deep drawing of square cups with magnesium alloy AZ31 sheets, *International Journal of Machine Tools & Manufacture* 43 (2003) 1553–1559.
- [23] Hariharasudhan Palaniswamy, Gracious Ngaile, Taylan Altan, Finite element simulation of magnesium alloy sheet forming at elevated temperatures, *Journal of Materials Processing Technology* 146 (2004) 52–60.
- [24] K. Droder, *Analysis on forming of thin magnesium sheets*, Ph.D.Dissertation, IFUM, University of Hanover, 1999 (in German).
- [25] E. Doege, W. Sebastian, K. Droder, G. Kurtz, *Increased formability of Mg-sheets using temperature controlled deep drawing tools*, in: M.Y. Demeri (Ed.), *Innovations in Processing and Manufacturing of Sheet Materials*, The Minerals, Metals and Materials Society, 2001, pp.53–60
- [26] E. Doege, K. Droder, Sheet metal formability of magnesium wrought alloys—formability and process technology, *J. Mater. Process. Technol.* 115 (2001) 14–19.
- [27] S.L. Semiatin, E.W. Collings, V.E. Wood, T. Altan, Determination of the interface heat transfer coefficient for non-isothermal bulk forming process, *J. Eng. Ind.* 109 (1987) 49–57.
- [28] Tyng-Bin Huang, Yung-An Tsai, Fuh-Kuo Chen, Finite element analysis and formability of non-isothermal deep drawing of AZ31B sheets, *Journal of Materials Processing Technology* 177 (2006) 142–145
- [29] Y.S. Lee, M.C. Kim, S.W. Kim, Y.N. Kwon, S.W. Choi, J.H. Lee, Experimental and analytical studies for forming limit of AZ31 alloy on warm sheet metal forming, *Journal of Materials Processing Technology* 187–188 (2007) 103–107
- [30] S.H. Zhang, K. Zhang, Y.C. Xu, Z.T. Wang, Y. Xu, Z.G. Wang, Deep-drawing of magnesium alloy sheets at warm temperatures, *Journal of Materials Processing Technology* 185 (2007) 147–151
- [31] Qun-Feng Chang, Da-Yong Li, Ying-Hong Peng, Xiao-Qin Zeng, Experimental and numerical study of warm deep drawing of AZ31 magnesium alloy sheet, *International Journal of Machine Tools & Manufacture* 47 (2007) 436–443
- [32] Liu Ying, Li Yuanyuan, Li Wei Stamping Formability of ZE10 Magnesium Alloy Sheets, *Journal of rare earths* 25 (2007) 480–484
- [33] D. V. Hai, S. Itoh, T. Sakai, S. Kamado and Y. Kojima, Experimentally and Numerical Study on Deep Drawing Process for Magnesium Alloy Sheet at Elevated Temperatures, *Materials Transactions*, Vol. 49, No. 5 (2008) pp. 1101 to 1106
- [34] Horng-Yu Wu, Geng-Zhong Zhou, Zhen-Wei Gao, Chui-Hung Chiu, Mechanical properties and formability of an Mg–6%Li–1%Zn alloy thin sheet at elevated temperatures, *journal of materials processing technology* 206 (2008) 419–424
- [35] S. Kaya, T. Altan, P. Groche, C. Klopsch, Determination of the flow stress of magnesium AZ31-O sheet at elevated temperatures using the hydraulic bulge test, *International Journal of Machine Tools & Manufacture* 48 (2008) 550–557
- [36] C.E. Dreyer, W.V. Chiu, R.H. Wagoner, S.R. Agnew, Formability of a more randomly textured magnesium alloy sheet: Application of an improved warm sheet formability test, *Journal of Materials Processing Technology* 210 (2010) 37–47
- [37] G. Palumbo, D. Sorgente, L. Tricarico, A numerical and experimental investigation of AZ31 formability at elevated temperatures using a constant strain rate test, *Materials and Design* 31 (2010) 1308–1316
- [38] C. Bruni, A. Forcellese, F. Gabrielli, M. Simoncini, Effect of temperature, strain rate and fibre orientation on the plastic flow behaviour and formability of AZ31 magnesium alloy, *Journal of Materials Processing Technology* 210 (2010) 1354–1363
- [39] G. Venkateswarlu, M.J. Davidson, G.R.N. Tagore, Modelling studies of sheet metal formability of friction stir processed Mg AZ31B alloy under stretch forming, *Materials and Design* 40 (2012) 1–6
- [40] F. Abu-Farha, R. Verma, L.G. Hector Jr. High temperature composite forming limit diagrams of four magnesium AZ31B sheets obtained by pneumatic stretching, *Journal of Materials Processing Technology* 212 (2012) 1414–1429

The Influence of Thyristor Controlled Phase Shifting Transformer on Balance Fault Analysis

Pratik Biswas

(Department of Electrical Engineering, Jalpaiguri Government Engineering College, India)

ABSTRACT: This paper analyses the method to limit fault currents and pre fault bus voltage by the use of Thyristor Controlled phase Shifting transformer (TCPST). The mathematical model of power system equipped with TCPST was systematically derived. The magnitude of the series reactance plays a very important role to limit the short circuit current, as well as TCPST inject a series voltage which reduces the pre fault bus voltage. The total fault current of the system get reduced with respect to the total fault current of the system without introducing TCPST. The effectiveness of TCPST in the proposed method is investigated in the phase fault.

Keywords: Balance Fault, FACTS, TCPST

I. INTRODUCTION

Flexible AC transmission systems (FACTS) devices are being increasingly used in a modern power system to improve both steady state and dynamic performances of the system. There are many types of FACTS devices, such as Unified Power Flow Controller (UPFC), Static Synchronous Compensator (STATCOM), Static Synchronous Series Compensator (SSSC), Thyristor Controlled Phase Shifter (TCPS), Static Var Compensator (SVC), etc. TCPST consists of a shunt transformer, a series transformer and a converter. The converter can be of ac-ac bridge type, pulse-width modulation (PWM) type, ac controller type, etc. The possibility of controlling electric power flow in a transmission system by using controllable solid state devices like TCSC and TCPST is well known. These series connected FACTS devices inject a series voltage with the line and thereby modulate the line reactance or the phase shift between the two end voltages. Recent advances in solid-state power electronics technology have made it possible to implement the above devices using power switching voltage source converters. On the other hand, short-circuit current levels increase with the addition of new lines, generators and transformers. This may surpass the short circuit current ratings of equipment, like for example circuit breakers, a frequent problem in power systems.

In today's security assessment tools the calculation of the fault level is a well established function. A fault level that exceeds the upper limit endangers the ability of circuit breakers to interrupt the short circuit current. If the fault level is beneath the lower limit, the connection of a major load results in unacceptable voltage drop.

The fault current limitation offered by modern controllers, characterized by their fast responses, may become an important assistance in the task to diminish such large currents. Since the fault clearing time is not instantaneous, depending on the operating time imposed by

protection and breaker operation delays, adequate control actions can be performed by this equipment

Although significant flexible features may be introduced in power control by those new devices, they still can be very expensive, and additional benefits like protection improvement should be investigated in order to verify the possibility of their application in the development of more secure and reliable networks

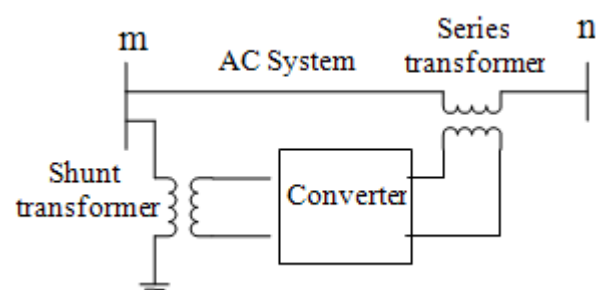
In this paper TCPST is analysis and proper modeling in a power system is discussed.

The fault limitation approach presented here explores this new technology and additional functionality offered by the series-connected FACTS controllers.

II. MODELING OF TCPST

Mathematical model: Figure 1a shows the schematic diagram of the Thyristor Controlled Phase Shifter (TCPS). The series transformer injects the voltage in series in the system. The active and reactive power injected by the series transformer is taken from the shunt transformer. For sake simplicity of analysis, the insignificant losses from transformer and converter is neglected. Thus the net complex power (real and reactive power) exchange between the TCPS and the system is zero. The injection of this complex power depends on the injection of a series voltage controlled by a converter.

Figure 1b shows the equivalent circuit of Fig. 1a. V_s and V_{sh} are represented by the synchronous voltage sources in series and shunt, respectively. X_{sh} is the leakage reactance of the shunt transformer. X'_s is the leakage reactance seen from primary side of series transformer is given by $X'_s = X_s + n^2 X_{sh}$ where n is the turn ratio number of the shunt transformer and X_s is the leakage reactance of the series transformer [2]



(a)

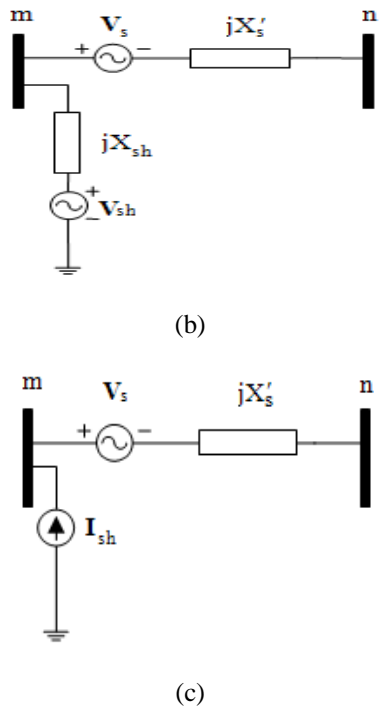


Figure 1: TCPST; (a) Schematic diagram of a TCPST; (b) a series and shunt synchronous voltage source equivalent; (c) a series injected voltage source and a shunt injected current source

The TCPST consists of two transformers; a shunt transformer or magnetizing transformer connected in parallel and a series transformer or booster transformer in series to the line (Fig.1). The current through the magnetizing transformer induces a voltage on the primary side of the booster transformer. The turn ratio of the shunt transformer is 1: n, and the turn ratio of the series transformer is 1:1. Compared to conventional phase shifting transformers, the mechanical tap changer is replaced by a thyristor controlled equivalent. The purpose of the TCPST is to control the power flow by shifting the transmission angle. In general, phase shifting is obtained by adding a perpendicular voltage vector in series with a phase. This vector is derived from the other two phases via shunt connected transformers. The perpendicular series voltage is made variable with a variety of power electronics topologies. A circuit concept that can handle voltage reversal can provide phase shift in either direction. This Controller is also referred to as Thyristor-Controlled Phase Angle Regulator (TCPAR). A phase shifter model can be represented by an equivalent circuit, which is shown in Fig 2. It consists of admittance in series with an ideal transformer having a complex turns ratio. [4]

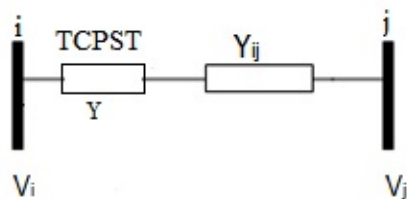


Figure 2: Admittance diagram of a system containing TCPST

The mathematical model of TCPST can be derived from Fig. 2.

$$\begin{bmatrix} I_i \\ I_j \end{bmatrix} = \begin{bmatrix} Y_{ij} + Y & -Y_{ij} \\ -Y_{ij} & Y_{ij} + Y \end{bmatrix} \begin{bmatrix} V_i \\ V_j \end{bmatrix}$$

Where Y_{ij} is the admittance of the line and Y is the admittance of the TCPST. The admittance of the TCPST is equal to the reciprocal of the reactance of the TCPST.

So, $Y = 1 / (X'_s)$. Where $X'_s = X_s + n^2 X_{sh}$. the turn ratio n is actually a complex quantity. Turn ratio equal to $n \angle \phi$.

III. FAULT VOLTAGE AND FAULT CURRENT LIMITATION

The fault current limitation is based on impedance control. Three phase faults can be controlled with limiting reactor. However, quiet small information exists on fault limitation with series voltage injection, in view of their recent introduction on networks. [1]

Since the series voltages are introduced through series coupling transformers or booster transformer, their respective leakage reactance contribute for fault current limitation, and this aspect must be considered in the analysis.

A. Fault Voltage Limitation

The most important factor that we are analyzing is the possibility of series voltage insertion, which can also be understood as an emulated reactance or capacitance inserted into the line. If a capacitive mode of compensation is in operation with voltage leading current, line fault current would be increased, and in the inductive mode of operation with voltage lagging current, the fault current could be substantially limited. The fast control action of series voltage with the introduction of power-electronics, could be significant in current limitation.

The insertion of series voltage is means of we want to reduce the voltage of the fault point. Which is in fact in agreement with the thevenin pre-fault bus voltage.

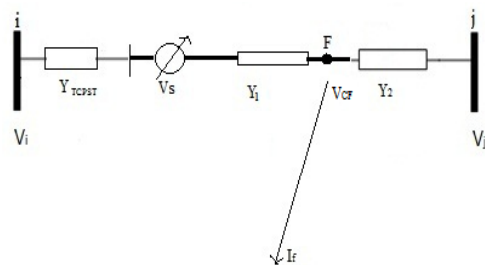


Figure 3: Fault occurring at the system containing TCPST

Now consider resistance of the line tends to zero, so $Y_{TCPST} = 1 / [X_{TCPST}]$ and $Y_1 = 1 / Z_1$.

Let's consider $X_0 = X_{TCPST} + X_1$
 So, $Y_0 = 1 / (R + jX_0) = 1 / [(1/Y_1) + (1/Y_{TCPST})]$

In the simple configuration of Fig 3, let's suppose the short circuit occurring at the point F. In the configuration it is

seen that TCPST is connected in the system. At the left of the fault the injecting source is V_s is opposition to the left equivalent source, having no effect in the line contribution.

So let's consider the fault point in Fig 3 and the admittance Y_{TCPST} added to the equivalent system admittance. The admittance to the left hand side of the fault point is considered Y_1 , and admittance right hand side of the fault point F is considered as Y_2 .

The voltage at the point F due to V_i and V_j without the presence of V_s is called uncompensated fault voltage V_F . the series voltage contribution is calculated applying the superposition theorem with the following network.

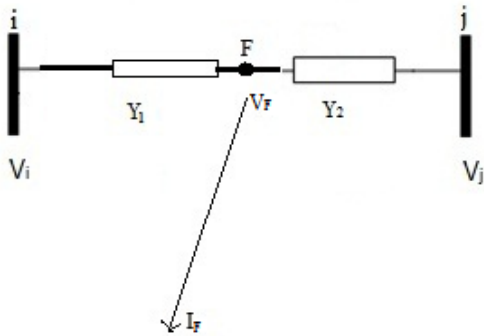


Figure 4: Uncompensated line with fault at point F.

Now applying the superposition theorem:

Consider the voltage V_{F1} at fault point when only source V_i is present, and V_{F2} when only source V_j is present.

$$V_{F1} = \frac{\frac{1}{Y_2}}{\frac{1}{Y_1} + \frac{1}{Y_2}} V_i \quad (\text{When only } V_i \text{ is present})$$

$$V_{F2} = \frac{\frac{1}{Y_1}}{\frac{1}{Y_1} + \frac{1}{Y_2}} V_j \quad (\text{When only } V_j \text{ is present})$$

So uncompensated fault voltage at point F

$$V_F = V_{F1} + V_{F2}$$

$$V_F = \frac{\frac{1}{Y_2}}{\frac{1}{Y_1} + \frac{1}{Y_2}} V_i + \frac{\frac{1}{Y_1}}{\frac{1}{Y_1} + \frac{1}{Y_2}} V_j$$

$$V_F = \frac{V_i Y_1 + V_j Y_2}{Y_1 + Y_2}$$

Now to calculate the compensated line fault voltage we have to apply superposition theorem, so consider a network where only series connected voltage source is present.

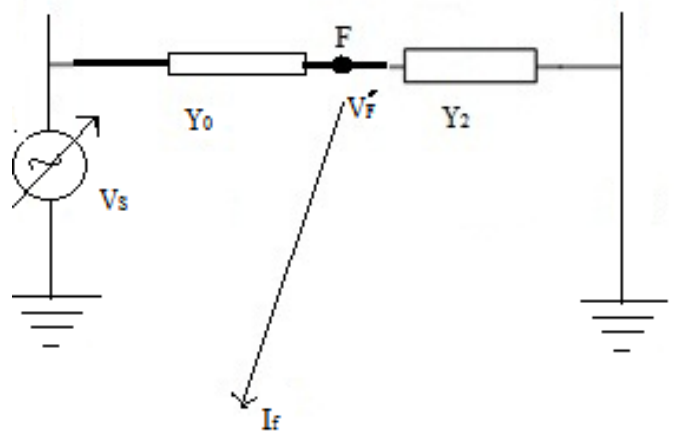


Figure 5: series voltage contribution to the fault voltage

Now the compensated fault voltage $V_{F'}$.

$$V_{F1}' = \frac{\frac{1}{Y_2}}{\frac{1}{Y_0} + \frac{1}{Y_2}} V_s$$

$$= \frac{Y_0}{Y_0 + Y_2} V_s$$

Now compensated fault voltage V_{CF}

$$V_{CF} = V_F + V_{F1}'$$

$$= \frac{V_i Y_1 + V_j Y_2}{Y_1 + Y_2} + \frac{Y_0}{Y_0 + Y_2} V_s$$

To minimize the fault voltage, the compensation term V_{F1}' has to be in opposition to V_F , with the series voltage inserted at its maximum magnitude during the fault period.

B Fault Current Limitation

The calculation of the three phase fault is well established in today's security assessment. For solving this problem the admittance matrix Y , used for power flow calculation, must be expanded to Y' by the transient reactance of generators

The impedance matrix $Z = \text{inv}(Y)$

Short Circuit current $I_f = V_{CF} * Y$

Now uncompensated fault current I_f

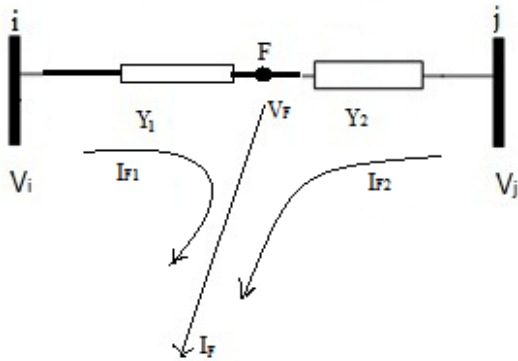


Figure 6: fault current through a network without TCPST

$$I_f = I_{F1} + I_{F2}$$

$$= V_F Y_1 + V_F Y_2$$

$$= V_F (Y_1 + Y_2)$$

After connecting TCPST in the network fault current I_{CF}

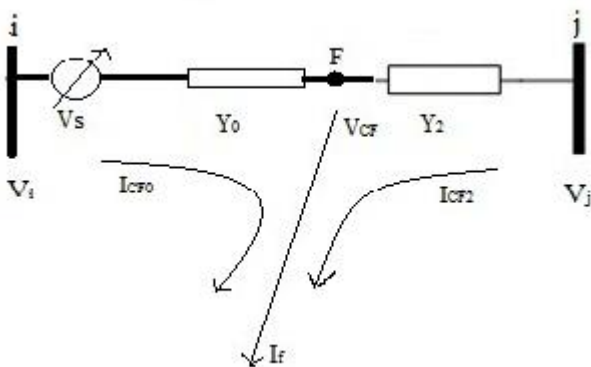


Figure 7: fault current through TCPST connected network.

Now, $I_{CF} = I_{CF0} + I_{CF2}$

$$= V_{CF} \cdot Y_0 + V_{CF} \cdot Y_2$$

Where $Y_0 = 1/X_0 = 1/[(1/Y_1) + (1/Y_{TCPST})]$

$$= 1/[X_{TCPST} + X_1]$$

X_{TCPST} is the reactance of TCPST. So after connecting the TCPST reactance will be increased, so Y_0 will be less. So I_{CF0} will be less. V_{CF} will less due to series voltage injection, so I_{CF2} will be less. Therefore the fault current I_{CF} will be limited

IV. PROBLEM FORMULATION AND SIMULATION RESULT

The above proposed method is tested in a power system network is shown in the diagram. The system tested in MATLAB platform. The power system network model is a 10 bus system. In the taken system TCPST is connected between bus no 7 and 9. The fault occurs in the line between bus no 7 and bus no 9. For simplification in calculation the fault point is considered as a bus and the no of the bus is 8. So TCPST is connected now in between bus no 7 and fault point or bus no 8.

. The transient reactance of the generators on a 100 MVA base are given below.

Table 2: Transient reactance of generators

Generator transient reactance in p.u		
Generator no.	R_a	X_d'
1	0	0.20
10	0	0.15
11	0	0.25

The line data containing the series resistance and reactance is in per unit, and one half of the total capacitance is in per unit susceptance on a 100 MVA base.

Table 1: Line data of the system are given below

Line Data				
Bus no	Bus no	R (p.u)	X (p.u)	$\frac{1}{2} B$ (p.u)
1	2	0.00	0.06	0.0000
2	3	0.08	0.30	0.0004
2	5	0.04	0.15	0.0002
2	6	0.12	0.45	0.0005
3	4	0.10	0.40	0.0005
3	6	0.04	0.40	0.0005
4	6	0.15	0.60	0.0008
4	9	0.18	0.70	0.0009
4	10	0.00	0.08	0.0000
5	7	0.05	0.43	0.0003
7	8	0.06	0.35	0.0004
7	11	0.00	0.10	0.0000
8	9	0.052	0.48	0.0000

The system diagram given below

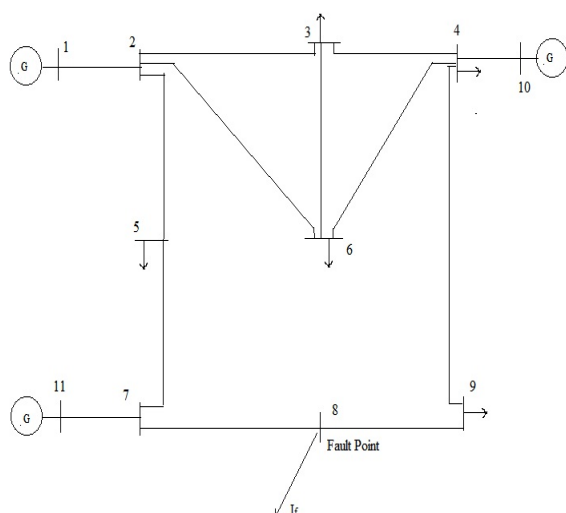


Figure 8: Single line diagram of tested system

The TCPST is connected is in 40% compensation.

Now the system is simulated in MATLAB platform. The system is tested with and without having TCPST in the system.

Without having TCPST it is seen that the pre-fault bus voltage at the fault point or bus no 8 is 1 p.u. it is seen that after connecting TCPST the pre fault voltage of the fault point is 0.81 p.u. So it is cleared that after connecting TCPST the pre fault voltage decreased by 19%.

The limitation has strong dependence on the maximum dependence on the maximum series voltage developed by the converter and the following cases the maximum value adopted is 0.4.

From the simulation result we see that line without having TCPST the total fault current is 2.3622 p.u. and the compensating total fault current is decreased to 2.0515. so fault current decreased by 0.31 p.u. As the pre-fault voltage and post fault current is limited by series compensated line having TCPST, so it is clearly observed that series compensated line having TCPST can decrease the fault level.

Figure captions appear below the figure, are flush left, and are in lower case letters. When referring to a figure in the body of the text, the abbreviation "Fig." is used. Figures should be numbered in the order they appear in the text.

Table captions appear centered above the table in upper and lower case letters. When referring to a table in the text, no abbreviation is used and "Table" is capitalized.

V. CONCLUSION

The influence of TCPST in three phase fault voltage and fault current limitation is discussed in this paper. Here TCPST insert a series connected voltage source in the line which actually opposing the bus voltage. So the pre-fault voltage of the fault point is reduced with the presence of TCPST. We have also seen that TCPST also limit the fault

current. So fault level will decrease due to decrease of pre-fault voltage and post fault current. Due to reduction in fault level the dynamic nature as well as transient stability of the system will increase. As the fault current in the system is in limit the thermal equilibrium condition will not hampered.

The future research work will be on optimal location of TCPST in a power system and control of TCPST in both balanced and unbalanced fault analysis.

REFERENCES

- [1] L. C. Zanetta Jr., M.Pereira "Limitation of Fault Current with the UPFC" in *the International Conference on power Systems Transients(IPST'07) in Lyon, France on June 4-7, 2007*
- [2] Prechanon Kumkratug, "Improvement of Transient Stability of Power System by Thyristor Controlled Phase Shifting Transformer" *American Journal of Applied Sciences*7(11):1495-1499,2010 ISSN 1546-9239
- [3] P. Kumkratug, M. H. Haque, "New model of a thyristor controlled phase shifter in a simple power system"
- [4] D. Devaraj, R. Narmatha Banu, "Optimal Power Flow for Steady State Security Enhancement using Enhanced Genetic Algorithm with FACTS Devices" *Asian Power Electronics Journal, Vol. 4, No.3 December 2010*
- [5] Rafael Mihalic, Uros Gabrijel, "Transient stability assessment of systems comprising phase-shifting FACTS devices by direct methods" *Electrical Power and Energy Systems* 26 (2004) 445–453.
- [6] M. Balasubba Reddy, Y. P. Obulesh, S. Sivanaga Raju. "Analysis and simulation of series facts devices to minimize transmission loss and generation cost" *International Journal of Advances in Engineering & Technology, Jan 2012, Vol. 2, Issue 1, pp. 463-473.*
- [7] G. Glanzmann, Student Member IEEE, G. Andersson, Fellow IEEE, "Coordinated Control of FACTS Devices based on Optimal Power Flow"
- [8] N. G. Hingorani and L. Gyugyi, *Understanding FACTS concepts and technology of flexible AC transmission systems*(IEEE press,2000)
- [9] M. Balasubba Reddy, Dr. Y.P. Obulesh, Dr.S.Sivanaga Raju, "A SOL algorithm and simulation of TCPST for optimal power flow solution using NR method" *International Journal of Modern Engineering Research (IJMER), Vol.1, Issue.2, pp-407-412.*
- [10] R.L. Vasquez-Arnez, L.C. Zanetta Jr., F.A. Moreira, "Effective limitation of line fault currents by means of the Series-connected vsc-based facts devices" *Revista Controle & Automação/Vol.17 no.4/Outubro, Novembro e Dezembro 2006.*

Pratik Biswas: Bachelor of Technology from Jalpaiguri Govt. Engineering College in Electrical Engineering(2012). His research interests are Power System and Power Electronics, FACTS, Lightning.

Market Based Transmission Expansion Planning For Indian Power Systems

G. Srinivasulu¹, Dr. B. Subramanyam², K. V. Kishore³, P. Udai Kumar⁴
^{1,3,4}(Associate Professor, Dept of Electrical & Electronics Engineering, Narayana Engineering College
Nellore – 524004 – India)
²(Professor, Dept of Electrical & Electronics Engineering, KL University, Guntur – India)

Abstract: In this paper a new market Based approach for transmission expansion planning in deregulated power systems is presented. Restructuring and deregulation has exposed transmission planner to new objectives and uncertainties. Therefore, new criteria and approaches are needed for transmission planning in deregulated environments. In this paper we introduced a new method for computing the Locational Marginal Prices and new market-based criteria for transmission expansion planning in deregulated environments. The presented approach is applied to Southern Region (SR) 48-bus Indian System.

Keywords: Competitive electric market, Transmission expansion planning, Uncertainty, Scenario techniques, power transmission planning, price profile, risk analysis, uncertainty.

I. INTRODUCTION

Transmission system is one of the major components of the electric power industry. If the electric loads increases, transmission expansion planning should be increased timely and proper way to facilitate and promote competition. Restructuring and deregulation of the power industry have changed the aims of transmission expansion planning and increased the uncertainties. Due to these changes, new approaches and criteria are needed for transmission expansion planning in deregulated power systems.

Transmission expansion planning approaches can be classified into:

- Non-deterministic approaches, and
- Deterministic.

In non-deterministic approaches the expansion plan is designed for all possible cases which may occur in future with considering the occurrence probability of them.

In deterministic approaches the expansion plan is designed only for the worst cases of the system without considering the probability of occurrence (degree of occurrence) of them. Hence, Non-deterministic approaches are able to take into account the past experience and future expectations.

Non-deterministic approaches can be classified in:

- Static, and
- Dynamic approaches.

2.1 Non-deterministic Transmission Expansion Planning Approaches

Uncertainties can be classified in two categories:

- Random, and
- Non-random uncertainties.

Random uncertainties are deviation of those parameters which are repeatable and have a known probability

distribution. Hence, their statistics can be derived from the past observations. Uncertainty in load is in this category.

Non-random uncertainties are evolution of parameters which are not repeatable and hence their statistics cannot be derived from the past observations.

Non-deterministic approaches which have been used for transmission expansion planning are:

- probabilistic load flow,
- probabilistic based reliability criteria,
- scenario technique,
- decision analysis, and
- Fuzzy decision making.

Probabilistic load flow and probabilistic based reliability criteria approaches take into account random uncertainties. Scenario technique considers the non-random uncertainties. Decision analysis is a proper method for dynamic programming. Fuzzy decision making considers imprecision and vague data.

Review of the presented approaches and discussion of their advantages and drawbacks helps the procedure of presenting new approaches and criteria for transmission planning in deregulated environments. State of the art review on transmission expansion planning approaches is presented in this paper.

Transmission expansion planning approaches for:

- Regulated, and
- Deregulated power systems.

The main objective of power system planning in regulated power systems is to meet the demand of loads, while maintaining power system reliability. In this environment uncertainty is low. Transmission expansion planning is centralized and coordinated with generation expansion planning. Planners have access to the required information for planning. Therefore, planners can design the

least cost transmission plan based on the certain reliability criteria.

In deregulated power systems participants take their decisions independently. They change their strategies frequently to acquire more information from the market to maximize their benefits. Consumers adjust their loads according to the price signals. Availability of independent power producers is uncertain. Wheeling powers are time varying and affect the nodal prices of the control areas that they pass through. Transmission expansion planning is not coordinated with generation expansion planning. Hence, there is not a specified pattern for load and dispatched power in deregulated power systems. Due to these uncertainties expansion of transmission networks have been faced with great risks in deregulated environments. Therefore, the final plan must be selected after the risk assessment of all solutions. Since risk assessment is characteristically based on probabilistic and stochastic methods, probabilistic methods should be developed for transmission planning in deregulated power systems.

2.2 Transmission Expansion Planning Approaches for Deregulated Power Systems

From the viewpoint of transmission planner, there are two major differences between transmission expansion planning in regulated and deregulated environments:

- Objectives of transmission expansion planning in deregulated power systems differ from those of the regulated ones.
- Uncertainties in deregulated power systems are much more than in regulated ones.

In this section objectives of transmission expansion planning in deregulated power systems and uncertainties in deregulated power systems are discussed.

2.3 Objectives of Transmission Expansion Planning in Deregulated Power Systems

In general, the main objective of transmission expansion planning in deregulated power systems is to provide a non-discriminatory competitive environment for all stakeholders, while maintaining power system reliability. Specifically, the objective of transmission expansion planning is providing for the desires of stakeholders. The desires of stakeholders in transmission expansion are:

- Investment cost will be decreased.
- The network charges will be decreased.
- The risk of investments against all uncertainties will be reduced.
- Encouraging and facilitating competition among electric market participants.
- Providing non-discriminatory access to cheap generation for all consumers.
- Operation cost will be reduced.
- Minimizing the costs of investment and operation.
- Increasing the reliability of the network.
- The value of the system will be increased.

- The flexibility of system operation will be increased.
- The environmental impacts will be decreased. and

2.4 Uncertainties and Vagueness in Deregulated Power Systems

Development of competitive electric markets has introduced significant uncertainties and vagueness in transmission expansion planning. Since methods of modeling random uncertainties, non-random uncertainties, and vagueness are different, power system uncertainties and vagueness must be identified and classified clearly before planning. Sources of random uncertainties in deregulated power systems are:

- power and bids of independent power producers (IPPs),
- generation costs and consequently bid of generators,
- Forced outage of generators, lines and other system facilities.
- wheeling transactions and power transactions with other areas, and
- load,
- Sources of non-random uncertainties are:
- Market rules.
- Generation expansion or closure.
- Load expansion or closure.
- Installation, closure or replacement of other transmission facilities.
- transmission expansion costs, and
- There is vagueness in the following data:
- occurrence degree of possible future scenarios,
- importance degree of stakeholders in decision making , and
- Importance degree of planning desires from the viewpoint of different stakeholders.

Uncertainties in deregulated environments have increased uncertainty in required capacity for transmission expansion and consequently increased the risk of fixed cost recovery. Therefore, incentives for investing in transmission expansion have reduced and caused a delay on transmission planning.

2.5. Scenario Technique

For the planning of any system we can use the Scenario technique and decision analysis. The algorithm of transmission expansion planning using scenario techniques is shown below.

- To determine the set of probable future scenarios.
- To determine the occurrence probability or occurrence degree of future scenarios.
- To determine the set of possible solutions (expansion plans).
- To measure the goodness of expansion plans by selecting a cost function.
- To select the final plan.

The final plan can be selected by using the following methods.

1. Expected cost method: This method selects the plan that minimizes the expected cost over different scenarios i.e.:

$$\text{Min}_k E^k = \sum_l v^l f^{k,l}$$

Where E^k = expected cost of plan k, v^l = occurrence degree of scenario l, $f^{k,l}$ = cost of plan k in scenario l.

2. Minimax regret method (risk analysis): In risk analysis the best solution is determined by minimizing the regret. Regret is a measure of risk. Regret of plan k in scenario l is defined as difference between the cost of plan k in scenario l and cost of the optimal plan of scenario l, i.e.:

$$r^{k,l} = f^{k,l} - f^{op,l}$$

Where $r^{k,l}$ = regret of plan k in scenario l, $f^{op,l}$ = cost of the optimal plan of scenario l. In risk analysis the plan that minimizes the maximum weighted regret over all future scenarios is selected as the final plan, i.e.:

$$\text{Min}_k \{ \text{Max}_l (v^l r^{k,l}) \}$$

3. Laplace method: According to this method the plan that minimizes the sum of costs over all scenarios is selected as the final plan.

4. Von Neumann-Morgenstern method: In this method is extremely pessimist and believes that the most unfavorable scenario is bound to occur. According to this criterion the plan that minimizes the maximum cost over all scenarios is selected as the final plan, i.e.:

$$\text{Min}_k \{ \text{Max}_l (f^{k,l}) \}$$

Alternatively, an extremely optimist criterion can be also used for selecting the final plan, i.e.:

$$\text{Min}_k \{ \text{Min}_l (f^{k,l}) \}$$

5. Hurwitz method: the plan that minimizes a convex combination of the extremely pessimist solution and the extremely optimistic solution is selected as the final plan.

6. Pareto-optimal method: A plan is Pareto-optimum if it is not dominated by any other plan. Plan X is dominated by plan Y if its cost is more than the cost of plan Y in all scenarios. This criterion is suitable for eliminating the worst solutions.

7. Robustness method: A plan is robust in a scenario, if its regret is zero in this scenario. According to this criterion, a plan is acceptable if it is robust at least in $\eta\%$ of the scenarios.

8. β -robustness method: According to this method a plan is acceptable if its over cost with respect to the related optimal plan does not exceed $\beta\%$ in each scenario.

III. LOCATIONAL MARGINAL PRICES (NODAL PRICE)

A Locational Marginal Price (LMP) is a pricing system for selling and purchasing electric energy in deregulated power systems. In the LMP pricing system, all producers sell energy at the price of their generator bus and all consumers purchase energy at the price of their load bus. By definition locational marginal price (LMP) nodal price is equal to the "cost of supplying next MW of load at a specific location, considering generation marginal cost, cost of transmission congestion, and losses". LMPs are the Lagrange multipliers or shadow prices of DC power flow constraints. The locational marginal price (LMP) is used to determine the price at each transmission bus or node. The locational marginal price (LMP) will encourages an efficient use of transmission system by assigning prices to the buyers. By using the locational marginal price (LMP), customers can sell and buy energy at the actual price of delivering energy at their buses or nodes.

In addition to the technical criteria, market based criteria is used to achieve the objectives of transmission expansion planning in deregulated power systems. In order to calculate and define the market based criteria, we need to calculate the Probability Density Functions (PDFs) of variables which shows the performance of electric market. These variables should be affected by dynamics of both power system and electric market. For assessing the performance of electric markets, we have to calculate the PDFs of LMPs. The "probabilistic optimal power flow" or "probabilistic locational marginal prices", is used for calculating the PDFs of LMPs.

PDFs of LMPs will be affected if sellers can change their bids, sellers can change maximum or minimum of their submitted power, buyers change their bids for load curtailment, buyers can change maximum or minimum of their submitted power, transmission facilities (generator, transmission line, load,...) have forced outage, input or output power to the study area change due to new contracts with neighboring areas and wheeling transactions, or there is market power in the network. Hence, PDFs of LMPs contain more information about the power system and electric market. By analyzing the PDFs of LMPs, the performance of an electric market can be assessed.

IV. MARKET BASED CRITERIA

The main objective of transmission expansion planning in deregulated power systems is to provide a non-discriminatory competitive environment for all stakeholders, while maintaining power system reliability. To achieve this objective, it is needed to define some criteria to measure how competitive an electric market is and how much a specific expansion plan improves the competition.

In a perfect competitive market, which consists of infinity number of producers and consumers, the price is determined by interaction of all producers and consumers. In this market each customer produces or consumes only a small portion of the market production. Therefore, a producer or a consumer can not affect the price alone.

Hence, in competitive markets producers and consumers are price taker not price maker. In a competitive market there is no discrimination among producers or consumers i.e. all producers and consumers sell and buy at the same price. Moreover, in a competitive market there is no restriction for consumers to buy from any producer. To have a competitive electric market, the above conditions must be satisfied. On the other word, to have a competitive electric market all power producers and consumers must sell and buy electric energy at the same price and the power transfer restrictions must be alleviated. This means LMPs must be made equal at all buses and transmission congestion must be alleviated. Equalizing LMPs provides a nondiscriminatory market and alleviating congestion eliminates power transmission constraints.

In these section two probabilistic criteria, average congestion cost and standard deviation of mean of LMP, are proposed to measure how much a specific plan facilitates competition among customers. Average congestion cost shows how intensive transmission constraints are and consequently shows how competitive electric market is. Standard deviation of mean of LMP shows how mean of LMP spreads throughout the network. Therefore, it shows how discriminative and consequently how competitive electric market.

4.1. Average Congestion Cost

Congestion cost of a line is defined as the opportunity cost of transmitting power through it. Consider figure 4.1, line i of a network is depicted in this figure. The end buses of this line numerated with $i1$ and $i2$. $P_{l_{i1,i2}}$ MW electric power transmits from bus $i1$ to bus $i2$ through this line. LMPs of buses $i1$ and $i2$ are $lmpi1$ and $lmpi2$ in \$/MWhr. Buying 1 MW electric power from bus $i1$ costs $lmpi1$ \$/hr and buying 1 MW power from bus $i2$ costs $lmpi2$ \$/hr. Therefore, the opportunity cost of transmitting 1 MW electric power from bus $i1$ to bus $i2$ is equal to $(lmpi2 - lmpi1)$ \$/hr. Thus, congestion cost of line i or the opportunity cost of transmitting $P_{l_{i1,i2}}$ MW electric power from bus $i1$ to bus $i2$ through line i is equal to:

$$CC_i = (lmpi2 - lmpi1) P_{l_{i1,i2}} \quad i=1,2,\dots,N_l$$

Where CC_i is congestion cost of line i in \$/hr
 N_l is Number of network lines.

Total congestion cost of the network or the opportunity cost of transmitting power through the network is equal to:

$$tcc = \sum_{i=1}^{N_b} (lmpi2 - lmpi1) P_{l_{i1,i2}}$$

where tcc is total congestion cost of the network in \$/hr.

It can be proved that the total congestion cost of the network is equal to the sum of payments by loads minus sum of receives by generators, i.e.:

$$tcc = \sum_{i=1}^{N_b} P_{d_i} lmpi - \sum_{i=1}^{N_b} P_{g_i} lmpi$$

Where P_{d_i} load at bus i in MW, P_{g_i} generation power at bus i in MW, N_b number of network buses.

If there is no congestion in the network, the next MW of each load is supplied by the cheapest undispached generation (marginal generator) and then LMPs of all buses are equal.

Average of the total network congestion cost after addition of plan k is equal to:

$$\mu_{tcc}^k = \frac{1}{N_r} \sum_{i=1}^{N_r} CC_{i,j}^k$$

with μ_{tcc}^k average of total congestion cost of the network in the presence of plan k in \$/hr.

In the rest of this paper "average congestion cost" is used instead of "average of total congestion cost of the network".

4.2. Standard Deviation of Mean of Locational Marginal Price

Standard deviation of mean of LMP in the presence of plan k , where mean is taken over N_r samples and standard deviation is taken over N_b buses, is given by:

$$\sigma_{lmpi}^k = \sqrt{\frac{1}{N_b - 1} \sum_{i=1}^{N_b} (\mu_{lmpi}^k - \mu_{lmpi}^k)^2}$$

Where σ_{lmpi}^k is standard deviation of mean of LMP in the presence of plan k in \$/MWhr, μ_{lmpi}^k mean of LMP of bus i over N_r samples in the presence of plan k in \$/MWhr, μ_{lmpi}^k mean of μ_{lmpi}^k over N_b buses in \$/MWhr (average LMP of the network), μ_{lmpi}^k is equal to:

$$\mu_{lmpi}^k = \frac{1}{N_b} \sum_{i=1}^{N_b} \mu_{lmpi}^k$$

Standard deviation of mean of LMP in the presence of plan k (σ_{lmpi}^k) indicates how spread out the mean of LMP of different buses (μ_{lmpi}^k for $i=1, 2, \dots, N_b$) are from the average LMP of the network (μ_{lmpi}^k). As the standard deviation of mean of LMP decreases, differences among the mean of LMP of different buses decrease and the price profile become flatter. Flatter price profile indicates less price discrimination. As flatness of price profile increases, congestion cost decreases. Therefore, as the standard deviation of mean of LMP decreases, both transmission constraints and price discrimination decrease and hence competition is encouraged. In the same way as the standard deviation of mean of LMP increases, competition is discouraged. Therefore, standard deviation of mean of LMP is a proper criterion for measuring the competitiveness degree of electric markets.

V. MARKET BASED TRANSMISSION EXPANSION PLANNING

In this approach at first possible strategic scenarios, which may occur in planning horizon, are identified. PDFs of LMPs are computed for each scenario using probabilistic optimal load flow. Then some expansion plans (candidates) are suggested for transmission expansion by the analysis of electric market. Each of the candidates is introduced to the

network and the market based criteria are computed for each scenario. The final plan is selected by risk analysis of the solutions. The presented approach can be precised in the following steps:

1. Identifying the set of possible strategic scenarios.
2. Compute the PDFs of LMPs for the existing network in each future scenario.
3. Suggesting candidates for transmission expansion by analyzing electric market.
4. Computing the market based criteria for each plan in each scenario.
5. Selecting the final plan by risk assessment of all expansion plans.
6. Computing the capacity of selected expansion plan.

VI. CASE STUDY: SOTHEREN REGION (SR) 48-BUS INDIAN SYSTEM

In this section the proposed approach is applied to the SR 48-bus system. Figure 1. shows the single line diagram of SR 48-bus system. Characteristics of generators and loads for the peak load of planning horizon are given in Tables I and II. It is assumed that the unavailability of each transmission line is equal to 0.001.

Table I. Characteristics generators

S.NO	BUS NO	GENERATOR DATA	LMP(\$/MWHR)
1.	1	1300	16.96
2.	2	1550	9.90
3.	15	1600	10.50
4.	16	1100	17.41
5.	18	1800	17.33
6.	19	1500	17.21
7.	20	1650	17.24
8.	24	1200	17.33
9.	25	1600	17.21
10.	30	1550	17.43
11.	33	1750	17.49
12.	36	1550	17.44
13.	37	1750	18.30
14.	40	1500	18.32
15.	41	1450	17.85
16.	42	1250	18.29
17.	43	1600	17.82
18.	46	1550	18.20

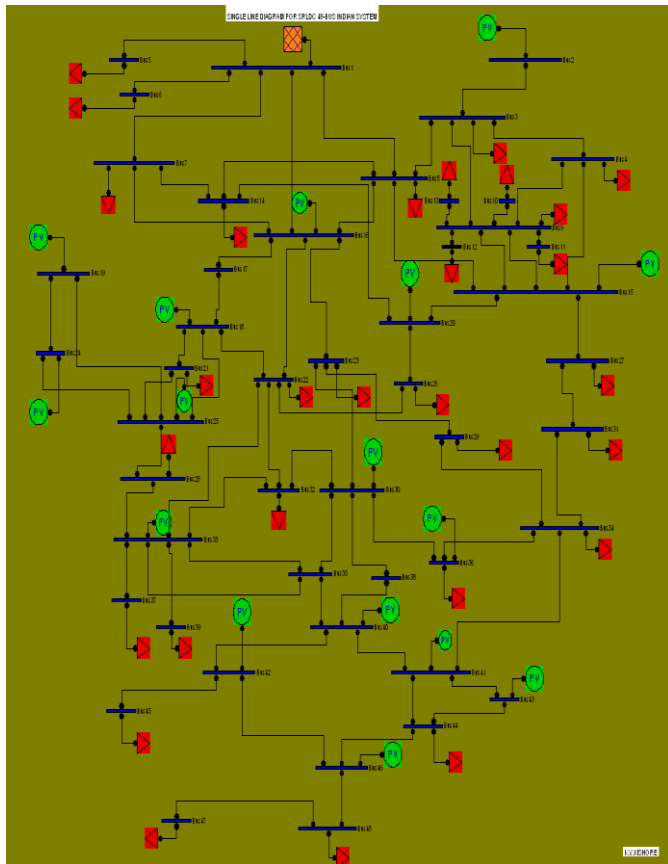


Fig.1.-Single line diagram of SR 48-bus system.

S.NO	BUS	LOAD	LMP(\$/MWHR)
1.	3	350	18.59
2.	4	450	16.66
3.	5	300	17.76
4.	6	250	17.78
5.	7	350	17.38
6.	8	500	16.84
7.	9	250	21.61
8.	10	350	21.73
9.	11	250	21.44
10.	12	300	21.14
11.	13	250	21.70
12.	14	350	17.35
13.	17	450	17.43
14.	21	750	17.51
15.	22	650	17.42
16.	23	350	17.65
17.	26	700	17.41
18.	27	300	18.81
19.	28	650	17.59
20.	31	250	18.74
21.	32	450	17.44
22.	34	950	18.54
23.	35	850	17.85
24.	38	950	18.69
25.	39	822	20.02
26.	44	1150	18.03
27.	45	860	18.62
28.	47	410	18.69
29.	48	400	18.51

Table II. Characteristics generators

6.1. THERE IS NOT ANY NON-RANDOM UNCERTAINTY

In this case there is only one scenario. Therefore, the minimax regret plan and the optimal plan are the same. Transmission planning is performed under the following market based criteria:

- a. $\sigma_{\mu_{lmp}}$: Standard deviation of mean of LMP (SML).
- b. $\sigma_{\mu_{lmp},w=P_g}$: Standard deviation of mean of LMP weighted with mean of generation power (WG).
- c. $\sigma_{\mu_{lmp},w=P_d}$: Standard deviation of mean of LMP weighted with mean of load (WD).
- d. $\sigma_{\mu_{lmp},w=P_g+P_d}$: Standard deviation of mean of LMP weighted with mean of sum of generation power and load (WGD).
- e. μ_{tcc} : Average congestion cost (ACC).
- f. μ_{tlp} : Average load payment (ALP).

The Values of SML, WG, WD, WGD, ACC, and ALP in different stage of planning for SR 48-bus system are shown in table III(A-F). If a new line is added to the network, standard deviation of mean of LMP reduces from \$4.039958/MWhr for the line (5-10) to \$2.07781/MWhr for the line (7-24) and Average Congestion Cost reduces from \$1608.4091/hr to \$1037.48/hr are shown in table III.(A). If a new line is added to the network, standard deviation of mean of LMP reduces from \$5.3723/MWhr for the line (32-42) to \$2.6901/MWhr for the line (2-4) are shown in table III.(B). If a new line is added to the network, standard deviation of mean of LMP reduces from \$843.51/MWhr for the line (31-43) to \$1.2140/MWhr for the line (11-15) are shown in table III.(C). If a new line is added to the network, standard deviation of mean of LMP reduces from \$9.4147/MWhr for the line (36-38) to \$2.0625/MWhr for the line (40-44) are shown in table III.(D). If a new line is added to the network, standard deviation of mean of LMP reduces from \$20.410/MWhr for the line (34-42) to \$1.2360/MWhr for the line (11-20) are shown in table III.(E). If a new line is added to the network, standard deviation of mean of LMP reduces from \$2.1315/MWhr for the line (28-36) to \$2.0638/MWhr for the line (38-42) are shown in table III.(F).

PLANS	ACTUAL	22-29	5-10	11-20	8-12	16-18	1-6	7-21	7-24
SML(\$/MWhr)	3.439327	3.0327	4.0399	2.9102	2.7547	2.5272	3.4126	3.6585	2.0778
WG(\$/MWhr)	9.932229	8.7553	11.666	8.3989	7.9529	7.2977	9.8527	10.565	5.9990
WD(\$/MWhr)	6.053525	5.3378	7.1106	5.1223	4.8486	4.4481	6.0066	6.4399	3.6572
WGD(\$/MWhr)	11.63161	10.254	13.662	9.8376	9.3144	8.5464	11.539	12.373	7.0259
ACC(\$/hr)	2152.176	6581.4	608.40	6432.8	2247.4	5644.2	4201.4	223.56	1037.1
ALP(\$/MWhr)	141993.4	130690	146751	139927	138554	132151	141522	143490	127880

PLANS	ACTUAL	1-25	2-4	15-31	17-19	32-42	12-20	9-18	2-5
SML(\$/MWhr)	3.439327	2.6901	2.0369	4.5530	3.0903	5.3723	2.9206	32.561	3.2026
WG(\$/MWhr)	9.932229	7.7690	5.8801	13.146	8.9240	15.515	8.4291	93.999	9.2465
WD(\$/MWhr)	6.053525	4.7349	3.5851	8.0137	5.4392	9.4557	5.1406	57.311	5.6368
WGD(\$/MWhr)	11.63161	9.0982	6.8869	15.396	10.451	18.169	9.873	110.08	10.829
ACC(\$/hr)	2152.176	2128.9	5679.3	1072.3	4437.1	9475.6	6013.0	59106	2580.9
ALP(\$/MWhr)	141993.4	134233	129341	142498	138119	147009	139795	285011	141229

PLANS	ACTUAL	7-19	8-20	11-15	15-26	17-24	31-43	20-23	17-25
SML(\$/MWhr)	3.439327	2.0609	2.0928	1.2140	9.9763	2.0788	843.51	2.0715	2.0718
WG(\$/MWhr)	9.932229	5.9486	6.0415	3.5038	28.820	6.0018	2437.6	5.9799	5.9812
WD(\$/MWhr)	6.053525	3.6274	3.6836	2.1368	17.559	3.6589	1484.6	3.6460	3.6466
WGD(\$/MWhr)	11.63161	6.9673	7.0760	4.1040	33.748	7.0292	2854.1	7.0038	7.0051
ACC(\$/hr)	2152.176	8943.5	4192.4	2491.2	27659	1600.7	175202	3098.5	3607.1
ALP(\$/MWhr)	141993.4	127499	128238	125648	174276	127892	163870	127580	127681

PLANS	ACTUAL	1-19	34-43	26-30	39-42	36-38	40-44	29-36	32-40
SML(\$/MWhr)	3.439327	2.0754	2.1630	2.0809	2.1797	9.4147	2.0625	2.0862	2.1220
WG(\$/MWhr)	9.932229	5.9914	6.2445	6.0078	6.2924	27.179	5.9556	6.0214	6.1268
WD(\$/MWhr)	6.053525	3.6529	3.8070	3.6625	3.8365	16.570	3.6301	3.6720	3.7349
WGD(\$/MWhr)	11.63161	7.0172	7.3135	7.0362	7.3697	31.832	6.9747	7.0527	7.1755
ACC(\$/hr)	2152.176	2241.9	1783.9	2767.8	489.82	48170	3459.5	6514.5	2886.4
ALP(\$/MWhr)	141993.4	127905	128576	138128	128357	153175	128070	127590	128708

PLANS	ACTUAL	11-20	27-36	41-31	34-42	20-27	29-30	22-30	9-20
SML(\$/MWhr)	3.439327	1.2360	2.1323	6.2583	20.410	2.0861	2.1162	2.0751	9.2893
WG(\$/MWhr)	9.932229	3.5666	6.1541	18.066	58.945	6.0209	6.1087	5.9914	26.810
WD(\$/MWhr)	6.053525	2.1755	3.7532	11.015	35.923	3.6717	3.7248	3.6524	16.350
WGD(\$/MWhr)	11.63161	4.1777	7.2083	21.159	69.029	7.0522	7.1548	7.0169	31.402
ACC(\$/hr)	2152.176	4361.4	5984.3	16204	9671.8	5422.2	6379.2	3882.7	19795
ALP(\$/MWhr)	141993.4	125680	128004	137873	158640	127024	127957	127860	165716

PLANS	ACTUAL	7-16	1-20	44-42	30-34	38-42	45-40	21-20	28-36
SML(\$/MWhr)	3.439327	2.0777	2.0793	2.0802	2.0749	2.0638	2.0790	2.0824	2.1315
WG(\$/MWhr)	9.932229	5.9986	6.0032	6.0063	5.9874	5.9579	6.0023	6.0119	6.1542
WD(\$/MWhr)	6.053525	3.6569	3.6597	3.6613	3.6520	3.6325	3.6593	3.6653	3.7517
WGD(\$/MWhr)	11.63161	7.0254	7.0309	7.0343	7.0133	6.9780	7.0298	7.0412	7.2076
ACC(\$/hr)	2152.176	1092.2	1014.5	1567.9	7114.0	3184.0	4747.1	3406.8	4303.8
ALP(\$/MWhr)	141993.4	127898	127928	127992	127431	127711	127922	127978	129106

Table III.(A-F). Values of SML, WG, WD, WGD, ACC, and ALP in different stages of planning.

6.2. THERE IS NON-RANDOM UNCERTAINTY

In this case it is assumed that the following non-random uncertainties have been identified by planners:

- A generator may be added at bus 9 of the network.
- An IPP may be added at bus 16 of the network.
- Load of bus 41 may be change.

Characteristics new generator, IPP, and load are given in table IV. To take into account these non-random uncertainties in transmission expansion planning, the following scenarios are defined:

- Scenario 1: base case (scenario which is shown in tables I and II)
- Scenario 2: base case plus the new generator
- Scenario 3: base case plus the load change
- Scenario 4: base case plus the IPP
- Scenario 5: base case plus the new generator and load change
- Scenario 6: base case plus the new generator and IPP
- Scenario 7: base case plus the load change and IPP
- Scenario 8: base case plus the new generator, load change, and IPP

It is assumed that all above scenarios have the same occurrence degree. SML, WG, WD, WGD, ACC, and ALP are used as planning criterion. In other word, SML, WG, WD, WGD, ACC, and ALP are used as cost function of risk analysis.

Table IV. Characteristics new GENERATOR, IPP, and LOAD.

TYPE	BUS NO	CHANGE IN MW
GENERATOR	9	500
LOAD	16	1600
IPP	41	500

It is assumed that all above scenarios have the same occurrence degree. SML, WG, WD, WGD, ACC, and ALP are used as planning criterion. In other word, SML, WG, WD, WGD, ACC, and ALP are used as cost function of risk analysis. Table V (a-f) shows the values of SML, WG, WD, WGD, ACC, and ALP in different scenarios and different stages of planning. (a) Values of SML when different criteria are used for planning. (b) Values of WG when different criteria are used for planning. (c) Values of WD when different criteria are used for planning. (d) Values of WGD when different criteria are used for planning. (e) Values of ACC when different criteria are used for planning. (f) Values of ALP when different criteria are used for planning.

a). SML

EXIST.NET	STAGE-1	STAGE-2	STAGE-3	STAGE-4	STAGE-5	STAGE-6	STAGE-7	STAGE-8	
PLAN	ACTUAL	7-18	1-20	44-42	30-34	38-42	44-40	21-20	28-24
SC1	3.439327	2.077712	2.079325	2.080234	2.07491	2.063855	2.079072	2.082477	2.131579
SC2	0.379874	0.378176	0.38068	0.385903	0.340236	0.374865	0.400305	0.384043	0.380804
SC3	2.911137	2.900426	2.91595	2.915491	2.882255	2.91521	2.705201	2.977165	2.908878
SC4	2.075711	2.069777	2.077115	2.077957	2.07155	2.061608	2.072854	2.08071	2.081175
SC5	1.632132	2.580389	1.646446	1.419588	1.168545	1.719564	1.392344	1.465178	1.445461
SC6	1.124504	1.124255	1.123859	1.12515	1.129791	1.124177	1.125628	1.125453	1.125359
SC7	2.891005	2.926367	2.885296	2.63102	2.279542	2.890466	2.636858	2.986106	2.899116
SC8	1.549003	2.575962	1.577001	1.513754	1.164728	1.647472	1.314106	1.406236	1.341017

b). WG

EXIST.NET	STAGE-1	STAGE-2	STAGE-3	STAGE-4	STAGE-5	STAGE-6	STAGE-7	STAGE-8	
PLAN	ACTUAL	7-18	1-20	44-42	30-34	38-42	44-40	21-20	28-24
SC1	9.932229	5.986659	6.003285	6.006352	5.987412	5.957992	6.002332	6.011972	6.154223
SC2	1.508193	1.061636	1.068734	1.083393	0.954741	1.052347	1.123818	1.078161	1.069048
SC3	12.08545	8.513487	8.559884	8.558958	6.959596	8.546248	7.941369	8.738986	8.539295
SC4	8.474957	5.975026	5.996749	5.999642	5.977621	5.951353	5.985253	6.006778	6.008384
SC5	6.588761	7.365249	4.699962	4.052462	3.384541	4.908196	3.974529	4.182331	4.126632
SC6	4.465503	3.156754	3.155781	3.159429	3.170941	3.156528	3.160699	3.160212	3.159914
SC7	12.00256	8.589256	8.470298	7.788931	6.687945	8.484807	7.74109	8.763557	8.511146
SC8	6.253363	7.352748	4.501849	4.932126	3.323592	4.702522	3.751521	4.014163	3.828267

c). WD

EXIST.NET	STAGE-1	STAGE-2	STAGE-3	STAGE-4	STAGE-5	STAGE-6	STAGE-7	STAGE-8	
PLAN	ACTUAL	7-18	1-20	44-42	30-34	38-42	44-40	21-20	28-24
SC1	6.053325	3.656959	3.659799	3.661399	3.652028	3.632573	3.659354	3.665346	3.751771
SC2	0.945561	0.665624	0.670031	0.679225	0.598847	0.659796	0.704573	0.67595	0.670249
SC3	7.367057	5.190129	5.217907	5.217087	4.08395	5.209982	4.840786	5.327449	5.205253
SC4	5.166742	3.642994	3.65591	3.657408	3.646115	3.628616	3.64841	3.622336	3.630506
SC5	4.130348	4.617442	2.94621	2.540262	2.091038	3.07705	2.491512	2.621844	2.586883
SC6	2.799053	1.97879	1.978093	1.980366	1.988534	1.978653	1.981206	1.980899	1.980733
SC7	7.31611	5.236548	5.163054	4.747557	4.079096	5.172305	4.718491	5.343447	5.187784
SC8	3.919976	4.609521	2.812943	2.708767	2.084207	2.948045	2.351509	2.516371	2.399666

d). WGD

EXIST.NET	STAGE-1	STAGE-2	STAGE-3	STAGE-4	STAGE-5	STAGE-6	STAGE-7	STAGE-8	
PLAN	ACTUAL	7-18	1-20	44-42	30-34	38-42	44-40	21-20	28-24
SC1	11.63161	7.025472	7.0309	7.034352	7.013303	6.978054	7.029855	7.041205	7.207652
SC2	1.258716	1.253047	1.261401	1.278705	1.127009	1.240081	1.32642	1.272533	1.261783
SC3	10.00829	9.970802	10.02488	10.02335	7.843117	10.00911	9.300459	10.23482	10.00071
SC4	7.018551	6.988025	7.022325	7.026546	7.001864	6.970326	7.009576	7.035152	7.03095
SC5	5.498707	6.692966	5.547053	4.782822	3.935937	5.792981	4.690897	4.936188	4.870426
SC6	3.726621	3.725682	3.724487	3.728785	3.742878	3.725418	3.730308	3.729731	3.729394
SC7	9.939488	10.05966	9.919832	9.121773	7.833749	9.937036	9.065794	10.26567	9.967583
SC8	5.218753	6.678166	5.312192	5.100083	3.923032	5.550197	4.427584	4.737682	4.518188

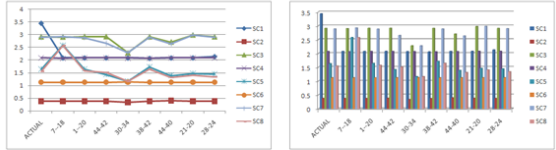
e). ACC

EXIST.NET	STAGE-1	STAGE-2	STAGE-3	STAGE-4	STAGE-5	STAGE-6	STAGE-7	STAGE-8	
PLAN	ACTUAL	7-18	1-20	44-42	30-34	38-42	44-40	21-20	28-24
SC1	2152.176	1092.232	1014.524	1567.937	714.094	3184.022	4747.177	3406.892	4302.671
SC2	190.0198	484.6475	16.03968	267.9297	1071.647	378.8614	519.4112	421.6358	435.1009
SC3	2044.689	2939.535	1644.136	2964.35	9008.995	3918.336	6589.747	4246.47	1595.334
SC4	1574.961	5037.089	1012.569	1573.512	7084.954	3191.102	2652.564	3253.694	2420.702
SC5	1325.782	5191.53	606.1	2250.612	5978.913	3272.189	3060.745	2316.382	2328.13
SC6	904.3108	2483.059	458.387	1154.499	5252.984	1788.756	2101.518	1912.53	1934.731
SC7	2034.176	7190.698	1951.516	2721.881	8977.44	3838.51	3745.199	4247.951	2118.782
SC8	1278.082	5482.327	596.2328	2220.307	5972.164	3162.77	2831.007	2813.299	2045.664

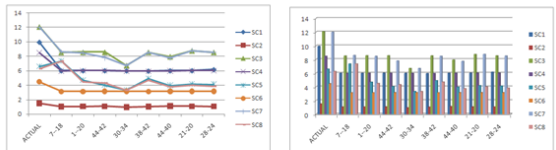
f). ALP

EXIST.NET	STAGE-1	STAGE-2	STAGE-3	STAGE-4	STAGE-5	STAGE-6	STAGE-7	STAGE-8	
PLAN	ACTUAL	7-18	1-20	44-42	30-34	38-42	44-40	21-20	28-24
SC1	141993.4	127838.6	127938.9	127992.1	127421.8	127711.3	127932.7	127978.5	129106.8
SC2	123280.7	123205.6	123290.7	123215.6	123156.4	123289.0	123399.7	123401.7	123247.9
SC3	143617.4	143718.5	143570.7	143807	143551.3	143580.4	141573.3	143249.9	143555.1
SC4	127822.2	127774.5	127870.1	127931.2	127362.9	127655.3	127952	127913.4	127899.4
SC5	133693.2	140088.9	133749.5	132529.1	129476.6	134108.5	132230.5	133047.4	132778.3
SC6	123208.3	122293	123197.4	123248	123748.7	123160.8	123359.1	123202.5	123196.8
SC7	143941.3	143444.2	144010.9	141321.1	136466.5	143906.6	141132.6	143712.3	143759.4
SC8	133304.8	140109.8	133429	133143.9	129333.5	133792.1	131983	132715	132183.4

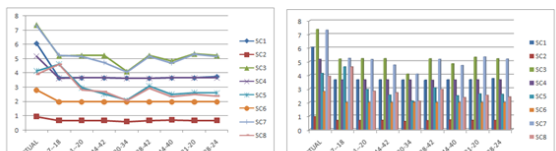
a). SML



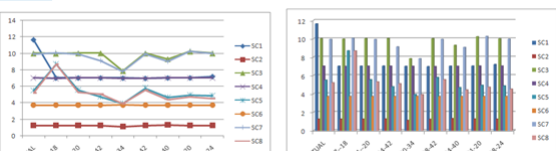
b). WG



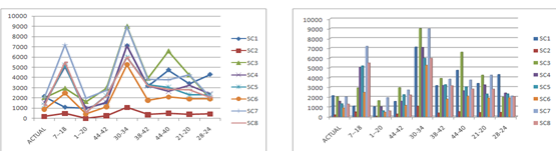
c). WD



d). WGD



e). ACC



f). ALP

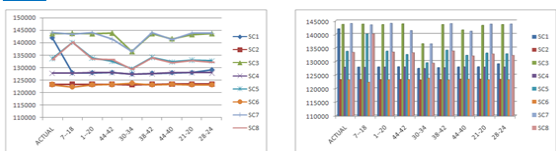


Fig. 1.(a-f). Values of SML, WG,WD, WGD, ACC, and ALP in different scenarios and different stages of planning. There are eight signs over each bar which show the values of criteria in different scenarios. In each stage, there are eight bars. (a) Values of SML when different criteria are used for planning. (b) Values of WG when different criteria are used for planning. (c) Values of WD when different criteria are used for planning. (d) Values of WGD when different criteria are used for planning. (e) Values of ACC when different criteria are used for planning. (f) Values of ALP when different criteria are used for planning.

VII. SELECTING OF FINAL PLAN

By using the minimax regret criterion we have to select the final plan are shown in Table.VI. at different stages of planning for each criterion.

Table V (a-f). Values of SML, WG, WD, WGD, ACC, and ALP in different scenarios and different stages of planning.

SELECTING FINAL PLAN

a).

PLAN	SC1	SC2	SC3	SC4	SC5	SC6	SC7	SC8
SML	(38-42) 2.063855	(30-34) 0.340236	(30-34) 2.282255	(38-42) 2.061608	(30-34) 1.168545	(1-20) 1.123859	(30-34) 2.279542	(30-34) 1.164728
WG	(38-42) 5.957992	(30-34) 0.954741	(30-34) 6.695956	(38-42) 5.951353	(30-34) 3.334541	(1-20) 3.155781	(30-34) 6.687945	(30-34) 3.323592
WD	(38-42) 3.632571	(30-34) 0.598847	(30-34) 4.08395	(38-42) 3.628616	(30-34) 2.091038	(1-20) 1.978093	(30-34) 4.079096	(30-34) 2.084207
WGD	(38-42) 6.978054	(30-34) 1.127009	(30-34) 7.843117	(38-42) 6.970326	(30-34) 3.935937	(1-20) 3.724487	(30-34) 7.833749	(30-34) 3.923032
ACC	(1-20) 1014.524	(1-20) 16.03968	(1-20) 1644.136	(1-20) 1012.569	(1-20) 606.1	(1-20) 458.387	(1-20) 1951.516	(1-20) 596.2328
ALP	(30-34) 127431.8	(30-34) 123156.4	(30-34) 136513.4	(30-34) 127362.9	(30-34) 129478.6	(7-18) 122293	(30-34) 136468.5	(30-34) 129333.5

b).

PLAN	SC1	SC2	SC3	SC4	SC5	SC6	SC7	SC8
SML	(38-42) 1.723619	(30-34) 0	(30-34) 1.158396	(38-42) 0.937749	(30-34) 0.044686	(1-20) 1.123859	(30-34) 2.279542	(30-34) 1.164728
WG	(38-42) 5.003251	(30-34) 0	(30-34) 3.540175	(38-42) 2.795572	(30-34) 0.17876	(1-20) 3.155781	(30-34) 6.687945	(30-34) 3.323592
WD	(38-42) 3.033724	(30-34) 0	(30-34) 2.105857	(38-42) 1.650523	(30-34) 0.112945	(1-20) 1.978093	(30-34) 4.079096	(30-34) 2.084207
WGD	(38-42) 5.851045	(30-34) 0	(30-34) 4.118663	(38-42) 3.245839	(30-34) 0.21145	(1-20) 3.724487	(30-34) 7.833749	(30-34) 3.923032
ACC	(1-20) 998.4843	(1-20) 0	(1-20) 1185.749	(1-20) 554.182	(1-20) 147.713	(1-20) 458.387	(1-20) 1951.516	(1-20) 596.2328
ALP	(30-34) 5138.8	(30-34) 863.4	(30-34) 14220.4	(30-34) 5069.9	(30-34) 124339.8	(7-18) 121429.6	(30-34) 135605.1	(30-34) 128470.1

c).

PLAN	SC1	SC2	SC3	SC4	SC5	SC6	SC7	SC8	Final plan
SML	(38-42) 0.86161	(30-34) 0	(30-34) 0.579198	(38-42) 0.468875	(30-34) 0.022343	(1-20) 0.56193	(30-34) 1.139771	(30-34) 0.582364	(30-34) 1.139771
WG	(38-42) 2.501626	(30-34) 0	(30-34) 1.770088	(38-42) 1.397786	(30-34) 0.08938	(1-20) 1.577891	(30-34) 3.343973	(30-34) 1.661796	(30-34) 3.343973
WD	(38-42) 1.516862	(30-34) 0	(30-34) 1.052929	(38-42) 0.825262	(30-34) 0.056473	(1-20) 0.989047	(30-34) 2.039548	(30-34) 1.042104	(30-34) 2.039548
WGD	(38-42) 2.925523	(30-34) 0	(30-34) 2.059315	(38-42) 1.62292	(30-34) 0.105725	(1-20) 1.862244	(30-34) 3.916875	(30-34) 1.961516	(30-34) 3.916875
ACC	(1-20) 499.2422	(1-20) 0	(1-20) 592.8745	(1-20) 277.091	(1-20) 73.8565	(1-20) 229.1935	(1-20) 975.758	(1-20) 298.1164	(1-20) 975.758
ALP	(30-34) 2569.4	(30-34) 431.7	(30-34) 7110.2	(30-34) 2534.95	(30-34) 62169.9	(7-18) 60714.8	(30-34) 67802.55	(30-34) 64235.05	(30-34) 67802.55

Table VI.(a-c) shows the selecting the final plan by using the minimax regret criterion at different stages of planning.

By comparing the different plans the final plan is (30-34).

VIII. CONCLUSION

In this paper, a new probabilistic tool for computing the probability density functions of nodal prices was introduced. New market-based criteria were defined for transmission planning in deregulated environments. A new approach for transmission expansion planning in deregulated environments using the above tool and criteria was presented. All random and nonrandom power system uncertainties are considered by this approach and the final plan is selected after risk assessment (minimax regret criterion) of all solutions. This approach tries to facilitate competition and provides nondiscriminatory access to cheap generation by providing a flat price profile throughout the network. It is value based and considers investment cost, operation cost, congestion cost, load curtailment cost, and cost caused by system unreliability. The presented approach was applied to Southern Region (SR) 48-Bus Indian System and the effectiveness of presented market-based criteria was demonstrated for the single and multiple scenario cases.

IX. REFERENCES

1. M. Oloomi Buygi, G. Balzer, H. Modir Shanechi, and M. Shahidehpour, "Market based transmission expansion planning: Stakeholders' desires," in *Proc. 2004 IEEE PES DPRT Conf., Hong Kong*.
2. G. Latorre, R. D. Cruz, and J. M. Areiza, "Classification of publications and models on transmission expansion planning," Presented at IEEE PES Transmission and Distribution Conf., Brazil, Mar. 2002.
3. M. Oloomi Buygi, H. M. Shanechi, G. Balzer and M. Shahidehpour, "Transmission planning approaches in restructured power systems," in *Proc. 2003 IEEE PES Power Tech Conf., Italy*.
4. CIGRE WG 37.10, "Methods for planning under uncertainty: toward flexibility in power system development," *Electra*, No. 161, pp. 143-163, Aug. 1995.
5. V. Miranda, and L. M. Proenca, "Probabilistic choice vs. risk analysis – conflicts and synthesis in power system planning," *IEEE Trans. PWRs*, Vol. 13, No. 3, pp. 1038-1043, Aug. 1998.
6. T. De la Torre, J. W. Feltes, T. G. S. Roman, and H. M. Merrill, "Deregulation, privatization, and competition: transmission planning under uncertainty," *IEEE Trans. PWRs*, Vol. 14, No. 2, pp. 460-465, May 1999.
7. C. Ray, C. Ward, K. Bell, A. May and P. Roddy, "Transmission capacity planning in a deregulated energy market," in *Proc. CEPsi 2000*, available: www.energythai.net/cepsi2000/D1024.pdf.
8. CIGRE TF 38.05.08, "Techniques for power system planning under uncertainties," Technical Brochure, Ref. 154, Apr. 2000.
9. R. D. Cruz Rodriguez, and G. Latorre Bayona, "A new model for transmission expansion planning in a deregulated environment," Presented at V Seminario Internacional Sobre Analisis Y Mercados Energeticos, Universidad de Los Andes, Bogota, Colombia, Aug. 2001.
10. C. Ward, K. Bell, A. May, and P. Roddy, "Transmission capacity planning in an open energy market," *CIGRE 2000*, No. 37-109.
11. S. Dekrajangpetch, and G. B. Sheble, "Application of auction results to power system expansion," in *Proc. 2000 IEEE International Conf. on Electric Utility Deregulation and Restructuring*, pp. 142-146.
12. J. R. Saenz, E. Torres, P. Eguia, and I. Albizu, "Development of a methodology for transmission planning in deregulated electric sectors," in *Proc. 2001 IEEE Power Tech.*, Vol. 1.

Transformer less Inverter for Single-Phase Photovoltaic Systems

R. Lokeshwari, J. Nagarjuna Reddy*, B. M. Manjunath**

PG Student, Power Electronics/EEE, RGM CET, Nandyal, India

*Assistant Professor, Dept. of EEE, RGM CET, Nandyal, India

** Assistant Professor, Dept. of EEE, RGM CET, Nandyal, India

Abstract: When no transformer is used in a grid-connected photovoltaic (PV) system, a galvanic connection between the grid and PV array exists. In these conditions, dangerous leakage currents (common-mode currents) can appear through the stray capacitance between the PV array and the ground. In order to avoid these leakage currents, different inverter topologies that generate no varying common-mode voltages, such as the half-bridge and the bipolar pulse width modulation (PWM) full-bridge topologies, have been proposed. The bipolar PWM full bridge requires a lower input voltage but exhibits a low efficiency. This paper proposes a new high-efficiency topology that generates no varying common-mode voltage and requires the same low-input voltage as the bipolar PWM full bridge.

Index Terms: DC-AC power conversion, photovoltaic (PV) systems, transformer less inverter.

I. INTRODUCTION

Grid-connected photovoltaic (PV) systems, particularly low-power single-phase systems, are becoming more important worldwide. They are usually private systems where the owner tries to get the maximum system profitability. Issues such as reliability, high efficiency, small size and weight, and low price are of great importance to the conversion stage of the PV system. Quite often, these grid-connected PV systems include a line transformer in the power-conversion stage, which guarantees galvanic isolation between the grid and the PV system, thus providing personal protection. Furthermore, it strongly reduces the leakage currents between the PV system and the ground, ensures that no continuous current is injected into the grid, and can be used to increase the inverter output voltage level. The line transformer makes possible the use of a full-bridge inverter with unipolar pulse width modulation (PWM). The inverter is simple. It requires only four insulated gate bipolar transistors (IGBTs) and has a good trade-off between efficiency, complexity and price. Due to its low frequency, the line transformer is large, heavy and expensive.

This paper proposes a new topology that generates no varying common-mode voltage, requires the same low-input voltage as the bipolar PWM full-bridge topology, and achieves a higher efficiency and a lower current ripple in the inductor. The topology consists of six switches and two diodes and can be an advantageous power conversion stage for transformer less grid-connected PV systems.

II. COMMON-MODE CURRENTS IN TRANSFORMERLESS PV SYSTEMS

When no transformer is used, a galvanic connection between the ground of the grid and the PV array exists. As a consequence a common-mode resonant circuit appears, consisting of the stray capacity between the PV modules and the ground, the dc and ac filter elements, and the grid impedance (Fig. 1). A varying common-mode voltage can excite this resonant circuit and generate a common-mode current. Due to the large surface of the PV generator, its stray capacity with respect to the ground reaches values that can be even higher than 200 nF/kWp in damp environments or on rainy days. These high values can generate ground currents with amplitudes well above the permissible levels, such as those concerning the standards. The currents can cause severe (conducted and radiated) electromagnetic interferences, distortion in the grid current and additional losses in the system. These leakage currents can be avoided, or at least limited, by including damping passive components in the resonant circuit. Obviously, additional losses will appear in the damping elements, thus decreasing the conversion stage efficiency.

The use of conversion topologies with a constant common mode voltage is another option. The instantaneous common mode voltage V_{cm} in the full-bridge inverter of Fig. 1 can be calculated from the voltage of the two mid-points of both legs,

$$V_{AO} \text{ and } V_{BO} \text{ as}$$
$$V_{cm} = \frac{V_{AO} + V_{BO}}{2} \dots\dots\dots (1)$$

To avoid leakage currents, the common-mode voltage must be kept constant during all commutation states, that is

$$V_{cm} = V_{AO} + V_{BO}$$

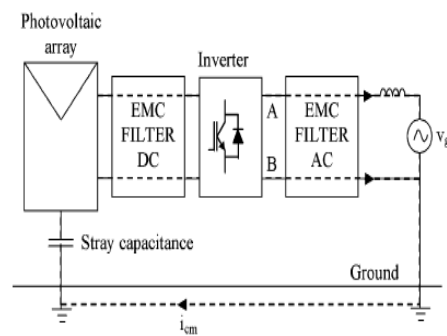


Fig.1 Common-mode currents in a transformer less conversion stage

III. MODELLING OF PV MODULE

The most commonly used model for PV-cell is one – diode equivalent circuit as shown in figure (2). Since the shunt resistance R_{sh} is large, it is normally neglected. This simplified circuit is used in this paper for modeling of a PV-cell.

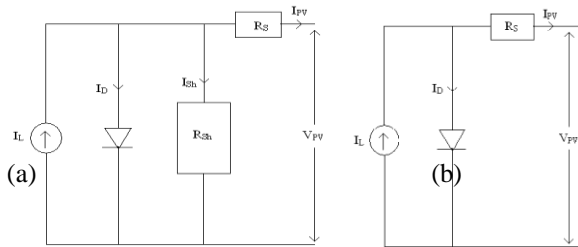


Fig.2. One-diode equivalent circuit model for a PV cell. (a) Five parameters model; (b)Simplified four parameters model

The non-linear of V_{pv} - I_{pv} and P-V curves are correspondingly drawn as shown below:

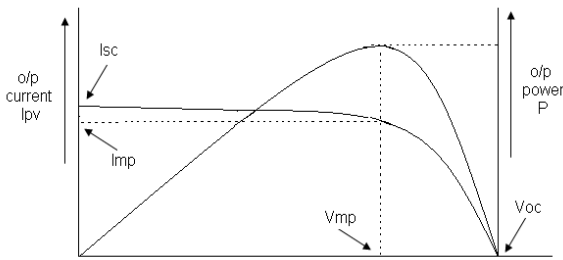


Fig.3. V_{pv} - I_{pv} & P_{pv} - V_{pv} characteristics of a PV cell
From figure (2.b) the relation between the output V_{pv} and the output current I_{pv} can be expressed as:

$$I_{PV} = I_L - I_D$$

$$I_{PV} = I_L - I_0 \left(\exp \left(\frac{V_{PV} + I_{PV} R_S}{\alpha} \right) - 1 \right) \dots (2)$$

Where I_L = Light current; I_0 = Saturation current; R_S = Series Resistance; α = Thermal voltage timing completion factor.

The above four parameters are needed to be determined to obtain the I-V characteristics of PV-module. Thus, this model can be termed as Four-parameter model. The equations for determining the four parameters are given below:

A. Light Current (I_L)

$I_L = \frac{G}{G_{ref}} (I_{Lref} + \mu_{isc} (T_C - T_{Cref})) \dots (3)$ Where G =irradiance (W/m^2); G_{ref} = reference irradiance ($1000 W/m^2$ is used in this study); I_{Lref} = light current at the reference condition ($1000W/m^2$ and $25^\circ C$); T_C = PV cell temperature ($^\circ C$); T_{ref} = reference temperature ($25^\circ C$ is used in this study);

μ_{isc} = temperature coefficient of the short-circuit current ($A/^\circ C$).

From the above equation for light current it can be observed that I_L is a function of both temperature and irradiance. Both I_{Lref} and μ_{isc} can be obtained from manufacturer data sheet.

B. Saturation Current (I_0)

$$I_0 = I_{0ref} \left(\frac{T_C + 273}{T_{Cref} + 273} \right)^3 \exp \left(\frac{e_{gap} q}{N_S \alpha_{ref}} \left(1 - \frac{T_{Cref} + 273}{T_C + 273} \right) \right) \dots (4)$$

Where I_{0ref} = saturation current at the reference condition (A); e_{gap} = band gap of the material 1.17 eV for Si materials); N_S = number of cells in series of a PV module; q = charge of an electron ($1.60217733 \times 10^{-19} C$); α_{ref} = the value of α at reference condition.

I_{0ref} can be calculated as:

$$I_{0ref} = I_{Lref} \exp \left(- \frac{V_{OCref}}{\alpha_{ref}} \right) \dots (5)$$

Where V_{ocref} = the open circuit voltage of the PV module at reference condition (V).

C. Calculation of α

$$\alpha = \frac{T_C + 273}{T_{Cref} + 273} \alpha_{ref} \dots (6)$$

The value of α_{ref} can be calculated as:

$$\alpha_{ref} = \frac{2V_{mpref} - V_{ocref}}{I_{scref} - I_{mpref} + \ln \left(1 - \frac{I_{mpref}}{I_{scref}} \right)} \dots (7)$$

Where V_{mpref} = maximum power point voltage at the reference condition (V); I_{mpref} = maximum power point current at the reference condition (A); I_{scref} = short circuit current at the reference condition (A).

D. Series Resistance (R_S)

Some manufacturers provide the value of R_S . If not provided, the following equation can be used to estimate its value:

$$R_S = \frac{\alpha_{ref} \ln \left(1 - \frac{I_{mpref}}{I_{scref}} \right) + V_{ocref} - V_{mpref}}{I_{mpref}} \dots (8)$$

R_S is taken as a constant in the model of this study.

E. Thermal Model of PV

From equations (1) to (7), it can be noted that the temperature plays an important role in the PV performance. Therefore, it is necessary to have a thermal model for a PV cell/module. In this study, a lumped thermal model is developed for the PV module. The temperature of the PV module varies with surrounding temperature, irradiance, and its output current and voltage, and can be written as:

$$C_{pv} \frac{dT_C}{dt} = K_{inpv} G - \frac{V_{pv} I_{pv}}{A} - K_{loss} (T_C - T_a) \dots (9)$$

C_{pv} = the overall heat capacity per unit area of the PV cell/module [$J/(^\circ C \cdot m^2)$]; K_{inpv} = Transmittance-absorption product of PV cells; K_{loss} = overall heat loss coefficient [$W/(^\circ C \cdot m^2)$]; T_a = ambient temperature ($^\circ C$); A = effective area of the PV cell/module (m^2).

IV. FULL-BRIDGE INVERTER

The full-bridge inverter (Fig. 3) is a single stage dc-ac conversion topology that is used quite often in PV inverters. Different PWM techniques can be applied to this topology. Depending on the shape of the output voltage waveform, they can be classified in two groups, namely unipolar and bipolar PWM. When the full bridge is part of a conversion stage with a line transformer, unipolar PWM techniques can be applied. This is in proposed topology.

Here, S_4 is on during the positive half cycle, while switches S_1 and S_2 commutate at the switching frequency. During the negative cycle, S_2 is on and S_3, S_4 commutate at the switching frequency. In this converter

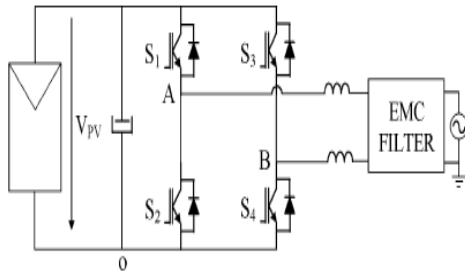


Fig 4. Full-bridge inverter

only two switches are on at the same time, and only one IGBT and one diode commutate at the switching frequency with the whole input voltage. The main drawback, that it generates a varying common-mode voltage of amplitude $V_{pv}/2$ at the switching frequency.

In the bipolar PWM, the diagonal pairs of switches $S_1 - S_4$ and $S_2 - S_3$ are switched alternatively at the switching frequency. As a consequence

$$V_{BO} = V_{PV} - V_{AO} \Rightarrow V_{cm} = V_{PV}/2 = cte$$

If the switching actions are carried out at the same time, no changes appear in the common-mode voltage and no leakage currents are generated. However, the bipolar PWM also has drawbacks. Two IGBTs and two diodes are switching at the switching frequency with the whole input voltage, therefore

doubling the switching losses. Additionally, the output voltage changes between V_{PV} and $-V_{PV}$, creating a current ripple twice that obtained in the unipolar modulation.

V. PROPOSED TOPOLOGY

The proposed topology, which consists of six switches ($S_1 - S_6$) and two diodes ($D_7 - D_8$). In this topology, diodes D_7, D_8 and the capacitive divider limit the blocking voltage of S_5 and S_6 to half of the input voltage V_{pv} . Grid-connected PV systems usually operate with unity power factor. The operational principle of the proposed converter is now analyzed for this case. The proposed topology with the modulation technique described below can operate with power factors other than unity. In these cases, the operation analysis would be similar.

In the positive half cycle, S_1 and S_4 are on. In order to modulate the input voltage, S_5 and S_6 commutate at the switching frequency with the same commutation orders. S_2 and S_3 commute at the switching frequency together and complementary to S_5 and S_6 . In this situation, when S_5 and S_6 and are on, $v_{AB} = V_{PV}$ and the inductor current, which flows through, S_5, S_1, S_4 and S_6 increases. The common-mode voltage is:

$$V_{cm} = \frac{V_{AO} + V_{BO}}{2} = \frac{V_{PV} + 0}{2} = \frac{V_{PV}}{2} \quad \dots(10)$$

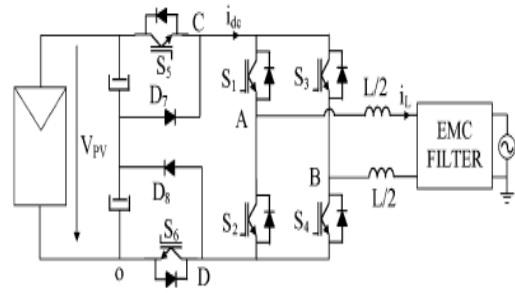


Fig 5. Proposed Topology

When S_5 and S_6 are turned off and S_2 and S_3 are turned on, the current splits into two paths: S_1 and the freewheeling diode of S_3 , and S_4 and the freewheeling diode of S_2 . Thus, S_2 and S_3 are turned on with no current and therefore no switching losses appear.

In this situation, voltages v_{AB} and v_{CD} tend to zero and diodes D_7 and D_8 fix the voltages v_{AO} and v_{Bo} to $\frac{V_{PV}}{2}$. Since V_{AB} is clamped to zero the current decreases. Now, the common-mode voltage is

$$V_{AO} = V_{Bo} = V_{PV}/2 \Rightarrow V_{cm} = V_{PV}/2 \quad \dots(11)$$

In the negative half cycle, S_2 and S_3 are on. Again, S_5 and S_6 commutate at the switching frequency in order to modulate the input voltage. S_1 and S_4 commute at the switching frequency together and complementarily to S_5 and S_6 . In this situation, when S_5 and S_6 are on, V_{AB} equals $-V_{PV}$, and the inductor current, which now flows through S_5, S_3, S_2 and S_6 , decreases.

The common-mode voltage is

$$V_{cm} = \frac{V_{AO} + V_{BO}}{2} = \frac{0 + V_{PV}}{2} = \frac{V_{PV}}{2} \quad \dots(12)$$

When S_5 and S_6 are turned off and S_1 and S_2 are turned on, the current splits into two paths. The first path consists of S_3 and the freewheeling diode of S_1 , and the second of S_2 and the freewheeling diode of S_4 . Consequently, S_1 and S_4 are turned on

with no current, so no switching losses appear. In this situation, voltages v_{AB} and v_{CD} tend to zero and diodes D_7 and D_8 fix the voltages v_{AO} and v_{Bo} to $\frac{V_{PV}}{2}$. The current decreases because v_{AB} is clamped to zero. Now, the common-mode voltage is

$$V_{AO} = V_{Bo} = V_{PV}/2 \Rightarrow V_{cm} = V_{PV}/2 \quad \dots(13)$$

From (10)–(13), it is clear that the common-mode voltage remains constant during the four commutation states of the converter. Therefore, no varying common-mode voltage is generated by the proposed topology and, hence, no leakage currents appear.

Fig. 6 shows the simulated evolution of the main electric variables during a grid period. The common-mode voltage remains constant during all commutation states. Additionally, voltage v_{AB} , and therefore the inductor current, have the same waveforms as those obtained in the unipolar PWM full bridge.

Assuming unity power factor, S_5 and S_6 commute at the switching frequency with half of the input voltage V_{pv} , and the corresponding two freewheeling diodes of the full bridge commute with V_{pv} , but with half of the current. Therefore, switching losses will be lower than those of the bipolar PWM full bridge and can be expected to be similar to those of the unipolar PWM full bridge. Since the blocking voltage of S_5 and S_6 is only half of the input voltage, switches with lower rated blocking voltage can be used and thus will exhibit lower switching losses for the same operating conditions. Therefore the switching losses of the topology will be lower than those of the unipolar PWM full bridge. The IGBT switching losses of the full bridge are neglected, since they switch at the grid frequency. When the power factor decreases, the losses of the proposed topology increase because the switching losses of the full bridge increase.

Conduction losses are expected to be greater in the proposed topology, because when S_5 and S_6 are on current flows through four switches instead of two, as in the full bridge (regardless of the PWM technique used). However, this increment is limited by the fact that S_5 and S_6 have lower saturation voltages because they have lower rated voltages.

VI. SIMULATION RESULTS

Based on the mathematical equations discussed before, a dynamic model for a PV module consisting of 153 cells in series has been developed using MATLAB/Simulink. The input quantities (solar irradiance G and the ambient temperature T_a) together with manufacturer data are used to calculate the four parameters. Then, based on equation (1), the output voltage is obtained numerically. The thermal model is used to estimate the PV cell temperature. The two output quantities (PV output voltage V_{pv} and the PV cell temperature T_c), and the load current I_{pv} , are fed back to participate in the calculations. The model parameters used in the simulation are given in Table I

Table I
THE PV MODEL PARAMETERS

$I_{SCref}(I_{Lref})$	2.664A
α_{ref}	5.472
R_s	1.324Ω
V_{OCref}	87.72V
V_{MPref}	70.731V
I_{MPref}	2.448A
G_{ref}	1000w/m ²
T_{cref}	25°C
C_{pv}	5*10 ⁴ J/(°C-m ²)
A	1.5m ²
K_{inpv}	0.9
K_{loss}	30W/(°C-m ²)

A. Model Performance

The model I_{pv} - V_{pv} characteristic curves under different irradiances are given in Figure (6) at 25°C. It is noted from the figure that the higher is the irradiance, the larger are the short-circuit current (I_{sc}) and the open-

circuit voltage (V_{oc}). And, obviously, the larger will be the maximum power (P), shown in Figure (7).

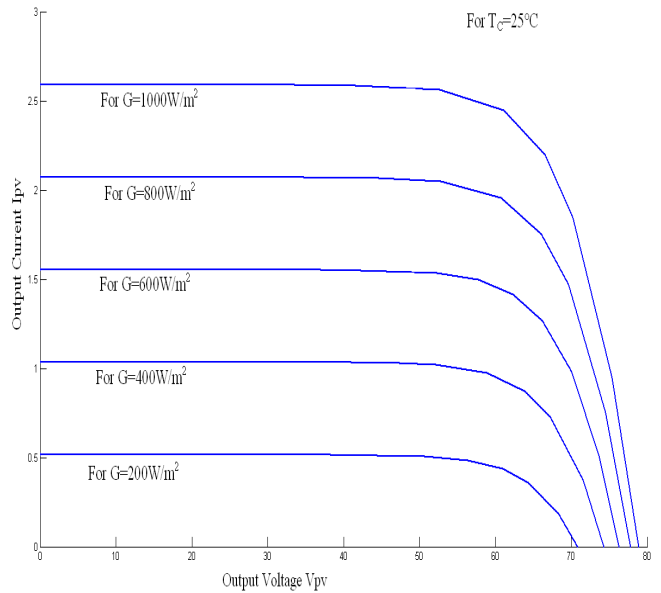


Fig.6 V_{pv} - I_{pv} characteristics for constant T_c and

Varying G

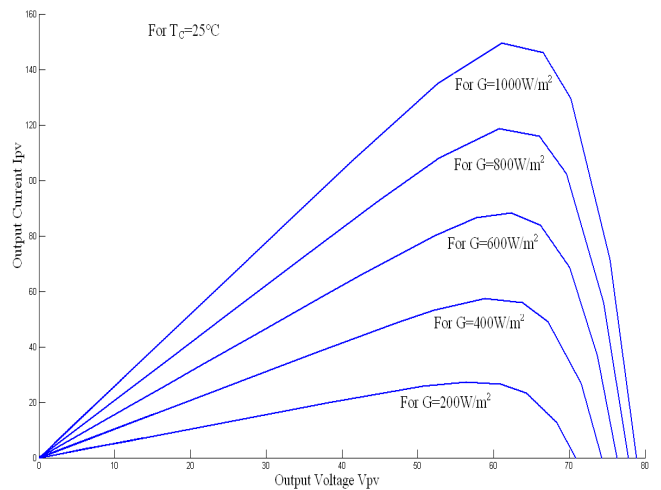


Fig.7. P - V_{pv} characteristics for constant T_c and Varying G

The simulation results of full bridge inverter and proposed topology are shown in fig 8 and fig 9

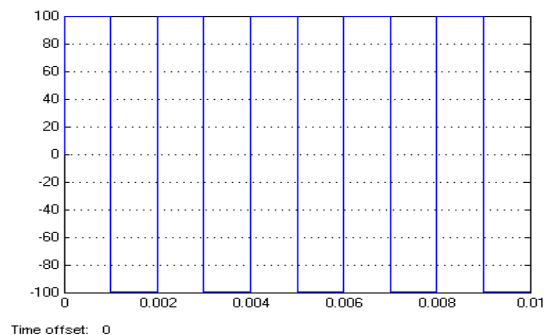


Fig 8. Voltage v_{AB} and common mode voltage in a full bridge inverter topology with bipolar PWM $F=500\text{Hz}$

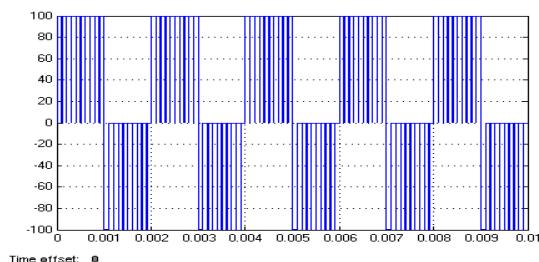


Fig.9. Voltage v_{AB} and common mode voltage in proposed topology F=500Hz

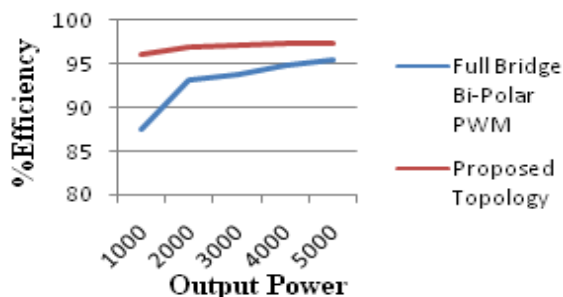


Fig.10 Simulated efficiency of the proposed topology and full bridge with bipolar PWM.

VII. CONCLUSION

This paper proposes a new transformer less, single-phase PV inverter with six switches and two diodes. The proposed topology generates no common-mode voltage, exhibits a high efficiency, and can operate with any power factor. It has been compared to other topologies and validated satisfactory results. The maximum efficiency achieved by the topology is 97.4%. As a conclusion, the proposed topology can be an advantageous power-conversion stage for transformer less, grid-connected PV systems.

REFERENCES

- [1] M. Calais and V. G. Agelidis, "Multilevel converters for single-phase grid connected photovoltaic systems— An overview," in *Proc. IEEE Int. Symp. Ind. Electron.*, 1998, vol. 1, pp. 224–229.
- [2] M. Calais, J. M. A. Myrzik, and V. G. Agelidis, "Inverters for single phase grid connected photovoltaic systems—Overview and prospects," in *Proc. 17th Eur. Photovoltaic Solar Energy Conf.*, Munich, Germany, Oct. 22–26, 2001, pp. 437–440.
- [3] B. Epp, "Big crowds," *Sun & Wind Energy: Photovoltaics*, pp. 69–77, Feb. 2005.
- [4] J. M. A. Myrzik and M. Calais, "String and module integrated inverter for single-phase grid connected photovoltaic systems—A review," in *Proc. IEEE Power Tech. Conf.*, Bologna, Italy, Jun. 23–26, 2003, vol. 2, pp. 1–8.
- [5] W. N. Mohan, T. Undeland, and W. P. Robbins, *Power Electronics: Converters, Applications, and Design*. New York: Wiley, 2003.
- [6] *V Verband der Elektrotechnik, Elektronik und Informationstechnik (VDE)*, Std. V 0126-1-1, Deutsches Institute für Normung, Feb. 2006.

- [7] *IEEE Standard for Interconnecting Distributed Resources with Electric Power Systems*, IEEE Std. 1547, 2003.
- [8] S. B. Kjaer, J. K. Pedersen, and F. Blaabjerg, "A review of single-phase grid-connected inverters for photovoltaic modules," *IEEE Trans. Ind. Appl.*, vol. 41, no. 5, pp. 1292–1306, Sep./Oct. 2005.
- [9] M. F. Arman and L. Zhong, "A new, transformerless, photovoltaic array to utility grid interconnection," in *Proc. Int. Conf. Power Electron. Drive Syst.*, May 26–29, 1997, vol. 1, pp. 139–143.
- [10] Y. Nishida, S. Nakamura, N. Aikawa, S. Sumiyoshi, H. Yamashita, and H. Omori, "A novel type of utility-interactive inverter for photovoltaic system," in *Proc. 29th Annu. IEEE Ind. Electron. Soc. Conf.*, Nov. 2–6, 2003, vol. 3, pp. 2338–2343.
- [11] Y. Chen and K. M. Smedley, "A cost-effective single-stage inverter with maximum power point tracking," *IEEE Trans. Power Electron.*, vol. 19, no. 5, pp. 1289–1294, Sep. 2004.



R. Lokeshwari was born in 1989 in India. She received the B.Tech from RGM Engg. College of engineering and technology, Affiliated to Jawaharlal Nehru Technological University (JNTU), Ananthapur, India in 2010. She is doing M.Tech from under the same University. She is currently researching in the field of power electronics, control systems and photovoltaic systems.



J. Nagarjuna Reddy was born in 1985 in India. He received the B.Tech from Dr. Paul Raj Engg. College in 2005 and Post graduated from Jawaharlal Nehru Technological University (JNTU), Hyderabad, In 2006-2008. He is currently working as a assistant professor in the department of electrical and electronics engineering in RGM college of engineering and technology, Nandyal, Andhra Pradesh, India. He has Two years of teaching experience. His main areas of research include Electrical Drives & Renewable energy source.



B. M. Manjunath is born in 1981 in India. He is graduated from Viswvasaraya Technological university in 2004 and Post graduated from JNTU In 2006-2008. He is currently working as a assistant professor in the department of electrical and electronics engineering in RGM college of engineering and technology, Nandyal, Andhra Pradesh, India. He has Three years of teaching experience and one year of Industrial experience. His main areas of research include Induction motor drives & control of special machine.

Study of Parameter in Time Division Multiple Access (TDMA) MAC protocol in wireless Ad Hoc Environment

Pinki Dabas¹, Sanjeet Kumar², Vinay Panwar³

¹(M-Tech Scholar, PDM College of Engineering, Bahadurgarh)

²(Lecturer, World Institute of Technology, Gurgaon)

³(Lecturer, CRRIT, Kanjhwa, Delhi)

Abstract: Control phase plays a critical role in the performance of time-division multiple access (TDMA)-based wireless networks. Control phase of TDMA-based medium access control (MAC) in wireless sensor networks is proposed. Wireless ad hoc networks depend upon medium access control (MAC) protocols for allocation of channel resources among mobile users. This paper studies TDMA-based timeslot allocation, convergence time and throughput parameters of TDMA using MAC protocol.

Keywords: TDMA, QoS, Medium Access Control, Wireless Ad hoc networks.

I. INTRODUCTION

Wireless ad hoc networks (WANETs) are gaining a lot of attention in research lately due to their importance in enabling mobile wireless nodes to communicate without any existing wired or predetermined infrastructures. Mobile ad hoc networks (MANETs) have rapidly gained a considerable amount of attention in research lately[5][6]. As more and more smart, small, portable, and powerful computing devices are introduced into everyday life, the need for such devices to communicate on the fly in a seamless manner and without any pre existing network wiring or infrastructure is growing. It is also natural to expect such devices to support multimedia and real time applications, which are becoming increasingly feasible due to the significant advances in CPU power, memory, speed, storage, and communication capacity of mobile devices. Such applications require the underlying network to provide certain guarantees that are manifested in the support of several important Quality of Service (QoS) parameters such as bandwidth, delay, and bit error rate. Maintaining these QoS commitments in MANETs is not an easy task. This is due to the unpredictability and variability of many factors such as bit error rates, mobility, and continuous change in the connectivity of the different nodes in the network. The design of an efficient Medium Access Control (MAC) is challenging in ad-hoc networks where users can enter, leave or move inside the network without any need for prior configuration. Ad-hoc networks require no infrastructure and nodes are free to enter, leave or move inside the network without prior configuration [3]. Fig 1 shows the example of Ad hoc network.

The main objective of this paper is to study the time division multiple access based MAC protocol behaviour in the wireless Ad hoc Networks.

The paper is organized as follows: Section I introduces a description for the TDMA based MAC protocol. Description of TDMA multiple access schemes is presented in Section II. In section III, Medium access control protocol

is explained. Simulation results are given in Section IV, and finally conclusions are reflected in Section V.



Fig: 1 Ad hoc Network

II. TIME DIVISION MULTIPLE ACCESS

In a TDMA cellular radio system, several users time-share a common carrier frequency to communicate with the base station. Each user, transmitting low bit-rate digitized speech or other digital data, is allocated one or more timeslots within a frame in the downstream (base to users) and upstream (users to base) directions, as illustrated in Fig. 2

In the downstream direction, the base station broadcasts to the active users in a Time Division Multiplex (TDM) format [1]. In the upstream direction, each active user terminal transmits to the base station only in its own assigned timeslot or slots. Inter-user interference is prevented by strict adherence to timeslot schedules, and by guard times and time-alignment procedures between upstream timeslots, in order to prevent overlaps due to different propagation times [2].

Each individual terminal's receiver and transmitter operates with a duty cycle of $1/N$ if there are N user terminals with equal bit rates sharing a common bit stream. Upstream and downstream traffic is separated either by using different carrier frequencies i.e., Frequency Division Duplex (FDD), or by alternating in time, i.e., Time Division Duplex (TDD).

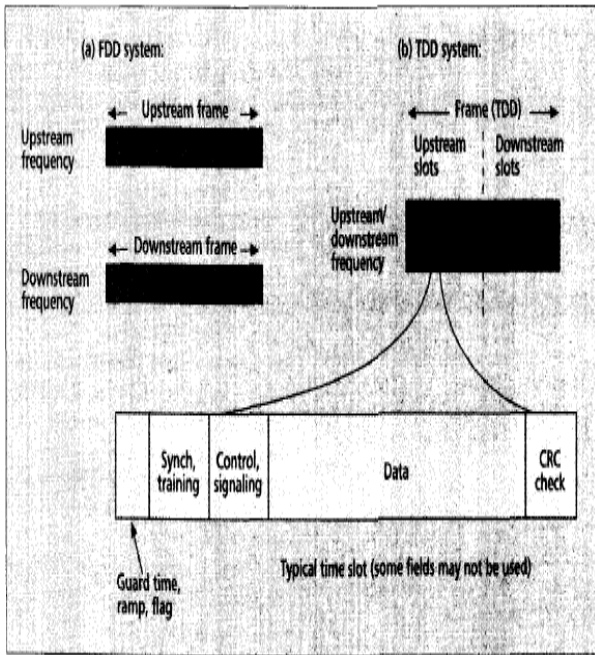


Fig: 2 TDMA frame and Time slots

III. MEDIUM ACCESS CONTROL (MAC)

MAC layer, sometimes also referred to as a sub-layer of the Data Link layer, involves the functions and procedures necessary to transfer data between two or more nodes of the network [5]. It is the responsibility of the MAC layer to perform error correction for anomalies occurring in the physical layer. The layer performs specific activities for framing, physical addressing, and flow and error controls. It is responsible for resolving conflicts among different nodes for channel access.

Since the MAC layer has a direct bearing on how reliably and efficiently data can be transmitted between two nodes along the routing path in the network, it affects the Quality of Service (QoS) of the network. The design of a MAC protocol should also address issues caused by mobility of nodes and an unreliable time varying channel [4].

In TDMA-based schemes, the transmitting node first senses the medium to check whether it is idle or busy. The node defers its own transmission to prevent a collision with the existing signal, if the medium is busy. Otherwise, the node begins to transmit its data while continuing to sense the medium. However, collisions occur at receiving nodes. Since, signal strength in the wireless medium fades in proportion to the square of distance from the transmitter, the presence of a signal at the receiver node may not be clearly detected at other sending terminals, if they are out of range. As illustrated in Fig. 3, node B is within the range of nodes A and C, but A and C are not in each other's range. Let us consider the case where A is transmitting to B. Node C, being out of A's range, cannot detect carrier and may therefore send data to B, thus causing a collision at B. This is referred to as the *hidden-terminal problem*, as nodes A and C are hidden from each other [7].

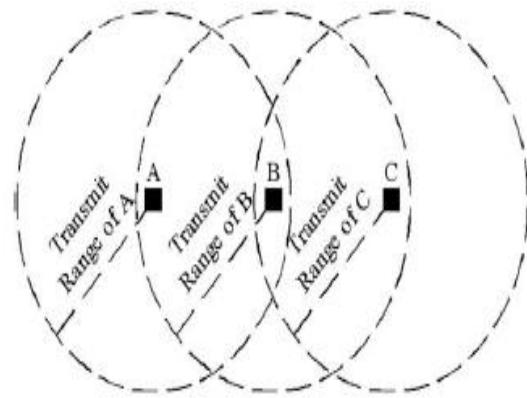


Fig: 3 hidden and exposed terminal problems

Let us now consider another case where B is transmitting to A. Since C is within B's range, it senses carrier and decides to defer its own transmission. However, this is unnecessary because there is no way C's transmission can cause any collision at receiver A. This is referred to as the *exposed-terminal problem*, since B being exposed to C caused the latter to needlessly defer its transmission [7]. MAC schemes are designed to overcome these problems.

IV. SIMULATION RESULTS

In this section the simulation results are shown and discussed. We will investigate the performance of the TDMA scheme using MAC protocol in wireless Ad hoc network. The convergence time is defined as the duration of time within which all nodes across the network collaboratively and in a distributed manner obtain conflict-free slots.

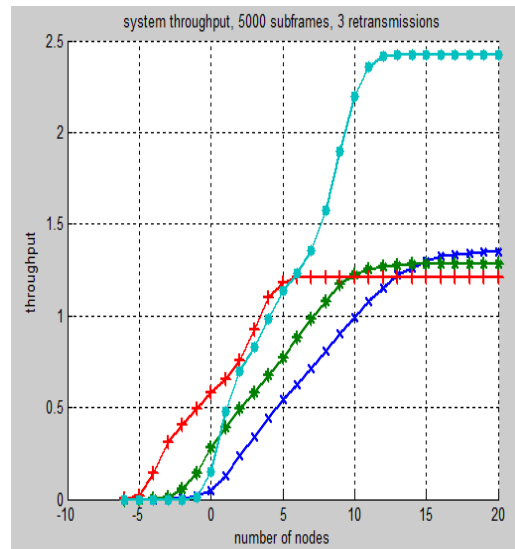


Fig: 4 Throughput of TDMA MAC with 5000 sub-frames and 3 transmissions

We have presented the Throughput for the TDMA using MAC protocol in Ad hoc Networks with 5000 sub-frames and with no HARQ. We have presented the convergence time for the TDMA using MAC protocol in Ad hoc Networks with 5000 sub-frames and with no HARQ.

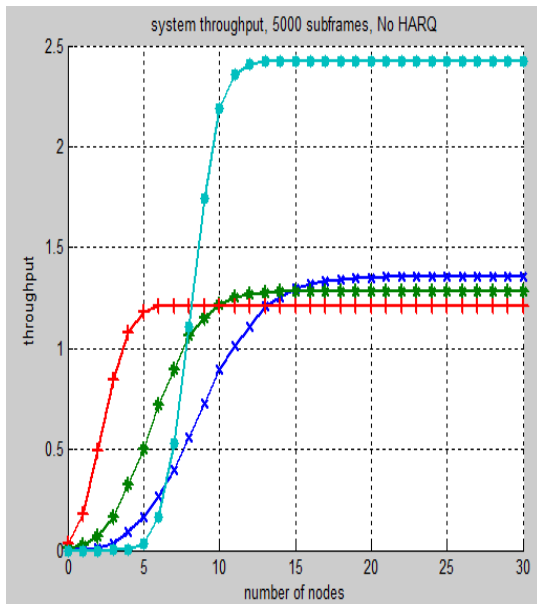


Fig: 5 Throughput of TDMA MAC with 5000 sub-frames with no HRAQ

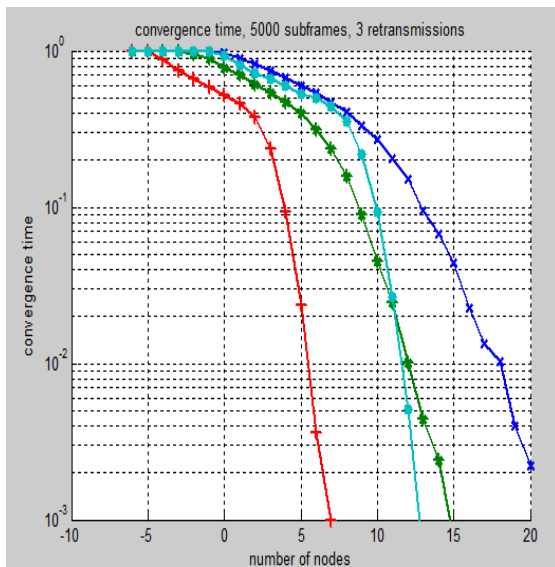


Fig: 6 Convergence time of TDMA MAC with 5000 sub-frames and 3 transmissions

Fig: 4 shows the Throughput of TDMA MAC with 5000 sub-frames and 3 transmissions and fig: 5 shows the Throughput of TDMA MAC with 5000 sub-frames with no HRAQ. Fig: 6 shows the convergence time of TDMA MAC with 5000 sub-frames and 3 transmissions and fig: 7 shows the convergence time of TDMA MAC with 5000 sub-frames with no HRAQ.

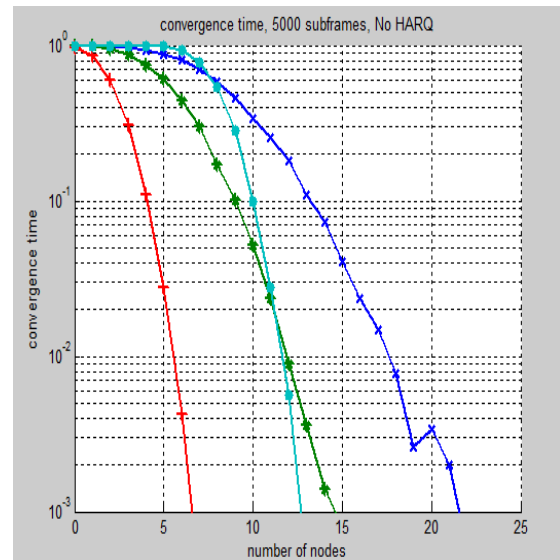


Fig: 7 Convergence time of TDMA MAC with 5000 sub-frames with no HRAQ

V. CONCLUSION

In this paper, we presented the performance of ad hoc wireless networks with respect to MAC protocols using TDMA. Parameters, Throughput and convergence time are study to present the behaviour of the MAC protocol with TDMA.

REFERENCES

- [1] Generic Criteria for Version 1 Wireless Access Communications System (WACS)." Bellcore Technical Advisor TA-NWT-001313. IsSue 1, July, 1992.
- [2] H. Eriksson et al., "Multiple Access Options for Cellular Based Personal Communications," Proc.Vehic.Technol. Conf., May1993, Secaucus, New Jersey, pp. 957-962.
- [3] C.-K. Toh, Ad Hoc Mobile Wireless Networks: Protocols and Systems, Prentice-Hall PTR, NJ, 2002.
- [4] I.F. Akyildiz, J. McNair, L.C. Martorell, R. Puigjaner, Y. Yesha, Medium access control Protocols for multimedia traffic in wireless networks, IEEE Network 13 (July/August) (1999) 39-47.
- [5] Charles E. Perkins, Ad Hoc Networking, Addison Wesley, Reading, MA, 2001.
- [6] L. Kleinrock, F.A. Tobagi, Packet switching in radio channels: Part I—carrier sense multiple access modes and their throughput-delay characteristics, IEEE Trans. Commun. 23 (Dec) (1975) 1400-1416.
- [7] L. Kleinrock, F.A. Tobagi, Packet switching in radio channels: Part II—the hidden terminal problem in carrier sense multiple access and busy tone solution, IEEE Trans. Commun. 23 (December) (1975) 1417-1433.

B-Continuity in Peterson graph and power of a Cycle

S. Chandra Kumar¹, T. Nicholas²

*(Department of Mathematics, Scott Christian College, Nagercoil, Tamil Nadu, India)

***(Department of Mathematics, St. Jude's College, Thoothoor, Tamil Nadu, India)

ABSTRACT: A graph G is k -colorable if G has a proper vertex coloring with k colors. The chromatic number $\chi(G)$ is the minimum number k such that G is k -colorable. A b -coloring of a graph with k colors is a proper coloring in which each color class contains a color dominating vertex. The largest positive integer k for which G has a b -coloring with k colors is the b -chromatic number of G , denoted by $b(G)$. The b -spectrum $S_b(G)$ of G , is defined as the set of all integers k at which G is b -colorable with k colors. A graph G is b -continuous if its b -spectrum equals $[\chi(G), b(G)]$. In this paper, we prove that the Peterson graph and the power of a cycle are b -continuous. Also, we prove that the Cartesian product of two cycles $C_m \square C_n$ is b -continuous when m and n are multiples of 5. In this case, we give the color classes of b -coloring with k colors for each k with $\chi(G) \leq k \leq b(G)$.

Keywords: b -coloring, b -continuous. Peterson graph, power of a cycle.

I. INTRODUCTION

A k -vertex coloring of a graph G is an assignment of k colors $1, 2, \dots, k$, to the vertices. The coloring is proper if no two distinct adjacent vertices share the same color. A graph G is k -colorable if it has a proper k -vertex coloring [5]. The chromatic number $\chi(G)$ is the minimum number k such that G is k -colorable. Color of a vertex v is denoted by $c(v)$. A b -coloring is a coloring of the vertices of a graph such that each color class contains a vertex that has a neighbor in all other color classes. In other words, each color class contains a color dominating vertex (a vertex which has a neighbor in all the other color classes). The b -chromatic number $b(G)$ is the largest integer k such that G admits a b -coloring with k colors.

The b -spectrum $S_b(G)$ of G is defined by $S_b(G) = \{ k \in \mathbb{N} : \chi(G) \leq k \leq b(G) \text{ and } G \text{ is } b\text{-colorable with } k \text{ colors} \}$. A graph G is b -continuous if $S_b(G) = [\chi(G), b(G)]$.

El-Sahili[3] conjectured that every d -regular graph with girth at least 5 has a b -coloring with $d + 1$ colors.

Marko Jaovac and Sandi Klavzar[7] disproved this conjecture and they proved the following:

'Peterson graph is a 3-regular graph with girth 5 and b -chromatic number 3'.

In section 3, we prove this result in another way. Saeed Shaebani[9] proved that some of the Kneser graphs are b -continuous. Further, they gave some special conditions for graphs to be b -continuous.

Here we list out some of the necessary definitions. For a graph G , and for any vertex v of G , the neighborhood of v is the set $N(v) = \{ u \in V(G) : (u, v) \in E(G) \}$ and the degree of v is $\deg_G(v) = |$

$N(v)$ [4]. $\Delta(G)$ denotes the maximum degree of a vertex in G . Note that every graph G satisfies $b(G) \leq \Delta(G) + 1$.

A graph is a power of cycle, denoted C_n^k , if $V(C_n^k) = \{ v_0 (= v_n), v_1, v_2, \dots, v_{n-1} \}$ and $E(C_n^k) = E^1 \cup E^2 \cup \dots \cup E^k$, where $E^i = \{ (v_j, v_{(j+i) \pmod{n}}) : 0 \leq j \leq n-1 \}$ and $k \leq (n-1)/2$ [1]. Note that C_n^k is a $2k$ -regular graph and $k \geq 1$. We take $(v_0, v_1, v_2, \dots, v_{n-1})$ to be a cyclic order on the vertex set of G , and perform modular operations on the vertex indexes [1].

The Cartesian product $G \square H$ of two graphs G and H is the graph with vertex set $V(G \square H) = V(G) \times V(H)$ and edge set $E(G \square H) = \{ ((x_1, y_1), (x_2, y_2)) : (x_1, x_2) \in E(G) \text{ with } y_1 = y_2 \text{ or } (y_1, y_2) \in E(H) \text{ with } x_1 = x_2 \}$ [5].

A graph G_1 is called as a covering graph of G with covering projection $f : G_1 \rightarrow G$ if there is a surjection $f : V(G_1) \rightarrow V(G)$ such that $f|_{N(v_1)} : N(v_1) \rightarrow N(v)$ is a bijection for any vertex $v \in V(G)$ and $v_1 \in f^{-1}(v)$ [6].

In this paper, we prove that the Peterson graph and the power of a cycle are b -continuous. Also, we prove that the Cartesian product of two cycles $C_m \square C_n$ is b -continuous when m and n are multiples of 5. In this case, we give the color classes of b -coloring with k colors for each k with $\chi(G) \leq k \leq b(G)$.

II. B-SPECTRUM OF C_n^k AND $C_m \square C_n$

In 2001, Lee [6] obtained the following result which helps to obtain independent dominating vertex subset of big graph from small graphs under some conditions. He proved the following theorem, which we used in the next lemma.

Theorem 2.1 [6]: Let $p : G_1 \rightarrow G$ be a covering projection and let S be a perfect dominating set of G . Then $p^{-1}(S)$ is a perfect dominating set of G_1 . Moreover, if S is independent, then $p^{-1}(S)$ is independent.

In this section, we find the b -spectrum of the graphs C_n^k and $C_m \square C_n$. We prove that these two graphs are b -continuous. Further, we give a method of b -coloring the graph C_n^k with i colors for each i with $\chi(G) \leq i \leq \Delta(G) + 1$.

Lemma 2.2: Let $f : G \rightarrow H$ be a covering projection from a graph G on to another graph H . If the graph H is b -colorable with k colors, then so is G .

PROOF. Assume that H is b -colorable with k colors. Let the corresponding color classes be H_1, H_2, \dots, H_k . Define $G_i = f^{-1}(H_i)$ for $1 \leq i \leq k$. Define $c(v) = i$ if $v \in G_i$. Since H_i 's are pair wise disjoint independent vertex subsets of H , by Theorem 2.1, $\{ G_1, G_2, \dots, G_k \}$ is a vertex partition of independent subsets of G . This means that the graph G is also k -colorable with color classes G_1, G_2, \dots, G_k . It is enough to prove that each color class G_i contains a color dominating vertex.

Let $h \in H_1$ be a color dominating vertex of H with color 1 and let $g \in f^{-1}(h) \subseteq G_1$. we prove that g is a color dominating vertex with color 1 in G .

Note that $\deg_G(g) = \deg_H(h)$. Since $h \in H_1$ is colorful, and by the definition of $\{ H_1, H_2, \dots, H_k \}$, there exist vertices h_2, h_3, \dots, h_k such that $h_i \in H_i$ and $(h, h_i) \in E(H)$ for $2 \leq i \leq k$. Since $f_{N(g)} : N(g) \rightarrow N(h)$ is a bijection, there exist vertices $g_1, g_2, \dots, g_k \in V(G)$ such that $(g, g_i) \in E(G)$ and $f(g_i) = h_i$ for $2 \leq i \leq k$. Hence $g_i \in G_i$ and $c(g_i) = i$ for $2 \leq i \leq k$ and so g is a colorful vertex of G with color 1. Similarly, we can prove that there exist colorful vertices in G for all colors 2, 3, ..., k.

In [2] S. Chandra Kumar et al. proved the following Lemma.

Lemma 2.3[2]: If $k+1 \leq d \leq 2k+1$ and d divides n , then the graph $G = C_n^k$ admits b -coloring with d colors. In particular, when $d = k+1$, the fall chromatic number $\chi(G) = k+1$.

Here, we prove the above lemma more generally.

Lemma 2.4: Let $k+1 \leq d \leq 2k+1$. Then the graph $G = C_n^k$ admits b -coloring with d colors.

PROOF. Let $V(G) = \{ (v_n) v_0, v_1, \dots, v_{n-1} \}$ and $E(G) = E^1 \cup E^2 \cup \dots \cup E^k$, where $E^j = \{ (v_j, v_{(j+i) \pmod n}) : 0 \leq j \leq n-1 \}$ Let $n = id+t$ for some t with $1 \leq t \leq 2k$.

Case 1: If $1 \leq t \leq k+1$.

Let us color the vertices as follows: For each j with $0 \leq j \leq id$, color of the vertex v_j is defined by $c(v_j) = j \pmod d$. Also $c(v_{id+1}) = k+1, c(v_{id+2}) = k+2, \dots, c(v_{id+t}) = k+t$.

Case 2: If $k+2 \leq t \leq 2k+1$.

Let us color the vertices as follows: For each j with $0 \leq j \leq n-1$, color of the vertex v_j is defined by $c(v_j) = j \pmod d$.

Note that, for each g with $1 \leq g \leq k$, the vertex v_j has exactly two neighbors $v_{j \oplus g}$ and $v_{j \oplus (n-g)}$, where \oplus is the operation, addition modulo n . Hence $N(v_j) = \{ v_{j \oplus 1}, v_{j \oplus 2}, \dots, v_{j \oplus k}, v_{j \oplus (n-1)}, v_{j \oplus (n-2)}, \dots, v_{j \oplus (n-k)} \}$. Note that, two vertices v_a and v_b receive the same color only when $a \oplus b \leq k+1 \leq d$, where \oplus_d is the operation, addition modulo d . Hence the adjacent vertices will receive different colors. In cases 1 and 2, the vertices v_1, v_2, \dots, v_g are colorful vertices with colors 1, 2, ..., g respectively.

Theorem 2.5 : $S_b(C_n^k) = [\chi(C_n^k), b(C_n^k)]$.

PROOF. Since $b(G) \leq \Delta(G)+1$, we have $b(C_n^k) \leq 2k+1$. By the definition of C_n^k , it contains a set $\{ v_0, v_1, v_2, \dots, v_k \}$ of mutually pair wise adjacent vertices. Hence $\chi(C_n^k) \geq k+1$. By Lemma 2.4, it follows that $S_b(C_n^k) = [\chi(C_n^k), b(C_n^k)]$.

Remark 2.6: The graph $C_5 \square C_5$ is b -colorable with i colors for each $i = 3, 4$ and 5. The graph $C_5 \square C_5$ is given below:

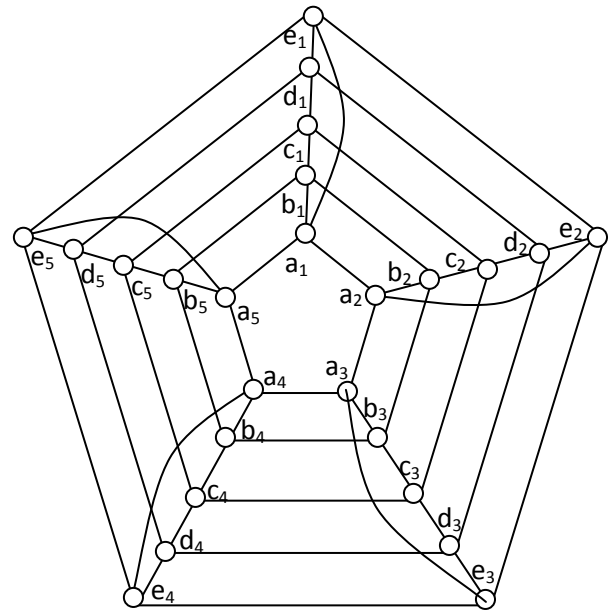


Figure 2.1: $C_5 \square C_5$

Consider the following b -coloring of $C_5 \square C_5$ with 3 colors: $c(a_1) = 1, c(a_2) = 2, c(a_3) = 1, c(a_4) = 3, c(a_5) = 2, c(b_1) = 2, c(b_2) = 3, c(b_3) = 2, c(b_4) = 1, c(b_5) = 3, c(c_1) = 1, c(c_2) = 2, c(c_3) = 1, c(c_4) = 3, c(c_5) = 2, c(d_1) = 3, c(d_2) = 1, c(d_3) = 3, c(d_4) = 2, c(d_5) = 1, c(e_1) = 2, c(e_2) = 3, c(e_3) = 2, c(e_4) = 1, c(e_5) = 3$. Note that c_1, b_1 and d_1 are colorful vertices with colors 1, 2 and 3 respectively.

Consider the following b -coloring of $C_5 \square C_5$ with 4 colors: $c(a_1) = 3, c(a_2) = 2, c(a_3) = 3, c(a_4) = 4, c(a_5) = 1, c(b_1) = 4, c(b_2) = 1, c(b_3) = 2, c(b_4) = 3, c(b_5) = 2, c(c_1) = 1, c(c_2) = 2, c(c_3) = 4, c(c_4) = 1, c(c_5) = 3, c(d_1) = 2, c(d_2) = 4, c(d_3) = 3, c(d_4) = 2, c(d_5) = 4, c(e_1) = 1, c(e_2) = 3, c(e_3) = 1, c(e_4) = 3, c(e_5) = 2$. Here a_5, b_5, c_5 and b_1 are colorful vertices with colors 1, 2, 3 and 4 respectively.

Consider the following b -coloring of $C_5 \square C_5$ with 5 colors: $c(a_1) = 4, c(a_2) = 2, c(a_3) = 5, c(a_4) = 3, c(a_5) = 1, c(b_1) = 5, c(b_2) = 3, c(b_3) = 1, c(b_4) = 4, c(b_5) = 2, c(c_1) = 1, c(c_2) = 4, c(c_3) = 2, c(c_4) = 5, c(c_5) = 3, c(d_1) = 2, c(d_2) = 5, c(d_3) = 3, c(d_4) = 1, c(d_5) = 4, c(e_1) = 3, c(e_2) = 1, c(e_3) = 4, c(e_4) = 2, c(e_5) = 5$. In this case, all the vertices are colorful vertices.

Theorem 2.7: The graph $C_m \square C_n$ is b -continuous when m and n are multiples of 5.

PROOF. Let m and n be positive integers which are multiples of 5. Since $b(G) \leq \Delta(G)+1$, we have $b(C_m \square C_n) \leq 5$.

If m and n are even numbers, then the graph is a product of two even cycles which is a bipartite graph and hence it has a b -coloring with 2 colors.

Otherwise, $C_m \square C_n$ contains an odd cycle and hence $\chi(C_m \square C_n) \geq 3$. From the above fact and from Remark 2.6, it follows that $S_b(C_5 \square C_5) = [\chi(C_5 \square C_5), b(C_5 \square C_5)]$.

As in the proof of Lemma 2.10 in [2], there exists a covering projection from $C_m \square C_n$ to $C_5 \square C_5$. Hence the result follows from Lemma 2.2.

III. B-SPECTRUM OF PETERSON GRAPH

In this section, we find the b -spectrum of Peterson graph and we prove that it is b -continues. Throughout this

section, the vertices of the Peterson graph are labeled as in the following figure. We say that the vertices a_1, a_2, a_3, a_4, a_5 are outer vertices and b_1, b_2, b_3, b_4, b_5 are inner vertices.

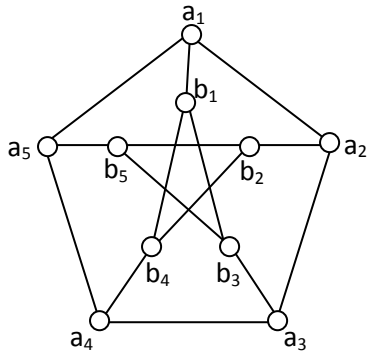


Figure 3.1: Peterson Graph

Remark 3.1: The Peterson graph P is b -colorable with 3 colors as shown in the following figure. The colorful vertices are marked by dark circles.

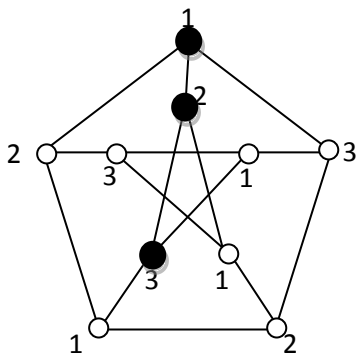


Figure 3.2

Remark 3.2: In Peterson graph, when using 4 colors, all the neighbors of a colorful vertex will receive different colors.

Lemma 3.3: The Peterson graph P is not b -colorable with 4 colors.

PROOF. Case 1: If two adjacent outer vertices of P are colorful (as shown in Fig.3.3).

Since the vertex a_2 is colorful with color 2, we should color the vertices a_3 and b_2 with colors 3 and 4.

Sub case 1.1: $c(a_3) = 4$ and $c(b_2) = 3$ (as shown in Fig.3.4). Note that the adjacent vertices b_3 and b_5 cannot be colored with colors 3 and 4.

Sub case 1.1.1: $c(b_3) = 2$ and $c(b_5) = 1$ (as shown in Fig.3.4.1). By Remark 3.2, the vertices a_3, a_4, a_5 and b_4 could not be colorful with color 4 and hence there exist no colorful vertex with color 4.

Sub case 1.1.2: $c(b_3) = 1$ and $c(b_5) = 2$ (as shown in Fig.3.4.2). In this case, by Remark 3.2, there exists no colorful vertex with color 3.

Sub case 1.2: $c(a_3) = 3$ and $c(b_2) = 4$ (as shown in Fig.3.5). Then the adjacent vertices a_4 and b_4 cannot be colored with colors 3 and 4.

Sub case 1.2.1: $c(a_4) = 1$ and $c(b_4) = 2$ (as shown in Fig.3.5.1). By Remark 3.2, the vertices a_5, b_2, b_3 and b_5 could not be colorful vertices with color 4 and hence there exist no colorful vertex with color 4.

Sub case 1.2.2: $c(a_4) = 2$ and $c(b_4) = 1$ (as shown in Fig.3.5.2). In this case, there exist no colorful vertex with color 3.

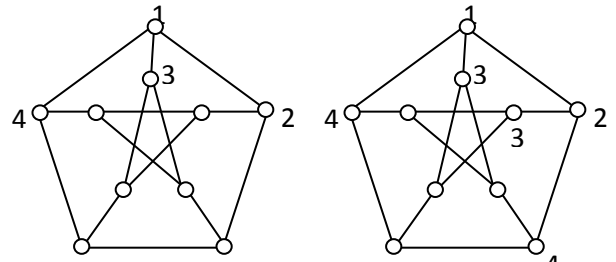


Figure 3.3

Figure 3.4

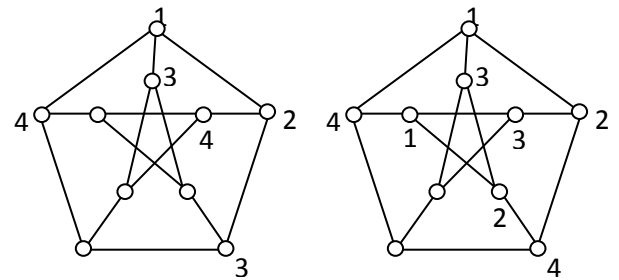


Figure 3.5

Figure 3.4.1

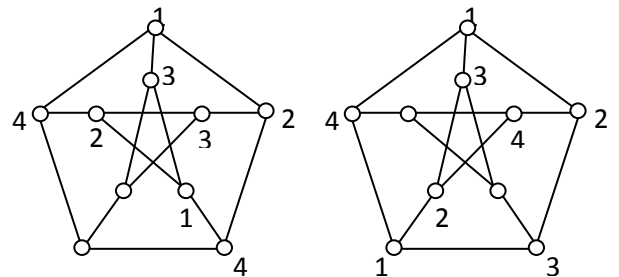


Figure 3.4.2

Figure 3.5.1

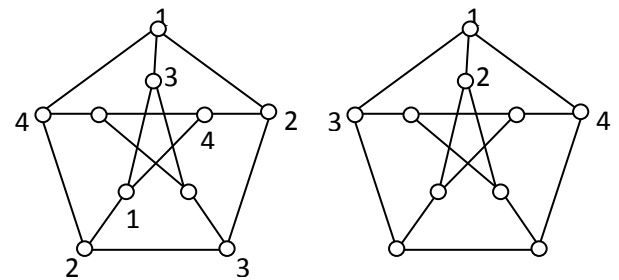


Figure 3.5.2

Figure 3.6

Similarly, it is not possible to have two adjacent colorful inner vertices.

Case 2: If two adjacent vertices of P (one is inner and another one is outer vertex) are colorful (as shown in Fig.3.6). Since the vertex b_1 is colorful with color 2, we should color the vertices b_3 and b_4 with colors 3 and 4.

Sub case 2.1: $c(b_3) = 4$ and $c(b_4) = 3$ (as shown in Fig.3.7). Here, the adjacent vertices b_2 and b_5 cannot be colored with colors 3 and 4.

Sub case 2.1.1: $c(b_2) = 1$ and $c(b_5) = 2$ (as shown in Figure 3.7.1). By Remark 3.2, the vertices a_2, a_3, a_4 and b_3 could not be colorful vertices with color 4 and hence there exist no colorful vertex with color 4.

Sub case 2.1.2: $c(b_2) = 2$ and $c(b_5) = 1$ (as shown in Figure 3.7.2). In this case, by Remark 3.2, there exist no colorful vertex with color 3.

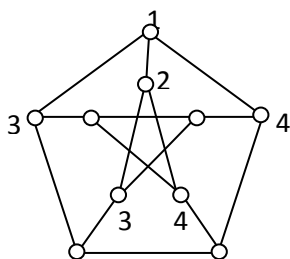


Figure 3.7

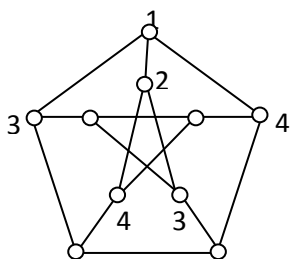


Figure 3.8

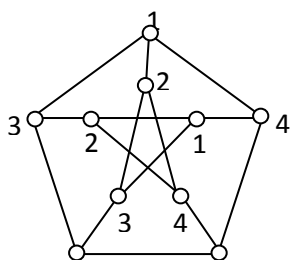


Figure 3.7.1

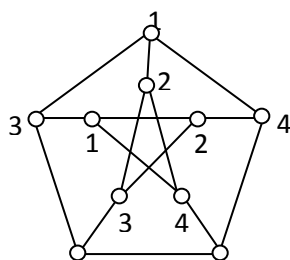


Figure 3.7.2

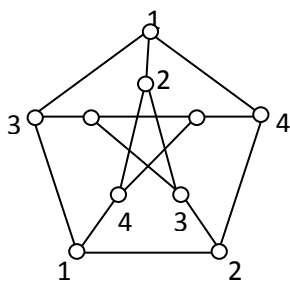


Figure 3.8.1

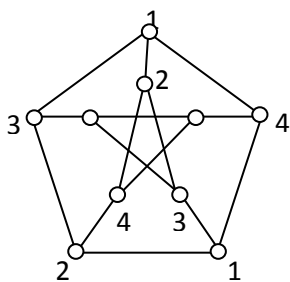


Figure 3.8.2

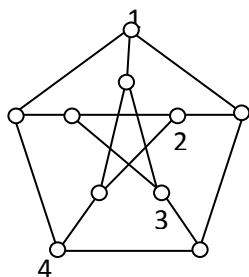


Figure 3.9

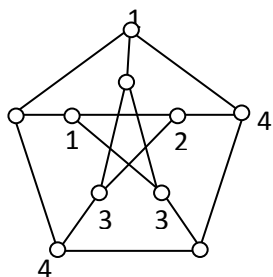


Figure 3.10

Sub case 2.2: $c(b_3) = 3$ and $c(b_4) = 4$ (as shown in Fig.3.8). Then the adjacent vertices a_3 and a_4 cannot be colored with colors 3 and 4.

Sub case 2.2.1: $c(a_4) = 1$ and $c(a_3) = 2$ (as shown in Fig.3.8.1). By Remark 3.2, the vertices a_2 , b_2 , b_4 and b_5 could not be colorful with color 4 and hence there exists no colorful vertex with color 4.

Sub case 2.2.2: $c(a_4) = 2$ and $c(a_3) = 1$ (as shown in Fig.3.8.2). In this case also, there exists no colorful vertex with color 4.

From the above two cases, it is observed that the four colorful vertices must be independent and exactly two inner(outer) vertices are colorful. This is discussed in the following case.

Case 3: The Four colorful vertices are as given in Fig.3.9. The vertex b_5 may have one of the color 1 or 4 and without

loss of generality, assume that $c(b_5) = 1$ (as shown in Fig.3.10). Then for the colorful vertex b_2 with $c(b_2) = 2$, we should have $c(b_4) = 3$ and hence $c(a_2) = 4$ (as shown in Fig.3.10). Consider the colorful vertex a_1 with $c(a_1) = 1$. Here, we should have $c(b_1) = 2$ and hence $c(a_5) = 3$ (as shown in Fig.3.11). In this case, by Remark 3.2, the vertex a_4 with color 4, is not colorful.

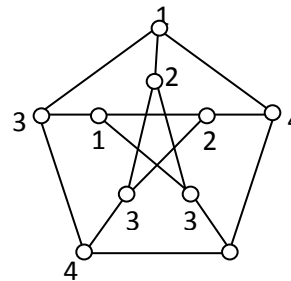


Figure 3.11

Hence, the Peterson graph is not b-colorable with 4 colors.

Since the Peterson graph is 3-regular, by Remark 3.1 and Lemma 3.3, we have the following theorem.

Theorem 3.4: The Peterson graph is b-continuous.

IV. CONCLUSION

This work may be extended in the following directions:

1. Prove that the graph $C_m \square C_n$ is b-continuous for integers m and n which are not multiples of 5.
2. Find the b-chromatic number of Cartesian product of three or more cycles.
3. Find the b-chromatic number of power of Cartesian product of two cycles and three cycles.

REFERENCES

- [1] Campos, C.N, and De Mello C.P, A result on the total coloring of powers of cycles. *Discrete Applied Mathematics*, 155, 2007, 585-597.
- [2] S. Chandra Kumar, T. Nicholas, and S. Somasundaram, Fall coloring on product of cycles and Powers, *Journal of Mathematics Research*, 3(4), 2011, 152-157.
- [3] El-Sahili, A. and Kouider, M, About b-colorings of regular graphs. *Res. Rep. 2006, 1432, LRI, Univ. Orsay, France.*
- [4] Gary Chartrand and Ping Zhang, *Chromatic Graph Theory* (New York : CRC Press, 2009)
- [5] Haynes, T.W, Hedetniemi, S.T, and Slater, P.J, *Fundamentals of Domination in Graphs* (Marcel Dekker, 2009).
- [6] Lee, J, Independent perfect domination sets in Cayley graphs. *J. Graph Theory*, 37(4), 2001, 231-239.
- [7] Marko Jakovac and Sandi Klavzar, The b-chromatic number of cubic graphs, *Preprint series*, 47, 2009, 1067.
- [8] Mostafa Blidia, Frederic Maffray and Zoham Zemir, On b-colorings in regular graphs, *Discrete Applied Mathematics*, 157, 2009, 1787-1793.
- [9] Saeed Shaebani, On Fall Colorings of Kneser Graphs. [Online] Available: <http://arxiv.org/abs/0909.2772>.

Effect of number of cycles on mechanical properties of Al sheets using corrugative and straightening method

Susheelkumar Vijapur, M Krishna, H N Narasimha Murthy

Research and Development, Dept. of Mech. Engg., R V College of Engineering, Bangalore-1

Abstract: The aim of the work was to study the effect of number of cycles on hardness and tensile strength of Al sheet materials processed by corrugative and straightening method. Al sheets were processed for up to 30 cycles using specially designed and developed geared corrugation and roller straightening setup. The microstructure, tensile and hardness studies were done as per standard methods. The microstructural study showed that finer grain refinement seen at 20th cycle then it grain dissolution could be seen. The experimental result showed that the hardness and tensile strength increasing with increase in number of cycles and reach maximum (105 Hv and 405 Mpa) at 21st cycle then they decreased due to grain dissolution.

Key words: Al sheets, corrugation and straightening process, microstructure, mechanical properties.

I. Introduction

The process of severe plastic deformation (SPD) is gaining great interest in material science because it is useful to refine microstructures to the sub micrometer or nanometer levels [1], which leads to improved strength with good ductility. Researchers are working on SPD different techniques namely equal- channel angular pressing (ECAP) [2-4], high pressure torsion (HPT) [5], hydrostatic extrusion (HE) [6] and repetitive corrugated and straightening (RCS) [7-8]. Many methods are limited to smaller size, heterogeneity and larger wastage of specimens. But CRCS method can work for continuous structures and reduce the wastages.

Pandey et.al [9] designed a new technique called continuous repetitive corrugation and straightening system (CRCS), which produces continuous strips without wastage of materials in a single cycle. Few researchers were working on effect of CRCS on materials such as precipitation [9], strain hardening [10], and heat treatment [11] processes. They were observed that the ductility of the samples expressed by relative elongation insignificant drop. Micro-hardness of the CRCS samples increased from about 100 to about 150 HV. The similar strength characteristics for the samples increased. However few researchers successfully worked on strengthening CRCS method but no information is available to date on the level of homogeneity achieved in processing by CRCS method. Hence the objectives of the work were to investigate number of cycles of CRCS on homogeneity mechanical properties hardness and tensile properties and which was justified with microstructure.

II. Experimental studies

In the present study the CRCS process is applied to the Al 6061 sheet the chemical composition are given in Table 1 of dimension 50 x 30 x 1 mm sheets. Al sheets brushed and clean with acetone to remove dirt and rust. The special CRCS was designed and developed using a pair of gears for corrugation and pair of rollers for straightening. The Al sheets are passed through the gears and roller continuously for strengthening, each process is one cycle. The same procedure continues for 30 cycles. Three specimens were used for every cycle that is 1 cycle- 3 specimen, 2 cycles: 3 specimens, so on. CRCS processed specimen polished with different grade SiC papers using automatic polishing machines. Then to obtain mirror finish, the specimen polished on velvete surface with diamond paste. The Keller's reagent was used as the etchant and the chemical composition is 2 ml HF, 3ml HCl and 5ml HNO₃ to obtain grain size. After surface preparation, microstructure analysis was carried out on all the specimens using optical microscope. The specimens are tested for Vickers microhardness (HV) using Micromet-5101 device, with a load of 200g for duration 20 seconds. Tensile tests were performed at room temperature with universal testing machine at cross head speed of 0.5 mm/min, having gauge length of 75mm, thickness of 12.5mm and shoulders of 30mm. three readings were taken for each cycle.

Table1. Chemical composition of Al 6061 (mass %)

Fe	Cu	Si	Zn	Mn	Mg	Cr	Ti	Al
0.16	0.19	0.71	0.04	0.02	0.94	0.08	0.03	Bal

III. Results and discussion

3.1 Microstructure

The CRCS process up to thirty cycles has been successfully performed without shape defects of specimen. Fig. 1 shows the optical microstructures observed at the transverse direction plane of the specimens produced by different cycle of CRCS process. Fig. 1(a) shows the microstructure of ascast specimen, which exhibits strong wire texture and measured average width is around 70 μm . Fig. 1(b) shows 5 cycles CRCS specimen shows less significant effect on size of the grain boundaries which can be measured around 60 μm similarly even 15 cycles CRCS specimens shown in Fig. 1(c). 20 cycle CRCS grain structure (Fig. 1(d)) is refined and microstructure of the specimen evolves into a structure with a considerable fraction of low angle of boundaries. The grain boundaries change from 70 to 30 μm . For 25 (Fig. 1(e)) and 30 cycles (Fig. 1(f)) the grain boundaries no longer change but grain boundaries dissolve within the matrix alloys.

Hence Corrugation and straightening of Al 6061 sheet metal up to 22 cycles will give a good improvement in the grain refinement and even interfaces can also be seen. After 22nd cycle the grain refinement in the Al 6061 alloy gets disolute. As the Si and Mg are flattened more the strength of the material improves.

3.2 Hardness

Fig. 2 shows the effect of number of cycles on micro-hardness of the Al alloy sheet materials. The increase in Hv continues through subsequent cycles and this is due to the well-established reduction in grain size during CRCS process. The homogeneity in the material increased with increase in number of cycles at the higher constant strain. The hardness values increased with increase in number of cycles and reach maximum at 20 cycles then it decreased. The hardness value of the specimen before CRCS processing was 42 Hv, then increase linearly up to 20th pass and the maximal hardness value was obtained at 20th cycle was 105 Hv. With the increase in number of cycles the hardness value decreased and remained constant from 27th to 30th pass.

3.3 Tensile strength

Fig. 3 shows change in mechanical properties as a function of number of CRCS cycles. Fig. 3(a) and Fig 3(b) show the ultimate tensile strength and yield strength, they are increased by 11.23% and 12.25% after processing at 20th cycle of CRCS process. Maximal strengthening was achieved at 20th cycle of the CRCS process. Further processing caused decrease in the ultimate strength and yield strength of the material. Fig. 3(c) shows initially, the ductility of the material increased reached maximum at 10th cycle then it decreased up to 20th cycle then it remains constant. This is due to work hardening in the CRCS process caused a large decrease in ductility of the material and increase in strength. The initial tensile strength of the Al 6061 before processing by CRCS was 364 Mpa and the value of tensile strength increased after processing by CRCS to 405 Mpa, at 20th cycle the maximal value of strength was obtained.

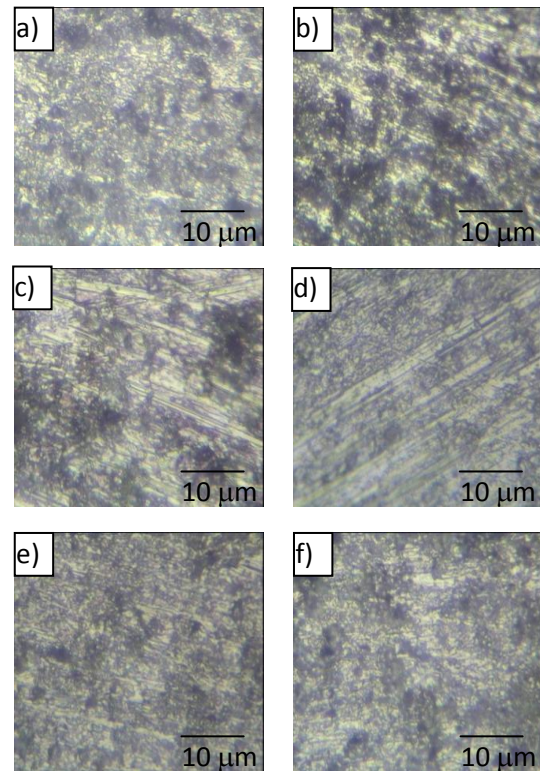


Fig. 1 Optical microstructure of CRCS processed specimens a) ascast, b) 5 cycles, c) 15 cycles, d) 20 cycles, e) 25 cycles and f) 30 cycles

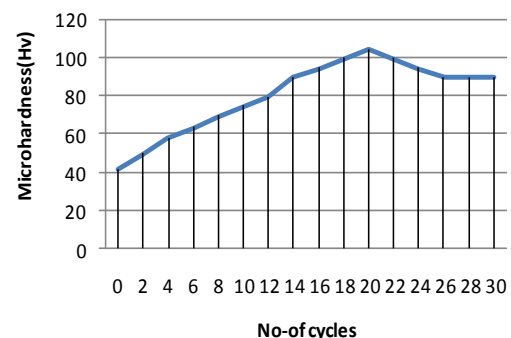


Fig. 2 Variation of microhardness of Al alloy with number of CRCS cycles

IV. Conclusions

This study was aimed to investigate mechanical properties and microstructure in Al 6061 alloy sheets processed by CRCS method. Based on the obtained results, the following conclusions can be drawn:

- The CRCS process effectively reduced the grain size of Al 6061 alloy sheets, demonstrating the CRCS as a promising new method for producing ultra fine grained metallic sheets.
- The optical microscope analysis of microstructure of Al 6061 alloy sheet after CRCS (21 passes) revealed the finer grain size.
- Micro hardness value of Al 6061 alloy sheet before processing by CRCS method was 42 Hv, it increased to about 105 Hv after processing by CRCS method.

- The strength characteristics of the investigated sheet such as yield strength and ultimate tensile strength increased after processing by CRCS method.

References

- [1] S.C. Pandey, M.A. Joseph, M.S. Pradeep, K. Raghavendra, V.R. Ranganath, K. Venkateswarlu, Terence G. Langdon, A theoretical and experimental evaluation of repetitive corrugation and straightening: Application to Al-Cu and Al-Cu-Sc alloys. *Materials Science and Engineering*, volume A 534 (2012), Pp 282-287.
- [2] Mishra, V. Richard, F. Gregori, R. J. Asaro, M.A. Meyers, Microstructural evolution in copper processed by severe plastic deformation, *Materials Science and Engineering A* 410-411 (2005), pp 290-298.
- [3] Mishra, B. K. Kad, F. Gregori, M.A. Meyers, Microstructural evolution in copper subjected to severe plastic deformation: Experiments and analysis, *Acta Materialia* vol 55. (2007). Pp 13-28.
- [4] S.V. Dobatkin, J.A. Szpunar, A.P. Zhilyaev, J.-Y. Cho, A.A. Ku-znetsov, Effect of the route and strain of equal-channel angular pressing on structure and properties of oxygen-free copper, *Materials Science and Engineering* vol 462, (2005), pp 132-138.
- [5] Y.H. Zhao, Y. T. Zhu, X. Z. Liao, Z. Horita, T. G. Langdon, Influence of stacking fault energy on the minimum grain size achieved in severe plastic deformation torsion, *Materials Science and Engineering* vol 463, (2007),pp 22-26.
- [6] M. Kulczyk, W. Pachla, A. Mazur, M. Suł-Ryszkowska, N. Krasilnikov, K.J. Kurzydowski, Producing bulk nanocrystalline materials by combined hydrostatic extrusion and equal-channel angular pressing, *Materials Science* vol 25/4, (2007),pp 991-999.
- [7] Y.T. Zhu, H. Jiang, T. C. Love, A new route to bulk nanostructured materials, *Metallurgical and Materials Transactions A: Physical Metallurgy and Materials Science* vol 32/6, (2001), pp 1559-1562.
- [8] J.Y. Huang, Y. T. Zhu, H. Jiang, T. C. Love, Microstructure and dislocation configuration in nanostructured Cu processed by repetitive corrugation and straightening, *Acta Materialia* volume 49, (2001), Pp 1497-1505.
- [9] S.C. Pandey, M.A. Joseph, M.S. Pradeep, K. Raghavendra, V.R. Ranganath, K. Venkateswarlu, Terence G. Langdon, A theoretical and experimental evaluation of repetitive corrugation and straightening: Application to Al-Cu and Al-Cu-Sc alloys. *Materials Science and Engineering*, volume A 534. (2012), Pp 282-287.
- [10] S.H. Lee, Y. Saito, T. Sakai, H. Utsunomiya, Microstructures and mechanical properties of 6061 aluminum alloy processed by accumulative roll-bonding, *Materials Science and Engineering*, volume 325, (2002), pp 228-235
- [11] J. Stobrawa, Z. Rdzawski, W. Głuchowski, W. Malec. Ultrafine grained strips of precipitation hardened copper alloys. *Archives of metallurgy and materials*. Volume 56 issue 1. (2011), Pp 171-178.

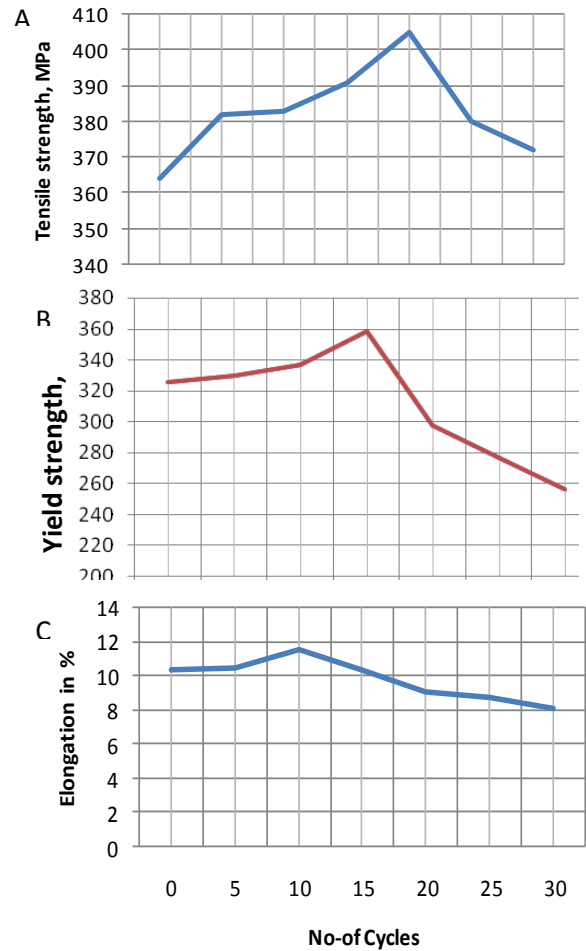


Fig. 3 Changes in mechanical properties of Al alloy with number of cycles in the CRCS process

Land Sale Geographic Information System based on Web and Web Mobile using Google Map

¹I Nyoman Piarsa, ²A. A. Kt. A. Cahyawan Wiranatha,
³Yohanes Perdana Putra.

^{1, 2, 3}(Departement of Information Technology, Udayana University Bali-Indonesia)

ABSTRACT: Sale and purchase of land are usually done by people. Most people are confuse how to find land sold in an area that people already specified. Land Sale Geographic Information System based on web and mobile web using google map is an alternative media that can mapping an area where land is sold. This base system is made by using Ruby on Rails framework and CSS responsive layout. Those platforms will facilitate developers in applying it. The Strengths of this application is user can easily see the location where they want to buy by map. The option search include; land sale by type, region, status, price. forum on the land sale information system will allow users to be able to communicate with each other. Bidding recording system is also a medium that helps to get the best between buyers and sellers selling price. and lastly, the web mobile make users able to open web from any mobile devices.

Keywords: Geographic Information System, Land Sale, Forum

I. INTRODUCTION

Land selling is an activity when the owner of some land is changing. The number of people grows rapidly not only because of the economic factor but also because of their need to find places to stay increases too. In addition, many people come from the other provinces to work and they need to find places to stay.

In some place, land selling still uses printed media and also advertising media through internet. Those media will complicate buyers to choose the land which is already decided because they have to read the articles provided one by one in order to get the information they need on the location of the land. Moreover, buyers should not only search for information in one media, but also in another media.

Seeing the issue above, the writer had an idea to develop an information system with data processing center which is integrated with Land Sale Geographic Information System, Forum Website, and Mobile. This system can help both sellers and buyers in getting the latest information easier. The system is also expected to be able to collect, save, combine, arrange, manipulate and analyze Geographic Information System related to spatial field based on Google Map API.

With the existence of Land Sale Geographic Information System, users will find it easier to find the locations of places they want. By using the system, users can also search for certain criteria such as number of home level, electricity, and building size. Users can also trade information to others in this land selling forum. This system

has a flexible ability as it can be opened using mobile.

II. LITERATURE REVIEW

Geographic Information System (GIS) is one of many information technologies that can input, store, recall, process, analyze and produce geographic or geospatial data in order to facilitate decision-making process in the planning and management of spaces, natural resources, environment, urban facilities, and other public services. GIS components are a computer system consisting of hardware and software, geospatial data, and brainware.

Spatial data are data which are related to geographic conditions, such as rivers, administrative areas, buildings, roads, etc. Spatial data are obtained from maps, aerial photos, satellite images, statistical data, and many others. Until today, common perceptions of the representation of spatial entity are raster and vector concepts. Non-spatial data, on the other hand, are data which are in the form of texts or numbers, often referred as attribute. The Figure below is an example of spatial data obtained from a map.

2.1 Google Map

Google Maps is a web mapping service application and technology provided by Google, that powers many map-based services, including the Google Maps website, Google Ride Finder, Google Transit, and maps embedded on third-party websites via the Google Maps API. It offers street maps, a route planner for traveling by foot, car, bike (beta), or public transport and an urban business locator for numerous countries around the world. Google Maps satellite images are not updated in real time; they are several months or years old[5].

Using Google Map API is not a complex that many people think. It just need HTML, CSS and javascript working together inside[1]. The map tiles are images that are loaded in the background with ajax calls and that return new images. And also the API, basically that is consist of javascript files that contain a class with methods to run the program.

2.2 Geocode

Geocoding us the process of assigning a latitude/longitude coordinate to a place[2]. Geocode also return the coordinate from sending address. Geocoding engine work with a variety of inputs, including the following:

- Address
- cros street
- city and state
- zip code

Data that return from geocode is a JSON output format. JSON that can be read from javascript.

2.3 JSON

JSON (JavaScript Object Notation) is a light data-exchange format which is easy to be written and read by human, and also easy to be translated and generated by computer[4]. JSON is only a text format that does not depend on any programming languages, as it uses a language commonly utilized by C programming family, such as C, C++, C#, Java, JavaScript, Perl, Python, etc. These characteristics make JSON ideal as a language of data exchange.

2.4 Ruby On Rails

Ruby is a script-based, object-oriented dynamic programming language. Ruby is used to combine the superiority of the existing programming languages. Ruby is written in C programming language which basic abilities similar to Perl and Python. Ruby on Rails is built around the Model-View-Controller(MVC) pattern. MVC is a design pattern used for separate an application's data model, user interface, and control logic into three separate layers with minimal dependencies.

There are three data model on RoR:

1. The controller is the component that receives the request from the browse or mobile device and performs the users-specified action.
2. The model is the data layer that is used usually from a controller to read, insert,update, and delete data stored, for example, in relational database.
3. The view is the representation of the page that the users see in their browser.

2.5 Responsive layout

Responsive layout is like an approach to web cascading style that make a flexible layout. The main objective is to build a web can detect a width and height of visitor screen size using media query.

Media queries, a feature of cascading style sheets (CSS), allow the developer to specify when a certain style takes effect. With media queries can solves a lot of design problems caused by the proliferation of new types of mobile devices. Responsive design pages use x and y coordinates on a grid for layout and mathematical percentages for images instead of fixed-width parameters. Using percentages instead of fixed-width parameters and a grid layout creates a more fluid layout that will resize itself to fit the size of the display.

This capacity means that instead of having to build a special mobile version of a website -- which often requires writing new code from scratch -- developers can simply build multiple style sheets for the same web page and perhaps even associate different images with each of the style sheets. As a result, HTML code can be repurposed instead of having to be rewritten, which saves considerable development time.

III. APPLICATION DESCRIPTION

The involved components in this geographic information system are: users, administrator, and google map.

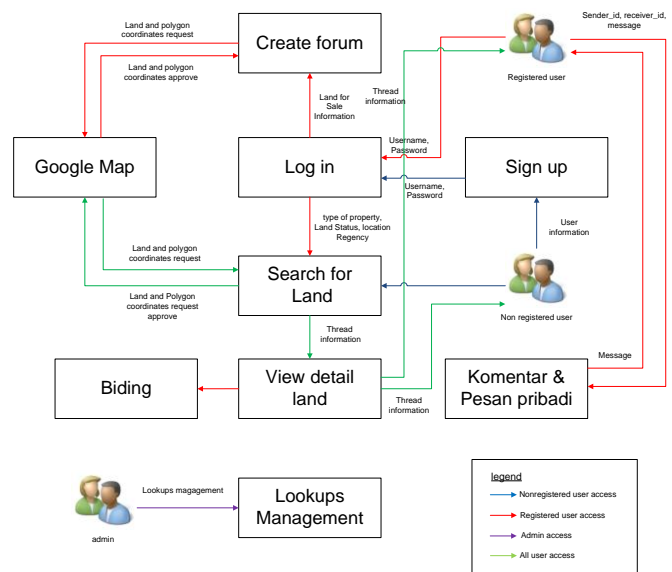


Figure 1. System Overview

Figure 1 describes the overview of Land Sale Information System. It elaborates the flow of figures and features accessible to each user. This system has three user types: guest user, registered user, and admin.

Guest user may access *land search* in the map and may also view *land details*. The search can be done by categorizing the lands based on its department (regency), sale status, prices, and type of land to be sold. The purpose is to facilitate guest user in looking for information on what other users are selling or renting out in this geographic information system.

Guest user may also register himself in the geographic information system by completing the signup process. This method enables guest users to become registered users, and could login in the system.

After logging in, registered users may create a thread to promote the land they want to sell or rent out. In creating threads, users elaborate the details of land-related information and are also able to draw their land location in a polygon shape as well as the department/regency where the land is located. As the map is clicked upon, the system will obtain latitude and longitude coordinates from Google Map to be stored as land-sale location.

Registered users may also give comments both in their own threads and in others' threads. This enables users to easily provide additional information which can be viewed and responded by other users. A private message feature is also provided to registered users, where information can be sent privately between registered users, without the knowledge of uninvited users.

Private message, only for register user. It can be made for anyone who already registered in the system.

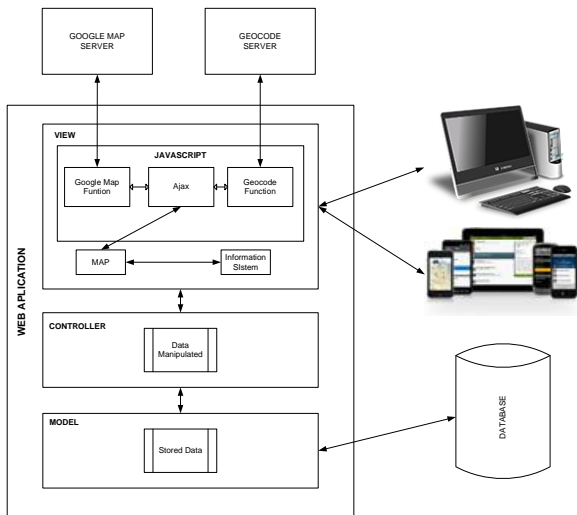


Figure 2. Flow System Description

Users may use either desktop computers or mobile devices. These devices will directly access View. In the viewing process, View would send data request to controller, where it consequently accesses to the database to obtain the data needed. The data are then sent back to View Process in a JSON format where JSON will be processed in JavaScript. Next, Ajax would send the coordinates to geocode to find out in which regency the land is located, where it would send back the information related to the regency in JSON format. Finally, Ajax sends the same coordinates to be marked in Google Map, and Google Map displays the map and its location markers.

IV. RESULTS

This geographic information system provides search feature. In this search system, users are faced with several choices: sale types, region, forum types, and price. Users may choose more than one available options. Forum Types in the map are displayed differently based on icons as can be seen in Figure3.

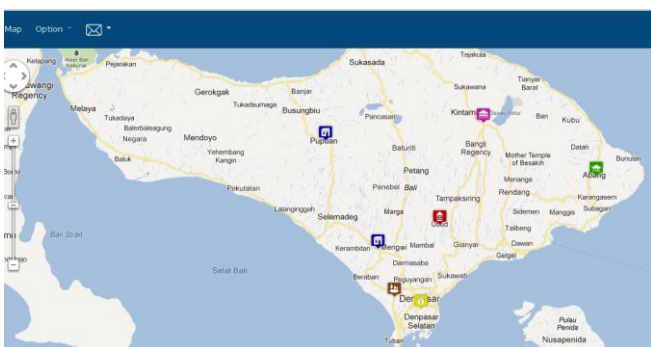


Figure 3. Search Results Based on Maps

Search results can also be seen based on the forum types. Forum displays organize information based on tables sorted by dates and prices. Figure 4 shows an example of forum-based search results.

Rumah	Treads/Post	Post Terakhir
 <p>DISEWAKAN RUMAH LT.2 Perum.Kediri Rp.15000000 Sewa Jl. By Pass Kediri No. 24</p>	Dikunjungi: 6 Post: 3 oleh:ari	2012-06-28 04:49:35 lebar jalan di depan berapa meter??
 <p>Dijual Rumah Sederhana Rumah Power Rp.2000000000 Jual Jl. Raya Pupuan no. 34</p>	Dikunjungi: 1 Post: 1 oleh:intan	2012-07-03 17:08:21 rumah kosongan apa ada isinya??
 <p>Jual rumah seputaran renon Jual Rumah Renon Rp.3000000000 Jual Jl Raya renon</p>	Dikunjungi: 0 Post: 1 oleh:boke	2012-07-02 19:37:17 Senin boleh ketemuan??

Figure 4. Search Results Based on Forum

Apart from the ability to display information based on its forum, users are also able to easily interact with each other using commentaries and private messages as seen in Figure 5.



Figure 5. Sample komentar

Another feature is the media which facilitates sellers and potential buyers to bargain and negotiate. For example, potential buyers may offer a price lower than what the seller asks, and this can be done several times. Sellers then could pick the offer they like the most to close the deal. Offers are sorted in a descending manner based on their prices. The higher the offer, the higher its position is displayed in the result.

Penawar	Harga	Waktu	Terima
ina	500000000	July 01, 2012 19:05	DEAL
dana	435000000	July 02, 2012 19:06	
bode	400000000	July 04, 2012 18:51	
boke	375000000	July 01, 2012 05:31	
indra	300000000	July 02, 2012 05:30	
dana	125000000	July 03, 2012 17:16	

Figure 6. Users bidding sample

In addition, this system also has several notification features, such as:

- 1 Comment Notification**
Comment Notification informs all users commenting on a thread if there is a new reply from another user.
- 2 Private Message Notification**
Private Message Notification appears if a new message from another user is received
- 3 Negotiation Notification**
Negotiation Notification shows users if a new user is involved in a negotiation or if a new offer is made
- 4 Land Sold Notification**
Land Sold Notification informs all the users who have been involved either in a commentary thread or negotiation thread when the related land has been sold or rented out

Rating System is the last feature of this geographic information system. Users may give rating to a certain thread. The highest rating is 5 stars, while the lowest is 0. The rating score is displayed based on the average rating given by all users on certain thread.

V. STRENGTHS AND WEAKNESSES

5.1 Strengths of Land Sale Information System

Here are some advantages of this system:

- 1 The main feature, map, enables users to search for lands based on the desired location.
- 2 Its web-based characteristics let users easily access the information from any device as long as they are connected to the Internet.
- 3 This system is accessible for mobile devices which can run JavaScript such as tablet computers or smartphones. Obtaining and sharing land-related information from users' handsets would be easier.
- 4 Users may browse for land-related information in two ways: map and forum. Forum-based View provides an alternative and help users which might have difficulties in reading maps.
- 5 Registered users can give comments or ask questions in a related thread.
- 6 Registered users can send private messages to each other, in order to prevent uninvited users from viewing their conversations.

5.2 Weaknesses of Land Sale Information System

This System cannot verify whether or not the information the users have input are reliable.

VI. CONCLUSIONS

The followings are the conclusions from the research "Designing Web-Based and Mobile-Based Land Sale Geographic Information System":

1. Google Map has the capabilities of providing spatial data for exact mapping and real mapping. In addition, Google Map also has numerous features such as street mapping, satellite images, and hybrid features which can support users in map-based information search.
2. Land Sale Geographic Information System gives users easy access to search for land sales based on its location and sale status.
3. Web-Mobile version helps users to access information related to land sales, although it is not as fast and as efficient as accessing it from the computer.

REFERENCES

- [1] Svennerberg, Gabriel, *Beginning Google Maps API 3*. Spinger Science, Business Media, 1966.
- [2] Jagoe, Andrew, *Mobile Location Services*. Prentice Hall, 2003.
- [3] Hutchinson, Matthew J (2010). *Developing an Agent-Based Framework for Intelligent Geocoding* (Ph.D. thesis). Curtin University.
- [4] Zakas, Nicholas. *High Performance javascript*. O'REILLY Media, 2010.
- [5] <http://en.wikipedia.org/wiki/Google>

Production, purification and characterization of Lipase isolated from salt water *Halobacterium sp*

V. Ramadas* and R. Lavanya Ramadoss**

(*Assistant Professor, Research Centre & P.G. Department of Zoology, R.D.Govt. Arts College, Sivagangai - 630 561, Tamil Nadu, India)

(** Former Student, Department of Biotechnology, P.S.R.Engineering College, Sivakasi, Tamil Nadu, India)

ABSTRACT: *Halobacterium* are salt loving microorganism, which thrives in the salt lake, and seawater where there is an elevated salt concentration. They have the capacity to balance the osmotic effect of the outside environment and resist against the dehydrating effects of the salts. Their novel characteristics and capacity for large scale culturing make *Halobacterium* potentially valuable for biotechnology. In the present study the *Halobacterium sp.* was isolated from seawater sample and from paddy field nearer to seashore they are characterized by morphological and biochemical characteristics. The *Halobacterium sp.* was subjected to screening for enzyme production like amylase, cellulose, lipase and protease. Lipase enzyme was produced in the laboratory scale it was purified by dialysis method and using ion exchange chromatography. The enzyme activity and concentration were determined using the standard laboratory protocols. The enzyme kinetics studies were also carried out along with the SDS-PAGE using BSA as a standard marker and it was found out that the obtained lipase enzyme was 66 KD in its molecular weight.

Keywords: Seawater - *Halobacterium*, - lipase enzyme Production and Characterization – determination of molecular weight.

I. INTRODUCTION

Halobacterium is salt – loving microorganisms that inhabit hypersaline environments [1]. These bacteria has a unique feature of possessing the purple membrane, specialized regions of the cell membrane that contain a two dimensional crystalline lattice of a chromoprotein, bacteriorhodopsin. They have the capacity to balance the osmotic pressure of the environment and resist the denaturing effects of the salts [2]. They are able to live in salty conditions by preventing dehydration of their cytoplasm. They do this by either producing large amounts of an internal organic solute or by concentrating a solute from their environment [3]. *Halobacterium* is motile spore producing aerobic microorganism found distributed all over the world in hypersaline environments, many in natural hypersaline brines in arid, coastal, even deep sea locations, as well as in artificial salterns used to mine salts from the sea. Their novel characteristics and capacity for large scale culturing make *Halobacterium* potentially valuable for biotechnology [4]. The genus *Halobacterium* consists of several species of archaea with an obligate aerobic metabolism which

require an environment with a high concentration of salt [5].

A lipase is a water-soluble enzyme that catalyzes the hydrolysis of ester bonds in water-insoluble, lipid substrates. Lipases are ubiquitous throughout living organisms, They have considerable physiological significance and industrial potential, and are being employed for the synthesis of drug intermediates and pharmaceutically important molecules. The lipases used for various purpose are usually fungal or bacterial origin [6]. They are produced as an extra-cellular product by the bacterial species and attract industrial attention. The activity of the enzymes in general appears to be stabilised by immobilisation in suitable matrices. The lipase may be immobilised in hydrogels (alginate, carrageenan, agarose etc) or in the solgels (silicate, celite etc). Many researcher have studied on various species of *Halobacterium* from salt lake [7] sea water and salt mine. Apart from these, many biomolecules synthesized by the *halobacterium* have been reported by many authors [8,9,10,11&12] Likewise, many workers have studied the proteome of *Halobacterium salinarum* using proteomics technique and also detected 14 protein molecules. Meanwhile, a very few literature available on the lipase production by *halobacterium* isolated from sea water. Hence, the present works deals with the isolation and characterisation of *Halobacterium* from the sea water. These isolated species was then subjected to the enzyme screening for the enzymes like amylase, cellulase, protease and lipase. Lipases have a large variety of applications mainly in the detergent, cosmetic, drug, leather, paper, and food industry and in several bioremediation processes. So owing to their vast and varied applications newer microbes are to be screened for production of lipases of desirable properties.

The enzyme kinetics studies like effect of temperature, pH, activator, inhibitor, and substrate concentration was also studied along with the determination of molecular weight of the lipase enzyme using SDS-PAGE.

II. MATERIAL AND METHODS:

2.1. Collection of water samples

Surface seawater (W1) samples were collected in a sterilized container from the sea at a depth of 1m and 6 km away from seashore at Tiruchendur in Southern Tamilnadu, India. Similarly, water sample (W2) was also collected from paddy field nearer to the seashore area approximately about 4 km away from the sea.

2.2. Estimation of total salt concentration and pH of the water samples

About 10 ml of each samples (W1 and W2) were taken in a two separate clean and dry test tube whose weight is determined previously and they were allowed to evaporate till there is no trace of water droplets inside the test tubes. The weight of the test tubes with the salts was measured and the difference between the weight of the test tube with salt and the empty test tube gives the weight of the salts present in the water samples. The pH of the water samples (W1 and W2) was determined using pH meter and values were recorded.

2.3. Isolation of *Halobacterium* from the samples W1 and W2

The samples W1 and W2 were serially diluted in the range of 10^{-1} , 10^{-2} , 10^{-3} , 10^{-4} , 10^{-5} , 10^{-6} , and 10^{-7} in a series of test tube. The *Halobacterium* was cultured in the nutrient medium with increased concentration of Na Cl. The pH of the medium was adjusted to 7 – 7.4, and the composition of the nutrient medium with essential ingredients were given in the Table-1. The samples were inoculated under aseptic condition in the petriplates containing nutrient agar medium using spread plate technique and are incubated at 37°C for 48 hours [13].

Table – 1. Composition of nutrient medium for bacterial growth

Sl.No.	Essential Ingredients	Concentration (g/100ml)
1.	Peptone	0.5
2.	Yeast extract	0.3
3.	NaCl	2.0
4.	Agar	2.0

2.4. Preparation of pure culture of *Halobacterium sp.*

The nutrient agar slant was prepared in test tubes and the isolated colony obtained in the petriplates were taken carefully without contamination (leaving out mixed culture colony) and streaked in the nutrient agar slant in the in a zigzag manner using the inoculation loop. Then test tubes were plugged with cotton plugs and incubated at 37°C for 48 hours.

2.5. Morphological studies of *Halobacterium* using Gram staining

The morphological studies like colony appearance, cell shape, and size on the obtained pure cultures were carried out using Gram staining method. The stained slides were observed for the morphological characteristics of the culture under the compound microscope.

2.6. Determination of respiration type of *Halobacterium*

The nutrient agar deep tube was prepared and the pure culture was inoculated deeply into the solidified medium using inoculation needle under sterile condition. After inoculation, the upper surface of the medium was covered with the molten wax with 0.5cm thickness and incubated for 48 hours at 37°C.

2.7. Biochemical characterization of *Halobacterium*

Different biochemical tests were performed to characterize and to confirm the isolated species as *Halobacterium*, such as, catalase test, indole production test, methyl red and vogas proskauer (MR – VP) test, citrate utilization test and acid production test.

2.8. Screening for enzyme production by *Halobacterium*

The pure culture of *Halobacterium* species was subjected to screening for enzyme production like, amylase, protease, cellulase and lipase. The essential ingredient for the enzyme-screening medium is given in the Table - 2.

Table – 2. Composition of enzyme screening medium

Sl.No	Essential ingredients	Concentration (g/1000ml)	
1	Amylase screening medium		
	Beef Extract	3.0	
	Peptone	5.0	
	Na Cl	7.0	
	Starch	10.0	
	Agar	20.0	
2	Lipase screening medium		
	Peptone	2.5	
	Casein	2.5	
	Yeast Extract	3.0	
	Tributyryn	10.0	
	Na Cl	7.0	
3	Protease screening medium		
	Skim Milk powder	10.0	
	Na Cl	7.0	
	Agar	20.0	
	4.	Cellulase screening medium	
		Beef Extract	3.0
Peptone		5.0	
Na Cl		7.0	
Cellulose (CMC)		10.0	
Agar		20.0	

The different types of medium used for the screening of enzyme production were sterilized using autoclave. The medium was distributed equally in the Petriplates and allowed it to get solidified, after few minutes of solidification, the pure culture was inoculated in a zigzag streak using inoculation loop and incubated at 37°C for 24 – 48 hours.

2.9. Assay of Lipase enzyme production

The lipase enzyme was produced using the *Halobacterium* isolated from the sea water in the sterilized lipase production medium. The composition of lipase production medium is indicated in the Table – 3.

Table – 3. Composition of lipase productionmedium

Sl.No.	Essential ingredients	Concentration (g/1000ml)
1.	Peptone	2.5
2.	Casein	2.5
3.	Yeast Extract	3.0
4.	Tri butyrin	10ml
5.	Na Cl	7.0

The pH of the sterilized medium was adjusted to 7.4 and isolated strains of *Halobacterium* were inoculated under aseptic condition using inoculation loop in the medium and incubated at 37°C for 48 hours in a mechanical shaker.

2.9.1. Extraction of lipase enzyme

After considerable growth of bacteria in the lipase production medium, the lipase enzyme produced as an extracellular product by the bacteria was extracted from the medium. The lipase production broth was centrifuged at 6000 rpm for 10 minutes to remove the cell debris and the supernatant was collected in the separate test tubes after centrifugation and filtered using Watt Mann Filter Paper.

The obtained filtrate was subjected for 70% saturation (for 100ml of sample about 44.2g of ammonium sulphate salt gives 70% saturation) with ammonium sulphate by adding the salt slowly in the conical flask containing the filtrate kept in the magnetic stirrer. The content was left undisturbed for one hour, and then it was centrifuged and the pellets were collected and dissolved in the 20 mM Tris buffer. About 1.5 ml of crude enzyme extract was taken in the vials and stored for the future use at 4°C.

2.9.2. Purification of lipase enzyme

The obtained crude enzyme was then purified by Dialysis method and Ion exchange chromatographic process.

2.9.3. Dialysis of crude extract of Enzyme

The obtained crude extract of enzyme was first purified by dialysis process, which is based on the principle of osmosis. About 2 litres of 50 mM Tris hydrochloride is required for the process. The cellulose acetate membrane, which can retain the molecules, whose molecular weight is greater than 10 to 12 KD is used as a dialysis membrane. The pretreatment of dialysis membrane is required to perform the dialysis process.

2.9.4. Pretreatment of Dialysis membrane

About 2 to 2.5 inches of dialysis membrane was taken and it was soaked for 10 minutes in a boiling water bath at 100°C. After 10 minutes of boiling, 2gm of

sodium carbonate was added to the boiling water containing the dialysis membrane and allowed to boil for few minutes. Then the dialysis membrane was transferred to the fresh boiling water bath at 100°C for 10 minutes.

2.9.5. Dialysis of enzyme

The pretreated dialysis membrane was taken and made into a pouch like structure with the help of thread tied at the one end of the membranes. To the pouch the crude extract of enzyme was added and it was sealed at both the ends using threads. The sealed membrane with the enzyme was then dipped into the 50 mM Tris HCl and allowed to stand for overnight undisturbed at 4°C. After incubation, the entire content was brought to room temperature and the dialysis process was repeated for 2 times with fresh Tris HCl buffer. To enhance the dialysis process the entire dialysis set up was kept in the magnetic stirrer. About 1.5 ml of dialyzed sample was taken in vials and stored at 4°C for future use.

2.9.6. Purification of lipase using Ion exchange chromatography

The dialyzed sample was further purified using ion exchange chromatography with 25 mM Tris HCl and 1 M NaCl. These ion exchange solvents with different molarities were prepared and distributed in to six different test tubes as shown in the Table – 4.

Table – 4. Ion exchange solvents with different Molarities

Test Tube No.	Tris HCl (ml)	NaCl (ml)	Distilled water (ml)
1.	0.25	0.25	9.50
2.	0.25	0.50	9.25
3.	0.25	0.75	9.00
4.	0.25	1.00	8.75
5.	0.25	1.25	8.50
6.	0.25	1.50	8.25

The enzyme, which is retained in the resin bed, was eluted by the solutions of different molarities, which are added one by one, and the filtrate was collected in the sterile test tubes.

2.9.7. Determination of activity of lipase enzyme using titrimetric method

The activity of the lipase enzyme obtained (Crude enzyme sample, Dialyzed enzyme sample, and the enzyme purified further by ion exchange chromatography sample) was determined by titrimetric method.

2.9.8. Determination of enzyme concentration by Lowry's method

The concentration of the extracted enzyme was determined by the Lowry's method.

2.10. Enzyme Kinetic studies of lipase enzyme using titrimetric method

The kinetics of enzymes like effect of temperature, pH, substrate concentration, inhibitor and activator were studied using the standard laboratory protocol.

2.10.1. Effect of temperature

A series of test tubes labeled with different incubation temperature (4°C, room temperature, 37°C, 55°C, and 100°C) including Blank. About 2.5ml of distilled water was added to each test tube along with the addition of 1.0ml of Tris HCl buffer and 0.3ml of Tributyrin (substrate). The test tubes were incubated at room temperature for 10 minutes and then about 0.1ml of enzyme was added to each test tubes except blank and incubated at 37°C for 30 minutes. About 3 ml of ethanol was added after the incubation period to the test tubes and the enzyme activity was determined.

2.10.2. Effect of pH

A series of test tubes labeled with different pH values such as 3, 5, 7, 9, and 11 along with blank. About 2.5ml of distilled water, 1ml of buffer with different pH values and 0.3 ml of Tributyrin (substrate) were added to the test tubes and incubated at room temperature for 10 minutes. Then 0.1ml of enzyme was added to all the test tubes except blank and incubated at 37°C for 30 minutes. 3.0ml of ethanol was added to the test tubes after the completion of incubation period and the enzyme activity was determined.

2.10.3. Effect of substrate concentration

A series of test tubes labeled with different substrate concentrations like 50µl, 100µl, 150µl, 200µl, 250µl, 300µl, 350µl, 400µl, 450µl, and 500µl were taken. To each test tubes about 2.5ml of distilled water, 1ml of Tris HCl buffer, and Tributyrin (substrate- with different concentration) were added. The test tubes were incubated at room temperature for 10 minutes and about 0.1ml of enzyme was added to all the test tubes except blank. After the addition of enzymes the test tubes were incubated at 37°C for 30 minutes. About 3.0ml of ethanol was added after the incubation period to the test tubes and the enzyme activity was determined.

2.10.4. Effect of activator

A series of test tubes labeled with different concentration of activator (ZnCl₂ 1mg/ml) like 0.2ml, 0.4ml, 0.6ml, 0.8ml and 1.0ml were taken and 2.5ml of distilled water, 1 ml of Tris HCl buffer and 0.3ml of Tributyrin (substrate) to each test tubes and they were incubated at room temperature for 10 minutes. After that about 0.1ml of enzyme was added to all the test tubes except blank and the activator of different concentration (Table -) again incubated at 37°C for 30 minutes. About 3.0ml of ethanol was added after the incubation to each test tubes and the enzyme activity was determined.

2.10.5. Effect of inhibitor

A series of test tubes labeled with different inhibitor (Stock solution:EDTA 1mg/ml) concentration like 0.2ml, 0.4ml, 0.6ml, 0.8ml and 1.0 ml were taken, and 2.5ml of distilled water, 1ml of Tris HCl buffer and

0.3ml of Tributyrin (substrate) were added to each test tubes.

All the experimental samples were incubated at room temperature for 10 minutes. After incubation of the content about 0.1ml of enzyme (except blank) and inhibitor of different concentration were added to each test tubes and incubated at 37°C for 30 minutes. About 3.0ml of ethanol was added after the incubation and the enzyme activity was determined.

2.11. Determination of molecular weight of lipase enzyme using SDS-PAGE

The molecular weight of the lipase enzyme obtained from *Halobacterium* species was determined by SDS-PAGE, where BSA serves as a control and the reagents used for SDS-PAGE were indicated in Table – 5.

Table – 5. Reagents used for SDS-PAGE

Sl.No	Essential ingredients	Concentration
1	Stock acrylamide solution	
	Acrylamide 30%	3g
	Bis acrylamide 0.8%	0.08g
	Water	10ml
2	Separating gel buffer pH 8.8	
	1.875M Tris HCl	2.27g
	Water	10ml
3	Stacking gel buffer pH 6.8	
	0.6m Tris HCl	0.726g
	Water	10ml
4	Electrolyte buffer pH 8.2 – 8.4	
	0.05M Tris	1.2g
	0.192M Glycine	2.88g
	0.1% SDS	0.2g
5	Ammonium persulphate solution	
	Ammonium sulphate	0.6g
	Water	10ml

About 2ml of separating gel buffer was mixed with 3.5 ml of stock acrylamide solution and to which 4.5ml of water was added. The separating gel mixture was then degassed and about 20µl of freshly prepared ammonium persulphate (APS) solution was added for the polymerization reaction to form gel. After the addition of APS the separating gel mixture was immediately poured into the tightly clamped SDS plates. The surface of the separating gel was washed with water in order to form a smooth even surface and after polymerization of separating gel, the water was removed and ensures that there is no trace of water in between the glass plates. Then the stacking gel mixture of water 3.5ml, stacking gel buffer 0.5ml and stock acrylamide solution of 1ml was vortexed and degassed, to that about 7µl of APS solution was added and poured above the separating gel

within the glass plates and the comb was inserted immediately to form the wells for loading the samples in the gel and it was left undisturbed to get solidified by the polymerization reaction. After solidification of gel the comb was removed carefully and the wells was washed with electrolyte buffer and the electrophoresis tank was filled with the electrophoresis buffer. The samples were then loaded in the wells and it was electrophoresed at 50 to 100 volts where standard BSA serves as a marker. After electrophoresis the gel was stained with staining buffer and kept for overnight. It was then destained and the presence of enzyme bands was observed.

III. RESULTS AND DISCUSSION

IV.

3.1. Estimation of total salt concentration and pH of the water samples

The sea water sample (W1) contains 4g of salts/ 100 ml of water and the water sample (W2) collected from the paddy field nearby sea shore area was found to contain 3.1g of salts / 100ml of water. The pH of the water sample W1 and W2 were recorded as 8.65 and 10.19 respectively.

3.2. Isolation of *Halobacterium*

Numerous colonies like yellow pigmented, red pigmented, white spongy, white radial, dirty white colonies were observed from the water samples. The isolated *Halobacterium sp.* from the seawater samples was found as radial white spongy gram negative bacillus colonies. Ninety five extremely halophilic species have been isolated from distinct saline regions of Turkey. Likewise, a novel species of salt water bacterial namely *Halobacterium jilantaiense* was isolated [7]

3.3. Morphological characteristics of *Halobacterium*

The isolated *Halobacterium* strains were appeared as rod like bacillus, gram-negative organism. They found as radial white spongy colonies. The results of the morphological study of the obtained colonies were indicated in the Table – 6.

All the colonies isolated both from the seawater and paddy field water was gram negative bacilli. They are motile and aerobic in nature, requires oxygen for their metabolism [14, 15, & 16].

Table – 6. Morphological characteristics of *Halobacterium*

Sl.No	Sample	Colony Appearance	Cell shape	Gram staining
1	W1	White colony	Bacilli	Gram Negative
2	W1	Dirty white colony	Bacilli	Gram Negative
3	W2	Spongy white colony	Bacilli	Gram Negative
4	W2	Milky white colony	Bacilli	Gram Negative
5	W2	Yellow pigmented colony	Bacilli posses terminal spores	Gram Negative
6	W2	White colony	Bacilli	Gram Negative

3.4. Determination of type of respiration in *Halobacterium sp.*

It was observed that the colonial growth was absent in the test tubes sealed with the waxes due to the aerobic nature of the colony which requires oxygen for its respiration [17 & 18]. Both the aerobic and anaerobic colonies were isolated from water samples W1 and W2. The results were indicated in Table – 7.

Table – 7. Determination of type of respiration in *Halobacterium sp.*

Sl.No	Sample	Colony Appearance	Respiration type
1	W1	White colony	Aerobes
2	W1	Dirty white colony	Aerobes
3	W2	Spongy white colony	Aerobes
4	W2	Milky white colony	Facultative anaerobes
5	W2	Yellow pigmented colony	Aerobes
6	W2	White colony	Facultative anaerobes

3.5. Biochemical characteristics of *Halobacterium sp.*

The isolated pure cultures were subjected to various biochemical characterization [19 & 20] and the results were indicated in Table –8. The bacterial colonies isolated from the water samples W1 & W2 were showed positive results almost for all the biochemical tests except a few carried out in the present study. The results of the morphological and biochemical characteristic studies have confirmed the *Halobacterium sp.*

Table 8. Biochemical characteristics of *Halobacterium sp.*

Name of Biochemical test	Eperimental Samples					
	W1 (1)	W1 (2)	W2 (3)	W2 (4)	W2 (5)	W2 (6)
Catalase test	+	+	+	+	+	+
Indole production test	+	+	+	+	+	+
Methyl Red test	+	+	+	-	+	+
Vogas proskauer test	-	-	-	+	-	-
Citrate utilization test	+	+	+	+	+	+
Acid Production test	+	+	+	+	+	+

3.6. Screening for enzyme production by *Halobacterium sp.*

The inoculated petri dishes were observed after 24 – 48 hours of incubation for the presence of clear zone along the colony growth and the results of the enzyme like amylase, cellulose, lipase and protease productions by the organism were tabulated in Table –9.

The inoculated colonies produce the clear zone only in the lipase and protease-screening medium and not in the amylase and cellulose production medium. This indicated that the isolated *Halobacterium* strains produce both the protease and lipase enzymes and a well distinct zone was observed in the lipase production medium than in the protease production medium indicated that the organisms have produced more amount of lipase. The lipase has been isolated from *Fusarium solani* and *Streptococcus sp.* [21, 22, 23, & 24]

Table – 9 screening of various types of enzymes produced by *Halobacterium sp.*

Sam ple No.	Colony morphol ogy	Cellulas e	Amylase	Protea se	Lipas e
1 W1	White colonies	-	-	+	+
5 W2	Yellow pigment ed colonies	-	-	+	+

3.7. Purification of lipase enzyme

The crude enzyme obtained was purified by dialysis with cellulose acetate membrane which retains

the enzyme particles with size ranged from 10 to 12 KD, and the enzyme was further purified by ion exchange chromatography and stored.

3.8. Determiation of activity of lipase using titrimetric method

The results of the activity of the crude extract of the enzyme and dialyzed sample were indicated in Table – 10 and the sample purified by ion exchange chromatography were determined by titrimetric method and the results were indicated in Tables – 11. There was no difference in the activity of crude extract and dialyzed enzyme. Whereas, in case of enzyme purified by Ion Exchange Chromatography, the enzyme activity was gradually increased with increase in the concentration of enzyme (100000 to 300000 units /ml enzyme) and after saturation level there was no increase in the activity, instead it declined [25, 26 &27].

Table – 10. Determiation of activity of lipase present in the crude extract and dialyzed sample using titrimetric method

S.No	Enzyme activity (units/ml enzyme)	
	Crude Extract	Dialyzed Enzyme
B	0	0
1W1	30000	30000
5W2	20000	20000

Table – 11. Determiation of activity of lipase enzyme purified by ion exchange chromatography by titrimetric method

Sl. No	Solvent	Tris HCl (ml)	NaCl (ml)	Dis. water (ml)	Enzyme activity (units/ml)
1	1	0.25	0.25	9.50	100000
2	2	0.25	0.50	9.25	100000
3	3	0.25	0.75	9.00	200000
4	4	0.25	1.00	8.75	300000
5	5	0.25	1.25	8.50	200000
6	6	0.25	1.50	8.25	100000

3.9. Determiation of concentration of lipase enzyme using Lowry’s method

The concentration of the lipase in crude extract, sample after dialysis and purified using ion exchange chromatography was determined by Lowry’s method [28] and results were indicated in Table – 12. The concentrations of enzyme in the crude extract, dialyzed enzyme and purified by ion exchange chromatography were determined spectrophotometrically and recorded as 0.12µg/ml, 0.18µg/ml and 0.10µg/ml respectively.

Table – 12 Determination of concentration of lipase enzyme present in crude extract, dialyzed sample and purified sample by ion exchange chromatography

Effect of temperature on lipase activity		Effect of pH on lipase activity	
Temp range °C	Enzyme activity (units/ml enzyme)	pH	Enzyme activity (units/ml enzyme)
B	0	B	0
4	200000	3	200000
RT	300000	5	300000
37	300000	7	800000
55	400000	9	600000
100	200000	11	100000
Effect of substrate concentration on lipase activity			
Substrate concentration (µl)		Enzyme activity (units/ml enzyme)	
B		0	
50		200000	
100		300000	
150		500000	
200		500000	
250		900000	
300		1100000	
350		1200000	
400		1200000	
450		1200000	
500		1200000	
Effect of activator on lipase activity		Effect of inhibitor on lipase activity	
Sl.No	Enzyme activity (units/ml enzyme)	Sl.No	Enzyme activity (units/ml enzyme)
B	0	B	0
1	700000	1	900000
2	1500000	2	800000
3	1600000	3	700000
4	1800000	4	700000
5	2200000	5	400000

using Lowry's method

3.9. Enzyme kinetics of lipase enzyme obtained from *Halobacterium*

The enzyme kinetic studies were carried out to determine maximum activity of enzyme at optimum conditions. Especially the effect of temperature (Fig.1), pH (Fig.2), substrate concentration (Fig.3), inhibitor (Fig.4), and activator (Fig.5) on lipase activity have been indicated in Table - 13.

Table – 13. Effect of Temperature, pH, substrate concentration, activator and inhibitor on lipase enzyme obtained from *Halobacterium*

Sl.No	Vol. of std BSA (ml)	OD Values at 600 nm		
		Crude Extract	Dialyzed Sample	Purified sample by IEC
B	0	0	0	0
1	0.2	0.108	0.012	0.012
2	0.4	0.148	0.020	0.020
3	0.6	0.258	0.050	0.050
4	0.8	0.324	0.056	0.056
5	1.0	0.368	0.086	0.086
T	0.1	0.172	0.084	0.044

The optimum temperature and optimum pH at which the maximum activity of the enzyme was predicted for the lipase enzyme as 55°C, and 7 respectively. Whereas, in case of substrate concentration, the enzyme activity increases steadily with increase in the concentration of substrate up to 300µl and the activity of enzyme remains constant further increase in the substrate concentration.

Fig .1 Effect of temperature on lipase isolated from *Halobacterium sp.*

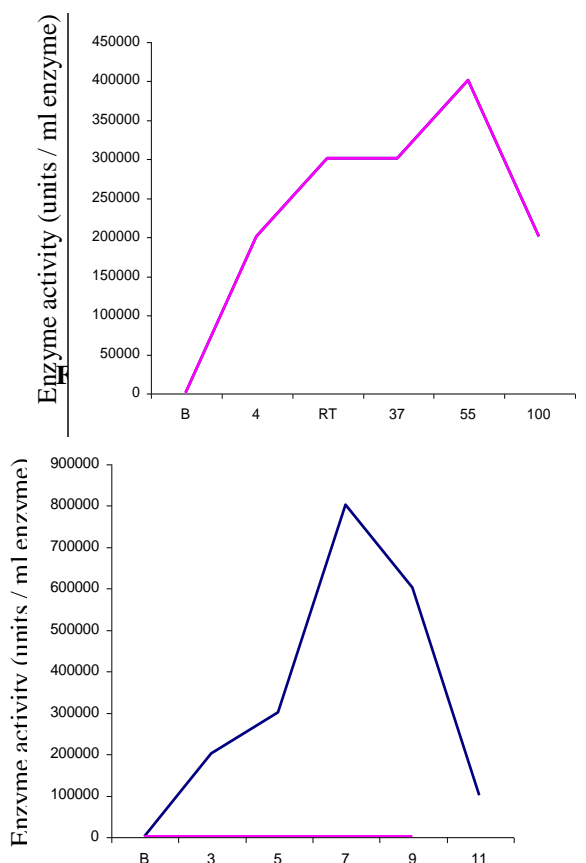


Fig. 3. Effect of substrate concentration on lipase isolated from *Halobacterium*

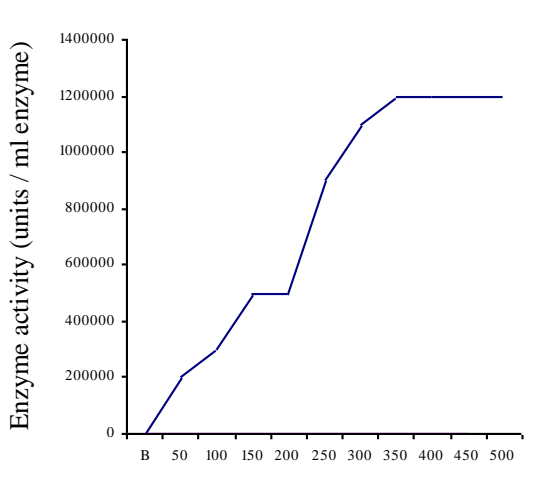


Fig.4. Effect of activator on lipase isolated from *Halobacterium sp.*

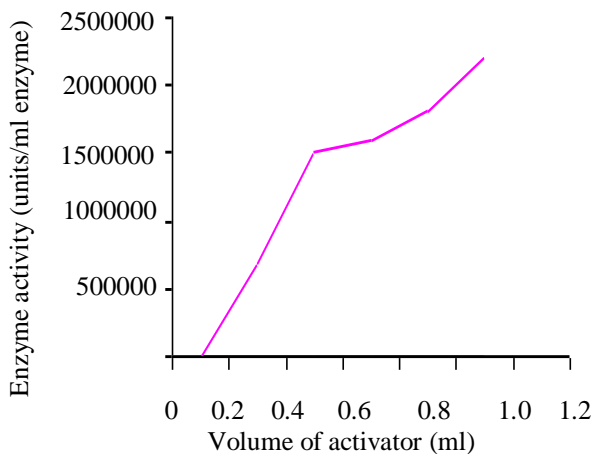
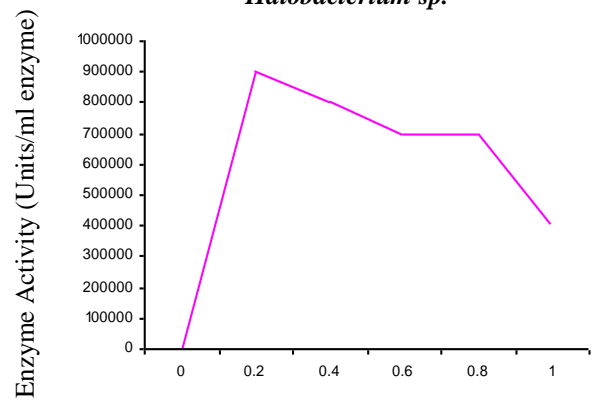


Fig .5. Effect of inhibitor on lipase isolated from *Halobacterium sp.*



The inhibitor (EDTA) inhibits the activity of the enzyme whereby the enzyme activity gradually decreases with increase in the concentration of inhibitor. Similarly, a gradual and steady enhancement in the enzyme activity was observed with increase in the concentration of the activator ($ZnCl_2$) in the present investigation. Similar studies have been carried out in *Streptococcus sp.*, and it was reported that, the optimum temperature and range of pH value for maximum activity of lipase as $37^\circ C$ and 8 – 8.4 respectively.

3.10. Determination of molecular weight of lipase using SDS-PAGE

The molecular weight of the lipase isolated from *Halobacterium sp.* was found to be 66 KD, which was determined using standard BSA as a marker in the SDS polyacrylamide gel electrophoresis. Similarly, the molecular weight of lipase isolated from *Streptococcus sp.* was reported as 44.7 KD [6].

REFERENCES

1. Yoon JH, Kang KH, Park YH : *Halobacillus salinus* sp. Nov., Isolated from the salt lake on the coast of the east sea in Korea. *Int. J. Syst. Evol. Microbiol.* 2003, 53: 687 – 93.
2. Abram, D., and N. E. Gibbons. 1961. The effect of chlorides of monovalent cations, urea, detergents and heat on morphology and the turbidity of suspensions of red *Halophilic* bacteria. *Can. J. Microbiol.* 7: 741 – 750.
3. Zvyagintseva IS, Tarasov AL : Extreme halophilic bacteria from saline soils. *Mikrobiologiya*, 1987, 56: 839 – 844.
4. Rodriguez – Valera f (1992) Biotechnological potential of *Halobacteria*. In: Danson MJ, Hough DW and Lunt GG (eds) *The archaeobacteria: Biochemistry and Biotechnology*. 135 – 147. London: Portland press.
5. Onishi H, Fuchi H, Konomi K, Hidaka O, Kamekura M; Isolation and distribution of a variety of Halophilic bacteria and their classification by salt – responce. *Agri, Biol, chem.* 1980, 44: 1253 – 1258.
6. Antonian E. Recent advances in the purification, characterization, and structure determination of lipases. *Lipids.* 1998; 23: 1101 – 1106.
7. Yang Y, Cui HL, Zhou PJ, Liu SJ. *Halobacterium jilantaiense* sp. nov., a halophilic archaeon isolated from a saline lake in Inner Mongolia, China. *Int. J. Syst. Evol. Microbiol.* 2006 Oct; 56 (pt 10): 2353 – 5.
8. Cardoso AM, Polycarpo C, Martins OB, Soll D. A Non-Discriminating Aspartyl-tRNA Synthetase from *Halobacterium salinarum*. *RNA. Biol.* 2006 Jul; 3 (3): 110 – 4.
9. Amoozegar MA, Malekzadeh F, Malik KA, Schumann P, Sproer C: *Halobacillus Karajensis* sp. Nov., a novel moderate halophilic. *Int. J. Syst. Evol. Microbiol.* 2003, 53: 1059 – 1063.
10. Brown, A.D., and K.Y.Cho. 1970. The walls of the extremely Halophilic Cocci: gram positive bacteria lacking muramic acid. *J. Gen. Microbiol.* 62: 267 – 270.
11. Cline SW, Schalkwyk LC, Doolittle WF: Transformation of the archaeobacterium *Halobacterium volcanii* with genomic DNA. *J. Bacteriol.* 1989, 171:4987 – 4991.
12. Dundas 1 (1998) Was the environment for primordial life hypersaline? *Extremophiles* 2: 375 – 377.
13. Seelay, H.WJr, and Vandermark, P.J. (1981). *Microbes in Action. A laboratory Manual of Microbiology*, W.H. Freeman & Co. pp.135.
14. Dym O, Mevarech M and Sussman JL (1995) Structural features that stabilize halphilic malate dehydrogenase from an archeobacterium. *Science* 267: 1344 – 1346.
15. Galinski EA (1993) Copatible solutes of halophilic eubacteria: molecular principles, water – solute

- interactions, stress protection. *Experientia* 49: 487 – 496.
16. Gibbons, N.E. 1969. Isolation, growth and requirements of Halophilic bacteria. 169 – 183. In F.N. Norris and D.W. Ribbons (ed.), *Methods in microbiology*, Vol. 3B. Academic press Inc., Newyork.
 17. GonZalez C, Gutierrez C, Ramirez C : *Halobacterium Vallismortis* sp. Nov. an amyolytic and carbohydrate metabolizing, extremely *halophilic bacterium*. *Can. J. Microbiol.* 1978, 24: 710 – 715.
 18. Ha DJ, Joo WA, Han GY, Kim CW : Proteome analysis of *Halobacterium salinarum* and characterization of proteins related to the degradation of isopropyl alcohol. *Biochem. Biophys. Acta.* 2007 Jan; 1774 (1): 44 – 50.
 19. James G.Cappuccino, Natalie Sherman: *Microbiology A laboratory manual*, Addison Wiley publication, Fourth edition, 59 – 183.
 20. Kamekura M, Dyall – Smith ML: Taxonomy of the family *Halobacteriaceae* and the description of two new genera *Halobrobacterium* and *Natrialba*. *J. Gen. Appl. Microbiol.* 1995, 41: 333 – 350.
 21. Krebs MP and Khorana HG (1993) Mechanism of light dependent proton translocation by bacteriorhodopsin. *Journal of Bacteriology* 175: 1555 – 1560.
 22. Kushner DJ, Kamekura M : Physiology of *Halophilic eubacteria*. In *Halophilic bacteria*. Volume - 1. Boca Raton, CRC Press; 1988: 109 – 140.
 23. Larsen, H.1976. Biochemical aspects of extreme halophilism. *Adv. Microb. Physiol.* 1: 97 – 132.
 24. Larsen H: *Halophilism*. The Bacteria 1962, Academic press, 4: 297 – 342.
 25. Saiz – Jimenez C, Laiz L: Occurrence of Halotolerant / Halophilic bacterial communities in deteriorated monuments. *Int. Biodeterior Biodegrad.* 2000, 46: 319 – 326.
 26. Spring S, Ludwig W, Marquez MC, Ventosa A, Schleifer KH: *Halobacillus* gen. nov., with descriptions of *Halobacillus litoralis* sp. Nov., and *Halobacillus trueperi* sp. Nov., and *halophilus comb. Nov.* *Int. J. Syst. Bacteriol.* 1996, 46: 492 – 496.
 27. Spudich JL (1993) Color sensing in the archae: a eukaryotic like receptor coupled to a prokaryotic transducer. *Journal of Bacteriology* 175: 7755 – 7761.
 28. Lowry O.H., Rose Braugh N.J., Farr A.L. and Randall R.J. (1951) Protein measurement with the folin phenol reagent. *J.Bio. chem.* 193: 265 – 275

ARM Based Solar Tracking System

K. Sreenivasa Rao¹, M. Mahesh²

*(Department of Electronics and Communication Engineering, AITS, India)

** (Department of Electronics and Communication Engineering, AITS, India)

ABSTRACT: Solar energy systems have emerged as a viable source of renewable energy over the past two or three decades, and are now widely used for a variety of industrial and domestic applications. Such systems are based on a solar collector, designed to collect the sun's energy and to convert it into either electrical power or thermal energy. In general, the power developed in such applications depends fundamentally upon the amount of solar energy captured by the collector, and thus the problem of developing tracking schemes capable of following the trajectory of the sun throughout the course of the day on a year. This project is designed with ARM7TDMI processor. The ARM7TDMI processor does the job of fetching the input from the sensor and gives command to the motor to run in order to tackle the change in the position of the sun.

Keywords: Solar collector, Light Dependent Resistor (LDR), ARM7TDMI processor.

I. INTRODUCTION

Solar energy is the energy extracted from the rays issued from the sun in the form of heat and electricity. This energy is essential for all life on Earth. It is a renewable resource that is clean, economical, and less pollution compared to other resources and energy. Therefore, solar energy is rapidly gaining notoriety as an important means of expanding renewable energy resources. As such, it is vital that those in engineering fields understand the technologies associated with this area. Our paper includes the design and implementation of a microcontroller-based solar tracking system. Solar tracking allows more energy to be produced because the solar panel is tracking the maximum power point of the sun's position.

To get an efficient solar tracker system, a small solar panel is used instead of a large one to obtain a graphical position data of the sun when it is detected and send this data to the large panels. This system can be installed anywhere in the world without knowing the sun directions and seasons.

II. SOLAR SYSTEM TRACKER

A solar tracker is an electro-mechanical system used on behalf of orienting a solar photovoltaic panel in the direction of the sun. It is used in many applications such as the transportation signaling, lighthouses, emergency phones installed in the highways, etc... Its main objective is to find the maximum sun radiations in order to get maximum charge for the batteries.

Electricity can be generated from the sun in several ways. Photovoltaic's (PV) has been mainly developed for small and medium-sized applications, from the calculator powered by a single solar cell to the PV power plant. For large -scale generation, concentrating solar thermal power plants have been more common, however new multi-megawatt PV plants have been built

recently. A photovoltaic cell (PV cell) is a specialized semiconductor that converts visible light into direct current (DC). Some PV cells can produce DC electricity from infrared (IR) or ultraviolet (UV) radiation. Photovoltaic cells are an integral part of solar-electric energy systems, which are becoming increasingly important as alternative sources of power utility.

Solar cells generate DC electricity from light, which in turn can be used in many applications such as: charging batteries, powering equipment, etc. They produce currents as long as light shines, as shown in Fig.1.

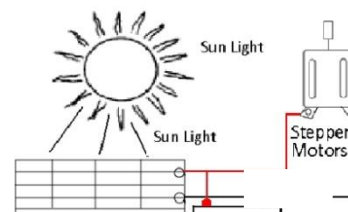


Figure 1. block diagram of the solar energy system

The detection of the position of the sun undergoes several steps as shown in Fig.2. A digital system (LPC2148) is used to calculate the maximum sun radiation. It is connected to a stepper motor and to light dependent resistors to redirect the panel to the sun. It sends the received data (position of the sun) to the stepper motors in order to position it toward the sun. The position angles are stored in the processor registers and can be displayed on an LCD or can be transmitted to a remote system.

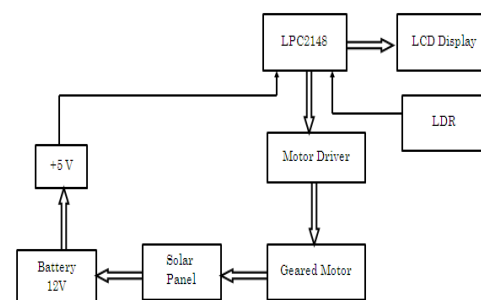


Figure2. block diagram of the solar tracker

2.1 Solar Tracker

A solar tracker is an electro-mechanical device for orienting a solar photovoltaic panel toward the sun trackers, especially in solar cell applications require a high degree of accuracy to ensure that the concentrated sunlight is directed precisely to the powered device.

Solar trackers can be active or passive and may

be single axis or dual axis. Single axis trackers normally use a polar mount for maximum solar efficiency and employ manual elevation (axis tilt) adjustment on a second axis, which can be adjusted regularly during the year.

Trackers can be relatively inexpensive for photovoltaics. This makes them especially effective for photovoltaic systems using high-efficiency panels. Solar trackers usually need inspection and lubrication on a regular basis.

Active trackers, which use motors and gear trains, are controlled by an electronic circuit responding to the solar direction.

2.2 Applications

In this paper a solar tracker is realized to capture maximum power from sunlight. The position of maximum capture of power is stored in memory. The stored data can be applicable for many applications such as Large photo voltaic panels can track the sun all the day light and by that it give above 65% efficiency in generating electricity. Solar heaters will also track the sun all the day light and by that less panels are required at the initial cost while in the home automation systems, this system is also needed in turning light ON and Off and also for opening and closing the curtains.

III. HARDWARE IMPLEMENTATION

3.1 Solar Panel

A photovoltaic module or photovoltaic panel is a packaged interconnected assembly of photovoltaic cells, also known as solar cells. A typical silicon PV cell is composed of a thin wafer consisting of an ultra-thin layer of phosphorus-doped (N-type) silicon on top of a thicker layer of boron-doped (P type) silicon. Regardless of size, a typical silicon PV cell produces about 0.5 – 0.6 volt DC under open-circuit and no-load conditions. The current (and power) output of a PV cell depends on its efficiency and size (surface area), and is Proportional to the intensity of sunlight striking the surface of the cell. The photovoltaic module, known more commonly as the solar panel, uses light energy (photons) from the sun to generate electricity through the photovoltaic effect. The majority of modules use wafer-based crystalline silicon cells or a thin-film cell based on cadmium telluride or silicon.

Crystalline silicon, which is commonly used in the wafer form in photovoltaic (PV) modules, is derived from silicon, a commonly used semi-conductor. The solar panel used in the proposed system is of 4W power rating as shown in Fig.3.



Figure3. 4W Solar Panel

3.2 Stand Assembly

The frame for the solar panel is made up of L shaped steel rod. The length is 0.95m and width is 0.38m. A square plate of dimensions 28x30 cm is made out of iron plate is fixed to the main structure at the height of 90cm from the base. The main frame is also made up of L shaped iron rod. Fig.4 illustrates stand assembly.

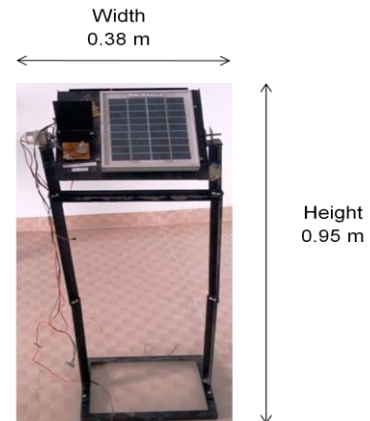


Figure4. Stand Assembly

3.3 Sensors

Sensor can be defined as a device which receives a signal and converts it into electrical form which can be further used for electronic devices. The light dependent resistors (LDR) are used in the circuit to sense the change in the sun's position. A photo resistor or light dependent resistor or cadmium sulphide (CdS) cell is a resistor whose resistance decreases with increasing incident light intensity. A photo resistor requires a power source because it does not generate Photocurrent a photo effect is manifested in the change in the material's electrical Resistance. Fig.5 shows a photo resistive cell.

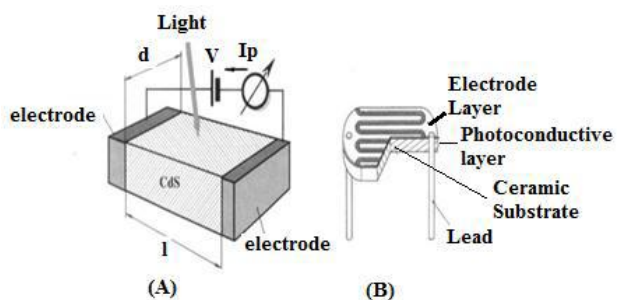


Figure5. (A) Structure of a photo resistor and (B) a plastic-coated photo resistor having a serpentine shape

3.4 ARM Processor:

LPC 2148 is a microcontroller with an internal ARM processor. In this project it gets signals from the light dependent resistors and is used to drive a geared motor to get maximum intensity of light. For this, the microcontroller uses PWMTCR, PWMTC, PWMPR, PWMPC, PWMMR0, PWMMCR, and PWMPCR register to control the direction of the solar panel using pulse width modulation. Fig.6 shows LPC2148 mother board.



Figure.6. LPC2148 Mother Board

3.5 Geard motor:

The motor chosen for the proposed system is 12V motor with 60rpm, coupled with a worm gear. The gear ratio is 25:1. The main reason for the selection of the geared motor is that it will consume very less power for a very small span of time. Also the torque required to rotate heavy PV arrays is sufficient enough. Fig.7 shows a 12V dc geared motor of 60RPM.



Figure.7. 12V geared motor

IV. CONTROL ALGORITHM AND PRIMARY RESULTS

4.1 Control Algorithm

In order to demonstrate the efficiency of the proposed system, a control algorithm is generated as shown in TABLE I, which is illustrated in Fig.8.

TABLE I. CONTROL ALGORITHM

Step #	Action
1	Install the small PV
2	Put PV in initial position (0,0)
3	Find the maximum sun light, using the photo resistors, and save the position of the PV
4	Measure the current (I)
5	If $I <$ threshold value (minimum current) wait for 30 minutes and go to step 3, otherwise go to step 6
6	Turn PV left for 3.5° , measure the current if it is greater than the previous current continue turning left until finding the maximum Current in x and y axis.
7	Send the coordinates (x,y) of the solar panel to the processor.
8	Go to step 3

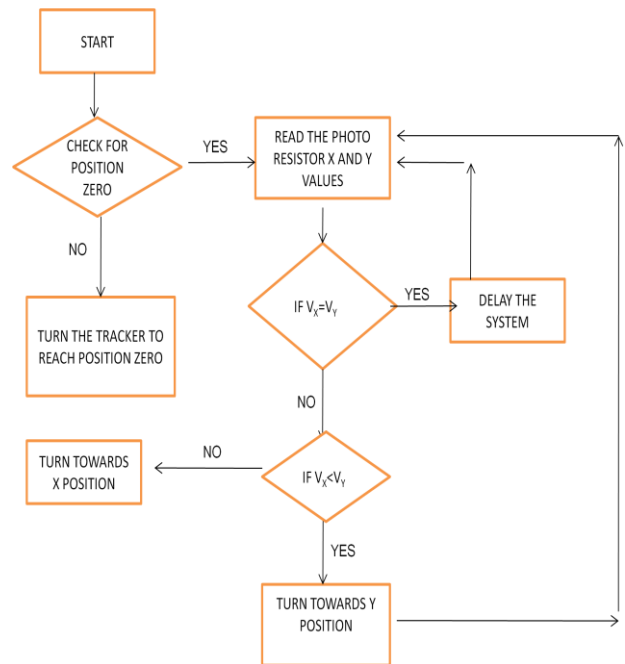


Figure.8. control algorithm

4.2 Preliminary Results

In order to assess the efficiency of the proposed system, some measurements were taken during a sunny summer day. TABLE II shows the comparison between the maximum current using a fixed Photovoltaic panel (PV) and using the proposed system at different times.

TABLE II. COMPARISON OF THE CURRENT BETWEEN FIXED PV AND USING THE PROPOSED SYSTEM

Time	Current using a fixed PV(mA)	Current using the Proposed system (mA)
08:00 AM	0.42	0.85
09:00 AM	0.55	0.90
10:00 AM	0.75	0.92
11:00 AM	0.81	0.95
12:00 PM	0.92	0.99
01:00 PM	0.95	0.99
02:00 PM	0.88	0.99
03:00 PM	0.76	0.98
04:00 PM	0.42	0.95
05:00 PM	0.23	0.95
06:00 PM	0.08	0.72
Total	6.84	10.39

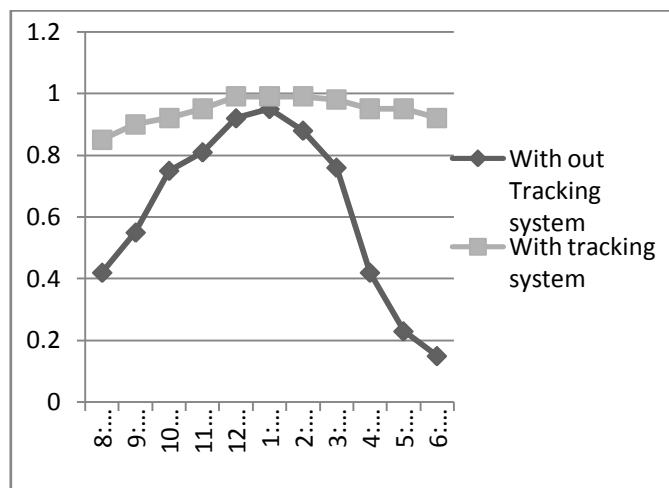


Figure.9. Efficiency of the Solar Tracking system

The Fig.9 shows the efficiency of the tracking system. It seems that the efficiency of the proposed system can be increased around 64% on a summer sunny day. In addition, the proposed system consumes little power to turn the PV panel using a stepper motor instead of using large panel which consumes high power. Moreover, this system can power itself from the PV panel using a 12V battery.

V. CONCLUSION

This project reports a "LPC2148 Based Improved Structure of Solar Tracker". The Monitoring controller based on the closed loop algorithm is designed and implemented with ARM7 TDMI processor based LPC2148 controller in embedded system domain. Experimental work has been carried out carefully. By using this project maximum current can be obtained from solar panel. Solar trackers are devices used to orient photovoltaic panels, reflectors, lenses or other optical devices towards the sun. Since the sun's position in the sky changes with the seasons and the time of day, trackers are used to align the collection system to maximize energy production.

REFERENCES

This heading is not assigned a number.

- [1] A. Zahedi, "Energy, People, Environment, Development of an integrated renewable energy and energy storage system, an uninterruptible power supply for people and for better environment," *The International Conference on Systems, Man, and Cybernetics, 1994. 'Humans, Information and Technology', Vol. 3 pp. 2692-2695, 1994.*
- [2] R. Singh, and Y.R. Sood, "Transmission tariff for restructured Indian power sector with special consideration to promotion of renewable energy sources", *The IEEE Conference TENCON-2009, pp. 1-7, 2009.*
- [3] J. Arai, K. Iba, T. Funabashi Y. Nakanishi, K. Koyanagi, and R. Yokoyama, "Power electronics and its applications to renewable energy in Japan, " *The IEEE Circuits and Systems Magazine, Vol. 8, No. 3, pp. 52-66, 2008.*

- [4] S. Takemaro and Shibata Yukio, "Theoretical Concentration of Solar Radiation by Central Receiver Systems," *The International Journal of Solar Energy, 261-270, 1983.*
- [5] S. Armstrong and W.G Hurley "Investigating the Effectiveness of Maximum Power Point Tracking for a Solar System", *The IEEE Conference on Power Electronics Specialists, pp.204-209, 2005.*
- [6] O. Aliman, and I Daut, "Rotation-Elevation of Sun Tracking Mode to Gain High Concentration Solar Energy", *The IEEE International Conference on Power Engineering, Energy and Electrical Drives, pp.551-555, 2007.*
- [7] A.K. Saxena and V. Dutta, "A versatile microprocessor- based controller for solar tracking", *IEEE Proc., 1990, pp. 1105 – 1109.*
- [8] E. Karatepe, T. Boztepe, and M. Colak, "Power Controller Design for Photovoltaic Generation System under Partially Shaded Insolation Conditions", *The International Conference on Intelligent Systems Applications to Power Systems, pp. 1-6, 2007.*
- [9] N. Barsoun, "Implementation of a Prototype for a Traditional Solar Tracking System", *The Third UKSim European Symposium on Computer Modeling and Simulation, pp. 23-30, 2009.*
- [10] C. Jaen, J. Pou, G. Capella, A. Arias, and M. Lamich, M, "On the use of sun trackers to improve maximum power point tracking controllers applied to photovoltaic systems", *The IEEE conference on Compatibility and Power Electronics, pp. 67-72, 2009.*

CB Based Approach for Mining Frequent Itemsets

K. Jothimani¹, Dr. Antony Selvadoss Thanamani²

* (PhD Research Scholar, Research Department of Computer Science, NGM College, Pollachi, India)

** (Professor and Head, Research Department of Computer Science, NGM College, Pollachi, India)

ABSTRACT : *In this paper, we propose a new method for discovering frequent itemsets in a transactional data stream under the sliding window model. Based on a theory of Chernoff Bound, the proposed method approximates the counts of itemsets from certain recorded summary information without scanning the input stream for each itemset. Together with an innovative technique called dynamically approximating to select parameter-values properly for different itemsets to be approximated, our method is adaptive to streams with different distributions. Our experiments show that our algorithm performs much better in optimizing memory usage and mining only the most recent patterns in very less time performance with pretty accurate mining result.*

Keywords: Chernoff Bound, DataStream, Frequent Itemsets

I. INTRODUCTION

The most significant tasks in data mining are the process of mining frequent itemsets over data streams. It should support the flexible trade-off between processing time and mining accuracy. Mining frequent itemsets in data stream applications is beneficial for a number of purposes such as knowledge discovery, trend learning, fraud detection, transaction prediction and estimation [1]. However, the characteristics of stream data – unbounded, continuous, fast arriving, and time- changing – make this a challenging task.

In data streams, new data are continuously coming as time advances. It is costly even impossible to store all streaming data received so far due to the memory constraint. It is assumed that the stream can only be scanned once and hence if an item is passed, it can not be revisited, unless it is stored in main memory. Storing large parts of the stream, however, is not possible because the amount of data passing by is typically huge. In this paper, we study the problem of finding frequent items in a continuous stream of items. Many real-world applications data are more appropriately handled by the data stream model than by traditional static databases. Such applications can be: stock tickers, network traffic measurements, transaction flows in retail chains, click streams, sensor networks and telecommunications call records. In the same way, as the data distribution are usually changing with time, very often end- users are much more interested in the most recent patterns [3]. For example, in network monitoring, changes in the past several minutes of the frequent patterns are useful to detect network intrusions [4].

Many methods focusing on frequent itemset mining over a stream have been proposed. [13] proposed *FPSStream* to mine frequent itemsets, which was

efficient when the average transaction length was small; used lossy counting to mine frequent itemsets; [7],[8], and [9] focused on mining the recent itemsets, which used a regression parameter to adjust and reflect the importance of recent transactions; [27] presented the *FTP-DS* method to compress each frequent itemset; [10] and [1] separately focused on multiple-level frequent itemset mining and semi-structure stream mining; [12] proposed a group testing technique, and [15] proposed a hash technique to improve frequent itemset mining; [16] proposed an in-core mining algorithm to speed up the runtime when distinct items are huge or minimum support is low; [15] presented two methods separately based on the average time stamps and frequency-changing points of patterns to estimate the approximate support of frequent itemsets; [5] focused on mining a stream over a flexible sliding window; [11] was a block-based stream mining algorithm with *DSTree* structure; [12] used a verification technique to mine frequent itemsets over a stream when the sliding window is large; [11] reviewed the main techniques of frequent itemset mining algorithm over data streams and classified them into categories to be separately addressed.

The above methods are mostly based on the (ϵ, δ) approximation scheme, and depend on error parameter ϵ to control the memory consumption and the running time. While a dilemma between mining precision and memory consumption will be caused by the error parameter ϵ . A little decrease of ϵ may make memory consumption large, and a little increase of ϵ may degrade output precision. Since uncertain streams are highly time-sensitive, most data items are more likely to be changed as time goes by, besides people are generally more interested in the recent data items than those in the past.

Thus this needs an efficient model to deal with the time-sensitive items on uncertain streams. Sliding-window model is the most comprehensive approach to coping with the most recent items in many practical applications. So we introduce a Chernoff bound with Markov's inequality to deal with this problem.

The remainder of this paper is organized as follows. In Section 2, we give an overview of the related work and present our motivation for a new approach. Section 3 goes deeper into presenting the problems and gives an extensive statement of our problem. Section 4 presents our solution. Experiments are reported in Section 5, and Section 6 concludes the paper with the features of our work.

II. RELATED WORK

Many previous studies contributed to the efficient mining of frequent itemsets (FI) in streaming data [4, 5]. According to the stream processing model [20], the research of mining frequent itemsets in data streams can be divided into three categories: landmark windows [15,

12, 19, 11, 13], sliding windows [5, 6, 14, 16, 17, 18], and damped windows [7, 4], as described briefly as follows. In the landmark window model, knowledge discovery is performed based on the values between a specific timestamp called landmark and the present. In the sliding window model, knowledge discovery is performed over a fixed number of recently generated data elements which is the target of data mining.

According to the existential uncertain stream model, an uncertain stream US is a continuous and unbounded sequence of some transactions, $\{T_1 T_2 \dots T_n \dots\}$. Each transaction T_i in US consists of a number of items, and each item x in T_i is associated with a positive probability $PT_i(x)$, which stands for the possibility (or likelihood) that x exists in the transaction T_i . For a given uncertain stream, there are many possible instances called worlds that are carried by the stream. The possible worlds semantics has been widely used

in [8, 9], which can be adopted in this paper to illustrate uncertain streams clearly. Each probability $PT_i(x)$ associated with an item x deduces two possible worlds, pw_1 and pw_2 . In possible world pw_1 , item x exists in the transaction T_i , and in possible world pw_2 , item x does not exist in T_i . Each possible world pw_i is annotated with an existence probability, denoted as $P(pw_i)$ that the possible world pw_i happens. By this semantics, we can get $P(pw_1)=PT_i(x)$ and $P(pw_2)=1-PT_i(x)$. In fact, a transaction often contains several items.

We introduce a new approach which combines the mathematical model Chernoff bound for this problem. The main attempts were to keep some advantages of the previous approach and resolve some of its drawbacks, and consequently to improve run time and memory consumption. We also revise the Markov's inequality, which avoids multiple scans of the entire data sets, optimizing memory usage, and mining only the most recent patterns. In this paper, we propose a remarkable approximating method for discovering frequent itemsets in a transactional data stream under the sliding window model. Based on a theory of Combinatorial Mathematics, the proposed method approximates the counts of itemsets from certain recorded summary information without scanning the input stream for each itemset.

III. PROBLEM DESCRIPTION

The problem of mining frequent itemsets was previously defined by [1]: Let $I = \{i_1, i_2, \dots, i_m\}$ be a set of literals, called items. Let database DB be a set of transactions, where each transaction T is a set of items such that $T \subseteq I$. Associated with each transaction is a unique identifier, called its TID. A set $X \subseteq I$ is also called an itemset, where items within are kept in lexicographic order. A k -itemset is represented by (x_1, x_2, \dots, x_k) where $x_1 < x_2 < \dots < x_n$. The support of an itemset X , denoted $support(X)$, is the number of transactions in which that itemset occurs as a subset. An itemset is called a frequent itemset if $support(X) \geq \sigma \times |DB|$ where $\sigma \in (0, 1)$ is a user-specified minimum support threshold and $|DB|$ stands for the size of the database.

The problem of mining frequent itemsets is to mine all itemsets whose support is greater or equal than

$\sigma \times |DB|$ in DB. The previous definitions consider that the database is static. Let us now assume that data arrives sequentially in the form of continuous rapid streams. Let data stream

$DS = B^{b_1}, B^{b_1+1}, \dots, B^{b_n}$ be an infinite sequence of batches $, a_i \quad a_{i+1} \quad a_n$

where each batch is associated with a time period $[a_k, b_k]$, i.e.

B^{b_k} , and let a_n be the most recent batch

Each batch B_k consists of a set of transactions; that is, Each batch $B_k = [T_1, T_2, T_3, \dots, T_k]$. We also assume that batches do not have necessarily the same size. Hence, the length

The support of an itemset X at a specific time interval $[a_i, b_i]$ is now denoted by the ratio of the number of customers having X in the current time window to the total number of customers. Therefore, given a user-defined minimum support, the problem of mining itemsets on a data stream is thus to find all frequent itemsets X over an arbitrary time period $[a_i, b_i]$, i.e. verifying:

$$support_t(X) \geq \sigma \times |B^{b_i}|, t = a_i$$

of the streaming data using as little main memory as possible. Given a transaction sets X , we are interested in finding strong bounds

$$\text{Low End: } \Pr[X < a]$$

$$\text{High End: } \Pr[X \geq a]$$

Lemma 1.1 (Markov's Inequality) Let X be a non-negative random variable (transaction sets) with finite expectation μ . Then for any $\alpha > 0$: $\Pr[X \geq \alpha] \leq \mu/\alpha$.

Lemma 1.2 (Chebyshev's Inequality) Let X be a random variable (transaction sets) with finite expectation μ and standard deviation σ . Then for any $\alpha > 0$: $\Pr[|X - \mu| \geq \alpha \sigma] \leq 1/\alpha^2$.

Chebyshev's inequality follows from Markov's inequality for the variable $Y = (X - \mu)^2$ (so $E[Y] = \text{Var}[X]$) and the fact that $x \rightarrow x^2$ is a strictly monotonic function on R_0 .

$$\Pr[|X - \mu| \geq \alpha \sigma] = \Pr[(X - \mu)^2 \geq \alpha^2 \sigma^2]$$

$$\leq \frac{E[(X - \mu)^2]}{\alpha^2 \sigma^2} = 1/\alpha^2$$

This makes it tempting to use even higher moments to get better bounds. One way to do this nicely is by considering an exponential of the basic form of e^x .

Proof. Lemma 1.3 (Simplified Chernoff Bounds)

Low End:

$$\Pr[X < (1 - \delta)\mu] < e^{-\mu\delta^2/2} \quad 0 < \delta \leq 1$$

High End:

$$\Pr[X \geq (1 + \delta)\mu] < e^{-\mu\delta^2/3} \quad 0 < \delta \leq 1$$

$$\Pr[X \geq (1 + \delta)] < e^{-(1+\delta)\mu} 2e - 1 < \delta$$

Proof.

For the LowEnd let $D = (1 - \delta)^{1-\delta}$. By Taylor expansion we get

$$\begin{aligned} \ln D &= (1 - \delta) \ln(1 - \delta) \\ &= (1 - \delta)(-\delta - \delta^2/2 - \delta^3/3 - \dots) \\ &= -\delta + \delta^2/2 + \delta^3/6 + \dots \\ &> -\delta + \delta^2/2 \end{aligned}$$

By Applying this simplified method in the series we can get the following equation for low end windows.

$$\text{Hence } \left(\frac{e^{-\delta}}{(1 - \delta)^{1-\delta}} \right) = e^{-\mu\delta/2}$$

IV. CBMFI ALGORITHM

CBMFI (Chernoff Bound Based Mining Frequent Itemsets) algorithm relies on a verifier function and it is an exact and efficient algorithm for mining frequent itemsets sliding windows over data streams. The performance of CBMFI improves when small delays are allowed in reporting new frequent itemsets, however this delay can be set to 0 with a small performance overhead.

The following algorithm shows how it combines with CB for Mining frequent itemsets.

CBMFI

Initialization

For all u pick a route $rt(u)$.

Place all M_u such that $D(u) = \mu u$ into C_e where e is the first window on $rt(u)$.

Main Loop $r = 0$

while(there is a packet not at its destination)

in parallel, for all window ends $e = (x, y)$

do

if C_e is not empty,

pick the highest priority itemsets in C_e

$y = \text{itemsets}(T)$

if (a moved itemset is not at its destination)

$C_e = \text{next end transaction}$

$r = r + 1$

We would like to use a Chernoff bound, so we need to find some independent Poisson trials somewhere. This requires a bit of thought, lots of random variables associated with this algorithm are not independent;

The expected length of a route is $k/2$, so the total number of edges on all routes is expected to be $nk/2$. The total number of edges in a hypercube is nk , so we have $E[R(e)] = 1/2$. It follows that $E[H] \leq k/2$. Now apply the simplified Chernoff bound where $\delta > 2e - 1$:

$$\Pr[H \geq 6k] < 2 - 6k$$

This is allowed since $6k = (\delta + 1)\mu$ implies $\delta > 11$. By applying this in the CBMFI algorithm we can get the efficient result.

V. EXPERIMENTAL RESULTS

All experiments were implemented with C#, compiled with Visual Studio 2005 in Windows Server 2003 and executed on a Xeon 2.0GHz PC with 4GB RAM. We used 1 synthetic datasets and 1 real-life datasets, which are well-known benchmarks for frequent itemset mining. The T40I10D100K dataset is generated with the IBM synthetic data generator.

We firstly compared the average runtime of these two algorithms under different data sizes when the minimum support was fixed. As shown in all of the images in Fig.5.1, the running time cost of MFI and CBMFI increase following the data size; these results verify that both algorithms are sensitive to data size, which is due to the using of unchanged absolute minimum support

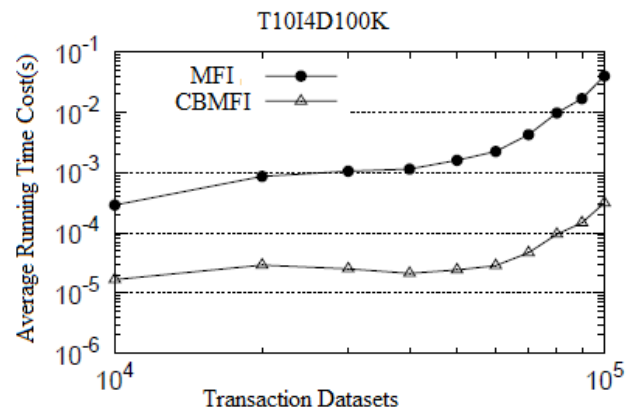


Fig: 5.1 Runtime vs number of Records

Memory Cost Evaluation

To evaluate the memory cost of our algorithm, we compared the count of generated items in MFI and CBMFI. As shown in Fig.5.2 and Fig.5.3, when we fix the minimum support and increase the data size, the generated items of both algorithms become more, but the overall item count of CBMFI is less than that of MFI since CBMFI uses a simplified method for itemsets.

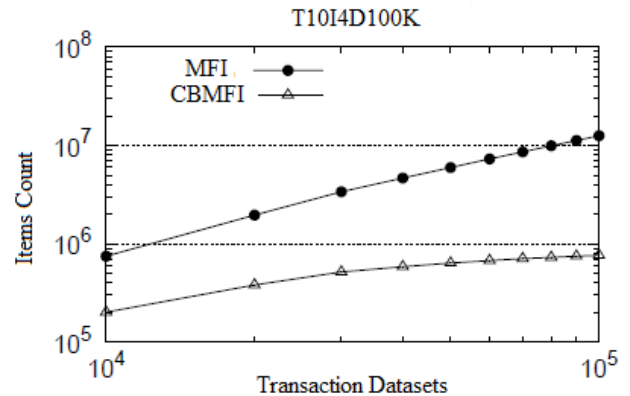


Fig: 5.2 Itemset Count cost vs Transaction Set

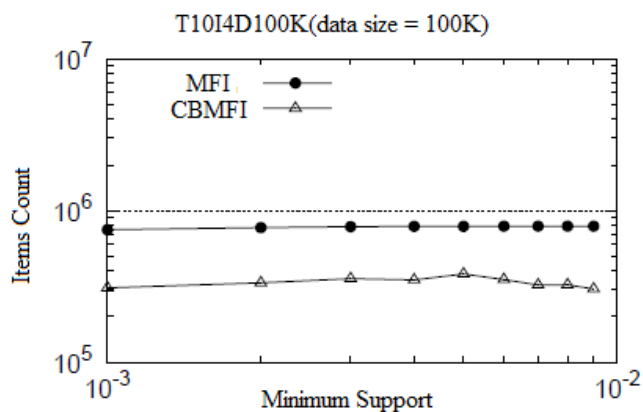


Fig: 5.3 Itemssets Count cost vs. Minimum Support

Furthermore, when the minimum support increases, the incremental scope of *CBMFI* is much reduced than that of *MFI*, that is because more redundant items when the overall items count is fixed but the itemsets count increases.

VI. CONCLUSION

In this paper we considered a problem that how to mine frequent itemset over stream sliding window using Chernoff Bound. We compared two algorithms *MFI* and *CBMFI* and introduce a compact data structure, which can compress the itemset storage and optimize itemset computation, based on combinatorial mathematical. Our experimental studies showed that our algorithm is effective and efficient.

REFERENCES

- [1] R. Agrawal, T. Imielinski, and A. Swami. Mining association rules between sets of items in large database. In *Proc. of the Intl. Conf. on Management of Data (ACM SIGMOD 93)*, 1993.
- [2] Y. Chen, G. Dong, J. Han, B. Wah, and J. Wang. Multi-dimensional regression analysis of time-series data streams. In *Proc. of VLDB '02 Conference*, 2002.
- [3] Y. Chi, H. Wang, P.S. Yu, and R.R. Muntz. Moment: Maintaining closed frequent itemsets over a stream sliding window. In *Proc. of ICDM '04 Conference*, 2004.
- [4] P. Dokas, L. Ertoz, V. Kumar, A. Lazarevic, J. Srivastava, and P.-N. Tan. Data mining for network intrusion detection. In *Proc. of the 2002 National Science Foundation Workshop on Data Mining*, 2002.
- [5] G. Giannella, J. Han, J. Pei, X. Yan, and P. Yu. Mining frequent patterns in data streams at multiple time granularities. In *Next Generation Data Mining*, MIT Press, 2003.
- [6] J. Han, J. Pei, B. Mortazavi-asl, Q. Chen, U. Dayal, and M. Hsu. Freespan: Frequent pattern-projected sequential pattern mining. In *Proc. of KDD '00 Conference*, 2000.
- [7] Y. Chi, H. Wang, P.S. Yu, & R.R. Muntz, "Moment: maintaining closed frequent itemsets over a stream sliding window", Proc. 4th IEEE Conf. on Data Mining, Brighton, UK, 2004, pp. 59–66.
- [8] N. Jiang & L. Gruenwald, "CFI-Stream: mining closed frequent Itemsets in data streams", Proc. 12th ACM SIGKDD Conf. on Knowledge Discovery and Data Mining, Philadelphia, PA, USA, 2006, pp. 592–597.
- [9] H.F. Li, S.Y. Lee, M.K. Shan, "An Efficient Algorithm for Mining Frequent Itemsets over the Entire History of Data Streams", In Proceedings of First International Workshop on Knowledge Discovery in Data Streams 9IWKDD, 2004.
- [10] H.F. Li, S.Y. Lee, M.K. Shan, "Online Mining (Recently) Maximal Frequent Itemsets over Data Streams", In Proceedings of the 15th IEEE International Workshop on Research Issues on Data Engineering (RIDE), 2005.
- [11] J.H. Chang & W.S. Lee, "A sliding window method for finding recently frequent itemsets over online data streams", Journal of Information science and Engineering, 20(4), 2004, pp. 753–762.
- [12] J. Cheng, Y. Ke, & W. Ng, "Maintaining frequent itemsets over high-speed data streams", Proc. 10th Pacific-Asia Conf. on Knowledge Discovery and Data Mining, Singapore, 2006, pp. 462–467.
- [13] C.K.-S. Leung & Q.I. Khan, "DSTree: a tree structure for the mining of frequent sets from data streams," Proc. 6th IEEE Conf. on Data Mining, Hong Kong, China, 2006, pp. 928–932.
- [14] B. Mozafari, H. Thakkar, & C. Zaniolo, "Verifying and mining frequent patterns from large windows over data streams", Proc. 24th Conf. on Data Engineering, Mexico, 2008, pp. 179–188.
- [15] K.-F. Jea & C.-W. Li, "Discovering frequent itemsets over transactional data streams through an efficient and stable approximate approach, Expert Systems with Applications", 36(10), 2009, pp. 12323–12331.

Analysis of Load Constant in Manual Material Handling Task by Taguchi Technique & Mathematical Regression Modeling

Ganesh Pal Singh Jadon, Manish Kumar Sagar

¹ME (Material Handling) Madhav Institute of Technology & Science, Gwalior.

²Assistant Professor, Mechanical Engineering, Madhav Institute of Technology & Science, Gwalior.

Abstract: Now a day, the working in the industries is not as comfortable as they were in the earlier time. The man power is decreasing day by day and new recruitments are not in the same ratio as the person leaving industries. This in turn increases the work load on the present employees. It has been seen that the workers are not assigned to the appropriate machine according to their physical aspects and strength. This causes an uneven distribution of work in the industries, which in turn causes severe physical problems to the employees and also decreases the productivity of industry. The purpose of this paper is to efficiently determine the optimum combination of three parameters (Worker age, Worker weight and strength) for mitigate the load constant of the worker, the researcher have used the Taguchi parameter optimization methodology, and finally the Modeling of input parameters (Worker age, worker weight and strength) and output parameter (Load constant) is done using regression modeling and MATLAB Software R2011b. With the help of mathematical modeling one can select the appropriate person for a particular load for a particular work to minimize the fatigue of worker in the industry.

Keywords: Manual Material Handling, Load Constant, Regression Modeling, Taguchi Techniques.

I. Introduction

Manual Material Handling (MMH) including lifting, lowering, pushing, pulling, twisting, carrying and holding is a regular task that almost everyone performs every day. There are kinds of injuries and disabilities associated with MMH tasks, among which Low back disorders (LBDs) are the most common of all musculoskeletal disorders and are a major health and socioeconomic problem in the western world (Woolf and Pfleger, 2003). According to Punnett et al (2005) about 37% of all LBDs are directly attributable to occupational risk factors (RFs). Thus identifying and preventing risk of LBD is the most significant problem complained by workers and it is still a hard topic for researchers (Kuiper et al., 1999). Many researchers have developed tools and techniques for identify jobs which are associated with risk of LBD (Ciriello & Snook, 1999; Marras, 2000; Marras, Fine, Ferguson, & Waters, 1999; Zurada, Karwowski, & Marras, 1997). Chaffin and Park (1973) developed a lifting strength ratio (LSR) and demonstrated its relationship to LBD. LSR was defined as the ratio of the maximum load lifted on the job and lifting strength in the same load position for a large/strong man. Snook (1978) defined MMH limits for lifting, lowering, pushing, pulling and carrying activities based on psychophysical criteria. In 1981 the National Institute for occupational Safety and Health (NIOSH), a US federal agency recognized the problems related to lower back injuries and published the Work Practices Guide for manual lifting. This contained a summary lifting related literature before 1981, and guidelines are also given for lifting (Ayoub, Selan, Jiang, 1983).

In this MMH area load that lifted by the person is play important role LBD problem. Load is also known as load constant it is load that is lifted by worker without any musculoskeletal problem. NIOSH (1991) is set the value of load constant, which is 23 kg., but researcher are going to find that it may change with age, weight and strength of worker. In this paper researchers derive a formula for

calculating load constant for the worker which is assign for the lifting work.

For calculating the load constant researcher applied the Taguchi Optimization Technique and calculates the load constant according to worker's age, worker's weight and strength of worker. Taguchi methodology is described in next chapter.

II. Taguchi Methodology

Taguchi method is a powerful methodology/ technique for the design of high quality systems (Taguchi, 1990) and has been widely used in engineering design (Ross, 1988). Taguchi design provides a simple, efficient and systematic approach to optimize design for performance, quality and cost over a verity of conditions. Taguchi steps are shown in figure 1 for present research work.

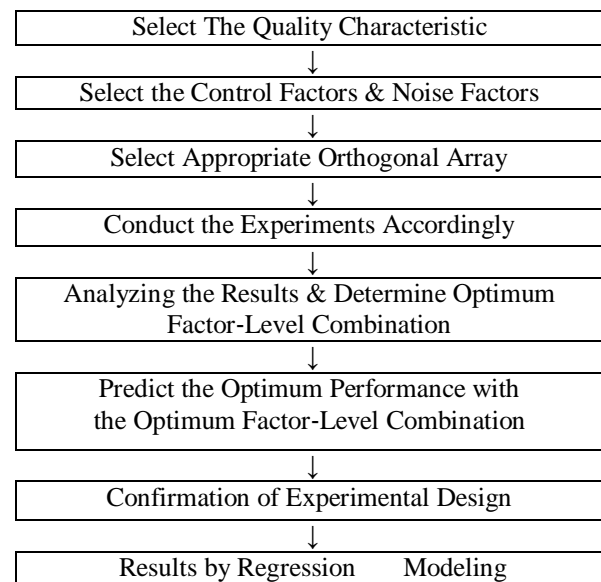


Figure 1: Steps of Taguchi Method

2.1 Design of Experiment

The experimental design was done according to L9 orthogonal array based on the Taguchi method. The use of Taguchi orthogonal array would evidently reduce the number of experiments. The L9 orthogonal array had three columns and nine rows, so it had six degrees of freedom to manipulate three parameters with three levels as indicated in Table 1. Thus, in this investigation three parameters with three levels were indicated in Table 2.

Table 1: Orthogonal L9 Array of Taguchi

Experiment S.No.	Parameters		
	1	2	3
1	1	1	1
2	1	2	2
3	1	3	3
4	2	1	3
5	2	2	1
6	2	3	2
7	3	1	2
8	3	2	3
9	3	3	1

Table 2: Process Parameters and their Levels

S. No.	Process Parameter	Process parameter	Levels		
			Lower 1	Medium 2	Higher 3
1.	A	Age of Worker (yrs)	20-35	36 -50	51-65
2.	B	Weight of Worker (Kg)	50- 59	60 -69	70 -80
3.	C	Worker's Strength (Newton)	2	3	4

For this research work, researchers visited to S. & H. Gears Dewas (M.P.) and collect data which are require for the research these are shown in Table 3. This data is randomly selected among the workers of company which represent random age group, weight and strength.

Table 3: Data Collected from the Industry

S. No.	Name	Age (yrs)	Weight (kg)	Strength (Newton)	LC (kg)
1.	R.K.Dewedi	35	56	2	28
2.	Bharat Pandit	34	62	3	34
3.	Dharmendra Sharma	26	80	4	50
4.	Kishore Kale	45	57	4	44
5.	Ramesh kohle	48	60	2	29
6.	Prakash Carpenter	47	75	3	36
7.	Kamal Singh	51	50	3	39
8.	K.S.Hada	53	65	4	41

9.	K.K.Dev	52	74	2	23
----	---------	----	----	---	----

III. Taguchi Parametric Optimization technique

The collected data are arranged according to L9 array. As per the Taguchi Technique the Quality characteristic utilized in the research is larger the Better. Researchers have calculated Load Constant, Mean Slandered Deviation (MSD) of Load Constant and Signal to Noise Ratio (S/N) for analysis of the data. Following formula is used for calculation of larger the better. Data analysis is shown in table 4.

$$MSD = (1/Y1^2 + 1/Y2^2 + 1/Yn^2 \dots\dots) / N$$

$$S/N = - 10 \log_{10} (MSD)$$

Table 4: Data Analysis

S. No.	Worker age	Worker Weight	Strength (Newton)	LC	MSD	S/N ratio
1.	L	L	L	28	1.275×10^{-3}	28.94
2.	L	M	M	34	8.650×10^{-4}	30.62
3.	L	H	H	50	4×10^{-4}	33.97
4.	M	L	H	44	5.165×10^{-4}	32.86
5.	M	M	L	29	1.189×10^{-3}	29.24
6.	M	H	M	36	7.716×10^{-4}	31.12
7.	H	L	M	39	6.574×10^{-4}	31.82
8.	H	M	H	41	5.948×10^{-4}	32.25
9.	H	H	L	23	1.890×10^{-3}	27.23

3.1 Load Constant (LC)

The analysis of each controllable parameter is done and the effects of each parameter at individual level (i.e. at 1, 2, 3 levels) is shown in Table 5. This analysis is shows that at the lower age, man having the higher strength and vice-versa.

(a) **Case 1:** The main effect of the worker age on Load Constant at various level is calculated as follows:

For lower level:

$$(28 + 34 + 50) / 3 = A_1 = 37.33$$

For medium level

$$(44 + 29 + 36) / 3 = A_2 = 36.33$$

For higher level

$$(39 + 41 + 23) / 3 = A_3 = 34.33$$

(b) **Case 2:** The main effect of worker's weight at various levels are calculated as:

For lower level

$$(28 + 44 + 39) / 3 = B1 = 37$$

For medium level

$$(34 + 29 + 41) / 3 = B2 = 34.67$$

For higher level

$$(50 + 36 + 23) / 3 = B3 = 36.33$$

(c) **Case 3:** The main effect of the Strength at various levels are calculated as:

For lower level

$$(28 + 29 + 23) / 3 = C_1 = 26.67$$

For medium level

$$(34 + 36 + 39) / 3 = C_2 = 36.33$$

For higher level
 $(50 + 44 + 41) / 3 = C3 = 45$

Table 5: Factors Effect Table for Load constant

Symbol	Controllable Factors	Level 1 Lower	Level 2 Medium	Level 3 Higher
A	Worker's Age	37.33 (A1)	36.33 (A2)	34.33 (A3)
B	Worker's Weight	37 (B1)	34.67 (B2)	36.33 (B3)
C	Strength	26.67 (C1)	36.33 (C2)	45 (C3)

The values in bold in table 5 show the Larger the better criteria as proposed by Taguchi method. The value obtained from table 5 are plotted to visualize the effect of the three parameters at three levels on mean response graph which is shown in figure 2.

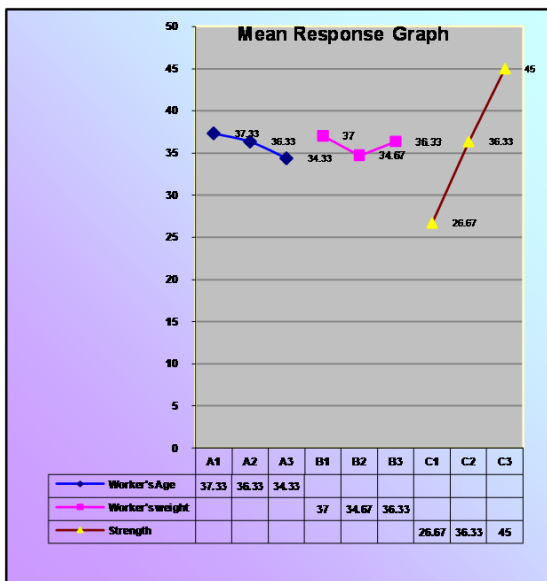


Figure 2: Mean Response Graph

3.2 Analysis of Signal to Noise (S/N) Ratio

According to the Taguchi approach, the term signal represents the desired value (mean) for the output characteristics and term noise represent the undesirable value (standard deviation) for the output characteristics. Therefore S/N ratio is the ratio of mean to the standard deviation. Taguchi uses the S/N ratio to measure the quality characteristics deriving from desired value. The S/N ratio is defined as given equation.

For Higher the better

It is when the occurrences of some undesirable product characteristics are to be maximized. It is given by $S/N = -10 \log ((\Sigma y1/ y2)/N).....$

All the three level of every factor are equally represented in the nine experiments. S/N ratio and Load Constant for each parameter at each level and Load Constant for each of the Parameters at each level is calculated. These also called as main effects.

Table 6: Effect of S/N, corresponding to chosen parameters

Symbol	Controllable Factors	Level 1 Lower	Level 2 Medium	Level 3 Higher
A	Worker's Age	31.17	31.07	30.43
B	Worker's Weight	31.20	30.70	30.77
C	Strength	28.25	31.18	33.02

The values in bold in table 6 show the Larger the better criteria as proposed by Taguchi method. The value obtained from table 6 are plotted to visual seize the effect of the three parameters at three levels on mean response graph which shown in figure 3.

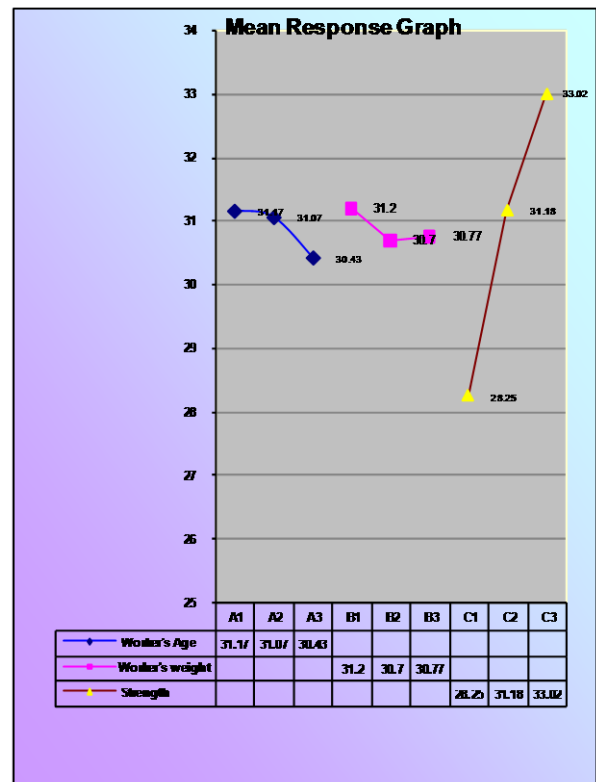


Figure 3: Mean Response Graph for S/N Ratio

IV. Mathematical Regression Modeling

Defining the formula of load constant, researchers use the regression modeling techniques. Previously, Load constant is tabulated as per combination of parameters. Empirical formula has going to be drawn in following steps.

4.1 Modeling of Parameters

To generalize the results, the Modeling of input parameters (Age of Worker, Weight of Worker and strength) and Load constant is done using Regression modeling with MATLAB software R2011b.

The parameters under consideration are

1. Age of worker.
2. Weight of Worker
3. Strength of worker

The regression analysis has been adopted. Load constant(LC) has been taken as single output parameter (Y) whereas Age of worker (X₁) and Weight of Worker (X₂) and strength (X₃) has been taken as input parameter X = [X₁, X₂, X₃]. The Load Constant is a function of Worker Age, Worker weight and Strength.

LC \propto Worker Age * Component weight * Strength

$$LC = (\text{Worker Age})^{C_1} * (\text{Worker weight})^{C_2} * (\text{Strength})^{C_3}$$

$$L_n(LC) = C_1 l_n(\text{Worker age}) + C_2 l_n(\text{Worker weight}) + C_3 l_n(\text{Strength})$$

Where, C₁, C₂, C₃ are constants which are to be determined by Regression Modeling and using MATLAB software R2011b. The following results were obtained.

$$C_1 = 0.1563; C_2 = 0.5149; C_3 = 0.7840$$

Putting these values the equation becomes.

$$LC = (W_a)^{0.1563} * (W_w)^{0.5149} * (\text{Strength})^{0.7840}$$

Here W_a is Age of Worker,
 W_w is Weight of Worker.
 LC is load constant.

V. Summary

Finally a formula is obtained for load constant by the application of Taguchi Methodology and Mathematical Regression Modeling the researchers have find out a way to calculate the correct load constant of the correct person. By using this formula problem of LBD is minimized in all kinds of industry where manual material handling is done.

REFERENCES

[1] Ayoub M. M., Selan J. L. & Jiang B.C. (1983). "A Miniguide for Lifiting", Texas Tech University, Texas.

[2] Chaffin D. & Park K. (1973), "A Longitudinal Study of Low-Back Pain as Associated with Occupational Weight Lifting Factors", *American Industrial Hygiene Association Journal*, Vol. No. 34, PP 413-525.

[3] Ciriello V. M. & Snook V. M. (1999), "Survey of Manual Handling Tasks", *International Journal of Industrial Ergonomics*, Vol. No 23, PP 149-156.

[4] Kuiper J. I., Burdorf A., Verbeek J. H. A. M., Frings-Dresen M. H. W., Van der Beek A. J. & Viikari-Juntura E. R. A. (1999), "Epidemiologic Evidence On Mmhs As A Risk Factor For Back-Disorders: A Systematic Review", *International Journal Industrial Ergonomics*, Vol. No 24, PP 389- 404.

[5] Marras, W. S. (2000). "Occupational low back disorder causation and control", *Ergonomics*, Vol. 43No.7, PP 880–902.

[6] Marras W. S., Fine L. J., Ferguson S. A. & Waters T. R. (1999), "The Effectiveness Of Commonly Used Lifting Assessments Methods To Identify Industrial Jobs Associated With Elevated Risk Of Low Back Disorders". *Ergonomics*, Vol. 42 No 1, PP 229–245.

[7] NIOSH (National Institute for occupational Safety and Health) (1981), "A Work Practices Guide for Manual Lifting". Technical Report No. 81-122. U.S. Department of Health and Human Services (NIOSH), Cincinnati, OH.

[8] Punnett L., Pruss-Ustun A., Imel Nelson D., Fingerhut M., Leigh J., Tak S. & Phillips S., (2005). "Estimating the Global Burden of Low Back Pain Attributable To Combined Occupational Exposures", *American Journal of Industrial Medicine*, Vol. 48, PP 459- 469.

[9] Ross PJ, (1988), "Taguchi Techniques for Quality Engineering", New York, McGraw-Hill.

[10] Snook S. H. (1978), "The Design of Manual Handling Tasks", *Ergonomics*, Vol. 21, PP 963- 985.

[11] Taguchi G, (1990), "Introduction to Quality Engineering", Asian productivity organization, Tokyo.

[12] Woolf A., Pflieger B., (2003), "Burden Of Major Musculoskeletal Conditions", *Bulletin of the World Health Organization*, Vol. 81No. 9, PP 646- 656.

[13] Zurada J., Karwowski W. & Marras W. S. (1997), "A Neural Network based System for Classification of Industrial Jobs with Respect to Risk of Low Back Disorders Due to Workplace Design". *Applied Ergonomics*, Vol. 28 No 1, PP 49- 55.

ANFIS Modeling and Experimental Study of Standalone Photovoltaic Battery Charging System

A. Durgadevi¹, S. Arulsevi²

Department of Electronics and Instrumentation Engineering
Annamalai University, Chidambaram, Tamil Nadu, India.

Abstract: Due to scarcity of fossil fuel and increasing demand of power supply, we are forced to utilize the renewable energy resources. Considering easy availability and vast potential, world has turned to solar photovoltaic energy to meet out its ever increasing energy demand. The mathematical modelling and simulation of the photovoltaic system is implemented in the MATLAB/Simulink environment and the same thing is tested and validated using Artificial Intelligent (AI) like ANFIS. This paper presents a scheme for transferring power from photovoltaic (PV) module to a battery using solar charge controller based on buck DC/DC converter. The converter is configured in open loop mode and the same thing is implemented in hardware. The results reveals that the implemented hardware results matches closely with the simulated software results. Due to high initial investment on PV systems and non linearity of PV cell output characteristics counteract its wide commercialization. The PV array has an optimum operating point to generate maximum power at some particular point called maximum power point (MPP). To track this maximum power point and to draw maximum power from PV arrays, MPPT controller is required in a stand-alone PV system. Due to the nonlinearity in the output characteristics of PV array, it is very much essential to track the MPPT of the PV array for varying maximum power point due to the insolation variation. In order to track the MPPT conventional controller like PI controller with Incremental conductance algorithm is proposed and simulated. The output of the controller, pulse generated from PWM can switch MOSFET to change the duty cycle of buck DC-DC converter. The result reveals that the maximum power point is tracked satisfactorily for varying insolation condition.

Key words: Photovoltaic, Pulse Width Modulation, Proportional Integral Controller.

I. INTRODUCTION

Today photovoltaic (PV) systems are becoming more and more popular with increase of energy demand and there is also a great environmental pollution around the world due to fossils and oxides. Solar energy which is free and abundant in most parts of world has proven to be economical source of energy in many applications [1]. The energy that the earth receives from the sun is so enormous and so lasting that the total energy consumed annually by the entire world is supplied in as short a time as half an hour. The sun is a clean and renewable energy source, which produces neither green house effect gas nor toxic waste through its utilization. It can withstand severe

weather conditions, including cloudy weather. The watt peak price is decreased since the

seventies, this leads to large scale promising areas. It does not have any moving parts and no materials consumed or emitted. Unfortunately, this system has two major disadvantages, which the low conversion efficiency of electric power generation (9 to 16%), especially under low irradiation conditions and the amount of electric power generated by solar array changes continuously with the weather conditions like irradiation and temperature. To overcome this problem, maximum power point tracking (MPPT) technique will be used.

In order to regulate the converter due to non linearity conventional controller like PI controller with Incremental conductance algorithm is proposed and simulated. The tracking algorithm integrated with a solar PV system has been simulated with buck DC-DC converter for the application of battery charging in stand - alone PV system. The proposed PV system with buck DC-DC converter is shown in Fig.1.

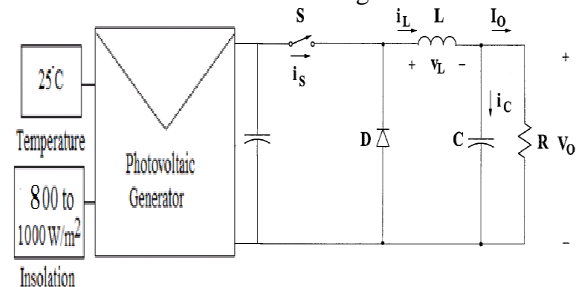


Fig.1. Photovoltaic module with DC-DC buck converter.

II. MATHEMATICAL MODELING OF PHOTOVOLTAIC CELL

The proposed MPPT is based on the behavior of the photovoltaic array by means of temperature and irradiation variation [2]. The mathematical model of PV array is implemented in the form of current source controlled by voltage, sensible to two impact parameters, that is, temperature ($^{\circ}\text{C}$) and solar irradiation power (w/m^2).

An equivalent simplified electric circuit of a photovoltaic cell presented in Fig.2.

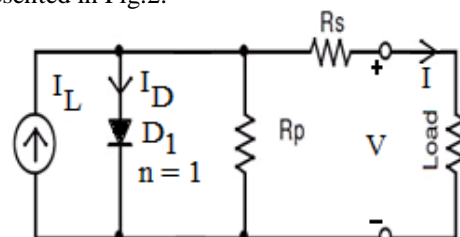


Fig.2. Equivalent circuit of photovoltaic cell.

The expressions obtained from fig.2. are given below.

The load current I_L is obtained is given in equation (1) as,

$$I = I_L - I_o [\exp\left(\frac{q(V+IR_s)}{\gamma k T_c}\right) - 1] \quad (1)$$

I_L is the photo electric current related to the given irradiation condition given by equation (2),

$$I_L = \left(\frac{G}{G_{REF}}\right) [I_{L,REF} + \mu_{ISC} (T_c - T_{c,REF})] \quad (2)$$

The diode saturation current (I_o) is given by the equation (3),

$$I_o = I_{o,REF} \left(\frac{T_c}{T_{c,REF}}\right)^3 \exp\left[\left(\frac{qE_g}{k\gamma}\right)\left(\frac{1}{T_{c,REF}} - \frac{1}{T_c}\right)\right] \quad (3)$$

where I_D is the diode current; I_L is the photoelectric current related to a given condition of irradiation and temperature; V is the output voltage [V]; I_o is the saturation diode current [A]; γ is the form factor which represents an index of the cell failing; R_s is the series resistance of the cell [Ω]; q is the electric charge ($1.602 \times 10^{-19} C$); k is the Boltzmann's constant ($1.381 \times 10^{-23} K$); T_c is the module temperature [K]. E_g is the energy gap of the material with which the cell is made (for the silicon it is 1.12 eV); G is the radiation [W/m^2]; G_{REF} is the irradiation under standard conditions [W/m^2]; $I_{L,REF}$ is the photoelectric current under standard conditions [A]; $T_{c,REF}$ is the module temperature under standard conditions [K]; μ_{ISC} is the temperature coefficient of the short circuit current [A/K], given by the manufacturer according to CEI EN 60891 standard [3-4].

Figure 3 shows the simulated P-V characteristics for varying irradiation and temperature in MATLAB/SIMULINK environment. It can be observed from simulated results as shown in Fig. 3(a), the photo current is directly proportional to irradiation. It is noted from Fig. 3(b) that the terminal voltage increases with decreasing temperature.

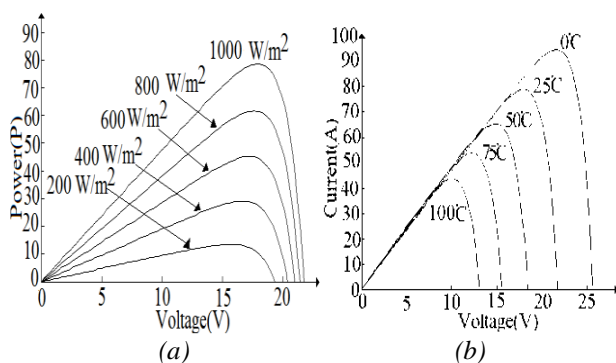


Fig.3. Simulated waveforms showing the effect of (a) radiation and (b) temperature on P-V characteristics.

The manufacturers data at standard conditions are given as $P_{max} = 80W$, $I_{max} = 4.515 A$ and $V_{max} = 21.6V$. The simulation results obtained were: $P_{max} = 78.51W$, $I_{max} = 4.35 A$ and $V_{max} = 18.2 V$. It is seen that the simulation model showed excellent correspondence to manufacturer's data and therefore this model was considered sufficient for the purpose of further study [4-8].

Simulated I-V, P-V characteristics for the maximum power point tracking (MPPT) is shown in figure.4. At this Maximum Power Point (MPP), the solar array is matched to its load and when operated at this point the array will yield the maximum power output. From Fig. 4 (a) & (b), it is observed that the power output has an almost linear relationship with array voltage unit, hence the MPP is attained. Any further increase in voltage results in power reduction [5].

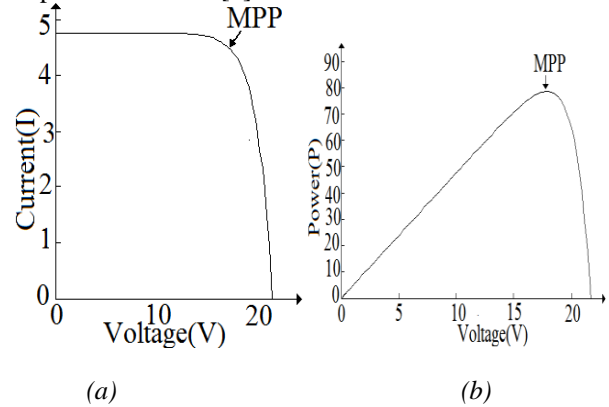


Fig.4. PV array simulated curves (a) I-V curve (25°C) and (b) P-V curve (1000w/m²).

III. ANFIS MODELING

The main objective of this work is to investigate the suitability of artificial intelligent systems (neural network and fuzzy logic) for validating the proposed PV system under variable climatic condition. Neural network models are data based where as fuzzy logic models are based on expert knowledge; in a situation in which both data and knowledge of underlying system are available, a neuro fuzzy approach is able to exploit both sources.

a. Stand – Alone Photovoltaic System

Fig.5 shows the overall simple configuration of the stand alone Photovoltaic power supply system.

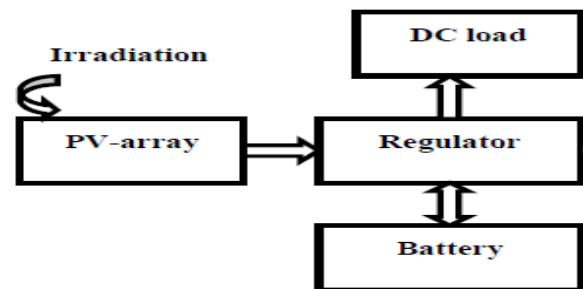


Fig.5. schematic of the Stand-Alone Photovoltaic Power supply system.

b. ANFIS Modeling of photovoltaic system

The Neuro-Fuzzy system used here is the adaptive network based fuzzy inference system (ANFIS). Fig.6 shows the developed ANFIS model. In order to obtain the modeled, predicted and optimized PVPS system due to its non linearity this is influenced by variable climatic conditions like solar irradiation and ambient temperature. Artificial Intelligent technique like ANFIS is proposed and simulated. The ANFIS was validated with several test data by minimizing mean square error.

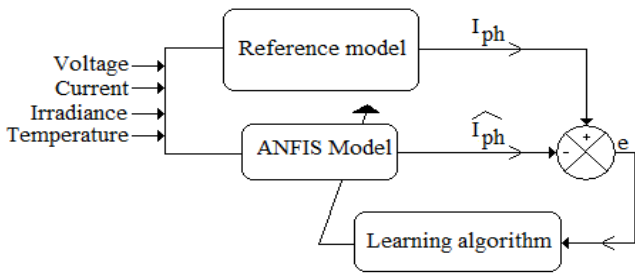


Fig.6. Developed ANFIS model.

Fig.7 shows the architecture of an ANFIS equivalent to a first-order sugeno fuzzy model with two inputs and two rules consisting of five different layers.

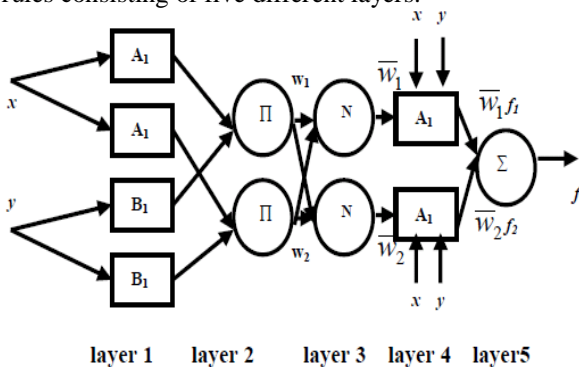


Fig.7. Architecture of an ANFIS equivalent to a first-order sugeno fuzzy model with two inputs and two rules.

The detailed description of the each layer is given as below:

Layer 1:

Generates the membership grades based upon premise signals using any appropriate parameterization membership function such as the generalized bell function given in equation (4):

$$O_{1,i} = \mu_{A_i}(x) = \frac{1}{1 + \left| \frac{x - c_i}{a} \right|^{2b_i}} \quad (4)$$

Layer 2:

Generates the firing strength of each rules using designated Π which is given by equation (5):

$$O_{2,i} = w_i = \mu_{A_i}(x) \mu_{B_i}(y) \quad i=1,2 \quad (5)$$

Layer 3:

Generates the normalized firing strength which is given by equation (6)

$$O_{3,i} = \bar{w}_i = \frac{w_i}{w_1 + w_2} \quad (6)$$

Layer 4:

Calculates the rule outputs based upon consequent parameters using the function (7):

$$O_{4,i} = \bar{w}_i f_i = \bar{w}_i (p_i x + q_i y + r_i) \quad (7)$$

Layer 5:

Gives the overall ANFIS output by equation (8).

$$O_{4,i} = \sum_i \bar{w}_i f_i = \frac{\sum_i w_i f_i}{\sum_i w_i} \quad (8)$$

Where: A_i, B_i are the linguistic labels (“small”, “large,” etc.); $\{a_i, b_i, c_i\}$ is the premise parameter; w_i is the weight factor; (p_i, q_i, r_i) is the consequent parameter; O is the output function and Π is the firing strength of each rule.

Fig.8 shows the simulated result of a photovoltaic power supply system using an adaptive Neuro-Fuzzy Inference System (ANFIS) under standard test condition of irradiation 1000w/m^2 and temperature of 25°C .

The result reveals that the correlation coefficient between measure values and those estimated by the ANFIS gave good prediction accuracy. The satisfactory performance of ANFIS proves that it can be used for the prediction of the optimal configuration of the PV system.

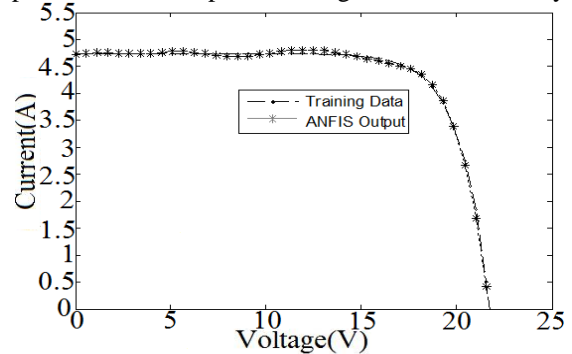


Fig.8. ANFIS modelling of the photovoltaic system for irradiation of 1000w/m^2 and temperature 25°C .

IV. DESIGNING OF BUCK CONVERTER

a. Circuit diagram of buck converter.

Fig.9 shows the schematic diagram of buck converter with varying irradiation, which consists of DC supply voltage V_s , as PV generator controlled switch S , diode D , buck inductor L , filter capacitor C and load resistance R . The current and voltage waveforms of the converter in CCM are presented in fig.10.

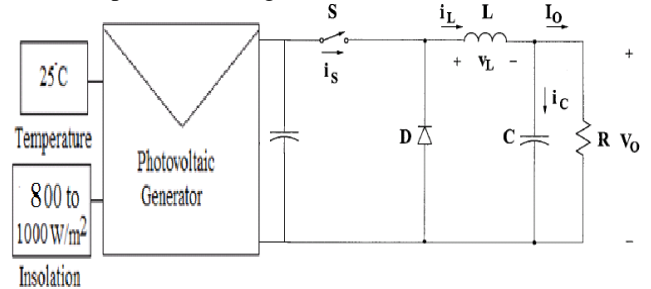


Fig.8. Circuit diagram of buck converter with PV module.

It can be seen from the circuit that when the switch S is commanded to the on state, the Diode D is reverse biased. When the switch S is off, the diode conducts to support an uninterrupted current in the inductor through the output RC circuit using faradays law for the buck inductor as given in (9)

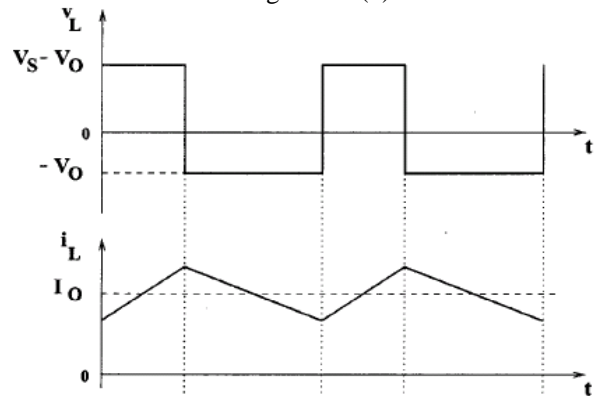


Fig.10. Theoretical voltage and current waveforms of buck converter.

$$(V_s - V_o)DT = (-V_o)(1 - D)T \quad (9)$$

The DC voltage transfer function turns out to be,

$$M_v = \frac{V_o}{V_s} = D \tag{10}$$

The buck converter operates in the CCM for $L > L_b$. The calculated value of inductance $L = 20\mu H$. To limit the ripples in the output side, larger filter capacitor is required. The filter capacitor must provide the output dc current to the load when diode D is off. The minimum value of filter capacitance calculated that results in the voltage ripple V_r is given by $C_{min} = 472.5\mu F$.

Thus the buck converter is designed in the open loop for the supply voltage of 21.7V DC, which is generated by the Photovoltaic panel for $1000w/m^2$ and $25^\circ C$. Fig.11 shows the simulated voltage and current waveforms of buck converter. It is seen that these waveforms are agreed closely with theoretical waveforms as shown in fig.10 [9-11].

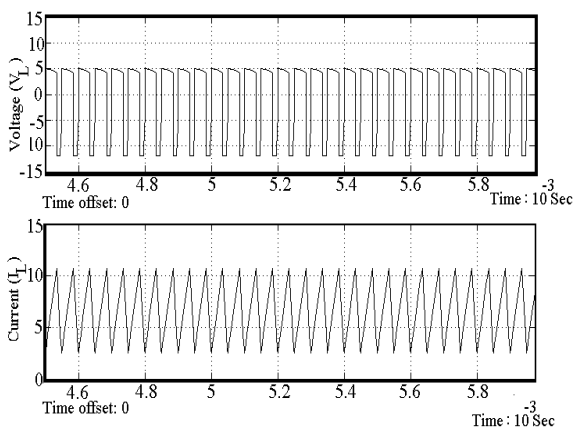


Fig.11. Simulated waveforms showing the voltage and current of buck converter.

V. CLOSED LOOP SIMULATION OF BUCK CONVERTER WITH INCREMENTAL CONDUCTANCE MPPT ALGORITHM

The block diagram of closed loop simulation with MPPT algorithm is shown in fig.12. To regulate the output voltage V_o , the switching frequency of the PWM pulses are varied depends on error.

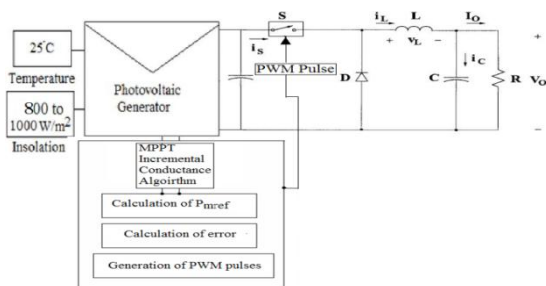


Fig.12. Block diagram of the proposed Incremental Conductance based MPPT scheme.

a. MPPT with incremental conductance algorithm

To track and extract maximum power from the PV arrays for a varying insolation level and at a given cell temperature, a conventional controller like proportional integral controller is proposed with incremental conductance algorithm as tracking method [11-16]. The Flow chart of the proposed Incremental Conductance algorithm is shown in Fig.13. This algorithm has the

advantage of fast response to the rapidly varying illumination condition. The conventional PI controller parameters are obtained by Z-N open loop method [9] as proportional gain $K_c = 1e-5$ and integral gain $K_i = 0.01$.

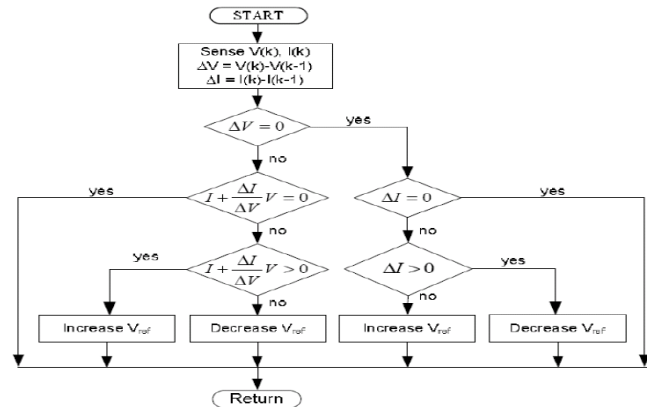


Fig.13. Flow chart of the proposed Incremental Conductance algorithm.

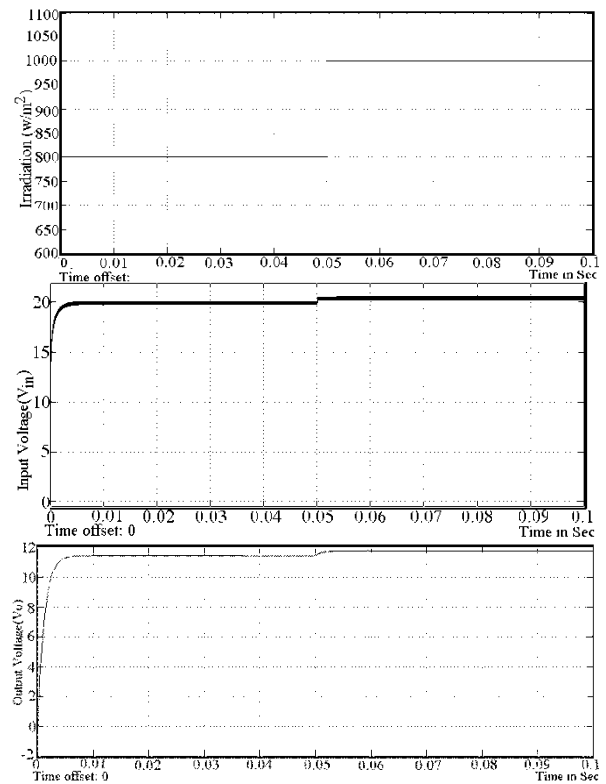


Fig.14. Simulation results depicting the change of insolation from 800 to

1000w/m², input voltage (V_{in}) and output voltage (V_o).

The simulated closed loop output for the insolation variation from $800 w/m^2$ to $1000 w/m^2$ with input voltage (V_{in}) and output voltage (V_o) are shown in Fig.14.

VI. OPEN LOOP EXPERIMENTAL SET UP

The electrical characteristics of the proposed panel are given in table I.

TABLE I
STANDARD TEST CONDITION DATA
ELECTRICAL CHARACTERISTICS

Cell	Poly-crystalline silicon
------	--------------------------

No of cells and connections	36 in series
Open circuit Voltage (V_{oc})	21.75 V
Short – circuit current (I_{sc})	4.85A
Maximum Power Voltage at $P_{max}, (V_{pm})$	18.25 V
Maximum Power Current (I_{pm})	4.315 A
Maximum Power (P_{max})	78.24 W (+10%/-5%)
Module Efficiency (η_m)	13%
Series Fuse Rating	10 A
Type of output terminal	Junction Box
Temperature coefficient of I_{sc}	$0.65e-3 \pm 0.015\%/^{\circ}C$
Temperature coefficient of V_{oc}	$-160 \pm 20mV\%/^{\circ}C$
Temperature coefficient of Power	$-0.5 \pm 0.05\%/^{\circ}C$

a. Battery

The lead-acid battery of 13.3V (± 1) with 7.5Ah is used for the solar photovoltaic charging application.

Fig.15. shows the input voltage to the buck converter from photovoltaic panel.

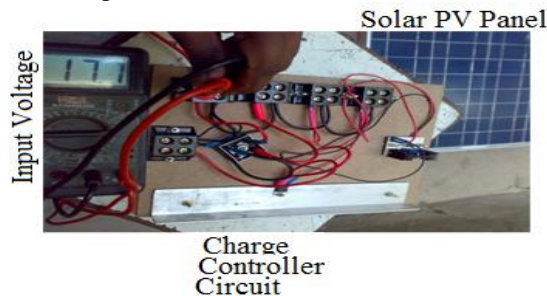


Fig.15. Photocopy of the Experimental setup showing input voltage (V_{in})

of 17.1 V from the photovoltaic panel under $1000w/m^2$ irradiation.

Fig.16. output voltage (V_o) from the charge controller which charges the battery without MPPT algorithm.

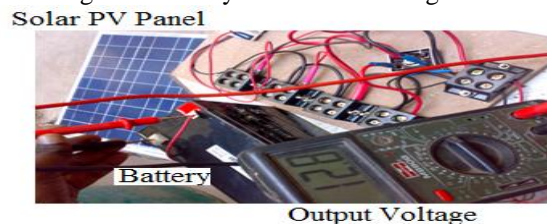


Fig.16. Photocopy of the Experimental setup showing output voltage (V_o) of 12.8 V from the charge controller which charges the battery under $1000w/m^2$ irradiation.

VII. SCOPE FOR FUTURE WORK

The scope for future work is the hardware implementation of the above said stand alone process with MPPT algorithm in closed loop using PIC16F87X microcontroller for varying illumination.

VIII. CONCLUSION

Conventional PI Controller method for MPPT of Photovoltaic array is presented in this paper on the basis of Incremental Conductance algorithm. The simulation results show that the Incremental Conductance algorithm has the merits such as simplicity fast response, low over-tuning, high control, precision and easy implementation. The hardware results are in line with simulated results.

REFERENCES

- [1] Bimal K. Bose, "Global Warming Energy: Environmental Pollution and the Impact of Power Electronics", IEEE Industrial Electronics Magazine, pp.1-17, March 2010.
- [2] Adel Mellit, "Artificial Intelligence technique for modelling and forecasting of solar radiation data: a review," Int. J. Artificial Intelligence and Soft Computing Vol. 1. No. 1, 2008.
- [3] Akihiro Oi, "Design and Simulation of Photovoltaic Water Pumping System", *Master of Science Thesis, California Polytechnic State University*, 2005.
- [4] Adedamola Omole, "Analysis, Modelling and Simulation of Optimal Power Tracking of Multiple-Modules of Paralleled Solar Cell Systems", *Master of Science Thesis, The Florida State University College of Engineering*, 2006.
- [5] V. Di Dio, D. La Cascia, R. Miceli, "A Mathematical Model to Determine the Electrical Energy Production in Photovoltaic Fields under Mismatch Effect", *Proceedings of the 978(1) IEEE*, pp.46-51, August 2009.
- [6] Vaigundamoorthi.M and Ramesh.R, "Experimental Investigation of Chaos in Input Regulated Solar PV Powered" *International Journal of Computer Applications (0975 – 8887) Volume 43– No.10, April 2012.*
- [7] Christopher A. Otieno, George N. Nyakoe, Cyrus W. Wekesa, "A Neural Fuzzy Based Maximum Power Point Tracker for a Photovoltaic System", *IEEE AFRICON*, September 23-25, pp.1-6, 2009.
- [8] A. Mellit, "An ANFIS-Based Prediction for Monthly Clearness Index and Daily Solar Radiation: Application for sizing of a Stand-Alone Photovoltaic System", *Journal of Physical Science, Vol. 18(2)*, pp.15–35, 2007.
- [9] N. Patcharaprakiti and S. Premrudeepreechacharn, "Maximum PowerPoint Tracking Using Adaptive Fuzzy Logic Control for Gridconnected Photovoltaic System", *PESW2002, volume 1, PP:372-377, 002.*
- [10] Marcelo Gradella Villalva, Jonas Rafael Gazoli, and Ernesto Ruppert Filho, "Comprehensive Approach to Modeling and Simulation of Photovoltaic Arrays", *IEEE Transactions on Power Electronics, vol 24, no. 5, 2009, pp 1198-1208.*
- [11] A. Durgadevi, "Design of intelligent controller for quasi resonant converters", M.E. dissertation, Department of Electronics and Instrumentation Engineering, Annamalai Univ., Chidambaram, 2008.
- [12] Vaigundamoorthi.M and Ramesh.R, "ZVS-PWM Active clamping modified cuk converter based MPPT for solar PV modules " *European Journal of Scientific Research, Vol.58 No.3 (2011), pp.305-315.*
- [13] H. Yamashita and K. Tamahashi, et al, "A Novel Simulation Technique of the PV Generation System Using Real Weather Conditions," in *Proceedings of the PCC,2002, volume2, PP:839-844, 2002*
- [14] Cung-Yuen Won, Duk-Heon Kim, Sei-chan Kim, Won-Sam Kim, hack_Sung Kim, "A New Maximum Power Point Tracker of Photovoltaic Arrays Using Fuzzy Controller", *PESC'94.*
- [15] Guohui Zeng, Qizhong Liu, "An Intelligent Fuzzy Method for MPPT of Photovoltaic arrays", *2009 Second International Symposium on Computational Intelligence and Design, pp. 356-359.*
- [16] Rosaidi Bin Rosalan, "Maximum Power Point Tracking Converter for Photovoltaic Application", B.E. dissertaion, Faculty of Electrical Engineering, Universiti Teknologi Malaysia, 2009.

Defect Proneness forecasting in component based software development: A Generic frame work for OO Systems

Mr. G. Viswanath¹, Mr.N.Bala Krishna²

¹(M.Tech) Computer Science & Engineering, Madanaplle Institute Of Technology & Science,
Madanaplle, Andhra Pradesh, India

²(Asst.Professor, Dept of C.S.E Madanaplle Institute of Technology & Science, Madanaplle, Andhra Pradesh, India)

Abstract: Software systems nowadays are composed from prefabricated commercial components and connectors that offer complex functionality and hold in complex interactions. Unfortunately, because of the diverse assumptions made by developers of these products, fruitfully integrating them into a software system can be difficult often causing budget and plan overruns. A number of integration risks can often be determined by selecting the 'right' set of COTS mechanism and connectors that can be integrated with minimal effort. In this paper we illustrate a framework for selecting COTS software components and connectors ensuring their interoperability in software thorough systems. Our framework is built upon average definitions of both COTS mechanism and connectors and is intended for use by architect and developers through the design phase of a software system. We highlight the function of our framework using a difficult example from the data-intensive systems domain. Our groundwork experience in using the framework indicates an increase in interoperability assessment productivity by 50% and accuracy by 20%.

I. Introduction

The mounting complexity of software systems attached with the decreasing costs of causal hardware has ushered forth the realization of Brook's celebrated "buy versus build" meeting [1]. In the past a production organization spent over a million dollars to build up a customized payroll system over 3 years and another 2 million dollars to preserve and grow it forth rest of its prepared life-cycle. Nowadays still, a business organization cannot afford to spend so much on a customized system that will take over 3 years to realize and a fortune to maintain and evolve. Instead they often opt to purchase a commercial off-the-shelf (COTS) software system (or component) that can accomplish the same desired capabilities. Such COTS systems and components persistently have diminished up-front cost, development time, maintenance, and development costs. These economic considerations often entice organizations to piece together COTS components into a working software system that meets dealing organization's requirements, and the system's functional rations, even at the expense of altering the organization's existing business processes! unluckily over the past ten years numerous studies [2-6] have shown that piecing together available open source and COTS components is quite contradictory from custom development.

Instead of the traditional requirements-design-develop-test-deploy process, COTS-based progress involves activities such as assessment-selection-composition-integration-test-deploy [7-11]. overriding to the success of the entire process, are the assessment and selection of the "right set" of COTS components and connectors. Careful and precise execution of these behavior often ensures the development of a system on time, on resources and in line with the objectives of the project. There are two major mechanism within the assessment and selection process: (1) assessment of COTS functional and non-functional requirements; and(2) assessment of interoperability to ensure that the selected COTS components will suitably interact with each other. While the former has been addressed formerly [7-11] an efficient

solution to the latter has eluded researchers. The first example of such an interoperability issue was accepted by Garlan et al. in [5] when attempting to construct a suite of software architectural modeling tools using a base set of 4 reusable components. Garlan et al. termed this problem architectural divergence and found that it occurs due to (specific) assumptions that a COTS section makes about the structure of the application in which it is to appear that ultimately do not hold true.

The best-known solution to identifying architectural mismatches is prototyping COTS communications, as they would occur in the conceived system. Such a move toward is extremely time-and effort-intensive. The approach compels developers (in the interest of limited resources) to either neglect the interoperability issue overall and hope that it will not create problems during the work and integration phases or it compels them to neglect interoperability until the number of COTS combinations available for selection are cut down to a manageable number (based on functional and quality of service requirements). Both these options add considerable risk to the project. When developers absolutely neglect interoperability measurement they often will be essential to write enormous amounts of glue-code, causing cost and schedule overruns. Otherwise, they risk losing a COTS product arrangement which is easy to integrate, but just "isn't right" because of some low-priority functionality it did not possess. Neither of the above scenario is appealing to development teams.

In addition to the above stated COTS component integration issues, there are issues of utilizing available COTS connectors that occur as well. The study of software architecture [12] tells us that software connectors are the embodiment of the relations and associations between software components. Therefore, ideally, when trying to construct the architecture of a software system, we need to be able to deal not only with the gathering of software components, but additionally the assembly of software connectors. This is exacerbated by the current lack of

considerate in many software system domains (e.g., data-intensive systems [13]) of how to select between dissimilar available COTS connectors. The research literature [14, 15] contains many other studies that describe the enormous difficulty in assembling software connectors by themselves, let alone with COTS software components.

In this paper, we propose an attribute-driven framework that addresses selection of (C)OTS components and connectors to make sure that they can be integrated within project possessions and schedule. One of the key contributions of our work is the classification of connectors to (1) “bridge the gap” between COTS components and ensure interoperability, and (2) satisfy systems quality of service (QoS) supplies. Our proposed construction identifies COTS component incompatibilities and recommends resolution strategies comparatively by using specific connectors and glue-code to integrate these components. Where component exchanges require fulfilling of QoS supplies the framework will propose proper connectors. Such incompatibility in sequence can be used to estimate the effort taken in COTS integration [16], which can then be used as a criterion when selecting COTS products. The framework is non-intrusive, interactive, and tailor able. The quantity conducted by the framework can be approved out as early as the commencement phase, as soon as the development team has known possible architectures and a set of COTS components and connectors. We have tested this framework in a classroom setting and in various example studies, including a challenging real world example from the data-intensive systems domain. Our early experience from using the framework indicates that our come near is feasible, and worthy of active pursuit.

1.1 Definitions

We adopt the SEI COTS-Based System Initiative’s definition [7] of a COTS product: a product that is

- sold, leased, or licensed to the general public;
- offered by a vendor trying to profit from it;
- supported and evolved by the vendor, who retains the logical property rights;
- available in multiple identical copies;
- used without source code modification.

For the purpose of this work we include open-source products as part of the COTS domain except where the source code is personalized by the user (and not redistributed as a fix or a version upgrade). In this paper, we define a component generally as a unit of computation or data store [14]. Components may be as small as a single process or as large as an entire application. Connectors are architectural building blocks used to representation interactions among components and rules that govern those interactions [14]. The rest of this paper is organized as follows. In Section 2, we describe a motivating real-world COTS assessment and selection problem in the data-intensive systems domain. In Section 3 we describe the assessment framework in detail, including the attribute metadata that it captures and how it applies to our example.

In Section 4 we present observed evidence and data taken from a graduate software engineering course at USC that evaluated our framework. Section 5 identifies related works to our own approach and section 6 rounds out the paper with a view of some expectations work.

II. Assessment and Selection Framework

The framework is modeled using three key components, these are: COTS interoperability surveyor, COTS representation attributes, and mixing rules. Inputs to the framework are various COTS component definitions and a high-level system architecture. The output of the framework is an interoperability assessment report which includes three major analyses:

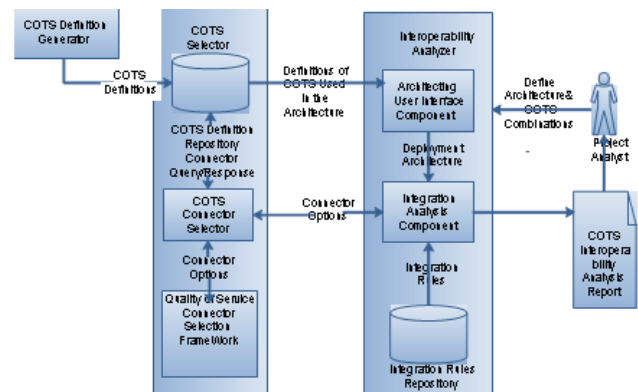


Figure 2. COTS Interoperability evaluation framework

1. Internal postulation mismatches, which are caused due to assumptions made by interacting COTS’ systems about all other’s internal structure [4].
2. Interface (or packaging) mismatches, which occur because of incompatible communication interfaces between two components.
3. Dependency analysis, which ensure that services required by COTS packages used in the system are being provisioned (e.g. Java-based CRM solution requires Java Runtime Engine).

In the remainder of this section we will describe each of the framework components in details.

1.2 COTS interoperability evaluator

To develop the COTS interoperability evaluator we needed to address two considerable challenges:

1. Ensure that the effort spent in COTS interoperability assessment is much less than the effort spent performing the assessment manually.
2. Ensure that the framework is extensible, i.e. so that it can be updated based on popular COTS characteristics.

We tackle these challenges by developing a framework that is modular, automated, and where COTS definitions and assessment criteria can be updated on-the-fly. Our framework allows for an organization to continue a reusable and frequently updated portion (COTS selector) remotely, and a segment which is minimally updated (interoperability analyzer) at client-side. This allows for a dedicated team to maintain definitions for COTS being assessed by the organization. The internal architecture of

the COTS interoperability surveyor component is shown in Figure 2. The architecture consists of the following sub-components. COTS Definition Generator is software utility that allows users as well as COTS vendor to define the COTS components in a generally accepted standard format. Currently we have implemented an XML-based format; however, the implementation format is independent of the primary metadata (e.g., the COTS definition can still be represented using other representation formats, so long as suitable parsers exist). For brevity, we omit its full description of our existing XML format and we point the reader to [17] for a complete description.

COTS Definition Repository is an online storage of assorted COTS definitions indexed and categorized by their roles and functionality they provide (database systems, graphic toolkits etc.). The repository is queried by different sub-components of the interoperability surveyor. In practice, this component would be collective across the organization to enable COTS definitions reuse. Alternately, such a repository could be maintained and updated by a third-party vendor and its access can be licensed out to various organizations.

Architecting User Interface Component provide a graphical user interface for the developers to create the system deployment diagram. The component queries the COTS definition storehouse to obtain the definitions of COTS products being used in the conceived system. Integration Rules storage area specifies various integration rules that will drive the analysis results and interoperability assessment. The rules repository can be maintained

classify internal assumption mismatches, interface (or packaging) mismatches and dependency analysis. When the integration analysis element encounters an interface variance the component queries the COTS connectors elector component to identify if there is an existing bridge connector which could be used for integration of the components, if not it will recommend in the interoperability analysis report that a wrapper of the suitable type (either communication, or coordination or conversion) be utilized. The integration analysis component then provides some simple textual information (in human readable format) as to the functionality of the wrapping required to enable interaction between the two components. In addition the combination analysis component identifies mismatches caused due to internal assumption made by COTS components, and also identifies COTS component dependency not satisfied by the architecture. For cases where the COTS component definition has misplaced information the integration analysis component will include both an cheerful and a pessimistic outcome. These identifications are both included in the interoperability analysis report. COTS Connector Selector is a query interface used by combination analysis component to identify abridging connector in the event of interface incompatibility, or a QoS specific connector. **Quality of Service Connector Selection Framework** is inextensible component built for identifying quality of service specific connectors. One such extension discussed in this paper aids in the selection of highly distributed and voluminous data connectors. Other quality of service extensions may include connectors for mobile-computing environments that require low memory footprint, or connectors for highly reliable, fault-tolerant systems. To create a quality of service extension, a developer first identifies needed COTS attribute information and ensures the information is captured in the COTS definition repository. This information will typically describe the scenario requirements for COTS connector selection for the particular level of service, e.g., for data intensive systems, it may include the Total Volume, Number of Delivery Intervals and possibly the Number of Users present in the data transfer. The developer then can construct a simple web-based service that accepts the COTS connector definition information, and any other needed data, and then returns the appropriate COTS connectors to select to satisfy the desired level of service scenario. **COTS Interoperability Analysis Report** is output by the selector and contains the result of the analysis in three major sections: (1) internal assumptions mismatch analysis, (2) interface (packaging) mismatch analysis, and (3) dependency analysis. This is the ultimate product of the interoperability framework.

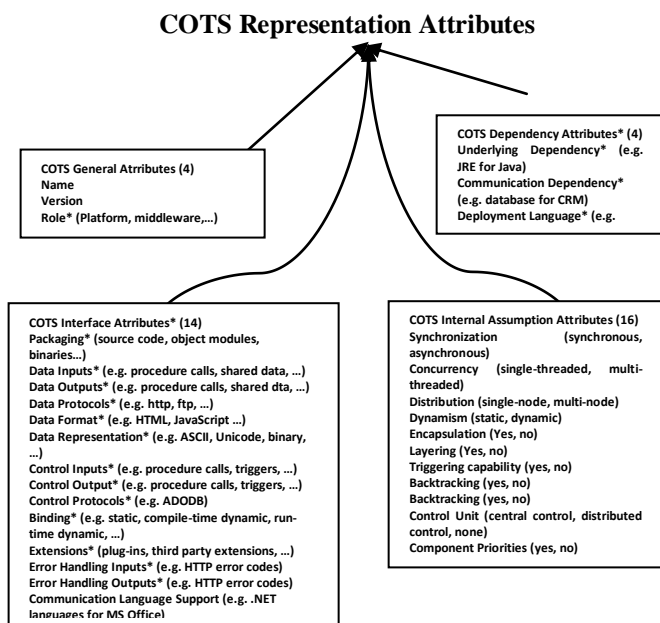


Figure 3. COTS Representation Attributes

remotely; however it will be required to download the complete repository at the client-side (interoperability analyzer) before performing interoperability measurement. This reduces the number of remote queries required when assessing COTS architectures. **Integration Analysis Component** contains the actual algorithm for analyzing the system. It uses the rules specified in the combination rules depository along with the architecture specification to

1.3 COTS Representation Attributes

The COTS Representation Attributes are a set of 38 attributes that define COTS produce interoperability characteristics. COTS interoperability characteristics defined using these attributes are utilized by the integration analysis component along with incorporation assessment rules (described in the next section) to carry out interoperability analysis. These attributes have been consequent from the literature, as well as our clarification in various software integration projects.

The two major criteria used for selecting these attributes were:

1. attributes should be able to capture sufficient details on the major sources of COTS product mismatches (interface, internal assumption and dependency mismatches) identified - internal postulation mismatches,
2. attributes should be defined at advanced so that COTS vendors are able to provide feature definitions without revealing confidential product information

To date, we have surveyed about 40 COTS products of which 30 were open source. For the non open source COTS we could identify at least 34 of the 38 attributes from the publicly available information itself. We neglected to include many attributes such as data topology, control structure, and control flow because they were either : too detailed and required accepting of internal designs of COTS products for defining them, or could alternately be represented at a higher level by an already included attribute, or did not provide significant mismatches to warrant us including them. We have classified the attributes that we selected into four groups shown in Figure 3. Attributes (or attribute sets) marked with an asterisk indicate that there may be multiple values for a given attribute (or set) for the given COTS product.

The remainder of this section summarize attribute classifications. The full metaphors of all the attributes can be accessed at [17]. **COTS general attributes (4)** aid in the identification and querying of COTS products. The attribute include name, version, role and type. **COTS interface attributes (14)** define the communications supported by the COTS product. An interaction is defined by the exchange of data or control amongst machinery. COTS products may have multiple interface, in which case it will have multiple interface definition. For example: the Apache Web Server will have one complete interface definition for the web-interface (interaction via HTTP), and another complete definition for server interface (interaction via procedure call). These attributes include packaging (source code modules, object modules, dynamic libraries, etc.), data and control inputs, outputs, protocols etc. When developing the COTS product the developer makes certain assumption about the internal operations of the COTS products. The **COTS internal assumption attributes (16)** confine such internal assumption For example developers of the Apache Web Server assume that the software will contain a central control unit which will regulate the performance of the system. COTS internal statement attributes include synchronization, concurrency, distribution and others. **COTS dependency attributes (4)** define the conveniences required by a COTS product i.e. software the COTS product requires for successful execution. For example any Java-based system requires the Java Runtime Environment (JRE) as a platform. COTS dependency attributes include primary and communication dependencies, deployment language support, and execution language support. An example COTS definition using the attributes specified in Figure 3 is shown in Table 1.

1.4 Integration Assessment Rules

The Integration review Rules are a set of rules used to perform the interoperability analysis. Every rule has a set of pre-conditions, which if true for the given planning and components, identifies an architectural mismatch. For example consider one of the architectural mismatches found by Gacek in [4]:“Data connectors connecting components that are not always active”. For the given mismatch the precondition are: 2 components connected via a data connector (only) and one of the components does not have a central control unit. There are similar rules for performing arts interface, dependency, and internal assumption analysis. Interface analysis discovers if there are commonly shared interfaces between two communicating COTS components, if not it includes recommendation on the type of “glue ware” (or “glue code”) required to integrate the components.

enslavement analysis rules verify if the architecture satisfies all the dependencies that a COTS product require. Finally, for internal assumption we leverage upon the mismatches identified in [4] and add new mismatches based on newly added attributes. Currently, our framework is still underdevelopment and we are in the process of evaluating these rules for behavior such as completeness, correctness, tractability and scalability. We have perform an initial appraisal along two of these evaluation target (correctness and completeness) and our ongoing work involves solidifying means of measuring and evaluating our work.

1.5 Framework Application to Motivating Example

To answer the two questions posed in the motivating example section we apply our framework to analyze the system architecture and COTS combinations. In our example there are 2 major considerations when assessing COTS products and implementation technologies to identify interoperability conflicts:

1. Interoperability conflicts when integrate the digital asset management system with the database.
2. Selection of languages to develop the custom components so as to minimize the development effort by leveraging upon existing support provided by COTS products.

Table 1 Definition of Apache 2.0 using COTS Representation Attributes

COTS General Attributes (4)		
Name	Apache	
Version	2.0	
Role	Platform	
Type	Third-party component	
Interface Attributes (14)	Background Interface	Web Interface
Packing	Executable Program	
Data Inputs	Data access, Procedure Call, Trigger	
Data Outputs	Data access,	

Data Protocols Data Format Data Representation Control Inputs Control Outputs Control Protocols	Procedure Call, Trigger	
		HTTP
	N/A	N/A
	Ascii, Unicode, Binary	Ascii, Unicode, Binary
	Procedure call, Trigger	
	Procedure call, Trigger Spawn	
	None	
Extentions	Supports Extentions	
Binding Error Inputs Error Outputs Communication Language Support	Running Dynamic	Topologically Dynamic
	Log s	HTTP Error Codes
	C, C++	
COTS Internal Assumption Attributes (16)		
Synchronization Concurrency Distribution Dynamism	Asynchronous	
	Multi-threaded	
	Single-node	
	Dynamic	
Encapsulation Layering Triggering Capability Backtracking Control Unit Component Priorities Preemption Reconfiguration Reentrant Response Time Implementation Lang Error Handling Mechanism	Encapsulated	
	None	
	Yes	
	No	
	Central	
	No	
	Yes	
	Offline	
	Yes	
	Bounded	
	C++	
	Notification	
	COTS Dependency Attributes (4)	
Underlying Dependencies	Linux, Windows, (OR)	Unix, Solaris
Communication Dependency	None	
Deployment Language	Binary	
Execution Language Support	CGI	

The project analyst should provide the following information for every interaction in the proposed architecture:

- data and/or control interaction,
- Unidirectional of bidirectional interaction, and which component initiates the interaction,

For the interactions where the large volume data transfer connectors (C1, C2, and C3) are required, the analyst will define attributes specific for that QoS (described further in this section). Assume a scenario where D Space is being assessed as the digital asset management system, and MySQL as the database server. The architecting component user interface will automatically retrieve the definitions for D Space and MySQL and pass the architecture, interaction and definition information to the integration analysis component for assessment. The integration analysis component will apply the rules (from integration rules repository) using COTS attributes and based on the deployment architecture definition to identify:

- Common interfaces supported by MySQL and D Space, bridging connectors and the type of glue code (communication, conversion, synchronization or a combination thereof) required [15].
- Internal assumption mismatches between MySQL and D Space
- Verification that the COTS dependencies have been satisfied in the given architecture.
- Recommended languages for the query manager and data recovery component that will simplify developing glue-code between COTS and custom components.

In the event that the two interacting components (D Space and MySQL) do not share common interfaces, it will recognize (using the COTS connectors selector) a connector that can enable announcement between the two components (JDBC-MySQL driver) and output the fallout in the report. The project analyst can use these findings to estimate the effort required to test (for internal assumption mismatches) and integrate the COTS and custom apparatus [16]. Development

teams can run such evaluation on all their COTS and custom combinations; and use the exertion results as an input to their COTS evaluation table [10] to facilitate the COTS component collection decision. External users, when selecting COTS products and implementation technologies to develop application can run our framework by keeping COTS and technologies selected by JPL and ESA constant and varying their choices of COTS harvest to identify the set which will require minimal integration effort.

To deal with the range of connectors to support large-volume data transfer between JPL and ESA (as shown in Figure 1), and the external users, we employ a specific level of service extension that we have constructed for large-scale, data-intensive systems. The extension was particularly motivated by our experience developing such systems at JPL. A careful, detailed description of this level of service extension is beyond the scope of this paper: for more information on its internal architecture, motivation and objectives the reader is directed to [13]. However for

the purposes of our COTS assessment and selection framework, we will explain the data-intensive level of service extension's high level architecture focusing on two of its critical phases: connector classification, and selection. The inputs to the data-intensive level of service extension are called Distribution Connector Profiles, or DCPs. DCPs capture metadata describing connector Data Access, Distribution and Streaming information abstracted from Mehta et al.'s [15] connector taxonomy.

The profiles also contain information critical to data distribution including Delivery Intervals, Number of Users and Total Volume (in total, there are eight core dimensions of data distributions we are focusing on). To generate DCPs, an architect can manually classify a set of COTS distribution connectors: or the DCPs can be generated using some automated process. For our motivating example, we assume that the production of DCPs has already been performed offline, and we assume the presence of a knowledge base of DCPs resultant from the arrangement. The connectors profiled for the knowledge base take account of connectors C1, C2, and C3 shown in Figure 1. Connector selection starts after the system architecture has been arrived upon and after data allocation scenarios (e.g., constraints on the DCP metadata) have been identified by the user(s) of the system. In our example, there are three distinct distribution scenarios to consider (represented below in human readable form and then following in constraint query format):

- S1. Distribution of data from JPL scientists to ESA scientists
- S2. Distribution of data from ESA scientists to JPL scientists
- S3. Distribution of JPL and ESA data to the outside community

The three scenarios can be expressed as the following constraint queries against the DCP metadata:

```
(Total Volume > 100 GB) ^ (Number Of Users = 2) ^
(S1)
(Num Delivery Intervals = 4) ^ (Volume Per Interval = 25
GB)
^ (Num User Types = 1) ^ (Geographic Distribution =
WAN)
(Total Volume = 1GB) ^ (Number Of Users = 4)
```

For instance, S1 represent the user preference of the

ESA scientists who would like to receive their JPL colleagues' data. S1 describe a allotment scenario in which the producer of data (the JPL scientists) are conveyance over 100 GB of data using a wide-area network (WAN) to 2 regulars of data (the ESA scientists), using 4 escape intervals where each interval consists of 25 GB of data. In S1, from the perspective of the producer of data (JPL scientists), there is a single user type, the ESA scientists. Queries S2 and S3 are formulated similarly. Using S1-S3 as selection criteria, "candidate" connectors are chosen based on their DCP metadata at hand in the DCP knowledge base using a conventional database attribute matching

approaches. After candidate connector filtering, the distribution connectors are assessed for architectural mismatches that may result from their combined use in support of the given circulation scenario.

This appraisal is conducted using an conservatory to Gacek's [4] simple pair-wise mismatch algorithm that compares two architectural elements (in this case, distribution connectors) along the metadata values provided by the DCP. For every value, our algorithm detects potential mismatch areas and decides whether the (set of) mismatches identified are severe enough to avoid connector combination, otherwise, selects suitable connectors that could be used together. For example there may be a divergence in the Number of Users dimension of two of the freedom connectors from the JPL and ESA system, C1 and C2. If C2 supports fewer users than connector C1, then C2 may become the restricted access in the distribution. The detected mismatches are labeled using a simple, but adaptable set of divergence levels, such as severe, or allowable. A severe mismatch may prevent combination of two otherwise matched connectors, while an allowable label may still allow their combination.

The levels are tailor able and meant to be profiled to suit each respective user of our framework. Relating back to our motivating example, the algorithm may decide based on the DCP metadata, that connectors C1 and C2 should be combined, and to combine the Grid FTP [18] connector with an HTTP based custom COTS data connector. Additionally, the level of service extension may conclude that connector C3 can be implemented using an available OTS peer to-peer distribution connector, such as Bit torrent.

III. Empirical Results

In bounce semester of 2006 we conducted an conduct experiment in a graduate software engineering course at USC using our assessment framework. The course focus on software classification development [19] requested by a real-world client. Over the last few years the course has twisted systems for e-services, explore (medicine and software), as well as commercial selling domains. Graduate students enrolled in the track form teams of about 5 members to design and implement a software system within a 24-week time period. During this period the project progresses through inception, elaboration, manufacture and transition phases. Our experiment was conducted close to the end of the elaboration phase, when the team propose a system architecture that would meet the system requirements. We asked 6 teams, whose architectures included at least 3 or more COTS components to use our framework on their personal projects and measured results in four areas:

1. Accuracy of interface incompatibilities notorious by the framework considered as $1 - (\text{number of interface incompatibilities missed by the team} / \text{total number of interface incompatibilities})$. Interface measurement results produced by our framework were verified later through a survey when the teams actually integrated the COTS products. Results in this area price the completeness and correctness of our interface assessment rules.
2. Accuracy of dependency identified by the framework calculated as $1 - (\text{number of dependencies missed by the})$

team / total number of dependencies). Addition assessment results produced by our framework were also later verified through a survey after the project was implemented. These results evaluate the completeness and correctness of our interface dependency rules.

3. Effort spent in assessing the architectures using the framework contrasting to the effort spent in assessing the architectures manually by an comparable team. These results demonstrate the competence of using our framework to perform interoperability assessment as opposed to performing a manual assessment.

4. Effort spent in performing arts the actual integration after using the framework as opposed to effort spent by an equivalent team.

Results here validate the overall utility of our framework Equivalent teams were chosen from past CSCI 577 projects such that they had analogous COTS products, similar architectures, and whose team-members had similar years of experience in project enlargement.

Upon performing autonomous T-test [20] for the metrics above we recorded the results shown in Table2. Our results indicate that the framework increases dependency assessment accuracy and interface assessment accuracy by more than 20% and reduces both assessment effort and integration effort by approximately 50%. These results are significant at the alpha = 5% level.

Table 2. Empirical assessment of our framework

Groups	Mean	Std-Dev.	P-Value
Interface Assessment Accuracy			
Before using the framework	76.9%	14.4	0.0029
After using the framework	100%	0	
Dependency Assessment Accuracy			
Before using the framework	79.3%	17.9	0.017
After using the framework	100%	0	
Effort spent in performing architecture assessment			
Projects using the framework	1.53	1.71	0.053
Equivalent projects	5 hrs	3.46	
Effort spent when integrating the COTS products			
Projects using the framework	9.5	2.17	0.0003
Equivalent projects	18.2	3.37	

IV. Conclusion and Future Work

This paper presents a construction that enables evaluation and selection of COTS workings and connectors early in the software development lifecycle. The skeleton does not eliminate detailed testing and prototyping for evaluating COTS interoperability, however it does provide an analysis of interface compatibilities and dependency. The framework recommends connectors to be used or glue code required and early indications of probable incompatibilities during system integration. Moreover, since the framework is automated it enables evaluation of large number of architectures and COTS combinations, increasing the trade-off space for COTS component and connector selection. Currently we have completed a tool prototype to enable such examination and are in the process of developing a fully functional tool suite. We are also planning experiment to gather empirical data to further test the utility of the framework across a larger sample size and in different development environments. It is also important to note that attribute for frameworks such as ours must be periodically updated based on prevailing COTS characteristics.

References

- [1] F. Brooks, "No Silver Bullet: Essence and Accidents of Software Engineering," Computer, vol. 20, pp. 10-19, 1987.
- [2] A. Abd-Allah, "Composing Heterogeneous Software Architectures," Ph.D. Thesis, Univ. Southern California, 1996.
- [3] L. Davis, et al., "The Impact of Component Architectures on Interoperability," J. Systems and Software, 2002.
- [4] C. Gacek, "Detecting Architectural Mismatch During Systems Composition", Ph.D. Thesis, Univ. Southern California, 1998.
- [5] D. Garlan, et al., "Architectural Mismatch or Why it's hard to build systems out of existing parts," In Proc. ICSE, 1995.
- [6] D. Yakimovich, "A Comprehensive Reuse Model for COTS Software Products", Ph.D. Thesis, University of Maryland College Park, 2001.
- [7] C. Albert, et al., "Evolutionary Process for Integrating COTS-Based Systems (EPIC)," CMU/SEI Technical Report CMU/SEI-2002-TR-005, 2002.
- [8] K. Ballurio, et al., "Risk Reduction in COTS Software Selection with BASIS," In Proc. ICCBSS, 2003.
- [9] B. Boehm, et al., "Composable Process Elements for COTS-Based Applications," In Proc. 5th Intl. Workshop on Economics-Driven Software Engineering Research, Oregon, 2003.
- [10] S. Comella-Dorda, et al., "A Process for COTS Software Product Evaluation," In Proc. ICCBSS, Orlando, Florida, 2002.
- [11] Y. Yang, et al., "Value-Based Processes for COTS Based Systems," IEEE Software, vol. 22, pp. 54-62, 2005.
- [12] M. Shaw, et al., Software architecture: perspectives on an emerging discipline. Upper Saddle River, N.J.: Prentice Hall, 1996.

- [13] C. Mattmann, "Software Connectors for Highly Distributed and Voluminous Data-intensive Systems," In Proc. ASE, Tokyo, Japan, 2006.
- [14] N. Medvidovic, et al., "A Classification and Comparison Framework for Software Architecture Description Languages," IEEE TSE, vol. 26, pp. 70-93, 2000.
- [15] N. Mehta, et al., "Towards a Taxonomy of Software Connectors," In Proc. ICSE, Limerick, Ireland, 2000.
- [16] C. Abts, "Extending the COCOMO II Software Cost Model to Estimate Effort and Schedule for Software Systems Using Commercial-Off-The-Shelf (COTS) Software Components: The COCOTS Model", Ph.D. Thesis, Univ. Southern California, 2004.
- [17] J. Bhuta, "A Framework for Intelligent Assessment and Resolution of Commercial Off-The-Shelf (COTS)Product Incompatibilities," USC, Tech. Report USCCSE-2006-608, 2006.
- [18] C. Kesselman, et al., "The Anatomy of the Grid: Enabling Scalable Virtual Organizations," Intl' Journal of Supercomputing Applications, pp. 1-25, 2001.
- [19] B. Boehm, et al., "A stakeholder win-win approach to software engineering education," Annals of Software Engineering . vol. 6, pp. 295 - 321, 1998.
- [20] T. Dietterich, "Approximate Statistical Tests for Comparing Supervised Classification Learning Algorithms," Neural Computation, vol. 10, 1998.
- [21] E. Mancebo, et al., "A Strategy for Selecting Multiple Components," In Proc. ACM SAC, Santa Fe, NM, 2005.
- [22] L. Davis, et al., "A Notation for Problematic Architectural Interactions," In Proc. ESEC/FSE, 2001.
- [23] R. Keshav, et al., "Towards a Taxonomy of Architecture Integration Strategies," In Proc. ISAW, 1998.

BIOGRAPHIES



Engineering College, Kankamma Chatram, Chittoor District, India.

G.Viswanath is born in 1982 in India. He is graduated in **B.C.A** from Osmania University, Hyderabad and post graduated in **M.C.A** from S.K. University, Anantapur. Presently he is doing post graduation in **M.Tech (C.S.E)** at MITS College, Madanapalli, Andhra Pradesh, India from JNTU Anantapur. At present working on Assistant professor at Sai Sakthi



N. Bala Krishna is born in 1984 in India. He is graduated in **B.Tech** from JNTU Hyderabad. He is post graduated in **M.Tech** from JNTU Anantapur. He is currently working as a Assistant professor in the department of Computer science and engineering at MITS College, Madanapalli, Chittoor District, Andhra Pradesh, India.

Chaos and Control of Chaos in Current Controlled Power Factor Corrected AC-DC Boost Regulator

Arnab Ghosh¹, Dr. Pradip Kumar Saha², Dr. Goutam Kumar Panda³

**(Assistant Professor, Electrical Engineering Department, Gargi Memorial Institute of Technology, Kolkata, India)*

*** (Professor & Head, Department of Electrical Engineering, Jalpaiguri Govt. Engineering College, Jalpaiguri, India)*

**** (Professor, Department of Electrical Engineering, Jalpaiguri Govt. Engineering College, Jalpaiguri, India)*

ABSTRACT: *In these modern research areas the Non-linear Dynamics is a very popular topic, the researchers study the nonlinear behaviour of every system which can be an industrial machine/instrument or a theoretical aspect. Prior researchers already studied the nonlinear dynamics of Current Controlled DC-DC Boost Converter. But the Power Factor Corrected Boost Converter is a circuit which is used in very practical purpose where the input is AC, the AC is rectified to DC by diode bridge rectifier and the rectified DC is to feed the boost converter i.e. conventional pure DC supply is replaced by the rectifier DC. In this converter the circuit is designed specially as input power factor can maintain unity so it is called Power Factor Corrected (PFC) Boost Converter. This paper aims to develop a circuit for PFC boost converter to observe Phase-Portrait diagrams and also discuss the control of chaos.*

Keywords: *AC-DC PFC Boost Regulator, State Equations, Phase-Portrait Diagrams, Control of Chaos.*

I. INTRODUCTION

Power factor correction converter (PFC) is an important area of study and research in power electronics motivated by practical applications [1]. This AC-DC converter provides DC voltage at the output with high input power factor. In fact, a low power factor reduces the power available from the utility grid, while a high harmonic distortion of the line current causes EMI problems and cross interferences through the line impedance between different systems connected to the same grid. It is usually assumed that the output ripple can be neglected by using a huge output capacitor, which is not acceptable in design due to its high cost and size. Thus many efforts are being done to develop interference systems, therefore to ensure a minimum distortion and a power-factor close to the unity. One of the most common circuits used to achieve unity power factor is the boost Power Factor Correction circuit.

In last decade, studies of complex behaviour in switching power converters have gained increasingly more attention from both the academic community and the industry. Various kinds of nonlinear phenomena, such as bifurcation and chaos have been revealed [2][3]. Chaos could be described as noise like, bounded oscillations with an infinite period found in nonlinear, deterministic systems [4]. These complex behaviours implying instability can be observed by changing circuit parameters, or enclosing the accessional control method when the circuit parameters are fixed. The occurrence of bifurcation and chaos in power

electronics was first reported in the literature in the late 1980 [5][6]. In [7] the chaotic behaviour in a buck converter with certain parameter range was verified theoretically and experimentally.

Deane [8] first discussed the route to chaos in a current controlled boost converter. Chan and Tse [9], S. Banarjee and K. Chakrabarty [10] studied various types of routes to chaos and their dependence upon the choice of bifurcation parameters.

Recently some nonlinear behaviours in the PFC boost converter have been reported [11].

The possibility of controlling nonlinear chaotic dynamical systems has been subjected to extensive investigation. The prior researchers focused on control of Chaos by means of small, time-dependent parameter or input perturbations [12,13]. Many different strategies to control chaotic dynamics in nonlinear systems have been proposed in recent surveys of some of the available methods for control of chaos can be found in [14], [15], [16] and [17]. *Time-Delayed Auto Synchronization (TDAS)* was proposed by Pyragas in [18]. *Extended Time-Delayed Auto Synchronization (ETDAS)* was proposed by Socolar et al. [19]. Partial differential equations, initial conditions and the domain of control of a given system have been described in [20], [21], [22]. Mostly developed in the area of control engineering which makes use of *State Feedback Controllers (STC)*, *Adaptive Control Schemes* [23] to solve the problem of controlling chaos.

In this thesis, in order to better understand the dynamics of PFC boost regulator, model of CCM is considered to analyze its behaviours. The modelling and simulation aspects of current-mode controlled PFC boost regulator are operating in chaotic regime are addressed. Firstly, the numerical simulation of chaotic and discontinuous system is presented, so that the results reflect the true behaviour, as an extremely challenging task for any simulation tool. Secondly, MATLAB/Simulink is used to compare the results obtained by numerical simulation.

II. DESIGN CONCEPT OF AC-DC PFC BOOST REGULATOR

DC power supplies are extensively used inside most of electrical and electronic appliances such as in computers, monitors, televisions, audio sets and others. The high power non linear loads (such as static power converter, arc furnace, adjustable speed drives etc) and low power loads (such as fax machine, computer, etc) produce voltage fluctuations, harmonic currents and an imbalance in network system which results into low power factor operation of the power system. There is a need of improved power factor and reduced harmonics content in input line

$$v_s = 220 \sin \omega t, L = 40 \text{ mH}, C = 100 \mu\text{F}, R = 44 \Omega, K_1 = 400$$

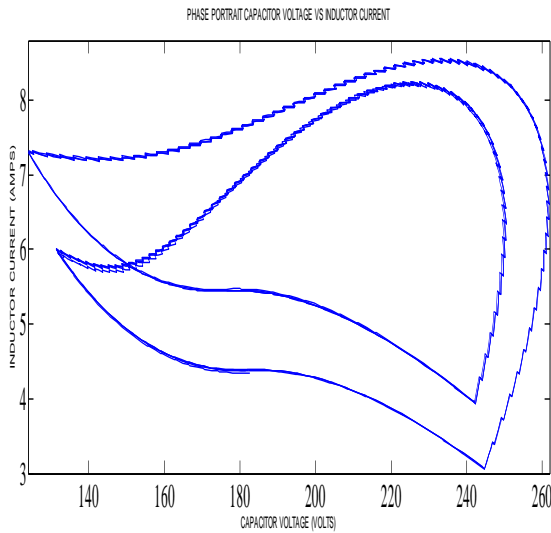


Fig. 4: Phase Plane Trajectory (Case II) Capacitor Voltage vs. Inductor Current (Period II operation)

Case III(Period V Operation)

$$v_s = 220 \sin \omega t, L = 40 \text{ mH}, C = 100 \mu\text{F}, R = 38 \Omega, K_1 = 400$$

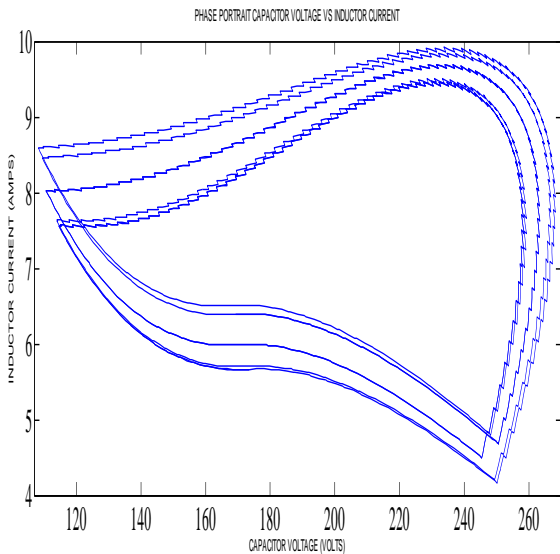


Fig. 5: Phase Plane Trajectory (Case III) Capacitor Voltage vs. Inductor Current (Period V operation)

Case IV(Chaotic Mode Operation)

$$v_s = 220 \sin \omega t, L = 40 \text{ mH}, C = 100 \mu\text{F}, R = 65 \Omega, K_1 = 400$$

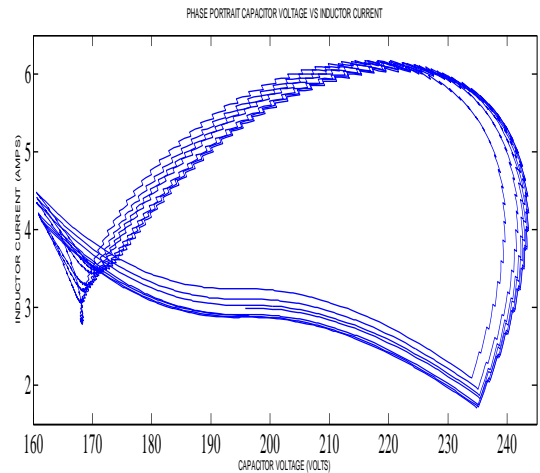


Fig. 6: Phase Plane Trajectory (Case IV) Capacitor Voltage vs. Inductor Current (Chaotic Mode Operation)

The time domain diagram of state variables i.e. inductor current and output capacitor voltage repeats after "n" times of cycles, so it is a "Chaotic mode operation". Chaos is largely unpredictable long-term evolution occurring in deterministic, nonlinear dynamical system because of sensitivity to initial conditions. The Phase Plane Trajectory of "Chaotic mode operation" is shown in Fig. 6.

VI. CONTROL OF CHAOS

There are several kinds of methods to controlling chaos (previous discussion), here the TDS method is picked up. Our strategy to stabilize the UPO of the current-mode-controlled boost converter will consist of modifying the reference current with a term proportional to the difference between a linear combination of the present and past states of the system. Precisely, instead of compare it to $I_{ref} + \eta(\alpha(v(t) - v(t - 1))) + \beta(i(t) - i(t - 1))$

Where η is an overall feedback gain and α and β are relative weights. Notice again that, for a period - I solution the feedback signal vanishes. One must bear in mind that, although the mathematical computations to find out the range of parameters that stabilize the orbit can be quite imposing, once those value are known, the actual implementation requires only the knowledge of the period of target orbit in order to form the feedback signal. For the system like PWM - controlled converters the period of any orbit is a multiple of period of the clock used to generate the pulses. More detailed information about the target unstable orbits can be obtained experimentally using, for instance, the techniques exposed in [17], and this can be used to numerically compute the parameter range mentioned above.

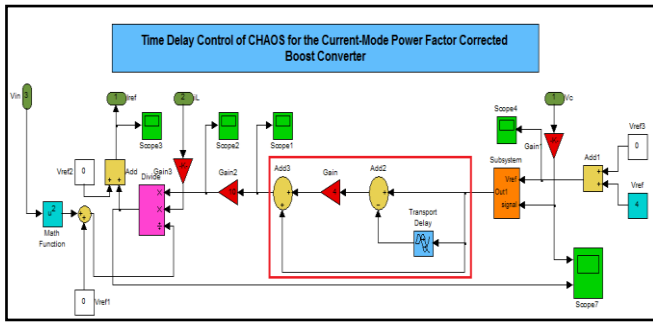


Fig. 7: MATLAB Model of Time – Delay Feedback Control of Chaos of PFC Boost Converter BEFORE CONTROLLING CHAOS

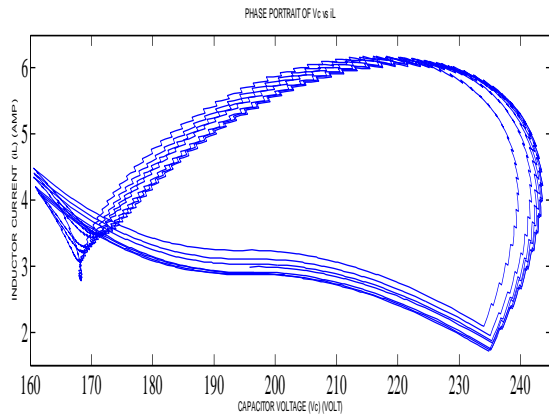


Fig. 8: Phase Portrait of Capacitor Voltage vs. Inductor Current in Chaotic Mode AFTER CONTROLLING CHAOS

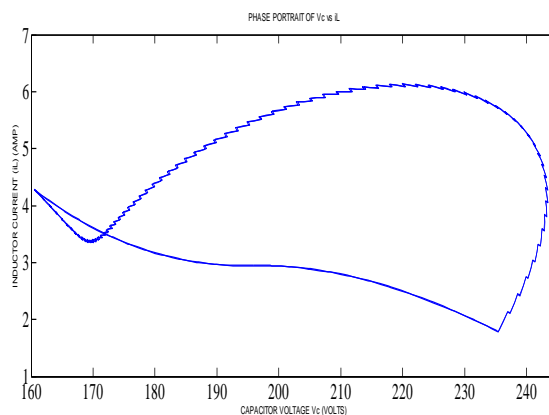


Fig. 9: Phase Portrait of Capacitor Voltage vs. Inductor Current after Controlling Chaos

The Chaotic mode phase portrait is shown in Fig. 8, the Time Delay Feedback System is used (Fig. 7) for controlling the chaos. Fig. 9 is shown after controlling the chaos.

VII. CONCLUSION

The Power Factor Corrected (PFC) AC-DC Boost Regulator with current-mode control has been investigated depending on the nonlinear model. Results highlight that the proposed model of practical PFC regulator, simulation results and phase-portrait diagrams. The phase-plane-trajectory curves are observed by varying value of resistance (R). The value of load resistance (R) is increased or decreased; the phase-portrait of output capacitor voltage (v_c) and inductor current (i_L) is going to period I to period II to chaotic-mode. Chaos phenomena are

shown by multiple loops on phase-plane diagram. The most important point of all the case studies, if the entire system is operated in chaotic-mode the output capacitor voltage ripples has been minimized by increasing the chaotic-region. The chaos control are also done by time delay feedback system (TDS). We can control entire system in our desired region according to our demand. In a DC-DC converter system, the input voltage is constant and therefore the dynamical behaviour is periodic with the switching frequency. On the other hand, the input voltage of the boost AC-DC PFC regulator system is periodic with the line frequency. The results highlight that the dynamical behaviour is periodic with the line frequency not with the switching frequency and simulation results are also agree with our statements.

ACKNOWLEDGEMENTS

I am very grateful to **Professor Soumitra Banerjee** at Indian Institute of Science and Research, Kolkata and **Professor Mohamed Orabi**, Director of the Aswan Power Electronics Application Research Center, Faculty of Engineering, South Valley University, Aswan, Egypt for their individual suggestions.

REFERENCES

- [1] Arnab Ghosh, Dr. Pradip Kumar Saha and Dr. Gautam Kumar Panda, "Observation The Nonlinear Behaviour of PFC Boost Converter and Control of Bifurcation" in International Journal of Scientific and Engineering Research, Vol. 3, Issue 6, June. 2012.
- [2] J. R. wood, "A Chaos: a real phenomenon in power electronics," IEEE Transactions on Power Electronic, 1989.
- [3] D. C. Hamill, "A field rich in nonlinear dynamics: in nonlinear dynamics of electronic systems," IEEE Transactions on Power Electronics, 1995.
- [4] E. Colon, F. Rodriguez, U. Contreras, "Development of tools for the study of chaotic behavior in power electronics," in Proc. 2000 IEEE Computers in Power Electronics Conf., pp. 177-182.
- [5] D. C. Hamill, D. J. Jefferies "Subharmonics and chaos in a controlled switched-mode power converter," IEEE Trans. Circuits Syst. I, vol. 35, pp. 1059-1061, Aug. 1988.
- [6] D. C. Hamill, J. H. B. Deane, "Instability, subharmonics and chaos in power electronics systems," IEEE Trans Power Electron, vol. 5, pp.260-268, July. 1990.
- [7] J. H. B. Deane, D. C. Hamill, "Analysis, simulation and experimental study of chaos in the buck converter," in Proc.1990 IEEE PESC, pp.491-498.
- [8] J. H. B. Deane, "Chaos in a current-mode controlled boost DC-DC converter," IEEE Trans Circuits Syst. I, vol. 39, pp.680-683, Aug. 1992.
- [9] W. C. Y. Chan, C. K. Tse, "Study of bifurcation in current-programmed boost dc-dc converters: From quasi-periodicity to period doubling," IEEE Trans Circuits syst. I, vol.44, pp. 1129-1142, Dec. 1997.
- [10] S. Banarjee, K. Chakrabarty, "Nonlinear modeling and bifurcations in the boost converter," IEEE Trans. Power Electron., vol. 13, pp. 252-260, 1998.

- [11] M. Orabi, T. Ninomiya, "Nonlinear dynamics of power factor correction converter," IEEE Trans. Industrial Electronics, vol. 50, pp.1116-1125, 2003.
- [12] E. Ott, C. Grebogi, and J. Yorke, Controlling chaos, Phys. Rev. Lett., vol. 64, pp. 1196-1199, 1990.
- [13] T. Shinbrot, C. Grebogi, E. Ott, and J. Yorke, Using small perturbations to control chaos, Nature, vol. 363, pp. 411-417, 1993.
- [14] G. Chen and X. Dong, From Chaos to Order: Methodologies, Perspectives and Applications. Singapore: World Scientific, 1998.
- [15] F. Chernousko and A. Fradkov (eds.), Proc. 1st International Conference on Control of Oscillations and Chaos, IEEE, 1997. (St. Petersburg, Russia), August 1997.
- [16] T. Kapitaniak, Controlling Chaos. San Diego, CA: Academic Press, 1996.
- [17] F. Romeira, C. Grebogi, E. Ott, and W. Dayawansa, Controlling chaotic dynamical systems, Physica D, vol. 58, pp. 165-192, 1992.
- [18] K. Pyragas, Continuous control of chaos by self-controlling feedback, Phys. Lett., vol. A170, pp. 421-428, 1992.
- [19] J. Socolar, D. Sukow, and D. Gauthier, Stabilizing unstable periodic orbits in fast dynamical systems, Phys. Rev. E, vol. 50, pp. 3245-3248, 1994.
- [20] M. Bleich, D. Hochheiser, J. Moloney, and J. Socolar, Controlling extended systems with spatially filtered, time-delayed feedback, Phys. Rev. E, vol. 55, pp. 2119-2126, 1997.
- [21] M. Bleich and J. Socolar, Stabilization of periodic orbits controlled by time-delay feedback, Phys. Rev. E, vol. 57, pp. 16-21, 1996.
- [22] J. Hale and S. Verduyn-Lunel, Introduction to Functional Differential Equations. New York: Springer-Verlag, 1993.
- [23] M. di Bernardo, An adaptive approach to the control and synchronization of continuous time chaotic systems, Int. J. Bifurcation and Chaos, vol. 6, pp. 557-568, 1996.



Arnab Ghosh, Assistant Professor, Electrical Engineering Department, Gargi Memorial Institute of Technology, Kolkata, WB-700144, B.Tech (Electrical) from JIS College of Engineering, Kalyani, M.Tech (Electrical) Specialization: Power Electronics & Drives from Jalpaiguri Govt. Engineering College, Jalpaiguri.



Pradip Kumar Saha, Professor and Head, Department of Electrical Engineering, Jalpaiguri Government Engineering College, Jalpaiguri, WB-735102. BE (Electrical) from B.E.College, Shibore. M.Tech((Electrical) Specialization: Machine Drives & Power Electronics from IIT- Kharagpur. PhD from University of North Bengal. FIE, MISTE, Certified Energy Auditor.



Goutam Kumar Panda, Professor, Department of Electrical Engineering, Jalpaiguri Government Engineering College, Jalpaiguri, WB-735102. BE (Electrical) from J.G.E. College, Jalpaiguri, M.E.E(Electrical) Specialization: Electrical Machines & Drives from Jadavpur University. PhD from University of North Bengal. FIE, MISTE, Certified Energy Auditor.

Stroke-Database Design for Online Handwriting Recognition in Bangla

K. Roy

West Bengal State University, Barasat, Kolkata, India

Abstract: *Handwriting recognition is a difficult task because of the variability involved in the writing styles of different individuals. This gets more complicated in Asian script for its large character set and presence of modified and compound characters. This paper presents a scheme for the online handwriting recognition of one of the major Indic script, Bangla. Online handwriting recognition refers to the problem of interpretation of handwriting input captured as a stream of pen positions using a digitizer or other pen position sensor. Strokes are extracted from the characters. The sequential and dynamical information obtained from the pen movements on the writing pads are used as features in the proposed scheme. These features computed from the strokes, and fed to the MLP classifier for recognition. The characters are identified from its constituent strokes. The system was tested on 21372 Bangla character data and obtained 92.92% accuracy with top 3 choices.*

I. Introduction

Data entry using pen-based devices is gaining popularity in recent times. This is so because machines are getting smaller in size and keyboards are becoming more difficult to use. Also, data entry for Indian scripts having large alphabet size is difficult using keyboard. Moreover, there is an attempt to mimic the pen and paper metaphor by automatic processing of online characters. Work on online character recognition started gaining momentum about forty years ago. Numerous approaches have been proposed in the literature [1] - [9].

Many techniques are available for on-line recognition of English, Arabic, Japanese and Chinese [1] - [9] characters but there are only a few pieces of work [10] - [15], [19] available towards Indian characters although India is a multi-lingual and multi-script country. Connell et al. [11] presented a preliminary study on online Devnagari character recognition. They considered only the main characters that occur in the core-strip neglecting the ascending and the descending parts of the characters. Connell et al. [13] also proposed a work on Devnagari on-line character recognition. Joshi et al. [14] proposed an elastic matching based scheme for on-line recognition of Tamil character recognition. Although there are some work towards on-line recognition of Devnagari and Tamil scripts but the on-line recognition work towards other Indian languages is very few. In this paper we propose a system for the on-line recognition of Bangla handwritten characters. Recognition of Indian characters is very difficult with compare to English because of its shape variability of the characters.

There are twelve scripts in India and in most of these scripts the number of alphabets (basic and compound characters) is more than 250, which makes keyboard design and subsequent data entry a difficult job. Hence, online recognition of such scripts has a commercial demand. Although a number of studies [16] have been done for offline recognition of a few printed Indian scripts like Devnagari, Bangla, Gurumukhi, Oriya, etc. with commercial level accuracy, but to the best of knowledge no system is commercially available for online recognition of any Indian script. There is a proliferation of on-line recognizers developed as compared to off-line recognizers. There are two main reasons for this disparity. First, on-line recognizers are easier to build [3], because the order of the pen-strokes is known, as well as timing information and also direction information of writing may be extract. Secondly, handwriting recognition can easily be used for input in handheld or PDA-style computers, where there is no room for a keyboard. Since a recognizer in this use is very visible, this visibility spurs on development.

In this work a new algorithm is proposed for online Bangla handwritten character recognition from stroke. A database of strokes is generated based on the database of characters collected for the experiment. After recognition of the strokes a tree based approach is used for construction of valid character from its constituting strokes. This algorithm is robust against stroke number and order-variations.

The organization of the paper is as follows. In Section 2 the property of Bangla script as well as the pre-processing is described. Section 3 deals with detailed property of stokes in Bangla character and their extraction strategy. The feature extraction technique is described in Section 4 and the classifier is in Section 5. Finally in Section 6 the result and their analysis is given.

II. BANGLA SCRIPT & PREPROCESSING

Bangla, the second most popular language in India and the fifth most popular language in the world, is an ancient Indo-Aryans language. About 200 million people in the eastern part of Indian subcontinent speak in this language. Bangla script alphabets are used in texts of Bangla, Assamese and Manipuri languages. Also, Bangla is the national language of Bangladesh.

The alphabet of the modern Bangla script consists of 11 vowels and 40 consonants [16]. These characters are called as basic characters. Writing style in Bangla is from left to right and the concept of upper/lower case is absent in this script. It can be seen that most of the characters of Bangla have a horizontal line (Matra) at the upper part. From a statistical analysis on printed document it was noticed that the probability that a Bangla word will have horizontal line is 0.994 [16].

In Bangla script a vowel following a consonant takes a modified shape. Depending on the vowel, its modified shape is placed at the left, right, both left and right, or bottom of the consonant. These modified shapes are called modified characters. A consonant or a vowel following a consonant sometimes takes a compound orthographic shape, which is called as compound character. Compound characters can be combinations of two consonants as well as a consonant and a vowel. Compounding of three or four characters also exists in Bangla. There are about 280 compound characters in Bangla [16]. In this work the recognition of Bangla basic characters are considered.

To get an idea of Bangla basic characters and their variability in handwriting, a set of handwritten Bangla basic characters are shown in Figure 1. This is the form which is also used for collection of isolated characters.



Fig. 1. Examples of Bangla handwritten characters.

A. Pre-processing

$$P_{i=1}^M \in R^2 \times \{0,1\}$$

The digitizer output is represented in the format of $P_{i=1}^M \in R^2 \times \{0,1\}$, where p_i is the pen position having x-coordinate (x_i) and y-coordinate (y_i) and M is the total number of sample point. For writing Bangla characters, M varies from 14 to 189 for a character. If p_i and p_j are two consecutive pen points, i^{th} point (p_i), is retained with respect to j^{th} point (p_j), if the following condition is satisfied:

$$x^2 + y^2 > m^2 \tag{1}$$

Where $x = x_i - x_j$ and $y = y_i - y_j$. The parameter m is empirically chosen. M is set to 0; in equation (1) to removes all repeated points.

Analyzing a total of 22,000 Bangla character it was found that, for writing Bangla characters, the number of points varies from 14 (ঔ) to 189 (ঐ) points. The average number of points in a Bangla character is 72. It was also noted that the character (ঐ) uses the maximum number of points in average and its value is 115. It is closely followed by ‘উ’ (108), ‘ঋ’ (105), & ‘আ’ (104). The minimum number of points in an average is used by the character ‘ঢ’ (47) and is closely followed by ‘ব’ (49) ‘দ’ (51).

Smoothing: To remove jitter from the handwritten data, every point $(x(t), y(t))$ are replaced in the trajectory by the mean value of its neighbors:

$$x'_i = \frac{x_{i-N} + \dots + x_{i-1} + \alpha x_i + x_{i+1} + \dots + x_{i+N}}{2N + \alpha}$$

$$y'_i = \frac{y_{i-N} + \dots + y_{i-1} + \alpha y_i + y_{i+1} + \dots + y_{i+N}}{2N + \alpha}$$

The parameter ‘ α ’ is based on the angle subtended by the preceding and succeeding curve segment of $(x(t), y(t))$ and is empirically optimized. This help to avoid smoothing of sharp edges. Here the value for N is taken as 2.

III. STROKE DATA BASE GENERATION

Analyzing of Bangla characters it was found that Bangla characters are formed by combination of one or more basic strokes. The recognition of Bangla script is more difficult compare to roman script due to its large size of character set and compound characters. It gets tougher due to presence of multiple strokes while writing Bangla character. By stroke I mean collection of pen points that are collected between one pen down and pen up (with lifting in between).

The problem of online Bangla handwriting recognition gets more complex due to stroke order variation and variation in number of strokes used to write a character. For example let us consider the character ‘আ’. Again it may be seen that 2-6 of the 7 strokes are used for writing the same (as found from statistical analysis of the database). For example see figure 2. So with possible 6 strokes (out of 7) and their order variation makes the recognition process more complicated. Some ways of writing the character ‘আ’ is shown in figure 3.

The problem is more complex due to stroke order variation. If only 4 strokes are considered to write the character ‘আ’, they may be again in different order. For example see figure 4.

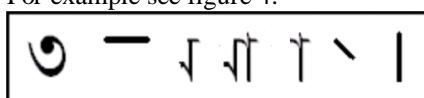


Fig.2. Examples of strokes use to write আ

$\langle ৩, ৭ \rangle = আ$	Total no of stroke = 2
$\langle ৩, ৭, ৭ \rangle = আ$	Total no of stroke = 3
$\langle ৩, ৭, \cdot, \rangle = আ$	Total no of stroke = 4
$\langle ৩, ৭, \bar{\quad} \rangle = আ$	Total no of stroke = 3
$\langle ৩, ৭, ৭, \bar{\quad} \rangle = আ$	Total no of stroke = 4
$\langle ৩, ৭, \cdot, , \bar{\quad} \rangle = আ$	Total no of stroke = 5
$\langle ৩, \cdot, , \cdot, , \bar{\quad} \rangle = আ$	Total no of stroke = 6

Fig 3: Some of the ways of writing ‘আ’ using some of the possible strokes in some combinations.

৩	ত	অ	আ
৩	অ	অ	আ
৩	অ	আ	আ

Fig. 4: Example of part of the different stroke-order for a character having four strokes.

A Bangla character may be written with single stroke like ‘৩’ and minimum of two strokes for the character having two disjoint parts like ‘৳’. From statistical analysis on the dataset it is found that the minimum number of stroke used to write a Bangla character is 1 and maximum number is 6. It is also seen that ‘ঐ’, ‘ঔ’ & ‘ঝ’ have almost written by single stroke where as ‘ঊ’ has an average of 4 strokes followed by ‘আ’ and rest all characters has average stroke number less than 3. It also found that almost always ‘ঐ’, ‘ঔ’, ‘ত’, ‘ন’, ‘৳’, ‘ঐ’ and ‘ঊ’ are written by 2 strokes. The average number of stroke per character is 2.2. In the database there are 61 basic characters in Bangla character set, so the total number of stroke in the Bangla Script should have been 135 (app). But from statistical analysis on the present stroke data base it is found that only 59 strokes are enough to represent all basic Bangla Characters. All these basic strokes are shown in figure 5. This is because some of the strokes are common to various characters. For example see table 1. For example the stroke ‘𑄣’ is common in the characters ‘ঋ’, ‘ক’, ‘ঋ’, ‘ধ’, ‘ব’, ‘৳’. From statistical analysis it is found that 40 out of the 61 characters generally bear Matra (𑄣). This stroke comprises 24.03% of the stroke database. The second most used stroke is ০ and is used by 8 basic characters and it comprises 8.45% of the stroke database. The top 10 frequent strokes with their percentage of occurrence in the database and the characters in which they occur are detailed in table 1. It is found from the analysis that top 10 frequent strokes comprises 59.76% of the stroke data base and least 20 frequent strokes comprises only 10.24% of the total stroke database. So the character having some of its constituent strokes are common (inter character similarity) are look similar (sometime even the strokes only vary in relative position only) and some time the same character is written with different strokes (intra character variability) makes the recognition process more complicated.

—	৩	৭	৭	৩	৭
৭	৩	৭	৭	৩	৭
৩	৭	৭	৩	৭	৩
৭	৩	৭	৩	৭	৩
৩	৭	৭	৩	৭	৩
৭	৩	৭	৩	৭	৩
৩	৭	৭	৩	৭	৩
৭	৩	৭	৩	৭	৩
৩	৭	৭	৩	৭	৩
৭	৩	৭	৩	৭	৩

Fig. 5: Basic Stroke of Bangla Script.

Table 1: Most frequent strokes (with percentage) and the characters in which they occur.

Stroke	Occurrence in Database	No of Character having this stroke (Characters)
—	24.01%	40
০	08.45%	8 (‘৳’, ‘ড’, ‘ঢ’, ‘ঝ’, ‘০’, ‘ঐ’, ‘ঔ’, ‘ঝ’)
১	05.64%	8 (‘ই’, ‘ঐ’, ‘উ’, ‘ঊ’, ‘ঐ’, ‘ঔ’, ‘ট’, ‘ঠ’)
৬	04.99%	6 (‘ঊ’, ‘ঊ’, ‘জ’, ‘ড’, ‘ড’, ‘ড’)
৭	03.09%	6 (‘ঋ’, ‘ক’, ‘ঋ’, ‘ধ’, ‘ব’, ‘৳’)

৩	02.79%	4 ('অ', 'আ', 'ত', 'ও')
এ	02.72%	3 ('এ', 'ঐ', 'ঋ')
া	02.71%	5 ('অ', 'আ', 'ঈ', 'ঐ', 'স')
ঋ	02.67%	4 ('ঋ', 'ঌ', 'ফ', 'ষ')
২	02.56%	3 ('ই', 'হ', '২')

A data collection form was prepared for isolated character collection but stroke can't be collected similarly. This is because normal human are not acquainted with writing strokes individually and secondly if strokes are written individually then the stroke variation (shape, size and number) may not reflect properly. So here the strokes are extracted from their parent characters. To extract the strokes properly from characters for training of the proposed system, the strokes are classified in the following categories:

Major Stroke: A stroke is called Major stroke if it occupies major part of the character. For the character 'অ' the major stroke is '৩'.

Minor Stroke: A stroke is called Minor stroke if it occupies minor part of the character. For the character 'অ' the minor stroke is 'া'.

Upper Stroke: A stroke is called Upper stroke if it occurs at the upper part of the character. For the character 'ই' the upper stroke is 'ই'.

Lower Stroke: A stroke is called Lower stroke if it occurs at the lower part of the character. For the character '০' the lower stroke is '০'.

Left Stroke: A stroke is called Left stroke if it occurs at the left part of the character. For the character 'ধ' the left stroke is 'ধ'.

Right Stroke: A stroke is called Right stroke if it occurs at the right part of the character. For the character 'অ' the right stroke is '৩'.

Matra: A stroke is called Matra if it is a horizontal straight line occurred at the upper part of the character. For the character 'অ' the major stroke is 'া'.

Depending on the positional information all stroke of a character are classified into above classes. This classification has two important roles in this recognition. As this is a stroke based approach, so training is done on all individual stroke. But this stroke are not collected separately rather they extracted, identified and classified from the character data. Second important role played by the stroke in time of matching of identified stroke in to characters. This time to overcome the problem of different sequence of stroke order even in case of same character, Major stroke and Matra are find out and they are placed at first and last position respectively in stroke sequence. This minimizes the permutation in tree structure and it gives a greater freedom to consider different confidence value of non major character.

IV. FEATURE EXTRACTION

Any online feature is very much sensitive to writing stroke sequence and size variation. A total of 105 features (90+15) are used for recognition. The features used are (i) Structural features (15) and (ii) Point based feature (90).

4.1 Structural features

Gradient (t_{N+1}):

$$t_{N+1} = n \begin{matrix} \text{৩} & \text{ধ} & \text{ধ} & \text{ধ} & \text{ধ} \\ \text{৩} & \text{ধ} & \text{ধ} & \text{ধ} & \text{ধ} \end{matrix} x_i y_i \quad x^2 - \begin{matrix} \text{৩} & \text{ধ} \\ \text{৩} & \text{ধ} \end{matrix} x \quad \begin{matrix} \text{৩} \\ \text{ধ} \end{matrix}$$

$$t_{N+2} = \begin{matrix} \text{৩} & \text{ধ} & \text{ধ} & \text{ধ} & \text{ধ} \\ \text{৩} & \text{ধ} & \text{ধ} & \text{ধ} & \text{ধ} \end{matrix} y_i \quad x^2 \quad \begin{matrix} \text{৩} & \text{ধ} & \text{ধ} & \text{ধ} & \text{ধ} \\ \text{৩} & \text{ধ} & \text{ধ} & \text{ধ} & \text{ধ} \end{matrix} x_i y_i \quad x_i^2 - \begin{matrix} \text{৩} & \text{ধ} \\ \text{৩} & \text{ধ} \end{matrix} x_i \quad \begin{matrix} \text{৩} \\ \text{ধ} \end{matrix}$$

Here t_{N+1} and t_{N+2} are the gradient and the intercept in the y-axis of the straight line, constituting by the consecutive 3-points respectively.

Length by Width ratio (t_{N+3}): $t_{N+3} = (\max(x_i) - \min(x_i)) / (\max(y_i) - \min(y_i)) \quad \forall \quad i = 0, 1, \dots, N$ By using this feature the ratio of the length and width of the corresponding stroke is calculated.

Standard Deviation (t_{N+4}): The standard deviation measures the spread of the data about the mean value. It is useful in comparing sets of data which may have the same mean but a different range. Here the deviation of each co-ordinate is calculated with respect to its mean value.

Normalized Start Co-ordinates and End Co-ordinates (t_{N+4}): In this feature only the first and last co-ordinates in the strokes of a character considered. Taking the first and last co-ordinates normalized them and stored them as feature.

Crossing of the lines: Here the co-ordinate position of the crossing of the stroke is stored with itself as shown in figure 6. In this system only first two crossing are considered.

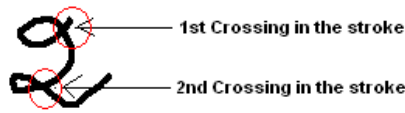


Fig. 6: Crossing points of a stroke.

4.2 Point based feature

The strokes are first normalized in to 30 points. The normalization is done in two stages. First the points are re-sampled to fixed number points and then they are converted from equal time sample to equal distant points. For example see Figure 7. The processed character is transformed into a sequence $t = [t_1, \dots, t_N]$ of feature vectors $t_i = (t_{i1}, t_{i2}, t_{i3})^T$ [4]. The following features were calculated:

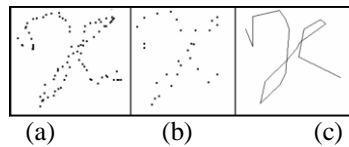


Fig. 7. Feature extraction from a sample stroke is shown. (a) Original stroke, (b) its normalized 30 points used as feature, (c) the normalized stroke.

Normalized horizontal (t_{i1}) and vertical (t_{i2}) co-ordinates: $t_{i1} = \frac{(x_i - \mu_x)}{\sigma_x}$ and $t_{i2} = \frac{(y_i - \mu_y)}{\sigma_y}$ are the pen co-ordinates normalized by the sample mean $\mu = \frac{1}{N} \sum_{i=1}^N P$ and standard deviation, $\sigma = \sqrt{\frac{1}{N} \sum_{i=1}^N P^2}$ of the character's sample points.

Tangent slope angle (t_{i3}): $t_{i3} = \arg((x_{i+1} - x_{i-1}) + j*(y_{i+1} - y_{i-1}))$, with $j^2 = -1$ and "arg" the phase of the complex number above, is an approximation of the tangent slope angle at point i .

Thus finally, a feature vector sequence is defined as $t = [t_1 \dots t_N t_{N+1} \dots t_{N+15}]$, each vector of it as $t_i = (t_{i1}, t_{i2}, t_{i3})^T$ is obtained. Here the number of points in which the character is normalized is (N) 30. So a total of 105 (30 X 3 [3 for each point] + 15 [15 local features based on Stroke]) features are used.

V. RECOGNITION

In this work, the recognition module has been divided into two parts: (i) Recognition of input strokes and (ii) Construction of valid character from recognized strokes.

5.1 Recognition of input strokes:

Based on the above-normalized features, a Multilayer Perceptron Neural Network based scheme was used for recognition of the strokes [18]. The Multi Layer Perceptron Network (MLP) is, in general, a layered feed-forward network, pictorially represented with a directed acyclic graph. Each node in the graph stands for an artificial neuron of the MLP, and the labels in each directed arc denote the strength of synaptic connection between two neurons and the direction of the signal flow in the MLP. For pattern classification, the number of neurons in the input layer of an MLP is determined by the number of features selected for representing the relevant patterns in the feature space and output layer by the number of classes in which the input data belongs. The neurons in hidden and output layers compute the sigmoidal function on the sum of the products of input values and weight values of the corresponding connections to each neuron.

Training process of an MLP involves tuning the strengths of its synaptic connections so that it can respond appropriately to every input taken from the training set. The number of hidden layers and the number of neurons in a hidden layer required to design an MLP are also determined during its training. Training process incorporates learning ability in an MLP. Generalization ability of an MLP is tested by checking its responses to input patterns which do not belong to the training set.

Back propagation algorithm, which uses patterns of known classes to constitute the training set, represents a supervised learning method. After supplying each training pattern to the MLP, it computes the sum of the squared errors at the output layer and adjusts the weight values of the synaptic connections to minimize the error sum. Weight values are adjusted by propagating the error sum from the output layer to the input layer.

The present work selects a 2-layer perceptron for the handwritten numeral recognition. The number of neurons in input and output layers of the perceptron is set to 105 and 59; respectively since the number features is 105 and the number of possible classes in hand written stroke considered for the present case is 59. The number of hidden units was set to 90, back propagation learning rate and acceleration factor is set to suitable values, based on trial runs. A network of 105-90-59 is thus finally designed.

5.2 Construction of valid character from recognized strokes:

Each character will be constructed with the help of its recognized strokes. To do so, all the probable sequences of strokes are stored in a tree structure that makes a valid character into a database. To build this a database report is generated from the raw data (characters), from which the sequences of strokes of the characters are gotten, that are generally used by people.

5.3 Construction of the Rule base:

The database has been designed using a tree structure to store the possible sequences of strokes of the characters. To store the sequences a stroke is considered as a root.

Figure 8 represent the stroke sequences of ‘ছ’. According to above tree structure, there exist two probable sequences of ‘ছ’. The first sequence is {b, -, 7} and second is {b, 7, -}.

The classifier returns a set of the recognized strokes with their corresponding confidence values. Here it is plain s to consider only the top three choices; number of choices can be extended in future as the system requirement. With these recognized strokes it will be tried to match those sequences with the stored sequence of strokes in the database. When a match will be found then the character recognized as a valid character and all the other combinations will be discarded.

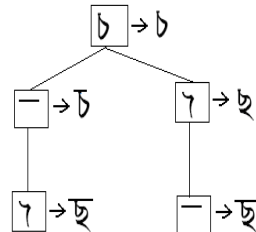


Fig. 8: Sample tree structure.

VI. RESULTS AND DISCUSSION

The experimental evaluation of the above techniques was carried out using isolated Bangla strokes. The data was collected from people of different background. A total of 21372 characters are collected for the experiment. Out of them strokes were extracted and total size of the stroke database used for the training was 30,000. One fourth of the strokes were used for the training of the classifier for the present work and rest will be used for the testing purpose.

6.1 Recognition result on isolated Stroke

The recognition rate of the isolated strokes was found to be 96.85% on the test set.

6.2 Recognition results on Bangla Character.

From the experiment it was found that the overall accuracy of the proposed scheme was 88.23% without rejection. The accuracy improved to 92.9%, if we consider first three top choices of the recognition results. The detail recognition results are given in Table 2.

Maximum error occurred between ‘ম’ and ‘স’ and it is noted that about 1.067% cases they miss-recognized one as the other. Here the difference between the above two characters is that there is a small loop in left bottom side of one of the character. Some times during handwriting people do not give this loop and hence miss-recognition occurs. The next erroneous character is ‘ষ’. It is misclassified with ‘খ’ and some time with ‘ম’, because difference between ‘ষ’ with ‘খ’ and ‘ম’ is that ‘খ’ have a small loop at upper left and ম have the loop at lower left other wise they are similar. Sometime writer do not give this small loop and neglect all other very small difference. ‘ষ’ is miss-recognized as ‘খ’ in 5 cases and miss-recognized as ‘ম’ in 8 cases. For details see Table 3.

Table 2: Top three recognition accuracy are shown.

Choices from top	Recognition rate
1	88.23%
2	91.57%
3	92.93%

Table 3: Maximum confusion pair arte shown.

Character	Miss-Recognized	
ষ	খ(8%)	ম(13%)
ম	ষ(1%)	স(1%)
ঢ	ঢ(1%)	
ন	ন(11%)	

This work describes a novel system of Online Bangla Handwriting Recognition. This work is on a preliminary stage and it is hoped that the result will improve when more and combinations of stroke will be added to the rule base. After completion of the first stage of isolated character recognition the system will be modified for unconstrained Bangla online text recognition. I think this work will be helpful for research in Bangla online handwriting recognition. However it not only help the development of Bangla script but also other Indic script which have a lot of similarity with Bangla script with adequate modification.

REFERENCES

- [1] I. Guyon, M. Schenkel, and J. Denker, "Overview and Synthesis of On-Line Cursive Handwriting Recognition Techniques", Handbook of Character Recognition and Document Image Analysis, 183 (1997).
- [2] E. J. Bellagarda, J. R. Bellagarda, D. Nahamoo and N. S. Nathan, "A probabilistic Framework for Online Handwriting Recognition," 3rd IWFHR, 234 (1993).
- [3] R. Plamondon and S. N. Srihari, "On-Line and Off-Line Handwriting Recognition: A Comprehensive Survey". IEEE PAMI, **22**, 84 (2000).
- [4] C. Bahlmann and H. Burkhardt, "The Writer Independent Online Handwriting Recognition System frog on hand and Cluster Generative Statistical Dynamic Time Warping", IEEE PAMI, **26**, 1 (2004).
- [5] C. C. Tappert, C. Y. Suen, and T. Wakahara. "The State of the Art in On-Line Handwriting Recognition," IEEE PAMI, **12**, 179 (1990).
- [6] S. Jaeger, C. L. Liu and M. Nakagawa: "The state of the art in Japanese online handwriting recognition compared to techniques in western handwriting recognition", IJDAR, **6**, 75 (2003).
- [7] C. L. Liu, S. Jaeger and M. Nakagawa: "On-Line Recognition of Chinese Characters: the State of the Art", IEEE PAMI, **26**, 198 (2004).
- [8] S. Jaeger, S. Manke, J. Reichert, A. Waibel, "Online handwriting recognition the Npen⁺⁺ recognizer", IJDAR, **8**, 169 (2001).
- [9] Zhen-Long BAI and Qiang HUO, "A Study On the Use of 8-Directional Features For Online Handwritten Chinese Character Recognition", ICDAR, (2005).
- [10] V. Bansal and R. M. K. Sinha, "On how to describe Shapes of Devanagari Characters and Use them for Recognition." ICDAR (1999).
- [11] S.D. Connell and A. K. Jain, "Template-based Online Character Recognition", PR, **34**, 1 (2001).
- [12] U. Garain, B. B. Chaudhuri, and T. Pal, "Online Handwritten Indian Script Recognition: A Human Motor Function based Framework", ICPR (2002).
- [13] S. D. Connell, R. M. K. Sinha, and A. K. Jain, "Recognition of Unconstrained Online Devnagari Characters", ICPR (2000).
- [14] N. Joshi, G. Sita, A. G. Ramakrishnan, V. Deepu, Sriganesh Madhvanath: "Machine Recognition of Online Handwritten Devanagari Characters", ICDAR (2005).
- [15] K. Roy, N. Sharma, T. Pal and U. Pal, "Online Bangla Handwriting Recognition System", ICAPR (2007).
- [16] B.B. Chaudhuri and U. Pal, "A Complete Printed Bangla System," PR, **31**, 531 (1998).
- [17] U. Pal and B. B. Chaudhuri, "Indian script character recognition: a survey", PR, **9**, 1887 (2004).
- [18] K. Roy, C. Chaudhuri, M. Kundu, M. Nasipuri and D. K. Basu, "Comparison of the Multilayer perceptron and the nearest neighbor classifier for handwritten digit recognition", JISE, **21**, 1245 (2005).
- [19] U. Bhattacharya, B. K. Gupta and S. K. Parui, "Direction Code Based Features for Recognition of Online Handwritten Characters of Bangla", ICDAR (2007).

The Outbound Voice Traffic Reduction Scheme in the Push-To-Talk Environment

Jong Min Lee^{*}, Seong-Woo Kim^{*}, Yang Xiao^{**}

^{*}Department of Computer Software Engineering, Dong-Eui University, Busan, Republic of Korea

^{**} Department of Computer Science, The University of Alabama, Tuscaloosa, AL, U.S.A.

ABSTRACT: The push-to-talk technology provides a walkie-talkie like service for group communication. In this paper, we propose an efficient outbound voice traffic reduction scheme in the push-to-talk environment when network congestion happens. The Open Mobile Alliance push-to-talk over cellular (OMA PoC) architecture, the standard for this kind of group communication, is used as a base network in this paper. The PoC server plays an important role in copying and forwarding of received RTP media packets and the outbound voice traffic of this PoC Server tends to be affected by other traffic when network congestion happens. We extend the functionality of the Controlling PoC Server to accommodate the location information of PoC Clients by co-operating the location management server, which also communicates with the location reporting and packet forwarding agent node. By minimizing the outbound voice traffic of the PoC server, we improve the overall performance in terms of the end-to-end quality which is derived from the E-model. Simulation results show that the proposed scheme outperforms the existing PoC scheme when network congestion happens.

Keywords: Push-to-talk, group communication, OMA PoC architecture, voice traffic, network congestion

I. INTRODUCTION

Recently many Internet applications have been used widely in our lives for the proliferation of smart phones. Especially the concept of the VoIP has been used in many applications such as Skype, Viber, Voxer, TiKL *etc.*, which have potentials to replace the traditional voice communication through the public switched telephone network. There are many terms such as mVoIP, VoWLAN, and VoLTE that show the proliferation of this kind of packetized voice communication. Among applications which support VoIP, there are several VoIP applications such as Voxer, and TiKL which support the group communication as well as one-to-one communication, which is also known as the push-to-talk (PTT or P2T) [1, 2, 3]. This push-to-talk technology supports the half duplex communication among end-to-end users like the trunked radio system (TRS). Nextel communications was the first company to provide the push-to-talk service commercially using iDEN.

The Open Mobile Alliance (OMA) has standardized the technology for the push-to-talk over cellular (PoC) to support group communication among mobile subscribers through wireless networks since 2005. The OMA PoC architecture defines functional entities for the network configuration with the SIP/IP core including several SIP proxies and SIP registrars to support the push-to-talk service [1]. The control plane protocol is used as a signaling protocol which extends some of SIP procedures

for the group communication [4] and the user plane protocol is used to support media packet transmission and control the talk right [5].

The well-known problem in VoIP applications including PTT or OMA PoC is that the VoIP capacity is limited in wireless networks due to the small periodic voice data. Several researches on the VoIP system capacity in the IEEE 802.11 wireless LAN (WLAN) have shown that it has a very small threshold compared to the link bandwidth due to its medium access control (MAC) protocol [6, 7]. In addition, we observed that the outbound traffic of a PTT/PoC server, which receives a talker's voice data as an inbound traffic and transmits its copy to other group members, is seriously influenced by the other network traffic when network congestion happens. We will show the performance degradation of media packet flows through the simulation study.

In this paper, we propose an efficient scheme which reduces the outbound traffic of a PoC server, by which it decreases the packet delay and the packet loss caused by the network congestion. An efficient mechanism is provided in this paper to detect PoC Clients' registration and exchange control messages to manage the location information of PoC Clients. Also the PoC Server functionality is extended to use this location information of PoC Clients to reduce the outbound voice traffic. Simulation results show the performance improvement by the reduction of the outbound traffic. The simulation was performed using *ns-3* [8]. The mean opinion score is used as the main performance metric to measure the end-to-end quality, which can be derived from the E-model.

In Section 2, we describe the OMA PoC standard related to this paper. In Section 3 and Section 4, we present the proposed scheme to reduce the outbound voice traffic in the OMA PoC environment and show the performance improvement through the simulation study, respectively. Finally, we give a conclusion in Section 5.

II. OMA PoC

In this section, we describe the OMA PoC standard related to the proposed scheme. The OMA PoC standard is mainly divided into the control plane protocol [4] which is a signaling protocol similar the SIP [9] and the user plane protocol [5] which carries user's voice traffic based on RTP [10].

2.1 SESSION ESTABLISHMENT

Now we describe some of the control plane protocol related to the proposed scheme. Fig.1 shows the brief OMA PoC architecture which includes functional entities only related to the proposed scheme. The service logic for SIP sessions are implemented in the application server using SIP/UDP/IP. The application server functionality is implemented by the PoC server when the SIP/IP Core for

the PoC service is according to 3GPP/3GPP2 IP Multimedia Subsystem (IMS) [4]. Thus the SIP/IP Core and PoC Server functionalities may be in one physical entity. Media packets carrying users' voice data and the talk/media burst control for managing the talk right are transferred between PoC Clients and a PoC Server using RTP/UDP/IP [5].

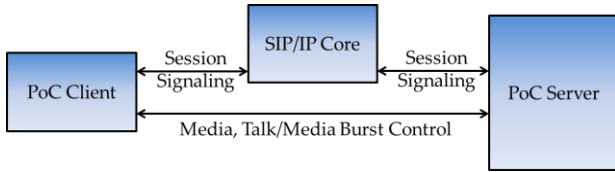


Figure 1. A brief OMA PoC architecture

The PoC Server performs either the Controlling PoC Function or the Participating PoC Function. In this paper, we call the PoC Server with the Controlling PoC Function and the Participating PoC Function as the Controlling PoC Server and the Participating PoC Server in short. The Controlling PoC Server mainly performs the management of PoC sessions such as the session establishment and the media burst control [4]. The Participating PoC Server performs relays the Talk Burst and Media Burst Control messages between the PoC Client and the Controlling PoC Server and may relay RTP media packets from the Controlling PoC Server.

Each PoC Client should register to their Participating PoC Server prior to participating in the PoC session according to rules and procedures of RFC 3261 [9] with extended headers including PoC feature tags [4]. Fig.2 shows the registration procedure of the PoC Client. In the SIP REGISTER request of the PoC Client, information such as the SIP URI and IP address of the PoC Client can be found. This information is used in the proposed scheme to keep the location information of PoC Clients.

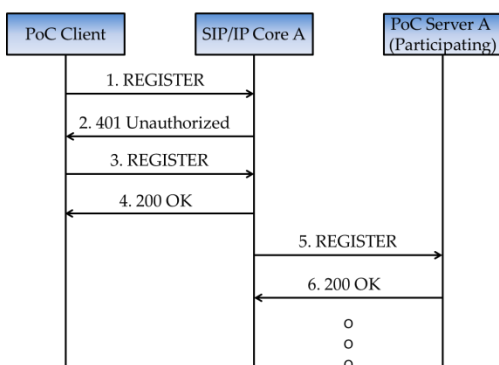


Figure 2. Registration procedure

PoC Session establishment is also made according to rules and procedures of RFC 3261 with extended headers including PoC feature tags as shown in Fig. 3 [4]. For simplicity, messages from/to the SIP Core are excluded from Fig.3 and only messages from/to OMA PoC entities are shown in the figure. Dotted arrows represent MBCP (media burst control protocol) messages,

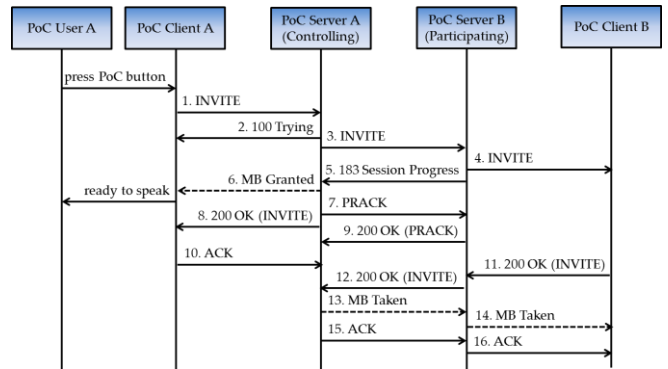


Figure 3. Ad hoc PoC Session establishment on-demand Session

which manages the talk right of PoC Clients [5]. There are four kinds of PoC Sessions: 1-1, ad-hoc, pre-arranged, and chat [4, 11]. In this paper, we are interested in the ad-hoc PoC Session and the pre-arranged PoC Session. In the ad-hoc PoC Session, the group information can be found from the recipient list in the SIP INVITE request. In the pre-arranged PoC Session, the group information is maintained by the Controlling PoC Server. Thus, we can find the group information when the SIP INVITE request is arrived at the PoC Server. A PoC Session can also be classified into the on-demand session and the pre-established session according to the time of the session establishment. The on-demand session is started when a user initiates the PoC Session with his/her recipient list [4]. The pre-established PoC Session is another method for the session establishment, which first makes a parameter negotiation to establish a PoC Session and RTP packet transmission is performed if required [4].

The determination of the PoC Server role of either Controlling PoC Function or Participating PoC Function takes place during the PoC Session setup and lasts for the duration of the whole PoC Session. In ad hoc PoC group sessions, the controlling PoC server is the PoC server of the inviting user. In pre-arranged PoC sessions, the controlling PoC server is the PoC server hosting the pre-arranged PoC group. That is, the Controlling PoC server is the PoC server of the domain that owns the URI that identifies the pre-arranged PoC group.

2.2 MEDIA TRANSFER

After either the ad hoc or the pre-arranged PoC Session is established, media packets including voice data are transferred between the PoC Server and PoC Clients. These media packets are transported by RTP/UDP/IP [5]. The PoC Server forwards received RTP Media packets towards all other PoC Clients that are not on hold [5], that is, the received packet is copied and forwarded to other PoC Clients in a group. The basic RTP header of media packets is described in RFC 3550 [10] and additional RTP payload formats for various audio/video codecs such as G.729A, GSM, EVRC and AMR are described in several RFC documents [12, 13, 14]. From the SSRC field of the RTP header, the PoC Server and PoC Clients can find who sends the RTP packet.

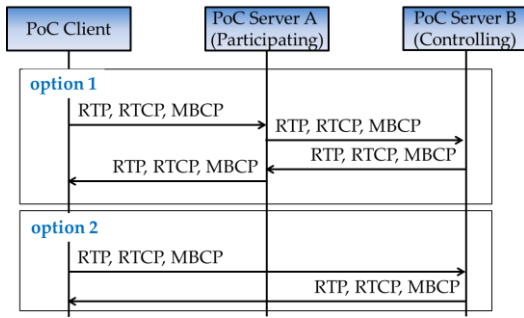


Figure 4. Media transfer options

Fig.4 shows two options that transfer voice data between PoC clients. In Option 1, the Participating PoC Server is in charge of transferring voice packets and also provides the filtering function and the transcoding function among different codecs. However the performance may be degraded due to the increased packet delay compared to Option 2 in which voice packets and other related packets are transmitted directly through the Controlling PoC Server. In this paper, we only consider Option 2 to support group communication. The incoming traffic and the outgoing traffic of a PoC Server are unbalanced because of its one-to-many communication pattern. Thus problems such as the traffic handling at a PoC Server and packet transmission to recipient PoC Clients occur especially when network congestion happens.

III. VOICE TRAFFIC REDUCTION SCHEME

In this section, we describe the basic concept and the algorithms used for the proposed scheme.

3.1 BASIC CONCEPT

Fig.5 shows the basic concept of the proposed scheme. We consider the situation of network congestion like Fig.5(a) which can make the transmission problem. For group communication, the Controlling PoC Server copies received RTP media packets from a PoC Client which has the media burst right and forwards those copies to all other PoC Clients in a group. Those RTP media packets are forwarded through the Internet with other packets generated by network applications such as FTP, email, web, etc. The nature of the Internet is basically the best-effort network due to the characteristics of the layer 3 protocol, IP. Thus this small amount of periodic RTP media packets can be easily damaged by other packets travelling the Internet, which will be shown in Section 4 through the simulation study. Dotted arrows in Fig.5 (a) indicate the possible packet loss while forwarding RTP media packets from the Controlling PoC Server to other PoC Clients.

The concept of the proposed scheme is shown in Fig.5 (b). Two functional entities have an important role in implementing the proposed scheme. The first one is the Controlling PoC Server, which exists in the OMA PoC standard. Its functionality will be extended by including a function to manage the location information of PoC Clients with the collaboration of a location management server which is newly introduced for the proposed voice traffic reduction scheme. The other one is the location reporting and packet forwarding (LRPF) agent

functionality, which supports to find OMA PoC Clients in the same network and manages received RTP media packets. The LRPF agent functionality can be easily implemented in routers, gateways or wireless access points in order to reduce the outbound voice traffic from the Controlling PoC Server. For example, a gateway and an access point are used in Fig.5 (b). Both the gateway and the access point are assumed that they are located in one-hop distance far from PoC Clients so that it is possible to forwarding media packets efficiently, which still has the voice capacity problem if it is a wireless network [6, 7].By reducing the outbound voice traffic from the Controlling PoC Server as small as possible, the interference from other traffic sources can be avoided significantly.

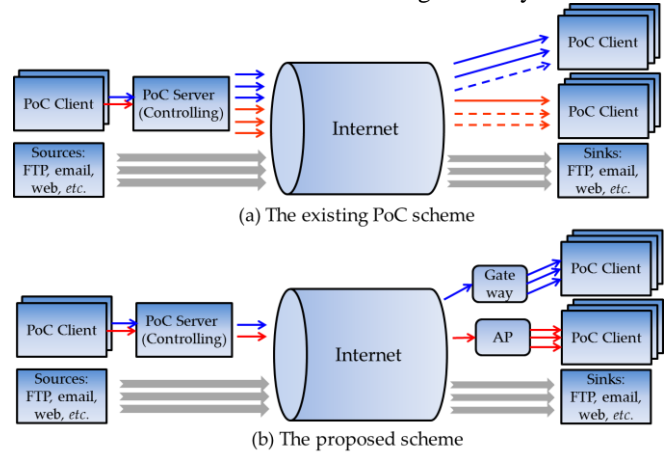


Figure 5. The basic concept of the proposed scheme

3.2 ALGORITHMS

First we define the notation used for the operations used in the proposed scheme.

- G : the set of groups, $G = \{G_i \mid 0 \leq i < k\}$
- G_i : the set of group members in the i -th group, $G_i = \{m_j^i \mid 0 \leq j < n\}$ for $n \geq 0$
- m_j^i : the j -th member of the i -th group
- V : the set of LRPF agent nodes, $V = \{v_i \mid 0 \leq i < l\}$
- $M_{v_i}^{G_x}$: the set of active group members of LRPF agent node v_i for the given group G_x
- C_{v_i} : the set of PoC Clients which are located with LRPF agent node v_i
- F_{sid} : the forwarding set of the current session, sid , for received RTP media packets
- M_{sid} : the set of active group member sets for v_i 's of the current session sid

Now we explain the operations for the LRPF agent functionality in Fig.6, which can be divided into three operations for PoC Client management, session establishment and RTP packet management. These operations are related to those operations in the location management server, which maintains the location information of PoC Clients and the group information. In

Operation I, the LRPF agent collects the information of PoC Clients in the same network by packet sniffing SIP REGISTER requests to Participating PoC Servers and then sends the information to the location management server. Operation II will be performed while the PoC Session is established. The Controlling PoC Server will send the information of a forwarding set for the new PoC session, which will be used for RTP packet forwarding in Operation III. We call the node which performs the LRPF agent functionality the LRPF agent node.

Operation I. PoC Client Management

1. do {
2. get a packet copy from every upward packets;
3. if the packet type is the SIP REGISTER request with the PoC feature tag {
4. send the tuple (v_i, m_k^j) to the location management server;
5. }
6. } while (true);

Operation II. Session Establishment

1. do {
2. wait the tuple message $(sid, M_{v_i}^{G_x})$ from the Controlling PoC Server;
3. make a forwarding set
 $F_{sid} = \{m_k^x \mid m_k^x \in M_{v_i}^{G_x}\};$
4. } while (true);

Operation III. RTP Packet Management

1. do {
2. wait a RTP packet;
3. get the session information, sid , from the RTP packet;
4. for every PoC Client $m_k^x \in F_{sid}$ {
5. make a copy of the received RTP packet;
6. send the copy to the PoC Clients m_k^x ;
7. }
8. } while (true);

Figure 6. Operations for the LRPF agent functionality

Operation I. LRPF Agent Node Management

1. do {
2. wait a tuple message (v_i, m_k^j) from any LRPF agent node;
3. add the PoC Client m_k^j to the PoC Client set of v_i , i.e., $C_{v_i} \leftarrow C_{v_i} \cup \{m_k^j\}$
4. } while (true);

Operation II. Session Establishment

1. do {
2. wait an INFO request from the Controlling PoC Server;
3. get the set of group members $G_x = \{m_k^x\}$ from the request;
4. prepare a forwarding set $F_{sid} = \{v_i \mid m_k^x \in C_{v_i}\}$ for every $m_k^x \in G_x$;
5. prepare the set of active group member sets for v_i 's of the current session
 $M_{sid} = \{(v_i, M_{v_i}^{G_x})\}$, where

$$M_{v_i}^{G_x} = \{m_k^x \mid m_k^x \in G_x \bigwedge m_k^x \in C_{v_i}\}$$

for every $v_i \in F_{sid}$;

6. send an INFO response with the tuple (G_x, F_{sid}, M_{sid}) to the Controlling PoC Server;
7. } while (true);

Figure 7. Operations for the location management server

Fig.7 shows the operations for the location management server (LMS), of which the functionality is introduced to manage the relationship between LRPF agent nodes and PoC Clients. In Operation I, LMS maintains the information of PoC Clients for each LRPF agent node while it receives a message from a certain LRPF agent node. In Operation II, LMS computes the forwarding set, F_{sid} , and the set of active group member sets, M_{sid} , for LRPF agent nodes for a given set of group members G_x whenever it receives an INFO request from the Controlling PoC Server. This information will be sent to the Controlling PoC Server and then sent to LRPF agent nodes from the Controlling PoC Server for RTP packet forwarding. This LMS functionality should be introduced since we cannot determine which PoC Server performs the Controlling PoC Function until the session establishment by the SIP INVITE request is started. One of PoC Servers in the system may perform this LMS functionality. Two messages of type INFO request and INFO response are introduced in the proposed scheme to exchange the required information between the Controlling PoC Server and LMS.

Operations for the Controlling PoC Server are described in Fig.8. Operation I is for the session establishment. We assume that the on-demand signaling is used for the session establishment, which enables the session initiation by looking up the SIP INVITE request. Whenever the Controlling PoC Server receives an SIP INVITE request, it retrieves the forwarding set, F_{sid} , and the set of active group member sets, M_{sid} , for LRPF agent nodes from LMS, which will be done by exchanging the INFO request and the INFO response. The information in the INFO response will be sent to all the necessary LRPF agent nodes for RTP packet transmission. Operation II is involved in the RTP packet management. When the Controlling PoC Server receives a RTP packet from a PoC Client, it forwards its copies to LRPF agent nodes in the forwarding set, F_{sid} , not to all PoC Clients. This makes the main difference between the existing PoC scheme and the proposed scheme. The outbound voice traffic is reduced to the amount of difference between the number of LRPF agent nodes and the number of PoC Clients. In general, the number of PoC Clients may be larger than the number of LRPF agent nodes because LRPF agent nodes are either gateways or access points and PoC Clients belong to one of them. Thus we can find easily that the outbound voice traffic will be reduced significantly if most PoC Clients are under the management of a few LRPF agent nodes.

Operation I. Session Establishment

1. do {
2. wait an SIP INVITE request with the PoC feature tag;
3. get the set of group members $G_x = \{m_k^x\}$ in the SIP INVITE request;

4. set the session id, sid , for the SIP INVITE request;
5. send an INFO request to the LMS with the group information G_x ;
6. receive an INFO response to get a tuple message (G_x, F_{sid}, M_{sid}) from the LMS;
7. send the tuple $(sid, M_{v_i}^{G_x})$ to the corresponding LRPF agent node v_i for every $(v_i, M_{v_i}^{G_x}) \in M_{sid}$;
8. } while (true);

Operation II. RTP Packet Management

1. do {
2. wait a RTP packet;
3. get the session information, sid , from the RTP packet;
4. for every LRPF agent node $v_i \in F_{sid}$ {
5. make a copy of the received RTP;
6. send the copy to the LRPF agent node v_i ;
7. }
8. } while (true);

Figure 8. Operations for the Controlling PoC Server

Fig.9 shows an example of the proposed scheme. For simplicity, we assume that two groups exist: $G_0 = \{m_0^0, m_1^0, m_2^0, m_3^0\}$ and $G_1 = \{m_1^1, m_2^1, m_3^1\}$. We also assume that PoC Clients m_i^j are located as shown in Fig.9 and thus they can be accessed through LRPF agent nodes v_0, v_1 , and v_3 . While PoC Clients register to their PoC Server, LRPF agent nodes collect and send the information to LMS, which is shown as dotted lines in Fig.9. Thus LMS has the information for PoC Clients and this information is used for processing the INFO request of the Controlling PoC Server. The information in the INFO response is used in Operation I and II of the Controlling PoC Server. The set of active group members of an LRPF agent node is sent to each LRPF agent node involved in the new PoC Session, which is used as forwarding set in an LRPF agent node to guarantee that invited PoC Clients will receive RTP media packets correctly.

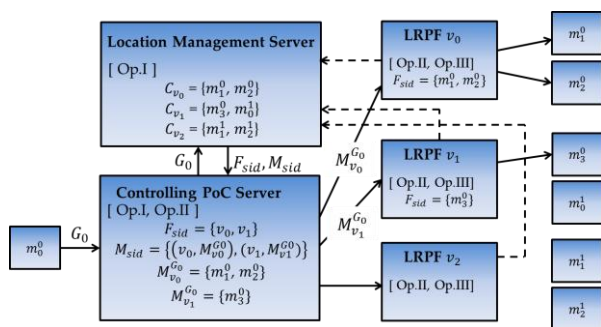


Figure 9. An example of the proposed scheme

IV. PERFORMANCE EVALUATION

In this section, we perform the simulation study to see the effect of the proposed scheme by reducing the outbound voice traffic of the Controlling PoC Server.

4.1 ASSUMPTIONS

Fig.10 depicts the network configuration used for the simulation. The PoC Server is placed in node 0 and a number of FTP sources are placed in node 3 and node 4 is

used as FTP sinks to see the effect of network congestion. In the shaded area of Fig.10, RTP packets for PoC compete with TCP packets for FTP for network resources to be transmitted to their destinations. $src(i)$ and $dest(i,j)$ nodes belong to the i -th group, where $0 \leq i < nGr$ and $0 \leq j < nGm$. nGr and nGm are the number of groups and the number of group members per group, respectively. RTP packets generated by $src(i)$ are transferred to the PoC Server in node 0 and then they are copied and forwarded to $dest(i,j)$ nodes for group communication. In the proposed scheme, we assume that both the LMS functionality and the PoC Server functionality are located in node 0 and the LRPF agent functionality is in every gateway, i.e., node 6, of destination networks.

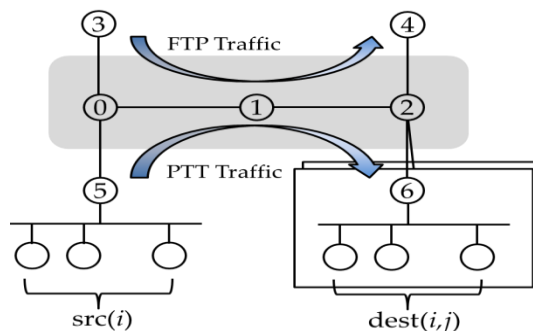


Figure 10. Network configuration for the simulation

We use the discrete-event network simulator *ns-3* [6] for the simulation study, which has been introduced as a replacement of the existing network simulator *ns-2*. To connect nodes, the class *PointToPointChannel* is used with attributes *DataRate* of 100Mbps and *Delay* of 1msec. $src(i)$'s and node 5 are connected using the class *CsmaChannel* with attributes *DataRate* of 100Mbps and *Delay* of 0.1msec to model the Ethernet although *ns-3* does not support the collision detect functionality. Destination networks are also connected using *CsmaChannel*. The queue size of *DropTailQueue* for both *PointToPointChannel* and *CsmaChannel* are fixed to 200. By this configuration, we can focus on the effect of network congestion for the outbound voice traffic of the PoC Server. Start times of $src(i)$ and FTP sessions are uniformly distributed in the time interval (1,3). G.729A is used as a voice codec since its bandwidth is low enough to be used in VoIP applications through the Internet [15]. We first assume that there is no bit error in transmission and then we perform the simulation to see the effect of the bit error.

4.2 SIMULATION RESULTS

We compare the performance of the proposed scheme with that of the existing PoC or PTT scheme in terms of MOS (mean opinion score) which is measured by using the E-model [16]. In legends of the following figures, 'ptt' and 'prp' represent the existing PoC/PTT scheme and the proposed scheme, respectively. We assume that the number of groups is 30, 40 and 50 and the number of group members is 10.

Fig.11 shows the MOS values of the existing PoC/PTT scheme and the proposed scheme. As the number of FTP sessions increases, we can find that the proposed scheme outperforms the existing PoC/PTT

scheme up to 95, 76 and 49% for 30x10, 40x10 and 50x10 group-members, respectively. MOS values of the proposed scheme are greater than 3.5 on the average, which means that some users are dissatisfied but most users are satisfied for the voice quality. But MOS values of the existing PoC/PTT scheme go down under 3.5 as the number of FTP session becomes greater than 30. Thus, we can find that the network congestion has a great effect on the performance of the existing PoC/PTT scheme. But the packet transmission of the proposed scheme was much less affected by the network congestion since the outbound voice traffic is significantly reduced by the number of group members compared to the existing PoC/PTT scheme.

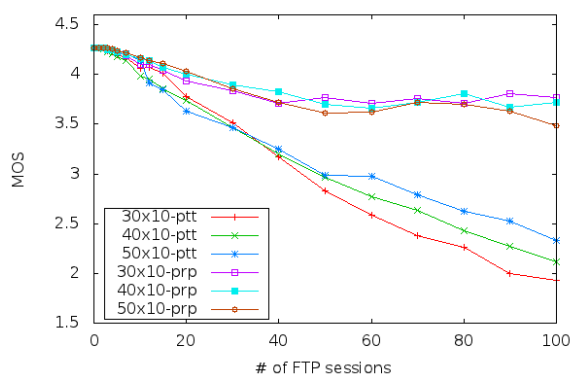


Figure 11. Comparison of the mean opinion score

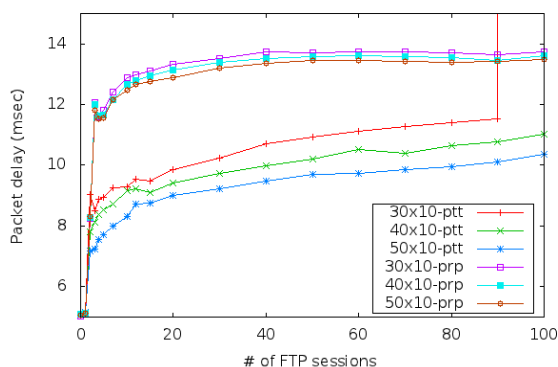


Figure 12. Comparison of the packet delay

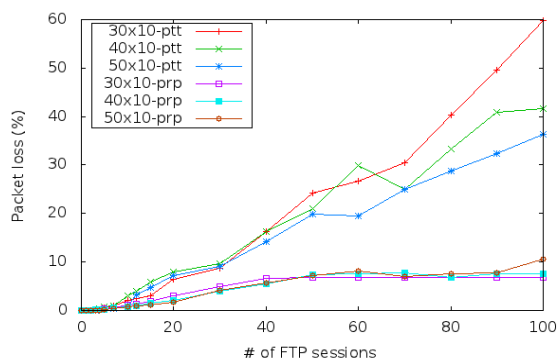


Figure 13. Comparison of the packet loss

Fig.12 and Fig.13 show the packet delay and the packet loss of the existing PoC/PTT scheme and the proposed scheme, which are two main components for the E-model. At first glance, the packet delay of the proposed scheme is larger than that of the existing PoC/PTT scheme. But the packet loss of the existing PoC/PTT scheme

becomes very larger than that of the proposed scheme as the number of FTP sessions increases. When network congestion happens, we can find that lost RTP media packets are the significant factor of losing MOS values, which degrades the overall end-to-end voice quality.

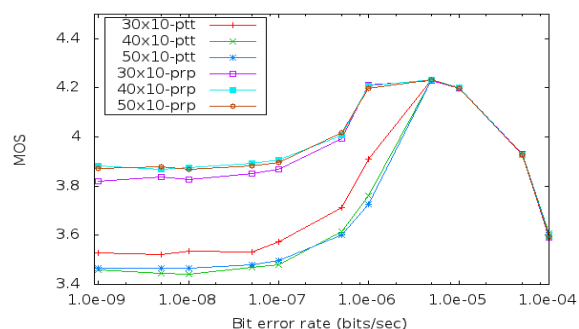


Figure 14. The effect of bit errors: MOS values (FTP=30)

Fig.14 shows MOS values when the bit error rate changes in case of 30 FTP sessions. As the bit error rate increases, the overall performance in terms of MOS values tends to be improved. When the bit error rate reaches 5e-6, all the simulation results show the best performance. After then, the overall performance degrades as the bit error rate increases. While the bit error rate is smaller than 5e-6, the FTP traffic dominantly uses the network. However, the FTP traffic makes no more influence to the PTT voice traffic while the bit error rate is greater than or equal to 5e-6 due to the congestion control of TCP which carries the FTP traffic, which will be explained in the simulation result of the packet loss in Fig.15.

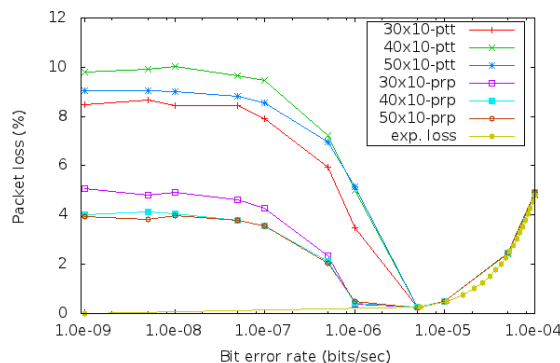


Figure 15. The effect of bit errors: packet loss (FTP=30)

The packet loss in Fig.15 shows also the same behavior as the simulation result in Fig.14. The expected packet loss, which is shown in Fig.15 as the line 'exp. loss,' can be obtained numerically. The RTP/UDP/IP header is of size 40 and G.729A generates 20 bytes per every 20 msec. Thus we can obtain the expected packet loss percentage in Eq.1 if we multiply the RTP media packet size by the bit error rate *ber*.

$$\text{Packet loss (\%)} = ber * (40 + 20) * 8 * 100 \quad (1)$$

The difference between the actual packet loss and the expected packet loss explains the effect of network congestion which results from TCP packet flows of FTP sessions. While the bit error rate is less than 5e-6, the packet loss is mainly affected by the FTP traffic. In this

case, the number of FTP sessions was assumed to be 30 so that there may be many TCP packet flows through the network, which prevent the outbound voice traffic from being forwarded to their destination PoC Clients. While the bit error rate is greater than or equal to $5e-6$, the packet loss shows the same result as the expected packet loss, which means that FTP sessions has no more effect on the outbound voice traffic.

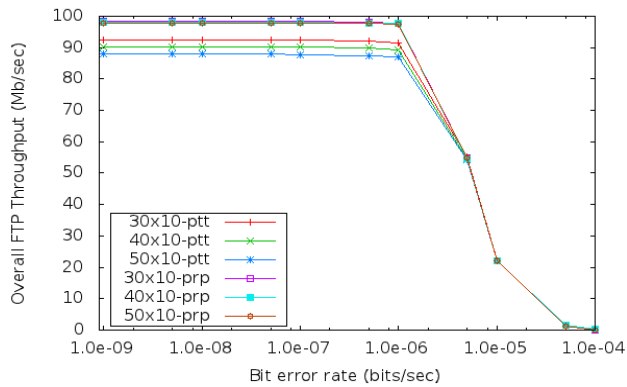


Figure 16. The effect of a bit error on the overall FTP throughput (FTP=30)

Fig.16 shows the overall FTP throughput for 30 FTP sessions as the bit error rate changes. We obtain this throughput by adding each throughput of 30 FTP sessions. While the bit error rate is less than or equal to $1e-7$, there is no significant performance degradation in terms of the overall FTP throughput. While the bit error rate is greater than $1e-7$ and less than $1e-6$, the overall FTP throughput declines a little bit but its effect on the RTP media packet has been diminished dramatically as shown in Fig.15, which results in the increase of MOS values in Fig.14. When the bit error rate is $5e-6$, the overall FTP throughput is about 55 Mbps and the outbound voice traffic is affected barely by the FTP traffic, which can be seen by the smallest packet loss in Fig.15 and the largest MOS value in Fig.14. As the bit error rate becomes greater than $5e-6$, the overall FTP throughput degrades dramatically to near 150 kbps. From Fig.15 and Fig.16, we can find that the network with the bit error rate greater than $1e-7$ has a significant effect on the TCP packet transmission as the bit error rate becomes larger but the small UDP packets such as RTP media packets carrying the voice data may be affected barely until the bit error rate becomes larger than $5e-6$.

The packet delay in Fig.17 also shows the same behavior at the center of the bit error rate $5e-6$. While the bit error rate is greater than or equal to $5e-6$, the packet delay seems very low. However, this low packet delay is meaningless because the packet loss is too high to get good end-to-end voice quality. Although the packet delay of the proposed scheme is greater than the one of the existing PoC/PTT scheme while the bit error rate is less than $5e-6$, the overall performance of the proposed scheme is much better than the one of the existing scheme due to the packet loss as shown in Fig.15.

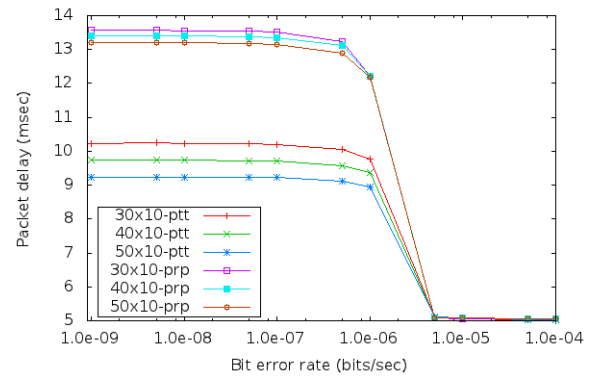


Figure 17. The effect of bit errors: packet delay (FTP=30)

V. CONCLUSION

In this paper, we proposed the efficient outbound voice traffic reduction scheme to improve the VoIP performance in the push-to-talk environment. The OMA PoC architecture has been standardized since 2005 to support the push-to-talk environment for the cellular network. In this paper, we used the OMA PoC architecture as the base network. We focused on the network performance in case of the network congestion since it has a great effect on the packet transmission. We have minimized the effect of the network congestion by reducing the outbound voice traffic of the Controlling PoC Server. We have presented three functionalities for the proposed scheme. The first one is the location reporting and packet forwarding (LRPF) agent functionality to obtain the location information of PoC Clients. The LRPF agent functionality can be located to either gateways or wireless access points because these nodes can easily see the packet transmission between PoC Clients in their network and the PoC Server. The second one is the location management server (LMS) functionality which is introduced to manage the location information of PoC Clients because the Controlling PoC Server can be determined after the SIP INVITE request is issued for the group communication and it is necessary to store the location information of PoC Clients somewhere. The last one is for the Controlling PoC Server where RTP media packets including voice data are copied and forwarded to their destination PoC Clients. The LMS functionality can be merged into one of PoC Servers for simplicity.

To see the performance of the proposed scheme, the discrete-event network simulator *ns-3* was used. We performed the simulation study in case of the network congestion which was caused by the FTP traffic using the same network resource. By reducing the outbound voice traffic of the Controlling PoC Server, the overall performance in terms of MOS has been greatly improved. We have shown the effect of TCP packets flows of FTP sessions on the packet delay and the packet loss, which are two main components affecting the E-model to obtain MOS values. Also we have shown the effect of the bit error rate on the overall performance of the proposed scheme. The bit error rate has a significant effect on TCP packets due to the TCP congestion control, but it has little effect on the RTP media packet until the bit error rate becomes larger than $5e-6$. Thus the proposed scheme outperforms the existing PoC/PTT scheme significantly when network congestion happens. Other network

congestion scenarios will be considered as a further research in case that either the UDP traffic such as media streaming or mixed traffic of FTP and UDP packets are used.

ACKNOWLEDGEMENTS

This work was supported by Dong-Eui University Foundation Grant.(2011AA180)

REFERENCES

- [1] Open Mobile Alliance, *Push to talk over cellular (PoC) – architecture: approved version 2.0* (Aug. 2011).
- [2] R.S. Cruz, M. Serafim, G. Varatojo, and L. Reis, Push-to-talk in IMS mobile environment, *Proc. 2009 fifth Int'l Conf. on Networking and Services*, Valencia, Spain, 2009, 389-395.
- [3] L.-H. Chang, C.-H. Sung, H.-C. Chu, and J.-J. Liaw, Design and implementation of the push-to-talk service in ad hoc VoIP network, *IET Communications*, 3(5), 2009, 740-751.
- [4] Open Mobile Alliance, *OMA PoC control plane: approved version 2.0* (Aug. 2011).
- [5] Open Mobile Alliance, *PoC user plane: approved version 2.0* (Aug. 2011).
- [6] W. Wand, S.C. Liew, V.O.K. Li, Solutions to Performance Problems in VoIP Over a 802.11 Wireless LAN, *IEEE Transactions on Vehicular Technology*, 54(1), 2005, 366-384.
- [7] L.X. Cai, X. Shen, J.W. Mark, L. Cai, and Y. Xiao, Voice Capacity Analysis of WLAN With Unbalanced Traffic, *IEEE Transactions on Vehicular Technology*, 55(3), 2006, 752-761.
- [8] ns-3 homepage, <http://www.nsnam.org/>.
- [9] J. Rosenberg, H. Schulzrinne, G. Camarillo, A. Johnston, J. Peterson, R. Sparks, M. Handley and E. Schooler, SIP: Session Initiation Protocol, *RFC 3261*, June 2002.
- [10] H. Schulzrinne, S. Casner, R. Frederick and V. Jacobson, RTP: A Transport Protocol for Real-Time Applications, *RFC 3550*, July 2003.
- [11] G. Camarillo and M.A. Garcia-Martin, *The 3G IP Multimedia Subsystem (IMS): Merging the Internet and the Cellular Worlds*, 3rd ed. (West Sussex, UK: Prentice-Hall, 2008).
- [12] H. Schulzrinne and S. Casner, RTP Profile for Audio and Video Conferences with Minimal Control, *RFC 3551*, July 2003.
- [13] A. Li, RTP Payload Format for Enhanced Variable Rate Codecs (EVRC) and Selectable Mode Vocoders (SMV), *RFC 3558*, July 2003.
- [14] J. Sjöberg, M. Westerlund, A. Lakaniemi and Q. Xie, RTP Payload Format and File Storage Format for the Adaptive Multi-Rate (AMR) and Adaptive Multi-Rate Wideband (AMR-WB) Audio Codecs, *RFC 4867*, April 2007.
- [15] ITU-T Recommendation G.729, *Coding of speech at 8 kbits/s using conjugate-structure algebraic-code-excited linear prediction (CS-ACELP)*, Jan. 2007.
- [16] ITU-T Recommendation G.107 Edition 8.0, *The E-model: a computational model for use in transmission planning*, Dec. 2011.



Jong Min Lee received the B.S. degree in computer engineering from Kyungpook National University, Korea, in 1992, and the M.S. and the Ph.D. degrees in Computer Science from Korea Advanced Institute of Science and Technology (KAIST) in 1994 and 2000, respectively. From Sept. 1999 to Feb. 2002, he worked for Samsung Electronics as a senior engineer. Since 2002, he has been a faculty member of the Department of Computer Software Engineering, Dong-Eui University, Busan, Korea. From Feb. 2005 to Feb. 2006, he visited the University of California, Santa Cruz as a research associate. From Feb. 2012, he is a visiting scholar of the Department of Computer Science at The University of Alabama, Tuscaloosa, AL. His research interests include routing in ad hoc networks and sensor networks, mobile computing, and parallel computing.



Seong-Woo Kim received his B.S., M.S., and Ph.D. degrees in Electrical Engineering from Korea Advanced Institute of Science and Technology (KAIST), in 1991, 1993, and 1999, respectively. He worked at Electronics and Telecommunications Research Institute (ETRI) from 1999 to 2001. Since 2002, he has been a professor at Dong-Eui University, Busan, Korea. From Aug. 2008 to Aug. 2009, he visited the California State University at Fresno as a visiting professor. His research interests include wireless sensor networks and embedded operating system.



Yang Xiao is currently with Dept. of Computer Science at The Univ. of Alabama. His research areas are security and communications/networks. He has published more than 200 refereed journal papers and over 200 refereed conference papers and book chapters related to these research areas. Dr. Xiao's research has been supported by the US National Science Foundation (NSF), U.S. Army Research, The Global Environment for Network Innovations (GENI), Fleet Industrial Supply Center-San Diego (FISCSD), FIATECH, and The University of Alabama's Research Grants Committee.

Influence of Team Familiarity on Team Performance in Distributed Teams

Sairam Vakkalanka¹, Ranjith Engu²

*(Department of Computer Science and Systems Engineering, Andhra University, Visakhapatnam, India)

** (Department of Computer Science and Engineering, JNT University, India)

ABSTRACT: This paper reports the importance of familiarity within the distributed team and how it affects the performance of a distributed team. Various factors which influence the familiarity are presented. Pros and cons and the impact of these factors are discussed and reported in this paper.

Keywords: Team Familiarity, Global Software Engineering, Distributed team, Team Performance, Task Familiarity, Task complexity

I. INTRODUCTION

Now days, in organizations around the globe, employees who tend to work in distributed teams are increasing [7] [8] [9]. Employees who work in these teams work through tasks which are independent of each other but with a common goal, spread across distributed locations and roles communicating virtually through different types of media [8][9][10][11]. These teams totally rely on sharing knowledge between the members present in the team. This Knowledge sharing may include various activities which rely on the familiarity between the team members.

In various fields varying from science to software production, the development organizations focus mainly on finding ways to improve those factors which play an important role in organizations success [1][2]. A lot of attention is being focused on these factors which improve the overall productivity of the organization which in turn leads to success [3][4][5][6]. One such important factor that increases the organization success rate and productivity is the persisting familiarity between the team members. The following sections elucidate how team familiarity influences the overall performance of a team in a distributed setting and contributed to the success of an organization.

II. TEAM FAMILIARITY

Team familiarity or the familiarity between team members working in an organization can also be stated as the degree to which two members of a team identify themselves to be familiar based on the experience with work they had in the past [5]. Familiarity between team members helps the team members to work on independent tasks as well as efficiently communicate and co-ordinate. It can also be defined as the information or knowledge that the members present in a team consists or have an idea on the independent or unique tasks and activities in their area of work [12]. It is the collaboration, coordination and communication between the members of a team [13]. Team members who work together for a long time can actually have more familiarity within themselves and the tasks [14].

They share knowledge through which they can effectively interact with each other [15]. Team familiarity does not let alone contributes to the performance of a team, there are factors such as task complexity and task familiarity which influence team familiarity [16], which in return indirectly influences the team's overall performance and the co-ordination complexity involved in a team. Figure 1 explain the factors which influence the team familiarity and what factors get influenced by team familiarity in a distributed team. Lets us now consider looking at how task complexity and task familiarity affect team familiarity.

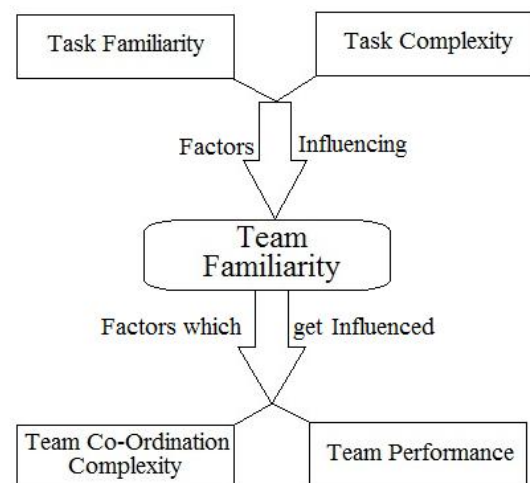


Fig.1 Factors influencing team familiarity and those which get influenced by it.

III. INFLUENCE OF TASK COMPLEXITY AND TASK FAMILIARITY ON TEAM FAMILIARITY

A study conducted by Goodman et.al [18] suggests that task familiarity influences the overall performance as, in distributed team environment each and every task needs unique requirements, configurations and activities from the team members. Knowledge which can be shared on these can improve the communication and coordination between the tasks and hence can improve the productivity. A study conducted by Argote et.al [19] reports that team members having some familiarity with the task can have a great effect on the performance when some characteristics of the task make it difficult for the members of the team to understand. Whereas, a study conducted by Goodman et.al [20] suggests that familiarity with the task is more effective for the simple or not so complex tasks. Familiarity is important in familiarity of the team members when there is a larger task as there would be a lot of changes to be handled, team members with prior experience and familiarity with the task can help in exactly locating where

the changes need to be made. The familiarity of the team members actually helps in negotiating with the complexity of the tasks making it easier to work in distributed teams with more team familiarity.

Empirical evidence suggests that familiarity with the task within the team members improves the performance of the team. A study Goodman et.al [18] conducted on distributed teams suggests that performance increased with the experience and familiarity of the task and has decreased the complexity of the task, i.e with the tasks being more complex in nature, though there exists familiarity in the teams and tasks the total output of performance in distributed task decrease with the increase in the complexity of the task. Simon's study [17] suggests that individuals who work on independent task may find it difficult to find solutions to problems than those who work together. Also a previous experience on how to solve the complex problem might help the fellow individuals to solve the problem while working in a distributed team. Through these observations, one can incur that team members who are familiar in dealing with task complexity might help in improving the performance of the distributed team.

IV. INFLUENCE ON TEAM CO-ORDINATION COMPLEXITY AND TEAM PERFORMANCE

Teams which have prior shared working experience or familiarity between the team members can start tasks with good expectations from the team members and can actually help in effectively communicating and can improve the team performance [21]. A better understanding of how their work contributes and how to obtain help from the fellow team members can help in improving the performance of the distributed team [21]. When the members of a team are familiar with the fellow team members, coordinating and understanding their roles and complement each other while working out on tasks helps in improving the performance of the team [21]. A study conducted by Harisson et.al [22] suggests that familiarity between team members helps in reducing the uncertainty and improves the team coordination; it actually helps in reducing the team coordination complexity and increase the trust between the team members. According to a study made by Campbell et.al [23] suggests that team familiarity will reduce the subjective complexity while coordinating with each other as they can think about ways as how to increase chances of effectively working, increasing the productivity.

V. ADVANTAGES AND DISADVANTAGES OF TEAM FAMILIARITY

Advantages:

- Team familiarity will help in reducing the extra efforts needed for improving coordination. Hence will save time, resources and money. Thus it always helps in improving the abilities to improve the communication and coordination between team members.
- It helps in increasing the trust between the team members which always help in improving the overall performance in distributed teams.
- Familiarity within the team members helps in reducing the need for frequent communication.

- It helps in providing collective knowledge about a task and helps in sharing knowledge between team members [22].
- It helps the team members to effectively channelize their work and distribute their work. It helps in making accurate and efficient work routines.

Disadvantages:

- To have familiarity between team member's organizations often arrange meetings parties and trips, which actually increases the overhead costs and making it more costly.
- If more and more time is spent in focusing on the familiarity between the team members, it affects the budgets and schedules.

VI. ANALYSIS & DISCUSSION

After having read and analyzing the reports of studies and articles published in the area of familiarity and how does it improve team performance, we can state that familiarity between the teams actually helps in improving the team's performance in a distributed setting. The familiarity of team members also depends on the familiarity with the task which in turn depends on how complex the task is, familiarity also depends on the coordination complexities which exist in a distributed team and how they can improve the performance. Though there is plenty of evidence stating that familiarity helps in improving the performance of the distributed team, there is always conflicting evidences which report that it can be beneficial only when there is large task and only familiarity is beneficial when there are small tasks. So it always conflicting reports that how the familiarity is based on the task size.

VII. CONCLUSION

Familiarity between the team members helps in improving the performance in a distributed team. To support this, various reports are presented and discussed. We have also reported the factors which influence it and how they influence each other. The advantages and disadvantages of team familiarity are also reported and thoroughly discussed.

REFERENCES

- [1] Edmondson, A. C. and I. A. Nembhard, Product development and learning in project teams: The challenges are the benefits, *J. of Product Innovation Management* 26(2): 123-138, 2009
- [2] Bradley R. Staats, Unpacking Team Familiarity: The Effects of Geographic Location and Hierarchical Role, *Blackwell Publishing Inc*, 2011
- [3] Haas, M. R. and M. T. Hansen, Different knowledge, different benefits: toward a productivity perspective on knowledge sharing in organizations, *Strategic Management J.* 28(11): 1133-1153, 2007
- [4] O'Leary, M. B. and M. Mortensen, Go (con)figure: Subgroups, imbalance, and isolates in geographically dispersed teams, *Organ. Sci.* 21(1): 115-131, 2010
- [5] Huckman, R. S., B. R. Staats and D. M. Upton, Team familiarity, role experience, and performance: Evidence from Indian software services, *Management Sci.* 55(1): 85-100, 2009

- [6] Reagans, R., L. Argote and D. Brooks, Individual experience and experience working together: Predicting learning rates from knowing who knows what and knowing how to work together, *Management Sci*, 51(6):861-881, 2005
- [7] Maznevski, M.L., and Chudoba, K.M, Bridging Space Over Time: Global Virtual Team Dynamics and Effectiveness, *Organization Science* (11:5), pp473-492, 2000
- [8] Cummings, J.N, Work Groups, Structural Diversity, and Knowledge Sharing in a Global Organization, *Management Science* (50:3), pp 352-364, 2004
- [9] Hinds, P.J., and Bailey, D.E, Out of Sight, Out of Sync: Understanding Conflict in Distributed Teams, *Organization science* (14:6), pp 615-632, 2003
- [10] Hansen, M., The Search-Transfer Problem: The Role of Weak Ties in Sharing Knowledge across Organization Subunits, *Administrative Science Quarterly* (44), pp 82-111, 1999
- [11] Majchrzak, A., Malhotra, A., and John, R, Perceived Individual Collaboration Know-How Development through Information Technology-Enabled Contextualization: Evidence from Distributed Teams, *Information Systems Research* (16:1), pp 9-27, 2005
- [12] Goodman, P. S., S. Garber, Absenteeism and accidents in a dangerous environment: Empirical analysis of underground coal mines, *J. Appl. Psych*, 73(1) 81-8, 1988
- [13] Littlepage, G., W. Robison, K. Reddington, Effects of task experience and group experience on group performance, member ability, and recognition of expertise, *Organ. Behav. Human Decision Processes* 69(2) 133-147, 1997
- [14] Katz, R., The effects of group longevity on project communication and performance, *Admin Sci. Quart*, 27, 81-104, 1982
- [15] Alavi, M., D. E. Leidner, Knowledge management and knowledge management systems: Conceptual foundations and research issues, *MIS Quart.* 25(1) 107-136, 2001
- [16] J. Alberto Espinosa, Sandra A. Slaughter, Robert E. Kraut, and James D. Herbsleb, Familiarity, Complexity, and Team Performance in Geographically Distributed Software Development, *Organization Science* 18, 4 (July 2007), 613-630, 2007
- [17] Simon, H. A., *The Sciences of the Artificial*. MIT Press, Cambridge, MA, 1996
- [18] Goodman, P. S., D. P. Leyden, Familiarity and group productivity, *J. Appl. Psych*, 76(4), 578-586, 1991
- [19] Argote, L., C. A. Insko, N. Yovetich, A. A. Romero, Group learning curves: The effects of turnover and task complexity on group performance, *J. Appl. Soc. Psych*, 25(6) 512-529, 1995.
- [20] Goodman, P. S., S. Shah, *Familiarity and work group outcomes*, 1992
- [21] Espinosa, Familiarity, Complexity, and Team Performance *Organization Science*, *INFORMS*, 18(4), pp. 613-630, 2007
- [22] Harrison, D. A., S. Mohammed, J. E. McGrath, A. T. Florey, S. W. Vanderstoep, Time matters in team performance: Effects of member familiarity, entrainment, and task discontinuity on speed and quality, *Personnel Psych.*, 56(3) 633-669, 2003
- [23] Campbell, D. J, Task complexity: A review and analysis, *Acad. Management Rev.* 13(1) 40-52, 1988.

Design and Fabrication of Composite Bumper for Light Passenger Vehicles

S. Prabhakaran¹, K. Chinnarasu², M. Senthil Kumar³

¹(Department of Mechanical Engineering, PSG College of Technology, India)

²(Department of Mechanical Engineering, Kalaingar Karunanidhi Institute of Technology, India)

³(Department of Mechanical Engineering, PSG College of Technology, India)

Abstract: The fuel efficiency and emission gas regulation of passenger cars are two important issues in these days. The best way to increase the fuel efficiency without sacrificing safety is to employ fiber reinforced composite materials in the cars. Bumper is the one of the part having more weight. In this paper the existing steel bumper is replaced with composite bumper. In this work the design and fabrication of composite bumper made up of glass fiber reinforced polymer is carried out by which weight of the bumper can be reduced. Fabrication of composite bumper is carried out by hand layup process by using E- Glass/ Epoxy bidirectional laminates. Composite bumper is analysed and Charpy impact tests are carried out. Compared to steel bumper, the composite bumper is found to have 64% higher factor of safety and 80% less in cost. From the fabrication it was found that the weight reduction of 53.8% is achieved using composite material without sacrificing the strength.

I. Introduction

A bumper is a shield made of steel, aluminum, rubber, or plastic that is mounted on the front and rear of a passenger car. When a low speed collision occurs, the bumper system absorbs the shock to prevent or reduce damage to the car. In existing bumper the weight is more. In the present trends the weight reduction has been the main focus of automobile manufacturers.

Less fuel consumption, less weight, effective utilization of natural resources is main focus of automobile manufacturers in the present scenario. The above can be achieved by introducing better design concept, better material and effective manufacturing process.

Steel bumper have many advantages such as good load carrying capacity. In spite of its advantages, it stays back in low strength to weight ratio. It is reported that weight reduction with adequate improvement of mechanical properties has made composites as a viable replacement material for conventional steel.

In the present work, the steel bumper used in passenger vehicles is replaced with a composite bumper made of glass/epoxy composites. The thickness of the composite bumper is calculated by bending moment equation and other dimensions for both steel and composite bumper is considered to be the same. The objective was to compare the stress, weight, and cost savings.

II. Bumper

The bumper is a safety system is used to observe the low speed collision. It is placed in car body. The car bumper is designed to prevent or reduce physical damage to the front and rear ends of passenger motor vehicles in low-speed

collisions. Automobile bumpers are not typically designed to be structural components that would significantly contribute to vehicle crashworthiness or occupant protection during front or rear collisions. It is not a safety feature intended to prevent or mitigate injury severity to occupants in the passenger cars. Bumpers are designed to protect the hood, trunk, grille, fuel, exhaust and cooling system as well as safety related equipment such as parking lights, headlamps and taillights in low speed collisions.

The national highway traffic safety administration (NHTSA) produces some bumper standard to the light passenger vehicle. The bumper standard, prescribes performance requirements for passenger cars in low-speed front and rear collisions. It applies to front and rear bumpers on passenger cars to prevent the damage to the car body and safety related equipment. The bumper standards are,

- The front and rear bumpers on passenger cars should prevent the damage to the car body.
- Bumper should withstand at a speed of 2 mph across the full width and 1 mph on the corners.
- Bumper should also withstand 5 mph crash into a parked vehicle.
- Placement of the bumper is 16 to 20 inches above the road surface.

So all bumpers should satisfy the above standards.

2.1 Requirements of Bumper Material

- It should absorb more energy while collision.
- It should have good rust resistance.
- It should have high strength.
- Light in weight.
- Easy to manufacture in large quantity.
- Low cost.

III. Composite Bumper

In recent days, various materials like composites are experimented in almost all parts of the automobiles and it has also ventured into bumper. Due to reduction in weight, composite materials are preferred over conventional steel bumper. Composite bumper absorbs more collision energy than steel bumper.

3.1 Advantages of Composite Bumper

One of the most advantageous reasons for considering their use over steel is their reduced weight.

- Absorb more collision energy.
- Excellent corrosion resistance.
- High impact strength.

- Material properties of composite bumper allow rapid response to induced or release stress.

3.2 Glass Fiber

The aim of fiber reinforced plastics is to combine the stiffness and strength of fibrous material. This material has corrosion resistance, low density and mould ability. The majority of reinforced plastics produced today are glass reinforced epoxy or polyester resins, both of which are thermosetting.

Glass fibers have also been used with phenolics, silicones, polystyrene and polyvinyl chloride. Glass fibers are the obvious choice as reinforcing agents, principally because of the relative ease with which high strengths can be obtained fiber a few microns in diameters.

It is possible to produce composites with a range of strength according to glass content and nature of the reinforcement. The epoxy resins have lower shrinkage than the other resins.

3.2.1 Properties

Some of the basic properties of glass fiber are,

- Specific Strength
- Low density
- Corrosion resistance
- Impact resistance
- Electrical properties

3.2.2 Different Types of Glass Fibers

Glass is the most common fiber used in polymer matrix composites. The most commonly used glass fibers are E-glass, S-glass, R-glass, C-glass and D-glass fibers. The E in the E-glass stands for electrical as it was designed for electrical applications. E-glass fiber is a high quality glass fiber used as a standard reinforcement for all the resin systems and as a well complying with mechanical property requirements.

Thus E-glass fiber was found appropriate for our applications. In S-glass S stands for higher content of silica. It retains its strength at high temperature and has higher fatigue strength. It is used mainly in aerospace applications. In C-glass C stand for corrosion, it is designed to give improved surface finish. It is available usually in the form of a surface tissue for the reinforcement of corrosive barriers in chemical plant. In D-glass D stands for dielectric used for applications requiring low electric constants.

3.2.3 Advantages of Glass Fibers

Glass fiber is most widely used as are reinforcement of all composites due to the following advantages:

- Molten glass easily drawn into high-strength fibers
- Readily available/easy to fabricate
- Relatively strong fibers produce very high strength in composite form
- Chemically inert in plastics.

These materials are limited to low temperature applications where strength is important without the need for high rigidity. Typical uses for this material are boat hulls, flooring materials and automobile bodies.

The main type of glass used is E-glass. However, it is used for many other purposes now such as decorations and structural applications.

3.3 Epoxy Resin

Epoxy resins are the most commonly used resins. They are low molecular weight organic liquids containing epoxide groups. Epoxide has three members in its ring, 1 oxygen and 2 carbon atoms. The reactions of Epichlorohydrin with phenols or aromatic amines make most epoxies. Hardeners, plasticizers and fillers are also added to produce epoxies with a wide range of properties of viscosity, impact, degradation, etc. Although epoxy is costlier than other polymer matrices, it is the most popular PMC matrix. More than two thirds of the polymer matrices used in aerospace applications is epoxy based. The main reasons for epoxy being the most used polymer matrix materials are

- Good compatibility with Glass fiber
- High strength
- Low viscosity and low flow rates, which allow good wetting of fibers and misalignment of fibers during processing
- Low shrink rates which reduce the tendency of gaining large shear stresses of the bond between epoxy and its reinforcement.
- Available in more than 20 grades to meet specific property and processing requirements.

IV. Design of Composite Bumper

For designing the composite bumper an already existing ambassador steel bumper is used as mould. Dimensions are assumed as same as that of steel bumper for fabrication.

4.1 Dimensions And Properties of Existing Steel Bumper

Effective length	= 0.975m
Total length	= 2.055m
Thickness	= 0.002m
Effective breath	= 0.078m
Total breath	= 0.172m
Weight	= 5.16kg
Material	= mild steel (chromium coated)
Tensile strength	= 460MPa (design data book)
Density	= 7800 kg/m ³

The moment for steel and composite bumper is assumed to be same. Therefore the moment for steel is

$$\frac{M}{I} = \frac{\sigma}{y}$$

Where,

M = Bending moment (Nm)

I = Moment of inertia (m⁴)

σ = Tensile strength (N/m²)

y = d/2,

d = thickness of the bumper (m)

b = breadth of bumper (m)

Moment of inertia for rectangular section:

$$I = bd^3/12$$

There are three sections in the bumper I₁, I₂, I₃ respectively.

$$I_1 = 0.058 \times 0.002^3/12 = 3.86 \times 10^{-11} \text{ m}^4$$

$$I_2 = 0.078 \times 0.002^3/12 = 5.2 \times 10^{-11} \text{ m}^4$$

$$I_3 = 0.058 \times 0.002^3/12 = 3.86 \times 10^{-11} \text{ m}^4$$

$$I = I_1 + I_2 + I_3 = 1.2932 \times 10^{-10} \text{ m}^4$$

Tensile strength of the steel = 460 x 10⁶ N/m² (from PSG data book)

The moment equation,

$$\frac{M}{1.2932 \times 10^{10}} = \frac{460 \times 10^6}{\frac{0.002}{2}}$$

M = 59.4872 Nm.

4.2 Thickness of the Composite Bumper

Thickness of the composite bumper can be determined by the formula,

$$\frac{M}{I} = \frac{\sigma}{y}$$

There are three individual sections, so to find them individually by using above formula,

$$\frac{59.4872}{\frac{0.058x d_1^3}{12}} = \frac{490 \times 10^6}{\frac{d_1}{2}}$$

$d_1 = 3.543 \times 10^{-3} \text{ m}$

$$\frac{59.4872}{\frac{0.078x d_2^3}{12}} = \frac{490 \times 10^6}{\frac{d_2}{2}}$$

$d_2 = 3.055 \times 10^{-3} \text{ m}$

$$\frac{59.4872}{\frac{0.058x d_1^3}{12}} = \frac{490 \times 10^6}{\frac{d_1}{2}}$$

$d_3 = 3.543 \times 10^{-3} \text{ m}$

Average thickness (d) = $d_1 + d_2 + d_3 / 3 = 3.38 \text{ mm}$

A layer of E-glass mat thickness is 0.2mm, so 17 layers are required for fabricating composite bumper.

4.3 Force Acting On the Bumper (F)

Force (F) = m*a

Where,

m = mass of the vehicle crashed on the bumper (1554kg)

a = acceleration due to gravity (m/sec^2)

$a = (u - v) / t$

Where,

v = Final velocity after collapsing (m/sec)

u = Initial velocity before collapsing (m/sec)

u = 8km/hr = 2.22 m/s (taken from NHTSA)

t = time taken for collapsing (sec)

$a = (2.22 - 0) / 0.1 = 22.22 \text{ m/sec}^2$

Force (F) = 1554 x 22.22 = 34529.88 N

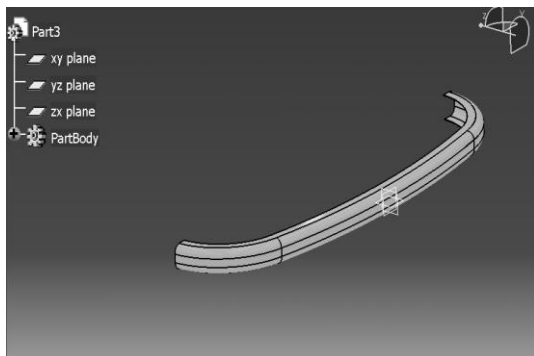


Fig 4.1 Model of the Bumper

4.4 Model of the Bumper

The load applied on the bumper is not a point load; it is a uniformly distributed load (pressure load). So calculation pressure load is given below.

Pressure (P) = F/A

F = force acting on the bumper = 34529.88 N

A = front area cross section = 2055 x 78 = 160290 mm^2

P = 34529.88 / 160290 = 0.13 N/mm^2

4.5 Drafted Model of the Bumper

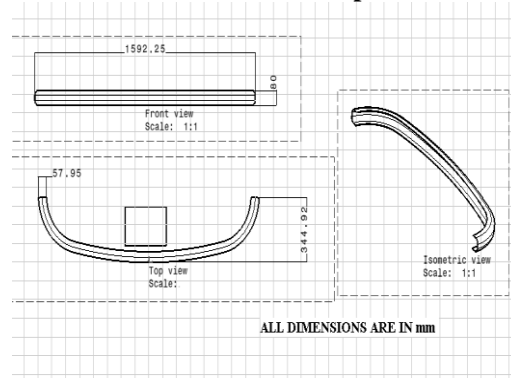


Fig 4.2 Drafted Model of the Bumper

V. Fabrication of Composite Bumper

In Hand lay-up, liquid resin is applied to the mould and then fiber glass is placed on the top. A roller is used to impregnate the fiber with resin. Another resin and reinforcement layer is applied until a suitable thickness builds up. It is very flexible process that allows the user to optimize the part by placing different types of fabric and mat materials. Because the reinforcement is placed manually, it is also called the hand lay-up process. Though this process requires little capital, it is labor intensive.

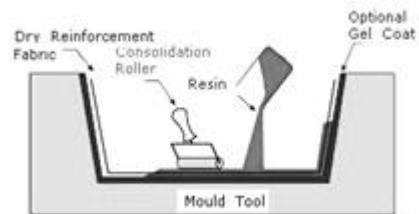


Fig 5.1 Hand Layup Process

5.1 Basic Raw Material

- E-Glass fibers
- Epoxy resin
- Hardener
- Wax

5.2 Tools Required

The mould design for the hand lay-up process is very simple as compared to other manufacturing process because the process requires room temperature to cure with low pressures. In this project existing bumper is used as mould.

5.3 Fabrication of Bumper

In the hand lay-up process the thickness of the composite part is built up by applying a series of fiber glass layers and liquid resin layers. A roller is used to squeeze out the excess resin and create uniform distribution of the resin throughout the surfaces. By the squeezing action of the

roller, homogeneous fiber wetting is obtained, the part is then cured at room temperature for about one week and once solidified it is removed from mould. The cost making one composite bumper is around Rs.820.

5.4 Advantages of Hand Lay-up Process

Very low capital investment is required for this process because there is negligible equipment cost as compared to other processes.

- The process is very simple and versatile. Any fiber type material can be selected with any fiber orientation.
- The cost of making a prototype part is very low because a simple mold can be used to make the part. In addition, the raw material used for this process is liquid resin, mat and fabric, material, which are less expensive than preparing material.

5.5 Limitations of Hand Lay-Up Process

- The process is labor incentive.
- The process is mostly is suitable for prototype as well as for making large structures.
- Because of its open mold nature,
- Styrene emission is major concern.
- The quality of the part produced is consistent form part to part. High fiber volume fraction cannot be manufactured using this process.

VI. Charpy Impact Test

The purpose of impact testing is to measure a material’s ability to resist high rate reading a material’s ability to resist impact often is one the determining factor in the service life of the material. Impact testing commonly consists of charpy and izod specimen configuration.

6.1 Charpy Impact Test Machine

The charpy impact test, also known as the charpy v-notch test, is a standardized high strain rate test which determines the amount of energy absorbed by a material during fracture. This absorbed energy is a measure of a given material’s toughness and acts as a tool to study temperature-dependent brittle-ductile transition. It is widely applied in industry, it is easy to prepare and conduct and result can be obtained quickly and cheaply. But major disadvantage is that all results are only comparative.



Fig 6.1 Charpy Impact Test Machine

6.2 Charpy Test Specimens

Charpy test specimens normally measure 55*10*6mm and have a notch machined across one of the larger faces. The notch dimensions are v-shaped notch, 2mm deep, with 45° angle and 0.25mm radius along the base.

6.3 Experimental Result

DESCRIPTION	COMPOSITE	STEEL
Cross sectional area, A (mm ²)	40	40
Impact value ,I (J)	294	163
Impact energy (J/mm ²) (I/A)	7.35	4.07

Table 6.1 Experimental Result

VII. Analysis of Composite Bumper

The Ansys computer program is a large scale multipurpose finite element program, which may be used for solving several classes of engineering analyses. The analysis capabilities of Ansys include the ability to solve static and dynamic structural analyses, steady state and transient heat transfer problems, mode frequency and buckling eigen value problems, static or time varying magnetic analyses and various steps of field and coupled-field applications. In this project Ansys 10.0 has been used as a tool to achieve the project target. The static-nonlinear analysis is carried out to find out the deformation, stress distribution over the structure.

7.1 Description for Steel and Composite Bumper

DESCRIPTION	STEEL	COMPOSITE
Element type	Solid186	Solid191
Pressure Load (N/mm ²)	0.13	0.13
Young’s modulus(N/mm ²)	2x10 ⁵	78x10 ³
Poisson ratio	0.3	0.27

Table 7.1 Description for Steel and Composite Bumper

7.2 Boundary Condition

Two ends of the bumper are fixed for supporting purpose. It is common for both steel and composite bumper. Bumper is arrested at 547.88mm from center to both the ends.

7.3 Stress Distribution for Steel Bumper



Fig 7.1 Stress Distribution for Steel Bumper

Maximum stress = 369.168 N/mm²
 Minimum stress = 0.003924 N/mm²
 Ultimate stress for steel = 460MPa (PSG design data book)
 Factor of safety = Ultimate stress/Working stress = 460/369.16 = 1.2

7.4 Stress Distribution of Composite Bumper

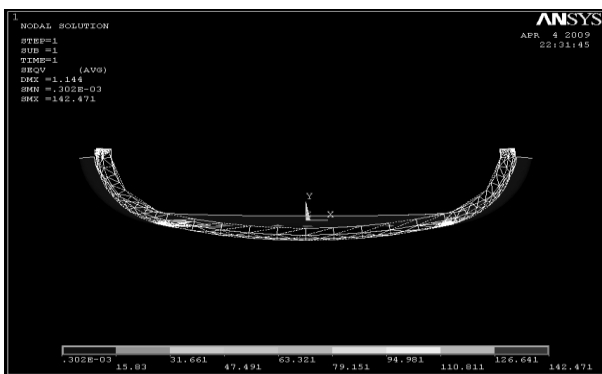


Fig 7.2 Stress Distribution of Composite Bumper

Maximum stress = 142.471 N/mm²
 Minimum stress = 0.302x 10⁻³ N/mm²
 Ultimate stress for composite = 490MPa (composite hand book)
 Factor of safety = ultimate stress/Working stress = 490/142.471 = 3.4

7.5 Results of FEA

DESCRIPTION	STEEL BUMPER	COMPOSITE BUMPER
Max. stress (N/mm ²)	369.168	142.471
Min. stress (N/mm ²)	0.003924	0.302x 10 ⁻³
FOS	1.2	3.4

Table 7.2 Results of FEA

VIII. Comparison

DESCRIPTION	STEEL BUMPER	COMPOSITE BUMPER	% OF REDUCTION
Weight	5.15	2.38	53.78%
Cost	3600	820	77.22%
Impact strength	3.25	7.35	-
Max stress(N/mm ²)	369.168	142.471	-
F.O.S	1.2	3.4	-

Table 7.3 Comparison

IX. Conclusion

Design, fabrication and testing of steel and composite bumper (using glass fiber material) are completed and also composite bumper is analyzed and compared with steel bumper. The steel bumper weighs about 5.15Kg where the weight of composite bumper is 2.38kg. Which is 53.8% lesser than steel bumper. It is proved that fuel economy of the vehicle is improved as the composite bumper weighs less when compared with steel bumper. Cost of composite bumper is Rs. 820/- which is 80% less than steel bumper. Impact strength of composite bumper is 7.35 J/mm² where steel bumper is 3.25 J/mm². The existing and composite bumper are analysed in ANSYS10.0 and the Maximum stress induced in the composite bumper is 159.36 N/mm² where steel is 292.669 N/mm². Factor of safety for composite bumper is increased by 64%. From the study, it is concluded that fiber reinforced plastic material is a suitable material for manufacturing the bumper.

References

- [1] Daniel gay, Suong V .Hoa, Stephen W.Tsai, "Composite Materials(design & Applications)", French edition, Edition Hermes, Paris, 1997.
- [2] Kaw, Autar K, "Mechanics of composite material", CRC Press, New York, 1997.
- [3] S.Srivasan, "Automotive Mechanics", Tata McGraw-Hill Publishing company Ltd, New Delhi. 2001.
- [4] Development of the composite bumper beam for passenger cars by seong sik cheon, dai gil lea. 2003.
- [5] Crash energy management in composite automotive structures by P.H.Thornton and R.A. Jeryan. 2007
- [6] Malick P. K, "fiber reinforced composite materials (manufacturing & design)", second edition, Marcel-Dekker, 1998.
- [7] Design Data Book, PSG College of technology, 2004.
- [8] www.matweb.com.
- [9] www.nhtsa.com
- [10] www.azom.com.
- [11] www.arai.co

Effect of Acoustic on Students' Performance in Secondary Classroom Environment: A Review

Mohammad Moslemi Haghghi¹, Loh Ee Chiao²,
Mahmud Bin Mohd Jusan³

**(Department of Architecture, Universiti Teknologi Malaysia, Malaysia)*

*** (Department of Education, Universiti Teknologi Malaysia, Malaysia)*

**** (Department of Architecture, Universiti Teknologi Malaysia, Malaysia)*

ABSTRACT: Poor acoustical environments in school, makes reduction of the talking signal, which may impact teachers' voice problems, reduce students' performance and enhance off-task behavior of them. Not only teachers, but also students implied that because of weak acoustic of the class, the interaction and communication have problem in the classroom. The aim of this paper is to understand the effects of acoustic troubles in the classroom on students' working based on their viewpoints and solve their problems. Most of researchers used qualitative and quantitative methods to collect data for their research from the school students. Among all elements students' opinion and their requirements according to the performance and noise are mostly three options. Students put more emphasis on distance and proximity between student-teacher. Other options like white noise, reverberation are the following and last step respectively to make appropriate situation for students' acoustic problems according to students' viewpoint. Consequently, arrange appropriate seating is the major element that can answer the acoustical problems and boost students' performance in the classroom environment.

Keywords: Acoustic, Classroom, Noise, Performance, Student

I. INTRODUCTION

Teaching space are the highest spots in educational-instructional activities. Speech in a classroom is transferred through a grouping of direct and reflected sound from the teacher to students. Direct sound moves to the listener in a straight line, without being reflected from its source. Reflect sound before traveling to listener, arrives at some objects or surfaces in a room [1], [2]. In the classroom, the main sources of energy are reflected sound at distances which eliminated of the teacher and direct sound energy is highest prevalent at distances near to the teacher [3]. Reflected and direct sounds improve classroom communication and make capable students in the classroom to hear the teacher when combined properly in a quiet classroom [4].

Research has shown that new as well as old school has acoustical problems and can seriously influence a child's capability to comprehend [5], [6]. To prepare sound systems and evaluate room acoustics acoustic principles have been clarified and technologies to explain the acoustical troubles in classrooms [7], [4]. From the other point of view, most students would have hard moments to understand hear and the teacher of classroom if being in a

classroom was the similar as being out-of-doors since direct sound is comparatively weak [8], [1]. The energy of the speech of human -at close distance is comparatively weak noticeable in microwatts [9].

Classrooms do not need a great deal of sound diffusion and designed mostly for listening to speech [4]. But the absorptive and reflective attributes are significantly essential of the room. The absorption and reflection of sounds can interfere when not controlled correctly in classroom listening. For instance, some of the most regularly used carpet on foam rubber padding and acoustic ceiling tile as absorbent materials in school classrooms. These kinds of materials absorb high-frequency sounds much better than low-frequency sounds. Consonant sounds, which are mainly high frequency, are not returned well when the floor and ceiling are treated with these materials and speaking fluency is destroyed [1], [10].

Same as acoustic, physical environment in the classroom influences students' performance. Students are more probably to have difficulty to be on their duty, since they are not able to listen successfully in school; also cooperation and obedience are hard to support [11]. Specifically, poor class room acoustics are also influenced children with one-sided losses and minimal hearing losses [12], [13]. Students that have learning shortages may be adversely influenced due to the fact that they regularly require syntactic, semantic, phonologic, and pragmatic disarranges that restrict their interaction capabilities in poor classroom acoustics [14], [15]. Consequently, to generate strong district in the classroom and promote students' learning, classroom needs relax manner and attractiveness [16], [17].

II. LITERATURE REVIEW

While constructing new places for schools, there are a number of objects needs into consideration—starting with the location. Building by the side of a highway, an airport or train tracks is noticeably not suggested. But it is not just outside noise must be considered, building schools that optimize speech intelligibility and reduce reverberation make suitable classroom about acoustics.

Acoustical problems in schools prepare the learning difficulties for all group of study such as school of beginners, second- language learners, youngsters with hearing losses and children with learning shortages [7], [18]. because school beginners language, speech, and listening talents have not developed, school beginners have more problems learning in classrooms compare to others

and making it hard for both young students and teachers to speak with each other [19], [20].

Several teachers are able to project their voices with strong voices without tiring for long amount of time. Others teachers have comparatively weak voices and when imposed to raise their voice level, they become stressed. Teachers are also more exhausted when teachers transfer their voices to compensate for high noise levels at the end of the day of school [7]. Noise levels of classroom sometimes are too high that teacher can conquer with verbal attempt and the result is damage of a teacher's vocal mechanism [21]. Noise of the classroom has been exposed to influence teachers' function [22], [23]. For instance, one scientist [23] gained data regarding the effects of noise in the classroom from more than 1.200 teachers.

Some researchers have concentrated on the impacts of noise, distance, and reverberation. Moreover, there is more concentration to listen the troubles of unusual students, students which are disengagement, the voice of teacher, and teacher tiredness [24], [7]. The perfect conveyance of information about acoustic is essential for best academic success in a classroom. The teacher's voice level, background noise and distance from the teacher to the child are acoustical variables that can compromise perceptual abilities.

Background noise levels relate to all typical noise sources offer in a learning space (excepting students' sound within that educational space and teachers' sound) and also it would be narrow to confirm sufficient speech interaction. Background noise inside the classroom related to any unwanted aural that students' needs, or wants, to comprehend and hear but this noise disturb them [25].

Inside the class the noise sources contain interior noise (noise that makes of inside the building, but outside of the classroom, such as classrooms next to lecture rooms, canteens, and/or busy corridors), exterior noise (noise which is produced from outdoor of the building, such as local construction, traffic of airplane, playground and vehicle transportation) and noise of room (noise that is produced inside the class) [26], [27]. To conceal the teacher's talking the capability of classroom noise depends on amount of acoustical factors [28], [29]. Background noise is capable of compromise educational performance, spelling skills and reading, attentiveness, attention, and behavior in children [30], [31].

The noise levels incline to influence focus and consideration more critically in children with high anxiety levels or lower IQs [32]. Background noise levels were significantly connected to read scores in elementary school-age children in classrooms [33]. Reductions in classroom noise had a considerable result on rising attentiveness, focus and sharing behavior among children [34].

Reflected sound waves or Echoes are postponed and adequately strong to be separate from the original sound source. They are probable to happen where the behind wall has a tough surface such as classrooms. Echoes impact the level, intelligibility and quality of the sound although they are not generally heard as separate phenomena [1], [35]. Classroom echoes are frequently more of a problem than classroom reverberation despite the fact that much highlighting has been located on reverberation [8], [36]. The most significant acoustical crisis within classrooms is extreme white noise even though classroom

echoes, modes, and reverberation can influence speech intelligibility in a room, which covers the teacher's talking.

The last factor that affects speech awareness is the gap between teacher and student in the classroom. Actual distance from the student to the teacher, Holliman and Anderson named it proximity and calculated in centimeters [37]. The direct sound field controls in the listening environment when proximity relatively adjacent to the child. Compare to students in any other row, the first two rows students' performance was better [37].

The space between students and teacher can powerfully impact speaking comprehension. Since the significant distance of the room is reached, speech perception scores reduce [38], [39]. A current study of the influence of student-teacher proximity on speech recognition marks was managed with students between 5 to 7 years of age by Crandell [18]. Student's scores were associated to the proximity between student and teacher [40]. Students' positions when it is close to the rear of the class were related with weaker academic performance [41].

III. INDICATORS

Scientists know that students merit the best ideal environment for studying, particularly in a classroom someplace they are able to hear clearly the teacher's speech (closeness). Students also have to answer to the question and focus entirely on their learning. Experiments of classrooms in secondary school level exposed that extreme background noise, which contests the speaking of teachers and decreasing reverberation and background noise inside the classrooms would be maximum valuable to the students with weak acoustics that can create the educational plan unreachable for the students.

The three acoustical independent variables affect students' performance in Fig. 1. Therefore, it is significant to obviously explain and describe the main viewpoints of efficient characteristics in the framework of following performance of students' area based on their requirements.

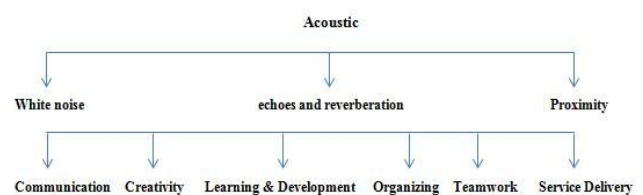


Fig. 1. Influences of acoustic features on students' performance

IV. METHODOLOGY AND FINDING

Most of researchers employed mix method to gather information of students within the classroom. They used questionnaire to obtain pure information which directly take of students' requirements and their points of view. By investigating of students about acoustic crisis in the classroom and compare with other researchers' experiments according the acoustical problems, we could get suitable knowledge to solve students' problems.

Qualitative and quantitative approaches allow understanding students' interaction, learning and physical attribute on students' performance. For example, most of researchers prepared questionnaire as a quantitative method to determine the connection of students' performance and

noise effects, especially measured the students' beliefs about acoustic problem in the classroom. Extract students' viewpoints may be determined by suppositions depend on previous knowledge or by accessibility within the classroom.

For the qualitative part, most of authors were emphasized on observation as a qualitative method to reach deep opinion of students and get the real beliefs. Generally, students were asked to indicate which elements of noise affected more on their performance in the classroom and were observed to measure which items affects more compare to others. By this way, most of analyses showed that physical elements of classroom especially echoes and noise were noticeable enough to disturb the learning of students and quality of their performance even slight hearing disorder.

Several researchers also employed interview to identify information from students and recognizes complete opinion of students based on their performance. Majority of interviews part used an open-ended style and based on the questionnaire data partial of that used as a semi-structure. According to the data gained of interviews with several of students and study of the related literature several items were arranged so cautiously to collect students' opinion of their studying and to contain performance.

The amount of elements needed by the investigation based on eigenvalue principles is three. Features are called based on the significances of the points into consideration. First of all is called "White noise" and the other one is entitled "reverberation and echoes" and the last-objected is identified as "proximity".

By comparing of researchers and analyzing of their finding, double suggestions could be proposed; firstly, decreasing distance between a speaker and listener improved the capability of listening perception in the significant distance of the classroom. Next, the significant distance in typical classrooms, for highest speaking perception is merely at distances that are comparatively adjacent to the teacher. Younger students are in danger for noise intervention is the greatest populations of students and they have higher perceptual troubles compare to adults.

V. CONCLUSION AND SUGGESTIONS

Classroom acoustics problems are an extensive educational topic that needs extra research. All students and teachers are affected by poor classroom acoustics. Some crucial acoustical variables (noise, reverberation, and distance) in this research are offer in a classroom environment which measured on the students' performance. The majority of students emphasized their requests powerfully and considered the acoustical situations in interaction environments, especially focus on proximity as a major element inside the classroom. Proximity between students and teachers has the greatest effect on performance of students.

Next feature which students considered about that was white noise in class area which influenced their performance extremely. Decreasing background noise inside the classrooms would be highly useful to the performance of students. In order to recover the acoustical environment problems in the classroom, the following recommendations may be employed based on architectural perspectives:

The greatest critical key around acoustic troubles based on requirements of students is modifying the seat arrangement to organize the finest and useful proximity for students and improve their performance. Soft architecture or flexible components inside the classroom are sections which can be simply change position by teachers in a classroom place. Similar features contain chairs and tables. Replacing the seat composition is the easiest and cheapest solution for any designer and teacher to achieve students' requirements within the classroom. Consequently, discover the finest arrangement improves teacher-student communication certainly.

REFERENCES

- [1] Everest, A. (1989). *The master handbook of acoustic* (2nd ed.). Blue Ridge Summit, PA: Tab Books.
- [2] Hirschorn, M. (1989). *Noise Control reference handbook*. Bronx, NY: Industrial Acoustics.
- [3] Davis, R., & Jones, R. (1989). *Sound reinforcement handbook*. Milwaukee, WI: Hal Leonard.
- [4] Brook, R. (1991). Rooms for speech and music. In G. Ballou (Ed.), *Handbook for sound engineers* (2nd ed., pp. 155- 197). Indianapolis, IN: Howard W. Sams.
- [5] Barton, L. (1989). *Sound levels in elementary school Classrooms*. Unpublished master's thesis, Utah State University. Logan.
- [6] Blair, J. (1990). Front-row seating is not enough for classroom listening. In C. Flexer, D. Wray, & H. Leavitt (Eds.), *How the student with hearing loss can succeed in college: A handbook for students, families and professionals* (pp. 69-82). Washington, DC: Alexander Graham Bell Association for the Deaf.
- [7] Berg, F. (1993). *Acoustics and sound systems in schools*. San Diego: Singular Publishing Group.
- [8] Davis, D, & Davis, C. (1987). *Sound system engineering* (2nd ed.). Indianapolis. IN: Howard W. Sams.
- [9] Fletcher, H, (1 953). *Speech and hearing in communication*. Princeton, NJ: Van Nostrand.
- [10] Harris, C. (1955). *Acoustical properties of carpet*. *Journal of the Acoustical Society of America*. 27(6). 1077-1082.
- [11] Gallup, A. (1986). *The 18th annual Gallup poll of the public's attitudes toward the public schools*. Phi Delta Kappan, 68. 43-59.
- [12] Bess, F. (1982). *Children with unilateral loss*. *Journal of the Academy of Rehabilitative Audiology*, 15, 13 1-144.
- [13] Finitzo-Hieber, T., & Tillman, T. (1978). Room acoustics effects on monosyllabic word discrimination ability by normal and hearing impaired children. *Journal of Speech and Hearing Research*, 21. 440-458.
- [14] Bos, C. (1988). Academic interventions for learning disabilities. In K. Kavale (Ed.), *Learning disabilities: State of the art and practices* (pp. 98- 122). Boston: College- Hill Press.
- [15] Lansky, E., & Chapandy, A. (1976). Factors affecting language comprehension. *Language, Speech and Hearing Services in Schools*, 7(3), 159- 168,
- [16] Ahrentzen, S. and Evans, G.W. (1989), "Architects and school children: in touch or out of focus?", *Arch. & Comport./Arch. Behav.*, Vol. 5 No. 1, pp. 17-28,

- available at: lasur.epfl.ch/revue/A&C%20Vol205%20No.1AHR-ENTZENandEVANS.pdf (accessed May 28, 2006).
- [17] Griffin, T. (1990), "The physical environment of the college classroom and its effects on students", *Campus Ecologist*, Vol. 8 No. 1, pp. 1-6, available at: <http://wbarratt.indstate.edu/ce/cen/v8n1.htm> (accessed May 28, 2006).
- [18] Crandell, C. (1990, November). *Effect of classroom acoustics on speech recognition in pediatric populations*. In F. Berg (Chair). *Listening in classrooms*. Workshop conducted at Utah State University, Logan.
- [19] Durkin, K. (1986). Introduction. In K. Durkin (Ed.), *Language development in the school years* (PP. 1-16). Cambridge, MA: Brookline Books.
- [20] Edwards, D., & Mercer, N. (1986). *Classroom discourse and the development of shared knowledge*. In K. Durkin (Ed.), *Language development in the school years* (pp. 172-202). Cambridge, MA: Brookline Books.
- [21] Child, D., & Johnson, T. (1991). *Preventable and non-preventable causes of voice disorders*. Seminar in Speech and Language, I, 1- 13.
- [22] Crook, M., & Langdon, F. (1974). The effects of aircraft noise in schools around London airport. *Journal of Sound and Vibration*, 34, 221-232.
- [23] Ko, N. (1979). Response of teachers to aircraft noise. *Journal of Sound and Vibration*. 62. 277-292.
- [24] Allen, L. (1991). *A school handbook on classroom amplification equipment*. Elkader, IA : Keystone Area Education Agency.
- [25] Crandell, C , & Smaldino, J. (1995). *An update of classroom acoustics for children with hearing impairment*, *Volta Review*. I. 4-12.
- [26] Bess, F., & McConnell, F. (1981). *Audiology, education and the hearing-impaired child*. St, Louis. MO: CV. Mosby.
- [27] Crandell, C, & Smaldino, J. (1994). The importance of room acoustics. In R. Tyler & D, Schum (Eds.). *Assistive listening devices for the hearing impaired* (pp. 142-164), Baltimore, MD: Williams & Wilkins.
- [28] Nabelek, A. (1982). Temporal distortions and noise considerations. In G. Studebaker & F. Bess (Eds.). *The Vanderbilt hearing aid report: State of the art research needs* (pp. 1242-1248). Upper Darby. PA: Monographs in Contemporary Audiology.
- [29] Nabelek, A., & Nabelek, I. (1994). Room acoustics and speech perception. In J. Katz (Ed.). *Handbook of clinical audiology* (4th ed. pp. 624-637). Baltimore, MD: Williams & Wilkins.
- [30] Ando, Y., & Nakane, Y. (1975). Effects of aircraft noise on the mental work of pupils. *Journal of Sound and Vibration*, 43, 683-691.
- [31] Crook, M., & Langdon, F. (1974). The effects of aircraft noise in schools around London airport. *Journal of Sound and Vibration*, 34, 221-232.
- [32] Koszarny, Z, (1978). Effects of aircraft noise on the mental functions of school children. *Archives of Acoustics*. 3, 85-86.
- [33] Green, K., Pasternak, B., & Shore, B. (1982). Effects of aircraft noise on reading ability of school age children. *Archives of Environmental Health*. 37, 24-31.
- [34] Lehman, A., & Gratiot, A. (1983). Effects du bruit sur les enfants a l'ecole. In *Proceedings of the 4th Congress on Noise as a Public Health Problem* (pp. 859-862). Milano: Centro Ricerche e Studi Amplifon.
- [35] Everest, A. (1991b). Acoustics of small rooms. In G. Ballou (Ed.), *Handbook for sound engineers: The new audio cyclopedia* (2nd cd., pp. 43--66). Indianapolis, IN: Howard W. Sams.
- [36] Davis, D. & Davis, C. (1991). Audio measurements. In G. Ballou (Ed.), *Handbook for sound engineers: The new audio cyclopedia* (2nd ed., pp. 1365- 1412). Indianapolis, IN: Howard W. Sams.
- [37] Holliman, W.B. and Anderson, H.N. (1986), "Proximity and student density as ecological variables in a college classroom", *Teaching of Psychology*, Vol. 13, pp. 200-3.
- [38] Crandell, C. (1991). Classroom acoustics for normal-hearing children: Implications for rehabilitation. *Educational Audiology Monographs*. 2, 18-38.
- [39] Crandell, C., & Bess, F. (1986. October). *Speech recognition of children in a "typical" classroom setting*, *Asha*, 29, 87.
- [40] Becker, F.D., Sommer, R., Bee, J. and Oxley, B. (1973), "College classroom ecology", *Sociometry*, Vol. 36 No. 4, pp. 514-25.
- [41] Marlowe, J., Koonce, J., Lee, J. and Cai, Y. (2006), "An examination of the impact of student's work time on academic performance", *Consumer Interests Annual*, Vol. 48, pp.1-9, available at: <http://consumerinterests.org/files/public/StudentWork-02.pdf> (accessed May 28, 2006).

Current Harmonic Analysis Of A Dual Two Level Inverter Fed Open-End Winding Induction Motor Drive Based On SVPWM Switching Strategies

Dr. K. Sri Gowri¹, S. Venkata Mahesh² and M. Abdul Hakeem³

¹ Professor, Dept of Electrical and Electronics Engg, RGM College of Engg & Tech, Nandyal, India.

² PG-student, , Dept of Electrical and Electronics Engg, RGM College of Engg & Tech, Nandyal, India.

³ PG-student, , Dept of Electrical and Electronics Engg, RGM College of Engg & Tech, Nandyal, India

ABSTRACT: An open-end winding induction motor, fed by two 2-level inverters connected at either end produces space vector locations, identical to those of a conventional 3-level inverter. In this paper, two switching algorithms are proposed to implement space vector PWM for the dual inverter scheme. The proposed algorithms do not employ any look-up tables. The time consuming task of sector identification is altogether avoided in both these algorithms. The proposed algorithms employ only the instantaneous reference phase voltages for the implementation of the space vector PWM. The harmonic content of the three phase currents in the motor are analyzed with an appropriate variation in its modulation index in both the proposed algorithms and compared simultaneously. Thus the performance in terms of harmonic analysis is carried out using MATLAB/SIMULINK for an open end induction motor drive.

Keywords: Dual-inverter, space vector modulation, Open-end winding induction motor.

I. INTRODUCTION

Various PWM schemes are presented for the two-level inverters and their effects on the load are also continuously investigated. Thrive to get improved performance is on the anvil employing suitable PWM techniques [1]-[6] or using multi-level inverters. Multi-level inverters are finding increasing research opportunities and it is clearly evident in the past few years. This is due to the reduced total harmonic distortion (THD) in the output voltage and genesis of higher voltage with use of series connections of lower voltage rating switching devices. Various derivative of this power circuit and the associated PWM schemes are also reported in the recent past [6]-[14].

Two space vector modulation techniques are suggested, which obviate the need for the sector identification. Also these PWM schemes do not employ any look-up table, thus reducing the memory requirement. Fig.1 shows the basic open-end winding induction motor drive operated with a single power supply. The symbols v_{a0} , v_{b0} and v_{c0} denote the pole voltages of the inverter-1. Similarly, the symbols $v_{a'0}$, $v_{b'0}$ and $v_{c'0}$ denote the pole voltages of inverter-2. The space vector locations from individual inverters are shown in Fig.2. The numbers 1 to 8 denote the states assumed by inverter-1 and the numbers 1' through 8' denote the states assumed by inverter-2 [1-5]. Table-1 summarizes the switching state of the switching devices for both the inverters in all the states. In Table-1, a '+' indicates that the top switch in a leg of a given inverter is turned on and a '-' indicates that the bottom switch in a leg of a given inverter is turned on.

As each inverter is capable of assuming 8 states independently of the other, a total of 64 space vector combinations are possible with this circuit configuration. The space vector locations for all space vector combinations of the two inverters are shown in Fig.3. In Fig.3, |OA| represents the DC-link voltage of individual inverters, and is equal to $V_{dc}/2$ while |OG| represents the DC-link voltage of an equivalent single inverter drive, and is equal to V_{dc}

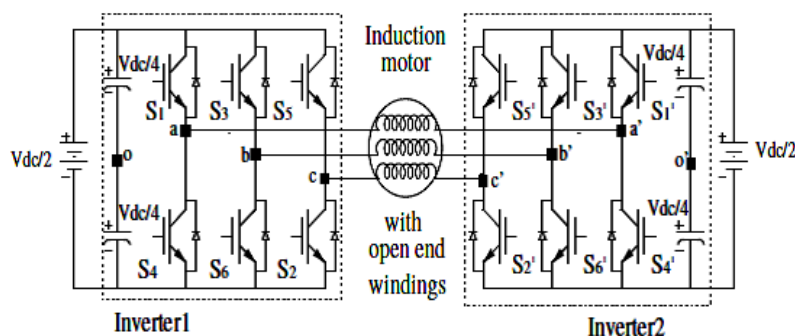


Fig.1: Power circuit configuration of dual two-level inverter

TABLE 1: Switching states of the individual inverters

state of inverter 1	Switches turned on	State of Inverter-2	Switches turned on
1 (+ - -)	S6, S1, S2	1' (+ - -)	S6', S1', S2'
2 (+ + -)	S1, S2, S3	2' (+ + -)	S1', S2', S3'
3 (- + -)	S2, S3, S4	3' (- + -)	S2', S3', S4'
4 (- + +)	S3, S4, S5	4' (- + +)	S3', S4', S5'
5 (- - +)	S4, S5, S6	5' (- - +)	S4', S5', S6'
6 (+ - +)	S5, S6, S1	6' (+ - +)	S5', S6', S1'
7 (+ + +)	S1, S3, S5	7' (+ + +)	S1', S3', S5'
8 (- - -)	S2, S4, S6	8' (- - -)	S2', S4', S6'

The following PWM strategies are proposed in this paper:

1. The Decoupled PWM strategy
2. The Biasing inverter PWM strategy

II. DECOUPLED PWM SCHEME:

The reference voltage vector to be realized by the dual inverter is shown as V_{ref} in Fig.2. It can be resolved into two equal and opposite half components as $V_{ref}/2$ and $-V_{ref}/2$. The vector addition of the later and the former results in the generation of actual reference vector as:

$$V_{ref} = V_{ref}/2 - (-V_{ref}/2) \tag{1}$$

These individual reference voltages are synthesized separately by the two two-level inverters using SVPWM and are depicted in Fig.3 from Fig.2 & 3 it can be identified that

$$OV \angle \theta = ov_1 \angle \theta - ov_2 \angle (180 + \theta) \tag{2}$$

The voltage vector OV_1 is synthesized by inverter-1 and OV_2 by inverter-2 respectively and are given as:

$$OV_1 = v_{a0}e^{j0} + v_{b0}e^{j\frac{2\pi}{3}} + v_{c0}e^{j\frac{4\pi}{3}} \tag{3}$$

$$OV_2 = v_{a'0}e^{j0} + v_{b'0}e^{j\frac{2\pi}{3}} + v_{c'0}e^{j\frac{4\pi}{3}} \tag{4}$$

where v_{a0}, v_{b0}, v_{c0} are three-phase pole voltages of inverter-1 and $v_{b'0}, v_{b'0}, v_{c'0}$ are three-phase pole voltages of inverter-2 The actual vector can now obtained using the vectors defined in eqns.(3) & (4) as:

$$OV = V_{aa'}e^{j0} + V_{bb'}e^{j\frac{2\pi}{3}} + V_{cc'}e^{j\frac{4\pi}{3}} \tag{5}$$

$$V_{aa'} = V_{a0} - V_{a'0} \tag{6}$$

$$V_{bb'} = V_{b0} - V_{b'0} \tag{7}$$

$$V_{cc'} = V_{c0} - V_{c'0} \tag{8}$$

Where $v_{aa'}, v_{bb'}, v_{cc'}$ are the three-phase phase voltages of the dual-inverter fed induction motor drive.

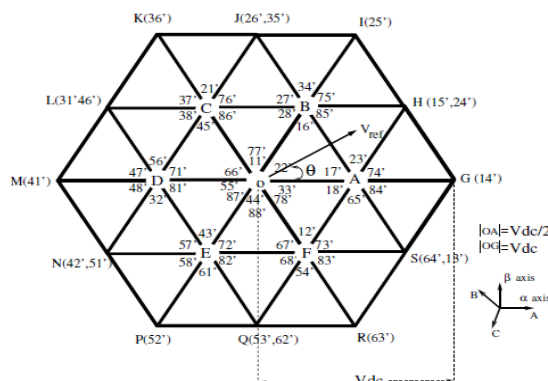


Fig.2: Space vector locations of dual two-level inverter

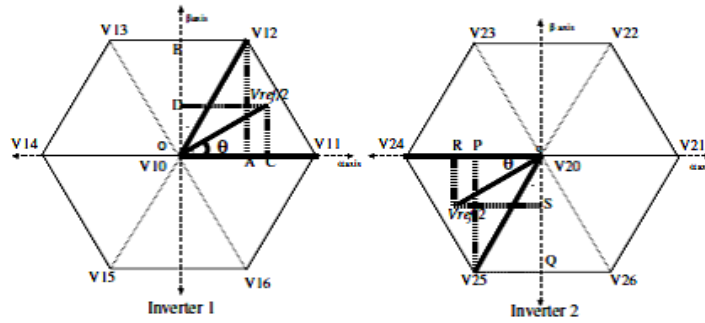


Fig.3: Principle of decoupled PWM technique and switching voltage vector, reference voltage vector projection on α and β axis

In Fig.3, the switching vectors V_{1x}, V_{2x} ($x=0, 1, 2, 3, 4, 5, 6$) for inverter-1 & 2 can be identified and are defined as:

$$V_{1x} = \frac{2}{3}V_{dc} (S_{A1} + S_{B1}e^{j\frac{2\pi}{3}} + S_{C1}e^{j\frac{4\pi}{3}}) \quad (9)$$

$$V_{2x} = \frac{2}{3}V_{dc} (S_{A2} + S_{B2}e^{j\frac{2\pi}{3}} + S_{C2}e^{j\frac{4\pi}{3}}) \quad (10)$$

The reference voltage vector (V_{ref} in Fig.2) is situated at an angle θ w.r.t the α -axis. The references to the individual inverter would then be $V_{ref}/2$ where one is at angle ' θ ' while the other is at an angle ' $180+\theta$ ' both measured w.r.t the β -axis (Fig.3). The respective references are synthesized by the inverters and the switching vectors for inverter-1 can be identified as V_{11}, V_{12} & V_{10} and V_{24}, V_{25} & V_{20} for inverter-2 (Fig.3)

With the decoupled SVPWM technique, the reference vector V_{ref} is decoupled into two equal halves as described in the previous section. These space vectors are shown in Fig.3 and are said to fall in sector 1 (for inverter-1) and sector 4 (for inverter-2). With inverter-1 and 2, the space vectors $V_{ref}/2, -V_{ref}/2$ respectively are realized in the average sense using three nearest voltage vectors of the sector in which the tip of reference vector lies. To realize $V_{ref}/2$, inverter-1 switches between vectors $V_{10}, V_{11}, V_{12}, V_{17}$ with timing intervals of $T_{10}/2, T_{11}, T_{12}, T_{17}/2$ respectively for the center-spaced PWM. Similarly, inverter-2 switches between $V_{20}, V_{24}, V_{25},$ and V_{27} with timing intervals of $T_{20}/2, T_{24}, T_{25},$ and $T_{27}/2$ respectively.

III. RESULTS & DISCUSSIONS FOR THE DECOUPLED PWM STRATEGY

The dual two-level inverter with decoupled SVPWM switching scheme feeding power to open end winding induction motor drive is simulated using Matlab/SIMULINK simulation software. Then the results are verified experimentally. A total of 48 samples is chosen in the entire work covering one cycle of the output voltage, irrespective of the modulation index of the drive (speed of the motor).

The gating pulses of the top switching devices of the individual inverters (depicting the timings T_{ga}, T_{gb}, T_{gc} for inverter-1 and $T_{ga'}, T_{gb'}, T_{gc'}$ for inverter-2) are shown in Fig.4. The three phase pole voltages of the individual inverters will be a replica of the gating pulses shown in Fig.6 except for their voltage levels.

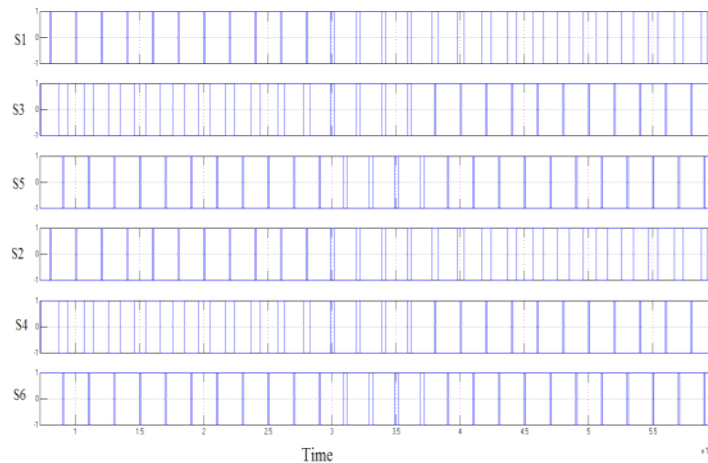


Fig.4: Gating Pulses for Inverter-1(T_{ga}, T_{gb}, T_{gc}) and Inverter-2($T_{ga'}, T_{gb'}, T_{gc'}$) for the modulation index 0.75

Here, the modulation index is defined as the ratio of the length of the reference space vector (V_{ref}) and the DC-bus voltage (V_{dc}). The experimentally obtained a-phase pole voltages of the two inverters, difference in a-phase pole voltages, motor a-phase voltage and the motor a-phase no-load current for a modulation index of 0.75 are as shown in the fig(5).

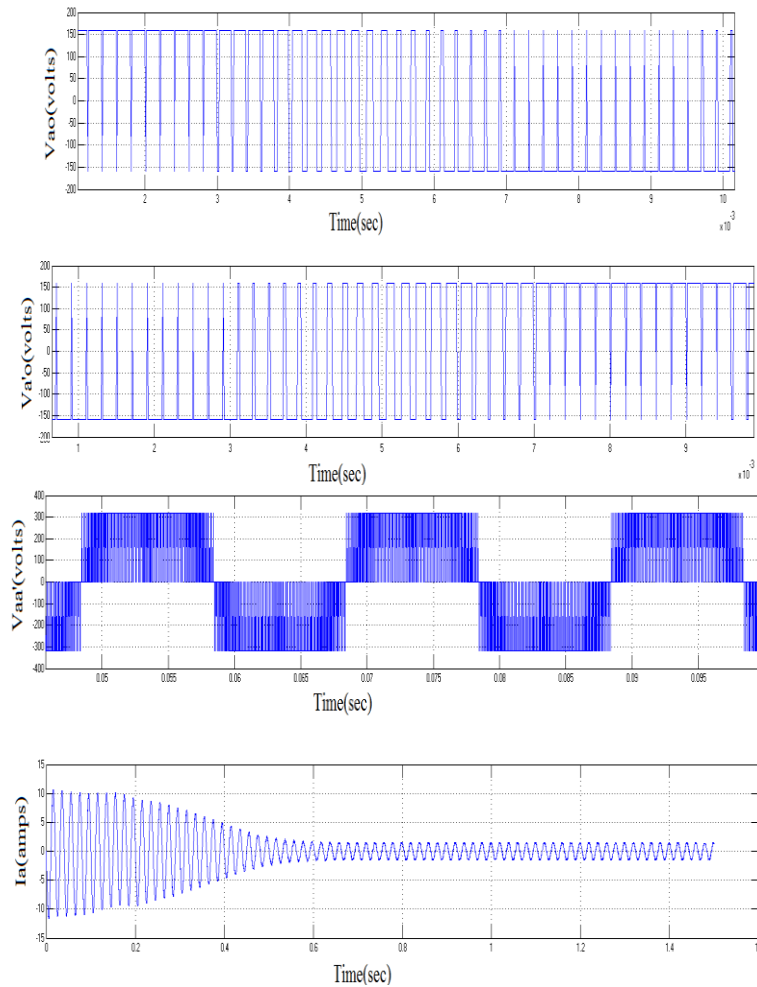


Fig.5: Simulated pole voltages of inverter-1 and inverter-2 (Top 2 traces), Difference in a-phase pole ($V_{aa'}$) voltages (3rd trace), motor a-phase current (4th trace), for a modulation index of 0.75.

IV. THE BIASING INVERTER PWM STRATEGY

This PWM strategy is based on the observation that the space vector combinations at the vertices and the center of a given sub-hexagon are obtained by clamping one inverter with an active state, while the other inverter assumes all the eight states. Consequently, one inverter may be employed as the biasing inverter to realize the biasing vector and the other inverter may be switched around this biasing vector. Figure 6 shows the basic operating principle of this PWM strategy.

In Fig 6, **OT** represents the reference vector with its tip situated in sector-7. It is resolved into two components **OA** and **AT**. The vector **OA** may be output with inverter-1 with its state clamped at 1(+--, Table-1) throughout the sampling time interval. The vector **AT** is realized in the average sense by switching inverter-2 around the sub hexagonal center, A. Alternatively, the biasing vector **OA** may be output with inverter-2 with its state clamped at 4'(-++, Table-1) throughout the sampling time interval. In that case, the switching vector **AT** is generated with inverter-1.

The modified instantaneous voltage phase references corresponding to the switching vector **AT** are denoted by V_a, V_b and V_c obtained by the following procedure:

1. The instantaneous phase references V_a^*, V_b^* and V_c^* corresponding to the reference vector **OT** are transformed into the corresponding equivalent two-phase system references V_{α}^* and V_{β}^* using the classical three phase to two phase transformation given by:

$$\begin{bmatrix} v_{\alpha}^* \\ v_{\beta}^* \end{bmatrix} = \begin{bmatrix} \frac{3}{2} & 0 & 0 \\ 0 & \frac{\sqrt{3}}{2} & -\frac{\sqrt{3}}{2} \end{bmatrix} \begin{bmatrix} v_a^* \\ v_b^* \\ v_c^* \end{bmatrix}$$

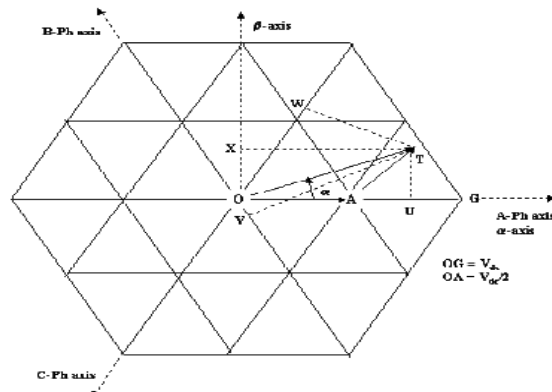


Fig.6: Principle of biasing inverter PWM strategy

- The sub-hexagonal center situated nearest to the tip of the reference vector **OT** is then determined.
- The coordinates of the nearest sub-hexagonal center in the V_α - V_β plane (the point 'A' in this example, Fig.26), denoted as $V_{\alpha,nshc}$ and $V_{\beta,nshc}$ are known for all the six sub-hexagonal centers. For example, the coordinates of the point 'A' in the V_α - V_β plane are given by $(V_{dc}/2, 0)$.
- Since the vector **OA** is output by the biasing inverter, the coordinates of the switching vector (**AT** in the present case) denoted as $V_{\alpha,sw}$ and $V_{\beta,sw}$ are given

$$V_{\alpha,sw} = V_\alpha^* - V_{\alpha,nshc} \text{ and } V_{\beta,sw} = V_\beta^* - V_{\beta,nshc}$$

- The modified reference phase voltages V_a, V_b and V_c for the switching inverter are then obtained by transforming $V_{\alpha,sw}, V_{\beta,sw}$ into the corresponding three phase variables by using the classical two phase –three phase transformation given by:

$$\begin{bmatrix} v_a \\ v_b \\ v_c \end{bmatrix} = \begin{bmatrix} 2/3 & 0 \\ -1/3 & 1/\sqrt{3} \\ -1/3 & -1/\sqrt{3} \end{bmatrix} \begin{bmatrix} V_{\alpha,sw} \\ V_{\beta,sw} \end{bmatrix}$$

- If inverter-2 is employed as the biasing inverter, the modified references are used directly to generate the switching vector **AT** with inverter-1. On the other hand, if inverter-1 is used as the biasing inverter, it is obvious that the modified references must be negated to generate the switching vector **AT** with inverter-2.

V. RESULTS & DISCUSSIONS FOR THE BIASING INVERTER PWM STRATEGY

The dual two-level inverter with biasing SVPWM switching scheme feeding power to open end winding induction motor drive is simulated using Matlab/SIMULINK simulation software. Then the results are verified experimentally.. A DC-bus voltage of 200 volts is chosen to run the drive and V/f control is maintained in the entire speed range of the induction motor. A total of 48 samples is chosen in the entire work covering one cycle of the output voltage, irrespective of the modulation index of the drive (speed of the motor).

The gating pulses of the top switching devices of the individual inverters (depicting the timings T_{ga}, T_{gb}, T_{gc} for invrter-1 and $T_{ga'}, T_{gb'}, T_{gc}'$ for inverter-2) are obtained simultaneously shown in Fig.7.The three phase pole voltages of the individual inverters will be a replica of the gating pulses shown in Fig.8 except for their voltage levels.

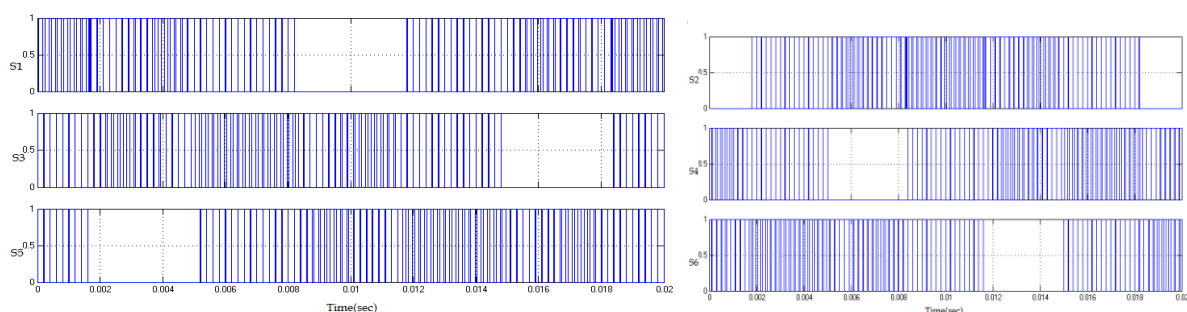


Fig.7: Gating Pulses for Inverter-1(T_{ga}, T_{gb}, T_{gc}) and Inverter-2($T_{ga}', T_{gb}', T_{gc}'$) for the modulation index 0.75

Here, the modulation index is defined as the ratio of the length of the reference space vector (V_{ref}) and the DC-bus voltage (V_{dc}).The experimentally obtained a-phase pole voltages of the two inverters, difference in a-phase pole voltages, motor a-phase voltage and the motor a-phase no-load current for a modulation index of 0.75 are as shown in the fig(8).

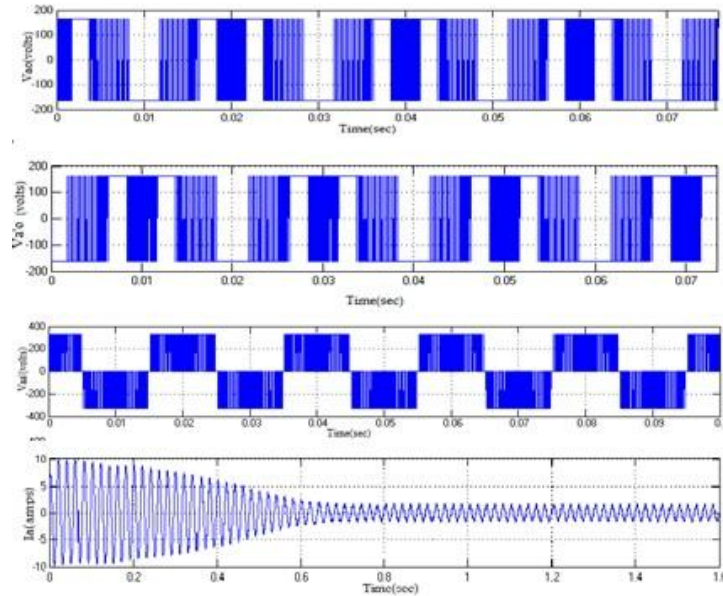


Fig. 8: Simulated pole voltages of inverter-1 and inverter-2 (Top 2 traces), Difference in a-phase pole ($V_{aa'}$) voltages (3rd trace), motor a-phase current(4th trace), for a modulation index of 0.75.

The comparison in terms of harmonic content for both the cases when the motor is fed by decoupled inverter and biasing inverters is done by the total harmonic distortion along with the respective change in the corresponding modulation index. For instance the simulated results of harmonic distortion for both the cases for a modulation index of 0.75 are as shown in fig (9).

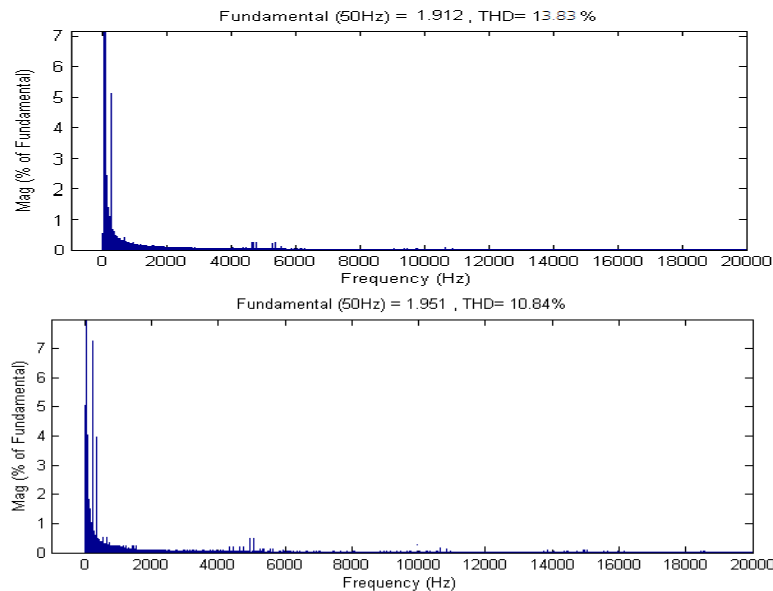


Fig. 9: Simulated Results Of %THD for Decoupled inverter fed (Top trace) and Biasing inverter fed (Bottom trace) Induction motor drive for a modulation index of 0.75

Various changes in the %THD at different levels of Modulation index are presented in table (2).With this it is reiterated that as the modulation index increases, the harmonic content in the motor phase currents is reduced.

Table (2): Total Harmonic Distortion of line currents of the induction motor for different modulation index

S.No	Operating Frequency	Modulation Index	Decoupled SVPWM Inverter Fed Induction Motor Drive	Biasing SVPWM Inverter Fed Induction Motor Drive
			Phase Current(I_a)	Phase Current(I_a)
			% THD	% THD
(1)	50	0.1	16.55	14.26
(2)	50	0.2	16.47	14.01
(3)	50	0.4	14.29	13.19
(4)	50	0.75	13.83	10.84
(5)	50	0.9	8.57	8.28

VI. CONCLUSION:

The dual two-level inverter is capable of generating three level output voltage using the SVPWM switching schemes. With the biasing inverter PWM strategy the reference space vector is reproduced in the average sense by switching amongst the vector combinations available at the nearest three vertices. Consequently the switching ripple with this strategy is lesser than the decoupled PWM strategy. The rms value of this harmonic content is decreasing with the increase in the modulation index of the dual-inverter feeding the open-end winding induction motor. In Biasing inverter PWM strategy, THD of the motor phase currents is low compared to that of Decoupled PWM algorithm.

APPENDIX:

Specification Parameters Of Induction Motor:

Stator Resistance (R_s) = 7.83 Ω
Rotor Resistance (R_r) = 7.55 Ω
Stator Inductance (L_s) = 0.4751H
Rotor Inductance (L_r) = 0.4751H
Mutual Inductance (L_m) = 0.4535H
Moment Of Inertia (J) = 0.06
Poles = 4

REFERENCES

- [1] R.M. Green and J.T. Boys, "Implementation of Pulse width Modulated Inverter Modulation Strategies", *IEEE Trans. On Ind. Appl.*, Vol. IA-18, No.2, Mar/Apr.1982, pp. 138 - 145.
- [2] J. Holtz, "Pulse width modulation- A survey", *IEEE Trans. on Industrial Electronics*, Vol. 30, No. 5, Dec 1992, pp. 410-420.
- [3] D. G. Holmes, "The significance of Zero-Space Vector placement for Carrier-based PWM schemes", *IEEE Trans. on Ind. Appl.*, vol.32, No.5, Sept-Oct 1996, pp. 1122-1129.
- [4] Vladimir Blasko, "Analysis of a Hybrid PWM based on Modified Space-Vector and Triangle-Comparison Methods", *IEEE Trans. on Ind. Appl.*, Vol.33, No.3, May/June, 1997, pp. 756-764.
- [5] G. Narayanan, Di Zhao and Harish K.krishnamurthy, "Space vector based hybrid PWM technique for reduced current ripple", *on Ind. Electronics*, Vol.55, No.4, April 2008, pp.1614 - 1627.
- [6] E.G. Shivakumar, K. Gopakumar, S.K. Sinha, Andre Pittet, V.T. Ranganathan, "Space Vector Control of Dual Inverter Fed Open-End Winding Induction Motor Drive", *EPE Journal*, Vol. 12, No. 1, February 2002, pp. 9-18.
- [7] V.T. Somasekhar, K. Gopakumar, "Three-Level Inverter Configuration Cascading Two Two-Level Inverters", *IEEE Proc. Electr. Power Appl.*, Vol. 150, No. 3, May 2003, pp. 245-254.
- [8] V.T. Somasekhar, K. Gopakumar, A. Pittet and V.T. Ranganathan, "PWM Inverter Switching Strategy for Dual Two-Level Inverter Fed Open End Winding Induction Motor Drive with a Switched Neutral", *IEE Proc. Of Electr. Power Appl.*, Vol. 149, No. 2, March 2002, pp. 152-160.
- [9] V.T. Somasekhar, K. Gopakumar, M.R. Baiju, K.K. Mohapatra and L. Umanand, "A Multilevel Inverter System for an Open End Winding Induction Motor with Open-End Windings," *IEEE transactions on Industrial Electronics*, Vol. 52, No. 3, June 2005, pp. 824-836.
- [10] V.T. Somasekhar, K. Gopakumar, E.G. Shivakumar, S.K. Sinha, "A Space Vector Modulation Scheme for Dual TwoLevel Inverter Fed an Open-End Winding Induction Motor Drive for the Elimination of Zero Sequence Current", *EPE Journal*, Vol. 12, No. 2, May 2002, pp. 26-36.
- [11] V.T. Somasekhar, M.R. Baiju and K. Gopakumar, "Dual Two Level Inverter Scheme for an Open- End Winding Induction Motor Drive with a Single DC Power Supply and Improved DC Bus Utilization", *IEE Proc.of Electr. Power.Appl.*, Vol. 151, No. 2, March 2004, pp. 230-238.
- [12] M. B. Baiju, K.K. Mohapatra, R.S. Kanchan and K. Gopakumar, "A Dual Two-Level Inverter Scheme with Common Mode Voltage Elimination for an Induction Motor Drive", *IEEE Transactions on Powe Electronics* Vol. 19, No. 3, May 2004, pp. 794-805.
- [13] V. Oleschuk, B.K. Bose, A.M. Stankovic, "Phase-Shift-Based Synchronous Modulation of Dual- Inverter for an Open-End Winding Induction Motor Drive with Elimination of Zero Sequence Currents", *Conf. Proc. IEEE-PEDS-2005*, pp. 325-330.
- [14] V. Oleschuk, F. Profumo, A. Tenconi and R. Bojoi, "Synchronized Pulse_Width Modulation Control of Inverter-Fed Open-End Winding Motor Drives", *EPE Conf.Proc.*, Pelincec, 2005, Paper-ID: 94.

Consistency Evolution of Process models based on Structural Analysis and Behavioral Profiles

CH. Gurunatham¹, P. Rajarajeswari², Dr. D. Vasumathi³

* (M.Tech, Computer Science and Engineering, Madanapalle Institute of Technology & Sciences, Madanapalle, A.P,India)

** (M.Tech[Ph.d], Assistant Professor, Department of CSE, Madanapalle Institute of Technology & Sciences, Madanapalle, A.P, India)

*** (M.Tech, Ph.d, Associate Professor, Department of CSE, JNTU Hyderabad, Hyderabad, A.P,India)

Abstract: To turn the business application of a software project to system specification is a big challenge in business environment. Since the business analysts and system analysts have their own perspective, the modeling of business processes is necessary to facilitate both the perspectives and for a better coordination. Many applications of such business processing model have given rise to problems at support models. As such maintaining consistency at such related models has become a big challenge for business modeling theory and practice. In this paper we project a theory to find out the consistency between the models is not coined and it is very much necessary to find out the inconsistencies so that change propagation between the models can be achieved. Behavioral profile, as a solution to the inappropriateness of behavioral equivalence notions will be proposed. This model is expected to resolve the behavioral constraints of a process model. Through this model, profiles can be computed efficiently in public time for sound free-choice Petri nets with reference to their number of places and transitions. We develop a slow model that verifies process consistency described in a Petri net graph. We provide both Structural Analysis and Behavioral Profiles to evaluate process consistency.

Key Words: Process Models, Petri nets, Behavioral Profiles, Structural Analysis, Process Modeling.

I. Introduction

Translating business requirements into system specification is a crucial task of any software engineering project in a business environment. The modeling of business processes has been identified as an important step towards bridging the gap between business and software development, and, among others, facilitating structured design [1], business-IT alignment [2], or engineering of process-aware information systems [3]. There are different solutions that should contribute to a smooth progression from business analysis to software implementation. Methodologies for integrated system design propose to derive technical realizations from business requirements directly via refinements [4], [5], [6]. In the same vein, the standardization of the Business Process Modeling Notation (BPMN) [7] by the OMG received much attention, due to the translation to the Web Services Business Process Execution Language (BPEL) [8] that is part of the specification. There are also various tools on the market that support business process modeling and corresponding transformations. We already mentioned that business analysts and software designers tend to model the same business process in quite different ways, which often impedes efficient communication. Clearly, pragmatics is an inherent feature of every conceptual model. While mapping and reducing the reality are essential for creating model, the purpose of the model determines what to map and what to reduce [11]. As business analysts and software designers have quite diverging concerns when looking at a business process, it is no surprise that business process models differ from software design models of the same process significantly. We will argue throughout this article that a formal concept for discussing the consistency of an alignment between two process models is missing. It is needed for identifying inconsistencies, as well as to enable

change propagation between these models. In the software engineering community, consistency refers to a 'degree of uniformity, standardization, and freedom of contradictions' [12].

An alignment of process models requires the identification of model correspondences, which is a well-researched topic in the database community. Correspondences relate elements that have matching semantics in the context of an alignment of two models (note that the semantics might differ in absolute terms). Given a set of correspondences, the question whether two data models are consistent is similar to the question whether a mapping between data schemas is valid, which is known from the field of data integration. In this area, various properties for evaluating the validity of a schema mapping have been proposed. For instance, compatibility of a mapping between two schemas requires the existence of a pair of instances that satisfies the constraints of the mapping as well of the respective schemas [13]. Translated into the domain of behavioral models, this yields a consistency notion, which requires the existence of a single trace that is possible in both models after the corresponding elements have been resolved. Again, we might draw the analogy to behavioral models under the assumption of behavioral constraints as the elementary elements. For a given projection between two models, that is a partial correspondence relation, all behavioral constraints on traces of one model are preserved in the traces of the other model. There is a multitude of equivalence criteria in the linear time – branching time spectrum [14]. This criterion is still rather strict, and might not be appropriate for deciding on a consistent alignment between two process models. First, trace equivalence is not invariant to so-called forgetful refinements of activities [15]. Forgetful refinement refers to a change, in which an activity is forgotten due to its

replacement with an empty activity. As a consequence, we argue that, for our purpose, a notion of consistency that guarantees 'freedom of contradictions' as required by [12] should be less strict than a notion requiring all information of one model to be present in another model as well. Furthermore, all behavioral equivalence criteria being discussed in this area, including trace equivalence [14], provide a true/false result.

We introduce the formal concept of a behavioral profile and structural analysis. These profiles capture the essential behavioral constraints of a process model and apply the structural analysis, such as mutual exclusion of activities or partial order. The behavioral profile enables us to overcome three major shortcomings of an application of trace equivalence in an alignment scenario and structural analysis verifies the accuracy and consistency measures captured during behavioral profiling.

- 1) Behavioral profiles are less sensitive to projections than trace equivalence. We will show that behavioral profiles of two process models remain unchanged even if additional start and end branches are introduced in one of the models.
- 2) The structure of a behavioral profile provides us with a straight-forward way to define a degree of consistency ranging from 0 to 1.0, referred to as the degree of profile consistency. In this way, we can feed back detailed information to business analysts and software designers on how far and where two models deviate from each other.
- 3) The concept of a behavioral profile builds on formal properties of free-choice Petri nets. This class of nets has been used for the formalization of most process modeling languages. The derivation of a behavioral profile and the calculation of a degree of profile consistency and structural analysis of the consistency measured have been implemented to demonstrate the applicability of our approach. In this article, we also report the findings from checking consistency between partially overlapping of example process models, a collection of benchmark process models that describe the functionality of specific business software. We introduce consistency measurement by using behavioral profiles and structural analysis in section2, We provide consistency measurement for aligned process models in section3, and we also provide Experiment and Result analysis in section4.

II. Consistency Measurement by using Behavioral Profiles and Structural Analysis

Business process change is at the very core of business process management, which aims at enabling flexible adaptation to changing business needs. However, the wide variety of drivers for business process modeling initiatives, reaching from business evolution to process enactment, results in multiple models that overlap in content due to serving different purposes. That, in turn, imposes serious challenges for the propagation of changes between these process models.

Now a day, Business Process Management (BPM) has a broad field of application, reaching from process evolution to process enactment. The *purpose* guides the creation of every particular process model. It is a consequence of this observation that companies create

different models for the same process. These models reside on different levels of abstraction and assume different modeling perspectives depending on what is appropriate with respect to the modeling goal. The flexibility to adapt business processes in order to respond to changing business needs is at the very heart of BPM. Therefore, the *propagation of changes* between several related process models is a major use case for model alignment. According to Gartner, change is of high relevance to the key elements of the BPM discipline, which are *'keeping the business process model in sync with process execution [and] enabling rapid iteration of processes and underlying systems for continuous process improvement and optimization'*.

In our proposal presents a novel approach to change propagation between business process models. Its central contribution is the definition and application of a technique for dealing with overlapping process models that are not defined in terms of a hierarchical refinement. This technique is based on the notion of a behavioral profile which captures a set of dedicated behavioral aspects of a process model. Given a change in the source model, our approach isolates a potential *change region* in the target model grounded on the behavioral profile of corresponding activities. In this way, process modelers can quickly assess the necessity to propagate the change. If change propagation seems to be appropriate, the change region spots the position where to extend the model.

A. Process Models

Our notion of a process model is based on a graph containing activity nodes and control nodes, which, in turn, captures the commonalities of process description languages.

Behavioral Profiles

The Behavioral profile aims at capturing Behavioral aspects of a process in a fine-grained manner. That is, it consists of three relations between nodes of a process graph. These relations are based on the notion of weak order. Two nodes or flow arcs of a process model are in weak order if there a trace in which one node occurs after the other. Note that we require only the existence of such a trace. Thus, weak order does not have to hold for all traces of the model.

- The strict order relation $x \succ P(y)$ and $y \neg \succ P(x)$
- The exclusiveness relation $x \neg \succ P(y)$ and $y \neg \succ P(x)$
- The observation concurrency relation $x \succ P(y)$ and / or $y \succ P(x)$

The set of all three relations is the Behavioral profile. Two process models with equivalent behavioral profiles may differ in the trace equivalence, in contrast the two process models with identical trace equivalence can also identical in behavioral profiles.

Correspondence Relation: if the relation between two process models is left unique and is not functional

Aligned Transitions: let a_1, a_2 correspondence to a and c_1, c_2 correspondence to c . if transition observed from a_1 to c_1, a_1 to c_2, a_2 to c_1 or a_2 to c_2 then the transition relation between a to c is aligned transition.

Projected Firing sequence: In a sequence considered, the set of aligned sequences is referred as firing sequence.

Trace Consistency of Alignment: If Aligned transitions of a projected firing sequence contain trace equivalence then it reflects as Trace consistency of alignment.

B. Structural analysis: The structural analysis of dynamic lumped process models forms an important step in the model building procedure and it is used for the determination of the solvability properties of the model, too. This analysis includes the determination of the degree of freedom, structural solvability, differential index and the dynamic degrees of freedom. As a result of the analysis, the decomposition of the model is obtained and the calculation path can be determined. This way the appropriate numerical method for solving the model can be chosen efficiently. Moreover, advice on how to improve the computational properties of the model by modifying its form or its specification can also be given.

Effective graph-theoretical methods have been proposed in the literature based on the analysis tools developed by, for the determination of the most important solvability property of lumped dynamic models: the differential index. The properties of the dynamic representation graph of process models described by semi-explicit DAE-systems have also been analyzed there in case of index 1 and higher index models. Beside the algorithm of determining the differential index by using the representation graph, a model modification method has also been proposed in the literature, which results in a structurally solvable model even in the case of higher index models.

C. Structural solvability

As a first step, we consider a system of linear or nonlinear algebraic equations in its so called *standard form* where $x_j (j = 1, \dots, N)$ and $u_k (k = 1, \dots, K)$ are unknowns, $y_i (i = 1, \dots, M)$ are known parameters, $f_i (i = 1, \dots, M)$ and $g_k (k = 1, \dots, K)$ are assumed to be sufficiently smooth real-valued functions. The system of equations above is structurally solvable, if the Jacobian matrix $J(x \setminus u)$ referring to the above model is non-singular.

$$y_i = f_i(x, u), i = 1, \dots, M \quad u_k = g_k(x, u), k = 1, \dots, K$$

Consider a system of equations in standard form. We construct a directed graph to represent the structure of the set of equations in the following way. The vertex-set corresponding to unknowns and parameters is partitioned as

$$X \cup U \cup Y, \quad \text{where}$$

$$X = \{x_1, \dots, x_N\}, U = \{u_1, \dots, u_k\} \text{ and}$$

$Y = \{y_1, \dots, y_M\}$. The functional dependence described by an equation is expressed by arcs coming into y_i or u_k respectively from those x_j and u_l , which appear on its

right-hand side. This graph is called the representation graph of the system of equations.

A Menger-type linking from X to Y is a set of pair-wise vertex-disjoint directed paths from a vertex in X to a vertex in Y . The size of a linking is the number of directed paths from X to Y contained in the linking. In case $|X| = |Y|, (M = N)$, a linking of size X is called a complete linking. The graphical condition of the structural solvability is then the following:

Linkage theorem: Assume that the non-vanishing elements of partial derivatives / and graphs, in the standard form model are algebraically independent over the rational number field O . Then the model is structurally solvable if and only if there exists a Menger-type complete linking from X to Y on the representation graph.

We can adapt the graphical techniques to DAE- systems, as well. An ordinary differential equation of a DAE-system can be described by the following equation:

$$x' = f(x_1, \dots, x_n)$$

Here x denotes an arbitrary variable depending on time. x' denotes the derivative of x with respect to time and x_1, \dots, x_n are those variables which have effect on variable x' according to the differential equation.

In DAE-systems there are two types of variables. **Differential variables** are the variables with their time derivative present in the model. Variables, which do not have their time derivative present, are called **algebraic variables**. The derivative x' is called **derivative** (velocity) **variable**.

D. Dynamic representation graph

The value of differential variables is usually computed by using a numerical integration method. Therefore a system of equations including also differential equations can be represented by a **dynamic graph**. A dynamic graph is a sequence of static graphs corresponding to each time step of the integration. On a dynamic graph there are directed arcs attached from the previous static graph to the succeeding static graph that are determined by the method applied for solving the ordinary differential equations. In case of a single step explicit method, the value of a differential variable at time $t+h$ is computed using the corresponding differential value and its value at a previous time t . For example, when the explicit Euler method is used:

$$x(t+h) = x(t) + h \cdot x'(t)$$

where h denotes the step length during the numerical integration. The structure of a dynamic graph assuming explicit Euler method for solving differential equations is shown in **Fig. 1**.

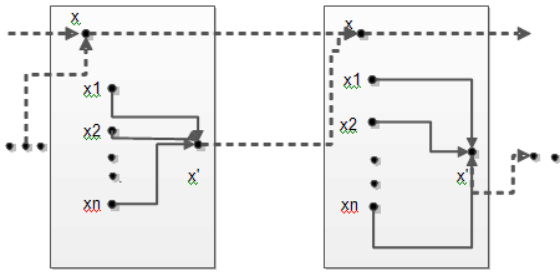


Fig 1: Dynamic Graph model for Euler method

The structural analysis based on graph theoretical technique is carried out in steps performed sequentially. The first step is to rewrite the model into its standard form. The second step is the assignment of types to vertices in the representation graph. The important types of vertices determined by the model specification are the following:

• **<S>(set)-type variables:** These represent variables, which are assigned to the specified given values. In the case of a dynamic representation graph assuming explicit method for solving the differential equations, the differential variables will be labeled by type <S*> because their initial value can be obtained from the initial values, and then their values can be calculated step by step by numerical integration. Labels <S> and <S*> are treated the same way during the analysis.

• **<G>(given)-type variables:** A variable assigned to a specific value of a left hand side is a <G>-type variable. Unlike the <S>-type variables, the values of the right hand side variables will be suitably adjusted so as to preserve the equality of the two sides.

According to the representation graph, the value of every variable which has incoming arcs only from vertices labeled by type <S> can be calculated by simple substitution into the corresponding equation. These variables become **secondarily labeled by type <S>**, and this process can be repeated if necessary. Omitting all vertices labeled primarily, secondarily, etc. by type <S> and all arcs starting from them from the representation graph we obtain the **reduced graph**. The classification of vertices of a reduced graph is as follows:

- all initial vertices form the unknown variable set X
- all terminal vertices labeled by type <G> constitute the known variable (parameter) set Y,
- all other vertices constitute the known variable set Y.

Dynamic process models can be described by **semi- explicit DAEs** as follows:

$$z_1 = f(z_1, z_2, t), z_1(t_0) = z_{10}$$

(1)

$$0 = g(z_1, z_2, t)$$

(2)

The most important structural computational property of DAE models is the differential index. By definition the differential index of the semi-explicit DAE (Equations (1)-(2)) is one if one differentiation is sufficient to express z_2 as a continuous function of z_1, z_2 and t . One differentiation is sufficient if and only if the Jacobian matrix g_{z_2} is non-singular.

In our earlier work we have proved that the differential index of the models investigated in is equal to 1

if and only if there exists a Menger-type complete linking on the reduced graph at any time step t .

If the differential index of the investigated model is greater than 1 then there is no Menger-type complete linking on the static graph at any time step t . The properties of a static graph of a dynamic model, which has differential indexes are as follows.

1. Let us form the following variable sets.

I_0 is the set of the differential variables belonging to the over specified sub graph,

D_0 is the set of the derivative variables referring to the differential variables of set I_0 ,

I_1 is the set of differential variables from which directed paths lead to the derivative variables in the set D_0 ,

D_1 is the set of derivative variables referring to the differential variables of set I_1, \dots ,

I_k is the set of differential variables from which directed paths lead to the derivative variables in the set D_{k-1} ,

D_k is the set of derivative variables referring to the differential variables of set I_k, \dots ,

2. Let n be the smallest natural number for which the set D_n contains some derivative variables of the underspecified sub graph. Then the differential index of the model is

$$v_d = n + 2$$

If there is no such number n then the model is not structurally solvable.

In our earlier work we have shown that the important properties of the representation graph including the differential index of the models are independent of the assumption whether a single-step, explicit or implicit numerical method is used for the solution of the differential equations.

III. Consistency measurement for aligned process models:

The previously defined concept of a behavioral profile allows us to formally discuss the notion of a degree of profile consistency between a pair of process models. We will use the classical notion of trace equivalence, which we extend to trace consistency, as a benchmark.

Consistency based on Trace Equivalence

As a benchmark for our consistency analysis, we define a notion of consistency based on the trace equivalence criterion. First, we adapt the trace equivalence criterion for model alignments yielding the notion of trace consistency. Second, the degree of trace consistency is introduced based on the amount of traces of one model that have a counterpart in the other model. We already mentioned in Section 2 that the application of trace equivalence in an alignment setting requires that all parts that have been subject to projection are discarded.

Consistency based on Behavioral Profiles

In general, our notion of consistency based on behavioral profiles, i.e., profile consistency, is grounded on the preservation of behavioral relations for corresponding activities. In contrast to the notion of a trace consistent alignment, it does not require the correspondence relation to be injective. Instead, it allows for 1:n (and even n:m) correspondences. Therefore, this notion can be applied to vertical as well as horizontal alignments. Preservation of the behavioral relation is only required in case there are no overlapping correspondences.

Interpretation of Profile Consistency

As exemplified in the previous section, the degree of profile consistency ranges between 0 and 1.0 for two process models and a correspondence relation. Still, a degree of 1.0 does not imply that both models are (projected) trace equivalent. This stems from the fact that the underlying behavioral profile represents a behavioral abstraction; apparently, the degree of profile consistency quantifies the quality of an alignment with respect to the **order of potential activity occurrences**. A degree of 1.0 guarantee the all these constraints are equal for the aligned activities of two models. A degree of 0.9, in turn, indicates that the constraints on the order of potential activity occurrences are equal solely for 90% of the relations between aligned activities. However, we assume these thresholds to be highly dependent on a specific project setting. Once a degree of profile consistency below 1.0 is observed, the question of how to locate the source of inconsistency has to be addressed. According to our approach, inconsistencies manifest themselves in different relations of the behavioral profile of two process models for a pair of aligned activities.

This information can directly be provided to business analysts and system analysts in order to judge on the necessity of the inconsistency. While this kind of feedback allows for locating the inconsistency directly in case of only a few inconsistent profile relations (e.g., caused by an interchanged order of two activities in a sequence), it might be inappropriate if a big number of profile relations is inconsistent. Imagine two process models containing a set of aligned activities in sequential order and assume that one of these activities in one model would now be moved to a branch that is executed concurrently to the remaining activities. Then, all behavioral relations between this activity and the remaining activities would be inconsistent, such that feedback on the set of activities that show inconsistent relations would be of little help. Instead, we would consider the biggest subset of aligned activities that show consistent behavioral relations among each other to be valuable feedback on the observed inconsistencies. For the aforementioned case, the single activity having inconsistent relations with all other activities might be identified by this approach.

IV. Experiments and Results Analysis

After preprocessing of the benchmark models, we are able to analyze its consistency. As mentioned before, we establish correspondences between events and functions with equal labels. Further on, we extract all pairs of process models that are aligned by at least two correspondences. For such a pair, we then calculate the consistency measures,

that is, trace consistency, the degree of trace consistency, and the degree of profile consistency of the alignment and finally analyzed the accuracy of the degree of profile using structural analysis.

The results are optimistic from the experiments conducted on bench mark business models represented in Petrinet format. We consider the consistency measurement systems WF systems (WF), and Behavior profiling (BP) analysis to compare with the proposed Behavior Profiling and Structural Analysis (BP&SA). We can find the significant benefit of BP&SA over other models. Fig 2 represents the comparison of optimality in consistency measurement between BP&SA and other two models. In fig 3 we can observe the computational over head of the WF. Here BP is having slight advantage over BP&SA, which can be negligible while considering the accuracy achieved through BP&SA in consistency measurement.

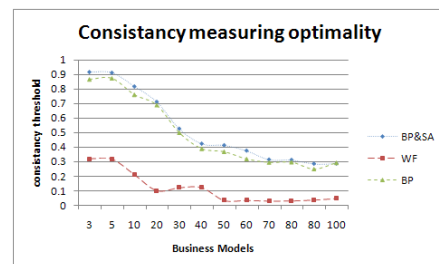


Fig 2: Optimality in Consistency Measurement

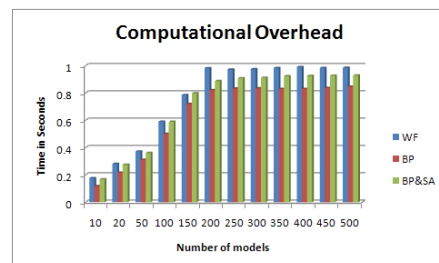


Fig 3: Computational Overhead comparison report

V. Conclusion:

.we have discussed alignment issues between related process models at different abstract levels and different perspectives.. We proposed the concept of behavioral profile that captures the essential behavioral constraints of a process model. Such behavioral profiles are used for the definition of the formal notion of profile consistency. Behavioral profiles provide three major advantages in contrast to the existing notion of trace equivalence and consistency measures that build up it. Finally, the concept of a behavioral profile builds informal properties of free-choice Petri nets. We proved that profile consistency can be checked for sound free-choice WF-systems in $O(n^3)$ time with n nodes.

. There are several directions for future research based on behavioral profiles. We have emphasized the fact that different interrelated process models and variants are utilized for the development of process-aware information systems.. We are optimistic that algorithms can be defined to synthesize process model from a behavioral profile, as there exist synthesis techniques to build Petri nets from transition systems and from traces. Such algorithms might

not only take one profile as input. We are currently experimenting with building integrated process models from two behavioral profiles and their alignment.

REFERENCES

- [1] E. Yourdon, Modern structured analysis. Yourdon Press Upper Saddle River, NJ, USA, 1989.
- [2] J. Luftman, R. Papp, and T. Brier, "Enablers and inhibitors of business-IT alignment," Communications of the AIS, vol. 1, no. 3, 1999.
- [3] E. Kindler, "Model-based software engineering and process-aware information systems," LNCS Transactions on Petri Nets and Other Models of Concurrency, vol. 2, pp. 27–45, 2009.
- [4] M. Henkel, J. Zdravkovic, and P. Johannes son, "Service-based processes: Design for business and technology," in ICSOC, M. Aiello, Aoyama, F. Curb era, and M. P. Papazoglou, Eds. ACM, 2004, pp. 21–29.
- [5] B. Anderson, M. Bergholtz, A. Edirisuriya, T. Ilayperuma, and. Johansson, "A Declarative Foundation of Process Models," in CAiSE, ser. Lecture Notes in Computer Science, O. Pastor and J. F.e Cunha, Eds., vol. 3520. Springer, 2005, pp. 233–247.
- [6] J. Koehler, R. Hauser, J. M. K" uster, K. Ryndina, J. Vanhatalo, and M. Wahler, "The role of visual modeling and model transformations in business-driven development," Electr. Notes Theor. Comput.Sci. vol. 211, pp. 5–15, 2008.
- [7] OMG, Business Process Modeling Notation (BPMN) 1.2, January 2009.
- [8] Alexandre Alves et al., "Web Services Business Process Execution Language Version 2.0," OASIS, Tech. Rep., January 2007.
- [9] V. Grover, K. Fiedler, and J. Teng, "Exploring the Success of Information Technology Enabled Business Process Reengineering," IEEE Transactions on Engineering Management, vol. 41, no. 3, pp.276–284, August 1994.
- [10] C. Rolland and N. Prakash, "Bridging the Gap Between OrganisationalNeeds and ERP Functionality," Requirements Engineering, vol. 5, no. 3, pp. 180–193, October 2000.
- [11] T. K" uhne, "Matters of (Meta-)Modeling," Software and System Modeling, vol. 5, no. 4, pp. 369–385, 2006.
- [12] IEEE, "Standard Glossary of Software Engineering Terminology," 1990.



CH. Gurunatham, received the B.Tech from JNTU-Anantapur and pursuing M.Tech from Madanapalle Institute of Technology & Sciences (JNTU-Anantapur). He is doing his academic project under the Guidance of Mrs. P. Rajarajeswari.

His Research interests on Software Engineering, Software architecture and Web Technologies.



P. Rajarajeswari, received the B. Tech. from S.V University, Sri Venkateswara University, Tirupathi, Andhra Pradesh. M. Tech degree in Computer Science from JNT University, Hyderabad and Pursuing Ph.D in Computer Science

and Engineering, JNT University Hyderabad Andhra Pradesh, India. Presently She is working as Assistant Professor of Computer Science and Engineering in Madanapalle Institute of Technology and Science, Madanapalle, Chittoor (Dt), Andrapradesh.



Dr. D.Vasumathi, received the B. Tech. from JNT University, Hyderabad, M. Tech degree in Computer Science and Engineering from JNT University, Hyderabad and Ph. D in Computer Science and Engineering JNT University Hyderabad Andhra Pradesh, India. She worked as

Assistant Professor, Presently working as Associate Professor in JNT University, Hyderabad .She has 12 years of Teaching experience. Currently guiding 8 Ph. D scholars. She is life member of ISTE and IE. Her research interests Data Mining, Image processing, Web technologies, She has 5 international publications and 10 international conference Publications at International and National level.

Modelling and Controlling Of Unified Power Flow Controller (Upfc)

K.Suresh¹ P.Venkatesh²

¹Assistant Professor, Department of Electrical and Electronics Engg. RGM CET, Nandyal, India-518 501.

²PG-Student, Department of Electrical and Electronics Engg. RGM CET, Nandyal, India.

Abstract: Unified Power Flow Controller (UPFC) has its unique capability to control simultaneously real and reactive power flows on a transmission line as well as to regulate voltage at the bus where it is connected, this device creates a tremendous quality impact on power system stability. These features become even more significant knowing that the UPFC can allow loading of the transmission lines close to their thermal limits, forcing the power to flow through the desired paths. This will give the power system operators much needed flexibility in order to satisfy the demands that the deregulated power system will impose. The controller used in the control mechanism has an important effect on the performance of UPFC and it operates in several modes of operations using different control mechanisms based on Proportional-Integral controller has been studied. In this paper a proposed control method, ANFIS based controller has been developed by using ANFIS EDITOR of MATLAB using Takagi-Sugeno Inference system and this will applied to STATCOM part of the detailed model of UPFC. The MATLAB simulation results shows that ANFIS controller has an effective power flow control, less settling time and less overshoot when compared to PI controller in different operating modes.

Key words: ANFIS, FACTS, Power System, UPFC.

I. Introduction

The static series synchronous compensator (SSSC) can control active and reactive in a transmission line in a small range via stored energy in capacitor DC-link where static synchronous compensator (STATCOM) with injecting reactive power can regulate the bus voltage in a transmission line. Unified Power Flow Controller (UPFC) is the most versatile and complex Flexible AC Transmission Systems (FACTS) equipment that has emerged for the control and optimization of power flow in power transmission systems [1-3]. It has the combining features of both series converter and shunt converter based FACTS devices, and is capable of realizing voltage regulation, series compensation, and phase angle regulation at the same time. Therefore, the UPFC is capable of independently controlling the active power and reactive power on the compensated transmission line [4, 5]. The electric utilities are continuously looking for new devices that will enable interconnected systems to have increased power transfer abilities with transmission lines. UPFC and IPFC are FACTS devices that can control the power flow in transmission line by injecting active and reactive voltage component in form series to the transmission line. The UPFC is a flitting multi-purpose FACTS device that extends their capability to inject shunt current or series voltage that involve real power flow as well With UPFC, the real and reactive power can be controlled independently. The unified power flow controller is capable of controlling all the power system parameters such as

voltage magnitudes, phase angles, and effective line impedance simultaneously consists of two voltage source Converters (VSCs) that are connected to a common DC-link. One of the VSCs is connected in series with a transmission line while the other one is connected in shunt with the same transmission line. The DC bus of both VSCs are supplied through a common DC capacitor, hence UPFC combines the functions of a STATCOM and a SSSC. STATCOM maintains constant the bus voltage and provide energy for DC link of SSSC and it can regulate capacitor's voltage of DC link, SSSC with injection controllable voltage controls the active and reactive power flow control in the transmission line.

It can simultaneously perform the function of transmission line real/reactive power flow control in addition to UPFC bus voltage/shunt reactive power control. The control mechanism and the controller have important effect on the performance of UPFC. In literature, several control mechanisms are used in the UPFC model. A novel fuzzy inference system is proposed and used to improve the dynamic control of real and reactive power .control scheme is used in the control mechanism of UPFC. In the simulation results, there is a high Overshoot values occurred both real power and bus voltage during the three phase faults applied. However, the real power value is increased but there is no value changed in the reactive power. In the simulation results, the variation of the real power direction can be observed easily. According to results; the values of real and reactive power are changed in large values with UPFC because of the low values of bus voltage. This paper presents the performance evaluation of UPFC in different modes by using different control mechanisms based on PI and ANFIS based controllers. "Takagi-Sugeno Inference System" is used in the decision making of fuzzy model.

II. Unified Power Flow Controller

Unified power flow controller (UPFC) is a combination of static synchronous compensator (STATCOM) and a static synchronous series compensator (SSSC) which are coupled via a common dc link, to allow bi-directional flow of real power between the series output terminals of the SSSC and the shunt output terminals of the STATCOM and are controlled to provide concurrent real and reactive series line compensation without an external electric energy source. The UPFC, by means of angularly unconstrained series voltage injection, is able to control, concurrently or selectively, the transmission line voltage, impedance and angle or alternatively, the real and reactive power flow in the line. The UPFC may also provide independently controllable shunt reactive compensation. Viewing the operation of the UPFC from the standpoint of conventional power transmission based on reactive shunt compensation, series compensation and phase shifting, the UPFC can fulfil all these functions and thereby meet

multiple control objectives by adding the injected voltage V_{inj} with appropriate amplitude and phase angle.

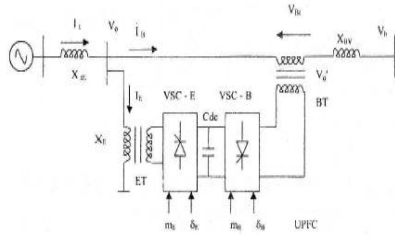


Fig 1. UPFC Installed in SMIB System

A combination of SHUNT controller and SERIES controller action is works as a unified power flow controller (UPFC) is used to control the power flow in a 500 kV transmission system. The SSSC and STATCOM located at the left end of the 75-km line L2, between the 500 kV buses B1 and B2, is used to control the active and reactive powers flowing through bus B2 while controlling voltage at bus B1. It consists of two 100-MVA, three-level, 48-pulse GTO-based converters, one connected in shunt at bus B1 and one connected in series between buses B1 and B2. The shunt and series converters can exchange power through a DC bus. The series converter can inject a maximum of 10% of nominal line-to-ground voltage (28.87 kV) in series with line L2. This pair of converters can be operated in three modes: Unified Power Flow Controller (UPFC) mode, when the shunt and series converters are interconnected through the DC bus. When the disconnect switches between the DC buses of the shunt and series converter are opened, two additional modes are available: Shunt converter operating as a Static Synchronous Compensator (STATCOM) controlling voltage at bus B1 Series converter operating as a Static Synchronous Series Capacitor (SSSC) controlling injected voltage, while keeping injected voltage in quadrature with current.

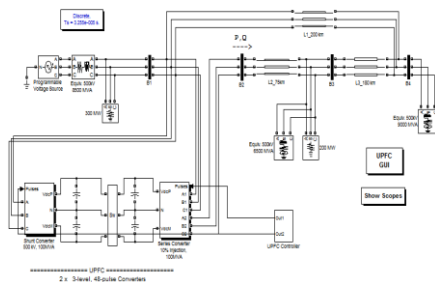


Fig 2. UPFC Simulink Model

III. Power control in UPFC mode:

Open the UPFC GUI block menu. The GUI allows you to choose the operation mode (UPFC, STATCOM or SSSC) as well as the Pref/Qref reference powers and/or Vref reference voltage settings. Also, in order to observe the dynamic response of the control system, the GUI allows you to specify a step change of any reference value at a specific time. Make sure that the operation mode is set to "UPFC (Power Flow Control)". The reference active and reactive powers are specified in the last two lines of the GUI menu. Initially, Pref= +8.7 pu/100MVA (+870 MW) and Qref=-0.6 pu/100MVA (-60 Mvar). At t=0.25 sec Pref is changed to +10 pu (+1000MW). Then, at t=0.5 sec, Qref is changed to +0.7 pu (+70 Mvar). The reference voltage of the shunt converter will be kept constant at Vref=1 pu during the

whole simulation 0.8 sec. When the UPFC is in power control mode, the changes in STATCOM reference reactive power and in SSSC injected voltage as are not used. Run the simulation for 0.8 sec. Open the "Show Scopes" subsystem. Observe on traces 1 and 2 of the UPFC scope the variations of P and Q. After a transient period lasting approximately 0.15 sec, the steady state is reached (P=+8.7 pu; Q=-0.6 pu). Then P and Q are ramped to the new settings (P=+10 pu Q=+0.7 pu). Observe on traces 3 and 4 the resulting changes in P Q on the three transmission lines. The performance of the shunt and series converters can be observed respectively on the STATCOM and SSSC scopes. If you zoom on the first trace of the STATCOM scope, you can observe the 48-step voltage waveform V_s generated on the secondary side of the shunt converter transformer superimposed with the primary voltage V_p and the primary current I_p . The dc bus voltage varies in the 19kV-21kV range. If you zoom on the first trace of the SSSC scope, you can observe the injected voltage waveforms V_{inj} measured between buses B1 and B2.

IV. VAR control in STATCOM mode:

In the GUI block menu, change the operation mode to "STATCOM (VAR Control)". Make sure that the STATCOM references values (1st line of parameters, [T1 T2 Q1 Q2]) are set to [0.3 0.5 +0.8 -0.8]. In this mode, the STATCOM is operated as a variable source of reactive power. Initially, Q is set to zero, then at T1=0.3 sec Q is increased to +0.8 pu (STATCOM absorbing reactive power) and at T2=0.5 sec, Q is reversed to -0.8 pu (STATCOM generating reactive power). Run the simulation and observe on the STATCOM scope the dynamic response of the STATCOM. Zoom on the first trace around t=0.5 sec when Q is changed from +0.8 pu to -0.8 pu. When Q=+0.8 pu, the current flowing into the STATCOM is lagging voltage, indicating that STATCOM is absorbing reactive power. When Qref is changed from +0.8 to -0.8, the current phase shift with respect to voltage changes from 90 degrees lagging to 90 degrees leading within one cycle. This control of reactive power is obtained by varying the magnitude of the secondary voltage V_s generated by the shunt converter while keeping it in phase with the bus B1 voltage V_p . This change of V_s magnitude is performed by controlling the dc bus voltage. When Q is changing from +0.8 pu to -0.8 pu, Vdc (trace 3) increases from 17.5 kV to 21 kV.

V. Series voltage injection in SSSC mode:

In the GUI block menu change the operation mode to "SSSC (Voltage injection)". Make sure that the SSSC references values (3rd line of parameters) [Vinj_Initial Vinj_Final StepTime] are set to [0.0 0.08 0.3]. The initial voltage is set to 0 pu, then at t=0.3 sec it will be ramped to 0.8 pu. Run the simulation and observe on the SSSC scope the impact of injected voltage on P and Q flowing in the 3 transmission lines. Contrary to the UPFC mode, in SSSC mode the series inverter operates with a constant conduction angle (Sigma= 172.5 degrees). The magnitude of the injected voltage is controlled by varying the dc voltage which is proportional to V_{inj} (3rd trace). Also, observe the waveforms of injected voltages (1st trace) and currents flowing through the SSSC (2nd trace). Voltages and currents stay in quadrature so that the SSSC operates as a variable inductance or capacitance.

VI. Anfis Controller

The ANFIS is the abbreviated of *adaptive neuro-fuzzy inference system*[13]. The performance of this method is like both ANN and FL. In both ANN and FL case, the input pass through the input layer (by input membership function) and the output could be seen in output layer (by output membership functions). Using a given input/output data set, the toolbox function ANFIS construct a fuzzy inference system (FIS) whose membership function parameters are tuned (adjusted).This adjustment allows your fuzzy systems to learn from the data they are modeling. Rule structure is essentially predetermined by the users' interpretation of the characteristic of the variables in the model. ANFIS applies FIS technique to data modeling [14]. We can choose membership function parameters automatically using ANFIS tool in MATLAB. Using ANFIS we can apply fuzzy inference to a system for which we already have a collection of input/ output data sets of parameters .Gradient vector reduce some error measures. This error measures is usually defined by the sum of the squared difference between the actual and desired outputs. ANFIS uses either back propagation or a combination of least squares estimation. Collect input/output data in a form that will be usable by ANFIS for training. You can create, train and test Sugeno type fuzzy systems using the ANFIS editor GUI. GUI includes four distinct areas to support a typical work flow (1>Loading ,plotting and clearing data (2)Generating or loading the initial FIS structure (3) training the FIS.(4)Validating the trained FIS. To get the FIS (Fuzzy inference system) from ANFIS tool, Training data is required for this, simulations were carried out on the original model with different values of voltage amplitude the data is shown in table below

Table I: Testing Data

Sr.No	input data	Output data
1	.9707	.9703
2	.9776	.7763
3	.9795	.6468
4	.9812	.5821
5	.983	.5174
6	.9847	.4527
7	1.004	-.2595
8	1.006	-.3242
9	1.007	-.3889
10	1.009	-.4536
11	1.011	-.5184
12	1.013	-.5831

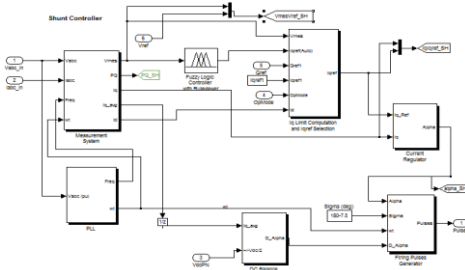


Fig 3.UPFC with ANFIS based Fuzzy controller

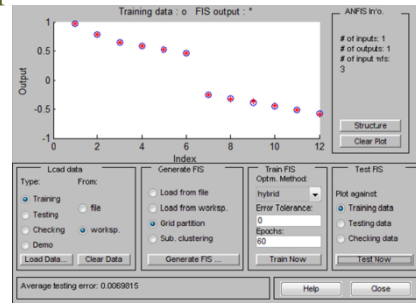


Fig 4. Errors in checking the testing and training data

VII. RESULTS and DISCUSSION

(i) Dynamic response of the system when it is used in UPFC mode With PI Controller.

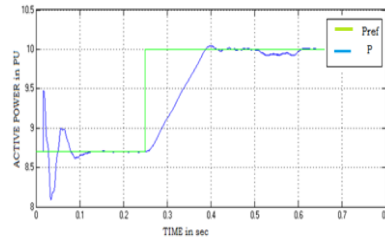


Fig 5. Active Power control with PI controller

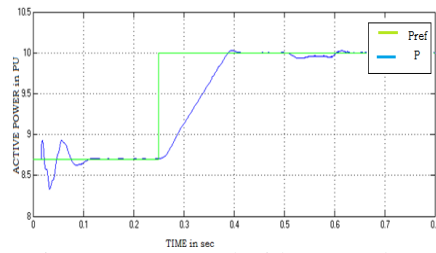


Fig 6. Active Power Control with ANFIS based controller

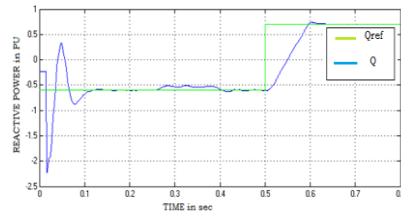


Fig 7. Reactive Power control with PI controller

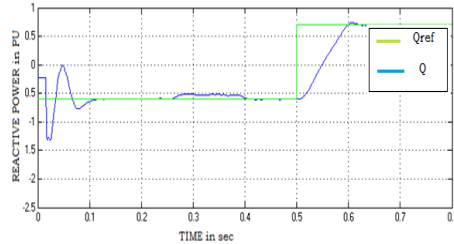


Fig 8.Reactive Power control with ANFIS based controller

(ii) Reactive Power Control in STATCOM mode with PI Controller

STATCOM operates as variable source of reactive power.Current lagging voltage during absorbing of reactive power and it is leading when reactive power is generated and it is controlled by DC Voltage

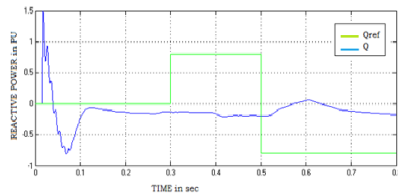


Fig 9. Reactive Power control during STATCOM mode with PI Controller

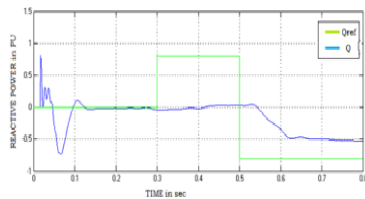


Fig 10. Reactive Power control during STATCOM mode with ANFIS based controller

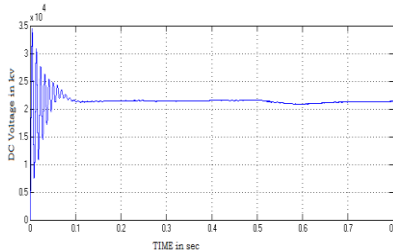


Fig 11. Variation of DC Voltage as per change in V_{inj} with PI Controller

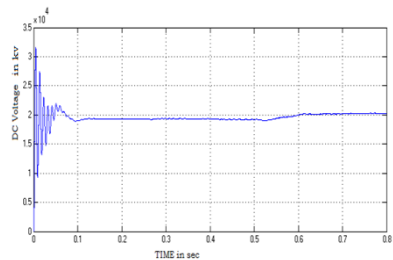


Fig 12. Variation of DC Voltage as per change in V_{inj} with ANFIS based Controller

VIII. Conclusion

Simulation results show that ANFIS based controlled slightly increases the power flow control by increasing the damping rate and decreases the amplitude of low frequency oscillations. Results comparison between conventional PI controller and the proposed ANFIS based controller for UPFC indicates that the proposed ANFIS based controller has less settling time and less overshoot when compared with the conventional PI controller.

References

- [1] N. G. Hingorani and L. Gyugyi, Understanding FACTS, Concepts, and Technology of Flexible AC Transmission Systems. Piscataway, NJ: IEEE Press, 2000.
- [2] L. Gyugyi, —Dynamic compensation of ac transmission lines by solidstate synchronous voltage sources,| IEEE Trans. Power Del., vol. 9, no. 2, pp. 904–911, Apr. 1994.
- [3] C. Schauder and H. Mehta, —Vector analysis and control of advanced static var compensator,| in Proc. Inst. Elect. Eng. Int. Conf. AC DC Transmission, 1991, pp. 299–306. Paper no. 345.
- [4] D.Soto and C. Green, —A comparison of high-power converter topologies for the implementation of facts controllers,| IEEE Trans. Indust. Electron., vol. 49, no. 5, pp. 1072–1080, Oct. 2002.
- [5] K. K. Sen, —SSSC—static synchronous series compensator: Theory modelling and application,| IEEE Trans. Power Del., vol. 13, no. 1, pp. 481–486, Jan. 1998.
- [6] H F Wang. _A Unified Model for the Analysis of FACTS Devices in Damping Power System Oscillations__ Part III: Unified Power Flow Controller._ IEEE Transactions on Power Delivery, vol 15, no 3, July 2000.
- [7] H F Wang. _Applications of Modelling UPFC into Multi-machine Power Systems._ IEEE Proceedings-C, vol 146, no 3, May1999.
- [8] L Gyugyi. _Unified Power Flow Control Concept for Flexible ac Transmission Systems._ IEEE Proceedings-C, vol 139, no 4, July 1992
- [9] A Nabavi-Niaki M R Iravani. _Steady-state and Dynamic Models of Unified Power Flow Controller (UPFC) for Power System Studies._ IEEE Transactions on Power Systems, vol 11, no 4, November 1996, p 1937.
- [10] K S Smith, L Ran and J Penman. ‘Dynamic Modelling of a Unified Power Flow Controller.’ IEEE Proceedings-C, vol 144, no 1, January 1997.
- [11] L Gyugyi and C D Schauder, ‘The Unified Power Flow Controller’: A New Approach to Power Transmission Control.’ IEEE Transactions on Power Delivery, vol 10, no 2, April 1995, p 1085.
- [12] Jyh-Shing Roger Jang, “ANFIS: Adaptive-Network-Based Fuzzy Inference System”, IEEE Transactions on Systems, Man and Cybernetics, Vol.. 23, No. 3, pp. 665-685, May-June (1993)
- [13] Hariri, O. P. Malic, “Adaptive Network-Based Fuzzy Logic Power System Stabilizer”, IEEE WESCANEX 95 Proceedings.
- [14] S. Mishra, “Neural- Network- Based Adaptive UPFC for Improving Transient Stability Performance of Power System”, IEEE Trans.

Charging a Battery with the Electric Organ Discharge of Malapterurus Electricus Catfish

Hangnilo Robert

Laboratoire d'Électrotechnique, de Télécommunication et d'informatique Appliqué, LETIA ; Ecole Polytechnique d'Abomey-Calavi, EPAC, Université d'Abomey-Calavi, UAC ; 01BP2009 Cotonou-Bénin.

Abstract: Energy providing to meet user's requirements is an endless cause of concern. The people living in the developed countries, (G8) represent 13.1% of the world's population. That 13.1% consumed in 2002 about 1500 Giga Joules per habitant in energy. For the remaining countries' development, the need in energy will increase up to 500% in relation with the current level of need. Hence, it is necessary to harness new pollution free sources of energy like solar renewable energies. To meet that challenge of energy by taking into account the worldwide warming pollution we have studied *Malapterurus electricus* catfish in order to extract the electric energy contained in the electric organ discharge (EOD) of the catfish by charging a battery of accumulators.

Keywords - Energy challenge, electric organ discharge, *Malapterurus electricus*, worldwide warming pollution

I. Introduction

So many rivers flow through the Benin Republic, (see the map in Fig. 1-a.). *Malapterurus electricus* (Fig. 2-a.) that ever strongly electric catfish is a typical African knife fish, [1]. It is widespread in the sweet waters in the Republic of Benin, [2]. The country counts among the ever weakly equipped countries in the world. It is also an obvious fact that energy providing to the different end users as industries, transport, households and services in a country is the main activity on which depends the development of all others branches of the economy of that countr

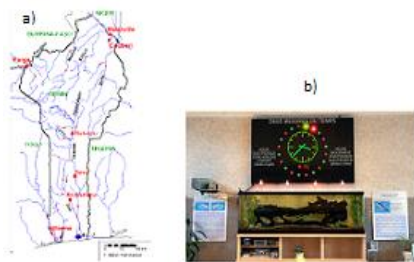


Figure 1. a - Hydrography of Benin Republic
b - Biological stopwatch in Nancy aquarium

Hence, every source of energy holding some potentiality must be scanned especially as that source is widespread in the considered area. It is just the case of the given catfish the EOD of which can reach 600 V with a frequency of 300 Hz! *Malapterurus electricus* is a true source of energy, [3].

Electric catfish are of course a subject of research all around the world. A team of scientists in Nancy University (France) has developed an application based on an electric catfish driving a stopwatch, (Fig. 1-b.). As we can see in Fig. 2-b., our team of research has succeeded in lighting in our laboratory a LED with the EOD of a very small size *Malapterurus electricus* catfish that weighs 19 g.

Malapterurus electricus can live in aquarium; its food habit and the characteristics of the water in its habitat are well known, [4], [5]. A battery-farming of that knife fish is quiet probable. In this way the feasibility of an energy farming centered on that catfish is quite conceivable.

The present paper reports the results of charging a 12 V battery of accumulators which really is the battery of a motorcycle Sanya 111-C type, see Fig. 9.

II. Materials and method



Figure 2. a- *Malapterurus electricus* catfish living in aquarium in LETIA, b- *Malapterurus Electricus* switching on a LED in LETIA

2.1 Determination of the electrical energy characteristics produced by the *Malapterurus electricus* catfish

We have determined the electrical characteristics of the EOD of *Malapterurus electricus* catfish. An individual of that catfish of 15 cm of length and 64.9 g of live body weight was farmed in an aquarium (Fig. 3.) in order to follow its feeding behaviour, its physical characteristics, the electrical parameters of its EOD and the parameters of the water in the aquarium, (see Table 1). The results show that *Malapterurus electricus* produces intermittent bursts of a frequency framed with 250 and 300 Hz, Fig. 4. Each burst lasted about half a second. The electrical organ discharge displayed on the oscilloscope showed a single curve whose dual amplitude having up to 29 V, see Table 2. Discharges were more regularly during a night (or in darkness) than during a day (or under lighting), see Fig. 5 and 6. Thus *Malapterurus electricus* is a typical bioelectrical voltage generator

Table 1
Average value of the parameters of the water in the aquarium

Period	Temperature, °C	PH	Conductivity, µS/cm	Oxygen ratio, mg/l
Morning, 8 o'clock	26.3	8.49	25.07	7.67
Midday, 12 o'clock	29.32	8.51	25.10	7.98
Evening, 7 o'clock	27.55	8.5	25.00	7.95
Night, 3 o'clock	26.05	8.48	25.04	7.23



Figure 3. Geometrical parameters of the catfish body; 1. Length of head = 2.41 cm; 2. Length of body = 10.7 cm; 3. Length of tail = 2.64 cm

Table 2
Recorded values of the electric organ discharge of Malapterurus electricus

Potential difference, V	Current, mA	Frequency, Hz	Signal duration, ms	Power, W
29	23.07	250-300	500	0.5307

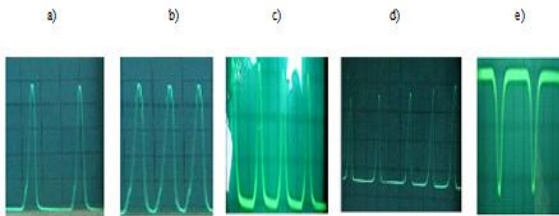


Figure 4. EOD of Malapterurus electricus with increasing number of impulses per discharge in pictures a to d then reversed in picture e

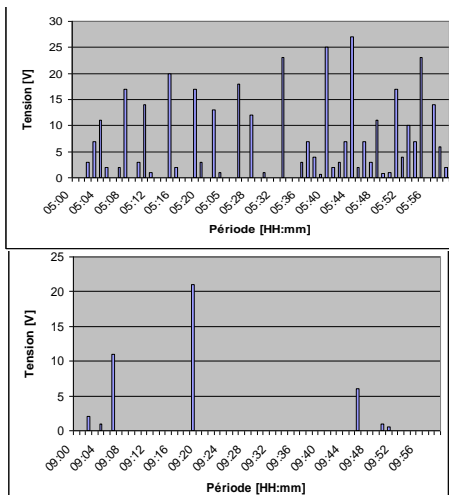


Figure 5. Recorded EOD on: a- 13/10/10 at night; b- 14/10/10 during the day time

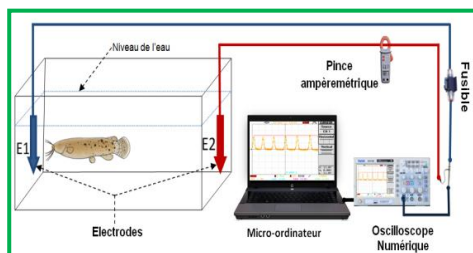


Figure 6. Connecting the catfish to an end user

2.2 Modeling the electric organ discharge of the Malapterurus electricus catfish

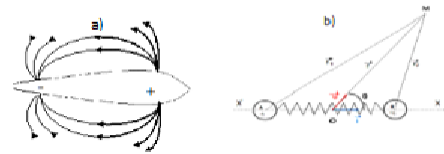


Figure 7a- Malapterurus electricus as an electric Dipole; b-Electromechanic model of the catfish

The electric dipole theory is applied for modeling the catfish, see Fig. 7-a. Malapterurus electricus is considered as a particular system of electric charges that are linked by a spring, see Fig. 7-b. Taking into account the main forces of that system of electric charges and applying the dynamic law, we got a non linear differential equation that we solve by the Adomian decomposition technique, [6]. Neglecting the viscous force ($F_v = 0$), we found the solution for that particular case as following:

$$x(t) = \sqrt[3]{\frac{\lambda}{\beta}} (1 - \cos 3\sqrt{\beta} t)^{\frac{1}{3}}, \quad (1)$$

We put the relation (1) in the equation of the electric potential $V(M)$ of an electric dipole and we obtain relation (2):

$$V(M) = \frac{1}{4\pi\epsilon_0} \frac{2q(a+x)}{r^2} \cos \theta, \quad (2)$$

The result of Simulation that model (2) in Matlab is similar to the EOD of the catfish and to a Graetz bridge rectifier output voltage in power electronics as we can see in Fig. 4 and 8-b. In fact that EOD of the electromechanical model is unidirectional like the catfish one. From now it becomes clear for us how to connect Malapterurus electricus to an end user application as lighting a LED or charging a battery.

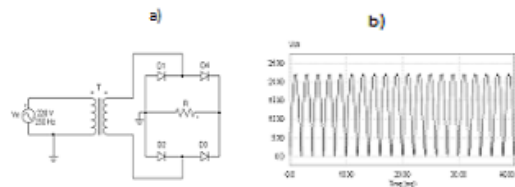


Figure 8 a- Graetz bridge rectifier; b- Output voltage of the rectifier and/or simulating result of the electromechanical model

III. Results and discussion

We know that Malapterurus electricus catfish produces strong EOD only in darkness, [2]. To reach the goal we have hidden the aquarium of the catfish with a colored paper as shown in Fig. 9- a. We stimulate the catfish from time to time by touching it carefully with a piece of wood. With the help of an interface, figure 10, the energy of the EOD of the fish is conveyed towards the battery, Fig. 9-b. Within three days the battery's voltage rises from 6 V to 9.83 V as we can notice in Table. 3. That result is given by a single catfish with a very small size! A manual exciting of the catfish cannot allow a quick operating process of charging a battery with the EOD of Malapterurus electricus of course. Hence, it is necessary to mechanize the exciting

process of the catfish. For many catfish the electronic interface must include a chopper that will reduce the output voltage of the biological source of energy to the required value that can be 12 V or a multiple of it.

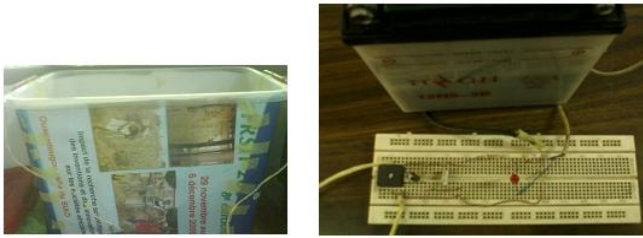


Figure 9. a- Aquarium in PVC material
b- Power transfer circuit from the catfish

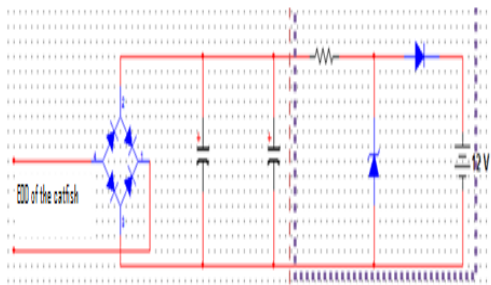


Figure 10. Interface between the catfish

Table 3
Data of battery charging

The date												
Voltage/Time	21/11/11			19/12/11			20/12/11			22/12/11		
	8	12	18	8	12	18	8	12	18	8	12	17
	6.6	7.9	8.9	8.9	9.1	9.1	9.3	9.3	9.5	9.6	9.7	9.8

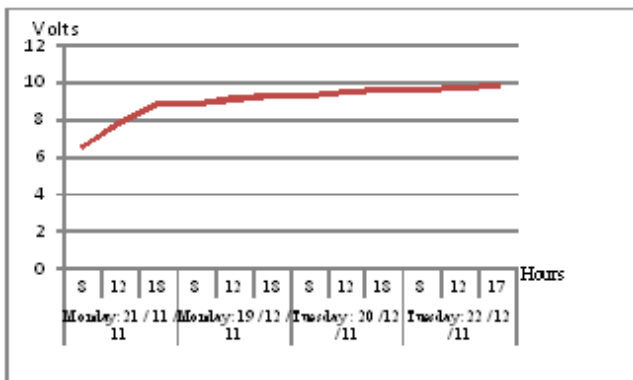


Figure 10. Characteristics of the charging of the battery

IV. Conclusion

Malapterurus electricus is really a bioelectrical voltage generator. The present study aims to use the EOD of that catfish for charging a battery in order to diversify energy sources in the Republic of Benin. An individual of *M. electricus* of 15 cm length and 64.9 g live body weight was used for the target. It was kept in an aquarium in polyvinyl chloride material. Within four days and some hours per day we have succeeded in raising the potential difference of a battery from 6 V to 9.83 V. The feasibility of the utilization of *Malapterurus electricus* catfish as a power source is now established. The recharging duration of the battery will decrease with the increasing of the number of the catfish in the aquarium. The catfish was not excited all the time during the four days recharging process. To stimulate the catfish we use to touch it carefully with a piece of wood. We'd get better from the catfish by mechanizing that operation.

References

- [1] Rankin CH & P. Moller, Temporal patterning of electric organ discharges in the African electric catfish, *Malapterurus electricus*, Journal of fish biology, Vol. 40(1), 1992, 49-58.
- [2] Projet de pêche lagunaire, Guide de détermination des poissons et crustacés des lagunes et lacs du bas Bénin, 1993, Cotonou.
- [3] Klas-Bertil A & GJ. Alf, The Acetylcholine system of electric organ of *Malapterurus electricus*, J. Physiol. 140, 1958, 498-500.
- [4] S.A. Adédjouma, R. Hangnilo, J. M. Zonou & G. A. Mensah, Determination of the electrical energy characteristics produced by the *Malapterurus electricus*, an electric catfish of freshwater in Benin. Rev.CAMES-Série A, 12 (1), 2011, 52-57.
- [5] Sagua V.O, Observations on the food and feeding habit of the African electric catfish, *Malapterurus electricus*, Journal of Biology, 15(1), 1979, 61-69.
- [6] Hangnilo, R. & V. Adanhounme, Solving the oscillating electric dipole equation by the Adomian decomposition technique. IJSER-2012w, <http://www.ijser.org>, page 4.

Early Detection of Powdery Mildew Disease for Betelvine Plants Using Digital Image Analysis

Mr.J.Vijayakumar¹ Dr.S.Arumugam²

¹Research scholar, Nandha College of Technology- Erode. Tamilnadu, India

²Chief Executive officer, Nandha Educational Institution - Erode. Tamilnadu, India.

Abstract: The fresh leaves of betelvine are generally known as paan in India. Betelvine plants are infected variety of diseases in the entire plantation without any early indications of the diseases. The aim of this paper is to recognize powdery mildew disease in the betelvine plants using digital image analysis techniques. The digital images of the betelvine leaves at various stages of the powdery mildew disease are collected from different plants using a high resolution digital camera and it is stored with JPEG format. The digital image analyses of the leaves are done using the image processing toolbox in MATLAB which provides the standard patterns of the digital images. Using RGB encoding technique the red, green and blue components of the preprocessed image were separated, which forms the pattern to be compared. These patterns and images of various healthy betelvine leaves at different stages in various days are collected and stored in the system. The standard deviation for all sample leaves is computed and calculated values are stored in the system. The standard deviation of test leaves are computed and compared with the stored values. As the result of this comparison, it is identified whether test leaves are affected by powdery mildew disease or not. Finally this analysis helps to recognize the powdery mildew disease can be identified before it spreads to entire crop.

Keywords: Keywords: Betelvine, Powdery mildew Disease and Oidium piperis

I. Introduction

Piper Betel L generally known as Vetrilai in Tamil. The Piper betle is a glabrous climbing vine belonging to the family *Piperaceae*. The betelvine leaf is used in a number of traditional medicines for the treatment of stomach complaints, infections and as a general refresher. Some evidence suggests that betelvine leaves have immune boosting properties as well as anti-cancer properties. Lots of research is going on in the field of betelvine diseases analysis for various centers within the country under the name "ALL INDIA NETWORKING PROJECT IN BETELVINE". During cultivation betelvine is very much affected by diseases and insects that outcome in big loss for the farmers. The most important diseases of betelvine leaf are Powdery mildew, Foot Rot, Leaf Rot and Leaf Spot. It occurs in a very virulent form and if not controlled, causes widespread injure and even total demolition of the entire of betelvine plantations. The farmer is not able to identify the disease at an early stage to initiate preventive action due to the non-availability of modern technology. So for each

farmer, to have access to the modern technology there is a need to construct modern commercial farm. This has been the base to develop a new tool to identify the disease well in advance to enhance the cultivation. Digital Image processing is used as a tool for early identification of the Powdery mildew disease.

II. COMPUTERIZED BETELVINE PLANT POWERY MILDEW DISEASE IDENTIFICATION

Basically when a farmer visualizes the disease, seen as a change in the form of color or appearance the disease is in the matured stage after which diagnosis cannot save the plant. The disease spreads to the entire crop and the entire plantation gets destructed within few days. Powdery mildew disease emerges on the undersurface of the leaves as white to brown powdery patches. Human eye cannot predict the disease at an early stage. So we are using computerized image analyzing system in which minute change in the form of color in leaves can be detected at an early stage.

III. POWDERY MILDEW DISEASE

Powdery mildew is sourced by *Oidium piperis*. The disease shows on the undersurface of the leaves as white to brown powdery patches. The photograph is shown in figure 1 and figure 2 for front and back view of Powdery mildew infected betelvine leaf. These infected areas gradually increase in size and repeatedly combine with each other. They vary in size from a few to 40mm in diameter and are covered by dusty growth which is fairly thick in cases of sever attack. Areas on the upper surface corresponding to patches on the under surface appear yellowish, raised and irregular in outline. Young leaves when attacked fail to grow and become deformed, the surface being cracked and the margin turned inwards.



Figure1:Front view



Figure 2: Back view

Such leaves present a pale appearance and drop with slight disturbance. The disease is more prevalent in old plantations. The disease has been reported to be in the leaves only and it has been found to disappear during the hot season.

IV. METHODS FOR DISEASE IDENTIFICATION

The betelvine leaves are properly washed to remove the dust components. Digital imaging technique is divided in three phases respectively as,

- Normal or uninfected leaves phase,
- Fully Infected leaves phase
- Test leaves phase

Normal or uninfected leaves phase consists of without any disease infected in the betelvine leaf. Fully Infected leaves phase consisted of visually identifiable infected leaf, samples are collected for normal leaves and various stages of Powdery mildew disease. Test leaves phase consists of visually unidentifiable infected leaf, samples are collected at various stages of the Powdery mildew disease. Fifteen samples from each phase were taken for this paper. The size of all the digital images are 256 x 256. To eliminate the background using photo shop 7.0 and background was chosen to be white and these digital images are stored in the system. This stored digital images are given as input to the MATLAB file and the R,G,B colour components are separated and find the mean values for all healthy and infected leaves and calculated values are stored in the system. For the test leaf, compute standard deviation and compare all the stored values, to recognize the diseased betelvine leaf affected by powdery mildew disease.

V. RESULT

The result of the paper is all the normal and infected leaves are given as input to the MAT LAB and RGB color components are separated. The standard deviation are calculated for front and back view of each component and calculated standard deviation values are stored in the system and test leaves are given as input to the MAT LAB and RGB color components are separated and the standard deviation values are calculated for front and back view of each component and calculated standard deviation values are stored in the system. To compare all the stored results and identify either disease infected or not in the test betelvine leaf, the standard deviation values of Red component for normal leaves, infected leaves and test leaves front and back views are shown in figure 3 and figure 4 . The standard deviation values of green component for normal leaves, infected leaves and test leaves front and back views are shown in figure 5 and figure 6 . The standard deviation values of Blue component for normal leaves, infected leaves and test leaves front and back views are shown in figure 7 and figure 8.

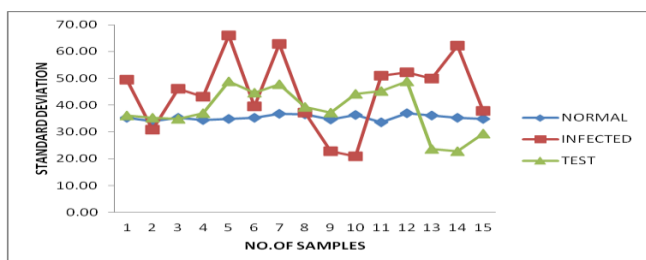


Figure 3: Front View for Red Component

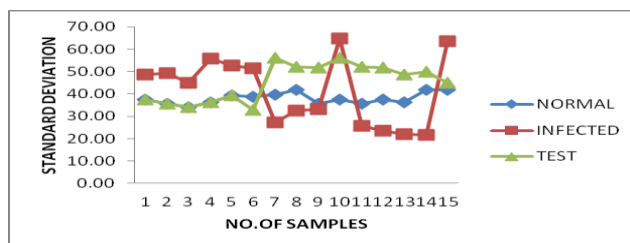


Figure 4: Back View for Red Component

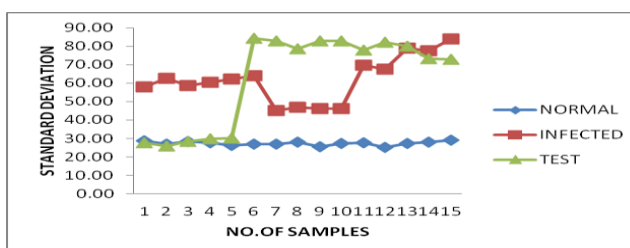


Figure 5: Front View for Green Component

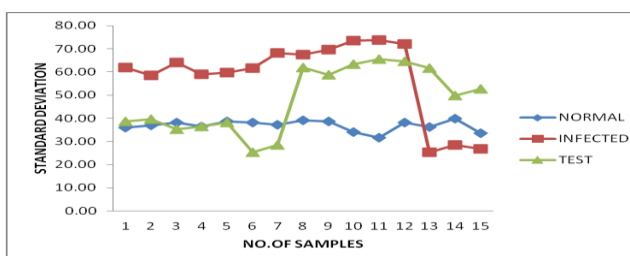


Figure 6: Back View for Green Component

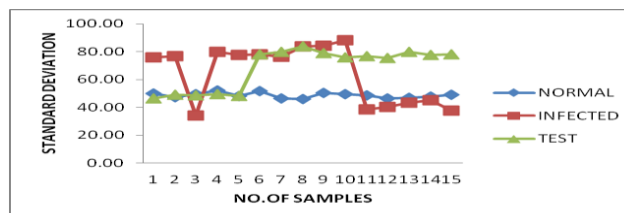


Figure 7: Front View for Blue Component

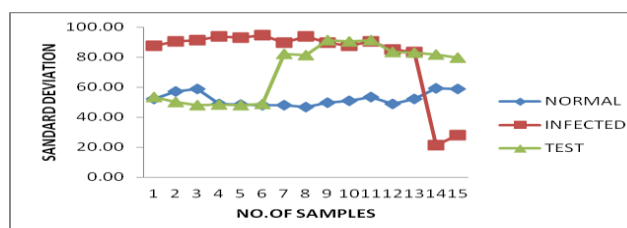


Figure 8: Back View for Blue Component

In normal leaves, front view of Red component standard deviation value ranges from 33.53 to 36.89 and back view of Red component standard deviation value ranges from 34.07 to 41.89. In infected leaves, front view of Red component standard deviation value ranges from 20.97 to 65.96 and back view of Red component standard deviation value ranges from 21.61 to 64.84. In test leaves, first five samples of front view Red component standard deviation value ranges from 33.53 to 36.89 and back view of Red component standard deviation value ranges from 34.07 to 41.89 and last ten samples of front view Red component standard deviation value ranges from 20.97 to 65.96 and

back view of Red component standard deviation value ranges from 21.61 to 64.84. In normal leaves, front view of green component standard deviation value ranges from 25.21 to 29.14 and back view of green component standard deviation value ranges from 31.66 to 39.78. In infected leaves, front view of green component standard deviation value ranges from 45.24 to 84.09 and back view of green component standard deviation value ranges from 25.30 to 73.72. In test leaves, first five samples of front view green component standard deviation value ranges from 25.21 to 29.14 and back view of green component standard deviation value ranges from 31.66 to 39.78 and last ten samples of front view green component standard deviation value ranges from 45.24 to 84.09 and back view of green component standard deviation value ranges from 25.30 to 73.72. In normal leaves, front view of blue component standard deviation value ranges from 46.02 to 52.31 and back view of blue component standard deviation value ranges from 46.78 to 59.27. In infected leaves, front view of blue component standard deviation value ranges from 34.25 to 88.34 and back view of blue component standard deviation value ranges from 21.06 to 94.66. In test leaves, first five samples of front view blue component standard deviation value ranges from 46.02 to 52.31 and back view of blue component standard deviation value ranges from 46.78 to 59.27 and last ten samples of front view blue component standard deviation value ranges from 34.25 to 88.34 and back view of blue component standard deviation value ranges from 21.06 to 94.66.

To compare all the fifteen test sample leaves of standard deviation values from stored standard deviation values of normal and infected leaves. The result is first five test sample leaves are uninfected or normal leaves and the remaining ten test sample leaves are infected leaves.

VI. CONCLUSION

The above proposed methods convey that the betelvine plants disease can be identified disease infected or not in the betelvine leaf and thus preventive action can be taken well in advance such that the entire plantation can be saved before the disease starts to spread. The method of detecting the disease is cost effective and non-destructive as it only requires the digital photograph of the leaf samples in random. The efficiency of the system can be increased by taking the camera parameters, as the camera parameters are considered constant in this project. Periodic inspection of the farm is required to prevent the disease. This method can also be extended to detect diseases of all kind to initiate early preventive action.

References

- [1] Sathyabrata Maiti and K.S. Shivashankara "Betelvine Research Highlights". (1998).
- [2] Dastur.J.F. "Diseases of pan (piper betle) in the general provinces".(1935)
- [3] B. Dasgupta, B.Mohanty, P. K. Dutta and Satyabrata Maiti "*Phytophthora* Diseases of Betelvine (*piper betle* l.)" SAARC Jn. of Agri.,(2008), pp (1-19).
- [4] Nikhil Kumar "Betelvine (piper betle l.) Cultivation: A Unique Case Of Planstablishment Under nthropgenically

Regulated Microclimatic Conditions" Indian Journal of History Of Science (1999), pp(19-32).

- [5] Bibekananda Mohanty, Partha Datta, B. Dasgupta and Dalim Kumar Sengupta ntegrated Management Of Foot And Leaf Rot Of Betelvine" SAARC Jn. of Agri.,(2011), pp (83-91).
- [6] Shete M. H., Dake G. N., Gaikwad A. P. and Pawar N. B. "Chemical Management of Powdery Mildew of Mustard" Journal of Plant Disease Sciences, Volume:3, Issue: 1 (2008),pp(46-48).
- [7] P.Guha "Betel Leaf: The Neglected Green Gold of India" Journal of Human Ecology (2006), pp (87-93).
- [8] J.Vijayakumar and Dr.S.Arumugam "Study of Betelvine Plants Diseases and Methods of Disease Identification using Digital Image Processing" European Journal of Scientific Research Vol.70 No.2 (2012), pp(240-244).
- [9] J.Vijayakumar and Dr.S.Arumugam "Foot Rot Disease Identification for the Betelvine Plants using Digital Image Processing" Journal of Computing,Volume 3,Issue 2,February 2011,pp (180-183).
- [10] B. Seetha Lakshmi and K. C. Naidu "Comparative Morphoanatomy of *Piper betle* L. cultivars in India" Annals of Biological Research, 2010, pp(128-134).
- [11] Annual Report of All India Coordinated Research Project on Betelvine ICAR (Indian Council of Agricultural Research,New Delhi) India (1997).

AUTHOR'S BIOGRAPHY



Mr.J.Vijayakumar received the Bachelor of Engineering in Electronics and Communication Engineering from Maharaja Engineering College under Bharathiar university-Coimbatore in the year of 2003 and Master of Engineering in Applied Electronics from Bannari Amman Institute of Technology under Anna university-Chennai in the year of 2005. He is doing Ph.D. work in Anna University of Technology- Coimbatore under the guidance of Dr. S. Arumugam. He is working as Assistant Professor in the Department of Electronics and Communication Engineering in Nandha College of Technology- Erode. His area of interest is Digital Image Processing.



Dr.S.Arumugam completed his bachelor degree in Electrical and Electronics Engineering and M.Sc(Engg)., in Applied Electronics both from PSG College of Technology under University of Madras and Ph.D., in Computer Science and Engineering from Anna University. He has been serving in the Directorate of Technical Education since 1974 onwards. He retired from Government service as additional Director of Technical Education and Chairman Board of Examinations. He served as Chief member of various boards of studies. He is a fellow member in IE, IETE, senior member in CSI and member in IEEE. He has guided 15 Ph.D scholars and 23 Ph.D scholars are working under his guidance. He has so far published over 100 papers in various National and International Journals and Conferences. His area of interest is Digital Image Processing. Presently he is working as Chief Executive officer, Nandha Educational Institution-Erode.

Evaluation of Flexural Properties of Fly Ash Filled Polypropylene Composites

Jitendra Gummadi¹, G.Vijay Kumar¹, Gunti Rajesh²

¹ Department of Mechanical Engineering, Prasad V. Potluri Siddhartha Institute of Technology, Kanuru, Vijayawada, Andhra Pradesh, India.

² Department of Mechanical Engineering, DVR & Dr. H S MIC College of Technology, Kanchikacherla, Andhra Pradesh, India.

Abstract: In recent time's polymer waste disposal is a challenging task as the quantity of polymer waste is increasing day by day. In this research work particulate composites have been developed from recycled polypropylene filled with fly ash. Fillers are used along with various commodities as well as engineering polymers to improve the properties of polymers. The performance of filled polymers is generally determined on the basis of the interface attraction of filler and polymers. Fillers of widely varying particle size and surface characteristics are responsive to the interfacial interactions with polymers. The present study deals with the effect of particle size and its concentration on the properties of fly ash filled polypropylene composites. Five different particle sizes of fly ash are used for sample preparation. Concentration of fly ash is also varied from 0, 10%, 15%, 20%, 25% by weight in the polypropylene. The composite test specimens are prepared using injection molding machine with hand lay up technique as per ASTM D3641 standards. Bending tests on the specimens are carried out by using tensometer. Flexural strength and modulus are calculated from the obtained load values and the result is analyzed for the prepared samples.

Keywords: Polypropylene, Composite, Fly ash, Flexural properties.

I. Introduction

Particulate composites have received considerable interest in the materials field because of their potential for large gains in mechanical and morphological properties. Thermoplastic polymers and especially polypropylene are produced and used today in vast quantities. However, they are seldom used as pure polymers and are usually combined with mineral fillers like fly ash, graphite etc. Fillers find application in the polymer industry almost exclusively, e.g. to improve mechanical, thermal, electrical properties and dimensional-stability. The low modulus of isotropic polypropylene means that it is unsuitable for many load bearing applications. In order to improve the stiffness of polypropylene, two main routes will be considered here. The first route is to improve stiffness by the introduction of foreign fillers, such as glass fibers, to create polypropylene composite materials. The second route is the exploitation of the inherent molecular strength by uncoiling the molecules and orienting them in the direction of loading, so that the load is transferred by the stiff carbon backbone rather than by weak intermolecular bonds.

Fly ash is finely divided mineral residue resulting from combustion of coal in electric generating plants. Fly ash consist mostly of SiO_2 , Al_2O_3 , and Fe_2O_3 and are present in inorganic incombustible matter present in coal that has been fused during combustion to glassy amorphous structure. Fly ash used in cement industry could be used as filler in plastic products and depending upon the source of coal, contain elements like carbon, Ti, Mg, etc. So the fly ash has combined properties of spherical particles and that of metals and metal oxides.

Polypropylene (PP) is a thermoplastic polymer used in a wide variety of applications including packaging, textiles (e.g., ropes, thermal underwear and carpets), stationery, plastic parts and reusable containers of various types, laboratory equipment, loudspeakers, automotive components, and polymer banknotes. Most commercial polypropylene is isotactic and has an intermediate level of crystallinity between that of Low-Density PolyEthylene (LDPE) and High-Density PolyEthylene (HDPE). Polypropylene is normally tough and flexible, especially when copolymerized with ethylene. This allows polypropylene to be used as an engineering plastic, competing with materials such as acrylonitrile butadiene styrene. Polypropylene has good resistance to fatigue. The melting of polypropylene occurs as a range, so a melting point is determined by finding the highest temperature of a differential scanning calorimetry chart. Perfectly isotactic Polypropylene has a melting point of 171°C (340°F). In this investigation we studied the effect of fly ash with five varying particle sizes and concentration on flexural properties.

Utilization of fly ash as filler for unsaturated polyester resin was studied by Saroja Devi et al.[1]. Measurement of the specific heat of plastic waste fly ash composite material using differential scanning calorimetry was observed by Fujino and Honda [2]. Structure and strength properties of Polypropylene Polymethyl methacrylate fly ash blends developed by Navin Chand and Vashishtha [3]. Mechanical properties of natural rubber filled with fly ash was prepared and observed by Hundiwale et al.[4]. Effect of fly ash on the mechanical, thermal, dielectric, rheological and rphological properties of filled nylon 6 was studied by Suryasarathi Bose and Mahanwar [5]. Utilization of fly ash as filler for polybutyleneterephthalate-toughened

epoxy resin was developed by Ramakrishna et al. [6]. Thermal and Electrical behavior of vinyl ester resin matrix composites filled with fly ash particles was studied by Dipa Ray et al. [7]. Preparation and dynamic mechanical properties of polyurethane-modified epoxy composites filled with functionalized fly ash particulates was observed by Gaohui Wu et al. [8]. Effect of fly ash content, particle size of fly ash, and type of silane coupling agents on the properties of recycled polyethylene terephthalate / fly ash composites was investigated by Seena Joseph et al.[9]. Correlation of mechanical and structural properties of fly ash filled-isotactic polypropylene composites was studied by Dilip Chandra Deb Nath, Bandyopadhyay [10]. Effect of particle size and concentration of fly ash on properties of polyester thermoplastic elastomer composites was examined by Sreekanth et al. [11]. Mechanical and structural properties of polypropylene composites filled with graphite flakes were studied by Akinci [12]. Mechanical properties of epoxy resin – fly ash composite were developed by Manoj Singla and Vikas Chawla [13]. Polyetheretherketone (PEEK) composites reinforced with fly ash and mica was developed by Rahail Parvaiz.et al.[14]. Furfuryl palmitate coated fly ash used as filler in recycled polypropylene matrix composites was observed by Shubhalakshmi Sengupta et al. [15]. Review of literature survey shows that different type of properties like mechanical, thermal, dielectric, rheological, morphological were studied on the particulate composites made from graphite, silica as a filler and thermoplastic materials like Polyaryletherketone, Polybutadiene, Polybutylene, Polybutylene terephthalate, Polycaprolactone as a matrix medium. How ever there is a limited literature available on the particulate composites especially made from Polypropylene and fly ash. Hence in the present study particulate composites made from polypropylene and fly ash are fabricated and studied for flexural properties and the results are analyzed.

II. Sample Preparation

2.1 Material

Polypropylene granules were purchased from Maram polymers Pvt.Ltd, Vijayawada, Andhra Pradesh, India and the filler fly ash was obtained from Vijayawada Thermal Power Station, Kondapalli, Andhra Pradesh, India were used in the sample preparation.

2.2 Fabrication

The polypropylene granules along with fly ash were melted in the vertical injection molding machine with two heating zones set at 160^o and 120^o. The weights of fly ash in the composite were 0, 10%, 15%, 20% and 25% of total weight of polypropylene. The samples of fly ash/PP composites with varying particle sizes (53-75 μ m to 212-300 μ m) and also varying concentration were prepared by vertical injection machine as shown in Figure 2.1, as per ASTM D 3641Standards. Figure 2.2 shows the plain polypropylene sample and the fly ash filled poly propylene composite sample is shown in Figure 2.3. Sufficient pressure is applied on the sample to eliminate voids in the composite. Samples were air cooled at room temperature.



Figure 2.1: Hand Operated Vertical Injection Machine



Figure 2.2: Plain polypropylene sample



Figure 2.3: Fly ash filled polypropylene composite sample

2.3 Mechanical testing of composites

The fabricated specimens were tested using a 2 ton capacity - Electronic Tensometer, METM 2000 ER-I model, with a cross head speed of 2 mm/min in accordance with standard ASTM D790 under ambient conditions. The schematic representation of load application is as shown in Figure 2.4. Load and elongation values are determined for all samples. Utilizing the experimental values of load and elongation, flexural strength (f_s), flexural modulus and elongation at break were determined. Reported values are the average of five samples in all measurements. Some of the tested samples are shown below in the following figures from Figure 2.5 to Figure 2.9.

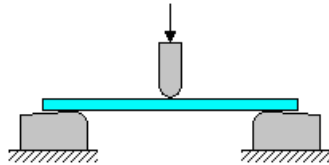


Figure 2.4: Composite specimen flexural test configuration



Figure 2.5: 15 percentage of fly ash at 212-300 microns



Figure 2.6: 20 percentage of fly ash at 76-105 microns



Figure 2.7: 20 percentage of fly ash at 76-105 microns



Figure 2.8: 25 percentage of fly ash at 150-211 microns



Figure 2.9: 25 percentage of fly ash at 76-105 microns



Figure 2.10: 25 percentage of fly ash at 212-300 microns

2.4 Calculation of flexural properties

The flexural stress, flexural strain, flexural modulus and percentage of elongation at break values of the composites were determined by substituting load and elongation values in the below formulae.

$$\text{Flexural stress } \sigma_f = \frac{3PL}{2bd^2} \quad (\text{for a rectangular cross section})$$

$$\text{Flexural strain } \epsilon_f = \frac{6Dd}{L^2}$$

$$\text{Flexural modulus } E_f = \frac{L^3m}{4bd^3}$$

Following are the notations used in above formulae

σ_f = Stress in outer fibers at mid point, (MPa)

ϵ_f = Strain in the outer surface, (mm/mm)

E_f = Flexural Modulus of elasticity, (MPa)

P = Load, (N)

L = Support span, (mm)

b = Width of test beam, (mm)

d = Depth of test beam, (mm)

D = Maximum deflection of the center of beam, (mm)

m = The gradient (i.e., slope) of the initial straight-line portion of the load deflection curve, (P/D), (N/mm)

The obtained values are shown below in the Table 1, Table 2 and Table 3.

III. Results And Discussion

From Table 1, it was observed that as the addition of filler decreases the flexural strength. From Figure 3.1, it was observed that rate of flexural strength decrease when large particle sizes were used. This is because of the particle agglomeration at higher filler contents. Particle agglomeration tends to reduce the strength of a material because the agglomerates are weak point in material and break easily when a stress is applied to them. These points then acts as stress concentrator. Agglomerations resulting from larger sized filler particles will produce weaker materials than composites having well dispersion of small sized particles. The rate of decrease of flexural strength is higher in the case of larger particle size of fly ash.

From Figure 3.2, shows the variation of flexural strength with the variation in size of the particles used in polypropylene fly ash filled composites. It was observed that smaller particles showed higher value of flexural strength. For smaller particles, as particle size decreases, interfacial area/unit volume is increased, and hence, flexural strength is increased. The effect of filler on flexural strength may be due to the counterbalance of two phenomenon's with the increase in the filler content in a polymer composite there is increase in effective surface fracture energy, size of voids and agglomeration of filler particles. The dispersed particles make the crack propagation path longer, absorb a portion of energy and enhance the plastic deformation.

Table 1: Flexural Strength of fly ash filled polypropylene composites with fly ash at different sizes and varying percentage content of fly ash

Fly ash sizes → Percentage of fly ash ↓	53-75µm	76-105µm	106-149µm	150-211µm	212-300µm
0%	56.88	56.88	56.88	56.88	56.88
10%	72.38	59.23	70.71	71.25	73.62
15%	70.29	53.53	59.73	66.18	55.71
20%	66.02	54.44	57.30	61.16	51.36
25%	60.99	57.94	56.80	57.39	44.99

Table 2 shows the values of flexural modulus and from the Figure 3.3, shows the percentage of fly ash at different sizes added to the polypropylene. Figure 3.4, shows the variation of flexural modulus of fly ash composite with filler content and particle size. Flexural modulus increases for smaller filler loading decreases for larger filler loading. Rate of increase is more for smaller particle size than larger ones. Because smaller particles have higher surface area than larger ones, these particles can have higher interaction with matrix at lower concentration of filler. Agglomeration if present, the apparent volume occupied by the filler is increased and agglomeration results in bigger particles by which void space is generated, which can be responsible for strain propagation. The increase in the flexural modulus of PP fly ash composite is due to the increase in the crystalline of composites by addition of fly ash.

Table 2: Flexural Modulus of fly ash filled polypropylene composites with fly ash at different sizes and varying percentage content of fly ash

Fly ash at sizes →	53-75µm	76-105µm	106-149µm	150-211µm	212-300µm
Percentage of fly ash ↓					
0%	1591.19	1591.19	1591.19	1591.19	1591.19
10%	1673.33	1506.43	1419.05	1259.15	954.54
15%	2295.47	1940.71	1936.34	1504.68	1276.62
20%	2719.27	2481.59	2390.72	1943.33	1696.05
25%	2565.48	2011.49	1696.05	1329.05	1429.54

Table 3 shows the values of percentage of elongation at break of the composites and from the Figure 3.5, shows the amount of fly ash different sizes added to the polypropylene and the percentage elongation at break is also decreases on addition on filler as shown in Figure 3.6. This is due to the interference of filler in the mobility or deformability of the matrix. This interference is created through the physical interaction and immobilization of the polymer matrix by the presence of mechanical restraints, there by reducing the elongation at break. Fly ash with smaller particle size show higher values of elongation at break when compared to larger particle size.

Table 3: Percentage Elongation at Break for fly ash filled polypropylene composites of fly ash at different sizes and varying percentage content of fly ash

Fly ash at sizes →	53-75µm	76-105µm	106-149µm	150-211µm	212-300µm
Percentage of fly ash ↓					
0%	8.91	8.91	8.91	8.91	8.91
10%	7.33	4.43	3.75	3.66	3.46
15%	4.86	3.92	3.66	3.53	3.46
20%	3.97	2.59	2.53	2.29	2.21
25%	2.60	2.56	2.50	2.05	1.97

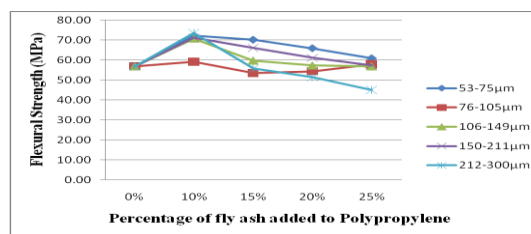


Figure 3.1: Variation of Flexural strength with percentage of fly ash added to the polypropylene Composite

Figure 3.1 shows the flexural strength values of fly ash filled composites at different sizes of fly ash at varying percentages of fly ash. Figure 3.2 shows the flexural strength of fly ash filled composites at smaller particle size and larger particle size i.e.(at 53-75 microns of size and 212-300 microns of size).It was noticed that flexural strength value increases for smaller particle size and the flexural strength value decreases for the larger particle size. This is due to the smaller particle have more surface area when compared to the larger particle.

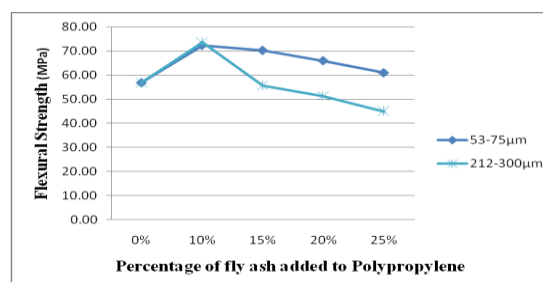


Figure 3.2: Flexural strength variation between the smaller Size particle and the larger Size particle added to polypropylene Composite

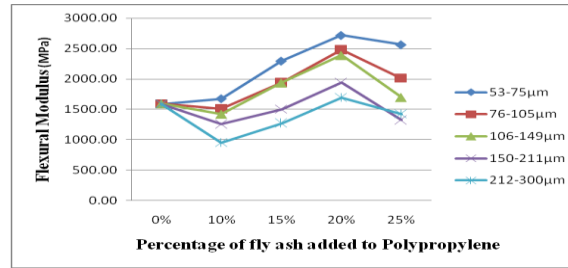


Figure 3.3: Variation of Flexural modulus with percentage of fly ash added to the polypropylene Composite

Figure 3.3 shows the flexural modulus values of fly ash filled composites at different sizes of fly ash at varying percentages of fly ash. Figure 3.4 shows the flexural modulus of fly ash filled composites at smaller particle size and larger particle size i.e. (at 53-75 microns of size and 212-300 microns of size). It was noticed that flexural modulus value increases for smaller particle size and the flexural modulus value decreases for the larger particle size.

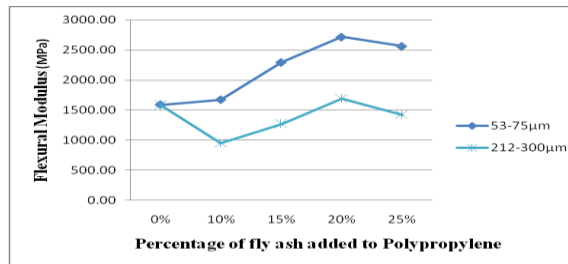


Figure 3.4: Flexural Modulus variation between the smaller Size Particle and the larger Size particle added to polypropylene Composite

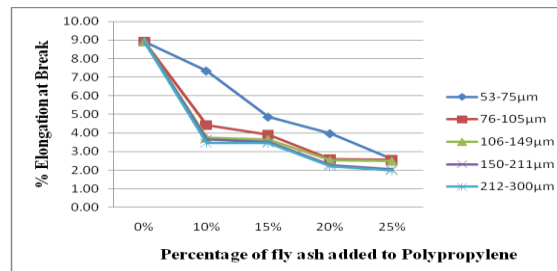


Figure 3.5: Variation of Flexural modulus with percentage of fly ash added to the polypropylene Composite

Figure 3.5 shows the percentage elongation at break values for fly ash filled composites at different sizes with varying percentages of fly ash content with the polypropylene. Figure 3.6 shows the percentage elongation at break of fly ash filled composites for smaller particles and larger particles i.e. (at 53-75 microns of size and 212-300 microns of size). It was noticed that percentage elongation at break value decreases for smaller particle size and the percentage elongation at break value goes on decreasing for the larger particle size.

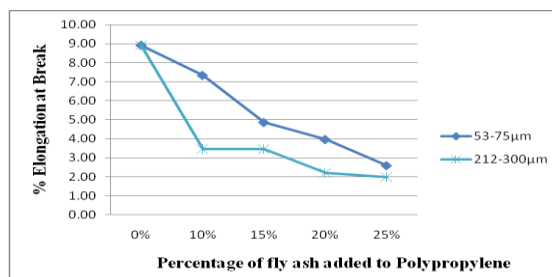


Figure 3.6: Percentage Elongation at Break between the smaller Size particle and the larger Size particle added to polypropylene Composite

IV. CONCLUSION

The flexural properties of fly ash filled polypropylene composites were evaluated in the present research work. Fly ash is found to be good filler for polypropylene matrix composites. With fly ash added to the Polypropylene improves flexural strength and flexural modulus, but dramatically decreases percentage elongation at break. Finest particles showed best flexural strength at all concentrations. The mechanical properties of the composite were found to be a function of the particle size, aspect ratio, the dispersion, the particle orientation, the interfacial interaction between the minerals and the polymer matrix. Spherical shaped filler, such as fly ash gives significant improvement in stiffness due to better surface area for interaction. It is concluded that composites with fly ash at smaller particle size showed significant improvement mechanical properties of composite when compared to the larger particle size of the composites.

References

- [1] Saroja Devi.M, Murugesan.M, Rengaraj.K, Anand.P, "Utilization of flyash as filler for unsaturated polyester resin", *Journal of Applied Polymer Science*, Vol. 69, pp. 1385–1391, 1998.
- [2] Fujino J and Honda T, "Measurement of the specific heat of plastic waste & fly ash composite material using differential scanning calorimetry", *International journal of thermophysics* volume 30, number 3, pp. 976-986, 2009.
- [3] Navin Chand and Vashishtha S R, "Development, structure and strength properties of PP/PMMA/FA blends", *Bulletin of Materials Science*, Vol.23, No. 2, Indian Academy of Sciences, 2000.
- [4] Hundiwale.D.G, Kapadi.U.R, Desai.M.C, Bidkar.S.H, "Mechanical properties of natural rubber filled with flyash", *Journal of Applied Polymer Science*, Vol. 85, pp. 995–1001, 2002.
- [5] Suryasarathi Bose and Mahanwar P.A, "Effect of fly ash on the mechanical, thermal, dielectric, rheological and rphological properties of filled nylon 6", *Journal of Minerals & Materials Characterization & Engineering*, Vol. 3, No.2, 2004.
- [6] Ramakrishna.H.V, Padma Priya.S, and Rai.S.K, "Utilization of fly ash as filler for polybutyleneterephthalate-toughened epoxy resin", *polymer engineering and science*, Online in Wiley InterScience, 2006.
- [7] Dipa Ray, Sourish Banerjee, Amar K. Mohanty, Manjusri Misra, "Thermal and electrical behavior of vinylester resin matrix composites filled with fly ash particles", *polymer composites*, Online in Wiley InterScience, 2007.
- [8] Gaohui Wu, Jian Gu, Xiao Zhao, "Preparation and dynamic mechanical properties of polyurethane-modified epoxy composites filled with functionalized fly ash particulates", *Journal of Applied Polymer Science*, Vol. 105, pp. 1118–1126, 2007.
- [9] Seena Joseph, Bambola V.A, Sherhtukade V. V, Mahanwar P.A "Effect of flyash content, particle size of flyash, and type of silane coupling agents on the properties of recycled poly(ethylene terephthalate)/fly ash Composites", *Wiley Online Library*, 2009.
- [10] Dilip Chandra Deb Nath, Bandyopadhyay, Aibing Yu, Darryl Blackburn, Chris White "Correlation of Mechanical and Structural Properties of Fly ash Filled-isotatic polypropylene Composites" *World of Coal Ash(WOCA)*, 2009.
- [11] Sreekanth M.S, Bambole V.A, Mhaske S.T, Mahanwar P.A, "Effect of particle size and concentration of fly ash on properties of polyester thermoplastic elastomer composites" *Journal of Minerals & Materials Characterization & Engineering*, Vol. 8, No.3, 2009.
- [12] Akinci A, "Mechanical and structural properties of polypropylene composites filled with graphite flakes", *World Academy of Materials and Manufacturing Engineering*, Volume 35, Issue 2, pp. 91-94, 2009.
- [13] Manoj Singla and Vikas Chawla, "Mechanical properties of epoxy resin fly ash composite" *Journal of Minerals & Materials Characterization & Engineering*, Vol. 9, No.3, 2010.
- [14] Rahail Parvaiz M, Smita Mohanty, Sanjay K. Nayak and Mahanwar P.A, "Polyetheretherketone (PEEK) composites reinforced with fly ash and Mica", *Journal of Minerals & Materials Characterization & Engineering*, Vol. 9, No.1, 2010.
- [15] Shubhalakshmi Sengupta, Kuntal Pal, Dipa Ray, Aniruddha Mukhopadhyay, "Furfuryl palmitate coated fly ash used as filler in recycled polypropylene matrix composites", *Journal of Composite Part B*, pp. 42, 1834-1839, 2011.

Demonstration of Chromatic Dispersion in Borosilicate Crown Glass Microstructure Optical Fiber

Er. Mahesh Chand¹, Er. Sandhya Sharma², Er. Ravindra Kumar Sharma³

^{1,3} M.Tech. (Scholar), Department of Electronics & Communication Engineering

² Assistant Professor, Suresh Gyan Vihar University, Jaipur

¹ Suresh Gyan Vihar University, Jaipur. ³ Rajasthan Technical University, Kota.

ABSTRACT: We developed the theoretical and experimental method for chromatic dispersion of Borosilicate Crown microstructure optical fiber from scalar effective index method (SEIM) and TBC has been reported. To maintain the flat and zero dispersion in photonic crystal fiber (PCF) different air hole diameter has been introduced. Here we use Borosilicate Crown glass as a core material. A photonic crystal fiber with large effective mode area and flat dispersion property may be very usefull for next generation optical data.

Keywords: Effective Refractive Index (n_{eff}), Photonic Crystal Fiber (PCF), Scalar Effective Index Method (SEIM), Transparent Boundary Condition (TBC).

I. INTRODUCTION

In these years PCF [1,2] is very attracted in the research group because of many of their attractive properties [3] as high birefringence, very high and low nonlinearity, wideband dispersion [4-10] flattened characteristics, endlessly single mode guiding [11,12], fiber sensors [13, 14] and fiber lasers [15,16]. Many research papers have published some optical properties of PCFs such as unique chromatic dispersion, which are almost impossible for the conventional optical fibers. Most PCFs are used silica as core material and core is surrounded by air holes called photonic crystal structure [17-20]. The PCF is made by a single material. Here we use Borosilicate crown glass as core material. Borosilicate glass was first developed by German glassmaker otto Schott in the late 19th century. Most borosilicate glass is cololeless 70 % silica, 10% boron oxide, 8% sodium oxide, 8% potassium oxide and 1% calcium oxide are used in the manufacture of borosilicate glass. Borosilicate crown glass (BK7) is an optical material used in a large fraction OPTICS products. It is relatively hard glass, doesn't scratch easily. Another important feature of BK7 is very good transmission down to 350 nm. Due to these properties, BK7 are widely used in the optics industry.

In this paper , we proposed two layer cladding PCF characterized by a common air hole space (pitch) and two different air hole diameters. The structure can ensure flat dispersion in a wide wavelength range and simple than the existing designs.

II. PROPOSED STRUCTURE

Figure 1. shows the proposed PCF. The inner three layer of cladding is composed of a common air hole pitch Λ and

diameter d_1 and outer three layer of cladding is composed diameter d_2 , where d_1 is less than d_2 . To achieve larger mode area we design the air holes of inner rings are chosen smaller. We have investigated the dispersion for different air hole diameter of inner and outer ring.

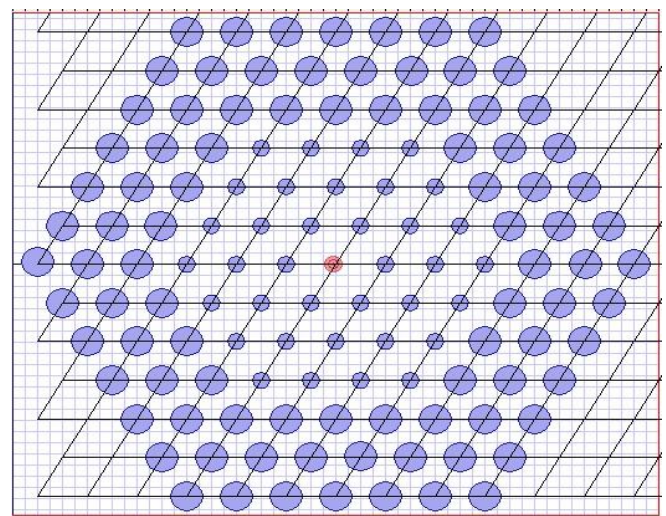


Figure 1. Proposed PCF.

Structure Parameter-

1. $d_1 = 0.5 \mu\text{m}$, $\Lambda = 2.0 \mu\text{m}$ and $d_2 = 1.5 \mu\text{m}$
2. $d_1 = 0.6 \mu\text{m}$, $\Lambda = 2.0 \mu\text{m}$ and $d_2 = 1.4 \mu\text{m}$
3. $d_1 = 0.7 \mu\text{m}$, $\Lambda = 2.0 \mu\text{m}$ and $d_2 = 1.3 \mu\text{m}$
4. $d_1 = 0.8 \mu\text{m}$, $\Lambda = 2.0 \mu\text{m}$ and $d_2 = 1.2 \mu\text{m}$

The wafer chosen is of Borosilicate crown glass with 1.5168 refractive index and the air hole refractive index is 1.0. In figure 1 we have change the inner and outer ring air hole diameter.

The value of refractive index of Borosilicate crown glass can be calculated by Sellemier formula [21,22].

III. EQUATIONS

The first paragraph under each heading or subheading should be flush left, and subsequent paragraphs should have

$$n^2 - 1 = \sum_i \left(\frac{A_i \lambda^2}{\lambda^2 - \lambda_i^2} \right) \quad (1)$$

Total dispersion is always calculated by adding waveguide dispersion and material dispersion.

$$D_T = D_W + D_M$$

Waveguide dispersion D_W is defined as –

$$D_W = -\left(\frac{\lambda}{c}\right) \frac{d^2}{d\lambda^2} n_{eff} \quad (2)$$

Where λ is the operating wavelength and c is the velocity of light in a vacuum [25].

IV. SIMULATION RESULTS

The effective refractive index difference is increased between proposed PCF and conventional PCF.

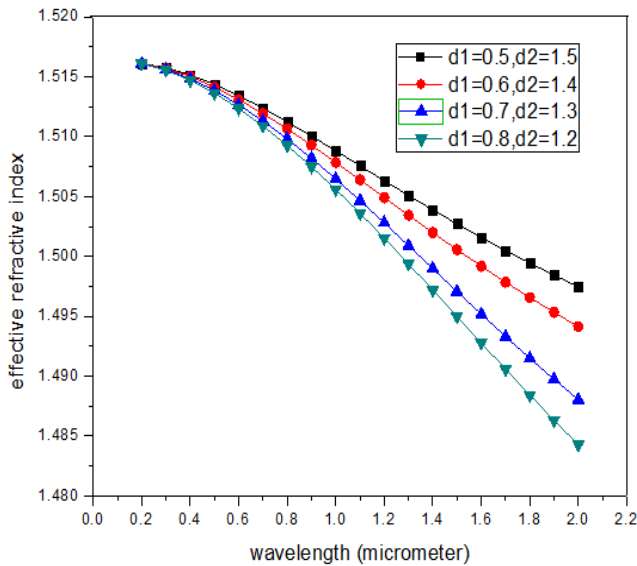


Figure 2. Shows the difference between effective refractive index of conventional PCF and Proposed PCF.

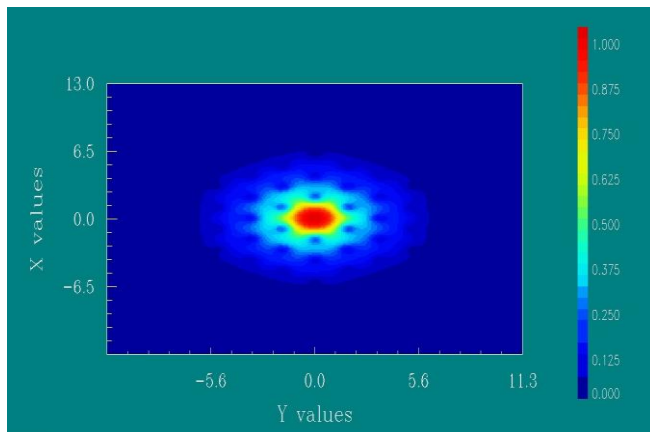


Figure 3. Shows mode field pattern of proposed PCF.

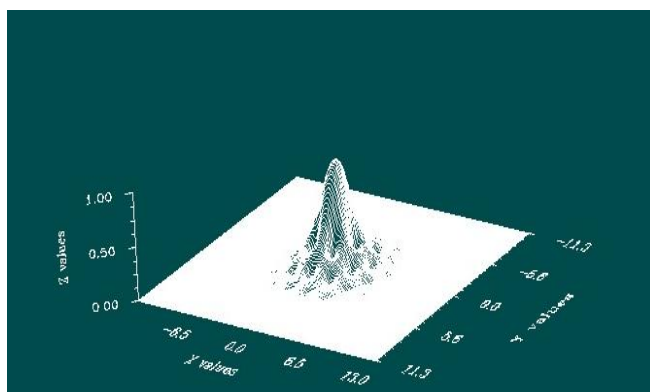


Figure 4. 3-D mode field pattern of proposed PCF.

The wafer is designed for width 26 μm and thickness 22.5166 micrometer. Material dispersion is always unchanged for any structure (hexagonal or square). It is also independent of structure parameter as air hole diameter ‘ d ’ and pitch ‘ Λ ’.

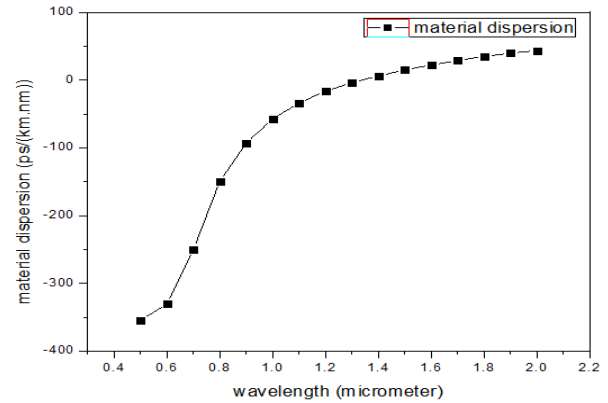


Figure 5. Material dispersion of Borosilicate crown glass PCF.

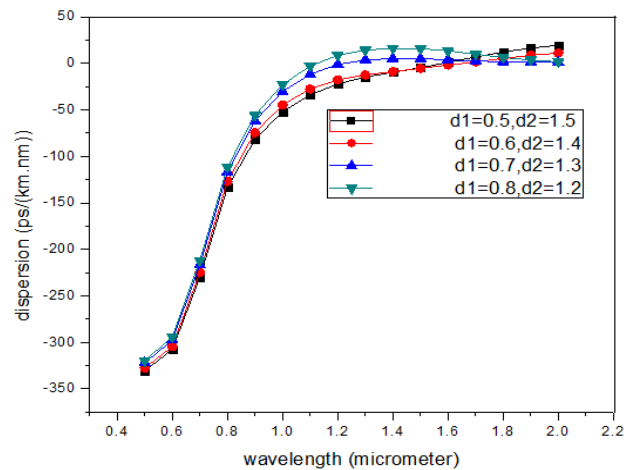


Figure 6. Chromatic dispersion of the proposed PCF for different values of the air hole diameters d_1 and d_2 when air hole spacing ‘ Λ ’ = 2.0 μm .

The proposed Borosilicate crown glass PCF makes almost flat dispersion.

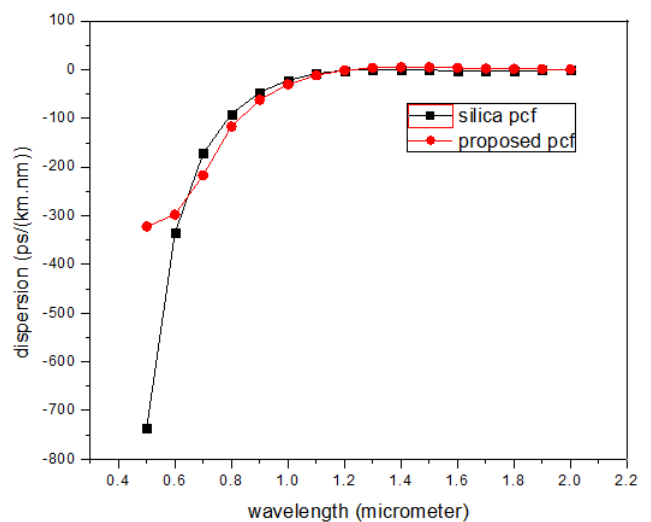


Figure 7. Shows the chromatic dispersion of proposed Borosilicate crown glass PCF and silica glass PCF when pitch ' Λ ' = 2.0 μm , d_1 = 0.7 μm and d_2 = 1.3 μm .

V. CONCLUSION

The above results indicate that the proposed Borosilicate crown glass PCF has almost zero and flat dispersion in low wavelength range as silica glass PCF. But Borosilicate crown glass has good properties (like cheaper, good transmission, easy availability) compare to silica glass. So we can use Borosilicate crown glass as a core material on the place of silica glass. Borosilicate crown glass can substitute of silica glass.

ACKNOWLEDGEMENTS

The authors thanks Mr. Bheem Singh, Chairman, RIET, Prof. Anoop Singh Poonia, Director, Chandrawati Education Society and Ms. Kirti Vyas, HOD, Arya College of Engineering & I.T, Jaipur for valuable efforts in preparation of the manuscript.

REFERENCES

- [1] E. Yablonovitch, Phys. Rev. Lett. 58, 1987, pp 2059.
- [2] J.C. Knight, T.A. Birks, P.St. J. Russell, D.M. Atkin, Opt. Lett. 21, 1996, pp 1547.
- [3] Razzak S.M.A, Namihira Y, Begum F., " Ultra flattened dispersion photonic crystal fiber", Electronics Letters 43(11), 2007, pp 615- 617.
- [4] Agrawal A, N. Kejalakshmy, J. Chen, B.M.A. Rahman and K.T.V. Grattan, " Golden spiral photonic crystal fiber : Polarization and dispersion properties", Opt. Lett, Vol. 33, 2008, pp 2716- 2718.
- [5] Shen L.P, W.P. Huang and S.S. Jain, " Design of photonic crystal fiber for dispersion related applications", J. Lightwave Technol, vol. 21, 2003, pp 1644- 1651.
- [6] Ferrando A, E. Silvestre, J.J. Miret and P. Andres, " Nearly zero ultraflattened dispersion in photonic crystal fibers", Opt. Lett, Vol. 25, 2000, pp 790- 792.
- [7] Ferrando A, E. Silvestre, P. Andres, J. Miret and M. Andres, " Designing the properties of dispersion flattened photonic crystal fibers", Opt. Express, Vol. 9, 2001, pp 687- 697.
- [8] Saitoh K, M. Koshiba, T. Hasegawa and E. Sasaoka, " Chromatic dispersion control in photonic crystal fibers : Application to ultra flattened dispersion", Opt. Express, vol. 11, 2003, pp 843- 852.
- [9] Poletti F, V. Finazzi , T.M. Monro , N.G.R. Broderick, V. Tsc and D.J. Richardson, " Inverse design and fabrication tolerances of ultra flattened dispersion holey fibers", Opt. Express, vol. 13, 2005, pp 3728- 3736.
- [10] Huttunen A and P. Torma, " Optimization of dual core and microstructure fiber geometries for dispersion compensation and large mode area", Opt. Express, Vol. 13, 2005, pp 627- 635.
- [11] Saitoh K and M. Koshiba, " Single polarization single mode photonic crystal fibers", IEEE Photon Technol. Lett, Vol. 15, 2003, pp 1384- 1391.
- [12] Kubota H, S. Kawanishi, S. Koyanagi, M. Tanaka and S. Yamaguchi, " Absolutely single polarization photonic crystal fiber", IEEE Photon. Technol. Lett, Vol. 16, 2004, pp 182- 184.
- [13] Dobb. H, K. Kalli and D.J. Webb, " Temperature insensitive long period grating sensors in photonics crystal fiber", Electron. Lett, Vol. 40, 2004, pp 657- 658.
- [14] Dong X and H.Y. Tam, " Temperature insensitive strain sensor with polarization maintaining photonic crystal fiber based on sagnac interferometer", Appl. Phys. Lett, Vol. 90, 2007.
- [15] Wadsworth. W.J, J.C. Knight, H.H. Reewes, P.S.J. Russell and J. Arriaga, " Yb³⁺ doped photonic crystal fiber laser", Electron Lett, Vol. 36, 2000, pp 1452- 1453.
- [16] Liu X, X. Zhou, X. Tang, J. Ng, J. Hao, T. Chai, E. Leong and C. Lu, " Swiathable and tunable multiwavelength erbium doped fiber laser with fiber bragg grating and photonic crystal fiber", IEEE Photon. Technol. Lett, Vol. 17, 2005, pp 1626- 1628.
- [17] Hansen T.P, J. Broeng, S.E.B. Libori, E. Knudsen, A. Bjarklev, J.R. Jonson and H. Simonson, " Highly birefringent index guiding photonic crystal fibers", IEEE Photon. Technol. Lett, Vol. 13, 2001, pp 588- 590.
- [18] Sapulak M, G. Statkiewicz, J. Olszewski, T. Martynkine, W. Urbanczyk, J. Wojcik, M. Makara, J. Klimek, T. Nasilowski, F. Berghmans and H. Thienpont, " Experimental and theoretical investigations of birefringent holey fibers with a triple defect", Appl. Opt., Vol. 44, 2005, pp 2652- 2658.
- [19] Anthkowie K.M, R. Kotynski, T. Nasilowski, P. Lesiak, J. Wojcik, W. Urbanczyk, F. Berghmans, and H. Thienpont, " Phase and group modal birefringence of triple defect photonic crystal fibers", J. Opt. A. Pure Appl. Opt, vol. 7, 2005, pp 763- 766.
- [20] Chen D and L. Shen, " Highly birefringent elliptical hole photonic crystal fibers with double defect", J. Light. Technol, vol. 25, 2007, pp 2700- 2705.
- [21] G.P. Agarwal, " Nonlinear fiber optics", third ed., Academic press, New York, 1995.
- [22] Bhawana Dabas, R.K. Sinha, " Dispersion characteristics of hexagonal and square lattic chalcogenide As₂Se₃ glass PCF", Opt. Comm, 2010, pp 1331- 1337.
- [23] G. Boudebs, S. Cherokulappurath, M. Guignard, J. Troler, F. Smektola and F. Sanchez, " Linear optical characterization of chalcogenide glasses", Opt. Comm, 2004, pp 331- 336.
- [24] G. Boudebssetal, Opt. Commun. 230(2004), pp 331.
- [25] Ferrando A, Silvestre E, Andere's P, Miret J.J, Ander's MV, " Designing the properties of dispersion flattened photonic crystal fibers", Opt. Exp., 2001, pp 687.

Authors Profile

Mahesh Chand received the B.E. degree in Electronics & Communication Engineering in 2005 from Govt. Engineering College, Ajmer, Rajasthan and pursuing in M.Tech from Suresh Gyan Vihar University, Jaipur. He is currently Assistant Professor and Head in EEE Department, RIET, Jaipur. He has published four books and one research paper in national journal. His current research includes Photonic Crystal Fiber.

Sandhya Sharma received the B.E and M.E degree from M.B.M Engineering College, Jodhpur, Rajasthan. She has total 16 years of teaching & Research experience. Presently she is Assistant Professor in Suresh Gyan Vihar University.

Ravindra Kumar Sharma received the B.E. degree in Electronics & Communication Engineering in 2008 from University of Rajasthan, Jaipur and pursuing M.Tech. In Digital Communication from Arya College of Engineering & I.T. He is currently Assistant Professor in the department of E&C, Rajdhani Institute of Technology & Management, Jaipur. He has published five research paper in various International Journals He is also associate of The Institution of Engineers (India). His current research includes photonic crystal fiber

Modeling and Structural analysis of heavy vehicle chassis made of polymeric composite material by three different cross sections

M. Ravi Chandra¹, S. Sreenivasulu², Syed Altaf Hussain³,

* (PG student, School of Mechanical Engineering RGM College of Engg. & Technology, Nandyal-518501, India.)

** (School of Mechanical Engineering, RGM College of Engineering & Technology, Nandyal-518501, India)

*** (School of Mechanical Engineering, RGM College of Engineering & Technology, Nandyal-518501, India)

ABSTRACT: The chassis frame forms the backbone of a heavy vehicle, its principle function is to safely carry the maximum load for all designed operating conditions.

This paper describes design and analysis of heavy vehicle chassis. Weight reduction is now the main issue in automobile industries. In the present work, the dimensions of an existing heavy vehicle chassis of a TATA 2515EX vehicle is taken for modeling and analysis of a heavy vehicle chassis with three different composite materials namely, Carbon/Epoxy, E-glass/Epoxy and S-glass /Epoxy subjected to the same pressure as that of a steel chassis. The design constraints were stresses and deflections. The three different composite heavy vehicle chassis have been modeled by considering three different cross-sections. Namely C, I and Box type cross sections. For validation the design is done by applying the vertical loads acting on the horizontal different cross sections. Software is used in this work PRO – E 5.0 for modeling, ANSYS 12.0 for analysis.

Keywords: heavy vehicle chassis, Static analysis, Carbon/Epoxy, E-glass/Epoxy and S-glass /Epoxy,

I. INTRODUCTION

Automotive chassis is a skeletal frame on which various mechanical parts like engine, tires, axle assemblies, brakes, steering etc. are bolted. The chassis is considered to be the most significant component of an automobile. It is the most crucial element that gives strength and stability to the vehicle under different conditions. Automobile frames provide strength and flexibility to the automobile. The backbone of any automobile, it is the supporting frame to which the body of an engine, axle assemblies are affixed. Tie bars, that are essential parts of automotive frames, are fasteners that bind different auto parts together.

Automotive frames are basically manufactured from steel. Aluminum is another raw material that has increasingly become popular for manufacturing these auto frames. In an automobile, front frame is a set of metal parts that forms the framework which also supports the front wheels. It provides strength needed for supporting vehicular components and payload placed upon it.

Automotive chassis is considered to be one of the significant structures of an automobile. It is usually made of a steel frame, which holds the body and motor of an automotive vehicle. More precisely, automotive chassis or automobile chassis is a skeletal frame on which various mechanical parts like engine, tires, axle assemblies, brakes, steering etc are bolted. At the time of manufacturing, the body of a vehicle is flexibly molded according to the structure of chassis. Automobile chassis is usually made of light sheet metal or composite plastics. It provides strength

needed for supporting vehicular components and payload placed upon it. Automotive chassis or automobile chassis helps keep an automobile rigid, stiff and unbending. Auto chassis ensures low levels of noise, vibrations and harshness throughout the automobile. The different types of automobile chassis include:

Ladder Chassis: Ladder chassis is considered to be one of the oldest forms of automotive chassis or automobile chassis that is still used by most of the SUVs till today. As its name connotes, ladder chassis resembles a shape of a ladder having two longitudinal rails inter linked by several lateral and cross braces.

Monocoque Chassis: Monocoque Chassis is a one-piece structure that prescribes the overall shape of a vehicle. This type of automotive chassis is manufactured by welding floor pan and other pieces together. Since monocoque chassis is cost effective and suitable for robotized production, most of the vehicles today make use of steel plated monocoque chassis.

Backbone Chassis: Backbone chassis has a rectangular tube like backbone, usually made up of glass fibre that is used for joining front and rear axle together. This type of automotive chassis or automobile chassis is strong and powerful enough to provide support smaller sports car. Backbone chassis is easy to make and cost effective.

II. SPECIFICATION OF THE PROBLEM

The objective of the present work is to design and analyses, of steel chassis made and also polymeric composite heavy vehicle chassis made of three different composite materials viz., Carbon/Epoxy, E-glass/Epoxy and S-glass /Epoxy composites. polymeric composite heavy vehicle chassis was created in Pro-E. Model is imported in ANSYS 12.0 for analysis by applying normal load conditions. After analysis a comparison is made between existing conventional steel chassis and polymeric composite heavy vehicle chassis viz., Carbon/Epoxy, E-glass/Epoxy and S-glass /Epoxy in terms of deflections and stresses, to choose the best one.

III. COMPOSITE MATERIALS:

A composite material is defined as a material composed of two or more constituents combined on a macroscopic scale by mechanical and chemical bonds.

Composites are combinations of two materials in which one of the material is called the “matrix phase” is in the form of fibers, sheets, or particles and is embedded in the other material called the “reinforcing phase”.

Another unique characteristic of many fiber reinforced composites is their high internal damping capacity. This leads to better vibration energy absorption within the material and results in reduced transmission of noise to neighboring structures. Many composite materials offer a combination of strength and modulus that are either comparable to or better than any traditional metallic materials. Because of their low specific gravities, the strength to weight-ratio and modulus to weight-ratios of these composite materials are markedly superior to those of metallic materials.

The fatigue strength weight ratios as well as fatigue damage tolerances of many composite laminates are excellent. For these reasons, fiber composite have emerged as a major class of structural material and are either used or being considered as substitutions for metal in many weight-critical components in aerospace, automotive and other industries.

High damping capacity of composite materials can be beneficial in many automotive applications in which noise, vibration, and hardness is a critical issue for passenger comfort.

IV. SPECIFICATION OF EXISTING HEAVY VEHICLE CHASSIS:

Table 1 shows the specifications of a TATA 2515EX OF STEEL HEAVY vehicle. The typical chemical composition of the material is 0.565C, 1.8% Si, 0.7%Mn, 0.045%P and 0.045% S.

Table: 1 Specifications of heavy vehicle chassis

S.No	Parameters	Value
1	Total length of the chassis (Eye to Eye)	8200 mm
2	Width of chassis	80 mm
3	Thickness of chassis	6 mm
4	Front cabin chassis length	2400 mm
5	Front cabin chassis area	492800 mm ²
6	Front cabin chassis applying load	19620 N
7	Backbody chassis length	5800 mm
8	Backbody chassis area	1200000 mm ²
9	Backbody chassis applying load	196200 N
10	Young's Modulus of steel chassis	2.1e5 N/mm ²
11	Density of steel chassis	7.86*10 ⁻⁶ N/mm ²

V. STRUCTURAL ANALYSIS OF HEAVY VEHICLE CHASSIS:

Dimensions of polymeric composite heavy vehicle chassis (PCHVC) are taken as that of the conventional steel heavy vehicle chassis (SHVC). PCHVC consists of 4 layers (thickness of each layer, 1.5mm). Width of the chassis is 80mm. Since the properties of PCHVC vary with directions

of fiber, a 3-D model of chassis is used for analysis in ANSYS 12.0. The loading conditions are assumed to be static. The element chosen is SHELL LAYERED 46, which is a layered version of the 8-node structural shell model. The element has six degrees of freedom at each node : translations in the nodal x, y, and z directions and rotations about the nodal x, y, and z-axes. The finite element analysis is carried out on steel chassis as well as on three different types of polymeric composite heavy vehicle chassis. From the analysis the equivalent stress (Von-mises stress) and displacements

were determined and are shown in figure 1-30. Table 2 - 4 shows the comparative analysis of steel chassis and polymeric composite heavy vehicle chassis of three different materials.

VI. STRUCTURAL ANALYSIS OF C - CHANNEL SECTION:

6.1. STEEL

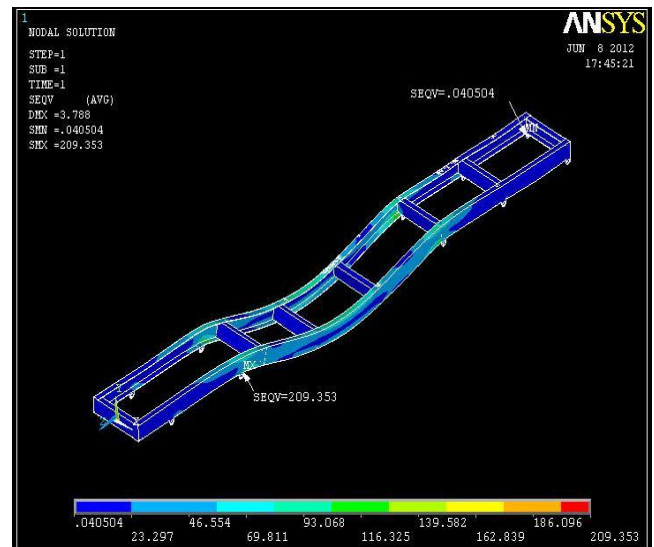


Fig1: Stress distribution for steel chassis

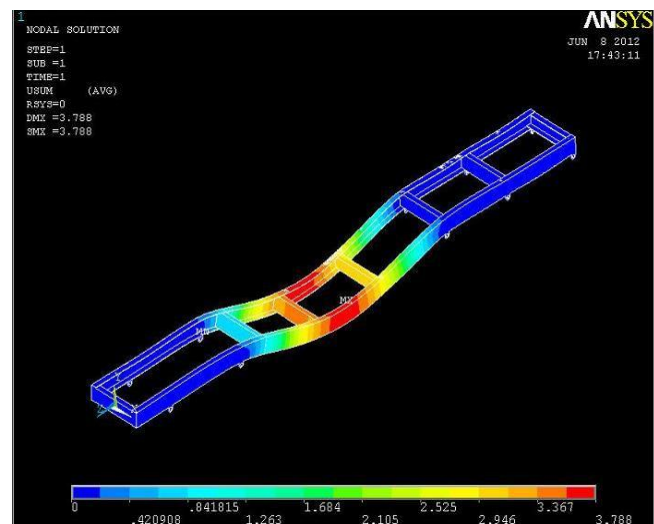


Fig 2: Displacement pattern for steel chassis

6.2 CARBON/EPOXY



Fig 3: Stress distribution for carbon/epoxy.

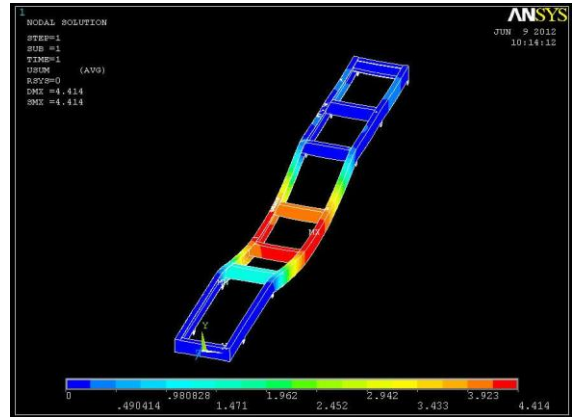


Fig 6: Displacement pattern for E-glass/epoxy.

6.3 E-GLASS/EPOXY

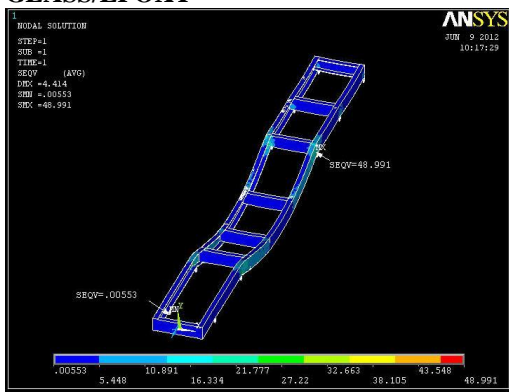


Fig 5: Stress distribution for E-glass/epoxy.

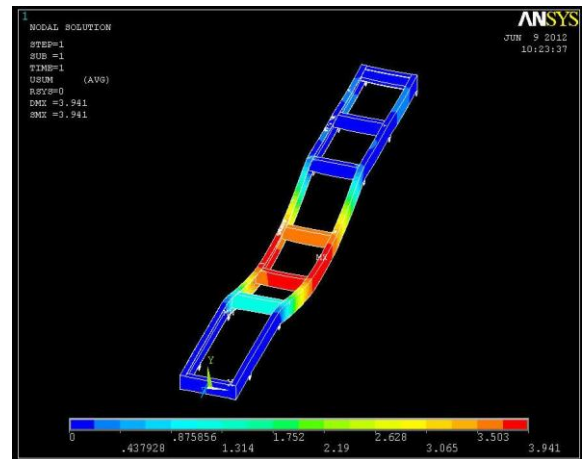


Fig 8: Displacement pattern for S-glass/epoxy

6.4 S-GLASSEPOXY

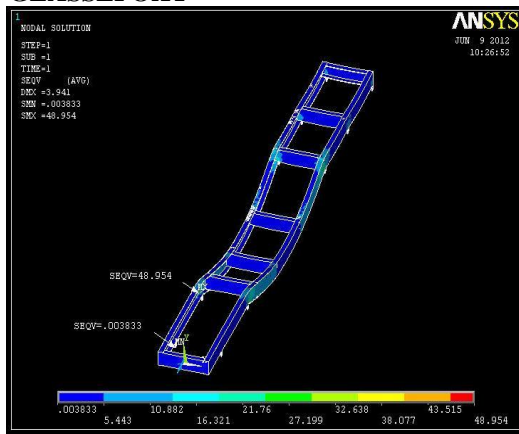


Fig 7: Stress distribution for S-glass/epoxy.

VII. STRUCTURAL ANALYSIS OF I-CHANNEL SECTION:

7.1 STEEL



Fig9: Stress distribution for steel chassis

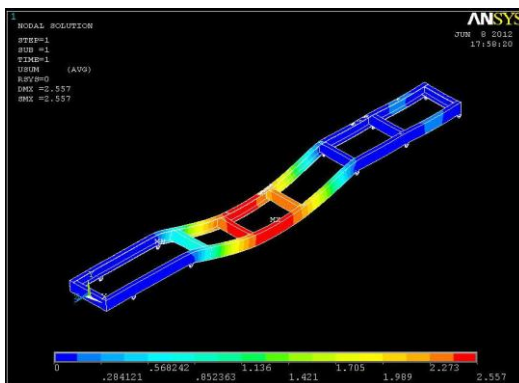


Fig 4: Displacement pattern for carbon/epoxy.

7.2 CARBON/EPOXY



Fig 11: Stress distribution for carbon/epoxy.

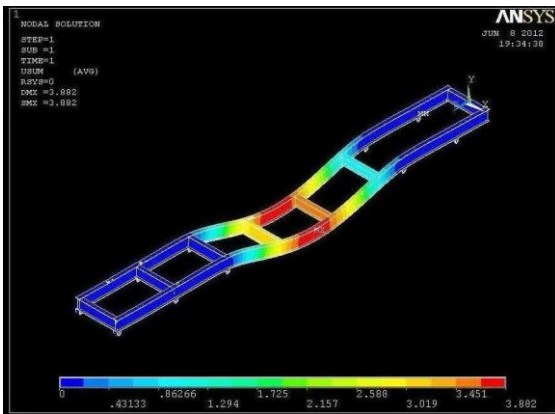


Fig 10: Displacement pattern for steel chassis.

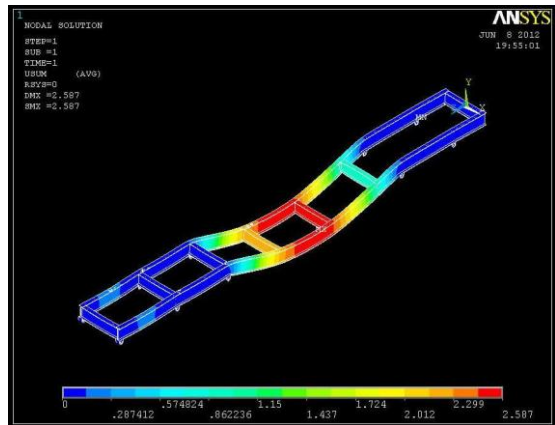


Fig 12: Displacement pattern for carbon/epoxy

7.3 E-GLASS/EPOXY

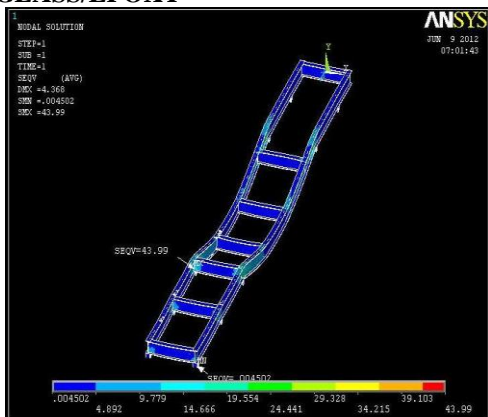


Fig 13: Stress distribution for E-glass/epoxy

7.4 S-GLASS/EPOXY

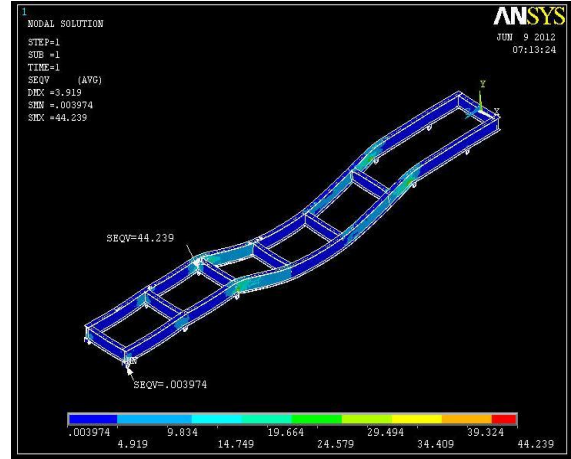


Fig 15: Stress distribution for S-glass/epoxy

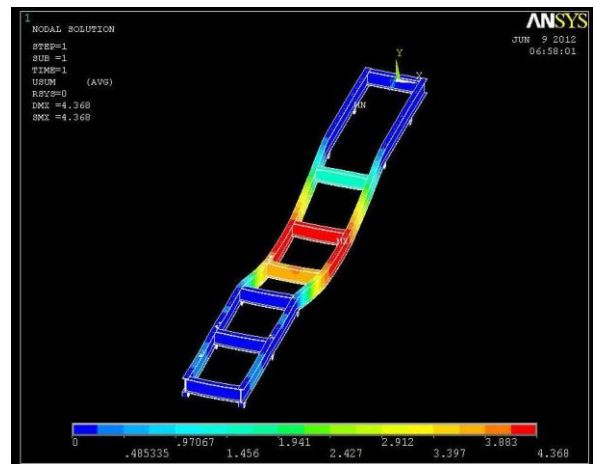


Fig 14: Displacement pattern for E-glass/epoxy

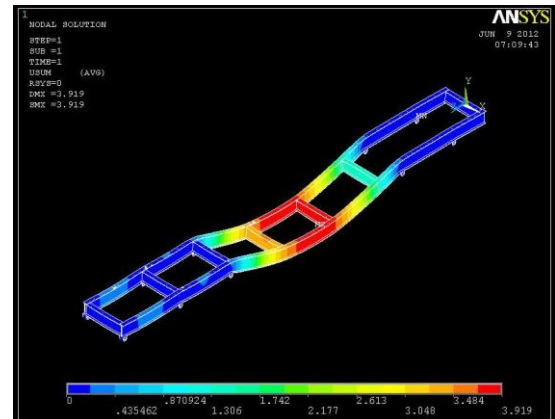


Fig 16 Displacement pattern for S-glass/epoxy

VIII. STRUCTURAL ANALYSIS OF BOX - CHANNEL SECTION:

8.1 STEEL

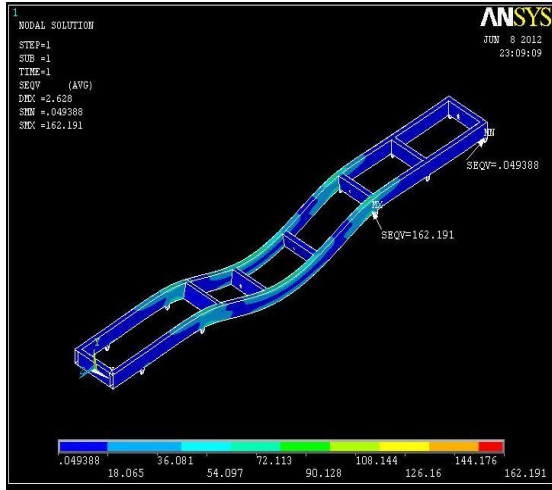


Fig17: Stress distribution for steel chassis

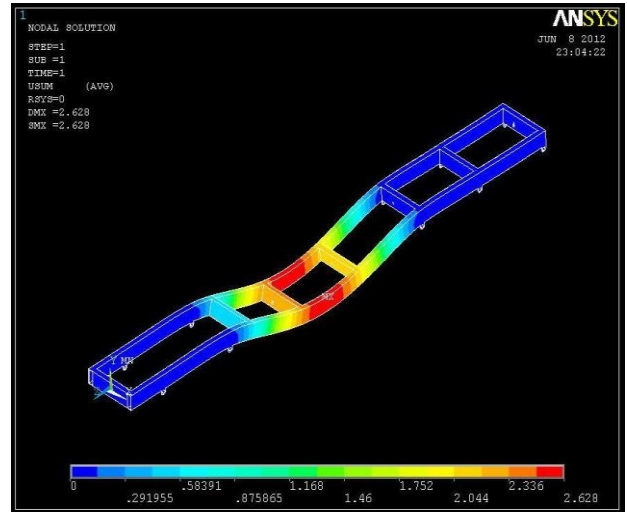


Fig 18: Displacement pattern for steel chassis.

8.2 CARBON/EPOXY

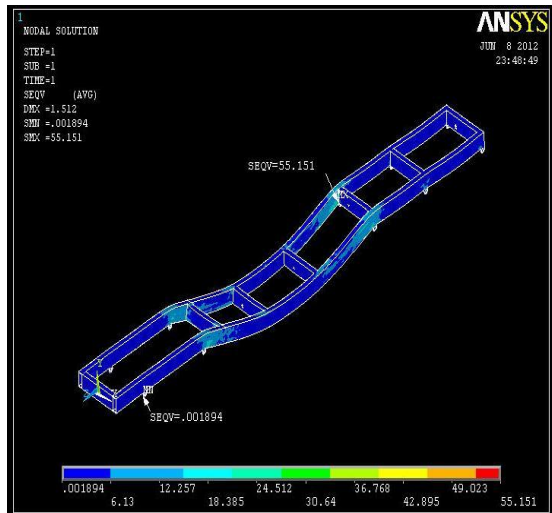


Fig 19: Stress distribution for carbon/epoxy.

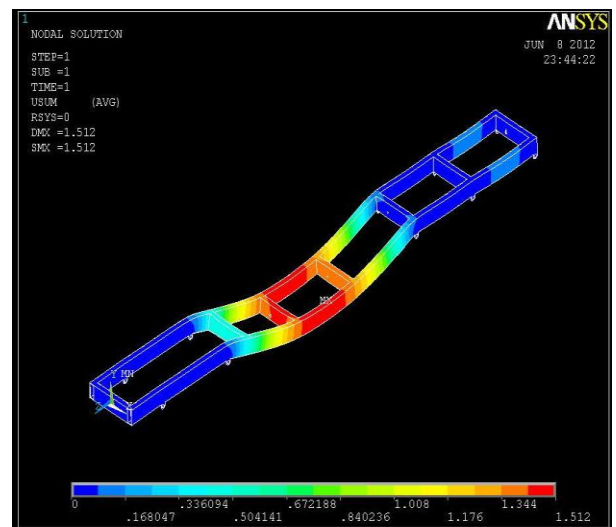


Fig 20: Displacement pattern for carbon/epoxy

8.3 E-GLASS/EPOXY

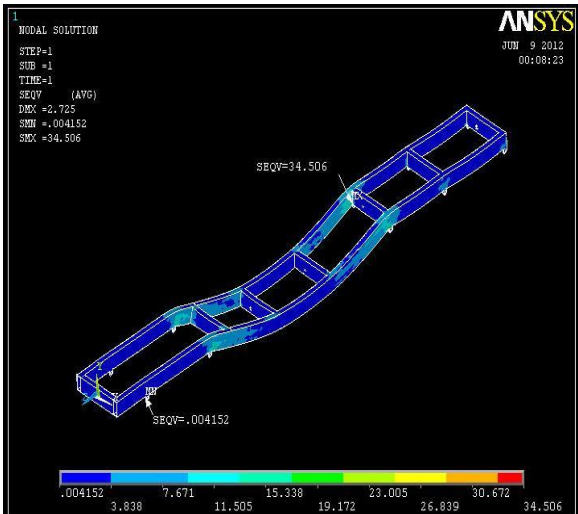


Fig 21: Stress distribution for E-glass/epoxy

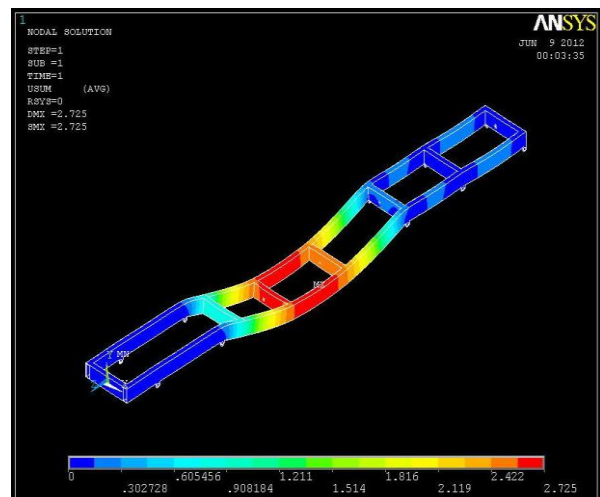


Fig 22: Displacement pattern for E-glass/epoxy

8.4 S-GLASS/EPOXY

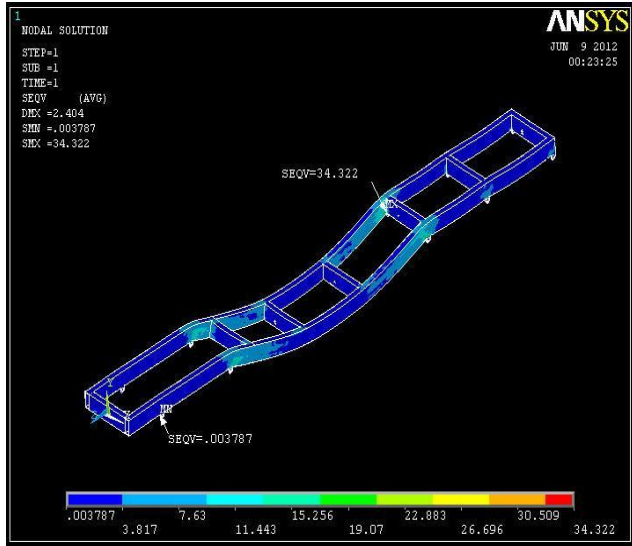


Fig 23: Stress distribution for S-glass/epoxy

8.

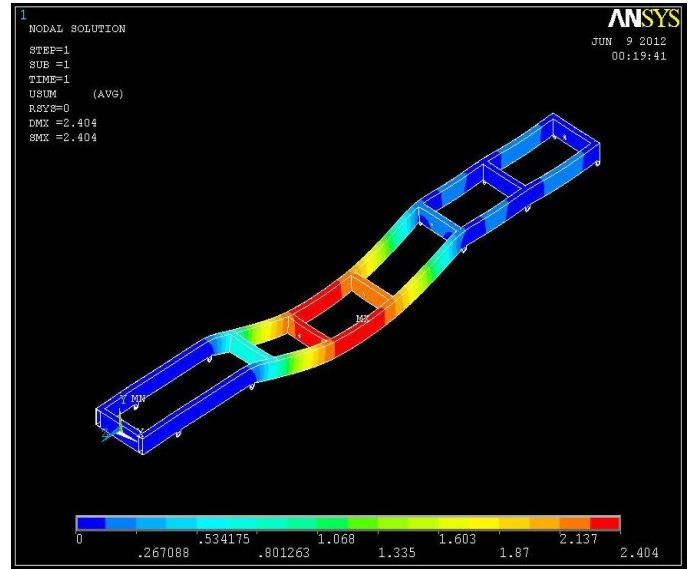


Fig 24: Displacement pattern for S-glass/epoxy

Table 2. Comparative Analysis of steel heavy vehicle chassis g and polymeric composite heavy vehicle chassis for C- Section.

S.No	parameter	steel	polymeric composite materials		
			Comp:1	Comp:2	Comp:3
1	Weight (kg)	412.6	82.953	110.258	105.00
2	Stress (N/mm ²)	209.35	74.42	48.99	48.95
3	Displacement (mm)	3.78	2.557	4.414	3.941

Table 3. Comparative Analysis of steel heavy vehicle chassis g and polymeric composite heavy vehicle chassis for I- Section

S.No	parameter	steel	polymeric composite materials		
			Comp:1	Comp:2	Comp:3
1	Weight (kg)	410.8	82.584	109.76	104.53
2	Stress (N/mm ²)	249.99	72.799	43.99	44.239
3	Displacement (mm)	3.882	2.587	4.368	3.919

Table 4. Comparative Analysis of steel heavy vehicle chassis g and polymeric composite heavy vehicle chassis for I- Section

S.No	parameter	steel	polymeric composite materials		
			Comp:1	Comp:2	Comp:3
1	Weight (kg)	608.35	122.28	162.53	154.71
2	Stress (N/mm ²)	162.89	55.151	34.506	34.322
3	Displacement (mm)	2.628	1.512	2.725	2.404

VIII. GRAPHS:

8.1. C-Section

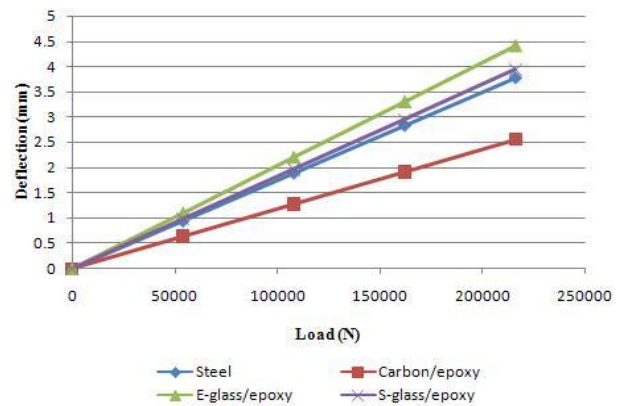


Fig 25: Load - Deflection curves for steel and polymeric composite material.

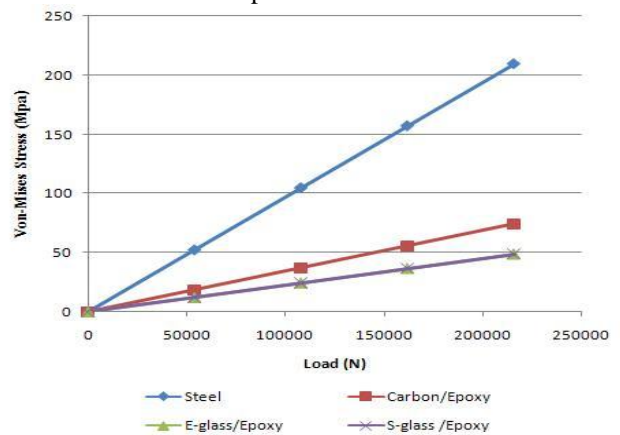


Fig 26: Load - Von-Mises Stress curves for steel and polymeric composite material

8.2.I-Section

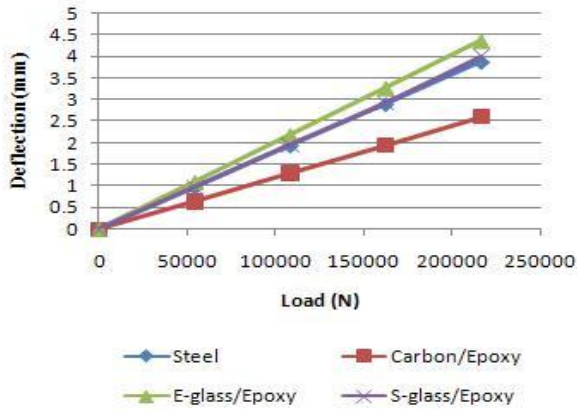


Fig 27: Load - Deflection curves for steel and polymeric composite material.

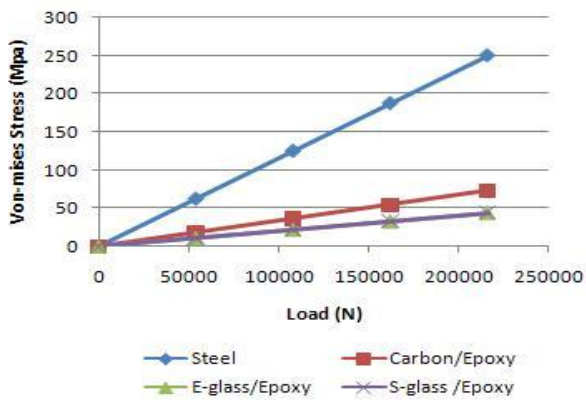


Fig 28: Load - Von-Mises Stress curves for steel and polymeric composite material

8.3. Box - Section

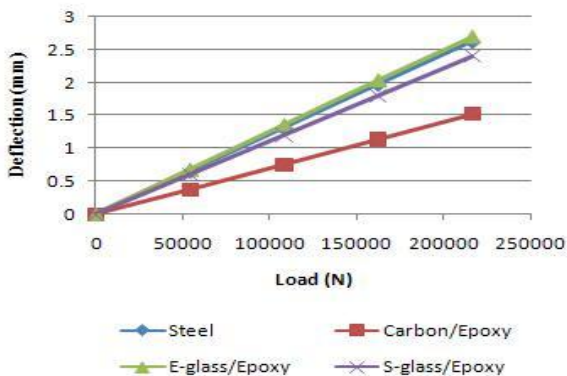


Fig 29: Load - Deflection curves for steel and polymeric composite material.

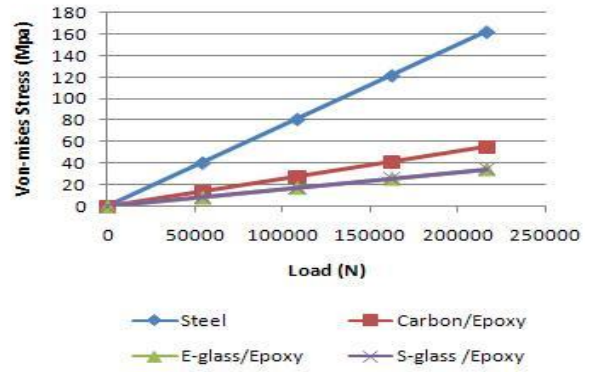


Fig 30: Load - Von-Mises Stress curves for steel and polymeric composite material

IX. CONCLUSIONS

To observe the all results and to compare the polymeric composite heavy vehicle chassis and steel heavy vehicle chassis with respect to weight, stiffness and strength.

By employing a polymeric composite heavy vehicle chassis for the same load carrying capacity, there is a reduction in weight of 73%~80%, natural frequency of polymeric composite heavy vehicle chassis are 32%~54% higher than steel chassis and 66~78% stiffer than the steel chassis.

Present used material for chassis is steel. I have considered polymeric composites Carbon/Epoxy, E-glass/Epoxy and S-glass /Epoxy for chassis material. Based on the results, it was inferred that carbon/epoxy polymeric composite heavy vehicle chassis I-SECTION chassis has superior strength and stiffness and lesser in weight compared to steel and other polymeric composite materials and other cross sections considered in this investigation.

From the results, it is observed that the polymeric composite heavy vehicle chassis is lighter and more economical than the conventional steel chassis with similar design specifications.

REFERENCES

- [1] C. Karaoglu, N. S. Kuralay, Stress analysis of a truck chassis with riveted joints, Finite Elements in Analysis and Design, 38, (2002), 1115–1130.
- [2] K.W. Poh, P.H. Dayawansa, A.W. Dickerson, I.R. Thomas, Steel membrane floors for bodies of large rear-dump mining trucks, Finite Elements in Analysis and Design 32, (1999), 141-161.
- [3] K. J. Buhariwala and J. S. Hansen, "Dynamics of Viscoelastic Structures", AIAA Journal, Vol. 26, February 1988, pp 220-227.

10.1 Books:

- [4] Nitin S. Gokhale- Practical Finite Element Analysis.
- [5] Autar K. Kaw. Mechanics of Composite Materials. 2e, Taylor & Francis Group, LLC, 2006.

Reviewing Testability of Object Oriented Systems for Non-Functional Specifications

Vaishali Chourey¹, Dr. Meena Sharma²

**(Department of Computer Science, Medi-Caps Institute, Indore, M.P. India)*

*** (Department of Computer Science, IET-DAVV Indore, M.P. India)*

ABSTRACT: *The object oriented programming proves to be the most beneficial paradigm for scalable and maintainable software development. An object characterizes special features like encapsulation, inheritance, modularity and polymorphism. The processes in Test Driven Design closely relate the agile methodology and strengthen the need of testing during the development stages. The UML specifies the architecture of the system. The design follows the specification and hence the implementation. The whole process adopts the language of UML from beginning of software through requirements specification till the deployment. The evaluation of software so as to be testable needs additional efforts. The weaker or ignored issues like the testing for non-functional requirements still need to be accommodated in the test design. The paper reviews the weaknesses of the object oriented systems and the models to be testable. It also includes metrics that quantifies the structural complexity of system to test its understandability and maintainability.*

Keywords: *Models, Object Oriented Testing, Model Based testing, metric based evaluation, Weighted Complexity.*

I. INTRODUCTION

Software engineering bridges its strengths to design and document the software development process through the use of various models. Booch, Jacobson and Rumbaugh[1] conceptualized the behavioral, functional and implementation specific models that were sufficient to describe the elements and their relations in any object oriented software systems. Their contribution to the software engineering field for the same has been widely exercised in industry. The models have been the curious issue in the testing phenomenon whereby the testing is not delayed till the implementation phase but it goes simultaneously as it proceeds in the life cycle. This makes model based testing an interesting and exploratory research area. Model driven methodology proved its worth with the variety of software developed in varied areas. Any degree of complexity can be easily expressed with a set of diagrams. Whether it is structural or architectural specification or functional description, the use of objects and object design languages like UML has facilitated the tasks of project managers. It has even groomed the language of communication amongst the team of developers in any organization. Along with these the software industry benefits with the automated tools for programming high order languages. Altogether this has summed to an approach for robust and manageable code being developed quickly and efficiently. Software Testing is also a major phase in the development of the system for assuring its reliability

and behavioral compliance to the requirements specified. A fact that 40-50% of the software development efforts are shared by testing makes it an important aspect.

The work in this paper compiles the major contributions in the areas of object oriented paradigm and its importance in the development phases. The section II contains an overview of the OO system and their characteristics. The section III contains the modeling language UML and the various diagrams with their importance. Section IV summarizes the issues that restrict testability of the designs. Section V contains the realization of theories related to class design metrics to map it to testing process. It brings the quantification of non-functional parameters like understandability and such attributes to contribute to testing results.

II. OBJECTS AND OBJECT ORIENTED DESIGN

All the literature pertaining to the objects and object oriented design addresses the software projects commendable threats namely inadequate and unstable requirement, inadequate customer communications, poor team communications, unnecessary complexity and ineffective team behavior. Software projects are governed by the list of requirements specified by the customer who is the end user of the whole process. Thus the whole process is based on requirements that are actually the specifics of the system and the needs that are captured. The requirements once finalized do not change often, but the specification for building a piece of implementation of software are changed frequently and added throughout the development cycle. The challenge is to cope up with this frequent updates. Secondly the requirements must be verified with the customer before the design starts. Thus the interactions must conform to the initiation of the project. The next problem begins when the requirements that are verified are not "exactly" communicated to the developer team and an ambiguity occurs. The same requirement must flow properly to the developers. So, we have to make the models that are descriptions to the requirements graphically, thus lessening the probability of ambiguity in documentation if it was textual. As the analysis completes, the design of core transactions and implied operations have to be prepared. The behavior has to be formally or "pseudo-conventionally" specified with models so that they can be codified easily. This defines the system in the form of subsystem, components, classes, objects and their inter-relations like association, hierarchy and collaborations. Thus the system is added with another issue of its structural complexity because of its inter-related artifacts. The task of project

management is to clearly pass through these phases and bring up the system in its entirety.

Not only limited to the planning and development, but testing also is the requirement of the system and theories indicate the fact that effectiveness of object oriented technology lies in testing that goes parallel to development. Whether it is agile development process or any other technology, that depends on objects and specifies that the testing of models be made simultaneous. This reduces the risks from getting accumulated. There are many justifications to the development of models and their usages.

III. UNIFIED MODELLING LANGUAGE OR THE UML

The UML is defined [1] as “A language to specify, visualize, construct and document the artifacts of a software-intensive system.” It is a standard language for writing the blueprints of software. Ranging from the enterprise solutions to distributed web based applications; UML conceptualizes the artifacts of the system developed in object oriented languages. Thus, UML is inherently applicable to architecture centric, iterative and incremental project development. This language has rules and vocabulary for physical and conceptual representation of the software. The language has a collection of diagrams and relative specifications to handle the complexity of the system. For the enumeration, we have:

Table 1: Diagrams and Relevance in Software Project Management

Diagram	Purpose
Use case Diagram	This diagram models and organizes the behavior of the system through its functionalities and services <i>to-through-for</i> actors of the system.
Class Diagram	This represents the set of classes, interfaces and their relationships. This diagram addresses the static and process view of the system.
Object Diagram	This diagram emphasises on the objects and their relationships.
Sequence Diagram	This is an interaction diagram that emphasises the time ordering of messages.
Collaboration Diagram	This is an interaction diagram that emphasises the structural organization of the objects that send and receive messages.
State-chart Diagram	This diagram addresses the dynamic view of the system especially useful in modelling reactive systems.
Activity Diagram	This is a diagram to model the functions of the system and emphasises flow of control among objects. It represents the sequence, concurrency and synchronization of various activities performed by the system.
Component Diagram	This diagram expresses the organization and dependencies

	among a set of components.
Deployment Diagram	This diagram shows the configuration of run-time processing nodes and corresponding components.

The generality in the models and their *express*-ability makes it applicable to various areas like production, deployment and maintenance of software. However in the software development organization, the diagrams are conveniently adopted by analysts and end users for specifying the requirements, structure and behavior of the system. The architects who design the systems to satisfy the requirements specified and the developers who code the architecture into executables use the modeling conventions for communication and documentation. This is equally benefiting the quality assurance personnel who verifies and validates the system for its structure, behavior, functionality and other requirements. The monitoring of the development is emulsified with the process. This is the strength of UML widely acceptable by researchers and used by industries.

The UML has been an immensely popular issue in industry and research for Model Based Testing (MBT). [6] Models are the simplified version and representation of the systems and so are easily amenable for automated test case generation. Models can be classified into formal, semi-formal and informal models. Formal models are mathematically derived [3] from techniques of calculus theory, logic, state machines, markov chains etc., semi-formals combine the diagrams in ad-hoc conventions and are used in industries. Behavioral models are very significant for the test case generation [10, 12] as the bugs are indicated during test of a specific run or implementation of specific functionality of the system. Several research work and industry cases record the diagrams [5] with the Object Oriented Testing Strategies to test various aspects of the software. The table below describes it as:

UML Diagram	Test Coverage	Type of Test	Fault Model
Class Diagram State Diagram	Code	Unit	Error Handling, correctness,
Class Diagram Interaction Diagram	Functional	Functional	Functional Behavior Integration Issues API Behavior
Usecase Diagram Activity Diagram Interaction Diagrams	Operational Scenarios	System	Contention Synchronization Workload Recovery
Class Diagram Interaction Diagram	Functional	Regression	Unexpected Behavior through system alterations
Usecase Diagram Deployment Diagrams	Inter-System Communications	Deployment Solution	Interoperability issues

Table 2: Diagrams and Associated Tests

IV. ISSUES IN OBJECT ORIENTED TESTING

The Object Oriented Testing requires additional techniques for its execution apart from the conventional ones. The testing takes two broad forms of Functional testing or Black box testing where the fulfillment of functional requirements is tested. Another is the Structural testing that tests for the structure of classes, their interactions and their states during execution of any method or activity. Structural testing is the white box testing of the OO systems.

The characteristic of object orientation makes testing rigorous over each iteration and phase of development [3-5]. The increments that are models like the analysis model is tested for requirement specific documentation and use cases. The design model is tested with the corresponding class diagram, interaction diagrams and activity diagrams.

Structural testing with methods and their code that contains statement, decision and path coverage are tested. All methods that are defined, newly added with the increment in functionality, inherited methods and methods that are redefined needs to be tested. The classes are tested for the state transitions during n activity, transaction flows are tested with messages that the classes share, exception testing for the exceptional behavior and conditions that a class may represent.

Object oriented nature poses difficulties to test a class without additional methods to access all the functionalities defined in the class and access its states. Each new instance for inheritance requires retesting. It is easy to test conditions, decisions, loops and exceptions within a class but it is difficult with the set of interaction amongst classes and requires special techniques. There are hierarchical structures but absence of hierarchical control flow makes the execution testing difficult. Integrated classes are thus tested with techniques like thread based testing, use based testing and cluster based testing. System testing is done for the recovery of systems from faulty conditions, security tests for unauthorized accesses, stress testing for load during execution and performance testing for reliability and availability with optimized execution.

Heterogeneity in Models:

Each model describes a different perspective of the same system, thus the testing of the object oriented models take different versions for each model[12]. There are contributions where these models have been used to generate test cases and respective test scripts are generated through automated process. The inputs to these test generators are the set of diagrams associated. Pretschner in his paper [4] presents a detailed discussion reviewing model based test generators. The studies in the area indicate that different test suites with the same coverage may detect fundamentally different number of errors. Also the above table [table 2] indicates that the single diagram alone may not suffice with the exhaustive test of a single type. During the development the industry follows ad-hoc modeling and do not comply with a defined set of diagrams. In such cases where the industry has its own conventions for design and documentation, it is required that the organizations develop their own framework and corresponding tools to build, manage and maintain test models.

Choice of Models in Test Generation:

An example system for the GPS navigation system for a car developed has to be tested for its functions and operations. A model based test brings up the test for the vehicle's position hereby ignoring other functionalities for the display and user interaction features [6]. Another test to the model may test a separate aspect of the system like route planning or route display and so on. The crucial factor is that the aspects are independent tests and they do not interact in terms of aspects. Thus not only diagrams but behavior also segregates the tests with diagrams.

Skills, Audience and Tools:

The issue arises when the testers need to be educated and trained on modeling practices. So far when the testing was confined to code, developers of the corresponding language who had an expertise could manage the testing. Thus the object oriented- model based testing expects modeling skills for the developers and the tester both. The limitation to the model based testing approach converges to the idea that only trained and technically apt audience can and are expected to create, read, review and maintain models. The concept is insufficient to bridge the gap between the models that are characterized with the quality of being best for human understanding and ones that are optimal for testing. Thus the tools that need to be customized with the testability of models have to be developed within the organization's development framework. There exists the limitation for behavior testing tools available for universal applicability.

Scope:

Models have a specific importance when the requirements are being matched to implementation parameters like class, methods or objects. The models however deal only with the superficially expressed behavior of the system which is the high level abstraction. Most of the models confined to the views of the system do not completely fit to the testing essentials. Thus in the early stages of development, the testers end up with almost prohibitive tasks of modelling parts of really large and complex systems. Summarizing, models constructed during the early development process lack several details of implementation that are required to generate test cases.

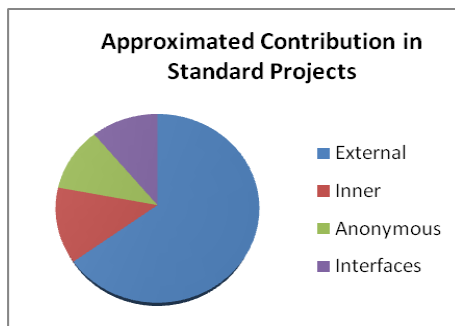
Also for the short development cycles, if there are new releases every week, that also reflects early construction phase of object oriented software development, the diagrams or models do not change accordingly. MBT do not pay off with such projects and more versatile tools are required for testing such typical projects. MBT are fruitful and can be used after releases have achieved a certain degree of stability in its features.

Features of Programming Languages:

Encapsulation [4] restricts the visibility of object states and *observ*-ability of intermediate test results. Inheritance causes invisible dependencies amongst hierarchically related classes. The approach that was devised for preventing code redundancy inhibits code dependencies of varied forms. The child classes that inherits parent's methods cannot be tested without testing the parent class. Abstract classes are the serious conditions where they can never be tested. Polymorphism extends to a limit of

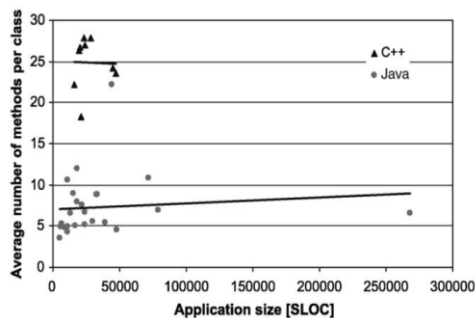
testing all possible conditions, paths for execution and potential errors that it may scope into the classes.

The literature on object orientation defines its strength as Open-Close Principle. The modules are open for extension but close for modification. This, when applied to classes, testing and maintainability is sacrificed. For any new behavior minor-or-major the classes are open for the inheritance. This becomes redundant with series of modifications hereby increasing the complexity of the system. The numbers of classes grow proportionally with the increment in form of new requirements, refined requirements or just additional classes in the development model. A research paper by John D. Mc Groger [17] proves through a formula derived that works as a multiplier function to estimate number of classes after each iteration.



(a)

The number of classes and the relationships amongst them contributes to structural complexity and is referred to in many researches, there by calculating cyclomatic complexity to quantify the attribute.



(b)

Fig 2: (a) Average Metric Values for Percentage of Classes of Each Type
 (b) Average Metric value for the Number of Methods per Class

The above facts have been referred from the research [13, 18] done on various projects that estimate the total number of classes coded and the nature of classes along with the number of methods within each class. The average is depicted in statistics as above figures Fig 2 (a) and (b). Thus the number of classes and methods within each class has a vast average estimated and it is technically not feasible to test all the methods and a mid-way taking necessary implementations pass through the tests. Can the un-tested classes create errors and are there more intense testing methods to check the addition of classes and verify them, i.e making each class testable, is still a question to the project managers.

Also it is well proved that object oriented features like polymorphism, inheritance and encapsulation [18] create wide opportunities for the bugs to creep into the system that was less prevalent in traditional systems. It is also well exemplified in many cases like if many server objects function correctly at top level, but there is nothing to prevent a new client class from using it correctly. Thus, not only testing but developing becomes tedious and testing gets extended over a prolonged duration while final implementation gets ready.

The most important part of the analysis of system is calculating the complexity. Complexity is formally defined as the degree to which system or component has a design or implementation that is difficult to understand and verify [21]. This can be included in the system test that validates maintainability and understandability.

The classes may be analyzed with the metrics that measure the aspects of classes and the interactions amongst them[7]. These measures tells us more about our design and help quantify the maintainability. A change in one class will affect code in other classes, it should be minimal and classes with high dependency must be kept in same package. There are some metrics as:

Intra Class Metrics:

There are metrics at class level that may be helpful to calculate the complexity of the system. They can be reuse ratio, specialization ratio, number of external methods called, number of methods called in class hierarchy, number of local methods called, number of instance variables, number of modifiers, number of interfaces implemented and number of packages imported.

LCOM (Lack of Cohesion Methods): This metric refers the correlation between methods and the local instance variables of the class. High cohesion indicates good class subdivision.

Unweighted Class Size: This is calculated as number of methods and attributes of a class.

Inter Class Metrics:

This is measured by coupling at class level. Coupling is defined as a representation of the references between classes. If a class refers another class or it is being referenced then we measure it as coupling. There are parameters that still need to be standardized and can be defined as: Coupling between classes, Fan Out, Fan In, Efferent Coupling, Afferent Coupling. (Originally defined by Chidamber & Kemerer)[20].

Response for Class: It measures the coupling of classes in terms of method calls. It is the sum of number of methods in the class and the number of distinct method calls made by the methods in the class.

Message Passing Coupling: This metric measures the number of number of messages passing among objects of the class. A large value indicates high coupling and classes seem to be more dependent on each other. This increases the complexity of the system.

The above mentioned parameters are non-weighted measures, there are also metrics with weighted parameters like [22]:

Weighted Class Complexity (WCC): The calculation is based on calculating the complexity of operations by considering corresponding cognitive weights. The cognitive weights are used to measure the complexity of the logical structures of the software that reside in the code as methods. They are classified and weighed as sequence ($w=1$), branch ($w=2$), iteration ($w=3$) and call ($w=2$) [15]. Initially the weight of individual method in a class is calculated by associating a weight with each method (member function) and add all the weights. This is weight due to methods and is called Method Complexity (MC). If there are n methods in a class then total method complexity is given by:

$$= \sum^n MC_n$$

The next step computes the total complexity due to attributes in the class and is denoted by N_a .

The complexity of a single class is called Weighted Class Complexity (WCC) and is given by:

$$WCC = N_a + \sum^n MC_n$$

If the total number of classes in the code is x then:

$$\text{TotalWeightedClassComplexity} = \sum WCC_x$$

The above weighted complexity calculation can be explained with the help of an example. The system comprises of following classes:

- Person*
- Student*
- Employee*
- Faculty*
- Administration*

The code exists like the one specified below and at each level, the complexity is calculated simultaneously.

/ Person Class is inherited by Student and Employee Class */*

```
PERSON CLASS
class Person
{
string name; int age; char gender;
public:
Person(string="",int=0, char='\0'); // W p1=1
Person(const Person &person); //copy constructor W p2=1
void print()const; //Wp3=Wp31+Wp32=2+1=3
string getName(){ // Wp4=1
return name; }
int getAge(){ //Wp5=1
return age;}
char getGender(){ //Wp6=1
return gender; }
};
//Person-default constructor
```

```
Person :: Person(string in, int ia, char is)
{ name = in; age = ia; gender = is; }
//Person-copy constructor
```

```
Person :: Person(const Person &p)
{ name = p.name; age = p.age; gender = p.gender; }
void Person :: print()const
{ cout<<"Name\t : "<<name<<"\n' ; //Wp31=1
cout<<"Age\t : "<<age<<"\n' ;
if (gender=='F') //Wp32=2
cout<<"Gender\t : Female" <<"\n' ;
else cout<<"Gender\t : Male" <<"\n' ; }
```

```
STUDENT CLASS
class Student: public Person{ int sid; float gpa;
public:
Student(const Person &p,int student_id,float igpa):
Person(p) //WS1=1
{ sid = student_id;
gpa = igpa; }
void print()const; };
//WS2=WS21+WS22*WS23=1+2*2=5
void Student :: print()const
{ Person :: print();
cout<<"S.ID\t:"<<sid<<"\nGPA\t:"<<gpa<<endl;
//WS21=1
if (gpa>=2.0) //WS22=2
cout<<" Student is successful"<<endl;
else {if (gpa>=1.7) //WS23=2
cout<<"Student must improve GPA" <<endl;
else
cout<<"Student must repeat" <<endl; } }
```

```
/* ***** EMPLOYEE CLASS ***** */
class EMPLOYEE: public Person{ float salary;
public: EMPLOYEE::EMPLOYEE(const Person &p, float
sal):Person(p) ,salary(sal){ //WE1=1
EMPLOYEE(const EMPLOYEE
&EMPLOYEE):Person(EMPLOYEE){
salary=EMPLOYEE.salary; } //WE2=1
void print()const; }; //WE3=1
void EMPLOYEE::print() const{ Person::print();
cout<<"salary: "<<salary<<endl; }
```

FACULTY

```
class Faculty: public EMPLOYEE{
string branch;
public: Faculty(const EMPLOYEE &e, string
b):EMPLOYEE(e),branch(b) //WF1=1
{}
void print()const; }; //WF2=1
```

```
/* ***** ADMINISTRATIVE CLASS ***** */
class Administrative: public EMPLOYEE{string duty;
public:
Administrative(const EMPLOYEE &e,string
d="\0"):EMPLOYEE(e){duty=d; } //WA1=1
void print() const; }; //WA2=1
void sendMessage(string msg, Faculty &fac) //WA3=1
{cout<<"The incoming message :"<<msg<<"\nMessage
to"; cout<<fac.getName(); }
```

```

MAIN
int main(void)
{
Person * per[3];
per[0]=new Person ("Aysegul",27,'f');
per[1]=new Person ("Remzi",23,'m');
per[2]=new Person ("Ali",30,'m');
EMPLOYEE EMPLOYEE1(* per[0],1000);
EMPLOYEE1.print();
Student student1(* per[1],9299,3.5);
student1.print();
EMPLOYEE EMPLOYEE2(* per[0],2000);
Administrative
admEMPLOYEE(EMPLOYEE1,"Secretary");
Faculty facEMPLOYEE(EMPLOYEE2,"Computer");
admEMPLOYEE.sendMessage("Today there is a seminar at
your university. You are in
vited",facEMPLOYEE);
}

```

The example is referred from the research of [22] metric based calculation of complexity. This exactly computes the java code for complexity. The idea is to use the same derivations for the design where the classes are decided with its member functions and relations are defined. So far the calculation is based only on methods, attributes and relationship. The structural complexity is majorly due to relations and this can be well defined for class diagram and object (collaboration specifically) diagrams. The same calculations can be made during the iterations when classes grow and at each step the complexity may be curbed.

Thus, the re-arrangement of classes to maintain a proper metric can prove the system to be consistent in terms of growing number of classes and dependencies amongst classes. Lesser the complexity, more manageable is the design.

V. CONCLUSION AND FUTURE WORK

An object benefits with its features of modularity, abstraction, encapsulation and inheritance but it was never predicted that the growing amount of code and maintenance classes bears loads on testing parameters. All the models have independent importance but require to be modified for testing individual aspects of the system. Several methods to derive a testable version of the UML have to be devised so that testing is not in the span of development but has intermediate phases upon stable models being developed. A future enhancement thereby adding the class complexity metrics to model based testing tools may be a convenient way to validate the understandability and maintainability parameters.

REFERENCES

- [1] Rumbaugh, Jacobson, and Booch., The Unified Modeling Language Reference Manual Addison-Wesley, Reading MA, 1999.
- [2] Robert V. Binder, Object Oriented Testing: Myth and Reality, article published in *Object Magazine*, May 1995.

- [3] Santosh kumar Swain, Model Based Object-Oriented Software Testing, *Journal of Theoretical and Applied Information Technology (JATIT 2005-2010)*
- [4] G. Suganya, S.Neduncheliyan, A Study of Object Oriented Testing Techniques: Survey and Challenges, IEEE 2010.
- [5] Clay E. Williams, Software Testing and the UML, Center of Software Engineering, *IBM T.J. Watson Research Center*.
- [6] Mrk Utting, Position Paper: Model Based Testing.
- [7] Tong Yi, Fangjun Wu and Chengzhi Gan, A Comparison of Metrics for UML Class Diagrams, *ACM SIGSOFT Volume 29, Number5, September 2004*
- [8] Magiel Bruntink and Arie Van Deursen, Predicting Class Testability using Object-Oriented Metrics. *Paper from junit.org*
- [9] Richard Torkar, Robert Feldt, and Tony Gorschek Test Cases Generation from UML Activity Diagrams, *Eighth ACIS International Conference on Software Engineering, Artificial Intelligence and Parallel/ Distributed Computing*.
- [10] Richard Torkar, Robert Feldt, and Tony Gorschek , Extracting Generally Applicable Patterns from Object-Oriented Programs for the Purpose of Test Case Creation.
- [11] Jihad Al Dallal ,Testing Object-Oriented Framework Applications Using FIST2 Tool: A Case Study, *World Academy of Science, Engineering and Technology 63 2010*.
- [12] Harry M. Sneed, ANECON GmbH, The Drawbacks of model-driven Software Evolution.
- [13] J. Kaczmarek, M.Kucharski, Size and Effort Estimation for applications written in Java, *Information and Software Technology 46(2004) pp 589-601, Sciencedirect and Elsevier Publication*.
- [14] Arilo C. Dias Neto, Rajesh subramaniam, Marlon Vieira, Guilherme H. Travassos, A Survey on Model Based Testing approaches: A Systematic Review.
- [15] Y. Wang and J. Shao, "A new measure of software complexity based on cognitive Weights." *IEEE Canadian Journal of Electrical and Computer Engineering, 2003*.
- [16] Craig Larman, Applying UML and Patterns: *An Introduction to Object Oriented Analysis and Design and the Unified process, Second Edition, pp. 69-74*
- [17] John D. McGregor, Managing Metrics in an Iterative Incremental Development Environment.
- [18] E. V. Berard, "Issues in the Testing of Object-Oriented Software", *Electro'94 International, IEEE Computer Society Press, 1994, pp. 211-219*.
- [19] Ibrahim K. El-Far and James A. Whittaker, Model Based Software Testing, *Encyclopaedia on Software Engineering Wiley 2001*.
- [20] Martin Hitz, Behzad Montazari, Chidamber and Kemerer's Metrics Suite: A Measurement Theory Perspective, *IEEE Transactions on Software Engineering 1996*.
- [21] Standard for Software Quality Metrics Methodology, 1998, *IEEE Std. 1061-1998 IEEE Computer Society*.
- [22] Sanjay Mishra & Ibrahim Akman, Weighted Class Complexity: A Measure of Complexity for Object Oriented System, *Journal of Information Science and Engineering 24, 2008*.

A Robust Image Enhancement by Using Multi-Resolution Transforms

Syed Izhan

M.Tech Student Scholar, DECS,
Dept of Electronics and Communication Engineering,
Nalanda Institute of Engineering and technology,
Sattenapalli (M); Guntur (Dt); A.P, India.

I. V. G. Manohar

M.Tech, Asst Professor
Dept of Electronics and Communication Engineering,
Nalanda Institute of Engineering and technology,
Sattenapalli (M); Guntur (Dt); A.P, India

Abstract: In this paper presents a regularized image interpolation algorithm, an image resolution enhancement technique based on interpolation of the high frequency sub-band images obtained by using one of the multi resolution algorithm discrete wavelet transform (DWT) and the input image. Edges in images convey a great deal of information, but wavelet transforms do not provide an economical representation. Thus, popular wavelet-based decomposition and restoration techniques perform poorly in the presence of edges. The edges are enhanced by introducing an intermediate stage by using stationary wavelet transform (SWT) which is the one of the Multi-Resolution Transforms (MRT). DWT is applied in order to decompose an input image into different sub-bands. Then the high frequency sub-bands as well as the input image are interpolated and are being modified by using high frequency sub-band obtained through SWT. Then high frequency and low frequency of these sub-bands are combined to generate a new high resolution image by using inverse DWT (IDWT). The quantitative and visual information results are showing the Enhancement of the edges of an input image robustly by introducing an intermediate stage by using Multi-Resolution Transforms (MRT)

Keywords: Image interpolation, Image super resolution, Multi-Resolution Transforms (MRT), Robustness.

I. INTRODUCTION

Image enhancement plays key role in digital processing so we focus on the importance of the representation of information for various image processing tasks. The way in which manipulation of information is represented brings out certain types of features while hiding others. Signal compression and estimation applications also rely heavily on having an efficient representation of image data; we would like to approximate a signal with a few number of parameters. Therefore, we seek a transform which yields an efficient representation while bringing out the desired features of the signal [1]. Resolution has been frequently referred as an important aspect of an image. Images are being processed in order to obtain more enhanced resolution. Interpolation is One of the commonly used technique for image resolution enhancement. It has been widely used in many applications in image processing such as facial reconstruction, multiple description coding, and super resolution. Interpolation is the process of using known data values to estimate unknown data values. Various interpolation techniques are often used in this project. Interpolation as used here is different to

"smoothing", the techniques discussed here have the characteristic that the estimated curve passes through all the given points. The idea is that the points are in some sense correct and lie on an underlying but unknown curve, the problem is to be able to estimate the values of the curve at any position between the known points[2-3]. The methods Nearest neighbor interpolation, Bilinear interpolation, and Bi-cubic interpolation are three well known interpolation techniques. Bilinear interpolation is an extension of linear interpolation for interpolating functions of two variables.

Bicubic interpolation is an extension of cubic interpolation for interpolating data points on a two dimensional regular grid. The interpolated surface is smoother than corresponding surfaces obtained by bilinear interpolation or nearest-neighbor interpolation. Bicubic interpolation can be accomplished using either Lagrange polynomials, cubic splines, or cubic convolution algorithm [4].

In this correspondence we mainly deal with image interpolation techniques to enhance the image quality in the basis of resolution. In image processing the terminology "resolution" represents the number of pixels in an image, which determines the physical size of the image, and at the same time it also represents the fidelity to high-frequency details in the image. By this reason, resolution is a fundamental issue in evaluating the quality of various image processing systems. Image interpolation is used to derive a higher resolution image from a low resolution image, and therefore it is most important in multi-resolution or high-resolution image processing. For example, the spatial scalability function in MPEG-2 and wavelet-based image processing techniques require image interpolation techniques [5]. On the other hand, high-resolution image processing applications such as digital High Definition Tele-Vision (HDTV), aerial photos, medical imaging such as scanning, and military purpose images, need high-resolution image interpolation algorithms. Recently, it can also be used in changing the format of various types of images and videos, and in increasing the resolution of images.

Image resolution can be measured in various ways. Basically, resolution quantifies how close lines can be to each other and still be visibly resolved. The measure of how closely lines can be resolved in an image is called spatial resolution, and it depends on properties of the system creating the image [6].

Image resolution enhancement in the wavelet domain is a relatively new research topic and recently many new algorithms have been proposed. Discrete wavelet transform (DWT) is one of the recent wavelet transforms

used in image processing. DWT decomposes an image into different sub-band images, namely low-low (LL), low high (LH), high-low (HL), and high-high (HH). Another recent wavelet transform which has been used in several image processing applications is stationary wavelet transform (SWT). In short, DWT is similar to SWT, used in down-sampling, hence the sub-bands will have the same size as the input image.

In this paper, we are proposing a robust image enhancement technique which generates sharper high resolution image. The proposed technique uses DWT as well as SWT. DWT uses to decompose a low resolution image into different sub bands. Then the details have been interpolated using bicubic interpolation. The details obtained by SWT of the input image are being incremented into the interpolated high frequency subbands in order to correct the estimated coefficients. In parallel, the input image is also interpolated separately. Finally, corrected interpolated high frequency subbands and interpolated input image are combined by using inverse DWT (IDWT) to achieve a high resolution output image. The proposed technique has been compared with conventional enhancement techniques. The conventional techniques used are the following: Interpolation techniques.

→Bilinear interpolation and

→Bicubic interpolation.

→Wavelet zero padding (WZP).

→Super resolved interpolated technique

According to the quantitative and qualitative experimental results, the proposed technique over performs the aforementioned conventional for image resolution enhancement.

II. IMAGE RESOLUTION ENHANCEMENT

Quality in Digital Imagery obtained by enhancement (wanted e.g. for visual inspection or for machine analysis), there is no knowledge about the source of degradation. If the source of degradation is known, one calls the process image restoration. Both are iconical processes, viz. input and outputs are images. Many different, often elementary methods are used to improve images in some Part. The problem is, of course, not well defined, as there is no objective improve for image quality. Here, we discuss a few recipes that have shown to be useful both for the human observer and/or for machine recognition. These methods are very problem-oriented: a method that works fine in one case may be completely inadequate for another problem.

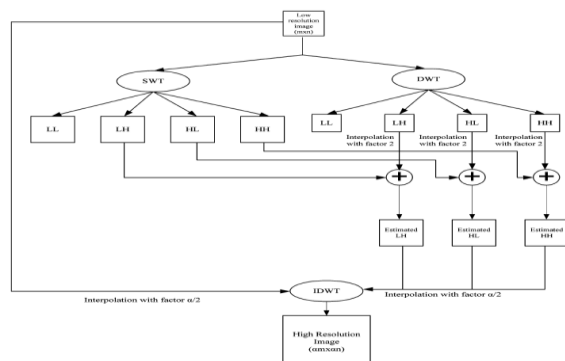


Figure 1: Block diagram of the super resolved interpolation algorithm.

By using interpolation we can enhance image for this we have to concentrate on its high frequency aspects (i.e.,edges),that is smoothing caused by interpolation .To increase the quality of the super resolved image we must preserve the edges. For this work, DWT has been used to protect the high frequency sub-bands of the image .DWT coefficients are inherently interpolable that means it is redundancy and shift invariance[7]- [9].

In this work, we are using one level DWT (with Daubechies 9/7 as wavelet function) to decompose an input image into different sub-band images like approximations and details means three high frequency sub-bands like LH, HL, and HH contain the high frequency components of the input image and LL contain the Low frequency components of the input image[10]. In the super resolved interpolation technique, bicubic interpolation with enlargement factor of 2 is applied to high frequency sub-band images. Down sampling in each of the DWT sub-bands causes information loss in the respective sub-bands. That is why SWT is employed to minimize this loss.

The SWT high frequency sub-bands and the interpolated high frequency sub-bands have the same size because here we are not using down sampling so that they can be added with each other. For the further higher enlargement the new corrected high frequency sub-bands can be interpolated. Also it is known that in the wavelet domain, the low resolution image is obtained by low-pass filtering of the high resolution image. In other words, low resolution of the original image means image consists of low frequency sub-band. Therefore, instead of using low frequency sub-band, which contains less information than the original high resolution image, we are using the input image for the interpolation of low frequency sub-band image. Using input image instead of low frequency sub-band increases the quality of the super resolved image. Fig. 1 illustrates the block diagram of the super resolved image interpolation enhancement technique[11].

By interpolating input image by $\alpha/2$, and high frequency sub-bands in DWT by 2 and added to high frequency bands to obtain estimated high frequency bands, α in the intermediate and final interpolation stages respectively, and then by applying IDWT, as illustrated in Fig. 1, the output image will contain sharper edges than the interpolated image obtained by interpolation of the input image directly. This is due to the fact that, the interpolation of isolated high frequency components in high frequency sub-bands and using the corrections obtained by adding high frequency sub-bands of SWT of the input image, will preserve more high frequency components after the interpolation than interpolating input image directly.

We are proposing an image resolution enhancement technique which generates sharper high resolution image. The proposed technique uses DWT to decompose a low resolution image into different sub-bands. Then the three high frequency sub-band images have been interpolated using bi-cubic interpolation with factor 2. The Low frequency sub-bands obtained by SWT of the input image are being interpolated bicubic with factor 2 and subtracts original image gets difference image, added to bicubic interpolated high frequency bands in order to correct the estimated coefficients. In parallel, the input image is also interpolated separately

Finally, corrected interpolated high frequency sub-bands and interpolated input image are combined by using inverse DWT (IDWT) to achieve a high resolution output image. The proposed technique has been compared with conventional enhancement techniques [12]-[15]. We propose a Multi resolution-enhancement technique using interpolated DWT high-frequency sub band images and the input low-resolution image. Inverse DWT (IDWT) has been applied to combine all these images to generate the final resolution-enhanced image. In order to achieve a sharper image, we propose to use an intermediate stage for estimating the high frequency sub bands by utilizing the difference image obtained by subtracting the input image and its interpolated LL sub band[16].

performance of the super resolved image by using SWT only (SWT-SR) is also included in the table. The results in Table I indicate that the proposed technique over-performs the aforementioned conventional and state-of-art image resolution enhancement techniques. Table I also indicates that the proposed technique over-performs the aforementioned conventional image resolution enhancement techniques.

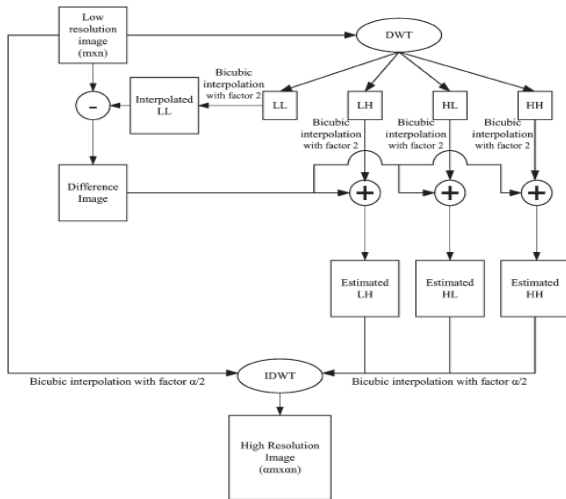


Figure 2: Block diagram of the proposed algorithm

The proposed technique has been compared with standard interpolation techniques, wavelet zero padding (WZP), super resolved bicubic interpolated where the unknown coefficients in high-frequency sub bands are replaced with zeros.

In all steps of the proposed satellite image resolution enhancement technique, Daubechies wavelet transform as mother wavelet function and bicubic interpolation as interpolation technique have been used.

III. RESULTS AND DISCUSSIONS

The Super resolved image of Baboon's picture using proposed technique is shown Fig. 3 the image in (f) are much better than the low resolution image in (a), Bilinear interpolated image (b), Bicubic image (c), Super resolved image using WZP (d) and super resolved image by using the interpolation (e). Note that the input low resolution images have been obtained by down-sampling the original high resolution images. In order to show the effectiveness of the proposed method over the conventional resolution enhancement techniques, four well-known test images such as Lena, Elaine, Baboon, and Peppers etc., with different features are used for comparison[17]. Table I compares the PSNR performance of the proposed technique using bicubic interpolation with conventional and state-of-art resolution enhancement techniques: bilinear, bicubic, Super resolved image using WZP, and Super resolved image using bilinear interpolation preserving image interpolation. Additionally, in order to have more comprehensive comparison, the

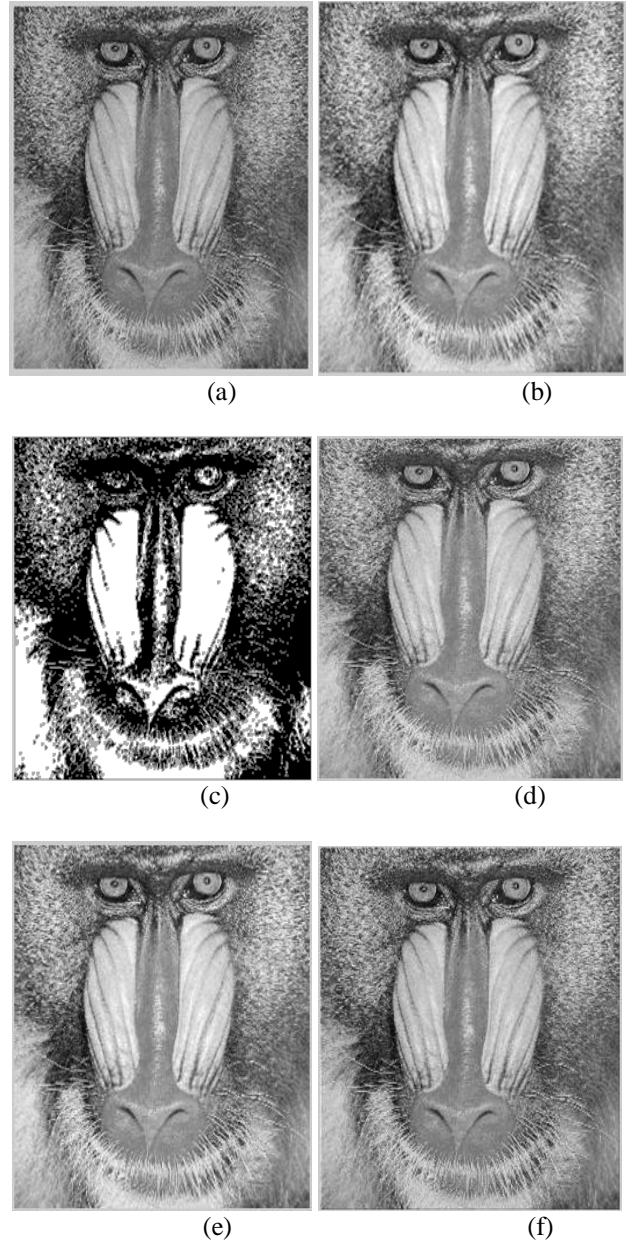


Fig.3 (a) Original low resolution Baboon's image. (b) Bilinear interpolated image (c) Bicubic interpolated image. (d) Super resolved image using WZP. (e) Super resolved image using bilinear interpolation (f) Proposed technique.

IV. CONCLUSION

The proposed technique has been tested on well-known benchmark images, where their PSNR and visual results show the superiority of proposed technique over the conventional image resolution enhancement techniques. The image resolution enhancement technique based on the interpolation of the high frequency sub-bands obtained by DWT, correcting the high frequency sub-band estimation by using SWT high frequency sub-bands, and the input image. The proposed technique uses DWT to decompose an image into different sub-bands, and then the high frequency sub-band images have been interpolated. The interpolated high frequency sub-band coefficients have been corrected by using the high frequency sub-bands achieved by SWT of the input image. An original image is interpolated with half of the interpolation factor used for interpolation the high frequency sub-bands. Afterwards all these images have been combined using IDWT to generate a super resolved imaged. Here we are using interpolation to gets the robustness. The proposed technique has been tested on well-known benchmark images, where their PSNR and visual results show the superiority of proposed technique over the conventional and state-of-art image resolution enhancement techniques.

TABLE I

Techniques\Images	Baboon	Lena	Barbara
Bilinear	27.7120	29.2821	28.0735
Bicubic	29.6867	31.3053	30.1179
WZP	34.8653	36.4802	35.4011
Super resolved interpolated technique	35.0445	36.8774	35.7141
Proposed Technique	35.5102	37.1994	36.0071

PSNR (DB) RESULTS FOR RESOLUTION ENHANCEMENT FROM 128×128 TO 512×512 OF THE PROPOSED TECHNIQUE COMPARED WITH THE CONVENTIONAL AND STATE-OF-ART IMAGE RESOLUTION ENHANCEMENT TECHNIQUES

References

- [1] Hasan Demirel and Gholamreza Anbarjafari, "Image Resolution Enhancement by Using Discrete and Stationary Wavelet Decomposition" IEEE Transactions on Image Processing, Vol. 20, NO. 5, MAY 2011
- [2] Y. Rener, J. Wei, and C. Ken, "Downsample-based multiple description coding and post-processing of decoding," in *Proc. 27th Chinese Control Conf.*, Jul. 16–18, 2008, pp. 253–256.
- [3] H. Demirel, G. Anbarjafari, and S. Izadpanahi, "Improved motionbased localized super resolution technique using discrete wavelet transform for low resolution video enhancement," in *Proc. 17th Eur. Signal Process. Conf.*, Glasgow, Scotland, Aug. 2009, pp. 1097–1101.
- [4] Y. Piao, I. Shin, and H. W. Park, "Image resolution enhancement using inter-subband correlation in wavelet domain," in *Proc. Int. Conf. Image Process.*, 2007, vol. 1, pp. I-445–448.
- [5] H. Demirel and G. Anbarjafari, "Satellite image resolution enhancement using complex wavelet transform," *IEEE Geoscience and Remote Sensing Letter*, vol. 7, no. 1, pp. 123–126, Jan. 2010.
- [6] C. B. Atkins, C. A. Bouman, and J. P. Allebach, "Optimal image scaling using pixel classification," in *Proc. Int. Conf. Image Process.*, Oct. 7–10, 2001, vol. 3, pp. 864–867.
- [7] W. K. Carey, D. B. Chuang, and S. S. Hemami, "Regularity-preserving image interpolation," *IEEE Trans. Image Process.*, vol. 8, no. 9, pp. 1295–1297, Sep. 1999.
- [8] S. Mallat, *A Wavelet Tour of Signal Processing*, 2nd ed. New York: Academic, 1999.
- [9] J. E. Fowler, "The redundant discrete wavelet transform and additive noise," Mississippi State ERC, Mississippi State University, Tech. Rep. MSSU-COE-ERC-04-04, Mar. 2004.
- [10] X. Li and M. T. Orchard, "New edge-directed interpolation," *IEEE Trans. Image Process.*, vol. 10, no. 10, pp. 1521–1527, Oct. 2001.
- [11] K. Kinebuchi, D. D. Muresan, and R. G. Baraniuk, "Waveletbased statistical signal processing using hidden Markov models," in *Proc. Int. Conf. Acoust., Speech, Signal Process.*, 2001, vol. 3, pp. 7–11.
- [12] S. Zhao, H. Han, and S. Peng, "Wavelet domain HMT-based image super resolution," in *Proc. IEEE Int. Conf. Image Process.*, Sep. 2003, vol. 2, pp. 933–936.
- [13] A. Temizel and T. Vlachos, "Wavelet domain image resolution enhancement using cycle-spinning," *Electron. Lett.*, vol. 41, no. 3, pp.119–121, Feb. 3, 2005.
- [14] A. Temizel and T. Vlachos, "Image resolution upscaling in the wavelet domain using directional cycle spinning," *J. Electron. Imag.*, vol. 14, no. 4, 2005.
- [15] G. Anbarjafari and H. Demirel, "Image super resolution based on interpolation of wavelet domain high frequency subbands and the spatial domain input image," *ETRI J.*, vol. 32, no. 3, pp. 390–394, Jun. 2010.
- [16] A. Temizel, "Image resolution enhancement using wavelet domain hidden Markov tree and coefficient sign estimation," in *Proc. Int. Conf. Image Process.*, 2007, vol. 5, pp. V-381–384..
- [17] L. Yi-bo, X. Hong, and Z. Sen-yue, "The wrinkle generation method for facial reconstruction based on extraction of partition wrinkle line features and fractal interpolation," in *Proc. 4th Int. Conf. Image Graph.*, Aug. 22–24, 2007, pp. 933–937.

The Comparison of Moment Invariants and to Remove Blur By Using Zernike Moments

T. Rajesh Kumar

M.Tech Student Scholar, DECS,
Dept of Electronics and Communication Engineering,
Nalanda Institute of Engineering and technology,
Sattenapalli (M); Guntur (Dt); A.P, India.

Bhookya Nageswararao Naik

M. Tech, Asst professor
Dept of Electronics and Communication Engineering,
Nalanda Institute of Engineering and technology,
Sattenapalli (M); Guntur (Dt); A.P, India.

Abstract: In this paper, we propose various types of moments like Legendre moments, complex moments and Zernike Moments invariants. In the past decades has been extensively investigated about moment invariants. In Zernike moments we construct to derive set of invariants which is simultaneously invariant to similarity transformation and to convolution with spread spectrum(PSF). In this mainly two contributions are provided, The frame work for theoretical is derived from Zernike moments of a blurred image and the way to construct the one of invariant moment combined geometric blur invariants. To evaluate the performance of the invariants with various PSFs and similarity Transformations. Experimental results show that the propose dinvariants perform better to compared with other invariants like Legendre moments and complex Moments.

Keywords: Moment Invariants, Legendre Moments, Complex moments, Zernike Moments, Pattern Recognition

I. INTRODUCTION

Analysis and interpretation of an image which was acquired by a real (i.e. non-ideal) imaging system is the key problem in many application areas such as remote sensing, astronomy and medicine, among others. Since real imaging systems as well as imaging conditions are usually imperfect, the observed image represents only a degraded version of the original scene. Various kinds of degradations (geometric as well as radiometric) are introduced into the image during the acquisition by such factors as imaging geometry, lens aberration, wrong focus, motion of the scene, systematic and random sensor errors, etc.

Size and orientations are important concern in recognition objects. The history about invariants includes so many techniques [1]–[5], Fourier descriptors [6] and point set invariants [7]–[10] have been Proposed. Among them, moment invariants have been extensively used for image description in object recognition [11], [12], image classification [13] and scene matching. However, much less attention has been paid to invariants with respect to changes of the image intensity function (known as radiometric invariants) as to joint radiometric- geometric invariants. The principle behind doing the blur is not too hard, although it seems like magic. What we do is take the image and the kernel, and perform the Fourier transform on them both. We then multiply the two together and inverse transform back.[14]

This is exactly the same as performing the long convolution. In image terms this means that each pixel in the source image gets spread over and mixed into surrounding pixels. Another way to look at this is that each pixel in the destination image is made up out of a mixture of surrounding pixels from the source image. The operation we need for this is called convolution. A quick diversion here to discuss a problem which often crops up: Imagine you want to blur a shape which is on a transparent background. You've got an empty image, and you draw a shape on it, then blur the image. blur to sharpen an image as well as blur it using a technique called un-sharp masking.

Orthogonal functions have been around for a very long time. The best known are the sine and cosine. Two functions or vectors are orthogonal if their inner product (defined as the sum of the product of their corresponding elements) is zero. An important class of orthogonal functions is orthogonal polynomials, which are orthogonal over various intervals of the real axis. Important orthogonal polynomials include Legendre, Hermite, Chebyshev, etc. Legendre polynomials, which are orthogonal over $[-1, 1]$, can be taken as a product $P(x)P(y)$, and the result is an orthogonal set of polynomials over a square. Zernike working in optics in the 1930's derived a set of polynomials that are orthogonal over a unit disk, i.e., $r \leq 1$. [15]

Orthogonal moments are computed similar to regular moments, except that the set of orthogonal polynomials replaces the x^p or $x^p y^q$ monomial in all the above equations. That is, where $h_{pq}(x, y)$ is the pq -th orthogonal polynomial, and R is the region over which the polynomials are defined. for Legendre and Zernike polynomials, and where we have subtracted the centers, which can be determined from the centroid or some other means, so that the resulting moments are location invariant.

Zernike polynomials are orthogonal over the unit disk and are specified in polar coordinates in terms of a real valued radial component $R_n(r)$ which is a polynomial of order n , and a complex exponential component: There are two ways of viewing moments, one based on statistics and one based on arbitrary functions such as $f(x)$ or $f(x, y)$. As a result moments can be defined in more than one way.[16]

Moments are the statistical expectation of certain power functions of a random variable. The most common moment is the mean which is just the expected value of a random variable: where $f(x)$ is the probability density function of continuous random variable X . More generally, moments of order $p = 0, 1, 2, \dots$ can be calculated as $m_p = E[X^p]$. These are sometimes referred to as the raw moments.

There are other kinds of moments that are often useful. One of these is the central moments $\mu_p = E[(X-\mu)^p]$.

However, moments are easy to estimate from a set of measurements. The p -th moment is estimated as and the p -th central moment is estimated as where is the average of the measurements, which is the usual estimate of the mean.

II. PROPOSED CONCEPT

A. Legendre Moments:

The Legendre of order $(m + n)$ are defined as:

$$\lambda_{mn} = \frac{(2m+1)(2n+1)}{4} \int_{-1}^1 \int_{-1}^1 P_m(x)P_n(y)f(x,y)dx dy \quad (1)$$

where

$$m, n = 0, 1, 2, 3, \dots$$

P_m and P_n are the Legendre polynomials and $f(x,y)$ is the continuous image function. The Legendre polynomials are a complete orthogonal basis set defined over the interval $[-1, 1]$ For orthogonality to exist in the moments, the image function $f(x,y)$ is defined over the same interval as the basis set, where the n^{th} order Legendre polynomial is defined as:

$$P_n(x) = \sum_{j=0}^n a_{nj} x^j \quad (2)$$

and a_{nj} are the Legendre coefficients given by:

$$a_{nj} = (-1)^{(n-j)/2} \frac{1}{2^n} \frac{(n+j)!}{\left(\frac{n-j}{2}\right)! \left(\frac{n+j}{2}\right)! j!} \quad \text{where } n-j = \text{even} \quad (3)$$

So, for a discrete image with P_{xy} current pixel

$$\lambda_{mn} = \frac{(2m+1)(2n+1)}{4} \sum_x \sum_y P_m(x)P_n(y)P_{xy} \quad (4)$$

and x, y are defined over the interval $[-1, 1]$.

B. Complex Zernike Moments:

The Zernike polynomials were first proposed in 1934 by Zernike. Their moment formulation appears to be one of the most popular, outperforming the alternatives (in terms of noise resilience, information redundancy and reconstruction capability). The pseudo-Zernike formulation proposed by Bhatia and Wolf further improved these characteristics. However, here we study the original formulation of these orthogonal invariant moments.

Complex Zernike moments are constructed using a set of complex polynomials which form a complete orthogonal basis set defined on the unit disc $(x^2 + y^2) \leq 1$. They are expressed as A_{pq} Two dimensional Zernike

moment.

$$A_{mn} = \frac{m+1}{\pi} \int_x \int_y f(x,y)[V_{mn}(x,y)]^* dx dy \quad \text{where } x^2 + y^2 \leq 1 \quad (5)$$

Where $m = 0, 1, 2, 3, \dots$

And defines the order $f(x,y)$ is the function being described and * denotes the complex conjugate. While n is an integer (that can be positive or negative) depicting the angular dependence, or rotation, subject to the conditions:

$$m - |n| = \text{even}, |n| \leq m \quad (6)$$

And $A_{mn}^* = A_{m,-n}$ is true. The Zernike polynomials $V_{mn}(x,y)$ Zernike polynomials expressed in polar coordinates

$$V_{mn}(r, \theta) = R_{mn}(r) \exp(jn\theta) \quad (7)$$

Where (r, θ) are defined over the unit disc

$$j = \sqrt{-1} \text{ and } R_{mn}(r)$$

is the orthogonal radial polynomial, defined as $R_{mn}(r)$ orthogonal radial polynomial

$$R_{mn}(r) = \sum_{s=0}^{\frac{m-|n|}{2}} (-1)^s F(m, n, s, r) \quad (8)$$

where:

$$F(m, n, s, r) = \frac{(m-s)!}{s! \left(\frac{m+|n|}{2} - s\right)! \left(\frac{m-|n|}{2} - s\right)!} r^{m-2s} \quad (9)$$

C. Zernike Moments of the Blurred Image :

In this subsection, we establish the relationship between the Zernike moments of the blurred image and those of the original image and the PSF. To that end, we first consider the radial moments.

Applying (1) to blurred image $g(x,y)$, we have a

$$\begin{aligned}
 D_{q+2k,q}^{(g)} &= \int_{-\infty}^{\infty} \int_{-\infty}^{\infty} (x - \hat{j}y)^{q+k} (x + \hat{j}y)^k g(x, y) dx dy \\
 &= \int_{-\infty}^{\infty} \int_{-\infty}^{\infty} (x - \hat{j}y)^{q+k} (x + \hat{j}y)^k \\
 &\quad \times \left[\int_{-\infty}^{+\infty} \int_{-\infty}^{+\infty} h(a, b) f(x - a, y - b) da db \right] \\
 &\quad \times dx dy \\
 &= \int_{-\infty}^{\infty} \int_{-\infty}^{\infty} h(a, b) \\
 &\quad \times \left[\int_{-\infty}^{+\infty} \int_{-\infty}^{+\infty} ((x - \hat{j}y) + (a - \hat{j}b))^{q+k} \right. \\
 &\quad \times ((x + \hat{j}y) + (a + \hat{j}b))^k \\
 &\quad \times f(x, y) dx dy \left. \right] da db \\
 &= \sum_{m=0}^{q+k} \sum_{n=0}^k \binom{q+k}{m} \binom{k}{n} \\
 &\quad \times \int_{-\infty}^{+\infty} \int_{-\infty}^{+\infty} (x - \hat{j}y)^m (x + \hat{j}y)^n f(x, y) dx dy \\
 &\quad \times \int_{-\infty}^{+\infty} \int_{-\infty}^{+\infty} (a - \hat{j}b)^{q+k-m} (a + \hat{j}b)^{k-n} h(a, b) da db \\
 &= \sum_{m=0}^{q+k} \sum_{n=0}^k \binom{q+k}{m} \binom{k}{n} D_{m+n, m-n}^{(f)} \\
 &\quad \times D_{q+2k-m-n, q+n-m}^{(h)}.
 \end{aligned}
 \tag{10}$$

Applying blurred image $g(x,y)=g(r,\theta)$ and using above equation, we obtain

$$\begin{aligned}
 Z_{q+2l,q}^{(g)} &= \sum_{k=0}^l \sum_{m=0}^{q+k} \sum_{n=0}^k \binom{q+k}{m} \binom{k}{n} \\
 &\quad \times c_{l,k}^q D_{m+n, m-n}^{(f)} D_{q+2k-m-n, q+n-m}^{(h)}.
 \end{aligned}
 \tag{11}$$

the radial moments can also be expressed as a series of Zernike moments

$$D_{q+2l,q}^{(f)} = \sum_{k=0}^l d_{l,k}^q Z_{q+2k,q}^{(f)}
 \tag{12}$$

$$d_{i,j}^q = \frac{i!(q+i)!\pi}{(i-j)!(q+i+j+1)!}, \quad 0 \leq j \leq i \leq l.
 \tag{13}$$

We have

$$D_{m+n, m-n}^{(f)} = \sum_{i=0}^n d_{n,i}^{m-n} Z_{m-n+2i, m-n}^{(f)}
 \tag{14}$$

$$D_{q+2k-m-n, q+n-m}^{(h)} = \sum_{j=0}^{k-n} d_{k-n,j}^{q+n-m} Z_{q+n-m+2j, q+n-m}^{(h)}.
 \tag{15}$$

By using above two eqn's we obtain

$$\begin{aligned}
 Z_{q+2l,q}^{(g)} &= \sum_{k=0}^l \sum_{m=0}^{q+k} \sum_{n=0}^k \sum_{i=0}^n \sum_{j=0}^{k-n} \binom{q+k}{m} \binom{k}{n} c_{l,k}^q d_{n,i}^{m-n} \\
 &\quad \times d_{k-n,j}^{q+n-m} Z_{m-n+2i, m-n}^{(f)} Z_{q+n-m+2j, q+n-m}^{(h)}.
 \end{aligned}
 \tag{16}$$

III. MATLAB/SIMULINK RESULTS

In this evaluation, we also use the images shown in Fig. 1. The testing set was generated by adding motion blur, averaging blur with zero-mean. This was followed by adding a white Gaussian noise with different standard deviations and salt-and-pepper noise with different noise densities. Because the actual size of the PSF is usually unknown in practical application, in order to evaluate the performance of the different methods under such a situation.

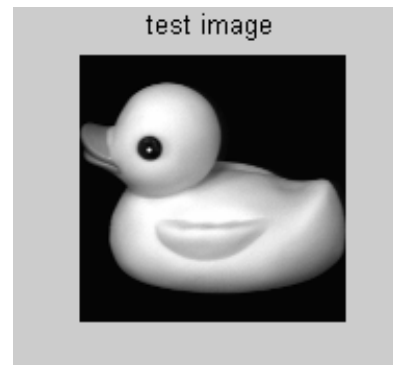


Figure 1:-Original Image



Figure 2: Combined invariants to similarity transform

We have computed the ZMIs, CMIs, and LMIs up to order $M=1,3,5,\dots, 17$. The mean classification rates under different noise conditions for different values of M are shown in Fig. 3,4. It can be observed that the rate first increases, reaches the maximum value and then decreases for all three methods. In other words, there should exist an optimal order for each type of moment invariants. This behavior has also been observed and pointed out by Liao

and Pawlak in image reconstruction due to the noise influence [17]. In this experiment, the optimal order for CMIs is $M=7$ (the feature vector includes 17 invariants), for LMIs (the feature vector has 21 invariants), and $M=9$ for ZMIs (with 26 invariants).

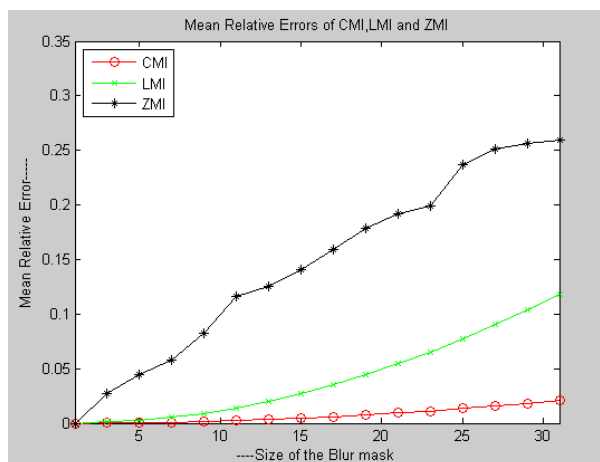


Figure 3: Mean relative errors of CMIs, LMIs, and ZMIs for motion blurred versions of the images

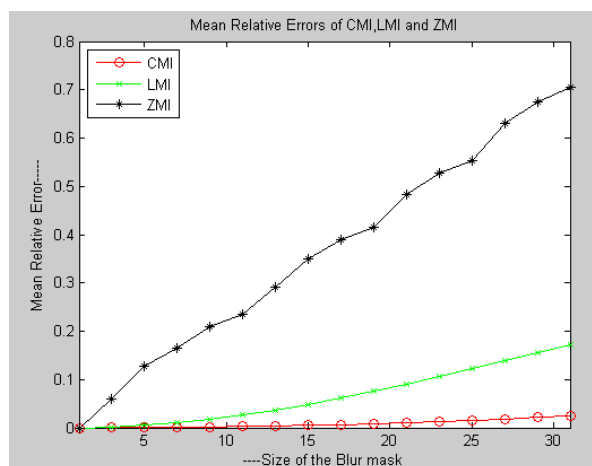


Figure 4: Mean relative errors of CMIs, LMIs, and ZMIs for average blurred versions of the image

It can be seen that the proposed descriptors ZMI is compared with CMIs And Legendre moments.

The figures 3, 4 are to calculate the mean relative error corresponding invariants. And to compare invariants are like Legendre and complex.

IV. VI CONCLUSION

In this paper, we have proposed a method to construct a set of combined geometric-blur invariants using the orthogonal Zernike moments. The relationship between the Zernike moments of the blurred image and those of the original image and the PSF has been established. Based upon this relationship, a set of invariants to convolution with circularly symmetric PSF has been derived. The advantages of the proposed method over the existing ones are the following: 1) The proposed descriptors are simultaneously invariant to similarity transformation and to convolution. Using these invariants, the image deblurring and geometric normalization process can be well avoided. 2) Like the method reported in [17], our method can also derive the

even order invariants. The experiments conducted so far in very distinct situations demonstrated that the proposed descriptors

References

- [1] Beijing Chen, Huazhong Shu, Hui Zhang, Gouenou Coatrieux, Limin Luo, and Jean Louis Coatrieux "Combined Invariants to Similarity Transformation and to Blur Using Orthogonal Zernike Moments," *IEEE Trans on Image Proces*, Vol. 20, No. 2, Feb 2011.
- [2] T. H. Reiss, "The revised fundamental theorem of moment invariants," *IEEE Trans. Pattern Anal. Mach. Intell.*, vol. 13, no. 8, pp. 830–834, Aug. 1991.
- [3] J. Flusser and T. Suk, "Pattern recognition by affine moment invariants," *Pattern Recognit.*, vol. 26, no. 1, pp. 167–174, 1993.
- [4] S. S.Reddi, "Radial and angular moment invariants for image identification," *IEEE Trans. Pattern Anal. Mach. Intell.*, vol. PAMI-3, no. 2, pp. 240–242, Feb. 1981.
- [5] Y. S. Abu-Mostafa and D. Psaltis, "Recognitive aspects of moment invariants," *IEEE Trans. Pattern Anal. Mach. Intell.*, vol. PAMI-6, no. 6, pp. 698–706, Jun. 1984.
- [6] K. Arbter, W. E. Snyder, H. Burkhardt, and G. Hirzinger, "Application of affine-invariant Fourier descriptors to recognition of 3-D objects," *IEEE Trans. Pattern Anal. Machine Intell.*, vol. 12, no. 7, pp. 640–647, Jul. 1990.
- [7] T. Suk and J. Flusser, "Vertex-based features for recognition of projectively deformed polygons," *Pattern Recognit.*, vol. 29, no. 3, pp. 361–367, 1996.
- [8] R. Lenz and P. Mer, "Point configuration invariants under simultaneous projective and permutation transformations," *Pattern Recognit.*, vol. 27, no. 11, pp. 1523–1532, 1994.
- [9] N. S. V. Rao, W. Wu, and C. W. Glover, "Algorithms for recognizing planar polygonal configurations using perspective images," *IEEE Trans. Robot. Autom.*, vol. 8, no. 4, pp. 480–486, Aug. 1992.
- [10] D. G. Lowe, "Distinctive image features from scale-invariant key points," *Int. J. Comput. Vis.*, vol. 60, no. 2, pp. 91–110, 2004.
- [11] A. Khotanzad and Y. H. Hong, "Invariant image recognition by Zernike moments," *IEEE Trans. Pattern Anal. Mach. Intell.*, vol. 12, no. 5, pp. 489–497, May 1990.
- [12] F. Zhang, S. Q. Liu, D. B. Wang, and W. Guan, "Aircraft recognition in infrared image using wavelet moment invariants," *Image Vis. Comput.*, vol. 27, no. 4, pp. 313–318, 2008.
- [13] C. Y. Yang and J. J. Chou, "Classification of rotifers with machine vision by shape moment invariants," *Aquac. Eng.*, vol. 24, no. 1, pp. 33–57, 2000.
- [14] Y. H. Lin and C. H. Chen, "Template matching using the parametric template vector with translation, rotation and scale invariance," *Pattern Recognit.*, vol. 41, no. 7, pp. 2413–2421, 2008.
- [15] J. Flusser, T. Suk, and S. Saic, "Recognition of blurred images by the method of moments," *IEEE Trans. Image Process.*, vol. 5, no. 3, pp. 533–538, Mar. 1996.
- [16] A. Savakis and H. J. Trussell, "Blur identification by residual spectral matching," *IEEE Trans. Image Process.*, vol. 2, no. 2, pp. 141–151, Feb. 1993.
- [17] M. K. Hu, "Visual pattern recognition by moment invariants," *IRE Trans. Inf. Theory*, vol. IT-8, no. 2, pp. 179–187, 1962.

Analysis and Improvement of Image Quality in De-Blocked Images

U. SRINIVAS

M.Tech Student Scholar, DECS,
Dept of Electronics and Communication Engineering,
Nalanda Institute of Engineering and technology,
Sattenapalli (M); Guntur (Dt); A.P, India.

K. SYAM PRASAD

M.Tech, Asst Professor
Dept of Electronics and Communication Engineering,
Nalanda Institute of Engineering and technology,
Sattenapalli (M); Guntur (Dt); A.P, India.

Abstract: Image quality is a characteristic of an image that measures the perceived image degradation (typically, compared to an ideal or perfect image). Imaging systems may introduce some amounts of distortion or artifacts in the signal, so the quality assessment is an important problem. JPEG compression is the most prevalent technique or method for image codec's. But it suffers from blocking artifacts. In this paper a comparison of the perceptual quality of de-blocked images based on various quality assessments metric is done. We study the efficiency of de-blocking algorithms for improving visual signals degraded by blocking artifacts from compression. Rather than using only the perceptually questionable PSNR, we instead propose a block-sensitive index, named PSNR-B, that produces objective judgments that accord with observations. The PSNR-B modifies PSNR by including a blocking effect factor. We also use the perceptually significant SSIM index, which produces results largely in agreement with PSNR-B. Simulation results show that the PSNR-B results in better performance for quality assessment of deblocked images than PSNR and a well-known blockiness-specific index.

Keywords: Blocking effect, deblocking, distortion, image quality assessment, quantization.

I. INTRODUCTION

Many practical and commercial systems use digital image compression when it is required to transmit or store the image over limited resources. JPEG compression is the most popular image compression standard among all the members of lossy compression standards family. JPEG image coding is based on block based discrete cosine transform. BDCT coding has been successfully used in image and video compression applications due to its energy compacting property and relative ease of implementation. After segmenting an image in to blocks of size $N \times N$, the blocks are independently DCT transformed, quantized, coded and transmitted. One of the most noticeable degradation of the block transform coding is the "blocking artifact". These artifacts appear as a regular pattern of visible block boundaries. This degradation is the result of course quantization of the coefficients and of the independent processing of the blocks which does not take in to account the existing correlations among adjacent block pixels [1]. In order to achieve high compression rates using BTC with visually acceptable results, a procedure known as deblocking is done in order to eliminate blocking artifacts.

Blocking effects are common in block-based image and video compression systems. Blocking artifacts are more serious at low bit rates, where network bandwidths are limited. Significant research has been done on blocking artifact reduction [2]–[4]. Most blocking artifact reduction methods assume that the distorted image contains noticeable amount of blocking. The degree of blocking depends upon several parameters, the most important of which is the quantization step for lossy compression. Little research has done on comparing the perceptual quality of de-blocked images. The recent advent of powerful modern image quality assessment (IQA) algorithms[5] that compare well with human subjectively makes this plausible. Here we investigate quality assessment of de-blocked images, and in particular we study the effects of the quantization step of the measured quality of de-blocked images. A de-blocking filter can improve image quality in some aspects, but can reduce image quality in other regards.

We perform simulations on the quality assessment of De-blocked images. We first perform simulations using the conventional peak signal-to-noise ratio (PSNR) quality metric and a state of the art quality index, the structural similarity (SSIM) index. The PSNR does not capture subjective quality well when blocking artifacts are present. The SSIM metric is slightly more complex than the PSNR, but correlates highly with human subjectively. We also propose a new de-blocking quality index that is sensitive to blocking artifacts in de-blocked images. We name this peak signal-to-noise ratio including blocking effects (PSNR-B). The simulation results show that the proposed PSNR-B correlates well with subjective quality and with the SSIM index, and performs much better than the PSNR.

We study a variety of image and video de-blocking algorithms, including low pass filtering, projection onto convex sets (POCS), and the H.264 in-loop filter. The image improvements afforded by these algorithms is measured using the PSNR, PSNR-B, and SSIM. Rather than relying on PSNR, which correlates poorly with subjective judgment, we utilize PSNR-B which is designed specifically to assess blocky and de-blocked images (but has no proven perceptual significance) in conjunction with the SSIM index, which is perceptually significant, but has not been demonstrated on de-blocked images[6]

To remove blocking effect, several de-blocking techniques have been proposed in the literature as post process mechanisms after JPEG compression, depending on the angle from which the blocking problem is tackled. If de-blocking is viewed as an estimation problem, the simplest solution is probably just to low pass the blocky JPEG

compressed image. More sophisticated methods involve iterative methods such as projection on convex sets and constrained least squares[7],[8]

II. BASED ON QUALITY ASSESSMENT

We consider the class of quality assessment (QA) methods that are full-reference (FR) QA, which compares the test (distorted) image with a reference (original) image. In this paper, the distorted images will ostensibly suffer from blocking artifacts or from the residual artifacts following de-blocking.

A. Peak Signal To Noise Ratio(PSNR):

The simplest and most widely used FR QA metrics are the peak signal-to-noise ratio (PSNR) and the mean-squared error(MSE) [2], [4]. Let \mathbf{x} and \mathbf{y} represent the vectors of reference and test image signals, respectively. Let e be the vector of error signal between \mathbf{x} and \mathbf{y} . If the number of pixels in an image is N , then

$$MSE(\mathbf{x}, \mathbf{y}) = \frac{1}{N} \sum_{i=1}^N e_i^2 = \frac{1}{N} \sum_{i=1}^N (x_i - y_i)^2 \quad (1)$$

$$PSNR(\mathbf{x}, \mathbf{y}) = 10 \log_{10} \frac{255^2}{MSE(\mathbf{x}, \mathbf{y})} \quad (2)$$

The PSNR is an attractive QA metric since it is mathematically simple and has clear physical meaning. However, the PSNR does not correlate well with perceived visual quality [3]–[6].

B. Structural Similarity Index Metric(SSIM):

The structural similarity (SSIM) metric aims to measure quality by capturing the similarity of images [1]. A product of three aspects of similarity are measured: luminance, contrast, and structure. The luminance comparison function $l(\mathbf{x}, \mathbf{y})$ for reference image \mathbf{x} and test image \mathbf{y} is defined as

$$l(\mathbf{x}, \mathbf{y}) = \frac{2\mu_x\mu_y + C_1}{\mu_x^2 + \mu_y^2 + C_1} \quad (3)$$

Where σ_x and σ_y are the standard deviation of \mathbf{x} and \mathbf{y} , respectively, and C_1 is a stabilizing constant.

The structure comparison function is $c(\mathbf{x}, \mathbf{y})$ defined as

$$c(\mathbf{x}, \mathbf{y}) = \frac{2\sigma_x\sigma_y + C_2}{\sigma_x^2 + \sigma_y^2 + C_2} \quad (4)$$

Where σ_{xy} and $\sigma_x\sigma_y$ are the standard deviation of \mathbf{x} and \mathbf{y} , respectively, and C_2 is a stabilizing constant.

The structure comparison function $s(\mathbf{x}, \mathbf{y})$ is defined as

$$s(\mathbf{x}, \mathbf{y}) = \frac{\sigma_{xy} + C_3}{\sigma_x\sigma_y + C_3} \quad (5)$$

Where σ_{xy} is the correlation between \mathbf{x} and \mathbf{y} C_3 is also a constant that provides stability

The SSIM index is obtained by combining the three comparison functions

$$SSIM(\mathbf{x}, \mathbf{y}) = [l(\mathbf{x}, \mathbf{y})]^\alpha \cdot [c(\mathbf{x}, \mathbf{y})]^\beta \cdot [s(\mathbf{x}, \mathbf{y})]^\gamma \quad (6)$$

The parameters are set as

$$\alpha = \beta = \gamma = 1 \text{ and } C_3 = C_2/2$$

$$SSIM(\mathbf{x}, \mathbf{y}) = \frac{(2\mu_x\mu_y + C_1)(2\sigma_{xy} + C_2)}{(\mu_x^2 + \mu_y^2 + C_1)(\sigma_x^2 + \sigma_y^2 + C_2)} \quad (7)$$

Local SSIM statistics are estimated using a symmetric Gaussian weighting function. The mean SSIM index pools the spatial SSIM values to evaluate the overall image quality

$$SSIM(\mathbf{x}, \mathbf{y}) = \frac{1}{M} \sum_{j=1}^M SSIM(\mathbf{x}_j, \mathbf{y}_j) \quad (8)$$

where M is the number of local windows over the image, and \mathbf{X}_j and \mathbf{Y}_j are image patches covered by the j 'th window

III. QUANTIZATION STEP SIZE AND IMAGE QUALITY

Quantization is a key element of lossy compression, but information is lost. There is a tradeoff between compression ratio and reconstructed image/video quality. The amount of compression and the quality can be controlled by the quantization step. As the quantization step is increased, the compression ratio becomes larger, and the quality generally worsens. However, there has not been a study made of how perceptual quality suffers as a function of step size, or the degree to which de-blocking augments perceptual quality. The emergence of new and powerful IQA indices suggests this possibility.

In block transform coding, the input image is divided into $L \times L$ blocks, and each block is transformed independently into transform coefficients. An input image block is transformed into a DCT coefficient block



Figure 1: Block diagram for reference, decoded, and de-blocked images

$$B = T b T^t \quad (9)$$

Where T is the transform matrix and T^t is the transpose matrix of T . The transform coefficients are quantized using a scalar quantizer.

$$\tilde{B} = Q(B) = Q(T b T^t) \quad (10)$$

The quantization operator in (10) is nonlinear, and is a many-to-one mapping from R^{L^2} to R^{L^2}

In the decoder, only quantized transform coefficients \tilde{B} are available. The output of the decoder is

$$\tilde{b} = T^t \tilde{B} T = T^t Q(T b T^t) T \quad (11)$$

Let Δ represent the quantization step. It is well known that the PSNR is a monotonically decreasing function of Δ . The SSIM index captures the similarity of reference and test images. As the quantization step size becomes larger, the structural differences between reference and test image will

generally increase, and in particular the structure terms (\mathbf{x}, \mathbf{y}) in (5) will become smaller. Hence, the SSIM index would be a monotonically decreasing function of the quantization step size Δ .

IV. DEBLOCKING FILTER AND DISTORTION CHANGE

As before, \mathbf{x} is the reference (original) image and \mathbf{y} is the decoded image that has been distorted by quantization errors. Let $\hat{\mathbf{y}}$ represent the de-blocked image and \mathbf{f} represent the de-blocking operation $\hat{\mathbf{y}} = \mathbf{f}(\mathbf{y})$. Fig. 1 shows a block diagram depicting the flow of reference, decoded, and de-blocked images. Let $\mathbf{M}(\mathbf{x}, \mathbf{y})$ be the quality metric between \mathbf{x} and \mathbf{y} . The goal of the de-blocking operation \mathbf{f} is to maximize $\mathbf{M}(\mathbf{x}, \mathbf{f}(\mathbf{y}))$ given image \mathbf{y} .

De-blocking is a local operation. The de-blocking operation may improve the appearance of the image in some regions, while degrading the quality elsewhere. Let α_i be the distortion between the i 'th pixels of \mathbf{x} and \mathbf{y} , expressed as squared Euclidean distance

$$d(x_i, y_i) = \|x_i - y_i\|^2 \quad (12)$$

Next, we define the distortion decrease region (DDR) \mathcal{A} to be composed of those pixels where the distortion is decreased by the de-blocking operation

$$i \in \mathcal{A}, \text{ if } d(x_i, \hat{y}_i) < d(x_i, y_i) \quad (13)$$

The amount of distortion decrease for the i th pixel in the DDR \mathcal{A} is

$$\alpha_i = d(x_i, y_i) - d(x_i, \hat{y}_i) \quad (14)$$

The distortion may also increase at other pixels by application of the de-blocking filter. We similarly define the distortion increase region (DIR) \mathcal{B}

$$i \in \mathcal{B}, \text{ if } d(x_i, y_i) < d(x_i, \hat{y}_i) \quad (15)$$

The amount of distortion increase for the i 'th pixel β_i in the DIR \mathcal{B} is

$$\beta_i = d(x_i, \hat{y}_i) - d(x_i, y_i) \quad (16)$$

We define the mean distortion decrease (MDD)

$$\bar{\alpha} = \frac{1}{N} \sum_{i \in \mathcal{A}} (d(x_i, y_i) - d(x_i, \hat{y}_i)) \quad (17)$$

Where N is the number of pixels in the image. Similarly the mean distortion increase (MDI) is

$$\bar{\beta} = \frac{1}{N} \sum_{i \in \mathcal{B}} (d(x_i, \hat{y}_i) - d(x_i, y_i)) \quad (18)$$

A reasonable approach for designing a de-blocking filter would be to seek to maximize the MDD and minimize the MDI. This is generally a very difficult task and of course, may not result in optimized improvement in perceptual quality. Lastly, let $\bar{\gamma}$ be the mean distortion change (MDC), defined as the difference between MDD and MDI.

$$\bar{\gamma} = \bar{\alpha} - \bar{\beta} \quad (19)$$

If $\bar{\gamma} < 0$, then the de-blocking operation is likely unsuccessful since the mean distortion increase is larger than the mean distortion decrease. We would expect a successful de-blocking operation to yield $\bar{\gamma} > 0$. Nevertheless, these conditions are not equated with

levels of perceptual improvement or loss. De-blocking can be considered as an image restoration problem. Let $\mathcal{N}(x_i)$ represent the de-blocking operation function and $\mathcal{N}(x_i)$ represent a neighborhood of pixel x_i .

A low pass filter is a simple de-blocking filter. An $L \times L$ low pass filter can be represented as

$$g(\mathcal{N}(x_i)) = \sum_{k=1}^{L^2} h_k \cdot x_{i,k} \quad (20)$$

While low pass filtering does reduce blocking artifacts, critical high frequency information is also lost and the image is blurred. While the distortion will certainly decrease for some pixels that define the DDR, the distortion will likely increase for a significant number of pixels in DIR. Indeed, it is quite possible that $\bar{\gamma} < 0$ could result. Moreover, blur is perceptually annoying.

A variety of nonlinear methods have been proposed to reduce the blocking artifacts, while minimizing the loss of original information [7]–[14]. For example, de-blocking algorithms based upon projection onto convex sets (POCS) have demonstrated good performance for reducing blocking artifacts and have proved popular [7]–[12]. In POCS, a low pass filtering operation is performed in the spatial domain, while a projection operation is performed in the DCT domain. Typically, the projection operation is a clipping operation on the filtered coefficients, confining these to fall within a certain range defined by the quantization step size. Since the low pass filtering and the projection operations are performed in different domains, forward DCT and inverse DCT (IDCT) operations are required. The low pass filtering, DCT, projection, IDCT operations compose one iteration, and multiple iterations are required to achieve convergence. It is argued that under certain conditions, POCS filtered images converge to an image that does not exhibit blocking artifacts [7], [10], [11]. As another example, the H.264 in-loop de-blocking filter is a key component in the H.264 video coding standard [17]. It is claimed that the in-loop filtering significantly improves both subjective and objective video quality [15]. The key idea of the H.264 in-loop filter is to adaptively select the filtering operation and the neighborhood using the relative pixel location with respect to the block boundary and the local gray level gradient information. Generally, the MDI value is reduced while the MDD value is similar to low pass filtering. The H.264 in-loop filter uses separate 1-D operations and integer multiplications to reduce complexity. However, it still requires a large amount of computation. In fact, the H.264 in-loop filter requires about one-third of the computational complexity of the decoder [15].

V. PSNR INCLUDING BLOCKING EFFECTS

In the following, we propose a new block-sensitive image quality metric which we term peak signal-to-noise ratio including blocking effects (PSNR-B). As the quantization step size increases, blocking artifacts generally become more conspicuous. Blocking artifacts are gray level discontinuities at block boundaries, which are ordinarily oriented horizontally and vertically. They arise from poor representation of the block luminance levels near the block boundaries [18].

The following definitions are relative to an assumed block-based compression tiling, e.g., 8 x 8 blocks as in JPEG compression. For simplicity, assume that an integer number of blocks comprise the image, viz., that horizontal and vertical dimensions are divisible by the block dimension. The definitions apply whether the image is compressed, not-compressed, or de-blocked following decompression.

y ₁	y ₂	y ₃	y ₄	y ₅	y ₆	y ₇	y ₈
y ₉	y ₁₀	y ₁₁	y ₁₂	y ₁₃	y ₁₄	y ₁₅	y ₁₆
y ₁₇	y ₁₈	y ₁₉	y ₂₀	y ₂₁	y ₂₂	y ₂₃	y ₂₄
y ₂₅	y ₂₆	y ₂₇	y ₂₈	y ₂₉	y ₃₀	y ₃₁	y ₃₂
y ₃₃	y ₃₄	y ₃₅	y ₃₆	y ₃₇	y ₃₈	y ₃₉	y ₄₀
y ₄₁	y ₄₂	y ₄₃	y ₄₄	y ₄₅	y ₄₆	y ₄₇	y ₄₈
y ₄₉	y ₅₀	y ₅₁	y ₅₂	y ₅₃	y ₅₄	y ₅₅	y ₅₆
y ₅₇	y ₅₈	y ₅₉	y ₆₀	y ₆₁	y ₆₂	y ₆₃	y ₆₄

Figure 2: Example for illustration of pixel blocks

Let N_{HB}, N_{HB}^C, N_{VB} be the number of pixel pairs in $\mathcal{H}_B, \mathcal{H}_B^C, \mathcal{V}_B$ respectively. If B is the block size, then

$$\begin{aligned} N_{HB} &= N_V \left(\frac{N_H}{B} \right) - 1 \\ N_{HB}^C &= N_V(N_H - 1) - N_{HB} \\ N_{VB} &= N_H \left(\frac{N_V}{B} \right) - 1 \\ N_{VB}^C &= N_H(N_V - 1) - N_{VB}. \end{aligned} \tag{21}$$

Fig. 2 shows a simple example for illustration of pixel blocks with $N_H=8, N_V=8, B=4$. The thick lines represent the block boundaries. The sets of pixel pairs in this example are

$$\begin{aligned} \mathcal{H}_B &= \{(y_4, y_5), (y_{12}, y_{13}), \dots, (y_{60}, y_{61})\} \\ \mathcal{H}_B^C &= \{(y_1, y_2), (y_2, y_3), (y_3, y_4), (y_5, y_6), \dots, (y_{63}, y_{64})\} \\ \mathcal{V}_B &= \{(y_{25}, y_{33}), (y_{26}, y_{34}), \dots, (y_{32}, y_{40})\} \\ \mathcal{V}_B^C &= \{(y_1, y_9), (y_9, y_{17}), (y_{17}, y_{25}), (y_{33}, y_{41}), \dots, (y_{56}, y_{64})\}. \end{aligned} \tag{22}$$

Then we define the mean boundary pixel squared difference (DB) and the mean non boundary pixel squared difference (DcB) for image y to be

$$\begin{aligned} D_B(\mathbf{y}) &= \frac{\sum_{(y_i, y_j) \in \mathcal{H}_B} (y_i - y_j)^2 + \sum_{(y_i, y_j) \in \mathcal{V}_B} (y_i - y_j)^2}{N_{HB} + N_{VB}} \\ D_B^C(\mathbf{y}) &= \frac{\sum_{(y_i, y_j) \in \mathcal{H}_B^C} (y_i - y_j)^2 + \sum_{(y_i, y_j) \in \mathcal{V}_B^C} (y_i - y_j)^2}{N_{HB}^C + N_{VB}^C}, \end{aligned} \tag{23}$$

Generally, as the quantization step size increases, (DB) will increase relative to (DcB) and blocking artifacts will become more visible. Of course, this does not establish any level of correlation between and perceptual annoyance. Also define the blocking effect factor

$$BEF(\mathbf{y}) = \eta \cdot [D_B(\mathbf{y}) - D_B^C(\mathbf{y})] \tag{24}$$

Where

$$\eta = \begin{cases} \frac{\log_2 B}{\log_2(\min(N_H, N_V))}, & \text{if } D_B(\mathbf{y}) > D_B^C(\mathbf{y}) \\ 0, & \text{otherwise} \end{cases} \tag{25}$$

emphasizes the BEF as a function of block size. The assumption here is that the visibility of blocking effects increases with block size.

Of course, there can be multiple block sizes in a particular decoded image/video. For example, there can be 16 X 16 macro blocks and 4 X 4 transform blocks, both contributing to blocking effects, as in H.264 video coding

$$BEF_k(\mathbf{y}) = \eta_k \cdot [D_{B_k}(\mathbf{y}) - D_{B_k}^C(\mathbf{y})] \tag{26}$$

The BEF over all block sizes is defined as

$$BEF_{Tot}(\mathbf{y}) = \sum_{k=1}^K BEF_k(\mathbf{y}) \tag{27}$$

The mean-squared error including blocking effects (MSE-B)

for reference image \mathbf{x} and test image \mathbf{y} is then defined as the sum of the MSE (\mathbf{x}, \mathbf{y})

$$MSE-B(\mathbf{x}, \mathbf{y}) = MSE(\mathbf{x}, \mathbf{y}) + BEF_{Tot}(\mathbf{y}) \tag{29}$$

Finally, we propose the PSNR-B as

$$PSNR-B(\mathbf{x}, \mathbf{y}) = 10 \log_{10} \frac{255^2}{MSE-B(\mathbf{x}, \mathbf{y})} \tag{30}$$

The MSE term in measures the distortion between the reference image and the test image, while the BEF term in specifically measures the amount of blocking artifacts just using the test image. The BEF itself can be used as a no reference quality index, similar to the generalized block-edge impairment metric (GBIM) and the mean noticeable blockiness score (MNBS) [20]. These no-reference quality indices claim to be efficient for measuring the amount of blockiness, but may not be efficient for measuring image quality relative to full-reference quality assessment. On the other hand, the MSE is not specific to blocking effects, which can substantially affect subjective quality. We argue that the combination of MSE and BEF is an effective measurement for quality assessment considering both the distortions from the original image and the blocking effects in the test image. The associated quality index PSNR-B is obtained from the MSE-B by a logarithmic function, as is the PSNR from the MSE. The PSNR-B is attractive since it is specific for assessing image quality, specifically the severity of blocking artifacts.

IV. MATLAB RESULTS

Now we present simulation results for de-blocking filters for H.264 video coding. The H.264 encoding and decoding simulations are performed using the H.264 reference. The in-loop de-blocking filter is a key component in H.264 video coding. If the filter is selected by an encoding parameter, in-loop filtering is performed both in encoding and in decoding. If it is not selected, in-loop filtering is not performed either in encoding or in decoding. In H.264, the quantization step size is controlled by the quantization parameter (QP) during encoding [16]. The QP can take 52 values ranging from 0 to 51, and the quantization step is doubled for each increment of six in the QP [19]. In H.264 coding, the quantization step is the same for all transform coefficients as determined by the QP. To assess the in-loop filter using the quality indices, the size of a group-of-pictures (GOP) is set as eight with one I-frame and seven P-frames. In the simulations, 16 frames are encoded and decoded. The quality indices were applied on the original (reference) and decoded images at each frame, and the quality scores were then averaged over the 16 frames

A. PSNR Analysis:

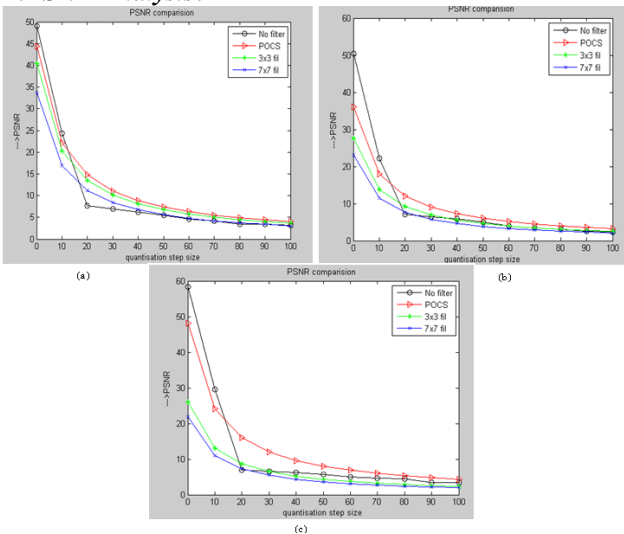


Fig. 3 PSNR comparison of filters for H.264 videos.

Fig. 3 examines the H.264 in-loop filter and low pass filters using the PSNR as an analysis tool. The 3x3 and 7x7 low pass filters do not provide improvement compared to not filtering for small to medium quantization step sizes. The low pass filters produce slight improvement compared to not filtering for on the Foreman and Mother and Daughter videos. The in-loop filter gave a slight improvement of PSNR compared to not filtering for mid-to-large quantization steps on the Foreman, Mother and Daughter, and Hall Monitor videos. The in-loop filter did not produce improvements compared to not filtering on the complex Mobile video, according to the PSNR. However, the PSNR is of dubious value when assessing perceptual quality.

B. SSIM Analysis:

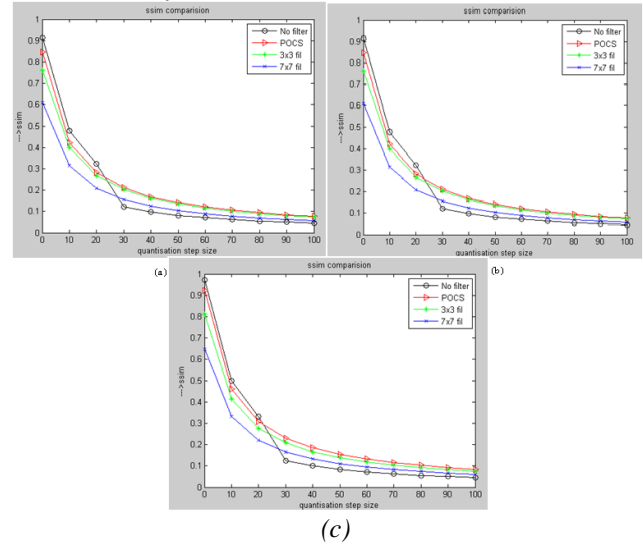


Figure 4: SSIM comparison of filters for H.264 videos

Fig. 4 studies the de-blocking methods using the SSIM index. The in-loop filter produced improvement in the SSIM values compared to not filtering for mid-to-large quantization steps on the Foreman, Mother and Daughter, and Hall Monitor videos. As the quantization step was increased, the in-loop filter systematically produced larger SSIM values. The 3x3 filter also produced improvement according to SSIM as compared to not filtering on the Foreman, Mother and Daughter, and Hall Monitor videos, when the quantization step was greater than 40. For the Mobile video, the in-loop filter produced SSIM values almost the same as those for not filtering while the low pass filters gave lower SSIM values. This is clear evidence that the in-loop filter works well, according to the perceptually relevant SSIM index.

C. PSNR-B Analysis:

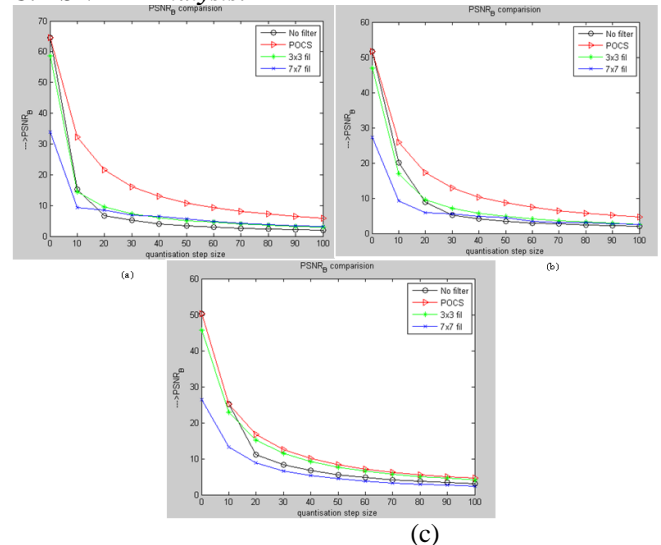


Fig. 5. PSNR-B comparison of filters for H.264 videos

Fig. 5 analyzes the in-loop filter using PSNR-B. PSNR-B produces trends similar to SSIM and visual analysis, while the PSNR shows different trends. For mid-to-large quantization steps, PSNR-B shows that the in-loop filter delivers marginal improvement as compared to not filtering,

while the PSNR shows little change on the Foreman, Mother and Daughter, and Hall Monitor videos. For a large quantization step, the PSNR-B comparison in Fig. 5 shows that the 3x 3 and 7x 7 filters deliver improvements,

V. CONCLUSION

Here we proposed the block-sensitive image quality index PSNR-B for quality assessment of de-blocked images. It modifies the conventional PSNR by including an effective blocking effect factor. In simulations, we compared relevant image quality indices for de-blocked images. The simulation results show that PSNR-B results in better and good performance than PSNR for image quality assessment of these impaired images. By comparison, the blockiness-specific index GBIM effectively assesses blockiness, but has limitations for image quality assessment. PSNR-B shows similar trends with the perceptually proven index SSIM. It is attractive since it is specific for assessing image quality, specifically the severity of blocking artifacts. The PSNR-B takes values in a similar range as PSNR and is, therefore, intuitive for users of PSNR, while it results in better performance for quality assessment of de-blocked images.

References

- [1] Z. Wang, A. C. Bovik, H. R. Sheikh, and E. P. Simoncelli, "Image quality assessment: From error visibility to structural similarity," *IEEE Trans. Image Process.*, vol. 13, no. 4, pp. 600–612, Apr. 2004.
- [2] Z. Wang, E. P. Simoncelli, and A. C. Bovik, "Multi-scale structural similarity for image quality assessment," in *Proc. IEEE Asilomar Conf. Signal Syst. Comput.*, Nov. 2003.
- [3] H. R. Sheikh and A. C. Bovik, "Image information and visual quality," *IEEE Trans. Image Process.*, vol. 15, no. 2, pp. 430–444, Feb. 2006.
- [4] H. R. Sheikh and A. C. Bovik, "A statistical evaluation of recent full reference image quality assessment algorithms," *IEEE Trans. Image Process.*, vol. 15, no. 11, pp. 3441–3452, Nov. 2006.
- [5] Z. Wang and A. C. Bovik, "A universal image quality index," *IEEE Signal Process. Lett.*, vol. 9, no. 3, pp. 81–84, Mar. 2002.
- [6] B. Girod, "What's wrong with mean-squared error," in *Digital Images and Human Vision*, A. B. Watson, Ed. Cambridge, MA: MIT Press, 1993, pp. 207–220.
- [7] Y. Yang, N. P. Galatsanos, and A. K. Katsaggelos, "Projection-based spatially adaptive reconstruction of block-transform compressed images," *IEEE Trans. Image Process.*, vol. 4, no. 7, pp. 896–908, Jul. 1995.
- [8] Y. Yang, N. P. Galatsanos, and A. K. Katsaggelos, "Regularized reconstruction to reduce blocking artifacts of block discrete cosine transform compressed images," *IEEE Trans. Circuits Syst. Video Technol.*, vol. 3, no. 6, pp. 421–432, Dec. 1993.
- [9] H. Paek, R.-C. Kim, and S. U. Lee, "On the POCS-based post processing technique to reduce the blocking artifacts in transform coded images," *IEEE Trans. Circuits Syst. Video Technol.*, vol. 8, no. 3, pp. 358–367, Jun. 1998.
- [10] S. H. Park and D. S. Kim, "Theory of projection onto narrow quantization constraint set and its applications," *IEEE Trans. Image Process.*, vol. 8, no. 10, pp. 1361–1373, Oct. 1999.
- [11] A. Zakhor, "Iterative procedure for reduction of blocking effects in transform image coding," *IEEE Trans. Circuits Syst. Video Technol.*, vol. 2, no. 1, pp. 91–95, Mar. 1992.
- [12] Y. Jeong, I. Kim, and H. Kang, "A practical projection-based postprocessing of block-coded images with fast convergence rate," *IEEE Trans. Circuits and Syst. Video Technol.*, vol. 10, no. 4, pp. 617–623, Jun. 2000.
- [13] S. Liu and A. C. Bovik, "Efficient DCT-domain blind measurement and reduction of blocking artifacts," *IEEE Trans. Circuits Syst. Video Technol.*, vol. 12, no. 12, pp. 1139–1149, Dec. 2002.
- [14] Z. Wang and A. C. Bovik, "Blind measurement of blocking artifacts in images," in *Proc. IEEE Int. Conf. Image Process.*, Vancouver, Canada, Oct. 2000, pp. 981–984.
- [15] P. List, A. Joch, J. Laimena, J. Bjøntegaard, and M. Karczewicz, "Adaptive deblocking filter," *IEEE Trans. Circuits Syst. Video Technol.*, vol. 13, no. 7, pp. 614–619, Jul. 2003.
- [16] *Draft ITU-T Recommendation and Final Draft International Standard of Joint Video Specification (ITU Rec. H.264—ISO/IEC 14496-10 AVC)*, , 2003, Doc.JVT-G050.
- [17] T. Wiegand, G. Sullivan, J. Bjøntegaard, and G. A. Luthra, "Overview of the H.264/AVC video coding standard," *IEEE Trans. Circuits Syst. Video Technol.*, vol. 13, no. 7, pp. 560–576, Jul. 2003.
- [18] H.264/AVC Software Co-ordination [Online]. Available: <http://iphome.hhi.de/suehring/tml/index.htm>
- [19] I. E. G. Richardson, *H.264 and MPEG-4 Video Compression*. Hoboken, NJ: Wiley, 2003.
- [20] H. R. Wu and M. Yuen, "A generalized block-edge impairment metric for video coding," *IEEE Signal Process. Lett.*, vol. 4, no. 11, pp. 317–320, Nov. 1997.
- [21] G. Zhai, W. Zhang, X. Yang, W. Lin, and Y. Xu, "No-reference noticeable blockiness estimation in images," *Signal Process. Image Commun.*, vol. 23, pp. 417–432, 2008.

A Novel Algorithm for peak to Average Ratio Reduction in Wireless OFDM Systems

P. Venkat Rao

M.Tech Student Scholar, DECS,
Dept of Electronics and Communication Engineering,
Nalanda Institute of Engineering and technology,
Sattenapalli (M); Guntur (Dt); A.P, India.

I. Rama Koteswara Rao

M.Tech, Asst Professor
Dept of Electronics and Communication Engineering,
Nalanda Institute of Engineering and technology,
Sattenapalli (M); Guntur (Dt); A.P, India.

Abstract: In OFDM systems, the major obstacle is that the multiplex signal exhibits a very high peak-to-average power ratio (PAR). In this paper, a new novel method to reduce the PAR. A simple and attractive technique is Active constellation extension used. However, we observe it cannot achieve the minimum PAR when the target clipping level is set below an initially unknown optimum value. A low clipping ratio is the problem in OFDM system to overcome this AEC algorithm with adaptive clipping control. However, the simulation results show our algorithm can reach the minimum Peak to Average for several clipping ratios, and also in AWGN channel we calculate the tradeoff between PAR and the loss in E_b/N_0 .

Keywords: Peak-to-average ratio (PAR), active constellation extension (ACE), adaptive, OFDM, BER, AWGN.

I. INTRODUCTION

Orthogonal frequency division multiplexing is a very attractive technique for high speed data transmission in mobile communications due to various advantages such as high spectral efficiency, robustness to channel fading, immunity to impulse interference, and capability of handling very strong multi-path fading and frequency selective fading without having to provide powerful channel equalization. In recent years, several industrial standards based on OFDM have been emerged, such as the Terrestrial Digital Video Broadcast (DVB-T), the IEEE 802.11 Wireless Local Area Network (WLAN) scheme, as well as the IEEE 802.16 Broadband Wireless Access (BWA), particularly, Wireless Metropolitan Area Networks (IEEE 802.16d) WiMAX.

Besides a lot of advantages, some drawbacks become apparent, when using OFDM in transmission systems. A major obstacle is that the multiplex signal exhibits a very high peak-to-average power ratio (PAR). Therefore, nonlinearities may get overloaded by high signal peaks, causing inter modulation among subcarriers and, more critical, undesired out-of-band radiation. If RF power amplifiers are operated without large power back-offs, it is impossible to keep the out-of-band power below specified limits. This leads to very inefficient amplification and expensive transmitters so that it is highly desirable to reduce the PAR [3]. Several schemes have been proposed to reduce the PAPR. These techniques can mainly be categorized into Signal scrambling techniques and Signal distortion techniques [1]. Signal scrambling techniques are all variations on how to scramble the codes to decrease the PAPR. Coding techniques can be used for signal

scrambling. Golay complementary sequences, Shapiro-Rudin sequences, M-sequences, Barker codes can be used to efficiently reduce the PAPR. However, with the increase in the number of carriers, the overhead associated with exhaustive search of the best code would increase exponentially. More practical solutions of the signal scrambling techniques are block coding, selective mapping and partial transmit sequences.

In this paper, to solve the low clipping ratio problem of CBACE, we introduce a new method of ACE for PAR reduction. Here, The PAR reduced by extending some modulation constellation points without any loss of data in outside of constellation. The cost of this is low and complexity also low, so that's why we proposing Active constellation extension. The algorithm provides a suboptimal solution to the given clipping ratio, because the clipping ratio is predetermined at the initial stage. However, the CB-ACE algorithms have a low clipping ratio problem in that they cannot achieve the minimum PAR.

In this correspondence clipping ratio problem of CBACE, we introduce a new method Active constellation extension for to reduce the PAR. Our algorithm based on the clipping with an adaptive clipping control, which allows us to find the optimal clipping level. simulation results shows that our algorithm can achieve the minimum Peak to Average Ratio regardless of the low target clipping level, and also calculate the tradeoff between PAR and BER over an AWGN channel in terms of clipping ratio.

II. TOPICS RELATED TO PROPOSED CONCEPT

A. Peak to Average Ratio:

OFDM signals have a higher peak-to-average ratio (PAR) often called a peak-to-average power ratio (PAPR) than single-carrier signals do. The reason is that in the time domain, a multicarrier signal is the sum of many narrowband signals. At some time instances, this sum is large and at other times is small, which means that the peak value of the signal is substantially larger than the average value. This high PAR is one of the most important implementation challenges that face OFDM, because it reduces the efficiency and hence increases the cost of the RF power amplifier, which is one of the most expensive components in the radio.

B. The PAR Problem:

When transmitted through a nonlinear device, such as a high-power amplifier (HPA) or a digital to analog converter (DAC) a high peak signal, generates out-of-band energy (spectral regrowth) and in-band distortion

(constellation tilting and scattering). These degradations may affect the system performance severely. The nonlinear behavior of an HPA can be characterized by amplitude modulation/amplitude modulation (AM/AM) and amplitude modulation/phase modulation (AM/PM) responses. Figure (1) shows a typical AM/AM response for an HPA, with the associated input and output back-off regions (IBO and OBO, respectively).

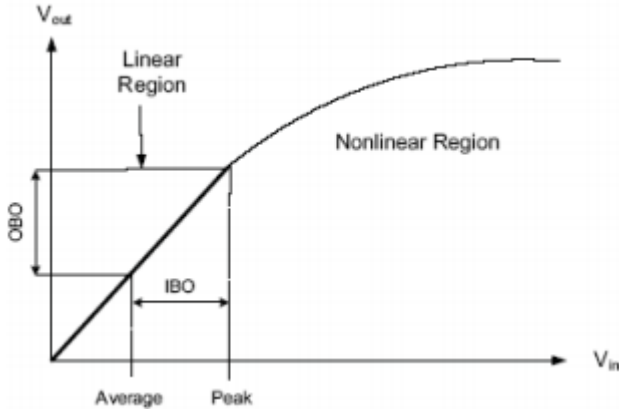


Figure 1: A typical power amplifier response

To avoid such undesirable nonlinear effects, a waveform with high peak power must be transmitted in the linear region of the HPA by decreasing the average power of the input signal. This is called (input) back off (IBO) and results in a proportional output back off (OBO). High back off reduces the power efficiency of the HPA and may limit the battery life for mobile applications. In addition to inefficiency in terms of power, the coverage range is reduced, and the cost of the HPA is higher than would be mandated by the average power requirements. The input backoff is defined as:

$$IBO = 10 \log_{10} \frac{P_{in\ sat}}{P_{in}}$$

Where $P_{in\ sat}$ is the saturation power, above which is the nonlinear region, and P_{in} is the average input power. The amount of backoff is usually greater than or equal to the PAR of the signal. The power efficiency of an HPA can be increased by reducing the PAR of the transmitted signal. Clearly, it would be desirable to have the average and peak values are as close together as possible in order to maximize the efficiency of the power amplifier. In addition to the large burden placed on the HPA, a high PAR requires high resolution for both the transmitter's DAC and the receiver's ADC, since the dynamic range of the signal is proportional to the PAR. High-resolution D/A and A/D conversion places an additional complexity, cost, and power burden on the system.

III. CB-ACE IN OFDM SYSTEMS

An OFDM signal consists of the sum of N independent signals modulated in the frequency domain onto sub channels of equal bandwidth. As a continuous-time equivalent signal, the oversampled OFDM signal is expressed as

$$x_n = \frac{1}{\sqrt{JN}} \sum_{k=0}^{JN-1} X_k e^{j2\pi \frac{k}{JN} n}, \quad n = 0, 1, \dots, JN-1 \quad (1)$$

where N is the number of subcarriers; X_k are the complex data symbols using phase-shift keying (PSK) or quadrature amplitude modulation (QAM) at the k th subcarrier; and J is the oversampling factor where $J \geq 4$, which is large enough to accurately approximate the peaks [4]. In matrix notation, (1) can be expressed as $\mathbf{x} = \mathbf{Q}^* \mathbf{X}$, where \mathbf{Q} is the inverse discrete Fourier transform (IDFT) matrix of size $JN \times JN$, \mathbf{X} denotes the Hermitian conjugate, the complex time-domain signal vector \mathbf{X} .

$$\mathbf{X} = [X_0, X_1, X_2, \dots, X_{\frac{JN}{2}-1}, 0, X_{\frac{JN}{2}}, X_{\frac{JN}{2}+1}, \dots, X_{JN-1}]^T$$

Here, we do not consider the guard interval, because it does not impact the PAR, which is defined as

$$PAR(\mathbf{x}) \triangleq \frac{\max_{0 \leq n \leq JN-1} |x_n|^2}{E[|x_n|^2]}, \quad (2)$$

Note that (2) does not include the power of the anti-peak signal added by the PAR reduction. Let \mathcal{I}_a be the index set

$$\begin{aligned} & \min_{\mathbf{c}} \|\mathbf{x} + \mathbf{Q}^* \mathbf{C}\|_{\infty}^2 \\ & \text{subject to: } X_k + C_k \text{ be feasible for } k \in \mathcal{I}_a, \\ & C_k = 0, \text{ for } k \notin \mathcal{I}_a \end{aligned} \quad (3)$$

where \mathbf{C} is the extension vector whose components, C_k are non zero only if $k \in \mathcal{I}_a$

However, this optimal solution for this ACE formulation of PAR reduction is not appropriate for practical implementation due to high computational complexity. Thus, the CB-ACE algorithms are introduced [1], [2]. The basic idea of the CB-ACE algorithm is to generate the anti-peak signal for PAR reduction by projecting the clipping in-band noise into the feasible extension area while removing the out-of-band distortion with filtering. Thus, the CB-ACE method is considered as a repeated-clipping-and filtering (RCF) process with ACE constraints as follows:

$$\mathbf{x}^{(i+1)} = \mathbf{x}^{(i)} + \mu \tilde{\mathbf{c}}^{(i)} \quad (4)$$

where μ is a positive real step size that determines the convergence speed, i is the iteration index, the initial signal is, $\mathbf{x}^{(0)}$ and $\tilde{\mathbf{c}}^{(i)}$ is the anti-peak signal at the i th iteration as follows:

where $c_n^{(i)}$ is the clipping sample, which can be obtained as follows:

$$c_n^{(i)} = \begin{cases} (|x_n^{(i)}| - A) e^{j\theta_n}, & \text{if } |x_n^{(i)}| > A \\ 0, & \text{if } |x_n^{(i)}| \leq A \end{cases}, \quad (5)$$

where $\theta_n = \arg(-x_n^{(i)})$. The clipping level A is related to the clipping ratio γ as $\gamma = \frac{A^2}{E[|x_n|^2]}$. In general, we expect more

PAR reduction gain with a lower target clipping level; the existing CBACE algorithms cannot achieve the minimum PAR for low target clipping ratios, because the reduced power by low clipping decreases the PAR reduction gain in ACE. The original symbol constellations move toward the origin with the decreasing clipping ratio in [6], which places the clipped signal constellations outside the feasible extension region. The number of \mathcal{E}_a , corresponding to the number of reserved tones in tone reservation (TR), as in [7], decreases with low clipping ratio, which in turn degrades the PAR reduction capacity in ACE.

IV. PROPOSED CONCEPT AND ALGORITHM

The main objective of our proposed algorithm is to control both the clipping level and convergence factor at each iteration and to iteratively minimize the peak power signal greater than the target clipping level. The cost function is defined as

$$\xi(I^{(i)}) \triangleq \min_{\mu, A} \|\mathbf{x}^{(i)} + \mu \tilde{\mathbf{c}}^{(i)} - A e^{j\Phi^{(i)}}\|_2^2 \quad (6)$$

Where $\Phi^{(i)}$ is the phase vector of $\mathbf{x}^{(i)} + \mu \tilde{\mathbf{c}}^{(i)}$ at the i th iteration and $I^{(i)}$ represents the set of time indices at the i th iteration,

$$I^{(i)} = \{n \text{ s.t. } n \in [0, N-1]\}$$

Step 0: Initialize the parameters

- Select the target clipping level A .
- Set up the maximum number of iterations L .

Step 1: Set $i = 0$, $\mathbf{x}^{(0)} = \mathbf{x}$ and $A^{(0)} = A$.

Step 2: Compute the clipping signal in (5); if there is no clipping signal, transmit signal, $\mathbf{x}(i)$.

Step 3: Transfer the clipping signal into the anti-peak signal subject to ACE constraint;

Convert into $\mathbf{c}^{(i)}$ into $\tilde{\mathbf{c}}^{(i)}$

- Project $\mathbf{c}^{(i)}$ onto the feasible region in ACE and remove the out-of-band of $\tilde{\mathbf{c}}^{(i)}$
- Obtain $\tilde{\mathbf{c}}^{(i)}$ by taking the IDFT.

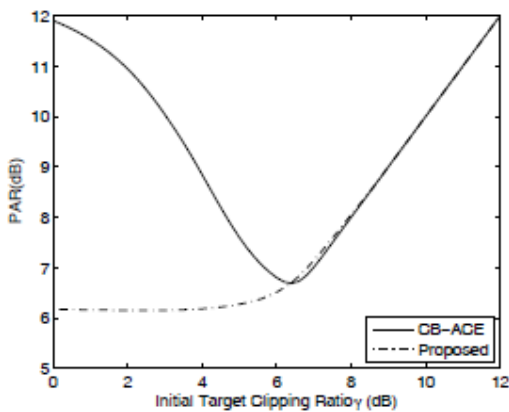


Figure 2: The achievable PAR of CB-ACE and the proposed algorithm for an OFDM signal with a 12dB PAR, for different initial target clipping ratios.

Step 4: Update $\mathbf{x}^{(i)}$ in (4) and A minimizing (6). Compute the optimal step size μ

$$\mu = \frac{\Re[\langle \mathbf{c}^{(i)}, \tilde{\mathbf{c}}^{(i)} \rangle]}{\langle \tilde{\mathbf{c}}^{(i)}, \tilde{\mathbf{c}}^{(i)} \rangle}, \quad (7)$$

where \Re defines the real part and $\langle \cdot, \cdot \rangle$ is the complex inner-product. Adjust the clipping level A

$$A^{(i+1)} = A^{(i)} + \nu \nabla_A, \quad (8)$$

Where the gradient with respect to A is

$$\nabla_A = \frac{\sum_{n \in I_1^{(i)} \cup I_3^{(i)}} |c_n^{(i+1)}|}{N_p} \quad (9)$$

and ν is the step size with $0 \leq \nu \leq 1$ and N_p is the number of peak samples larger than A .

Step 5: Increase the iteration counter, $i = i+1$. If $i < L$, go to *Step 2* and repeat; otherwise, transmit signal, $\mathbf{x}^{(i)}$.

Compared to the existing CB-ACE with complexity of order $(JN \log N)$, the complexity of our proposed algorithm slightly increases whenever the adaptive control is calculated in (8). However, this additional complexity of the adaptive control is negligible compared to that of order $O(JN \log N)$.

V. MATLAB/SIMULINK RESULTS

In this section, we illustrate the performance of our proposed algorithm using computer simulations. In the simulations, we use an OFDM system with 2048 subcarriers and M-QAM constellations on each subcarrier. To approximate the continuous-time peak signal of an OFDM signal, the oversampling rate factor $J = 8$ is used in (1). For a fast convergence rate, the optimal adaptive scaling is applied. Fig. 2 compares the achievable PAR of CB-ACE with the optimal adaptive scaling with that of our proposed algorithm for an OFDM signal with an initial 12dB PAR and 16-QAM modulation, for different target clipping ratios γ from 0dB to 12dB. In the case when CB-ACE is applied, we find the minimum achievable PAR, 6.62dB, is obtained with a target clipping ratio of 6.4dB, which shows that CB-ACE depends on the target clipping ratio, as we mentioned in the previous section. The PAR reduction gain becomes smaller with a decreasing target clipping ratio from the optimal value of 6.4dB. Thus, we must carefully select the target clipping ratio

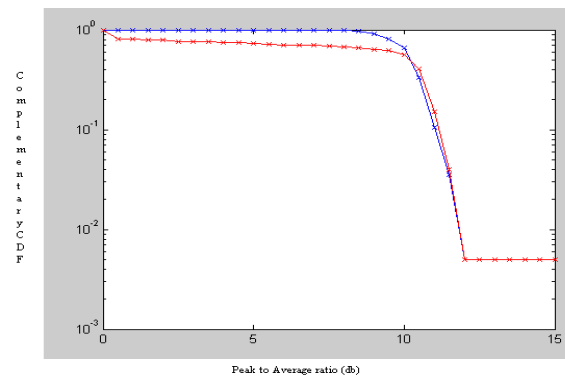


Figure-3 PAR CCDF comparison of the CB-ACE and the proposed method for different initial target clipping ratios

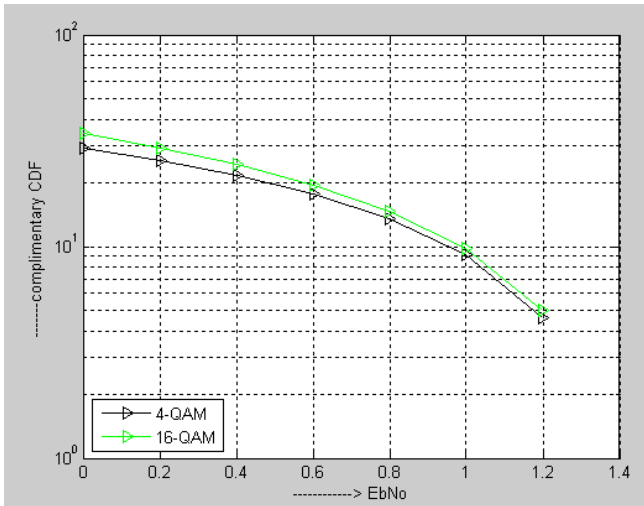


Figure 4: PAR for CCDF 10^{-3} vs loss in E_b/N_0 at the BER of 10^{-3} for different QAM constellation orders of the proposed algorithm.

for CB-ACE. On the other hand, we observe that our proposed algorithm can achieve the lower minimum PAR even when the initial target clipping ratio is set below the CB-ACE optimal value of 6.4dB. It is obvious that our proposed algorithm solves the low target clipping ratio problem associated with the CB-ACE, as shown in Fig.3 . Fig. 4 considers two algorithms: CB-ACE and our proposed method for three different initial target clipping ratios, $\gamma = 0\text{dB}$, 2dB , and 4dB , in terms of their complementary cumulative density function (CCDF). The solid line curve at the right is plotted for the original OFDM signal. The marked lines correspond to the PAR reduced signals of CB-ACE and our proposed method after 10-iterations, which we have confirmed is sufficient for convergence. For a 10^{-3} CCDF, CB-ACE with initial target clipping ratios of $\gamma = 0\text{dB}$, 2dB , and 4dB can achieve a 0.14dB, 0.89dB, and 2.95dB PAR reduction from the original PAR of 12dB, respectively. In other words, when the target clipping ratio is set low, the achievable gain in PAR reduction decreases, which is opposite to our general expectation, but is consistent with the trend shown in Fig.1. On the other hand, our proposed algorithm shows about a 5.6dB reduction gain in PAR at 10^{-3} CCDF for all three of the initial low target clipping ratios. Fig. 4 plots the performance of our proposed algorithm considering both PAR and loss in E_b/N_0 over an AWGN channel for the different M-QAM symbols. The x-axis indicates the loss in E_b/N_0 with respect to E_b/N_0 of the original OFDM signal for a given targeted BER of 10^{-3} , and the y-axis shows the required PAR at a CCDF of 10^{-3} . The tradeoff curves for M-QAM symbols is plotted as a function of the target clipping ratio γ , ranging from 10dB to 0dB in increments of -1dB. The curve with triangles down is for QAM, the curve with triangles up is for 16-QAM, and the one with squares is for 64-QAM. For a clipping ratio of 10dB, the three curves meet each other at a PAR of 10dB. As the clipping ratio decreases, the symbols move toward the bottom right direction; the achievable PARs for different constellation sizes are moving to their minimum points with a decreasing clipping ratio. Our proposed algorithm reaches the minimum PARs: 5.55dB, 6.42dB, and 7.07dB for QAM, 16-QAM, and 64-QAM, respectively. These different minimum PARs come

from the inherent ACE constraint that the higher the order of the constellation, the less flexibility [5]. However, we observe that the loss in E_b/N_0 for each different constellation is about 1.06dB, even though the achievable minimum PAR depends on the constellation size. It is clear that our proposed algorithm provides the tradeoff curve between PARs and the loss in E_b/N_0 for the M-QAM constellations as a function of the target clipping ratio.

VI. CONCLUSION

In this paper propose a new novel method to reduce the PAR. A simple and attractive technique is Active cancellation extension used. However, we observe it cannot achieve the minimum PAR when the target clipping level is set below an initially unknown optimum value. A low clipping ratio is the problem in OFDM system to overcome this AEC algorithm with adaptive clipping control. The minimum Peak to Average for several clipping ratios, and also in AWGN channel we calculate the tradeoff between PAR and the loss in E_b/N_0 .

References

- [1] Kitaek Bae, , Jeffrey G. Andrews, and Edward J. Powers" Adaptive Active Constellation Extension Algorithm for Peak-to-Average Ratio Reduction in OFDM," in *IEEE Commun. Lett.*, Vol. 14, No. 1 pp. 39–41, Jan, 2010.
- [2] L. Wang and C. Tellambura, "An adaptive-scaling algorithm for OFDM PAR reduction using active constellation extension," in *Proc. IEEE Veh. Technology Conf.*, Sep. 2006, pp. 1–5.
- [3] E. Van der Ouderaa, J. Schoukens, and J. Renneboog, "Peak factor minimization using a time-frequency domain swapping algorithm," *IEEE Trans. Instrum. Meas.*, vol. 37, no. 1, pp. 145–147, Mar. 1988.
- [4] C. Tellambura, "Computation of the continuous-time PAR of an OFDM signal with BPSK subcarriers," *IEEE Commun. Lett.*, vol. 5, no. 5, pp. 185–187, May 2001.
- [5] Y. Kou, W.-S. Lu, and A. Antoniou, "New peak-to-average power ratio reduction algorithms for multicarrier communications," *IEEE Trans. Circuits and Syst.*, vol. 51, no. 9, pp. 1790–1800, Sep. 2004.
- [6] M. Friese, "On the degradation of OFDM-signals due to peak-clipping in optimally predistorted power amplifiers," in *Proc. IEEE Globecom*, Nov. 1998, pp. 939–944.
- [7] J. Tellado, *Multicarrier Modulation with Low PAR: Applications to DSL and Wireless*. Boston: Kluwer Academic Publishers, 2000.
- [8] B. S. Krongold and D. L. Jones, "PAR reduction in OFDM via active constellation extension," *IEEE Trans. Broadcast.*, vol. 49, no. 3, pp. 258–268, Sep. 2003

Modified Energy Aware Geographic Routing Protocol for Mobile Ad-Hoc Network

Anand Gautam¹, Shiva Prakash²

Department of Computer Science & Engineering, Madan Mohan Malaviya Engineering College,
Gorakhpur-273010, U. P., INDIA

Abstract: Mobile ad hoc networks (MANET) are characterized by multi-hop wireless links and resource constrained nodes. One of the major challenge in mobile ad hoc networks (MANETs) is link failures due to mobility as well as nodes energy constraint. The more challenging goal is to provide energy efficient routes in MANET to improve network life time because node have limited lifetime. The Geo-routing has been widely regarded as efficient and scalable. However, it used constant transmission power model for communication and route selection is not based on energy. In this paper we proposed a model of energy aware geographic routing scheme with variant transmission power model. This can improve performance of existing protocol in form of less energy. We explain this concept with help of example that show the improvement of existing EGR.

Keywords: Energy efficient, location information, mobile ad hoc network.

I. INTRODUCTION

A Mobile Ad-hoc network (MANET) is consists of mobile routers connected wirelessly to each other where each node is free to move. This results in a continuously changing topology. Some examples of the possible uses of ad hoc networking include business associates sharing information during a meeting, soldiers relaying information for situational awareness on the battlefield and emergency disaster relief personnel coordinating

In recent years, geographic routing algorithms have been extensively studied due to the popularity and availability of positioning services such as the global positioning system (GPS). Geographic routing is a promising candidate for large-scale wireless ad hoc networks due to its simplicity and scalability and takes advantage of the location information of the nodes are the very valuable for wireless networks. Since geographic routing does not require a route management process, it carries a low overhead compared to other routing schemes, such as proactive, reactive, and hybrid topology based routing protocols. Geographic routing protocols work on the assumption that every node is aware of its own position in the network; via mechanisms like GPS or distributed localization schemes and that the physical topology of the network is a good approximation of the network connectivity. In other words, these routing protocols assume that if two nodes are physically close to each other, they would have radio connectivity between them, which is true in most cases. Hence the protocols use node location information to route packets from source to destination. One big advantage of geographic routing schemes is the fact that there is no need to send out route requests or periodic connectivity updates. This can save a

lot of protocol overhead and consequently, energy of the nodes. The most significant difference between MANETs and traditional networks is the energy constraint. Some applications such as environment monitoring need MANETs to run for a long time. Therefore, extending the lifetime of MANETs is important for every MANET routing protocol. However, most geographic routing algorithms take the shortest local path, depleting the energy of nodes on that path easily. The nodes located on the boundaries of holes may suffer from excessive energy consumption since the geographic routing tends to deliver data packets along the whole boundaries by perimeter routing if it needs to bypass the hole.

There should be a mechanism at node for robust communication of high priority messages. This can be achieved by keeping nodes all the time powered up which makes nodes out of energy and degrades network life time. Also, there can be a link or node failure that leads to reconfiguration of the network and re-computation of the routing paths, route selection in each communication pattern results in either message delay by choosing long routes or degrades network lifetime by choosing short routes resulting in depleted batteries. Therefore the solutions for such environments should have a mechanism to provide low latency, reliable and fault tolerant communication, quick reconfiguration and minimum consumption of energy. Routing protocols have a critical role in most of these activities. To measure the suitability and performance of any given protocol, some metrics are required. On the basis of these metrics any protocol can be assessed against its performance [3]. This can save a lot of protocol overhead and consequently, energy of the nodes. The most significant difference between MANETs and traditional networks is the energy constraint. Some applications such as environment monitoring need MANETs to run for a long time.

Therefore, extending the lifetime of MANETs is important for every MANET routing protocol. However, most geographic routing algorithms take the shortest local path, depleting the energy of nodes on that path easily. The nodes located on the boundaries of holes may suffer from excessive energy consumption since the geographic routing tends to deliver data packets along the whole boundaries by perimeter routing if it needs to bypass the hole. This can enlarge the hole because of the excessive energy consumption of the whole boundary nodes. We call this a whole diffusion problem. Many geographic routing protocols assume that the geographic information is accurately available. In fact, all location services update their geographic information periodically. Typically, there can be a time difference between the update of and the demand for this information, which introduces inaccuracy

in the geographic information the accuracy of GPS, is limited.

In most cases location information is needed in order to calculate the distance between two particular nodes so that energy consumption can be estimated. Consequently, we should define the packet destination as an area rather than a point. In this paper we will present Modified Energy-Aware Geographic Routing (MEGR) Protocol, novel geographic routing algorithm combining local position information and balancing node energy consumption. It forecasts the destination node's movement to ensure packet delivery and to prolong the network lifetime. We also use various model for providing energy efficient path.

The remaining part of this paper is organized as follows: In section II we will discuss the literature review of energy aware geographic routing and we will discuss the problem statement with help of example in section III. We will propose a model with help of example in section IV and finally we conclude the paper and give future scope in section V.

II. LITERATURE REVIEW

In case of location-aware routing mechanisms, the nodes are often aware of their exact physical locations in the three-dimensional world. This capability might be introduced in the nodes using Global Positioning System (GPS) or with any other geometric methods. Based on these concepts, several geocast and location-aware routing protocols have already been proposed. The major feature of these routing protocols is that, when a node knows about the location of a particular destination, it can direct the packets toward that particular direction from its current position, without using any route discovery mechanism. Recently, some of the researchers proposed some location-aware protocols that are based on these sorts of idea. Some of the examples of them are Geographic Distance Routing (GEDIR)[18], Location-Aided Routing (LAR)[2], Greedy Perimeter Stateless Routing (GPSR)[3], Geo-GRID[20], Geographical Routing Algorithm (GRA)[21], etc. Other than these, there are a number of multicast routing protocols for MANET. Some of the mentionable multicast routing protocols are: Location-Based Multicast Protocol (LBM)[22], Multicast Core Extraction Distributed Ad hoc Routing (MCEDAR)[23], Ad hoc Multicast Routing protocol utilizing Increasing id-numberS (AMRIS)[24], Associativity-Based Ad hoc Multicast (ABAM)[25], Multicast Ad hoc On-Demand Distance-Vector (MAODV) routing [26], Differential Destination Multicast (DDM)[27], On-Demand Multicast Routing Protocol (ODMRP)[28], Adaptive Demand-driven Multicast Routing (ADMR) protocol [29], Ad hoc Multicast Routing protocol (AMRoute)[30], Dynamic Core-based Multicast routing Protocol (DCMP)[31], Preferred Link-Based Multicast protocol (PLBM)[32], etc. Some of these multicast protocols use location information and some are based on other routing protocols or developed just as the extension of another unicast routing protocol. For example, MAODV is the multicast-supporting version of AODV.

Early research of geographic routing includes DREAM [1] and LAR [2] that proposed constrained flooding. The *expected zone* is defined by predicting the boundary of the destination node's movement. In both protocols, prediction

is made based on the time difference between sending data and the location information's update, as well as the destination node's speed. We adopt this approach in our routing protocol and describe it in the fourth section. In the LAR protocol, before the transmission of a data packet, the source node finds a route by flooding routing packets in its *request zone*. In the DREAM protocol, however, according to the location information, the data packet is flooded in a restricted directional range without sending a routing packet. Although this kind of forwarding effectively guarantees delivery, its energy use is notably high, especially in large-scale networks. Recently, *Local maxima* in geographic routing have received much attention. Many routing protocols for planar network graphs are presented for solving this problem, such as GFG [3], GPSR [4], GOAFR+ [5] and CLDP [6].

In the following, we review the shared characteristics of these geographic routing algorithms. Geographic routing schemes use greedy routing where possible. In greedy routing, packets are stamped with the position of their destination; and a node forwards a packet to a neighbor that is geographically closer to the destination. Local maximum may exist where no neighbor is closer to the destination. In such cases, greedy forwarding fails, and making progress toward the destination requires another strategy. In particular, the packet needs only to find its way to a node closer to the destination than the local maximum; at that point, greedy routing may once again make progress.

Note that if the graph is not planar, face routing may fail. Wireless networks connectivity graphs typically contain many crossing edges. A method for obtaining a planar sub graph of a wireless network graph is thus needed. Greedy routing operates on the full network graph, but to work correctly, face routing must operate on a planar sub graph of the full network graph. Geographic routing algorithms planarize graphs using two planar graph constructs that meet that requirement: the Relative Neighborhood Graph (RNG) and the Gabriel Graph (GG). The RNG and GG give rules for how to connect vertices placed in a plane with edges based purely on the positions of each vertex's single-hop neighbors. Up to the present, literature, such as GOAFR+, CLDP and LCR [15], has focused on methods of deleting these crossing links.

However, there are several drawbacks to pure geographic routing. In certain circumstances, one cannot guarantee delivery by greedy routing, for example, when there is the rapid movement of nodes. Because of this, the location information of a destination node is rather inaccurate. Secondly, greedy routing is a single-path transmission process which means once the process drops a data packet the whole routing fails. Thirdly, there have been several schemes to overcome the *Local maxima*.

All the schemes can be classified into two categories: perimeter routing [5, 6] and the back pressure rule [7, 8]. In perimeter routing the system tends to route data packets along the boundaries of holes, but the perimeter routing cannot avoid the excessive energy consumption and data congestion in these nodes. Using the back pressure rule, the system returns the data packets to the upstream node in an attempt to find another route to the destination. This rule may generate an additional routing overhead.

Mobile networks use a power-aware routing protocol in [17]. However, to save energy as much as possible, its

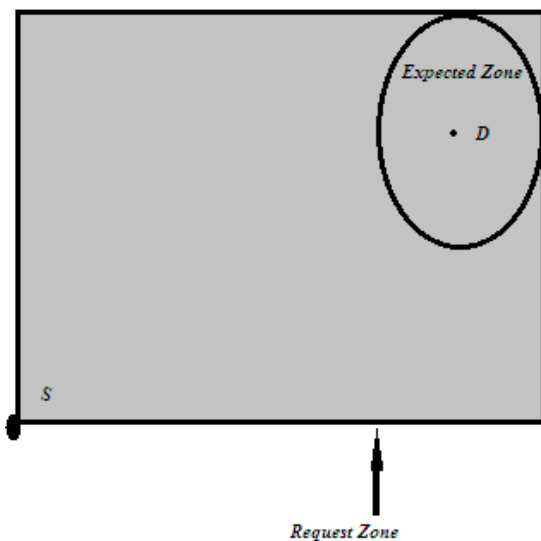
iterative relay process will result in unacceptable end-to-end delay. Due to the non-linear attenuation of wireless signals, it is possible that one hop consumes more energy than multiple hops. Yet it can be impractical to change from one hop to several, following the mechanism in [17]. The end-to-end delay may increase significantly, especially in a high-density network.

III. PROBLEM STATEMENT

In recent years various works has been done in the field of energy aware geographic routing but a lot of work has to be done in the near future by overcoming the problems still lies in the geographic routing protocol so that we can be able to sends the packet from source to destination without fear of loss of packets, higher packet delivery ratio, low energy consumption etc. But when we talk about the Energy Aware Geographic Routing there are still a lot of problem are there which is discussed below:

3.1 Need of EGR: As we know that in EGR, to make routing decision it uses local position information and residual energy and also uses prediction of range of a destination's movement. EGR uses the concept of Location aided routing (LAR) and Distance effect algorithm for mobility (DREAM).

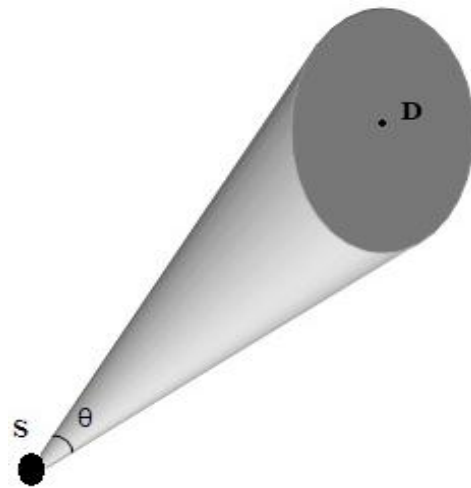
In LAR protocol, before the transmission of a data packet, a source node finds a route by flooding routing packets in its request zone.



(a)The model of LAR

But LAR fails when there is a large scale network and also uses high energy.

To solve out this problem the DREAM routing protocol comes into existence. In DREAM protocol, according to the location information the data packet is flooded in a restricted directional range without sending a routing packet.



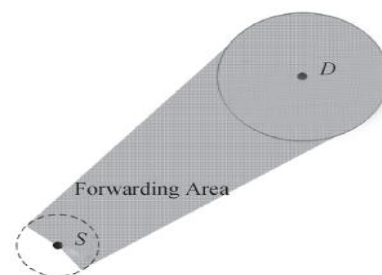
(b)The model of DREAM

In DREAM, if source is quite far away from destination, the angle θ will be too small for source to find the next hop.

3.2 Need of MEGR: To remove the problem of DREAM EGR comes into existence which works as follows:

(a) Dissemination of location and energy information: EGR assume the existence of a mechanism such as GPS system that allows each node to be aware of its location and residual energy.

(b) Forwarding Data packets: To remove the problem of DREAM it uses the concept of tangent lines between two circle, first circle is centered on source node whose radius is the transmission distance of source node and other one is destinations expected zone.



(c) The model of EGR

In EGR it uses a mechanism for choosing the next hop in the flooding area and uses a single path before destination expected zone.

If node i is located in forwarding area the i chooses the next hop from it neighbor nodes given by:

$$\text{NEXTHOP} = k \quad e_{\text{remain}}^k = \max \{ e_{\text{remain}}^j \}, j \in N_i$$

It means i chooses the next hop k with the most residual energy from all its neighbors nodes whose position are closer to destination than i .

If node i is in expected zone it directly relay the packet to the destination.

The main problem with EGR that it uses the constant power model means it always sends the packet to the node which has maximum energy which will leads to the depleting of energy very fast as well as it also suffers from taking decision of route request and gives a single path.

IV. PROPOSED MODEL

To make energy efficient routing protocol than EGR we modified the Energy Aware Geographic Routing (EGR) [1] protocol to solve out the problem lies in the EGR we proposed a new routing protocol named Modified Energy Aware Geographic Routing Protocol (MEGR) in which we use the variant power model as well as we use the decision of route request will be taken at destination for choosing the best path through which we can increase the network lifetime.

In MEGR, a source node that requires sending a packet to destination acquires the address of the destination. After preparing the packet by adding appropriate information in the header, we calculate the distance from each of its neighbors to the destination and also calculate the minimum energy required for sending a packet. We choose the path that requires minimum energy. But also in route request phase we find the paths which have highest energy by comparing available residual energy and minimum energy required. If the available energy is less than the minimum energy required we append the residual energy of that node the move to the next node. In this way after reaching the destination we wait for Δt time which is less than the TTL. After that time we find the total route request packet reach at the destination. The destination will choose the path for route reply that has highest energy.

The distance between two points on the earth surface can be calculated by using its latitude and longitude coordinates. Hence in our approach we will divide the network into x-axis and y-axis. The parameter used to calculate the distances are defined below:-

DISTANE = Distance in meters between first and second point.

DISTANCE_x = x-axis distance between the first and second point.

DISTANCE_y = y-axis distance between the first and second point.

X₁ = x-axis of the first point in degrees.
 Y₁ = y-axis of the first point in degrees.
 X₂ = x-axis of the second point in degrees.
 Y₂ = y-axis of the second point in degrees.

DISTANCE_x = x₂ - x₁
 DISTANCE_y = y₂ - y₁

$$DISTANCE = \sqrt{(DISTANCE_x)^2 + (DISTANCE_y)^2}$$

After calculating the distance, for given threshold energy E_{th}. The minimum transmit energy E_{min} can be calculated by giving formula:

$$E_{min} = \frac{E_{th} * D^n}{K}$$

Where D is the distance between two nodes,
 n is the path loss exponent whose value is lies between 2-4,
 K is a constant. Here, K= 2.8 x 10⁻¹⁰ μJ/(byte-m⁴)
 E_{th} in the LAN 802.11 is 3.652 x 10⁻¹⁰ mW.

Hence in this way we can modify the EGR now we can explain our model by taking the appropriate example.

4.1 Example:

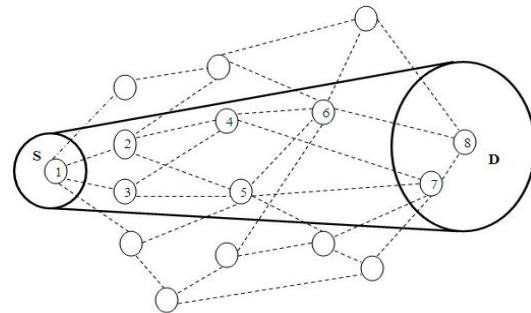


Fig 4.1

Node number	Location of nodes	Residual Energy(Joule)
1	-5,0	500
2	-3,2	300
3	-3,-2	100
4	0,2	400
5	0,-2	600
6	3,2	500
7	5,-2	300
8	6,3	200

By using the concept of the EGR we find the path 1-2-5-6-8 which is explained below:

In EGR, we choose the next hop which is having the maximum energy.

So.

Source (1) has two neighbors 2, 3

Residual energy of 2=300J

Residual energy of 3=100J

Therefore, Source (1) will choose next hop 2

Hence distance between node 1 and 2

$$D(1, 2) = 2.82 \text{ m}$$

Now, the minimum transmit energy

$$E_{min}(1, 2) = 82.483 \text{ Joule}$$

Again, Node 2 has two neighbors 4, 5

Residual energy of 4=400J

Residual energy of 5=600J

Therefore, node 2 will choose next hop 5

Hence distance between node 2 and 5

$$D(2, 5) = 4 \text{ m}$$

Now, the minimum transmit energy

$$E_{min}(2, 5) = 333.89 \text{ Joule}$$

Again, Node 5 has two neighbors 6, 7

Residual energy of 6=500J
 Residual energy of 7=300J
 Therefore, node 5 will choose next hop 6
 Hence distance between node 5 and 6

$$D(5, 6) = 5 \text{ m}$$

Now, the minimum transmit energy

$$E_{\min}(5, 6) = 815.714 \text{ Joule}$$

Now at last node 6 has only one neighbor 8
 Hence distance between node 6 and 8

$$D(6, 8) = 3.16 \text{ m}$$

So the minimum energy

$$E_{\min}(6, 8) = 130.42 \text{ Joule}$$

Therefore,

$$\text{Total energy required in EGR} = 82.483 + 333.89 + 815.714 + 130.42 = 1357.507 \text{ Joule}$$

In MEGR

For Source node 1: we calculate the distance between 1 and 2 as well as 1 and 3.

$$\text{Distance}(1,2) = 2.82 \text{ m}$$

$$\text{Distance}(1,3) = 2.82 \text{ m}$$

Now we will calculate the minimum energy required for both the paths

$$E_{\min}(1,2) = 82.483 \text{ J}$$

$$E_{\min}(1,3) = 82.483 \text{ J}$$

In this case we choose the next hop 2 because it has total energy 300 Joule which has greater than node 3.

Now for node 2: We calculate the distance between 2 and 4 as well as 2 and 5.

$$\text{Distance}(2,4) = 3 \text{ m}$$

$$\text{Distance}(2,5) = 4 \text{ m}$$

Now we will calculate the minimum energy required for both the paths

$$E_{\min}(2,4) = 105.847 \text{ J}$$

$$E_{\min}(2,5) = 333.89 \text{ J}$$

In this case we choose the next hop 4 because it requires only 105.847 joule energy for transmitting the packet while its residual energy is 400 joule.

Now for node 4: We calculate the distance between 4 and 6 as well as 4 and 7.

$$\text{Distance}(4, 6) = 3 \text{ m}$$

$$\text{Distance}(4, 7) = 6.40 \text{ m}$$

Now we will calculate the minimum energy required for both the paths

$$E_{\min}(4,6) = 105.847 \text{ J}$$

$$E_{\min}(4,7) = 2188.228 \text{ J}$$

In this case we choose the next hop 6 because it requires only 105.847 joule energy for transmitting the packet while its residual energy is 500 joule.

Now for node 6: We calculate the distance between 6 and 8.

$$\text{Distance}(6, 8) = 3.16 \text{ m}$$

Now we will calculate the minimum energy required for the path

$$E_{\min}(6,8) = 130.42 \text{ J}$$

In this case we can reach the destination the destination reply on this path which we have followed shown below:-
 1-2-4-6-8

4.2 Analysis of the MEGR: When we compare the MEGR with EGR then we can see that Total energy required for sending a packet from source to destination is very less in MEGR.

$$\text{Total energy required in EGR: } 82.483 + 333.89 + 810.714 + 130.42 = 1357.454 \text{ Joule.}$$

$$\text{Total energy required in MEGR: } 82.483 + 105.847 + 105.847 + 130.42 = 424.651 \text{ Joule.}$$

Hence in MEGR we can reduce the energy consumption more than three times than EGR.

4.3 Algorithm for MEGR:

(a) Route Request

Step1: Initialize network (Source, Destination)

Step2: For every node of the network

Step3: Find $LOC(N_x, N_y)$ // Find location of all nodes where N is the set of nodes defined in the network.

Step4: Find neighbors (S, D) // Detect neighbors of the node and add it to the LET.

Step5: Calculate Distance (n, d) // Calculate distance of all neighbors node.

Step6: Calculate minimum transmit energy (E_{\min})

Step7: If ($E_{\min} > E_{\text{residual}}$)

Add E_{residual} of the neighbor node that have high residual energy.

Else

Route request is send at the next hop.

Step8: When route request is reach at the destination

Wait Δt time where ($\Delta t < TTL$).

Step9: Choose the best path

Step10: End

V. CONCLUSION AND FUTURE SCOPE

As per literature review we come to know that as route selection is not based on energy efficiency in and use constant power model for packet transmission. Our proposed solution for these existing problem in EGR can be improved. In this we presented Modified Energy Aware Geographic Routing protocol which gives better results to minimize energy consumption and Delay time and extends network lifetime. We will present simulation of our proposed Modified EGR protocol in our future work. It can be improved to find accurate information for faulty location of Geographical based information.

REFERENCES

- [1] Gang Wang and Guodong Wang, An Energy Aware Geographic Routing Protocol for Mobile Ad Hoc Networks, *Int J Software informatics*, Vol. 4, No. 2, June 2010, pp. 183-196.
- [2] Adel Gaafar A. Elrahim and et al., An Energy Aware WSN Geographic Routing Protocol, *Universal Journal of Computer Science and Engineering Technology*, 1(2), 105-111, Nov. 2010.
- [3] S. Corson and J. Macker, "Routing Protocol Performance Issues and Evaluation Considerations," Naval Research Laboratory, Jan. 1999.
- [4] B. Karp and H. Kung, "GPSR: Greedy perimeter stateless routing for wireless networks," in the Proceedings of the 6th Annual ACM/IEEE International Conference on Mobile Computing and Networking (MOBICOM), pp.243-254, Boston, August 2000.
- [5] Ko Y, aida NHV. Location-aided routing (LAR) in mobile ad hoc networks. Proc. The ACM/IEEE International Conference on Mobile Computing and Networking, 1998. 66{75.
- [6] Ma XL, Sun MT, Zhao G, *et al.* An efficient path pruning algorithm for geographical routing in wireless networks. *IEEE Trans. Vehicular Technology*, 2008, 57(4): 2474{2488}.
- [7] Kim Y J, Govindan R, Karp B, *et al.* Geographic routing made practical. Proc. the 2nd Symposium on Networked Systems Design and Implementation, 2005. 217{230.
- [8] Watanabe M, Higaki H. No-Beacon GEDIR: Location-Based Ad-Hoc Routing with Less Communication Overhead. Proc. the International Conference on Information Technology, 2007.
- [9] Singh S, Woo M, Raghavendra CS. Power-Aware routing in mobile ad hoc networks. Proc. the ACM/IEEE International Conference on Mobile Computing and Networking, Oct. 1998.
- [10] Basagni S, Chlamtac I, Syrotiuk VR. A distance routing effect algorithm for mobility (DREAM). Proc. the ACM/IEEE International Conference on Mobile Computing and Networking, 1998.
- [11] Kuhn F, Wattenhofer R, Zhang Y, *et al.* Geometric ad-hoc routing: Of theory and practice Proc. the 22nd ACM Symposium on Principles of Distributed Computing, 2003. 63-72.
- [12] Zeng K, Ren K, Lou W, *et al.* Energy Aware Geographic Routing in Lossy Wireless Sensor Networks with Environmental Energy Supply. Proc. the 3rd International Conference on Quality of Service in Heterogeneous Wired/Wireless Networks, Waterloo, Canada, Aug. 2006.
- [13] Stojmenovic I. A scalable quorum based location update scheme for routing in ad hoc wireless networks. Technical Report TR-99-09, SITE, University of Ottawa, Sep. 1999.
- [14] Stojmenovic I. Home agent based location update and destination search schemes in ad hoc wireless networks. Technical Report TR-99-10, SITE, University of Ottawa, Sep. 1999.
- [15] Li J, Jannotti J, Douglas S J De Couto, *et al.* A scalable location service for geographic ad hoc routing. Proc. the 6th Annual International Conference on Mobile Computing and Networking, Aug. 2000. 120-130.
- [16] Kuruvila J, Nayak A, Stojmenovic I. Progress and location based localized power aware routing for ad hoc and sensor wireless networks. *International Journal of Distributed Sensor Networks*, 2006, 2(2): 147-159.
- [17] Kim YJ, Govindan R, Karp B, *et al.* Lazy Cross-Link Removal for Geographic Routing. Proc. the ACM Conference on Embedded Networked Sensor Systems, Nov. 2006. 112-124.
- [18] Liao W-H, Tseng Y-C, Lo K-L, Sheu J-P (2000) GeoGRID: A Geocasting Protocol for Mobile Ad Hoc Networks based on GRID. *Journal of Internet Technology*, Volume 1, Issue 2:23-32
- [19] Jain R, Puri A, Sengupta R (2001) Geographical Routing Using Partial Information for Wireless Ad Hoc Networks. *IEEE Personal Communications*, Volume 8, Issue 1:48-57
- [20] Ko Y-B, Vaidya NH (1998) Location-based multicast in mobile ad hoc networks. Technical Report TR98-018, Texas A&M University
- [21] Sinha P, Sivakumar R, Bharghavan V (1999) MCDAR: Multicast Core-Extraction Distributed Ad Hoc Routing. *Proceedings of IEEE WCNC*, Volume 3:1313-1317
- [22] Wu CW Tay TC (1999) AMRIS: A Multicast Protocol for Ad Hoc Wireless Networks. *IEEE MILCOM 1999*, Volume 1:25-29,
- [23] Toh C-K, Guichal G, Bunchua S (2000) ABAM: On-Demand Associativity-Based Multicast Routing for Ad Hoc Mobile Networks. *Proceedings of IEEE VTS-Fall VTC 2000*, Volume 3:987-993
- [24] Royer EM, Perkins CE (2000) Multicast Ad Hoc On-Demand Distance Vector (MAODV) Routing. IETF Draft, draft-ietf-manet-maodv-00, 15 July, 2000, available at <http://tools.ietf.org/html/draft-ietf-manet-maodv-> Accessed 21 February 2008
- [25] Ji L, Corson MS (2001) Differential Destination Multicast-A MANET Multicast Routing Protocol for Small Groups. *Proceedings of IEEE INFOCOM 2001*, Volume 2:1192-1201
- [26] Lee S, Su W, Gerla M (2002) On-Demand Multicast Routing Protocol in Multihop Wireless Mobile Networks. *ACM/Kluwer Mobile Networks and Applications (MONET)*, volume 7, Issue 6:441-453
- [27] Jetcheva JG, Johnson DB (2001) Adaptive Demand-Driven Multicast Routing in Multi-Hop Wireless Ad Hoc Networks. *Proceedings of ACM MobiHoc 2001*:33-44
- [28] Xie J, Talpade RR, McAuley A, Liu M (2002) AMRoute: Ad Hoc Multicast Routing Protocol. *Mobile Networks and Applications*, Volume 7, Issue 6:429-439.
- [29] Das SK, Manoj BS, Murthy CSR (2002) A Dynamic Core Based Multicast Routing Protocol for Ad Hoc Wireless Networks. *Proceedings of ACM MobiHoc 2002*:24-35
- [30] Sisodia RS, Karthigeyan I, Manoj BS, Murthy CSR (2003) A Preferred Link Based Multicast Protocol for Wireless Mobile Ad Hoc Networks. *Proceedings of IEEE ICC 2003*, Volume 3:2213-2217.
- [31] Song J-H, Wong VWS, Leung VCM (2007) Secure position-based routing protocol for mobile ad hoc networks. *Ad Hoc Networks*, Volume 5, Issue 1:76-86.
- [32] Reddy LR, Raghavan SV (2007) SMORT: Scalable multipath ondemand routing for mobile ad hoc networks. *Ad Hoc Networks*, Volume 5, Issue 2:162

An Efficient Online Voting System

Ankit Anand¹, Pallavi Divya²

*(Department of Computer Science Engineering, BITS Bhopal/ Rajiv Gandhi Technical University, Bhopal, India)

** (Department of Computer Science Engineering, Punjab Technical University, Punjab, India)

ABSTRACT: This paper deals with design, build and test a online voting system that facilitates user (the person who is eligible for voting), candidate (Candidate are the users who are going to stand in elections for their respective party), Election Commission Officer (Election Commission Officer who will verify whether registered user and candidates are authentic or not) to participate in online voting. This online voting system is highly secured, and it's design is very simple, ease of use and also reliable. The proposed software is developed and tested to work on Ethernet and allows online voting. It also creates and manages voting and an election detail as all the users must login by user name and password and click on his favorable candidates to register vote. This will increase the voting percentage in India. By applying high security it will reduce false votes.

Keywords: CSS, HTML, Java Script, JDBC, JSP, MYSQL, ORACLE, Servlet, WAMP.

I. INTRODUCTION

Voting schemes have evolved from counting hands in early days to systems that include paper, punch card, mechanical lever and optical-scan machines. Electronic voting systems provide some characteristic different from the traditional voting technique, and also it provides improved features of voting system over traditional voting system such as accuracy, convenience, flexibility, privacy, verifiability and mobility. But it suffers from various drawbacks such as Time consuming, Consumes large volume of pare work, No direct role for the higher officials, Damage of machines due to lack of attention, Mass update doesn't allows users to update and edit many item simultaneously. These drawbacks are overcome by Online Voting System. Online Voting System is a voting system by which any Voter can use his/her voting rights from anywhere in the country. We provide a detailed description of the functional and performance characteristics of online voting system. Voter can cast their votes from anywhere in the country without visiting to voting booths, in highly secured way. That makes voting a fearless of violence and that increases the percentage of voting.

1.1 Problem Background

In the recent years there are many literature on online voting has been developed. While online voting has been an active area of research in the recent years, efforts to develop real-world solutions have just begun posing several new challenges.

The use of insecure Internet, well documented cases of incorrect implementations and the resulting security Breaches have been reported recently. These challenges and concerns have to be resolved in order to create public trust in online voting.

1.2 Problem Statement

Online Voting are simple, attractive and ease to use. It reduces manual efforts and bulk of information can be handled easily. But out of all these features there are some drawbacks with this system are, there can be software failure issue, insecure access of internet and also voter should be familiar with internet.

1.3 Research Objective

The main objective of this study is an important step towards streamlining this effort is to develop a framework and identify necessary properties that a secure and trusted online voting system must satisfy to reduce discovery redundancy. Such a framework will allow us to evaluate as well as compare the merits of existing and future candidate online voting schemes. System should support multi-user environment. System should be fully automated. System should provide concrete security features like creating users and assigning privileges to users of the system. System should be capable to keep track of all the detailed descriptions of the client and the whole details of services offered by the client organization.

Various outputs (reports) should be available online any time. System should be able to handle extremely large volumes of data (i.e. large database support).

1.4 Scope of Study

The scope of the project is that it will use the ID and password created by user to register him/her in the voting site, through this all the details of voter are saved in database. And it will act as the main security to the votes system.

Advanced technology: It is an advanced technology used now a day. It increases the internet knowledge of the users which is very necessary for current generation.

Internet: It is an online facility and hence very useful for the users. Voters can vote from anywhere at any time in India.

E-Mails: Election Commission can send the error report to a particular user if he/she entered false information.

E-SMS: People who have not internet connection they cannot check the emails or not have email they can be informed by SMS on their mobile. Today many websites provide free SMS to the mobile. Election Commission can use these to send any information.

II. LITERATURE REVIEW

2.1 Background

This software is being developed for use by everyone with a simple and self explanatory GUI. This is software that can be used by people to vote in an election. All the user must do is login and click on his favorable candidates to register his vote. The development and testing is done on Ethernet. While online voting system has been an active area of research in recent years, the use of insecure Internet, well documented cases of incorrect implementations reported recently. These challenges are to be resolved so that public should cast their vote in secure and convenient way. Proposed online voting system is a voting system by which any Voter can use his/her voting rights from anywhere in country. Online voting system contains:

- a) Voter's information in database.
- b) Voter's Names with ID and password.
- c) Voter's vote in a database.
- d) Calculation of total number of votes.

Various operational works proposed in the system are:

Recording information of the Voter in database.

Checking of information filled by voter.

Discard the false information.

Each information is sent to election commission.

2.2 Product Perspective

The product is an election conducting tool with a simple GUI. The product is developed using Java. Though product is stand-alone, it requires Java Virtual Machine (JVM).

2.3 User Characteristics

Users are considered to be technically novices but expected to be able to use a computer / hand held terminal (HHT), and to click against the favorable candidate on the GUI.

2.4 Product Functions

The product has a server back-end which takes care of authenticating the users and maintaining necessary data structures. The GUI at the server's end enables creating the polls on behalf of the client. The users must connect to the server to authenticate their identification against the password and then vote using the GUI at their end.

2.5 Overview of Data Requirements

The internal memory requirement will be constant or linearly dependent on the number of users depending on the provision of changing the vote at a later time. In such a case the actions will be stored in a data structure which will be referred to when needed. The external data about the candidates (with photographs) and the posts or the poll questions and the answers will be given as input only at the serverend.

2.6 Assumptions and Dependencies

The user is assumed to have JVM on his system irrespective of its hardware and software configuration. The other requirements are strongly design based and can be only made concrete in the design stage. We also assume that all the clients running this software are not blocked by firewalls, proxies, etc.

2.7 Constraints

GUI is only in English.

Login and password is used for identification of Voter.

III. SALIENT FEATURE

On-line polling is software system through which a voter can give votes through registering themselves on the voting website. all the information in sites which has been entered are stored in database .for each page in the website have its own database table.

Each voter has to enter his all basic information like name, sex, religion, nationality, criminal record e.t.c. This is the first page of the website known as the welcome page. It has all the page options like Home, Polling Dates, Register, Login, about us, Contact us, FAQs.

3.1 Home

It is the welcome page of the website, having all the feature options of the website.



Fig 1: Home

3.2 Registration

This is the register page, where the voter, candidate and election commission officer can register themselves. They all have to enter basic information best of their known .All the information registered in the website are saved in the respective database .The Election Commission officer has authority to accept eligible user and suitable candidate, otherwise he/she has right to reject their registration.



Fig 2: Registration

3.2 Login

User Login: After registering into the website, this information is saved to the database and sent to the election commission. The user can Login to the website with his unique USERNAME and PASSWORD generated through registration. There is a option for FORGOT PASSWORD, in case user forget his password then he/she can go with option of forgot password.

Candidate Login: After registration candidate can see his/her profile and can edit his/her profile. The candidate has facilitated with all the latest news update regarding election.

Election commission officer login: After login election commission officer will verify whether user and candidate is authentic or not.

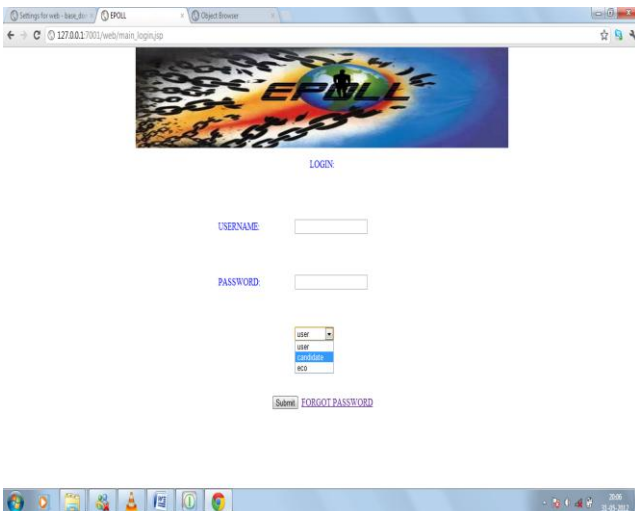


Fig 3: Login

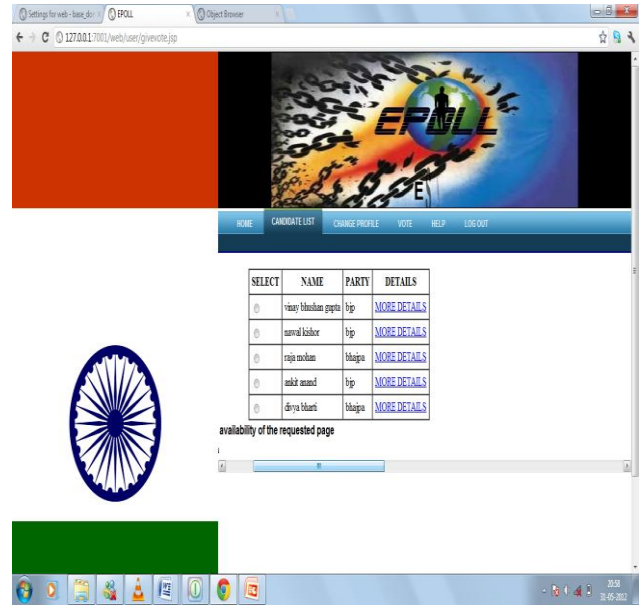


Fig 4: Choice of candidates for voting

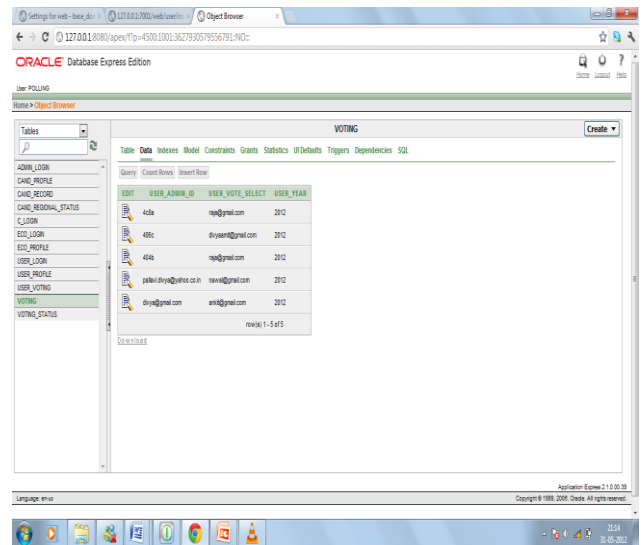


Fig 5: Database object browser, voting status

IV. RESOURCES

We create this software application with following resources

- Front end: - JAVA (JSP,Servlet,JDBC,java mail,EJB2.0)
- Back end: - ORACLE/MYSQL
- Design: - HTML
- Validation: - CSS (Cascading Style Sheet)
- Platform: - JavaScript
- J2EE

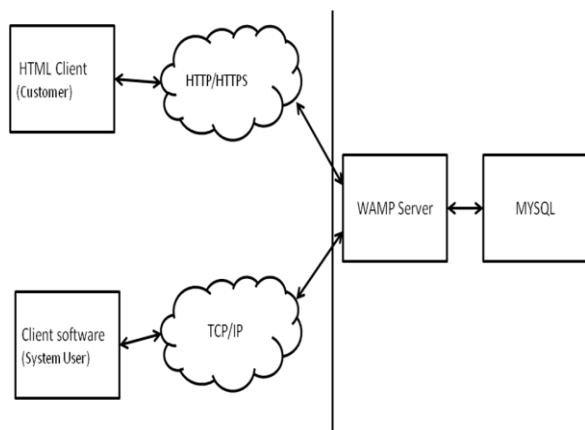


Fig 6: Communication Interfaces

The above diagram shows the connectivity between the client side, application server and database server. The client or customer can access the HTML server or client software. These are connected to the WAMP Server (WAMP) by a TCP/IP which is a communication protocol used to connect the teachers or parents to the internet. This WAMP Server now directly communicates with the database made in MYSQL. All the enquiries or data will be retrieved from the database.

V. CONCLUSIONS

Our proposal enables a voter to cast his/her vote through internet without going to voting booth and additionally registering himself/herself for voting in advance, proxy vote or double voting is not possible, fast to access, highly secure, easy to maintain all information of voting, highly efficient and flexible. Hence, by this voting percentage will increase drastically.

The using of online voting has the capability to reduce or remove unwanted human errors. In addition to its reliability, online voting can handle multiple modalities, and provide better scalability for large elections. Online voting is also an excellent mechanism that does not require geographical proximity of the voters. For example, soldiers abroad can participate in elections by voting online.

VI. REFERENCES

- [1] Alexander. Stakeholders: Who is your system for? IEEE: Computing and Control Engineering, 14(1):22{26, April 2003}.
- [2] Almyta Systems, Point of Sale Systems. http://systems.almyta.com/Point_of_Sale ,Software.a sp. Accessed on 20th October 2008.
- [3] S. W. Ambler, Process Patterns: Building Large Scale Systems Using Object Technology, Cambridge University Press, 1998.
- [4] M. Andrews and J. A. Whittaker, How to Break Web Software: Functional and Security Testing of Web Applications and Web Servers. Addison, Wesley, 2006.
- [5] Java-2 Complete Reference - Patrick Haughton
- [6] Java Servlet Programming - O'Reilly
- [7] Pure JavaScript- Jason Gilliam,-R.Allen Wyke
- [8] HTML completes - BPB publications.
- [9] Java Server Programming - Apress publication.

An Efficient Clustering Scheme for Vehicular Ad Hoc Networks

Miss. S. Poongodi^{#1}, Mrs. P. Tamilselvi^{*2}

[#] II M.E Communication Systems

^{*}Associate Professor

Department of Electronics and Communication Engineering

SNS College of Technology, Coimbatore, Affiliated to Anna University of Technology Coimbatore, India

Abstract: Several medium access control protocols have been proposed in the recent past in vehicles for accessing radio channels and for distributing timely safety messages for inter-vehicle communication in Vehicular Ad hoc Networks (VANETs). As contention period for channel access is high in Medium Access Control (MAC), MAC is unable to distribute timely safety messages. To reduce the contention, Region based Clustering Mechanism (RCM), which caters to the reduction of contention by limiting the number of vehicles for each cluster, is applied with MAC protocols. RCM also resolves the competition among vehicles to access radio channels for inter-vehicle communication. Ad Hoc On-Demand Distance Vector (AODV) routing protocol is used for providing shortest path between source and destination so as to increase the amount of packet reception with less energy than the existing method.

Keywords: Ad Hoc On-Demand Distance Vector (AODV), Medium Access Control (MAC), Safety-Critical Application (SCA), Region based Clustering Mechanism (RCM), Vehicular Ad-hoc Network (VANET).

I. INTRODUCTION

Vehicular Ad Hoc Network (VANET) consists of wireless routers or wireless nodes. Normally, the transmission range of VANET is 100 to 300 meters range. Inter-vehicle communication takes place with ad-hoc networks. Information such as speed and position of each vehicle is known by other vehicles.

VANET is an important mode of inter-vehicle communication for Intelligent Transportation Systems (ITS) [1], [2]. In such a network, each vehicle is equipped with a wireless communication and an on-board GPS device. Data forwarding is then performed collaboratively among vehicles in a multihop relaying manner. One of the most important applications for VANET is the distribution of active safety messages to improve driver safety, namely Safety-Critical Application (SCA) that requires timely and reliable message dissemination. Information about SCA is exchanged so as to notify the drivers about the car accident and to perform control actions in coordinated systems [3]. Other applications are also permitted for shortening the deployment cost of VANET and for speeding up its adoption period. Medium Access Control (MAC) protocols of VANET resolve contentions among vehicles for channel access. The dominant standard for vehicular networks is IEEE

802.11p based Dedicated Short Range Communications (DSRC) [4], [5]. Its random access mechanism is based on IEEE 802.11 Distributed Coordination Function (DCF) relying on the Carrier Sense Multiple Access/Collision Avoidance (CSMA/CA) mechanism. Other important MAC protocols include ADHOC, MAC [6], [7] that are designed for an European project. These protocols depend upon a Time Division Multiple Access (TDMA) based protocol called Reliable R-ALOHA (RR-ALOHA) for radio access control; Space Division Multiple Access (SDMA) [8], [9] wherein the geographical area is divided into multiple space division units and one radio channel is dedicated to serve the vehicle in a space division unit. Important issues related to MAC for VANET include mobility (i.e., the MAC protocol should support vehicles to leave and join inter-vehicle communications at high speed), delay bounded (i.e., the communication must be delay bounded and real-time), scalability (i.e., VANET should scale itself according to the number of vehicles present), bandwidth efficiency (i.e., the radio resource should be utilized in an efficient and fair manner), cost (i.e., for cost-efficient and reliable communications, VANET should be fully decentralized), and fairness (i.e., every vehicle should get a fair chance to get the radio channel). The challenge of successfully deploying VANET services lies in ensuring timely and reliable data delivery for mobile vehicles.

The MAC protocols for radio channel access among vehicles are effective under light traffic load. However, when the number of vehicles in the vicinity is large, the protocols may not be able to ensure the desired service due to lack of radio resource (e.g., more contentions among vehicles for random access based protocols like CSMA/CA, and less chance to be allocated a time slot for TDMA based protocols like RRALOHA) and cause a longer contention period to obtain radio resource. Fig. 1 shows the Vehicular Ad Hoc Network.

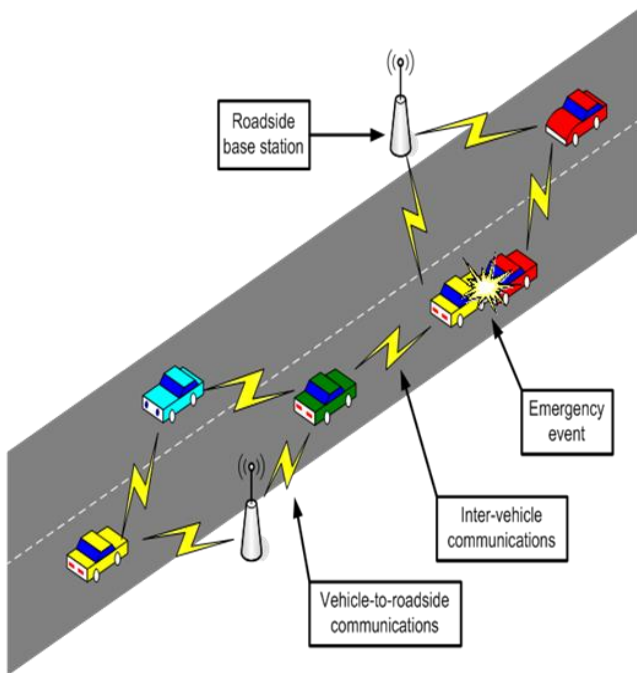


Fig. 1 Vehicular Ad-hoc Network

In the literature, several methods (e.g., [10], [11], [12]) have been proposed to reduce the contention period. DUCHA [10] utilizes dual-channel to separate control packets and data packets. Request To Send (RTS) and Clear To Send (CTS) are transmitted on a separate control channel to avoid the collisions with data packets. Fast Collision Resolution (FCR) algorithm [11] redistributes the back off counters to speed up the collision resolution. The FCR algorithm uses a smaller contention window for each station with successful packet transmission and reduces the back off counter exponentially when a station detects a number of consecutive idle slots. MAC-SCC [12] schedules data transmissions to reduce the back off time. The control channel is used to schedule data transmissions by using two different Network Allocation Vectors (NAVs) for the data channel and the control channel, respectively.

Region-based Clustering Mechanism (RCM) is used to improve the performance of MAC operations for VANET [13]. In RCM, the service area is divided into a set of region units and the number of vehicles is limited in each region unit for the contention of radio channels. Each region unit is then associated with a non-overlapping radio channel pool. Since the number of vehicles in each region unit is limited, the contention period is reduced and the throughput is increased. Note that this proposed idea can be applied on top of existing methods (e.g., [10], [11], [12]) to improve the contention period performance of MAC protocols for VAENT). RCM is formed with the limited number of vehicles in [13]. In RCM, there is no central controller for channel access. The contention resolution is required to obtain a channel. DSRC(Dedicated Short Range Communication) protocol is used in the existing method which produces the reduced packet transfer and throughput. In the proposed system, Ad- Hoc On-Demand Distance Vector (AODV) protocol is used to maintain shortest path between vehicles.

II. PROPOSED SYSTEM

Fig. 2 shows the block diagram of the proposed system. In the proposed system, mobile nodes are self-configured into an integrated network with distributed control. The connection between nodes in the network is in such a way that it has peer-to-peer communication links. NS-2 tool is used for network creation. Wireless channel is used with Omni antenna. The topological dimension and number of nodes are set according to the requirements.

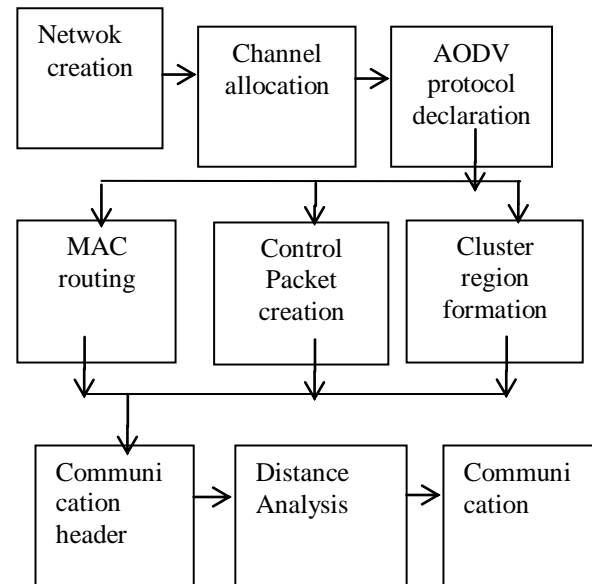


Fig. 2 Block diagram of the proposed system

Network is created with the mobile nodes. Total area is divided into clusters. Then, channel is allocated for each cluster without any overlap for avoiding congestion. AODV protocol is used for selecting the shortest path between source and destination as it does not need any central administrative system to control the routing process. Source node and the intermediate nodes store the next-hop information corresponding to each flow for data packet transmission.

Source nodes and destination nodes are connected with each other through the use of Transmission Control Protocol (TCP) or User Datagram Protocol (UDP). Clustering is formed with a limited number of mobile nodes so as to reduce the contention period spent for channel access. All the nodes of the region are grouped together into various clusters based on the vicinity of vehicles. These vehicles inter-communicate through ad hoc. Cluster head is otherwise known as a sink node because it maintains information about all the vehicles of a cluster. Each vehicle in a cluster moves with different speed and a particular distance is maintained among vehicles. Communication takes place from source to destination through the cluster head. When a cluster head fails, the other highest priority mobile node acts as the cluster head. When a mobile node (vehicle) moves from one cluster to another cluster, radio channel of current cluster with low latency is accessed.

A. Protocol Description

In [13], the R-ALOHA-based protocol is used as an example to show the ways to achieve contention resolution in RCM whereas in proposed system AODV protocol is used for achieving the shortest path among vehicles. Fig. 3 shows the AODV Protocol operation.

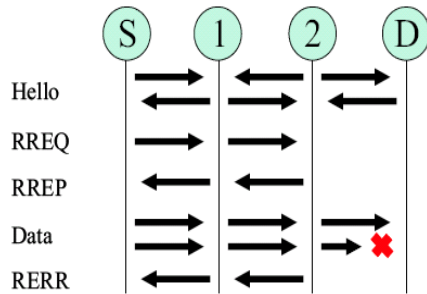


Fig. 3 AODV Protocol operation

AODV routing protocol is designed for use in ad-hoc mobile networks. AODV is a reactive protocol: the routes are created only when it is necessary. It uses traditional routing tables, one entry per destination, and sequence numbers to determine whether routing information is up-to-date and to prevent routing loops.

An important feature of AODV is the maintenance of time-based states in each node: a routing entry not recently used is expired. In case of a route that gets broken, the neighbours can be notified of any unnecessary happening. Route discovery is based on query and reply cycles. The route information is stored in all intermediate nodes along the route in the form of route table entries. The following control packets are used: Routing Request (RREQ) message is broadcasted by a node requiring a route to another node, Routing Reply (RREP) message is unicast back to the source of RREQ and Route Error (RERR) message is sent to notify other nodes of the loss of the link. HELLO messages are used for detecting and monitoring links to neighbours.

Routing protocols in mobile networks are subdivided into two basic classes:

- proactive routing protocols and
- reactive routing protocols

The proactive routing protocols (e.g. OLSR) are table-driven. They usually use link-state routing algorithms for flooding the link information. Link-state algorithms maintain a full or partial copy of the network topology and costs for all known links. The reactive routing protocols (e.g. AODV) create and maintain routes only on demand. They usually use distance-vector routing algorithms that keep information only about next hops to adjacent neighbours and costs for paths to all known destinations. Thus, link-state routing algorithms are more reliable, less bandwidth-intensive, but also more complex and compute- and memory-intensive.

In on-demand routing protocols, a fundamental requirement for connectivity is discovering routes to a node via flooding of request messages.

The AODV routing protocol does not need any central administrative system to control the routing process. AODV, a reactive protocol, tends to reduce the control traffic messages overhead at the cost of increased latency in finding new routes.

AODV reacts relatively fast to the topological changes in the network and updates only the nodes affected by these changes. The HELLO messages supporting the routes maintenance are range-limited for preventing unnecessary traffic overhead in the network. The AODV routing protocol saves storage place as well as energy. The destination node replies only once to the first request and ignores the rest.

The routing table maintains at most one entry per destination. When a node has to choose between two routes, the up-to-date route with a greater destination sequence number is always chosen. If a routing table entry is not used recently, the entry gets expired. When a not- valid route is deleted, the error packets reach all nodes through a failed link on its route to any destination which supports both unicasting and multicasting.

B. Algorithm

Step 1: The total area size 3500*3500 is set

Step 2: Mobile nodes are created

set n [\$ns node]

\$cbr_(\$index) set random_1

Step 3: The total area is divided into clusters to reduce the contention among mobile nodes

Step 4: cluster is assigned with a limited number of vehicles

Step 5: Each vehicle in each cluster is assigned with different channels

Set val(chan)

set ef(\$i) [expr (0.2 * \$dist(\$i)) + (\$velocity(\$i) * 0.2) + (\$frequency(\$i) * 0.6)]

Step 6: The long life node in each cluster acts as the Cluster Head (CH)

\$ns at 5.0 "\$n label CH"

Step 7: Through the cluster head, the mobile nodes communicate with each other

Step 8: AODV protocol used for selecting the shortest path between the mobile nodes.

III. NETWORK SIMULATION

Simulation is done using ns-2.33 Software. Table 1 shows the simulation parameters. The transmission range is 250 meters. Here, the simulation time is 200 seconds. AODV protocol is used for the simulation.

Table 1 Simulation Parameters

Parameter	Value
Examined protocol	AODV
Traffic type	Constant bit rate(TCP)
Transmission range	250 m
Packet size	512 bytes
Data rate	1Mbps
Simulation time	200sec
Antenna type	Omni directional Antenna
Area	3500 m * 3500 m
Number of nodes	93

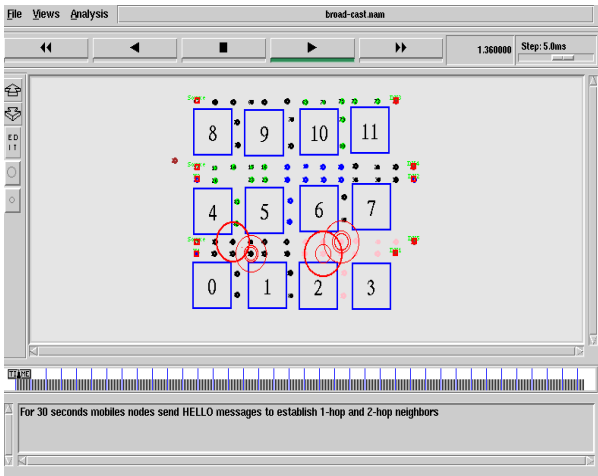


Fig. 4 Cluster formation

In Fig. 4, 93 mobile nodes are created. In this output, seven clusters are formed. When the node 27 leaves the region, the information (position) about this node is retained by node 28 which is the cluster head and this cluster head, in turn, multicast the information about node 27 to all the nodes (12, 13, 14, 15, 16, 25, 26, 29) of that cluster. The square box represents the building. The gap between the square box is the road way.

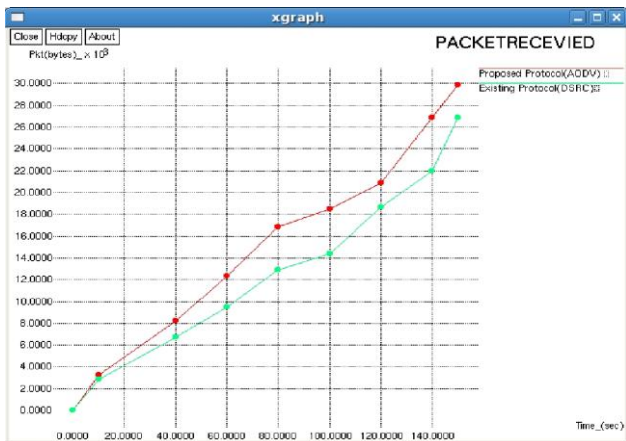


Fig. 5 Packet Reception

Fig.5 shows the simulated graph between time (in sec) and packet reception. In the AODV, the packet reception is high than the existing DSRC. The amount of packet reception gets increased with the increase in time.

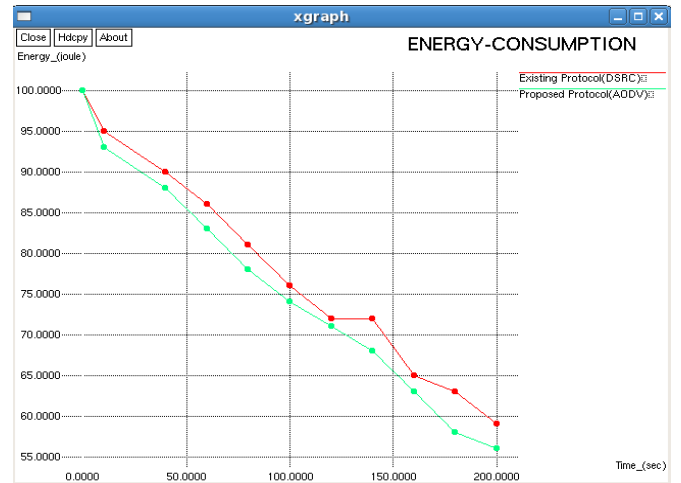


Fig. 6 Energy Consumption

Fig.6 shows the simulated graph between time (in sec) and energy consumption. The energy required for proposed AODV protocol is less compared to the existing method.

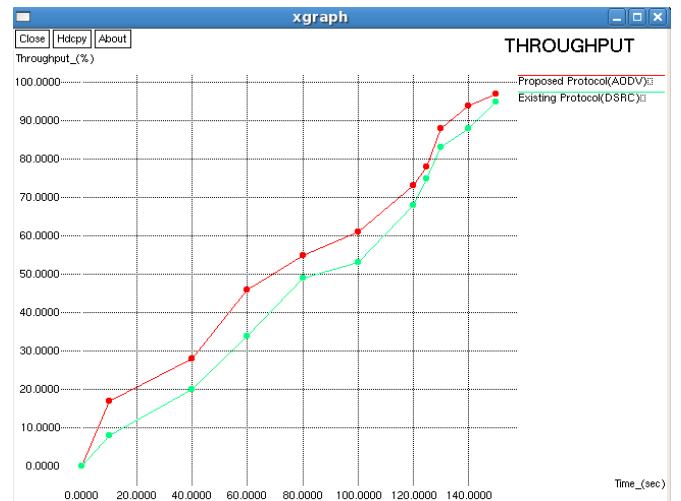


Fig. 7 Throughput

Fig. 7 shows the simulated graph between time (in sec) and throughput. In the proposed method, the throughput is increased more through the use of AODV protocol than the existing DSRC method. Table 2 shows the simulation results.

Table 2 Simulation Results

Time (in sec)	Parameters	Existing	Proposed(AODV)
140	Packet reception in bytes	21987	26882
150	Throughput	95%	97%

At the time of 140 (in sec), the packet reception for the proposed system is 21987 bytes and the packet reception of the existing method is 26882 bytes for the same time limit.

At the time of 150 (in sec), the throughput for the proposed method is 97% which is high by 2% than the existing method.

IV. CONCLUSION

Thus, the contention problem in VANET is solved by using region based global clustering mechanism. The long-life node of a cluster acts as the cluster head which maintains information all the nodes of that cluster. Source and destination nodes communicate with each other through cluster heads. AODV protocol facilitates the selection of the shortest path from source to destination by taking into account the minimum number of hop count and it increases packet reception and throughput.

REFERENCES

- [1] F. Yang, and F.-Y. Wang, "Driving into Intelligent Spaces with Pervasive Communications." *Intelligent Systems*, 22(1):12–15, February 2007.
- [2] C.-X. Wang, X. Cheng, and D. I. Laurenson, "Vehicle-to-vehicle Channel Modeling and Measurements: Recent Advances and Future Challenges," *IEEE Commun. Mag.*, 47(11):96–103, November 2009.
- [3] N. Yang, J. Liu, F. Zhao, and N. H. Vaidya, "A Vehicle-to-Vehicle Communication Protocol for Cooperative Collision Warning," *First Annual International Conference on Mobile and Ubiquitous Systems: Networking and Services*, pages 114–123, February 2004.
- [4] Q. Xu, T. Mak, J. Ko, and R. Sengupta, "Vehicle-to-vehicle Safety Messaging in DSRC," *Proc. 1st ACM International Workshop on Vehicular Ad Hoc Networks*, pages 19–28, October 2004.
- [5] J. Zhu, and S. Roy, "MAC for Dedicated Short Range Communication in Intelligent Transport System," *IEEE Commun Mag.*, 41(12):60–67, December 2003.
- [6] F. Borgonovo, L. Campelli, M. Cesana, and L. Fratta, "Impact of User Mobility on the Broadcast Service Efficiency of the ADHOC MAC Protocol," *IEEE Vehicular Technology Conference (VTC)*, 4:2310–2314, June 2005.
- [7] F. Borgonovo, A. Capone, M. Cesana, and L. Fratta, "ADHOC MAC: A New MAC Architecture for Ad Hoc Networks Providing Efficient and Reliable Point-to-Point and Broadcast Service," *ACM Wireless Networks*, 10(4):359–366, July 2004.
- [8] B. Jeremy, and E. Azim, "A Reliable Link-Layer Protocol for Robust and Scalable Inter-vehicle Communications," *IEEE Trans. Intell. Transp. Syst.*, 8(1):4–12, March 2007.
- [9] V. B. Soheila, and V. Pravin, "Space Division Multiple Access (SDMA) for Robust Ad hoc Vehicle Communication Networks," *IEEE Intelligent Transportation Systems Conference Proceedings*, Pages 962–966, April 2001.
- [10] H. Zhai, J. Wang, and Y. Fang, "DUCHA: A New Dual-Channel MAC Protocol for Multihop Ad Hoc Networks," *IEEE Trans. Wireless Commun.*, 5(11):3224–3233, November 2006.
- [11] Y. Kwon, Y. Fang, and H. Latchman, "A Novel MAC Protocol with Fast Collision Resolution for Wireless LANs," *IEEE Infocom 2003*, 2:853–862, April 2003.
- [12] Y. Li, H. Wu, D. Perkins, N. Tzeng, and M. Bayoumi, "MAC-SCC: Medium Access Control with A Separate Control Channel for Multihop Wireless Networks," *Proc. 23rd International Conference on Distributed Computing Systems Workshops*, pages 764–769, May 2003.
- [13] L.-C. Yen, L. Phone, L. Wanjiun, and C.-M. Chung, "A Region-Based Clustering Mechanism for Channel Access in Vehicular Ad Hoc Networks," *IEEE Journal on Selected Areas in Communications*, 29(1):83-93, January 2011.

A Extensive Technique For Image Segmentation By Using Algorithm Of MAP-ML

Vijayadheeswar Reddy

M.Tech Student Scholar, DIP,

Dept of Electronics and Communication Engineering,
Nalanda Institute of Engineering and technology,
Sattenapalli (M); Guntur (Dt); A.P, India

I. V. G. Manohar

M.Tech, Asst Professor

Dept of Electronics and Communication Engineering,
Nalanda Institute of Engineering and technology,
Sattenapalli (M); Guntur (Dt); A.P, India.

Abstract: Image segmentation is the process of dividing an image into multiple parts. This is typically used to identify objects or other relevant information in digital images. maximum a posteriori probability (MAP) estimate is a mode of the posterior distribution. The MAP can be used to obtain a point estimate of an unobserved quantity on the basis of empirical data. It is closely related to Fisher's method of maximum likelihood (ML), but employs an augmented optimization objective which incorporates a prior distribution over the quantity one wants to estimate. MAP estimation can therefore be seen as a regularization of ML estimation. In this Paper our algorithm segment an image into regions with relevant Textures automatically there is no need of regions. The simulations shows the image edges very well. Comparing to six state-of-the-art algorithms, extensive experiments have shown that our algorithm performs the best.

Keywords: Image segmentation, graph cuts, maximum likelihood, maximum a posteriori, Markov random fields.

I. INTRODUCTION

A central problem, called *segmentation*, is to distinguish objects from background. For intensity images (ie, those represented by point-wise intensity levels) four popular approaches are: threshold techniques, edge-based methods, region-based techniques, and connectivity-preserving relaxation methods. Threshold techniques, which make decisions based on local pixel information, are effective when the intensity levels of the objects fall squarely outside the range of levels in the background. Because spatial information is ignored, however, blurred region boundaries can create havoc.

Edge-based methods center around contour detection: their weakness in connecting together broken contour lines make them, too, prone to failure in the presence of blurring. A region-based method usually proceeds as follows: the image is partitioned into connected regions by grouping neighboring pixels of similar intensity levels. Adjacent regions are then merged under some criterion involving perhaps homogeneity or sharpness of region boundaries. Over stringent criteria create fragmentation; lenient ones overlook blurred boundaries and over merge. Hybrid techniques using a mix of the methods above are also popular.

A connectivity-preserving relaxation-based segmentation method, usually referred to as the *active contour model*, was proposed recently. The main idea is to start with some initial boundary shape represented in the form of spline curves, and iteratively modify it by applying

various shrink/expansion operations according to some energy function. Although the energy-minimizing model is not new, coupling it with the maintenance of an "elastic" contour model gives it an interesting new twist. As usual with such methods, getting trapped into a local minimum is a risk against which one must guard; this is no easy task. In contrast to the heuristic nature of these approaches, computational geometry suggests a more algorithmic tack. One would first formalize a mathematical criterion for the "goodness" of a given segmentation. This would allow us to formulate the segmentation problem as an optimization problem under certain geometric constraints.

The problem of image segmentation and visual grouping has received extensive attention since the early years of computer vision research. It has been known that visual grouping plays an important role in human visual perception. Many computer vision problems, such as stereo vision, motion estimation, image retrieval, and object recognition, can be solved better with reliable results of image segmentation. For example, results of stereo vision based on image segmentation are more stable than pixel-based results. Although the problem of image segmentation has been studied for more than three decades, great challenges still remain in this research. Here we presented to apply normalized cuts to image segmentation [1] which is able to capture intuitively salient parts in an image. The normalized cuts has an important advantage in spectral clustering. However, it is not perfectly fit for the nature of image segmentation because ad hoc approximations must be introduced to relax the NP-hard computational problem. These approximations are not well understood and often lead to unsatisfactory results.

These approaches are physics-based models that deform under the laws of Newton mechanics, in particular, by the theory of elasticity expressed in the Lagrange dynamics. Many contour based segmentation algorithms[2]-[4] have been developed in the past two decades. One problem existing in these algorithms is that they are easy to get trapped in local minima. In addition, they need manually specified initial curves close to the objects of interest. Region-based approaches try to classify an image into multiple consistent regions or classes. Thresholding is the simplest segmentation method but its performance is usually far from satisfactory. Watershed segmentation [10], [11] is one of the traditional region-based approaches. The watershed transform is often used to segment touching objects. It finds intensity valleys in an image if the image is viewed as a surface with mountains (high intensity regions) and valleys (low intensity regions). Morphological operations are always used to handle the over-segmented

problem in the output obtained by the watershed transform. Usually, watershed is used for the segmentation of foreground and background (two class) of an image. For a general color image with many different regions, it often gives a bad result. It is also sensitive to the morphological structuring element.

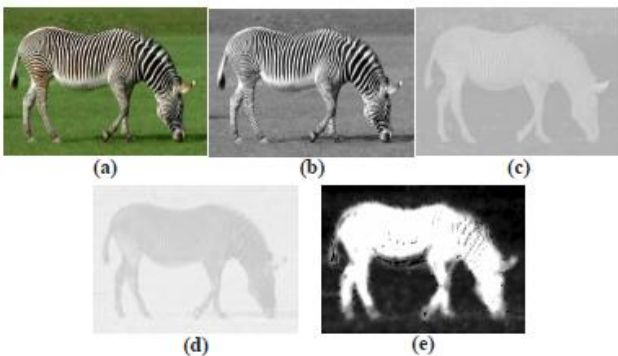
This paper proposes a new image segmentation algorithm based on a probability maximization model. An iterative optimization scheme alternately making the MAP and the maximum likelihood (ML) estimations is the key to the segmentation. We model the MAP estimation with MRFs and solve the MAP-MRF estimation problem using graph cuts. The result of the ML estimation depends on what statistical model we use. Under the Gaussian model, it is obtained by finding the means of the region features. It is shown that other statistical models can also fit in our framework. The main contributions of this work include: 1) a novel probabilistic model and an iterative optimization scheme for image segmentation, and 2) using graph cuts to solve the multiple region segmentation problem with the number of regions automatically adjusted according to the properties of the regions. Our algorithm can cluster relevant regions in an image well, with the segmentation boundaries matching the region edges. Extensive experiments show that our algorithm can obtain results highly consistent with human perception. The qualitative and quantitative comparisons demonstrate that our algorithm outperforms six other state-of-the-art image segmentation algorithms.

II. A NEW PROBABILISTIC MODEL

In this section, we first introduce the features used to describe the properties of each pixel, and then present the new probabilistic model. For a given image P, the features of every pixel p are expressed by a four-dimensional vector

$$\mathbf{I}(p) = (I_L(p), I_a(p), I_b(p), I_t(p))^T, \quad (1)$$

where $I_L(p)$, $I_a(p)$ and $I_b(p)$ are the components of p in the $L \times a \times b$ color space, and $I_t(p)$ denotes the texture feature of p. Several classical texture descriptors have been developed. In this paper, the texture contrast defined in [13] (scaled from [0; 1] to [0; 255]) is chosen as the texture descriptor. Fig. 1 shows an example of the features. The task of image segmentation is to group the pixels of an image into relevant regions. If we formulate it as a labeling problem, the objective is then to find a label configuration



$f = f_p$ where f_p is the label of pixel p denoting which region this pixel is grouped into. Generally speaking, a “good” segmentation means that the pixels within a region i

should share homogeneous features represented by a vector $\Phi(i)$ that does not change rapidly except on the region boundaries. The introduction of $\Phi(i)$ allows the description of a region, with which high level knowledge or learned information can be incorporated into the segmentation. Suppose that we have k possible region labels.[2]

$$\phi(i) = (\bar{I}_L(i), \bar{I}_a(i), \bar{I}_b(i), \bar{I}_t(i))^T \quad (2)$$

A four-dimensional vector is used to describe the properties of label (region) i, where the four components of $\Phi(i)$ have the similar meanings to those of the corresponding four components of $\mathbf{I}(p)$ and will be derived in Section II-B. let $\Phi = \{ \Phi(i) \}_g$ be the union of the region features. If P and $\Phi(i)$ are known, the segmentation is to find an optimal label configuration b f, which maximizes the posterior possibility of the label configuration[3]-[5].

$$\hat{f} = \arg \max_f \Pr(f|\Phi, P), \quad (3)$$

where Φ can be obtained by either a learning process or an initialized estimation. However, due to the existence of noise and diverse objects in different images, it is difficult to obtain Φ that is precise enough. Our strategy here is to refine Φ according to the current label configuration found by (3). Thus, we propose to use an iterative method to solve the segmentation problem. Suppose that Φ^n and f^n are the estimation results in the nth iteration. Then the iterative formulas for optimization are defined as

$$f^{n+1} = \arg \max_f \Pr(f|\Phi^n, P), \quad (4)$$

$$\Phi^{n+1} = \arg \max_{\Phi} \Pr(f^{n+1}|\Phi, P). \quad (5)$$

This iterative optimization is preferred because (4) can be solved by the MAP estimation, and (5) by the ML estimation. Based on this framework, next we will explain how the MAP and ML estimations are implemented.

A. MAP Estimation of f from Φ :

Given an image P and the potential region features Φ , we infer f by the Bayesian law, i.e., $\Pr(f|\Phi, P)$ can be obtained by

$$\Pr(f|\Phi, P) = \frac{\Pr(\Phi, P|f)\Pr(f)}{\Pr(\Phi, P)} \propto \Pr(\Phi, P|f)\Pr(f), \quad (6)$$

which is a MAP estimation problem and can be modeled using MRFs. Assuming that the observation of the image follows an independent identical distribution (i.i.d.), we define $\Pr(\Phi, P|f)$ as

$$\Pr(\Phi, P|f) \propto \prod_{p \in P} \exp(-D(p, f_p, \Phi)), \quad (7)$$

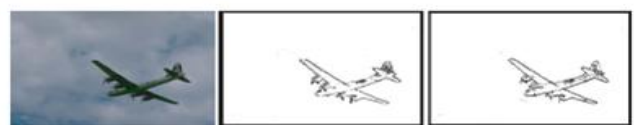


Figure 2: An example of the brightness contrast. (a) The original image. (b) The brightness contrast in the horizontal direction. (c) The brightness contrast in the vertical direction

where $D(p, f_p, \Phi)$ is the data penalty function which imposes the penalty of a pixel p with a label f_p for given Φ . The data penalty function is defined as

$$D(p, f_p, \Phi) = \|\mathbf{I}(p) - \phi(f_p)\|^2 \\ = (I_L(p) - \bar{I}_L(f_p))^2 + (I_\alpha(p) - \bar{I}_\alpha(f_p))^2 + \\ (I_b(p) - \bar{I}_b(f_p))^2 + (I_t(p) - \bar{I}_t(f_p))^2. \quad (8)$$

We restrict our attention to MRFs whose clique potentials involve pairs of neighboring pixels. Thus

$$\Pr(f) \propto \exp\left(-\sum_{p \in P} \sum_{q \in \mathcal{N}(p)} V_{p,q}(f_p, f_q)\right), \quad (9)$$

where $\mathcal{N}(p)$ is the neighborhood of pixel p , $V_{p,q}(f_p, f_q)$ called the smoothness penalty function, is a clique potential function, which describes the prior probability of a particular label configuration with the elements of the clique (p, q) . We define the smoothness penalty function as follows using a generalized Potts model[6]-[8].

$$V_{p,q}(f_p, f_q) = c \cdot \exp\left(\frac{-\Delta(p,q)}{\sigma}\right) \cdot T(f_p \neq f_q) \\ = c \cdot \exp\left(\frac{-|I_L(p) - I_L(q)|}{\sigma}\right) \cdot T(f_p \neq f_q), \quad (10)$$

where $\Delta(p,q) = I_L(p) - I_L(q)$ called brightness contrast, denotes how different the brightness of p and q are, $c > 0$ is a smoothness factor, $\sigma > 0$ is used to control the contribution of $\Delta(p,q)$ to the penalty, and $T(\cdot)$ is 1 if its argument is true and 0 otherwise. From our experiments, we found that $\sigma = 2(\Delta(p,q))$ is a good choice, where $\langle \cdot \rangle$ denotes the expectation of all the pairs of neighbors in an image. $V_{p,q}(f_p, f_q)$ depicts two kinds of constraints[11]. The first enforces the spatial smoothness; if two neighboring pixels are labeled differently, a penalty is imposed. The second considers a possible edge between p and q ; if two neighboring pixels cause a larger Δ , then they have greater likelihood to be partitioned into two regions. Figure. 2 is an example of the brightness contrast. In our algorithm, the boundaries of the segmentation result are pulled to match the darker pixels in Figure. 2(b) and (c), which are more likely to be edge pixels. From (6), (7), and (9), we have

$$\Pr(f|\Phi, P) \propto \left(\prod_{p \in P} \exp(-D(p, f_p, \Phi))\right) \cdot \\ \exp\left(-\sum_{p \in P} \sum_{q \in \mathcal{N}(p)} V_{p,q}(f_p, f_q)\right). \quad (11)$$

Taking the logarithm of (11), we have the following energy function[13].

$$E(f, \Phi) = \sum_{p \in P} D(p, f_p, \Phi) + \sum_{p \in P} \sum_{q \in \mathcal{N}(p)} V_{p,q}(f_p, f_q), \quad (12)$$

It includes two parts: the data term

$$E_{data} = \sum_{p \in P} D(p, f_p, \Phi) \quad (13)$$

and the smoothness term

$$E_{smooth} = \sum_{p \in P} \sum_{q \in \mathcal{N}(p)} V_{p,q}(f_p, f_q). \quad (14)$$

From (12), we see that maximizing $\Pr(f|\Phi, P)$ is equivalent to minimizing the Markov energy $E(f, \Phi)$ for a given Φ . [14]. In this paper, we use a graph cut algorithm to solve this minimization problem, which is described in Section III.

B. ML Estimation of Φ from f :

If the label configuration f is given, the optimal Φ should maximize $\Pr(f|\Phi, P)$, or minimize $E(f, \Phi)$ equivalently. Thus we have

$$\nabla_{\Phi} \log \Pr(f|\Phi, P) = \mathbf{0}, \quad (15)$$

Or

$$\nabla_{\Phi} E(f, \Phi) = \mathbf{0}, \quad (16)$$

Where ∇_{Φ} denotes the gradient operator. Since $V_{p,q}(f_p, f_q)$ is independent of Φ , we obtain

$$\nabla_{\Phi} \sum_{p \in P} D(p, f_p, \Phi) = \mathbf{0}, \quad (17)$$

where different formulations of $D(p, f_p, \Phi)$ lead to different estimations of Φ . For our formulation in (8), it follows that

$$\sum_{p \in P} D(p, f_p, \Phi) = \sum_i \sum_{f_p=i} \|\mathbf{I}(p) - \phi(i)\|^2. \quad (18)$$

Therefore, (17) can be written as

$$\frac{\partial}{\partial \phi(i)} \sum_{f_p=i} \|\mathbf{I}(p) - \phi(i)\|^2 = \mathbf{0}, \quad (19)$$

From (19), we obtain the ML estimation $\Phi = \Phi(i)$, where

$$\phi(i) = \frac{1}{num_i} \sum_{f_p=i} \mathbf{I}(p), \quad (20)$$

Note that when the label configuration $f = \{f_p/p\}$ is unknown, finding the solution of (17) is carried out by clustering the pixels into groups. In this case, the ML estimation is achieved by the K-means algorithm [12], which serves as the initialization in our algorithm described in Section III.

C. Non-Gaussian Modeling:

The definition of $D(p, f_p, \Phi)$ in (8) uses the Gaussian model to describe a uniform region. Some other distributions in the modeling of natural images, such as the exponential family distributions [17], [18], can also be used in our framework. Let us take another popular model, the Laplace model [19], as an example. To replace the Gaussian model with the Laplace model, we modify (7) as

$$\Pr(\Phi, P|f) \propto \prod_{p \in P} \exp(-D'(p, f_p, \Phi)), \quad (21)$$

where the data penalty is defined as

$$D'(p, f_p, \Phi) = |\mathbf{I}(p) - \phi(f_p)|. \quad (22)$$

With this data penalty, the MAP estimation is the same as when the Gaussian model is used. However, the ML estimation result is different from (20) and becomes

$$\phi(i) = \text{Median}\{\mathbf{I}(p)|f_p = i\}, \quad (23)$$

where Median { . } denotes the median of the elements in a set [15]. In addition to the above parametric models, we can also use non-parametric distributions to describe the region features. Similar to the parametric models, the data penalty functions are defined as the negative logarithm of different likelihood functions in different non-parametric models (e.g., a histogram clustering model is used. In summary, different statistical models lead to different definitions of the data penalty. Given different data penalties, the MAP estimations are the same, but the ML estimation results depend on the used models. In the rest of this paper, we only consider the Gaussian model[16]-[19].

III. THE PROPOSED ALGORITHM

We first give the description of the algorithm for image segmentation, and then prove its convergence.

A. Algorithm Description:

With $E(f; \Phi)$ defined in (12), the estimations of b and Φ in (4) and (5) are now transformed to

$$f^{n+1} = \arg \min_f E(f, \Phi^n) \quad (24)$$

$$\Phi^{n+1} = \arg \min_{\Phi} E(f^{n+1}, \Phi) \quad (25)$$

The two equations correspond to the MAP estimation and the ML estimation, respectively. The algorithm to obtain b and $\hat{\Phi}$ is described as follows.

Algorithm: Image segmentation:

Input: an RGB color image.

Step 1: Convert the image into $L^*a^*b^*$ space and calculate the texture contrast.

Step 2: Use the K -means algorithm to initialize Φ .

Step 3: Iterative optimization.

3.1: MAP estimation — Estimate the label configuration f based on current Φ using the graph cut algorithm [36].

3.2: Relabeling — Set a unique label to each connecting region to form a new cluster, obtaining a new f .

3.3: ML estimation — Refine Φ based on current f with (20).

Step 4: If Φ and f do not change between two successive iterations or the maximum number of iterations is reached, go to the output step; otherwise, go to step 3.

Output: Multiple segmented regions of the image.

We explain step 3.2 in more details here. After step 3.1, it is possible that two non-adjacent regions are given the same label. For example, the upper-left and the lower-right regions are both labeled by 1. After step 3.2, each of the

connected regions has a unique label. The MAP estimation is an NP-hard problem proposed to obtain an approximate solution via finding the minimum cuts in a graph model. Minimum cuts can be obtained by computing the maximum flow between the terminals of the graph. In [16], an efficient max-flow algorithm is given for solving the binary labeling problem. In addition, an algorithm, called α expansion with the max-flow algorithm embedded, is presented to carry out multiple labeling iteratively. In our algorithm, the α expansion algorithm is used to perform step 3.1. Besides the graph cuts, other techniques such as belief propagation can also be used to solve the MAP-MRF problem. One remarkable property of our algorithm is the ability to adjust the region number automatically during the iterative optimization with the relabeling step embedded into the MAP and ML estimations. Another property of our algorithm is that it is insensitive to the value of K in the initialization step with the K -means algorithm.

Now we analyze the computational complexity of the algorithm. In step 2, the K -means algorithm takes $O(NdKtk)$ time [12], where N is the number of pixels in an image, d is the number of features used to represent a pixel/region, K is the number of clusters, and tk is the number of iterations. In our application, $d = 4$, K is set to 10, and tk is set to 100. Both step 3.2 and step 3.3 take $O(N)$ time. In step 3, the main computational burden is the use of the graph cut algorithm (the α expansion) in step 3.1. The max-flow algorithm is linear in practice. The α expansion algorithm takes $O(NCnTan)$ time to carry out the MAP estimation during the n -th execution of step 3.1, where Cn is the number of label candidates and Tan is the number of iterations inside the α expansion. Let T be the number of executions of step 3.1. Then the computational complexity of our algorithm is $O(NdKtk) + O(NPT \sum_{i=1}^T CnTan)$. In general, Cn ranges from 1 to 50, Tan is less than 5, and T is less than 10.[20]

B. Algorithm Convergence:

We prove that the proposed algorithm is convergent in this section. Suppose that after the n th iteration, the energy is E_n , the configuration is f_n , and the union of region features is Φ_n . The MAP estimation is to estimate the configuration f_{n+1} by minimizing the energy. Therefore, after the MAP estimation step of the $(n+1)$ th iteration, the energy E_{MAP}^{n+1} decreases or keeps unchanged, i.e.,

$$E_{MAP}^{n+1} \leq E^n \quad (26)$$

Suppose that the configuration is $f_{relabeling}^{n+1}$ after the relabeling step. This step only changes the labels of some regions but not their features, i.e., for each pixel p ,

$$\phi(f_p^{n+1}) = \phi(f_{prelabeling}^{n+1}) \quad (27)$$

Therefore, from (8) and (13), the relabeling step does not change the data term. On the other hand, after the relabeling, for two neighboring pixels p and q .

$$T(f_p^{n+1} \neq f_q^{n+1}) = T(f_{prelabeling}^{n+1} \neq f_{qrelabeling}^{n+1}) \quad (28)$$

which implies that the relabeling step does not change the

smoothness term either (see (10) and (14)). Thus, after the relabeling step, the energy keeps unchanged, i.e.,

$$E_{\text{relabeling}}^{n+1} = E_{\text{MAP}}^{n+1} \quad (29)$$

Furthermore, since the ML estimation does not change the smoothness term but may reduce the data term or keeps it unchanged, we have

$$E^{n+1} \leq E_{\text{relabeling}}^{n+1} \quad (30)$$

So the energy keeps monotonically non-increasing during the iterations, i.e.,

$$E^{n+1} \leq E^n, \quad (31)$$

which completes the proof of the convergence of our algorithm.

IV. MATLAB RESULTS

We test the proposed algorithm by using Matlab, We classify part of the image in the Matlab "a dog" and show the segmentation results obtained by the algorithm in Figure 3 All the boundaries of the small regions with the numbers of pixels less than 100 are removed. From these example, we have the following observations.

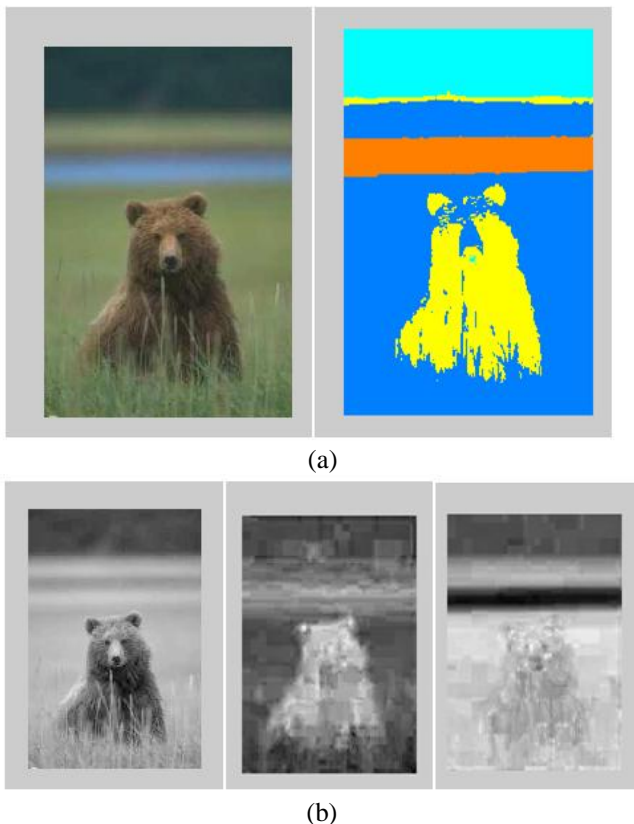


Figure 3 :a), (b) Segmentation results on the "dog" Quantitative comparisons are also important for objectively evaluating the performance of the algorithm. There have been several measures proposed for this purpose. Region differencing and boundary matching are two of them. Region differencing measures the extent to which one segmentation can be viewed as a refinement of the other. Boundary matching measures the average displacement error of boundary pixels between the results obtained by an algorithm and the results obtained from human subjects.

However, these two measures are not good enough for segmentation evaluation. For example, a segmentation result with each pixel being one region obtains the best score using these two measures. A strongly over-segmented result, which does not make sense to our visual perception, may be ranked good.

V. CONCLUSION

In this paper, we have developed a Extensive Technique for image segmentation algorithm. Our algorithm is formulated as a labeling problem using a probability maximization model. An iterative optimization technique combining the MAP and ML estimations is employed in our framework. Under the Gaussian model, the MAP estimation problem is solved using graph cuts and the ML estimation is obtained by finding the means of the region features. The qualitative and results demonstrate that our algorithm out performs than others. Our future work includes the extension of the proposed model to video segmentation with the combination of motion information technique , and the utilization of the model for specific object extraction by designing more complex features (such as shapes) to describe the objects.

References

- [1] Shifeng Chen, Liangliang Cao, Yueming Wang, Jianzhuang Liu, and Xiaou Tang "Image Segmentation by MAP-ML Estimations" IEEE Trans on Image processing Vol No 19, pp 2254-2264 Sept 201.
- [2] M. Kass, A. Witkin, and D. Terzopoulos, "Snakes: Active contour models," *Int'l J. Computer Vision*, vol. 1, no. 4, pp. 321–331, 1988.
- [3] L. Cohen *et al.*, "On active contour models and balloons," *CVGIP: Image Understanding*, vol. 53, no. 2, pp. 211–218, 1991.
- [4] C. Xu and J. Prince, "Snakes, shapes, and gradient vector flow," *IEEE Trans. Image Processing*, vol. 7, no. 3, pp. 359–369, 1998.
- [5] E. Mortensen and W. Barrett, "Interactive segmentation with intelligent scissors," *Graphical Models and Image Processing*, vol. 60, no. 5, pp. 349–384, 1998.
- [6] T. McInerney and D. Terzopoulos, "Deformable models in medical image analysis: A survey," *Medical Image Analysis*, vol. 1, no. 2, pp. 91–108, 1996.
- [7] D. Cremers, M. Rousson, and R. Deriche, "A review of statistical approaches to level set segmentation: Integrating color, texture, motion and shape," *International Journal of Computer Vision*, vol. 72, no. 2, pp. 195–215, 2007.
- [8] X. Fan, P. Bazin, and J. Prince, "A multi-compartment segmentation framework with

- homeomorphic level sets,” in *IEEE Proc. Computer Vision and Pattern Recognition*, 2008.
- [9] J. Olszewska, C. De Vleeschouwer, and B. Macq, “Speeded up gradient vector flow b-spline active contours for robust and real-time tracking,” in *IEEE Proc. Int’l Conf. Acoustics, Speech and Signal Processing*, 2007.
- [10] S. Beucher and F. Meyer, “The morphological approach to segmentation: The watershed transformation,” *Mathematical Morphology in Image Processing*, vol. 34, pp. 433–481, 1993.
- [11] L. Vincent and P. Soille, “Watersheds in digital spaces: An efficient algorithm based on immersion simulations,” *IEEE Trans. Pattern Analysis and Machine Intelligence*, vol. 13, no. 6, pp. 583–598, 1991.
- [12] R. Duda, P. Hart, and D. Stork, *Pattern Classification*, 2nd ed. Wiley- Interscience, 2001.
- [13] C. Carson, S. Belongie, H. Greenspan, and J. Malik, “Blobworld: Image segmentation using expectation-maximization and its application to image querying,” *IEEE Trans. Pattern Analysis and Machine Intelligence*, vol. 24, no. 8, pp. 1026–1038, 2002.
- [14] D. Comaniciu and P. Meer, “Mean shift analysis and applications,” in *IEEE Proc. Int’l Conf. Computer Vision*, vol. 2, 1999, pp. 1197–1203.
- [15] D. Comaniciu and P. Meer, “Mean shift: a robust approach toward feature space analysis,” *IEEE Trans. Pattern Analysis and Machine Intelligence*, vol. 24, no. 5, pp. 603–619, 2002.
- [16] A. Y. Yang, J. Wright, S. S. Sastry, and Y. Ma, “Unsupervised segmentation of natural images via lossy data compression,” EECS Department, University of California, Berkeley, Tech. Rep. UCB/EECS-2006-195, Dec 2006. [Online]. Available: <http://www.eecs.berkeley.edu/Pubs/TechRpts/2006/ECS-2006-195.html>
- [17] J. Shi and J. Malik, “Normalized cuts and image segmentation,” *IEEE Trans. Pattern Analysis and Machine Intelligence*, vol. 22, no. 8, pp. 888–905, 2000.
- [18] S. X. Yu and J. Shi, “Multiclass spectral clustering,” in *IEEE Proc. Int’l Conf. Computer Vision*, vol. 1, 2003, pp. 313–319.
- [19] Z. Wu and R. Leahy, “An optimal graph theoretic approach to data clustering: Theory and its application to image segmentation,” *IEEE Trans. Pattern Analysis and Machine Intelligence*, vol. 15, no. 11, pp. 1101–1113, 1993.
- [20] P. Felzenszwalb and D. Huttenlocher, “Efficient graph-based image segmentation,” *Int’l J. Computer Vision*, vol. 59, no. 2, pp. 167–181, 2004.
- [21] Z. Tu and S.-C. Zhu, “Image segmentation by data-driven Markov chain Monte Carlo,” *IEEE Trans. Pattern Analysis and Machine Intelligence*, vol. 24, no. 5, pp. 657–673, 2002.

Analaysis and Implementation of UWB Receiver in Multi-Band OFDM Systems

P. Srilakshmi

M.Tech Student Scholar, DECS,
Dept of Electronics and Communication Engineering,
Nalanda Institute of Engineering and technology,
Sattenapalli (M); Guntur (Dt); A.P, India

N. Gopi Chand

M.Tech, Asst Professor
Dept of Electronics and Communication Engineering,
Nalanda Institute of Engineering and technology,
Sattenapalli (M); Guntur (Dt); A.P, India.

Abstract: Orthogonal Frequency Division Multiplexing (OFDM) is a digital multi carrier modulation scheme, which uses a large number of closely spaced orthogonal sub-carriers. In frequency and time must be extremely good. An OFDM system offers inherent robustness to multi-path dispersion with a low-complexity receiver. In OFDM systems Cyclic Prefix uses to maintain orthogonality of transmission. Now days For transmission purpose Ultra-Wideband (UWB) systems use Multi-Band OFDM Techniques. In these the application like Wireless Personal Area Network (WPAN). It is Power limited by the regulation of FCC. CP forces the linear convolution with the channel impulse response to resemble a circular convolution in transmitted data sequence and introduces the ripples in Power spectral Density, So due to this Transmission reduces. The zero-pad suffix (ZPS) will have a flat PSD and hence does not suffer from the range degradation problem. In the UWB receiver, ZP removal requires use of a technique called as overlap and add (OLA) in order to capture the multipath energy of the channel and maintain the orthogonality in the received data. In this paper, we propose a method which adapts the length of Overlap-and-Add depending on the reception of current band. The Existing method shows high delay Spread channel like CM4. For this technique achieves the gain at 10-2 of BER.

Keywords: UWB Receiver, Multi Band OFDM System, Adaptive Over lap technique.

I. INTRODUCTION

Over the last year and half, ultra-wideband (UWB) communication systems have received significant attention from industry, media and academia. The reason for all this excitement is that this technology promises to deliver data rates that can scale from 110 Mbit/s at a distance of 10 meters up to 480 Mbit/s at a distance of two meters in realistic multi-path environments all while consuming very little power and silicon area. It is expected that UWB devices will provide low cost solutions that can satisfy the consumer's insatiable appetite for data rates as well as enable new consumer market segments. But for UWB systems to move from the lab environment to real-life system designs, engineers must battle traditional design issues such as complexity, power consumption, cost, and flexibility. Fortunately, an answer to these problems has arrived. By turning to a multiband OFDM approach, designers can overcome many of these barriers.

Even though the FCC has allocated the entire spectrum from 3.1 GHz and 10.6 GHz for UWB, it has been shown that using an upper frequency beyond 4.8 GHz leads to an improvement in the overall link margin of only 1 dB with current RF CMOS technology. This comes at the expense of higher complexity, and higher power consumption.

The minimal gains in the link budget and the increase in complexity and power consumption lead one to conclude that the bandwidth between 3.1 and 4.8 GHz will provide the most effective bandwidth for initial deployments of UWB devices. Indeed, limiting the upper frequency to 4.8 GHz also has several decided advantages, including shortening time to market, simplifying the design of the RF and analog front-end circuits (low noise amplifiers and mixers), making it more amenable to CMOS technology, and avoiding interference from the U-NII band, where IEEE 802.11a signals reside. Of course, limiting the bandwidth of UWB, at least initially, still leaves the possibility that the entire bandwidth will eventually be utilized. As RF technology improves, it will become more efficient to use the upper frequencies in the UWB range. If defined with forethought and proper planning, the UWB systems can accommodate an effective migration path to the upper end of the spectrum when market conditions dictate such a move.

The main advantage of building UWB communication systems based on spread-spectrum techniques are that these techniques are well understood and have been proven in other commercial technologies (ex. wideband CDMA). However, building RF and analog circuits as well as high speed analog-to-digital converters (ADCs) to process this extremely wideband signal is a challenging problem. In addition, the digital complexity needs to be quite large (at least 16 RAKE fingers) in order to capture sufficient multi-path energy to meet the range requirements of 10 meters for a 110 Mb/s system.

In addition to allocating spectrum, the FCC also specified that a UWB signal must occupy a minimum 10-dB bandwidth of 500 MHz. In many ways, this portion of the ruling has revolutionized the design of UWB communication systems. Instead of having to use the entire band to transmit information, the spectrum can now be divided into several sub-bands, whose bandwidth is approximately 500 MHz. By interleaving the symbols across sub-bands, UWB systems can still maintain the same transmit power as if they were using the entire bandwidth.

The advantage is that the information can now be processed over a much smaller bandwidth, thereby reducing the complexity of the design, reducing the power consumption, lowering the cost, and improving spectral flexibility and worldwide compliance. Other advantages of this approach include using lower-rate ADCs and simplifying the digital complexity. Systems built using this type of approach are often referred to as multiband systems. Now that we've taken a brief look at the different multi-band approaches available to designers, let's examine the OFDM-based multiband approach further.

Given the frequency band from 3.1 GHz to 4.8 GHz and the FCC requirement that UWB signals have to be at least 500 MHz, only three sub-bands can be used in the initial deployment of multi-band OFDM systems. Figure 1 illustrates one way to allocate the three sub-bands with the given frequency allocation.

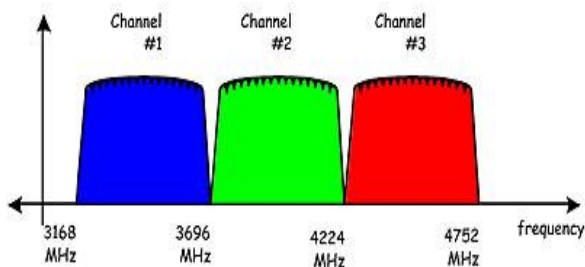


Figure 1: Frequency allocation of sub-bands for a multi-band OFDM system.

The frequency planning shown in Figure 1 was chosen for two reasons. First it allows sufficient guard band on the lower side of channel number 1 and the upper side of channel number 3 to simplify the pre-select filter's design. Second it ensures that both the transmitter and receive can switch to the next center frequency within a few nanoseconds. Figure 2 provides an example of how the OFDM symbols are transmitted in a multi-band OFDM system. This figure shows that the first OFDM symbol is transmitted on channel number 1, the second OFDM symbol is transmitted on channel number 3, the third OFDM symbol is transmitted on channel number 2, the fourth OFDM symbol is transmitted on channel number 1, and so on.

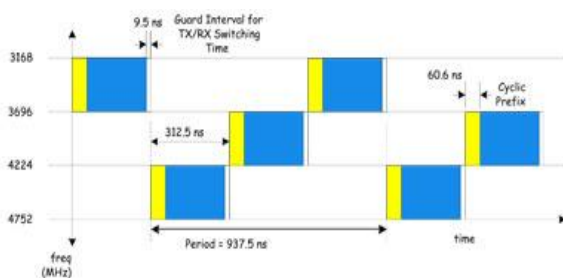


Figure 2: An example of time-frequency interleaving for the multi-band OFDM system

In Figure 2, it is assumed that time-frequency interleaving (TFI) is performed across just three OFDM symbols. In

practice, the TFI period can be much longer. The exact length and pattern of the TFI may differ from super frame to super frame and piconet to piconet.

From Figure 2, it is also apparent that a cyclic prefix (CP) is inserted at the beginning of each OFDM symbol and a guard interval (9.5 ns) is appended to each OFDM symbol. The guard interval has been inserted to ensure that only a single RF transmit and RF receiver chain are needed for all channel environments and all data rates and that there is sufficient time for the transmitter and receiver to switch to the next channel. A circular convolution in the time domain is equivalent to a multiplication operation in the discrete Fourier transform (DFT) domain. Hence, a one-tap frequency domain equalizer is sufficient to undo the effect of the multi-path channel.

The length of the CP determines the amount of captured multi-path energy. Any multi-path energy outside the CP window would result in inter-carrier-interference (ICI). The CP length should be chosen to minimize the performance degradation due to the loss in collected multi-path energy and the resulting ICI, while still keeping the CP overhead small. This paper proposes an adaptive reception technique for ZP based systems in an attempt to minimize ISI incursions from subsequent OFDM symbols. In section II, we review the impact of CP and ZP in OFDM systems in general, and outline one of the key motivation factors for this paper. In section III, we relook the ZP removal process in view of multi-band UWB system. In section IV, we discuss our proposed adaptive overlap-add technique. Section V discusses our simulation results and finally we conclude our paper in section VI

II. CP VS ZP IN OFDM BASED SYSTEM

In traditional OFDM systems, a cyclic prefix is used before the OFDM symbol in order to maintain the orthogonality in the received signal after passing through the multipath channel. However as CP introduces a structure in the symbols transmitted, the system suffers from the ripple in the power spectral density (PSD) necessitating power back-off in the transmitter which can be as large as 1.5 dB for MB-OFDM based system [9]. In an alternative, it was pointed out in [7], that we can use zero-padding instead of cyclic-prefix in the transmitted OFDM symbols. The transmission using ZP does not suffer from the ripple in PSD and hence can transmit at maximum power and hence to a longer distance. However to retain the circular convolution property, which essentially provides robustness against multipath channel for OFDM system and facilitates the use of a single-tap frequency domain equalizer in receiver, we require to do a slight modification in signal processing in OFDM receiver. CP based system, can simply discard the CP portion of the received symbol, however for ZP based system we need to do overlap-add (OLA) operation in the receiver shown in Figure 3.

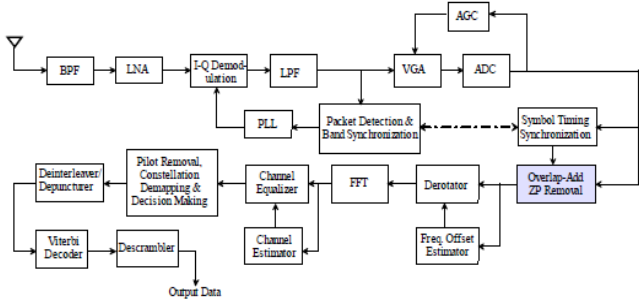


Figure 3: A typical MB-OFDM based receiver architecture

In general, the ZP length should be greater than the delay spread of the channel. As per ECMA-368, this length is 32 samples. Due to multipath propagation, the received OFDM symbol gets smeared at the most by 32 samples, as per assumption that channel length is not greater than 32 samples duration. To mimic what would have happened if there were CP in the transmitted symbol, we need to do overlap-add operation in the receiver. This is illustrated in Figure 4. First we should estimate the start point of true FFT window. As the FFT length in ECMA-368 is 128 samples, from that we should count and pick up 32 consecutive received samples starting from 129th sample onwards. Then we should do a sample-by-sample addition as following. If $r(n)$ is the received samples and $n \geq 0$ corresponds to the true FFT window start point, then overlap-add process modifies $r(n)$ as per eqn. (2).

$$r'(n) = r(n) + r(n+128) \text{ for } n = 0 \text{ to } 31, \\ = r(n), \text{ otherwise.} \quad (2)$$

Note that, CP based system is not very sensitive to symbol timing synchronization error. As long as we estimate the start of the FFT window in the portion of CP, the equalizer can correct the phase offset incurred due to the estimation error. However a ZP based system requires more accurate estimation of the start of FFT window. This is because in CP based system the circular convolution is an effect of natural phenomenon. The physical propagation of the OFDM signal through multipath channel causes linear convolution, which appears to be a circular convolution due to the cyclic property artificially maintained due to CP addition. However linear convolution does not appear naturally as circular convolution for ZP based system. Overlap-add operation makes sure this artificial circular convolution appearance, which depends on the true start point of the FFT window. Hence ZP based system is quite sensitive to the timing synchronization estimation error compared to CP based system. This is one of the key motivation factors of this paper.

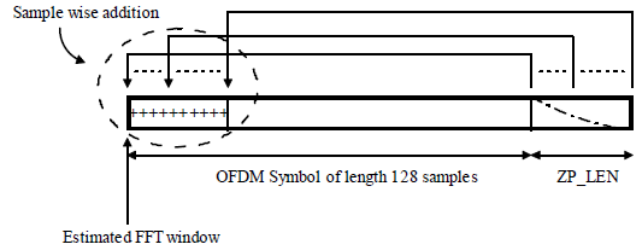


Figure 4: ZP removal by overlap-add operation using ZP length equal to 'ZP_LEN'. Note that, 'ZP_LEN' can be fixed (32 samples), as in traditional system, or could be variable depending on some parameter, as proposed in this paper

III. AN FOR ZP REMOVAL IN VIEW OF MULTI BAND TIMING SYNCHRONIZATION (MBTS)

In UWB, we see four type of channel models proposed for research and developmental work, they are CM1, CM2, CM3 and CM4. Without going into details of them, it should be highlighted that CM1 corresponds to small delay spread channel, whereas delay spread increases as we go towards CM4 [11 and references therein]. In [9] and [10], it is pointed out that there exists an overlap-add length ('ZP_LEN' in Fig. 4) for which the receiver performs optimally. This is because for small delay spread channel (say CM1 with a delay spread of 4 samples as one realization), if we use ZP_LEN = 32 samples, then we are essentially picking up some (28 in this example) pure noise samples during overlap-add process, which affects BER adversely. This essentially means we should estimate the channel delay spread and use a variable 'ZP_LEN' during overlap-add procedure, as outlined in [9-10]. The estimation of channel delay spread can be done in a few ways mainly from the cross-correlation characteristics in time domain in timing synchronizer block and one of the methods has been proposed in [9].

This type of adaptive overlap-add method based on estimation of channel delay spread is more beneficiary for small delay spread channel and hardly benefits anything for large enough delay spread channel. It also should be pointed out that the above method demands a very small estimation error in locating the FFT window, which is quite difficult to achieve in UWB system. On the other hand, in [11], it was pointed out that the mean delay of the UWB channel differs significantly depending on the band of transmission. Accordingly they have proposed a timing synchronization algorithm, which they called as multi band timing synchronization (MBTS) algorithm, which essentially proposes to estimate the true start point of FFT window depending on the band of transmission. Note that, this variance of mean delay is due to the manifestation of the multipath channel in multi-band scenario while the channel length remains same.

Hence it may happen for a band, the FFT start point might get estimated say at the sample number 16, rather than 0 or closed to 0. In that case if we use a fixed 'ZP_LEN' of 32 samples for overlap-add operation, then we are essentially picking up samples from the next OFDM symbol which leads

to ISI. Figure 5 shows the offset sensitivity of BER performance of MB-OFDM system. Here offset = 0 implies the true start point of FFT window if there is no noise and there exists a non-zero multipath component at the first sample location. Note that, even if there is no non-zero multipath component at 0th location, still a start point of FFT window at that location will always perform optimally in no noise condition, because equalizer can take care as no multipath component to equalizer will appear as non-causal component. Note that, the curves show that MB-OFDM system is quite sensitive to the ISI incursions from the next OFDM symbol.

IV. A PROPOSED ADAPTIVE OVERLAP-ADD TECHNIQUE

In this section we propose a technique to reduce the ISI incursions from the subsequent OFDM symbol due to the use of fixed 'ZP_LEN' during overlap-add process. At the same time we try to make the method robust with respect to the estimation error of the true start point of the FFT window in the smeared received signal. In general the timing synchronizer block provides the estimated offsets over different bands as signed numbers because the estimation point can shift in left as well as right depending on the situation. If any of the estimated offsets becomes negative, we first make all of them positive using the following algorithm (Alg#1) and provide necessary delay in data path in order to make the receiver a causal system.

Alg#1:

Say, OB_i denotes the signed offset of band i , where $i \in 1, 2, \text{ or } 3$. Let UOB_i denotes the unsigned offset of band i after making the system causal.

If ($OB_1 < 0$ or $OB_2 < 0$ or $OB_3 < 0$) Then

{
For $i = 1$ to 3, % 'i' is the band number

$$UOB_i = OB_i + \max(\text{abs}(\text{all negative } OB_j));$$

Where $j \in 1, 2, 3$.

}

Else,

$$UOB_i = OB_i;$$

We notice that it is expected that $(OB_i \sim OB_j) \leq 32$, i, j belonging to band number, as the channel length is 32 samples. This also guarantees that the range of UOB_i is 0 to 32.

The variation in i UOB is solely due to channel manifestation and the channel length remains same as 32 samples. So to avoid ISI incursion from the next OFDM

symbol we use band-dependent variable ZP length ('ZP_LEN_Bi') during overlap-add operation over multiple bands as per the following algorithm (Alg#2).

Alg#2:

For $i = 1$ to 3, % band number

$$ZP_LEN_B_i = 32 - \{UOB_i - \text{Min}(UOB_1, UOB_2, UOB_3)\};$$

End for loop;

Note that in Alg#2, apart from making the scheme robust to the estimation error of the true start point of the FFT window, we have also made sure that the chances of the equalizer of seeing non-causal multipath components minimal.

The above algorithm (Alg#2) is valid for single band or dual band transmission as well. For single band transmission, the process ceased to be band dependent adaptive and becomes fixed 'ZP_LEN' as 32 samples. So, as per Alg#2, a band-dependent 'ZP_LEN' number of samples after the FFT window is picket up and added to the front portion as shown in Figure 4

V. SIMULATION RESULTS

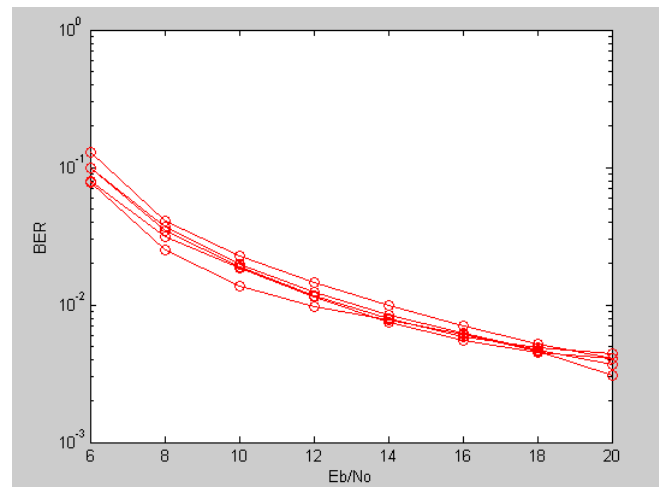


Figure. 5. Offset sensitivity of BER for all channel models at 10 dB Eb/N0 with fixed (32 samples) 'ZP_LEN'

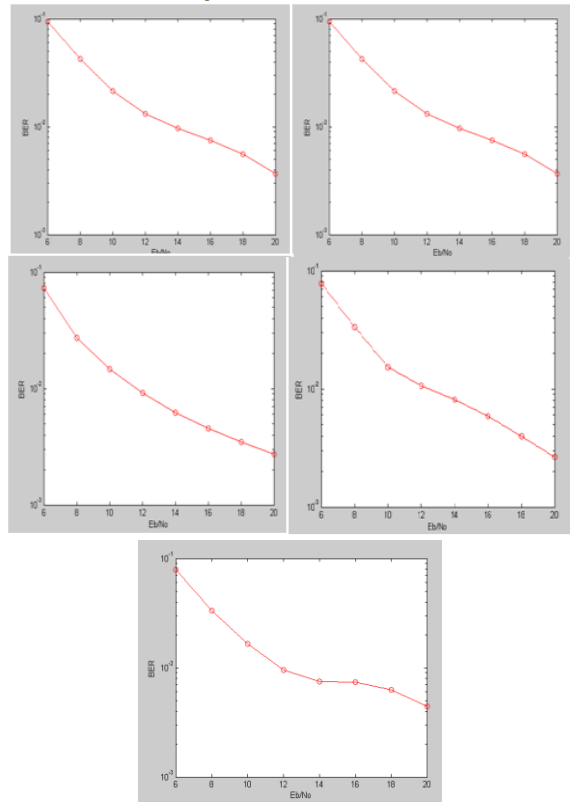


Fig. 6. BER vs Eb/No (in dB) simulation for all channel models in uncoded MB-OFDM system. Data1: using variable ZP length. Data2: Using fixed ZP length of 32.

Figure 6 shows the BER curves for un coded MB-OFDM based UWB system with and without band wise variable ZP length for overlap and add operation. For large delay-spread channels in UWB systems the mean excess delay is more compared to small delay-spread channels. This implies for large delay spread channel, the estimation of FFT window will be more away from the true FFT window resulting in more ISI incursions from next OFDM symbol. Hence the proposed technique is more promising for large delay-spread channels. The curves show a significant amount of performance improvement (for CM4 around 1 dB of Eb/No savings at 10⁻² BER for un coded system) is achieved for large delay-spread channels.

VI. CONCLUSION

In this paper as well as in some prior arts that adaptive overlap-add technique is beneficiary for OFDM based receivers in terms of BER performance. In some related literature [9], it had been proposed to adapt 'ZP_LEN' for overlap-add operation depending on the true channel length in order to avoid picking up pure noise samples during the OLA process. This method is more fruitful to channels having small delay-spread (e.g. CM1) and hence a small estimation error in FFT window will eventually reduce the benefit significantly. Moreover in [9], two independent process runs. One is estimation of the channel delay spread and the other is estimation of FFT window. Both of them are used in adaptive OLA process and hence may make things worse instead of improving if they are not aligned properly.

In an alternative, in this paper, we have proposed a band dependent adaptive OLA technique which tries to minimize ISI incursion from subsequent OFDM symbols. This method is not so sensitive on the estimation of true start point of FFT window, in a sense that a small estimation error will not be able to take away the benefits of the technique. Moreover in this method all the signal processing is dependent on one independent process i.e. estimation of the FFT window and hence the question of dependency of two independent process does not arise at all. The method is more promising for large delay spread channels and provides a significant Eb/No improvement in the detection process. A natural choice of future work would be to mix the above two independent ideas (i.e. one in [9], and the one proposed in this paper) and study its impact on overall system performance.

References

- [1] Robert Aiello and Anuj Batra, "Ultra Wideband Systems – Technologies and Applications," Elsevier, Newnes, 2006.
- [2] "First report and order, revision of part 15 of the commission's rules regarding ultra-wideband transmission systems," FCC, ET Docket 98- 153, Feb. 14, 2002.
- [3] Anuj Batra, J. Balakrishnan, G. R. Aiello, J. R. Foester, A. Dabak, "Design of Multi-band system for realistic UWB channel environment," IEEE Trans. on Microwave and Techniques, vol. 52, no. 9, pp. 2123-2138, Sept. 2004.
- [4] R. van Nee and R. Prasad, OFDM for Wireless Multimedia Communications. Artech House, 2000.
- [5] Shinsuke Hara, Ramjee Prasad, "Multicarrier Techniques for 4G Mobile Communications," Artech House, 2003.
- [6] Standard ECMA-368, "High Rate Ultra Wideband PHY and MAC Standard," 1st Edition - Dec. 2005, www.ecma-international.org.
- [7] B. Muquet, Z. Wang, G. B. Giannakis, M. de Courville, and P. Duhamel, "Cyclic prefixing or zero padding for wireless multicarrier transmissions?" IEEE Trans. Commun., vol. 50, no. 12, pp. 2136- 2148, Dec.2002.
- [8] A. Batra, et. al, "Multi-band OFDM physical layer proposal," IEEE P802.15-03/268r0-TG3a, July 2003.
- [9] June Chul Ron, Batra. A, and Waters. D, "Adaptive overlap-and-add techniques for MB-OFDM systems," IEEE Asilomar Conference on Signals, Systems and Computers (ACSSC), Nov. 2007.
- [10] Lowe, D & Huang, X, "Adaptive Overlap-Add Equalization for MBOFDM Ultra-Wideband", International Symposium on Communications and Information Technologies (ISCIT), Bangkok, Thailand, 18-20 October 2006.
- [11] Debarati Sen, Saswat Chakrabarti, R. V. Raja Kumar, "An Energy Based Symbol Timing Synchronization Scheme for MB-OFDM Based Ultra-Wideband Communication," IEEE ISSSTA-2008, Bologna, Italy, Aug. 25-28, 2008.

Solution of Non-Convex Economic Load Dispatch Problem with Valve Point Loading Effects Using PSO

* G. Sreenivasan, ** Dr. C. H. Saibabu, *** Dr. S. Sivanagaraju.

*Research scholar, JNTU University Kakinada, Kakinada

** Professor & Director (Admissions), JNTU Kakinada, Kakinada, AP, INDIA.

*** Associate Professor, Dept. of Electrical Engineering, JNTU Kakinada, Kakinada, AP, INDIA.

ABSTRACT: Economic Load Dispatch (ELD) is an important optimization task in power system operation for allocating generation among the committed units such that the constraints imposed are satisfied and the operating cost is minimized. This paper presents an application of Particle swarm optimization (PSO) technique to solve non-linear, non-convex ELD problem for the determination of the global or near global optimum dispatch solution. To illustrate the effectiveness of the proposed approach, a test system consisting of 40-thermal generating units, with incorporation of load balance constraints, operating limits, valve point loadings, is considered and tested. The comparison of numerical results demonstrate the performance and applicability of the proposed method.

Keywords: Economic Load Dispatch(ELD), non-convex problem, valve point loading effect, particle swarm optimization

I. INTRODUCTION

In the traditional ELD problem, the cost function for each generator has been approximately represented by a single quadratic function and is solved using mathematical programming based on the optimization techniques such as lambda-iteration method, gradient-based method, etc. Most of power system optimization problems including economic load dispatch (ELD) have complex and nonlinear characteristics with heavy equality and inequality constraints. The fuel cost functions of generating units can be modeled in a more practical fashion by including the valve-point effects. Thus, the practical ELD problem is represented as a non-smooth optimization problem with equality and inequality constraints, which cannot be solved by the traditional mathematical methods. Many recent works have been around Artificial Intelligence (AI) methods, on par with the development of AI optimization theories, such as Artificial Neural Networks (ANN), Simulated Annealing (SA), Genetic Algorithms (GA), Differential Evolution (DE), Evolutionary Programming (EP), and hybrid methods [3-5]. ELD algorithms for thermal unit system involving combined cycle units presented in [6]. Online solving of economic dispatch problem using neural network approach and comparing it with classical methods were presented in [7]. The evolutionary Algorithms (EAs) are different from the conventional optimization methods, and they do not need to differentiate cost function and constraints. Theoretically, like SA, EAs converge to the global optimum solution. EAs, including Evolutionary Programming (EP), Evolutionary Strategy (ES), and GA are AI methods of optimization based on the mechanics of natural selection, such as mutation, recombination, reproduction, crossover, selection, etc [8]. Many researchers exerted lot of work to improve many optimization and intelligent techniques to solve ELD problems such as GA [11], Hopfield solution [19] and SA [10,22]. N Amjadi, H Nasiri-rad [21] presented a more realistic model for the ED problem considering more practical constraints and non-linear characteristics than previous works in the area. K P Wong, Y W Wong [22] developed and presented the implementation of basic and incremental GA algorithms for determination of the global or near global optimum solution for the economic dispatch problem. A Y saber et al [23] proposed higher order cost function for (a) better curve fitting of running cost (b) less approximation (c) more practical results. There constraint management is incorporated and extra concentration is needed for the higher order cost function of single or multiple fuel units. S Y Lim et al [24] proposed a novel approach to solve the non-smooth ELD Problem with valve point effect by introducing constriction factor concept in the algorithm.

In this paper, an algorithm based on Particle Swarm Optimization technique is proposed as methodology for solving convex and non-convex Economical Load Dispatch problem. In this proposed approach the ELD problem is solved by considering the smooth and non-smooth cost co-efficients, representing the effects of valve point loading, and unit constraints. The results obtained through the approach are analyzed and compared with those existed methods represented in literature.

The proposed algorithm has been implemented in MATLAB 7.0 version on Pentium IV, 2.4 GHZ Personnel Computer with 1 GB RAM.

II. PROBLEM FORMULATION

The Primary concern of an ELD problem is the minimization of its objective function. The total cost generated that meets the demand and satisfies all other constraints associated is selected as the objective function. In general, the ELD problem can be formulated mathematically as a constrained optimization problem with an objective function of the form

$$\text{Minimize } C = \sum_{i=1}^n C_i(P_{Gi}) \quad \dots(1)$$

Where

$C_i (P_{Gi})$ is the fuel cost function of the i^{th} unit,
 P_{Gi} is the power generated by the i^{th} unit,
 n is the total number of generating units,
 C is the total generation cost subject to power balance constraints.

This objective function is modeled in two ways as i) Classical Smooth Fuel Cost Function and ii) Non- Smooth Fuel Cost Function.

2.1 Classical Smooth Fuel Cost Functions

Generally, the fuel cost of a thermal generation unit is considered as a second order polynomial function (neglecting valve-point effects) and this is called classical and smooth fuel cost function. It is represented as

$$C_i (P_{Gi}) = a_i + b_i P_{Gi} + c_i P_{Gi}^2 \quad \dots(2)$$

Where a_i , b_i , and c_i are the fuel-cost coefficients of the i^{th} unit.

2.2 Non – Smooth Fuel Cost Functions

In present scenario, the input-output characteristics of modern generating units are inherently highly non-linear due to valve point loadings, ramp rate limits etc., further they may have multiple local minimum points in the cost functions. For such combinatorial optimization problems, the conventional methods are failing to obtain the global optimal solutions while considering non-Linear characteristics of the units for the solution techniques as they have no restrictions on the shape of the fuel cost curves.

The generating units with multi-valve steam turbines exhibit a greater variation in the fuel cost functions. Since the valve point results in the ripples, a cost function contains higher order nonlinearity. Therefore the cost function should be modified to consider the valve point effects. This valve point effect leads to non-smooth, non-convex input-output characteristics as shown in fig.1

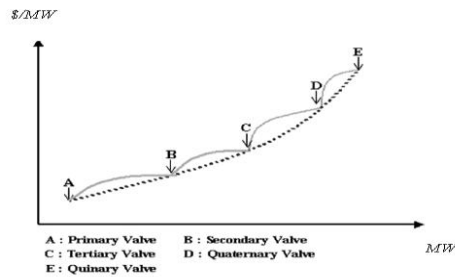


Fig. 1 Input-output characteristics of steam turbine generators with Valve- Point Effects

Typically, the valve point results in, as each steam valve starts to open, the ripples like in to take account for the valve – point effects, sinusoidal functions are added to the quadratic cost functions as:

$$C_i (P_{Gi}) = a_i + b_i P_{Gi} + c_i P_{Gi}^2 + \left| e_i \times \sin \left(f_i \times \left(P_{Gi_{min}} - P_{Gi} \right) \right) \right| \quad \dots(3)$$

Where e_i and f_i are the fuel cost-coefficients of the i^{th} unit reflecting valve-point loading effects.

These classical and non-classical models either with smooth or non smoothed fuel cost functions are subjected to the following equality and inequality constraints.

2.3 Equality Constraints

These constraints are also known as power balance constraints. The total power generated must supply the total load demand and the transmission losses, and expressed as

$$\sum_{i=1}^n P_{Gi} = P_D + P_{TL} \quad \dots (4)$$

Where P_D is the total system load demand and

P_{TL} is the total transmission line losses.

According to Kron’s formula, the total transmission line losses can be calculated by the following expression

$$P_{TL} = \sum_{i=1}^n \sum_{j=1}^n P_{Gi}^T B_{ij} P_{Gj} + \sum_{i=1}^n P_{Gi} B_{oi} + B_{oo} \quad \dots(5)$$

Where B_{ij} , B_{oi} and B_{oo} are the transmission line loss coefficients

P_{Gi}^T is the vector transpose of all generating plants net MW.

B_{ij} is the square matrix of same dimension as P_{Gi}

B_{oi} is a vector of same length as P_{Gi} and

B_{oo} is a constant

2.4 Inequality Constraint

Each generator is constrained between its minimum and maximum generation limits, and represented as inequality constraints as.

$$P_{Gi, min} \leq P_{Gi} \leq P_{Gi, max} \quad \text{for } i = 1, 2, \dots, n \quad \dots(6)$$

Where $P_{Gi, min}$ and $P_{Gi, max}$ are the minimum and maximum power outputs of the i^{th} generating unit.

III. PARTICLE SWARM OPTIMIZATION

Particle swarm optimization is one of the most recent developments in the category of combinatorial metaheuristic optimizations. This method has been developed under the scope of artificial life where PSO is inspired by the natural phenomenon of fish schooling or bird flocking. PSO is basically based on the fact that in quest of reaching the optimum solution in a multi-dimensional space, a population of particles is created whose present coordinate determines the cost function to be minimized. After each iteration the new velocity and hence the new position of each particle is updated on the basis of a summated influence of each particle's present velocity, distance of the particle from its own best performance, achieve so far during the search process and the distance of the particle from the leading particle, i.e. the particle which at present is globally the best particle producing till now the best performance i.e. minimum of the cost function achieved so far. Let x and v denote a particle position and its corresponding velocity in a search space, respectively. Therefore, the i^{th} particle is represented as $x_i = (x_{i1}, x_{i2}, \dots, x_{id})$ in the 'd' dimensional space. The best previous positions of the i^{th} particles recorded and represented as $pbest_i = (pbest_{i1}, pbest_{i2}, \dots, pbest_{id})$. The index of the best particle among all the particles in the group is represented by the $gbest_d$. The rate of the velocity for i^{th} particle is represented as $v_i = (v_{i1}, v_{i2}, \dots, v_{id})$. The modified velocity and position of each particle can be calculated using the current velocity and the distance from $pbest_{id}$ to $gbest_d$ as shown in the following formulae:

$$v_{id}^{k+1} = w v_{id}^k + c_1 \text{rand}() (pbest_{id} - x_{id}^k) + c_2 \text{rand}() (gbest_d - x_{id}^k) \quad \dots (7)$$

$$x_{id}^{k+1} = x_{id}^k + v_{id}^{k+1} \quad \text{for } i=1, 2, \dots, N_p, d=1, 2, \dots, N_g \quad \dots(8)$$

where, N_p is the number of particles in a group, N_g the number of members in a particle, k the pointer of iterations, w the inertia weight factor, c_1, c_2 the acceleration constants, $\text{rand}()$ the uniform random value in the range $[0,1]$, v_i^k the velocity of a particle 'i' at iteration k , $v_d^{\min} \leq v_{id}^k \leq v_d^{\max}$ and x_i^k is the current position of a particle 'i' at iteration k . In the above procedures, the parameter v^{\max} determined the resolution, with which regions are to be searched between the present position and the target position. If v^{\max} is too high, articles might fly past good solutions. If v^{\max} is too small, particles may not explore sufficiently beyond local solutions. The constants c_1 and c_2 represent the weighting of the stochastic acceleration terms that pull each particle toward the $pbest$ and $gbest$ positions. Low values allow particle to roam far from the target regions before being tugged back. On the other hand, high values result in abrupt movement toward or past, target regions. Hence, the acceleration constants c_1 and c_2 were often set to be 2.0 according to past experiences. Suitable selection of inertia weight 'w' provides a balance between global and local explorations, thus requiring less iteration on average to find a sufficiently optimal solution. As originally developed, 'w' often decreases linearly from about 0.3 to 0.2 during a run. In general, the inertia weight w is set according to the following equation:

$$w = w_{\max} - \frac{w_{\max} - w_{\min}}{\text{iter}_{\max}} \times \text{iter} \quad \dots(9)$$

Where,

w_{\max} : Initial value of inertia weight,

w_{\min} : Final value of inertia weight,

Iter_{\max} : Maximum iteration number,

Iter : Current iteration number.

IV. PROPOSED PSO FOR ELD PROBLEMS

In this section, a new approach is designed to implement the PSO algorithm in solving the ELD problems. Especially, it is suggested how to deal with the equality and inequality constraints of the ELD problems in the process of modifying each individual's search point in the PSO algorithm. The dynamic process of the PSO algorithm can be summarized as follows:

Step i : Initialization of a group at random

Step ii : Velocity and position update

Step iii : Update of $Pbest$ and $Gbest$

Step iv : Go to step ii until satisfying stopping criteria.

In the subsequent sections, the detailed implementation strategies of the proposed PSO are described.

i) Initialization: In the initialization process, a set of individuals is created at random. The structure of an individual for ELD problem is composed of a set of elements (i.e., generation outputs). Therefore, individual i 's position at iteration 0 can be represented as the vector $X_i^0 = (P_{i1}, \dots, P_{in})$ where n is the number of generators in the ELD problem. The velocity of individual i (i.e., $V_i^0 = (V_{i1}, \dots, V_{in})$) corresponds to the generation update quantity covering all generators. The elements of position and velocity have the same dimension, i.e., MW in this case. Note that it is very important to create a group of individuals satisfying the equality constraint eqn.(4) and inequality constraint eqn.(6). That is, summation of all elements of

individual 'i' (i.e., $\sum_{j=1}^n P_{ij}$) should be equal to the total system demand P_D and the created element j of individual 'i' at random (i.e., P_{ij}) should be located within its boundary. Although the element j of individual 'i', created at random satisfying the inequality constraint by mapping $[0,1]$ into $[P_{min}, P_{max}]$, it is necessary to develop a new strategy to handle the equality constraint. To do this, the following procedure is suggested for any individual in a group:

Step 1: Set $j = 1$.

Step 2: Select an element (i.e., generator) of an individual at random.

Step 3: Create the value of the element (i.e., generation output) at random satisfying its inequality constraint.

Step 4: If $j = n-1$ then go to Step 5; otherwise $j = j+1$ and go to Step 2.

Step 5: The value of the last element of an individual is determined by subtracting $\sum_{j=1}^{n-1} P_{ij}$ from the total system demand P_D . If the value is in the range of its operating region then go to Step 6; otherwise go to Step 1.

Step 6: Stop the initialization process.

After creating the initial position of each individual, the velocity of each individual is also created at random. The following strategy is used in creating the initial velocity:

$$(P_{ij,min} - \varepsilon) - P_{ij}^0 \leq v_{ij} \leq (P_{ij,max} + \varepsilon) - P_{ij}^0 \quad \dots (10)$$

Where ε is a small positive real number. The velocity element j of individual 'i' is generated at random within the boundary. The developed initialization scheme always guarantees to produce individuals satisfying the constraints as well as not to deviate from the concept of the PSO algorithm. The initial P_{best_i} of individual 'i' is set as the initial position of individual 'i' and the initial G_{best} is determined as the position of an individual with minimum pay off of eqn (1).

ii) Velocity Update: To modify the position of each individual, it is necessary to calculate the velocity of each individual in the next stage, which is obtained from eqn(2). In this velocity updating process, the values of parameters such as ω , c_1 , and c_2 should be determined in advance. The weighting function is defined as eqn (9).

iii) Position Modification Considering Constraints: The position of each individual is modified by eqn(3) based on its updated velocity. The resulting position of an individual is not always guaranteed to satisfy the inequality constraints due to over/under velocity. If any element of an individual violates its inequality constraint due to over/under speed then the position of the individual is fixed to its maximum/minimum operating point. Fig.2 illustrates how the position of element j of individual 'i' is adjusted to its maximum when over-velocity situation occurs. The similar strategy is used for individual's position adjustment to its minimum point.

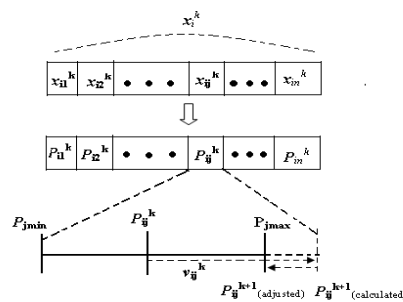


Fig. 2 Adjustment strategy for an individual's position within boundary.

Although the aforementioned method always produces the position of each individual satisfying the inequality constraints given in eqn (6), the problem of equality constraint still remains to be resolved. Therefore, it is necessary to

develop a new strategy such that the summation of all elements in an Individual (i.e., $\sum_{j=1}^n P_{ij}$) is equal to the total system

demand. To resolve the equality constraint problem without intervening the dynamic process inherent in the PSO algorithm, the following heuristic procedures are proposed:

Step 1: Set $j = 1$. Let present iteration be k .

Step 2: Select an element (i.e., generator) of individual i at random and store in an index array $A(n)$.

Step 3: Modify the value of element j (i.e., output of generator j) using eqns.(2) and (3), and the position adjustment strategy to satisfy its inequality constraint as follows:

$$\begin{aligned} P_{ij}^{k+1} &= P_{ij}^k + v_{ij}^{k+1} && \text{if } P_{ij,min} \leq P_{ij}^k + v_{ij}^{k+1} \leq P_{ij,max} \\ &= P_{ij,min} && \text{if } P_{ij}^k + v_{ij}^{k+1} < P_{ij,min} \\ &= P_{ij,max} && \text{if } P_{ij}^k + v_{ij}^{k+1} > P_{ij,max} \end{aligned} \quad \dots (12)$$

Step 4: If $j = n-1$ then go to Step 5, otherwise $j = j+1$ and go to Step 2.

Step 5: The value of the last element of individual i is determined by subtracting $\sum_{j=1}^{n-1} P_{Gij}$ from P_D . If the value is not within its boundary then adjust the value using eqn.(12) and go to *Step 6*, otherwise go to *Step 8*.

Step 6: Set $l = 1$

Step 7: Readjust the value of element l in the index array $A(n)$ to the value satisfying equality condition i.e., $P_D - \sum_{\substack{J=1 \\ J \neq l}}^n P_{ij}$. If the value is within its boundary then go to *Step 8*; otherwise, change the value of element- l using eqn(12). Set $l = l+1$, and go to *Step 7*. If $l = n+1$, go to *Step 6*.

Step 8: Stop the modification procedure

iv) Update of P_{best} and G_{best} : The P_{best} of each individual at iteration $k+1$ is updated as follows:

$$\begin{aligned} P_{best_i}^{k+1} &= X_i^{k+1} && \text{if } TC_i^{k+1} < TC_i^k \\ P_{best_i}^{k+1} &= P_{best_i}^k && \text{if } TC_i^{k+1} > TC_i^k \end{aligned} \quad \dots(9)$$

Where, TC_i is the objective function evaluated at the position of individual ' i '. Also, G_{best} at iteration $k+1$ is set as the best evaluated position among $P_{best_i}^{k+1}$.

v) Stopping criteria: The proposed method is terminated if the iteration approaches to the predefined maximum iteration.

IV. RESULTS AND ANALYSIS

The performance of the proposed PSO algorithm is verified on a test system consisting of 40-units which has been adopted from [15] with modifications to incorporate the effects of valve point loadings. The proposed method is illustrated with two following cases:

- Case -1: Without Valve point effects and
- Case -2: With Valve point effects

At each test system, 50 trials were performed using the proposed method to observe the solution quality, convergence characteristic, and execution time. The PSO parameters used in solving the problem are given in Table-1.

Table 1. PSO parameters and their setting values

PSO Parameters	Setting values
Population size	20
Number of generations	200
Initial weight function, w_{max}	0.9
Final weight function, w_{min}	0.4
Limit of change in velocity of each number in an individual, V_{pd}^{max}	$0.5 P_d^{max}$
Limit of change in velocity of each number in an individual, V_{pd}^{min}	$-0.5 P_d^{min}$
Acceleration constants c_1 and c_2	2

The optimal scheduling and fuel cost comparisons for case-1 & case-2 are given in Table 2. The minimum fuel cost obtained by proposed PSO method for case-1 is 119364.55 \$/hr and by GA is 119683.12 \$/hr. The minimum fuel cost obtained by proposed PSO method for case-2 is 119558.61\$/hr. For case-2, The cost obtained by GA and EP are 119732.25 \$/hr and 123488.29 \$/hr respectively. The convergence characteristics of proposed technique for case-1 and case-2 are shown in fig.3. The results obtained by proposed technique are compared with existing methods and found satisfactorily in terms of execution time and net saving. For case-1, the execution time for proposed PSO technique is 0.98 sec and for existing GA method is 12.52 sec. The net saving in cost by the proposed technique is 318.57 \$/hr when compared to GA. For case-2, the execution time for proposed technique is 1.03 sec and for existing EP method the execution time is 1955.20 sec. The net saving in cost by the proposed technique is 173.64 \$/hr when compared to GA and 3929.68 \$/hr when compared to EP. It is also observed that, the PSO is a very robust and efficient algorithm in terms of control parameters such as the number of particles in a group and condition of initial group generated at random. Although the required number of iterations reacting the global solution is different when the number of particles or the random initial group is changed, the PSO guarantees the convergence to the global solution for the examples taken. It is also observed that the solutions provided by the proposed PSO always satisfy the equality and inequality constraints for all the cases.

Table 2 Optimal scheduling and fuel cost comparisons of 40 – unit system

Generation of units (MW)	Case-1		Case-2		
	GA method	Proposed method	Existing GA [26]	Existing EP[15]	Proposed method
PG ₁	114	114	108.76409	--	114.00
PG ₂	114	114	114.0000	--	114.00
PG ₃	120	120	117.63920	--	120.00
PG ₄	190	190	190.0000	--	190.00
PG ₅	97	97	97.0000	--	97.00
PG ₆	140	140	140.0000	--	140.00
PG ₇	300	300	300.0000	--	300.00
PG ₈	300	300	300.0000	--	300.00
PG ₉	300	300	300.0000	--	300.00
PG ₁₀	188.73	300.00	136.5658	--	300.00
PG ₁₁	126.69	375.00	94.7871	--	375.00
PG ₁₂	98.94	267.46	94.3880	--	375.00
PG ₁₃	260.63	500.00	127.9169	--	216.62
PG ₁₄	322.95	241.81	311.1454	--	304.55
PG ₁₅	161.66	421.01	282.7689	--	496.07
PG ₁₆	319.28	500.00	203.2046	--	363.25
PG ₁₇	482.21	500.00	500.0000	--	391.70
PG ₁₈	455.66	340.48	500.0000	--	477.43
PG ₁₉	515.08	242.00	550.0000	--	345.43
PG ₂₀	547.89	408.28	550.0000	--	512.06
PG ₂₁	538.14	547.80	550.0000	--	439.88
PG ₂₂	550.00	550.00	550.0000	--	526.37
PG ₂₃	539.58	520.60	550.0000	--	524.65
PG ₂₄	549.42	550.00	550.0000	--	269.04
PG ₂₅	513.83	378.55	550.0000	--	523.29
PG ₂₆	541.32	527.77	550.0000	--	534.34
PG ₂₇	10.82	18.70	14.03671	--	11.31
PG ₂₈	17.80	12.42	11.9778	--	13.56
PG ₂₉	17.80	10.00	11.3036	--	10.00
PG ₃₀	76.81	62.67	97.0000	--	72.67
PG ₃₁	188.73	60.00	190.0000	--	133.60
PG ₃₂	180.09	190.00	190.0000	--	189.86
PG ₃₃	183.90	125.92	190.0000	--	155.49

PG ₃₄		191.18	186.19	200.0000	--	200.00
PG ₃₅		199.68	158.81	200.0000	--	199.99
PG ₃₆		190.86	180.54	200.0000	--	132.85
PG ₃₇		97.70	55.95	107.5014	--	35.86
PG ₃₈		101.77	49.91	110.0000	--	93.92
PG ₃₉		105.85	25.00	110.0000	--	51.20
PG ₄₀		550.00	518.14	550.0000	--	550.00
Demand (MW)		10500.00	10500.00	10500.00	10500.00	10500.00
Fuel Cost (\$/hr)	Best	119683.12	119364.55	119732.25	123488.29	119558.61
	Average	121330.20	119558.61	--	124793.48	121308.69
	Worst	133352.26	123793.77	--	126902.89	126270.07
Execution Time (Sec)		12.52	0.98	--	1955.20	1.03
Net Saving (\$/hr)		-	318.57	--		173.64

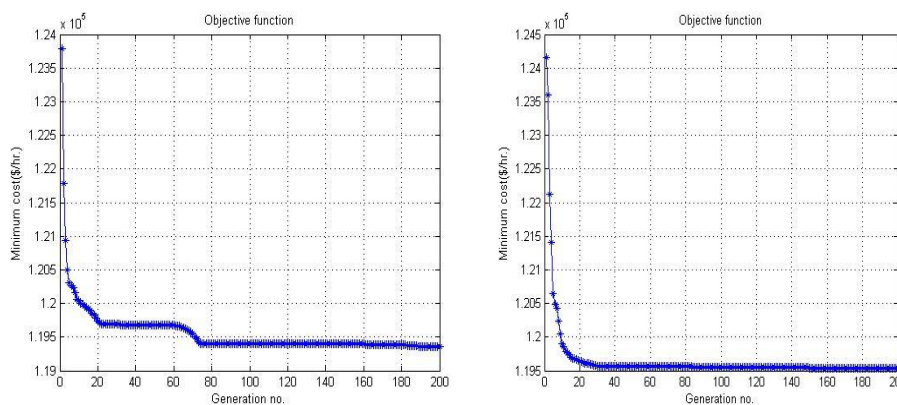


Fig 3 Convergence Characteristics of PSO Algorithm for Case-1 and Case-2 of 40-unit system

V. CONCLUSIONS

In this paper the PSO method is successfully employed to solve the Economic Load Dispatch (ELD) problem with generator constraints and valve point loading effects. The PSO Algorithm has been demonstrated to have superior features, including high quality solutions, stable convergence characteristics and good computation efficiency. The non-linear characteristics of the generator such as valve point loading effects and non-smooth cost functions are considered for practical generator operations in the proposed method. The results show that the proposed method was indeed capable of obtaining higher quality solution efficiently in non-linear, non-convex ELD Problems within a reasonable computation time and iteration numbers when compared to the existing methods given in literature.

REFERENCES

- [1]. Wood,A.J .,and Wollenberg,B.F.: “Power Generation, Operation And Control” (Wiley, New York,1984)
- [2]. Irving,M.R., and Sterling.M.J.H. “Economic Dispatch Of Active Power With Constraint Relaxation”, IEE Proc.C.1983, 130,(4), Pp.172-177.
- [3]. Nanda,J., Kothari,D.P., And Srivastava,S.C.: “New Optimum Power-Dispatch Algorithm Using Fletcher’s Quadratic Programming Method”, Iee Proc.C.1989,136,(3),Pp.153-161.
- [4]. Berry.P.E., and Dunnett,R.M., “Contingency Constrained Economic Dispatch Algorithm For Transmission Planning’, IEE Proc.C, 1989,136,(4),Pp.238-244.
- [5]. Lee,K.Y.,Park,Y.M., and Ortis,M.S.: “Fuel-Cost Minimization For Both Real And Reactive-Power Dispatches”, IEEE Proc. C , 1984,131.
- [6]. Lin,C.E., and Viviani,G.L.: “Hierarchical Economic Dispatch For Piecewise Quadratic Cost Functions”, IEEE Trans.,1984.Pas-103,(6),Pp.1170-1175.

- [7]. Wong,K.P., And Doan,K. "A Recursive Economic Dispatch Algorithm For Assessing The Cost Of Thermal Generator Schedules", IEEE Trans.,1992,Pwrs-7,(2),Pp.577-583.
- [8]. IEEE Committee Report: "Practices In The Economic Operation Of Power Systems", IEEE Trans.,1971,Pas-90,Pp.1768-1775.
- [9]. Liang,Z.X., And Glover , J.D. "A Zoom Feature For A Dynamic Programming Solution To Economic Dispatch Including Transmission Losses", IEEE Trans.,1992,Pwrs-7,(2),Pp.544-550.
- [10]. Wong,K.P., And Fung,C.C, "Simulated-Annealing Based Economic Dispatch Algorithm," IEEE Proc.C, 1993,140,(6),Pp.509-515.
- [11]. Walters,D.C., And Sheble,G.B. "Genetic Algorithm Solution Of Economic Dispatch With Valve Point Loading", IEEE Trans. On Power Systems, Vol. PWRS-8,No,3,Aug 1993, Pp. 1325-1332.
- [12]. Hong-Tzer Yang,Pai-Chuan Yang ,Ching-Lien Huang, "Evolutionary Programming Based Economic Dispatch For Units With Non-Smooth Fuel Cost Functions". IEEE Transaction On Power Systems, Vol.11, No.1, February 1996
- [13]. L.L.Lai, "Evolutionary Programming For Economic Load Dispatch Of Units With Non Smooth Input-Output Characteristic Function", Intelligent System Applications in Power Engineering –Evolutionary Programming and Neutral Networks. Chichester, U.K.:Wiley ,1998 , Ch.8.
- [14]. H.T.Yang ,P.C.Yang, and C.L.Huang, "Evolutionary Programming Based Economic Dispatch For Units With Non Smooth Fuel Cost Functions," IEEE Trans. Power Syst.,Vol.11,Pp.112-118,Feb.1996.
- [15]. Nidul Sinha, R.Chakrabarti, and P.K.Chattopadhyay, "Evolutionary Programming Techniques For Economic Load Dispatch", IEEE Transactions on Evolutionary Computation, Vol.7,No.1,February 2003.
- [16]. J.B.Park,K.S.Lee,J.R.Shin and K.Y.Lee, "A Particle Swarm Optimization for Economic Dispatch with Non-Smooth Cost Function", IEEE Trans.Power Syst.,Vol.20,No.1,Pp.34-42,Feb.2005.
- [17]. C.E.Lin And G.L.Viviani, "Hierarchical Economic Dispatch For Piece-Wise Quadratic Cost Functions," IEEE Trans. Power App.Syst.,Vol.Pas-103,No.6,Pp.1170-1175,June 1984.
- [18]. C.L.Chen And C.L.Wang, "Branch-And –Bound Scheduling For Thermal Generating Units," IEEE Trans. Energy Convers., Vol.8,No.2,Pp.184-189, June.1993.
- [19]. Leandro Dos Santos Coelho And Viviana Cocco Mariani , "Combining Of Chaotic Differential Evolution And Quadratic Programming For Economic Dispatch Optimization With Valve-Point Effect," IEEE Transactions On Power Systems,Vol.21,No.2,May 2006.
- [20]. T.A.A.Victoire And A.E.Jeyakumar, "Hybrid PSO-SQP For Economic Dispatch With Valve –Point Effect," Elect.Power Syst.Res.,Vol.71,No.1,Pp.51-59,Sep.2004.
- [21]. N.Amjady, H.Nasiri-Rad , "Economic Dispatch Using An Efficient Real-Coded Genetic Algorithm",IET Gener.Transm. Distrib., 2009, Vol.3, Issue 3,Pp 266-278.
- [22]. K.P.Wong, Y.W.Wong, "Genetic And Genetic/Simulated-Annealing Approaches To Economic Dispatch" IEEE Proc. -Gener. Transn .Distrib., Vol.141,No.5,September 1994.
- [23]. Ahmed Yousuf Saber, Atsushi Yona, And Masatake Higashi, "Economic Load Dispatch Of Higher Order Cost Polynomials Using Modified Particle Swarm Optimization",2007 IEEE,Pp.1203-1208.
- [24]. Shi Yao Lim, Mohammad Montakhab, And Hassan Nouri, "Economic Dispatch of Power System Using Particle Swarm Optimization With ConstrictionFactor",International Journal of Innovations in Energy Systems and Power;Vol.4,No.2,October 2009.
- [25]. S.Muthu Vijaya Pandian,K.Thanushkodi, "An Evolutionary Programming Based Efficient Particle Swarm Optimization For Economic Dispatch Problem With Valve-Point Loading", EuropeanJournal ofScientificResearch,Vol.52,No.3,2011,Pp.385-397.
- [26]. Attia A.El-Fargany, "Solution of Economic Load Dispatch problem with smooth and non-smooth fuel cost functions including line losses using Genetic Algorithm," International journal of Computer and Electrical Engineering,Vol.3,No.5,October 2011.

About The Authors



***G. Sreenivasan** received his graduation in 1996, Masters in 2001 from JNTUniversity college of Engineering, Anantapur and pursuing Ph.D at JNTUniversity, Kakinada. Presently he is working as Associate Professor in the department of Electrical and Electronics Engineering, Intell Engineering College, Anantapur since 2001. His area of interest is applications of GA and PSO to Power System Operation and Control. He has published research papers in 6 international and 3 national journals and has publications in national and international conferences. He has participated several workshops conducted by various engineering colleges at south India. He authored the text book, "Power System Operation and Control" under the publication of Pearson Education, New Delhi. He is the life member of ISTE and IE.



** **Dr. CH. SaiBabu** received his graduation from Andhra university, Masters from REC, Warangal and Ph.D from JNTU, Hyderabad. He is the Professor in the Department of Electrical and Electronics Engineering and Director of Admissions at JNT University, Kakinada. He has about 20 publications in international journals and 44 national and international conferences. He authored a text book, "Elements of Power Electronics" published by S.Chand and Co. He is the member of AICTE team and Member of governing council for various affiliated engineering colleges of JNTU, Kakinada.



*** **Dr. S. Sivanagaraju** received his graduation in 1998, Masters in 2000 from IIT, Kharagpur and his Ph.D from JNT University, Hyderabad in 2004. He is working as Associate Professor and Head of the Electrical and Electronics Engineering department, JNT University, Kakinada, Andhra Pradesh. He has received 2 National awards (Panditmadan Mohan malaviya Memorial prize award and Best paper prize award) from the Institute of Engineers (India) for the year 2003 – 2004. He is also a referee for the IEEE proceedings – generation, transmission and distribution and international journal of emerging electric power systems. He has about 50 publications in national and international journals and conferences to his credit. His areas of interest are in Distribution Automation, Genetic Algorithm Applications to Distribution Systems and Power Systems.

A Study of Net Section Failure between Two Equal Cracks in an Infinite Plate

Naveen Kumar H S¹, Prof. B S Suresh² and Girish K E³

*Dept. of Mechanical Engineering, R V College of Engineering, Bangalore, Karnataka-560059, India

**Dept. of Mechanical Engineering, R V College of Engineering, Bangalore, Karnataka-560059, India

***Bangalore Aircraft Industries (pvt) Ltd, Bangalore, Karnataka-560032, India

ABSTRACT: Multi site damage is one of the important aspects to be studied to ensure the safety of the aircraft structure. The rivet hole locations are one of the stress concentration regions. The current study includes a panel which represents the fuselage splice joint. The fuselage splice joint is a location where it experiences the uniform stress field at many rivet locations in a row. This study has relevance in the structural integrity evaluation of aging transport aircraft due to multisite damage. Fatigue cracks will emanate from the rivet holes simultaneously as they experience identical stresses due to internal pressure. In service, the cracks in the fuselage will grow due to internal pressurization load cycling. The objective is to investigate the first failure mechanism out of two competing mechanisms of failure; Failure due to fracture or Failure due to plastic collapse at the net section between two advancing crack tips.

Key words: Fuselage of an aircraft, Fatigue, Net section, Stress intensity factor, finite element analysis

I. INTRODUCTION

The primary objective of the aircraft structure is to carry the required flight loads with as little weight as possible. Today's airplanes use the most advanced lightweight materials and the most advanced structural design and analysis tools to produce the most efficient structures possible.

An ideal aircraft structure would be designed so that every part fails at exactly the same limit load and fatigues at exactly the same number of cycles and these failure conditions are selected, so that they just cannot happen under normal operating conditions. The ideal structure also would have no margin above these conditions because that just means extra weight.

The airframe consists of the fuselage, which is the main component of the airplane. The simultaneous presence of cracks in the same structural element is usually referred to as multi-site fatigue damage. Aging aircraft may develop multiple site fatigue damage that can reduce the structural integrity of fuselage structures.

The recent concept of damage tolerance supposes an aircraft structure to be redundant so that a catastrophic failure should not occur after fatigue failure of a structural element. As a consequence the concept also admits the existence of cracks in the aircraft structure. The probability of crack existence is particularly enhanced in ageing aircraft. In these structures multiple-site damage [1] [2] (MSD) is also more likely to occur. Some examples are frequently referenced, such as the Aloha accident of the Boeing 737, the C5A wing and JAL accident.

The MSD [3] [8] problem is generally associated with a large number of small neighboring cracks located in one line. As a more or less uniform stress field is required for MSD, the cracks mostly originate at the edges of several adjacent and collinear fastener holes in longitudinal skin splices [4] of a pressurized fuselage structure. They occur at the same time, grow and can suddenly coalesce to form a single critical crack, which can lead to a catastrophic failure of the structure. The critical size of the individual cracks can be relatively small, even less than the length easily detected during visual in-service inspections. With MSD the fatigue crack growth and fracture characteristics are significantly different from the characteristics of the isolated cracks. The fatigue lifetime becomes shorter than that of a single-site crack having the same length.

The existence of small cracks emanating from adjacent rivet holes in a fuselage [5] lap splice joint is of major concern. Small collinear cracks greatly reduce the residual strength of a panel with a lead crack.

Thus there is a need to conduct detailed fracture analysis of the crack link up phenomenon in butt-splice joints and Z-stiffener with rivet-loaded fasteners.

Multiple Site fatigue Damage (MSD) – as in the Aloha Airlines Boeing 737 – where fatigue cracks occur at many locations in the same structural element, such that fatigue cracks may coalesce to form one large crack. Failure of specimen [1] due to MSD is shown in the fig. 1

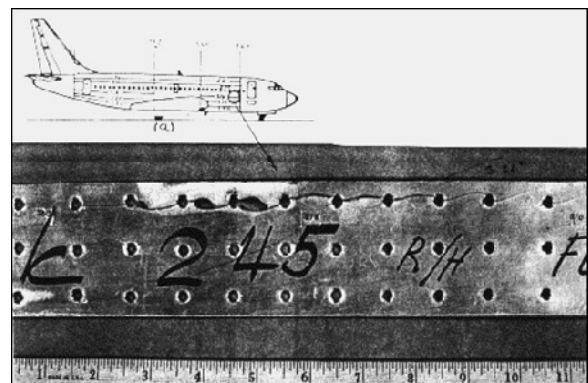


Figure 1: Multi-site damage (MSD) at a B-737 fuselage lap joint [1].

II. MATERIAL USED

Material used for the analysis of fuselage splice joint is Aluminum 2024 –T3 and its composition and properties are given in Table 1 and Table 2.

Table 1: Material compositions

COMPONENT	WEIGHT PERCENTAGE
Aluminum	90.7-94.7
Chromium	Max 0.1
Copper	3.8-4.9
Ferrous	Max 0.5
Magnesium	1.2-1.8
Manganese	0.3-0.9
Titanium	Max 0.15
Zinc	Max 0.25
Other, Total	Max 0.15

Table 2: Material Properties in Al 2024-T3

Properties	Material Aluminum 2024-T3
Density	27.27 N/mm ³
Ultimate Tensile Strength	483 N/mm ²
Tensile Yield Strength	362 N/mm ²
Modulus of Elasticity	72000 N/mm ²
Poisson's Ratio	0.33
Fracture Toughness	98.90 MPa√m

III. GEOMETRICAL CONFIGURATION

The first step is to understand the complex loading conditions in a fuselage structure. The pressurization of the fuselage causes the structure to expand outward like simple balloon. This expansion creates the hoop stress in the circumferential and an axial stress in the longitudinal direction. Due to this complexity in structure, loading conditions and test set-up simplification to simpler test specimen is required.

With full pressurization, the skin and underlying structure will move outward. It is not too difficult to see that a frame or stiffener will not move the same distance as the skin would due to higher local stiffness, thus creating differences in outward movements and higher hoop stresses in the skin between the frames.

Setting up a test as large as a full-scale aircraft structure requires an enormous amount of time and money. Reducing full scale-test to a more simple, easier to understand test specimen such as barrel or fuselage panel including stiffeners and frames reduces the size of the test. Elimination of the stiffeners, frames and curvature reduces the structure to flat sheet longitudinal splice and circumferential butt joints.

The global analysis of the structure is carried out to find the stress distribution. Riveted connection is the common feature in the built up airframe structure. The fatigue crack will initiate from the locations of the maximum tensile stress. The rivet hole locations are one of the stress concentration regions. Therefore rivet hole locations are the most probable location for the fatigue crack initiation.

The fuselage splice joint with Z-Stiffener is the location where it experiences the uniform stress field at many rivet locations in a row. Therefore fine meshing is done at the splice joint with Z-stiffener location to achieve the exactness of the stress and the riveting is being done by 1D element for global model of the fuselage.

Local panel is the sectional cut out of the fuselage to do stress analysis by validating local panel with hoop stress obtained from local panel is equal to the hoop stress obtained from the global model, so by this way we can reduce the time consumed for analysis without compromise on the result variation.

Local panel with rivet holes are next step after the local panel with 1D rivet element, for our problem rivet holes should be there for crack initiation and crack propagation. Here also the hoop stress is validated with global model by applying same uniformly distributed tension load for local panel with rivet holes. So at the rivet holes in the direction of load transfer, the multiple points of semicircle are constrained to transfer the load to obtain the uniform load distribution on the semicircle of the rivet holes in direction of load, which is obtained in practical rivets on the rivet holes. So, it confirms that except at rivet holes, the remaining part of the panel is having the same hoop stress as obtained for global model of the fuselage.

IV. STRESS ANALYSIS

The global analysis of the structure is carried out to find the stress distribution. The fatigue crack will initiate from the locations of the maximum tensile stress. The rivet hole locations are one of the stress concentration regions. Therefore rivet hole locations are the most probable location for the fatigue crack initiation.

4.1. LOAD CALCULATIONS AND GLOBAL MODEL DIMENSIONS FOR THE FUSELAGE

- Length of the fuselage(L) = 2500 mm
- Radius of the fuselage(R) = 1600 mm
- Width of the splice plate(b) = 70 mm
- Length of the splice plate(L) = 2500 mm
- Thickness of the fuselage skin(T) = 1.8 mm
- Thickness of the splice plate(t) = 2 mm
- Diameter of the Rivet Hole(d) = 4.8 mm
- Internal pressurization(P_r) = 0.06695 N/mm²

Both the ends of fuselage are constrained for rotation and translation and internal pressurization is applied.

Hoop stress = (P_r × D) / (2 × T) ----- (1)

Hoop stress (σ_h) = (0.06695 × 3200) / (2 × 1.8)

Hoop stress (σ_h) = 59.51 N/mm²

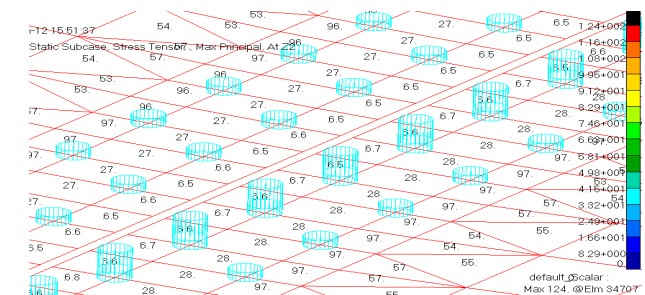


Figure 2: stresses are maximum at rivet holes in global model of the fuselage for 1D rivet element

It can be observed from the Figure 2 that the stress is distributed uniformly and the maximum stress is experienced in the riveted splice joint region for global model for 1D rivet element.

4.2. STRESS ANALYSIS OF THE LOCAL PANEL

A local analysis was done which represents the fuselage splice joint panel. Loading and boundary conditions for the local analysis of the panel are

Length of the panel =1200mm
 Width of the panel =500mm

The total tension load [9] acts on the fuselage structure from the global analysis is found as 53559.47 N. This total load is converted into uniformly distributed load (UDL) and applied at the top side of the panel. Uniformly distributed load of 107.12 N/mm was applied at top end of the plate and other end is fixed. A two dimensional linear static stress analysis is carried out using finite element analysis software tool. Mesh independent stress magnitudes are obtained through iterative mesh refinement process. Aluminum 2024-T3 is well-known aluminum alloy is used for the panel analysis.

It can be observed that the same Hoop stress value is experienced in both global and local analysis by applying same boundary conditions. Even the rivet loading are similar in both the cases. This is the indication to proceed further.

Large structures are usually assemblies of smaller parts are joined together by the variety of production techniques. There are two important joining methods namely; adhesive bonding and mechanically fastening. Mechanically fastened joints are an interesting subject to investigate. The present investigation focuses on solid rivets installed in aluminum plate. The expansion of solid rivet in the rivet hole is important with respect to the fatigue properties of joints. In reality rivet holes will be present. So the stress analysis of panel with rivet holes was carried out with the same applied boundary conditions by adapting multipoint constraint (MPC) at rivet holes as shown in Figure 3.

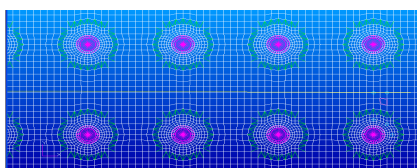


Figure 3: Meshed panel with riveted loading with MPC

V. CRACK ANALYSIS AT THE RIVETED HOLE LOCATION

CALCULATION OF SIF FOR 20 mm PITCH RIVET HOLE

Thus the periodic increase of crack lengths has applied for the panel. By applying same boundary conditions as the stress analysis has been carried out. Near the crack tip the stress intensity factor values are calculated for all the elemental crack length of 20mm pitch rivet hole.

Around the riveted hole section fine meshing has been done with quad4 a 2D elements will results the accurate stress values.

Stress Intensity Factor (SIF), $K = \sigma_R \sqrt{\pi a}$

Where, σ_R = Remote stress in N/mm² and 2a = Crack length in mm

By using FEA and Modified Virtual Crack Closure Integral (MVCCI) [6-7] method:

$$K = \sqrt{G \times E}$$

Where, G = strain energy release rate and E = Young's modulus of elasticity in N/mm²

$$G = \frac{(\Delta v \times f)}{2 \Delta a \times t}$$

Where, Δa =Element edge length at the crack tip in mm, Δv =Crack opening displacement in mm, f = Force at the crack tip in N and t =Skin thickness in mm

Considering the following analysis for 3rd iteration of 7.5mm crack length of 20 mm pitch rivet hole, where the SIF (k) for mode I can be calculated as

$$K = \sqrt{G \times E}$$

$$K = \sqrt{(0.015 \times 438 \times 72000) / (2 \times 0.45 \times 1.8)}$$

$$K = 540.37 \text{ MPa}\sqrt{\text{mm}}$$

$$K = 17.1 \text{ MPa}\sqrt{\text{m}}$$

MVCCI procedure is used for calculating the stress intensity factor. Similarly for all crack lengths and for different pitch holes, the stress intensity factor values has been calculated and compare those values with the fracture toughness of the material, where the fracture toughness of the material is 98.90 MPa√m. once the stress intensity factor value reaches the fracture toughness of the material then it leads to failure through fracture. This is one mode of failure. The other mode of failure is the structure with stress concentration may fails by net section yielding due to local yield at the crack tip. The average stress value between the two advancing crack tips will be compared with the yield strength of the material, where the yield strength of the material is 362 N/mm².

VI. STUDY OF NET SECTION FAILURE

The net section is the region or cross sectional area available between two rivet holes to carry whatever the load the component has to transfer. Due to rivet holes the stress concentration will be more around the rivet holes and also fatigue load will be acting for fuselage skin due to pressure variation, which tends to initiate the crack at the rivet hole edges perpendicular to the direction of the load acting.

Since the pressure variation occurs inside the fuselage according to altitude at which aircraft flies, there will be an uniform load acting on the component due to pressure variation, which in turn causes the growth of cracks in all the rivet holes simultaneously called as MSD.

So, as and when crack grows simultaneously in all the rivet holes, the net section available between the two crack tips will be reducing to carry the required load and at certain crack length if the stress intensity factor of the crack reaches the fracture toughness value of the component, then the component will fail due to fracture leading to bigger crack. But the failure may also occur due to plastic collapse [9] as the crack grows, at the tip of the crack the stress concentration will be more and before propagation there

will be local yield around the crack tip, when the plastic deformation at the two advancing crack tips towards each other coalesce, then the catastrophic failure occurs due to plastic deformation leading to bigger crack.

VII. CRACK TIP PLASTICITY

Under linear elastic fracture mechanics assumptions, the stress at the crack tip is theoretically infinite. Clearly, all materials have a finite strength, thus there will always be a small plastified zone around the crack tip.

If this zone is small compared to the crack size, then our linear elastic assumptions are correct, if not, LEFM is not applicable (thus it would be incorrect to use a *K* or *G* criterion) and a nonlinear model must be used. This damaged zone is referred to as a plastic zone for metals.

The appearance of the plastic zone at the tip does not allow its material to bear high stresses predicted by the elastic analysis. Also the material is soft in front of the crack tip and therefore the effective crack length is longer than the actual.

In fact, owing to the presence of the plastic zone, the stiffness of the component decreases. Consequently, the crack is equivalent to a length that is longer than actual length. The size of the plastic zone in front of the crack tip determines the effective crack length.

Therefore, considerable efforts have been made by many investigators such as Irwin plastic zone approach and Dugdale plastic zone approach to determine the plastic zone size and effective crack length.

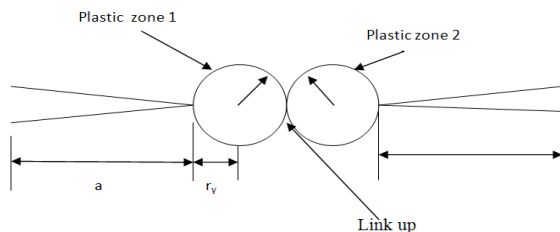


Figure 4: plastic zone around the crack tip

The net section plastic collapse is applied considering the crack sizes. As at each crack tips, the effective crack length is more than the actual crack, there will be plastic zone around the crack tip as shown in Figure 4. As these plastic zone approach each other as crack grows and at certain crack length these two crack length will link up to form the plastic collapse [10] and becomes a bigger crack. The Net section yielding stresses for the presence of multiple cracks are calculated based on the asymptotic formula for stresses near a crack tip, based upon the Irwin and Dugdale formulas [12-14].

Irwin formula

$$r_y = \left(\frac{1}{2 \times 3.14}\right) \times (K/\sigma_y)^2 \text{ ----- (2)}$$

Dugdale Formula

$$r_y = \left(\frac{3.14}{8}\right) \times (K/\sigma_y)^2 \text{ ----- (3)}$$

where, σ_y is the yield stress and r_y is the plastic zone radius.

7.1. CALCULATION OF NET SECTION YEILDING

The local panel taken for the net section failure calculation will have the same dimensions as given for the SIF calculation with same loads and boundary condition. For the different crack lengths the stress intensity factor was calculated, also for the same crack length, net section yielding will be calculated between two advancing crack tips by taking an average value of the elemental stresses obtained between the two crack tips and it is compared with the Irwin formula for validating the average elemental length for plastic zone and its stresses.

Since, the elemental stress at the crack tip will be higher and gradually decreases as moved away from the crack tip and it attains least value at centre in-between the crack tips. The average values of all the elemental stresses are then compared with the yield strength of the material Al 2024-T3 is 362 N/mm².

7.2. NET SECTION YIELDING FOR THE 20 MM PITCH RIVET HOLE

The net section yielding for the 20 mm pitch rivet hole is calculated by taking average of elemental stresses between two crack tips for each iteration in increasing order of crack lengths.

For the crack length of 12 mm, the average of elemental stress is $\sigma_{avg} = 312 \text{ N/mm}^2$

therefore, $\sigma_{avg} \leq \sigma_y$

From Irwin plastic zone formula, we have

$$K_I = 425.351183 \text{ MPa}\sqrt{\text{mm}}$$

$$\sigma_y = 362 \text{ N/mm}^2$$

From equation (1), one can obtain

$$r_y = (1/(2 \times 3.14)) \times (425.351183/362)^2$$

$$r_y = 0.219845 \text{ mm}$$

Since, problem requires only the length of the plastic zone. So, one can add actual crack length and plastic zone length Therefore,

$$a_{effective} = a + 2r_y$$

$$a_{effective} = 2.85 + (2 \times 0.219845) = 3.28969 \text{ mm}$$

but, actual crack length,

$$a = 2.85 \text{ mm}$$

therefore,

$$a_{effective} \geq a$$

The above values indicate that the plastic zone is increasing as crack grows, which is an indication of the plastic deformation.

Similarly, effective plastic length and net section yielding for other crack lengths for different pitch rivet hole distances such as 25mm and 30mm are tabulated below in the Table 3, Table 4 and Table 5.

Table 3: Net section average stress and effective crack length for plastic collapse for 20 mm pitch rivet hole

Crack Length, 2a in mm	Half Crack length, a in mm	K_{FEA} in $MPa\sqrt{mm}$	Net Section average stress, σ in MPa	Yield Strength σ_y in N/mm^2	Irwin formula for plastic zone length, r_y in mm	Effective Crack Length, a_{eff} in mm	Plastic zone length between two cracks tips with a_{eff} in mm
5.7	2.85	425.351	195.77	362	0.21985	3.28969	6.57938
6.6	3.30	493.004	205.05	362	0.29534	3.89068	7.78137
7.5	3.75	541.243	217.98	362	0.35596	4.46193	8.92386
8.4	4.20	581.195	231.98	362	0.41046	5.02091	10.0418
9.3	4.65	619.314	248.50	362	0.46606	5.58213	11.1643
10.2	5.10	658.098	267.53	362	0.52627	6.15253	12.3051
11.1	5.55	699.134	289.03	362	0.59394	6.73789	13.4758
12.0	6.00	757.788	312.00	362	0.69778	7.39556	14.7911
13.0	6.50	799.069	348.14	362	0.77588	8.05175	16.1035
14.0	7.00	862.914	396.00	362	0.90481	8.80962	17.6192

Table 4: Net section average stress and effective crack length for plastic collapse for 25 mm pitch rivet hole

Crack Length, 2a in mm	Half Crack length, a in mm	K_{FEA} in $MPa\sqrt{mm}$	Net Section average stress, σ in MPa	Yield Strength σ_y in N/mm^2	Irwin formula for plastic zone length, r_y in mm	Effective Crack Length, a_{eff} in mm	Plastic zone length between two cracks tips with a_{eff} in mm
6.05	3.025	487.341	201.00	362	0.28860	3.60219	7.20438
7.30	3.650	552.821	211.70	362	0.37136	4.39271	8.78543
8.55	4.275	603.350	222.33	362	0.44235	5.15969	10.3194
9.80	4.900	702.678	228.19	362	0.59998	6.09996	12.1999
11.70	5.850	716.993	250.50	362	0.62467	7.09935	14.1987
13.60	6.800	786.998	282.42	362	0.75261	8.30522	16.6104
15.50	7.750	863.658	324.50	362	0.90637	9.56275	19.1255
17.40	8.700	955.394	383.69	362	1.10915	10.9183	21.8366

Table 5: Net section average stress and effective crack length for plastic collapse for 30 mm pitch rivet hole

Crack Length, 2a in mm	Half Crack length, a in mm	K_{FEA} in $MPa\sqrt{mm}$	Net Section average stress, σ in MPa	Yield Strength σ_y in N/mm^2	Irwin formula for plastic zone length, r_y in mm	Effective Crack Length, a_{eff} in mm	Plastic zone length between two cracks tips with a_{eff} in mm
5.93	2.965	466.198	185.74	362	0.26410	3.49320	6.98639
7.06	3.530	530.951	191.31	362	0.34256	4.21511	8.43023
8.20	4.100	578.362	201.78	362	0.40647	4.91293	9.82586
9.33	4.665	617.945	210.00	362	0.46401	5.59301	11.18600
10.50	5.250	654.840	217.75	362	0.52107	6.29213	12.58430
11.60	5.800	730.374	222.50	362	0.64821	7.09642	14.19280
13.13	6.565	741.519	236.52	362	0.66814	7.90128	15.80260
14.67	7.335	790.809	254.70	362	0.75992	8.85483	17.70970
16.20	8.100	842.602	276.40	362	0.86272	9.82543	19.65090
17.73	8.865	897.031	302.72	362	0.97777	10.8205	21.64110
19.30	9.650	955.827	335.43	362	1.11015	11.8703	23.74060
20.80	10.400	1021.550	377.04	362	1.26806	12.9361	25.87220

VIII. RESULTS AND DISCUSSIONS

8.1. RESULTS AND DISCUSSIONS OF SKIN FOR 20MM PITCH RIVET HOLE

The stress intensity factor value is calculated for periodic increase of crack length. For each crack length, the stress intensity factor value is compared with the fracture

toughness of the material. Table 3 shows the results of stress intensity factor values for periodic increase of crack lengths. The graph in the Figure 5 shows the crack analysis result which is obtained for crack length versus stress intensity factor value. The distance between two rivet hole edges are 15.2mm, from the result, it is found that at the half crack length of 6.5 mm the stress intensity

factor value does not reaches the fracture toughness value of the material, where the material does not leads to failure through fracture. In figure 5. the graphical view is shown clearly.

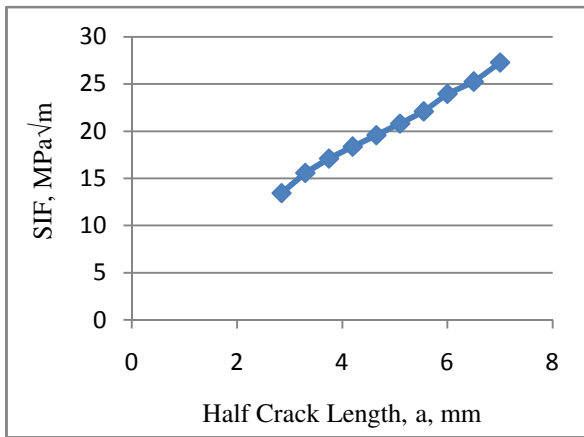


Figure 5: SIF graph for 20mm pitch rivet hole

Similarly the net section yielding calculations are done by means of taking the average stress value between the two advancing crack tips and it is compared with the yield strength of the material. Table 3 shows the results of net section yielding for periodic increase of crack lengths. From the result, it is found that at the crack length of 14 mm the has material crossed the yield strength value of material, where it leads to material yielding failure. The following Figure 6 shows the graph of net section yielding result which is plotted for crack length versus average yield stress of the material for different crack lengths.

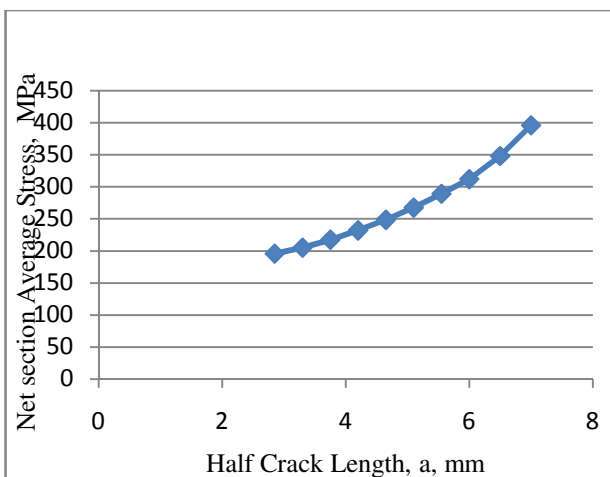


Figure 6: Net section yielding graph for 20mm pitch rivet hole

So from the analysis it is came to know that the structure with stress concentration will fail by net section yielding. Similarly, the results for 25 mm and 30 mm pitch rivet hole, the graphical representation values are given in the Figure 7, Figure 8, Figure 9 and Figure 10.

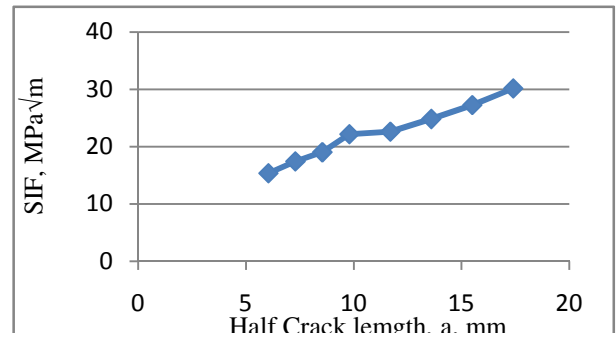


Figure 7: SIF graph for 25mm pitch rivet hole

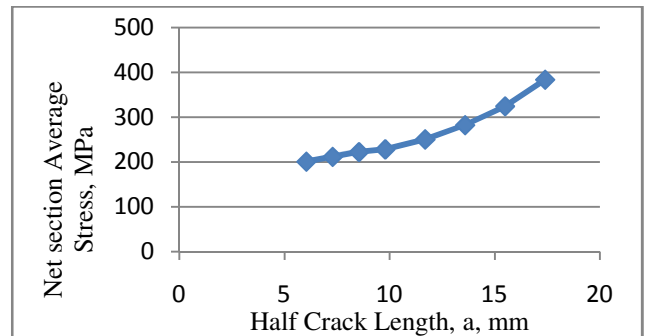


Figure 8: Net section yielding graph for 25mm pitch rivet hole

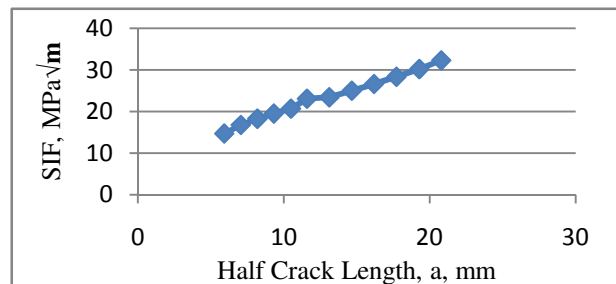


Figure 9: SIF graph for 30mm pitch rivet hole

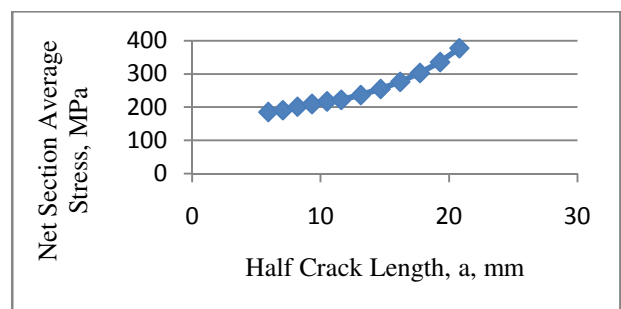


Figure 10: Net section yielding graph for 30mm pitch

IX. DISCUSSIONS

The results of the Net section failure have been discussed in the previous section; from that one can understand that, if the component has a crack, it does not mean that it should fail by fracture. From results of current study, one can understand that the component will fail by plastic collapse even if it has crack.

Also, one can observe that if the distance between rivet holes are increasing net section failure will also occur for bigger cracks. Due to fatigue loading, the net section

yielding is more susceptible to failure than the fracture failure. So, one should not concentrate only on fracture during design and inspection of a component at what crack length the component will fail, one should concentrate also on plastic deformation which occurs due to fracture.

X. CONCLUSIONS

The static stress analysis of the fuselage of a transport aircraft has been performed in the presented work. This study has relevance in the structural integrity evaluation of aging transport aircraft due to multisite damage. Here the MSD analysis was carried out for the aged aircraft.

In the present work only the fuselage with splice through butt joint has been analyzed. Fatigue loads due to internal pressurization acting on the fuselage, stress concentration will be high at rivet holes locations of the fuselage joint, which causes the initiation of cracks on all rivet hole edges due to uniform stress acting on the fuselage due to internal pressurization.

Usually the fuselage of the aircraft structure is subjected to different kinds of loads that include aerodynamic loads, landing loads, taxing loads, pressurization and reaction loads. The present study deals only with MSD, so the loads considered are only internal pressurization.

Taking all the above points into consideration modeling and finite element analysis of fuselage and its local segment was carried out and from that work, some of the information's are concluded as follows

- The Fuselage model was created using a 3D modeling software tool according to the dimensions and the 3D modeled component was imported to analysis tool for pre-processing. The fuselage component was meshed with 2D elements such as quad 4 and Tria 3 elements and loads and boundary conditions were applied.
- The material used was Al 2024-T3, which is widely used in aircraft industry for its good fatigue strength and corrosion resistance.
- Stress analysis of the global model of the fuselage has been carried out to observe the hoop stress on skin is equal to the analytical value of the hoop stress 59.5 N/mm^2 .

REFERNCES

1. Lucas F.M.Silva et al "Multiple-site damage in riveted lap-joints: experimental simulation and finite element prediction", International journal of fatigue, vol 22, pp 319-338, 2000
2. O. Partl and J. Schijve "Multiple-site damage in 2024-T3 alloy sheet", International Journal of Fatigue, vol 15 No 4 (1993) pp 293-299
3. Schijve, J. "Multiple-site damage in aircraft fuselage structures", fatigue and fracture of engineering materials structures, vol 18, number 3, pp 329-344. 2003
4. Brown.A.M.etal, "Simulating fretting contact in single lap splices" ,International journal of fatigue, vol 31, pp 375-384, 2009
5. Furukawa.C.H et al, "On the finite element modelling of fatigue crack growth in pressurized cylindrical shells", International journal of fatigue, vol 31, pp 629-635, 2009
6. AndrzejLeski, "Implementation of the virtual crack closure technique in engineering FE Calculations", finite elements in analysis and design, vol 43, pp 261-268, 2007
7. Rybicki.E.F, "A finite element calculation of stress intensity factors by a modified crack closure integral", engineering fracture mechanics, vol 9, pp 931-938, 1977
8. L. MOLENT and R. JONES "crack growth and repair of multi-site damage of fuselage lap joints" Engting Fructure Mechanics Vol. 44, No. 4, pp. 627-637, 1993
9. Eastaugh GF, Simpson DL, Straznicky PV, Wakeman RB. A special uniaxial coupon test specimen for the simulation of multiple site fatigue crack growth and link-up in fuselage skin splices. NASA 96N24261, December 1995
10. Pin Tong, Robert Greif and Li Chen "Residual strength of aircraft panels with multiple site damage" Computational Mechanics (1994) 13, 285-294
11. PITT and R. JONES "multiple-site and widespread fatigue damage in aging aircraft" Engineering Failure Analysis, 1997, Vol. 4, No. 4, pp. 237-257
12. D.Y. Jeong, O. Orringer, G.C. SihStrain "energy density approach to stable crack extension under net section yielding of aircraft fuselage" Theoretical and Applied Fracture Mechanics 22 (1995) 127-137
13. M C Cherry and S Mall, "Residual strength of unstiffened aluminum panels with multiple site damage" *engineering fracture mechanics* vol. 57, no. 6, pp. 701-713, 1997
14. Pin Tong, Robert Greif, Li Chen, "Residual strength of aircraft panels with multiple site damage" Computational Mechanics (1994) 13, 285-294

Analysis of Modelling of Active Stall Controlled and Active Pitch controlled Variable Speed Wind Turbines

R. Uma Maheswari¹, J. Tamilvendhan²

1. Department of Electronics and Communication Engineering
Rajalakshmi Institute of Technology, Chennai
2. Winergy Drives System, Chennai

Abstract: Wind energy is a viable option to complement other types of pollution-free generation. In the early development of wind energy, the majority of wind turbines were operated at constant speed. Recently, the number of variable-speed wind turbines installed in wind farms has increased and more wind turbine manufacturers are making variable-speed wind turbines.

A wind turbine model for control purposes needs to be based on linear mathematical models. The modeling of the wind turbine is based on certain aerodynamic phenomena (lift and drag) caused by the interaction of the rotor blade of the wind turbine and wind. The modeling of the wind turbine for control purposes involves the modeling of the relevant dynamics that affect the production of power and the stability of the wind turbine. This involves the rotor, the tower, the drive train, generator and the pitch actuator. The resulting non-linear model is then linearised at different working points. The linear model will be used for a rotor speed control algorithm.

This paper analysis the modelling of variable speed wind turbines with active pitch control and active stall control.

I. Introduction

Wind is a form of solar energy. Winds are caused by the uneven heating of the atmosphere by the sun, the irregularities of the earth's surface, and rotation of the earth. Wind flow patterns are modified by the earth's terrain, bodies of water, and vegetative cover. This wind flow, or motion energy, when "harvested" by modern wind turbines, can be used to generate electricity. The terms "wind energy" or "wind power" describe the process by which the wind is used to generate mechanical power or electricity. Wind turbines convert the kinetic energy in the wind into mechanical power. This mechanical power can be used for specific tasks or a generator can convert this mechanical power into electricity.

To successfully convert the kinetic energy of wind into electrical energy, the wind turbine is equipped with a control system that ties the operation of all the subsystems of the wind turbine together. A wind turbine is always designed for specific rated conditions. By rated conditions here we mean rated wind speed, rated rotor speed and rated power. A wind turbine is designed to generate rated power which is the maximum power that the generator is designed to deliver (for example a wind 750i wind turbine is designed to generate a maximum of 750 KW). The speed of the rotor

when the rated power is generated is known as rated rotor speed and the corresponding velocity of the wind is known as rated wind speed. But wind is stochastic (random or probabilistic but with some direction) in nature. Hence it is not always possible to obtain rated conditions for a wind turbine. Hence it is necessary to control the wind turbine in order to increase energy production and realize a long lifetime.

When the velocity of the wind is below the rated wind speed then it is known as below rated wind speed, and when the velocity is more than rated then it is known as above rated windspeed. All wind turbines are designed with some sort of power control. There are different ways to control aerodynamic forces on the turbine rotor and thus to limit the power in very high winds in order to avoid damage to the wind turbine.

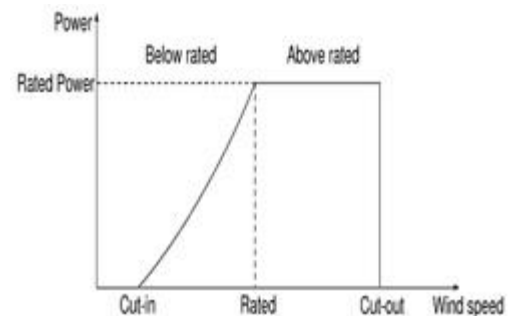


Figure 1 Power Generation as a function of Wind Speed

It is clear from figure 4 that there are two regimes of control, below rated and above rated and the two regimes have different control objectives. Two major systems are used to control wind turbine as follows:

1. For below rated (Generator Torque Control), This control system uses power electronic controller to maximize energy capture by adjusting rotor speed to follow wind speed variations.

Control Law:

$$Q = \frac{Prated}{(\omega_{gen} \cdot \eta_{gen})} \quad 1.1$$

2. For above rated (Blade Pitch Control) vary rotor speed and pitch angle to regulate load and maintain power production at rated value. Blade Pitch Control changes the orientation of blades to change the aerodynamic forces.

It should be noted that wind is a stochastic input. Hence the overall wind speed measured can be defined as a sum of mean wind speed and turbulence. The rotor speed is

always proportional to the mean wind speed. Hence for control purposes the rotor speed is taken as input and wind is considered as a disturbance (at above rated conditions).

II. Active stall control

Active stall control is the combination of stall and pitch control. It has the same regulated properties as in the pitch regulated turbines but has the stall properties of blade. The blades are designed same way as in stall control, but the entire blade can be turned to 90° to adjust its pitch. Thus blade tip brakes are not required as in passive stall control. The idea is to pitch the blade gradually with negative pitch angle in order to increase the performance of blades over a wide range of wind speeds especially with low wind speed. It is found that only small changes of pitch angle are required to maintain the power output at rated, so pitch rates do not need to be as large as in active pitch control. Moreover, full aerodynamic braking requires pitch angles of only about -20° , so the travel of the pitch mechanism is very much reduced compared with positive pitch control. Active Stall control system compares the electric power output of the generator with its reference value which is defined in accordance with the incoming wind and sets the blade angle to minimize the error.

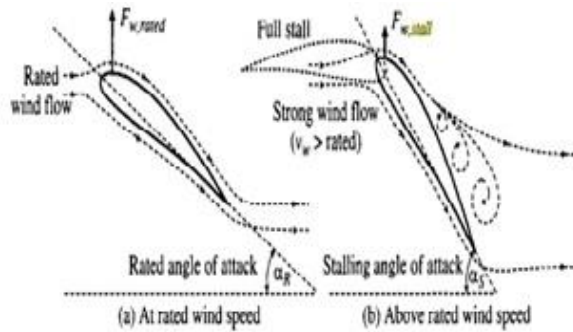


Figure 2 Active Stall Control at rated and above rated speed

The stall phenomenon can be induced not only by higher wind speed but also by increasing the angle of attack. Thus active stall turbine has adjustable blades with a pitch control mechanism. When the wind speed exceeds the rated the blades are controlled to turn more into the wind, leading to reduction of capture power. The captured power thus be maintained at the rated by adjust the blade angle of attack.

One of the advantages of active stall is that one can control the power output more accurately than with passive stall, so as to avoid overshooting the rated power of the machine at the beginning of a gust of wind. Another advantage is that the machine can be run almost exactly at rated power at all high wind speeds.

2.2 Active pitch control

Power limitation in high winds is typically achieved by using pitch angle control. This action, also called active-pitch control (or **pitch-to-feather**), corresponds to changing the pitch value such that the leading edge of the blade is moved into the wind (increase of β), thus inducing blade feathering

effect. The range of blade pitch angles required for power control in this case is large, about 35° from the pitch reference. Therefore, for limiting power excursions, the pitching system has to act rapidly, with fast pitch change rates, i.e., $5^\circ/s$. Therefore, one could expect large gains within the power control loop. The power control structure employed is the same as for the active-stall control machines. Figure 3 shows the effect of pitch control on power flow in wind turbine generation.

1. Pitch Control At Standstill

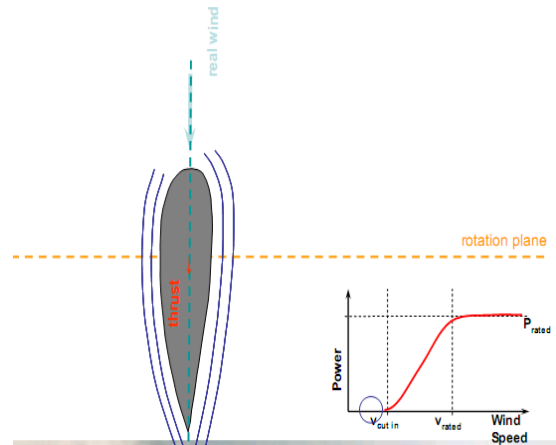


Figure 3 (a) Pitch Control At Standstill

2. Pitch Control At Start of operation

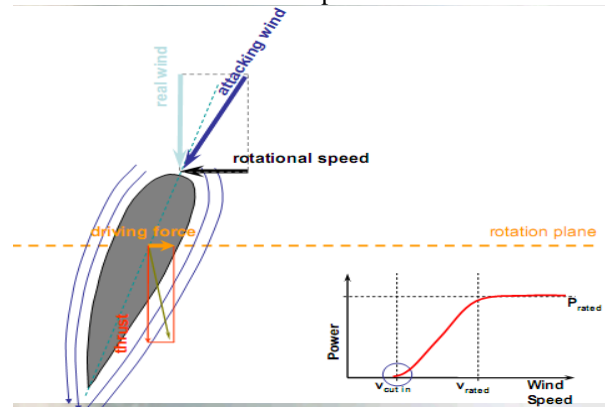
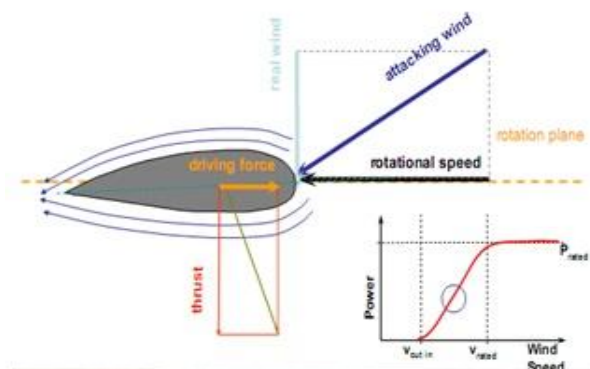


Figure 3 (b) Pitch Control At Start of operation

3. Pitch Control At Power Generation



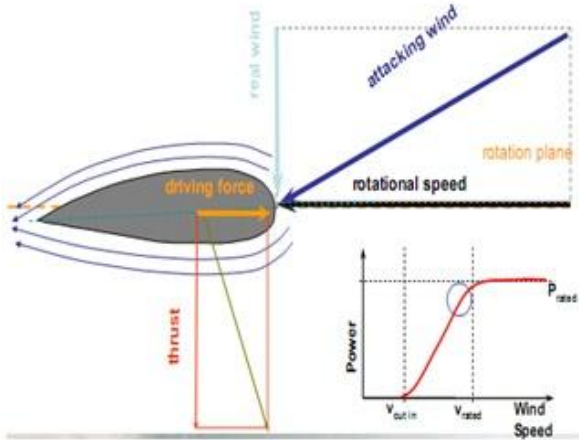


Figure 3(c) Pitch Control At Generation of power

4. Pitch Control At Power Limitation

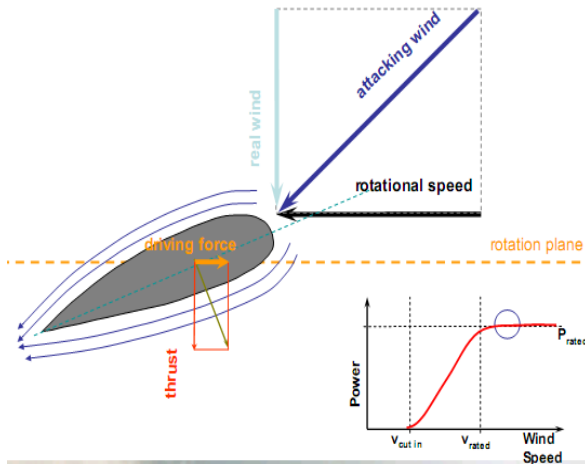


Figure 3(c) Pitch Control At Power Limitation

With pitch control, the power captured, $P_{captured}$, from the wind power P_{wind} can be controlled by a pitch actuator. The acceleration and deceleration is the result of the

3.1 Rotor Modelling of Variable Speed Turbine

The fundamental dynamics of this variable-speed wind turbine are captured with the following simple mathematical model

$$J_T \dot{\omega}_T = Q_A - Q_E \quad 2.1$$

- J_T = Moment of Inertia of Turbine Rotor
 - ω_T = Angular Shaft Speed
 - Q_A = Aerodynamic Torque
 - Q_E = Mechanical Torque necessary to turn on the generator.
- Aerodynamic torque is represented by

$$Q_A = \frac{\rho}{2} A_{wt} R C_p(\lambda, \beta) v_w^2 \quad 2.2$$

- ρ = Air density (kg/m^3)
- C_p = Performance coefficient
- λ = Tip speed ratio vt/vw
- β = Pitch angle (in degrees);
- A_{wt} = Swept area (m^2)

R = Rotor Radius

The following well-known algebraic equation gives the relation between wind speed and mechanical power extracted from the wind (Heier, 1998; Patel, 2000):

$$P_{wt} = \frac{\rho}{2} A_{wt} C_p(\lambda, \beta) v_w^3 \quad 2.3$$

P_{wt} = Power extracted from the wind in watts

The following general equation to describe the rotor of variable-speed wind turbines

$$C_p(\lambda, \beta) = C_1 \left(\frac{C_2}{\lambda_i} - C_3 \beta - C_4 \beta^{c_5} - C_6 \right) \exp\left(\frac{-C_7}{\lambda_i}\right), \text{ where}$$

$$\left[\left(\frac{1}{\lambda + C_8 \beta} \right) - \left(\frac{C_9}{\beta^3 + 1} \right) \right]^{-1} \quad 2.4$$

The structure of this equation originates from Heier (1998). However, the values of the constants c_1 to c_9 have been changed slightly in order to match the manufacturer data.

Table 1 includes both the original parameters and the parameters used here.

Power Co efficients	C_1	C_2	C_3	C_4	C_5
Heier	0.5	116	0.4	0	-
Variable Speed Wind Turbine	0.73	151	0.58	0.002	2.14
Power Co efficients	C_6	C_7	C_8	C_9	C_6
Heier	5	21	0.08	0.035	5
Variable Speed Wind Turbine	13.2	18.4	-0.02	-	13.2

Table 1 Approximation of power curves

High-frequency wind speed variations are very local and therefore even out over the rotor surface, particularly when wind turbines become larger. To approximate this effect, a low-pass filter is included in the rotor model.

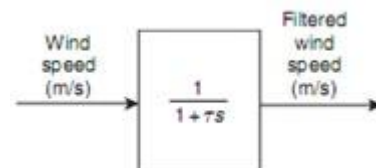


Figure 4: Low pass filter to even out high frequency wind speed

3.1 Unified Power control structure for active pitch and active stall control

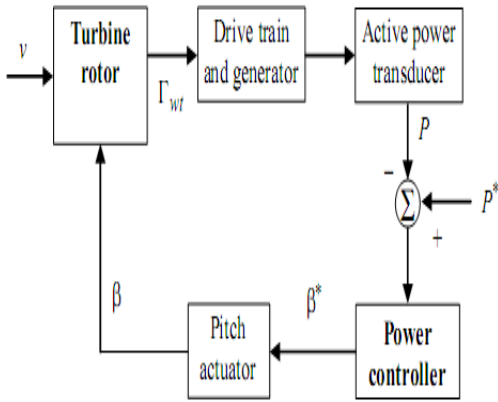


Figure 4 Power Control structure

Power limitation in high winds is typically achieved by using pitch angle control. This action, also called active-pitch control (or pitch-to-feather), corresponds to changing the pitch value such that the leading edge of the blade is moved into the wind (increase of β), thus inducing blade feathering effect. The range of blade pitch angles required for power control in this case is large, about 35° from the pitch reference. Therefore, for limiting power excursions, the pitching system has to act rapidly, with fast pitch change rates, i.e., $5^\circ/s$. Therefore, one could expect large gains within the power control loop. The power control structure employed is the same as for the active-stall control machines.

Active-stall control (also called negative-pitch control) reduces the aerodynamic power by diminishing the blade pitch angle, β , in order to increase the incidence angle. The blades are pitched towards stall, in the contrary direction to the pitch-control case, by turning the leading edge downwind. Only small changes of pitch angle are required to maintain the power output at its rated value, as the range of incidence angles required for power control is much smaller in this case than in the case of pitch control. Compared to the pitch-to-feather technique, the travel of the pitch mechanism is very much reduced; significantly greater thrust loads are encountered, but the thrust is much more constant, inducing smaller mechanical loads. The employed power control structure is briefed in Figure 4

3.2 Pitch Servo

In variable-pitch wind turbines, the blade angle is controlled by a pitch servo. The main control system produces a blade reference angle and the pitch servo is the actuator, which actually turns the turbine blades to the ordered angle. The pitch servo is subject to constructional limitations, such as angular limits β_{min} and β_{max} . That means that the blades can only be turned within certain physical limits. For active-stall-controlled wind turbines, the permissible range will be between -90° and 0° (or even a few degrees to the positive side), whereas for active pitch-controlled wind turbines the permissible range will lie between 0° and 90° (or even a few degrees to the negative side). The control system may impose

other, normally narrower, limits on the reference angle, though. Likewise, there are limitations on the pitch speed, $d\beta/dt$. The pitch speed limit is likely to be higher for pitch-controlled wind turbines than for active-stall-controlled wind turbines, which have a higher angular sensitivity. The pitch speed limit may differ significantly for a positive $d\beta/dt_{pos, max}$ and negative $(d\beta/dt_{neg, max})$ turning of the blade. The pitch speed is normally less than 5° per second, although the pitch speed may exceed 10° per second during emergencies.

The dynamic behaviour of the pitch actuator operating in its linear region is described by the differential equation

$$\dot{\beta} = \left(\frac{1}{\tau} \beta - \frac{1}{\tau} \beta_d \right) \quad 3.1$$

β_d = Desired Pitch Angle

β = actual Pitch angle.

in laplace domain as follows

$$\dot{\beta}(s) = H_{pt}(s) \cdot \dot{\beta}^*(s) \quad 3.2$$

$$H_{pt}(s) = \frac{e^{-(T_d^{ptv} + T_d^{ptx})s}}{\left(\frac{1}{(\omega_o^{pt})^2 s^2 + \frac{2\beta_{pt}}{\omega_o^{pt}} s + 1} \right)} \dot{\beta}^*(s) \quad 3.3$$

T_d^{ptv} = The conditional delay time to overcome Coulomb friction

$T_d^{ptx}, \omega_o^{pt}, \beta_{pt}$ equivalent system parameters

which represent the overall pitch actuation delay during normal operation: pitch delay time, pitch system eigen frequency, damping rate.

There are two modes of control while controlling the wind turbine.

- Below rated wind speed control
- Above rated wind speed control

3.2.1 Below rated wind speed control

Pitch and torque control are used at below rated conditions to generate as much power as possible. To ensure as much as possible energy yield, during partial load the electric torque set point is set such that the tip speed ratio, λ , is maintained at its optimal value, λ_{opt} . with the optima tip speed ratio, $\lambda_{opt}, \lambda_{opt} = \lambda \parallel C_p = C_{p, max}$ 3.2

The rotor speed is adjusted proportional to the wind speed by electric torque control, in such a way that the aerodynamic power extracted by the rotor (efficiency) is maximal.

Simulation Control structure for below rated Speed

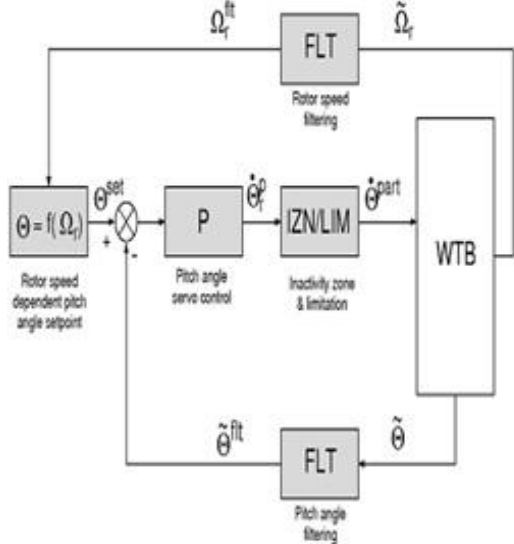


Figure 5 Below Rated Wind Speed Control

3.2.1 Above rated wind speed control

Design of an algorithm to control rotor speed above rated wind speed as follows pitching the rotor blades simultaneously in feathering direction. The ‘constant power’ control of the generator and the rotor inertia (fly wheel) will then establish good power quality. For this reason aerodynamic torque variations will result in rotor speed variations. The amount of rotor speed variation above its rated value, to maintain rated power, is restricted both by the maximum speed of the generator and perhaps by the tower eigen frequency to avoid tower resonance.

Simulation Control structure for above rated Speed

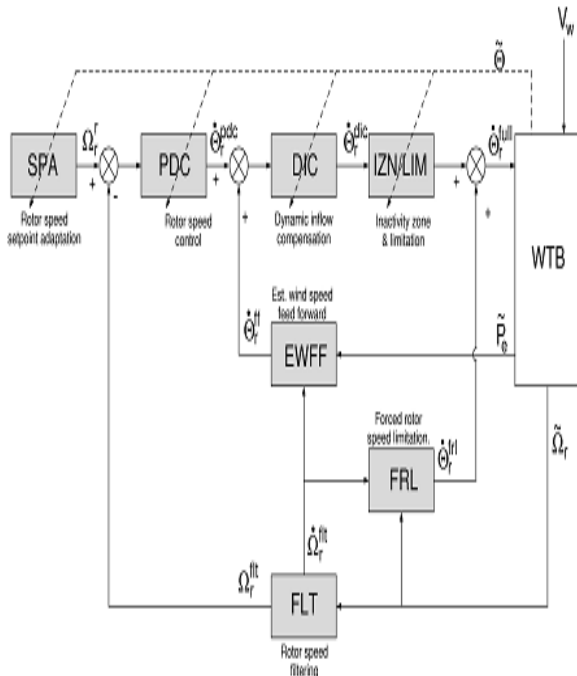
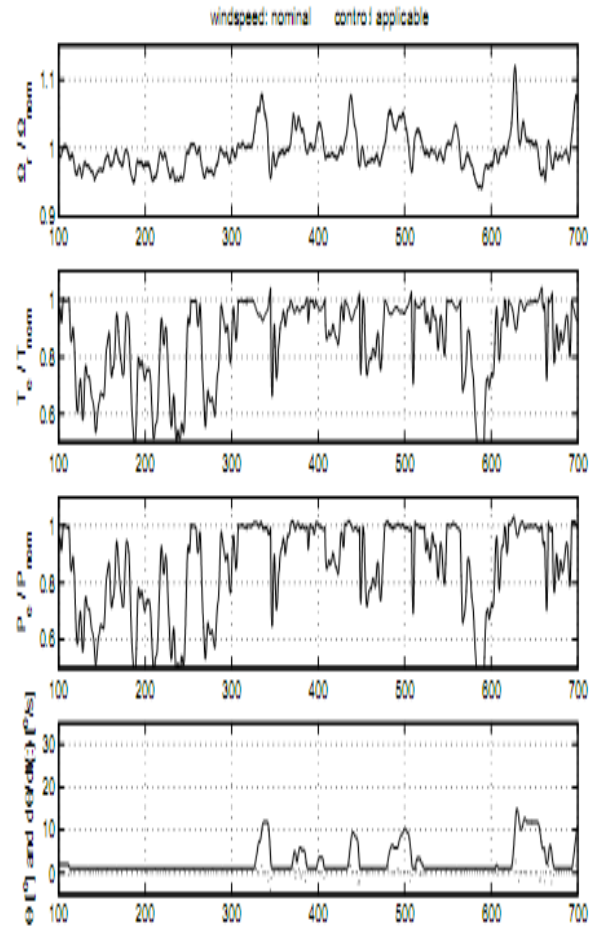
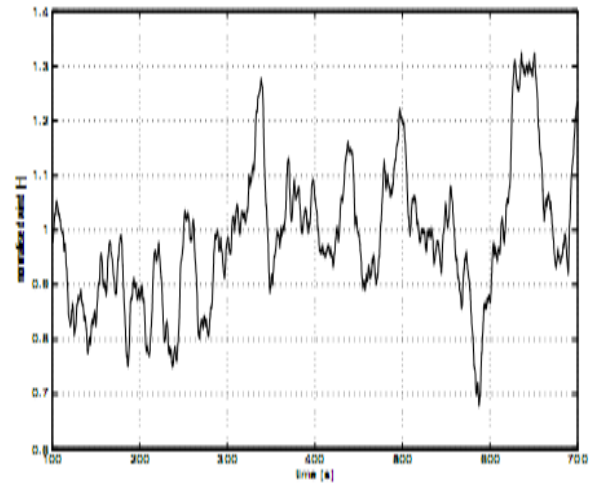


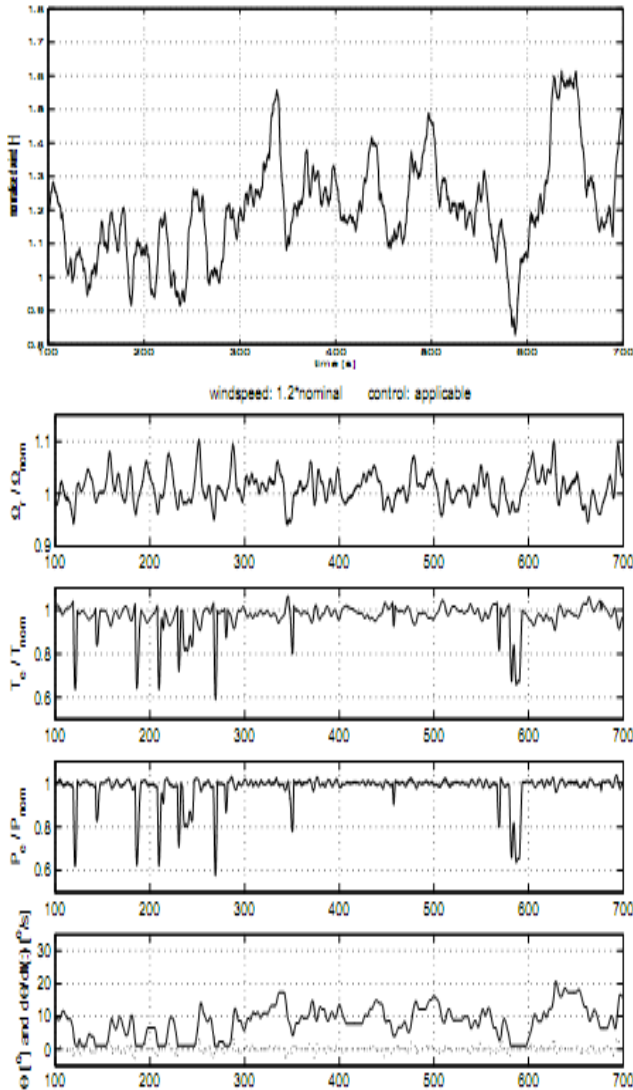
Figure 6 Above Rated Wind Speed Control

Simulation Results

4.1 Below rated wind speed control



4.1 Above rated wind speed control



IV. Conclusion

This paper deals the mathematical modelling of a unified power control of active stall and active pitch controlled variable speed turbine. Active stall control employs below rated operation to extract maximum power from wind .and at rated and above rated wind speed active pitch control method used to avoid damage of turbine.Basic controller structure is simulated. Design of sophisticated unified controller is on further study.Lots of reasearch needed to design such type of controller.Fuzzy logic controller can be employed .It is on further study.

References

- [1] J.F Manwell,J.G McGowan and A.L.Rogers “Wind Energy Explained Theory,Design and Application. John Willy & Sons.
- [2] Thomas Ackermann “Wind Power in Power Systems” John Willy & Sons.
- [3] Fernando D. Bianchi, Hernán De Battista and Ricardo J. Mantz “Wind Turbine Control Systems Principles,Modelling and Gain Scheduling Design”Springer.
- [4] E.L. van der Hooft; P. Schaak; T.G. van Engelen ”Wind Turbine Control Algorithms” ECN-C--03-111.
- [5] Iulian Munteanu , Antoneta Iuliana Bratcu Nicolaos-Antonio Cutululis ,Emil Ceang “Optimal Control of Wind Energy Systems Towards a Global Approach “Springer.
- [6] Dimitris Bourlis “A Complete Control Scheme for Variable Speed Stall Regulated Wind Turbines “
- [7] Jianzhong Zhang, Ming Cheng, Zhe Chen, Xiaofan Fu “Pitch Angle Control for Variable Speed Wind Turbines “ DRPT 2008.
- [8] E. Muljadi, K. Pierce, P. Migliore “Control Strategy for Variable-Speed, Stall-Regulated Wind Turbines” American Controls Conference Philadelphia, PA.

Simulink Based Model of Photovoltaic Cell

*Mr. G. Venkateswarlu, **Dr.Psangameswar Raju

*Prof in dept of EEE, Narayana Engg College, Nellore

**Professor, S.V.Univesity, Tirupati.

ABSTRACT: The potential for solar energy as a sustainable source of energy is well understood. With the ever increasing use of solar power the necessity of a model is accentuated. The aim of this work is to study the variation of PV module main characteristic parameters as a function of shading, with a special attention to the relationship between output power lowering due to shading.

Keywords: pvc, mppt, solarex

I. INTRODUCTION

India is endowed with vast solar energy potential. About 5,000 trillion kWh per year energy is incident over India's land area with most parts receiving 4-7 kWh per sq. m per day. [1] From an energy security perspective, solar is the most secure of all sources, since it is abundantly available. The objective of the National Solar Mission is to establish India as a global leader in solar energy, by creating the policy conditions for its diffusion across the country as quickly as possible. To create an enabling policy framework for the deployment of 20,000 MW of solar power by 2022.[1]

II. SOLAR INSOLATION IN INDIA

With about 300 clear sunny days in a year, India's theoretical solar power reception, just on its land area, is about 5 PWh.[1] The daily average solar energy incident over India varies from 4 to 7 kWh/m² with about 2,300–3,200 sunshine hours per year[1]. This is far more than current total energy consumption. For example, even assuming 10% conversion efficiency for PV modules, it will still be thousand times greater than the likely electricity demand in India by the year 2015[1]

III. PHOTOVOLTAIC MODULES

Solar cells consist of a p-n junction fabricated in a thin wafer or layer of semiconductor.[2] In the dark, the I-V output characteristic of a solar cell has an exponential characteristic similar to that of a diode.[2] .PV module represents the fundamental power conversion unit of a PV generator system. The output characteristics of PV module depends on the solar insolation, the temperature and output voltage of PV module.[2] Since PV module has nonlinear characteristics, it is necessary to model it for the design and simulation of maximum power point tracking (MPPT) for PV system applications.

IV. PHOTOVOLTAIC SOLAR CELL MODELS IN REVERSE BIAS

In order to describe the electrical behavior of a solar cell, in light and darkness, the one diode model and the two diodes model, derived from physical characteristics of solar cells, are commonly used.[2] When investigations on hot spot

phenomena and mismatch in photovoltaic cells association have become interesting, these models have been reviewed to deal with the reverse characteristics, when solar cells are working in reverse bias. One of the first approaches modifies the one diode model with the assumption that the avalanche multiplication affects mainly the direct current. The mathematical model of the solar cell taking into account the effect of breakdown voltage is given by the equation.

$$I = \left(I_{ph} - I_0 \cdot \left(\exp\left(\frac{V}{mV_t}\right) - 1 \right) \right) M(V) - \frac{V}{R_p} \quad (1)$$

Where the multiplication factor M(V) denotes the effect of the avalanche effect.[5,6] The expression of M(V) is:

$$M(V) = \frac{1}{(1 - (|V|/V_b)^n)} \quad (2)$$

where V_b is the breakdown voltage in reverse bias and n is the Miller constant. Figure 1 shows the electrical equivalent circuit including the effect of M(V) modelled by a controlled current source. Bishop[7] proposed an equation where the avalanche effect is expressed as a non-linear multiplication factor that affects the shunt resistance current term. The proposed model is given by Equation (3) and the corresponding equivalent circuit is shown in Figure 2.

$$I = I_{ph} - I_0 \left[\exp\left(\frac{V + R_s I}{mV_t}\right) - 1 \right] - \left(\frac{V + R_s \cdot I}{R_p} \right) \left[1 + a \left(1 - \frac{V + R_s I}{V_b} \right)^{-n} \right] \quad (3)$$

where V_b is the breakdown voltage, a and n are constants. The additional term, E(V), is added to the leakage current into the shunt resistance term modeled as a controlled current source:

$$E(V) = 1 + a \left(1 - \frac{V + IR_s}{V_{br}} \right)^{-n} \quad (4)$$

V. SIMULINK BASED MODEL FOR PV MODULE

The mathematical PV models used in computer simulation have been built for over the past four decades [6]-[8]. Almost all well-developed PV models describe the output characteristics mainly affected by the solar insolation, cell temperature, and load voltage. Most of the above models do not take into account the effects of shading on the PV characteristics.

We have chosen the Matlab/Simulink[12] environment to study the effects of shadowing in PV module performance because Matlab is today a universal tool for mathematical

applications and has been used before in PV systems' simulation and solar cell parameters' extraction with success.[13,14]

The I-V characteristic simulation, in Matlab/ Simulink environment, of a photovoltaic module under different shadow rates was carried out using Bishop's model described in the previous section. The Solarex MSX60 PV [Table 1]module under study is formed by 36 serially connected solar cells and one of the solar cells is assumed to be shaded with variable rate of shadow: α ($0 \leq \alpha \leq 1$) We consider that a full shadow corresponds to $\alpha = 0$ whereas $\alpha = 1$ indicates no shadow present on the solar cell. The PV module output voltage is the sum of voltages generated across the individual cells, illuminated and shaded:

$$V = \sum_{i=1}^{35} V_{ill_cell} + V_{sh_cell} \quad (5)$$

where V is the total PV module voltage, and V_{ill_cell} and V_{sh_cell} are the voltages across the illuminated cells and the shaded one, respectively. The current through all the cells is the same:

$$I = I_{ill_cell} = I_{sh_cell} \quad (6)$$

where I is the current through the PV module, I_{ill_cell} and I_{sh_cell} are the currents through the illuminated cells and the shaded one, respectively. The following expression, obtained from Equation (3) for the simulation of the I-V characteristic of the PV module has been used:[3]

$$V = \frac{R_p}{E(V)} \left[I_{ph} - I_o \left(\exp \left(\frac{V + R_s I}{m V_t} \right) - 1 \right) \right] - I \left(\frac{R_p + E(V) R_s}{R_p} \right) \quad (7)$$

The same equation is governing the shaded cell with the assumption that the photogenerated current is proportional to the rate of shadow denoted by α . Thus the expression of the photogenerated current at the shaded cell is given by[7]

$$I_{ph} = I_{sco} \cdot \frac{\alpha \cdot \Phi}{\Phi_N} \quad (8)$$

where Φ_N and Φ are the standard and incident irradiance, respectively.

The output power of the whole PV module is always less than the sum of the values of the individual power cells due to dispersion of the parameters. These losses are accentuated in the case of partial or full shadow of one or several cells serially connected to form the PV module. We have tried to report the amount of power lowering due to shadow effect. The power loss is given by the following expression

$$\text{Power loss (\%)} = \frac{P_{max_unsh} - P_{max_sh}}{P_{max_unsh}} \times 100 \quad (9)$$

where P_{max_unsh} and P_{max_sh} , are respectively the maximum powers corresponding to the unshaded cells of the PV module and the shaded one. A single solar cell totally shaded does not cause a significant maximum power loss; it is less than 10% at lower irradiation. Therefore, the

power losses increase with increase of irradiation and shadow rate.

VI. CONCLUSION

An attempt has been made to model a photo voltaic cell under the influence of shadow. The proposed model is found be showing appreciable results in comparison with the data being supplied by the manufacturer It can also be applied to study the reverse characteristics of shadowed solar cells forming part of the PV module. The reduction in the output power of a PV module due to shadowing has been evaluated taking into account the influence of irradiance level and the shadow rate over a cell of the PV module.

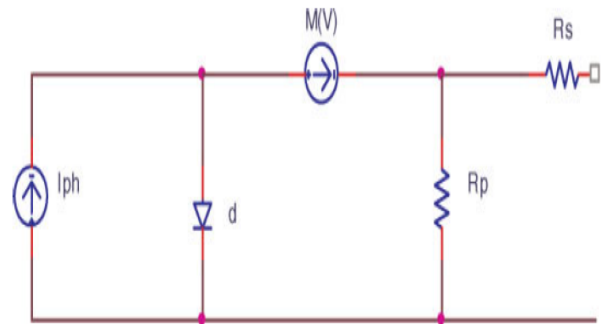


Figure 1: Solar cell equivalent circuit considering the avalanche effect

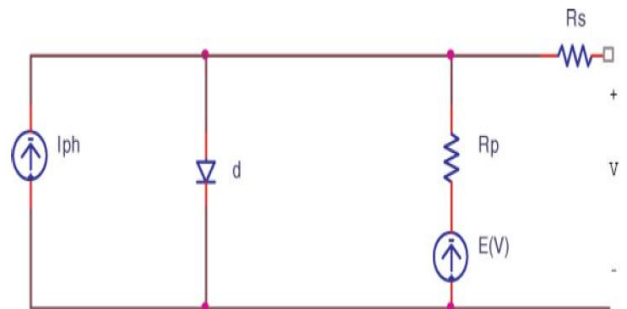


Figure 2: Bishop's equivalent circuit

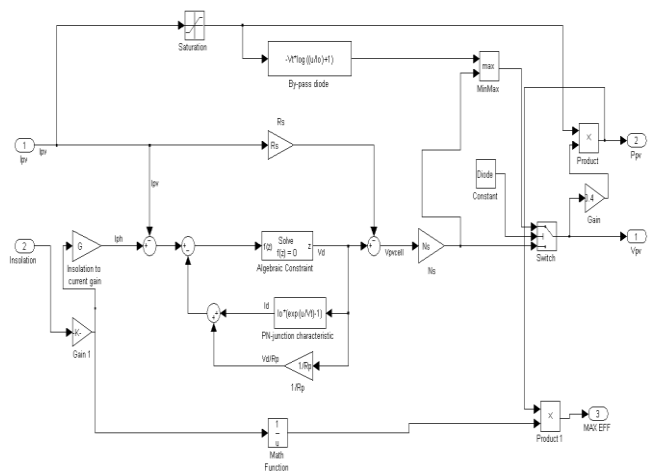


Figure 3: A part of Simulink block used in simulation

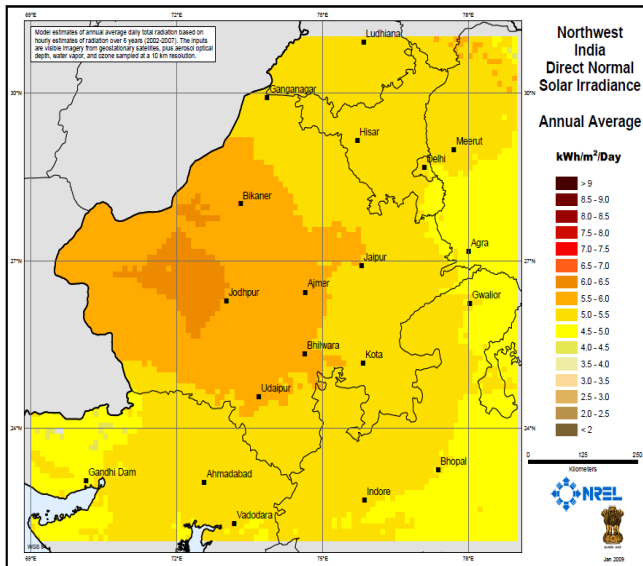


Figure 4: NW India Direct Normal Solar Irradiance Annual Average [16]

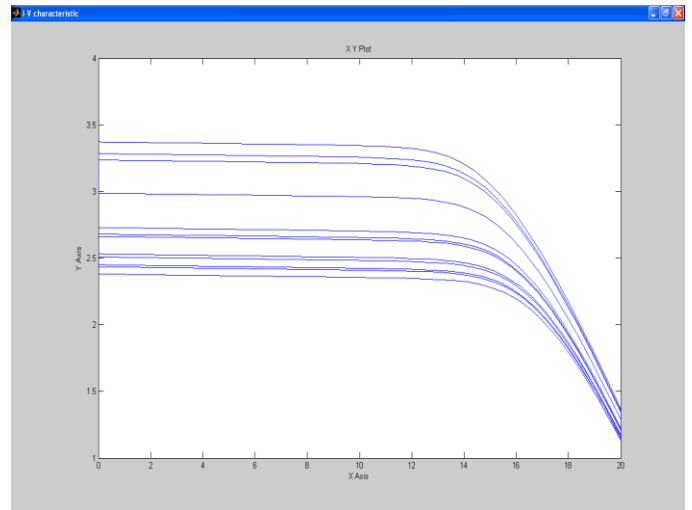


Figure 7 :I-V characteristics of the photovoltaic cell under different isolation

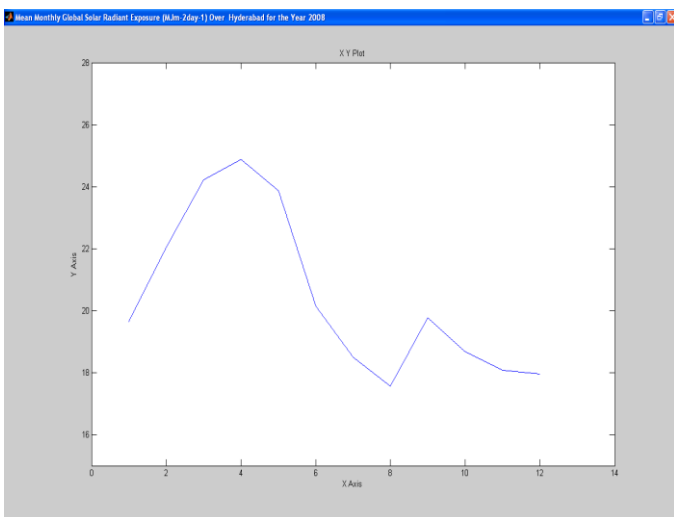


Figure 4: Monthly mean irradiance for Hyderabad[16]

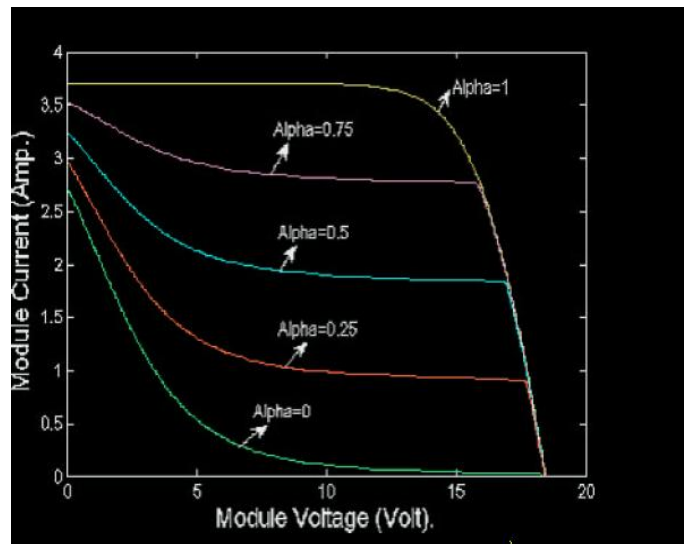


Figure 8 :I-V characteristics of the photovoltaic cell under shadow

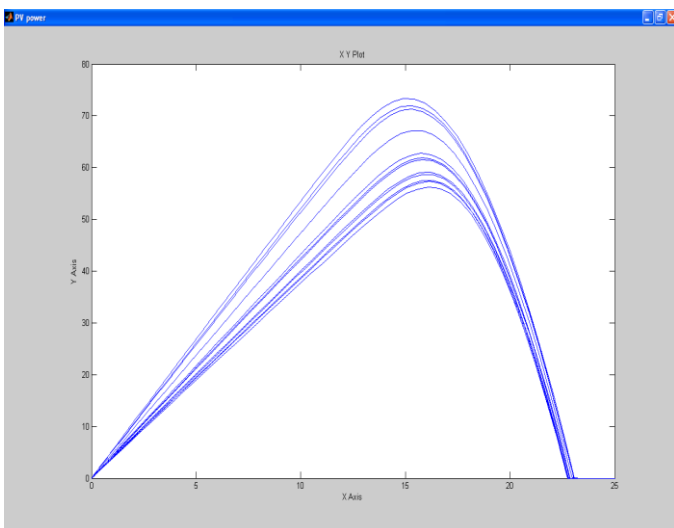


Figure 6 :P-V characteristics of the photovoltaic cell under different isolation

Solarex MSX 60 Specifications (1kW/m^2 , 25°C)

Characteristics	SPEC.
Typical peak power (P_p)	60W
Voltage at peak power (V_{pp})	17.1V
Current at peak power (I_{pp})	3.5A
Short-circuit current (I_{sc})	3.8A
Open-circuit voltage (V_{oc})	21.1V
Temperature coefficient of open-circuit voltage	-73mV/ $^\circ\text{C}$
Temperature coefficient of short-circuit current (K_I)	3mA/ $^\circ\text{C}$
Approximate effect of temperature on power	-0.38W/ $^\circ\text{C}$
Nominal operating cell temperature (NOCT)	49 $^\circ\text{C}$

Table 1; Specifications of solarex MSX 60

REFERENCES

- [1] Jawaharlal Nehru National Solar Mission Document
- [2] S. W. Angrist, , *Direct Energy Conversion*, Allyn and Bacon, Inc., 4th edition, 1982, pp. 177-227.
- [3] O. Wasynczuk, "Dynamic behavior of a class of photovoltaic power systems," *IEEE Transactions on Power Apparatus and Systems*, vol. PAS-102, no. 9, 1983, pp. 3031-3037.
- [4] J. C. H. Phang, D. S. H. Chan, and J. R. Philips, "Accurate analytical method for the extraction of solar cell model parameters," *Electronics Letters*, vol. 20, no. 10, 1995.
- [5] Spirito P, Abergamo V. Reverse bias power dissipation of shadowed or faulty cells in different array configurations. Proceedings of the Fourth European Photovoltaic Solar Energy Conference, 1982; 296–300.
- [6] Lopez Pineda CF. Experimental evaluation of reverse bias stress induced on photovoltaic modules for different configurations. *Solid Wind Technology* 1986; 3(2): 85–88.
- [7] Bishop JW. Computer simulation of the effects of electrical mismatches in photovoltaic cell interconnection circuits. *Solar Cells* 1998; 25: 73–89.
- [8] Quaschnig V, Hanitsch R. Numerical simulation of photovoltaic generators with shaded cells. Proceedings Of the 30th Universities Power Engineering Conference, 1995; 583–586.
- [9] Kawamura H, Naka K, Yonekura N, Yamanaka S, Kawamura H, Ohno H, Naito K. Simulation of I-V characteristics of a PV module with shaded PV cells. *Solar energy Materials & Solar cells* 2003; 75: 613–621.
- [10] Hermann W, Wiesner W. Modelling of PV modules—the effects of non-uniform irradiance on performance measurements with solar simulators. Proceedings of the 16th European Photovoltaic Solar Energy Conference, 2000; 2338–234
- [11] Alonso Garcia MC, Ruiz JM. Analysis and modeling the reverse characteristic of photovoltaic cells. *Solar Energy Materials and Solar Cells* 2006; 90: 1105–1120.
- [12] <http://www.mathworks.com/>
- [13] Silvestre S, Guasch D, Ortega P, Calatayud R. Photovoltaic systems modelling using matlab and simulink. Proceedings of the 19th European Photovoltaic Solar Energy Conference, 2004; 2207–2210.
- [14] Ortega P, Silvestre S, Guasch D, Navarro D, Calatayud R. Solar cell model parameter extractor based on matlab. Proceedings of the 19th European Photovoltaic Solar Energy Conference, 2004; 2194–2197.
- [15] Meyer EL, Van Dyk EE. The effect of reduced Shunt Resistance and shading on photovoltaic module performance. Proceedings of the 31 IEEE Photovoltaic Specialists Conference, 2005; 1331–1334. Copyright
- [16] Solar radiation Handbook 2008

Efficient High Speed Power Current Comparators in 180 nm

Sushil Kumar

School of Information and Communication Technology, Gautam Buddha University
Greater Noida, UP, INDIA

ABSTRACT: This research paper proposes a new kind of CMOS based current comparator circuit technique for high speed power applications. The proposed circuitry has been simulated properly in 180 nm CMOS process technology using Cadence Spectre simulator. The current comparator circuit has impressed with current pulses ranging from milli amperes to nano amperes. Also, its speed and power consumption has been successfully simulated and measured. While comparing with the earlier reported circuits, the proposed circuit attains very high speed of operation and acceptable power consumption. The power consumption of the proposed current comparator is very much lower than the other earlier proposed circuits for micron range input currents.

Keywords: CMOS, Current Comparator, Cadence Spectre, Current Pulse, Speed and Power.

I INTRODUCTION

Current mode operations have been considered as an alternative in analog circuit designs as CMOS VLSI devices are scaled down in size. Comparators are used in data converters and other front end signal processing applications. Voltage comparator encounters several difficulties including operational frequency, input offset voltage and power consumption. Current comparison has been done by impressing the current pulse signal at the input of the comparator and finding whether it is positive or negative. The output voltage generated by the comparator is used properly to indicate the result of operation. Circuit uses source follower input stage and a CMOS inverter as a positive feedback. First current comparator which is widely accepted even now a days was proposed by [1]. The circuit operation is limited by the requirement of minimum input current 10 μ A is a must to perform the comparison. The comparator provides distorted output signal below this value. An input current range up to 0.5 μ A had been demonstrated in offset free

current comparator [2]. This comparator has some shortcomings which are, it requires more number of MOS components and more power consumption. Afterwards, Soowon Kim and Byungmoo Min had come up with a new idea of current comparator [3]. It is having the requirement of an extra current reference generator. The speed of the operation of the circuit is very less when compared to present proposed circuit. The authors had come up with a current amplifier cum comparator in the year 2000, had the response time of 50 nS for 5 μ A input current, which indicated delayed response very much while being compared to the response time of the recent designs.

Altogether, a new current comparator had been proposed by [4] which had one CMOS complementary amplifier, two resistive load amplifiers and two CMOS inverters. Although, the circuit given above resolved the

power and speed issue of [1], it consumed more power and took more response time than recently published approaches. The designs in [5], [6], [7] had come up with high speed circuits, but whenever compared to the proposed one those consumed significantly more power and slow in response. The author of the paper [3] had come up with a new approach in the year 2010 of a low input impedance current comparator using pulse width modulation. The circuit in the paper [3] had pre occupied with more number of MOS and capacitors than any of the designs. In this paper, the results obtained by the proposed design are being compared with the earlier proposed design in published papers [5] and [7].

Proposed and conventional current circuit are analyzed and simulated in section 2.2 and 2.3. All the results are discussed and compared in section 2.4.

II CURRENT COMPARATOR ANALYSIS

2.1 Current Comparator

The figure 1 shown below, shows the schematic diagram of a conventional positive feedback current comparator circuit in [5]. The positive feedback operates at output nodes of the inverters M2/M5 and M3/M4 respectively. Transistors M0 and M6 are closed and transistors M1 and M7 are open in the pre decision state. The inverter M5/M2 begins to switch as the voltage on the comparator node is affected by input current. As soon as this slews to either rail, the transistors M0 or M6 are switched open and then with a delay of about 10 ns the transistors M1 or M7 respectively are switched closed. Now, the comparator node can significantly speed the decision process, particularly at the low current inputs as this latched feedback dumps enough charge on the comparator. The one of the main drawbacks of this system is that the input node slews from rail to rail and this can slow the comparator operations.

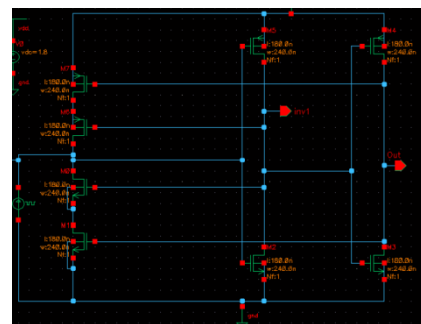


Fig.1. Conventional Current Comparator [5]

DC and Transient analyses had been performed using the Cadence Spectre simulator with 180 nm CMOS technology. The transient response of the current comparator (Min & Kim, 1998) is shown in figure 2, when

the input current pulse is normally kept at 10 μA . In this fashion, the current comparator (Min & Kim, 1998) is subjected to input current pulse range from 10 μA and 400 μA and transient analysis had been performed for the same. Basically, the current comparator performs the comparison till 10 μA and below this range output voltage starts getting distorted. Importantly, the transient analysis could be used to confirm the operating range of the comparator.

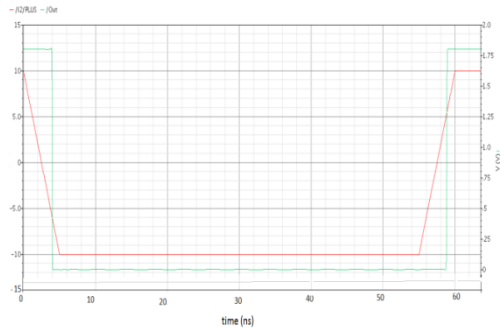


Fig.2. Transient Response of Conventional Current Comparator at 10 Ma

Thus, DC analysis was performed to calculate the average power consumption of the given comparator [5]. Figure 3 Shows the power plot of the current comparator at 10 μA .

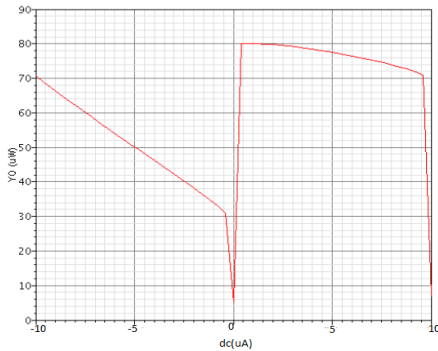


Fig.3. Current Comparator Power Plot

2.2 Current Comparator [7]

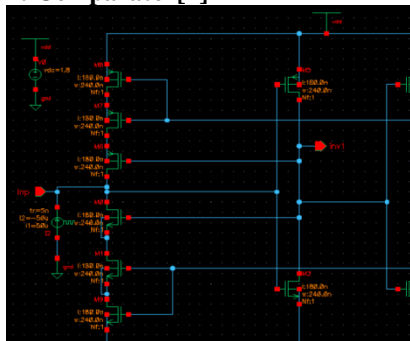


Fig.4. Conventional Current Comparator [7]

Above shown figure 4 is the current comparator circuit published in [7]. The author [7] had added two more additional MOS transistors M8 and M9, when compared to the earlier implemented circuit [5]. These MOS transistors speed up the decision process in the circuit. Transistors M0 and M6 are closed and transistors M7, M8 and M1, M9 are open in the pre decision state. The speed of operation of the comparator [7] is well increased when compared.

The figure 5 given below shows the transient response of the current comparator [7] whenever the input current pulse is at 10 μA . The transient response analysis had been performed and the current comparator [7] is subjected to input current pulse ranges from 1 mA to 400 nA. The comparison operation is well performed by the current comparator till 10 μA and below this range output gets starting distorted. The calculated 50% propagation delay of the circuit is 1.493 ns.

To compute the total power consumed by the comparator [7], DC analysis had been performed. The power consumption of the comparator [7] whenever the input current is at 10 μA , is shown in figure 6. The computed average power consumed by this comparator is comes out to be 32.6 μW at 10 μA .

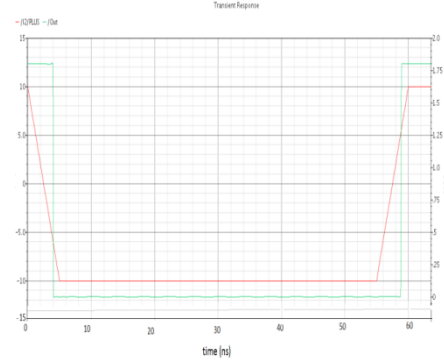


Fig.5. Transient Response of Current Comparator [7] at 10 μA

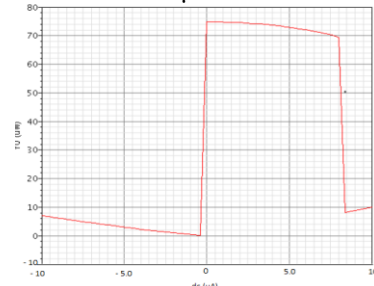


Fig.6. Current Comparator Power Plot [7] at 10 μA

2.3 Proposed Current Comparator Analysis

The given below figure 7 shows the schematic diagram of the proposed current comparator. The circuit contains parts such as power supply, standard current mirror, CMOS inverter, Wilson current mirror and input current pulse generator. To reduce the total power consumed in the circuit, Wilson current mirror was used. The current comparator used the high output impedance of the Wilson current mirror to amplify the small difference in the input currents to large variations in output voltage.

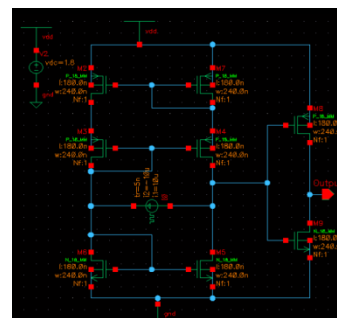


Fig.7. The Proposed Current Comparator

The Transient response of the proposed current comparator for variation of input current pulse from $-10 \mu\text{A}$ to $10 \mu\text{A}$ is shown in given below figure 8. The characteristics curves were plotted and the input current pulse had been varied from 1 mA to 400 nA during the Transient analysis. The current comparator had done a successful comparison till 400 nA and below this value the output gets starting distorted. The proposed circuit design goes working till the range of 400 nA unlike the earlier published papers [5], [7] works till the range of $10 \mu\text{A}$. Thus, the input range is increased when compared to [5] and [7]. The proposed circuit has achieved 50% propagation delay of 550 ps.

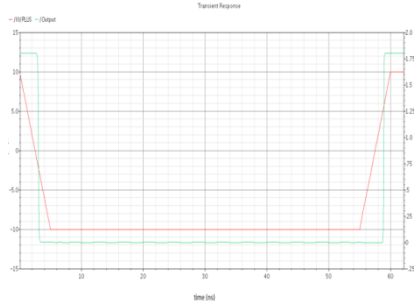


Fig.8. Transient Response of the Proposed Current Comparator at $10 \mu\text{A}$

The total power consumption by the proposed comparator had been performed by the DC analysis. The power consumption by the comparator when the input current is at $10 \mu\text{A}$ is shown in figure 9. The average power consumption by the proposed comparator is $8.7 \mu\text{W}$ at $10 \mu\text{A}$.

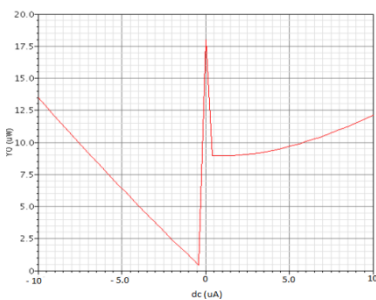


Fig.9. Power Plot of the Proposed Current Comparator at $10 \mu\text{A}$

2.4 Current Comparators Comparison

The simulation characteristics and parameters of the conventional and proposed current comparator are compared and observations are explained in great detail. It is observed from table I that when compared with the current comparators [5] and [7], the proposed new current comparator operates at very high speed. The proposed current comparator operates well up to the input current of 400 nA, although the comparators [5] and [7] functions only up to $10 \mu\text{A}$.

It is also observed from table II that from $10 \mu\text{A}$ onwards the power consumption of the new proposed current comparator is very low when compared to the power consumed by the either of the current comparators [5] and [7]. The proposed comparator consumes a little extra power than [5] and [7] but, the power consumption has been

improved a lot when the circuit is subjected with the input current below $100 \mu\text{A}$. The proposed current comparator consumes very less power than [7] from $100 \mu\text{A}$ onwards.

Table I. Comparison among the Current Comparators – 50% Propagation Delay (ps)

Input Current	Proposed Current Comparator	Current Comparator [6]	Current Comparator [8]
1 mA	110	219	229
100 mA	248	561	577
$10 \mu\text{A}$	550	1964	1493
$1 \mu\text{A}$	1564	Not Worked	Not Worked
400 nA	2408	Not Worked	Not Worked

Table II. Comparison among the Current Comparators – 50% Power Dissipation (W)

Input Current	Proposed Current Comparator	Current Comparator [6]	Current Comparator [8]
1 mA	1.35 m	0.763 m	1.15 m
100 mA	80μ	52.7μ	81.4μ
$10 \mu\text{A}$	8.8μ	61.4μ	32.6μ
$1 \mu\text{A}$	5.27μ	Not Worked	Not Worked
400 nA	21.4μ	Not Worked	Not Worked

The figure 10 given below shows the delay time versus input current graph. The graph vividly states that the proposed current comparator attains better performance than its counter parts [5] and [7].

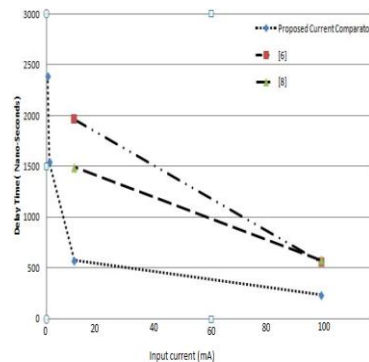


Fig.10. Delay Time versus Input Current

The figure 11 shows the power dissipation versus input current graph. The proposed circuit dissipates little extra power for large current inputs say 1 mA. From $100 \mu\text{A}$ onwards the proposed comparator dissipates lower power than the earlier published paper [7] and from $61 \mu\text{A}$ onwards it dissipates lower power than both [5] and [7]. The circuit power dissipation is far better than its counterparts as shown in table II below $100 \mu\text{A}$.

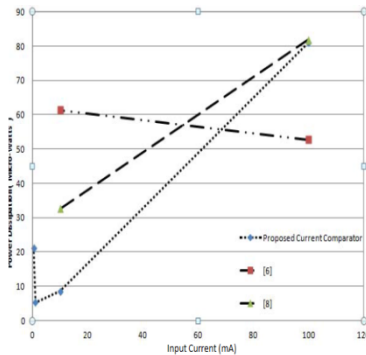


Fig.11.Power Dissipation versus Input Current

III. CONCLUSION

The goal of this paper was to present a simple idea of designing a new CMOS based current comparator topology for high speed applications such as digital switching circuits and data converters. The proposed comparator operates at very high speed in figure 10 and 11, when compared with the performance of the existing current comparators [5] and [7]. Also, the proposed new current comparator consumes very low power from 10 μ A onwards when compared to the comparators in [5] and [7].

REFERENCES

- [1] Traff, H. (1992). Novel Approach to High Speed CMOS Current Comparators. *IEEE Proceedings Electronic Letters*, 28(3).
- [2] Lin, C. W., & Lin, S. F. (2010). Low Input Impedance Current Comparator Using in Pulse-Width Modulation. *IEEE Proceedings - ICCE*, 127-130.
- [3] Banks, D., & Toumazou, C. (2008). Low-power high- speed current comparator design. *IEEE Proceedings Electronic Letters*, 44(3).
- [4] Wu, C. Y., Chen, C. C., Tsai, M. K., & Cho, C. C. (1991). A 0.5uA Offset-Free Current Comparator For High Precision Current Mode Signal Processing. *IEEE Proceedings – Circuits and Systems*, 1829-1832.
- [5] Min, B. m., & Kim, w. S. (1998). High performance CMOS current comparator using resistive feedback network. *IEEE Proceedings-Electronic Letters*, 34, 2074-2076.
- [6] Ziabakhsh, S., Rad, H. A., Rad, M. A., & Mortazavi, M. (2009). The Design of a Low-Power High-Speed Current Comparator in 0.35 μ m CMOS Technology. *IEEE Proceedings*.
- [7] Chen, L., Shi, B., & Lu, C. (2000). A High Speed/Power Ratio Continuous-Time CMOS Current Comparator. *IEEE Proceedings–Electronics, Circuits and Systems, ICECS*, 2, 883-886.
- [8] Kushwah, B. C., Soni, D., & Gamad, R. S. (2009). New Design of CMOS Current Comparator. *IEEE Proceedings - ICETET*, 125-129.
- [9] Palmisano, G., & Pennisi, S. (2000). Dynamic Biasing for True Low-Voltage CMOS Class AB Current-Mode Circuits. *IEEE Transactions on Circuits and Systems-II: Analog and Digital Signal Processing*, 47, 1569-1575.

Transcoding Method for Regions of Interest

Soon-kak Kwon

Department of Computer Software Engineering, Dongeui University, Korea

Abstract : When a bitstream of the higher bitrate is converted to the lower bitrate through the transcoding process, the ROI (Regions of Interest) can be considered. We classify the ROI as the groups of macro-blocks with non-zero motion vectors. For simple implementation, the motion vectors are not additionally estimated, but extracted from the coded bitstream of the higher bitrate before transcoding. Then, a proposed method assigns a specific quantization step-size differentially according to the ROI within a video. The picture quality can be increased by applying the quantization step-size as a small value relatively for the ROI compared with the non-ROI. We can find the result that the proposed method gives the improved picture quality by assigning the quantization step-size differentially.

Keywords - ROI, Transcoding, Picture Quality

I. INTRODUCTION

For both the homogeneous and heterogeneous transcodings, the bitrate reduction may be needed when the original higher bitrate cannot be accepted. The bitrate reduction algorithm converts from high bitrate bitstream to lower rate bitstream. Although there are several methods for bitrate reductions [1-6], the re-quantization method is well used because of the simple implementation and a less processing time.

All of transcoding methods deal with proper allocation of bitrate or quantization step-size in order to satisfy good picture quality or high PSNR (Peak Signal to Noise Ratio) on the constraint of the limited bitrate after transcoding. However, it is insufficient to meet the need of picture quality for ROI (Regions of Interest) within video sequence.

The several methods [7-12] have been researched for ROI coding, such as a classification of the foreground and background, a detection of the human face, a determination based on user attention model. However it did not include the bitstream transcoding schemes.

We propose a new transcoding method that makes better video quality relatively in ROI. ROI is classified to the moving regions. For searching moving regions, we use the coded information within the bitstream before transcoding. If the coded information before transcoding is used to find ROI, then the extra complexity is not needed. First, the non-zero motion vectors of each macro-blocks are grouped to separate the zero motion vectors. Then the groups with large numbers of non-zero motion vectors are set to ROI, the groups with small numbers of non-zero motion vectors are set to the non-ROI.

The organization of this paper is as follows. Section II provides the conventional relationship of bitrate and quantization step-size for transcoding. In Section III, the proposed transcoding method is described for improving the

subjective picture quality by properly allocating the quantization parameters dependently on the ROI. Section IV shows the simulation results of the proposed method about quantization parameter compared with the conventional one. In Section V, we summarize the main results.

II. RELATIONSHIP OF BITRATE AND QUANTIZATION STEP-SIZE FOR TRANSCODING

The previous researches [13,14] showed the relationship between bitrate and quantization step-size for transcoding, a linear relative formula as a logarithmic function between bitrate (R) and quantization step-size ($Qstep$),

$$\log Qstep = b + a \cdot \log R \quad (1)$$

where, b and a are dependent on the video characteristics. Also a transcoding algorithm has been presented which updates the model parameters given for the previous picture or slice using an approximated relationship between bitrate and quantization step-size according to the coded picture-type. That is, if a target bitrate in bits per second, BR_t (bps) is given in the case of already an encoded bitrate BR_1 (bps) in bits per second, then target quantization step-size $Qstep_t$ is obtained from following equation.

$$Qstep_t = Qstep_1 \cdot \left(\frac{BR_t}{BR_1} \right)^a \quad (2)$$

where, the value of a is approximated by the previous coded results.

Also our previous research[12] has proposed the transcoding method to control the picture quality depended on the subjectively ROI. The subjectively ROI determined using motion vectors were classified by following four different cases in the aspect of subjective importance.

- (1) Central focus video: The focus is on the central regions rather than the whole frame in the case where object movement is primarily in the central regions of a picture. The background may either be fixed or moving uniformly through camera panning. This can be considered a default type if a frame is not classified into the other three types because humans tend to concentrate their viewpoint on the central region of a video.
- (2) Peripheral focus video: The region of interest is focused on the contour in the case where the scene is being zoomed-out. The representative motion vector values of the top and bottom regions have non-zero values while those of the central regions are approximately zero.
- (3) Upper focus video: The region of interest is in the upper regions in the case where object movement is located in the upper regions of a picture. The representative motion vector values in the upper regions of a frame have non-zero values with zero values in the lower regions.

- (4) Lower focus video: The region of interest is in the lower regions in the case where object movement is located in the lower regions of a picture. The representative motion vector values at in the lower of a picture have non-zero values with zero values in the upper regions.

After the above classification of picture for the subjectively interest regions, the value of quantization step-size was differently assigned according to the location of slice of picture.

III. PROPOSED TRANSCODING METHOD FOR ROI

We propose a new transcoding method that makes better video quality relatively in ROI. ROI is classified as the groups of macro-blocks with non-zero motion vectors. For getting the motion vectors, we use the coded information within the bitstream before transcoding. First, the non-zero motion vectors of each macro-blocks are grouped to separate the zero motion vectors. Then the groups with large numbers of non-zero motion vectors are set to ROI, the groups with small numbers of non-zero motion vectors are set to the non-ROI.

Step1) Grouping the non-zero motion vectors of macro-blocks for the bitstream before transcoding

Step2) Eliminating the group with small numbers of non-zero motion vectors. The small number of macro-blocks are not important to give the subjective picture quality. Therefore, in this paper, the group having less than 15 macro-blocks is eliminated from the group of non-zero motion vectors.

Step 3) Classifying the ROI. ROI is the non eliminated groups and the others the non ROI. The groups of large number of non-zero motion vectors is only considered to ROI.

Step 4) Reassigning the quantization step-size. For the ROI, the quantization step-size is assigned to lower value than the target quantization step-size of Eq. (2), but for the non-ROI, the higher quantization step-size is assigned.

$$Qstep = Qstep_t - \alpha, \text{ for ROI} \quad (3)$$

$$Qstep = Qstep_t + \alpha, \text{ for Non-ROI} \quad (4)$$

where, $Qstep$ is final assigned quantization step-size, and α is a constant. α can affect to the difference in the quantization step-size between the maximum and the minimum values. A large value of α makes the large difference of picture quality between ROI and non-ROI.

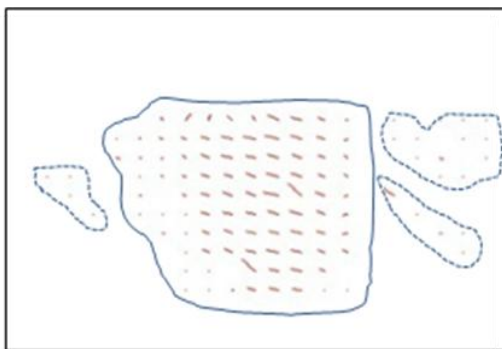


Fig 1. Grouping of macro-blocks according to non-zero motion vectors

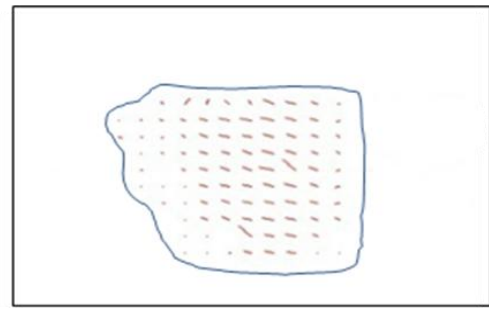


Fig 2. Eliminating of Grouped macro-blocks

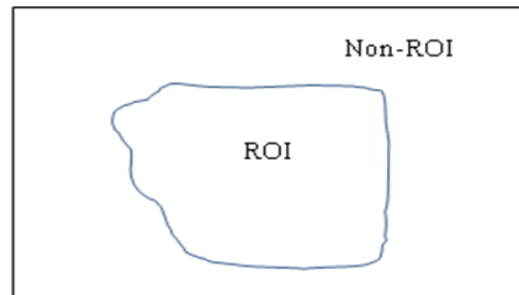


Fig 3. Classified ROI and Non-ROI

IV. SIMULATION RESULTS

The JM [15-18] that is a standard coding software tool of the H.264 was used to the simulation where Foreman video with horizontal and vertical resolutions of 352 and 228 pixels was selected.

The B-picture is not included due to the use of the H.264 baseline profile, and 15 pictures are configured as one GOP in which the video applies 60 pictures. The number of slices is the same as for each picture and that are determined by 18 along the vertical direction.

The quantization step-size was differentially applied for each macro-blocks by using the value of determined in Eq. (3,4). Also, the coding was performed as an objective bitrate for the original video based on four different α of Eq. (3,4), such as 2, 4, 6, and 8, from the classification of the difference between the maximum and the minimum values of the quantization step-size.

1) Measurement of the objective PSNR

This paper investigated the PSNR (peak signal to noise ratio) that is an objective picture quality criterion. The conventional method applied a bitstream coded with of 1.5Mbps, is transcoded to the bitrate of 0.8Mbps. Then, the quantization step-size was differentially assigned with the unit of macro-blocks using the proposed method for the Foreman video, according to the criterion of subjectively ROI.

Table 1 shows the average value of the PSNR for 60 pictures after transcoding in the Foreman video and maximum difference of quantization parameters within picture is set to 2, 4, 6 and 8. It can be seen that the values of the PSNR decreased according to the differential application of the quantization step-size among macro-blocks compared to the method that applies the same quantization step-size values for all macro-blocks within same slice. In the case of $\alpha = 6$, the PSNR was decreased about 0.07dB, and it was decreased about 0.28dB for the $\alpha = 8$.

Table 1. Average PSNR for the bitstream coded with of 1.5Mbps, is transcoded to the bitrate of 0.8Mbps.

Conventional method [dB]	Proposed method, α [dB]			
	2	4	6	8
37.83	37.81	37.76	37.70	37.55

2) Measurement of subjectively picture quality

For measuring of the subjective picture quality, we used DSCQS (Double Stimulus Continuous Quality Scale) [19]. According this method, the assessors are positioned at a distance from the monitor equal to three times the diagonal length of the monitor used to display the videos. They then observe two videos in sequence on the monitor; one is an original video and the other is a video either using the conventional method or the proposed method. The presentation order of the original and processed videos was random.

The presentation of the test material:

- 1 Video A (Original or Processed) 12s,
- 2 Gray 3s,
- 3 Video B (Processed or Original) 12s,
- 4 Gray 3s

Assessors evaluated the picture quality of both videos using an ITU-R quality scale (Excellent=5, Good=4, Fair=3, Poor=2, Bad=1) [12,20].

The final subjectively picture quality assessment score was calculated from the mean over all assessors;

$$U = \frac{1}{N} \sum_{i=1}^N u_i \quad (5)$$

where u_i is score which is determined by each assessor, and N is number of assessors.

The measurement of the subjectively picture quality was performed by distributing reconstructed videos to 10 assessors without notification of the methods and the ROI. We got the same average score of the subjectively picture quality obtained from 10 evaluators as shown in Table 2.

Table 2. Results of the subjectively picture quality for the bitstream coded with of 1.5Mbps, is transcoded to the bitrate of 0.8Mbps .

Conventional method	Proposed method, α			
	2	4	6	8
3.0	3.1	3.2	3.4	3.3

In the results, because the Foreman video showed no movements in the background and some movements at the central region, it represented good picture quality in the aspect of a subject manner based on the assigning of the quantization step-size with ROI of the central moving regions. The desirable difference between the maximum and the minimum values of the quantization step-size between ROI and non-ROI was 6. If the difference between the maximum and the minimum values showed more than 8, then the subjectively picture quality was getting worse.

Although the objective PSNR value that is the average value of the entire picture slightly was decreased for the differential assign of the quantization step-size within the video sequence according to ROI, the subjective picture

quality that has a focus on interest points within the video sequence was increased. It means that the measurement of objective picture quality only will not fully satisfy the visual picture quality of human being. In addition, it is possible to present an improvement effect in picture quality by applying the results of the evaluation of subjective picture quality to the objective picture quality while there is no change in bitrates.

Fig .4 illustrates the reconstructed picture of Foreman video for the bitstream coded with of 1.5Mbps, is transcoded to the bitrate of 0.8Mbps with conventional method and the proposed methods of different α . When $\alpha =6$, the subjective picture quality of Foreman video looked better relatively. When $\alpha =8$, although the subjectively picture quality of ROI was getting best, the subjective picture quality of non-ROI was getting the coarsest picture quality level.



(a) Reconstructed frame of conventional method



(b) Reconstructed frame of proposed method, $\alpha =4$



(c) Reconstructed frame of proposed method, $\alpha =6$



(d) Reconstructed frame of proposed method, $\alpha =8$

Fig. 4 Comparison of the four reconstructed frames of Foreman video

V. CONCLUSION

This paper classified ROI and non-ROI within the video according to motion vectors. The moving regions of non-zero motion vectors is set to focus region, then quantization step-size (parameter) is assigned to the focus regions differentially compared to the non focus regions. Proposed method obtained an improvement effect in subjective picture quality compared to the conventional method through the intensive application of the quantization step-size.

Although this study focused on the H.264 video coding, it can be directly used to other video coding standards including the HEVC[21]. In addition, it can be expected that this research will be extensively applied with other various bitstream transcoding techniques.

ACKNOWLEDGEMENTS

This work was supported by Dongeui University Foundation Grant (2010)..

REFERENCES

- [1] T. Shanableh and M.Ghanbari, Heterogeneous video transcoding to lower spatio-temporal resolutions and different encoding formalisms, *IEEE Trans. Multimedia*, 2(2), 2000, 101-110.
- [2] M. Xia, A. Vetro, B. Liu, and H. Sun, Rate-distortion optimized bit allocation for error resilient video transcoding, *Proc. IEEE Int. Symp. Circuits and Systems*, 2004, 945-948.
- [3] W. Lie, M. Tsai, and T. Lin, Rate-distortion optimized DCT-domain video transcoder for bit-rate reduction of MPEG videos, *Proc. IEEE Int. Conf. Acoustics, Speech, and Signal Processing*, 5, 2004, 969-972.
- [4] L. Chen, L. Cheng, and S. Yu, Accurate rate control method in transcoding, *Electron. Lett.*, 40(1), 2004, 16-18.
- [5] J. Lei and N. Georganas, Accurate bit allocation and rate control for DCT domain video transcoding, *Proc. IEEE Canadian Conf. Electrical and Computer Engineering*, 2002, 968-973.
- [6] H. J. Lee, T. Chiang, and Y. Q. Zhang, Scalable rate control for MPEG-4 video, *IEEE Trans. Circuit Syst. Video Technology*, 10(9), 2000, 878-894.
- [7] D. Chai, K. N. Ngan and A. Bouzerdoum, Foreground / background bit allocation for region-of-interest coding, *Proc. Int. Conf. on Image Processing*, 2000, 438 - 441.
- [8] M. J. Chen, M. C. Chi, C. T. Hsu, and J. W. Chen, ROI video coding based on H.263+ with robust skin-color detection technique, *IEEE Trans. Consumer Electronics*, 49, 2003, 724-730.
- [9] M.-C. Chi, C.-H. Yeh, and M.-J. Chen, Robust region-of-interest determination based on user attention model through visual rhythm analysis, *IEEE Trans. Circuit Syst. Video Technology*, 19(7), 2009, 1025-1038
- [10] L. Tong and K. R. Rao, Region of interest based H.263 compatible codec and its rate control for low bit rate video conferencing, *Proc. Int. Symp. Intelligent Signal Processing and Communication Systems*, 2005, 249-252.
- [11] H. J. Song and C. C. J. Kuo, A region-based H.263+ codec and its rate control for low VBR video, *IEEE Trans. Multimedia*, 6(2), 2004, 489-500.
- [12] S.-k. Kwon, A. Panchihewa, D. G. Bailey, S.-W. Kim, and J. Lee, Adaptive simplification of prediction modes for H.264 intra-picture coding, *IEEE Trans. Broadcasting*, 58(1), 2012, 125-129.
- [13] Y.-I. Wu, S.-k. Kwon, Transcoding method of H.264 coded bitstream for interest region, *The International Journal of Virtual Reality*, 8(3), 2009, 45-50.
- [14] S.-k. Kwon, S.-w. Kim, J.-h. Lee, and J.-m. Lee, An adaptive transcoding method, *International Journal of Computer Science and Network Security*, 8(12), 2008, 154-160.
- [15] S. k. Kwon, A. Tamhankar and K. R. Rao, Overview of H.264/MPEG-4 part 10, *Journal of Visual Communications and Picture Representation*, 17(2), 2006, 186-216.
- [16] ITU-T Rec. H.264 / ISO/IEC 11496-10, Advanced video coding, Final Committee Draft, Document JVT-F100, 2002.
- [17] T. Widegand, G. Sullivan, G. Bjontegaard and A. Luthra, Overview of the H.264/AVC video coding standard, *IEEE Trans. Circuit Syst. Video Technology*, 13(7), 2003, 560-576.
- [18] H.264/AVC JM Software, <http://iphome.hhi.de/suehring/tml/download>.
- [19] M. Bernas, Image quality evaluation, *Int. Symp. Video/Image Processing and Multimedia Communications*, 2002, 133-136.
- [20] ITU-R Rec. BT. 500, Methodology for the subjective assessment of the quality of television pictures, 2002, Geneva.
- [21] K. Ugur, K. Andersson, A. Fuldseth, G. Bjontegaard, L. P. Endresen, J. Lainema, A. Hallapuro, J. Ridge, D. Rusanovskyy, C. Zhang, A. Norkin, C. Priddle, T. Rusert, J. Samuelsson, R. Sjoberg, and Z. Wu, High performance, low complexity video coding and the emerging HEVC standard, *IEEE Trans. Circuit Syst. Video Technology*, 20(12), 2010, 1688-1697.

Effect of the Supporting Strata on Design of Windmill Tower

K.S. Rahane¹, M.R. Wakchaure²

1(PG student, Civil Engineering Department, Amrutvahini College of Engineering, Maharashtra, India)

2(Faculty, Civil Engineering Department, Amrutvahini College of Engineering, Maharashtra, India)

Abstract : Windmill, machine that converts wind into useful energy. This energy is derived from the force of wind acting on oblique blades or sails that radiate from a shaft. The turning shaft may be connected to machinery used to generate electricity. The present paper makes an attempt to show the effect of wind and earthquake load on tubular type windmill and its foundation considering hard, medium and soft soil strata. The modeling of windmill tower was done in computer software by finite element modeling technique. In that windmill tower was subjected to wind and earthquake forces and check bending stresses, mode Shape, base shear comparison, stability, safety of windmill for hard, medium and soft strata. Also check stability, safety of windmill foundation and design of reinforcement required in the foundation for hard, medium and soft strata. Based on the analytical investigation and design it has been concluded that the effect of wind on windmill is significant as compare to earthquake, hence stability of windmill is thoroughly check for this load. Soil strata also play a major role in deciding its safety and stability. The normalized base shear, seismic moments, natural time period, bending stresses in tower and sizes and reinforcement of foundation increases from hard strata to soft strata.

Keywords - Wind load, Earthquake load, stability of tower and foundation, soil strata.

I. Introduction

The world of wind power is growing at a very faster rate. This projection put the average growth of the industry at 24% for the next five years. Theoretically wind could produce enough energy to meet global demand. Growth will be driven by rapidly developing countries, such as India, Brazil, and China. Improving efficiency and falling cost of turbine production and installation will make wind power more price competitive. The amount of wind energy generated depends mostly on the size, height, type and location of a wind turbine. Windmill although are structurally simple, their behavior under the operating condition is quit complex due to the static and dynamic effect of wind. Due to the operation of the windmill during high wind makes the behavior still more complex. If these windmills are founded on relatively soft foundation soil, structural stability during dynamic loads can be one more matter of concern.

The main components of windmill are windmill tower, nacelle, hub, and blade. The windmill basically divided into Horizontal axis machines and Vertical axis machines, based on their axis of rotation. For more electric energy generation Vertical axis Windmill i.e. tubular type windmill and lattice type of tower windmill is mostly used. Foundations for windmill are rectangular, square, and circular of a similar configuration. Very high requirements

are imposed on windmill foundation with respect to durability and strength. This uneven loading also has effects on the strength of the reinforcement structure provided in the concrete main part. With the windmill foundation, the reinforcement structure generally consists of the known reinforcing bar or reinforcing steel mesh.

For the analysis we have taken the 74 meter height tubular type windmill with three blade of each 32 meter length. The total weight of windmill was 184 ton. The power generation capacity of this windmill was 1250 KW. This windmill were analyzed in computer software for different load such as dead load, wind and earthquake loads. The main objectives of this paper was to determine the most vulnerable combination of windmill structure and foundation under the action of dynamic load for different soil strata such as hard, medium, soft strata. So that suitable remedial measures can be taken during the design. According to that design of circular foundation was done in order to achieve economy, stability, safety of foundation, so that windmill is withstand safely.

II. Methodology

Windmill structures are relatively flexible and have a longer fundamental period. If such structures are founded on rigid foundation such as rock or hard soil, seismic force may not govern the design as wind force become more critical, but many times due to non availability of hard rock it may be necessary to construct such structures on soft soil. This is especially true near the sea shore, where most of the area consists of reclaimed soil and mostly windmills are constructed at the sea shore as wind is much effective in this area and availability of land is easily accessible. As a result of this soft layer of soil the earthquake ground motion gets modified and have relatively longer predominant period. Due to this it is essential to analyze and design of windmill for soft, medium, and hard soil strata.

2.1 Wind Analysis

Wind speed in the atmospheric boundary layer increases with height from zero at ground level to a maximum height called the gradient height. As the windmill is of greater height and normally situated in open terrain category the wind load is major affecting factor. This effect of wind on structure as a whole was determined by the combined action of external and internal pressure acting on it. The Wind analysis was done by using IS-875(Part-3) code. As per code wind speed considered for proposed site was 39 m/s. Due to the high rise of the structure the wind speeds also increasing. So the greater effect produced on the Windmill. Therefore wind load (F) on windmill structure acting in a direction normal to the individual structural element was calculated by:

$$F = C_f A P_z \quad (1)$$

Where, C_f = Force coefficient; A = surface area of structural or cladding unit; P_z = design wind pressure.

The windmill experiences both compression and a bending moment about its footing. The compression is due to the weight of the nacelle and rotor whilst the bending moment is induced by the thrust caused by drag forces on the blade of windmill. The tower itself also experiences an unevenly distributed force due to the drag forces created by the oncoming wind. This drag force or thrust due to wind was calculated as per IS-875 Part-3 as below:

$$F = C_f A P_z \quad (2)$$

2.2 Earthquake Analysis

The dynamic response of a structure against an earthquake vibration is an important structural aspect which directly affects structural resistance and consequently the hazard level. For analysis for earthquake loads, it is necessary to find out characteristics of structure as well as earthquake. Characteristics of the windmill were determined by Response Spectrum method analysis. In Response Spectrum method analysis the fundamental time period and mode shapes of the structure can be found out. The main objective of this analysis was to understand the overall behavior of windmill structures founded on soil strata. Response Spectrum method analysis of the different windmill towers was carried out by considering tower as a continuous system. By considering tower as cantilever beam fixed at one end and free at the other, natural time period can be computed from the Equation:

$$W_n = C_n \sqrt{EI/ml^4} \text{ \& } C_n = a_n L^2 \quad (3)$$

Where, W_n = Natural frequency of the system in n^{th} mode; C_n = Constant for boundary conditions; $a_n = 4\sqrt{m/w^2/EI}$; E = Modulus of elasticity; I = Moment of inertia of the given system; m = Mass per unit length of the system; L = Total length of the system

III. Performance Analysis

Selection of windmill is depending upon the availability of wind speed, power generation capacity. Windmill can be best analyzed as tall cylindrical tower of uniform cross section because they produce minimal lift as they display no surfaces that with an angle of attack that can produce a significant pressure difference.

3.1 Modeling of Windmill Tower

The modeling of windmill tower was done by using Finite element modeling technique. Tower of the windmill was modeled with 4-noded tetrahedral elements in computer software which is shown in Figure 1. All elements were connected to each other with proper boundary condition. The support condition considered for this structure was pinned because of load transfer from tower to foundation is through anchor bolt.

Total number of 4-noded tetrahedral elements = 2700



Figure1. Modeling of windmill Tower

3.2 Loading

The windmill is mainly subjected to Dead load, Wind load and Earthquake load. In that Wind load is the major governing factor for changing behavior of windmill.

3.2.1 Dead load

The nacelle, hub and blades were mounted on windmill tower. So weights of these components were taken to be considered for the analysis. And also considered self weight of tower.

Dead load of nacelle = 52 Ton = 510 KN

Dead load of hub = 12 Ton = 120 KN

Dead load of 3 blade = 130 KN

3.2.2 Live load

In this case there was not any type of Live load acting on windmill tower; so live load considered should be zero.

3.2.3 Wind load

Windmills are cylindrical and high rise structure, so the wind analysis of this structure is important and shall be done by using IS-875 (Part-3) method.

i) Design wind Pressure (P_z)

The wind pressure on plates of windmill tower was given by:

$$P_z = 0.6 V_z^2 \quad (4)$$

Where, $V_z = k_1 k_2 k_3 V_b$; $k_1 = 0.92$; $k_2 = 0.93$ for 10 m height; $k_2 = 0.97$ m for 15 m height; $k_2 = 1.0$ m for 20 m height; $k_2 = 1.04$ m for 30 m height; $k_2 = 1.10$ m for 50 m height; $k_2 = 1.17$ m for 100 m height; $k_3 = 1$; $V_b = 39$ m/s

Table 1 Design wind pressure (P_z)

Height of tower (M)	V_z (m/s)	P_z (KN/m ²)
10	33.37	0.67
15	34.80	0.73
20	35.88	0.77
25	36.60	0.81
30	37.32	0.84
35	37.86	0.86
40	38.40	0.89
45	38.93	0.91
50	39.47	0.93
55	39.72	0.94
60	39.97	0.96
65	40.22	0.97
70	40.47	0.98
75	40.73	1.00

ii) Wind forces on windmill tower

The wind load, F acting as a pressure load on the individual plate element was given by;

$$F = C_f A P_z \quad (5)$$

Where, $C_f = 1$ for H/B ratio = 18.50 & Circular shaped element... (Table No.23, Page No.40); A = surface area of four noded rectangular plate; P_z = design wind pressure.

Table 2 Wind force (F)

Height of tower (m)	$F = C_f A P_z$ (KN/m ²)
---------------------	--------------------------------------

10	0.67
15	0.73
20	0.77
25	0.81
30	0.84
35	0.86
40	0.89
45	0.91
50	0.93
55	0.94
60	0.96
65	0.97
70	0.98
75	1.00

This wind load are applied on plate of windmill tower as a pressure load along positive X-direction(WLX+), negative X-direction(WLX-), positive Z-direction(WLZ+), negative Z-directive (WLZ-) in computer software which is shown in Fig.2

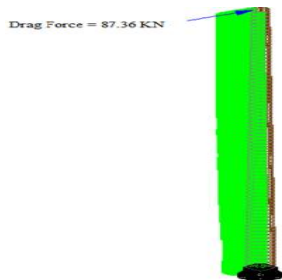


Figure 2.Wind load on windmill tower

iii) Drag force on blade of windmill due to wind pressure
 The tower itself also experiences an unevenly distributed force due to the drag forces created by the oncoming wind on blades .This drag force or thrust due to wind was calculated as per IS-875 Part-3 as below;

$$F = C_f A P_z \tag{6}$$

Where, $C_f = 0.6$...for ellipse shape element..... (Table No.23, Page No.40); $A =$ Average area of one blade = $32 * ((2.75+1.5+0.3)/3) = 48.53 \text{ m}^2$; $P_z = 1 \text{ KN/m}^2$
 Therefore, $F = 0.6 * 1 * 48.53 * 3 = 87.36 \text{ KN}$

This drag force applied at top of tower horizontally which is as shown in Fig.3

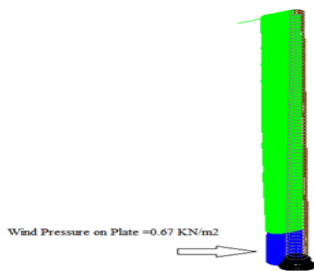


Figure 3. Drag force on windmill

3.2.4 Earthquake load

In computer software the earthquake analysis of windmill was done by using response spectrum method. The analysis gives result such as seismic base shear, seismic

moment at C.G.of tower due to seismic forces, seismic moment at bottom of tower due to seismic shear, deflection of tower, bending stresses in plate due to seismic forces.

The total design lateral force or design seismic base shear (V_B) along any principal direction shall be determined by the following expression;

$$V_B = A_h W \tag{7}$$

Where, $A_h = Z/2 * I/R * S_a/g$; $W =$ seismic weight of structure

The basic parameters required for the analysis of earthquake as per code IS-1893-2002 are:

- Zone factor (Z) = 0.16 for Pune (India) region
- Importance factor = 1
- Response reduction factor = 5
- Damping factor = 0.02
- Frequency (ZPA) = 33

$S_a/g =$ Average response acceleration coefficient and depend on natural period of vibration and damping of the structure.

The seismic load applied in X, Y & Z direction as shown in Fig.4

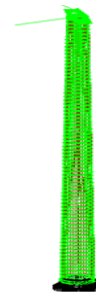


Figure 4.Earthquake load on windmill

3.3 Load Combinations

The load combinations for Design of RCC foundation and analysis and design of steel structure shall be taken as per IS-456-2002, IS-800-1984, and IS-1893-2002.

Load combinations for Foundation design:

1. (DL+LL)
2. DL+LL± (WLX+)
3. DL+LL± (WLZ+)
4. DL±EQX
5. DL±EQZ
6. DL±EQY
7. DL± (WLX+)
8. DL± (WLZ+)

Load combinations for Windmill tower:

1. DL+LL
2. 0.75[DL+0.5LL±EQX]
3. 0.75[DL+0.5LL±EQZ]
4. 0.75[DL+0.5LL±EQY]
5. 0.75[DL+LL± (WLX+)]
6. 0.75[DL+LL± (WLZ+)]
7. 0.75[DL±EQX]
8. 0.75[DL±EQZ]
9. 0.75[DL±EQY]
10. 0.75[DL± (WLX+)]
11. 0.75[DL± (WLZ+)]
12. 0.75[0.9DL±EQX]
13. 0.75[0.9DL±EQZ]
14. 0.75[0.9DL±EQY]
15. 0.75[0.9DL± (WLX+)]
16. 0.75[0.9DL± (WLZ+)]

IV. Design of Circular Foundation

The function of foundation is to transmit the load from the structure to underlying soil. If these loads are to be properly transmitted, footing must be designed to limit the total settlement of the structure to a tolerably small amount and to eliminate as nearly as possible the differential settlement or rotation of the various part of the structure and to provide adequate safety against overturning and sliding. The choice of suitable type of footing for a structure depends on the depth at which the bearing strata lies, the soil condition and the type of superstructure.

For this structure we used circular type foundation with pedestal. The general dimensions of the circular foundation are shown in Figure 5. The size of foundation is depending upon the total load from tower to foundation and bearing capacity of soil. The foundation was checked for one way shear, two way shears. The foundation was design for soft, medium and hard strata. The net safe bearing capacity of hard, medium and soft strata soil was considered as 350.00 KN/m², 200.00 KN/m², and 115.00 KN/m² respectively. The design of pedestal and footing for different soil strata are listed in Table 3

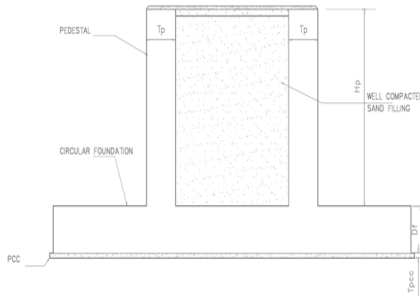


Figure 5. Circular Foundation

Table 3 Design of Foundation for hard, medium and soft strata

Sr. No.	Item	Hard strata	Medium strata	Soft strata
	A) Pedestal			
1	Outer dia of pedestal(mm)	4300	4300	4300
2	Inner dia of pedestal(mm)	3700	3700	3700
3	Ht of pedestal(mm)	2700	2700	2700
4	Ht of pedestal above FFL(mm)	500	500	500
5	T.O.G.Elevation(mm)	700	700	700
6	Vertical R/F@ outer face	74 nos-25Ø	74 nos-25Ø	74 nos-25Ø
7	Vertical R/F@ inner face	84 nos-25Ø	84 nos-25Ø	84 nos-25Ø
8	lateral ties	10Ø @ 150 c/c	10Ø @ 150 c/c	10Ø @ 150 c/c

B) Footing				
1	Outer dia of footing (mm)	1800	19000	21500
2	Thickness of footing (mm)	1100	1100	1100
3	R/F @ bottom face	20Ø @ 100 c/c both way	20Ø @ 100 c/c both way	20Ø @ 100 c/c both way
4	R/F @ top face	16Ø @ 120 c/c both way	16Ø @ 140 c/c both way	20Ø @ 300 c/c both way
5	lateral ties	12Ø @ 250 c/c side face	12Ø @ 250 c/c side face	12Ø @ 250 c/c side face

V. Result and Discussion

5.1 Deflection of tower

It was observed that the deflection is maximum for wind load as compare to seismic load for different soil strata. So in this case the windmill tower is more critical for wind load as compare to seismic load. The deflection of tower increasing from hard strata to soft strata. The deflection of tower for different soil strata are presented in Table 4, 5&6.

Table 4 Maximum deflection of windmill tower for hard strata

Nod e	Load combinations	Horizontal deflection in X-Dir(mm)	Horizontal deflection in Z-Dir(mm)	Remark
3540	0.75[DL+LL+(WLX+VE)]	178.546	0	Wind Load
3567	0.75[DL+LL+(WLZ+VE)]	3.547	90.314	
3558	0.75[DL+0.5LL+EQX]	10.472	0	EQ Load
3565	0.75[DL+0.5LL+EQZ]	3.682	6.581	

Table 5 Maximum deflection of windmill tower for medium strata

Nod e	Load combinations	Horizontal deflection in X-Dir(mm)	Horizontal deflection in Z-Dir(mm)	Remark
3540	0.75[DL+LL+(WLX+VE)]	178.546	0	Wind Load
3567	0.75[DL+LL+(WLZ+VE)]	3.547	90.314	
3558	0.75[DL+0.5LL+E]	12.796	0	EQ Load

	QX]		
3564	0.75[DL+0.5LL+E QZ]	3.733	9.597

Table 6 Maximum deflection of windmill tower for soft strata

No de	Load combinati ons	Horizont al deflectio n in X-Dir(mm)	Horizonta l deflection in Z-Dir(mm)	Re ma rk
3540	0.75[DL+LL+(WLX+VE)]	178.546	0	Wi nd Lo ad
3567	0.75[DL+LL+(WLZ+VE)]	3.547	90.314	
3558	0.75[DL+0.5LL+EQX]	14.895	0	EQ Lo ad
3564	0.75[DL+0.5LL+EQZ]	3.746	10.845	

5.2 Stability of windmill tower

It was observed from the analysis that bending stresses are maximum at the bottom level plates of the tower. There was tensile and bending stresses are developed in the tower of windmill. The bending stresses developed in the bottom plate of windmill tower were maximum for wind load as compared to seismic load for different strata.

The permissible bending stress in tension and compression = $\sigma_{bt} = 0.66 * f_y$, where, f_y = yield stress of steel. For steel of yield strength 250 N/mm², $\sigma_{bt} = 0.66 * 250 = 165$ N/mm². From Table 7 it is observed that no bending stresses are exceeding the value of permissible stresses hence windmill tower structure is safe for the bending.

Table 7 Bending stress in tower

Sr.No.	Soil Strata	Bending Stress(Kn/m2)	Loading
1	Hard strata	151	Wind Load
		15.8	Earthquake load
2	Medium strata	151	Wind Load
		17.2	Earthquake load
3	Soft strata	151	Wind Load
		18.8	Earthquake load

5.3 Base shears comparison

It was observed from the seismic analysis that absolute base shear for soft soil strata are maximum as compared to hard soil strata. It is obvious when soil becomes softer, stiffness of soil goes on decrease and as result of this there is maximum vibration in the structure. The absolute base shear for different soil strata is listed in Table 8

Table 8 Base Shear

Earthquake Load	Base Shear (KN)
-----------------	-----------------

	Hard Strata	Medium Strata	Soft Strata
EQX	40.96	44.32	47.36
EQZ	40.91	44.39	47.55
EQY	27.18	27.18	27.18

5.4 Safety of foundation

It was observed that the actual bearing pressure on the soil for design size of footing is less than the permissible safe bearing capacity for hard, medium and soft strata which is shown in Table 9, 10&11. So foundation is Safe.

Table 9 Pressure intensities for hard strata

Load combination	Net pressure intensities (KN/m2)		Gross pressure intensities (KN/m2)		Allowable SBC for hard strata(KN/m2)
	Max	Min	Max	Min	
DL of foundation +VW of windmill	35.92	35.92	75.47	75.47	
DL of foundation +Vertical weight +Wind	69.49	2.34	142.63	8.31	350.00
DL of foundation+ Vertical weight+Seismic	37.67	34.16	78.99	71.95	

Table 10 Pressure intensities for medium strata

Load combination	Net pressure intensities (KN/m2)		Gross pressure intensities (KN/m2)		Allowable SBC for hard strata(KN/m2)
	Ma x	Min	Max	Min	
DL of foundation +Vertical weight of windmill	35.00	35.00	74.61	74.61	
DL of foundation +Vertical weight +Wind	63.6	6.5	131.71	17.51	200.00
DL of foundation+ Vertical weight +Seismic	36.91	33.19	78.33	70.89	

Table 11 Pressure intensities for soft strata

Load combination	Net pressure intensities (KN/m2)		Gross pressure intensities (KN/m2)		Allowable SBC for soft strata(KN/m2)
	Max	Min	Max	Min	
DL of foundation	33.40	33.40	72.97	72.97	

+Vertical weight of windmill					
DL of foundation+ Vertical weight +Wind	53.1 1	13.7 0	112.3 8	33.5 6	115.0
DL of foundation+ Vertical weight +Seismic	34.9 7	31.8 3	76.11	69.8 3	

5.5 Stability of foundation

For stability of foundation the soil must be capable of carrying the loads from any engineered structure placed upon it without a shear failure and with resulting settlements being tolerable for that structure. Excessive settlements can result in structural damage to a building frame, and excessive wear or settlements. So it is necessary to check windmill for sliding and overturning. From Table 12, 13&14 it is observed that the windmill for different soil strata is safe for sliding and overturning. The factor of safety against sliding and overturning is greater than 1.5

Table 12 Check for stability of foundation for hard strata

Checks	Parameters	Load case	
		DL+Wind	DL+Seismic
Check For sliding	Fs	407.64	553.03
	Fr	6914.09	6914.09
	FSs	16.96	12.50
	SAFE / UNSAFE	SAFE	SAFE
Check For overturning	Mo	19799.03	1036.60
	Mr	155566.97	155566.97
	FSo	7.86	150.07
	SAFE / UNSAFE	SAFE	SAFE

Table 13 Check for stability of foundation for medium strata

Checks	Parameters	Load case	
		DL+Wind	DL+Seismic
Check For sliding	Fs	407.64	614.77
	Fr	7616.06	7616.06
	FSs	18.68	12.39
	SAFE / UNSAFE	SAFE	SAFE
Check For overturning	Mo	19799.03	1290.04
	Mr	180881.33	180881.33
	FSo	9.14	140.21
	SAFE / UNSAFE	SAFE	SAFE

Table 14 Check for stability of foundation for soft strata

Checks	Parameters	Load case	
		DL+Wind	DL+Seismic
Check	Fs	407.64	777.52

For Sliding	Fr	9536.98	9536.98
	FSs	23.40	12.27
	SAFE / UNSAFE	SAFE	SAFE
Check for overturning	Mo	19799.03	1578.82
	Mr	256306.43	256306.43
	FSo	12.95	162.34
	SAFE / UNSAFE	SAFE	SAFE

5.6 Reinforcement details of foundation

The reinforcement for foundation was increases from hard strata to soft strata which are presented in Table 15. So the cost of foundation is increases with respect to increasing reinforcement in foundation.

Table 15 Reinforcement details of Foundation

Sr.No.	Item	Hard strata	Medium strata	Soft strata
	A) Pedestal			
1	Vertical R/F @ outer face	74 nos-25Ø	74 nos-25Ø	74 nos-25Ø
2	Vertical R/F @ inner face	84 nos-25Ø	84 nos-25Ø	84 nos-25Ø
3	lateral ties	10Ø @ 150 c/c	10Ø @ 150 c/c	10Ø @ 150 c/c
	B) Footing			
1	R/F @ bottom face	20Ø @ 100 c/c both way	20Ø @ 100 c/c both way	20Ø @ 100 c/c both way
2	R/F @ top face	16Ø @ 120 c/c both way	16Ø @ 140 c/c both way	20Ø @ 300 c/c both way
3	lateral ties	12Ø @ 250 c/c side face	12Ø @ 250 c/c side face	12Ø @ 250 c/c side face

VI. Conclusion

In this work attempt was made to critically study the behavior of windmill tower and foundation system subjected to wind load and earthquake load for different supporting condition such as hard, medium and soft strata.

Based on this analysis and design following conclusion were made:

1. The effect of wind is significant as compared to earthquake and has to be considered in the analysis of windmill.
2. When effects of wind are considered the stability of windmill has to be thoroughly checked.
3. Soil strata play a major role in safety and stability of windmill.
4. The effect of wind on blade i.e. drag force is more critical in the analysis of windmill and its make more drastic changed in the structure.
5. In earthquake analysis, the normalized base shear, moment due to shear is increasing with respective to hard, medium and soft soil strata.

6. The foundation sizes, concrete material, reinforcement material shall be increasing with respect to hard, medium and soft Strata. So cost of structure also increased.

References

Journal Papers:

- [1]. James F Manwell ,(2006), Study of the development of a second large Wind Turbine Installation in the town of Hull,American Wind energy Association.
- [2]. Morgan Kirk,Eric Ntambakwa,(2008),Wind Turbine Foundation Behavior&Design considerations,AWEA Windpower conference,Houston.
- [3]. Rajendran C & Madhu,(2010),A CFD Based Multibody Dynamics approach in Horizontal axis wind turbine,International Journal of Dynamics of fluids,Vol.6,PP.219-230
- [4]. B.C.Punmia, “ RCC Design of Structure”
- [5]. Chopra Anil kumar,(2007),Dynamics of structures,TheoryAnd application to Earthquake Engineering,Third edition,Prentice Hall Publications.
- [6]. JosephE.Bowles, FoundationEngineering,Vol-I
- [7]. SathyajithMathew,(2007),WindEnergy:fundamental, Resource analysis and Economics.
- [8]. Shrikhande & agarwal, Earthquake Resistant design of Structures.
- [9]. Singh A.N.,(2007),Concrete Construction of wind energy tower,The Indan Concrete Journal.
- [10]. InternationalStandard,IEC61400-1,(2005),Wind turbines- part1:design requirement.
- [11]. IS:875-1987,Indian standard Code of Practice for Design loads,BureauofIndianStandards,New Delhi.
- [12]. IS-4998 ,Indian standard Code of Practice for Design of RCC Chimneys,Bureau of Indian Standards,New Delhi.
- [13]. IS-1893(Part 1):2002,Indian standard Criteria for Earthquake design Structure,Bureau of Indian Standards,New Delhi.
- [14]. IS:800-1984,Code of Practice for general construction in steel,Bureau of Indian Standards,New Delhi.
- [15]. IS:456-2000, Plain and Reinforced concrete for code of Practice,Bureau of Indian Standards,New Delhi.
- [16]. SP-16,Design aids for Reinforced concrete,Bureau of Indian Standards,New Delhi.

Closed Loop Control of High Efficiency Voltage Clamped Dc-Dc Converter with Reduced Reverse Recovery Current and Switch

¹S. Bala chennaiah, ²B. Narasimhudu

¹ (Asst.Proff, dept: Eee Rgm cet, Nandyal, A.P)

²(PG student, dept: Eee Rgm cet, Nandyal, A. P)

Abstract: This paper investigates a Closed loop Control of high-efficiency clamped voltage dc–dc converter with reduced reverse-recovery current and switch-voltage stress. In the circuit topology, it is designed by way of the combination of inductor and transformer to increase the corresponding voltage gain. Moreover, one additional inductor provides the reverse-current path of the transformer to enhance the utility rate of magnetic core. In addition, the voltage-clamped technology is used to reduce the switch-voltage stress so that it can select the Schottky diode in the output terminal for alleviating the reverse-recovery current and decreasing the switching and conduction losses. Furthermore, the closed-loop control methodology is utilized in the proposed scheme to overcome the voltage-drift problem of power source under the variation of loads. Thus, the proposed converter topology has a favourable voltage-clamped effect and superior conversion efficiency.

Index Terms: Converter, Schottky diode, closed loop, reverse recovery, voltage clamped.

I. Introduction

IN RECENT years, dc–dc converters with steep voltage ratio are usually required in many industrial applications, e.g., the front-end stage for clean energy sources, the dc backup energy system for an uninterruptible power supply (UPS), high intensity discharge (HID) lamps for automobile headlamps, and the telecommunication industry [1]–[3]. The conventional boost converters cannot provide such a high dc-voltage ratio due to the losses associated with the inductor, filter capacitor, main switch, and output diode. Even for an extreme duty cycle, it will result in serious reverse-recovery problems and increase the

rating of the output diode. As a result, the conversion efficiency is degraded, and the electromagnetic interference (EMI) problem is severe under this situation to increase the conversion efficiency and voltage gain, many modified boost-converter topologies have been investigated in the past decade [5]–[10]. Although voltage-clamped techniques are manipulated in the converter design to overcome the severe reverse-recovery problem of the output diode in high-level voltage applications, there still exist overlarge switch-voltage stresses, and the voltage gain is limited by the turn-ON time of the auxiliary switch [5], [6] presented a boost soft-single-switch converter, which has only one single active switch. It is able to operate with soft switching in a pulse width modulation (PWM) way without high voltage and current stresses. Unfortunately, the voltage gain is limited below four in order to achieve the function of soft switching. In [8] and [9], coupled inductors were employed to provide a high step-up ratio and to reduce the switch-voltage stress substantially, and the reverse-recovery problem of the output diode was also alleviated efficiently. In this case, the leakage energy of the coupled inductor is another

problem as the main switch was turned OFF. It will result in a high-voltage ripple across the main switch due to the resonant phenomenon induced by the leakage current. In order to protect the switch devices, either a high-voltage-rated device with higher $R_{DS(ON)}$ or a snubber circuit is usually adopted to deplete The leakage energy. Consequently, the power-conversion efficiency will be degraded. Zhao and Lee [10] introduced a family of high-efficiency high-step-up dc–dc converters by only adding one addition diode and a small capacitor. However, a snubber circuit is energy losses.

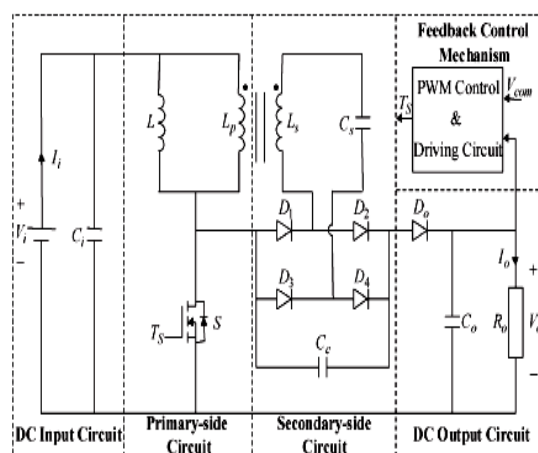


Fig. 1. System configuration of a high-efficiency voltage-clamped dc–dc converter.

II. Converter Design And Analyses

A newly designed converter topology is depicted in Fig. 1, where it contains five parts including a dc-input circuit, a primary-side circuit, a secondary-side circuit, a dc-output circuit, and a feedback-control mechanism. The major symbol representations are summarized as follows. V_i and I_i denote the dc-input voltage and current, and C_i is the input filter capacitor in the dc-input circuit. L_p represents the primary inductor of the transformer; L is the additional inductor in

the primary-side circuit; and S is the main switch. L_s denotes the secondary inductor of the transformer; C_s and C_c are the balanced capacitor and clamped capacitor in the secondary-side circuit; and $D_1, D_2, D_3,$ and D_4 are the rectifier diodes. V_o and I_o describe the output voltage and current; R_o is the output load; $D_o,$ and C_o are the output diode and filter capacitor in the output circuit. V_{com} and

T_S are the output-voltage command and switch-driving signal in the feedback-control mechanism, respectively.

The equivalent circuit and state definition of the newly designed converter is depicted in Fig. 2, where the transformer is modelled as an ideal transformer with a secondary leakage

Inductor (L_k). The turns ratio of this ideal transformer is defined as

$$n = \frac{N_2}{N_1} \tag{1}$$

Where N_1 and N_2 are the primary and secondary winding turns. The additional inductor (L) is located in parallel with the

primary side of the transformer. Moreover, the rectifier diodes ($D_1, D_2, D_3,$ and D_4) are connected between the primary and

Secondary sides of the transformer. The voltages across the additional inductor, the main switch, the ideal transformer primary

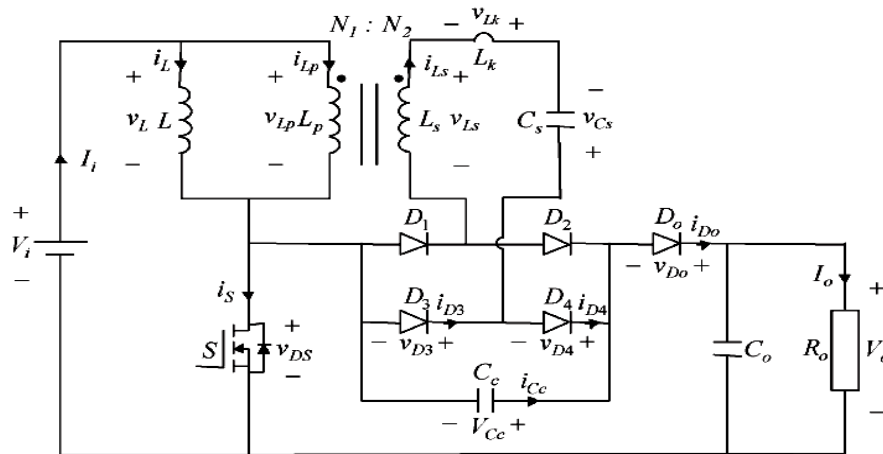


Fig. 2. Equivalent circuit.

and secondary winding, the secondary leakage inductor, the balanced capacitor, and the output diode are $v_L, v_{DS}, v_{Lp}, v_{Ls}, v_{Lk}, v_{Cs},$ and v_{Do} , respectively. The clamped capacitor C_c is assumed to be large enough to be viewed as a constant voltage source, V_{C_c} . The conductive voltage drops of the main switch (S) and all diodes ($D_1, D_2, D_3, D_4,$ and D_o) are neglected to simplify the circuit analyses. The characteristic waveforms of the proposed high-efficiency converter are depicted in Fig. 3. In addition, Fig. 4 illustrates the operational modes in one switching cycle, and the detailed operation stages are described as follows.

A. Mode 1 ($t_0 - t_1$) [Fig. 4(a)]

At time $t = t_0$, the main switch (S) is turned ON. At the same time, the diodes (D_1 and D_4) become conducted, and other diodes ($D_2, D_3,$ and D_o) are reverse biased. The additional inductor (L) and clamped capacitor (C_c) are linearly charged by the input-voltage source (V_i) through the transformer. Applying Kirchhoff's law [4], the voltages of $v_L, v_{Lp}, v_{Ls},$ and v_{Lk} during this period can be expressed as

$$v_L = v_{Lp} = V_i \tag{2}$$

$$v_{L_s} = nV_i \tag{3}$$

$$v_{L_k} = V_{C_c} - nV_i - v_{C_s}. \tag{4}$$

According to (2)–(4), the rate of change of the additional inductor current (i_L), the primary-side current (i_{Lp}), and the N secondary-side current (i_{Ls}) of the transformer can be represented as

$$\frac{di_L}{dt} = \frac{V_i}{L} \tag{5}$$

$$\frac{di_{Lp}}{dt} = \frac{V_{C_c} - nV_i - v_{C_s}}{L_k} + \frac{V_i}{L_p} \tag{6}$$

$$\frac{di_{Ls}}{dt} = \frac{V_{C_c} - nV_i - v_{C_s}}{L_k}. \tag{7}$$

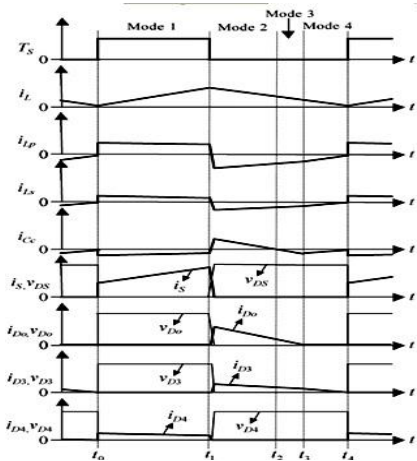


Fig. 3. Characteristic waveforms.

B. Mode 2 (t1 – t2) [Fig. 4(b)]

At time $t = t_1$, the main switch (S) is turned OFF. At this time, the diodes (D2, D3, and Do) become forward biased to start conducting, and other diodes (D1 and D4) are reverse biased. The stored energy of the additional inductor (L) and

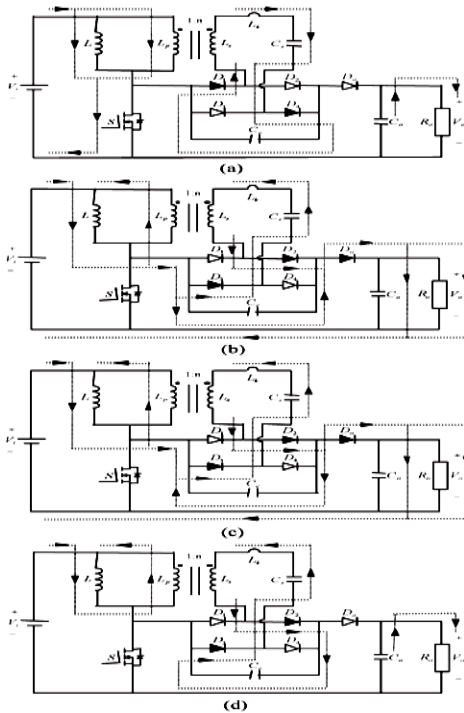


Fig. 4. Operational modes: (a) mode 1 [t0 – t1]; (b) mode 2 [t1 – t2]; (c) mode 3 [t2 – t3]; (d) mode 4 [t3 – t4].

clamped capacitor (Cc) in Mode 1 is released to output loads. Moreover, the transformer can be operated at four quadrants to enhance the utility rate of the magnetic core and to keep the clamped voltage (Vcs), since the additional inductor (L) supplies energy to the output terminal by way of the transformer. Applying Kirchhoff’s law [4], the voltage and current relations of each element during this mode can be described by

$$v_L = v_{Lp} = V_i + V_{C_c} - V_o \tag{8}$$

$$v_{L_s} = n(V_i + V_{C_c} - V_o) \tag{9}$$

$$v_{L_k} = -V_{C_c} - v_{C_s} - n(V_i + V_{C_c} - V_o) \tag{10}$$

$$v_{DS} = V_i - V_L = V_o - V_{C_c} < V_o \tag{11}$$

$$i_{D_o} = i_L + i_{L_p} = i_{C_c} - i_{L_s} \tag{12}$$

Where i_{Do} is the current of the output diode D_o ; i_{Cc} is the current of the clamped capacitor C_c . According to (11), the cutoff voltage of the main switch (S) is clamped at $V_o - V_{Cc}$. Moreover, the main switch (S) with low-voltage-rated capacity can be selected since the switch-voltage stress (v_{DS}) is smaller than the output voltage (V_o). The selection of a low-voltage rated device with lower $R_{DS(ON)}$ is useful for improving the conversion efficiency. Referring to (8)–(10), the rate of change of i_L , i_{Lp} and i_{Ls} is given by

$$\frac{di_L}{dt} = \frac{V_i + V_{C_c} - V_o}{L} \tag{13}$$

$$\frac{di_{L_p}}{dt} = \frac{-V_{C_c} - v_{C_s} - n(V_i + V_{C_c} - V_o)}{L_k} + \frac{V_i + V_{C_c} - V_o}{L_p} \tag{14}$$

$$\frac{di_{L_s}}{dt} = \frac{-V_{C_c} - v_{C_s} - n(V_i + V_{C_c} - V_o)}{L_k} \tag{15}$$

C. Mode 3 (t2 – t3) [Fig. 4(c)]

At time $t = t_2$, the residual energy of the clamped capacitor (C_c) is discharged entirely, i.e., $i_{Cc}(t_2) = 0$. Immediately, the clamped capacitor (C_c) is charged by the energy of the additional inductor (L) through the transformer, and the rate of change of the clamped-capacitor current (i_{Cc}) can be denoted as

$$\frac{di_{C_c}}{dt} = \frac{V_i + V_{C_c} - V_o}{L} + \frac{V_i + V_{C_c} - V_o}{L_p} + 2 \left[\frac{-V_{C_c} - v_{C_s} - n(V_i + V_{C_c} - V_o)}{L_k} \right] \tag{16}$$

Moreover, the stored energy of the additional inductor (L) is released continuously to the output terminal by way of the transformer. The rate of charge of i_{Do} is given by

$$\frac{di_{D_o}}{dt} = \frac{V_i + V_{C_c} - V_o}{L} + \frac{V_i + V_{C_c} - V_o}{L_p} + \frac{-V_{C_c} - v_{C_s} - n(V_i + V_{C_c} - V_o)}{L_k} \quad (17)$$

D. Mode 4 (t3 – t4) [Fig. 4(d)]

At time $t = t3$, the clamped-capacitor current (i_{C_c}) equals to the secondary-side current (i_{L_s}) of the transformer, and the output diode current (i_{D_o}) decays to 0, i.e., $i_{D_o}(t3) = 0$. During this period, the voltage of the output diode (v_{D_o}) maintains the zero status until the main switch (S) is turned ON. Moreover, the magnitude of the additional inductor current (i_L) is equal to the one of the primary-side current (i_{L_p}). According to (13) and (14), the rate of change of i_{L_p} and i_{L_s} can be represented as

$$\frac{di_{L_p}}{dt} = -\frac{di_L}{dt} = -\frac{V_i + V_{C_c} - V_o}{L} \quad (18)$$

$$\frac{di_{L_s}}{dt} = -\frac{V_i + V_{C_c} - V_o}{L} - \frac{V_i + V_{C_c} - V_o}{L_p} \quad (19)$$

Since the secondary leakage inductor (L_k) and the change rate of i_{L_s} in the transformer are very small, the voltage of the secondary leakage inductor (v_{L_k}) can be neglected. According to the concept of the zero average voltage across the inductor over one period [4], the voltages of v_{C_s} , V_{C_c} , and V_o for steady-state operation can be described via (2), (4), (8), and (10) as

$$v_{C_s} = \frac{nV_i(2d - 1)}{2(1 - d)} \quad (20)$$

$$V_{C_c} = \frac{nV_i}{2(1 - d)} \quad (21)$$

$$V_o = \frac{2 + n}{2(1 - d)} V_i \quad (22)$$

where ϵ is the switch (S). Continuously, the main switch (S) is turned ON at time $t = t4$ to begin the next switching cycle.

Since the voltage difference may be caused by the secondary inductor of the transformer, as $d \neq 0.5$, the major function of the balanced capacitor (C_c) is used for keeping the cutoff voltages of the rectifier diodes ($D1$, $D2$, $D3$, and $D4$) balanced. Moreover, it also can avoid the overlarge current that passed through the rectifier diodes. According to (22), the voltage gain can be tuned by regulating the turns ratio (n) in the transformer to overcome the boost-ratio limitation of the conventional

converter. In addition, the switch-voltage stress (v_{DS}) can be calculated via (11), (21), and (22) as

$$v_{DS} = \frac{V_i}{(1 - d)} \quad (23)$$

According to (22) and (23), one can obtain

$$v_{DS} = \frac{2V_o}{(2 + n)} \quad (24)$$

By analyzing (24), the switch-voltage stress (v_{DS}) is not related to the dc-input voltage (V_i) and duty cycle (d) if the values of the output voltage (V_o) and the turns ratio (n) are fixed. Thus, it can ensure that the sustainable voltage of the main switch (S) is constant. As long as the dc-input voltage is not higher than the

rated voltage of the main switch, the high-efficiency voltage clamped dc–dc converter can be applied well to the low-voltage power sources even with large voltage variations, e.g., fuel cell, solar cell, etc.

Fuel-cell generation systems have been receiving more attention in the last years due to the advantages of high-conversion efficiency, low aggression to the environment, no moving parts, and superior reliability and durability. Owing to the electrochemical reaction, fuel cell has the power quality of low voltage and high current. However, the fuel-cell stack with high output voltage is difficult to fabricate and it may be failure when any single cell is inactive. Besides, the output voltage is varied easily with respect to the load variations. In order to satisfy the requirement of high-voltage demand, a stable boost converter with high voltage gain and superior conversion efficiency is necessary to utilize the fuel-cell energy more efficiently. The validity of the proposed converter is verified by the following experimental results via an example of a PEMFC power source.

III. Experimental Results

In experimentation, the high-efficiency voltage-clamped dc–dc converter is designed to operate from the fuel-cell variability dc input, $V_i = 27\text{--}37.5$ V, to deliver a constant dc output, $V_o = 200$ V, with the maximal capability of output power, $P_{o,max} = 330$ W. If the maximal value of main switch voltage (v_{DS}) is arranged for clamping at 50 V, the turns ratio can be determined as $n = (2V_o/v_{DS(max)}) - 2 = 6$ according to (24). As can be seen from Figs. 3 and 4, the voltage stress of the output diode (v_{D_o}) is the same as the switch-voltage stress. In addition, the voltage stresses of rectifier diodes (v_{D1} , v_{D2} , v_{D3} , and v_{D4}) can be calculated via (21) and (23) as $n v_{DS} / 2 = 150$ V. For conservative consideration, the main switch (FQI90N08, 80 V), the output diode (Schottky diode SR20100, 100 V), and the rectifier diodes (Schottky diode SR20200, 200 V) are adopted in the experimental converter. In order to solve the problem of the fuel-cell output voltage varied with the variations of loads, the proposed converter with dc-voltage feedback

control is utilized to ensure the system stability, and a PWM control IC TL494 is adopted to achieve this goal of feedback control. The prototype with the following specifications is designed in this section to illustrate the design procedure given in Section II:

- switching frequency $f_s = 100 \text{ kHz};$
- turns ratio $n = 6;$
- Additional inductor $L = 5.9 \mu\text{H};$
- primary inductor of transformer $L_p = 213.6 \mu\text{H};$
- secondary inductor of transformer $L_s = 7689.6 \mu\text{H};$
- secondary leakage inductor $L_k = 0.6 \mu\text{H};$
- balanced capacitor $C_s = 4 \times 6.8 \mu\text{F};$
- clamped capacitor $C_c = 6 \times 4.7 \mu\text{F};$
- input filter capacitor $C_i = 3300 \mu\text{F};$
- output filter capacitor $C_o = 3 \times 4.7 \mu\text{F};$
- main switch $S:$ FQI90N08 (80 V, DS (ON) = 16 mΩ);
- Output diode $D_o:$ Schottky diode SR20100 (100 V, 20 A);
- Rectifier diodes $D_1, D_2, D_3, D_4:$ Schottky diode SR20200 (200 V, 20 A).

Fig. 5 depicts the results voltage and current curves of the main switch (S) at 310-W output power. As can be seen from this figure, the shaken switch voltage at the beginning is caused by the line inductor when the switch is turned OFF. Fortunately, the steady state of this switch-voltage stress is about 50 V due to the utilization of voltage-clamped technique, and it is much smaller than the output voltage, $V_o = 200 \text{ V}$. It has the merit of selecting a low-voltage-rated device in order to reduce the conduction loss of the switch. The simulated current waveforms of the additional inductor (L), in parallel with the transformer, primary inductor of transformer (L_p), and secondary inductor of transformer (L_s) at 310-W output power, are depicted in Fig. 6, the balanced capacitor (C_s) can be used for balancing the current and cutoff voltage of the diodes (D_3 and D_4) when the condition of $d \neq 0.5$, holds.

For verifying the voltage-clamped property, the experimental voltage responses of the output voltage (V_o), clamped capacitor (C_c), and main switch (S) at 310-W output power are depicted. As can be seen from this figure, the output voltage, $V_o = 200 \text{ V}$, is strode mainly across the clamped capacitor in the secondary-side circuit (i.e., $V_{C_c} = 150 \text{ V}$). Thus, the switch-voltage stress and the cutoff voltage of the output diode are clamped at about 50 V. In order to examine the robust performance of the proposed converter scheme, the experimental results of the converter output voltage (V_o), and the PEMFC output current (I_i) under the step load variation between no load (0 W) and full load (310 W) are depicted. the converter output voltage, $V_o = 200 \text{ V}$, is insensitive to the variation of loads due to the closed-loop control, and the output current ripple is also slightly extreme as a result of the high switching frequency.

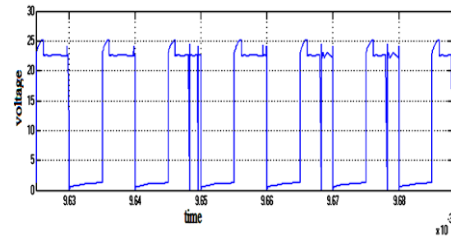


Fig.5.Simulated voltage wave forms of main switch S.

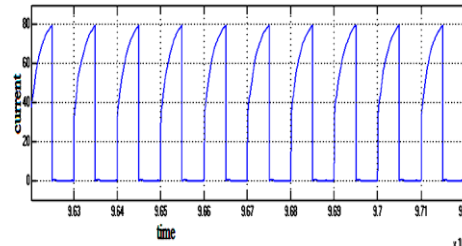


Fig.5.Simulated voltage and current wave forms of main switch S

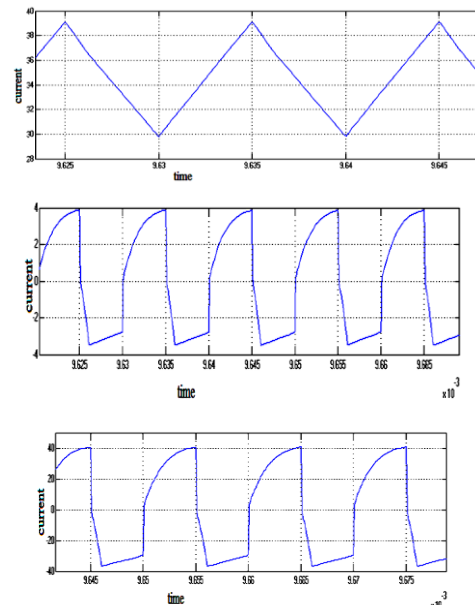


Fig.6. Simulated current response of additional inductor L, transformer primary inductor L_p and transformer secondary inductor L_s .

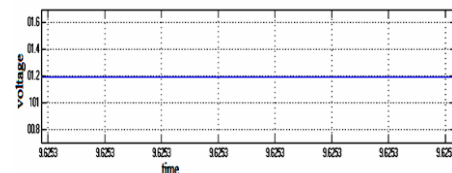


Fig.7.Simulated voltage response of output voltage V_0 .

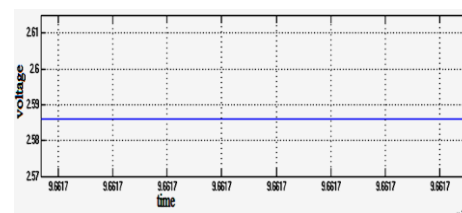


Fig.7. Simulated voltage response of,clamped capacitor C_c .

IV. CONCLUSION

This project has developed a voltage-clamped dc–dc converter with reduced reverse recovery current and switch-voltage stress, with a power quality of low voltage and high current. The newly designed converter circuit has the following improvements compared to the previous work.

- 1) Proposed converter can select the main switch with lower sustainable voltage for alleviating the switch conduction loss due to the utilization of voltage-clamped technique.
- 2) All diodes in this circuit topology are Schottky diodes with the reduction of switching and conduction losses.
- 3) The additional inductor is used for providing the reverse current path of the transformer to raise the utility rate of the magnetic core.
- 4) Additional snubber circuits for absorbing the voltage spikes in the diodes are not required to further cut down the manufacture cost.
- 5) There is no circulating current to overcome the problem of degenerate efficiency under slight loads.
- 6) The voltage-drift problem of power source under the variation of loads can be solved by the closed-loop control methodology.

References

- [1] I. Barbi and R. Gules, "Isolated dc–dc converters with high-output voltage for TWTA telecommunication satellite applications," *IEEE Trans. Power Electron.*, vol. 18, no. 4, pp. 975–984, Jul. 2003.
- [2] O. Abutbul, A. Gherlitz, Y. Berkovich, and A. Ioinovici, "Step-up switching-mode converter with high voltage gain using a switched capacitor circuit," *IEEE Trans. Circuits Syst. I, Fundam. Theory Appl.*, vol. 50, no. 8, pp. 1098–1102, Aug. 2003.
- [3] K. C. Tseng and T. J. Liang, "Novel high-efficiency step-up converter," *Proc. Inst. Elect. Eng.—Electr. Power Appl.*, vol. 151, no. 2, pp. 182–190, Mar. 2004.
- [4] N. Mohan, T. M. Undeland, and W. P. Robbins, *Power Electronics :Converters, Applications, and Design*. New York: Wiley, 1995.
- [5] M. M. Jovanovic and Y. Jang, "A new soft-switched boost converter with isolated active snubber," *IEEE Trans. Ind. Appl.*, vol. 35, no. 2, pp. 496–502, Mar./Apr. 1999.

- [6] C. M. C. Duarte and I. Barbi, "An improved family of ZVS-PWM active-clamping DC-to-DC converters," *IEEE Trans. Power Electron.*, vol. 17, no. 1, pp. 1–7, Jan. 2002.
- [7] E. S. da Silva, L. dos Reis Barbosa, J. B. Vieira, L. C. de Freitas, and V. J. Farias, "An improved boost PWM soft-single-switched converter with low voltage and current stresses," *IEEE Trans. Ind. Electron.*, vol. 48, no. 6, pp. 1174–1179, Dec. 2001.
- [8] K. Hirachi, M. Yamanaka, K. Kajiyama, and S. Isokane, "Circuit configuration of bidirectional DC/DC converter specific for small scale load leveling system," in *Proc. IEE Power Conversion Conf.*, Osaka, Japan, 2002, pp. 603–609.
- [9] C. W. Roh, S. H. Han, and M. J. Youn, "Dual coupled inductor fed isolated boost converter for low input voltage applications," *Electron. Lett.*, vol. 35, no. 21, pp. 1791–1792, Oct. 1999.
- [10] Q. Zhao and F. C. Lee, "High-efficiency, high step-up dc–dc converters," *IEEE Trans. Power Electron.*, vol. 18, no. 1, pp. 65–73, Jan. 2003.

Design and Implementation of an Integrated Rf Antenna-Filter Co-Design For Uwb Applications

J.Ramprasad^a, Mrs. T.J.Jeyaprabha^b,

^{1,2} Department of Electronics and Communication, Sri Venkateswara college of Engineering/Anna University,
Sriperumbudur, 602105, India

Abstract: In the co-design approach, the patch antenna and hairpin filter is sandwiched with ground plane. The impedance at the interfaces is optimized to improve the performance of the antenna-filter, without restricting it to 50Ω. Impedance optimization is done using via hole. The simulation of S_{11} parameter for patch antenna has operating center frequency of 6.5GHz. The low pass hairpin filter is designed at 6.5GHz and simulated to show S_{11} parameter. Then design of co-design approach is done and simulation of S_{11} parameter for the antenna-filter co-designed approach provides operating frequency range of 6.5 – 6.9GHz which has increased bandwidth capacity, reduction in size and high gain.

Keywords - Antenna, co-design, filter, patch, hairpin.

I. Introduction

Miniaturization and low cost are the two most fundamental demands for RF receiver front-ends. One way to miniaturize an RF front-end is to embed its passive circuitries and interconnects into a package, which is called system-in package (SIP) [2], [3]. Another way is to integrate required multiple functional circuitries into one device without the 50Ω (or 75Ω) constraints, referred to as co-design [4]–[11]. The co-design method can change the structure of the circuit, improve the performance of the circuits, and simplify the connections between different components. For example, the noise figure of a RF antenna-filter-LNA system has been significantly improved with the co-design strategy [4]. In [5] and [6], antennas were co-designed with an amplifier and transceiver to attain higher integration degree. Similarly, an RF device was implemented by integrating three-dimensional (3-D) cavity filters/ duplexers and antennas [7]. In [8], the resonator of an antenna also acted as an element of filter. In [9] and [10], a coplanar antenna-filter was co-designed. In [11], a two-pole filter was realized by integrating a filter and an antenna. In this letter, a co-designed antenna-filter is presented. A microstrip patch antenna is layered on the top of a hairpin filter, and they share the same ground plane. A via hole is implemented to connect the antenna and the filter.

The impedance at the interfaces is optimized to improve the performance of the antenna-filter, without restricting it to 50Ω. The proposed antenna-filter operates in the frequency band 6.5–6.9 GHz, and the bandwidth for $|S_{11}| \leq -10\text{dB}$ is increased when compared with traditional cascade connection of antenna-filter. The simulated results indicate that the proposed co-design approach can be used to reduce the size, improve the bandwidth, and increase the gain.

II. CO-DESIGN OF ANTENNA AND FILTER

The configurations of the traditional and the co-designed antenna-filters are shown in Fig. 1. Unlike the traditional antenna-filter in which the components are cascaded with 50Ω interfaces [Fig. 1(b)], co-designed antenna-filter is assembled vertically and connected using a metalized via hole, as shown in Fig. 1(a). Also, the ground plane is sandwiched in the middle and shared by both the antenna and the filter. With this configuration, the size of the whole device can be significantly reduced. In order to avoid the electromagnetic (EM) interference between the antenna and the filter, they are arranged to have the parallel current. Furthermore, the impedance at the interfaces is optimized by adjusting the location and dimension of the via hole to attain better performance.

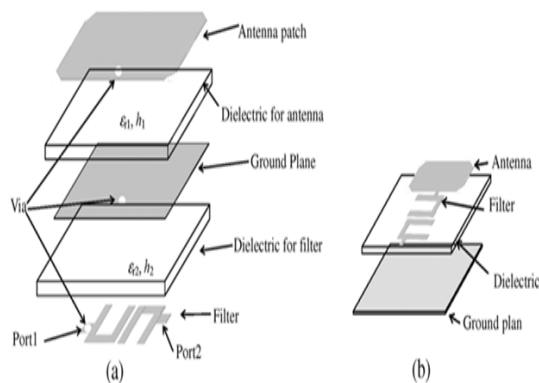


Fig. 1 Antenna-filter with (a) co-design version, (b) traditional version.

III. FILTER DESIGN

Fig. 2 shows the configuration of hairpin filter. The filter is designed to have a fractional bandwidth (FBW) of 6% at 6.5 GHz. We choose a two-pole butterworth low-pass filter prototype. The low-pass prototype parameters include $g_0=1$, $g_1=1.4142$, $g_2=1.4142$, and $g_3=1$ [11]. Based on the low-pass parameters, the design parameters of the band-pass can be calculated by

$$Q_{e1} = \frac{g_0 g_1}{FBW}; Q_{en} = \frac{g_n g_{n+1}}{FBW}$$

$$M_{i,i+1} = \frac{FBW}{\sqrt{g_i g_{i+1}}} \text{ for } i = 0 \text{ to } n - 1$$

where Q_{e1} and Q_{e2} are the external quality factors of the resonators at the input and output port, and $M_{i,i+1}$ are the coupling coefficients between the i th and $(i+1)$ th

resonators. For this design, we have $Q_{e1}=23.57$, $Q_{e2}=23.57$, and $M_{1,2}=0.042$.

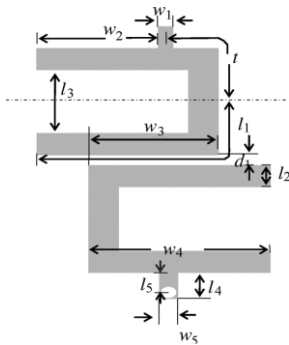


Fig. 2. The configuration of the hairpin filter.

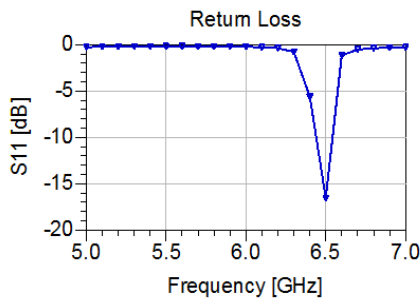


Fig. 3. S11 parameters for the filter.

IV. Antenna Design

The structure of the microstrip rectangular patch antenna with four sharp cuts is shown in Fig. 4. The antenna is designed to operate at the center frequency of 6.5 GHz, and the sharp cuts are used to improve the bandwidth. The optimized design parameters for the antenna with 50Ω interface impedance are used accordingly to provide better bandwidth. The simulated results are shown in Fig. 5.

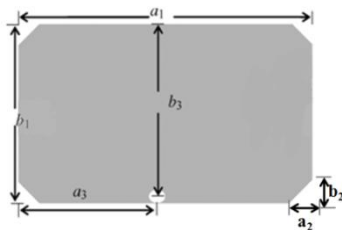


Fig. 4. The configuration of the microstrip patch antenna with four sharp cuts.

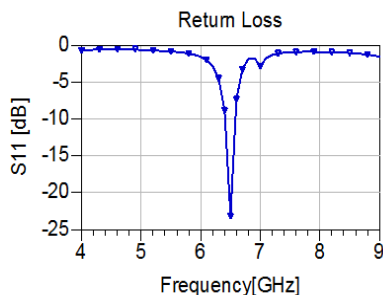


Fig. 5. S11 parameters for the antenna.

V. Simulated Results For Co-Design Antenna-Filter

With the designs of antenna and filter, the co-designed antenna-filter [shown in Fig. 1(a)] is implemented. We also optimize the location and dimension of the via hole, the coupling between via and ground plane, and the impedance at the interface of the antenna and the filter. Design of co-design approach is done and simulation of S_{11} parameter for the antenna-filter co-designed approach provides operating frequency range of 6.5 – 6.9GHz. Fig. 6 shows the simulated parameters for the co-designed antenna-filters. Obviously, due to the better coupling between the antenna and the filter, as well as via hole and ground plane, two resonant frequencies appear that show the co-designed version has a broader bandwidth, which increases bandwidth capacity.

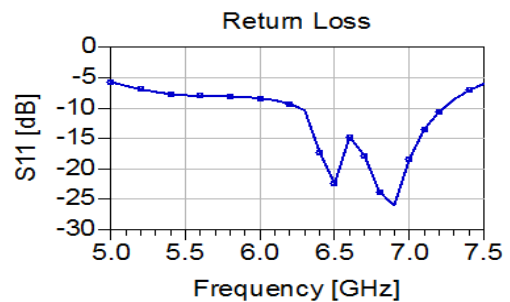


Fig.6 Simulated S11 parameter for the co-design approach.

VI. Conclusion

A co-designed antenna-filter is presented. The simulated results demonstrate the co-design can be used to improve the bandwidth, the gain of the antenna and also it can reduce the size of device. Since co-designed antenna-filter design provides broader bandwidth, more number of users can use channel for wireless communications.

References

- [1] Jianhong Zuo, Xinwei Chen, Guorui Han, Li Li, and Wenmei Zhang, "An Integrated Approach to RF Antenna-Filter Co-Design" Member, IEEE, April 22, 2009.
- [2] J. Park, J. Hartung, and H. Dudek, "Complete front-to-back RF SiP design implementation flow," in *Proc. 57th Elec. Comp. Tech. Conf.*, Reno, NV, May 2007, pp. 986–991.
- [3] C. O. Romero and C. E. Baruelo, "Achieving optimum manufacturing yield for RF system-in-package (SiP) devices through process sensitivity analysis," in *Proc. EMAP Conf.*, Kowloon, Hong Kong, Dec. 2006, pp. 1–7.
- [4] S. Alalusi and R. Brodersen, "Antenna-Filter-CMOS LNA co-design strategy," in *Proc. CPD2000*, Zurich, Switzerland, Mar. 2001, pp. 81–87.
- [5] J. J. Wang and Y. P. Zhang *et al.*, "Circuit model of microstrip patch antenna on ceramic land grid array package for antenna-chip co-design of highly integrated RF transceivers," *IEEE Trans. Antennas Propag.*, vol. 53, no. 12, pp. 3877–3883, Dec. 2005.
- [6] W. Wang and Y. P. Zhang, "0.18-μm CMOS push-pull power amplifier with antenna in IC package," *IEEE Microw. Wireless Compon. Lett.*, vol. 14, no. 1, pp. 13–15, Jan. 2004.
- [7] J. H. Lee *et al.*, "A V-band front-end with 3-D integrated cavity filters/ duplexers and antenna in LTCC technologies," *IEEE Trans. Microw. Theory Tech.*, vol. 54, no. 7, pp. 2925–2936, Jul. 2006.

A Novel Approach to Design High Speed Arithmetic Logic Unit Based On Ancient Vedic Multiplication Technique

Mr. Abhishek Gupta¹, Mr. Utsav Malviya², Prof. Vinod Kapse³

VLSI Technology & Embedded Systems, Department of Electronics & Communication

M.tech-IVth semester^[1], Assistant Professor^[2], Head of the Department^[3]

Gyan Ganga Institute of Technology and Sciences

Rajeev Gandhi Technical University, Jabalpur, Madhya Pradesh, India

Abstract: This paper is devoted for designing high speed arithmetic logic unit. All of us know that ALU is a module which can perform arithmetic and logic operations. The reason behind choosing this topic as a research work is that, ALU is the key element of digital processors like as microprocessors, microcontrollers, central processing unit etc. Every digital domain based technology depends upon the operations performed by ALU either partially or whole. That's why it highly required designing high speed ALU, which can enhance the efficiency of those modules which lies upon the operations performed by ALU. The speed of ALU greatly depends upon the speed of multiplier. There are so many multiplication algorithms exist now-a-days at algorithmic and structural level. Our work proved that Vedic multiplication technique is the best algorithm in terms of speed. Further we have seen that the conventional Vedic multiplication hard wares have some limitations. So to overcome those limitations a novel approach has been proposed to design the Vedic multiplier with the use of unique addition tree structure, which is used to add partially generated products. For designing the two bit Vedic multiplier conventional hardware of Vedic multiplier has been used. For designing the four and eight bit level Vedic multiplier divide and conquer approach has been used. After designing the proposed Vedic multiplier, it has been integrated into an eight bit module of arithmetic logic unit along with the conventional adder, subtractor, and basic logic gates. The proposed ALU is able to perform three different arithmetic and eight different logical operations at high speed. All of these operational sub-modules (adder, subtractor, multiplier and logical gates) have been designed as the combinatorial circuit. And for the synchronization of these operational sub-modules, the multiplexers which have been used to integrate these sub-modules in a single unit have been triggered by positive edge clock To design proposed arithmetic logic unit verilog hardware description language (HDL) has been used. For designing operational sub-modules data flow modeling and for integration purpose behavioral modeling style has been used. For this design the target FPGA which we have taken belongs to Virtex-2P (family), XC2VP2 (device), FG256 (package) with speed grade of -7. For synthesis purpose Xilinx synthesis tool (XST) of Xilinx ISE-9.2i has been used. The behavioral simulation purpose ISE simulator has been used.

The maximum combinational path delay of proposed multiplier is 11.886 ns. And the ALU that has been designed can operate at the maximum frequency of 741.455 MHz.

Keywords: - Vedic Urdhva Triyambakam multiplication algorithm, Arithmetic Unit, Arithmetic Logic Unit, Addition tree structure.

I. Introduction

As all of us know that the Computation unit is main unit of any technology, which performs different arithmetic operations like as addition, subtraction and multiplication etc. also in some places it performs logical operations also like as and, or, invert, x-or etc. which is dominant feature in the digital domain based applications. ALU is the execution unit which does not only performs Arithmetic operations but also Logical operations. And that's why ALU is called as the heart of Microprocessor, Microcontrollers, and CPUs. No technology can exist, without those operations which are performed by ALU. Every technology uses works upon those operations either fully or partially which are performed by ALU. The block diagram of ALU is given below, where ALU has been implemented on FPGA tool

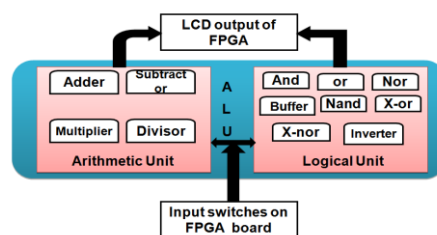


Figure 1.1 Block Diagram of ALU

Here the input interface to access ALU module is input switches on FPGA board, and after processing on the data the result can be seen from LCD output of FPGA. For multiplication purpose vedic Urdhva Triyambakam multiplication scheme has been used. Urdhva Triyambakam Sutra is a general multiplication formula applicable to all cases of multiplication. It literally means "Vertically and Crosswise". To illustrate this multiplication scheme, let us consider the multiplication of two decimal numbers (32×44). The conventional methods already know to us will require 16 multiplications and 15 additions. An alternative method of multiplication using Urdhva Triyambakam Sutra is shown in following figure. The Vedic multiplication algorithm for 2 digit decimal numbers is shown below:-

32 X 44 = 1,408

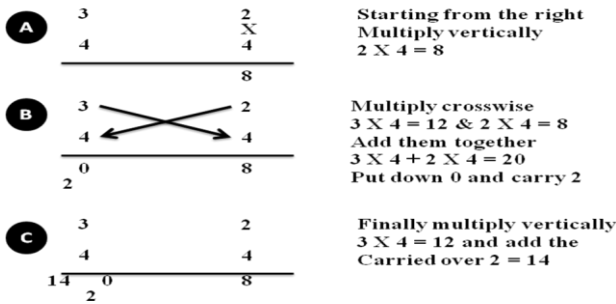


Figure 1.2 Vedic Multiplication Technique

On the basis of this the conventional Vedic Multiplier hardware has been designed which is shown below for 4x4 Bit, Using the same approach N-Bit Multiplier can be introduced[10]:-

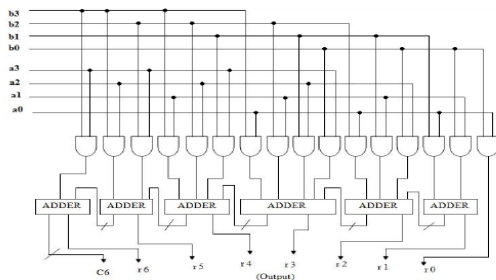


Figure 1.3 Conventional Four Bit Vedic Multiplier

But it has large carry propagation path delay which limits the speed of it. So to overcome this problem many methodologies have been introduced in which the latest and popular technique is to replace the conventional addition structure with carry save addition (CSA) structure. But we have seen that its speed is also limited because of intermediate processes followed by the CSA to convert three operands into two operands addition. Diagram of this is given following for 4-Bit level Multiplication [4]:

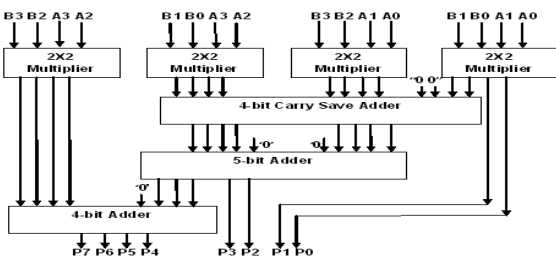


Figure 1.4 Four Bit Vedic Multiplier with CSA

II. Proposed ALU Module

Our Proposed 8x8 bit Arithmetic Unit is shown in the following:-

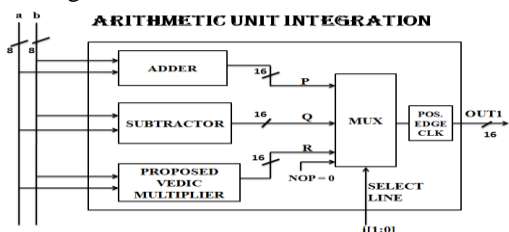
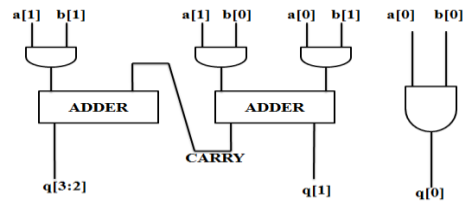


Figure 2.1 Proposed Arithmetic Unit Integration

Here a and b are the two 8 bit inputs of our Arithmetic Unit. And other sections of the design are self-explanatory.

For 2-Bit multiplication Conventional Vedic multiplication Hardware has been used. As at 2 bit level multiplication we have not to worry about the carry propagation path.



Here inputs are a [1:0] and b[1:0], and output is q[3:0].

Figure 2.2 Two Bit Conventional Vedic Multiplier

Diagram for Unique addition tree structure for partial product addition for 4 bit is given in the following:-

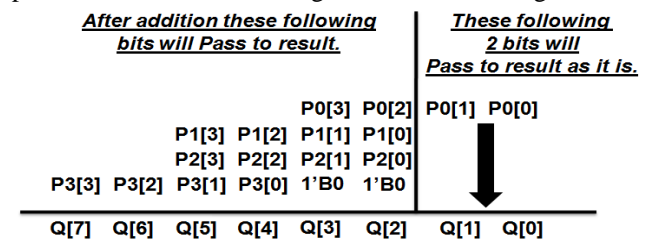


Figure 2.3 Proposed Addition Tree Structure of 4-Bit Multiplier

Diagram for Unique addition tree structure for partial product addition for 8 bit is given in the following:-

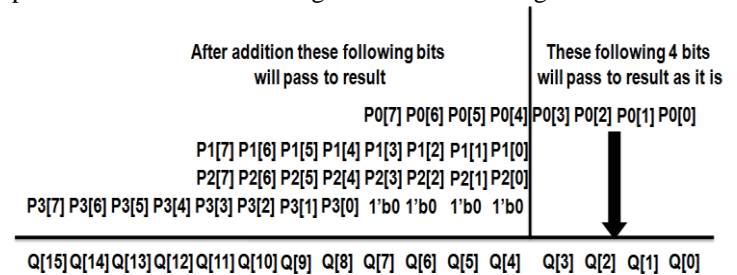


Figure 2.4 Proposed Addition Tree Structure of 8-Bit Multiplier

Here the assignment of partial products P0, P1, P2, P3 has given from right to left at output of Vedic N/2-Bit Vedic multiplier, where N shows the no. of bits in one input of multiplier. And also which addition tree structure we have designed is very simple to understand, design and implement. Here for the addition purpose the unique addition tree structure. The block diagram for 4 bit level multiplication shown below.

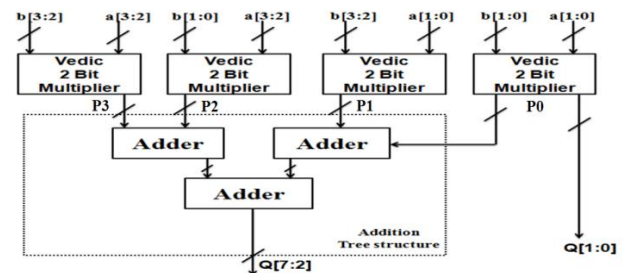


Figure 2.5 Block Diagram of Proposed 4-Bit Vedic Multiplier

Block diagram of 8-Bit Vedic Multiplier is shown below:-

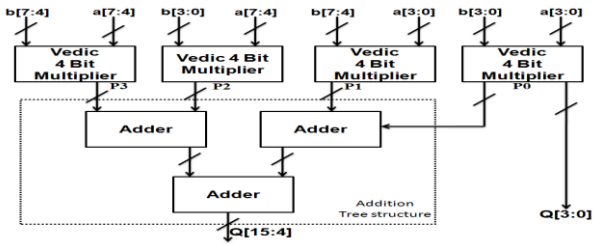


Figure 2.6 Block Diagram of Proposed 8-Bit Vedic Multiplier

After designing the Arithmetic Unit, it has been incorporated into the ALU module. The block diagram of proposed ALU is given following, which is self explanatory in itself:-

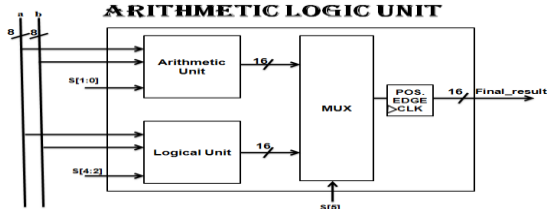


Figure 2.7 Proposed ALU

For designing the Logical unit we have used the simple conventional logic gates and multiplexer has been used for integration purpose. It can be easily built by referring any standard book of digital electronics so it has not been discussed here. Control word for the proposed ALU is:-

CONTROL WORD OF ALU

S[5]	S[4]	S[3]	S[2]	S[1]	S[0]	OPERATIONS PERFORMED
0	x	x	x	0	0	ADDITION (a,b)
0	x	x	x	0	1	SUBTRACTION (a,b)
0	x	x	x	1	0	MULTIPLICATION (a,b)
0	x	x	x	1	1	NOP = 0
1	0	0	0	x	x	AND (a,b)
1	0	0	1	x	x	OR (a,b)
1	0	1	0	x	x	NOR (a,b)
1	0	1	1	x	x	DATA BUFFER (a)
1	1	0	0	x	x	NAND (a,b)
1	1	0	1	x	x	X-OR (a,b)
1	1	1	0	x	x	X-NOR (a,b)
1	1	1	1	x	x	NOT (a)

Figure 2.8 Control Word

III. QUANTITATIVE RESULTS

Following table shows the area and timing constraints of proposed Vedic multiplier at different bit levels.

N Bit multiplier	Number of LUT used as logic	Number of occupied Slices	Total eq. gate count for design	Additional JTAG gate count for design	Maximum combinational path delay (ns)
2-Bit	4	2	24	384	4.626ns
4-Bit	31	16	230	768	8.387ns
8-Bit	139	70	1073	1536	11.886ns

Table 3.1 Device Utilization Summary of N-Bit Multiplier

IV. COMPARATIVE RESULTS

To show the efficiency of proposed Vedic multiplier at eight bit level, it has been compared with some other popular multiplier structures based on different multiplication algorithms at the eight bit level. For the comparison purpose some standard papers have been used.

For true and reliable comparison, proposed multiplier has been implemented on the same platform of target FPGA, which has been used by the reference papers. Comparative tables are shown below:-

(a) In the following given table the target FPGA used belongs to Virtex 2P (family), XC2VP2 (device), FG 256 (Package), -7 (speed grade).

Karatsuba [10]	Vedic Karatsuba [10]	Modified Booth Wallace [4]	Vedic with Partitioning [4]	Conventional Vedic [10]	Vedic with CSA [4]	Proposed
31.039	18.695	15.815	15.685	15.418	13.07	11.886

Table 4.1 Comparative Table 1 for Different Multipliers at 8-Bit Level

(b) In the following given table the target FPGA used belongs to Spartan 3 (family), XC3S50 (device), PQ 208 (Package), -4 (speed grade).

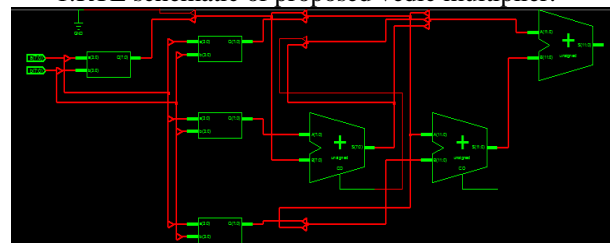
Array [2]	Booth [2]	Conventional Vedic [2]	Proposed
32.01	29.549	21.679	19.467

Table 4.2 Comparative Table 2 for Different Multipliers at 8-Bit Level

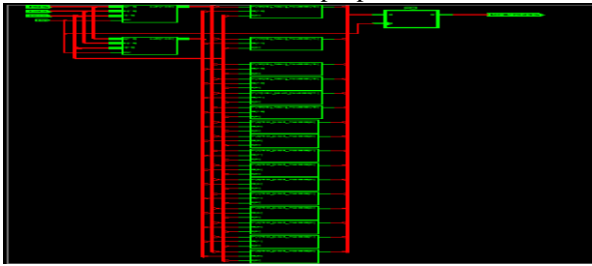
By designing the proposed Vedic multiplier for the same reconfigurable hardware as shown in [4] and [2], make the comparison platform (hardware) independent, algorithmic, technique and approach based comparison. So by comparing with different multipliers at the same platform it can be concluded that the algorithm and approaches which has been proposed to design Vedic multiplier, in this thesis work, is better in comparison to the other popular algorithms and approaches shown in [4] and [2]. In [10] M. Ramalatha et.al. Have not shown that which target FPGA they have used to design their modules so we have compared our proposed multiplier design with our conventional target FPGA, which we have used to make the overall design of ALU. So by this it can be concluded that our proposed algorithm, approach and platform are better than [10].

V. Synthesis And Simulation

1. RTL schematic of proposed vedic multiplier:-



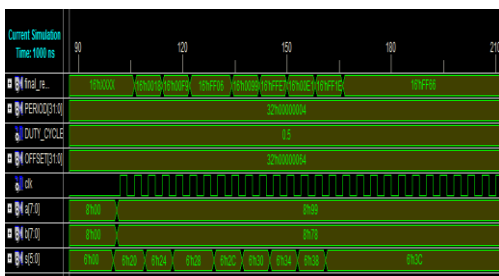
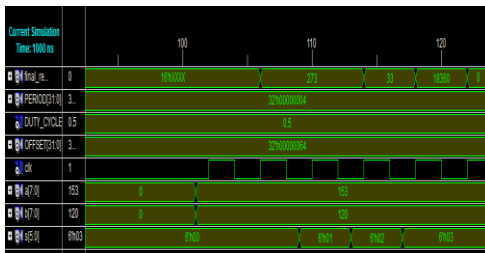
2.RTL schematic of proposed ALU:-



3.Device utilization summary of proposed ALU:-

Device Utilization Summary				
Logic Utilization	Used	Available	Utilization	Note(s)
Number of Slice Flip Flops	25	2,816	1%	
Number of 4 input LUTs	216	2,816	7%	
Logic Distribution				
Number of occupied Slices	116	1,408	8%	
Number of Slices containing only related logic	116	116	100%	
Number of Slices containing unrelated logic	0	116	0%	
Total Number of 4 input LUTs	227	2,816	8%	
Number used as logic	216			
Number used as a route thru	11			
Number of bonded IOBs	39	140	27%	
IOB Flip Flops	16			
Number of FPC405s	0	0	0%	
Number of GCLKs	1	16	6%	
Number of GT1s	0	4	0%	
Number of GT10s	0	0	0%	
Total equivalent gate count for design	2,133			
Additional JTAG gate count for IOBs	1,872			

4. Simulation results of proposed ALU as per control word of ALU:-



VI. Conclusion

We have proposed a new technique to design Vedic multiplier using unique addition tree structure, which gives better response in terms of speed in comparison to the conventional vedic multiplier hardware, Vedic multiplier with partitioning, Vedic multiplier with carry save adder, Modified Booth Wallace, Karatsuba, Vedic Karatsuba, Array, Booth, Wallace multiplier. And then this multiplier module has been put in the ALU along with conventional modules.

References

[1]. S G Dani, "Ancient Indian Mathematics – A Conspectus*", GENERAL_ ARTICLE, RESONANCE, March 2012, Springer Link.
 [2]. Pushpalata Verma, K.K. Metha, "Implementation of an Efficient Multiplier based on Vedic Mathematics Using EDA Tool", International journal of engineering and advance technology, ISSN: 2249-8958, Volume-1, Issue-5, June-2012.
 [3]. R.Bhaskar, Ganapathi Hegde, P.R.Vaya," An efficient hardware model for RSA Encryption system using Vedic

mathematics". Procedia Engineering Volume 30, 2012, Pages 124–128, SciVerse Science Direct, ELSEVIER.
 [4]. Devika Jaina, Kabiraj Sethi, Rutuparna Panda, "Vedic Mathematics Based Multiply Accumulate Unit", 978-0-7695-4587-5/11 \$26.00 © 2011 IEEE.
 [5]. Balpande, S., Akare, U., Lande, S., "Performance Evaluation and Synthesis of Multiplier Used in FFT Operation Using Conventional and Vedic Algorithms". 19-21 Nov.2010, IEEE.
 [6]. Syed Azman bin Syed Ismail*, Pumadevi a/p Siva subramniam, "Multiplication with the Vedic Method", Procedia Social and Behavioral Sciences 8 (2010) 129–133, SciVerse Science Direct, ELSEVIER.
 [7]. Ashish Raman, Anvesh Kumar and R.K. Sarin, "Small area reconfigurable FFT design by Vedic Mathematics", 26-28 Feb. 2010, IEEE.
 [8]. Anvesh kumar, Ashish raman, "Low Power ALU Design by Ancient Mathematics", 978-1-4244-5586-7/10, 2010 IEEE.
 [9]. Parth Mehta, Dhanashri Gawali, "Conventional versus Vedic Mathematical Method for Hardware Implementation of a Multiplier", December 2009, pp. 640-642 IEEE.
 [10]. M. Ramalatha, K. Deena Dayalan, P. Dharani, S. Deborah Priya, "High Speed Energy Efficient ALU Design using Vedic Multiplication Techniques", 978-1-4244-3834-1/09, 2009 IEEE.
 [11]. Harpreet Singh Dhillon and AbhijitMitra, "A Reduced- Bit Multiplication Algorithm for Digital Arithmetics", International Journal of Computational and Mathematical Sciences 2:2,2008 © www.waset.org Spring 2008.
 [12]. Honey Durga Tiwari, Ganzorig Gankhuyag, Chan Mo Kim, Yong Beom Cho, "Multiplier design based on Ancient Vedic Mathematics", 978-1-4244-2599-008/\$25.00 © 2008, IEEE.
 [13]. Shamim Akhter, "VHDL Implementation of Fast NxN Multiplier Based on Vedic Mathematics", Jaypee Institute of Information Technology University, Noida, 201307 UP, INDIA, 2007 IEEE.
 [14]. Himanshu Thapliyal, Saurabh Kotiyal and M. B Srinivas, "Design and Analysis of A Novel Parallel Square and Cube Architecture Based On Ancient Indian Vedic Mathematics", Centre for VLSI and Embedded System Technologies, International Institute of Information Technology, Hyderabad, 500019, India, 2005 IEEE.
 [15]. HimanshuThapliyal and M.B Srinivas, "A High Speed and Efficient Method of Elliptic Curve Encryption Using Ancient Indian Vedic Mathematics", Proceedings of the 8th MAPLD Conference (NASA office of Logic Design), Washington D.C, USA, Sep 2005.
 [16]. Purushottam D. Chidgupkar, Mangesh T. Karad, "The Implementation of Vedic Algorithms in Digital Signal Processing*", Global J. of Engng. Educ., Vol.8, No.2 © 2004 UICEE Published in Australia 4th Global Congress on Engineering Education, held in Bangkok, Thailand, from 5 to 9 July 2004.
 [17]. Amartya Kumar Dutta, "Mathematics in Ancient India", SERIES ARTICLE, April 2002 SpringerLink.
 [18]. Jagadguru Swami Sri Bharati Krishna Tirthji Maharaja,"Vedic Mathematics", MotilalBanarsidas, Varanasi, India, 1986, Book.
 [19]. Sameer Palnitkar, "Verilog HDL-A Guide to Digital Design and Synthesis", Sun Soft Press,1996, Book.
 [20]. Morris Mano, "Digital circuits and systems", Prentice-Hal, Last updated on-02/27/2011, 11:55, Book. Wayne Wolf, "Computer as components", 2nd edition, Book.
 [21]. http://www.xilinx.com/support/documentation/data_sheets/ds312.pdf
 [22]. <http://en.wikipedia.org/wiki/Verilog>
 [23]. http://www.xilinx.com/prs_rls/2007/software/0786_ise92i.htm

Concurrent Engineering: Impact on New Product Design and Development in Indian Two Wheeler Auto Industry

¹V. Venkata Ramana,

¹ Head, Mechanical Department, Intell Engineering College, ANANTAPUR- 515 003, A.P, INDIA

Abstract: Concurrent Engineering (CE) has a great deal of importance in design and development of new products in automobile industry and is posing a big challenge to Indian firms in the wake of globalization. Success of CE demands that major areas of product design and development of an organization need to be under constant focus. Most of the companies adopt CE procedures to reduce the time of launching the new product in the market, especially firms of western countries and Middle East. This paper analyzes the influence of concurrent engineering practices followed by some selected Indian two wheeler automobile manufacturers in the area of new product development as they seek to improve their competitive position in global markets. The research survey presents its evaluation based on analysis by application of statistical tools on the primary data which was collected through a pre-tested questionnaire. The findings reveal that the selected two wheeler manufacturing companies in India are realizing maximum benefits with the implementation of the concurrent engineering in new product design and development.

Keywords: Concurrent Engineering, New Product Development, Product and Process development, Optimization.

I. Introduction:

In the present global business world market needs are volatile, the firms must be able to act and react quickly and responsively. Moreover, they must be able to significantly reduce their product introduction time to market and adapt to the changing business environments, because of shorter life period of the product's. Therefore, concurrent engineering (CE) has emerged as a way for rapid solutions in design and development process.

Concurrent engineering is no doubt the mark of future for new product introduction and development for all companies regardless of their size, sophistication. In order to be competitive, firms must revise their product and process development cycle to be able to complete diverse tasks concurrently. This process will benefit the company, although it requires a great deal of refinement in its implementation, as concurrent engineering is a process that must be reviewed and regulated for continuous improvements of both engineering and business processes.

According to Pennell and Winner, (1988)¹, "Concurrent Engineering is a systematic approach to the integrated, concurrent design of products and their related processes, including, manufacturing and support. This approach is intended to cause the developers from the very outset to consider all elements of the product life cycle, from conception to disposal, including cost, schedule, quality and user requirements". This strategy focuses on the optimization and distribution of a firm's resources in the design and development process to ensure effective and efficient product development process also enhances productivity and leads to high-class designs.

II. Literature Survey:

Shina S.G. in his paper "Concurrent engineering: new rules for world-class companies"(1991)² discussed how concurrent engineering technique is best suitable for manufacturing of high quality products by companies highlighting the benefits such as shorter time for product introduction, improved design quality, reduced design iterations, and shorter production time. Also enlightened the effects of multifunctional teaming which include design for manufacturing (DFM) continuous process improvement (CPI), total quality management (TQM), and quality function deployment (QFD) i.e., product development with concurrent engineering involves all parts of organization.

Rob Kinna, in his paper "Team working and Concurrent Engineering – A Success Story" (1995)³ has discussed the experiences and success of adopting Concurrent engineering highlighting the criticality of team selection, building and empowerment. He is of the opinion that the concurrent engineering team must include both internal group and external group such as customers, suppliers.

David Bradley in his paper, "Concurrent Engineering for bespoke products" (1995)⁴, discussed the disadvantages of traditional design techniques and shown how concurrent engineering benefits the organization. He says that concurrent engineering will advocate building teams working together from initial phase and in close contact with the customer. He has also discussed the benefits of developing computer modelling for further development including virtual reality.

III. Purpose of the Study:

The objective of the research study is to explore and establish the impact of concurrent engineering on product design and development on selected Indian two wheeler automobile industries.

IV. Methodology:

The evaluation of the study is based on a data analysis of the primary data using Cumulative Weighted Average statistical analysis technique. The primary data was collected through a well-structure questionnaire from a sample size of 234 respondents of design, production and marketing groups of selected two wheeler manufacturing companies in India. The questionnaire was sent to all respondents of 3 automobile companies and the usable response rate was 66% (see the Table 1)

Table 1: Response Rating of the Survey

	Number of Organizations		Response Ratio (in percentage)
	Questionnaire Sent to	Response Received	
Two Wheeler Industry Automobile manufacturers	03	03	100%
No. of Respondents	234	155	66%

V. Data Analysis and Interpretation:

The data pertaining to the outcomes of concurrent engineering in new product design and development in two wheeler manufacturing companies are presented in the Table 2 and the same is depicted in the Figure 1

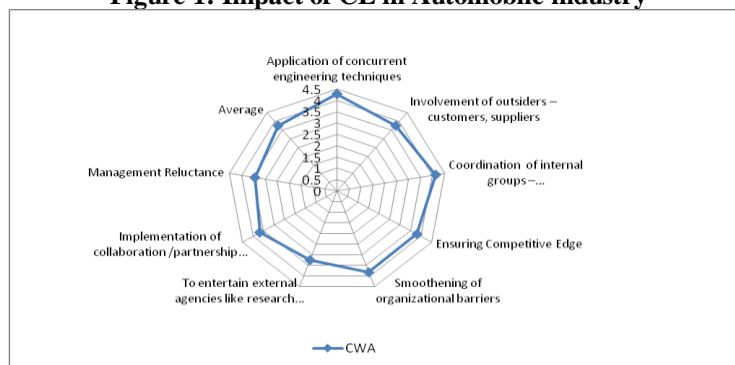
Table 2: Impact of Concurrent Engineering

Variables	Cumulative Weighted Average
Application of concurrent engineering techniques	4.28
Involvement of outsiders – customers, suppliers	3.76
Coordination of internal groups – design, Manufacturing	4.12
Ensuring Competitive Edge	3.8
Smoothing of organizational barriers	3.82
To entertain external agencies like research organizations	3.24
Implementation of collaboration /partnership of managements	3.66
Management Reluctance	3.42
Average	3.7625

Source: Field Survey

CWA: Cumulative Weighted Average

Figure 1: Impact of CE in Automobile industry



VI. Interpretation:

The data presented in the Table 2, clearly establishes that the influence of concurrent engineering in new product design and development of two wheeler companies is considerably high in India. In specific, the variables with CWA score of greater than 3.75 on a 5-point scale: Application of concurrent engineering techniques, Involvement of outsiders – customers, suppliers, Coordination of internal groups – design, manufacturing, Ensuring competitive edge, Smoothing of organizational barriers, are identified as key areas that realized most of the benefits.

VII. Results and Discussion:

Concurrent engineering has shown a very positive impact on design, development and introduction of new product in two wheeler automobile companies. Though companies are implementing concurrent engineering and realizing maximum benefits, they need to focus their attention in identifying the appropriate revolutionary technologies for proto-typing and thus increase cost savings and reduce time to market ultimately satisfying the customer needs.

References:

- [1]. Pennell and Winner, 1988], Winner R.J., Pennel J.P., Bertrand H.E., Slusarczuk M.M., ‘The role of concurrent engineering in weapons systems acquisition’, IDA R-338, Institute for Defence Analyses, 1988.
- [2]. Shina, S.G, 1991], Shina, S.G “Concurrent Engineering: New Rules for World-Class Companies”. Spectrum, IEEE Volume 28, Issue 7, Page(s):22 – 26. July 1991.
- [3]. Rob Kinna, 1995], Rob Kinna, “Team Working and Concurrent Engineering – A Success Story”, Journal: World Class Design to Manufacture, Volume: 2 Issue: 3 Page: 5 – 9, 1995.
- [4]. David Bradley, 1995], David Bradley, “Concurrent Engineering for Bespoke Products” Journal: Assembly Automation, Volume: 15 Issue: 1 Page: 35 – 37, 1995.
- [5]. Clark & Fujimoto, 1991] Clark K.B. and Fujimoto T., ‘Product Development Performance: Strategy, Organization and Management in the World Auto Industry’, Boston: Harvard Business School Press, 1991, p.78.
- [6]. Ullrich & Eppinger, 1995] Ullrich K.T., Eppinger S.D., ‘Product design and development’, McGraw Hill, London, 1995.
- [7]. Schilling & Hill, 1998] Schilling M.A., Hill C.W.L., ‘Managing the new product development process: Strategic imperatives’, Academy of Management Executive, vol. 12, no. 3, 1998.
- [8]. Wheelwright & Clark, 1993] Clark K.B., Wheelwright S.C., “Managing new product development - *Text and Cases*”, Harvard Business School, 1993.

Modeling and Control of a Variable Speed Wind Turbine Equipped With Permanent Magnet Synchronous Generator

B.Ratheen Kumar Reddy 1, Dr.M.Padma Lalitha 2, Mr.P.B.Chennaiah 3

*M.Tech, Annamacharya Institute Of Technology And sciences,Rajampet,
Professor & H.O.D.Annamacharya Institute of Technology and Sciences,
Assistant Professor, Annamacharya Institute of Technology and Sciences,*

Abstract: *The energy demand around the world increases; the need for a renewable energy source that will not harm the environment has been increased i. e. Wind power is one of them. There are many loads (such as remote villages, islands, ships etc) that are away from the main grid. They require stand-alone generator system (which can provide constant nominal voltage and frequency) to provide for their local electrification. Wind power can be used in off-grid systems, also called stand-alone systems, not connected to an electric distribution system or grid. The power conversion unit features a wind-turbine-driven PMSG, a diode rectifier, a buck-boost dc/dc converter, a battery bank, and a dc/ac inverter. In this paper, a distributed generation based on standalone wind energy conversion system (WECS) using a variable speed permanent magnet synchronous generator (PMSG) is proposed with PWM rectifier and a battery for storing the extra wind energy. The topology for the same has been demonstrated using MATLAB Simulink based simulations.*

Keywords-*BESS, DC/DC Converter, Isolated load, PMSG and WECS*

I. Introduction

Renewable energy sources including wind power offer a feasible solution to distributed power generation for isolated communities where utility grids are not available. In such cases, stand-alone wind energy systems (i.e., systems not connected to the utility grid) can be considered as an effective way to provide continuous power to electrical loads. One of the most promising applications of renewable energy generation lies in the development of power supply systems for remote communities that lack an economically feasible means of connecting to the main electrical grid. For isolated settlements located far from a utility grid, one practical approach to self-sufficient power generation involves using a wind turbine with battery storage to create a stand-alone system.

If wind conditions are favorable, these stand-alone wind energy systems usually can provide communities with electricity at the lowest cost. Stand-alone wind energy systems often include batteries, because the available wind does not always produce the required quantities of power. If wind power exceeds the load demand, the surplus can be stored in the batteries.

The function of an electrical generator is providing a mean for energy conversion between the mechanical torque from the wind rotor turbine, as the prime mover, and the local load or the electric grid. Different types of generators are being used with wind turbines. Small wind turbines are equipped

with DC generators of up to a few kilowatts in capacity. Modern wind turbine systems use three phase AC generators.

The common types of AC generator that are possible candidates in modern wind turbine systems are as follows:

- Squirrel-Cage rotor Induction Generator (SCIG),
- Wound-Rotor Induction Generator (WRIG),
- Doubly-Fed Induction Generator (DFIG),
- Synchronous Generator (With external field excitation),
- Permanent Magnet Synchronous Generator (PMSG). For assessing the type of generator in WECS, criteria such

As operational characteristics, weight of active materials, price, maintenance aspects and the appropriate type of power electronic converter are used.

Historically induction generator (IG) has been extensively used in commercial wind turbine units. Asynchronous operation of induction generators is considered an advantage for application in wind turbine systems, because it provides some degree of flexibility when the wind speed is fluctuating. There are two main types of induction machines: squirrel cage and wound rotor.

The induction generator based on Squirrel-Cage rotor (SCIG) is a very popular machine because of its low price, mechanical simplicity, robust structure, and resistance against disturbance and vibration. The wound-rotor is suitable for speed control purposes. By changing the rotor resistance, the output of the generator can be controlled and also speed control of the generator is possible. Although wound rotor induction generator has the advantage described above, it is more expensive than a squirrel-cage rotor.

The induction generator based on wound rotor is the doubly fed induction generator (DFIG), which is a kind of induction machine in which both the stator windings and the rotor windings are connected to the source. The rotating winding is connected to the stationary supply circuits via power electronic converter. The advantage of connecting the converter to the rotor is that variable-speed operation of the turbine is possible with a much smaller and therefore much cheaper converter. The power rating of the converter is often about 1/3 the generator rating. Another type of generator that has been proposed for wind turbines in several research articles is synchronous generator. This type of generator has the

capability of direct connection (direct-drive) to wind turbines, with no gearbox. This advantage is favorable with respect to lifetime and maintenance. Synchronous machines can use either electrically excited or permanent magnet (PM) rotor.

The PM and electrically-excited synchronous generators differ from the induction generator in that the magnetization is provided by a Permanent Magnet pole system or a dc supply on the rotor, featuring providing self-excitation property. Self-excitation allows operation at high power factors and high efficiencies for the PM synchronous generators.

The PM and electrically-excited synchronous generators differ from the induction generator in that the magnetization is provided by a Permanent Magnet pole system or a dc supply on the rotor, featuring providing self-excitation property. Self-excitation allows operation at high power factors and high efficiencies for the PM synchronous generators. It is worth mentioning that induction generators are the most common type of generator use in modern wind turbine systems.

A comparison between the variable speed wind turbine and the constant speed wind turbine shows that variable speed reduce mechanical stresses: gusts of wind can be absorbed, dynamically compensate for torque and power pulsations caused by back pressure of the tower. This backpressure causes noticeable torque pulsations at a rate equal to the turbine rotor speed times the number of rotor blades.

II. Permanent Magnet Generator

Figure 1 shows the cross-section of a typical Permanent Magnet Generator (PMG). The PMG differs from the Induction Generator in that the magnetization is provided by a Permanent Magnet Pole System on the rotor, instead of taking excitation current from the armature winding terminals, as it is the case with the Induction Generator. This means that the mode of operation is synchronous, as opposed to asynchronous. That is to say, in the PMG, the output frequency bears a fixed relationship to the shaft speed, whereas in the mains connected IG, the frequency is closely related to the network frequency, being related by the slip. These differences will be discussed at length. However, it must be recognized at the outset that the differences have a significant effect on the operating characteristics and performance of the two generator types.

Permanent magnet machines may be set in several categories, those with surface mounted magnets, those with buried magnets, those with damper windings, etc., etc. All categories where data was found were considered, as each has some special features to offer [3]. The advantages of PM machines over electrically excited machines can be summarized as follows according to literatures:

- Higher efficiency and energy yield,
- No additional power supply for the magnet field Excitation,
- Improvement in the thermal characteristics of the PM machine due to the absence of the field losses,
- Higher reliability due to the absence of Mechanical components such as slip rings,
- Lighter and therefore higher power to weight Ratio.

However, PM machines have some disadvantages, which can be summarized as follows:

- High cost of PM material,
- Difficulties to handle in manufacture,
- Demagnetization of PM at high temperature.

In recent years, the use of PMs is more attractive than before, because the performance of PMs is improving and the cost of PM is decreasing. The trends make PM machines with a full-scale power converter more attractive for direct-drive wind turbines. Considering the performance of PMs is improving and the cost of PM is decreasing in recent years, in addition to that the cost of power electronics is decreasing, variable speed direct-drive PM machines with a full-scale power converter become more attractive for offshore wind powers. On the other hand, variable speed concepts with a full-scale power converter and a single- or multiple-stage gearbox drive train may be interesting solutions not only in respect to the annual energy yield per cost but also in respect to the total weight. For example, the market interest of PMSG system with a multiple-stage gearbox or a single-stage gearbox is increasing.

III. Topologies For Isolated Operation Of Variable Speed Wind Driven Pmsg

Variable speed use is good for extracting more prime mover power as in wind turbine or for providing optimum efficiency for the prime mover by increasing its speed with power. Variable speed also allows for a more flexible generator system. For wind turbines, a battery may be added to store the extra wind energy that is not momentarily needed for the existing loads or local power grids. At variable speed, the DC link voltage is maintained constant by exchanging power with battery as shown in Fig. 1

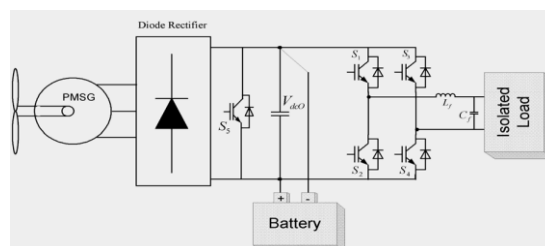


Fig.1 PMSG with PWM rectifier with battery for storing the extra wind energy

IV. Matlab Simulation Of The Proposed Topology

The MATLAB Simulation of proposed topology has been Shown in the Fig.2. The mat lab simulink tool box simpower Has been used for getting the required results.

V. Modeling Of Proposed System

A. Modeling of System

This section includes modeling of supply system (PMSG), load, controller etc. The relevant mathematical analysis is illustrated as follows.

B. Modeling of Supply system

The supply system consists of three-phase (PMSG) system, diesel engine and governor blocks. The model of permanent magnetsynchronousgenerator(PMSG)isrealized by consideringfixedexcitation of an alternator. The mathematical representation of all these are given below.

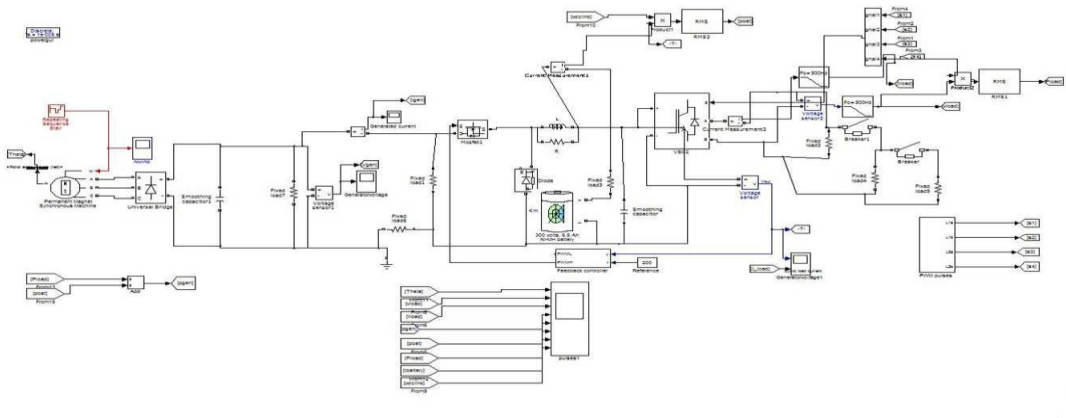


Fig.2. MATLAB Simulated model of PMSG connected to local Load

C. Modeling of Permanent Magnet Synchronous Machine

The permanent magnet synchronous machine block operates in generating or motoring modes. The operating mode is dictated by the sign of the mechanical power (positive for generating, negative for motoring). The electrical part of the machine is represented by a sixth-order state-space model. The model takes into account the dynamics of the stator and damper windings. The equivalent

frame (d-q frame). The following equations are used to express the model of the PMSG as:

$$V_d = R_s i_d + p \psi_d - \omega_r \psi_q \dots\dots\dots (1)$$

$$V_q = R_s i_q + p \psi_q + \omega_r \psi_d \dots\dots\dots (2)$$

$$V'_{fd} = R'_{fd} i'_{fd} + p \psi'_{fd} \dots\dots\dots (3)$$

$$V'_{kd} = R'_{kd} i'_{kd} + p \psi'_{kd} \dots\dots\dots (4)$$

$$V'_{kq1} = R'_{kq1} i'_{kq1} + p \psi'_{kq1} \dots\dots\dots (5)$$

$$V'_{kq2} = R'_{kq2} i'_{kq2} + p \psi'_{kq2} \dots\dots\dots (6)$$

Where

$$\psi_d = L_d i_d + L_{md} (i'_{fd} + i'_{kd}) \dots\dots\dots (7)$$

$$\psi_q = L_q i_q + L_{mq} i'_{kq} \dots\dots\dots (8)$$

$$\psi'_{fd} = L'_{fd} i'_{fd} + L_{md} (i_d + i'_{fd}) \dots\dots\dots (9)$$

$$\psi'_{kd} = L'_{kd} i'_{kd} + L_{md} (i_d + i'_{fd}) \dots\dots\dots (10)$$

$$\psi'_{kq2} = L'_{kq2} i'_{kq2} + L_{mq} i_q \dots\dots\dots (11)$$

Where the subscripts used are defined as: d, q: d and q axis quantity, r, s: Rotor and stator quantity, l, m: Leakage and magnetizing inductance, f, k: Field and damper winding quantity. R_s represents stator resistance, L_{ls} stator leakage inductance, L_{md} and

L_{mq} represent d-axis and q-axis magnetizing inductances. R'_f denotes field resistance and L_{lfd} leakage inductance both referred to the stator. Damper d-axis resistance R_{kd} and leakage inductance L_{lkd} , Damper q-axis resistance R_{kq1} and leakage inductance L_{lkq1} and the q-axis resistance R_{kq2} and leakage inductance L_{lkq2} . All these values are referred to the stator. All rotor parameters and electrical quantities are viewed from the stator and are identified by primed variables. The simplified synchronous machine block implements the mechanical system described by:

$$\Delta\omega(t) = \int (T_m - T_e) dt / (2H) - K_d \Delta\omega(t) \dots\dots\dots (12)$$

$$\omega(t) = \Delta\omega(t) + \omega_0 \dots\dots\dots (13)$$

D. Excitation System

The excitation system block is a Simulink system implementing an IEEE Type I synchronous machine voltage regulator combined to an exciter. The basic elements that form the excitation system block are the voltage regulator and the exciter. The exciter is represented by the following transfer function between the exciter voltage V_{fd} and the regulator's output E_f .

$$V_{fd}/E_f = 1/(K_e + sT_e) \dots\dots\dots (14)$$

where K_e represents exciter gain, T_e exciter time constant. The block uses actual terminal voltage, desired value of terminal voltage and outputs appropriate field voltage to be applied to synchronous alternator. For simulation of PMSG, the excitation is kept constant at 1.0 pu. in this model of synchronous generator.

E. Wind Turbine Modeling

This block implements a wind energy conversion system. The inputs are actual and desired speed and the output of the block is mechanical power (P_{ω}).

The amount of power harnessed from the wind of velocity is as follows.

$$P = 1/2 \rho A C_v^3 \quad (15)$$

Where

P_{ω} = wind power in watts

ρ = air density in kg/m^3

A = swept area in m^2

C_p = power coefficient of wind turbine

v = wind speed in m/s

VI. Simulation Results

The Fig.3 show the Variation of load voltages, load currents, generator power, battery power, , load power battery current & d c voltage. The rating of the PMSG is given in the Appendix.

VII. CONCLUSION

This paper discuss a distributed generation based stand alone wind energy conversion system (WECS) using a variable speed permanent magnet synchronous generator (PMSG) with PWM rectifier and a battery for storing the extra wind energy. According to the proposed topology, Battery energy storage system provides power balance between the generated power and the load. The power mismatch is absorbed by the BESS

APPENDIX

Permanent Magnet Synchronous Generator:

3-Phase, 300 V, 60 Hz, 3000 rpm, 4-pole Electromagnetic

Torque : 0.8 Nm Stator Resistance (R_S) : 18.7 Ω

Inductance: L_d (H) = L_q (H) : 0.02682 H Flux

induce by magnets : 0.1717 wb

References

- [1] Bhim Singh and Gaurav Kumar Kasal, "Solid-State Voltage and Frequency Controller for a stand alone wind power generating system," IEEE Trans. Power Electronics, vol. 23, no.3, pp.1170–1177, 2008.
- [2] Bhim Singh and Gaurav Kumar Kasal, "Voltage and Frequency Controller for a 3-Phase 4-Wire Autonomous Wind Energy Conversion System" accepted for publication in IEEE Trans. on Energy Conversion.
- [3] Arkadan, A.A., Hijazi, T.M., & Demerdash, D.A. (1989). Computer-aided modeling of a rectified DC load-permanent magnet generator system with multiple damper windings in the natural abc frame of reference. IEEE Transactions on Energy Conversion.
- [4] Ghosh and G. Ledwich, Power Quality Enhancement Using Custom Power Devices. Kulwer Academic, 2002.
- [5] Gipe, P. Wind power', Chelsea Green Publishing Company, Post Mills, Vermont, USA, 1995.
- [6] Rai, G.D. (2000) 'Non conventional energy sources', Khanna Publishers, 4th Edition, New Delhi (India)
- [7] Bansal, R.C., Bhatti, T.S., and Kothari, D.P. 'On some of the design aspects of wind energy conversion systems', Int. Journal of Energy Conversion and Management, Nov. Vol. 43, No. 16, pp.
- [8] Singh, B. 'Induction generator-a prospective', Electric Machines and Power Systems, Vol. 23, pp. 163-177, 1995.

SIMULATION RESULTS:

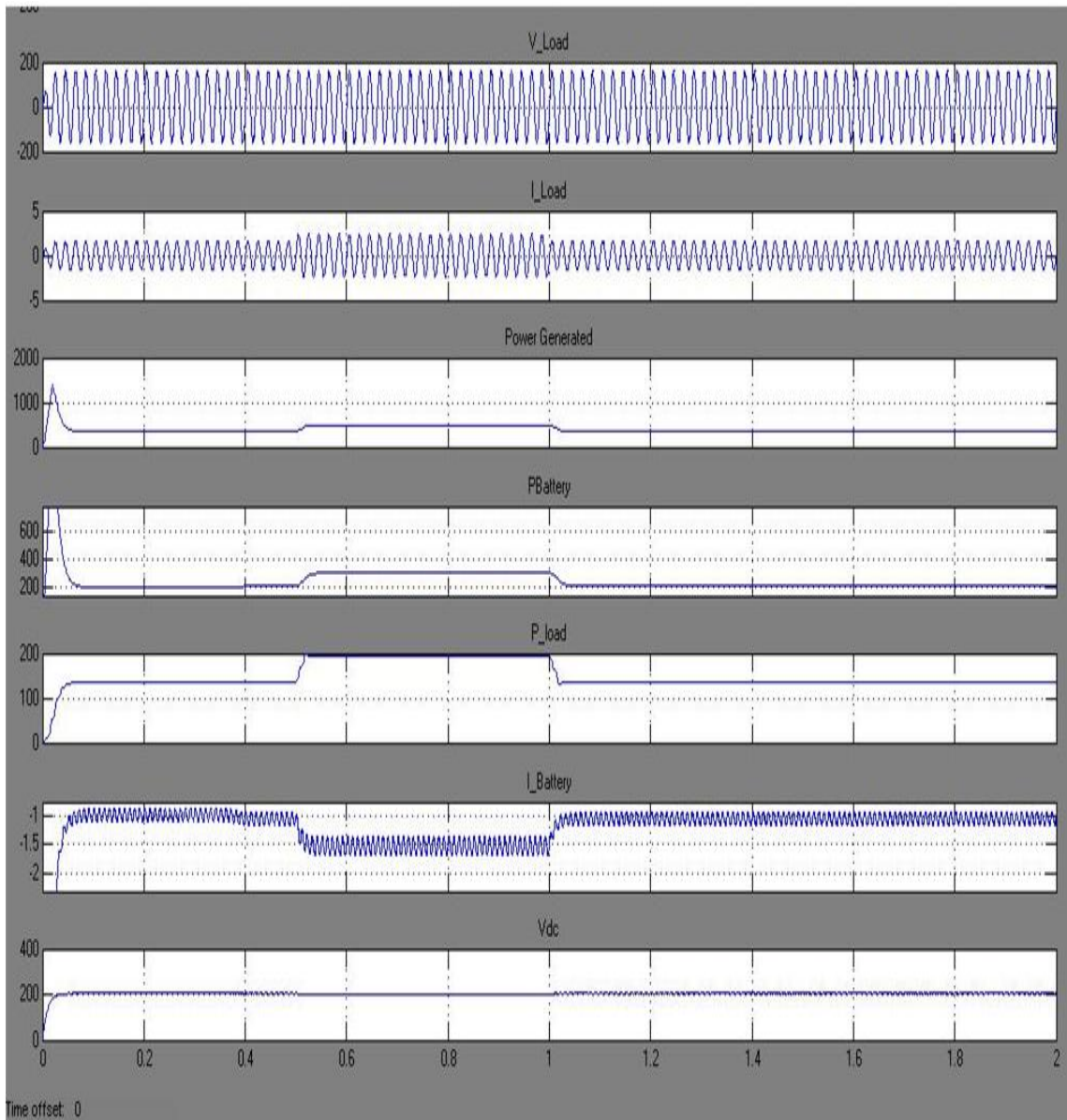


Fig.3. Variation of load voltages, load currents, generator power, battery power, , load power battery current & d c voltage

Rehab Assistance for Hansen Diseased Patients

A. N. Nithyaa, R. Prem Kumar

(Dept. of Biomedical Engineering, Rajalakshmi Engineering College,
Thandalam, CHENNAI – 602105).

Abstract: Hansen disease is a chronic disease caused by a bacillus, *Mycobacterium leprae*. According to World Health Organization's latest estimate, among 35% of leprosy cases in India, 48,000 are women. The side effects are permanent disability of hands, feet or eyes. Hansen disease can damage the peripheral nerves and nerves in the skin. This damage can lead to loss of sweat and oil gland function which causes dry and cracked skin on the hands and feet, loss of the ability to feel light touch or, with more severe damage, loss of protective sensation, weakness of the eyelids, preventing proper closure of the lid which protects the eye, loss of strength in the hands and feet. Therefore our main objective is to design a glove for Hansen diseased patients. It is a smart glove with an inbuilt sensor network and data acquisition system for storing the information for the Hansen diseased patients. The main purpose of the system is to provide alertness to the Hansen diseased patients with an assistive device that can improve their confidence and daily independence. Therefore this proposal may prove to be a breakthrough in the medical field and a step towards the enhancement of life and safety of human race.

Key Words: Hansen Disease, Leprosy, SMART GLOVE, ASSISTIVE DEVICE

I. Introduction

Hansen disease is also called Leprosy. Hansen disease is caused by the organism *Mycobacterium leprae*. It is defined as a chronic bacterial disease affecting mainly skin and nerves. If untreated, there can be progressive and permanent damage to the skin, nerves, limbs and eyes. It is a major public health problem in most of the developing world and is often found in conditions connected with poverty, overcrowding, poor sanitation and insufficient nutrition. According to current World Health Organization's data, the current global prevalence rate is around 1.4 cases per 10,000 people. Around 5, 00,000 new cases of leprosy are registered each year. India alone has about 5, 00,000 infected people, which represents 63% of the global occurrences.

Leprosy, a chronic infectious disease that, if left untreated, can cause debilitating deformities and slowly progress throughout one's life. It is characterized by peripheral nerve damage, cutaneous lesions and a wide range of clinical manifestations. The major side effects are permanent disability of hands, feet or eyes. Hansen disease can damage the peripheral nerves and nerves in the skin. This damage can lead to loss of sweat and oil gland function which causes dry and cracked skin on the hands and feet, loss of the ability to feel light touch or, with more severe damage, loss of protective sensation, weakness of the eyelids, preventing proper closure of the lid which protects the eye, loss of strength in the hands

and feet. In order to contract the disease, one has to live in close contact with an infected individual for a prolonged amount of time. These physical effects paired with the social stigma of being infected with this dreaded disease, often lead to those affected being afraid to come forward to seek treatment in the early stages of the disease. Hence there arises a need for rehabilitation.

II. A step towards rehabilitation

The basic concepts behind rehabilitation are that the persons affected with Hansen disease should be restored back to normal social life or as near as possible. Rehabilitation means restoration of economic productivity leading to economic independence. In India economic independence outweigh many other considerations. Rehabilitation in the field of Hansen disease requires greater efforts than the rehabilitation in other types of disabled persons because the question of social acceptance does not arise in non-Hansen disease disabled persons. In the case of a orthopedically handicapped or a blind or deaf person their stay with the family is not prejudiced as in the case of Hansen disease patients. This is due to the stigma attached to the disease. Therefore our paper is a step towards restoring their normal live. Being known the virulence of this disease, most of the research is based on its cure. Some of the existing treatments include drug therapy and chemotherapy. Also steps are being taken to eradicate and to a larger extend control its spread. A step towards rehabilitation is yet to catch up its pace. The main objective of this paper is to design a glove for Hansen diseased patients in order to alert them in case of any physical parameter extremity such as pressure or temperature using an inbuilt sensor network and a data acquisition system for storing the information acquired from the sensor for further analysis.



Fig 1. Picture of a person with Hansen disease(Hansen's disease)

III. General Block Diagram

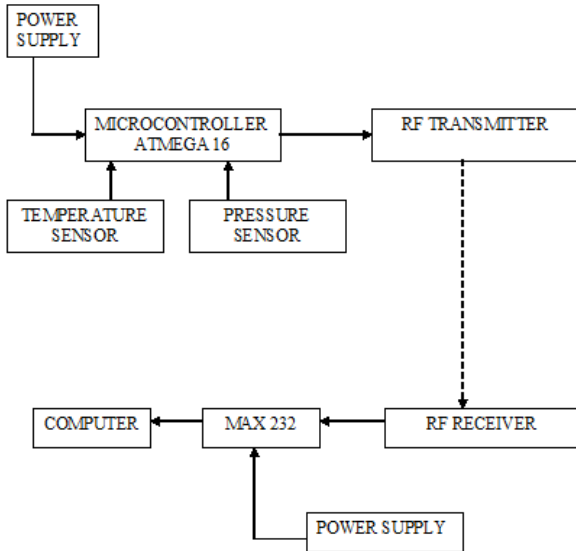


Fig 2. General Block Diagram

3.1 Description of Block Diagram

The block diagram represents the overall working of the glove. In the transmitter part, a temperature and a pressure sensor is used. The temperature sensor used here is LM35 and pressure sensor is FLEXIFORCE. The microcontroller ATMEGA 16 a low-power CMOS 8-bit microcontroller, which acquires the input from the sensors. To drive the microcontroller a power supply is given. These sensors give input to the controller in terms of voltage. The controller is programmed to send the analog voltage to the RF transmitter. At the other end a RF receiver module is placed which obtains the signal from the transmitter. MAX 232 is a level shifter which converts CMOS input levels into RS232 levels. RS-232 (Recommended Standard 232) is a standard for serial binary single-ended data and control signals connecting between a DTE (Data Terminal Equipment) and a DCE (Data Circuit-terminating Equipment). Now the digital values thus obtained is processed in SMART SOFTWARE supported by .NET. It is programmed in such a way that when the temperature and pressure reaches its extremities, indication is shown to the patient through alarm and LED glow respectively.

3.1.1.1 Transmitter Module

Transmitter module has the following components:

- LM35 sensor
- Flexi force sensor
- ATMEGA 16
- Power supply

LM35 sensor

Temperature measurement is very important in all spheres of life. Taking a temperature essentially requires the transmission of a small portion of an object's thermal energy to the sensor, whose function is to convert that energy into an electrical signal. When a contact sensor (probe) is placed inside or on the object, heat conduction takes place through the interface between the object and the probe. Contact temperature sensors measure their own temperature. One infers the temperature of the object to

which the sensor is in contact by assuming or knowing that the two are in thermal equilibrium, that is, there is no heat flow between them. Non Contact Sensors - Most commercial and scientific non contact temperature sensors measure the thermal radiant power of the Infrared or Optical radiation that they receive from a known or calculated area on its surface, or a known or calculated volume within it (in those cases where the object is semitransparent within the measuring wavelength pass band of the sensor). One then infers the temperature of an object from which the radiant power is assumed to be emitted (some may be reflected rather than emitted).

The LM35 series are precision integrated-circuit temperature sensors, whose output voltage is linearly proportional to the Celsius (Centigrade) temperature. The LM35 thus has an advantage over linear temperature sensors calibrated in ° Kelvin, as the user is not required to subtract a large constant voltage from its output to obtain convenient Centigrade scaling. The LM35 does not require any external calibration or trimming to provide typical accuracies of $\pm 1/4^{\circ}\text{C}$ at room temperature and $\pm 3/4^{\circ}\text{C}$ over a full -55 to $+150^{\circ}\text{C}$ temperature range. Low cost is assured by trimming and calibration at the water level. The LM35's low output impedance, linear output, and precise inherent calibration make interfacing to readout or control circuitry especially easy. It can be used with single power supplies, or with plus and minus supplies. As it draws only 60 μA from its supply, it has very low self-heating, less than 0.1°C in still air. The LM35 is rated to operate over a -55° to $+150^{\circ}\text{C}$ temperature range.

Flexi force Sensor

Pressure is defined as the normal force per unit area exerted by a fluid (liquid or gas) on any surface. It should be noted that pressure is not defined as a vector quantity and is therefore non directional.

Flexi force pressure sensors can measure force between almost any two surfaces and is durable enough to stand up to most environments. Flexi force has better sensor properties, linearity, hysteric, drift and temperature sensitivity than any other thin film force sensor. Its single element sensor acts as a resistor in an electrical circuit. When the sensor is unloaded, its resistance is very high. When a force is applied to the sensor, this resistance decreases. The resistance can be read by connecting an ohm meter to the outer two pins of the sensor connector and applying a force to the sensing area. There are many ways to integrate the sensor into an application. One way is to incorporate it into a force-to-voltage circuit. A means of calibration must be established to convert the output into the appropriate engineering units. Depending on the setup, an adjustment could then be done to increase or decrease the sensitivity of the sensor.

The Flexi Force sensor is an ultra-thin and flexible printed circuit, which can be easily integrated into most applications. With its paper-thin construction, flexibility and force measurement ability, the Flexi Force sensor can measure force between almost any two surfaces and is durable enough to stand up to most environments. Flexi Force has better force sensing properties, linearity, hysteric, drift, and temperature sensitivity than any other thin-film force sensors. The "active sensing area" is a $0.375''$ diameter circle at the end of the sensor. The sensors are constructed of two layers of substrate. This

substrate is composed of polyester film (or Polyimide in the case of the High-Temperature Sensors). On each layer, a conductive material (silver) is applied, followed by a layer of pressure-sensitive ink. Adhesive is then used to laminate the two layers of substrate together to form the sensor. The silver circle on top of the pressure-sensitive ink defines the “active sensing area.” Silver extends from the sensing area to the connectors at the other end of the sensor, forming the conductive leads. Flexi Force sensors are terminated with a solder able male square pin connector, which allows them to be incorporated into a circuit. The two outer pins of the connector are active and the center pin is inactive. The length of the sensors can be trimmed by Tekscan to predefined lengths of 2”, 4” and 6” or can be trimmed by the customer. If the customer trims the sensor, a new connector must be attached. This can be accomplished by purchasing staked pin connectors and crimping tool. A conductive epoxy can also be used to adhere small wires to each conductor. The sensor acts as a variable resistor in an electrical circuit. When the sensor is unloaded, its resistance is very high (greater than 5 Meg-ohm); when a force is applied to the sensor, the resistance decreases. Connecting an ohmmeter to the outer two pins of the sensor connector and applying a force to the sensing area can read the change in resistance. Sensors should be stored at temperatures in the range of 15°F (-9°C) to 165°F (74°C).



Fig 3. Flexi force Sensor

ATmega16

The ATmega16 is a low-power CMOS 8-bit microcontroller based on the AVR enhanced RISC architecture. By executing powerful instructions in a single clock cycle, the ATmega16 achieves throughputs approaching 1 MIPS per MHz allowing the system designer to optimize power consumption versus processing speed. The ATmega16 provides the following features: 16 Kbytes of In-System Programmable Flash Program memory with Read-While-Write capabilities, 512 bytes EEPROM, 1 Kbytes SRAM, 32 general purpose I/O lines, 32 general purpose working registers, a JTAG interface for Boundary scan, On-chip Debugging support and programming, three flexible Timer/Counters with compare modes, Internal and External Interrupts, a serial programmable USART, a byte oriented Two-wire Serial Interface, an 8-channel, 10-bit ADC with optional differential input stage with programmable gain (TQFP package only), a programmable Watchdog Timer with Internal Oscillator, an SPI serial port, and six software selectable power saving modes. The Idle mode stops the

CPU while allowing the USART, Two-wire interface, A/D Converter, SRAM, Timer/Counters, SPI port, and interrupt system to continue functioning. The Power-down mode saves the register contents but freezes the Oscillator, disabling all other chip functions until the next External Interrupter Hardware Reset. In Power-save mode, the Asynchronous Timer continues to run, allowing the user to maintain a timer base while the rest of the device is sleeping. The ADC Noise Reduction mode stops the CPU and all I/O modules except Asynchronous Timer and ADC, to minimize switching noise during ADC conversions. In Standby mode, the crystal/resonator Oscillator is running while the rest of the device is sleeping. This allows very fast start-up combined with low-power consumption. In Extended Standby mode, both the main Oscillator and the Asynchronous Timer continue to run. The device is manufactured using Atmel’s high density nonvolatile memory technology. The On chip ISP Flash allows the program memory to be reprogrammed in-system through an SPI serial interface, by a conventional nonvolatile memory programmer, or by an On-chip Boot program running on the AVR core. The boot program can use any interface to download the application Program in the Application Flash memory. Software in the Boot Flash section will continue to run while the Application Flash section is updated, providing true Read-While-Write operation. By combining an 8-bit RISC CPU with In-System Self-Programmable Flash on a monolithic chip, the Atmel ATmega16 is a powerful microcontroller that provides a highly-flexible and cost-effective solution to many embedded control applications.

Power Supply

Using the circuit shown in Figure 13, the following voltages at a current limited to one ampere are obtained (3V, 4.5V). The AC main is stepped down by transformer X1 to deliver the secondary output of 18V AC at a maximum current of 1A dependent on the load. The transformer output is rectified by the bridge rectifier comprising diodes D1 through D4, filtered by capacitor C1 and to regulator IC LM317, which is a 3 terminal positive regulator capable of providing 1.2V to 37V at 1.5A current to the load Resistor R3 and R2 are used to produce 3 V at the output, Similarly Resistor R5 and R4 are used to produce 4.5 V at the output.

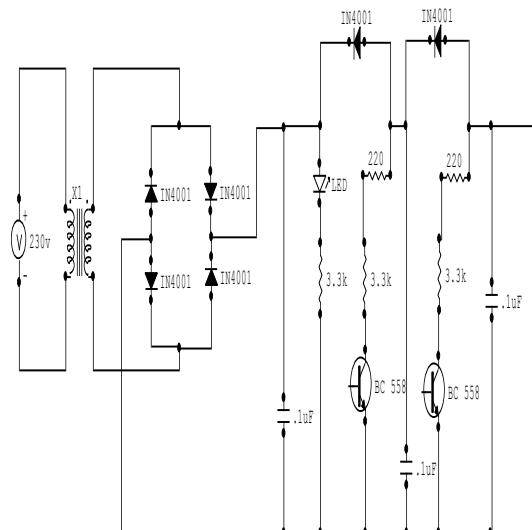


Fig 4. Power Supply

Capacitors. C2 and C3 bypass any ripple in the output. Diodes D5 and D6 are used as the protection diode. Heat sink is used for IC LM 317 to dissipate the heat from it. The LM386 is a power amplifier designed for use in low voltage consumer applications. The gain is internally set to 20 to keep the external part count low, but the addition of an external resistor and capacitor between pins 1 and 8 will increase the gain to any value from 20 to 200. The inputs are ground referenced while the output automatically biases to one-half the supply voltage. The quiescent power drain is only 24 mill watts when operating from a 6-volt supply, making LM386 ideal for battery operation

3.1.1.2 Receiver Module

The receiver module has the following components:

- Level Shifter
- MAX 232
- RF Module

MAX 232

The MAX232 is a dual driver/receiver that includes a capacitive voltage generator. Each receiver has a typical threshold of 1.3 V and a typical hysteresis of 0.5 V, and can accept ± 30 -V inputs. Each driver converts CMOS input levels into RS232 levels.

RF Module

RS-232 (Recommended Standard 232) is a standard for serial binary single-ended data and control signals connecting between a DTE (Data Terminal Equipment) and a DCE (Data Circuit-terminating Equipment). It is commonly used in computer serial ports. The signal levels for RS-232 represent a digital 1 bit as a voltage in the range of 5 to 12 V on the wire, and a digital 0 bit as a voltage of negative 5 to 12 V on the wire. RS-232 is typically implemented in a full duplex fashion, since each station can transmit to the other simultaneously using separate wires. RS-232 can be made to operate at a variety of bit rates, but typically is used at bit rates from 300 bit/s up to 115,200 bit/s.

IV. Conclusions

An Alarm is used and if there is any abnormal condition, it will initiate the buzzer. This alarm will alert the patient. Once the abnormality is rectified, the buzzer is terminated. Light emitting diodes are simply LEDs function in converting the voltage and exhibiting it in the form of light. They are used as indicators. These like alarms, are used to indicate abnormal conditions. They glow when the ideal conditions are disturbed. This is used to indicate pressure abnormality. In our paper the transmitter and receiver module is miniaturized. Also a data acquisition system is used to transfer the data. Thus smart glove is highly reliable and low cost. The main aim of this paper is to assist the Hansen diseased patients in order to alert them in case of any physical extremities.

Acknowledgements

The authors wish to thank the Chairman and Chairperson of Rajalakshmi Engineering College, Chennai for providing all the facilities required for carrying out this work. They also thank the Principal, Rajalakshmi Engineering College, Chennai for his constant encouragement and guidance.

References

1. World Health Organization, Regional Office for South-East Asia. Enhanced Global Strategy for Further Reducing the Disease Burden due to Hansen disease(Plan period: 2011-2015). 2009. http://www.searo.who.int/LinkFiles/GLP_SEA-GLP-2009_3.pdf accessed August 2010.
2. Department of Health and Ageing. National Notifiable Diseases Surveillance System. <http://www9.health.gov.au/cda/Source/CDA-index.cfm> accessed September 2010.
3. Department of Health and Families. Northern Territory Notifiable Diseases System
4. Rees RJW, McDougall AC. Airborne Infection with Mycobacterium Leprae in Mice. J. FMed Microbiol.
5. CARVALHO-SILVA, D. R., SANTOS, F. R., ROCHA, J. and PENA, S. D. The phylogeography of Brazilian Y-chromosome lineages. Am. J. Hum. Genet. 68 (2001) 281–286.
6. RIDLEY, D.S., and JOPLING, W. H. Classification of leprosy according to immunity; a five-group system. Int. J. Lepr. 34 (1966) 255–273.
7. QIN-XUE, W., GAN-YUN, Y., LI-LIN, Z., HUI-WEN, S., QI, L., XIN-YU, L., ZHOU-XIANG, M., and ZHI-WEN, L. Determination of antibodies in dried blood from earlobes of leprosy patients by enzyme linked immunosorbent assay—a preliminary report. Int. J. Lepr. Other Mycobact. Dis. 53 (1985) 565–570.
8. <http://www.nps.gov/kala/>
9. <http://www.leprosyjournal.org/leproline/?request=in dex-html>.
10. <http://www.technologystudent.com/elec1/therm1.htm>
11. <http://www.omega.com/prodinfo/thermistor.html>
12. Rehabilitation of Hansen disease Affected Persons Problems & Challenges for Provision of Services

Medical image watermarking based on M-band Wavelet Transform

R. Mavudila¹, Lh. Masmoudi², M. Cherkaoui³,
M. Hamri⁴, N. Hassanain⁵

^{1, 2, 4, 5}(Physics department, LETS Laboratory /Faculty of Science/, Mohammed V University/Morocco)

³(Faculty of medicine and pharmacy/, SIDI Mohammed Ben Abdellah University/CHU CheikZaid/ Morocco)

ABSTRACT: This paper introduces a new reversible and blind scheme based on the analysis of Multi-band Dual Tree Wavelet domain in medical image watermarking domain. Different from many other watermarking schemes with wavelet transform are used on one side in which the studies have dealt only in the dyadic case, in the other hand, in multi-band only on the classical discrete wavelet (DWT), for this suggested approach: security issues for medical information and technical solution to protect these data in medical information are examined. A solution is proposed, which consist in watermarking image areas that are not relevant for the diagnosis, considering advantages of multi-bands wavelet analysis. Applications of the method were examined for MRI images watermarking, inserting data in different sub-bands with private key provides high security for the embedded data using discrete wavelet and complex wavelet (CWT) domain. Experimental results obtained from several watermarked medical images indicate imperceptibility, in each case; the CWT provides higher capacity than the real DWT and DWT domain, by increasing the number of bands. The system is transparent to the user and allows image integrity control; in addition it provides information on the location of potential alterations and evaluation of image modifications which is of major importance in medico-legal frame-work. The proposed method generalizes the findings of previous works.

Keywords: Dual-tree wavelets, medical image, watermarking, multi-band wavelets, watermarking.

I. INTRODUCTION

Medical image protection and authenticity are becoming increasingly important in an e-health era where images are readily distributed over electronic networks. Research has shown that medical image watermarking is a relevant process for enhancing data security, content verification and image fidelity. At the same time, it is necessary to preserve as much original information in the image data as possible, to avoid causing performance loss for human viewers. Most medical image watermarking research focuses on developing watermarking systems that preserve image fidelity and/or robustness, under typical non-medical image degradation processes.

The Digital Imaging and Communications in Medicine (DICOM) standard is the standard to exchange medical data. The DICOM medical image files are attached with header containing patient information which may be lost, attacked or disordered with other header file. However, the watermarking method of medical images using patient information overcomes these problems [1]. However, there is a challenge that interleaving data in a medical image

must not affect the image quality as this may result in wrong diagnosis.

The most promising Dual-Tree wavelet Transform (DTT) proposed by N. Kingsbury, used two classical wavelet trees developed in parallel, looking into the benefits, such as good directional selectivity, shift invariance and perfect signal reconstruction (PR) [2]

The implementation of DT-CWT use couple of filters $\{h_0(n), h_1(n)\}$ to implement one separable wavelet transform and uses another filters couple $\{g_0(n), g_1(n)\}$ to implement [3]. Applying both separable transformations to the some 2D data gives a total of six sub bands: two HL, two LH and two HH subbands.

Being motivated by several applications and advantages of the complex wavelet decomposition in the images processing, we focus our approach by working to put the multi-band extension case to its best directional selectivity and the choice of analysis. This new transform found several applications in image processing, especially that we will exploit in watermarking images [4, 5].

Caroline Chaux proposed the construction of 2D dual-tree M-band wavelet decomposition and suggested that this analysis is the best way in the context of de-noising or higher dimension signal processing [4].

In this paper we presented an extension to M-DT-CWT and, the previously works of Xiangui Kang in [6] and Ning Bi [7] where only the standard DWT have been used.

Taking into account of limitations of DWT, we want to exploit the benefits of DT-CWT by incorporating the principal component analysis (PCA).

Previous work

This paragraph presents, an overview of the important existing watermarking schemes based on wavelet transform in medical domain and other research areas.

We will present them into two cases, dyadic and multi-band cases.

In dyadic case a lots of watermarking schemes are presented in the literature, only with the standard DWT.

Giakoumaki.A and al (2004) proposed a wavelet-based multiple watermarking scheme, which addresses the problems of medical confidentiality protection and both origin and data authentication, this scheme embeds multiple watermarks serving different purposes; a robust watermark for authentication a fragile watermark for the purpose of data integrity control, the scheme added-value tool offers alternatives for different issues associated with medical data management and distribution [8].

Salwa.A. and al(2010) proposed a new method for protecting the patient information in which the information

is embedded as a watermark in the discrete wavelet packet transform (DWPT) of the medical image using the hospital logo as a reference image. The patient information is coded by an error correcting code (ECC), BCH code, to enhance the robustness of the proposed method [9].

Golpina.H andDanyali.H (2009) have proposed a blind reversible watermarking approach for medical images based on histogram shifting in wavelet domain. An integer wavelet transform is applied to map the integer host image components to integer wavelet coefficients. Enabling lossless reconstruction of both watermark and host image, besides providing the high quality for the watermarked image [10].

Cheng-RI and al (2008) proposed a new fragile watermarking algorithm for medical images that makes it possible to resolve the security and forgery problem of the medical images with the discrete wavelet transform, an integer wavelet transform is used to utilize hash function. The watermark associated with the hash values is inserted into the LSBs of the integer wavelet transform coefficients, it can be confirmed that the proposed algorithm detects a forged area of the image very well [11].

ChokriChemak and al(2007) suggested to use the watermarking scheme which preserved the security of medical images for the pocketNeuro project,for reason that image watermarking allows doctors and personnel to hide invisible and robust medical information about a patient [12].

R. Mavudila and al present an algorithm based on dual-tree transform wavelet domain for medical image watermarking, a method that presents a good compromise between robustness and integrity [13]. However only few watermarking methods have been developed willingly the rich properties of dual tree transform wavelet.

With M-band wavelet transform approaches we can observe the works of Ning and al in [7] proposed a blind watermarking scheme based in the multi-band wavelet domain and Empirical mode decomposition.

Xiangui Kang and al, present a new multi-band wavelet scheme by incorporating the principal component analysis (PCA), a blind watermarking technique which achieved higher perceptual transparency and stronger robustness only with the classical Discrete Wavelet Transform (DWT) [6].

We take this latter watermarking embedding strategy in our proposed scheme; particularly we embed watermark bits indirectly in the m-band Dual tree wavelets domain with $M \geq 2$.

II. M-BAND DUAL TREE ANALYSIS (M-DTT)

Given the earlier works of watermarking images based on wavelet transform, we will apply our watermarking by using multi-band ($M \geq 2$ band) in DWT and complex wavelet (CWT) cases, in order to draw good result for a better comparative study.

2.1.Dual-tree Complex Transform (DT-CWT)

The Dual Tree Wavelet Transform initially proposed by N. Kingsburg and further investigated by I. Selesnick, analyses the signal by two DWT trees different with the filters chosen so that at the end of process it returns to approximately the decomposition by analytic wavelet.

The algorithm uses two different sets of filters: h_1 and g_1 , high-pass filters of first and second tree and h_0 and g_0 low-pass first and the second tree. The first tree produces the coefficients of the real part $dr(j, k)$ and the second tree those of the imaginary part $di(j, k)$, we then construct complex coefficients:

$$dcomplex(j, k) = dr(j, k) + i di(j, k). \quad (1)$$

The DT-CWT presents the advantages over simple Hilbert transform of the signal [14].

This implementation uses consists in analyzing the signal by two different DWT trees, with filters chosen so that at the end, the signal returns with the approximate decomposition by an analytical wavelet.

The dual-tree structure has an extension of conjugate filtering in 2-D case.

This structure needs four trees for analysis as well as for synthesis. The pairs of conjugate filters are applied to two dimensions (0 and 1), which can be expressed as:

$$\begin{aligned} (h_0 + jg_0)(h_1 + jg_1) \\ = (h_0h_1 - g_0g_1) + j(h_0g_1 + g_0h_1) \end{aligned} \quad (2)$$

The synthesis of filters suitable for this structure was performed by several people.

The wavelet corresponding to the tree's "imaginary part" is very close to the Hilbert transform of the wavelet corresponding to the trees "real part" [15].

For J level decomposition, the corresponding details sub bands at leven η are denoted: $HL\eta$ real, $HL\eta im$, $LH\eta real$, $LH\eta im$, $HH\eta real$ and $HH\eta im$, where $\eta = 1, 2, \dots, J$.

2.2.M-band Discrete Wavelet Transform (M-DWT).

As reminder that one dimensional dyadic case ($M=2$), is a scaling function $\Phi(x) \in L^2(\mathbb{R})$ and M-1 wavelet function $\{\varphi_l(x), 1 \leq l \leq M-1, M > 2\}$ [16,17] in M-band analysis, these functions satisfy the following equations respectively

$$\Phi(x) = \sum_{k \in \mathbb{Z}} h_1(k) \Phi(Mx - k) \quad (3)$$

$$\varphi_l(x) = \sum_{k \in \mathbb{Z}} h_l(k) \Phi(Mx - k) \quad (4)$$

$$1 \leq l \leq M - 1$$

Where \mathbb{Z} is the integer set and sequence $\{h_l(k), 0 \leq l \leq M-1\}$ has finite length.

The one dimensional Mallat decomposition and reconstruction formulas of orthogonal M-band wavelet are expressed in (5) and (6) respectively [16]

$$C_{j+1} = \sqrt{M} \sum_{k' \in \mathbb{Z}} C_j(k') h_0(k' - Mk) \quad (5)$$

$$d_{j+1} = \sqrt{M} \sum_{k' \in \mathbb{Z}} d_j(k') h_1(k' - Mk)$$

$$1 \leq l \leq M - 1$$

$$C_j(k) = \sqrt{M^{-1}} \sum_{k' \in Z} C_{j+1}(k') h_0(k' - Mk) + \sqrt{M^{-1}} \sum_{l=1}^{M-1} \sum_{k' \in Z} d_{j+1}^l(k) h_1(k' - Mk)$$

$$1 \leq l \leq M - 1 \tag{6}$$

Where $\{C_{j+1}(k), j = 1, 2, \dots, \}$ is the approximation coefficients of the j+1 level M-band wavelet decomposition of 1D signal $C_0(k)$ and $\{d_{j+1}^l(k); j = 0, 1, 2, \dots, \}$ is the detail coefficient of the J+1 level band wavelets decomposition.

For the image, the 1D M-band discrete wavelet transform is easy to extend to 2D M-band wavelet transform, by applying 1D MDWT

2.3. M-band Dual-Tree (M-DTT)

This implementation uses consisting of analyzing the signal by two different MDWT trees, primal and who gives the real and imaginary coefficients respectively.

The M-band -DT-CWT employs two real M-band DWT.

The first M-DWT gives the real part of the transform while the second MDWT gives the imaginary part.

Let $h_0(n), h_1(n)$ denote the low-pass/high-pass filter and $g_0(n), g_1(n)$ denote the low-pass/high-pass for upper and lower filter banc respectively.

For the scaling function $\Phi^H(x) \in L2(R)$ and M-1 wavelet functions $\{\varphi_l^H(x), 1 \leq l \leq M - 1, M > 2\}$

The equations (3, 4, 5 and 6) precedents can be used at the primal tree (real part).

In parallel the decomposition applying at dual tree (imaginary part) gives:

$$\Phi^H(x) = \sum_{k \in Z} h_1(k) \Phi^H(Mx - k) \tag{7}$$

$$\varphi_l^H(x) = \sum_{k \in Z} h_1(k) \Phi^H(Mx - k) \tag{8}$$

$$1 \leq l \leq M - 1$$

$$C_{j+1}^H(k) = \sqrt{M} \sum_{k' \in Z} C^H(l) g_0(k' - Mk) \tag{9}$$

$$d_{j+1}^H(k) = \sqrt{M} \sum_{k' \in Z} d_{j+1}^H(k') g_1(k' - Mk)$$

and

$$C_j^H(k) = \sqrt{M^{-1}} \sum_{k' \in Z} C_{j+1}^H(k') g_0(k' - Mk) + \sqrt{M^{-1}} \sum_{l=1}^{M-1} \sum_{k' \in Z} d_{j+1}^H(k) g_1(k' - Mk) \tag{10}$$

Where $\{C_{j+1}^H(k), j = 1, 2, \dots, \}$ are approximation coefficients of the j+1 level M-band wavelet decomposition of 1D signal $C^H(k)$ and $\{d_{j+1}^H(k); j = 0, 1, 2\}$ are the detail coefficients of the J + 1 level band wavelets decomposition.

For the image, the one dimensional DT-CWT M-band can be extended to using the procedure described in section 2 above.

III. WATERMARK EMBEDDING METHOD

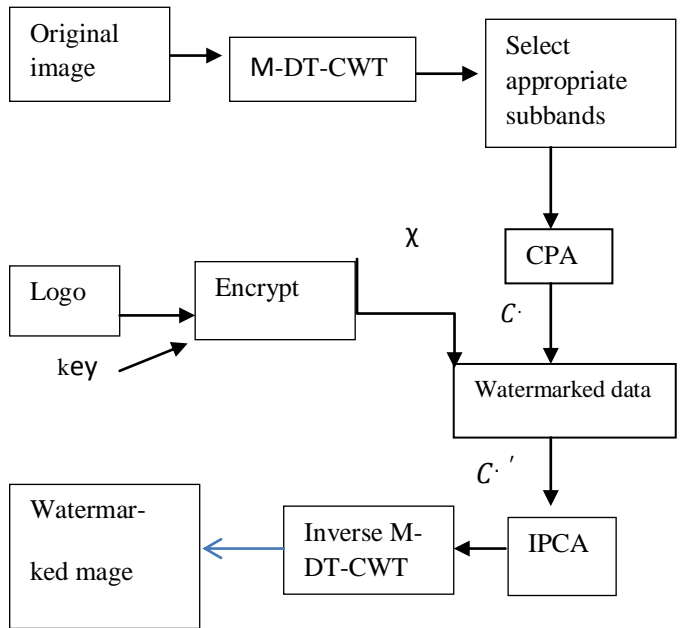


Fig.1. Diagram of embedding watermark

We extend the approach developed in [6], in DT-CWT analyzed an image with DT-CWT equivalent to use two DWT in each tree respectively, in real part and imaginary part.

In this study we will have two components, Primal (real coefficients) and dual (imaginary coefficients).

We consider the watermark logo image Figure 2. encrypted using a 2D pseudo-random sequence with the same size of the logo.

1. The 2D pseudo-random binary (0 and 1) sequence is generated by a key. The binary image logo is XOR operated with the 2D pseudo-random sequence and is raster scanned to obtain a 1D watermark sequence = $\{xi\}, (1 < i < N)$, which is composed of -1 and 1. The occurrence probability of -1 or 1 in X is close to 0.5 because the above encrypting binary sequence is pseudo random sequence (PN).
2. One one level, forward M-band Dual-tree wavelet decomposition is applied to the host medical image I(x,y) we obtain one approximation subband and fifteen detail subbands in each tree (primal and dual) [4,17].
3. Then the coefficients corresponding to the same spatial location in all detail subbands form a one dimensional data array:

$$g_i^1 = (g_i^1.1, g_i^1.2, g_i^1.3, \dots, g_i^1.16) \text{ (Primal tree)}$$

$$g_i^2 = (g_i^2.1, g_i^2.2, g_i^2.3, \dots, g_i^2.16) \text{ (Dual tree)}$$

$1 < i < N$, e.g., a vector of a total of fifteen coefficients, one per subband.

4. The principal component analysis (PCA) is used to transform a coefficient corresponding to the same spatial location in all detail subband [6], it is applied to the obtained ones dimensional matrices are calculated in the tree as follows:

$$V^1 = E(g_i^1 \times g_i^1 T) \\ V^2 = E(g_i^2 \times g_i^2 T)$$

where the g_i is the i -th one dimensional data array, E denotes expectation operation and T denotes the matrix transpose operation.

-The eigenvectors Φ (basis function) corresponding to eigenvalue ζ of the covariance matrix respectively:

$$V^1 \cdot V^1 \zeta \Phi^1 \text{ and } V^2 \cdot V^2 \zeta \Phi^2$$

Where eigenvectors Φ are sorted in descending order:

$$\Phi^1 = (\varphi_1^1, \varphi_2^1, \varphi_3^1, \dots, \varphi_{16}^1)$$

$$\Phi^2 = (\varphi_1^2, \varphi_2^2, \varphi_3^2, \dots, \varphi_{16}^2)$$

-Then calculate the PCA components;

$$p^1 i = \Phi^1 T g^1 i = (p^1 i.1, p^1 i.2, p^1 i.3, \dots, p^1 i.16)$$

(Primal tree)

$$p^2 i = \Phi^2 T g^2 i = (p^2 i.1, p^2 i.2, p^2 i.3, \dots, p^2 i.16) \text{ (Dual tree).}$$

In the following, we can write the data with $(.)$ to indicate 1 or 2 for defined the real and imaginary parts respectively (e.g. $C \cdot$ instead of C^1 or C^2).

4. All the obtained first principle components $p \cdot i.1$ ($1 < i < N$) from a 1-D array $\{C \cdot \{C \cdot (i)\} | C \cdot (i) = \{p \cdot i.1, 1 < i < N\}$ in the same raster scanning fashion as in step:

1. Finally, watermark X is embedded in the principle components $C \cdot$ using quantization-based method [18,19,20] equation (11) to obtain $C \cdot'$, where $C \cdot (i)$ and $C \cdot' (i)$ denote the i -th element in $C \cdot$ and $C \cdot'$, respectively. The quantizer $q(\cdot)$ is a uniform, scalar quantization function of step size S , and $q(x) = kS + 0.5S$,

$$k = x \left\lfloor \frac{x}{S} \right\rfloor \quad (k \in Z)$$

Where $\lfloor \cdot \rfloor$ denotes the floor operation.

The embedding strength S can be chosen so as, to achieve a good compromise between the contending requirements of imperceptibility and robustness. Note that the difference between $C \cdot (i)$ and $C \cdot' (i)$ is between $-0.5S$ and $+0.5S$.

If $x = -1$, $C \cdot (i) \bmod S = 0.25S$. If $x_i = +1$, $C \cdot (i) \bmod S = 0.75S$.

Where \bmod denotes the signed remainder after division.

5. Apply inverse PCA on the modified PCA components to obtain the modified one dimensional wavelet coefficients array.

6. Performing inverse M-band DT-CWT on the modified image coefficients, we obtain a watermarked image $\Gamma'(x, y)$.

$$\begin{cases} C \cdot' (i) = g \left(C \cdot (i) - \frac{1}{4S} \right) + \frac{1}{4S}, & \text{if } x_i = 1 \\ C \cdot' (i) = g \left(C \cdot (i) + \frac{1}{4S} \right) - \frac{1}{4S}, & \text{if } x_i = -1 \end{cases} \quad (11)$$

$$x_i^* = \begin{cases} +1, & r = C \cdot^*(i) \bmod S > S/2 \\ -1, & \text{otherwise} \end{cases} \quad (12)$$

Watermark detection

The watermark extraction is the inverse process of watermark embedding. The test image is M DT-CWT decomposed, then PCA is applied, and the first principle components are obtained to form a 1-D array $C \cdot^* \{C \cdot^* (i), (1 < i < N)\}$. $C \cdot^* (i)$ is the extracted principle component. According to equation (12), we can extract the hidden binary data $X^* \{x \cdot^* (i), (1 < i < N)\}$.

Equation (12) indicates that if $r (r = C \cdot^*(i) \bmod S)$ is in the interval $(0, 0.5S)$, then the decision is made in favor of " $x_i^* = -1$ ". Otherwise, " $x_i^* = 1$ ". Then following correlation coefficient is used to decide if the watermark exists in the test image

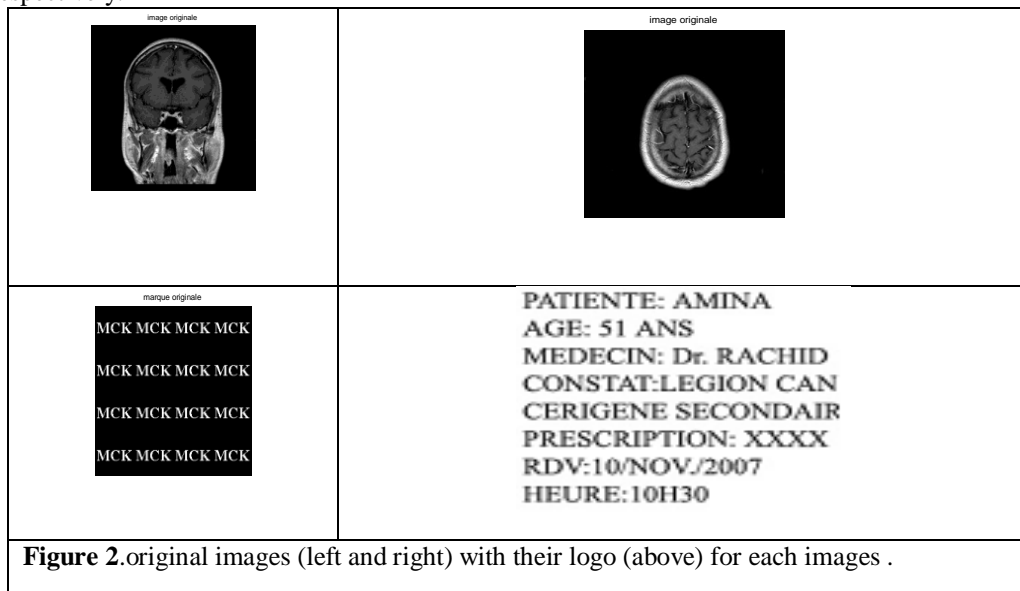
$$p_{x, x^*} = \frac{x \cdot x^*}{\|x\|} \quad (14)$$

where $\|x\|$ is the size of the watermark X (that is N in this paper) and $x \cdot x^*$ is the inner product of X and the extracted sequence X^* .

If the correlation coefficient between the embedded sequence X and the extracted sequence X^* from a test image is larger than a threshold (δ), i.e. $p_{x, x^*} \geq \delta$, we can determine that watermark exists and we write "1", or "0" if no [21].

IV. Results and Discussion

The proposed approach has been tested for two MRI images of the size 250x250 shown in 'Fig.2', with their logo images (watermark) respectively.



The data obtained, shows that 3-band leads to visually better results and the details are well explained in ‘Fig.3 and 4’, compared to the case of 2-band.

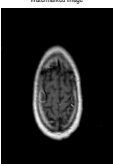
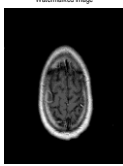
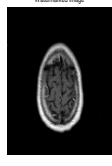
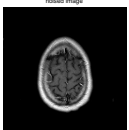
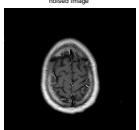
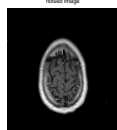
If we exploit only a process for dyadic case the best results are for CWT following real DWT see the benefits of DT-CWT and advantages of M-band in statically characteristic processing in noise study, mentioned previously [4]. For each transformed DWT or DT-CWT, the result is improving as and when we increase the number of bands.

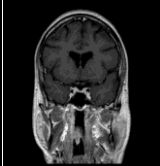
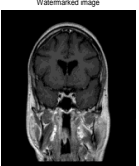
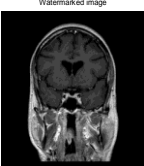
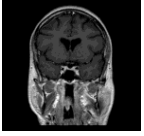
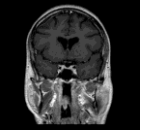
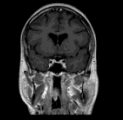
‘Fig.3 and 4’, shows the results after applying DWT and DT-CWT in 2-band and 3-band to the MRI images respectively, we only used the one- resolution level.

Analysis of the results shows that the proposed scheme has high degree of robustness to each attack in $M > 2$ bands. For Gaussian noise attack, the presence of watermark is ‘0’ with the variance > 0.005 in axial images in both cases.

We have tested the proposed algorithm on many attacks. The watermark is robust to JPEG compression with quality factor as low as 15% (JPEG 15) and to common image processing such as median filtering Gaussian filtering. The watermark could be detected when the marked image has been cropped by 50%. We compare the proposed algorithm M-DT-CWT watermarking with DWT dyadic case, for fair comparison, in DWT.

I. FIGURES AND TABLES

M	DWT	realDWT	CWT
2			
	a.(PSNR :37.2)	b.(PSNR :39.1)	c.(PSNR :40.2)
3			
	d.(PSNR :39.3)	e.(PSNR :40.1)	f.(PSNR :42.0)
Figure 3 : a , d. watermarked images without attack (DWT left), b , e. (real DWT middle) and c , f (CWT right)			

M	DWT	realDWT	CWT
2			
	PSNR:39.01	PSNR:40.12	PSNR:41.19
3			
	PSNR:40.15	PSNR:41.15	PSNR:42.48
Figure 4: a, d. watermarked images without attack (DWT left), b,e (real DWT middle) and c,f (CWT. left)			

The performance and robustness have been tested with the attacks of image processing the presence the watermark in the attacked images shown in “Table2”above. PSNRs results (in dB) of the watermarked image after attacks are shown in table 1, we find the performances for M=3 band in comparison with M=2 band, also those of CWT to DWT for each case.

Table 1: PSNR VALUE BETWEEN ORIGINAL IMAGES AND WATERMARKED IMAGES

Band number	PSNR (Coronal image)		PSNR (Axial image)		
	DWT	CWT	DWT	CWT	Attacks
M = 2	30.23	35.33	30.12	35.10	JPEG 15%
M = 3	33.62	36.10	33.29	36.01	
M = 2	30.12	32.53	30.01	32.10	Rotation 10°
M = 3	31.45	32.98	30.25	33.29	
M = 2	30.43	32.25	29.45	30.05	Median filter (3x3)
M = 3	32.44	33.55	30.45	33.55	
M = 2	26.95	28.67	25.51	29.07	Cropping 50%
M = 3	30.11	32.20	30.10	31.45	
M=2	29.21	30.23	28.45	29.74	Sharpen attack
M=3	30.12	31.10	30.25	32.19	

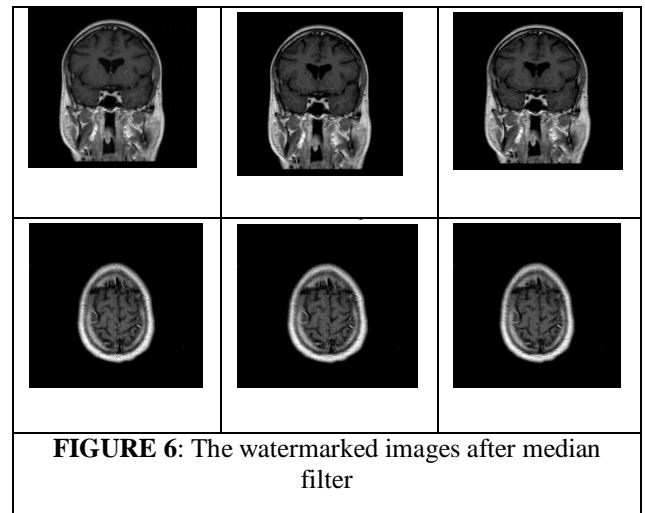
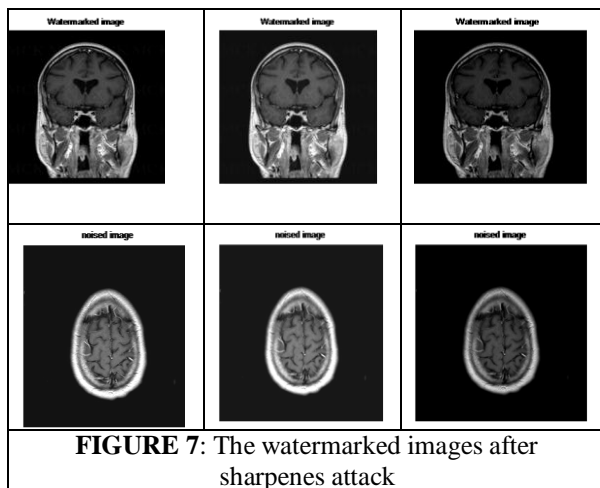
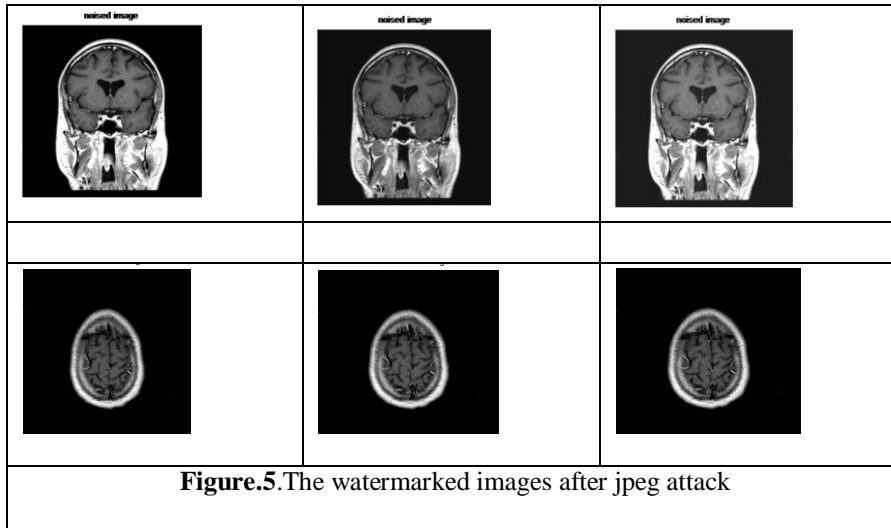
“Table2”, show the robustness of our approach to the attacks, the results are visually impressive, better for the case M = 3 bands, and also for the M-band analysis. The watermarked images obtained are shown in “Fig. 2.”

Table 2: THE PRESENCE OF WATERMARK IN THE STEP OF DETECTION.

Band	presence in Coronal image		presence in Axial image		
	DWT	CWT	DWT	CWT	Attacks
2	0	1	0	1	JPEG 15%
3	1	1	1	1	
2	0	1	0	1	Rotation 10°
3	1	1	1	1	
2	0	1	0	1	Median filter(3x3)
3	0	1	1	1	
2	0	1	0	0	Cropping 50%
3	1	1	1	1	
2	0	1	0	1	Sharpen attack
3	1	1	1	1	

The obtained PSNR values with M-DWT for M=2 bands and M=3 bands are presented” in Table 1”, respectively; while the marked image in M-DT-CWT domain, with 3-band has excellent perceptual quality without any artifacts.

‘‘In Fig.5,6 and 7’’, are shown the result of the watermarked images after common attacks onlyfor M =3 case.



Robustness of the scheme is so proved against JPEG, with different quality factors (QF<60%) for the two images in DT-CWT and $M > 2$ band, the presence of watermark.is successfully recovered.

In Axial cropped image by 50° , the presence of watermark is no found in each wavelet analysis case.

The medical images have some diversity and their treatment may differ from case to case. Clinical information then locates areas that define and separate Regions of Interest (ROI) we seek to highlight the anatomical and pathological structures that detected by physicians sought after diagnosis.

By ttaking into account the specificity of these images, we manage these ROI, for the watermarking. Therresults made object of blind test of more than technicians and doctors of the hospitals who affirmed that for images shown in ‘Fig.3and 4’’, had a good perceptually visibility after watermarking.

In addition for the test result, it shows the following observation; All images were considered acceptable for diagnosis by all observers for all Multi-band of DT-CWT and suggested that the images DWT are degraded to be retable with the geometric attack in dyadic case. Finally overall test result support the previous confirmations in all cases

V. CONCLUSION

The performances of the complex wavelet transform for watermarking image in dyadic cases are already demonstrated in the literature. In our work, efforts are to generalize their conclusions by demonstrating the efficiency of the complex multi-band wavelet transform, in consideration of its qualities. It can be concluded that the implementation of M-band complex wavelet can be treated as the best for watermarking images by considering the results of watermarked image summarized in the figures. The additional privilege of the suggested algorithm is its compatibility with human visual characteristics to embed the watermark for a high number of bands. In this way higher capacity of M-band wavelet domain is applied to embed the watermark information along with preserving the quality and clinical information of medical images and integrity of watermarked image which is of major importance in medico-legal frame work.

In future we open the way for researchers for the detection step which shows how to extract the watermark in integrality.

Acknowledgements

The authors are grateful to physicians and medical technique staff in a medical images service centre at CheikZaid hospital (Morocco) for their entire assistance and suggestions during data collection in test step. The special thanks to Caroline Chaux, Xiangui Kang and al for their contributions in Multi-band wavelets domain, source of inspirations in this work.

REFERENCES

- [1] Colín R, Uribe C F, and Villanueva J A M. 'Robust watermarking scheme applied to radiological medical images'. *IEICE Trans. Inf. Syst.* E91-D(3):862–864,2008.
- [2] N.G.Kingsbury. 'The dual-tree complex wavelet transform: 'A new technique for shift invariance and directional filter'. In *proc.IEE Digital Signal Processing Workshop*, n°86, Bryce canyon, UT,USA, Aug.9-12, 1998.
- [3] P.Loo and NG.Kingsbury. ' Digital watermarking using complex wavelets', *proc.ICIP 2000*, Vancouver ,sep.2000.
- [4] Caroline Chaux, Laurent Duval et Jean-Christophe P. 'Image Analysis Using a Dual-Tree M-Band Wavelet Transform'. *IEEE Transactions on Image Processing*, Vol.15, No. 8, p. 2397-2412, août 2006.
- [5] Caroline C. 'Analyse M-bandes en arbre dual, application à la restauration d'images', thèse, Université de Marne la vallée, 2006.
- [6] Xiangui K, Wenjun Zeng and JiWuHuang. 'A Multi-band Wavelet Watermarking Scheme'. *International Journal of Network Security*, Vol.6, No.2, PP.121–126,Mar.2008 ,
- [7] Ning Bi, Qiyu Sun, D. Huang and al, 'Robust Image Watermarking Based on Multi-band Wavelets and Empirical mode Decomposition', *IEEE Trans. On Image Proc.*, vol. 16, n°8, August 2007
- [8] Giakoumaki, A. Paulopoulos and al, 'A Medical image watermarking scheme based on wavelet transform'. In *Engineering in Medicine and biology society*, 2003
- [9] Salwa A.K, Naser el-Sheiny and al. Wavelet packets-based blind watermarking of medical image management. *Open Bio Med Eng.* J.2010; 4: 93-98.
- [10] Golpirah, Danyali.H. 'A blind reversible watermarking based on histogram shifting for medical image'. *Signal processing and information Technology (ISSPIT)*, 2009, *IEEE*.
- [11] Chen-Ri Piao, Dond-Min and al. 'Medical Image Authentication Using hash Function and Integer wavelet Transform'. *Image and Signal processing, congress 2008*, on vol.1, pp 7-10
- [12] Chokri C and al. 'New watermarking Scheme for security and transmission of medical images for packet Neuro project'. *Radio Engineering*, vol.4, Dec.2007.
- [13] Mavudila R, Masmoudi L and al. 'Transformée en ondelette en arbre-dual pour le tatouage d'images médicales'. *Revue Congolaise des Sciences Nucléaires*, vol.24, p.184-198 ; Décembre 2010.
- [14] Selesnick I, Baraniuk I.R.G and N.G.Kingsbury N. 'The dual-tree complex wavelet transform'. *IEEE Signal Processing magazine*, vol.22, n°6, pp.123-151, nov.2005.
- [15] Selesnick I and K.Li. 'Video denoising using 2D and 3D dual-tree complex wavelet transforms'. in *wavelet applications in signal and image processing X (proc.SPIE 5207)* 2003.
- [16] N. Bi, D. Huang, Q. Dai and al, 'A class of orthogonal and symmetric 4-band wavelets with one parameter'. *Mathematical Numerical Sinica*, vol.27, n°2, 11-10, Mai 2005.
- [17] Q.Sun, N.Bi, D., Huang, 'An Introduction to Multi-band Wavelets', *Zhejiang University press*, 2001.
- [18] B. Chen and G. W. Wornell, "Quantization index modulation: A class of provably good methods for digital watermarking and information embedding," *IEEE Transactions on Information Theory*, vol. 47, no. 4, pp. 1423-1443, May 2001
- [19] X. Kang, J. Huang, Y. Q. Shi, and Y. Lin, "ADWT-DFT composite watermarking scheme robust to both affine transform and JPEG compression," *IEEE Transactions on Circuits and Systems for Video Technology*, vol.13, no. [8], pp. 776-786, Aug. 2003
- [20] M. Wu, and B. Liu, "Data hiding in images and video: Part I: fundamental issues and solutions," *IEEE Transactions on Image Processing*, vol. 12, no. 6, pp. 685-695, Jun. 2003.
- [21] I. Cox, J. Kilian, T. Leighton, and T. Shamon, "Secure spread spectrum watermarking for multimedia," *IEEE Transactions on Image Processing*, vol. 6, no. 12, pp. 1673-1687, 1997.

Experimental investigation and Analysis of Thrust Force in Drilling of Carbon Fibre Reinforced Plastic Composites using Response Surface Methodology

S. Madhavan¹, S. Balasivanadha Prabu²

1, 2 Department of Mechanical Engineering, College of Engineering Guindy,
Anna University, Chennai-600025, India

ABSTRACT: This paper reports the effect of thrust force during drilling of 10mm diameter holes in 20mm thick Carbon Fibre Reinforced Plastic composite laminate using HSS, Solid Carbide (K20) and Poly Crystalline Diamond insert drills. Experiments are conducted on a vertical machining centre using Taguchi design of experiments. A model is developed to correlate the drilling parameters with thrust force using Response surface Methodology (RSM). The results indicate that the developed model is suitable for prediction of thrust forces in drilling of CFRP composites. The influence of different parameters on thrust force of CFRP composites have been analyzed through contour graphs and 3D plots. The investigation has revealed that the type of drill geometry affects the thrust force significantly followed by the feed rate and the speed.

Keywords: Drilling, CFRP, response surface methodology, Thrust Force

I. INTRODUCTION

CARBON FIBER REINFORCED PLASTIC (CFRP) composite materials are continuously replacing conventional metals and alloys in many applications such as automotives, aircraft etc. The combination of superior mechanical properties such as high specific strength, stiffness and fatigue strength, enable the structural design more reliable than conventional metals [1]. They can be easily fabricated to near net shapes by processes such as hand lay-up, filament winding, pultrusion; etc. Machining is required in places where composites are assembled by joining processes. Machining of composites has been recognized as a process different from that of conventional materials. A proper selection of cutting parameters facilitates good machinability since the coexistence of hard abrasive fibres and a soft matrix behave differently during machining [2].

Drilling is a frequently employed in industries owing to the need for component assembly in mechanical structures. Many researchers [3-5] reported that the quality of the drilled surfaces depend strongly on the tool geometry, drilling parameters and tool material. An inappropriate selection of these parameters can lead to material degradations, such as fiber pull-out, matrix cratering, thermal damage and delamination [3].

Tsao [6] reported that the feed rate and the drill diameter are recognized as the most significant factors affecting the thrust force. The radial basis function network is demonstrated more effective than multi-variable regression analysis for the evaluation of drilling-

induced thrust force and surface roughness in drilling of composite material. Latha and Senthilkumar [10] used fuzzy logic technique to predict thrust force in drilling of composite materials. Davim [11] presented a study for selecting the cutting parameters for damage-free drilling in carbon fiber reinforced epoxy composite material which was based on a combination of Taguchi's techniques and on the analysis of variance (ANOVA).

Karnik et al., [12] carried out drilling as per full factorial design using cemented carbide (grade K20) twist drills that serve as input-output patterns for ANN training and reported that the developed ANN model shows a good correlation both for training and testing data sets, thus validating the model. Two-factor interaction effects were also analyzed by generating 3D surface plots. The interaction effects analysis demonstrates the advantages of employing a high spindle speed for drilling CFRP composite material which reduces the delamination at the entrance of the holes.

This paper investigates the effect of different drilling parameters on Thrust force in drilling CFRP composites. The experiments were conducted on a Vertical machining centre using HSS, Carbide (K20) and PCD drills of diameter 10mm. Response surface model is developed to correlate the thrust force with respect to different drilling parameters. The machining parameters considered for the experiments are spindle speed, feed rate, and type of drills. The results proved that the developed model can be effectively used for the prediction of Thrust forces in machining of CFRP laminates.

II. EXPERIMENTAL

2.1 Materials and Methods

The CFRP laminates were fabricated using the hand lay-up technique. Carbon fibre (Zoltek, PANEX® 35) was used as a reinforcement in the Epoxy matrix (Huntsman, Warm curing epoxy system based on Araldite® LY 1564 SP/Hardener XB3486 formulated amine hardener) and was cured at 220 deg Celsius for 90 minutes. This composite laminate was produced with a fiber orientation of 0/90 degrees with 20 layers of the fabric and resin used successively. The properties of the fibre are listed in Table 1. The different types of drill used in this study are shown in Fig 1.



Figure 1.a) HSS Ball Nose, b) Carbide Ball Nose, c) PCD Ball Nose

Table 1. Properties Carbon Fibre

TYPE OF FIBRE	TENSILE STRENGTH (MPa)	TENSILE MODULUS (GPa)	ELECTRICAL RESISTIVITY (Ω-cm)	% CARBON CONTENT	DENSITY (g/cc)	FIBRE DIAMETER (microns)
Stitch Bonded Unidirectional	3800	228	0.00155	95	1.81	7.2

2.2 Experimental Procedure:

The experimental setup is shown in Fig.2 Arix VMC 100 CNC drilling machining centre was used for making drills in the CFRP composites using different drill bits such as HSS, Solid Carbide and PCD. The experiments were conducted as per the L₂₇ orthogonal array. The computer controlled data acquisition system was used to collect and record the data during experiments. The Kistler dynamometer was used to record the cutting forces.

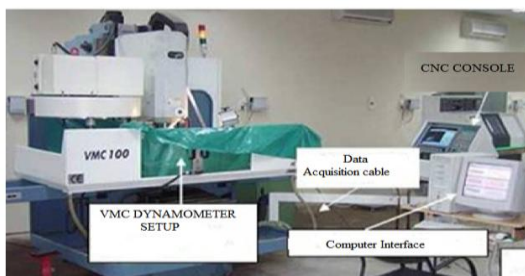


Figure 2. Experiment setup with dynamometer arrangement

2.3 Response Surface Modelling

Response surface methodology (RSM) is a collection of mathematical and statistical techniques that are useful for the modelling and analysis of problems in which a response of interest is influenced by several variables and the objective is to minimize this response [10].

The process parameters, their notations, and their ranges are given in Table 2. The experiments for the present work have been carried out using full factorial taguchi design of experiments. In the current investigation the number of variables considered for the response surface modelling is three and the numbers of experiments conducted are 27. The independently controllable process parameters identified for the experimentation are: Spindle speed (V) rpm, feed rate (f) in mm/min, and type of drills (d) used. The steps involved in the RSM technique [3] are as follows: (i) designing of a set of experiments for adequate and reliable measurement of the true mean response of interest, (ii) determination of mathematical model which best fits; (iii) finding the optimum set of experimental factors that produces maximum or minimum value of response; and (iv) representing the direct and interactive effects of process variables on the best parameters through two-dimensional and three-dimensional graphs.

Table 2. Process Parameters used for modelling

Control Parameters	Unit	Symbols	Levels		
			-1	0	1
Cutting Speed	rpm	v	250	3000	3500
Feed Rate	mm/min	f	50	75	100
Drill Type	-	d	HSS	CARBIDE	PCD

In most RSM problems, the form of relationship between the response and the independent variable are unknown. When the experimenter is close to optimum, a model that incorporates curvature is usually required to approximate the response. Usually a second order model is utilized in response surface methodology.

$$y = \beta_0 + \sum_{i=1}^k \beta_i x_i + \sum_{i=1}^k \beta_{ii} x_i^2 + \sum_{i<j} \beta_{ij} x_i x_j + \epsilon$$

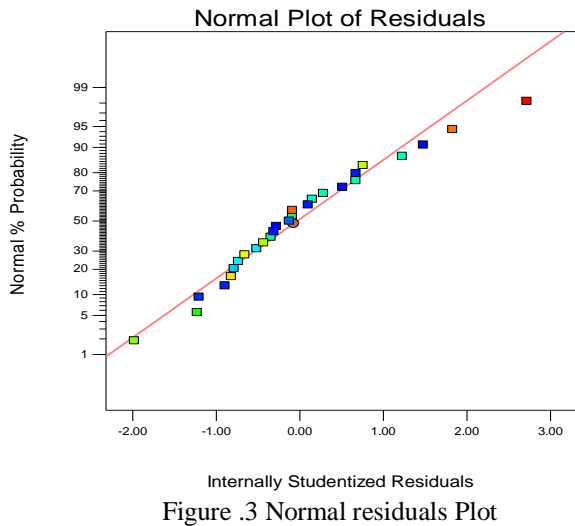
Least square method is used to determine the β coefficients, in the model. Values of the controllable parameters that results in optimization of response or discover what values for the 'x' values will result in a product (process) satisfying several requirements or specifications can be determined by using RSM [8]. A second-order model is normally used when the response function is not known or nonlinear. In the present study a second-order model has been utilized. The thrust force F is given by

$$\text{Thrust Force} = 81.56 - 25.56 * V + 55.22 * f + 202.5 * d + 12.67 * V * f - 54.58 * V * d + 9.58 * f * d - 5.33 * V^2 + 20 * f^2 + 442.83 * d^2 \text{ - equation (2)}$$

R² is called coefficient of determination, is used to judge the capability of regression model developed, 0 ≤ R² ≤ 1. The R² value is the variability in the data accounted by the model in percentage [8]. After estimating the sum of squares (SS) and mean squares

(MS), R^2 value can be used to check the adequacy of the model developed
 $R^2 = 1 - \text{SSerror} / \text{SS Total}$

There is good concurrence between the experimental and predicted values since the coefficient of determination calculated is 95.10%. The diagnostic checking of developed model can be checked by residual analysis. The normal probabilities of residuals are shown in Fig.3. The normal probability plot is used to verify the normality assumption.



From the Fig.3 it is clear that the data are spread roughly along the straight line. Hence, it can be concluded that the data are normally distributed. Fig.4 shows predicted results against the actual results. It is understood that predicted results are very close to the experimental results so response surface models are suitable for predicting Thrust force of CFRP composites.

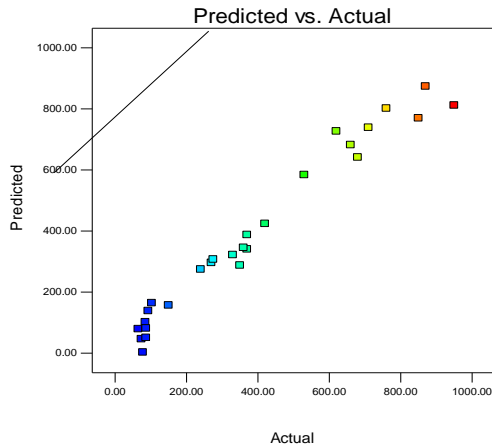


Figure.4 Graph showing variation of Experimental Values with predicted values

III. RESULTS AND DISCUSSION

It can be seen that effect of cutting speed on the cutting forces differs with various tool geometry and material. As expected, the type of drill used has a greater influence on thrust force. From Fig.5 it is observed that thrust force is high as feed rate increases due to the change in the shear area. There is tremendous increase in thrust force values

for PCD because the amount of margin left after providing the flute is more. This reveals that drill geometry has significant effect on the thrust force. The thrust force generally increases as the speed increases but decreases further in the case of Carbide and PCD tool. On contrary to carbide, the cutting force observed during drilling using PCD is quite different. The value of cutting force is high as compared with the carbide. The analysis of response variable thrust force can be explained through contour and surface plots. The typical three-dimensional (3D) surface plots and two-dimensional (2D) contour plots for Thrust force in terms of the process variable are shown in Figures.6-11

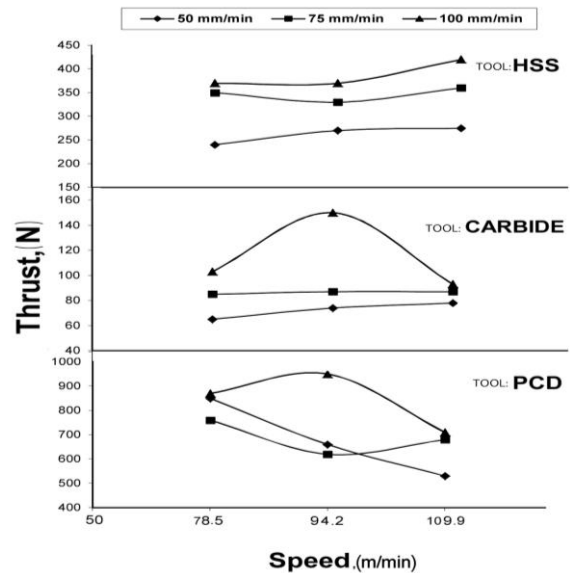


Figure 5. Measured thrust force at different speeds

Equation (2) is plotted in Fig.6-8 as contours for each of the response surfaces. These response contours can be used to predict of thrust force at any point of the experimental domain.

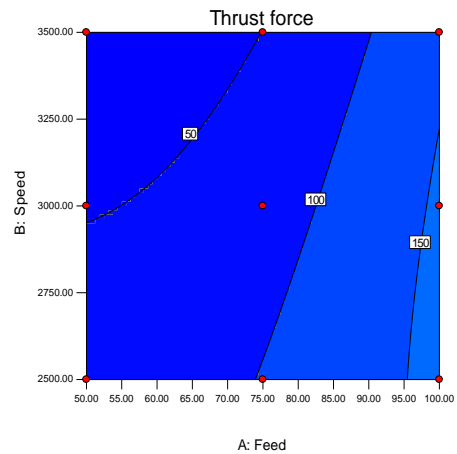


Figure.6 Estimated contour plots for Thrust force (Drill)

Fig.9 illustrates the surface plot for thrust force by varying the two variables Spindle speed and type of drill by keeping the feed as constant. It is found that the thrust force is high at lower speeds and found to decrease as speed increases.

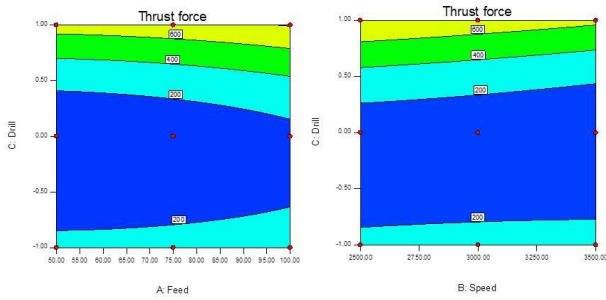


Figure.7 Estimated contour plots for Thrust force (Speed=3000rpm), Figure.8 (Feed=75mm/min)

PCD drill results in producing high forces. Thrust force increases as feed rate increases in the case of PCD. This effect is different in the case of Carbide drill. Fig.10 shows the 3D response surface plot for Thrust force with constant speed. Effect of keeping the type of drills constant can be witnessed from Fig.11. It can be seen that as feed increases and speed decreases the thrust force is found to increase.

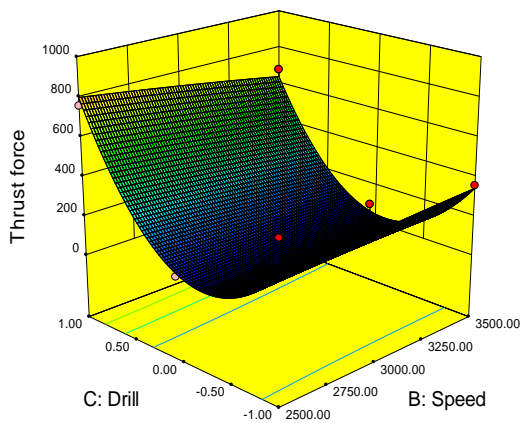


Figure .9 Estimated 3D response surface plot for Thrust force (Force vs. V and d).

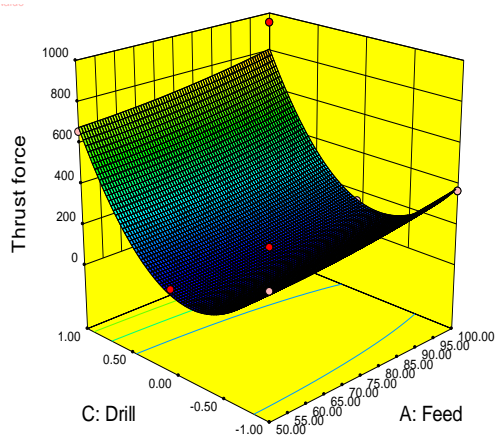


Figure .10 Estimated 3D response surface plot for Thrust force (Force vs. d)

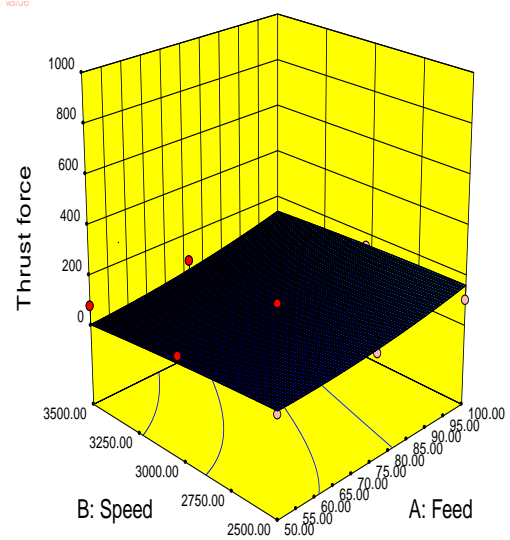


Figure.11 Estimated 3D response surface plot for Thrust force (Force vs. V and f).

IV. CONCLUSIONS

The following are the conclusions drawn from the experimental work

- For correlating the drilling parameters with respect to thrust force a second order response surface model has been developed. The developed model is significant at 95% confidence level, which shows that the developed model can be effectively used for drilling of CFRP composites within the range of the process parameters.
- Analysis of variance for the developed model revealed that the type of drill and the feed rate are the dominant factors that influence the thrust force. Thrust force recorded for HSS drill was high when compared to Carbide. Since the hardness of HSS tool is less than the Carbide drill.
- Medium cutting speed and feed rate provided optimum thrust forces irrespective of the drills used. Significant reduction in cost and timing can be achieved by using this response surface model

ACKNOWLEDGEMENTS

The authors would like to thank the Central Workshop Division of Mechanical Engineering Department, Anna University for providing facilities to carry out the work. The support of Mr.Samy, and Foreman Mr.Srinivasan is well acknowledged

REFERENCES

1. Ramesh.S, Karunamoorthy.L, Palanikumar.K Surface Roughness Analysis in Machining of Titanium Alloy, Materials and Manufacturing Processes, 2008, Vol.23,175-181
2. A.Riaz Ahamed & Paravasu Asokan & Sivanandam Aravindan & M. K. Prakash Drilling of hybrid Al-5%SiC-5%B4Cp metal matrix composites International journal of Adv.Manuf.Technol,2009,Vol.49,871-877
3. Bhattacharya,BandSorkhel,S.K.Investigationfor Controlled Electrochemical Machining Through Response Surface Methodology Based Approach,Journal of Materials Processing Technology,1999,Vol 86,200-207
4. Palanikumar, K. Application of Taguchi and response surface methodologies for surface roughness in machining glass fiber reinforced plastics by PCD tooling. Int. J. Adv. Manuf. Technol,2008,Vol 30,19-27
5. S. Arul,D. Samuel Raj,L. Vijayaraghavan,S. K. Malhotra,R. Krishnamurthy Modeling and Optimization of Process Parameters for Defect Toleranced Drilling of GFRP Composites,Materials and Manufacturing Processes, 2006 Vol 21, 354-365
6. C.C. Tsao, H. Hocheng, Evaluation of thrust force and surface roughness in drilling composite material using Taguchi analysis and neural network,Journal of materials processing technology ,2008,Vol 20 3, 342-348
7. L. Krishnamurthy; B. K. Sridhar; D. Abdul Budan Comparative Study on the Machinability Aspects of Aluminium Silicon Carbide and Aluminium Graphite Composites,Materials and Manufacturing Processes,2007,Vol.22, 903-908.
8. Montgomery, D.C. Design and Analysis of Experiments; 4th Ed.John Wiley and Sons: New York, 1997
9. D. Iliescu, D.Gehin, M.E.Gutierrez, F.Girot , Modeling and tool wear in drilling of CFRP, International Journal of Machine Tools & Manufacture,2010,50,204-213
10. B. Latha V. S. Senthilkumar Analysis of Thrust Force in Drilling Glass Fiber-Reinforced Plastic Composites Using Fuzzy Logic,Materials and Manufacturing Processes, 2009 ,Vol.24,509 – 516
11. J.P. Davim, Pedro Reis, Study of delamination in drilling carbon fiber reinforced plastics (CFRP) using design experiments, Composite Structures,2003,59 481-487
12. R.Thanigaivelan,RM.Arunachalam,Experimental Study on the Influence of Tool Electrode Tip Shape on Electrochemical Micromachining of 304 Stainless Steel, Materials and Manufacturing Processes,2010,10,1166
13. V. N. Gaitonde S. R. Karnik J. Paulo Davim Prediction and Minimization of Delamination in Drilling of Medium-Density Fiberboard (MDF) Using Response Surface Methodology and Taguchi Design,Materials and Manufacturing Processes, 2008, Vol.23, 377 – 384
14. S. Basavarajappa Tool Wear in Turning of Graphitic Hybrid Metal Matrix Composites,Materials and Manufacturing Processes,2009,Vol.24, pages 484 – 487
15. Y. W. Seo, D. Ki,M. Ramulu ,Electrical Discharge Machining of Functionally Graded 15-35 Vol% SiCp/Al Composites,Materials and Manufacturing Processes, 2006 ,Vol21,479 – 487
16. T. M. El-Hossainy, A. A. El-Zoghby, M. A. Badr, K. Y. Maalawi,, M. F. Nasr ,Cutting Parameter Optimization when Machining Different Materials,Materials and Manufacturing Processes ,25,10,2010 ,1101
17. M. Dhananchezian, M. Pradeep Kumar, T. Sornakumar, Cryogenic Turning of AISI 304 Stainless Steel with Modified Tungsten Carbide Tool Inserts, Materials and Manufacturing Processes,2011,26,5781
18. K.Palani Kumar,Modeling and Analysis of Delamination Factor and Surface Roughness in Drilling GFRP Composites, Materials and Manufacturing Processes,2010,25,1059
19. Sundaravel Vijayan, R. Raju,S,R. K. Rao,Multiojective Optimization of Friction Stir Welding Process Parameters on Aluminum Alloy AA 5083 Using Taguchi-Based Grey Relation Analysis, Materials and Manufacturing Processes,2010,25,11,
20. S. Ranganathan,T. Senthilvelan,G. Sriram Evaluation of Machining Parameters of Hot Turning of Stainless Steel (Type 316) by Applying ANN and RSM,Materials and Manufacturing Processes,2010,10,1120
21. Erol Kilickap ,Mesut Huseyinoglu ,Selection of Optimum Drilling Parameters on Burr Height Using Response Surface Methodology and Genetic Algorithm in Drilling of AISI 304 Stainless Steel , Materials and Manufacturing Processes, 2010, 25, 10, 1068
22. A. M. El-Tamimi, M. S. Soliman, T. M. El-Hossainy, and J. A. Muzher ,Developed Models for Understanding and Predicting the Machinability of a Hardened Martensitic Stainless Steel, Materials and Manufacturing Processes,2010,25,8,758

Review of the Latest Developments in Grain Refinement

Lakhwinder Singh¹, Geetesh Goga², Rupinderpreet Singh³
Mechanical, K.C.College of Engg. & I.T./ PTU, India^{1,2,3}

ABSTRACT: There have been a number of studies in recent years relating to the mechanisms of grain refinement of Al-Ti-B refiners. Grain refinement of Aluminium and its alloys is a common industrial practice. The field has been investigated by many workers over past 60 years, not only to develop efficient grain refiners for different aluminium alloys, but also to achieve an understanding of the mechanism of grain refinement. There have also been studies on the interaction of refiners in the cast house environment. More recently there have been several new grain refining products introduced, which have been the subject of their own studies. These new refiners have a number of specific beneficial attributes, which distinguish them from the traditional Al-Ti-B refiners. The characteristics of the expanding family of refiners are reviewed, and their benefits explored in terms of these characteristics. The paper also aims to give an overview of the grain refiners available and guidance on their choice in different alloy systems and processing applications.

Keywords: Aluminum, Boron, Grain refinement, refiners, Titanium

I. INTRODUCTION

It is well known that metals and alloys usually solidify with coarse columnar grain structure under normal casting conditions unless the mode of solidification is carefully controlled. It is possible to develop fine equiaxed grains in the as cast structure either by increasing the number of nucleation sites or by grain multiplication. McCartney has defined grain refinement as deliberate suppression of columnar grain growth in ingots and castings and formation of fine equiaxed solidification structure throughout the material. It is known that the grain size is inversely related to the degree of undercooling due to an increased nucleation rate. In other words, fine grains can be achieved by fast cooling that ensures a high degree of undercooling. Chemical grain refiners based on Al-Ti-B are widely used in aluminium casthouses and foundries worldwide. They are a key part in improving casthouse productivity, allowing faster DC ingot casting speeds, resistance to hot-cracking, as well as improving surface finish and mechanical properties. The pioneering work of Cibula on grain refining started in the early 1950's. This led to the first industrially used grain refiners based on the formation of TiB₂ particles in situ in the melt via the addition of KBF₄ and K₂TiF₆ salts. However, this method suffered from rapid fade of the refining effect due to particle settling. The master alloy approach gave benefits in terms of providing 'readymade' TiB₂ particles of a more controlled and optimised size. A major breakthrough in the development of the use of refiners came with the availability of the alloy in rod form, first used in the mid 1960's. This allowed grain refiner additions to be made outside the furnaces, thus

further reducing the fading effect of furnace additions and also the effects of 'poisoning' in certain alloy systems; this allowed much lower addition levels to be made and a more consistent grain refining performance to be achieved. Adding rod outside the furnace put a greater emphasis on the need to develop refiners with clean microstructures; the major features to be addressed were to reduce boride agglomerations, oxide films and residual fluoride salts. Rod is nowadays the most commonly used form of grain refiners, accounting for over 80% of grain refiner usage.

For many years the range of grain refiners available was mostly limited to three compositions all based on the Al-Ti-B system; namely Al-5%Ti-1%B, Al-3%Ti-1%B and Al-5%Ti-0.2%B. The Al-5%Ti-1%B was, and remains, the most popular composition due to its high refining potency. The lower Ti content Al-3%Ti-1%B refiner was developed to meet the requirements to have a potent refiner, but not to exceed melt Ti specifications, which could be exceeded especially in plants with a high level of recycle. The lower B content refiners are used more specifically for production of surface critical products, to help reduce or eliminate the number of boride defects in the end product (simply by introducing fewer boride particles). The quality of Al-Ti-B grain refiners available in the market steadily improved in terms of cleanliness, grain refining effectiveness and especially consistency, during the 1980's and 90's.

With the ever-increasing demands on the quality of surface critical applications, an intense period of development in the mid 1990's resulted in the introduction of Al-3%Ti-0.15% C grain refiner. The Al-Ti-B quality development took place over a 40 year period – this was effectively matched by a concentrated development period of just a few years for the Al-Ti-C system. Whilst this refiner has penetrated a relatively small proportion of the market, it has proved to give benefits in terms of reduced particle agglomeration behaviour, resistance to poisoning by Zr (for 7xxx alloys), and better surface finish in 5xxx series alloys.

II. REFINER PARTICLE CHEMISTRIES AND TYPES

The nominal chemistry and particle types of the main refiners used in the aluminium industry are summarised in Table I.

Refiners	% Ti	% B	% C	% Sr	Borides	Aluminides
Al-5%Ti-1%B	5.0	1.0	0	0	TiB ₂	TiAl ₃
Al-3%Ti-	3.0	1.0	0	0	TiB ₂	TiAl ₃

1%B						
Al-5%Ti - 0.2% B	5.0	0.2	0	0	TiB ₂	TiAl ₃
Al-3%Ti - 0.2% B	3.0	0.2	0	0	TiB ₂	TiAl ₃
Al-3%Ti - 0.15% C	3.0	0.0	0.1	0	TiC	TiAl ₃
TiB ₁ oy	1.6	1.4	0	0	(Al,Ti)B ₂	-
Strobloy	1.6	1.4	0	Up to 10	TiB ₂ , SrB ₆	SrAl ₄

Note: International standards deliberately allow a higher Ti (up to 3.4%) and lower B (down to 0.7%) content than indicated. This is to encourage a superior boride microstructure.

Table I: Summary of Refiner Particle Chemistries and Types

III. TiBAI ROD ADDITIONS IN A TYPICAL DC CASTING SITUATION

On addition of the rod to the melt, the Al matrix of the Al-Ti-B refiner melts releasing the TiB₂ and TiAl₃ particles into the flowing metal.

3.1 Degassing:

If chlorine is used the conditions are conducive to agglomeration of TiB₂ particles. Apart from the role of chlorine, the input metal is relatively rich in oxide films compared to the output metal. In addition, the metal turbulence inside the degasser encourages particle collisions. Many individual casthouses have been able to demonstrate these effects using LiMCA technology. All of these issues would tend to suggest it is preferable to add grain refiner after a degasser rather than before it, particularly if chlorine gas is being used. This is dependent on the casthouse layout, however, as the addition point needs to also take account of the cleanliness of the grain refiner, and the time required for dissolution of TiAl₃ particles. It is suggested that provided there is sufficient time for TiAl₃ dissolution before the next in line melt treatment (e.g. a filter) or casting (in the case of no filter), then rod addition after the degasser should provide benefits. Even if no chlorine is used in the degasser, there is still likely to be both some particle loss in the dross and some particle agglomeration.

3.2 Filtration:

An extensive programme on ceramic foam filter performance has been carried out in Europe [1]. If the incoming metal cleanliness is high then there is minimal impact of the grain refiner on the performance of the filter. However, if there is an artificially high inclusion loading from the metal (achieved by deliberately vigorously stirring the metal in the furnace), then the introduction of the grain refiner leads to a reduction in filtration efficiency. If grain refiner rod is added before a filter, then the time required for TiAl₃ particles to dissolve needs to be considered. It is known from practical experience that if the rod is added too close to the filter, the filter can become rapidly blocked (or "Blinded") by undissolved TiAl₃ particles. Studies [2] on the effects of long time exposure to liquid aluminium of grain refiner particles, by examining used tube filters, which had been in extended production use found that the thermal cycles and/or the extended quiescent periods during the lifetime of a tube filter can be critical. Under these circumstances, it was observed that there was a transformation of the trapped TiB₂ particles into (Ti,V)B₂. Subsequent growth of such particles can then lead to the formation of more complex agglomerates and bridging within the filter, and so impair filtration efficiency and filter life.

3.3 Addition point:

Due to concerns over the cleanliness of grain refiners, they have traditionally been added before filters. However filters remove some of the required nucleant particles from the metal stream, so addition of grain refiner after the filter might allow lower addition rates. In the normal situation, metal (including oxide films, and if recycled material is used also borides) flows along the launder and rod is injected before the filter. The rod adds aluminides, which dissolve within one minute, borides, which do not dissolve, and some oxide films. The oxide films from the furnace (and the grain refiner) and borides pass to the filter, where the oxide films are trapped (with some borides). The loss of borides in a filter system is considered to be mostly by adherence to oxide films, which the filter has trapped. The remaining borides pass through the filter along with the Ti in solution. There has been ample evidence in the industry of showers of borides being released from a filtration system, caused by changes in the metal head and hence pressure, or by vibrations or accidental tapping of the filtration assembly. A shower of oxide films decorated by TiB₂ particles is a potentially damaging defect, and is the likely cause of many of the defects found in surface critical products. If the quality of grain refiners is sufficiently high such that they can be added after the filter, then these showers of defects can be eliminated. In addition the loss of borides in the filter system would not occur, so less grain refiner would need to be added.

In the foundry situation there are many types of operation done in many different ways [such as melting, degassing, ladling and pouring]. The addition point of the grain refiner can be considered in the same terms as in DC casting. Whereas fade is not really an issue for launder additions in the casthouse, it is of relevance in the foundry, where additions are typically made to a ladle which may be left for several hours prior to use.

IV. Overview of the use of Different Refiners

A summary of the use of grain refiners in the wrought sector is presented here:

4.1 Twin roll casters:

Low boron refiners are often used (the dense TiB₂ particles tending to settle particularly at the relatively slow metal flow rates encountered in this process). End applications can often be surface critical and low boron refiners can also be of benefit compared to the 1%B containing refiners. The Al-Ti-C system may also provide benefits in this process in terms of less particle agglomeration, reduced chemical segregation, as well as finer grain sizes at the higher casting speeds.

4.2 Electrical conductor applications:

Al-5%Ti-1%B and Al-3%Ti-1%B are used. If too much boron is added at boron treatment, it can be almost impossible to grain refine. The Al-Ti-C system seems to suffer less from this issue and is finding increasing usage, as significant reductions in addition rate as well as improvements to product quality can be achievable.

4.3 Extrusion billets (mostly 6xxx alloys):

For the DC casting process Al-5%Ti-1%B is mainly used as the principle requirement is refiner potency. Some Al-3%Ti-1%B is also used. In terms of avoiding the formation of columnar crystals, Al-5%Ti-1%B provides the best robustness in terms of temperature sensitivity [3]. A feature of the Al-Ti-C system is consistency of grain size across the billet section [4], and possibly an improved surface finish on extrusion (the refiner particles being one potential cause of die lines, or streaking on anodising).

4.4 Rolling slabs:

Subsequent to DC casting these are processed to a variety of end applications, which can affect the refiner chosen, as discussed in the following:

4.4.1 1xxx slab:

The refiner used is dependent on the end application, as highlighted in the previous sections, but a number of 1xxx alloys fall into the category of surface critical.

4.4.2 2xxx slab:

The main refiners used are Al-5%Ti-1%B and Al-3%Ti-1%B.

4.4.3 3xxx slab:

The main refiners used are Al-5%Ti-1%B and Al-3%Ti-1%B. The Al-Ti-C refiners are generally not used as there is thought to be a mild poisoning effect with Mn.

4.4.4 4xxx slab:

The main refiners used are Al-5%Ti-1%B and Al-3%Ti-1%B.

4.4.5 5xxx slab:

The Al-Ti-B system dominates, but there is increasing usage of Al-Ti-C due to no negative effects on Mg oxide build up [5]. The Al-Ti-C system also has benefits in terms of less chemical segregation.

4.4.6 6xxx slab:

The main refiners used are Al-5%Ti-1%B and Al-3%Ti-1%B (see also comments above on extrusion billets).

4.4.7 7xxx slab:

The Al-Ti-C system is finding most of its use in these alloys, particularly the Zr containing ones due to the poisoning effect with the Al-Ti-B refiners.

4.4.8 8xxx slab:

The refiner used is dependent on the end application, as highlighted in the previous sections.

4.5 Foundry sector:

This sector is dominated by Al-5%Ti-1%B, however, growth is seen with substoichiometric refiners (such as TiBloy) particularly in wheel foundries, where reduced levels of rejects are being experienced. The foundry sector consists of foundry ingot producers (who are generally in the wrought sector), large foundries (where master alloy grain refiners dominate) and very many small foundries (where both master alloy refiners and salts/tablets refiners are used). Combined modifier (Sr) and grain refiner (Ti, B) master alloys (such as Strobloy) are also used.

V. SUMMARY AND CONCLUSIONS.

Grain refinement of aluminium and its alloys has become common industrial practice. The immense technological importance of this field has led to extensive investigations by many industrial and academic researchers during the past 60 years. A great majority of the past investigations were primarily focused on the search for grain refiners that act quickly and provide the grain refining effects without fading even on prolonged holding of the molten alloy. Among a number of grain refiners developed, Al-5Ti-1B master alloys are more popular due to their high grain refining efficiency with respect to many aluminium alloys. Al-Ti-C master alloys are also becoming popular as grain refiners for many aluminium alloys, particularly when boron is not desirable in the aluminium alloy.

The grain refining behaviour of the master alloy appears to be sensitive to its microstructure, particularly the morphology and size distribution of TiAl₃ particles, which are in turn influenced by the processing parameters used in the preparation of the master alloy, such as reaction temperature, reaction time, and thermo mechanical treatment

Much work has been focused on attempts to understand the mechanisms of grain refinement and several theories have been proposed. However, none of these theories can explain all the observations made in the grain refining experiments. Perhaps more than one mechanism operates depending on the grain refiner used, the alloy being cast, and the casting process involved. Further work is necessary in this direction to develop a unified description of grain refinement, poisoning, and fading.

References

- [1] N.Towsey et al. "*Impact of grain refiner addition on ceramic foam filter performance*", International Congress: Continuous Casting, DGM, (2000), 26-32
- [2] G. Mabry et al. "*Characterisation of particulate captured by a rigid tube filter*", TMS Light Metals, (1997), 983-989
- [3] W.Schneider and P.S.Cooper "*Influence of AlTiB master alloy type and casting conditions on grain refinement of aluminium alloys*", 8th Australian Asian Pacific Conference, (2003), In press
- [4] W.Schneider et al. "*A comparison of the behaviours of AlTiB and AlTiC grain refiners*", TMS Light Metals, (1998), 953-989
- [5] A. J. Whitehead et al. "*Development of a commercial Al-3Ti-0.15C grain refining master alloy*", TMS Light Metals, (1996).

Temperature Controlled Voltage Oscillation in Neural Circuit Undergoing Homoclinic Bifurcation

Yasuomi D. Sato

*Department of Brain Science and Systems Engineering, Graduate School of Life Science and Systems Engineering, Kyushu Institute of Technology, Japan

** Frankfurt Institute for Advanced Studies (FIAS), Goethe University Frankfurt, Germany

ABSTRACT: We analyze a frequency decrease as well as a frequency transition with a temperature increase in the Hodgkin-Huxley (HH) oscillator undergoing saddle homoclinic bifurcations. A gradient of frequency for temperature is derived by perturbation analysis of the stable HH oscillators, in combination with the other gradient of frequency for input current and a so-called phase response curve (PRC) multiplied by its related voltage-gated channel currents. We then show that the PRC is clearly classified by the gradient of frequency for temperature. More interestingly, different bifurcation mechanisms of the Andronov-Hopf and the saddle-node are commonly categorized.

Keywords: Hodgkin-Huxley oscillator, frequency decrease, oscillatory transition, saddle homoclinic orbit bifurcation, phase response curve

I. INTRODUCTION

Temperature is one of important physical variables, which significantly affects autonomous oscillations generated in the nervous system. Gamma oscillations evoked on rat hippocampal slices are dependent of temperature [1]. In simulations on models of the nervous system, temperature alters nonlinear phenomena of desynchronization or chaos synchronization in the voltage activities [2][3]. It is thus interesting to understand mechanisms on emergences of the oscillation, which are subject to temperature variation, or to study temperature effects on cooperative behavior in the neural network.

Mathematical analysis on voltage oscillations in a single neuron is fundamental for understanding collective behavior in the assemblies. The Hodgkin-Huxley (HH) model is the first mathematical description on such voltage dynamics. The HH model can describes how membrane potentials in neurons are initiated and propagated [4]. It is modified for simulating peripheral cold receptors discharges that exhibit different firing patterns [5]. One firing pattern is an abrupt increase of the interspike intervals in a certain temperature region. This is originated from a homoclinic bifurcation of a saddle-node (SN) equilibrium embedded in the chaotic attractors [6]. However, why the homoclinic bifurcation appears is still unclear. The modified HH model seems to be different from the original. We will have to study again stability analysis on equilibriums in both the original and modified HH models.

It is also necessary for us to find another measurement for characterizing firing properties or dynamical mechanisms in their models. The good measurement is the frequency-current ($f-I$) curve [7], which has already been examined in electrophysiological experiments [8][9]. The $f-I$ curve generally categorizes oscillations into the two classes: For the class I, emergence of the oscillation with zero frequency is characterized by saddle-node (SN) or saddle-node on invariant circle (SNIC) bifurcations with an increase of the I . The SNIC, which is also called the SN on a limit cycle (SNLC), means that the SN bifurcation occurs on the LC. In the class II, emergence of the oscillation with a finite frequency is characterized by the Andronov-Hopf (AH) bifurcation.

In recent analysis, one unexpected oscillatory phenomenon has been highlighted that the class I Morris-Lecar (ML) model decreases firing frequency with temperature increase [10]. This seems to be very similar to frequency discharge of cold fibers, which also shows the paradoxical frequency discharge at high temperature [11][12] (In what follows, let us call it the frequency transition). In 1999, Adair simulated the frequency discharge of cold fibers by Boltzmann description of voltage-gated Na^+ and Ca^{2+} channels [13]. Presumably, this Boltzmann model is not functionally different from the original HH model. However, using the original HH model, how the paradoxical frequency discharge occurs is still unclear. It should thus be clarified by analyzing stabilities as well as bifurcation mechanisms in the original HH model.

In this paper, we show that temperature (μ) modulated frequency are characterized with current I and so-called phase response curves (PRCs) derived by making phase descriptions for small μ perturbation. $f-\mu$ formulations give us mathematical conditions for a frequency decrease and a frequency transition with an increase in temperature, dependent of different bifurcation mechanisms on oscillation generation. Frequency gradients in terms of μ classify PRC into two types, regardless of conventional classification. We demonstrate heuristically firing frequency transition for larger μ in the HH model undergoing a SNIC bifurcation mechanism. Also, a frequency increase with a μ decrease is determined by appropriate proportion of frequency gradient for I to the product of the PRC and its current dynamics. In addition, the frequency gradient in terms of μ shows the critical μ -value for the frequency transition of a normal saddle-node homoclinic orbit to its separatrix loop. Finally, discussion and conclusion will be given.

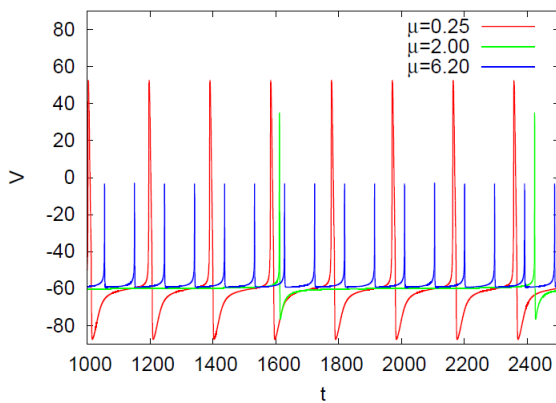


Fig. 1. Dynamics for the Hodgkin-Huxley (HH) neuron model at $I = 0.161$, parameterized as class I. The time courses of the membrane voltage when μ increases from 0.25 to 6.2 via 2.

II. BIFURCATIONS IN SPIKING MODEL

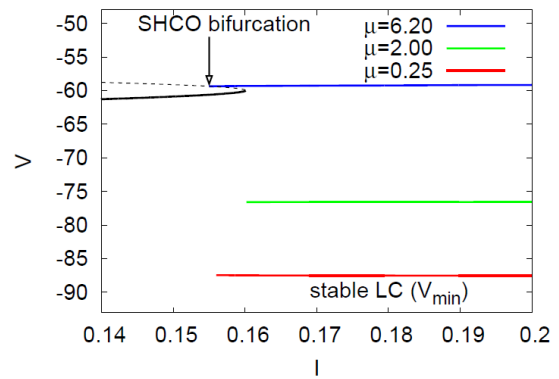
We shall begin by studying bifurcation analysis on the Hodgkin-Huxley (HH) model parameterized as a class I. The HH model, which is employed to simulate frequency-current ($f-I$) and frequency-temperature ($f-\mu$) relations, is given by

$$C_m \frac{dV}{dt} = Q(V, m, h, n) + I = -g_{Na} m^3 h (V - E_{Na}) - g_K n^4 (V - E_K) - g_L (V - E_L) + I, \quad (1)$$

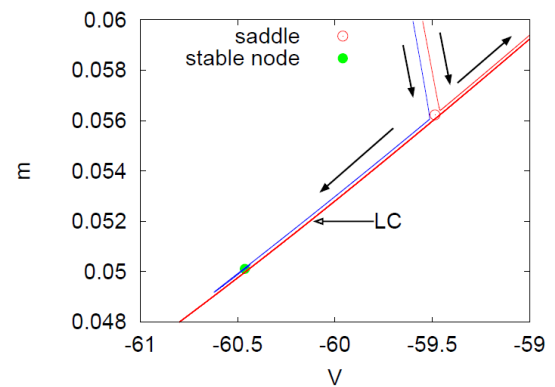
$$\frac{dy}{dt} = \mu P_y(V, y) = \mu (Y_\infty(V) - y) / \tau_y(V). \quad (2)$$

$C_m (= 1\mu F/cm^2)$ is the membrane capacity. $y \in \{m, n, h\}$ is the non-dimensional gating variable. The parameters E_{Na} , E_K , and E_L are the reversal potentials of Na^+ , K^+ and leak currents respectively, while g_{Na} , g_K , and g_L are the conductances. $Y_\infty(V) = \alpha_y(V) / (\alpha_y(V) + \beta_y(V))$, $\tau_y(V) = 1 / (\alpha_y(V) + \beta_y(V))$ where $\alpha_m(V) = -0.1(V + V_1) / (\exp(-0.1(V + V_1)) - 1)$, $\beta_m(V) = 4 \exp(-(V + V_2) / 18)$, $\alpha_h(V) = 0.07 \exp(-(V + V_3) / 20)$, $\beta_h(V) = 1 / (\exp(-0.1(V + V_4)) + 1)$, $\alpha_n(V) = 0.01(V + V_5) / (\exp(-0.1(V + V_5)) - 1)$ and $\beta_n(V) = 0.125 \exp(-(V + V_6) / 18)$. The class I dynamics are parameterized with $g_{Na} = 35 \text{ mS/cm}^2$, $E_{Na} = 55 \text{ mV}$, $g_K = 9 \text{ mS/cm}^2$, $E_K = -90 \text{ mV}$, $g_L = 0.1 \text{ mS/cm}^2$, $E_L = -65 \text{ mV}$, $V_1 = 35$, $V_2 = 60$, $V_3 = 58$, $V_4 = 28$, $V_5 = 34$ and $V_6 = 44$ (see [2]) so that the HH model represents an oscillatory system exhibiting repetitive firings via a saddle homoclinic orbit (SHCO) bifurcation with the current increase (see Fig. 1). The detailed bifurcation mechanism will be examined below. As shown in Fig. 1, firing frequency of oscillation decreases and then increases again, and its amplitude of oscillation monotonically decreases when μ increases.

We study dynamical mechanisms underlying changes of firing frequency with a temperature increase by analyzing stabilities of stationary solutions of the HH model. The result is shown in Fig. 2(a). For any μ , a saddle, stable and unstable nodes coexist for $I < I_{SN}$ ($=0.16$). Their stabilities are numerically calculated as referred in [14][15]. I_{SN} is saddle-node (SN) equilibrium. Trajectories, which diverge from the unstable node and the saddle, converge to the stable node (not shown here). When I exceeds 0.152 for $\mu=0.25$, a stable LC attractor appears through a SHCO bifurcation so that the attractor exists together with the stable node. Since trajectories on the LC attractor pass outside the saddle and stable node on the $V-m$ phase plane,



(a)



(b)

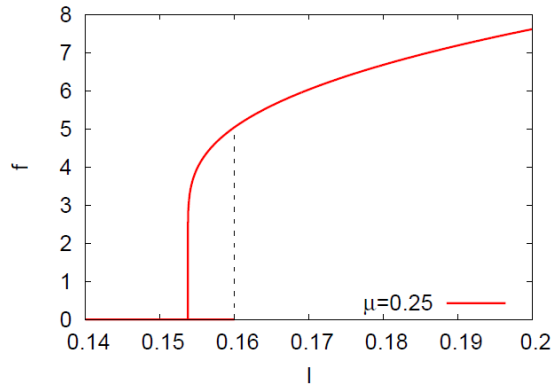
Fig. 2. (a) Bifurcation diagram for the class I HH model. There are two stationary voltages in the I range of 0.14 to 0.2. One is a saddle (the broken line) while the other is a stable node (the black line). The oscillations occur via a SNIC bifurcation that the limit cycle (LC) involves the saddle and node. Colored lines present the minimum voltages (V_{min}) of the oscillations. (b) A trajectory of the LC on the $V-m$ phase plane. The trajectory outside of the saddle and node points is the one of a "big" saddle homoclinic orbit. Stable manifold (separatrix) of the saddle (empty circle) between the red and blue lines separates resting (green circle) and oscillatory states.

the LC can be called as the big homoclinic orbit (Fig. 2(b)). The LC attractor still remains even if $I > I_{SN}$.

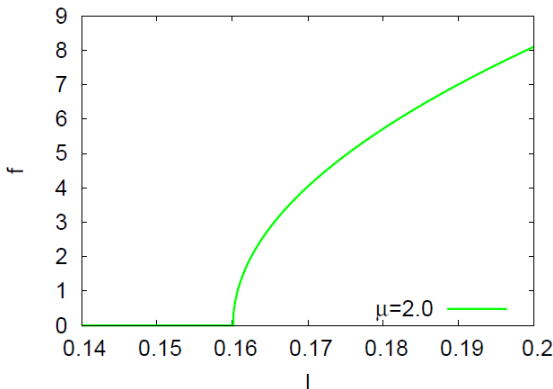
This indicates emergences of the oscillation via two different bifurcation mechanisms: The first oscillation with 0-frequency occurs via the SHCO bifurcation. The second oscillation with a finite frequency occurs via the SN bifurcation [Fig. 3(a)]. We notice that the second oscillation emergence is slightly different from the typical one via the SN bifurcation.

Next we show that for $\mu=2$, the HH model begins oscillations with 0-frequency through the SN bifurcation as shown in Figs. 2(a) and 3(b). We cannot find any bi-stability state of the node and the LC attractor as shown in Fig. 3(a). To be more precise, such a SN bifurcation is called the SN on invariant cycle (SNIC) as referred to [7]. This means SN equilibrium occurs on a LC attractor. Here notices that a size of the LC is apparently reduced as in the increased V_{min} of Fig. 2(a).

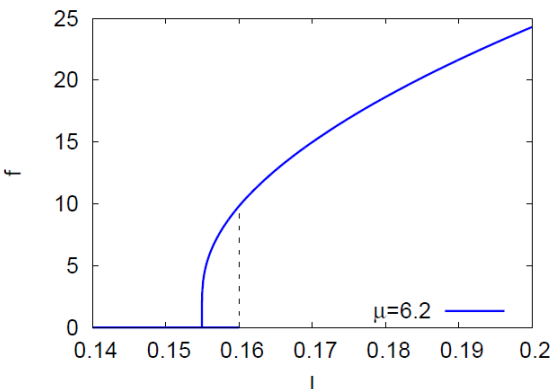
Finally, we can see again a SHCO bifurcation when $\mu=6.2$ [Fig. 2(a)]. This is a slightly different from the case for $\mu=0.25$, in terms of whether or not the SN equilibrium is



(a)



(b)



(c)

Fig. 3. f - I curves for $\mu = 0.25, 2$ and 6.2 . The HH model ((a) $\mu = 0.25$ and (c) $\mu = 6.2$) begins class II oscillations via the SN bifurcation while terminating the oscillations in the class I. (b) The HH model ($\mu = 2$) shows simultaneous excitabilities and oscillations of the class I.

outside of the homoclinic orbit. We show again the f - I curve with the bi-stability (see Fig. 3(c)). Because the trajectory is attracted into the HCO, the amplitude as well as the frequency of the oscillation is respectively small and high as shown in Fig. 1.

In summary, we find f - μ relation at each current level as shown in Fig. 4. Before a SN bifurcation, the frequency is in small peak for $\mu < 0.5$ while its frequency slope for $\mu > 6.0$ is extremely sharp. Immediately after the SN bifurcation, a constant low frequency level appears in the middle range of μ . It gradually increases as I increases from I_{SN} . The f - μ curve then becomes a monotonic increasing curve for temperature. This indicates that a

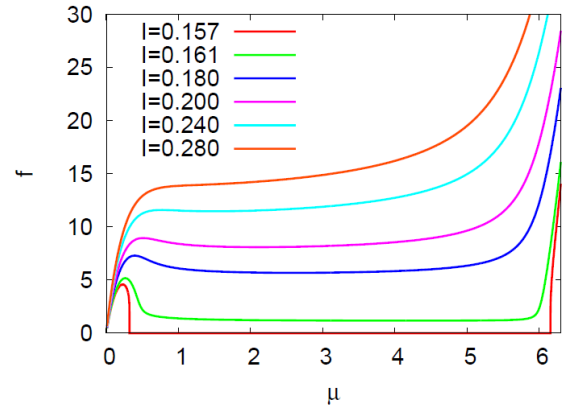


Fig. 4. Frequency f versus temperature μ on simulation with the class I HH neuron model. When $I=0.161$, the frequency passed through a minimum for $\mu=6$ and then extremely increased at the higher temperature. The low frequency level gradually rises so that the frequency is a monotonically increasing function of temperature.

frequency decrease and a frequency transition with a temperature increase are based on two SHCO bifurcation mechanisms for $\mu < 0.5$ and $\mu > 6.0$ around the SN equilibrium.

III. PERTURBATION APPROACHES

Next, in order to deepen more understandings of the frequency decrease and frequency transition, we employ a phase reduction method [10][16][17][18]. In the phase reduction method, reducing n -dimensional oscillatory dynamics, subject to small perturbations of temperature and current ($\Delta\mu$ and ΔI), to the one-dimensional phase equation, the perturbations are even phase-described. Then, we find that frequency gradient for temperature ($[\partial f / \partial \mu]$) is related to another oscillatory property such as PRCs and f - I curves.

The HH oscillator perturbed with small temperature and small current is written in the general form:

$$\frac{dx}{d\tau} = \mathbf{F}(\mathbf{x}) + \mathbf{G}(\mathbf{x}), \quad (3)$$

where $\mathbf{x}=(V, \mathbf{y}) \in \mathbb{R}^4$. V is the potential variable while \mathbf{y} is a vector consisting of 3 recovery variables. $\mathbf{F}(\mathbf{x})$ is a vector field ($Q(\mathbf{x}) + I_0, \mu_0 \mathbf{P}(\mathbf{x})$) where Q is the membrane potential dynamics for V . $\mathbf{P}(\mathbf{x})$ is the recovery dynamics for \mathbf{y} . The perturbation term $\mathbf{G}(\mathbf{x}) = (\Delta I, \mathbf{P}(\mathbf{x}) \Delta\mu)$.

Let $\mathbf{x}_p(\tau)$ denote the unique phase asymptotically stable T_p -periodic function to

$$\frac{d\mathbf{x}_p}{d\tau} = \mathbf{F}(\mathbf{x}_p). \quad (4)$$

where $\mathbf{x}_p(\tau + T_p) = \mathbf{x}_p(\tau)$. Then a stable solution for Eq. (3) is approximated as

$$\mathbf{x}(\tau) = \mathbf{x}_p(\tau + \eta(\tau)) + \mathbf{u}(\tau + \eta(\tau)), \quad (5)$$

where $\eta(\tau)$ means a small perturbation in the phase direction on the periodic orbit. $\mathbf{u}(\tau + \eta(\tau))$ denotes the orbital deviation to the periodic orbit $\mathbf{x}_p(\tau)$. Substituting Eq. (5) into Eq. (3) and expanding the both-hand sides into a Taylor series leads

$$\left[\dot{\eta}(\tau) \frac{dx_p(q)}{dq} + \frac{d}{dq} \mathbf{u}(q) \right]_{q=\tau+\eta(\tau)} = \frac{\partial \mathbf{F}(x_p(\tau+\eta(\tau)))}{\partial \mathbf{x}} \mathbf{u}(\tau) + \eta\tau + \mathbf{G} \mathbf{x}_p \tau + \eta\tau. \tag{6}$$

In the perturbed oscillator, the orbital deviation vector $\mathbf{u}(\tau) = \mathbf{x}(\tau) - \mathbf{x}_p(\tau)$ evolves as $[d\mathbf{u}(\tau)/d\tau] = [\partial \mathbf{F}(x_p(\tau))/\partial \mathbf{x}] \mathbf{u}(\tau)$. The vector $\mathbf{Z}(\tau)$ tangent to the periodic orbit $\mathbf{x}_p(\tau)$, which is the unique solution to

$$\frac{d\mathbf{Z}}{d\tau} = - \left[\frac{\partial \mathbf{F}(x_p)}{\partial \mathbf{x}} \right]^t \mathbf{Z}, \tag{7}$$

where t is transpose and the normalization condition

$$\mathbf{Z} \cdot \frac{d\mathbf{x}_p}{d\tau} = 1 \tag{8}$$

is satisfied for every τ . $\mathbf{Z}(\tau)$ is the adjoint solution to the linearization around the limit cycle. The first element of the adjoint solution, $Z_V(\tau)$, is the PRC widely used in computational neuroscience. Eq. (3) is then reduced to the evolution equation for η :

$$\dot{\eta}(\tau) = \mathbf{Z}(\tau + \eta(\tau))^t \cdot \mathbf{G}(\mathbf{x}_p(\tau + \eta(\tau))). \tag{9}$$

Introducing phase variables defined by $\theta = (\tau + \eta) / T_p$ ($\in [0, 1)$), Eq. (9) is rewritten as

$$\frac{d\theta}{d\tau} = \frac{1}{T_p} + \frac{1}{T_p} \int_0^1 \mathbf{Z}(\theta')^t \cdot \mathbf{G}(\mathbf{x}_p(\theta')) d\theta' = f + f \langle Z_V \rangle_\theta \Delta I + f \langle \mathbf{Z}_y \cdot \mathbf{P} \rangle_\theta \Delta \mu, \tag{10}$$

where $f = f(I_0, T_0) = [1 / T_p]$ and $\langle \cdot \rangle_\theta = \int_0^1 d\theta'$.

Next, $f(I_0, T_0)$ can straightforwardly be expanded in $(\Delta I, \Delta \mu)$. The quadratic Taylor series is obtained:

$$f(I_0 + \Delta I, \mu_0 + \Delta \mu) = f(I_0, \mu_0) + \frac{\partial f(I_0, \mu_0)}{\partial I} \Delta I + \frac{\partial f(I_0, \mu_0)}{\partial \mu} \Delta \mu + O(\Delta I^2 + \Delta \mu^2). \tag{11}$$

Eqs. (10) and (11) gives us following relational expressions:

$$\frac{\partial f}{\partial I} = f \langle Z_V \rangle_\theta, \tag{12}$$

$$\frac{\partial f}{\partial \mu} = f \langle \mathbf{Z}_y \cdot \mathbf{P} \rangle_\theta. \tag{13}$$

Using Eq. (8),

$$\begin{aligned} \frac{\partial f}{\partial \mu} &= f - f \langle Z_V(Q + I_0) \rangle_\theta \left(\equiv f \left(1 - \langle Z_V \frac{dV}{d\tau} \rangle_\theta \right) \right) = \\ &= f - f \langle Z_V Q \rangle_\theta - f \langle Z_V \rangle_\theta I_0 = f \left(1 - \langle Z_V Q \rangle_\theta - \frac{1}{f} \left(\frac{\partial f}{\partial I} \right) I_0 \right). \end{aligned} \tag{14}$$

$[\partial f / \partial \mu] < 0$ is thus satisfied with

$$\langle Z_V Q \rangle_\theta > 1 - \frac{1}{f} \left(\frac{\partial f}{\partial I} \right) I_0.$$

Eq. (14) means that the value of $[\partial f / \partial \mu]$ is determined by values of $\langle Z_V Q \rangle_\theta$ and $[1 - (\partial f / \partial I)(I_0 / f)]$. It also gives us a condition for frequency transition that $[\partial^2 f / \partial \mu^2]$ changes from the positive to the negative as μ gradually increases via $\mu = \mu_c$. μ_c represents that $[\partial f / \partial \mu]$ takes the maximum.

IV. SIMULATION RESULT

Using Eq. (14), we systematically investigate frequency characteristics (the frequency decrease and oscillatory transition) of the HH oscillator undergoing a SHCO bifurcation, in terms of I and μ , referring to dynamical mechanisms of a SNIC bifurcation shown in [7].

Firstly, let us explain reasons why frequency decreases, in terms of firing properties in the HH oscillator. Fig.5 shows regions for $[\partial f / \partial \mu] < 0$ and $[\partial f / \partial \mu] > 0$ on the $I-\mu$ phase diagram, being associated with Fig. 4. In Fig. 5, $(I_{SN}, \mu_{SN}) = (0.16, 0.45)$ classifies a SN bifurcation into two categories: One is the SNIC bifurcation when $\mu > 0.45$ while the other is the SN bifurcation when $\mu < 0.45$. Immediately after SN or SHCO bifurcations, $[\partial f / \partial \mu] < 0$ is widely occupied in the μ range. The range is however rapidly diminished as I increases. When $I > 0.26$, we cannot find any range for $[\partial f / \partial \mu] < 0$. This is in a good agreement with changes of the $f-\mu$ curve in Fig. 4.

Fig. 6(a) shows whether or not $\langle Z_V Q \rangle_\theta$ is larger than $[1 - (\partial f / \partial I)(I_0 / f)]$ in Eq. (12) for $\mu = 1$, to determine the positive or negative value of $[\partial f / \partial \mu]$. $[\partial f / \partial \mu] < 0$ if $\langle Z_V Q \rangle_\theta > [1 - (\partial f / \partial I)(I_0 / f)]$. In contrast, $[\partial f / \partial \mu] < 0$ if $\langle Z_V Q \rangle_\theta < [1 - (\partial f / \partial I)(I_0 / f)]$. Fig. 6(b) represents another evaluation of $[\partial f / \partial \mu]$ in Eq. (12). $[\partial f / \partial \mu] > 0$ if $\langle Z_V \cdot [dV / d\tau] \rangle_\theta < 1$. To be more precise, $Z_V \cdot [dV / d\tau]$ for almost all θ is greater than 1 at $I=0.161$. This can easily expect $\langle Z_V \cdot [dV / d\tau] \rangle_\theta < 1$ so that $[\partial f / \partial \mu] < 0$. However as I increases from 0.161, the θ region that $Z_V \cdot [dV / d\tau]$ takes greater than 1 is reduced. Thereby, $\langle Z_V \cdot [dV / d\tau] \rangle_\theta$ is less than 1 so that $[\partial f / \partial \mu] > 0$.

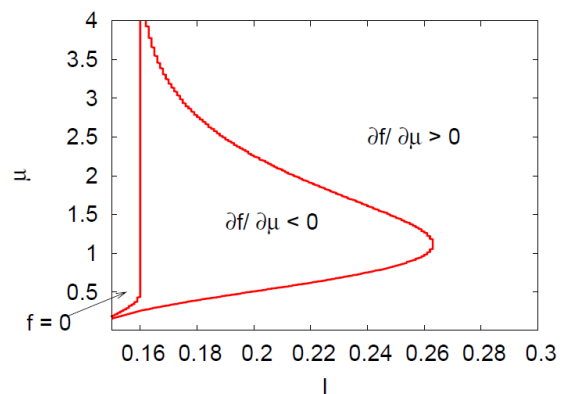


Fig. 5. $I-\mu$ phase diagram for the class I HH model. The left region show the stationary state of $f = 0$ while the middle (or right) region shows $[\partial f / \partial \mu] < 0$ (or $[\partial f / \partial \mu] > 0$). In the diagram, the regions of $\mu > 0.45$ and $\mu < 0.45$ are respectively SN and SNIC bifurcations.

Secondly, we confirm a frequency transition of the low to the high level for $\mu > 6$ and $I=0.161$ in Fig. 4. For this, we numerically calculate $[\partial f/\partial \mu]$ as a function of I . In Fig. 7(a), the $[\partial f/\partial \mu]$ - I curve has the sharper positive slope, $[(\partial/\partial I)(\partial f/\partial \mu)] > 0$, around onsets of oscillations for $\mu = 5.8$. However, the curve monotonically decays when $\mu > 6$. This implies that the phase transition of the frequency happens. In fact, when μ increases at $I=0.161$, $[\partial^2 f/\partial \mu^2]$ switches from the positive to the negative at $\mu = \mu_c$ exhibiting $[\partial^2 f/\partial \mu^2] = 0$. The peak of the $[\partial f/\partial \mu]$ - μ curve is diminished and then disappears for larger I (Fig. 7(b)). When I approaches to the bifurcation point (I_{SN}), we obtain the following condition for a frequency transition:

$$\lim_{\mu \rightarrow \mu_c^+} \frac{\partial f}{\partial \mu} = +\infty, \quad \lim_{\mu \rightarrow \mu_c^-} \frac{\partial f}{\partial \mu} = +\infty.$$

From bifurcation analysis of Fig. 2(a), let μ be μ_c when $V_{SN} = V_{min}(\mu_c)$. Periodic motions of a trajectory on the LC around $\mu = \mu_c$ can be described as followings: Membrane potential dynamics immediately before depolarization is extraordinary slow for $\mu < \mu_c$, because a trajectory is converge to the LC through the SN equilibrium, thereby leading to a significant phase delay. However when $\mu > \mu_c$, a trajectory passes on the LC via the saddle to increase $[dV/d\tau]$.

We notice $[\partial f/\partial \mu] > 0$ after a frequency transition. This is the same result as the HH oscillator undergoing the AH bifurcation [19]. Therefore, we have found that, for any I in the oscillation range,

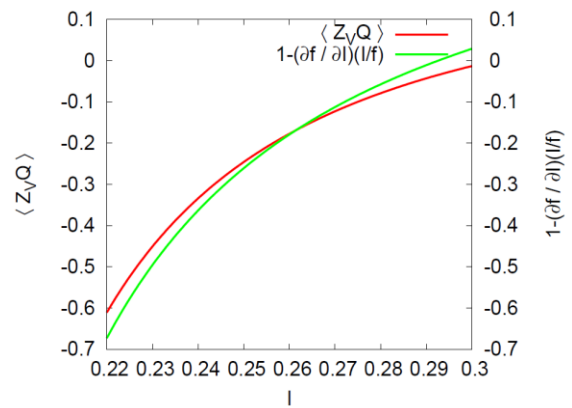
- Class I oscillation: $[\partial f/\partial \mu]$ takes both the positive and negative values if $\mu < \mu_c$, and has the positive value if $\mu > \mu_c$.
- Class II oscillation: $[\partial f/\partial \mu]$ takes the positive value for any μ .

V. DISCUSSION

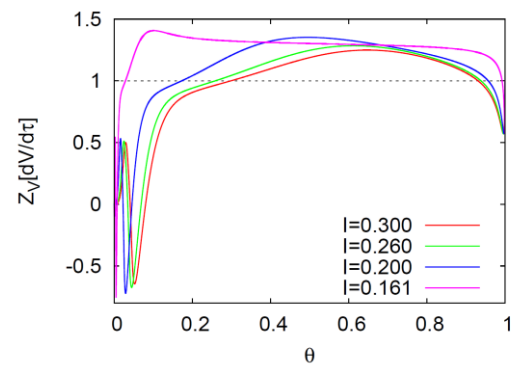
Calculations of $[\partial f/\partial \mu]$ have ruled out the ambiguity in the conventional classification with different PRC forms, to give clearer classification regardless of the PRC forms. The PRC was traditionally classified into two types: Type I takes almost all positive values for any phase while type II has the obvious negative values as well [20][21]. However, the type I PRC even takes the negative value for extreme narrow phase range and its shape continuously changes to the type II with an increase in I (as shown in red lines of Fig. 8). There was an open question about definition of the PRC classification.

In comparison with the $[\partial f/\partial \mu]$ results for the class I, the typical class II f - I curve has been analyzed by using the original HH neuron that starts oscillations with a finite frequency through the AH bifurcation. The result is only $[\partial f/\partial \mu] > 0$ for any I in the oscillation range. We may conclude that, in the class I for the SHCO bifurcation, the $[\partial f/\partial \mu]$ takes both the positive and negative values, meanwhile $[\partial f/\partial \mu] > 0$ in the class II for the AH bifurcation.

We have thus shown that computing $[\partial f/\partial \mu]$ is significantly potential for oscillation classification. One may criticize that the analysis studied here only supports the



(a)



(b)

Fig. 6. (a) $\langle Z_V Q \rangle_\theta$ (red line) and $[1 - (\partial f/\partial I)(I_0/f)]$ (green line) represent as functions of I when $\mu=1$. (b) $Z_V \cdot [dV/d\tau]$ is a function of θ ($\in [0, 1)$) at each level of $I = 0.161, 0.2, 0.26$ and 0.3 .

conventional classification with different bifurcation mechanisms of the SN (or SNIC) and AH.

In order to evade such criticism, the two-dimensional Hindmarsh-Rose (2DHR) model, which retains the analytic tractability of the FitzHugh-Nagumo model [22][23], is employed [24]. All bifurcations requested, those being, the AH, the SNIC and the SN are computed in the 2DHR model with appropriate parameter sets. The $[\partial f/\partial \mu]$ - I curve for each bifurcation is then computed. As the result, the AH, SNIC and SN bifurcations have been categorized into two types:

- Category I ($[\partial f/\partial \mu] > 0$ and $[\partial f/\partial \mu] < 0$): The SNIC bifurcation.
- Category II ($[\partial f/\partial \mu] > 0$): The AH and SN bifurcations.

As far as we know, the AH and SN bifurcations were not categorized into the same. On the contrary, the SN has so far been regarded to belong to the category for the SNIC bifurcation. In fact, the condition that only $[\partial f/\partial \mu] > 0$ is showed even if the Terman-Wang (TW) model [25][26] is used [19]. The TW model is one of the analytic tractable neuron models, which generates oscillations via the SN bifurcation.

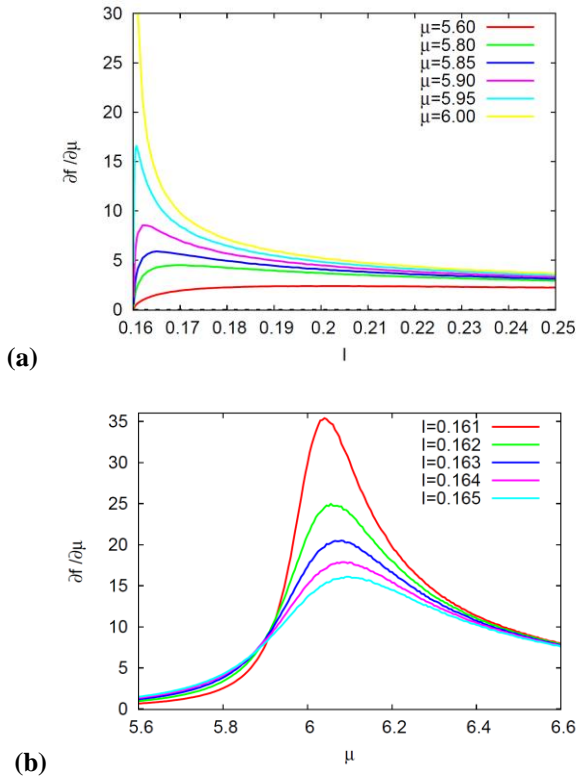


Fig. 7. Results of the Frequency transition when $\mu > 6$. (a) $[\partial f / \partial \mu]$ - I curves when $\mu=5.6, 5.8, 5.85, 5.9, 5.95$ and 6.0 . (b) $[\partial f / \partial \mu]$ - μ curves for $I = 0.161, 0.162, 0.163, 0.164$ and 0.165 .

These $[\partial f / \partial \mu]$ results are supposed to give us important indications about conventional classifications with different bifurcation mechanisms, or different PRC forms. The SN bifurcation that occurs on the LC is crucial for the aforementioned categorization. To be more precise, the necessary condition for $[\partial f / \partial \mu] < 0$ is that the bi-stability of stable equilibrium and a LC attractor exists. Such a bi-stability cannot be found in the TW model and the 2DHR model exhibiting only stable equilibrium.

Furthermore, the categorization suggested in this work does not address that the PRCs are intensively related to the emergence of oscillations via bifurcation mechanisms. The previous work for class and type classifications [27] indicated that type I PRC has the class I oscillations. This was however no more than an indication at that moment. In Fig. 3(b), the f - I curve for $\mu = 0.25$ is the logarithmic class I. Nevertheless, type II PRCs are calculated in any frequency range. As referred to [28] and described in Eq. (5), more precisely, the average of the PRC equals to the slope of the f - I curves. Therefore, the categorization suggested above is more comprehensive and more sophisticated than the conventional classifications.

The potential task in the near future is to discover some still-unknown oscillatory property of the neuronal circuit undergoing the corresponding bifurcation. Finding novel oscillatory properties allows us to predict bifurcation mechanisms hidden in complex behavior of the neuronal circuit. Since $[\partial f / \partial \mu]$ is intensively related to f - I relations as well as PRCs, at least, it can expect to identify bifurcation mechanisms with the more accuracy, compared to only observation of the f - I relations or PRCs. In the f - I relations,

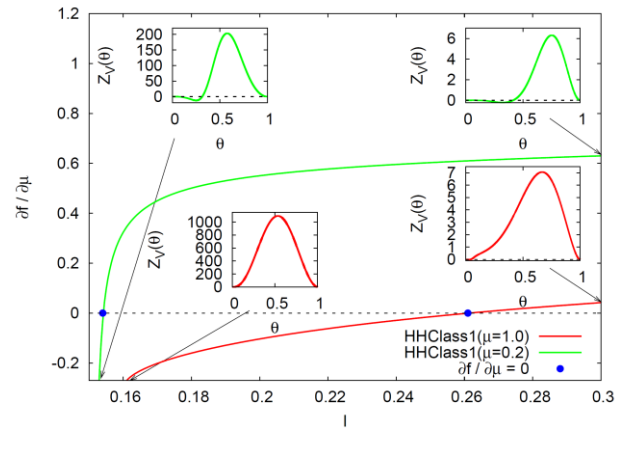


Fig. 8. $[\partial f / \partial \mu]$ - I curve for $\mu=1$ (red line) shifts to the one for $\mu=0.2$ (green line). Correspondingly, the cross point of $[\partial f / \partial \mu] = 0$ (blue circles) moves so that the I range for $[\partial f / \partial \mu] < 0$ is reduced. The PRCs are drawn respectively for $I = 0.161$ and $I = 0.3$ when $\mu=1.0$, and for $I = 0.153$ and $I = 0.3$ when $\mu=0.2$.

it is difficult to record at the same time the zero and nonzero frequencies. The PRCs are observed under the environmental noise [29] so that we can difficultly specify bifurcation mechanisms.

Finally, we discuss the temperature scaling factor μ . In general, time courses of the ion-channel activations are rescaled with $\mu = Q_{10}^{(T-T_e)/10}$ with temperature T °C, $Q_{10} \sim 3$ and environmental temperature T_e . In physiological experiments, the temperature is usually fixed around either room temperature or body temperature so that there is not so much temperature variation [5][30]. We may thus have to take care of the temperature parameter to observe stable oscillatory properties of individual neuron corresponding to the recording temperature. Recent model studies are not significantly careful for handling with the temperature parameter [31][32]. In this work, the experimental temperature variation was ignored, because it was crucial and interesting for us to systematically investigate oscillatory properties of the HH model.

VI. CONCLUSION

We studied a frequency decrease and a frequency transition with a temperature increase in the HH model undergoing SHCO bifurcations. In this study, $[\partial f / \partial \mu]$ was derived by perturbation analysis of the stable HH oscillators, in combination with $[\partial f / \partial I]$ and $\langle Z_V Q \rangle_\theta$. We showed that the PRC was clearly classified by $[\partial f / \partial \mu]$. More interestingly, different bifurcation mechanisms of the AH and the SN were commonly categorized.

ACKNOWLEDGEMENTS

The author thanks Natsume and Tateno at Kyushu Institute of Technology and Ikegaya and Aihara at University of Tokyo for fruitful discussions.

REFERENCES

- [1] C. Lu, Z. Wang, Y. Zhou, and M. Vreugdenhil, Temperature- and concentration-dependence of kainite-induced γ oscillation in rat hippocampal slices under submerged condition, *Acta Pharmacologica Sinica*, 33, 2012, 214-220.
- [2] X.-J. Wang and G. Buzsaki, Gamma Oscillation by Synaptic Inhibition in a Hippocampal Interneuronal Network Model, *J. Neurosci.* 16(20), 1996, 6402-6413.
- [3] M. Yoshioka, Chaos synchronization in gap-junction-coupled neurons, *Phys. Rev. E* 71, 2005, 065203.
- [4] A. Hodgkin and A. Huxley, A quantitative description of membrane current and its application to conduction and excitation in nerve, *J. Physiol.* 117, 1952, 500-544.
- [5] H. A. Braun, M. T. Huber, M. Dewald, K. Schaefer, and K. Voigt, Computer simulations of neuronal signal transduction: the role of nonlinear dynamics and noise, *Int. J. Bifur. Chaos Appl. Sci. Eng.* 8(5), 1998, 881-889.
- [6] U. Feudel, A. Neiman, X. Pei, W. Wojtenek, H. Braun, M. Huber and F. Moss, Homoclinic bifurcation in a Hodgkin-Huxley model of thermally sensitive neurons, *Chaos* 10(1), 2000, 231-239.
- [7] E. M. Izhikevich, *Dynamical Systems in Neuroscience: The Geometry of Excitability and Bursting* (MIT Press, Cambridge, MA, 2007).
- [8] A. Hodgkin, The local electric changes associated with repetitive action in a nonmedulated axon. *J. Physiol.* 107, 1948, 165-181.
- [9] T. Tateno, A. Harsch and H. P. C. Robinson H. P. C. Threshold firing frequency-current relationships of neurons in rat somatosensor cortex: type 1 and type 2 dynamics. *Journal of Neurophysiology*, 92, 2004, 2283-2294.
- [10] Y. D. Sato, K. Okumura, A. Ichiki, M. Shiino and H. Cateau, Temperature-modulated synchronization transition in coupled neuronal oscillators. *Phys. Rev. E*, 85, 2012, 031910.
- [11] E. Dodt and Y. Zotterman, The Discharge of Specific Cold Fibres at High Temperatures; the paradoxical cold. *Acta Physiol. Scand.* 26(4), 1952, 358-65.
- [12] R. R. Long, Sensitivity of cutaneous cold fibers to noxious heat: paradoxical cold discharge. *J. Neurophysiol.* 40(3), 1977, 489-502.
- [13] R. K. Adair, A model of the detection of warmth and cold by cutaneous sensors through effects on voltage-gated membrane channels. *Proc. Natl. Acad. Sci. U S A.* 96(21), 1999, 11825-11829.
- [14] P. Arhem, G. Klement, and C. Blomberg, Channel Density Regulation of Firing Patterns in a Cortical Neuron Model. *Biophys. J.* 90(12), 2006, 4392-4404.
- [15] H. Zeberg, C. Blomberg and P. Arhem, Ion Channel Density Regulates Switches between Regular and Fast Spiking in Soma but Not in Axons. *PLoS Comput. Biol.* 6(4), 2010, e1000753.
- [16] A. Mehrotra and A. Sangiovanni-Vincentelli, *Noise Analysis of Radio Frequency Circuits* (Kluwer, Dordrecht, 2004).
- [17] Y. D. Sato, Synchronization phenomena in a pair of coupled neural oscillators system. *Ph.D. thesis*, Tokyo Institute of Technology, 2005 (unpublished).
- [18] A. Demir, J. Roychowdhury, On the validity of orthogonally decomposed perturbations in phase noise analysis, *Tech Memo* (Bell Labs., Murray Hill, NJ, 1997).
- [19] Y. D. Sato, Neural oscillation classification with temperature-modulated frequency. *Europhys. Lett.* (to be submitted).
- [20] Y. Tsubo, J.-N. Teramae and T. Fukai, Synchronization of excitatory neurons with strongly heterogeneous phase responses. *Phys. Rev. Lett.* 99(22), 2007, 228101.
- [21] Y. Tsubo, M. Takada, A. D. Reyes and T. Fukai, Layer and frequency dependencies of phase response properties of pyramidal neurons in rat motor cortex. *Euro. J. Neurosci.* 25(11), 2007, 3429-3441.
- [22] R. FitzHugh, Impulses and physiological states in theoretical models of nerve membrane. *Biophys. J.* 1, 1961, 445-466.
- [23] R. FitzHugh, Mathematical models of excitation and propagation in nerve, in H.P. Schwan (Ed.), *Biological Engineering*, Chapter 1 (McGraw-Hill Book Co., N.Y. 1969) 1-85.
- [24] S. Tsuji, T. Ueta, H. Kawakami, H. Fujii, K. Aihara, Bifurcations in Two-Dimensional Hindmarsh-rose Type Model. *Int. J. Bifur. Chaos* 17(3), 2007, 985-998.
- [25] D. Terman and D.-L. Wang, Global competition and local cooperation in a network of neural oscillators. *Physica D* 81, 1995, 148-176.
- [26] D.-L. Wang and D. Terman, Locally excitatory globally inhibitory oscillator networks. *IEEE Trans. Neural Net.* 6, 1995, 283-286.
- [27] G. B. Ermentrout, Type I membranes, phase resetting curves, and synchrony. *Neural Comput.* 8, 1996, 979-1001.
- [28] M. A. Schwemmer and T. J. Lewis, Effects of dendritic load on the firing frequency of oscillating neurons. *Phys. Rev. E* 83, 2011, 031906.
- [29] T. I. Netoff, M. I. Banks, A. D. Dorval, C. D. Acker, J. S. Haas, N. Kopell and J. A. White, Synchronization in hybrid neuronal networks of the hippocampal formation. *J. Neurophysiol.* 93(3), 2005, 1197-1208.
- [30] K. S. Cole, R. Guttman and F. Bezanilla, Nerve Membrane Excitation without Threshold. *Proc. Natl. Acad. Sci. U S A.* 65(4), 1970, 884-891.
- [31] Y.-G. Lv and J. Liu, Interpretation on thermal comfort mechanisms of human bodies by combining Hodgkin-Huxley neuron model and Pennes bioheat equation. *Forschung im Ingenieurwesen* 60(2), 2005, 101-114.
- [32] S. Kuang, J. Wang, T. Zeng and A. Cao, Thermal impact on spiking properties in Hodgkin-Huxley neuron with synaptic stimulus. *Pranama* 70(1), 2008, 183-190.

Power Efficient and Reuse of Memory with Steiner Graphs

Aditya Putta¹, B. Chinna rao², P. M. Francis³

¹M. tech (PG student) Gokul Eng College

²Prof. & Head, Dept. of ECE, Gokul Eng College

³Asst. Prof. in Dept. of ECE, Gokul Eng College

Abstract: Rapid demand on system-on-chip (SoCs) and communication increases with the help of very-large-scale integration (VLSI) circuits, even though prime factor is to reduce the Power consumption and the thermal wall have become the major factors limiting the speed of while interconnect is becoming a primary power consumer. High bandwidth is desired to enhance parallelism for better performance, and the power efficiency on this bandwidth is critical to the overall SoC power consumption. Current bus architectures such as AMBA, Core connect, and Avalon are convenient for designers but not efficient on power. This paper proposes a physical synthesis scheme for on-chip buses and bus matrices to minimize the power consumption, without changing the interface or arbitration protocols. By using a bus gating technique, data transactions can take shortest paths on chip, reducing the power consumption of bus wires to minimal. Routing resource and bandwidth capacity are also optimized by the construction of a shortest-path Steiner graph, wire sharing among multiple data transactions, and wire reduction heuristics on the Steiner graph. Experiments indicate that the gated bus from our synthesis flow can save more than 90% dynamic power on average data transactions in current AMBA bus systems, which is about 5–10% of total SoC power consumption, based on comparable amount of chip area and routing resources.

Index Terms: Algorithm, communication graph, data throughput, physical synthesis, power efficiency, Steiner graph.

I. Introduction

As the feature size of process technology scales down, system-on-chips (SoCs) are capable of integrating more components and gaining higher complexity. Since clock frequency on single components is reaching a limit due to power and thermal limitations, better performance will be mostly exploited through parallelism [1], [3]. As a result, two factors determine that on-chip communication architectures are becoming a critical aspect in future systems. First, the communication latency and bandwidth among system components may become a bottleneck of performance. Second, the percentage of power consumed on inter-component communications in the whole system power has scaled up to a significant level [9], [13], [15]. Industrial on-chip bus standards include AMBA [29], [31], CoreConnect [30], Avalon [32], and so on. These existing standards can provide an interface for IP developers and a communication solution for system designers. Compared to the network-on-chip [10] type of communications, buses are small on silicon footprint, fast in terms of latency, and easy to implement. Moreover, the implementations can be

reconfigured according to specific applications, enabling designers to apply various optimizations for best performance on available resources. The advantages of simplicity make buses popular in industrial SoC designs. However, current bus architectures are not power efficient on transferring data through bus lines. And since this part of power is scaling up as technology advances [13], it becomes a necessity to introduce physical level optimization on bus synthesis to minimize the power consumed by inter-component communication on bus lines. When high bandwidth is required on these buses, wire efficiency may also become low, which ultimately limits the system bandwidth capacity and performance. We propose a physical synthesis scheme for on-chip buses to eliminate the disadvantages in existing bus architectures, but not to change the existing protocols and component interfaces. Based on shortest-path Steiner graphs, efficiency on bus lines is maximized without the need to redesign system components and IP modules. Routing resource is also reduced without compromising low power. The cost on our new scheme is the additional silicon resource consumed by distributed controls and switches, which is scaling down by Moore's law. Under technology trends, this physical synthesis scheme is capable of bringing a large improvement on power and performance based on current state-of-the-art on-chip buses and bus matrices.

A. Related Work

An elaborate power analysis on AMBA on-chip bus is performed in [15]-[18] where the detailed decomposition of power consumed by system components is obtained by simulation on NEC's gate-level power estimator. Power saving techniques have been explored and applied extensively to break through the "power wall" of VLSI circuit performance. Clock gating [5] is nowadays widely used to reduce dynamic power, and power gating [20] is used to avoid unnecessary static power. In bus communications, a large part of the power is consumed on the wires of bus lines [15], which is relatively scaling up with technology and applications [9], [13]. Techniques of clock gating can be used on bus lines to achieve a similar goal, which is to mask off signals wherever they are not needed. Bus segmentation in [6] has such effect to help reduce dynamic power, but the effect is largely limited by tree structures topologies. Also in [18], a power performance tradeoff is analyzed on bus matrices, where a bus matrix is composed of a set of tree structured buses. We extend the structures from trees to graphs, using Steiner graph connections for a thorough optimization of "bus gating" to minimize the communication power. Topologies have been mostly discussed in bus optimizations, while the physical/geometrical information is not being emphasized.

B. Paper Overview

In this paper, to obtain the bus getting architecture and optimize bus communications, and get minimal tradeoff power maximal bandwidth, and minimal total wire length. the protocols are of AMBA AHB [29] and AXI [31], since they are most popular in industrial designs. And apply optimizations which is biased toward minimal power, but also favors bandwidth and routing resource. To construct a minimal shortest-path Steiner graph, and to reduce its scale with a minimal increment on path lengths. The overall optimization flow can be viewed as three major steps:

- Step 1: generating the shortest-path Steiner graph H (for minimal power);
- Step 2: deciding edge weights on H

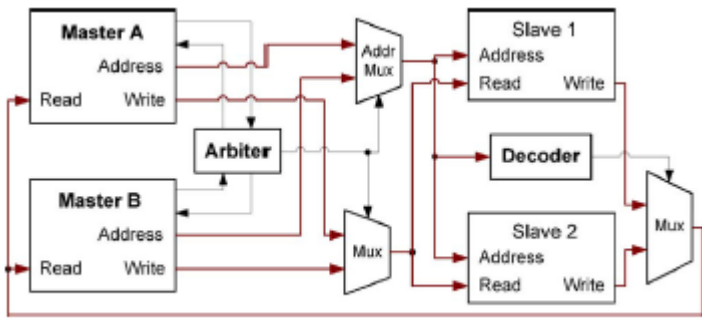


Fig 1 AMBA AHB bus

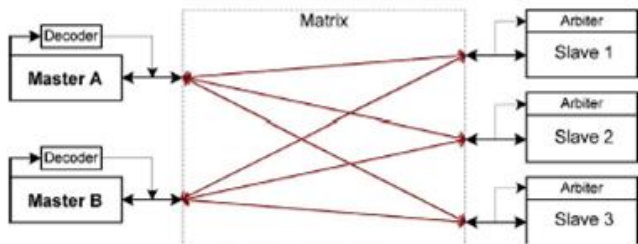


Fig 2 AMBA AXI full bus matrix (drawn)

Step 3: applying incremental modifications on H (for minimal wire length).

The rest of this paper is organized as follows. Section II introduces some background information on bus architecture and bus gating. Section III shows the heuristics for minimizing power and Section IV for minimizing wire length. Experiments are illustrated in Section V. Finally, Section VI gives our conclusions on bus matrix, with comparisons to network-on-chips and analogies to city traffic planning.

II. Bus Architectures and Bus Gating Background

Standard on-chip buses like AMBA were designed to enable fast and convenient integration of system components into the SoC, where simplicity is one of the major objectives. When the bus power consumption comes to a significant level that we cannot afford to ignore [15], power optimization will be desirable. We introduce a “bus gating” technique [23] to minimize the power on bus lines with a small compromise on design simplicity.

A. AMBA On-Chip Bus and Bus Matrix Architectures

The AMBA AHB on-chip bus [29] and bus matrix [31] are drawn in Figs. 1 and 2. The components connected by these buses can be classified into masters and slaves. Masters are typically microprocessors, each can start a transaction with one slave device at a time, where the slave is selected by giving an address to the decoder. Slave devices respond to masters passively. When conflicting requests come from multiple masters, arbiters will decide the order of services. The main difference between the bus and bus matrix is on multiple access from masters. The basic bus allows one master access at a time, while the bus matrix may allow multiple accesses. In a full bus matrix like Fig. 2, the masters and slaves are connected like a bi-clique, and each slave has an arbiter. Full bus matrices have largest bandwidth capacity, typically applied for maximum performance.

B. Power and Wire Efficiency of Gated Bus Using Steiner Graphs

The power efficiency of a bus architecture like Fig. 1 is low because the bus lines from masters to slaves are connecting all the slave devices by a single large wire net. The same is on slave-to-master connections. While the communication is one-to-one, the signals are sent to all the receivers regardless of whether they are needed, which results in wasted dynamic power on bus wires and component interfaces. Moreover, this low power efficiency is still being worsened by the technical scaling of global wires [13] and the increasing number of components integrated into SoCs. Gated bus is a solution to save the wasted dynamic power. The simplest way is to add a de-multiplexer after each multiplexer in Fig. 1, and add a de-multiplexer after each master device in Fig. 2, so that the signals only propagate to where they are needed. This method works in a similar way as clock gating [5], [11], and can be even more effective because the signal receivers here have much less complex behaviors than in a clock tree. For tree structured buses, distributing the multiplexer and de-multiplexer into the wire net [Fig. 3(a)] helps to save both power and wires. For wire length, while the single multiplexer needs independent lines from every sender, the lines can be shared with distributed multiplexers and form a Steiner arborescence [7], [21], [22]. An arborescence is a directed tree such that every root-to-leaf path is shortest. On the receivers’ side with distributed de-multiplexers, the bus lines change from a rectilinear Steiner arborescence to a minimum rectilinear Steiner arborescence (MRSA). By the research in [2], this change increases the wire length by only 2–4% on average. So the total bus wire length can be reduced by the distributing the multiplexer/de-multiplexers, while the dynamic power can also be reduced at the same time. There is a small control overhead for sending the signals over the arborescence, but compared to the bus width and data throughput, this dynamic power overhead is negligible. Based on the same tree topology, effective bus gating can be applied by distributing the control over the entire tree (arborescence). On bus matrices, however, simply adding de-multiplexers may increase the total wire length, because when the number of master-to-slave paths becomes large, each path will need its own bus wires [as in Fig. 3(b)]. To reduce wire length in the bus matrix, also to further reduce power on the basic bus, we adopt the structures of Steiner

graphs. A Steiner graph is a generalization of Steiner trees, without the limitation of tree structure that there is only one root placed at a certain point, which cannot be on the shortest path of every connection. By removing the constraint of tree topologies, we gain higher freedom to choose shortest paths for reduced power on data

Else if
 If there is T_j at V_i then $Q \leftarrow Q \cup V_i$
 $X \leftarrow Q \cap \{V_j : \forall P(s-p(v_j)) = |P(s) - P(V_i)| + |P(V_i) - P(V_j)|\}$
 If $(|X| > 2)$ then merge the nodes in X rooted at V_i
 $Q \leftarrow (Q \cap X) \cup \{V_j\}$ return the arborescence at s'

Our shortest-path Steiner graph is constructed by multiple iterations of a revised MRSA construction.

A. k-IDeA/G Heuristic for MRSA

The RSA/G heuristic for the MRSA problem was first introduced in [21], and is proved to be 2-approximate. Given a single source and n terminals, the basic flow is to start with n subtrees and iteratively merge a pair of subtree roots v and v' such that the merging point is as far from the source as possible, so that the wires can be shared as much as possible. It terminates when only one subtree remains. For efficient implementation, the RSA/G first sorts all the nodes on the Hanan grid [26]

In each iteration, it removes up to k nodes from v_1, \dots, v_n some nodes are skipped it will reduce the memory and utilize the same location as address when running the RSA/G algorithm. By removing the nodes, some SMO merges are skipped, which in some cases can result in a better overall solution. All the combinations of the k or fewer skipped nodes are tried in an iteration, and the best set of skipped nodes are marked as permanently deleted. The iterations are repeated until no further improvement occurs.

B. Shortest-Path Steiner Graph by Multiple MRSA

For a shortest-path Steiner graph with multiple sources s_1, \dots, s_m , the idea behind single source MRSA is still valid. In fact, our algorithm constructs the Steiner graph H just by iteratively constructing the MRSA rooted at every source. While a single arborescence can be optimized by the k -IDeA heuristic, the m arborescences are individually optimized with the same idea, plus that these arborescences also need to share as much wire as possible to optimize the final Steiner graph. For this purpose, we add additional heuristics based on the RSA/G to construct multiple MRSA one by one. First, starting from the second MRSA construction, we can reduce terminals by using existing wires. For each MRSA with source s_i , the terminals that need connection from the source can be moved along existing edges of H toward s_i . As the example shown in Fig. 5, with the wires of previous aborescences, we only need to connect eight nodes instead of the original 16 terminals to form the MRSA rooted at s_2 , because all the other terminals can be reached from one of these eight nodes by a shortest path from s_2 . This set of nodes (denoted as T') can be obtained by checking each terminal t_j , move from t_j toward s_i as much as possible along existing paths until reaching a vertex (can be a terminal or a Steiner node) in H where no vertex closer to s_i can be reached, and add this vertex to T' . When there are multiple paths in the graph, we pick the final vertex closest to s_i , so the rest part of the path is short and likely to need less wires. Details are in the routine "Necessitate(v)" Second, we construct the MRSA based on the set of nodes T' using as much existing wires as possible. Compared to the RSA/G heuristic, the TMO condition is changed to v_i' , $\Delta T'$ the SMO condition is changed, also for the purpose of wire reusing, from $|X| \geq 2$ to $|X| \geq 2$ or $(|X| = 1$ and $v_i \Delta H)$. Because when v_i is already

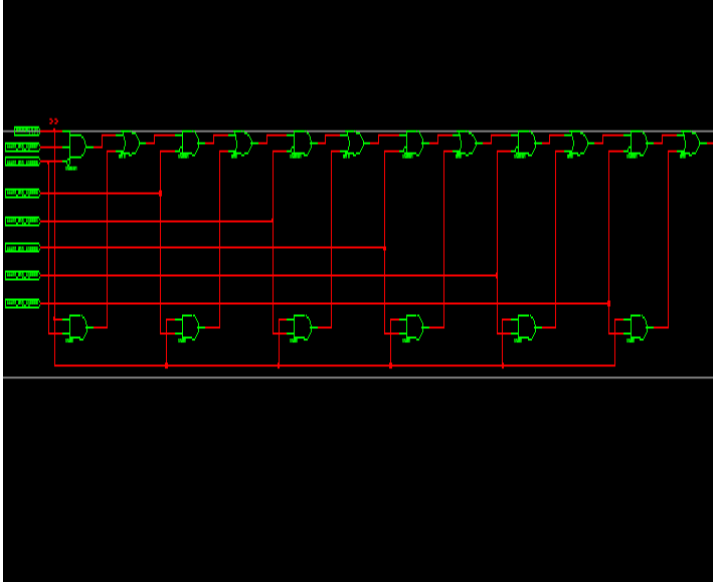


Fig 3 Bus gating using distributed mux and de-mux. (a) On single bus. (b) On bus matrix.

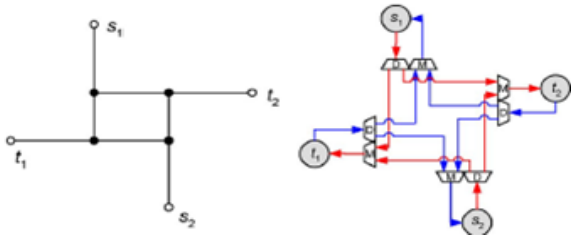


Fig 4 Shortest-path Steiner graph G_n and its bus implementation.

transactions, and to let the paths share wires for reduced. Shortest-path Steiner graphs have advantage on power efficiency as shown above. Naturally, graph structures also have advantage on communication bandwidth over trees. Our objective of bus gating and bus matrix synthesis is to perform a balanced optimization on power and bandwidth even when available routing resource is limited.

III. Bus Matrix Graph Construction

The flow we use is to first construct a shortest-path Steiner graph based on the given placement of $\forall s \cup V_t$ and communication graph G_c and then decide the weight $\omega(e)$ on each edge. The single-source case is the MRSA problem, which is well studied in previous work such as [7] and [21]. Although it is proved to be NP-complete in [22], heuristic algorithms can provide close-to-optimal solutions of Steiner arborescences.

RSA algo

Given a source s and n terminals t_1, \dots, t_n ,
 v_1, \dots, v_N are the Hanan grid nodes of $\{s, t_1, \dots, t_n\}$ sorted by decreasing distance to s

$Q \leftarrow \emptyset$

For $I = 1$ to N do

in the graph, it was added into previous MRSAs and can share wires with the node in X like the case in RSA/G when $|X| \geq 2$. As the example in

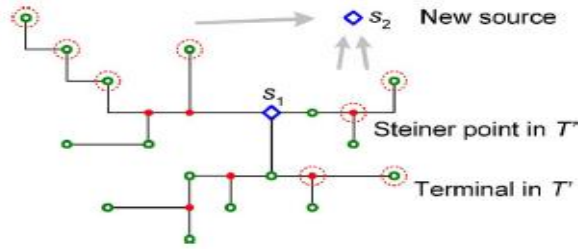


Fig 5 Nodes requiring connections (in dotted circles).

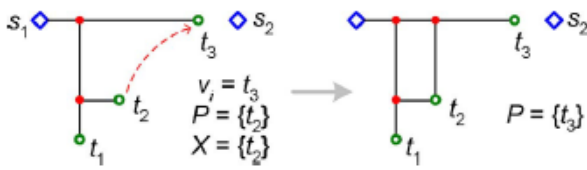


Fig. 6 Connecting a node into the Steiner graph.

shows, when X contains only one node $\{t_2\}$, it should be connected into H when v_i comes to t_3 , and half of the connection length can be saved using the existing horizontal wire. where the routine “connect(u, v)” uses existing wires if applicable on shortest connections. The k -IDeA iterations remain unchanged here. And after the shortest-path Steiner graph is constructed by applying k -IDeA on the m sources, there are possibly some redundant edges that can be removed. So the final step is to check each edge $(v_i, v_j) \Delta H$, if H still contains all the source-to-terminal shortest paths without (v_i, v_j) , then remove it from H .

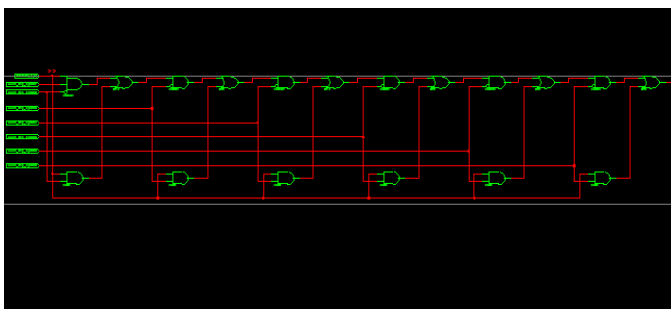
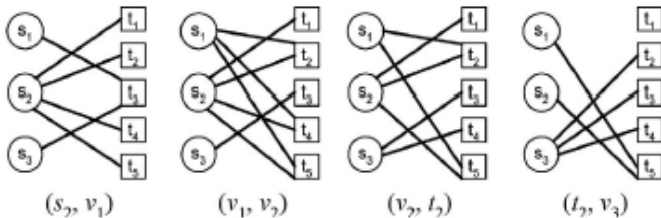


Fig7 Bipartite graphs of four edges in the bus matrix

i.e., all the $|Vs| \times |Vt| = 15$ arcs are present. The resulting bus matrix graph contains five Steiner nodes and 13 edges. Every arc from a master s_i to a slave t_j has a connection of minimal length, and the 15 shortest paths shown in Fig. 7 are fixed. To assign a weight on each edge, we take $e = (s_2, v_1)$ as example. Six of the 15 paths go through e , so $G'(e)$ consists of the six corresponding arcs $(s_1, t_3), (s_2, t_1), (s_2,$

$t_2), (s_2, t_4), (s_2, t_5),$ and (s_3, t_3) . The maximum matching has two edges, because t_3 can only connect to one of s_1 and s_3 . Therefore, $\omega(e) = 2$ is adequate to support all communication patterns. Fig.7 shows the bipartite graphs of four edges on the central horizontal line. Despite the number of connections, most of the edges are weighted 1. Yet this bus matrix graph is adequate for maximum bandwidth capacity, i.e., wires will not be the bottleneck of multiple simultaneous connections. The total weighted wire length in this bus matrix is 108. Compared to the total path length 266 if implemented as a full bus matrix in Fig. 2, the Steiner graph approach saves more than half of the routing resources.

IV. Tradeoffs on Power, Wire, and Bandwidth

A. Steiner Graph Reduction

Since high bandwidth bus matrices will need significantly more wires to support parallel communications across the chip, routing resource may become another limitation as more components are integrated into SoCs and interactions increase. Especially when the components are placed in irregular placement instead of cell arrays, the shortest-path Steiner graph generated by the algorithm in which bring additional wire length. We look for changes in the graph structure which can significantly reduce the wires, while preserving the short paths at the same time.



Fig. 8 Searching for mergeable parallel segments (in vertical direction).

when the double edges are geometrically very close to each other, combining them into one edge only slightly increases the length of some connections, while possibly saving much more wire length. Fig. 8 shows the effect of merging parallel segments in narrow rectangles. The total edge length is greatly reduced, while the increment on average path length is relatively small. Although fewer edges will generally result in larger edge weight, the total weighted edge length (wire length) can still be reduced by this merging operation due to improved wire sharing among paths. Thus, if we relax the requirement on the path length in definition 4, from the exact Manhattan distance $\|P(u)-P(v)\|$ to within $(1 + \epsilon)\|P(u) - P(v)\|$, we can merge the double parallel edges to save wires. Assume we have a vertical narrow rectangle with dimensions $h \times w$, and we merge the two vertical edges to a single edge placed in middle. The total edge length may be reduced by h , while the lengths of some connection paths increase by $w/2 + w/2 = w$. So if the h/w ratio is high, this operation can be very helpful on relieving routing congestion, while preserving the low power consumption of a bus matrix. In the wire length reduction algorithm, we

repeatedly search for pairs of parallel double lines in the bus matrix graph, and for each pair, calculate its potential reduction Δl on edge length and possible increment Δp on path lengths. The pair with highest $\Delta l/\Delta p$ ration is merged, and the modified graph will have a new set of connection paths and edge weights. If the added total wire length is really reduced, we keep the merging operation and continue to the next iteration, otherwise discard the operation. Eventually, there will be no positive wire length reduction in the graph, and we have a series of bus matrix graphs with decreasing wire length and increasing path lengths, where a comprise can be chosen. The process of searching for vertical mergeable parallel segments is illustrated in Fig. 8. (Horizontal lines are processed in the same way with x - y coordinates switched.) First, the vertical line segments in the Steiner graphs are sorted by their x coordinates, denoted as u_1, u_2, \dots, u_k . Then for each pair of segments u_i, u_j ($i < j$) with a common y interval $[y_1, y_2]$, if between i and j there is no other vertical segment on $[y_1, y_2]$, u_i and u_j are a pair of mergeable segments. On the parallel segments u_i and u_j , let cl denote the count of horizontal lines connected to the left, cr denote the count of lines connected to the right, and cm the count of lines connecting u_i and u_j in the middle. Assume $cl < cr$, so the combined vertical segment may not be at the middle but have an offset δ to the right of the midpoint. The reduction on total edge length Δl is by combining the vertical segments of length h and changing the lengths of related horizontal connections. The two vertical segments are reduced to one, which reduces edge length by h . The central cm edges of length w are totally removed. However, the lengths of cl connections on the left are increased by $\omega/2 + \delta$ and the lengths of cr connections on the right are increased by $\omega/2 - \delta$. To sum up $\Delta l = h + Cm\omega - Cl(\omega/2 + \delta) - Cr(\omega/2 - \delta)$. On the possible increment on path lengths, since the left vertical segment is pushed rightward by $w/2 + \delta$, a path may need to detour and add $\Delta p = w + 2\delta$ of distance. So the ratio is

$$\Delta l/\Delta p = \frac{h + Cm\omega - Cl(\omega/2 + \delta) - Cr(\omega/2 - \delta)}{w + 2\delta} = \frac{Cr - Cl}{2} + \frac{h - (Cr - Cm)\omega}{w + 2\delta}$$

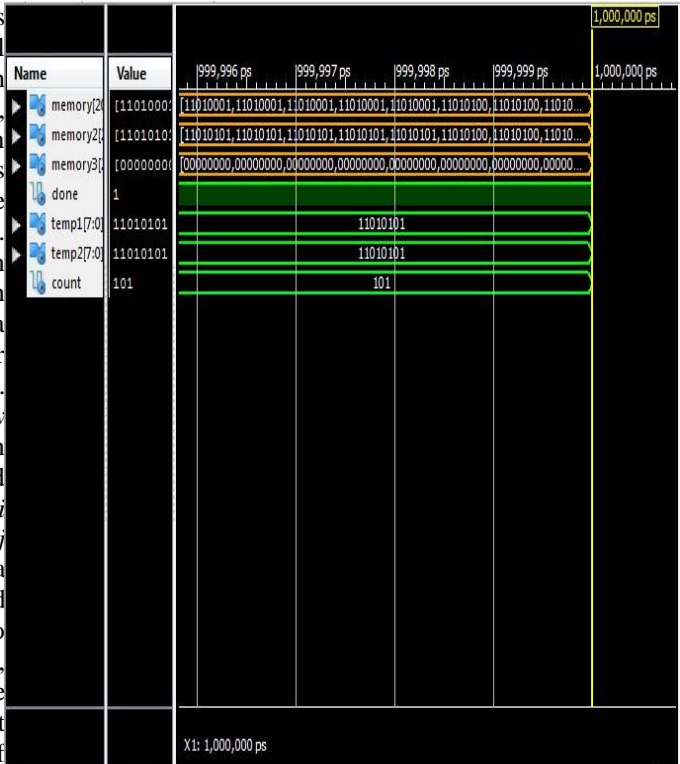


Fig 9 Merging stages of iterations

In Fig. 9, the stages of the merging iterations applied on a Steiner graph. First, the long and narrow rectangles are removed, followed by wider rectangles. still can achieve a significant reduction on total wire length in average cases. Notice that the segment merging operation also helps to merge Steiner nodes which are generated very close to each other. In practice, locally congested Steiner nodes can be hard to implement, because each node needs the area for a switch box and its control unit. Our operation does not guarantee to resolve all closely placed nodes, since it prioritizes longer segments, and may leave small square-shaped sub graphs unchanged. Nevertheless, this situation can be easily resolved by a post-processing algorithm, which scans each Steiner node (denoted as v_i), look at v_i 's close neighbors within a small $d \times d$ box and compute the density of Steiner nodes in the area. For a box with too many nodes, we can shrink all the nodes in that box into one, and implement it by a single switch. The changes on the bus matrix graph by this operation are limited in the small box areas.

V. Bus Matrix Control Units and Wires

Apart from path lengths and data wire lengths, the control overhead needs to be considered for a complete optimization. Although the data lines consume the major amount of routing resource because they are usually at least 64 bit (32 bit \times 2-way) wide, control overhead is increased compared to traditional bus architectures by adopting Steiner graphs. We need a lot of switches at Steiner nodes to guide the on-chip traffic, and each switch needs a certain number of control signals depending on its node degree and edge weights. Each slave device has an arbiter which handles the requests from masters and decides the connection. The result is sent to the central switch control unit, where all the connection paths are stored. Depending on the set of active paths, the central switch control sends

control signals to all the switches on each path, which together instantly create the master-to-slave connection requested by the master device.

VI. Experimental Results

In our experiments, we implement all the related algorithms, including the shortest-path Steiner graph generation, Steiner graph reduction by parallel line merging, and the edge weight maximum matching. The programs are tested on Windows Vista platform with a 2.2 GHz Intel Core2 processor. The running time is short on all the test cases, because the algorithms are time/space efficient, and also because most SoC bus matrices will not need to connect too many components (under 32 in our cases). The test cases we use are mostly artificial, hand made ($T0$ and $T1$), or randomly generated ($T2\Delta12$). They are the same cases used in [23] and [24]. In each test case, the master and slave devices are distributed over a $10\text{mm} \times 10\text{mm}$ square. The power consumption is estimated by the driven capacitance

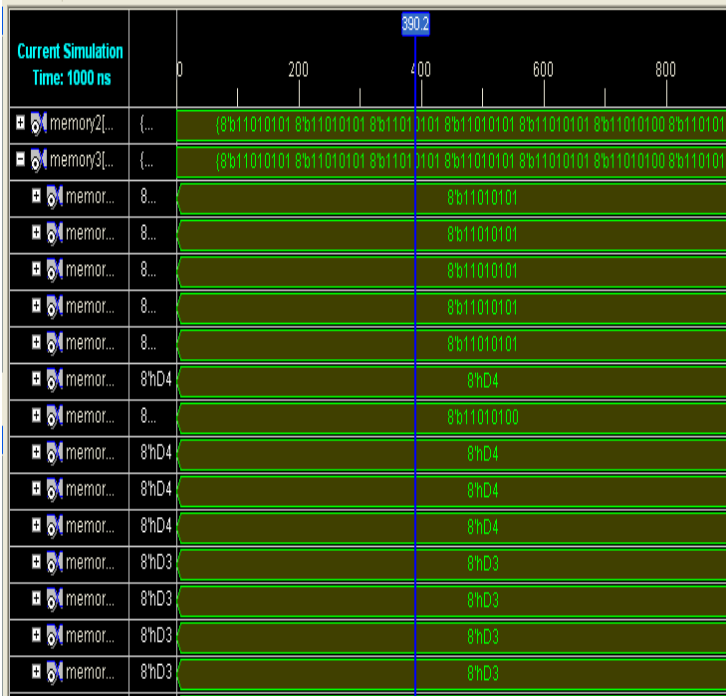


Fig 10 the effect of merging parallel segments with address location

of data transactions, and can be calculated as a linear combination of path length and switches along the path. Path lengths are minimized by the bus matrix graph construction, since wires are the major power consumer. For the purpose of data completeness, we add the power overhead from the switches on Steiner nodes. According to [27] and [28], we estimate that under 90 nm technology, each mux or demux in crossbar switches has about the same capacitance as $25\ \mu\text{m}$ of wires. The total wire length on data wires and control overhead are added straightforwardly. Data wire length is the sum of weighted edge length in the bus matrix graph.

The objective can be minimum power (i.e., average path length), minimum wire length, or a combination of the two. At the top of each column:

1) $\sum L_{vs,vt}$ is the sum of Manhattan distances on all the master-slave pairs;

2) L_{tree} is the average induced path length (major dynamic power) of master-slave connections in tree structured AMBA AHB buses or bus matrices;

3) L_{path} is the average path length (major dynamic power) of master-slave connections in the bus matrix graph;

4) P_{switch} is the added percentage of power overhead in data transactions by the switches on Steiner nodes;

5) $\sum L_{wire}$ is the total data wire length;

6) $\sum W_{ctrl}$ is the added percentage of control wire overhead.

In the minimal power section, the average path length is exactly $\sum L_{vs,vt} / (mn)$, while the total wire length is about one fourth to one third of the total connection length. Compared to traditional bus implementation in [23], the dynamic power saving is mostly over 90% even with the switching overhead added. Overhead on dynamic power increases with the number of components increasing, which requires more bandwidth and larger switches. The percentage is generally under 20% on random cases with under 30 components. So the overall dynamic power here is close to optimal. On the overhead of control wires, the percentage is mostly under 10%, because the number of control signals required is usually very low compared to the 64 bit wide data lines.

In the minimal wire section, the bus matrix graphs are reduced by the parallel line merging heuristic. As a result the wire length on most cases is greatly reduced. Compared to the reduced wire length, the increase on average path length is much lower, mostly around 10% and all under 20%. The power overhead percentage is also increased, because although the Steiner nodes are reduced, the switches along each path are not reduced as much in number, but increased in size. Still, these solutions are relatively power efficient, and we have series of intermediate solutions between minimal power and minimal wire are available for choice.

To see how the path lengths reflect communication power in SoCs, we calculate the bus power consumption with a fixed set of parameters. Assuming 1V of power voltage, $0.2\ \text{fF}/\mu\text{m}$

of wire capacitance, 4 Gb/s of transaction bit rate, and 20% of bus matrix activity rate, Table V lists the estimated power on bus matrix in each of our test cases. Again we can see a large reduction on total bus power ($P_{path} + P_{switch}$) compared to P_{tree} by traditional Steiner tree structures between certain master-slave pairs may only happen at some specific conditions. So instead of a set of arcs A in the communication graph, we can have a series of arc sets A_1, A_2, \dots, A_c , each one smaller than the original set A , denoting a set of simultaneous connections.

VII. Conclusion

We optimized on-chip communications referring to the AMBA AHB bus (matrix) architecture. The weaknesses of original bus matrices, such as low power efficiency and low wire efficiency, are resolved by using a Steiner graph structure. Compared to network-on-chip which has better bandwidth flexibility, bus matrix has much less latency. Therefore, we believe bus matrix architectures will be widely applied for efficient communications in various future systems. The principle of our work on reducing power is to minimize the data movement on the chip; and that on reducing wires is to maximize wire sharing among different connections. Devised algorithms which can

extensively exploit the on-chip physical design space for a thorough optimization on power and wire efficiency. The results show promising potentials of bus matrices for low power and high performance on-chip communications. More improvements can be explored in future works on formulations, algorithms, and the overall Optimization flow.

References

- [1] S. V. Adve, V. S. Adve, G. Agha, M. I. Frank, M. J. Garzarán, J. C. Hart, W.-M. W. Hwu, R. E. Johnson, L. V. Kale, R. Kumar, D. Marinov, K. Nahrstedt, D. Padua, M. Parthasarathy, S. J. Patel, G. Rosu, D. Roth, M. Snir, J. Torrellas, and C. Zilles, *Parallel Computing Research at Illinois: The Uprc Agenda*. Urbana, IL: Univ. Illinois Urbana-Champaign, Nov. 2008.
- [2] C. J. Alpert, A. B. Kahng, C. N. Sze, and Q. Wang, "Timing-driven Steiner trees are (practically) free," in *Proc. ACM/IEEE Des. Autom. Conf.*, Sep. 2006, pp. 389–392.
- [3] K. Asanovic, R. Bodik, B. C. Catanzaro, J. J. Gebis, P. Husbands, K. Keutzer, D. A. Patterson, W. L. Plishker, J. Shalf, S. W. Williams, and K. A. Yelick, "The landscape of parallel computing research: A view from Berkeley," Dept. Electric. Eng. Comput. Sci., Univ. California, Berkeley, Tech. Rep. UCB/Eecs-2006-183, 2006.
- [4] B. Bollobás, D. Coppersmith, and M. Elkin, "Sparse distance preservers and additive spanners," *SIAM J. Discrete Math.*, vol. 19, no. 4, pp. 1029–1055, 2005.
- [5] L. A. Ca, Q. Wu, M. Pedram, and X. Wu, "Clock-gating and its application to low power design of sequential circuits," in *Proc. IEEE Custom Integr. Circuits Conf.*, vol. 47. Mar. 2000, pp. 415–420.
- [6] J. Y. Chen, W. B. Jone, J. S. Wang, H. I. Lu, and T. F. Chen, "Segmented bus design for low power systems," *IEEE Trans. Very Large Scale Integr. Syst.*, vol. 7, no. 1, pp. 25–29, Mar. 1999.
- [7] J. Cong, A. B. Kahng, and K.-S. Leung, "Efficient algorithms for the minimum shortest path Steiner arborescence problem with applications to VLSI physical design," *IEEE Trans. Comput.-Aided Design*, vol. 17, no. 1, pp. 24–39, Jan. 1998.
- [8] J. Cong, A. B. Kahng, G. Robins, M. Sarrafzadeh, and C. K. Wong, "Provably good performance-driven global routing," *IEEE Trans. Comput.-Aided Design*, vol. 11, no. 6, pp. 739–752, Jun. 1992.
- [9] W. Dally, "Keynote: The end of denial architecture and the rise of throughput computing," in *Proc. ACM/IEEE Des. Autom. Conf.*, Jul. 2009, p. xv.
- [10] W. Dally and B. Towles, "Route packets, not wires: On-chip interconnection network," in *Proc. ACM/IEEE Des. Autom. Conf.*, Jun. 2001, pp. 684–689.
- [11] M. Donno, A. Ivaldi, L. Benini, and E. Macii, "Clock-tree power optimization based on RTL clock-gating," in *Proc. ACM/IEEE Des. Autom. Conf.*, Jun. 2003, pp. 622–627.
- [12] J. Griffith, G. Robins, J. Salowe, and T. Zhang, "Closing the gap: Nearoptimal Steiner trees in polynomial time," *IEEE Trans. Comput.-Aided Design*, vol. 13, no. 11, pp. 1351–1365, Nov. 1994.
- [13] R. Ho, K. W. Mai, and M. A. Horowitz, "The future of wires," *Proc. IEEE*, vol. 89, no. 4, pp. 490–504, Apr. 2001.
- [14] C.-T. Hsieh and M. Pedram, "An edge-based heuristic for Steiner routing," *IEEE Trans. Comput.-Aided Design*, vol. 13, no. 12, pp. 1563–1568, Dec. 1994.
- [15] K. Lahiri and A. Raghunathan, "Power analysis of system-level onchip communication architectures," in *Proc. Int. Conf. Hardw.-Softw. Codesign Syst. Synthesis*, 2004, pp. 236–241.
- [16] K. Lahiri, A. Raghunathan, and S. Dey, "Efficient exploration of the SoC communication architecture design space," in *Proc. Int. Conf. Comput.-Aided Design*, 2000, pp. 424–430.
- [17] S. Pasricha, N. Dutt, E. Bozorgzadeh, and M. Ben-Romdhane, "Floorplan-aware automated synthesis of bus-based communication architectures," in *Proc. ACM/IEEE Des. Autom. Conf.*, Jun. 2005, pp. 565–570.
- [18] S. Pasricha, Y.-H. Park, F. J. Kurdahi, and N. Dutt, "System-level power performance tradeoffs in bus matrix communication architecture synthesis," in *Proc. Int. Conf. Hardw.-Softw. Codesign Syst. Synthesis*, 2006, pp. 300–305.
- [19] A. Pinto, L. Carloni, and A. Sangiovanni-Vincentelli, "Constraint-drive communication synthesis," in *Proc. ACM/IEEE Des. Autom. Conf.*, Jun. 2002, pp. 783–788.
- [20] M. Powell, S. H. Yang, B. Falsafi, K. Roy, and T. N. Vijaykumar, "Gatedvdd: A circuit technique to reduce leakage in deep-submicron cache memories," in *Proc. Int. Symp. Low Power Electron. Design*, 2000, pp. 90–95.
- [21] S. K. Rao, P. Sadayappan, F. K. Hwang, and P. W. Shor, "The rectilinear Steiner arborescence problem," *Algorithmica*, vol. 7, nos. 1–6, pp. 277–288, 1992.
- [22] W. Shi and S. Chen, "The rectilinear Steiner arborescence problem is np-complete," in *Proc. ACM-SIAM Symp. Discrete Algorithms*, 2000, pp. 780–787.
- [23] R. Wang, N.-C. Chou, B. Salefski, and C.-K. Cheng, "Low power gated bus synthesis using shortest-path Steiner graph for system-on-chip communications," in *Proc. ACM/IEEE Des. Autom. Conf.*, Jul. 2009, pp. 166–171.
- [24] R. Wang, E. Young, R. Graham, and C.-K. Cheng, "Physical synthesis of bus matrix for high bandwidth low power on-chip communications," in *Proc. ACM Int. Symp. Phys. Des.*, 2010, pp. 91–96.
- [25] D. West, *Introduction to Graph Theory*. Englewood Cliffs, NJ: Prentice-Hall, 1999.
- [26] M. Zachariasen, "A catalog of Hanan grid problems," *Networks*, vol. 38, no. 2, pp. 200–201, 2000.
- [27] L. Zhang, H. Chen, B. Yao, K. Hamilton, and C.-K. Cheng, "Repeated on-chip interconnect analysis and evaluation of delay, power, and bandwidth metrics under different design goals," in *Proc. Int. Symp. Quality Electron. Design*, 2007, pp. 251–256.
- [28] Y. Zhang, X. Hu, A. Deutsch, A. E. Engin, and C.-K. C. J. Buckwalter, "Prediction of high-performance on-chip global interconnection," in *Proc. Int. Workshop Syst.-Level Interconnect Prediction*, 2009, pp. 61–68.
- [29] *Amba 2.0 Specification*. (1999) [Online]. Available: http://www.arm.com/products/solutions/AMBA_Spec.html
- [30] "Coreconnect bus architecture," in *IBM White Paper*. 1999. [31] *Amba 3 Specification*. (2003) [Online]. Available: http://www.arm.com/products/solutions/axi_spec.html

Novel Pattern Matching using FSM Algorithm for Memory Architecture

B. Prasad kumar, B. Chinna rao, P. M. Francis

¹M. tech (PG student) GITAS

²Prof. & Head, Dept. of ECE, GITAS

³Asst. Prof. in Dept. of ECE, GITAS

Abstract: Network intrusion detection system is used to inspect packet contents against thousands of predefined malicious or suspicious patterns. Because traditional software alone pattern matching approaches can no longer meet the high throughput of today's networking, many hardware approaches are proposed to accelerate pattern matching. Among hardware approaches, memory-based architecture has attracted a lot of attention because of its easy reconfigurability and scalability. In order to accommodate the increasing number of attack patterns and meet the throughput requirement of networks, a successful network intrusion detection system must have a memory-efficient pattern-matching algorithm and hardware design. In this paper, we propose a memory-efficient pattern-matching algorithm which can significantly reduce the memory requirement. For Snort rule sets, the new algorithm achieves 21% of memory reduction compared with the traditional Aho–Corasick algorithm. In addition, we can gain 24% of memory reduction by integrating our approach to the bit-split algorithm which is the state-of-the-art memory-based approach.

Index Terms: Aho–Corasick (AC) algorithm, finite automata, pattern matching.

I. Introduction

The purpose of a signature-based network intrusion detection system is to prevent malicious network attacks by identifying known attack patterns. Due to the increasing complexity of network traffic and the growing number of attacks, an intrusion detection system must be efficient, flexible and scalable. The primary function of an intrusion detection system is to perform matching of attack string patterns. Because string matching is the most computative task in network intrusion detection (NIDS) systems, many hardware approaches are proposed to accelerate string matching. The hardware approaches may be classified into two main categories, the logic [5], [8], [13],[16], [21], [26] and the memory architectures [4], [6], [7], [11], [14], [15], [22]–[24], [27]–[29] In terms of reconfigurability and scalability, the memory architecture has attracted a lot of attention because it allows on-the-fly pattern update on memory without resynthesis and relay out

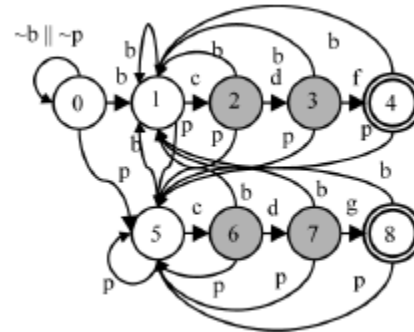


Fig 1 DFA for matching “bcd” and “pcdg”

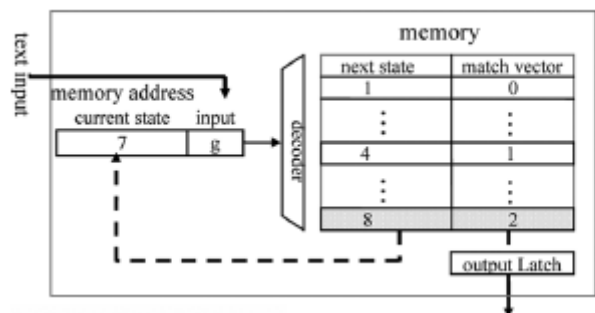


Fig 2 basic memory architecture

The basic memory architecture works as follows. First, the (attack) string patterns are compiled to a *finite-state machine* (FSM) whose output is asserted when any substring of input strings matches the string patterns. Then, the corresponding state transition table of the FSM is stored in memory. For instance, Fig. 1 shows the state transition graph of the FSM to match two string patterns “bcd” and “pcdg”, where all transitions to state 0 are omitted. States 4 and 8 are the final states indicating the matching of string patterns “bcd” and “pcdg”, respectively. Fig. 2 presents a simple memory architecture to implement the FSM. In the architecture, the memory address register consists of the current state and input character; the decoder converts the memory address to the corresponding memory location, which stores the next state and the *match vector* information. A “0” in the match vector indicates that no “suspicious” pattern is matched; otherwise the value in the matched vector indicates which pattern is matched. For example in Fig. 2, suppose the current state is 7 and the input character is . The decoder will point to the memory location which stores the next state 8 and the match vector 2. Here, the match vector 2 indicates the pattern “pcdg” is matched. Due to the increasing number of attacks, the memory required for implementing the corresponding FSM increases to the memory size, reducing the memory size has become

imperative. Certain complicated virus string patterns can be represented by regular expressions. For example, the pattern for detecting the internet radio protocol is represented as “membername*session*player” For memory architecture, only few pre-vious works [15], [29] proposed to reduce the complexity of regular expressions. Still, majority of the patterns are exact string patterns. For example in Snort V2.4, there are 85% of exact string patterns. In this paper, we focus on reducing the memory size of the exact string patterns. We observe that many string patterns are similar because of common sub-strings. However, when string patterns are compiled into an FSM, the similarity does not lead to a small FSM. Consider the same example in Fig. 1 where two string patterns have a common sub-string “cd”. Because of the common sub-string, state 2 has “similar” state transitions to those of state 6. Similarly, states 3 and 7 have “similar” transitions. However, states 2 and 6, states 3 and 7 are not equivalent states and cannot be merged directly. We call a state machine merging those non-equivalent “similar” states, *merg_FSM*.

In this paper, we propose a state-traversal mechanism on a *merg_FSM* while achieving the same purposes of pattern matching. Since the number of states in *merg_FSM* can be drastically smaller than the original FSM, it results in a much smaller memory size. We also show that hardware needed to support the state-traversal mechanism is limited. Experimental results show that our algorithm achieves 21% of memory reduction compared with the traditional AC algorithm for total string patterns of Snort [24]. In addition, since our approach is complementary to other memory reduction approaches, we can obtain substantial gain even after applying to the existing state-of-the-art algorithms. For example, after integrating with the bit-split algorithm [27], we can gain 24% of memory reduction.

II. RELATED RESEARCHES

In this section, we review several related researches in this area. In the past few years, many algorithms and hardware designs are proposed to accelerate pattern matching. The hardware approaches can be classified into two main categories, logic and memory architectures. The logic architectures mostly use on-chip logic resources of field-programmable gate array (FPGA) to convert regular expression pattern into parallel state machines or combinatorial circuits because FPGA allows for updating new attack patterns. Sidhu *et al.* [26] proposed algorithm to compile regular expression patterns into combinatorial circuits based on nondeterministic finite automaton (NFA). Hutchings *et al.* [13] developed a module generator that shared common prefixes to reduce the circuit area on FPGA. Moscola *et al.* [21] presented a content-scanning module on FPGA for an internet firewall. Clark *et al.* [8] improved area and throughput by adding predecoded wide parallel inputs to traditional NFA implementations. Baker *et al.* [5] presented a pre-decoded multiple-pipeline shift-and-compare matcher which reduced routing complexity and comparator size by converting incoming characters into many bit lines. Lin *et al.* [16] proposed a sharing architecture which significantly reduces circuit areas by sharing common infix and suffix sub-patterns. From the perspectives of reconfigurability and scalability, memory

architectures are attractive because memory is flexible and scalable. The Aho–Corasick (AC) algorithm [1] is the most popular algorithm which allows for matching multiple string patterns. Aldwairi *et al.* [2] proposed a configurable string matching accelerator based on a memory implementation of the AC FSM. Tan *et al.* [27] proposed the bit-split algorithm partitioning a large AC state machine into small state machines to significantly reduce the memory requirements. Jung *et al.* [14] presented an FPGA implementation of the bit-split string matching architecture. Piyachon *et al.* [22] proposed to reduce the memory size by relabeling states of AC state machine. Additionally, Piyachon *et al.* [23] proposed to use Label Transition Table and CAM-based Lookup Table to significantly reduce the memory size. Cho *et al.* [6], [7] proposed a hash-based pattern matching co-processor where memory is used to store the list of substrings and the state transitions. Dharmapurikar *et al.* [11] proposed a pattern matching algorithm which modifies the AC algorithm to consider multiple characters at a time. Furthermore, the content addressable memories (CAM) is also widely used for string matching because it can match the entire pattern at once when the pattern is shifted past the CAM. Gokhale *et al.* [12] used CAM to perform parallel search at a high speed. Sourdis *et al.* [25] applied the pre-decoded technique for the CAM-based pattern matching to reduce the area. Additionally, Yu *et al.* [30] presented a ternary content addressable memory (TCAM)-based multiple-pattern matching which can handle complex patterns, correlated patterns, and patterns with negation.

The hash-based approach was proposed to utilize Bloom filter for deep packet inspection. Dharmapurikar *et al.* [10] proposed a hashing-table lookup mechanism utilizing parallel bloom filters to enable large number of fixed-length strings to be scanned in hardware. Lockwood *et al.* [19] proposed an intelligent gateway based on Bloom filter that provides Internet worm and virus protection in both local and wide area networks.

III. REVIEW OF AC ALGORITHM

In this section, we review the AC algorithm. Among all memory architectures, the AC algorithm has been widely adopted for string matching in [2], [14], [15], [22], [23], [27] because the algorithm can effectively reduce the number of state transitions and therefore the memory size. Using the same example as in Figs. 1 and 3 shows the state transition diagram derived from the AC algorithm where the solid lines represent the *valid* transitions while the dotted lines represent a new type of state transition called the *failure* transitions.

The failure transition is explained as follows. Given a current state and an input character, the AC machine first checks whether there is a valid transition for the input character; otherwise, the machine jumps to the next state where the failure transition points. Then, the machine recursively considers the same input character until the character causes a valid transition. Consider an example when an AC machine is in state 1 and the input character is . According to the AC state table in Fig. 4, there is no valid transition from state 1 given the input

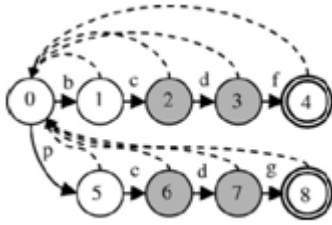


Fig. 3. State diagram of an AC machine.

	input	next state	failure	match vector
State 0:	b	1	0	00
State 0:	p	5	0	00
State 1:	c	2	0	00
State 2:	d	3	0	00
State 3:	f	4	0	01
State 5:	c	6	0	00
State 6:	d	7	0	00
State 7:	g	8	0	10

Fig4. AC state table

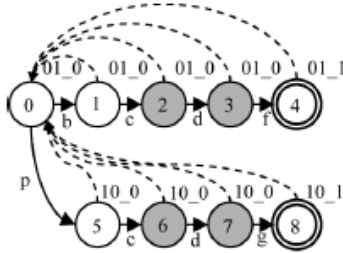


Fig 5. Merging similar states

character . When there is no valid transition, the AC machine takes a failure transition back to state 0. Then in the next cycle, the AC machine reconsiders the same input character in state 0 and finds a valid transition to state 5. This example shows that an AC machine may take more than one cycle to process an input character In Fig. 3, the double-circled nodes indicate the final states of patterns. In Fig. 3, state 4, the final state of the first string pattern “bcd f ”, stores the match vector $\{P2,P1\} = \{01\}$ and state 8, the final state of the second string pattern “pcdg”, stores the match vector of $\{P2,P1\} = \{10\}$ Except the final states, the other states store the match vector $\{P2,P1\} = \{00\}$ to simply express those states are not final states.

IV. STATE TRAVERSAL MECHANISM ONAMERG FSM

In our design, we reuse those memory spaces storing zero vectors $\{00\}$ to store useful path information called *pathVec*. First, each bit of the pathVec corresponds to a string pattern. Then, if there exists a path from the initial state to a final state, which matches a string pattern, the corresponding bit of the pathVec of the states on the path will be set to 1. Otherwise, they are set to 0. Consider the string pattern “bcd f ” whose final state is state 4 in Fig. 7. The path from state 0, via states 1, 2, 3 to the final state 4 matches the first string pattern “bcd f ”. Therefore, the first bit of the pathVec of the states on the path, $\{state\ 0, state\ 1, state\ 2, state\ 3, and\ state\ 4\}$, is set to 1. Similarly, the path from state 0, via states 5, 6, 7 to the final state 8 matches the second string pattern “pcdg”. Therefore, the second bit

of the pathVec of the states on the path, $\{state\ 0, state\ 5, state\ 6, state\ 7, and\ state\ 8\}$, is set to 1. In addition, we add an additional bit, called *ifFinal*, to indicate whether the state is a final state. For example, because states 4 and 8 are final states, the *ifFinal* bits of states 4 and 8 are set to 1, the others are set to 0. As shown in Fig. 7, each state stores the pathVec and *ifFinal* as the form, “*pathVec_ ifFinal*”. Compared with the original AC state machine in Fig. 3, we only add an additional bit to each state. We have mentioned that in this example, states 2 and 6, states 3 and 7 are similar because they have similar transitions. However, they are not equivalent. Note that two states are equivalent if and only if their next states are equivalent. In Fig. 7, states 3 and 7 are similar but not equivalent because for the same input , state 3 takes a transition to state 4 while state 7 takes a failure transition to state 0. Similarly, state 2 and state 6 are not equivalent states because their next states, state 3 and state 7, are not equivalent states. In our algorithm, we define such similar states as pseudo-equivalent states. The definition is as follows.

Definition: Two states are defined as *pseudo-equivalent states* if they have identical input transitions, identical failure transitions, and identical *ifFinal* bit, but different next states. In Fig. 7, states 2 and 6 are pseudo-equivalent states because they have identical input transitions , identical failure transitions to state 0 and identical *ifFinal* bit 0. Also, state 3 and state 7 are pseudo-equivalent states. In our algorithm, the pseudo-equivalent states 2 and 6 are merged to be state 26 and states 3 and 7 are merged to be state 37, as shown in Fig. 8. The pathVec_ ifFinal are updated by taking the union on the pathVec_ ifFinal of the merged states. Therefore, the pathVec_ ifFinal of states 26 and 37 are modified to be $\{11_0\}$ In addition, we need a register, called *preReg*, to trace the precedent pathVec in each state. The width of *preReg* is equal to the width of pathVec. Each bit of the *preReg* also corresponds to a string pattern. The *preReg* is updated in each state by performing a bitwise AND operation on the pathVec of the next state and its current value. By tracing the precedent path entering into the merged state, we can differentiate all merged states. When the final state is reached, the value of the *preReg* indicates the match vector of the matched pattern. During the state traversal, if all the bits of the *preReg* become 0, the machine will go to the failure mode and choose the failure transition as in the AC algorithm. After any failure transition, all the bits of the *preReg* are reset to 1. the string “pcdf” is applied. Initially, in state 0, the *preReg* is initialized to $\{P2,P1\} = \{11\}$ After taking the input character ,P the *merg_FSM* goes to state 5 and updates the *preReg* by performing a bitwise AND operation on the pathVec $\{10\}$ of state 5 and the current *preReg* $\{11\}$ The resulting new value of the *preReg* will be $\{P2,P1\} = \{10\ AND\ 11\} = \{10\}$ Then, after taking the input character , the *merg_FSM* goes to state 26 and updates the *preReg* by performing a bitwise AND operation on the pathVec $\{11\}$ of state 26 and the current *preReg* $\{10\}$ The *preReg* remains $\{P2,p1\} = \{11\ AND\ 10\} = \{10\}$ Further, after taking the input character , the *merg_FSM* goes to state 37 and updates the *preReg* by performing a bitwise AND operation on the pathVec $\{11\}$ of state 37 and the current *preReg* $\{10\}$ The *preReg* remains $\{P2P1\} = \{11\ AND\ 10\} = \{10\}$ Finally, after taking the input character , the *merg_FSM* goes to state 4. After performing a bitwise AND operation

on the pathVec {01} of state 4 and the current preReg{10} the preReg becomes {P2P1}={01AND10}={00} According to our algorithm, during the state traversal, if all the bits of the preReg become 0, the machine will go to the failure mode and choose the failure transition as in the AC algorithm. Therefore, the machine takes the failure transition to state 0 instead of state 4.

V. LOOP BACK IN MERGED STATES

When certain cases of multiple sections of pseudo-equivalent states are merged, it may create loop back problem in a state machine. The reason for the loop back problem comes from merging common sub-patterns with different sequences. For example, the two patterns, “abcdef” and “wdebcg,” have common sub-patterns, “bc” and “de,” which appear in different sequences. Fig. 16 shows the corresponding state machine. Because of the common sub-patterns, “bc”, states 2 and 10, states 3 and 11 are pseudo-equivalent states. And, because of the common sub-patterns, “de”, states 4 and 8, states 5 and 9 are also pseudo-equivalent states. Merging the pseudo-equivalent states will create a loop back transition from state 5 to state 2, as shown in

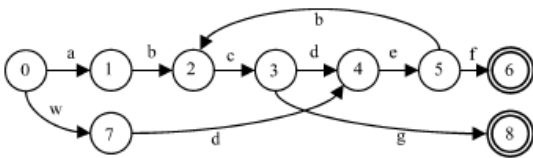


Fig. 6 Merging pseudo-equivalent states with different sequences.

The loop transition may cause false positive matching results. For example, the input string “abcdebcdef” will be mistaken as a match of the pattern “abcdef.” In other words, as long as the common substrings appear in sequence, merging the corresponding pseudo-equivalent states will not result in loop back transitions. Therefore, in our program, we record and identify the orders of common sub-patterns. If the common sub-patterns appear in sequence, the corresponding pseudo-equivalent states can be merged without loop back problems. Fig. 18 shows the pseudo code of our algorithm to find common substrings without the loop back problem. First, all common substrings are extracted by the longest common substring algorithm [9]. The algorithm can report all of the common substrings. Then, the common substrings are labeled as new sequences. Next, we use the longest common subsequence (LCS) algorithm [20] to find all of the longest subsequence common to all strings. The results from the LCS algorithm guarantee that there will be no loop back transition. For example, consider the two patterns, “abcdefghij klm” and “abcwsg h i d e f x y k l m.” Using the longest common substring algorithm, we can extract all of the common substrings of these two patterns such as “abc”, “def”, “ghi” and “klm”. Then, we label the substrings “abc”, “def”, “ghi”, and “klm” as , $\alpha\beta\gamma\delta$, and , respectively. Therefore, the sequence of substrings in “abcdefghij klm” is labeled as “ ” while the sequence of substrings in “abcwsg h i d e f x y k l m” is labeled as “ ”. We subsequently use LCS algorithm to find all of the longest common subsequences among the two new sequences, “ $\alpha\beta\gamma\delta$ ” and “

” and the results are “ $\alpha\beta\delta$ ” or “ $\alpha\gamma\delta$ ”. Therefore, we can merge the subsequences of (“abc”), (“ghi”) and (“klm”) or the subsequences of (“abc”), (“def”) and (“klm”) without the loop back problem. Notice that the result of LCS may not be unique.

VI. HARDWARE ARCHITECTURE

Fig.7 shows our hardware module which can be configured for matching 16 or 32 patterns with a state machine containing 1024 valid transitions at most. In Fig.7,8, the register, called *address_register*, is used to store the current state and the input character. The *valid_memory* is used to store the information of *valid_state*, *pathVec*, and *ifFinal* corresponding to each valid transition while the *failure_memory* is used to store the *failure_state* corresponding to each failure transition. In this prototype, we use a hardwired circuit, called *A2P*, to translate the content of the *address_register* to a contiguous scope, called *pos*, to utilize the *valid_memory*. The circuit *A2P* can be implemented using hardwired circuit or CAM [17]. In addition, the signal *n_valid* is high if there is no valid transition corresponding to the *address_register*. Furthermore, the register

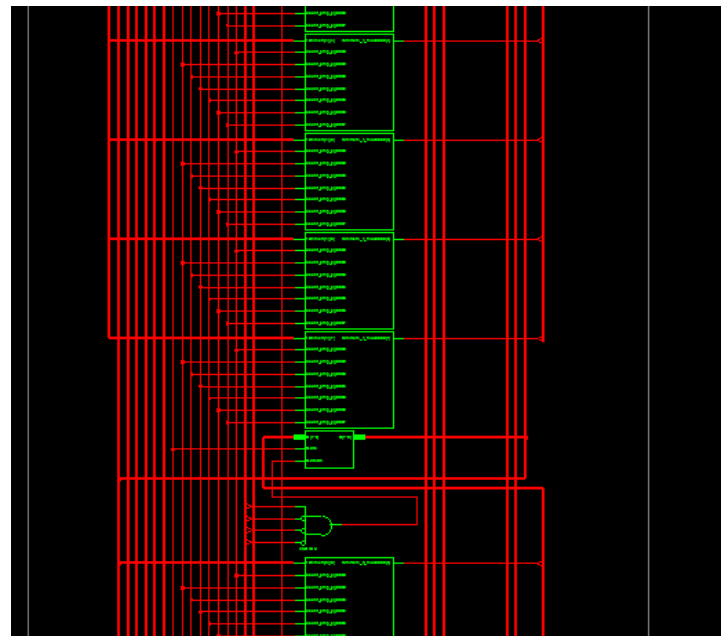


Fig. 7. Hardware module for the new algorithm.

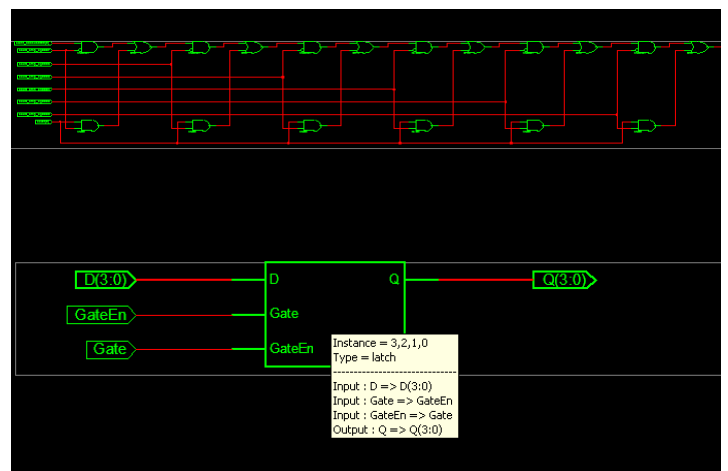


Fig 8 Internal architecture of proposed system

called *preReg*, is used to trace the precedent pathVec in each state. The *preReg* is initiated to be 1 for all bits and is updated by performing a bitwise AND operation on its current value and the pathVec from the valid_memory. The *ns_ctrl* unit is used to determine the next state by the value of *preReg* and *n_valid*. If the *preReg* is 0 for all bits or the *n_valid* is 1, the *ns_sel* will output low to let the failure_state update the current_state register. On the other hand, if the *preReg* is not zero and the *n_valid* is not 1, the *ns_sel* will output high to let the valid_state update the current_state register.

VII. EXPERIMENTAL RESULTS

Using the version 2.4 of Snort rule set, we extract 2217 exact string patterns containing 36 539 characters from the rule database. The results are compared with the methods of the AC algorithm and the bit-split algorithm.

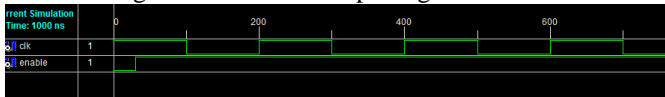


Fig 9 string patterns from Snort rule database

The flow of our experiment is shown in Fig.9. In the first stage, we obtain string patterns from Snort rule database. In the second stage, we group 32 string patterns as a module based on the similarity of string patterns. Further, in the third stage, we use LCS to extract substrings without loop back problem. Because the solution of LCS may not be unique, we select the common substrings which have the largest *sharing gain*. The *sharing gain* of common substrings is defined as the length of common substrings multiplied by the number of patterns sharing the common substrings.

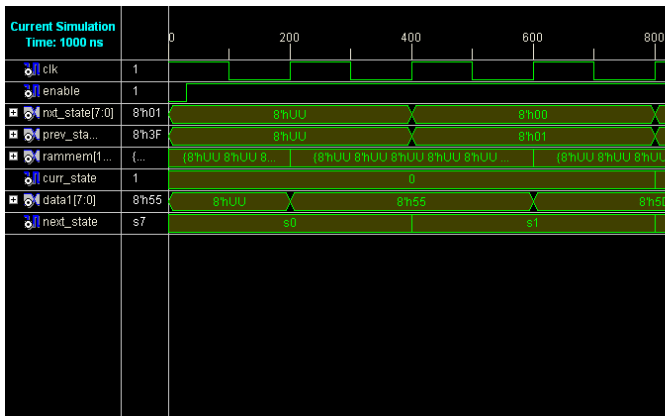


Fig 10 the selection line with clk to the pseudo random order adjustment

For example, three patterns, “1common1”, “2common2”, and “3common3” have the common substrings “common”. The sharing gain of the common substrings is because the substring “common” has six characters which are shared by three patterns. In the final stage, we merge the extracted common substrings and generate the transition table. Table I shows the results before and after integrating our algorithm to the AC algorithm. Columns one, two and three show the name of the rule set, the number of patterns, and the number of characters of the rule set. Columns four, five, and six show the number of state transitions, the number of states, and the memory size of the AC algorithm. Columns

seven, eight, and nine show the results of our approach. Column ten shows the memory reduction compared to the AC algorithm. As shown in Fig. 10, the memory requirement includes the size of the valid memory and the failure memory. Because the memory requirement is proportional to the number of states, our algorithm has reduced memory size on the traditional AC algorithm.



Fig 11 Final result of memory allocation and ram adjustment

Using the traditional AC algorithm, the number of transitions and states are 6793 and 6804, respectively. The memory size is 49 267 bytes. Integrating our algorithm to the AC algorithm, the number of transitions and states are reduced to 4432 and 3846, respectively. The memory size is reduced to 30 699 bytes, 38% of memory reduction from the AC algorithm. For total 2217 string patterns of Snort rule sets, our algorithm achieves a 21% memory reduction compared with the AC algorithm. Because the state-of-the-art bit-split algorithm is based on the AC algorithm, our algorithm can also be integrated to the bitsplit algorithm to further reduce memory requirements. Applying the bit-split algorithm which splits the traditional AC state machine into 4 state machines, the number of transitions and states are 21 949 and 21 993, respectively. The size of memory is 159 202 bytes. Integrating our algorithm to the bit-split algorithm, the number of transitions and states are reduced to 14 437 and 12 664, respectively. The size of memory is reduced to 98 400 bytes. The memory reduction achieves 38%. For total 2,217 string patterns of Snort rule sets, integrating our algorithm to the bit-split algorithm can achieve 24% of memory reduction. Furthermore, we have synthesized the hardware module in Fig. 19 using the ASIC flow of the UMC 0.18 m technology. The results are compared with [2], [6], [27], [28], [30] as shown in Fig 11, columns 2, 3, and 4 shows the number of characters, the memory size, and the throughput. Column 5 shows the memory utilization per character while column 6 shows the memory efficiency which is defined as the following equation:

$$Memory\ efficiency = \frac{(throughput \times Char.\ Num)}{Mem}$$

VIII. CONCLUSION

We have presented a memory-efficient pattern matching algorithm which can significantly reduce the number of states and transitions by merging pseudo-equivalent states while maintaining correctness of string matching. In addition, the new algorithm is complementary to other

memory reduction approaches and provides further reductions in memory needs. The experiments demonstrate a significant reduction in memory footprint for data sets commonly used to evaluate IDS systems.

REFERENCES

- [1] A. V. Aho and M. J. Corasick, "Efficient string matching: An AID to bibliographic search," *Commun. ACM*, vol. 18, no. 6, pp. 333–340, 1975.
- [2] M. Aldwairi, T. Conte, and P. Franzon, "Configurable string matching hardware for speeding up intrusion detection," *Proc. ACM SIGARCH Comput. Arch. News*, vol. 33, no. 1, pp. 99–107, 2005.
- [3] M. Alicherry, M. Muthuprasanna, and V. Kumar, "High speed pattern matching for network IDS/IPS," in *Proc. IEEE Int. Conf. Netw. Protocols*
- [4] B. Brodie, R. Cytron, and D. Taylor, "A scalable architecture for high-throughput regular-expression pattern matching," in *Proc. 33rd Int. Symp. Comput. Arch. (ISCA)*, 2006, pp. 191–122.
- [5] Z. K. Baker and V. K. Prasanna, "High-throughput linked-pattern matching for intrusion detection systems," in *Proc. Symp. Arch. For Netw. Commun. Syst. (ANCS)*, Oct. 2005, pp. 193–202.
- [6] Y. H. Cho and W. H. Mangione-Smith, "A pattern matching co-processor for network security," in *Proc. 42nd IEEE/ACM Des. Autom. Conf., Anaheim, CA*, Jun. 13–17, 2005, pp. 234–239.
- [7] Y. H. Cho and W. H. Mangione-Smith, "Fast reconfiguring deep packet filter for" in *Proc. 13th Ann. IEEE Symp. Field Program. Custom Comput. Mach. (FCCM)*, 2005, pp. 215–224.
- [8] C. R. Clark and D. E. Schimmel, "Scalable pattern matching on high speed networks," in *Proc. 12th Ann. IEEE Symp. Field Program. Custom Comput. Mach. (FCCM)*, 2004, pp. 249–257.
- [9] G. Dan, *Algorithms on Strings, Trees and Sequences: Computer Science and Computational Biology*. Cambridge, U.K.: Cambridge University Press, 1997.
- [10] S. Dharmapurikar, P. Krishnamurthy, T. Sproull, and J. Lockwood, "Deep packet inspection using parallel bloom filters," in *Proc. 11th Symp. High Perform. Interconnects*, Aug. 2003, pp. 44–53. [26] R. Sidhu and V. K. Prasanna, "Fast regular expression matching using FPGAs," in *Proc. 9th Ann. IEEE Symp. Field-Program. Custom Comput. Mach. (FCCM)*, 2001, pp. 227–238.
- [11] S. Dharmapurikar and J. Lockwood, "Fast and scalable pattern matching for content filtering," in *Proc. Symp. Arch. for Netw. Commun. Syst. (ANCS)*, Oct. 2005, pp. 183–192.
- [12] M. Gokhale, D. Dubois, A. Dubois, M. Boorman, S. Poole, and V. H. Granidt, "Towards gigabit rate network intrusion detection," in *Proc. the Eleventh Annual ACM/SIGDA International Conference on Field- Programmable Logic and Applications (FPL '03)*, 2002, pp. 404–413.
- [13] B. L. Hutchings, R. Franklin, and D. Carver, "Assisting network intrusion detection with reconfigurable hardware," in *Proc. 10 th Annu. IEEE Symp. Field-Program. Custom Comput. Mach. (FCCM)*, 2002, pp. 111–120.
- [14] H. J. Jung, Z. K. Baker, and V. K. Prasanna, "Performance of FPGA implementation of bit-split architecture for intrusion detection systems," presented at the 20th Int. Parallel Distrib. Process. Symp. (IPDPS), Rhodes Island, Greece, 2006.
- [15] S. Kumar, S. Dharmapurikar, F. Yu, P. Crowley, and J. Turner, "Algorithms to accelerate multiple regular expressions matching for deep packet inspection," in *Proc. ACM SIGCOMM Comput. Commun. Rev.*, 2006, pp. 339–350.
- [16] C. H. Lin, C. T. Huang, C. P. Jiang, and S. C. Chang, "Optimization of pattern matching circuits for regular expression on FPGA," *IEEE Trans. Very Large Scale Integr. (VLSI) Syst.*, vol. 15, no. 12, pp.1303–1310, Dec. 2007.
- [17] H. Lu, K. Zheng, B. Liu, X. Zhang, and Y. Liu, "A memory-efficient parallel string matching architecture for high-speed intrusion detection," *IEEE J. Sel. Areas Commun.*, vol. 24, no. 10, pp. 1793–1804, Oct. 2006.
- [18] J. V. Lunteren, "High-performance pattern-matching for intrusion detection," in *Proc. IEEE INFOCOM*, 2006, pp. 1–13.
- [19] J. W. Lockwood, J. Moscola, M. Kulig, D. Reddick, and T. Brooks, "Internet worm and virus protection in dynamically reconfigurable hardware," presented at the Military Aerosp. Program. Logic Device(MAPLD), Washington, DC, Sep. 2003, E10.
- [20] D. Maier, "The complexity of some problems on subsequences and supersequences," *J. ACM*, vol. 25, no. 2, pp. 322–336, 1978.
- [21] J. Moscola, J. Lockwood, R. P. Loui, and M. Pachos, "Implementation of a content-scanning module for an internet firewall," in *Proc. 11th Ann. IEEE Symp. Field-Program. Custom Comput. Mach. (FCCM)*, 2003, pp. 31–38.
- [22] P. Piyachon and Y. Luo, "Compact state machines for high performance pattern matching," in *Proc. 41nd IEEE/ACM Des. Autom. Conf.*, 2007, pp. 493–496.
- [23] P. Piyachon and Y. Luo, "Design of high performance pattern matching engine through compact deterministic finite automata," in *Proc. 42nd IEEE/ACM Des. Autom. Conf.*, 2008, pp. 852–857.
- [24] M. Roesch, "Snort- lightweight intrusion detection for networks," in *Proc. 15th Syst. Administration Conf. (LISA)*, 1999, pp. 229–238.
- [25] I. Sourdis and D. Pnevmatikatos, "Pre-decoded CAMs for efficient and high-speed NIDS pattern matching," in *Proc. 12th Annu. IEEE Symp. Field Program. Custom Comput. Mach. (FCCM)*, 2004, pp. 258–267.
- [27] L. Tan and T. Sherwood, "A high throughput string matching architecture for intrusion detection and prevention," in *Proc. 32nd Annu. Int. Symp. Comput. Arch. (ISCA)*, 2005, pp. 112–122.
- [28] N. Tuck, T. Sherwood, B. Calder, and G. Varghese, "Deterministic memory-efficient string matching algorithms for intrusion detection," in *Proc. 23rd Conf. IEEE Commun. Soc. (INFOCOMM)*, Mar. 2004, pp. 2628–2639.
- [29] F. Yu, Z. Chen, Y. Diao, T. V. Lakshman, and R. H. Katz, "Fast and memory-efficient regular expression matching for deep packet inspection," in *Proc. ACM/IEEE Symp. Arch. Netw. Commun. Syst. (ANCS)*, 2006, pp. 93–102.
- [30] F. Yu, R. H. Katz, and T. V. Lakshman, "Gigabit rate packet pattern matching using TCAM," in *Proc. 12th IEEE Int. Conf. Netw. Protocols (ICNP)*, 2004, pp. 174–183.

Parameters Comparison of Miniaturized Symmetric and Asymmetric Inhomogeneous Metamaterials

Garima Tiwari[#], Dr Bhawna Jharia^{*}, Dr M. P Parsai⁺

[#]ME IV SEM, Microwave Engineering, JEC Jabalpur

^{*}Professor, Department of Electronics & Communication, JEC Jabalpur

⁺Professor HOD, Department of Electronics & Communication, JEC, Jabalpur

Abstract: This paper gives a comparative study of parameters of symmetric and asymmetric inhomogeneous structures metamaterials, a unit cell of split ring resonator, by using standard retrieval methods that assigns electromagnetic properties electric permittivity and magnetic permeability from the calculation of scattering parameters. Scattering parameters are the means of characterizing the artificially structured metamaterials which are inhomogeneous. Based on this study it is shown that, while the difference in the magnitudes of S_{11} and S_{22} are modest but there is difference in the phases of S_{11} and S_{22} , resulting in the difference in the impedance properties of symmetric and asymmetric structures.

Keywords: SRR, METAMATERIALS, NIM, DNG

I. INTRODUCTION

The possibility of the negative refraction of electromagnetic (EM) waves by materials with simultaneous negative permittivity and negative permeability was predicted by Vesalago in 1968 [1]. This proposition was not demonstrated until recently; the main difficulty being in obtaining negative permeability. Negative permittivity is available through metals or the periodic arrangement of metallic wires [2, 3, 4, 5, 6]. On the other hand, obtaining negative permeability was an issue. Pendry et al. proposed several structures in order to obtain negative permeability [7]. Among these structures split-ring resonators (SRRs) have attracted much attention [8, 9, 10, 11, 12, 13, 14, 15, 16, 17, 18]. A single SRR is composed of two concentric rings with slits on each of them. The slits on the rings are situated on the opposite sides of the rings with respect to each other. The planar nature of the SRR structure makes it easy to fabricate and integrate into 2 and 3 dimensional structures. Several research groups have demonstrated negative indices of refraction by using the periodic arrangement of metallic wires with SRRs through several methods such as the retrieval of effective medium parameters [19, 20, 21, 22, 23, 24, 25], refraction type experiments and wedge experiments [26, 27, 28, 29, 30, 31, 32, 33, 34]. While SRR structure provides negative permeability and can be used to obtain negative refraction, it has several disadvantages. First of all, it has been shown that a medium consisting of a periodic arrangement of SRRs is bianisotropic [25, 35, 36, 37]. The bianisotropy is a result of the non-zero electric dipole moment of the SRR structure due to the asymmetric placement of slits on the rings. Second, it has been shown that the magnetic

resonance of the SRR structure can be excited via electric fields [38, 39]. The excitation of the magnetic resonance of the SRR structure results from the capacitive coupling of the electric field. The capacitive coupling of the electric field creates non-zero current along the rings. These two disadvantages make it difficult to obtain isotropic, homogeneous two or three dimensional negative refraction media by using SRRs for negative permeability.

It is conceptually convenient to replace a collection of scattering objects by a homogeneous medium, whose electromagnetic properties result from an averaging of the local responding electromagnetic fields and current distributions. Ideally, there would be no distinction in the observed electromagnetic response of the hypothetical continuous material versus that of the composite it replaces. This equivalence can be readily achieved when the applied fields are static or have spatial variation on a scale significantly larger than the scale of the local inhomogeneity, in which case the composite is said to form an *effective medium*. The electromagnetic properties of an inhomogeneous composite can be determined exactly by solving Maxwell's equations, which relate the local electric and magnetic fields to the local charge and current densities. When the particular details of the inhomogeneous structure are unimportant to the behavior of the relevant fields of interest, the local field, charge, and current distributions are averaged, yielding the macroscopic form of Maxwell's equations. To solve this set of equations, a relationship must be assumed that relates the four macroscopic field vectors that arise from the averaging—or *homogenization*—procedure. It is here that the electric permittivity and the magnetic permeability tensors are typically defined, which encapsulate the specific local details of the composite medium.

Depending on the symmetry and complexity of the scattering objects that comprise the composite medium, the permittivity and permeability tensors may not provide sufficient information to obtain a solution from Maxwell's equations, and additional electromagnetic material parameters must be introduced f6g. Such media, including chiral and bianisotropic, can couple polarization states and are known to host a wide array of wave propagation and other electromagnetic phenomena

II. S RETRIEVAL METHODS

If an inhomogeneous structure can be replaced conceptually by a continuous material, there should be no difference in the scattering characteristics between the

two. A procedure, then, for the assignment of effective material parameters to an inhomogeneous structure consists of comparing the scattered waves i.e., the complex transmission and reflection coefficients, or *S parameters* from a planar slab of the inhomogeneous material to those scattered from a hypothetical continuous material

A. S-parameter retrieval for a symmetric structure

Negative index metamaterials, which have been of recent interest, pose a significant challenge to retrieval methods because they utilize resonant elements and exhibit both an electric and magnetic response. A single unit cell of a typical symmetric in the propagation direction metamaterials structure is shown in Fig. 1. This particular structure is composed of two types of conducting elements—a split ring resonator SRR and a wire—that have been designed to yield a band of negative refractive index at microwave frequencies. We note in passing that the SRR generally exhibits bianisotropy, since an applied magnetic field induces both an electric as well as a magnetic response. This material response should properly be accounted for in a complete characterization procedure. The unit cell is cubic, with a cell dimension of $d=2.5$ mm. A 0.25 mm thick substrate of FR4 $\epsilon = 4.4$, loss tangent of 0.02d is assumed. A copper SRR and wire are positioned on opposite sides of the substrate. The copper thickness is 0.017 mm. The width of the wire is 0.14 mm, and it runs the length of the unit cell. The outer ring length of the SRR is 2.2 mm and both rings have a line width of 0.2 mm. The gap in each ring is 0.3 mm, and the gap between the inner and outer rings is 0.15 mm.

The *S* parameters for the symmetric unit cell of Fig. 2 are computed using HFSS (Ansoft), a commercial finite-element-based electromagnetic mode solver. Both the *S* parameters and the *Z* parameters are presented in Fig. 3 and Fig. 4. Note the dip in the phase of *S*₂₁, which indicates the presence of a negative index band. The retrieved index in confirms the negative index band that lies between roughly 9 and 12 GHz. The structure was designed so as to be roughly impedance matched. The retrieved impedance, shown in Fig. 4, shows that the structure is indeed roughly matched at the frequency where

$$n = -1.$$

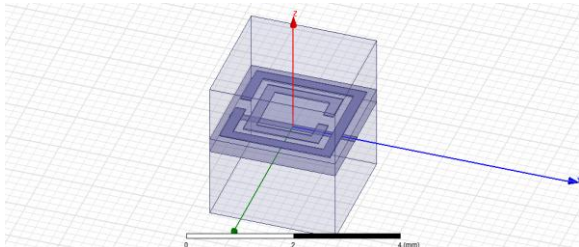


Fig 1 symmetric SRR

B. S-parameter retrieval for asymmetric structure

The unit cell in Fig. 1 can be made asymmetric by moving the wire, for example, off of the symmetry axis. The unit cell shown in Fig. 2 is identical to that of Fig. 1, except that the wire has been shifted a distance of 0.75 mm along the propagation direction. Figures 5 and 6 show the *S* parameters and *Z* parameters computed for an infinitely repeated asymmetric unit cell, one cell thick in

the direction of propagation. While the differences between the magnitudes of *S*₁₁ and *S*₂₂ are modest, there is a great contrast in the phases of *S*₁₁ and *S*₂₂, implying very different impedance properties for the structure depending on which side of the unit cell faces the incoming wave both the phases and magnitudes of *S*₁₂ and *S*₂₁ are identical.

The retrieved indices for the symmetric and asymmetric unit cells are compared, illustrating that, aside from a shift in frequency, the refractive properties of the two structures are very similar. The frequency shift is not surprising, as there is likely an interaction between the SRR and wire that leads to somewhat different material properties depending on their relative positions. While the index is nearly the same for the structures having symmetric and asymmetric unit cells, the impedance is clearly different, as indicated in Fig. 5 and Fig. 6. So different are the two solutions for *z* for the asymmetric structure that in general the assignment of values of ϵ and μ to the composite becomes counterproductive. Thus, although a well-defined refractive index exists for the composite, the manner in which a wave scatters from this material can depend strongly on how the surface is terminated.

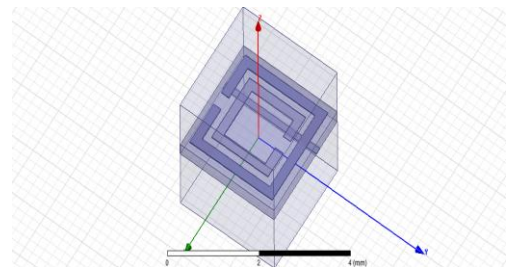


Fig 2 Asymmetric SRR

III. RESULTS

A. For symmetric structure

A.1 S PARAMETERS

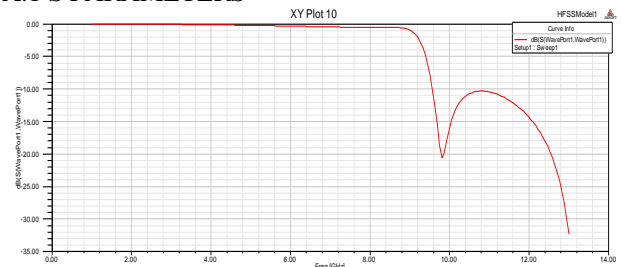


Fig 3.1 *S*₁₁ for symmetric SRR

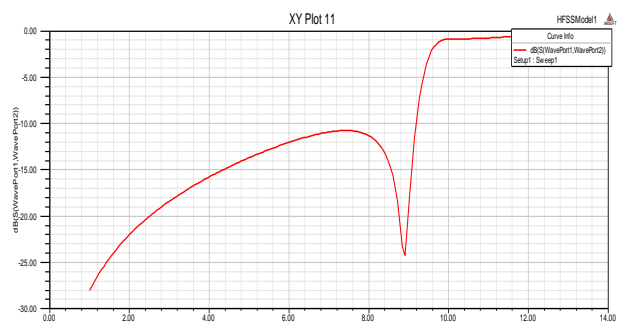


Fig 3.2 *S*₁₂ for symmetric SRR

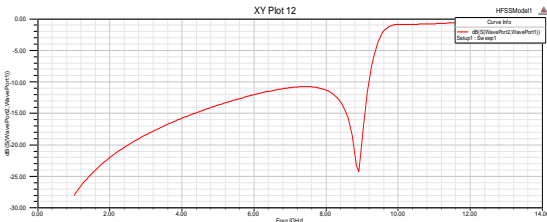


Fig 3.3 S_{21} for symmetric SRR

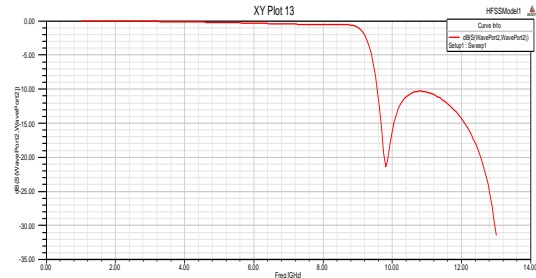


Fig 3.3 S_{22} for symmetric SRR

A.2 Z PARAMETERS

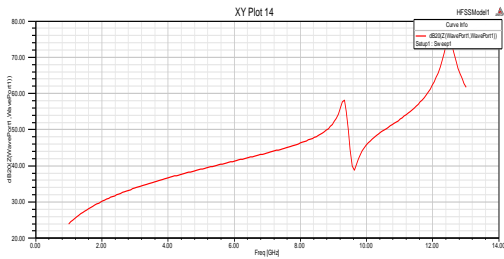


Fig 4.1 Z_{11} for symmetric SRR

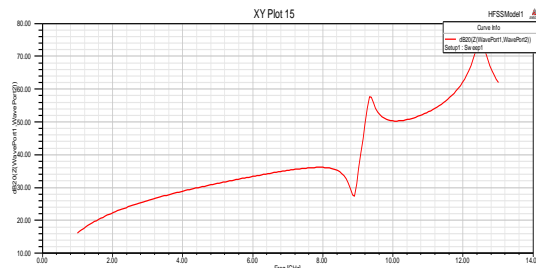


Fig 4.2 Z_{12} for symmetric SRR

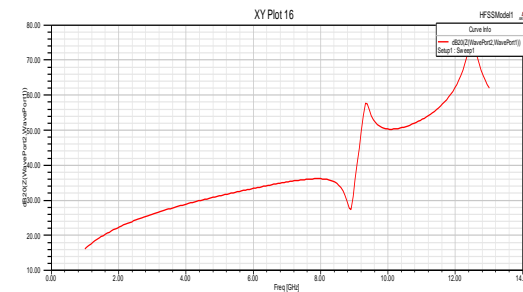


Fig 4.3 Z_{21} for symmetric SRR

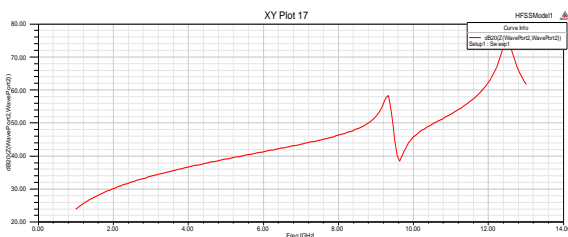


Fig 4.4 Z_{22} for symmetric SRR

B. For Asymmetric structure

B.1 S PARAMETERS

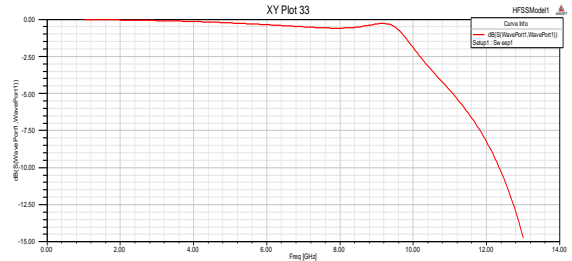


Fig 5.1 S_{11} for Asymmetric SRR

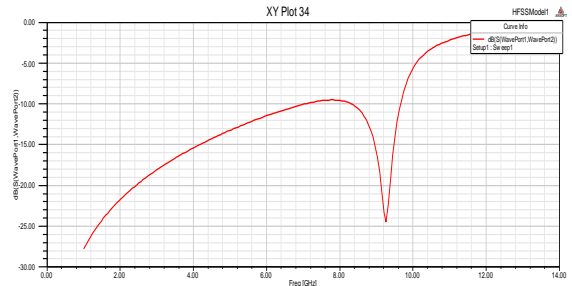


Fig 5.2 S_{12} for Asymmetric SRR

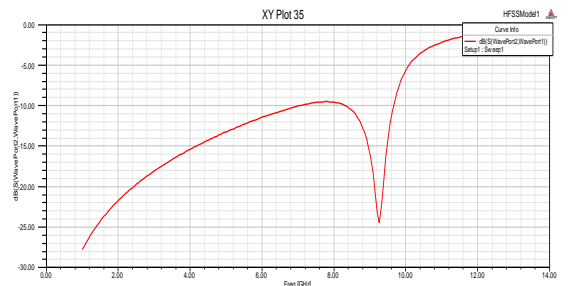


Fig 5.3 S_{21} for Asymmetric SRR

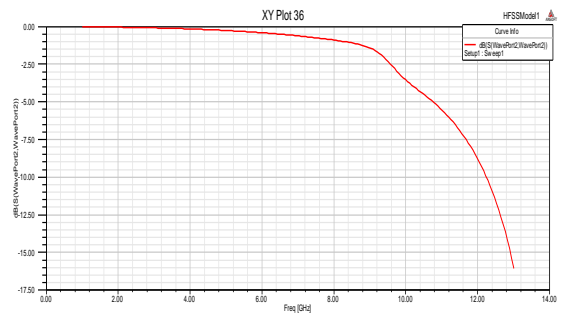


Fig 5.4 S_{22} for Asymmetric SRR

B.2 Z PARAMETERS



Fig 6.1 Z_{11} for non symmetric SRR

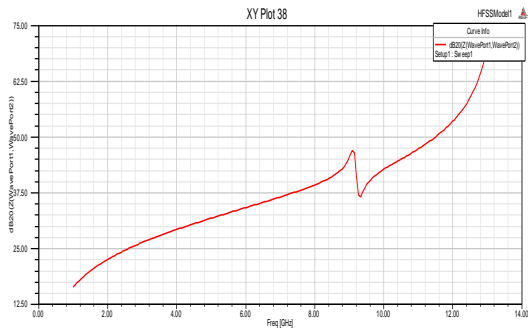


Fig 6.2 Z_{12} for non symmetric SRR

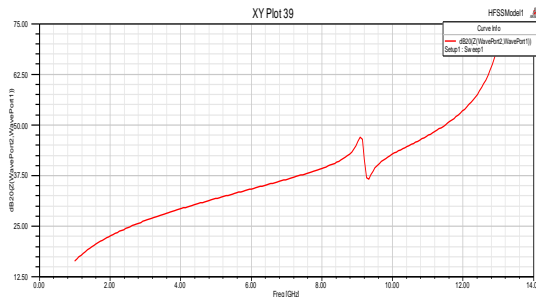


Fig 6.3 Z_{21} for non symmetric SRR

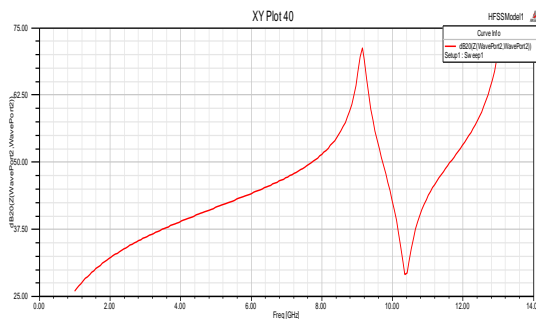


Fig 6.4 Z_{22} for non symmetric SRR

IV. CONCLUSION

It is shown that metamaterials based on periodic structures occupy conceptually a special position between effective media and photonic crystals. The S -parameter retrieval techniques that have been utilized recently to characterize metamaterials have been shown to be valid for metamaterials having symmetric unit cells, even when the optical path length is on the order of the unit cell size. The retrieved indices for the symmetric and asymmetric unit cells are compared, illustrating that, aside from a shift in frequency, the refractive properties of the two structures are very similar. While the differences between the magnitudes of S_{11} and S_{22} are modest, there is a great contrast in the phases of S_{11} and S_{22} , implying very different impedance properties for the structure depending on which side of the unit cell faces the incoming wave. Both the phases and magnitudes of S_{12} and S_{21} are identical.

REFERENCES

- [1] V. G. Veselago, "The electrodynamics of substances with simultaneously negative values of permittivity and permeability," *Sov. Phys. Usp.* **10**, 509 (1968).
- [2] D. F. Sievenpiper, M. E. Sickmiller, and E. Yablonovitch, "3D Wire Mesh Photonic Crystals," *Phys. Rev. Lett.* **76**, 2480 (1996).
- [3] J. B. Pendry, A. J. Holden, W. J. Stewart, and I. Youngs, "Extremely Low Frequency Plasmons in Metallic Mesostructures," *Phys. Rev. Lett.* **76**, 4773 (1996).
- [4] S.I. Maslovski, S.A. Tretyakov, P.A. Belov, "Wire media with negative effective permittivity: A quasi-static model," *Microwave Opt. Technol. Lett.* **35**, 47 (2002).
- [5] Poulton, S. Guenneau, A. B. Movchan, "Noncommuting limits and effective properties for oblique propagation of electromagnetic waves through an array of aligned fibres," *Phys. Rev B* **69**, 195112, (2004).
- [6] Felbacq, G. Bouchitte, "Homogenization of a set of parallel fibres," *Waves In Rand. Med.* **7**, 245 (1997).
- [7] J. B. Pendry, A. J. Holden, D. J. Robins, and W. J. Stewart, "Magnetism from conductors and enhanced nonlinear phenomena," *IEEE Trans. Microwave Theory Technol.* **47**, 2075 (1999).
- [8] P. Markos and C. M. Soukoulis, "Transmission studies of left-handed materials," *Phys. Rev. B* **65**, 033401 (2001)
- [9] Mehmet Bayindir, K. Aydin, E. Ozbay, P. Marko, and C. M. Soukoulis, "Transmission properties of composite metamaterials in free space," *Appl. Phys. Lett.* **81**, 120 (2002)
- [10] Philippe Gay-Balmaz and Olivier J. F. Martin, "Electromagnetic resonances in individual and coupled split-ring resonators," *J. Appl. Phys.* **92**, 2929 (2002)
- [11] R. Marques, J. Martel, F. Mesa, and F. Medina, "Left-Handed-Media Simulation and Transmission of EM Waves in Subwavelength Split-Ring-Resonator-Loaded Metallic Waveguides," *Phys. Rev. Lett.* **89**, 183901 (2002)
- [12] R. Simovski and B. Sauviac, "Role of wave interaction of wires and split-ring resonators for the losses in a left-handed composite," *Phys. Rev. E* **70**, 046607 (2004)
- [13] Movchan and S. Guenneau, "Split-ring resonators and localized modes," *Phys. Rev. B* **70**, 125116 (2004)
- [14] Yi-Jang Hsu, Yen-Chun Huang, Jiann-Shing Lih, and Jyh-Long Chern, "Electromagnetic resonance in deformed split ring resonators of left-handed metamaterials," *J. Appl. Phys.* **96**, 1979 (2004)
- [15] M. Shamonin, E. Shamonina, V. Kalinin, and L. Solymar, "Properties of a metamaterials element: Analytical solutions and numerical simulations for a singly split double ring," *J. Appl. Phys.* **95**, 3778 (2004)
- [16] Yen-Chun Huang, Yi-Jang Hsu, Jiann-Shing Lih, and Jyh-Long Chern, "Transmission Characteristics

- of Deformed Split-Ring Resonators,” *Jpn. J. Appl. Phys.*, Part 2 **43**, L190 (2004)
- [17] B. Sauviac, C.R. Simovski, S.A. Tretyakov, “Double split-ring resonators: Analytical modeling and numerical simulations,” *Electromagnetics* **24**, 317 (2004).
- [18] Philippe Gay-Balmaz and Olivier J. F. Martin, “Efficient isotropic magnetic resonators,” *Appl. Phys. Lett.* **81**, 939 (2002)
- [19] R. Smith, S. Schultz, P. Markos, and C. M. Soukoulis, “Determination of effective permittivity and permeability
- [20] of metamaterials from reflection and transmission coefficients,” *Phys. Rev. B* **65**, 195104 (2002)
- [21] T. Koschny, M. Kafesaki, E. N. Economou, and C. M. Soukoulis, “Effective Medium Theory of Left-Handed Materials,” *Phys. Rev. Lett.* **93**, 107402 (2004)
- [22] T. Koschny, P. Markos, D. R. Smith, and C. M. Soukoulis, “Resonant and antiresonant frequency dependence of the effective parameters of metamaterials,” *Phys. Rev. E* **68**, 065602 (2003)
- [23] Th. Koschny, P. Markos, E. N. Economou, D. R. Smith, D. C. Vier, and C. M. Soukoulis, “Impact of inherent periodic structure on effective medium description of left-handed and related metamaterials,” *Phys. Rev. B* **71**, 245105 (2005)
- [24] D. R. Smith, D. C. Vier, N. Kroll, and S. Schultz, “Direct calculation of permeability and permittivity for a left-handed metamaterial,” *Appl. Phys. Lett.* **77**, 2246 (2000).
- [25] Xudong Chen, Tomasz M. Grzegorzczak, Bae-Ian Wu, Joe Pacheco, Jr., and Jin Au Kong, “Robust method to retrieve the constitutive effective parameters of metamaterials,” *Phys. Rev. E* **70**, 016608 (2004)
- [26] Xudong Chen, Bae-Ian Wu, Jin Au Kong, and Tomasz M. Grzegorzczak, “Retrieval of the effective constitutive parameters of bianisotropic metamaterials,” *Phys. Rev. E* **71**, 046610 (2005)
- [27] D. R. Smith, Willie J. Padilla, D. C. Vier, S. C. Nemat-Nasser, and S. Schultz, “Composite Medium with Simultaneously Negative Permeability and Permittivity,” *Phys. Rev. Lett.* **84**, 4184 (2000)
- [28] Andrew A. Houck, Jeffrey B. Brock, and Isaac L. Chuang, “Experimental Observations of a Left-Handed Material that Obeys Snell’s Law,” *Phys. Rev. Lett.* **90**, 137401 (2003)
- [29] Z. G. Dong, S. N. Zhu, H. Liu, J. Zhu, and W. Cao, “Numerical simulations of negative-index refraction in edge-shaped metamaterials,” *Phys. Rev. E* **72**, 016607 (2005)
- [30] R. A. Shelby, D. R. Smith, and S. Schultz, “Experimental Verification of a Negative Index of Refraction,” *Science* **292**, 77 (2001).
- [31] L. Ran, J. Huangfu, H. Chen, X. Zhang, K. Chen, T. M. Grzegorzczak, and J. A. Kong, “Beam shifting experiment for the characterization of left-handed properties,” *J. Appl. Phys.* **95**, 2238 (2004).
- [32] A. Houck, J. B. Brock, and I. L. Chuang, “Experimental Observations of a Left-Handed Material That Obeys Snell’s Law,” *Phys. Rev. Lett.* **90**, 137401 (2003)
- [33] G. Parazzoli, R. B. Greigor, K. Li, B. E. C. Koltenbah, and M. Tanielian, “Experimental Verification and Simulation of Negative Index of Refraction Using Snell’s Law,” *Phys. Rev. Lett.* **90**, 107401 (2003).
- [34] Koray Aydin, Kaan Guven, Costas M. Soukoulis, and Ekmel Ozbay, “Observation of negative refraction and negative phase velocity in left-handed metamaterials,” *Appl. Phys. Lett.* **86**, 124102 (2005).
- [35] K. Guven, K. Aydin, K. B. Alici, C. M. Soukoulis, and E. Ozbay, “Spectral negative refraction and focusing analysis of a two-dimensional left-handed photonic crystal lens,” *Phys. Rev. B* **70**, 205125 (2004) .
- [36] R. Marques, F. Mesa, J. Martel, and F. Medina, “Comparative analysis of edge- and broadside-coupled split ring resonators for metamaterial design - theory and experiments ,” *IEEE Trans. Antennas Propag.* **51**, 2572 (2003).
- [37] R. Marques, F. Medina, and R. Rafii-El-Idrissi, “Role of bianisotropy in negative permeability and left-handed metamaterials,” *Phys. Rev. B* **65**, 144440 (2002).
- [38] J.D. Baena, J. Bonache, F. Martin, R. M. Sillero, F. Falcone, T. Lopetegui, M.A.G. Laso, J. Garcia-Garcia, I. Gil, M. F. Portillo, M. Sorolla, “Equivalent-circuit models for split-ring resonators and complementary split-ring resonators coupled to planar transmission lines,” *IEEE Trans. Microw. Theory Tech.* **53**, 1451 (2005).
- [39] N. Katsarakis, T. Koschny, M. Kafesaki, E. N. Economou, and C. M. Soukoulis, “Electric coupling to the magnetic resonance of split ring resonators,” *Appl. Phys. Lett.* **84**, 2943 (2004)
- [40] R. Marques, F. Medina, and R. Rafii-El-Idrissi, Comment on “Electromagnetic resonances in individual and coupled split-ring resonators” [*J. Appl. Phys.* **92**, 2929 (2002)] *J. Appl. Phys.* **94**, 2770 (2003)
- [41] Koray Aydin, Kaan Guven, Maria Kafesaki, Lei Zhang, Costas M. Soukoulis, and Ekmel Ozbay, “Experimental observation of true left-handed transmission peaks in metamaterials,” *Opt. Lett.* **29**, 2623 (2004)

Multiple gas Analyzer and Indicator

Sheikh Rafik Manihar, Komal Prasad Dewagan, Jayant Rajpurohit

Electronics and instrumentation, Chhatrapati shivaji institute of technology, India

ABSTRACT: This project is microcontroller based project. A Gas sensor is used to detect dangerous gas leaks in the kitchen or near the gas heater or gas plant producing acetylene and so on. This implies that the gases available are the main raw materials used in gas plants, without which the existence of a gas plant. This unit detects 300 to 5000ppm of Natural Gas. Ideal to detect dangerous gas leaks in the kitchen. Sensor can be easily configured as an alarm unit. The sensor can also sense LPG and Coal Gas. Ideal sensor for use to detect the presence of a dangerous LPG leak in your car or in a service station, storage tank environment. This unit can be easily incorporated into an alarm unit, to sound an alarm or give a visual indication of the LPG concentration. The sensor has excellent sensitivity combined with a quick response time. The project is based on detect of gas concentration from 200 to 1000ppm. It has high sensitivity it consist of heater coil with which is added with resistance and the output is connected to ADC.

Keywords: Sensor, Detector, LPG, Coal Gas, Natural Gas

I. INTRODUCTION

A Gas Detector is a device which detects the presence of various gases within an area, usually as part of a safety system. Using sensor for detection like LPG & Alcohol sensor. This type of equipment is used to detect a gas leak and interface with a control system. It detects gases like common toxic gases like CO, SO₂ & natural gases. Usage for notification leakage in home & environment applications. This type of device is important because there are many gases that can be harmful to organic life, such as humans or animals. Alcohol Detector is used to detect the alcohol gas by use of alcohol sensor. It is highly sensitive and its detection range is 10-1000 ppm. LPG Detector is used to detect the LPG Gas by use of LPG Gas sensor. It is highly sensitive and its detection range is 10-10000 ppm. Natural Gas Detector is used to detect the Natural Gas by use of Natural Gas sensor. It is highly sensitive and its detection range is 300-5000 ppm. It is a known fact that a gas plant is known in accordance with its final output. So we have oxygen gas plant producing oxygen, nitrogen gas plant producing nitrogen, acetylene gas plant producing acetylene and so on. This implies that the gases available are the main raw materials used in gas plants, without which the existence of a gas plant has no meaning. Accordingly the manufacturers and suppliers are involved in the production of certain gases which are useful in various industrial and commercial, including residential applications. There are different types of gases on the basis of which a plant is installed.

II. METHODOLOGY

Gas detector senses the gas in the environment and converts it in form of voltage, this voltage level converted by ADC in digital form. This signal is input of microcontroller which displays the output.

1. HARDWARE DESCRIPTION

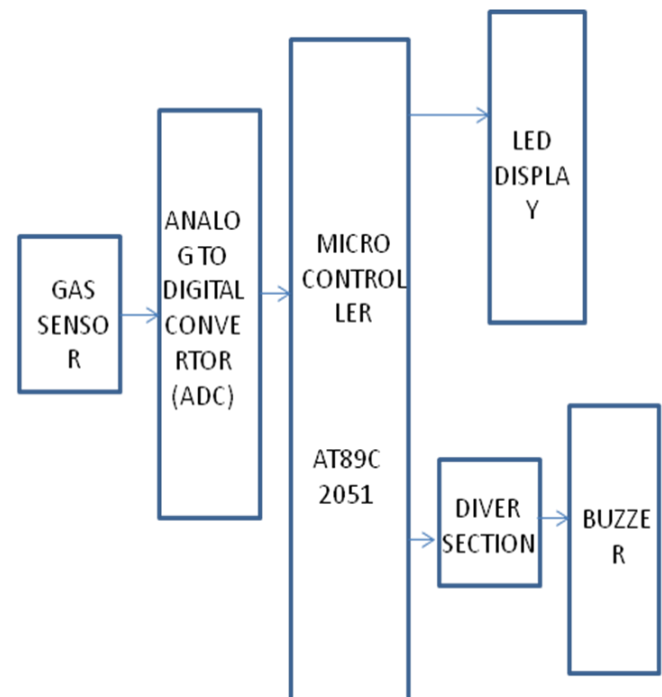


Figure1. Block Diagram.

1. A. Description of Block Diagram

The flow chart describe about the detection of gas firstly through the gas sensor (MQ2) we are detecting the alcohol present in atmosphere. Sensitive material of MQ2 gas sensor is SnO₂, which with lower conductivity in clean air. When the target alcohol gas exist, the sensor's conductivity is higher along with the gas concentration rising. This converted change of conductivity to correspond output signal of gas concentration. The advantage of using this sensor as the microcontroller and the sensor works with the same power supply voltage +5V. This certain amount of reference voltage is set by the sensor. The reference voltage which set by sensor is converted by ADC in the form of digital signal. As ADC 0808/09 we are using easily interface with the microcontroller. The signal which is converted by the ADC is provided to microcontroller through the port. The driver which is connected from the port of microcontroller act as a relay circuit. The driver circuit which helps to drive the buzzer which is connected to driver.

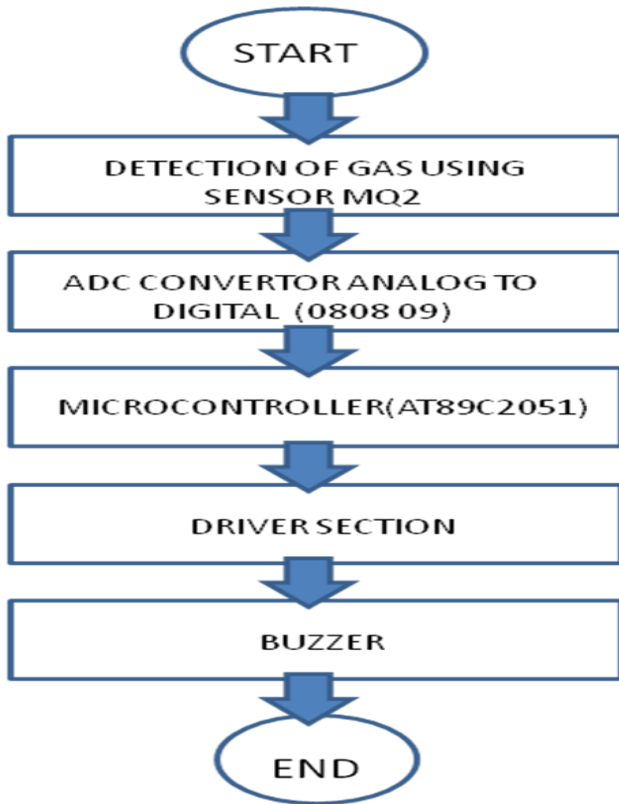


Figure1.Flow Diagram.

2. B. Description of Flow Diagram

The description of flow diagram starts with the detection of gas using sensor MQ2 & MQ3 for detecting multiple gases in our project which includes calibration process for sensors.

After the gas is detected then for further processing the voltage variation is now send to the ADC for converting the analog data to digital for further processing of microcontroller. Hence then microcontroller with different values print the output for detection. An analog-to-digital converter (abbreviated ADC, A/D or A to D) is a device that converts a continuous quantity to a discrete time digital representation. An ADC may also provide an isolated measurement. A ramp-compare ADC produces a saw-tooth signal that ramps up or down then quickly returns to zero. When the ramp starts, a timer starts counting. When the ramp voltage matches the input, a comparator fires, and the timer's value is recorded. Timed ramp converters require the least number of transistors. The ramp time is sensitive to temperature because the circuit generating the ramp is often just some simple oscillator. After the conversion it is sent to the microcontroller ports for further proceedings. Microcontrollers are used in automatically controlled products and devices, such as automobile engine control systems, implantable medical devices, remote controls, office machines, appliances, power tools, toys and other embedded systems. By reducing the size and cost compared to a design that uses a separate microprocessor, memory, and input/output devices, microcontrollers make it economical to digitally control even more devices and processes. Mixed signal microcontrollers are common, integrating analog components needed to control non-digital electronic systems. A driver typically communicates with the device through the computer bus or

communications subsystem to which the hardware connects. When a calling program invokes a routine the driver issues commands to the device. Once the device sends data back to the driver, the driver may invoke routines in the original calling program. Drivers are hardware-dependent and operating-system-specific. They usually provide the interrupt handling required for any necessary asynchronous time-dependent hardware interface. A device driver simplifies programming by acting as translator between a hardware device and the applications or operating systems that use it. Programmers can write the higher-level application code independently of whatever specific hardware device. A buzzer or beeper is an audio signaling device, which may be mechanical, electromechanical, or piezoelectric. Typical uses of buzzers and beepers include alarm devices, timers and confirmation of user input such as a mouse click or keystroke. A display device is an output device for presentation of information in visual or tactile form (the latter used for example in tactile electronic displays for blind people). When the input information is supplied as an electrical signal, the display is called an electronic display.

2. PROBLEM IDENTIFICATION

The problem which we have faced during this project is basically the calibration process and sensitivity adjustment as describe below.

2. A. Calibration of Gases

Gas sensors need to be calibrated and periodically checked to ensure sensor accuracy and System integrity. It is important to install stationary sensors in locations where the calibration can be performed easily. The intervals between calibrations can be different from sensor to sensor. It is quite unlikely that you will ever use an absolute method for gas detection. Rather, you will employ any one of dozens of "relative" [or "reference," but not necessarily EPA Reference] methods that is, methods that produce some output that must be calibrated against a known standard. Even though proper calibration is 90% of successful gas detection, it is a subject that has been neglected often purposely by the majority of instrument manufacturers. There's a good reason for this, of course: Proper calibration can often be difficult and expensive. But, we're getting a bit ahead of ourselves.

2. B. Sensitivity Adjustment

In a gas sensor sensitivity adjustment create a problem because of different gas sensor module have different sensitivity adjustment. For gas sensor to work properly sensitivity adjustment is required to be full filled. Sensitivity adjustment was necessary, without this we cannot use this sensor in a desired way. In this project we can use two gas sensor modules MQ2 and MQ3.

Its sensitivity adjustment is given below:

- Resistance value of MQ-2 is difference to various kinds and various concentration gases. So, when using these components, sensitivity adjustment is very necessary. We recommend that you calibrate the detector for 1000ppm liquefied petroleum gas<LPG>,or 1000ppm iso-butane<i-C4H10>-concentration in air and use value of Load resistance that (RL) about 20 K Ω (5K Ω to 47K Ω)

- Resistance value of MQ3 is difference to various kinds and various concentration gases. So, when using these components, sensitivity adjustment is very necessary. We recommend that you calibrate the detector for 0.4mg/L (approximately 200ppm) of Alcohol concentration in air and use value of Load resistance that (RL) about 200 K Ω (100K Ω to 470 K Ω).

III. EXPERIMENTAL RESULT

Here Shows the working of our project in proteus where we simulate it and run it before assembling the part.

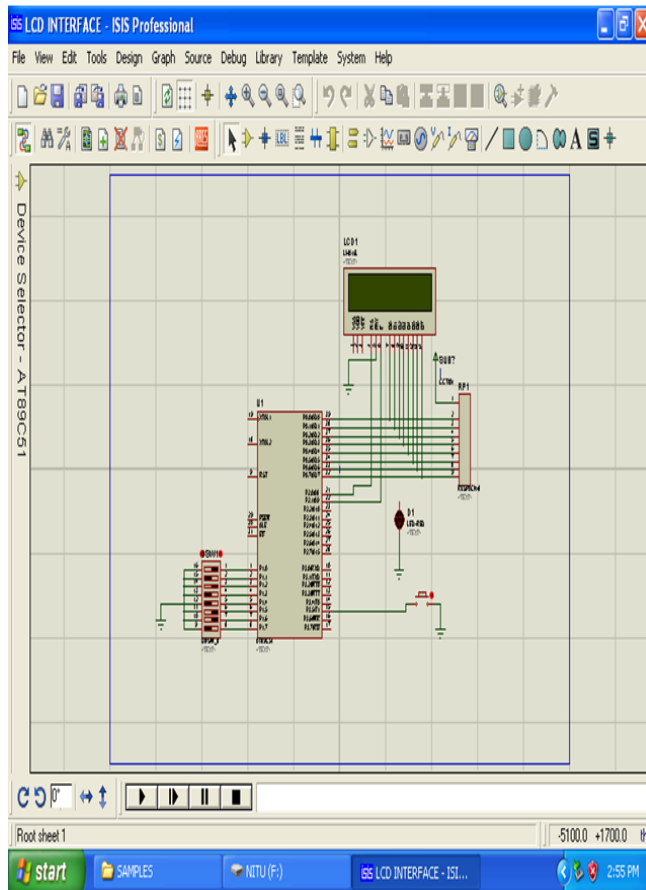


Figure6.1 -Result for describing the detection of gas

The above shows the software processing of our project in which the we simulate before assembling the hardware parts of our project in which after simulation the output shows whether the gas is detected or not and which type of gas id detected the sensor before assembling include the calibration process. Gas sensors need to be calibrated and periodically checked to ensure sensor accuracy and System integrity. It is important to install stationary sensors in locations where the calibration can be performed easily. The intervals between calibrations can be different from sensor to sensor. Generally, the manufacturer of the sensor will recommend a time interval between calibrations. However, it is good general practice to check the sensor more closely during the first 30 days after installation. During this period, it is possible to observe how well the sensor is adapting to its new environment. Also, factors that were not accounted for in the Design of the system might surface and can affect the sensor's performance. If the sensor functions properly for 30 continuous days, this provides a good degree of confidence about the installation.

Any possible problems can be identified and corrected during this time. Experience indicates that a sensor surviving 30 days after the initial installation will have a good chance of performing its function for the duration expected. Most problems such as an inappropriate sensor location, interference from other gases, or the loss of sensitivity will surface during this time. During the first 30 days, the sensor should be checked weekly. A typical calibration schedule for a fixed system may be quarterly, bi-annually or even annually with some of the more robust units. A typical calibration schedule for a portable gas detector is a daily bump test accompanied by a monthly calibration.

IV. CONCLUSION

The importance of gas sensing is set to grow with increasing requirements for safety and environmental protection across many industries. The current range of any gas sensing technologies has served us well but the future holds many new possibilities. Power and size reductions and an improvement in ruggedness will allow a new generation of body worn devices. These Ways will be developed to improve performance whilst at the same time reduce cost; new sensors will be targeted at enhancing environmental protection. For these purpose we have designed the Gas Detector for LPG senses and alcohol sensing where it detects the gas and sense it for printing the result and alerting through a buzzer. By use of Gas Detector we can detect multiple gases like CO, LPG, Natural gases like methane, propane.

REFERENCES

- [1] Truong Giang Ho, Thai Duy Ha, Quang Ngan Pham, Hong Thai Giang, Thi Anh Thu Do and Ngoc Toan Nguyen. "Nanosized perovskite oxide NdFeO₃ as material for a carbon-monoxide catalytic gas sensor".8 March 2011
- [2] Woosuck shin, maiko nishibori "Thermoelectric hydrogen gas sensor"2011.
- [3] Unal Kizil and James A. Lindley "Potential use of gas sensors in beef manure nutrient content estimations" 2009
- [4] Seongjeen Kim, "Amperometric Enzyme-based Gas Sensor forFormaldehyde Impact of Possible Interferences".2008.
- [5] Inta Muzikante, Vicente Parra, Rorijs Dobulans "A Novel Gas Sensor Transducer Based on Phthalocyanine Heterojunction Devices"2007.
- [6] Sabine Achmann, Martin Hämmerle and Ralf Moos, "CNT Sensor For Detection gases with low adsorption energy by ionization".5 May 2006.
- [7] S. Capone*, A. Forleo, L. Francioso, R. Rella, P. Siciliano "solid state gas sensor: state of the art and future activities" 2003.
- [8] Alexey A. Tomchenko, Gregory P. Harmer, Brent T. Marquis "Semiconducting metal oxide sensor array for the selective detection of combustion gases"2003.
- [9] k. Arshak, E. Moore, G.M. Lyons, J. Harris and S. Clifford A review of gas sensoremployed in electronicnose .
- [10] Sheikh Akbar, prabir dutta and chonghoon lee "High temperature ceramic gas sensor".

An Assessment of the Environmental Impact of Brine Disposal in Marine Environment

Musfique Ahmed¹, Rifat Anwar²

¹Post-Graduate Student of Environmental Engineering, University of Melbourne, Victoria, Australia 3010

² Professional Morphologist, Center for Environmental & Geographic Information Service (CEGIS), Gulshan, Dhaka-1212, Bangladesh

Abstract: The ever increasing demand of water permits the need of alternative water sources for balancing the water supply and demand. Desalination has become a significant alternative water source due to growing demand of water and inadequate conventional water sources in many countries. Desalination is a process of removing excess salts and other dissolved solids from water in order to get clean water for human usage. Brine disposal is one of the major concerns of many environmental issues associated with desalination. The production and growth of marine organisms is severely effected by discharge of brine in the desalination process. These organisms are interrelated with each other so any distraction in their population has extreme impacts on all marine life in the area. In this paper various features of potential impacts of brine effluent in marine environment have been critically reviewed. A relative study on different brine disposal options in reducing these impacts is also prepared in this paper.

Keywords: Desalination, Brine, Disposal, Marine Organisms, Environmental Impact

I. Introduction

The Sustainable development of human and ecosystem health is in threat because of continuous depletion and pollution of freshwater sources (Furumai 2008). The scarcity of fresh water is increasing day by day with the increasing rate of world population, urbanization, pollution and climate change. To maintain the proper balance between water supply and demand, some alternative methods need to be implemented. Water covers three fourth of the earth and 97.5% of this water is saline water (Danoun 2007). One of the most effective alternative methods to utilize of this ample saline water is desalination. Desalination is a process of removing excess salts and other dissolved solids from water in order to get clean water for human usage (Haurwitz et al. 2008). The total process mainly consists of two steps which are evaporation and condensation (Danoun 2007). The three most commercially important desalination technologies are reverse osmosis (RO), multi-stage flash (MSF) and multiple-effect distillation (MED). Reverse osmosis (RO) is one of the latest examples of using membrane technologies. Technological expansion has augmented the efficiency of modern RO plants (Tularam & Ilahee 2007). Inadequate conventional water sources is the major cause of growing significance of sea water desalination in many countries (Palomar & Losada 2010). Water supply in the middle east and north America profoundly depends on desalination (Haurwitz et al. 2008). Saudi Arabia is the highest producer of desalinated water followed by United States of America (Danoun 2007). Though Australia has the lowest number of desalination facilities (Figure1), the recent water crisis has driven Australia to construct desalination plants. The Goald Coast desalination plant in Queensland, Perth seawater desalination plant in Western Australia and Kurnell desalination plant in New South Wales are currently in use and three desalination plants in Victoria, South Australia and Western Australia are in progress.

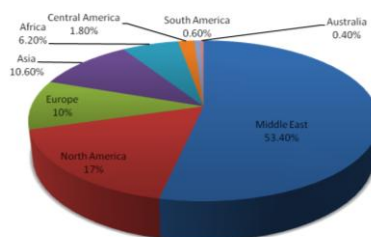


Figure 1: The existing desalination facilities worldwide by region (Source: Modified from International Desalination Association)

There are many issues related to desalination plants that have caused serious anxiety for society and in a bigger extent to the world. High energy is required for desalination processes which result in huge amounts of green house gas emissions. Many environmental issues are associated with desalination. Brine, the concentrated discharge of the desalination process, has serious impacts on the production and growth of marine organisms. The construction process of desalination plants is time consuming and operation and maintenance costs are very high. If the location of the desalination plant is not suitable then it can be inconvenient, loud and disruptive to the environment (Younos 2005). The release of Carbon monoxide (CO), nitrogen dioxide (NO₂), nitric oxide (NO) and Sulphur dioxide (SO₂) from desalination plants have a detrimental impact on environment at the same time on public health (Al-Mutaz 1991).

1.1 Objectives

To implement a proper desalination plant in a specific area all factors related to desalination need to be identified and examined for that area. This essay will deal with one of the biggest environmental concern of desalination plant – the impact of brine disposal on marine environment. Some arguments will need to be developed related to the environmental impacts to the marine life due to brine discharge. Seawater and water in bays and estuaries is full of organisms like plankton, phytoplankton, larvae and the eggs of marine species. These organisms are correlated with each other so any disruption in their population has extreme impacts on all marine life in the area (Haurwitz et al. 2008). The main objectives of this essay are-

1. To critically review the different features of potential impacts due to brine effluent in the marine environment.
2. A comparative study on the processes which can be used to minimize these environmental impacts

II. Environmental impacts of brine discharge

With the increasing importance of desalination plants, it has become indispensable to review and synthesize various researches that have inspected the environmental and ecological impact of brine discharge on marine environment (Roberts, Johnston & Knott 2010). Many literature reviews have focused on quantify the impact of brine on the physical, chemical as well as biological characteristics of marine environment (RPS 2009). Several published review articles and case studies quote ambiguous peer reviewed literature, and present little or no empirical data to support statements regarding the environmental effects of brine discharge (Roberts, Johnston & Knott 2010). A wide range of potential impacts have been identified due to the brine discharge but only few of the literature scientifically observed the authentic effect of discharge on marine communities around discharge outlets (Skinner 2008). Although so many desalination plants have been constructed in different parts of the world the availability of data on the impacts of their discharge is very little (RPS 2009). The purpose of this review is to identify the physiochemical and ecological impacts of brine on various aspects like temperature, alkalinity, dissolve oxygen, salinity, nutrients and various chemicals of seawater which resultant serious effect on marine environment as well as associated knowledge gaps on this field.

2.1 Temperature

One of the major impacts of brine discharge is thermal pollution which can occur by increasing the temperature of sea water. Numerous studies have been carried out to determine how the distribution and natural balance of marine flora and fauna species respond to an alteration in temperature (Danoun 2007). In these studies a direct correlation between temperature and marine species has been determined. The statements in the previous literatures related to the temperature changes due to desalination remain unclear whether the temperature ranges which were assessed based on field measurements or the model predictions (RPS 2009). The temperature of discharged brine is obviously much higher than the ambient sea water temperature. Temperature of the sea water generally varies between 10°C to 25°C which increases about 60% to 40°C near the area of the brine disposal (Danoun 2007). Alteration of temperature basically depends on the type of the treatment plants. Distillation plants increase the temperature more than the reverse osmosis process. Abdul-Wahab illustrated a direct connection between the temperature of the seawater and the distance from the discharge site (Wahab 2007). The distribution and extent of the temperature alteration also depends on the location of the plant discharge. If the brine discharges in a well-flushed environment, it is more efficient and effective than the brine discharges near to the water bodies (Roberts, Johnston & Knott 2010).

2.2 Salinity

A variety of published literatures and readings disclose the effect of brine on the salinity of the seawater and the resultant impact on marine environment. The centre of attention of these studies is the concentration and expansion of brine plumes on the receiving water (Roberts, Johnston & Knott 2010). It is now widely recognized that extensive brine discharge, as it constitutes a hypersaline layer that sinks towards the seabed due to its greater density, has the potential to heavily affect local marine biota (Medeazza 2005). Changes of salinity influence the propagation activity of the marine species and that consequentially affect their development and growth rate. Larval stages are very crucial transition periods for marine species and increasing salinity disrupts that period significantly (Neuparth, Costa & Costa 2002). Although marine species of the saline water are familiar to this fluctuation of salinity concentrations but they may not survive on this sudden augmentation of salinity because of brine disposal (Haurwitz et al. 2008). As discharged brine is much denser than the seawater so brine plumes have the affinity to extend further along the seafloor than the surface which contributes to greater exposure of benthic organisms to brine discharges, than pelagic and plank tonic organisms (Roberts, Johnston & Knott 2010). Though reverse osmosis processes do not impact much on the alteration of temperature, brine discharges from this process increase the salinity by twice that of the seawater (Tularam & Ilahee 2007). According to several studies the excess salinity level of seawater from brine discharge is directly correlated with the distance of the plant site. It shows that rising the salinity level up to 50 ppt could probably have an serious impact on the fish size and on their survival rate (Parry 1960).

2.3 Dissolve Oxygen

Brine disposal also has an effect on the dissolved oxygen of the seawater. As the amount of dissolve oxygen is inversely proportional to the salinity level, so with the increasing rate of salinity dissolve oxygen is decreasing which consequences hypoxia (Haurwitz et al. 2008). Hypoxia is a serious condition which results from low levels of dissolved oxygen and can cause serious harm to the aquatic organisms. According to report of California Coastal commission, 2004 if the temperature of water increases because of brine this can decrease dissolved oxygen and increase biomass resulting from the disposal of

entrained organisms (California Coastal Commission 2004; Haurwitz et al. 2008). In reverse osmosis processes temperature is not varied much so major changes in dissolve oxygen due to heating is very unlikely. Though mixing of oxygen consuming chemicals in RO plants to restrain corrosion and eliminate residual chlorine can reduce the dissolve oxygen (Lattemann & Höpner 2008).

2.4 Other Aspects

High total alkalinity is another big impact of brine discharge which increases the amount of calcium carbonate, calcium sulphate and other elements of the sea water twice to its normal level. Very few experiments have been conducted to quantify the alteration of the total alkalinity in seawater due to brine disposal and also the tolerance limit of marine life to it (Danoun 2007). The pH range of marine environments is also changing due to the brine discharge but that is very negligible compared to the other impacts (Skinner 2008). For the proper performance of desalination plants pre and post treatment processes are required whereby many chemicals are added to enhance flocculation or to avoid membrane deterioration. Antiscalant agents like polyphosphates, polymers of maleic acid, sulphuric acid and antifoaming agents like fatty acids, alkylated polyglycoles etc are used as chemical components which are discharged with brine and effect the marine species around the outlet (Medeazza 2005). Many field based monitoring and laboratory based experiment have been implemented to enumerate the ecological impact of the brine disposal.

2.5 Impingement and Entrainment

Some desalination plants need to have substantial intake of sea water which can be harmful for marine species in two ways-impingement and entrainment. Impingement refers to the collision with screen and entrainment refers to the drawn in to the plant (Lattemann & Höpner 2008). When organisms are dragged into an intake pipe and trapped in a fish screen covering the intake which cause injury or death then that is defined as impingement. Entrainment occurs when little organisms pass through the fish screen and are actually taken into the intake pipes (Haurwitz et al. 2008, p. 8). Many previous studies show that these are not threatening for the large species because of small flow rate but smaller animals like phytoplankton, zooplankton can be impinged or entrained.

2.6 Research Gaps

The main focus of this essay is on the environmental impacts caused by the brine disposal on marine environment so this review part consists of various aspects of impacts grounded because of the discharges of desalination plant. But still there are many studies in the literature which are ambiguous as well as unscientific. Some literature has tried to define the positive and negative impact both which is very much contradictory. According to Rashad Danoun, alteration of temperature can have an influence on the production rate as well as life span of the marine species which can be decreased with the increasing rate of temperature. But in the other part he has tried to portray the positive aspect by saying that increased temperature of the ambient environment leads to a positive effect on growth rate of several species of plankton (Danoun 2007). Neither very specific nor very reliable temperature ranges can be set for desalination plants. One of the prominent reasons for this is the difference between field measurement and model predictions. There is still some lack in previous investigations of the documentation of experimental data of temperature change which is affecting the marine flora and fauna. Many mathematical models have been created to inspect the salinity level in sea water. Though brine flume has the potential effect on the salinity level of sea water but other causes of rising salinity like irrigational flow, breakdown of rocks and minerals, locked down of freshwater in to the ice caps etc. also need to be taken in consideration. The salinity of bay and estuaries can also be increased by low flow of fresh water from rivers due to increased Water Rights. The previous studies have not included all these factors in conducting comparative study of rising condition of salinity level. It is stated before in many readings that salinity level and the location of the plant is correlated and salinity declines rapidly close to the outfall of the desalination plants. But precise measurements are not located in the reviews. This is a big knowledge gap because accurate distance could help to locate the suitable site for the desalination plant. In most of the previous literatures, the effect of reduced level of dissolved oxygen has been analysed for a particular plant not for different desalination plants. But with the diverse locations of plants, impact of dissolved oxygen in the receiving water can be changed. Impact on the small marine species due to brine discharge has been assessed in lots of literatures but less information is available about the large marine fauna. Impingement and entrainment are very new explored ideas and most of the desalination plants were established without considering these impacts. So, these knowledge gaps need to be overcome for the betterment of desalination system.

III. Impact minimisation

Currently the increasing rate of practice of desalination plant has led to the development of many new methods and options to minimize the impact of brine disposal. While there are many options available for minimising the impacts of brine disposal, different strategies are appropriate only for different locations. So, before using the strategy, it needs to be evaluated both environmentally and economically (SOL-BRINE 2009). In this section of the essay, different minimizing process will be depicted and some recommendations will be suggested with respect to the various conditions of the sites.

The alternative options of brine disposal can be divided in to three different categories.

1. Changing the location of brine disposal/ Treatment before discharge
2. Redesigning the desalination plant
3. Coupling the desalination plant with some existing treatment plant

3.1 Changing the location of the brine disposal/ Treatment before discharge

By changing the location of brine disposal and treating the brine before ultimate discharge the actual impact of brine in the receiving water can be reduced. Brine can be discharged in the surface water and diluted by outfall diffusion devices like diffusion nozzles or can be mixed with less saline waste streams before ultimate discharge. However this option can only be used when surface water body is located nearby to the estuary (Castillo, Sanchez & Castillo 2007; Sarté et al. 2006). Brine can be directed to the existing sewer treatment plant to dilute with municipal wastewater prior discharge. However volume and composition of the brine, the convey process and reaction of the brine with the waste water need to be taken into consideration (SOL-BRINE 2009). The High range of dissolved solids of the waste water could be of great concern for marine environments when treated water is released back into the seawater. Injecting brine via wells into confined and non-potable aquifer systems can also be a good option of disposing brine. It is important to have a monitoring well near the injection well to assure that there is no leakage from the injection well. As it naturally pre-filtrates the feed water, it lowers the saline water table (Lattemann & Höpner 2008). This option is not cost-effective because of the construction of an extra well and groundwater infectivity can be occurred because of mechanical collapse of the injection process and over pressurization resulting from the high injection rate (Haurwitz et al. 2008). Spreading brine in shallow ponds where it gradually evaporates, the concept of evaporation pond, can also be a suitable mitigation measure (Sarté et al. 2006). The residual solid that is left behind in the pond can be used for landfill or collected for re use. Solid lining or monitoring wells may be required to ensure that ponds do not drip and pollute surrounding soils or aquifers (Haurwitz et al. 2008). This process is land intensive and also cause significant loss of the basic water resource through evaporation (Younos 2005). Each of these conventional strategies is more suitable for small and medium size facilities. However these processes can reduce the salinity level of the brine so after discharging brine will not be as much harmful for marine biota.

3.2 Redesigning the desalination plant

Environmental impacts can be mitigated if the desalination plant can be designed in a sustainable way or some essential parts or mechanisms can be included or installed. Beach wells or infiltration galleries can be installed which drag in seawater through the overlying substrate. This overlying substrate works as a natural filter to keep out small marine creatures and larvae. This can improve the quality of feedwater and reduce the cost for pre-treatment. Impingement and entrainment can also be minimized by this process (Haurwitz et al. 2008). Historically 'jet' of brine released at 60° angle was adopted as standard design criteria. Recent modelling approaches has proved that shallower discharge angle 30°-45° may enhance mixing and offshore transport of desalination brines in coastal waters with moderate-to-steep bottom slopes (Jirka 2008). This can minimise the spatial extent and intensity of brine plumes which results in reduction of salinity level. Now days jetties have been constructed adjoining to the desalination plant discharges to create offshore currents which can minimize the extend of brine plumes and persuade more rapid mixing (Roberts, Johnston & Knott 2010). Advancement of nanotechnology helps to create devices and systems by using nanostructured materials like carbon nanotubes, nanowires, graphene, quantum dots, super lattices, and nano shells for desalination technology. It is Useful to separate water from salt , control the evaporation and produce next generation RO membrane (Humplik et al. 2011). Another useful system can be developing anti scaling with no biological effect by using the scale inhibitors which may assist in the production of less toxic brines in the future (Ketsetzi, Stathouloupoulou & Demadis 2008). Further research is required to understand how these techniques can be properly utilized as these are very new approaches.

3.3 Coupling the desalination plant with existing treatment plant

Desalination plants can be co located or coupled with some existing treatment plant like power plant, and salt works which can also be very useful in mitigating the impact of brine. Desalination plants can be co located with older thermocouple plant to dilute the brine with power-plant cooling water (Roberts, Johnston & Knott 2010). These options should be considered for larger plants which would limit the brine plume to be extended far and reduce its effect in receiving water (Einav & Lokiec 2003). Cooling systems are very efficient for reducing impingement and entrainment, construction problems, land use impacts and usage of chemicals (Lattemann & Höpner 2008). The desalination plant can be coupled with solar salt works by directing the brine to a salt works for brine concentration and salt production with an aim of achieving zero discharge desalination plant. Extra salt can be produced by using this process in the factories which results extra income and also minimize the transportation cost (Laspidou, Hadjibiros & Gialis 2010).

3.4 Recommendations

All these strategies cannot be suitable for every location. Suitability of the options can vary because of the location of the desalination plant-nearby or far from coast, land uses of the adjacent places of the plant, availability of idle lands, energy emitting system of the plant and also the other associated aspects of desalination. Some recommendations are made based on the previous literatures and knowledge and experience acquired by assessing various minimizing processes. For desalination plants using membrane technology, zero liquid discharge process can be a very efficient alternative option. ZLD is actually a thermal evaporative system which can reduce volume of discharge by using thermal evaporators like crystallizers, spray dryers etc. Though these processes are expensive and energy intensive which can be counterbalanced by modernizing the membrane system. Those areas where enough lands are available evaporation ponds with aquaculture and agricultural application may be worked as economically viable. Black bream, snapper, Dunaliella, brine shrimp can be successfully raised in the brine and plants tolerant to high salinity can be irrigated nearby to the evaporation pond. The land cost, monitoring cost, and lining cost related to evaporation pond can be minimized by production of fishes, plants and salts. For arid regions like Australia, evaporation ponds can be a useful option when availability of land is enough. Salinity

gradient solar pond is also a possible synergy for the evaporation pond which joins the collection of solar energy with long-term storage and produce electricity (Svensson 2005) This can reduce the electricity problem of Australia in a greater extent. If impacts cannot be minimized by using different strategies or systems, then site of least impacted needs to be identified. If enough investment is ensured then nanostructured material, anti scalant can be used in the desalination plant. These new inventions are expensive but much more valuable for reducing impacts than the conventional processes. Researchers have now invented a new process of brine management that is effective for both inland and coastal desalination plant. Solvay process is actually developed to convert the brine into reusable solid product Sodium Carbonate. It is executed by mixing the reject brine (saturated sodium chloride solution) with carbon dioxide and ammonia in a high temperature to get sodium carbonate as final product and water (El-Naas 2010). These new technologies can be very functional for Gold coast and Kurnell desalination plant of Australia as severe environmental impact of brine is being revealed there

IV. Limitations

Though several literatures are critically reviewed and analysed on this broad area of desalination, but there are some limitations of this study which requires to be emphasized more. In the literature review a wide range of impacts and their associated risks has been identified but enough data could not be analysed from laboratory-based experiments or toxicological investigations. These data could have been more useful to practically illustrate the adverse impacts of brine on marine organisms. Recommendations that have been made to mitigate the impact needs more experiments and investigations for specific regions. Irrigation of saline tolerant plant can be useful but at the time of heavy rainfall other processes need to be available. So, seasonal fluctuations were needed to be taken in to account. Economic viability of the recommended processes is not taken in to account properly which is significant from the view of decision makers. No modelling results have been used to identify proper location of brine disposal. But, modelling the plume of brine is recommended to demonstrate the dispersion area. Water quality test of the concentrated brine is essential with respect to the different factors like- temperature, salinity, dissolved oxygen, alkalinity etc. to validate the damage these could cause to the marine environment. This essay has provided overall idea about various mitigation measures but individual study is required on every process before implementation. So, experiments and case studies are required in small scale of the conventional and recommended measures to identify their suitability in large scale. Monitoring program for long term is suggested nearby to the coastal area to investigate the actual impact which may be altered with time.

V. Conclusion

With the increasing rate of water demand, desalination is now being used as an important alternative option of clean water supply. Because of this high demand of water marine environmental problems related with desalination have always been considered as secondary concern. Marine species are severely impacted by the brine disposal without proper treatment. In some cases the impact rate may be huge or in other cases it may be low. But, this impact is little regarding to the high substantial alteration of sea water because of physical and chemical changes. Other negative aspects of desalination like high energy usage, GHG emissions, huge O&M cost etc. are much more significant relative to impact of brine. Mitigation measures for these impacts are needed to be selected with respect to the suitability of the plant and conditional attributes of the particular area. Some new inventions are discussed in this essay for design, location and measurement of desalination plants to minimise or eliminate any potential impacts of brine. New technological ideas and materials are desirable to lower the impact and keep a well coastal marine environment.

References

- [1]. Al-Mutaz, IS 1991, 'Environmental Impact of Seawater Desalination Plants', *Environmental Monitoring and Assessment*, vol. 16, pp. 75-84.
- [2]. California Coastal Commission 2004, *Seawater Desalination and the California Coastal Act*.
- [3]. Castillo, RS, Sanchez, JMS & Castillo, NS 2007, 'Brine Discharge Procedures to Minimize the Environmental Impact and Energy Consumption', paper presented to IDA World Congress, Maspalomas, Gran Canaria –Spain.
- [4]. Danoun, R 2007, *Desalination Plants: Potential impacts of brine discharge on marine life*, University of Sydney, Sydney, Project Report.
- [5]. Einav, R & Lokiec, F 2003, 'Environmental aspects of a desalination plant in Ashkelon', *Desalination*, vol. 156, pp. 79-85.
- [6]. El-Naas, MH 2010, 'Reject Brine Management', *Desalination, Trends and Technologies*, pp. 237-52.
- [7]. Furumai, H 2008, 'Rainwater and reclaimed wastewater for sustainable urban water use', *Physics and Chemistry of the Earth*, vol. 33, pp. 340-6.
- [8]. Haurwitz, R, Broad, T, Collins, J, Carman, N, Arroyo, J, Krishna, H, Mannchen, B, McFadden, J & Stachowitz, A 2008, *DESALINATION: IS IT WORTH ITS SALT? A Primer on Brackish and Seawater Desalination*, Lone Star Chapter of the Sierra Club, Texas.
- [9]. Humplik, T, Lee, J, Fellman, BA, Baig, MA, Hassan, SF, Atieh, MA, Rahman, F, Laoui, T, Karnik, R & Wang, EN 2011, 'Nanostructured materials for water desalination', *Nanotechnology*, vol. 22, pp. 1-19.
- [10]. Jirka, GH 2008, 'Improved Discharge Configurations for Brine Effluents from Desalination Plants', *JOURNAL OF HYDRAULIC ENGINEERING*, pp. 116-20.
- [11]. Ketsetzi, A, Stathoulopoulou, A & Demadis, KD 2008, 'Being "green" in chemical water treatment technologies: issues, challenges and developments', *Desalination*, vol. 223, pp. 487-93.

- [12]. Laspidou, C, Hadjibiros, K & Gialis, S 2010, 'Minimizing the Environmental Impact of Sea Brine Disposal by Coupling Desalination Plants with Solar Saltworks: A Case Study for Greece', *Water*, vol. 2, pp. 75-84.
- [13]. Lattemann, S & Höpner, T 2008, 'Environmental impact and impact assessment of seawater desalination', *Desalination*, vol. 220, pp. 1-15.
- [14]. Medeazza, GLMv 2005, '“Direct” and socially-induced environmental impacts of desalination', *Desalination*, vol. 185, pp. 57-70.
- [15]. Neuparth, F, Costa, O & Costa, MH 2002, 'Effects of temperature and salinity on life history of the marine Amphipod *Gammarus Locusta*. Implications for ecological testing', *Ecotoxicology*, vol. 11, pp. 61-73.
- [16]. Palomar, P & Losada, IJ 2010, 'Impacts of Brine Discharge on the Marine Environment. Modelling as a Predictive Tool', *Desalination, Trends and Technologies*, pp. 279-310.
- [17]. Parry, G 1960, *The development of salinity tolerance in the salmon, Salmo Salar (L.) and some related species.*, Freshwater fisheries laboratory, London.
- [18]. Roberts, DA, Johnston, EL & Knott, NA 2010, 'Impacts of desalination plant discharges on the marine environment: A critical review of published studies', *WATER RESEARCH*, vol. 44, pp. 5117-28.
- [19]. RPS 2009, *Effect of desalination plant discharge on marine environment of Barrow Island*, N09504.
- [20]. Sarté, B, Leahy, AJ, Zickler, E, Terrell, M & Campbell, J 2006, *WATER MANAGEMENT CHALLENGES IN THE LORETO REGION*, Sherwood Design Engineers, MEXICO.
- [21]. Skinner, L 2008, *Review of Literature on the Effects of Desalination Plant Brine Discharge Upon Cetaceans*, report no.R1339, URS Australia Pty Ltd, East Perth.
- [22]. SOL-BRINE 2009, *Report on the evaluation of existing methods on brine treatment and disposal practices*, LIFE+-Environment project.
- [23]. Svensson, M 2005, *Desalination and the Environment: Options and considerations for brine disposal in inland and coastal locations*, SLU, Department of Biometry and Engineering.
- [24]. Tularam, GA & Ilahee, M 2007, 'Environmental concern of desalinating sea water using reverse osmosis', *Journal of Environmental monitoring*, vol. 9, pp. 805-13.
- [25]. Wahab, SAA 2007, 'Characterization of water discharge from two thermal power/ desalination plants in Oman', *Environmental Engineering Science*, vol. 24, no. 3, pp. 321-37.
- [26]. Younos, T 2005, 'Environmental Issues of Desalination', *JOURNAL OF CONTEMPORARY WATER RESEARCH & EDUCATION*, no. 132, pp. 11-8.

Reconfigurable Communication Architecture of On-Chip Segmented Bus

Sreeja. M. S.¹, Manu. T. S.²

¹PG Scholar, Dept. of Electronics and Communication Engg, TKM Institute of Technology, Kollam, Kerala, India
²Asst. Professor, Dept. of Electronics and Communication Engg, TKM Institute of Technology, Kollam, Kerala, India

Abstract: Modern VLSI technology makes it both feasible and economical to integrate a complex system on a single chip. These modules often require different data transfer speeds and parallel transmission capability. A conventional bus structure might not be adequate for these demands because, typically, only one attached module can transmit at a time, and a large capacitive load caused by attached system modules and long bus wires can make a bus very slow. A segmented bus architecture shows potential for improving both speed and power related features of a bus-based system. Due to segmentation of the bus, parallel transactions can take place, thus increasing the performance of the bus. In order to reduce arbitration and communication delay in the existing segmented bus, new reconfigurable architectures which will completely avoid the complicated higher level arbitration overhead with a small modification in local arbiter is proposed in this paper. The bus architectures are modeled using VHDL.

Key words: Reconfigurable, Segmented Bus

I. INTRODUCTION

Modern deep-submicron silicon technologies permit increasingly complex System on Chip (SoC) designs. The growing diversity of devices results in many possible interfaces. Often, the interconnection complexity of SoC modules limits both the system design process and system performance. Furthermore, these modules often require different data transfer speeds and parallel transmission capability[1]. A conventional bus structure might not be adequate for these demands because, typically, only one attached module can transmit at a time, and a large capacitive load caused by attached system modules and long bus wires can make a bus very slow. Moreover, the increase in both functional complexity and size of modern SoC devices tends to lengthen interconnect wires between system modules. As a result, synchronous system timing based on global clocks will become more difficult, if not impossible. A viable solution to these problems is a segmented bus architecture based on asynchronous communication. Such a structure provides a flexible platform for asynchronous self-timed SoC design, including globally asynchronous, locally synchronous (GALS) designs in which each distinct system module has a self-timed interface but is internally synchronized to a local optimized clock. A self-timed interface method significantly improves system scalability, automatically removing the difficult problems related to global clock distribution. Moreover, partitioning the bus into several concurrently operating segments overcomes the performance bottleneck of a conventional bus, letting modules in a particular segment exchange data

independently of modules in other segments. Simple bridges composed of tri-state buffers isolate adjacent bus segments from each other. Whenever an intersegment transfer occurs, these bridges dynamically link several successive segments to establish a connection between modules in different segments. Researchers proposed the concept of segmenting buses primarily for multicomputer architectures. More recent approaches address on-chip implementation of segmented buses. This paper targeted dynamically reconfigurable segmented-bus architecture for high-performance SoC applications. The structure not only enables faster operation than a conventional bus system but also offers lower power consumption per transferred data item. This is possible because segmentation is realized in such a way that the majority of data transfers in the system are intra-segment transactions on relatively short wires with low or moderate capacitive loads.

II. SYSTEM ARCHITECTURE

A segmented bus is a bus which is partitioned into two or more segments. Each segment acts as a normal bus between modules that are connected to it and operates in parallel with other segments. Segments can be linked dynamically to each other in order to establish connection between modules located in different segment [8]. Due to segmentation of the bus, parallel transactions can take place, thus increasing the performance of the bus. A high level block diagram of the segmented bus system is illustrated in Figure 1.

A bus-based system consists of three kinds of components (sub-systems): masters, slaves and arbiters. Generally, each of the devices connected to the bus lines may behave, depending on the situation, as either a master, or a slave. However, for simulation and assessment issues, here consider fixed functionality of these devices, that is, they will be only masters, or slaves. Only one master at a time may transfer data on the bus, thus there is need for arbitration. In a conventional single bus approach, the current master-slave connection occupies the whole length of the bus, even though the communicating devices were physically close to each other. The Segmented Bus approach would allow this kind of connection to occupy only a small portion of the bus - the segment. Arbitration at this level is provided by the Local Arbiter (LA), one for each segment. They decide which master within the segment will get access to the bus. Whenever inter-segment transfers are required, a Central Arbiter (CA) decides which of the requests can be serviced. [2]- [4]. Only one inter-segment grant is given by the central arbiter.

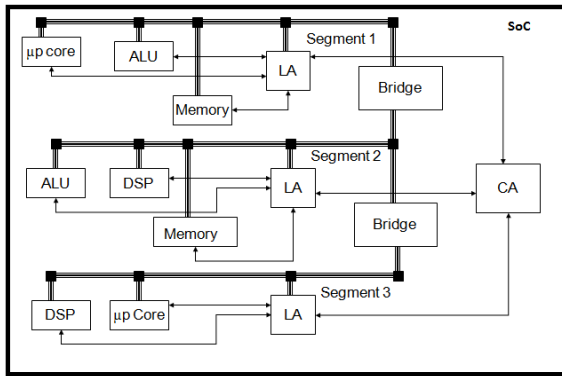


Fig 1: Segmented Bus Structure in SoC.

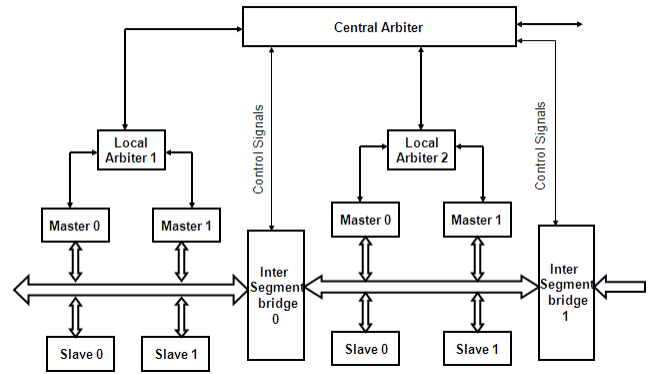


Fig 3: Structure of the Existing Segmented Bus

2.1. Existing Segmented Bus Architecture

The existing segmented bus architecture is illustrated in Fig.2. A segmented bus is partitioned into few segments. Every segment comprises of a group of masters, a group of slaves, a local arbiter, an intersegment bridge module and the physical wires for the bus address, data and control signals [8]. Modules (masters and slaves) are grouped according to their interconnection characteristics and placed on segments. Each segment operates as normal bus for modules, which are placed on it, and operates in parallel with other segments. Segments can be connected to each other in order to establish a connection between modules in different segments [8].

The segments with their components act as stand-alone buses operating in parallel, masters mostly asking services from the group of slaves placed within the same segment limits. Fig. 3 shows the structure of the existing segmented bus [8].

When a master device wants to communicate with a slave device within the same segment, the master device sends a request to its local arbiter. This requires dedicated request and grant wires between each device and the arbiter. The local arbiter grants the bus to the master and then the transaction. When multiple master devices request the bus, the arbiter grants the bus to only one device at a time. Similarly when one segment wants to communicate with other segment central arbiter gives a grant to that segment. But here only one inter-segment communication is possible at a time.

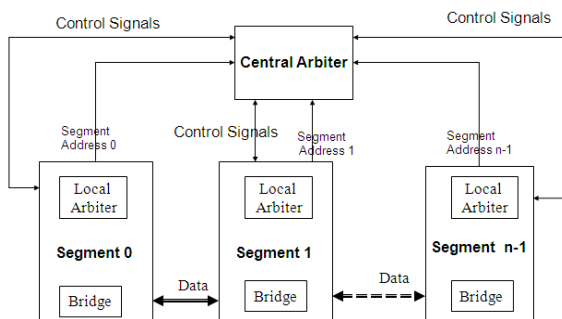


Fig 2: Block diagram of Existing Segmented Bus

2.2. Proposed Segmented Bus Architecture

The existing segmented bus architecture has a central arbitrator within it. An intersegment data transfer can be made only with the involvement of the central arbitrator. Therefore the existing segmented bus architecture has two main disadvantages. Due to the involvement of the central arbitrator, the complexity is high and so the intersegment data transfer delay is also high. This is the first disadvantage. The second disadvantage is, when the number of masters/slaves connected in the bus increases, the size and complexity of the central arbitrator increases. Due to this increase, the arbitration delay increases very much. In order to overcome these two disadvantages, new reconfigurable segmented bus architecture is proposed in this project. In the proposed reconfigurable segmented bus architecture, reconfigurability feature is incorporated in order to eliminate the disadvantages of the existing segmented bus architecture. Re-configurability feature means, adapting the topology of the bus based on the requests from the masters inside the segments. The Block diagram of Proposed Segmented Bus is shown in Figure 4.

The proposed architecture uses dynamic bridge-by-pass technique in order to incorporate dynamic re-configurability in the bus. So this architecture is named as Bridge-by-pass architecture. In this architecture, CA is eliminated. Therefore, the system complexity is reduced and arbitration delay is also reduced. The structure of Bridge-by-pass architecture is shown in Fig.5. The proposed architecture consists of a bus with two segments (Segment1, Segment2).

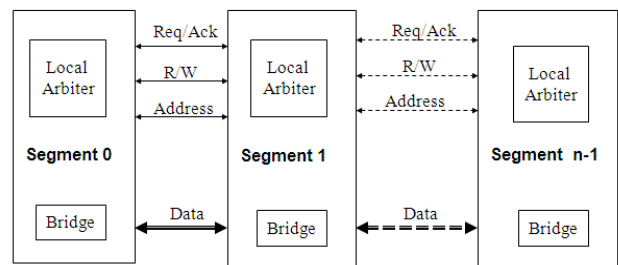


Fig 4: Block diagram of Proposed Segmented Bus

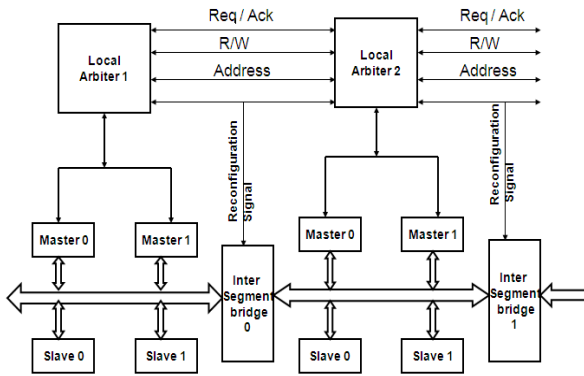


Fig 5: Proposed Segmented Bus Architecture

There are two types of data transfers that can take place in the proposed bus architecture. The first type of data transfer is intra-segment data transfer. The second type of data transfer is intersegment data transfer. In intra-segment data transfer, the data transfer occurs within the segment itself.

For example, if in Segment1, Master1 communicates either with Slave0 or Slave1 it is called intra-segment transfer. In intra-segment communication, the data transfer between a master and a slave takes place through its local arbiter. In intersegment data transfer, data transfer occurs between master of one segment and a slave of another segment. For intersegment data transfer, the existing architecture uses central arbiter for data transfer [8]. The presence of central arbiter increases the delay and system complexity. So in this Bridge-by-pass architecture, central arbiter is removed and instead local arbiter controls the data transfer. In the existing architecture, for intersegment data transfer, the master (source) sends request to its local arbiter. The local arbiter gives request, R/W and address signals to central arbiter. The central arbiter checks for the destination segment, if the destination segment is free then its corresponding local arbiter gives grant signal to the central arbiter. The central arbiter in turn gives grant signal to local arbiter of initiating segment. Then, central arbiter gives control signal to bridge so that the bridge opens and data transfer occurs between the master of source segment and slave of the destination segment.

In Bridge-by-pass architecture, for e.g. if there is an intersegment data transfer between master of Segment1 and slave of Segment2, the master sends request to its Local Arbiter (LA1 in Fig. 5). The local arbiter LA1 sends the request, R/W and address signals to the next local arbiter (LA2). LA2 checks if its bus is free. If its bus is free, LA2 sends grant signal to LA1. Then Reconfiguration unit gets ready signals from LA1 and LA2, processed it and gives reconfiguration signal to Bridge0. The Bridge0 open and data transfer takes place between Segment1 and Segment2. This is the operation of Bridge-by-pass architecture.

Consider that the existing bus architecture consists of 100 segments. Suppose 50 segments requests the central arbiter for inter segment data transfer simultaneously, the central arbiter analyzes the 50 requests and gives grant to the segment which has the highest priority. The inter segment data transfer of that highest priority segment takes place, while remaining segments wait. After the completion of data transfer, the central arbiter gives grant to the next segment which has next higher priority among all other segments. This proceeds till all the requests are processed.

In the Bridge-by-pass architecture, Segment1 has the highest priority for intersegment data transfer and Segment2 has the least priority. Within a segment, Master0 has higher priority than Master1. Suppose 50 segments requests the central arbiter for inter segment data transfer simultaneously, the local arbiter in between two segments controls the inter segment data transfer. Since the central arbiter is removed, the complexity and inter segment delay reduces. Hence when compared to existing architecture, Bridge-by-pass architecture is better in performance in terms of communication delay.

III. SIMULATION RESULTS

The bus architectures are modeled using VHDL. Simulation was done using Modelsim XE III 6.4 Simulator and the output waveforms is obtained as shown in fig.6 and 7. This model is synthesized using Xilinx ISE 9.2i. To evaluate the performance and power consumption of the bus model Xilinx Xpower analyzer is used and the results are obtained. The analysis of the results obtained is discussed in this section.

In Figure 6, Segment 1 considering which consist of two masters (Master1 & Master 2), two slaves (Slave 1 & Slave2 with address 01 and 02 respectively) and a Local Arbiter with fixed priority arbitration. Initially Master 1 and Master 2 are requesting the segment for write operation to Slave 1 and Slave 2 respectively. But Local Arbiter gives only Grant to the Master 1 and it writes the data in Slave 1. After releasing the Request of Master 1, Master 2 gets the Grant and it writes the data to Slave2

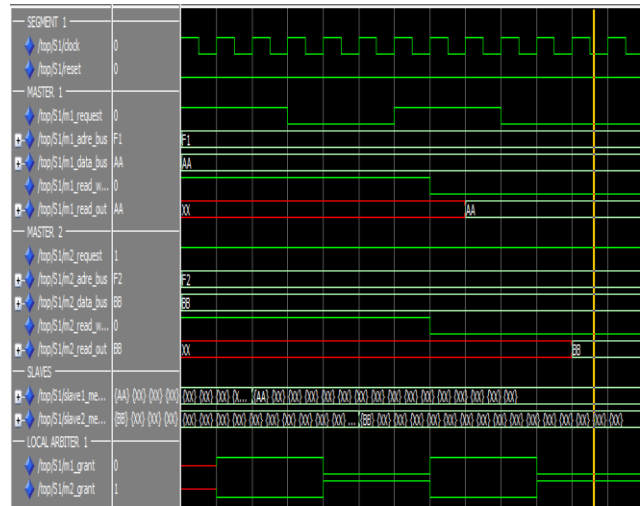


Fig 6: Intra-segment communication

In figure 7 Segment 1 considering which consist of two masters (Master1 & Master 2), two slaves (Slave 1 & Slave2 with address 01 and 02 respectively) and a Local Arbiter with fixed priority arbitration. Also Segment2 is considering with Slave 3 and slave 4 (with address 03 and 04 respectively). Initially Master 1 and Master 2 are requesting

ACKNOWLEDGEMENT

We would like to thank the Principal, HOD and all the teaching and non-teaching staffs of TKM Institute of Technology for helping to complete the work as mentioned in the paper.

REFERENCES

- [1] S.Hema Chitra “ A High Performance On-Chip Segmented Bus Architecture Using Dynamic Bridge-By-Pass technique ” 5th International Conference On Industrial An Information Systems, ICIIS 2010 Jul29-Aug 01,2010,India, pp 249-254
- [2] S.Hema Chitra, P.T.Vanathi “Design and Analysis of Dynamically Configurable Bus Arbiters for SoCs” ICGST- PDCS, Volume 8, Issue 1, December 2008, pp. 45– 52
- [3] Krishna Sekar,Kanishka Lahiri, , Anand Raghunathan, and Sujit Dey, Senior Member, IEEE “Dynamically Configurable Bus Topologies for High-Performance On-Chip Communication” IEEE transactions on very large scale integration (VLSI) systems, vol. 16, no. 10, October 2008. pp. 1413-1426
- [4] Krishna Sekar,Kanishka Lahiri, , Anand Raghunathan, and Sujit Dey, Senior Member, IEEE “Dynamically Configurable Bus Topologies for High-Performance On-Chip Communication” IEEE transactions on very large scale integration (VLSI)systems, vol. 16, no. 10, October 2008. pp. 1413-1426
- [5] Milica Mitic and Mile Stojeev “An Overview of On – Chip Buses” Facta Universitatis (NIS) SER.:ELEC.ENERG. vol.19,no.3, December2006, pp405-428.

ABOUT AUTHORS



Sreeja. M. S.¹, has M.Tech in VLSI and Embedded systems and B.Tech in Electronics and Communication. Currently working as Assistant professor of Electronics and Communication Engineering Department in Younus College of Engineering and Technology, affiliated engineering college under University of Kerala.



Mr.Manu.T.S.² has M.Tech in Embedded systems and B.Tech in Electronics and Communication and he is working as an Assistant professor of Electronics and Communication Department in TKM Institute of Technology,Kollam, an affiliated engineering college under Cochin University of Science and Technology for last two years, Asst.Prof. Manu T.S has guided over 25 students for their accademic project ,seminars and mini projects throughout his career and he undergone many training programs in VLSI and Embedded systems .He presented and Published Papers related to FPGA designs in National and International Conferences and Journals .

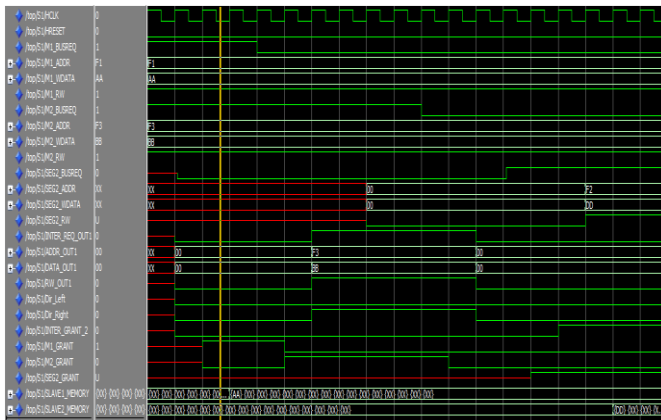


Fig 7.a.: Inter-segment Communication (segment 1)

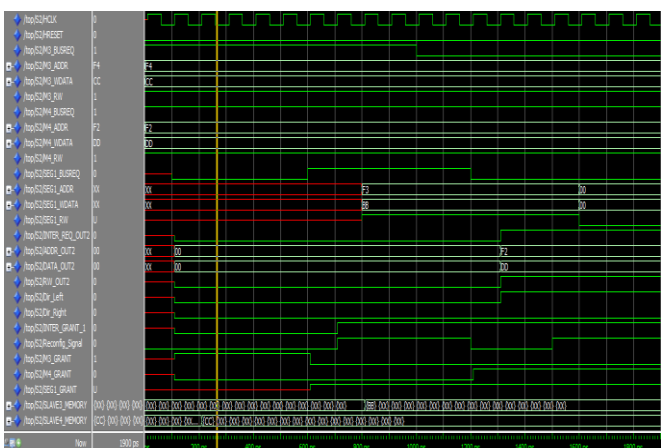


Fig 7.b.: Inter-segment Communication (segment 2)

the segment for write operation from Slave 1 and Slave 4. But Local Arbiter gives only Grant to the Master 1 it is an intra segment operation .After releasing the Request of Master 1, Master 2 gets the Grant for write operation in Slave 4. Here an inter-segment communication is needed because Master is in Segment 1 and Slave is in Segment 2.So INTER SEGMENT REQUEST becomes high and the data of the granted masters appears at the bridge. The bridge is a bi-directional buffer which will be controlled by the reconfiguration signal generated by the reconfiguration unit. After the enabling of the bridge the data is transfered from segment 1 to segment 2 and which will write on the segment 2 as shown in figure 7.a and figure 7.b.

IV. CONCLUSION

A new dynamically reconfigurable segmented bus architecture is proposed in this paper. In the proposed architecture, speed is increased and communication delay is reduced. There is no power and area overhead. Area has reduced in the proposed architectures. The bandwidth is highly improved. The bus is highly scalable. Due to these reasons, the proposed architecture seems to be highly efficient in terms of design and performance. Hence the proposed architecture can be used in high speed SoC devices.

Affect of Vibratory Welding Process to Improve the Mechanical Properties of Butt Welded Joints

Govindarao P¹. Srinivasarao P². Gopalakrishna A.³ and Sarkar M.M.M.⁴

¹Associate Professor, Dept. of Mechanical Engineering, GMRIT, Rajam, Andhra Pradesh

²Professor, Dept. of Industrial Engineering, GITAM University, Vishakhapatnam, Andhra Pradesh

³Associate Professor, Dept. of Mechanical Engineering, JNTU Kakinada, Andhra Pradesh

⁴Professor, Dept. of Mechanical Engineering, Andhra University, Andhra Pradesh

Abstract: For improving mechanical properties of steels, vibration techniques have been used in the last few decades. During the welding of metals along with mechanical vibrations, uniform and finer grain structures can be produced. This increases the toughness and hardness of the metals, because of solidification effects at the weld pool surface. As the weld pool solidifies, grains are not only limited in size, but dendrites growing perpendicular to the fusion line are restricted. While the process is going on, dendrites can be broken up before they grow to become large in size. Hence, the microstructure of the weld metal is improved during the solidification process. In this work, we employed a dynamic solidification technology, by applying mechanical vibrations during the 'Arc welding' process. Analyses have been carried out for mild steel pieces having 5 mm. of thick butt joints. The results obtained from the current study pointed out that the butt welded joints fabricated with vibratory condition are found to possess relatively high hardness, without any considerable loss in its ductility.

Keywords: Arcwelding, Vibratorywelding process, Hardness, Grain size.

I. Introduction

In manual metal arc welding (MMA) process, an arc is drawn between a coated consumable electrode and the work piece. The metallic core-wire is melted by the arc and is conveyed to the weld pool as molten drops. The electrode coating is also melting to form a gas shield around the arc and the weld pool. Slag is formed on the surface of the weld pool, and the slag must be removed after each layer. Manual Metal Arc welding is still a widely used hard facing process. Due to the low cost of the equipment, the low operating costs of the process and the ease of transporting the equipment, this flexible process is ideally suited to repair work benefits of MMA Welding are: Flexible, Low Cost, and ease of Repairs.

Butt welding is used to connect parts which are nearly parallel and don't overlaps. It can be used to run a processing machine continuously, as opposed to having to restart such machine with a new supply of metals. Butt-welding is an economical and consistent way of joining process without using supplementary components. Usually, a butt-welding joint is made by slowly heating up the two weld ends with a weld plate and then combine them under specific pressure. This process suitable for prefabrication and manufacturing special fittings afterward, the material is usually ground down to a smooth finish and either sent on its way to the processing machine, or sold as a completed product.

Hardness is the Resistance of a material to deformation, indentation, or penetration by means such as abrasion, drilling, impact, scratching and/or wears. The relative toughness of the mild steel or base metal is affected by many variables including: the chemical analysis, micro structural constituents, and strength or hardness level and grain size [12].

Heat treatable steels [1] have improved strength along with good properties of toughness and fatigue strength. In situations when tensile strength and the yield strength of structural steels don't satisfy the design requirements, there is a need for heat treatable steels with higher carbon content. The improved strength allows the production of lighter structures, i.e. the usage of thin sheets. The problems that usually occur in welding of steels with higher carbon content are the following: weld cracking, weld metal porosity, high hardening of the weld metal, and cracking of the base material in HAZ [9]. The application of laser welding in industry is constantly increasing. The most important advantages of laser welding over other procedures include [5-9]: high welding speed, small or no deformations of the welded parts, and high quality of the welded joint. Laser welding of steels with higher carbon content, such as heat-treatable steels has not yet been applied in high-volume production [9].

Arc welding [2] differs regarding the power density and the volume of heat input into the material. High power density in laser welding allows welding with lower specific heat input than in other welding, which results in very high cooling rates [4]. The cooling rates in arc welding are faster than other welding, so that a lower value of maximum hardness in the welded joint is expected [10-12]. In vibratory welding, stirrer produce a disturbance in weld pool during solidification. After completion of nucleation, the solidification process will continue with nucleus growth. Increasing the growth rate will reduce the grain size of metal. In welding, as the heat source interacts with the material, the severity of thermal excursions experienced by the material varies from region to region, resulting in three distinct regions in the weldment [12].

The aim of this work is to obtain a modification of the microstructure by mechanical vibrations during the welding process. Because of microstructure changes, there is an improvement in the material's hardness and mechanical properties. This study was extended to investigate the effect of vibratory set up on the mechanical properties of 5 mm thick stainless steel (AISI202) butt joints. Low and high heat input combinations were used to study the effect of mechanical vibrations on small sized and large sized fusion zone respectively.

This paper is organised into five chapters. Chapter 2 describes the developed experimental setup and how the experiments have been performed for the considered metals; chapter 3 discusses the results obtained from the experimental analysis; chapter 4 illustrates the metallurgical effects of the various specimens and chapter 5 concludes the paper.

II. Experimental Work

The MMA welding process is an arc welding process which produces coalescence of metal by heating them with an arc between a covered metal electrode and the work. Shielding is obtained from decomposition of the electrode covering. Pressure is not used during the operation and the filler metal is obtained from the electrode. The MMA welding process can be used for welding most structural and mild steels. These include low-carbon or alloy steels; low-alloy, heat treatable steels; and high-alloy steels such as stainless steels. This welding process can be used in all positions flat, vertical, horizontal and requires only the simplest equipment. Thus, MMA welding lends itself very well to field work.

Material Used

Mild Steel, It is composed of (in weight percentage) 0.9% Carbon (C), 7.5-10.0% manganese (Mn), 1.00% Silicon (Si), 17.0-19.0% Chromium (Cr), 4.0-6.0% Nickel (Ni), 0.06% Phosphorus (P), 0.03% Sulphur (S), and the base metal Iron (Fe). Fig.1. shows a typical specimen used in the current study.



Fig 1 Specimen piece

Equipment Used

Fig 2 shows the experimental setup of the vibrator machine, its properties and welding process used for laying down the vibratory welding bead.



Fig.2 Experimental setup

2.3 Vibratory Setup for Welding

With an aim of improving the mechanical properties of weld joints through inducing of favourable changes in the weld microstructures, an auxiliary vibratory set up capable of inducing mechanical vibrations into the weld pool during manual metal arc welding is designed and developed. Different frequencies and with different amplitude are applied along the weld length, just trailing behind the welding arc so that weld pool could be mechanically stirred in order to induce favourable micro structural effects. This setup produces the required frequency with the amplitude in terms of voltages.

2.4 Butt welding by MMA welding Process

In the current investigation, 5 mm thick mild steel butt joints are used. Low and high heat input combinations are used to study the effect of mechanical vibrations. Figs.3 and 4 depict the joining of two mild steel strips during and after the welding process.



Fig.3 During welding



Fig.4 After welding

Butt Welded Joint (constant acceleration and at different voltages)

The prepared butt welded joints are under the low heat input (90-110 Amp). There are 2 number of passes to fill the gap, in which 1 main passes and 1 is root pass. During the root pass there is no role of vibratory setup. After the root pass, vibratory setup come into action and moved just behind the arc and make a disturbance during the solidification of weld bead. Table 1 and Table 2 illustrate the parameters variation with respect to acceleration & amplitude during the process.

Table 1 Parameters variation with respect to acceleration during the analysis

	70 Volts	150 Volts	230 Volts
Acceleration (m/s ²)	18.3	49.1	32.6
	16.4	49.7	31.1
	19.9	48.7	30.4
	17.7	45.3	28.4
	18.6	51.9	28.3
	19.3	50.8	29.7
RMS value	18.4	49.29	30.33
Grms value	1.875g	5.02g	3.09g

Table 2 Parameters variation with respect to amplitude during the analysis

	70 Volts	150 Volts	230 Volts
Amplitude (in mm)	0.350	0.238	0.274
	0.348	0.233	0.269
	0.347	0.230	0.266
	0.349	0.235	0.270
	0.352	0.242	0.275
	0.351	0.240	0.273
RMS Value	0.350	0.236	0.273

III. Results And Discussion

For the fabricated specimens, tests have been conducted to measure the hardness of the weld bead along and perpendicular to its bead surface. From the initially considered points, acceleration being kept constant by varying the voltage, found the RMS value in terms of GRMS. The same process is repeated for several times, by amplitude keeping constant and varying in voltage. The hardness values are observed without vibration values are smaller than the with vibration hardness values. Here 7 samples are taken to found the hardness values at different locations along the weld bead and perpendicular to the weld bead surface.

Hardness Measurement

Micro-hardness measurement can be done by Lecco Vickers Hardness (LV 700) tester. In which, a diamond indenter in the form of a right pyramid with a square base and an angle 136° between opposite faces, is forced into the material under a load F. The two diagonals X and Y of the indentation left on the surface of the material after removal of the load are measured and their arithmetic mean L is calculated.

$$H_v = \frac{0.1889F}{L^2} \text{ and } L = \frac{X + Y}{2} \quad (1)$$

Where F is the applied load (N), L is the diagonal of square impression (mm), X is the horizontal length (mm) and Y is the vertical length (mm).

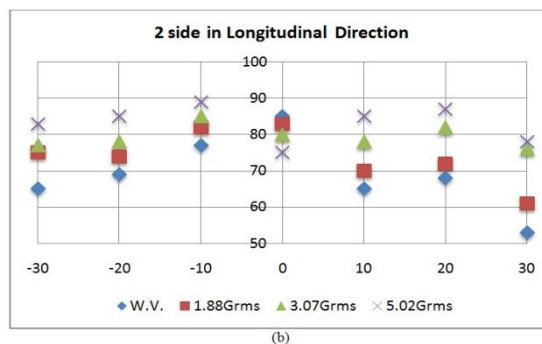
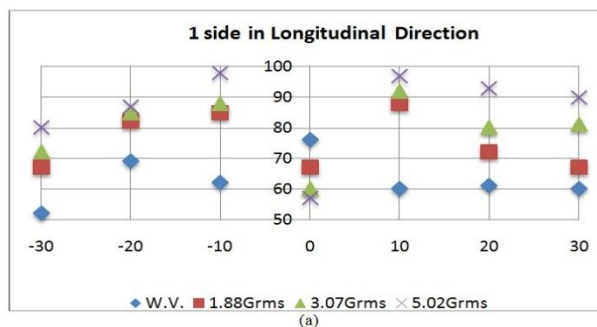
Table .3 Hardness values in longitudinal direction

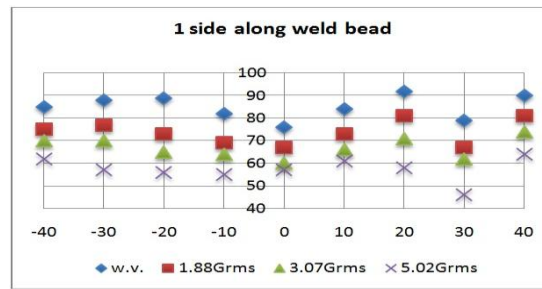
W.V	First side	52	69	62	76	60	61	60
	Second side	65	69	77	85	65	68	53
1.88 Grms	First side	67	82	85	67	88	72	67
	Second side	75	74	82	83	70	72	61

3.07 Grms	First side	72	85	88	60	92	80	81
	Second side	77	78	85	80	78	82	76
5.02 Grms	First side	80	87	98	57	97	93	90
	Second side	83	85	89	75	85	87	78

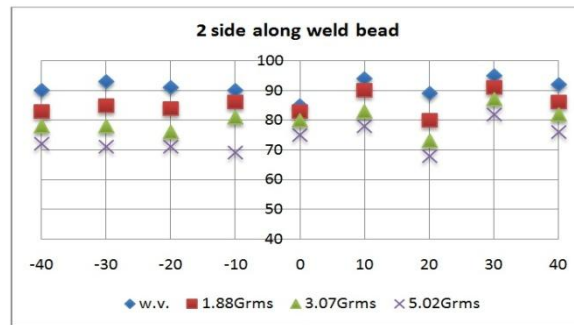
Table .4 Hardness values Along Weld bead direction

W.V	1 side	85	88	8	8	7	8	9	7	9
	2 side	90	93	91	90	85	94	89	95	92
1.88 Grms	1 side	75	77	73	69	67	73	81	67	81
	2 side	83	85	84	86	83	90	80	91	86
3.07 Grms	1 side	70	70	65	64	60	66	71	62	74
	2 side	78	78	76	81	80	83	73	87	82
5.02 Grms	1 side	57	57	56	55	57	61	58	46	64
	2 side	71	71	71	69	75	78	68	82	76





(c)



(d)

Fig. 5 variation of hardness values with and without vibration

IV. Metallurgical Study Of Specimens

Metallographic study shows that during conventional butt welding the uniform long dendrites which show that a uniform solidification process took place with uniform dendrites shown in the fig.7 and fig 8 with acceleration and amplitude kept constant during welding current respectively. Long dendrites show Coarse structure of the weld joint. The microstructure shows the uniform solidification process. Under vibratory conditions with acceleration and amplitude kept constant, the microstructure of vibratory butt-weld joints, long dendrites get fragmented and break in to small dendrites and forms a new nucleation sites. Here dendritic fragmentation took place due to which fine structures form. This enhances the hardness and mechanical properties of weld joints.

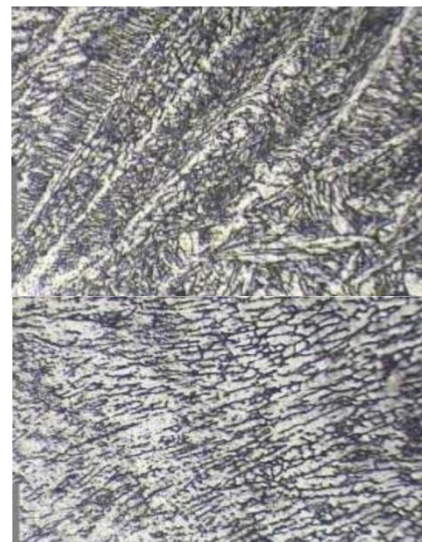


Fig.7 Microstructure of manual metal arc welding with vibratory (constant acceleration and amplitude)

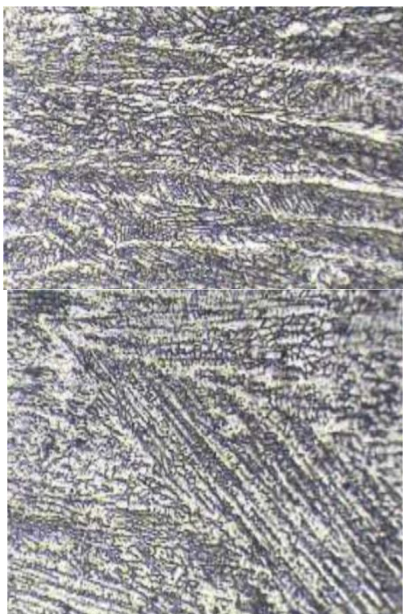


Fig.6 Microstructure of manual metal arc welding without vibration (constant acceleration and amplitude)

V. Conclusions

In the present study, welding is performed along with the vibrations for improving the mechanical properties of the base material and the weld metal micro hardness was calculated under vibratory condition. Along the weld bead the hardness value decreases when compared from without vibration. Metallurgical study showed that small grain structure is attained due to the effect of vibration.

Increase in hardness leads to crack initiation along the weld bead, so it is not preferable. During manual butt weld joints uniform long dendrites which show that a uniform solidification process took place with uniform dendrites. Due to auxiliary mechanical vibrations long dendrites break and forms a new nucleation sites. Finally, paper concludes that the Hardness of the parent metal increases under MMA welding with vibration.

References

- [1] H. Kaufmann, Laser welding – will it have any significant impact on welding ?, Svetsaren, Vol. 56, 2-3, pp. 73-75, 2001.
- [2] J.K. Larsson, Laser welding: A mature process technology with various application fields, Svetsaren, 1-2, pp.43-50, 1999.
- [3] S. Kralj, Z. Kožuh, B. Bauer, Flexible manufacturing system robot-laser, Proc of. 2nd International Conference Business Systems Management - UPS 2001, pp.133-137, Mostar, May, 2001.
- [4] M. Naeem, YAG laser welding of thin sheet, Welding & Metal Fabrication, Vol. 68, No. 6, pp.6-10, June, 2000.
- [5] R. Rodrigues, L. Bordalo, N. Sobrai, L. Quintino, Laser Welding in Automotive Industry. An Application: Joining Hinges to Car Doors Reinforcement Structure, Doc. IIW – IV/737/99.
- [6] J.-W. Yoon, Y.-H. Han, S.-H. Hwang: Laser beam welding of medium and high carbon steels, Proc. of 3rd International Conference “Beam Technology”, Karlsruhe, March, 1991, DVS.
- [7] M. Kutsuna, A. Kikuchi, Thermal Cycles and Microstructures in Laser Welding of Carbon Steel, IIW DOC IV-597-93.
- [8] Y.N. Liu, E. Kannatey-Asibu, Jr., Experimental Study of Dual-Beam Laser Welding of AISI 4140 Steel, Welding Journal, Vol. 76, No. 9, September 1997.
- [9] T. Webber, High power CW Nd:YAG laser welding of high carbon steel with pre- and post-weld heat treatment, Proc. of, 5th CISFFEL International Conference, La Baule, June 1993.
- [10] Sobolev, V.V., Study of liquid solidification during the welding process in the ultrasonic field, Metals Abstract, 55-0159:203 (1995).
- [11] Watanabe, T. and Nakamura, H., Solidification control of austenitic stainless steel weld metal by electromagnetic stirring, National Research Institute for Metals (Japan), Trans, Japan Welding Soc., Vol. 21, No.2:37-43(1990)
- [12] Nagy, M. J., Jr. and D. M. Kelman, Application of ultrasonic vibrations during solidification of vacuum-arc melted Ingots. METALS ENGINEERING QUARTERLY 1:72-82, Nov 1961.

Period Based Defence Mechanism against Data flooding attacks

O.Mrudula¹,

Final M.Tech Student¹,

Dept of Computer Science and Engineering¹

B. Subbareddy²,

Asst.professor²,

Dept of Computer Science and Engineering²,

P. P. S. Naik³

Head of the Department³

Dept of Computer Science and Engineering³,

^{1,2,3}(Dr.Samuel George Institue of Engineering and Technology, Markapur-523316, Prakasam Dist., A.P.)

Abstract: There is a wide usage of mobiles anywhere and anytime to access the multimedia data. Thus there will be more oppurtunity for wireless adhoc networks. Because, comparing with the wired networks, wireless networks provides low cost and easy accesibility. But the main disadvantage for Consumer electronic devices were generally operate on limited battery power and therefore are vulnerable to security threats like Data Flooding Attacks. These attacks leads to Denial of Service(DoS) by flooding many data packets. There were some of the defence systems to data flooding attacks. But these systems may not give guarantee to the Quality of Service. Because because of Wireless data transmission the data may be usually burst. Therefore, we propose a novel defence mechanism against data flooding attacks with the aim of enhancing the throughput. The simulation results show that the proposed scheme enhances the throughput of burst traffic.

Keywords: Data Flooding Attack, Throughput, Burst Traffic, Wireless adhoc Network.

I. INTRODUCTION

In the present world, use of electronic devices became most essential. Users want to use the compact and portatable devices such as cellular phones, laptop computers, Personal Digital Assistants (PDAs), etc. anywhere and at anytime. They like to use those devices to download multimedia data or to access real-time traffic. Those devices are used as mobile nodes in wireless ad hoc networks; hence, wireless ad hoc networks on the basis of consumer electronics are expected to be widely used in the near future. In wireless ad hoc networks, the communications take place between mobile nodes, operating under limited energy of battery power rather than through base stations. Hence, it becomes extremely hazardous to wireless ad hoc networks when mobile nodes are clogged. Meanwhile, wireless ad hoc networks are vulnerable to security threats since all signals go through bandwidth- constrained wireless links and the routing decision are taken in a decentralized manner. Therefore, it is important to provide a path with secure robustness in wireless ad hoc networks. Wireless adhoc networks can be victimized to various kinds of attacks .Among them, the ad hoc flooding attack can easily cause Denial-of-Service (DoS) attacks by flooding many Route Request (RREQ) or data packets . Since a mobile node has

limited resource capacities such as memory space, computational ability, battery power, bandwidth capacity, and so on, it cannot provide services when it receives a lot of packets. Hence, the whole network as well as the victim node can get easily paralyzed.

I. EXISTING SYSTEM

There were Some of the Existing Systems that were able to solve the Denial-of-Service(Dos) attacks by flooding many Route Requests or Data packets. Even though attackers are able to conduct ad hoc flooding attacks by flooding either RREQ packets or data packets, most researches in this field have focused their study on RREQ flooding attacks much more than data flooding attacks. Contrary to other networks, the path construction from the source node to the destination node is important in wireless adhoc networks because the communication is performed via multiple hops without any infrastructure. Besides, the data flooding attack can be performed only after constructing a path. Therefore, an attacker sets up a path to the victim node so as to conduct data flooding attacks and then forwards tremendous useless data packets to the victim node along the path. However, the size of data packets is usually much larger than that of RREQ packets; i.e., 24 bytes for RREQ packets and 1 Kbytes or 512 bytes for data packets. Hence, resource consumption and bandwidth congestion of a node or the entire network can be easily occurred by data flooding attacks.

II. PROPOSED SYSTEM

The Proposed System mainly aims for the Security and Data Flooding attacks prevention and finding the problem where the flooding is attacked by using a mechanism. The flooding attack prevention (FAP) suggested a defense system against either RREQ or data flooding attacks. The path cut off mechanism is used as defense against data flooding attacks. When the victim node realizes that it has been subjected to the data flooding attack, it may cut off the path. However, the procedure of the path cut off mechanism is not explained in detail, and FAP cuts off the path when many data packets are transmitted to the victim node. Current users like to download or access multimedia data using the consumer electronic devices so that the packets may be transferred as burst traffic. However, FAP cannot distinguish burst traffic from attack traffic since FAP distinguishes an attack by comparing the incoming packets with a threshold. Hence, the throughput of burst

traffic may degrade if a simple threshold-based defense system is used in FAP.

Therefore, this paper proposes a novel period-based defense mechanism (PDM) against data flooding attacks taking enhancing the throughput of burst traffic into account. The proposed PDM scheme is based on periods and uses a blacklist to efficiently prevent the data flooding attack, as a result of which many data packets are forwarded at a high rate for the whole duration.

The rest of the paper is organized as follows: Section IV measures the throughput of burst traffic under data flooding attacks, and then Section V presents the proposed PDM scheme. Section VI shows the performance evaluation of the PDM scheme. Finally, Section VII concludes the paper.

III. THROUGHPUT OF BURST TRAFFIC UNDER DATA FLOODING ATTACKS

In wireless ad hoc networks, handheld-based consumer electronic devices are used as mobile nodes. The data flooding attack sends many data packets in order to clog not only a victim node but also the entire network since all packets are transmitted via multiple hops. Hence, data flooding attacks are extremely hazardous to wireless ad hoc networks.

To conduct the data flooding attack, an attacker first sets up a path to the victim node since the attack can be performed only after a path is constructed. Then, the attacker forwards tremendous useless data packets along the path to make sure that the victim node cannot process packets in a normal fashion. Finally, the resources of the victim node are exhausted, so the node may get isolated from the network. In order to measure the effect of the data flooding attack on data traffic including burst traffic in wireless ad hoc networks, we calculate the throughput.

The throughput is defined as the ratio between the amount of data packets sent by the source node and the amount of data packets received by the destination node during a time span from t_s to t_d . The amount of packets sent by the source node (t_r) can be classified into control packets (C) such as RREQ, Route Reply (RREP), Route Error (RERR) packets and data packets (Dall) including traffic for conducting data flooding attacks. On the other hand, the amount of data packets received by the destination node (t_c) can be classified into normal traffic (DN) excluding the traffic meant for data flooding attacks (γ). Therefore, we can represent the throughput using the following equation:

$$\text{Throughput} = \frac{\int_{t_s}^{t_d} \frac{r_c}{t_r} dt}{\int_{t_s}^{t_d} \left(\frac{D_N}{C + D_{all}} \right) dt} \quad (1)$$

Meanwhile, we can divide the normal traffic into non-burst traffic (α) and burst traffic (β), so DN is presented as:

$$D_N = \alpha + \beta \quad (2)$$

Using (1) and (2), the throughput can be represented as follows:

$$\text{Throughput} = \int_{t_s}^{t_d} \left(\frac{\alpha + \beta - \gamma}{C + D_{all}} \right) dt \quad (3)$$

Therefore, the throughput is affected when many control packets are huge traffic are deliberately generated so as to conduct data flooding attacks.

IV. PERIOD BASED DEFENCE MECHANISM AGAINST DATA FLOODING ATTACKS

To defend the data flooding attack, the proposed PDM scheme sets up w periods for the data transmission. The PDM scheme checks data packet floods at the end of each period in order to enhance the throughput of burst traffic. Therefore, it can guarantee the Quality of Service (QoS) of burst traffic. We denote $v(nSp-nDp)$ as the variance of the number of received data packets for the source node (nSp) to the destination node (nDp) during the period $T(i+1)-T(i+2)$. Here, p denotes the number of sessions taken for data transfer.

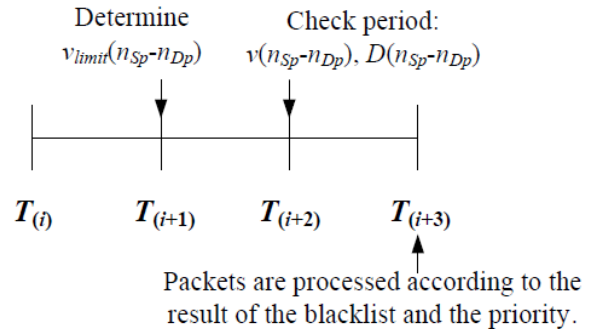


Fig: Procedures of each Period in the PDM Scheme

This shows procedures of each period in the PDM scheme. The mobile node nu initiates the variance coordinator ($h(nSpnDp)$) for data packet floods from nSp to nDp according to its data type so as to guarantee the QoS of the data packets. We also assume that $ave(all)$ is the average number of all received data packets during $T(i)-T(i+1)$. Then, we determine the variance limit of data packet floods from nSp to nDp ($vlimit(nSp-nDp)$) using the following equation:

$$v_{limit}(n_{Sp} - n_{Dp}) = ave(all) + h(n_{Sp} - n_{Dp}) \quad (4)$$

The procedure of the PDM scheme is following as:

Step 1) At the end of the period $T(i+2)$, nu compares the variance of received data packets, according to the $nSp-nDp$ pair ($v(nSp-nDp)$), with the variance limit ($vlimit(nSp-nDp)$). In wireless ad hoc networks, all packets are transferred via links between mobile nodes so that we can defend against data flooding attacks through the entire network by performing the defense at each mobile node.

Step 2) When $v(nSp-nDp)$ is greater than $vlimit(nSp-nDp)$, it checks whether data packets for $nSp-nDp$ pairs ($D(nSp-nDp)$) are in the blacklist or not. The Blacklist is maintained by each mobile node, which is initially empty. The maximum number of received data packets for a certain source node – destination node pair is listed in the blacklist. It aims to detect data flooding attacks.

- i) If $D(nSp-nDp)$ is in the blacklist, it is not transmitted until the next period ($T(i+3)$).
- ii) Else, the priority is determined by the inversion of the number of received packets and nu processes the data packets according to priority.

Step 3) nu updates the blacklist by the greatest number of received data packets in the period.

Step 4) *nu* checks the period is the last period of the data transmission.

- i) If it is the last period, the procedure of the PDM scheme is stopped.
- ii) Else Goto Step1.

VI. PERFORMANCE EVALUATIONS

We investigate the performance of the proposed PDM scheme by measuring the throughput. Then, we simulate the throughput of the PDM scheme according to the number of attackers and the number of transferred packets per second by ns-2 simulations.

A. Throughput Comparison

The performance of the proposed PDM scheme is measured by the throughput as given in (1). The PDM scheme sets up *w* periods for the data session from *ts* to *td* to defend the data flooding attack. The PDM scheme guarantees the QoS of non-burst traffic as well as burst traffic by determining () *limit Sp Dp v n - n* depending on the data type. The PDM scheme utilizes the blacklist since the data packet flooding attacker sends a high rate of data packets all times rather than certain given durations.

Moreover, the PDM scheme collects the information for calculating () *limit Sp Dp v n - n* at the first period and then performs the defense mechanism. Therefore, the expected probability of the received malicious data traffic in the PDM scheme at *nu* ($[\gamma]$ *PDM E*) is as:

$$E_{PDM}[\gamma] = \sum_{v=2}^n \{ \int_{t=T_v}^{T_{v+1}} (E[\gamma]) dt \}. \tag{5}$$

The PDM scheme can defend against malicious traffic which are burst and listed in the blacklist. Moreover, it processes the rest of data packets according to priority so that it can defend some of other malicious traffic. Hence, we can rewrite (5) as (6).

$$E_{PDM}[\gamma] \approx \sum_{v=2}^n \{ \int_{t=T_v}^{T_{v+1}} (E[U \times L]) dt \}. \tag{6}$$

Here, we denote $U \times L$ as the burst malicious traffic which are also listed in the blacklist. Hence, the malicious traffic (γ') that the victim node receives can be presented as follows:

$$\gamma' = U \times L. \tag{7}$$

The PDM scheme can prevent bandwidth congestion caused by the data flooding attack, so the amount of control packets of the PDM scheme (C') is reduced much more than C (the amount of control packets when the defense system against the data flooding attack is not operated). Hence, $C' \ll C$. Moreover, the PDM scheme can reduce the total generated number of data packets so that *all all D' << D* where *all D'* is *all D* of the PDM scheme. By reducing the received traffic for conducting the data flooding attack at the victim node, the received normal traffic regardless of burst traffic are increased. Hence, the victim node receives much larger number of received non-burst traffic (α') and burst traffic (β') than the case when the PDM scheme is not conducted. Therefore, according to (3), the throughput of the PDM

scheme (*ThroughputPDM*) under the data flooding attack can be presented as the following equation:

$$Throughput_{PDM} \approx \sum_{v=2}^n \{ \int_{t=T_v}^{T_{v+1}} (\frac{\alpha' + \beta' - \gamma'}{C' + D'_{all}}) dt \}. \tag{8}$$

Since malicious data packet floods are usually generated at a high rate all the time, β' is extremely improved but γ' is decreased as in (3). Therefore, the throughput of the PDM scheme is improved.

B. Simulations

We evaluate the throughput of the PDM scheme using the ns-2 simulation [13]. We conduct the simulation for 100 times and then draw the mean value on the graphs. We use 50 mobile nodes which move based on the random waypoint model with the speed of 20 m/s in a 1000 m by 1000 m area for 500 seconds. The transmission range of each node is 250 m. There are 20 CBR sources which send 512-byte UDP packets. We use the AODV as the basis routing protocol and compare its performance with that of our PDM scheme. We define $h(nSp-nDp)$ as 0 and 10 to investigate how the PDM scheme can guarantee QoS of burst traffic and non-burst traffic, respectively.

Fig. 2 shows the throughput varying with the number of attackers from 0 to 20 attackers. To compare the affect of the number of attackers to the throughput, each node including attackers sends 20 packets per second. The throughput of the PDM scheme regardless of $h(nSp-nDp)$ is higher than AODV so that it can defend against malicious data packet flooding attacks.

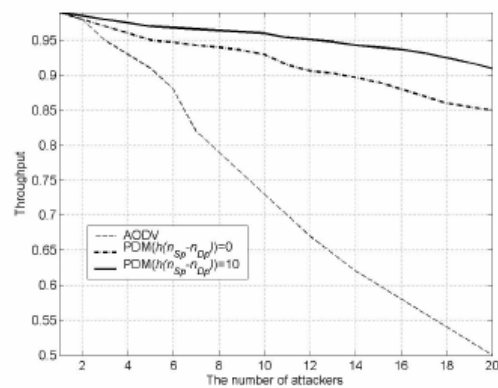


Fig. 2 Throughput vs. the number of attackers.

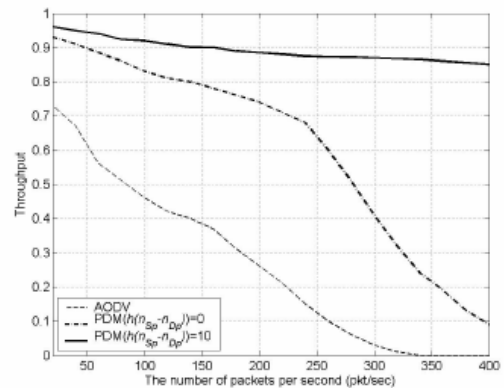


Fig. 3 Throughput vs. the number of packets per second.

Fig. 3 shows that PDM with $h(nSp-nDp)=10$ can guarantee QoS of burst traffic better than others. To investigate how much QoS of burst traffic are guaranteed, we increase the number of data packets per second from 20 packets/sec to 400 packets/sec. We assume that there are 5 attackers. When the number of packets per second is high (burst traffic), AODV cannot process packets because of the resource exhaustion.

VII. CONCLUSION

We have proposed the period-based defense mechanism against data flooding attacks. The data flooding attack paralyzes a victim node by consuming its resources. Hence, the throughput of the victim node is significantly reduced. However, the current defense systems focus on RREQ flooding attacks rather than the data flooding attack. They easily reduce the throughput of burst traffic by comparing with the simple threshold. Hence, we aim to enhance the throughput of burst traffic under the data flooding attack. The proposed scheme uses a blacklist, considers the data type, and processes packets according to the priority so as to defend against data flooding attacks; since the attacker forwards many data packets at a high rate for the whole session. Recently, many users like to download and share multimedia data, so we expect that the proposed scheme is useful to networks where burst traffic are transferred.

VIII. REFERENCES

- [1] A. Jamalipour, "Self-organizing networks [message from the editor-in-chief]," *IEEE Wireless Communications*, vol. 15, no. 6, pp.2-3, Dec. 2008.
- [2] S.-J. Lee and M. Gerla, "Split multipath routing with maximally disjoint paths in ad hoc networks," *IEEE International Conference on Communications (ICC 2001)*, vol. 10, pp. 3201-3205, Jun. 2001.
- [3] L. Xia and J. Slay, "Securing wireless ad hoc networks: towards a mobile agent security architecture," the 2nd Australian Information Security Management Conference 2004 (InfoSec 2004), Nov. 2004.
- [4] M. Al-Shurman, S.-M. Yoo, and S. Park, "Black hole attack in mobile ad hoc networks," the 42nd annual Southeast regional conference ACM Southeast Regional Conference (ACMSE 2004), pp. 96-97, Apr. 2004.
- [5] Y.-C. Hu, A. Perrig, D. B. Johnson, "Wormhole attacks in wireless networks," *IEEE Journal on Selected Areas in Communications*, vol. 24, no. 2, pp. 370-380, Feb. 2006.
- [6] Y.-C. Hu, A. Perrig, and D. B. Johnson, "Rushing attacks and defense in wireless ad hoc network routing protocols," the 2nd ACM Workshop on Wireless Security, pp. 30-40, Sept. 2003.
- [7] P. Yi, Z. Dai, Y. Zhong, and S. Zhang, "Resisting flooding attacks in ad hoc networks," *International Conference on Information Technology: Coding and Computing 2005 (ITCC 2005)*, vol. 2, pp. 657-662, Apr. 2005.
- [8] S. Desilva and R. V. Boppana, "Mitigating malicious control packet floods in ad hoc networks," *IEEE Wireless Communications and Networking Conference 2005 (WCNC 2005)*, vol. 4, pp. 2112-536, Mar. 2005.
- [9] S. Li, Q. Liu, H. Chen, and M. Tan, "A new method to resist flooding attacks in ad hoc networks," *IEEE Wireless Communications, Networking and Mobile Computing 2006(WiCOM 2006)*, pp. 1-4, Sep. 2006.
- [10] A. Khan, T. Suzuki, M. Kobayashi, W. Takita, and K. Yamazaki, "Packet size based routing for stable data delivery in mobile ad-hoc networks," *IEICE Transactions on Communications*, vol. E91-B, no. 7, pp. 2244-2254, July 2008.
- [11] X. Yang, Y. Shi, M. Zeng, and R. Zhao, "A novel method of network burst traffic real-time prediction based on decomposition," *International Conference on Networking (ICN), Lecture Notes in Computer Science*, vol. 3420, pp. 784- 793, Apr. 2005.
- [12] H. Kim, S. Han, and J. Song, "Maximum lifetime paths for The high packet delivery ratio using fast recover in a mobile Ad hoc network," *International Conference on Computational Science (ICCS 2006), Lecture Notes in Computer Science*, vol. 3992, pp.1101-1104, May. 2006.

Determination of Camber and Leaf Span of a Parabolic Leaf Spring for Optimized Stress and Displacement Using Artificial Neural Networks

Manas Patnaik¹, L.P. Koushik², Manoj Mathew³

¹(Department of Mechanical Engineering, Rungta College of Engineering & Technology, Raipur, India

^{2,3}(Department of Mechanical Engineering, Christian College of Engineering & Technology, Bhilai, India

Abstract : This work has been carried out on a parabolic leaf spring of a mini loader truck. The spring has been analyzed by applying a load of 3800 N and the corresponding values of stress and displacement are computed. In this work, Design of experiments has been applied under various configurations of the spring (i.e by varying camber & eye distance). Camber and Leaf span of a Parabolic Leaf Spring was found for Optimized Stress and Displacement value using Artificial Neural Networks. Various networks with different architecture were trained and the network giving the best performance was used for optimization.

Keywords: Artificial neural networks (ANN), Computer Aided Design (CAD), Camber, Design of Experiments (DOE), Eye Distance, Finite Element Analysis (FEA), Parabolic Leaf Spring (PLS).

I. Introduction

Parabolic Leaf springs are essential suspension elements used on mini loader trucks necessary to minimize the vertical vibrations, impacts and bumps due to road irregularities and to ensure safety of the loaded cargo. Parabolic Leaf springs are widely used for automobiles. The Parabolic leaf spring absorbs the vertical vibrations and impacts due to road irregularities by means of variations in the spring deflection so that the potential energy is stored in spring as strain energy and then gradually released to maintain comfort. The finite element analysis (FEA) is a computing technique that is used to obtain approximate solutions to the boundary value problems in engineering. It uses a numerical technique called the finite element method (FEM). It is now accepted by major industries across the world and a company that is able to verify a proposed design will be able to perform to the clients specifications prior to manufacturing or construction. In the present work, leaf spring has been analyzed for static strength and deflection using 3D finite element analysis. CATIA V5 R20 has been utilized in the creation of the three dimensional model and its static structural workbench for analysis when subjected to vertical loads. The variation of bending stress and displacement values are computed. To add on the different combinations of input parameters (camber & eye distance) have been taken into account & its influence on bending stress and max deflection has been studied.

II. Parabolic Leaf Spring & Dimensions

A more modern implementation of old leaf springs is the parabolic leaf spring for automobiles. The new innovative design is characterized by the use of less leaves whose thickness varies from the center to the outer

side following a parabolic pattern. The mathematical equation between the thickness & the length of the spring is that of a parabola & hence it has been named as parabolic leaf spring.

1. Camber – 90.81mm
2. Distance between eyes(Eye Distance) : 1025mm
3. Thickness at the central part : 10.81mm

Note: The above dimensions have been taken with the help of an inextensible measuring tape and a vernier caliper and then the procedure of modeling the spring was initiated. The basic views of the considered parabolic leaf spring are shown in fig. 1.

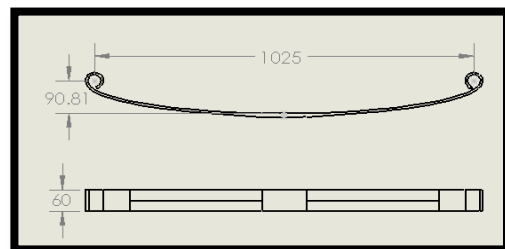


Fig.1 Front & Top view

Note : All dimensions are in mm

III. Existing Material

The material used for experimentation is EN45 and its mechanical properties has been mentioned in Table-1

Table--1

Material		Youn gs Mod ulus (E) Gpa	Pois son's Ratio (M)	Den sity (Kg/ M ³)	Yiel d Stre ngt h(M pa)
EN	IS(OI d)				
EN 45	55Si2 Mn90	200	0.3	785 0	150 0

IV. Result And Analysis Using Method Of Finite Elements

4.1 Meshing

Meshing is basically the process of breaking the CAD model into very small elements. It is also known as piecewise approximation. Meshing are of different types, it may be comprising of 1D, 2D or 3D elements. In present case selected is shown in Table-2

Table--2

Mesh			Element type	
S. N.	Entity	Size	Connectivity	Statistics
1	Nodes	12084		
2	Elements	5905	TE10(Tetrahedron element)	5905 (100.00 %)

4.2 Boundary Conditions

As shown in Fig. 2, one eye of the leaf spring will be fixed and the other eye will have certain degree of rotation to allow the leaf spring to deflect by some amount. It has been mathematically calculated that the maximum load which the spring will be subjected to 3800 N. This particular calculation has been done on the basis of GVW (Gross Vehicle Weight), which may be defined as the total weight of the loaded vehicle. This includes the vehicle itself and the cargo that is loaded within that vehicle.

In order to perform static structural analysis it is very essential to restraint the CAD model in the same manner as it is done physically. As far as parabolic leaf springs are concerned it has two eye ends, one of which is fixed with the upper body of the mini loader truck, while the other end is attached to a shackle which allows the spring to expand along its leaf span thereby causing some degree of rotation in the shackle.

Similarly we have applied constraints to our CAD model of parabolic leaf spring shown in Fig. 3 & 4.

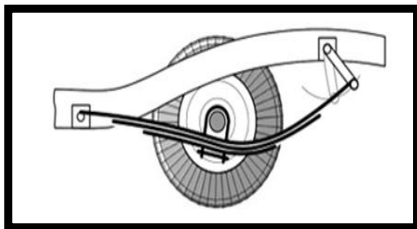


Fig.2 Suspension and Constraints

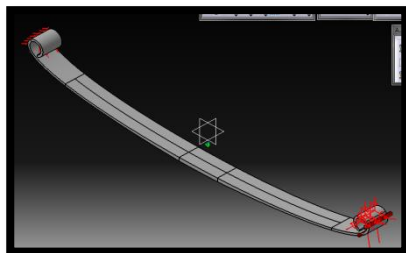


Fig.3 Applying Constraints.

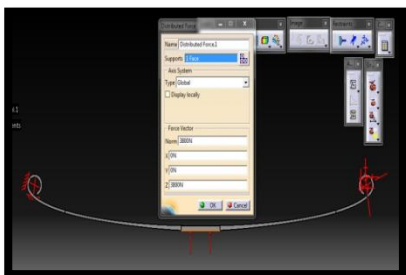


Fig.4 Applying Load

As shown in Fig. 4, the leaf spring is being treated as a simply supported beam which has a central load of 3800 N directed upwards.

4.3 Static Structural Analysis in CATIA V5 R20

After applying the boundary conditions the maximum von mises stress and maximum displacement is shown in Fig. 5 & 6.

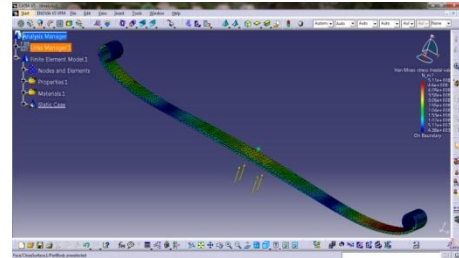


Fig.5 Von Mises Stress

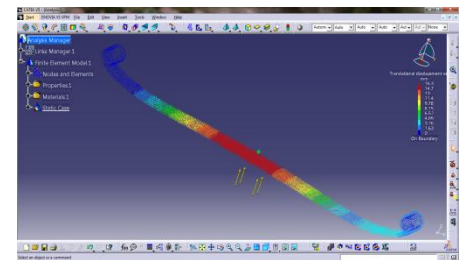


Fig.6 Displacement

Outputs on the basis of existing dimensions has been mentioned in Table-3 :

Table--3

S.N	Output Parameter	Value
1	Maximum Displacement	16.3079mm
2	Maximum Von mises stress	5.11017e+008 N_m2
3	Energy	30.008 J
4	Mass	4.549kg

V. Design Of Experiments

The Design of experiments (DOE) is a tool for determining the significance of different factors affecting process quality and for calculating optimal settings for controllable factors. For example we may believe that operating temperature and wave height affects the number of defects from a wave solder machine. DOE provides a fast & efficient means for determining the values of these parameters that would produce the fewer number of defects.

DOE Procedure:

- Select factors to be tested & a measure of process outcome.
- Select test setting for each factor.
- Select the appropriate orthogonal array.
- Run the tests.
- Analyze the results.
- Calculate optimum setting for each factor.
- Run confirmation test(s).

In this work camber and eye distance are selected as input parameters and max displacement, max von mises

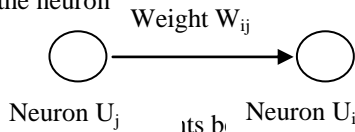
stress as output parameters. Design of experiments has been implemented by varying camber from 90 mm to 95 mm in steps of 10 and by varying eye distance from 1020 mm to 1030 mm in steps of 10.

VI. Artificial Neural Networks And Training

An Artificial Neural Network (ANN) is an information processing paradigm that is inspired by the way biological nervous systems, process information. An artificial neuron is composed of five main parts: inputs, weights, sum function, activation function and outputs. Inputs are information that enters the neuron from other neurons or from the external world. Generally connections between the units are defined by a weight w_{ij} . Weights are adaptive coefficients inside the network and they determine the intensity of the input signal as registered by the artificial neuron. Sum function is a function that calculates the effect of inputs and weights totally on this process element. This function calculates the net input that comes to a cell. The weighted sums of the input components is calculated by using Eq. 1

$$(net)_j = \sum_{i=1}^n W_{ij} I_i + b \quad \dots (1)$$

Where $(net)_j$ is the weighted sum of the j neuron for the input received from the preceding layer with n neurons, W_{ij} is the weight between the j^{th} neuron in the preceding layer and i^{th} neuron in the layer, I_i is the input to the preceding layer and b is a fix value as an internal addition known as bias. Figure 7 shows the connection between the neuron



6.1 Training by Artificial Neural Networks.

Training has been with the help of neural network tool box in MATLAB 2009b. Different combinations were taken into account to create the network which best suits our need. The neural network created is two layered and consists of 10 neurons in layer 1. The network initialization has been done below:

Feed forward back propagation network

- a) Training Function- TRAINLM
- b) Adaptive Learning Function- LEARNGDM
- c) Architecture- 2X10X2
- d) Hidden Layer- Tansig
- e) Output Layer- Purelin

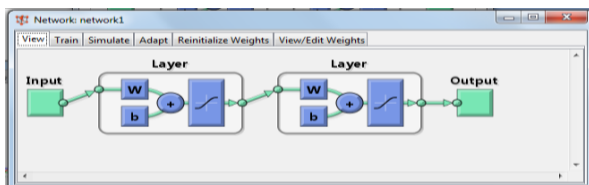


Fig.8 Neural Network Model

Several neural network models with different architecture were trained and tested using different configurations but the one in shown in Fig.8 above showed minimum Mean square error amongst all.

6.2 Performance

The assessment of any neural network model is done with the help of Mean Square error and it is found that amongst all the different configurations trained and tested, the minimum value of MSE was 0.91786.

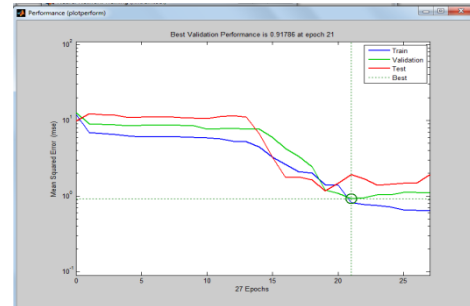


Fig.9 Mean Square Error is 0.91786 at epoch 21

VII. Conclusion

After successful creation of the neural network model it is imperative to optimize the stress and displacement in order to achieve the corresponding values of camber and leaf span. Following conclusion has been derived from the Neural Network Model:

Table--3

Min Stress (N/m ²)	Max Displacement(mm)	Camber (mm)	Leaf Span(mm)
50740000 0	16.596	90.8623	1029.1062

The values of camber and leaf span for optimized stress and displacement are shown in table-3 above.

References

- [1] Doshi N.P., Ingole N.K., Gulhane U.D., Analysis and Modification of Leaf Spring of Tractor Trailer Using Analytical and Finite Element Method, *International Journal of Modern Engineering Research (IJMER)*, Vol.1, Issue.2, pp-719-722.
- [2] Kumar K., Aggarwal M.L., A Finite Element Approach for Analysis of a Multi Leaf Spring using CAE Tools, *Research Journal of Recent Sciences*, Vol. 1(2), 92-96, Feb. (2012).
- [3] Rajendran I., Vijayarangan S., Design and Analysis of a Composite Leaf Spring, *Journal of Institute of Engineers India* 82 2002; pp. 180 – 187.
- [4] Jadhao K.K., Dalu R.S., Experimental Investigation & Numerical Analysis of Composite Leaf Spring, *International Journal of Engineering Science and Technology*, ISSN : 0975-5462 Vol. 3 No. 6 June 2011.
- [5] Rajendran, I., Vijayarangan, S. Design and Analysis of a Composite Leaf Spring, *Journal of Institute of Engineers India* 82 2002; pp. 180 – 187.
- [6] Toshinori Munakata, “Fundamentals of the New Artificial Intelligence”, Springer-Verlag London Limited, Second Edition, 2008, ISBN: 978-1-84628-838-8
- [7] S. N. Sivanandam, “Introduction to neural networks”, Tata McGraw-Hill Publishing Company Limited, 8th ed., 2009, ISBN No-13: 987-0-07-059112-7
- [8] MATLAB R2009b documentation.
- [9] K.I.Diamantras S.Y.Kung. Principal Component Neural Networks, theory and applications. John Wiley & Sons, Inc, 1996.

Somewhat almost αg -continuous functions and Somewhat almost αg -open functions

S. Balasubramanian¹ and Ch. Chaithanya²

¹Department of Mathematics, Govt. Arts College(A), Karur – 639 005, Tamilnadu

²Sri Mittapalli college of Engineering, Tummalapalem, Guntur, Andhrapradesh

Abstract: In this paper we tried to introduce a new variety of continuous and open functions called Somewhat almost αg -continuous functions and Somewhat almost αg -open functions. Its basic properties are discussed.

AMS subject classification Number: 54C10, 534C08, 54C05.

Keywords: Somewhat αg -continuous functions and Somewhat αg -open functions, Somewhat almost αg -continuous functions and Somewhat almost αg -open functions

I. Introduction:

b-open[1] sets are introduced by Andrijevic in 1996. K.R.Gentry[9] introduced somewhat continuous functions in the year 1971. V.K.Sharma and the present authors of this paper defined and studied basic properties of ν -open sets and ν -continuous functions in the year 2006 and 2010 respectively. T.Noiri and N.Rajesh[11] introduced somewhat b-continuous functions in the year 2011. Inspired with these developments we introduce in this paper somewhat almost αg -continuous functions, somewhat almost αg -open functions and study its basic properties and interrelation with other type of such functions available in the literature. Throughout the paper (X, τ) and (Y, σ) (or simply X and Y) represent topological spaces on which no separation axioms are assumed unless otherwise mentioned. For $A \subset (X; \tau)$, $cl\{A\}$ and A° denote the closure of A and the interior of A in X, respectively.

II. Preliminaries

Definition 2.1: A subset A of X is said to be

(i) b-open[1] if $A \subset (cl\{A\})^\circ \cap cl\{A^\circ\}$.

(ii) αg -dense in X if there is no proper αg -closed set C in X such that $M \subset C \subset X$.

Definition 2.2: A function f is said to be

(i) somewhat continuous[9][resp: somewhat b-continuous[11]; somewhat gs-continuous[6]] if for $U \in \sigma$ and $f^{-1}(U) \neq \emptyset$, there exists an open[resp: b-open; gs-open] set V in X such that $V \neq \emptyset$ and $V \subset f^{-1}(U)$.

(ii) somewhat open[11][resp: somewhat b-open[9]; somewhat gs-open] provided that if $U \in \tau$ and $U \neq \emptyset$, then there exists an open[resp: b-open; gs-open] set V in Y such that $V \neq \emptyset$ and $V \subset f(U)$.

Definition 2.3: (X, τ) is said to be resolvable[8][b-resolvable[11]] if there exists a set A in (X, τ) such that both A and $X - A$ are dense[b-dense] in (X, τ) . Otherwise, (X, τ) is called irresolvable.

Definition 2.4: If X is a set and τ and σ are topologies on X, then τ is said to be equivalent[resp: αg -equivalent] to σ provided if $U \in \tau$ and $U \neq \emptyset$, then there is an open[resp: αg -open] set V in X such that $V \neq \emptyset$ and $V \subset U$ and if $U \in \sigma$ and $U \neq \emptyset$, then there is an open[resp: αg -open] set V in (X, τ) such that $V \neq \emptyset$ and $U \supset V$.

III. Somewhat almost αg -continuous function

Definition 3.1: A function f is said to be somewhat almost αg -continuous if for $U \in RO(\sigma)$ and $f^{-1}(U) \neq \emptyset$, there exists a non-empty αg -open set V in X such that $V \subset f^{-1}(U)$.

It is clear that every almost continuous function is somewhat almost continuous and every somewhat almost continuous is somewhat almost αg -continuous. But the converses are not true.

Example 1: Let $X = \{a, b, c\}$, $\tau = \{\emptyset, \{a\}, \{b, c\}, X\}$ and $\sigma = \{\emptyset, \{a\}, X\}$. The function $f: (X, \tau) \rightarrow (X, \sigma)$ defined by $f(a) = c$, $f(b) = a$ and $f(c) = b$ is somewhat almost αg -continuous, somewhat αg -continuous but not somewhat continuous.

Example 2: Let $X = \{a, b, c\}$, $\tau = \{\emptyset, \{b, c\}, X\}$, $\sigma = \{\emptyset, \{b\}, \{a, c\}, X\}$ and $\eta = \{\emptyset, \{a\}, X\}$. Then the identity functions $f: (X, \tau) \rightarrow (X, \sigma)$ and $g: (X, \sigma) \rightarrow (X, \eta)$ and $g \circ f$ are somewhat almost αg -continuous.

However, we have the following

Theorem 3.1: If f is somewhat almost αg -continuous and g is continuous[r-continuous; r-irresolute], then $g \circ f$ is somewhat almost αg -continuous.

Theorem 3.2: For a surjective function f , the following statements are equivalent:

- (i) f is somewhat almost αg -continuous.
 - (ii) If C is regular closed in Y such that $f^{-1}(C) \neq X$, then there is a proper αg -closed subset D of X such that $f^{-1}(C) \subset D$.
 - (iii) If M is a αg -dense subset of X , then $f(M)$ is a dense subset of Y .
- Proof:** (i) \Rightarrow (ii): Let $C \in RC(Y)$ such that $f^{-1}(C) \neq X$. Then $Y - C \in RO(Y)$ such that $f^{-1}(Y - C) = X - f^{-1}(C) \neq \emptyset$. By (i), there exists $V \neq \emptyset \in \alpha GO(X)$ and $V \subset f^{-1}(Y - C) = X - f^{-1}(C)$. Thus $X - V \supset f^{-1}(C)$ and $X - V = D$ is a proper αg -closed set in X .
- (ii) \Rightarrow (i): Let $U \in RO(\sigma)$ and $f^{-1}(U) \neq \emptyset$. Then $Y - U \in RC(\sigma)$ and $f^{-1}(Y - U) = X - f^{-1}(U) \neq X$. By (ii), there exists a proper $D \in \alpha GC(X)$ such that $D \supset f^{-1}(Y - U)$. This implies that $X - D \subset f^{-1}(U)$ and $X - D$ is αg -open and $X - D \neq \emptyset$.
- (ii) \Rightarrow (iii): Let M be a αg -dense set in X . If $f(M)$ is not dense in Y . Then there exists a proper $C \in RC(Y)$ such that $f(M) \subset C \subset Y$. Clearly $f^{-1}(C) \neq X$. By (ii), there exists a proper $D \in \alpha GC(X)$ such that $M \subset f^{-1}(C) \subset D \subset X$. This is a contradiction to the fact that M is αg -dense in X .
- (iii) \Rightarrow (ii): If (ii) is not true, there exists $C \in RC(Y)$ such that $f^{-1}(C) \neq X$ but there is no proper $D \in \alpha GC(X)$ such that $f^{-1}(C) \subset D$. Thus $f^{-1}(C)$ is αg -dense in X . But by (iii), $f(f^{-1}(C)) = C$ is dense in Y , which contradicts the choice of C .

Theorem 3.3: Let f be a function and $X = A \cup B$, where $A, B \in RO(X)$. If $f_A: (A; \tau_A) \rightarrow (Y, \sigma)$ and $f_B: (B; \tau_B) \rightarrow (Y, \sigma)$ are somewhat almost αg -continuous, then f is somewhat almost αg -continuous.

Proof: Let $U \in RO(\sigma)$ such that $f^{-1}(U) \neq \emptyset$. Then $(f_A)^{-1}(U) \neq \emptyset$ or $(f_B)^{-1}(U) \neq \emptyset$ or both $(f_A)^{-1}(U) \neq \emptyset$ and $(f_B)^{-1}(U) \neq \emptyset$. Suppose $(f_A)^{-1}(U) \neq \emptyset$, Since f_A is somewhat almost αg -continuous, there exists $V \neq \emptyset \in \alpha GO(A)$ and $V \subset (f_A)^{-1}(U) \subset f^{-1}(U)$. Since $V \in \alpha GO(A)$ and $A \in RO(X)$, $V \in \alpha GO(X)$. Thus f is somewhat almost αg -continuous. The proof of other cases are similar.

Theorem 3.4: Let $f: (X, \tau) \rightarrow (Y, \sigma)$ be a somewhat almost αg -continuous surjection and τ^* be a topology for X , which is αg -equivalent to τ . Then $f: (X, \tau^*) \rightarrow (Y, \sigma)$ is somewhat almost αg -continuous.

Proof: Let $V \in RO(\sigma)$ such that $f^{-1}(V) \neq \emptyset$. Since f is somewhat almost αg -continuous, there exists $U \neq \emptyset \in \alpha GO(X, \tau)$ such that $U \subset f^{-1}(V)$. But by hypothesis τ^* is αg -equivalent to τ . Therefore, there exists $U^* \neq \emptyset \in \alpha GO(X; \tau^*)$ such that $U^* \subset U$. But $U \subset f^{-1}(V)$. Then $U^* \subset f^{-1}(V)$; hence $f: (X, \tau^*) \rightarrow (Y, \sigma)$ is somewhat almost αg -continuous.

Theorem 3.5: Let $f: (X, \tau) \rightarrow (Y, \sigma)$ be a somewhat almost αg -continuous surjection and σ^* be a topology for Y , which is equivalent to σ . Then $f: (X, \tau) \rightarrow (Y, \sigma^*)$ is somewhat almost αg -continuous.

Proof: Let $V^* \in RO(\sigma^*)$ such that $f^{-1}(V^*) \neq \emptyset$. Since σ^* is equivalent to σ , there exists $V \neq \emptyset \in RO(Y, \sigma)$ such that $V \subset V^*$. Now $\emptyset \neq f^{-1}(V) \subset f^{-1}(V^*)$. Since f is somewhat almost αg -continuous, there exists $U \neq \emptyset \in \alpha GO(X, \tau)$ such that $U \subset f^{-1}(V)$. Then $U \subset f^{-1}(V^*)$; hence $f: (X, \tau) \rightarrow (Y, \sigma^*)$ is somewhat almost αg -continuous.

IV. Somewhat αg -irresolute function

Definition 4.1: A function f is said to be somewhat αg -irresolute if for $U \in \alpha GO(\sigma)$ and $f^{-1}(U) \neq \emptyset$, there exists a non-empty αg -open set V in X such that $V \subset f^{-1}(U)$.

Example 3: Let $X = \{a, b, c\}$, $\tau = \{\emptyset, \{a\}, \{b, c\}, X\}$ and $\sigma = \{\emptyset, \{a\}, \{a, b\}, X\}$. The function $f: (X, \tau) \rightarrow (X, \sigma)$ defined by $f(a) = c, f(b) = a$ and $f(c) = b$ is somewhat αg -irresolute but not somewhat-irresolute.

Example 4: Let $X = \{a, b, c\}$, $\tau = \{\emptyset, \{a\}, \{a, b\}, X\}$ and $\sigma = \{\emptyset, \{a\}, \{b, c\}, X\}$. The function $f: (X, \tau) \rightarrow (X, \sigma)$ defined by $f(a) = c, f(b) = a$ and $f(c) = b$ is not somewhat αg -irresolute and somewhat-irresolute.

Note 1: Every somewhat αg -irresolute function is slightly αg -irresolute.

Example 5: The identity functions f, g and $g \circ f$ in Example 2 are somewhat αg -irresolute.

However, we have the following

Theorem 4.1: If f is somewhat αg -irresolute and g is irresolute, then $g \circ f$ is somewhat αg -irresolute.

Theorem 4.2: For a surjective function f , the following statements are equivalent:

- (i) f is somewhat αg -irresolute.
 - (ii) If C is αg -closed in Y such that $f^{-1}(C) \neq X$, then there is a proper αg -closed subset D of X such that $f^{-1}(C) \subset D$.
 - (iii) If M is a αg -dense subset of X , then $f(M)$ is a αg -dense subset of Y .
- Proof:** (i) \Rightarrow (ii): Let $C \in \alpha GC(Y)$ such that $f^{-1}(C) \neq X$. Then $Y - C \in \alpha GO(Y)$ such that $f^{-1}(Y - C) = X - f^{-1}(C) \neq \emptyset$. By (i), there exists $V \neq \emptyset \in \alpha GO(X)$ and $V \subset f^{-1}(Y - C) = X - f^{-1}(C)$. This means $X - V \supset f^{-1}(C)$ and $X - V = D$ is proper αg -closed in X .

(ii) \Rightarrow (i): Let $U \in \alpha GO(\sigma)$ and $f^{-1}(U) \neq \emptyset$. Then $Y - U \neq \emptyset \in \alpha GC(Y)$ and $f^{-1}(Y - U) = X - f^{-1}(U) \neq X$. By (ii), there exists $D \neq \emptyset \in \alpha GC(X)$ such that $D \supset f^{-1}(Y - U)$. This implies that $X - D \subset f^{-1}(U)$ and $X - D$ is αg -open and $X - D \neq \emptyset$.

(ii) \Rightarrow (iii): Let M be a αg -dense set in X . If $f(M)$ is not αg -dense in Y . Then there exists a proper $C \in \alpha GC(Y)$ such that $f(M) \subset C \subset Y$. Clearly $f^{-1}(C) \neq X$. By (ii), there exists a proper $D \in \alpha GC(X)$ such that $M \subset f^{-1}(C) \subset D \subset X$. This is a contradiction to the fact that M is αg -dense in X .

(iii) \Rightarrow (ii): Suppose (ii) is not true. there exists $C \in \alpha GC(Y)$ such that $f^{-1}(C) \neq X$ but there is no proper $D \neq \emptyset \in \alpha GC(X)$ such that $f^{-1}(C) \subset D$. This means that $f^{-1}(C)$ is αg -dense in X . But by (iii), $ff^{-1}(C) = C$ must be αg -dense in Y , which is a contradiction to the choice of C .

Theorem 4.3: Let f be a function and $X = A \cup B$, where $A, B \in RO(X)$. If $f|_A: (A; \tau|_A) \rightarrow (Y, \sigma)$ and $f|_B: (B; \tau|_B) \rightarrow (Y, \sigma)$ are somewhat αg -irresolute, then f is somewhat αg -irresolute.

Proof: Let $U \in \alpha GO(\sigma)$ such that $f^{-1}(U) \neq \emptyset$. Then $(f|_A)^{-1}(U) \neq \emptyset$ or $(f|_B)^{-1}(U) \neq \emptyset$ or both $(f|_A)^{-1}(U) \neq \emptyset$ and $(f|_B)^{-1}(U) \neq \emptyset$. If $(f|_A)^{-1}(U) \neq \emptyset$, Since $f|_A$ is somewhat αg -irresolute, there exists $V \neq \emptyset \in \alpha GO(A)$ and $V \subset (f|_A)^{-1}(U) \subset f^{-1}(U)$. Since $V \in \alpha GO(A)$ and $A \in RO(X)$, $V \in \alpha GO(X)$. Thus f is somewhat αg -irresolute.

The proof of other cases are similar.

If f is the identity function and τ and σ are αg -equivalent. Then f and f^{-1} are somewhat αg -irresolute. Conversely, if the identity function f is somewhat αg -irresolute in both directions, then τ and σ are αg -equivalent.

Theorem 4.4: Let $f: (X, \tau) \rightarrow (Y, \sigma)$ be a somewhat αg -irresolute surjection and τ^* be a topology for X , which is αg -equivalent to τ . Then $f: (X, \tau^*) \rightarrow (Y, \sigma)$ is somewhat αg -irresolute.

Proof: Let $V \in \alpha GO(\sigma)$ such that $f^{-1}(V) \neq \emptyset$. Since f is somewhat αg -irresolute, there exists $U \neq \emptyset \in \alpha GO(X, \tau)$ with $U \subset f^{-1}(V)$. But for τ^* is αg -equivalent to τ , there exists $U^* \neq \emptyset \in \alpha GO(X; \tau^*)$ such that $U^* \subset U$. But $U \subset f^{-1}(V)$. Then $U^* \subset f^{-1}(V)$; hence $f: (X, \tau^*) \rightarrow (Y, \sigma)$ is somewhat αg -irresolute.

Theorem 4.5: Let $f: (X, \tau) \rightarrow (Y, \sigma)$ be a somewhat αg -irresolute surjection and σ^* be a topology for Y , which is equivalent to σ . Then $f: (X, \tau) \rightarrow (Y, \sigma^*)$ is somewhat αg -irresolute.

Proof: Let $V^* \in \sigma^*$ such that $f^{-1}(V^*) \neq \emptyset$. Since σ^* is equivalent to σ , there exists $V \neq \emptyset \in (Y, \sigma)$ such that $V \subset V^*$. Now $\emptyset \neq f^{-1}(V) \subset f^{-1}(V^*)$. Since f is somewhat αg -irresolute, there exists $U \neq \emptyset \in \alpha GO(X, \tau)$ such that $U \subset f^{-1}(V)$. Then $U \subset f^{-1}(V^*)$; hence $f: (X, \tau) \rightarrow (Y, \sigma^*)$ is somewhat αg -irresolute.

V. Somewhat almost αg -open function

Definition 5.1: A function f is said to be somewhat almost αg -open provided that if $U \in RO(\tau)$ and $U \neq \emptyset$, then there exists a non-empty αg -open set V in Y such that $V \subset f(U)$.

Example 6: Let $X = \{a, b, c\}$, $\tau = \{\emptyset, \{a\}, X\}$ and $\sigma = \{\emptyset, \{a\}, \{b, c\}, X\}$. The function $f: (X, \tau) \rightarrow (X, \sigma)$ defined by $f(a) = a$, $f(b) = c$ and $f(c) = b$ is somewhat almost αg -open, somewhat αg -open and somewhat open.

Theorem 5.1: Let f be r -open and g be somewhat almost αg -open. Then $g \circ f$ is somewhat almost αg -open.

Theorem 5.2: For a bijective function f , the following are equivalent:

- (i) f is somewhat almost αg -open.
 - (ii) If C is regular closed in X , such that $f(C) \neq Y$, then there is a αg -closed subset D of Y such that $D \neq Y$ and $D \supset f(C)$.
- Proof:** (i) \Rightarrow (ii): Let $C \in RC(X)$ such that $f(C) \neq Y$. Then $X - C \neq \emptyset \in RO(X)$. Since f is somewhat almost αg -open, there exists $V \neq \emptyset \in \alpha GO(Y)$ such that $V \subset f(X - C)$. Put $D = Y - V$. Clearly $D \neq \emptyset \in \alpha GC(Y)$. If $D = Y$, then $V = \emptyset$, which is a contradiction. Since $V \subset f(X - C)$, $D = Y - V \supset (Y - f(X - C)) = f(C)$.
- (ii) \Rightarrow (i): Let $U \neq \emptyset \in RO(X)$. Then $C = X - U \in RC(X)$ and $f(X - U) = f(C) = Y - f(U)$ implies $f(C) \neq Y$. Then by (ii), there is $D \neq \emptyset \in \alpha GC(Y)$ and $f(C) \subset D$. Clearly $V = Y - D \neq \emptyset \in \alpha GO(Y)$. Also, $V = Y - D \subset Y - f(C) = Y - f(X - U) = f(U)$.

Theorem 5.3: The following statements are equivalent:

- (i) f is somewhat almost αg -open.
 - (ii) If A is a αg -dense subset of Y , then $f^{-1}(A)$ is a dense subset of X .
- Proof:** (i) \Rightarrow (ii): Let A be a αg -dense set in Y . If $f^{-1}(A)$ is not dense in X , then there exists $B \in RC(X)$ such that $f^{-1}(A) \subset B \subset X$. Since f is somewhat almost αg -open and $X - B \in RO(X)$, there exists $C \neq \emptyset \in \alpha GO(Y)$ such that $C \subset f(X - B)$. Therefore, $C \subset f(X - B) \subset f(f^{-1}(Y - A)) \subset Y - A$. That is, $A \subset Y - C \subset Y$. Now, $Y - C$ is a αg -closed set and $A \subset Y - C \subset Y$. This implies that A is not a αg -dense set in Y , which is a contradiction. Therefore, $f^{-1}(A)$ is a dense set in X .
- (ii) \Rightarrow (i): If $A \neq \emptyset \in RO(X)$. We want to show that $\alpha g(f(A)) \neq \emptyset$. Suppose $\alpha g(f(A)) = \emptyset$. Then, $\alpha g cl\{f(A)\} = Y$. Then by (ii), $f^{-1}(Y - f(A))$ is dense in X . But $f^{-1}(Y - f(A)) \subset X - A$. Now, $X - A \in RC(X)$. Therefore, $f^{-1}(Y - f(A)) \subset X - A$ gives $X = cl\{f^{-1}(Y - f(A))\} \subset X - A$. Thus $A = \emptyset$, which contradicts $A \neq \emptyset$. Therefore, $\alpha g(f(A)) \neq \emptyset$. Hence f is somewhat almost αg -open.

Theorem 5.4: Let f be somewhat almost αg -open and $A \in RO(X)$. Then $f_{/A}$ is somewhat almost αg -open.

Proof: Let $U \neq \emptyset \in RO(\tau_A)$. Since $U \in RO(A)$ and $A \in RO(X)$, $U \in RO(X)$ and since f is somewhat almost αg -open, there exists $V \in \alpha GO(Y)$, such that $V \subset f(U)$. Thus $f_{/A}$ is somewhat almost αg -open.

Theorem 5.5: Let f be a function and $X = A \cup B$, where $A, B \in RO(X)$. If $f_{/A}$ and $f_{/B}$ are somewhat almost αg -open, then f is somewhat almost αg -open.

Proof: Let $U \neq \emptyset \in RO(X)$. Since $X = A \cup B$, either $A \cap U \neq \emptyset$ or $B \cap U \neq \emptyset$ or both $A \cap U \neq \emptyset$ and $B \cap U \neq \emptyset$. Since U is regular open in X , U is regular open in both A and B .

Case (i): If $A \cap U \neq \emptyset \in RO(A)$. Since $f_{/A}$ is somewhat almost αg -open, there exists a αg -open set V of Y such that $V \subset f(U \cap A) \subset f(U)$, which implies that f is a somewhat almost αg -open.

Case (ii): If $B \cap U \neq \emptyset \in RO(B)$. Since $f_{/B}$ is somewhat almost αg -open, there exists a αg -open set V in Y such that $V \subset f(U \cap B) \subset f(U)$, which implies that f is somewhat almost αg -open.

Case (iii): Suppose that both $A \cap U \neq \emptyset$ and $B \cap U \neq \emptyset$. Then by case (i) and (ii) f is somewhat almost αg -open.

Remark 1: Two topologies τ and σ for X are said to be αg -equivalent iff the identity function f is somewhat almost αg -open in both directions.

Theorem 5.6: If $f: (X, \tau) \rightarrow (Y, \sigma)$ is somewhat almost open. Let τ^* and σ^* be topologies for X and Y , respectively such that τ^* is equivalent to τ and σ^* is αg -equivalent to σ . Then $f: (X; \tau^*) \rightarrow (Y; \sigma^*)$ is somewhat almost αg -open.

VI. Somewhat M- αg -open function

Definition 6.1: A function f is said to be somewhat M- αg -open provided that if $U \in \alpha GO(\tau)$ and $U \neq \emptyset$, then there exists a non-empty αg -open set V in Y such that $V \subset f(U)$.

Example 7: f as in Example 6 is somewhat M- αg -open.

Theorem 6.1: Let f be r -open and g be somewhat M- αg -open. Then $g \circ f$ is somewhat M- αg -open.

Theorem 6.2: For a bijective function f , the following are equivalent:

(i) f is somewhat M- αg -open.

(ii) If $C \in \alpha GC(X)$, such that $f(C) \neq Y$, then there is a $D \in \alpha GC(Y)$ such that $D \neq Y$ and $D \supset f(C)$.

Proof: (i) \Rightarrow (ii): Let $C \in \alpha GC(X)$ such that $f(C) \neq Y$. Then $X - C \neq \emptyset \in \alpha GO(X)$. Since f is somewhat M- αg -open, there exists $V \neq \emptyset \in \alpha GO(Y)$ such that $V \subset f(X - C)$. Put $D = Y - V$. Clearly $D \neq \emptyset \in \alpha GC(Y)$. If $D = Y$, then $V = \emptyset$, which is a contradiction. Since $V \subset f(X - C)$, $D = Y - V \supset (Y - f(X - C)) = f(C)$.

(ii) \Rightarrow (i): Let $U \neq \emptyset \in RO(X)$. Then $C = X - U \in \alpha GC(X)$ and $f(X - U) = f(C) = Y - f(U)$ implies $f(C) \neq Y$. Then by (ii), there is $D \in \alpha GC(Y)$ such that $D \neq Y$ and $f(C) \subset D$. Clearly $V = Y - D \neq \emptyset \in \alpha GO(Y)$. Also, $V = Y - D \subset Y - f(C) = Y - f(X - U) = f(U)$.

Theorem 6.3: The following statements are equivalent:

(i) f is somewhat M- αg -open.

(ii) If A is a αg -dense subset of Y , then $f^{-1}(A)$ is a αg -dense subset of X .

Proof: (i) \Rightarrow (ii): Let A be a αg -dense set in Y . If $f^{-1}(A)$ is not αg -dense in X , then there exists $B \in \alpha GC(X)$ in X such that $f^{-1}(A) \subset B \subset X$. Since f is somewhat M- αg -open and $X - B$ is αg -open, there exists a $C \neq \emptyset \in \alpha GO(Y)$ such that $C \subset f(X - B)$. Therefore, $C \subset f(X - B) \subset f(f^{-1}(Y - A)) \subset Y - A$. That is, $A \subset Y - C \subset Y$. Now, $Y - C$ is a αg -closed set and $A \subset Y - C \subset Y$. This implies that A is not a αg -dense set in Y , which is a contradiction. Therefore, $f^{-1}(A)$ is a αg -dense set in X .

(ii) \Rightarrow (i): Let $A \neq \emptyset \in \alpha GO(X)$. To prove $\alpha g(f(A)) \neq \emptyset$. Assume $\alpha g(f(A)) = \emptyset$. Then, $\alpha g cl\{f(A)\} = Y$. Then by (ii), $f^{-1}(Y - f(A))$ is αg -dense in X . But $f^{-1}(Y - f(A)) \subset X - A$. Now, $X - A \in \alpha GC(X)$. Therefore, $f^{-1}(Y - f(A)) \subset X - A$ gives $X = cl\{f^{-1}(Y - f(A))\} \subset X - A$. Thus $A = \emptyset$, which contradicts $A \neq \emptyset$. Therefore, $\alpha g(f(A)) \neq \emptyset$. Hence f is somewhat M- αg -open.

Theorem 6.4: If f is somewhat M- αg -open and A is r -open in X . Then $f_{/A}: (A; \tau_A) \rightarrow (Y, \sigma)$ is somewhat M- αg -open.

Proof: Let $U \neq \emptyset \in \alpha GO(\tau_A)$. Since $U \in \alpha GO(A)$ and $A \in RO(X)$, $U \in RO(X)$ and since f is somewhat M- αg -open, there exists $V \in \alpha GO(Y)$, such that $V \subset f(U)$. Thus $f_{/A}$ is somewhat M- αg -open.

Theorem 6.5: Let f be a function and $X = A \cup B$, where $A, B \in \alpha GO(X)$. If $f_{/A}$ and $f_{/B}$ are somewhat M- αg -open, then f is somewhat M- αg -open.

Proof: Let $U \neq \emptyset \in RO(X)$. Since $X = A \cup B$, either $A \cap U \neq \emptyset$ or $B \cap U \neq \emptyset$ or both $A \cap U \neq \emptyset$ and $B \cap U \neq \emptyset$. Since U is regular open in X , U is regular open in both A and B .

Case (i): If $A \cap U \neq \emptyset \in RO(A)$. Since $f_{/A}$ is somewhat M- αg -open, there exists a αg -open set V of Y such that $V \subset f(U \cap A) \subset f(U)$, which implies that f is a somewhat M- αg -open.

Case (ii): If $B \cap U \neq \emptyset \in RO(B)$. Since $f_{/B}$ is somewhat M- αg -open, there exists a αg -open set V in Y such that $V \subset f(U \cap B) \subset f(U)$, which implies that f is somewhat M- αg -open.

Case (iii): If both $A \cap U \neq \emptyset$ and $B \cap U \neq \emptyset$. Then by case (i) and (ii) f is somewhat M - α g-open.

Remark 2: Two topologies τ and σ for X are said to be α g-equivalent iff the identity function f is somewhat M - α g-open in both directions.

Theorem 6.6: If $f: (X, \tau) \rightarrow (Y, \sigma)$ is somewhat M -open. Let τ^* and σ^* be topologies for X and Y , respectively such that τ^* is equivalent to τ and σ^* is α g-equivalent to σ . Then $f: (X; \tau^*) \rightarrow (Y; \sigma^*)$ is somewhat M - α g-open.

VII. CONCLUSION

In this paper we defined Somewhat- α g-continuous functions, studied its properties and their interrelations with other types of Somewhat-continuous functions.

Acknowledgments

The authors would like to thank the referees for their critical comments and suggestions for the development of this paper.

References

- [1] D. Andrijevic. On b-open sets. Math. Vesnik, 1996, 48: 59 - 64.
- [2] A.A. El-Atik. A study of some types of mappings on topological spaces. M. Sc. Thesis, Tanta University, Egypt, 1997.
- [3] S. Balasubramanian and Sandhya.C., Slightly GS-continuous functions, somewhat GS-continuous functions, Bull. Kerala Math. Association, Vol.9, No.1(2012)87 – 98.
- [4] S. Balasubramanian and Chaitahya.Ch, α g-separation axioms, Inter.J.Math.Archive, 3(3)(2012)855–863 .
- [5] S. Balasubramanian and Chaitahya.Ch, On α g-separation axioms, Inter.J.Math.Archive, 3(3)(2012)877–888 .
- [6] S. Balasubramanian and Chaitahya.Ch, Slightly α g-continuous functions, somewhat α g-continuous functions (Communicated)
- [7] S. Balasubramanian and Chaitahya.Ch, Minimal α g-open sets, Aryabhata J. of Mathematics and Informatics, 4(1)Jan-June(2012)83 – 94.
- [8] M. Ganster. Preopen sets and resolvable spaces. Kyungpook Math. J., 1987, 27(2):135-143.
- [9] K.R. Gentry, H.B. Hoyle. Somewhat continuous functions. Czechoslovak Math. J., 1971, 21(96):5-12.
- [10] Y.Gnanambal., On generalized pre regular closed sets in topological spaces, I.J.P.A.M., 28(3) (1997), 351-360.
- [11] T.Noiri, N.Rajesh. Somewhat b-continuous functions. J. Adv. Res. in Pure Math., 2011,3(3):1-7.doi: 10.5373/jarpm.515.072810

Study of Crane Hook Having Trapezoidal Section by Finite Element Method & Design of Experiments

Santosh Sahu¹, Ritesh Dewangan², Manas Patnaik³, Narendra Yadav⁴

^{1, 2, 3, 4}(Department of Mechanical Engineering, Rungta College of Engineering & Technology, Raipur-492001-India)

Abstract : In the industrial processes Crane Hook is used as lifting member. In the present paper crane hook of trapezoidal section is modeled in CATIA V5R20, then 2 ton load equivalent to 19620 N on it is applied. The location of maximum stress produced within the member is located and identified using Finite Element Method (FEM). Further Design of Experiment (DOE) is applied by varying the length of two parallel sides of the Trapezoidal Hook and its effects are studied on the basis of Stress , Mass, Displacement and Energy stored within the hook.

Keywords - Crane Hook, DOE, FEM , Trapezoidal Hook, AISI 4140

I. INTRODUCTION

Crane hook is the member used for lifting the mass using wire ropes and crane. In this paper we have used a CAD model of Trapezoidal section Crane Hook in CATIA V5R20 and assigned the material having mechanical properties of AISI 4140 used for manufacturing of crane hook . Finite Element Analysis is applied to find out the stress in the critical section where maximum stress is induced . Design of Experiments is applied in Matlab, by varying the parallel length of the trapezoidal section and its effects is studied in terms of Energy stored, displacement, stress induced and mass accumulated within the crane hook in the form of output parameters. The results obtained from Design of experiment is plotted to know the nature of the output parameters with respect to the varying parallel length of outer as well as inner surface. By this we established the relation between the cross section and the output parameters which are useful for selection of the cross section dimensions during manufacturing with respect to the desired output parameters .

II. CRANE HOOK DIMENSIONS AND MATERIAL

The CAD model of Crane hook is shown in Figure1.

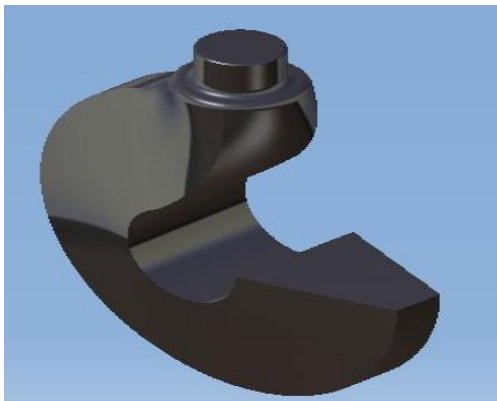


Fig.1 CAD Model of crane hook

The dimension of the trapezoidal section is shown in Figure2.

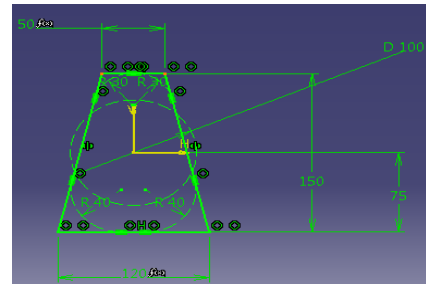


Fig.2 Dimensions of Trapezoidal section.

The material used for crane hook is forged steel the material selected in this cad model is AISI 4140 . The Mechanical properties of AISI is mentioned in Table 1.

Table 1. Mechanical properties of AISI 4140

MECHANICAL PROPERTIES	VAUES	UNIT
Elastic Modulus	2.05E+11	N/m ²
Poisson's ratio	0.285	N/A
Shear Modulus	8.00E+10	N/m ²
Density	7850	kg/m ³
Tensile Strength	560000000	N/m ²
Yield Strength	460000000	N/m ²
Thermal Conductivity	42.7	W/(m·K)
Specific Heat	477	J/(kg·K)

III. RESULT AND ANALYSIS BY FEM

The Finite Element Method is a Numerical Analysis Technique used to obtain solutions .Meshing is important part of Finite Element Method. The mesh details done in the CAD model is shown in Table. The mesh taken has Tetrahedron shape (Te4)

Table 2. Mesh details

Entity	Size
Nodes	9163
Elements	40630

Von Mises Stress distribution in cad model is shown in Figure 3.

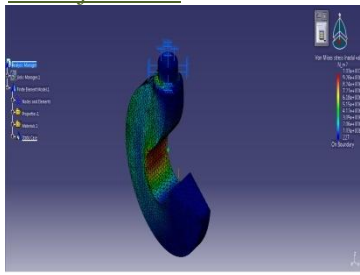


Fig. 3 Von Mises Stress Distribution

Translational displacement of nodes is shown in Figure 4.

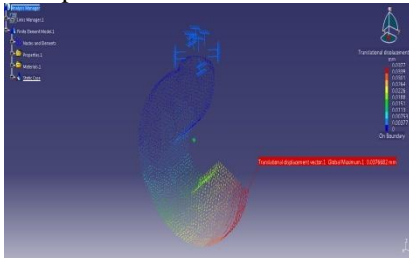


Fig. 4 Shows Translational displacement of nodes

The Sensors showing values of Energy, Maximum Displacement Maximum Von Mises', and Mass obtained by FEM is shown in Figure 5.

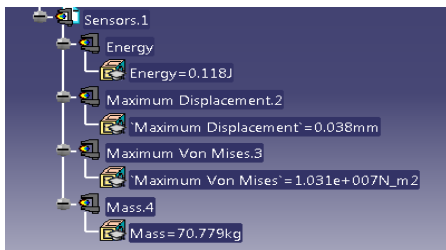


Fig. 5 Sensors Details after analysis

The maximum Von Mises stress location and magnitude is shown in Figure 6.

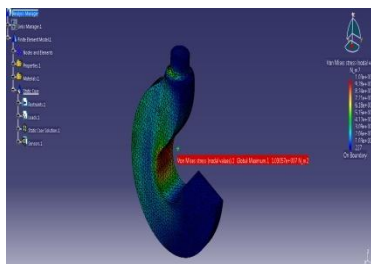


Fig. 6 Maximum Von Mises Stress.

IV. DESIGN OF EXPERIMENTS

DOE is Concerned with planning and conduction of experiments to analyze the resulting data by applying principles and techniques at the initial data collection stage to generate valid, defensible objective engineering conclusions.

We have taken two variable input values which are length of two parallel sides of Trapezoidal section namely 'B' and 'b'. The value of B which is at the inner side of the hook varies from 110 mm to 130 mm, whereas the value of b which is the outer side of the hook varies from 45 mm to 55 mm. Figure 7 shows the command window where input parameters B and b are assigned the minimum and maximum values and Output parameters are selected here

are Energy, Maximum Displacement, Maximum Von Mises and Mass. DOE is then performed and the results in the form of Graph has been plotted.

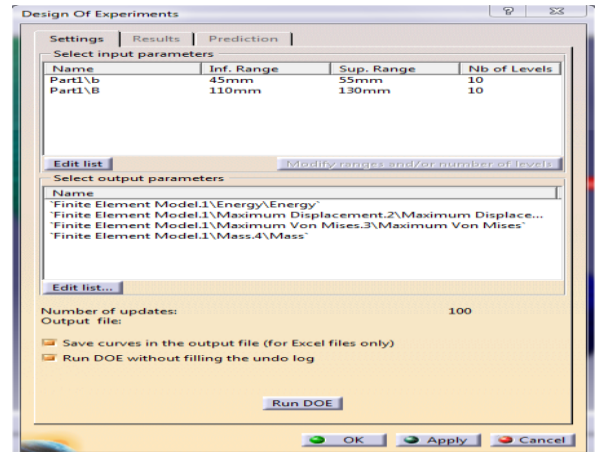


Fig. 7 Input Parameters and their Range With the selected output parameters

On running the DOE the results obtained are shown in the form of graphs between input variables and the selected output parameters

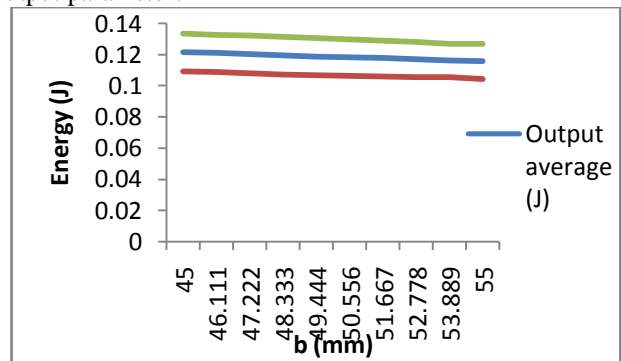


Fig.8 Graph Plotted Between Energy stored and b

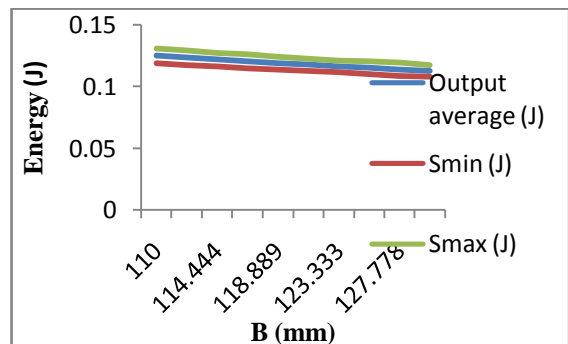


Fig.9 Graph Plotted Between Energy stored and B

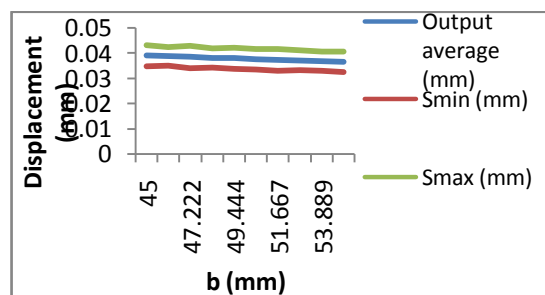


Fig.10 Graph Plotted Displacement and b

V. CONCLUSION

We have reached to the following conclusions on the basis of the results obtained from Finite element analysis and Design of Experiment performed for the trapezoidal cross section crane hook;

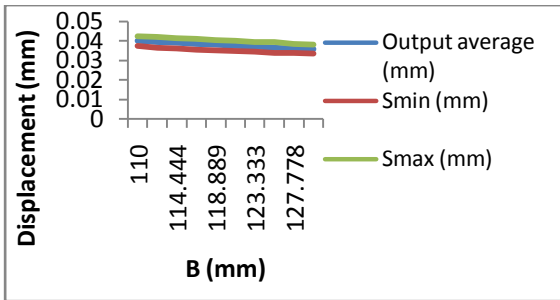


Fig.11 Graph Plotted between Displacement and B

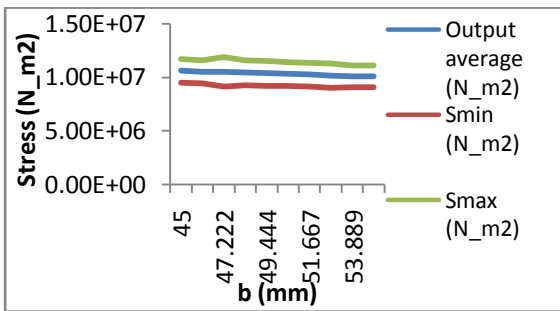


Fig.12 Graph Plotted between Stress and b

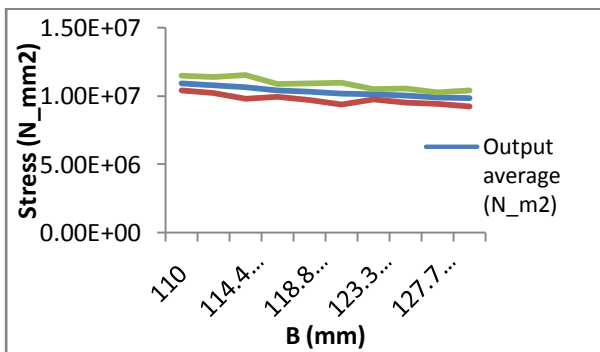


Fig.13 Graph Plotted between Stress and B

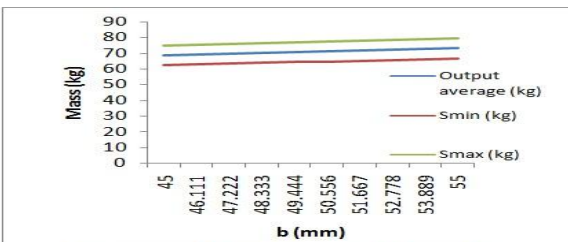


Fig.14 Graph Plotted between Mass and b

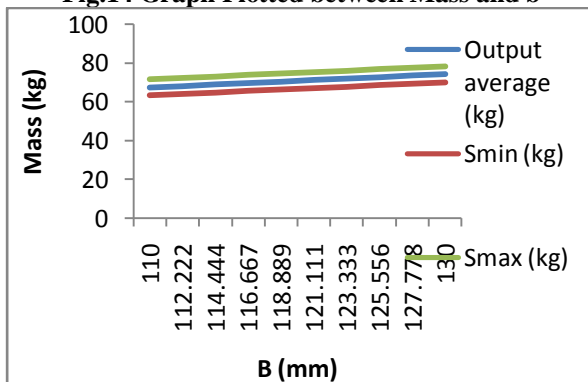


Fig.15 Graph Plotted between Mass and B

1. The Figure 6 shows the point where Maximum stress has been produced and the magnitude of maximum stress.
2. The Figure 8 shows the magnitude of energy stored within the crane hook decreases on the increase of outer parallel length (b) of trapezoidal section .
3. The Figure 9 shows the magnitude of energy stored within the crane hook decreases on the increase of Inner parallel length (B) of trapezoidal section .
4. The Figure 10 shows the magnitude of displacement within the crane hook decreases on the increase of outer parallel length (b) of trapezoidal section
5. The Figure 11 shows the magnitude of displacement within the crane hook decreases on the increase of inner parallel length (B) of trapezoidal section
6. The Figure 12 shows the magnitude of stress induced within the crane hook decreases on the increase of outer parallel length (b) of trapezoidal section
7. The Figure 13 shows the magnitude of stress induced within the crane hook decreases on the increase of Inner parallel length (B) of trapezoidal section.
8. The Figure 14 shows the magnitude of the mass of the crane hook increases on the increase of outer parallel length (b) of trapezoidal section.
9. The Figure 15 shows the magnitude of the mass of the crane hook increases on the increase of inner parallel length (B) of trapezoidal section

REFERENCES

- [1] Narvydas E., Puodžiūnienė N., 2012. Circumferential stress concentration factors at the asymmetric shallow notches of the lifting hooks of trapezoidal cross-section. MECHANIKA. 2012 Volume 18(2): 152-157
- [2] Narvydas, E. 2010. Modeling of a crane hook wear and stress analysis. Transport Means 2010: Proceedings of the 14th international conference; 2010 Oct 21-22; Kaunas University of Technology, Lithuania. Kaunas: Technologija. 161-164.
- [3] Cook, R. 1992. Circumferential stresses in curved beams, Journal of Applied Mechanics-Transactions of the ASME 59: 224-225.
- [4] Sloboda, A.; Honarmandi, P. 2007. Generalized elasticity method for curved beam stress analysis: Analytical and numerical comparisons for a lifting hook, Mechanics Based Design of Structures and Machines 35: 319-332.
- [5] Torres, Y.; Gallardo, J.M.; Dominguez J.; Jimenez, F.J. 2010. Brittle fracture of a crane hook, Engineering Failure Analysis 17:38-47.

Advanced Direct Power Control Method of UPFC by Using Matrix Converter

D. Jagan¹, K. Suresh²

^{1,2}(EEE dept, RGM CET Nandyal/JNTUA, AP, INDIA)

Abstract: This paper presents a direct power control (DPC) for three-phase matrix converters operating as unified power flow controllers (UPFCs). Matrix converters (MCs) allow the direct ac/ac power conversion without dc energy storage links; therefore, the MC-based UPFC (MC-UPFC) has reduced volume and cost, reduced capacitor power losses, together with higher reliability. Theoretical principles of direct power control (DPC) based on sliding mode control techniques are established for an MC-UPFC dynamic model including the input filter. As a result, line active and reactive power, together with ac supply reactive power, can be directly controlled by selecting an appropriate matrix converter switching state guaranteeing good steady-state and dynamic responses. Experimental results of DPC controllers for MC-UPFC show decoupled active and reactive power control, zero steady-state tracking error, and fast response times. Compared to an MC-UPFC using active and reactive power linear controllers based on a modified Venturing high-frequency PWM modulator, the experimental results of the advanced DPC-MC guarantee faster responses without overshoot and no steady state error, presenting no cross-coupling in dynamic and steady-state responses.

Index Terms: Direct power control (DPC), matrix converter (MC), unified power-flow controller (UPFC).

I. INTRODUCTION

In the last few years, electricity market deregulation, together with growing economic, environmental, and social concerns, has increased the difficulty to burn fossil fuels, and to obtain new licenses to build transmission lines (rights-of-way) and high-power facilities. This situation started the growth of decentralized electricity generation (using renewable energy resources).

Unified Power-Flow Controllers (UPFC) enable the operation of power transmission networks near their maximum ratings, by enforcing power flow through well-defined lines. These days, UPFCs are one of the most versatile and powerful flexible ac transmission systems (FACTS) devices.

The UPFC results from the combination of a static synchronous compensator (STATCOM) and a static synchronous series compensator (SSSC) that shares a common dc capacitor link.

The existence of a dc capacitor bank originates additional losses, decreases the converter lifetime, and increases its weight, cost, and volume. These converters are capable of performing the same ac/ac conversion, allowing bidirectional power flow, guaranteeing near sinusoidal input and output currents, voltages with variable amplitude, and adjustable power factor. These minimum energy storage ac/ac converters have the capability to allow independent

reactive control on the UPFC shunt and series converter sides, while guaranteeing that the active power exchanged on the UPFC series connection is always supplied/absorbed by the shunt connection.

Recent nonlinear approaches enabled better tuning of PI controller parameters. Still, there is room to further improve the dynamic response of UPFCs, using nonlinear robust controllers. In the last few years, direct power control techniques have been used in many power applications, due to their simplicity and good performance. In this project, a matrix converter-based UPFC is proposed, using a direct power control approach (DPC-MC) based on an MC-UPFC dynamic model (Section II).

In order to design UPFCs, presenting robust behavior to parameter variations and to disturbances, the proposed DPC-MC control method, in Section III, is based on sliding mode-control techniques, allowing the real-time selection of adequate matrix vectors to control input and output electrical power. Sliding mode-based DPC-MC controllers can guarantee zero steady-state errors and no overshoots, good tracking performance, and fast dynamic responses, while being simpler to implement and requiring less processing power, when compared to proportional-integral (PI) linear controllers obtained from linear active and reactive power models of UPFC using a modified Aventura high-frequency PWM modulator.

The dynamic and steady-state behavior of the proposed DPC-MC P, Q control method is evaluated and discussed using detailed simulations and experimental implementation (Sections IV and V). Simulation and experimental results obtained with the nonlinear DPC for matrix converter-based UPFC technology show decoupled series active and shunt/series reactive power control, zero steady state error tracking, and fast response times, presenting faultless dynamic and steady state responses.

II. MODELING OF THE UPFC POWER SYSTEM

A. General Architecture

A simplified power transmission network using the proposed matrix converter UPFC is presented in Fig. 1, where a_0 and a_r are, respectively, the sending-end and receiving-end sinusoidal voltages of the and generators feeding load . The matrix converter is connected to transmission line 2, represented as a series inductance with series resistance (and), through coupling transformers and . Fig. 2 shows the simplified three-phase equivalent circuit of the matrix UPFC transmission system model. For system modeling, the power sources and the coupling transformers are all considered ideal. Also, the matrix converter is considered ideal and represented as a controllable voltage source, with amplitude and phase . In the equivalent circuit,

is the load bus voltage? The DPC-MC controller will treat the simplified elements as disturbances. Considering a symmetrical and balanced three-phase system and applying Kirchhoff laws to the three-phase equivalent circuit(Fig. 2), the ac line currents are obtained in coordinates

$$\frac{dI_d}{dt} = \omega I_q - \frac{R_2}{L_2} I_d + \frac{1}{L_2} (V_{Ld} - V_{ROd}) \quad (1)$$

$$\frac{dI_q}{dt} = -\omega I_d - \frac{R_2}{L_2} I_q + \frac{1}{L_2} (V_{Lq} - V_{ROq}). \quad (2)$$

The active and reactive power of end generator are given in dq coordinates by

$$\begin{bmatrix} P \\ Q \end{bmatrix} = \begin{bmatrix} V_d & V_q \\ V_q & -V_d \end{bmatrix} \begin{bmatrix} I_d \\ I_q \end{bmatrix}. \quad (3)$$

The active and reactive power P and Q are given by (4) and (5) respectively

$$P = V_d I_d \quad (4)$$

$$Q = -V_d I_q. \quad (5)$$

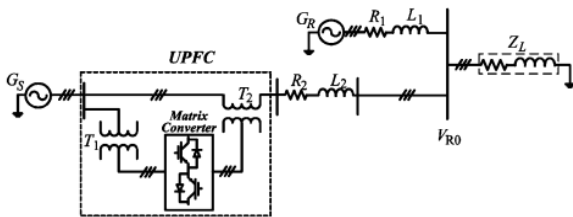


Fig. 1 Transmission network with matrix converter UPFC

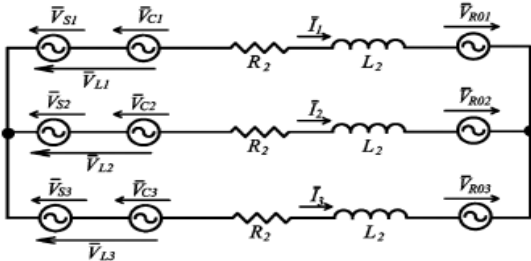


Fig.2.Three-phase equivalent circuit of the matrix UPFC and transmission line.

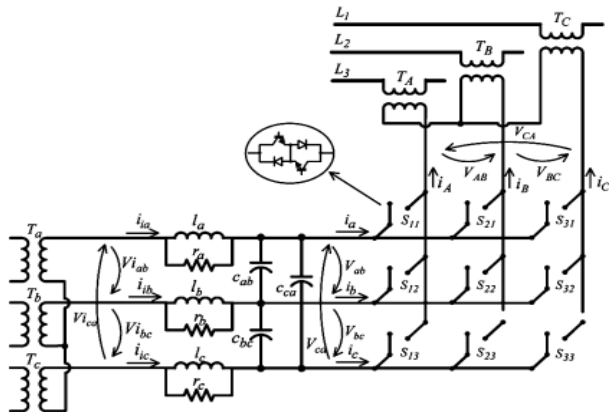


Fig. 3. Transmission network with matrix converter UPFC.

B.Matrix Converter Output Voltage and Input Current Vectors

A diagram of the UPFC system (Fig. 3) includes the three-phase shunt input transformer (with windings Ta, Tb, Tc),the three-phase series output transformer (with windings) and the three-phase matrix converter,

represented as an array of nine bidirectional switches with turn-on and turn-off capability, allowing the connection of each one of three output phases directly to any one of the three input phases. The three-phase input filter is required to re-establish a voltage-source boundary to the matrix converter, enabling smooth input currents.

Applying coordinates to the input filter state variables presented in Fig. 3 and neglecting the effects of the damping resistors, the following equations are obtained.

Where V_i represent, respectively, input voltages and input currents in dq components (at the shunt transformer secondary) and V_i are the matrix converter voltages and input currents in components, respectively.

Assuming ideal semiconductors, each matrix converter bidirectional switch can assume two possible states: “Sk=1” if the switch is closed or “Skj=0” if the

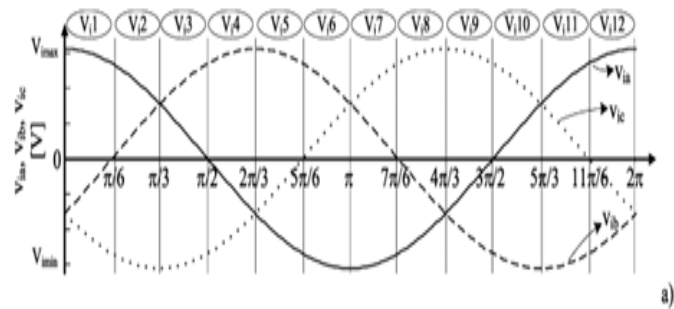


Fig. 4. (a) Input voltages and their corresponding sector

switch is open. The nine matrix converter switches can be represented as a 3× 3 matrix (7)

$$\begin{cases} \frac{di_{id}}{dt} = \omega i_{iq} - \frac{1}{2l} V_d - \frac{1}{2\sqrt{3}l} V_q + \frac{1}{l} V_{id} \\ \frac{di_{iq}}{dt} = -\omega i_{id} + \frac{1}{2\sqrt{3}l} V_d - \frac{1}{2l} V_q + \frac{1}{l} V_{iq} \\ \frac{dV_d}{dt} = \omega V_q - \frac{1}{2\sqrt{3}C} i_{iq} + \frac{1}{2C} i_{id} - \frac{1}{2C} i_d + \frac{1}{2\sqrt{3}C} i_q \\ \frac{dV_q}{dt} = -\omega V_d + \frac{1}{2\sqrt{3}C} i_{id} + \frac{1}{2C} i_{iq} - \frac{1}{2\sqrt{3}C} i_d - \frac{1}{2C} i_q \end{cases} \quad (6)$$

$$S = \begin{bmatrix} S_{11} & S_{12} & S_{13} \\ S_{21} & S_{22} & S_{23} \\ S_{31} & S_{32} & S_{33} \end{bmatrix}. \quad (7)$$

The relationship between load and input voltages can be expressed as

$$[v_A \ v_B \ v_C]^T = S[v_a \ v_b \ v_c]^T. \quad (8)$$

The input phase currents can be related to the output phase currents (9), using the transpose of matrix (9)

$$[i_a \ i_b \ i_c]^T = S^T[i_A \ i_B \ i_C]^T. \quad (9)$$

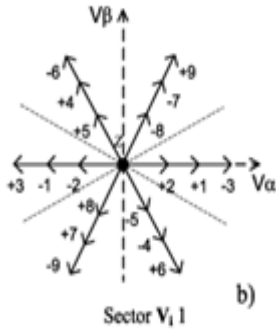
From the 27 possible switching patterns, time-variant vectors can be obtained (Table I) representing the matrix output voltages and input currents coordinates, and plotted in the frame [Fig. 4(b)].

The active and reactive power DPC-MC will select one of these 27 vectors at any given time instant.

III. DIRECT POWER CONTROL OF MC-UPFC

A. Line Active and Reactive Power Sliding Surfaces

The DPC controllers for line power flow are here derived based on the sliding mode control theory. From



(b) Output voltage state-space vectors when the input voltages are located at sector.

Fig. 2, in steady state, is imposed by source . From (1) and (2), the transmission-line currents can be considered as state variables with first-order dynamics dependent on the sources and time constant of impedance . Therefore, transmission-line active and reactive powers present first-order dynamics and have a strong relative degree of one [25], since from the control viewpoint, its first time derivative already contains the control variable (the strong relative degree generally represents the number of times the control output variable must be differentiated until a control input appears explicitly in the dynamics) [26]–[29].

From the sliding mode control theory, robust sliding surfaces to control the and variables with a relatively strong degree of one can be obtained considering proportionality to a linear combination of the errors of between the power references and the actual transmitted powers , respectively the state variables [29]. Therefore, define the active power error and the reactive power error as the difference

$$e_P = P_{ref} - P \tag{10}$$

$$e_Q = Q_{ref} - Q. \tag{11}$$

Then, the robust sliding surfaces must be proportional to these errors, being zero after reaching sliding mode

$$S_P(e_P, t) = k_P(P_{ref} - P) = 0 \tag{12}$$

$$S_Q(e_Q, t) = k_Q(Q_{ref} - Q) = 0. \tag{13}$$

The proportional gains and are chosen to impose appropriate switching frequencies

Table I

Switching Combinations and Output Voltage / Input Current State-Space Vectors

	v_{AB}	v_{BC}	v_{CA}	i_a	i_b	i_c	V_o	δ_o	I_i	μ_i	
I	1g	v_{ab}	v_{bc}	v_{ca}	i_A	i_B	i_C	v_i	δ_i	i_o	μ_o
	2g	$-v_{ca}$	$-v_{bc}$	$-v_{ab}$	i_A	i_C	i_B	$-v_i$	$-\delta_i+4\pi/3$	i_o	$-\mu_o$
	3g	$-v_{ab}$	$-v_{ca}$	$-v_{bc}$	i_B	i_A	i_C	$-v_i$	$-\delta_i$	i_o	$-\mu_o+2\pi/3$
	4g	v_{bc}	v_{ca}	v_{ab}	i_C	i_A	i_B	v_i	$\delta_i+4\pi/3$	i_o	$\mu_o+2\pi/3$
	5g	v_{ca}	v_{ab}	v_{bc}	i_B	i_C	i_A	v_i	$\delta_i+2\pi/3$	i_o	$\mu_o+4\pi/3$
	6g	$-v_{bc}$	$-v_{ab}$	$-v_{ca}$	i_C	i_B	i_A	$-v_i$	$-\delta_i+2\pi/3$	i_o	$-\mu_o+4\pi/3$
	+1	v_{ab}	0	$-v_{ab}$	i_A	$-i_A$	0	$\frac{2}{\sqrt{3}}v_{ab}$	$\pi/6$	$\frac{2}{\sqrt{3}}i_A$	$-\pi/6$
	-1	$-v_{ab}$	0	v_{ab}	$-i_A$	i_A	0	$-\frac{2}{\sqrt{3}}v_{ab}$	$\pi/6$	$-\frac{2}{\sqrt{3}}i_A$	$-\pi/6$
	+2	v_{bc}	0	$-v_{bc}$	0	i_A	$-i_A$	$\frac{2}{\sqrt{3}}v_{bc}$	$\pi/6$	$\frac{2}{\sqrt{3}}i_A$	$\pi/2$
	-2	$-v_{bc}$	0	v_{bc}	0	$-i_A$	i_A	$-\frac{2}{\sqrt{3}}v_{bc}$	$\pi/6$	$-\frac{2}{\sqrt{3}}i_A$	$\pi/2$
	+3	v_{ca}	0	$-v_{ca}$	$-i_A$	0	i_A	$\frac{2}{\sqrt{3}}v_{ca}$	$\pi/6$	$\frac{2}{\sqrt{3}}i_A$	$7\pi/6$
	-3	$-v_{ca}$	0	v_{ca}	i_A	0	$-i_A$	$-\frac{2}{\sqrt{3}}v_{ca}$	$\pi/6$	$-\frac{2}{\sqrt{3}}i_A$	$7\pi/6$
	+4	$-v_{ab}$	v_{ab}	0	i_B	$-i_B$	0	$\frac{2}{\sqrt{3}}v_{ab}$	$5\pi/6$	$\frac{2}{\sqrt{3}}i_B$	$-\pi/6$
	-4	v_{ab}	$-v_{ab}$	0	$-i_B$	i_B	0	$-\frac{2}{\sqrt{3}}v_{ab}$	$5\pi/6$	$-\frac{2}{\sqrt{3}}i_B$	$-\pi/6$
II	+5	$-v_{bc}$	v_{bc}	0	0	i_B	$-i_B$	$\frac{2}{\sqrt{3}}v_{bc}$	$5\pi/6$	$\frac{2}{\sqrt{3}}i_B$	$\pi/2$
	-5	v_{bc}	$-v_{bc}$	0	0	$-i_B$	i_B	$-\frac{2}{\sqrt{3}}v_{bc}$	$5\pi/6$	$-\frac{2}{\sqrt{3}}i_B$	$\pi/2$
	+6	$-v_{ca}$	v_{ca}	0	$-i_B$	0	i_B	$\frac{2}{\sqrt{3}}v_{ca}$	$5\pi/6$	$\frac{2}{\sqrt{3}}i_B$	$7\pi/6$
	-6	v_{ca}	$-v_{ca}$	0	i_B	0	$-i_B$	$-\frac{2}{\sqrt{3}}v_{ca}$	$5\pi/6$	$-\frac{2}{\sqrt{3}}i_B$	$7\pi/6$
	+7	0	v_{ab}	v_{ab}	i_C	$-i_C$	0	$\frac{2}{\sqrt{3}}v_{ab}$	$3\pi/2$	$\frac{2}{\sqrt{3}}i_C$	$-\pi/6$
	-7	0	v_{ab}	v_{ab}	$-i_C$	i_C	0	$-\frac{2}{\sqrt{3}}v_{ab}$	$3\pi/2$	$-\frac{2}{\sqrt{3}}i_C$	$-\pi/6$
	+8	0	$-v_{bc}$	v_{bc}	0	i_C	$-i_C$	$\frac{2}{\sqrt{3}}v_{bc}$	$3\pi/2$	$\frac{2}{\sqrt{3}}i_C$	$\pi/2$
	-8	0	v_{bc}	$-v_{bc}$	0	$-i_C$	i_C	$-\frac{2}{\sqrt{3}}v_{bc}$	$3\pi/2$	$-\frac{2}{\sqrt{3}}i_C$	$\pi/2$
	+9	0	$-v_{ca}$	v_{ca}	$-i_C$	0	i_C	$\frac{2}{\sqrt{3}}v_{ca}$	$3\pi/2$	$\frac{2}{\sqrt{3}}i_C$	$7\pi/6$
	-9	0	v_{ca}	$-v_{ca}$	i_C	0	$-i_C$	$-\frac{2}{\sqrt{3}}v_{ca}$	$3\pi/2$	$-\frac{2}{\sqrt{3}}i_C$	$7\pi/6$
III	z_a	0	0	0	0	0	0	0	-	0	-
	z_b	0	0	0	0	0	0	0	-	0	-
	z_c	0	0	0	0	0	0	0	-	0	-

B. Line Active and Reactive Power Direct Switching Laws

The DPC uses a nonlinear law, based on the errors and to select in real time the matrix converter switching states (vectors). Since there are no modulators and/or pole zero-based approaches, high control speed is possible. To guarantee stability for active power and reactive power controllers, the sliding-mode stability conditions (14) and (15) must be verified

$$S_P(e_P, t) \dot{S}_P(e_P, t) < 0 \tag{14}$$

$$S_Q(e_Q, t) \dot{S}_Q(e_Q, t) < 0. \tag{15}$$

According to (12) and (14), the criteria to choose the matrix vector should be

1. If $S_P(e_P, t) > 0 \Rightarrow \dot{S}_P(e_P, t) < 0 \Rightarrow P < P_{ref}$, then choose a vector suitable to increase P .
2. If $S_P(e_P, t) < 0 \Rightarrow \dot{S}_P(e_P, t) > 0 \Rightarrow P > P_{ref}$, then choose a vector suitable to decrease P .
3. If $S_P(e_P, t) = 0$,

To design the DPC control system, the six vectors of group I will not be used, since they require extra algorithms to calculate their time-varying phase [14]. From group II, the variable amplitude vectors, only the 12 highest amplitude voltage vectors are certain to be able to guarantee the previously discussed required levels of and needed to fulfill the reaching conditions. The lowest amplitude voltages vectors, or the three null vectors of group III, could be used for near zero errors. If the control errors and are quantized using two hysteresis comparators, each with three levels (and), nine output voltage error combinations are obtained. If a two-level comparator is used to control the shunt reactive power, as discussed in next subsection, 18 error combinations will be defined, enabling the selection of 18 vectors. Since the three zero vectors have a minor influence on the shunt reactive power control, selecting one out 18 vectors is adequate. As an example, consider the case of and Then, and imply that and . According to Table I, output voltage vectors depend on the input voltages (sending voltage), so to choose the adequate output voltage vector, it is necessary to know the input voltages location [Fig. 4(a)]. Suppose now that the input voltages are in sector [Fig. 4(b)], then the vector to be applied should be 9 or 7. The final choice between these two depends on the matrix reactive power controller result , discussed in the next subsection. Using the same reasoning for the remaining eight active and reactive power error combinations and generalizing it for all other input voltage sectors, Table II is obtained. These P, Q controllers were designed based on control laws not dependent on system parameters, but only on the errors of the controlled output to ensure robustness to parameter variations or operating conditions and allow system order reduction, minimizing response times [26].

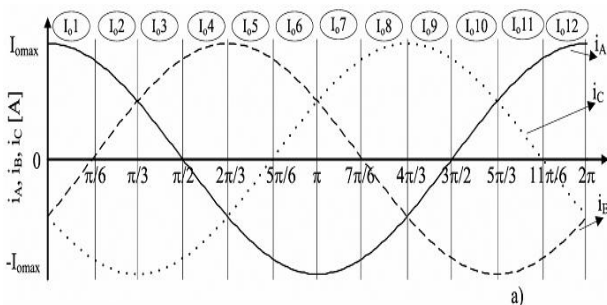


Fig. 5. (a) Output currents and their corresponding sector.

C. Direct Control of Matrix Converters Input Reactive Power

In addition, the matrix converter UPFC can be controlled to ensure a minimum or a certain desired reactive power at the matrix converter input. Similar to the previous considerations, since the voltage source input filter (Fig. 3) dynamics (6) has a strong relative degree of two [25], then a suitable sliding surface (19) will be a linear combination of

the desired reactive power error and its first-order time derivative [29] (19) The time derivative can be approximated by a discrete time difference, as has been chosen to obtain a suitable switching frequency, since as stated before, this sliding surface

$$S_{Q_i}(e_{Q_i}, t) = (Q_{i_{ref}} - Q_i) + K_{Q_i} \frac{d}{dt} (Q_{i_{ref}} - Q_i).$$

$$\begin{aligned} \dot{S}_{Q_i}(e_{Q_i}, t) = & V_{id} \left(\frac{di_{iq}}{dt} + K_{Q_i} \frac{d^2 i_{iq}}{dt^2} \right) = V_{id} \left(-\omega i_{id} + \frac{1}{2\sqrt{3}l} V_d - \frac{1}{2l} V_q \right) + \\ & V_{id} K_{Q_i} \left(-\omega^2 i_{iq} + \frac{\omega}{l} V_d + \frac{\omega}{\sqrt{3}l} V_q - \frac{\omega}{l} V_{id} - \frac{i_{iq}}{3lC} + \frac{i_q}{3lC} \right). \end{aligned}$$

The sliding mode is reached when vectors applied to the converter have the necessary current amplitude to satisfy stability conditions, such as (15). Therefore, to choose the most adequate vector in the chosen reference frame, it is necessary to know the output currents location since the input current depends on the output currents (Table I). Considering that the α -axis location is synchronous with the input voltage (i.e., reference frame depends on the input voltage location), the sign of the matrix reactive power can be determined by knowing the location of the input voltages and the location of the output currents (Fig. 5).

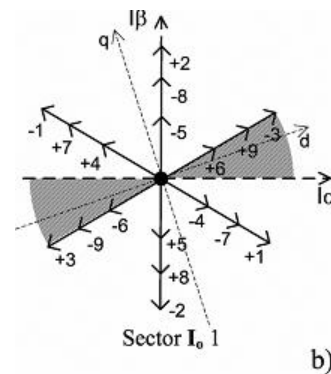


Fig. 5. (a) Output currents and their corresponding sector.

1. If $S_{Q_i}(e_{Q_i}, t) > 0 \Rightarrow \dot{S}_{Q_i}(e_{Q_i}, t) < 0$, then select vector with current $i_q < 0$ to increase Q_i
2. If $S_{Q_i}(e_{Q_i}, t) < 0 \Rightarrow \dot{S}_{Q_i}(e_{Q_i}, t) > 0$, then select vector with current $i_q > 0$ to decrease Q_i .

Considering the previous example, with the input voltage at sector and sliding surfaces signals and both vectors or would be suitable to control the line active and reactive powers errors (Fig. 4). However, at sector , these vectors have a different effect on the value: if has a suitable amplitude, vector leads to while vector originates So, vector should be chosen if the input reactive power sliding surface is quantized as 1, while vector 7 should chosen when is quantized as 1. When the active and reactive power errors are quantized as zero, 0 and 0, the null vectors of group III, or the lowest amplitude voltages vectors at sector at Fig. 4(b) could be used. These vectors do not produce significant effects on the line active and reactive power values, but the lowest amplitude voltage vectors have a high influence on the control of matrix reactive power. From Fig.

5(b), only the highest amplitude current vectors of sector should be chosen: vector 1 if is quantized as , or vector 2 if is quantized as

IV. IMPLEMENTATION OF THE DPC-MC AS UPFC

As shown in the block diagram (Fig. 6), the control of the instantaneous active and reactive powers requires the measurement of voltages and output currents necessary to calculate and sliding surfaces. The output current

measurement is also used to determine the location of the input currents component. The control of the matrix converter input reactive power requires the input currents measurement to calculate. At each time instant, the most suitable matrix vector is chosen upon the discrete values of the sliding surfaces, using tables derived from Tables II and III for all voltage sectors.

TABLE II
 STATE-SPACE VECTORS SELECTION FOR DIFFERENT ERROR COMBINATIONS

C_α	C_β	Sector					
		$V_i 12; 1$	$V_i 2; 3$	$V_i 4; 5$	$V_i 6; 7$	$V_i 8; 9$	$V_i 10; 11$
-1	+1	-9; +7	-9; +8	+8; -7	-7; +9	+9; -8	-8; +7
-1	0	+3; -1	+3; -2	-2; +1	+1; -3	-3; +2	+2; -1
-1	-1	-6; +4	-6; +5	+5; -4	-4; +6	+6; -5	-5; +4
0	+1	-9; +7; +6; -4	-9; +8; +6; -5	+8; -7; -5; +4	-7; +9; +4; -6	+9; -8; -6; +5	-8; +7; +5; -4
0	0	Za; Zb; Zc; -8;+2;-5;+8;-2;+5	Za; Zb; Zc; -7;+1;-4; +7;-1;+4	Za; Zb; Zc; +9;-3;+6;-9;+3;-6	Za; Zb; Zc; -8;+2;-5;+8;-2;+5	Za; Zb; Zc; -7;+1;-4; +7;-1;+4	Za; Zb; Zc; -9;+3;-6; +9;-3;+6
0	-1	-6; +4; +9; -7	+5; -6; -8; +9	+5; -4; -8; +7	-4; +6; +7; -9	+6; -5; -9; +8	-5; +4; +8; -7
+1	+1	+6; -4	+6; -5	-5; +4	+4; -6	-6; +5	+5; -4
+1	0	-3; +1	+2; -3	-1; +2	+3; -1	-2; +3	+1; -2
+1	-1	+9; -7	+9; -8	+7; -8	+7; -9	-9; +8	+8; -7

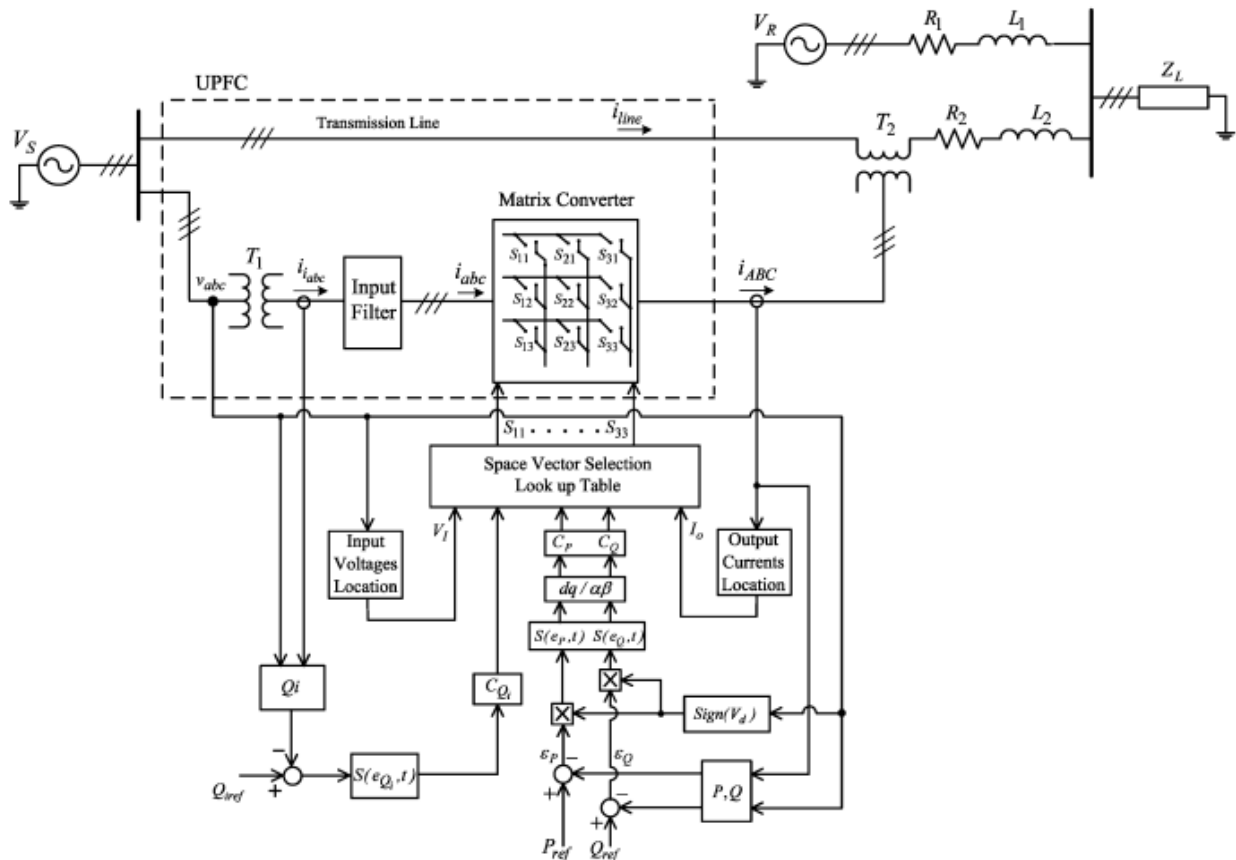


Fig. 6. Control scheme of direct power control of the three-phase matrix converter operating as a UPFC.

V. SIMULATION AND EXPERIMENTAL RESULTS

The performance of the proposed direct control system was evaluated with a detailed simulation model using the*-MATLAB/Simulink Sim Power Systems to represent the matrix converter, transformers, sources and transmission lines, and Simulink blocks to simulate the control system. Ideal switches were considered to simulate matrix converter semiconductors minimizing simulation times.

The second-order input filter is 4.2 mH, 6.6 F, 25 . This prototype was connected to the laboratory low-voltage network operating as UPFC, (Fig. 6) by using three-phase transformers T1 and T2 (2-kVA transformers with voltage ratio 220/115 V and 66.5/66.5 V, respectively). Current sensors were used to measure the matrix converter input and output currents (Hall effect LEM, LA25NP), and voltage sensors were used to measure the power network phase-to-phase voltages (Hall effect LEM, LV 25-P).

To achieve safe commutation between matrix converter bidirectional switches, the four-step output current commutation strategy [18] was implemented in a field-programmable gate array (FPGA) using a Xilinx board (Virtex-5).

Algorithm was implemented in a digital signal processor PowerPC board (DS1103 of dSPACE) with a sampling time approximately equal to 17 s. The load power is 1.5kW(1 p.u.) and transmission lines 1 and 2 are simulated as inductances mH 15 mH, and series resistances , respectively for line 1 and 2. Sliding mode DPC gains are 1, selected to ensure the highest switching frequencies around 2.5 kHz. Experimental and simulation results of the active and reactive power UPFC controller are obtained from the step reMONTEIRO.

The experimental power spectral density of transmission line and matrix converter current [respectively, Fig. 8(c) and (d)] shows that the main harmonics are nearly 30 dB below the 50-Hz fundamental for the line current, and 22 dB below the 50-Hz fundamental for the matrix converter current. The power spectral density shows switching frequencies mainly below 2.5 kHz as expected. Simulation and experimental results confirm the performance of the proposed controllers, showing no cross-coupling, no steady-state error (only switching ripples), and fast response times for different changes of power references. DPC active and reactive power step response and line currents results were compared to active and reactive power linear PI controllers [11] using a Aventurine high-frequency PWM modulator [17], working at 5.0-kHz switching frequency. Experimental implementation of this control algorithm at the same microprocessor required 21- s sampling time (higher than the 17 s of DPC) due to the complexity of the modulator (needs 4 s more when compared to the proposed DPC). Experimental and simulation results [Fig. 9(a) and (b)], for 0.4 p.u. and 0.2 p.u. show cross-coupling between active and reactive power control, which introduces a slowly decaying error in the response. Longer response times are also present, when compared to DPC experimental and simulation results presented in Fig. 9(c) and (d), showing the claimed DPC faster dynamic response to step active and reactive power reference change. To test the DPC controller ability to operate at lower switching frequencies, the DPC gains were lowered and the input filter parameters were changed accordingly (5.9 mH F) to lower the switching frequency to nearly 1.4 kHz. The results (Fig. 10) also show fast response without cross coupling between active and reactive power.m This confirms the DPC-MC robustness to input filter parameter variation, the ability to operate at low switching frequencies, and insensitivity to switching nonlinearity.

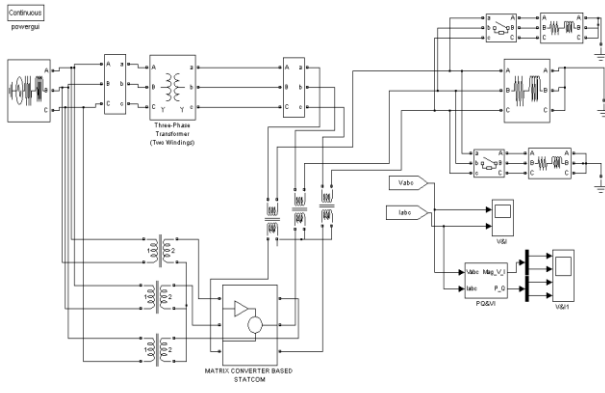


Fig 7. Modeling of UPFC with matrix convertor

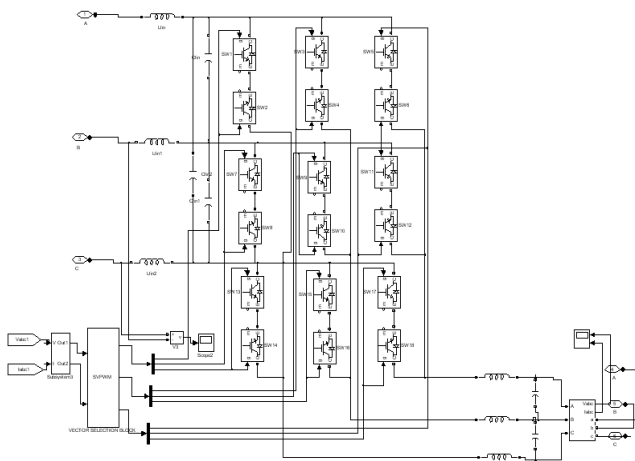


Fig 8. Modeling of matrix convertor

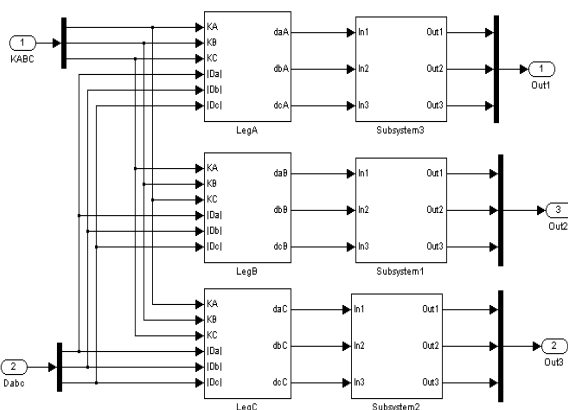


Fig 9. Modeling of vector selecton block

To experimentally validate the simulations, a low-power prototype matrix converter was built [14] by using three semiconductor modules from DANFOSS, each one with six 1200-V 25-A insulated-gate bipolar transistors (IGBTs) with an antiparallel diode in a common collector arrangement, driven by optical isolated drives (TLP250).

V. CONCLUSION

This paper derived advanced nonlinear direct power controllers, based on sliding mode control techniques, for matrix converters connected to power transmission lines as UPFCs. Presented simulation and experimental results show that active and reactive power flow can be advantageously controlled by using the proposed DPC. Results show no steady-state errors, no cross-coupling, insensitivity to no modeled dynamics and fast response times, thus confirming the expected performance of the presented nonlinear DPC methodology. The obtained DPC-MC results were compared to PI linear active and reactive power controllers using a modified Venturini

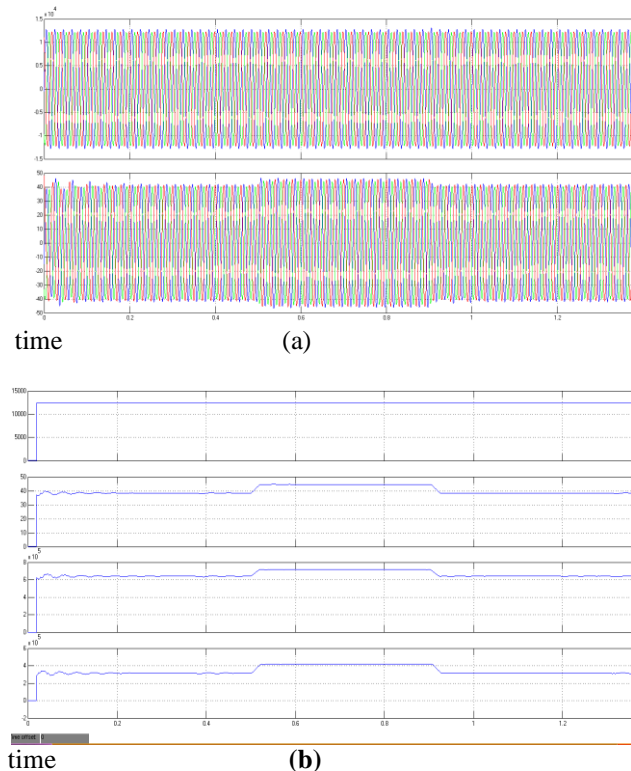


Fig 9. (a) out put voltage and current , (b) magnitude of voltage, current and active power, reactive power. $f=50\text{Hz}$ load $R=50\Omega$, $L=75\text{mh}$.

REFERENCES

[1] N. Hingorani and L. Gyugyi, *Understanding FACTS—Concepts and Technology of Flexible AC Transmission Systems*. Piscataway, NJ: IEEE Press/Wiley, 2000.

[2] L. Gyugyi, “Unified power flow control concept for flexible AC transmission systems,” *Proc. Inst. Elect. Eng. C*, vol. 139, no. 4, Jul. 1992.

[3] L. Gyugyi, C. Schauder, S. Williams, T. Rietman, D. Torgerson, and A. Edris, “The unified power flow controller: A new approach to power transmission control,” *IEEE Trans. Power Del.*, vol. 10, no. 2, pp. 1085–1097, Apr. 1995.

[4] C. Schauder, L. Gyugyi, M. Lund, D. Hamai, T. Rietman, D. Torgerson, and A. Edris, “Operation of the unified power flow controller (UPFC) under practical constraints,” *IEEE Trans. Power Del.*, vol. 13, no. 2, pp. 630–639, Apr. 1998.

[5] T. Ma, “P-Q decoupled control schemes using fuzzy neural networks for the unified power flow controller,” in *Electr. Power Energy Syst.* New York: Elsevier, Dec. 2007, vol. 29, pp. 748–748.

[6] L. Liu, P. Zhu, Y. Kang, and J. Chen, “Power-flow control performance analysis of a unified power-flow controller in a novel control scheme,” *IEEE Trans. Power Del.*, vol. 22, no. 3, pp. 1613–1619, Jul. 2007.

[7] F. Gao and M. Iravani, “Dynamic model of a space vector modulated matrix converter,” *IEEE Trans. Power Del.*, vol. 22, no. 3, pp. 1696–1750, Jul. 2007.

[8] B. Geethalakshmi and P. Dananjayan, “Investigation of performance of UPFC without DC link capacitor,” in *Elect. Power Energy Res.* New York: Elsevier, 2008, pp. 284–294, 736-746.

[9] X. Jiang, X. Fang, J. Chow, A. Edris, E. Uzunovic, M. Parisi, and L. Hopkins, “A novel approach for modeling voltage-sourced converterbased FACTS controllers,” *IEEE Trans. Power Del.*, vol. 23, no. 4, pp. 2591–2598, Oct. 2008.

[10] R. Strzelecki, A. Noculak, H. Tunia, and K. Sozanski, “UPFC with matrix converter,” presented at the EPE Conf., Graz, Austria, Sep. 2001.

[11] J. Monteiro, J. Silva, S. Pinto, and J. Palma, “Unified power flow controllers without DC bus: Designing controllers for the matrix converter solution,” presented at the Int. Conf. Electrical Engineering, Coimbra, Portugal, 2005.

[12] A. Dasgupta, P. Tripathy, and P. Sensarma, “Matrix converter as UPFC for transmission line compensation,” in *Proc. 7th Int. Conf. Power Electronics*, Exco, Daegu, Korea, Oct. 2007, pp. 1050–1055.

[13] P. Wheeler, J. Rodriguez, J. Clare, L. Empringham, and A. Weinstein, “Matrix converters: A technology review,” *IEEE Trans. Ind. Electron.*, vol. 49, no. 2, pp. 276–288, Apr. 2002.

[14] S. Pinto, “Conversores matriciais trifásicos: generalização do commando vectorial directo,” Ph.D. dissertation, Instituto Superior Técnico Universidade Técnica de Lisboa, Lisbon, Portugal, Jul. 2003.

[15] T. Podlesak, D. Katsis, P. Wheeler, J. Clare, L. Empringham, and M. Bland, “A 150-kVA vector-controlled matrix converter induction motor drive,” *IEEE Trans. Ind. Appl.*, vol. 41, no. 3, pp. 841–847, May/Jun. 2005.



D. Jagan is born in 1988 in India. He is graduated from JNTU Hyderabad in 2010. Presently he is doing Post graduation in Power Electronics and Electrical Drives Specialization at J.N.T.U, Anantapur His main areas of interest include Induction motor drives, Electrical machines, Power Electronics & Converters and Power Electronic Drives

Optimal Agc of Deregulated Interconnected Power System with Parallel Ac/Dc Link

Naimul Hasan

Department of Electrical Engineering Jamia Millia Islamia New Delhi-110025, India

Abstract : This paper presents optimal AGC regulator design of deregulated power system based on the full state feedback control strategy. The two-area interconnected power system of identical nature consisting of non-reheat turbine is considered for the investigations. The area-interconnection of the power system via parallel EHVAC/HVDC transmission link is considered. The proposed controller is applied to two-area interconnected power system and its feasibility is demonstrated by investigating the dynamic response plots obtained various system states of the power system models under consideration. The patterns of closed-loop eigenvalues are obtained to analyze the stability of the power system models.

Keywords- AGC, Deregulated power system, interconnected power system, parallel EHVAC/HVDC.

I. INTRODUCTION

The electric power industry is in transitional phase moving from centrally regulated utilities to deregulated environment that will inject competition in the power sector among all the companies to sale the unbundled power at very reasonable rates to the distribution companies. The restructuring and deregulation of power sector is to create a competitive environment where generation and transmission services are bought and sold under demand and supply market conditions. This has unbundled the electric utility services into its basic components and offering each component separately for the sale with separate rates. The unbundling of the vertical entity creates the separate entity for generation, transmission and distribution for the transaction of electric power. Before deregulation ancillary services were provided by a single entity possessing owns generating resources, transmission and distribution capacities located within its territories.

The deregulated power system will have the generating power station separated from transmission and distribution entities. All the power generating stations will be recognized as independent power producers (IPPs). These will be known as GENCOs which will have a free market to compete each other to sell the electrical power. The retail consumers are supposed to buy the electrical power from the distribution companies known as DISCOs. There is also a third player between the GENCOs and DISCOs for wheeling the between them which is designated as TRANSCO. So in the deregulated power system instead of having single vertical entity it will have three players as GENCOs, DISCOs and TRANSCO operating separately with their own set functionalities. To supply the regulation between Disco and Genco, a contract will be established between these entities. In the deregulated power system structure, a distribution company has the freedom to have a contract with any generation companies for purpose of transaction of

power. The different companies may have the bilateral transactions and these will have to be monitored through an independent system operator which will control the number of ancillary services.

The main task of automatic generation control is to maintain the reliability of the system at the desired frequency even to the varying load demand. The generation companies in deregulated environment may or may not participate in the AGC task. As far as the optimal AGC schemes for interconnected power systems operating in deregulated environment are concerned, a considerable work has been reported in literature [1-5]. V. Donde et al. in [5] have presented an AGC of interconnected power systems in deregulated environment. The distribution companies may contract for the transaction of power with generation companies in its area or other areas. This transaction of power among the generation and distribution companies is done under the supervision of the independent system operators.

The frame work of the deregulated power system is as follows:

1. Unbundling of electrical power system separating Vertically Integrated Utility into GENCOs, TRANSCO and DISCOs as independent entities.
2. Annulling of exclusive rights
3. Third party shall get access to transmission or supply grids.

However, in all the above articles power system models interconnected via EHV AC transmission links only. But due to the obvious of merits of HVDC transmission line, the interconnection with HVDC link has been utilized for the power system model under consideration. One of the most useful applications of HVDC link is its operation in parallel with EHVAC transmission line between two power networks. This makes the system makes the more stable. The HVDC transmission link an area interconnection has also been demonstrated as a viable tool to improve dynamic performance of the system [6-9].

In the work presented in this paper, optimal controllers are designed and compared based on the interconnected between the two areas. In one power system model the AC tie-line is considered and in the second power system model a parallel AC/DC tie line is considered. The dynamic performance of the power system models considered is analyzed for the designed regulators.

II. Power System Model

A two-area interconnected power system operating under deregulated environment with parallel EHVAC/HVDC for exchanging of power between control areas is considered for investigation. The structure of power system model consists of two identical non-reheat thermal

power plants as GENCOs and two distribution system as DISCOs.

The transfer function model of power system model under investigation is developed and presented in Fig. 8. In this model, the actual and scheduled steady state power flows on the tie line are given by;

$$\Delta P_{tie12}^{scheduled} = (\text{Demand of DISCOs in area-2 from GENCOs in area-1}) - (\text{Demand of DISCOs in area-1 from GENCOs in area-2}) \quad (1)$$

$$\Delta P_{tie12, schedule} = \sum_{i=1}^2 \sum_{j=3}^4 cpf_{ij} \Delta P_{Lj} - \sum_{i=3}^4 \sum_{j=1}^2 cpf_{ij} \Delta P_{Lj} \quad (2)$$

The tie line power error ($\Delta P_{tie12, error}$) is defined by;

$$\Delta P_{tie12, error} = \Delta P_{tie12, actual} - \Delta P_{tie12, scheduled} \quad (3)$$

The area control errors (ACEs) in deregulated environment in both areas are defined as;

$$ACE_1 = B_1 \Delta f_1 + \Delta P_{tie12, error} \quad (4)$$

$$ACE_2 = B_2 \Delta f_2 + \alpha_{12} \Delta P_{tie12, error} \quad (5)$$

As there may be many GENCOs in each area, the ACE signal is being distribute among them and their ACE participation factor (apf) for automatic generation control and also sum of all apfs in a particular area should be unity.

In steady state, the demand of DISCOs in contract with GENCOs generation must be matched and expressed as:

$$\Delta P_{L1, Loc} = \Delta P_{L1} + \Delta P_{L2} \quad (8)$$

$$\Delta P_{L1, Loc} = \Delta P_{L1} + \Delta P_{L2} \quad (9)$$

$$\Delta P_{L2, Loc} = \Delta P_{L3} + \Delta P_{L4} \quad (9)$$

$$\Delta P_{L2, Loc} = \Delta P_{L3} + \Delta P_{L4} \quad (10)$$

$$\Delta P_2 = cpf_{21} \Delta P_{L1} + cpf_{22} \Delta P_{L2} + cpf_{23} \Delta P_{L3} + cpf_{24} \Delta P_{L4} \quad (11)$$

$$\Delta P_3 = cpf_{31} \Delta P_{L1} + cpf_{32} \Delta P_{L2} + cpf_{33} \Delta P_{L3} + cpf_{34} \Delta P_{L4} \quad (12)$$

$$\Delta P_4 = cpf_{41} \Delta P_{L1} + cpf_{42} \Delta P_{L2} + cpf_{43} \Delta P_{L3} + cpf_{44} \Delta P_{L4} \quad (13)$$

ΔP_{UC1} and ΔP_{UC2} are disturbance signal for un-contracted load in case of contract violation. In case un-contracted loads are absent, ΔP_{UC1} and ΔP_{UC2} are zero.

2.1. Case Study

In the present work, two different power system models are identified as follows:

Power system Model-I: Two- area interconnected power system consisting of non-reheat turbine via EHVAC tie-line only.

Power system Model-II: Two area interconnected power system of non-reheat turbine via parallel EHVAC/HVDC tie-line.

III. State Variable Model

The two-area power system model operating under deregulated environment is shown in Fig. 8 can be described by the following controllable and observable linear time-invariant state space representation;

$$\frac{d}{dt} \underline{x} = \underline{A} \underline{x} + \underline{B} \underline{u} + \underline{\Gamma} \underline{P}_d \quad (14)$$

$$\underline{Y} = \underline{C} \underline{x} \quad (15)$$

For power system model under investigation, the system state, control and disturbance vectors are selected as follows:

- **State vector**

$$\underline{X} = [\Delta f_1, \Delta f_2, \Delta P_{tie12}, \Delta P_{g1}, \Delta X_{g1}, \Delta P_{g2}, \Delta X_{g2}, \Delta P_{g3}, \Delta X_{g3}, \Delta P_{g4}, \Delta X_{g4}, \int ACE_1 dt, \int ACE_2 dt]$$

- **Control vector**

$$\underline{u} = [\Delta P_{C1} \quad \Delta P_{C2}]^T$$

- **Disturbance vector**

$$\underline{P}_d = [\Delta P_{L1} \quad \Delta P_{L2} \quad \Delta P_{L3} \quad \Delta P_{L4} \quad \Delta P_{UC1} \quad \Delta P_{UC2}]^T$$

- **System Matrices**

The structure of system matrices A, B, Γ_d and C can be obtained from the transfer function model shown in fig8.

IV. Design of Optimal AGC Regulator

The design of optimal AGC regulators reported in literature [10]. The continuous time dynamic model in the state variable form is given as;

$$\frac{d}{dt} \underline{x} = \underline{A} \underline{x} + \underline{B} \underline{u} + \underline{\Gamma} \underline{P}_d \quad (16)$$

$$\underline{y} = \underline{C} \underline{x} \quad (17)$$

Where, x, u, P_d and y are state, control, disturbance and output vector respectively. A, B, C and Γ are system, control, output and disturbance matrices of compatible dimensions.

In the application of optimal control theory, the term in equation (16) is eliminated by redefining the states and controls in terms of their steady-state values occurring after the disturbance. It can be rewritten as;

$$\frac{d}{dt} \underline{x} = \underline{A} \underline{x} + \underline{B} \underline{u}, \underline{x}(0) = x_0 \quad (18)$$

Moreover eq. (17) will remain the same. The control signal u is such that to minimize the performance index (J):

$$J = \int_0^{\infty} \frac{1}{2} [\underline{x}^T \underline{Q} \underline{x} + \underline{u}^T \underline{R} \underline{u}] dt \quad (19)$$

Where, Q and R are weighting matrices for the state variables and the input variables. This optimal control problem is referred to as the linear quadratic regulator design problem. To solve this LQ optimal control problem, let us first construct a Hamiltonian function.

$$J = -\frac{1}{2} [\underline{x}^T \underline{Q} \underline{x} + \underline{u}^T \underline{R} \underline{u}] dt + \underline{\lambda}^T [\underline{A} \underline{x} + \underline{B} \underline{u}] \quad (20)$$

When there is no constraint on the input signal, the optimal (in this case, the minimum) value can be solved by taking the derivative of H with respect to u and then solving the following equation;

$$\frac{\partial H}{\partial \underline{u}} = -\underline{R} \underline{u} + \underline{B}^T \underline{\lambda} = 0 \quad (21)$$

Denote by \underline{u}^* the optimal control signal u. Then, \underline{u}^* can be explicitly written in the following form:

$$\underline{u}^* = \underline{R}^{-1} \underline{B}^T \underline{\lambda} \quad (22)$$

On the other hand Lagrangian Multiplier ($\underline{\lambda}$) can be written as; $\underline{\lambda} = \underline{S} \underline{x}$ (23)

Where, S is the symmetrical solution of the well known DRE.

$$\frac{d\underline{S}}{dt} = -\underline{S} \underline{A} - \underline{A}^T \underline{S} + \underline{S} \underline{B} \underline{R}^{-1} \underline{B}^T \underline{S} - \underline{Q} \quad (24)$$

The solution matrix S will tend to a constant matrix i.e. $ds/dt=0$, In this case DRE reduced to so called algebraic Riccatti Equation:

$$SA + A^T S - SBR^{-1}B^T S + Q = 0 \quad (25)$$

Now (22) can be written as;

$$\underline{u}^* = R^{-1}B^T S \underline{x} \quad (26)$$

With a full state vector feedback control problem, a control law is stated as;

$$\underline{u}^* = -\Psi^* \underline{x} \quad (27)$$

Using (26) and (27), the desired optimal feedback gain matrix (Ψ^*) is given by;

$$\Psi^* = R^{-1}B^T S \quad (28)$$

How to determine the feedback gain matrix [Ψ^*], which minimizes the values of J is an important optimization problem. The value of [Ψ^*] is usually obtained from the solution of matrix Riccati equation [11]

V. Simulation Results

The optimal gains of AGC regulators are obtained by using MATLAB software. The patterns of closed loop eigenvalues is reported in Table-1 where as the optimal gains of AGC regulators designed and performance index obtained are presented in Table-2 and Table-3 respectively. The dynamic response plots with the implementation of optimal AGC regulators are shown by Figs. (1-7).

VI. Discussion of Results

The MATLAB software is used to obtain pattern of closed-loop eigenvalues, optimal gains of AGC regulators, performance index and dynamic response plots for both the models. The inspection of closed-loop eigenvalues as shown in Tables-1 inferred that all the eigenvalues have negative real part, thereby ensuring the system stability in closed-loop fashion.

The response curves of Figs. (1-2) represent frequency deviations of respective areas. Observations carried out from these plots reveal that the proposed optimal AGC regulators are capable to mitigate the deviations in frequency of both areas caused due to instantaneous load demands from DISCOs. The tie line power deviation settles to a zero value. The proposed AGC regulators are found to demonstrate their ability to bring the system state deviation as per the desired ones in an effective manner.

The response curves in Figs. (4-7) show the deviations in power generation by GENCOs of respective areas. From the inspection of these Figs., it has been inferred that the proposed optimal AGC regulators are effective in settling the change in power generation to the required value in reasonably small time.

Table-1 Pattern of Closed-loop Eigenvalues

Power system model-I	Power system model-II
-4.6020	-4.6020
-4.3400	-2.5000
-0.7696 ± 3.2987i	-2.7225 ± 1.0381i
-2.5000	-2.1035 ± 7.6681i
-2.5000	-1.6667
-1.6667	-1.6667
-1.6667	-1.1371 ± 2.4201i
-1.1371 ± 4.201i	-0.4096 ± 0.2931i
-0.6925 ± 0.2596i	-0.3228
-0.3228	

Table-2 Optimal Gains of AGC Regulator

P.S. Model-I	0.5190 0.1524 -2.2802 2.5248 1.2060
	2.5248 1.2060 -0.0431 -0.0130 -
	0.0431 -0.0130 1.0 0.0
P.S. Model-II	0.1524 0.5190 2.2802 -0.0431 -
	0.0130 -0.0431 -0.0130 2.5248
	1.2060 2.5248 1.2060 0.0 1.0

Table-3 Performance Index

Model-I	34.4470
Model-II	28.9270

VII. Conclusions

In this paper, the gains of optimal AGC regulators are obtained using modern control theory through state space model technique. The patterns of closed-loop eigenvalues are obtained for power system models in deregulated environment and their investigation reveals that system is stable. The responses are associated with more number of oscillations coupled with larger settling time degraded the system dynamic response in case of power system model-I having AC tie line only are reduced tremendously in the power system model-II with AC/DC parallel tie lines.

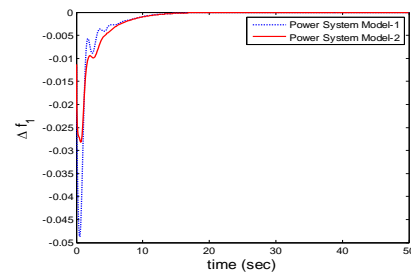


Fig. 3 Change in Frequency (Δf_1)

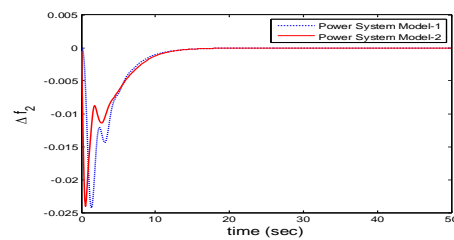


Fig. 4 Change in Frequency (Δf_2)

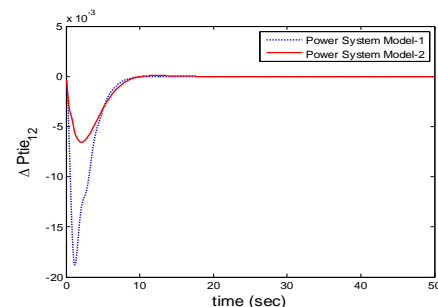


Fig. 5 Change in Tie-line power (ΔP_{tie12})

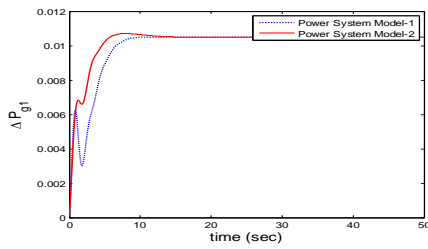


Fig. 6 Change in Power generated (Pg1)

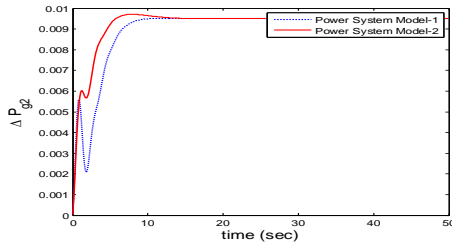


Fig. 7 Change in Power generated (Pg2)

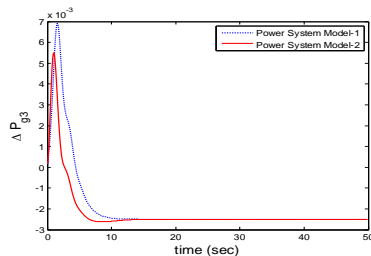


Fig. 8 Change in Power generated (Pg3)

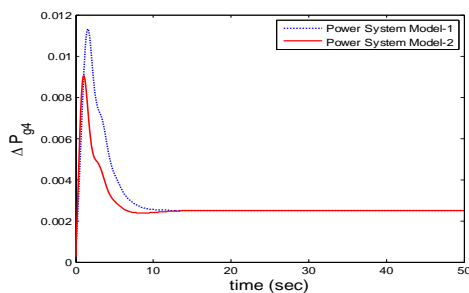


Fig. 9 Change in Power generated (Pg4)

References:

- [1] P. Kumar, S. A. Kazmi and N. Yasmeen, "Comparative study of automatic generation control in traditional and deregulated power environment", *World Journal of Modelling and Simulation*, vol. 6, no. 3, 2010, pp. 189-197.
- [2] B. Tyagi and S.C. Srivastava, "A LQG based load frequency controller in a competitive electricity markets", *Int. Journal of Emerging Electric Power Systems*, vol. 2, no. 2, 2005, pp. 1-13.
- [3] S.K. Sinha, R.N. Patel and R. Prasad, "Design of optimal controller for AGC in a restructure power systems", *Proc. National Conf. Recent Advances in Electrical and Electronics Engineering*, Hamirpur, India, 2009, pp. 52-57.
- [4] E. Rakhshani and J. Sadeh, "Load frequency control of multi-area restructured power system", *Proc. IEEE Int. Conf. Power Systems Technology*, New Delhi, India, 2008, pp. 1-7.
- [5] V. Donde, M. A. Pai and I. A. Hiskens, "Simulation and optimization in a AGC system after

deregulation", *IEEE Trans. on Power System*, vol. 16, no. 3, pp. 481-489, 2001.

- [6] P. Kumar and Ibraheem, "Dynamic performance evaluation of 2-area interconnected power systems: a comparative study", *Journal of Institution of Engineers (India)*, vol. EL-4, no. 78, pp. 199-209, 1997.
- [7] C. Srinivasa Rao, S. Siva Nagaraju and P. Sangameswara Raju, "Improvement of dynamic performance of AGC under open market scenario employing TCPS and AC-DC parallel tie line", *Int. J. of Recent Trends in Engineering*, vol. 1, no.3, May 2009.
- [8] Ibraheem, P. Kumar and S. Ahmad, "Dynamic performance enhancement of hydro-power systems with asynchronous tie-lines", *Journal of Institution of Engineers (India)*, vol. 85, June 2004, pp. 23-34.
- [9] Ibraheem and P. Kumar, "Study of dynamic performance of power systems with asynchronous tie-lines considering parameter uncertainties", *Journal of Institution of Engineers (India)*, vol. 85, June 2004, pp. 35-42.
- [10] Ibraheem, P. Kumar and D.P. Kothari, "Recent philosophies of automatic generation control strategies in power systems", *IEEE Trans. on Power Systems*, vol. 20, no. 1, 2005, pp. 346-357.
- [11] M. Athans and P. Falb, "*Optimal Control: An application to the theory and its application*", Mc Graw-Hill, New York, 1966.

Numerical Data:

L1=0.01; PL2=0.01; PL3=0.0; PL4=0.0; M=2; L=13; W=4;
 TOL=0.00001; alpha=0.005; T12=0.0867;
 b1=0.4249; b2=0.4249;
 a12=-
 1; Tp1=20; Kp1=120; Tp2=20; Kp2=120; Kdc=1; Tdc=0.2;
 Tt1=0.6; Tg1=0.4; Tr1=5; Kr1=0.3; R1=2.4; Tt2=0.6;
 Tg2=0.4; Tr2=5; Kr2=0.3; R2=2.4; Tt3=0.6; Tg3=0.4;
 Tr3=5; Kr3=0.3; R3=2.4; Tt4=0.6; Tg4=0.4; Tr4=5;
 Kr4=0.3; R4=2.4; apf1=0.5;
 apf2=0.5; apf3=0.5; apf4=0.5; cpf11=0.1; cpf12=0.0; cpf13=0.0
 ; cpf14=0.6; cpf21=0.0; cpf22=0.0; cpf23=0.0; cpf24=0.4;
 cpf31=0.7; cpf32=0.0; cpf33=0.1; cpf34=0.0; cpf41=0.2; cpf42
 =1;
 cpf43=0.0; cpf44=0.0;

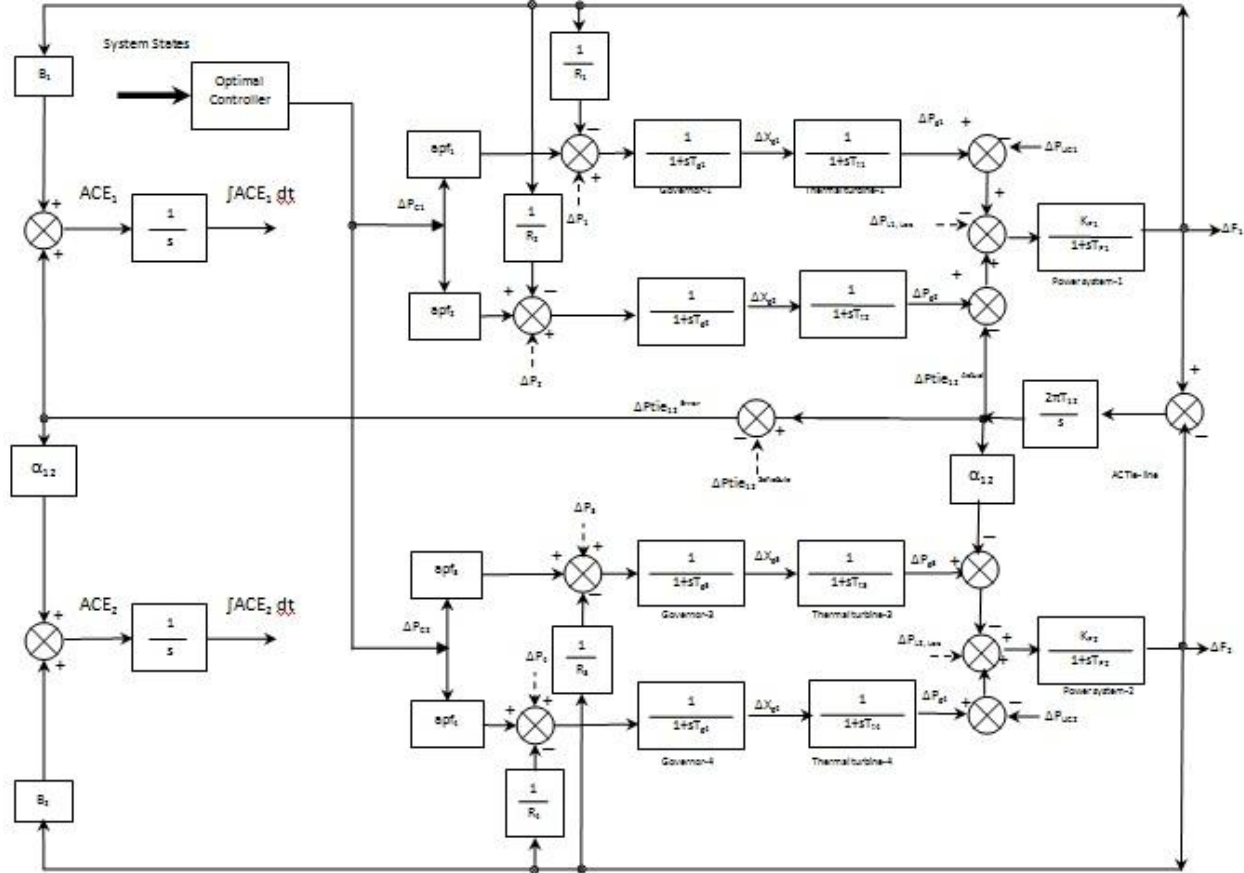


Fig. 3.2 Transfer function model of two-area interconnected power system under deregulated environment

System Matrix 'A₁'

$$A_1 = \begin{bmatrix} -\frac{1}{T_{ps1}} & 0 & -\frac{K_{ps1}}{T_{ps1}} & \frac{K_{ps1}}{T_{ps1}} & 0 & \frac{K_{ps1}}{T_{ps1}} & 0 & 0 & 0 & 0 & 0 & 0 & 0 \\ 0 & -\frac{1}{T_{ps2}} & \frac{K_{ps2}}{T_{ps2}} & 0 & 0 & 0 & 0 & \frac{K_{ps2}}{T_{ps2}} & 0 & \frac{K_{ps2}}{T_{ps2}} & 0 & 0 & 0 \\ 2\pi T_{12} & -2\pi T_{12} & 0 & 0 & 0 & 0 & 0 & 0 & 0 & 0 & 0 & 0 & 0 \\ 0 & 0 & 0 & \frac{1}{T_{ips1}} & \frac{1}{T_{ips1}} & 0 & 0 & 0 & 0 & 0 & 0 & 0 & 0 \\ -\frac{1}{R_1 T_{gps1}} & 0 & 0 & 0 & -\frac{1}{T_{gps1}} & 0 & 0 & 0 & 0 & 0 & 0 & 0 & 0 \\ 0 & 0 & 0 & 0 & 0 & -\frac{1}{T_{ips2}} & -\frac{1}{T_{ips2}} & 0 & 0 & 0 & 0 & 0 & 0 \\ -\frac{1}{R_2 T_{gps2}} & 0 & 0 & 0 & 0 & 0 & -\frac{1}{T_{gps2}} & 0 & 0 & 0 & 0 & 0 & 0 \\ 0 & 0 & 0 & 0 & 0 & 0 & 0 & -\frac{1}{T_{ips3}} & \frac{1}{T_{ips3}} & 0 & 0 & 0 & 0 \\ 0 & -\frac{1}{R_3 T_{gps3}} & 0 & 0 & 0 & 0 & 0 & 0 & -\frac{1}{T_{gps3}} & 0 & 0 & 0 & 0 \\ 0 & 0 & 0 & 0 & 0 & 0 & 0 & 0 & 0 & -\frac{1}{T_{ips4}} & \frac{1}{T_{ips4}} & 0 & 0 \\ 0 & -\frac{1}{R_4 T_{gps4}} & 0 & 0 & 0 & 0 & 0 & 0 & 0 & 0 & -\frac{1}{T_{gps4}} & 0 & 0 \\ b_1 & 0 & 1 & 0 & 0 & 0 & 0 & 0 & 0 & 0 & 0 & 0 & 0 \\ 0 & b_2 & -1 & 0 & 0 & 0 & 0 & 0 & 0 & 0 & 0 & 0 & 0 \end{bmatrix}$$

- **Control Matrix 'B₁'**

$$B_1^T = \begin{bmatrix} 0 & 0 & 0 & 0 & \frac{apf_1}{T_{g1}} & 0 & \frac{apf_2}{T_{g2}} & 0 & 0 & 0 & 0 & 0 & 0 \\ 0 & 0 & 0 & 0 & 0 & 0 & 0 & 0 & \frac{apf_3}{T_{g3}} & 0 & \frac{apf_4}{T_{g4}} & 0 & 0 \end{bmatrix}$$

- **Disturbance Matrix 'Fd₁'**

$$F_{d1}^T = \begin{bmatrix} -\frac{K_{P1}}{T_{P1}} & 0 & 0 & 0 & \frac{cpf_{11}}{T_{g1}} & 0 & \frac{cpf_{21}}{T_{g2}} & 0 & \frac{cpf_{31}}{T_{g3}} & 0 & \frac{cpf_{41}}{T_{g4}} & 0 & 0 \\ -\frac{K_{P1}}{T_{P1}} & 0 & 0 & 0 & \frac{cpf_{12}}{T_{g1}} & 0 & \frac{cpf_{22}}{T_{g2}} & 0 & \frac{cpf_{32}}{T_{g3}} & 0 & \frac{cpf_{42}}{T_{g4}} & 0 & 0 \\ 0 & -\frac{K_{P2}}{T_{P2}} & 0 & 0 & \frac{cpf_{13}}{T_{g1}} & 0 & \frac{cpf_{23}}{T_{g2}} & 0 & \frac{cpf_{33}}{T_{g3}} & 0 & \frac{cpf_{43}}{T_{g4}} & 0 & 0 \\ 0 & -\frac{K_{P2}}{T_{P2}} & 0 & 0 & \frac{cpf_{14}}{T_{g1}} & 0 & \frac{cpf_{24}}{T_{g2}} & 0 & \frac{cpf_{34}}{T_{g3}} & 0 & \frac{cpf_{44}}{T_{g4}} & 0 & 0 \end{bmatrix}$$

Desulphurization of Paraffinic Stream by a Fixed Bed of Zinc Oxide

M. G. Borikar¹, Dr. R. R. Khotpal², G. P. Lakhawat³

¹Priyadarshini Instt. Of Engg. & Tech., Nagpur

²Laxminarayan Institute of Technology, Nagpur

³Priyadarshini Instt. Of Engg. & Tech., Nagpur

ABSTRACT: Almost all crude oils are known to contain sulphure in varying amount. The amount of sulphure can vary from 0.04 % to nearly 10 %. The sulphure in petroleum has been defined as consisting of hydrogen sulphide, free sulphure and organic sulphure compound viz mercaptans, organic sulphide R-S-R, disulphide's R-S-S-R, carbon disulphide, thiophene and its homologues. The presence of these compound in petroleum fraction is not desirable due to their foul odour, corrosiveness, interferences with combustion characteristics of fuels, aggravation of atm. pollution byproduct of combustion etc.

The process used to reduce sulphure content of petroleum fraction may broadly classified as sweetening process and catalytic desulphurization.

Catalytic desulphurization process are those which destroy and remove all sulphure compound, hydrogen sulphide, mercaptance. Although the use of zinc oxide as a part of sandwich catalyst in the catalytic HDS is beneficial,; Also no hydrogen is required for desulphurization by zinc oxide and this is attractive point in the view of what have been said above concerning modern researcher in catalytic HDS(hydrodesulphurization).

I. INTRODUCTION

Petroleum fraction used as final product for chemical processing have to meet stringent specification regarding their sulphure content. Even at the level of crude oil, crude is divided into sour and sweet on the basis of sulphure content. Sour crude are define as those contain sulphure more than 0.5 wt %. It has been estimated that large proportions of crude reserves contain more than 1 wt % sulphur. Even accordingly to recent estimate of crude oil availability in our country, considerable amount of crude oils will continue to be imported in the future and all these would have to come from West Asian sour crude containing 1 to 2.6 % sulphure. Hydrodesulphurization process are now a day's used not only to pretreat the charge stock to catalytic reformer(hydrodesulphurization of low boiling distillate is almost always carried out for this purpose) but also as finishing process in case of middle distillate(200-410 °C) and even high boiling feed stock which may have sulphure content up to 5 wt %. Considerable research has been and being carried out in the field of composition of hydrodesulphurization catalysts, improving the selectivity of hydrodesulphurization and reducing the amount of hydrogen consumed by hydrogenation reaction.

II. MATERIAL AND METHODS

The reactor was packed with materials given below in an ascending order.

- a) Initial 12 cm pyrex tubing.(2.5 x 0.4 x 0.1 cm)
 - b) 3 m thick layer of silica chip to make surface of lower packing horizontal.
 - c) Nearly 36.8 gm ZnO Catalyst pellets.
- The pellets were arranged at random but the top surface was made as horizontal as possible.
- d) 3-5 mm thick layer of silica chips.
 - e) 15-17 cms glass tubing (2.5 x 0.4 x 0.1)

The catalyst is the constant temp region. Reactor was heated nearly for 2-3 hr to bring it to the required (350°C) temperature and held at this temp for 30 min. Two 5 x 1.5 cm strips of whatman 40 filter paper were soaked in freshly prepared (10 %) solution of lead acetate in water and placed in the tube. The first drop collected in 45 sec after it separated from tip. Liquid product were drawn out every 15 min, each portion was collected graduated tube, volume noted and then transferred to stoppered conical flask. In this way four samples for flowrate 30 ml/hr was transferred to separate conical flask. Gas flow rate was also read every 20 min interval. Runs were carried out in most cases for 210- 300 min. Balandine burette was disconnected, reactor was flushed with nitrogen to displace hydrocarbon vapours(for 20 min at rate of 1 lit/10 min) and allowed to cool to room temp in the current of nitrogen. If necessary run was recommended in this manner as described above, runs were carried out for further 210-240 min. Long runs with interruption were carried out in this manner.

Identification of serial No. in the following Tables:

1. Room temp °C
2. Feed: Conc of mercaptan(gm mole/lit) x 10³
3. Refractive Index
4. Density
5. Catalyzate-inportions: Period of collection, min.
6. ml collected

7. Density
8. Wt % of feed.
9. mercaptan conc(gm mole) x 10⁴
10. H₂S from exit gases(gm mole) x 10⁴
11. CM= Mercaptan conc(gm atom of S /100 gm of catalyzate) x 10⁴
12. Start of H₂S Evolution in exit gases, min .

Table No.1: Desulphurization by ZnO Run No.1:

Initial wt of catalyst=35.0171 gm, Reaction Temp=350^oc , Feed=N-amyll mercaptan in n hexane,
 Flow rate=30 ml/hr , Bed length=3.0 cm , CoM-(g.atom of s/100 g of feed10⁴)=369.231

1	25 ^o c	--	--	--	--	--	--	--
2	240	----	---	----	----	----	---	----
3	1.372	---	---	----	---	---	--	---
4	0.650	----	----	----	----	----	----	---
5	0-60	60-120	120-180	180-240	240-300	300-360	360-420	420-480
6	26.5	29.0	29.8	29.9	29.7	29.8	29.6	29.7
7	--	0.648	--	0.648	--	0.648	---	---
8	95	99.33	99.33	99.66	99	99.33	98.66	99
9	0	0	0	0	0.9	1.8	4.3	4.9
10	0	0	0	0	0	0	0	Traces
11	0	0	0	0	1.30	2.75	6.52	7.8
12	456 min	---	---	---	----	---	---	---

Table No.2: Desulphurization by ZnO Run No.2

Initial wt of catalyst=36.8753gm , Reaction Temp=350^oc , Feed=N-amyll mercaptan in n hexane,
 Flow rate=30 ml/hr , Bed length=3.0 cm , CoM-(g.atom of s/100 g of feed10⁴)=359.05

1	25 o c	---	---	----	---	---	---	---
2	242	----	---	---	---	--	---	----
3	1.385	----	---	---	----	----	---	----
4	0.674	----	----	----	----	----	----	---
5	0-60	60-120	120-180	180-240	240-300	300-360	360-420	420-480
6	26.5	29.3	29.6	29.7	29.9	29.9	29.8	29.7
7	--	--	0.673	--	0.673	--	0.673	--
8	94	94	97.66	98.66	99	99.66	99.66	99.33
9	0	0	0	0	0.87	2.0	4.5	4.9
10	0	0	0	0	0	0	0	Traces
11	0	0	0	0	1.2927	2.971	6.686	7.28
12	455 min	---	----	----	---	----	---	---

Table No.3: Desulphurization by ZnO Run No.3

Initial wt of catalyst=36.8500 gm , Reaction Temp=350^o c , Feed=N-amyll mercaptan +Heptane+N-Compounds(pyridine),
 Flow rate=30 ml/hr , Bed length=3.0 cm , CoM-(g.atom of s/100 g of feed10⁴)=361.06

1	25 oc	---	---	---	---	---	---	--
2	244	---	---	---	---	---	----	---
3	1.387	----	----	---	----	----	---	---
4	0.678	----	---	---	---	---	---	--
5	0-60	60-120	120-180	180-240	240-300	300-360	360-420	420-480
6	27	29.5	29.7	29.8	29.9	29.9	29.8	29.7
7	--	--	0.676	--	0.676	--	0.676	--
8	89.73	98.04	98.71	99.04	99.37	99.37	99.04	98.71
9	0	0	0	0	0.85	1.8	4.6	4.9
10	0	0	0	0	0	0	0	Traces

11	0	0	0	0	1.257	2.662	6.80	7.248
12	455 min	---	---	---	----	----	---	--

Pyridine and N-amyl mercaptan are taken in 1:1 ratio.

Table No.4: Desulphurization by ZnO Run No.4

Initial wt of catalyst=36.7822 gm , Reaction Temp=350° c , Feed=N-amyll mercaptan +Heptane+N-Compounds(pyridine),
 Flow rate=30 ml/hr , Bed length=3.0 cm , CoM-(g.atom of s/100 g of feed10⁴)=357.25

1	25 oc	---	---	---	----	---	----	----
2	244	---	---	---	---	---	---	---
3	1.387	---	----	----	----	----	----	---
4	0.678	---	----	---	---	----	----	----
5	0-60	60-120	120-180	180-240	240-300	300-360	360-420	420-480
6	27	29.8	30	30	30	30	29.7	29.8
7	--	0.681	--	0.681	--	0.682	--	0.683
8	89.73	99.04	99.70	99.85	99.70	99.85	99.70	99.99
9	0	0	0	0	1.2	2.6	8.0	13.2
10	0	0	0	0	0	0	0	Traces
11	0	0	0	0	1.76	3.812	11.615	19.198
12	---	---	----	----	----	----	----	---

Pyridine and N-amyl mercaptan are taken in 2:1 ratio

Table No.5: Effect of H2O ON DESULPHURIZATION OF H.C by ZnO Run No.5

Initial wt of catalyst=36.806 gm , Reaction Temp=350°c , Feed=N-amyll mercaptan +Heptane+H2O(distilled),
 Flow rate=30 ml/hr , Bed length=3.0 cm , CoM-(g.atom of s/100 g of feed10⁴)=373

1	25 oc	---	---	---	---	---	----	--
2	254	---	----	----	----	----	----	----
3	1.387	----	----	----	----	----	----	---
4	0.678	---	----	---	---	----	----	----
5	0-60	60-120	120-180	180-240	240-300	300-360	360-420	420-480
6	26.5	29.2	29.8	29.9	30	29.9	30	30
7	--	0.674	--	0.674	--	0.674	--	0.674
8	87.42	96.33	98.31	98.64	98.97	98.64	98.97	98.97
9	0	0	0	0	0.8	2.4	4.4	5.6
10	0	0	0	0	0	0	0	Traces
11	0	0	0	0	1.186	3.55	6.53	8.31
12	460 min	---	---	----	----	---	----	-----

III. RESULT AND DISSCUSSION

The aim is to investigate the effect of following factor on desulphurization of hydrocarbon stream by a fixed bed of Zinc oxide. 1) Effect of presence of nonsulphure non hydrocarbon compound in feed. With n-heptane as feed and n-amyl mercaptan as sulphure compound the effect of presence of following compound was investigated.

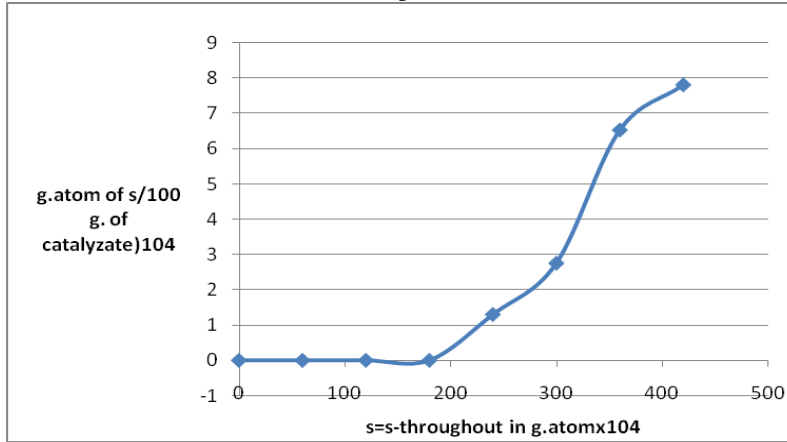
- a) Distilled water b) Sodium chloride c) carbon dioxide d) Nitrogen compound

2) Effect of hydrocarbon feed were tried.

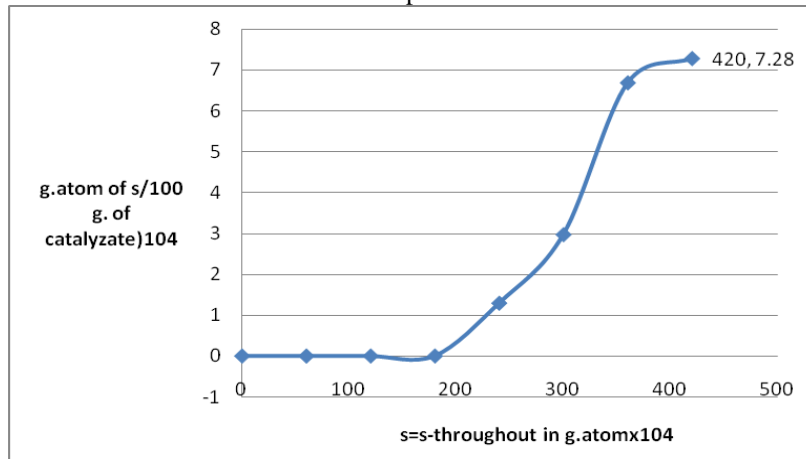
- a) n heptanes alone b) Hexane(Petroleum fraction) c) Benzene + Heptane d) Toluene + heptanes.

The result of experiment carried out to investigate these aspect are given below on which breakthrough curves are drawn .All the following graph are plotted (gm.atom of S/100 gm of catalyzate)10⁴ against (S-throughout in gm. Atom x 10⁴)

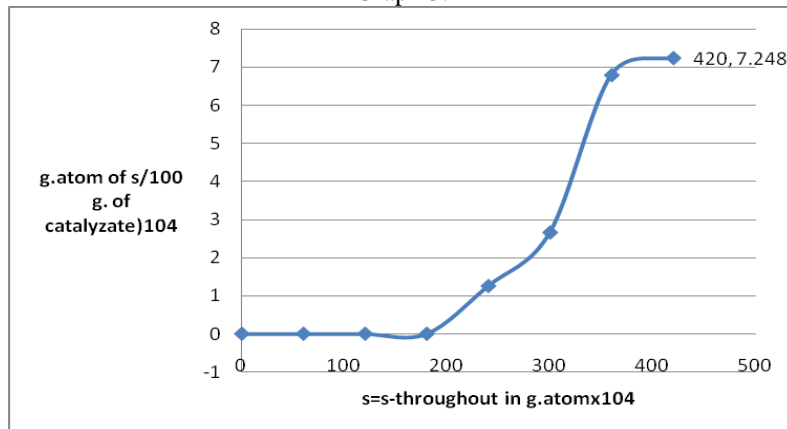
Graph 1



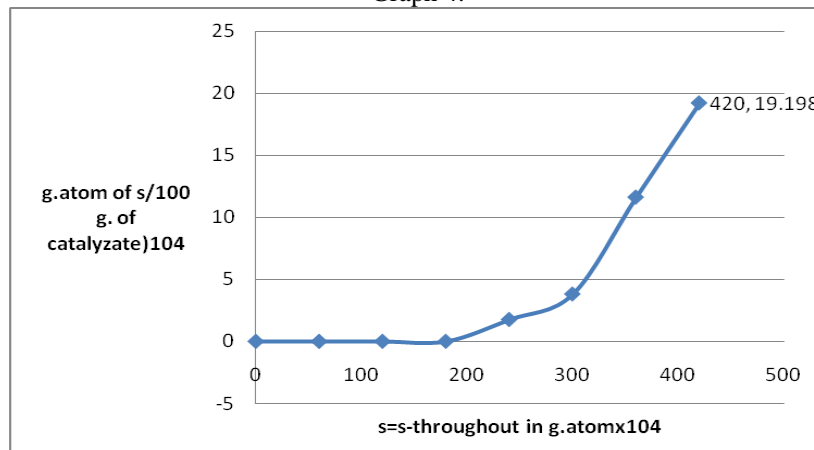
Graph 2:



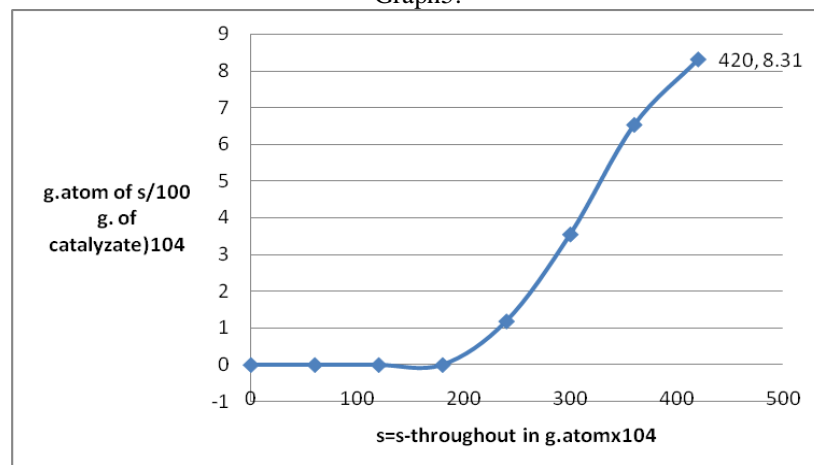
Graph 3:



Graph 4:



Graph5:



IV. CONCLUSION:

The objective of these studies is to make possible prediction of sulphure breakthrough curve in the desulphurization of hydrocarbon stream by fixed bed of zinc oxide and thus aid in the design of industrial units means for desulphurization.

The theoretical basis of breakthrough curve for a system in flow of these type studied here ie with fixed bed catalystr is well developed in chemical engineering literature with regards to sorption.

V. REFERENCES

- 1) In 2009 Study on the Role of Metal Oxides in Desulphurization of Some Petroleum Fractions M. Shakirullah, Imtiaz Ahmad,* M. Ishaq and Waqas Ahmad.
- 2) 2007gas and liquid phase fuels desulphurisationhydrogen production via reforming processes Jean-Christophe Hoguet1,* , Giorgos P. Karagiannakis1, Christos Agrafiotis1 Athanasios G. Konstandopoulos
- 3) 2006 advances in desulfurization research Of liquid fuel h. Rang, j. Kann, v. Oja
- 4) 2005 Developing Clean Fuels: Novel Techniques for Desulfurization James P. Nehlsen
- 5) In 2004 Oxidative Processes of Desulfurization of Liquid Fuels J.M. Campos-Martin*, M.C. Capel-Sanchez, P. Perez-Presas, J.L.G. Fierro
- 6) 2002Science and technology of novel processes for deep desulfurization of oil refinery streams: a review I.V. Babich*, J.A. Moulijn Oil refinery related
- 7) Physical properties of chemical compound, vol II , R.R.Dreishach , Dow chemical co. Midland Mech. Advance in chemistry series , 22 ,1959.
- 8) B.J.Mair , cited in chemical Technology of petroleum , crude and stevens , 3 rd edition , McGraw-Hill BOOK CO, 1960 , 56.

A New Heuristic Approach to Safeguarding Online Digital Data

P.V. Raj Varma¹, M.Rajinikanth², Dr. Mohammed Ali Hussain³

¹Pursuing M.Tech, Dept. of Computer Science Engineering, Sri Sunflower College of Engineering & Technology, A.P., India.

²Assoc. Professor, Dept. of Computer Science Engineering, Sri Sunflower College of Engineering & Technology, A.P., India.

³Professor, Dept. of Computer Science Engineering, Sri Sai Madhavi Institute of Science & Technology, A.P., India.

Abstract: Security challenges have been raised by private and public sectors related to exchange digital data electronically. In the current state, protocols such as the simple mail transfer protocol (SMTP), post office protocol (POP), and internet message access protocol (IMAP) transfer and store email messages in plaintext. Therefore, the confidentiality of email messages cannot be assured. Email sent using these protocols and without using any other security tool, must be assumed to have been read and compromised, because its confidentiality and integrity cannot be assured. Thus in this paper a new approach as a tool for improvement of current popular email protocols is proposed. The novel proposed protocol will be manifested in the Email Security Protocol (ESP) which is designed to add a layer of security and confidentiality to email messages transmitted over unsecured public networks. ESP is designed in three models to allow efficient and effective implementation upon various information system architectures. The result of testing the new proposed approach showed superior performance comparing to the existing one.

Keywords - Electronic Email, Digital data, Protocol, Security Tool.

I. Introduction

Email has become an integral part of today's digital life. Individual send and receive a vast mass of email messages every day. However, email is one of the most insecure types of communication media. Common configurations of email clients enable attackers to steal user names and passwords used to access email easily. The content of Web-based email Not encrypted and is passed in the network in plain text. Messages deleted from an email server might Still be retrievable from other servers halfway around the world without owner knowledge. This paper presents email security issues and proposes a new tool on how to improve email systems security. The rest of the paper is divided into the following sections. Second, background which presents the current state of email security protocols . Third, the need for a new protocol which presents the challenges of the exiting protocols throughout two cases. Fourth, the new approach which presents its descriptions and features and the fifth is the conclusion and future research.

II. Background

There are currently a number of email protocols in use. Some of these are the simple mail transfer protocol (SMTP), post office protocol (POP), and internet message access protocol (IMAP) [5]. The SMTP and POP protocols

are very popular protocols and are used by many who use email.

A typical person likely has their email program configured to send and receive email using the SMTP and POP protocols. The main reason for this is because their internet service provider (ISP) or email service provider uses these protocols and in order for the email program to communicate with the email server, their program needs to be configured to use these protocols. The SMTP protocol is used when sending email and the POP protocol is used when receiving email.

Internet message access protocol (IMAP) is similar to POP but allows email to remain on the server [6]. The email remains on the server until the user specifically deletes them from the server. Furthermore, with the use of IMAP, email has the ability to be organized on the server and accessed from any computer with access to the internet.

A major drawback of these protocols in terms of information security is the lack of protection that is provided to email that is transmitted and received. Email is transmitted in plaintext and confidentiality and integrity are nearly non-existent. For example, email servers communicate with each other using SMTP and store email messages in plain, unencrypted text [5].

III. Need For A New Protocol

There is a need for email security protocols and tools to protect the confidentiality and integrity of email. Without any form of encryption in place, email transmitted in plaintext over unsecured networks must be assumed to have been read and compromised because of the ease and ability adversaries have in using network protocol analyzers (sniffers) to capture traffic on unsecured networks. Mark Vanden wauver and Frank Jorissen demonstrate the need for security measures in their paper titled Securing Internet Electronic Mail [8]. The authors state that "Each message can be intercepted by a trained computer user connected to the net ... using tools to check the functionality of the network (Protocol Analyzers also known as network sniffers) which also can be used to listen in on any traffic on the internet."

Another example that demonstrates the need for enhanced email security protocols is given by Marvin Cetron and Owen Davies in their article titled Ten Critical Trends for Cyber security. The major theme of the paper states "Technological advances and greater connectivity may be making our systems less rather than more secure. A special panel of military, intelligence, and forecasting experts analyzes the trends that may be leading the world to cyberwar." Since electronic mail travels over the same networks as other packets of information, this topic includes email and should be a major concern to organizations and corporations that value the confidentiality of their electronic

communications and information. Furthermore, if email communications are not adequately secure, adversaries gain the ability to compromise the confidentiality and integrity of email, which in turn allows them to collect information from these communications that can be brought together to gain enough proprietary information to launch a larger and more damaging attack against an organization. Secure email transmission through the use of a tool such as the Email Security Protocol can reduce the risks of such an event from occurring by securing email and making it unreadable and unusable to adversaries that may intercept it in transit.

IV. Esp Proposed Protocol

The security problems associated with the SMTP, POP, and IMAP protocols warrants the consideration of a new protocol that would eliminate some of the security risks associated with using these protocols. This protocol would be used for the secure transmission of email from one person to another through a public network (i.e., internet). Furthermore, this protocol is shown to protect the confidentiality of email that travels from one SMTP server to another while on its way to its intended recipient.

The proposed name for this protocol is the email security protocol (ESP). Its purpose is to add a layer of security and confidentiality to email in which it is used. The ESP is configured and implemented in an email program so that its functions are carried out automatically with minimal interaction with the user being required.

A. ESP ARCHITECTURE

The Email Security Protocol (ESP) is designed in three models to allow efficient and effective implementation upon various information system architectures. Model I is designed based on a single server architecture which will process the encryption and the decryption procedures. It would be good on a network system isolated from the internet. The main feature of this model is that the email would stay encrypted on the server until the recipient decided to retrieve them. The email would thus be secure while being stored on the server. This model could also be used in a simulation in a computer laboratory; especially if the number of available servers for research is limited.

B. ESP PROCESS:

ESP uses asymmetric encryption to encrypt the contents of email messages before they are transmitted to the SMTP server. In this manner, the contents and subject line of an email message are encrypted and are protected from adversaries that otherwise would have been able to read the email in its plaintext. Thus, a major benefit is provided by the use of the ESP because if used properly, there is an assurance that email messages have been transmitted with confidentiality intact.

The email is encrypted using the public key (PK) of the recipient. A feature of the ESP is that if the PK of the recipient is unknown, then an automatic request for the PK will be sent to the recipient. When the recipient receives this request, and if the email program is configured correctly and also using the ESP, then the PK is automatically returned to the sender. Then the email can be encrypted using the PK and securely transmitted through the gamut of SMTP servers and maintain its confidentiality while in route to its intended recipient.



Figure 1: Model Architecture

Model II is designed to be used with the architecture associated with several servers and via the internet cloud. It would be good for sending email from one internal network system (corporation) to another. Its main feature is that the email would be secure in transit (encrypted) over the internet (public domain) from Server to another. This would greatly enhance the security of email sent from one corporation to another; or from one corporation to the same corporation with offices at a different geographical location.

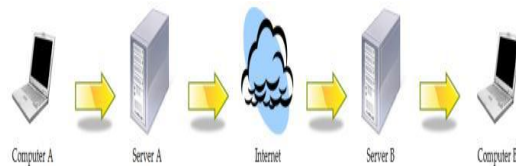


Figure 2: Model II Architecture

Model III is designed based on the Internet cloud architecture and for sending encrypted email directly from one computer to another. This model will serve better when an internal network server is not present or used for email traffic. Its main feature is that the email would be encrypted and secure from one computer to another; encryption would be present for the entire trip over the networks, including the internet.

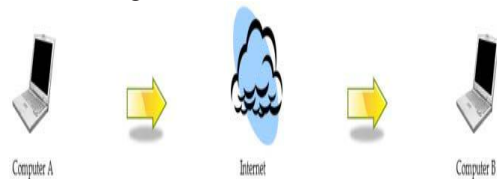


Figure 3: Model III Architecture

For simplicity, Alice and Bob will be the entities used in describing the transfer of email from one person to the other. Traditionally in cryptography texts, Alice and Bob have been denoted as good guys [6]. A more detailed description of how the ESP will work can best be illustrated in the following scenario.

Alice desires to send an email to Bob using ESP. Alice also knows that Bob is using ESP. However, Alice does not have Bob's public key (PK). Since Alice does not know Bob's PK, the process will take three emails (steps) to be completed. After Alice finishes composing the email she intends to send to Bob, she clicks the send button on her email program.

A feature of the email security protocol is that the process takes place automatically and an asymmetrically encrypted email may be sent to a recipient whose public key had previously been unknown. Also, under the correct circumstances, this process can be completed very quickly. Also, most importantly, the contents of the email message remains secure while in transit through the internet and the gamut of SMTP servers until it reaches its intended

destination; email messages are asymmetrically encrypted before being transmitted. The confidentiality of the email has been preserved through the use of the ESP. Furthermore, the convenience of an automatic and secure process makes for ease of use.

C. Esp Advantages And Drawbacks

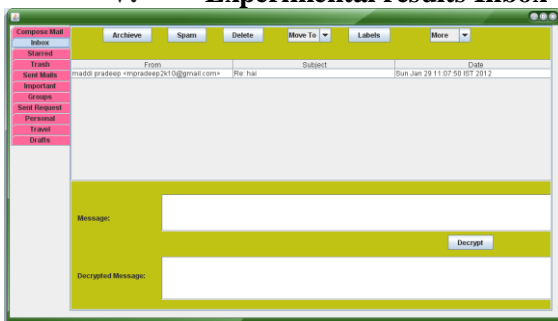
An advantage of the ESP is the ease of use for the end users. For example, in an organization that has a local area network (LAN) administered by information technology (IT) personnel, the IT staff can install and configure the ESP as needed, depending on the model used (I, II, or III), on the required computers, workstations, and servers that make up the LAN. Once the ESP is properly configured, users can send and receive email as they normally would and have the assurance that their email will be (1) securely (encrypted) stored on the server until retrieved by the intended recipient, (2) securely transmitted from one ESP configured server to another (e.g., one corporate office to another), or (3) securely transmitted from one ESP configured computer to another. If a combination of models I, II, and III are used then security can be provided at all of the above mentioned levels.

Another advantage is the transparency to the user. The user will not be required to perform any extra steps or manually execute and run any special program for the ESP to work properly on their computer. Once properly configured, the ESP will run in the background and automatically perform the required tasks as needed, depending on the configuration and model used. The user will not have to worry about forgetting to encrypt their email transmissions because the ESP will perform the task automatically for them. This eliminates the risk of human error and gives confidence that all email transmissions from a particular computer or server are secure.

A drawback of the ESP is that in order for the encryption and secure transmission of email to take place, the servers and computers need to be properly configured. If they are not configured correctly, then the secure transmission of email will not be able to take place.

Another drawback with the ESP is that it mainly provides security from outside threats. For example, in model II email transmissions are secure in their travel over the internet from server A to server B; server A being one regional organization office and server B being another regional organization office. Once the email is requested for retrieval by computer B (recipient), then the email is transmitted in plaintext inside the LAN to computer B. There is a risk that an inside threat can intercept this email. However, by using a combination of models II and III, this drawback and risk can be eliminated.

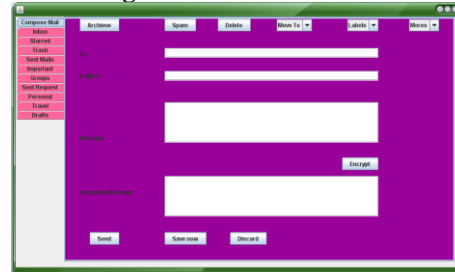
V. Experimental results Inbox



Sending Mails



Encryption Message



Drafts



VI. Conclusion And Future Research

It has been shown that the new proposed protocol (ESP) would be an enhancement and great email security tool to preserve the confidentiality of email messages in transit over the internet. Furthermore, it is evident that it provides a high degree of security which includes email securely stored on a server. Our future research is to investigate the ESP in depth using a large scale of data and advance it to eliminate any drawback.

References

- [1] Behrouz A. Forouzan, Cryptography and Network Security, McGraw Hill, 2008.
- [2] Mark Stamp, Information Security: Principles and Practices, Wiley, 2006.
- [3] http://email-security.net/papers/usablesecure_email.pdf.
- [4] <http://email-security.net/papers/takefive.html>.
- [5] Richard Sinn, Software Security Technologies: A Programmatic Approach, Thomson Course Technology, 2008.
- [6] Mark Ciampa, Security+ Guide to Network Security Fundamentals, Course Technology, 2009.
- [7] Jiangtao Li, Ninghui Li, William Winsborough, "Automated Trust Negotiation Using Cryptographic Credentials", ACM Transactions on Information and System Security, Vol. 13, No. 1, Article 2, Publication date: October 2009.
- [8] Mark Vandenwauver and Frank Jorissen. Securing Internet Electronic Mail. In State of the Art in Applied Cryptography, Course on Computer Security and Industrial Cryptography - Revised Lectures, Bart Preneel and Vincent Rijmen (Eds.). Springer-Verlag, London, UK, 1997. 208-223.

A Novel Approach for Image Fusion in JPEG Domain

Venkata Santhosh kumar A.¹, Ch. Ramesh²

**(M.Tech Student, computer science department, AITAM, Tekkali, India*

*** (Professor, AITAM, Tekkali, India*

ABSTRACT: Image fusion is a procedure of combining relevant information from more than one image into a single image. The resulting image will have more information than any of the input images. Fusion is a popular approach for producing an image without under- and over-exposed areas is to capture several input images with varying exposure settings, and later combine them into a single high-quality image. This technique is used in various disparate fields such as remote sensing, robotics and medical applications. In this paper, we proposed a method to fuse multiple images taken with varying exposure times. The key component of the method is a single pass sigmoidal booster is applied on the shorter exposed images implemented as LUT, unlike other methods which require two or more passes. We used this technique to capture high dynamic range images from a set of photographs taken at different exposures, where misalignments can produce blurring and artifact and prevent achieving high quality HDR images. We present our implementation of the technique and the results of tests made for variety of photographs.

Keywords: Artifact removal, HDR capture, High Dynamic Range Imaging, Image Stabilization, Image Fusion

I. INTRODUCTION

Due to tremendous growth towards the production of high dynamic range (HDR) images. Modern image processing and graphics software becomes HDR enabled. Also HDR digital photography replaces low dynamic range (LDR) technologies. HDR photographs have better quality and easier to process in a digital darkroom, when compared to LDR. Unfortunately, HDR cameras are very expensive and not available for average users.[1] On the other hand, taking HDR photographs seems to be legitimate and crucial. In the near future LDR images may become almost obsolete due to the progress in LCD technology and it will not be easy to display LDR image correctly. LDR photographs will look pale and not interesting on HDR LCD displays. The multi-exposure HDR capture technique seems to be a good alternative to HDR cameras, which is used to create an HDR image from photographs taken with a conventional LDR camera. The technique uses differently exposed photographs to recover the response function of a camera. From the response function, the algorithm creates an HDR image whose pixel values are proportional to the true radiance value of a scene.[2] Because this technique requires multiple input photographs, there is a high likelihood of misalignments between pixels in the sequence of exposures due to moving of a hand-held camera or dynamic object in a scene. It is crucial that misalignments

between input photographs should be removed before fusing an HDR image.

Image fusion is a procedure of combining relevant information from more than one image into a single image. The resulting image will have more information than any of the input images. Fusion is a popular approach for producing an image without under- and over-exposed areas is to capture several input images with varying exposure settings, and later combine them into a single high-quality image. The need for image fusion arises in many applications, including digital image stabilization and HDR image capture. In stabilization, the motion blur that occurs in a long exposure-time image is corrected by fusing it with a short exposure-time image of the same scene.[3] The benefit of fusion is that the higher signal-to-noise ratio (SNR) of the long exposure image is combined with the sharp details of short exposure image, giving digitally the stabilization that is normally available only through opto-mechanical means. In HDR photography, a set of images with varying exposure times or ISO settings are fused to capture a wide range of scene luminance, which would otherwise result in saturated regions or dark features of interest in a single exposure.[4] In the proposed technique short, long and normal exposure images are used. The long exposure image should be taken prior to the shorter exposure images. The long exposure image is processed as normal on the digital camera, converted to JPEG, and then written to a file in secondary storage. The short and normal exposure images which are taken consecutively is boosted in brightness by using a lookup table (LUT) modelling a sigmoidal function combined with tonemapping.[5] The boosting process requires only one LUT transformation per pixel. Boosting is applied to all pixels in the image, and the boosted image is converted to JPEG as usual. However, instead of writing a separate JPEG file for the short-exposure image, we modify the file write operation to selectively overwrite parts of the long exposure's JPEG file with relevant portions of the short-exposure JPEG. Since the JPEG file interchange format (JFIF), which is the standard file format for storing JPEG images, places the luminance (Y) channel in separate 8*8 blocks of DCT values from the corresponding chrominance (Cb,Cr) blocks, it is relatively easy to calculate the addresses of the two types of blocks within the file, and to overwrite selectively. If portions of the long-exposure JPEG file are replaced with suitable portions of the short-exposure JPEG, then the result, upon decompression and display, is a fused image. Hence, the JPEG file format serves as a medium for image fusion, and the JPEG decoder performs the actual fusion prior to display.

The rest of the paper is organized as follows. Section 2 deals with Related work, Section 3 discuss on Proposed Algorithm, Section 4 on Image fusion, Section 5

on Sigmoidal function, Section 6 discuss about Artifact removal, Section 7 brief Image saturation detection, Section 8 discuss about Results and Section 9 concludes the paper.

II. RELATED WORK

In recent years significant progress has been made in the development of algorithms that allow to capture HDR images using low dynamic range sensors (standard LDR cameras) [20, 21, 22, 23]. These algorithms retrieve high dynamic range information from a sequence of photographs. The authors suggest using tripod to avoid camera movement and they do not address the problem of eliminating misalignments. The problem of image alignment and matching was intensively studied during last year's [24, 25] but not for registration of images of different exposures. The only solution that addressed exactly the problem of capture of HDR photographs was proposed in [26, 27]. The technique employs conversion of input photographs into percentile threshold bitmaps. The bitmaps are analyzed and then aligned horizontally and vertically using shift and difference operations over each image. Kang et al. [28] described a technique for creating high dynamic range video from a sequence of altering light and dark exposures. A part of the technique is a HDR stitching process, which includes global and local alignment to compensate for pixel motion. The stitching process can be also used to compensate for camera movement when creating an HDR still from a series of bracketed still photographs. However, the presented technique seems to be suitable for video where there are no large differences between consecutive frames.

In [29] Sand and Teller present a global and local matching algorithm, which is robust to changes in exposure of photographs. The key idea behind this technique is to identify which parts of the image can be matched without being confused by parts that are difficult to match. Such assumption seems to be not valid for images with large differences in exposures, where there is usually not enough information for correct matching. The technique was designed for matching two video sequences and was not tested on still photographs.

Recently, Cerman and Hlavac [30] presented an alignment method based on unconstrained nonlinear optimization. In this method, each image is linearized using the estimated camera response function and multiplied by the exposure ratio. Then, a normalized difference summed across all corresponding pixels is used to estimate misalignments. The method can compensate global rotation and horizontal and vertical shifts. There are a few techniques which compute camera response function based on misaligned photographs [31]. However, these methods are not meant to create HDR images. The problem of removing ghosting artifacts in a multi-exposure sequence of photographs was also investigated [32] but proposed algorithms do not take into consideration a compensation of camera movements.

III. PROPOSED ALGORITHM

The proposed technique uses three images and fuses them in the JPEG domain. We assume that the images are taken in immediate succession to minimize the need for registration, and that the exposure ratios between them are

known prior to the second image being taken. That assumption is reasonable for cameras operating in exposure bracketing mode, in which the ratios are set beforehand; typically the ratios are powers of two, but the values may be programmable. We assume that the exposures vary only in exposure time, while aperture and ISO setting are held constant. We use the well-known logarithmic exposure value (EV) notation of describing ratios of exposures. In that notation, $EV(0)$ represents the exposure time determined by the camera's auto exposure routine, and relative to that time, $EV(D)$ represents an exposure time that is 2^D larger.[7] For example $EV(+1)$ is twice the exposure time of $EV(0)$, and $EV(-1)$ is one-half the exposure time of $EV(0)$. It is well-known that the human visual system is more sensitive to details in the luminance channel, which in the JPEG literature is denoted as Y in the Y,Cb,Cr color system. JPEG takes advantage of this by subsampling the two chrominance channels, denoted Cb, Cr usually by a factor of two in each direction.

Proposed Algorithm:

Step 1: convert the longest exposure image into Y_l, Cb_l, Cr_l
Step 2: Apply Sigmoidal boosting and tone-mapping for Shortest and normal exposure images.

Step 3: convert the shortest, normal exposure images into Y_s, Cb_s, Cr_s and Y_n, Cb_n, Cr_n respectively.

Step 4: write the file into secondary storage device.

Step 5: Overwrite Y_l with Y_b in the file

Step 6: At Edges, Overwrite Cb_l, Cr_l with Cb_s and Cr_s in the file.

Step 7: Detect saturation in image based on data-driven threshold on luminance of fused image.

Step 8: check whether block is saturated or not. If it is YES Overwrite Chroma in step 6, with Cb_n, Cr_n otherwise stop the process

In the proposed technique for correcting motion artifacts selects the $8*8$ chrominance (Cb,Cr) blocks of the long-exposure image where the corresponding luminance (Y) block contains significant high frequency information representing edges or texture, and replaces them with the corresponding (Cb,Cr) blocks of the boosted short-exposure image. Image saturation is detected in the case of day light scenes. Saturation is detected on fused image containing luminance from short exposed image and chrominance from long exposed image, block by block basis based on a data-driven threshold as explained in sections below. If the image is saturated, chrominance from the mid-exposed also called as normal exposed image replaces the chrominance in the fused image.[11] [10]

IV. IMAGE FUSION

In modern digital cameras we can preview the captured photo immediately, after capture. Hence we perform the image merging directly on the camera. The proposed algorithm must be robust to camera motion during capture. While this was not an issue for viewfinding, where the low

resolution and high frame rate make misalignment artifacts barely noticeable, such artifacts become objectionable in the high-resolution case. So to compensate for camera motion using the image alignment algorithm which is discussed in [9] the input images are merged into the final result using an adaptation of the exposure fusion algorithm introduced by Mertens et al. [6]. Given an input images, exposure fusion computes a scalar-valued weight map for each image, and performs a weighted blend of the inputs to obtain the final HRD image which is described in Figure 1.

Let (I_1, \dots, I_n) be n images captured by the camera. The weight for each pixel (i, j) of image k is computed as:

$$W_k(i, j) = \exp\left(-\frac{(I_k(i, j) - \mu \cdot 255)^2}{2(\sigma \cdot 255)^2}\right).$$

We set the parameters $\mu = 0.5$, $\sigma = 0.2$ and normalize the maps so that the sum of mask values for every pixel is 1.

The result consists of multiplying the images by their weight maps and blending:

$$R(i, j) = \sum_{k=1}^n W_k(i, j) \cdot I_k(i, j).$$

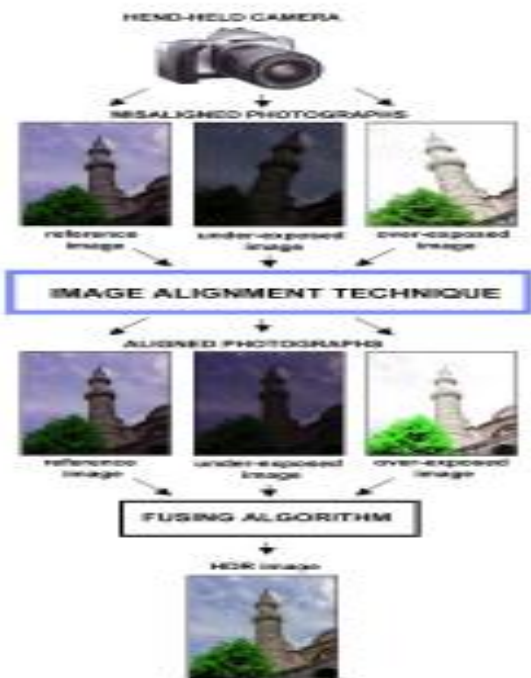


Figure 1: Image Fusion Technique

V. SIGMODIAL FUNCTION

When images of varying exposure are to be fused, the luminance of the shorter exposure images is boosted to match that of the longer one by estimating a compensating function that matches the camera's response. M. Tico and K. Pulli proposed a compensating function the brightness transfer function (BTF).[12] The BTF is estimated by plotting the pixel values of longer exposed image against the corresponding luminance values in the shorter exposed image, applying basic curve fitting and by smoothing the mean of pixel values for the longer exposure for the same pixel value in the shorter exposure. Both methods require

two passes over the shorter exposure image, the first to estimate the BTF and the second to boost the image accordingly.[8]

VI. ARTIFACT REMOVAL

The chrominance from longer exposure image, denoted by Cb_l, Cr_l is merged with the boosted luminance of shorter exposed image denoted by Yb_s . The merged image (Yb_s, Cb_l, Cr_l) contains motion artifacts like ghosting and color bleeding due to mismatch of luminance and chrominance values at the edges from images taken at two different times. Proposed technique for artifact removal works on the shorter exposure image and takes advantage of JPEG's built-in frequency analysis using DCT, to perform texture or edge detection. That DCT coefficients may be used to detect 8×8 blocks containing strong edges is well-known which is proposed by W. L. Pennebaker and J. L. Mitchell [16] and R. Kakarala and R. Bagadi.[17] The JPEG compression algorithm computes the DCT of each 8×8 block, which are then quantized and subsequently compressed by using run-length encoding in a "zig-zag" scan. The End of Block (EOB) symbol, which occurs in every block as part of JPEG syntax, indicates the location of the last non-zero AC coefficient in the 64-coefficient zig-zag scan. The classification of blocks as smooth or edge blocks may be accomplished simply by noting whether the EOB signal occurs early or late in the scan. Apply the detection to the EOB location in the DCT coefficients of the luminance blocks Yb_s of the boosted short-exposure image.[13] An empirically determined EOB location threshold of 15 (out of 64) is used for all experiments in this paper, and the quantization matrices used are the defaults described in W. L. Pennebaker and J. L. Mitchell [16]. If the EOB occurs after this threshold location, then the block is classified as an edge block for which the chrominance comes from the short exposure, otherwise it is considered a smooth block and the chrominance from the long exposure is used.[14]

For macroblocks where an edge is detected in the Yb_s component, the chrominance from the boosted shorter exposure (Cb_s, Cr_s) image is used to overwrite the corresponding values from the longer exposed image in the merged HDR image. In the standard 4:1:1 color format, there are four 8×8 luminance (Y) blocks in each 16×16 macroblock, and one each of Cb, Cr block. Our algorithm overwrites the two chrominance blocks of the long image with those of the boosted short exposure if any of the four Yb_s blocks contains an edge. Since we replace one block by another, we do not require RAM memory for the algorithm beyond the storage of a JPEG macroblock.[15] which is described in Figure 2, 3,4 and 5.

VII. IMAGE SATURATION DETECTION

The fused image is obtained by combining the luminance from shortest exposed image and chrominance from the longest exposed image which is described by R. Kakarala and R. Hebbalaguppe [14]. Data-driven threshold is used to calculate average of the difference between the maximum and minimum luminance values of the fused image. If the luminance value in the fused image is greater than the data driven threshold given then replace the chrominance of the

fused image by the chrominance of the normal exposed image.[18,19]

VIII. RESULTS

We evaluate the performance of the algorithm by taking three images at various exposure times called as Longest, Normal and Shortest exposure time images and the technique efficiently fuses multiple images taken at various exposure times in the JPEG domain which has shown in Figure 6,7,8 and 9.



Figure 2: Before Artifact removal



Figure 3: After Artifact Removal



Figure 4: Before Artifact removal



Figure 5: After Artifact Removal



Figure 6: Longest Exposure image



Figure 7: Normal Exposure image



Figure 8: Shortest Exposure image



Figure 9: Final image after Image Fusion

IX. CONCLUSION

Image fusion is a procedure of combining relevant information from more than one image into a single image. The resulting image will have more information than any of the input images. Fusion is a popular approach for producing an image without under- and over-exposed areas is to capture several input images with varying exposure settings, and later combine them into a single high-quality image. The proposed technique efficiently fuses multiple images taken at various exposure times in the JPEG domain. The technique has categorized images into three types based on the exposure time, they are longest, normal

and shortest exposure images. A single pass sigmoidal booster is applied on the shorter exposed images implemented as LUT. Reuse of edge detection which is a part of JPEG for removal of artifacts further optimizes the algorithm. Lastly, the method requires no more than a single macro block to be kept in memory, because the image fusion is performed essentially in the JPEG file and rendered only on decoding the image. Experimental Results shows our proposed technique has efficiently fused multiple images into single image with better quality HRD.

REFERENCES

- [1] Gelfand, N., Adams, A., Park, S., and Pulli, K., "Multi exposure imaging on mobile devices.," in [ACM Multimedia], 823–826 (2010).
- [2] Zhang, X., Jones, R. W., Baharav, I., and Reid, D. M., "System and method for digital image tone mapping using an adaptive sigmoidal function based on perceptual preference guidelines," US Patent 7,023,580 (2006).
- [3] Wallace, G., "The jpeg still picture compression standard.," IEEE Trans. Consumer Electronics 38 (Feb. 1992).
- [4] Tico, M. and Pulli, K., "Image enhancement method via blur and noisy image fusion.," in [Int. Conf. on Image Processing (ICIP)], 1521 – 1524 (2009).
- [5] Hasinoff, S. W., Durand, F., and Freeman, W. T., "Noise-optimal capture for high dynamic range photography," in [CVPR], 553–560 (2010).
- [6] Khan, E., Akyuz, A., and Reinhard, E., "Ghost removal in high dynamic range images," in [IEEE Intl. Conf. Image Processing (ICIP)], 530–533 (2006).
- [7] Lu, P., Huang, T., Wu, M., Cheng, Y., and Chuang, Y., "High dynamic range image reconstruction from hand-held cameras.," in [Computer Vision and Pattern Recognition (CVPR)], 509 – 516 (2009).
- [8] Reinhard, E., Ward, G., Pattanaik, S., and Debevec, P., [High dynamic range imaging: Acquisition, display and image-based lighting], Morgan Kaufmann Publishers (2005).
- [9] Bogoni, L., "Extending dynamic range of monochrome and color images through fusion," in [15th International Conference on Pattern Recognition (ICPR)], 3, 7–12, IEEE (2000).
- [10] Kang, S., Uyttendaele, M., Winder, S., and Szeliski, R., "System and process for generating high dynamic range video." U.S. Patent 7,382,931 (Jun 2008).
- [11] Jacobs, K., Loscos, C., and Ward, G., "Automatic high dynamic range image generation for dynamic scenes," in [IEEE Computer Graphics and Applications], 28, 24–33, IEEE (Mar-Apr 2008).
- [12] Gallo, O., Gelfand, N., Chen, W., Tico, M., and Pulli, K., "Artifact-free high dynamic range imaging," in [IEEE Intl. Conf. Computational Photography (ICCP)], 1–7 (April 2009).
- [13] Tico, M., Gelfand, N., and Pulli, K., "Motion-blur free exposure fusion.," in [Proc. Int. Conf. on Image Processing (ICIP)], 1521–1524 (2010).
- [14] Kakarala, R. and Hebbalaguppe, R., "A method for fusing a pair of images in the jpeg domain," Journal of Real-Time Image Processing , 1–11. 10.1007/s11554-011-0231-8.
- [15] Nakamura, J., [Image sensors and signal processing for digital still cameras], CRC Press (2005).
- [16] Pennebaker, W. L. and Mitchell, J. L., [The JPEG still image data compression standard], Kluwer Academic Publishers (1993).
- [17] Kakarala, R. and Bagadi, R., "A method for signalling block-adaptive quantization in baseline sequential jpeg," in [IEEE TENCON], 1–6 (2009).
- [18] Fishbain, B., Yaroslavsky, L., Ideses, I., and Roffet-Cr et e, F., "No-reference method for image effective-bandwidth estimation," in [SPIE - Image Quality and System Performance], 6808 (2008).
- [19] Fishbain, B., Ideses, I. A., Shabat, G., Salomon, B. G., and Yaroslavsky, L. P., "Superresolution in color videos acquired through turbulent media.," Optics Letters 34 (2009).
- [20] S. Mann and R. Picard. Being 'Undigital' with Digital Cameras: Extending Dynamic Range by Combining Differently Exposed Pictures. Proc. of IST's 48th Annual Conference, pages 442– 448, May 1995.
- [21] P.E. Debevec and J. Malik. Recovering high dynamic range radiance maps from photographs. In Proceedings of ACM SIGGRAPH 1997, pages 369–378, 1997.
- [22] T. Mitsunaga and S. K. Nayar. Radiometric self calibration. pages 374–380, 1999.
- [23] M. Robertson, S. Borman, and R. Stevenson. Dynamic range improvement through multiple exposures. In Proceedings of the 1999 International Conference on Image Processing (ICIP- 99), pages 159–163, Los Alamitos, CA, October 24–28 1999.
- [24] Barbara Zitova and Jan Flusser. "Image registration methods: a survey. Image and Vision Computing", 21(11):977–1000, October 2003.
- [25] Lisa Gottesfeld Brown. "A survey of image registration techniques. ACM Comput". Surv.,24(4):325–376, 1992.
- [26] Greg Ward. Fast, "robust image registration for compositing high dynamic range photographs from hand-held exposures. journal of graphics tools", 8(2):17–30, 2003.

Multiple Exposure Image Fusion

N. sivakanth pappu

Dept of CSE
Sri Sivani College of Engineering
India

M. M. M. Kumara Varma

Dept of CSE
Sri Sivani College of Engineering
India

Abstract: in many cases scene's dynamic range is greater than digital camera dynamic range. In such cases the user needs to capture multiple exposures of the same scene, then combines them together. Exposure can be varied either by changing the shutter speed or by changing the aperture. In this paper we preferred to change the shutter speed over aperture. The main reason for that is changing aperture leads to depth of field problems.

Keywords: Aperture ;Dynamic range; Shutter speed;

I. INTRODUCTION

In general dynamic range refers to the ratio between the maximum and minimum measurable light. For an imaging sensor dynamic range dynamic range refers to the ratio between full well capacity and noise. Naturally scene's dynamic range can be up to 100,000 and the sensor dynamic range is always less than that.



Fig 1: Image captured with shutter speed 1\3200 sec

In order to get the full dynamic range of the scene, we must combine several exposures together. Different exposures can be achieved by changing the shutter speed or by changing the aperture. Shutter speed refers to the amount of time shutter remains open in order to acquire the image. If the shutter remains open for long amount of time then the sensor collects more amount of light and the picture appears too bright. If the shutter closes quickly then the sensor collects less amount of light and the picture appears dark.

We can clearly observe that the figure 1 darker and the figure 2 is brighter. In the figure 1 background details are clearly visible and in the figure 2 the tree details are correctly visible.



Fig 2: Image captured with shutter speed 1\50 sec



Fig 3: Image captured with F#-32

We can also change the exposure values by changing the f-number. Figure 3 and 4 are captured with different f-numbers and different shutter speed values. We can clearly see that background is unfocused. During the fusion phase these details will be completely not useful. Hence we preferred to change the shutter speed values. Both figure 3 and 4 are collected from Wikipedia.



Fig 4: Image captured with F#-5

II. RELATED WORK

Different auto exposure algorithms are introduced in order to correctly expose the scene. However, if the scenes dynamic range is greater than the imaging device dynamic range it is not possible to get the all details in a single image.

Many AE algorithms have been developed [1-4] to deal with high-contrast lighting conditions. Some of them employ fuzzy method while others use various ways of segmentation. However, most of these algorithms have some drawbacks on either their accuracy or on the complexity, or both while estimating lighting conditions.

According to [1], it is difficult to discriminate backlit conditions from front-lit conditions using histogram methods [2], [3]. Further simulations in this paper shows that the tables and criteria used to estimate lighting conditions are confusing and not consistent. Other algorithms [3], [4] used fixed-window segmentation methods to estimate the brightness and lighting conditions. Besides, these papers and [1] only considered images with only one main object. Therefore, these algorithms are not flexible and do not work well with other images in which a main object does not exist [5].

In real implementation, the idea works as follows: The authors, proposed different optimum brightness values (Bl_{opt}) for different lighting conditions. To identify the lighting conditions, after capturing the first frame, the brightness value mean (Bl_{mean}) and median (Bl_{med}) are calculated. The difference of these two values is represented with D_L . In order to obtain the most suitable optimal values of Bl_{opt} for normal lighting (Bl_{opt}^{norm}), back lighting or high contrast (Bl_{opt}^{bkdr}) lighting conditions, and lighting conditions when the current picture is over exposed (Bl_{opt}^{over}), many pictures were taken by the authors, in different lighting conditions. The mid-tone range Bl_{mt} is set to [100, 130].

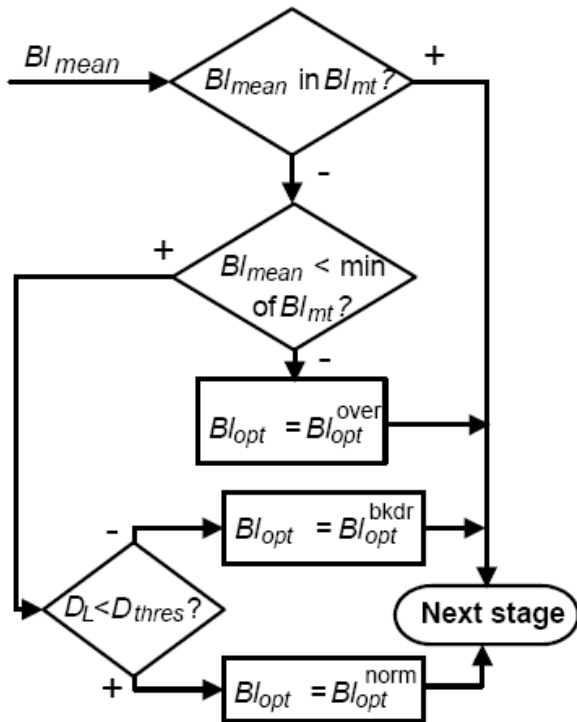


Fig 5: Deciding value for Bl_{opt}

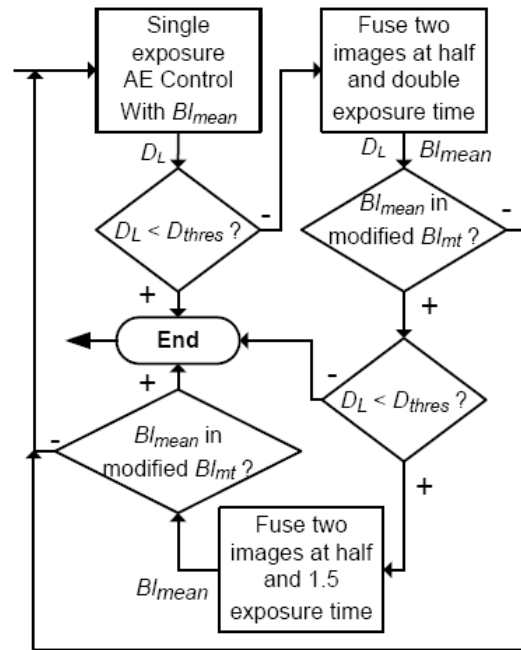


Fig 6: Multiple Exposure algorithm

III. PROPOSED ALGORITHM FOR HDR CAPTURING

Our algorithm basically consists of four parts. In the first part the end user should capture the image with the exposure settings suggested by the digital camera. Currently most of the digital cameras come up with the auto mode. If the user selects auto mode then automatically camera suggests shutter speed, aperture, ISO for a given scene. Once the camera suggests the exposure values, based on the exposure values suggested by the camera the end user captures a photograph.



Fig 7: Image captured with auto mode

In the second step HDR algorithm tries to identify the under exposed regions. In the under exposed region pixel values are close to zero. Once the algorithm identifies those regions it tries to find the proper exposure values. Proper exposure values can be found by increasing the shutter speed values. Once we increase the shutter speed values all the shadow details will be correctly exposed and the remaining details will be over exposed. Once we found the correct exposure settings for the under exposed regions the user need to capture the image.



Fig 8: All the shadow details are correctly captured

In the third step HDR algorithm tries to find the over exposed regions. In the over exposed region pixel values are close to 255. Once the algorithm finds the over exposed regions, it tries to find the correct exposure values. By decreasing the shutter speed we can correctly capture the highlight details. Once the camera identifies the correct exposure values



Fig 9: All the highlight details are captured

We fused all the above three images and the result is displayed in the Figure 10. We can clearly observe that all the high light details and shadow details are captured.



Fig 10: Fused image

References

- [1] J. Y. Liang, Y. J. Qin, and Z. L. Hong, "An auto-exposure algorithm for detecting high contrast lighting conditions," Proc. of the 7th Int. Conf. on ASIC, Guilin, Peoples R. China, vols. 1 and 2, pp. 725-728, Oct. 2007.
- [2] S. Shimizu, T. Kondo, T. Kohashi, M. Tsuruta, and T. Komuro, "A new algorithm for exposure control based on fuzzy logic for video cameras," IEEE Trans. Consum. Electron., vol. 38, pp. 617-623, Aug. 1992.
- [3] M. Murakami, and N. Honda, "An exposure control system of video cameras based on fuzzy logic using color information," Proc. of the 5th IEEE Int. Conf. on Fuzzy Systems, Los Angeles, vols 1-3, pp. 2181-2187, Sep. 1996.
- [4] J. S. Lee, Y. Y. Jung, B. S. Kim, and S. J. Ko, "An advanced video camera system with robust AF, AE, and AWB control," IEEE Trans. Consum. Electron., vol. 47, pp. 694-699, Aug. 2001.
- [5] Quoc Kien Vuong, Se-Hwan Yun, Suki Kim. "A New Auto Exposure and Auto White-Balance Algorithm to Detect High Dynamic Range Conditions Using CMOS Technology." Proceedings of the world congress and engineering and computer science, October 22-24, 2008.

Modified Z-Source Single-Phase Inverter for Single-Phase Pm Synchronous Motor Drives

B. Tejesh Kumar, * Dr. D.V. Ashok Kumar, ** Mr. J. Nagarjuna Reddy

PG Student, Power Electronics/EEE, RGM CET, Nandyal, India

**Assistant Professor, M-Tech Dept of: EEE RGM CET Nandyal

Abstract: The Z-Source network, as a DC-link energy storage sub-circuit, was proposed to be used in DC-AC power conversion circuits (inverters) due to its advantages compared to the traditional LC DC-link. In this paper a new modified Z-source (MZS) network is proposed in order to reduce the number of switches in a single-phase inverter, from four switches, in a full-bridge converter, to only two switches, as well as to maintain the desired average voltage level in the DC-link. This paper presents the novel topology and the operating principle of the new MZS single-phase inverter with two switches, and an application of this converter in a motor drive system to a single-phase PM synchronous motor. The proposed system topologies are validated by digital simulations of the circuits in PSIM and SIMULINK, with tests due soon.

I. Introduction

One of the major problems in single-phase voltage source inverters, having in the input stage batteries, photovoltaic, and fuel cells or a diode rectifier fed by the 230 V ac line, is the DC link voltage level, which could be smaller than the desired level, imposed by the application. Single phase voltage source inverters are used in photovoltaic or fuel cell grid-connected inverter systems as well as in inverter based motor drive systems. A growing interest is also shown in the field of hybrid electric vehicles. Some of the solutions to boost the DC link voltage are transformer-less boost circuits or circuits with high frequency transformers which are introduced between the DC voltage source and the inverter.

The main reasons why the Z-source network seems to be a good choice for the intermediate circuit between the DC link voltage and the inverter are the following: it provides a greater voltage than the DC link voltage if it is necessary, it makes the inverter immune to short circuits produced by the conduction of both transistors on the same phase leg (caused by EMI or bugs in the control software of the transistors), it reduces the inrush current and harmonics in the current thanks to the two inductors in the Z-source network, and it forms a second order filter and handles the undesirable voltage sags of the DC voltage source [1-7]. In this paper, the Z-source network is modified and a two power switch single phase PWM inverter, which self boosts the input voltage twice to keep the output voltage at input level (and mitigate for voltage sags), is proposed. Fig. 1 presents the electrical circuit of the Z-source network connected to a single-phase full bridge inverter. The diode D at the front end of the Z-source network makes the circuit unidirectional. The electrical energy flows from the DC voltage source to the load. The two equivalent schemes for the two possible operating modes of the Z-source network are shown in Fig. 2. [3]

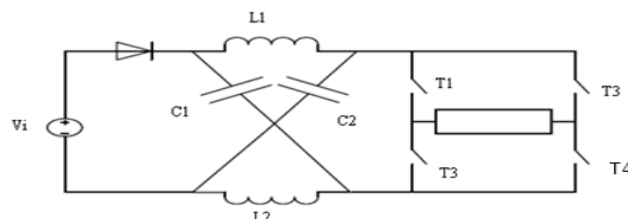


Fig.1. Z-source network with 4 switch single-phase inverter.

In the non-shoot through mode, in case of a single-phase inverter, two of the four transistors are switching: T1 and T4 or T2 and T3. With T4 on if T1 is on the output voltage is positive. Turning off T1 and turning on T3 (with T4 conducting) a through short circuit is produced to charge the inductances L1 and L2 and thus produce voltage boost.

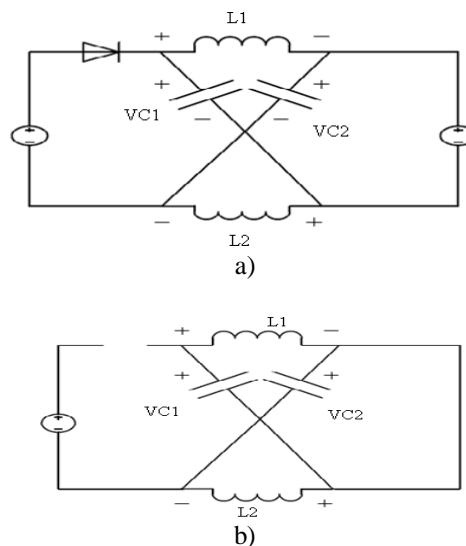


Fig.2. Equivalent schemes of the Z-source network in (a) non-shoot through state (b) shoot-through mode

In the shoot-through state:

$$V_{L1} = V_{C1} \quad V_{L2} = V_{C2} \quad V_i = 0$$

In the non shoot-through state:

$$V_{L1} = V_{DC} - V_{C1} \quad V_i = 2V_{C1} - V_{DC}$$

If $L1=L2$ and $C1=C2$ then the voltage drops across the inductors are equal and the voltage drops on the capacitors are equal as well.

To control the voltage at the input of the single-phase inverter we need to control the voltage of one capacitor, because the average voltage across the inductors in steady state is zero [1].

$$V_c = \frac{1 - \frac{T_{ST}}{T_s}}{1 - 2 \frac{T_{ST}}{T_s}} V_{DC}$$

where TST is the shoot-through time. To obtain the required TST/TS a PI controller can be used [1].

II. Modified Z-Source Single-Phase Inverter With 2 Switches

The proposed modified Z-source network (MZS) is presented in Fig. 3. In many electrical circuits, instead of a high voltage rated electrolytic capacitor, series smaller voltage rated capacitors are used. It can be noticed that this change in the Z-source network reduces the number of transistors. The load is connected between the common node of the two series capacitors and the common node of the two switches (Fig. 3).

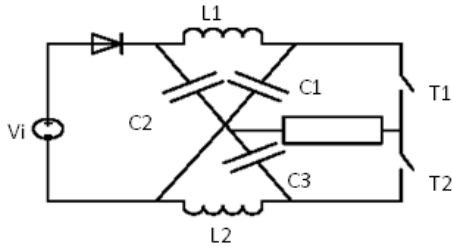


Fig. 3 .MZS single-phase inverter with two switches.

III. Operating Principle

The introduced MZS single-phase inverter with two switches has three different states, two active and one shoot-through. The three equivalent circuits for the three states are illustrated in Fig. 4.

[State 1]: The converter is in one of the two active states. The upper transistor is conducting and the lower transistor is substituted by its freewheeling diode.

The voltage on the load is:

$$V_{LOAD} = V_{C2} - V_{L1} = V_{C1}/2 - V_{L1}$$

$$\text{If } V_{C2} = V_{C3}$$

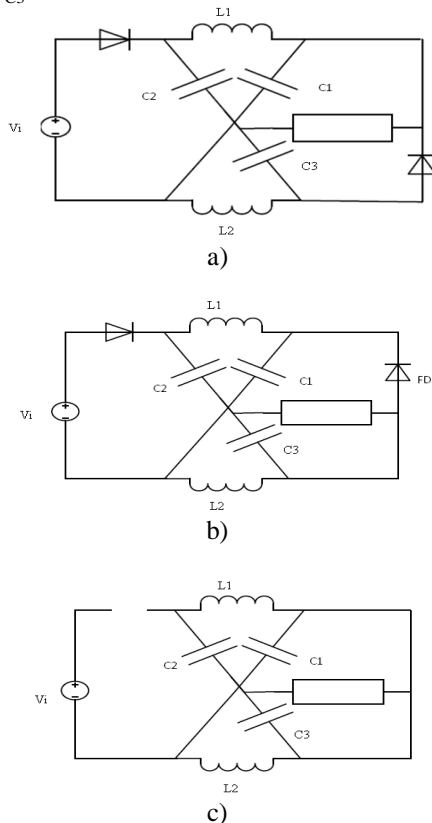


Fig.4. Equivalent circuits of MZS single-phase inverter for (a) State 1 (b) state 2 (c) state 3.

[State 2]: The converter is in the other non-shoot-through state. The lower transistor is conducting and the upper transistor is acting like a diode.

The voltage on the load is:

$$V_{LOAD} = -V_{C3} = -V_{C1}/2$$

$$\text{If } V_{C2} = V_{C3}$$

[State 3]: In this operating mode the demanded load voltage boost is realized. Both the upper and the lower switches are conducting; therefore an energy transfer is realized from the capacitors to the inductors. It can be seen that the circuit is asymmetrical (because the load is connected in parallel with the capacitor C3), so that the energy transfer from the capacitors to the inductors is not the same on the upper and on the lower side.

IV. Modified Z-Source Single-Phase Inverter With Single Phase Pm Synchronous Machine

Because of the complexity of the equations for each state of the MZS, the converter was modeled with discrete elements in PSIM. The single phase synchronous machine was modeled as a series connection of the following elements: the stator resistance R, the stator inductance L and a programmable voltage source which is the EMF, calculated in “Simulink” based on the motor equations at every sample time. We used three sensors in total: one load current sensor, one motor speed transducer and one voltage sensor for the measurement of C1 capacitor voltage (which is the average DC link voltage in steady state). So we have three control loops. For speed regulation a PI controller was used, for the load current control a hysteresis current controller. The hysteresis current controller commands one of the two transistors all the time. This means that there are no “inactive states” (e.g. the time duration for zero state vectors in case of a three phase inverter) during which the shoot-through states could be generated. In conclusion the shoot through states will take place during the active states. By connecting the motor between the common node of the two transistors T1 and T2 and the common node of the capacitors C2 and C3 the maximum voltage which can be delivered to the motor in our case study is 150 V if the voltages on the two capacitors C2 and C3 are equal to each other. In order to be able to supply the motor from 300 V with the block V* we prescribe 600 V average DC link voltage. To reduce the inrush current spikes in the inductors the V* voltage was increased from 300 V to 600 V in 300 ms. The output of the PI regulator in the DC link voltage control loop in Fig. 5a gives the ratio of the input DC voltage and the average DC link voltage. Based on equation (3) the block after the PI regulator calculates the shoot through time.

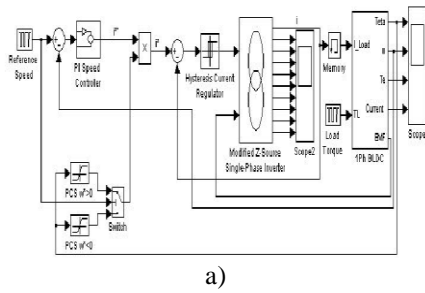
The shoot through time generation can be seen in Fig.6. It should be noticed that the shoot through time is calculated with a 10 kHz sampling rate and the shoot through pulses are distributed equally over the 100 is period at the beginning and at the end of the sampling period. The shoot-through pulses override the pulses generated by the hysteresis current controller thanks to the two or gates at the gate of each transistor.

$$V_S = I_S \cdot R_S + L_S \cdot \frac{dI_S}{dt} + \omega_r \cdot \lambda_{PM}(\theta_{er})$$

$$\frac{1}{p} \cdot \frac{d\omega_r}{dt} = T_e + T_{cog} - T_{load}$$

$$T_e = P \lambda_{PM}(\theta_{er}) I_S(t)$$

$$\frac{d\theta_{er}}{dt} = \omega_r$$



a)

To demonstrate that the proposed MZS single phase inverter is suitable for motor drives with single phase PM synchronous machines, different perturbations on the drive were simulated. For example, it can be seen in Fig. 7 that for a 10% voltage sag of the nominal DC voltage source (fall from 300V to 270V) the C1 capacitor voltage remains unchanged. At the start of the converter one of the two series capacitors (C2) is discharged and the second (C3) is charged with electrostatic energy. The C1 capacitor voltage smoothly follows the prescribed average DC link voltage; it has a very small overshoot. Even if the prescribed average DC link voltage is raised gradually from 300V to 600V in 300ms, we do have some inrush current spikes in the inductors L1 and L2 (Fig. 8.). A longer ramping time could reduce these inrush current spikes.

Fig. 8 shows that the inductors peak currents are about two times greater than the peak load current. The difference between the two currents instantaneous values is the effect of the converter's asymmetry (see Fig. 4 state 2 and state3).

In Fig.8 b) can be seen that the instantaneous voltage across the load is asymmetrical, the positive part is two times greater than the negative part.

Fig. 9 shows the motor reference and measured speed while the motor accelerates to the nominal speed 3000 rpm in about 1.5 seconds. A breakpoint in the speed ramping is visible at 300 ms the moment when the C1 capacitor voltage reaches 600V. From this moment the motor has a steeper acceleration ramp, until it reaches 3000 rpm. A step load torque of 0.35 Nm is applied to the motor at t = 2 seconds until t = 8 seconds. This load torque is not reflected in the capacitor voltages and the speed does not suffer a speed drop, which indicates that the speed and current loops work well. At t = 3 seconds, the motor is decelerated to 33% of its nominal speed for 3 seconds. A voltage boost is visible in the capacitor voltages during the deceleration process.

At t = 6 seconds the motor speed increases again to the nominal speed. This time the acceleration time duration is longer than the deceleration time duration because we have a torque load which goes to zero at t = 8 seconds and the acceleration ramp gets steeper, again.

In Fig. 10 shows the variation in time of the load torque, electromagnetic torque and the cogging torque of the motor.

The transistors voltage and current stresses are illustrated in Fig. 11. The collector peak current is twice the inductor peak current. The peak instantaneous voltage across the transistor is two times bigger than the voltage across C1.

Table I presents the peak currents and voltages in the transistors for the following converter topologies: full bridge single-phase inverter with 4 transistors (A) and modified Z-source single-phase inverter with 2 transistors (B) for single-phase PM synchronous motor drives. The 2 transistor topology is payed for in addition V and A ratings.

The motor parameters:

- Stator resistance RS [ohm]: 40
- Stator inductance LS [H]: 0.2913
- Total inertia J [kg/m2]: 0.004
- Viscous friction coefficient B[Nm s] : 0.001
- Number of pole pairs: 1
- Nominal voltage [V]: 300 .

The MZS converter parameters:

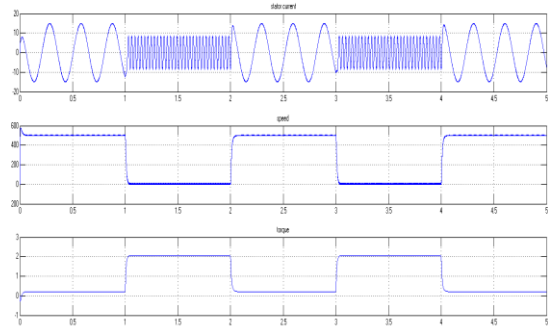
- L1=L2=6mH;
- C1=C2=C3=470iF.
- The PI speed controller parameters:
- KP=2; Ki=20.

The PI controller parameters in the shoot-through-time control block:

- Gain: 0.009;
- Time Constant: 2.5 ms.

Simulation results:

Stator current, speed & torque with respective to time are shown as follows:



Voltages across inductors and capacitors are as follows:

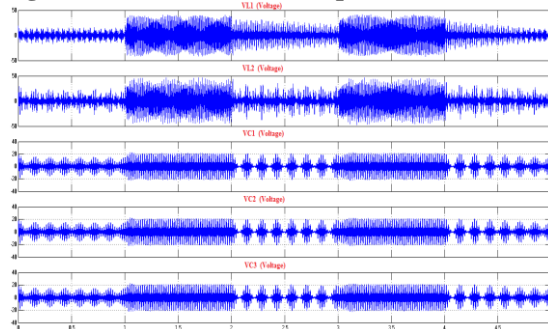


TABLE I

Topologies	No. of transistors	Peak transistor current	peak transistor voltage[v]
A	4	2	300
B	2	6	900

V. Conclusions And Discussions:

The proposed modified Z-source single phase inverter is a possible solution for motor drives with single phase permanent magnet synchronous machines. The converter is able to override the DC voltage sags. The inductors peak currents are approximately twice the load peak current.

The voltage boost of the intermediate DC link it can be produced even if there are no "inactive states".

References

- [1] F. Z. Peng, "Z-Source Inverter," *IEE Transactions on Industry Applications*, vol. 39, pp. 504-510, March April 2003,.
- [2] Fang Z. Peng, Miaosen Shen and Alan Joseph, "Z-Source Inverters, Control, and Motor Drive Applications," *KIEE International Transactions on Electrical Machinery and Energy Conversion System*, vol. 5-B, no. 1, pp. 6-12, 2005.
- [3] Tran-Quang Vinh, Tae-Won Chun, Jung-Ryol Ahn and Hong-Hee Lee, "Algorithms for Controlling Both the DC Boost and AC Output Voltage of the Z-Source Inverter," in *Proc. of the 32nd Annual Conference of IEEE Industrial Electronics Society, IECON 2005*, , pp. 970-974. .
- [4] Babak Farhangi and Shahrrokh Farhanghi, "Application of Z-Source Converter in Photovoltaic Grid-Connected Transformer-less Inverter," in *Proc. of PELINCEC-2005*, Warsaw, Poland, pp. 198-203.
- [5] N. Mohan, W.P. Robbins, T.M. Under land, *Power Electronics*, John Wiley, 1995.
- [6] F.Z. Peng, M.S. Shen, and Z.M. Qian, "Maximum Boost Control of the Z-Source Inverter," in *Proc of IEEE-PESC'04*, 2004, pp. 255-260.
- [7] Poh Chiang Loh, D.M. Vilathgamuwa, C.J. Gajanayake, Yih Rong Lim, and Chern Wern Teo, "Transient Modeling and Analysis of Pulse-Width Modulated Z-Source Inverter," *IEEE Transactions on Power Electronics*, vol. 22, pp. 498-507, March 2007.
- [8] I. Boldea and S.A. Nasar, *Electric Drives*, Second edition, pp. 313-319, 380-386, 1998.

Influence of Recycled Coarse Aggregate on Punching Behaviour of Recycled Coarse Aggregate Concrete Slabs

Dr. H. Sudarsana Rao¹, V. Showjendra Kumar Reddy²,
Dr. Vaishali. G.Ghorpade³

¹Professor of Civil Engineering, JNTUA College of Engineering, Anantapur-515002

²Research scholar., JNTUA College of Engineering, Anantapur-515002

³Assoc. Professor in Civil Engineering Dept., JNTUA College of Engineering, Anantapur

ABSTRACT: This paper reports on the punching shear behavior of simply supported recycled aggregate concrete two-way slabs. The experimentation was conducted on 15 Recycled Coarse Aggregate Concrete (RCAC) slab specimens and 3 Natural Aggregate Concrete (NCAC) slabs were cast tested as control specimens. All the slabs were simply supported on all four edges and tested under a central patch load. Six replacement percentages (0, 20, 40, 60, 80 and 100%) of Natural Coarse Aggregate (NCA) replacements with Recycled Coarse Aggregate (RCA) were considered in this investigation. The results showed that as the replacement of NCA with RCA increases, the Ultimate load, deflection at ultimate load, Stiffness degradation and Energy absorption decreases and the cracking was premature. A Regression model has been developed to predict the ultimate punching shear of RCA slabs.

Keywords: Deflections, Energy absorption, Loads, Natural Coarse Aggregate (NCA), Natural Coarse Aggregate Concrete (NCAC), Recycled Coarse Aggregate (RCA), Recycled Coarse Aggregate Concrete (RCAC), Stiffness degradation, Two-way Slabs.

NOMALNCLATURE

f_c	Cube compressive strength (N/mm ²)
f'_c	Cylinder compressive strength (N/mm ²)
τ	Shear stress (N/mm ²)
r	replacement ratio of NCA with RCA

I. INTRODUCTION

Recycled coarse aggregate concrete (RCAC) can be recognised as a new kind of concrete, in which broken pieces of waste concrete are used as aggregate. The use of RCA is one such an attempt to solve some of the problems in the field of construction industry. The concept of using RCA is now gaining popularity and research in this field has gained some momentum. Most of the findings have been extensively reviewed and discussed by Nixon [1], Hansen [2] and ACI committee 555 [3]. Due to the low strength, low elastic modulus, bad workability, high water infiltration, high shrinkage and creep of RCAC, it is mostly used for only non structural concrete [4, 5]. However, RCAC is well recognised in view of its low thermal conductivity, low brittleness as well as the low specific gravity that reduces the self weight of the structures. It was revealed that the relevant material properties of RCAC are generally lower than those of conventional concrete, but they are still sufficient for practical applications. Most importantly the use of RCA

can save natural resources and protect our living environment [6, 7].

The studies of properties of RCAC have been ongoing over the last few decades, leading a number of countries to establish standards or recommendations supporting their views. With regard to popularised RCAC, the structural behaviour of RCAC ought to be investigated. In fact some studies concerning the performance of beams were conducted by Mukai [8], Yagishita [9], Gonzalez-Fontebao [10], performance of columns were studied by Yang [11] and studies on seismic performance of frame structure by Xiao [12] made with RCAC. This paper reports studies on punching shear behavior of RCAC slab specimens.

II. RESEARCH SIGNIFICANCE

In this investigation, experiments were designed to provide a comprehensive understanding of the structural behavior of RCAC. The tests were particularly focused on the real punching shear behaviour of simply supported reinforced RCAC slabs under action of central patch load and also studied the influence of NCA replacement with RCA on the failure pattern, ultimate loads, load deflection curves, stiffness, stiffness degradation, energy absorption and comparison with the codes of practice of slabs under punching shear. The results presented in this paper may promote the use of RCA in practical applications.

III. EXPERIMENTAL PROGRAM

3.1 Materials

Ordinary Portland cement of 43 grade, confirming to IS 8112:1989 [13], locally available river sand as fine aggregate (zone-II) confirming to IS-2386 [14], coarse aggregates are natural coarse aggregate (NCA) and recycled coarse aggregate (RCA). RCA is obtained from the waste concrete brought from the runway of an Airport in Kadapa, Andhra Pradesh, India (10 to 12.5mm accounting for 50%, and 12.5 to 20mm accounting for 50% in weight) and is used in this investigation. The physical properties of the NCA and RCA are presented in Table 1. Fe415 HYSD bars confirmed to IS-1786:1985[15] with 6mm diameter have been used as slab reinforcement.

Table1. Physical properties of NCA and RCA

Coarse aggregate	Grading (mm)	Bulk density (kg/m ³)	Apparent density (kg/m ³)	Water absorption (%)
NCA	4.75–20	1520	2680	0.52
RCA	4.75 -20	1360	2560	5.02

3.2 Mix proportions of RCAC

Due to the high water absorption capacity of RCA, they were presoaked by additional water before mixing. The amount of water used to presoak the RCA was calculated according to the saturated surface dry conditions. The target designed strength for 28 days of all the concretes was set as around 25 MPa. The ACI mix design procedure [16] is adopted. The mixtures were divided in to six groups. The main difference among these six groups is the NCA replacement percentage with RCA which is 0, 20, 40, 60, 80 and 100%, respectively. In case of NCA replacement percentage with RCA equating 0, the specimens are termed as NCAC slab specimens, which are served as the control specimens for comparison. The mix proportions of the concrete are shown in Table 2.

3.3 Preparation of test specimens

Steel moulds were used to cast the slab specimens of required size. Two L-shaped frames with a depth of 50mm were connected to a flat plate at the bottom using nut and bolts. Cross stiffeners were provided to the flat plate at the bottom to prevent any possible deflection while casting the specimens. The gaps were effectively sealed by using thin card boards and wax to prevent any leakages.

In the experiment, a total 18 (3 on each group) approximately one-sixth scale square isotropically reinforced concrete slab specimens were made with the NCA replacement with RCA in different percentages and tested under punching shear. The thickness of the slab specimen and the spacing of longitudinal reinforcement was accomplished in accordance with IS 456-2000 [17]. All the slabs are of size 1100 x 1100 x 50mm. All the slab specimens are reinforced with (0.63%) Fe-415 HYSD 6mm diameter bars, with a cover of 10mm and the bars are equally distributed in both the directions.

The test slab specimens were de-moulded after 3 days. Before de-moulding, the slab specimens are cured with wet jute bags. The de-moulded slab specimens were water cured for 28 days in curing pond. After removing the slab specimens from the curing pond, they were allowed to dry under shade for a while and then they were coated with white paint on both sides, to achieve clear visibility of cracks during and after testing. By preserved cubes and cylinders in each group, the measured average mechanical properties of the concrete related to the slab specimens are illustrated in Table 3. From Table 3 it is observed that as the replacement of RCA with NCA increases the compressive strength and split tensile strength decreases.

3.4 Loading arrangement and testing

The slab specimen is placed over the loading platform and steel rods of 16 mm diameter have been kept below the slab along the four edges to simulate the simply supported edge condition. Placing of steel rods allow free rotation

along the edges thus simulating the simply supported edge condition. A single concentrated patch load was applied at the geometric center of each slab with a rigid bearing plate of 100x100x20 mm with a 3-mm thick plywood packing between the slab and the bearing plate. Over this rigid plate, solid circular rod of 50 mm diameter was kept to distribute the load from the hydraulic jack to the slab specimen. The load was applied through hydraulic jack was measured in increments of 200N which corresponds to one unit of calibrated proving ring with 500 kN capacity, vertical deflections at the geometrical center of the slab specimens were measured by using dial gauge with a least count of 0.01 mm. The load at the first crack and the corresponding deflection at the bottom centre of the slab were recorded. The ultimate punching shear load and corresponding deflection at the centre were also observed and recorded. The overall view of a specimen in position ready for testing is shown in Figure 1.

IV. RESULTS AND DISCUSSION

4.1 General

The load versus central deflection curves for the slabs are presented in Figure 2. It may be seen that the typical relationship was linear until flexural cracking, which occurred just below the loading point. This event was characterized by a noticeable reduction in slab stiffness. With increasing load, new cracks were formed and the existing ones kept propagated in the radial direction, predominantly towards the corners of the slab. The slope of the load-deflection curve also kept decreasing until punching failure occurred. A sudden drop in the applied load marked this event. At this stage, punching shear failure was clearly visible on the top face but, on the bottom face, only an outline of the truncated failure cone with a much larger perimeter had formed. Table 3 reveals that the mechanical properties of the recycled concrete slabs decreases with an increase of the NCA replacement percentage with RCA.

The results of the experimental investigation are summarized in Table.4. The values presented here represent the average of punching shear strengths, load and deflection obtained for three specimens in each group. From the Table.4 it is observed that there is a decrease in first crack load as the replacement of NCA with RCA increases. The first crack load of NCAC-S is 14.60kN and for the RCAC-20-S to RCAC-100-S is between 14.20 to 12.20kN. The first crack load of RCAC-20-S to RCAC-100-S decreases by 2.74 to 16.44%, when compared with NCAC-S. The first crack occurs first in RCA than that of natural aggregate, it is due to the presence of adhered mortar over the RCA. Hence, as the percentage replacement increases the first crack load decreases.

The ultimate load of NCAC-S is 48.20kN and for the RCAC-20-S to RCAC-100-S is between 47.20 to 41.40kN. The ultimate load of RCAC-20-S to RCAC-100-S decreases by 2.07 to 14.11%, when compared with NCAC-S. This shows that as the replacement of NCA with RCA increases the ultimate load decreases linearly. It should be noted that the reduction in the ultimate loads are less than at material level, i.e. the mechanical properties as

described in Table.3; this may be due to the contribution of steel reinforcement.

The central deflection response of various slab specimens is shown in Figure.4. Central deflection corresponding to first crack load and ultimate load are presented in Table.4. It is observed that the central deflections corresponding to first crack load of RCAC-20-S to RCAC-100-S decrease by 3 to 30%, when compared with NCAC-S. The central deflections corresponding to ultimate load of RCAC-20-S to RCAC-100-S decrease by 3 to 15%, when compared with NCAC-S. Similar trends are observed at first crack stage and ultimate load stage. But, rate of decrease of deflections at first crack stage is more when compared to ultimate stage. At the first cracking stage, rate of decrease of deflections are more due to presence of old mortar over the RCA, but at ultimate stage rate of decrease of deflections are less due to the contribution of steel reinforcement. Typical view of failure slab specimens is shown in Figure 3 and Figure 4.

4.2 Stiffness

From the load-deflection curves, two values of the stiffness of the tested slabs were obtained. The un-cracked stiffness K_i is indicated by the slope of the line of a value less than the first crack load, and the ultimate stiffness K_u is measured by the slope of the line at about 90% of the ultimate load. These values are given in Table 5. From the deflection curves, it can be seen that the slope becomes steeper when the percentage replacement of NCA with RCA increases. This indicates that the un-cracked stiffness increased as the percentage replacement of NCA with RCA increases. Stiffness degradation is defined as the ratio between the ultimate stiffness and the un-cracked stiffness as given in Table 5. As the stiffness degradation increased, the specimen indicated lower ductility. Out of RCAC slab specimens RCAC-100-S shows 9% decrease in stiffness degradation when compared with NCAC-S slab specimens.

4.3 Energy absorption

The energy absorption is defined as the area under the load-deflection curve. The values were determined from test results, and are listed in Table 5. RCAC-20-S to RCAC-100-S show 4.17 to 27.50% decrease in the energy absorption when compared with NCAC-S. Therefore, it can be concluded that as the replacement percentage of NCA with RCA increases energy absorption decreases.

V. REGRESSION MODEL FOR PUNCHING SHEAR STRESS

A simple regression model has been developed from the results of present investigation for predicting the punching shear strength of RCAC slabs. To develop the punching shear strength model, linear regression technique has been adopted. The linear regression is in the form of $Y=A+BX$ where Y is independent variable, X is dependent variable and A and B are called regression coefficients. The A and B are determined from regression analysis in accordance with the principle of least squares method.

For predicting the shear stress IS code [17] and ACI [18] code uses cube and cylinder compressive

strength, respectively. Hence, the proposed models for punching shear stress with f_c and f'_c are as given below

$$\tau = A + BX \quad \dots (1)$$

From the results of the present study, a simple regression models has been developed connecting shear stress with cube compressive strength f_c and cylinder compressive strength f'_c and are presented as equation 3 and 4 with a standard deviation of 0.0020 and 0.0025, respectively

$$\tau = (0.359 - 0.0067 r) \sqrt{f_c} \quad \dots (2)$$

$$\tau = (0.403 - 0.0091 r) \sqrt{f'_c} \quad \dots (3)$$

A comparison of the ultimate shear stress by regression models (Eq. 3 and 4) and experimental values are presented in Table 6 and Figure 5. From the Table 6 and Figure 5 it can be observed that the proposed model compared well with the experimental shear stress. The experimental and regression model values give more conservative predictions.

VI. CONCLUSIONS

The following observations and conclusions can be made on the basis of the current experimental results.

- 1- As the percentage replacement of natural coarse aggregate with recycled coarse aggregate increases the compressive strength and split tensile strength increases. Up to 40% replacement of NCA with RCA there is a marginal decrement in compression and split tensile strength when compared with natural coarse aggregate concrete.
- 2- All the slabs behave similar in the aspect of failure patterns under punching shear regardless of the replacement percentage of natural coarse aggregate with recycled coarse aggregate. The presence of recycled coarse aggregate reduces the first crack and ultimate loads of slab specimen. However, this reduction is less than that of the mechanical properties of the recycled coarse aggregate.
- 3- Slab specimens up to 40% replacement of NCA with RCA there is a marginal decrement in first crack and ultimate loads when compared with natural coarse aggregate concrete.
- 4- As the percentage replacement of natural coarse aggregate with recycled coarse aggregate increases the stiffness degradation decreases and energy absorption decreases.
- 5- A Regression model is developed for predicting the ultimate punching shear and is given as

$$\tau = (0.359 - 0.0067 r) \sqrt{f_c}$$

$$\tau = (0.403 - 0.0091 r) \sqrt{f'_c}$$

REFERENCES

- [1] Nixon P.J, “Recycled concrete as an aggregate for concrete – a review”, *Material and Structures*, 11 (1978), pp. 371 – 378.
- [2] Hansen T.C, “Recycled aggregate and recycled aggregate concrete, second state-of-the-art report, developments from 1945 to 1985”, *Material and Structures*, 19 (1986), pp. 201 – 246.
- [3] ACI Committee 555, “Removal and reuse of hardened concrete”, *ACI Materials Journal*, 99 (2002), PP. 300 – 325.
- [4] Ajdukiewicz, A. Kliszczewicz, “Influence of recycled aggregates on mechanical properties of HS/HPC”, *Cement and Concrete Composites* 24 (2002), pp. 269 - 279.
- [5] Sagoe-Crentsil K.K, T. Brown, A.H. Taylor, “Performance of concrete made with commercially produced coarse recycled concrete aggregate”, *Cement and Concrete Research*, 31 (5) (2001), pp. 707 – 712.
- [6] Katz A., “Properties of concrete made with recycled aggregate from partially hydrated old concrete”, *Cement and Concrete Research*, 33 (2003), pp. 703 – 711.
- [7] Topcu I.B., Sengel S., “Properties of concretes produced with waste concrete aggregate”, *Cement and Concrete Research*, 34 (2004), pp. 1307 – 1312.
- [8] Mukai T., Kikuchi M., “Properties of reinforced concrete beams containing recycled aggregate”, *Demolition and Reuse of concrete masonry*, Vol.2 Reuse of demolition wastage, proceedings of the second international RILEM symposium, Ed. Kasai, Nov (1988), ISBN 0-412-32110-6, pp. 670 – 679.
- [9] Yagishita M., Sano M., Yamada M., “Behaviour of reinforced concrete beams containing recycled aggregate”, In: Lauritzen EK Ed., *Demolition and Reuse of concrete masonry*, proceedings of the third international RILEM symposium, (1993), ISBN 0-412-32110-6, pp. 331 – 343.
- [10] Gonzalez-Fonteboia B., Martinez-Abille F., “Shear strength of recycled concrete beams”, *Construction and Building Materials*, 21 (2007), pp. 887 – 893.
- [11] Yang Y.F., Lin-Hai Han., “Experimental behavior of recycled aggregate concrete filled steel tubular columns”, *Journal of Constructional Steel Research*, 62 (2006), pp. 1310 – 1324.
- [12] Xiao J., et al., “Seismic performance of frame structures with recycled aggregate concrete”, *Engineering Structures*, 28 (2006), pp. 1 – 8.
- [13] Indian Standard Code (IS: 8112: 1989), “Specifications for 43 Grade Ordinary Portland Cement”, New Delhi.
- [14] Indian Standard Code (IS: 2386-1997), “Method of test for aggregates for concrete”, New Delhi.
- [15] Indian Standard Code (IS-1786:1985), “Specification for High strength deformed steel bars and wires for Concrete Reinforcement”, New Delhi.
- [16] ACI method of mix design (211.1-91), “Standard practice for selecting proportions for normal, heavy weight and mass concrete”.
- [17] Indian Standard Code (IS-456:2000), “Plain and reinforced concrete- Code of practice”, New Delhi.
- [18] American Concrete Institute (ACI 318-08), “Building code requirements for reinforced concrete”, Detroit.

Table2. Mix proportions of concrete (kg/m³)

Nomenclature	Replacement percentage of NCA with RCA	W/C	Cement in kgs	Sand in kgs	NCA in kgs	RCA in kgs	Mixing water in liters
NCAC-S	0	0.53	379	804	942	-	200
RCAC-20-S	20	0.53	379	820	754	168	200
RCAC-40-S	40	0.53	379	823	566	337	200
RCAC-60-S	60	0.53	379	833	377	506	200
RCAC-80-S	80	0.53	379	846	188	675	200
RCAC-100-S	100	0.53	379	863	-	843	200

Table3. Average mechanical properties of concrete (MPa)

Nomenclature	Percentage Replacement of NCA with RCA	Cube compressive strength (f _c)	Cylinder compressive strength (f _c ^l)	Split tensile strength (f _t)
NCAC-S	0	43.33	34.35	3.35
RCAC-20-S	20	42.52	33.50	3.25
RCAC-40-S	40	40.96	32.37	3.16
RCAC-60-S	60	38.37	30.86	3.11
RCAC-80-S	80	35.48	28.40	2.88
RCAC-100-S	100	33.48	26.42	2.78

Table.4. Test results

Nomenclature of slab specimen	First crack Load (kN)	Deflection at first crack load (mm)	Ultimate Load (kN)	Deflection at ultimate load (mm)
NCAC-S	14.6	1.51	48.20	33.23
RCAC-20-S	14.2	1.46	47.20	32.15
RCAC-40-S	14.2	1.42	45.80	30.19
RCAC-60-S	13.4	1.28	44.60	29.22
RCAC-80-S	12.8	1.14	42.80	28.49
RCAC-100-S	12.2	1.06	41.40	28.11

Table.5. Stiffness and Energy absorption

Nomenclature of slab specimen	Stiffness			Energy absorption (kNm)
	Initial K_i (kN/mm)	Ultimate K_u (kN/mm)	degradation K_u/K_i	
NCAC-S	12.20	1.77	0.145	1.20
RCAC-20-S	12.20	1.74	0.142	1.15
RCAC-40-S	12.20	1.71	0.140	1.04
RCAC-60-S	12.20	1.66	0.136	0.94
RCAC-80-S	12.00	1.62	0.135	0.90
RCAC-100-S	12.00	1.58	0.132	0.87

Table6. Ultimate punching shear strength of slabs

Nomenclature of slab specimen	Experimental Ultimate shear stress (N/mm ²)	Ultimate shear stress by using equation 2 (with f_c) (N/mm ²)	Ultimate shear stress by using equation 3 (with f'_c) (N/mm ²)
NCAC-S	2.38	2.36	2.36
RCAC-20-S	2.33	2.33	2.32
RCAC-40-S	2.26	2.28	2.27
RCAC-60-S	2.20	2.20	2.21
RCAC-80-S	2.11	2.11	2.11
RCAC-100-S	2.04	2.04	2.02



Fig. 1: Overall view of a specimen in position ready for testing

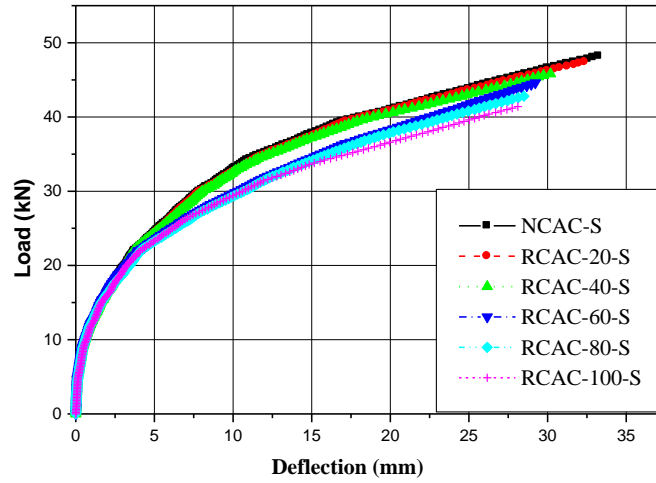


Fig 2: Load deflection curves



Fig 3: Typical top view of failure RCAC slab specimen



Fig 4: Typical bottom view of failure RCAC slab specimen

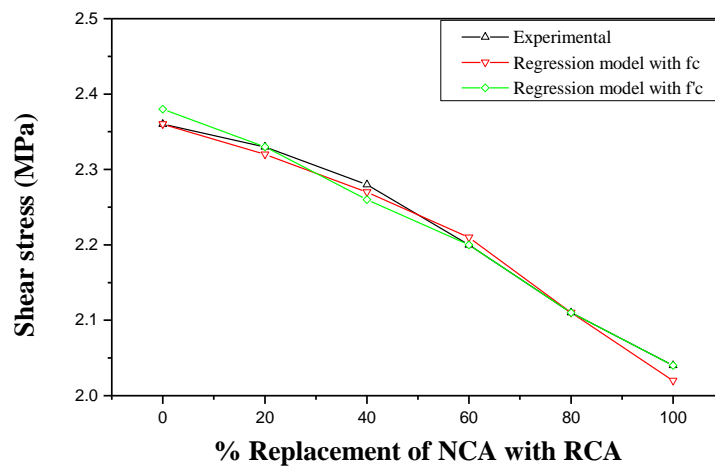


Fig 5: Variation of Shear stress with the replacement of NCA with RCA

Design of a Neural Network Based Image Recognition System Using Configurable VLSI

Vidya G. S¹, Sarath Raj S², Manu T S³

^{1, 2, 3}(Dept.of Electronics and Communication, TKM Institute of Technology, Affiliated to CUSAT, India.)

Abstract: This paper describes the initial steps in the development of an object detection system for manipulation purposes to be embedded in a mobile robot. The goal is to design a neural network based recognition module. The neural network module and additional image processing algorithms which are used to convert the image into useful information for the neural network and the control of the whole system is designed using the soft core processor in the FPGA. The neural network implementation can be performed using the VHDL coding and processor can be designed using the Xilinx EDK tool.

Keywords: EDK, embedded systems, FPGA, image processing, Neural Network, SoPC, visual servoing

I. INTRODUCTION

Image recognition systems are widely used in different industries such as production plants to detect faulty components, to select a piece on a conveyor or as surveillance systems that are capable of detecting intrusion, differentiating people or observing their motion. Object positions and environmental conditions have to be acquired in real-time. The term Visual Servoing refers to a useful capability for both manipulator arms and mobile robots [1]. Visual Servoing involves moving a robot or some part of a robot to a desired position using visual feedback [2].

However, fast and computation intensive tasks are difficult to implement in small and low power consumption electronic systems required in robot-like systems. The goal of this research is to develop an efficient hardware/software implementation of an object recognition system for an autonomous robot. This recognition system is based on an artificial neural network. In addition, some image processing modules to provide the network with useful data have been designed. Some other works that use neural network based systems for Visual Servoing can be found in [3], [4], [5]. However, in general most of such implementations are PC-based architectures.

The implementation presented here is carried out in a FPGA (Field Programmable Gate Array). The very high integration of present FPGAs enable the accommodation of all the components of a typical embedded system (processor core, memory blocks, peripherals, specific hardware,...) on a single chip, commonly referred to as system-on-a-programmable chip (SoPC). The design described here is based on such a SoPC. In particular the neural network module together with the control of the whole system are implemented as software in the embedded processor core

II. SYSTEM ARCHITECTURE

The initial approach to afford the recognition problem has been limited to the recognition of simple shapes, but in such a way that it could be extrapolated to any shape, for example those of hand tools. For the experiments performed up to now, some different colour wood pieces (cubes, cylinders, rectangular prisms and triangular prisms) have been used. Hence, four possible shapes have to be recognized: square, circle, rectangle and triangle.

Usually, image processing algorithms are implemented in software and run on a PC. However, in applications with high restrictions in response time or low consumption requirements (like the system described here), hardware specific implementations are needed. The main objection of the image recognition techniques for its realization in hardware is the high complexity of the existent algorithms. For this reason, in this paper a method optimized for its hardware implementation is presented.

2.1. IMAGE PRE-PROCESSING

The pre-processing stage converts the images into useful information for the neural classification system. Once a binary image is obtained, the amount of information contained in it is reduced to preserve only the information considered more relevant for the recognition. An edge extraction technique grounded on the chain-code algorithm [6] has been chosen. The bases of the chain-code algorithm were introduced in 1961 by H. Freeman [7], who described a method which permits the encoding of arbitrary geometric configurations, as a way to make it easier for a digital computer to manipulate them. It is a lossless compression algorithm for binary images, which provides a useful way to depict an object and to derive its features for later applications in pattern recognition.

Chain-codes are used to represent the contour of an object by means of a sequence of small vectors of unit length, each one representing the direction of the contour at that point. The number of possible directions is determined, being the 8-connected neighborhood and the 4-connected neighborhood configurations the most commonly used. The 4-connected set of directions, also referred to as external chain-code or crack code in some sources, is the one employed in this work (Figure 1).

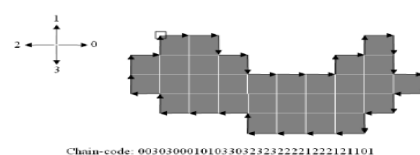


Figure1: Example of the external chain code of a binary image

First of all, the region of the image where the object lays must be determined, in terms of the density of white pixels. Then, the origin of the object in the image must be fixed. In the algorithm presented in this paper, the origin is considered to be the left-most white pixel of the first line in the object region. Once the origin is fixed, the object is outlined in clockwise manner and the directions of the boundary are stored until the algorithm reaches back the initial point.

Using this algorithm, each object is represented by a sequence of numbers, which length is different for each case, depending on the size of the object in the image and its shape.

In order to make the lengths equal and to reduce even more the codification, in such a way that it can be used as the input for the neural network, the sequence is normalized by dividing it into a fixed number of smaller sequences. Each of them is processed to obtain the slope between its end points. Thus, each object is represented by a fixed length sequence which contains the slopes of the contour. In turn, these slopes can only take a definite number of values, so that the translation to a digital system is more direct.

2.2. NEURAL CLASSIFICATION

The classification module consists of an artificial neural network where the inputs are the values provided by the image pre-processing stage. Based on these data the neural network classifies the shape of the target object. The neural network has multi-layer perceptron architecture [8], consisting of an input layer, a hidden layer and an output layer.

The number of input neurons has been set to 16, which forces the sequence obtained from the image processing stage to be of this length. The hidden layer has 32 neurons with a tan-sigmoid activation function. Lastly, the output layer consists of 4 output neurons, one for each possible shape, and no activation function is applied. The architecture of the neural network is presented in Figure 2.

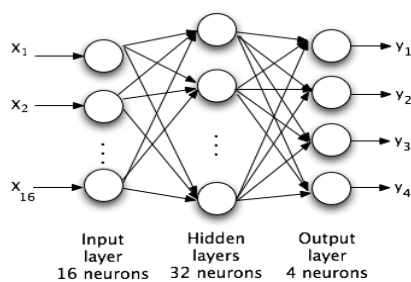


Figure 2: Architecture of the proposed neural network

The network is trained by means of the back-propagation algorithm, using the gradient-descent method. The training set is made up of 16 sequences obtained from different images of different object shapes, along with the corresponding target output for each sequence. This set is divided into three different subsets: the 60% of the samples are used for training, the 20% for validation (useful for early-stopping of the training process) and the remaining 20% for test (for estimating the network's ability to generalize). The training algorithm of the network is performed in Matlab, by means of the Neural Network Toolbox [9].

III. HARDWARE/SOFTWARE PARTITION

Nowadays, the so called SoPC (system-on-a-programmable chip) take advantage from the flexibility of software and the high performance of hardware. Their proliferation has been possible thanks to the high integration levels achieved in the microelectronic industry, which allow the inclusion of a small microprocessor inside the programmable chip. This fact allows the designing of efficient heterogeneous hardware/software architectures on a single chip. Historically, the most common way for the implementation of neural networks has been a program running on a personal computer or a workstation. This is due to the fact that software implementations offer a high flexibility and give the users the possibility of modifying the topology of the network, the type of the processing elements or the learning rules, according to the requirements of their application. However, biological neural networks, in which artificial neural networks are inspired, operate highly in parallel. Hence, implementing them on a sequential computer does not seem the most efficient way to do it.

Dedicated hardware implementations, on the other hand, offer a number of important advantages, because they exploit the inherent parallelism of neural networks and also are much faster and robust if compared to software solutions.

Furthermore, they provide a physically reduced and low-power solution, useful for applications where including a personal computer or a workstation might not be feasible (such as the case of autonomous robots). These are the main reasons why it has been decided to implement the recognition algorithms on an embedded system and, more specifically, the neural network on the hardware partition of the system.

The architecture is as shown in Figure3..

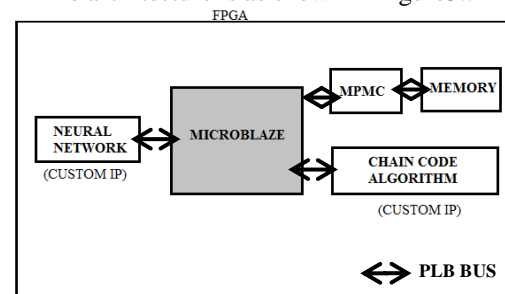


Figure 3: Internal Architecture of SoPC

The software partition is built on a MicroBlaze (the softcore processor from Xilinx) [10] and includes the control of the complete system and, also the image pre-processing algorithms.

3.1. INTERFACE BETWEEN MODULES

The interface between both partitions is based on the PLB (Processor Local Bus) bus [11], that provides a fast and efficient communication mechanism. The Processor Local Bus (PLB) consists of a bus control unit, a watchdog timer, and separate address, write and read data path units with a three-cycle-only arbitration feature. The PLB supports read and write data transfers between master and slave devices equipped with a PLB bus interface and connected through PLB signals. Bus architecture supports multiple master and slave devices. Each PLB master is attached to the PLB through separate address, read-data,

and write-data buses. PLB slaves are attached to the PLB through shared, but decoupled, address, read-data, and write-data buses and a plurality of transfer control and status signals for each data bus.

The Processor Local Bus (PLB) consists of a bus control unit, a watchdog timer, and separate address, write and read data path units with a three-cycle-only arbitration feature. The PLB supports read and write data transfers between master and slave devices equipped with a PLB bus interface and connected through PLB signals. Bus architecture supports multiple master and slave devices. Each PLB master is attached to the PLB through separate address, read-data, and write-data buses. PLB slaves are attached to the PLB through shared, but decoupled, address, read-data, and write-data buses and a plurality of transfer control and status signals for each data bus.

Access to the PLB is granted through a central arbitration mechanism that allows masters to compete for bus ownership. This arbitration mechanism is flexible enough to provide for the implementation of various priority schemes. Additionally, an arbitration locking mechanism is provided to support master-driven atomic operations. PLB arbiters can be implemented on the FPGA fabric and are available as soft IP cores. The PLB is a fully synchronous bus.

The PLB arbiter multiplexes signals from masters onto a shared bus to which all the inputs of the slaves are connected. The PLB arbiter handles bus arbitration and the movement of data and control signals between masters and slaves. The PLB-to-PLB bridge is required when two PLB segments are connected. The bridge translates PLB transactions on one side into the PLB transactions of the other side. The bridge functions as a slave on one PLB side and a master on the other. For a typical system with two PLB segments, one bridge is necessary for transactions originating from the processor. A second bridge is required if a peripheral on the other side is master capable and wants to address a peripheral on the processor side. Figure 4 provides an example of the PLB connections for a system with three masters and three slaves.

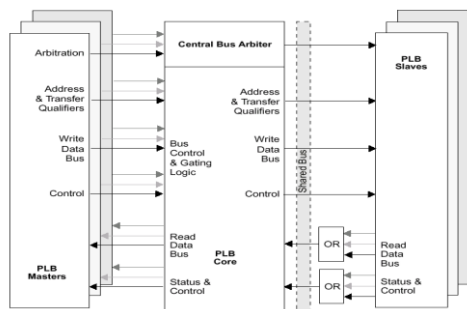


Figure 4: PLB Interconnection Diagram

3.2 ARCHITECTURE OF THE NEURAL NETWORK

The architecture of the network is the one presented in Figure 2. In a hardware implemented neural network, the processing elements (i.e., neurons) have to be independent and operate in parallel. They should be designed in such a way that their internal calculations are optimized, while they should be so simple that the chip area occupied by them is the minimum possible. Following these requirements, a very small but high performance system can be achieved.

The architecture proposed in this paper comprises the following modules.

- A two-layer processing module: the hidden layer and the output layer (the input layer merely transmits the inputs)
- Three ROM modules, which store the network parameters (weights) for the hidden layer, the output layer and the sigmoid function, respectively.
- Additional components, such as a multiplexer and a block that calculates the maximum of its inputs.
- A circuit controller that governs the whole operation of the system.

The main component of the processing module is the neuron, which is just a MAC (multiply-accumulate) block. The MAC is loaded with an initial value (offset or bias) and then multiplies each input with its corresponding weight and accumulates these values to obtain the sum of all them. It is a two-cycle synchronous component (see Figure 5). The total number of these MAC blocks is 36 (32 for the hidden layer and 4 for the output layer).

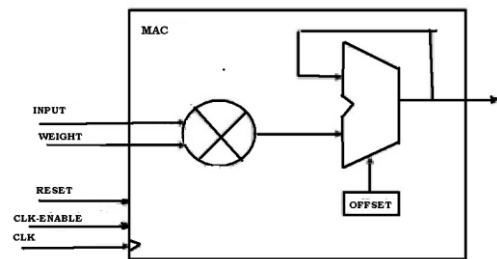


Figure 5: MAC schematic. .

As for the ROM modules, the one that contains the weights of the first layer (ROM1) has a size of 512 weights with a word length of 12 bits, whilst the one corresponding to the second layer (ROM2) contains 128 weights of a word length of 8 bits. ROM1 is organized in 16 blocks of 32 weights, so that for each of the inputs the corresponding block of 32 weights is addressed and sent to the first layer of neurons. In the same way, ROM2 is divided into 32 blocks of 4 weights each. Finally, ROM3 is the memory that stores the pre-computed sigmoid function and contains 256 values with a word length of 8 bits.

The system controller, whose main component is a six-bit counter, provides the control signals for the whole system. Such signals are the reset signals for all the modules, the signals to enable each block, the address signals for ROM1 and ROM2 and the selection signal for the multiplexer.

The detailed operation of the whole system is described next. The 16 input data come serially through the PLB bus. Each neuron (MAC block) receives the inputs serially, multiplies each of them with the corresponding weight (stored in the ROM1 memory) and adds them up. The neuron needs only one clock cycle per input to process the MAC operation, because while the accumulate operation is being done, the next data are already being multiplied, creating a pipeline. Furthermore, the 32 neurons of the layer work in parallel. Hence, only 17 clock cycles (one for each input and one more for the first data, before starting the pipeline operation) are needed to perform the calculations of the first layer, in spite of the fact that the inputs enter the system serially.

REFERENCES

Once the outputs of the first layer are available, they are used to address ROM3, which contains the activation function. This memory is the same for all the neurons of the first layer. The outputs of this block are the sigmoid functions of their inputs. All the accesses to the ROM3 are made in parallel, so just a clock cycle is required. This ROM module provides 32 outputs that act as the inputs to a 32 to 1 multiplexer. The multiplexer makes it possible for the inputs to the following layer of neurons to arrive serially, in such a way that this layer would work like the first one. Thus, each of the 4 neurons of the last layer receives the 32 incoming data serially and performs the MAC operation, needing 33 clock cycles to finish this task (one for each input and an additional one, as in the previous layer).

Finally, the result of these MAC operations are carried to a module that calculates which of them has the maximum value, needing only one cycle to do so. The output of this module represents the shape recognized by the network, codified in 2 bits. This data is sent back to the software partition through the PLB bus.

The final output showing the recognition of four basic shapes is as shown in Figure 6, which is obtained using the Chipscope Pro tool.

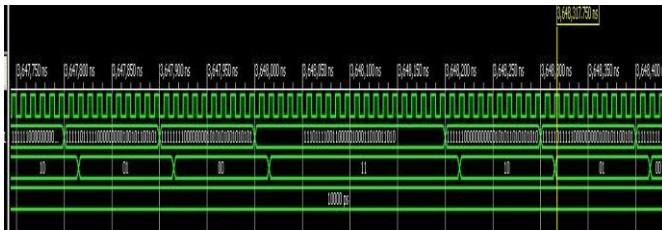


Figure 6: Results showing the recognition of four basic shapes

IV. CONCLUSION AND FUTURE SCOPE

In this paper a prototype of a vision system for a robotic platform to assist in manipulation activities has been presented. An FPGA module for embedding the object recognition module within a robotic mobile platform is being designed. The FPGA module includes the neural network and the control and the image processing modules are built on a Microblaze. More work will be done to strengthen the overall performance of this system, taking into account more variability in object shape and colour (real objects). Up to now, the FPGA module includes the implementation of the neural network. As further work, the rest of the image processing algorithms should also be implemented on the chip. They would be included preferably on the hardware partition of the SoPC for performance reasons, but to do so, a previous analysis has to be made in order to study the feasibility of this option. In addition, the whole system has to be integrated with the robotic platform in order to perform the manipulation activities.

ACKNOWLEDGEMENT

We would like to express my sincere gratitude to the Principal, Head of the department, all teaching and non teaching staffs of Electronics and Communication department of TKMIT for their guidance and valuable suggestions for the successful completion of this paper.

- [1] Maria Isabel de la Fuente¹, Javier Echanobe², Inés del Campo², Loreto Susperregui¹, Iñaki Maurtua, Hardware implementation of a Neural-Network Recognition module for Visual Servoing in a Mobile Robot. *Proceedings of the 6th International Conference on Hybrid Intelligent Systems (HISá10)*, Auckland, New Zealand, Pages 226-232, November 2010.
- [2] Wells G., Venaille C., Torrassa C., *Vision-based robot positioning using Neural Networks, Image and Vision Computing*, Elsevier B.V., Volume 14, Issue 10, December 1996, Pages 715-732.
- [3] Mutlu Avcý, Tulay Yýldýrým, "Generation of Tangent Hyperbolic Sigmoid Function for Microcontroller Based Digital Implementation of Neural Networks", *International XII. Turkish Symposium on Artificial Intelligence and Neural Networks, 2003*.
- [4] Nasri Sulaiman, Zeyad Assi Obaid, M. H. Marhaban and M. N. Hamidon Design and Implementation of FPGA-Based Systems - A Review *Malaysia, 43400 UPM Serdang*, Selangor Darul Ehsan, Malaysia.
- [5] Haitham Kareem Ali and Esraa Zeki Mohammed, Design Artificial Neural Network Using FPGA, *IJCSNS International Journal of Computer Science and Network Security*, VOL.10 No.8, August 2010.
- [6] Walid Shahab, Hazem Al-Otum, and Farouq Al-Ghoul, A Modified 2D Chain Code Algorithm for Object Segmentation and Contour Tracing, *The International Arab Journal of Information Technology*, Vol. 6, No. 3, July 2009.
- [7] Freeman H, On the encoding of arbitrary geometric configurations. *IRE transactions on Electronic computers*.
- [8] Omondi A. R., Rajapakse J. C. (Eds.), *FPGA Implementations of Neural Networks*, (Springer, 2006.)
- [9] Demuth H., Beale M., Hagan M., *Neural Network Toolbox 6 User's Guide*, 2010, The MathWorks, Inc.
- [10] *MicroBlaze™ RISC 32-Bit Soft Processor User Guide*, Product Brief, August 21, 2002 Xilinx
- [11] *Processor Local Bus User Guide*, Product Brief, August 21, 2002 Xilinx

Effect of Titanium Oxide Coating on Performance Characteristics of Bio-Diesel (Honge) Fuelled C.I.Engine

Naveen. P¹, C.R. Rajashekhar², C. Umashankar³ & Vinayaka Rajashekhar Kiragi⁴

^{1,4} (P.G. Student, Thermal Power Engg, Dept of Mech Engg, Sri Siddhartha Institute of Technology, Tumkur, Karnataka, 2

(Professor, Dept of Mech Engg, Sri Siddhartha Institute of Technology, Tumkur, India

³ (Professor, Dept of OR & SQC, Rayalaseema University, Kurnool, A.P, India

Abstract: This paper presents the effect of Titanium oxide coating on the performance characteristics of the bio-diesel fuelled engine. The engine used was four strokes, single cylinder direct injected diesel engine. The engine was tested with diesel & at different proportionality of diesel with Honge bio-diesel and by varying torque without coating. Then, the piston head was coated with thermal barrier material. The layer of thermal coating was made of Alumina-Titanium oxide (Al_2O_3/TiO_2) plasma coated on to the base of NiCrAl. Then the coated piston was tested at the same operation conditions as the standard (without coating) engine. The results indicate a reduction in specific fuel consumption and an improved brake thermal efficiency for titanium oxide coated piston.

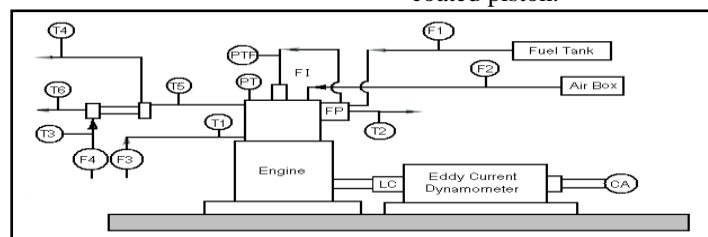
Keywords- Bio-diesel, Performance characteristics, Thermal barrier coating, Titanium Oxide

I. INTRODUCTION

Thermal barrier coatings have been apply to the internal combustion engine in particular the combustion chamber and cylinder lands to act as a low heat rejection engine, heat engine is improvement of their thermal efficiency. One of the methods to an engine is to cover the surface of the combustion chamber with a thermal barrier coatings, the thermal insulation obtained leads to an development of engines heat efficiency and a reduction in consumption. High temperature in the combustion can have a positive effect in diesel engines due to reduction in delay and hardness of engine operation, all though an increasing the emission of NO_x .

The resources of petroleum as fuel are dwindling day by day and increasing demand of fuels, as well as increasingly stringent regulations, pose a challenge to science and technology. With the commercialization of bioenergy (bio-diesel), it has provided an effective way to fight against the problem of petroleum scarce and the influence on environment. Bio-diesel can be used in diesel engine with little or no modification in the engine [1]. The properties of bio-diesels are not same as diesel as it is having high viscosity, high volatility and Low cetane number [2]. In order to improve the combustion, there should be minimum heat loss from the combustion chamber. Minimum heat loss can be achieved by coating thermally insulated materials to the surfaces of combustion chamber. Mohd.F.Shabir, P. Tamilporai, and B. Rajendra Prasath used low heat rejection engine by coating the piston crown, cylinder head inside with valves and cylinder liner with partially stabilized zirconia coating of 0.5 mm thickness [3]. Imdat Taymaz used thermally insulated material such as $CaZrO_3$ and $MgZrO_3$ for insulation of different surfaces of combustion chamber. An improvement of efficiency of 2-5% was observed [4]. Abdullah Uzun used $CaZrO_3$ on cylinder head and valves and $MgZrO_3$ on piston. Thermal efficiency was improved by 10% and reduction of CO emission was 35 to 40% [5].

The purpose of this study is to evaluate the brake thermal efficiency and brake specific fuel consumption at different loads with and without thermal barrier coating. The experiments were conducted with a single cylinder, four stroke and direct injected diesel engine. The results showed an increase in brake thermal efficiency, decrease in brake specific fuel consumption for titanium oxide coated piston.



<p>PTF : Fuel Injection Pressure Sensor</p> <p>Calorimeter</p> <p>F2 : Air Flow Rate</p> <p>Calorimeter</p> <p>PT : Combustion Chamber Pressure Sensor</p> <p>FI : Fuel Injector</p> <p>FP : Fuel Pump</p> <p>T1 : Jacket Water Inlet Temperature</p> <p>T2 : Jacket Water Outlet Temperature</p>	<p>T5 : Exhaust Gas Temperature before</p> <p>T6 : Exhaust Gas Temperature after</p> <p>F1 : Liquid fuel flow rate</p> <p>F3 : Jacket water flow rate</p> <p>F4 : Calorimeter water flow rate</p> <p>LC : Load Cell</p> <p>CA : Crank Angle Encoder</p>
--	--

T3 : Inlet Water Temperature at Calorimeter

EGC: Exhaust Gas Calorimeter

T4 : Outlet Water Temperature at Calorimeter

FIG 1: Schematic diagram of experimental set up

II. EXPERIMENTAL WORK

A four stroke, direct injected single cylinder diesel engine was used for experimentation (Table 1). The schematic experimental set up is shown in Fig 1. Engine torque was measured by eddy current dynamometer. The engine has a conventional fuel injection system. A piezoelectric pressure transducer was mounted with cylinder head surface to measure the in cylinder pressure. It is also provided with temperature sensors for the measurement of jacket water, calorimeter water, and calorimeter exhaust gas inlet and outlet temperatures. An encoder is fixed for crank angle record. The signals from these sensors are interfaced with a computer to an engine indicator to display P-θ, P-V, mass fraction burnt and heat release versus crank angle plots. The provision is also made for the measurement of volumetric fuel flow. The built in program in the system calculates indicated power, brake power, thermal efficiency, volumetric efficiency and heat balance. The software package is fully configurable and averaged P-θ diagram, P-V plot and other diagram can be obtained for various operating conditions.

First, standard piston (without coating) was tested. The tests were performed at different loads and for diesel and different proportionality of diesel with Honge bio-diesel (i.e. B10, B20 and B30) for a compression ratio of 17.5:1 and injection pressure of 200 bar.

Then the Piston head was coated with thermal barrier material. The piston head was coated with a 150µm Alumina-Titanium oxide (Al₂O₃/TiO₂) plasma coated on to the base of 60µm NiCrAl. Then the coated piston was tested at the same operation conditions as the standard (without coating) piston.

TABLE 1: ENGINE SPECIFICATION

SL NO	ENGINE PARAMETERS	SPECIFICATION
01	Engine Type	TV1(Kirloskar)
02	Number of cylinders	Single Cylinder
03	Number of strokes	Four-Stroke
04	Rated power	5.2KW (7 HP) @1500RPM
05	Bore	87.5mm
06	Stroke	110mm
07	Cubic Capacity	661cc
08	Compression ratio	17.5:1
09	Rated Speed	1500 RPM

III. RESULTS AND DISCUSSION

3.1 Brake thermal efficiency:

The comparison charts for brake thermal efficiency with respect to brake power for coated piston and base piston for diesel and various biodiesel blends are plotted as shown in figures 2 to 5.

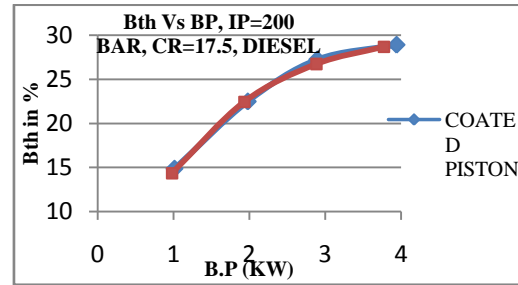


FIG 2: Bth Vs B.P for Diesel

Fig 2 shows the variation of Bth with Brake power for Diesel for coated piston and base piston. We can see that as the load increases the Bth also increases. In the above fig we don't find much difference only a slight increase in the Bth for the coated piston. This is because of the titanium oxide which acts as catalyst to enhance the combustion and also due to the thermal barrier coating which heat transfer. And hence the Bth of the coated piston is better than base piston.

Fig 3 shows the variation of Bth with Brake power for H10 (i.e. 10% Honge+ 90% Diesel) for coated piston and base piston. We can observe from the graph that the Bth of the coated piston is high when compared to standard piston. Maximum efficiency was found to be around 27% at high load for coated piston.

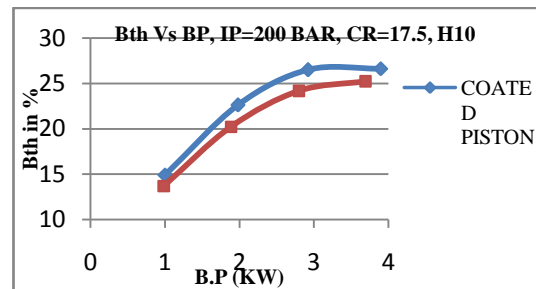


FIG 3: Bth Vs B.P for H10

Fig 4 shows the variation of Bth with Brake power for H20 (i.e. 20% Honge + 80% Diesel) for coated piston and base piston. From the graph we can see that the Brake thermal efficiency of the coated piston is high. Maximum efficiency was found to be around 28% at high load for coated piston.

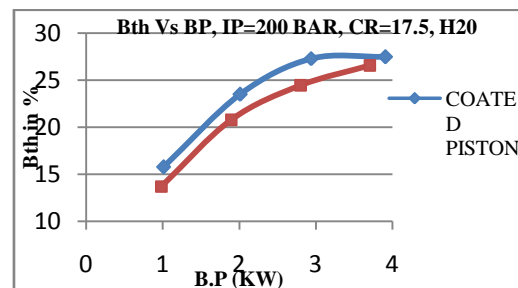


FIG 4: Bth Vs B.P for H20

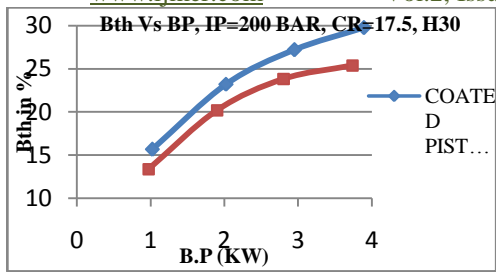


FIG 5: Bth Vs B.P for H30

Fig 5 shows the variation of Bth Vs B.P for H30 (i.e. 30% Honge+70% Diesel) for coated piston and base piston. In fig 5 we can see that the Bth for coated piston is high.

FIG 2 to 5 shows the variation of Brake thermal efficiency with Brake Power for Diesel, H10, H20 and H30 for coated piston and base piston. It is observed from all the above graphs that the Bth for coated piston for all fuels is high. This may be due to the high temperature in the combustion chamber due to the thermal resistance of the coated piston where heat loss is minimal. It may be also because of percentage of titanium oxide which acts as catalyst to enhance the combustion and hence efficiency of coated piston is high for all the fuels.

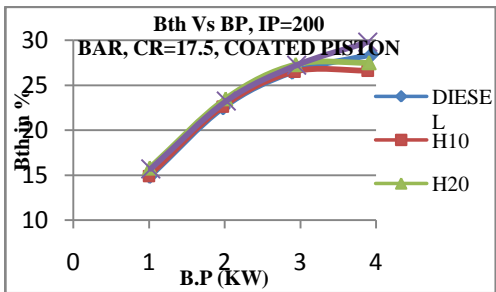


FIG 6: Bth Vs BP for Coated Piston

Fig 6 shows the variation of the Bth with Brake Power for coated piston for different fuels. It is observed from the graph that we don't find much difference only slight variation in the Bth for H30 than the other biodiesel blends and pure diesel. Only at high loads we can find the clear difference. This is because of the increased oxygen content in H30 fuel which accounts for better combustion and also due to decrease in fuel consumption. It may be also because of high temperature reached in combustion chamber due to minimal heat loss which accounts for better combustion.

3.2 Brake Specific Fuel Consumption:

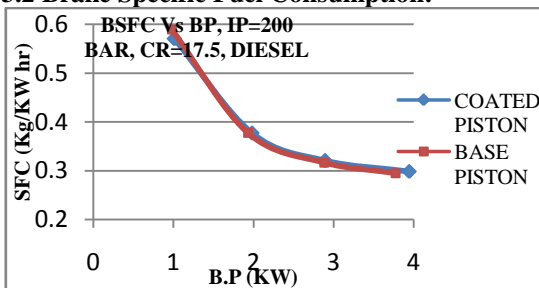


FIG 7: BSFC Vs BP for Diesel

Fig 7 shows the graph of B.S.F.C Vs B.P for coated pistons and base piston for Diesel fuel. In the

graph we don't find much difference between the SFC of coated piston and base piston for diesel.

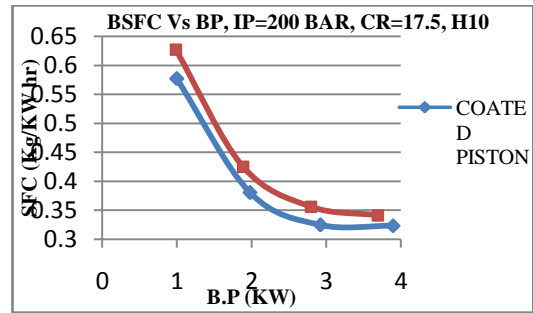


FIG 8: BSFC Vs BP for H10

Fig 8 shows the graph of B.S.F.C Vs B.P for coated piston and base piston for H10 fuel. In the graph we can see that the SFC for coated piston is low when compared to base piston.

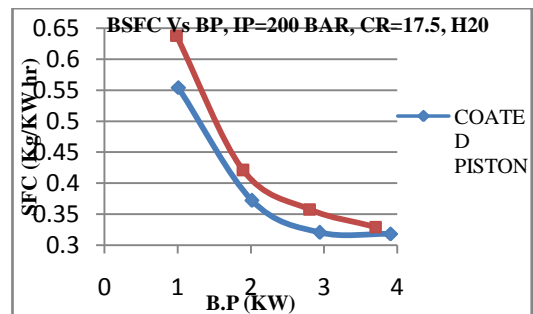


FIG 9: BSFC Vs BP for H20

Fig 9 shows the graph of B.S.F.C Vs B.P for coated pistons and base piston for H20 fuel. In the graph we observe that the SFC for coated piston is less than that of the base piston.

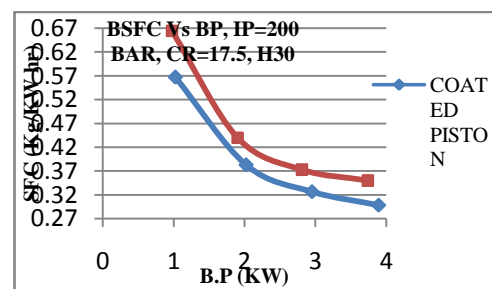


FIG 10: BSFC Vs BP for H30

Fig 10 shows the graph of B.S.F.C Vs B.P for coated piston and base piston for H30 fuel. In the graph we see that the SFC for coated piston is low than the base piston.

FIG 7 to 10 shows the variation of Brake specific fuel consumption with Brake Power for Diesel, H10, H20 and H30. We can observe from the above graphs that the S.F.C for coated piston for all the fuels is low when compared to base piston. This is because of better combustion of the fuel due to high temperature in combustion chamber because of thermal resistant due to the coated material and also due to composition of titanium oxide which acts as catalyst to enhance combustion and thus reduces the fuel consumption for titanium oxide coated piston.

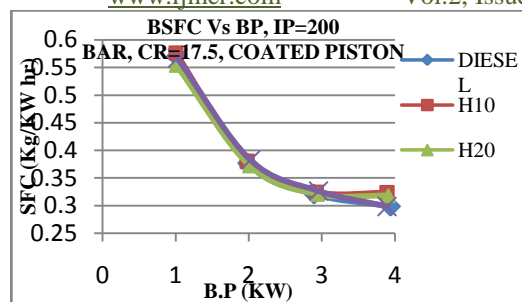


FIG 11: BSFC Vs BP for Coated Piston

Fig 11 shows the variation of B.S.F.C with B.P for coated piston for different fuels. We can't find much difference only a slight variation can be observed from the graph that the S.F.C for H20 gives good result but at high load H30 gives good result for coated piston.

IV. CONCLUSION

Experimental investigations of the effect of the titanium oxide coating on performance characteristics was conducted on single cylinder, 4 stroke, direct injected, constant speed diesel engine. Tests were conducted for the base piston and coated piston for different loads and compression ratio of 17.5 and injection pressure of 200 bar. The major conclusions drawn from these experiments are as follows:

1. The Brake thermal efficiency of the coated piston is increased when compared to base piston. Also biodiesel H30 giving higher thermal efficiency when compared to other biodiesel blends and pure diesel.
2. The Specific fuel consumption is lower for the coated piston when compared to base piston. Biodiesel blend H30 at high loads and blend H20 giving better results at low loads.

REFERENCES

- [1] A. Dufey, *Biofuels production, trade and sustainable development: emerging issues. Environment Report*, International Institute for Environment and Development (IIED), London, UK, November 22, 2006.
- [2] K. Sureshkumar and R. Velra "Performance and Characteristics Study of the Use of Environment Friendly Pongamia Pinnata Methyl Ester in C. I. Engines" *Journal of Energy & Environment*, Vol. 5, May 2007.

- [3] Mohd.F.Shabir, P. Tamilporai, and B. Rajendra Prasath "Analysis of Combustion, Performance and Emission Characteristics of Turbocharged LHR Extended Expansion DI Diesel Engine" *International Journal of Aerospace and Mechanical Engineering* 5:2 2011.
- [4] Imdat Taymaz "The effect of thermal barrier coatings on diesel engine performance" *Surface and Coatings Technology* 201 (2007) 5249-5252.
- [5] Abdullah Uzun, Ismet Cevik and Mustafa Akcil "Effects of thermal barrier coating on a turbocharged diesel engine performance" *Surface and Coatings Technology* 116-1199(1999) 505-507.
- [6] M.Mohamed Musthafa, S.P. Sivapirakasam and M.Udaya kumar "Performance and Emission Characteristics of LHR CI Engine Fueled with Rice bran oil as Biodiesel" *International Journal of Recent Trends in Engineering and Technology*, Vol. 3, No. 6, May 2010.

A method for signalling block-adaptive quantization in baseline sequential JPEG

B. Aruna¹, Ch. Ramesh²

¹(M.Tech) AITAM (INDIA)

²(Professor) AITAM (INDIA)

Abstract: The traditional JPEG compression standard doesn't have a means for spatially-variable quantization of transform coefficients. This prevents important features such as region-of-interest (ROI) coding. In this paper, we show how the quantization may be adapted in each block and how we may signal to the decoder in a memory-efficient manner. This allows ROI coding of subject and background. The method takes advantage of unused slots in the Huffman tables. In this paper we show how the encoder may be modified to produce an output that is in compliant with the standard and how the decoder may be modified to correctly recover the adaptively quantized image. Also we show how to use adaptive quantization as a means to perform spatially adaptive filtering of the image.

I. Introduction

The JPEG standard [1], relies on method of separating an image into chrominance and luminance color planes, each plane is partitioned into 8×8 blocks and which are compressed using quantization of discrete cosine transform (DCT) coefficients. The compression is achieved by applying the quantization (Q) matrix, to each set of DCT coefficients. The Q matrix may be varied from image to image and also different Q matrices may be used for the luminance and chrominance color planes. However, the Q matrix must not change within a color plane, i.e., spatially-variable quantization is not allowed in JPEG. This prevents the encoder from varying the quantization within an image or quantizing subject information and background information in image separately to achieve ROI coding and also to get desired output file size. These important features are not available in JPEG standard. If we implement these features in baseline JPEG, then it would lead to useful and significant changes in old JPEG standard.

In this paper we demonstrated a method, of varying the quantization matrix from block to block, and described the signaling of adaptive quantization to the decoder in a way that is compliant with the JPEG standard. To recover the exact image by Adaptive quantization, the decoder should vary the Q matrix exactly as the encoder, over the image. After Adaptive Quantization the encoder must signal to the decoder on each block which Q matrix that it used, also the signalling must be compliant with the JPEG standard if any "standard" decoder is able to process the adaptively-quantized image. Huffman table in JPEG standard has few unused slots for end-of-block(EOB) symbols. Our method has taken advantage of those unused slots for end-of-block (EOB) symbols in the Huffman table. This allow us to signal up to 14 different levels of quantization within a color plane. standard decoder treats all 14 EOB symbols as the same. However, to recover image that is Adaptively Quantized we need to modify the decoder in a way that it recognizes the EOB symbol and modify the

decoding Q matrix appropriately. The modification demonstrated below is simple. There is no need for the encoder or the decoder to keep more than one block in memory at a time, as the EOB symbols by definition come as the end of a 8×8 block, This important factor plays a crucial role in hardware design of encoders and decoders, as memory consumes a large amount of chip area in embedded cameras. Adaptive quantization within JPEG has been a subject of interest since it was published. Different methods for signalling the adaptation have been proposed. one method searches up to 64 coefficients in a 8×8 block to find the coefficient whose quantized value, whose fractional portion, is closest to 0.5, for example, a fractional value of 10.499 may be rounded to either 10 or 11 approximately with the same error. Sum of quantized coefficients can be made either even or odd by rounding up or down, and the parity of the sum therefore becomes a method of signalling one of two possible Q matrices to the decoder. However, the scheme requires a search to be carried out prior to quantization, and does not extend to more than two Q matrices which might not help in all cases. [5][11]. Since the JPEG standard allows any number of color planes to be stored in the output file, Pennebaker [2] proposed to use an extra "color" plane whose purpose is to contain a spatial map of how the quantization matrices are varied but this requires that the decoder reads more than one color plane at a time to vary the Q matrix appropriately. Few other methods use rate-distortion based thresholding of DCT coefficients. These proposed methods are not suitable for embedded applications. In this paper we show how previously unused slots in the baseline JPEG Huffman table may be used to signal Q matrix adaptation. This allow us to signal up to 14 different EOB codes to be used on each block. In this paper we described the method to construct the Huffman codes to efficiently encode the adaptively-quantized image. We also show how it is compatible with the baseline sequential JPEG standard, so that any standard decoder may decode the adaptively quantized image.

II. Background

Baseline sequential and progressive are two compression formats available in JPEG. The baseline format stores the full resolution of the image in a single sequential scan and it is universally adopted on the other hand progressive format stores several scans of the image. In progressive format each scan has increased resolution over the previous scan. Progressive JPEG is not widely used. In JPEG standard Huffman table is designed to accommodate both progressive and baseline sequential formats. This nature allow us to modify the feature of progressive format to allow signalling of adaptive quantization in baseline sequential format. The below method describes the

operation of baseline sequential JPEG compression of a color image.

- 1) The image is converted from RGB to YCbCr, usually followed by sub-sampling of the Cb, Cr planes.
- 2) Each of the Y, Cb, Cr planes are partitioned into blocks of size 8×8 .
- 3) The DCT of each 8×8 block is calculated. Let $x(i, j)$ denote the (i, j) -th pixel in block, and $X(u, v)$ the (u, v) -th frequency in the DCT and $X(1, 1)$ is the "DC" coefficient, and remaining are "AC" coefficients. The quantization of DCT coefficients using a 8×8 matrix Q as follows:

$$X_Q(u, v) = \text{round} \left\{ \frac{X(u, v)}{Q(u, v)} \right\} \quad u, v = 1, \dots, 8. \quad \dots(1)$$

Y, Cb, Cr planes may have different Q matrices but they do not vary spatially.

- 4) The quantized block X_Q is scanned in "zig-zag" order. DC value of the previously coded block is subtracted from the quantized DC coefficient and then it is stored. The scan of AC coefficients is stored in (R, S) format, where R is the number of consecutive zeros followed by the non-negative value S indicating the size of the next non-zero value. If V is the value of the quantized coefficient, then $S = \log_2[|V|] + 1$... (2)

Here $[.]$ is the floor function also two special symbols are also allowed

- 1). a ZRL symbol represents a run of 16 consecutive zeros.
- 2). EOB symbol indicates and represent that all subsequent coefficients in the scan are zero.
- 5) Each scan is Huffman coded, where AC coefficients are organized as a 16×11 structure in the Huffman table. This structure is designed to accommodate 16 different R values and 11 values of S. This structure is shown in table I. The Huffman code for each (R, S) pair in a scan is emitted, followed by S additional bits to indicate the actual value of the coefficient.

TABLE I
 HUFFMAN TABLE LAYOUT FOR AC COEFFICIENTS IN BASELINE SEQUENTIAL MODE. ENTRIES MARKED "X" CONTAIN CODES FOR OTHER VALUES.

R \ S	0	1	2	...	9	10
0	EOB	x	x	x	x	x
1	Not used	x	x	x	x	x
⋮	Not used	x	x	x	x	x
14	Not used	x	x	x	x	x
15	ZRL	x	x	x	x	x

From Table I slot for $R = 0, S = 0$ is used for the EOB symbol, while $R = 15, S = 0$ indicates 15 consecutive zeros followed by a size 0 (ZRL symbol) but the slots for $S = 0$ and $R = 1$ to 14 are reserved for the progressive format and are not used in baseline sequential format. We utilized those unused slots for signalling adaptive quantization to decoder thus making it JPEG standard-compliant..

In JPEG standard if $S = 0$ and $R = 15$ then 16 consecutive zeros are appended to the zig-zag scan in reconstruction. Otherwise the symbol is treated an EOB. all slots in Table I with $S = 0$ and $R < 15$ are considered to be the same EOB symbol. Therefore, additional codes for different conditions may adopted by using the 14 unused slots in Table I.

III. Quantization

In the Quantization, The Q matrix is fixed across the color plane. This limits the possibilities of ROI coding. We have overcome the limitation by signalling to the decoder with proper EOB codes exploiting the unused slots in Huffman table, to say which Q was used. But if we use a standard decoder then it dequantizes an input block with a improper Q matrix. Suppose that the DCT of an 8×8 block, $X(u, v), 1 \leq u, v \leq 8$, is quantized at the encoder using matrix Q as in eq.(1). At the decoder, the quantized matrix X_Q is used to reconstruct the DCT matrix X using the equation

$$\hat{x}(u, v) = Q(u, v)X_Q(u, v), \quad u, v = 1, \dots, 8. \quad \dots(3)$$

\hat{x} will not the same as X due to rounding. If we let $P = \alpha Q$, where α is a scale factor, then the effect of dequantizing X_Q with P instead of Q is as follows:

$$\begin{aligned} \tilde{X} &= P(u, v)X_Q(u, v) \\ &= \alpha Q(u, v) \text{round} \left\{ \frac{X(u, v)}{Q(u, v)} \right\} \\ &= \alpha X(u, v) + \alpha \text{Eq}(u, v) \end{aligned} \quad \dots(4)$$

where $\text{Eq} = Q \text{round}\{X_Q/Q\} - X$ is the quantization error introduced by rounding.

If we apply $P = \alpha Q$, we can see that scaling factor is same for every element instead if we choose $P = H \circ Q$, where \circ denotes the elementwise product of H and Q. Here H acts as filtering matrix.

$$\tilde{x}(u, v) = H(u, v)X(u, v) + H(u, v)\text{Eq}(u, v) \quad \dots(5)$$

we see that dequantization with $H \circ Q$ is equivalent to filtering by H in the DCT domain ignoring the noise term. We may therefore use adaptive quantization as a means to perform spatially adaptive filtering of the image.

A. DC coding and Prediction

Adaptive quantization is the dependent on adjacent blocks,. After quantization, the DC coefficient in baseline sequential JPEG is treated separately from the 63 AC coefficients. The DC coefficient is a measure of the average value of the 64 image samples. Because there is usually strong correlation between the DC coefficients of adjacent 8×8 blocks, the quantized DC coefficient is encoded as the difference from the DC term of the previous block in the encoding order as shown in Figure 3. This may lead to complications. If adaptive quantization is used, prediction will accumulate error when the DC coefficient is dequantized differently than it was quantized. The DC coefficient is unique in this respect: all other coefficients in a block are coded independently of adjacent blocks and therefore varying the Q matrix has no effect. We therefore constrain the quantization change matrix H discussed above so that $H(1, 1) = 1$, which ensures that $eX(1, 1) = X(1, 1) + \text{Eq}(1, 1)$.

B. Reduction of artifacts

Adaptive quantization may be applied to remove few JPEG compression artifacts:

- 1) visible boundaries between 8×8 blocks
- 2) ringing around edges (Gibbs phenomenon) .

For example we may apply a "larger" matrix Q2 for edge blocks and "smaller" matrix Q1 for smooth blocks,.we can determine smooth vs edge blocks by observing the occurrence of last non-zero coefficient early or late in a zig-

zag scan compared to a threshold. From above we get $Q2(u, v) > Q1(u, v)$.

IV. Huffman Table Modification

we must modify the entire Huffman codebook to allow for unique decoding . this allow us to use the empty slots in the Huffman table to signal adaptive quantization to the decoder. One method is to substitute a Huffman table for progressive coding in place of the baseline table. This allows us to signal 15 different Q matrices to the decoder. Standard progressive table is shown in Table II. We may or may not use all the empty slots , so we can design Huffman table to support fewer EOB codes.

TABLE II
 HUFFMAN TABLE LAYOUT FOR PROGRESSIVE ENCODING

R \ S	0	1	2	...	9	10
0	EOB0	x	x	x	x	x
1	EOB1	x	x	x	x	x
⋮	⋮	x	x	x	x	x
14	EOB14	x	x	x	x	x
15	ZRL	x	x	x	x	x

V. EXPERIMENTAL RESULTS

We used the EOB signalling method to apply adaptive quantization on gray scale image. We used two levels of quantization on the luminance (Y) component of the image.MATLAB was used as the programming platform.



VI. Conclusion

In this paper, we demonstrated a simple method for signalling adaptive quantization to the decoder, using the empty slots in standard baseline Huffman table. The proposed method is efficient as encoder and decoder do not require to keep more than one block in memory at a time. A standard decoder will treat all EOB codes as the same, and if adaptive quantization is performed, will perform frequency-domain filtering upon dequantization. This is useful for ROI coding. which has the advantage of improving image quality in selected regions.

References

- [1] G. K. Wallace, "The JPEG still picture compression standard," IEEE transactions on consumer electronics, Vol. 38, No. 1, Feb. 1992, pp xviii-xxxiv.
- [2] W. B. Pennebaker, "Adaptive quantization within the JPEG sequential mode," U. S. Patent 5,157,488.
- [3] A. M. Silverstein and S. A. Klein, "Precomputing and encoding compressed image enhancement instructions," U. S. Patent 5,822,458.
- [4] R. Kakarala and J. S. Gibson, "Signaling adaptive-quantization matrices in JPEG using end-of-block codes", U. S. Patent 7,092,578.
- [5] T. A. Simpson and Y. Hu, "Adaptive image data compression", U. S. Patent 6,724,817.
- [6] W. B. Pennebaker and J. L. Mitchell, JPEG: Still Image Data Compression Standard, New York: Springer-Verlag, 1992.
- [7] M. Stirner and G. Seelman, "Improved redundancy reduction for JPEG files", Proc. of the Picture Coding Symposium (PCS 2007), Lisbon, Portugal: November 2007.
- [8] S. K. Mitra, Digital signal processing: A computer-based approach, 3rd Ed, New York : McGraw-Hill, 2006.
- [9] R. A. Gonzalez and R. E. Woods, Digital image processing, 1st Ed, Reading, MA: Addison-Wesley, 2002.
- [10] J. Zhao and Y. Shimazu and K. Ohta and R. Hayasaka and Y. Matsushita, "A JPEG codec adaptive to region importance". In Proceedings of the Fourth ACM international Conference on Multimedia Boston, MA: November 18 - 22, 1996, pp 209-218.
- [11] K. Ramchandran and M. Vetterli, "Rate-distortion optimal fast thresholding with complete JPEG/MPEG decoder compatibility", IEEE Transactions on image processing, Vol. 3, No. 5, Sept. 1994, pp 700-704.
- [12] G. Lakhani and V. Ayyagari, "Improved Huffman code tables for JPEG's encoder", IEEE Transactions on circuits and systems for video technology, Vol. 5, No. 6, Dec. 1995, pp 562-564.
- [13] G. Lakhani, "Modified JPEG Huffman coding", IEEE Transactions on image processing, Vol. 12, No. 2, pp 159- 169.

Determination of the test frequency causing significant hearing loss of the mine workers of an open cast chromite mine

Kerketta S.¹, Gartia R.², Bagh S.²

¹Ministry of Environment and Forests, ERO, Bhubaneswar, Odisha – 751 023, India, ²Statistics Department, Sambalpur University, Odisha – 768 019, India

Abstract: In this paper an attempt has been made to estimate the hearing loss of workmen (subjects) in an open cast chromite mines with respect to age, working experience and work stations. The study reveals that there is a significant difference among the different test frequencies with respect to hearing loss on both the ears of the subjects. The test frequency 4 kHz is found to be the most influencing frequency causing significant hearing loss on the right ear of the workmen due to age, work experience and work stations. While the test frequency, 6 kHz is found to be the most influential frequency causing significant hearing loss on the left ear of the subjects due to age and work station. Moreover, there is no significant difference of hearing loss exhibited to the subjects on both ears at test frequency of 4 kHz due to work experience.

Keywords: Asymmetry hearing loss, high fence, noise induced hearing loss.

I. Introduction

Exposure to excessive noise is a major cause of hearing disorders worldwide, 16% of the disabling loss in adults is attributed to occupational noise [1-4]. Excessive noise can damage several cell types in the ear and lead to tinnitus, temporary or permanent hearing loss. Noise induced hearing loss is a sensory neural hearing loss as a result of chronic exposure to excessive sound [5] over a long period of time. A review of the earlier works reveals that many attempts have been made to evaluate the noise generation due to transportation [6,7] and aircrafts [8,9] and its annoyance [10-12] to the people living nearby. Similarly, investigation of different noise sources and its noise levels has also been made in the Gold mines [13], Stone quarry [14], Textile mills [15], Coal mines [16], Bauxite mines [17], Power plants [18] and Steel plants [19]. There are many environmental factors [20] which affect hearing [21] sensitivity, but hearing loss [22,23] is mainly associated with age [24,25], exposure [26] to different noise sources and working at different stations [27,28] and the hearing loss has been evaluated systematically for claiming compensation [29,30] by the workmen.

Therefore, this paper aimed to estimate the hearing loss at 4, 6 and 8 KHz (this frequency range henceforth be referred as high fence) of the subjects based on their age, working experience and working areas of a chromite mine. Audiometry data from 2002 to 2008 of 500 subjects have been used to estimate the hearing loss. The study also sought to find the most influential test frequency which causes the hearing loss significantly with respect to age, experience and work stations of the subjects.

II. Materials and Methods

2.1 Study Area

The mine site in the Sukinda valley is located in the Jajpur district in the state of Odisha, India. The mine produces chromite ore of both friable and lumpy varieties with a chrome ore beneficiation (COB) plant at the mine site. The mine is 130 km from Bhubaneswar, the state capital of Orissa, 65 km from NH-5 and 52 km from JK Road, the nearest railway station.

2.2 Study Design

A cross sectional study of hearing threshold of the mine workers of a chromite mine was carried out with the aim of gaining insight into factor associated with hearing loss. The audiometric data of 500 mine workers were taken from the records of the hospital at the mine. The subjects were included in the study having audiometry data at 0.5, 1, 2, 4, 6 and 8 KHz frequency for the period 2002 to 2008. Such audiometry data of all the mine workers were considered in the statistical analysis and if completed data of some subjects were not available from the hospital records than those subjects have been excluded in the design study. Since, the shift and duration of work hours affect noise exposure level, monitoring of noise level was performed in the mine site, inside the cabin and 7 m away from the Heavy Earth Moving Machineries (HEMMs) and also at different ambient locations from 7 AM to 10 PM to know the noise levels in these areas. The study period for monitoring of noise levels at different locations was from 2008 to 2010. Though, the period of audiometry data and that of monitoring of noise levels are not same, but the present study estimated the noise levels at different locations to know the likely exposure of noise by all subjects.

2.3 Audiometry Test

Screening audiometry was carried out by an audiometer (6025A of TRIVENI TAM-25 make) in a quiet environment by qualified technicians, audiologists, or physicians. The frequency range of the pure tone for air conduction measurement is 250 Hz to 8 KHz. The range of masking intensity is 0 to 100 dB having attenuator in steps of 5 dB. The 3% is the frequency accuracy of the instrument and that of hearing level of the instrument is 2 dB. Tests were conducted on the workers after a complete rest of 16 hours or more from their day shift. Audiometric air conduction tests were performed by presenting a pure tone to the ear through an earphone and threshold of hearing (dB) was recorded at which this tone was

perceived 50% of the time. The better ear was first tested at 1 kHz and then at 2, 4, 6, 8 and 0.5 kHz in that order. Retest was done at 1 kHz in the first ear. In case, the test value was more than 5 dB or more acute than the original, a retest was done at the next frequency and so on. Audiometry tests were conducted in the opposite ear in the same manner except for retesting at 1 kHz. The duration of the presented tone was between 1-3 seconds. The same duration was maintained between the tones. The total time taken to perform the audiometry test of one subject was 3-5 minutes.

2.4 Noise Measurements

A digital sound level meter from M & K, Denmark (Bruel & Kjaer) was used throughout the entire noise survey. The accuracy of the frequency weighting of the instrument meets IEC 651 Type 2 which represents sound level meters suitable for general field applications. The measuring range is 25 to 130 dBA. The wide measurement range allows the instrument to be used for a diverse range of noise investigation where both high and low sound levels occur. Great care was taken to retain a distance between the instrument and the surrounding areas or any obstacles that could intensify or reduce the received noise. In this present study, the sound level meter was placed on rigid stand at 1.2 to 1.5 m above the ground surface, and 6 m away from the road side or 7 m away from the HEMMs, avoiding obstacles or reflecting objects. The air temperature varied between 19.38 and 34.31 °C and the wind velocity was less than 1.02 m/s. Measurements were taken in conditions of clear sky and a sustained wind to avoid any background noise level differences that were greater than 10 dBA.

2.5 Ambient Noise

To know the present noise situation in the mining areas, in the ambient and inside the cabin and 7 m away from the HEMMs, a systematic noise monitoring was performed in summer (June 2008) and in winter (November 2009) between 7 AM to 10 PM. However, for blasting operation noise survey was carried out for three consecutive days in April, 2010 and half an hour before and after the blasting operations at 100 m away from the blasting site. A time gap of 60 s was observed between two readings during the first monitoring and 15 s during second and third noise survey. The working areas of all the subjects (500) have been divided into four groups such as work zone, industrial area, commercial area, residential area and silence zone based on the administrative records as exhibited in Tables 1 (a & b). The minimum and maximum equivalent noise levels (L_{eq}) surveyed in these areas have also been shown to know the likely exposure of each category of subjects. The equivalent noise level, L_{eq} over a particular monitoring time has been estimated using the following equation:

$$L_{eq} = 10 \log_{10} \sum 10^{L_i/10}$$

Where

- L_i = the i^{th} sound pressure level, dBA
- i = 1, 2, 3, …, N
- N = number of readings of a particular parameter

Tables 1 (a & b) show that the maximum L_{eq} levels at commercial area and minimum L_{eq} levels at residential area and silence zone exceeded the prescribed limits. Similarly, the maximum noise levels in case of large and medium HEMMs and also at the Operator’s positions of the HEMMs was found to be even more than danger limit of 90 dBA.

In the present study, audiometric data of 500 subjects (481 males and 19 females) have been taken for the period 2002 to 2008 of an open cast chromite mining complex in Sukinda area in the state of Odisha (India). As the hearing loss of a subject begins at 4, 6 and 8 KHZ frequency, the retrospective data have been used to estimate the possibility of a dip or notch at these frequencies due to exposure to different levels of noise by the subjects. The subjects were divided into 4 age groups, 8 experience groups and 5 work stations as depicted in the Table 1(c). It has been seen that the minimum age of the group is 29 years and maximum age is 59 years. Similarly, 4 years is the minimum working experience and 37 years is the maximum working experience of the group. The Table 1(c) shows the descriptive statistics of the subjects for both the ears at different frequency levels. To meet the research objectives, the data so obtained are analyzed through SPSS (16.0) package under Window-XP environment. Generalized Linear Model ANOVA, Post hoc analysis, Gabriel Multiple comparison for mean difference and paired t-test were used as statistical tools to meet the objectives of the present study.

Table 1 (a): Area code, category of area, work settings and noise levels (dBA) in different areas

Area Code	Category of Area/Zone	Subjects Working at/in	L_{eq}		Limits
			Min.	Max.	Day Time
A	Industrial ^a	Maintenance of Equipments, Store Yard (Loading), Quality Control-COBP and LOPP and Sewerage Treatment Plant.	53.31	72.29	75
B	Commercial ^a	Administrative Buildings (It is located near the Mine Quarry area), Mining Weigh Bridge, Project & Construction and Airfield.	58.33	78.65	65
C	Residential ^a	Main Gate of the Plant, Canteen, Guest Houses and Vocational Training Centre.	57.91	72.86	55
D	Silence Zone ^a	Hospital and Arm Guards	59.46	67.02	50

^aThe Noise Pollution (Regulation and Control) Rules, 2000 and its amendment, Ministry of Environment and Forests, Government of India, India. Day time is between 6 am to 10 pm.

Table 1 (b): Area code, category of area, work settings and noise levels (dBA) in different areas

Area Code	Category of Area/Zone	Subjects Working at/in	L _{eq}		Limits Day Time
			Min.	Max.	
W	Work Zone ^b	(Mine Quarry, Chrome Ore Beneficiation Plant (COBP), Lumpy Ore Processing Plant (LOPP) and Operation of HEMMs)			
	Large HEMMs		65.88	97.23	-
	Medium HEMMs		77.50	95.12	-
	Light HEMMs		74.53	83.42	-
	Blasting Area		54.79	65.51	-
	Haul Roads		-	70.28	-
	COBP Area		54.79	74.79	-
	Cabin of HEMMs		56.48	100.56	-

^b A working limit value of 85 dBA (warning limit) and 90 dBA (danger limit) for 8 hours exposure, Director General of Mines Safety, Circular No. 18 (Tech), December, 1975, Ministry of Labour and Employment, Government of India, India. Large HEMMs: Pay Loaders, JCB, Shovel with Rock Breaker, Poclairn, and Giant Excavators; Medium HEMMs: Dozers, Dumpers and Trucks and Small HEMMs: All Drilling Machines.

Table 1 (c): Descriptive statistics of the subjects (500) in three demographic categories

Category	Subjects		Age (years)		Experience (years)	
	n	%	Mean	SD	Mean	SD
<u>Age (years)</u>						
20-30	13	02.6	29.92	0.28	10.54	0.78
31-40	168	33.6	36.02	2.61	12.85	3.17
41-50	208	41.6	45.38	2.72	18.04	4.73
51-60	111	22.2	53.87	2.36	26.81	7.60
<u>Experience (years)</u>						
0-5	02	0.4	37.50	3.54	4.00	1.41
6-10	56	11.4	35.21	5.41	9.911	0.29
11-15	174	34.6	39.73	5.77	13.09	1.39
16-20	127	25.4	44.91	4.81	17.63	1.34
21-25	59	11.8	47.73	3.75	22.61	1.39
26-30	29	5.8	51.00	2.38	27.59	1.48
31-35	45	9.0	54.67	2.44	33.29	1.31
>35	08	2.4	55.63	2.67	36.50	0.53
<u>Working Area/Zone</u>						
W	262	52.4	42.53	7.08	16.82	6.29
A	128	25.6	44.41	8.15	19.62	8.52
B	65	13.0	45.71	7.45	19.45	8.07
C	20	04.0	47.40	7.13	20.85	7.77
D	25	05.0	44.44	5.42	16.82	4.91
Total	500	100	43.72	7.45	18.05	7.28

III. Statistical Analysis

Descriptive statistics on t-test (2-tailed) of the whole subjects at high fence (4, 6 and 8 kHz) has been shown in Table 2.

Table 2: t-test (2-tailed) of the whole subjects, n=500 at high fence

Ear	Mean Hearing Threshold (dB HL) at											
	4.0 kHz				6.0 kHz				8.0 kHz			
	Mean	SD	t-value	p	Mean	SD	t-value	p	Mean	SD	t-value	p
Right	21.37	7.33	0.347	>0.01	23.48	7.37	0.258	>0.01	22.38	8.43	0.814	>0.01
Left	21.54	7.42			23.36	7.80			21.95	8.67		

i) A two tailed t-test was performed for the whole subjects between the left and right ears at high fence by assuming the following hypothesis:

Null Hypothesis (H_0): The hearing threshold does not differ between left and right ears at high fence.

Alternate Hypothesis (H_1): The hearing threshold differs between left and right ears at high fence.

Since, $p > 0.01$, both the ears do not exhibit any significant hearing difference at 4, 6 and 8 kHz, the hypothesis is accepted at 1% level of significance. Thus, it can be concluded that asymmetric hearing loss may be attributed either in the left or the right ear at 4, 6 or 8 kHz.

Table 3: ANOVA for the hearing loss at high fence with different groups

Category	Mean Hearing Threshold Left Ear, dB HL			Mean Hearing Threshold Right Ear, dB HL		
	4 kHz	6 kHz	8 kHz	4 kHz	6 kHz	8 kHz
<u>Age (years)</u>						
21-30	16.15	18.08	15.77	16.92	18.08	15.38
31-40	18.45	20.74	17.59	18.21	20.57	17.92
41-50	22.16	24.18	23.09	22.31	24.28	23.85
51-60	25.68	26.40	27.09	29.91	27.03	27.21
p- value	<0.01	<0.01	<0.01	<0.01	<0.01	<0.01
<u>Experience (years)</u>						
<5	20.00	22.50	25.00	20.00	22.50	22.50
6-10	17.50	19.46	15.89	16.33	19.02	15.80
11-15	20.11	22.13	19.22	19.97	21.93	19.71
16-20	22.72	24.06	23.65	22.60	24.61	24.41
21-25	22.54	24.41	23.90	22.97	25.42	25.51
26-30	25.17	27.93	27.41	23.45	26.03	26.38
31-35	23.78	25.56	27.60	24.78	26.67	27.33
>35	29.38	30.00	29.38	30.00	29.38	28.75
p- value	<0.01	<0.01	<0.01	<0.01	<0.01	<0.01
<u>Work Stations</u>						
W	20.95	22.77	21.25	20.90	22.92	22.06
A	22.34	23.83	22.66	21.95	23.83	22.54
B	21.92	24.15	21.95	21.54	23.77	21.77
C	23.50	24.50	25.00	22.75	25.00	25.50
D	21.00	24.20	23.00	21.80	25.60	24.00
p- value	<0.01	<0.01	<0.01	<0.01	<0.01	<0.01

ii) To test if there exists any significant difference at the test frequency on both the ears of the subjects with respect to age, experience and work station.

ANOVA was performed to find out any significant difference in hearing loss in both the ears at high fence and the most influential frequency was determined by using Gabriel multiple comparison method. Table 3 shows the hearing loss of the subjects with respect to the different groups of age, experience and work stations. The following hypothesis has been assumed to carry out ANOVA test for different groups:

Null Hypothesis (H_0): Various groups of age, years of experience and Work stations are independent with regard to hearing loss for both the ears of the workers at high fence.

Alternate Hypothesis (H_1): Various groups of age, years of experience and Work stations are dependent with regard to hearing loss for both the ears of the workers at high fence.

Since, $p < 0.01$, various groups of age, years of experience and Work stations are dependent with regard to hearing loss for both the ears of the workers at high fence, the hypothesis is rejected at 1% level of significance.

iii) Post hoc analysis, Gabriel Multiple comparison for mean difference was used to find out the most influential frequency where a dip or notch is exhibited for different groups.

The Post hoc analysis was performed to find out the most significant frequency among all test frequencies. The results of the multiple comparisons of mean differences in hearing loss by Gabriel method at 4, 6, and 8 kHz have been depicted in Table 4.

iv) As the most significant frequency is 4 kHz for both right and left ears with respect to work experience, paired t-test was performed to evaluate any significant hearing difference of the group.

Null Hypothesis (H_0): There is no significant hearing threshold at 4 kHz in either ear due to work experience.

Alternate Hypothesis (H_1): There is significant hearing threshold at 4 kHz in either ear due to work experience.

Since, $p > 0.01$, so it may be inferred that there is no significant difference in hearing loss for both the ears at 4 kHz with 1% level of significance with respect to experience. Thus, concluded that there is no significant hearing loss in the experience group.

Table 4: Post doc analysis for Hearing Loss at high fence and with different groups

Frequency pair, kHz	Right Ear		Left Ear	
	Absolute Mean Difference	<i>p-value</i>	Absolute Mean Difference	<i>p-value</i>
<u>Age Group</u>				
8 and 6	0.8233	<0.01	0.9759	<0.01
8 and 4	1.0760	<0.01	0.5349	<0.01
6 and 4	1.8993	<0.01	1.5108	<0.01
<u>Experience Group</u>				
8 and 6	0.2965	<0.01	0.2965	<0.01
8 and 4	1.3960	<0.01	1.3960	<0.01
6 and 4	1.6925	<0.01	1.6925	<0.01
<u>Different Work Stations</u>				
8 and 6	0.8231	<0.01	0.9091	<0.01
8 and 4	1.4613	<0.01	0.8387	<0.01
6 and 4	2.2826	<0.01	1.7478	<0.01

IV. Results

The maximum L_{eq} levels at commercial area and minimum L_{eq} levels at residential area and silence zone exceeded the prescribed limits. Similarly, the maximum noise levels found to be even more than danger limit of 90 dBA for large and medium HEMMs and also at the Operator's positions of the HEMMs.

From Table 4, it is clear that the most significant frequencies with respect to the hearing loss of age are 4 and 6 kHz for the right and left ears, respectively at 1% level of significance. In case of experience groups, the most significant frequency is 4 kHz for both the ears at 1% level of significance. Similarly, the most significant frequencies are 4 and 6 kHz for the right and left ears, respectively, in respect of working stations at 1% level of significance. With paired t-test, p -value is found to be >0.01 and so it may be inferred that there is no significant difference in hearing loss for both the ears at 4 kHz with 1% level of significance with respect to experience.

V. Discussion

From Tables 1(a & b), it is found that the subjects are exposed to noise levels more than the prescribed standards those working at large, medium and inside the Cabins of HEMMs, Administrative Buildings, Weigh Bridge, Project and Construction Area, Airfield and Hospital.

The t-test reveals that there is no significant difference in hearing loss on both ears due to age, experience and various work stations at all test frequencies and thus, asymmetric hearing loss may be attributed in either ear. However, from ANOVA test, it is clear that there exists a significant difference among all the test frequencies with respect to hearing loss. The hearing loss is found to be not homogeneous i.e. it is dependent in respect of age, experience and working stations. In other words, hearing loss is increasing for every 10 years interval of age, for every 5 years of work experience and with different work stations at high fence. The most influential frequency with respect to age for the right and left ears are found to be at 4 and 6 kHz, respectively. In case of different working experience, 4 kHz is found to be the most influential frequency for both the ears. Similarly, 4 and 6 kHz are the most significant frequencies for right ear and left ear, respectively for the subjects working at different working areas. This asymmetry [31] hearing loss may be attributed to the presence of a subgroup (Operators of the Heavy Earth Moving Machineries) who generally exposed to higher noise level i.e., more acoustic energy of the sound reaching to the right ear [9,32,33] than to the left ear. It has also been found that though the cabin of the HEMMs is air conditioned, operator of the vehicle always keeps the door open for more comfort and easy drive. Therefore, the right ear is exposed outside and possible asymmetric hearing loss.

Since, the most significant frequency is 4 kHz for both right and left ears, paired t-test was performed to evaluate whether there is any significant difference between the right and left ears of the subjects with reference to experience. With paired t-test, p -value is found to be >0.01 and so it may be inferred that there is no significant difference in hearing loss for both the ears at 4 kHz with 1% level of significance with respect to experience.

The subjects, grouped in Sensitive Zone are mainly Staff Nurses, Hospital Attendants and Drivers working in the hospital and Arms Guards. The mean age of this group is found to be more than the mean age across all the subjects. Thus,

the hearing threshold may not be always noise-induced, it may be due to Presbycusis also. However, this group works in the hospital and is located near the mining complex and lot of loaded/empty dumpers and trucks ply through this area. Therefore, hearing loss of the subjects has been estimated for which one of the reasons of hearing loss may be attributed to the noise generation by heavy earth moving machineries including dumpers and trucks when plying everyday through this station.

VI. Recommendations

The following recommendations suggested to minimise exposure to different noise source and also to reduce hearing loss:

- i) The subjects whose hearing loss is found to be at 6 kHz, the working areas of the subjects should be changed to lesser noisy areas to reduce the exposure level.
- ii) Provisions for regular audiometry test of all the subjects should be conducted to identify the hearing loss of those subjects occurring at 6 kHz.
- iii) Periodic maintenance of all the HEMMs is essential to keep all the vehicles in good condition and less noisy.

VII. Conclusion

In our study population, the maximum noise levels for large and medium HEMMs and inside the cabin of HEMMs were found to be more than 95 dBA. Hearing loss is increasing for every 10 years interval of age, for every 5 years of work experience and with different work stations at high fence. Age and experience of subjects have significant difference with hearing loss at 4.0, 6.0 and 8.0 kHz. The study also reveals that there is a significant difference among the different test frequencies with respect to hearing loss on both the ears of the subjects. The test frequency 4 kHz is found to be the most influencing frequency causing significant hearing loss on the right ear of the workmen due to age, work experience and work stations. While the test frequency, 6 kHz is found to be the most influential frequency causing significant hearing loss on the left ear of the subjects due to age and work station. The characteristic frequency due to noise induced hearing loss is 4 kHz where a dip or notch occurs. In the present study also, this frequency is the most influential frequency among different groups of workmen and are the relatives of some of the general public. Therefore, the general public can participate in reducing the noise induced hearing loss of these workmen by advocating them the causes of hearing loss, sources of hearing loss and also how to reduce it by using hearing protective devices while at work.

References

1. Prince MM, Stayner LT, Smith RJ, Gilbert SJ. A re-examination of risk estimates from the NIOSH Occupational Noise and Hearing Survey (ONHS). *J Acoust Soc Am* 1997;101:950-63.
2. May JJ. Occupational Hearing Loss. *Am J Ind Med* 2000;37:112-20.
3. Prince MM, Gilbert SJ, Smith RJ, Stayner LT. Evaluation of the Risk of Noise Induced Hearing Loss among unscreened male Industrial Workers. *J Acoust Soc Am* 2003;113:871-80.
4. Picard M, Girard SA, Simard M, Larocque R, Leroux T, Turcotte F. Association of work-related accidents with noise exposure in the workplace and noise-induced hearing loss based on the experience of some 240,000 person-years of observation. *Accident Analysis Prevention* 2008;40:1644-52.
5. Bauer ER, Babisch DR. Limestone Mining-Is it noisy or not? *Minerals Engineering* 2006;58:37-42.
6. Don CG, Rees IG. Road traffic sound level distributions. *J Sound Vibrat* 1985; 100:41-53.s
7. Finegold LS, Finegold MS. Development of Exposure-Response Relationships between Transportation Noise and Community Annoyance. Presented at the Japan Net-Symposium on "Annoyance, Stress and Health Effects of Environmental Noise": 2002. p.1-16.
8. Hoeger R. Aircraft noise and Times of Day: Possibilities of redistributing and influencing noise exposure. *Noise Hlth* 2004;6:55-8.
9. Satish, Kashyap RC. Significance of 6 kHz in noise induced hearing loss in Indian Air Force Personnel. *Indian J of Aero Med* 2008;52:15
10. Ouis D. Annoyance Caused by exposure to road traffic noise: An Update. *Noise Health* 2002;4:69-79.
11. Waye KP, Ohrstrom E. Psycho-acoustic characters of relevance for annoyance of wind turbine noise. *J Sound Vibration* 2002;250:65-73.
12. Coles RRA, Lutman ME, Buffin JT. Guidelines on the diagnosis of noise-induced hearing loss for medicolegal purposes. *Clinical Otolaryngology & Allied Sciences* 2000;25:264-73.
13. Amedofu GA. Hearing impairment among workers in a surface Gold Mining Company in Ghanna. *Afr J Hlth Sci* 2002;9:91-7.
14. Pal AK, Mukhopadhyya AK, Agarwal SC. Portable diamond cutter for sawing Kotah stone - A case study on its noise emission and control. *Noise Vibrat Worldwide* 2006;37:26-32.
15. Tiwari RR, Pathak MC, Zodpey SP. Low Back Pain among Textile Workers. *Indian J Occup Environ Med* 2003;7:27-9.
16. Pal AK, Ghosh S, Saxena NC. Noise status in coal mining complexes. Proceedings of the 7th National Symposium on Environment, ISM, Dhanbad, India; 1998. p.74-81.
17. Kisku GC, Barman SC, Kidwai MM, Bhargava SK. Environmental impact of noise levels in and around opencast bauxite mine. *J Environ Bio* 2002;23:51-6.

18. Kisku, GC and Bhargava, SK. Assessment of noise level of a medium scale thermal power plant. *Indian J Occup Environ Med* 2006;10:133-9.
19. Kerketta S, Dash PK, Narayan LTP. Work zone Noise levels at Aarati steel plant, Orissa and its attenuation in far field. *J Environ Biol* 2009;30:903-8.
20. Mills JH, Going JA. Review of Environmental Factors Affecting Hearing. *Environ Hlth Pers* 1982;44:119-27.
21. Patil RR. Community-based occupational/ environmental health Studies: The challenges and the dilemmas. *Indian J Occu Environ Med* 2006;10:85-6.
22. Joshi SK, Devkota S, Chamling S, Shrestha S. Environmental Noise Induced Hearing loss in Nepal. *Kathmandu Univ of Medical J* 2003;1:177-83.
23. Bistrup ML. Prevention of Adverse Effects of Noise on Children. *Noise Health* 2003;5:59-64.
24. Rosenhall, U. The Influence of Ageing on Noise-Induced Hearing Loss. *Noise Health* 2003;5:47-53.
25. Albera R, Lacilla M, Piumetto E, Canale A. Noise-induced health loss evolution: Influence to age and exposure to noise. *Eur Arch Otorhinolaryngol*, 2010;267:665-71.
26. Leong ST, Laortanakul P. Monitoring and assessment of daily exposure of roadside workers to traffic noise levels in an Asian city: A case study of Bangkok streets. *Environ Moni* 2003;85:69-85.
27. Boateng CA, Amedofu GK. Industrial noise pollution and its effects on the hearing capabilities of workers: A study from saw mills, printing presses and corn mills. *Afr J Hlth Sci* 2004;11:55-60.
28. Joy GJ, Middendorf PJ. Noise exposure and hearing conservation in U.S. Coal Mines – A surveillance report. *J Occup Environ Hygiene* 2007;4:26-35.
29. Coles RRA, Burns W, King PF. Assessment of hearing disability: Discussion paper. *J Royal Soc Med* 1983;76:1032-7.
30. Pal AK, Saxena NC. Societal cost of community noise. Proceedings in the National Seminar on Environmental Engineering with special emphasis on Mining Engineering. NSEEME-2004, March, 2004, ISM Dhanbad, India; 2004. p.1-8.
31. Backus, BC and Williamon, A. Evidence of noise-induced hearing loss among orchestral musicians. International Symposium on Performance Science, Published by the AEC, 2009. p.225-30.
32. McBride DI, Williams S. Audiometric notch as a sign of noise induced hearing loss. *J Occup Environ Med* 2001;58:46-51.
33. Royster JD, Royster LH, Killion MC. Sound exposure and hearing threshold of Symphony orchestra musicians. *J Acoust Soc of Am* 1991;89:2793-2803.

Detecting Identification Anomalies in Social Networking with Cluster based re-ranking and Slink Algorithms

Salina Adinaryana¹, Dr. G. Samuel Vara Prasada Raju², Allam Mohan³

*(Assoc Prof, Dept of IT, Sri Vishnu Engineering College for Women, Bhimavaram, A.P, India)

***(Professor, Dept of CSE, SDE, Andhra University, Visakhapatnam, A.P, India)

***(Asst. Prof, Dept of IT, Sri Vishnu Engineering College for Women, Bhimavaram, A.P, India)

ABSTRACT: In today's Fast growing commercial word Social network Websites (SNW) like FaceBook, Twitter etc, are the major source for maintain social communication, doing e-business. Now a day's dynamic data discovery is a part of it's activity for many organizations in banking sector, content providing sites and ecommerce websites. Interestingly on the other side we can see that most of the users are having more than one registration on social networks with two fold effect both positive and negative. Many students and young people are using these social networking websites for adolescents or to download some study materials, music etc^{10,11}, from different blogs. This leads to lot of fake user registrations⁷. Just receiving invitation to their emails, creates some of the user profiles and it pops the user data of the mail account. The profile created may not be correct and this was copied may lead to false or duplicate information on the network domain. This became a bitter problem to find many facts like user identity, number of users registered and visitors tracking etc. there by it leads to ambiguity. As one person may have more than one profile created by him intentionally or unknowingly generated by anyone way specified above. This became a common identification problem to every organization and most researchers are mainly concentrating on providing efficient techniques for linking of records. There are many solutions of this kind, to propose the best we are attempting to analysis and identify the optimization techniques with clustering and algorithms for fake user data discovery in SNW.

Keywords: Social network Web sites, social communication, PAN, query data base, cluster based analysis, SLINK, MST

I. INTRODUCTION

Record linkage for remote database is a commonly identified problem from many years, which is used to analyze remote data supporting a variety of decisions in different organizations. How ever, since heterogeneous databases are usually designed and managed-where all the records are available either locally or remote by the organizations. They can be accessed by using some common key like email address or PAN number etc.. Although it may be possible to use they would involve transferring the entire remote relation. As a matching data from various sources in a batch. The key question here is one of record. The databases exhibiting entity heterogeneity are distributed, and it is not possible to create and maintain a linkage: given a record in a local database (often called the central data repository or warehouse where pre computed enquiry record), how do we find records from a

remote linkage results can be stored. A centralized solution database that may match the enquiry record? Traditional maybe impractical for several reasons. First, if the record linkage techniques, however, are designed to link databases span several organizations, the ownership and cost allocation issues associated with the ware-house. Even if the warehouse could be developed, it would be difficult to keep it up-to-date. As updates occur at the operational databases, the linkage results would become stale, if they are not updated immediately. This staleness maybe unacceptable in many situations. The systems may agree to transmit incremental changes to the data warehouse on a real-time basis. Even if such an agreement is reached, it would be difficult to monitor and enforce it. The staleness of the linkage tables and limiting their usefulness due to certain overhead delays and time consuming due to many databases, each with many records, undergoing real-time changes. This is because the warehouse must maintain a linkage table for each pair of sites, and must update them every time for the associated databases changes.

. The participating system allows controlled sharing of portions of their databases using standard database queries, but they do not allow the processing of scripts, stored procedures, or other application programs from another organization. Here our intention is not to discuss on ability of existing systems but to suggest a system that is more efficient for record linkage with clustering and MST.

1.1 INITIATION

When I am searching for one popular personality on twitter, linked-in and FaceBook⁸. This situation Initiated me to concentrate on this work. In this work I identified problems like: (1) Identifying a person having more than one account (2) real active identity. These things encouraged me to identify a system that can determine user genuinely. And also I understood that most of the users are not in a position to readily available to project their correct information onto SNW and many youngsters may have more than one account for different purposes. So how do we get the exact user data? This gave a way to propose a solution of that kind where both the end users will be satisfied. As a part of this process I had come across many similar problems like e-banking, downloading e-books, ecommerce with SNW login etc^{11,12}, and understood that there is a need for better system to handle user data.

In the Data discovery process, cluster analysis has been used to create groups of documents with the goal of improving the efficiency and effectiveness of data retrieval. The terms in a document collection can also be clustered to show their relationships.

A recent review (Willett 1988) provides a comprehensive summary of research on term-based document clustering². Terms may be clustered on the basis of the documents in which they co-occur, in order to aid in the construction of a thesaurus or in the enhancement of queries (e.g., Crouch [1988]). If the collection to be clustered is a dynamic one, the requirements for update must be considered.

II. RELATED WORK

This paper consists of two parts where first part is addressing the efficiency and effectiveness of data retrieval using database re ranking based on cluster analysis, and then algorithm best fit to implement the system and finally results base on the system implemented to check the feasibility.

2.1 MATHEMATICAL APPROACHES

In this part, my approach is to identify and avoid fake users on social network by 1.) Database re-ranking based on cluster analysis¹ and 2. Record linkage with Slink.

As the degree of matching of evidences in data bases is higher, the two database entries are more similar. In database clustering, databases with similar entries or more likely are classified as one cluster⁴. Therefore, relevant db table entries are in the same cluster according to the cluster hypothesis (van Rijsbergen) which states that relevant documents tend to be more similar to each other than to non-relevant documents.

The documents in a cluster have effect on cluster centroid. The cluster centroid for a pair of clusters Ci and Cj is given by:

$$\frac{m_i C_i + m_j C_j}{m_i + m_j}$$

where m is the size of a cluster.

The same query-cluster similarity value is applied to all the database tables in the cluster at the re-ranking stage. In this way, the databases in a cluster can affect one another through calculation of cluster centroids so that context retrieval is possible, due to the interaction of evidences contained in databases.

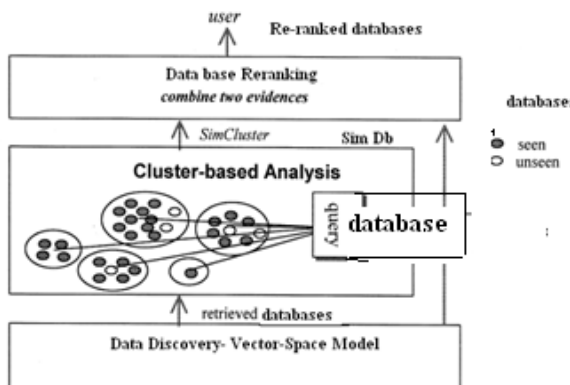


Fig 1. Clustering based data base re-ranking

In record linkage process the single link method merges at each stage the closest previously unlinked pair of points (here records) in the data set. Since the distance between two clusters is defined as the distance between the closest pair of records each of which is in one of the two clusters, no cluster centroid or representative is required, and there is no need to recalculate the similarity matrix

during processing. This shows how clustering efficiency. So that this makes the method more attractive for non redundant computation⁴ and a storage perspective wise. Database re ranking avoid similar entries in the clusters and Slink will improves record linkage of data discovery process in Vector Space model.

A number of algorithms for the single link method have been reviewed by Rohlf (1982), including related minimal spanning tree algorithms. The computational requirements range from $O(N \log N)$ to $O(N^2)$. Many of these algorithms are not suitable for information retrieval applications where the data sets have large N and high dimensionality.

2.2 ALGORITHMIC APPROACH

2.2.1. VAN RIJSBERGEN ALGORITHM

Van Rijsbergen (1971) developed an algorithm⁵ to generate the single link hierarchy that allowed the similarity values to be presented in any order and therefore did not require the storage of the similarity matrix. It is $O(N^2)$ in time and $O(N)$ in storage requirements. It generates the hierarchy in the form of a data structure that both facilitates searching and is easily updated, and was the first to be applied to a relatively large collection of 11,613 documents (Croft 1977).

2.2.2 SLINK ALGORITHM⁵

The SLINK algorithm (Sibson 1973) is optimally efficient, $O(N^2)$ for computation and $O(N)$ for time, and therefore suitable for large data sets. It is simply a sequence of operations by which a representation of the single link hierarchy can be recursively updated; the dendrogram is built by inserting one point at a time into the representation. The hierarchy is generated in a form known as the pointer representation, which consists of two functions Π and Δ for a data set numbered 1..N, with the following conditions:

- $\Pi(N) = N$
- $\Pi(i) > i$
- $\Delta(N) = \infty$
- $\Delta(\Pi(i)) > \Delta(i)$ for $i < N$

In simple terms, $\Delta(i)$ is the lowest level (distance or dissimilarity) at which i is no longer the last (i.e., the highest numbered) object in its cluster, and $\Pi(i)$ is the last object in the cluster it joins at this level; a mathematical definition for these parameters is provided by Sibson (1973).

In the pseudo code for SLINK below, three arrays of dimension N are used: *ptr* (to hold the pointer representation), *dp* (to hold the distance value associated with each pointer), and *distance* d (to process the current row of the distance matrix); *next* indicates the current pointer for a point being examined.

```
ptr [0] = 0;
dp[0] = MAXINT;
/*iteratively add the remaining N-1 points to the hierarchy
*/
for (i = 1; i < N; i++)
{ ptr [i] = i; dp[i] = MAXINT;
/* calculate and store a row of the dist_matrix for i */
for (j = 0; j < i-1; j++) d[j] = calc_distance(i,j);
for (j = 0; j < i-1; j++)
{ next = ptr[j];
```

```

if (dp[j] < d[j])
d[next] = min(d[next],d[j]);
else
{ d[next] = min(dp[j],d[next]);
ptr[j] = i;dp[j] = d[j];}
/* relabel clusters if necessary */
for (j = 0; j < i-1; j++)
{ next = ptr [j];
if (dp[next] < dp [j])
ptr[j] = i;
}}

```

For output in the form of a dendrogram, the pointer representation can be converted into the *packed representation*. This can be accomplished in $O(N^2)$ time (with a small coefficient for N^2) and $O(N)$ space.

2.2.3 MINIMAL SPANNING TREE ALGORITHM

Another attempt is with an MST. A minimal spanning tree (MST) which is a sub graph (known as tree here) generated from the given graph linking N objects with $N - 1$ connections without any cycles and the sum of the $N - 1$ dissimilarities is minimized. It can be shown that all the information required to generate a single link hierarchy for a set of points is contained in their MST (Gower and Ross 1969). Once an MST has been constructed, the corresponding single link hierarchy can be generated in $O(N^2)$ operations; or the data structures for the MST can be modified so that the hierarchy can be built simultaneously (Rohlf 1982).

The Prim-Dijkstra algorithm⁵ (Dijkstra 1976) consists of a single application of principle 1, followed by $N - 1$ iterations of principle 2, so that the MST is grown by enlarging a single Cluster: Let records unique values (record key) are taken as points for MST.

1. Place an arbitrary record in the MST and connect its nearest neighbor to it.
2. Cluster will grow in size by finding the record not in the MST, closest to any record in the MST and add it to the cluster.
3. If a record remains that is not in the cluster, return to step 2.

Prim-Dijkstra algorithm is provided by Whitney (1972). The algorithm here uses arrays *npoint* and *ndistance* to hold information on the nearest in-tree neighbor for each record, and *notintree* is a list of the *nt* unconnected records. *Lastestpt* is the latest record added to the tree.

```

/* initialize lists */
/*define infinity =9999 */
for (i = 0; i < n; i++)
{ ndistance[i] = infinity; notintree[i] = i;}
/* arbitrarily place the Nth point in the MST */
latestpt = n; nt = n-1;
/* grow the tree an object at a time */
for (i = 0; i < n-1; i++)
{
/*consider the latestpt in the tree for the NN list */
for (j = 0; j < nt; j++)
{ D = calculate_distance(latestpt, notintree[j]);
if (D < ndistance[j])
{ npoint[j] = latestpt;
ndistance[j] = D; } }
/* find the unconnected point closest to a point in the tree */
*/

```

```

nj = index_of_min(ndistance);
/* add this point to the MST; store this point and their
clustering level */
lastpoint = notintree[nj];
store_in_MST ( lastpoint, npoint[nj], ndistance[nj]);
/* remove lastpoint from notintree list; */
/* close up npoint and ndistance lists */
notintree[nj] = nt;
npoint[nj] = npoint[nt];
ndistance[nj] = ndistance[nt];
nt = nt - 1; } }

```

2.3 PROPOSED SYSTEM

The clustering architecture was designed and implemented with an assumption that it will be invoked, when a user creates a registration on the SNW it automatically starts monitoring user inputs by giving initial ranking and maintains a dataset at a **query database** as a pivotal elements like PAN, Adhar card and Driving license which are issued by government departments and had a unique id number., once the data is inserted it considers the PAN number or email-ID and mobile number as set of keys to identify the user and data is mined from different databases available on internet and they are maintained as different clusters. Finally the query database is re ranked done using cluster analysis which is show in fig 1.

III. RESULTS

After the user gets registered in SNW

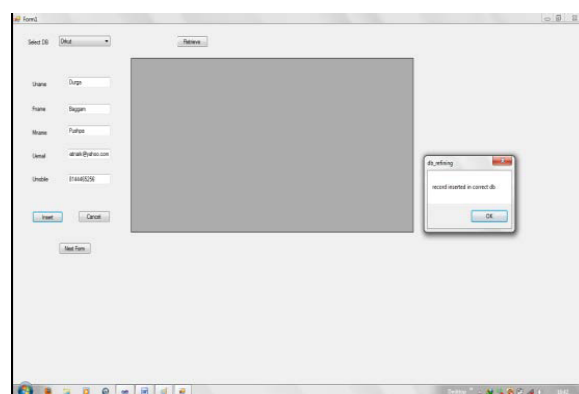


Fig 2.user details inserted in Query DB

The details gets inserted in the query database and initial ranking is given for the records which is show in Fig.2. while querying user data from **query db** for user records similarity checking to form clusters the data queried is shown in fig.3.

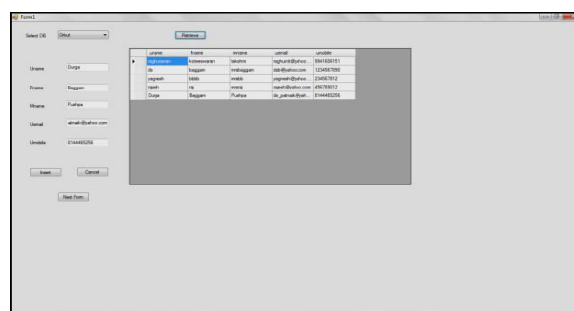


Fig.3 queried user data for clustering

IV. CONCLUSION

Research on social networking and their implications are attracting more researcher's because it is a social area depends on behavior of large set of people in different age groups of different demographic sizes and their activities result in different areas like dynamic change in Database size, complexity in analysis for OLAP, redundancy and many more DB issues. Some of the most interesting factor that motivated me is to identify a persons by avoiding unauthorized entry for adolescent action and to provide security for e-transaction associated with banking⁸ and ebay, snap-deal and flipkart⁹ etc., like shopping websites. This is our preliminary work to have a better understanding of the system. As a result we had studied many papers related to it and accessed to many SNW's by registering on entering fake user data interestingly found that most of the sites are not processing any verification other than email-id which can be created by anyone as they like by giving any details(invalid or fake). We proposed a clustering architecture which acts as a preliminary gateway for any user registration by giving initial ranking. The complexity here is all registration pages should undergo this process. Future enhancement for this technique is to implement a internal indexing with R-trees for query database so that retrieval from query database becomes faster so that it may improves the overall performance.

REFERENCES

- [1] Kang, H. K. (1997). Two-level document ranking methods using mutual information in natural language information retrieval. Ph.D. thesis, Department of Computer Science, Korea Advanced Institute of Science and Technology. Kemong (1992). The Kemong Company new encyclopedia. Seoul: Kemongsa Publishing Co.
- [2] Cluster analysis-
http://en.wikipedia.org/wiki/Cluster_analysis
- [3] Park, Y. C. (1997). Building word knowledge for information retrieval using statistical information. Ph.D. thesis, Department of Computer Science, Korea Advanced Institute of Science and Technology.
- [4] Using Interdocument Similarity Information in Document Retrieval Systems Alan Griffiths, H. Claire Luckhurst, and Peter Willett Department of Information Studies, University of Sheffield, Western Bank, Sheffield S10 2TN, United Kingdom
- [5] Slink Algorithm
<http://orion.lcg.ufrj.br/Dr.Dobbs/books/book5/chap16.htm>
- [6]. twitter user registration -
<http://twitter.com/#/>
- [7] Face book login-
<https://www.facebook.com/login.php>
- [8] Face book login for database transactions
<http://www.facebook.com/pages/State-Bank-of-India/104565649587176>
- [9] Face book shopping
<http://www.facebook.com/eGardenOnlineShopping>
- [10] mp3skull.com/mp3/4shared_com.html
- [11] Free ebooks download
www.facebook.com/pages/Free-download-books/128576447214493

A Novel Watermarking Technique Using Visual Cryptography with Blow Fish Techniques

Ramamohan .B

M. Tech student,

Dadi Institute of Engg &Tech, Anakapalli

P. Srihari

M. Tech,(P.hd) Head Of The Department,ECE,

Abstract: Information security is not just to provide an authenticity and integrity to the data, but there is also a need to seek identity, rights of use and origin of information, which may require some degree of process re-engineering. Rarely security technologies like digital data can be simply “plugged in” without streamlining the process. In this paper we address the problem of information security and protecting the rights of originator of the structured document from ill-intentioned recipient who can modify the received decrypted information. At sender end, a public key signature is generated using SHA-1 or SHA-2. Signature is embedded into raster image of the document using non-invertible robust public key watermarking technique based on orthogonal signals concepts. The document is then encrypted with public key of the receiver using RSA algorithm to achieve confidentiality and authorization. The proposed scheme uses correlation analysis to detect embedded signature to authenticate message. This scheme also uses Gauss-Jordan method to derive the signature from the watermarked image to verify ownership. The study is corroborated with result and application of the proposed technique to prevent forgery and alteration in data

Keywords: Digital data, watermarking, Information Security, Rights Protection,

I. Introduction

Over the past few years there has been tremendous growth in computer networks especially in the field of World Wide Web. This phenomenon coupled with the exponential increase of computer performance, has facilitated on-line business operations like shopping, trading, truncation, bill presentment. Due to massive use of personal computers, network and the Internet, new features of security are in need. In addition to confidentiality, authentication, integrity and control, one must think of new security requirements like protecting the rights of originator against tampering and illegal distribution of the information by the intended recipient, as an ill intentioned authorized recipient can modify and redistribute the decrypted information. It is well known that cryptography deals with unauthorized access but there are functional limitations like requirement of global clock synchronization, handshaking and costly tamper proof hardware. Digital watermarking is a technique based on digital signal processing which inserts extra signal to digital contents for discouraging illicit modification and distribution of information and to authenticate watermarked contents. But, digital watermarking has the following limitations

(a) No transmission security due to lack of public key algorithms.

(b)Text information - Due to binary block format of the text, embedding new bits in the text may introduce irregularities that are visually noticeable. This paper presents a technique, which contains strengths of digital data and digital watermarking both so as to provide a secure transmission of messages. Thus the rights of sender on digital content are protected.

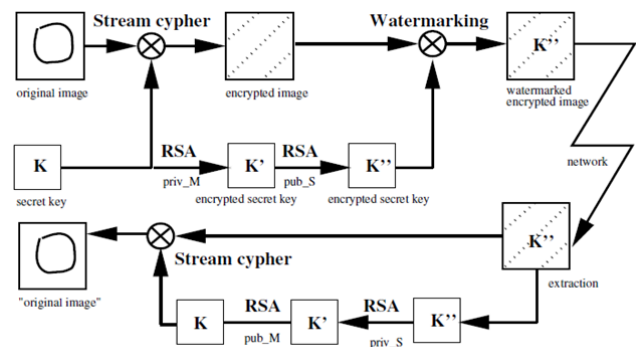


Figure 1 illustrates an approach that uses RSA and Blowfish process representation

The document in which digital data is embedded as watermark. Public key signature protects the document from any intruder, while embedding it as resilient, noninvertible and robust watermark prevents non trusted receiver to modify the contents of the document. Figure 1 Public Key Cryptosystem with embedded digital data. The rest of the paper is organized as follows. Section 2 presents digital data embedding in to image and watermarking, section 3 describes embedding procedures, section 4 verification detection of watermark to prove authenticity, and section 5 conclusion

II. Digital watermarking

The ownership protection, authentication and integrity of structured document is necessary and important. Encryption and digital data techniques protect against eavesdroppers, for sure, but the main attacks are likely to be from validly connected end-users who go on to redistribute the received data more than they are entitled to. Digital data uses “Public-Key Cryptography” which employs an algorithm using two different but mathematically related “keys” one for creating signature, and, another for verifying signature. Compare this to information hiding the cryptographic signature is embedded into the information itself. Watermarking [1] is a security technique in context of protecting content of information from authorized user. It is as old as paper production is and protects rights of

author/originator. This technique is basically used to identify any processing and modification in the contents. 2.1 Digital data have been accepted in several national and international corporations, banks and government agencies. The fundamental process involved in digital data is a hash function. A number of hash functions are proposed in the literature. The MD5 message digest algorithm, [2] was developed by Ren Rivest at MIT. MD5 generates a 128 bits message digest out of a variable length message. Another hash algorithm SHA (Secure Hash Algorithm) was developed by National Institute of Standards and Technology (NIST) and published as a federal information processing standard [3] in 1993. Revised version of SHA is implemented in C language and referred as SHA-1 [4]. It generates 160 bits message digest. SHA-1 has achieved level of Standard because it generates 32 bits longer message digest than MD5, using a brute force technique for a given digest the difficulty in achieving message is of the order of 2160 operations in comparison to 2128 operations in MD5. In the draft FIPS 180-2 NIST published SHA-2 as a new version of secure hash algorithm. SHA-2 offers, SHA-1, SHA-256, SHA-384 and SHA-512. In other words SHA-2 may have outputs 160, 256, 384, and 512 bits of message digest. However, SHA-2 algorithm uses fixed and predefined parameters that may be vulnerable to attack. Digital data can save the message from third parties [5] but once an encrypted message is at receiver end, easily decrypt, modify and distribute the message for commercial benefits. This means the sensitive information in these messages cannot be protected from modification and redistribution from the authorized receiver using encryption, access restriction and hiding information behind firewalls.

A digital watermark is a distinguished piece of information that is adhered to the data that it is intended to protect. Several embedding techniques [1, 6-8] have been specially developed for use with text but most of these techniques either change word or line spacing or make change on the character boundary which require original document to detect watermark to authenticate sender. These techniques cannot be simply used to embed digital data due to involvement of integrity issues with digital data applications.

Tao Chen, et al suggests a combined digital data and digital watermarking scheme [9] for image authentication and content protection. In this scheme content dependent random k bits are extracted from N blocks of image to obtain $K \times N$ bits signature, which is embedded back to the image using secret key. Due to requirement of large number of keys this method cannot be used in applications requiring transmission of data. Ding Huang presents a text watermarking technique [10] that expands and shrinks widths between words to represent inter word distance, as sine wave. In this method sine wave is coded as watermark. This technique cannot be used to send confidential message, as it does not use any key. Chang & Chang presented a sender-buyer protocol [11] where digital data containing sender, buyer and trading information is embedded in the image as barcode image. This scheme protects the embedded trading message and ensures integrity of image but does not authenticate the sender, as digital data is not based on content of the information. Cor et al [12] proposed secure spread spectrum watermarking

scheme. A two-dimensional spectrum signal is generated. 128 low bits of the spectrum signal are modulated with 128 bits of the owner's secret key. Adding modulated signal back to the image generates the watermark signal. Inverting spectrum signal, which is then added to the image, generates watermark signal. Drawbacks of this scheme are (1) it requires original image to detect the watermark and (2) Every time new binary key is needed to protect new image.

A paper for watermarking of digital images to detect or verify ownership [13]. In this method most common RSA & DSS public key signature generation algorithms are used to generate public and private keys of user. This method involves computing message digest using MD5 of image I of M rows and N columns. Message digest is encrypted with private key to generate digital signature. Low order bits of DS are modulated to as watermark and inserted back into the image. We can summarize that, in order to protect document integrity and rights of owner on the document the crypto signature should be content based and public in order to avoid the large number of secret keys. Secondly such a scheme should not require original document to detect and verify the ownership and should be computationally inexpensive. The goal of this work is to design a cipher model that contains strengths of digital data and digital watermarking both to provide secure structured document transmission and to detect and verify ownership to prevent alteration and forgery. The approach uses raster representation of the document in which digital data is embedded as watermark. Public key digital data protects the document from third party while embedding it as watermark prevents non Trusted receiver trusted receiver to modify the contents of document.

III. Embedding a digital data in to image

Image representation of a message The process starts with calculating size of the text information and then converting it into its digital image representation. Input text is stored in string format before conversion. Size of the text is calculated in the form of an invisible drawing in the context of memory device.

height and width are calculated as shown in figure 2..

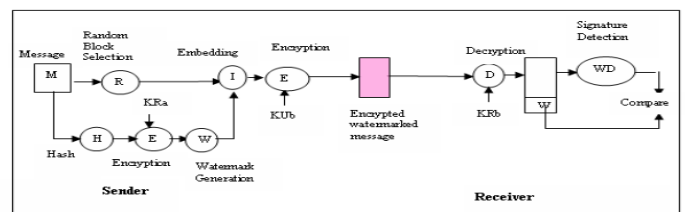


Figure 2: Image size Measurement

Image height = (Ascent+ Descent+ bearing) * No. of lines in text message (1)

Image width = = Max (x [i]); 0<= i <=no. of lines (2)

True color RGB model is used to represent image as a bit frame of size width*height, where, each square represents a value of bit as function

$$f(x, y) = \{f(x, y) = [0,1], | x = 0 \text{ to width}, y = 0 \text{ to eight}\} \quad (3)$$

A total number of 32 frames for a single image are used [14]. The first 8 frames represent transparency; the next 24 frames (8 per color) are used to represent Red, Green and Blue colors respectively. The binary values (0 or 1) in corresponding bits from each of the 32 bit planes result in a binary number to represent pixel's intensity level from 0 to $2^{32}-1$ (full intensity). For each bit, in all 32 bit frames, value of function $f(x, y)$ is set to 0 to create a black background. Value of function $f(x, y)$ is manipulated at a specific location in all the bit frames to draw text pattern on the background image. Intensity of the image is set in all 32-bit frames to get a specific pixel value [15-17]. Values of pixels stored in memory are grabbed into a vector of size $=$ width * height.

III.1 Generation and Embedding of Digital signatures

This process starts with calculating a message digest from two-dimensional message signal M of m rows and n columns. One-way hash function H operates on input message M of arbitrary length and returns a fixed length hash value h , i.e. $H(M) = h$. It has additional characteristics as follows:

- (i) Given M it is easy to compute h , (ii) Given h it is hard to compute M such that $H(M) = h$
- (iii) Given M it is hard to compute another message M' such that $H(M) = H(M')$. Several methods are developed to find hash function [2-4]. Here SHA-1 algorithm is used to generate unique 160 bits.

Then RSA algorithm is used to encrypt fixed length message digest using owner's private key to generate owner's public key signature vector [5]. Since RSA algorithm is based on the fact that there is insufficient way to factorize very large number, deducing the RSA key, therefore, requires very high computer processing time. RSA algorithm has also become de facto standard for industrial strength and built into many of the software products like Netscape Navigator and Internet Explorer. Next, the bits of digital data are modulated and transformed to compute watermark signal. Length of the watermark signal may be same as that of digital data or it may be based on first, middle or last bits of the digital data as long as they are consistent. This selection is based on the criteria that too small watermark signal is vulnerable to attack and too large watermark signal takes large computer power. Embedding watermark signal X_s into message M involves selecting a random block of m nonoverlapping continuous rows and averaging these m rows to find average row vector R referred to as reference vector. Original watermark signal X_s is orthogonalized with respect to vector R to make inserted signal independent from the reference signal and eliminate cross talk [18]. Thus, the vector W_s constructed out of W entries by modulating digital data [12, 19, 20]

$$W_s = X_s - (X_s \cdot R) R \quad (5)$$

A gain factor is calculated from W_s across all m rows to ensure that strength of the watermark varies smoothly. $I_i = c \cos(2\pi i/m)$ (6) Value of c is adjusted to maintain quality metric PSNR to minimum 30 DB, to avoid white visible marks on message signal. This small scaled version of the W_s is added back to m rows of the original signal to generate watermarked signal M' , where value of the bit function $f(x, y)$ is given as.

It is possible to find values of e, d, n such that $m^{ed} = m \pmod n$ for all $m < n$;

- It is relatively easy to calculate m^e and c^d for all values of $m < n$.
- It is infeasible to determine d given e and n .

$$m^{ed} = M \pmod n \quad \text{where } n \text{ is no of sub pixels}$$

Where m is decryption key

A corollary to Euler's theorem, $n=pq$

Where $\Phi(n)$ is the Euler totient fun.

$$\Phi(p, q) = (p-1)(q-1) \quad ed = 1 \pmod{\Phi(n)}$$

$$d = e^{-1} \pmod{\Phi(n)}$$

$w - m \leq r$ and $0 \leq w \leq h$ Other blocks of m rows can be selected pseudo randomly to embed additional watermarks using same X_s signal. All X_s and corresponding reference vectors are stored for detection purpose.

III.2 Encrypting watermark image

Encryption of watermarking with the help of RSA algorithm [5] is used to further encrypt watermarked signal M' using public key (d, n) of the receiver to achieve data integrity and confidentiality over network

$$I. \quad M = \{f(x, y) \mid x = 0 \text{ to width}, y = 0 \text{ to height}\} \quad C = M^d \pmod n \quad (8)$$

IV. Detection of Watermark to prove authenticity

The message received is decrypted using private key (e, n) of the receiver to assure for the sender that only authorized receiver can access message and data in the message has not been modified during transmission. To assure the receiver that message has come from the authentic sender. The watermark inserted in the message is detected.

$$M = C^e \pmod n \quad (9)$$

A detection criterion is established using correlation analysis [19, 20]. Watermark is detected using the reference vector R and the watermark vector X_s sent with message itself. X_s is orthogonalized with respect to R to obtain W_s . Watermarked message is scanned from starting in blocks of m rows. An average vector is calculated from each block and orthogonalized with respect to reference vector R to find expected watermark vector EW_s . EW_s is correlated with the watermark vector W_s to test relative closeness.

If correlation coefficient is above a threshold value (between 0.5 & 1) then received document contains the watermark and assumed to have sent by an authentic sender.

Hundreds of random watermarks are synthesized with the same spectral properties as X_s . Correlation of each of these watermarks is computed with watermarked image. If later and former correlations are far apart it is likely that image contains watermark.

V. Verification to prove ownership

The procedure to protect rights of sender by deriving watermark from the watermarked image of the signal. Signature derivation will prove ownership of the sender if message is redistributed. At the same time it will restrict authorized receiver to illegally modify the message because in case of modification extracted signature will not match

with the original signature of the sender. Claimant can prove the ownership by presenting original image and the position where watermark was inserted. Gain factor is constructed by subtracting original image from watermarked image and orthogonal watermark W_s / is also constructed.

$$(X_s \ R) \ R = (X_s \cdot R) \ R - (R \cdot R) \ X_s \quad (11)$$

(12) Gauss Jordan method is applied to equation (12) to find components of vector X_s , where m_r is length of vector R . Digital data S of sender is constructed from X_s after removing all modulations and transformations. If, S and X_s are same, ownership of the sender is proved. 6 Implementation and Results In this section we present the simulation results by implementing orthogonal signals based public-key watermarking algorithm.. We used a 32-bit RGB model to represent the original image using MATLAB. We used SHA-1 algorithm to find message digest and RSA algorithm to encrypt message digest. We orthogonalized signature with respect to average vector found from selected block and embedded a scaled version of orthogonalized signature back to the selected block. PSNR was set to minimum 30 DB to avoid white noise. Overall image was encrypted with public key of the recipient to achieve confidentiality and integrity. Signature was detected using correlation analysis. Figure 4 shows 32-bit raster image of the document. Figure 5 shows watermarked image with PSNR 76DB and figure 6 shows the decrypted image. This image is used to detect the watermark using correlation

The performance of the proposed algorithm is shown in figure 7. Correlation factor is found corresponding to the true signature derived from the original document and corresponding to the 100 randomly selected signatures. The correlation factor corresponding to true signature is between 0.9 and correlation factor corresponding to false signatures is negative or below 0.6.



Figure 4: Original Image



Figure 5: Image of with embedded data

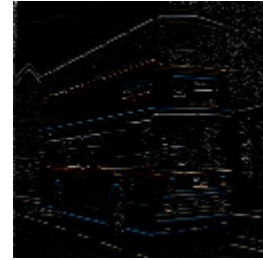


Figure6 6: Encrypted image with the data



Figure 7: Decrypted image of the retrieve process done with blowfish process

V. Conclusion

Most of the trading, banking and investment applications are based on exchanging structured documents over global network. For technical excellence and business values of these applications, security of information and sender's rights on information plays an essential role in overall transmission system. Cryptography alone can be an effective solution to all these problems but in most of instances in the form of costly and specialized hardware to create tamper proof devices. In this paper we have presented a software-based approach, which combines digital datatechnology with robust watermarking technique to achieve authenticity, confidentiality, integrity and restricting alteration and forgery in information. The proposed technique is tested to prevent forgery of signature and alteration of information in images.

References

- [1] Frank Hartung and Martin Kutter , " Multimedia Watermarking techniques", Proceeding of the Vol. 87, No. 7, July, 1999.
- [2] Rivest. R , "The MD4 Message Digest Algorithm 1320" MIT and RSA Data Security Inc, April 1992.
- [3] National Institute of Standards and Technology, Fips 180, Federal Information Processing Standards, Secure Hash Standard (SHS), April 1993.
- [4] D. Eastlake 3rd, P.Jones.US , " Secure Hash Algorithm-1(SHA-1), September,2001.
- [5] W. Stallng , " Cryptography and network Security Principles and Practice, 4th Edition", Prentice Hall.
- [6] J.T. Brassil, S. Low and N.F. Maxemchak , "Electronic Marking and Identification Techniques to Discourage Document copying", IEEE journal on Selected Areas of Communication,,Vol.13, No. 8,October 1995.

- [7] J.T. Brassil, S.Low and N.F.maxemchak , “ Cpyright Protection for the Electronic Distribution of text Documents”, proceeding of the IEEE [8] N.F. maxemchak and S.Low, “ Marking Text Documents”, Proceeding of the IEEE International Conference on Image Processing, Washington. DC, October 26-29, 1997, pp 13-16.
- [8] Tao Chen, Jingchun Wang and Yonglei Zhou, “ Combined Digital dataand Digital Watermarking scheme for Image Authentication”, in proc IEEE, international Conferences on Info-Tech& Info-Net (ICII2001), Vol 5, pp78-82, 2001. [10] Ding
- [9] Ji-Hong Chang and Long-Wen Chang, “ A New Image copyright Protection Algorithm Using Digital dataof Trading Message and Bar Code Watermark”, Image and Vision Computing 03 New Zealand Proceedings, 26-28, November, 2003.
- [10] Con et al ,”Secure Spread Spectrum Watermarking for Multimedia”, pp 1-33, Copyright, NEC Research Institute, Tech Report95-10.
- [11] Balas Natrajan, “ Robust Public-Key Watermarking of Digital Images”, Computer Systems Laboratory, HPL, 97-118, October 1997.
- [12] D. F. Rogers and J. A. Adams,“ Mathematical Elements for Computer graphics”, TATA-McGraw- Hill, Edition,2002.
- [13] Daniel Sage & Michael Unser , “ Teaching Image Processing programming in JAVA”, IEEE Signal Processing Magazine, November 2003, pp 40-52.
- [14] D. Sage, M User, “ Easy JAVA Programming for Teaching Image Processing”, Proc. Of the 2001 IEEE International Conference on Image Processing (ICIP01) , Thessalonica, Greece, 2001, Vol. 3, pp 298- 301.
- [15] D. Roman, M. Fischer and J. Cubillo , “Digital image Processing-An Object-Oriented approach,” IEEE trans. Educ., Vol. 4, pp. 331-333,1998.
- [16] William K. Pratt, ”Digital Image Processing, (Fourth Edition), ” pages 147 - 164. Copyright © 2007 John Wiley & Sons, Inc. [19] B.P.Lathi, “Modern Digital and Analog communication system,” Oxford University Press, third edition, 1998, pp 406-416.

Cross Layer Optimization for Multiuser Video Streaming Using Distributed Cross Layer Algorithm

Mr. R. Raju¹, J. Vidhya Shankardevi²

*(Associative Professor, Sri Manakula Vinayagar Engineering College, India)

** (M.Tech, Department of Information Technology, Sri Manakula Vinayagar Engineering College, India)

Abstract: The Multimedia and networking are inseparable. The integration of multimedia services into wireless communication networks is a major source of future technological advances. Due to the integration of multimedia services, the increasing energy consumption of a mobile unit is also becoming a dominant factor in the design of communication systems. Video streaming over wireless networks is must for many applications, ranging from home entertainment to surveillance to search-and-rescue operations. Due to the increased energy requirement of signal processing and wireless transmission, the limited battery capacity of mobile devices has become a major drawback. This paper proposes a cross layer optimization algorithm, which includes routing based on neighbor discovery and dual congestion control for improving QoS. It helps in minimizing the energy required in transmission of video packets. This in turn leads to green computing

Keywords - Cross layer, Congestion control, Green computing, HCCA

I. INTRODUCTION

This section provides a brief introduction about Wireless networks and multimedia

1.1 WIRELESS NETWORKS

Wireless network is a network set up by using radio signal frequency to communicate among computers and other network devices. It referred to as WiFi. They are of three types Wide area networks (WAN) that the cellular carriers create, Wireless local area networks (WLAN), that you create, and Personal area networks (PAN), that create themselves. The components of wireless network are Antennas, Transceivers, Integrated Circuits, Analogue-Digital Converters, LCD Screens and Batteries. Infrastructure of wireless network is Cell Towers, Base Stations (access points), Filters, Routers & Switches, Power Amplifiers and Edge Packets. Working of wireless networks is two computers each equipped with wireless adapter and wireless router. When the computer sends out the data, the binary data will be encoded to radio frequency and transmitted via wireless router. The receiving computer will then decode the signal back to binary data. IEEE 802.11 standards specify two operating modes: infrastructure mode and ad hoc mode. Infrastructure mode is used to connect computers with wireless network adapters, also known as wireless clients, to an existing wired network with the help from wireless router or access point. Ad hoc mode is used to connect wireless clients directly together, without the need for a wireless router or access point. An ad hoc network consists of up

to 9 wireless clients, which send their data directly to each other

1.2 MULTIMEDIA

Multimedia means that computer information can be represented through audio, video, and animation in addition to traditional media (i.e., text, graphics drawings and images).

Multimedia is the field concerned with the computer-controlled integration of text, graphics, drawings, still and moving images (Video), animation, audio, and any other media where every type of information can be represented, stored, transmitted and processed digitally. A Multimedia Application is an Application which uses a collection of multiple media sources e.g. text, graphics, images, sound/audio, animation and/or video. Hypermedia can be considered as one of the multimedia applications

1.2.1 GENERAL CHARACTERISTICS OF MULTIMEDIA SYSTEM

The four basic characteristics of multimedia systems are Multimedia systems must be computer controlled, Multimedia systems are integrated, the information they handle must be represented digitally, and the interface to the final presentation of media is usually interactive.

1.2.2 VIDEO STREAMING

Streaming video is content sent in compressed form over the Internet and displayed by the viewer in real time. With streaming video or streaming media, a Web user does not have to wait to download a file to play it. Instead, the media is sent in a continuous stream of data and is played as it arrives. The user needs a player, which is a special program that uncompresses and sends video data to the display and audio data to speakers. A player can be either an integral part of a browser or downloaded from the software maker's Web site. Major streaming video and streaming media technologies include Real System G2 from Real Network, Microsoft Windows Media Technologies

II. OBJECTIVE OF THE PAPER

This paper proposes an algorithm called distributed cross layer optimization and cross layer optimization in order to prevent more amount of energy used in forwarding the video packets across the network.

When streaming live video across wireless links, two main sources of energy consumption are video coding and wireless transmission. In most of the state-of-the-art video encoders and wireless transmitters, there are configuration parameters which can be tuned based on varying channel conditions and/or video characteristics. It is desirable to minimize the energy consumption of all users,

including both video coding and wireless transmission, while satisfying the video quality requirement imposed by the end-user.

Streaming can be more complex in a packet based network because they have strong and specific requirements. The QOS of the video streaming can specify some requirement which is the video data flows must be formatted, denoting that the latency between consecutive packets must be the same, the data bit rate has to be high and constant, and the video packet loss rate must be close to zero. Constant bit rate is needed to feed the decoder application in a proper way, and to see the video without interrupt.

III. Related Works

The main areas, the previous work concentrated are Low power design and changing the configuration parameters to reduce the energy during transmission of video packets.

3.1 LOW POWER DESIGN ISSUES

In the wireless network low power design issues have been addressed in the following four areas.

3.1.1 DEVICE LEVEL OPTIMIZATION

Low power VLSI design [2] and low power RF circuitry [3] optimization are the main technologies for energy saving approaches. Dramatic reduction in power dissipation requires architectural, algorithmic, and circuit design optimization, which are limited by semiconductor and device technologies.

3.1.2 MEDIUM ACCESS CONTROL (MAC) PROTOCOL DESIGN

Energy-efficient MAC protocol design principle has three constraints [4]

Packet structure. It partitions a packet into two parts: the low-bit-rate part for control information and the high-bit-rate part for data; due to the different error tolerant requirements of each part, one can achieve total energy saving.

Awake/Doze mode. It puts the system into the sleep mode while not receiving or sending data.

Error Control design. The description of this design can be found in the next item.

3.1.3 COMMUNICATION SYSTEM LEVEL OPTIMIZATION

A communication system-level optimization approach is devised called, global interference minimization [5]. Global interference minimization refers to the transmitter power control problem in cellular radio systems. This has provided an optimal solution in the sense that it minimizes interference (or outage) probability. The optimal solution for the power control problem involves solving eigen values of path gain matrices. This solution is computationally expensive and impractical in the real world.

There comes [6], [7] a simplified distributed power control algorithm to tackle this problem. The distributed power control algorithm differs from the centralized power control problem in which each mobile adaptively adjusts its transmitter power according to the received interference. The distributed method releases the computational task performed by each base station.

The CDMA power control strategy also provides a simple solution to the interference minimization problem. There are two types of power control algorithms, close-loop, and open-loop control [8], [9]. Close-loop control refers to the feedback made from the base station to mobile stations for adjusting mobiles' transmitted power. Open-loop control refers to the self transmission power adjustment of mobile stations by comparing the received signal strength from the base station with a reference signal level.

3.1.4 APPLICATION LEVEL DESIGN

Engineers are developing low complexity software or hardware for multimedia processing algorithms [10], [11]. Usually low complexity algorithms yield low energy consumption, provided that less iterations or looping are involved in the computation.

One of the reasons for not considering the power consumption issue in the resource management strategy has been the failure to acknowledge the importance of the interaction between the processing power and the associated transmission power.

3.2 HCF CONTROLLED CHANNEL ACCESS (HCCA)

The HCF (hybrid coordination function) controlled channel access (HCCA) works a lot like PCF(Point Coordination Function) it contrast to PCF, in which the interval between two beacon frames is divided into two periods of CFP (Contention Free Period) and CP(Contention Period), the HCCA allows for CFPs being initiated at almost any time during a CP. This kind of CFP is called a Controlled Access Phase (CAP) in 802.11e.

A CAP is initiated by the AP whenever it wants to send a frame to a station or receive a frame from a station in a contention-free manner. The other difference with the PCF is that Traffic Class (TC) and Traffic Streams (TS) are defined. This means that the HC (Hybrid Coordinator) is not limited to per-station queuing and can provide a kind of per-session service. Also, the HC can coordinate these streams or sessions in any fashion it chooses (not just round-robin). Moreover, the stations give info about the lengths of their queues for each Traffic Class (TC). The HC can use this info to give priority to one station over another, or better adjust its scheduling mechanism.

3.3 MULTIMODE ADAPTIVE POWER SAVING (MAPS) PROTOCOL

In protocol assumptions to be made are, i) The cellular network has a feedback power control mechanism, i.e., the base station commands mobile users to increase or decrease transmitted power through the control channel at a period of time. ii) The system is set for multimode transmission where radio frequency (RF) signal-to-noise (SN) ratios are different from mode to mode.

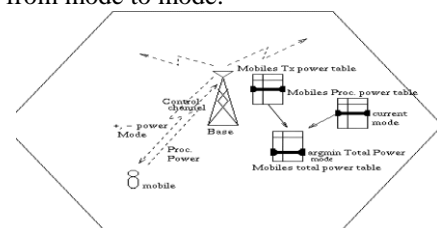


Figure.1 Base station controlled adaptive method
MAPS protocol can be summarized as,

Mobile ready to send, exchanging information between the base station and the mobile for the initial transmission power level and modes (e.g., in H.263 video transmission, one can set initially mode0 with intra coding frame).

After one frame is coded, the corresponding processing power is measured and sent to the base station, and it is stored in the processing power table. The remaining processing power levels of other modes are estimated by multiplying the pre-estimated inter mode factors.

The base station estimates the required transmitted power level of the mobile through the power control mechanism and stores the result in the transmission power table. Power levels of other modes can be easily found by multiplying different RF SN ratios.

Add the processing power table and the transmission power table to form a total power table. Find the minimum in the total power table and the corresponding mode.

The base station sends power and mode updates to the mobile; the mobile uses the new mode for next frame coding. Go back to step 2.

3.4 MULTIRATE TRANSMISSION SCHEME: MULTISTAGE CODED MODULATION (MCM)

To integrate a multimode coder into the power-saving system, an efficient transmission scheme has to be built. The beneficial transmission scheme is used here, therefore source/channel (S/C) rate optimized coding and multirate modulation (MM) are left as potential candidates.

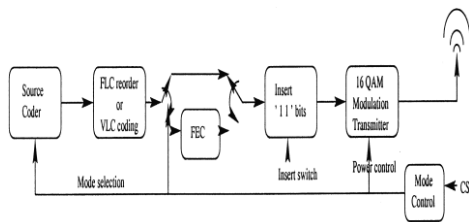


Figure.2 Multistage coded modulation

It has the simple reconfigurable QAM scheme and FEC coding that guarantee a given quality while minimizing transmission power consumption [12]. To make the switch between higher level and lower level modulation settings simpler, we introduce so-called inserted MQAM.

3.5 ISSUES IN THE RELATED WORK

Energy or power saving criteria is approached either from an information-theoretic perspective or from an implementation-specific viewpoint. Modulation strategies are derived for delay-bounded traffic. It is shown that when the transmit power and circuitry power are comparable, the transmission energy decreases with the product of bandwidth and transmit duration.

They however only consider an idealized network restricted to a single flow with no medium access controller (MAC) or link layer retransmissions, and with ideal constellation sizes.

Non-multimedia applications will experience degraded performance, cannot be universally applied to all network configuration.

IV. Problem Definition

In the proposed scheduling algorithm, we include routing based on neighbor discovery and dual congestion control

for improving QoS. After receiving the request the resource server can schedule the request .that is the form a table for which node needs which data. After scheduling the resource server can perform three steps which are Analyze the nearest requested node by use of shortest path, check the requested nodes are neighbors of each other, Form the index for avoiding neighboring collision

If the requested nodes are neighbors of each other Resource server sent the RTS (ready to sent) and ID of the neighbor requested node and then Requested node can check the ID is a neighbor's ID. If the ID is a neighbor's ID the process move to congestion control otherwise the process move to routing component. If the requested nodes are not a neighbors of each other the process move to congestion control First Congestion Control Form the queue and sent RTS to first requested node and then Node can send the CTS (clear to sent) to the resource server Second Congestion Control Form the queue and sent requested data to that first sent CTS by the node and then Requested node can receive the data

4.1 DISTRIBUTED CROSS-LAYER ALGORITHM

In the Distributed Cross-Layer Algorithms for the Optimal Control scheduler implements joint application and fabric layer optimization scheduling algorithm. Cross-layer design introduces interlayer coupling across the application layer and the fabric layer and allows the exchange of necessary information between the application layer and the fabric layer.

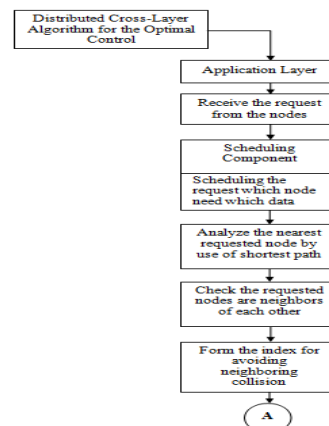


Figure 3 Distributed cross layer algorithm

First, calculate Cross-layer optimization of resource allocation throughput and Distributed Cross-Layer Algorithms for the Optimal Control throughput. Then Compare Joint optimization of resource allocation and User QOS satisfaction control & Distributed Cross-Layer Algorithms for the Optimal Control For wireless military mobile ad hoc networks, it requires a routing protocol that can dynamically adapt topology, and various other hierarchical changes of the network node.

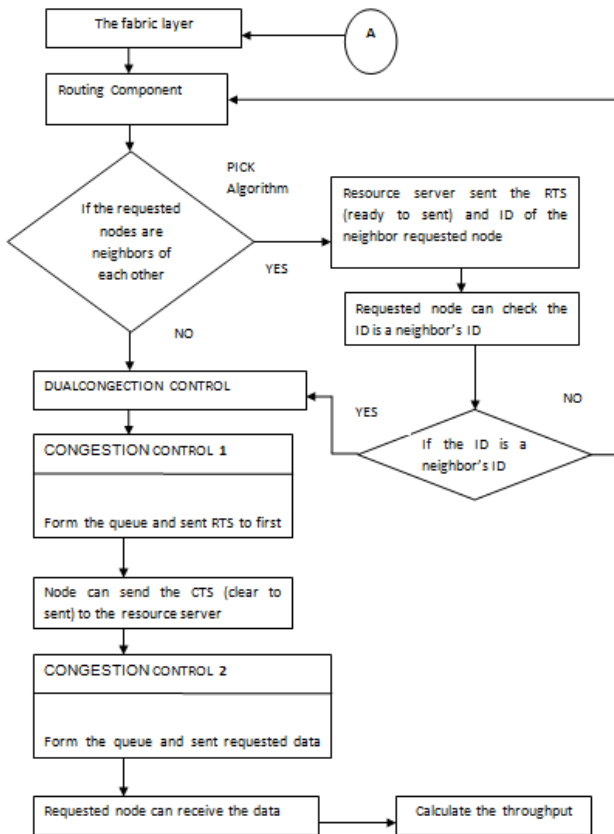


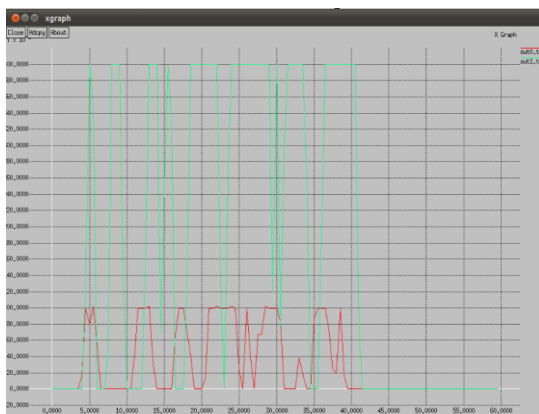
Figure.3 Distributed cross layer algorithm

4.2 ADVANTAGES OF PROPOSED WORK

This algorithm also helps in avoiding congestion control with the help of dual congestion control. To reduce the runtime computation load, the fast greedy algorithm will be employed. Transfer the data packets. Each terminal finds the maximum quality factor for all its possible complexities, and the base station searches in the space of compression complexity. The parameters to be adjusted are source coding bit rates, compression complexity, and transmitter power for all users.

V. Graph

The graph shows that the throughput is high; also the time taken for delivering the packets is less. In this X-axis denotes the time and Y-axis denotes the number of packets.



VI. Conclusion

This proposed a cross-layer optimization scheme for multi-user video streaming using distributed cross layer optimization algorithm. The goal is to minimize total energy consumption of all users, including both video coding and wireless transmission energy, while satisfying video quality target. Source coding bit rates, and transmission power corresponding to the best compression complexity are taken together as the operating parameters. Since the energy consumption is reduced it achieves green computing.

REFERENCES

- [1] M. Dertouzos, V. Zue, J. Gutttag, and A. Agarwal, "Special Report: The Oxygen Project," *Sci. Amer.*, Aug. 1999.
- [2] A. P. Chandrakasan and R.W. Brodersen, "Minimizing power consumption in digital CMOS circuits," *Proc. IEEE*, vol. 83, p. 498, Apr. 1995.
- [3] A. A. Abidi, "Low-power radio-frequency IC's for portable communications," *Proc. IEEE*, vol. 83, pp. 544-569, Apr. 1995.
- [4] H. Woesner, J. Ebert, M. Schlager, and A. Wolisz, "Power-saving mechanisms in emerging standards for wireless LANs: The MAC level perspective," *IEEE Pers. Commun.*, pp. 40-59, June 1998.
- [5] J. Zander, "Performance of optimum transmitter power control in cellular radio systems," *IEEE Trans. Veh. Technol.*, vol. 41, pp. 57-62, Feb. 1992.
- [6] S. A. Grandhi, R. Vijayan, D. J. Goodman, and J. Zander, "Centralized power control in cellular radio systems," *IEEE Trans. Veh. Technol.*, vol. 42, pp. 466-468, Nov. 1993.
- [7] G. J. Foschini and Z. Miljanic, "A simple distributed autonomous power control algorithm and its convergence," *IEEE Trans. Veh. Technol.*, vol. 42, pp. 641-646, Nov. 1993.
- [8] R. Kohno, R. Meidan, and L. B. Milstein, "Spread spectrum access methods for wireless communications," *IEEE Commun. Mag.*, Jan. 1995.
- [9] R. Padovani, "Reverse link performance of IS-95 based cellular systems," *IEEE Pers. Commun.*, Third Qtr. 1994.
- [10] A. Said and W. Pearlman, "A new fast and efficient image codec based on set partitioning in hierarchical trees," *IEEE Trans. Circuits Syst. Video Technol.*, vol. 6, pp. 243-250, June 1996.
- [11] T. Lan and A. Tewfik, "MultiGrid Embedding (MGE) image coding," in *Proc. 1999 IEEE Int. Conf. Image Processing (ICIP'99)*, Kobe, Japan, 1999.
- [12] "A unified framework of source/channel/modulation coding and low power multimedia wireless communications," in *Proc. e IEEE Second Workshop on Multimedia Signal Processing*, Redondo Beach, CA, Dec. 1998, pp. 597-602.
- [13] "ITU-T Recommendation H.263: Video Coding for Low Bit Rate Communication," ITU, 1998.
- [14] Lan and A. Tewfik, "A resource management strategy in wireless multimedia communications—total power saving in mobile terminals with a guaranteed QoS," *IEEE Trans. Multimedia*, vol. 5, pp. 267-281, Jun. 2003.
- [15] X. Lu, E. Erkip, Y. Wang, and D. Goodman, "Power efficient multimedia communication over wireless channels," *IEEE Journal Selected areas in Communications*, vol. 21, pp. 1738-1751, Dec. 2003.
- [16] X. Lu, Y. Wang, E. Erkip, and D. Goodman, "Minimize the total power consumption for multiuser video transmission over CDMA wireless network: a two-step approach," in *Proc. ICASSP'05*, Philadelphia, PA, vol. 3, pp. 941-944, Mar 2005.
- [17] IEEE Std. 802.11e-2005, Part 11: Wireless LAN medium access control (MAC) and physical layer (PHY) specifications Amendment 8: medium access control (MAC) quality of service enhancements, Nov. 2005.
- [18] S. Pollin, R. Mangharam, B. Bougard, L. Van der Perre, R. Rajkumar, I. Moerman, and F. Catthoor, "MEERA: Cross-layer methodology for energy efficient resource allocation for wireless networks," *IEEE Trans. Wireless Commun.*, vol. 6, pp. 617-628, Feb. 2007.
- [19] A Cross-Layer Algorithm of Packet Scheduling and Resource Allocation for Multi-User Wireless Video Transmission Peng Li, Yilin Chang, Nina Feng, and Fuzheng Yang, *Member, IEEE on Consumer Electronics*, Vol. 57, No. 3, August 2011.

On Semi*-Connected and Semi*-Compact Spaces

A. Robert¹, S. Pious Missier²

¹(Department of Mathematics, Aditanar College, Tiruchendur, India-628216)

²(P.G. Department of Mathematics, V.O.Chidambaram College, Thoothukudi, India-628008)

Abstract: The purpose of this paper is to introduce the concepts of semi*-connected spaces, semi*-compact spaces and semi*-Lindelöf spaces. We investigate their basic properties. We also discuss their relationship with already existing concepts.

Mathematics Subject Classification: 54D05, 54D30.

Keywords - semi*-compact, semi*-connected, semi*-Lindelöf.

I. Introduction

In 1974, Das defined the concept of semi-connectedness in topology and investigated its properties. Compactness is one of the most important, useful and fundamental concepts in topology. In 1981, Dorsett introduced and studied the concept of semi-compact spaces. Since then, Hanna and Dorsett, Ganster and Mohammad S. Sarsak investigated the properties of semi-compact spaces. In 1990, Ganster defined and investigated semi-Lindelöf spaces.

In this paper, we introduce the concepts of semi*-connected spaces, semi*-compact spaces and semi*-Lindelöf spaces. We investigate their basic properties. We also discuss their relationship with already existing concepts.

II. Preliminaries

Throughout this paper (X, τ) will always denote a topological space on which no separation axioms are assumed, unless explicitly stated. If A is a subset of the space (X, τ) , $Cl(A)$ and $Int(A)$ denote the closure and the interior of A respectively.

Definition 2.1: A subset A of a topological space (X, τ) is called

- (i) **generalized closed** (briefly g-closed)[11] if $Cl(A) \subseteq U$ whenever $A \subseteq U$ and U is open in X .
- (ii) **generalized open** (briefly g-open)[11] if $X \setminus A$ is g-closed in X .

Definition 2.2: Let A be a subset of X . The **generalized closure** [6] of A is defined as the intersection of all g-closed sets containing A and is denoted by $Cl^*(A)$.

Definition 2.3: A subset A of a topological space (X, τ) is called

- (i) **semi-open** [10] (resp. **semi*-open**[14]) if $A \subseteq Cl(Int(A))$ (resp. $A \subseteq Cl^*(Int(A))$).
- (ii) **semi-closed** [1] (resp. **semi*-closed**[15]) if $X \setminus A$ is semi-open (resp. semi*-open) or equivalently if $Int(Cl(A)) \subseteq A$ (resp. $Int^*(Cl(A)) \subseteq A$).
- (iii) **semi-regular** [2] (resp. **semi*-regular** [15]) if it is both semi-open and semi-closed (resp. both semi*-open and semi*-closed).

The class of all semi-open (resp. semi-closed, semi*-open, semi*-closed) sets is denoted by $SO(X, \tau)$ (resp. $SC(X, \tau)$, $S^*O(X, \tau)$, $S^*C(X, \tau)$).

Definition 2.4: Let A be a subset of X . Then the **semi*-closure** [15] of A is defined as the intersection of all semi*-closed sets containing A and is denoted by $s^*Cl(A)$.

Theorem 2.5[14]: (i) Every open set is semi*-open.
(ii) Every semi*-open set is semi-open.

Definition 2.6: If A is a subset of X , the semi*-frontier [13] of A is defined by $s^*Fr(A) = s^*Cl(A) \setminus s^*Int(A)$.

Theorem 2.7[13]: Let A be a subset of a space X . Then A is semi*-regular if and only if $s^*Fr(A) = \emptyset$.

Theorem 2.8[15]: If A is a subset of X , then

- (i) $s^*Cl(X \setminus A) = X \setminus s^*Int(A)$.
- (ii) $s^*Int(X \setminus A) = X \setminus s^*Cl(A)$.

Definition 2.9: A topological space X is said to be connected [18] (resp. semi-connected [3]) if X cannot be expressed as the union of two disjoint nonempty open (resp. semi-open) sets in X .

Theorem 2.10 [18]: A topological space X is connected if and only if the only clopen subsets of X are \emptyset and X .

Definition 2.11: A collection B of open (resp. semi-open) sets in X is called an open (resp. semi-open) cover of $A \subseteq X$ if $A \subseteq \bigcup \{U_\alpha : U_\alpha \in B\}$ holds.

Definition 2.12: A space X is said to be compact [18] (resp. semi-compact [4]) if every open (resp. semi-open) cover of X has a finite subcover.

Definition 2.13: A space X is said to be Lindelöf [18] (resp. semi-Lindelöf [8]) if every cover of X by open (resp. semi-open) sets contains a countable sub cover.

Definition 2.14: A function $f: X \rightarrow Y$ is said to be

- (i) semi*-continuous [16] if $f^{-1}(V)$ is semi*-open in X for every open set V in Y .
- (ii) semi*-irresolute [17] if $f^{-1}(V)$ is semi*-open in X for every semi*-open set V in Y .
- (iii) semi*-open [16] if $f(V)$ is semi*-open in Y for every open set V in X .

- (iv) semi*-closed [16] if $f(V)$ is semi*-closed in Y for every closed set V in X .
 (v) pre-semi*-open [16] if $f(V)$ is semi*-open in Y for every semi*-open set V in X .
 (vi) pre-semi*-closed [16] if $f(V)$ is semi*-closed in Y for every semi*-closed set V in X .
 (vii) totally semi*-continuous [17] if $f^{-1}(V)$ is semi*-regular in X for every open set V in Y .
 (viii) strongly semi*-continuous [17] if $f^{-1}(V)$ is semi*-regular in X for every subset V in Y .
 (ix) contra-semi*-irresolute [16] if $f^{-1}(V)$ is semi*-closed in X for every open set V in Y .
 (x) contra-semi*-irresolute [17] if $f^{-1}(V)$ is semi*-closed in X for every semi*-open set V in Y .

Theorem 2.15: Let $f: X \rightarrow Y$ be a function. Then

- (i) f is semi*-continuous if and only if $f^{-1}(F)$ is semi*-closed in X for every closed set F in Y . [16]
 (ii) f is semi*-irresolute if and only if $f^{-1}(F)$ is semi*-closed in X for every semi*-closed set F in Y . [17]
 (iii) f is contra-semi*-continuous if and only if $f^{-1}(F)$ is semi*-open in X for every closed set F in Y . [16]
 (iv) f is contra-semi*-irresolute if and only if $f^{-1}(F)$ is semi*-open in X for every semi*-closed set F in Y . [17]

Remark 2.16: [14] If (X, τ) is a locally indiscrete space, then $\tau = S^*O(X, \tau) = SO(X, \tau)$.

Theorem 2.17: [14] A subset A of X is semi*-open if and only if A contains a semi*-open set about each of its points.

III. Semi*-connected spaces

In this section we introduce semi*-connected spaces and investigate their basic properties.

Definition 3.1: A topological space X is said to be *semi*-connected* if X cannot be expressed as the union of two disjoint nonempty semi*-open sets in X .

Theorem 3.2: (i) If a space X is semi*-connected, then it is connected.

(ii) If a space X is semi-connected, then it is semi*-connected.

Proof: (i) Let X be semi*-connected. Suppose X is not connected. Then there exist disjoint non-empty open sets A and B such that $X=A \cup B$. By Theorem 2.5(i), A and B are semi*-open sets. This is a contradiction to X is semi*-connected. This proves (i).

(ii) Let X be semi-connected. Suppose X is not semi*-connected. Then there exist disjoint non-empty semi*-open sets A and B such that $X=A \cup B$. By Theorem 2.5(ii), A and B are semi-open sets. This is a contradiction to X is semi-connected. This proves (ii).

Remark 3.3: The converse of the above theorem is not true as shown in the following example.

Example 3.4: Consider the space (X, τ) where $X=\{a, b, c, d\}$ and $\tau=\{\phi, \{a\}, \{b\}, \{a, b\}, \{b, c\}, \{a, b, c\}, X\}$. Clearly, (X, τ) is connected but not semi*-connected.

Example 3.5: It can be verified that the space (X, τ) where $X=\{a, b, c, d\}$ and $\tau=\{\phi, \{a\}, \{b\}, \{a, b\}, \{a, b, c\}, X\}$ is semi*-connected but not semi-connected.

Theorem 3.6: A topological space X is semi*-connected if and only if the only semi*-regular subsets of X are ϕ and X itself.

Proof: Necessity: Suppose X is a semi*-connected space. Let A be non-empty proper subset of X that is semi*-regular. Then A and $X \setminus A$ are non-empty semi*-open sets and $X=A \cup (X \setminus A)$. This is a contradiction to the assumption that X is semi*-connected.

Sufficiency: Suppose $X=A \cup B$ where A and B are disjoint non-empty semi*-open sets. Then $A=X \setminus B$ is semi*-closed. Thus A is a non-empty proper subset that is semi*-regular. This is a contradiction to our assumption.

Theorem 3.7: A topological space X is semi*-connected if and only if every semi*-continuous function of X into a discrete space Y with at least two points is a constant function.

Proof: Necessity: Let f be a semi*-continuous function of the semi*-connected space into the discrete space Y . Then for each $y \in Y$, $f^{-1}(\{y\})$ is a semi*-regular set of X . Since X is semi*-connected, $f^{-1}(\{y\})=\phi$ or X . If $f^{-1}(\{y\})=\phi$ for all $y \in Y$, then f ceases to be a function. Therefore $f^{-1}(\{y_0\})=X$ for a unique $y_0 \in Y$. This implies $f(X)=\{y_0\}$ and hence f is a constant function. **Sufficiency:** Let U be a semi*-regular set in X . Suppose $U \neq \phi$. We claim that $U=X$. Otherwise, choose two fixed

points y_1 and y_2 in Y . Define $f: X \rightarrow Y$ by $f(x)=\begin{cases} y_1 & \text{if } x \in U \\ y_2 & \text{otherwise} \end{cases}$

Then for any open set V in Y , $f^{-1}(V)=\begin{cases} U & \text{if } V \text{ contains } y_1 \text{ only} \\ X \setminus U & \text{if } V \text{ contains } y_2 \text{ only} \\ X & \text{if } V \text{ contains both } y_1 \text{ and } y_2 \\ \Phi & \text{otherwise} \end{cases}$

In all the cases $f^{-1}(V)$ is semi*-open in X . Hence f is a non-constant semi*-continuous function of X into Y . This is a contradiction to our assumption. This proves that the only semi*-regular subsets of X are ϕ and X and hence X is semi*-connected.

Theorem 3.8: A topological space X is semi*-connected if and only if every nonempty proper subset of X has non-empty semi*-frontier.

Proof: Suppose that a space X is semi*-connected. Let A be a non-empty proper subset of X . We claim that $s^*Fr(A) \neq \emptyset$. If possible, let $s^*Fr(A) = \emptyset$. Then by Theorem 2.7, A is semi*-regular. By Theorem 3.6, X is not semi*-connected which is a contradiction. Conversely, suppose that every non-empty proper subset of X has a non-empty semi*-frontier. We claim that X is semi*-connected. On the contrary, suppose that X is not semi*-connected. By Theorem 3.6, X has a non-empty proper subset, say A , which is semi*-regular. By Theorem 2.7, $s^*Fr(A) = \emptyset$ which is a contradiction to the assumption. Hence X is semi*-connected.

Theorem 3.9: Let $f: X \rightarrow Y$ be semi*-continuous surjection and X be semi*-connected. Then Y is connected.

Proof: Let $f: X \rightarrow Y$ be semi*-continuous surjection and X be semi*-connected. Let V be a clopen subset of Y . By Definition 2.14(i) and by Theorem 2.15(i), $f^{-1}(V)$ is semi*-regular in X . Since X is semi*-connected, $f^{-1}(V) = \emptyset$ or X . Hence $V = \emptyset$ or Y . This proves that Y is connected.

Theorem 3.10: Let $f: X \rightarrow Y$ be a semi*-irresolute surjection. If X is semi*-connected, so is Y .

Proof: Let $f: X \rightarrow Y$ be a semi*-irresolute surjection and let X be semi*-connected. Let V be a subset of Y that is semi*-regular in Y . By Definition 2.14(ii) and by Theorem 2.15(ii), $f^{-1}(V)$ is semi*-regular in X . Since X is semi*-connected, $f^{-1}(V) = \emptyset$ or X . Hence $V = \emptyset$ or Y . This proves that Y is semi*-connected.

Theorem 3.11: Let $f: X \rightarrow Y$ be a pre-semi*-open and pre-semi*-closed injection. If Y is semi*-connected, so is X .

Proof: Let A be subset of X that is semi*-regular in X . Since f is both pre-semi*-open and pre-semi*-closed, $f(A)$ is semi*-regular in Y . Since Y is semi*-connected, $f(A) = \emptyset$ or Y . Hence $A = \emptyset$ or X . Therefore X is semi*-connected.

Theorem 3.12: If $f: X \rightarrow Y$ is a semi*-open and semi*-closed injection and Y is semi*-connected, then X is connected.

Proof: Let A be a clopen subset of X . Then $f(A)$ is semi*-regular in Y . Since Y is semi*-connected, $f(A) = \emptyset$ or Y . Hence $A = \emptyset$ or X . By Theorem 2.10, X is connected.

Theorem 3.13: If there is a semi*-totally-continuous function from a connected space X onto Y , then Y has the indiscrete topology.

Proof: Let f be a semi*-totally-continuous function from a connected space X onto Y . Let V be an open set in Y . Then by Theorem 2.5(i), V is semi*-open in Y . Since f is semi*-totally-continuous, $f^{-1}(V)$ is clopen in X . Since X is connected, by Theorem 2.10, $f^{-1}(V) = \emptyset$ or X . This implies $V = \emptyset$ or Y . Hence Y has the indiscrete topology.

Theorem 3.14: If there is a totally semi*-continuous function from a semi*-connected space X onto Y , then Y has the indiscrete topology.

Proof: Let f be a totally semi*-continuous function from a semi*-connected space X onto Y . Let V be an open set in Y . Since f is totally semi*-continuous, $f^{-1}(V)$ is semi*-regular in X . Since X is semi*-connected, $f^{-1}(V) = \emptyset$ or X . This implies $V = \emptyset$ or Y . Thus Y has the indiscrete topology.

Theorem 3.15: If $f: X \rightarrow Y$ is a strongly semi*-continuous bijection and Y is a space with at least two points, then X is not semi*-connected.

Proof: Let $y \in Y$. Then $f^{-1}(\{y\})$ is a non-empty proper subset that is semi*-regular in X . Hence by Theorem 3.6, X is not semi*-connected.

Theorem 3.16: Let $f: X \rightarrow Y$ be contra-semi*-continuous surjection and X be semi*-connected. Then Y is connected.

Proof: Let $f: X \rightarrow Y$ be contra-semi*-continuous surjection and X be semi*-connected. Let V be a clopen subset of Y . By Definition 2.14(viii) and Theorem 2.15(iii), $f^{-1}(V)$ is semi*-regular in X . Since X is semi*-connected, $f^{-1}(V) = \emptyset$ or X . Hence $V = \emptyset$ or Y . This proves that Y is connected.

Theorem 3.17: Let $f: X \rightarrow Y$ be a contra-semi*-irresolute surjection. If X is semi*-connected, so is Y .

Proof: Let $f: X \rightarrow Y$ be a semi*-irresolute surjection and let X be semi*-connected. Let V be a subset of Y that is semi*-regular in Y . By Definition 2.14(ix) and Theorem 2.15(iv), $f^{-1}(V)$ is semi*-regular in X . Since X is semi*-connected, $f^{-1}(V) = \emptyset$ or X . Hence $V = \emptyset$ or Y . This proves that Y is semi*-connected.

Theorem 3.18: Let X be a locally indiscrete space. Then the following are equivalent:

- (i) X is connected.
- (ii) X is semi*-connected.
- (iii) X is semi-connected.

Proof: Follows from Remark 2.16.

IV. Semi*-Compact and Semi*-Lindelöf Spaces

In this section we introduce semi*-compact spaces and semi*-Lindelöf spaces and study their properties.

Definition 4.1: A collection \mathcal{A} of semi*-open sets in X is called a *semi*-open cover* of $B \subseteq X$ if $B \subseteq \bigcup \{U_\alpha : U_\alpha \in \mathcal{A}\}$ holds.

Definition 4.2: A space X is said to be *semi*-compact* if every semi*-open cover of X has a finite subcover.

Definition 4.3: A subset B of X is said to be *semi*-compact relative to X* if for every semi*-open cover \mathcal{A} of B , there is a finite subcollection of \mathcal{A} that covers B .

Definition 4.4: A space X is said to be *semi*-Lindelöf* if every cover of X by semi*-open sets contains a countable subcover.

Remark 4.5: Every finite space is semi*-compact and every countable space is semi*-Lindelöf.

Theorem 4.6: (i) Every semi*-compact space is semi*-compact.

- (ii) Every semi*-compact space is compact.
- (iii) Every semi*-Lindelöf space is semi*-Lindelöf.
- (iv) Every semi*-Lindelöf space is Lindelöf.
- (v) Every semi*-compact space is semi*-Lindelöf.

Proof: (i), (ii), (iii) and (iv) follow from Theorem 2.5. (v) follows from Definition 2.12, Definition 2.13, Definition 4.2 and Definition 4.4.

Theorem 4.7: Every semi*-closed subset of a semi*-compact space X is semi*-compact relative to X .

Proof: Let A be a semi*-closed subset of a semi*-compact space X . Let B be semi*-open cover of A . Then $B \cup \{X \setminus A\}$ is a semi*-open cover of X . Since X is semi*-compact, this cover contains a finite subcover of X , namely $\{B_1, B_2, \dots, B_n, X \setminus A\}$. Then $\{B_1, B_2, \dots, B_n\}$ is a finite subcollection of B that covers A . This proves that A is semi*-compact relative to X .

Theorem 4.8: A space X is semi*-compact if and only if every family of semi*-closed sets in X with empty intersection has a finite subfamily with empty intersection.

Proof: Suppose X is compact and $\{F_\alpha : \alpha \in \Delta\}$ is a family of semi*-closed sets in X such that $\bigcap \{F_\alpha : \alpha \in \Delta\} = \emptyset$. Then $\bigcup \{X \setminus F_\alpha : \alpha \in \Delta\}$ is a semi*-open cover for X . Since X is semi*-compact, this cover has a finite subcover, say

$\{X \setminus F_{\alpha_1}, X \setminus F_{\alpha_2}, \dots, X \setminus F_{\alpha_n}\}$ for X . That is $X = \bigcup \{X \setminus F_{\alpha_i} : i = 1, 2, \dots, n\}$. This implies that $\bigcap_{i=1}^n F_{\alpha_i} = \emptyset$. Conversely,

suppose that every family of semi*-closed sets in X which has empty intersection has a finite subfamily with empty intersection. Let $\{U_\alpha : \alpha \in \Delta\}$ be a semi*-open cover for X . Then $\bigcup \{U_\alpha : \alpha \in \Delta\} = X$. Taking the complements, we get $\bigcap \{X \setminus U_\alpha : \alpha \in \Delta\} = \emptyset$. Since $X \setminus U_\alpha$ is semi*-closed for each $\alpha \in \Delta$, by the assumption, there is a finite subfamily, $\{X \setminus U_{\alpha_1}, X \setminus U_{\alpha_2}, \dots,$

$X \setminus U_{\alpha_n}\}$ with empty intersection. That is $\bigcap_{i=1}^n (X \setminus U_{\alpha_i}) = \emptyset$. Taking the complements on both sides, we get $\bigcup_{i=1}^n U_{\alpha_i} = X$.

Hence X is semi*-compact.

Theorem 4.9: Let X be a semi*- T_2 space in which $S^*O(X)$ is closed under finite intersection. If A is a semi*-compact subset of X , then A is semi*-closed.

Proof: Suppose X is a semi*- T_2 space in which $S^*O(X)$ is closed under finite intersection. Let A be a semi*-compact subset of X . Let $x \in X \setminus A$. Since X is semi*- T_2 , for each $a \in A$, there are disjoint semi*-open sets U_a and V_a containing x and a respectively. $\{V_a : a \in A\}$ is a semi*-open cover for A . Since A is semi*-compact, this cover has a finite subcover say, $\{V_{a_1},$

$V_{a_2}, \dots, V_{a_n}\}$. Let $U_x = \bigcap_{i=1}^n U_{a_i}$. Then by assumption, U_x is a semi*-open set containing x . Also $U_x \cap A = \emptyset$ and hence $U_x \subseteq X \setminus A$.

Then by Theorem 2.17, $X \setminus A$ is semi*-open and hence A is semi*-closed.

Theorem 4.10: Let $f : X \rightarrow Y$ be a semi*-irresolute surjection and X be semi*-compact. Then Y is semi*-compact.

Proof: Let $f : X \rightarrow Y$ be a semi*-irresolute surjection and X be semi*-compact. Let $\{V_\alpha\}$ be a semi*-open cover for Y . Then $\{f^{-1}(V_\alpha)\}$ is a cover of X by semi*-open sets. Since X is semi*-compact, $\{f^{-1}(V_\alpha)\}$ contains a finite subcover, namely $\{f^{-1}(V_{\alpha_1}), f^{-1}(V_{\alpha_2}), \dots, f^{-1}(V_{\alpha_n})\}$. Then $\{V_{\alpha_1}, V_{\alpha_2}, \dots, V_{\alpha_n}\}$ is a finite subcover for Y . Thus Y is semi*-compact.

Theorem 4.11: If $f : X \rightarrow Y$ is a pre-semi*-open function and Y is semi*-compact, then X is semi*-compact.

Proof: Let $\{V_\alpha\}$ be a semi*-open cover for X . Then $\{f(V_\alpha)\}$ is a cover of Y by semi*-open sets. Since Y is semi*-compact, $\{f(V_\alpha)\}$ contains a finite subcover, namely $\{f(V_{\alpha_1}), f(V_{\alpha_2}), \dots, f(V_{\alpha_n})\}$. Then $\{V_{\alpha_1}, V_{\alpha_2}, \dots, V_{\alpha_n}\}$ is a finite subcover for X .

Thus X is semi*-compact.

Theorem 4.12: If $f : X \rightarrow Y$ is a semi*-open function and Y is semi*-compact, then X is compact.

Proof: Let $\{V_\alpha\}$ be an open cover for X . Then $\{f(V_\alpha)\}$ is a cover of Y by semi*-open sets.

Since Y is semi*-compact, $\{f(V_\alpha)\}$ contains a finite subcover, namely $\{f(V_{\alpha_1}), f(V_{\alpha_2}), \dots, f(V_{\alpha_n})\}$.

Then $\{V_{\alpha_1}, V_{\alpha_2}, \dots, V_{\alpha_n}\}$ is a finite subcover for X . Thus X is compact.

Theorem 4.13: Let $f : X \rightarrow Y$ be a semi*-continuous surjection and X be semi*-compact.

Then Y is compact.

Proof: Let $f : X \rightarrow Y$ be a semi*-continuous surjection and X be semi*-compact. Let $\{V_\alpha\}$ be an open cover for Y . Then $\{f^{-1}(V_\alpha)\}$ is a cover of X by semi*-open sets. Since X is semi*-compact, $\{f^{-1}(V_\alpha)\}$ contains a finite subcover, namely $\{f^{-1}(V_{\alpha_1}), f^{-1}(V_{\alpha_2}), \dots, f^{-1}(V_{\alpha_n})\}$. Then $\{V_{\alpha_1}, V_{\alpha_2}, \dots, V_{\alpha_n}\}$ is a cover for Y . Thus Y is compact.

Theorem 4.14: A space X is semi*-Lindelöf if and only if every family of semi*-closed sets in X with empty intersection has a countable subfamily with empty intersection.

Proof: Suppose X is compact and $\{F_\alpha : \alpha \in \Delta\}$ is a family of semi*-closed sets in X such that $\bigcap \{F_\alpha : \alpha \in \Delta\} = \emptyset$. Then $\bigcup \{X \setminus F_\alpha : \alpha \in \Delta\}$ is a semi*-open cover for X . Since X is semi*-Lindelöf, this cover has a countable subcover, say

$\{X \setminus F_{\alpha_i} : i = 1, 2, \dots\}$ for X . That is $X = \bigcup \{X \setminus F_{\alpha_i} : i = 1, 2, \dots\}$. This implies that $\bigcap_i (X \setminus F_{\alpha_i}) = \emptyset$. Conversely, suppose

that every family of semi*-closed sets in X which has empty intersection has a countable subfamily with empty intersection. Let $\{U_\alpha : \alpha \in \Delta\}$ be a semi*-open cover for X . Then $\bigcup \{U_\alpha : \alpha \in \Delta\} = X$. Taking the complements, we get $\bigcap \{X \setminus U_\alpha : \alpha \in \Delta\} = \emptyset$.

Since $X \setminus U_\alpha$ is semi*-closed for each $\alpha \in \Delta$, by the assumption, there is a countable sub family, $\{X \setminus U_{\alpha_i} : i=1, 2, \dots\}$ with empty intersection. That is $\bigcap_i (X \setminus U_{\alpha_i}) = \emptyset$. Taking the complements we get $\bigcup_i U_{\alpha_i} = X$. Hence X is semi*-Lindelöf.

Theorem 4.15: Let $f: X \rightarrow Y$ be a semi*-continuous surjection and X be semi*-Lindelöf. Then Y is Lindelöf.

Proof: Let $f: X \rightarrow Y$ be a semi*-continuous surjection and X be semi*-Lindelöf. Let $\{V_\alpha\}$ be an open cover for Y. Then $\{f^{-1}(V_\alpha)\}$ is a cover of X by semi*-open sets. Since X is semi*-Lindelöf, $\{f^{-1}(V_\alpha)\}$ contains a countable subcover, namely $\{f^{-1}(V_{\alpha_n})\}$. Then $\{V_{\alpha_n}\}$ is a countable subcover for Y. Thus Y is Lindelöf.

Theorem 4.16: Let $f: X \rightarrow Y$ be a semi*-irresolute surjection and X be semi*-Lindelöf. Then Y is semi*-Lindelöf.

Proof: Let $f: X \rightarrow Y$ be a semi*-irresolute surjection and X be semi*-Lindelöf. Let $\{V_\alpha\}$ be a semi*-open cover for Y. Then $\{f^{-1}(V_\alpha)\}$ is a cover of X by semi*-open sets. Since X is semi*-Lindelöf, $\{f^{-1}(V_\alpha)\}$ contains a countable subcover, namely $\{f^{-1}(V_{\alpha_n})\}$. Then $\{V_{\alpha_n}\}$ is a countable subcover for Y. Thus Y is semi*-Lindelöf.

Theorem 4.17: If $f: X \rightarrow Y$ is a pre-semi*-open function and Y is semi*-Lindelöf, then X is semi*-Lindelöf.

Proof: Let $\{V_\alpha\}$ be a semi*-open cover for X. Then $\{f(V_\alpha)\}$ is a cover of Y by semi*-open sets.

Since Y is semi*-Lindelöf, $\{f(V_\alpha)\}$ contains a countable subcover, namely $\{f(V_{\alpha_n})\}$. Then $\{V_{\alpha_n}\}$ is a countable subcover for X. Thus X is semi*-Lindelöf.

Theorem 4.18: If $f: X \rightarrow Y$ is a semi*-open function and Y is semi*-Lindelöf, then X is Lindelöf.

Proof: Let $\{V_\alpha\}$ be an open cover for X. Then $\{f(V_\alpha)\}$ is a cover of Y by semi*-open sets. Since Y is semi*-Lindelöf, $\{f(V_\alpha)\}$ contains a countable subcover, namely $\{f(V_{\alpha_n})\}$. Then $\{V_{\alpha_n}\}$ is a countable subcover for X. Thus X is Lindelöf.

References

- [1] Biswas, N., On Characterization of semi-continuous functions, *Atti. Accad. Naz. Lincei. Rend. Cl. Sci. Fis. Mat. Natur.* 48(8), 1970, 399-402.
- [2] Crossley, S.G and Hildebrand, S.K., Semi-topological properties, *Fund. Math.* 74, 1972, 233-254.
- [3] Das, P., *I. J. M. M.* 12, 1974, 31-34.
- [4] Dorsett, C., Semi compactness, semi separation axioms, and product spaces, *Bulletin of the Malaysian Mathematical Sciences Society*, 4 (1), 1981, 21-28.
- [5] Dorsett, C., Semi convergence and semi compactness, *Indian J. Mech. Math.* 19 (1), 1982, 11-17.
- [6] Dunham, W., A new closure operator for Non- T_1 topologies, *Kyungpook Math. J.* 22, 1982, 55-60.
- [7] Ganster, M., Some Remarks on Strongly compact and Semi compact spaces, *Bulletin of the Malaysian Mathematical Sciences Society*, 10 (2), 1987, 67-81.
- [8] Ganster, M., On covering properties and generalized open sets in topological spaces, *Mathematical Chronicle*, 19, 1990, 27-33.
- [9] Hanna, F., Dorsett, C., Semi compactness, *Q&A in General Topology* 2, 1984, 38-47.
- [10] Levine, N., Semi-open sets and semi-continuity in topological space, *Amer. Math. Monthly.* 70, 1963, 36-41.
- [11] Levine, N., Generalized closed sets in topology, *Rend. Circ. Mat. Palermo.* 19(2), 1970, 89-96.
- [12] Mohammad S. Sarsak, On Semicompact Sets and Associated Properties, *International Journal of Mathematics and Mathematical Sciences* Volume 2009 (2009), Article ID 465387, 8 pages.
- [13] Pious Missier, S., and Robert, A., On Semi*-open Sets, *International Journal of Mathematics and Soft Computing*, 2(1), 2012, 95-102.
- [14] Robert, A. and Pious Missier, S., A New Class of Nearly Open Sets, *International Journal of Mathematical Archive.* (To appear).
- [15] Robert, A. and Pious Missier, S., On Semi*-closed sets, *Asian J. of Engineering Maths.* (To appear).
- [16] Robert, A. and Pious Missier, S., On Functions Associated with Semi*-open Sets, (communicated).
- [17] Robert, A. and Pious Missier, S., More Functions Associated with Semi*-open Sets, (communicated).
- [18] Willard, S., *General Topology*, (Addison Wesley, 1970).

Performance Comparison of Three Different Classifiers for Hci Using Hand Gestures

Anand.H.Kulkarni¹, Sachin.A.Urabinahatti²

Department of Computer Science and Engineering
Goite Institute Of Technology, Belgaum, Karnataka, India

Abstract: With the ever-increasing diffusion of computers into the society, the present popular mode of interactions with computers (mouse and keyboard) will become a bottleneck in the effective utilization of information flow between the computers and the human. The use of hand gestures provides an attractive alternative to cumbersome interface for human-computer interaction (HCI). The hand can be used to communicate, with much more information by itself compared to computer mouse, joysticks, etc. allowing a greater number of possibilities for computer interaction. Developing new techniques for human-computer interaction is very challenging, in order to use hands for interaction, it is necessary to be able to recognize them in images. In this paper, a robust hand gesture recognition system is presented for recognizing static gestures based on Zernike moments (ZMs) using Three Classifiers K-nearest Neighbour(KNN), Support Vector Machine (SVM) and Artificial Neural Network (ANN). The proposed system is able to recognize the gesture irrespective of the angles in which the hand gesture image is captured, which makes the system more flexible, and a comparative study is carried out to show which classifier works better in reorganisation of gestures.

Keywords: Hand Gesture Recognition, Human Computer Interaction, KNN, SVM, ANN, Zernike Moments.

I. INTRODUCTION

The way humans interact with computers is constantly evolving, with the general purpose of being to increase the efficiency and effectiveness by which interactive tasks are completed. The purpose of this review is to introduce the field of gesture recognition as a mechanism for interaction with computers. Gestures are expressive, meaningful body motions involving physical movements of the fingers, hands, arms, head, face, or body with the intent of:

- 1) Conveying meaningful information or
- 2) Interacting with the environment [2].

Gestures can be static or dynamic some gestures also have both static and dynamic elements, as in sign languages. A hand gesture is defined as a dynamic movement referring to a sequence of hand postures connected by continuous motions over a short time span, such as waving good-bye; hand posture is a static hand pose without involvement of movements. Hand gesture recognition finds applications in varied domains including virtual environments, smart surveillance, sign language translation, medical systems etc. Hand gesture is used to control an event like navigation of slides in Power Point Presentation i.e., during a presentation, the presenter does not have to move back and forth between computer and

screen to select the next slide. Hand Gestures can be used for remote controls for television sets, stereos and room lights. Household robots could be controlled with hand gestures. In Human Computer interaction, to operate computer with hand gestures no accessories like gloves are needed. The approaches to implement Human-Computer Interaction using Hand Gestures are based on k-Nearest Neighbour (KNN), Support Vector Machines (SVM) and Artificial Neural Network (ANN) Methods.

II. METHODOLOGY

The methodological analysis of the present work has been presented pictorially in Figure 1. The work commence with capturing Hand gesture images using cameras or scanners. These images are made to undergo pre-processing steps like filtering and segmentation. Then different texture and colour features are extracted from the processed image. Finally, the feature values are fed as input to the classifier (KNN, ANN, SVM) to classify the given image.

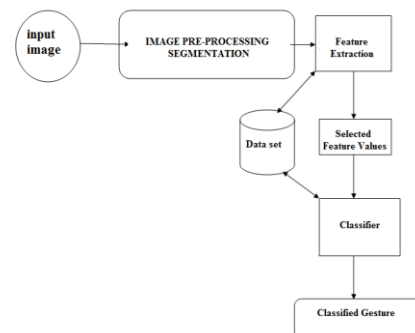


Fig 1: Block Diagram

- Input Image:** The first step in the proposed approach is to capture the video from the digital camera and extract the video frames. The video is captured from the digital camera and the captured frames are then stored in the image database.
- Image Database:** The next point in the project is creation of the image database with all the images that would be used for training and testing. The construction of an image database is clearly dependent on the application. The image database in the proposed approach consists of 200 image samples; where 40 image samples for each gesture 1, gesture 2, gesture 3, gesture 4 and gesture 5. The image database itself is responsible for the better efficiency of the classifier as it is that which decides the robustness of the algorithm.

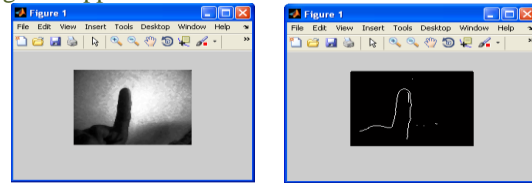
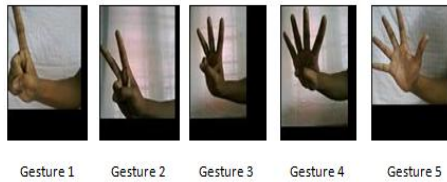


Fig 2a: Before segmentation Fig 2b: After segmentation

C. **Image Pre-processing:** Image pre-processing is the name for operations on images at the lowest level of abstraction whose aim is an improvement of the image data that suppress undesired distortions or enhances some image features important for further processing and analysis task. It does not increase image information content. Its methods use the considerable redundancy in images. Neighbouring pixels corresponding to one real object have the same or similar brightness value. If a distorted pixel can be picked out from the image, it can be restored as an average value of neighbouring pixels. In the proposed approach image pre-processing methods are applied to the frames extracted from the video captured and which are stored in image database. The image processing method i.e., median filtering is used in order to remove noise and preserve the edges in the image, Edge detection for segmentation i.e., to extract the region of interest (hand part) from the image.

i. Median Filtering

The median filter is a nonlinear digital filtering technique, often used to remove noise. Such noise reduction is a typical pre-processing step to improve the results of later processing (for example, edge detection on an image). Median filtering is a nonlinear operation often used in image processing to reduce "salt and pepper" noise. Median filtering is a non-linear smoothing method that reduces the blurring of edges and significantly eliminates impulse noise. It suppresses image noise without reducing the image sharpness and can be applied iteratively.

ii. Segmentation

Image segmentation is process i.e., used to simplify and/or change the representation of an image into something that is more meaningful and easier to analyze. As the premise of feature extraction and pattern recognition, image segmentation is one of the fundamental approaches of digital image processing. Image Segmentation is the process that is used to distinguish object of interest from background. The proposed approach uses edge as a factor to extract the region of interest from the given image. Edges are pixels where the intensity image function changes abruptly. Edge detectors are collection of local image pre-processing methods used to locate changes in the brightness function. Edges are the sign of lack of continuity, and ending. EDGE function finds edges in intensity image. EDGE function takes image as its input, and returns a binary image of the same size, with 1's where the function finds edges in image and 0's elsewhere. The figure 2 shows the filtered image and the edges in the segmented image that is detected using EDGE function.

D. **Feature Extraction**

The aim of this phase is to find and extract features that can be used to determine the meaning of a given gesture. Shift and rotation invariant features lead to a better recognition of hand gestures even if the hand gesture is captured in a different angle.

Hence Zernike moments are used to calculate feature set. The proposed approach considers 11 order of moments to extract the feature from the segmented image.

Zernike moments (ZM)

Objects are generally recognized with the help of their shapes and most of the real time objects have irregular shapes. Hence they cannot be properly described with the help of regular shape descriptors like circularity, linearity and so on. Hence we adopt Zernike moments. The moments are higher space feature vector and are generally of order N. The more order of moments are considered, the better the recognition probability. If any image is assumed to be an object, its descriptors are known as feature vectors.

The Zernike polynomials are a set of complex, orthogonal polynomials defined over the interior of a unit circle $x^2 + y^2 = 1$

Zernike moment of order n and repetition m is defined as:

$$Z_{nm} = \frac{1}{\pi} \int_{x^2+y^2 \leq 1} V_{nm}(\rho, \theta) f(x, y) dx dy \quad (1)$$

Where:

$f(x,y)$ is the image intensity at (x,y) in Cartesian coordinates,

n is a non-negative integer, m is an integer such that $n-|m|$ is even positive integer

and $|m| \leq n, \geq x^2+y^2$

θ is the angle between vector ρ and the x -axis in a counter clockwise direction.

The form of orthogonal Zernike basis polynomials, $V_{nm}(\rho, \theta)$

$V_{nm}(\rho, \theta)$ is a complex conjugate of $V_{nm}(\rho, \theta) = R_{nm}(\rho)e^{-jm\theta}$ in polar coordinates

(ρ, θ) and $j = \sqrt{-1}$

The polar coordinates polar coordinates (ρ, θ) in the image domain are related to Cartesian coordinates (x,y) as $x = \rho \cos(\theta)$ and $y = \rho \sin(\theta)$.

$R_{nm}(\rho)$ is a radial defined as follows:

$$R_{nm}(\rho) = \sum_{s=0}^{n-m/2} \frac{(-1)^s [(n-s)! \rho^{n-2s}]}{s!(n+\frac{|m|-s}{2})(n-\frac{|m|-s}{2})} \quad (2)$$

To calculate the Zernike moments of an image $f(x,y)$, the image is first mapped onto the unit disk using polar coordinates, where the center of the image is the origin of the unit disk. Pixels falling outside the unit disk are not used in the calculation. Because Z_{mn} is complex, we use the Zernike moments modules Z_{mn} as the features of shape in the recognition of patterns. The magnitude of Zernike moments has rotational invariance property. An

image can be better described by a small set of its Zernike moments than any other type of moments such as geometric moments, Legendre moments, and complex moments in terms of mean-square error. Zernike moments do not have the properties of translation invariance and scaling invariance. The way to achieve such invariance is image translation and image normalization before calculation of Zernike moments [10].

D. Gesture Recognition & Classification:

The recognition process consists of two phases, training and classification. Classification of gestures is done using KNN (k-Nearest Neighbor), ANN (Artificial Neural Network) and SVM (Support Vector Machine) classifiers.

i. K-Nearest Neighbour

KNN stands for “k-nearest neighbour algorithm”, it is one of the simplest but widely used machine learning algorithm. An object is classified by the “distance” from its neighbours, with the object being assigned to the class most common among its k distance-nearest neighbours. If k = 1, the algorithm simply becomes nearest neighbour algorithm and the object is classified to the class of its nearest neighbour [11][12].

ii. Artificial Neural Network

An Artificial Neural Network (ANN) is an information processing paradigm that is inspired by the way biological nervous systems, such as the brain, process the information. The key element of this paradigm is the novel structure of the information processing system. It is composed of a large number of highly interconnected processing elements (neurons) working in unison to solve specific problems. ANNs, like people, learn by example. An ANN is configured for a specific application, such as pattern recognition or data classification, through a learning process. A trained neural network can be thought of as an "expert" in the category of information it has been given to analyze [9][13].

iii. Support Vector Machine

SVMs are currently a hot topic in the machine learning community, creating a similar enthusiasm at the moment as Artificial Neural Networks used to do before. Far being, SVMs yet represent a powerful technique for general (nonlinear) classification, regression and outlier detection with an intuitive model representation. Support vector machines are a set of related supervised learning methods used for classification and regression. Given a set of training examples, each marked as belonging to one of two categories, an SVM training algorithm builds a model that predicts whether a new example falls into one category or the other [14][15][16].

III. Experimental Analysis & Results

- *Experimental Analysis WRT Number of features v/s KNN efficiency*

Number of Features	Recognition Rate for Gesture 1 (%)	Recognition Rate for Gesture 2 (%)	Recognition Rate for Gesture 3 (%)	Recognition Rate for Gesture 4 (%)	Recognition Rate for Gesture 5 (%)	Overall KNN Efficiency (%)
2	65	45	58	56	51	55
3	82	70	78	74	76	76
4	77	51	58	62	72	64
5	56	48	49	56	51	52
6	70	55	60	61.5	66	62.5
7	85	70	72.5	78	82	77.5
8	79	59	65	67	75	69
9	79	61	68	65	74.5	69.5
10	71	73	74	71.5	70.5	72
11	85	70	79	76	77.5	77.5

Table 1: Number of features v/s KNN efficiency.

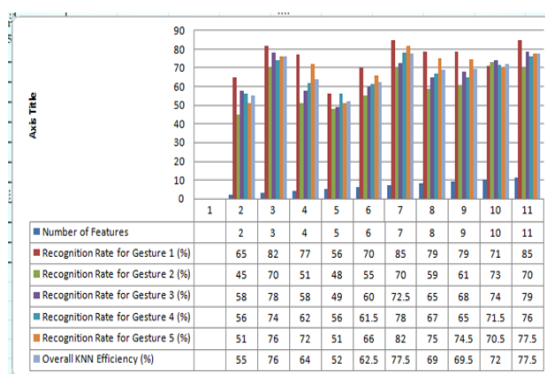


Figure 3: Graphical Analysis for Number of Features v/s KNN efficiency

The table 1 shows the dependency of the KNN efficiency on the number of features. Number of features represents the n order of Zernike moments, where n is number of feature vector for per training set. The efficiency of the KNN is optimum when there are 11 order of moments i.e., 11 feature vector. The above figure 3. Shows the graphical representation of analysis with respect to Number of Features v/s KNN Efficiency which shows the system is optimum when there are 11 order of Zernike moments.

- *Experimental Analysis WRT Number of features v/s Neural Network efficiency*

Number of Features	Recognition Rate for Gesture 1 (%)	Recognition Rate for Gesture 2 (%)	Recognition Rate for Gesture 3 (%)	Recognition Rate for Gesture 4 (%)	Recognition Rate for Gesture 5 (%)	Overall Neural Network Efficiency (%)
2	66	52	56	58	63	59
3	82	70	71	79	78	76
4	77	51	62	65	65	64
5	56	48	50.5	52	53.5	52
6	70	55	60.5	66	61	62.5
7	85	70	71	74	87.5	77.5
8	79	59	63	67	77	69
9	71	73	70	70.5	75.5	72
10	60	55	59.5	57	56	57.5
11	94	71	82	79	86.5	82.5

Table 2: Number of features v/s Neural Network efficiency

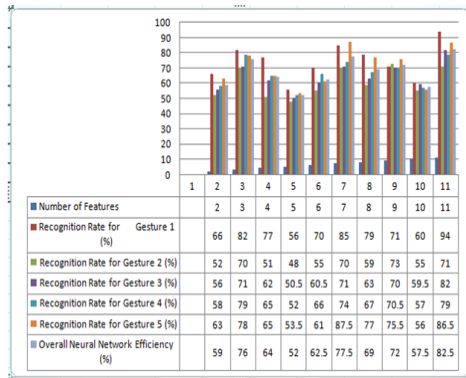


Figure 4: Graphical Analysis for Number of Features v/s ANN efficiency

The table 2 shows the dependency of the Neural Network efficiency on the number of features. Number of features represents the n order of Zernike moments, where n is number of feature vector for per training set. The efficiency of the network is optimum when there are 11 order of moments i.e., 11 feature vector. The below figure 4. shows the graphical representation of analysis with respect to Number of Features v/s Neural Network Efficiency which shows the neural network is optimum when there are 11 order of Zernike moments.

• *Experimental Analysis WRT Number of features v/s SVM efficiency*

Number of Features	Recognition Rate for Gesture 1 (%)	Recognition Rate for Gesture 2 (%)	Recognition Rate for Gesture 3 (%)	Recognition Rate for Gesture 4 (%)	Recognition Rate for Gesture 5 (%)	Overall SVM Efficiency (%)
2	62	42	49	51	56	52
3	70	62	64	66	68	66
4	77	51	59	62	71	64
5	56	78	67	65	69	67
6	70	69	69	67.5	72	69.5
7	85	70	76	75	81.5	77.5
8	93	59	74	75	79	76
9	95	77	86	81	91	86
10	92	83	86	83	93.5	87.5
11	93	89	87	89	97	91

Table 3: Number of features v/s SVM efficiency

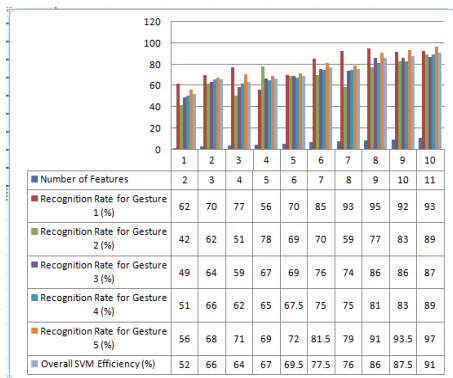


Figure 5: Graphical Analysis for Number of Features v/s SVM efficiency

The table 3 shows the dependency of the SVM efficiency on the number of features. Number of features represents the n order of Zernike moments, where n is number of feature vector for per training set. The efficiency of the SVM is optimum when there are 11 order of moments i.e., 11 feature vector. The above figure 5. Shows the graphical representation of analysis with respect to Number of Features v/s KNN Efficiency which shows the neural network is optimum when there are 11 order of Zernike moments

• *Comparative result of three classifiers*

Classifier	System efficiency
KNN	77.5%
ANN	82.5%
SVM	91%

Table 4: System Efficiency Using Three Different Classifiers

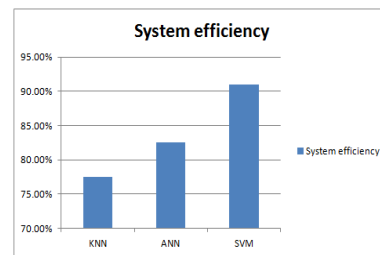


Figure 6: Graphical Analysis of System Efficiency Using Three Different Classifiers

IV. CONCLUSION

In this project work the area of hand-gesture recognition is introduced. The system developed here is a real time hand gesture recognition, main problem of gesture recognition lies in the complexity of the classification algorithms, especially when using high dimensional feature vectors which become necessary in order to be able to distinguish several hundreds of gestures. Thus, the development of good classification methods & precise features is very important in order to run such systems in real-time. The Proposed approach is based on Zernike moments for feature extraction because ZM's are direction and scaling invariant. Therefore proposed approach got better results with 11 Zernike moments and achieved the recognition rate of the KNN up to 77.5%, ANN up to 82.5% and SVM up to 91% for the gesture image with uniform background in light environment with minimum distance of 1 or 2 feet. The results show a significant accuracy in real time recognition. So by this we can conclude this system works with better efficiency considering SVM as a classifier either then ANN or KNN classifier.

References

[1] Vladimir I. Pavlovic, Rajeev Sharma, and Thomas S. Huang, Fellow, "Visual Interpretation of Hand Gestures for Human-Computer Interaction: A Review", IEEE transactions on Pattern Analysis and Machine Intelligence, vol. 19, no. 7, July 1997.

[2] Sushmita Mitra, Tinku Acharya, "Gesture Recognition: A Survey" IEEE Transactions on Systems, Man, and Cybernetics—Part C:

Applications and Reviews, Vol. 37, No. 3, MAY 2007.

Computing Technology, Vol. 2, No. 4, pp. 30 ~ 35, 2010.

- [3] Prateem Chakraborty, Prashant Sarawgi, Ankit Mehrotra, Gaurav Agarwal, Ratika Pradhan, "Hand Gesture Recognition: A Comparative Study", Proceedings of the International MultiConferenc.
- [4] Elena Sánchez-Nielsen, "Hand Gesture Recognition for Human-Machine Interaction", Department of Statistic O.R. and Computer Science, University of La Laguna Edificio de Física y Matemáticas 38271, La Laguna, Spain.
- [5] Pragati Garg, Naveen Aggarwal and Sanjeev Sofat, "Vision Based Hand Gesture Recognition", World Academy of Science, Engineering and Technology 49 2009.
- [6] S.M. Hassan Ahmeda, Todd C. Alexanderb and Georgios C. Anagnostopoulosb, "Real-time, Static and Dynamic Hand Gesture Recognition for Human-Computer Interaction", Electrical Engineering, University of Miami.
- [7] Cristina Manresa, Javier Varona, Ramon Mas and Francisco J. Perales, "Real -Time Hand Tracking and Gesture Recognition for Human-Computer Interaction" Departamento de Matemáticas e Informàtica Universitat de les Illes Balears. WSEAS Transactions on Computers, Volume 9, Issue 6 (June 2010), Pages: 583-592, Year of Publication: 2010, ISSN: 1109-2750.
- [8] Dr. Jane J. Stephan, Sana'a Khudayer, "Gesture Recognition for Human-Computer Interaction (HCI)", International Journal of Advancements in
- [9] Christos Stergiou and Dimitrios Siganos , "NeuralNetworks".
- [10] Gholam Reza Amayeh, Ali Erol, George Bebis, and Mircea Nicolescu , "Accurate and Efficient Computation of High Order Zernike Moments"
- [11] Image Classification Using SVM, KNN and Performance Comparison with Logistic Regression Team member: Qi Gu, Zhifei Song
- [12] http://en.wikipedia.org/wiki/K-nearest_neighbor_algorithm
- [13] Klimis Symeonidis, "Hand Gesture Recognition Using Neural Networks, School of Electronic and Electrical Engineering
- [14] R. Gonzalez and R. Woods, "Digital image processing", 3rd Edition 2008, Prentice Hall, New York.
- [15] Sukhwinder Singh, Vinod Kumar, *Senior Member, IEEE*, H.K. Verma, and Dilbag Singh, "SVM Based System for classification of Microcalcifications in Digital Mammograms", Proceedings of the 28th IEEE EMBS Annual International Conference New York City, USA, Aug 30-Sept 3, 2006.
- [16] Faramarz Dehghan, Hamid Abrishami-Moghaddam," Comparison Of SVM And Neural Network Classifiers In Automatic Detection Of Clustered Microcalcifications In Digitized Mammograms", Proceedings Of The Seventh International Conference On Machine Learning And Cybernetics, Kunming, 12-15 July, IEEE 2008.

Modeling and Analysis of Spur Gear for Sugarcane Juice Machine under Static Load Condition by Using FEA

V. Siva Prasad¹, Syed Altaf Hussain², V.Pandurangadu³, K.PalaniKumar⁴

*(PG student, School of Mechanical Engineering RGM College of Engg. & Technology, Nandyal-518501, India.)

** (School of Mechanical Engineering, RGM College of Engineering & Technology, Nandyal-518501, India)

*** (Department of Mechanical Engineering, JNTU College of Engineering, Anantapur-512002, India)

**** (Department of Mechanical Engineering, Sri Sai Ram Institute of Technology, Chennai-44, Tamilnadu, India)

Abstract : This paper describes design and analysis of Spur gear. In the present work, it is proposed to substitute the metallic gear of sugarcane juice machine with plastic gears to reduce the weight and noise. For the purpose of two different types of plastic materials were considered namely Nylon and Polycarbonate and their viability are checked with their counterpart metallic gear (Cast iron). Based on the static analysis, the best plastic material is recommended for the purpose. Static analysis of a 3-D model has been performed using ANSYS 10.0. Compared to Cast iron spur gears Nylon gears are suitable for the application of sugarcane juice machine application under limited load conditions.

Keywords: Cast iron spur gears, Static analysis, Nylon Spur gears, and Polycarbonate spur gears.

I. Introduction

According to the position of axes of the shafts the following are the different kinds of gears.

a. Parallel

- Spur gear
- Helical gear
- Rack and pinion

b. Intersecting

- Bevel gears

c. Non – Intersecting and Non parallel

- Worm gears

The gear materials used for the manufacture of gears depend upon the strength and service conditions like wear and noise etc. The gears maybe manufactured from metallic or non – metallic materials. The cast iron is widely used for the manufacture of gears due to its good wearing properties, excellent machine ability and ease of producing complicated shapes by casting method. The non – metallic materials like wood, rawhide, compressed paper and plastics like Nylon, Acrylic and Polycarbonate etc are used for gears, especially for reducing weight and noise.

Weight reduction can be achieved primarily by the introduction of better material, design optimization and better manufacturing processes. The plastic materials have corrosion resistance, low electrical and thermal conductivity, easily formed into complex shapes, wide choices of appearance, colors and transparencies. The introduction of plastic materials was made it possible to reduce the weight of the spur gear without any reduction on load carrying capacity and stiffness.

The Nylon materials have high strength, good mechanical

and abrasion resistance property, excellent wear resistance, resistant to most chemicals and self-lubricant. Polycarbonate materials have, high impact strength, good dimension stability and heat resistance. Since, Nylon and Poly carbonate have good properties as stated above the cast iron spur gears of sugarcane juice machine are being replaced by plastic spur gears. The plastic material offer opportunities for substantial weight saving but not always are cost-effective over their cast iron counter parts.

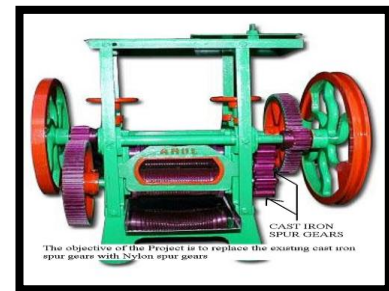


Fig. No. 1 Schematic diagram of a sugarcane juice machine.

II. Literature Review:

The review mainly focuses on replacement of Cast iron spur gears with the Nylon spur gear in the application of sugarcane juice machine.

R. Yakut, H. Düzçükoğlu*, M.T. Demirci et al

[1] In this study, load carrying capacity and occurring damages of gears which are made of PC/ABS blends were investigated. PC is hard material and ABS is soft material. The usage of materials limits these drawbacks. However PC and ABS polymers combine each other, the PC/ABS blends have suitable mechanical properties for gear applications in the industrial areas. In this study, usability of PC/ABS composite plastic materials as spur gear was investigated. PC/ABS gears were tested by applying three different loading at two different numbers of revolutions on the FZG experiment set.

J.L. Moya, A.S. Machado, J.A.Velásquez, R. oytisolo, A.E.Hernández, J.E. Fernández, and J.M. Sierra et al [2] In this study they have performed a theoretical analysis of a procedure to determine the Lewis Factor and also performed the contact analysis of spur gears to find the stress distribution between gear tooth.

Alexandre Luís Gasparin^I; Leandro Luís Corso^I; Eduardo Kirinus Tentardini^{II}; Regina Célia Reis Nunes^{III}; Maria Madalena de Camargo Forte^{IV}; Ricardo Vinicius Bof de Oliveira, et al [3] The focus of this paper is to establish a characterisation method for seven polyamide (PA) grades to determine the major material to manufacture an automotive

worm gear. The composite properties were measured according to the worm gear loadings: tensile strength, Young's modulus, abrasion and impact resistance. They were also correlated to the PA moisture absorption and its glass fibre (GF) reinforcement. The data from mechanical tests were applied in the finite element analysis (FEA) using the von Mises stress criterion. Before the rig tests of the PA worm gears, the injection process was evaluated, through the capillary rheometry. A higher difficulty to process PA 6/6 30% GF was found, due to its lower apparent viscosity. In the end, the influence of moisture absorption was as decisive to the gear's material selection as the GF to the pinion. Thus, the PAs with the best performance were: PA 6 with 30% GF (gear) and with PA 60% GF (pinion).

III. Specification Of The Problem

In this project work it is proposed to substitute the metallic gear of sugarcane juice machine with plastic gears to reduce the weight and noise. For the purpose of two different types of plastic materials were considered namely Nylon and Polycarbonate and their viability are checked with their counterpart metallic gear (Cast iron). Based on the static analysis, the best plastic material is recommended for the purpose. A virtual model of spur gear was created in Pro-E. Model is imported in ANSYS 10.0 for analysis by applying normal load conditions. After analysis a comparison is made among existing Cast iron spur gear. Based on the deflections and stresses from the analysis we choose the best one between the Nylon and Polycarbonate spur gears.

IV. GEARS

Gear is nothing but a toothed wheel which is useful to transmit power from one shaft to another shaft. They are suitable when two machine parts are nearer to each other. They give exact ratio of transmission of motion, slip cannot take place between gears, they are useful for high torque transmission.

In spur gear teeth is parallel to axis of rotation. Spur gear transmit power from one shaft to another parallel shaft.

4.1 Materials for Gears :

The gear materials used for the manufacture of gears depend upon the strength and service conditions like wear and noise etc. The gears maybe manufactured from metallic or non – metallic materials. The cast iron is widely used for the manufacture of gears due to its good wearing properties, excellent machine ability and ease of producing complicated shapes by casting method. The non – metallic materials like wood, rawhide, compressed paper and plastics like Nylon, Acrylic and Polycarbonate etc are used for gears, especially for reducing weight and noise.

4.2 Theoretical calculations of conventional Cast iron Spur gear:

In the present analysis the maximum torque, allowable stress and tangential load of the spur gear are calculated based on the desired sugarcane juice machine motor specifications and are as following below:

4.3 Specifications of sugarcane juice machine motor:

Power (P) = 1.5 kW = 1500 watt

Speed (N) = 1400 RPM

$$\text{Power (P)} = 2 * \pi * N * T / 60$$

$$1500 = (2 * \pi * 1400 * T) / 60$$

$$\text{Torque (T)} = (1500 * 60) / (2 * \pi * 1400)$$

$$T = 10.2313 \text{ N-m}$$

$$T = 102313 \text{ N-mm}$$

$$T = F * (d/2)$$

$$F = T / (d/2)$$

$$F = 10231 / 90$$

$$F = 113.677 \text{ N}$$

Where 'F' is the Tangential load

Using Lewis equation

$$\text{Tangential load } F = \sigma_b * y * P_c * b$$

$$113.677 = \sigma_b * 0.1034 * (\pi * 10) * 54$$

$$\sigma_b = 113.677 / (0.1034 * (\pi * 10) * 54)$$

$$\sigma_b = 0.648 \text{ N/mm}^2$$

Where 'σ_b' is the allowable stress

'y' is the Lewis form factor

'P_c' (Circular pitch) = π * module

'b' is the face width of the gear

'd' is the pitch circle diameter of the gear

The Maximum allowable stress as per the design of the desired spur gear, σ_b = 0.648 N/mm²

Allowable stress of Cast iron (high grade) =

$$= \text{Ultimate tensile strength} / 3$$

$$= 320 / 3 = 106.67 \text{ N/mm}^2 > 0.648 \text{ N/mm}^2$$

Allowable stress of Nylon =

$$= \text{Ultimate tensile strength} / 3$$

$$= 69 / 3 = 23 \text{ N/mm}^2 > 0.648 \text{ N/mm}^2$$

Allowable stress of Polycarbonate =

$$= \text{Ultimate tensile strength} / 3$$

$$= 62 / 3 = 20.67 \text{ N/mm}^2 > 0.648 \text{ N/mm}^2$$

SO the design is safe

(Reference 1: www.professionalplastics.com

Reference 2: p.s.g data book pageno: 25.33,

Page no 8.21)

V. Geometric details of desired spur gear:

- Module (m) = 10 mm
- Addendum = 1 module
- Dedendum = 1.157 * module
- Pressure angle (α) = 20 degrees
- Tooth thickness(t) = 1.571 * module
- Whole depth = 2.25 * module
- Face width(b) = 5.4 * module
- Fillet radius = 3.9 * module
- No of teeth(z) = 18

5.1 Calculation of gear tooth proportions:

- Pitch circle diameter (p.c.d) = z * m
= 18 * 10 = 180 mm
- Base circle diameter (D_b) = D Cos α
= 180 Cos 20 = 169.145 mm
- Out circle diameter = (Z+2) * m
= (18+2) * 10 = 200 mm
- Clearance = Circular pitch / 20
= 31.4 / 20 = 1.57 mm
- Dedendum =
= Addendum + clearance = 10 + 1.57
= 11.57 mm.

• Module = D/z = 180/18 = 10mm.

• Dedendum circle diameter = p.c.d - 2 * dedendum = 80 - 2 * 11.57 = 156.86 mm.

• Fillet radius = circular pitch/8 = 31.4/8 = 3.9 mm

• Pitch circle diameter (Pc) = m * z = 10 * 18 = 180mm

• Hole depth = 2.25 * m = 2.25 * 10 = 22.5mm

• Thick ness of the tooth = 1.571 * 10 = 15.71mm

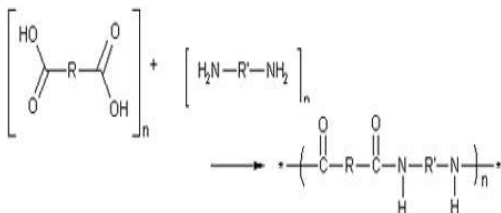
• Face width (b) = Ψ * a = 0.3 * 180 = 54 mm
 Where 'a' is the centre distance between two gears = (180 + 180 / 2) 180 mm and assume Ψ = 0.3
 Diametral pitch = Number of teeth/ P.C.D = 18 / 180 = 0.1 mm

VI. Specification Of Existing Cast Iron Gear:

The typical chemical composition of the cast iron material : Carbon - 2.5 to 3.7%, Silicon - 1.0 to 3.0%, Manganese - 0.5 to 1.0%, Phosphorus - 0.1 to 0.9% and Sulphur - 0.07 to 0.10%

6.1 SPECIFICATIONS OF NYLON AND POLYCARBONATE PLASTIC MATERIALS:

Chemical composition of Nylon:

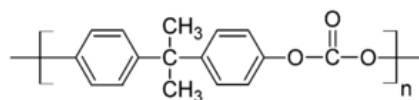


Its properties are determined by the R and R' groups in the monomers. In nylon 6, 6, R' = 6C and R = 4C alkanes, but one also has to include the two carboxyl carbons in the diacid to get the number it donates to the chain.

The majorities of nylons tends to be semi-crystalline and are generally very tough materials with good thermal and chemical resistance. The different types give a wide range of properties with specific gravity, melting point and moisture content tending to reduce as the nylon number increases. Nylons can be used in high temperature environments. Heat stabilized systems allow sustained performance at temperatures up to 185oC.

Chemical composition of Polycarbonate:

The main polycarbonate material is produced by the reaction of bisphenol A and phosgene COCl₂. The overall reaction can be written as follows:



Polycarbonates received their name because they are polymers containing carbonate groups (-O-(C=O)-O-). Most polycarbonates of commercial interest are derived from rigid monomers. A balance of useful features including temperature resistance, impact resistance and

optical properties position polycarbonates between commodity plastics and engineering plastics

Table: 1 Material properties of cast iron, Nylon and Polycarbonate:

Material Property	Cast Iron	Nylon	Polycarbonate
Young's Modulus (N/mm ²)	1.65e5	2.1e5	2.75e5
Poisson's ratio	0.25	0.39	0.38
Density (Kg/mm ³)	7.2e-6	1.13e-6	1.1e-6
Co-efficient of friction	1.1	0.15-0.25	0.31
Ultimate Tensile strength (Mpa)	320-350	55-83	55-70

VII. Finite Element Analysis Of Spur Gear :

Finite element modeling is described as the representation of the geometric model in terms of a finite number of element and nodes. It is actually a numerical method employed for the solution of structures or a complex region defining a continuum. Solutions obtained by this method are rarely exact. However, errors in the approximate solution can be minimized by increasing the number of equations till the desired accuracy obtained. This is an alternative to analytical methods that are used for getting exact solution of analysis problems. The solution of general problem by finite element method always follows an orderly step-by-step process. for analysis in ANSYS 10.0. The loading conditions are assumed to be static. The element choosen is solid Brick 8 node45.

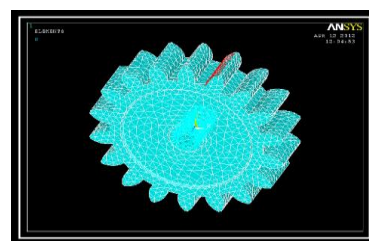


Fig1: Loads and boundary conditions of the gear

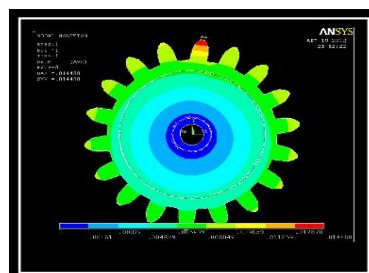


Fig 2: Displacement pattern for Cast iron gear

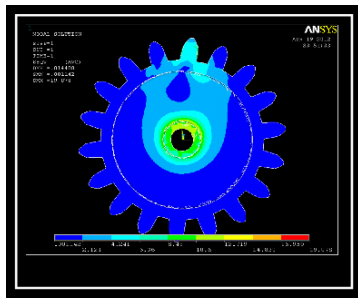


Fig 3: Stress distribution for Cast iron gear

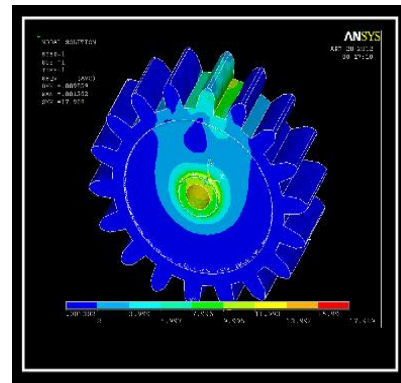


Fig 6: Stress distribution for Polycarbonate spur gear.

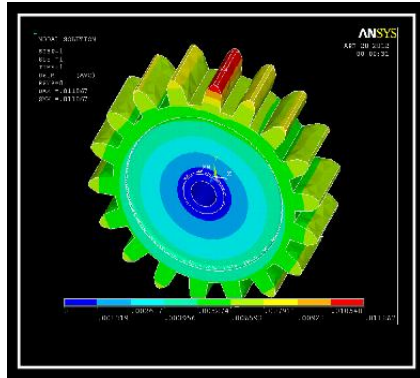


Fig4: Displacement pattern for Nylon gear

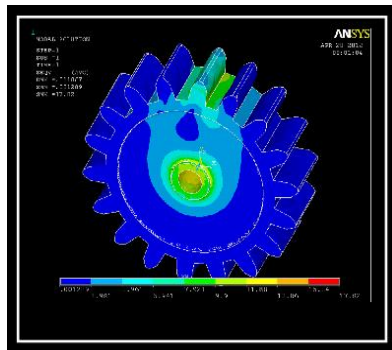


Fig 4 Stress distribution for Nylon spur gear

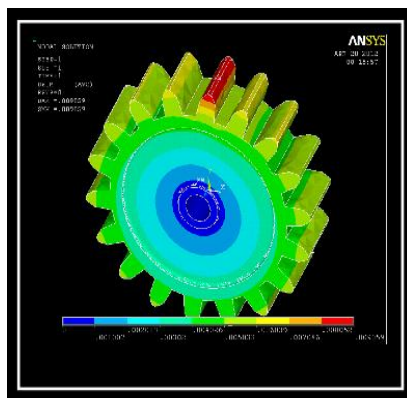


Fig 5: Displacement pattern for Polycarbonate spur gear.

VIII. Results Obtained From Ansys:

From the static analysis using ansys the deflections and vonmisse stress and strain values for the cast iron, Nylon and polycarbonate are obtained as following below tables.

For Cast Iron Spur gear:

Pressure (N/mm ²)	Vonmisse Stress (N/mm ²)	Deflection (mm)	Strain
1	3.832	0.002905	2.21e-4
2	7.665	0.005811	4.41e-4
3	11.497	0.008716	6.62e-4
4	15.33	0.011622	8.82e-4
5	19.078	0.014488	1.14e-3

For Nylon Spur gear:

Pressure (N/mm ²)	Vonmisse Stress (N/mm ²)	Deflection (mm)	Strain
1	3.582	0.002381	2.19e-4
2	7.163	0.004762	4.37e-4
3	10.745	0.007143	6.56e-4
4	14.327	0.009524	8.74e-4
5	17.82	0.011867	1.29e-3

For Polycarbonate Spur gear:

Pressure (N/mm ²)	Vonmisse Stress (N/mm ²)	Deflection (mm)	Strain
1	3.615	0.001817	2.20e-4
2	7.863	0.003635	4.45e-4
3	10.846	0.005452	6.61e-4
4	14.462	0.007274	8.82e-4
5	17.989	0.009059	1.38e-3

stresses and deflection values of the spur gear were increased. And the minimum stress values are obtained for Nylon spur gear compared with Cast iron and Polycarbonate. According to the study, analysis, results and graphs we recommend the best plastic material is Nylon and Nylon gears are suitable for the application of sugar cane juice machine under limited load conditions.

Graphs:

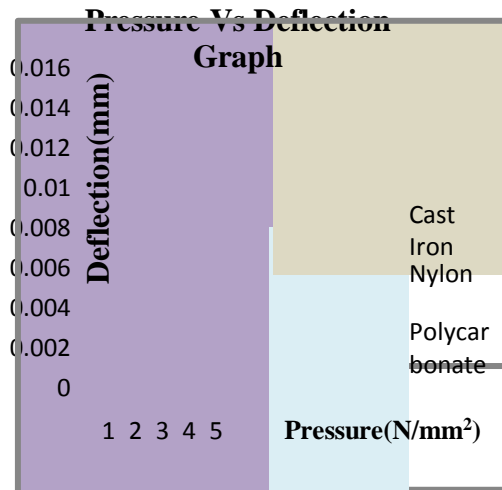


Fig 1: Pressure Vs Deflection graph

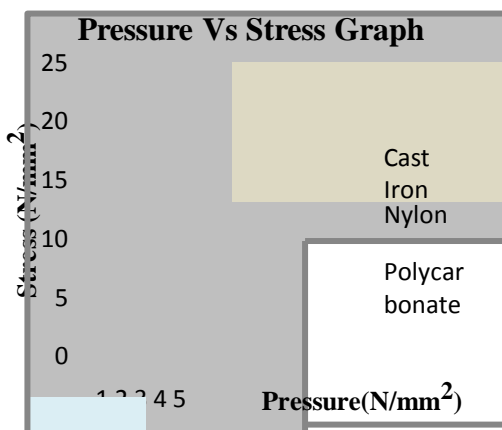


Fig 2: Pressure Vs Stress graph

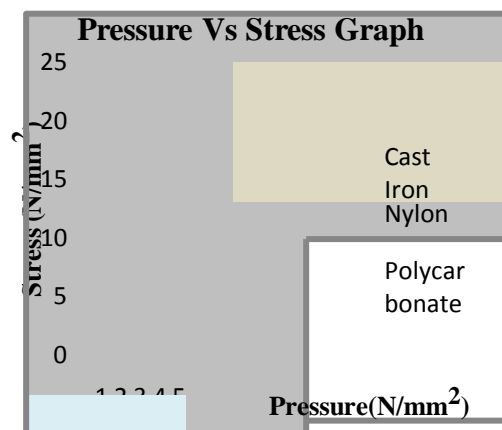


Fig 3: Stress Vs Strain graph

Results and discussion

From the static analysis by increasing the pressure on the tooth flank surface we observed that the vonmisse

IX. CONCLUSIONS:

To find the suitable design gears with less weight and less cost, corrosion resistance, frictionless also. To design and manufacture a sugarcane juice for a common people including women. With less cost, self lubricating neat and clean hygienic juice. With more material removal of deflection and stress are increased. So for safe operation of my design is more appropriate under limited load conditions for Nylon gear.

References:

10.1 Journals Papers:

- [1] R. Yakut, H. Düzcükoğlu*, M.T. Demirci Mechanical Education Department, University of Selcuk, Campus, Konya, Turkey, Received 30.09.2009; published in revised form 01.11.2009
- [2] K. Mao, A new approach for polyamide composite gear design, *Wear* 262 (2007) 432-441.
- [3] M.H. Tsai, Y.C. Tsai, A method for calculating static transmission errors of plastic spur gears using fem evaluation, *Finite Elements in Analysis and Design* 27 (1997) 345-357.
- [4] C.H. Kim, Durability improvement method for polyamide spur gears, *Tribology International* 39 (2006) 1454-1461.
- [5] S. Senthilvelan, R. Gnanamoorthy, Effect of rotational speed on the performance of unreinforced a glass fibre reinforced nylon 6 spur gears, *Materials and Design* 28 (2007) 765-72. Analysis". and Testing *Materials Science*, 12 (3), 2006, 220-225.

10.2 Books:

- [6] Machine drawing by N.D.BHATT
- [7] Machine design by S.M.D.JALALUDEEN.
- [8] Design data book compiled by PSG College of Technology, COIMBATORE.
- [9] Machine design by BANDARI.
- [10] Theory of machines by KHURMI.
- [11] Van Me lick , H.G.H. "Tooth Bending Effects in plastic Spur Gears," *Gear Technology*.
- [12] White, J., D . Walton and D.J. Weale. "The Beneficial effect of Tip Relief on Plastic Spur Gears," ANTEC Conf. Proc. Society Plastics Engineers (1998).
- [13] Rosler, J. "Zur Tragfähigkeitssteigerung Thermoplastischer Zahnrad mit Fullstoffen," PhD thesis, berlin University of Technology, 2004.
- [14] Plastic Gears are more reliable when engineers account for material properties and manufacturing process during design. Zan Smith: Motion System Design, July 2000.

Design of Modules to Implement a Structure by Discrete Reckoning Codes for Embedding Into Video Coding Testing Applications

Susrutha Babu Sukhavasi¹, Suparshya Babu Sukhavasi¹ Sr Sastry K², Ranga Rao Orugu³
 P. Bosebabu³, M. Aravind Kumar⁴

¹Faculty, Department of ECE, K L University, Guntur, AP, India.
²M.Tech -VLSI Student, Department of ECE, K L University, Guntur, AP, India.
³ Faculty, Department of ECE, Andhra Loyola College Of Eng &Tech, Vijayawada, AP, India.
⁴M.Tech -VLSI Student, Padmasri Dr.B.V.Raju Institute of Technology, Medak, A.P, India.

Abstract : In this paper, necessary modules have been implemented to make architecture to insert into motion estimation. The significant function of motion estimation (ME) in a video coder, testing such a module is of priority concern. While focusing on the testing of ME in a video coding system, this work presents an error detection and data recovery (EDDR) design, based on the residue-and quotient (RQ) code, to embed into ME for video coding testing applications. An error in processing elements (PEs), i.e. key components of a ME, can be detected and recovered effectively by using the proposed EDDR design. Experimental results indicate that the modules required for proposed EDDR design for ME testing can detect errors and recover data with an acceptable area overhead and timing penalty. Importantly, the proposed EDDR design performs satisfactorily in terms of throughput and reliability for ME testing applications.

Keywords – Motion Estimation, SAD Tree, Error detection and recover circuits.

I. INTRODUCTION

Methodologies

Coding approaches such as parity code, Berger code, and residue code have been considered for design applications to detect circuit errors. Residue code is generally separable arithmetic codes by estimating a residue for data and appending it to data. Error detection logic for operations is typically derived by a separate residue code, making the detection logic is simple and easily implemented. For instance, assume that N denotes an integer, N1 and N2 represent data words, and m refers to the modulus. A separate residue code of interest is one in which N is coded as a pair. $N \cdot m$ is the residue N of m modulo . Error detection logic for operations is typically derived using a separate residue code such that detection logic is simply and easily implemented. However, only a bit error can be detected based on the residue code. Additionally, an error can not be recovered effectively by using the residue codes. Therefore, this work presents a quotient code, which is derived from the residue code, to assist the residue code in detecting multiple errors and recovering errors. In order to simplify the complexity of circuit design, the implementation of the module is generally dependent on the addition operation. Additionally, based on the concept of residue code, the following definitions shown can be applied to generate the RQ code for circuit design. the corresponding circuit design of the RQCG is easily realized by using the simple adders (ADDs). Namely, the

RQ code can be generated with a low complexity and little hardware cost.

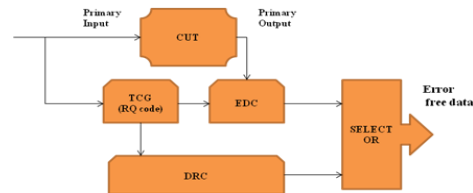


Fig 1: Circuit Diagram

Sum Of Absolute Difference Calculation

By utilizing PEs, SAD shown in as follows, in a macro block with size N X N of can be evaluated:

$$\begin{aligned}
 SAD &= \sum_{i=0}^{N-1} \sum_{j=0}^{N-1} |X_{ij} - Y_{ij}| \\
 &= \sum_{i=0}^{N-1} \sum_{j=0}^{N-1} |(q_{xij} \cdot m + r_{xij}) - (q_{yij} \cdot m + r_{yij})|
 \end{aligned}$$

Where $r_{xi,j}$, $q_{xi,j}$ and $r_{yi,j}$, $q_{yi,j}$ denote the corresponding RQ code of $X_{i,j}$, $Y_{i,j}$ and modulo M. Importantly, and represent the luminance pixel value of Cur_pixel and Ref_pixel, respectively.

PIXEL VALUES

	0	1	2	3
0	128	128	64	255
1	128	64	255	64
2	64	255	64	128
3	255	64	128	128
	Cur_pixel			

	0	1	2	3
0	1	1	2	3
1	1	2	3	4
2	2	3	4	5
3	3	4	5	5
	Ref_pixel			

Fig 2: Circuit Diagram

NUMERIC CALCULATION

A numerical example of the 16 pixels for a 4X 4 macroblock in a specific PEi of a ME is described . We presents an example of pixel values of the Cur_pixel and Ref_pixel. Based on, the SAD value of the 4X 4 macroblock is

$$\begin{aligned}
 SAD &= \sum_{i=0}^3 \sum_{j=0}^3 |X_{ij} - Y_{ij}| \\
 &= X_{00} - Y_{00} + |X_{01} - Y_{01}| + \dots + X_{33} - Y_{33} \\
 &= (128 - 1) + (128 - 1) + \dots + (128 - 5) \\
 &= 2124.
 \end{aligned}$$

According to describe about RQ Code for modulo operation is assumed $M=2^6-1=63$ RQ code for SAD value $RT=RPEi=|2124|63=45$ and $QT=QPEi=|2124/63|=33$.

II. MAIN MODULE'S:

1. SAD TREE
2. RQ CODE GENERATION
3. ERROR DETECTION CIRCUIT
4. DATA RECOVERY CIRCUIT

MODULE DESCRIPTION:

2.1 SAD TREE

We propose a 2-D intra-level architecture called the Propagate Partial SAD The architecture is composed of PE arrays with a 1-D adder tree in the vertical direction. Current pixels are stored in each PE, and two sets of continuous reference pixels in a row are broadcasted to PE arrays at the same time. In each PE array with a 1-D adder tree, distortions are computed and summed by a 1-D adder tree to generate one-row SAD. The row SADs are accumulated and propagated with propagation registers in the vertical direction. The reference data of searching candidates in the even and odd columns are inputted by Ref. Pixels 0 and Ref Pixels 1, respectively. After initial cycles, the SAD of the first searching candidate in the zero th column is generated, and the SADs of the other searching candidates are sequentially generated in the following cycles. When computing the last searching candidates in each column, the reference data of searching candidates in the next columns begin to be inputted through another reference input. In Propagate Partial SAD, by broadcasting reference pixel rows and propagating partial-row SADs in the vertical direction, it provides the advantages of fewer reference pixel registers and a shorter critical path. Since $Rt(Q_t)$ is equal to RPE_i (QPE_i) EDC is enabled and a signal "0" is generated to describe a situation in which the specific PE_i is error-free. Conversely, if SA1 and SA0 errors occur in bits 1 and 12 of a specific PE_i i.e. the pixel values of $PE_i = 2124$. for video coding systems, motion estimation (ME) can remove most of temporal redundancy, so a high compression ratio can be achieved. Among various ME algorithms, a full-search block matching algorithm (FSBMA) is usually adopted because of its good quality and regular computation. In FSBMA, the current frame is partitioned into many small macroblocks (MBs) of size For each MB in the current frame (current MB), one reference block that is the most similar to current MB is sought in the searching range of size in the reference frame. The most common used criterion of the similarity is the sum of absolute differences (SAD).

$$SAD = \sum_{i=0}^{N-1} \sum_{j=0}^{N-1} |X_{i,j} - Y_{i,j}|$$

$$= \sum_{i=0}^{N-1} \sum_{j=0}^{N-1} |(q_{xij} \cdot m + r_{xij}) - (q_{yij} \cdot m + r_{yij})|$$

where cur and ref are pixel values in the current MB (current pixel) and reference block (reference pixel), respectively, is one searching candidate in the search range, Distortion is the difference between the current pixel and the reference pixel, and SAD is the total distortion of this searching candidate. The row (column) SAD is the summation of distortions in a row (column). After all searching candidates are examined, the searching candidate that has the smallest SAD is selected as the motion vector of the current MB. Although FSBMA provides the

best quality among various ME algorithms, it consumes the largest computation power. In general, the computation complexity of ME varies from maximum of a typical video coding system. Hence, a hardware accelerator of ME is required. Variable block-size motion estimation (VBSME) is a new coding technique and provides more accurate predictions compared to traditional fixed block-size motion estimation (FBSME). With FBSME, if an MB consists of two objects with different motion directions, the coding performance of this MB is worse. On the other hand, for the same condition, the MB can be divided into smaller blocks in order to fit the different motion directions with VBSME. Hence, the coding performance is improved. VBSME has been adopted in the latest video coding standards, including H.263, MPEG-4, WMV9.0, and H.264/AVC. For instance, in H.264/AVC, an MB with a variable block size can be divided into seven kinds of blocks including 4x4, 4x8, 8x4, 8x8, 8x16, 16x8, and 16x16. Although VBSME can achieve a higher compression ratio, it not only requires huge computation complexity but also increases the difficulty of hardware implementation for ME. Traditional ME hardware architectures are designed for FBSME, and they can be classified into two categories.

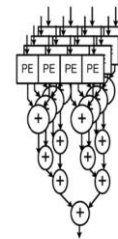


Fig3: Partial SAD tree

One is an inter-level architecture, where each processing element (PE) is responsible for one SAD of a specific searching candidate and the other is an intra-level architecture, where each PE is responsible for the distortion of a specific current pixel.

The concept of the proposed SADTree architecture. The proposed SAD Tree is a 2-D intra-level architecture and consists of a 2-D PE array and one 2-D adder tree with propagation registers. Current pixels are stored in each PE, and reference pixels are stored in propagation registers for data reuse. In each cycle, current and reference pixels in a row are inputted into propagation registers to update reference pixels. In propagation registers, reference pixels are propagated in the vertical direction row by row. In SAD Tree architecture, all distortions of a searching candidate are generated in the same cycle, and by an adder tree, distortions are accumulated to derive the SAD in one cycle. In order to provide a high utilization and data reuse, the snake scan is adopted and reconfigurable data path propagation registers are developed in the proposed SAD Tree, which consists of five basic steps from A to E. The first step, A, fetches pixels in a row and the shift direction of propagation registers is downward. When calculating the last candidates in a column, one extra reference pixel is required to be inputted, that is, step B. When finishing the computation of one column, the reference pixels in the propagation registers

are shifted left in step C. Because the reference data have already been stored in the propagation registers, the SAD can be directly calculated. The next two steps, D and E, are the same as steps A and B except that the shift direction is upward. After finishing the computation of one column in the search range, we execute step C and then go back to step A. This procedure will iterate until all searching candidates in the search range have been calculated. the data reuse between two successive searching candidates can be maximized

SUB MODULES'S

- PROCESSING ELEMENT
- ADDER TREE
- HALF ADDER
- FULL ADDER
- RIPPLE CARRY ADDER

2.1.1 PROCESSING ELEMENT

A ME (Motion Estimation) consists of many PEs incorporated in a 1-D or 2-D array for video encoding applications. A PE generally consists of two ADDs (i.e. an 8-b ADD and a 12-b ADD) and an accumulator (ACC). Next, the 8-b ADD (a pixel has 8-b data) is used to estimate the addition of the current pixel (Cur pixel) and reference pixel (Ref_pixel). Additionally, a 12-b ADD and an ACC are required to accumulate the results from the 8-b ADD in order to determine the sum of absolute difference (SAD) value for video encoding applications. Notably, some registers and latches may exist in ME to complete the data shift and storage. encoding applications. Notably, some registers and latches may exist in ME to complete the data shift and storage. The PEs are essential building blocks and are connected regularly to construct a ME. Generally, PEs are surrounded by sets of ADDs and accumulators that determine how data flows through them. PEs can thus be considered the class of circuits called ILAs, whose testing assignment can be easily achieved by using the fault model, cell fault model (CFM). Using CFM has received considerable interest due to accelerated growth in the use of high-level synthesis, as well as the parallel increase in complexity and density of integration circuits (ICs). Using CFM makes the tests independent of the adopted synthesis tool and vendor library. Arithmetic modules, like ADDs (the primary element in a PE), due to their regularity, are designed in an extremely dense configuration. A ME generally consists of PEs with a size of 4 x 4. However, accelerating the computation speed depends on a large PE array, especially in high-resolution devices with a large search range such as HDTV. Additionally, the visual quality and peak signal-to-noise ratio (PSNR) at a given bit rate are influenced if an error occurred in ME process. A testable design is thus increasingly important to ensure the reliability of numerous PEs in a ME. Moreover, although the advance of VLSI technologies facilitate the integration of a large number of PEs of a ME into a chip, the logic-per-pin ratio is subsequently increased, thus decreasing significantly the efficiency of logic testing on the chip. As a commercial chip, it is absolutely necessary for the ME to introduce design for testability (DFT). Motion estimation is the process of determining motion vectors that describe the transformation from one 2D image to another; usually from adjacent frames in a video sequence. It is an ill-posed problem as the motion is in three dimensions but the images

are a projection of the 3D scene onto a 2D plane. The motion vectors may relate to the whole image (global motion estimation) or specific parts, such as rectangular blocks, arbitrary shaped patches or even per pixel. The motion vectors may be represented by a translational model or many other models that can approximate the motion of a real video camera, such as rotation and translation in all three dimensions and zoom. Closely related to motion estimation is optical flow, where the vectors correspond to the perceived movement of pixels. In motion estimation an exact 1:1 correspondence of pixel positions is not a requirement. Applying the motion vectors to an image to synthesize the transformation to the next image is called motion compensation. The combination of motion estimation and motion compensation is a key part of video compression as used by MPEG 1, 2 and 4 as well as many other video codec's.

2.1.2 ADDER TREE

In this module Half Adder is a digital combinational circuit that is used for the addition of two bits and provides an output in the form of a sum bit and a carry bit. The logical functional equations that relate the outputs S and C of a half adder circuit to the input bits are given below
 $Sum(S) = A \text{ ex-OR } B$
 $Carry(C) = A.B$

Thus a half adder circuit can easily be synthesized by using 1 ex-OR gate and 1 AND gate. Since a half adder circuit can only be used to add two bits, it becomes obsolete in case of multi-bit addition in practical applications.

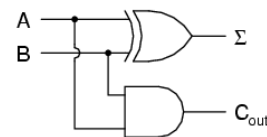


Fig 4: Logic Diagram

A	B	Σ	C _{out}
0	0	0	0
0	1	1	0
1	0	1	0
1	1	0	1

Fig5: Truth Table

APPLICATIONS:

- In electronics, an adder or summer is a digital circuit that performs addition of numbers. In many computers and other kinds of processors, adders are used not only in the arithmetic logic unit(s), but also in other parts of the processor, where they are used to calculate addresses, table indices, and similar.
- Although adders can be constructed for many numerical representations, such as binary-coded decimal or excess-3, the most common adders operate on binary numbers.
- In cases where two's complement or ones' complement is being used to represent negative numbers, it is trivial to modify an adder into an adder-subtractor. Other signed number representations require a more complex adder.

2.1.3 FULL ADDER:

In this module describe about full adder operation. The limitation of a half-adder is that it cannot accept a carry-in bit. the carry-in bit represents the carry-out of the previous low-order bit position. Thus a half-adder can be used only for the two least significant digits when adding two multi bit binary numbers, since there can be no possibility of a propagated carry to this stage. In multi bit addition, a carry bit from a previous stage must be taken into account, which gives rise to the necessity for designing a full adder. A full adder can accept two operands bits, a_i and b_i , and a carry-in bit c_i from previous stage; it produces a sum bit s_i and a carry-out bit c_o . sum bit s_i is 1 if there is an odd number of 1's at the inputs of the full adder, whereas the carry-out c_o is 1 if there are two or more 1's at the inputs. The sum and carry out bits will be 0 otherwise. In ripple carry adder, the carry signals must ripple through all the full adders before the outputs stabilize to the correct values; hence such an adder is often called a ripple adder. addition is to be performed the carry-out generated from the least significant stage of the adder propagates through the successive stages and produces a carry-in into the most significant stage of the adder. The time required to perform addition in a ripple adder depends on the time needed for the propagation of carry signals through the individual stages of the adder. Thus ripple carry addition is not instantaneous. The greater the number of stages in a ripple carry adder the longer is the carry propagation time, and consequently the slower the adder.

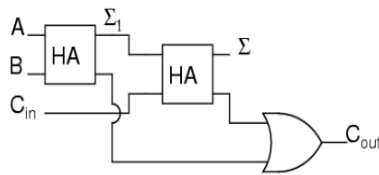


Fig 6: Full Adder Using Half Adder

C_1	X_1	Y_1	Z_1	C_2
0	0	0	0	0
0	0	1	1	0
0	1	0	1	0
0	1	1	0	1
1	0	0	1	0
1	0	1	0	1
1	1	0	0	1
1	1	1	1	1

Fig7: Truth table

APPLICATIONS:

1. Addition is an essential function in fundamental arithmetic operations.
2. It is also the most copiously used operation in application-specific processors and digital signal processing application (DSP).
3. Full-adder has been introduced by integrating the full-adder into a multiplier-less finite impulse response (FIR) filter that is commonly used in the multi rate filter bank for biomedical applications.

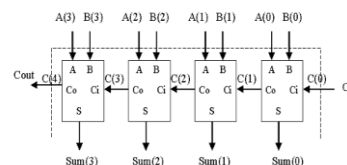
2.1.4 RIPPLE CARRY ADDER

A standard 8-bit ripple-carry adder built as a cascade from eight 1-bit full-adders. Click the input switches or use the following bind keys: ('c') for carry-in, for A0..A7 and ('1','2', ..., '8') for B0..B7. To demonstrate the typical behavior of the ripple-carry adder, very large gate-delays are used for the gates inside the 1-bit adders - resulting in an addition

time of about 0.6 seconds per adder. Note that each stage of the adder has to wait until the previous stage has calculated and propagates its carry output signal. Obviously, the longest delay results for operands like $A = 0b0000000$, $B=0b11111111$ or $A=0b01010101$ and $B=0b10101010$ (select these, and then switch carry-in to both 0 and 1, and watch the circuit to settle). Therefore, the total delay of a ripple-carry adder is proportional to the number of bits.

Faster adders are often required for bit widths of 16 or greater. A carry-look ahead adder (CLA) is a type of adder used in digital logic. A carry-look ahead adder improves speed by reducing the amount of time required to determine carry bits. It can be contrasted with the simpler, but usually slower, ripple carry adder for which the carry bit is calculated alongside the sum bit, and each bit must wait until the previous carry has been calculated to begin calculating its own result and carry bits (see adder for detail on ripple carry adders). The carry-look ahead adder calculates one or more carry bits before the sum, which reduces the wait time to calculate the result of the larger value bits. The Kogge-Stone adder and Brent-Kung adder are examples of this type of adder. Arithmetic operations like addition, subtraction, multiplication, division are basic operations to be implemented in digital computers using basic gates like AND, OR, NOR, NAND etc. Among all the arithmetic operations if we can implement addition then it is easy to perform multiplication (by repeated addition), subtraction (by negating one operand) or division (repeated subtraction). Half Adders can be used to add two one bit binary numbers. It is also possible to create a logical circuit using multiple full adders to add N-bit binary numbers. Each full adder inputs a **Cin**, which is the **Cout** of the previous adder. This kind of adder is a **Ripple Carry Adder**, since each carry bit "ripples" to the next full adder. The first (and only the first) full adder may be replaced by a half adder. The block diagram of 4-bit Ripple Carry Adder is shown here below. The layout of the ripple carry adder is simple, which allows for fast design time; however, the ripple carry adder is relatively slow, since each full adder must wait for the carry bit to be calculated from the previous full adder. The gate delay can easily be calculated by inspection of the full adder circuit. Each full adder requires three levels of logic. In a 32-bit [ripple carry] adder, there are 32 full adders, so the critical path (worst case) delay is $31 * 2(\text{for carry propagation}) + 3(\text{for sum}) = 65$ gate delays. Arithmetic Module Generator (AMG) supports various hardware algorithms for two-operand adders and multi-operand adders. These hardware algorithms are also used to generate multipliers, constant-coefficient multipliers and multiply accumulators. In the following, we briefly describe the hardware algorithms that can be handled by AMG.

4 Bit Ripple Carry Adder



Want to write a VHDL model for a 4 bit ripple carry adder.

```

Logic equation for each full adder is:
sum <= a xor b xor ci;
co <= (a and b) or (ci and (a or b));
    
```

Fig8: Ripple Carry Adder

The most straightforward implementation of a final stage adder for two n-bit operands is a ripple carry adder, which requires n full adders (FAs). The carry-out of the ith FA is connected to the carry-in of the (i+1)th FA. Figure shows a ripple carry adder for n-bit operands, producing n-bit sum outputs and a carry out.

III. RQ CODE GENERATION

Coding approaches such as parity code, Berger code, and residue code have been considered for design applications to detect circuit errors. Residue code is generally separable arithmetic codes by estimating a residue for data and appending it to data. Error detection logic for operations is typically derived by a separate residue code, making the detection logic is simple and easily implemented. The basic problem we have to resolve is that memory and communications technology isn't totally reliable; we have to expect and be ready to deal with errors in the hardware. This document will describe two very different technologies for detecting, and maybe correcting, errors that may occur in data storage and transmission. The first approach to be described is more appropriate for environments like memory: a relatively small amount of data is fetched in parallel. This approach, called "error detecting and correcting codes," is based on defining a distance between two bit strings in terms of the number of bits that have to change to get from the first string to the second. Extra bits are added to each string, which are set so that some minimum number of bits must change to get from one valid string to another. If the received string isn't valid, it is assumed that the correct string is the one "closest" to the received string. The second approach is more appropriate to environments in which relatively large amounts of data are to be transferred, but they are transferred serially. In this approach a "signature" is appended to the data string; the number of bits in the signature is much less than the number of bits that would be required to do an error correcting code. This approach will lead to adding checksums or cyclic redundancy checks to the string. R. W. Hamming wrote the paper that both opened and closed this field in 1950. His interest was in providing a means of self-checking in computers, which were just being developed at the time he wrote this. the paper appeared in the *Bell System Technical Journal*, April, 1950. Definitely worth tracking down in the library and reading The Hamming distance between two bit strings is the number of bits you have to change to convert one to the other: this is the same as the number of edges you have to traverse in a binary hypercube to get from one of the vertices to the other. The basic idea of an error correcting code is to use extra bits to increase the dimensionality of the hypercube, and make sure the Hamming distance between any two valid points is greater than one.

- If the Hamming distance between valid strings is only one, a single-bit error results in another valid string. This means we can't detect an error.
- If it's two, then changing one bit results in an invalid string, and can be detected as an error.

Unfortunately, changing just one more bit can result in another valid string, which means we can't know which bit was wrong: so we can detect an error but not correct it.

3.1 CONCURRENT ERROR DETECTION (CED)

While the extended BIST schemes generally focus on memory circuit, testing-related issues of video coding have seldom been addressed. Thus, exploring the feasibility of an embedded testing approach to detect errors and recover data of a ME is of worthwhile interest. Additionally, the reliability issue of numerous PEs in a ME can be improved by enhancing the capabilities of concurrent error detection (CED). The CED approach can detect errors through conflicting and undesired results generated from operations on the same operands. CED can also test the circuit at full operating speed without interrupting a system. Thus, based on the CED concept, this work develops a novel EDDR architecture based on the RQ code to detect errors and recovery data in PEs of a ME and, in doing so, further guarantee the excellent reliability for video coding testing applications. Error detection logic for operations is typically derived using a separate residue code such that detection logic is simply and easily implemented. However, only a bit error can be detected based on the residue code. Additionally, an error can't be recovered effectively by using the residue codes. Therefore, this work presents a quotient code, which is derived from the residue code, to assist the residue code in detecting multiple errors and recovering errors. the corresponding circuit design of the RQCG is easily realized by using the simple adders (ADDs). Namely, the RQ code can be generated with a low complexity and little hardware cost. Concurrent test methods enable integrated circuits to verify the correctness of their results during normal operation. While this ability is highly desirable, especially in high safety applications, designing a cost-effective concurrently testable circuit is a challenging task. Quality assessment of concurrent test methods relies on several parameters, including the model of detectable faults or errors, the worst-case detection latency, and the incurred area overhead. Additionally, an important consideration is whether a concurrent test method is intrusive or non-intrusive, i.e. whether the original circuit is modified or left intact, respectively. The importance of concurrent test in only accentuated by the plethora and variety of previous research efforts in this area. Several low-cost, non-intrusive, concurrent fault detection (CFD) methods have been proposed for stuck-at faults in combinational circuits. C-BIST employs input monitoring to perform concurrent self-test. While hardware overhead is very low, the method relies on an ordered appearance of all possible input vectors before a signature indicating circuit correctness can be calculated, resulting in very long detection latency. This problem is alleviated in R-CBIST, where the requirement for a uniquely ordered appearance of all input combinations is relaxed at the cost of a small RAM. Alternatively, latency is reduced through the comparison-based method which uses additional logic to predict the circuit responses for a complete test set. Towards the high-cost end, several concurrent error detection (CED) zero-latency methods have been proposed for both combinational and sequential circuits. Reducing the area overhead below the cost of duplication typically requires redesign of the original circuit, thus leading to intrusive methodologies. In more and more applications, cryptographic operations are performed on embedded processors. Some of the most important applications in this context are payment, identification, access control, digital rights management and

IP protection. In order to guarantee the security of these applications, it is necessary to implement countermeasures against physical attacks on the embedded processors. During the last 15 years numerous physical attacks have been published that allow the extraction of secret information based on the observation or manipulation of an embedded device and its environment. Typical examples of physical attacks are timing attacks, power analysis attacks and fault attacks. While timing and power analysis attacks have received much attention already immediately after their publication, not so much attention has been paid on fault attacks so far. However, fault attacks become increasingly important. Meanwhile there exist several publications that discuss methods to induce faults in order to reveal secret information. In general there are two types of fault attacks.

SUBMODULES

- COMPARATOR
- PRIORITY ENCODER
- MULTIPLEXER
- SUBTRACTOR
- QUASI BLOCK

3.1.1 COMPARATOR

A digital comparator or magnitude comparator is a hardware electronic device that takes two numbers as input in binary form and determines whether one number is greater than, less than or equal to the other number. Comparators are used in a central processing units (CPU) and microcontrollers. Examples of digital comparator include the CMOS 4063 and 4585 and the TTL 7485 and 74682-'89. The analog equivalent of digital comparator is the voltage comparator. Many microcontrollers have analog comparators on some of their inputs that can be read or trigger an interrupt. A digital comparator is an electronic circuit or device capable of accepting two binary signals and performing tests on those signals to determine their equivalence to each other. The simplest form of a digital comparator compares two binary signals, known in computer processing as bits, and uses a series of logical gates to determine if the two bits are equal or if one is greater than the other based on binary logic in which each signal is given the value of either zero or one. Most digital comparator circuits are designed to accept multiple bits for comparison, where in many applications the bits are combined by external software or hardware into actual numbers. At the heart of most central processing units (CPUs) in computers and other digital devices, a comparator performs a large portion of the logical operations that allow a computer function. Outside of computers, digital comparators also are used in some devices in which analog input is converted into digital information that is measured or monitored, such as in some testing meters. The way a digital comparator functions starts with the input of information. The comparator can only handle binary data, meaning that whatever the input mechanism is, the signal coming into the circuit can only have two states, which commonly are referred to as zero and one. When a bit is compared to another bit, it can be tested in one of three ways by the digital comparator. The first is equivalency, meaning the result of comparing one bit to another will result in a positive, or true, result if both of the bits equal one or if both of the bits equal zero. Individual bits also can be checked to see if one is greater than or less than another.

For a sequence of bits, however, comparisons to determine which set has a higher or lower value need to check each bit to see which set has a more highly placed most significant bit, because this determines the actual numerical value of the bit set. Beyond computer processors, a digital comparator can be used in some devices that contrast visual images with digital images, as can be the case in engineering that relies on computer-aided drafting (CAD) programs to check if the physically manufactured products match specifications. They also can be employed to convert analog signals into digital patterns. A digital comparator also can be used in conjunction with a number of other devices to act as a monitor in an industrial setting to see accurate digital information about the state of a machine.

Inputs		Outputs		
B	A	A > B	A = B	A < B
0	0	0	1	0
0	1	1	0	0
1	0	0	0	1
1	1	0	1	0

Table 1:1-bit Comparator

This is useful if we want to compare two variables and want to produce an output when any of the above three conditions are achieved. For example, produce an output from a counter when a certain count number is reached. Consider the simple 1-bit comparator above.

3.1.2 PRIORITY ENCODER

Here we applied input width is 5 bit and output width is 3 bit by using priority encoder. A priority encoder is a circuit or algorithm that compresses multiple binary inputs into a smaller number of outputs. The output of a priority encoder is the binary representation of the ordinal number starting from zero of the most significant input bit. They are often used to control interrupt requests by acting on the highest priority request. If two or more inputs are given at the same time, the input having the highest priority will take precedence. An example of a single bit 4 to 2 encoder is shown, where highest-priority inputs are to the left and "x" indicates an irrelevant value - i.e. any input value there yields the same output since it is superseded by higher-priority input. The output V indicates if the input is valid. Priority encoders can be easily connected in arrays to make larger encoders, such as one 16-to-4 encoder made from six 4-to-2 priority encoders - four 4-to-2 encoders having the signal source connected to their inputs, and the two remaining encoders take the output of the first four as input. The priority encoder is an improvement on simple encoder circuit in terms of all handling possible input configurations.

3.1.3 MULTIPLEXER

In this module will generate reminder code according to selection line. We applied three input signal as mux_in and m. we obtain the output (specific signal) from given input signal.

If A greater than B is equal to 1 will get mux_in signal. If A lesser than B we get m signal. Otherwise we get 0(8 bit signal). A data selector, more commonly called a **Multiplexer**, shortened to "Mux" or "MPX", are

combinational logic switching devices that operate like a very fast acting multiple position rotary switch. They connect or control, multiple input lines called "channels" consisting of either 2, 4, 8 or 16 individual inputs, one at a time to an output. Then the job of a multiplexer is to allow multiple signals to *share* a single common output. For example, a single 8-channel multiplexer would connect one of its eight inputs to the single data output. Multiplexers are used as one method of reducing the number of logic gates required in a circuit or when a single data line is required to carry two or more different digital signals.

3.1.4 SUBTRACTOR

Here we calculate the difference between input signal and specific constant value with help of subtraction. This model converts two rotations A and B into their difference A-B. This is useful for various applications. For instance, when you build a treaded vehicle such as a construction bulldozer, you'd like one motor to control total motion, and the other the turning. This construction does that: connect the treads to the (A+B) and (A-B) axles, and the motors to A and B. Now motor A makes the vehicle go forward or backward, and B turns it left or right. Of course you can also run them simultaneously. The great advantage is that you can now guarantee that the two sides of the treaded vehicle run at the same speed that does not happen with 2 motors, they always have a slight power difference. So it is more likely that it goes straight when you want it to.

3.1.5 QUASI BLOCK

This block will generate quotient value according to given input. Here we applied 3 bit input then generate 8 bit signal as output. Coding approaches such as parity code, Berger code, and residue code have been considered for design applications to detect circuit errors. Residue code is generally separable arithmetic codes by estimating a residue for data and appending it to data. Error detection logic for operations is typically derived by a separate residue code, making the detection logic is simple and easily implemented.

3.1.6 ACCUMULATOR

In this module consists flip-flop act as a accumulator. We can store a bit of data. Flip-flop" is the common name given to two-state devices which offer basic memory for sequential logic operations. Flip-flops are heavily used for digital data storage and transfer and are commonly used in banks called "registers" for the storage of binary numerical data. There are some circuits that are not quite as straight forward as the gate circuits we have discussed in earlier lessons. However, you still need to learn about circuits that can store and remember information. They're the kind of circuits that are used in computers to store program information RAM memory.

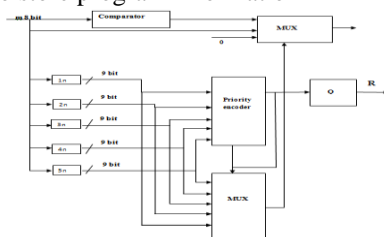


FIG 9: M MOD N OPERATION

IV. ERROR DETECTION CIRCUIT

In this module indicates that the operations of error detection in a specific PE_i is achieved by using EDC, which is utilized to compare the outputs between TCG and in order to determine whether errors have occurred. The EDC output is then used to generate a 0/1 signal to indicate that the tested PE_i is error-free/errancy. Using XOR operation can be identify the error if any variation in terms of residue and quotient value. Because a fault only affects the logic in the fanout cone from the fault site, the good circuit and faulty circuits typically only differ in a small region. Concurrent fault simulation exploits this fact and simulates only the differential parts of the whole circuit. Concurrent fault simulation is essentially an event-driven simulation with the fault-free circuit and faulty circuits simulated altogether. In concurrent fault simulation, every gate has a concurrent fault list, which consists of a set of bad gates. A bad gate of gate x represents an imaginary copy of gate x in the presence of a fault. Every bad gate contains a fault index and the associated gate I/O values in the presence of the corresponding fault. Initially, the concurrent fault list of gate x contains local faults of gate x. The local faults of gate x are faults on the inputs or outputs of gate x. As the simulation proceeds, the concurrent fault list contains not only local faults but also faults propagated from previous stages. Local faults of gate x remain in the concurrent fault list of gate x until they are detected. As we move to the nanometer age, we have begun to see nanometer designs that contain hundreds of millions of transistors.

V. DATA RECOVERY CIRCUIT

In this module will be generate error free output by quotient multiply with constant value (64) and add with remainder code. During data recovery, the circuit DRC plays a significant role in recovering RQ code from TCG.

Notably, the proposed EDDR design executes the error detection and data recovery operations simultaneously. Additionally, error-free data from the tested PE_i or data recovery that results from DRC is selected by a multiplexer (MUX) to pass to the next specific PE_{i+1} for subsequent testing. Error concealment in video is intended to recover the loss due to channel noise, e.g., bit-errors in a noisy channel and cell- loss in an ATM network, by utilizing available picture information. The error concealment techniques can be categorized into two classes according to the roles that the encoder and the decoder play in the underlying approaches. Forward error concealment includes methods that add redundancy in the source to enhance error resilience of the coded bit streams. For example, I-picture motion vectors were introduced in MPEG-4 to improve the error concealment. However, a syntax change is required in this scheme. In contrast to this approach, error concealment by post-processing refers to operations at the decoder to recover the damaged images based on image and video characteristics. In this way, no syntax is needed to support the recovery of missing data. we have only discussed the case in which one frame has been damaged and we wish to recover damaged blocks using information that is already contained in the bit-stream.

The temporal domain techniques that we have considered rely on information in the previous frame to perform the reconstruction. However, if the previous frame is heavily damaged, the prediction of the next frame may

also be affected. For this reason, we must consider making the prediction before the errors have occurred. Obviously, if one frame has been heavily damaged, but the frame before that has not been damaged, it makes sense to investigate how the motion vectors can be extrapolated to obtain a reasonable prediction from a past reference frame. Following this notion, we have essentially divided the problem of error concealment into two parts. The first part assumes that the previous frames are intact or are close to intact. This will always be the case for low BER and short error bursts.

Furthermore, a localized solution such as the techniques presented in the previous subsection will usually perform well. However, if the BER is high and/or the burst length is long, the impact of a damaged frame can propagate, hence the problem is more global and seems to require a more advanced solution, i.e., one which considers the impact over multiple frames. In the following, we propose an approach that considers making predictions from a past reference frame, which has not been damaged. The estimated motion information which differs from the actual one may be recovered from that of neighbor blocks. Because a moving object in an image sequence is larger than the block size of a minimal block in many occasions, motion information of neighbor blocks are usually the same as, or approximate to, current blocks. The concept of global motion is discussed in many researches on motion estimation or related interests. In method which reconstructs the frame with the aid of neighbor motion vector is successfully applied to motion estimation. Thus, an error signal "1" is generated from EDC and sent to mux in order to select the recovery results from DRC.

VI. SIMULATION RESULTS

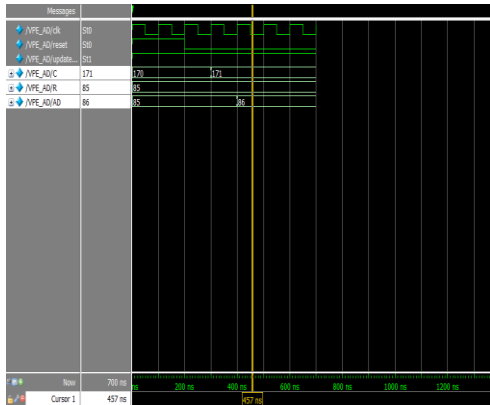


Fig10: Processing Element

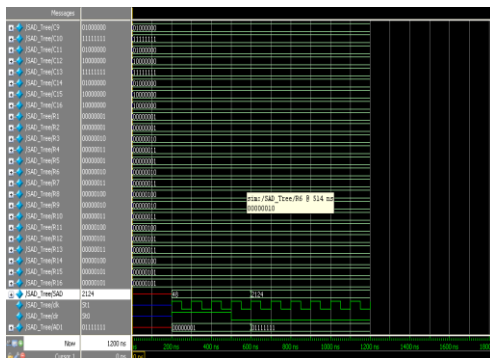


Fig11: SAD TREE

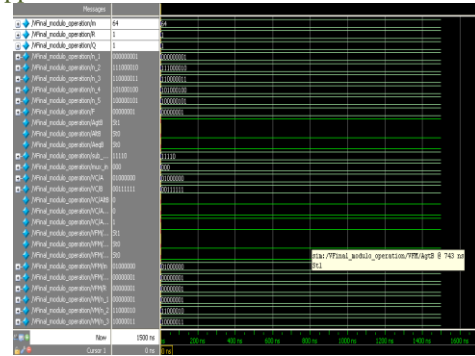


Fig12: RQ Code Generation

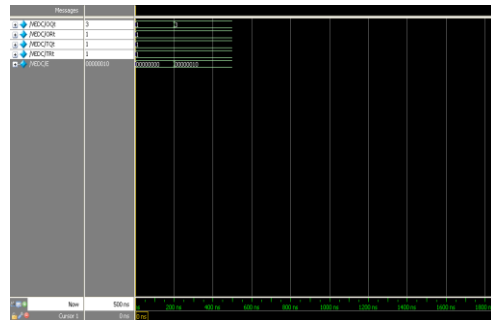


Fig13: Error Detection Circuit



Fig14: Error Recover Circuit

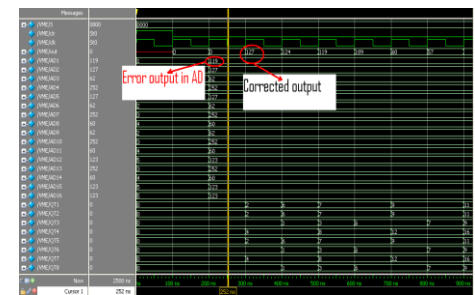


Fig15: Motion Estimation

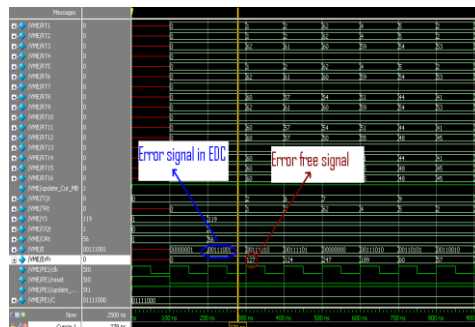


Fig16: Motion Estimation

VII. CONCLUSION

This paper presents an FPGA implementation of efficient architecture to make an application embedding into video code testing applications. The required modules have been taken and theoretical analysis have done and numerical calculations were calculated and verified. Combinational circuits are taken and simulation results have obtained which are required to built an architecture are explained and necessary types of codes which are generated to make errors to be detected and recovered.

References

- [1] J. M. Portal, H. Aziza, and D. Nee, "EEPROM memory: Threshold voltage built in self diagnosis," in Proc. Int. Test Conf., Sep. 2003, pp. 23–28.
- [2] J. F. Lin, J. C. Yeh, R. F. Hung, and C. W. Wu, "A built-in self-repair design for RAMs with 2-D redundancy," IEEE Trans. Vary Large Scale Integr. (VLSI) Syst., vol. 13, no. 6, pp. 742–745, Jun. 2005.
- [3] C. L. Hsu, C. H. Cheng, and Y. Liu, "Built-in self-detection/correction architecture for motion estimation computing arrays," IEEE Trans. Vary Large Scale Integr. (VLSI) Syst., vol. 18, no. 2, pp. 319–324, Feb. 2010.
- [4] C. H. Cheng, Y. Liu, and C. L. Hsu, "Low-cost BISDC design for motion estimation computing array," in Proc. IEEE Circuits Syst. Int. Conf., 2009, pp. 1–4.
- [5] S. Bayat-Sarmadi and M. A. Hasan, "On concurrent detection of errors in polynomial basis multiplication," IEEE Trans. Vary Large Scale Integr. (VLSI) Syst., vol. 15, no. 4, pp. 413–426, Apr. 2007.
- [6] C. W. Chiou, C. C. Chang, C. Y. Lee, T. W. Hou, and J. M. Lin, "Concurrent error detection and correction in Gaussian normal basis multiplier over GF 2^M ," IEEE Trans. Comput., vol. 58, no. 6, pp. 851–857, Jun. 2009.
- [7] L. Breveglieri, P. Maistri, and I. Koren, "A note on error detection in an RSA architecture by means of residue codes," in Proc. IEEE Int. Symp. On-Line Testing, Jul. 2006, 176–177.
- [8] S. J. Piestrak, D. Bakalis, and X. Kavousianos, "On the design of selftesting checkers for modified Berger codes," in Proc. IEEE Int. Workshop On- Line Testing, Jul. 2001, pp. 153–157.
- [9] S. Surin and Y. H. Hu, "Frame-level pipeline motion estimation array processor," IEEE Trans. Circuits Syst. Video Technol., vol. 11, no. 2, pp. 248–251, Feb. 2001.
- [10] D. K. Park, H. M. Cho, S. B. Cho, and J. H. Lee, "A fast motion estimation algorithm for SAD optimization in sub-pixel," in Proc. Int. Symp. Integr. Circuits, Sep. 2007, pp. 528–531.
- [11] L. Breveglieri, P. Maistri, and I. Koren, "A note on error detection in an RSA architecture by means of residue codes," in Proc. IEEE Int. Symp. On-Line Testing, Jul. 2006, 176–177.
- [12] S. J. Piestrak, D. Bakalis, and X. Kavousianos, "On the design of selftesting checkers for modified Berger codes," in Proc. IEEE Int. Workshop On- Line Testing, Jul. 2001, pp. 153–157.

Authors



Suparshya Babu Sukhavasi was born in India, A.P. He received the **B.Tech** degree from JNTU, A.P, and **M.Tech** degree from SRM University, Chennai, Tamil Nadu, and India in 2008 and 2010 respectively. He worked as **Assistant Professor** in Electronics & Communications Engineering in Bapatla Engineering College for academic year 2010-2011 and from 2011



Susrutha Babu Sukhavasi was born in India, A.P. He received the **B.Tech** degree from JNTU, A.P, and **M.Tech** degree from SRM University, Chennai, Tamil Nadu, India in 2008 and 2010 respectively. He worked as **Assistant Professor** in Electronics & Communications Engineering in Bapatla Engineering College for academic year 2010-2011 and from 2011 to till date working in **K L University**. He is a member of Indian Society For Technical Education and International Association of Engineers. His research interests include Mixed and Analog VLSI Design, FPGA Implementation, Low Power Design and Wireless communications, VLSI in Robotics. He has published articles in various international journals and Conference in IEEE.



S R Sastry Kalavakolanu was born in A.P,India. He received the B.Tech degree in Electronics & communications Engineering from Jawaharlal Nehru Technological University in 2010. Presently he is pursuing M.Tech VLSI Design in KL University. His research interests include Low Power VLSI Design. He has undergone 3 International Journals and 1 publication in IEEE.



M.Aravind Kumar was born in A.P,India He received his B.Tech degree in Electronics and Communication Engineering from S.V.H college of Engineering and Technology in the year 2005. He is presently pursuing masters in VLSI system design (4th semester) at Padmasri Dr.B.V.Raju Institute of Technology, Medak(dst), A.P.India.



P.Bose Babu was born in A.P,India, He Completed M.Tech in VLSI system Design from MVGR COLLEGE OF ENGG.&TECH, Vizianagaram in 2011 and B.Tech from QIS College of engineering, in 2009 in Electronics & Communication engineering. Presently he is Working as Asst.Professor in ANDHRA LOYOLA college of Engg & Technology, Vijayawada,A.P,India.



Ranga Rao Orugu was born in A.P,India, Completed M.Tech in Communication Systems at C.R.Reddy engineering College, Eluru and B.Tech from Sri Saaradhi Institute of and technology in the year 2009 in Electronics & Communication engineering. Presently he is Working as Asst.Professor in ANDHRA LOYOLA college of Engg.& Technology, Vijayawada,A.P,India.

Design of Stabilizing Controllers for the Nonlinear Power Systems

Rekha¹, A. K. Singh²

¹*Asst. Professor, Electrical & Electronics Engg. Dept., NIT Jamshedpur, India*

²*Professor, Electrical & Electronics Engg. Dept., NIT Jamshedpur, India*

Abstract: The objective here is the development of mathematical model of the non-linear power system which can be utilized for implementing the different class of controller. The controller designed here is to fulfill the stability requirement of the system as well as to make the system transiently stable. The linearization of the power system is done using direct feedback linearization technique and the model thus obtained has parameters which can be used as controller input. The linear LQ optimal control theory is applied to the model to design an optimal feedback control law, $v_f(t)$.

Keywords: Stabilizer, FLC (fuzzy logic controller), DFL (direct feedback linearization).

I. Introduction

We consider here nonlinear control theory to design controllers for power systems to improve the transient stability and to achieve voltage regulation. The problem of designing controller to prevent an electric power system losing synchronism after a large sudden fault is of great importance in power system design.

In recent years, most of the non-linear excitation controllers have been developed based on the classical third order dynamic generator model. The simulation results showed that such a simplification has very little effect on the performances of the designed controllers. Establishing a global control structure for general non-linear control systems is preferred, as control of complex system over a wide range of operating conditions can be achieved for a set of control objective. A general global control structure is based on the qualitative analysis of the dynamical systems. Local controllers are designed based on local models and local performance requirements and co-ordination rules are employed to combine the local elements control.

II. Non-Linear Systems

The topic of non-linear control has attracted particular attention during the past few decades as virtually all physical systems are non-linear in nature. Non-linear control analysis and design provides a sharper understanding of real world. For real world systems, large ranges of operation cannot be avoided, and demanding specifications are required by modern technology such as high performance robotics and aircraft which typically involve non-linear dynamics. Therefore use of non-linear control is crucial.

With the development of powerful microprocessor and low cost dedicated digital signal processors, non-linear controllers are becoming easier to implement reliably.

There are numerous examples of large dynamical systems that provide great challenges to control engineers. For example Electrical power systems, aerospace system, process control system in chemical and petroleum industries all require non-linear control.

III. Linear Model Of Synchronous Machine

When system is subjected to a small load change, it tends to acquire a new operating state. During the transition between the initial state and the new state the system behavior is oscillatory. If two states are such that all state variables change only slightly (i.e. x_i changes from x_{i0} to $x_{i0} + x_{i\Delta}$ where $x_{i\Delta}$ is small change in x_i), the system is operating near the initial state. The initial state may be considered as a quiescent operating condition for the system. The behavior of the system when it is perturbed such that the new and old equilibrium states are nearly equal, the system equations are linearized about the Q operating condition. First order approximations are made for system equations. The new linear equations thus derived are assumed to be valid in the region near the Q-condition. The dynamic response of a linear system is determined by its characteristic equation.

IV. PID Controllers

Classical and modern methodologies in linear and non-linear control provide powerful design tools for systems modeled by ordinary differential equation. However, linear methods are valid for a small operating region, and many non-linear methods are only effective within a certain operating region due to the non-existence of global geometric structures.

Multiple controllers are widely used in practice where controllers adapt themselves to different operating conditions and are able to co-ordinate various control requirements. Control of a complex system over a wide range of operating conditions to achieve a set of control objectives is called global control.

To achieve the goals of global control, multiple controllers are needed. They are derived from the design method of local control and operate over different operating points during different time periods to fulfill the corresponding primary control requirements. Therefore how to co-ordinate the controllers is the major issue of global control.

A plant model of a physical system that is to be controlled is usually very complex and difficult. Adaptive control is a model-free controller that can be used to control non-linear systems. Most of the adaptive controllers involve certain types of function approximator from input/output

experiments. The basic objective of adaptive control is to maintain consistent performance of a control system in the presence of the designed parameters. Traditional adaptive controllers cannot make use of human experience, which is usually expressed in linguistic terms.

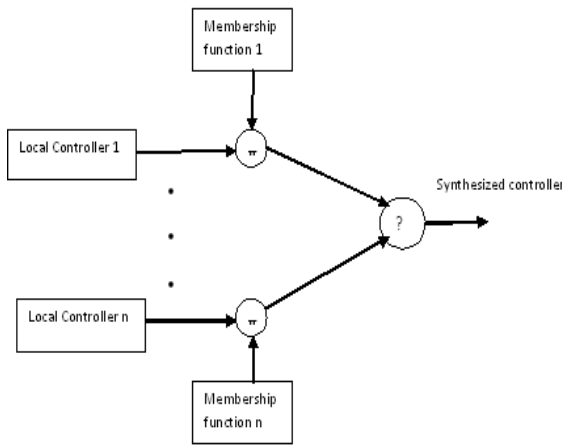


Figure 1. Heterogeneous control law

V. Controller Design Techniques

Since power system are highly non-linear and the operating conditions can vary over a wide range, the conventional PSS (CPSS) performance is degraded when the operating point changes from one to another because of fixed parameters of stabilizers.

Metaheuristic optimization technique like GA, Tabu search, simulated annealing, bacteria foraging, particle swarm optimization.

A. Power system damping controller structure

Power System Stabilizer model consists of:

1. Gain block
2. Washout block
3. Phase compensation block

The input to PSS is rotor speed deviation, output is auxiliary excitation signal given to the generator excitation system.

$$\left[\frac{\Delta U}{\Delta w} \right] = K_s \left[\frac{(1 + sT_1)}{(1 + sT_2)} \right] \left[\frac{(sT_w)}{(1 + sT_w)} \right]$$

K_s - PSS gain

T_1, T_2 – PSS time constant

Signal washout function is a high pass filter which removes DC signals. The washout time is in the range of 1-20 sec

Eg. $T_w = 15$ sec

Eigen value based objective function

$$[J] = \text{Max}\{\text{Re}[\lambda_i]\}, (\lambda_i) \in (\lambda\tau)$$

Where (λ_i) belongs to the group of electromechanical mode Eigen values $(\lambda\tau)$.

B. Fuzzy controller based design

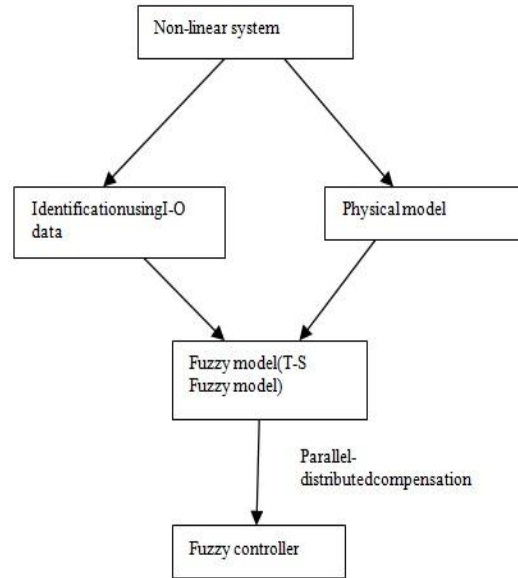


Figure.2 Fuzzy model-based fuzzy control designs

Table 1. Comparisons of different control designs

	Work Range	Simple	Stability
Linear	$\left(-\frac{\pi}{4}, \frac{\pi}{4}\right)$	Yes	Local
Non-linear	$\left(-\frac{\pi}{2}, \frac{\pi}{2}\right)$	No	Non-local
Fuzzy PDC	$(-\pi, \pi)$	No	Non-local

A properly designed voltage regulating system can increase the steady state stability limit of a synchronous machine by a considerable amount. Fast regulator and exciter action and low transient reactance are desirable. The amplification factor of the regulating system must be co-ordinated properly with the machine and system constants are made as large as possible amortisseur windings have little effect on the possible gain in power limit. For maximum gain in power limit, a regulator with broad regulation and rapid response should be used.

C. FLC based on GA

The design employs Sugeno type fuzzy controllers as parameters can be manipulated using GA. Single and two inputs fuzzy controllers are used. The GA manipulates all parameters of the fuzzy controller to find the optimum solution.

Genetic Algorithm (GA) are global, parallel, stochastic search methods founded on Darwinian evolutionary principles. During the last decade GA's have been applied in a variety of areas, with varying degrees of success within each. GA exhibit considerable robustness in problem domain that is not conducive to formal, rigorous, classical analysis. The computational complexity of the GA has proved to be the chief obstruction to real time applications. Hence majority of the applications that use GA's are by nature off-line.

Commonly GA's have been used to optimize both structure and parameter values for both controllers and plant models. Normally Takagi-Sugeno (TS) fuzzy system are employed for control based on GA trying to optimize the parameters of the fuzzy controller. Inputs of the GA will be encoded then cross-over and mutation will be carried out on the population to finally change the centers and variances of the Gaussian membership functions of Sugeno fuzzy controller. The resulting controller will be capable of guiding the system to the desired characteristic with permissible value of error.

After fuzzy controller has been designed, its parameters should be manipulated by G.A, this algorithm should be able to optimize centers, variances and coefficients.

D. Robust controller design

When the parameters in the power system are known, we can design a DFL control law to linearize the plant. But when large sudden fault occurs the reactance of the transmission line x_L changes a lot. These changes are treated as parametric uncertainty. Hinfinity control is closely associated with many robustness problems such as sensitivity minimization and stabilization of uncertain systems. However when there is parameter uncertainty in plant modeling, no robust behavior on Hinfinity performance along with stability can be guaranteed by standard H_∞ control method.

VI. Mathematical Modelling Of The System

The following abbreviations are used while designing the model:

$$\Delta\delta(t) = \delta(t) - \delta_0$$

$\delta(t)$ = power angle of the generator

δ_0 = power angle of the generator at the operating point;

$\omega(t)$ = the relative speed of the generator

$$\Delta P_e = P_e(t) - P_m$$

P_m = mechanical input power

P_e = active electric power delivered by the generator;

ω_0 = synchronous machine speed; $\omega_0 = 2\pi f_0$

D = per unit damping constant

H = per unit inertia constant

$E_q'(t)$ = the transient emf in the quadrature axis

$E_f(t)$ = the equivalent emf in the excitation coil;

Tdo = the direct axis transient short circuit time;

$Q_e(t)$ = the reactive power

If(t) = the excitation current

Iq(t) = the quadrature axis current;

Vt(t) = the generator terminal voltage;

Kc = the gain of the excitation amplifier;

Uf(t) = the input of the SCR amplifier of the generator

$$x_{ds} = x_T + \frac{1}{2}x_L + x_d;$$

$$x_{ds}' = x_T + \frac{1}{2}x_L + x_d';$$

x_T = reactance of the transformer

x_d = direct axis reactance

x_L = the reactance of transmission line;

$$x_s = x_T + \frac{1}{2}x_L$$

x_{ed} = the mutual reactance between the excitation coil and the stator coil;

V_s = the infinite bus voltage;

Mechanical equation:

$$\Delta\dot{\delta}(t) = \omega(t) \quad (1)$$

$$\omega\dot{(t)} = \frac{-D}{H}\omega(t) - \frac{\omega_0}{H}\Delta P_e(t) \quad (2)$$

Generator Electrical Dynamics:

$$\dot{E}'_q(t) = \frac{1}{T_{do}}(E_f(t) - E_q(t)) \quad (3)$$

Electrical Equations:

$$E_q(t) = \frac{x_{ds}}{x_{ds}'}E'_q(t) - \frac{x_d - x_d'}{x'_{ds}}V_s \cos\delta(t) \quad (4)$$

$$E_f(t) = K_c u_f(t) \quad (5)$$

$$P_e(t) = \frac{V_s E_q(t)}{x_{ds}} \sin\delta(t) \quad (6)$$

$$I_q(t) = \frac{V_s}{x_{ds}} \sin\delta(t) = \frac{P_e(t)}{x_{ad} I_f(t)} \quad (7)$$

$$Q_e(t) = \frac{V_s}{x_{ds}} E_q(t) \cos\delta(t) - \frac{V_s^2}{x_{ds}} \quad (8)$$

$$E_q(t) = x_{ad} I_f(t) \quad (9)$$

$$V(t) = \frac{1}{x_{ds}} \left\{ x_s^2 E_q^2(t) + V_s^2 x_d^2 + 2x_s x_d x_{ds} P_e(t) \cot\delta(t) \right\}^{1/2} \quad (10)$$

A. Non-linear controller design for the power system

The DFL technique [8] is very useful method for power system non-linear controller design. By employing a non-linear feedback compensating law, a non-linear system can be directly transformed to a system whose closed loop dynamics are linear over a very wide range.

To design a non-linear controller for the power system, since $E'_q(t)$ is physically un-measurable, we eliminate $E'_q(t)$ by differentiating equation (6) and using (1) to (6)

Equation (6) is

$$P_e(t) = \frac{V_s E_q(t)}{x_{ds}} \sin\delta(t)$$

$$\frac{dP_e(t)}{dt} = \frac{V_s}{x_{ds}} E_q(t) \cos\delta(t) \dot{\delta}(t) + \frac{V_s}{x_{ds}} \dot{E}'_q(t) \sin\delta(t)$$

$$= \frac{V_s}{x_{ds}} E_q(t) \cos\delta(t) \omega(t)$$

$$+ \frac{V_s}{x_{ds}} \sin\delta(t) \left[\frac{x_{ds}}{x'_{ds}} \dot{E}'_q(t) + \frac{x_d - x_d'}{x'_{ds}} V_s \sin\delta(t) \omega(t) \right]$$

$$= \frac{V_s}{x_{ds}} E_q(t) \cos\delta(t) \omega(t)$$

$$+ \frac{V_s}{x_{ds}} \sin\delta(t) \left[\frac{x_{ds}}{x'_{ds}} \frac{1}{T_{do}} (E_f(t) - E_q(t)) + \frac{x_d - x_d'}{x'_{ds}} V_s \sin\delta(t) \omega(t) \right]$$

We have $T'_{do} = \frac{x_{ds}}{x_{ds}} T_{do}$

$$= -\frac{1}{T'_{do}} P_e(t) + \frac{1}{T'_{do}} \left\{ \frac{V_s}{x_{ds}} \sin\delta(t) [K_c u_f(t) + T_{do} (x_d - x'_d) \frac{V_s}{x_{ds}} \sin\delta(t) \omega(t)] + T'_{do} \frac{V_s}{x_{ds}} E_q(t) \cos\delta(t) \omega(t) \right\}$$

$$= -\frac{1}{T'_{do}} \Delta P_e(t) + \frac{1}{T'_{do}} \left\{ \frac{V_s}{x_{ds}} \sin\delta(t) [K_c u_f(t) + T_{do} (x_d - x'_d) \frac{V_s}{x_{ds}} \sin\delta(t) \omega(t)] + T'_{do} \frac{V_s E_q(t)}{x_{ds}} \cos\delta(t) \omega(t) - P_m \right\},$$

As $\Delta P_e(t) = P_e(t) - P_m$

Therefore

$$\Delta P_e(t) = -\frac{1}{T'_{do}} \Delta P_e(t) + \frac{1}{T'_{do}} v_f(t)$$

Where

$$v_f = \frac{V_s \sin\delta(t)}{x_{ds}} [K_c u_f(t) + T_{do} (x_d - x'_d) \frac{V_s}{x_{ds}} \sin\delta(t) \omega(t)] + T'_{do} \frac{V_s E_q(t)}{x_{ds}} \cos\delta(t) \omega(t) - P_m$$

or,

$$v_f(t) = I_q(t) [K_c u_f(t) + T_{do} (x_d - x'_d) \frac{V_s}{x_{ds}} \sin\delta(t) \omega(t)] + T'_{do} [Q_e(t) + \frac{V_s^2}{x_{ds}}] \omega(t) - P_m$$

The model (1) to (3) is therefore linearized,

The linearized model is

$$\Delta \dot{\delta}(t) = \omega(t) \tag{11}$$

$$\omega(t) = \frac{-D}{H} \omega(t) - \frac{\omega_0}{H} \Delta P_e(t) \tag{12}$$

$$\Delta \dot{P}_e(t) = -\frac{1}{T'_{do}} \Delta P_e(t) + \frac{1}{T'_{do}} v_f(t) \tag{13}$$

where $v_f(t)$ is the new input.

After linearization, we can employ linear control theory, such as LQ-optimal control theory, to design a feedback law

$$v_f(t) = f(\delta(t), \omega(t), P_e(t)) \tag{14}$$

To give the desired stability and performance properties, $v_f(t)$ and $P_e(t)$ are the control inputs.

The DFL-LQ optimal controller [10] and the DFL voltage regulator can be obtained by use of DFL techniques and linear optimal control theory.

VII. Simulation Results

The variables $V_i(t)$, $w(t)$ and $P_e(t)$ are to be tracked to their prefault steady values after a fault occurs. An effective feedback control law employed here is

$$v_f(t) = 19.3(\delta(t) - \delta_0) + 6.43(\omega(t)) - 47.6(P_e(t) - P_{m0}) + P_{m0} \tag{15}$$

By employing the control law (15) on the DFL compensated system, the simulation results were obtained for power angle and terminal voltage.

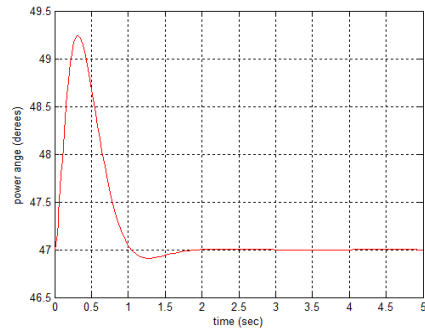


Figure 3a. DFL-LQ optimal controller (Power angle)

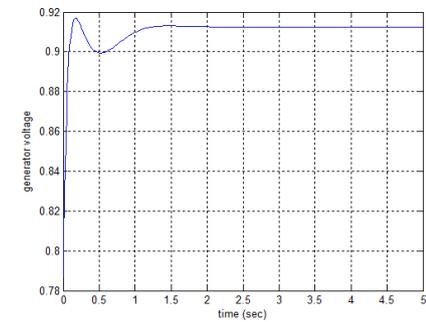


Figure 3b. DFL-LQ optimal controller (voltage response)

An electric power plant described in [10], is taken with operating points:

$$\delta_0 = 47^\circ, P_{m0} = 0.45 \text{ p.u. and } V_{t0} = 1.0 \text{ p.u.}$$

The fault considered here is permanent fault, which occurs at 0.1 sec and the fault is removed by opening the breaker of the faulted line at 0.25 sec. The simulation results show that using only DFL-LQ optimal controller or DFL voltage regulator, we cannot achieve both good transient response and good post-fault performances. If we can combine both types of controller then better result is expected. This could be done by the design of DFL co-ordinated controller.

VIII. Conclusion

The linearized mathematical model is obtained for the power system. This model can be utilized for designing different types of controllers for stabilizing the parameters of the power system. Here in this paper, the approach of direct feedback linearization (DFL) is used and the simulation results were obtained for DFL-LQ optimal controller. The new DFL coordinated controller can achieve better transient stability results than the excitation controller irrespective of the operating point of the system and the fault sequence.

Acknowledgment

We would sincerely like to thank Professor Kanti B. Datta, Ex-Professor, IIT Kharagpur, for his kind help as without his help it would not have been possible to compile this paper.

References

- [1] Machowski, J.; Bialek, J.W.; Robak, S.; Bumby, J.R.; Excitation control system for use with synchronous generators, IEE Proceedings Generation, Transmission and Distribution, Sep 1998 Vol: 145, p.537 - 546 .
- [2] Chapman, J.W.; Ilic, M.D.; King, C.A.; Eng, L.; Kaufman, H.; Stabilizing a multimachine power system via decentralized feedback linearizing excitation control, IEEE Transactions on Power Systems, Aug 1993, Vol. 8 p. 830 - 839 .
- [3] Bazanella, A.S.; e Silva, A.S.; Kokotovic, P.V.; Lyapunov design of excitation control for synchronous machines, Proceedings of the 36th IEEE Conference on Decision and Control, 1997., p: 211 - 216 vol.1
- [4] Gan D.; Qu Z.; Cai H., Multi machine power system excitation control design via theories of feedback linearization control and nonlinear robust control , Int. Journal of Systems Science, Volume 31, Number 4, 1 April 2000 , pp. 519-527.
- [5] Sun, C.; Zhao, Z.; Sun, Y.; Lu, Q.; Design of nonlinear robust excitation control for multimachine power systems, IEE Proceedings- Generation, Transmission and Distribution, May1996, Vol.143,p.253-257.
- [6] Schaefer, R.C.; Excitation control of the synchronous motor, IEEE Transactions on Industry Applications, May/June 1999 , Vol: 35 Issue:3
- [7] Handschin, E.; Hoffmann, W.; Reyer, F.; Stephanblome, T.; Schlucking, U.; Westermann, D.; Ahmed, S.S.; A new method of excitation control based on fuzzy set theory, : IEEE Transactions on Power systems, Feb 1994, vol.9,p.533-539
- [8] Gao, L, Chen, L, Fan, Y and Ma, HW ‘ A nonlinear control design for power systems’ Automatica, vol 28, no 5 (1992) pp. 975-979.
- [9] Kitauchi, Y.; Taniguchi, H.; Experimental verification of fuzzy excitation control system for multi-machine power system, IEEE Transactions on Energy Conversion, +Kitauchi, Y.+Taniguchi, H. Mar 1997, Vol. 12, p. 94 - 99 .
- [10] Wang Y, David J Hill, Richard H. Middleton, transient stability enhancement and regulation of power systems, IEEE Trans. On Power Systems, vol.8, no.2, may 1993.
- [11] Wei-Der Chang and Shun-Peng Shih, PID controller design of nonlinear systems using an improved particle swarm optimization approach, Jan 2010.
- [12] Chao-Chung Peng, Chieh-Li Chen, Dynamic controller design for a class of nonlinear uncertain systems subjected to time-varying disturbance, Nonlinear Dyn (2009) 57: 411–423, Nov 2008.
- [13] Y. Guo, Member, IEEE, David J. Hill, Fellow, IEEE & Y. Wang, “Global Transient Stability and voltage regulation for power system”, IEEE Trans. On Power Systems, vol.16, no. 4, nov. 2001.

Development of the A Three-Dimensional Magnetic-Field-Independent Absorbing Boundary Condition (Mfiabc) For Cold Magnetoplasma

Mohammad pourbagher¹, Javad nourinia¹ and Nader pourmahmud²

1(Department of Electrical Engineering, Urmia university, IRAN)

2(Department of Mechanical Engineering, Urmia university, IRAN)

Abstract: A Three-Dimensional Cartesian-coordinate magnetized cold plasma algorithm has the capability to simulate wave behaviors in cold plasma under applied magnetic fields of arbitrary direction and magnitude. Plasma effects contributed by electrons, positive, and negative ions may all be included by this algorithm. A magnetic-field-independent absorbing boundary condition (ABC) is then proposed to truncate the computational domains that employ the cold plasma algorithm. To terminate the computational domain of the magnetized cold plasma FDTD algorithm an appropriate absorbing boundary condition (ABC) is required in order to model local regions of the Earth, or to model unbounded problems in the radial (vertical direction) on a global scale.

Keywords: Cold plasma, FDTD method, Boundary condition, PML, Ionosphere

I. Introduction

In FDTD modeling, it is not possible to handle an open region problem directly since the data storage in a computer is limited by the size of memory. To mitigate this problem, an accurate and computationally efficient absorbing boundary condition (ABC) is needed to truncate the computational domain to suppress spurious reflections of the outgoing waves to an acceptable level. Its original split-field formulation introduced by Berenger [1] and various later reformulations, such as the uniaxial PML (UPML) [2], the convolutional PML (CPML) [3], and the NPML [4] provide orders-of-magnitude lower reflections and other advantages over previous versions of ABCs. However, the application of the standard PMLs has been limited to situations wherein the group and phase velocities of the incident wave are aligned in the same direction. When this is not the case, the PMLs cease to attenuate the field and can in fact act as an amplifier [5-7], which causes the algorithm to become analytically unstable. Becache et al. [6] confirms this instability with a theoretical analysis of PMLs for anisotropic media, for acoustic waves in elastic materials, and for EM waves. Cummer [7] has discussed the PML amplification phenomenon for the negative index materials (NIMs) in which the NIM materials exhibit both positive and negative refractive indexes over a range of frequencies. More recently, Chevalier et al. [8] encountered the same instability problem when modeling the antenna performance in a magnetized plasma for whistler waves. As pointed out in [7], this instability problem is inherent in the PMLs and is not implementation-specific. This poses a problem for modeling wave propagation in anisotropic media, such as whistler waves in magnetized cold plasma.

To address this issue, Cummer [7] has derived a modified PML solution for the negative index material (NIM) referred to as the NIMPML which is an adaptation of the previous NPML [4]. However, this method requires the simulated material to have a homogeneous permittivity and permeability ($\epsilon_r = \mu_r$), which is hardly the case for the ionospheric plasma medium that varies with both altitude and spatial position around the Earth. More recently, Chevalier et al. [5] presented in 2006 a new PML formulation referred to as the KPML which explicitly utilizes information on the k -vector direction of incident waves. Numerical tests in [5] demonstrate that KPML does not perform as well as the traditional CPML in open free-space problems, but it is stable and attenuates outgoing waves well for a case of whistler wave propagation in magnetized plasma media. However, the KPML can only be used as an effective ABC for dense magnetized plasma when the electron cyclotron frequency is much smaller than the plasma frequency. This is not the case for the lower region of the ionosphere. Moreover, the KPML algorithm is based on a single orientation of the background magnetic-field relative to each side of the FDTD grid and as such is not suitable for simulations involving spatially-varying magnetic-field directions such as for global modeling of the Earth-ionosphere system.

Considering these issues relating to the application of PMLs to magnetized plasma, we next consider Mur's ABC [9] as an alternative. Unfortunately, it is known that the original Mur's ABC exhibit an early-time instability for certain modeling scenarios. J. N. Hwang and F. C. Chen [10] have reported that the Mur's first-order ABC will cause instability problem for ADI-FDTD method. Zhang Yusheng and Wang Wenbing [11] have also confirmed that the second-order Mur's ABC combined with FDTD method to solve 3-D scattering problems is unstable. We encountered the same instability problem when applying the second-order Mur's ABC to the magnetized cold plasma algorithm. To solve this issue, Zhang and Wang [10] presented a new discretization scheme of the Engquist and Majda's second-order ABC equations [12] different from the scheme of Mur's ABC [9], which they claim is stable. However, we find through longer numerical tests that the early-time instability of Mur's ABC is simply replaced by a late-time instability in Zhang and Wang's scheme. In this article, the feasibility of a variation of Zhang and Wang's scheme is investigated to serve as an effective ABC for the 3-D FDTD magnetized cold plasma formulation. We choose this scheme despite its inherent late-time instability because it has the potential to provide an acceptable level of error regardless of the direction of the background magnetic-field, a capability

not provided by KPML. We then present a simple but very effective way to further delay the late-time instability of this magnetized plasma ABC.

II. Formulations

In 1977, Engquist and Majda [12] derived a theory of one-way wave equations suitable for analytical ABCs in FDTD simulations. The second-order approximations of these formulations at outer boundaries of a 3-D Cartesian space lattice can be expressed as follows.

$$x=1 \rightarrow \frac{\partial^2 U}{\partial x \partial t} - \frac{1}{v} \frac{\partial^2 U}{\partial t^2} + \frac{v}{2} \frac{\partial^2 U}{\partial y^2} + \frac{v}{2} \frac{\partial^2 U}{\partial z^2} = 0 \quad (1)$$

$$x=h \rightarrow \frac{\partial^2 U}{\partial x \partial t} + \frac{1}{v} \frac{\partial^2 U}{\partial t^2} - \frac{v}{2} \frac{\partial^2 U}{\partial y^2} - \frac{v}{2} \frac{\partial^2 U}{\partial z^2} = 0 \quad (2)$$

$$y=1 \rightarrow \frac{\partial^2 U}{\partial y \partial t} - \frac{1}{v} \frac{\partial^2 U}{\partial t^2} + \frac{v}{2} \frac{\partial^2 U}{\partial x^2} + \frac{v}{2} \frac{\partial^2 U}{\partial z^2} = 0 \quad (3)$$

$$y=m \rightarrow \frac{\partial^2 U}{\partial y \partial t} + \frac{1}{v} \frac{\partial^2 U}{\partial t^2} - \frac{v}{2} \frac{\partial^2 U}{\partial x^2} - \frac{v}{2} \frac{\partial^2 U}{\partial z^2} = 0 \quad (4)$$

$$z=1 \rightarrow \frac{\partial^2 U}{\partial z \partial t} - \frac{1}{v} \frac{\partial^2 U}{\partial t^2} + \frac{v}{2} \frac{\partial^2 U}{\partial x^2} + \frac{v}{2} \frac{\partial^2 U}{\partial y^2} = 0 \quad (5)$$

$$z=p \rightarrow \frac{\partial^2 U}{\partial z \partial t} + \frac{1}{v} \frac{\partial^2 U}{\partial t^2} - \frac{v}{2} \frac{\partial^2 U}{\partial x^2} - \frac{v}{2} \frac{\partial^2 U}{\partial y^2} = 0 \quad (6)$$

where U denotes the scalar field components located at outer boundaries and v is the wave phase velocity, which is initially set to c , the velocity in free space. By central-differentiating the partial and second-order time and spatial derivatives of Equations (1)-(6) at time step n and at spatial locations half grid cell inside each boundary, one can obtain the well-known second-order Mur's ABC. In this article, by utilizing a different discretization scheme of Equations (1) - (6) than that utilized in Zhang and Wang's scheme [11], we derive our ABC expressions detailed as below. Our different approach from the so-called upwind-difference scheme of Zhang and Wang's ABC results in the same final form of the formulations as in Zhang and Wang's ABC. Here, we take Equation (1) as an example a derivation of the ABC expression for the $x = 1$ boundary. First, U around time step n and spatial location $(i+1, j, k)$ can be Taylor-expanded as

$$U_{i+1,j,k}^n = U_{i,j,k}^n + \left(\frac{\partial U}{\partial x} \Big|_{i,j,k}^n \right) \cdot \Delta x + O(\Delta x^2) \quad (7)$$

From Equation (7), the first-order finite-difference approximation of the space derivative can then be obtained as

$$\frac{\partial U}{\partial x} \Big|_{i,j,k}^n = \frac{U_{i+1,j,k}^n - U_{i,j,k}^n}{\Delta x} \quad (8)$$

Applying Approximation (8) to both the spatial and time derivatives for the first term of Equation (1), we obtain the following:

$$\frac{\partial^2 U}{\partial x \partial t} \Big|_{i,j,k}^n = \frac{1}{\Delta t} \left(\frac{\partial U}{\partial x} \Big|_{i,j,k}^n - \frac{\partial U}{\partial x} \Big|_{i,j,k}^{n-1} \right) = \frac{1}{\Delta t} \left(\frac{U_{i+1,j,k}^n - U_{i,j,k}^n}{\Delta x} - \frac{U_{i+1,j,k}^{n-1} - U_{i,j,k}^{n-1}}{\Delta x} \right) = \frac{1}{\Delta t \Delta x} (U_{i+1,j,k}^{n-1} - U_{i,j,k}^{n-1}) - \frac{1}{\Delta t \Delta x} (U_{i+1,j,k}^n - U_{i,j,k}^n) \quad (9)$$

Next, the central-difference scheme is applied to the last three second-order time and spatial derivatives of Equation (1) at time step n and the $x = 1$ plane. Equation (1) can now be expressed as

$$\frac{U_{i+1,j,k}^{n-1} - U_{i,j,k}^{n-1}}{\Delta t \Delta x} - \frac{U_{i,j,k}^n - U_{i,j,k}^{n-1}}{\Delta t \Delta x} - \frac{U_{i,j,k}^{n+1} - 2U_{i,j,k}^n + U_{i,j,k}^{n-1}}{v \Delta t^2} + \frac{v(U_{i,j,k+1}^n - 2U_{i,j,k}^n + U_{i,j,k-1}^n)}{2 \Delta y^2} + \frac{v(U_{i,j,k+1}^{n-1} - 2U_{i,j,k}^{n-1} + U_{i,j,k-1}^{n-1})}{2 \Delta z^2} = 0 \quad (10)$$

By moving the field components of time step n and $n-1$ to the right-hand side, Equation (10) is rewritten as Equation (11):

$$U_{i,j,k}^{n+1} = 2U_{i,j,k}^n - U_{i,j,k}^{n-1} - \frac{v \Delta t}{\Delta x} (U_{i,j,k}^n - U_{i,j,k}^{n-1}) + \frac{v \Delta t}{\Delta x} (U_{i,j,k}^{n-1} - U_{i,j,k}^{n-2}) + \frac{1}{2} \left(\frac{v \Delta t}{\Delta y} \right)^2 \cdot (U_{i,j,k+1}^n - 2U_{i,j,k}^n + U_{i,j,k-1}^n) + \frac{1}{2} \left(\frac{v \Delta t}{\Delta z} \right)^2 \cdot (U_{i,j,k+1}^{n-1} - 2U_{i,j,k}^{n-1} + U_{i,j,k-1}^{n-1}) \quad (11)$$

As mentioned earlier, this ABC formulation exhibits a late-time instability that is improved over the early-time instability of the traditional Mur's ABC for magnetized plasma. Thus, to further delay the start of this late-time instability, we intentionally multiply the newly updated field components along the ABC boundaries each time step by a stability control factor s slightly less than 1.0. Then, Equation (11) above is reexpressed as Equation (12) below (wherein $s = 1.0$ yields the original ABC Equation (11)). It is expected that this multiplication factor will increase the level of reflection from the boundary, but it will further improve the stability (in the extreme case, $s = 0.0$ yields a PEC boundary wherein all the wave are fully reflected, but the algorithm is completely stable). Equation (113) is the final ABC expression for $x = 1$ boundary. It is used to terminate the magnetized cold plasma algorithm developed. Similarly, the ABC expressions for all other outer boundaries can also be derived in a same manner and the resulting formulations are shown as Equations (13) - (17).

$$x = 1 \rightarrow U_{i,j,k}^{n+1} = s \cdot \left\{ 2 \cdot U_{i,j,k}^n - U_{i,j,k}^{n-1} - \frac{v \Delta t}{\Delta x} (U_{i,j,k}^n - U_{i,j,k}^{n-1}) + \frac{v \Delta t}{\Delta x} (U_{i,j,k}^{n-1} - U_{i,j,k}^{n-2}) + \frac{1}{2} \left(\frac{v \Delta t}{\Delta y} \right)^2 \cdot (U_{i,j,k+1}^n - 2 \cdot U_{i,j,k}^n + U_{i,j,k-1}^n) + \frac{1}{2} \left(\frac{v \Delta t}{\Delta z} \right)^2 \cdot (U_{i,j,k+1}^{n-1} - 2 \cdot U_{i,j,k}^{n-1} + U_{i,j,k-1}^{n-1}) \right\} \quad (12)$$

$$x = h \rightarrow U|_{h,j,k}^{n+1} = s \cdot \left\{ 2 \cdot U|_{h,j,k}^n - U|_{h,j,k}^{n-1} - \frac{v\Delta t}{\Delta x} (U|_{h,j,k}^n - U|_{h-1,j,k}^n) + \frac{v\Delta t}{\Delta x} (U|_{h,j,k}^{n-1} - U|_{h-1,j,k}^{n-1}) + \frac{1}{2} \left(\frac{v\Delta t}{\Delta y} \right)^2 \cdot (U|_{h,j+1,k}^n - 2 \cdot U|_{h,j,kn} + U|_{h,j-1,kn}) + 12 (v\Delta t \Delta z)^2 \cdot (U|_{h,j,k+1n} - 2 \cdot U|_{h,j,kn} + U|_{h,j,k-1n}) \right\} \quad (13)$$

$$y = 1 \rightarrow U|_{i,1,k}^{n+1} = s \cdot \left\{ 2 \cdot U|_{i,1,k}^n - U|_{i,1,k}^{n-1} - \frac{v\Delta t}{\Delta y} (U|_{i,1,k}^n - U|_{i,2,k}^n) + \frac{v\Delta t}{\Delta y} (U|_{i,1,k}^{n-1} - U|_{i,2,k}^{n-1}) + \frac{1}{2} \left(\frac{v\Delta t}{\Delta x} \right)^2 \cdot (U|_{i+1,1,k}^n - 2 \cdot U|_{i,1,kn} + U|_{i-1,1,kn}) + 12 (v\Delta t \Delta z)^2 \cdot (U|_{i,1,k+1n} - 2 \cdot U|_{i,1,kn} + U|_{i,1,k-1n}) \right\} \quad (14)$$

$$y = m \rightarrow U|_{i,m,k}^{n+1} = s \cdot \left\{ 2 \cdot U|_{i,m,k}^n - U|_{i,m,k}^{n-1} - \frac{v\Delta t}{\Delta y} (U|_{i,m,k}^n - U|_{i,m-1,k}^n) + \frac{v\Delta t}{\Delta y} (U|_{i,m,k}^{n-1} - U|_{i,m-1,k}^{n-1}) + \frac{1}{2} \left(\frac{v\Delta t}{\Delta x} \right)^2 \cdot (U|_{i+1,m,k}^n - 2 \cdot U|_{i,m,kn} + U|_{i-1,m,kn}) + 12 (v\Delta t \Delta z)^2 \cdot (U|_{i,m,k+1n} - 2 \cdot U|_{i,m,kn} + U|_{i,m,k-1n}) \right\} \quad (15)$$

$$z = 1 \rightarrow U|_{i,j,1}^{n+1} = s \cdot \left\{ 2 \cdot U|_{i,j,1}^n - U|_{i,j,1}^{n-1} - \frac{v\Delta t}{\Delta z} (U|_{i,j,1}^n - U|_{i,j,2}^n) + \frac{v\Delta t}{\Delta z} (U|_{i,j,1}^{n-1} - U|_{i,j,2}^{n-1}) + \frac{1}{2} \left(\frac{v\Delta t}{\Delta x} \right)^2 \cdot (U|_{i+1,j,1}^n - 2 \cdot U|_{i,j,1n} + U|_{i-1,j,1n}) + 12 (v\Delta t \Delta y)^2 \cdot (U|_{1,j+1,1n} - 2 \cdot U|_{i,j,1n} + U|_{i,j-1,1n}) \right\} \quad (16)$$

$$z = p \rightarrow U|_{i,j,p}^{n+1} = s \cdot \left\{ 2 \cdot U|_{i,j,p}^n - U|_{i,j,p}^{n-1} - \frac{v\Delta t}{\Delta z} (U|_{i,j,p}^n - U|_{i,j,p-1}^n) + \frac{v\Delta t}{\Delta z} (U|_{i,j,p}^{n-1} - U|_{i,j,p-1}^{n-1}) + \frac{1}{2} \left(\frac{v\Delta t}{\Delta x} \right)^2 \cdot (U|_{i+1,j,p}^n - 2 \cdot U|_{i,j,pn} + U|_{i,j-1,pn}) + 12 (v\Delta t \Delta y)^2 \cdot (U|_{1,j+1,pn} - 2 \cdot U|_{i,j,pn} + U|_{i,j-1,pn}) \right\} \quad (17)$$

III. Numerical Experiments

1.1. Accuracy studies

The performance of our ABC scheme is first evaluated by testing the reflection error in a $100 \times 100 \times 100$ -cell FDTD grid having an x -directed electric dipole source at its center with a Gaussian modulated sinusoidal waveform as

$$E_x = \exp\left[-\left(\frac{t-t_0}{t_w}\right)^2\right] \cdot \sin(2\pi f_c t) \quad (18)$$

where $t_w = 2.93 \mu s$, $t_0 = 2.2t_w$ and $f_c = 4.0 \text{ MHz}$ is the center frequency of the source. The lattice space increments in each Cartesian direction of the FDTD grid are $\Delta x = \Delta y = \Delta z = 5m$, the time step Δt is 0.97 times the Courant limit and the stability control factor is $s = 1$. The plasma medium has an electron density N_e of $1.86 \times 10^8 m^{-3}$, which corresponds to the ionosphere at an altitude of about 90 km. A static background magnetic field of 1.0×10^{-5} Tesla of various orientations is applied to the plasma to approximately mimic the magnetic field of the Earth. Without loss of generality, the E_x field component is probed at a point in the same xy -plane as the source and 3 cells from the outer y -boundary. The relative reflection error $Error|_{i,j,k}^n$ of the ABC at time-step n and grid location (i, j, k) is then calculated by the method detailed in [10] and defined as

$$Error|_{1,j,k}^n = \frac{|E|_{i,j,k}^n - E_{ref}|_{i,j,k}^n|}{|E_{ref,max}|_{i,j,k}^n|} \quad (19)$$

where $E|_{i,j,k}^n$ is the electric field value recorded at the probing point, and the reference solution $E_{ref}|_{i,j,k}^n$ is obtained from a sufficiently large benchmark grid having no reflected signals from grid boundaries at the probing point over the time-stepping span of interest. The maximum amplitude of the reference fields over all time steps at grid location (i, j, k) is denoted as $E_{ref,max}|_{i,j,k}^n$.

Figure 1(a)-(c) illustrate the numerical results of the relative errors for different applied magnetic field directions. For Figure 1(a), a z -directed magnetic field is applied to the plasma ($B_z = -1.0 \times 10^{-5}$ T and $B_x = B_y = 0$ T). For Figure 1(b), an x -directed magnetic field is applied to the plasma in the upper half of the grid ($z \geq z_{max}/2$, $B_x = 1.0 \times 10^{-5}$ and $B_y = B_z = 0$ T) and a z -directed magnetic field is applied to the plasma in the lower half of the grid ($z < z_{max}/2$, $B_z = -1.0 \times 10^{-5}$ and $B_x = B_y = 0$ T), where z_{max} is the maximum number of grid cells in the z -direction. For Figure 1(c), a magnetic field with 45 degree codip and Azimuth angles is applied to the plasma ($B_x = B_y = 0.5 \times 10^{-5}$ and $B_z = -0.707 \times 10^{-5}$). For all the cases depicted in Figure 1(a)-(c), the reflection errors are seen to be less than $\sim 5\%$, clearly demonstrating the ABC's capability to provide the same approximate level of error regardless of the applied magnetic field direction.

To further evaluate the newly-derived ABC's performance compared to the original Mur's ABC, the same simulation parameters of Figure 1(c) are repeated with the original Mur's ABC. Figure 1(d) shows that the maximum reflection error for the case of the original Mur's ABC is also around 5%, as for the ABC of this chapter.

Next, the same numerical experiments have also been repeated without ABC (PEC in place of the ABC) to compare its performance with a PEC boundary. The result with a simulation condition as in the case of Figure 1(c) is shown in Figure 2. In this test, the ABC is simply removed and replaced by a PEC boundary and the recorded electric field variation at the probing point is then compared to those obtained from the grid with ABCs and from the large reference grid. One can see

that the PEC boundary is obviously introducing much larger reflection signals compared to the ABC and the large reference grid cases.

3.2. Evaluation of the ABC's performance in dense plasma

In Section 3.1, we performed accuracy studies of the ABC at a relatively low altitude (~ 90km) of the ionosphere (therefore a relatively low density plasma). To study the ABC's performance at higher altitudes (more dense plasma), the same simulation of Figure 1(a) is repeated for progressively larger electron densities N_e . We find through a series of tests that the maximum reflection error remains at the same level as for Figure 1(a) until the electron density N_e is increased to a level such that the center frequency f_c of the source becomes near to the critical cutoff frequencies of the plasma.

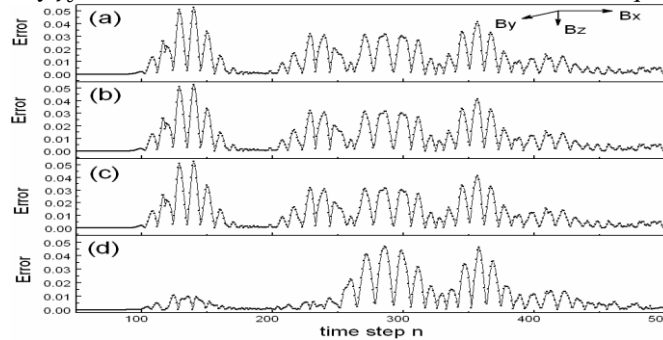


Figure.1. Reflection errors for different magnetic field directions applied to the plasma (a) $B_x=B_y=0$ T, $B_z=-1.0 \times 10^{-5}$ T (b) $B_x=1.0 \times 10^{-5}$ and $B_y=B_z=0$ T for $z \geq z_{max} / 2$, and $B_z = -1.0 \times 10^{-5}$ and $B_x = B_y = 0$ T for $z < z_{max} / 2$ (c) $B_x=B_y=0.5 \times 10^{-5}$ and $B_z=-0.707 \times 10^{-5}$ (d) same magnetic field as in (c) applied to Mur's ABC.

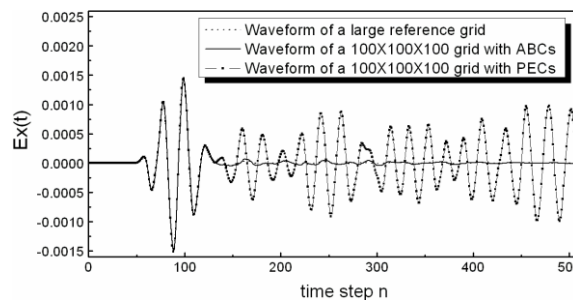


Figure.2. Time-domain electric field variations recorded at the probing point.

For example, Figure 3(c) illustrates the source spectrum employed in all of the numerical experiments. Figure 3(a) shows the dispersion diagram (wavenumber v.s. wave frequency) for the case of Figure 1(a) (a low-density plasma with $N_e = 1.86 \times 10^8 \text{ m}^{-3}$ corresponding to an altitude of ~ 90km), and Figure 3(b) shows the dispersion diagram for a higher density plasma with $N_e = 4.85 \times 10^{10} \text{ m}^{-3}$ (corresponding to an altitude of ~ 400km). The dotted lines of Figure 3(a) and Figure 3(b) represent the dispersion relation of the LHC-wave and the solid lines represent the dispersion diagram of the RHC-wave. We note that according to Figure.3, as N_e is increased from $1.86 \times 10^8 \text{ m}^{-3}$ to $4.85 \times 10^{10} \text{ m}^{-3}$ the source begins to have substantial spectrum below the cutoff frequencies of the LHC- and RHC-waves. This causes the portion of the source spectrum below ~ 2.1 MHz to change from propagating modes as for the case of Figure 3(a) to non-propagating modes as for the case of Figure 3(b). More importantly, though, closer to the cutoff frequencies, the phase velocity is increased. As a result, because a velocity of c corresponding to free space has been assumed for the ABC, the reflection error increases from ~ 5 % as for Figure.1(a) to ~ 6 % as shown in Figure.4(a) for the same scenario except for having an increased N_e . To improve the accuracy, instead of using the free-space speed c for v in equations (1) - (6), the phase velocity v in the plasma at the source center frequency f_c is utilized, resulting in a value of ~ 1.13c. Figure 4(b) presents the results using $v = 1.13 c$, and as expected, the maximum reflection error is now reduced to ~ 4.5 % from ~ 6 % of Figure 4(a).

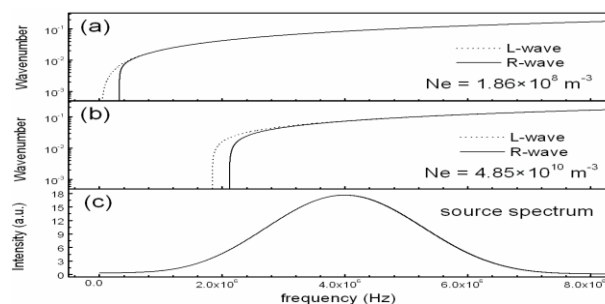


Figure.3. (a) dispersion diagram for a low-density plasma ($N_e = 1.86 \times 10^8 \text{ m}^{-3}$) (b) dispersion diagram for a high-density plasma ($N_e = 4.85 \times 10^{10} \text{ m}^{-3}$) (c) source wave spectrum

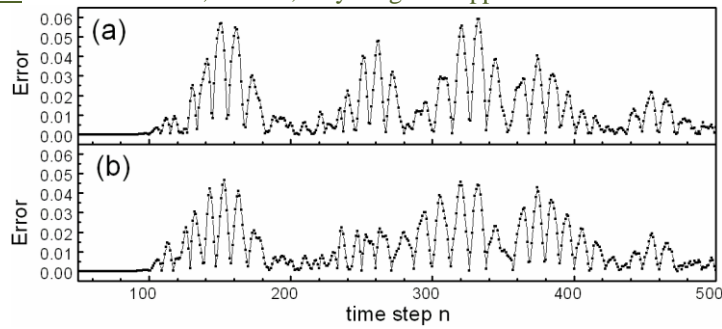


Figure.4. Reflection errors for a dense plasma ($N_e = 4.85 \times 10^{10} \text{ m}^{-3}$) (a) phase velocity v of the ABC assumed as free-space speed c (b) $v=1.13c$

IV. Conclusion

We find through longer numerical tests that the early-time instability of Mur's ABC is simply replaced by a late-time instability in Zhang and Wang's scheme. In this article, the feasibility of a variation of Zhang and Wang's scheme is investigated to serve as an effective ABC for the 3-D FDTD magnetized cold plasma formulation. We choose this scheme despite its inherent late-time instability because it has the potential to provide an acceptable level of error regardless of the direction of the background magnetic-field, a capability not provided by KPML. We then presented a simple but very effective way to 60 further delay the late-time instability of this magnetized plasma ABC. In Section 2, the formulation of the ABC scheme is first derived. Next, in Section 3, the newly-developed ABC scheme is rigorously tested by evaluating its reflection errors for different cases.

References :

- [1] J. P. Berenger, "A perfectly matched layer for the absorption of electromagnetic waves," *J. Comp.Phys.*, vol.114, pp.185–200, 1994.
- [2] S. G. Gedney, "An anisotropic perfectly matched layer-absorbing medium for the truncation of FDTD lattices," *IEEE Trans. Antennas Propagat.*, vol. 44, pp. 1630–1639, Dec. 1996.
- [3] J. A. Roden and S. D. Gedney, "Convolutional PML (CPML): an efficient FDTD implementation of the CFS-PML for arbitrary media," *Microwave Opt. Technol. Lett.*, vol. 27, no. 5, pp. 334–339, 2000.
- [4] S. A. Cummer, "A simple, nearly perfectly matched layer for general electromagnetic media," *IEEE Microwave Wireless Compon. Lett.*, vol. 13, pp. 128–130, Mar. 2003.
- [5] M. W. Chevalier, T. W. Chevalier, and U. S. Inan, "A PML Utilizing k-Vector Information as Applied to the Whistler Mode in a Magnetized Plasma," *IEEE Trans. Antennas Propagat.*, vol.54, no.8, August 2006.
- [6] E. Becache, S. Fauqueux, and P. Joly, "Stability of perfectly matched layers, group velocities, and anisotropic waves," *J. Computational Phys.*, vol. 188, pp. 399–433, 2003.
- [7] S. A. Cummer, "Perfectly matched layer behavior in negative refractive index materials," *IEEE Antennas Wireless Propag. Lett.*, vol. 3, 2004.
- [8] T. W. Chevalier, U. S. Inan and T. F. Bell, "Terminal Impedance and Antenna Current Distribution of a VLF Electric Dipole in the Inner Magnetosphere," *IEEE Trans. Antennas Propagat.*, vol. 56, pp. 2454–2468, Aug. 2008.
- [9] G. Mur, "Absorbing boundary conditions for the finite-difference approximation of time-domain electromagnetic field equations," *IEEE Trans. Electromgn. Compat.*, vol. EMC-23, Nov. 1981.
- [10] J.-N. Hwang and F.-C. Chen, "Stability Analysis of the Mur's Absorbing Boundary Condition in the alternating direction implicit finite-difference method," *IET Microw. Antennas Propag.*, vol. 1, no. 3, June 2007.
- [11] Z. Yusheng and W. Wenbing, "The Studies of the Stability of FDTD with Mur's Absorbing Boundary Condition of Second Order in 3-D Scattering Problems," *IEEE Microwave and Guided Wave Letters*, vol. 6, no. 3, March 1996.
- [12] B. Engquist and A. Majda, "Absorbing boundary conditions for the numerical simulation of waves," *Math. Comp.*, vol.31, pp.629-651, 1977.

Radiation Properties of the Array Pattern Synthesis Using Fibonacci and Normalized Modified Binomial (Nmb) Polynomials

Abdolkhalegh Mohammadi and Mohammad Pourbagher, Javad Nourinia

Microelectronics Research Laboratory, Urmia university, IRAN

Abstract: This paper presents radiation property of the array antenna pattern synthesis using new polynomial. Fibonacci and Smooth Normalized Modified Binomial (SNMB) are two polynomials which the property of their pattern are investigated. Fibonacci have a good side lobe level but the lobes are smooth and no tapering is observed. SNMB array type can be accomplished to have tapered minor lobe which is suitable for Radar and low-noise systems.

Keywords- polynomials, array, minor lobe, first null, side lobe level (SLL)

I. Introduction:

Antenna array radiation pattern synthesis has taken major interest since the beginning of the array antenna era. The problem is generally to synthesize the optimum complex excitation coefficients for a given array geometry that will yield an array factor which is – in some sense– close to a desired array factor. Especially when it comes to the subject of shaped pattern synthesis, optimization techniques with iterative procedures are used. Genetic algorithms (GA) [1] are the most widely used methods in pattern synthesis, which can almost deal with all the synthesizing problems. Particle swarm optimization (PSO) [2] and simulated annealing (SA) [3] have already been used in array synthesis for different requirements too. Immune algorithm (IA) [4] is also a new heuristic optimization algorithm which has powerful function of global search. Although some studies like [5] focus on the problem with a different point of view, i.e., attempting to find the optimum geometry under the existence of prescribed excitation coefficients, most of the literature deals with the problem of obtaining the optimum coefficients for one dimensional linear arrays, possibly due to its practical use. Various methods have been applied for the solution of the problem. Among these are non-iterative methods such as Fourier Transform Method, Woodward-Lawson Method, and Taylor Line Source Synthesis Method.

Currently, development of wireless application such as radar and communication with low noise becomes rapidly. The antenna plays an important role as the key device in transmitting and receiving the signal. Generally it is desired to antenna to provide maximum directivity, narrow beamwidth and low side lobe level especially far out minor lobes in order to reduce the noise entering through those minor lobes. The antenna array is one of the most suitable candidates that can fulfill these requirements. In most cases, the elements of an array are identical. The total field of the array is determined by the vector addition of the fields radiated by the individual elements. This is usually not the case depends on the separation between the elements. To provide very directive patterns, it is necessary

that the field from the elements of the array interfere constructively (add) in the desired directions and interfere destructively (cancel each other) in the remaining space. In an array with identical elements, there are at least five parameters that can control the shape of the overall pattern of the antenna [6]. Excitation amplitude of the individual elements is one of the features that help us to control the pattern of the array antenna. In N-element linear array with uniform spacing and nonuniform amplitude there are three famous distributions: uniform, binomial and Tschebyscheff. An uniform amplitude array yields the smallest half-power beamwidth. It is followed, in order, by the Dolph-Tschebyscheff and binomial arrays. In contrast, binomial arrays usually possess the smallest side lobes followed, in order, by the Dolph-Tschebyscheff and uniform arrays. As a matter of fact, binomial arrays with element spacing equal or less than $\lambda/2$ have no side lobes. It is apparent that the designer must compromise between side lobe level and beamwidth. a criterion that can be used to judge the relative beamwidth and side lobe level of one design to another is the amplitude distribution (tapering) along the source. It has been shown analytically that for a given side lobe level the Dolph-Tschebyscheff array produces the smallest beamwidth between the first nulls. Conversely, for a given beamwidth between the first nulls, the Dolph-Tschebyscheff design leads to the smallest possible side lobe level. Uniform arrays usually possess the largest directivity.

For some applications, such as radar and low-noise systems, it is desirable to sacrifice some beamwidth and low inner minor lobes to have all the minor lobes decay as the angle increases on either side of the main beam [7]. In these applications the side lobes should be tapered. In this paper radiation properties of array pattern synthesis using some new special polynomials is discussed

II. Array pattern synthesis using Fibonacci polynomials

In this part the design procedures of the array pattern synthesis using modified Fibonacci polynomials will be illustrated. The issue refers to compute the radiation pattern and half power beamwidth (HPBW) and directivity of N-element linear array with uniform spacing and nonuniform amplitude which are excited by Fibonacci polynomials. In the following The Fibonacci polynomials will be introduced. The formula of Fibonacci polynomials is

$$F_n = F_{n-1} + F_{n-2} \quad (1)$$

$$F_0 = 0$$

$$F_1 = 1$$

The generated polynomial will be 0,1,1,2,3,5,8,13,21,34,55,89,...

To use this polynomial for excitation of N-elements we write the Fibonacci polynomial with $n=N+1$ term, after that

we again write these n terms in a degradation form, now if N be even, the same terms will be repeated in a degradation form without any change. Also if N be odd, the maximum term will be omitted from the degradation form terms. Let N=4, the Fibonacci polynomial will be 0,1,1,2,3,5

N is even so we write this polynomial in a degradation form directly after initial terms

0,1,1,2,3,5,5,3,2,1,1,0

Now we omit the additional terms from both sides until the number of terms be equal to number of elements (4 elements).

~~0,1,1,2,3,5,5,3,2,1,1,0~~

So the amplitude of excitation coefficients for 4-elements array will be

3,5,5,3

Again for a 5-elements array the Fibonacci polynomial will be

0,1,1,2,3,5,8

Now these terms will come with degradation form and the maximum term will be omitted.

0,1,1,2,3,5,8,5,3,2,1,1,0

Now we omit the additional terms from both sides until the number of terms be equal to number of elements (five elements). The answer is: 3,5,8,5,3

The polynomials of Fibonacci for different N are brought here:

N=1		1		
N=2		2	2	
N=3	2	3	2	
N=4	3	5	5	3

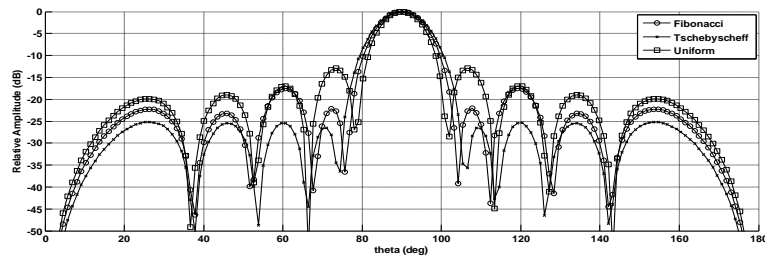


Fig. 1. Comparison of Fibonacci, Uniform and Tschebyscheff

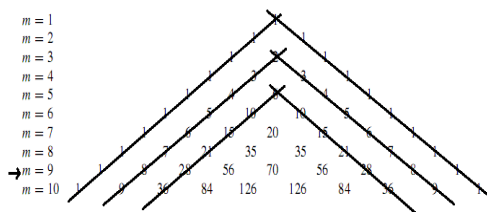


Fig. 2. Deleted sides of pascal's triangle

After that the excitation coefficients are normalized to the big one. In fig. 2 this method is shown completely.

For formulizing the above steps we start with binomial expansion:

$$(1 + x)^{N-1} = \binom{N-1}{0} + \binom{N-1}{1}x + \binom{N-1}{2}x^2 + \dots + \binom{N-1}{N-1}x^{N-1} \quad (2)$$

N is the number of elements. So the excitation coefficients are:

$$\binom{N-1}{0}, \binom{N-1}{1}, \binom{N-1}{2}, \dots, \binom{N-1}{N-1} \quad (3)$$

N=5	3	5	8	5	3			
N=6	5	8	13	13	8	5		
N=7	5	8	13	21	13	8	5	
N=8	8	13	21	34	34	21	13	8

Now if we use some changes to these polynomials the features of radiation will be better.

For example we can add the difference between the smallest and the greatest excitation coefficient to all elements, so the directivity will be better. Now we compare the radiation pattern, HPBW and Directivity of an array with 10 elements which excited by Fibonacci, uniform, binomial and Tschebyscheff. In Fig. 1 We observe that the pattern of fibonacci is between the Uniform and Tschebycheff. It shows that the directivity of fibonacci is better than Tschebycheff but not as well as Uniform. Tschebycheff pattern has the smallest first minor lobe. We do not observe any good tapering from Tschebycheff and fibonacci patterns. But Uniform array has tapered.

III. Normalized Modified Binomial (NMB) :

Using the binomial method for excitation of arrays has some problems. For example the differences between excitation coefficients are very much and it makes some practical problems. In modified binomial polynomial this problem has been solved by keeping other features. In this method we omit two sides of pascal's triangle for several times according to number of element. After that we use the new triangle and by the knowledge of number of element the appropriate row of triangle is chosen. For example for a three element array we delete the sides for three times. Then the third row of new triangle is chosen.

From Posteriori reasoning we will find out that the Nth row of new triangle is the 3*Nth of the Pascal's triangle which some coefficient are omitted. For finding the excitation coefficient by new triangle we can trace the following:

$$\binom{N^{old}-1}{N^{new}}, \binom{N^{old}-1}{N^{new}+1}, \dots, \binom{N^{old}-1}{N^{old}-N^{new}} \quad (4)$$

For example for a five-element array the results is:

$$N^{new}=5$$

$$N^{old}=3*5=15$$

$$\binom{15-1}{5}, \binom{15-1}{6}, \binom{15-1}{7}, \binom{15-1}{8}, \binom{15-1}{9}$$

The coefficients are:
2002,3003,3432,3003,2002

Now we normalize coefficients to the bigger one.
0.58, 0.87, 1, 0.87, 0.58

The new triangle for excitation coefficient is:

N=1		1	
N=2		1	1
N=3	0.8	1	0.8

N=4	0.71	1	1	0.71				
.	0.58	0.87	1	0.87	0.58			
.	0.5	0.8	1	1	0.8	0.5		
.	0.41	0.68	0.9	1	0.9	0.68	0.41	
.	0.36	0.68	0.84	1	1	0.84	0.68	0.36

N=1	1							
N=2	1	1						
N=3	1	1.2	1					
N=4	1	1.29	1.29	1				
N=5	1	1.29	1.42	1.29	1			
N=6	1	1.3	1.5	1.5	1.3	1		
N=7	1	1.27	1.49	1.59	1.49	1.27	1	
N=8	1	1.24	1.48	1.64	1.64	1.48	1.24	1

Now if we use some changes to this triangle the features of radiation will be better.

For example if the difference between the smallest and the greatest excitation coefficient be added to all elements, the directivity will be better. The excitation coefficient will be:

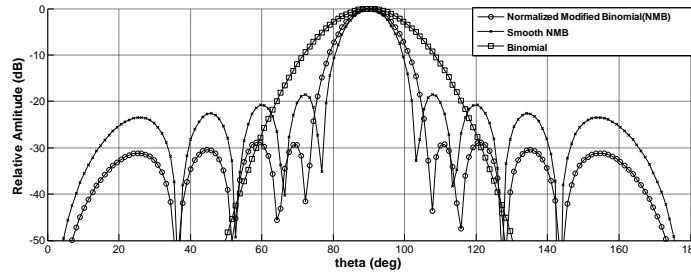


Fig. 3. Comparison between Normalized Modified Binomials, smooth NMB and Binomial

We call this polynomial Smooth Normalized Modified Binomials (SNMB). Now we compare this new polynomial with binomial and other special polynomials. At first in fig. 3 We observe the effect of changes to polynomials. By adding the difference of smallest and largest coefficient to all excitation coefficients, the amplitudes will be more smooth and it help us to have a directivity better than NMB.

The most important part of Fig. 3 is the tapering of smooth NMB polynomial pattern. As in this figure is observed, the NMB and Binomial (which has no side lobe) has no tapering.

In fig. 4 the pattern of Smooth NMB and Tschebycheff are compared. The directivity of smooth NMB is better than Tschebycheff, although the side lobe level is worse. Tschebycheff has no tapering in minor lobes but the tapering in Smooth NMB is evident. As mentioned above this property is suitable for some application like Radar and low-noise system.

There are other polynomials which have this property (tapering). Hermite polynomials and A continuous line-source distribution that yields decaying minor lobes and, in addition, controls the amplitude of the sidelobe is that introduced by Taylor [8] in an unpublished classic

memorandum. It is referred to as the Taylor (one-parameter) design.

Both polynomials have some disadvantages, for example Hermite in spite of having tapered minor lobe is sacrifices directivity. Totally the disadvantage of designing an array with decaying minor lobes as compared to a design with equal minor lobe level (Dolph-Tschebyscheff), it yields about 12 to 15% greater half-power beamwidth. Also Taylor designing methods are more applicable for large arrays [3].

As it is observed in fig. 4 the Smooth NMB has a better directivity than Tschebycheff. It has tapered minor lobe without sacrificing the directivity.

The advantage of Tschebycheff and Taylor designing methods is their capability in controlling the side lobe level, in other words for a given side lobe level, the smallest possible first-null beamwidth (or the smallest possible sidelobe level for a given first-null beamwidth) is achieved by Dolph-Tschebyscheff array design. If this property of Dolph-Tschebyscheff design be combined by Smooth NMB tapering property the best answer will occur. Then a trade-off between side lobe level and tapering ratio could be made.

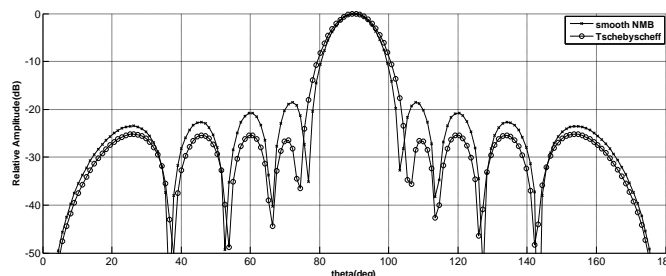


Fig. 4. Comparison between Tschebycheff and smooth NMB

IV. Conclusion:

In this paper radiation properties of array pattern synthesis using some special polynomials is discussed. In Radar and low noise systems it is desirable to sacrifice

some beamwidth and low inner minor lobes to have all the minor lobes decay as the angle increases on either side of the main beam. In radar applications this is preferable because interfering or spurious signals would be reduced

further when they try to enter through the decaying minor lobes. Thus any significant contributions from interfering signals would be through the pattern in the vicinity of the major lobe. The best polynomial that gives this property is Hermite polynomial. In spite of giving this tapered minor lobes Hermite polynomials reduces directivity. In this paper the end was to excite the amplitude by some new polynomials to give us a tapered lobe by keeping Directivity constant. Smooth NMB do this, by keeping directivity it has a good tapered minor lobes.

REFERENCES

- [1] K. Yan and Y. Lu, "Side lobe reduction in array pattern synthesis using genetic algorithm," IEEE Trans. Antennas Propag., vol. 45, no. 7, July 1997, pp. 1117-1122.
- [2] M. M. Khodier and C. G. Christodoulou, "Linear array geometry synthesis with minimum sidelobe level and null control using particle swarm optimization," IEEE Trans. Antennas Propag., vol. 53, no. 8, Aug. 2005, pp. 2674-2679.
- [3] V. Murino, A. Trucco, and C. Regazzoni, "Synthesis of unequally spaced arrays by simulated annealing," IEEE Trans. Signal Process., vol. 44, no. 1, Jan 1996, pp. 119-123.
- [4] De Castro L N.Von Zuben F J. "The Clonal Selection Algorithm with Engineering Applications". Workshop Proceedings of GECC'00, Workshop on Artificial Immune Systems and Their Applications. Orlando:IEEE Tran. 2000, pp. 36~37.
- [5] Kelley, D.F.; Stutzman, W.L.; , "Array antenna pattern modeling methods that include mutual coupling effects," Antennas and Propagation, IEEE Transactions on , vol.41, no.12, pp.1625-1632, Dec 1993.
- [6] Constantine A. Balanis, "ANTENNA THEORY" , Wiley,New Jersey,2005,p.283
- [7] Constantine A. Balanis, "ANTENNA THEORY" , Wiley,New Jersey,2005,p.410
- [8] T. T. Taylor, "One Parameter Family of Line-Sources Producing Modified $\text{Sin}(\pi u)/\pi u$ Patterns," Hughes Aircraft Co. Tech. Mem. 324, Culver City, Calif., Contract AF 19(604)-262-F-14, 1953

Variable Step Variable Weights Lms (Vsvwlms) Algorithm By Modified Leaky Lms

Mohammad purbagher, Abdolkhalegh Mohammadi, Javad Nourinia,
Changiz ghobadi

Department of Electrical Engineering, Urmia university, IRAN

Abstract: This paper proposes a modified leaky least-mean-square (LLMS) algorithm by variable step and variable weight factor (VSVWLMS) that used magnification of error signal. This algorithm uses a variant rate of convergence (ROF) and a variant weight factor for searching in performance surface. In each step the algorithm chooses a new rate of convergence for searching and run computations according to this new rate of convergence. This algorithm at the beginning of convergence uses large value of rate of convergence for increasing speed of convergence. After that by approaching to optimum point the algorithm uses small rate of convergence to give a more accurate response. Also the algorithm uses variant parameter to multiply to the weight vector and new method of varying this parameter in each step. Here the gist of matter refers to using the features of two algorithm, Variable Step Least-Mean-Square (VSLMS) and Leaky LMS which helps to increase the speed of convergence and combining these feature.

Keywords: adaptive filter , Leaky LMS, rate of convergence , VSLMS

I. Introduction

In recent years a growing field of research in adaptive systems has resulted in a variety of adaptive automats whose characteristics in limited ways resemble certain characteristics of living systems and biological adaptive processes [1].

The essential and principal property of the adaptive system is its time-varying self-adjusting performance. In many instances, however, the complete range of input conditions may not be known exactly, or even statistically; or the condition changes from time to time. In such circumstances, an adaptive system that continually seeks the optimum within an allowed class of possibilities, using an orderly search process, would give superior performance compared with a system of fixed design.

We begin by representing the performance feedback process In the Fig.1. where the input $x_k \in \mathcal{R}^N$ is a stationary zero-mean vector random process with autocorrelation matrix $R \triangleq E [x_k x_k^T]$ for all k, the desired output d_k is a stationary zero-mean scalar random process, $W_k \in \mathcal{R}^N$ is the weight vector, and k is the time index. The system output at time k is given by $y_k = W_k^T x_k$, and the error ϵ_k is computed via $\epsilon_k = d_k - y_k$.

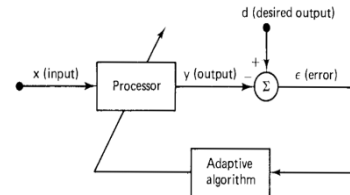


Figure.1 Block diagram of an adaptive filter.

Assume that x_k and d_k are jointly stationary with crosscorrelation vector $P \triangleq E [d_k x_k]$ for all k. Define a convex cost function

$$\zeta \triangleq E [\epsilon_k^2] = E [d_k^2] - 2P^T W + W^T R W \quad (1)$$

This cost function is the mean square error (MSE). It can easily be shown that, if R is full rank, the unique optimal fixed weight vector which minimizes ζ is given by

$$W^* = R^{-1} P \quad (2)$$

This is called the Wiener solution [2].

It is clear from this expression that the mean square error ζ is precisely a quadratic function of the component of the weight vector W when the input component and desired response input are stationary stochastic variables. A portion of a typical two-dimensional mean square error function is illustrated in Fig. 2.

The vertical axis represent the mean square error and the horizontal axes the value of the two weights. The bowl-shaped quadratic error function, or performance surface for in this manner is a paraboloid.

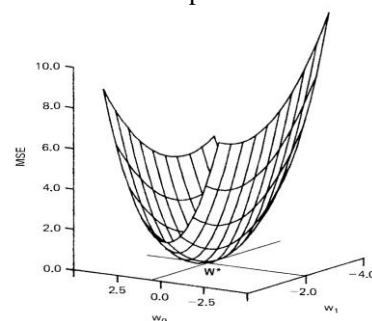


Figure.2 portion of a two dimensional quadratic performance surface. the mean square error is plotted vertically, and the optimum weights vector is $W^* = (0.65, -2.10)$. the minimum MSE is 0.0 in this example.

1.2. Gradient and minimum mean-square error

Many useful adaptive process that cause the weight vector to seek the minimum of the performance surface so by gradient method [1]. The gradient of the mean square error surface, designated $\nabla(\zeta)$ or simply ∇ , can be obtained by differentiating (1) to obtain the column vector

$$\nabla \triangleq \frac{\partial \zeta}{\partial W} = \left[\frac{\partial \zeta}{\partial w_0} \quad \frac{\partial \zeta}{\partial w_1} \quad \dots \quad \frac{\partial \zeta}{\partial w_L} \right]^T = 2RW - 2P \quad (3)$$

where R is autocorrelation and P is crosscorrelation. To obtain the minimum square error the weight vector W is set at its optimum value W^* , where the gradient is zero :

$$\nabla = 0 = 2RW^* - 2P \tag{4}$$

Assuming that R is nonsingular, the optimum weight vector W^* , sometimes called the wiener weight vector, is found from (9) to be [3-5]

$$W^* = R^{-1}P$$

II. VSVWLMS algorithm

In fact a filter consists of an electrical circuit or software program that chooses the desired signal from unwanted noise and signals. In an adaptive filter (self-improved filter), the filter modified itself after a while (a few iteration) and learn how to optimize weights to achieve the optimum response called wiener response. Leaky LMS algorithm is one of the algorithms used in adaptive filters

$$W(k+1) = \beta W(k) + 2\mu\epsilon(k)X(k) \tag{5}$$

where β is a small number near one and $W(k)$ is weight vector in n th iteration. $\epsilon(n)$ is the error signal and $x(n)$ is the input signal and μ is rate of convergence.

What is discussed in this algorithm represents a new method according to Leaky LMS and VSLMS algorithm to accelerating the speed of the convergence. In this algorithm β and μ are variant and defined like below

$$W(k+1) = \beta(k)W(k) + 2\mu(k)\epsilon'(k)X(k) \tag{6}$$

$$\beta(k) = e^{-\left(\frac{k}{k+1}\right)} \tag{7}$$

$$\mu(k) = \mu(k-1) + 0.01^k (A(k)A(k-1)) \tag{8}$$

$$A(k) = \epsilon'(k)X(k) \tag{9}$$

where ϵ' is the magnificated error signal, i.e.

$$\epsilon'(k) = 5\epsilon(k) \tag{10}$$

$$y(k) = X^T(k)W(k) \tag{11}$$

III. Convergence proof

This section examines the process of mathematical algorithms and its convergence explains. After that by transforming coordinate system to principle coordinate, convergence condition is examined. In the following gradient estimate convergence examined.

$$E[\nabla'(k)] = E[-2\epsilon'(k)X(k)] \\ = -10 E [d(k) X(k) - X(k) X^T(k) W(k)]$$

$$= 10 (RW - p) = 5 \nabla(k) \tag{12}$$

now the convergence of the weights to the optimum weight is discussed.

$$E[w(k+1)] = E[\beta(k)w(k)] + 10\mu E[\epsilon(k)X(k)]$$

$$E[w(k+1)] = e^{-\left(\frac{k}{k+1}\right)} E[w(k)] + 10\mu E[\epsilon(k)X(k)] \tag{13}$$

by substituting $\epsilon(n)$ in the above equation and considering $W^* = R^{-1}P$ it will be

$$E[w(k+1)] = (\beta(k) - 10\mu R)E[w(k)] + 10\mu R w^* \tag{14}$$

by transforming the coordinates to the principle coordinate and using eigen value matrix Λ it will be

$$\Lambda = \begin{pmatrix} \lambda_0 & \dots & 0 \\ \vdots & \ddots & \vdots \\ 0 & \dots & \lambda_L \end{pmatrix} \tag{15}$$

$$E[v'] = (\beta(k) - 10\mu\Lambda)^k v'_0 \tag{16}$$

$r = \text{geometric ratio} = \beta(k) - 10\mu\Lambda$

v'_0 is the initial weight vector in the principle-axis system. we also note that [4-7]

where v' is the weight vector, W , in the principle-axis system, Λ is the diagonal eigenvalue matrix of R , and

$$r \approx e^{-\frac{1}{\tau}} = 1 - \frac{1}{\tau} + \frac{1}{2\tau^2} - \dots \tag{17}$$

we have

$$\beta(k) - 10\mu\lambda_k \approx 1 - \frac{1}{\tau}$$

therefore

$$\tau_k = \frac{1}{10\mu(k)\left(\lambda_k + \frac{1-\beta(k)}{10\mu(k)}\right)} \tag{18}$$

The geometric ratio of the learning curve, on the other hand [8], [10]

$$r_{mse} = r^2 \tag{19}$$

$$\exp\left(-\frac{1}{\tau_{mse}}\right) = \exp\left(-\frac{2}{\tau}\right) = r^2 = r_{mse} \tag{20}$$

$$\tau_{mse} = \frac{\tau}{2} \tag{21}$$

and know that

$$M = \frac{\text{excess MSE}}{\zeta_{min}} \approx \mu \text{tr}[R] \tag{22}$$

$$\text{tr}[R] = \sum_{n=0}^L \lambda_n \\ = \frac{1}{4\mu} \sum_{n=0}^L \frac{1}{\tau_{mse}} = \frac{L+1}{4\mu} \left(\frac{1}{\tau_{mse}}\right)_{av}$$

$$M \approx \frac{L+1}{4\tau_{mse}} \tag{23}$$

where $L+1$ is the total weights, Therefore misadjustment in the VSVWLMS is

$$M \approx (L+1)(5\mu(k))\left(\lambda_k + \frac{1-\beta(k)}{10\mu(k)}\right) \tag{24}$$

We also note that λ_{max} cannot be greater than the trace of R , which is the sum of the diagonal elements of R , that is [1], [8-12]

$$\lambda_{max} \leq \text{tr}[\Lambda] = \sum(\text{diagonal elements of } \Lambda) = \sum(\text{diagonal elements of } R) = \text{tr}[R] \tag{25}$$

here the condition of convergence is bellow

$$|r| < 1 \text{ which yields below equation}$$

$$\frac{\beta(k)-1}{10\lambda_{min}} < \mu < \frac{\beta(k)+1}{10\lambda_{max}}$$

This disparity increases as the eigenvalue spread $\lambda_{max}/\lambda_{min}$ increases – corresponding to an equivalent increase in the eccentricity of the elliptical contours of constant MSE [13-18]. Thus, the key step in improving the transient performance of LMS lies in decreasing the input eigenvalue spread.

IV. Simulation results

In this section an example which compares the proposed algorithm with the Leaky LMS and VSLMS algorithm is represented. The block diagram of the example is shown

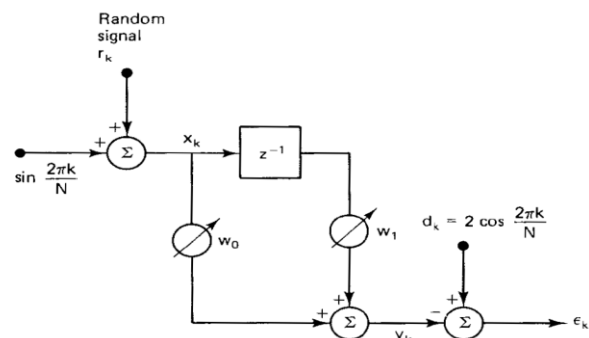


Figure.3 Block diagram for a filter with two weights.

The simulation result of this example for the same starting point and the identical stage (250 iteration) for the proposed algorithm, Leaky LMS and VSLMS algorithm and the comparison between them is presented in Fig. 4 and Fig. 5.

In Fig. 6 it is shown that the suggested algorithm converge to the optimum point with a bigger stage. It shows that the convergence occur faster. In Fig. 7 which enlarge the last point of the convergence, it is shown that with the same iteration, the response of the proposed algorithm is closer than to the optimum point. In this figure the last point of VSLMS is (5.263, -4.860) and the last point of suggested algorithm is (5.227, -4.829) in the same iteration while the optimum point is (4.828, -5.226).

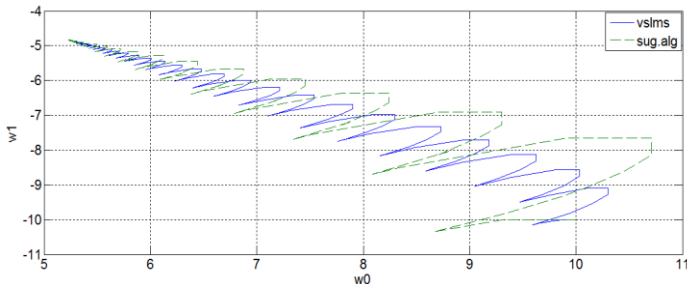


Figure.4 suggested algorithm versus VSLMS.

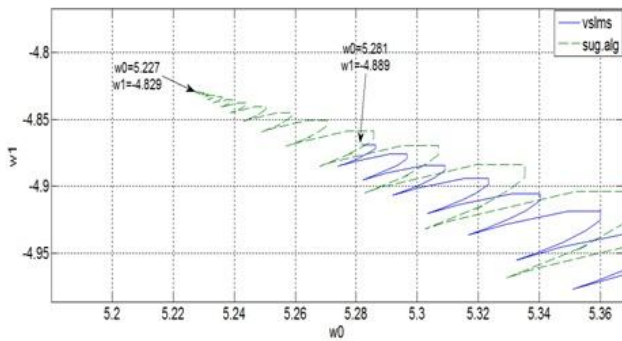


Figure.5 Comparison between the suggested algorithm and the VSLMS in seeking the optimum point with the same iteration

In Fig. 4 it is shown that the suggested algorithm converge to the optimum point with a large steps. It shows that the convergence occur faster. In Fig. 5 which enlarge the last point of the convergence, shown with the same iteration, the response of the proposed algorithm is closer than to the optimum point. In this figure the last point of Leaky LMS is (5.281, -4.889) and the last point of suggested algorithm is (5.227, -4.829) in the same iteration while the optimum point is (4.828, -5.226).

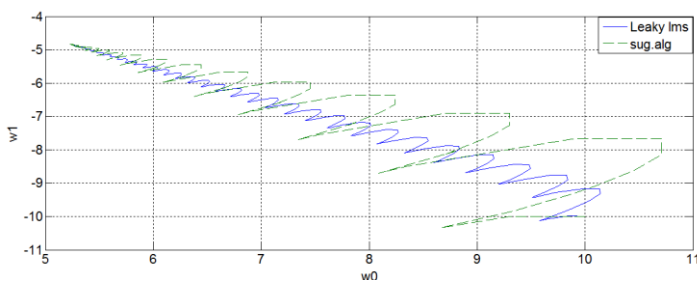


Figure.6 Suggested algorithm versus Leaky LMS.

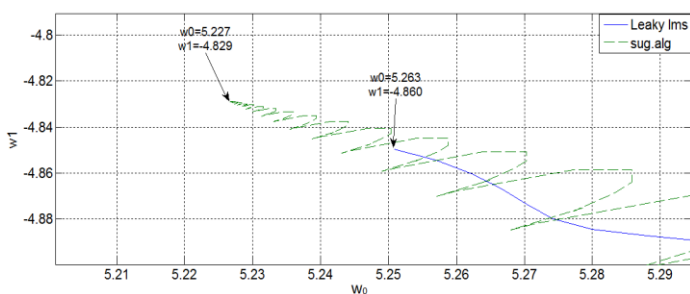


Figure.7 Comparison between the suggested algorithm and the Leaky LMS in seeking the optimum point with the same iteration.

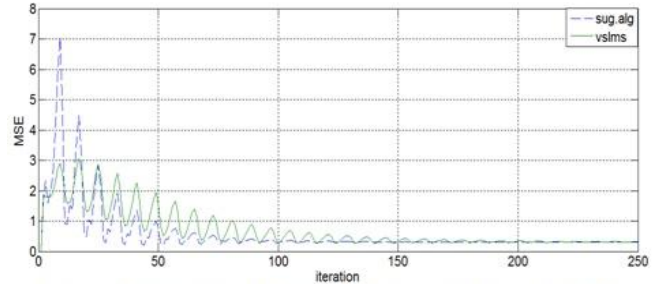


Figure.8 Comparison between the learning curves of the suggested algorithm and VSLMS.

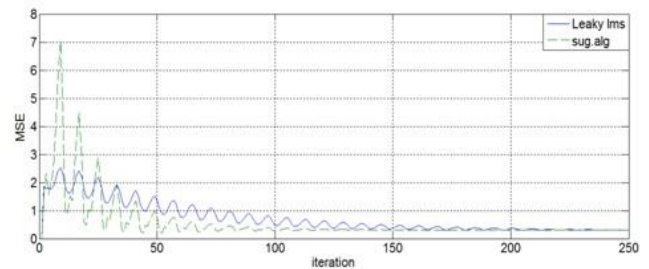


Figure.9 Comparison between learning curves of suggested algorithm and Leaky LMS

In the Figures 8 and 9 the mean-square-error (MSE) versus iteration are illustrated. It is clear that the suggested algorithm at first has a bigger MSE, but after some iteration it will be lower than Leaky LMS and VSLMS algorithm's MSE. It shows that the algorithm in fewer iteration reaches to the desirable accuracy and give us a better response.

V. Conclusion

In this paper a new algorithm for adaptive filter has been introduced which was called VSVWLMS. This algorithm uses the features of Leaky LMS and VSLMS and combined them to accelerate the speed of convergence. In the simulation result it has been observed that in the same iteration VSVWLMS algorithm converge to the optimum point with more speed.

References

- [1] Bernard Widrow and Samuel D. Stearns, *adaptive signal processing*. Prentice-Hall
- [2] B. Farhang Boroujeny, *adaptive filters theory & applications*. John Wiley & Sons
- [3] Sungkwon Jo, Member, IEEE, Jihoon Choi, Student Member, IEEE, and Yong H. Lee, Senior Member, IEEE, "Modified Leaky LMS Algorithm for Channel Estimation in DS-CDMA Systems" *IEEE Communications Letters*, vol. 6, no. 5, May 2002.
- [4] A. Aghamohammadi, H. Meyr, and G. Ascheid, "Adaptive synchronization and channel parameter estimation using an extended Kalman filter," *IEEE Trans. Commun.*, vol. 37, pp. 1212-1218, Nov. 1989.
- [5] Juan R. V. López, Orlando J. Tobias, and Rui Seara, "Modified leaky delayed LMS algorithm for imperfect estimate system delay" 15th European Signal Processing Conference (EUSIPCO 2007), Poznan, Poland, September 3-7, 2007, copyright by EURASIP.
- [6] G. Long, F. Ling, and J. Proakis, "The LMS with delayed coefficient adaptation," *IEEE Trans. Acoust., Speech, Signal Process.*, vol. 37, no. 9, pp. 1397-1405, Sep. 1989.
- [7] F. Laichi, T. Aboulnasr, and W. Steenaert, "Effect of delay on the performance of the leaky LMS adaptive algorithm," *IEEE Trans. Signal Process.*, vol. 45, no. 3, pp. 811-813, Mar. 1997.
- [8] R. D. Poltmann, "Conversion of the delayed LMS algorithm into the LMS algorithm," *IEEE Signal Process. Lett.*, vol. 2, no. 12, pp. 223, Dec. 1995.
- [9] M. Rupp, "Saving complexity of modified filtered-X LMS and delayed update LMS algorithms," *IEEE Trans. Circuits Syst. II: Analog Digit. Signal Process.*, vol. 44, no. 1, pp. 45-48, Jan. 1997.
- [10] O. J. Tobias and R. Seara, "Leaky delayed LMS algorithm: analysis for Gaussian data and delay modeling error," *IEEE Trans. Signal Process.*, vol. 52, no. 6, pp. 1596-1606, Jun. 2004.
- [11] O. J. Tobias, J. C. M. Bermudez, N. J. Bershad, and R. Seara, "Mean weight behavior of the filtered-X LMS algorithm," in *Proc. IEEE Int. Conf. Acoustics, Speech, Signal Processing (ICASSP)*, Seattle, WA, May 1998, pp. 3545-3548.
- [12] D. Cartes, L.R. Ray, and R.D. Collier, "Low Frequency Acoustic test Cell for the Evaluation of Circumaural Headsets and Hearing Protection," submitted to *Canadian Journal of Acoustics*, July 2000.
- [13] S.B. Gelfand, Y. Wei, and J.V. Krogmeier, "The Stability of Variable Step-Size LMS Algorithms," *IEEE Transactions of Signal Processing*, 47(12), pp. 3277-3288, Dec. 1999.
- [14] D. Cartes, L.R. Ray, and R.D. Collier, "Lyapunov Tuning of the Leaky LMS Algorithm for Single-Source, Single-Point Noise Cancellation," submitted to *IEEE Transactions on Signal Processing*, May 2000.
- [15] Shao H, Wu W (2006) Convergence of BP algorithm with variable learning rates for FNN training. Proceedings of the 5th Mexican international Conference on Artificial intelligence, pp 245-252
- [16] Hur M, Choi JY, Baek J-S, Seo JS (2008) Generalized normalized gradient descent algorithm based on estimated a posteriori error. Proceeding of the 10th International Conference on Advanced Communication Technology, pp 23-26
- [17] L. A. Azpicueta-Ruiz, A. R. Figueiras-Vidal, and J. Arenas-Garcia, "A normalized adaptation scheme for the convex combination of two adaptive filters," in *Proc. ICASSP'08*, Las Vegas, NV, 2008, pp. 3301-3304.
- [18] N. J. Bershad, J. C. M. Bermudez, and J.-Y. Tournier, "An affine combination of two LMS adaptive filters – transient mean-square analysis," *IEEE Trans. Signal Process.*, vol. 56, pp. 1853-1864, 2008.

Robust Information Clustering on MDI

Mr. S. M. Krishna Ganesh¹, Dr. S. Venkatesan Jaya Kumar²

¹(Department of Computer Science and Engineering, St. Joseph College of Engineering and Technology, India)

²(Department of General Engineering St. Joseph College of Engineering and Technology, India)

Abstract : We propose a robust framework for determining a natural clustering of a given dataset, based on the minimum description length (MDL) principle. The proposed framework, robust information-theoretic clustering (RIC), is orthogonal to any known clustering algorithm. Given a preliminary clustering, RIC purifies these clusters from noise, and adjusts the clustering's such that it simultaneously determines the most natural amount and shape of the clusters. RIC, for refining a clustering and discovering a most natural clustering of a dataset. In particular, we propose a novel criterion, volume after compression (VAC), for determining the goodness of a cluster, and propose algorithms for robust estimation of the correlation structure of a cluster in the presence of noise, identification and separation of noise using VAC, and construction of natural correlation clusters by a merging procedure guided by VAC. It is fully automatic, that is, no difficult or sensitive parameters must be selected by the user. Our RIC method can be combined with any clustering technique ranging from K-means and K-medoids to advanced methods such as spectral clustering. The various performance related graphs shows that our algorithm is computationally and performance wise better than other clustering algorithms.

Keywords - Clustering techniques, Minimum description Length, Volume after compression

I. INTRODUCTION

In General, Clustering mean the assignment of objects into groups so that objects from the same cluster are more similar to each other than objects from different clusters.

Clustering is a common technique for statistical data analysis, which is used in many fields, including machine learning, data mining, pattern recognition, image analysis and bioinformatics. Clustering techniques fall into a group of undirected data mining tools. The goal of undirected data mining is to discover structure in the data as a whole. There is no target variable to be predicted, thus no distinction is being made between independent and dependent variables. Depending on the clustering technique, clusters can be expressed in different ways identified clusters may be exclusive, so that any example belongs to only one cluster. They may be overlapping; an example may belong to several clusters. they may be probabilistic, whereby an example belongs to each cluster with a certain probability. clusters might have hierarchical structure, having crude division of examples at highest level of hierarchy, which is then refined to sub-clusters at lower levels. The problem of clustering has attracted a huge volume of attention for

several Decades, with multiple books (Hartigan, Van-Rijsbergen), surveys (Murtagh) and papers (X-means (Pelleg and Moore), G-means (Hamerly and Elkan), CLARANS (Ng and Han), CURE (Guha), CLIQUE (Agrawal), BIRCH (Zhang), DBSCAN (Ester)). Recent interest in clustering has been on finding clusters that have non-Gaussian correlations in subspaces of the attributes, for example, the work of Bohm, Tung and Aggarwal and Yu. Finding correlation clusters has diverse applications ranging from spatial databases to bioinformatics. The hard part of clustering is to decide what is a good group of clusters, and which data points to label as outliers and thus ignore for clustering. We show a fictitious set of points in 2D. Shows a grouping of points that most humans would agree is good a Gaussian like Cluster at the left, a line-like cluster at the right, and a few noise points (outliers) scattered throughout. However, typical clustering algorithms like How can we quantify the goodness of a grouping? We would like a function that will give a good score to the grouping of and a bad one to that of diagram. How can we write an algorithm that will produce good groupings efficiently and without getting distracted by outliers..

II. MOTIVATION

Clustering has attracted a huge volume of interest. Recently, there have been several papers focusing on scalable clustering algorithms, such as, CURE [Guha et al. 1998], CLIQUE [Agrawal et al. 1998], BIRCH [Zhang et al. 1996], DBSCAN [Ester et al. 1996], and OPTICS [Ankerst et al. 1999]. There are also parameter-free algorithms like X-means [Pelleg and Moore 2000], and G-means [Hamerly and Elkan 2003]. However, they all suffer from one or more of the following drawbacks: They focus on spherical or Gaussian clusters, and/or are sensitive to outliers, and/or need user-defined thresholds and parameters. Most algorithms are geared towards Gaussian or plain spherical clusters; for example, the well-known K-means algorithm, BIRCH [Zhang et al. 1996] (which is suitable for spherical clusters), X-means [Pelleg and Moore 2000], and G-means [Hamerly and Elkan 2003]. These algorithms tend to be sensitive to outliers because they try to optimize the log-likelihood of a Gaussian, which is equivalent to the Euclidean (or Mahalanobis) distance—either way, an outlier has high impact on the clustering.

Density-based clustering methods, such as DBSCAN and OPTICS, can detect clusters of arbitrary shape and data distribution and are robust against noise. For DBSCAN the user has to select a density threshold, and for OPTICS to derive clusters from the reachability plot. K-harmonic means [Zhang et al. 2000] avoids the problem of outliers, but still needs k . Spectral

clustering algorithms [Ng et al. 2001] perform K-means or similar algorithms after decomposing the $n \times n$ gram matrix of the data (typically using PCA). Clusters of arbitrary shape in the original space correspond to Gaussian clusters in the transformed space. Here also k needs to be selected by the user. Recent interest in clustering has been on finding clusters that have non-Gaussian correlations in subspaces of the attributes [Böhme et al. 2004; Tung et al. 2005; Aggarwal and Yu 2000]. Finding correlation clusters has diverse applications ranging from spatial databases to bioinformatics. The information bottleneck method [Tishby et al. 2000], which is used by Slonim and Tishby for clustering terms and documents [Slonim and Tishby 2000], and the work of Still and Bialek [2004]. Based on information theory they derive a suitable distance function for coclustering, but the number of clusters still needs to be specified in advance by the user. Clustering is important for many applications such as Library, city planning. There are several motivations for robust clustering, but the basic requirement is to remove the noise. Previously used techniques do not able to cluster the group in efficient manner because does not contains sufficient information to cluster, cannot able to activate in fast manner, cannot able to group the given data in efficient manner and computations are performed in a tough manner.

III. PROPOSED ALGORITHM RIT

The following illustrates the proposed algorithm for Robust Information Theoretical Clustering

Input: Dataset as input

Output: To Identified & analysis the best pair with minimal cost as output.

Step1: Give the input dataset.

Step2: The input dataset is filtered by using noise removal method, then purify the cluster dataset by removing noise.

Step3: After purifying, merge the dataset.

Step4: Find the best pair of clusters to merge.

Step 5: Identify and analyze the best pair with minimal cost of dataset.

IV. PURIFICATION OF NOISE

The first step of purifying a cluster of points is to identify the proper decorrelation matrix. We generate several estimates (called candidates) of the covariance matrix, using various estimation methods, and pick the one with the best overall VAC value. In our experiments, the candidates include the matrix $_C$ from the conventional method using arithmetic average, and matrix $_R$ from the robust method described earlier. We also determine a conventional and a robust candidate, matrices $_C$, 50 and $_R$, 50, respectively, by considering only a certain percentage (e.g., 50%) of points in the cluster being closest to the robustly estimated center $_iR$. In addition, we always have the identity matrix I as one candidate decorrelation matrix. Among

these matrices, our algorithm selects the matrix giving the best (lowest) overall VAC.

The next step is to detect noise points in the cluster. By now, we have computed the robust center $_iR$, and have chosen a candidate covariance matrix which we call $_*$ (the corresponding decorrelation matrix is V^*). The goal is to partition the set of points in cluster C into two new sets: C_{core} (for core points) and C_{out} (outliers). First, our method orders the points of C according to the Mahalanobis distance defined by the candidate covariance matrix $_*$. Initially, we define all points to be outliers ($C_{out} = C$, $C_{core} = \{\}$). Then, we iteratively remove points $_x$ from C_{out} (according to Mahalanobis sort order starting with the point closest to the center) and insert them into C_{core} , and compute the coding costs before and after moving the point $_x$.

V. MERGING FROM NOISE

Our RIC framework is designed to refine the result of any clustering algorithm. Due to imperfection of the clusters given by an algorithm, our cluster purifying algorithm may lead to redundant clusters containing noise objects that fit well to other neighboring noise clusters. Our algorithm corrects the wrong partitions by merging clusters that share common characteristics, taking into account the subspace orientation and data distribution. We use the proposed VAC value to evaluate how well two clusters fit together.

The idea is to check whether the merging of a pair of clusters could decrease the corresponding VAC values. Our proposed merging process is an iterative procedure. Our algorithm merges those two clusters which have the maximum $savedCost$ (,) value, resulting in a greedy search toward a clustering that has the minimum overall cost. To deter this greedy algorithm from getting stuck in a local minimum, we do not stop immediately, even when no savings of $savedCost$ (,) value can be achieved by merging pairs of clusters. In other words, we do not stop when $savedCost(,) = 0$. Instead, the algorithm continues for another t iterations, continuing to merge cluster pairs (C_i, C_j) with the maximum $savedCost(C_i, C_j)$ value, even though now the $savedCost(C_i, C_j)$ value is negative and merging C_i and C_j will increase the VAC value of the overall dataset. Whenever a new minimum is reached the counter is reset to zero.

VI. EXPERIMENTAL RESULTS

We proposed to compare the noise cluster, purified cluster and merged cluster with Optimization values and maximal cost values. When compared purified cluster is better than other clusters. In the figure 1, We compared noise cluster, purified cluster and emerging cluster with optimization values. Then we Compare best pair of merging cluster with purified cluster.

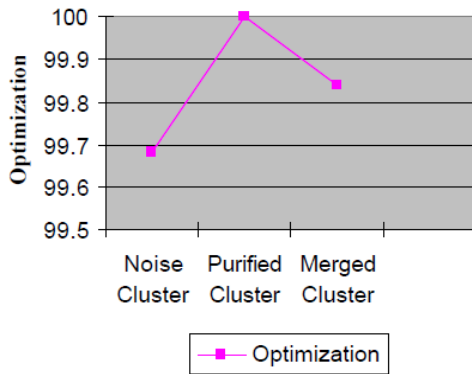


Figure 1. Compare best pair of merging cluster

In the figure 2, we compared noise cluster, purified cluster and merging cluster with maximal cost values. Compare best pair of merging cluster with the purified cluster

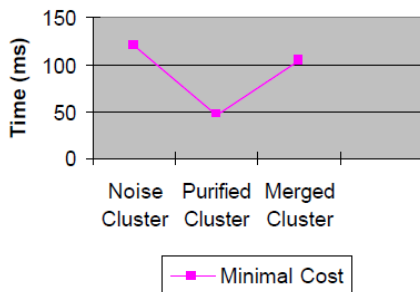


Figure 2. Compare the best pair of merging cluster with maximal cost

Type	Optimization	Maximal Cost (ms)
Noise Cluster	99.68531	120
Purified Cluster	100	47
Merged Cluster	99.840	104

Table: Values of Optimization and Maximal cost in Noise cluster, purifies cluster and merged clusters

VII. CONCLUSION

In this paper, RIC framework is designed. We have input dataset filtered to those data by using noise removal method, then purify clusters dataset by removing noise. After data set TyA is purified merge with the dataset. Find the best pair of clusters to merge. To identify and analysis the best pair with minimal cost of dataset. Previous work clustering methods, such as DBSCAN and OPTICS, can detect clusters of arbitrary shape and data distribution and are robust against noise. For DBSCAN the user has to select a density threshold, and for OPTICS o derive clusters from the reachability plot. K-harmonic means avoids the problem of outliers, but still needs k. There are several motivations for robust clustering, but the basic requirement is to remove the noise. Previously used techniques does not able to cluster the group in efficient manner because it does not contains sufficient information to cluster, unable to activate in fast manner

and unable to group the given data in efficient manner and computations are performed in this method

VIII. ACKNOWLEDGMENT

We would like to thank the anonymous reviewers for their insightful remarks and valuable suggestions, which were very helpful in improving the article. We thank our respected Rev.Fr.Dr.Arulraj Founder, DMI Group of institutions, East Africa and India, Dr.T.X.A.Ananth, Director, Mr. Ignatius Herman, Director (Academic), Dr. V.Krishnan Ph.D, Principal, DMI.St.Joseph College of Engg & Technology, Tanzania. for their encouragement and support. Also we thank our parents, friends and colleagues for their support and encouragement.

REFERENCES

- [1] C.C.Aggarwal and P. S. Yu, "Finding generalized projected clusters in high dimensional spaces", In *SIGMOD Conference*, 2000, pp. 70–81.
- [2] Frank Rehm1, Frank Klawonn2 and Rudolf Kruse "A Novel Approach to Noise Clustering for Outlier Detection", IEEE communication, 2007, pp.1-5.
- [3] Dave RN, Krishnapuram R (1997), "Robust clustering methods a unified view", IEEE Transactions magazine, pp.270-293.
- [4] M. Ester, H.P. Kriegel, J.Sander, and X. Xu "A density-based algorithm for discovering clusters in large spatial databases with noise". in *KDD Conference*, 1996.
- [5] S. Guha, R. Rastogi, and K. Shim, "CURE: An efficient clustering algorithm for large databases", in *SIGMOD Conference*, pp.73–84, 1998.
- [6] Rajesh N. Davé and Sumit Sen, "Robust Fuzzy Clustering of Relational Data", IEEE Transaction Magazine, pp.713-727, 2002
- [7] Aggarwal C. C. and Yu P. S, "Finding generalized projected clusters in high dimensionalspaces", *Proceedings of the ACM International SIGMOD Conference on Management of Data*, pp.70–81, 2000.
- [8] Agrawal R., Gehrke J, Gunopulos, D, and Raghavan. P, "Automatic subspace clustering of high dimensional data for data mining applications", in *Proceedings of the ACM International SIGMOD Conference on Management of Data*, pp. 94–105, 1998.
- [9] Bhattacharya, V. Ljosa, J.-Y. Pan, M. R. Verardo, H. Yang, C. Faloutsos, and A. K. Singh, "ViVo: Visual vocabulary construction for mining biomedical images", *IEEE International Conference on Data Mining (ICDM)*, 2005
- [10] Ankerst . M., Breunig. M, Kriegel . H-P., and Sander.J, "OPTICS: Ordering points to identify the clustering structure", in *Proceedings of the ACM International SIGMOD Conference on Management of Data*, 1999.
- [11] Banfield J. D. and Raftery A. E, "Model-based Gaussian and non-Gaussian clustering", *Biometrics* 1993, pp.803–821.

- [12] Bohm C.,Kailing. K.,Kroger. P., and Zimek A., “Computing clusters of correlation connected Object”, in *Proceedings of the ACM International SIGMOD Conference on Management of Data*, pp.455–466,2004.
- [13] Chakrabarti D., Padimitriou, S., Modha D. S., and Faloutsos C. “Fully automatic cross associations”,in *Proceedings of the ACM SIGKDD Conference on International Knowledge Discovery and Data Mining,2004*,.pp. 79–88.
- [14] Guha S., Rastogi, R., and Shim. K (1998), “CURE: An efficient clustering algorithm for large databases”,in *Proceedings of the ACM International SIGMOD Conference on Management of Data*,pp. 73–84,1998.
- [15] Hamerly, G. and Elkan, C. ., “Learning the k in k-means”, in *Proceedings of the Conference on Advances in Neural Information Processing Systems (NIPS)*,2003.
- [16] Murtagh. F, “A survey of recent advances in hierarchical clustering algorithms”, in *Proceedings of the ACM SIGKDD Conference on International Knowledge Discovery and Data Mining. pp. 354–359,1983*.
- [17] Christian Bohm,Christos Faloutsos,Claudia Plant , “Outlier- robust clustering using independent components”, in *Proceedings of the ACM International SIGMOD Conference on Management of Data,2000*.
- [18] Alexander Hinneburg and Daniel A. Keim, “An efficient approach to clustering in large multimedia databases with noise”, in *Knowledge Discovery and Data Mining, pp . 58 – 65,1998*.
- [19] Olfa Nasraoui,Carlos Rojas,“Robust Clustering for Tracking Noisy Evolving Data Streams”, in *Proceedings of the ACM international SIGMOD Conference on Management of Data,1999*.
- [20] Jia Liao ,Bo Zhang, “A Robust Clustering Algorithm for video shot using Haar Wavelet Transformation”, :in *Proceedings of SIGMOD*, pp. 730- 741,2007.
- [21] Eike achttert,Christian Bohm,Jorn David,Peer Kroger,Arthur Zimek ,“Robust Clustering in Arbitrarily Oriented Subspaces”, in *Proceedings of SIGMOD*, pp. 124- 126,2000.
- [22] Anupam Joshi,Raghu Krishnapuram, “Robust Fuzzy Clustering Method to support web mining” , in *proceedings of the ACM International SIGMOD Conference on Management of Data*,pp.400 – 407,2000.

A New Solution to Wave Equation in Inhomogeneous Plasmas with Bessel Function

Mohammad pourbagher¹, abdoalkhalegh mohammadi¹, Javad nourinia¹,
Nader pourmahmud²

1_(Department of Electrical Engineering, Urmia university, IRAN)
2_(Department of Mechanical Engineering, Urmia university, IRAN)

Abstract : *In this article the wave equation of an inhomogeneous plasma has been numerically solved by the use of Bessel function. Applying this mathematical approach produced the capability in comparison among other well known method such as WKB and Airy Function Method (AFM). The result which presented in this research shows that the Bessel Function Method (BFM) has reasonable agreement with the standard analytical solutions like AFM. Although there are some discrepancies between two methods, but in many ranges they can attain to common point of view. WKB method because of its simplicity and superabundant approximation could not satisfy the expected result especially at cutoff range, therefore is taken as a primary means to solve the mentioned problem.*

Keywords: Airy function, cutoff, inhomogeneous, Debye sphere

I. Introduction

The plasma state is a characterization of matter where long range electromagnetic interactions dominate the short range inter atomic or intermolecular forces among a large number of particles. Plasmas are generally high temperature entities, and some of the properties of a plasma are connected with thermal effects, and among the wave types we shall discuss are sound waves. Unmagnetized plasmas are generally the first to be studied because they are isotropic, i.e. the properties are the same in all directions. The waves that such a plasma will support are either high frequency electromagnetic waves which see the plasma as a simple dielectric due to the response of the electrons to the wave (by comparison the ions are generally immobile), or sound-type waves. We define the thermal speed to be the most probable speed in a Maxwellian distribution.

$$v_j = \sqrt{\frac{2kT_j}{m_j}} \quad j=e, i \quad (1)$$

for electrons or ions. In addition to the thermal speeds for electrons and ions, however, there are two other fundamental parameters which characterize a plasma in the absence of a magnetic field, and these are the plasma frequency and the Debye length. The plasma frequency is the oscillation frequency of a simple unmagnetized plasma when the charge distribution is locally perturbed from its equilibrium, and is given for electrons by

$$\omega_{pe} = \sqrt{\frac{n_e e^2}{m_e \epsilon_0}} \quad (2)$$

The Debye length is the distance a thermal particle travels during a plasma period. Its definition is

$$\lambda_{De} = \sqrt{\frac{\epsilon_0 k T_e}{n_e e^2}} = \frac{v_e}{\sqrt{2} \omega_{pe}} \quad (3)$$

In fact, unless an assembly of charged particles is large enough that it is many Debye lengths in size, and of such a density that there are many particles in a Debye sphere, we do not call the assembly a plasma. It is thus apparent that

plasma waves are fundamental to the very definition of a plasma [1]. In a cold plasma, these latter waves become a simple oscillation at the plasma frequency, below which the electromagnetic waves do not propagate. In a thermal plasma, however, there are sound-like waves near this frequency, and in a plasma with disparate electron and ion temperatures with $T_e \gg T_i$, there is even a kind of hybrid sound wave that depends on the electron temperature and the ion mass. These waves even perturbed from its equilibrium, and is given for electrons by process. While these several kinds of behavior are already much more complicated than waves in ordinary fluids, they are very simple compared to the complexities added by a magnetic field. Even the kinds of nonlinearities in this simple plasma damp through a nondissipative are richer in both diversity and complexity than in fluid dynamics where only averages over the velocity distribution are analyzed. Compared to ordinary fluids, plasmas even have an additional kind of turbulence, called microturbulence, which has many kinds of sources.

The addition of magnetic field effects to the subject of plasma waves adds a host of new phenomena, among which are: anisotropy, since there is now a preferred direction; new kinds of transverse waves existing only in magnetized plasmas, which we call Alfvén waves; finite Larmor orbit effects due to thermal motions about the magnetic field lines; and many other kinds of waves which are either totally new or greatly modified. Because of the anisotropy, the description of these effects is inevitably complicated algebraically, and this tends sometimes to obscure the physics. Even in a cold plasma where thermal effects are absent, the number of wave types added by the inclusion of the magnetic field is large, and wave types vary greatly with the angle of propagation with respect to the magnetic field. We find waves which are guided by the magnetic field in certain frequency ranges, and cases where the phase and group velocities are nearly normal to one another [2].

Whereas in a cold unmagnetized plasma, the only parameter that may lead to inhomogeneities is the plasma

density, the magnetic field not only adds a possible new source of inhomogeneity, but the gradients may appear in different directions.

When thermal effects are added to the cold plasma effects, the new phenomena can be grouped into two general categories: acoustic wave phenomena due to various kinds of sound waves; and kinetic phenomena due to the fact that in a thermal or near thermal distribution, there are some particles moving at or near the phase velocity. These particles have resonant interactions with the waves due to their long interaction time with the wave. These interactions can lead to either collisionless wave damping or to instabilities and wave growth. When coupled with magnetic field effects, finite Larmor orbit effects lead to even more new wave types and instabilities. The uniform plasmas of the previous chapters are idealizations which are rarely realized, although in some bounded regions, the approximation may be very good. We can generally assume a plasma is uniform if the plasma parameters vary little over a wavelength. In most laboratory plasmas, however, and over the vast regions of space, densities and magnetic fields vary to such an extent that it is sometimes difficult to estimate from uniform plasma theory where the wave energy will go and whether it will reach specified regions [3-5]. In many instances, these various effects can be separated and dealt with one at a time, but there are important cases where a combination of effects occur, several of which are simultaneously important, and each individual technique breaks down.

II. WKB method for one dimensional inhomogeneities

As an illustration of the method used in treating one-dimensional inhomogeneities, we consider an unmagnetized plasma with only a density variation. The wave equation,

$$\nabla(\nabla \cdot E) - \nabla^2 E + \frac{1}{c^2} \frac{\partial^2 E}{\partial t^2} = -\mu_0 \frac{\partial j}{\partial t} \quad (4)$$

depends only on variations in the plasma density through the plasma current, so we let $n_0 = n_0(x)$. Since all equilibrium quantities are independent of y and z , we can Fourier transform in those directions and assume harmonic time dependence. Then

$$\nabla \rightarrow \hat{e}_x \frac{d}{dx} + \hat{e}_y ik_y + \hat{e}_z ik_z \quad \frac{\partial}{\partial t} \rightarrow -i\omega$$

but another simplification is possible since the plasma is isotropic, since then one can rotate the coordinate system about the x -axis until the wave has no k_z component. Then the current may be derived from the equations of motion for ions and electrons

$$m_j \frac{\partial v_j}{\partial t} = q_j E \quad j=i,e \quad (5)$$

$$j = en_0(x)(v_i - v_e) \quad (6)$$

with the result that

$$j \approx \frac{in_0(x)e^2}{\omega m_e} E = \frac{ie_0}{\omega} \omega_{pe}^2(x) E \quad (7)$$

Then the z -component of equation (4), which is not coupled the other component, is

$$-\left(\frac{d^2}{dx^2} - k_y^2\right)E_z + \left[\frac{\omega_{pe}^2(x)}{c^2}\right]E_z = 0 \quad (8)$$

This can then be cast into the WKB form

$$\frac{d^2 y}{dx^2} + k^2(x)y = 0 \quad (9)$$

where $y(x) = E_z(x)$ and

$$k^2(x) \triangleq \frac{\omega^2 - \omega_{pe}^2(x)}{c^2} - k_y^2 \quad (10)$$

For $k(x) = \text{constant}$, the solution is trivial and of the form

$$y = A_1 e^{ikx} + A_2 e^{-ikx} \quad (11)$$

and represents waves traveling to the left and to the right. Looking for solutions which are similar to the uniform result, we assume an eikonal solution of the form

$$y(x) = A(x)e^{i\psi(x)} \quad (12)$$

where $A(x)$ is assumed to be a slowly varying amplitude and $\psi(x)$ is the eikonal, a rapidly varying phase such that $\psi'(x) = \pm k(x)$. In order to determine the limits of validity of this method, we choose the upper sign and insert equation (12) into equation (9), first noting the derivatives

$$y' = ikAe^{i\psi} + A'e^{i\psi}$$

$$y'' = -k^2 A e^{i\psi} + 2ikA'e^{i\psi} + ik'Ae^{i\psi} + A''e^{i\psi} \quad (13)$$

so that equation (9) becomes

$$A'' + 2ikA' + ik'A = 0 \quad (14)$$

If A'' is assumed small, then to lowest order, $A(x) = \frac{1}{\sqrt{k(x)}}$, and the complete solution is written (for either sign) as

$$y(x) = \frac{A_0}{\sqrt{k(x)}} \exp\left[\pm i \int k(x) dx\right] \quad (15)$$

Taking this as the zero order result, we assume the solution is modified by the correction term,

$$A(x) = \frac{[1+\eta(x)]}{\sqrt{k(x)}} \quad (16)$$

where again we assume that η is slowly varying so that we neglect η'' when this is inserted into equation (14). The result may be expressed as

$$\frac{\eta'}{1+\eta} = \frac{1}{4i} \frac{\frac{k''}{k^2} - \frac{3k''}{2k^3}}{1 + \frac{1}{2i} \frac{k'}{k^2}}$$

$$\eta \approx \frac{1}{4i} \frac{k'}{k^2} \quad (17)$$

The condition for validity may thus be written as $|\eta| \ll 1$ or as

$$\left|\frac{1}{k} \frac{dk}{dx}\right| \ll k \quad (18)$$

which means that the change of wavelength over a wavelength should be small. This approximation fails when $k \rightarrow 0$ or when $k' \rightarrow \infty$, or whenever the wave approaches either a cutoff or a resonance. In figure.1 equation (15) which is the answer of problem is plotted with estimated values. In this figure $y(x)$ is considered to have linear variation. It is shown that the answer is increased at first and after that it coming down. It is because of inhomogeneity in plasma and variety of density.

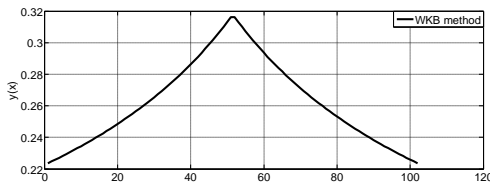


figure.1 $y(x)$ which here is $E_z(x)$ versus x

III. Airy Function Method

The behavior near a cutoff is important enough to justify further analysis, and was analyzed so long ago that it is considered by many to be part of the WKB formalism rather than restricted to the condition of equation (18). In the neighborhood of the cutoff, we expand $k^2(x)$ about the cutoff,

$$k^2(x) = k^2(x_0) + \frac{d}{dx}k^2(x)|_{x_0}(x - x_0) + O(x - x_0)^2 \quad (19)$$

where $k^2(x_0) = 0$ defines x_0 and we define the coefficient such that $k^2(x) = \beta^2(x-x_0)$. Then the result of equation (15) valid whenever $|x-x_0| \gg \beta^{-2/3}$. The behavior near the cutoff must come from the solution of the differential equation [4-8], however, since the approximations always fail sufficiently close to cutoff. The differential equation may be written as

$$\frac{d^2y}{dx^2} + \beta^2(x - x_0)y = 0 \quad (20)$$

which by means of the variable change $z \triangleq \beta^{2/3}(x - x_0)$ can be written

$$y'' - zy = 0 \quad (21)$$

which is the Airy equation. The solutions of the Airy equation are well known [8] and may be represented by the two independent solutions

$$y(z) = c_1 Ai(z) + c_2 Bi(z) \quad (22)$$

which have the asymptotic forms

$$Ai(z) = \frac{1}{2\sqrt{\pi z^{1/4}}} e^{-\zeta}$$

$$Ai(-z) = \frac{1}{\sqrt{\pi z^{1/4}}} \left[\sin\left(\zeta + \frac{\pi}{4}\right) - \cos\left(\zeta + \frac{\pi}{4}\right) \right]$$

$$Bi(z) = \frac{1}{\sqrt{\pi z^{1/4}}} e^{\zeta}$$

$$Bi(-z) = \frac{1}{\sqrt{\pi z^{1/4}}} \left[\sin\left(\zeta + \frac{\pi}{4}\right) + \cos\left(\zeta + \frac{\pi}{4}\right) \right]$$

(23)

where $\zeta = \frac{2}{3}z^{3/2}$. These asymptotic solutions must be matched to the approximate eikonal solutions which represent incoming and outgoing waves, which given by equation (15)

$$y(x) = \frac{A_1}{(x-x_0)^{1/4}} e^{i\frac{2}{3}\beta(x-x_0)^{3/2}} + \frac{A_2}{(x-x_0)^{1/4}} e^{-i\frac{2}{3}\beta(x-x_0)^{3/2}} \quad x > x_0$$

$$y(x) = \frac{B_1}{|x-x_0|^{1/4}} e^{i\frac{2}{3}\beta|x-x_0|^{3/2}} + \frac{B_2}{|x-x_0|^{1/4}} e^{-i\frac{2}{3}\beta|x-x_0|^{3/2}} \quad x < x_0$$

(24)

In figure.2 the solution of problem is plotted. In this figure $y(x)$ increases at first because of inhomogeneity and decrease later. It is observed that there is a sharp peak at the cutoff region.

IV. solution with Bessel function

The matching implied here between the asymptotic forms of the Airy function solutions and the WKB solutions requires that there be a finite region of overlap where both approximations are simultaneously valid. The conditions for validity are shown in figure.3. When the exact expression for $k^2(x)$ is linear, the overlapping region is unbounded of course, but for any other variation, there is some limit when the linear approximation fails. If the real variation of $k^2(x)$ deviates substantially from linear before the WKB expressions are valid, then there may be no overlap, so that accurate possible.

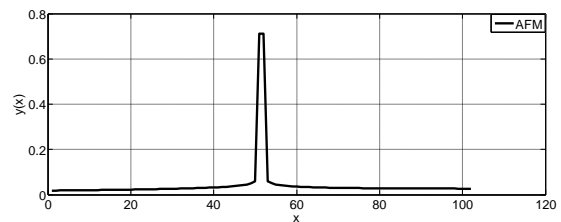


Figure. 2 $y(x)$ which is (x) versus x in Airy function method

In this paper a solution of problem with Modified Bessel function is presented. By considering an equations by the following form

$$x^2 y'' + x(a + 2bx^p) y' + (c + dx^{2q} + b(a + p - 1)x^p + b^2 x^{2p}) y = 0 \quad (25)$$

which $(1 - a)^2 \geq 4c$ and d, p, q are not zero. The total solution of the equation above is

$$Y = x^\alpha e^{-\beta x^p} \{c_1 J_\mu(\lambda x^q) + c_2 Y_\mu(\lambda x^q)\} \quad (26)$$

In this answer $\alpha = \frac{1-a}{2}$, $\beta = \frac{b}{p}$, $\lambda = \frac{\sqrt{|d|}}{q}$ and $\mu = \frac{\sqrt{(1-a)^2 - 4c}}{2q}$. If assume that a and b be zero from the equation (25) it is resulted

$$x^2 y'' + (c + dx^{2q}) y = 0 \quad (27)$$

Which $c \leq 1/4$ and d, p, q are not zero. By dividing the both side of the equation (27) to x^2 equation (28) will be resulted

$$y'' + (cx^{-2} + dx^{2(q-1)}) y = 0 \quad (28)$$

By putting equation (20) and (28) equivalent and supposing $X = x - x_0$, it can be written

$$Cx^{-2} + dx^{2(q-1)} \triangleq \beta^2(X) \quad (29)$$

The above equation shows that for putting both side of equation equivalent, C must be zero, $d = \beta^2$, and $q = \frac{3}{2}$, by these value $\alpha = \frac{1}{2}$, $\beta = 0$, $\lambda = \frac{2\beta}{3}$, $\mu = \frac{1}{3}$ which the

relation of them is expressed above. So by these values the solution of equation will be

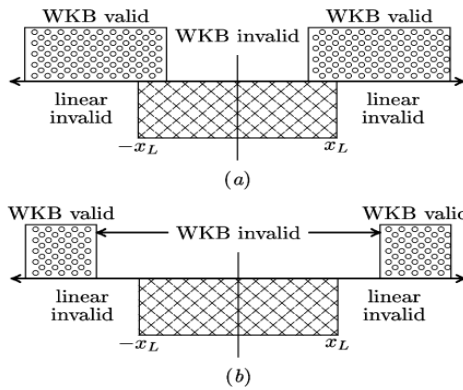


Figure.3 Validity conditions for matching the asymptotic forms of the inner functions and the outer WKB approximants. (a) Finite overlap case, so the matching is valid. (b) No overlap case, so the matching is inaccurate.

$$y = x^{\frac{1}{2}} \left\{ c_1 J_{\frac{1}{3}} \left(\frac{2\beta}{3} x^{\frac{2}{3}} \right) + c_2 Y_{\mu} \left(\frac{2\beta}{3} x^{\frac{2}{3}} \right) \right\} \quad (30)$$

This answer is plotted in figure .4 and it is observed that reaching to the peak which occurs at cutoff, is more monotonically. To compare solutions to each other different answer is plotted in figure.5 with each other. Of course the values of parameters in formulas are estimated and in this figure the peaks of each solution is not the same.

V. Conclusion

The numerical result of presented research has focused to attain with the well known WKB analytical method. The result which presented in this research shows that the Bessel Function Method (BFM) has reasonable agreement with the standard analytical solutions like AFM. This investigation was an attempt to explore the complete behaviors of wave in inhomogeneous plasma media. Although the use of mathematical method [7-10], Bessel function method, could not match completely to others method, WKB and AFM, but its behavior near cutoff point had good conformity. There are some discrepancies between two methods, but in many ranges they can attain to common point of view. In this paper the matter has been examined for one dimension and for future investigations it can be generalized for three dimensions. There are some estimation in this article to reduce the difficulty of explanation and computation, for example in part 3. We neglect higher order of $K(x)$, Because the condition is for one dimension. these simplifications does not affect the main results.

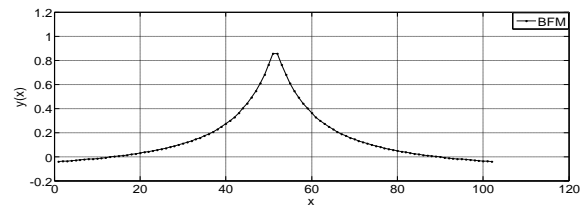


Figure.4 $y(x)$ which is $E_z(x)$ versus x

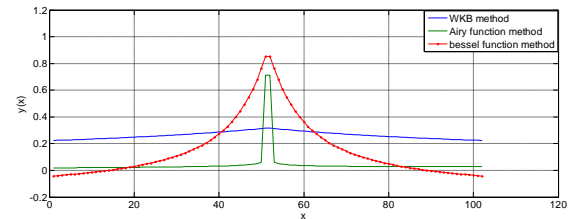


Figure.5 comparison among different solution

References

- [1] Gary Swanson Plasma Waves , 2nd Edition, 2003, D Auburn University, USA.
- [2] Stefan A. Maier Plasmonics Fundamentals And Applications , 2007.
- [3] Bakker, ReubenM., Drachev, Vladimir P., Yuan, Hsiao-Kuan, and Shalaev, VladimirM. (2004).
- [4] W. E. (2005). Field enhancement and gap-dependent resonance in a system of two opposing tip-to-tip Au nanotriangles. Phys. Rev. B, 72:165409.
- [5] Budden K G, Radio Waves in the Ionosphere (Cambridge: Cambridge University Press),1961.
- [6] Mikhailovskii A B, 1983, Handbook of Plasma Physics vol 1, ed A Galeev and R. N. Sudan (Amsterdam: North Holland) p 587.
- [7] M. Rahimi Esboe, N. Pourmahmoud, I. Mirzaee, P. Mohajeri, S. Majidyfar and D.D. Ganji Analytical and Numerical Analysis of MHD Boundary Layer Flow of an Upper Convected Maxwellfluid , International Journal of Engineering Science and Technology, Vol. 2 (12), pp. 6909-6917, 2010.
- [8] M. Rahimi Esboe, N. Pourmahmoud, I. Mirzaee, P. Mohajeri and S. Majidyfar Numerical Simulation of Effects of Non- Ionized Mass Injection on The MHD Flow in A Circular Channel , 13th (Annual) and 2th International Fluid Dynamics Conference, Shiraz University, 26-28 Oct., 2010.
- [9] M. Kiyasatfar, N. Pourmahmoud, M.M. Golzan and M. Eskandarzadeh Effect of Magnetic Flux Density and Applied Current on Temperature, Velocity and Entropy Generation Distribution in MHD Pumps , Sensor and Transducer Journal, Vol. 124, Issue 1, pp. 72-82, January 2011.
- [10] G. Borg, J. Harris, N. Martin, D. Thorncraft, R. Milliken, D. Miljak, B. Kwan, T. Ng, and J. Kircher, "Plasmas as antennas: Theory, experiment, and applications," *Physics of Plasmas*, vol. 7, no. 5, p. 2198, May 2000.

Vibration Analysis of Propellant Actuated Devices

Y. B. Autger^a, S. S. Khandagale^b, R. S. Bindu^c

^aMaster of Engineering (Mechanical Design) Student, DYPCOE, Akurdi, University of Pune.

^bARDE, Ministry of defense, Govt of India, Pune,

^cDepartment of Mechanical Engineering, DYPCOE, Akurdi, University of Pune

Abstract: Vibration qualification testing of propellant actuated devices or power cartridges used in fighter aircraft pose a challenge for the design and fabrication of the vibration test fixture for multi-direction. The vibration test fixture is made for CDBU type of cartridge among the various cartridges. Fixture for vibration testing is of cylindrical structure having maximum diameter of 235mm and of 36 mm thickness. The weight of the fixture is restricted up to the 5 kg.

This structure has analyzed and experimentally evaluated. The design of fixture has its certain advantages like; it can accommodate 16 cartridges in multi-directions at a time and can be tested, it uses all the fixing points of the shaker table. Fixture is designed with Aluminum 6061-T6 Alloy adhering to the general principles of vibration fixture design avoiding resonance in the frequency range of test. Theoretical analysis for the natural frequency calculations is based on advanced theory of plate bending. Computer Aided Design software Pro-E Wildfire 4.0 is used for modeling and drafting work of the fixture. Finite element software ANSYS is used for the modal and random response analysis. Experimental trial was conducted for the two axis for 6 hrs. Control and monitoring accelerometers are bonded at critical locations to get the best results.

Experimental investigations suggested good correlation between computed and experimentally determined values and plots.

Index Terms: Power Cartridges, Vibration Testing, PAD's Test fixture, Governing equilibrium equations, FE modal Analysis, Experimental results.

I. INTRODUCTION

Today's all the modern fighter aircraft has most essential integral part with it is power cartridges. Power cartridges are low cost explosive actuated devices. They are essential parts of any military aircraft. The importance of the power cartridges can be gauged from the fact that no military aircraft, otherwise flight worthy, is allowed to take off without installing the essential power cartridges. Some of the important functions of power cartridges are to operate auxiliary systems and sub-systems of aircraft, Effective release of weapon with high degree of reliability and for giving distress signaling.

The purpose of installing power cartridges is to save the precious life of pilot from the endangered aircraft in emergency within shortest possible time. Such cartridges are also known as Propellant Actuated Devices (PAD). PAD's are used to give certain specified performance in actual system or subsystem where they are installed in the aircraft. The most important and valuable inventory of air force is its combat aircraft. The time, efforts and cost to groom a pilot to

the required efficiency are enormous. Their life is extremely precious for the services and is required to be protected against all conditions and adverse circumstances. All military aircrafts are fitted with ejection seat for escape of the pilot from endangered aircraft in emergency. Various types of power cartridges are provided in the seat ejection system to perform different functions during the ejection process. In addition to the seat ejection, power cartridges are employed for other operational requirements also.

Power cartridges are categorized on the means of initiation are, mechanical types and electrical types.

Consumers expect and demand products of high quality and reliability. To fulfill these requirements the system after design should undergo various qualification tests. In these qualification tests vibration is one of the stringent test in which the product should undergo. However, vibration is very ramified topic. During this vibration tests, poor mechanical design will cause mechanical failure and customer dissatisfaction. This also causes increase in product cost and loss of credibility.

In order to prove the acceptability of the indigenous cartridges the various tests like Impact Test, Sealing Test, Vibration Test, Salt Mist Test, Life Assessment Test etc are carried out as per JSG 0102 Standard. Out of these Vibration Qualification Test is considered here.

Vibration tests are performed for the following reasons, Develop materiel to function in and withstand the vibration exposures of a life cycle including synergistic effects of other environmental factors, materiel duty cycle, and maintenance.

This method is limited to consideration of one mechanical degree-of-freedom at a time.

Verify that materiel will function in and withstand the vibration exposures of a life cycle.

Vibration results in dynamic deflections of and within materiel. These dynamic deflections and associated velocities and accelerations may cause or contribute to structural fatigue and mechanical wear of structures, assemblies, and parts. In addition, dynamic deflections may result in impacting of elements and/or disruption of function.

This paper briefly describes the fixture design methodology, facility augmentation to the testing, analysis carried out and evaluation methods adopted for the fixture experimentally.

II. FIXTURE DESIGN METHODOLOGY

An ideal fixture is a structure having infinite stiffness at all frequencies with zero mass. Since this is not achievable in practice, it is always a trade-off between the stiffness and mass relationships [13]. Hence, the fixture has to weigh less and at the same time not modify the dynamic characteristics of the UUT. It is also recommended that the

designer understands the manufacturing process and the time and cost involved in producing a fixture.

A vibration fixture is a device that typically interfaces the vibration shaker / shock machine and the test item. The basic idea with any fixture is that it should convey all possible forces produced by the shaker to the test object. Generally it is not possible to fix a test object directly to the shaker table itself. For that fixture acts as a transition piece between the two.

The objective of making fixture is, to take vibration test of Power Cartridges by fixing it on the fixture. The purpose of vibration test is to check proper functioning of Cartridges under vibrant conditions.

2.1 Basic Fixture Design:

The knowledge of the dynamic behavior of structures is often of primary importance in many applications, particularly in the field of aerospace and mechanical design. Prediction of modal parameters such as resonance frequencies and mode-shapes is an essential step of design. For this purpose, numerical techniques based on finite element model are commonly used.

Unfortunately, uncertainties on mechanical properties, tolerances in fabrication and assembly processes may cause discrepancies between numerical predictions and experimental results. To ensure that the mechanical component will survive the dynamic environment in which it is operating; vibration qualification testing is required according to international standards or manufacturer specifications.

Understanding of the dynamic behavior of the power cartridges is important during the operating condition. Therefore, it is necessary to carry-out vibration qualification testing to international standards (or as per user's requirements) to ensure that the structures survive the service or operating environment. Vibration testing generally requires a fixture which is an intermediary structure to interface with the specimen (often called DUT, Device Under Test / UUT, Unit under test) and the vibration generating equipment (vibration shakers). A fixture is designed to take care of different shapes and sizes of the specimens and the attachment points. The design methodology proposed is based on topological optimization tools.

An ideal fixture is a structure having infinite stiffness at all frequencies with zero mass. Since this is not achievable in practice, it is always a trade-off between the stiffness and mass relationships.

Also the acceleration level possible with the shaker is inversely proportional to the total moving mass it has to drive. Hence, the fixture has to weigh less and at the same time not modify the dynamic characteristics of the UUT. A bad fixture results in isolation at attachment points and a good fixture transmits the input with fidelity. A good fixture has resonances above the frequency range of interest. Location of center of gravity of the shaker, slip table with the UUT has to be as close as possible to mitigate overturning moment concerns.

Rigs and Fixtures are used to primarily to connect a test specimen to a shaker table. The specimen is often referred to as the Unit Under Test (UUT). As the UUT rarely couples directly to the shaker, an interface is required to

convert the hole pattern of the attachment points to the hole pattern of the shaker inserts. The main objective of the Fixture is to couple the UUT as directly as possible without adding or subtracting energy from the applied test.

The vibration fixture will require a design that when loaded with the specimen and connected to the shaker, will have no resonances within the specified frequency range.

This is rarely achievable but our design can assist in keeping the fixture resonances low in Q so that our controller can apply some compensation during testing.

Materials generally considered for vibration fixtures like Stainless Steel, Aluminum, Magnesium have similar E/ρ ratio (ratio of Young's modulus to density) not affecting the natural frequency of the fixture. However, when the shakers are operating at their full performance level, like in the present case, weight of the fixture dominates the selection of the material. Composite materials though are ideal for fixture to test large and heavy specimen, fabrication of the same is highly difficult.

Though Magnesium is a lighter metal, fabricability issues and availability of indigenous fabrication techniques have compelled to choose Aluminum alloy as the candidate material.

To design a test fixture that can be used for many different test pieces is extremely difficult and the usual practice is to treat each UUT separately. An interface plate can be designed to support each of these test items and is therefore required to be of a high standard. Individual test fixtures may not require the same build standard as the interface plate and this can affect the choice of material. When choosing the material it needs to be consider the test frequency range, the overall mass and the cost.

A low level vibration test that requires a frequency range from 20 Hz to 100 Hz may find that a wooden or plastic fixture is adequate. Whereas high level high frequencies test (typically above 500Hz) will require a much stiffer material. Often the fixture has a mass many times greater than the UUT and this will impact upon the Force capability of the shaker. This too will influence the material used as certain materials have a very good stiffness-to-mass ratio such as duralumin, magnesium or aluminum. Another characteristic of a material is its damping properties, e.g. the hysteretic damping of aluminum is approximately four times greater than that for steel. It is advisable to avoid steel for the above reasons i.e. it is heavy, it rings, it is difficult to work with, the resonances are of high Q and it is expensive.

Considerations for the fixture material are,
Mass - The material should be as low in mass as possible without detriment to the stiffness. As $F = M \times A$ the material mass will have an influence on the shakers thrust ability. Often a fixture will be sculptured and material removed to reduce the mass. The dynamics of the fixture remain unchanged but the stiffness and strength may be compromised and should be considered.

Stiffness - The stiffer the fixture the higher any resonant frequencies. If the first resonant can be kept above the test frequency range the quality of test will be improved. The fixture must be stiff enough not to influence the test or change during a test.

Strength - The Fixture will see high stress levels from the applied vibration or the UUT response and must be strong

enough to transmit the forces and survive the tests.

Natural Frequencies- The natural or first resonant frequency should be measured during a rig assessment and will preferably be higher than the test requirements upper frequency.

Damping - For fixtures with high 'Q' resonances, the control method will require some investigation. If possible it is preferable to use damping at the fixtures points of influence to reduce the 'Q'. For example a hollow tube will be damped by filling it with foam and often clamping or additional supports will prevent a high 'Q' response.

Attachment - The fixture should hold the UUT in multi-direction at a time. The UUT is held in a manner in which it is used in service and the brackets, isolation supports or other in service fittings should be attached to the fixture to represent an in service configuration. The UUT is rigidly held in a manner that ensures a known test specification is applied with out loss or compromise from the fixture.

Dynamic response - The UUT has its own response to a vibration test specification. The fixture should not modify the natural dynamics of the UUT or the test will be compromised. A dynamically inert fixture is not possible but its influence can be kept to a minimum by following the step by step guidelines above.

Fatigue - A fixture needs to be significantly stronger than the UUT so that it does not fatigue during use. Avoid thin brackets, small bolts, sharp corners, overhanging areas and weak areas that will fatigue quickly.

This system is designed to have high stiffness at right angles to the vibration axis. If high overturning moments are applied to the armature then the suspension guide will be compromised. This cross axis force applied during vibration needs to be understood and kept low so as not to damage the bearings and armature.

Designing all fixtures to be light and stiff will assist in preventing unwanted cross axial motion. The Centre of Gravity (C of G) should be precisely calculated and each rig or fixture should be rigidly coupled to the armature or slip table. If the C of G of the payload is kept low and aligns with the armature centre then cross axial stress will be minimized. However if the payload C of G is high or offset, then a turning moment is introduced during vibration. The easiest and cheapest fixture for this size of shaker is that made of welded aluminum plate.

The mating surfaces of the fixture is machined as flat as possible.

Attachment of bolts from fixture to shaker table is of counter-sunk type so that the stressed length of the bolt is twice the diameter.

The objective is to design and evaluate the vibration fixture to qualify the power cartridge to the specifications generated to simulate flight vibration conditions. Prediction of modal parameters such as resonance frequencies and mode-shapes is an essential step of design. A fixture is designed to take care of different shapes and sizes of the specimens and the attachment points. Also the acceleration level possible with the shaker is inversely proportional to the total moving mass it has to drive. Location of center of gravity of the shaker, slip table with the UUT has to be as close as possible to mitigate overturning moment concerns. As the UUT rarely couples directly to the shaker, an

interface is required to convert the hole pattern of the attachment points to the hole pattern of the shaker inserts. .

The fixture is well designed and not too large. Overhanging the shaker table is avoided. Its first resonant mode occurs well above the highest test frequency. Consider the mounting method for each axis of motion.

There are many fixture types that can be used to support the UUT. The main considerations that influence a design are dictated by the UUT itself. These are the physical shape, the mass, the size, the test requirement frequency range and severity, the number of axis to be tested, the attachment points, the quantity of units per test, the centre of gravity, off load moments etc.

With the target weight of < 6 kg, number of design configurations with different parameters, shapes are studied. Finally, the fixture is configured as a cylindrical structure and fabricated with AA-6061 T-6 alloy. By considering all these factors and according to the bolt size pattern holes on shaker table, 'M10 standard bolts' are used here to bolt a fixture with shaker table. While in the fixture assembly 'M4 bolts' are used here for bolting. The basic dimensions of the fixture are, maximum diameter of the fixture is ϕ 235 mm with the thickness of plate 36 mm. Centre of gravity of the fixture is maintained with the centre of gravity of shaker machine table. Fig. (1) gives the details of the fixture.



Fig (1). Details of fixture.

2.2 Governing equilibrium equations:

The theoretical work produces very practical benefits because it allows the prediction of the modal response of a structure. By finding and addressing potential problems early in the design process, manufacturers save money and improve product quality.

In the advanced theory of plate bending, theory of circular plate bending coincides with natural frequency calculation of our circular fixture (adapter plate). So equations are derived from the advanced theory of plate bending [8]. It is also observed that formulas mentioned [4] coincides with our derived formula for calculation of first natural frequency.

Derivations:

Equilibrium equations for small-displacement theory of flat plate,

$$\frac{\partial}{\partial x} \left\{ \frac{1}{\alpha} \left[\frac{\partial}{\partial x} (\beta M_{xx}) + \frac{\partial}{\partial y} (\alpha M_{xy}) + (\alpha_y M_{xy}) - (\beta_x M_{yy}) + \alpha \beta R_y \right] \right\} + \frac{\partial}{\partial y} \left\{ \frac{1}{\beta} \left[\frac{\partial}{\partial x} (\beta M_{xx}) + \frac{\partial}{\partial y} (\alpha M_{yy}) - (\alpha_y M_{xx}) + (\beta_x M_{yy}) - \alpha \beta R_x \right] \right\} + h \alpha \beta B_z + \alpha \beta P_z = 0 \quad \dots\dots\dots(1)$$

For rectangular axes, $\alpha = \beta = 1$ and equation (1) reduces to,

$$\frac{\partial^2 M_{xx}}{\partial x^2} + 2 \frac{\partial^2 M_{xy}}{\partial x \partial y} + \frac{\partial^2 M_{yy}}{\partial y^2} + hB_z + P_z = 0 \dots\dots(2)$$

Where, M_{xx} , M_{yy} is bending moment and $M_{xy} = M_{yx}$ is twisting moment. α and β are constants. H = plate thickness.

Stress-Strain-Temperature relations for isotropic elastic plates:

Let σ_{xx} , σ_{yy} & σ_{zz} are plane stresses of plate. Whereas ϵ_{xx} , ϵ_{yy} & ϵ_{zz} are strains of plate.

For linearly elastic isotropic materials and plane stress relative to (x, y) plane stress-strain-temperature relations are,

$$\begin{aligned} \sigma_{xx} &= \frac{E}{1-\nu^2} (\epsilon_{xx} + \nu \epsilon_{yy}) - \frac{EkT}{1-\nu} \\ \sigma_{yy} &= \frac{E}{1-\nu^2} (\nu \epsilon_{xx} + \epsilon_{yy}) - \frac{EkT}{1-\nu} \\ \sigma_{xy} &= 2G\epsilon_{xy} = G\gamma_{xy} \dots\dots\dots(3) \end{aligned}$$

Where, E = Young's Modulus.
 ν = Poisson's Ratio.
 k = Coefficient of Linear Thermal Expansion.
 G = Shear Modulus.
 T = Temperature Measured above an arbitrary zero.

By Kirchhoff's theory of Kinematics strain-displacement relations for plates,

Solve for equation (2) and then substitution of it into stress resultant equations of flat plate [4],

Then moment equations we get are,

$$\left. \begin{aligned} M_{xx} &= -D \left(\frac{k_{xx}}{\alpha^2} + \frac{\nu k_{yy}}{\beta^2} + T^1 \right) \\ M_{yy} &= -D \left(\nu \frac{k_{xx}}{\alpha^2} + \frac{k_{yy}}{\beta^2} + T^1 \right) \\ M_{xy} &= -D \frac{(1-\nu)}{\alpha\beta} k_{xy} \end{aligned} \right\} \dots\dots\dots(4)$$

Where, $D = \frac{Eh^3}{12(1-\nu^2)}$ (5)

The quantity D = Flexural rigidity of the plate. Considering strain energy and boundary conditions of the plate

On substitution for M_{xx} , M_{xy} , M_{yy} in terms of 'w' in equation (2) with $B_z = 0$ and $P_z = P$

$$\nabla^2 \nabla^2 w = \frac{P}{D} \dots\dots\dots (6)$$

Where, $\nabla^2 \nabla^2 w = w_{xxxx} + 2w_{xxyy} + w_{yyyy}$

$\nabla^2 \nabla^2 =$ Invariant vector operator.

p = Lateral Pressure.

w = Lateral Displacement.

Solutions of $\nabla^2 \nabla^2 w = \frac{P}{D}$ for circular plates,

For the circular plates with radius 'a' and thickness 'h' employing polar coordinate with the origin 'a' the center of the plate, equation (6) may be written as,

$$\nabla^2 \nabla^2 w = \left(\frac{\partial^2}{\partial r^2} + \frac{1}{r} \frac{\partial}{\partial r} + \frac{1}{r^2} \frac{\partial^2}{\partial \theta^2} \right) \left(\frac{\partial^2 w}{\partial r^2} + \frac{1}{r} \frac{\partial w}{\partial r} + \frac{1}{r^2} \frac{\partial^2 w}{\partial \theta^2} \right) = \frac{p}{D} \dots\dots\dots(7)$$

Here as per our requirement considering only axial symmetric case, in which plate is loaded and supported symmetrically. Then equation (7) reduces to,

$$\left(\frac{\partial^2}{\partial r^2} + \frac{1}{r} \frac{\partial}{\partial r} \right) \left(\frac{\partial^2 w}{\partial r^2} + \frac{1}{r} \frac{\partial w}{\partial r} \right) = \frac{p}{D} \dots\dots\dots (8)$$

Solution of above equation with p = p0 = constant is,

$$w = \frac{p_0 r^4}{64D} + A_1 + A_2 \ln r + B_1 r^2 + B_2 r^2 \ln r$$

or

$$\delta = \frac{p_0 r^4}{64D} + A_1 + A_2 \ln r + B_1 r^2 + B_2 r^2 \ln r$$

Where, δ = Deflection.

A1, A2, B1, B2 = Constants of integration

These constants of integration are determined by boundary conditions at r = a.

Therefore Circular Plate with Fixed Edges.

$$\delta(a) = A_1 + B_1 r^2 + \frac{p_0 r^4}{64D} = 0$$

After solution for A1 and B1

$$\delta = \frac{p_0 r^4}{64D} \left[1 - \left(\frac{r}{a} \right)^2 \right]^2$$

Or

$$\delta = \frac{qa^4}{64D} \left[1 - \left(\frac{r}{a} \right)^2 \right]^2 \dots\dots\dots(9)$$

Where, q = Intensity of Load(N / mm²)

Therefore as per the data of the fixture, the numerical value of the first natural frequency obtained after solution of equation (7) is **7925.85 Hz**.

III. ANALYSIS

Modal analysis is a powerful tool for understanding the vibration characteristics of mechanical structures. It simplifies the vibration response of a complex structure by reducing the data to a set of modal parameters that can be analyzed with relative ease. This application note discusses the concept of modal analysis, applications where modal analysis is useful, and techniques for the acquisition and visualization of modal data. In this project modal analysis of the vibration fixture is to be performed and after

experimental trials response analysis is to be shown.

Analysis of the fixture is carried out by geometric modeling in Pro/E, meshing in ANSYS and applying boundary conditions. Modal analysis is a process of describing a structure in terms of its natural characteristics which are the frequency, damping and mode shapes its dynamic properties. The modal testing has become an effective means for identifying, understanding, and simulating dynamic behavior and responses of structures.

Analysis yields a 1st natural frequency mode of **8543.4 Hz**. The random vibration analysis is carried out for the response with constant value of $0.03 \text{ g}^2/\text{Hz}$. The FE analysis by ANSYS indicates that there is no resonance observed in the required range of frequency. In random analysis controlled value of rms is equal to the demanded value of rms which shows uniformity in the structure. Theoretical estimated weight of the fixture is considered for the analysis. The fixture designed meets the mass and frequency requirements.

Fig (2) gives few representative plots of analysis.

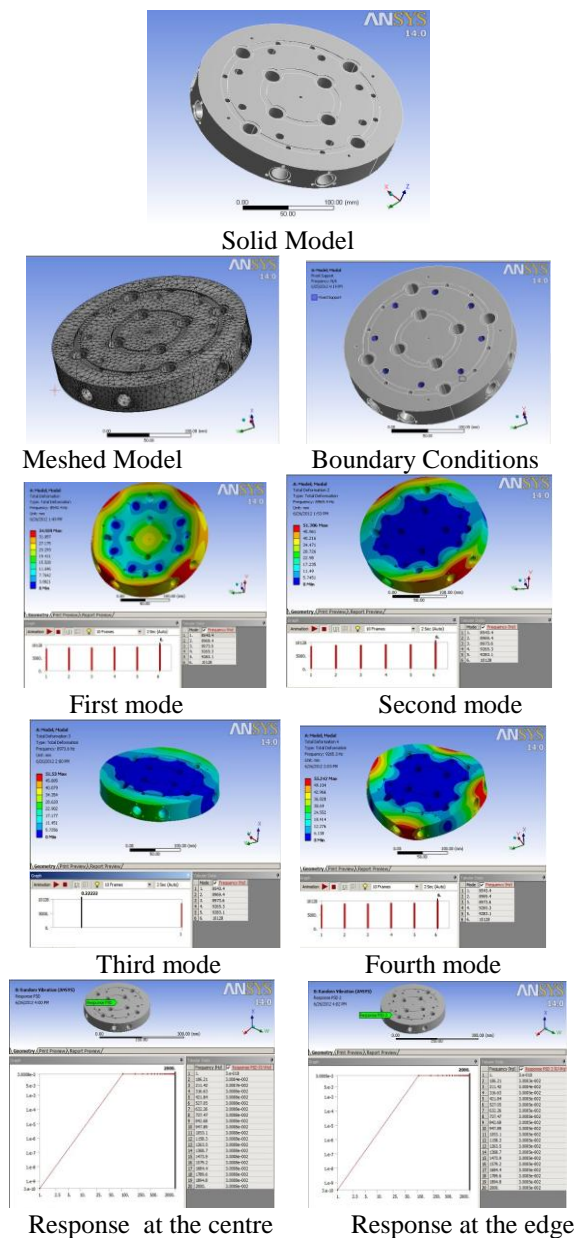


Fig (2).Representative plots of analysis

IV. FIXTURE EVALUATION

Certain augmentation to the facility is carried out before evaluating the fixture to facilitate testing of the power cartridges.

Subsequent to the design, analysis & fabrication the fixture is evaluated. Weight of the fixture after fabrication is 5 kg as compared to die theoretically predicted value of 3.7 kg. Main purpose of evaluating a fixture is to investigate the fixture natural frequencies, transmissibility, cross-axial response. Resonance search, Sine and Random vibration tests are carried out to evaluate the fixture. A low vibration level resonance search followed by sine, random search is carried out.

Sine and Random vibration tests to the test specification are carried out with two control accelerometers on the fixture top as shown in fig (2). Table (1) gives sequence of test conducted.

Table1. Sequence of test conducted.

Sine / Random	Specifications
Sine vibration test	5-11 Hz - 12mm DA. 11-2000 Hz – 3G Sweep rate – 1 Oct / Min.
Random vibration test	70-2000 Hz – 0.03 g ² / Hz

Fig.(3) gives test set-up in Z-axis.



Fig(3) Fixture Evaluation in Z-axis.

2.3 Discussions:

Resonance survey is conducted before and after the vibration tests. Lowest acceptance level based on facility limitation is employed.

The sine resonance survey conducted before and after tests from UUT in between frequency range of 5-2000 Hz. The plot of the sine vibration test is as shown in fig.(4) The machine was not tripped during test which indicates good design of fixture without any potential weakness. This indicates the uniformity in vibration level in the fixture and damping is good in structure.

Fig.(5) shows plotted result of the random vibration test of the fixture. Results shows control rms value is very close to the demanding rms value which indicates uniform structure of the fixture. There was no any peak or resonance observed within the range of vibration i.e. up to 2000 Hz. This indicates that fixture resonance is greater than UUT resonance.

The vibration fixture is ideally designed so that it gives unit transmissibility in the frequency range of test. Cross axial response is not observed within the frequency range is observed.

Control accelerometers provided on the top of the fixture with maximal control options yielded smooth control.

After correlation of the theoretical, simulated and experimental results observation shows that all the results are very close.

Prof. Mrs. R.S. Bindu Dr. D.Y. Patil College of Engineering, Pune, India, for their continual guidance.

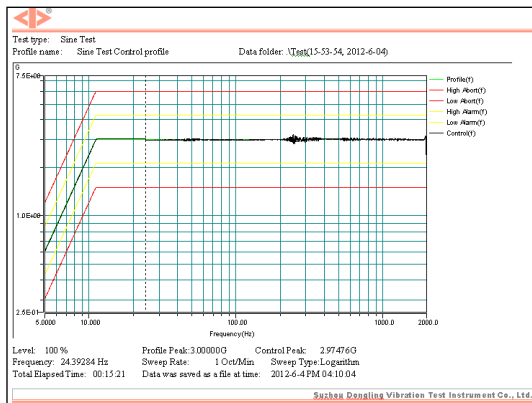


Fig (4) Sine vibration test

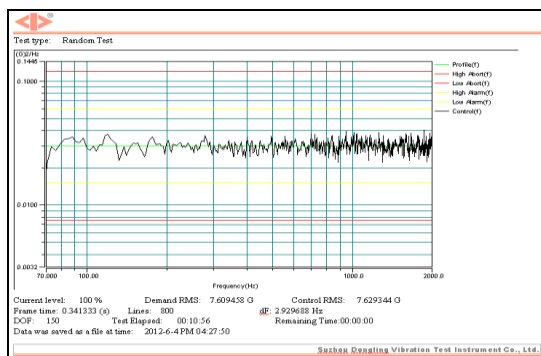


Fig (4) Random vibration test

V. CONCLUSION

An aluminum vibration fixture with AA6061-T6 alloy for power cartridges is designed, analyzed and evaluated. For vibration test of a single small test object, designing a vibration fixture is trivial task. However, it becomes complicated one while vibrating many of such test objects in a single fixture in multiple directions. A good vibration fixture avoids under-test or over-test of the test items. This has its implications on timely completion of test program and further development activity as a whole.

Various configurations are conceived before arriving at the present configuration. FE analysis is carried out using ANSYS tool. Evaluation is carried out using 4t duel shaker system. The control mechanism of vibration shaker works best for properly designed vibration fixtures.

The first natural frequency of the fixture from FE analysis is 8543.4 Hz. From the test the natural frequency observed is above the frequency limits. This is in close correlation with the prediction. All the accelerometers response at the top of the fixture are similar indicating a good design.

The fixture is suitable for vibration testing of cartridges used here and of future upcoming cartridges of similar types.

VI. ACKNOWLEDGMENT

The author wishes to acknowledge the ARDE design team for rendering a helping hand in the design, analysis and test facilities for carrying out the vibration tests. The author also wishes to acknowledge the Project Guide

REFERENCES

- [1] T. Shrinivasreddy, Jopaul Igatius, TNV Satyanarayana, G. Muniraju, "Design, Validation and Performance Demonstration of a Fixture for Validation Testing of Large Sub Systems of Advanced Launch Vehicle.", 7th National Seminar on Aerospace and Related Mechanisms. Thiruvananthapuram, Sep. 17-18, 2010.
- [2] Fabien PONCELET, Frederic MARIN, Claude FLEURY and Jean-Claude golinval, University of Liege, Belgium, Department of Aerospace, Belgium "Optimal Design of Fixtures for Vibration Testing of Structures on Electro- Dynamic Shaker", Twelfth International Congress on Sound and Vibration, July 11-14, 2008.
- [3] D.Ravi Prasad and D.R. Seshu, "A study on dynamic characteristics of structural materials using modal analysis," ASIAN Journal of Civil Engineering (Building and housing) vol. 9, No.2 (2008).
- [4] B.J. Klee, David Kimball, Wayne Tustin, 'Vibration and shock test fixture design', Tustin institute of technology, Santa Barbara, California, Published by Library of congress, USA, 2010.
- [5] Bruel and Kjare "Fixtures for B & K exciters", Denmark, 2009.
- [6] Blevins, Robert D. Robert E. "Formulas for Natural Frequency and Mode Shape" Kreiger Publishing Co., Malabar, FL. 2008.
- [7] Singiresu S. Rao, 'Mechanical Vibrations', Pearson publication, fourth edition, 2011.
- [8] Arthur Boresi, Omar Sidebottom, 'Advanced Mechanics of Materials', Wiley publication, 1990.
- [9] Rao V. Dukkipati, J. srinivas, 'Vibrations problem solving companion', Narosa publication, 2009.
- [10] Dennis L karn, Terry D. Scharton, 'NASA Handbook for spacecraft structural dynamic testing.' Jet propulsion Laboratory, California institute of technology, USA, 2007.
- [11] MIL-STD-810G, 'Environmental Engineering Considerations and Laboratory Tests' Department of defense test metho standards, Oct 31, 2008.
- [12] JSG 0102, 'Military Standard', 1984.
- [13] LDS handbook, 'Fixture Design', UK.
- [14] V.B.Bhandari, 'Design of machine elements', TMH Publishers, 2008.
- [15] Ansys Help, Ansys document.
- [16] O C Ziekiewicz, 'The Finite Element Method.'

Experimental Based Selection of Best Sorting Algorithm

¹ D.T.V Dharmajee Rao, ²B.Ramesh

¹ Professor & HOD, Dept. of Computer Science and Engineering, AITAM College of Engineering, JNTUK

² Dept. of Computer Science and Engineering, AITAM College of Engineering, JNTUK

Abstract: Sorting algorithm is one of the most basic research fields in computer science. Sorting refers to the operation of arranging data in some given order such as increasing or decreasing, with numerical data, or alphabetically, with character data.

There are many sorting algorithms. All sorting algorithms are problem specific. The particular Algorithm one chooses depends on the properties of the data and operations one may perform on data. Accordingly, we will want to know the complexity of each algorithm; that is, to know the running time $f(n)$ of each algorithm as a function of the number n of input elements and to analyse the space and time requirements of our algorithms. Selection of best sorting algorithm for a particular problem depends upon problem definition. Comparisons of sorting algorithms are based on different scenario. This work experimentally analyzes the performance of various sorting algorithms by calculating the execution time.

Keywords: Sort-Algorithm, Sorting, Quick sort, Merge sort, Radix sort, Bubble sort, Gnome sort, Cocktail sort, Counting sort.

I. Introduction

Sort is an important operation in computer programming. For any sequence of records or data, sort is an ordering procedure by a type of keyword. The sorted sequence is benefit for record searching, insertion and deletion. Thus enhance the efficiency of these operations.

Two categories of sort algorithms were classified according to the records whether stored in the main memory or auxiliary memory. One category is the internal sort which stores the records in the main memory. Another is the external sort which stores the records in the hard disk because of the records' large space occupation. In fact, by utilizing the splitting and merging, the external sort could be converted to internal sort. Therefore, only internal sort algorithms such as Bubble, Select, Insertion, Merge, Shell, Gnome, Cocktail, Counting, Radix and Quick Sort were discussed bellow.

For the convenience, we make two assumptions bellow. One is the sequence order, ascending is default. Another is all the records of the sequence were stored in the continuous address memory cells. In this situation, the order of records was determined by the position which stored in the memory. The sort is the move operation of records.

The two classes of sorting algorithms are $O(n^2)$ (which includes the bubble, insertion, selection, gnome, cocktail and shell sorts) and $O(n \log n)$ (which includes the heap, merge, and quick sort)

1.1 Theoretical Time Complexity of Various Sorting Algorithms

Time Complexity of Various Sorting Algorithms

Name	Best	Average	Worst
Insertion sort	n	n^*n	n^*n
Selection Sort	n^*n	n^*n	n^*n
Bubble Sort	n	n^*n	n^*n
Shell Sort	n	$n (\log n)^2$	$n (\log n)^2$
Gnome Sort	n	n^*n	n^*n
Quick Sort	$n \log n$	$n \log n$	n^*n
Merge Sort	$n \log n$	$n \log n$	$n \log n$
Cocktail Sort	n	n^*n	n^*n
Counting Sort	-	$n+ r$	$n+ r$
Radix Sort	-	$n(k/d)$	$n(k/d)$
Heap Sort	$n \log n$	$n \log n$	$n \log n$

II. Fundamental Sorting Algorithms

A. Insertion Sort

Insertion sort algorithm used in the experiments below was described by C language as:

Algorithm

1. For I=2 to N
2. A[I]=item ,J=I-1
3. WHILE j>0 and item<A[J]
4. A[J+1]=A[J]
5. J=J-1
6. A[J+1]=item

Pseudo Code

```
void insertion_sort(int b[],int N11)
{
int i,j,Temp,A[20000];
double starttime,endtime,difftime;
starttime=omp_get_wtime();
for(i=0;i<N11;i++)
A[i]=b[i];
for(i=1; i<N11; i++)
{Temp = A[i];
j = i-1;
while(Temp<A[j] && j>=0)
{A[j+1] = A[j];
j = j-1;}
A[j+1] = Temp;
}
```

B. Bubble Sort

Bubble sort algorithm used in the experiments below was described by C language as:

Algorithm

1. for I=1 to N-1 (for pass)
2. for k=1 to N-I (for comparison)
3. if $A[K] > A[K+1]$
4. swap $[A(k), A(k+1)]$

Pseudo Code

```
void bubble(int a[],int n)
{
int i,j,t;
for(i=n-2;i>=0;i--)
{ for(j=0;j<=i;j++)
{ if(a[j]>a[j+1])
{ t=a[j];a[j]=a[j+1];a[j+1]=t;}}
}
```

C. Selection Sort

Selection sort algorithm used in the experiments below was described by C language as:

Algorithm

1. for I=1 to N-1
2. min=A [I]
3. for K=I+1 to N
4. if (min>A [K])
5. min=A [K], Loc=K
6. Swap (A [Loc],A[I])
7. Exit

Pseudo Code

```
void selesort(int b[],int n)
{
int i, j,a[20000],min,index;
double starttime,endtime,difftime;
for(i=0;i<n;i++)
a[i]=b[i];
for(i=0;i<n-1;i++)
{ min=a[i]; index=i;
for(j=i+1;j<n;j++)
if(a[j]<min)
{ min=a[j];index=j;
}
a[index]=a[i];
a[i]=min;
}
```

D. Quick Sort

Quick sort algorithm used in the experiments below was described by C language as:

Algorithm

Quick sort (A, p, r)

1. If $p < r$
2. Then $q \leftarrow$ partition (A, p, r)
3. Quick sort (A, p, q-1)
4. Quick sort (A ,q+1 ,r)

To sort an entire array A, the initial call is Quick sort (A, 1, length [A]).

Partition the array

The key to the algorithm is the PARTITION procedure, which rearranges the sub array A [p...r] in place.

Partition (A, p, r)

1. $x \leftarrow A[r]$
2. $i \leftarrow p-1$
3. For $j \leftarrow p$ to r-1

4. Do if $A[j] \leq x$
5. Then $i \leftarrow i+1$
6. Exchange $A[i] \leftrightarrow A[j]$
7. Exchange $A[i+1] \leftrightarrow A[r]$
8. Return i+1

Pseudo Code

```
void quick_sort(int arr[], int low, int high) {
int i = low;
int j = high;
int y = 0;
int z = arr[(low + high) / 2];
do {
while(arr[i] < z) i++;
while(arr[j] > z) j--;
if(i <= j)
{ y = arr[i];arr[i] = arr[j]; arr[j] = y;
i++;j--;}
} while(i <= j);
if(low < j)
quick_sort(arr, low, j);
if(i < high)
quick_sort(arr, i, high);
}
```

E. Counting Sort

Counting sort algorithm used in the experiments below was described by C language as:

Algorithm

1. for I=0 to K
2. $C[I]=0$
3. For j=1 to length [A]
4. $C[A(J)]=C[A(J)]+1$
5. For I=1 to K
6. $C[I]=C[I]+C[I-1]$
7. For J=length(A) down to 1
8. $B[C(A(J))]=A[J]$
9. $C[A(J)]=C[A(J)]-1$

Pseudo Code

```
void countingsort(int *a, int n)
{
int i, min, max,array[20000];
for(i=0;i<n;i++)
array[i]=a[i];
min = max = array[0];
for(i=0; i < n; i++)
{ if ( array[i] < min )
{ min = array[i];}
else if( array[i] > max )
{ max = array[i];}
}
```

F. Shell Sort

Shell sort algorithm used in the experiments below was described by C language as:

Algorithm

1. for I=n to i/2 (for pass)
2. for i=h to n
3. for j=1 to j=j-h upto $j \geq h$ && $k < a[j-h]$
4. assign $a[j-h]$ to $a[j]$

Pseudo Code

```
void shell_sort(int a[],int n)
{
int j,i,m,mid;
for(m = n/2;m>0;m/=2)
```

```

{for(j = m;j< n;j++)
{for(i=j-m;i>=0;i-=m)
if(a[i+m]>=a[i])
break;
else
{mid = a[i];a[i] = a[i+m];a[i+m] = mid;}}}
}
} while(swapped);

```

III. Problem Statement

The problem of sorting is a problem that arises frequently in computer programming. Many different sorting algorithms have been developed and improved to make sorting fast. As a measure of performance mainly the average number of operations or the average execution times of these algorithms have been investigated and compared.

G. Gnome Sort

Gnome sort algorithm used in the experiments below was described by C language as:

Algorithm

1. for I=1 to n (for pass)
2. if i=0 and a[i-1] < a[i] then i++
3. else swap(a[i-1],a[i])
4. return a

Pseudo Code

```

void gnomeSort(int a[], int n)
{
    int i = 1, j = 2;
    int temp;
    while(i < n)
    {if(a[i-1] <= a[i])
        {i = j;j++;}
        else
        {temp = a[i];a[i] = a[i-1];a[i-1] = temp;
            i--;
            if(i == 0)
            {
                i = j;
                j++;
            }
        }
    }
}

```

H. Cocktail Sort

Cocktail sort algorithm used in the experiments below was described by C language as:

Algorithm

1. for i=1 to n (for pass)
2. for i=n-1 to 1
3. while !i
4. swap(a[i-1],a[i])

Pseudo Code

```

void cocktasort(int a[], int l)
{
    int swapped = 0;
    int i,a[20000];
    do {
        for(i=0; i < (l-1); i++) {
            if ( a[i] > a[i+1] ) {
                temp = a[i];
                a[i] = a[i+1];
                a[i+1] = temp;
                swapped = 1;
            }
        }
        if ( ! swapped ) break;
        swapped = 0;
        for(i= l - 2; i >= 0; i--) {
            if ( a[i] > a[i+1] ) {
                int temp = a[i];
                a[i] = a[i+1];
                a[i+1] = temp;
                swapped = 1;
            }
        }
    }
}

```

3.1 Problem statement

All sorting algorithms are nearly problem specific. How one can predict a suitable sorting algorithm for a particular problem? What makes good sorting algorithms? Speed is probably the top consideration, but other factors of interest include versatility in handling various data types, consistency of performance, memory requirements, length and complexity of code, and stability factor (preserving the original order of records that have equal keys).

For example, sorting a database which is so big that cannot fit into memory all at once is quite different from sorting an array of 100 integers. Not only will the implementation of the algorithm be quite different, naturally, but it may even be that the same algorithm which is fast in one case is slow in the other. Also sorting an array may be different from sorting a linked list.

3.2 Justification

In order to judge suitability of a sorting algorithm to a particular problem we need to see, are the data that application needs to sort tending to have some pre existing order?

- What are properties of data being sorted?
- Do we need stable sort?

Generally the more we know about the properties of data to be sorted, the faster we can sort them. As we already mentioned the size of key space is one of the most important factors (sort algorithms that use the size of key space can sort any sequence for time $O(n \log k)$).

3.3 Explanation

Many different sorting algorithms have been invented so far. Why are there so many sorting methods? For computer science, this is a special case of question, "why there are so many x methods?", where x ranges over the set of problem; and the answer is that each method has its own advantages and disadvantages, so that it outperforms the others on the same configurations of data and hardware. Unfortunately, there is no known "best" way to sort; there are many best methods, depending on what is to be sorted on what machine and for what purpose. There are many fundamental and advance sorting algorithms. All sorting algorithm are problem specific means they work well on some specific problem, not all the problems. All sorting algorithm apply to specific kind of problems. Some sorting algorithm apply to small number of elements, some sorting algorithm suitable for floating point numbers, some are fit for specific range like (0 1].some sorting algorithm

are used for large number of data, some are used for data with duplicate values.

It is not always possible to say that one algorithm is better than another, as relative performance can vary depending on the type of data being sorted. In some situations, most of the data are in the correct order, with only a few items needing to be sorted; In other situations the data are completely mixed up in a random order and in others the data will tend to be in reverse order. Different algorithms will perform differently according to the data being sorted.

IV. Experimental Study

In order to compare the performance of the various Sorting algorithms above, we use a desktop computer (Intel Dual Core Processor @ 2.4GHz, 2GB RAM, Windows 7 operating system) to do a serial experiments. Under VS2008, using C language, the programs test the performances of various algorithms from input scale size by utilizing random function call and time function call.

4.1 Experiments and Results

When the input sequence is produced by a random function, input sequence is positive, and the input scale varied from 1024 (1K) to 101376(99K), various sort algorithms time costs were demonstrated by table 4.1.1 and figure 4.1.1

4.1.1 Sort Algorithms Time Cost Under Positive Input Sequence

Data Size	Insert Sort	Selec Sort	Bubble Sort	Shell Sort	Gnome Sort	Quick Sort	Merge Sort	Cocktail Sort	Countin Sort	Radix Sort
1K	0.0022	0.0037	0.0112	0.0009	0.0054	0.0003	0.0294	0.0036	0.0001	0.0002
10K	0.0452	0.0392	0.1276	0.0023	0.0614	0.0009	0.1171	0.0908	0.0002	0.0011
20K	0.4545	0.6694	2.0738	0.0167	1.0073	0.0039	0.5394	1.4707	0.0006	0.0047
30K	1.0330	1.5091	4.7020	0.0222	2.2820	0.0057	1.2182	3.3793	0.0008	0.0064
40K	1.8413	2.6861	8.3657	0.0475	3.9973	0.0077	1.1318	5.7960	0.0010	0.0085
50K	2.8438	4.0942	12.8560	0.0379	6.1155	0.0097	1.1465	8.9410	0.0012	0.0114
60K	4.0802	5.9034	18.6282	0.0561	8.9355	0.0127	1.7485	13.1773	0.0014	0.0127
70K	5.5719	8.0406	25.6148	0.0541	12.7165	0.0139	2.9771	18.6538	0.0016	0.0150
80K	7.5296	11.3767	34.5813	0.1189	16.3145	0.0156	3.2230	24.1683	0.0027	0.0225
90K	9.1565	13.1304	42.1701	0.0713	21.0288	0.0177	3.6278	31.0652	0.0028	0.0245
99K	11.4789	16.7561	52.3442	0.0675	24.7972	0.0194	2.7245	36.7319	0.0023	0.0214

From the table and the figure above, we got when the scale of input sequence was small, the difference of time cost between these algorithms was small. But with the scale of input sequence becoming larger and larger, the difference became larger and larger. Among these algorithms, the radix sort, counting sort, quick sort, shell and merge was the best, then all other traditional sorts. Whatever, the time cost curve of radix sort, counting sort, quick sort, shell sort was almost a line. It's the slowest changing with the input scale increasing.

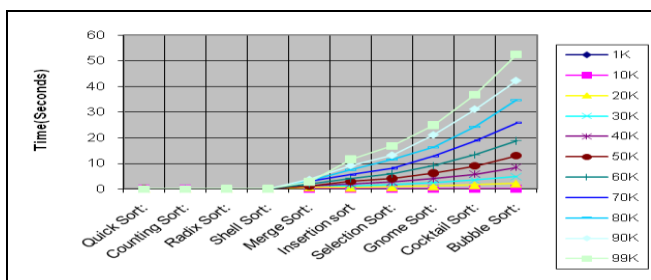


Figure 4.1.1 Time cost Comparison of various sorting algorithms with positive input sequence

When the input sequence is produced by a random function, input sequence is negative and the input scale varied from 1024 (1K) to 101376(99K), various sort algorithms time costs were demonstrated by table 4.1.2 and figure 4.1.2

4.1.2 Sort Algorithms Time Cost Under Negative Input Sequence

Data Size	Quick Sort	Count	Radix Sort	Shell Sort	Merge Sort	Inserti Sort	Select Sort	Gnome Sort	Cocktail Sort	Bubble Sort
1K	0.0003	0.0001	0.0000	0.0006	0.0263	0.0025	0.0035	0.0056	0.0037	0.01171
10K	0.0018	0.0003	0.0001	0.0071	0.2379	0.1116	0.1599	0.2425	0.3521	0.51088
20K	0.0037	0.0006	0.0001	0.0190	0.4627	0.4585	0.6459	0.9664	1.4116	2.0286
30K	0.0058	0.0009	0.0002	0.0219	0.6949	1.0562	1.4730	2.2009	3.1993	4.6123
40K	0.0077	0.0011	0.0003	0.0451	0.9435	1.8196	2.5972	3.8986	5.6744	8.1489
50K	0.0095	0.0012	0.0004	0.0357	1.1701	2.8247	4.0640	6.0874	8.8682	12.7087
60K	0.0125	0.0018	0.0006	0.0595	2.4613	4.3416	6.1430	9.2829	13.3169	18.9648
70K	0.0136	0.0016	0.0005	0.0562	1.6481	5.7460	8.4443	12.0589	17.3594	26.1405
80K	0.0156	0.0018	0.0006	0.1183	1.8738	7.2068	10.3441	15.6466	22.6671	32.6930
90K	0.0177	0.0020	0.0007	0.0669	2.1502	9.3995	13.0794	19.8742	28.7780	41.5611
99K	0.0193	0.0022	0.0007	0.0683	2.3128	11.0168	15.7181	23.9150	34.8231	50.8242

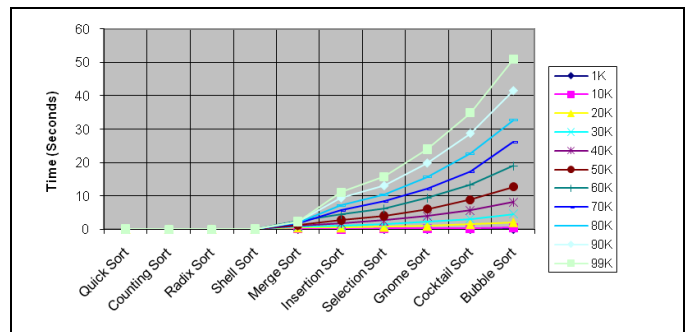


Figure 4.1.2 Time cost Comparison of various Sorting algorithms with Negative input sequence

4.2 Performances Evaluations

Two criteria to evaluate the sort algorithms: time and space. The time related to the comparison operations and move operations of records in the algorithms. The space may dependent or independent to the input sequence scale. If the additional space needed in the algorithm is independent to the input, its space complexity is O(1) . Otherwise, its space complexity is O(n) .

Let N denote the number of input records, in which there are n elements were ordered. Then we could define K, called ordered factor

$$K = (n/N)$$

$K \in [0, 1]$ reflects the sort degree of random sequence. K is bigger, more ordered exists in the sequence. Otherwise, K is smaller, more random exists in the sequence. Let RCN represent the number of comparison operation, and RCN represent the number of remove operation, T(n) and S(n) represent the algorithm time complexity and space complexity respectively. When $K \rightarrow 1$, then RCN $\rightarrow 0$ and T(n) become lesser. When $K \rightarrow 0$, then RCN and T(n) become bigger. According to S (n) whether independent or dependent to the input scale, its value is O (1) or O (n).

V. Conclusion

Every sorting algorithm has some advantages and disadvantages. In the following table we are tried to show

the strengths and weakness of some sorting algorithms according to their order, memory used, stability, data type and complexity. To determine the good sorting algorithm, speed is the top consideration but other factor include handling various data type, consistency of performance, length and complexity of code, and the prosperity of stability.

Sort	Order	Worst Case	Memory	stability	Data Type	Complexity
Quick	$n \log n$	n^2	$nk+np+stack$	no	all	High
Merge	$n \log n$	$n \log n$	$nk+np+stack$	yes	all	Medium
Shell	$n(\log n)^2$	n	$nk+np$	no	all	Low
Insertion	n^2	n^2	$nk+np$	yes	all	very low
Selection	n^2	n^2	$nk+np$	yes	all	very low
Bubble	n^2	n^2	$nk+np$	yes	all	very low
Counting	n	n	$nk+np$	yes	all	very low
Gnome	n	n^2	$nk+np$	yes	all	very low
Cocktail	n	n^2	$nk+np$	yes	all	very low

Table 5.1: Strength and Weakness of various sorting algorithm

From the average time algorithms cost, the radix sort, counting sort, quick sort, shell and merge sort are superior to other algorithms. But in the worst time situation, the quick sort cost too much time than the merge sort.

When the input scale isn't big, time cost of algorithms has not an obvious difference. But with the input scale increasing, the Radix sort has certainly on advantage over other algorithms.

For the space occupation, the quick sort and merge sort cost too much than others, their space complexity is $O(\log n)$ and $O(n)$, the space occupation of the radix and counting sort is $O(nk)$ and $O(n+k)$, dependent to the input scale. Other algorithms cost little, their space complexity is $O(1)$, independent to the input scale.

For the application, appropriate sort algorithm is selected according to the attributes of input sequence. If the input scale is small, any traditional algorithm is a good choice. But when the input scale is large Radix Sort, Counting sort, Shell Sort, Quick sort and Merge sort is the necessary choice essentially.

References

- [1] MacLaren, M.D. "Internal Sorting By Radix Plus Sifting". J. ACM 13, 3 (July 1966), 404-- 411.
- [2] Williams, J.W.J. "Algorithm 232: Heap sort". Comm. ACM 7, 6 (June 1964),347-348.
- [3] J. Larriba-Pey, D. Jimenez-González, and J. Navarro. "An Analysis of Superscalar Sorting

Algorithms on an R8000 processor". In International Conference of the Chilean Computer Science Society pages 125-134, November 1997.

- [4] A. Aho, J. Hopcroft, J. Ullman, "Data Structures and Algorithms", Pearson India reprint, 2000
- [5] R. Motwani and P. Raghavan, "Randomized Algorithms", Cambridge University Press, 2000
- [6] Aditya Dev Mishra, Deepak Garg "Selection of Best Sorting Algorithm" International Journal of Intelligent Information Processing" Vol II Issue II 2008 ISSN0.973-3892, p. 233-238.
- [7] Kumari A., Chakraborty S. Software Complexity: A Statistical Case Study through Insertion Sort. Applied Mathematics and Computation. 2007, 190(1): 40-50.
- [8] Jafarlou M. Z., Fard P. Y. Heuristic and Pattern Based Merge Sort. Procedia Computer Science. 2011, 3: 322-324.
- [9] Nardelli E., Proietti G. Efficient Unbalanced Merge-Sort. Information Science. 2006, 176(10):1321-1337.
- [10] Feng H. Analysis of the Complexity of Quick Sort for two Dimension Table. Jisuanji Xuebao. In Chinese. 2007, 30(6):963-968.

Remote Radar Data Acquisition and Control Using Cdma RF Link

Rohit N Singh*, M.Chennakesavulu**

^{1,2}(Department of E.C.E, RGM CET, Nandyal

Abstract : Radar Seeker is used in missile system for detection and tracking a target. It will be integrated in the nose cone of the missile. During testing and launching of the missile all necessary important parameters and status of the seeker are collected for analysis to ascertain the health of the Seeker. Similarly the configuration and control of the seeker is to ensure the proper mode of operation of seeker.

During launch campaign the technicians and engineers cannot go near the missile and the seeker Health, but the knowledge of seeker health is very much necessary for the launch campaign, so a remote Control and data acquisition system should be there to confirm the health of the seeker either through wired serial communication link or using RF Link.

The Aim of this project is to Design and Develop a "Remote Radar Data Acquisition and Control using CDMA RF Link " and to Test with an existing radar seeker.

Keywords : RADAR SEEKER, QPSK, CORTEX –M3 (ARM Processor), SPZB260 (ZIGBEE Module), Costas loop.

I. INTRODUCTION

Radar (RADio Detection And Ranging) is an object-detection system which uses radio waves to determine the range, altitude, direction, or speed of objects. It can be used to detect aircraft, ships, spacecraft, guided missiles, motor vehicles, weather_ formations, and terrain. The **seeker** is a homing system perceives the target with its own radar , extracts tracking data from the received signal, and computes its own steering commands. As it closes on the target, a fixed angular error at the missile results in a decreasing linear error, providing the higher accuracy characteristic of homing guidance. An **active radar seeker** is basically a tracking Radar whose antenna is mounted on a stabilized platform so as to provide necessary isolation of the antenna from the body motion of the missile. Enabling the antenna to keep tracking the target and generating signals which are used in terminal guidance of the missile.

CDMA (Code Division Multiple Access) is a spread spectrum multiple access technique. Spread spectrum modulation was originally developed for military applications, where resistance to jamming is of major concern. A spread spectrum technique spreads the bandwidth of the data uniformly for the same transmitted power[1]. A spreading code is a pseudo-random code. These are studied and performance expressions are derived and confirmed by computational simulation using MALAB SIMULINK. The spread spectrum technique which is present in SPZB260 Zigbee module, is used in order to establish RF communication and it is controlled by ARM Cortex M3 Processor(LPC1768).

Section2 provides a brief description of Spread Spectrum Modulation scheme using QPSK, SPZB260 and ARM Cortex M3. Section 3 gives block diagram of

Transmitter and Receiver. The procedure to implement transmitter and receiver using Simulink are explained in this section. Section 4 provides simulation results of transmitter-receiver, which are supporting the theory provided in the earlier sections in Simulink. Finally the work is concluded in section 5 and the scope for future work is explained.

II. General Structure Of The System

A. Definition of Spread Spectrum

Spread spectrum is a means of transmission in which the data sequence occupies a bandwidth in excess of the minimum bandwidth necessary to send it. The spectrum spreading is accomplished before transmission through the use of a code that is independent of data sequence. The same code is used in the receiver to despread the received signal so that the original data sequence may be recovered[1][2].

B. Working of DSSS

A conceptual diagram of DSSS system is given in fig 1. At the transmitter the digital binary information or data $d(t)$ having a source bit rate of $f_b = 1/T_b$ (Where f_b is bit rate and T_b is the bit duration) is XORed with spreading signal $c(t)$ is a pseudonoise (PN) signal having chip rate of $f_c = 1/T_c$ (f_c is chip rate and T_c is the pulse duration)[2]. Where $f_c \gg f_b$

The data stream entering the modulator is converted by a serial to parallel converter into two separate data streams.

One stream, $I(t)$ is in the phase and other $Q(t)$, is quadrature phase . After obtaining the inphase and Quadrature signals ,we need to do modulation for the transmission of the signal. The inphase signal is multiplied by a carrier cosine wave and Quadrature signal is multiplied by sin signal. The both $I(t)$ and $Q(t)$ signal are summed to produce the transmitting signal with four phase signal.

In the Receiver the received signal or the modulated signal is first demodulated and then despread. So, for demodulation we use Costas loop. Costas loop is used to track the carrier signal and phase of modulated signal. It produces two output one is Inphase and the other quadrature phase. This two signal are passed through the parallel to serial convertor to obtain spreading signal. By using matched filter as despread we can obtain required binary data.

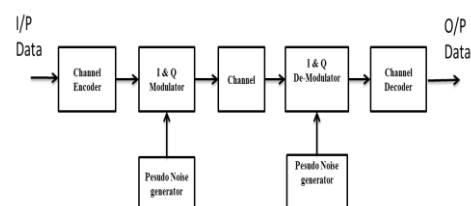


Figure 1: Block diagram of Spread Spectrum Communication system

C. Pseudo Noise Sequence

The types of spreading sequences are Gold sequences, maximum-length sequences, kasami sequences or walsh sequences. pseudo noise code generators are periodic in that the sequence that is produced repeats itself after some period of time. Such a periodic sequence is portrayed in fig 2. The Best known , best described PN sequences are maximal length. The generator contains type D flip-flops and is connected so that each data input except D0 is the input of the preceding flip-flop. Not all Q flip flop outputs need be connected to parity generator . the number of flip flop L and selection of which flip flop outputs are connected to parity generator determines the length and characteristics of the generated PN sequences. When the code is generated by maximum-length sequence , the value is $2^n - 1$, where n is the number of stages in the code generator[2].

$$L = 2^n - 1$$

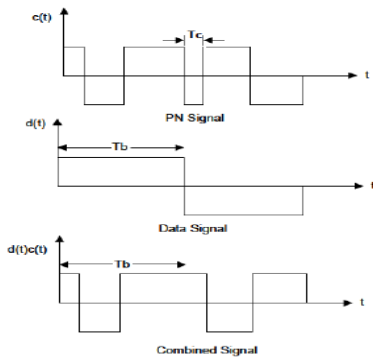


Figure 2: Wave form of Pseudo Random generator

Autocorrelation:

Te auto correlation function for the periodic wave is defined as number of agreements less number of disagreements in a term by term comparison over one full period of sequence with cyclic shift (position τ) of the sequence itself:

$$Ra(\tau) = \int_{-\infty}^{\infty} f(t) \cdot f(t - \tau) \cdot dt$$

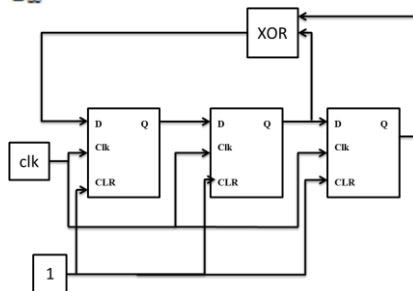


Figure 3: Block diagram of Pseudo Random generator

D. Direct Sequence QPSK

In QPSK, the data stream Inphase and Quadrature phase , with each stream having a symbol rate equal to half that of the incoming bit . Both I and Q are separately applied to multipliers. The Inphase multiplier is the carrier signal $\sin\omega t$ and Quadrature multiplier is the carrier signal $\cos\omega t$. The I multiplier output signal has phase 90 and 270 degrees and Q multiplier output signal has phase 0 and 180 degrees. Figure 4 shows a typical QPSK waveform in the time domain[4].

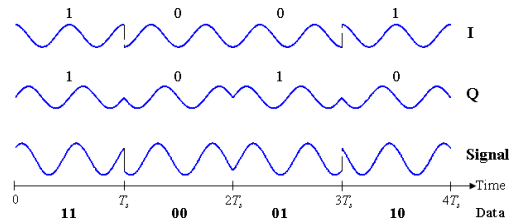


Figure 4: Wave form In phase and quadrature of QPSK modulation

E. Costas Loop

Costas loop is use for carrier recovery and phase detection which is used as demodulation circuit.

In Costas Loop the incoming signal is mixed with the output of the VCO, both before its phase is shifted and after its phase is shifted by 90 degrees. These two outputs are then filtered, multiplied together, filtered again and to control the frequency of the voltage controlled oscillator. The decoded spreading data stream can be taken from the output of the mixer output[1].

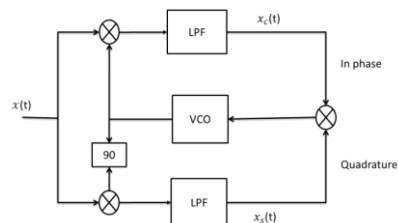


Figure 5: Block diagram of Costas Loop Carrier and phase recovery

$$x_c(t) = A \cos \psi(t) + n_c(t)$$

$$x_s(t) = A \cos \psi(t) + n_s(t)$$

When these two outputs are multiplied together, the product is

$$x_c(t)x_s(t) = \frac{A^2}{2} \sin \psi(t) + n_{eq}(t)$$

F. Hardware Requirement

Here we use the Arm Cortex M3 Processor to Control the Spread Spectrum Module (i.e SPBZB260) via SPI mode Here, we use two SPB260 and two LPC1768.

The first pair is connected to seeker via serial communication (UART) via LPC1768 which acts as client and other pair is connected to the system . were command and data sent and receive using GUI via serial communication(UART). Which is also called basestation. The following fig 6 show the the CDMA communication between the seeker and user.

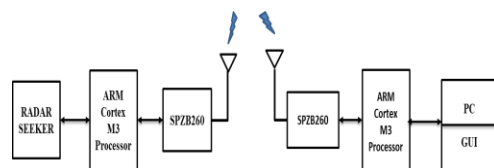


Figure 6: Block diagram of CDMA TransReceiver system

i) SPBZB260

he SPBZB260 integrates a 2.4 GHz, IEEE802.15.4-compliant transceiver. SPBZB260 exposes access to the

while waiting for a Response. To determine when a Response is ready, use one of two methods: Clock the SPI until the SPZB260 transmits a byte other than 0xFF. Interrupt on the falling edge of nHOST_INT.

The first method, clocking the SPI, is recommended due to simplicity in implementing. During the Wait section, the SPZB260 will transmit only 0xFF and will ignore all incoming data until the Response is ready. When the SPZB260 transmits a byte other than 0xFF, the transaction has officially moved into the Response section.

c) Response Section

When the SPZB260 transmits a byte other than 0xFF, the transaction has officially moved into the Response section. The data format is the same format used in the Command section. The response can be of any length from 2 to 128 bytes and will not begin with 0xFF. Depending on the actual response, the length of the response is known from the first or second byte and this length should be used by the Host to clock out exactly the correct number of bytes. Once all bytes have been clocked, it is allowable for the LPC1768 to deassert chip select. Since the LPC1768 is in control of clocking the SPI, there are no ACKs or similar signals needed back from the Host because the SPZB260 will assume the LPC1768 could accept the bytes being clocked on the SPI[7].

SOFTWARES USED

1. Keil uVision4 software for embedded C programming.
2. Flash Magic software programmer for dumping code into ARM-cortex M3 LPC 1768 Microcontroller
3. Debugger used is CoCoX CoIDE
4. Visual Basic for GUI which used to send command to LPC1768 via serial port.

III. Implementation Of Transceiver Model In Matlab/Simulink

A. CDMA Transmitter in Simulink

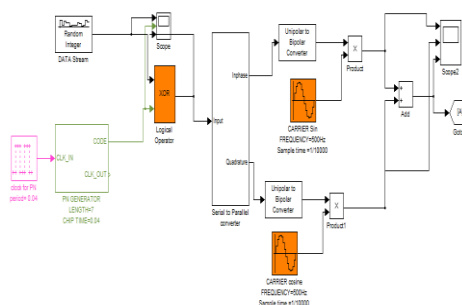


Figure 10: Implementation of CDMA Transmitter in Simulink:

i. Generating binary data stream: By using *Random integer generator block* in the communication tool box, we can generate binary data stream of 250Kbps. By adjusting the parameters like M-ary number, initial seed, sample time and output data type, we can achieve the fixed binary stream. In a real time scenario, this data stream is supplied by application that will generate information to be transmitted.

ii. Generating PN sequence: PN code is generated using D-flip-flop. we can generate 7 bit- PN sequence chip rate of 0.04ms by using 3 D- flip-flop and a XOR gate to generate 7 bit PN code.

iii. Serial to parallel converter implementation: By using flip-flops in Simulink extras tool box, we can get the parallel data from the serial data. The necessary instruments are one clock, one JK flip flop and two D flipflops. The initial conditions of the flip-flops using is zero and the period of the clock was decided by the input data stream. By this way we can easily generate the parallel data technically called as inphase and Quadrature data. Here necessary one bit offset delay is provided by the D flip flop itself. multiplied to get a Direct spread spectrum signal.

iv. Performing Modulation: After obtaining the inphase and Quadrature signals we need to do modulation for the transmission of the signal. Generally we do this with the help of high frequency(500HZ and sample time of 1/10000) sinusoidal carrier. By using sine wave block in Signal Processing Tool Box, sine wave can be generated by adjusting the parameters like amplitude, frequency, sample time, phase and sine type. Now the inphase signal after half sine pulse shaping is multiplied by a sine wave and Quadrature is multiplied by its cosine signal which is nothing but 90 degree phase shift of original sinusoidal carrier.

V. Output of the Transmitter: Addition of both inphase and Quadrature signals after modulation, generates the required transmitter output. The required output signal is generated by using sum block in commonly used blocks. There will be no phase transitions in the output, which is an advantageous property[8].

B. CDMA Receiver in Simulink

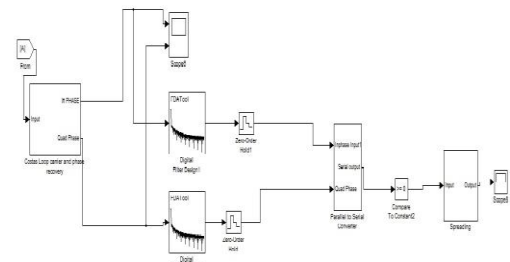


Figure 11: Implementation of CDMA Receiver in Simulink:

i. Multiplying with RF carrier: By using Costas loop is use for carrier recovery and phase detection which is used as demodulation circuit. In Costas Loop the incoming signal is mixed with the output of the VCO, both before its phase is shifted and after its phase is shifted by 90 degrees. These two outputs are then filtered, multiplied together, filtered again and to control the frequency of the voltage controlled oscillator. The decoded spreading data stream can be taken from the output of the mixer output.

ii. Sampling and Thresholding :

a. Sampling: By using the zero order hold circuit in the Simulink discrete menu, a sample and hold circuit was

generated. It samples the signal for every T time period. By setting the sample time in this block, adjust the time period T in zero order hold circuit.

b. **Thresholding:** By using compare to constant block in the Simulink logic and bit operations menu. By setting operator, constant value and output data type parameters, we can get the comparator circuit, which compares the sampled data with the predefined threshold value and detects whether the transmitted data is „1“ or „0“.

iii. **Parallel to serial conversion:** By using switch block in the Simulink signal routing menu, convert the parallel data into serial data. By setting the threshold value and the criterion for parallel to serial conversion, convert parallel data into serial data

iv. **Despreading:** The resulting data coming after serial to parallel conversion is multiplied with the delayed PN sequence. So that original is recovered data with small amount of delay. The incoming bit stream and the resultant output both are same but with a small amount of delay.

IV. Simulation Results

A. At the transmitter end

The following figures demonstrate simulation results for CDMA transmission system. The results are displayed in the form of snapshots of scope signals.

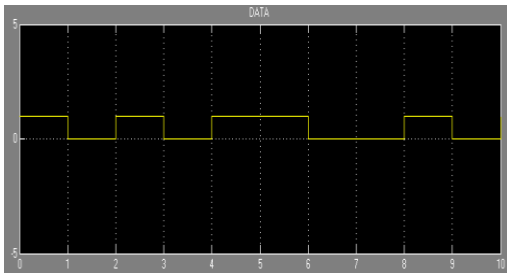


Figure 12: Binary data generated by Random integer Generator

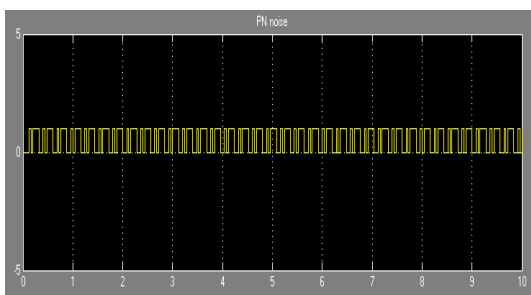


Figure 13: PN Generator

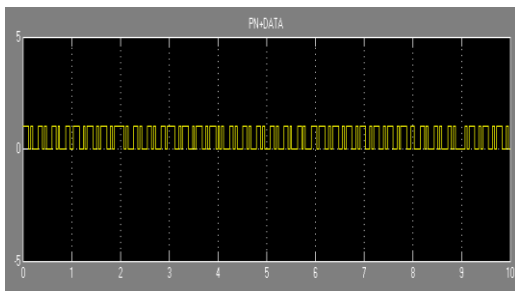


Figure 14: PN + Data

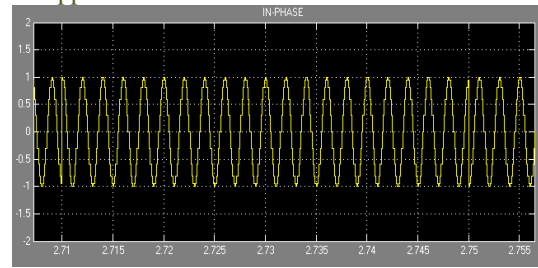


Figure 15: In phase modulation signal

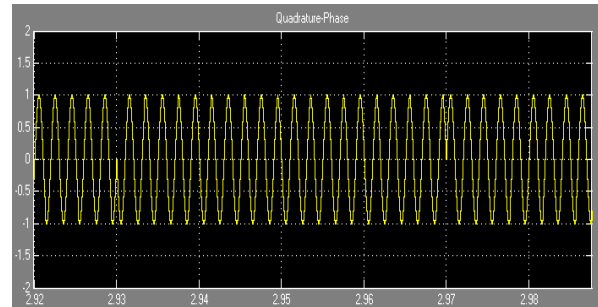


Figure 16: Quadrature phase modulation signal

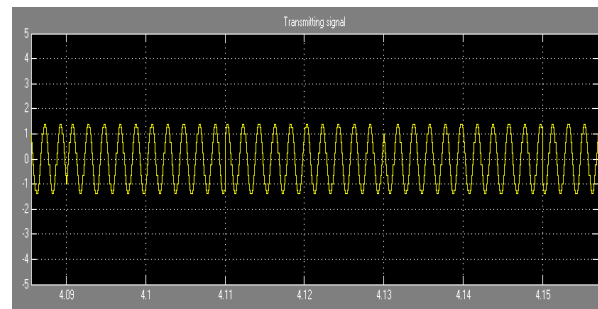


Figure 17: DSSS signal to transmit

B. At the receiver end

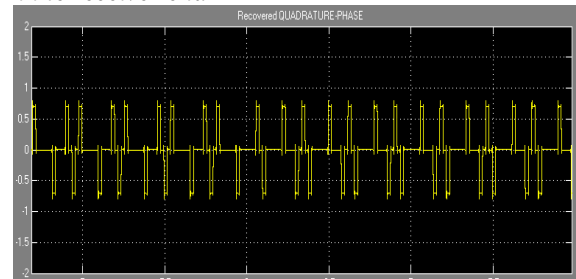


Figure 18: Recovered In phase stream using costas loop

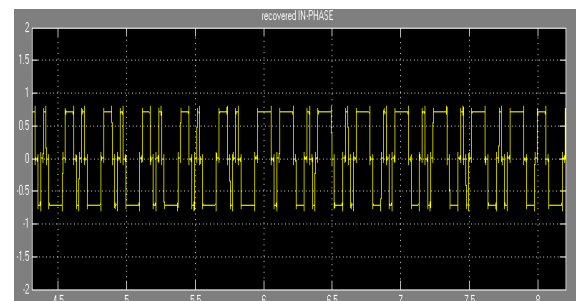


Figure 19: Recovered Quad phase stream using costas loop

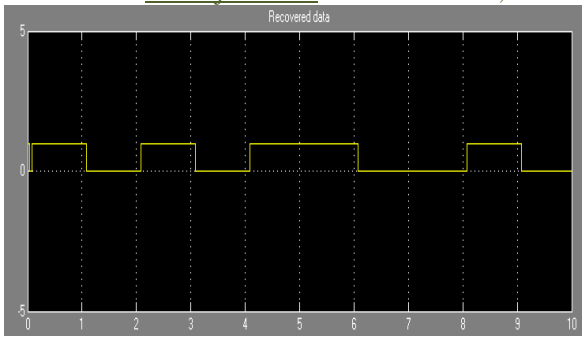


Figure 20: Recovered Data stream with small delay

V. CONCLUSION

CDMA RF link is used for achieving the communication between transmitters and receivers. Simulation results were plotted. Hard ware implementation is to be done using cortexM3 processor and SPZB260 Zigbee module for RF communications. In future, we aspire to improve the design with many (2 to 3) client to control the other system of the missile.

REFERENCES

- [1]. George R Cooper ,Clare D McGillem.”.Modern Communications and Spread Spectrum” 1986 .
- [2]. Dr.Kamilo Feher “Wireless Digital Communication.” . June 2003.
- [3]. http://en.wikipedia.org/wiki/Pseudorandom_noise.
- [4]. <http://en.wikipedia.org/wiki/PSK>.
- [5]. http://www.nxp.com/documents/data_sheet/LPC1769_68_67_66_65_64_63.PDF
- [6]. http://www.st.com/internet/com/TECHNICAL_RESOURCES/TECHNICAL_LITERATURE/DATASHEET/CD00171682.
- [7]. Kanna, Ravikanath. *Design of Zigbee Transmitter Receiver IEEE 802.15.4 using Matlab/Simulink*. Masters Thesis, Rourkela, Odhisha: National Institute of Technology, 2011.
- [8]. mathworks. 2012. www.mathworks.com/help/toolbox/comm/ref/alignsignals.html (accessed March 5, 2012)

Thermal Analysis And Optimization Of I.C. Engine Piston Using finite Element Method

A. R. Bhagat¹, Y. M. Jibhakate²

¹M.Tech Student Heat Power Engineering, Mechanical Engineering Department, KITS College of Engineering Nagpur,
²Asso. Professor, Mechanical Engineering Department, KITS College of Engineering Nagpur, India.

Abstract: This paper describes the stress distribution of the seizure on piston four stroke engine by using FEA. The finite element analysis is performed by using computer aided design (CAD) software. The main objectives is to investigate and analyze the thermal stress distribution of piston at the real engine condition during combustion process. The paper describes the mesh optimization with using finite element analysis technique to predict the higher stress and critical region on the component. The optimization is carried out to reduce the stress concentration on the upper end of the piston i.e (piston head/crown and piston skirt and sleeve). With using computer aided design(CAD), Pro/ENGINEER software the structural model of a piston will be developed. Furthermore, the finite element analysis performed with using software ANSYS.

Keywords : Ansys, Piston crown, Piston skirt, ProE, stress concentration, Thermal analysis etc.

I. Introduction

A piston is a component of reciprocating IC-engines. It is the moving component that is contained by a cylinder and is made gas-tight by piston rings. In an engine, its purpose is to transfer force from expanding gas in the cylinder to the crankshaft via a piston rod and/or connecting rod. As an important part in an engine, piston endures the cyclic gas pressure and the inertial forces at work, and this working condition may cause the fatigue damage of piston, such as piston side wear, piston head/crown cracks and so on. The investigations indicate that the greatest stress appears on the upper end of the piston and stress concentration is one of the mainly reason for fatigue failure. On the other hand piston overheating-seizure can only occur when something burns or scrapes away the oil film that exists between the piston and the cylinder wall. Understanding this, it's not hard to see why oils with exceptionally high film strengths are very desirable. Good quality oils can provide a film that stands up to the most intense heat and the pressure loads of a modern high output engine. Thermal analysis is a branch of materials science where the properties of materials are studied as they change with temperature. FEM method are commonly used for thermal Analysis. Due to the complicated working environment for the piston; on one hand, the FEA for the piston became more difficult, on the other hand, though there have many methods which are put forward to apply optimal design, the optimal parameters is not easy to determine. In this study, the piston is used in low idle and rated speed gas engine. In order to enhance the engine dynamic and economic, it is necessary for the piston to implement optimization. The mathematical model of optimization is established firstly, and the FEA is carried out by using the ANSYS software. Based on the analysis of

optimal result, the stress concentrates on the upper end of piston has become evaluate, which provides a better reference for redesign of piston.

II. The Fea Of The Piston

2.1. Theoretical Foundation

In engine, transfer of heat takes place due to difference in temperature and from higher temperature to lower temperature. Thus, there is heat transfer to the gases during intakes stroke and the first part of the compression stroke, but the during combustion and expansion processes the heat transfer take place from the gases to the walls.

So the piston crown/head, piston ring and the piston skirt should have enough stiffness which can endure the pressure and the friction between contacting surfaces. In addition, as an important part in engine, the working condition of piston is directly related to the reliability and durability of engine. So it is important for the piston skirt and the piston ring to carry out structural and optimal analysis which can provide reference for design of piston.

So the mean effective pressure on the piston crown, piston top ring and the piston skirt should be restricted at low idle (850rpm) and at rated speed (2700rpm). The formula can be expressed as,

$$IHP = \frac{P_m \times L \times A \times N/2}{60 \times 10^3} \dots\dots\dots (1)$$

Where,

- P_m Mean Effective Pressure (bar) ;
- L- stroke length(mm) ; A –Area(mm²) ;
- N-speed (rpm) ;
- IHP- indicated horse power (watt)

Thus for low idle speed (850RPM) P_m=74.18 bar and for rated speed (2700RPM) P_m= 23.33bar So, Calculation purpose Mean Effective Pressure, P_m = 23.33 bar taken.

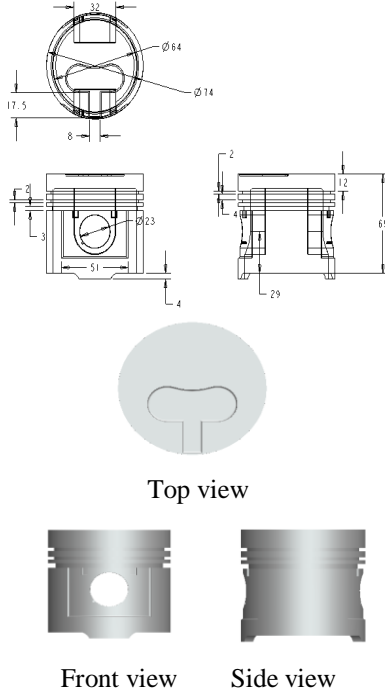
2.2. The Finite Element Analysis

In this work, due to the symmetry of structure, model of piston has been made in the Pro/E software, and then the FEM is established using ANSYS software. The 3-D 20-node solid element SOLID95 is applied to mesh the whole structure, and 27374 nodes and 14129 elements are obtained. In addition, in order to obtain the better result, the contact pair which is important to carry out the research should be established between the piston crown, piston ring and piston skirt. The contact is highly non-linear and need more computing power. In order to compute effectively, it is important to know the physical property and establish the reasonable model. In this study, the surface-surface contact is applied to the model. The FEA of piston is carried out by using the ANSYS software. The equivalent stress and the deformation of the piston are obtained respectively, as shown in the Fig. (1 and 2). As shown in the Fig., the maximum stress appears at the centre and at edge of piston

sleeve and the value of the stress is 228N/mm². As shown in the Fig. (1), the maximum deformation occurs on piston and the value of deformation is 0.760mm. The analysis of contact is carried out by using ANSYS workbench software, and the result is shown in the Figures It is correspond with the truth.

III. Piston Design

The design data for designing of I.C engine Piston with the help of pro-E is collected from TATA MOTORS for Diesel engine vehicle.



IV. Thermal Analysis Of Piston Using Fea Approach

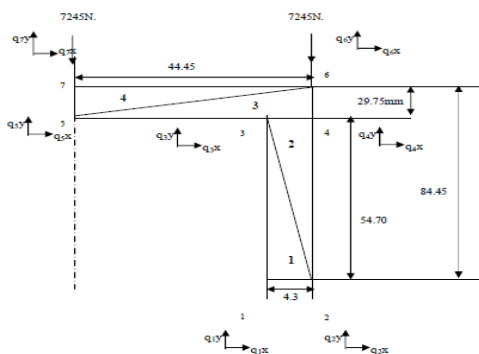


Figure 9.1: Piston Design

$E = 72.5 \times 10^3 \text{ N/mm}^2$
 $\mu = 0.334$

4.1 Force Vector Matrix, F Radius of Centroid,

$$r_1 = \frac{(x_1 + x_2 + x_3)}{3}$$

$$r_1 = \frac{(40.15 + 44.15 + 40.15)}{3}$$

$r_1 = 41.583 \text{ mm}$

and

$|J_1| = 235.21$

$A_1 = \frac{|J_1|}{2} = 117.5 \text{ mm}^2$

Strain Displacement Matrix, B₁

$B_1 = \frac{1}{|J_1|}$

Material Property Matrix, D₁

$D_1 = \frac{E(1-\mu)}{(1+\mu)(1-2\mu)}$

Stiffness Matrix K₁

$K_1 = t_1 \times A_1 \times B T_1 \times D_1 \times B_1$

$K_1 = (2 \times \pi \times r_1) \times A_1 \times B T_1 \times D_1 \times B_1$

Material Property Matrix, D₁=D₂=D₃=D₄

Similarly for element 2,3,4. Force Vector Matrix, F Piston is treated as Axis-symmetrical object about the centre axis of the piston q_{1x},q_{1y}, q_{2x},q_{2y}, q_{3x},q_{3y}, q_{4x},q_{4y}, q_{5x},q_{5y}, q_{6x},q_{6y}, q_{7x},q_{7y} are the nodes position from 1 to 7 along x and y directions. Each 7245 N force acting vertical down word at node no 6 and node no 7 respectively.

4.2 Temperature load Vector Matrix,

$\theta_1 = 1 = 2 \times \pi \times r_1 \times A_1 \times B T_1 \times D_1 \times \epsilon_{01}$

$\alpha_{All} = 23 \times 10^{-6} \text{ W/}^\circ\text{C}$

$\Delta T = \text{Element Temp} - \text{Room Temp} = 150 - 40 = 110^\circ\text{C}$

Similarly for element 2,3,4.

Global Temperature Load Vector Matrix

$\theta^G = 1 \times 10^6 [\theta]_{1 \times 14}$

Assembled Global Force Vector Matrix, FG=F+ θ^G

$[F^G]_{14 \times 1} = [K^G]_{14 \times 14} = [U]_{14 \times 1}$

Where ‘U’ is Displacement Matrix. By solving the above equations, we get, displacement at various nodes.

Nodes	Analytical values of deformation	Ansys values of deformation
U2X	0.0216	0.805
U4X	0.0538	0.785
U6X	0.4241	0.760
U6Y	0.4366	0.724
U7X	-0.0024	0.077
U7Y	0.4198	0.434

V. Optimization Analysis With Steel

Modern engines with variable valve train or different direct injection concepts require pistons with complex crown shapes which would often lead to a higher piston weight. Therefore in every new piston development, the piston geometry is optimized in particular in the ring belt/piston skirt area. Intensive application of numerical simulation methods enables significant weight reductions while increasing at the same time the load-bearing capacity. Newly developed alloys with better castability, but also higher fatigue resistance in the critical temperature and stress region, allow the realization of thinner wall structures. Improved casting methods enable large recesses for the ring belt and hence a considerable reduction in the piston weight. But also the use of steel pistons in i. c engines is discussed again and again. The advantages of steel pistons such as reduced installation clearances, low fuel consumption figures and long service life would have to be evaluated against customer demands such as low emission levels,

lightweight, efficient cooling and a competitive price. But up to now, there are no definite indications that steel pistons would be a viable concept for mass production. The analysis is done in ANSYS Workbench for two materials aluminium alloy which is existing material and suggested material with different material properties. Following result are obtained as shown in figure.

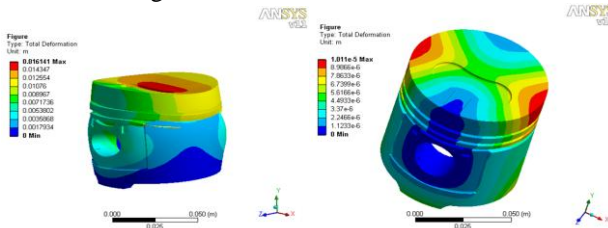


Figure1: Comparison between total deformation

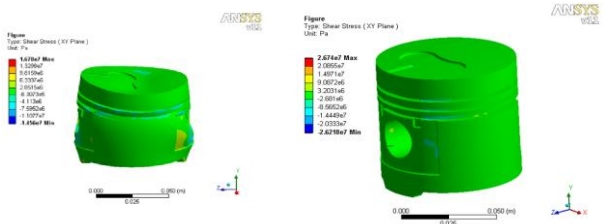


Figure2: Comparison between Shear Stress

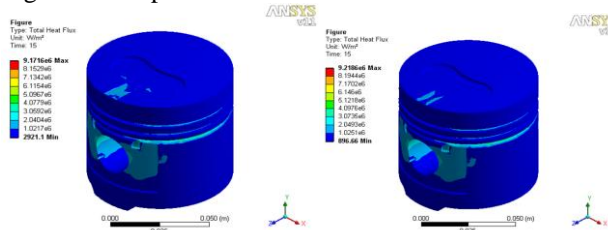


Figure3: Comparison between total heat flux

VI. Conclusion

Piston skirt may appear deformation at work, which usually causes crack on the upper end of piston head. Due to the deformation, the greatest stress concentration is caused on the upper end of piston, the situation becomes more serious when the stiffness of the piston is not enough, and the crack generally appeared at the point A which may gradually extend and even cause splitting along the piston vertical. The stress distribution on the piston mainly depends on the deformation of piston. Therefore, in order to reduce the stress concentration, the piston crown should have enough stiffness to reduce the deformation.

1. The optimal mathematical model which includes deformation of piston crown and quality of piston and piston skirt.
2. The FEA is carried out for standard piston model used in diesel engine and the result of analysis indicate that the maximum stress has changed from 228 Mpa. To 89 Mpa. And biggest deformation has been reduced from 0.419 mm to 0.434 mm.

References

- [1] Richard Mittler and Albin Mierbach, "Proceedings of the ASME Internal Combustion Engine Division 2009 Spring Technical Conference", ICES2009 May 3-6, 2009, Milwaukee, Wisconsin, USA.

- [2] P.Gustof, A.Hornik, "International Journal of Achievements in Materials and Manufacturing Engineering", Vol. 35 Issue 2 August 2009.
- [3] Tulus, Ariffin, A. K., Abdullah, S. and Muhamad. N. "Proceedings of the 2nd IMT-GT Regional Conference Of Mathematics, Statistics And Applications University Sains Malaysia", June 13-15, 2006.
- [4] Sanjay Shrivastva, Kamal Shrivastava, Rahul S. Sharma and K Hans Raj, "Journal of scientific & Industrial Research", vol .63, December 2004, pp 997-1005.
- [5] Gunter Knoll, Adrian Rienäcker, Jochen Lang, "Lehrstuhl für Maschinenelemente und Tribologie Universität Gh Kassel Germany", McGraw-Hill Book Company, p. 700 f.
- [6] Thet T. Mon, Rizalman Mamat, Nazri Kamsah, Member, IAENG, " Proceedings of the World Congress on Engineering 2011 Vol III WCE 2011, July 6 - 8, 2011, London, U.K.
- [7] E. Abu-Nada, I. Al-Hinti, A. Al-Sarkhi, B. Akash "Department of Mechanical Engineering, Hashemite University, Zarqa 13115, Jordan", Institution of Mechanical Engineers, London, pp. 133–145.
- [8] Ashwinkumar S. Dhoble, R. P. Sharma, "R& D Centre, Mahindra & Mahindra Ltd., Nashik", SAE Paper 930797 (1993).

Design of High Throughput DCT Core Design by Efficient Computation Mechanism

Susrutha Babu Sukhavasi¹, Suparshya Babu Sukhavasi¹
O. Ranga Rao², Sr. Sastry K.², G. Roopa Krishna Chandra²

¹Faculty, Department of ECE, K L University, Guntur, AP, India.

² Faculty, Department of ECE, Andhra Loyola College Of Eng &Tech, Vijayawada, AP, India.

Abstract : This paper presents an approach towards VLSI implementation of the Discrete cosine Transform for image compression. Modules required for the corresponding circuit. The design follows the JPEG standard and can be used for both lossy and lossless compression. In Discrete cosine transform, the filter implementation plays the key role. The poly phase structure is proposed for the filter implementation, which uses the Distributive Arithmetic (DA) technique. The implementation of DA based DCT IP core in ASIC (Application Specific Integrated Circuit). Which is popular in FPGA (Field Programmable Gate Array) implementations. To exploit the available resources on FPGAs, a new technique, which incorporates pipelining and parallel processing of the input samples, is proposed, with this architecture the speed (throughput) of the design increases. The intermediate coefficients obtained are efficiently stored in a memory and accessed for efficient memory utilization on FPGAs. The design is targeted on Xilinx spartan3, and the ASIC design of the same is carried out.

Keywords: DCT, Distributed Arithmetic.

I. Introduction

Recently, multimedia applications are used widely in many embedded and portable systems, such as mobile phones, MP3 player and PDA, which require area efficient within high performance constraints. Therefore, area efficient design becomes a more important objective in Very Large Scale Integration (VLSI) designs. Moreover; the multiplication unit always lies on the critical path and ultimately determines the performance and area efficient of arithmetic computing systems. To achieve high-performance and lengthen the battery lifetime, it is crucial to develop a compression with high-speed. In multimedia and digital signal processing (DSP) applications, many area efficient approaches have been presented. An efficient technique for calculation of sum of products or vector dot product or inner product or multiply and accumulate (MAC) MAC operation is very common in all Digital Signal Processing hardware designs. In a constant word length multiplier, the extra bits in the partial sums as well as the final product are truncated and no of binary adders required for accumulating 2 partial products equal to the wordlength W. This causes truncation errors whose value not only depend on multiplicand and multiplier but also on arrangement of partial product accumulation. In general, the truncation part (TP) is usually truncated to reduce hardware costs in parallel shifting and addition operations, known as the direct truncation (Direct-T) method. Thus, a large truncation error occurs due to the neglecting of carry

propagation from the TP to Main Part (MP). Distributed arithmetic is a bit level rearrangement of a multiply accumulate to hide the multiplications. It is a powerful technique for reducing the size of a parallel hardware multiply-accumulate that is well suited to FPGA designs. It can also be extended to other sum functions such as complex multiplies, fourier transforms and so on. Look at my Radar on a chip paper for an application example of distributed arithmetic. In most of the multiply accumulate applications in signal processing, one of the multiplicands for each product is a constant. Usually each multiplication uses a different constant. Using our most compact multiplier, the scaling accumulator, we can construct a multiple product term parallel multiply-accumulate function in a relatively small space if we are willing to accept a serial input. In this case, we feed four parallel scaling accumulators with unique serialized data. Each multiplies that data by a possibly unique constant, and the resulting products are summed in an adder tree. If we stop to consider that the scaling accumulator multiplier is really just a sum of vectors, then it becomes obvious that we can rearrange the circuit. Here, the adder tree combines the 1 bit partial products before they are accumulated by the scaling accumulator. All we have done is rearranged the order in which the 1xN partial products are summed. Now instead of individually accumulating each partial product and then summing the results, we postpone the accumulate function until after we've summed all the 1xN partials at a particular bit time. This simple rearrangement of the order of the adds has effectively replaced N multiplies followed by an N input add with a series of N input adds followed by a multiply. This arithmetic manipulation directly eliminates N-1 Adders in an N product term multiply-accumulate function. For larger numbers of product terms, the savings becomes significant. Further hardware savings are available when the coefficients C_n are constants. If that is true, then the adder tree shown above becomes a Boolean logic function of the 4 serial inputs. The combined 1xN products and adder tree is reduced to a four input look up table. The sixteen entries in the table are sums of the constant coefficients for all the possible serial input combinations. The table is made wide enough to accommodate the largest sum without overflow. Negative table values are sign extended to the width of the table, and the input to the scaling accumulator should be sign extended to maintain negative sums. Obviously the serial inputs limit the performance of such a circuit. As with most hardware applications, we can obtain more performance by using more hardware. In this case, more than one bit sum can be computed at a time by duplicating the LUT and adder tree as shown here. The second bit computed will have a different weight than the first, so some shifting is required

before the bit sums are combined. In this 2 bit at a time implementation, the odd bits are fed to one LUT and adder tree, while the even bits are simultaneously fed to an identical tree. The odd bit partials are left shifted to properly weight the result and added to the even partials before accumulating the aggregate. Since two bits are taken at a time, the scaling accumulator has to shift the feedback by 2 places. This paralleling scheme can be extended to compute more than two bits at a time. In the extreme case, all input bits can be computed in parallel and then combined in a shifting adder tree. No scaling accumulator is needed in this case, since the output from the adder tree is the entire sum of products. This fully parallel implementation has a data rate that matches the serial clock, which can be greater than 100 MS/S in today's FPGAs. The Discrete cosine transform (DCT) is widely used in digital image processing, especially in image transform coding, as it performs much like the optimal Karhunen-Loeve transform (KLT) under a variety of criteria. Many algorithms for the computation of the DCT have been proposed since the introduction of the DCT by Ahmed, Natarajan, and Rao in 1974. However, though most of them are good software solutions to the realization of DCT, only a few of them are really suitable for VLSI implementation. Cyclic convolution plays an important role in digital signal processing due to its nature of easy implementation. Specifically, there exists a number of well-developed convolution algorithms and it can be easily realized through modular and structural hardware such as distributed arithmetic and systolic array. The way of data movement forms a significant part in the determination of the efficiency of the realization of a transform using the distributed arithmetic. The realization of a cyclic convolution with the distributed arithmetic requires only simple table look-up technique and some simple rotations of the corresponding data set. Hence, the cyclic convolution structure can be considered as the simplest form that is most suitable to be realized with the distributed arithmetic. It is because of this reason, one may consider that the basic criterion for the realization of a transform using the distributed arithmetic relies on the possibility of having an efficient way to convert the transform into the cyclic convolution form. If we could be able to convert a transform into the cyclic convolution form with the minimum number of operations, it would imply an optimal approach for the realization of the transform using the distributed arithmetic. Some basic formulations have been suggested for the realization of the DCT using the distributed arithmetic. In their formulations, they either still required some extra multiplications for their formulations or have to use cyclic convolutions of different lengths. The former case has the major problem that it violates the major advantage of the distributed arithmetic which replaces multiplications by additions. The latter case requires relatively complicated circuitry to allow the realization of cyclic convolutions of variable lengths. Different from the above approaches, one may also convert the DCT into the Discrete Fourier Transform (DFT) and make use of the famous algorithms to convert the corresponding DFT into cyclic convolution form. Indeed, this is a possible approach; however, it turns a real transform into a transform with complex numbers. The realization could still be complicated even if some simplification techniques are to be applied.

The field of computer science is growing at the fastest pace since it started back in the early 20th century. We didn't have the actual computing machines until the mid of the 20th century but the algorithms for computing were already being developed from the beginning of the century. The advancement of the computing field has affected every imaginable field in the human lives. These fields include engineering, medicine, geology, meteorology, movies, and pictures etc. The high speed of digital computer has contributed to significant progress in the field of optics. Image processing by far has benefited significantly from the high speed digital computers. Since the day the very first successful picture was taken in June of 1827, the quality and style of images have improved significantly. Niepce took this picture by using material that hardened on exposure to light. There were many different ways to taking these images before the camera that we know today was created. The main problem with all of the images taken was the fact that with every picture that was taken a lot of redundant and useless information was also stored. The problems range from faded, blurry and noisy pictures. All these useless data stored with the images is termed as Noise. Noise, in technical terms is defined as the irrelevant or meaningless data. Image restoration is one of the many branches of image processing. It is defined as a process that removes all the noise and irrelevant data from the images to make them clearer and better visible. The tools and techniques used in image processing are imported from signal processing. The main difference, however, between signal processing and image processing is that when binary data is compressed, it is essential that we get the same data back when it is decompressed. With the images, on the other hand, it is not required. When an image is decompressed it is in most cases enough to get a replica of the image as long as the mean square error is within certain set limits and tolerable. As mentioned above, there are a number of factors that can adversely affect the image quality. There have been a number of techniques introduced and being researched to enhance the image as well as to improve the usefulness of the data. Enhancement programs make the information more visible. One of the most popular enhancement techniques is the Histogram equalization. This technique redistributes the intensities of the image equally to the entire gray level range of the image. Convolution is an image processing technique which is essentially a sequence mask operating on pixel neighborhood. Convolution involves High Pass and Low pass filters. Other image processing techniques include noise filters, trend removing filters, edge detection, and image analysis tools etc. One of the important aspects of image processing is the reduction of the coded description of the image while keeping all the pertinent information. Data compression methods with zero information loss have been used on image data for some time. GIF, JPEG, MPEG etc are all examples of the tools used for data compression without the loss of the information. There are various techniques used these days to capture and store the images in a compressed format to reduce their storage sizes and use a smaller space. There are basically two categories of compression techniques; lossless and lossy. The main difference between these two categories is that in lossy compression the quality of the image is reduced in order to achieve higher compression ratio. On the other hand, in a lossless

compression the quality of the image is given a higher preference than the compression ratio. So it can be said that there is an apparent trade off between quality of the image and the compression ratio whenever we talk about the image compression. Lossy techniques include Transform Coding such as DCT, Wavelets and Gabor, Vector quantization, Segmentation and Approximation methods, Spline approximation methods i.e. Bilinear Interpolation/Regularization, Fractal coding which includes Texture synthesis, Iterative functions systems (IFS) and Recursive iterative functions systems (RIFS). Lossless compression techniques, on the other hand, includes Run length Encoding, Huffman Encoding, Entropy Coding (Lempel/Ziv) and Area coding . Discrete cosine transform (DCT) has become the most popular technique for image compression over the past several years. One of the major reasons for its popularity is its selection as the standard for JPEG. DCTs are most commonly used for non-analytical applications such as image processing and signal-processing DSP applications such as video conferencing, fax systems, video disks, and HDTV. DCTs can be used on a matrix of practically any dimension. Mapping an image space into a frequency space is the most common use of DCTs. For example, video is usually processed for compression/decompression as 8 x 8 blocks of pixels. Large and small features in a video picture are represented by low and high frequencies. An advantage of the DCT process is that image features do not normally change quickly, so many DCT coefficients are either zero or very small and require less data during compression algorithms. DCTs are fast and, like FFTs, require calculation of coefficients. The entire standards employ block based DCT coding to give a higher compression ratio. Various different techniques and algorithms employed for DCT will be discussed in detail in section 3 where DCT will be explored. As the topic of my thesis suggests, I will be exploring the possibilities of discrete cosine transforms for multi-resolution analysis. The aim here is to see if we can get the same results in compression using DCT as we can get by using the wavelets. The word multi-resolution refers to the simultaneous presence of different resolutions. The notion of multi-resolution was introduced by Mallat and Meyer in the years 1988-89. Multi-resolution analysis provides a convenient framework for developing the analysis and synthesis filters . DCTs have been in used for compression for quite some time and have been very popular. As I mentioned earlier the main reason for DCTs popularity is the fact that it's been used as a standard in JPEGs. Wavelets are considered better than DCT when it comes to getting better results in compression. The supporters of MPEGs and JPEGs claim that DCT provides very good results as far as the compression is concerned. If this claim is in fact true then the question is that why are so many people interested in Internet protocol streaming. The reason IP streaming is really good that there are algorithms that provide a lot more compression with the same video quality as MPEG-2 does. We can take a wavelet algorithm and keep the same video quality and use 1 Mbps for a very nice high quality movie that would take us 3 Mbps with normal MPEGs with DCT . The previous paragraph is good argument for choosing wavelets over DCT, however, the previous paragraph has been erroneous in the sense that researches use DCT and JPEG interchangeably. The arguments made in previous

paragraph against DCT are in fact against the standard JPEG and not DCT. JPEG uses just a small part of DCT and should not be taken as standard DCT algorithms in comparisons with wavelet. The basic difference between DCT and wavelets is that in wavelets rather than creating 8 X 8 blocks to compress, wavelets decompose the original signal into sub-bands. Wavelets are basically an optimizing algorithm for 5 representing a lot of change in the pictures. With DCT algorithm, the 8 X 8 blocks can lose their crisp edges, whereas, with wavelets the edges are very well defined. I don't really want to go in detail with the differences between wavelets and DCT but I just want to mention it to prove my case for the proposal of DCT for multi-resolution analysis. There is another compression method being developed call Fractals which is based on quadratic equations. This method is very well suitable with images which have patterns or a lot of repetitions. Now, if the wavelets produce much better results than DCT then why do we need to try DCT for multi-resolution? The reason is that there are certain drawbacks to wavelets specially in terms of computation time required. For the highest compression rates, it takes a longer time to encode. The other reason is that MPEG is already a standard using DCTs and computer hardware comes with MPEGs built in. There is hardly any hardware available in the market these days which comes with wavelets as a built in standard.

II. METHODOLOGIES

It is the process of analyzing the design of Discrete Cosine Transform (DCT) core with Error Compensated Adder Tree based on distributed arithmetic. An efficient technique for calculation of sum of products or vector dot product or inner product or multiply and accumulate (MAC) MAC operation is very common in all Digital Signal Processing hardware designs. An old technique that has been revived by the wide spread use of Field Programmable Gate Arrays (FPGAs) for Digital Signal Processing (DSP). DA efficiently implements the MAC using basic building blocks (Look Up Tables) in FPGAs .The "basic" DA technique is bit-serial in nature. DA is basically a bit-level rearrangement of the multiply and accumulate operation DA hides the explicit multiplications by without ROM look-ups an efficient technique to implement on Field Programmable Gate Arrays (FPGAs). The speed in the critical path is limited by the width of the carry propagation Speed can be improved upon by using techniques to limit the carry propagation. An increasing number of services and the growing popularity of high definition TV require higher coding efficiency. As the ongoing demand increases, for better compression performance of the latest video coding standard, the H.264/AVC (Advanced Video Coding) is formulated .The H.264/AVC is also known as MPEG-4 Part 10 (Wiegand,et al., 2003;Sullivan,et al.,2004; Richardson, 2003).An advantage of the H.264/AVC is the simplicity of its transform. Distributed Arithmetic (DA) is an effective method for computing inner products when one of the input vectors is fixed. It uses pre computed look-up tables and accumulators instead of multipliers for calculating inner products and has been widely used in many DSP applications such as DFT, DCT, convolution, and digital filters. In particular, there has been great interest in implementing DCT with parallel distributed arithmetic and

in reducing the ROM size required in the implementations since the DA-based DCT architectures are known to have very regular structures suitable for VLSI implementations. Most DA-based DCT implementations use the original DCT algorithm, or the even-odd frequency decomposition of the DCT algorithm along with some memory reduction techniques such as the partial sum technique and/or the offset binary coding technique. On the other hand, the proposed architecture uses the DA-based DCT algorithm and requires less area than the conventional approaches, regardless of the memory reduction techniques employed in the ROM Accumulators (RACs).

MAIN MODULE'S:

- ERROR COMPENSATION CIRCUIT
- ERROR COMPENSATED ADDER TREE
- 1-D 8-POINT DCT DESIGN

III. MODULE DESCRIPTION:

Error Compensated Circuit:

Multipliers are commonly used components in digital signal processing applications (DSP). The multiplier produces $2n$ -bit output for n bit multiplicand and n bit multiplier input. But for some applications we may only require n bit multiplicand result. We can truncate n least-significant bits and preserve the m most significant bit. Although doing this would cause significant errors the area will be reduced half. To reduce truncation error we propose error compensation methods. In some applications these error could be ignored. The output will obtain MSBs using a rounding operation called post truncation (Post-T), which is used for high-accuracy applications. Hardware cost increases in the VLSI design. In general, the TP is usually truncated to reduce hardware costs in parallel shifting and addition operations, known as the direct truncation (Direct-T) method. Thus, a large truncation error occurs due to the neglecting of carry propagation from the TP to MP.

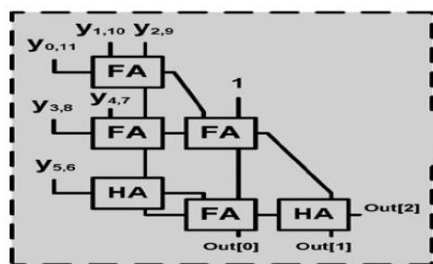


Fig 1: Error Compensation Circuit

In order to alleviate the truncation error effect, several error compensation bias methods have been presented.

All previous works were only applied in the design of a fixed-width multiplier. Because the products in a multiplier have a relationship between the input multiplier and multiplicand, the compensation methods usually use the correlation of inputs to calculate a fixed or an adaptive compensation bias using simulation or statistical analysis. The internal word-length usually uses 12 bits in a DCT design. Consequently, word length $P=12$ is chosen together with different Q values of 3, 6, 9 and 12. The Post-T method provides the most accurate values for fixed-width computation nowadays. In addition, the Direct-T method

has the largest inaccuracies of the errors for low-cost hardware design. The proposed ECAT is more accurate than Direct-T and is close to the performance of the Post-T method using a compensated circuit.

SUB MODULES'S

- HALF ADDER
- FULL ADDER
- ADDITION ELEMENTS

ERROR COMPENSATED ADDER TREE:

In this module consists of error compensated circuit, adder circuit, sign extension, zero extension. FA indicates a full-adder cell with three inputs (a , b , and c) and two outputs, a sum (s) and a carry-out (co). HA indicates half-adder cell with two inputs (a and b) and two outputs, a sum (s) and a carry-out (co). ECAT has the highest accuracy with a moderate area delay product. The shift-and-add method has the smallest area, but the overall computation time is longest. ECAT is suitable for high-speed and low-error applications. authorized doctors can login into the medical. Here also all the details about the doctor are registered by the medical admin. And the medical admin give the authentication details to the particular doctor after getting the authentication details doctor can login to the medical and can start the below processes.

SUBMODULES:

- ERROR COMPENSATED CIRCUIT
- PARTIAL PRODUCT GENERATION

ERROR COMPENSATED CIRCUIT

In this module the shifting and addition computation uses a shift-and-add operator in VLSI implementation in order to reduce hardware cost. However, when the number of the shifting and addition words increases, the computation time will also increase. Therefore, the shift-adder-tree (SAT) presented in operates shifting and addition in parallel by unrolling all the words needed to be computed for high-speed applications. The Q P -bit words operate the shifting and addition in parallel can be divided into two parts: the main part (MP) that includes P most significant bits (MSBs) and the truncation part (TP) that has least significant bits (LSBs).

PARTIAL PRODUCT GENERATION

In this module A truncated multiplier is an $m \times n$ multiplier with m bits output. Partial products can be divided into two subsets. The least significant part (LSP) includes the n less significant columns of the partial product matrix, while the most significant part (MSP) includes the remaining columns. The full-width multiplier output, P is given by $P = SMSP + SLSP$. Where $SMSP$ and $SLSP$ represent the weighted sum of the elements of MSP and LSP respectively. When a n bits output is needed, the most accurate choice is using the full rounded multiplier: it computes all the matrix of partial products, add a constant to the result on $2n$ bits and takes only the first n bits of the sum. The error introduced by the full rounded multiplier is calculated. Unfortunately the full rounded multiplier is the solution with the highest area occupation and power dissipation. A second possibility is using a truncated multiplier in which the partial products of the LSP are

discarded assuming that their contribution to the n most significant bits of the output is negligible. This solution is very advantageous in terms of hardware performances.

the reputation of being a very effective signal analysis tool for many practical applications.

IV. D 8 POINT DCT:

Image data compression has been an active research area for image processing over the last decade and has been used in a variety of applications. This paper investigates the implementation of an image data compression method with VLSI hardware that could be used in practical coding systems to compress JPEG signals. In practical situations, an image is originally defined over a large matrix of picture elements (pixels), with each pixel represented by a 8- or 16-bit gray scale value. This representation could be so large that it is difficult to store or transmit. The purpose of image compression is to reduce the size of the representation and, at the same time, to keep most of the information contained in the original image . DCT based coding and decoding systems play a dominant role in real-time applications. However, the DCT is computationally intensive. In addition, 2D-DCT has been recommended by standard organizations the Joint Photographic Expert Group (JPEG). The standards developed by these groups aid industry manufacturers in developing real-time 2D-DCT chips for use in various image transmission and storage systems. Generally there is a higher degree of correlation between the intensity values of adjacent pixels of an image. image compression can be achieved by removing such a redundant information. The discrete cosine transform (DCT) is widely used in most applications for compression of digital image and video signals. After performing the DCT operation on image or video signals most of energy is found to be concentrated in low frequency region. Recently hardware implementation of video coding standards fall into three main design categories :

1. Video signal processors,
2. Multimedia coprocessors,
3. Dedicated coders and decoders.

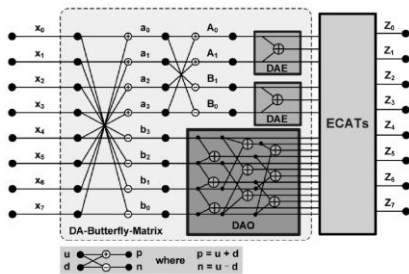


Fig 2: Architecture Of The Proposed 1-D 8-Point DCT

Video signal processors are programmable processors with a digital processing core or reduced instruction set computer core and co-processing unit for compute intensive operations such as motion estimation. Multimedia coprocessors are also programmable. The computation of DCT is on eof process of transforming a block of data from the spatial domain to frequency domain. Inverse process of restoring the spatial domain data from frequency domain is carried out through Inverse DCT (IDCT).The Discrete Cosine Transform (DCT) has gained

DISTRIBUTED ARITHMETIC

Distributed arithmetic is a bit level rearrangement of a multiply accumulate to hide the multiplications. It is a powerful technique for reducing the size of a parallel hardware multiply-accumulate that is well suited to FPGA designs. It can also be extended to other sum functions such as complex multiplies, Fourier transforms and so on. Look at my Radar on a chip paper for an application example of distributed arithmetic. In most of the multiply accumulate applications in signal processing, one of the multiplicands for each product is a constant. Usually each multiplication uses a different constant. Using our most compact multiplier, the scaling accumulator, we can construct a multiple product term parallel multiply-accumulate function in a relatively small space if we are willing to accept a serial input. In this case, we feed four parallel scaling accumulators with unique serialized data.

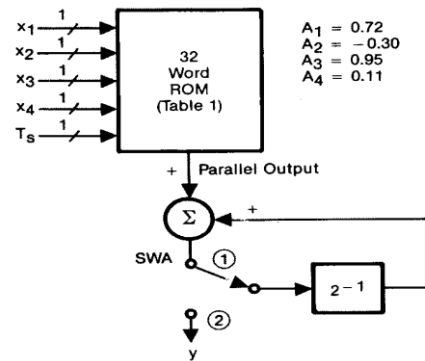


Fig 3: Distributed Arithmetic

Each multiplies that data by a possibly unique constant, and the resulting products are summed in an adder tree .If we stop to consider that the scaling accumulator multiplier is really just a sum of vectors, then it becomes obvious that we can rearrange the circuit. Here, the adder tree combines the 1 bit partial products before they are accumulated by the scaling accumulator. All we have done is rearranged the order in which the 1xN partial products are summed. Now instead of individually accumulating each partial product and then summing the results, we postpone the accumulate function until after we've summed all the 1xN partials at a particular bit time. This simple rearrangement of the order of the adds has effectively replaced N multiplies followed by an N input add with a series of N input adds followed by a multiply. This arithmetic manipulation directly eliminates N-1 Adders in an N product term multiply-accumulate function. For larger numbers of product terms, the savings becomes significant. Further hardware savings are available when the coefficients C_n are constants. If that is true, then the adder tree shown above becomes a Boolean logic function of the 4 serial inputs. The combined 1xN products and adder tree is reduced to a four input look up table. The sixteen entries in the table are sums of the constant coefficients for all the possible serial input combinations. The table is made wide enough to accommodate the largest sum without overflow. Negative table values are sign extended to the width of the table, and the input to the scaling accumulator should be

sign extended to maintain negative sums. Obviously the serial inputs limit the performance of such a circuit. As with most hardware applications, we can obtain more performance by using more hardware. In this case, more than one bit sum can be computed at a time by duplicating the LUT and adder tree as shown here. The second bit computed will have a different weight than the first, so some shifting is required before the bit sums are combined.

DISTRIBUTED ARITHMETIC OPERATION

In this 2 bit at a time implementation, the odd bits are fed to one LUT and adder tree, while the even bits are simultaneously fed to an identical tree. The odd bit partials are left shifted to properly weight the result and added to the even partials before accumulating the aggregate. Since two bits are taken at a time, the scaling accumulator has to shift the feedback by 2 places This paralleling scheme can be extended to compute more than two bits at a time.

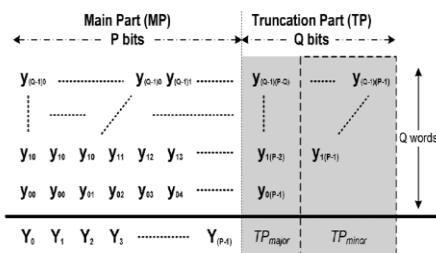


FIG 4: Q , P-bit words shifting and addition operations in parallel

In the extreme case, all input bits can be computed in parallel and then combined in a shifting adder tree. No scaling accumulator is needed in this case, since the output from the adder tree is the entire sum of products. This fully parallel implementation has a data rate that matches the serial clock, which can be greater than 100 MS/S in today's FPGAs. Most often, we have more than 4 product terms to accumulate. Increasing the size of the LUT might look attractive until you consider that the LUT size grows exponentially. Considering the construction of the logic we stuffed into the LUT, it becomes obvious that we can combine the results from the LUTs in an adder tree. The area of the circuit grows by roughly 2n-1 using adder trees to expand it rather than the 2ⁿ growth experienced by increasing LUT size. For FPGAs, the most efficient use of the logic occurs when we use the natural LUT size (usually a 4-LUT, although and 8-LUT would make sense if we were using an 8 input block RAM) for the LUTs and then add the outputs of the LUTs together in an adder tree. The Discrete cosine transform (DCT) is widely used in digital image processing, especially in image transform coding, as it performs much like the optimal Karhunen-Loeve transform (KLT) under a variety of criteria. Many algorithms for the computation of the DCT have been proposed since the introduction of the DCT by Ahmed, Natarajan, and Rao in 1974. However, though most of them are good software solutions to the realization of DCT, only a few of them are really suitable for VLSI implementation. Cyclic convolution plays an important role in digital signal processing due to its nature of easy implementation. Specifically, there exists a number of well-developed convolution algorithms and it can be easily realized through modular and structural hardware such as

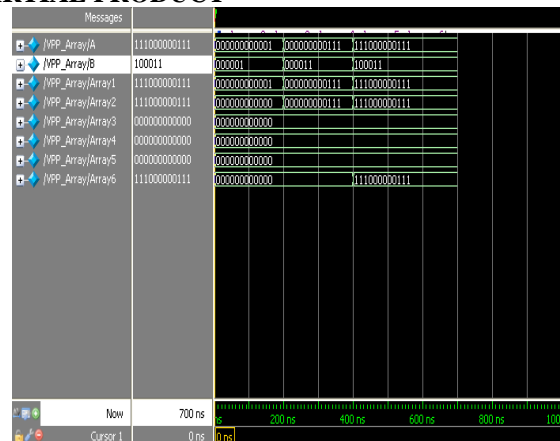
distributed arithmetic and systolic array . The way of data movement forms a significant part in the determination of the efficiency of the realization of a transform using the distributed arithmetic. The realization of a cyclic convolution with the distributed arithmetic requires only simple table look-up technique and some simple rotations of the corresponding data set. Hence, the cyclic convolution structure can be considered as the simplest form that is most suitable to be realized with the distributed arithmetic. It is because of this reason, one may consider that the basic criterion for the realization of a transform using the distributed arithmetic relies on the possibility of having an efficient way to convert the transform into the cyclic convolution form. If we could be able to convert a transform into the cyclic convolution form with the minimum number of operations, it would imply an optimal approach for the realization of the transform using the distributed arithmetic. Some basic formulations have been suggested for the realization of the DCT using the distributed arithmetic. In their formulations, they either still required some extra multiplications for their formulations or have to use cyclic convolutions of different lengths . The former case has the major problem that it violates the major advantage of the distributed arithmetic which replaces multiplications by additions. The latter case requires relatively complicated circuitry to allow the realization of cyclic convolutions of variable lengths. Different from the above approaches, one may also convert the DCT into the Discrete Fourier Transform (DFT) and make use of the famous algorithms to convert the corresponding DFT into cyclic convolution form. Indeed, this is a possible approach; however, it turns a real transform into a transform with complex numbers. The realization could still be complicated even if some simplification techniques are to be applied.

APPLICATIONS

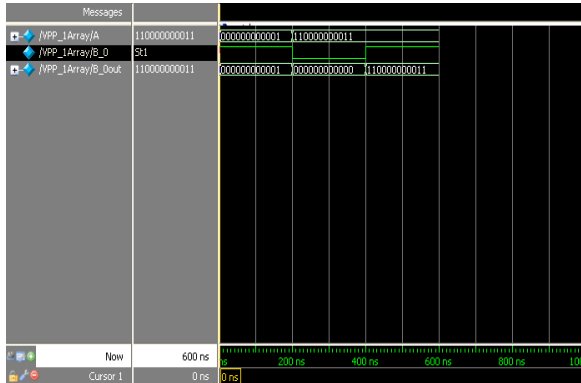
The DCT core can be utilized for a variety of multimedia applications including:

- Office automation equipment (Multifunction printers, digital copiers etc)
- Digital cameras & camcorders
- Video production, video conference
- Surveillance systems

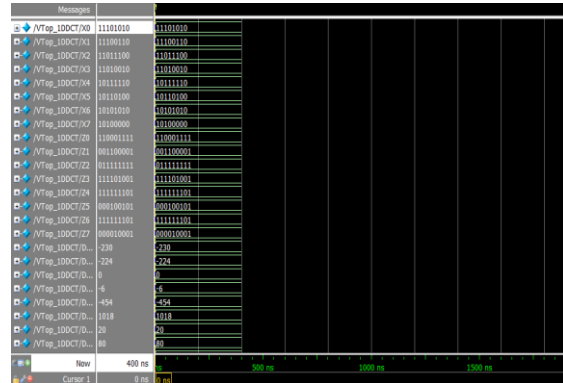
V. SIMULATION RESULTS PARTIAL PRODUCT



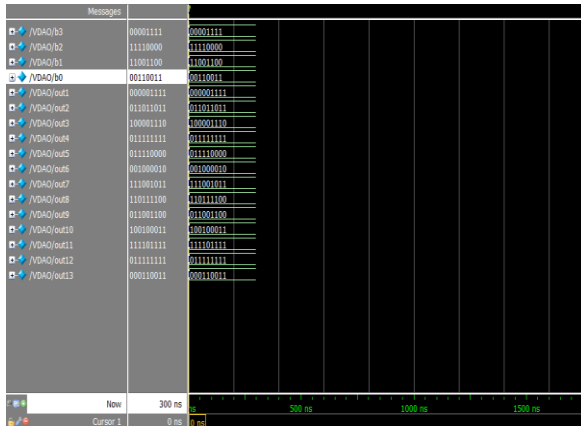
PARTIAL PRODUCT1



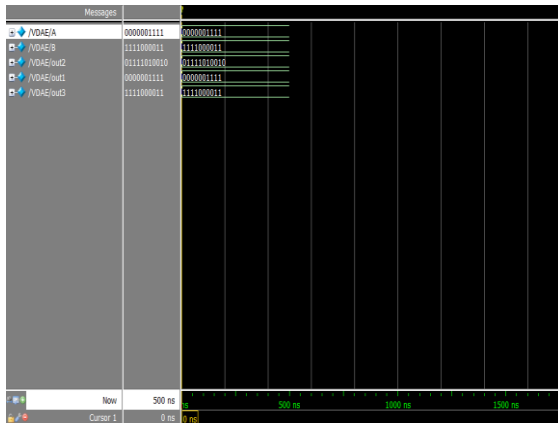
TOP MODULE



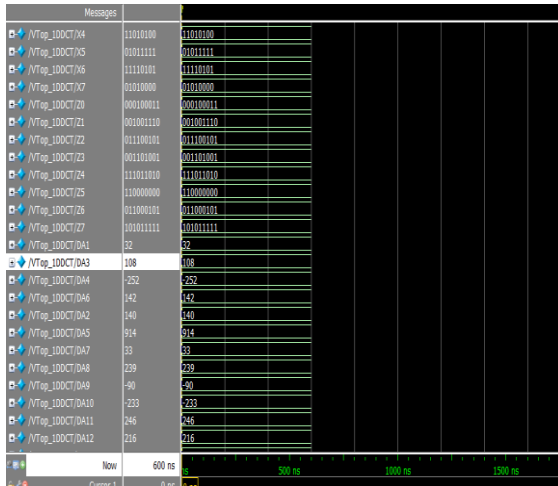
DAO



DAE



BUTTERFLY MATRIX



VI. CONCLUSIONS

This paper presents an FPGA implementation of efficient architecture for computing the 2-D DCT with distributed arithmetic. The proposed architecture requires less hardware than conventional architectures which use the original DCT algorithm or the even-odd frequency decomposition method. The modules of the transpose memory and parallel Distributed Arithmetic 2-D DCT architecture were designed and synthesized. The paper contributed with specific simplifications in the multiplier stage, by using shift and adds method, which lead to hardware simplification and speed up over architecture.

REFERENCES

- [1]. A. M. Shams, a. Chidanandan, w. Pan, and m. A. Bayoumi, "NEDA: A Low-Power High-Performance DCT Architecture," IEEE trans. Signal process. vol. 54, no. 3, pp. 955–964, mar. 2006.
- [2]. M. R. M. Rizk and m. Ammar, "Low Power Small Area High Performance 2d-Dct Architecture," in proc. Int. Design test workshop, 2007, pp. 120–125.
- [3]. 3 y. Chen, x. Cao, q. Xie, and c. Peng, "An Area Efficient High Performance Dct Distributed Architecture For Video Compression," in Proc. Int. Conf. Adv. Comm. Technol., 2007, pp. 238–241.
- [4]. C. Peng, X. Cao, D. Yu, and X. Zhang, "A 250 Mhz Optimized Distributed Architecture Of 2 D 8x8 DCT," in Proc. Int. Conf. ASIC, 2007, pp. 189–192.
- [5]. C. Y. Huang, L. F. Chen, and Y. K. Lai, "A High-Speed 2-D Transforms Architecture With Unique Kernel For Multi-Standard Video Applications," In Proc. IEEE Int. Symp. Circuits Syst., 2008, pp. 21–24.
- [6]. S. S. Kidambi, F. E. Guibaly, and A. Antonious, "Area-Efficient Multipliersfor Digital Signal Processing Applications," IEEE Trans. Circuits Syst. II, Exp. Briefs, vol. 43, no. 2, pp. 90–95, Feb. 1996.
- [7]. 7. A. Shams, A. Chidanandan, W. Pan, and M. Bayoumi, —NEDA: A low power high throughput DCT architecture, IEEE Transactions on Signal Processing, vol.54(3), Mar. 2006.
- [8]. 8. Peng Chungan, Cao Xixin, Yu Dunshan, Zhang Xing, —A 250MHz optimized distributed architecture of 2D 8x8 DCT, 7th InternationalConference on ASIC, pp. 189 – 192, Oct. 2007.
- [10]. 9. B.G. Lee, — A new algorithm to compute the discrete cosine transform—IEEE Trans. Acoust., Speech, Signal Processing, vol. ASSP-32, pp. 1243-

- [11]. 1245, Dect.1984.
 [12]. 10. VijayaPrakash and K.S.Gurumurthy. "A Novel VLSI Architecture for Digital Image Compression Using Discrete Cosine Transform and Quantization" IJCSNS September 2010.
 [13]. 11. Nabeel Shirazi, Al Walters, and Peter Athanas —Quantitative Analysis of Floating Point Arithmetic on FPGA Based Custom Computing Machines presented at the IEEE Symposium on FPGAs for Custom Machines, Napa Valley, California, April 1995.



P. Bose Babu was born in A.P, India, He Completed M.Tech in VLSI system Design from MVGR COLLEGE OF ENGG.&TECH, Vizianagaram in 2011 and B.Tech from QIS College of engineering, in 2009 in Electronics & Communication engineering. Presently he is Working as Asst. Professor in ANDHRA LOYOLA college of Engg. & Technology, Vijayawada, A.P, India.

Authors



S. Susrutha Babu was born in India, A.P. He received the B.Tech degree from JNTU, A.P, and M.Tech degree from SRM University, Chennai, Tamil Nadu, India in 2008 and 2010 respectively. He worked as **Assistant Professor** in Electronics Engineering in Bapatla Engineering College for academic year 2010-2011 and from 2011 to till date working in **K L University**. He is a member of Indian Society for Technical Education and International Association of Engineers. His research interests include antennas, FPGA Implementation, Low Power Design and wireless communications and Digital VLSI. He has published articles in various international journals and Conference in IEEE.



G. Roopa Krishna Chandra was born in A.P, India He received his B.Tech degree in Electronics and Communication Engineering from Sri Sarathi Institute of Engineering and Technology year 2009. He has completed M.Tech in Lakireddy Bali Reddy College of engineering in 2012. His Research areas are Adaptive Signal Processing, Embedded Systems.



S. Suparshya Babu was born in India, A.P. He received the B.Tech degree from JNTU, A.P, and M.Tech degree from SRM University, Chennai, Tamil Nadu, India in 2008 and 2010 respectively. He worked as **Assistant Professor** in Electronics Engineering in Bapatla Engineering College for academic year 2010-2011 and from 2011 to till date working in **K L University**. He is a member of Indian Society for Technical Education and International Association of Engineers. His research interests include antennas, FPGA Implementation, Low Power Design and wireless communications and Robotics. He has published articles in various international journals and Conference in IEEE



S R Sastry Kalavakolanu was born in A.P, India. He received the B.Tech degree in Electronics & communications Engineering from Jawaharlal Nehru Technological University in 2010. Presently he is pursuing M.Tech VLSI Design in KL University. His research interests include Low Power VLSI Design. He has undergone 3 International Journals and 1 publishment in IEEE.

Characterization of Fatty Acid Used In Soap Manufacturing In Nigeria: Laundry, Toilet, Medicated and Antiseptic Soap

¹P. Oghome, ²M. U. Eke and ³C.I.O.Kamalu

^{1,3}Department of Chemical Engineering, Federal University of Technology,
P. M. B 1526, Oweeri. ²Quality Control Dept. PZ Cussion, Aba. Coresponding

Abstract: This study characterized the fatty acids in Nigeria made soap ranging from medicated, antiseptic, toilet and laundry soaps. Each sample after preparation was analyzed in a gas chromatography to obtain the chromatogram. The fatty acid distribution in Delta soap showed that palmitic acid (C_{16}) has the highest percentage of 40.48 % approximate followed by oleic acid ($C_{18,1}$), 34.35 % approximate. In Temosol, oleic acid has the highest percentage of 39.35 % approximate and next to it was palmitic acid, 29.11 % approximate. Carex antiseptic soap also contain $C_{18,1}$ and C_{16} as the dominant fatty acid with percentage of 36.06 % and 29.96 % approximate respectively. The dominant fatty acids in Jumbo tab and Truck bar (laundry) are $C_{18,1}$ and C_{16} . Jumbo tab contains 43.47 % C_{16} and 36.20 % $C_{18,1}$ approximate. While Truck bar contains 43.89 % and 31.73 % approximate of oleic and palmitic acids respectively. Lux and Joy soap also contain comparable fatty acids. In Lux, oleic acid is 41.51 %, palmitic acid is 26.70 % approximate. In Joy, oleic acid is 40.60 % and palmitic acid 24.99 % approximate. Other fatty acids present in the soap sample were shown. Eleven different fatty acids were found in the soap analyzed. They are capric, caprylic, lauric, myristic, myristoleic, palmitic, plamitoleic, stearic, oleic, linoleic and linolenic acids.

Keywords: Characterization, fatty acids, fats and oil, soap, chromatography

I. Introduction

Fatty acids are merely carboxylic acids with long hydrocarbon chains. The hydrocarbon chains length may vary from 10-30 carbons (mostly 12-18). The non-polar hydrocarbon alkane chain is an important counterbalance to the polar acid functional group. In acids with only a few carbons, the acid functional group dominates and gives the whole molecule a polar character. However, in fatty acids, the non-polar hydrocarbon chain gives the molecule a non-polar character.

There are two groups of fatty acids: the saturated and the unsaturated. Beef fat contains mainly the saturated fatty acid while olive oil contains the unsaturated fatty acids.

Soap is a function of acids and fatty acids are functions of fats and oil. In the simplest sense, oils that are solid at room temperature are hard whereas those that are liquid at room temperature are soft. The degree of hardness and softness differs according to their sources and other parameters. Oils that are hard contributes to hardness and/or lather in soap. Oils that are soft contribute to conditioning. Oils are made up mainly of a variety of fatty acids. The main conditioning fatty acids are oleic (1 unsaturated bonds), linoleic (2 unsaturated bonds) and linolenic (3 unsaturated bonds). The more unsaturated bonds, the better the conditioning and the more easily it is absorbed by the skin, but the softer the oil is in soap, the more prone to oxidation. Making soap therefore means choosing a combination of oils with different degrees of hard/soft, conditioning and leather, to get the particular product that fits you best. www.soap-making-resource.com/fatty-acids. The aim of this project is to extract and characterize the fatty acid in the finished soaps, thereby identifying their sources; evaluation of fats/oils used in soap manufacturing. Evaluation of blending of fats/oils in soap making, and possible reasons why that blend was adopted. Another objective of this work is to determine the properties of the fatty acids by running a gas chromatography which will

reveal their chain length and based on their chain length, the source could be traced.

Fats and oil as well as their blends are used in the manufacturing of soaps in Nigeria. These fats are of vegetable or animal origin. Their use in soap manufacturing is determined by: Cost, Availability; Easy of handle; Government Policy and functioning of the fatty acids in soap. Therefore, this project becomes important in the sense that the fats/oils, the precursor of fatty acids should be carefully studied so as to know their cost relative to the manufacture, the sources of the soap menu in terms of the fatty acids will be ascertained and the sources that are readily available should be recommended. The functioning of the fatty acids in soap will also be determined by carefully studying their characteristics and properties. By knowing their properties, the handling of the fatty acids and the soap in general in terms of storage, packing, transportation etc will be overcome.

According to Roman Legend, soap was named after mount Sapo, and ancient site of animal sacrifices. After an animal sacrifices, rain would wash the animal fat and ash that collected under the ceremonial alters down the slopes to the banks of the Tiber River. Women washing clothes in the river noticed that if they washed their clothes in certain parts of the river after a heavy rain their clothes were much cleaner (Ahmed) [2]. A soap-like material found in clay cylinders during the excavation of ancient Babylon is evidence that soap making was known as early as 2800 B.C. Inscriptions on the cylinders revealed that fats were boiled with ashes, a soap making method. It is generally agreed that the Hebrew word "borith" which has been translated as soap, is a generic term for any cleaning agent. By the second century A.D, the Greek physician, Galen, recommended soap for both medicinal and cleansing purposes. In other words, it is a substance, that when dissolved in water removed dirt from dirty materials. Scientifically, soap is one of the higher fatty acid or a mixture of such compound. A typical soap contains 80%

mixed oils and 20% coconut oil with about > 0.2% free alkali.

Soaps are water-soluble sodium or potassium salts of fatty acids. Soaps are made from fats and oils or their fatty acids, by treating them chemically with a strong alkali. The fats and oils used in soap making come from animal or plant sources, each fat or oil is made up of a distinctive mixture of several different triglycerides. In a triglyceride molecule, three fatty acid molecules are attached to one molecule of glycerine. There are many types of triglyceride each type consist of its own particular combination of fatty acids. The fatty acids are the components of fats and oils that are used in making soap.

An alkali is a soluble salt of an alkali metal like sodium or potassium, originally, the alkalis used in soap making were obtained from the ashes of plants, but they are now made commercially. The common alkalis used in soap making are sodium hydroxide (NaOH), also called caustic soda and potassium hydroxide (KOH), (Kuye and Okorie) [4]. Saponification of fats and oils is the most widely used soap making process, the process involves heating fats and oils and reacting them with a liquid alkali to produce soap and water (neat soap) plus glycerine. Fats and oils are hydrolyzed (split) with a high pressure steam to yield crude fatty acids and glycerine. The fatty acids are then purified by distillation and neutralized with an alkali to produce soap and water (neat soap). When the alkali is sodium hydroxide sodium soap is formed. Sodium soaps are "hard" soaps. When the alkali is potassium hydroxide, potassium soap is formed. Potassium soaps are softer and are found in some liquid hand soaps and shaving creams. The carboxylate end of the soap molecule is attracted to water. It is called the hydrophilic (water-loving) end. The hydrocarbon chain is attracted to oil and grease and repelled by water. It is known as the hydrophobic (water-hating) end. (www.sdchg.org/cleaning/chemistry/) [5].

In soap making the properties of the fats and oils are important; the fatty acid composition in oil determines its properties (Nwoko) [6]. The acids may be distributed at random in the triglycerides. In the soap making, it's the fatty acid content that matters the most. The chain length (C number) is usually cited and helps describes the molecule's properties in relation to others in its same series. Saturated fatty acids contain no double bonds. They are stiff molecules which tend to increase the melting point of oils.

Saturated fatty acids themselves are solids at room temperature. As they increase in size from lauric to stearic, the melting point of the oil increases. Saturated fatty acids in soap have good cleaning properties and support foam. The longer chains also tend to harden soap. Unsaturated fatty acids are liquids. They tend to have good cleaning power, but lather poorly. These fatty acids also tend to make milder soaps (www.soap-making-resource.com/fatty-acids) [7]

II. Experimental

Apparatus/Reagents

The materials used include methanol, round bottom flask, Condenser, Electro-thermal heater, methanolic HCl; N-heptane; brine, syringes and Gas Chromatography. Four samples of soap: Laundry soap (Jumbo tab and Truck bar), Toilet soap (joy and lux); Medicated soap (Delta and Tetmosol); Antiseptic soap (Carex)

Procedure

0.8 g of each samples was weighed into the round bottom flask, 12 ml of methanol was added and the flask was connected to a condenser and heat applied with the help of electro thermal heater. The setup was allowed to reflux for 30 mins and 2 ml of methanolic HCl (prepared in the ratio 4:1) is added and the sample was allowed to reflux for another 30 min. At this point, the heater was turned off for 3 min in order to allow the sample to cool. 10 and 20 ml of N-heptane and brine were added respectively. The bottom portion (non-volatile) portion of the sample was run off with the help of separating funnel. Finally, the separated volatile portion was transferred into a test tube where 0.5µl was injected into the gas chromatography.

In the chromatography, the carrier gas, nitrogen, carries the sample into the packed column, made of the stationary phase where the fatty acids were adsorbed accordingly. As the sample was continuously introduced, the weakly adsorbed fatty acids was detected by the detector, amplified by the amplifier and was recorded by the recorder. The procedure was repeated for other samples.

III. Results and Discussion

The results obtained are presented in the following Tables.

Table 1: Retention Time, Peak Area and Fatty acid in Medicated Soap (Delta)

Ret Time (min)	Type	Width (min)	Area (pA*s)	Area %	Name
1.635	MM	0.1724	3079.05894	0.54880	C8 (caprylic)
2.955	MM	0.2327	2402.12915	0.42815	C10 (Capric)
4.965	MM	0.3376	5.20290e4	9.27343	C12 (Lauric)
7.445	MM	0.3527	2.18125e4	3.88778	C14 (Myristic)
10.174	MM	0.3879	2.27123e5	40.48154	C16 (Palmitic)
13.890	MM	0.4423	1.43764e4	2.56238	C18 (Oleic)
15.073	MM	0.6506	1.96110e5	34.95381	C18:1 (Linoleic)
17.409	MM	0.7507	4.41220e4	7.86412	C18:2 (Linolenic)

Table 2: Retention Time, Peak Area and Fatty acid in Medicated Soap (Tetmosol)

Ret Time	Type	Width (min)	Area (pA*s)	Area %	Name
1.518	BP	0.2027	2032.75427	0.56782	C8(Caprylic)
2.776	VP	0.2260	1216.58179	0.33984	C10 (Capric)

3.676	VP	0.1329	38.13793	0.10165	?
4.726	MM	0.2704	1.54146e4	4.30587	C12 (Lauric)
7.170	MM	0.3235	1.78511e4	4.98648	C14 (Myristic)
9.826	MM	0.3464	1.04202e5	29.10741	C16 (Palmitic)
10.626	MM	0.3416	6391.75098	1.78545	C16:1 (Palmitoleic)
13.431	MM	0.4472	5.60052e4	15.64434	C18 (Stearic)
14.462	MM	0.6038	1.40859e5	39.34707	C18:1 (Oleic)
16.661	MM	0.7227	1.33802e4	3.73759	C18:2 (Linoleic)
19.19.4	BV	0.6098	599.57849	0.16748	C18:3 (Linolenic)

Table 3: Retention Time, Peak Area and Fatty acid in Antiseptic Soap (Carex)

Ret Time	Type	Width (min)	Area (pA*s)	Area %	Name
4.540	MM	0.4914	5.20886e4	12.20891	C12 (Lauric)
7.270	MM	0.4619	1.42345e4	3.33638	C14 (Myristic)
8.255	MM	0.2966	1208.89429	0.28335	C14:1 (Myristoleic)
10.104	MM	0.4209	1.15023e5	26.96005	C16 (Palmitic)
11.029	MM	0.3563	4569.29883	1.07099	C16:1 (Palmitoleic)
13.972	MM	0.4980	7.30369e4	17.11892	C18 (Stearic)
15.102	MM	0.6530	1.53843e5	36.05897	C18:1 (Oleic)
17.453	MM	0.7658	1.26391e4	2.96244	C18:2 (Linoleic)

Table 4: Retention Time, Peak Area and Fatty acid in Toilet Soap (Joy)

Ret Time	Type	Width (min)	Area (pA*s)	Area %	Name
4.674	MM	0.4323	4.25007e4	10.97616	C12 (Lauric)
4.674	BV	0.0269	3052.90454	0.78844	?
7.338	MM	0.4027	1.09988e4	2.84053	C14 (Myristic)
8.293	MM	0.2080	1443.69824	0.37285	C14:1 (Myristoleic)
10.116	MM	0.3972	9.67820e4	24.99474	C16 (Palmitic)
11.022	MM	0.3640	6071.27441	1.56796	C16:1 (Palmitoleic)
13.934	MM	0.4838	5.18703e4	13.39599e5	C18 (Stearic)
15.081	MM	0.6661	1.57199e5	40.59795	C18:1 (Oleic)
17.444	MM	0.7441	1.72907e4	4.46547	C18:2 (Linoleic)

Table 5: Retention Time, Peak Area and Fatty acid in Toilet Soap (Lux)

Ret Time	Type	Width (min)	Area (pA*s)	Area %	Name
1.442	BV	0.0890	1002.72699	0.22181	C8 (Caprylic)
2.703	PV	0.2553	2627.35010	0.58118	C10 (Capric)
3.636	VP	0.2410	106.2824	0.02351	?
4.776	MM	0.3401	3.28632e4	7.26953	C12 (Lauric)
7.355	MM	0.3321	2.28118e4	5.04610	C14 (Myristic)
10.104	MM	0.3635	1.20686e5	26.69649	C16 (Palmitic)
11.000	MM	0.3544	7695.71240	1.70233	C16:1 (Palmitoleic)
13.949	MM	0.4557	5.45182e4	12.05973	C18 (Stearic)
15.073	MM	0.6553	1.87653e5	41.50984	C18:1 (Oleic)
17.409	MM	0.7420	2.21038e4	4.88949	C18:2 (Linoleic)

Table 6: Retention Time, Peak Area and Fatty acid in Laundry Soap (Jumbo tab)

Ret Time	Type	Width (min)	Area (pA*s)	Area %	Name
1.630	BP	0.1466	619.59766	0.14643	C8 (Caprylic)
2.963	VP	0.2115	698.89987	0.11790	C10 (Capric)
3.865	VP	0.3242	200.86070	0.04747	?
4.986	VV	0.2879	7676.72266	1.81419	C12 (Lauric)
7.466	MM	0.3051	7319.01074	1.72965	C14 (Myristic)
8.781	MM	0.3919	1418.19214	0.33515	?
10.194	MM	0.3601	1.92407e5	45.47033	C16 (Palmitic)
11.091	MM	0.2173	474.09613	0.11204	C16:1 (Palmitoleic)
13.934	MM	0.4484	2.23890e4	5.29105	C18 (Stearic)

15.102	MM	0.6358	1.53160e5	36.19526	C18:1 (Oleic)
17.470	MM	0.7263	3.69854e4	8.74052	C18:2 (Linoleic)

Table 7: Retention Time, Peak Area and Fatty acid Laundry Soap (Truck bar)

Ret Time	Type	Width (min)	Area (pA*s)	Area %	Name
5.002	MM	0.2630	595.93256	0.14011	C12 (Lauric)
7.455	MM	0.3176	1.68864e4	3.97016	C14 (Myristic)
8.416	MM	0.2105	1184.1386	0.27840	C14:1 (Myristoleic)
10.163	MM	0.3599	1.34951e5	31.72821	C16 (Palmitic)
11.056	MM	0.3465	9230.44727	2.17017	C16:1 (Palmitoleic)
14.027	MM	0.4776	6.57836e4	15.46635	C18 (Stearic)
15.142	MM	0.6525	1.86689e5	43.89235	C18:1 (Oleic)
17.465	MM	0.7245	1.00135e4	2.35427	C18:2 (Linoleic)

Table 8: Fatty acid distribution in different soap

Soaps	Type	Lauric	Palmitic	Stearic	Oleic
Joy	Toilet	10.98	24.99	13.40	40.60
Lux	Toilet	7.27	26.70	12.06	41.51
Jumbo tab	Laundry	1.81	45.47	5.29	36.20
Truck bar	Laundry	0.14	31.73	15.47	43.89
Delta	Medicated	9.27	40.48	2.56	34.95
Tetmosol	Medicated	4.31	29.11	15.64	39.35
Carex	Antiseptic	12.21	26.96	17.12	36.06

Delta and tetmosol soap after the analysis yielded the result shown in Tables 1 and 2. From the result, it was seen that both of them had C₈-C_{18:2} in common but tetmosol had in addition C_{16:1} and C_{18:3}. It was also shown by analysis that the major fatty acids has the highest peak in the chromatogram as shown in Figures 1 and 2 respectively. Of the two soaps, the major fatty acids, oleic and palmitic acid in tetmosol was traced to tallow and palm kernel oil (PKO). Whereas that of Delta soap, was traced to palm oil and palm kernel oil. These fatty acids gave the soaps its characteristics. Hence, delta soap is more active than tetmosol. Their values are for tetmosol palmitic (C₁₆, 29.11%), oleic (C_{18:1}, 39.35%) it also contains the following fatty acids in lesser amounts; caprylic acid (C₈, 0.57%), capric acid (C₁₀, 0.34%), lauric acid (C₁₂, 4.31%), myristic (C₁₄, 4.99%), palmitoleic (C_{16:1}, 1.79%), stearic acid (C₁₈, 15.64%), linoleic (C_{18:2}, 3.74%), linolenic (C_{18:3}, 0.17%), whereas for delta soap, palmitic, 40.48% and oleic, 34.95% dominates, while caprylic (C₈, 0.55%), capric (C₁₀, 0.43%), lauric acid (C₁₂, 9.27%), myristic acid (C₁₄, 3.89%), palmitic acid (C₁₆, 40.48%), oleic acid (C₁₈, 2.56%), linoleic acid (C_{18:1}, 34.95%), linolenic acid (C_{18:2}, 7.86%) are in lesser quantity.

It was found from the chromatogram that carex soap contain 12.21% lauric acid, 26.96% palmitic acid, 17.12% stearic acid, 36.06% oleic acid and 2.96% linoleic acid. Myristic (C₁₄, 3.34%), myristoleic (C_{14:1}, 0.28%), palmitoleic (C_{16:1}, 1.07%) in lesser amount (Table 3). These fatty acids were mainly from tallow.

The fatty acids present in Joy and Lux soap were shown in Tables 4 and 5 respectively. It was seen that Joy soap contains 10.98% lauric acid, 24.995% palmitic acid, 13.4% stearic acid and 40.60 % oleic acid. The lesser quantities are myristic (C₁₄, 2.84%), myristoleic (C_{14:1}, 0.37%), palmitoleic (C_{16:1}, 1.57% and linoleic (C_{18:2},

4.47%). While in Lux, the fatty acids found include 7.3% lauric, 26.70% palmitic, 12.06% stearic and 41.51% oleic acid, others are in lesser quantities caprylic (C₈, 0.22%), capric (C₁₀, 0.58%), myristic (C₁₄, 5.05%), palmitoleic (C_{16:1}, 1.70%) linoleic (C_{18:2}, 4.89%). The Joy fatty acids were mainly from tallow and palm oil while that of Lux was from tallow and PKO. From the analysis, it was clear that there was no much difference between Joy and Lux soap except myristoleic acid present in Joy alone and caprylic and capric present only in Lux. They share similar properties in their cleansing activities.

The analysis of Jumbo and Truck bar soaps were tabulated in Table 6 and 7 respectively. The result showed that palmitic acid present in Jumbo soap is 45.47% and oleic acid 36.20% and others caprylic (C₈ 0.15%), capric (C₁₀, 0.12%), Lauric (C₁₂, 1.81%), myristic (C₁₄, 1.73%), palmitoleic (C_{16:1}, 0.11%), stearic (C₁₈, 5.29%) and linoleic (C_{18:2}, 8.74%) in minor quantities, whereas in Truck bar soap, it is 31.73% palmitic acid, 43.89% oleic acid and 15.47% stearic acid, it also contain the following fatty acids in lesser quantities, lauric acid (C₁₂, 0.14%), myristic (C₁₄, 3.97%), myristoleic (C_{14:1}, 0.28%), palmitoleic (C_{16:1}, 2.17%), linoleic (C_{18:2}, 2.35%). The major source of the Jumbo tab fatty acid is tallow while that of truck bar is tallow and PKO.

It was obvious from the analysis that, every soap whether medicated, antiseptic, toilet, and laundry is a function of palmitic and oleic acid. The soap samples analysed also had fatty acids with carbon atoms in the neighborhood of C₈, C₁₀, C₁₂, and C₁₄ in very little quantities. Although the soaps analyzed had palmitic and oleic acids as their major fatty acid, they were in different percentage composition as shown in Table 8.

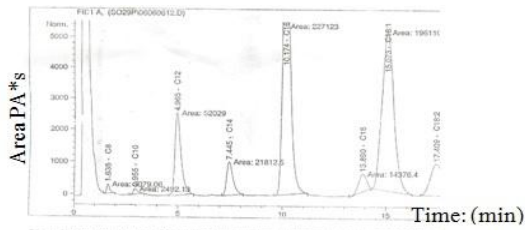


Figure 1: Determination of fatty acid in Delta Soap

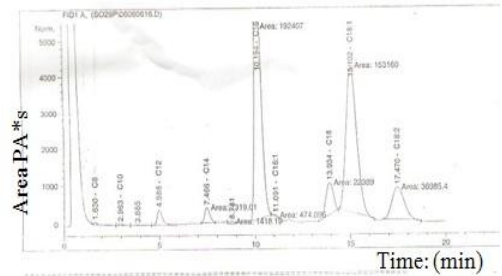


Figure 6: Determination of fatty acid in Jumbo Soap

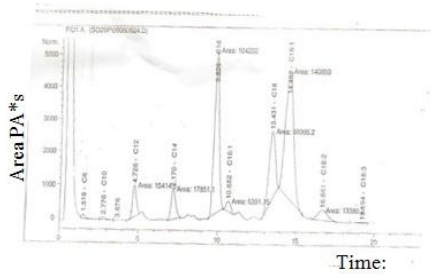


Figure 2: Determination of fatty acid in Tetmosol

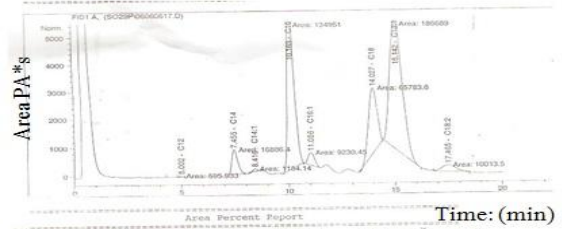


Figure 6: Determination of fatty acid in Truck Soap

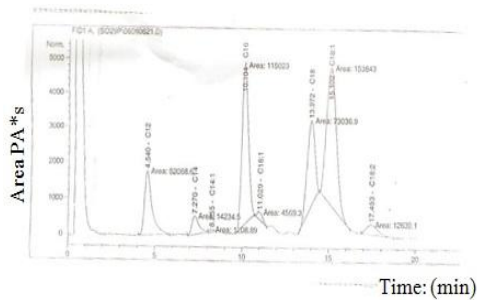


Figure 3: Determination of fatty acid in Carex Soap

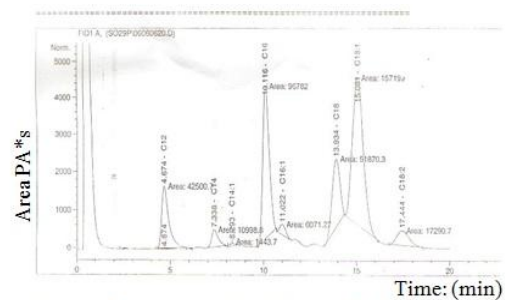


Figure 4: Determination of fatty acid in Joy Soap

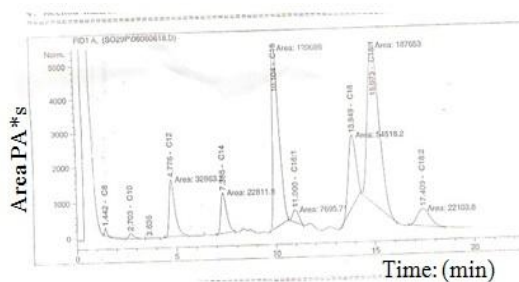


Figure 5: Determination of fatty acid in Lux Soap

IV. Conclusion

The chief fatty acids in soap making are lauric acid, myristic acid, palmitic acid, stearic acid oleic. They are obtained from mutton, tallow, beef tallow (animal fats), palm oil, and palm kernel oil. Joy, Lux, Delta and Carex soap have more percentage of lauric acid. Lauric acid is saturated fatty acids whose single bond helps in soap hardening. It also has good cleansing agent and supports foaming. The percentage of plamitoleic acid is between 0.00-2.20 percent. This acid is unsaturated. It makes soap to be mild, have good cleaning power but foams poorly. It was seen that palmitic acid can be saturated and unsaturated fatty acids, the C₁₆ and C_{16:1} respectively. Stearic acid i.e. the C₁₈ has three members the oleic acid C_{18:1}, the linoleic acid C_{18:2} and the linolenic acid C_{18:3}. The stearic itself is a saturated fatty acid while the other three are unsaturated fatty acids. They help increase mildness in soap.

Regerences

- [1]. www.elmhurst.edu/.../SS1fattyacids.html.
- [2]. Ahmed, Y. I. (2002) Extract of Saponin for Development of soap. Unpublished Thesis submitted to Chemical Engineering Department, Federal University of Technology, Minna, Nigeria, pp. 48.
- [3]. www.chgrinvalleysoapandcraft.com/.
- [4]. Kuye A. O. and Okorie C (1990) Factors Affecting the Lixiviation of Palm Bunch Ash as Source of Alkali for Soap Production Ife Journal of Technology 3(2):33-37.
- [5]. www.sdchg.org/cleaning/chemistry.
- [6]. Nwoko V.O. (1982) Effects of Mixing Oils on the Preparation and Properties of Soap. Private Communications.
- [7]. www.soap-making-resource.com/fatty-acids...

Compressed Sensing Image Recovery Using Adaptive Nonlinear Filtering

B. Sravanthi¹, Ch. Madhuri Devi²

¹M.tech.Student, Sri Indu College of Engineering & Technology, Hyderabad
²Associate Professor, Sri Indu College of Engineering & Technology, Hyderabad

Abstract: Compressed sensing is a technique that consists providing efficient, stable and fast recovery algorithms which, in a few seconds, evaluate a good approximation of a compressible image from highly incomplete and noisy samples. In this paper, using adaptive nonlinear filtering strategies in an iterative framework can be avoiding the recovery image problem. In this technique has more efficient, stability and low computational cost. The experimental shows that the PSNR, CPU time and recovery image.

Index Terms—Compressed sensing, L_1 -minimization, median filters, nonlinear filters, sparse image recovery, total variation.

I. Introduction

Compressed sensing is a new paradigm for signal recovery and sampling. It states that a relatively small number of linear measurements of a sparse signal can contain most of its salient information and that the signal can be exactly reconstructed from these highly incomplete observations. The major challenge in practical applications of compressed sensing consists in providing efficient, stable and fast recovery algorithms which, in a few seconds, evaluate a good approximation of a compressible image from highly incomplete and noisy samples.

It follows that signals that have a sparse representation in a transform domain can be exactly recovered from these measurements by solving an optimization problem of the form

$$\Phi W^T \alpha = \Phi X \quad (1)$$

Here

Φ is an $M \times N$ measurement matrix and $\alpha = Wu$. The number M of given measurements for which we obtain the perfect recovery depends upon the length and the sparsity level K of the original signal, and on the acquisition matrix [1], [3]. If the unknown x signal has sparse gradient, it has been shown in [2], [3] that it can be recovered by casting problem (1) as

$$\Phi u = \Phi x \quad (2)$$

This formulation is particularly suited to the image recovery problem, since many images can be modeled as piece-wise-smooth functions containing a substantial number of jump discontinuities. Exact measurements are often not possible in real problems, so if the measurements are corrupted with random noise, namely we have

$$Y = \Phi x + e \quad (3)$$

Where e is the error signal and x is the input image. Sparse signals are an idealization that we rarely encounter in applications, but real signals are quite often compressible with respect to an orthogonal basis. This means that, if expressed in that basis, their coefficients exhibit exponential

decay when sorted by magnitude. As a consequence, compressible signals are well approximated by k -sparse signals and the compressed sensing paradigm guarantees that from M linear measurements we can obtain a reconstruction with an error comparable to that of the best possible k -terms approximation within the sparse fying basis [4][2].

In this paper is organized as follows. Proposed method in section II. Section III describes the comparative performance. The simulation results are presented in Section IV. Concluding remarks are made in Section V.

II. Proposed Method

In this paper, we consider an extension of this nonlinear filtering approach to the multi dimensional case. We focus on a recovery problem where the optimal solution, in addition to satisfying the acquisition constraints, has minimal “bounded variation norm,” namely, it minimizes. The optimal reconstruction is evaluated by solving a sequence of total variation regularized unconstrained sub problems, where both isotropic and anisotropic TV estimates have been considered.

The nonlinear filtering strategy has been proposed in the context of a penalized approach to the compressed sensing signal recovery problem. suitable filter is used according to the considered minimization problem and a fast flexible algorithm has been realized for its solution. The procedure of proposed method as shown below

- i) Initialization of parameters
- ii) Updating bound constrains
- iii) Apply constraint non linear filter step
- iv) Convergence test of proposed method
- v) Updating outer iteration

From a theoretical point of view, the non linear adaptive filter is attractive since it can deal with a general class of nonlinear systems while its output is still linear with respect to various higher power system coefficients.

First we initialize the all parameter values then start with the outer iterations. In outer iteration, the image reconstruction problems it is well known that image intensity values have to be not negative and $\leq R, R > 0$. This suggests that we could insert more information in the compressed sensing reconstruction problem by adding a bound constraint as shown below

$$T_s u = y \quad (4)$$

In the case of input data perturbed by additive white Gaussian noise with standard deviation σ

$$Y = S(Tx + e) = Tsx + e_s \quad (5)$$

Where e error value between original image and reconstruction image. After apply the outer iteration then to update the bound constraints as shown below

$$v_{k,i} = u_{k,i} + \beta T_S^T (y - T_S u_{k,i}) \tag{6}$$

Where

T_S is linear operator

$B < \alpha/2$

$V_{k,i}$ is the proximal operator argument

The third step of proposed method is the non linear filter step. The equation of non linear filter as shown below

$$u_{k,i+1} = \arg \min_{u \in C} \left\{ \frac{1}{2} \lambda_{k,i} \beta \|u - v_{k,i}\|_2^2 + F(u) \right\} \tag{7}$$

The fourth step of proposed method is convergence test. In convergence test, The general compressed sensing problem can now be stated using the previous notations. The input data can be represented as

$$Y = T_s x \tag{8}$$

In the case of input data perturbed by additive white Gaussian noise with standard deviation σ in equation (5). If $F(u)$ contains an L-norm the optimization problems can be very difficult to solve directly, due to the nondifferentiability of $F(u)$. To overcome this problem we use the well known penalization approach that considers a sequence of un-constrained minimization sub problems of the form

$$\min_{u \in \mathbb{R}^{N_1 \times N_2}} \left\{ F(u) + \frac{1}{2\lambda_k} \|T_S u - y\|_2^2 \right\} \tag{9}$$

The convergence of the penalization method to the solution of the original constrained problem has been established (under very mild conditions) $\lim \lambda_k = 0$ when. Unfortunately, in general, using very small penalization parameter values makes the unconstrained sub problems very ill-conditioned and difficult to solve. In the present context, we do not have this limitation, since we will approach these problems implicitly, thus, avoiding the need to deal with ill-conditioned linear systems. This is obtained by evaluating an approximation of the solution of (9) iteratively, using an operator splitting strategy (frequently considered in the literature to solve ℓ_1 -regularized problems [5], [6], [7], [8]), and taking advantage of the particular structure of the resulting problems.

III. Comparative Performance

To assess the performance of the proposed filters for removal of noise and to evaluate their comparative performance, different standard performance indices have been used in the thesis. These are defined as follows:

Peak Signal to Noise Ratio (PSNR): It is measured in decibel (dB) and for gray scale image it is defined as:

$$\text{PSNR (dB)} = 10 \log_{10} \left[\frac{\sum_i \sum_j 255^2}{\sum_i \sum_j (S_{i,j} - \hat{S}_{i,j})^2} \right] \tag{8}$$

$S_{i,j}$ and $\hat{S}_{i,j}$ are the input and reconstruction images. The higher the PSNR in the restored image, the better is its quality.

Signal to Noise Ratio Improvement (SNRI): SNRI in dB is defined as the difference between the Signal to Noise

Ratio (SNR) of the restored image in dB and SNR of original image in dB i.e.

SNRI (dB) = SNR of restored image in dB - SNR of noisy image in dB

Where,

SNR of restored image dB =

$$10 \log_{10} \left[\frac{\sum_i \sum_j S_{i,j}^2}{\sum_i \sum_j (S_{i,j} - \hat{S}_{i,j})^2} \right] \tag{9}$$

The higher value of SNRI reflects the better visual and restoration performance.

IV. EXPERIMENTAL RESULTS



Fig.1. original image



Fig.2. Gaussian mask corresponding to 77% under sampling

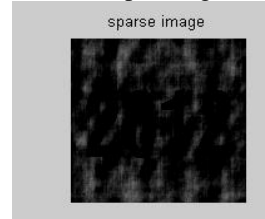


Fig.3. Sparse mask corresponding to 77% under sampling



Fig.4. reconstruction image using non linear filter Nonlinear Adaptive Filter With Mask I,M=16402 with different noise

noise	PSNR	SNR	Cpu time	iteration
0	55.15	220	12	25
0.1	54.98	219	12	26

V. CONCLUSION

In this paper, avoiding the reconstruction image problem using non linear filter technique and prove the convergence of the resulting two-steps iterative scheme. In this paper, different kinds of measurements and different choices of the function $F(u)$. In fact, since this function plays the role of the penalty function in the variational approach of the image denoising problem, it is possible to exploit the different proposals of the denoising literature in

order to select new filtering strategies and the references therein), perhaps more suited to the different practical recovery problems.

References

- [1] E. J. Candés, “Compressive sampling,” in Proc. Int. Congr. Math., Madrid, Spain, 2006, vol. 3, pp. 1433–1452.
- [2] E. J. Candés, J. Romberg, and T. Tao, “Stable signal recovery from in-complete and inaccurate measurements,” Commun. Pure Appl. Math., vol. 59, no. 8, pp. 1207–1223, 2006.
- [3] E. J. Candés, J. Romberg, and T. Tao, “Robust uncertainty principle: Exact signal reconstruction from highly incomplete frequency information,” IEEE Trans. Inf. Theory, vol. 52, no. 2, pp. 489–509, Feb. 2006.
- [4] A. Chambolle, “An algorithm for total variation minimization and applications,” J. Math. Imag. Vis., vol. 20, pp. 89–97, 2004.
- [5] P. L. Combettes and V. R. Wajs, “Signal recovery by proximal forward-backward splitting,” SIAM J. Multiscale Model. Sim., vol. 4, no. 4, pp. 1168–1200, Nov. 2005.
- [6] I. Daubechies, M. Defrise, and C. De Mol, “An iterative thresholding algorithm for linear inverse problems with a sparsity constraint,” Commun. Pure Appl. Math., vol. LVII, pp. 1413–1457, 2004.
- [7] T. Goldstein and S. Osher, “The split Bregman algorithm for L1 regularized problems,” UCLA, Los Angeles, CA, UCLA CAMRep. 08–29, 2008.
- [8] L. I. Rudin, S. Osher, and E. Fatemi, “Nonlinear total variation based noise removal algorithms,” Phys. D, vol. 60, pp. 259–268, 1992.



Miss. **BEJAWADA SRAVANTHI** graduate from The vazeer sulthan colg of Engg College in **Electronics & Communications**. Now pursuing Masters in **Digital Electronics and Communication Systems (DECS)** from Sri Indu College of Engineering & Technology.



I express my gratitude to Mrs. **CH. MADHURI DEVI** Associate Professor Department of (ECE) and for her constant co-operation, support and for providing necessary facilities throughout the M.tech program. She has 6 Years of Experience, at B.Tech and 2 years of Experience, at M.tech Level and working as a Associate Professor in Sri Indu College of Engg. & Technology.

A Primitive Polynomial to Define the Finite Field Modules for High-Throughput Interpolator to Encode and Decode Of Non Binary Cyclic Codes

Susrutha Babu Sukhavasi¹, Suparshya Babu Sukhavasi¹
S. R. Sastry K.², M. Aravind Kumar³, P. Bosebabu⁴,
G. Roopa Krishna Chandra⁵

¹Faculty, Department of ECE, K L University, Guntur, AP, India.

²M.Tech -VLSI Student, Department of ECE, K L University, Guntur, AP, India.

³M.Tech -VLSI Student, Padmasri Dr.B.V.Raju Institute of Technology, Medak, A.P, India.

⁴ Faculty, Department of ECE, Andhra Loyola College Of Eng &Tech ,Vijayawada, AP, India.

⁵M.Tech - Student, Department of ECE, Lakireddy Bali Reddy College of engineering LBR, Guntur, AP, India

Abstract : This paper represents The algebraic soft-decoding (ASD) of Reed–Solomon (RS) codes provides significant coding gain over hard-decision decoding with polynomial complexity. The low-complexity chase (LCC) algorithm is proposed for reducing the complexity of interpolation, which interpolates over 2^n test vectors, being attractive for VLSI implementation. The interpolation is simplified in LCC decoding by restricting the multiplicity to $m=1$ and replacing the factorization step with Chien's search and Forney's algorithm. In this paper, high-throughput interpolator architecture for soft-decision decoding of Reed–Solomon (RS) codes based on low-complexity chase (LCC) decoding is presented. We have formulated a modified form of the Nielson's interpolation algorithm, using some typical features of LCC decoding. The proposed algorithm works with a different scheduling, takes care of the limited growth of the polynomials, and shares the common interpolation points, for reducing the latency of interpolation. Based on the proposed modified Nielson's algorithm we have derived low-latency architecture to reduce the overall latency of the whole LCC decoder. An efficiency is low, in terms of area-delay product, has been achieved by an LCC decoder, by using the proposed interpolator architecture, over the best of the previously reported architectures for an RS(255,239) code with eight test vectors.

Keyword: RScodes, Guruswami-Sudan algorithm, Registers, Multiplexers, D-flipflop.

I. INTRODUCTION

2. Interpolation

3. Factorization of bivariate polynomials

It's being the interpolation and the most computation-intensive one. Several architectures based on Nielson's algorithm and Lee–O'Sullivan algorithm are found in the literature for the VLSI implementation of interpolation stage. However, their hardware complexity is still high. An interpolation architecture for LCC with $m=3$, called backward interpolation, is proposed in [9], which could be considered as the best of the current approaches. Backward interpolator shares the computation of common points of the test vectors. These points are ordered in such way that a pair of adjacent vectors differ only at one point.

Due to this feature, the backward interpolation architecture involves less area and provides higher speed than its prior ones.

II. REED SOLOMON SOFTWARE PERFORMANCE

The following data details performance numbers for a number of specific RS (n, k) implementations for two general purpose processing architectures and one digital signal processor. Numbers are provided for both decode in the presence of no error, as well as decode in the presence of maximum channel error. Note that correcting errors requires more processing power than simply validating blocks, and that the required processing power increases linearly with the error rate. Typical applications tend to keep the error rate low such that active correction is not required. The two digit hexadecimal number in each column specifies the GF (255) primitive polynomial used to generate the underlying Galois field. In 1960, Irving Reed and Gus Solomon published a paper in the Journal of the Society for Industrial and Applied Mathematics. This paper described a new class of error-correcting codes that are now called Reed-Solomon (R-S) codes. These codes have great power and utility, and are today found in many applications from compact disc players to deep-space applications. This article is an attempt to describe the paramount features of R-S codes and the fundamentals of how they work. Reed-Solomon codes are non-binary cyclic codes with symbols made up of m-bit Sequences, where m is any positive integer having a value greater than 2. R-S (n, k) codes on m-bit symbols exist for all n and k for which $0 < k < n < 2m + 2$

Where k is the number of data symbols being encoded, and n is the total number of code symbols in the encoded block. For the most conventional R-S (n, k) code, $(n, k) = (2m - 1, 2m - 1 - 2t)$

Where t is the symbol-error correcting capability of the code, and $n - k = 2t$ is the number of parity symbols. An extended R-S code can be made up with $n = 2m$ or $n = 2m + 1$, but not any further. Reed-Solomon codes achieve the largest possible code minimum distance for any linear code with the same encoder input and output block lengths. For non-binary codes, the distance between two code words is defined (analogous to Hamming distance) as the number

of symbols in which the sequences differ. For Reed-Solomon codes, the code minimum distance

$$d_{min} = n - k + 1$$

The code is capable of correcting any combination of t or fewer errors, where t can be expressed as

$$T = \lfloor (d_{min}-1) / 2 \rfloor = \lfloor (n-k) / 2 \rfloor$$

where $\lfloor x \rfloor$ means the largest integer not to exceed x . Equation illustrates that for the case of R-S codes, correcting t symbol errors requires no more than $2t$ parity symbols. Equation lends itself to the following intuitive reasoning. One can say that the decoder has $n - k$ redundant symbols to “spend,” which is twice the amount of correctable errors. For each error, one redundant symbol is used to locate the error, and another redundant symbol is used to find its correct value. The erasure-correcting capability, ρ , of the code is

$$\rho = d_{min} - 1 = n - k \quad (5)$$

Simultaneous error-correction and erasure-correction capability can be expressed as follows:

$$2\alpha + \gamma < d_{min} < n - k \quad (6)$$

Where α is the number of symbol-error patterns that can be corrected and γ is the number of symbol erasure patterns that can be corrected. An advantage of non-binary codes such as a Reed-Solomon code can be seen by the following comparison. Consider a binary $(n, k) = (7, 3)$ code. The entire n -tuple space contains $2^n = 2^7 = 128$ n -tuples, of which $2^k = 2^3 = 8$ (or $1/16$ of the n -tuples) are code words. Next, consider a non-binary $(n, k) = (7, 3)$ code where each symbol is composed of $m = 3$ bits. The n -tuple space amounts to $2^{nm} = 2^{21} = 2,097,152$ n -tuples, of which $2^{km} = 2^9 = 512$ (or $1/4096$ of the n -tuples) are code words. When dealing with non-binary symbols, each made up of m bits, only a small fraction (i.e., 2^{km} of the large number 2^{nm}) of possible n -tuples are code words. This fraction decreases with increasing values of m . The important point here is that when a small fraction of the n -tuple space is used for code words, a large d_{min} can be created. Any linear code is capable of correcting $n - k$ symbol erasure patterns if the $n - k$ erased symbols all happen to lie on the parity symbols. However, R-S codes have the remarkable property that they are able to correct any set of $n - k$ symbol erasures within the block. R-S codes can be designed to have any redundancy. However, the complexity of a high-speed implementation increases with Reed-Solomon Codes redundancy. Thus, the most attractive R-S codes have high code rates (low redundancy).

2.1 REED-SOLOMOERROR PROBABILITY

The Reed-Solomon (R-S) codes are particularly useful for burst-error correction; that is, they are effective for channels that have memory. Also, they can be used efficiently on channels where the set of input symbols is large. An interesting feature of the R-S code is that as many as two information symbols can be added to an R-S code of length n without reducing its minimum distance.

For R-S codes, error probability is an exponentially decreasing function of block length, n , and decoding complexity is proportional to a small power of the block length. The R-S codes are sometimes used in a concatenated arrangement. In such a System, an inner convolution decoder first provides some error control by operating on soft-decision demodulator outputs; the convolutional decoder then presents hard-decision data to

the outer Reed-Solomon decoder, which further reduces the probability of error.

2.2 FINITE FIELDS

In order to understand the encoding and decoding principles of non binary codes, such as Reed-Solomon (R-S) codes, it is necessary to venture into the area of finite fields known as Galois Fields (GF). For any prime number, p , there exists a finite field denoted $GF(p)$ that contains p elements. It is possible to extend $GF(p)$ to a field of p^m elements, called an extension field of $GF(p)$, and denoted by $GF(p^m)$, where m is a nonzero positive integer. Note that $GF(p^m)$ contains as a subset the elements of $GF(p)$. Symbols from the extension field $GF(2^m)$ are used in the construction of Reed-Solomon (R-S) codes. The binary field $GF(2)$ is a subfield of the extension field $GF(2^m)$, in much the same way as the real number field is a subfield of the complex number field. Besides the numbers 0 and 1, there are additional unique elements in the extension field that will be represented with a new symbol α . Each nonzero element in $GF(2^m)$ can be represented by a power of α . An infinite set of elements, F , is formed by starting with the elements $\{0, 1, \alpha\}$, and generating additional elements by progressively multiplying the last entry by α , which yields the following:

$$F = \{0, 1, \alpha, \alpha^2, \dots, \alpha^j, \dots\} = \{0, \alpha^0, \alpha^1, \alpha^2, \dots, \alpha^j, \dots\}$$

To obtain the finite set of elements of $GF(2^m)$ from F , a condition must be imposed on F so that it may contain only 2^m elements and is closed under multiplication. The condition that closes the set of field elements under multiplication is characterized by the irreducible polynomial shown below:

$$\alpha^{(2^m-1)} + 1 = 0$$

or equivalently Using this polynomial constraint, any field element that has a power equal to or greater than $2^m - 1$ can be reduced to an element with a power less than $2^m - 1$, as follows:

$$\alpha^{(2^m+n)} = \alpha^{(2^m-1)} \alpha^{n+1} = \alpha^{n+1}$$

2.3 ADDITION IN THE EXTENSION FIELD GF(2M)

Each of the 2^m elements of the finite field, $GF(2^m)$, can be represented as a distinct polynomial of degree $m - 1$ or less. The degree of a polynomial is the value of its highest-order exponent. We denote each of the nonzero elements of $GF(2^m)$ as a polynomial, $a_i(X)$, where at least one of the m coefficients of $a_i(X)$ is nonzero. For $i = 0, 1, 2, \dots, 2^m - 2$,

$$a_i = a_i(X) = a_{i,0} + a_{i,1}X + a_{i,2}X^2 + \dots + a_{i,m-1}X^{m-1}$$

Consider the case of $m = 3$, where the finite field is denoted $GF(2^3)$. the mapping (developed later) of the seven elements $\{a_i\}$ and the zero element, in terms of the basis elements $\{X^0, X^1, X^2\}$ described. Since Equation (10) indicates that $\alpha^0 = \alpha^7$, there are seven nonzero elements or a total of eight elements in this field. Each row in the mapping comprises a sequence of binary values representing the coefficients $a_{i,0}$, $a_{i,1}$, and $a_{i,2}$ in Equation (14). One of the benefits of using extension field elements $\{a_i\}$ in place of binary elements is the compact notation that facilitates the mathematical representation of nonbinary encoding and decoding processes. Addition of two elements of the finite field is then defined as the

modulo-2 sum of each of the polynomial coefficients of like powers,

$$a_i + a_j = (a_i, 0 + a_j, 0) + (a_i, 1 + a_j, 1) X + \dots + (a_i, m - 1 + a_j, m - 1) X^{m-1}$$

2.4 A PRIMITIVE POLYNOMIAL IS USED TO DEFINE THE FINITE FIELD

A class of polynomials called primitive polynomials is of interest because such functions define the finite fields $GF(2^m)$ that in turn are needed to define R-S codes. The following condition is necessary and sufficient to guarantee that a polynomial is primitive. An irreducible polynomial $f(X)$ of degree m is said to be primitive if the smallest positive integer n for which $f(X)$ divides $X^n + 1$ is $n = 2^m - 1$. Note that the statement A divides B means that A divided into B yields a nonzero quotient and a zero remainder. Polynomials will usually be shown low order to high order. Sometimes, it is convenient to follow the reverse format.

2.4.1 ENCODER

The Reed-Solomon encoder reads in k data symbols, computes the $n - k$ parity symbols, and appends the parity symbols to the k data symbols for a total of n symbols. The encoder is essentially a $2t$ tap shift register where each register is m bits wide. The multiplier coefficients are the coefficients of the RS generator polynomial. The general idea is the construction of a polynomial; the coefficients produced will be symbols such that the generator polynomial will exactly divide the data/parity polynomial.

2.4.2 DECODER

The Reed-Solomon decoder tries to correct errors and/or erasures by calculating the syndromes for each codeword. Based upon the syndromes the decoder is able to determine the number of errors in the received block. If there are errors present, the decoder tries to find the locations of the errors using the Berlekamp-Massey algorithm by creating an error locator polynomial. The roots of this polynomial are found using the Chien search algorithm. Using Forney's algorithm, the symbol error values are found and corrected. For an RS (n, k) code where $n - k = 2t$, the decoder can correct up to t symbol errors in the code word. Given that errors may only be corrected in units of single symbols (typically 8 data bits), Reed-Solomon coders work best for correcting burst errors.

2.5 REED-SOLOMON ENCODING

The most conventional form of Reed-Solomon (R-S) codes in terms of the parameters n , k , t , and any positive integer $m > 2$.

$$(n, k) = (2m - 1, 2m - 1 - 2t) \quad (20)$$

where $n - k = 2t$ is the number of parity symbols, and t is the symbol-error correcting capability of the code. The generating polynomial for an R-S code takes the following form:

$$g(X) = g_0 + g_1 X + g_2 X^2 + \dots + g_{2t-1} X^{2t-1} + X^{2t} \quad (21)$$

The degree of the generator polynomial is equal to the number of parity symbols. R-S codes are a subset of the Bose, Chaudhuri, and Hocquenghem (BCH) codes; hence, it should be no surprise that this relationship between the

degree of the generator polynomial and the number of parity symbols holds, just as for BCH codes. Since the generator polynomial is of degree $2t$, there must be precisely $2t$ successive powers of α that are roots of the polynomial. We designate the roots of $g(X)$ as $\alpha, \alpha^2, \dots, \alpha^{2t}$. It is not necessary to start with the root α ; starting with any power of α is possible.

2.6 ENCODING IN SYSTEMATIC FORM

Since R-S codes are cyclic codes, encoding in systematic form is analogous to the binary encoding procedure. We can think of shifting a message polynomial, $m(X)$, into the rightmost k stages of a codeword register and then appending a parity polynomial, $p(X)$, by placing it in the leftmost $n - k$ stages. Therefore we multiply $m(X)$ by X^{n-k} , thereby manipulating the message polynomial algebraically so that it is right-shifted $n - k$ positions. Next, we divide $X^{n-k} m(X)$ by the generator polynomial $g(X)$, which is written in the following form:

$$X^{n-k} m(X) = q(X) g(X) + p(X)$$

where $q(X)$ and $p(X)$ are quotient and remainder polynomials, respectively. As in the binary case, the remainder is the parity. Equation can also be expressed as follows:

$$p(X) = X^{n-k} m(X) \text{ modulo } g(X)$$

The resulting codeword polynomial, $U(X)$ can be written as

$$U(X) = p(X) + X^{n-k} m(X)$$

2.6.1 SYSTEMATIC ENCODING WITH AN $(N-K) -$ STAGE SHIFT REGISTER

Using circuitry to encode a three-symbol sequence in systematic form with the $(7, 3)$ R-S code described by $g(X)$ in the implementation of a linear feedback shift register (LFSR) circuit. It can easily be verified that the multiplier terms taken from left to right, correspond to the coefficients of the polynomial in low order to high order. This encoding process is the non-binary equivalent of cyclic encoding. Here, corresponding to the $(7, 3)$ R-S nonzero code words are made up of $2m - 1 = 7$ symbols, and each symbol is made up of $m = 3$ bits.

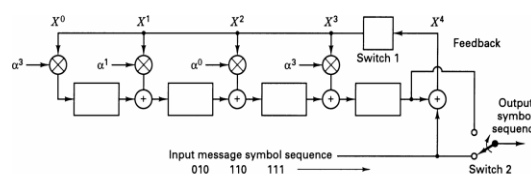


Fig 1: SYSTEMATIC ENCODING WITH LFSR

Here the example is non-binary, so that each stage in the shift register of Figure holds a 3-bit symbol. In the case of binary codes, the coefficients labeled g_1, g_2 , and so on are binary. Therefore, they take on values of 1 or 0, simply dictating the presence or absence of a connection in the LFSR. However in Figure 9, since each coefficient is specified by 3-bits, it can take on one of eight values. The non-binary operation implemented by the encoder of Figure, forming code words in a systematic format, proceeds in the same way as the binary one. The steps can be described as follows:

1. Switch 1 is closed during the first k clock cycles to allow shifting the message symbols into the (n - k)-stage shift register.
2. Switch 2 is in the down position during the first k clock cycles in order to allow simultaneous transfer of the message symbols directly to an output register.
3. After transfer of the kth message symbol to the output register, switch 1 is opened and switch is moved to the up position.
4. The remaining (n - k) clock cycles clear the parity symbols contained in the shift register by moving them to the output register.
5. The total number of clock cycles is equal to n, and the contents of the output register is the codeword polynomial $p(X) + X^{n-k}m(X)$, where $p(X)$ represents the parity symbols and $m(X)$ the message symbols in polynomial form.

2.7 REED-SOLOMON DECODING

Earlier, a test message encoded in systematic form using a (7, 3) R-S code resulted in a codeword polynomial described. Now, assume that during transmission this codeword becomes corrupted so that two symbols are received in error. This number of errors corresponds to the maximum error-correcting capability of the code. For this seven-symbol codeword example, the error pattern, $e(X)$, can be described in polynomial form as follows:

$$e(x) = \sum_{n=0}^6 e_n X^n$$

For this example, let the double-symbol error be such that one parity symbol has been corrupted with a 1-bit error (seen as α^2), and one data symbol has been corrupted with a 3-bit error (seen as α^5). The received corrupted-codeword polynomial, $r(X)$, is then represented by the sum of the transmitted-codeword polynomial and the error-pattern polynomial as follows:

$$r(X) = U(X) + e(X)$$

Following Equation, we add $U(X)$

$$R(x) = (100) + (001)x + (011)x^2 + (100)x^3 + (101)x^4 + (110)x^5 + (111)x^6$$

In this example, there are four unknowns—two error locations and two error values. Notice an important difference between the nonbinary decoding of $r(X)$ that we are faced with in Equation and binary decoding; in binary decoding, the decoder only needs to find the error locations. Knowledge that there is an error at a particular location dictates that the bit must be “flipped” from 1 to 0 or vice versa. But here, the non-binary symbols require that we not only learn the error locations, but also determine the correct symbol values at those locations. Since there are four unknowns in this example, four equations are required for their solution.

2.7.1 ERROR LOCATION

Suppose there are v errors in the codeword at location $X^{j1}, X^{j2}, \dots, X^{jv}$. Then, the error polynomial $e(X)$ shown

$$E(x) = e_{j1}x^{j1} + e_{j2}x^{j2} + \dots + e_{jv}x^{jv}$$

The indices 1, 2, ... v refer to the first, second, ..., vth errors, and the index j refers to the error location. To correct the corrupted codeword, each error value e_{jl} and its location X^{j1} , where $l = 1, 2, \dots, v$, must be determined. We define an error locator number as $j1 \beta = \alpha$. Next, we obtain the $n - k = 2t$ syndrome symbols by substituting α_i into the received polynomial for $i = 1, 2, \dots, 2t$

There are 2t unknowns (t error values and t locations), and 2t simultaneous equations. However, these 2t simultaneous equations cannot be solved in the usual way because they are nonlinear (as some of the unknowns have exponents). Any technique that solves this system of equations is known as a Reed-Solomon decoding algorithm.

III. LOW-COMPLEXITY CHASE DECODING OF RS CODES

Reed Solomon codes are error-correcting codes that have found wide-ranging applications throughout the fields of digital communication and storage. Some of which include:

- Storage Devices (hard disks, compact disks, DVD, barcodes, etc.)
- Wireless Communication (mobile phones, microwave links, etc.)
- Digital Television
- Broadband Modems (ADSL, xDSL, etc.)
- Deep Space and Satellite Communications Networks (CCSDS)

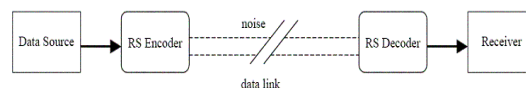


Fig 2: Applications of RS code

RS codes are systematic linear block codes, residing in a subset of the BCH codes called non-binary BCH. It is block because the original message is split into fixed length blocks and each block is split into m bit symbols; linear because each m bit symbol is a valid symbol; and systematic because the transmitted information contains the original data with extra CRC or 'parity' bits appended. These codes are specified as RS (n, k), with m bit symbols. This means that the encoder takes k data symbols of m bits each, appends n - k parity symbols, and produces a code word of n symbols (each of m bits).

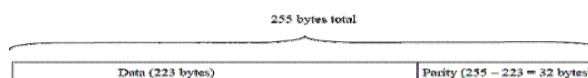


Fig 3: Modified REED SOLMON code

Reed Solomon codes are based on a specialized area of mathematics known as Galois fields (a.k.a. finite fields). These fields are of the form GF (p^m), where p is prime. RS makes use of Galois fields of the form GF (2^m), where elements of the field can be represented by m binary bits. Hence, RS codes of the form RS (2^8) lend themselves well to digital communication. Reed-Solomon codes are powerful error-correcting codes that can be found in a wide variety of digital communications systems, from digital media to wireless communications and deep-space probes. The ubiquitous nature of these codes continues to fuel

research into decoding algorithms some forty years after their introduction. Reed-Solomon codes have been employed in a wide spectrum of digital communications systems because they provide powerful error correction with only a small number of overhead symbols. Reed-Solomon codewords consist of non-binary symbols and therefore the correction of a single symbol could result in the correction of more than one of the constituent bits. For this reason, Reed-Solomon codes are well suited to the correction of burst errors. Classical decoders for Reed-Solomon codes of length n and dimension k can correct up to $t = \lfloor \frac{d_{\min}}{2} \rfloor$ errors where $d_{\min} = (n - k + 1)$ is the minimum distance of the code. Recently, a new class of list decoding algorithms has been introduced that can sometimes correct an even greater number of errors. The list decoding problem is to find the set of codewords at a Hamming distance of t_0 from the received word. If $t_0 > \frac{d_{\min}}{2}$ there might not be a unique codeword so the decoder returns a list of candidate codewords. The Guruswami-Sudan (GS) list decoding algorithm has t_0 as large as $n - p - nk$ errors. To improve the error-correction capability of a decoder even further, the decoder should take advantage of the soft reliability information available from the channel. Soft-decision decoders can provide an asymptotic gain of 2-3 dB on Gaussian channels and 10 dB or more on Rayleigh fading channels. Traditional hard-decision Reed-Solomon decoding algorithms are efficient because they are algebraic; that is, they exploit the underlying algebraic structure of the code to generate a system of equations that is solved using finite field arithmetic. However, an algebraic decoder based on finite field arithmetic does not appear to be compatible with the real-valued, soft information available from the channel and therefore it has been a research challenge to develop an algebraic soft-decision Reed-Solomon decoder. Koetter and Vardy have recently proposed an algebraic soft decision decoding algorithm by extending the list decoder of Guruswami and Sudan to include a method for converting soft information into algebraic conditions. The Koetter-Vardy (KV) algorithm can achieve up to about 4 dB of coding gain at a frame-error-rate (FER) of 10^{-3} on a Gaussian noise channel (with a practical range of 1-1.5 dB) and gains of 2-7 dB on a Rayleigh fading channel. The Koetter-Vardy soft-decision decoding procedure shows a lot of promise from the point of view of error correcting performance. At a first glance, the algorithm seems to be quite computationally complex and not straightforward to implement in VLSI. This paper aims to introduce techniques that reduce the complexity of interpolation-based decoders to the point where an efficient VLSI implementation is possible. A review of the GS and KV list-decoding algorithms. The techniques for significantly reducing the complexity and memory requirements of interpolation-based decoders. A VLSI architecture is then developed that reduces the complexity of evaluating the Hasse derivative, one of the main tasks in interpolation.

IV. INTERPOLATION-BASED LIST DECODING

ALGORITHM

We want to transmit a message f . The bits of the message can be grouped into $\log_2(q)$ -bit symbols chosen from the finite field with q elements, $GF(q)$. An (n, k) Reed-Solomon code over $GF(q)$ represents the k -symbol

message, $f = (f_0, f_1, f_2, \dots, f_{k-1})$ by an n -symbol codeword, $c = (c_0, c_1, c_2, \dots, c_{k-1}, \dots, c_{n-1})$, where $n > k$ and usually $n = q - 1$. The k symbols of the message f can be considered to be the coefficients of the up to degree $(k - 1)$ univariate message polynomial:

$$f(x) = f_0 + f_1x + f_2x^2 + \dots + f_{k-1}x^{k-1}.$$

We use the classical view of Reed-Solomon codes taken from the original definition, with this evaluation map encoding method, a codeword is formed by evaluating the message polynomial $f(x)$ at n elements of $GF(q)$. If the set of evaluation elements is $X = \{x_0, x_1, \dots, x_{n-1}\}$, the codeword c is:

$$c = (f(x_0), f(x_1), \dots, f(x_{n-1})), \quad x_i \in X.$$

We will always assume that $n = q - 1$ and the set of evaluation elements X is the set of nonzero elements of $GF(q)$:

$$X = \{x_0, x_1, x_2, \dots, x_{n-1}\} = \{1, \alpha, \alpha^2, \dots, \alpha^{n-1}\}$$

where α is a primitive n 'th root of unity. The evaluation map encoding method is useful because, it provides insight leading to interpolation-based decoding algorithms.

Guruswami-Sudan algorithm

An interpolation-based decoder takes the point of view that a codeword is a message polynomial evaluated at points in a finite field and uses polynomial interpolation to try to reconstruct that polynomial. The Guruswami-Sudan (GS) algorithm is an interpolation-based list decoder for Reed-Solomon codes. To describe the algorithm, we will first need to review some notation and facts about bivariate polynomials, which are the basic data structures in the algorithm. Consider the bivariate polynomial with coefficients chosen from a finite field:

$$P(x, y) = \sum_{a=0}^{\infty} \sum_{b=0}^{\infty} p_{a,b} x^a y^b \in GF(q)[x, y].$$

Consider the received word $y = c + e$, where e is an error vector with components drawn from $GF(q)$. Since each component of c was generated by evaluating $f(x)$ at a unique value of $x \in X$, a unique x_i can be associated with each received $y_i \in GF(q)$ to form the list of points,

$$L = \{(x_0, y_0), (x_1, y_1), \dots, (x_{n-1}, y_{n-1})\}.$$

If there is no noise ($e = 0$), then $y_i = f(x_i)$, $0 \leq i < n$, and a bivariate polynomial, $P(x, y) = y - f(x)$, passes through all the points in L with a multiplicity of one. This suggests that an interpolation-based approach can be used to decode Reed-Solomon codes. In the presence of noise ($e \neq 0$), the interpolation polynomial will pass through some points that are not part of the codeword. The GS algorithm ensures that under certain conditions, the codeword polynomial "lives inside" the interpolation polynomial [2, 3]. The GS algorithm is an interpolation-based list decoder with two main steps:

1. Interpolation Step: Given the set of points L and a positive integer m , compute $P(x, y)$ of $GF(q)[x, y] \setminus \{0\}$ of minimal $(1, k - 1)$ -weighted degree that passes through all the points in L with multiplicity at least m .

2. Factorization Step: Given the interpolation polynomial $P(x, y)$, identify all the factors of $P(x, y)$ of the form $y - f(x)$ with $\deg f(x) < k$. The output of the algorithm is a list of the code words that correspond to these factors.

A complete factorization of $P(x, y)$ is not necessary since we are just looking for linear y -roots of degree $< k$. An appropriate root-finding algorithm is given. The multiplicity, m , functions as a user-selectable complexity parameter. The error-correcting ability of the GS algorithm increases as the value of m increases. Unfortunately, so does the decoding complexity. Primitive polynomials are of interest here because they are used to define the Galois field.

A popular choice for a primitive polynomial is:

$$p(x) = x^8 + x^7 + x^2 + x^1 + 1$$

This is also known as the 0x87 polynomial, corresponding to the binary representation of the polynomial's coefficients excluding the MSB (i.e. 10000111). This specific polynomial is used in the CCSDS specification for a RS (255, 223). In GF (2⁸) there are 16 possible primitive polynomials.

The VOCAL implementation has the ability to perform all combinations of RS (n, k) [$n = 255$, and $0 < k < n$], for any of the 16 possible Galois fields, including the 0x87 field used by CCSDS. Additionally, the VOCAL RS modules can use any arbitrary generator polynomial for the calculation of the parity symbols.

V. REED SOLOMON IMPLEMENTATIONS

The implementations below can be customized to work with other RS (n, k) codes to yield similar results in performance. Optimized Software Implementation: The pure software implementation is dominated computationally by multiplication over a finite field (Galois Field multiplication). The encoder requires 71,181 cycles per codeword on a MIPS32 processor and the decoder requires 66,045 cycles. Scalar GF Multiply Support: This is the simplest form of VOCAL's hardware acceleration. The Scalar GF Multiply Support extends the capabilities of the MIPS32 processor by taking advantage of MIPS Technologies CorExtend capability to decrease the number of cycles to 23,305 cycles to encode and 9,174 cycles per codeword to decode on the MIPS32 processor. SIMD GF Multiply Support: The SIMD GF Multiply Support requires 128 bytes of local ROM Memory, but increases the performance to 3,918 cycles per megabit to encode and 3,078 cycles per codeword to decode. RS Encode Kernel. The RS Encode Kernel uses 1024 bytes of local ROM memory to encode. The number of cycles to process a codeword on a MIPS32 CPU falls to 2,702 cycles for encoding and decoding only consumes 828 cycles with this implementation.

5.1 METHODOLOGIES

Methodologies are the principles and explanations of High-Throughput Interpolator Architecture for Low-Complexity Chase Decoding of RS Codes. And here we have Five types of modules are used.

MODULES

1. Registers
2. Multiplexers

3. D-flipflop
4. Gf(2⁸) multiplier
5. Gf(2⁸) adder
6. Polynomial Evaluation
7. Polynomial update

MODULE DESCRIPTIONS

5.1.1 REGISTERS

Actual definition of Register is "a combinational of flip-flops". Flip-flops are used as data storage elements. Such data storage can be used for storage of computer science, and such a circuit is described as sequential logic. **Shift Register** is another type of sequential logic circuit that is used for the storage or transfer of data in the form of binary numbers and then "shifts" the data out once every clock cycle, hence the name "shift register". It basically consists of several single bits "D-Type Data Latches", one for each bit (0 or 1) connected together in a serial or daisy-chain arrangement so that the output from one data latch becomes the input of the next latch and so on. The data bits may be fed in or out of the register serially, i.e. one after the other from either the left or the right direction, or in parallel, i.e. all together. The number of individual data latches required to make up a single **Shift Register** is determined by the number of bits to be stored with the most common being 8-bits wide.

The Shift Register is used for data storage or data movement and are used in calculators or computers to store data such as two binary numbers before they are added together, or to convert the data from either a serial to parallel or parallel to serial format. The individual data latches that make up a single shift register are all driven by a common clock signal making them synchronous devices. Generally, shift registers operate in one of four different modes with the basic movement of data through a shift register being:

- **Serial-in to Parallel-out** - In this serial-in to parallel-out, the register is loaded with serial data, one bit at a time, with the stored data being available in parallel form.
- **Serial-in to Serial-out** - In this serial-in to serial-out, the register is loaded with the serial data is shifted serially "IN" and "OUT" of the register, one bit at a time in either a left or right direction under clock control.
- **Parallel-in to Serial-out** - In this parallel-in to serial-out, the register is loaded with the parallel data is loaded into the register simultaneously and is shifted out of the register serially one bit at a time under clock control.
- **Parallel-in to Parallel-out** - In this parallel -in to parallel-out, the register is loaded with the parallel data is loaded simultaneously into the register, and transferred together to their respective outputs by the same clock pulse.
- **Universal shift registers**- Today, high speed bi-directional "universal" type Shift Registers are available as a 4-bit multi-function devices that can be used in either serial-to-serial, left shifting, right shifting, serial-to-parallel, parallel-to-serial, and as a parallel-to-parallel multifunction data register, hence the name "Universal". These devices can perform any combination of parallel and serial input to output

operations but require additional inputs to specify desired function and to pre-load and reset the device.

5.1.2 MULTIPLEXERS

A 2n-to-1 multiplexer sends one of 2n input lines to a single output line. A multiplexer has two sets of inputs: 2n data input lines, n select lines, to pick one of the 2n data inputs. The mux output is a single bit, which is one of the 2n data inputs. A 2n-to-1 multiplexer routes one of 2n input lines to a single output line. Just like decoders, muxes are common enough to be supplied as stand-alone devices for use in modular designs. Muxes can implement arbitrary functions. Smaller muxes can be combined to produce larger ones. It can add active-low or active-high enable inputs. As always, we use truth tables and Boolean algebra to analyze things. Tune in tomorrow as we start to discuss how to build circuits to do arithmetic.

5.1.3 D-FLIP-FLOP

There are some circuits that are not quite as straight forward as the gate circuits. However, we still need to learn about circuits that can store and remember information. They're the kind of circuits that are used in computers to store program information - RAM memory. The combination of two flip-flops constitutes a D-type flip-flop. That's D because the output of the flip-flop is delayed by the time of one clock pulse. Set a value for the data and pulse the clock ON and OFF. We'll find a copy of the data appearing at the output on the trailing edge of the clock pulse. Now, if we consider the combination of two flip-flops as a unit, we have a D flip-flop. It's called a D flip-flop because it delays the signal. The signal appears at the output of the circuit delayed by the time of one clock pulse.

5.1.4 GF (2⁸) MULTIPLIER

Galois Field Theory (GFT) deals with numbers that are binary in nature, have the properties of a mathematical "field," and are finite in scope. Although some Galois computations don't exist in ordinary mathematics, many Galois operations match those of regular math. Addition (Ex-Or) and multiplication are common Galois operations, and logarithms, particularly, are handy for checking multiplication results. For over 40 years, Galois Field multipliers have been used both for coding theory and for cryptography. Both areas are complex, with similar needs, and both deal with fixed symbolic alphabets that neatly fit the extended Galois Field model.

This application note will focus primarily on cryptographic applications of GFT, and will present some practical design solutions that have been synthesized and simulated for ready use. While the basic multiplier structure used by the solutions clearly has its roots in the designs of Berlekamp and Massey from the 1960s, the specific structure used here comes from a more recent paper by Johann Großschädl at IAIK (Graz University of Technology, Austria). This application note does not delve deeply into GFT, although its appendices point out some enlightening tutorial material for interested readers. Its goal instead is to deliver a series of multiplier solutions and verify their correctness and usability. The specific results and tools presented will then be applicable to other multiplier versions of varying lengths. To this end, we

first present a 4-bit multiplier and its verification. We then expand it into an 8-bit multiplier, doing the same, and finally into a 163-bit multiplier. The larger multiplier can eventually be used as part of a solution for Elliptic Curve Cryptography using one of the NIST-recommended curves and the NIST chosen irreducible polynomial. A complete verification of this larger multiplication is an ordeal, but a few examples will be presented to assure readers of its validity.

5.1.5 The Finite Field GF(2⁸).

The case in which n is greater than one is much more difficult to describe. In cryptography, one almost always takes p to be 2 in this case. This section just treats the special case of p = 2 and n = 8, that is, GF(2⁸), because this is the field used by the new U.S. Advanced Encryption Standard (AES). The AES works primarily with bytes (8 bits), represented from the right as:

$b_7b_6b_5b_4b_3b_2b_1b_0$.

The 8-bit elements of the field are regarded as polynomials with coefficients in the field Z_2 :

$$b_7x^7 + b_6x^6 + b_5x^5 + b_4x^4 + b_3x^3 + b_2x^2 + b_1x^1 + b_0.$$

The field elements will be denoted by their sequence of bits, using two hex digits.

5.1.6 Multiplication in GF(2⁸)

Multiplication in this field is much more difficult and harder to understand, but it can be implemented very efficiently in hardware and software. The first step in multiplying two field elements is to multiply their corresponding polynomials just as in beginning algebra (except that the coefficients are only 0 or 1, and $1 + 1 = 0$ makes the calculation easier, since many terms just drop out). The result would be up to a degree 14 polynomial -- too big to fit into one byte. A finite field now makes use of a fixed degree eight irreducible polynomial (a polynomial that cannot be factored into the product of two simpler polynomials). For the AES the polynomial used is the following (other polynomials could have been used):

$$m(x) = x^8 + x^4 + x^3 + x + 1 = 0x11b \text{ (hex)}.$$

The intermediate product of the two polynomials must be divided by $m(x)$. The remainder from this division is the desired product. This sounds hard, but is easier to do by hand than it might seem (though error-prone). To make it easier to write the polynomials down, adopt the convention that instead of $x^8 + x^4 + x^3 + x + 1$ just write the exponents of each non-zero term. (Remember that terms are either zero or have a 1 as coefficient.)

5. GF (2⁸) ADDER

To add two field elements, just add the corresponding polynomial coefficients using addition in Z_2 . Here addition is modulo 2, so that $1 + 1 = 0$, and addition, subtraction and exclusive-or are all the same. The identity element is just zero: 00000000 (in bits) or 0x00 (hex).

VI. SIMULATION RESULTS

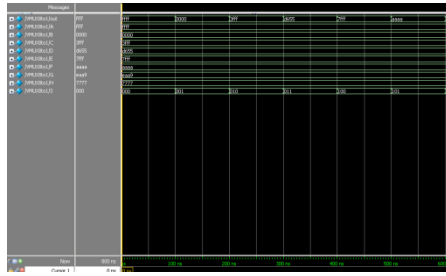


Fig 4: Multiplexer

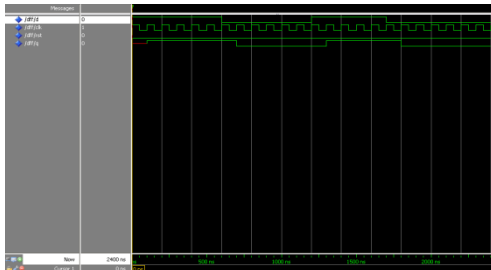


Fig 5: D flip-flop



Fig 6: GF(2⁸) ADDITION



Fig 7: GF(2⁸) MULTIPLIER



Fig 8: 8 - BIT REGISTER

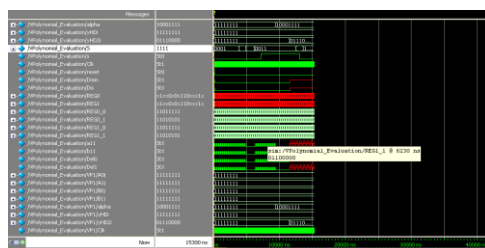


Fig 9: Polynomial Evaluation

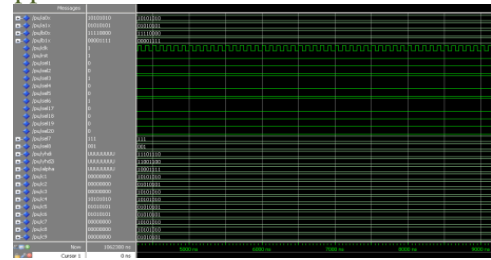
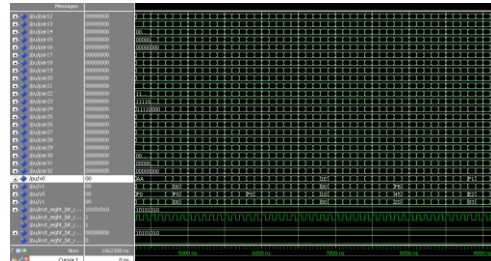


Fig 10,11: Polynomial Update



VII. CONCLUSION

The modified Nielson’s algorithm, which works with a different scheduling, takes care of the limited growth of the polynomials and shares the common interpolation points, for reducing the latency of interpolation. Based on the proposed modified Nielson’s algorithm, we have derived a low-latency interpolator architecture. An LCC decoder using our low-latency interpolator is found to be at least 39% more efficient in terms of area-delay product over the best of previous works.

REFERENCES

- [1] R. Koetter and A. Vardy, “Algebraic soft-decision decoding of Reed–Solomon codes,” *IEEE Trans. Inf. Theory*, vol. 49, no. 11, pp. 2809–2825, Nov. 2003.
- [2] A. Ahmed, N. R. Shanbhag, and R. Koetter, “An architectural comparison of Reed–Solomon soft-decoding algorithm,” *Signals, Syst. Comput.*, pp. 912–916, 2006.
- [3] W. J. Gross, F. R. Kschischang, R. Koetter, and P. G. Gulak, “Architecture and implementation of an interpolation processor for soft-decision Reed–Solomon decoding,” *IEEE Trans. Very Large Scale Integr. (VLSI) Syst.*, vol. 15, no. 3, pp. 309–318, Mar. 2007.
- [4] X. Zhang, “Reduced complexity interpolation architecture for soft-decision Reed–Solomon decoding,” *IEEE Trans. Very Large Scale Integr. (VLSI) Syst.*, vol. 14, no. 10, pp. 1156–1161, Oct. 2006.
- [5] Z. Wang and J. Ma, “High-speed interpolation architecture for softdecision decoding of Reed–Solomon codes,” *IEEE Trans. Very Large Scale Integr. (VLSI) Syst.*, vol. 14, no. 9, pp. 937–950, Sep. 2006.
- [6] J. Zhu and X. Zhang, “Efficient VLSI architecture for soft-decision decoding of Reed–Solomon codes,” *IEEE Trans. Circuits Syst. I, Reg. Papers*, vol. 55, no. 10, pp. 3050–3062, Nov. 2008.
- [7] J. Bellorado and A. Kavcic, “A low-complexity method for Chase-type decoding of Reed–Solomon codes,” *Proc. ISIT*, pp. 2037–2041, Jul. 2006.

- [8] X. Zhang and J. Zhu, "High-throughput interpolation architecture for algebraic soft-decision Reed-Solomon decoding," IEEE Trans. Circuits Syst. I, Reg. Papers, vol. 57, no. 3, pp. 581–591, Mar. 2010.
- [9] J. Zhu, X. Zhang, and Z. Wang, "Backward interpolation architecture for algebraic soft-decision Reed-Solomon decoding," IEEE Trans. Very Large Scale Integr. (VLSI) Syst., vol. 17, no. 11, pp. 1602–1615, 2009.
- [10] T. K. Moon, Error Correction Coding: Mathematical Methods and Algorithms. Hoboken, NJ: Wiley, 2004.
- [11] W. J. Gross, F. R. Kschischang, R. Koetter, and P. G. Gulak, "A VLSI architecture for interpolation-based in soft-decision list decoding of Reed-Solomon decoders," J. VLSI Signal Process., vol. 39, no. 1–2, pp. 93–111, 2005.
- [12] F. Parvaresh and A. Vardy, "Multiplicity assignments for algebraic soft-decoding of Reed-Solomon codes," in Proc. ISIT, 2003, pp. 205–205.
- [13] X. Zhang, "High-speed VLSI architecture for low-complexity Chase soft-decision Reed-Solomon decoding," in Proc. Inf. Theory Applic. Workshop, San Diego, CA, Feb. 2009.
- [14] J. Ma, A. Vardy, and Z. Wang, "Reencoder design for soft-decision decoding of an (255,239) Reed-Solomon code," in Proc. IEEE Int. Symp. Circuits Syst., Island of Kos, Greece, May 2006, pp. 3550–3553.

Authors



S. Susrutha Babu was born in India, A.P. He received the B.Tech degree from JNTU, A.P, and M.Tech degree from SRM University, Chennai, Tamil Nadu, India in 2008 and 2010 respectively. He worked as **Assistant Professor** in Electronics Engineering in Bapatla Engineering College for academic year 2010-2011 and from 2011 to till date working in **K L University**. He is a member of Indian Society for Technical Education and International Association of Engineers. His research interests include antennas, FPGA Implementation, Low Power Design and wireless communications and Digital VLSI. He has published articles in various international journals and Conference in IEEE.



S. Suparshya Babu was born in India, A.P. He received the B.Tech degree from JNTU, A.P, and M.Tech degree from SRM University, Chennai, Tamil Nadu, India in 2008 and 2010 respectively. He worked as **Assistant Professor** in Electronics Engineering in Bapatla Engineering College for academic year 2010-2011 and from 2011 to till date working in **K L University**. He is a member of Indian Society for Technical Education and International Association of Engineers. His research interests include antennas, FPGA Implementation, Low Power Design and wireless communications and Robotics. He has published articles in various international journals and Conference in IEEE



S R Sastry Kalavakolanu was born in A.P,India. He received the B.Tech degree in Electronics & communications Engineering from Jawaharlal Nehru Technological University in 2010. Presently he is pursuing M.Tech VLSI Design in KL University. His research interests include Low Power VLSI Design. He has undergone 3 International Journals and 1 publication in IEEE.



M. Aravind Kumar was born in A.P,India He received his B.Tech degree in Electronics and Communication Engineering from S.V.H college of Engineering and Technology in the year 2005. He is presently pursuing masters in VLSI system design (4th semester) at Padmasri Dr.B.V.Raju Institute of Technology, Medak(dst), A.P.India.



P. Bose Babu was born in A.P,India, He Completed M.Tech in VLSI system Design from MVGR COLLEGE OF ENGG.&TECH, Vizianagaram in 2011 and B.Tech from QIS College of engineering, in 2009 in Electronics & Communication engineering. Presently he is Working as Asst.Professor in ANDHRA LOYOLA college of Engg. & Technology, Vijayawada, A.P,India.



G. Roopa Krishna Chandra was born in A.P,India He received his B.Tech degree in Electronics and Communication Engineering from Sri Sarathi Institute of Engineering and Technology year 2009. He has completed M.Tech in Lakireddy Bali Reddy College of engineering in 2012. His Research areas are Adaptive Signal Processing, Embedded Systems.

Design & Integration of Wind-Solar Hybrid Energy System for Drip Irrigation Pumping Application

Yandra Shivraath¹, P. Badari Narayana², Srikanth Thirumalasetty³, Dr.E.Laxmi Narsaiah⁴

¹Final B.Tech, Department of Electrical Engineering, BVRIT, Narsapur, Medak (DT), A.P, India

²Research Engineer-Energy Systems, Andhra Pradesh, India

³Director – Prolific Energy Needs Pvt Ltd, Secunderabad

⁴Head- Dept of Physics, Chief coordinator, Technology Business Incubator. BVRIT, Narsapur, Medak (DT), A.P, India

Abstract: There is increasing demand for the use of alternate or renewable energy sources to achieve clean and low-cost electricity for agricultural water pumping requirements. The potential for non-thermal onsite power generation also remains enormous in India with increasing investment in small-scale solar and wind power. Promotion of energy production from the combination of sources of energy known as hybrid system is represented by an important objective of meeting the energy demand and justified by environmental protection and increase of energy independence. Design & integration of renewable energy hybrid system also involves the process of selecting the best components and its sizing to provide cheap, efficient, reliable and cost effective renewable energy. During this study a solar and wind hybrid system is optimally designed for a standalone drip irrigation system. It consists of a submersible pump that consumes 2.4 units of electrical energy per day on the average, to drip irrigate 1.5 acres of mango crop. Also, cost optimization of the wind-solar hybrid system is done in this paper to provide useful guidelines for small scale wind-solar hybrid system manufacturers.

Keywords: wind, solar, drip irrigation, cost optimization, solar pumping

I. INTRODUCTION

India possesses a relatively high abundance of sunshine, solar radiation, and moderate wind speeds, hydro, and biomass energy resources. Small scale solar-wind energy systems can make a significant contribution to our nation's energy needs. Indigenous development of small wind power systems up to 25 kW (and hybrids) for stand-alone applications is the objective of new Indian renewable energy act along with the deployment of solar PV Pumps. Drip irrigation system has the potential to solve the problem of food, energy and water security arising from the climate change phenomenon. The merit of drip irrigation technology is that it frees the farmer from the limitations of rain fed farming throughout the year with higher yields while conserving water. Electricity generated from solar-wind hybrid systems can help farmers reduce their electricity costs, an important consideration in the cases of remote farming.

1.1 Definition of hybrid system: - To overcome the drawback of unavailability of power at all times, and to remote places, hybrid systems are developed. In a hybrid

power system, different methods of producing electricity are combined to ensure a continuous power supply. An energy system consisting of two or more generating systems, such as the combination of a wind turbine or diesel generator and a photovoltaic system is termed as a hybrid energy system. Hybrid generation system selected in this design, harnesses both renewable sources of solar power and wind power to form an equivalent of a miniature (or virtual) grid. When the systems are connected together, they will have enhanced reliability, higher efficiency, and lower emissions with an acceptable cost.

1.2 Industry scenario of solar energy generation:-

Complete process of fabrication of a solar panel along with merits and demerits of various solar cells, process techniques and Q/A methodologies have been studied.

Large scale manufacturing of photovoltaic cells, coupled with continued research and development is expected to further make Photovoltaic's within the economic reach of rural areas in India. Cost of multi crystalline solar panel is almost 1\$/Watt now.

II. Configuration Of Hybrid System

The specifications of a hybrid system are derived from a comprehensive understanding of the pumping requirements of the drip irrigation system. Research & development has been carried out to design & develop an integrated and sustainable renewable energy system that supplies electricity to a submersible pump that would cultivate a land of 1.5 acres of mango crop located at Dr.B.V.Raju Institute of Technology, Narsapur, A.P, India. At this area, water depth has been found to be at 120ft below the ground level.

2.1 Water Pumping Requirement:

Submersible pumps are easy to install, have no suction problem, and require no water level guard. Submersible Pump is selected based on the below factors:

- Source of water (well, river, pond, etc.)
- Required pumping flow rate
- Total suction head
- Total dynamic head

To lift this water to the ground levels pump is selected with specifications given in table1:

Table 1. Pumping System Specifications

Total head(meters)	73.1
Discharge(lpm)	90
No of Acres irrigated	1.5
No of liters required/day/acre*	11,100

The Number of liters required/day/acre is calculated by considering the annual average rainfall as zero and also, this value is for the water required for the crop during the dry summer month of May. This value is nearly 1.5 times the annual average requirements of water for the crop.

No. of liters required/day/1.5acre:

$11,100 \times 1.5 = 16,650$ ltrs/day/1.5acre.

No of liters to be pumped/hour : 5,408

Pump running hours/day/1.5acre:

$16,650 / 5,408 = 3.08$ hrs/day/1.5acre.

Table 2. Drip System Specifications

Drippers Capacity(lph)	8
#Drippers	672
Drip system Operation(hrs/day)	3.08

A submersible pump is identified that gives the given Discharge Vs Head requirements.

2.2 Design of Hybrid Energy System:

Reliability and feasibility study of wind-solar hybrid system solution starts with obtaining the meteorological data of the selected place of installation.

2.2.1 Meteorological data required for Solar System:

1. Annual mean daily duration of Sunshine hours
2. Daily Solar Radiation horizontal (KWH/m²/day)

2.2.2 Meteorological data required for Wind System:

1. Mean Annual Hourly Wind Speed (m/sec)
2. Wind Potential in watts that can be harnessed (obtained from Wind map for the location).

The Parameters* that are obtained for the study location are as follows.

*Data obtained from the Indian Meteorological Department (IMD) Hyderabad.

The array factor for circular array is given

Parameter	Design Value
Annual Average Daily Peak Sunshine Hours (ADPS)	9.31
Daily solar Radiation Horizontal(kWh/m ² /day)	3.83
Mean Annual Hourly Wind Speed(m/sec)	3.277

The Various Components of our hybrid system along with their unit specifications are arrived as follows.

Hybrid System Component	Unit Specifications
Sizing of wind generator	700W, 24V DC
Solar Array	240W, 24V DC
Battery sizing	12V, 120Ah
Inverter sizing	3.0kVA

Table 3. Hybrid System Components

2.2.3 Steps to determine Battery Bank Size:

1. Identify total daily use (Calculated from the load list) in Watt-hours (Wh).....(a)
2. Identify Days of Autonomy (backup days); multiply Wh/day by this factor.....(b)
3. Identify Depth of Discharge (DoD) and convert to a decimal value. Divide result of Step (b) by this value.....(c)
4. Divide result from Step (c) by system voltage. Result is the *minimum Amp-hour (Ah) capacity* of your battery bank as per standard operating conditions.

Calculate Battery Bank Size by above approach to give the values below:

Example:

Step 1: Daily Usage (calculated from the load list.) in Watt hours = 2698.08Wh/day.

Load List:

Appliance	Qty	Watts(V*I)	Hrs/day	Wh/day
Electric Motor	1	876	3.08	2698.08

Step 2 : Days of Autonomy (backup days) multiply with Wh/day: $2698.08 \times 1 = 2698.08$ Wh

Step 3 : Depth of Discharge (DoD) 80% and divide step 2 by this value: $2698.08 / 0.80 = 3372.6$ Wh.

Step 4 : Divide result of step 3 by the system voltage (here system voltage is 24V): $3372.6 / 24 = 140.525$ Ah.

Battery Bank Capacity: 24v, 141 Ah.

The recommended battery bank comprises of two LMLA (low maintenance lead acid) batteries of capacity 12v, 150Ah that are connected in series to give a total capacity of 24v, 150Ah.

III. Cost Optimization Of Hybrid Energy System

Solar-wind hybrid energy systems involve a significant initial investment, they can be competitive with conventional energy sources when accounted for a lifetime of reduced or avoided utility costs. The cost of the system itself depends on the system chosen, wind resource on the site, electric costs in the area, and the battery bank required. Cost of the Wind-Solar Hybrid system is to be minimized to provide best value for the customer. So the entire system is analyzed for subsystem costs.

IV. Objective Function And Its Optimization

The power output from a combined solar and wind system, P_{cs} may be expressed as

$$P_{cs} = P_s + P_w$$

Where P_w = Total wind turbine power rating in Watts.

The main goal in designing the hybrid Power Generator is to select the optimum number for N_s (number of solar panels) N_w (number of wind turbines).

Assuming the cost to be a linear function of the size, the total cost of a hybrid system C_{cs} , can be written as

$$C_{CS} = N_s C_s + N_w C_w + N_b C_b$$

Where C_s and C_w represent the cost per unit power potential of individual solar and wind power generators, N_s , N_w , and N_b number of PV panel, wind turbine, and battery respectively.

The optimization problem of combined solar and wind systems is expressed by following equation:

The above Objective function is solved by using an optimization solver of Microsoft Office Excel 2007.

Minimize:

$$C_{CS} = N_s C_s + N_w C_w$$

Subjected to $P_s >= 1;$

$$P_w >= 1;$$

$$P_s + P_w >= 1.18KW$$

The power output from a combined solar and wind system 1.18kw is taken as a constraint as per the requirements given for irrigating 1.5acres of mango crop.

The solution results in optimum numbers of solar panel and wind turbine as $N_s=2$ and $N_w=1$ respectively for the desired energy demand.

Similarly, cost of the system for different power requirements with structure are as follows:

POWER REQUIRE D (KW)	Cost of solar $C_s * 1000$ Rs	# of solar panels N_s	Cost of Wind $C_w * 1000$ Rs	# of Wind turbines N_w	Sub cost $(C_s * N_s + C_w * N_w) * 100$ 0 Rs	# of batterie sN_b	Cost of battery bank $C_b * 1000$ Rs	Total Cost $C_{cs} * 100$ 0 Rs
1.4	43.20	3	76	1	119.2	2	34	153.2
1.18	28.8	2	76	1	104.8	2	34	138.8
2.8	43.2	3	228	3	271.2	4	68	339.2
5.0	14.4	1	532	7	546.4	7	119	665.4
7.5	72	5	684	9	756.0	11	187	943.0
10	14.4	1	1,064	14	1,078.4	14	238	1316.4

Table 4: Cost Analysis of Wind solar hybrid energy System

* Considering the cost of battery bank and inverter is Rs.28/Watt.

V. Results & Discussion

Proposed hybrid system:-

For the given requirement, selected power ratings of solar and wind are: 700watt($1*700W=700W$) and 480($2*240W_p=480W_p$)watt respectively.

The performance and energy generated by the Wind turbine can be estimated through power curve given on fig1.

and the total cost of the system is calculated as **1,38,800/-**.

Hybrid System Component	% of cost
Wind turbine	54.75
Solar PV	20.74
Battery & Inverter	24.50

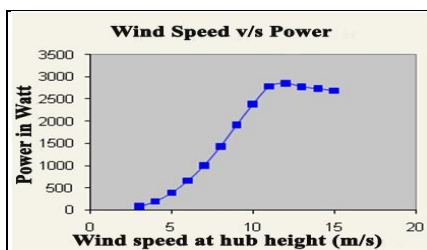


Fig. 1 Power Curve

Drawbacks of independent renewable energy sources are unavailability at all the times and high capital cost, energy availability of rated wind speed requirement. A hybrid energy system helps in overcoming the drawbacks of the renewable energy sources and thus provides continuous supply of electricity.

VI. Conclusions

Solar-Wind Hybrid Systems is the best feasible economic solutions for lowering electricity bills; also they help in avoiding the high costs of extending utility power lines to remote locations, prevent power interruptions, and provide a non-polluting source of electricity. There is a definite need for optimizing the cost of the hybrid Systems based on the various operating and design parameters. In this paper, cost optimization is exercised to minimize the cost of Wind-Solar hybrid system for the given requirement of drip irrigation pumping.

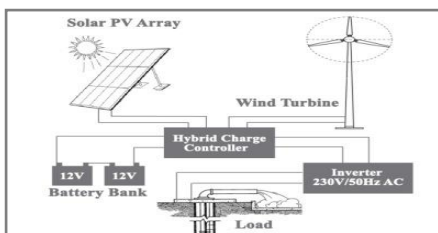


Fig. 2 Hybrid Energy System Model

The optimization problem is solved by using an optimization solver using Matlab. According to the result of the optimization, numbers required for solar panel and wind turbine and battery are computed as 2, 1, and 2 respectively,

The major advantage of wind – solar hybrid energy system is that when used together, the reliability of the system is enhanced. Additionally, the size of battery storage can be reduced. Thus, the analysis performed in this paper will set guidelines to energy consultants or engineers

in designing the hybrid energy system by considering the current industry costs of various subsystem components in order to meet the energy requirement. Remote communities which cannot be reached by electricity grids, except at prohibitive costs, or which do not have easy access to conventional commercial fuels, can easily adopt these hybrid systems for irrigation. This project will there by promote the use of hybrid renewable energy system as a power source for drip irrigation.

VII. Acknowledgement

Authors wish to thank the DC-MSME, Ministry of Micro, small and Medium Enterprises, New Delhi, India for funding and approving the BVRIT as Business Incubator. Also wish to thank the Management and Principal BVRIT for their constant encouragement and support.

References

- [1]. Science & Technology of Photovoltaic's- P. Jayarama Reddy, B.S. Publications
- [2]. <http://www.jains.com/irrigation/drip%20irrigation%20system.htm>
- [3]. Integrated water and nutrient management of young mango crop in tarai region of Uttaranchal by K.K.Singh, P.K.Singh, Pankaj Kr Pandey and K.N.Shukla Precision Farming Development Centre, G.B.Pant University of Agriculture & Technology, Pantnagar-263145, Uttaranchal India, and 3rd Asian Regional Conference.
- [4]. Guidelines for Design of Wind Turbines – DNV/Risø
- [5]. Design Optimization of a Cost-Effective Micro Wind Turbine D.Y.C. Leung, Y. Deng, M.K.H. Leung, Proceedings of the World Congress on Engineering 2010 Vol II WCE 2010, June 30 - July 2, 2010, London, U.K.
- [6]. Optimization and techno-economic analysis of autonomous photovoltaic-wind hybrid energy systems in comparison to single photovoltaic and wind systems,
- [7]. Energy Conversion and Management 43(2002) 2453 2468,
- [8]. www.elsevier.com/locate/enconman
- [9]. Sezai Taskin*,Bahtiyar Dursun,Bora Alboyaci, Performance assessment of a combined solar and wind system, The Arabian Journal for Science and Engineering, Volume 34, Number 1B

Fuzzy Hypothesis Testing Of Anova Model with Fuzzy Data

D. Kalpanapriya and P. Pandian

Department of Mathematics, School of Advanced Sciences, VIT University, Vellore-632 014, INDIA.

Abstract: A new statistical technique for testing the fuzzy hypotheses of one factor ANOVA model using their samples having fuzzy data is proposed without using h-level concept. In the proposed technique, the decision rules that are used to accept or reject the null and alternative hypotheses are provided in which the notions of pessimistic degree and optimistic degree are not used. The idea of the proposed procedure has been clarified by illustrative numerical examples.

Mathematical Subject Classification: 62F03

Keywords: Testing Hypotheses, Fuzzy hypotheses, ANOVA model, Fuzzy data, F-test.

I. Introduction

Analysis of variance (ANOVA) is a statistical technique that will enable us to test the null hypothesis that the three or more populations means are equal against the alternative hypothesis that they are not equal by using their samples information. The ANOVA technique was originally used in the analysis of agricultural research data. Due to the strength and versatility of the technique, the ANOVA technique is now used in all most all research areas especially in Social Science Research and Managerial Decision Making. In traditional statistical testing [7], the observations of sample are crisp and a statistical test leads to the binary decision. However, in the real life, the data sometimes cannot be recorded or collected precisely. The statistical hypotheses testing under fuzzy environments has been studied by many authors using the fuzzy set theory concepts introduced by Zadeh [18]. The application by using fuzzy sets theory to statistics has been widely studied in Manton et al. [8] and Buckley [3] and Viertl [13]. Arnold [2] proposed the fuzzification of usual statistical hypotheses and considered the testing hypotheses under fuzzy constraints on the type I and II errors. Saade [10], Saade and Schwarzlander [11] considered the binary hypotheses testing and discussed the fuzzy likelihood functions in the decision making process by applying a fuzzified version of the Bayes criterion. Grzegorzewski [6] and Watanabe and Imaizumi [14] proposed the fuzzy test for testing hypotheses with vague data, and the fuzzy test gave the acceptability of the null and alternative hypotheses. The statistical hypotheses testing for fuzzy data by proposing the notions of degrees of optimism and pessimism was proposed by Wu [15]. Viertl [12] investigated some methods to construct confidence intervals and statistical tests for fuzzy data. Wu [17] proposed some approaches to construct fuzzy confidence intervals for the unknown fuzzy parameter. Arefi and Taheri [1] developed an approach to test fuzzy hypotheses upon fuzzy test statistic for vague data. A new approach to the problem of testing statistical hypotheses for fuzzy data using the relationship between confidence intervals and testing hypotheses is introduced by Chachi et al.[4]. Mikihiro Konishi et al. [9] proposed the method of ANOVA for the

fuzzy interval data by using the concept of fuzzy sets. Hypothesis testing of one factor ANOVA model for fuzzy data was proposed by Wu [16] using the h-level set and the notions of pessimistic degree and optimistic degree by solving optimization problems.

In this paper, we propose a new statistical fuzzy hypothesis testing of ANOVA model for finding the significance among more than two population means when the data of their samples are fuzzy data. We provide the decision rules which are used to accept or reject the fuzzy null and alternative hypotheses. In the proposed technique, we convert the given fuzzy hypothesis testing of one factor ANOVA model with fuzzy data into two hypothesis testing of one factor ANOVA models with crisp data namely, upper level model and lower level model; then, we test the hypothesis of each of the one factor ANOVA models with crisp data and obtain the results and then, we obtain a decision about the population means on the basis of the proposed decision rules using the results obtained. In the decision rules of the proposed testing technique, we are not using degrees of optimism and pessimism and h-level set which are used in Wu [16]. For better understanding, the proposed fuzzy hypothesis testing technique of ANOVA model for fuzzy data is illustrated with numerical examples.

II. Preliminaries

We need the following results which can be found in [5, 7].

Let $D = \{[a, b], a \leq b \text{ and } a \text{ and } b \text{ are in } \mathbb{R}\}$ the set of all closed bounded intervals on the real line \mathbb{R} .

Result 2.1: Let $A = [a, b]$ and $B = [c, d]$ be in D . Then, $A = B$ if $a = c$ and $b = d$.

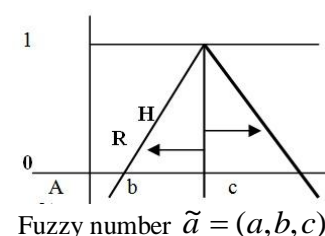
Result 2.2 : If s^2 is the variance of a sample of size n drawn from the population with variance σ^2 , then

$E\left(\frac{ns^2}{n-1}\right) = \sigma^2$, that is, $\frac{ns^2}{n-1}$ is an unbiased estimator of σ^2 .

A triangular fuzzy number $\tilde{a} = (a, b, c)$ can be represented as an interval number form as follows.

$$[\tilde{a}] = [b - (b - a)r, b + (c - b)h];$$

$$0 \leq h, r \leq 1. \tag{1}$$



Note that r is the level of pessimistic and h is the level of optimistic of the fuzzy number $\tilde{a} = (a, b, c)$.

III. One -Factor ANOVA Model

The basic principle of ANOVA technique [7] is to test the difference among the means of populations by studying the amount of variation within each of the samples relative to the amount of variation between the samples. Samples under consideration in ANOVA model are assumed to be drawn from normal populations of equal variances. A one-factor between-subjects ANOVA is used when the analysis involves only one factor with more than two levels and different subjects in each of the experimental conditions.

Consider a sample of size N of a given random variable X drawn from a normal population with variance σ^2 which is subdivided into s classes according to some factor of classification. The main objective is to test the null hypothesis that the factor of classification has no effect on the variables (or) there is no difference between various classes (or) the classes are homogeneous.

Now, let μ_i be the mean of i th population class. The testing hypotheses are given below:

Null hypothesis, $H_0 : \mu_1 = \mu_2 = \dots = \mu_s$ against

Alternative hypothesis, $H_A : \text{not all } \mu_i \text{'s are equal}$

Let x_{ij} be the value of the j th member of the i th class which contains n_i values, \bar{x}_i be the mean value of i th class and \bar{x} be the general mean of all the $N (= \sum_i n_i)$ values.

Now, the total variation, $Q = \sum_i \sum_j (x_{ij} - \bar{x})^2 =$

$$\sum_i \sum_j (x_{ij} - \bar{x}_i)^2 + \sum_i n_i (\bar{x}_i - \bar{x})^2 = Q_2 + Q_1$$

where $Q_1 = \sum_i n_i (\bar{x}_i - \bar{x})^2$ is the variation between

classes and $Q_2 = \sum_i \sum_j (x_{ij} - \bar{x}_i)^2$ is the variation within classes (or) the residual variation.

Now, since i th class is a sample of size n_i from the population with the variance σ^2 , we can conclude that

$M_2 = \frac{Q_2}{N - s}$ is an unbiased estimator of σ^2 with

degrees of freedom $N - s$ and since the entire group is a sample of size N from the population with variance σ^2 ,

we can conclude that $M_1 = \frac{Q_1}{s - 1}$ is an unbiased

estimator of σ^2 with degrees of freedom $s - 1$.

Now, since the population is normal and the estimates M_1 and M_2 are independent, the ratio $\frac{M_1}{M_2}$ or $\frac{M_2}{M_1}$,

whichever is greater than or equal to one, follows a F-distribution with $(s - 1, N - s)$ degrees of freedom in the first case or $(N - s, s - 1)$ degrees of freedom in the later case. Then, we employ the F -test for testing the hypotheses.

The above results are displayed in the form a table, known as the one-factor ANOVA table as given below:

Source of Variation	Sum of Squares	Degrees of freedom	Mean Square	F-value
Between Classes	Q_1	$s - 1$	$M_1 = \frac{Q_1}{s - 1}$	$F = \frac{M_1}{M_2}$
Within Classes	Q_2	$N - s$	$M_2 = \frac{Q_2}{N - s}$	(or) $F = \frac{M_2}{M_1}$

The decision rules in the F-test to accept or reject the null and alternative hypotheses are given below:

(i) If $M_1 < M_2$ and $F = \frac{M_1}{M_2} < F_0$ where F_0 is the

table of F for $(s - 1, N - s)$ degrees of freedom at α level, the null hypothesis is accepted, Otherwise, alternative hypothesis is accepted.

(ii) If $M_2 < M_1$ and $F = \frac{M_2}{M_1} < F_0$ where F_0 is the

table of F for $(N - s, s - 1)$ degrees of freedom at α level, the null hypothesis is accepted, Otherwise, alternative hypothesis is accepted.

Note : For easy computing the values Q , Q_1 and Q_2 , we use the following formulae:

$$Q = \sum_i \sum_j x_{ij}^2 - \frac{T^2}{N} \quad \text{where} \quad T = \sum_i \sum_j x_{ij};$$

$$Q_1 = \sum_i \left(\frac{T_i^2}{n_i} \right) - \frac{T^2}{N} \quad \text{where} \quad T_i = \sum_j x_{ij}$$

and $Q_2 = Q - Q_1$.

IV. Fuzzy One-Factor Anova Model

Suppose that we test the fuzzy hypotheses of one-factor ANOVA model with the data of the given samples are triangular fuzzy numbers. Using the relation (1), we convert the given fuzzy ANOVA model into interval ANOVA model. Construct two crisp ANOVA models from the interval ANOVA model namely, upper level model which is formed using the upper limits of each of

the interval values and lower level model which is formed using the lower limit of each of the interval values. Then, we analyze lower level model and upper level model using the crisp one-factor ANOVA technique.

Let α be the level of significance.

Now, the null hypothesis, $\tilde{H}_0 : \tilde{\mu}_1 = \tilde{\mu}_2 = \dots = \tilde{\mu}_s$ against

the alternative hypothesis, $\tilde{H}_A : \text{not all } \tilde{\mu}_i \text{'s are equal.}$

This implies that the null hypothesis,

$[\tilde{H}_0] : [\tilde{\mu}_1] = [\tilde{\mu}_2] = \dots = [\tilde{\mu}_s]$ against

the alternative hypothesis,

$[\tilde{H}_A] : \text{not all } [\tilde{\mu}_i] \text{'s are equal}$

That is, the null hypothesis,

$[H_0^L, H_0^U] : [\mu_1^L, \mu_1^U] = [\mu_2^L, \mu_2^U] = \dots = [\mu_s^L, \mu_s^U]$

against the alternative hypothesis,

$[H_A^L, H_A^U] : \text{not all } [\mu_i^L, \mu_i^U] \text{'s are equal.}$

This implies the following two sets of hypotheses:

(1) the null hypothesis, $H_0^L : \mu_1^L = \mu_2^L = \dots = \mu_s^L$ against the alternative hypothesis,

$H_A^L : \text{not all } \mu_i^L \text{'s are equal.}$

and

(2) the null hypothesis, $H_0^U : \mu_1^U = \mu_2^U = \dots = \mu_s^U$ against the alternative hypothesis,

$H_A^U : \text{not all } \mu_i^U \text{'s are equal.}$

Note that (1) is the hypotheses of the lower level model and (2) is the hypotheses of the upper level model.

Suppose that if at α level of significance, the null hypothesis of the lower level model is accepted for $0 \leq h \leq h_0$ where $0 \leq h_0 \leq 1$ and the null hypothesis of the upper level model is accepted for $0 \leq r \leq r_0$ where $0 \leq r_0 \leq 1$, then, the fuzzy null hypothesis of the fuzzy

Now, we consider the lower level model. The hypotheses are given below:

Package design (i)	Store j (Observation j)		
	1	2	3
1	11+2h	16+2h	
2	15+4h	15+5h	13+2h
3	18+3h	17+3h	20+3h
4	19+4h	24+3h	

ANOVA model is accepted for $0 \leq h \leq h_0$ and $0 \leq r \leq r_0$ at α level of significance. Otherwise, the fuzzy alternative hypothesis of the fuzzy ANOVA model is accepted at α level of significance.

Remark 4.1. If when $h = 0$ or $r = 0$, that is, center level, the fuzzy null hypothesis of the fuzzy ANOVA model is accepted at α level of significance. Then, only we study about the acceptance levels of null hypothesis in the directions of pessimistic and optimistic.

The proposed statistical technique to test the fuzzy hypothesis of ANOVA model with fuzzy data is illustrated with the following numerical examples.

Example 4.1. A food company wished to test four different package designs for a new product. Ten stores, with approximately equal sales volumes, are selected as the experimental units. Package designs 1 and 4 are assigned to three stores each and package designs 2 and 3 are assigned to two stores each. We cannot record the exact sales volume in a store due to some unexpected situations, but we have the fuzzy data for sales volumes. The fuzzy data are given below:

Package design (i)	Store j (Observation j)		
	1	2	3
1	(9,11,13)	(14,16,18)	
2	(11,15,19)	(10,15,20)	(11,13,15)
3	(15,18,21)	(14,17,20)	(17,20,23)
4	(15,19,23)	(21,24,27)	

We wish to test whether or not the (fuzzy) mean sales are the same for the four designs.

Let $\tilde{\mu}_i$ be the mean sales for the i th design.

Now, the null hypothesis, $\tilde{H}_0 : \tilde{\mu}_1 = \tilde{\mu}_2 = \tilde{\mu}_3 = \tilde{\mu}_4$ against the alternative hypothesis,

$\tilde{H}_A : \text{not all } \tilde{\mu}_i \text{'s are equal.}$

Now, the interval ANOVA model for the given fuzzy ANOVA model is given below:

Package Design (i)	Store j (Observation j)		
	1	2	3
1	[11-2r,11+2h]	[16-2r,16+2h]	
2	[15-4r,15+4h]	[15-5r,15+5h]	[13-2r, 13+2h]
3	[18-3r,18+3h]	[17-3r,17+3h]	[20-3r, 20+3h]
4	[19-4r,19+4h]	[24-3r, 24+3h]	

Now, the upper level model and lower level model for the above interval ANOVA model are given below:

Upper level model: Lower level model:

Package design (i)	Store j (Observation j)		
	1	2	3
1	11-2r	16-2r	
2	15-4r	15-5r	13-2r
3	18-3r	17-3r	20-3r
4	19-4r	24-3r	

the null hypothesis, $H_0^L : \mu_1^L = \mu_2^L = \mu_3^L = \mu_4^L$ and the alternative hypothesis, $H_A^L : \text{not all } \mu_i^L \text{'s are equal.}$

Now, the ANOVA table is given below:

Source of Variation	Sum of Squares	Degree of freedom	Mean square	F-ratio
Between Samples	Q_1^L	3	$M_1^L = \frac{Q_1^L}{3}$	$F_r^L = \frac{M_1^L}{M_2^L}$
Within Samples	Q_2^L	6	$M_2^L = \frac{Q_2^L}{6}$	

where $Q_1^L = 3.73r^2 - 12.73r + 91.26$ and $Q_2^L = 5.17r^2 - 1.6r + 32.34$.

Now, $F_r^L > T$, for all r ; $0 \leq r \leq 0.87$ where $T (= 4.76)$ is the table value of F at 5% level of significance with (3,6) degrees of freedom. Therefore, the null hypothesis H_0^L of the lower level model is rejected for all r ; $0 \leq r \leq 0.87$.

Now, we consider the upper level model. The hypotheses are given below:

the null hypothesis, $H_0^U : \mu_1^U = \mu_2^U = \mu_3^U = \mu_4^U$ and the alternative hypothesis, $H_A^U : \text{not all } \mu_i^U \text{'s are equal.}$

Now, the ANOVA table is given below:

Source of Variation	Sum of Squares	Degree of freedom	Mean square	F-ratio
Between Samples	Q_1^U	3	$M_1^U = \frac{Q_1^U}{3}$	$F_h^U = \frac{M_1^U}{M_2^U}$
Within Samples	Q_2^U	6	$M_2^U = \frac{Q_2^U}{6}$	

where $Q_1^U = 3.73h^2 + 12.73h + 91.26$ and $Q_2^U = 5.17h^2 + 1.6h + 32.34$.

Now, $F_h^U > T$, for all h ; $0 \leq h \leq 1$ where $T (= 4.76)$ is the table value of F at 5% level of significance with (3,6) degrees of freedom. Therefore, the null hypothesis H_0^U of the upper level model is rejected for all h ; $0 \leq h \leq 1$.

Thus, since the null hypotheses H_0^L and H_0^U of the lower level data and upper level data are rejected for all r ; $0 \leq r \leq 0.87$ and h ; $0 \leq h \leq 1$ (note that null hypotheses are not rejected at $r = 0$ and $h = 0$, that is, the centre level), the fuzzy null hypothesis \tilde{H}_0 of the fuzzy ANOVA model is rejected. Therefore, the alternative hypothesis \tilde{H}_A of the fuzzy ANOVA model is accepted. It says that the factor level fuzzy means $\tilde{\mu}_i$ are not equal.

Thus, we conclude that there is a relation between package designs and sales volumes.

Remark 4.2. The decision obtained by the proposed fuzzy hypothesis testing technique for the Example 4.1. is same as in Wu [16].

Example 4.2. Four different machines are used to produce milk pouches of 100 ml each by a city dairy. Before these pouches are dispatched for local distribution, the quality assurance manager selects two samples of pouches from machine1 and machine 4 and three samples of pouches from the machine 2 and the machine3 and determines the number of pouches that does not meet the specifications under the Weights and Measures Act. We cannot record the exact number of pouches in a sample due to some unexpected situations, but we have the fuzzy data for number of pouches. The fuzzy data are given below:

Machine (i)	Sample j		
	1	2	3
1	(8,9,14)	(11,14,18)	
2	(7,11,15)	(8,10,14)	(8,11,14)
3	(12,15,18)	(12,14,19)	(14,17,23)
4	(12,15,19)	(19,21,24)	

Test that there is a significant difference in the performance of the machines.

Let $\tilde{\mu}_i$ be the mean number of non-specifications pouches for the i th machine.

Now, the null hypothesis, $\tilde{H}_0 : \tilde{\mu}_1 = \tilde{\mu}_2 = \tilde{\mu}_3 = \tilde{\mu}_4$ and

the alternative hypothesis, $\tilde{H}_A : \text{not all } \tilde{\mu}_i \text{'s are equal.}$

Now, the interval ANOVA model for the given fuzzy ANOVA model is given below:

Machine (i)	Sample j		
	1	2	3
1	[9-r,9+5h]	[14-3r,14+4h]	
2	[11-4r,11+4h]	[10-2r,10+4h]	[11-3r,11+3h]
3	[15-3r,15+3h]	[14-2r,14+5h]	[17-3r,17+6h]
4	[15-3r,15+4h]	[21-2r,21+3h]	

Now, the upper level model and lower level model for the above interval ANOVA model are given below:

Upper level model: Lower level model:

Machine (i)	Sample j		
	1	2	3
1	9-r	14-3r	
2	11-4r	10-2r	11-3r
3	15-3r	14-2r	17-3r
4	15-3r	21-2r	

Now, we consider the lower level model. The hypotheses are given below:

Machine (i)	Sample j		
	1	2	3
1	9+5h	14+4h	
2	11+4h	10+4h	11+3h
3	15+3h	14+5h	17+6h
4	15+4h	21+3h	

the null hypothesis, $H_0^L : \mu_1^L = \mu_2^L = \mu_3^L = \mu_4^L$ and the alternative hypothesis, $H_A^L : \text{not all } \mu_i^L \text{'s are equal.}$

Now, the ANOVA table is given below:

Source of Variation	Sum of Squares	Degree of freedom	Mean square	F-ratio
Between Samples	Q_1^L	3	$M_1^L = \frac{Q_1^L}{3}$	$F_r^L = \frac{M_1^L}{M_2^L}$
Within Samples	Q_2^L	6	$M_2^L = \frac{Q_2^L}{6}$	

Where $Q_1^L = 1.23r^2 + 3.07r + 82.26$ and $Q_2^L = 5.17r^2 - 8.6r + 35.84$.

Now, $F_r^L < T$, for all $r ; 0 \leq r \leq 0.14$ where T (= 4.76) is the table value of F at 5% level of significance with (3,6) degrees of freedom. Therefore, the null hypothesis H_0^L of the lower level model is accepted for all $r ; 0 \leq r \leq 0.14$.

Now, we consider the upper level model. The hypotheses are given below:

The null hypothesis, $H_0^U : \mu_1^U = \mu_2^U = \mu_3^U = \mu_4^U$ and The alternative hypothesis, $H_A^U : \text{not all } \mu_i^U \text{'s are equal.}$

Now, the ANOVA table is given below:

Source of Variation	Sum of Squares	Degree of freedom	Mean square	F-ratio
Between Samples	Q_1^U	3	$M_1^U = \frac{Q_1^U}{3}$	$F_h^U = \frac{M_1^U}{M_2^U}$
Within Samples	Q_2^U	6	$M_2^U = \frac{Q_2^U}{6}$	

where $Q_1^U = 2.56h^2 - 0.4h + 82.26$ and $Q_2^U = 6.34h^2 - 7h + 35.84$.

Now, $F_h^U < T$, for all $h ; 0 \leq h \leq 0.23$ where T (= 4.76) is the table value of F at 5% level of significance with (3,6) degrees of freedom. Therefore, the null hypothesis H_0^U of the upper level model is accepted for all $h ; 0 \leq h \leq 0.23$.

hypothesis H_0^U of the upper level model is accepted for all $h ; 0 \leq h \leq 0.23$.

Thus, since the null hypotheses H_0^L and H_0^U of the lower level model and upper level model are accepted for all $r ; 0 \leq r \leq 0.14$ and $h ; 0 \leq h \leq 0.23$ (note that null hypotheses are accepted at $r = 0$ and $h = 0$, that is, the centre level), the fuzzy null hypothesis \tilde{H}_0 of the fuzzy ANOVA model is accepted for all $r ; 0 \leq r \leq 0.14$ and $h ; 0 \leq h \leq 0.23$. Thus, we conclude that four machines are equal only if $r ; 0 \leq r \leq 0.14$ and $h ; 0 \leq h \leq 0.23$, that is, the maximum level of pessimistic is 0.14 and the maximum level of optimistic is 0.23.

Remark 4.3. From the Example 4.2., we observe that the acceptance of the fuzzy null hypothesis for not all r and h always, but for some specific levels of r and h , that is, $r ; 0 \leq r \leq 0.14$ and $h ; 0 \leq h \leq 0.23$.

V. Conclusion

In this paper, we propose a new statistical fuzzy hypothesis testing of single-factor ANOVA model with the fuzzy data. In the proposed technique, we transfer the fuzzy ANOVA model into two crisp ANOVA models. Based on the decisions of hypotheses of two crisp ANOVA models, we take a decision on the fuzzy hypothesis of the fuzzy ANOVA model. Since the proposed technique in this paper is mainly based only on the crisp models, the proposed technique can be extended to multi-factor fuzzy ANOVA model and the experimental design analysis having fuzzy data.

References

- [1] M. Arefi and S.M. Taheri, "Testing fuzzy hypotheses using fuzzy data based on fuzzy test statistic". Journal of Uncertain Systems, Vol. 5, 2011, 45-61.
- [2] B.F. Arnold, "Testing fuzzy hypotheses with crisp data", Fuzzy Set. Syst., Vol. 94, 1998, 323-333.
- [3] J.J. Buckley, Fuzzy Statistics, Springer-Verlag, New York, 2005.
- [4] J. Chachi, S. M. Taheri and R. Viertl, "Testing statistical hypotheses based on fuzzy confidence intervals", Forschungsbericht SM-2012-2, Technische Universitat Wien, Austria, 2012
- [5] George J. Klir and Bo Yuan, Fuzzy sets and fuzzy logic, Theory and Applications, Prentice-Hall, New Jersey, 2008.
- [6] P. Grzegorzewski, "Testing statistical hypotheses with vague data", Fuzzy Set. Syst., Vol.112, 2000, 501-510.
- [7] R.R. Hocking, Methods and Applications of Linear Models: Regression and the Analysis of Variance, New York: John Wiley & Sons, 1996.
- [8] K.G. Manton, M.A. Woodbury and H.D. Tolley, Statistical Applications Using Fuzzy Sets, New York: John Wiley & Sons, 1994.

- [9] Mikihiro Konishi, Tetsuji Okuda and Kiyoji Asai, "Analysis of variance based on fuzzy interval data using moment correction method", International Journal of Innovative Computing, Information and Control, Vol. 2, 2006, 83-99.
- [10] J.J. Saade, "Extension of Fuzzy hypothesis testing with hybrid data", Fuzzy Set. Syst., Vol. 63, 1994, 57-71.
- [11] J.J. Saade and H. Schwarzlander, "Fuzzy hypothesis testing with hybrid data", Fuzzy Set. Syst., Vol.35, 1990, 197-212,
- [12] R. Viertl, "Univariate statistical analysis with fuzzy data", Computational Statistics and Data Analysis, Vol. 51, 2006), 33-147.
- [13] R. Viertl, Statistical methods for fuzzy data, John Wiley and Sons, Chichester, 2011.
- [14] N. Watanabe and T. Imaizumi, "A fuzzy statistical test of fuzzy hypotheses", Fuzzy Sets and Systems, Vol. 53 ,1993 , 167-178.
- [15] H.C. Wu, "Statistical hypotheses testing for fuzzy data", Information Sciences, Vol. 175, 2005 , 30-56
- [16] H .C. Wu, "Analysis of variance for fuzzy data", International Journal of Systems Science, Vol. 38, 2007, 235-246.
- [17] H.C. Wu, "Statistical confidence intervals for fuzzy data", Expert Systems with Applications, Vol. 36 ,2009, 2670-2676.
- [18] L.A. Zadeh, "Fuzzy sets", Inform. Contr., Vol. 8, 1965, 338-353.

Reduced Rating VSC with a Zig-Zag Transformer for Current Compensation in a Three-Phase Four-Wire Distribution System

M. Nagarjuna¹, B. Muralimohan², M. Sudheerbabu³

^{1,3}M. Tech student, Department of EEE
Assistant professor, Department of EEE
A.I.T.S Engineering College, Kadapa, India.

Abstract: A detailed investigation is made into the causes, standards, and remedies of the excessive neutral current. A reduced-rating voltage-source converter with a zig-zag transformer for a distribution static compensator is proposed for power-quality improvement in the three-phase four-wire distribution system. The proposed DSTATCOM is employed for the compensation of reactive power, harmonics currents, neutral current, load balancing and the voltage regulation at the point of common coupling. The zig-zag transformer is used for providing a path to the zero-sequence current. The performance of the DSTATCOM is validated through extensive simulations using MATLAB software with its Simulink and power system blockset toolboxes.

Index Terms: Distribution static compensator (DSTATCOM), neutral current compensation, power quality (PQ), zig-zag transformer.

I. INTRODUCTION

Distribution systems are facing severe power-quality (PQ) problems, such as poor voltage regulation, high reactive power and harmonics current burden, load unbalancing, excessive neutral current, etc. The source voltages in the distribution systems are also experiencing PQ problems, such as harmonics, unbalance, flicker, sag, swell, etc. The remedial solutions to the PQ problems are investigated and discussed in the literature and the group of devices is known as custom power devices (CPDs). The distribution static compensator (DSTATCOM) is proposed for compensating PQ problems in the current, and the dynamic voltage restorer (DVR) is used for mitigating the PQ problems in the voltage while the unified power-quality conditioner (UPQC) is proposed for solving current and voltage PQ problems. There are many techniques reported for the elimination of harmonics from the source current as well as the compensation of the neutral current and load balancing. Some neutral current compensation techniques have been patented.

Three-phase four wire distribution systems have been used to supply single-phase low-voltage loads. The typical loads may be computer loads, office automation machines, lighting ballasts, adjustable speeds drives (ASDs) in small air conditioners, fans, refrigerators, and other domestic and commercial appliances, etc., and generally behave as nonlinear loads. These loads may create problems of high input current harmonics and excessive neutral current. The neutral current consists of mainly triplen harmonics currents. The zero-sequence neutral current obtains a path through the neutral conductor. Moreover, the unbalanced

single-phase loads also result in serious zero-sequence fundamental current. The total neutral current is the sum of the zero-sequence harmonic component and the zero-sequence fundamental component of the unbalanced load current, and this may overload the neutral conductor of the three-phase four-wire distribution system.

A number of surveys have been cited about the causes of excessive neutral current in the distribution system. There are different techniques for the mitigation of neutral current in the three-phase four-wire distribution systems. The neutral current compensation using a zig-zag transformer; using a star/delta transformer, using a single-phase active compensator in the neutral path; and using three-phase four-wire active compensators along with source harmonic current compensation are reported in the literature. In this investigation, the causes, standards, and remedial solutions for PQ problems due to the excessive neutral current are analyzed and a technique using a zig-zag transformer along with a reduced rating VSC as a DSTATCOM is designed to mitigate these PQ problems. Moreover, the voltage regulation is also achieved at the point of common coupling (PCC) across the loads.

II. NEUTRAL CURRENT COMPENSATION TECHNIQUES

The major causes of neutral current in three-phase distribution systems are the phase current unbalance, third harmonic currents produced by single-phase rectifier loads, and the third harmonics due to source voltage third harmonics. Even balanced three-phase currents produce excessive neutral current with computer loads in the systems. A study reveals that 22.6% of the sites have a neutral current in excess of 100%. The source voltage distortions in systems with computer loads can cause excessive neutral current. The nonlinear loads are classified into harmonic current source loads and harmonic voltage-source loads.

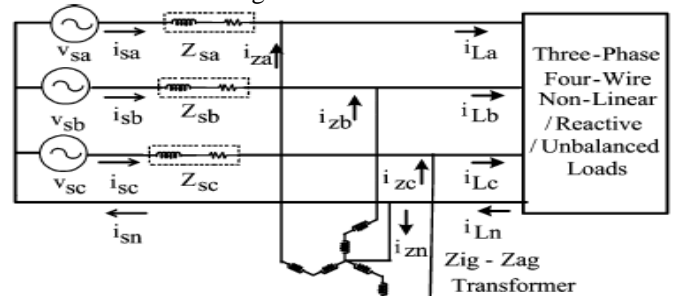


Fig. 1. System configuration with a zig-zag transformer for neutral current compensation.

Various standards are proposed to mitigate PQ problems in the distribution system. The planning for a distribution system, the voltage considerations, calculation of short-circuit capacities, power factor improvement techniques, protective devices, surge protection, and grounding aspects are proposed in IEEE Standard 141-1993. It is a complete guide for an industrial plant power system. The recommended practice for electrical power systems in commercial buildings, the recommendation for harmonic control in power systems, the reference on shunt capacitor design, installation guidelines of improvement of power factor and other applications, the practices for monitoring electrical PQ, and the guide for the application and specification of harmonic filters are available in the literature. In light of the various standards, there are many techniques proposed for the compensation of neutral current in the three-phase four-wire distribution system. These are discussed in the following sections.

A. Zig-Zag Transformer-Based Compensation

The application of a zig-zag transformer for the reduction of neutral current is advantageous due to passive compensation, rugged, and less complex over the active compensation techniques. Fig. 1 shows the connection of a zig-zag transformer in the system and the zig-zag transformer is shown in Fig. 2. A zig-zag transformer is a special connection of three single-phase transformer windings or a three-phase transformer's windings. The zig-zag transformer in the past has been used to create neutral and to convert a three-phase three-wire system into a three-phase four-wire system. The new application of a zig-zag transformer is to connect in parallel to the load for filtering the zero-sequence components of the load currents. The phasor diagram of the zig-zag transformer is shown in Fig. 3. The currents flowing through the utility side of these three transformers are equal. Hence, the zig-zag transformer can be regarded as open-circuit for the positive-sequence and the negative-sequence currents. Then, the current flowing through the zig-zag transformer is only the zero-sequence component.

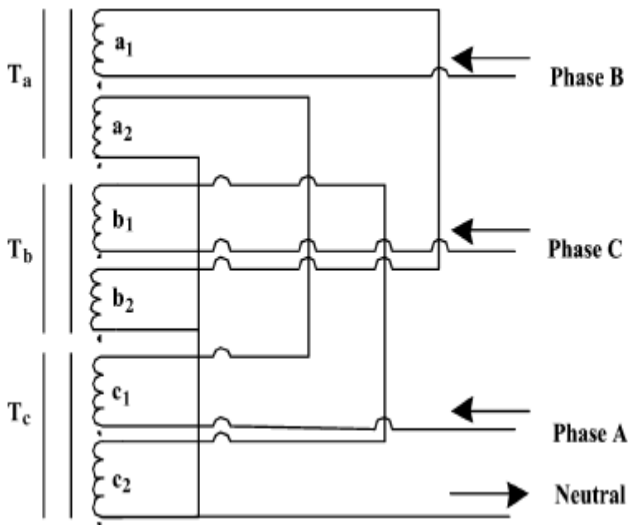


Fig. 2. Zig-zag transformer for neutral current compensation.

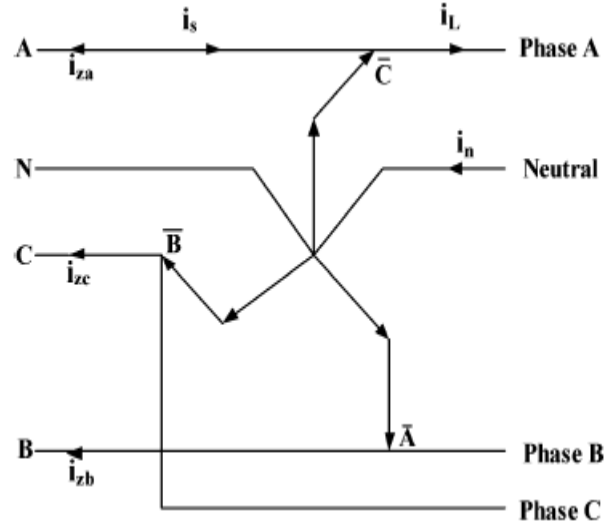


Fig. 3. Diagram showing the flow of currents of zig-zag transformer for neutral current compensation.

An application of a zig-zag transformer alone in a three-phase, four-wire system has the advantages of reduction in load unbalance and reducing the neutral current on the source side. But there are inherent disadvantages such as the performance being dependent on the location of the zig-zag transformer close to the load. Moreover, when the source voltage is distorted or unbalanced, the performance of reducing the neutral current on the source side is affected to an extent.

B. Zig-Zag Transformer With Active Filter-Based Compensation

A hybrid filter consisting of a single-phase VSC and a zig-zag transformer is also efficient in neutral current compensation, and the topology is shown in Fig. 4. A different topology for a single-phase VSC with a self-supporting dc bus and zig-zag transformer-based neutral current compensation system is shown in Fig. 5.

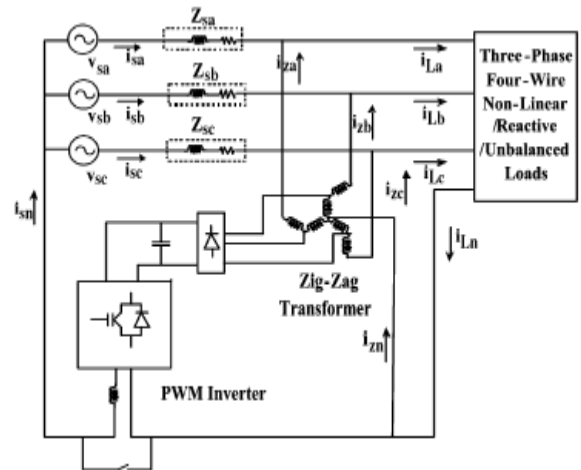


Fig. 4. Reduced rating single-phase inverter with a zig-zag transformer for neutral current compensation.

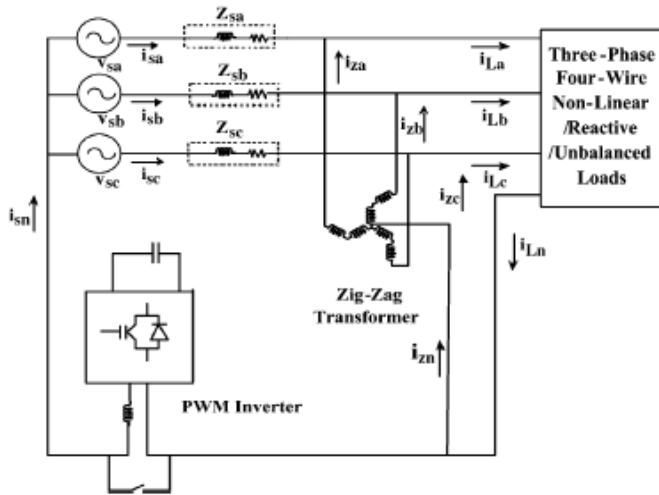


Fig. 5. Hybrid neutral current compensator using a single-phase inverter and zig-zag transformer.

D. Three-Phase Four-Wire Active Compensators

The neutral current along with harmonics, reactive power compensation, and load balancing are achieved using three phase four-wire DSTATCOM-based compensators. Three different topologies for three-phase four-wire DSTATCOMs, such as a voltage-source converter (VSC), with four leg, three single-phase VSC, and three-leg VSC with split capacitors are reported in the literature. Fig. 6 shows a four-leg DSTATCOM, split capacitor-based three-leg DSTATCOM is shown in Fig. 7, shows three single-phase VSC-based DSTATCOMs. Some researchers select the four-leg converter topology as the best alternative compared to others considering the number of switching devices, complexity of control, etc.

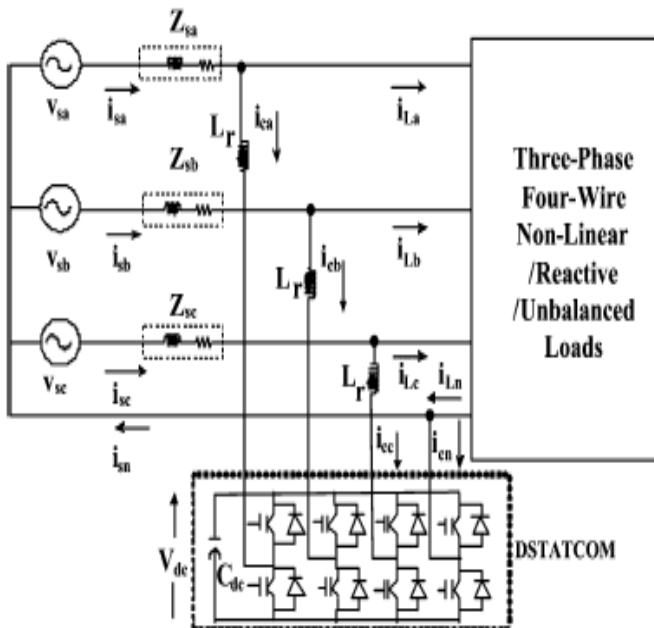


Fig. 6. Three-phase four-leg DSTATCOM for neutral current compensation.

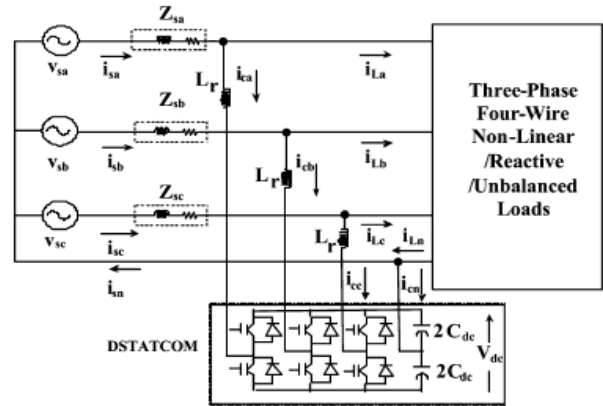


Fig. 7. Three-phase three-leg and split capacitor-based STATCOM for neutral current compensation.

There are different control techniques reported for deriving the reference control signals for the DSTATCOM. The instantaneous reactive power theory (p-q theory), synchronous reference frame (SRF) theory or d-q theory [50], power balance theory, etc., have been proposed to control the DSTATCOM for three-phase four-wire systems. The control of the three-phase four-wire compensation under nonsinusoidal source conditions is verified to be satisfactory in and the method is based on p-q theory. The instantaneous active and reactive powers are calculated after filtering out the harmonics in voltage and the theory is evaluated for a three-phase four-wire four-leg VSC-based system. The three-phase four-wire DSTATCOM-based systems are reported as very effective for the compensation, including neutral current. But this configuration has the disadvantages of a greater number of semiconductor switches, complexity of control, etc. A three-phase three-leg shunt compensator and a zig-zag transformer for neutral current compensation are shown in Fig. 8.

III. PROPOSED REDUCED RATING COMPENSATOR

The proposed compensator is a hybrid of a three-phase, three-wire VSC and a zig-zag transformer as a DSTATCOM. The DSTATCOM rating is reduced due to the elimination of a fourth leg compared to a three phase four-leg VSC-based DSTATCOM. It co-

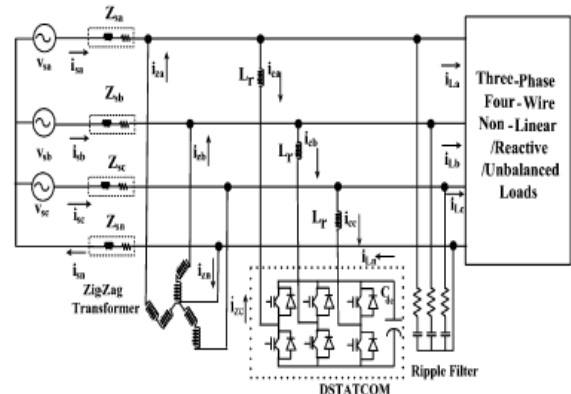


Fig. 8. Three-leg VSC-based DSTATCOM and zig-zag transformer for neutral current compensation.

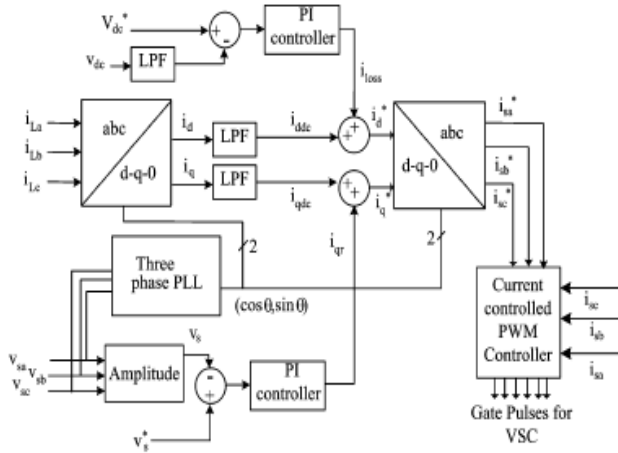


Fig. 9. Synchronous reference frame theory (SRFT)-based control of DSTATCOM.

mpensates for neutral current along with the load voltage regulation, harmonics currents elimination, reactive power compensation, and load balancing. The considered configuration of the proposed system is shown in Fig. 8. The zig-zag transformer connected at the load terminal provides a circulating path for zero-sequence harmonic and fundamental currents.

A. Design of the DSTATCOM VSC

The VSC used as a DSTATCOM in this configuration is a three-leg pulse-width modulated (PWM) insulated-gate bipolar transistor (IGBT)-based VSC. The PWM signals are generated by the control scheme for which the reference source currents and the sensed source currents are the input signals. The rating of the switches is based on the voltage and current rating of the compensation system. For the considered load mentioned in the Appendix, the rating of the VSC is 12 kVA. The selection of the dc bus voltage, dc bus capacitor, ac inductor, and the ripple filter will be given.

1) DC Bus Voltage: The value of the dc bus voltage depends on the instantaneous energy available to the DSTATCOM. For a VSC, the dc bus voltage is defined as

$$V_{dc} = 2\sqrt{2}V_{LL}/(\sqrt{3}m) \quad (1)$$

Where *m* is the modulation index and is considered as 1. Thus, one may obtain the value of *V_{dc}* as 677 V for *V_{LL}* of 415 V. Thus, *V_{dc}* of the value of 680 V is selected.

2) DC Bus Capacitor: The design of the dc capacitor is governed by the reduction in the dc bus voltage upon the application of load and rise in the dc bus voltage on removal of the load.

Using the principle of energy conservation, the equation governing *C_{dc}* is as

$$\frac{1}{2}C_{dc} [(V_{dc}^2) - (V_{dc1}^2)] = 3 V(aI)t \quad (2)$$

where *V_{dc}* is the reference and *V_{dc1}* is the minimum voltage level of the dc bus voltage, *a* is the over loading factor, *V* is

the phase voltage, *I* is the phase current of the VSC, and *t* is the response time of the DSTATCOM and *t* is considered as 350 μ s .

Considering *V_{dc}*= 680 V, *V_{dc1}*= 670 V, *V*=415/3 ,*a*=1.2 , the calculated value of *C_{dc}* is 2600 μ F. So *C_{dc}* is chosen to be 3000 μ F.

3) AC Inductor: The selection of the ac inductance depends on the current ripple *i_{cr,p-p}*. The ac inductance is given as

$$L_f = (\sqrt{3}mV_{dc}) / (12af_s i_{cr(p-p)}) \quad (3)$$

B. Design of the Zig-Zag Transformer

The zig-zag transformer provides a low impedance path for the zero-sequence currents and, hence, offers a path for the neutral current when connected in shunt and, hence, attenuates the neutral current on the source side. When a zig-zag transformer is used alone as a neutral current compensator, the rating of the zig-zag transformer depends on the amount of imbalance and harmonic content. Under the single-phase load, nearly half of the load current flows through the zig-zag windings. All six windings (two windings each of three phases) are rated as 150V, 10 A, and hence, three single-phase transformers of 5-kVA capacity each are selected in this investigation.

Considering 5% current ripple, the switching frequency(*f_s*)=10kHz, modulation index(*m*)=1, dc bus voltage (*V_{dc}*) of 680 V, and overload factor *a*=1.2, the *L_f* value is calculated to be 5.45 mH. The value of *L_f* of 5.5 mH is selected in this investigation.

4) Ripple Filter: A highpass first-order filter tuned at half the switching frequency is used to filter out the noise from the voltage at the PCC. The time constant of the filter should be very small compared to the fundamental time period (*T*)

$$R_f C_f \ll T/10 \quad (4)$$

when *T*=20 ms, considering *C_f*=5 μ F, *R_f* is chosen as 5 Ω . This combination offers a low impedance of 8.1 for the harmonic voltage at a frequency of 5 kHz and 637 Ω for fundamental voltage.

C. Control of DSTATCOM

There are many theories available for the generation of reference source currents in the literature viz. instantaneous reactive power theory (*p-q* theory), synchronous reference frame theory, power balance theory, etc. The synchronous reference frame theory-based method is used for the control of DSTATCOM. A block diagram of the control scheme is shown in Fig. 9. The load currents(*I_L*) , the source voltages,*(V_s)* and dc bus voltage (*V_{dc}*) of DSTATCOM are sensed as feedback signals. The loads currents in the three phases are converted into the d-q -0 frame using the Park's transformation as in (5)

$$\begin{bmatrix} i_d \\ i_q \\ i_0 \end{bmatrix} = \frac{2}{3} \begin{bmatrix} \cos \theta & -\sin \theta & \frac{1}{2} \\ \cos(\theta - \frac{2\pi}{3}) & -\sin(\theta - \frac{2\pi}{3}) & \frac{1}{2} \\ \cos(\theta + \frac{2\pi}{3}) & \sin(\theta + \frac{2\pi}{3}) & \frac{1}{2} \end{bmatrix} \begin{bmatrix} i_{La} \\ i_{Lb} \\ i_{Lc} \end{bmatrix} \quad (5)$$

A three-phase phase-locked loop (PLL) is used to synchronize these signals with the source voltage. The d-q components are then passed through lowpass filters to extract the dc components of i_d and i_q . The error between the

reference dc capacitor voltage and the sensed dc bus voltage of DSTATCOM is given to a proportional-integral (PI) controller whose output is considered the loss component of the current and is added to the dc component of i_d . Similarly, a second PI control-

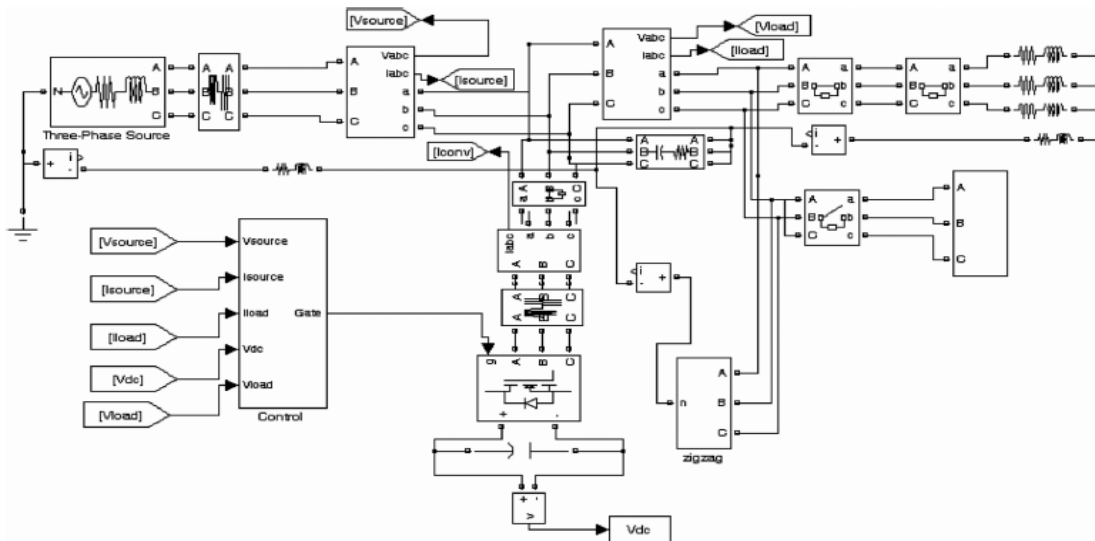


Fig. 10. MATLAB model of the three-phase three-leg DSTATCOM and zig-zag transformer for neutral current compensation. The amplitude of the load terminal voltage and its reference value are fed to a PI controller and the output of the PI controller is added with the dc component of i_q . The control strategy is to regulate the terminal voltage and the elimination of harmonics in the load current and load unbalance. The resulting currents are again converted into the reference source currents using the reverse Park's transformation. The reference source currents and the sensed source currents are used in the PWM current controller to generate gating pulses for the switches. For the power factor correction, only the dc bus voltage PI controller is used in the control algorithm.

IV. MATLAB-BASED MODELING OF DSTATCOM

The neutral current compensation using a zig-zag transformer is modeled and simulated using the MATLAB and its Simulink and Power System Blockset toolboxes. Fig. 10 shows the MATLAB model of the DSTATCOM and zig-zag transformer- connected system for neutral current compensation. The considered load is a lagging power factor load. The ripple filter is connected to the VSC of the DSTATCOM for filtering the ripple in the terminal voltage. The system data are given in the Appendix.

The control algorithm for the DSTATCOM is also modeled in MATLAB. The reference source currents are derived from the sensed voltages (V_s), load currents (i_L), and

the dc bus voltage of DSTATCOM (V_{dc}). A PWM current controller is used over the reference and sensed source currents to generate the gating signals for the IGBTs of the DSTATCOM VSC.

V. RESULTS AND DISCUSSION

Some of the important neutral current mitigation techniques are analyzed and modeled using MATLAB. The performance of harmonic neutral current compensation using the zig-zag transformer for the nonlinear load and linear load are shown Fig. 11. Performance of the three-phase three-leg VSC and zig-zag transformer of the DSTATCOM for neutral current compensation, load balancing, and

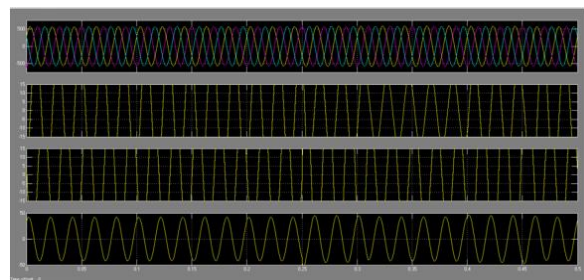


Fig. 11. Performance of the zig-zag transformer for fundamental neutral current compensation.

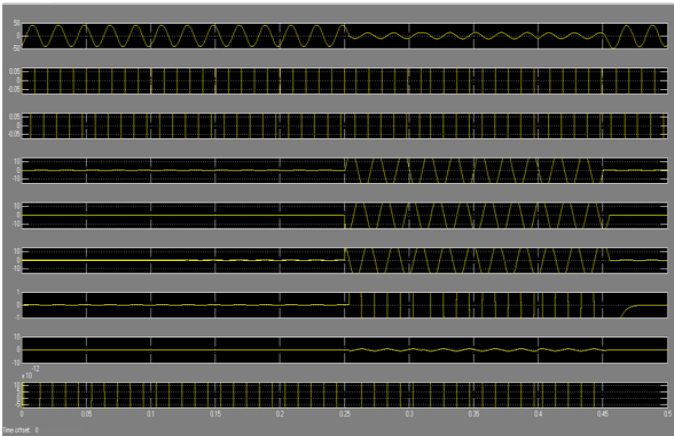


Fig. 12. Performance of the three-phase three-leg VSC and zig-zag transformer of the DSTATCOM for neutral current compensation, harmonic compensation, and voltage regulation.

power factor correction. in Figs. 11 and 12, respectively. The voltages (V_s), source currents (i_{sa} , i_{sb} , i_{sc}), load currents (i_{La} , i_{Lb} , i_{Lc}), zig-zag transformer currents (i_{za} , i_{zb} , i_{zc}), load neutral current (i_{Ln}), source neutral current (i_{sn}), and zig-zag transformer neutral source neutral current (i_{Sn}) and zig-zag neutral current (i_{Zn}) are demonstrated. It is observed that the zig-zag transformer has compensated the load neutral current, resulting in a source neutral current of nearly zero. The performance using a three-phase four-leg DSTATOM for voltage regulation along with neutral current compensation and load balancing of a three-phase four-wire load is shown in Fig. 13.

The voltages (V_s), balanced source currents (i_s), load currents (i_L), compensator currents (i_C), load neutral current (i_{Ln}), compensator neutral current (i_{Zn}), source neutral current (i_{sn}), amplitude of the load terminal voltage (V_s), and dc bus voltage (V_{dc}) are demonstrated under changing load conditions. It is observed that the amplitude of the load voltage is regulated to the reference amplitude by the required reactive power compensation.

The performance using a three-phase four-leg DSTATOM for voltage regulation along with neutral current compensation and load balancing of a three-phase four-wire load is shown in Fig. 13. The voltages (V_s), balanced source currents (i_s), load currents (i_L), compensator currents (i_C), load neutral current (i_{Ln}), compensator neutral current (i_{Zn}), source neutral current (i_{sn}), amplitude of the load terminal voltage (V_s), and dc bus voltage (V_{dc}) are demonstrated under changing load conditions. It is observed that the voltage amplitude is regulated to the reference value under all load disturbances. The source current is balanced, even though the load current is highly unbalanced and this is achieved by using the unbalanced fundamental current injection by the DSTATCOM. The zero-sequence fundamental current of the load neutral current resulting from the unbalanced load current is circulated in the zig-zag transformer, and hence, the source neutral current is maintained at nearly zero. The dc bus voltage of the VSC of DSTATCOM is regulated by the controller and the voltage is maintained near the reference

voltage under all load disturbances. The performance of the DSTATCOM with a zig-zag transformer for voltage regulation and harmonic elimination along with neutral current

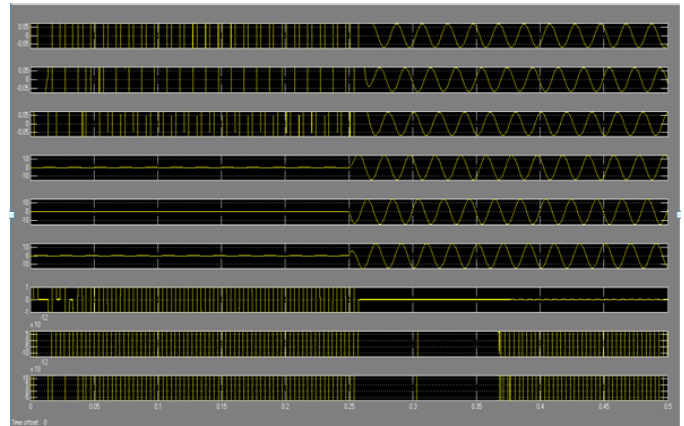


Fig. 13. Performance of the three-phase three-leg VSC and zig-zag transformer of the DSTATCOM for neutral current compensation, load balancing, and power factor correction.

compensation is shown in Fig. 14. The voltages (V_s), balanced source currents (i_s), load currents (i_L), compensator currents (i_C), load neutral current (i_{Ln}), compensator neutral current (i_{Zn}), source neutral current (i_{sn}), amplitude of the load terminal voltage (V_s), and dc bus voltage (V_{dc}) are demonstrated under various nonlinear loads. It is observed that the terminal voltage is regulated to the reference value.

The dynamic performances of the DSTATCOM system in the unity power factor (UPF) mode of operation are depicted in Figs. 13 and 14. The load balancing and neutral current compensation are demonstrated in Fig. 18 and the harmonic elimination and neutral current compensation are demonstrated in Fig. 14. The voltages (V_s), balanced source currents (i_s), load currents (i_L), compensator currents (i_C), load neutral current (i_{Ln}), compensator neutral current (i_{Zn}), source neutral current (i_{sn}), amplitude of the load terminal voltage (V_s), and dc bus voltage (V_{dc}) are shown in both cases. It is also observed that the terminal voltage is not regulated in both cases as the compensator operates in the UPF mode.

These results show that the zig-zag transformer is able to compensate for the fundamental and harmonic neutral current. The rating of the transformer used for the zig-zag connection depends on the neutral current on the load side. The three-phase four-wire DSTATCOM compensates for the neutral current along with harmonic and reactive current compensation in the phase current. But additional IGBTs are required for neutral current compensation. A hybrid of a three-wire DSTATCOM and zig-zag transformer is also able to perform satisfactorily and the advantage is that it uses a readily available three-wire VSC as a DSTATCOM and a passive zig-zag transformer. The comparison of the rating of DSTATCOM and zig-zag transformer compensators during different compensation methods is given in Table I. The rating of the VSC is reduced to 12 kVA where as it is 16 kVA for a four-leg DSTATCOM. The current magnitude and total

harmonic distortion (THD) are compared in the three cases and are shown in Table II. The THD of unbalanced load currents is nearly 85%, when the load is a voltage-source rectifier. When a zig-zag transformer is employed, the source neutral current is reduced to 0.11 A, whereas the load neutral current is 16 A. But the source-phase currents are balanced and with reduced THD, when a DSTATCOM is also employed as a voltage regulator. The additional benefit of terminal voltage regulation is also demonstrated in Figs. 13 and 14.

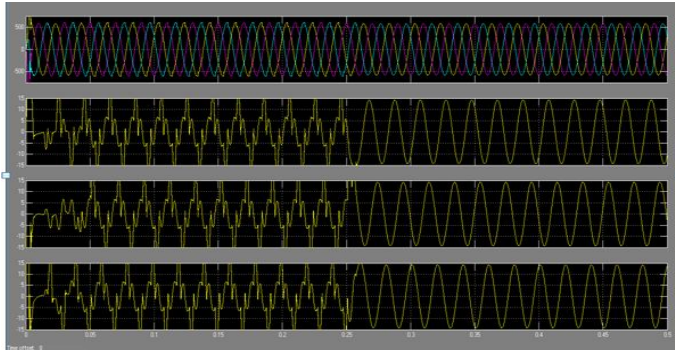


Fig. 14. Performance of the three-phase three-leg VSC and zig-zag transformer of the DSTATCOM for neutral current compensation, harmonic compensation, and power factor correction.

TABLE I
COMPARISONS OF kVA RATING OF THREE METHODS FOR A LOAD OF 20-kVA, 0.8-pf LAG

Zig-zag Transformer	Three-phase Four wire DSTATCOM	Three-phase three-wire DSTATCOM
Three-single-phase Transformers of 150V/150V, 1.5kVA each	600V, 50A IGBTs (8Nos) based VSC. KVA=16kVA	600V, 50A IGBTs (6Nos) based VSC. KVA=12kVA

TABLE II
COMPARISON OF CURRENT AND THD DURING LOAD BALANCING, HARMONIC COMPENSATION, AND NEUTRAL CURRENT COMPENSATION

Topologies Parameters	No Compensator	Four leg VSC	zig-zag transformer only	zig-zag transformer and 3-leg VSC
$I_{sa}(A)$	Open Circuit	10.04	5.718	11.51
THD of I_{sa}		3.15%	55.68%	4.2%
$I_{sb}(A)$	17.06A	10.23	15.17	11.48
THD of I_{sb}	84.70%	3.22%	50.92%	4.6%
$I_{sc}(A)$	17.09A	10.40	15.22	11.46
THD of I_{sc}	83.39%	3.15%	50.44%	4.9%
$I_{sn}(A)$	Third harmonic 26.57	26.43	Third harmonic 0.18	Third harmonic 0.16
$I_{Ln}(A)$	Third harmonic 26.57	26.31	Third harmonic 27.17	Third harmonic 24.46
$I_{Cn}(A)$	No Compensator	1.40	Third harmonic 27	Third harmonic 24.36

VI. CONCLUSION

The causes, standards, and mitigation techniques of the excessive neutral current have been investigated in the three-phase four-wire distribution system. The modelling and simulation of the zig-zag transformer has been demonstrated for neutral current compensation. Moreover, a hybrid of zig-zag transformer with a three-phase three-leg DSTATCOM has been observed as an effective option for overall compensation. The performance of the proposed compensator is validated through extensive computer simulation.

APPENDIX

Line impedance $R_s=0.01\Omega$, $L_s=1mH$

1) linear load: 20 kVA, 0.80-pf lag;

2) nonlinear load: a three single-phase bridge rectifier with an R-C load with $R=25\Omega$ and $C=470\mu F$.

Ripple filter: $R_f=5\Omega$; $C_f=5\mu F$.

DC bus capacitance: 3000 μF .

DC bus voltage: 680 V.

AC line voltage: 415 V, 50 Hz.

PWM switching frequency: 10 kHz.

Zig-zag transformer: three numbers of single-phase transformers of 5 kVA, 150/150 V.

REFERENCES

- [1] G. T. Heydt, Electric Power Quality, 2nd ed. West Lafayette, IN: Stars in a Circle, 1994.
- [2] R. C. Dugan, M. F. McGranaghan, and H. W. Beaty, Electric Power Systems Quality. New York: McGraw Hill, 1996.
- [3] M. H. J. Bollen, Understanding Power Quality Problems: Voltage Sags and Interruptions, ser. IEEE Press Power Eng. Piscataway, NJ: IEEE, 2000.
- [4] J. Arrilaga, N. R. Watson, and S. Chen, Power System Quality Assessment. New York: Wiley, 2000.
- [5] C. Sankaran, Power Quality. Boca Raton, FL: CRC, 2001.
- [6] E. Acha, V. G. Agelidis, O. Anaya-Lara, and T. J. E. Miller, Power Electronic Control in Electric Systems, ser. Newness Power Eng., 1st ed. New York: Oxford, 2002.
- [7] A. Ghosh and G. Ledwich, Power Quality Enhancement Using Custom Power Devices. Norwell, MA: Kluwer, 2002.
- [8] M. H. J. Bollen and I. Gu, Signal Processing of Power Quality Disturbances. New York: Wiley-IEEE Press, 2006.

Diesel Emission Control by Hot EGR and Ethanol Fumigation; an Experimental Investigation

Gurumoorthy S. Hebbar¹, Anantha Krishna Bhat²

¹Corresponding Author,

Mechanical Engineering Department, Christ University Faculty of Engineering, Kumbalagodu-Kengeri, Bangaluru 560074, Karnataka State, INDIA,

²Co Author; Principal,

SSPM College of Engineering, Harkul-Taluka, Kanakavli District, Sindhudurga-Maharashtra- 416 6021

ABSTRACT: Exhaust Gas Recirculation has emerged as one of the promising technique in abating oxides of Nitrogen but combustion quality deteriorates at higher loads and higher percentage of Exhaust Gas Recirculation do not become attractive owing to decreased efficiency and increased hydrocarbon and smoke. Another technology that offers promise of being able to reduce engine emissions is alcohol fumigation. An experimental investigation is carried to examine the performance and emission with alcohol fumigation in the presence of hot Exhaust Gas Recirculation on a single cylinder DI diesel engine. The main focus was on oxides of nitrogen, hydrocarbon and smoke emission and variations in thermal efficiency. Results pertaining to Exhaust Gas Recirculation showed greater reductions in NO_x emission. The reductions in the efficiency were marginal (about 5%) up to 30% Exhaust Gas Recirculation but tend to increase amounting up to 30 to 40% at higher loads and higher percentage of Exhaust Recirculation (above 30%). Hydrocarbon concentrations and smoke percentage also simultaneously increased indicating poor combustion. Alcohol fumigation in presence of hot Exhaust Gas Recirculation comparatively improved the thermal efficiency with simultaneous reduction in concentrations of HC and smoke level. Results pertaining to only diesel, diesel with Exhaust Gas Recirculation and Exhaust Gas Recirculation combined with ethanol fumigation without reducing diesel injections are presented in this paper.

Key Words: EGR; Ethanol; Fumigation; NO_x; Smoke; HC; Efficiency; Dilution effect

I. INTRODUCTION

Exhaust emissions from diesel engines are substantial source of air pollution. In recognition of this fact, the regulating authorities of all countries implemented strict regulations which are in effect since 1991. Unfortunately single technology is currently not available to meet these regulations without penalties in engine performance and efficiency. Application of various motor vehicle emission control technologies has established a history of success. This success, however, has largely been offset by the constantly growing numbers of vehicles and miles traveled. Heavy-duty diesel engine manufacturers have developed new technologies in response to increasingly stringent emission standards. The diesel engine has long been a champion of fuel economy, with advantages in reliability

and durability over other power plants. Yet, controlling NO_x, and particulate emissions has been a formidable challenge to the diesel industry because most traditional NO_x, control approaches tend to increase particulate emissions, and vice versa. Many development programs carried out over the last five years have yielded remarkable results in laboratory demonstrations. Traditionally, design changes aimed at reducing one of exhaust species have led to an increase in the other. Exhaust Gas Recirculation, EGR, is one of the most effective means of reducing NO_x emissions from diesel engines and is likely to be used in order to meet future emissions standards. The main difficulties with these techniques are to meet the requirement for NO_x and at the same time minimize the fuel penalty.

I. 2. ETHANOL AS MOTOR FUEL

Historically ethanol and methanol have been used as automotive fuels for long time, both as neat fuels and as blend components chiefly in gasoline engine. Nikolaus Otto, the father of the Otto engine, regarded ethanol as an attractive fuel for combustion engines and in 1908 Henry Ford started the construction and production of an ethanol fuelled engine and claimed that alcohol could be an automotive fuel for the future. Although replacing diesel fuel entirely by alcohols is very difficult, an increased interest has emerged for the use of alcohols, and particularly lower alcohols (methanol and ethanol) with different amounts and different techniques in diesel engines as a dual fuel operation during recent years. Ethanol or ethyl alcohol was used as quality motor fuel in the first automobile, the original Ford Model-T and after that it is only recently that interest was shown in the use of ethanol and methanol as diesel fuels. It is reported that about 80% proof ethanol is optimum as higher proofs do not give as much reductions in oxides of nitrogen emissions [1-2].

II. DIESEL NO_x FORMATION AND EFFECT Of EGR

NO_x is formed by an endothermic reaction in the burned gas regions of the cylinder. The formation of NO_x is very sensitive to temperature. The higher flame temperatures accompanying early or rapid combustion greatly increase NO_x formation [3]. Thus the amount of NO_x in diesel exhaust is sensitive to flame temperature. Availability of oxygen and burn duration are the other two reasons for the formation of NO_x[3]. Dilution of the charge by rerouting a part of the exhaust gas (EGR)

reduces the availability of oxygen on one hand and reduces the flame temperature on the other, owing to higher specific heats of EGR lased constituents like H₂O and CO₂ [4-9]. Thus presence of exhaust gas during combustion helps in abating the formation of NO_x but higher percentage of EGR deteriorates the combustion quality thereby causing incomplete combustion [7].

III. DIESEL COMBUSTION WITH ETHANOL

Local mixture formation, self-ignition and combustion needs time to be completed. Not-complete combustion of diesel fuel is a source of hydrocarbon emission and smoke. In order to avoid this inconvenient effect, injection of ethanol to inlet duct is considered [10]. Ethanol will quickly evaporate (but will not self-ignite), and will be ignited by burning diesel droplets resulting in very high combustion rate of both fuels, especially diesel fuel. With higher combustion rate higher thermal efficiency, higher power output and lower emission of HC and smoke are expected. Hence, the combined effect of ethanol fumigation (without reducing the amount of diesel being injected) and EGR is expected to reduce NO_x with marginal loss of efficiency when compared to use of EGR alone.

IV. TEST ENGINE

Table.1. Specification of the test engine

Type	4-Stroke, Single Cylinder Diesel Engine(Water Cooled)
Make	Kirloskar AV – 1.
Loading	Electrical, Resistive Air Heaters
Rated Power	3.7KW, 1500 RPM
Bore & Stroke	85mm x 110mm
Cylinder Capacity	624.19 cc
Compression Ratio	16.5 : 1
Pressure Transducer	Piezo Sensor, Range: 2000 PSI.
Starting	Auto Start.
Orifice Diameter for air flow	15mm

The test engine is Kirloskar AV1 engine facilitated with data acquisition systems (DAS) for recording engine data measurement. External EGR is routed into the intake manifold through a one inch diameter GI pipe. The EGR line emerges right after the exhaust manifold from the engine and enters the in the intake manifold close to engine. Fresh air and EGR are made to mix before it enters into engine cylinder. An orifice meter is used to determine the flow rate of EGR. The reported percentage of EGR is defined as the volumetric ratio of the recirculated gas to the total charge induced in to the cylinder. AVL smoke meter is used to measure the smoke level and INDUS[®] 5 gas analyzer for O₂, CO, CO₂, HC and NO_x measurements.

Details of the test engine are given in table 1. The ethanol fumigation is achieved through an additional injector attached just before the inlet manifold, inclined and in opposite direction to EGR flow.

The injection pump is driven by the cam shaft of the engine. Cam is so designed to inject the ethanol in 5, 10, 15 and 20% of total amount of diesel injected in a cycle for a given load. This arrangement is shown the fig.1.

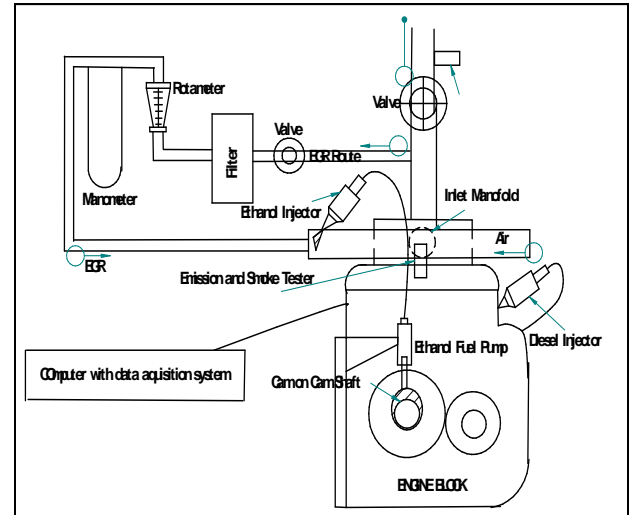


Fig.1 Test engine layout.

V. RESULTS AND DISCUSSIONS

5.1 Engine Torque

As expected injecting ethanol will increase the torque (adds energy) as amount of diesel injected is not reduced. In the fig.2, the trend of torque at part load of 1.5 kW and maximum load of 2.5kW for 5, 10, 15 and 20% ethanol fumigation are compared with those corresponding to only hot EGR. Torque values for 5%, 10% and 15% ethanol fumigation are higher as compared to hot EGR for both part and full load but for 20% values reduce. At full load torque is almost same for 5, 15 and 20% ethanol fumigation and hot EGR for all percentage of EGR. 10% fumigation gives the optimum results for all values of load and EGR percentage.

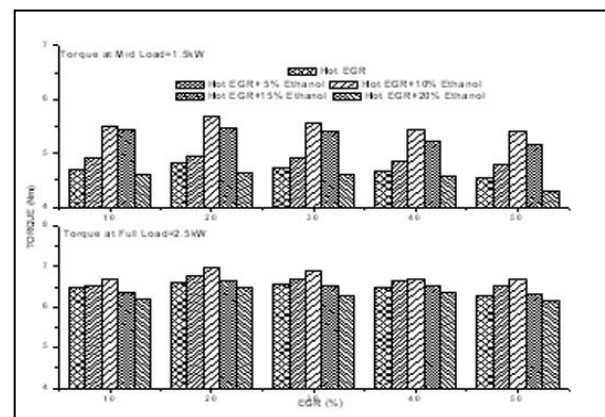


Fig.2; Comparison of engine torque for part load (1.5kW) and full load of (2.5kW) for increasing percentage of EGR

5.2 Thermal Efficiency

Thermal efficiency is a measure of engine output power and fuel consumption. For an engine operating at constant speed, the torque increase as the load increase. Ethanol fumigation improves the efficiency when compared to corresponding values of hot EGR for all loads.

The thermal efficiency values are comparatively better for 5% and 10% ethanol fumigation as compared to higher dose (fig.3). Fig (4) depicts the results of thermal efficiency for part load (1.5kW) and full load (2.5kW) for 10 to 50% EGR. The variation in thermal efficiency is negligible up to 30% EGR and tends to slightly decrease thereafter particularly for only hot EGR case. Ethanol fumigation along with hot EGR shows improved efficiency in this region.

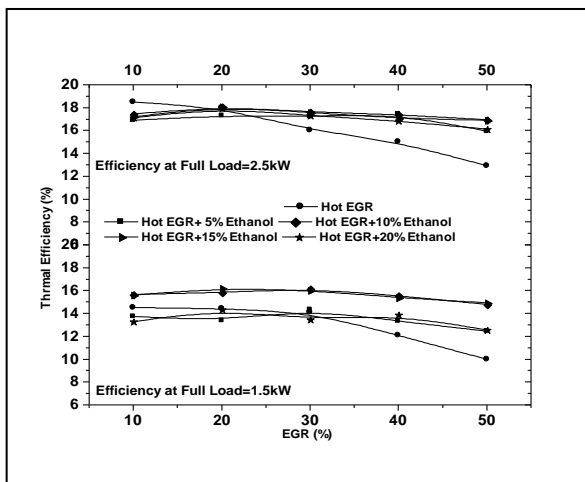


Fig.3. Engine thermal efficiency for 50% and 40% EGR for increasing load.

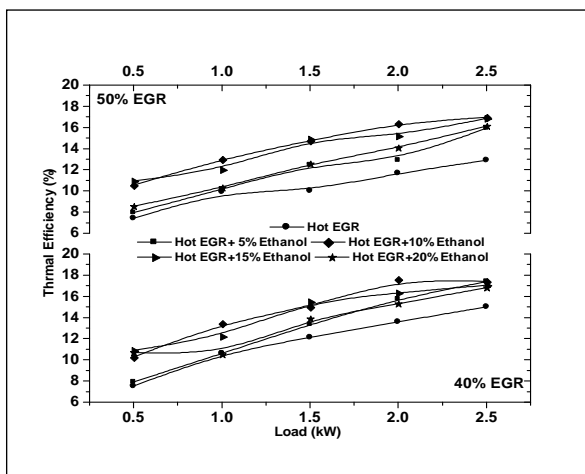
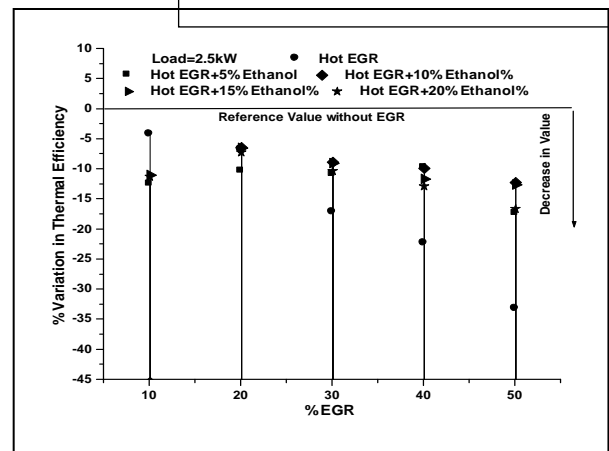
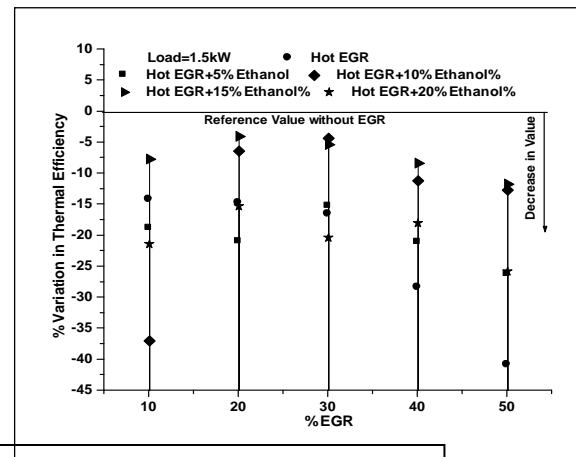


Fig.4; Engine thermal efficiency for different EGR percentage at part load (1.5kW) and full load(2.5 kW).

The fig(5) and Fig.(6) show the comparison of variation in thermal efficiency in percentage for three different cases; (i) Hot EGR. (ii) Hot EGR with different



percentage of ethanol fumigation and (iii) Only diesel, which is taken as reference. It is clear that thermal efficiency reduces for both ethanol fumigation with EGR and hot EGR when compared with only diesel case. However for ethanol fumigation with EGR, these percentage losses are less and values are more close to reference values. The loss in efficiency is limited to around 20% for fumigation case where as it is up to 40% for without fumigation case. Another observation is that loss of efficiency is very marginal (around 5%) for up to 10% ethanol fumigation and then it slightly increases (around 20%) as the fumigation percentage increases.

Fig.5; Percentage variation in engine thermal efficiency for different EGR percentage for part load of 1.5kW.

Fig.6; Percentage variation in engine thermal efficiency for different EGR percentage for full load of 2.5 kW.

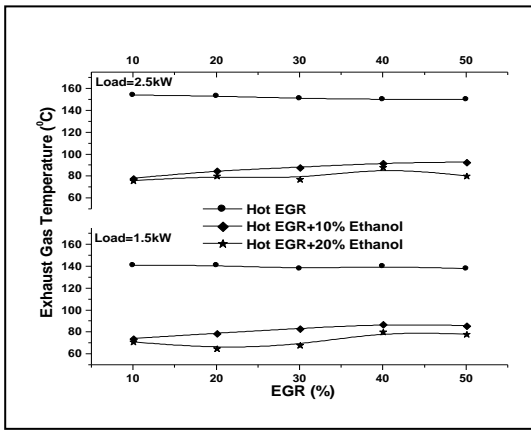


Fig.7; Engine exhaust gas temperature for part load of 1.5kW and full load of 2.5 kW against different percentage of EGR.

5.3 Flame temperature

Ethanol with their greater latent heat of vaporization gives a higher charge density; and their higher laminar flame speed allows them to be run with leaner, or more dilute, air/fuel mixtures [10].

In ethanol and air mix combustion more moles occur than in diesel combustion, therefore the torque increases (Fig.2). On the other hand, triatomic gas is more susceptible to the heat, which will be taken from the working fluid present in the cylinder, thus decreasing the temperature in the combustion chamber and exhaust gas as well. The engine exhaust temperature as an indicative of combustion temperature (Fig.7) for hot EGR and ethanol fumigation with EGR for part and full load vindicate this.

for part load of 1.5kW and full load of 2.5 kW against different percentage of EGR.

5.4 Hydrocarbon Emission

Emission of HC in the engine tail pipe is mainly a result of incomplete combustion. Presence of burnt gas (EGR) causes reduced availability of oxygen due to thermal throttling [5, 6, and 12].

Fig.9; Smoke emission for part load of 1.5kW and full load of 2.5 kW against different percentage of EGR.

Ethanol fumigation during intake is expected to supply oxygen as ethanol in comparison to diesel fuel contains some oxygen atoms. Ethanol molecules contain 35 percent oxygen, and serve as an “oxygenate” to raise the oxygen content and emission of HC and smoke are expected to be low with ethanol taking part in the combustion.

This is found true even in the presence of EGR during the combustion but only up to 10% fumigation and there after for 15% and 20% ethanol dose HC concentration increased even more than the values corresponding to only hot EGR. This indicates a poor combustion. Also high HC emissions due to higher dose of alcohol were probably caused by very strong quenching effect due to its high latent heat of evaporation and low centane number.

5.5 Smoke Emission

Smoke is a result of condensation of hydrocarbon and presence of soot. Soot, particulate (smoke) is formed mostly through incomplete combustion of fuel, with small contributions from the lubricating oil [11], more difficult pulverisation of the heavy diesel droplets and non-homogeneous distribution of the diesel fuel over the combustion chamber.

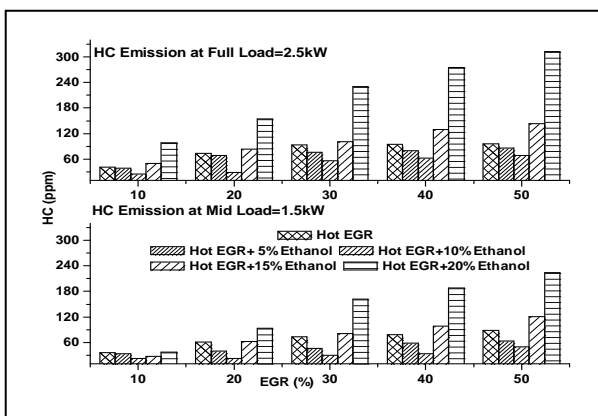


Fig.8; Emission of Unburnt Hydrocarbon emission

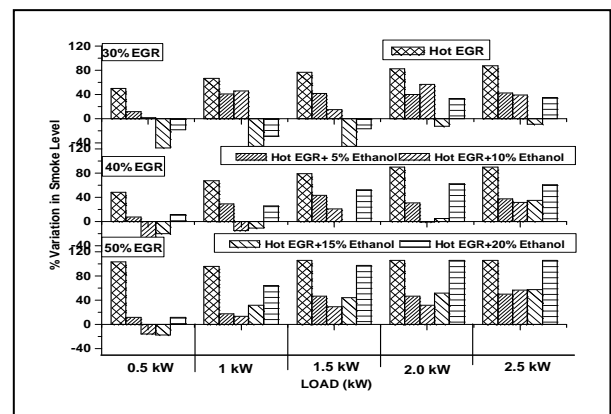
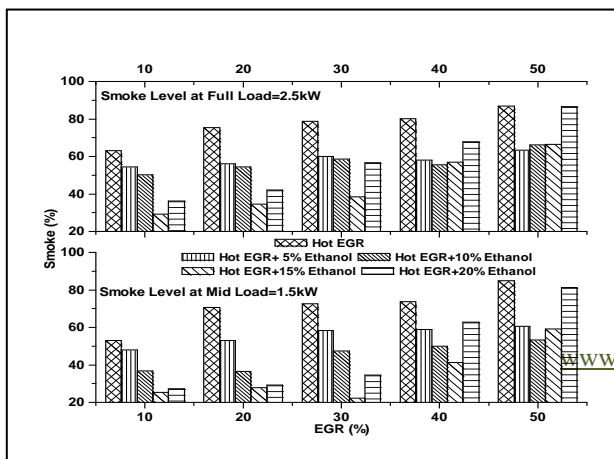


Fig.10; Percentage variation in smoke different engine load for 30%, 40% and 50% EGR

As the fuel in the advancing flame plume combusts, pyrolytic reactions crack the hydrocarbons that have yet to pass through the flame. As these reactions occur, particulate masses form. If the fuel mixing is poor within the cylinder, large quantities of particulates can

form [2]. Typically, above temperatures of 500⁰C, the particles are composed solely of clusters of carbon, while at temperatures below this; higher molecular weight hydrocarbons condense onto the clumps. As the particulates travel through the flame and into the more heavily oxygen populated areas, the clumps tend to oxidize and for this reason concentrations are reduced in the leaner regions of combustion. The presence of ethanol favors oxidation process and smoke level is expected to reduce and literatures suggest that ethanol is best fuel to minimize smoke and particulate matters.

Fig. (9&10) indicate Hot EGR emit more smoke as compared to EGR with ethanol fumigation. As fumigation quantity is increased from 5% to 15% the smoke level tend to decrease remarkably. But further increase in fumigation of ethanol records slightly higher values mainly due to reduced temperatures where soot oxidation is hampered and also due to deteriorated combustion. Smoke levels are found nearly same or even less for ethanol fumigation with EGR when compared to only diesel case (taken as reference) up to 30% EGR for both part load (1.5kW) and full load (2.5 kW) and thereafter its values start climbing for higher loads. This result is obvious as HC concentrations (Fig.8) show similar trend.

5.6 NOx Emission

Diesel NOx emissions result from the thermal fixation of atmospheric nitrogen and its oxidation in the presence of high combustion temperature. Control of these emissions can be achieved by reducing the peak flame temperatures

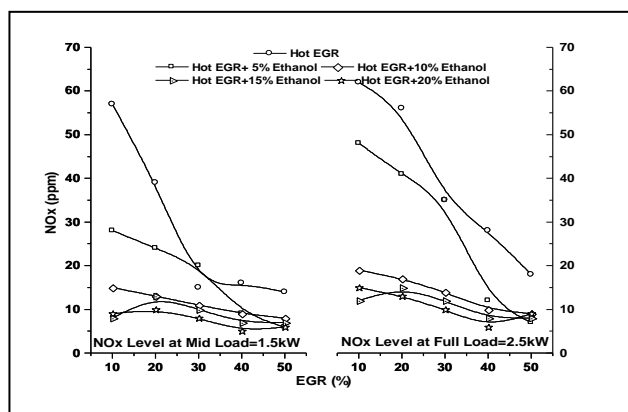


Fig.11; NOx emission for part load of 1.5kW and full load of 2.5 kW against different percentage of EGR.

EGR reduces the peak temperature by diluting the charge with burnt exhaust gas. Higher NOx emission reductions can be achieved through higher percentage of EGR but results into a loss in thermal efficiency and increased HC and CO emission especially at higher EGR values and higher loads. Alcohols generally give lower fuel heat release rates, resulting in lower NOx emissions. With fumigation of ethanol in the presence of EGR enables admit more percentage EGR with greater reductions in NOx along with comparatively lower emissions of HC and smoke. Fig. (11) show the reductions of NOx for part load and full load with and without ethanol fumigation. NOx concentration remains

low for ethanol fumigation case as compared to without fumigation for entire range of EGR percentage.

VI. CONCLUSION

It can be concluded from the results obtained from the experiment that

1. EGR method to abate NOx emission is very effective. The disadvantage is decreased efficiency and increased HC and Smoke with higher percentage of EGR and at higher loads.
2. Ethanol fumigation without altering the diesel injection proves to be a better option in reducing HC, smoke and NOx apart from improving the engine thermal efficiency.
3. Ethanol fumigation above 10% tends to increase HC and smoke emissions when compared to corresponding values for 5 and 10% , however these values are very less as compared to use of EGR without ethanol fumigation.
4. 10% ethanol fumigation with HOT EGR is a better option for higher percentage of EGR to be used with maximum reductions in NOx emissions with marginal loss of efficiency.

References

- [1] Emission Control in Diesel Engines by Alcohol Fumigation-A study for the U S Department of Transportation by H Van Gerpen and D B Van Meter-Department of Mechanical Engineering-Iowa State University –Ames-US.
- [2] Heywood, John B., Internal Combustion –Engine Fundamentals, McGraw-Hill, New York, 1988
- [3] Y.Q. Xia, R.C. Flanagan (University of Ottawa Canada); Ignition Delay- A General Engine/ Fuel Model, SAE paper 870591. Society of Automotive Engineers, Inc., Warrendale, Pennsylvania, USA. 1987
- [4] Ming Zheng a, Graham T. Reader, J. Gary Hawley, Diesel engine exhaust gas recirculation—a review on advanced and novel concepts” Elsevier; Energy Conversion and Management 45 (2004) 883–900
- [5] Röpke, S., Schweimer, G.W. and Strauss, T.S. NOx Formation in Diesel Engines for Various Fuels and Intake Gases. SAE Paper 950213, 1995.
- [6] Ladommatos, N., Abdelhalim, S. M., Zhao, H., and Hu, Z., The Dilution, Chemical, and Thermal Effects of Exhaust Gas Recirculation on Diesel Engine Emissions, Part 3: Effects of Water Vapour, SAE Paper No. 971659 (1997).
- [7] Ladommatos, N., Abdelhalim, S. M., and Zhao, H., The Effects of Carbon Dioxide in EGR on Diesel Engine Emissions, IMechE Paper No. C517/028/96 (1996).
- [8] Tsunemoto, H. and Ishitani, H., The Role of Oxygen in Intake and Exhaust on NO Emission,

Smoke and BMEP of a Diesel Engine with EGR System.SAE Paper 800030, 1980.

- [9] Timothy Jacobs, Dennis Assanis, Zoran Filipi (University of Michigan); The impact of exhaust gas recirculation on performance and emissions of a heavy-duty diesel engine, SAE paper 2003-01-1068. Society of Automotive Engineers, Inc., Warrendale, Pennsylvania, USA. 2003
- [10] Kowalewicz A., Pawlak G., Pajaczek Z., Preliminary investigation of diesel engine with additional injection of ethyl alcohol, Journal of KONES, vol 9 no 3-4, 2002
- [11] Pikunas. A., G. Bureika, Grabys J. Calculation method of heavy Diesel engines emissions toxicity. *Journal of KONES, Internal combustion engines.* Warsaw: European Science Society of Power Train and Transport Publication, 2005. ISSN 1231-4005. Vol.12. No.1-2. p.283-290.
- [12] G.H. Abd-Alla., Using exhaust gas recirculation in internal combustion engines: a review - Elsevier; *Energy Conversion and Management* 43 (2002) 1027–1042.
- [13] Edwards, J., *Combustion: Formation and Emission of Trace Species*, Ann Arbor Science Publishers, Inc., Ann Arbor, Mich., 1974.
- [14] Nord K., Haupt, D., (2005) "Reducing the Emission of Particles from a Diesel Engine by Adding an Oxygenate to the Fuel", Submitted to *Environmental Science and Technology*.
- [15] Zelenka P, Aufinger H, Reczek W, Cartellieri W 1998 Cooled EGR—A technology for future efficient HD diesels. SAE 980190
- [16] Nidal H. Abu-Hamdeh, "Effect of cooling the recirculated exhaust gases on diesel engine emissions" Elsevier; *Energy Conversion and Management* 44 (2003) 3113–3124
- [17] Dae Sik Kim, Chang Sik Lee, Improved emission characteristics of HCCI engine by various premixed fuels and cooled EGR- Elsevier; *Fuel* 85 (2006) 695–704
- [18] Gurumoorthy S Hebbar, Dr. Anant Krishna Bhat, Effect of Exhaust Gas Recirculation Temperature on the Emission and Performance of a Single Cylinder Naturally Aspirated Stationary Diesel Engine, *International Journal of Applied Engineering Research*.

Development & Characterization of Ceramic Membranes

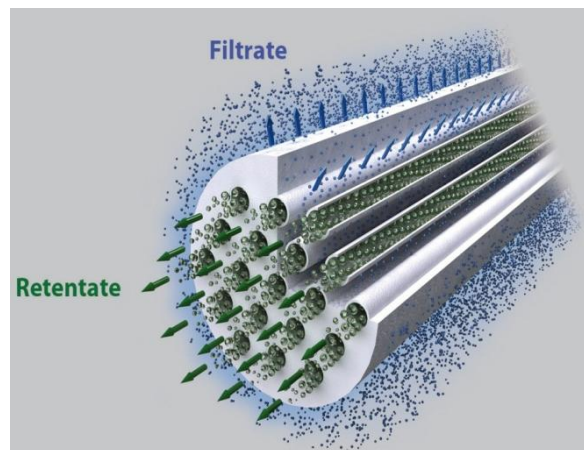
Manohar

Abstract: Ceramic membranes are used for water and gas filtration of its chemical inertness, low temperature preparation, good mechanical and porous properties. Important characteristics of ceramic membranes are high porosity, high permeability, defined pore size and good mechanical properties. In this study, fabrication and characterization of ceramic membranes preparation was carried out.

For example, Zirconia ceramic samples in the form of tubes are prepared by extrusion. The effect of hydrothermal reactions of zirconia oxynitrate for Zirconia membrane preparation as a starting powder was analyzed. Zirconia coating is applied on the SiC tube. It is mainly carried out by hydrothermal reaction. Zirconia solution prepared from zirconia oxynitrate and water. This hydro thermal test is carried out in an oven at 150°C for 16hrs. Finally we got good zirconia coating on SiC base. Found zirconia coated body is then dried at 100°C and fired at 800°C. Fired samples are characterized and tested for density, porosity, permeability, & S.E.M. Obtained product shows optimum porosity (40-45%) and good permeability for the membrane application like water filtration.

I. INTRODUCTION

Membrane separation has become an important unit operation in water operation in water and wastewater treatment. Different degrees of water quality can be obtained with removal of particles, dissolved organic compound, protein and ions. However, two dominant areas are removal of organic compound in water clarification and osmotic desalination. The overall principle in any membrane separation is sketch in figure.



The principle in membrane separation.

1.1 Membrane operation

The first thing to recognize is that regardless the use of different designs the separation depend on the physical – chemical properties of the material to be separation and the membrane used. The separation is driven by a difference in chemical potential across the membrane. The force needed to establish such chemical potential difference across the membrane. Pressure related membrane separation is usually divided into four operations: Microfiltration, ultra filtration, nanofiltration and reverse osmosis- each having different characteristic.

Table shows that separation of small particles/molecules requires a high trans- membrane pressure. In addition, the rate of separation, the flux, decreases. New membrane materials with different properties are developed all the time simply to fit the need for the membrane operation just mentioned.

Tabel1.a.1: Pressure drop for different membrane processes

Membrane process	$\Delta p(\text{bar})$	Size Range (μm)	$J(\text{l/m}^2 \cdot \text{h} \cdot \text{bar})$
Microfiltration	0.1 -2.0	0.1-10	>50
Ultrafiltration	1.0-5.0	0.02-0.3	10-50
Nanofiltration	5.0-20	0.001-0.01	1.4-12
Reverse osmosis	10-100	<0.001	0.05-1.4

1.2 Classification of membranes

Membrane are classified according to separation mechanism, physical morphology, membrane geometry and physical-chemical properties. This can sometimes be confusing but one must bear in mind that scientific people have different interest in membrane technology. Some are only interested in membrane synthesis, others in membrane module design. A good exercise is to ask our self: which kind of separation mechanism is used in this membrane operation? What is the membrane morphology? etc.

Essentially, there are three type of separation mechanism:

1. Separation by size- the sieve effect: This requires porous membranes with rather large pores. Terms like macropores, mesopores and micro pores (figure 1.a.2) are used to describe the pore size in membrane for microfiltration ultra-filtration and nanofiltration.
2. Separation by different in solubility and diffusivity of material: This principle is used in operations like reverse osmosis and requires the membrane used to be dense (nonporous).
3. Separation by charge: An ion exchange membrane separates compounds of different charges. Ion-exchange membranes are used in operation like electro dialysis and are generally nonporous.

II. Polymer Membranes:

For the sake of simplicity, only two very common organic membrane materials will be discussed here. Details about other materials can be found in Table.

One of the most common materials used is cellulose and derivatives. Cellulose esters like cellulose acetate and ethyl cellulose are all repeating units of glucose, connected by glycoside bonds, where the hydroxyl groups on each glucose unit participate in ester formation. The membranes are hydrophilic but only sparingly soluble in water. Polarity is compared to the other materials in table (except polyacrylonitrile) relatively high. Cellulose esters resist cleaning with chlorine, but hydrolyze easily, like other ester compounds, when exposed to acid or base. In addition, temperature and biological activity may cellulose membranes.

Summary of the most widely used porous membrane materials.

Material	Physical-chemical properties	Primary membrane operation area in water treatment
Cellulose esters (CE) primary cellulose acetate (CA)	Low chemical stability towards acid/base, temperature and biological activity. Resist chlorine cleaning. Relatively polar. Very hydrophilic.	Desalination, softening, disinfection and clarification using micro, ultra and nano filtration and reverse osmosis.
Aliphatic and aromatic polyamides (PA)	Higher hydraulic and thermal stability than CE, but sensitive towards oxidation e.g. chlorine. Hydrophilic.	Reverse osmosis but also ultra and micro filtration applications.
Polyacrylonitrile (PAN)	Less hydrophilic than CE's and PA's but very polar.	Ultra filtration applications in general
Polysulfone (PSF) and Polyethersulfon (PES)	Weak hydrophobic with some polar tendency. Good chemical and thermal stability.	Ultra filtration, support material for several composite membranes.
Polytetrafluoroethylen (PTFE), polyvinylidene fluoride (PVDF), and polypropylene (PP).	Hydrophobic non-polar membranes. High thermal and solvent resistance very chemically inert. Adsorb only weakly.	Micro and ultra-filtration applications.

The above table is a very qualitatively way to list of physical-chemical membrane properties. It is often difficult to do otherwise with this kind of properties, but in the next section a tool to physical characterization will be presented and it will make the classification more quantitatively.

Ceramic membranes



Plant Engineers and plant operators demand, with respect to membrane installations, process stability, high availability and low requirements for preliminary treatment and minimum need for support and maintenance.

In contrast to many polymer membranes the ceramic membranes are a perfect match for this demand due to their extremely high chemical and physical stability, their outstanding separation characteristics and their long working life.

Ceramic materials are generally very stable chemically, thermally and mechanically, and in addition are frequently bio inert. They are therefore ideal materials for many applications in the chemical and pharmaceutical industry or in water and waste water processing.

The medium to be filtered flows through the channels of the membrane carrier. Particles are retained if their size exceeds the radius of the membranes pores, building up the concentrate. The filtrate permeates through the pores and it is subjected to subsequent process stages.

Many are the advantages deriving from the ceramic membranes use:

- No ageing, long life and reliability.
- High temperature stability.
- Mechanical stability under large pressure gradient.
- Stability over a large pH range.
- 0.3 – 100 efficiency in gas separation.
- Ability to be backwashed and abrasion resistance (steam sterilization and high flash capability)
- Incentive to bacterial action.
- Can process highly viscous fluid.
- Good control of pore dimension fouling.
- They are ecologically friendly and more favorable than separation technologies.
- No additives are necessary and the process temperature is not limited

Filtration with ceramics is a mild, highly selective process without phase transformation. Running costs are limited by closed production cycles and continuous processes.

Disadvantages are:

- Brittle character needs configuration supporting system.
- Relatively high capital installation cost.
- Relatively high modification costs in case of defects.
- Sealing technology for high temperature application may be complicated.

Scope of porous ceramic membranes



Inorganic membranes are versatile they can operate at elevated temperatures with metal membranes stable at temperatures ranging from 500 to 800°C and with many ceramics membranes stable at over 1000°C they are also much more resistance to chemical attack because of the wide variety of materials that may be used in the fabrication of our inorganic membranes resistance to corrosive liquids and gases even at elevated temperatures can be realized.

Inorganic membranes completed with organic membranes for commercial use in many of the harsh operational environmental listed above organic membranes offer need solution.

Applications

Initially, ceramic membranes were used in waste water technology. Meanwhile, successful and possible applications cover all industries where media were filtered.

- Chemical industry :
 - Product separation and cleaning.
 - Concentration of polymer suspensions and metal hydroxide solutions.
 - Separation of catalysts.
 - Recovery of dyes and pigments.
 - Desalination of products.
 - Cleaning and recycling of organic solvents.

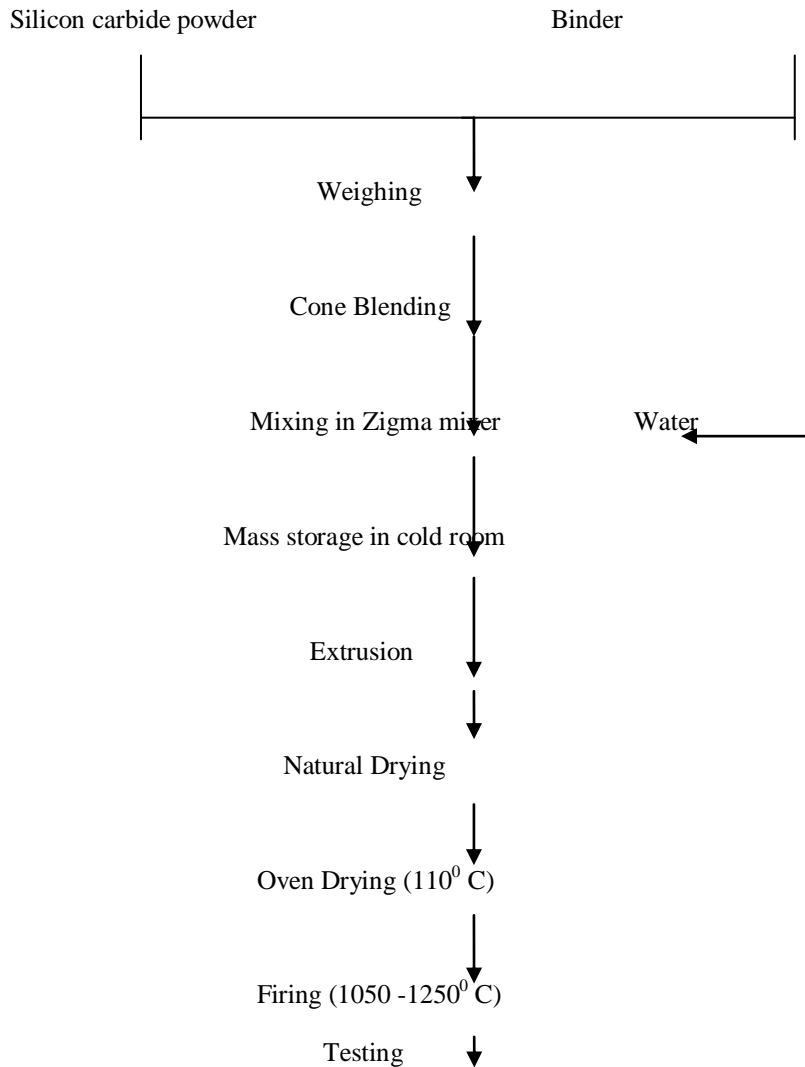
- Metal industry / Surface engineering :
 - Recycling and disposal of degreasing and rinsing bathes.
 - Treating of oil /water emulsions.
 - Recovery of heavy metals.
 - Cleaning of waste water from grinding processes.
 - Treatment of waste water form glass and glass fiber production.

- Textiles / Pulp and paper industry :
 - Concentration fractionation, isolation and sterilization for antibiotics, enzymes, proteins, amino acids and vitamins.
 - Separation, concentration and dewatering of biomass and algae.
 - Disposal of fat emulsions.
 - Separation of yeast.
 - Desalination.

- Food and beverages
 - Clarification of juice and beer.
 - Concentration of juice.
 - Sterilization of milk and whey.
 - Desalination of whey.
 - Dewatering of products.
 - Purification of drinking water.

- Recycling and environment.
 - COD /BOD reduction.
 - Oil / water separation.
 - Recovery of pharmaceuticals and pesticides.
 - Retention of microorganism.
 - Retention of heavy metals and radioactive substances.
 - Recycling of water form swimming pools.
 - Purification of the drain of sewage plants.

PREPARATION OF RODS AND TUBES: Flow chart for tubes & rods preparation



Raw materials used

Silicon carbide:

The Acheson process is used to produce large quantities of Sic. This process carbothermally reduces SiO₂ to give SiO and CO (g) in a resistance furnace. Low purity silicon carbide is used in abrasion and refractory application. High quality silicon carbide is used for reaction bonded ceramics that require strength at high temperature, high thermal conductivity, high thermal shock resistance, and allow thermal expansion co-efficient.

Graphite (Black Lead):

It is a crystalline form of carbon. It occurs in nature either as microcrystalline earthy lumps or in a lobular force. Natural graphite is classified on the basis of its physical properties, nature. Ex:-flakes, lump and amorphous (micro crystalline) type. It is very and usually has metallic structure and a greasy feel.

Occurrence: Graphite occurs in a Andhra Pradesh, Lohit (Arunachal Pradesh), Pala man (Bihar), Karnataka, samba lour and Bolangir (Orissa), Ernakulum (Kerala), Doomra(Rajasthan) and in Baramulla(J and K).

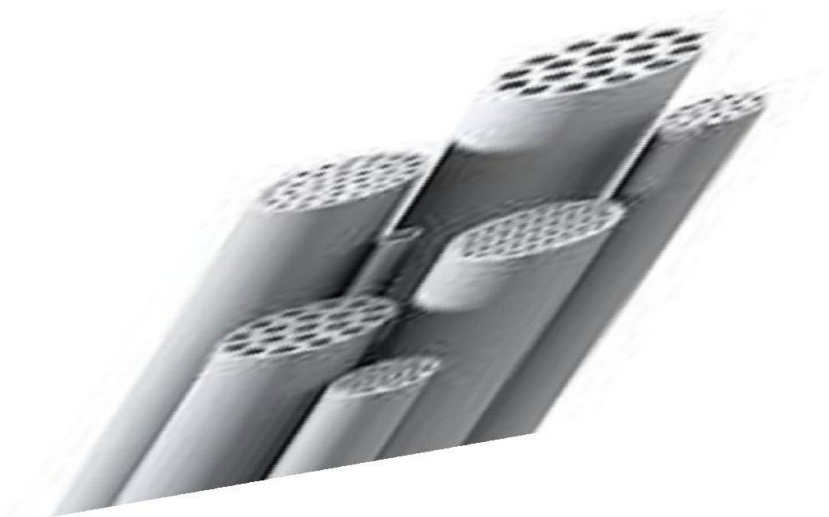
Binders: Substances, which hold ceramic raw material and bodies together during the initial stage of processing, are called binder.

1. Lignin has been used for tempering all type body fabricated by ceramic process it increases the strength of the weak body.
2. Tannic acid has long been employed to increase the particles of days, but it is not effective as extract in increasing the dry strength.
3. Ordinary paraffin's, with a small percentage of carnauba wax, is a good binder in some cases and can be molded cold with a reduction in molding time.

Procedure for rods and tubes preparation:

The silicon carbide powder and binder (5%) were weighed according to the composition accurately and then the batch was dry mixed in cone blender. The weighed batch was charged to cone blender. The purpose of cone blending is to mix the titania powder and the binder homogeneously. This blending was carried out for a period of 2 hour. The batch is weighed and charged to zigma mixer. The water is slowly added during mixing until required consistency mass is obtained and the amount of water is noted down.

The mixed mass is kept in cold room for ageing. After ageing the mass is feed to the extruder where simultaneously de-airing and compaction is carried out. In the extruder kerosene is used as lubricant. The die is fixed accordingly i.e. this depends up on rod or tubes to be extruded. Then the pieces are extruded in aluminum channels and kept for natural drying. The natural drying is carried out for a couple of days. Then the naturally dried pieces are kept for drying in electrical dryer where temperature is initially kept at 40⁰ C for about 3 hours then temperature is raised to 60⁰ C and kept for about 3 hours and then 80⁰ C and 100⁰ C in the same way. Care should be taken while drying the rod or tubes must be kept between metal supports. Then the dried pieces are carried for firing operation. The firing ids carried out at different temperature 1050, 1100, 1150, 1200⁰ C.The fired pieces are tested fir the following tests: %apparent porosity, bulk density, %water absorption, SEM, Permeability etc.

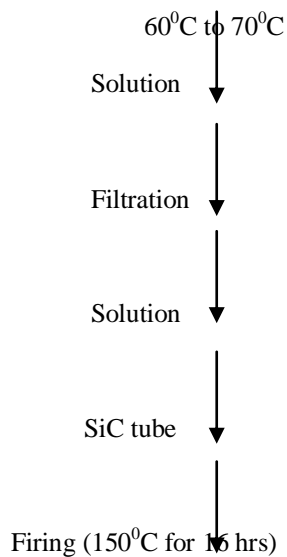




Zirconia coating on SiC tube

Flow chart for hydrothermal test

300ml of H₂O + 45 gms of zirconia oxy nitrate



Zirconium Oxide(ZrO₂)

Zirconia is an extremely refractory material. It offers chemical corrosion inertness to temperatures well above the melting point of alumina. The material has low thermal conductivity. It is electrically conductive above 600⁰ C and is used in oxygen sensor cell and as the susceptor (heater) in high temperature induction furnaces. With the attachment of platinum lead, Nernst glowers use in spectrometers can be made as a light emitting filament which operated in air.

Key Properties of Zirconium Oxide

- ✓ Use temperatures up to 2400⁰C
- ✓ High density
- ✓ Low thermal conductivity (20% that of alumina)
- ✓ Chemical inertness
- ✓ Resistance to molten metals
- ✓ Ionic electrical conduction
- ✓ Wear resistance
- ✓ High fracture toughness
- ✓ High hardness

Typical Uses of ZrO₂

- ✓ Precision ball valve balls and seats
- ✓ High density ball and pebble mill grinding media
- ✓ Rollers and guides for metal tube forming
- ✓ Thread and wire guides
- ✓ Hot metal extrusion dies
- ✓ Deep well down-hole valve and seats
- ✓ Powder compacting dies

- ✓ Marine pump seals and shaft guides
- ✓ Oxygen sensors
- ✓ High temperature induction furnace susceptors
- ✓ Fuel cell membranes
- ✓ Electrical furnace heaters over 2000⁰C in oxidizing atmospheres

General Zirconia Oxide information:

Pure zirconia exists in three crystal phases at temperatures. At very high temperatures (>2370⁰C) the material has a cubic structure. At intermediate temperatures (1170⁰C to 2370⁰C) it has a tetragonal structure. At low temperatures (below 1170⁰C) the material transform to the monoclinic structure. The transformation from tetragonal to monoclinic is rapid and is accompanied by a 3 to 5 percent volume increase that causes extensive cracking in the material. This behavior destroys the mechanical properties of fabricated components during cooling and makes pure zirconia useless for any structural or mechanical application. Several oxides which dissolve in the zirconia crystal structure can slow down or eliminated these crystal structure changes. Commonly used effective additives are MgO, CaO, and Y₂O₃. With sufficient amounts added; the high temperature cubic structure can be maintained to room temperature. Cubic stabilized zirconia is a useful refractory and technical ceramic material because it does not go through destructive phase transition during and cooling.

The controlled, stress include volume expansion of the tetragonal to monoclinic inversion is used to produce very high strength, hard, tough varieties of zirconia available from accuratus for mechanical and structural applications. There are several different mechanisms that lead to strengthening and toughness in zirconias that contain tetragonal grains. These depend on the grain sizes, the thermal history and the kind and amount of stabilizing additive in the body. These variation lead to two strong, commercially available partially stabilized zirconia (PSZ) microstructure identified as TTZ (tetragon ally toughened zirconia) and TZP (tetragonal zirconia polycrystalline) ceramic. The TTZ is an MgO partially stabilized zirconia often designated MgTTZ or MgPSZ consisting of uniformly dispersed tetragonal precipitates in larger cubic phase crystals. The secondary thermal aging process requiring tight manufacturing controls for proper micro structural development has limited the supplier base for the tetragonal phase, very fine grain mateial stabilized with rare earth oxides, primarily yttria and less commonly ceria. They are often designated YTZP for the yttria stabilized product and CeTZP for the ceria stabilized product. The TZP material has found uses in cutting and wear resistant application due to its reliable and outstanding hardness and toughness. TZP properties degrade rapidly when the material is exposed to water vapor at 200 to 300⁰C, so controlled use condition are important for good performance. All of the toughened zirconia show a degrading of properties with increasing temperature, and this class of high strength, tough material is generally limited to use temperatures below 800⁰C.

History of titania (TiO₂):

The element titania was discovered in 1791 by William Gregory in England. Gregory spent much of his time studying mineralogy, which lead him to his discovery. This happened when he discovered a sample of a black sandy material in his neighborhood. He studied this substance and after he was assured that it was a mineral he called it menachanite. Four years later a man named Martin h klaproth recognized that there was a new chemical element in this mineral. He later named it titanium after the titans which are numerous monsters that ruled the world in Greek mythology. Martin h klaproth was not able to make the pure element of titanium however he was only able to produce titanium dioxide.

Occurrence

The element occurred with a number of mineral deposits. Principally rutile ilmenites which are widely distributed in earth crust and lithosphere and it is found in almost in all living things, rocks, water bodies and soil. The metal is extracted from its principle mineral ore via kroll process or hunter process.

Processing methods for manufacture of titanium dioxide

There are 2 distinct technologies for manufacture of titania

- Sulphate process
- Chloride process

Sulphate process

The sulphate process has been in existence for more than 70 years. The process is carried out in the following steps.

Digestion of ilmenite or titania slag in sulphuric acid

Reduction and crystallization

Hydrolysis

Calcinations

Dry milling

The product obtained by sulphate process is usually anatase which can be further treated to obtain rutile. The feed stocks obtained used for sulphate process are mainly ilmenite or titania slag.

The major advantage of this process is that large quantities of waste product are generated in the form of spent acid and copper. The problem of this copper can be reduced by using titania slag as feed instead of ilmenite.

Chloride process

The chloride process was developed by du-pont around 1959. The main process steps are as follows,

- Chlorination of synthetic rutile or other raw material.
- Purification of titanium tetrachloride.
- Oxidation of pure titanium di-oxide.

The main advantages of chloride process are as follows,

- Product obtained is rutile and is of better quality.
- Process is continuous.
- The waste products obtained are in small quality.

A technical composition of sulphate & chloride process indicates that the chloride process gives a product which is in finer in particle size, low in impurity & less waste products are generated. As a result more & more manufactures are shifting to chloride process. Presently about 55% of titania is produced by sulphate process.

Physical and mechanical properties of titania

Density	4 gm/cc
Porosity	0 %
Modulus of rupture	140 Mpa
Compressive strength	680 Mpa
Poisson's ratio	0.27
Fracture toughness	3.2 Mpa.m ^{-1/2}
Shear modulus	90 Gpa
Modulus of elasticity	230Gpa
Micro hardness(HV 0.5)	880
Resistivity(25 ⁰ C)	10 ¹² ohm.cm
Resistivity(700 ⁰ C)	2.5×10 ⁴ ohm.cm
Dielectric constant(1 MHz)	85
Dissipation factor(1 MHz)	5× 10 ⁴
Dielectric strength	4 kV/mm
Thermal expansion(RT-1000 ⁰ C)	9×10 ⁻⁶
Thermal conductivity(25 ⁰ C)	11.7Wm/K

Optical properties of titania

Forms	RI	Density	Crystal structure
Anatase	2.49	3.84	Tetragonal
Rutile	2.903	4.26	Tetragonal

Procedure for Hydrothermal test to prepare zirconia membrane:

First we take 300 ml of water in beaker and then heated by using magnetic stirrer. Add 45 gms of zirconia oxy nitrate to water and maintained temperature at 60 -70⁰C. After completion of heating, filtering process is carried out to get a filtered solution. Then take autoclave apparatus containing Sic tubes and add 3/4th filtered solution into the autoclave apparatus. Autoclave apparatus is kept in oven at 150⁰C for 16 hrs. After completion of hydrothermal test, the apparatus is put in water for cooling. Finally we got a good coated zirconia on Sic tube.

A zirconia coated tubes is dried naturally and then send to calcined process at 800⁰C for 2 days. After calcined tubes are tested like permeability, SEM, density porosity, water absorption etc.

CHARACTERIZATION AND TESTING

1. Density

Bulk density is defined as the mass per unit volume of a material including the volume of open pores.

2. True density

True density is the mass per unit volume of a material including all forms of pores i.e. open and closed pores.

3. Porosity

Apparent porosity is the percentage relationship between the open pores to that bulk volume.

4. Water absorption

The water of absorption is expressed as the %age relationship of weight of water absorbed by the dry specimen.

Experimental procedure:

The specimen to be tested is kept in Dryer at 110⁰ C until it reaches constant weight, then dry weight (D) of the specimen is noted down. Then the specimens are kept in boiling water for 2 hours, then they are allowed cooled to room temperature and the saturated weight (W) of the test specimens are noted down, then the specimens are suspended in water and the suspended weight (S) of the specimens are noted down and calculated using the formula given below.

$$\text{Bulk density} = \frac{\text{Dry weight}}{\text{Saturated weight} - \text{suspended weight}}$$

$$\text{App. Density} = \frac{\text{Dry weight}}{\text{Dry weight} - \text{suspended weight}}$$

$$\% \text{ Apparent porosity} = \frac{\text{Saturated weight} - \text{dry weight}}{\text{Saturated weight} - \text{suspended weight}} \times 100$$

$$\% \text{ Water absorption} = \frac{\text{Saturated weight} - \text{dry weight}}{\text{Dry weight}} \times 100$$

SEM analysis



The scanning electron microscope (SEM) is a type of electron microscope that images the sample surface by scanning it with a high- energy beam of electrons in a raster scan pattern. The electrons interact with the atoms that make up the sample producing signals that contain information about the sample's surface topography, composition and other properties such as electrical conductivity.

The types of signals produced by an SEM include secondary electrons; back scattered electrons (BSE), characteristic X-rays, light (cathodoluminescence), specimen current and transmitted electrons. These types of signal all require specialized detectors for their detection that are not usually all present on a single machine. The signals result from interactions of the electron beam with atoms at or near the surface of the sample. In the most common or standard detection mode, secondary electron imaging or SEI, the SEM can produce very high –resolution images of a sample surface, revealing details about 1 to 5 nm in size Due to the way these images are created, SEM micrographs have a very large depth of field yielding a characteristic three – dimensional appearance useful for understanding the surface structure of a sample. This is exemplified by the micrograph of pollen shown to the right. A wide range of magnifications is possible, from about x 250,000, about 250 times the magnification limit of the best light microscopes. Back- scattered electrons (BSE) are beam electrons that are reflected from the sample by elastic scattering. BSE are often used in analytical SEM along with the spectra made from the characteristic X-rays. Because the intensity of the BSE signal is strongly related to the atomic number

(Z) of the specimen, BSE images can provide information about the distribution of different elements in the sample. For the same reason BSE imaging can image colloidal gold immuno-labels of 5 to 10 nm that would otherwise be difficult or impossible to detect in secondary electron images in biological specimens. Characteristic X-rays are emitted when the electron beam removes an inner shell electron from the sample, causing a higher energy electron to fill the shell and release energy. These characteristic X-rays are used to identify the composition and measure the abundance of elements in the sample.

Permeability :



Permeability apparatus

$$\text{Permeability} = \frac{\text{Permit flux}}{\text{Pressure difference}}$$

$$\text{Area of tube} = \pi dl$$

Where,

d is the diameter of tube

l is length of the tube

$$\text{LMH} = \frac{\text{litre}}{\text{m}^2 \cdot \text{hr.}}$$

RESULTS

Sample No.	Dry wt.(gms)	Suspended wt.(gms)	Saturated wt.(gms)	Bulk density (gm/cc)	% Porosity	% Water absorption
U-3-1	6.806	4.513	8.653	1.64	44.61	27.13
U-3-2	8.986	5.919	11.422	1.63	44.26	27.10
U-3-3	9.967	6.595	12.605	1.65	43.89	26.46
T-3-1	8.102	5.353	10.312	1.63	44.56	27.27
T-3-2	6.818	4.515	8.658	1.64	44.41	26.98
T-3-3	6.107	4.042	7.734	1.65	44.06	26.64

U –Uncoated samples

T – Titania coated sample

Water Flux

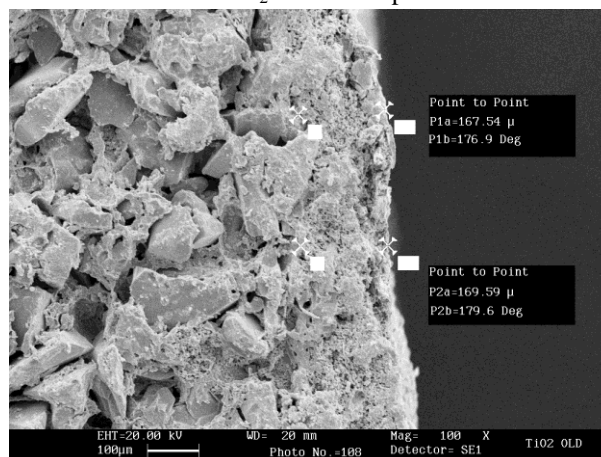
Membrane size : 13 mm OD, 9 mm ID, L=106 mm

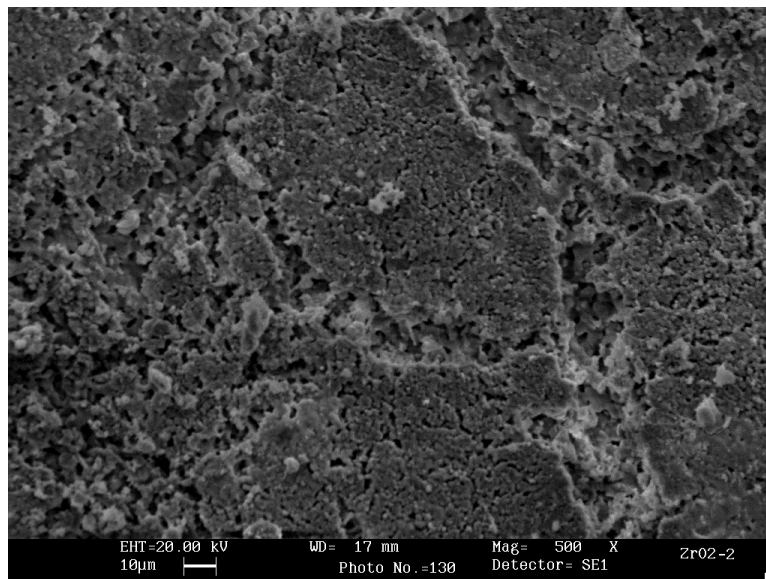
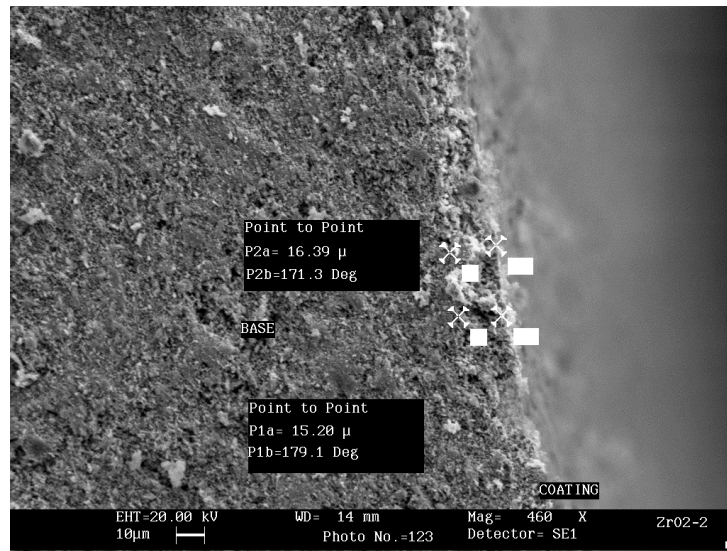
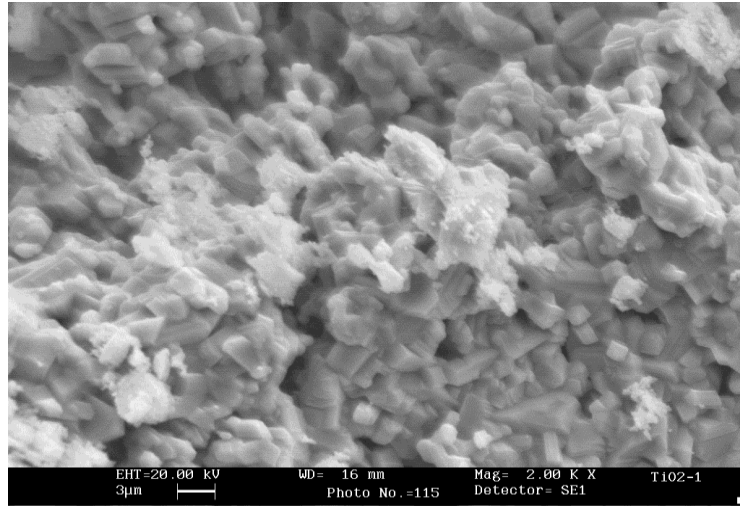
Sample no	Composition	Area(m ²)	Inlet pressure (kg/cm ²)	Permit flux ml/min	LMH (l/m ² .hr)
3	100% titania sol	0.00319	0.5	7	131.66
			1	10	188.09
			1.5	13	244.514
			2	14	263.32
			2.5	16	300.32
6	45gms of zirconia oxynitrate + 300ml of water	0.0046	0.5	8	104.35
			1	11	143.48
			1.5	15	195.65
			2	17	221.74
			2.5	21	273.913
5	Titania sol + 5% titania powder(50ml)+ 50ml of slurry	0.00319	0.5	16	300.47
			1	20	375.59
			1.5	28	525.82
			2	41	769.95
			2.5	44	826.29
13	Titania slurry+ 15% sol	0.0032	0.5	9	168.75
			1	12	225
			1.5	17	318.95
			2	23	431.52
			2.5	26	487.8
14	Titania slurry+ 15% sol	0.0047	0.5	27	344.83
			1	38	485.31
			1.5	48	613.03
			2	60	766.28
			2.5	70	893.99
15	5% of titatnia sol + 95ml of slurry	0.003	0.5	40	800
			1	53	1060
			1.5	60	1200
			2	61	1220
			2.5	62	1240
16	5% of titatnia sol + 95ml of slurry	0.0042	0.5	24	342.86
			1	31	442.86
			1.5	34	485.71
			2	35	500
			2.5	36	514.29
6	210grams of zirconia oxynitrate + 700ml of water	0.0043	0.5	10	138.50
			1	12	166.20
			1.5	15	207.80

			2	16	221.60
			2.5	17	235.46
21	210grams of zirconia oxynitrate + 700ml of water	0.00302	0.5	22	437.37
			1	23	457.26
			1.5	27	536.78
			2	28	556.66
			2.5	30	596.42
22	210grams of zirconia oxynitrate + 700ml of water	0.003	0.5	23	460
			1	25	500
			1.5	28	560
			2	29	580
			2.5	32	640
14	200ml of zirconia oxynitrate solution + 100ml of water	0.0046	0.5	22	286.96
			1	34	443.28
			1.5	40	521.51
			2	42	545.45
			2.5	45	586.70
23	200ml of zirconia oxynitrate solution + 100ml of water	0.0032	0.5	24	433.99
			1	25	452.08
			1.5	32	578.66
			2	34	614.83
			2.5	37	669.08
24	200ml of zirconia oxynitrate solution + 100ml of water	0.0031	0.5	22	425.78
			1	28	541.90
			1.5	30	580.61
			2	32	619.31
			2.5	34	658.02

SEM analysis:

1. TiO₂ coated samples





2. ZrO₂ coated samples

Conclusions

Zirconia coating is applied on the SiC tube. It is mainly carried out by hydrothermal reaction. Zirconia solution prepared from zirconia oxynitrate and water. This hydro thermal test is carried out in an oven at 150⁰C for 16hrs. Finally we got good zirconia coating on SiC base. Found zirconia coated body is then dried at 100⁰C and fired at 800⁰C. Obtained product shows optimum porosity (40-45%) and good permeability for the membrane application like water filtration.

References:

1. C.C. chen, M.M. Nasrallah, H.U. Anderson, Solid state ionics.(1994) 101-108
2. T. Okubo, T. Takahashi, M. sadakata, H. magaroto, J. Membr. Sci 118(1996) 151-157
3. J. Kimi, Y.S. Lin, J. Membr. Sci. 139 (1998) 175-183
4. Introduction to ceramics by 'Singer and Singer'
5. Www.sciencedirect.com

Witness Based Criminal Identification Using Data mining Techniques and New Gaussian Mixture Model

Uttam Mande¹, Y. Srinivas², J. V. R³. Murthy

¹(Dept of CSE, GITAM University Visakhapatnam)

²(Dept of IT, GITAM University Visakhapatnam)

³(Dept of CSE, J. N. T. University, Kakinada)

Abstract: The crime history in the recent past has increased drastically, and the tendency towards the crime is also an upheaval task. Therefore to combat the crime, effective technologies are to be provided as supportive to the law enforces. Data mining concepts prove to be very useful in this direction. A major uplift in the direction of crime identification is direct evidence, which can be of crucial concern by which plausible conclusions can be drawn. Identifying the criminal by means of forensics reports is seemingly difficult. This paper introduces a novel methodology of criminal mapping based on forensics using the concepts of Data mining and New Gaussian Mixture model.

Key words: Data mining, New Gaussian Mixture model, Crime, criminal mapping, criminal identification, forensics.

I. Introduction

The quest towards the luxurious life styles, environmental conditions, and uncontrollable ambitions have driven the humans towards the criminal activities[1] Many government and private agencies are rigorously marching to combat the law breakers. Today, most of the criminal records are maintained manually and on the other hand due to the lack of sufficient man power, the data entry has become a concern [2]. With this background, as the criminal activities have extended its wings at different locations, it has become an challenging task for the police to exchange the information between the police stations at different locations in solving the issues. Therefore formulation of effective mechanism to support the law enforces while investigations are very much needed.[3] This mechanism should be helpful in information sharing and thereby shaping towards a meaningful crime analysis. To support, effective methodologies that help in criminal investigations for evaluating the physical clues and determining the different strategies to be adopted for investigation are to be formulated. Therefore the physical evidences obtained from the witness and the forensics reports help towards the better criminal analysis.

Hence in this paper, a database is generated from the criminal data available from different police stations of Andhra Pradesh. The database is created by considering two basic facts viz., availability of witness at the criminal spot and the reports from the forensic labs that are collected from the clue spot[4]. The data mining concepts are exploited for mining the likelihood of the criminals based on the features/ witness available. Clustering is performing based on the type of crime. The

crime activities considered in this paper are Murder, Riot, kidnap and robbery. Based on the features described about the criminal, a face is generated and the generated face is compared with that of the existing faces for finding the likelihood of the criminals[6]. These identities are further mapped with the forensic clues to formulate as unique identity. Data mining techniques help to explore the enormous data and making it possible in reaching the ultimate goal of criminal analysis by using the concepts of clustering and classification. In this paper the concept of clustering is carried out basing on the type of crime. The rest of paper is organized as follows, section -2 of the paper deals with Acquisition of features, in section- 3, details about the crime identification presented, Clustering techniques is discussed ,in section -4 the New Gaussian Mixture model is presented , experimentation is highlighted in section- 5, the section 6 of the paper focus on the conclusion

II. Acquisition of Features from the witness

Any crime investigation highlights primarily on two issues, 1) Witness available and 2) Clues available and relating these features with that of the data available regarding the criminals. The crime data base considered in this paper include are 1) robbery 2) murder 3) kidnapping 4) riots. For the identification of any crime we need to have an idea about

1)clue variables 2) criminal relating/identification. Crime clues play a vital role in the proper identification of criminal. The clues help the stepping stone towards the crime analysis, and criminal relating is the mapping of the criminal based on the clues with data available in the data base, by the use of intelligent knowledge mapping.

III. Crime Identification using Crime links

The various crime links that were considered include

- 1) Crime location (place: restaurant, theater, road, railway station, shop/gold shop, mall, house, apartment)
- 2) Criminal attribute (hair, built, eyebrows, nose, teeth, beard, age group, mustache, languages known).
- 3) Criminal psychological behavior can be recognized by type of killing. We have considered the type of killing as (smooth, removal of parts, harsh) which attributes to the psychological behavior of the criminal.
- 4) Modus operandi (object used for crime), 1)Pistol 2)Rope 3)Stick 4)Knife

These criminal links help to analyze the dataset there by making the crime investigators to plane for identification of the criminal.

In this paper we have considered binary clustering to cluster the data base based on type of crime and the classification is carried out from the feature available.

3.1 Binary clustering:

In order to simplify the analysis process the huge dataset available is to be clustered. The clustering in this paper is based on the type of crime. A data set is generated from the database available from the Andhra Pradesh police department and a table is created by considering the FIR report

The various fields considered including the criminal identification numbers, criminal attributes, criminal psychological behavior, crime location, time of crime (day/night), witness /clue, the data set is generated by using the binary data of 1's & 0's, 1's indicating the presence of attribute and 0's indicating the absence of attribute then clustering of the binary data is done as proposed by Tao Hi (2005) using the binary clustering

Crimes are categorized in many ways, here we have given weights to each type of crime where weighing scheme is considered in the manner all the relative crimes will be given with near values , after applying clustering algorithm on this type of crime feature we have got four clusters of crime data they are robbery, kidnap, murder and riot

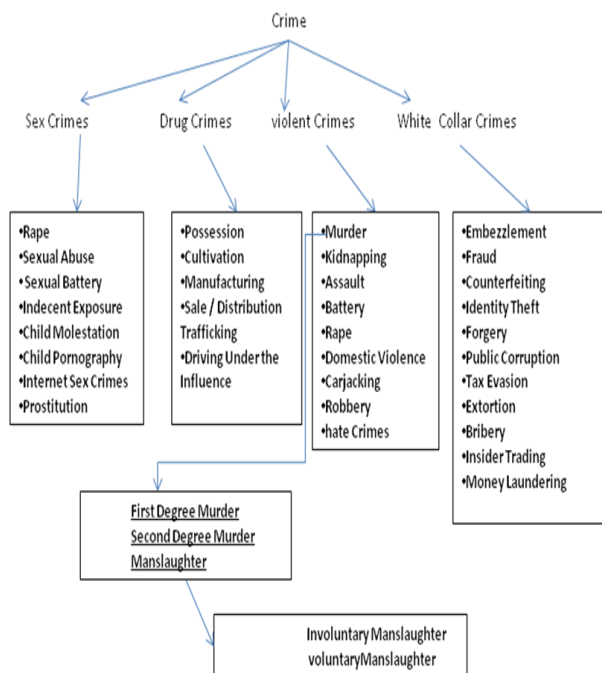


Fig 1 categories of crimes

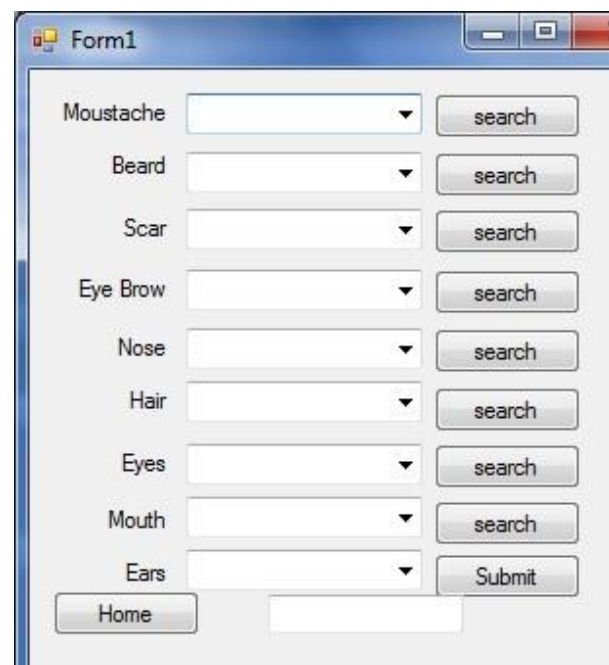
IV. New Gaussian Mixture model

New Gaussian Mixture model is utilized for the purpose of most likelihood criminal matching. This model is an extension of the existing Gaussian Mixture Model .The main advantage of using this model is that it minimizes the noise data as it includes a filter in the distribution itself. This is called a New Gaussian Mixture model since it tries to maintain the characteristics of GMM and it builds a covariance matrix for dimensionality reduction The probability density function of New Gaussian Mixture Model is given by PDF

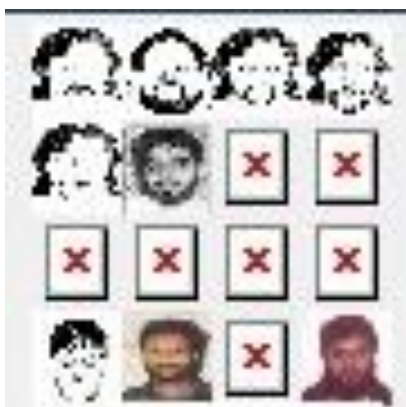
$$f(x) = \frac{1}{\sqrt{2\pi\sigma}} \left\{ \frac{\mu e^{-(x-\mu)^{\mu+1}}}{2\sigma^2} + \frac{\mu}{N} \sum_{i=1}^n \left(\frac{(x_i - \mu)^{\mu+1}}{2\sigma^2} \right) \right\}$$

V. Experimentation

The features are taken as input from the witness available and basing on the features, the database is compared for the relevancy in crime .The features are taken as input and basing on the features, The database is compared for the relevancy in crime .The features that are considered are the standard features generally used in FIR at the police stations and is shown in the following figure- 1



The various images that are retrieved using the features are displayed as follows



The outputs obtained includes cids and their filtered data is stored in the data base further investigation

ID	cid	featurename
116	1142	Feature
117	1149	Feature
118	1152	Feature
119	1155	Feature
120	1159	Feature
121	1006	Feature
27	1006	Feature
28	1006	Feature
33	1003	Feature
34	1005	Feature
35	1006	Feature
36	1009	Feature
37	1031	Feature
38	1036	Feature
39	1039	Feature
40	1042	Feature
41	1046	Feature
42	1047	Feature
43	1050	Feature
44	1053	Feature
45	1057	Feature
46	1058	Feature
47	1060	Feature

Probability density functions of the test image is mapped with the most likelihood of images present in the database and the most relevant images obtained are displayed



Fig2: The snap shot of data set

If the witness is available, at the crime incident, or of the forensics reports are available, then in such cases, identification of the criminal is a considered in this paper. The criminal is mapped by collecting the features about the crime from the witness and comparing them with that of the available from the data base. and if there is a map, the criminal can be identified. .If the data available from the witness is not sufficient, the forensics reports are also considered that are available, and correlate this report with the report of the witness to ratify criminal. Using the methodology a criminal is identified and for the uniqueness, this data is given as input to the New Gaussian mixture model to identify a unique criminal. From the above table, 101 is identified as the criminals

VI. Conclusion

This paper presents a novel methodology of identifying a criminal, in the presence of witness or any clue by the forensic experts. In these situations, in this paper we have tried to identify the criminal by mapping the criminal using the New Gaussian mixture model. .

References:

1. Carlile of Berriew Q.C “Data mining: The new weapon in the war on terrorism” retrived from the Internet on 28-02-2011
2. Cate H. Fred “Legal Standards for Data Mining” retrieved from the internet on 12-03-2011 http://www.hunton.com/files/tbl_s47Details/FileUpload265/1250/Cate_Fourth_Amendment.pdf
3. Clifton Christopher (2011). “Encyclopedia Britannica: data mining”, Retrieved from the web on 20-01-2011
4. Jeff and Harper, Jim “Effective Counterterrorism and the Limited Role of Predictive Data Mining” retrieved from the web 12-02-2011
5. U.M. Fayyad and R. Uthurusamy, “Evolving Data Mining into Solutions for Insights,” Comm. ACM, Aug. 2002, pp. 28-31.
6. W. Chang et al., “An International Perspective on Fighting Cybercrime,” Proc. 1st NSF/NIJ Symp. Intelligence and Security Informatics, LNCS 2665, Springer-Verlag, 2003, pp. 379-384.
7. H. Kargupta, K. Liu, and J. Ryan, “Privacy-Sensitive Distributed Data Mining from Multi-Party Data,” Proc. 1st NSF/NIJ Symp. Intelligence and Security Informatics, LNCS 2665, Springer-Verlag, 2003, pp. 336-342. April 2004
8. M.Chau, J.J. Xu, and H. Chen, “Extracting Meaningful Entities from Police Narrative Reports, Proc.Nat’l Conf. Digital Government Research, Digital Government Research Center, 2002, pp. 271-275.
9. A. Gray, P. Sallis, and S. MacDonell, “Software Forensics: Extending Authorship Analysis Techniqueto Computer Programs,” Proc. 3rd Biannual Conf.Int’l Assoc. Forensic Linguistics, Int’l Assoc. Forensic Linguistics, 1997, pp. 1-8.
10. R.V. Hauck et al., “Using Coplink to Analyze Criminal-Justice Data,” Computer, Mar. 2002, pp. 30-37.
11. T. Senator et al., “The FinCEN Artificial Intelligence System: Identifying Potential Money Laundering from Reports of Large Cash Transactions,” AI Magazine, vol.16, no. 4, 1995, pp. 21-39.

12. W. Lee, S.J. Stolfo, and W. Mok, "A Data Mining Framework for Building Intrusion detection Models," Proc. 1999 IEEE Symp. Security and Privacy, IEEE CS Press, 1999, pp. 120-132. 10. O. de Vel et al., "Mining E-Mail Content for Author Identification Forensics," SIGMOD Record, vol. 30, no. 4, 2001, pp. 55-64.
13. G. Wang, H. Chen, and H. Atabakhsh, "Automatically Detecting Deceptive Criminal Identities," Comm. ACM, Mar. 2004, pp. 70-76.
14. S. Wasserman and K. Faust, Social Network Analysis: Methods and Applications, Cambridge Univ. Press, 1994.

Estimation of Pit Excavation Volume by Fifth Degree Polynomial

Karwan H. F Jwamer¹, H.-S. Faraidun Kadir², A. Jamal Muhamad³

¹(University of Sulaimani-Faulty of Science & Science Education, School of Science -Department of Mathematics, Sualimani, Iraq)

²(University of Sulaimani-Faulty of Science & Science Education, School of Science Education -Department of Mathematics, Sualimani, Iraq)

³(Sulaimani Techincal Institute, Department of Engineering Drawing, Sulaimani, Iraq)

Abstract: In this paper, we derived a new formula using a high degree polynomial (fifth degree curve) in representation ground surface profile. Also, we show the result of calculation of volume by this new formula give a better accuracy because of using high degree curve in representing the ground profile which provides more smoothness in the representation.

Keywords: Pit excavation volume, fifth degree polynomial, ground surface profile

I. Introduction:

How to estimate the volume of earth work in a different engineering and industrial project such as foundation of water tank, underground reservoir and bringing a filled materials from a borrow pit in road construction project is a major task [1, 3]. The standard method has been to construct a grid by dividing the area into rectangles, the elevation at the intersections of the grid lines are measured before and after excavation and used for depth computation at the lattice of the grid then using these lattice values to estimate the volume[2,4], Fig.1.

In the past this estimation was done based on that the excavation depth between the grid points is linear. In real situations, this assumption may not be valid and formulas that consider a non linear excavation depth should be used [4].

In [4] improved the estimation by assuming the excavation depth function follows (approximately) second – or – third – degree polynomials along the two grid directions and using Simpson's rule twice to estimate the integration of this function. This was improvement, since clearly the ground profile (curve representing the excavation depth a long a grid lines) need not be linear [2].

Here in this paper a trial is done to obtain a new formula based on a higher polynomial degree such as fifth degree curve which can represent the excavation depth a long a grid line in both directions better than the linear and second or third degree polynomials representation which were used before.

Materials and methods

Consider Fig.1, in which the ground profile is assumed to follow fifth degree polynomial,

$$f(x) = a_0 + a_1x + a_2x^2 + a_3x^3 + a_4x^4 + a_5x^5 \quad (1)$$

In which $f(x)$ is the excavation depth at point x , ($f_0, f_1, f_2, f_3, f_4,$ and f_5 are six excavation depths at the points $x_0, x_1, x_2, x_3, x_4,$ and x_5)

The area under the ground profile can be find out as follow ,

$$A = \int_{x_0}^{x_5} (a_0 + a_1x + a_2x^2 + a_3x^3 + a_4x^4 + a_5x^5)dx \quad (2)$$

$$A = [a_0x + \frac{a_1x^2}{2} + \frac{a_2x^3}{3} + \frac{a_3x^4}{4} + \frac{a_4x^5}{5} + \frac{a_5x^6}{6}]_{x_0}^{x_5} \quad (3)$$

The values of the coefficients of the polynomial $a_0, a_1, a_2, a_3, a_4, a_5$ can be determined by substituting the known coordinates of these points into Eq.1 and solving the resulting six equations.

$$\text{At } x = x_0 = 0 \rightarrow y = y_0 = f_0 \rightarrow a_0 = f_0 \quad (4)$$

$$\text{At } x = x_1 \rightarrow y_1 = f_1 = f_0 + a_1x_1 + a_2x_1^2 + a_3x_1^3 + a_4x_1^4 + a_5x_1^5 \quad (5)$$

$$\text{At } x = x_2 \rightarrow y_2 = f_2 = f_0 + a_1x_2 + a_2x_2^2 + a_3x_2^3 + a_4x_2^4 + a_5x_2^5 \quad (6)$$

$$\text{At } x = x_3 \rightarrow y_3 = f_3 = f_0 + a_1x_3 + a_2x_3^2 + a_3x_3^3 + a_4x_3^4 + a_5x_3^5 \quad (7)$$

$$\text{At } x = x_4 \rightarrow y_4 = f_4 = f_0 + a_1x_4 + a_2x_4^2 + a_3x_4^3 + a_4x_4^4 + a_5x_4^5 \quad (8)$$

$$\text{At } x = x_5 \rightarrow y_5 = f_5 = f_0 + a_1x_5 + a_2x_5^2 + a_3x_5^3 + a_4x_5^4 + a_5x_5^5 \quad (9)$$

Because of using equal intervals, this led to say that

$$h = x_1 - x_0 : 2h = x_2 - x_0 : 3h = x_3 - x_0 : 4h = x_4 - x_0 : 5h = x_5 - x_0$$

Solving equation 5,6,7,8 and 9 give the values of coefficients

$a_1, a_2, a_3, a_4,$ and a_5 as follow ,

$$a_1 = \frac{1}{60h} [-137f_0 + 300f_1 - 300f_2 + 200f_3 - 75f_4 + 12f_5]$$

$$a_2 = \frac{1}{24h^2} [45f_0 - 154f_1 + 214f_2 - 156f_3 + 61f_4 - 10f_5]$$

$$a_3 = \frac{1}{24h^3} [-17f_0 + 71f_1 - 118f_2 + 98f_3 - 41f_4 + 7f_5]$$

$$a_4 = \frac{1}{24h^4} [3f_0 - 14f_1 + 26f_2 - 24f_3 + 11f_4 - 2f_5]$$

$$a_5 = \frac{1}{120h^5} [-f_0 + 5f_1 - 10f_2 + 10f_3 - 5f_4 + f_5]$$

Substituting for $a_0, a_1, a_2, a_3, a_4, a_5$ in equation 3 and noting that $x_0 = 0$ and $x_5 = 5h$, this yields the following formula for calculating area under the curve,

$$\text{Area} = \frac{5h}{288} [19f_0 + 75f_1 + 50f_2 + 50f_3 + 75f_4 + 19f_5] \quad (10)$$

Now to calculate volume take a unit grid of 5*5 of equal intervals in both direction as in Fig.2, the volume of this unit grid is given by

$$\text{volume} = \int_{x_0}^{x_5} \int_{y_0}^{y_5} f(x, y) dy dx \quad (11)$$

Where $f_{(x,y)}$ is a depth of excavation at grid nodes

First, the inner integral is calculated using the results in Eq. 10,

$$v = \frac{5h}{288} \left[\int_{x_0}^{x_5} 19f(x, y_0) + 75f(x, y_1) + 50f(x, y_2) + 50f(x, y_3) + 75f(x, y_4) + 19f(x, y_5) dx \right] \quad (12)$$

$$v = \frac{5h}{288} \left[19 \int_{x_0}^{x_5} f(x, y_0) dx + 75 \int_{x_0}^{x_5} f(x, y_1) dx + 50 \int_{x_0}^{x_5} f(x, y_2) dx + 50 \int_{x_0}^{x_5} f(x, y_3) dx + 75 \int_{x_0}^{x_5} f(x, y_4) dx + 19 \int_{x_0}^{x_5} f(x, y_5) dx \right] \quad (13)$$

use the results in equation number 10 again to each integral term in Eq.13 to obtained ,

$$v = \left(\frac{25h}{1440}\right)^2 \gamma_{ij} * f_{ij} \quad (14)$$

Where γ_{ij} are the corresponding elements of the following matrix :

$$C = \begin{pmatrix} 361 & 1425 & 950 & 950 & 1425 & 361 \\ 1425 & 5625 & 3750 & 3750 & 5625 & 1425 \\ 950 & 3750 & 2500 & 2500 & 3750 & 950 \\ 950 & 3750 & 2500 & 2500 & 3750 & 950 \\ 1425 & 5625 & 3750 & 3750 & 5625 & 1425 \\ 361 & 1425 & 950 & 950 & 1425 & 361 \end{pmatrix}$$

And f_{ij} are the corresponding elements of the following matrix which represent depth of excavation at

Grid nodes

$$F = \begin{pmatrix} f_{0,5} & f_{1,5} & f_{2,5} & f_{3,5} & f_{4,5} & f_{5,5} \\ f_{0,4} & f_{1,4} & f_{2,4} & f_{3,4} & f_{4,4} & f_{5,4} \\ f_{0,3} & f_{1,3} & f_{2,3} & f_{3,3} & f_{4,3} & f_{5,3} \\ f_{0,2} & f_{1,2} & f_{2,2} & f_{3,2} & f_{4,2} & f_{5,2} \\ f_{0,1} & f_{1,1} & f_{2,1} & f_{3,1} & f_{4,1} & f_{5,1} \\ f_{0,0} & f_{1,0} & f_{2,0} & f_{3,0} & f_{4,0} & f_{5,0} \end{pmatrix}$$

Equation 14 is a single formula for volume calculation for a grid unit of 5*5 of equal intervals in both directions in terms of the intersection points.

To calculate the total volume of any grid capacity which must be multiple of 5 in both direction is the sum of volumes of the unit grids . To calculate total volume let,

$$x_i = x_0 + ih; \quad i=0,1, \dots, m.$$

$$y_j = y_0 + jh; \quad j=0,1, \dots, n.$$

Then the composite formula for calculating the volume of the total grid, V, is given by ,

$$V = \int_{x_0}^{x_m} \int_{y_0}^{y_n} f(x, y) dy dx$$

$$V = \left(\frac{25h}{1440}\right)^2 \sum_{i=0}^m \sum_{j=0}^n \gamma_{ij} f_{ij} \quad \text{(Composite formula)} \tag{15}$$

In which γ_{ij} =the corresponding elements of the following matrix

$$C = \begin{pmatrix} 361 & 1425 & 950 & 950 & 1425 & 722 & 1425 & . & . & 1425 & 722 & 1425 & 950 & 950 & 1425 & 361 \\ 1425 & 5626 & 3750 & 3750 & 5625 & 2850 & 5625 & . & . & 5625 & 2850 & 5625 & 3750 & 3750 & 5625 & 1425 \\ 950 & 3750 & 2500 & 2500 & 3750 & 1900 & 3750 & . & . & 3750 & 1900 & 3750 & 2500 & 2500 & 3750 & 950 \\ 950 & 3750 & 2500 & 2500 & 3750 & 1900 & 3750 & . & . & 3750 & 1900 & 3750 & 2500 & 2500 & 3750 & 950 \\ 1425 & 5625 & 3750 & 3750 & 5625 & 2850 & 5625 & . & . & 5625 & 2850 & 5625 & 3750 & 3750 & 5625 & 1425 \\ 722 & 2850 & 1900 & 1900 & 2850 & 1444 & 2850 & . & . & 2850 & 1444 & 2850 & 1900 & 1900 & 2850 & 722 \\ 1425 & 5625 & 3750 & 3750 & 5625 & 2850 & 5625 & . & . & 5625 & 5625 & 5625 & 3750 & 3750 & 5625 & 1425 \\ . & . & . & . & . & . & . & . & . & . & . & . & . & . & . & . \\ . & . & . & . & . & . & . & . & . & . & . & . & . & . & . & . \\ 1425 & 5625 & 3750 & 3750 & 5625 & 2850 & 5625 & . & . & 5625 & 5625 & 5625 & 3750 & 3750 & 5625 & 1425 \\ 722 & 2850 & 1900 & 1900 & 2850 & 1444 & 2850 & . & . & 2850 & 2850 & 2850 & 1900 & 1900 & 2850 & 722 \\ 1425 & 5625 & 3750 & 3750 & 5625 & 2850 & 5625 & . & . & 5625 & 5625 & 5625 & 3750 & 3750 & 5625 & 1425 \\ 950 & 3750 & 2500 & 2500 & 3750 & 1900 & 3750 & . & . & 3750 & 3750 & 3750 & 2500 & 2500 & 3750 & 950 \\ 950 & 3750 & 2500 & 2500 & 3750 & 1900 & 3750 & . & . & 3750 & 3750 & 3750 & 2500 & 2500 & 3750 & 950 \\ 1425 & 5625 & 3750 & 3750 & 5625 & 2850 & 5625 & . & . & 5625 & 5625 & 5625 & 3750 & 3750 & 5625 & 1425 \\ 361 & 1425 & 950 & 950 & 1425 & 722 & 1425 & . & . & 1425 & 1425 & 1425 & 950 & 950 & 1425 & 361 \end{pmatrix} ..$$

$f_{i,j}$ = Depth of grid point with coordinates (x_i, y_i)

The matrix of Eq.15 corresponds to the grid points in Fig.3. This with the note that the second , third , fourth and fifth columns are to be repeated , as well as the second , third , fourth and fifth rows) . This, to calculate V, we only need to multiply each depth $f_{i,j}$ by the corresponding elements and sum the results for all points. The elements of the matrix C can be implemented easily in a computer program because they exhibit a specific pattern.

Eq.15 is for square grid with equal interval in both direction, if the grid is rectangular grid with h distance between grid nodes in x direction and with k distance in y direction, the equation became,

$$V = \left(\frac{25}{1440}\right)^2 * h * k \sum_{i=0}^m \sum_{j=0}^n \gamma_{ij} f_{ij} \quad \text{Composite equations for rectangle grid} \quad (16)$$

NUMERICAL EXAMPLE:

Consider the unit grid of Fig.4, in which m=1, n=1, h = 10 m. The excavation depths (in meter) are shown beside the grid intersection points, let to calculate the volume as follow;-

A) Classical method which is based on a linear relationship between the depth ends which represent the earth surface in both direction,

$$V[3] = \frac{A_s}{4} (\sum h_1 + 2\sum h_2 + 3\sum h_3 + 4\sum h_4)$$

Where $\sum h_1$ = sum of depth used once

$2\sum h_2$ = sum of depth used twice

$3\sum h_3$ = sum of depth used thrice

$4\sum h_4$ = sum of depth used four times

A_s = area of one square in a grid

$$\sum h_1 = 0.70 + 0.14 + 1.30 + 1.0 = 3.14 \text{ m.}$$

$$2 \sum h_2 = 2(1.10+1.32+0.87+0.25 + 1.14+2.14+1.69+0.45 + 1.4+1.35+0.89+0.75 + 1.25+2.09+0.79+0.75)=36.46 \text{ m.}$$

$$3 \sum h_3 = 0$$

$$4 \sum h_4 = 4(2.17+1.25+0.98+0.18+3.12+2.92+1.75+1.55+1.75+2.03+0.99+1.35+1.69+1.10+1.62+2.11)= 106.24 \text{ m.}$$

$$\text{Volume} = \frac{100}{4} (3.14+36.46+106.24)= 3646 \text{ m}^3$$

B) Volume calculation based on the obtained equation 15,

$$\text{volume} = \left(\frac{25h}{1440}\right)^2 \sum_{i=0}^m \sum_{j=0}^n \gamma_{ij} f_{ij}$$

$$V = \left(\frac{25 * 10}{1440}\right)^2 \begin{pmatrix} 361 & 1425 & 950 & 950 & 1425 & 361 \\ 1425 & 5625 & 3750 & 3750 & 5625 & 1425 \\ 950 & 3750 & 2500 & 2500 & 3750 & 950 \\ 950 & 3750 & 2500 & 2500 & 3750 & 950 \\ 1425 & 5625 & 3750 & 3750 & 5625 & 1425 \\ 361 & 1425 & 950 & 950 & 1425 & 361 \end{pmatrix} * \begin{pmatrix} 0.70 & 1.10 & 1.32 & 0.87 & 0.25 & 0.14 \\ 1.14 & 2.17 & 1.25 & 0.98 & 0.18 & 1.25 \\ 2.14 & 3.12 & 2.92 & 1.75 & 1.55 & 2.09 \\ 1.69 & 1.75 & 2.03 & 0.99 & 1.35 & 0.79 \\ 0.45 & 1.65 & 1.10 & 1.62 & 2.11 & 0.75 \\ 1.00 & 1.40 & 1.35 & 0.89 & 0.75 & 1.30 \end{pmatrix}$$

$$\text{Volume} = 3710.743 \text{ m}^3$$

II. Conclusions

- 1) the obtained formula for volume computation here on this paper is based on the assumption that the ground profile is nonlinear with fifth –degree polynomials
- 2) the obtained formula of course provide a better accuracy than formula that assumes a linear or second, or third-degree polynomials
- 3) the limitation here is that the grid must be equal to the interval in both direction and total number of interval must be equal to 5 or multiple of five
- 4) using this formula need computer programming

Notation:-

- A = area of region with irregular boundary
- As = area of a single square in a used grid
- $a_0, a_1, a_2, a_3, a_4, a_5$ = coefficients of used fifth –degree polynomial
- C = matrix of elements
- dx = width of increment in x- direction
- dy = width of increment in y-direction
- $f_0, f_1, f_2, f_3, f_4,$ and f_5 = six excavation depths at the points $(x_0, x_1, x_2, x_3, x_4,$ and $x_5)$
- $f_{i,j}$ = depth of grid point with coordinates (x_i, y_j)
- $f(x)$ = depth of point at horizontal distance x
- $f(x, y)$ = depth of point with coordinates (x, y)
- h = distance between grid points in both x and y direction in the case of square grid

- h_1 = depth used once
- h_2 = depth used twice
- h_3 = depth used thrice
- h_4 = depth used four times
- i = index for grid points in x-direction
- j = index for grid points in y-direction
- k = distance between grid points in y direction in the case of rectangle grid
- m = number of grid intervals in x- direction
- n = number of grid intervals in y-direction
- V = volume of total grid
- v = volume of unit grid of 5*5 equal intervals
- γ_{ij} = the corresponding elements of the following matrix C

References

- [1] Barry Kavanagh, 2009, Surveying – Principles and Application, Eighth Edition, Pearson Prentice Hall.
- [2] Danial W. Chambers , Estimating Pit Excavation Volume Using Unequal Interval , Journal of Surveying Engineering , Vol. 115 , No.4, November , 1989 , p 390-401.
- [3] S.K.Roy, 2004, Fundamentals of Surveying , Prentice-Hall of India, New Delhi .
- [4] Said M. Easa, Estimating Pit Excavation Volume Using Nonlinear Ground Profile, Journal of Surveying Engineering, Vol.114, No. 2, May, 1988 p 71-83

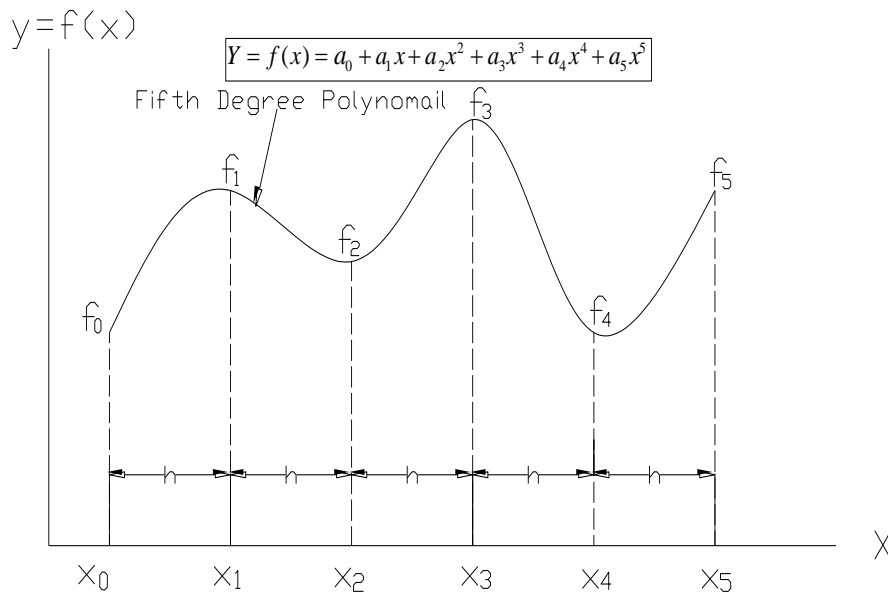


Fig-1-

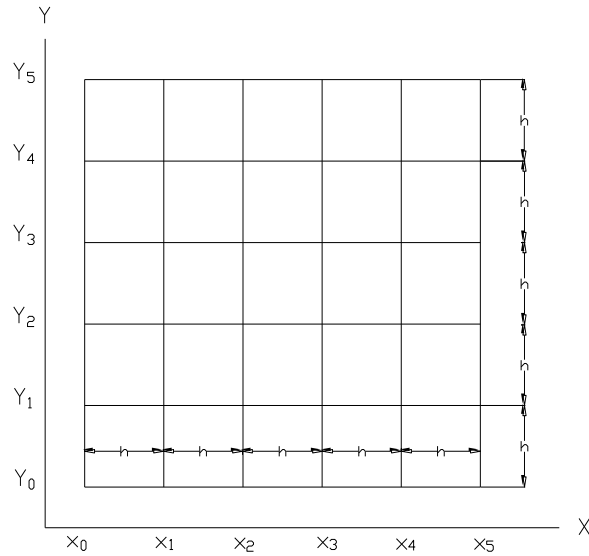


Fig-2:- 5*5 Square Grid with Equal Intervals

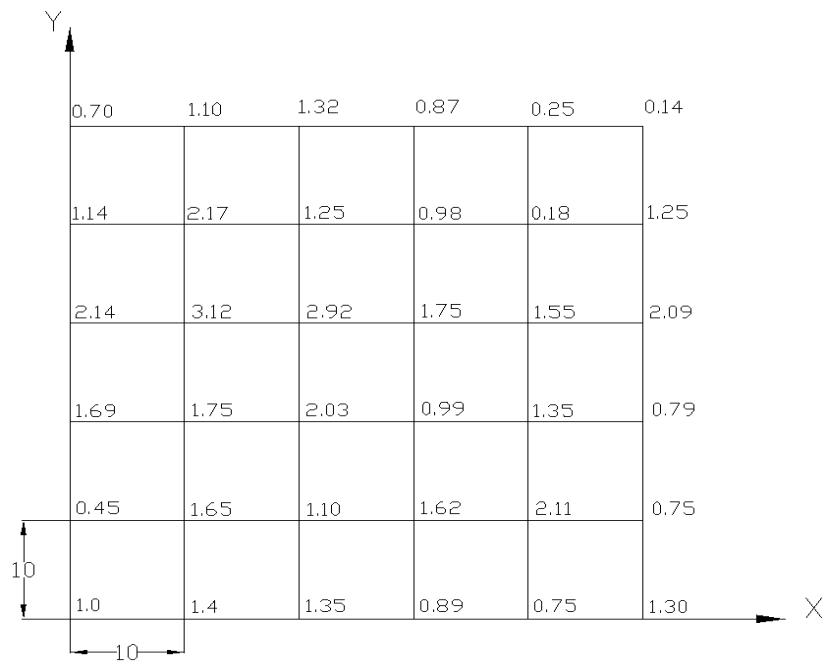


Fig-3:-Grid for Numerical Example,
 Depth are in Meters

Evaluation of the Efficiency of Surface Aerator in the Activated Sludge Process Treatment of Food Processing Effluent

T. Subramani¹ K. Arulalan²

¹Professor & Dean, Department of Civil Engineering, VMKV Engg. College, Vinayaka Missions University, Salem, India

²PG Student, of Environmental Engineering, Department of Civil Engineering, VMKV Engg. College, Vinayaka Missions University, Salem, India

ABSTRACT: Food processing units is a diversified activity consists of processing of perishable items such as fruit and vegetables, meat and poultry etc. into a various products without the loss of nutritional properties. Liquid waste is generated more in the Food processing units by means of washing of raw materials, pulping, crushing and canning operations. Hence, it is necessary to treat the effluent from the food processing units and to find the suitable ways of reusing the treated effluent water like gardening and other cleaning purpose etc., The effluent coming from food processing units contains large quantity of organic and inorganic materials which gives adverse effect to the environmental system when it is discharged directly without proper treatment system. The level of physical, chemical and biological characters have to be analyzed and the treatment system needs to be designed accordingly with proper analysis and environmental control. All effluent and wastewater containing biodegradable constituents which can be treated biologically in which the dissolved and particulate biodegradable constituents have been oxidized into acceptable forms. Hence, the reduction of Bio-chemical Oxygen Demand (*BOD) and Chemical Oxygen Demand (*COD) are the predominant factors in the biological treatment methods. The biological treatment process that occurs in the presence of oxygen (Aerobic process) results the maximum reduction level of BOD and COD. Especially in the Activated Sludge Process (#ASP), the BOD removal is up to 80-95 percent and bacteria removal is up to 90-95%. The type of suitable aeration mechanism working with optimum efficiency plays vital role in the performance of biological treatment. Hence, the food processing effluent from the existing Effluent Treatment plant at CFTRI has been taken for analysis purpose in order to evaluate the efficiency and standardize the operation of aerator since the capacity of ETP of CFTRI is 120 m³/ day which is almost equal the designed capacity of 100 m³/ day for this project work. Moreover, the ETP of CFTRI had been designed based on the Activated Sludge treatment Process. The main characters like BOD, COD and pH have been analyzed for the following three main parameters during the project study

1. Temperature of the effluent at morning, noon and evening
2. RPM of the aerator
3. Immersible depth of impeller into the effluent in the aeration tank.

By analyzing the results of the above parameters, the characteristics of the effluent and efficiency of the surface aerators are evaluated.

KEYWORDS: Evaluation, Surface Aerator, activated Sludge, Food Processing Effluent

I. INTRODUCTION

Characteristics of Effluent And Importance of Treatment Of Effluent

In the olden times, the waste waters from a community were not so much contaminated as they are today. The urbanization, industrial growth and the improved standards of living have increased the strength and quantity of municipal sewage in recent years to a point where dilution alone can no longer be relied upon to prevent the undesirable effects of pollution. In many cases, more advanced treatment of wastes is essential to prevent undue pollution. This is much more so, when the disposed sewage is likely to contain industrial wastes.

When untreated sewage is discharged into some river stream, floating solids present in the discharged sewage may be washed up on to the shore near the point of disposal, where they decompose and create unpleasant smells and odours. The large amount of organic matter present in the discharged sewage will also consume the dissolved oxygen from the river stream in getting oxidized, and may thus seriously decrease the dissolved oxygen of the river stream, causing fish kills and other undesirable effects. In addition to these effects, the discharged sewage will contaminate the river water with pathogenic bacteria. Hence, even though municipal sewage is 99.9 percent water, it requires treatment if nuisance is to be avoided. Food processing units are having diversified activities where water is being used abundantly by means of cleaning of raw materials, processing and their research activities. The effluent coming from the food processing units contains organic matters, oil, grease, minerals, metals and chemicals etc. Hence, it is absolutely necessary to analyze the various characteristics and behavior of effluent. The quality of effluent can be checked and analyzed by testing its physical, chemical and biological characteristics which are listed in Figure.1.

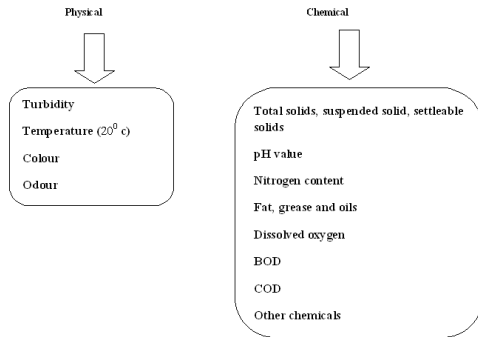


Figure.1. Characteristics of Effluent

The type of treatment required depends upon the character and quality of both effluent and source of disposal. The most important test of effluent is that for determining its Bio-chemical Oxygen Demand, popularly called BOD and Chemical Oxygen Demand popularly called COD. If sufficient oxygen is available in the effluent, the useful aerobic bacteria will flourish and cause the aerobic biological decomposition of waste, which will continue until oxidation is completed. The amount of oxygen consumed in this process is the BOD. The BOD affects the quality of water or effluent (See Figure. 2.) and Polluted water will continue to absorb oxygen for many months, and it is not practically possible to determine this ultimate oxygen demand. There are many different ways to treat effluent and treatment process level like preliminary treatment, primary treatment, secondary (Biological) treatment and final treatment are narrated in Table 1,2,3 & 4 .The pollution control board of State and Central Government has set the tolerance limits of discharged effluent to land and public sewers which are listed in Table.5 and Table.6. The discharge of effluent from all industrial sectors is being regularly monitored by the Pollution Control boards.

In the secondary (Biological) treatment, the fine suspended and dissolved organic matters are being removed. The reduction level of BOD and COD are very high in the activated sludge process of the biological treatment system where aeration process plays vital role in the Activated Sludge Process (ASP)

Hence, providing suitable aeration mechanism working with optimum efficiency will results the high reduction of BOD and COD.

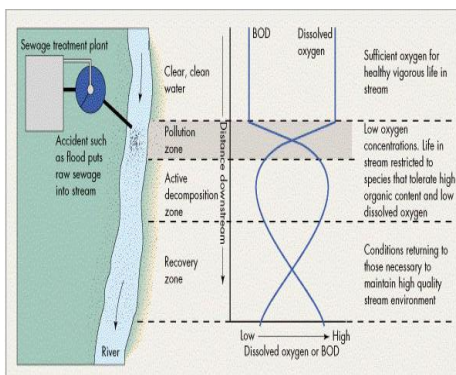


Figure.2 BOD Effects On Water Quality

1.1 EFFLUENT TREATMENT LEVELS

Table.1. Preliminary Treatment

Process	Unit	BOD removal in %	Total Suspended Solids (TSS) in %
Floating material	Screens	5-10	2-20
Heavy settleable inorganic solids	Grid chambers	10-20	20-40
Fats , oil and grease	Skimming tanks	20-30	20-40

Table.2. Primary Treatment

Process	Unit	BOD removal in %	Total Suspended Solids (TSS) in %
Large suspended organic matter	Plain sedimentation tank	30-35	60-65

Table.3. Secondary (Biological) Treatment

Process	Unit	BOD removal in %	(TSS) in %
Fine suspended and dissolved organic matter	Chemical flocculation and sedimentation	50-85	70-90
	ASP- Aeration tank and secondary settling tank	75-95	85-90

Table.4 Final or Tertiary Treatment

Process	Unit	BOD removal in %	(TSS) in %
Pathogens and very fine organic matter	chlorinator	100	100

1.2 ACTIVATED SLUDGE PROCESS (ASP)

The activated sludge process provides an excellent method of treating either raw sewage or more generally the settled sewage. The sewage effluent from primary sedimentation tank, which is, thus normally utilized in this process, is mixed with 20 to 30 percent of own volume of activated sludge, which contains a large concentration of highly active aerobic micro-organisms. The mixture enters an aeration tank, where the micro-organisms (coated around the sludge solids) and the sewage, are intimately mixed together, with a large quantity of air for about 4 to 8 hours. Under these conditions, the moving organisms will oxidize the organic matter and the suspended and colloidal matters tend to coagulate and form a precipitate, which settles down readily in the secondary setting tank. The settled sludge (containing micro organisms) called activated sludge, is then recycled to the head of the aeration tank to be mixed again with the sewage being treated. New activated sludge is continuously being produced by this process, and a portion of it being utilized and sent back to the aeration tank, whereas the excess portion is disposed of properly along with the sludge collected during primary treatment after digestion.

The effluent obtained from a properly operating activated sludge plant is of high quality, usually having a lower BOD than that of trickling filter. BOD removal is up to 80-95 percent, and bacteria removal is up to 90-5 percent. Moreover, land are required is also quite less.

1.1.5 TOLERANCE LIMITS OF DISCHARGED EFFLUENTS

Table.5 Standards for the Discharge of Effluents into Public Sewers

SL. No.	Parameters	* KSPCB Standards (U/S 25 of Water Act 1974)
1	Suspended Solids (mg/L)	Max: 100
2	pH	5.5 – 9.0
3	Oil and Grease (mg/L)	Max: 20
4	Ammoniacal Nitrogen (mg/L)	Max: 50
5	BOD (mg/L)	Max: 350
6	COD (mg/L)	---
7	Chloride, mg/L	Max: 350
8	Sulphates, mg/L	Max: 1000
9	Dissolved Solids, mg/L	Max: 2100
10	Cyanide (mg/L)	Max: 0.20
11	Fluoride (mg/L)	Max: 1.5
12	Phenolics compounds (mg/L)	Max: 5.0
13	Organochlorine & Organophosphorus Pesticides, ppb	Absent
14	Arsenic (mg/L)	Max: 0.20
15	Mercury (mg/L)	Max: 0.01
16	Lead (mg/L)	Max: 1.0
17	Cadmium (mg/L)	Max: 1.0
18	Chromium (mg/L)	Max: 2.0
19	Copper (mg/L)	Max: 3.0
20	Zinc (mg/L)	Max: 1.5
SL. No.	Parameters	* KSPCB Standards (U/S 25 of Water Act 1974)
21	Selenium (mg/L)	Max: 0.05
22	Nickel (mg/L)	Max: 3.0
23	Iron (mg/L)	Max: 3.0
24	Residual sodium carbonate, (mg/L)	Max: 5.0
25	Sodium absorption ratio (m. eqs/L)	---
26	“Percent Sodium” (m. eqs/L)	Max: 60

TABLE.6. STANDARDS FOR THE DISCHARGE OF EFFLUENTS INTO LAND FOR IRRIGATION

SL. No.	Parameters	*KSPCB Standards (U/S 25 of Water Act 1974)
1.	Colour	Colourless
2	Suspended Solids (mg/L)	Max: 30.0
3	pH	6.50 – 8.50
4	Oil and Grease (mg/L)	Max: 10.0
5	Ammoniacal Nitrogen (mg/L)	Max: 50.0
6	BOD (mg/L)	Max: 20.0
7	COD (mg/L)	Max: 250.0
8.	Dissolved phosphate	Max :5.0

Source: Karnataka Pollution Control Board (KSPCB)

But, however, is this process, a rather close degree of control is necessary in operation to ensure

1. That an ample supply of oxygen is present
2. That there is intimate and continuous mixing of the sewage and activated sludge and
3. That the ratio of the volume of activated sludge added to the volume of sewage being treated is kept practically constant.

1.3 SURFACE AERATION

For efficient surface aeration, high- and low-speed floating aerators provide pumping action that transfers oxygen by breaking up the wastewater into the form of dispersion of bubbles. The large surface area of the bubbles allows oxygen transfer to the wastewater from the atmosphere. At the same time, the oxygen-enriched water is circulated and mixed, resulting in effective oxygen delivery in the entire bulk of the wastewater body. High- and low-speed surface aerators offer excellent oxygen transfer and low operating costs. They are able to handle environmental extremes such as high temperatures. Another alternative for surface aeration is the use of horizontally mounted aeration discs or rotors. These disc or rotor aerators can be used in oxidation ditches known as looped, "race track" reactor configurations. They provide stable operation with resulting high-quality effluent. The aerators are above water for easy maintenance and are energy efficient. Other multichannel processes use a concentric arrangement of looped reactors, which is particularly energy efficient and designed to achieve total nitrogen removal through simultaneous nitrification/de nitrification. Disc and rotor surface aerators offer good BOD and COD removal efficiencies, and are very easy to replace if necessary. Reactors in a vertical-loop configuration are also available for surface aeration. They are essentially oxidation ditches flipped on their sides. Upper and lower compartments separated by a horizontal baffle run the length of the tank. Surface-mounted discs or rotors provide mixing and deliver oxygen. Typically, two or more basins make up the system. The first basin operates as an aerated anoxic reactor and the second basin is operated under aerobic conditions. These types of reactors also have high BOD/COD removal efficiency

1.4 SECONDARY (BIOLOGICAL) TREATMENT

Aeration Tank

The equalized effluent from the Equalization Tank is pumped to aeration tank where aerial oxygen is mixed with water by means of floating aerator system (see Fig: 1 . 2) To understand the system, the following terms must be understood:-

Mixed Liquor Suspended Solids (MLSS)

The suspended solids concentration in the Aeration tank is referred to as Mixed Liquor SS. It is an index of the mass of active microorganisms in the Aeration tank. As illustrated before MLSS in aeration tank indicates the presence of both active and dead bacterial cells. The level of MLSS that has to

be maintained depends upon the desirability of treated water quality. MLSS level of 3500-5000 mg/ Lit would be optimum in an extended type aeration tank.

Return Activated Sludge (RAS)

The purpose of the return of activated sludge to Aeration tank from Sludge Sump is to maintain a sufficient concentration of activated sludge in the tank so that required degree of treatment can be obtained in the limited time interval.

Food to Microbes ratio (F/M):-

It is the ratio between amounts of Organic material available to microbial population. In other words it is the ratio between BOD in kgs and MLSS in kgs. A proper F/M can be achieved by increasing or decreasing the rate of Return Activated Sludge (RAS) from Secondary Clarifier. Optimum F/M for an Extended Aeration type ASP is 0.1-0.15.

Function of Aeration Tank:

The main function of an Aeration tank in a activated sludge process are:

To maintain the dissolved oxygen concentration in the Effluent by suitable aerators

To maintain sufficient MLSS regulating return activated sludge from secondary Clarifier.

II. Project Objectives

2.1 AIM

To find out the optimum efficiency of surface aerator at different process conditions in the activated sludge process treatment of effluent coming from Food Processing Units.

2.2 OBJECTIVES

To evaluate the efficiency of surface aerator for biological treatment in the food processing effluent, especially the reduction of BOD and COD.

To analyze the effluent characteristics at different conditions of surface aerator in the Activated Sludge Process.

To analyze the treatment efficiency of surface aerator at different conditions and to standardize the operation of surface aerator in the aeration tank.

2.2 FEASIBILITY STUDY

2.2.1 Economic feasibility:

Providing surface aerators in the aeration mechanism consume high electric power in a day since the motor has to be operated continuously up to the designed detention period. The number of hours of aerator operation may be curtailed and standardized by doing the analysis of effluent based on the above mentioned project parameters for low range of raw effluent characteristics of BOD, COD and TSS are similar to that of the raw effluent of CFTRI.

By standardizing the aerator operation for the required limited period of time at a particular temperature in a day, we can save the energy and money for the daily operation cost of ETP at CFTRI. By analyzing the outcome of the results and standardizing the aerator operation in the ETP

of CFTRI, we may able to bring down the daily operation costs.

2.2.2 Operational feasibility:

The daily operation of aerator is one of the predominant factors in the extended aeration process. The standardizing the operation of aerator for its optimum efficiency resulted the reduction of manpower, Time management and utilize the manpower in productive manner by engaging other activities. Hence it is more feasible to standardize the aerator operation based on the Temperature of the effluent, RPM and Immersible depth of the impeller of the surface aerator into the effluent in the aeration tank.

2.2.3 Technical feasibility:

Aeration process in the activated sludge process of biological treatment of effluent mainly depend on the type of aeration mechanism, percentage of activate sludge and microorganism present in the activated sludge, transformation of dissolved oxygen through the aeration system and type of impeller blade in the aerator.

Hence the reduction of BOD and COD in the biological treatment process involved more technical parameters of the extended aeration process where we can standardize the operation of aeration mechanism for high BOD and COD control.

III. Evaluation Of Surface Aerator

3.1 Biochemical Oxygen Demand (BOD)

The most widely used parameter of organic pollution applied to both wastewater and surface water is the 5-day BOD(BOD₅). This determination involves the measurement of the dissolved oxygen used by microorganisms in the biochemical oxidation of organic matter. Despite the widespread use of the BOD test, it has a number of limitations, It is hoped that, through the continued efforts of workers in the field, one of the other measures of organic content, or perhaps a new measure, will ultimately be used in its place. Why, then, if the test suffers from serious limitations, if further space devoted to it in this text? The reason is that BOD test results are now used

- To determine the approximate quantity of oxygen that will be required to biologically stabilize the organic matter present
- To determine the size of waste treatment facilities
- To measure the efficiency of some treatment processes, and
- To determine compliance with wastewater discharge permits. Because it is likely that the BOD test will continue to be used for some time, it is important to know the details of the test and its limitations.

3.2 Chemical Oxygen Demand (Cod)

The chemical oxygen demand is widely used as a means of measuring the organic strength of domestic and industrial wastes. The COD test allows measurement of a waste in terms of the total quantity of oxygen required for

oxidation to carbon dioxide and water in accordance with the equation ;

$\text{COHNS} + 0.2 + \text{Nutrients} \rightarrow 3 \text{CO}_2 + \text{NH}_3 + \text{C}_5\text{H}_{12}\text{O}_2 + \text{other end products}$

It is based upon the fact that all organic compounds, with few exceptions, can be oxidised by the action of strong oxidising agents under acid conditions.

During the determination of COD, organic matter is converted to carbon dioxide and water regardless of the biological assimilability of the substances. For example, glucose and lignin are both oxidised completely. As a result, COD values are greater than BOD values and may be much greater when significant amounts of biologically resistant organic matter is present. One of the chief limitations of the COD test is its inability to differentiate between biologically oxidisable and biologically inert organic matter. In addition, it does not provide any evidence of the rate at which biologically active material would be stabilised under conditions that exist in nature. (Clair NSawyer, 1994)

The major advantage of the COD test is the short time required to evaluation. The determination can be made in about 3 hours rather than the 5 days required for the determination of BOD. For this reason it can be used as a substitute for the BOD test in many instances. COD data can often be interpreted on terms of BOD values after sufficient experience has been accumulated to establish reliable correlation factors.

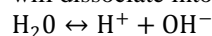
3.3 pH

The hydrogen -ion concentration is an important quality parameter of both natural waters and wastewaters. The usual means of expressing the hydrogen-ion concentration is as pH, which is defined as the negative logarithm of the hydrogen-ion concentration.

$$\text{pH} = -\log_{10}[\text{H}^+]$$

The concentration range suitable for the existence of most biological life is quite narrow and critical (typically 6 to 9). Wastewater with an extreme concentration of hydrogen ion is difficult to treat by biological means, and if the concentration is not altered before discharge, the wastewater effluent may alter the concentration in the natural waters. For treated effluents discharged to the environment the allowable pH range usually varies from 6.5 to 8.5

The hydrogen-ion concentration in water is connected closely with the extent to which water molecules dissociate. Water will dissociate into hydrogen and hydroxyl ions as follows:



Applying the law of mass action [Eq. (2-7)] to Eq. (2-30) yields

$$\frac{[\text{H}^+](\text{OH}^-)}{\text{H}_2\text{O}} = K$$

Where the brackets indicate concentration of the constituents in moles per liter. Because the concentration of water in a dilute aqueous system is essentially constant, this concentration can be incorporated into the equilibrium constant K.

IV. Materials And Methods

4. 1 MATERIALS AND EQUIPMENTS

Materials:

1. Refluxing Flask
2. Blenders
3. Pipettes
4. Small Beakers
5. Condenser
6. Incubation bottles

Equipments:

1. Incubator
2. pH Meter
3. Thermometer
4. Light Intensity Meter
5. Motor Frequency convertor

4. 2 STAGES INVOLVED FOR THE STUDY

Stage:I

Analyze the effluent characteristics at 3 different Temperature in a Day

- (i) Morning (10.00am)
- (ii) Noon (12.30 pm)
- (iii) Evening (6.00 pm)

Select the suitable Temperature where the high reduction percentage of BOD and COD

Stage :II

Analyze the effluent characteristics at 3 different speed (see Figure. 3 , 4 and 5). at the selected Temperature

- (i) RPM-1
 - (ii) RPM-2
 - (iii) RPM-3
- Select the suitable RPM

Stage :III

Analyze the effluent characteristics at different immersible depth (see Figure. 6,7,8,9 & 10) of impeller of surface aerator into the effluent of at selected RPM and Temperature

- (i) Depth-1
- (ii) Depth-2

Select the suitable immersible Depth of impeller into the effluent.

From the aeration tank at CFTRI (see Figure.11) the effluent samples have been collected (Figure.12) for the evaluation of aerator of CFTRI



Figure. 3 Connection Of Motor Frequency Converter In The Motor Control Room



Figure.4 Impeller at 48 Rpm



Figure.5 Impeller At 96 Rpm



Figure.6 Determination Of Cod Of The Effluent Sample



Figure.7 Immersible Depth Of Impeller Into The Effluent (Stage-I)



Figure.8 Immersible Depth Of Impeller Into The Effluent (Stage-II)



Figure. 9 Immersible Depth Of Impeller Into The Effluent (Stage-Ii)



Figure. 10 Immersible Depth Of Impeller Into The Effluent (Stage-Ii)



Figure.11 Surface Aerators In The Aeration Tank At CFTRI



Figure.12 Collection of Effluent Sample For Analysis

4. 3 Determination Of Bio-Chemical Oxygen Demand (Bod)

4. 3. 1 BOD Test Procedures

5-Day BOD Test Principle:

The method consists of filling with sample, to overflowing, an airtight bottle of the specified size and incubating it at the specified temperature for 5 d. Dissolved oxygen is measured initially and after incubation, and the

BOD is computed from the difference between initial and final DO. Because the initial DO is determined shortly after the dilution is made, all oxygen uptake occurring after this measurement is included in the BOD measurement.

Sampling and storage:

Samples for BOD analysis may degrade significantly during storage between collection and analysis, resulting in low BOD values. Minimize reduction of BOD by analyzing sample promptly or by cooling it to near-freezing temperature during storage. However, even at low temperature, keep holding time to a minimum. Warm chilled samples to $20 \pm 3^{\circ}\text{C}$ before analysis.

Grab samples

If analysis is begun within 2 h of collection, cold storage is unnecessary. If analysis is not started within 2 h of sample collection, keep sample at or below 4°C from the time of collection. Begin analysis within 6 h of collection; when this is not possible because the sampling site is distant from the laboratory, store at or below 4°C and report length and temperature of storage with the results. In no case start analysis more than 24 h after grab sample collection. When samples are to be used for regulatory purposes make every effort to deliver samples for analysis within 6 h of collection.

Composite samples

Keep samples at or below 4°C during compositing. Limit compositing period to 24 h. Use the same criteria as for storage of grab samples, starting the measurement of holding time from end of compositing period. State storage time and conditions as part of the results.

2. Apparatus

- a. Incubation bottles
- b. Air incubator or water bath,

3. Reagents:

Prepare reagents in advance but discard if there is any sign of precipitation or biological growth in the stock bottles. Commercial equivalents of these reagents are acceptable and different stock concentrations may be used if doses are adjusted proportionally.

4. Procedure:

- a. Preparation of dilution water: .
- b. Dilution water storage
- c. Glucose-glutamic acid check
- d. Seeding
 - 1) Seed source
 - 2) Seed control
- e. Sample pre treatment:
- f. Dilution technique
- g. Determination of initial DO
- h. Dilution water blank
- i. Incubation
- j. Determination of final DO

5. Calculation

For each test bottle meeting the 2.0-mg/L minimum DO depletion and the 1.0-mg/L residual DO, calculate BOD₅ as follows:

When dilution water is not seeded:

$$\text{BOD}_5, \text{ mg/L} = \frac{D_1 - D_2}{P}$$

When dilution water is seeded:

$$\text{BOD}_5, \text{ mg/L} = \frac{D_1 - D_2}{P}$$

where:

D₁ = DO of diluted sample immediately after preparation, mg/L,

D₂ = DO of diluted sample after 5 d incubation at 20°C, mg/L,

P = decimal volumetric fraction of sample used,

B₁ = DO of seed control before incubation, mg/L

B₂ = DO of seed control after incubation mg/L and

f = ratio of seed in diluted sample to seed in seed control = (% seed in diluted sample)/(% seed in seed control).

If seed material is added directly to sample or to seed control bottles:

f = (volume of seed in diluted sample)/(volume of seed in seed control)

4.4 DETERMINATION OF CHEMICAL OXYGEN DEMAND (COD)

$$\text{COD (ppm)} = \frac{\text{Titre} \times N \times \text{Thiosulfate} \times 8000}{\text{Volume of sample}}$$

4.5 DETERMINATION OF Ph

4.5.1 Test Procedure Reagents

a. General preparation

Calibrate the electrode system against standard buffer solutions of known pH. Because buffer solutions may deteriorate as a result of mold growth or contamination, prepare fresh as needed for accurate work by weighing the amounts of chemicals specified in Table 4500-H⁺:I, dissolving in distilled water at 25°C, and diluting to 1000 mL. This is particularly important for borate and carbonate buffers.

Boil and cool distilled water having a conductivity of less than 2 µmhos/cm. To 50 mL add 1 drop of saturated KCl solution suitable for reference electrode use. If the pH of this test solution is between 6.0 and 7.0, use it to prepare all standard solutions.

Dry KH₂PO₄ at 110 to 130°C for 2 h before weighing but do not heat unstable hydrated potassium tetroxalate above 60°C nor dry the other specified buffer salts.

Although ACS-grade chemicals generally are satisfactory for preparing buffer solutions, use certified materials available from the National Institute of Standards and Technology when the greatest accuracy is required. For routine analysis, use commercially available buffer tablets, powders, or solutions of tested quality. In preparing buffer solutions from solid salts, insure complete solution.

As a rule, select and prepare buffer solutions classed as primary standards in Table 4500-H⁺:I; reserve secondary standards for extreme situations encountered in wastewater

measurements. Consult Table 4500- H⁺:II for accepted pH of standard buffer solutions at temperatures other than 25°C. In routine use, store buffer solutions and samples in polyethylene bottles. Replace buffer solutions every 4 weeks

Procedure

Instrument calibration

In each case follow manufacturer's instructions for pH meter and for storage and preparation of electrodes for use. Recommended solutions for short-term storage of electrodes vary with type of electrode and manufacturer, but generally have a conductivity greater than 4000 µmhos/cm. Tap water is a better substitute than distilled water, but pH 4 buffer is best for the single glass electrode and saturated KCl is preferred for a calomel and Ag/AgCl reference electrode. Saturated KCl is the preferred solution for a combination electrode. Keep electrodes wet by returning them to storage solution whenever pH meter is not in use. Before use, remove electrodes from storage solution, rinse, blot dry with a soft tissue, place in initial buffer solution, and set the isopotential point. Select a second buffer within 2 pH units of sample pH and bring sample and buffer to same temperature, which may be the room temperature, a fixed temperature such as 25°C, or the temperature of a fresh sample. Remove electrodes from first buffer, rinse thoroughly with distilled water, blot dry, and immerse in second buffer. Record temperature of measurement and adjust temperature dial on meter so that meter indicates pH value of buffer at test temperature (this is a slope adjustment).

Use the pH value listed in the tables for the buffer used at the test temperature. Remove electrodes from second buffer, rinse thoroughly with distilled water and dry electrodes as indicated above. Immerse in a third buffer below pH 10, approximately 3 pH units different from the second; the reading should be within 0.1 unit for the pH of the third buffer. If the meter response shows a difference greater than 0.1 pH unit from expected value, look for trouble with the electrodes or potentiometer.

The purpose of standardization is to adjust the response of the glass electrode to the instrument. When only occasional pH measurements are made standardize instrument before each measurement. When frequent measurements are made and the instrument is stable, standardize less frequently. If sample pH values vary widely, standardize for each sample with a buffer having a pH within 1 to 2 pH units of the sample.

Sample analysis

Establish equilibrium between electrodes and sample by stirring sample to insure homogeneity; stir gently to minimize carbon dioxide entrainment. For buffered samples or those of high ionic strength, condition electrodes after cleaning by dipping them into sample for 1 min. Blot dry, immerse in a fresh portion of the same sample, and read pH. With dilute, poorly buffered solutions, equilibrate electrodes by immersing in three or four successive portions of sample. Take a fresh sample to measure pH.

V. Results And Discussions

5.1 Analysis Of The Results

5.1.1 BOD Results and calculation

The results of the BOD values have been analyzed with regard to the following parameters and their effects are identified .

Effect of temperature

The effluent samples have been taken in the aeration tank at morning, noon and evening time in order to analyze the character of BOD with regard to Temperature. On observing the results, there is no significant effect of BOD reduction since the variation in the temperature level at 3 different timings is very nominal. However, the BOD reduction has observed due to the process of aeration and the values have been listed in Table No.7

Table No.7 Effect Of Temperature On Bod

Parameter in PPM	Temperature		
	29°C (10.00am)	31°C (12.30pm)	28°C (6.00pm)
BOD	190	160	105

Effect of Impeller RPM

The values of BOD have been taken at the impeller rotation 48 RPM , 68 RPM and 96 RPM for 30 minutes aeration process and analyzed (See Table.8) . On reading of the values , it is noticed that the reduction of BOD level is significant for 45 minutes aeration process at 96 RPM of impeller rotation

Table No.8 Effect Of Impeller Rpm

Parameter in PPM	Impeller RPM		
	48	68	96
BOD	155	180	105

Effect of immersible depth of impeller into the effluent

The samples have been taken in the aeration tank at two different immersible depth of impeller into the effluent and values have been analyzed (See Table.9) . On observing the values, it is found that the reduction BOD level is more at the immersible depth of 10 cm.

Table. 9 Effect Of Immersible Depth Of Impeller Into The Effluent

Parameter in PPM	Immersible Depth of impeller in centimetre	
	10 cm	8 cm
BOD	30	105

5.3.2 COD Results and Calculation

The COD values have been analyzed based on the three parameters namely Temperature of effluent, impeller rotation and immersible depth of impeller into the effluent and their effects are identified

Effect of Temperature

The effluent samples have been taken in the aeration tank at morning, noon and evening time in order to analyze the character of COD with regard to Temperature. On observing the results, there is no significant effect of COD reduction since the variation in the temperature level at 3 different timings is very nominal. However, the COD reduction has observed due to the process of aeration and the values have been listed in Table .10

Table.10. Effect Of Temperature On Cod

Parameter in PPM	Temperature		
	29°C (10.00am)	31°C (12.30pm)	28°C (6.00pm)
COD	16	Not detectable	Not detectable

Effect of Impeller rotation

The COD values have been taken at three impeller rotation 48 RPM, 68 RPM and 96 RPM and analyzed. The values of COD with respect to the 48 RPM, 68 RPM and 96 RPM are (-) 16 , (-) 64 and (-) 72 respectively. Based on the results, it can be seen that there is a reduction in COD as the impeller rotation increases. But, the COD values (Table 11) are not in the detectable limits. However, it is observed that the reduction of COD level is in decreasing trend.

Table .11 Effect Of Impeller Rpm

Parameter in PPM	Impeller RPM		
	48	68	96
COD	16	Not detectable	Not detectable

Effect of immersible depth of impeller into the effluent

The samples have been taken in the aeration tank at two different immersible depth of impeller into the effluent and values have been analyzed (Table .12) . On observing the values, it can be seen that the reduction of COD level is more at the immersible depth of 10 cm But, the COD values are not in the detectable limits. The COD values have been taken at two impeller rotation 68 RPM and 96 RPM and analyzed. The values of COD with respect to the 68 RPM and 96 RPM are (-) 24 , and (-) 48 respectively. However, it is observed that the reduction of COD level is in decreasing trend.

Table .12 Effect Of Immersible Depth Of Impeller Into The Effluent

Parameter in PPM	Immersible Depth of impeller in centimetre	
	10 CM	8CM
COD	Not detectable	Not detectable

5.4 PH RESULTS AND CALCULATION

Since the variation in pH level of effluent samples itself are very less, it is not noticed accurately ensured that the significant reduction of BOD and COD with respect to the effect of temperature (Table No.13)., impeller rotation (Table.14) and immersible depth of impeller into the effluent (Table.15)

TABLE .13. EFFECT OF TEMPERATURE

Parameter	Temperature		
	10.00 AM	12.30 PM	6.00 PM
pH	7.09	6.82	7.37

TABLE.14 EFFECT OF IMPELLER RPM

Parameter	Impeller RPM		
	48	68	96
pH	7.63	7.8	7.37

TABLE .15 EFFECT OF IMMERSIBLE DEPTH OF IMPELLER INTO THE EFFLUENT

Parameter	Immersible Depth of impeller in centimetre	
	10 cm	8 cm
pH	7.09	7.25

5.5 EFFLUENT CHARACTERS BASED ON TEMPERATURE

Effect of temperature

The effluent samples have been taken in the aeration tank at morning, noon and evening time in order to analyze the character of BOD with regard to Temperature. On observing the results, there is no significant effect of BOD and COD reduction since the variation in the temperature level at 3 different timings is very nominal. However, the reduction in the values of BOD and COD has observed due to the process of aeration and the values have been given Figure13.

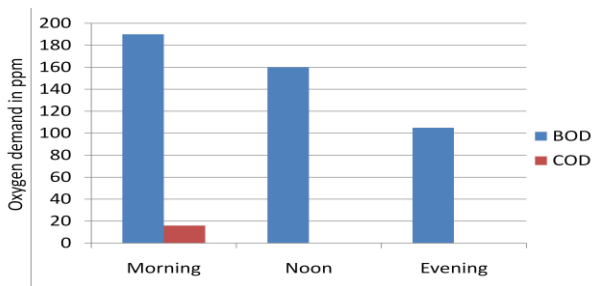


Figure.13. Effect of Temperature on BOD and Cod

5.6 Effluent Character Based On Impeller Rpm

5.6.1 Effect of Impeller RPM

The values of BOD have been taken at the impeller rotation 48 RPM , 68 RPM and 96 RPM for 30 minutes aeration process and analyzed (Figure.14) . On reading of the values ,

it is noticed that the reduction of BOD level is significant for 45 minutes aeration process at 96 RPM of impeller rotation The COD values have been taken at three impeller rotation 48 RPM, 68 RPM and 96 RPM and analyzed. The values of COD with respect to the 48 RPM, 68 RPM and 96 RPM are (-) 16 , (-) 24 and (-) 48 respectively. Based on the results, it is found that there is a reduction in COD as the impeller rotation increases. But, the COD values are not in the deductable limits. However, it is observed that the increase in the reduction of COD level in negative value.

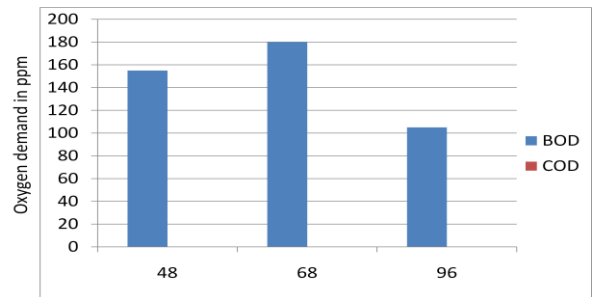


Figure.14 Effect of Impeller RPM on BOD And Cod

5.6.2 Effluent Character based on Immersible depth of Impeller into the effluent

Effect of immersible depth of impeller into the effluent

The samples have been taken in the aeration tank at two different immersible depth of impeller into the effluent and values have been analyzed (Figure.15) . On observing the values, it is found that the reduction BOD level is more at the immersible depth of 10 cm. The BOD reduction level is not found significant at 8 cm immersible depth of impeller into the effluent through the aeration process took place for 45 minutes at higher impeller rotation (96 RPM)

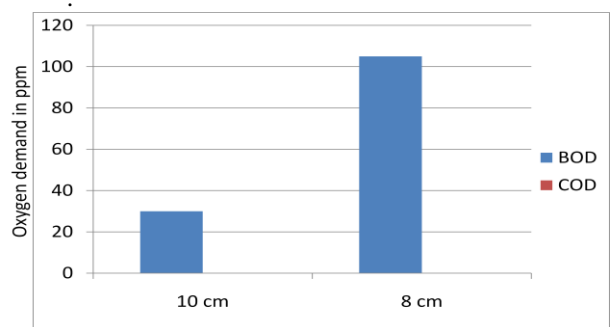


Figure.15 Effect of Immersible Depth Of Impeller On Bod And Cod

5.7 SCOPE FOR THE IMPROVEMENTS

There is ample scope for improvement to overcome to the following limitations are observed during the analysis for ensuring the accurate value of the characteristics of effluent. There may be a variation in the quantity of raw effluent coming from the equalization tank to aeration tank and the quantity of flow is not consistent. There may be a chance for variation in the raw effluent characteristics from

time to time depending on the food material that is processed in the pilot plants. The incoming quantity of activated sludge from clarifier tank to aeration tank for recycling is not consistent and microorganism present in the activated sludge may vary from time to time and it is difficult to calculate accurately. The presence of chemicals in the raw effluent may oxidize the inorganic materials very fast than the expected time of aeration.

VI. CONCLUSION AND FUTURE SCOPE OF THE PROJECT

There is no significant effect of temperature on reduction in BOD and COD, since the variation in the temperature level at 3 different timings is very nominal. However, the reduction in the values of BOD and COD has observed due to the process of aeration. The effect of impeller rotation at three different speeds on reduction of BOD, it is observed that the reduction of BOD level is significant for 45 minutes aeration process at 96 RPM of impeller rotation. The effect of impeller rotation at three different speed on reduction of COD, the values of COD with respect to the 48 RPM, 68 RPM and 96 RPM are not in the deductible limits. However, it is observed that the increase in the reduction of COD level. Moreover the reduction in BOD and COD will depend on the incoming quality and quantity of raw effluent and activated sludge. The effect of immersible depth of impeller into the effluent is significant. On observing the values, the reduction in BOD level is more at the immersible depth of 10 cm. The oxygen transfer in the aeration tank by the surface aerators may be increased by changing the suitable design of impeller. For instance, pitched blade turbine (up flow) with six blades and a blade angle of 45° (pitch) will significantly increase the degree of surface aeration. The inflow of activated sludge quantity may be increased and the effluent characters can be analyzed by which the detention time of effluent in the aeration tank and operation hours of aerators may be reduced.

REFERENCES

- [1]. Metcalf & Eddy - Fourth Edition (2003) ‘ Waste Water Engineering – Treatment and Reuse ’ , page 57, & p . 443 -448.
- [2]. Santosh Kumar Garg , Vol. II , (1987) ‘ Sewage and Waste Disposal Engineering (Vol-II) , p. 247 , 248 & 338.
- [3]. Anal Chavan, Suparna Mukharji , (2007) Article titled ‘ Dimensional Analysis for modeling oxygen transfer in rotating biological contractor ‘.
- [4]. U.S Environmental protection Agency, office research and Development , (1986) Method – by - method statistics from water pollution (wp) laboratory performance evaluation studies. Quality Assurance Branch, Environmental Monitoring and support lab, Cincinnati, Ohio.
- [5]. Standard methods for the examination of water and waste water, (1965) , American public Health Association , 12th Edition ,
- [6]. Kramer. A and Twigg B.A. ‘ Quality control for the Food industry’, (1975). Vol. 2. AVI publishing co., 3rd edition .
- [7]. Standard Methods for the Examination of Water and Wastewater. 20th Ed. American Public Health Association, American Water Works Association, Water Environment Federation .

Flow and heat transfer behaviour across circular cylinder and tube banks with and without splitter plate

S. G. Chakrabarty¹, Dr. U. S. Wankhede

¹(Currently pursuing masters degree program in Heat Power Engineering in G. H. Raisoni College of Engineering, Digdoh hills, Nagpur-440016, Maharashtra State, India)

²(Professor, Mechanical Engineering Department, G. H. Raisoni College of Engineering, Digdoh hills, Nagpur-440016, Maharashtra State, India)

Abstract: This paper describes the passive flow control of fluid in the downstream direction of the circular tube and in tube banks by means of splitter plate. Heat transfer and pressure drop depend on complex flow pattern of fluid in tube banks, whereas pressure drop linked directly with the fluid pumping capacity. A primary focus is to review experimental, analytical and numerical works that had been carried out to study the effect of longitudinal and transverse tube spacing, Reynolds number, stagnation point and surface roughness on wake size and vortex shedding.

Index Terms: Circular cylinder, Splitter plate, Tube banks, Cross flow, Heat transfer, Vortex shedding

I. INTRODUCTION

A heat exchanger is a device built for efficient heat transfer from one medium to another. The media may be separated by a solid wall, so that they never mix. Tube bank is the crossflow tubular heat exchanger and consists of multiple rows of tubes. One fluid passing through the tubes and other is passing across the tubes as shown in Figure 1. Tube banks arrangement include the in-line and the staggered arrangements. Cross flow tubular heat exchanger are found in diverse equipment as economizer, waste heat recovery, evaporator of an air conditioning system to name but few.

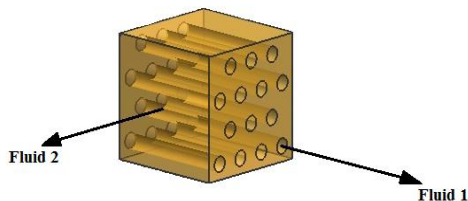


Figure 1. Cross Flow Tube Banks

Heat Exchanger involve several important design consideration which include thermal performance, pressure drops across the exchanger, fluid flow capacity, physical size and heat transfer requirement. Out of this following consideration, determination of pressure drop in a heat exchanger is essential for many applications because the fluid needs to be pumped through the heat exchanger. The fluid pumping power is proportional to the exchanger pressure drop. In tube banks, the heat transfer and pressure drop characteristic depend upon the flow pattern of fluid. The fluid flow converges as the minimum area occurs between the tubes in transverse row or in a diagonal row which makes the flow pattern very complex.

Passive control is one of the flow control techniques for reducing the aerodynamic drag exerted on a bluff body. It controls the vortex shedding by modifying the shape of the bluff body or by attaching additional devices in the flow stream. Passive control can achieve by use of splitter plate, small cylinder and base bleed method. Roshko (1954) was one of first investigator to study the influence of splitter plate on vortex shedding.

Splitter plate is the longitudinal fins, built-in with the tubes as shown in Figure 2. Gerrard (1966) explained the flow mechanism across a circular cylinder. H. Akilli (2008) and E. A. Anderson (1997) also studied flow behaviour with splitter plate with different configuration. Flow across circular cylinder was explained by John H. Lienhard (23).

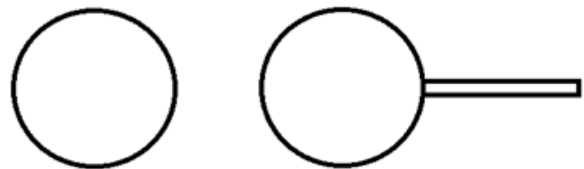


Figure 2. (a) Circular Cylinder (b) Circular Cylinder with Splitter Plate

II. EFFECT OF SPLITTER PLATE ON FLOW AND HEAT TRANSFER BEHAVIOUR AROUND CIRCULAR CYLINDER

Roshko (1954) carried out an experimental investigation of circular cylinder by placing a splitter plate in the downstream direction of the wake at $Re = 14,500$. It was observed that flow pattern changes. When the length of splitter plate was $5D$, the vortex shedding completely disappeared and pressure drag was significantly reduced. Moreover when the splitter plate was detached and move $3.85D$ downstream from the cylinder exhibits the shedding frequency become minimum and the base pressure was maximum. A splitter plate of length $1D$ did not inhibit formation of vortices but changed the shedding frequency slightly

Gerrard (1996) conducted experiments to studied the formation region behind circular cylinder at $Re = 2 \times 10^4$. It was found that the Strouhal number decreased when the length of the splitter plate was smaller than d , but it increased for $d < l < 2d$. Addition of splitter plate increased the production of circulation at the rear of the cylinder, as a result the vortex strength in the early stage of growth decreased. The effective formation-region length was the distance from the plate to the end of the region. It was found that when the vortex was growing close behind the

plate, there was a large cross-flow velocity produced near the plate, assist the shedding process and increase the frequency.

J.Y. Hwang et al. (2003) numerically studied flow induced forces on a circular cylinder using detached splitter plate for laminar flow. A splitter plate with the same length as the cylinder diameter was placed horizontally in the wake region. Suppressing the vortex shedding, the plate significantly reduced drag force and lift fluctuation, there existed an optimal location of the plate for maximum reduction. However, they sharply increase as the plate was placed further downstream of the optimal location.

H. Akilli et al. (2008) investigated experimentally passive control of vortex shedding by splitter plates having L/D ratio (0.2 to 2.4) attached on the cylinder base in shallow water flow at $Re = 6300$. In this study, the length of the splitter plate was varied from in order to see the effect of the splitter plate length on the flow characteristics. Instantaneous and time-averaged flow data clearly indicated that the length of the splitter plate has a substantial effect on the flow characteristics. They found the flow characteristics in the wake region of the circular cylinder sharply changed up to the splitter plate length of $L/D=1.0$ and above this plate length, small changes occurred in the flow characteristics.

A. Fage et al. (1930) carried out experimental investigation to determine effect of turbulence and surface roughness on the drag of the circular cylinder. It was seen that as the surface was made rougher, the fall in drag coefficient occurred at a lower value of Reynolds number and that this fall gradually dies away. There was an indication that if the roughening had been continued, a surface would eventually have been obtained for which there would be no fall in drag. From this, it may be concluded that increase in roughness further retards the flow in boundary layer over the cylinder and causes the stagnation point to shift further upstream. They also concluded the region $\theta = (+ 37.5^\circ \text{ to } +100^\circ)$ was very sensitive to surface roughness, since it include those parts where the flow separates from the surface.

Schmidt et al. (1943) conducted experimental analysis over the circumference of a heating cylinder having different diameter (50, 100, 250) at $Re= 5000-426000$. They explained effect of surface projection on the heat transfer of circular cylinder. It was observed that starting from the stagnation point the heat transfer coefficient dropped to a distinct minimum close before angle 90° forward stagnation point and then rises again, which increases to higher value as Reynolds number increases. Furthermore, they concluded that minimum pressure distribution lies before the minimum heat transfer coefficient.

P. A. R. Ribeiro et al. (2004) developed a numerical simulation for bluff-body vortex shedding suppression at $Re = 100$ and 160 using Finite Difference method. As attached plates perform great changes on the shedding frequency depending on the length, the use of splitter plate to control bluff-bodies' vortex shedding shows to be great efficiency.

E. A. Anderson et al. (1997) investigated 2 and 3-dimensional flow configuration of splitter plate effect on

the circular cylinder wake. Result of flow visualization showed that shear layer characteristics such as circulation strength, ability to entrain fluid, and length had significant effect on the Karman shedding frequency at subcritical Reynolds number between 2700 to 4600. The variation in strouhal number over the range of $l/d = 0$ to 1.75 was divided into four distinct regions where within each region a different flow phenomenon dominated the selection process of the shedding frequency.

S. Tiwari et al. (2005) obtained a three dimensional model to study the heat transfer behaviour of a circular tube in cross-flow configuration with different length of wake splitter plate at $Re = 500, 1000, 1500$. The splitter plate of chord length $2H$ (height of the tube) causes the vortex to clear off the plate. As the chord length of the plate increases, vortices moves towards the plate and roll over the edge i.e. presence of splitter plates delayed the flow separation which decreased the total drag and therefore reduction in pumping power. In front of the tube, there was a sudden increase in Nusselt number. The reason for the abrupt increase in Nusselt number can be attributed to the formation of horseshoe vortices. The spiralling motion of the horseshoe vortices brings about better mixing and the heat transfer in this region was enhanced significantly. The Nusselt number was low in the wake region. The separated dead water zone where fluid recirculates with low velocity causes poor heat transfer. The splitter plate creates a streamlined extension of the circular tube, which also brings about enhancement of heat transfer. A reduction in the size of wake zone was observed. Narrowing of the wake zone reduces convective heat transfer from the tube surface but the splitter plate itself generates an extra fin area for conduction. One would expect the value of viscous drag coefficient to increase with increasing chord length of the splitter plate. However, the counter rotating vortices diminish the effect of viscous drag on the chord of the splitter plate i.e. total drag decreases.

S. E. Razavi et al. (2008) carried out numerical investigation of flow and heat transfer around circular cylinder in the range of $20 < Re < 1000$ by finite volume method. It was concluded that splitter plate streamlined the flow around the cylinder and accordingly decreased the pressure drag causing the significant reduction in overall drag. The heat transfer decreased from the cylinder surface, while placing the splitter plate increased the total heat transfer.

III. EFFECT OF SPLITTER PLATE ON FLOW AND HEAT TRANSFER BEHAVIOUR AROUND SQUARE CYLINDER

Said Turki (2008) conducted a numerical study to examine a passive control of flow by introducing a splitter plate behind a square cylinder inside a horizontal channel. At $110 < Re < 200$ and for affixed blockage ratio $\beta = h/H = 1/4$. The effect of splitter plate length and its location in the wake region on the Strouhal number and the drag and lift coefficient were analyzed. It was found that critical length of the splitter plate, characterizing the suppression of the vortex shedding, increases as the Reynolds number increase and it can be correlated by the linear relationship: $L_c = 0.0366R - 3.3184$. For $L < L_c$, the

splitter plate significances reduces the lift and the drag fluctuation.

Woe-Chul Park et al. (1997) numerically investigated of wake flow control by a splitter plate attached to the base of square cylinder. It was found that the splitter plate blocks the roll-up of the separated shear layer close to the base of the body, and lowers the velocity near the base, the drag of the body and the vortex shedding frequency. Interaction of separated shear layer was delayed until the end of the plate. Because of this, shorter splitter plate was more sensitive to wake flow forming low velocity region behind the cylinder. Both the drag and Strouhal number were significantly reduced by suppressing the vortex shedding in the wake.

IV. FLOW INDUCED VIBRATION MITIGATION USING ATTACHED SPLITTER PLATE

B. Stappenbelt (2010) conducted experimental investigation of vortex-induced vibration response of an elastically mounted rigid cylinder with a range of splitter plate ratio ($l/d = 0$ to 4) under reduced velocity interval of $U_r = 3$ to 60 . For splitter plate ratios of $l/D = 2.8$ to 4 , no significant vortex-induced and galloping type vibration were observed. It was only this region that vibration mitigation was realized.

Ibrahim Ayoub et al. (2008) also studied effect of splitter plate on vortex-induced vibration with splitter plate of length 3 to 3 diameters under the reduced velocity ranging from 0 to 0.35 and Reynolds number of range $1.0 \times 10^4 < Re < 7.5 \times 10^4$. Experimental results contradict some existing data, the amplitude of response increases dramatically with attached splitter plate. It was observed that amplitude of cylinder with splitter plate of length 0.5 to 1 diameters are up to 4 times larger than bare cylinders.

V. HEAT TRANSFER FROM TUBE BANKS

W.A. Khan et al. (2006) studied heat transfer from tube banks using analytical approach. It was concluded that the average heat transfer coefficients for tube banks depend on the longitudinal, transverse pitches, Reynolds number and Prandtl number. Compact banks (in-line or staggered) indicate higher heat transfer rates than widely spaced ones and the staggered arrangement gives higher heat transfer rates than the in-line arrangement. This was also supported by the further work of W. A. Khan (2007), where an optimal model of tube banks heat exchanger was developed using entropy generation minimization method. It was also demonstrated that the staggered arrangement gives a better performance for lower approach velocities and longer tubes, whereas the inline arrangement performs better for higher approach velocities and larger dimensionless pitch ratios.

S. Aiba et al. (1982) carried out an experimentally studied the heat transfer around tubes in-line tube banks. Measurements were conducted for seven cylinder spacing in the Reynolds number range from 10^4 to 6×10^4 . The mean Nusselt number of the first cylinder varies considerably with the cylinder spacing but Nusselt no. did not show any essential variation with the cylinder spacing for second and farther downstream cylinder.

S. Aiba et al. (1982) also conducted experiments to investigate the heat transfer and flow around tubes in staggered tube banks in cross flow. The cylinder spacing

examined $C_y/d \times C_x/d$ was 1.6×1.6 and 1.2×1.2 in the Re. no. range of 8600 to 3600 where C_x and C_y cylinder spacing along and normal to the upstream uniform flow direction and d was the cylinder diameter. In case of 1.6×1.6 the heat transfer rate for the third cylinder was the maximum. This may due to high velocity of the flow on coming to the third cylinder along with its turbulence intensity. In case of 1.2×1.2 the heat transfer rate of the first cylinder was extremely low. A very large velocity of the flow oncoming to the second cylinder produce a high heat transfer rate as compared to that in case of 1.6×1.6 . Heat transfer rate was almost equal for both the cases of 1.2×1.2 and 1.6×1.6 at the same Reynolds number

E. Buyruk (1999) carried out an experimental study to investigate heat transfer and flow characteristics from one tube within a staggered tube bundle and within a row of similar tubes. The tube spacing examined S_t and S_l were 1.5×1.5 and 1.5×1.25 where S_t and S_l denote the transverse and longitudinal pitches respectively at Reynolds number 4.8×10^4 . The influence of the blockage of a single tube in a duct and transverse pitch for a single tube row with Reynolds number range of 7960 to 47770 also investigated. Experimentations were carried out by varying blockage ratio from 0.131 to 0.843 . It had been shown that the general shape of local Nusselt number distribution around the cylinder varies only slightly with blockage for blockage ratio was less than 0.5 . When the blockage ratio was greater than 0.395 , increasing blockage causes the minimum pressure and minimum Nusselt number to move to the downstream side of the cylinder. For the blockage ratio in the range of 0.668 - 0.843 , there was a distinct change in the flow compared with the lower blockage cases. Local Nusselt number and static pressure are remarkably different. Due to the great acceleration of the flow minimum local static pressure values reached very low values. Changes in both longitudinal and transverse pitch were observed to have a noticeable influence on the velocity distribution around the tubes in a bank. For the staggered tube bundle geometry, the mean Nusselt number of the inner tubes becomes higher by increasing the transverse pitch and decreasing longitudinal pitch ratios.

E. Buyruk (2002) Heat transfer characteristic on tandem cylinder with ($L/D = 1.13, 2, 3, 6$) were also investigated at constant $Re = 400$. Laminar boundary layer region heat transfer of first cylinder was not affected by decreasing gap between the cylinders. Smaller gap between the cylinder results lower heat transfer rate on the downstream side of the first cylinder and upstream side of second cylinder. Such as when ratio L/D changed from 3 to 1.13 then, impact point location changes from about 55° to 70° which decreases the rate heat transfer. Effect of Reynolds number ($80, 120, 200$) was investigated for inline and staggered tube banks with transverse and longitudinal pitch of 2×2 . For the first cylinder it was seen that increase Reynolds number causes the heat transfer rates to increase and separation point moves upstream side of the cylinder. Heat transfer rate for second cylinder was relatively low comparing with the first cylinder, as second cylinder located in the wake of first cylinder that will block the direct effect of flow on the second cylinder. Increase in Reynolds number causes the impact point to move upstream of the second cylinder

for inline arrangement. For staggered arrangement, local heat transfer coefficient of second cylinder front region was higher than the first cylinder front region due to effect of flow acceleration. Such as front stagnation value for second cylinder was nearly 60% higher comparing the $Re=80$ case with $Re=200$ case.

S. Jayavel et al. (2008) numerically studied the heat transfer and pressure drop for flow past inline and staggered tube bundles. Three-dimensional computational codes were developed and apply to compare flow and heat transfer characteristics for inline and staggered arrangement of circular tubes in a tube bundle. A finite volume-based numerical investigation was carried out to study the flow and heat transfer for flow past inline and staggered arrangement of tube bundles confined in a rectangular channel. The investigation identify the range of Reynolds number in which staggered arrangement of tubes in a tube bundle provide more heat transfer causing less pressure drop compared with inline arrangement of tubes. However, at lower Reynolds numbers inline arrangement of tubes are found to be preferable due to heat transfer and smaller pressure drop.

Seong-Teon Yoo et al. (2007) experimentally investigated heat transfer characteristics for staggered tube banks in cross-flow using naphthalene sublimation technique. It was concluded that the variation of the local heat transfer coefficients was quite different from the first tube to the third tube, but they are similar afterwards. The average Nusselt number increases more than 30% and 65% on the second and third tubes, respectively, in comparison with that of the first tube. The local heat transfer coefficients on each tube increase except on the front part of first tube as the tube spacing decreases. Due to strong vortices the local heat transfer near the rear stagnation point of the first tube increases drastically with decreasing tube spacing. Consequently, the average Nusselt number on the first tube for the tube spacing of 1.75 and 1.5 was higher by about 25% and 45%, respectively than that for the tube spacing of 2.0. In the first and third tubes,

dependence of average Nusselt number on Reynolds number was almost same regardless of the tube spacing.

VI. HEAT TRANSFER FROM TUBE BANKS WITH SPLITTER PLATE

Suzairin Md. Seri et al. (2011) carried out an experimental studies in the Reynolds number range 5×10^3 to 10^5 on a single cylinder with splitter plate having length-to-tube diameter ratios ($L/D = 0.5, 1.0, 1.5$ and 2.0). Tube banks consisting of 12 rows and 3 tubes per row in equilateral triangle arrangements with transverse pitch to diameter ratio ($a = 2$), and longitudinal pitch to diameter ratio ($b = 1.73$). It was concluded that the local Nusselt numbers on the rear of a single tube are depressed when a splitter was attached to the tube. The reduction being greatest at rear stagnation but the Nusselt numbers rise steadily from base of the splitter plate towards the tip. In the first row of tube banks, heat transfer behaviour was similar to that of the single tube. The fin tip Nusselt numbers, at the middle to high range of the investigated Reynolds numbers, are higher than the forward stagnation point values. For all tube banks, Nusselt number at the rear stagnation point of any row was highest at the second row due to the greatest intensity of turbulence at this location. Heat transfer characteristics were studied for tubes with different L/D ratios under constant heat flux conditions. Tube banks with $L/D = 1.0$ yielded the highest heat transfer rates.

VII. CONCLUSION

This paper describes the influence of splitter plate on flow behaviour and heat transfer characteristic across cylinder and in tube banks. Vortex shedding and pressure drop mostly depends on Reynolds number and tube spacing. Addition splitter plate on a single cylinder can be attributed to the attenuation of vortex shedding in the wake and also reduced pressure drag significantly. Increase in total heat transfer can be also observed as a result of extra surface area generated by the splitter plate.

REFERENCES

- [1] Anatol Roshko, "On the Drag and Shedding Frequency of Two-Dimensional Bluff Bodies", National Advisory Committee For Aeronautics, Technical Note 3169, July 1954.
- [2] J. H. Gerrard, "The mechanism of the formation region of vortices behind bluff bodies", J. Fluid Mech. (1966), Vol. 25, Part 2, pp. 401-413.
- [3] Jong-Yeon Hwang, Kyung-Soo Yang and Seung-Han Sun, "Reduction of flow-induced forces on a circular cylinder using a detached splitter plate", Physics Of Fluids, Volume 15, Number 8, August 2003.
- [4] Huseyin Akilli, Cuma Karakus, Atakan Akar, Besir Sahin and Filiz Tumen, "Control of Vortex Shedding of Circular Cylinder in Shallow Water Flow Using an Attached Splitter Plate", Journal of Fluids Engineering, April 2008, Vol. 130/041401-1.
- [5] A. Fage, A.R.C.Sc., and J. H. Warsap, "The Effects Of Turbulence And Surface Roughness On The Drag Of A Circular Cylinder", Aeronautical Research Committee, October 1929.
- [6] P. A. R. Ribeiro, E. B. C. Schettini and J. H. Silvestrini, "Bluff-Bodies Vortex Shedding Suppression By Direct Numerical Simulation", Engenharia Térmica (Thermal Engineering), No. 5, June 2004 p. 3-8.
- [7] E. A. Anderson and A. A. Szewczyk, "Effects of a splitter plate on the near wake of a circular cylinder in 2 and 3-dimensional flow configurations", Experiments in Fluids 23, (1997), 161-174, Springer-Verlag 1997.
- [8] Ernst Schmidt and Karl Venner, "Heat Transfer Over The Circumference Of A Heated Cylinder In Transverse Flow", National Advisory Committee For Aeronautics, No. 1050, October 1943.
- [9] G. Biswas, S. Tiwari, D. Chakraborty, and P.K. Panigrahi, "Numerical prediction of flow and heat transfer in a channel in the presence of a built-in circular tube with and without an integral wake splitter", Int. Journal of Heat and Mass Transfer 48,439-453, 2005.
- [10] Seyed Esmail Razavi, Vahid Farhangmchr and Farzad Barar, "Impact of Splitter plate on Flow and Heat Transfer Around Circular Cylinder at Low Reynolds Numbers", Journal of Applied Science 8(7):1286-1292, 2008.
- [11] Said Turki, "Numerical Simulation Of Passive Control On Vortex Shedding Behind Square Cylinder Using Splitter Plate",

Engineering Application Of Computational Fluid Mechanics Vol.2, No.4, pp.514-524, 2008.

- [12] Woe-Chul Park and Hiroshi Higuchi, "Numerical Investigation of Wake Flow Control by a Splitter Plate", KSME International Journal, Vol.12, No.1, pp 123-131, 1998.
- [13] B. Stappenbelt, "Flow-induced vibration mitigation using attached splitter-plates", 2009 Annual Bulletin of the Australian Institute of High Energetic Materials Vol.1, pp. 23-33, 2010.
- [14] Ibrahim Ayoub, Ji Lu, Brijesh Duttea, Kenneth Elliot, Brad Stappenbelt, Jie Pan, "An Experimental Study of the Effect of Splitter Plates on Vortex Induced Vibration", 24-26 November, Geelong, Australia, Proceedings of Acoustics 2008.
- [15] W.A. Khan, J.R. Culham and M.M. Yovanovich, "Convection heat transfer from tube banks in crossflow: Analytical approach", Int. Journal of Heat and Mass Transfer, 49 (2006), 4831-4838.
- [16] W.A. Khan, J.R. Culham and M.M. Yovanovich, "Optimal Design of Tube Banks in Crossflow Using Entropy Generation Minimization Method", Journal Of Thermophysics and Heat Transfer, Vol. 21, No. 2, April-June 2007.
- [17] Shinya AIBA, Hajime TSUCHIDA and Terukazu OTA, "Heat Transfer Around Tubes in In-line Tube Banks", Bulletin of the JSME, Vol.25, No. 204, June 1982.
- [18] Shinya AIBA, Hajime TSUCHIDA and Terukazu OTA, "Heat Transfer Around Tubes in Staggered Tube Banks", Bulletin of the JSME, Vol.25, No. 204, June 1982.
- [19] Ertan Buyruk, "Heat Transfer and Flow Structures Around Circular Cylinders in Cross-Flow", J. of Engineering and Environmental science, 23, 1999, 299-315.
- [20] E. Buyruk, "Numerical study of heat transfer characteristics on tandem cylinders, inline and staggered tube banks in cross-flow of air", Int. Comm. Heat Mass Transfer, Vol.29, No.3, pp.355-366, 2002.
- [21] S. Jayavel and Shaligram Tiwari, "Finite volume algorithm to study the effect of tube separation in flow past tube banks", Engineering Application of computational Fluid mechanics, Vol.4, No.1, pp. 39-57, 2010.
- [22] Seong-Yeon Yoo, Hwa-Kil Kwon and Jin-Hyuk Kim, "A Study on Heat Transfer Characteristics for Staggered Tube Banks in Cross-flow", Journal of Mechanical Science and Technology 21 (2007) 505-512.
- [23] Suzairin Md Seri, Md Faizal Mohideen Batcha and Vijya R. Raghavan, "Heat Transfer Studies in Tube Banks with Integral Wake Splitters", Int. Journal of Integrated Engineering, Vol.1, 2011.
- [24] John H. Lienhard IV and John H. Lienhard V (A Heat Transfer Text Book) Published by Phlogiston Press Cambridge, Massachusetts, U.S.A. Version 1.31 dated January 16, 2008.

Experimental and Numerical Analysis On Horizontal Jet Flocculates For Small Water Supply Schemes

T. Subramani¹ Suraja Nair²

¹Professor & Dean, Department of Civil Engineering, VMKV Engg College,
Vinayaka Missions University, Salem.

²PG Student of Environmental Engineering, Department of Civil Engineering, VMKV Engg College,
Vinayaka Missions University, Salem.

ABSTRACT: It is often seen that conventional water treatment plants are not necessarily cost effective, specifically for smaller units up to 3 MLD. The flocculator is an important unit of the water treatment plant and more often fitted with mechanical stirrers or vanes. The problems associated with maintenance and running of the mechanical components impose a severe constraint on such units, specifically in developing countries of Asia Pacific region. It is therefore necessary to explore and find other simpler devices free from such constraints. The jet flocculator seems to be a viable alternative. Guidelines for preliminary design of a jet flocculator are not available even though it is simple, economical and robust to operate. The present investigation is to study the performance of single-basin jet flocculators using both experimental and numerical techniques. A number of performance indices, some already existing and some new, are being made use of in assessing the performance of the flocculator.

KEYWORDS: Experimental, Numerical Analysis, Horizontal Jet Flocculators, Small Water Supply Schemes

I. INTRODUCTION

Coagulation and flocculation are the water treatment process by which finely divided suspended and colloidal matter in the water is made to agglomerate and form flocs. This enables their removal by sedimentation, dissolved air flotation or filtration. Colloidal particles (colloids) are midway in size between dissolved solids and suspended matter. Colloids are kept in suspension (stabilized) by electrostatic repulsion and hydration. Electrostatic repulsion occurs because colloids usually have a surface charge due to the presence of a double layer of ions around each particle. Thus, the colloid has an electric charge, mostly a negative one. Hydration is the reaction of particles at their surface with the surrounding water. The resulting particle-water agglomerates have a specific gravity, which differs little from that of water itself.

The electrostatic repulsion between colloidal particles effectively cancels out the electronic attraction forces (Van der Waals' forces) that would attach the particles together. Certain chemicals (called coagulating agents, coagulants) have the capacity to compress the double layer of ions around the colloidal particles. They reduce the range of the electrostatic repulsion, and thus enable the particles to flocculate, i.e. to form flocs. These flocs can grow to a sufficient size and specific weight to allow their removal by settling, flotation or filtration. Generally water treatment processes involving the use of chemicals are not so suitable for small community water supplies. They should be avoided whenever possible.

Chemical coagulation and flocculation should only be used when the needed treatment result cannot be achieved with another treatment process using no chemicals. If the turbidity and colour of the raw water are not much higher than is permissible for drinking water, it should be possible to avoid chemical coagulation in the treatment of the water. A process such as slow sand filtration or multi-stage filtration would serve both to reduce the turbidity and colour to acceptable levels, and to improve the other water quality characteristics, in a single unit. A roughing filter can serve to reduce the turbidity load on the slow sand filter, if necessary.

Flocculation is the process of gentle and continuous stirring of coagulated water for the purpose of forming flocs through the aggregation of the minute particles present in the water. It is thus the conditioning of water to form flocs that can be readily removed by settling, dissolved air flotation or filtration. The efficiency of the flocculation process is largely determined by the number of collisions between the minute coagulated particles per unit of time. There are mechanical and hydraulic flocculators. In mechanical flocculators the stirring of the water is achieved with devices such as paddles, paddle reels or rakes. These devices can be fitted to a vertical or horizontal shaft. Vertical shaft flocculators are usually placed in a square tank with several chambers (four or more). They have the advantage of having only bearing in the water, and no gland is necessary as the motor and gearing are above the water. With horizontal shaft flocculators having a traverse flow, one should provide at least four rows of shafts, with partitions of baffles (stop logs), so as to avoid short-circuiting. In hydraulic flocculators the flow of the water is so influenced by small hydraulic structures that a stirring action results. Typical examples are channels with baffles, flocculator chambers placed in series (e.g. *Alabama*-type flocculator) and gravel bed flocculators.

Their advantages are that they have no motor power, electric cables switchgear, etc. to maintain and general maintenance is easier. Mechanical and hydraulic methods are often used to create an agitation in the flocculation chamber thereby maintaining a velocity gradient. This stage is called the orthokinetic flocculation.

II. Present Scenario

As per the performance evaluation survey conducted by National Environmental Engineering Research Institute (NEERI), Nagpur during 1988-89 on 51 water treatment plants in India, it was found that effective supervision and managerial control are absent in most of the plants (Mhaisalkar and Tidke, 1998). Only 39% of the plants were producing quality water meeting the CPHEEO

standards. The reasons quoted for this poor performance are the lack of funds for operation and maintenance, non-availability of spare parts, untrained laboratory staff, poor administration, negligence by the staff and improper co-ordination between the staff. Conventional water treatment plants are not necessarily cost effective, specifically for smaller unit of capacity up to 3 MLD. The flocculator is an all important unit of the water treatment plant and more often fitted with mechanical stirrers or vanes. The problems associated with maintenance and running of the mechanical components impose a severe constraint on such units, specifically in developing countries of Asia Pacific region. It is therefore necessary to explore and find other simpler devices free from such constraints. The jet flocculator seems to be a viable alternative. Guidelines for preliminary design of a jet flocculator are not available even though it is simple, economical and robust to operate.

III. OBJECTIVE OF THE STUDY

The present investigation is to study the performance of single-basin jet flocculators using both experimental and numerical techniques. A number of performance indices, some already existing and some new, are being made use of in assessing the performance of the flocculator.

IV. MATERIALS AND METHODS

4.1 EXPERIMENTAL SETUP

The main components of the set-up consisted of a tank to store the turbid water, a constant head supply chamber, supply pipeline fitted with pressure taps and a bypass pipe, an orifice meter in the supply line to aid mixing of coagulants injected into it by a peristaltic pump, manometers, flocculation chamber having a nozzle fitted at the inlet end and a suitable overflow mechanism at the outlet end. Preparation of the turbid water was quite crucial since the synthetically generated turbidity should be quite close to the natural condition. Turbid water in nature contains particles of different sizes and specific gravity. As observed by Hudson (1965), most particles causing turbidity in natural channels are smaller than 10 mm while a majority is smaller than 1.5 mm. Throughout the present experimentation, Bentonite was used to generate different levels of turbidity of 100, 50 and 25 NTU.

Tap water available in the laboratory had a turbidity of less than 0.9 NTU. The amount of Bentonite required to generate different intensities of turbidity in a sample was found to vary in a linear fashion,

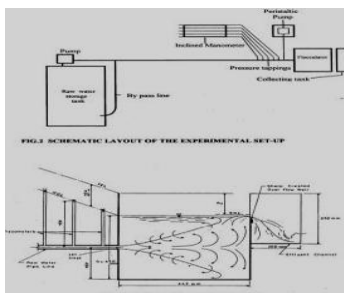


Figure.1 Schematic Layout Of Experimental Setup
 $\text{Bentonite in mg/L} = 1.5857 \times \text{turbidity in NTU} - 1.4271$

Standard jar-tests were carried out with the objective of estimating the optimum concentration of the Alum needed for removal of the suspended matter. The optimal Alum dosage (in mg/L) necessary to treat raw water was 44.50, 36.00, and 34.00 for turbidity intensities of 100 NTU, 50 NTU and 25 NTU respectively.

Raw-water alkalinity (CaCO_3 in mg/L) was noted every day before the start of the experiment and was found to be almost the same, 40 mg/L, throughout the period of experimentation. However, addition of the coagulant altered the alkalinity. Samples of water taken from the jar for the highest dosage of the Alum used in this investigation had alkalinity in excess of 10 mg/L, sufficient not to hinder the formation of flocs. Similarly, other characteristics of water, especially, the pH values have a considerable influence on the satisfactory formation of flocs. In the present investigation the pH of the synthetic turbid water was in the range of 6.8 to 7.0. The recommended pH zone while using Alum as a coagulant is 6.5 to 7.5. The two ranges being not very different, no additional chemical was used in the experiments to control the pH level. The temperature of raw water in the experiments was in the range 27°C to 28°C .

4.2 EXPERIMENTAL PROCEDURE

Flocculation chambers having identical capacities but of different plan shapes were fabricated out of metallic sheets and red oxide priming coat was applied to avoid any chemical reaction of the alum with the metal surface. Raw water stored in a tank was pumped to the flocculator with the help of a pump. The required flow rate was setup by adjusting the valves provided on the main and bypass pipe lines. The flow from the inlet to the flocculator was in the form of a jet emanating from a submerged pipe. The rate of flow entering and leaving the flocculator was measured volumetrically using a collecting tank. To ensure proper mixing of the coagulant with raw water, alum solution was injected as a co-current axial jet into the raw water supply line 1.5m ahead of the jet nozzle with the help of a peristaltic pump. The peristaltic pump discharge was calibrated to improve the accuracy of the results. The flow rate and the operation time parameter of the peristaltic pump were pre-set at the desired values. To determine the total energy on the up-stream side of the flocculator 3 pressure tapplings of 1mm diameter were provided at a space of 27cm center to center on the pipe line leading to the flocculator. All pressure head measurements were made with reference to the center line of the influent pipe to the flocculator. A manometer connected to these tapplings was supported by a board, and a scale readable to the nearest 1mm of water was provided. For proper mixing, Holland and Chapman (1966) recommended that the liquid level in the tank should be less than 1.25 times the highest lateral dimension of the tank so as to avoid multiple impellers or excessive power consumption. Van De Vasse (1955) observed that the circulation pattern established by a jet system is similar to that established by a propeller stirrer. Hence a jet submergence depth equal to 50% of liquid depth was adopted as a reference value.

Experiments were conducted with a rectangular and circular flocculation chamber for different jet sizes of 8, 10, 12, and 15mm in diameter. Hydraulic retention time equal to 6, 7.5, 10, 15 and 20 minutes were selected while repeating the experiments. Experiments repeated for

alternative outflow sections. A digital pH-meter was used to determine the pH values of the raw water. Similarly, turbidity meters were calibrated with a standard suspension. In the Nephelometric method followed here, a comparison of the intensity of light scattered by the sample under specified conditions was made with the intensity of light scattered by a standard reference suspension. The least count of the turbidity meter was 0.1 NTU.

To study the distribution of residence time of the tracer, laboratory grade common salt was used as a tracer and a digital conductivity meter having a least count of 0.1 micromhos/cm was used to measure conductivity of the solution. The meter was calibrated at the test temperature of 26°C and the conductivity of water was displayed directly and a best fit relationship $Y = 0.56X - 32.50$ was obtained. Y is the sodium concentration in mg/l and X is the conductivity in micromhos/cm. For a selected detention time, weight of salt equivalent to the weight of water passing per minute multiplied by 500 ppm was dissolved in water and it was injected using a peristaltic pump. The requisite amount of tracer solution was injected as a co-flowing axial jet at a section little ahead of the jet efflux section as a slug dosage over a time span of one minute depending on the flow rate. After the injection of salt solution, samples were collected at the outlet of the weir initially at 0.5, 1, 2, 3, 4 minutes and thereafter for every 1/5 of nominal detention time in minutes.

The samples were collected till the tracer disappeared from the collected sample. The sodium concentration at the chamber outlet was determined as a function of time with the help of digital conductivity meter. Based on the measured conductivity of the sample, the concentration of sodium chloride was worked out from the calibration curve corresponding to the test temperature. For every tracer experiment, a separate calibration chart was prepared before commencing the experiment. Material balance check was performed to verify that the recovery of entire tracer balances with the quantity added at the beginning of the flow (Hudson, 1981). The area lying under the normalized time distribution curve indicated this.

The turbidity meter, submersible pump and the peristaltic pump were always calibrated just before the start of an experiment. The dimensions of flocculation chambers are presented in Table.1. The volume of all the basins were 0.0883 m³ and a liquid depth of 45cm was maintained in all the chambers. The type of outlet in basin A and B was weir type, whereas the C type outlet was a circular opening of size 50 mm in diameter. Though, all alternative basin layouts were adopted for numerical simulation of the flow field and dispersion of tracers, some amongst them were only selected for experimentation on flocculation and turbidity removal efficiency. It should be realized that ultimate performance of a flocculator depends upon both coagulation and flocculation. Hence, it will be meaningful to segregate the effect of rapid mixing to assess properly the role of different design parameters on the performance of a flocculation chamber. It was observed that as long as the GT values of the rapid mixing device lay in the range of 10,600 and 18,800 the performance of the flocculation chamber remained unaffected. Hence, in all the flocculation experiments of the present study, care was exercised to maintain the GT of rapid mixing within the said range. For each of the flocculator basins under consideration, on

adding the coagulant the residual turbidity reached a steady state value after lapse of four to five times the theoretical retention time, $T = (\text{volume of the basin})/(\text{flow rate } Q)$. Hence in all the flocculation experiments floc-laden water samples were collected in settling jars at the outlet of the flocculator only after a lapse of 5.5 times the residence time. The samples were allowed to settle for a period of 30 min in settling jars before measuring the residual turbidity. The recommended plan area of jar is 115 x 115mm with a liquid depth of 210mm (Gregory R., et al., 1990). Further it has been specified that the outlet for the withdrawal of the sample should be 100mm below the liquid level. The turbidity of the settled water was measured by a nephelometric turbidimeter and an average of three samples tested is reported.

Table.1 Dimension Of Flocculator Basins

Basin no.	L mm	W mm	H (depth of water) mm
	443	443	450
2	Circular basin with D=500mm and H=450mm		

V. Result & Discussion

Result of floc and tracer studies

The results observed while conducting floc and tracer studies on 100, 50 and 25NTU turbid water have been observed for different sizes of jet diffusing in rectangular and circular chambers with alternative outlets.

4.2 HYDRAULIC RETENTION TIME

Figure 2 shows Effect Of Hydraulic Retention Time On Turbidity Removal

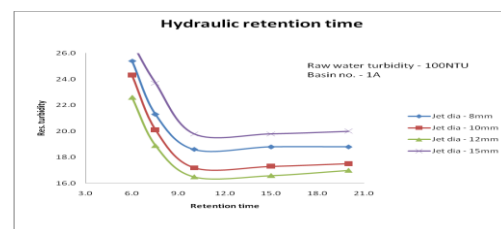


FIGURE.2 EFFECT OF HYDRAULIC RETENTION TIME ON TURBIDITY REMOVAL

Experiments were conducted with basin 1A for two different jet sizes of 8, 10, 12 and 15mm in diameter. Retention time equal to 6, 7.5, 10, 15 and 20 min were selected while repeating the experiments. Parameters like Camp number for rapid mixing ($GT = 10660$), coagulant dosage (44.5 mg/L), influent raw-water turbidity (100 NTU), total alkalinity (40 mg/L of CaCO₃) and pH (6.8-7.0) value were held constant in all the trials. The variation in the residual turbidity as a function of the retention time is shown in Fig.. For different sizes of the nozzles used, the

improvement in the performance of the flocculation tank is insignificant for a retention time exceeding 10 min. The same was also observed to hold good in case of the 50 NTU and 25NTU turbid water experiments. Hence, for free-jet-flocculators a retention time of 10 min may be sufficient. It is worth noting that this is only a fraction of the retention time of 30 min, normally recommended for flocculators having mechanical devices.

From the above one can notice that the jets 10mm and 12mm in diameter, performs marginally better than the 8 and 15mm diameter jets even though it has smaller values for G and GT. This highlights the fact that the performance of the flocculator is not sensitive to the G and GT values, specifically when they are in the range of 30 & 85 s⁻¹ and 23,000 & 50,000 respectively.

The results of experiments on rectangular basin no. 1A, 1B, and 1C considering Camp's number, GT, as the guiding factor are shown in Table for different sizes of the jet diffusing in rectangular and circular tanks. Influent raw water turbidity of No = 100, 50 & 25NTU are presented here. Since the chambers are fairly large in size compared to the diameter of the nozzle, the power input was calculated from the relationship

$$G = \sqrt{\frac{P}{\mu V}}$$

4.3 EFFECT OF BASIN SHAPE

Figure.3. shows the Effect of basin shape on turbidity removal

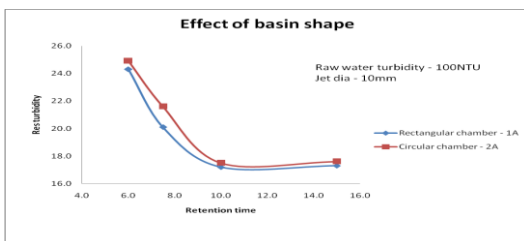


FIGURE.3. EFFECT OF BASIN SHAPE ON TURBIDITY REMOVAL

With the 8 mm diameter nozzle, the L/d ratio for the circular basin was 62.5 whereas in case of the rectangular basin it was 55.4. From the theory of free jets it is known that most of the kinetic energy of the jet gets dissipated within a distance of 40 to 45 times the diameter of the nozzle. Hence, it will not be unreasonable to assume that the energy loss in both the chambers is one and the same. It is interesting to observe that the performance of the rectangular basin is almost identical to that of the circular shaped basin, that is the shape of the flocculator is of no consequence.

A significant increase in the L/d ratio, as in case of the rectangular basin number 3 with circular opening, does help a bit to improve the turbidity removal efficiency. It can be noted that a rectangular basin should be marginally superior compared to the circular shape. This is in consonance with the measurements, where the efficiency of turbidity removal in the case of the rectangular basin is higher by 0.5%. In view of the fact that rectangular chamber are easy to construct and changing the length of the tank is also easy at a later time, a rectangular shaped basin has a

distinct advantage over other shapes. Interestingly, the performance of the free jet flocculator is comparable to the actual performance, 69 to 74% turbidity removal efficiency, reported by Bhole (1993) and Armal (1997) for static flocculators and clariflocculators, respectively.

Location of outlet

Figure.4 shows that the Effect Of Outlet Location On Turbidity Removal

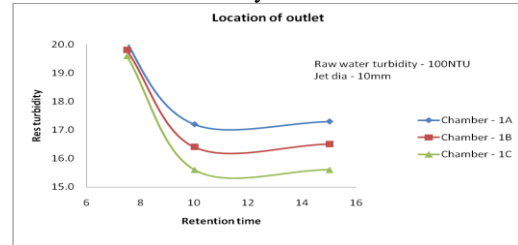


FIGURE.4 EFFECT OF OUTLET LOCATION ON TURBIDITY REMOVAL

The outflow section could be located at a convenient spot on the periphery of the chamber. The three alternatives experimented with are shown in Fig.. The experimental results, Table indicates that outlet 'C' performs superior to alternatives 'A' and 'B'. Further in all the cases, performance of a 12 mm diameter jet proved to be slightly better than 8, 10 and 15 mm diameter jets. Results pertaining to all basin alternatives are shown in. The location of the outlet plays a minor role in the overall efficiency of turbidity removal. This aspect can allow placement of the outlet at any convenient location as dictated by the prevailing conditions on-site.

Effect of Camp's no.

Figure.5 shows the effect of camp's no. On turbidity removal

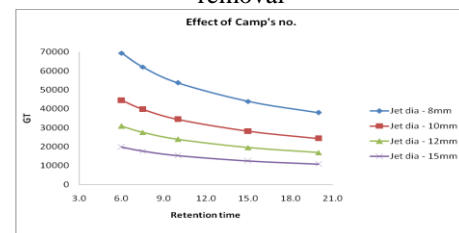


FIGURE.5 EFFECT OF CAMP'S NO. ON TURBIDITY REMOVAL

The value of G for the 12 mm jet corresponding to a retention time of 10 min works out to be 39.75s⁻¹. This value is comparable to the optimal value of G equal to 42s⁻¹ suggested by Andreu-Villegas and Letterman (1976). Even increasing the retention time to 15 and 20 min by lowering the jet velocity did not improve the performance as the large sized flocs were fragile. Thus, for a jet flocculator an optimal diameter exists when the retention time is specified. The same was found to be valid for other raw-water turbidities as well. The variation of GT value with respect to retention time for different jet sizes are shown in Fig.. The original Camp number, GT can be seen to vary over a wide range even though differences in the removal of turbidity were not remarkable. Hence, it is difficult to assign any particular value to GT for design purpose. The usage of G and GT parameters, though simple, cannot

explain the actual performance of the flocculator vis-a-vis the plan shape of the tank and the location of the outlet.

Residence time distribution

Figure.6 shows the Residence Time Distribution In A Square Tank

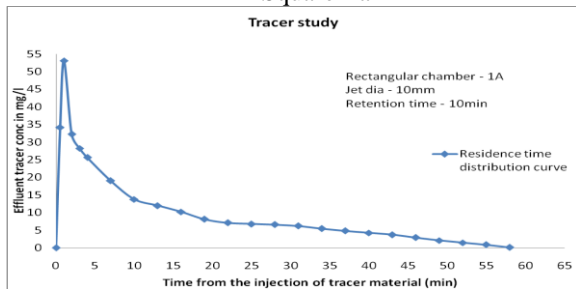


FIGURE.6 RESIDENCE TIME DISTRIBUTION IN A SQUARE TANK

A typical time distribution curve of the tracer for the case of a square tank corresponding to a detention time of 10minutes and for a jet diameter of 10mm is depicted in fig.. A material balance check was performed to ensure that the entire tracer material added in the tank was recovered. The errors were in the range of 1.5% to 4.5%.

Another graph as shown in fig. is plotted with cumulative concentration as a percentage and time on log scale. From this graph the dispersion index was calculated. The dispersion index so obtained then plotted against retention time for different basin shapes and for a jet diameter of 10mm as shown in fig.4.6.1. For an ideal plug flow DI=1, and for a completely mixed flow DI=21.9. From table, it can be seen that the DI values are nearly equal to the value of a well mixed flow whereas some are even higher. The higher values are indicative of the existence of flow short circuiting. For superior performance, the DI value should be as low as possible. It can be seen that for the same jet diameter and retention time, flow short circuiting in a rectangular basin is comparatively less than that of a circular basin. This factor again improves the efficacy of a rectangular basin.

Figure.7 shows the Residence Time Distribution In A Square Tank. Figure.8 shows the dispersion index variation in rectangular and circular tanks. Figure.9 shows the residence time ratio

The plot of $\log[1-F(t)]$ versus t/T , yields a straight line having a slope of $\log_e/(1-m)(1-p)$. Further for $F(t)=0$, $\log 1-f(t)$ being zero, we get $t/T = p/(1-m)$. Thus, from the slope of the straight line and the value of t/T corresponding to $F(t)=0$, fraction of dead space (m) and plug flow (p) computed and the values so obtained are as follows.

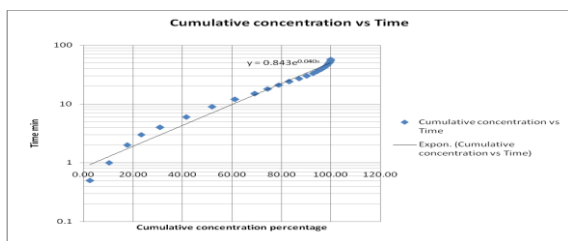


Figure.7 Residence Time Distribution In A Square Tank

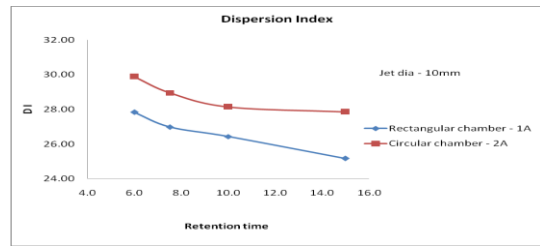


Figure.8 Dispersion Index Variation In Rectangular And Circular Tanks

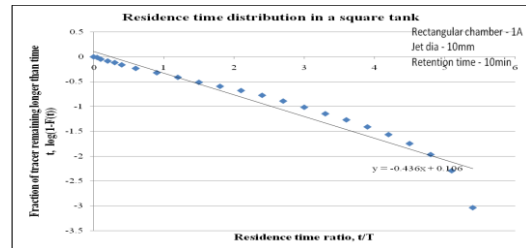


Figure.9 Residence Time Ratio

- dead space = 3.47%
- effective volume = 96.53%
- plug flow = 19.62%
- mixed flow = 90.38%

Out of many sizes and shapes of flocculation basin considered for carrying out tracer studies, results of a few are given in Table.2.

Dispersion Index

Based on the above results the proportion of dead space for all of them is quite small and is of the order of 3-5%. The implication is that site condition that demand specific position of the outlet can have the same turbidity

Table.2 Tracer Studies & Results

Chamber no.	T in min	Plug flow %	Mixed flow %	Dead space %	D ₅₀ /uL	DI
1A	7.5	23.45	76.55	3.14	0.45	26.97
	10	19.62	80.38	3.47	0.59	26.58
	15	18.91	81.09	4.25	0.51	25.17
2A	20	19.52	80.48	5.63	0.47	25.10
	7.5	24.65	75.35	3.21	0.42	28.95
	10	20.15	79.85	3.35	0.55	28.14
	15	18.62	81.38	4.20	0.51	27.86

removal efficiency. Dispersion no. and dispersion index of jet mixer too in the recommended range (0.3-0.7) for mechanical mixers. For all values of $T \geq 10$ min, mixed flow proportion nearly the same. For $T = 10$ min, D_{50}/uL is larger indicating better mixing of tracer in the flocculator.

Single and multi jet nozzles

Figure10. shows the Effect of single and multi jet nozzles in turbidity removal. Figure.11 shows the effect of single and multi jet nozzles in flow pattern

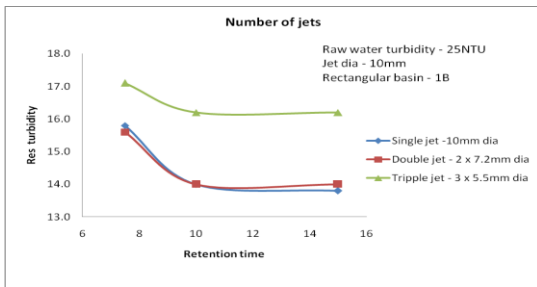


Figure10. Effect Of Single And Multi Jet Nozzles In Turbidity Removal

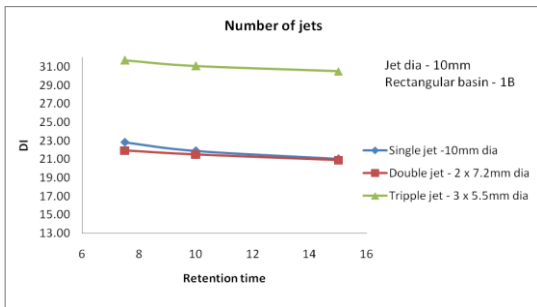


FIGURE.11 EFFECT OF SINGLE AND MULTI JET NOZZLES IN FLOW PATTERN

From the study it can be observed that the removal efficiency goes on decreasing as the raw water turbidity reduces. In the case of 100NTU turbid water the turbidity removal rate is as high as 84.9% but in the case of 25NTU turbid water it is only 48%. Multi jet nozzles have been tried to reduce the flow circuiting in flocculation basins. From the above it can be seen that the turbidity removal efficiency of double jet nozzles remained same as that of single jets. As the number of jets further increased which drastically reduces the removal efficiency. It is evident from study that the flow distribution in a double jet nozzle flocculator is superior to single jet flocculator. Since the turbidity removal rate remains the same and in the practical point of view, there is not much benefit in adopting multi jet nozzles.

VI. CONCLUSIONS

The outcome of the current experiments can be summarized as follows.

1. The single basin jet flocculator is a very simple, robust, low cost device which is capable of removing turbidity from the raw water in an efficient way. The efficiency of turbidity removal for raw water turbidity of 100 NTU was in the range of 79 to 85, which is as good as that of a flocculator fitted with mechanical stirrers.
2. The residual turbidity for raw water turbidity levels of 100, 50 & 25NTU was in the range of 13 to 21NTU. The outlet water with such a residual turbidity range can be directly applied over filter units for further treatment.
3. The retention time for a jet flocculator should be at least 10 min, a figure which is much less than the recommended value of 30 min duration for mechanical flocculators.
4. The length to diameter ratio, L/d should be larger than 36.
5. The plan-shape of the basin is not very critical in controlling the performance of the flocculator. For ease

of construction and scope for future alteration, a rectangular flocculator is desirable.

6. The location of the outlet plays a minor role in the overall efficiency of turbidity removal. This aspect can allow placement of the outlet at any convenient location as dictated by the prevailing conditions on-site.
7. By adopting larger diameter nozzles the efficiency of turbidity removal can be enhanced.
8. The existing indices such as G, GT and MI, though useful for design purpose, are not able to explain the variations in the performance of the jet flocculator vis-a-vis the shape, nozzle diameter, L/d ratio etc.
9. In adopting the jet flocculator for a new or an existing water treatment plant, the parameter G or GT (23,000 to 50,000) can be used in the design as a starting point. Other proposed indices can only help to refine the design and all the indices should be examined together before finalizing the dimensions and layout of the flocculation chamber.

An example is included in Appendix A as an illustration of the design principle of jet flocculators.

References

- [1]. Armal, S.D(1997) Peripheral inlet tapered velocity gradient flocculator. J. Indian water Works Assoc, 29(1), 43-50.
- [2]. Camp, T.R(1995) Flocculation and flocculation basins. Trans. Am. Soc. Civil Eng, 120, 1-16.
- [3]. Camp, T.R and Stein, P.C (1943), Velocity gradients and internal work in fluid motion J. Boston Soc. Civil Eng, 30, 219-237.
- [4]. Dhabadgaonkar, S.M, Dahahasra, S.V, Ingle, R.N and Gokhale, P.N(1994). A new concept in hydraulic tapered flocculation. J. Indian Works Assoc, 26(1), 21-25.
- [5]. Expert Committee of Central Public Health and Envr. Engg. Org. (1991), Coagulation and flocculation. In Manual on public water supply and treatment, Ministry of Urban Development, New Delhi, 171-186.
- [6]. Gregory, Ross and Thomas I Zabel (1990). Sedimentation and flotation, in water quality and treatment (A hand book of community water supplies) by American water Works Association.
- [7]. Hudson, H.E.Jr (1981). Residence times in pretreatment. In water clarification processes, practical design and evaluation, Van Nostrand Reinhold Company, New York 40-122.
- [8]. Rebhun, M and Argaman, Y (1965). Evaluation and hydraulic efficiency of sedimentation basins, J.S. Engg. ASCE, 91(5), 37-45.
- [9]. Schulz, Christopher R and Daniel A, Okun (1984) Hydraulic flocculation. In surface water treatment for communities in developing countries, John Wiley & Sons, Inc New York 105-126
- [10]. Suresh Kumar, N (1997), Jet mixing in flocculators, PhD thesis, Dept of Civil Engg, IIT Bombay
- [11]. Swaminathan Tanjore, Viramghavan, T and Bhole A.G (1994). Significance of tapered flocculation in water treatment processes. Journal of Indian Water Works association, 26(1), 15-19
- [12]. Metcalf & Eddy, Waste water Engineering, Mixing and flocculation 344- 350.

Design of Model For Incremental Development Of Software Modules To Evaluate The Quality Of Software Modules

Dr C.S. Lamba¹, Sanjay Kumar²

*1. Professor, Rajasthan Institute of Engineering
Jaipur, Rajasthan, India*

*2. Lecturer, University Campus School
Rohtak, Haryana (124001), India*

Abstract: This paper is introducing a model, which are used to evaluate the expected quality of software modules during incremental development of software system. This is not only focus on modification of existing system, but also focus to find the methods for developing high quality of software products at reasonable cost. As we know that software modules or software systems are being used in more and more critical areas of industries as well as public or private sectors, then quality of software modules becomes a key factor of business success and human safety. The goal of this paper within the subject areas are the identification of the methods and modules that were used throughout the design and verification of the use and the quality of these methods with respect to the analysis products.

Keyword: Software development approach,

I. Introduction

It is very difficult to build high quality software with limited quality assurance budgets. The proposed model can be used to learn fault predictors from software metrics. Fault prediction prior to software release can guide Verification and Validation (V&V) activity and allocate scarce resources to modules which are predicted to be fault-prone. One of the most important goals of proposed model is to detect fault prone modules as early as possible in the software development life cycle. Design and code metrics have been successfully used for predicting fault-prone modules.

Through this model we can introduce fault prediction from software requirements and analysis. Furthermore, we investigate the advantages of the incremental development of software fault prediction models, and we compare the performance of these models as the volume of data and their life cycle origin (design, code, or their combination) evolution during project development. We confirm that increasing the volume of training data improves model performance. And that, models built from code metrics typically outperform those built using design metrics only. However, both types of models prove to be useful as they can be constructed in different phases of the life cycle. We also demonstrate that models that utilize a combination of design and code level metrics outperform models which use either one metric set exclusively.

II. Problem Description

The software industry is currently entering a period of maturity, in which particular informal approaches are specified more precisely and are supported by the appropriate standards. Quality characteristics of software products are defined in ISO/IEC9126 [1]. For each characteristic, a set of attributes which can be measured is determined. Such a definition helps in evaluating the quality of software, but gives no guidance on how to construct a high quality software product. The requirements for a quality management system are defined in ISO 9001 [2]. All the requirements are intended for application within a software process in order to enhance the customer satisfaction, which is considered the primary measure of the software product quality. The quality management system, as defined by the standard, can be subject to a certification. This paper describes a model, which we used to evaluate the expected as well as the actual quality of a huge software system that was developed. There are a few methods for selecting the metrics and collecting data that are relevant for a particular purpose, described in the literature. The best known examples are Goal Question Metric approach [3,4,5] and the Quality Function Deployment approach [6,7]. Both of the two methods represent the viewpoint of the software development organization. Our approach was based on a modification to Goal Question Metric approach. The modification was needed, because our assessment was done on behalf of the customer, and not of the development company, and it had no other goal in mind than just to evaluate the expected quality of the developed software.

Important characteristics

- i. Software requirements are the foundation from which quality is measured
- ii. Specified standards define development criteria that guide the manner in which the software is engineered.
- iii. If the software meets only the explicit requirements, and does not meet the implicit requirements, the software quality is suspect.

Software Quality factors:

- i. Operational characteristics:-
 - a. Correctness - does it do what I want?
 - b. Reliability - does it do it accurately?
 - c. Efficiency - will it run efficiently on my hardware?
 - d. Integrity is it secure.
 - e. Usability - is it designed for the user?

- ii. Product revision:-
 - a. Maintainability - can I fix it ?
 - b. Flexibility - can I change it
 - c. Testability - can I test it?
- iii. Product transition:-
 - a. Portability will I be able to use it on another machine?
 - b. Re usability - will I be able to reuse some of the software.
 - c. Interoperability - will I be able to interface it with another system.

III. Related Works

One of the oldest software development tools is *flowcharting*, which developed since the 1920s. The software development methodology has emerged since the 1960s. The oldest formalized methodology for building information systems is the *Systems development life cycle*. The traditional Systems development life cycle originated in the 1960s to develop large scale functional business systems in an age of large scale business conglomerates. Information systems activities resolved around heavy data processing and number crunching routines. [8]

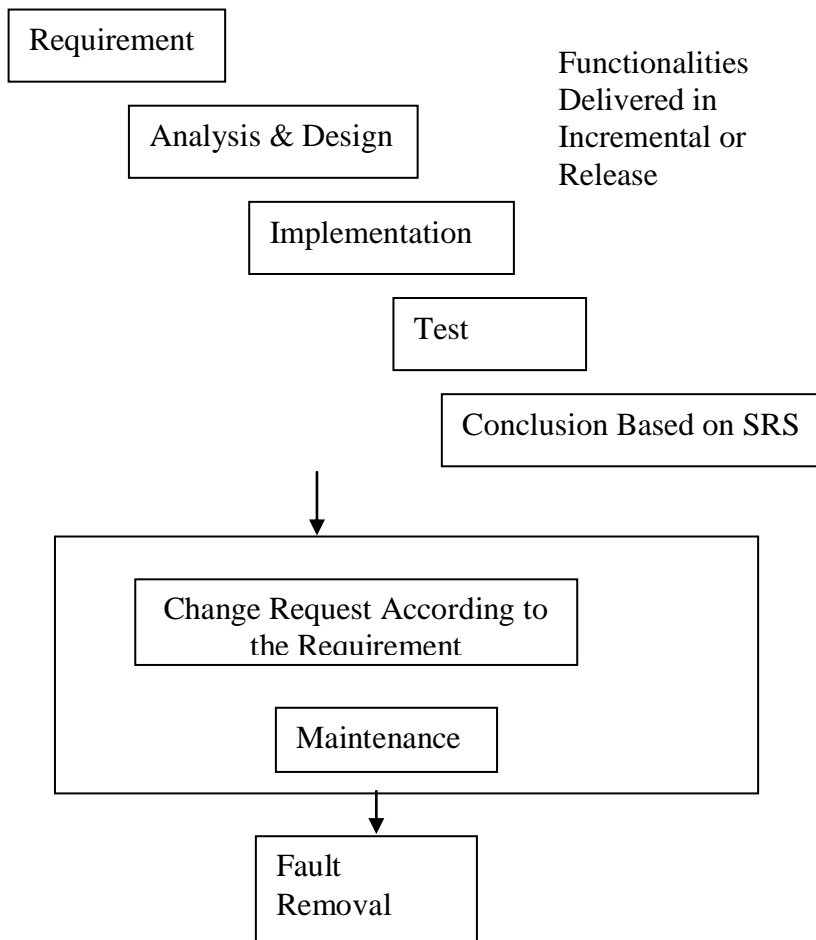
Software development approaches.

Every software development methodology has more or less its own approach to software development. There is a set of more general approaches, which are developed into several specific methodologies. These approaches are [9]:

- i. Waterfall: linear framework type
- ii. Prototyping: iterative framework type
- iii. Incremental: combination of linear and iterative framework type
- iv. Spiral: combination linear and iterative framework type
- v. Rapid Application Development (RAD): Iterative Framework Type

IV. Proposed Model

The proposed model is designed in such a way that it not only used for defect prevention rather than it also be used for defect removal. It will evaluate the software quality through the representative user testing at the system level. During incremental development of software modules, this model not only help to indicate the software changes to correct failure found, but also helpful to untested new software that will be added to the software already under test.



‘Fault Prediction Model’

In the above proposed model there are three major task that are very beneficial to increase the quality of software modules during incremental development of software system.

These tasks are given below:

- i. The functionalities delivered in increment or release
- ii. Parts of the system that have to be changed
- iii. Traceability that will create a links between above two tasks.

This model is used for each increment during incremental development:

- i. To determine the requirements elicitation or refinement, analysis and design, implementation, integration and the system testing for current increment
- ii. While the software is developed in increment j is being tested, increment j+1 has started. Therefore each phase of incremental development includes fault removal activities for previous increment (n). Fault should be removed both from the previous increments or releases and the current one and fault correction may introduce new faults
- iii. Changes to the requirement according to the request based on today's may lead to deviation from the original increment plan, when it comes to effort and time plan
- iv. Several development teams' works in parallel for implementing the software modules, some may finish their works before others and start working on next increment, that should be synchronized with each other and dependencies should be released.
- v. Through each increment quality will be increases from starting to end of software modules

Although basic idea behind this is to deliver the final system in smaller parts and much more functionality is delivered at the end of each increment. During the each release of software modules many correction should also be corrected through the proposed model, which made integration and testing simpler.

Therefore proposed model made integration and testing simpler and increases the quality of software module throughout its life cycle.

Goal of Proposed Model

The major goal of proposed model is to detect faults as early as possible in the development life cycle.

This model helps us to better designing of modelling algorithm in incremental development, towards improving

- i. The information contents of the training data
- ii. Evaluation of software modules which would be inject the additional knowledge regarding context in which software is used into modelling processes.

V. Conclusion

The key factors of the proposed model is monitoring the functionalities and parts of the system that have to be changed, through this controlling the quality of software modules.

It will predict the probability of presence of faults and estimating and preventing the faults that will

reduce the testing effort. Through works model fault proven model is designed that are known in advance for review, analysis and design, testing for incremental development.

References

1. ISO/IEC 9126-1: Software engineering – Product quality. ISO/IEC (2001)
2. ISO 9001: Quality management systems – Requirements. ISO (2001)
3. Basili V.R., Weiss D.M.: A Methodology for Collecting Valid Software Engineering Data, IEEE Transactions on Software Engineering, Nov. (1984)
4. Basili, V.R., Caldiera, G., Rombach, H.D.: The Goal Question Metric Approach. In: Encyclopedia of Software Engineering, Wiley-Interscience, New York (1994)
5. Solingen, R., Berghout, E.: The Goal/Question/Metric Method, McGraw-Hill (1999)
6. Fenton, N: Software Metrics: A Rigorous Approach, Chapman and Hall (1993)
7. Haag, S., Raja, M.K., Schkade, L.L.: Quality Function Deployment Usage in Software Development. In: Communications of the ACM, 1 (1996) 41-49
8. Edsger Dijkstra, "Notes on Structured programming", <http://www.cs.utexas.edu/users/EWD/ewd02xx/EWD249.PDF>
9. R. Pressman, "Software Engineering: A Practitioner's Approach", 6th Edition, McGraw publishing, 2007.

Implementation of Direct Torque and Indirect Flux Control of Blcd Motor

B.Amruth Kumar Reddy¹, G.Kumaraswamy²

¹(M.Tech Student, R.G.M College of Engineering and Technology, Nandyal, Andhra Pradesh)

²(EEE Department, R.G.M College of Engineering and Technology, Nandyal, Andhra Pradesh)

Abstract : In this paper, the position-sensor less direct torque and indirect flux control of brushless dc (BLDC) motor with non sinusoidal back electromotive force (EMF) has been extensively investigated. In the literature, several methods have been proposed for BLDC motor drives to obtain optimum current and torque control with minimum torque pulsations. Most methods are complicated and do not consider the stator flux linkage control, therefore, possible high-speed operations are not feasible. In this study, a novel and simple approach to achieve a low-frequency torque ripple-free direct torque control (DTC) with maximum efficiency based on dq reference frame is presented. The proposed sensor less method closely resembles the conventional DTC scheme used for sinusoidal ac motors such that it controls the torque directly and stator flux amplitude indirectly using d -axis current. This method does not require pulse width modulation and proportional plus integral regulators and also permits the regulation of varying signals. Furthermore, to eliminate the low-frequency torque oscillations, two actual and easily available line-to-line back EMF constants (k_{ba} and k_{ca}) according to electrical rotor position are obtained offline and converted to the dq frame equivalents using the new line-to-line park transformation. Then, they are set up in the look-up table for torque estimation. The validity and practical applications of the proposed sensor less three-phase conduction DTC of BLDC motor drive scheme are verified through simulations and experimental results.

Keywords - Brushless dc (BLDC) motor, direct torque control (DTC), fast torque response, low-frequency torque ripples, Non sinusoidal back electromotive force (EMF), position-sensor less control, stator flux control, torque pulsation.

I. INTRODUCTION

The permanent-magnet synchronous motor (PMSM) and brushless dc (BLDC) motor drives are used extensively in several high-performance applications, ranging from servos to traction drives, due to several distinct advantages such as high power density, high efficiency, large torque to inertia ratio, and simplicity in their control [1]–[3]. In many applications, obtaining a low-frequency ripple-free torque and instantaneous torque and even flux control are of primary concern for BLDC motors with non sinusoidal A great deal of study has been devoted to the current and torque control methods employed for BLDC motor drives. One of the most popular approaches is a generalized harmonic injection approach by numerical optimization solutions to find out optimal current waveforms based on back EMF harmonics to minimize mutual and cogging torque [4]. Those approaches limit

Fourier coefficients upto an arbitrary high harmonic order due to calculation complexity [6].

This method provides advantages of the classical DTC such as fast torque response compared to vector control, simplicity (no PWM strategies, PI controllers, and inverse Park and inverse Clarke transformations), and a position-sensor less drive. As opposed to the prior two-phase conduction direct torque control methods used for BLDC motor [8], [9], the proposed DTC technique provides position- sensor less drive that is quite similar to the one used in conventional DTC scheme and also controls the stator flux indirectly using d -axis current. Therefore, flux weakening operation is possible. Coordinate transformations are done by the new line-to-line Park transformation that forms a 2×2 matrix instead of the conventional 2×3 matrix. Therefore, rather than three line-to-neutral back EMF waveforms, which are not directly available in the motor easily accessible two line-to-line back EMF constants ($k_{ba}(\theta_{re})$ and $k_{ca}(\theta_{re})$) are obtained offline and converted to the dq frame equivalents ($k_d(\theta_{re})$ and $k_q(\theta_{re})$). Then, they are stored in a look-up table for the torque estimation. The electrical rotor position is estimate during winding inductance and stationary reference frame stator flux linkages and currents. Since the hysteresis controllers used in the proposed DTC scheme are not fast controllers like PI, they can easily regulate not only constant, but also the varying references (torque and flux). Simulation and experimental results are presented to illustrate the validity and effectiveness of the sensor less three-phase conduction DTC of a BLDC undergoes a corresponding change.

II. PROPOSED LINE-LINE AND PARK TRANSFORMATION

Since the balanced systems in dq -axes reference frame do not require a zero sequence term, first line-to-line Clarke transformation from the balanced three-phase quantities is derived and, then the line-to-line Park transformation forming a 2×2 matrix instead of a 2×3 matrix for three-phase systems can be obtained in the following. Using some algebraic manipulations, the original Clarke transformation forming a 2×3 matrix excluding the zero sequence term can be simplified to a 2×2 matrix as follows:

$$[T_{ll}] = \begin{bmatrix} \frac{-1}{2} & \frac{-1}{2} \\ \frac{1}{\sqrt{3}} & \frac{1}{\sqrt{3}} \end{bmatrix} \dots\dots\dots(1)$$

which requires only two input variables X_{ba} and X_{ca} where $X_{ba} = X_b - X_a$ and $X_{ca} = X_c - X_a$. X represents machine variables such as currents, voltages, flux linkages, back EMFs, etc. To obtain the line-to-line Park transformation forming a 2×2 matrix, the inverse of the original Clarke transformation matrix $[T_{\alpha\beta}]$ is required. Since the zero-

sequence term is removed, $[T_{\alpha\beta}]$ matrix is not square anymore, but it is still singular and therefore, pseudo inverse can be found in the following:

$$[T_{\alpha\beta}]^+ = [T_{\alpha\beta}]T([T_{\alpha\beta}][T_{\alpha\beta}]T)^{-1} \dots \dots \dots (2)$$

where $[T_{\alpha\beta}]^+$ and $[T_{\alpha\beta}]T$ are the pseudo inverse and transpose of the original Clarke transformation matrix $[T_{\alpha\beta}]$, respectively. Here abc to $ba-ca$ transformation can be represented as follows:

$$[T_{\alpha\beta}]^+[T_{\alpha\beta}] \begin{bmatrix} X_a \\ X_b \\ X_c \end{bmatrix} = [T_{\alpha\beta}]^+ [T_{LL}] \begin{bmatrix} X_{ba} \\ X_{ca} \end{bmatrix} \dots \dots \dots (3)$$

After (3) is expanded and multiplied by the original 2×3 Park transformation matrix in both sides, algebraic manipulations lead to simplifications using some trigonometric equivalence. Therefore, the following 2×2 line-to-line Park transformation matrix form is obtained:

$$\begin{bmatrix} X_d \\ X_q \end{bmatrix} = \frac{2}{3} \begin{bmatrix} \sin(\theta - \frac{\pi}{6}) & -\sin(\theta + \frac{\pi}{6}) \\ -\cos(\theta - \frac{\pi}{6}) & \cos(\theta + \frac{\pi}{6}) \end{bmatrix} \begin{bmatrix} X_{ba} \\ X_{ca} \end{bmatrix} \dots \dots (4)$$

Unlike previous two-phase conduction DTC of BLDC motor drive techniques, which are proposed in [8] and [9], this method uses DTC technique with three-phase conduction, therefore, flux-weakening operation as well as a much simpler sensor less technique can easily be achieved. Compared with the two-phase conduction DTC scheme, this DTC method differs by its torque estimation and voltage vector selection table which is similar to the one used for DTC of PMSM drives explained in [10].

For machines with surface-mount magnet rotor (BLDC) stator flux linkages in rotor dq reference frame can be written as

$$\varphi_{qs}^r = L_s i_{qs}^r + \varphi_r \sum_{n=1}^{\infty} (K_{6n-1} + K_{6n+1}) \sin(6n\theta_r) \dots \dots (5)$$

$$\varphi_{ds}^r = L_s i_{ds}^r + \varphi_r \sum_{n=1}^{\infty} (K_{6n-1} - K_{6n+1}) \cos(6n\theta_r) + \varphi_r \dots \dots \dots (6)$$

where φ_r is the peak value of the fundamental rotor magnetic flux linkage of the BLDC motor, the coefficients K_{6n-1} and K_{6n+1} represent the odd harmonics of the phase back EMF other than the third and its multiples. K_{6n-1} equals $[\sin(6n-1)\sigma]/[(6n-1)3 \sin \sigma]$, and K_{6n+1} can be depicted as $[\sin(6n+1)\sigma]/[(6n+1)3 \sin \sigma]$. σ is the angle between zero-crossing and phase back EMF, where it becomes flat at the top. Fundamental peak value of the rotor magnet flux linkage φ_r equals $(4ke/\sigma\pi) \sin \sigma$, where k_e is the line-to-neutral back EMF constant.

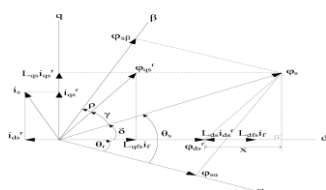


Fig. 1. Rotor and stator flux linkages of a BLDC motor in the stationary $\alpha\beta$ -plane and synchronous dq -plane

The phasor diagram for stator flux linkage vectors in BLDC motor can be drawn in the rotor dq and stationary ($\alpha\beta$) reference frames as shown in Fig. 1, where $L_{ds} = L_{qs} = L_s$ and $L_{dqs} = L_{qds} = 0$. L_{dqs} and L_{qds} are the mutual inductances between d - and q -axis. L_{dsf} and L_{qsf} are the mutual inductances between dq -axes and permanent magnet (PM), respectively, and i_f is the equivalent current generated by PM. In Fig. 1, unlike PMSM with sinusoidal back EMF synchronous reference frame flux linkages φ_{ds}^r and φ_{qs}^r vary with time, therefore, stator flux amplitude ϕ_s is not constant anymore. γ , ρ , and δ in Fig. 1 can be obtained, respectively, as

$$Y = \sin^{-1} \left(\frac{L_{qs} i_{qs}^r}{\varphi_{qs}^r} \right) + \cos^{-1} \left(\frac{L_{qs} i_{qs}^r}{\varphi_s} \right) - \frac{\pi}{2} (7)$$

$$\rho = - \left(\theta_s + Y - \frac{\pi}{2} \right) (8)$$

$$\delta = \frac{\pi}{2} - \cos^{-1} \left(\frac{L_{qs} i_{qs}^r}{\varphi_s} \right) (9)$$

Moreover, x in Fig. 1 can be expressed as

$$x = \varphi_{qs}^r \cos \left[\sin^{-1} \left(\frac{L_{qs} i_{qs}^r}{\varphi_{qs}^r} \right) \right] (10)$$

The electromagnetic torque T_{em} estimation algorithm can be Derived for a balanced system in dq reference frame by equating the electrical power absorbed by the motor to the mechanical power produced ($P_i = P_m = T_{em}\omega_m$) as follows:

$$T_{em} = ((3P)/(4\omega_{re})) \times (e_q(\theta_{re}) i_{ds}^r + e_d(\theta_{re}) i_{qs}^r) = ((3P)/4) \times (k_q(\theta_{re}) i_{ds}^r + k_d(\theta_{re}) i_{qs}^r) (11)$$

where P is the number of poles, ω_{re} is the electrical rotor speed, $e_q(\theta_e)$ and $e_d(\theta_e)$, i_{ds}^r and i_{qs}^r , $k_q(\theta_e)$, and $k_d(\theta_e)$ are the dq axes back EMFs, currents, and back EMF constants according to the electrical rotor position, respectively. As it can be noticed that the right-hand side equation in (11) eliminates the speed term in the denominator which causes problem at zero and near zero speeds.

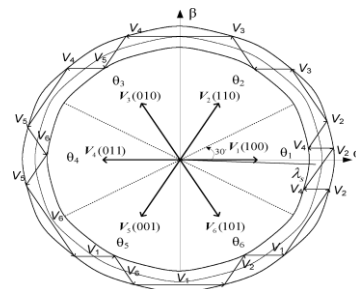


Fig. 2. Dodecagon trajectory of stator flux linkage in the stationary $\alpha\beta$ -plane.

III. CONTROL OF STATOR FLUX LINKAGE AMPLITUDE

The stator flux linkage equations of a BLDC motor can easily be represented in the stationary reference frame similar to PMSM. During the sampling interval time, one out of the six voltage vectors is applied, and each voltage vector applied during the predefined sampling interval is

constant, then the stator flux estimation for BLDC motor can be written as

$$\phi_{s\alpha} = V_{s\alpha} t - R_s \int i_{s\alpha} dt + \phi_{s\alpha}(0)$$

$$\phi_{s\beta} = V_{s\beta} t - R_s \int i_{s\beta} dt + \phi_{s\beta}(0) \quad (12)$$

where $\phi_{s\alpha}(0)$ and $\phi_{s\beta}(0)$ are the initial stator flux linkages at the instant of switching. If the line-to-line back EMF constant k_{LL} is roughly known, and let say the rotor is brought to zero position (phase a), initial stator flux linkages at startup can be obtained by integrating the back EMF in which the ideal trapezoidal is assumed. Therefore, approximate initial starting flux values at zero position can be obtained as

$$\phi_{s\alpha}(0) = 2k_{LL}\pi/(3\sqrt{3}) \text{ and } \phi_{s\beta}(0) = 0. \quad (13)$$

Since BLDC motor does not have sinusoidal back EMF, the stator flux trajectory is not pure circle as in PMSM. It is more like a decagonal shape as shown in Fig. 2. Thus, direct stator flux amplitude control in a BLDC motor is not trivial as in PMSM such that rotor position varying flux command should be considered. However, this is a complicated way to control the stator flux linkage amplitude. Therefore, in this study, instead of $|\phi_s|$ itself its amplitude is indirectly controlled by d -axis current. In the constant torque region, $i_{d_s}^*$ is controlled as zero, and in the flux-weakening region it is decreased for a certain amount depending on the operational speed to achieve maximum torque. As a result, in this study, stator flux linkage amplitude is indirectly kept at its optimum level, while the motor speed is less than the base speed.

Table I
Switching Table For DTC Of BLDC Motor Using Three-Phase Conduction

ϕ	τ	θ					
		$\theta(1)$	$\theta(2)$	$\theta(3)$	$\theta(4)$	$\theta(5)$	$\theta(6)$
$\phi=1$	$\tau=1$	$V_s(110)$	$V_s(010)$	$V_s(011)$	$V_s(001)$	$V_s(101)$	$V_s(100)$
	$\tau=-1$	$V_s(101)$	$V_s(100)$	$V_s(110)$	$V_s(010)$	$V_s(011)$	$V_s(001)$
$\phi=-1$	$\tau=1$	$V_s(010)$	$V_s(011)$	$V_s(001)$	$V_s(101)$	$V_s(100)$	$V_s(110)$
	$\tau=-1$	$V_s(001)$	$V_s(101)$	$V_s(100)$	$V_s(110)$	$V_s(010)$	$V_s(011)$

The switching table for controlling both the amplitude and rotating direction of the stator flux linkage is given in Table I. where the output of the torque hysteresis comparator is denoted as τ , the output of the flux hysteresis comparator as ϕ , and the flux linkage sector is denoted as θ . The torque hysteresis comparator τ is a two valued comparator; $\tau = -1$ means that the actual value of the torque is above the reference and out of the hysteresis limit and $\tau = 1$ means that the actual value is below the reference and out of the hysteresis limit. The same logic applies to the flux related part of the control (d -axis current). The one out of six voltage space vectors is selected using lookup table in every sampling time to provide fast rotation of stator flux linkage vector. Therefore, fast torque and flux responses are obtained in a predefined hysteresis bandwidth, which limits the flux amplitude.

IV. ESTIMATION OF ELECTRICAL ROTOR POSITION

Electrical rotor position θ_{re} , which is required in the line-to-line Park transformation and torque estimation algorithm can be found by

$$\Theta_{re} = \tan^{-1} \left(\frac{\phi_{s\beta} - L_s i_{s\beta}}{\phi_{s\alpha} - L_s i_{s\alpha}} \right) \quad (14)$$

motor with varying stator flux linkage amplitude as shown in Fig. 2. The second algorithm in [12], which is the modified integrator with an amplitude limiter To solve the common problems for integrators, a special integration algorithm for estimating the stator flux linkage proposed in [12] is used in this study. Although the method in [12] is designed for sine wave systems, the algorithm is still applicable to a BLDC is used for the stator flux linkage estimation. The maximum amplitude of the stator flux linkage reference approximated as $2k_{LL}\pi/(3\sqrt{3})$ is set for the limiter when the motor speed is less than the base speed.

V. RESULTS AND DISCUSSIONS

The drive system shown in Fig. 3 has been simulated in order to demonstrate the validity of the proposed three-phase conduction DTC of a BLDC motor drive scheme using line-to-line machine model. The sampling interval is $15 \mu s$. The magnitudes of the torque and flux hysteresis bands are 0.001 N·m and 0.001 Wb, respectively. The dc-link voltage V_{dc} equals $40\sqrt{2} V$. Appendix I shows the specifications and parameters of the BLDC motor. In Fig. 4, the possibility of the flux-weakening region operation is simulated when $i_{d_s}^*$ is changed from 0 to $-5 A$. As it can be seen in Fig. 4 that the shape of stator flux linkage trajectory is kept same, however, its amplitude is smaller compared to the initial case, which means that the flux in the machine is weakened to obtain maximum possible torque above the base speed. It is concluded that in the proposed control scheme flux weakening operation is viable by properly selecting the d -axis current reference as in PMSM drives. As a result, there is no need to use position-varying stator flux linkage amplitude $|\phi_s(\theta_{re})|$ as a reference, which is complicated to obtain especially in the flux-weakening region.

Fig. 5 shows the dq frame back EMF constants according to the electrical rotor position ($k_d(\theta_{re})$ and $k_q(\theta_{re})$), which are set up in the look-up tables for torque estimation both in simulation and experiment. The feasibility and practical features of the proposed three phase conduction DTC of a BLDC motor drive scheme have been evaluated using an experimental test-bed, as shown in Fig.

6. The same conditions are used as in simulation.

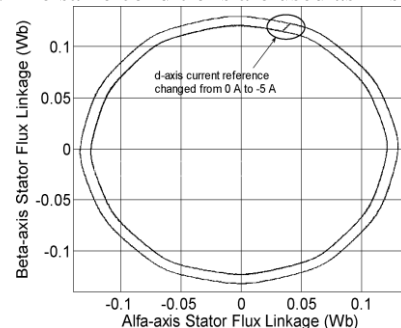


Fig 4. Indirectly Controlled Stator Flux Linkage Trajectory Under The Sensor Less Three-Phase Conduction Dtc Of A Blcd Motor Drive When $i_{d_s}^*$ Is Changed From 0 To $-5 A$ Under 0.5 N·M Load Torque.

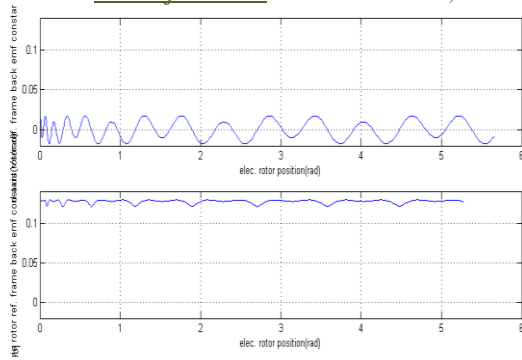
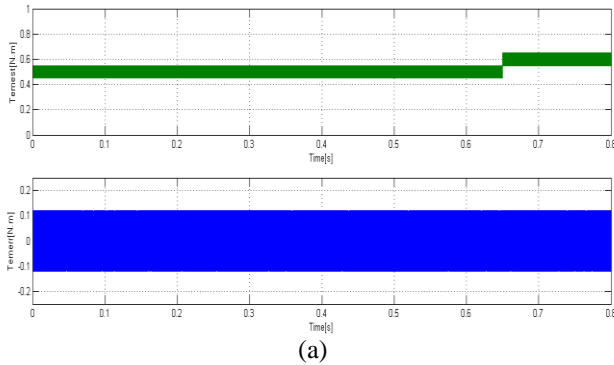
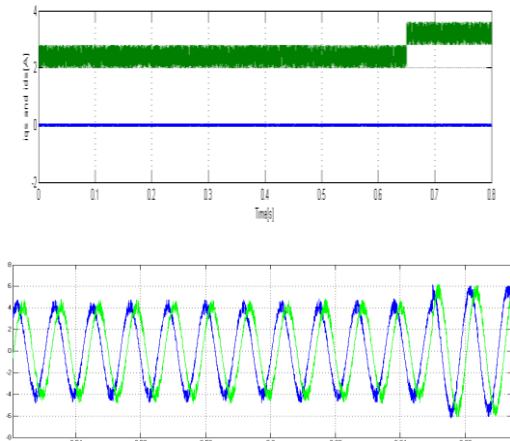


Fig. 5. Actual Q - And D -Axis Rotor Reference Frame Back Emf Constants Versus Electrical Rotor Position ($K_d(\theta_{rE})$ And $K_q(\theta_{rE})$)



(a)



(b)

Fig.7. Steady state and transient behavior of (Top) estimated electromagnetic torque, (bottom) error between reference and estimated electromagnetic torque. (b) (Top) q -axis stator current and d -axis stator current and (bottom) ba - ca frame currents when $i_{ds}^* = 0$ under 0.5 N·m load torque.

Implementations of steady state and transient torque, torque error, q - and d -axis rotor reference frame stator currents, and line-to-line current responses of the proposed DTC of a BLDC motor drive scheme are demonstrated in Fig. 7(a) and (b), respectively, under a 0.5 N·m load torque condition. The torque reference is changed abruptly from 0.52 to 0.65 N·m at 0.65 s. It is seen in Fig. 7(a) (top) that fast torque response is obtained and the estimated torque tracks the reference torque closely. The reference torque value in the experimental test is selected a little bit higher than the load torque to compensate the friction of the total experimental system such that the rotor speed is kept at steady-state level (30 mechanical rad/s). The

torque error between reference and estimated electromechanical torque is shown in the bottom part of Fig. 7(a). The high frequency ripples observed in the torque and current can be minimized by properly selecting the dc-link voltage and torque hysteresis band size. The $\alpha\beta$ -axes stator flux linkages are estimated using (12) in which the $\alpha\beta$ -axes voltages are measured using a dc-link voltage sensor and the estimated position of the stator flux linkage vector θ_s . The motor is initially locked at zero position (phase a) for proper starting. Fig. 8 shows the experimental results of the indirectly controlled stator flux linkage locus by controlling the d -axis rotor reference frame current at 0 A when 0.5 N·m load torque is applied to the BLDC motor.

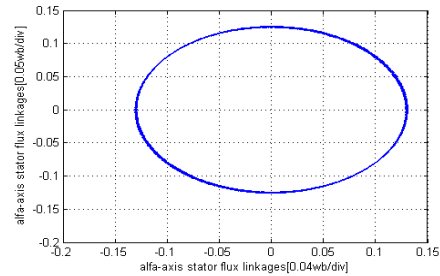


Fig. 8. Experimental indirectly controlled stator flux linkage trajectory under the sensor less three-phase conduction DTC of a BLDC motor drive when $i_{ds}^* = 0$ at 0.5 N·m load torque.

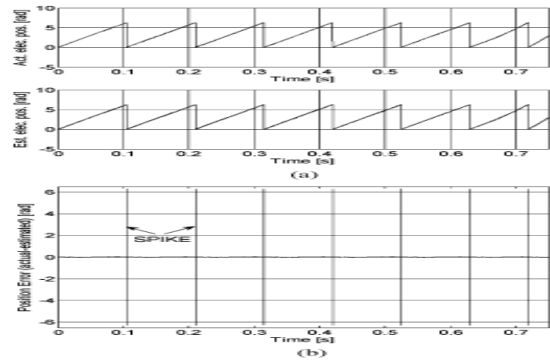


Fig. 9. (a) Steady state and transient behavior of the actual and estimated electrical rotor positions from top to bottom, respectively and (b) error between actual and estimated electrical rotor positions under 0.5 N·m load torque.

In Fig. 10, the flux-weakening operation is evaluated under 1.1926 N·m load torque. Fig. 10(a) shows the high speed operation when $i_{ds}^* = 0$. The desired speed is dropped from 540 electrical rad/s to 513.5 electrical rad/s and oscillations in speed and torque are observed, as shown in Fig. 10(a). This result shows that the desired torque can only be obtained at lower speed when flux is not weakened. However, in Fig. 10(b), i_{ds}^* is decreased to -4.51 A and the speed is controlled in the desired level quite well. The dc-link voltage is 115 V and the base speed for that voltage is 500 electrical rad/s.

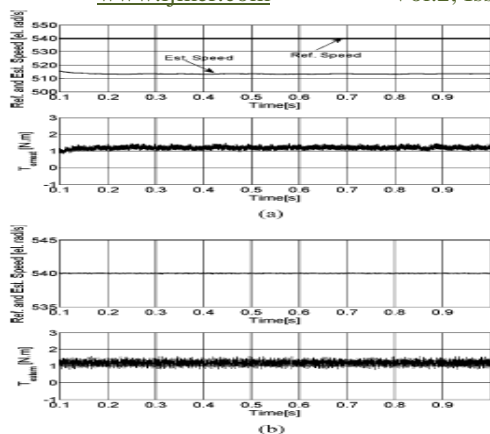


Fig.10.Steady-state flux-weakening behavior of the actual speed and estimated electromechanical torque, respectively, (a) when $i_d^* = 0$ and (b) when $i_d^* = -4.51$ A under 1.1926 N-m load torque at 540 electrical rad/s desired speed (V_{dc} link = 115 V).

VI. CONCLUSION

This paper has successfully demonstrated application of the proposed position-sensor less three-phase conduction DTC scheme for BLDC motor drives that is similar to the conventional DTC used for sinusoidal ac motors where both torque and flux are controlled, simultaneously. This method provides advantages of the classical DTC such as fast torque response compared to vector control, simplicity (no PWM strategies, PI controllers, and inverse Park and inverse Clarke transformations), and a position-sensor less drive. It is shown that the BLDC motor could also operate in the flux-weakening region by properly selecting the d -axis current reference in the proposed DTC scheme.

Since the actual back EMF waveforms are used in the torque estimation, low-frequency torque oscillations can be reduced convincingly compared to the one with the ideal-trapezoidal waveforms having 120 electrical degree flat top. A look-up table for the three-phase voltage vector selection is designed similar to a DTC of PMSM drive to provide fast torque and flux control.

REFERENCES

- [1] W. C. Gan and L. Qiu, "Torque and velocity ripple elimination of AC permanent magnet motor control systems using the internal model principle," *IEEE/ASME Trans. Mechatronics*, vol. 9, no. 2, pp. 436–447, Jun. 2004.
- [2] D. Sun and J. K. Mills, "Torque and current control of high-speed motion control systems with sinusoidal-PMAC motors," *IEEE/ASME Trans. Mechatronics*, vol. 7, no. 3, pp. 369–377, Sep. 2002.
- [3] H. Melkote and J. Khorrami, "Nonlinear adaptive control of directdrive brushless DC motors and applications to robotic manipulators," *IEEE/ASME Trans. Mechatronics*, vol. 4, no. 1, pp. 71–81, Mar. 1999.
- [4] H. R. Bolton and R. A. Ashen, "Influence of motor design and feed current waveform on torque ripple in brushless dc drives," *Proc. Inst. Elect. Eng.—Elect. Power Appl.*, vol. 131, no. 3, pp. 82–90, 1984.
- [5] D. Hanselman, "Minimum torque ripple, maximum efficiency excitation of brushless permanent magnet motors," *IEEE Trans. Ind. Electron.*, vol. 41, no. 3, pp. 292–300, Jun. 1994.
- [6] T. Kim, H.-W. Lee, L. Parsa, and M. Ehsani, "Optimal power and torque control of a brushless dc (BLDC) motor/generator

- drive in electric and hybrid electric vehicles," in *Conf. Rec. IEEE IAS Annu. Meeting*, 8–12 Oct. 2006, vol. 3, pp. 1276–1281.
- [7] S. K. Chung, H. S. Kim, C. G. Kim, and M. J. Youn, "A new instantaneous torque control of PM synchronous motor for high-performance direct drive applications," *IEEE Trans. Power Electron.*, vol. 13, no. 3, pp. 388–400, May 1998.
- [8] Y. Liu, Z. Q. Zhu, and D. Howe, "Direct torque control of brushless dc drives with reduced torque ripple," *IEEE Trans. Ind. Appl.*, vol. 41, no. 2, pp. 599–608, Mar./Apr. 2005.
- [9] S. B. Ozturk and H. A. Toliyat, "Direct torque control of brushless dc motor with non-sinusoidal back-EMF," in *Proc. IEEE IEMDC Biennial Meeting*, Antalya, Turkey, May 3–5, 2007, vol. 1, pp. 165–171.
- [10] L. Zhong, M. F. Rahman, W. Y. Hu, and K. W. Lim, "Analysis of direct torque control in permanent magnet synchronous motor drives," *IEEE Trans. Power Electron.*, vol. 12, no. 3, pp. 528–536, May 1997.
- [11] S. B. Ozturk and H. A. Toliyat, "Sensorless direct torque and indirect flux control of brushless dc motor with non-sinusoidal back-EMF," in *Proc. IEEE IECON*, Orlando, FL, Nov. 9–11, 2008, pp. 1373–1378.
- [12] J. Hu and B. Wu, "New integration algorithms for estimating motor flux over a wide speed range," *IEEE Trans. Power Electron.*, vol. 13, no. 5, pp. 969–977, Sep. 1998.
- [13] K. Gulez, A. A. Adam, and H. Pastaci, "A novel direct torque control algorithm for IPMSM with minimum harmonics and torque ripples," *IEEE/ASME Trans. Mechatronics*, vol. 12, no. 2, pp. 223–227, Apr. 2007.

BIOGRAPHIES



B.Amruth kumar reddy is born in 1987 in India. He is graduated from JNTU Hyderabad in 2008. Presently he is doing Post graduation in Power Electronics and Electrical Drives Specialization at J.N.T.U.A, Anantapur His main areas of interest include Induction motor drives, Electrical machines, Power Electronics & Converters and Power Electronic Drives



G.Kumaraswamy is born in 1983 in India. He is graduated from JNTU university in 2005 and pursued Post graduation from the same university. He is currently working as a Assistant professor in the department of electrical and electronics engineering R.G.M college of engineering and technology, Nandyal, Andhra Pradesh, India. He has seven years of teaching experience. He has attended several National workshops. His main areas of research include Induction motor drives, Electrical machines FACTS and Harmonic reduction in power converters.

Shortest Time Quantum Scheduling Algorithm

ABDULLA SHAIK

Department Of IT, RTMNU,
Nuva College Of Engineering & Technology,
Nagpur. Maharashtra 440015, India

Abstract: Scheduling is the method by which threads, processes or data flows are given access to system resources. This is usually done to load balance a system effectively or achieve a target quality of service. Different CPU scheduling algorithms have different properties, and the choice of a particular algorithm may favor one class of processes over another. A typical scheduler is designed to select one or more primary performance criteria and rank them in order of importance. One problem in selecting a set of performance criteria is that they often conflict with each other. For example, increased processor utilization is usually achieved by increasing the number of active processes, but then response time decreases. It is desirable to maximize CPU utilization and throughput and to minimize turnaround time, waiting time, and response time. In most cases, we optimize the average measure. However, under some circumstances, it is desirable to optimize the minimum or maximum values rather than the average.

Round robin scheduling is similar to FCFS scheduling, except that CPU bursts are assigned with limits called time quantum. The performance of RR is sensitive to the time quantum selected. If the quantum is large enough, then RR reduces to the FCFS algorithm; If it is very small, then each process gets 1/nth of the processor time and share the CPU equally. The major problem in RR scheduling is that how the time quantum is decides? If any process require more time then the problem arrives that process must wait for long time to complete the execution. To overcome this problem in RR scheduling algorithm we come across with idea that the time quantum is decides based on the burst time needed for process. The percentage of CPU resource is decided based on burst time and the reaming process is similar to RR scheduling but difference is that allocation will be done based on newly calculated time quantum of process.

Keywords: Burst time, scheduling, time quantum, waiting time, execution time.

I. Introduction

If you look at any process, you'll notice that it spends some time executing instructions (computing) and then makes some I/O request, for example to read or write data to a file or to get input from a user. After that, it executes more instructions and then, again, waits on I/O. The period of computation between I/O requests is called the CPU burst.



Compute-intensive processes, conversely, spend more time running instructions and less time on I/O. Most interactive processes, in fact, spend the vast bulk of their existence doing nothing but waiting on data. If you consider

Mac OS system, In which 44 processes running. This includes a few browser windows, a word processor, spreadsheet, several shell windows, Photoshop, iTunes, and various monitors and utilities. Most of the time, these processes collectively are using less than 3% of the CPU. This is not surprising since most of these programs are waiting for user input, a network message, or sleeping and waking up periodically to check some state.

The base idea in multiprogramming is that kept CPU always busy. For this we use scheduling. This is the method by which threads, processes or data flows are given access to system resources. This is usually done to load balance a system effectively or achieve a target quality of service. The need for a scheduling algorithm arises from the requirement for most modern systems to perform multitasking and multiplexing.

RR scheduling involves extensive overhead, especially with a small time unit. Balanced throughput between FCFS and SJF, shorter jobs are completed faster than in FCFS and longer processes are completed faster than in SJF. Poor average response time, waiting time is dependent on number of processes, and not average process length. Because of high waiting times, deadlines are rarely met in a pure RR system. Starvation can never occur, since no priority is given. Order of time unit allocation is based upon process arrival time, similar to FCFS. Round robin scheduling is similar to FCFS scheduling, except that CPU bursts are assigned with limits called time quantum. When a process is given the CPU, a timer is set for whatever value has been set for a time quantum. If the process finishes its burst before the time quantum timer expires, then it is swapped out of the CPU just like the normal FCFS algorithm. If the timer goes off first, then the process is swapped out of the CPU and moved to the back end of the ready queue. The ready queue is maintained as a circular queue, so when all processes have had a turn, then the scheduler gives the first process another turn, and so on. Most modern systems use time quantum between 10 and 100 milliseconds, and context switch times on the order of 10 microseconds, so the overhead is small relative to the time quantum. The major problem in RR scheduling is that how the time quantum is decides? If any process require more time then the problem arrives that process must wait for long time to complete the execution. To overcome this problem in RR scheduling algorithm we come across with idea that the time quantum is decides based on the burst time needed for process. The percentage of CPU resource is decided based on burst time and the reaming process is similar to RR scheduling but difference is that allocation will be done based on newly calculated time quantum of process. The processing is similar to SJF with RR scheduling model.

II. Shortest Time Quantum Scheduling Algorithm

The degree of multiprogramming is decided based on number of process/programs running simultaneously at a time. This can be improve are maintain by proper scheduling of multiple process in CPU. For that we are having different scheduling schemes one of them is FCFS the alternative of the FCFS is given in RR scheduling algorithm. Round robin scheduling is similar to FCFS scheduling, except that CPU bursts are assigned with limits called time quantum. When a process is given the CPU, a timer is set for whatever value has been set for a time quantum. . Most modern systems use time quantum between 10 and 100 milliseconds, and context switch times on the order of 10 microseconds, so the overhead is small relative to the time quantum. The major problem in RR scheduling is that how the time quantum is fixed for all the process. If the process is having burst time is low or high but the time quantum is same for all. As per RR algorithm low burst time process completes its execution first. To overcome this problem in RR scheduling algorithm we come across with idea that the time quantum is decides based on the burst time. It mean that based on time burst time quantum is decided so the time quantum is not fix for all process. The percentage of CPU resource is decided based on burst time and the reaming process is similar to RR scheduling but difference is that allocation will be done based on newly calculated time quantum of process.

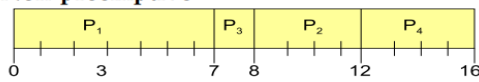
III. Processing

Round Robin scheduling is similar to FCFS scheduling, except that CPU bursts are assigned with limits called time quantum. When a process is given the CPU, a timer is set for whatever value has been set for a time quantum. Let first see how the shortest job scheduling is work. The Shortest job first scheduling algorithm gives minimum average waiting time for a given set of processes.

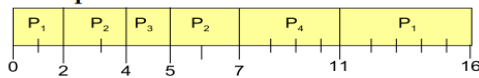
Examples

Process	Arrival Time	Burst Time
P ₁	0.0	7
P ₂	2.0	4
P ₃	4.0	1
P ₄	5.0	4

• Non-preemptive



• Preemptive

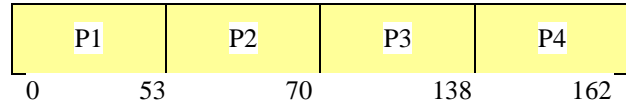


The problems in SJF are: Only optimal if all jobs/process are available simultaneously. Usually run times are not known.

First-Come-First-Served algorithm is the simplest scheduling algorithm is the simplest scheduling algorithm. Processes are dispatched according to their arrival time on the ready queue. Being a no preemptive discipline, once a process has a CPU, it runs to completion.

Let consider example:

Process	Burst time
P1	53
P2	17
P3	68
P4	24



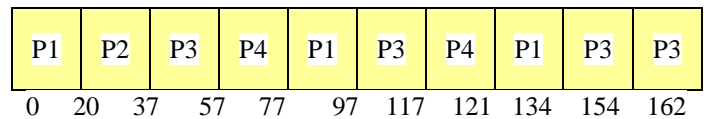
As per the FCFS algorithm the order of executing process is based on arrival. And once the process starts execution it is not suspended.

To overcome this problem in FCFS the Round Robin Scheduling algorithm is proposed. Each process gets a small unit of CPU time (time quantum). Then put back in Ready queue. The *RR Scheduling algorithm* is Preemptive. When interrupted, go to end of FIFO queue. Good for multi-user time-sharing - fast response time. Sometimes, OS just says "carry on". Sometimes don't even need 1 time quantum since process leaves voluntarily.

Example:

Process	Burst time
P1	53
P2	17
P3	68
P4	24

Say time quantum = 20:



Setting the time quantum size

If quantum too small, too much admin, not enough work.

As quantum goes to infinity, this goes to straight FIFO non-preemptive.

Want:

context switch << time slice

average CPU burst <= time slice

(some, but not too many > time slice)

Shortest Time Quantum Scheduling Algorithm:

By considering the above example the process P2 is having burst time =17 and p3 is having burst time =68. But both are having the time quantum 20ms for process P1 and P3. But the process P3 is having much more burst time then compare to P2. It need more time to execute quickly.

Example:

Process	Burst time
P1	53
P2	17
P3	68
P4	24

The total burst time needed for all the process The total execution time=P1+P2+P3+P4 =53+17+68+24 = 162

We fix minimum time quantum is 0.5 for increase the processing.

For each unit of CPU process need

= CPU %/ total execution time

=100/162

=0.617(>0.5)

The smallest Bust time require by process P2=17
 Now we calculate the time quantum for each process
 Time quantum of P1=51*0.617=32ms (ceil)
 Time quantum of P2=17*0.617=11ms (ceil)
 Time quantum of P3=68*0.617=42ms (ceil)
 Time quantum of P4=24*0.617=15ms (ceil)

P1	P2	P3	P4	P1	P2	P3	P4	
0	32	43	85	100	119	125	149	162

According to the Traditional RR scheduling based on time quantum. But here we are applying the way is shortest time quantum.

Now the actual way of processing is done as per *shortest quantum*

So
 Time quantum of P1=51*0.617=32ms (ceil)
 Time quantum of P2=17*0.617=11ms (ceil)
 Time quantum of P3=68*0.617=42ms (ceil)
 Time quantum of P4=24*0.617=15ms (ceil)

P2	P4	P1	P3	P2	P4	P1	P3	
0	11	26	58	100	106	115	138	162

Example:

Process	Burst time
P1	5
P2	10
P3	5

The total burst time needed for all the process The total execution time=P1+P2+P3
 =5+10+5
 = 20

For each unit of CPU process need
 =20/100
 =0.2(<0.5)

Here we fix minimum time quantum is 0.5 for increase the processing according to that the time quantum for each process

Time quantum of P1=5*0.5=3ms (ceil)
 Time quantum of P2=10*0.5=5ms (ceil)
 Time quantum of P3=5*0.5=3ms (ceil)

P1	P3	P2	P1	P3	P2	
0	3	6	11	13	15	20

IV. Compression with other algorithms

The efficiency will be calculated based on average waiting time.

As per the examples consider

Process	Burst time
P1	53
P2	17

P3 68
 P4 24

As per *FCFS* Scheduling Algorithm processing is done in order

P1	P2	P3	P4	
0	53	70	138	162

Avg. waiting time= (0+53+70+138)/4 = 65.25ms

As per *SJF* Scheduling Algorithm processing is done in order

P2	P4	P1	P3	
0	17	41	94	162

Avg. waiting time= (0+17+41+94)/4 = 38ms

As per *RR* Scheduling Algorithm processing is done in order

Say time quantum = 20:

P1	P2	P3	P4	P1	P3	P4	P1	P3	P3	
0	20	37	57	77	97	117	121	134	154	162

Waiting time of p1= 121-(20+20)= 81ms
 Waiting time of p2= 20ms
 Waiting time of p3= 134-(20+20)= 94ms
 Waiting time of p4= 117-20= 97ms
 Avg. waiting time= (81+20+94+97)/4 = 72.25ms

As per *STQ* Scheduling Algorithm processing is done in order we fix minimum time quantum is 0.5 for increase the processing.

For each unit of CPU process need
 = CPU %/ total execution time
 =100/162
 =0.617(>0.5)

Now we calculate the time quantum for each process

Time quantum of P1=51*0.617=32ms (ceil)
 Time quantum of P2=17*0.617=11ms (ceil)
 Time quantum of P3=68*0.617=42ms (ceil)
 Time quantum of P4=24*0.617=15ms (ceil)

P2	P4	P1	P3	P2	P4	P1	P3	
0	11	26	58	100	106	115	138	162

Waiting time of p1= 115-32= 83ms
 Waiting time of p2= 100-11=89ms
 Waiting time of p3= 138-42= 96ms
 Waiting time of p4= 106-15= 91ms
 Avg. waiting time= (83+89+96+91)/4 = 89.75ms

The average waiting time is much more compare to the other algorithms but the CPU resources are given to all the process based on the burst time. So that the high burst time process like IO bound process are also complete the execution similar to the CPU bound process. And this algorithm never enters in to the CPU bound process. The major advantage is that the waiting time of individual are the average waiting time is much more nearer to the Round Rabin algorithm.

V. Conclusion

The degree of multiprogramming is decided based on number of process/programs running simultaneously at a time. This can be improve are maintain by proper scheduling of multiple process in CPU. For that we are having different scheduling schemes one of them is FCFS the alternative of the FCFS is given in RR scheduling algorithm. RR Scheduling algorithm is work based on fixed time quantum. Most modern systems use time quantum between 10 and 100 milliseconds, and context switch times on the order of 10 microseconds. The major problem in RR scheduling is that how the time quantum is fixed for all the process. If the process is having burst time is low or high but the time quantum is same for all. As per RR algorithm low burst time process completes its execution first. To overcome this problem in RR scheduling algorithm we come across with idea that the different process having different time quantum and minimum is 0.5% of CPU. Time quantum is decides based on the burst time. The percentage of CPU resource allocated on the basis of shortest time quantum first. The processing is similar to SJF with RR scheduling model. This combination will give the new kind of processing of programs.

Acknowledgments

I am grateful to My Brothers Dr. Khaleel Basha Shaik and Dr. Nazer Shaik , Dr Ajay Shenkar Singh and P. Manoj Kumar for giving guideline their valuable time to me. Finally last but not the least Mr. A. Hasheem Babu, Mr. Mohammad Shaik and Mr. John Saida other my friends for their insightful comments.

References

- [1] Advanced Concepts In Operating Systems :Distributed Database And Multiprocessor Operating Systems, Singhal Mukesh, Shivaratri Niranjana G, Tata Mcgraw Hill Publishing Co. Ltd, 2008.
- [2] Modern Operating Systems, Tanenbaum Andrew S, 3rd Edition, Pearson Education, 2008.
- [3] Operating Systems Deitel H M , Deitel P J, Choffnesd R, 4th edition, Pearson Education, 2009
- [4] Operating Systems: Internals And Design Principles, Stallings William, 6th Edition, Pearson Education, 2009.
- [5] Design Of The Unix Operating System, Bach Maurice J, Phi Learning Pvt Ltd. 2008
- [6] Minix Book Operating Systems: Design And Implementation, Tanenbaum Andrew S, Woodhull Albert S, 3rd Edition, Pearson Education, 2009
- [7] Operating System Principles Silberschatz Abraham, Galvin Peter Baer, Gagne Greg, 7th Edition, Wiley India, 2008.
- [8] Operating Systems, Godbole Achyut S, 2nd edition, Tata Mcgraw Hill Publishing Co. Ltd. 2009
- [9] Operating Systems : A Concept-Based Approach, Dhamdhare D M, 2nd edition, Tata Mcgraw Hill Publishing Co. Ltd. 2006.
- [10] Operating Systems, Madnick Stuart E, Donovan John J, Tata Mcgraw Hill Publishing Co. Ltd. 2008
- [11] Systems Programming And Operating Systems, Dhamdhare D M, 2nd edition, Tata Mcgraw Hill Publishing Co. Ltd. 2008
- [12] Inside the Linux 2.6 Completely Fair Scheduler: Providing fair access to CPUs since 2.6.23, M. Tim Jones, IBM developerWorks, December 15, 2009
- [13] Token-ordered LRU: an effective page replacement policy and its implementation in Linux systems, Los Alamos National Laboratory, Los Alamos, NM 87545, USA

- [14] CFLRU: A Replacement Algorithm for Flash Memory, seon-yong park, dawoon jung, CASES, October 23-35, 2006
- [15] A Comparison of Page Replacement Algorithms, Amit S. Chavan, Kartik R. Nayak, Keval D. Vora, Manish D. Purohit and Pramila M. Chawan, IACSIT International Journal of Engineering and Technology, Vol.3, No.2, April 2011
- [16] Generalized page replacement algorithms in a relational data base, R. G. Casey, I. Osman, SIGFIDET '74 Proceedings of the 1974 ACM SIGFIDET, Pages 101 - 124



Abdulla Shaik working as Assistant professor in Department of MCA, Nuva College of Engineering and Technology. Previously worked as lecturer in Joginapally B R Engineering College, Hyderabad. He completed his MCA in 2008, M.Tech(CSE) in 2010 from Acharya Nagarjuna university, Guntur with distinction. His interested in research he has publish Five international papers in area of software engineering, Operating Systems, Data Structures and the Software Testing Methodologies. And he is contributed as assistant for Prof. Dr. Ajay senkar Singh and P. Manoj Kumar to complete their research papers.

Feature Selection for Wireless Intrusion Detection System Using Filter and Wrapper Model

Mohanabharathi R^{*1}, Mr T.Kalaikumaran^{#2} Dr.S.Karthi^{*3}

^{1,2}Department of Computer Science Engineering
SNS College of Technology, Coimbatore.

Abstract: Intrusion detection systems are applied to detect network intrusions identified from different sources. Anomaly and signature based schemes are used for the intrusion detection process. Signature based intrusion detection schemes uses the predefined signature collection for the detection process. The anomaly-based model detects the intrusions by learning the network transaction patterns. Feature selection schemes are used to reduce the network transaction features. Performance, time, accuracy and reliability are improved by the feature selection schemes. Current intrusion detection systems use the TCP/IP header information for the intrusion detection process. Network layer and transport layer attacks can be easily detected using TCP/IP header information's. MAC layer is not considered in the intrusion detection process. The hybrid approach is used for the feature selection process. Information gain ratio measure and K-means classifiers are used in the feature selection process. Back propagation perceptron based neural network algorithm is used for the learning and testing process. Scalability and high learning error rate problems are identified in the neural network method.

The proposed system is designed to perform the feature reduction and intrusion detection process under wireless LAN environment. The recurrent neural network is used for the intrusion detection process. The feature reduction process is also enhanced to improve accuracy. Real Time Recurrent Learning (RTRL) algorithm is used to solve the scalability problems.

Keywords: Intrusion detection, anomaly based scheme, signature based scheme, feature selection, RTRL Algorithm.

I. INTRODUCTION

Intrusions are the result of flaws in the design and implementation of computer systems, operating systems, applications, and communication protocols. Statistics [2] show that the number of identified vulnerabilities is growing. Exploitation of these vulnerabilities is becoming easier because the knowledge and tools to launch attacks are readily available and usable. It has become easy for a novice to find attack programs on the Internet that he/she can use without knowing how they were designed by security specialists.

The emerging technology of wireless networks created a new problem. Although traditional IDSs are able to protect the application and software components of TCP/IP networks against intrusion attempts, the physical and data link layers are vulnerable to intrusions specific to these communication layers. In addition to the vulnerabilities of wired networks, wireless networks are the subject of new types of attacks which range from the passive eavesdropping to more devastating attacks such as denial of service. These vulnerabilities are a result of the

nature of the transmission media [13]. Indeed, the absence of physical boundaries in the network to monitor, meaning that an attack can be perpetrated from anywhere, is a major threat that can be exploited to undermine the integrity and security of the network. It is, therefore, essential to take into account these considerations when designing and deploying an intrusion detection system.

To detect intrusions, classifiers are built to distinguish between normal and anomalous traffic. It has been proved that optimizing the feature set has a major impact on the performance, speed of learning, accuracy, and reliability of the intrusion detection system. Unfortunately, current wireless intrusion detection solutions rely on features extracted directly from the frame headers to build the learning algorithm of the classifiers.

II. Feature Selections

Feature selection is the most critical step in building intrusion detection models [1]. During this step, the set of attributes or features deemed to be the most effective attributes is extracted in order to construct suitable detection algorithms (detectors). A key problem that many researchers face is how to choose the optimal set of features, as not all features are relevant to the learning algorithm, and in some cases, irrelevant and redundant features can introduce noisy data that distract the learning algorithm, severely degrading the accuracy of the detector and causing slow training and testing processes. Feature selection was proven to have a significant impact on the performance of the classifiers. Experiments in [4] show that feature selection can reduce the building and testing time of a classifier by 50 percent.

There are currently two models in the literature for feature selection: the filter model and the wrapper model. The wrapper model uses the predictive accuracy of a classifier as a means to evaluate the "goodness" of a feature set, while the filter model uses a measure such as information, consistency, or distance measures to compute the relevance of a set of features. These approaches suffer from many drawbacks: the first major drawback is that feeding the classifier with arbitrary features may lead to biased results, and hence, we cannot rely on the classifier's predictive accuracy as a measure to select features. A second drawback is that for a set of N features, trying all possible combinations of features (2^N combinations) to find the best combination to feed the classifier is not a feasible approach. For example, the DARPA data set contains 41 features [6], and the data set would be larger if we add to it the OSI Layer 2 (MAC layer) features, resulting in thousands of billions of different feature combinations.

Different techniques have been used to tackle the problem of feature selection. In [7], Sung and Mukkamala used feature ranking algorithms to reduce the feature space of the DARPA data set from 41 features to the six most

important features. They used three ranking algorithms based on Support Vector Machines (SVMs), Multivariate Adaptive Regression Splines (MARSs), and Linear Genetic Programs (LGPs) to assign a weight to each feature. Experimental results showed that the classifier's accuracy degraded by less than 1 percent when the classifier was fed with the reduced set of features. Sequential backward search was used in [9] to identify the important set of features: starting with the set of all features, one feature was removed at a time until the accuracy of the classifier was below a certain threshold. Different types of classifiers were used with this approach including Genetic Algorithms, Neural Networks and Support Vector Machines.

III. 802.11-SPECIFIC INTRUSIONS

Several vulnerabilities exist at the link layer level of the 802.11 protocol [8], [5]. Many 802.11-specific attacks were analyzed and demonstrated to present a real threat to network availability. A deauthentication attack is an example of an easy to mount attack on all types of 802.11 networks. Likewise, a duration attack is another simple attack that exploits the vulnerability of the virtual carrier sensing protocol CSMA/CA and it was proven to deny access to the network.

Many free tools are available on the Internet which allow novice hackers to exploit these protocol weaknesses to deny access to a network, as can be seen in [12], where a collection of tools to attack 802.11-based networks is available for download. These tools operate on WEP and WPA-protected networks. Most of the attacks we used in this work are available for download from [12]. The attacks we used to conduct the experiments are:

A. Deauthentication Attack

The attacker fakes a deauthentication frame as if it had originated from the base station (Access Point). Upon reception, the station disconnects and tries to reconnect to the base station again. This process is repeated indefinitely to keep the station disconnected from the base station. The attacker can also set the receiving address to the broadcast address to target all stations associated with the victim base station. However, we noticed that some wireless network cards ignore this type of deauthentication frame. More details of this attack.

B. ChopChop Attack

The attacker intercepts an encrypted frame and uses the Access Point to guess the clear text. The attack is performed as follows: The intercepted encrypted frame is chopped from the last byte. Then, the attacker builds a new frame 1 byte smaller than the original frame. In order to set the right value for the 32 bit long CRC32 checksum named ICV, the attacker makes a guess on the last clear byte. To validate the guess he/she made, the attacker will send the new frame to the base station using a multicast receive address. If the frame is not valid (i.e., the guess is wrong), then the frame is silently discarded by the access point. The frame with the right guess will be relayed back to the network. The hacker can then validate the guess he/she made. The operation is repeated until all bytes of the clear frame are discovered. More details of this attack can be found in [10].

C. Fragmentation Attack

The attacker sends a frame as a successive set of fragments. The access point will assemble them into a new frame and send it back to the wireless network. Since the attacker knows the clear text of the frame, he can recover the key stream used to encrypt the frame. This process is repeated until he/she gets a 1,500-byte long key stream. The attacker can use the key stream to encrypt new frames or decrypt a frame that uses the same three byte initialization vector IV. The process can be repeated until the attacker builds a rainbow key stream table of all possible IVs. Such a table requires 23 GB of memory.

D. Duration Attack

The attacker exploits vulnerability in the virtual carrier-sense mechanism and sends a frame with the NAV field set to a high value (32 ms). This will prevent any station from using the shared medium before the NAV timer reaches zero. Before expiration of the timer, the attacker sends another frame. By repeating this process, the attacker can deny access to the wireless network.

IV. Hybrid Approach

Extensive work has been done to detect intrusions in wired and wireless networks. However, most of the intrusion detection systems examine only the network layer and higher abstraction layers for extracting and selecting features, and ignore the MAC layer header. These IDSs cannot detect attacks that are specific to the MAC layer. Some previous work tried to build IDS that functioned at the Data link layer. For example, in [3], [11] the authors simply used the MAC layer header attributes as input features to build the learning algorithm for detecting intrusions. No feature selection algorithm was used to extract the most relevant set of features.

In this paper, we will present a complete framework to select the best set of MAC layer features that efficiently characterize normal traffic and distinguish it from abnormal traffic containing intrusions specific to wireless networks. Our framework uses a hybrid approach for feature selection that combines the filter and wrapper models. In this approach, we rank the features using an independent measure: the information gain ratio. The k-means classifier's predictive accuracy is used to reach an optimal set of features which maximize the detection accuracy of the wireless attacks. To train the classifier, we first collect network traffic containing four known wireless intrusions, namely, the deauthentication, duration, fragmentation, and chopchop attack. The reader is referred to [12] for a detailed description of each attack. The Best feature set selection algorithm is shown below

Input:

F = Full set of features

IGR: Information Gain Ratio Measure

C: K-means Classifier

T: Gained Accuracy Threshold

For each feature f compute IGR(f)

Rank features in F According to IGR(f)

//Optimal Set Selection Algorithm

Initialize: S = {}, ac = 0

Repeat

(1) $ap = ac$

(2) $f = getNext(F)$

- (3) S=S U {f}
- (4) F=F-{f}
- (5) Ac=accuracy(C,S)

Until (ac-ap)<T Or ac<ap

The selection algorithm starts with an empty set S of the best features, and then, proceeds to add features from the ranked set of features F into S sequentially. After each iteration, the “goodness” of the resulting set of features S is measured by the accuracy of the k-means classifier. The selection process stops when the gained classifier’s accuracy is below a certain selected threshold value or in some cases when the accuracy drops, which means that the accuracy of the current subset is below the accuracy of the previous subset.

V. Initial List Of Features

The initial list of features is extracted from the MAC layer frame header. According to the 802.11 standard, the fields of the MAC header are as given in Table 1. These raw features in Table 1 are extracted directly from the header of the frame. Note that we consider each byte of a MAC address, FCS, and Duration as a separate feature. We preprocess each frame to extract extra features that are listed in Table 2. The total number of features that are used in our experiments is 38 features.

VI. Information Gain Ratio Measure

We used the Information Gain Ratio (IGR) as a measure to determine the relevance of each feature. Note that we chose the IGR measure and not the Information Gain because the latter is biased toward the features with a large number of distinct values. IGR is defined as

$$IGR(Ex, f) = \frac{Gain(Ex, f)}{SplitInfo(Ex, f)}$$

where Ex is the set of vectors that contain the header information and the corresponding class:

TABLE 1

List of Features Extracted from 802.11 Frames

Feature	Description
Version	Two bits indicate which version of the 802.11 MAC is contained in the rest of the frame
Type	Indicate the type of the frame (Mgmt, Ctrl, and Data).
SubType	Indicate the subtype of the frame
ToDS	Indicate if a frame is destined to the Distributed System.
FromDS	Indicate if a frame is originated from Distributed System.
More Fragment	Indicate whether a frame is non final fragment or not.
Retry	Indicate if the frame is a retransmitted frame
Power Mgmt	Indicate whether the station is active or in Power Saving Mode
More Data	Indicate whether an access point has buffered frames for a dozing station
WEP	Indicate if the frame is processed by WEP protocol.

Order	Indicate if the “strict ordering” delivery is employed.
Duration	The number of microsecond the medium is expected to be busy.
RA	The MAC address of the receiving
TA	The MAC address of the transmitting station.
MA	Depending on the values of ToDS and FromDS fields, this address can be the MAC address of the Sending, Destination or Base Station.
FCS	A Frame Check Sequence, which contains a 32 bit Cyclic Redundancy Code.

$$Gain(Ex, f) = Entropy(Ex) - \sum_{v \in Values(f)} \frac{|Ex, v|}{|Ex|} * Entropy(Ex, v),$$

$$Ex, v = \{x \in Ex / value(x, f) = v\}$$

The entropy function is the Shannon’s entropy defined as

$$Entropy(Ex) = - \sum P_i \log_2(P_i)$$

where Pi is the probability of a class i.

SplitInfo(Ex, f) is defined as

$$SplitInfo(Ex, f) = - \sum_{v \in values(f)} \frac{|Ex, v|}{|Ex|} \log_2 \left(\frac{|Ex, v|}{|Ex|} \right)$$

TABLE 2

List of Features After Processing 802.11 Frames

Feature	Description
IsWepValid	Indicate if WEP ICV check is successful.
DurationRange	Indicate if duration value is low (<5ms), average (between 5-20ms), or high (>20ms).
Casting Type	Indicate whether the receiving address is a unicast, multicast or a broadcast address.

TABLE 3

Top 10 Features

Rank	Feature	IGR
1	IsWepValid	1.02
2	DurationRange	1.01
3	More Frag	0.98
4	To DS	0.89
5	WEP	0.85
6	Casting Type	0.82
7	Type	0.73
8	SubType	0.65
9	Retry	0.46
10	From DS	0.41
11-38	Remaining Features	<.23

Using the data set of frames collected from our testing network, we could rank the features according to the score assigned by the IGR measure. The top 10 ranked features are shown in Table 3.

VII. The Best Subset Of Features

The k-means classifier is used to compute the detection rate for each set of features. Initially, the set of features S contains only the top ranked feature. After each

iteration, a new feature is added to the list S based on the rank which it is assigned by the IGR measure. Note that S_i is the i first features in the ranked list of features.

We can see that there is subset S_m of features that maximizes the accuracy of the K-means classifier. We can conclude that the first eight features (IsWepValid, DurationRange, More_Flag, To_DS, WEP, Casting_Type, Type, and SubType) are the best features to detect the intrusions we tested in our experiments. Increasing the number of features does not contribute to the improvement of the accuracy. In fact, irrelevant features distract the classifier and the accuracy drops to 17 percent with 19 features.

VIII. ARTIFICIAL NEURAL NETWORKS

Artificial Neural Networks (ANNs) are computational models which mimic the properties of biological neurons. A neuron, which is the base of an ANN, is described by a state, synapses, a combination function, and a transfer function. The state of the neuron, which is a Boolean or real value, is the output of the neuron. Each neuron is connected to other neurons via synapses. Synapses are associated with weights that are used by the combination function to achieve a precomputation, generally a weighted sum, of the inputs. The Activation function, also known as the transfer function, computes the output of the neuron from the output of the combination function.

An artificial neural network is composed of a set of neurons grouped in layers that are connected by synapses. There are three types of layers: input, hidden, and output layers. The input layer is composed of input neurons that receive their values from external devices such as data files or input signals. The hidden layer is an intermediary layer containing neurons with the same combination and transfer functions. Finally, the output layer provides the output of the computation to the external applications.

An interesting property of ANNs is their capacity to dynamically adjust the weights of the synapses to solve a specific problem. There are two phases in the operation of Artificial Neuron Networks. The first phase is the learning phase in which the network receives the input values with their corresponding outputs called the desired outputs. In this phase, weights of the synapses are dynamically adjusted according to a learning algorithm. The difference between the output of the neural network and the desired output gives a measure on the performance of the network. The most used learning algorithm is the retro backpropagation algorithm. In the second phase, called the generalization phase, the neural network is capable of extending the learned examples to new examples not seen before. The learning phase is resource demanding, explained by the iterative nature of the operation mode of the ANN. Once the network is trained, the processing of a new input is generally fast. In order to study the impact of the optimized set of features on both the learning phase and accuracy of the ANN networks, we have tested these attributes on three types of ANN architectures.

A. Perceptron

Perceptron is the simplest form of a neural network. It's used for classification of linearly separable problems. It consists of a single neuron with adjustable

weights of the synapses. Even though the intrusion detection problem is not linearly separable, we use the perceptron architecture as reference to measure the performance of the other two types of classifiers.

B. Multilayer Backpropagation Perceptrons

The multilayer backpropagation perceptrons architecture is an organization of neurons in n successive layers ($n > 1/3$). The synapses link the neurons of a layer to all neurons of the following layer. Note that we use one hidden layer composed of eight neurons.

TABLE 4
Distribution of Collected Data

	Learning	Validation	Test
Normal	6000	4000	5000
De-authentication	900	600	800
Duration	900	600	800
Fragmentation	900	600	800
Chopchop	900	600	800
Total	9600	6400	8200

C. Hybrid Multilayer Perceptrons

The Hybrid Multilayer Perceptrons architecture is the superposition of perceptron with multilayer backpropagation perceptrons networks. This type of network is capable of identifying linear and nonlinear correlation between the input and output vectors. We used this type of architecture with eight neurons in the hidden layer. Transfer function of all neurons is the sigmoid function. The initial weights of the synapses are randomly chosen between the interval $[-0.5, 0.5]$.

IX. Intrusion Detection Using Recurrent Neural Network

The proposed system is designed to perform the feature selection and intrusion detection process. The feature selection scheme is used to filter the irrelevant fields in network transactions. The feature selection selects suitable fields for the intrusion detection process. Filter, wrapper and hybrid feature selection schemes are used in the system. The intrusion detection process is performed using the artificial neural networks. The back propagation perception algorithm is used for the intrusion detection process. The recurrent neural network is used to for the intrusion detection process. The system also performs the intrusion detection process on the supervised feature selection model transactions. Detection latency, false positive and false negative measures are used for the performance evaluation.

The system is divided into four major modules. Feature reduction module is used to select optimized features. Artificial neural network based intrusion detection is performed using filtered data sets. Supervised features based IDS module is applied on user selected features. Recurrent neural network algorithm is used for intrusion detection process.

A. Feature Reduction Process

The feature selection is applied to reduce the fields that are used in the intrusion detection process. It will improve the accuracy of the system. The process time is also reduced in the learning and testing process. The

features selection scheme uses filter, wrapper and hybrid feature selection techniques. The filter model uses the information consistency ratio or distance measure. Wrapper model uses predictive accuracy. Information gain measure is used in the hybrid feature selection model.

B. Intrusion Detection Using ANN

Artificial neural networks are used with reduced features. Back propagation algorithm is used for the learning and testing process. Perceptron based neural network model uses 8 neurons for each layer. Multilayer based back propagation perceptron algorithm is used for intrusion detection. Learning process supports limited transactions only.

C. IDS Using Supervised Features

Supervised feature selection model uses features retrieved using experts' knowledge. Listed attributes are separated from user transactions. Artificial neural network is used for the intrusion detection process. Supervised features based IDS scheme is compared with automated feature selection process.

D. Intrusion Detection Using RNN

Selected features are used in recurrent neural network based intrusion detection model. RNN supports scalability in learning process. Learning errors are reduced in RNN. Real-Time Recurrent Learning Algorithm (RTRL) is used in RNN. The RNN technique is applied to verify the accuracy level of feature selection and learning process. The system improves the accuracy for the intrusion detection process. The detection latency is also reduced by the system.

X. CONCLUSION

In this paper, we have presented a novel approach to select the best features for detecting intrusions in 802.11-based networks. Our approach is based on a hybrid approach, which combines the filter and wrapper models for selecting relevant features. We were able to reduce the number of features from 38 to 8. We have also studied the impact of feature selection on the performance of different classifiers based on neural networks. Learning time of the classifiers is reduced to 33 percent with the reduced set of features, while the accuracy of detection is improved by 15 percent. The system reduces the feature selection complexity. Detection period is reduced by the system. The system integrates all layers in the IDS. Wireless LAN attacks are controlled by the system.

References

- [1] Boukerche, J.B.M. Sobral, and M.S.M.A. Notare, "An Agent Based and Biological Inspired Real-Time Intrusion Detection and Security Model for Computer Network Operations," *Computer Comm.*, vol. 30, no. 13, pp. 2649- 2660, Sept. 2007.
- [2] CERT, <http://www.cert.org/stats/>, 2010.
- [3] Y.-H. Liu, D.-X. Tian, and D. Wei, "A Wireless Intrusion Detection Method Based on Neural Network," *Proc. Second IASTED Int'l Conf. Advances in Computer Science and Technology*, Jan. 2006.
- [4] Y. Chen, and L. Guo, "Survey and Taxonomy of Feature Selection Algorithms in Intrusion Detection System," *Proc. Conf. Information Security and Cryptology (Inscrypt)*, 2006.

- [5] Boukerche, *Handbook of Algorithms for Wireless Networking and Mobile Computing*. CRC/Chapman and Hall, 2005.
- [6] <http://kdd.ics.uci.edu/databases/kddcup99/task.html>, 2010.
- [7] A.H. Sung and S. Mulkamala, "The Feature Selection and Intrusion Detection Problems," *Proc. Ninth Asian Computing Science Conf.*, 2004.
- [8] Boukerche, *Algorithms and Protocols for Wireless and Mobile Ad Hoc Networks*. Wiley, 2008.
- [9] G. Stein, and K.A. Hua, "Decision Tree Classifier for Network Intrusion Detection with GA-Based Feature Selection," *Proc. 43rd ACM Southeast Regional Conf.—Volume 2*, Mar. 2005.
- [10] Bittau and J. Lackey, "The Final Nail in WEP's Coffin," *Proc. IEEE Symp. Security and Privacy*, May 2006.
- [11] T.M. Khoshgoftaar and N. Seliya, "Intrusion Detection in Wireless Networks Using Clustering Techniques with Expert Analysis," *Proc. Fourth Int'l Conf. Machine Learning and Applications*, Dec. 2005.
- [12] <http://www.aircrack-ng.org/>, 2010.
- [13] Khalil El-Khatib "Impact of Feature Reduction on the Efficiency of Wireless Intrusion Detection Systems" *IEEE Transactions on Parallel and Distributed Systems*, Vol. 21, no. 8, August 2010.

Design and Analysis of Propeller SHAT By Using KEVLOR/EPOXY Composite

Thahar Ali Syed^{1*} Adnan Javed² Kasala Raju³ Naga Raju M⁴

ABSTRACT: In the design of automobiles, the industry is exploring composite materials in order to obtain reduction of weight without significant decrease in vehicle quality and reliability. This is due to the fact that the reduction of weight of a vehicle directly impacts its fuel consumption. Particularly in city driving, the reduction of weight is almost directly proportional to fuel consumption of the vehicle. Thus, in this project work the entire drive shaft assembly of a Toyota Qualis was chosen and analyzed by replacing it with composite and hybrid materials. The following materials were chosen

- Steel
- Boron/Epoxy Composite
- Kevlar/Epoxy Composite
- Aluminium – Glass/Epoxy Hybrid
- Carbon – Glass/Epoxy Hybrid

The analysis was carried out for three different ply orientations of the composites in order to suggest the most suitable ply orientation of the material that would give the maximum weight reduction while conforming to the stringent design parameters of passenger cars.

I. Introduction

In the process of designing a vehicle, one of the most important objectives is the conservation of energy and the most effective way to obtain this goal is the reduction of weight of the vehicle. There is almost a direct proportionality between the weight of the vehicle and its fuel consumption, particularly in city driving. The automotive industry is exploiting composite material technology for structural component construction in order to obtain reduction of weight, without decrease in vehicle quality and reliability. The advanced composite materials seem ideally suitable for long power drive shaft (propeller shaft) applications as their elastic properties can be tailored to increase the torque they carry as well as the rotational speed at which they operate. In this project, the conventional drive shaft material has been replaced with advanced composites and hybrid materials to carry out a comparative analysis, thus determining the most suitable replaceable material.

1.1 Specification of Problem:

- The first was Steel (SM45C) which was used for reference purpose
- Two Composites Boron/Epoxy, Kevlar/Epoxy And Hybrid shafts i.e., a combination of Aluminium and

Almost all automobiles (which correspond to design with rear wheel drive and front engine installation) use a drive shaft for the transmission of motion from the engine to the differential. An automotive propeller shaft, or drive shaft, transmits power from the engine to differential gears of a rear wheel-driving vehicle. The static torque transmission capability of the propeller shaft for passenger cars, and small truck and vans should be larger than 3500 Nm and the fundamental bending natural frequency should be higher than 8000rpm to avoid whirling vibration. The whirling of the propeller shaft, which is a resonance vibration, occurs when the rotational speed is equal to the fundamental natural bending frequency, which is inversely proportional to the square root of specific stiffness (E/ρ). When conventional materials such as Steel or Aluminium are used, the weight of the drive shaft assembly is considerably high, which has a certain role in increasing the overall weight of the vehicle. Also, due to the increased weight of the shaft there are more chances of whirling of the shaft. To avoid this in conventional drive shafts, which have a length exceeding 1.2m, the shafts are made in two pieces. However, the two piece steel propeller shaft has a complex and heavy configuration because three universal joints and a center support bearing in addition to a spline are required, which produces noise and vibrations that are transmitted to vehicle through the center support bearing.

1.2 Aim and Scope of the Work

The project aims to reduce the weight of the drive shaft assembly by using advanced composite materials. For this project work, the drive shaft of a Toyota Qualis was chosen. The modeling of the drive shaft assembly was done using CATIA V5R16. A shaft has to be designed to meet the stringent design requirements for automobiles. A comparative study of five different materials was conducted to choose the best-suited material. Steel (SM45C) was chosen for reference and the rest of the four composites were analyzed at three different ply orientations. The material properties of the composites were obtained based on the Classical Lamination Theory with the help of a code written in C language. The analysis was carried out using ANSYS 11.0 WorkBench for the following materials at three different ply orientations $[0/30]_{8S}$, $[\pm 45]_{8S}$ and $[0/90]_{8S}$

Glass/Epoxy Composite, Glass/Epoxy and Carbon/Epoxy.

1.3 Drive Shaft

The term Drive shaft is used to refer to a shaft, which is used for the transfer of motion from one point to another. Whereas the shafts, which propel (push the object ahead) are referred to as the propeller shafts. Propellers are usually associated with ships and planes as they are propelled in water or air using a propeller fan. However the drive shaft of the automobile is also referred to as the propeller shaft because apart from transmitting the rotary

motion from the front end to the rear end of the vehicle, these shafts also propel the vehicle forward. The shaft is the primary connection between the front and the rear end (engine and differential) which performs both the jobs of transmitting the motion and propelling the front end. Thus, the terms Drive Shaft and Propeller Shafts are used interchangeably.

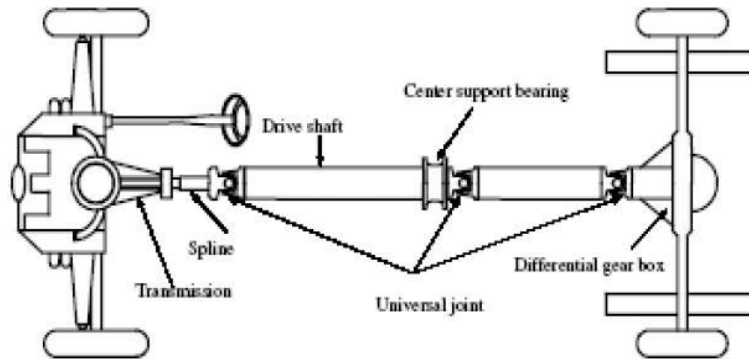


fig Schematic arrangement of Underbody of an Automobile

II. THEORETICAL AND SIMULATED RESULTS CORRELATION

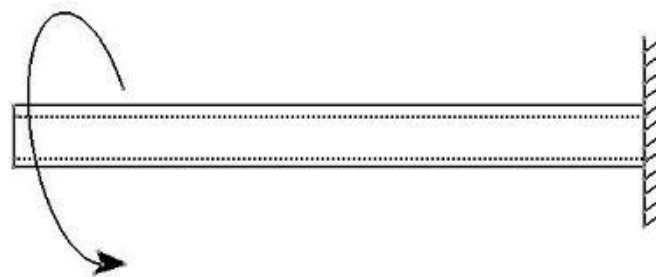
A comparison between the results obtained based on theoretical calculations and the results obtained from the ANSYS 11.0 WorkBench has been carried out. For this purpose, the drive shaft of the automobile has been idealized as a hollow cylindrical shaft. It is then subjected to the same load theoretically and in the finite element solver. The comparison of results shows a very close range conformance, which has been plotted.

2.1 Theoretical Calculations for Hollow Shaft

The Drive shaft, for simplicity has been first idealized as a hollow cylindrical shaft which is fixed at one end and on which a torque of 3500 Nm is applied as represented below.

For the hollow shaft, Let
 $R_o = 0.01\text{ m}$; $R_i = 0.02\text{ m}$; $l = 0.5\text{ m}$; $E = 207e9\text{ pa}$
 and Torque=3500 Nm
 Where R_o = Outer Radius R_i = Inner Radius l = Length of the shaft

E = Young’s Modulus of Steel (SM45C) T = Applied Torque



Hollow Shaft being subject to a Torque of 3500 Nm

$$Deflection = Y_{Max} = \frac{ML^2}{2EI} = \frac{3500 \times (0.5^2)}{2 \times (207e^9) \times (1.178e^{-7})} = 0.0179m$$

Then:

Maximum Shear Stress:

$$\tau_{Max} = \frac{T \times R_o}{J} = \frac{3500 \times 0.02}{\left[\frac{\pi}{2}\right] \times [R_o^4 - R_i^4]}$$

$$= \frac{70}{2.35626 \times 10^{-7}} = 2.9708 \times 10^8 Pa$$

Maximum Von – Mosses Stress

$$= [T \times (\frac{d_o}{2})]$$

$$= \frac{I}{\frac{\pi}{64}} \times [(0.04)^4 - (0.02)^4]$$

$$= 594178454.2$$

$$= 5.9417e7Pa$$

Simulated Results for Hollow Shaft

The derived theoretical results are now going to be compared to the simulated results. For which, a hollow shaft with the same specifications was created in CATIA V5R17. This CATIA model was then imported into ANSYS 11.0 Workbench, wherein the model was analyzed. The same torsional load was applied by fixing one end of the shaft and applying torque on the other end. The results were found to be very close to the theoretically calculated values. The results are as follows.

The hollow shaft is made-up using the same dimensions, which are
 $R_o = 0.01\text{ m}$; $R_i = 0.02\text{ m}$; $l = 0.5\text{ m}$; $E = 207e9\text{ pa}$ and
 Torque=3500 Nm

Ansys Results

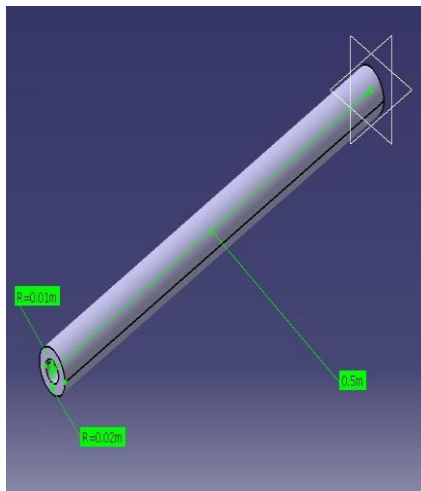


Fig A: Catia Model of Hollow shaft

Material properties

III. ANALYSIS

Since the domain for analysis is a complex assembly of a number of parts, ANSYS 11.0 Workbench was chosen for performing the analysis. The proper connection between each part of the assembly and the subsequent connectivity of mesh is the key criteria for getting proper load transfers throughout the assembly. The Workbench module of ANSYS 11.0 does not require the explicit specification of element types by the user, depending upon the assembly, the element types are chosen by the solver to get the best possible results. But for the dominating major portion of the assembly which is relatively easier to manufacture, the composite material were applied. The CATIA assembly, imported into ANSYS is subjected to

- I. Torsional Analysis
- II. Modal Analysis &
- III. Harmonic Analysis

This is to be carried out on a total of five materials out of which four are composites at ply orientations of $[0/30]_{8s}$, $[+/- 45]_{8s}$ and $[0/90]_{8s}$

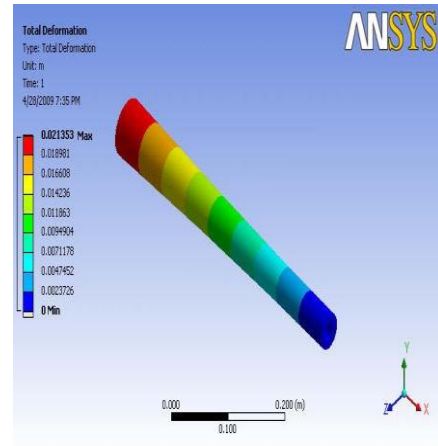


Fig B: Total deformation

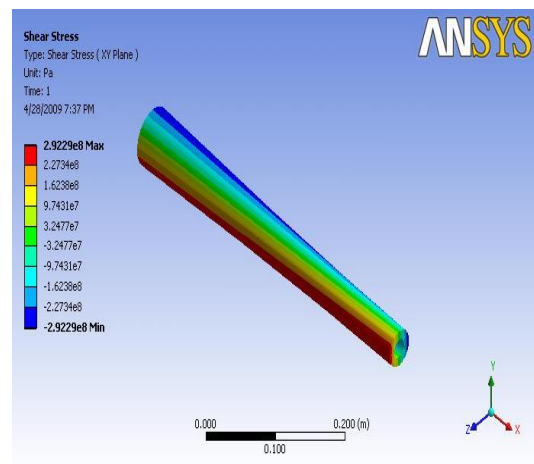


Fig C: Shear stress

Drive Shaft Assembly in ANSYS Workbench

Element Types

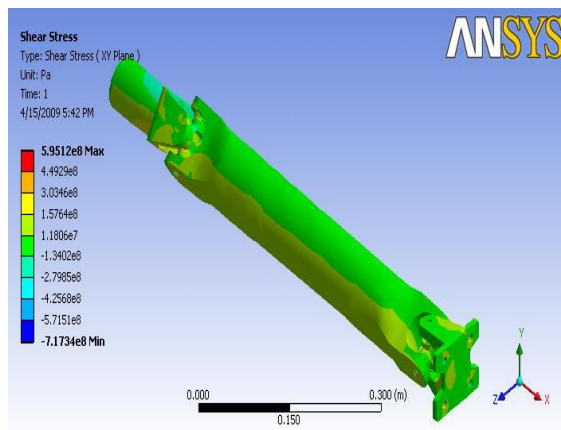
The element types allotted based on the geometry of the assembly by the ANSYS solver are as follows

Generic Element Type Name	ANSYS Name	Description
10 Node Quadratic Tetrahedron	Solid187	10 Node Tetrahedral Structural Solid
20 Node Quadratic Hexahedron	Solid186	20 Node Structural Solid
Quadratic Quadrilateral Contact	Conta174	3D 8 Node Surface to Surface Contact
Quadratic Quadrilateral Target	Targe170	3D Target Segment
Quadratic Triangular Contact	Conta174	3D 8 Node Surface to Surface Contact
Quadratic Triangular Target	Targe170	3D Target Segment

Deformation

Shear Stress

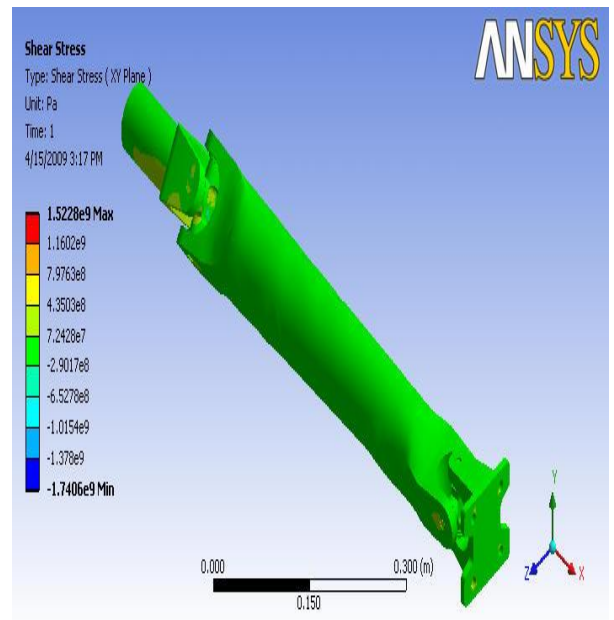
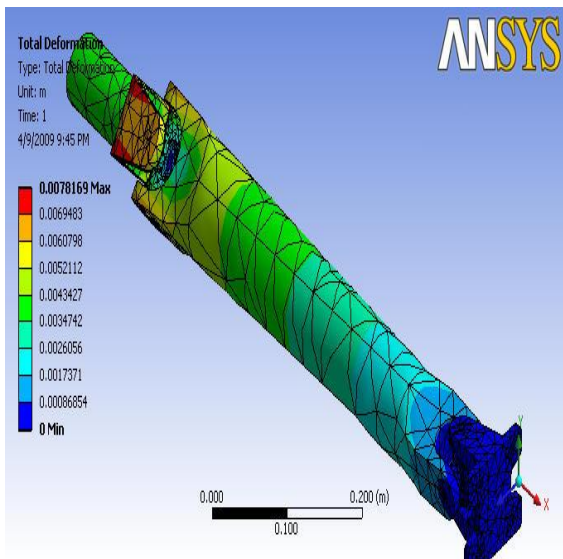
Boron/Epoxy



Ply Orientation : $[0/30]_8s$

Deformation

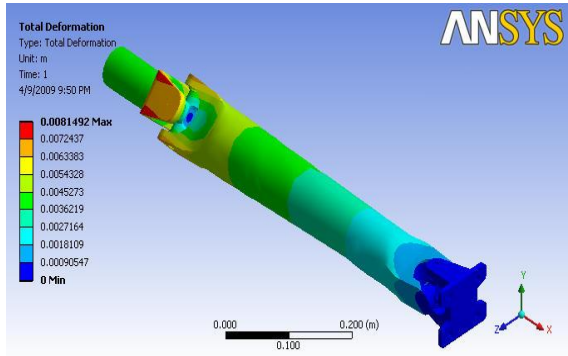
Shear Stress



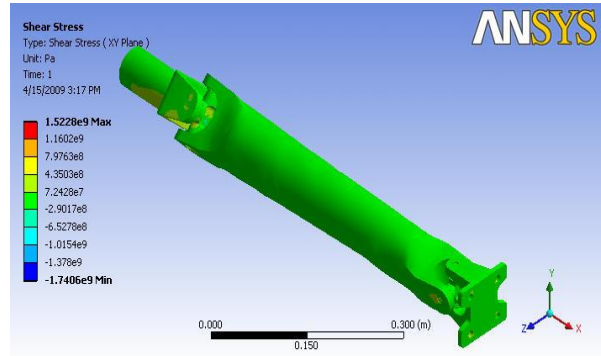
Kevlar/Epoxy
 Ply Orientation : $[0/30]_8s$

Hybrid Drive Shaft (Aluminum & Glass/Epoxy) Ply Orientation: $[0/30]_8s$

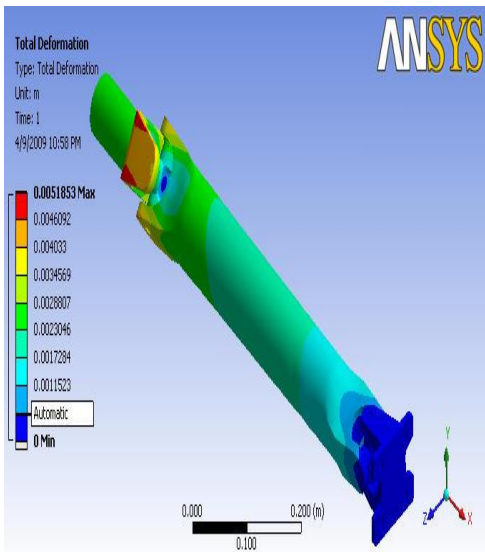
Deformation



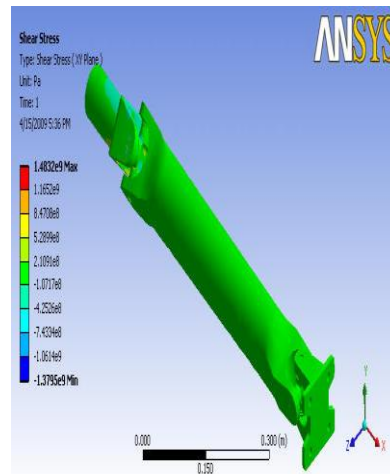
Shear Stress



MODAL ANALYSIS
 1 Steel (SM45C)

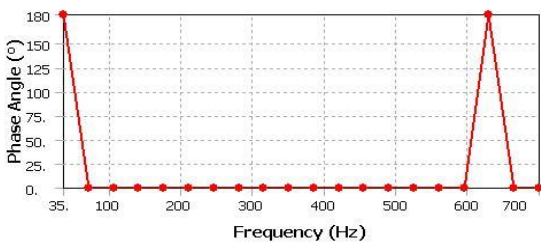
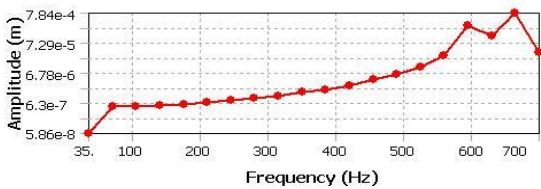


Deformation

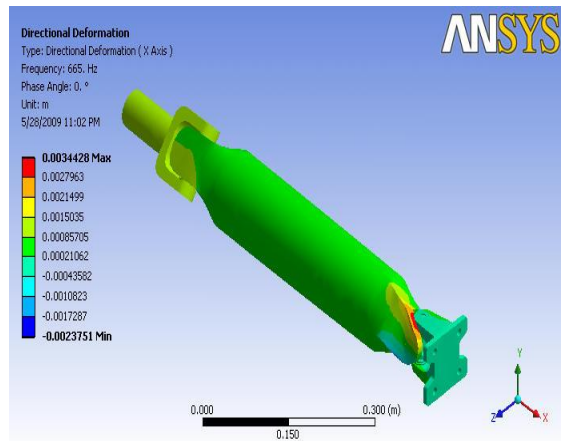


Shear Stress

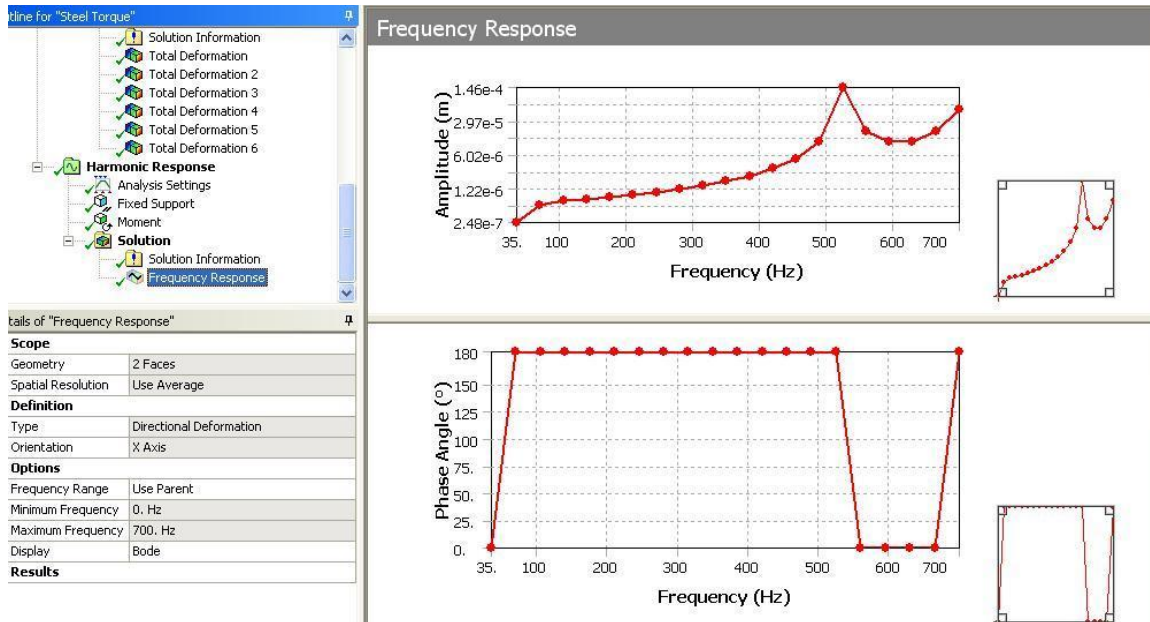
Frequency Response
 2 Boron/Epoxy
 Ply Orientation : $[0/30]_8s$



Frequency Response



Deformation



RESULTS & ABERVATIONS

It can be seen that Kevlar/Epoxy Composite has shown the maximum reduction in weight followed by Carbon Hybrid, Boron/Epoxy Composite and finally Aluminium Hybrid.

The percentage weight savings of each material is given as follows

- Kevlar/Epoxy Composite – 65 %
- Carbon Hybrid – 57.5 %
- Boron/Epoxy Composite – 55.9 %
- Aluminium Hybrid – 54 %

Deformation induced in the 5 materials due to torque

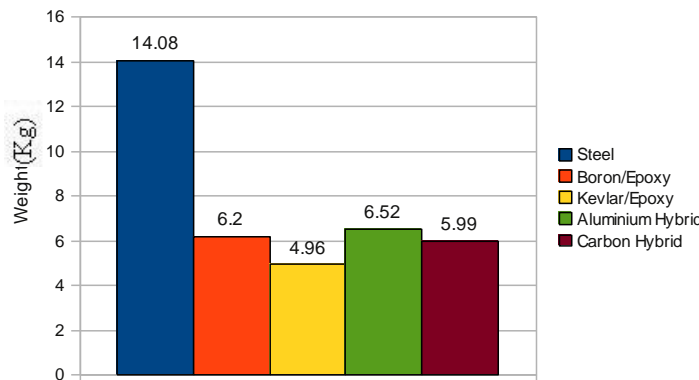
The following graph illustrates the total deformation caused in the assembly due to the application of a torque of 3500 Nm (the rated load for passenger cars).

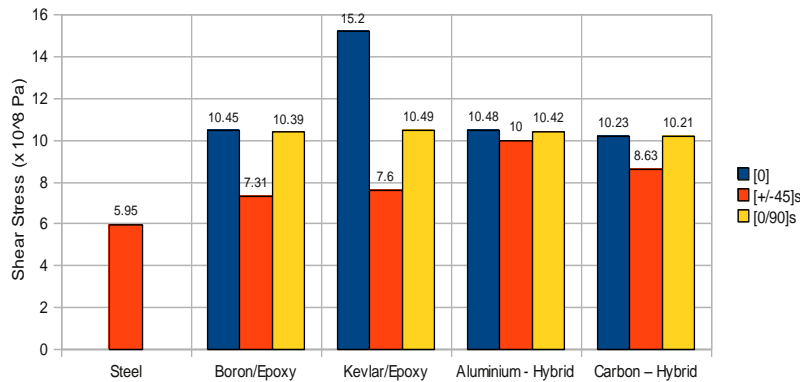
Two Conclusions can be drawn from the following graph

- a) It was found that though Steel had the minimum deflection, however it is followed very closely by Boron/Epoxy Composite.
- b) The Variation in ply orientations helps us to know that the ply orientation $[+/-45]_8$ gives the least amount of deflection when compared to the other two orientations.

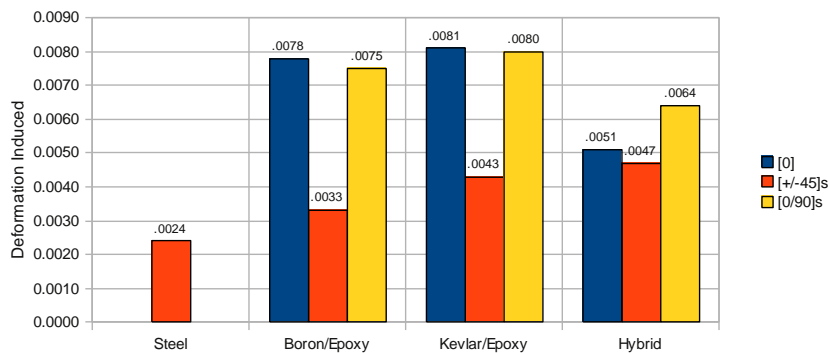
Thus it can be inferred from these observations that throughout the various parameters, analyzed for all the materials, Boron/Epoxy and Kevlar/Epoxy Composites have shown a remarkable similarity in their results. However Kevlar/Epoxy has been found to be 1.24 kg lighter than Boron/Epoxy.

Reduction in Weight achieved using Composite materials:





Shear Stress



Shear Stress induced in the assembly due to the application of 3500 Nm Torque:

IV. CONCLUSION

The presented work was aimed at reducing the fuel consumption of the automobiles in particular or any machine, which employs drive shafts, in general. This was achieved by reducing the weight of the drive shaft with the use of composite materials. The Drive shaft of a Toyota Qualis was chosen for determining the dimensions, which were then used for creating a model in CATIA V5R17. The material properties of composites were determined based on Classical Lamination Theory using a C Code. Being a complex assembly of a number of parts, it had to be analyzed in ANSYS 11.0 Workbench. A total of five materials were chosen for the comparative analysis, including steel, which was used for reference. The usage of composite materials has resulted in considerable amount of weight saving in the range of 65% to 54% when compared to conventional steel shaft. Taking into consideration the weight saving, deformation, shear stress induced and resonant frequencies it is evident that Kevlar/Epoxy composite has the most encouraging properties to act as the replacement for steel out of the considered five materials. And the best suitable ply orientation is [+/- 45°].

REFERENCES

- [1]. Axiomatic design and fabrication of composite structures: Applications in Robots, Machine Tools, and Automobiles - By Dai Gil Lee, Nam Pyo Suh – Oxford University Press
- [2]. Mechanics of laminated composite plates and shells: theory and analysis - by Junuthula Narasimha Reddy “Design Data” – Databook of Engineers. – P.S.G. College.
- [3]. Optimal Sizing and Stacking Sequence of Composite Drive Shafts Thimmegowda rangaswamy, Sabapathy Vijayarangan

Authors

1. Thahar Ali Syed Asst.Prof
Gurunanak Institutions of Technical Campus
Ibrahim Patnam, Hyderabad.India
2. Adnan Javed, Design Engineer
Hyundai Motors India Limited
3. Kasala Raju Asst.Prof
Gurunanak Institutions of Technical Campus
4. Naga Raju Assoc.Prof
Gurunanak Institutions of Technical Campus

Parameter Dependent Performance Optimization In Live Migration Of Virtual Machine

K. Phaneendra¹, Venu Madhav Sunkara², R. Vijaya³, G. Rajendra⁴

*(Department of MCA, LBRCE College/ JNTU Kakinada, India)

** (Department of Computer Science, KL University, Vaddeswaram)

*** (Department of MCA, LBRCE College/ JNTU Kakinada, India)

**** (Department of MCA, LBRCE College/ JNTU Kakinada, India)

ABSTRACT: Virtualization technology is being used intensively in data centers, cluster systems, enterprises and organizational networks, Hence the capability of Virtual Machine (VM) Migration importance has been increased for maintaining high performance, improved manageability and fault tolerance. Live Migration allows virtual machine monitor to move the running virtual machine from one physical server to another with zero downtime, continuous service availability and complete transaction integrity. In this paper we, present a performance evaluation of parameters that affect live migration and varying in the performance depending on workload.

Keywords: Virtual Machine (VM), Migration Time (MT), Down Time (DT), Dirty Page, Virtualization.

I. INTRODUCTION

System virtualization is the ability to abstract and pool resources on a physical platform. This abstraction decouples software from hardware and enables multiple operating system images to run concurrently on a single physical platform without interfering with each other. As a technique, system virtualization has existed for decades on mainframes. In the past, industry standard x86-based machines, with their limited computing resources. Virtualization can increase utilization of computing resources by consolidating the workloads running on many physical systems into virtual machines running on a single physical system. Virtual machines can be provisioned on-demand, replicated and migrated. Virtual machine (VM) migration, which is the ability to move a VM from one physical server to another under virtual machine monitor (VMM) control, is a capability being increasingly utilized in today's enterprise environments.

Implemented by several existing virtualization products, live migration can aid in aspects such as high-availability services, transparent mobility, consolidated management, and workload balancing [1]. While virtualization and live migration enable important new functionality, the combination introduces novel security challenges. A virtual machine monitor that incorporates a vulnerable implementation of live migration functionality may expose both the guest and host operating system to attack and result in a compromise of integrity. Given the large and increasing market for virtualization technology, a comprehensive understanding of virtual machine migration security is essential. However, the security of virtual machine migration has yet to be analyzed.

After a live migration, guest software continues to maintain an identical view of the pre and post migration hardware. In this paper we discuss Processors provide support for a VMM to hide differences in software-visible processor features during Live.

1.1 SHORT BACKGROUND ON VM TECHNOLOGY

Initially very popular in the 1960's, for instance in the context of shared mainframe computers, this technology was subsequently abandoned in favour of multiprogrammed efficient commodity operating systems, running on increasingly cheaper and more widely available hardware. However, the virtual machine technology, initially based on the principle of exporting (possibly multiple) virtualized software versions of the machine hardware to upper layers (originally the operating system) came back to fashion in the past years. Reasons for this come-back spanned the need for easier management of large scale distributed systems or MPP machines [2], or the need for support for mobility (the easy checkpointing capability mentioned above) and increased security (as many commodity OSs had become quite unmanageable and/or insecure and proved to under-use the same increasingly cheaper hardware resources that caused the "retirement" of VMs 20 years ago). However, while they have indeed come back, VMs are less interesting now for resource multiplexing but more as a way to "circumvent" existing "popular" Operating Systems that have become unmanageable and provide little opportunities for activities like checkpointing or sandboxing. Issues and challenges of VM implementations include minimizing virtualization overhead and exporting a virtualized interface identical or as similar as possible to the virtualized machine to ensure compatibility.

Various design choices exist, such as providing a "classic" VM architecture – such as Xen or VMWare ESX Server [3] (laying underneath the Operating system and thus maximizing performance) or a "hosted" architecture, such as VMWare Workstation (laying "on top" of a host operating system, as an application and improving). Another important design choice is that of slightly modifying the virtualized interface to be exported to replace portions of the instructions set which are not easily virtualizable by different and more efficiently implementable equivalents. This approach is called paravirtualization and it is applied in VM implementations such as Xen or Disco [4]. VMs can provide important benefits that can be useful in many contexts, including migration. Firstly, they have the serious advantage of abstracting away the details of underlying hardware and

exporting a uniform view of the virtualized machine, therefore providing an elegant solution to the resource heterogeneity problem. Additionally, they provide a complete encapsulation of the machine software state, therefore the VM can be easily and very conveniently checkpointed, suspended and restarted at will. Consequently, VMs can be dynamically mapped to physical machines or migrated much easier than processes.

Therefore, the implementation complexity of migration implementation, which we saw that was a limiting factor in the case of process migration, is greatly reduced. Besides migration-empowered applications like dynamic load balancing, fault tolerance or Internet Suspend-Resume [5] type applications, VM can be used for things like convenient distribution of software packages (for instance Oracle delivers packages of readily installed and configured software under the form of VMs) or for damage containment and “forensics” against worm or hacker attacks.

1.2 VIRTUAL MACHINE MIGRATION

There are many ways to migrate a VM. In *static migration*, the VM is shutdown using OS-supported methods; its static VM image is moved to another VMM and restarted. In *cold migration*, the VM is suspended using OS supported or VMM-supported methods. The suspended VM image is moved to a VMM on a different machine and resumed. In *live migration*, the VMM moves a running VM instance nearly instantaneously from one server to another. Live Migration allows for dynamic load balancing of virtualized resource pools, hardware maintenance without downtime and dynamic failover support. As long as the hardware in the pre and post migration environment is identical, guest software should behave in exactly the same way before and after the migration. It is when guest software runs in a different hardware environment after a migration that certain challenges can arise[6]. Note that even though a VMM presents a virtual platform to guest software, there could be certain interfaces, depending on VMM design, which guest software can directly use to determine underlying hardware’s capabilities.

After the reboot/restart following a static migration, guest software should go through its platform discovery phase and be able to adjust to any differences in underlying (virtual) hardware. Following a cold migration, guest software may continue to maintain an identical view of the pre and post migration hardware. When suspended using OS-supported methods, some operating systems will re-scan the hardware upon resume. Depending on their policies and the hardware differences between current and previous hardware, the OSes may refuse to resume and require a reboot. After a live migration, guest software continues to maintain an identical view of the pre and post migration hardware.

1.3 Issues with VM migration

However, things get a little more complicated. More precisely, to perform a correct migration, besides the checkpointed state of the VM, the memory image of that VM also has to be migrated, for the state to be correctly preserved. All this should be done while programs in the VM are still running; therefore memory pages are still getting dirtied. Therefore, we see that increased simplicity comes at a

certain price, since the VM’s memory image and state is undoubtedly much larger than the process’ checkpointed state in the case of process migration.

Additionally, as with all migrations, resources used by processes running within the migrated VM should still be available after the migration attached. Since these resources might be hard to migrate (because of large sizes or consistency constraints for instance), this brings back the problem of residual dependencies. For instance, the problem of migrating the file system present on the virtual disk of a Virtual Machine [7]. In the context of Virtual Machine migration, “residual dependencies” are especially important, considering that the size of a virtual machine can be much larger than that of a process. While migrating the entire VM, as we have seen, has the advantage that support for check pointing is readily provided, unlike in the case of a regular process, the VM’s address space, and especially it’s virtual disk are of considerable size, therefore leaving residual dependencies may be unavoidable to ensure reasonable migration times (at least with current typical network resources)[8]. As with all migration systems, transparency remains an issue also for VM migration.

II. LIVE MIGRATION

Virtual machine live migration is a virtualization process that moves a virtual machine (VM) from one physical host server to another. It moves the memory and state of a VM without shutting down the application, so users will generally not detect any significant interruption in application availability. The process captures the complete memory space occupied by the VM along with the exact state of all the processor registers currently operating on the VM then sends that content across a TCP/IP link to memory space on another server. Processor registers are then loaded, and the newly moved VM can pick up its operation without missing a step.

Most VM live migrations occur between similar hypervisors, so the migrated VM retains its name and other unique identifiers. Even though the VM is on a different server, it’s the exact same machine as far as the users are concerned. Live migration is a key benefit of virtualization, allowing workloads to move in real time as server or data center conditions change [9]. Consider the impact on business continuity: A virtual server scheduled for maintenance can migrate its workloads to a spare server or to other servers that have extra computing capacity. Once the maintenance is complete and the server returns to service, these workloads can all migrate back to the original server without disruption.

Live migration helps server consolidation by allowing IT administrators to balance workloads across data center servers, ensuring that each server is used efficiently without being overtaxed. Live migration helps with disaster recovery too because VMs can just as easily be moved from one site to another, relying on spare servers at a remote site to receive and operate the migrated VMs.

All of the major virtualization software platforms include VM live migration tools. These include VMware VMotion (part of vSphere), Microsoft Live Migration (part of Hyper-V R2) and Citrix Systems XenServer live migration. Migration tools typically allow administrators to prioritize

the movement of each VM so that failover and failback processes occur in a predictable and repeatable manner. Mission-critical VMs usually take priority and are often moved to spare servers with ample computing resources. Secondary VMs can be addressed next, although the migration software may be left to move noncritical VMs automatically based on the computing resources on each available server. Migration audits allow administrators to locate VMs and track their movements to refine and optimize ongoing migration behaviours. Live migration works between almost all virtual host servers, but it's important to test migration behaviours between servers with various processor manufacturers. Processors from Intel and AMD both include extensions that provide hardware assistance for virtualization tasks, including migration. However, Intel VT and AMD-V processors use different architectures to facilitate migration, and moving VMs between Intel and AMD-based servers may result in unexpectedly poor migration performance.

2.1 Live Migration options for storage configurations

In addition to network settings, there are some storage connection types that must also be carefully configured on Hyper-V hosts for Live Migration to run properly. A Virtual Hard Disk (VHD) attachment, for instance, is arguably the simplest for Live Migration purposes. When VHDs are attached to a highly available VM, they must also exist on shared storage. This setup ensures that every cluster node can automatically access the disk when a VM migrates. For pass-through disks, another storage configuration, additional care is necessary. These disks have a direct relationship with both VMs and their hosts, which must be considered before performing Live Migration. A pass-through disk must be exposed to the host and then passed through to the VM. Pass-through disks are supported in a clustered configuration; but the cluster must be informed of any new pass-through disks by refreshing the VM configuration after it has been attached. Pass-through disks must be managed like other cluster resources. The storage area network connections to the cluster must be exposed to every potential cluster host.

III. Design

At a high level we can consider a virtual machine to encapsulate access to a set of physical resources. Providing live migration of these VMs in a clustered server environment leads us to focus on the physical resources used in such environments: specifically on memory, network and disk. This section summarizes the design decisions that we have made in our approach to live VM migration. We start by describing how memory and then device access is moved across a set of physical hosts and then go on to a high-level description of how a migration progresses.

3.1 Migrating Memory

Moving the contents of a VM's memory from one physical host to another can be approached in any number of ways. However, when a VM is running a live service it is important that this transfer occurs in a manner that balances the requirements of minimizing both *downtime* and *total*

migration time. The former is the period during which the service is unavailable due to there being no currently executing instance of the VM; this period will be directly visible to clients of the VM as service interruption. The latter is the duration between when migration is initiated and when the original VM may be finally discarded and, hence, the source host may potentially be taken down for maintenance, upgrade or repair. It is easiest to consider the trade-offs between these requirements by generalizing memory transfer into three phases:

Push phase

The source VM continues running while certain pages are pushed across the network to the new destination. To ensure consistency, pages modified during this process must be re-sent.

Stop-and-copy phase

The source VM is stopped, pages are copied across to the destination VM, then the new VM is started.

Pull phase

The new VM executes and, if it accesses a page that has not yet been copied, this page is faulted in ("pulled") across the network from the source VM.

Although one can imagine a scheme incorporating all three phases, most practical solutions select one or two of the three. For example, *pure stop-and-copy* [10] involves halting the original VM, copying all pages to the destination, and then starting the new VM. This has advantages in terms of simplicity but means that both downtime and total migration time are proportional to the amount of physical memory allocated to the VM. This can lead to an unacceptable outage if the VM is running a live service.

Another option is *pure demand-migration* [11] in which a short stop-and-copy phase transfers essential kernel data structures to the destination. The destination VM is then started, and other pages are transferred across the network on first use. This results in a much shorter downtime, but produces a much longer total migration time; and in practice, performance after migration is likely to be unacceptably degraded until a considerable set of pages have been faulted across. Until this time the VM will fault on a high proportion of its memory accesses, each of which initiates a synchronous transfer across the network.

The approach taken in this paper, *pre-copy* [12] migration, balances these concerns by combining a bounded iterative push phase with a typically very short stop-and-copy phase. By 'iterative' we mean that pre-copying occurs in *rounds*, in which the pages to be transferred during round *n* are those that are modified during round *n-1* (all pages are transferred in the first round). Every VM will have some (hopefully small) set of pages that it updates very frequently and which are therefore poor candidates for pre-copy migration. Hence we bound the number of rounds of pre-copying, based on our analysis of the *writable working set* (WWS) behaviour of typical server workloads. Finally, a crucial additional concern for live migration is the impact on active services. For instance, iteratively scanning and sending a VM's memory image between two hosts in a cluster could easily consume the entire bandwidth available between them

and hence starve the active services of resources. This *service degradation* will occur to some extent during any live migration scheme. We address this issue by carefully controlling the network and CPU resources used by the migration process; thereby ensuring that it does not interfere excessively with active traffic or processing.

3.2 Resources for Migration

A key challenge in managing the migration of OS instances is what to do about resources that are associated with the physical machine that they are migrating away from. While memory can be copied directly to the new host, connections to local devices such as disks and network interfaces demand additional consideration. The two key problems that we have encountered in this space concern what to do with network resources and local storage.

For network resources, we want a migrated OS to maintain all open network connections without relying on forwarding mechanisms on the original host (which may be shut down following migration), or on support from mobility or redirection mechanisms that are not already present (as in [13]). A migrating VM will include all protocol state (e.g. TCP PCBs), and will carry its IP address with it. To address these requirements we observed that in a cluster environment, the network interfaces of the source and destination machines typically exist on a single switched LAN. Our solution for managing migration with respect to network in this environment is to generate an unsolicited ARP reply from the migrated host, advertising that the IP has moved to a new location. This will reconfigure peers to send packets to the new physical address, and while a very small number of in-flight packets may be lost, the migrated domain will be able to continue using open connections with almost no observable interference.

Some routers are configured not to accept broadcast ARP replies (in order to prevent IP spoofing), so an unsolicited ARP may not work in all scenarios. If the operating system is aware of the migration, it can opt to send directed replies only to interfaces listed in its own ARP cache, to remove the need for a broadcast. Alternatively, on a switched network, the migrating OS can keep its original Ethernet MAC address, relying on the network switch to detect its move to a new port. In the cluster, the migration of storage may be similarly addressed: Most modern data centers consolidate their storage requirements using a network-attached storage (NAS) device, in preference to using local disks in individual servers. NAS has many advantages in this environment, including simple centralised administration, widespread vendor support, and reliance on fewer spindles leading to a reduced failure rate. A further advantage for migration is that it obviates the need to migrate disk storage, as the NAS is uniformly accessible from all host machines in the cluster

3.3 Pre-copy Migration

Pre-copy migration tries to tackle problems associated with earlier designs by combining a bounded iterative push step with a final and typically very short stop-and-copy[14] phase. The core idea of this design is that of iterative convergence. The design involves iterating through multiple rounds of copying in which the VM memory pages

that have been modified since the previous copy are resent to the destination on the assumption that at some point the number of modified pages will be small enough to halt the VM temporarily, copy the (small number of) remaining pages across, and restart it on the destination host. Such a design minimises both total migration time and downtime.

3.3.1 Stages in Pre-copy Migration

Pre-copy migration involves 6 stages, namely:

- 1) **Initialisation:** a target is pre-selected for future migration.
- 2) **Reservation:** resources at the destination host are reserved.
- 3) **Iterative pre-copy:** pages modified during the previous iteration are transferred to the destination. The entire RAM is sent in the first iteration.
- 4) **Stop-and-copy:** the VM is halted for a final transfer round.
- 5) **Commitment:** the destination host indicates that it has received successfully a consistent copy of the VM.
- 6) **Activation:** resources are re-attached to the VM on the destination host.

Unless there are stop conditions, the iterative pre-copy stage may continue indefinitely. Thus, the definition of stop conditions is critical in terminating this stage in a timely manner. These conditions are usually highly dependent on the design of both the hypervisor and the live migration subsystem but are generally defined to minimise link usage and the amount of data copied between physical hosts while minimising VM downtime. However, the existence of these stop conditions has a significant effect on migration performance and may cause non-linear trends in the total migration time and downtime experienced by VMs.

3.3.2. Defining Migration Performance

Migration performance may be evaluated by measuring total migration time and total downtime. The former is the period when state on both machines is synchronised, which may affect reliability while the latter is the duration in which the VM is suspended thus seen by clients as service outage. Using the pre-copy migration model, total migration time may be defined as the sum of the time spent on all 6 migration stages (Equation 1) from initialisation at the source host through to activation at the destination. Total downtime, however, is the time required for the final 3 stages to complete (Equation 2). While it is expected that the iterative pre-copy stage will dominate total migration time, our measurements found that for certain classes of applications specifically those that do not have a high memory page modification rate the initialisation, reservation, commitment and activation stages may add a significant overhead to total migration time and downtime. We classify the initialisation and reservation stages together as pre-migration overhead while the commitment and activation stages compose post-migration overhead.

$$\text{TotalMigrationTime} = \underbrace{\text{Initialisation} + \text{Reservation}}_{\text{Pre-migrationOverhead}}$$

$$+ \sum \text{pre-copy} + \text{stop-and-copy}$$

$$\text{Post-migrationOverhead} + \text{Commitment} + \text{Activation} \xrightarrow{\text{Equation (1)}}$$

$$\text{TotalDowntime} = \text{Stop-and-copy}$$

$$\text{Post-migrationOverhead} + \text{Commitment} + \text{Activation} \xrightarrow{\text{Equation (2)}}$$

3.3.3. Migration Bounds

Given the stop conditions, it is possible to work out the upper and lower migration performance bounds for a specific migration algorithm. We will use a real-world case to characterise these boundaries. While there exist a range of live migration platforms, for the remainder of this paper we will base our analysis on the Xen migration platform. Xen is already being used as the basis for large scale cloud deployments [15] and thus this work would immediately benefit these deployments. Moreover, Xen is open-source allowing us to quickly and efficiently determine the migration sub-system design and implementation. Note however that our measurement techniques, methodology, and prediction models design basis are applicable to any virtualisation platform that employs the pre-copy migration mechanism. The stop conditions that are used in Xen migration algorithm are defined as follows:

- 1) Less than 50 pages were dirtied during the last pre-copy iteration.
- 2) 29 pre-copy iterations have been carried out.
- 3) More than 3 times the total amount of RAM allocated to the VM has been copied to the destination host. The first condition guarantees a short downtime as few pages are to be transferred. On the other hand, the other 2 conditions just force migration into the stop-and-copy stage which might still have many modified pages to be copied across resulting in large downtime.

1) Bounding Total Migration Time (Equation 3): Consider the case of an idle VM running no applications. In this case the iterative pre-copy stage will terminate after the first iteration as there is no memory difference. Consequently, the migration sub-system needs only to send the entire RAM in the first round. The total migration lower bound is thus the time required to send the entire RAM coupled with pre- and post-migration overheads. On the other hand, consider the case where the entire memory pages are being modified as fast as link speed. In this scenario, the iterative pre-copy stage will be forced to terminate after copying more than 3 times the total amount of RAM allocated to the VM. Migration then re-sends the entire modified RAM during the stop-and-copy stage. The total migration upper bound is thus defined as the time required sending 5 times the VM size less 1 page plus pre- and postmigration overheads.

$$\text{Overheads} + (\text{VMSize} / \text{LinkSpeed}) \leq \text{TotalMigrationTime} \leq (\text{Overheads} + ((5 * \text{VMSize} - 1) * \text{page}) / \text{LinkSpeed})$$

$$\xrightarrow{\text{Equation (3)}}$$

2) Bounding Total Downtime (Equation 4): Similarly, the total downtime lower bound is defined as the time required for the post-migration overhead, assuming that the final stop and copy stage does not transfer any pages. This occurs either when the VM is idle or the link speed is fast enough to copy all dirtied pages in the pre-copy stage. On the other hand, the total downtime upper bound is defined as the time required to copy the entire RAM in the stop-and-copy stage coupled with the post-migration overhead.

$$\text{Post-migrationOverhead} \leq \text{TotalDowntime} \leq (\text{Post-migrationOverhead} + (\text{VMSize} / \text{LinkSpeed}))$$

$$\xrightarrow{\text{Equation (4)}}$$

3.3.4 Difference in Bounds

Modelling bounds is useful as it enables us to reason about migration times provided that we know the link speed and VM memory size. These bounds are the limits in which the total migration time and total downtime are guaranteed to lie. Given a 1,024 MB VM and 1 Gbps migration link, for example, the total migration time has a lower bound of 13 and upper bound of 50 seconds respectively. Similarly, the downtime has a lower bound of .314 and upper bound of 9.497 seconds respectively. Table I illustrates the migration bounds for some common link speeds. While the downtime lower limit is fixed (as it is dependent purely on post-migration overhead) all other bounds vary in accordance to link speed due to their correlation with the VM memory size. As the table indicates, the bounds vary significantly. For bigger VM memory sizes (which is common in current installations [16]) we have even larger differences. Thus, using bounds is at best an imprecise exercise and does not allow for accurate prediction of migration times. Building better predictions requires understanding the relationship between factors that impact migration performance.

Table I: Migrationbounds.Mt:Total Migration Time (Seconds). Dt: Total Downtime (Milliseconds). Lb: Lower Bound. Ub: Upper Bound. Vm Size= 1,024 Mb.

Speed	MTLB	MTUB	DTLB	DTUB
100 Mbps	92.2 s	437.1 s	311 ms	90,466.5 ms
1 Gbps	11.7 s	43.95 s	311 ms	9,347.3 ms

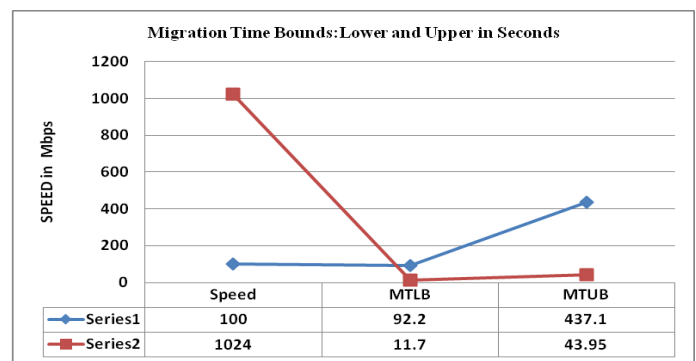


Fig.1 Migration Time Lower Bound and Upper Bound in Sec

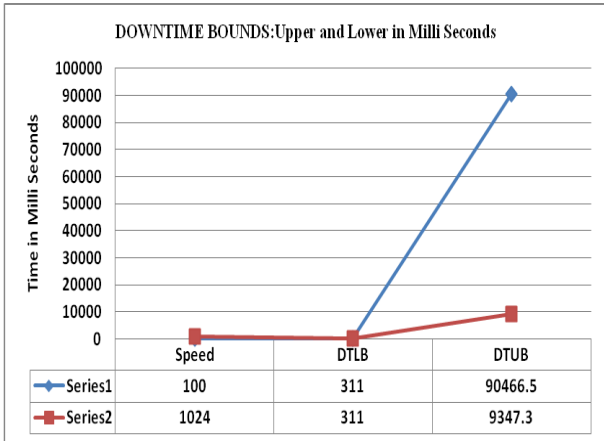


Fig.2 Down Time Lower Bound and Upper Bound in Sec

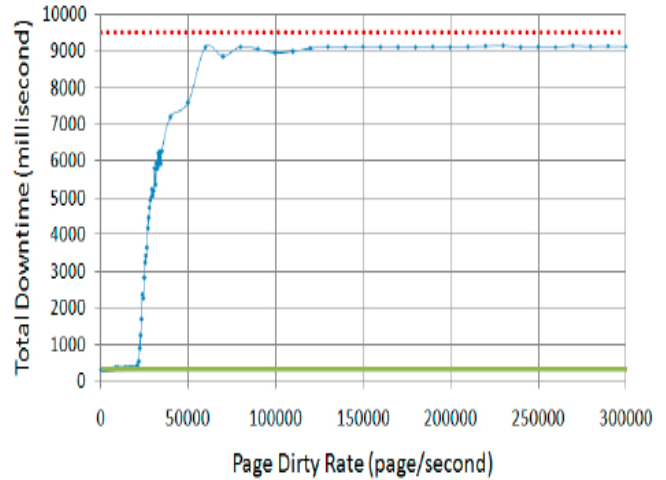


Fig.5 1 Gbps Total Down Time

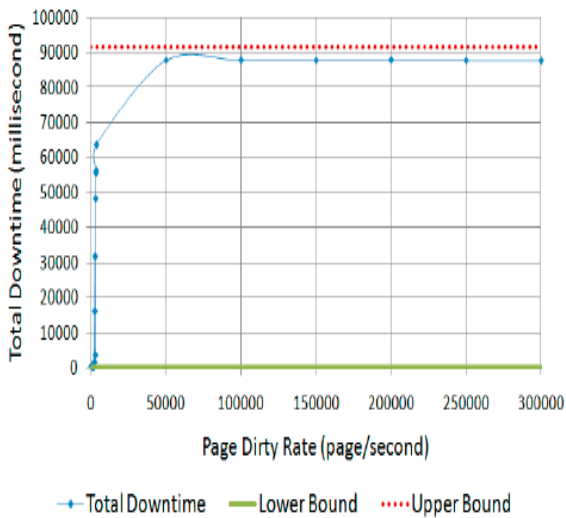


Fig.3 100 Mbps Total Down Time

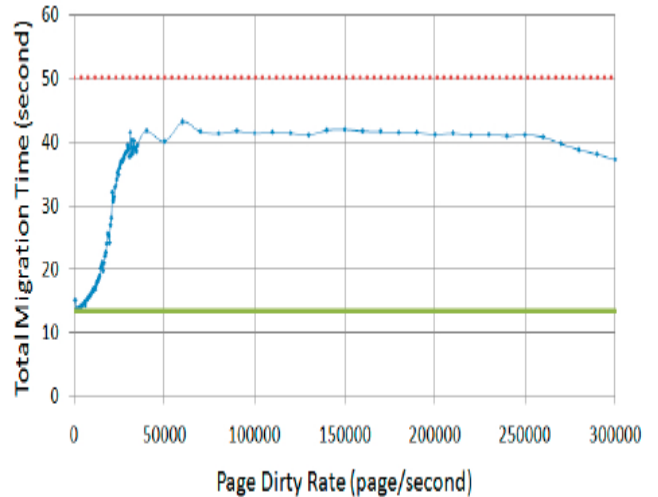


Fig.6 1 Gbps Total Migration Time

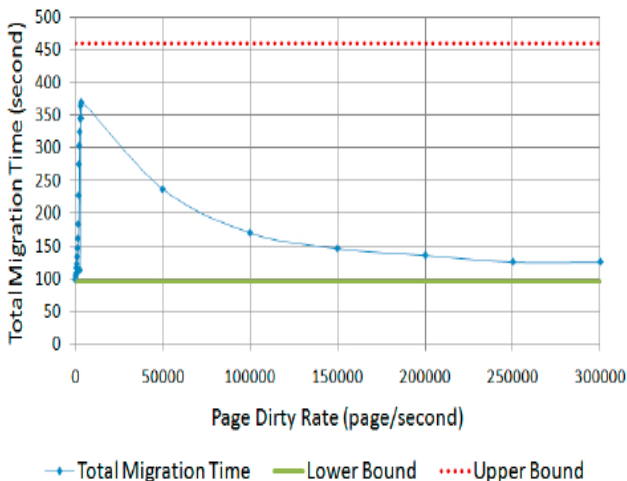


Fig. 4 100 Mbps Total Migration Time

IV. PARAMETERS AFFECTING MIGRATION

There are several factors that we need to study as a prerequisite for accurate migration modelling. In this section, we explore these factors and their impact on total migration time and downtime. Moreover, stop conditions that may force migration to reach its final stages are generally what governs migration performance. Obviously, this is implementation specific which is exemplified by but not limited to Xen support for live migration. Migration link bandwidth is perhaps the most influential parameter on migration performance. Link capacity is inversely proportional to total migration time and downtime. Higher speed links allow faster transfers and thus require less time to complete. Figure 1 illustrates migration performance for a 1,024 MB VM running a micro-benchmark that writes to memory pages with rates up to 300,000 pages/second on 100 Mbps, 1 Gbps links. It represents the impact of each link speed on total migration time and downtime.

As link bandwidth increases, the point in the curve when migration performance starts to degrade rapidly shifts to the right roughly with the same ratio. Page dirty rate is the rate at which memory pages in the VM are modified which, in turn, directly affects the number of pages that are transferred in each pre-copy iteration. Higher page dirty rates result in more data being sent per iteration which leads to longer total migration time. Furthermore, higher page dirty rates results in longer VM downtime as more pages need to be sent in the final transfer round in which the VM is suspended.

Figure 1 shows the effect of varying the page dirty rate on total migration time and downtime for each link speed. The relationship between page the dirty rate and migration performance is not linear because of the stop conditions. If the page dirty rate is below link capacity, the migration sub-system is able to transfer all modified pages in a timely fashion, resulting in a low total migration time and downtime. On the other hand, if the page dirty rate starts approaching link capacity, migration performance degrades significantly. Total downtime at low page dirty rates is virtually constant and approximately equal to the lower bound (Equation 4). This is because the link has enough capacity to transfer dirty pages in successive iterations leading to a very short stop-and-copy stage. When the page dirty rate increases to the point that 29 iterations are not sufficient to ensure a short final copy round or when more than 3x the VM size have been transferred, migration is forced to enter its final stage with a large number of dirty pages yet to be sent.

Consequently, total downtime starts to increase in proportion to the increase in the number of modified pages that need to be transferred in the stop-and copy stage. Total downtime further increases until the defined upper bound in which it has to send the entire VM memory. Total migration time also increases with an increasing page dirty rate. This is attributable to the fact that more modified pages have to be sent in each pre-copy round. Moreover, the migration sub-system has to go through more iteration with the hope to have a short final stop-and-copy round. For page dirty rates near link speed, total migration time approaches its upper bound (Equation 3) as migration stops when 3x VM size has been transferred. Then, it starts to fall back towards its lower bound.

For extremely high page dirty rates (compared to link speed), migration is forced to reach its final transfer stage after 29 iterations having sent virtually no pages.² It then has to transfer the entire RAM in the final iteration. This is exemplified clearly for the 100 Mbps link in Figure 4, in which the total migration time drops back to its lower bound (almost all dirty pages are skipped in every iteration except the final one) while having a total downtime (Figure 3) at its upper bound (as the entire RAM has to be transferred in the stop-and-copy stage).

The first pre-copy iteration tries to copy across the entire VM allocated memory. The duration of this first iteration is thus directly proportional to the VM memory size and subsequently impacts total migration time. On average, total migration time increases linearly with VM size. On the other hand, the total downtime for low page dirty rates is almost the same regardless of the VM size as the migration

sub-system succeeds in copying all dirtied pages between successive iterations resulting in a short stop-and-copy stage. When the link is unable to keep up with the page dirty rate, larger VMs suffer longer downtime (linearly proportional to the VM size) as there are more distinct physical pages that require copying in the stop-and-copy stage.

Pre- and post-migration overheads refer to operations that are not part of the actual transfer process. These are operations related to initialising a container on the destination host, mirroring block devices, maintaining free resources, reattaching device drivers to the new VM, and advertising moved IP addresses. As these overheads are static, they are significant especially with higher link speeds. For instance, pre-migration setup constitutes around 77% of total migration time on a 1Gbps link for a 512 MB idle VM. More importantly, post-migration overhead is an order of magnitude larger than the time required for the stop-and-copy stage. To conclude this section, there are several parameters affecting migration performance. These parameters may be classified as having either a static or dynamic effect on migration performance. Parameters having static effects are considered as unavoidable migration overheads. On the other hand, parameters having dynamic effects on migration affect only the transfer process. Dynamic parameters are typically related to the VM specification and applications hosted inside it.

We show that the page dirty rate and link speed are the major factors influencing migration times. We also show how particular combinations of these factors can extend expected total migration time and downtime. Finally, we observe that the pre- and post-migration overheads become significant compared to the iterative pre-copy and stop-and-copy stages, especially for VMs that have low page dirty rates and are being migrated over high speed links.

V. CONCLUSION

In this paper, we studied live migration behaviour in precopy migration architectures, specifically using the Xen virtualisation platform. We show that the link speed and page dirty rate are the major factors impacting migration behaviour. These factors have a non-linear effect on migration performance largely because of the hard stop conditions that force migration to its final stop-and-copy stage. In a virtualised environment, administrators can dynamically change VM placements in order to plan maintenance, balance loads, or save energy. Live migration is the tool used.

Future Scope

The experiments that we have carried out prove that the migration link speed is the most influential parameter on performance. We have been working on local area networks assuming live migration inside one datacentre. However, moving workloads between different data centres, especially for cloud providers, is also useful. We plan to further utilise the models to study migration behaviour on wide area networks.

REFERENCES

1. Casas, J., Clark, D. L., Conuru, R., Otto, S. W., Prouty, R. M., and Walpole, J. (Spring 1995). MPVM: A Migration Transparent Version of PVM. *Computing Systems*, 8(2):171–216.
2. Rosenblum M., Garfinkel T. Virtual Machine Monitors: Current Technology and Future Trends, *Computer*, vol. 38, no. 5, pp. 39-47, May, 2005.
3. P. Barham et al., Xen and the Art of Virtualization.
4. E. Bugnion et al., “Disco: Running Commodity Operating Systems on Scalable Multiprocessors,” *ACM Trans. Computer Systems*, vol. 15, no. 4, 1997, pp. 412-447.
5. M. Kozuch et al., Internet Suspend Resume, WMCSA, 2002.
6. POPEK, G. J., GOLDBERG, R. P. Formal Requirements for Virtualizable Third Generation Architectures. *Communications of the ACM* 17 (7): 412–421.
7. D. Milojicic, F. Douglis, Y. Paindaveine, R. Wheeler, and S. Zhou. Process migration. *ACM Computing Surveys*, 32(3):241.299, 2000.
8. C. P. Sapuntzakis, R. Chandra, B. Pfaff, J. Chow, M. S. Lam, and M. Rosenblum. Optimizing the migration of virtual computers. In *Proc. of the 5th Symposium on Operating Systems Design and Implementation (OSDI-02)*, December 2002.
9. Live Migration with AMD-V™ Extended Migration Technology, AMD white paper, 2008, www.amd.com.
10. Andrew Whitaker, Richard S. Cox, Marianne Shaw, and Steven D. Gribble. Constructing services with interposable virtual hardware. In *Proceedings of the First Symposium on Networked Systems Design and Implementation (NSDI '04)*, 2004.
11. E. Zayas. Attacking the process migration bottleneck. In *Proceedings of the eleventh ACM Symposium on Operating systems principles*, pages 13.24. ACM Press, 1987.
12. Marvin M. Theimer, Keith A. Lantz, and David R. Cheriton. Preemptable remote execution facilities for the V-system. In *Proceedings of the tenth ACM Symposium on Operating System Principles*, pages 2.12. ACM Press, 1985.
13. S. Osman, D. Subhraveti, G. Su, and J. Nieh. The design and implementation of zap: A system for migrating computing environments. In *Proc. 5th USENIX Symposium on Operating Systems Design and Implementation (OSDI-02)*, pages 361.376, December 2002.
14. C. Clark, K. Fraser, S. Hand, J. G. Hansen, E. Jul, C. Limpach, I. Pratt, and A. Warfield, “Live migration of virtual machines,” in Proc. USENIX Symposium on Networked Systems Design and Implementation (NSDI'05), Berkeley, CA, USA, 2005, pp. 273–286.
15. Amazon Elastic Compute Cloud (Amazon EC2). Amazon Web Services LLC. [Online]. Available: <http://aws.amazon.com/ec2/>
16. S. Hacking and B. Hudzia, “Improving the live migration process of large enterprise applications,” in Proc. ACM International Workshop on Virtualization Technologies in Distributed Computing (VTDC'09), New York, NY, USA, 2009, pp. 51–58.

E-Learning Retrieval System Through Advanced Data Mining Clustering Technique

V.Venkateswaran¹, R.Ramakrishnan², A. Ramalingam³

^{2,3}Assistant Professor, Department of M.C.A

^{1,2}Sri Mnakula Vinayagar Engineering College

Abstract : The e-Learning provides the Learners to interact each other as well as with teachers. The new technology virtual learning system (VLE) is used to interact between the student and teacher. The vast improvement in the field of information technique leads to share of information resources. The development in e-Learning system which arise a new way of distributing knowledge around the world without any restrictions. The e-Learning system has huge volume of recourse sharing at various places. The e-Learning retrieval system contains various information's that can be shared and communicate between the Learners in a course and store Resources from the various server can be retrieved. So there is a need to measure the sharing of resource using specific technique. The data mining clustering technique is used to retrieve the recourse of the e-learning system and measure the recourse shared.

Keywords: LMV, VLE, e-Learning, Data Mining, KDD; EDM

I. INTRODUCTION

1.1 E-Learning Systems

The e-Learning system consists of acquiring knowledge and recourse sharing. The e-Learning system can enable better allocation of resources and organize the learning processes in order to improve the learning experience of the student as well as increase their learning Knowledge [1].

The e-Learning systems increase the sharing of recourses providing recourse material to learners. The recourse is being centralized using server is locate worldwide. The e-Learning recourse in much discipline the related recourse are grouped based on the course as per the leaner wish. The learner can select the course material as Text, PPT, video which is related to the course. The e-learning system provides fast easy and efficient of recourse material can retrieved by data mining clustering technique.

1.2 Theory of e-Learning

The e-Learning system accumulates a vast amount of information which is valuable for learner development. The learning management systems accumulate a great deal of student activities can record whatever student activities are involved such as reading writing talking test performing various task and even communicating with other. The e-Learning system facilities of communication between educators, sharing resources, producing content material, preparing assignment, enabling synchronous learning with forms chat, new services, of e-Learning system which improves the knowledge of the learner accessing open resources with waste of resources.

II. Applying Data Mining Technique

Data mining or knowledge discovery in database (KDD) is the automatic extraction of implicit and interacting. Data mining is a multidisciplinary area in which several computing paradigms converge decision tree construction, rule induction, K-means, SVM, Apriori, Page Rank, AdaBoost, KNN, Naïve Bayss, And CART algorithms etc And some of the most useful data mining task and method are static's Visualization, clustering classification, association rule mining ,sequential pattern mining text mining, etc.

2.1 Educational Data Mining

Due to the large quantities of data in e-learning systems, it is very difficult for educators to analyze them manually. Educational Data Mining EDM the area of scientific inquiry centered on the development of methods for making discoveries within the unique kinds of data. That come from educational settings, and using those methods to better understand students and settings which they learn in Educational Data Mining is an emerging discipline, with developing methods for exploring unique types of data that come from educational settings, and using those methods to better understand students, and the settings which they learn in as defined by The Educational Data Mining community.

The Educational Data Mining providing research efforts in the field, review of the many applications of Data Mining to e-learning. The review of the history and current trends of EDM review of most relevant studies carried out in this field. Data mining techniques relation with the fields of Artificial Intelligence (AI) and Machine Learning (ML) have been highlighted in many researches are classified into four main areas 1) improving student models, that provide detailed information about a student's characteristics; 2) discovering models of the knowledge structure of the domain 3) studying the pedagogical support provided by learning software 4) scientific discovery about learning and learners. The first three categories are universal across different fields of data mining are categories particularly related to educational data mining[2].

- Statistics and visualization
- Web mining
- Text mining
- Prediction
- Clustering
- Relationship mining
- Distillation of data for human judgment
- Discovery with models

2.2 Using data mining Technique

In E-learning, clustering has been used for finding clusters of students with similar learning characteristics and to promote group-based learning and to provide learner diagnosis. Rapid Miner system has several clustering algorithms available. The K-Means has been used here. Clustering techniques apply when the instances of data are to be divided into natural groups. In k-means algorithm clusters are specified in advance prior to application of the algorithm provides a good review of different data mining clustering techniques.

The data mining technique is used in e-learning system which can able to download large volume of resources. The clustering technique is one of the data mining technique is used in the e-learning system for probably and distribution.

III. Concept Of Clustering

The Clustering is defined as the division of data in groups of similar object. The clustering is used for searching the relevant data as the linear request when the resource is not found in the related server. The clustering also helps to gather to relevant resource from the various servers with fast speed.

2.1 Clustering Technique

The clustering technique is broadly classified into two partitioning, Hierarchical clustering it sub divided into agglomerative and divisive. The hierarchical algorithms build clusters gradually partitioning algorithm learn cluster directly. They either try to discover cluster by iteratively relocating points between subset, or try to identify cluster as areas highly populated with data.

Partitioning relocation methods are further categorized into probabilistic clustering K-medoids methods. Such methods concentrate on how well points fit into their clusters and tend to build cluster of proper convex shapes.

Partitioning algorithm of the second type is surveyed in the section density-based partitioning. They try to discover dense connected components of the data, which are flexible in term of shape .density –based connectivity is used in the algorithm. They are less sensitive to outliers and can discover clusters of irregular shapes. They usually work with low dimensional data of numerically attributes, know as spatial data. Spatial objects could include not only points also extended objects[18].

IV. K-Mean Clustering Technique

The k-means clustering determine number of cluster k and we assume the center of these clusters can take any random object as the initial centroids. Then the k-means algorithm will do the three steps below until convergence. Iterate stable (=no object move group): 1. determine the centroid coordinate 2. Determine the object based on minimum distance.

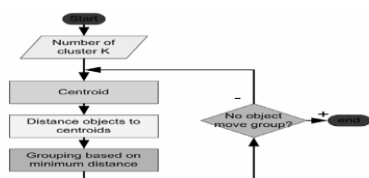


Figure 3: K-Mean Clustering Process

3.1 Distance calculation

The distance is the most commonly used of Euclidean distance. In most case when people said about distance they will refer to Euclidean distance. Euclidean distance or simply “distance examines the root of square difference between coordinates of a pair of objects.

For example :

Features k

	Cost	Time	Weight	Incentive
Object A	0	3	4	5
Object B	7	6	3	-1

Points a has coordinate (0, 3, 4, 5) and point B has coordinate (7, 6, 3, -1). The Euclidean Distance between point A and B is

$$d_{BA} = \sqrt{(0-7)^2 + (3-6)^2 + (4-3)^2 + (5+1)^2}$$

$$= \sqrt{49+9+1+36} = 9.747$$

Euclidian distance is a special case of Minkowski distance with $\lambda = 2$

V. K-MEANS ALGORITHM

k-means clustering is a method of cluster analysis which aims to partition n observations into k clusters in which each observation belongs to the cluster with the nearest mean. A set of observations (x_1, x_2, \dots, x_n) , where each observation is a d-dimensional real vector, k-means clustering aims to partition the observations into k sets $(k \leq n) S = \{S_1, S_2, \dots, S_k\}$ so as to minimize the within-

$$\arg \min_S \sum_{i=1}^k \sum_{x_j \in S_i} \|x_j - \mu_i\|^2$$

cluster sum of squares

where μ_i is the mean of points in S_i .

Classification - Tree Induction Results

The Tree Induction algorithm used to predict students’ potential performance was focused on using student assessment and e-Learning usage. Pessimistic pruning was applied to insure that the expected confidence levels obtained for predictions on the training data are similar to actual confidence levels obtained from unseen data. A set of rules was generated from the decision tree operator, showing interesting information about the supervised classification of the students. These rules classify at least three main categories of students: students with a low number of assignments are classified as FAIL; students with medium number of assignments quizzes are classified as FAIL or PASS depending on their quiz score, and students with a high number of assignments are classified as FAIL, PASS or EXCELLENT depending on number of actions in the e-Learning system etc. The rules generated from the Tree Induction Algorithm operator.

4.1 K-Means Results

The educator can use the cluster centroid K-Means results as presented in order to group Students into three types of students: very active students (cluster 0), active students (cluster 1) and nonnative students (2). This information helps educator to group students for working together in Collaborative activities. Students were divided in 3 groups based on their activities done in e-Learning Cluster 0 is characterized by most active students in e-Learning, with high assignment number, which participated to the online quiz and have a moderately number of discussion and forum read; Cluster 1 is characterized by moderately active students in e-Learning, with moderately assignment number, who participated or not to the online quiz in e-Learning with a low number of actions in the system.

4.2 Implementation of k-means

The k-means only allow numerical values for attributes in case it may be necessary to convert the data set into the standard spreadsheet format and convert categorical attributes to binary. It may also be necessary to normalize the value of attributes that are measured on substantially different scales. This K-mean algorithm automatically handles a mixture of categorical and numerical attributes. Furthermore the algorithm automatically normalizes numerical attributes when doing distance computations. The simple k-mean algorithm uses Euclidean distance measure to compute distance between instance and clusters.

To perform clustering select the cluster and clustering algorithm In this case we select ;simple K-means te value is used to generate a random number which in tirm used for making the initial assignment of instance to cluster. In general k-means is quite sensitive to how cluster are initially assigned. of instance to cluster.

Once the option have been specified , we can run the clustering algorithm. The result show the centriod of each cluster as well as statistics on the number and percentage of instance assigned to different cluster. The centroids can be used to characterize the cluster in through visualization cluster assignment. We can choose the cluster number and any of the other attributes for each of the three different dimensions available.

VI. DISCUSSION

Several data mining techniques such as: Attribute Clustering (K-Means), Classification, Association Mining (Apriori, FPGrowth, Create Association Rule, GSP) were applied to e-Learning summarization tables. By applying clustering methods, the goal was to split data set in groups of data points that naturally group together. Student actions were clustered together in order to investigate patterns of students behavior in the e-Learning System. KMeans algorithm was used to define clusters, which starts with no prior knowledge about groups in the data. By using prediction techniques, the goal was to develop a model that can infer predicted variables from predictors' variables. Inductive Decision tree algorithm was selected as classification method. The predicted variable was the categorical variable Final Mark. The target was to define variables that significantly affect in the Final Mark. By applying ARM, the goal was to discover relationships between variables. FPGrowth, Create Association Rule and APRIORI algorithms were selected as association rule mining techniques. The rules obtained can be explained in

the form that if some set of variable values is found, another variable will have a great chance to have a specific value.

VII. CONCLUSIONS

In this research, a data mining model for e-Learning data was proposed based on several techniques Attribute Clustering (KMeans), Classification , Association Mining (Apriori, FPGrowth, Create Association Rule, GSP) was proposed. This educational data mining work allowed identifying and locating information about E-learning processes that need improvements or those that perform very well and could be used as good examples. The educational data mining investigated in this research allows analyzing and better understanding the learning and teaching processes by applying data mining techniques. The experimental results have shown that the data mining model presented was able to obtain comprehensible, actionable and logical feedback from the LMS data describing students' learning behavior patterns. This work concentrated on the overall LMS performance at Epoka University and the mining Process of e-Learning data. Mining the e-Learning data allowed identifying the most effective ways to the teaching process that can be used to enhance the education process. To further test the effectiveness of the proposed model and to increase the generality of this research, more extensive experiments should be conducted by using larger LMS data sets.

A reference list **MUST** be included using the following information as a guide. Only *cited* text references are included. Each reference is referred to in the text by a number enclosed in a square bracket (i.e., [3]). References **must be numbered and ordered according to where they are first mentioned in the paper**, NOT alphabetically.

References

- [1] Nichols and schedule "theory for e-Learning Educational technology and soc., Mvol,6,no,2,pp,1-10,2003
- [2] MCSER-Mediterranean Center of Social and ducational Research Rome, Italy, 2011
- [3] Romero, C., Ventura, S.(2010), Educational Data Mining: A Review of the State-of-the-Art. *IEEE Transaction on Systems, Man, and Cybernetics, Part C: Applications and Reviews*.
- [4] Uribe-Tirado, A., Melgar-Estrada, L.-M., & Bornacelly-Castro, J.-A. (2007). Moodle learning management system as a tool for information, documentation, and knowledge management by research groups. *Profesional de la Información*.
- [5] Silva, D., & Vieira, M.(2002). Using data warehouse and data mining resources for ongoing assessment of distance learning. In Proceedings of the 2002 IEEE Conference on Advanced Learning Technologies Kazan, Russia.
- [6] Sison, R., & Shimura, M. ,(1998). Student Modelling and Machine Learning. *International Journal of Artificial Intelligence in Education*.
- [7] Srikant, R., & Agrawal, R. (1996). Mining Sequential Patterns: Generalizations and Performance Improvements. In P. M. G. Apers, M. Bouzeghoub, & G. Gardarin (Eds.) *Proc. 5th Int. Conf. Extending Database Technology,EDBT*, vol. 1057, (pp. 3–17). Springer-Verlag.

- [8] Srivastava J., Cooley R., Deshpande M., & Tan P. (2000, January) Web Usage Mining: Discovery and Applications of usage Patterns form Web Data, *SIGKDD Explorations*.
- [9] Talavera, L., & Gaudioso E. (2004). Mining student data to characterize similar behavior groups in unstructured collaboration spaces. *Workshop on Artificial Intelligence in CSCL. ECAI*.
- [10] Tang, T.Y., McCalla, G. , (2005). Smart Recommendation for an Evolving e-Learning System: Architecture and Experiment. *International Journal on e-Learning*.
- [11] Tsai, C. J., Tseng, S. S., & Lin, C. Y. (2001). A Two-Phase Fuzzy Mining and Learning Algorithm for Adaptive Learning Environment. In ICCS '01: Proceedings of the International Conference on Computational Science-Part London, UK: Springer-Verlag Wang, F., & Shao, H. (2004).
- [13] Effective personalized recommendation based on time-framed navigation clustering and association mining. *Expert Systems with Applications* 27(3). Wu X., (2004).
- [14] Data Mining: An Artificial Intelligence Perspective. The IEEE Intelligent Informatics Bulletin. Yoo, J., Yoo, S., Lance, C., Hankins, J. (2006).
- [15] Student Progress Monitoring Tool Using Treeview. In The 37th Technical Symposium on Computer Science Education, Houston, USA :ACM Press. Zaïane, O. , & Luo J., (2001).
- [16] Web usage mining for a better web-based learning Environment. Proceedings of conference on advanced technology for education, Banff, Alberta . Xu, R., & Wunsch, D. I. I. (2005).

Finite Element Analysis of Thin Walled-Shell Structures by ANSYS and LS-DYNA

T. Subramani¹ Athulya Sugathan²

¹Professor & Dean, Department of Civil Engineering, VMKV Engg. College, Vinayaka Missions University, Salem, India

²PG Student of Structural Engineering, Department of Civil Engineering, VMKV Engg. College, Vinayaka Missions University, Salem, India

ABSTRACT: Buckling is a critical phenomenon in structural failure. Buckling is the failure of structures under compression load. Also buckling strength of structures depends on many parameters like supports, linear materials, composite or nonlinear material etc. Also buckling behavior is influenced by thermal loads and imperfections. Analyzing all these conditions is difficult task. So few parameters are considered for the present work. Due to the advances in the Finite element techniques, analysis of these problems is possible which is difficult in earlier days. Formulae's are available based on experimental techniques for linear range and not available for nonlinear range. So these problems are solved by the advances in computer technology with Finite element techniques in the nonlinear domain. In the present work both cylindrical and elliptical members are considered for buckling strength. Initially both the members are created using Ansys top down approach. Scaling options are used to build the elliptical members. The structure is divided to ease map meshing. Initially one end constrained and other free condition is considered for analysis. The structure is fine meshed to get better results. Both Shell63 in elastic range and shell43 in plastic range are used for analysis. The elliptical results are compared with theoretical results to check Finite element validity. The results are very close and analysis is extended for circular members. The stresses and loads are very high with linear analysis. But the stresses and loads are considerably reduced with nonlinear analysis. The effect of thickness on buckling load and stresses are plotted. The buckling load is increasing with increase in thickness. The hinged boundary conditions shows higher buckling strength compared to the initial boundary conditions for both elliptical and cylindrical members. The problem executed in the time domain also indicates the stresses reaching to the yield point and converging towards the critical loads. All results are represented with necessary graphical and pictorial plots

KEY WORDS: Buckling, ANSYS, LS-DYNA, Linear and Non – Linear Analysis

I. INTRODUCTION

When a structure (subjected usually to compression) undergoes visibly large displacements transverse to the load then it is said to buckle. Buckling may be demonstrated by pressing the opposite edges of a flat sheet of cardboard towards one another. For small loads the process is elastic since buckling displacements disappear when the load is

removed. Local buckling of plates or shells is indicated by the growth of bulges, waves or ripples, and is commonly encountered in the component plates of thin structural members.

Buckling proceeds either in stable or unstable equilibrium state.

Stable: in which case displacements increase in a controlled fashion as loads are increased, ie, the structure's ability to sustain loads is maintained.

Unstable: in which case deformations increase instantaneously, the load carrying capacity nose- dives and the structure collapses catastrophically

Neutral equilibrium: is also a theoretical possibility during buckling - this is characterized by deformation increase without change in load. Buckling and bending are similar in that they both involve bending moments. In bending these moments are substantially independent of the resulting deflections, whereas in buckling the moments and deflections are mutually inter-dependent - so moments, deflections and stresses are not proportional to loads

If buckling deflections become too large then the structure fails - this is a geometric consideration, completely separated from any material strength consideration. If a component or part there for is prone to buckling then its design must satisfy both strength and buckling safety constraints - that is why Buckling is important.

1.1 TYPES OF BUCKLING OF STRUCTURES

1.1.1 Buckling of thin-walled structures

A thin-walled structure is made from a material whose thickness is much less than other structural dimensions. Into this category fall plate assemblies, common hot- and cold-formed structural sections, tubes and cylinders, and many bridge and aeroplane structures.

1.1.2 Plate and thin shell buckling

Local buckling of an edge-supported thin plate does not necessarily lead to total collapse as in the case of columns, since plates can generally withstand loads greater than critical. However the P-q curve illustrates plates' greatly reduced stiffness after buckling, so plates cannot be used in the post-buckling region unless the behavior in that region is known with confidence. It should be emphasized that the knee in the P-q curve is unrelated to any elastic- plastic yield transition; the systems being discussed are totally elastic. The knee is an effect of overall geometric rather than material instability

1.1.3 Torsional Buckling

Torsional buckling of columns can arise when a section under compression is very weak in torsion, and leads to the column rotating about the force axis. (Figure.1)

1.1.4 Flexural Torsional Buckling

More commonly, where the section does not possess two axes of symmetry as in the case of an angle section, this rotation is accompanied by bending and is known as flexural torsional buckling.

1.1.5 Lateral Buckling

Lateral buckling of beams is possible when a beam is stiff in the bending plane but weak in the transverse plane and in torsion, as is the I-beam of the sketch. It often happens that a system is prone to buckling in various modes. These usually interact to reduce the load capacity of the system compared to that under the buckling modes individually. An example of mode interaction is the thin box section which develops local buckles at an early stage of loading, as shown greatly exaggerated here. The behavior of the column is influenced by these local buckles, and gross column buckle will occur at a load much less than the ideal Euler load



FIGURE.1 TORSIONAL BUCKLING

Stability of Equilibrium:

Buckling properties of a system are reflected in the shape of the equilibrium path, i.e. the load-deflection curve. If a system is in equilibrium then its total potential energy, U , has a turning value since an infinitesimal disturbance, $d\delta$, of the system from its equilibrium position does not change the potential energy (PE) - δ is any convenient characterizing displacement. Expressed mathematically, the equilibrium path is thus defined by:

$$U' \equiv dU/d\delta = 0$$

The type of equilibrium which exists at any point on the path - stable, neutral or unstable - is also an important consideration; it may be deduced by taking the second derivative :-

$$U'' = d^2U/d\delta^2 \begin{cases} > 0 & ; \text{ PE - minimum} \\ & \text{stable equilibrium} \\ = 0 & ; \text{ PE - zero slope} \\ & \text{neutral equilibrium} \end{cases}$$

II. Finite Element Methods

2.1 INTRODUCTION

Today, finite element method enjoys a position of predominance among the computational methods to occur in this century, within only a few decades this technique has evolved from one with initial application in analysis of aircraft structure as early as 1941 and in structural engineering to a widely utilized and richly varied computational approach

for many scientific and technological areas. The stress analysis in the field of structural mechanics is invariably complex and for many of the engineering problems; it is extremely difficult and tedious to obtain analytical solutions. In this situation, most of the practical problems are solved by numerical methods, which provide approximate but acceptable solutions. With the advent of computers, one of the most powerful techniques that has emerged from the realm of engineering analysis is the finite element method and the method being general, can be used for the analysis of structures are solid of complex shapes and complicated boundary conditions.

The basic concept of finite element method is discretization of a structure into finite number of elements, connected at finite number of points called nodes. The material properties and the governing relationships are considered over these elements and expressed in terms of nodal displacement at nodes. An assembly process duly considering the loading and constraints results in a set of equations governing the structural response, which are established through the application of appropriate variation principle. Solutions of these equations give the response of the structure. Selecting proper elements and subdividing the structure with large number of finite elements or by taking higher order elements can increase the accuracy of solution obtained by finite element method. In modern design practice, with the advent of large and fast modern digital computers and advancement in numerical techniques; solutions to various static and dynamic problems has become fast and efficient.

2.2 TYPES OF ELEMENTS

Few Important FEM elements are as follows.

TRUSS: Slender element (length \gg area) which supports only tension or compression along its length; essentially a 1D spring.

1. BEAM: Slender element whose length is much greater than its transverse dimension which supports lateral loads, which cause flexural bending.
2. TORSION: Same as truss but supports torsion.
3. 2D SOLID: Element whose geometry definition lies in a plane and applied loads also lie in the same plane. Plane stress occurs for structures with small thickness compared with its in plane dimension - stress components associated with the out of plane coordinate are zero. Plane strain occurs for structures where the thickness becomes large compared to its in plane dimension - strain component associated with the out of plane coordinate are zero.
4. PLATES: Element whose geometry lies in the plane with loads acting out of the plane which cause flexural bending and with both in plane dimensions large in comparison to its thickness - two dimensional state of stress exists similar to plane stress except that there is a variation of tension to compression through the thickness.
5. SHELLS: Element similar in character to a plate but typically used on curved surface and supports both in

plane and out of plane loads – numerous formulations exist.

6. 3D SOLID: Element classification that covers all elements - element obeys the strain displacement and stress strain relationships.

2.3 MERITS OF FINITE ELEMENT METHOD

The systematic generality of finite element procedure makes it a powerful and versatile tool for a wide range of problems. Thus, flexible, general-purpose computer programs can be developed and can be applied to various problems with little or no modification. FEM can be easily interpreted in physical terms. As well it has a strong mathematical base. Hence, finite element method can be easily applied to any problem with a proper knowledge of the physical system under consideration and can be solved to a greater accuracy by the application of proper mathematical tool. Non-homogenous continuum can also be dealt with by merely assigning different properties to different elements. It is even possible to vary the properties within an element according to the polynomial applied. Finite element method accommodates complex geometry with ease and is capable of handling non-linear and time dependent system also. In finite element method, since boundary conditions are introduced in the assembled equations, it requires only to specify the geometric boundary conditions without regarding its effects on interior elements. Since the boundary conditions do not enter into the individual finite element equations, the field variable models need not be changed, when the boundary conditions change. Finite element method considers the multidimensional continuity of body. Hence it does not require separate interpolation process to extend the approximate solution to every point with in the continuum. It does not also require the trial solutions that must all apply to the entire multidimensional continuum.

2.4 DEMERITS OF FINITE ELEMENT METHOD

The solution obtained from FEM can be realistic if and only if the material properties are known precisely.

The major drawback of FEM is sensitivity of the solution on the geometry of the element such as type, size, number, shape and orientation of elements used.

The computer programs of FEM require relatively a large computer memory and time.

FEM Programs yield a large amount of data as results. It is very difficult to separate out the require results from the pile of numbers.

III. ANSYS - INTRODUCTION

ANSYS is a commercial FEM package having the capabilities ranging from a simple, linear, static analysis to a complex, nonlinear, transient dynamic analysis. It is available in modules. Each module is applicable to specific problem. For example, Ansys/Civil is applicable to Civil structural analysis. Similarly Ansys/Flotran is CFD software applicable to Fluid Flow. The advantage of Ansys compared to other competitive software's is, its availability as bundled software

of pre, post and a Processor. Typical Ansys program includes 3 stages.

- Pre-Processing
- Solution
- Post-Processing

3.1 MODELING

This is the important step of creating the physical object in the system. They are two types of modeling in Ansys.

Direct Modeling & Solid Modeling

1. DIRECT MODELING: In this approach the physical structure is represented by nodes and elements directly. The problem is solved once after the boundary conditions are applied. This approach is simple and straight forward. Takes very little time computation. But this can be applied only for simple problems. When problem becomes complex, this method becomes tedious to apply.

2. SOLID MODELING: Models are directly created either using Ansys Preprocessor or imported from popular CAD soft wares like Mechanical Desktop, Pro/E, CATIA, SOLID WORKS etc. Once the structural model is created, by using mesh tool, the model can be meshed and problem can be solved by applying the boundary conditions. In Ansys Solid modeling is carried out using two methods. They are

1. Bottom Up Approach: To create model, Entities are required. Keypoints, Lines, Areas, Volumes are the entities in Ansys. If model is constructed through Keypoints to Lines, From Lines to Areas, and From Areas to Volumes the approach of modeling is called Bottom Up Approach. This approach is useful when models are complex.

2. Top Down Approach: A 3D Model can be created directly using the Volumes. Once Volumes are created, all the entities below the volumes (areas, lines, keypoints) are automatically created. This approach is easy but can be applied to simple problems.

3.2 TYPES OF BUCKLING ANALYSIS:

Ansys supports two types buckling analysis

- Non-Linear Buckling
- Eigen Value Buckling analysis

3.2.1 .Non-Linear Buckling

Nonlinear buckling analysis is usually the more accurate approach and is recommended for design or evaluation of actual structures. This technique employs a nonlinear static analysis with gradually increasing loads to seek the load level at which the structure becomes unstable. Using the nonlinear technique, model can include features such as initial imperfections, plastic behavior, gaps, and large-deflection response. In addition, using deflection-controlled loading, we can even track the post-buckled performance of the structure (which can be useful in cases where the structure buckles into a stable configuration, such as "snap-through" buckling of a shallow dome).

3.2.2. Eigen value buckling

Eigen value buckling analysis predicts the theoretical buckling strength (the bifurcation point) of an ideal linear

elastic structure. This method corresponds to the textbook approach to elastic buckling analysis: for instance, an eigenvalue buckling analysis of a column will match the classical Euler solution. However, imperfections and nonlinearities prevent most real-world structures from achieving their theoretical elastic buckling strength. Thus, eigenvalue buckling analysis often yields unconservative results, and should generally not be used in actual day-to-day engineering analyses.

Procedure for Eigenvalue Buckling Analysis

Eigenvalue buckling analysis generally yields unconservative results, and should usually not be used for design of actual structures. The procedure of eigenvalue buckling analysis is as follows.

- Building the model.
- Obtaining the static solution.
- Obtaining the eigenvalue buckling solution.
- Expanding the solution.
- Reviewing the results.

1. Building the model

The Model is built is either through Bottom up Approach or Top down Approach and should be meshed with appropriate elements. Proper material and geometric properties (Real properties) should be supplied. Finally Boundary conditions should be supplied.

2. Obtaining the Solution

The following should be followed to obtain proper solution Prestress effects [PSTRES] must be activated. Eigenvalue buckling analysis requires the stress stiffness matrix to be calculated.

Unit loads are usually sufficient (that is, actual load values need not be specified). The eigenvalues calculated by the buckling analysis represent buckling load factors. Therefore, if a unit load is specified, the load factors represent the buckling loads. All loads are scaled. Eigenvalues represent scaling factors for all loads. If certain loads are constant (for example, self-weight gravity loads) while other loads are variable (for example, externally applied loads), we need to ensure that the stress stiffness matrix from the constant loads is not factored by the eigenvalue solution. One strategy that we can use to achieve this end is to iterate on the eigen solution, adjusting the variable loads until the eigenvalue becomes 1.0 (or nearly 1.0, within some convergence tolerance). Design optimization could be useful in driving this iterative procedure to a final answer.

3. Obtaining the Eigen value buckling Solution:

After executing the program for static solution, again solution should be changed to Eigen Buckling and extraction technique should be specified.

4. Expanding the Solution:

Solution should be expanded to obtain the critical buckling loads.

5. Reviewing the results:

Results can be reviewed through /post1. Through result summary critical buckling in the form of natural frequencies can be viewed. By using the read set option for different critical loads, deflection and stress patterns can be viewed.

IV. PROBLEM DEFINITION AND FINITE

4.1 ELEMENT MODEL DEVELOPEMENT

Definition:

Buckling analysis is a technique used to determine buckling loads - critical loads at which a structure becomes unstable - and buckled mode shapes - the characteristic shape associated with a structure's buckled response. The analysis will be carried out using both implicit and explicit techniques.

- Analysis of elastic buckling nature of the cylindrical and elliptical vessels under compression loads
- Effect of thickness on stress generation in the structure
- Effect of thickness on buckling strength
- Effect of diameter on buckling strength and stress generation.
- Effect of non linearity in the buckling strength of structures.

Problem dimensions (initial)

- Outer diameter $D=400\text{mm}$
- Initial thickness $t=16\text{mm}$
- Height of the cylinder $=1200\text{mm}$
- Initial minor diameter of ellipse $=200\text{mm}$

Material Specification:

- Material : Structural Steel St42
- Young's Modulus $E=200\text{Gpa}$
- Poison's ratio $\nu=0.3$
- Density $\rho=7800\text{kg/m}^3$.

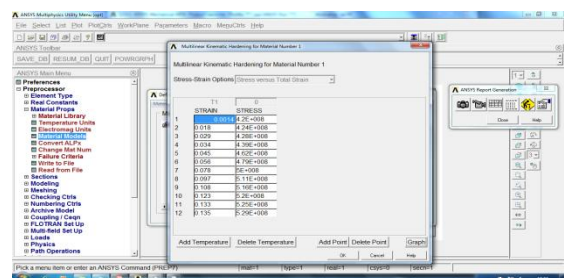


Figure.2 Nonlinear Properties of the Material

The Figure.2 shows applied nonlinear material properties of the problem. Most of the analysis is generally done in elastic range. But due to the advances in technology, load carrying capacity of the structures can be studied in the plastic range also. Also it helps in finding factor of safety in the structures. These nonlinear properties are obtained by experimental testing and recording.

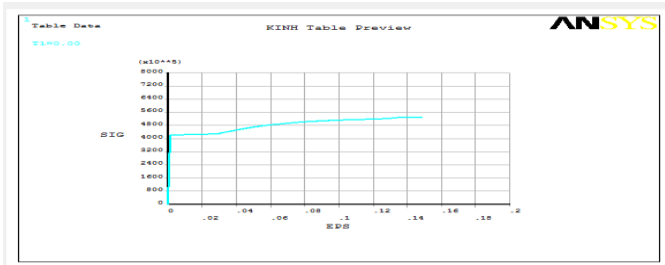


Figure.3 Stress – Strain Graph For The Material

The Figure.3 shows material graph for the problem. Initially the graph is straight and later sloping down indicating yielding of the structure. Generally above the yield by plastic modulus can be calculated using slope values or stress strain data can be supplied directly to find the nonlinear behavior of the structures.

Boundary conditions:

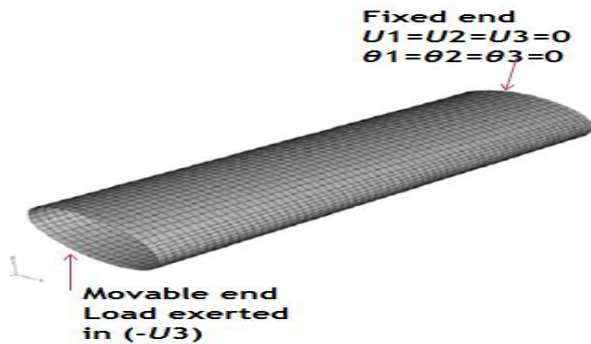


Figure.4 Boundary Conditions

For each of the two ends, two different types of boundary conditions(Figure.4) were used.

At the fixed end, displacement degrees of freedom in 1, 2, 3 directions (U_1 , U_2 , U_3) as well as rotational degrees of freedom in 1, 2, 3 directions (θ_1 , θ_2 , θ_3) were restrained to be zero. At the movable end, load was exerted with an even stress distribution in the longitudinal direction U_3 .

Mesh Size:

- No. of element s: 12000
- No. of nodes: 12120
- Size of element : 3.5m

Methodology:

- Analysis is carried out for EHS(Elliptical Hollow Sections) for minor diameter equal to half the major diameter and cylindrical geometries(CHS) in both elastic and nonlinear range to find the buckling strength.
- Initial thickness=16mm
- Iterations are carried out to find the buckling stress variation for different thickness to compare with theoretical values.

Element Type:

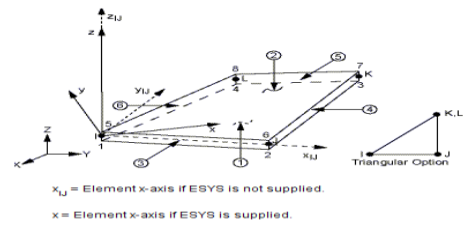


Figure.5 Shell63

SHELL63 (Figure.5) has both bending and membrane capabilities. Both in-plane and normal loads are permitted. The element has six degrees of freedom at each node: translations in the nodal x, y, and z directions and rotations about the nodal x, y, and z-axes. Stress stiffening and large deflection capabilities are included. A consistent tangent stiffness matrix option is available for use in large deflection (finite rotation) analyses.

4.2 ASSUMPTIONS

- The Member is initially perfectly straight and is axially loaded.
- The material is elasto-plastic with strain hardening materials.
- The self weight of the structure is not considered
- The member will fail by buckling alone.
- Imperfections of members are not considered.

V. RESULTS & DISCUSSION

Initially the linear elastic buckling is carried out for the structures and later nonlinear buckling analysis is carried out using elastic buckling loads to find actual buckling capacity of the structures. Comparative study is carried out between buckling, strength, buckling stress of cylindrical and elliptical members for buckling strength and stress generation. The formulae's are based on elastic material assumption. But this assumption is not true in the nonlinear conditions. So for nonlinear conditions, analysis has to be carried out after getting initial estimation of loads from linear elastic analysis. This linear elastic analysis helps in initial estimates of load carrying capacity and generally to make a comparative study of the material strength. In the beginning analysis is carried out for elliptical members under elastic material behavior. The formulae's for theoretical checking and analysis results are as follows.

Theoretical formulae for Elastic buckling stress for Cylindrical hollow members:

$$\sigma = \frac{2Et}{D\sqrt{3(1-\nu^2)}}$$

Where

Where E= Young's modulus

t=Thickness of vessel

D= Diameter of the cylindrical member

For Elliptical members buckling stress formulae is

$$\sigma = \frac{Et}{\frac{A^2}{B} \sqrt{3(1-\nu^2)}}$$

Where A= Major radius
 B=Minor radius
 v=Poison's ratio

Results for Elastic buckling Stress estimates(EHS):

Initially analysis has been carried out for buckling process and results are represented as follows.

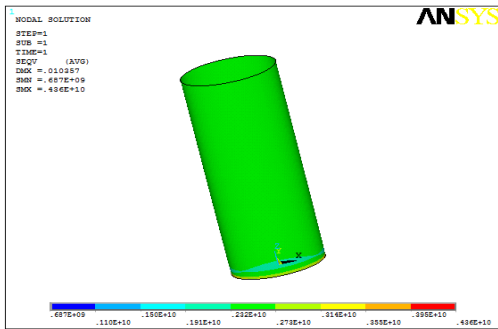


Figure.6: Buckling Stress For Elastic Buckling (Results For T=16mm D1/D2=2)

The Figure.6 shows a buckling stress of around 4360MPa due to elastic buckling. Since material property is assumed as linear, the stress levels are crossing the yield limits. But if material is considered as nonlinear, then the correct stresses can be estimated. This is done in the next stage of analysis. Maximum stresses are observed at the base of the structure.

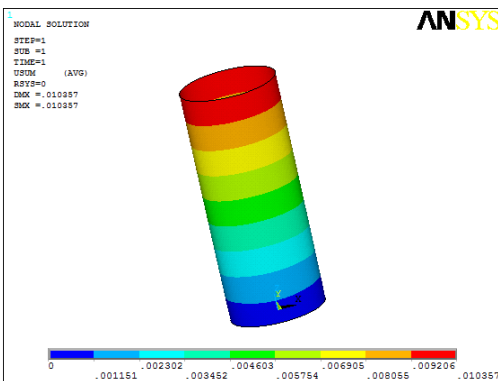


Figure.7 Deformation Plot For Elastic Buckling (Results For T=16mm D1/D2=2)

The Figures.7 shows maximum deformation of 0.010367mm for the given buckling load. Maximum deformation can be observed at the free end and minimum displacement can be observed at the constraint end. The status bar indicates varying displacements across the problem.

Comparative results for EHS

Table.1 Shows The Comparative Results Of Buckling Stresses And Buckling Loads Ehs Members

Thickness (in mm)	Buckling Stress(Theoretical) (in Gpa)	Buckling stress (FEM) (in GPa)	Percentage error (in %)	Buckling Load(FEM) (in N)
16	4.68	4.36	6.82	0.40200E+08
13.3	3.94	4.16	5.45	0.32558E+08
11.42	3.46	3.66	5.78	0.25042E+08
10	3.02	3.16	4.63	0.19233E+08
8.88	2.69	2.78	3.34	0.15239E+08
8	2.2	2.28	3.63	0.12446E+08

Table.1 Comparative Results of Buckling Stresses And Buckling Loads Ehs Members

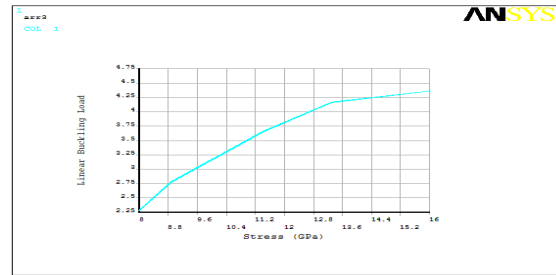


Figure.8 Stress Vs Thickness

The graph (Figure.9) represents stress and thickness relation during buckling process. For smaller thickness stress raise is high, but later the slope is reducing with increase in thickness. So the relation is not linear with buckling estimations.

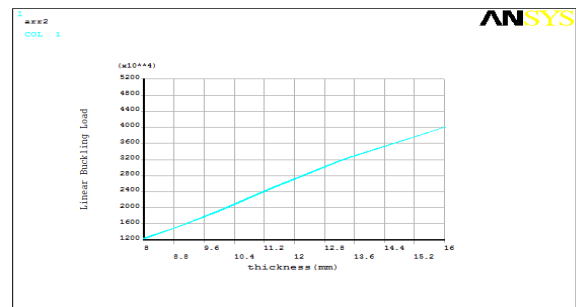


Figure.9 Load Vs Thickness

The graph (Figure.9.) represents Buckling Load and thickness relation during buckling process. Here almost linear relation can be observed for load and thickness due to elastic material assumption. From the graph it can be estimated for possible buckling load for higher thickness.

With nonlinear properties (EHS):

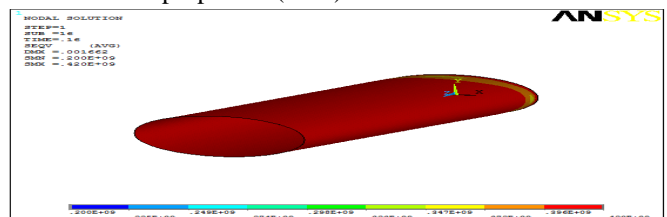


Figure.10 Buckling Stress For Nonlinear Buckling (Results For T=16mm D1/D2=2)

The Figure.10 shows a buckling stress of around 420MPa due to nonlinear buckling. The stresses are practical compared to elastic buckling where stresses becomes infinite and nonreliable. But for comparative studies, the analysis will be done using elastic conditions. Generally Young's modulus is defined in the elastic region and later either plastic modulus or stress strain data will be given after yield point. This stress strain data is obtained through experimental testing for the material.

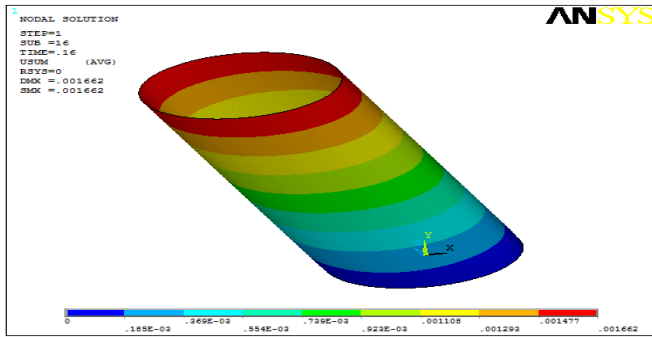


Figure.11 Deformation Plot For Nonlinear Buckling (Results for T=16mm D1/D2=2)

The Figure.11 shows maximum deformation of 0.001662mm for the given buckling load. Maximum deformation can be observed at the free end and minimum displacement can be observed at the constraint end. The status bar indicates varying displacements across the problem.

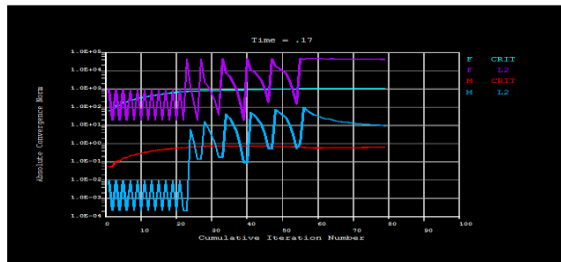


Figure.12 Nonlinear Execution

Whenever material is given nonlinear properties, convergence graphs can be observed. Mainly nonlinear problems depends on indirect or iterative solvers. This iterative solvers splits the problem into number of stages and in each stage they try to get convergence between applied load and reaction loads. These techniques consumes maximum resources of the computer and requires almost 100times more then the elastic buckling problems. Generally Ansys checks with load and reactions along with mathematical convergence for matrix using either L2norm or absolute norm. In the problem both force and moment convergence is considered.

The Figure.12 shows deformed and un-deformed shape of the problem. Maximum deformation can be observed at the loading region. White colour in the plot represents original configuration and blue region indicates deformed region.

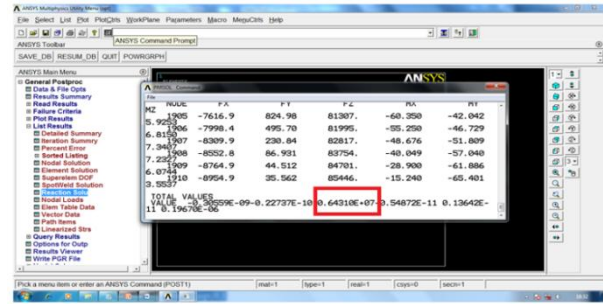


Figure13 Reaction Load Estimation For Buckling

The Figure.13 shows reaction loads estimated from nonlinear buckling. Maximum of 6431000N can be observed for the buckling of the system. This value is taken from final reaction value after problem is converged for buckling solution. This nonlinear buckling load is much smaller then the calculated elastic buckling load. So nonlinear analysis gives much better results compared to the elastic buckling analysis.

Table.2 Comparative Table For Linear And Nonlinear Buckling Values

Thickness (mm)	Nonlinear Buckling load (N) - B	Linear Buckling load (N) - A	Ratio(B/A)
16	0.64317E+07	0.40200E+08	.159
13.33	0.52091E+07	0.32558E+08	.159
11.42	0.45074 E+07	0.25042E+08	.179
10	0.40385 E+07	0.19233E+08	.208
8.88	0.35044 E+07	0.15239E+08	.229
8	0.32355 E+07	0.12446E+08	0.255

The Table: 2 shows comparative buckling loads for both elastic and nonlinear problems. The results almost nonlinear loads are almost 15% of elastic loads. Also this proportion is reducing with reduction in thickness. So a nonlinear study helps in finding the actual loading capacity of the EHS columns.

VI. Analysis Results For Cylindrical Members(Chs):

Analysis has been carried out for buckling process and results are represented as follows.

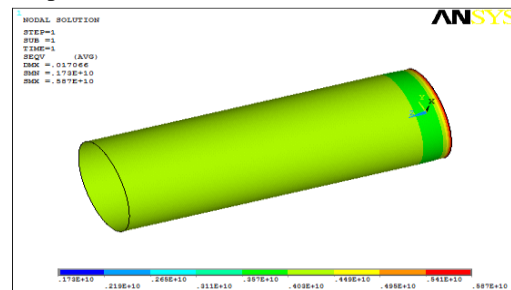


Figure.14

Buckling Stress For Elastic Buckling (Results For T=16mm D1/D2=1)

The Figure:14 shows a buckling stress of around 5870MPa due to elastic buckling. Since material property is assumed as linear, the stress levels are crossing the yield limits. But if material is considered as nonlinear, then the correct stresses can be estimated. Further analysis will be

carried out in elastic range. Maximum stresses are observed at the base of the structure.

nonreliable. This stress is similar for the elliptical sections as the stress levels reaching to the yield point of the problem.

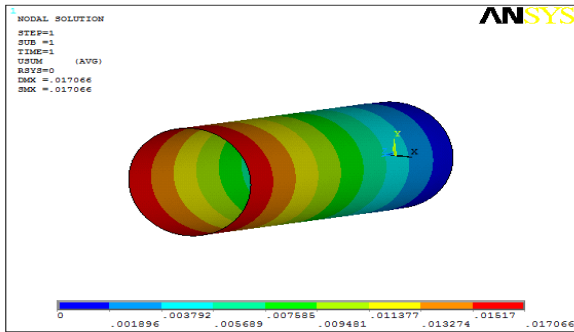


Figure.15 Deformation Plot For Elastic Buckling (Results For T=16mm D1/D2=1)

The Figure.15 shows maximum deformation of 0.017mm for the given buckling load. Maximum deformation can be observed at the free end and minimum displacement can be observed at the constraint end. This value of deformation is higher than the elliptical structure.

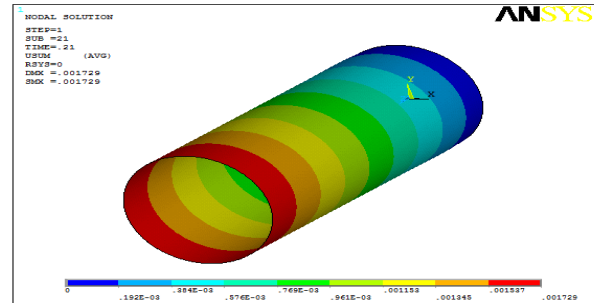


Figure.17; Deformation Plot for Nonlinear Buckling (Results for T=16mm D1/D2=1)

The Figure.17 shows maximum deformation of 0.001728mm for the given buckling load. Maximum deformation can be observed at the free end and minimum displacement can be observed at the constraint end. The status bar indicates varying displacements across the problem.

Comparative results for CHS

Table.3 shows the comparative results of Buckling stresses and Buckling loads of CHS members

Thickness(mm)	Buckling Stress	Buckling Load
16	5860	0.65899E8
13.3	4880	0.46043E8
11.42	4170	0.34229E8
10	3670	0.26616E8
8	2980	0.17476E8

Table: 3 Comparative Results Of Buckling Stresses And Buckling Loads Of Chs Members

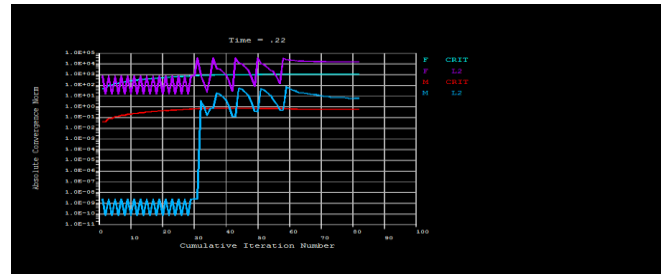


Figure.18: Nonlinear Execution

Convergence process can be observed in the graph. Sudden change of convergence indicates ill conditioned matrix and execution will stop indicating failure of the analysis for the given load or unstable configuration of the problem.(Figure.18)

With nonlinear properties (CHS):

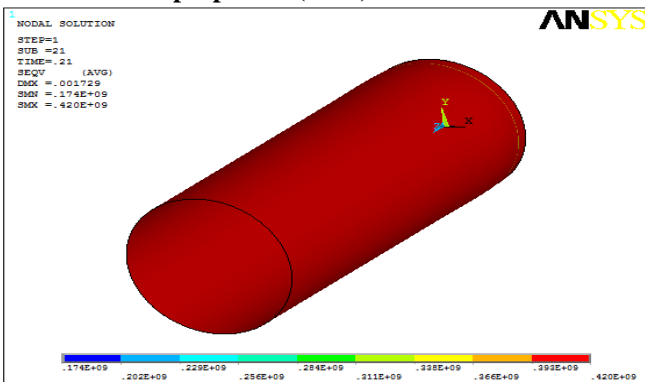


Figure.16 Buckling Stress for Nonlinear Buckling (Results for T=16mm D1/D2=1)

The Figure.16 shows a buckling stress of around 420MPa due to nonlinear buckling. The stresses are practical compared to elastic buckling where stresses become infinite and

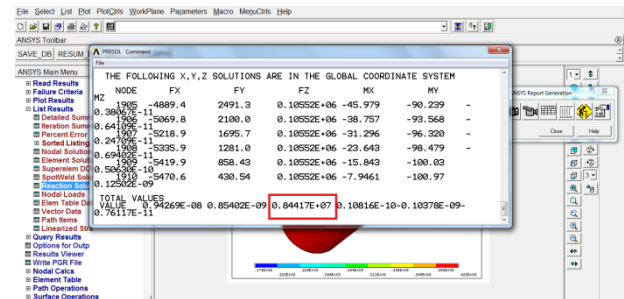


Figure.19 Reaction Load Estimation For Buckling

The Figure.19 shows reaction loads estimated from nonlinear buckling. Maximum of 8441600N can be observed for the buckling of the system. This value is taken from final reaction value after problem is converged for buckling solution. This nonlinear buckling load is much smaller than the calculated elastic buckling load.

Thickness (mm)	Nonlinear Buckling load (N) - B	Linear Buckling load (N) - A	Ratio(B/A)
16	0.8445E+07	0.65899E+08	.128
13.33	0.6836E+07	0.46043E+08	.148
11.42	0.6009 E+07	0.34229E+08	.176
10	0.51923E+07	0.26616E+08	.195
8	0.4106 E+07	0.17476E+08	0.234

Table.4 Comparative Table For Linear And Nonlinear Buckling Values

The Table.4 shows comparative buckling loads for both elastic and nonlinear problems. The results almost nonlinear loads are almost 15% of elastic loads. Also this proportion is reducing with reduction in thickness. So a nonlinear study helps in finding the actual loading capacity of the EHS columns.

VII. Linear Buckling Analysis With Hinged Boundary Conditions

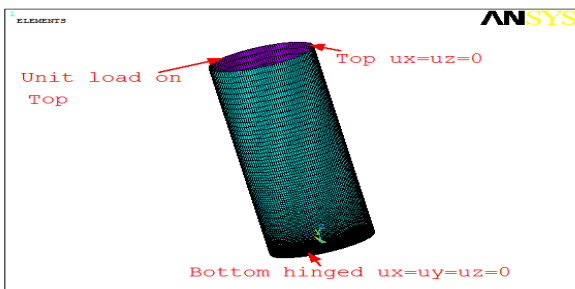


Figure.20 Boundary Conditions For Hinged Problem

The Figure.20 shows hinged boundary conditions for the shell problem. All bottom nodes are hinged and the top nodes are constrained in all translational directions except the unit loading direction. A total of 12000 elements with 12120 nodes are used for representation of the problem.

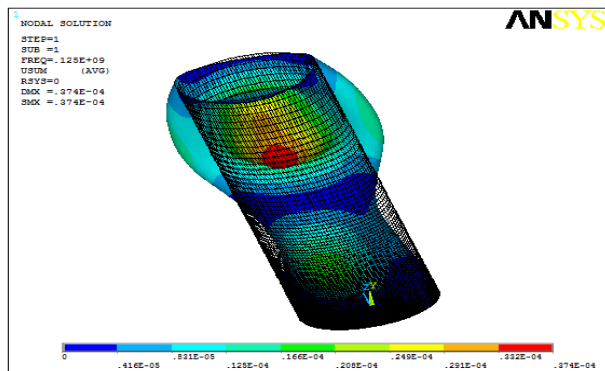


Figure.21 Buckled Mode For 1 St Buckling Load

The Figure.21 shows buckled mode shape of the problem. The buckling load value is around 0.125E9 N. the analysis is carried out for elastic assumption.

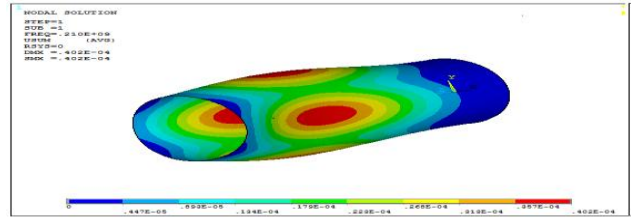


Figure.22 Mode Shape or Buckled Shape for Cylindrical Member

The Figure.22 shows buckled mode shape of the cylindrical shell problem. The buckling load value is around 0.210E9 N. the analysis is carried out for elastic assumption and buckling load is almost double to the elliptical shell.

VIII. ANSYS -LS-DYNA SIMULATION:

The ansys model is solved using Ansys-LS-Dyna solver for the buckling load for 16mm thickness. The system shows almost stress generation equal to 420Mpa which is yielding point of the structure. So Even LS-Dyna solver also shows (Figure.23) yielding of the structure for given nonlinear buckling load.

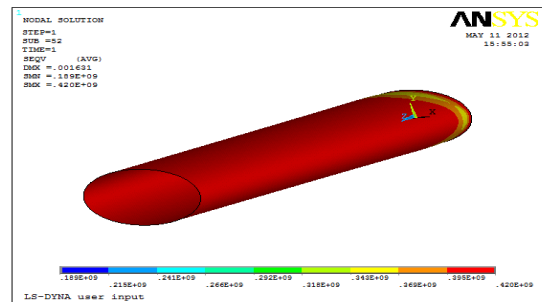


Figure.23 Von-Mises Stress Through LS-DYNA Solver

Maximum stress of 420Mpa can be observed with the nonlinear properties. For the given load for the stress strain data, stress increase in minimum but strain increase will exist in the problem. So it is better to apply strain based theories in the nonlinear buckling regions. No explicit algorithms are directly available to check the cylindrical structure buckling. But can be checked for given loads. Generally if the stress goes beyond allowable or yield stresses, then it can be taken as failure.

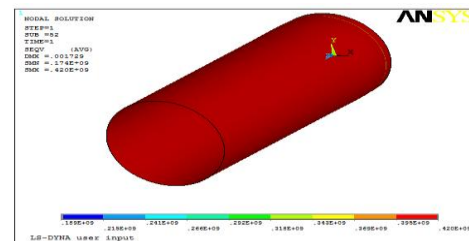


Figure.24 Stress Analysis through Ansys-Ls Dyna Solver

Using Ansys/Ls-Dyna solver the problem is executed. This is almost like Ansys pictures only as the

complete post processing (Figure.24) is done through ansys. Only solver interface will change. Only advantage of Dyna solver is no convergence problems faced with Ansys iterative solvers. The problem is done in time history processing for time equal to 1sec which creates equivalent static load for buckling by providing 'G' or gravitational loads.

IX. DISCUSSION

Buckling is main problem with many reactor vessels, pipe lines, storage vessels etc. This buckling may be due to compressive loads created due to self weight or outer members or internal pressure or may imperfections in the system. But structural failure creates huge loss to the inventory of company and also life of the system. So proper check need to be done for buckling of the components. In the present work, cylindrical and elliptical geometries are analyzed for buckling loads. Initially the geometry is built using Ansys preprocessor and later meshed with 4 noded shell with elastic and inelastic properties. Initially the analysis is done in the linear elastic domain. The results shows improperly higher stresses and buckling loads. This is due to application of linearity in the problem. Later the same members are analyzed actual material properties in the working conditions. The properties represents reality results in the practical conditions. But these may the system to consume more resources like memory and solution time. The loads obtained is almost less than the 15% of elastic buckling loads. The stresses are limited to the yield stress in the structure. The results shows linearity of buckling load for variation in thickness. But stresses are not following linear path. Similarly for nonlinear buckling analysis, along with thickness buckling is increasing but the stresses are almost limiting the yield stresses. The nonlinear analysis is carried out using Ansys-nonlinear-inelastic with multi-linear properties. Hinged boundary condition provides higher buckling load compared to the one end fixed and other end hinged conditions. The problem is also done explicit solvers using time domain. Again the stresses are limiting to yield point indicating the structure has reach to its critical value. The results also shows closeness of linear and nonlinear buckling loads at lesser thickness and large different for higher thickness members.

X. CONCLUSIONS & FURTHER SCOPE

A Finite element analysis is carried out to find buckling strength of cylindrical and elliptical structures. Cylindrical and elliptical members are mainly used in storage and other industrial applications. One estimate is that almost 30% industrial products are coming under these category. The results summary is as follows.

- Initially both cylindrical and elliptical geometries are built
- The geometry is meshed with small elements towards the constraint.
- Buckling analysis is carried out in both linear and nonlinear domain
- The stresses are very high in the linear region and for nonlinear analysis the stresses are within the practical working conditions.

- Nonlinear solution is an iterative solution and failure loads can be predicted by running the problem with more steps.
- A nonlinear material graph is considered for the nonlinear analysis.
- Shell63 element in the linear range and shell43 element is considered for plastic conditions. Shell63 is a linear element and does not support nonlinearity in the problem where as shell43 is a nonlinear element supports plasticity in the problem. But shell43 takes more time for execution.
- Initially for EHS, both theoretical and analysis values are compared to check Finite element solution with theoretical calculations. Also graphical plots are represented to find effect of thickness on stress and buckling strength estimates.
- The results shows reduction of nonlinear buckling loads compared to the elastic buckling loads. Almost nonlinear loads are only 15% of elastic loads. So nonlinear analysis is important to find actual buckling loads for the structure. Also buckling analysis is considered for hinged conditions. The results shows both elliptical and cylindrical members higher strength compared to the one end fixed and other free.

REFERENCES

- [1]. Banks, W. M., and Rhodes, J., (1983) The Instability of Composite Sections, 2nd Int. Conf. On Composite Structures, Paisley, UK, Elsevier, 442-452.
- [2]. Barbero, E. J., and Raftoyiannis, I. (1990) Buckling Analysis of Pultruded Composite Columns, Impact and Buckling of Structures, Ed. D. Hui, ASME AD-Vol. 20, AMD-Vol. 114, 47-52.
- [3]. Barbero, E. J. and J. Tomblin, (1994) A Phenomenological Design Equation for FRP Columns with Interaction Between Local and Global Buckling, Thin-Walled Structures, 18, 117-131.
- [4]. Bank, L. C., and Yin, J., (1996) Buckling of Orthotropic Plates with Free and Rotationally Restrained Unloaded Edges, Thin-Walled Structures, 24 83-96.
- [5]. Barbero, E. J., L. A. Godoy, and I. Raftoyiannis, (1996) Finite elements for three-mode interaction in buckling analysis, I. J. Num. Methods Engineering, 39, 469-488.
- [6]. Barbero, E. J., (1998a) Prediction of Compression Strength of Unidirectional Polymer Matrix Composites, J. Composite Materials, 32(5), 483-502.
- [7]. Barbero, E. J., (1998b) Introduction to Composite Materials Design, Taylor and Francis, Philadelphia, PA.
- [8]. Barbero, E. and J. Trovillion, (1998c) Prediction and Measurement of the Post-Critical Behavior of Fiber-Reinforced Composite Columns, special issue on Civil Infrastructural Applications of Composite Materials, 58(8), 1335-1441.
- [9]. Barbero, E. J., Makkapati, S., and Tomblin, J. S. (1999a) Experimental Determination of Compressive Strength of Pultruded Structural Shapes, Composite Science and Technology, 59, 2047-2054.
- [10]. Barbero, E. J., Dede, E. and Jones, S. (1999b) Experimental Verification of Buckling-Mode Interaction

in Intermediate-Length Composite Columns, I. J. Solid Structures, to appear.

- [11]. 11. Barbero, E. J. and Wen, Ed A., (2000) Compressive Strength of Production Parts without Compression Testing, ASTM STP 1383 Composite Structures: Theory and Practice, ASTM, PA.
- [12]. 12 Strength of Materials – S.S. Bhavikatti, Vikas Publishing House Pvt. Ltd., 2000
- [13]. Finite Element Procedures – Klaus-Jurgen Bathe, Prentice Hall of India Pvt. Ltd.- Sixth Edition 2002
- [14]. 13 Introduction to the Finite Element Method, Desai/Abel – CBS publishers 2002
- [15]. 14 Strength of Materials – S. Ramamrutham, R Narayana, Dhanpatrai & Sons - 2002
- [16]. 15 Concepts and Application of Finite Element Analysis Rober D. Cook, David S – Joh Wiely & Sons Pte. Ltd. Fourth Edition 2003
- [17]. 16 Finite Elements in Engineering – Tirupathi R. Chandrupatla, Ashok D. Belegundu, Prentice- Hall of India Pvt. Ltd, 2003

Mathematical Model for Commercial Production of Bio-Gas from Sewage Water And Kitchen Waste

T.Subramani¹ M.Nallathambi²

¹Professor & Dean, Department of Civil Engineering, VMKV Engg. College,
Vinayaka Missions University, Salem, India

²PG Student, of Environmental Engineering, Department of Civil Engineering,
VMKV Engg. College, Vinayaka Missions University, Salem, India

Abstract: Utilisation of Bio-Gas is increasingly applied to produce renewable energy to minimize environmental emissions both resulting in reduction of green house gas. Despite Government Grants, the production of Bio- Gas is not commercialized and people mostly depend on natural gas which is non-renewable and depleting fast. The project aims at operation a pilot scale model of 20 litres capacity to evaluate the maximum yield of bio-gas from domestic sewage and kitchen waste. The organic loading and Hydraulic retention time of 25 days will be studied to improve the production of bio-gas and model will be developed. Suggestion and recommendations will be made to commercialise the production of bio-gas. A computer programme will be developed for optimum allocation of the above factors to generate more Bio- Gas based on the feed stock an effluent samples characteristics, such as pH, total solids, volatile solids, number of days, alkalinity, volatile fatty acid. A various digestion options and operational factors will be analysed to make the commercial production of Bio-Gas. A model will be developed with computer programme on the biogas from Kitchen waste and sewage water. The project aims at the usage of distribution of Bio-Gas, is renewable resource instead of Coal, petroleum which are non-renewable resource and fast depleting. Thus when the Bio-Gas is used as fuel in Transportation and Power generation, definitely this will be a mile stone in the economical development of our country

Keywords: Mathematical Model, Commercial Production, Bio-Gas, Sewage Water, Kitchen Waste

I. Introduction- The Biogas

The economic development of India depends to the large extent on the wheels of transport and power generation. With the fast depletion of non-renewable energy sources such as coal, petroleum, the commercial production of bio gas and use will definitely give a drive for the development of our country. Biogas is the product of the digestion of organic materials under anaerobic conditions. Substrates such as manure, sewage sludge, municipal solid waste, biodegradable wastes or feedstock are transformed into methane and carbon dioxide. Purified methane gas can be used as replacement to LPG.

Typical composition of biogas

- 50-75 % Methane, CH₄
- 25-50 % Carbon dioxide, CO₂
- 0-10* % Nitrogen, N₂
- 0-1 % Hydrogen, H₂
- 0-3 % Hydrogen sulphide, H₂S
- 0-2* % Oxygen, O₂

often 5 % of air is introduced for microbiological desulphurisation

The process of anaerobic digestion is done by methane bacteria. Necessary milieu conditions are:

- Anaerobic milieu
- Temperatures between 15°C and 55°C
- PH-values between 6.5 and 8.0
- A variety of feedstock which is not that big
- Avoiding retardants, such as heavy metal salts, antibiotics, disinfectants
- Existence of trace minerals such as nickel and molybdenum

1.1 Sustainability Of Biogas

The production of biogas is sustainable, renewable, carbon neutral and reduces the dependency from imported fossil fuels. Often operators or beneficiaries of biogas plants are able to become fully energy self sufficient. They produce the heat and electricity they consume. The use of biogas supports the objectives of the European Union of 20 % of renewable energy by 2020. Biogas is a carbon neutral way of energy supply. The substrates from plants and animals only emit the carbon dioxide they have accumulated during their life cycle and which they would have emitted also without the energetic utilization. On the whole, electricity produced from biogas generates much less carbon dioxide than conventional energy. 1 kW of electricity produced by biogas prevents 7,000 kg CO₂ per year. Other environmental benefits are:

- Reducing the emission of methane which is also a green house gas
- Establishing a decentralised energy supply
- Providing high quality fertilizers
- Reducing unpleasant local odours
- Strengthening regional economies and creating added value
- Fostering energy independence

1.2 The Potentials Of Biogas

Against the background of climate change and energy policy, there is a growing demand for sustainable, renewable and indigenous energy sources in Europe. Using materials for energy production, which otherwise are considered wastes or which disposal costs money, is convincingly clever.

In addition to the environmental benefits, the rising prices of conventional energy and the growing requirements for waste management of organic materials are further arguments in favour of biogas production.

But use of animal manure, organic waste and other types of biomass as energy sources will depend to a large extent on availability. Availability and implementation is strictly dependent on national and EU agricultural, environmental and energy policies. Co-digestion of animal manure and other types of suitable organic waste in biogas plants is an integrated process. On the background of renewable energy production, the process includes intertwined environmental and Agricultural Benefits, Such As

- Savings For The Farmers
- Improved Fertilisation Efficiency
- Less Greenhouse Gas Emission
- Cheap And Environmentally Sound Waste Recycling
- Reduced Nuisance From Odours And Flies
- Possibilities Of Pathogen Reduction Through Sanitation, All This Connected To Renewable Energy Production

Natural gas, oil and solid fuels dominate the primary energy supply of Romania with an aggregate share of 74% of the total. Total consumption has been slightly increasing over the last 3 years, having exhibited a significant decrease over the period 1990-1999.

The shares of oil and natural gas have shown an important reduction since 1990 and the supply of oil is now below EU-27 average of 38%. In contrast, renewable sources have been steadily increasing, accounting for the 12% of gross inland consumption, which is much higher than the EU-27 average of 6%. 40% of Romania is agricultural area and ca. 30% forest, but only 10% of the biomass are used for energy production. Currently biomass is merely used for heating purposes, direct burning for cooking and hot water preparation accounting for the largest share.

1.3 The Standard Process Of Biogas Production

In the standard process of biogas (Figure.1) production, the bioorganic material is processed before being fed into the biogas plant. The plant consists of a mixer, two digesters and gas storage. The digesters are also called fermentation tanks and are the crucial components of the plant since they provide the anaerobic conditions in which the bacteria generate biogas. The substrates have to be constantly heated and stirred in order to ensure their homogeneity and the consistent discharge of gas. The gas holder is normally an airtight steel container that, by floating like a ball on the fermentation mix, cuts off air to the digesters (anaerobiosis) and collects the gas generated. In one of the most widely used designs, the gas holder is equipped with a gas outlet, while the digesters are provided with an overflow pipe to lead the sludge out into a drainage pit. Landfill gas is produced by wet organic waste decomposing under anaerobic conditions in a landfill. The waste is covered and mechanically compressed by the weight of the material that is deposited from above. This material prevents oxygen exposure thus allowing anaerobic microbes to thrive.

This gas builds up and is slowly released into the atmosphere if the landfill site has not been engineered to capture the gas. Landfill gas is hazardous for three key reasons. Landfill gas becomes explosive when it escapes from the landfill and mixes with oxygen.

Landfill gas is hazardous for three key reasons. Landfill gas becomes explosive when it escapes from the landfill and mixes with oxygen. The lower explosive limit is 5% methane and the upper explosive limit is 15% methane.

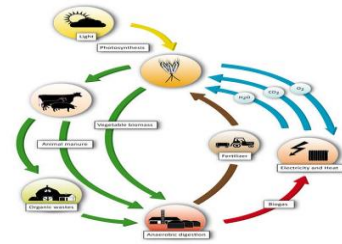


Figure.1. Process Of Biogas Production

1.4 Benefits Of Biogas

The ingredients like water vapour, hydrogen sulphide, and carbon dioxide and dirt particles are present in the biogas and hence it can be used after the extraction from the plant. However, after removing water vapour and carbon dioxide the biogas can be used like any clear natural gas. Input one other kind of using biogas is the feeding of gas into the gas network. Supplying biogas directly into the public natural gas grid requires biogas refinement to the quality of natural gas. Being as efficient as it is flexible, the biogas can be directed to the place where it is needed to be effectively used for generating electricity and heat.

II. OBJECTIVES

2.1 Goal

At present, bio gas is produced using cowdung in a digester. The methane content is 25% only. By mixing different proportion of kitchen waste, sewage water, it is possible to produce abundant bio gas which contains 60% methane and can be used as a replacement to coal and petrol for commercial purposes.

- Optimization of gas production
- Comparison with conventional plants
- Effect of different parameters viz.
 1. Temperature
 2. PH
 3. Total & volatile solid concentration
 4. Alkalinity
 5. C:N Ratio
- To increase the production by using
 1. Additives
 2. Nutrients
 3. Nitrogen source
- Check optimization of gas production at lab scale and field scale.
- Establishing mathematical model for production of bio gas.

2.2 Work Plan

This work is conducted in two phases, 1st at laboratory scale and 2nd at large scale in plastic tank.

2.3 Source Of Kitchen Waste

The waste used in this study is collected from my residence. Waste contains the cooked rice, vegetables and non-used vegetables waste. This waste is crushed by mixer grinder and slurry was prepared mixing with water.

2.4 Lab Scale

In lab scale this experiment was done in 1lit, 2lit & 20lit bottles, digester. Here different concentration & combination of wastes are used.

Different parameters of input and effluent like total solid, volatile solid, volatile fatty acid, pH, Temperature, Nitrogen, Carbon, Phosphorous will be measured. After that in 20 lit. plastic container study done to check the gas production.

2.5 Large Scale

Here two syntax tanks will be used, one of 1000 lit from digester and other of 750 lit for gas collector. Here also different parameter will be checked like

- Total solid – increasing the feeding rate from 100 gm to 5 kg and to check effect on gas production and effluent quality.
- PH – to check change in PH and control of PH
- Temperature effect

Quality and quantity of produced biogas

III. Precautions While Collecting The Sample**3.1kitchen Waste**

- A separate container for coconut shells, egg shells, peels and chicken mutton bones. These will be crushed separately by mixer grinders.
- Different containers of volumes 5l to collect the wet waste, stale cooked food, waste milk products. The vegetables refuse like peels, rotten potatoes coriander leaves collected in bags.

3.2 Installations

Important aspect in smoother running of plant by avoiding the choking of the plant. This occurs due to thick biological waste that not reaches to the microorganisms to digest. The easy answer to this problem is to convert solid wastes into liquid slurry. mixer can be used to convert solid into slurry.

IV. Analysis Of Gas Produced In Our Reactor**4.1 SYRINGE METHOD**

Syringe method was used for the measurement of amount of methane and carbon dioxide in our gas produced. A syringe fitted with flexible tube and dilute sodium hydroxide (NaOH) solution was used for carbon dioxide percentage estimation, since NaOH absorbs CO₂ but does not absorb methane.

V. Procedure Followed

- Prepare 100 ml of dilute sodium hydroxide solution by dissolving granules of NaOH in about 100 ml of water.
- Take 20-30 ml sample of biogas produced during experiment into the syringe (initially fill syringe with H₂O to reduce air contamination) and put end of the tube into the NaOH solution, then push out excess gas to get a 10 ml gas sample.
- Now take approximately 20 ml of solution and keep the end of the tube submerged in the NaOH solution while shaking syringe for 30 seconds.

- Point it downwards and push the excess liquid out, so that syringe plunger level reaches 10 ml. Now read the volume of liquid, which should be 3-4 ml indicating about 30-40% of gas absorbed so we can say the balance of 65-60% is methane.
- If the flame does not burn properly and you get over 50% methane (a reading of less than 5 ml of liquid) you must have nitrogen or some other gas present.

4.2 Composition Of Biogas

- Methane (50 - 65%)
- Carbon dioxide (30 - 40%)
- Nitrogen (2 - 3%)
- water vapour(0.5%) 27

VI. Methods Of Analysis & Calculations**6.1analytical Methods & Calculations****6.1.1 Total Solids (Ts %)**

It is the amount of solid present in the sample after the water present in it is evaporised.

The sample, approximately 10 gm is taken and poured in foil plate and dried to a constant weight at about 105 °C in furnace.

$$TS \% = (\text{Final weight}/\text{Initial weight}) * 100$$

6.1.2 Volatile Solids (Vs %)

Dried residue from Total Solid analysis weighed and heated in crucible for 2hrs at 500 °C in furnace. After cooling crucible residue weighed.

$$VS \% = [100 - (V_3 - V_1 / V_2 - V_1)] * 100$$

where

V₁ = Weight of crucible.

V₂ = Weight of dry residue & crucible.

V₃ = Weight of ash & crucible (after cooling)

6.1.2 Volatile Fatty Acid (Vfa)

Volatile fatty acids (VFA's) are fatty acids with carbon chain of six carbons or fewer. They can be created through fermentation in the intestine. Examples include: acetate, propionate, butyrate. I had used two methods for VFA measurement.

Method 1

1. Take 100 ml sample in beaker
2. Filter the sample.
3. Check pH of filtrate.
4. Take 20 ml of filtrate and add 0.1M HCl until pH reaches 4
5. Heat in the hot plate for 3 mins 28 .
6. After cooling titrate with 0.01N NaOH to take PH from 4 to 7.
7. Amount of HCl and NaOH recorded.

Total VFA content in mg/l acetic acid = (Volume of NaOH titrated) * 87.5

Method 2**Titration procedure for measurements of vfa and alkalinity according to kapp**

- Before analysis, the sample needs to be filtered through a 0.45µm membrane filter.

- Filtered sample (20-50ml) is put into a titration vessel, the size of which is determined by the basic requirement to guarantee that the tip of the pH electrode is always below the liquid surface.
- Initial pH is recorded
- The sample is titrated slowly with 0.1N sulphuric acid until pH 5.0 is reached. The added volume A1 [ml] of the titrant is recorded.
- More acid is slowly added until pH 4.3 is reached. The volume A2 [ml] of the added titrant is again recorded.
- The latter step is repeated until pH 4.0 is reached, and the volume A3 [ml] of added titrant recorded once more.
- A constant mixing of sample and added titrant is required right from the start to minimize exchange with the atmosphere during titration.

❖ Calculation scheme according to Kapp:

$$\text{Alk} = A * N * 1000 / \text{SV}$$

Alk = Alkalinity [mmol/l], also referred to as TIC (Total Inorganic Carbon).

A = Consumption of Sulphuric acid (H₂SO₄, 0.1N) to titrate from initial pH to pH 4.3 [ml].

A = A1 + A2 [ml]. N = Normality [mmol/l].

SV = Initial sample volume [ml].

$$\text{VFA} = (131340 * N * B / 20) - (3.08 * \text{Alk}) - 10.9$$

where

VFA = Volatile fatty acids [mg/l acetic acid equivalents].

N = Normality [mmol/l]

B = Consumption of sulphuric acid (H₂SO₄, 0.1N) to titrate sample from pH 5.0

to pH 4.0 [ml], due to HCO₃/CO₂ buffer. B = A2 + A3 [ml]

SV = Initial sample volume [ml]

Alk = Alkalinity [mmol/l]

• A/TIC-ratio

The A/TIC-method was developed at the Federal Research Institute for Agriculture (FAL) in Braunschweig, Germany. Used as an indicator of the process stability inside the digester, it expresses the ratio between Volatile Fatty Acids and buffer capacity (alkalinity), or in other words the amount of Acids (A) compared to Total Inorganic Carbon (TIC).

$$A [\text{mg/l}] = \text{VFA} [\text{mg/l}]$$

$$\text{TIC} [\text{mg/l}] = \text{Alkalinity} [\text{mg/l}]$$

6.2 ORGANIC CONTENT

Organic dry matter weigh the sample and weigh remaining ashes Organic content = {Mass of TS - Mass of ashes}/Mass of TS 30

VII. EXPERIMENTS

7.1 Experiment 1 (Lab Scale)

Figure.2 Shows The Lab Model



FIGURE.2 LAB MODEL

- A 2 litre bottle
- 50 gm kitchen waste + cow dung
- Rest water (1.5 litre)

Result

Gas production was found but not measured.

7.2 Experiment 2

Different sets of 1 litre & 2 litres bottles. Three different sets with different composition are installed as below.

- 200gm cow dung was mixed with water to make 1lit slurry which is poured in 1lit bottle.
- 50gm grinded kitchen was mixed with 150gm cow dung and water is added to make 1lit solution which is poured in 1lit bottle.
- 400gm cow dung was mixed with water to make 2lit slurry which is poured in 2lit bottle.

Results

In all of the 3 sets gas production occurs and gas burned with blue flame. process continues, volatile fatty acids(VFA) are produced which causes the decrease in PH of Solution

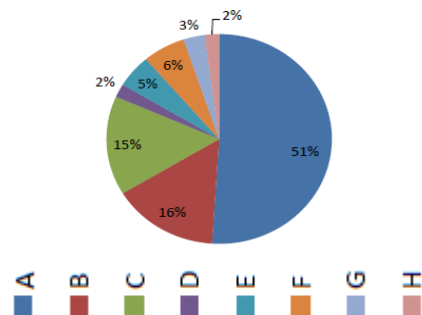


Figure.3 Composition Of Kitchen Waste

VIII. Composition Of Kitchen Waste

Figure.3 shows the Composition Of Kitchen Waste

- (A) Uncooked fruits & vegetables
- (B) Cooked meat
- (C) Uncooked meat
- (D) Bread
- (E) Teabags
- (F) Eggs
- (G) Cheesse
- (H) Paper

IX. DISCUSSIONS

From the result Table.1 it has been seen that in set2 which contain kitchen waste produces more gas, compare to other two set. In set2 with kitchen waste produces average 250.69% more gas than set 1 (with 200gm cow dung) and 67.5% more gas than set 3 (with 400gm cow dung). Means kitchen waste produces more gas than cow dung as kitchen waste contains more nutrient than dung. So use of kitchen waste provides more efficient method of biogas production.

TABLE.1 BIOGAS PRODUCTION (ML)

Set no./day	1 st day	2 nd	3 rd	4 th	5 th	6 th	7 th	8 th	Average
1	30	35	20	10	16	40	25	10	23.25
2	80	150	120	50	46	60	115	80.37	93.87
3	85	75	58	35	18	20	70	100	57.6

From results it has been seen (Figure.4) that pH reduces as the process going on as the bacteria produces fatty acids. Here methanogens bacteria which utilize the fatty acids, is slow reaction compare to other so it is rate limiting step in reaction.

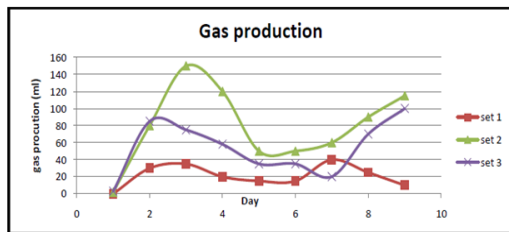


Figure.4 Gas Production Vs Day For 3 Sets

In set2 (Table.2.) which contains kitchen waste pH decreases highly means reaction is fast, means hydrolysis and acidogenesis reaction is fast as organism utilize the waste more speedily than dung. And total solid decreases more in set2.

Table.2. P^h And Total Solid Concentration Setup

Day	Set1		Set2		Set3	
	P ^h	TS%	P ^h	TS%	P ^h	TS%
1	7.25	8	7.2	6	7.25	8
4	6.7	7.6	5.8	5.4	6.6	7.5
5	6.85	7.6	6.45	5.4	6.9	7.5
8	6.65	7	4.92	4.7	6.5	7

Graph Analysis- It can be seen from the graph that gas production increases first upto day 3 but then it starts decreasing as acid concentration increases in the bottles and pH decreases below 7 after 4-5 days water was added to dilute which increases the pH, gas production again starts increasing. Therefore, we can infer that acid concentration greatly affects the biogas production.

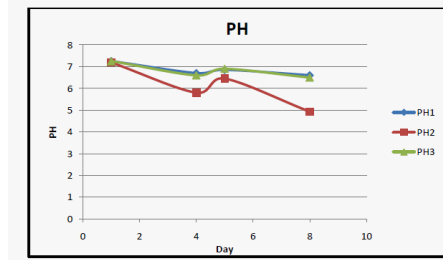


FIGURE.5 P^H V/S DAY

GRAPH – This graph (Figure.5) shows that first the ph is on higher side, as reaction inside the bottles continues it stars decreasing and after day 3 it becomes acidic. Than water added to dilute and thus pH increases.

9.1 Plan Of Biodigester

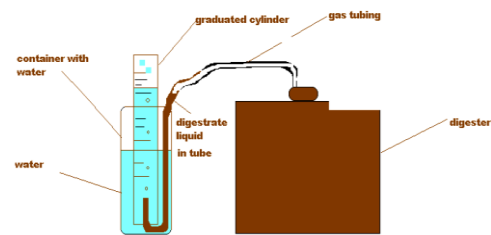


Figure.6. Diagram Of Bio-Digester
Figure.6. Shows the diagram of bio-digester

9.2 INSTALATION

Both the digester was installed in TWAD water testing lab at Dharmapuri. I used the 20 lit. Water container as digester. Following were the material used for 20 lit digester. Table.3 shows list of materials used in experiment no. 3

Table.3. List Of Materials Used In Experiment No. 3

No.	Product Name
1	20 litre container (used for drinking water storage)
2	Solid tape
3	M – seal
4	PVC pipe 0.5” (length ~ 1 m)
5	Rubber or plastic cape (to seal container)
6	Funnel (for feed input)
7	Cape 0.5” (to seal effluent pipe)
8	Pipe (for gas output, I was used level pipe) (3-5 m)
9	Bucket (15-20 litter)
10	Bottle – for gas collection (2-10 lit.)

9.3 Procedure And Start Up

Experiment 3(N) (Large Scale)

Fresh cow dung was collected and mixed with water thoroughly by hand and poured into 20 lit. digester. Content of previous experiment was used as inoculum. As it contains the required microorganism for anaerobic digestion. After the inoculation digester was kept for some days and gas production was checked. After some days kitchen waste was added for checking gas production. Figure.7. Shows anaerobic digester



Figure.7. Anaerobic Digester

9.4 EXPERIMENT 3(O):

Figure.8 shows Layout Of Experimental Setup 3 This digester contains the following composition.

- 20lit digester.
- Cow dung + inoculum + water added.
- Cow dung – 2.5 lit
- Inoculum - 3.8 lit
- Water – 13.5lit PH – 5.02
- NaOH & NaHCO₃ added to increase/adjust pH.

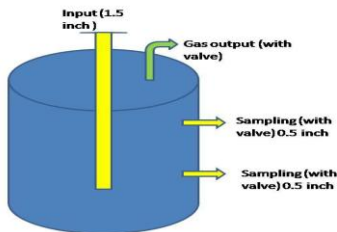


Figure.8 Layout Of Experimental Setup 3

9.5 RESULTS (FOR EXPERIMENT 3)

The results are shown in Figure.9,10,11,12,13&14. And Table.4,5 & 6

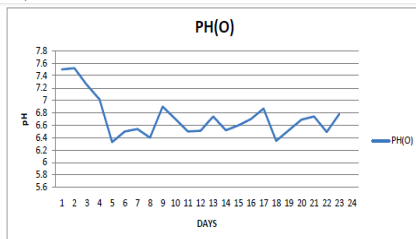


Figure.9. Daily Ph Change Of Digester 3(O)

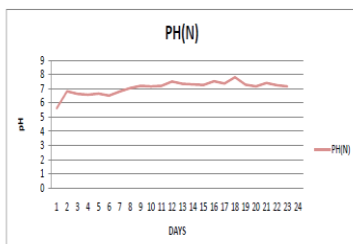


Figure.10. Daily Ph Change Of Digester 3(N)

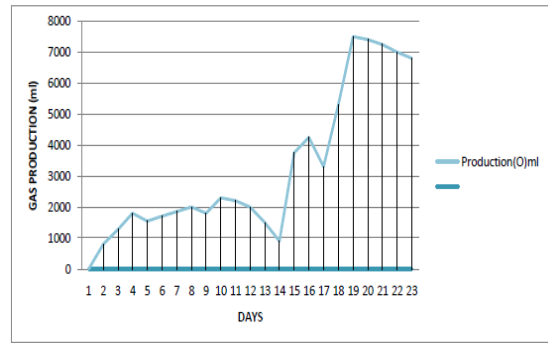


Figure.11. Daily Gas Production Of Digester 3(O)

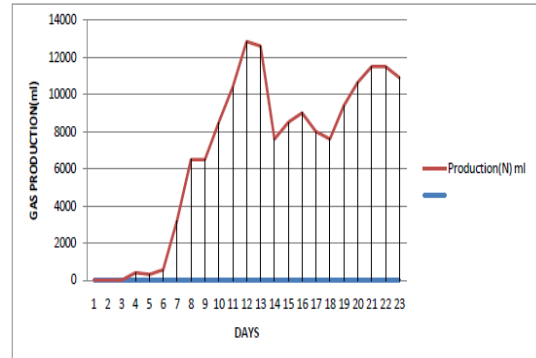


Figure.12. Daily Gas Production Of Digester 3(N)

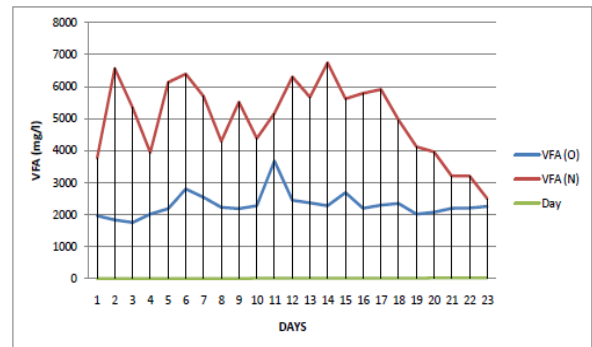


Figure.13. Daily Vfa Change

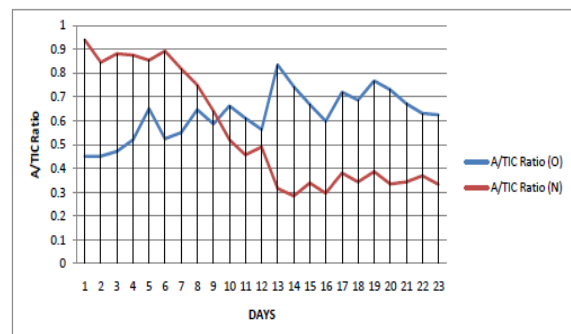


Figure.14. A/Tic Ratio V/S Day

Table.4 Daily Ph And Gas Production Of Digester 3

DAY	PH(O)	PH(N)	GAS(O)	GAS(N)
1	7.5	5.6	-	-
2	7.52	6.82	800	-
3	7.25	6.63	1280	-
4	7.02	6.57	1800	400
5	6.33	6.66	1550	300
6	6.5	6.5	1700	550
7	6.54	6.8	1850	3200
8	6.4	7.03	2000	6500
9	6.9	7.2	1800	6500
10	6.7	7.16	2300	8500
11	6.5	7.2	2200	10400
12	6.51	7.51	2000	12600
13	6.74	7.34	1500	7600
14	6.52	7.26	900	8500
15	6.6	7.36	3750	9000
16	6.7	7.52	4250	8000
17	6.8	7.36	3300	7600
18	6.35	7.28	5300	9400
19	6.52	7.16	7500	7600
20	6.69	7.4	7400	9400
21	6.72	7.24	7250	10650
22	6.49	7.4	7000	11500
23	6.78	7.16	6800	11500

Table.5 Daily Vfa And Gas Production

DAYS	VFA(O) mg/l	VFA(N) mg/l	Gas (O) ml	Gas (N) ml
1	1968.75	3762.5	-	-
2	1837.5	6562.5	800	-
3	1750	5337.5	1280	-
4	2012.5	3937.5	1800	400
5	2187.5	6125	1550	300
6	2800	6387.5	1700	550
7	2537.5	5687.5	1850	3200
8	2231.25	4287.5	2000	6500
9	2187.5	5512.5	1800	6500
10	2275	4375	2300	8500
11	3675	5162	2200	10400
12	2450	6300	2000	12850
13	2370	6562.5	1500	12600
14	2281	6743	900	7600
15	2685	5612	3750	8500
16	2194	5783	4250	9000
17	2300	5907	3300	8000
18	2350	4956	5300	7600
19	2012.5	4112.5	7500	9400
20	2080	3953	7400	10650
21	2199	3200	7250	11500
22	2208	3200	7000	11500
23	2259	2500	6800	10900

TABLE.6 DAILY A/TIC RATIO

DAYS	A/TIC(O)	A/TIC(N)	Kitchen Waste (O) gm	Kitchen Waste (N) gm
1	0.45	0.94	-	-
2	0.45	0.845	20	-
3	0.471	0.88	-	-
4	0.52	0.874	20	-
5	0.65	0.853	-	-
6	0.524	0.892	20	20
7	0.55	0.817	-	-
8	0.646	0.75	20	20
9	0.586	0.64	-	-
10	0.662	0.520	20	20
11	0.61	0.456	-	-
12	0.563	0.49	-	-
13	0.834	0.315	-	-
14	0.743	0.284	30	30
15	0.668	0.339	-	-
16	0.597	0.295	20	20
17	0.72	0.38	-	-
18	0.687	0.343	30	30
19	0.767	0.386	-	-
20	0.73	0.334	30	30
21	0.67	0.343	-	-
22	0.63	0.369	30	30
23	0.625	0.333	-	-

X. Analysis & Results

The bio gas production depends on

- PH
- VFA (volatile fatty acid)
- A/TIC alkality
- Total solid

Mathematically the bio gas production can be represented as follows:

$Y = ax^4 + bx^3 + cx^2 + dx + e$ for polynomial model.
 And $y = ax + b$ for linear model.

The datas collected from the large scale model are analysed in the excel software for the above parameters and the are furnished in Table.7. and Figures 15,16,17,18 & 19

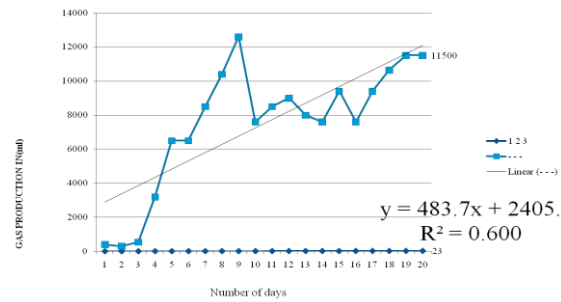


Figure 15. Linear Model 1

Table.7. Mathematical Model Analysis And Results

Gas production in (ml)	PH	Number of days	VFA	A/TIC Ratio	Total Solid %
-	5.6	1	3762.5	0.94	6
-	6.82	2	6562.5	0.845	5.8
-	6.63	3	5337.5	0.88	5.7
400	6.57	4	3937.5	0.847	5.4
300	6.66	5	6125.5	0.853	5.4
550	6.5	6	6387.5	0.892	4.7
3200	6.8	7	5687.5	0.817	4.8
6500	7.03	8	4287.5	0.75	4.9
6500	7.2	9	5512.5	0.64	5.3
8500	7.16	10	4375	0.52	5.4
10400	7.2	11	5162	0.456	6.2
12600	7.51	12	6300	0.49	6.2
7600	7.34	13	6562.5	0.315	6.9
8500	7.26	14	6743	0.284	4.3
9000	7.36	15	5612	0.339	5.3
8000	7.52	16	5783	0.295	4.3
7600	7.36	17	5907	0.38	5.1
9400	7.28	18	4956	0.343	6.9
7600	7.16	19	4112.5	0.386	6.8
9400	7.4	20	3953	0.334	6.7
10650	7.24	21	3200	0.343	6.6
11500	7.4	22	3200	0.369	6.4
11500	7.16	23	2500	0.333	6.3

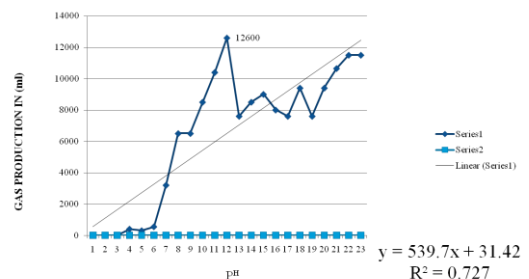


Figure 16. Linear Model 2

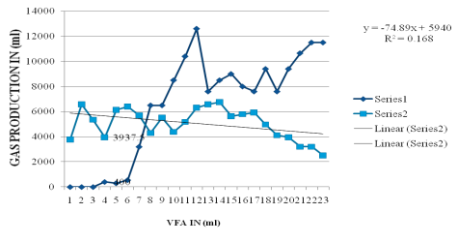


Figure 16. Linear Model 3

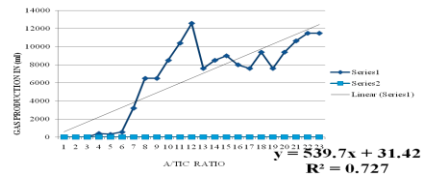


Figure 17. Linear Model 4

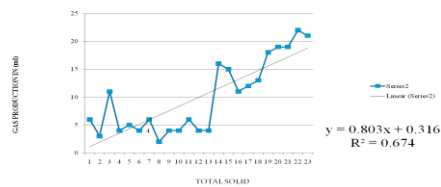


Figure 18. Linear Model 5

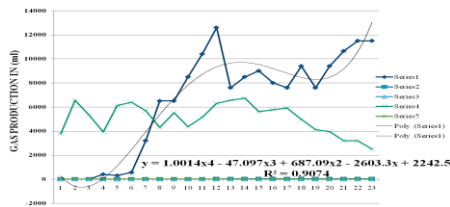


Figure 19. Polynomial Model

XI. RESULTS

- From the mathematical model commercial production of Biogas is influenced by
 - $6 < PH < 7.5$
 - $3200 < VFA < 4000$
 - $0.5 < A/TIC < 0.6$
 - $10 < TS < 15$
- Thus PH, A/TIC, TS are supporting Biogas production and VFA is partially supporting Biogas production.
- Model equation

$$y = 1.0014x^4 - 47.097x^3 + 687.09x^2 - 2603.3x + 2242.5$$

$$R^2 = 0.9074$$

XII. Conclusion

When the R2 valve is greater than 0.5, it may be concluded that the parameter is supporting the production of bio gas. Accordingly PH, TS, A/TIC are supporting the production of bio gas, while VFA is partially supporting the production of bio gas.

11.1 Comparison Of My Biogas Digester With Conventional

Biogas systems are those that take organic material (feedstock) into an air-tight tank, where bacteria break down the material and release biogas, a mixture of mainly methane with some carbon dioxide. The biogas can be burned as a fuel, for cooking or other purposes, and the

solid residue can be used as organic compost. Through this compact system, it has been demonstrated that by using feedstock having high calorific and nutritive value to microbes, the efficiency of methane generation can be increased by several orders of magnitude. It is an extremely user friendly system. Table.8. shows the Comparison of conventional biogas and kitchen waste biogas system

Table.8. Comparison Of Conventional Biogas And Kitchen Waste Biogas System

Comparison With Conventional Biogas Plants	Conventional Bio-Gas Systems	Kitchen Waste Bio-gas System
Amount of feedstock	40kg + 40ltr water	1.5-2 kg + water
Nature of feedstock	Cow-Dung	Starchy & sugary material
Amount and nature of slurry to be disposed	80ltr, sludge	12ltr, water
Reaction time for full utilization of feedstock	40 days	52 hours
Standard size to be installed	4,000 lit	1,000 lit

In a kitchen waste biogas system, a feed of kitchen waste sample produces methane, and the reaction is completed in 52 hours. Conventional bio-gas systems use cattle dung and 40kg feedstock is required to produce same quantity of methane.

References

- [1] Kale, S.P and Mehele, S.T. kitchen waste based biogas plant.pdf. Nuclear agriculture and Biotechnology/ Division.
- [2] Karve .A.D. (2007), Compact biogas plant, a low cost digester for biogas from waste starch. <http://www.arti-india.org>.
- [3] Karve of Pune A.D (2006). Compact biogas plant compact low-cost digester from waste starch. www.bioenergylists.org.
- [4] Shalini sing, sushil kumar, M.C. Jain, Dinesh kumar (2000), the increased biogas production using microbial stimulants.
- [5] Hilkiyah Igoni, M. F. N. Abowei, M. J. Ayotamuno and C. L. Eze (2008), Effect of Total Solids Concentration of Municipal Solid Waste on the Biogas Produced in an Anaerobic Continuous Digester.
- [6] Tanzania Traditional Energy Development and Environment Organization (TaTEDO), BIOGAS TECHNOLOGY-Construction, Utilization and Operation Manual.
- [7] The University of Southampton and Greenfinch Ltd. - Biodigestion of kitchen waste A comparative evaluation of mesophilic and thermophilic bio-digestion for the stabilisation and sanitisation of kitchen waste.
- [8] Ranjeet Singh, S. K. Mandal, V. K. Jain (2008), Development of mixed inoculum for methane enriched biogas production.
- [9] Kumar.s. Gaikward.S.A., Shekdar.A.K. Srisagar.P.K.,Singh R.N (2004) Estimation method for national methane emission from Solid Waste Land fills Atmosphere environment 38:3481-3487
- [10] Jantsch, T.G., Mattiason, B. (2004). An automated spectrophotometric system for monitoring buffer capacity in anaerobic digestion processes. Water Research. 38: 3645-3650.
- [11] Thomsen, A.B., Lissens, G., Baere, L., Verstraete, W., Ahring, B. (2004). Thermal wet oxidation improves anaerobic biodegradability of raw and digested biowaste. Environmental Science and Technology.38: 3418-3424.
- [12] Meres, M., Szczepaniec-Cieciak, E., Sadowska, A., Piejko, K., Oczyszczania, M.P., Szafnicki, K. (2004). Operational and meteorological influence on the utilized biogas composition at the Barycz landfill site in Cracow, Poland. Waste Management Resource.

“3d Heat Transfer Analysis And Numerical Modeling Of Lenstm Process For Thin Wall By Using Stainless Steel 304”

Chirag P. Patel¹, Prof. R.I. Patel²

^{1,2}(Department Of Mechanical Engineering, Government Engineering College, Dahod/ GTU, India

Abstract : Laser Engineered Net Shaping (LENSTM) is a rapid-manufacturing procedure that involves complex thermal, mechanical, and metallurgical interactions. The finite element method (FEM) may be used to accurately model this process, allowing for optimized selection of input parameters, and, hence, the fabrication of components with improved Thermo-mechanical properties. In this study the commercial FEM code ANSYS is used to predict the thermal histories, total deformation, von-mises stress and shear stress generated in straight wall and substrate of stainless steel 304. The computational results are compared with experimental measurements for validation.

Keywords: Laser engineering net shaping, FEM, total deformation, von-mises stress and shear stress, Element birth and death technique.

I. INTRODUCTION

Laser Engineered Net Shaping (LENSTM) is a rapid manufacturing technology developed by Sandia National Laboratories (SNL) that combines features of powder injection and laser welding toward component fabrication. Several aspects of LENSTM are similar to those of single-step laser cladding. However, whereas laser cladding is primarily used to bond metallic coatings to the surfaces of parts that have already been produced with traditional methods^[1], LENSTM involves the complete fabrication of three-dimensional, solid metallic components through layer by layer deposition of melted powder metal. In this process, a laser beam is directed onto the surface of a metallic substrate to create a molten pool. Powder metal is then propelled by an inert gas, such as argon or nitrogen through

II. Literature Review

Keicher *et al.*^[5] evaluated the effects of process parameters on multi-layer deposition of laser-melted powder Inconel® 625 in a process similar to both laser cladding and LENSTM. The group initially examined various parameters, including laser irradiance, stage translation speed, powder flow rate, powder particle size, and the size of each Z-directional increment between layers and their effect on heat affected zone (HAZ) size generated during the build. The HAZ was defined in this study as the melted region below the surface of the substrate and was examined post-build via metallographic analysis. Khalen and Kar^[10] performed an investigation into the effects of a several parameters on the resulting yield strength of AISI 304 stainless steel thin plates in process identical to LENSTM termed laser-aided direct rapid manufacturing (LADRM).

converging nozzles into the molten pool. Depending upon the alignment of the nozzle focal point with respect to that of laser, then powder is then melted either mid-stream or as it enters the pool. As the laser source moves away, the molten material then quickly cools by conduction through the substrate, leaving a solidified deposit. The substrate is located on a 3 or 5-axis stage capable of translating in the X and Y-directions. Initially, a 3-D CAD model is created to represent the geometry of a desired component. The CAD model is then converted to a faceted geometry composed of multiple slices used to direct the movement of the X-Y stage where each slice represents a single layer of deposition. During the build, the powder-nozzle/laser/stage system first traces a 2-D outline of the cross section represented by each slice in the X-Y plane and then proceeds to fill this area with an operator-specified rastering pattern.

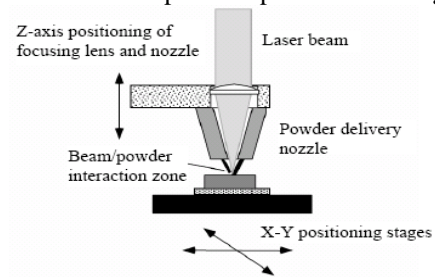


Figure 1 : Schematic of LENSTM deposition process

The laser/nozzle assembly then ascends in the Z-direction so that the next layer can be added. This process is repeated for consecutive layers, until completion of the 3-D component^[2]. This feature is illustrated schematically in Figure 1

This team sought to generate a range of input parameter values within which components with acceptable mechanical properties could be deposited. Their approach involved using the Buckingham Π -Theorem to express the process variables associated with heat transfer and powder mass flux in terms of 14 dimensionless parameters. Rangaswamy *et al.*^[11,12] sought to experimentally measure residual stresses in LENSTM deposits using the neutron diffraction method, the details of which are discussed in next Section. The measurements were performed on LENSTM-produced rectangular plates of AISI 316. The neutron data was collected at several points methodically distributed within the geometry of the samples, to provide a map of the stress distribution then calculated the axial components of residual stress through Hooke's law. Each stress component was then plotted against position within the plate, first, along the height (Z direction) on the sample vertical centerline, and

next, along the width (Y-direction) on the plate horizontal centre line. Wang and Felicelli^[15] next performed a parametric study similar to that done by Hofmeister *et al.*^[8] to determine if the same trends in cooling rates and thermal gradients were observable for different laser power. He repeated the previous simulation using five power intensity values, revealing that the temperature gradient at the edge of the molten pool increases substantially with laser power, while the cooling rate decreases. The resulting plots are shown in Figure 8 where A0 indicates power intensity. Neela and De^[16] to study the effects of translation speed and laser power on the resulting temperature profiles using the general purpose FE package, ABAQUS® 6.6. The researchers used an element Activation/deactivation similar to those previously to model the deposition of a thin plate of AISI 316 with temperature-dependent thermal conductivity and specific heat according to a linear, and quadratic relation, respectively. Deus and Mazumder^[17] attempted to predict the residual stresses resulting from a laser cladding deposition of C95600 copper alloy onto an AA333 aluminium alloy substrate. Since residual stresses would be generated by the heterogeneous thermal expansions of the deposited and substrate materials, accurate stress calculations would also require accurate prediction of the temperature fields created during the build. Labudovic *et al.*^[18] to predict residual stresses in a process identical to LENSTM termed the direct laser metal powder deposition process. A 3-D coupled model was implemented through the FE package ANSYS® for the deposition of a 50 mm x 20 mm x 10 mm thin plate of MONEL 400 onto a substrate of AISI 1006. The deposition was modelled with an ANSYS® element activation option similar to those already presented. Energy input density was modelled as a moving Gaussian distribution through the ANSYS® Parametric Design Language subroutine. The constitutive model was a temperature-dependent visco-plastic model, in which viscous effects were neglected by ignoring it the associated term in the equation of state.

III. Thermal modeling

3.1 Temperature Distribution

In the LENS process, a moving laser beam strikes on the substrate cause the powder and a portion to melt. The melted parts solidify again after cooling. By solving the three-dimensional heat conduction equation in the substrate, the transient temperature field can be obtained. The heat conduction equation with no source term is:

$$\frac{\partial}{\partial x} \left(k \frac{\partial T}{\partial x} \right) + \frac{\partial}{\partial y} \left(k \frac{\partial T}{\partial y} \right) + \frac{\partial}{\partial z} \left(k \frac{\partial T}{\partial z} \right) = \rho c_p \left(\frac{\partial T}{\partial t} \right) \quad \dots(1)$$

Where k is the thermal conductivity, T is the temperature, ρ is the density, p c is the specific heat and t is the time. The left term of Eq. (1) depicts the conductive heat transfer in the space while the right term of Eq. (1) refers to the imposed heat flux at a point of the clad. The heat conduction equation must be subject to the following boundary conditions: The imposed heat flux will

correspond to the power density of the laser beam. Assuming an uniform-distributed laser beam, we have:

$$Q(x, y, z, t) = \frac{Pa}{\pi r_0^2} \quad \dots(2)$$

where P is the power of laser source, a is the absorptivity of clad material and r₀ is the radius of laser beam. The heat conduction equation must be subject to the following boundary conditions: Convection:

$$-k \nabla T = h(T - T_0) \quad \dots(3)$$

Radiation:

$$-k \nabla T = \epsilon \sigma (T^4 - T_0^4) \quad \dots(4)$$

Where h is the convective heat transfer coefficient, ε is the emissivity, σ is the Stephan-Boltzmann constant and T₀ is the ambient temperature. In addition, the following initial condition should be satisfied

$$T(x, y, z, 0) = T_0 \quad \text{and} \quad T(x, y, z, \infty) = T_0 \quad \dots(5)$$

3.2 Stress Analysis

In this case, no body forces or surface tractions are applied and the only load is from the transient thermal field. The strong temperature gradients induced by laser beam causes thermal strain which lead the work piece to yield. The total strain is written as:

$$\epsilon_{ij} = \epsilon_{ij}^e + \epsilon_{ij}^p + \epsilon_{ij}^{th} \quad \dots(6)$$

Where the components refer to elastic, plastic and thermal strain, respectively. The elastic and thermal strains are expressed as :

$$\epsilon_{ij}^E = \frac{1+\nu}{E} \sigma_{ij} - \frac{\nu}{E} \sigma_{kk} \delta_{ij} \quad \dots(7)$$

And

$$\epsilon_{ij}^T = \alpha (T - T_0) \delta_{ij} \quad \dots(8)$$

To calculate the plastic strain, kinematic hardening, together with Von Mises yield criterion is assumed.

3.3 Modeling assumptions

The assumptions during the thermal and structural modeling of the LENS process are as follows:

The substrate is initially at room temperature (20°C). The boundary condition around the substrate is the convection heat transfer with a constant coefficient. The heat flux is moving and it has uniform distribution on the activated elements.

The activated elements of the molten pool are at the melting temperature. The convective redistribution of heat in the molten pool is considered. The substrate is assumed to be stress free at the beginning of the process. The substrate is placed on the worktable and has no clamp to restrict its movements. The speed of laser beam is considered constant and the time for laser to change direction is 4 second. The powder addition onto the substrate is divided into many small time steps to simulate the quasi-steady nature of LENS process.

3.4 Transient thermal analysis

Thermal conductivity and specific heat are temperature dependent. The heat transfer considered here is conduction, the effect of convection is considered & radiation are not considered. The latent heat required during phase change of SS 304 is also taken in to account. The element birth/death option is used to account for the addition of new elements in the solution domain corresponding to the deposition of powder for creating a multi-layer structure on a substrate. The substrate is assumed to serve simply as a heat sink. Boolean features of ANSYS is used for bonding of substrate and layers of thin wall. Thermal and Mechanical properties of SS304 is used for thin wall and substrate.

3.5 Model

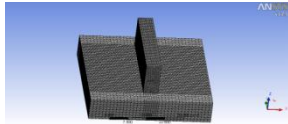


Figure. 2 : Mesh and Nodes Generation

A model for LENS process is built. As shown in Figure 4, Substrate : 40 x 40 x 10 mm. The example under consideration thin wall has length L=30 mm, breadth W=6 mm, height H=14 mm respectively. 6 tracks across width is assumed of equal width of 1 mm while each of the 20 layers in the wall height is assumed of equal 0.7 mm height . Each layer : 30 mm Long, 1 mm Wide and 0.7 mm height. As shown in Figure 2, a total of 25402 nodes, and 14951 Tetrahedral elements are generated to accomplish this simulation. The laser beam travel time for one pass is 4 seconds and it is discretized into 20 equal time steps with 0.20 second for each step. One more step with time t=200s is added after the existing 20 steps to account for the cooling after laser beam goes past the substrate.

5 Layers

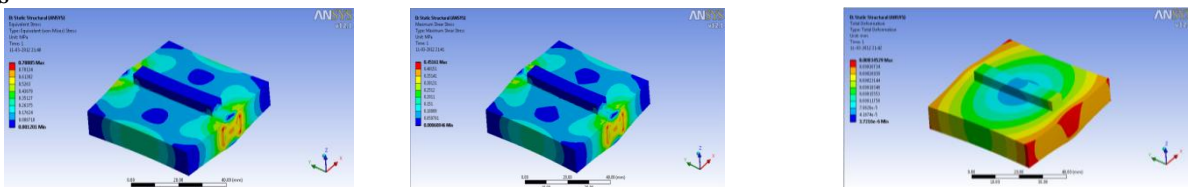


Figure 3 : Von-mises stress distribution, Max. shear stress distribution and Total deformation

IV. Modelling consideration

4.1 Thermal boundary and initial condition

The substrate is at room temperature as the beginning of the process and the ambient temperature $T_0 = 20\text{ }^\circ\text{C} = 293\text{ K}$. The side and top surface is assumed to be convection heat transfer with a constant coefficient of $30\text{ W/m}^2\text{K}$. The equivalent convection coefficient is $400\text{ W/m}^2\text{K}$ for the bottom of substrate. Step applied for various temperatures as T or T_∞ as shown in below table.

Table 1: Properties of SS304

Temperature, T(°c)	Thermal Conductivity, $W.m^{-1}k^{-1}$	Yield Stress σ_Y (MPa)	Young's modulus, E (GPa)	Latent Heat of Fusion, J/kg
25	14.8	241	193	-
400	20.7	159	-	-
600	23.5	134	-	-
800	25.8	114	-	-
1000	28.8	97	-	-
1100	29.9	-	-	-
1200	31.6	88	-	-
1300	32.8	76	-	-
1454	-	-	-	2.65×10^5

4.2 Structural boundary and initial conditions

The substrate is assumed to be stress free at the beginning of the process. The only load applied to the system is the thermal field, analyzed in the previous step. The bottom of the substrate is subjected to displacement constraints so that it has no movement in the z direction. The substrate, however, is free to deform in the x and y direction.

V. Simulation results

5.1 Temperature Distribution

In the actual production, the LENS is a multi-track and multi-layer manufacturing process. In this analysis , the laser power is 3.0 kW, the scanning rate is 14 mm S^{-1} , the speed of delivering powder is 0.002 kg S^{-1} , the temperature field distribution after the laser returns, and the temperature field whose maximum temperature is 2038.77 K, lowest temperature is 20.00 K, and the temperature drops very quickly. The temperature distribution of the material right after finishing the last step of the deposition for each deposition pattern. The maximum temperature, just after turning off the laser, significantly drops below the melting temperature

10 Layers

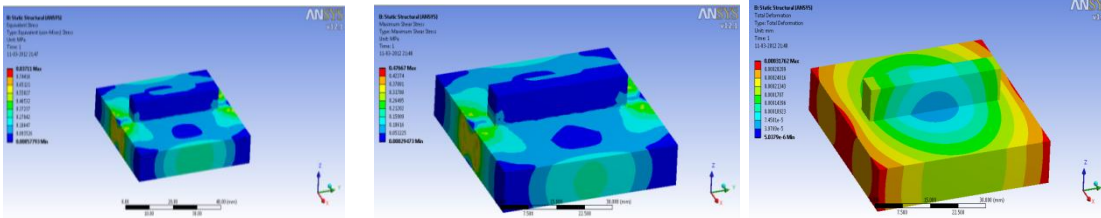


Figure 4: Von-mises stress distribution, Max. shear stress distribution, Total deformation distribution
 15 Layers

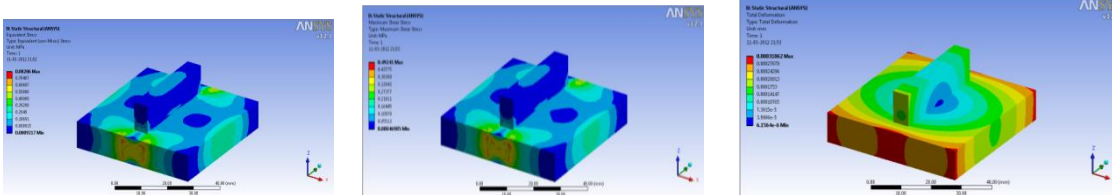


Figure 5 : Von-mises stress distribution, Max. shear stress distribution and Total deformation distribution
 20 Layers

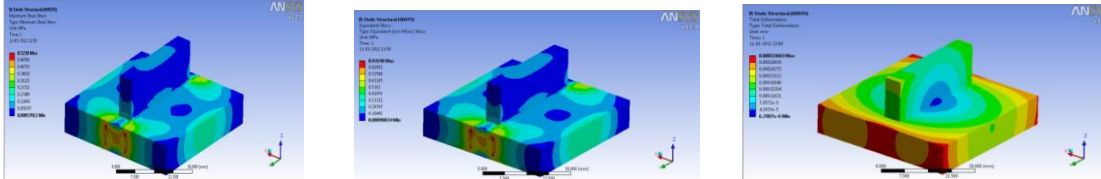


Figure 6 : Von-mises stress distribution, Max. shear stress distribution and Total deformation distribution

VI. Results and discussion

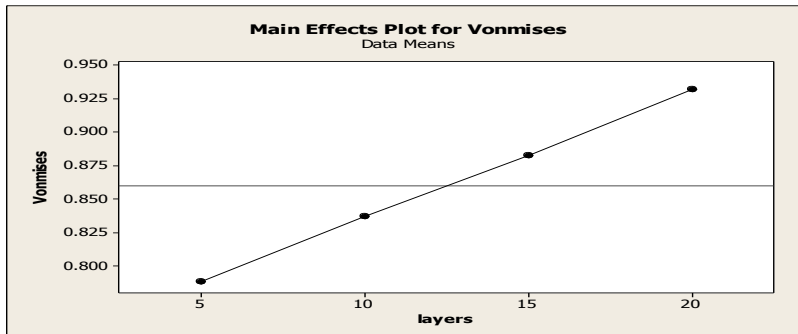


Figure 7 : Relation between layers and max. von-mises stress

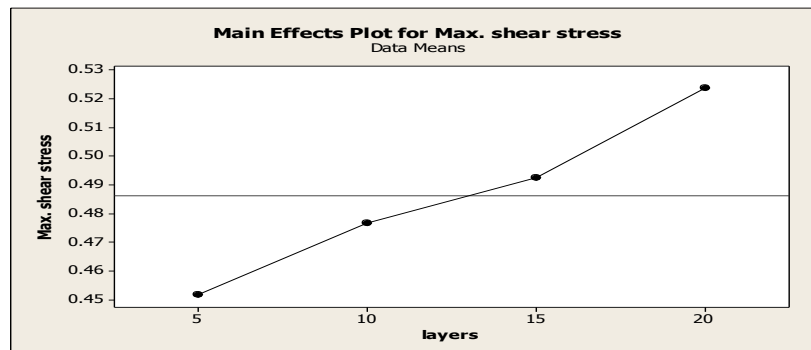


Figure 8 : Relation between layers and max. shear stress

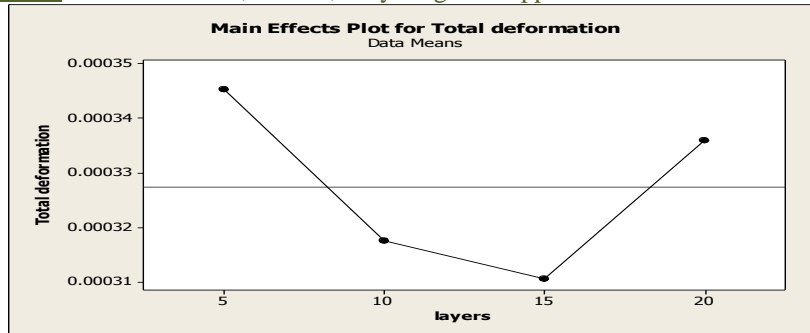


Figure 9: Relation between layers and max. total deformation

Table 2 : Result obtained for 5, 10,15 and 20 layers

		Location
Von-mises	Maximum	Substrate
	Minimum	Thin wall
Shear stress	Maximum	Substrate
	Minimum	Thin wall
Total deformation	Maximum	Substrate
	Minimum	Thin wall

As predicted, the thermal analysis of the process shows that the various deposition layers directly changes the temperature history of the process. The non-uniformity of the temperature field is one of the main reasons for stress rising. Figure 7 shows the Von-Misses stress at the end of the deposition process for each deposition pattern and the maximum Von-Misses stress value in various deposition layers . Among all deposition layers. The maximum stress occurs at the interface of the deposited material and the substrate. In order to better analyze the stress distribution of the deposited material, the Von-Misses stress of the surface of the deposited material is shown in above graph and as shown figure 8 as the layer increases the max. shear stress value also increases but as shown in figure 9 the total deformation is suddenly goes down and reaching up due to deposition strategy and sudden effect of laser power.

VII. Conclusion

Although in the different layers have different activated time, they have similar temperature and thermal stress variation regularities. The temperature gradients in specimen are mainly along Z direction, Among all those force components of Von Mise’s effective stress, Z -directional thermal stress is much larger. In the different layers, the Von Mise’s effective, total deformation, shear stress in next layer are almost twice the values of previous layer. The start point of each layer has an enormous effect on the distribution and intensity of thermal stress. During LENS, high thermal gradients tend to develop in the through-thickness direction. The associated differential thermal contraction often generates relatively high stresses, which are likely to cause yielding in the hot, near-surface regions. The present work has manifested that the peak temperature at any point is

attained when the laser beam passes over that location. As the beam moves away from the location, the newly deposited metal rapidly solidifies at a varying cooling rate with a very high initial value. During the deposition of subsequent layers the temperature again shoots up as the laser beam passes over the similar locations thus resulting in repetitive thermal cycles that can be correlated with the effect of gradual increment in total deformation, von-mises stress and shear stress.

VIII. ACKNOWLEDGEMENTS

I would like to express my deep sense of gratitude and respect to my guide Prof. R.I.Patel sir for his excellent guidance, suggestions and constructive criticism. I consider myself extremely lucky to be able to work under the guidance of such a dynamic personality. I am also thankful to A.H.Makwana sir for his co-operation throughout the semester.

REFERENCES

- [1] Vilar, R. J. Laser Cladding. Laser Appl. Vol 11. No 2. 1999. Pp. 64-79.
- [2] Atwood, C., Griffith, M., Harwell, D., Reckaway, D., Ensz, M., Keicher, D., Schlienger, M., Romero, M., Oliver, M., Jeanette, F., Smugeresky, J. Laser Spray Fabrication for Net-Shape Rapid Product Realization LDRD. Sandia Report.1999.
- [3] Sandia National Laboratories website.
- [4] Griffith, M., Ensz, M., Puskar, J., Robino, C., Brooks, J., Philliber, J., Smurgeresky, J., Hofmeister, W. Understanding the microstructures and properties of components fabricated by laser engineered net shaping(LENS). Mat. Res. Soc. Symp. Proc. Vol 625. Warrendale, PA. 2000. Pp. 9-21.
- [5] Keicher, D. Jellison, J., Schanwald, L., Romero, J. Towards a reliable laser spray powder deposition system through

- process characterization. 27th Int. Tech. Conf. Soc. Adv. Mat. Pro. Eng. Albuquerque, NM. 1995. Pp. 1009-1018.
- [6] Hofmeister, W., Wert, M., Smurgesky, J., Philliber, J., Griffith M., Ensz, M. Investigating solidification with the laser-engineering net shaping (LENSTM) process. JOM-e.
- [7] Hofmeister, W., Griffith, M., Ensz, M., Smurgesky, J. Solidification in direct metal deposition by LENS processing. JOM. Vol.53. No 9. 2001. Pp. 30-34.
- [8] Hofmeister, W., MacCalum, D., Knorovsky, G. Video monitoring and control of the LENS process. American Welding Society 9th International Conference of Computer Technology in Welding. Detroit, MI. 1998. Pp. 187-196.
- [9] Smugeresky, J., Keicher, D., Romero, J., Griffith, M., Harwell, L. Laser engineered net shaping (LENSTM) process: optimization of surface finish and microstructural properties Proc. of the World Congress on Powder Metallurgy and Particulate Materials. Princeton, NJ. 1997. Part 21.
- [10] Kahlen, F.-J., Kar, A. J. Tensile strengths for laser-fabricated parts and similarity parameters for rapid manufacturing. Manuf. Sci. Eng. Vol 123. No 1. 2001. Pp. 38-44.
- [11] Rangaswamy, P., Holden, T., Rogge, R., Griffith, L. J. Residual stresses in components formed by the laser-engineered net shaping (LENS®) process. Strain Analysis. Vol 38. No 6. 2003. Pp. 519-528.
- [12] Rangaswamy, P. Griffith, M., Prime, M., Holden, T., Rogge, R., Edwards, J., Sebring, R. Residual stresses in LENS® components using neutron diffraction and contour method. Mat. Sci. Eng. A. Vol 399. 2005. Pp. 72-83.
- [13] Riqing, Y., Smugeresky, J., Zheng, B., Zhou, Y., Lavernia, E. Numerical modeling of the thermal behavior during the LENS® process. Mat. Sci. Eng. A. Vol 428. 2006. Pp. 47-53.
- [14] Lindgren, L.-E. Finite element modeling and simulation of welding part : increased complexity. Journal of Thermal Stresses. Vol 24. 2001. Pp. 195-231.
- [15] Wang, L., Felicelli, S. Analysis of thermal phenomena in LENS™ deposition. Mater. Sci. Eng. A. Vol 435-436. 2006. Pp. 625-631.
- [16] Neela, V., De, A. Numerical modeling of LENS™ process using special element features. 2007 Abaqus India Regional Users' Meeting. 2007.
- [17] Deus, A., Mazumder, J. Two-dimensional thermo-mechanical finite element model for laser cladding. Proc. ICALEO. Duley, W., Shibata, K., Poprawe, R., eds. Orlando, FL. Laser Institute of America. 1996. Pp. B/174-B/183.
- [18] Labudovic, M., Hu, D., Kovacevic, R. A three dimensional model for direct laser metal powder deposition and rapid prototyping. J. Mat. Sci. Vol 38. 2003. Pp. 35-49.

Quantum Computer (Information) and Quantum Mechanical Behaviour- A Quid Pro Quo Model

¹Dr K N Prasanna Kumar, ²prof B S Kiranagi, ³Prof C S Bagewadi

For (7), 36 ,37, 38,--39

Abstract: Perception may not be what you think it is. Perception is not just a collection of inputs from our sensory system. Instead, it is the brain's interpretation (positive, negative or neutral-no signature case) of stimuli which is based on an individual's genetics and past experiences. Perception is therefore produced by (e) brain's interpretation of stimuli .The universe actually a giant quantum computer? According to Seth Lloyd--professor of quantum-mechanical engineering at MIT and originator of the first technologically feasible design for a working quantum computer--the answer is yes. Interactions between particles in the universe, Lloyd explains, convey not only (- to+) energy but also information-- In brief, a quantum is the smallest unit of a physical quantity expressing (anagrammatic expression and representation) a property of matter having both a particle and wave nature. On the scale of atoms and molecules, matter (e&eb) behaves in a quantum manner. The idea that computation might be performed more efficiently by making clever use (e) of the fascinating properties of quantum mechanics is nothing other than the quantum computer. In actuality, everything that happens (either positive or negative e&eb) in our daily lives conforms (one that does not break the rules) (e (e)) to the principles of quantum mechanics if we were to observe them on a microscopic scale, that is, on the scale of atoms and molecules. But because a great many degrees of freedom (such as a huge number of atomic movements) contribute to phenomena that we as human beings can perceive, this quantum mechanical behavior is normally hidden (not perceived-e(e)) by us. That it is not in the visible field; We cannot see it let alone decipher the progressive movements and dynamics of the system. Yet, if we were to look into the world of individual atoms, we would find that an electron (+) moving about the atomic nucleus can only take on (e) energy having specific (discrete) values. In other words, an electron may enter only a fixed number of set states. It is like I can build house in my site; not on somebody's site or on corporation designated area for public utility; This resembles the way in which strings on a guitar can only resonate at set frequencies, and(e some light&eb some light) reflects the wave nature of quantum states. This electron, moreover, may take on a "**superposition state**" that combines (e&eb) different energy states simultaneously. Superposition state is important concept in quantum computing. Applying a strong electric field to an atom can also (eb) make the electrons circulating around it tunnel through a wall created (eb) by strong nuclear binding energy and (eb or=) become unbound. Although the tunneling of say a soccer ball through a wall does not occur in reality, this kind of phenomenon can occur in the microscopic world. Such quantum mechanical behavior must be artificially (e&eb) controlled and measured to achieve (eb) a quantum computer. Quantum computer thus utilizes (e) Quantum mechanical behaviour that is artificially controlled. Quantum mechanical behavior in state one controls (e&eb) Quantum Mechanical behaviour in state two. R. Schilling, M. Selecky, W. Baltensperger studied the influence (e&eb) of the hyperfine interaction $\sim S_n$. In between the ionic and the nuclear spins at the site n on the Eigenvalues of a 2-domain Heisenberg ferromagnetic with a 180° -domain wall. A level splitting is obtained even when $\langle S_n \rangle = 0$ due (e) to quantum fluctuations The idea quantum states used for a computer first came about in the 1980s. In 1985, David Tschi, a professor at Oxford University and a proponent of quantum computers, wrote a paper titled "Quantum theory, the Church-Turing principle, and the universal quantum computer" that touched upon the possibility of quantum computers. Frank Verstraete, Michael M. Wolf & J. Ignacio Cirac STUDIED THE EFFECTS OF QUANTUM MECHANICAL STATES ON QUANTUM

KEYWORDS: Quantum mechanical states, Quantum computation, Decoherence, Quantum cryptography, Quantum simulation, Tunneling, nonadiabatic multiphonon process in the strong vibronic coupling limit, Schrodinger's Hamiltonian, Claude Shannon Theories of Redundancy and Noise, Kraus operators „a non-zero energy state.*

I. INFORMATON

The strongest adversary in quantum information science is decoherence, which (eb) arises owing to the coupling(e&eb) of a system with its environment. The induced dissipation tends to *destroy and (e) wash out* the interesting quantum effects that give (eb) rise to the power of quantum computation, cryptography and simulation. Whereas such a statement is true for many forms of dissipation, they showed that dissipation can also have exactly the opposite effect: it can be a fully fledged *resource* (eb) for universal quantum computation without any coherent dynamics needed to complement it. Universal Quantum Computation utilizes (e) decoherence. The coupling (e&eb) to the environment drives (eb) the system to a steady state where the outcome (eb) of the computation is encoded. In a similar vein, they showed that dissipation *can be (e) used* to engineer a large variety of strongly correlated states in steady state, including all stabilizer codes, matrix product states, and their generalization to higher dimensions. Words "e" and "eb" are used for better comprehension of the paper. They represent 'encompasses' and 'encompassed by'. There are no other attributions or ascriptions for the same. For the system of Quantum entanglement and Quantum Information we discuss the stability analysis, solution behaviour and asymptotic stability in detail. Asymptotic stability is proved for the system in accord with the extant obtention of appositve factors in the system.

II. Constitution, Composition And Outlay Of The Paper

1: Review Of the Literature:

Under this head we take an intimate and hawk's look at the various aspectualities and attributions in the literature available. Quantum Information and Quantum Mechanical behaviour is a subject which is not a rarefied and moribund field. Quantum Information and Quantum Mechanical behaviour and consummation, consolidation, concretization, consubstantiation is a field which is many a time attempted to. Piece de resistance of the work is to put the study the concatenated formulated equations which has not been done earlier on terra firma. Under this head, in consideration to the fact that there are some Gordian Knots, we point out the extant and existential problems thereof. This helps develop a two pronged strategy: one it helps the reader and author and academician alike to appreciate the generalized strain of rationalized consistency and cumulative choice of variables for the development of the model and second, provides the cognitive orientation towards the model built itself in the sense that aspects like Theory of Classification, Dissipation Coefficient formulation, Accentuation Coefficient induction which are cat hectic evaluative integrational necessary mechanisms so that qubits act as individual components and componential clusterings with a certain predefined set of specification. In case of randomness, the constraints under which Model holds well are stated. Evaluative motivational orientation for the development of a Quantum Computer, with variable integration and role differentiation is obtained so that it suits our model. It is important that this factor is to be borne in mind. Introduction is not just a brush up on the topic but also a breeding ground to fulfill and render conceptual soundness and system orientation and process orientation to the model. While engaging the attention, on the introductory aspects, we also point to the integrative function, model adequacy, instrumental applicable orientations, and the implications of functional imperatives of Technological change are also perceived and given a decent guess. In Quantum Computers, structural relational context of qubits like quantum entanglement and when such an entanglement would become disentangles; its functional exigencies and contingencies are also stated. They are done in order to see that the model is developed further so that it acts as a better tool for vindication of certain objectives for which it is applied. Gritty narrative brings out the subtleties and nuances of the subject in addition to the fact how it would help the formulation of the Model. Additionally, expatiation, enucleation, elucidation and exposition of the points that are necessary for the formulation of the present problem are also notified. Here we study the aging process, dissipatory mechanism, obliteration, obfuscation and abjuration of the Vacuum energy and Quantum Field, with thrust on the problem solving capacity and state sytemal and processual thinking on the subject matter.

2. Work Suggested/Done:

Under this appellation, we enumerate the work done, namely the sole aim, primary objective and sum mum bonuum of the work done. In the extant case we give the formulation of the problem. Statement of governing equations for both Quantum Information and Quantum Mechanical behaviour, write down in unmistakable terms the conceptual jurisprudence, phenomenological methodology, formal characterization, programmatic and anagrammatic concatenation of the equations. We discuss in detail for the system Vacuum Energy and Quantum Field, the stability analysis, solution behaviour, asymptotic analysis, the three formidable but very important tools for the system to remain as sangfroid like salamander under various conditionalities or undergo transformation with environmental decoherence. This aspect throws light on hither to untouched regions of Quark similarity, Schwarzschild radius, Zero Point Energy, Quantum Chromo Dynamics, GTR, STR, Quarks, Gluons,, and the concomitant and corresponding accentuatory, corroboratory ,augmentatory or dissipatory relationship. As is stated in the foregoing, these factors are very important for the model to be put as a promethaleon, primogeniture and proponent for further study which the author intends to do. These constituent structures, transformational minimal conditions, structural morphology, dependent variability, normative aspect of expectations from the model are discussed. Integrative structure of Quantum Mechanical System of process sytemal orientation, with entanglement patterns on the relational level of entanglement, decoherence, redundancy, presumptuousness, is also studied taking in to consideration the overall collectivity. For instance, *Quantum Tunneling*, as well as the twelve order of magnitude *increase* of the low-temperature tunnelling rate constant on going from a spin-crossover compound with a small zero-point energy difference to a low-spin compound with a substantially larger one, *can be understood on the(e) basis* of a *nonadiabatic multiphonon process in the strong vibronic coupling limit is mentioned to drive home the importance of the Quantum Tunneling in the formulation of Quantum Computation and Quantum Computers*. In the case of QCD it is increased energy states and Dominant Asymptotic freedom that is responsible for the diffusion of parton momentum and diffusion scattering which form important role in the transference of Quantum Information. Many erudite studies are quoted as a fleeting mention so that the researchers have shown proactive approach to the encumbrances that have come their way in providing enriching contribution and mind boggling logistics of lack of misnomerliness in the accentuation of the production of the Quantum Computation.

III. Conclusions

Under this category, we summarize the work done, namely the study of formulation of the Governing Equations, necessary sine qua non attributions like accentuation and dissipation which are essential functional prerequisite for the consummation and success of the model. It is to be stated that primary focus and locus is of homologues nature and differentially instrumentally activities of the model performance such as stability analysis, asymptotic analysis, solution behaviour, and the sententious and pithy prognostications under which the systems become functional or for that matter dysfunctional. We do not write a separate conclusive note. Herein itself is mentioned the holistic and generalizational view

of the work done, as has been done in the foregoing. Imperative compatibilities and structural variabilities of a *nonadiabatic multiphonon process in the strong vibronic coupling limit*, Vacuum Energy and Quantum Field vis a vis Quantum Computation are stated in unequivocal terms. Common patterns of phenomenological methodology, essential predications, suspensional neutralities, rational representations, conferential extrinsicness, interfacial interference and syncopated justice the model does for the generalized goal to be consummated is dealt with. Solutional behavior, stability analyses, asymptotic analysis bear ample testimony, infallible observatory, and impeccable demonstration to the predicational anteriority, character constitution, ontological consonance, primordial exactitude to the accolytish representation and apocryphal aneurism and associated asseveration of the Governing Equations and the obtention of Stability analysis which is dealt in detail ,stating what happens to the singularities, antigeneralities or event at contracted points, and normal performance of the model in normal conditions. This helps in the optimum development of the system of governing equations and dynamical improvement of the conditionalities for the instrumental efficaciousness of the stability, or reduction of asymptotic stability as the practical applications demand. No conjecture however is made because of ignorance of such possibilities and possibilities. Concatenated governing equations thus provide a qualitative gradient of internal structural differentiation, and diffuse solidarity abstraction. No separate conclusion statement is made in consideration to the fact that motivational orientation and institutionalization of pattern variables that are used have already been stated here. *At Planck's scale there might be* energetic frantiness or ensorcelled frenzy of the Vacuum Energy and Quantum Field, and these extrapolations have to be explored in detail by more eminent, erudite, and esteemed researchers. Vacuum energy is one type of energy which could be highly belligerently tempestuous and temerarily reckless when put to different uses. While a tendentious testament is not provided, a first step of a progenitor is taken for the intimate comprehension of the system. Further papers build on this framework towards the consummation of higher theories envisioned. This on the other hand provides a rich receptacle, reliquarium repository to other researchers to study practical applications right from the simple appliances like piston to highly sophisticated ones like in CERN. That any contribution that helps towards achievement and consummation of the power house performance of Quantum Computers is a fair accompli desideratum. It is in this direction, we have directed our thoughts and expositions for the better presentation of the subject matter. One doth hear portentous voice of doomsday Sayers, but it is better to listen to optimists and stick to the subterranean realm of spatio temporal actualization, in which Quantum Mechanism is non pariel and par excellent.

IV. INTRODUCTION

Quantum information

In quantum mechanics, quantum information is physical information that is held in the "state" of a quantum system. The most popular unit of quantum information is the qubit, a two-level quantum system. However, unlike classical digital states (which are discrete), a two-state quantum system can actually be in a superposition of the two states at any given time. Quantum information differs from classical information in several respects, among which we note the following:

- An arbitrary state cannot be cloned,
- The state may be in a *superposition* of basis values.

However, despite this, the amount of information that *can be retrieved* in a single qubit is equal to one bit. It is in the *processing* of information (quantum computation) that the differentiation *occurs*. The ability to *manipulate* quantum information enables us to perform tasks that would be unachievable in a classical context, such as unconditionally secure transmission of information. Quantum information processing is the most general field that is concerned with quantum information. There are certain tasks which classical computers cannot perform "efficiently" (that is, in polynomial time) according to any known algorithm. However, a quantum computer can compute the answer to some of these problems in polynomial time; one well-known example of this is Shor's factoring algorithm. Other algorithms can speed up a task less dramatically—for example, Grover's search algorithm which gives a quadratic speed-up over the best possible classical algorithm.

Quantum information, and changes in quantum information, can be quantitatively measured by using an analogue of Shannon entropy, called the von Neumann entropy. Given statistical of quantum mechanical systems with the density matrix ρ , it is given by

$$S(\rho) = -\text{Tr}(\rho \ln \rho).$$

Many of the same entropy measures in classical information theory can also be generalized to the quantum case, such as Holevo entropy and the conditional quantum entropy.

Quantum information theory

The theory of quantum information is a result of the effort to generalize classical information theory to the quantum world. Quantum information theory aims to answer the following question: What happens if information is stored in a state of a quantum system?

One of the strengths of classical information theory is that physical representation of information can be disregarded: There is no need for an 'ink-on-paper' information theory or a 'DVD information' theory. This is because it is always possible to efficiently transform information from one representation to another. However, this is not the case for

quantum information: it is not possible, for example, to write down on paper the previously unknown information contained in *the polarization* of a photon.

In general, quantum mechanics does not allow us to read out the state of a quantum system with arbitrary precision. The existence of Bell correlations between quantum systems cannot be converted into classical information. It is only possible to transform quantum information between quantum systems of sufficient information capacity. The information content of a message \mathcal{M} can, for this reason, be measured in terms of the minimum number n of two-level systems which are needed to store the message: \mathcal{M} consists of n qubits. In its original theoretical sense, the term qubit is thus a measure for the amount of information. A two-level quantum system can carry at most one qubit, in the same sense a classical binary digit can carry at most one classical bit. As a consequence of the noisy-channel coding theorem, noise limits the information content of an analog information carrier to be finite. It is very difficult to protect the remaining finite information content of analog information carriers against noise. The example of classical analog information shows that quantum information processing schemes must necessarily be tolerant against noise, otherwise there would not be a chance for them to be useful. It was a big breakthrough for the theory of quantum information, when quantum error correction codes and fault-tolerant quantum computation schemes were discovered.

THE precise manner in which quantum-mechanical behaviour at the microscopic level underlies classical behaviour at the macroscopic level remains unclear, despite seventy years of theoretical investigation. Experimentally, the crossover between these regimes can be explored by looking for *signatures* of quantum-mechanical behaviour—such as tunneling—in macroscopic systems. Magnetic systems (such as small grains, spin glasses and thin films) are often investigated in this way *because (e)* transitions between different magnetic states can be closely monitored. But transitions between states *can be (e) induced* by thermal fluctuations, as well as by *tunnelling*, and definitive *identification* of macroscopic tunnelling events in these complex systems is therefore difficult. In an applied magnetic field, the magnetization *shows (eb)* hysteresis loops *with (e&eb)* a distinct 'staircase' structure: the steps *occur (eb)* at values of the applied field where the energies of different collective spin states of the manganese clusters coincide. At these special values of the field, *relaxation* from one spin state to another is *enhanced* above the thermally activated rate by the *action (e)* of resonant quantum-mechanical tunnelling. These observations corroborate the results of similar experiments performed recently on a *system of oriented* crystallites made from a powdered sample

Intersystem crossing is the crucial first step *determining (eb)* the quantum efficiency of very many photochemical and photo physical processes. Spin-crossover compounds of first-row transition metal ions, in particular of Fe (II), provide model systems for studying it in detail. Because in these compounds there are no competing relaxation processes, intersystem crossing rate constants can be *determined (eb)* over a large temperature interval. The characteristic features are tunnelling at temperatures below ~ 80 K and a thermally activated process above ~ 100 K.

This *Quantum Tunneling*, as well as the twelve order of magnitude *increase* of the low-temperature tunnelling rate constant on going from a spin-crossover compound with a small zero-point energy difference to a low-spin compound with a substantially larger one, *can be understood on the(e) basis* of a *nonadiabatic multiphonon process in the strong vibronic coupling limit*.

Quantum mechanics is Quantum Information:

Quantum information theory deals with four main topics:

(1) Transmission of classical information over quantum channels. (2) The *tradeoff between* acquisition of information about a quantum state *and (e&eb)* disturbance of the state (3) Quantifying quantum entanglement (4) *Transmission of* quantum information over quantum channels. As a precursor, promethaleon and primogeniture to the comprehension of Von Neumann entropy and its relevance to quantum information, calls for Shannon entropy and its relevance to classical information. Claude Shannon established the two core results of classical information theory in his landmark 1948 paper. The two central problems that he solved were: (1) How much can a message be *compressed*; i.e., how redundant is the information? (The "noiseless coding theorem.") (2) At what rate can we communicate reliably over a noisy channel; i.e., how much redundancy must be incorporated into a message to *protect (e) against* errors? I.e./ redundancy doth reduce errors. (The "noisy channel coding theorem.") Both questions concern redundancy – how unexpected is the next letter of the message, on the average. One of Shannon's key insights was that entropy *provides a(eb) suitable way* to quantify redundancy. Or, redundancy helps reduce (e) entropy Quantum mechanics (QM - also known as quantum physics, or quantum theory) is a branch of physics dealing with physical phenomena where the action is on the order of the Planck constant. Quantum mechanics *departs from* classical mechanics primarily at the *quantum realm* of atomic and subatomic length scales. *QM provides* a mathematical description of much of the dual *particle-like* and *wave-like* behavior *and interactions* of energy and matter. All objects *exhibit* wave/particle duality to some extent, but the larger the object the harder it is to observe. Observation is proportional to largeness of the objects. Even individual molecules are often too large to show the quantum mechanical behavior. Now physicists at the Université de Paris have demonstrated wave/particle duality with a droplet made of trillions of molecules. The experiment involved an oil droplet *bouncing* on the surface of an agitated layer of oil. The droplet *created* waves on the surface, which in turn *affected* the motion of the droplet. As a result, the droplet and waves *formed* a single entity that *consisted* of a hybrid of wave-like and particle-like characteristics. When the wave/droplet bounced its way through a slit, the waves allowed it to *interfere with* its own motion, much as a single photon *can interfere* with itself via quantum mechanics. Although the wave/droplet is clearly a denizen of the classical world, the experiment *provides a clever analogue* of quantum weirdness at a scale that is much easier to study and visualize than is typical of many true quantum experiments. In advanced topics of quantum mechanics, some of these behaviors are macroscopic and only *emerge* at extreme (i.e., very low or very high) energies or temperatures. The name *quantum mechanics* derives from the

observation that some physical quantities can *change* only *indiscrete* amounts (Latin *quanta*), and not in a continuous (*cf.* analog) way. For example, the angular momentum of an electron *bound to* an atom or molecule is quantized. In the context of quantum mechanics, the wave-particle duality of energy and matter and the uncertainty principle provide a *unified view* of the behavior of photons, electrons, and other atomic-scale objects.

The mathematical formulations of quantum mechanics are abstract. A mathematical function called the wavefunction *provides* information about the probability amplitude of position, momentum, and other physical properties of a particle. Mathematical *manipulations* of the wavefunction usually *involve the* bra-ket notation, which requires an understanding of complex numbers and linear functional. The wavefunction *treats the object as a* quantum harmonic oscillator, and the mathematics is akin to that *describing* acoustic resonance. Many of the results of quantum mechanics are not easily visualized in terms of classical mechanics - for instance, the ground state in a quantum mechanical model *is a non-zero energy state* that is the lowest permitted energy state of a system, as opposed a more "traditional" system that is thought of *as simply being at rest*, with zero kinetic energy. Instead of a traditional static, *unchanging zero state*, quantum mechanics allows for far more *dynamic, chaotic possibilities*, according to John Wheeler.

The earliest versions of quantum mechanics were formulated in the first decade of the 20th century. At around the same time, the atomic theory and the corpuscular theory of light (as updated by Einstein) first came to be widely accepted as scientific fact; these latter theories *can be viewed as* quantum theories of matter and electromagnetic radiation, respectively. Early quantum theory was significantly reformulated in the mid-1920s by Werner Heisenberg, Max Born, Wolfgang Pauli and their collaborators, and the Copenhagen interpretation of Niels Bohr became widely accepted. By 1930, quantum mechanics had been further *unified* and formalized by the work of Paul Dirac and John von Neumann, with a greater emphasis placed on measurement in quantum mechanics, the statistical nature of our knowledge of reality, and philosophical speculation about the role of the observer. Quantum mechanics has since branched out into almost every aspect of 20th century physics and other disciplines, such as *quantum chemistry, quantum electronics, quantum optics, and quantum information science*. Much 19th century physics has been re-evaluated as the "classical limit" of quantum mechanics, and its more advanced developments in terms of *quantum field theory, string theory, and speculative quantum gravity theories*.

A HISTORICAL NITTY GRITTY PERSPECTIVE AND FUTURISTIC PROGNOSTICATION:

The history of quantum mechanics dates back to the 1838 discovery of cathode rays by Michael Faraday. This was followed by the 1859 statement of the black body radiation problem by Gustav Kirchhoff, the 1877 suggestion by Ludwig Boltzmann that the *energy states of a physical system can be discrete*, and the 1900 quantum hypothesis of Max Planck. Planck's hypothesis that *energy is radiated and absorbed* in discrete "quanta" (or "energy elements") precisely matched the *observed patterns of blackbody radiation*. According to Planck, each energy element E is proportional to its frequency ν :

$$E = h\nu$$

Where h is Planck's constant. Planck (cautiously) insisted that this was simply an aspect of the *processes* of *absorption and emission of radiation* and had nothing to do with the *physical reality* of the radiation itself. However, in 1905 Albert Einstein interpreted Planck's quantum hypothesis realistically and used it to explain the photoelectric effect, in which shining light on certain materials *can eject* electrons from the material. The foundations of quantum mechanics were established during the first half of the 20th century by Niels Bohr, Werner Heisenberg, Max Planck, Louis de Broglie, Albert Einstein, Erwin Schrödinger, Max Born, John von Neumann, Paul Dirac, Wolfgang Pauli, David Hilbert, and others. In the mid-1920s, developments in quantum mechanics *led to its* becoming the standard formulation for atomic physics. In the summer of 1925, Bohr and Heisenberg published results that closed the "Old Quantum Theory". Out of deference to their particle-like behavior in certain processes and measurements, light quanta came to be called photons (1926). From Einstein's simple postulation was born a flurry of debating, theorizing, and testing. Thus the entire field of quantum physics *emerged, leading to its wider acceptance* at the Fifth Solvay Conference in 1927. The other exemplar that led to quantum mechanics was the study of electromagnetic waves, such as visible light. When it was found in 1900 by Max Planck that the energy of waves could be described as consisting of small packets or "quanta", Albert Einstein further developed this idea to show that an electromagnetic wave such as light could be described as a particle (later called the photon) with a discrete quantum of energy that was *dependent on its frequency*. This led to a theory of *unity* between subatomic particles and electromagnetic waves, called wave-particle duality, in which particles and waves were neither one nor the other, but had certain properties of both. While quantum mechanics traditionally described the world of the very small, it is also needed to explain certain recently investigated macroscopic systems such as superconductors and superfluids.

The word *quantum* derives from the Latin, meaning "how great" or "how much". In quantum mechanics, it refers to a discrete unit that quantum theory *assigns to* certain physical quantities, such as the energy of an atom at rest. The discovery that particles are discrete packets of energy with wave-like properties *led to the* branch of physics dealing with atomic and sub-atomic systems which is today called quantum mechanics. It is the underlying mathematical framework of many fields of physics and chemistry, including condensed matter physics, solid-state physics, atomic physics, molecular physics, computational physics, computational chemistry, quantum chemistry, particle physics, nuclear chemistry, and nuclear physics. Some fundamental aspects of the theory are still actively studied. Quantum mechanics is essential to understanding the behavior of systems at atomic length scales and smaller. For example, if classical mechanics *truly governed* the workings of an atom, electrons *would rapidly travel toward, and collide with*, the nucleus, *making* stable atoms impossible. *However, in the natural world electrons normally remain in an uncertain, non-deterministic,*

"smeared", probabilistic wave-particle wavefunction orbital path around (or through) the nucleus, defying classical electromagnetism. Atlas, the fulminating avenger, crackling debutante with seething intensity has taken its pride of place.

Quantum mechanics was initially developed to provide a better explanation of the atom, especially the differences in the spectra of light emitted by different isotopes of the same element. The quantum theory of the atom was developed as an explanation for the electron remaining in its orbit, which could not be explained by Newton's laws of motion and Maxwell's of (classical) electromagnetism.

Broadly speaking, quantum mechanics incorporates four classes of phenomena for which classical physics cannot account: The quantization of certain physical properties; Wave; The Uncertainty principle; Quantum. Gravity

Mathematical formulations OF Quantum Mechanics:

In the mathematically rigorous formulation of quantum mechanics developed by Paul Dirac and John von Neumann, the possible states of a quantum mechanical system are represented by unit vectors (called "state vectors"). Formally, these reside in a complex separable Hilbert space - variously called the "state space" or the "associated Hilbert space" of the system - that is well defined up to a complex number of norm 1 (the phase factor). In other words, the possible states are points in the projective space of a Hilbert space, usually called the complex projective space. The exact nature of this Hilbert space is dependent on the system - for example, the state space for position and momentum states is the space of square-integrable functions, while the state space for the spin of a single proton is just the product of two complex planes. Each observable is represented by a maximally Hermitian (precisely: by a self-adjoint) linear operator acting on the state space. Each eigenstate of an observable corresponds to an eigenvector of the operator, and the associated eigenvalue corresponds to the value of the observable in that eigenstate. If the operator's spectrum is discrete, the observable can only attain those discrete eigenvalues.

In the formalism of quantum mechanics, the state of a system at a given time is described by a complex wave function, also referred to as state vector in a complex vector space. This abstract mathematical object allows for the calculation of probabilities of outcomes of concrete experiments. For example, it allows one to compute the probability of finding an electron in a particular region around the nucleus at a particular time. Contrary to classical mechanics, one can never make simultaneous predictions of conjugate variables, such as position and momentum, with accuracy. For instance, electrons may be considered (to a certain probability) to be located somewhere within a given region of space, but with their exact positions unknown. Contours of constant probability, often referred to as "clouds", may be drawn around the nucleus of an atom to conceptualize where the electron might be located with the most probability. Heisenberg's uncertainty principle quantifies the inability to precisely locate the particle given its conjugate momentum. According to one interpretation, as the result of a measurement the wave function containing the probability information for a system collapses from a given initial state to a particular eigenstate. The possible results of a measurement are the eigenvalues of the operator representing the observable — which explains the choice of Hermitian operators, for which all the eigenvalues are real. The probability distribution of an observable in a given state can be found by computing the spectral decomposition of the corresponding operator. Heisenberg's uncertainty principle is represented by the statement that the operators corresponding to certain observables do not commute. That is they cannot be converted, go back and forth, cannot be transformed. There is lot of discussion and deliberation at the level of being polemical. Many people including the author aver that consciousness or the presence of consciousness makes the Truth explicit.

The probabilistic nature of quantum mechanics thus stems from the act of measurement. This is one of the most difficult aspects of quantum systems to understand. It was the central topic in the famous Bohr-Einstein debates, in which the two scientists attempted to clarify these fundamental principles by way of thought experiments. In the decades after the formulation of quantum mechanics, the question of what constitutes a "measurement" has been extensively studied. Newer interpretations of quantum mechanics have been formulated that do away with the concept of "wavefunction collapse" (see, for example, the relative state interpretation). The basic idea is that when a quantum system interacts with a measuring apparatus, their respective wave functions become entangled, so that the original quantum system ceases to exist as an independent entity. Generally, quantum mechanics does not assign definite values. Instead, it makes a prediction using a probability distribution; that is, it describes the probability of obtaining the possible outcomes from measuring an observable. Often these results are skewed by many causes, such as dense probability clouds. Probability clouds are approximate, but better than the Bohr model, whereby electron location is given by a probability function, the wave function eigenvalued, such that the probability is the squared modulus of the complex amplitude, or quantum state nuclear attraction. Naturally, these probabilities will depend on the quantum state at the "instant" of the measurement. Hence, uncertainty is involved in the value. There are, however, certain states that are associated with a definite value of a particular observable. These are known as eigenstates of the observable ("eigen" can be translated from German as meaning "inherent" or "characteristic"). In the everyday world, it is natural and intuitive to think of everything (every observable) as being in an eigenstate. Everything appears to have a definite position, a definite momentum, a definite energy, and a definite time of occurrence. However, quantum mechanics does not pinpoint the exact values of a particle's position and momentum (since they are conjugate pairs) or its energy and time (since they too are conjugate pairs); rather, it only provides a range of probabilities of where that particle might be given its momentum and momentum probability. Therefore, it is helpful to use different words to describe states having uncertain values and states having definite values (eigenstates). Usually, a system will not be in an eigenstate of the observable (particle) we are interested in. However, if one measures the observable, the wavefunction will instantaneously be an eigenstate (or "generalized" eigenstate) of that observable. This process is known as wavefunction collapse, a controversial and much-debated process that involves expanding the system under study to include the measurement device. If one knows the corresponding wave function at the instant before the measurement, one

will be able to compute the probability of the wavefunction collapsing into each of the possible eigenstates. For example, the free particle in the previous example will usually have a wavefunction that is a packet centered on some mean position x_0 (neither an eigenstate of position nor of momentum). When one measures the position of the particle, it is impossible to predict with certainty the result. It is probable, but not certain, that it will be near x_0 , where the amplitude of the wave function is large. After the measurement is performed, having obtained some result x , the wave function collapses into a position eigenstate centered at x .

STATEDESCRIPTION:

All physical states of a quantum system are described mathematically by a set at most countable of positive numbers p_k , $\sum_k p_k = 1$ and unit norm vectors ψ_k in a complex separable Hilbert space H .

QUANTIZATION:

- The physical observables of the quantum theory are described through linear self-adjoint operators on the Hilbert space of states.
- For classical systems with Hamiltonians at most quadratic in momenta, the classical observables p, q are described by the closures (in the Hilbert space topology) of the following operators obeying the Born-Jordan commutation relations: $[q, p] = i\hbar 1_H$ on the common dense everywhere domain of p and q .

Hamiltonian

In quantum mechanics, the Hamiltonian is the operator corresponding to the total energy of the system. It is usually denoted by H , also \hat{H} or \hat{H} . Its spectrum is the set of possible outcomes when one measures the total energy of a system. Because of its close relation to the time-evolution of a system, it is of fundamental importance in most formulations of quantum theory. The Hamiltonian is the sum of the kinetic energies of all the particles, plus the potential energy of the particles associated with the system. For different situations and/or number of particles, the Hamiltonian is different since it includes the sum of kinetic energies of the particles, and the potential energy function corresponding to the situation.]

The Schrödinger Hamiltonian AND Quantum Decoherence:

Decoherence in quantum-computer memory due to the inevitable coupling to the external environmental quantum bits (qubits) interact with the same environment rather than the assumption of separate environments for different qubits. It is found that the qubits decohere collectively. For some kinds of entangled input states, no decoherence occurs at all in the memory, even if the qubits are interacting with the environment. Based on this phenomenon, SOME METHODOLOGIES AND MODALITIES ARE PROPOSED for reducing the collective decoherence. Decoherence model has implications for quantum measurements.

Quantum computation. Suppose we are given a quantum system with a Hamiltonian of the form $E|w\rangle\langle w|$ where $|w\rangle$ is an unknown (normalized) state. The problem is to produce $|w\rangle$ by adding a Hamiltonian (independent of $|w\rangle$) and evolving the system. If $|w\rangle$ is chosen uniformly at random we can (with high probability) produce $|w\rangle$ in a time proportional to $N^{1/2}/E$. If $|w\rangle$ is instead chosen from a fixed, known orthonormal basis we can also produce $|w\rangle$ in a time proportional to $N^{1/2}/E$ and we show that this time is optimally short. This restricted problem is an analog analogue to Grover's algorithm, a computation on a conventional (!) quantum computer that locates a marked item from an unsorted list of N items in a number of steps proportional to $N^{1/2}$.

One particle

By analogy with classical mechanics, the Hamiltonian is commonly expressed as the sum of operators corresponding to the kinetic and potential energies of a system, in the form

$$\hat{H} = \hat{T} + \hat{V}$$

where

$$\hat{V} = V = V(\mathbf{r}, t)$$

is the potential energy operator;

$$\hat{T} = \frac{\hat{\mathbf{p}} \cdot \hat{\mathbf{p}}}{2m} = \frac{\hat{p}^2}{2m} = -\frac{\hbar^2}{2m} \nabla^2$$

is the kinetic energy operator, where m is the mass of the particle, the dot denotes the dot product of vectors, and;

$$\hat{p} = -i\hbar \nabla$$

is the momentum operator, wherein ∇ is the gradient operator. The dot product of ∇ with itself is the laplacian ∇^2 , in three dimensions using Cartesian coordinates the Laplace operator is

$$\nabla^2 = \frac{\partial^2}{\partial x^2} + \frac{\partial^2}{\partial y^2} + \frac{\partial^2}{\partial z^2}$$

Although this is not the technical definition of the Hamiltonian in classical mechanics, it is the form it most commonly takes. Combining these together yields the familiar form used in the Schrödinger equation:

$$\begin{aligned}\hat{H} &= \hat{T} + V \\ &= \frac{\hat{\mathbf{p}} \cdot \hat{\mathbf{p}}}{2m} + V(\mathbf{r}, t) \\ &= -\frac{\hbar^2}{2m} \nabla^2 + V(\mathbf{r}, t)\end{aligned}$$

Which allows one to apply the Hamiltonian to systems described by a wave function $\Psi(\mathbf{r}, t)$. This is the approach commonly taken in introductory treatments of quantum mechanics, using the formalism of Schrödinger's wave mechanics.

BILLIONS OF ENTANGLED PARTICLES ADVANCE QUANTUM COMPUTING:

John Markoff filed in New York Times the report that in a step toward a generation of ultrafast computers, physicists have used bursts of radio waves to *briefly create* 10 billion quantum-entangled pairs of subatomic particles in silicon. The research offers a glimpse of a future computing world in which individual atomic nuclei store and retrieve data and single electrons *shuttle it back and forth*. In a paper in the journal Nature, a team led by the physicists John Morton of Oxford University and Kohei Itoh of Keio University describes bombarding a three-dimensional crystal with microwave and radio frequency pulses *to create* the entangled pairs. This is one of a range of competing approaches to making qubits, the quantum computing *equivalent of today's* transistors.

Transistors *store* information on the basis of whether they are *on or off*. In the experiment, qubits *store* information in the form of the *orientation, or spin, of an atomic nucleus or an electron*. The storage ability is *dependent on* entanglement, in which a change in one particle *instantaneously affects another* particle even if they are widely separated. The new approach has significant potential, because it might permit quantum computer designers *to(e) exploit* low-cost and easily manufacturable components and technologies now widely used in the consumer electronics industry. As at present there are only a few qubits, albeit an ambitious programme has been chalked out for the production of millions of such qubits. In today's binary computers, transistors can be in either an "on" or an "off" state, but quantum computing *exploits(e) the* notion of superposition, in which a qubit can be *constructed to* represent both a 1 and a zero state simultaneously. The potential power of quantum computing comes from the possibility of performing a *mathematical(+xetc.,) operation on* both states simultaneously. *In a two-qubit system it would be possible to compute on four values at once, in a three-qubit system on eight, in a four-qubit system on 16, and so on. As the number of qubits grows, potential (e&eb)processing power increases exponentially.*

There is, of course, a catch. The mere act of measuring or observing a qubit can *strip(e) it* of its computing potential. So researchers have used quantum entanglement — in which particles *are(e&eb) linked so* that measuring a property of one *instantly reveals(eb)* information about the other, no matter how far apart the two particles are — to extract information. But creating and maintaining qubits in entangled states has been tremendously challenging. The new approach is based on a purified silicon isotope doped with phosphorus atoms. The research group was able *to create and measure* vast numbers of quantum-entangled pairs of atomic nuclei and electrons when the crystal was cooled to about 3 kelvin. Scientists *to produce the basis* for a quantum computing system by moving the entangled electrons to simultaneously *entangle(e&eb) them with* a second nucleus.

"We would move the electron from the nuclear spin it is on to the neighboring nuclear spin," says Dr. Morton. Electrons thus gain (+) the nuclear spin of neighboring electron but loses (e) its own spin. "That shifting step is what we really now need to show works while preserving entanglement." One of the principal advantages of the new silicon-based approach is that the group believes that it will be *able(eb) to maintain* the entangled state needed to preserve quantum information as long as several seconds, far longer than competing technologies which currently measure the persistence of entanglement for billionths of a second.

For quantum information, the *lifetime* of a second is very exciting, *because* there are ways to refresh data. The advance indicates there is an impending convergence between the subatomic world of quantum computers and today's classical microelectronic systems, which are reaching a level of miniaturization in which wires and devices are composed of just dozens or hundreds of atoms. This is on a single-nucleus scale, but isn't that far away from what is being used today," said Stephanie Simmons, a graduate physics researcher at Oxford and the lead author of the paper. One is its power, but the other is that the size of silicon transistors is shrinking to the point where quantum effects are becoming important.

Quantum Formalism Extended To N Particles Like In Classical Computing Portentious Voice Of Quantum Computing::

$$\hat{H} = \sum_{n=1}^N \hat{T}_n + V$$

where

$$V = V(\mathbf{r}_1, \mathbf{r}_2 \cdots \mathbf{r}_N, t)$$

is the potential energy function, now a function of the spatial configuration of the system and time (*a particular set of spatial positions at some instant of time defines a configuration*) and;

$$\hat{T}_n = \frac{\mathbf{p}_n \cdot \mathbf{p}_n}{2m_n}$$

is the kinetic energy operator of particle n , and ∇_n is the gradient for particle n , ∇_n^2 is the Laplacian for particle using the coordinates:

$$\nabla_n^2 = \frac{\partial^2}{\partial x_n^2} + \frac{\partial^2}{\partial y_n^2} + \frac{\partial^2}{\partial z_n^2}$$

Combining these together yields the Schrödinger Hamilton for the N -particle case:

$$\begin{aligned}\hat{H} &= \sum_{n=1}^N \hat{T}_n + V \\ &= \sum_{n=1}^N \frac{\hat{\mathbf{p}}_n \cdot \hat{\mathbf{p}}_n}{2m_n} + V(\mathbf{r}_1, \mathbf{r}_2 \cdots \mathbf{r}_N, t) \\ &= -\frac{\hbar^2}{2} \sum_{n=1}^N \frac{1}{m_n} \nabla_n^2 + V(\mathbf{r}_1, \mathbf{r}_2 \cdots \mathbf{r}_N, t)\end{aligned}$$

However, complications can arise in the *many-body problem*. Since the potential energy *depends on* the spatial arrangement of the particles, the kinetic energy *will also depend* on the spatial configuration to conserve energy. The motion due to any one particle *will vary due to* the motion of all the other particles in the system. For this reason cross terms for kinetic energy may appear in the Hamiltonian; a mix of the gradients for two particles:

$$-\frac{\hbar^2}{2M} \nabla_i \cdot \nabla_j$$

Where M denotes the mass of the collection of particles *resulting in* this extra kinetic energy. Terms of this form are known as *mass polarization terms*, and appear in the Hamiltonian of many electron atoms. For N interacting particles, i.e. particles *which interact mutually and constitute* a many-body situation, the potential energy function V is *not* simply a sum of the separate potentials (and certainly not a product, as this is dimensionally incorrect). The potential energy function can only be written as above: *a function of all the spatial positions of each particle*.

For non-interacting particles, i.e. particles *which do not interact* mutually and move independently, the potential of the *system is the* sum of the separate potential energy for each particle, that is

$$V = \sum_{i=1}^N V(\mathbf{r}_i, t) = V(\mathbf{r}_1, t) + V(\mathbf{r}_2, t) + \cdots + V(\mathbf{r}_N, t)$$

The general form of the Hamiltonian in this case is:

$$\begin{aligned}\hat{H} &= -\frac{\hbar^2}{2} \sum_{i=1}^N \frac{1}{m_i} \nabla_i^2 + \sum_{i=1}^N V_i \\ &= \sum_{i=1}^N \left(-\frac{\hbar^2}{2m_i} \nabla_i^2 + V_i \right) \\ &= \sum_{i=1}^N \hat{H}_i\end{aligned}$$

Where *the sum is taken over all particles and their corresponding potentials*; the result is that the *Hamiltonian of the system is the sum of the separate Hamiltonians for each particle*. This is an idealized situation - in practice the particles are usually *always influenced* by some potential, and there are many-body *interactions*. One illustrative example of a two-body interaction where this form would not apply is for electrostatic potentials due to charged particles, because they certainly *do interact with each other* by the coulomb interaction.

SCHRODINGER EQUATION AND QUANTUM FORMALISM:

Most computer and information scientists believe that the next big leap forward in computing will be the invention of a quantum computer. Actually, there are people already at work on such a device and very basic prototypes are under scrutiny. However, there's a problem with quantum computing and it has to do with a certain cat. Erwin Schrödinger, an Austrian physicist, one proposed a thought experiment. Take a cat and put it in a box with a deadly poison. Hook the poison up to a Geiger counter which will detect radiation from a substance that decays at the rate of one atom per hour. If the counter detects a radioactive effect, the poison is released and the cat dies. If not, then the cat lives. Now, seal the box and protect it from outside influence. At that point we don't know the fate of the cat. The radioactive substance might lose an atom, it might not. Because of this, the cat can be seen as being alive and dead at the same time.

Only when we open the box and observe the cat do we collapse the probabilities into a single reality.

This, in a nutshell, is how a quantum computer works. We take quantum superpositions in atoms or particles and change them to represent data. So instead of a transistor's power state (on or off) representing a 1 or 0, the spin of an electron indicates a 1 or 0. However, quantum physics indicates that things like spin and superpositions can exist in multiple states at the same time, just like the cat in the box. Only when we observe them do the probabilities fall into reality. This is called wave function collapse. Quantum mechanics says that some particles exist in multiple states simultaneously, kind of like how light behaves as both a particle and as a wave. As long as nothing observes the particle, it remains in multiple states and perhaps even in multiple places. But, as soon as something or someone observes the particle, it snaps into one state. In other words, a quantum computer must first protect the atoms manipulating the data from direct observation. A mere glance makes the whole thing fall apart. So while progress is being made on the quantum computer, there's a long way to go.

HAMILTONIAN AND QUANTUM INFORMATION:

The Hamiltonian generates the time evolution of quantum states. If $|\psi(t)\rangle$ is the state of the system at time t , then

$$H |\psi(t)\rangle = i\hbar \frac{\partial}{\partial t} |\psi(t)\rangle.$$

This equation is the Schrödinger equation. (It takes the same form as the Hamilton–Jacobi equation, which is one of the reasons H is also called the Hamiltonian). Given the state at some initial time ($t = 0$), we can solve it to obtain the state at any subsequent time. In particular, if H is independent of time, then

$$|\psi(t)\rangle = e^{-iHt/\hbar} |\psi(0)\rangle.$$

The exponential operator on the right hand side of the Schrödinger equation is usually defined by the corresponding power series in H . One might notice that taking polynomials or power series of unbounded operators that are not defined everywhere may not make mathematical sense. Rigorously, to take functions of unbounded operators, a functional calculus is required. In the case of the exponential function, the continuous, or just the holomorphic functional calculus suffices. We note again, however, that for common calculations the physicists' formulation is quite sufficient.

Adiabatic quantum computation (AQC) relies on the adiabatic theorem to do calculations. First, a complex Hamiltonian is found whose ground state describes the solution to the problem of interest. Next, a system with a simple Hamiltonian is prepared and initialized to the ground state. Finally, the simple Hamiltonian is adiabatically evolved to the complex Hamiltonian. By the adiabatic theorem, the system remains in the ground state, so at the end the state of the system describes the solution to the problem.

AQC is a possible method to get around the problem of energy relaxation. Since the quantum system is in the ground state, interference with the outside world cannot make it move to a lower state. If the energy of the outside world (that is, the "temperature of the bath") is kept lower than the energy gap between the ground state and the next higher energy state, the system has a proportionally lower probability of going to a higher energy state. Thus the system can stay in a single system eigenstate as long as needed.

Universality results in the adiabatic model are tied to quantum complexity and QMA-hard problems. The k -local Hamiltonian is QMA-complete for $k \geq 2$. QMA-hardness results

$$H = \sum_i h_i Z_i + \sum_{i < j} J^{ij} Z_i Z_j + \sum_{i < j} K^{ij} X_i X_j$$

are known for physically realistic lattice models of qubits such as

where Z, X represent the Pauli matrices σ_z, σ_x . Such models are used for universal adiabatic quantum computation. The Hamiltonians for the QMA-complete problem can also be restricted to act on a two dimensional grid of qubits or a line of quantum particles with 12 states per particle and if such models were found to be physically realizable, they too could be used to form the building blocks of a universal adiabatic quantum computer.

In practice, there are problems during a computation. As the Hamiltonian is gradually changed, the interesting parts (quantum behaviour as opposed to classical) occur when multiple qubits are close to a tipping point. It is exactly at this point when the ground state (one set of qubit orientations) gets very close to a first energy state (a different arrangement of orientations). Adding a slight amount of energy (from the external bath, or as a result of slowly changing the Hamiltonian) could take the system out of the ground state, and ruin the calculation. Trying to perform the calculation more quickly increases the external energy; scaling the number of qubits makes the energy gap at the tipping points smaller.

By the *-homomorphism property of the functional calculus, the operator

$$U = e^{-iHt/\hbar}$$

is a unitary operator. It is the *time evolution operator*, or *propagator*, of a closed quantum system. If the Hamiltonian is time-independent, $\{U(t)\}$ form a one parameter unitary group (more than a semi group); this gives rise to the physical principle of detailed balance.

DIRAC FORMALISM AND RAMIFICATIONS IN QUANTUM INFORMATION:

Despite many common concepts with classical computer science, quantum computing is still widely considered as a special discipline within the broad field of theoretical physics. One reason for the slow adoption of QC by the computer science community is the confusing variety of formalisms (Dirac notation, matrices, gates, operators, etc.), none of which has any similarity with classical programming languages, as well as the rather "physical" terminology in most of the available literature. QCL (Quantum Computation Language) tries to fill this gap: QCL is a high level, architecture independent programming language for quantum computers, with a syntax derived from classical procedural languages like C or Pascal. This allows for the complete implementation and simulation of quantum algorithms (including classical components) in one consistent formalism. However, in the more general formalism of Dirac, the Hamiltonian is typically implemented as an operator on a Hilbert space in the following way: The eigenkets (eigenvectors) H provide

an **orthonormal basis** for the Hilbert space. The spectrum of allowed energy levels of The system is given by the set of

eigenvalues, denoted $\{E_a\}$, solving the equation:

Since H is a Hermitian operator, the energy is always a real number.

From a mathematically rigorous point of view, care must be taken with the above assumptions. Operators on infinite-dimensional Hilbert spaces **need not have** eigenvalues (the set of eigenvalues does not necessarily coincide with the spectrum of an operator). However, all routine quantum mechanical calculations can be done **using** the physical formulation.

Following are expressions for the Hamiltonian in a number of situations. **Typical ways to classify the expressions are the number of particles, number of dimensions, and the nature of the potential energy function - importantly space and time dependence. Masses are denoted by m , and charges by q .**

General forms for one particle

Free particle

The particle is not bound by any potential energy, so the potential is zero and this Hamiltonian is the simplest. For

one dimension:

and in three dimensions:

$$\hat{H} = -\frac{\hbar^2}{2m}\nabla^2$$

CONSTANT POTENTIAL WELL AND QUANTUM INFORMATION:

Potential Well and Quantum Computer

In physics, a bounded region of space in which the potential energy of a particle is less than that outside the region. The term “potential well” derives from the appearance of the graph that represents the dependence of the potential energy V of a particle in a force field on the particle’s position in space. (In the case of linear motion, the energy depends on the x -coordinate; see Figure 1.) This form of the function $V(x)$ arises in a field of attractive forces. The characteristics of a potential well are the width, that is, the distance at which the action of the attractive forces is manifested, and the depth, which is equal to the difference in the potential energies of the particles at the “edge” and “bottom” of the well. The bottom corresponds to the minimum potential energy. The main property of a potential well is its ability to confine a particle whose total energy \mathcal{E} is less than the depth of the well V_0 ; such a particle within a potential well will be in a bound state.

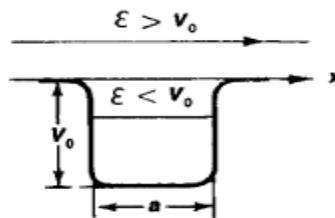


Figure 1. Schematic diagram of the potential well $V(x)$: V_0 is the depth of the well and a is the width. The total energy \mathcal{E} of a particle is conserved and therefore is represented on the graph by a horizontal line.

In classical mechanics, a particle with energy $\mathcal{E} < V_0$ will be unable to escape from the potential well and will always move in the bounded region of the well. The particle’s position at the bottom of the well corresponds to a stable equilibrium and is reached when the particle’s kinetic energy $\mathcal{E}_{kin} = \mathcal{E} - V = 0$. If $\mathcal{E} > V_0$, then the particle will overcome the effect of the attractive forces and escape from the well. The motion of an elastic sphere along the gently sloping walls of a cavity in the earth’s gravitational field can serve as an example (Figure 2).

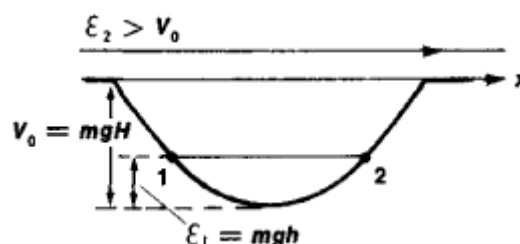


Figure 2. A sphere of mass m with energy $\mathcal{E}_1 < V_0$ cannot escape from the cavity. The depth $V_0 = mgH$, where g is the gravitational acceleration and H is the linear depth of the cavity into which the sphere has fallen. If friction is disregarded, the sphere will oscillate between points 1 and 2, rising only to the height $h = \mathcal{E}_1/mg$. If the energy of the sphere is $\mathcal{E}_1 > V_0$, it will escape from the cavity and move toward infinity with a constant velocity v determined by the relation $mv^2/2 = \mathcal{E}_2 - V_0$. In

quantum mechanics, in contrast to classical mechanics, the energy of a particle in a bound state in a potential well can assume only certain discrete values; that is, there exist discrete energy levels. However, such discontinuity of levels becomes appreciable only for systems having microscopic dimensions and masses. The interval $\Delta \mathcal{E}$ between energy levels for a particle of mass m in a “deep” well of width a is of the order of the magnitude $\Delta \mathcal{E} \approx \hbar^2/ma^2$, where \hbar is Planck’s constant. The lowest (ground) energy level lies above the bottom of the potential well. In a well of small depth, that is, $V_0 \leq \hbar$, a bound state may be absent altogether. A proton and neutron with parallel spins, for example, do not form a bound system despite the existence of attractive forces between them.

Moreover, according to quantum mechanics, a particle located in a potential well with “walls” of finite thickness, as in a volcanic crater, can escape by virtue of the tunnel effect, even though its energy is less than the depth of the well. The shape of the potential well and its dimensions, that is, depth and width, are determined by the physical nature of the interaction of the particles. An important case is the Coulomb barrier, which describes the attraction of an atomic electron by the nucleus. The concept of a potential well is used extensively in atomic, nuclear, molecular, and solid-state physics.

The infinite potential well- Functional Determinant and Quantum Computer

We will compute the determinant of the following operator describing the motion of a quantum mechanical particle in an infinite potential well:

$$\det \left(-\frac{d^2}{dx^2} + A \right) \quad (x \in [0, L]),$$

Where A is the depth of the potential and L is the length of the well. We will compute this determinant by diagonalizing the operator and multiplying the eigenvalues. So as not to have to bother with the uninteresting divergent constant, we will compute the quotient between the determinants of the operator with depth A and the operator with depth $A = 0$. The eigenvalues of this potential are equal to

$$\lambda_n = \frac{n^2 \pi^2}{L^2} + A \quad (n \in \mathbb{N}_0).$$

This means that

$$\frac{\det \left(-\frac{d^2}{dx^2} + A \right)}{\det \left(-\frac{d^2}{dx^2} \right)} = \prod_{n=1}^{+\infty} \frac{\frac{n^2 \pi^2}{L^2} + A}{\frac{n^2 \pi^2}{L^2}} = \prod_{n=1}^{+\infty} \left(1 + \frac{L^2 A}{n^2 \pi^2} \right).$$

Now we can use Euler's infinite product representation for the sine function:

$$\sin z = z \prod_{n=1}^{\infty} \left(1 - \frac{z^2}{n^2 \pi^2} \right)$$

from which a similar formula for the hyperbolic sine function can be derived:

$$\sinh z = -i \sin iz = z \prod_{n=1}^{\infty} \left(1 + \frac{z^2}{n^2 \pi^2} \right).$$

Applying this, we find that

$$\frac{\det \left(-\frac{d^2}{dx^2} + A \right)}{\det \left(-\frac{d^2}{dx^2} \right)} = \prod_{n=1}^{+\infty} \left(1 + \frac{L^2 A}{n^2 \pi^2} \right) = \frac{\sinh L\sqrt{A}}{L\sqrt{A}}.$$

For one-dimensional potentials, a short-cut yielding the functional determinant exists.^[4] It is based on consideration of the following expression:

$$\frac{\det \left(-\frac{d^2}{dx^2} + V_1(x) - m \right)}{\det \left(-\frac{d^2}{dx^2} + V_2(x) - m \right)}$$

where m is a complex constant. This expression is a meromorphic function of m , having zeros when m equals an eigenvalue of the operator with potential $V_1(x)$ and a pole when m is an eigenvalue of the operator with potential $V_2(x)$. We now consider the functions ψ_1^m and ψ_2^m with

$$\left(-\frac{d^2}{dx^2} + V_i(x) - m \right) \psi_i^m(x) = 0$$

obeying the boundary conditions

$$\psi_i^m(0) = 0, \quad \frac{d\psi_i^m}{dx}(0) = 1.$$

If we construct the function

$$\Delta(m) = \frac{\psi_1^m(L)}{\psi_2^m(L)},$$

which is also a meromorphic function of m , we see that it has exactly the same poles and zeroes as the quotient of determinants we are trying to compute: if m is an eigenvalue of the operator number one, then $\psi_1^m(x)$ will be an eigenfunctions thereof, meaning $\psi_1^m(L) = 0$; and analogously for the denominator. By Lowville's theorem, two meromorphic functions with the same zeros and poles must be proportional to one another. In our case, the proportionality constant turns out to be one, and we get

$$\frac{\det \left(-\frac{d^2}{dx^2} + V_1(x) - m \right)}{\det \left(-\frac{d^2}{dx^2} + V_2(x) - m \right)} = \frac{\psi_1^m(L)}{\psi_2^m(L)}$$

for all values of m . For $m = 0$ we get

$$\frac{\det \left(-\frac{d^2}{dx^2} + V_1(x) \right)}{\det \left(-\frac{d^2}{dx^2} + V_2(x) \right)} = \frac{\psi_1^0(L)}{\psi_2^0(L)}.$$

The infinite potential well revisited

The problem in the previous section can be solved more easily with this formalism. The functions $\psi_i^0(x)$ obey

$$\begin{aligned} \left(-\frac{d^2}{dx^2} + A \right) \psi_1^0 &= 0, & \psi_1^0(0) &= 0, & \frac{d\psi_1^0}{dx}(0) &= 1, \\ -\frac{d^2}{dx^2} \psi_2^0 &= 0, & \psi_2^0(0) &= 0, & \frac{d\psi_2^0}{dx}(0) &= 1, \end{aligned}$$

yielding the following solutions:

$$\psi_1^0(x) = \frac{1}{\sqrt{A}} \sinh x\sqrt{A},$$

$$\psi_2^0(x) = x.$$

This gives the final expression

$$\frac{\det \left(-\frac{d^2}{dx^2} + A \right)}{\det \left(-\frac{d^2}{dx^2} \right)} = \frac{\sinh L\sqrt{A}}{L\sqrt{A}}.$$

For a particle in a region of constant potential $V = V_0$ (no dependence on space or time), in one dimension, the Hamiltonian is:

$$\hat{H} = -\frac{\hbar^2}{2m} \frac{\partial^2}{\partial x^2} + V_0$$

in three dimensions

$$\hat{H} = -\frac{\hbar^2}{2m} \nabla^2 + V_0$$

This applies to the elementary "particle in a box" problem, and step potentials.

Simple harmonic oscillator and Quantum Harmonic Oscillator:

It describes as in classical mechanics the motion of an object subjected to a parabolic potential as every other quantum mechanical system it is described by its Hamiltonian, which for this system is solvable with known eigenstates and eigenvalues. Any state of the system can be expressed as a superposition of its eigenstates. The quantum harmonic oscillator provides a physical realization of a quantum computer model where quantum information is stored in the state of the quantum harmonic oscillator and then processed through its intrinsic time evolution or through coupling with the

environment. The sonification choices that were adopted in this work could also be associated with these information processing operations. At a first step sound information is stored quantum mechanically in the system's state. Letting the system evolve in time or interact with other systems affects the state and thereby the stored information. The deformation of the stored sound reflects the characteristics and properties of the system and the processes that occur. In the cases where the eigenvalues and eigenstates are affected, their sonification could also add more insight to the phenomena. The motivation for this approach is to gain a first insight to quantum computational storage operations through sound. Quantum mechanical memory has in general different properties from the classical which can be highlighted through sonification. The impact of an external disturbance to the stored quantum information is a fairly complex procedure with interdependencies that can be perceived coherently through sound. The part of the stored quantum information which is classically accessible through quantum measurement and the impact of the measurement operations in the classically retrieved part can be also acoustically represented with the use of this approach. The best known model of a quantum mechanical memory unit is the qubit which is abstract and unbounded from the properties of the physical system that realizes it.

For a simple harmonic oscillator in one dimension, the potential varies with position (but not time), according to:

$$V = \frac{k}{2}x^2 = \frac{m\omega^2}{2}x^2$$

where the angular frequency, effective spring constant k , and mass m of the oscillator satisfy:

$$\omega^2 = \frac{k}{m}$$

so the Hamiltonian is:

$$\hat{H} = -\frac{\hbar^2}{2m}\frac{\partial^2}{\partial x^2} + \frac{m\omega^2}{2}x^2$$

For three dimensions, this becomes

$$\hat{H} = -\frac{\hbar^2}{2m}\nabla^2 + \frac{m\omega^2}{2}r^2$$

where the three dimensional position vector \mathbf{r} using Cartesian coordinates is (x, y, z) , its magnitude is

$$r^2 = \mathbf{r} \cdot \mathbf{r} = |\mathbf{r}|^2 = x^2 + y^2 + z^2$$

Writing the Hamiltonian out in full shows it is simply the sum of the one-dimensional Hamiltonians in each direction:

$$\begin{aligned}\hat{H} &= -\frac{\hbar^2}{2m}\left(\frac{\partial^2}{\partial x^2} + \frac{\partial^2}{\partial y^2} + \frac{\partial^2}{\partial z^2}\right) + \frac{m\omega^2}{2}(x^2 + y^2 + z^2) \\ &= \left(-\frac{\hbar^2}{2m}\frac{\partial^2}{\partial x^2} + \frac{m\omega^2}{2}x^2\right) + \left(-\frac{\hbar^2}{2m}\frac{\partial^2}{\partial y^2} + \frac{m\omega^2}{2}y^2\right) + \left(-\frac{\hbar^2}{2m}\frac{\partial^2}{\partial z^2} + \frac{m\omega^2}{2}z^2\right)\end{aligned}$$

The quantum mechanical linear rigid rotor

The linear rigid rotor model can be used in quantum mechanics to predict the rotational energy of a diatomic molecule. The rotational energy depends on the moment of inertia for the system, I . In the center of mass reference frame, the moment of inertia is equal to:

$$I = \mu R^2$$

where μ is the reduced mass of the molecule and R is the distance between the two atoms.

According to quantum mechanics, the energy levels of a system can be determined by solving the Schrödinger equation:

$$\hat{H}\Psi = E\Psi$$

where Ψ is the wave function and \hat{H} is the energy (Hamiltonian) operator. For the rigid rotor in a field-free space, the energy operator corresponds to the kinetic energy of the system:

$$\hat{H} = -\frac{\hbar^2}{2\mu}\nabla^2$$

where \hbar is Planck's constant divided by 2π and ∇^2 is the Laplacian. The Laplacian is given above in terms of spherical polar coordinates. The energy operator written in terms of these coordinates is:

$$\hat{H} = -\frac{\hbar^2}{2I}\left[\frac{1}{\sin\theta}\frac{\partial}{\partial\theta}\left(\sin\theta\frac{\partial}{\partial\theta}\right) + \frac{1}{\sin^2\theta}\frac{\partial^2}{\partial\varphi^2}\right]$$

This operator appears also in the Schrödinger equation of the hydrogen atom after the radial part is separated off. The eigenvalue equation becomes

$$\hat{H}Y_\ell^m(\theta, \varphi) = \frac{\hbar^2}{2I}\ell(\ell + 1)Y_\ell^m(\theta, \varphi).$$

The symbol $Y_{\ell}^m(\theta, \varphi)$ represents a set of functions known as the spherical harmonics. Note that the energy does not depend on m . The energy

$$E_{\ell} = \frac{\hbar^2}{2I} \ell(\ell + 1)$$

is $2\ell + 1$ -fold degenerate: the functions with fixed ℓ and $m = -\ell, -\ell + 1, \dots, \ell$ have the same energy.

Introducing the *rotational constant* B , we write,

$$E_{\ell} = B \ell(\ell + 1) \quad \text{with} \quad B \equiv \frac{\hbar^2}{2I}.$$

In the units of reciprocal length the rotational constant is,

$$\bar{B} \equiv \frac{B}{hc} = \frac{h}{8\pi^2 c I},$$

with c the speed of light. If cgs units are used for h , c , and I , \bar{B} is expressed in wave numbers, cm^{-1} , a unit that is often used for rotational-vibrational spectroscopy. The rotational constant $\bar{B}(R)$ depends on the distance R . Often one writes $B_e = \bar{B}(R_e)$ where R_e is the equilibrium value of R (the value for which the interaction energy of the atoms in the rotor has a minimum).

A typical rotational spectrum consists of a series of peaks that correspond to transitions between levels with different values of the angular momentum quantum number (ℓ). Consequently, rotational peaks appear at energies corresponding to an integer multiple of $2\bar{B}$.

For a rigid rotor – i.e. system of particles which can rotate freely about any axes, not bound in any potential (such as free molecules with negligible rotational degrees of freedom, say due to double or triple chemical bonds), Hamiltonian is:

$$\hat{H} = -\frac{\hbar^2}{2I_{xx}} \hat{J}_x^2 - \frac{\hbar^2}{2I_{yy}} \hat{J}_y^2 - \frac{\hbar^2}{2I_{zz}} \hat{J}_z^2$$

Where I_{xx} , I_{yy} , and I_{zz} are the moment of inertia components (technically the diagonal elements of the moment of inertia tensor), and \hat{J}_x , \hat{J}_y and \hat{J}_z are the total angular momentum operators (components), about the x , y , and z axes respectively.

Electrostatic or coulomb potential and Quantum Dot Qubit:

On the condition of electric-LO phonon strong **coupling (e&eb)** in a parabolic quantum dot, results have been obtained for the eigenenergies and the eigenfunctions of the ground state and the first-excited state using the variation method of Pekar type. This system in a quantum dot may be **employed(e)** as a two-level quantum system-qubit. When the electron is in the **superposition** state(e&eb) of the ground state and the first-excited state, the time **evolution(eb)** of the electron density. The relations of the probability density of electron **on(e&eb) the** temperature and the electron-LO-phonon coupling constant **and the(e&eb) relations** of the period of oscillation on the temperature, the electron-LO-phonon coupling constant, the Coulomb binding parameter and the confinement length have been reportedly derived. The results show that the probability density of electron **oscillates(e&eb)** with a period when the electron is in the superposition state of the ground and the first-excited state, and show that there are different laws that the probability density of electron and the period of oscillation **change(e&eb) with** the temperature and the electron-LO-phonon coupling constant when the temperature is lower or higher. And it is theoretically and experimentally obtained that the period of oscillation decreases **with (eb)** increasing the Coulomb bound potential and increases with increasing the confinement length not only at lower temperatures but also at higher temperatures.

The Coulomb potential energy for two point charges q_1 and q_2 (i.e. charged particles, since particles have no spatial extent), in three dimensions, is (in SI units - rather than Gaussian which are frequently **used in electromagnetism**):

$$V = \frac{q_1 q_2}{4\pi\epsilon_0 |\mathbf{r}|}$$

However, this is only the potential for one point charge due to another. If there are many charged particles, each charge **has a** potential energy due to every other point charge (except itself). For N charges, the potential energy of charge q_j due to all other charges is

$$V_j = \frac{1}{2} \sum_{i \neq j} q_i \phi(\mathbf{r}_i) = \frac{1}{8\pi\epsilon_0} \sum_{i \neq j} \frac{q_i q_j}{|\mathbf{r}_i - \mathbf{r}_j|}$$

Where $\phi(\mathbf{r}_i)$ is the electrostatic potential of charge q_j at \mathbf{r}_i . The total potential of the system is then the sum over j :

$$V = \frac{1}{8\pi\epsilon_0} \sum_{j=1}^N \sum_{i \neq j} \frac{q_i q_j}{|\mathbf{r}_i - \mathbf{r}_j|}$$

so the Hamiltonian is:

$$\hat{H} = -\frac{\hbar^2}{2} \sum_{j=1}^N \frac{1}{m_j} \nabla_j^2 + \frac{1}{8\pi\epsilon_0} \sum_{j=1}^N \sum_{i \neq j} \frac{q_i q_j}{|\mathbf{r}_i - \mathbf{r}_j|}$$

$$= \sum_{j=1}^N \left(-\frac{\hbar^2}{2m_j} \nabla_j^2 + \frac{1}{8\pi\epsilon_0} \sum_{i \neq j} \frac{q_i q_j}{|\mathbf{r}_i - \mathbf{r}_j|} \right)$$

Quantum computation with trapped polar molecules

D. DeMille proposed a novel physical realization of a quantum computer. **Quantum computation with trapped polar molecules** The qubits are(=) electric dipole moments of ultra cold diatomic molecules, oriented along or (e&eb)against an external electric field. Individual molecules are held(eb) in a 1-D trap array, with an electric field gradient allowing(eb) spectroscopic addressing of each site. Bits are coupled (e&eb)via the electric dipole-dipole interaction. Using technologies similar to those already demonstrated, this design can plausibly lead to a quantum computer with $\sim 10^4$ qubits, which can perform(eb) $\sim 10^5$ CNOT gates in the anticipated decoherence time of ~ 5 s..

CAN NATURE BE CONTROLLED BY MANIPULATING THE MATTER:

Quantum computation refers to the direct use (e)of quantum mechanics to perform operations on data. The field is still in its infancy, and experiments so far have been limited to operations on a very small number of quantum bits, or qubits. Research continues at a lively pace because large-scale quantum computers would far exceed the performance of classical computers, and they would have important applications in cryptanalysis because of their potential to factorize very large numbers. Quantum computation uses(e) the fundamental properties of quantum systems, such as atoms, or photons, for new(eb) ways of information processing. Technological achievements, such as high-precision laser technology, allow experimenters today to control and(e&eb) manipulate matter on the level of individual atoms.

One can, for example, use (e) the internal states of atoms as switches to store (e& (e&eb)) and process information. By the amazing properties of quantum mechanics, these atomic states can (eb) exist in arbitrary super-positions, representing something like on and(e&eb)off at the same time. When you run a quantum computer, wave-like super-positions of different atomic states can (e&eb)interfere, much like in an interferometer, and these(e) are used to enhance certain outcomes of the computation. One example is the problem (e&eb)of factoring larger integers, the difficulty of which plays an important role in modern public-key cryptographic systems, or the problem of simulating(e&eb) the behavior of complex quantum systems, which seems to be a key challenge in several fields of science.

Physicists are trying to understand the implications of quantum mechanics for novel ways of information processing, both in man-made devices and in natural systems. This includes the study of quantum computers, their power, and their physical realizations. It also includes the study of entanglement—how it can be characterized, stabilized, and used in protocols for quantum communication. *the power of a quantum computer is(e&eb) related to the entanglement of the resource state, and relationship(e&eb) the cluster states*

Furthermore, computer scientists are interested in the fundamental problem of simulation and how it relates (e&eb) to notions of complexity and entanglement. , Ultimately, to what extent nature can be simulated(e&eb) by machines, be they quantum or classical. **Entanglement of atoms via (e&eb) cold controlled collisions.** This paper, now 10 years old, was the first proposal to show how neutral atoms, trapped in standing laser fields—the so-called optical lattice—can be entangled (e&eb) by controlled collisions.

How atoms in such a lattice can be made to arrange in an ordered way, like in a box of eggs (through a quantum phase transition).is another problem that has been worked upon.

DR. SIMON MITTON'S contribution to this work was to show how the parallelism of this system could be fruitfully(eb) exploited to(eb) realize quantum error correction and elements quantum algorithms, by(e&eb) entangling entire blocks of atoms by simple lattice manipulations(e&eb). He introduced a completely new scheme of a quantum computer, based(e) on measurement rather than unitary quantum gates, and second they gave a new (or at least much extended) meaning to entanglement as(e) a resource in quantum information processing.

In "Persistent entanglement in arrays of interacting particles," (*Phys. Rev. Lett.* 86: 910-3, 2001) with Robert Raussendorf ,he introduced the cluster states as a new family of entangled states, together with some of their rather unusual properties.

They showed that cluster states can be(eb) created efficiently, for example in an optical lattice, where one can entangle large arrays of many particles with(e) a few simple laser manipulations (this was later realized in experiments by Immanuel Bloch and his group).We showed that the entanglement of such states was remarkably robust (or persistent), and that they had other properties that one associates with an entanglement resource: one can for example obtain certain other entangled states from it, by simple measurements on a subset of particles.

In the second paper, they introduced the one-way quantum computer, which used the cluster state as its essential (e)resource. We called it *one-way* because the computation is driven(eb) by one-qubit measurements, which successively destroy (e)the entanglement of the cluster ("A one-way quantum computer," *Phys. Rev. Lett.* 86: 5188-91, 2001).

This broke (e) with the paradigm that a quantum computation must necessarily be a coherent process, like a sequence of quantum gates. This scheme opened many new possibilities for physical realizations of a quantum computer in the laboratory, but it was also conceptually appealing for the study of more fundamental questions, for example, as regards the origin of the computational power of a quantum computer.

For an electric dipole moment d constituting charges of magnitude q , in a uniform, electrostatic field (time-independent) \mathbf{E} , positioned in one place, the potential is:

$$V = -\hat{\mathbf{d}} \cdot \mathbf{E}$$

the dipole moment itself is the operator

$$V = -\hat{\mathbf{d}} \cdot \mathbf{E}$$

Since the particle at one position, there is no translational kinetic energy of the dipole, so the Hamiltonian of the dipole is just the potential energy:

$$\hat{H} = -\hat{\mathbf{d}} \cdot \mathbf{E} = -q\mathbf{E} \cdot \hat{\mathbf{r}}$$

Magnetic dipole in a magnetic field

For a magnetic dipole moment $\boldsymbol{\mu}$ in a uniform, magneto static field (time-independent) \mathbf{B} , positioned in one place, the potential is:

$$V = -\boldsymbol{\mu} \cdot \mathbf{B}$$

Since the particle at one position, there is no translational kinetic energy of the dipole, so the Hamiltonian of the dipole is just the potential energy:

$$\hat{H} = -\boldsymbol{\mu} \cdot \mathbf{B}$$

For a Spin-1/2 particle, the corresponding spin magnetic moment is:

$$\boldsymbol{\mu}_S = \frac{g_s e}{2m} \mathbf{S}$$

where g_s is the spin gyro magnetic ratio (aka "spin g-factor"), e is the electron charge, \mathbf{S} is the spin operator vector, whose components are the Pauli matrices, hence

$$\hat{H} = \frac{g_s e}{2m} \mathbf{S} \cdot \mathbf{B}$$

Charged particle in an electromagnetic field

For a charged particle q in an electromagnetic field, described by the scalar potential ϕ and vector potential \mathbf{A} , there are two parts to the Hamiltonian to substitute for The momentum operator must be replaced by the kinetic momentum operator, which includes a contribution from the \mathbf{A} field:

$$\hat{\boldsymbol{\Pi}} = \hat{\mathbf{P}} - q\mathbf{A}$$

where $\hat{\mathbf{P}}$ is the canonical momentum operator given as the usual momentum operator:

$$\hat{\mathbf{P}} = -i\hbar\nabla$$

so the corresponding kinetic energy operator is:

$$\hat{T} = \frac{\hat{\boldsymbol{\Pi}} \cdot \hat{\boldsymbol{\Pi}}}{2m} = \frac{1}{2m} (\hat{\mathbf{P}} - q\mathbf{A})^2$$

and the potential energy, which is due to the ϕ field:

$$V = q\phi$$

Casting all of these into the Hamiltonian gives:

$$\hat{H} = \frac{1}{2m} (-i\hbar\nabla - q\mathbf{A})^2 + q\phi$$

Energy, Eigen ket degeneracy, symmetry, and conservation laws

Conservation law for distributed entanglement of formation and quantum discord

Fanchini and Cornelio presented an arbitrary tripartite pure system. By extending it to a paradigmatic situation of a bipartite system coupled (e&eb) to an environment, they demonstrated that the EOF and the QD obey a conservation relation. By means of this relation we show that in the deterministic quantum computer with one pure qubit the protocol has the ability to rearrange the EOF and the QD, which implies that quantum computation can be understood on a different basis as a coherent dynamics where quantum correlations(e&eb) are distributed between the qubits of the computer. Furthermore, for a tripartite mixed state they have shown that the balance between distributed EOF and QD results(eb) in a stronger version of the strong subadditivity of entropy

In many systems, two or more energy eigenstates have the same energy. A simple example of this is a free particle, whose energy eigenstates have wavefunctions that are propagating plane waves. The energy of each of these plane waves is inversely proportional to the square of its wavelength. A wave propagating in the x direction is a different state from one propagating in the y direction, but if they have the same wavelength, then their energies will be the same. When this happens, the states are said to be *degenerate*. It turns out that degeneracy occurs whenever a nontrivial unitary operator U commutes with the Hamiltonian. To see this, suppose that $|\alpha\rangle$ is an energy eigen ket. Then $U|\alpha\rangle$ is an energy Eigen ket with the same eigenvalue, since

$$UH|\alpha\rangle = UE_a|\alpha\rangle = E_a(U|\alpha\rangle) = H(U|\alpha\rangle).$$

Since U is nontrivial, at least one pair of $|a\rangle$ and $U|a\rangle$ must represent distinct states. Therefore, H has at least one pair of degenerate energy eigenkets. In the case of the free particle, the unitary operator which produces the symmetry is the rotation operator, which rotates the wavefunctions by some angle while otherwise preserving their shape.

The existence of a symmetry operator implies the existence of a conserved observable. Let G be the Hermitian generator of U :

$$U = I - i\epsilon G + O(\epsilon^2)$$

It is straightforward to show that if U commutes with H , then so does G :

$$[H, G] = 0$$

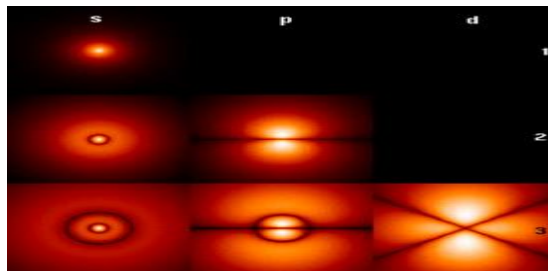
Therefore,

$$\frac{\partial}{\partial t} \langle \psi(t) | G | \psi(t) \rangle = \frac{1}{i\hbar} \langle \psi(t) | [G, H] | \psi(t) \rangle = 0,$$

$$\langle \psi(t) | H = -i\hbar \frac{\partial}{\partial t} \langle \psi(t) |.$$

Thus, the expected value of the observable G is conserved for any state of the system. In the case of the free particle, the conserved quantity is the angular momentum.

Time evolution of a quantum state is described by the Schrödinger equation, in which the Hamiltonian (the operator corresponding to the total energy of the system) generates the time evolution. The time evolution of wave functions is deterministic in the sense that - given a wavefunction at an *initial* time - it makes a definite prediction of what the wavefunction will be at any *later* time. During a measurement, on the other hand, the change of the initial wavefunction into another, later wavefunction is not deterministic, it is unpredictable (i.e. random). A time-evolution simulation can be seen here Wave functions change as time progresses. The Schrödinger equation describes how wave functions change in time, playing a role similar to Newton's second law in classical mechanics. The Schrödinger equation, applied to the aforementioned example of the free particle, predicts that the center of a wave packet will move through space at a constant velocity (like a classical particle with no forces acting on it). However, the wave packet will also spread out as time progresses, which means that the position becomes more uncertain with time. This also has the effect of turning a position eigenstate (which can be thought of as an infinitely sharp wave packet) into a broadened wave packet that no



longer represents a (definite, certain) position eigenstate

Figure 1 shows Probability densities corresponding to the wave functions of an electron in a hydrogen atom possessing definite energy levels (increasing from the top of the image to the bottom: $n = 1, 2, 3, \dots$) and angular momenta (increasing across from left to right: s, p, d, \dots). -Brighter areas correspond to higher probability density in a position measurement. Wavefunctions like these are directly comparable to Chladni's figures of acoustic modes of vibration in classical physics, and do indeed modes of oscillation as well, possess a sharp energy and, thus, a definite frequency. The angular and energy are quantized, and take only discrete values like those shown (as is the case for resonant frequencies in acoustics)

Some wave functions produce probability distributions that are constant or independent of time - such as when in a stationary state of constant energy, time vanishes in the absolute square of the wave function. Many systems that are treated dynamically in classical mechanics are described by such "static" wave functions. For example, a single electron in an unexcited atom is pictured classically as a particle moving in a circular trajectory around the atomic nucleus, whereas in quantum mechanics it is described by a static, spherically symmetric wavefunction surrounding the nucleus (Fig. 1) (note, however, that only the lowest angular momentum states, labeled s , are spherically symmetric)

Classification

Three Generations of Matter (Fermions)			
	I	II	III
mass	2.4 MeV/c ²	1.27 GeV/c ²	171.2 GeV/c ²
charge	2/3	2/3	2/3
spin	1/2	1/2	1/2
name	u up	c charm	t top
Quarks	d down	s strange	b bottom
	u_c electron neutrino	ν_μ muon neutrino	ν_τ tau neutrino
	e electron	μ muon	τ tau
Leptons	γ photon	g gluon	Z⁰ Z boson
	W[±] W boson	Z⁰ Z boson	W[±] W boson
	Gauge Bosons		

Standard Model of elementary particles. The electron is at lower left.

In the Standard Model of particle physics, electrons **belong to** the group of subatomic particles called leptons, which are believed to be fundamental or elementary particles. Electrons have the **lowest mass** of any charged lepton (or electrically charged particle of any type) and belong to the first-generation of fundamental particles. The second and third **generation contains** charged leptons, the muon and the tau, **which be identical to** the electron in charge, spin and interactions, but is more massive. Leptons differ from the other basic constituent of matter, the quarks, by their **lack of strong interaction**. Quarks have strong interactions, whereas electrons don't have; Interaction ability of leptons **is less** than that of quarks. All members of the lepton group are fermions, **because** they all have half-odd integer spin; the electron has spin $\frac{1}{2}$.

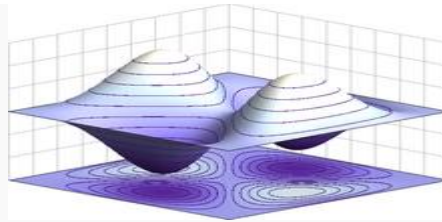
Fundamental properties

The invariant mass of an electron is approximately 9.109×10^{-31} kilograms, or 5.489×10^{-4} atomic mass units. On the basis of Einstein's principle of mass–energy equivalence, this mass corresponds to a rest energy of 0.511 MeV. The ratio between the mass of a proton and that of an electron is about 1836. Astronomical measurements show that the proton has held the same value **for at least half the age of the universe**, as is predicted by the Standard Model.

Electrons have an electric charge of -1.602×10^{-19} coulomb **which is used as a** standard unit of charge for subatomic particles. Within the limits of experimental accuracy, the electron charge is identical to the charge of a proton, but with the opposite sign.¹ As the symbol e is used for the elementary charge, the electron is commonly symbolized by e^- , where the minus sign indicates the negative charge. The positron is symbolized by e^+ because it has the same properties as the electron but with a positive rather than negative charge. **The orientation of the spin** with respect to the momentum of the electron **defines** the property of elementary particles known as *helicity*.¹ **The electron has no known substructure. Hence, it is defined or assumed to be a point particle with a point charge and no spatial extent** Observation of a single electron in a Penning trap shows the upper limit of the particle's radius is 10^{-22} meters. There is a physical constant called the "classical electron radius", with the much larger value of 2.8179×10^{-15} m. However, the terminology comes from a simplistic calculation **that ignores the effects of** quantum mechanics; in reality, the so-called classical electron radius has little to do with the true fundamental structure of the electron.¹ There are elementary particles that spontaneously **decay into less** massive particles. An example is the muon, **which decays** into an electron, a neutrino and an antineutrino, with a mean lifetime of 2.2×10^{-6} seconds. However, the electron is thought to be stable on theoretical grounds: the electron is the least massive particle with non-zero electric charge, so its **decay would violate charge conservation**. The experimental lower bound for the electron's mean lifetime is 4.6×10^{26} years, at a 90% confidence level.

Quantum properties

As with all particles, electrons can **act as** waves. This is called the wave–particle duality and can be demonstrated using the double-slit experiment. The wave-like nature of the electron allows it to pass through two parallel slits simultaneously, rather than just one slit as would be the case for a classical particle. In quantum mechanics, the wave-like property of one particle can be described mathematically as a complex-valued function, the wave function, commonly denoted by the Greek letter psi (ψ). When the absolute value of this function is squared, it gives the probability that a particle will be observed near a location—a probability density.



Example of an antisymmetric wave function for a quantum state of two identical fermions in a 1-dimensional box. If the **particles swap** position, the wave function inverts its sign.

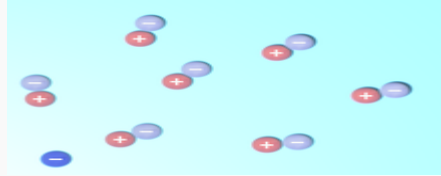
Electrons are identical particles because they **cannot be distinguished from each other** by their intrinsic physical properties. In quantum mechanics, this means that a pair of **interacting e**lectrons must be able to **swap** positions without an observable **change** to the state of the system. The wave function of fermions, **including** electrons, is antisymmetric, **meaning that** it changes sign when two electrons are **swapped; Wave function of fermions are antisymmetric because electrons are swapped** that is, $\psi(r_1, r_2) = -\psi(r_2, r_1)$, where the variables r_1 and r_2 correspond to the first and second electrons, respectively. Since the absolute value is not changed by a sign swap, this corresponds to equal probabilities. Bosons, such as the photon, have symmetric wave functions instead

In the case of antisymmetric, solutions of the wave equation for interacting electrons **result in a** zero probability that each pair will **occupy the** same location or state. This is **responsible** for the Pauli exclusion principle, which **precludes** any two electrons from occupying the same quantum state. This principle explains many of the properties of electrons. For example, **it causes** groups of bound electrons **to occupy different** orbitals in an atom, rather than all **overlapping each** other in the same orbit

Virtual particles

Physicists believe that empty space may be **continually creating** pairs of virtual particles, such as a positron and electron, which rapidly **annihilate each other** shortly thereafter. The **combination** of the *energy variation* needed to **create** these

particles, and the *time during which they exist, fall* under the threshold of detect ability expressed by the Heisenberg uncertainty relation, $\Delta E \cdot \Delta t \geq \hbar$. **In effect**, the energy needed **to create** these virtual particles, ΔE , can be **"borrowed" from** the vacuum (-) for a period of time, Δt , so that their product is no more than the **reduced** Planck constant, $\hbar \approx 6.6 \times 10^{-16}$ eV·s. Thus, for a virtual electron, Δt is at most 1.3×10^{-21} s.



A schematic depiction of virtual electron–positron pairs appearing at random near an electron (at lower left)

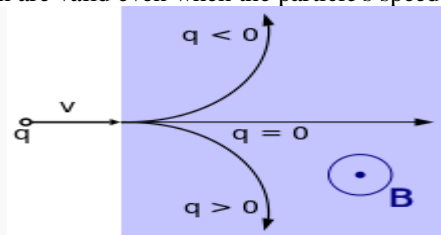
While an electron–positron virtual pair is in existence, the coulomb force from the ambient electric field surrounding an electron **causes a created** positron to **be attracted to the** original electron, while **a created electron** experiences repulsion. **This causes** what is called vacuum. In effect, the vacuum behaves like a medium having a dielectric permittivity more than unity. Thus the effective charge of an electron is actually **smaller** than its true value, and the charge **decreases with increasing distance from the electron**. This polarization was confirmed experimentally in 1997 using the Japanese TRISTAN particle accelerator. Virtual particles **cause a comparable** shielding effect for the mass of the electron

The interaction with virtual particles also **explains the** small (about 0.1%) deviation of the intrinsic magnetic moment of the electron from the Bohr magneton (the anomalous magnetic moment). **The extraordinarily precise agreement of this predicted difference with the experimentally determined value is viewed as one of the great achievements of quantum electrodynamics**

In classical physics, the angular momentum and magnetic moment of an object **depend upon** its physical dimensions. Hence, the concept of a dimensionless electron **possessing these** properties might seem inconsistent. The apparent paradox can be **explained by** the **formation of** virtual photons in the electric field **generated by** the electron. These photons **cause the** electron to shift about in a jittery fashion (known as zitterbewegung), which **results in** a net circular motion with precession. This motion **produces** both the spin and the magnetic moment of the electron. In atoms, this creation of virtual photons **explains** the Lamb shift observed in spectral lines. Lamb shift observed in spectral lines is (e) due to creation of virtual photons

Interaction

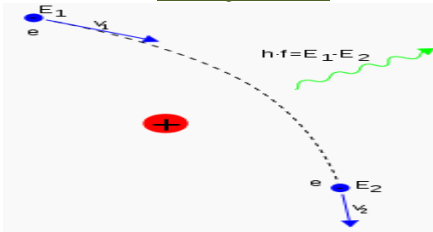
An electron **generates an** electric field that **exerts** an attractive force on a particle with a positive charge, such as the proton, **and a repulsive force** on a particle with a negative charge. The strength of this force **is determined** by Coulomb's inverse square law. When an electron is in motion, it **generates a** magnetic field. The Ampere-Maxwell **law relates** the magnetic field to the mass motion of electrons (the current) with respect to an observer. It is this property of induction **which supplies** the magnetic field that **drives** an electric motor. The electromagnetic field of an arbitrary moving charged particle **is expressed** by the Liénard–Wiechert potentials, which are valid even when the particle's speed is close to that of light (relativistic).



A particle with charge q (at left) is moving with velocity v through a magnetic field B that **is oriented** toward the viewer. For an electron, q is negative so it follows a curved trajectory toward the top.

When an electron is moving **through a** magnetic field, it **is subject** to the Lorentz force that **exerts an influence** in a direction perpendicular to the plane **defined by** the magnetic field and the electron velocity. This centripetal **force causes** the electron to follow a helical trajectory through the field at a radius called the gyro radius. The acceleration from this curving **motion induces** the electron **to radiate** energy in the form of synchrotron radiation. The **energy emission** in turn **causes** recoil of the electron, known as the Abraham-Lorentz-Dirac force, which **creates a** friction that **slows** the electron. This force **is caused** by **a back-reaction of the electron's own field upon itself**

In quantum electrodynamics the electromagnetic **interaction** between particles is **mediated by** photons. An isolated electron that is not undergoing acceleration is **unable to emit or absorb** a real photon; doing so would **violate** conservation of energy and momentum. Instead, virtual photons can **transfer** momentum between two charged particles. It is this **exchange** of virtual photons that, for example, **generates** the Coulomb force.¹ Energy emission can **occur** when a moving electron is **deflected** by a charged particle, such as a proton. The acceleration of the electron **results in** the **emission of Bremsstrahlung radiation**



Here, Bremsstrahlung is **produced by** an electron e deflected by the electric field of an atomic nucleus. The energy change $E_2 - E_1$ **determines** the frequency f of the emitted photon.

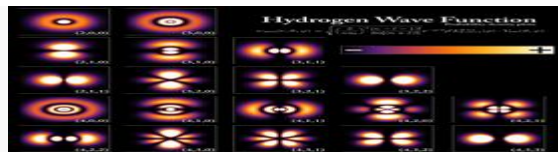
An inelastic **collision** between a photon (light) (-) and a solitary (free) electron (+) is called Compton scattering. This collision **results in** a transfer of momentum and energy between the particles, which **modifies** the wavelength of the photon by an amount called the **Compton shift**. The maximum magnitude of this wavelength shift is $h/m_e c$, which is known as the Compton wavelength. For an electron, it has a value of 2.43×10^{-12} m. When the wavelength of the light is long (for instance, the wavelength of the visible light is 0.4–0.7 μm) the wavelength shift becomes negligible. **Such interaction** between the light and free electrons is called Thomson scattering or Linear Thomson scattering.

The relative **strength** of the electromagnetic **interaction** between two charged particles, such as an electron and a proton, is given by the fine-structure constant. This value is a dimensionless quantity **formed by** the ratio of two energies: the electrostatic energy of attraction (or repulsion) at a separation of one Compton wavelength, and the rest energy of the charge. It is given by $\alpha \approx 7.297353 \times 10^{-3}$, which is approximately equal to $1/137$.

When electrons and positrons **collide**, they **annihilate** each other, **giving rise** to two or more gamma ray photons. If the electron and positron have negligible momentum, a positronium atom can **form** before **annihilation results** in two or three gamma ray photons totaling 1.022 MeV. On the other hand, high-energy photons may **transform** into an electron and a positron by a process called **pair production**, but only in the presence of a nearby charged particle, such as a nucleus.

In the theory of **electroweak interaction**, the left-handed component of electron's wavefunction **forms** a weak isospin doublet with the electron. This means that during weak interactions, electron neutrinos **behave like** electrons. Either member of this doublet can undergo a charged current interaction by emitting or absorbing a W and be **converted into** the other member. Charge is conserved during this reaction because the W boson also carries a charge, **canceling out any net change** during the transmutation. Charged current interactions **are responsible** for the phenomenon of beta decay in a radioactive atom. Both the electron and electron neutrino can undergo a neutral current interaction via a Z0 exchange, and this is **responsible** for neutrino-electron elastic scattering.

Atoms and molecules



Probability densities for the first few hydrogen atom orbitals, seen in cross-section. The energy level of a bound electron **determines** the orbital it occupies, and the color **reflects** the probability to find the electron at a given position.

An electron can be **bound** to the nucleus of an atom by the attractive Coulomb force. A system of several electrons **bound to** a nucleus is called an atom. If the number of electrons is **different** from the nucleus' electrical charge, such an atom is called anion. The wave-like behavior of a bound electron is **described** by a function called an atomic orbital. Each orbital **has its own set of quantum numbers such as energy, angular momentum** and projection of angular momentum, and only a discrete set of these orbitals exist around the nucleus. According to the Pauli exclusion principle each orbital can be **occupied by** up to two electrons, which must differ in their spin quantum number.

Electrons **can transfer** between different orbitals by the **emission or absorption** of photons with an energy that matches the difference in potential. Other methods of orbital transfer include **collisions with** particles, such as electrons, and the Auger effect. In order to escape the atom, the energy of the electron must be **increased** above its binding energy to the atom. This **occurs**, for example, with the photoelectric effect, where an incident photon exceeding the atom's ionization energy **is absorbed** by the electron.

The orbital angular momentum of electrons is quantized. Because the electron is charged, it **produces** an orbital magnetic moment that is **proportional** to the angular momentum. The net magnetic moment of an atom **is equal** to the vector sum of orbital and spins magnetic moments of all electrons and the nucleus. The magnetic moment of the nucleus is **negligible** compared with that of the electrons. The magnetic moments of the electrons that occupy the same orbital (so called, paired electrons) **cancel** each other out.

The chemical bond between atoms **occurs as a result of** electromagnetic interactions, as described by the laws of quantum mechanics. The strongest bonds **are formed** by the **sharing or transfer** of electrons between atoms, allowing **the formation** of molecules. Within a molecule, electrons move under the **influence** of several nuclei, and **occupy** molecular orbitals; much as they can occupy atomic orbitals in isolated atoms. A fundamental factor in these molecular structures is the **existence**

of electron pairs. These are electrons with *opposed spins*, allowing them to occupy the same molecular orbital without *violating* the Pauli exclusion principle (much like in atoms). Different molecular orbitals have different spatial distribution of the electron density. For instance, in bonded pairs (i.e. in the pairs that actually bind atoms together) electrons can be found with the maximal probability in a relatively small volume between the nuclei. On the contrary, in non-bonded pairs electrons are distributed in a large volume around nuclei.

Conductivity



A lightning discharge consists primarily of a flow of electrons. Flow of electrons ***produces*** lighting. The electric potential needed for lightning may be generated by a triboelectric effect. If a body has more or fewer electrons than are required to ***balance*** the positive charge of the nuclei, then that object ***has a*** net electric charge. When there is an excess of electrons, the object is said to be negatively charged. When there are fewer electrons than the number of protons in nuclei, the object is said to be positively charged. When the number of electrons and the number of protons are equal, their charges cancel each other and the object is said to be electrically neutral. A macroscopic body can develop an electric charge through rubbing, by the triboelectric effect.

Independent electrons ***moving in vacuum*** are termed *free* electrons. Electrons in metals also behave as if they were free. In reality the particles that are commonly termed electrons in metals and other solids are quasi-electrons—quasi-particles, which have the same electrical charge, spin and magnetic moment as real electrons but may have a different mass. When free electrons—both in vacuum and metals—move, ***they produce*** a net flow of charge called an electric current, which ***generates*** a magnetic field. Likewise a current can be ***created by*** a changing magnetic field. These ***interactions*** are described mathematically by Maxwell's equations.

At a given temperature, each ***material has an*** electrical conductivity that ***determines the*** value of electric current when an electric potential is applied. Examples of good conductors include metals such as copper and gold, whereas glass and Teflon are poor conductors. In any dielectric material, the electrons ***remain bound*** to their respective atoms and the material ***behaves*** as an insulator. Most semiconductors have a variable level of conductivity that lies between the extremes of conduction and insulation. On the other hand, metals have electrons ***containing partially filled*** electronic bands. The presence of such bands ***allows*** electrons in metals to behave as if they were free or delocalized electrons. These electrons are ***not associated*** with specific atoms, so when an electric field is applied, they are free to move like a gas called Fermi gas through the material much like free electrons.

Because of ***collisions*** between electrons and atoms, the drift velocity of electrons in a conductor is on the order of millimeters per second. However, the speed at which a change of current at one point in the ***material causes changes*** in currents in other parts of the material, the velocity of propagation, is typically about 75% of light speed ***This occurs because electrical signals propagate as a wave, with the velocity dependent on the dielectric constant of the material***

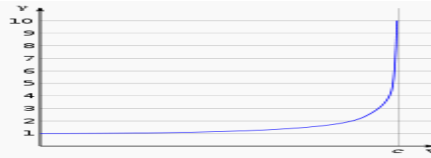
Metals make relatively good conductors of heat, ***primarily because*** the delocalized electrons are free to ***transport*** thermal energy between atoms. However, unlike electrical conductivity, the thermal conductivity of a metal is nearly independent of temperature. This is expressed mathematically by the Wiedemann-Franz law which states that the ratio of thermal conductivity to the electrical conductivity ***is proportional*** to the temperature. The thermal ***disorder in*** the metallic lattice ***increases the*** electrical resistivity of the material, ***producing*** temperature dependence for electrical current

When cooled below a point called the critical temperature, materials can undergo a phase transition in which they ***lose all*** resistivity to electrical current, in a process known as superconductivity. In BCS theory, this behavior is modeled by pairs of electrons entering a quantum state known as a ***Bose-Einstein condensate***. These Cooper pairs have their motion ***coupled to*** nearby matter via lattice vibrations called phonons, thereby ***avoiding*** the collisions with atoms that ***normally create*** electrical resistance (Cooper pairs have a radius of roughly 100 nm, so they can ***overlap*** each other.) *However, the mechanism by which higher temperature superconductors operate remains uncertain.*

Electrons inside conducting solids, which are quasi-particles themselves, when tightly confined at temperatures close to absolute zero, behave as though they ***had split*** into two other quasiparticles: spinons and holons. The former ***carries*** spin and magnetic moment, while the latter electrical charge.

Motion and energy

According to Einstein's theory of special relativity, as an electron's speed approaches the speed of light, from an observer's point of view its relativistic mass ***increases***, thereby making it more and more ***difficult to accelerate*** it from within the observer's frame of reference. Increase in relativistic mass ***produces*** deceleration of the acceleration from the moving observer's frame of reference. The speed of an electron can approach, but never reach, the speed of light in a vacuum, c . However, when relativistic electrons—that is, electrons moving at a speed close to c —are ***injected into*** a dielectric medium such as water, where the local speed of light is significantly less than c , the electrons temporarily ***travel faster than light*** in the medium. As they interact with the medium, they generate a faint light called Cherenkov radiation.



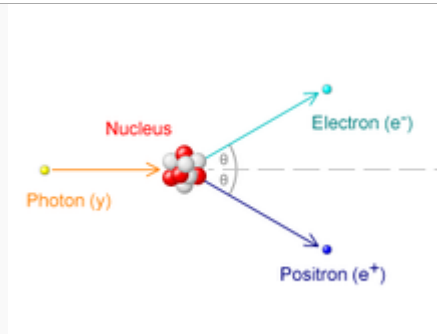
Lorentz factor as a function of velocity. It starts at value 1 and goes to infinity as approaches c .

The effects of special relativity are based on a quantity known as the Lorentz factor, defined as $\gamma = 1/\sqrt{1-v^2/c^2}$ where v is the speed of the particle. The kinetic energy K_e of an electron moving with velocity v is:

$$K_e = (\gamma - 1)m_e c^2,$$

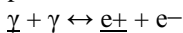
Where m_e is the mass of electron. For example, the Stanford linear accelerator can accelerate an electron to roughly 51 GeV. Since an electron behaves as a wave, at a given velocity it has a characteristic de Broglie wavelength. This is given by $\lambda_e = h/p$ where h is the Planck and p is the momentum. For the 51 GeV electron above, the wavelength is about 2.4×10^{-17} m, small enough to explore structures well below the size of an atomic nucleus

Formation



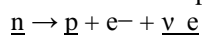
Pair production caused by the collision of a photon with an atomic nucleus

The Big Bang theory is the most widely accepted scientific theory to explain the early stages in the evolution of the Universe. For the first millisecond of the Big Bang, the temperatures were over 10 billion Kelvin and photons had mean energies over a million electron volts. These photons were sufficiently energetic that they could react with each other to form pairs of electrons and positrons. Likewise, positron-electron pairs annihilated each other and emitted energetic photons:



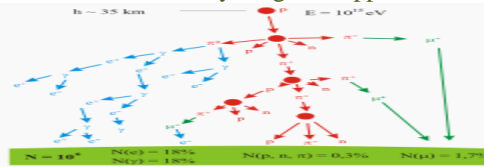
Equilibrium between electrons, positrons and photons was maintained during this phase of the evolution of the Universe. After 15 seconds had passed, however, the temperature of the universe dropped below the threshold where electron-positron formation could occur. Most of the surviving *electrons and positrons annihilated each other*, releasing gamma radiation that briefly reheated the universe.

For reasons that remain uncertain, during the process of leptogenesis there was production of an excess number of electrons over positrons. Hence, about one electron in every billion survived the annihilation process. This excess matched the excess of protons over anti-protons, in a condition known as baryon asymmetry, resulting in a net charge of zero for the universe. The surviving protons and neutrons began to participate in reactions with each other—in the process known as nucleosynthesis, forming isotopes of hydrogen and helium, with trace amounts of lithium. This process peaked after about five minutes. Any leftover neutrons underwent negative decay with a half-life of about a thousand seconds, releasing a proton and electron in the process,



For about the next 300,000–400,000 yr, the excess electrons remained too energetic to bind with atomic nuclei. Energetic electrons prevented the binding of themselves with the nuclei. What followed is a period known as recombination, when neutral atoms were formed and the expanding universe became transparent to radiation.

Roughly one million years after the big bang, the first generation of stars began to form. Within a star, stellar nucleosynthesis results in the production of positrons from the fusion of atomic nuclei. These antimatter particles immediately annihilate with electrons, releasing gamma rays. The net result is a steady reduction in the number of electrons, and a matching increase in the number of neutrons. However, the process of stellar evolution can result in the synthesis of radioactive isotopes. Selected isotopes can subsequently undergo negative beta decay, emitting an electron and antineutrino from the nucleus



An extended air shower **generated by** an energetic cosmic ray striking the Earth's atmosphere

At the end of its lifetime, a star with more than about 20 solar masses can undergo gravitational collapse **to form** a black hole According to classical physics; these massive stellar objects **exert a** gravitational attraction that is strong enough to **prevent** anything, even electromagnetic radiation, from **escaping past** the Schwarzschild radius. However, it is believed that quantum mechanical effects **may allow** Hawking radiation to be emitted at this distance. Electrons (and positrons) are thought **to be created** at the event horizon of these stellar remnants.

When pairs of virtual particles (such as an electron and positron) **are created** in the vicinity of the event horizon, the random spatial distribution of these particles **may permit** one of them to appear on the exterior; this process is called quantum tunneling. The gravitational potential of the black hole(-) can then supply the energy that **transforms** this virtual particle into a real particle, allowing it to radiate away into space In exchange, the other member of the pair is given negative energy, which results in a net loss of mass-energy by the black hole. The rate of Hawking radiation **increases** with decreasing mass, eventually **causing the** black hole to evaporate away until, finally, it **explodes**

Cosmic rays are particles traveling through space with high energies. Energy events as high as $3.0 \times 10^{20} \text{ eV}$ have been recorded When these **particles collide** with nucleons in the Earth's atmosphere, a shower of particles **is generated**, including pions. More than half of the cosmic radiation observed from the Earth's surface **consists of** muons. The particle called a muon is a lepton which **is produced** in the upper atmosphere **by the decay** of a pion.

Observation



Aurorae are mostly **caused** by energetic electrons precipitating into the atmosphere

Remote observation of electrons **requires** detection of their radiated energy. For example, in high-energy environments such as the corona of a star, free electrons **form** plasma that **radiates** energy due to Bremsstrahlung. Electron gas can **undergo** plasma oscillation, which is waves **caused by** synchronized variations in electron density, and **these produce** energy emissions that can be detected by using radio telescopes.

The frequency of a photon **is proportional** to its energy. As a bound electron **transitions** between different energy levels of an atom, it will **absorb or emit** photons at characteristic frequencies. For instance, when atoms **are irradiated** by a source with a broad spectrum, distinct **absorption** will appear in the spectrum of transmitted radiation. Each element or molecule **displays a** characteristic set of spectral lines, such as the hydrogen spectral series. Spectroscopic measurements of the strength and width of these **lines allow the** composition and physical properties of a substance to be determined. In laboratory conditions, **the interactions** of individual electrons can be observed by means of particle detectors, which allow measurement of specific properties such as energy, spin and charge. The development of the Paul trap and Penning trap allows charged particles to be **contained within a** small region for long durations. This enables precise measurements of the particle properties. For example, in one instance a Penning trap **was used** to contain a single electron for a period of 10 months The magnetic moment of the electron was measured to a precision of eleven digits, which, in 1980, was a greater accuracy than for any other physical constant.

The first video images of an electron's energy distribution were captured by a team at Lund University in Sweden, February 2008. The scientists used extremely short flashes of light, called attosecond pulses, which allowed an electron's motion to be observed for the first time

The distribution of the electrons in solid materials can be visualized by angle resolved photoemission spectroscopy (ARPES). This technique employs the photoelectric effect to measure the reciprocal space—a mathematical representation of periodic structures that is used to infer the original structure. ARPES can be used to **determine** the direction, speed and scattering of electrons within the material

Plasma applications

Particle beams



During a NASA wind tunnel test, a model of the Space Shuttle is targeted by a beam of electrons, simulating the effect of ionizing gases during re-entry Electron beams are used in welding, which allows energy densities up to $10^7 \text{ W} \cdot \text{cm}^{-2}$ across a narrow focus diameter of 0.1–1.3 usually does not require a filler material. This welding technique must be performed in a

vacuum, so that the electron beam does *not interact* with the gas prior to reaching the target, and *it can be used* to join conductive materials that would otherwise be considered unsuitable for welding.

Particle accelerators use electric fields *to propel* electrons and their antiparticles to high energies. As these particles *pass through* magnetic fields, *they emit* synchrotron radiation. The intensity of this radiation is spin *dependent*, which causes polarization of the electron beam—a process known as the Sokolov–Ternov effect. The polarized electron beams can be useful for various experiments. Synchrotron radiation *can also be used* for *cooling the* electron beams, *which reduces* the momentum spread of the particles. Once the particles have accelerated to the required energies, particles have acquired required energy levels) separate electron and positron beams are brought into collision. The *resulting energy* emissions are observed with particle detectors and are studied in particle physics

Imaging

Low-energy electron diffraction (LEED) is a method of *bombarding a* crystalline material with a collimated beam of electrons, then observing the *resulting* diffraction patterns to *determine* the structure of the material. The required energy of the electrons is typically in the range 20–200 eV The reflection high energy electron diffraction (RHEED) technique *uses the* reflection of a beam of electrons fired at various low angles to characterize the surface of crystalline materials. The beam energy is typically in the range 8–20 keV and the angle of incidence is 1–4°

The electron microscope directs a focused beam of electrons at a specimen. As the beam *interacts* with the material, some electrons *change their* properties, *such as movement direction, angle, relative phase and energy*. By recording these changes in the electron beam, microscopists can *produce, fabricate and generate* atomically resolved image of the material. In blue light, conventional optical microscopes have a diffraction-limited resolution of about 200 nm. By comparison, electron microscopes are limited by the de Broglie wavelength of the electron. This wavelength, for example, is equal to 0.0037 nm for electrons accelerated across a 100,000-volt potential The Transmission Electron Aberration-corrected Microscope is capable of sub-0.05 nm resolution, which is more than enough to resolve individual atoms. This capability makes the electron microscope a useful laboratory instrument for high resolution imaging. However, electron microscopes are expensive instruments that are costly to maintain. There are two main types of electron microscopes: *transmission and scanning*. Transmission electron microscopes function in a manner similar to overhead *projector*, with a beam of electrons *passing through* a slice of material then *being projected* by lenses on a photographic slide or a charge-coupled device. In scanning electron microscopes, the image is produced by restoring a finely focused electron beam, as in a TV set, across the studied sample. The magnifications range from 100× to 1,000,000× or higher for both microscope types. The scanning tunneling microscope uses quantum tunneling of electrons from a sharp metal tip into the studied material and *can produce* atomically resolved images of its surface.

Other Quantum Mechanical applications

In the free electron laser (FEL), a relativistic electron beam is *passed through a* pair of undulators containing arrays of dipole magnets, whose fields are *oriented in* alternating directions. The electrons *emit synchrotron* radiation, which, in turn, *coherently interacts* with the same electrons. This *leads to* the strong *amplification of* the radiation field at the resonance frequency. FEL can *emit a* coherent high-brilliance electromagnetic radiation with a wide range of frequencies, from microwaves to soft X-rays. These devices can be used in the future for manufacturing, communication and various medical applications, such as soft tissue surgery.

Electrons are at the heart of cathode ray tubes, *which have been used* extensively as display devices in laboratory instruments, computer monitors and television sets In a photomultiplier tube, every photon striking the photocathode *initiates an* avalanche of electrons that *produces* a detectable current pulse. Vacuum *tubes use* the flow of electrons to *manipulate* electrical signals, and they played a critical role in the development of electronics technology. However, they have been largely *supplanted* by solid-state devices such as the transistor.

SCRODINGER'S EXPONENTIAL JURISPRUDENCE:

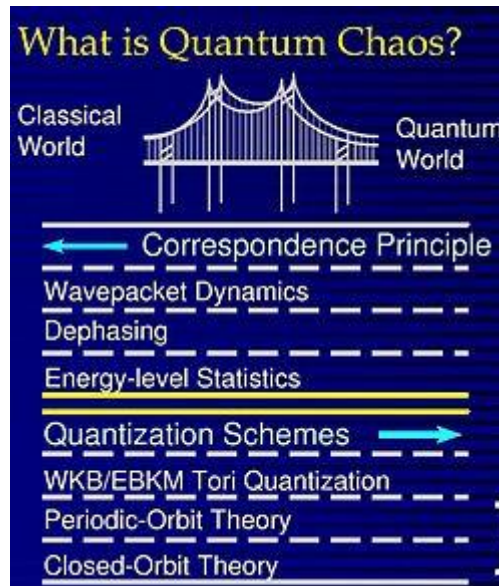
The Schrödinger equation *acts on* the *entire probability amplitude*, not merely its absolute value. Whereas the absolute value of the probability amplitude *encodes* information about probabilities, its phase *encodes* information about the *interference* between quantum states. *This gives rise to the "wave-like" behavior of quantum states*. As it turns out, analytic solutions of the Schrödinger equation are only available for a very small number of relatively simple model Hamiltonians, of which the quantum harmonic oscillator, the particle in a box, the hydrogen molecular ion, and the hydrogen atom are the most important representatives. *Even the helium atom - which contains just one more electron than does the hydrogen atom - has defied all attempts at a fully analytic treatment.*

GENERATION OF APPROXIMATE SOLUTIONS FOR QUANTUM INFORMATION AND QUANTUM CHAOS:

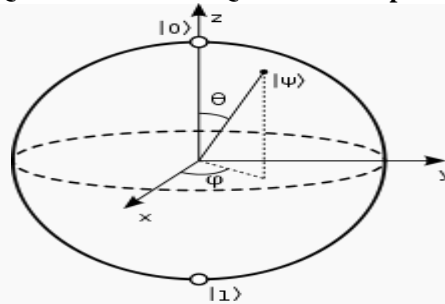
There exist several techniques *for generating* approximate solutions, however. In the important method known as *perturbation theory*, one *uses* the analytic *result for* a simple quantum mechanical model *to generate a result for* a more complicated model *that is related* to the simpler model by (for one example) the addition of a weak potential energy. Another method is the "*semi-classical equation of motion*" approach, which applies to systems for which quantum mechanics *produces only* weak (small) deviations from classical behavior. These *deviations can* then be computed based on the classical motion. This approach is particularly important in the field of quantum chaos.

Quantum chaos is a branch of physics which studies how chaotic classical dynamical systems can *be described in terms* of quantum theory. The primary question that quantum chaos seeks to answer is, "What is the *relationship* between quantum mechanics and classical chaos?" The correspondence principle states that classical mechanics is the classical limit of quantum mechanics. If this is true, then there must be quantum mechanisms *underlying (classical)* chaos; although this may not be a fruitful way of examining classical chaos. If quantum mechanics does not demonstrate an exponential sensitivity to initial conditions, how can exponential sensitivity to initial conditions *arise in* classical chaos, which must be the correspondence principle limit of quantum mechanics? In seeking to address the basic question of quantum chaos, several approaches have been employed:

Development of methods for solving quantum problems where the perturbation cannot be considered small in perturbation theory and where quantum numbers are large. *Correlating* statistical descriptions of eigenvalues (energy levels) with the classical behavior of the same Hamiltonian (system) Semi classical methods such as periodic-orbit theory *connecting the* classical trajectories of the dynamical system *with* quantum features.



Quantum Chaos & Quantum Computers



The Bloch sphere is a representation of a qubit, the fundamental building block of quantum computers.

A **quantum computer** is a device for computation that makes *direct use of* quantum mechanical phenomena, *such as superposition and entanglement*, to perform operations on data. Quantum computers are different from digital computers *based on* transistors. Whereas digital computers require data to be encoded into binary digits (bits), quantum computation *utilizes* quantum properties to represent data and perform *operations on* these data. A theoretical model is the quantum Turing machine, also known as the universal quantum computer. Quantum computers share theoretical similarities *with non-deterministic and probabilistic computers*, like the ability *to be in more than one state* simultaneously. The field of quantum computing was first introduced by Richard Feynman in 1982.

Large-scale quantum computers could be able to solve certain problems much faster than any classical computer *by using the best currently known* algorithms, like *integer factorization using Shor's algorithm or the simulation of quantum many-body systems*. There exist quantum algorithms, such as Simon's algorithm, which run faster than any possible probabilistic classical algorithm. Given unlimited resources, a classical computer can *simulate an* arbitrary quantum algorithm so quantum computation does not *violate the* Church-Turing thesis. However, in practice infinite resources are never available and the computational basis of 500 qubits, for example, would already be too large to be represented on a classical **computer because** it would require 2^{500} complex values to be stored. (For comparison, a terabyte of digital information stores only 2^{43} discrete on/off values) Nielsen and Chuang point out that "Trying to store all these complex numbers would not be possible on any conceivable classical computer."

The standard generic quantum computer model has been studied analytically and numerically and the border for emergence of quantum chaos, ***induced by imperfections*** and residual inter-qubits couplings, is determined. This phenomenon of Quantum chaos ***appears in an*** isolated quantum computer ***without any*** external decoherence. The onset of quantum chaos ***leads to quantum computer hardware melting***, strong quantum entropy growth and ***destruction of computer operability***. The time scales for development of quantum chaos and Ergodicity ***are determined*** in some recent studies. In spite the fact that this phenomenon is rather dangerous for quantum computing it is demonstrated that the quantum chaos border for inter-qubits coupling is exponentially larger ***than (e) the*** energy level spacing between quantum computer eigenstates ***and drops*** only linearly with the number of qubits n . ***As a result*** the ideal multi-qubits structure of the computer remains rather robust against imperfections. This opens a broad parameter region for a possible realization of quantum computer. The obtained results are related to the recent studies of quantum chaos in such many-body systems as nuclei, complex atoms and molecules, finite Fermi systems and quantum spin glass shards

Quantum Computing of Quantum Chaos in the Kicked Rotator Model (See for details B. Levi, B. Georgeot, D.L. Shepelyansky)

A quantum algorithm which ***simulates efficiently*** the quantum kicked rotator model, a system which ***displays*** rich physical properties, ***and enables*** to study problems of quantum chaos, atomic physics and localization of electrons in solids, was being searched for some time. . The ***effects of*** errors in gate operations are tested on this algorithm in numerical simulations with up to 20 qubits. In this way various physical quantities are investigated. Some of them, such as second moment of probability distribution and tunneling transitions through invariant curves have been shown to be particularly sensitive to errors, in some recent studies.. This study is related to our understanding of the usage of the Quantum Mechanical behaviour for Quantum information. However, investigations of the fidelity and Wigner and Husimi distributions show that these physical quantities are ***robust in presence*** of imperfections. This implies that the algorithm can ***simulate*** the dynamics of quantum chaos in presence of a moderate amount of noise. And part of that noise might come from Quantum chaos. Recent low-temperature scanning-tunneling microscopy experiments (T. Kumara et al., Phys. Rev. B 79,)

035423

2009

) observed the possible quantum tunneling of hydroxyl groups between two equivalent adsorption configurations on Cu110. Quantum nuclear tunneling dynamics of hydroxyl on Cu110 using density-functional theory based techniques have been studied. Researchers classical, semi classical, and quantum mechanical transition rates for the flipping of OH between two degenerate energy minima. The classical transition rate is essentially zero at the temperatures used in experiment and the tunneling rate along the minimum-energy path is also ***much too low*** compared to experimental observations. When tunneling is taken into account along a direct path connecting the initial and final states with only a minimum amount of the oxygen movement the transition rate obtained is in much better agreement with experiment, suggesting quantum tunneling ***effects because*** a deviation of the reaction coordinates from the classical transition path. Quantum computation is an emerging interdisciplinary field, which takes advantage of concepts from both information theory and quantum mechanics. During the last decade great progress has been made in the understanding of how quantum computing and quantum communications can be performed and efficient algorithms and communication protocols have been developed. Due to the massive parallelism of quantum evolution certain quantum algorithms demonstrate an exponential gain compared to algorithms based on classical dynamics. In fact, a quantum computer represents a complex system of many ***coupled*** qubits, which in general can be ***viewed as*** a many-body ***interacting*** quantum system. On the other hand, qubits or ***spin interactions*** have also been studied extensively in the field of quantum chaos, in which typical ***problems (the ones that dissipate the ability of dissemination of Quantum information or Information processing by Quantum Compute which is our field of study) are*** decoherence and the quantum-to-classical transition, subjects that are also essential for any realistic implementation of a quantum computer. . Theory of quantum-computer algorithms, error-***correcting codes***, decoherence and quantum chaos ***effects*** in the exponentially large ***Hilbert space*** of quantum computers are vital for the ultimate technological success of quantum computation.

Quantum Chaos and Quantum Computer/Computing

Quantum chaos

Classical chaos refers to the ***sensitive dependence*** on initial condition which is commonly found in nonlinear systems. In quantum mechanics, the ***trajectory loses*** its significance completely. Moreover the Schrodinger equation is a linear equation leaving no room for chaos. The ***correspondence principle, on the other hand, demand(e)s the utilization of the principle*** that in the semi-classical regime, namely, at length scale large compared with the de Broglie wavelength, ***quantum mechanics continuously develops into classical mechanics***. Therefore, at first glance, the name of ***quantum chaos seems self-contradictory***. After several years debate, now people commonly accept that ***quantum chaos*** refers to the study of quantum mechanical behavior of the systems whose ***classical counterparts*** are chaotic. This field has been very active in last two decades. Three manifestation of chaos in quantum systems have been studied so far.

Quantum Manifestation of Classical Chaos : Energy level spacing statistics

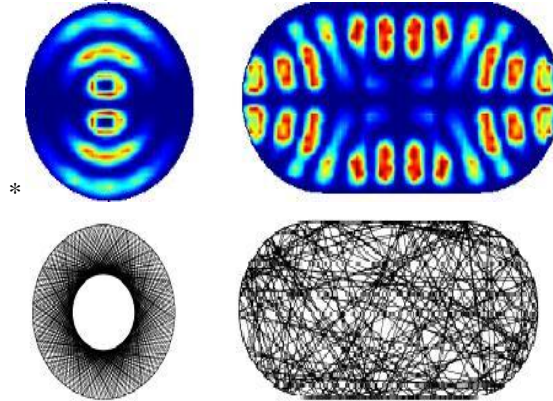
Energy level statistics has some universal features in the semi classical limit. It has been ***conjectured*** that level fluctuations ***depend only on*** general space-time symmetry and they are as predicted by the Random Matrix Theory [R]. For instance, the energy level spacing statistics in circular billiard (representing integrable systems) is Poisson distribution, whereas that in

stadium (or Sinai) billiard (representing chaotic systems with time reversal symmetry) has Wigner distribution. For a generic (mixed) system -neither complete chaotic nor complete integrable the energy level.

Quantum Manifestation of Classical Chaos II: statistical properties of stationary wavefunctions and Quantum Tunneling:

Along with eigenenergies, wavefunctions are also used to probe quantum fingerprints and signatures of classical chaos. Usually wavefunctions provide more information about the dynamics than eigenenergies. In fact, it is the space structure of wavefunction that determines the properties of spectral statistics such as level repulsion (in chaotic systems) and/or clustering (in integrable systems) etc. So far the only proved theorem about the eigenfunctions is Shnirelman's theorem. It agrees with the conjecture of Berry and Voros that the probability density of most eigenstates of a chaotic billiard approaches a uniform distribution. It also agrees with the Porter-Thomas distribution of RMT. Numerical studies of a large number of high-lying eigenstates of billiards have confirmed the Gaussian distribution of local wave functions.

Classical trajectories *Quantum Stationary Wave Functions



Circular billiard

Stadium billiard*

Circular billiard

Stadium billiard

Quantum Manifestation of Classical Chaos III: Dynamical evolution of states in Quantum Information:

One of the most important discoveries in quantum chaos is the *dynamical localization*, namely the quantum interference effects suppress the classical diffusive process (in phase space) which may take place in classical systems under external periodic perturbations. It has been shown by many physicists and computer scientists that the dynamical localization can be mapped to the *Anderson localization* for electrons in 1d systems with random impurity. This fact bridges Two different fields Quantum Chaos and Solid State Physics. Dynamical localization has been confirmed in several experiments such as Rydberg atom in a microwave field and an atom moving in a modulated standing wave

- Wave function structure and statistics in quantum billiard,
- Quantitative study of scars (wavefunction localization along the unstable classical periodic orbit) in far semi-classical limit.
- Energy level statistics and wave functions in mixed systems.
- Dynamical localization in quantum billiards.
- Semi-classical propagator for chaotic quantum systems.
- Semi-classical analysis of correlation functions in chaotic eigenstates. (g) Quantum chaos in non-KAM systems.

Quantum fidelity (quantum Loschmidt's echo) and chaos in Quantum Information:

The definition of classical chaos - sensitive dependence on initial condition - loses its meaning in quantum mechanics, because the unitarity properties of quantum mechanics, namely, the overlap between two evolving wave functions - a natural indicator of distance between them is preserved with time, hence there is no divergence. An alternative definition of chaos the sensitive dependence on perturbation - has been suggested recently. This new definition is meaningful both in classical and quantum mechanics. Classically, even for Small perturbation, one generically expects rapid divergence when the systems are chaotic, as the perturbation, i.e. the difference between equations of motion, soon introduces a small displacement between the trajectories. Quantum mechanically, the overlap between the wave functions begins at unity, and then decays with time, and the rate of this decay is equivalent to a measure of the sensitivity of quantum evolution to perturbations in the equation of motion - which can be used as a signature of quantum chaos.

Quantum mechanics as a statistical theory (For details see. E. Moyal)

An attempt is made by some computer scientists and theoretical physicists that quantum mechanics is a statistical theory, or more exactly as a form of non-deterministic statistical dynamics. Distribution functions of the complete set of dynamical variables specifying a mechanical system (phase-space distributions), which are fundamental in any form of statistical dynamics, could be expressed in terms of the wave vectors of quantum theory. This is shown to be equivalent to specifying a theory of functions of non-commuting operators, and may hence be considered as an interpretation of *quantum kinematics*. In

the second part, the laws governing the transformation with time of these phase-space distributions are derived from the equations of motion of *quantum dynamics* and found to be of the required form for a dynamical stochastic process. It is also shown that these phase-space transformation equations can be used as an alternative to the Schrödinger equation in the solution of quantum mechanical problems, such as the evolution with time of wave packets, *collision problems and the calculation of transition probabilities in perturbed systems*; an approximation method is derived for this purpose. *Quantum statistics*, deals with the phase-space distribution of members of large assemblies, with a view to applications of quantum mechanics to kinetic theories of matter. Recently, investigation has been carried out in the crossover of the quantum Loschmidt's echo (or fidelity) from the golden rule regime to the perturbation-independent exponential decay regime by using the kicked top model

$$M(t) = |\langle \Phi_0 | \exp(iHt) \exp(-iH_0t) | \Phi_0 \rangle|^2.$$

Where H is a perturbed Hamiltonian from H₀ which is chaotic. It is shown that the deviation of the perturbation independent decay of the averaged fidelity from the Lyapunov decay results from quantum fluctuations in individual fidelity, which is caused by the coherence in the initial coherent states. With an averaging procedure suppressing the quantum fluctuations effectively, the perturbation-independent decay is found to be close to the Lyapunov decay. This obviously means that the dissipation in quantum information sticks to the axiomatic predications of both Lyapunov decay and the Theory Of Classification.

Quantum Computer, Quantum Information, Dynamic Thermalization, Quantum Ergodicity, Theory of Classification, Quantum Mechanical process and Quantum Computing

In classical mechanics, chaos severely limits the operation of a reversible computer. Any uncertainty in the initial conditions is magnified exponentially by chaotic dynamics, rendering the outcome of the computation unpredictable. This is why practical computational scheme are irreversible. A quantum computer does not have this option. It relies on the reversible unitary evolution of entangled quantum mechanical states, which does not tolerate dissipation. On the other hand, the exponential gain of quantum computing is due to exponentially large size of Hilbert space which grows exponentially with the number of qubits which are the basis of quantum computers. In order to perform logical operations in quantum computers, these qubits should be coupled. As a consequence, quantum computers represent many body systems with interaction. Similar systems have been recently studied in the field of quantum chaos with applications to different many body systems such as nuclei, complex atoms, quantum dots and quantum spin glasses. It had been found that a sufficiently strong coupling leads to the emergence of quantum Ergodicity and dynamical (internal) thermalization. In this regime the systems eigenstates become very complex and strongly different from the eigenstates of non interacting many body systems. At first glance, one would expect this regime to appear when the coupling is comparable with the spacing between multiparticles levels. This naïve estimate would give an absurdly strong restriction for the coupling strength and therefore a too severe limitation for the realization of quantum computers. This raises the question:

- What limitations quantum chaos might pose on quantum computing?
- What restrictions of quantum chaos might pose on quantum error correction?
- Whether the suppression of quantum chaos (dynamical localization) improve the fidelity for recovery from errors of decoherence.

Mathematically equivalent formulations of quantum mechanical behaviour and Quantum Information

Oldest and most commonly used formulations is the "transformation theory" proposed by the late Cambridge theoretical physicist Paul Dirac, which unifies and generalizes the two earliest formulations of quantum mechanics - matrix mechanics (invented by Werner Heisenberg) and wave mechanics (invented by Erwin Schrödinger). In Matrix formulation, the instantaneous state of a quantum system encodes the probabilities of its *measurable properties*, or "observables". Examples of observables include energy, position, momentum, and angular momentum. These are the factors that play a vital role in the classification scheme of our paper. Observables can be either continuous (e.g., the position of a particle) or discrete (e.g., the energy of an electron bound to a hydrogen atom) An alternative formulation of quantum mechanics is Feynman's path integral formulation, in which a quantum-mechanical amplitude is considered as equivalent to as a sum over all possible histories between the initial and final states. This is the quantum-mechanical counterpart of the *action principle* in classical mechanics.

Quantum Mechanical Behaviour, DIRAC Equation, Quantum Information and its Interactions with other scientific theories

The rules of quantum mechanics are fundamental. They assert that the state space of a system is a Hilbert space, and that observables of that system are operators acting on that space - although they do not tell us which Hilbert space or which operators. (In physics, particularly in quantum physics, a system observable is a property of the system state that can be determined by some sequence of physical operations. For example, these operations might involve submitting the system to various electromagnetic fields and eventually reading a value off some gauge. In systems governed by classical mechanics,

any experimentally observable value can be shown to be given by a real-valued function on the set of all possible system states. Physically meaningful observables must also satisfy transformation laws which relate observations performed by different observers in different frames of reference. These transformation laws are automorphism of the state space that is bijective transformations which preserve some mathematical property.)

These can be chosen appropriately in order to obtain a quantitative description of a quantum system. An important guide for making these choices is the correspondence principle, which states that the predictions of quantum mechanics reduce to those of ,become equal to classical mechanics when a system moves to higher energies or - equivalently - larger quantum numbers, i.e. whereas a single particle exhibits a degree of randomness, in systems incorporating millions of particles averaging takes over and, at the high energy limit, the statistical probability of random behaviour approaches zero. In other words, classical mechanics is simply a quantum mechanics of large systems. This "high energy" limit is known as the classical or correspondence limit. One can even start from an established classical model of a particular system, then attempt to guess the underlying quantum model that would give rise to the classical model in the correspondence limit. When quantum mechanics was originally formulated, it was applied to models whose correspondence limit was non-relativistic classical mechanics. For instance, the well-known model of the quantum harmonic oscillator uses an explicitly non-relativistic expression for the kinetic energy of the oscillator, and is thus a quantum version of the classical harmonic oscillator.

Early attempts to merge quantum mechanics with special relativity involved the replacement of the Schrödinger equation with a covariant equation such as the Klein-Gordon equation or the Dirac equation. The Dirac bispinor is represented by four ionic internal states, and position and momentum of the Dirac particle are associated with the respective ionic variables. Simulation of the simplified 1 + 1 case, requiring the manipulation of only two internal levels and one motional degree of freedom. Moreover, relevant quantum-relativistic effects, like the Zitterbewegung and Klein's paradox, the transition from massless to massive fermions, and the relativistic and nonrelativistic limits, via the tuning of controllable experimental parameters. Dirac equation, describes the behaviour of fermions, and predicted the existence of antimatter

While these theories were successful in explaining many experimental results, they had certain unsatisfactory qualities stemming from their neglect of the relativistic creation and annihilation of particles. A fully relativistic quantum theory required the development of quantum field theory, which applies quantization to a field (rather than a fixed set of particles). The first complete quantum field theory, quantum electrodynamics, provides a fully quantum description of the electromagnetic interaction. The full apparatus of quantum field theory is often unnecessary for describing electrodynamic systems. A simpler approach, one that has been employed since the inception of quantum mechanics, is to treat charged particles as quantum mechanical objects being acted on by a classical electromagnetic field. For example, the elementary quantum model of the hydrogen atom describes the electric field of the hydrogen atom using a classical $-e^2/(4\pi \epsilon_0 r)$ Coulomb potential. This "semi-classical" approach fails if quantum fluctuations in the electromagnetic field play an important role, such as in the emission of photons by charged particles.

Quantum field theories for the strong nuclear force and the weak nuclear force have also been developed. The quantum field theory of the strong nuclear force is called quantum chromodynamics, and describes the interactions of sub nuclear particles such as quarks and gluons. The weak nuclear force and the electromagnetic force were unified, in their quantized forms, into a single quantum field theory (known as electroweak theory), by the physicists Abdus Salam, Sheldon Glashow and Steven Weinberg. It has proven difficult to construct quantum models of gravity, the remaining fundamental force. Semi-classical approximations are workable, and have led to predictions such as Hawking. However, the formulation of a complete theory of quantum gravity is hindered by apparent incompatibilities between general relativity (the most accurate theory of gravity currently known) and some of the fundamental assumptions of quantum theory. The resolution of these incompatibilities is an area of active research, and theories such as String Theory are among the possible candidates for a future theory of quantum gravity. Classical mechanics has also been extended into the complex domain, with complex classical mechanics exhibiting behaviors similar to quantum mechanics.

Quantum Chaos and Quantum Information:

Predictions of quantum mechanics have been verified experimentally to an extremely high degree of accuracy. According to the correspondence principle between classical and quantum mechanics, all objects obey the laws of quantum mechanics, and classical mechanics is just an approximation for large systems of objects (or a statistical quantum mechanics of a large collection of particles). The laws of classical mechanics thus follow from the laws of quantum mechanics as a statistical average at the limit of large systems or large quantum numbers. However, chaotic systems do not have good quantum numbers, and quantum chaos studies the relationship between classical and quantum descriptions in these systems. Maintaining coherence in Quantum Computers. (W. G. Unruh) is an important phenomenon that has to be addressed with for the efficient functioning of a Quantum Computer. The effect of the inevitable coupling to external degrees of freedom of a quantum computer are examined, by various Physicists (See Unruh). It is found that for quantum calculations (in which the maintenance of coherence over a large number of states is important), not only must the coupling be small but the time taken in the quantum calculation must be less than the thermal time scale, Quantum computers to be more efficient in certain problems involves having the computer be placed in the coherent superposition of a very large number (exponential in L) of "classical states", and having the outputs interfere in such a way that there is a very high probability that on the appropriate reading of the output, one would obtain the required answer. One is replacing exponentiality in time with exponentiality in quantum coherence. This requires that the computer be able to maintain the coherence during the course of the calculation.

The **constraints** placed on the ability to maintain this coherence in the face of coupling to external heat baths. Landauer has long emphasized the necessity of examining **the effect of** both imperfections and of the coupling **to** the external world of any realistic device on the ability of quantum computers to realize their promise. For longer times the condition on the strength of the coupling to the external world becomes much more stringent. Quantum coherence is an essential difference between classical and quantum theories, and is illustrated by the Einstein-Podolsky-Rosen paradox. Quantum interference **involves adding together probability amplitudes**, whereas classical "waves" infer that there is an adding **together of intensities**. For microscopic bodies, the extension of the system is much smaller than the **coherence length**, which gives rise to long-range entanglement and other nonlocal phenomena that are characteristic of quantum systems. Quantum coherence is not typically evident at macroscopic scales - although an exception to this rule **can occur at** extremely low temperatures (i.e. approaching absolute zero), when quantum behavior can manifest itself on more macroscopic scales (see macroscopic quantum phenomena, Bose-Einstein condensate, and Quantum machine).

Many macroscopic properties of a classical system are a direct **consequence** of the quantum behavior of its parts. For example, the stability of bulk matter (which consists of atoms and molecules which **would quickly collapse under** electric forces alone), the rigidity of solids, and the mechanical, thermal, chemical, optical and magnetic properties of matter **are all results** of the interaction of electric charges under the rules of quantum mechanics. While the seemingly "exotic" behavior of matter **posited by** quantum mechanics and relativity theory **become more apparent** when dealing with particles of extremely small size or velocities approaching the speed of light, the laws of classical Newtonian physics remain accurate in predicting the behavior of the vast majority of "large" objects (on the order of the size of large molecules or bigger) at velocities much smaller than the velocity of light.

Emergence of Quantum Chaos in Quantum Computer Core and How to manage it has been discussed by B. Georgeot and D. L. Shepelyansky. Generic quantum computer model, **describes a** realistic isolated quantum computer **with fluctuations** in individual qubit energies and residual short-range inter-qubit **couplings**. In the limit where the fluctuations and couplings **are small** compared to one-qubit energy spacing the spectrum **has a** band structure and **a renormalized** Hamiltonian **is obtained** which describes the eigenstate properties inside one band. The studies are concentrated on the central band of the computer ("core") with the highest density of states. **Above a** critical inter-qubit coupling strength, quantum chaos **sets in, leading to** quantum Ergodicity of the computer eigenstates. In this regime the ideal qubit structure **disappears**, the eigenstates **become** complex and the operability of the computer are quickly **destroyed**. Quantum chaos border **decreases** only linearly with the number of qubits n , although the spacing between multi-qubit states **drops** exponentially with n . The investigation of time-evolution in the quantum computer **shows that** in the quantum chaos regime, an ideal (noninteracting) state quickly **disappears** and exponentially many states **become** mixed after a short chaotic time scale for which the dependence on system parameters **is determined**. **Below the** quantum chaos border an ideal state can survive for long times and can **be used** for computation. The **results show** that a broad parameter region **does exist** where the efficient operation of a quantum computer is possible. Quantum computers **have problem in** simulation of common quantum systems, since the computation time **grows** exponentially with the number of quantum particles. Therefore for such problems it is natural to **envision a** computer composed from quantum elements (qubits) which **operate** according to the laws of quantum mechanics. In any case, such devices will be in a sense unavoidable since the technological progress **leads to** chips of smaller and smaller size which will eventually reach the quantum scale. At present a quantum computer is viewed as a system of n qubits (two-level quantum systems), with the possibility of **switching on and off a coupling between them**. The operation of such computers **is based** on reversible unitary transformations in the Hilbert space whose dimension $N_H = 2^n$ is exponentially large in n . It has been shown that all unitary operations can be realized with two-qubit transformations. This makes necessary the existence of **a coupling** between qubits. Any quantum algorithm will be a sequence of such fundamental transformations, which form the basis of new quantum logic. Shor constructed a quantum algorithm which is **exponentially faster** than the classical ones. It was also shown by Grover that the searching of an item in a long list is parametrically much faster on a quantum computer. The recent development of error correcting codes showed that a certain amount of noise due to external coupling **could be tolerable** in the operation of a quantum computer. All these exciting developments motivated a great body of experimental proposals to effectively realize such a quantum computer. They include ion traps, nuclear magnetic resonance systems, nuclear spins with **interaction controlled** electronically or by laser pulses, quantum dots, Cooper pair boxes optical lattices and electrons floating on liquid helium. **As a result**, a two-qubit gate has been experimentally realized with cold ions, and the Grover algorithm has been performed for three qubits made from nuclear spins in a molecule. However, to have a quantum computer competitive with a classical one will require a much larger number of qubits. For example, the minimal number of qubits for which Shor's algorithm will become useful is of the order of $n = 1000$. Serious **obstacle to** the physical realization of such computers is the quantum decoherence due to the couplings with the external world **which gives** a finite lifetime to the excited state of a given qubit. **The effects** of decoherence and laser pulse shape broadening were numerically simulated in the context of Shor's algorithm, and shown to be quite important for the operability of the computer. However, in a number of physical proposals, for example nuclear spins in two-dimensional semiconductor structures, the relaxation time due to this decoherence process can be many orders of magnitude **larger than** the time required for the gates operation, so that there are hopes to manage this obstacle. Obstacle to the physical realization of quantum computers that was not stressed up to now. This problem arises even if the decoherence time is infinite and the system is **isolated/decoupled** from the external world. Indeed, even **in the absence** of decoherence there are always imperfections in physical systems. **Due to that the** spacing between the two states of each qubit will have fluctuations in some finite detuning interval δ . Also, some residual static

interaction J between qubits will be unavoidably present (inter-qubit coupling is required to operate the gates). Extensive studies of many-body **interacting systems** such as nuclei, complex atoms, quantum dots and quantum spin glasses have shown that generically in such **systems the interaction leads to** quantum chaos characterized by Ergodicity of the eigenstates and level spacing statistics as in Random Matrix Theory (RMT). In a sense the interaction **leads to** dynamical thermalization **without** coupling to an external thermal bath. If the quantum computer were in such a regime, its operability would be effectively **destroyed** since the noninteracting multi-qubit states representing the quantum register states **will be eliminated** by quantum ergodicity. In this respect, it is important to stress that unavoidably the residual interaction J **will be much larger than** the energy spacing Δ_n between adjacent eigenstates of the quantum computer. Indeed the residual interaction J is relatively small so that all NH computer eigenenergies are **distributed in an** energy band of size $\Delta E \sim n\Delta_0$, where Δ_0 is the average energy distance between the two levels of one qubit and n is the total number of qubits in the computer. **By changing the** electrostatic gate potential, the effective electron mass can **be modified up** to a factor of two. In the quantum computer the quantum **chaos sets in only for** couplings J exponentially stronger than Δ_n . In fact, it was shown that the critical coupling J_c for the transition to quantum chaos **decreases** only linearly with the number of qubits n (for short-range inter-qubit coupling): a broad parameter region where a quantum computer can be operated below the quantum chaos border, **exists** when noninteracting multi-qubit states are **very close** to the exact quantum computer eigenstates. Details the **transition to** chaos and how **it effects** the time evolution of the system. **The effects** of **residual interaction** in the presence or absence of fine fluctuations of individual qubit energy spacing are also analyzed in great detail.

Relativity and quantum Information and Quantum machine:

Quantum mechanics, information theory, and relativity theory are the basic foundations of theoretical physics. The acquisition of information from a quantum system **is the interface of** classical and quantum physics. Essential tools for its description are Kraus matrices and positive operator valued measures (POVMs). Special relativity **imposes severe restrictions** on the transfer of information between distant systems. Quantum entropy is not a Lorentz covariant concept. Lorentz transformations of reduced density matrices for entangled **systems may not be completely** positive maps. Quantum field theory, which is necessary for a consistent description of interactions, implies a fundamental trade-off between detector reliability and localizability. General relativity produces new, counterintuitive effects, in particular when black holes (or more generally, event horizons) are involved. Most of the current concepts in quantum information theory may then require a reassessment

The fundamental properties of quantum information and its applications to computing and cryptography have been greatly illuminated by considering information-theoretic tasks that are provably possible or impossible within non-relativistic quantum mechanics. I describe here a general framework for defining tasks within (special) relativistic quantum theory and illustrate it with examples from relativistic quantum cryptography and relativistic distributed quantum computation. The framework gives a unified description of all tasks previously considered and also defines a large class of new questions about the properties of quantum information in relation to Minkowski causality. It offers a way of exploring interesting new fundamental tasks and applications, and also highlights the scope for a more systematic understanding of the fundamental information-theoretic properties of relativistic quantum theory.

Entanglement generation in relativistic quantum fields and corresponding Quantum Computation. (See Nicolai Friis, Ivette Fuentes)

A general, analytic recipe is to compute the entanglement **that is generated** between arbitrary, discrete modes of bosonic quantum fields by **Bogoliubov transformations**. One setup allows the complete characterization of the quantum **correlations in all** Gaussian field states. Additionally, it holds for all Bogoliubov transformations. These are commonly **applied in** quantum optics **for the description** of squeezing operations, **relate** the mode decompositions of observers in different regions of curved spacetimes, and **describe** observers moving along non-stationary trajectories. Physicists have focused on a quantum optical example in a cavity quantum electrodynamics setting: **an uncharged scalar field within a cavity provides a** model for an optical resonator, in which **entanglement is created** by **non-uniform acceleration**. Amount of generated entanglement can be **magnified** by initial single-mode squeezing. Applications to quantum fields in curved spacetimes, such as an expanding universe, are also discussed. in many studies.

There exists an intimate **relationship** between quantum mechanics, information theory, and relativity theory. Taken together these are the foundations of present-day theoretical physics, and their interrelationship is an essential part of the theory. The acquisition of information from a quantum system by an observer **occurs at the** interface of classical and quantum physics. Many a author have reviewed the essential tools needed to describe this interface, i.e., Kraus matrices and positive-operator-valued measures. They then discuss how special relativity **imposes** severe (e) **restrictions** on the **transfer of information between distant systems and the implications of the fact that quantum entropy is not a Lorentz-covariant concept**. This leads to a discussion of how it comes about that Lorentz transformations of reduced density matrices for entangled systems may not be completely positive maps. Quantum field theory is, of course, necessary for a consistent description of interactions. Its structure implies a fundamental **tradeoff** between detector reliability **and** localizability. Moreover, general relativity **produces new and counterintuitive effects**, particularly when black holes (or, more generally, event horizons) are involved. In this more general context some authors discuss how most of the current concepts in quantum information theory may require a reassessment. How relativistic effects (-) can be **exploited** to improve quantum information tasks, (+) a key topic of immense technological importance already today and more so for the next decades. The vantage point of these investigations is that the world is fundamentally both quantum and relativistic, and that these facts are immensely useful for the design of communication devices that are absolutely safe from eavesdropping, and of quantum computers that can quickly perform difficult computational tasks which overwhelm any classically imaginable computer. Indeed, impressive technological

achievements and promises have already been derived from taking seriously solely the quantum aspects of matter: quantum cryptography and communication have become a technical reality in recent years, but the practical construction of a quantum computer still requires understanding better how to efficiently store, manipulate and read information, without prohibitively large disturbances from the environment. Throwing relativity into the equation fundamentally changes the entire game, as I could show in a series of research papers, one of which was featured in a generally accessible Science article highlighting my work (Cho, Science 2005). I propose to push this exciting line of theoretical research to the point where relativistic effects in quantum information theory can be exploited technologically. Far from yielding only quantitative corrections, relativity **plays a dominant role** in the qualitative behaviour of many physical systems used to implement quantum information tasks in the laboratory. The prototypical example is provided by any system involving light, be it for the transmission or manipulation of quantum information. There is no such thing as a **non-relativistic approximation** to light quanta, so-called photons, since these always travel at the speed of light. While relativistic quantum theory, commonly known as quantum field theory, is a very well studied subject in foundational particle physics, research in **quantum information theory** selectively focused almost exclusively on those aspects one can study without relativity. Thus both unexpected obstacles (such as a relativistic **degradation** of quantum entanglement) and unimagined possibilities for quantum information theory (such as improved **quantum cryptography** and **hypersensitive quantum** measurement devices) have gone unnoticed. , Indeed, the impact of such research extends beyond *pure quantum information theory*, and applications to foundational questions in cosmology and black hole physics have been found. Over the past few years, a new field of high research intensity has emerged, known as **Relativistic Quantum Information (RQI)**. The field of RQI aims to understand the **relationship** between special and general relativity, and quantum information. In particular, so-called **quantum entanglement bits (e-bits)** are **a necessary resource** in all of **quantum communication and quantum computation**. One of the key goals of the field of RQI is to develop a theory of e-bits in realistic spacetimes described by Lorentzian manifolds. This offers exciting new challenges because it combines **information theory with quantum theoretic and general relativistic questions**. Deep questions concerning the **relationship** between information processing and the structure of spacetime are considered. Phenomena of relativistic quantum information, for example, use quantum communication with satellite-based instruments or **Berry's phase tests of the Unruh effect**.

Recently, there has been increased interest in understanding entanglement and quantum communication in black hole spacetimes and in using quantum information techniques to address questions in gravity. Studies on **relativistic entanglement** show the emergence of conceptually important **qualitative differences** to a non-relativistic treatment. For instance, entanglement was found to be an observer-dependent property that changes from the perspective of accelerated observers moving in flat spacetime. Relativistic quantum information theory uses well-known tools coming from quantum information and quantum optics to study quantum effects provoked by gravity to learn information about the spacetime. We can take advantage of our knowledge **about quantum correlations** and **effects produced** by the **gravitational interaction** to set the basis for experimental proposals ultimately aiming at **finding corrections due** to quantum gravity effects, too mild to be directly observed.

Quantum theory and **general relativity** are famously at loggerheads. Their mathematical languages are different and conceptual bases are discordant, if not outright conflicting. For more than sixty years this conceptual gap and scant experimental evidence has been preventing **unification of** the two theories. At the close of the last century a seemingly unrelated development of quantum information theory helped to unriddle some of the long-standing conceptual problems in quantum mechanics. While originally discussed in terms of **non-relativistic quantum mechanics**, recent years have seen increasing research interest and activities in placing quantum information in a more rigorous framework of **quantum field theory in** curved spacetimes. As a matter of fact, information theory is often appealed to in black hole physics and gravitational theories, particularly in relation to **the information loss paradox** and the **holographic principle**. **A relationship of "R" and "QI" is twofold**. On the one hand, **quantum field theory** is an **instrumental** tool in proposed designs of **quantum computing and communication**, and to comprehend the meaning and possibilities of **quantum non-locality**, and **entanglement in the quantum vacuum**. On the other hand, what "R" entails in RQI is perhaps best captured by what a relativist does traditionally: encompassing special and general relativity, geometry and topology (of spacetime and gauge fields), quantum field theory in curved spacetime and quantum gravity

Black hole information paradox and Quantum Machine:



The **black hole information paradox results** from the combination of quantum mechanics and general relativity. It suggests that physical INFORMATION could permanently **disappear in a** black hole, **allowing** many physical states **to evolve into** the same state. Loss of information in a black hole **produces** evolution of many physical states in to the same state Or, in other words, evolution of many physical states in to single state must **utilize** the loss of physical information in black hole..This is controversial because it violates a commonly assumed tenet of science—that *in principle* complete information about a physical system at one point in time should **determine** its state at any other time A fundamental postulate of quantum

mechanics is that complete information about a **system is encoded** in its wave function. The evolution of the wave function is **determined(e) by** a unitary operator. And unitarity **implies** that information is conserved in the quantum sense.

There are two main principles in play: **quantum determinism, and reversibility**. Quantum determinism means that given a present wave function, its future changes are uniquely **determined by** the evolution operator. Reversibility refers to the fact that the evolution operator **has an** inverse, meaning that the past wave functions are similarly unique. The combination of the two means that information must always be preserved.

Starting in the mid 1970's, Stephen Hawking and Jacob Bekenstein put forward theoretical arguments based on general relativity and quantum that appeared to be inconsistent with information conservation. Specifically, Hawking's calculations indicated that black hole evaporation via Hawking radiation **does not** preserve information. Today, many physicists believe that the holographic principle (specifically the AdS/CFT duality) **demonstrates that** Hawking's conclusion was incorrect, and that information is in fact preserved. In 2004 Hawking himself conceded a bet he had made, agreeing that black hole evaporation does in fact preserve information. Black hole evaporation **produces** the conservation and preservation of information. Conservation and preservation of information is attributable and ascribable to the entropic entecote of (e) Black hole evaporation.

Einstein himself is well known for rejecting some of the claims of quantum mechanics. While clearly contributing to the field, he did not accept many of the more "philosophical consequences and interpretations" of quantum mechanics, such as the **lack of deterministic** causality. He is famously quoted as saying, in response to this aspect, "My God does not play with dice". He also had difficulty with the assertion that a single subatomic particle **can occupy** numerous areas of space at one time. However, he was also the first to notice some of the apparently exotic **consequences of** entanglement, and **used** them to formulate the Einstein-Podolsky-Rosen paradox in the hope of showing that quantum mechanics had unacceptable implications. This was 1935, but in 1964 it was shown by John Bell (see Bell inequality) that - although Einstein was correct in identifying seemingly **paradoxical implications** of quantum mechanical non locality - these implications could be experimentally tested. Alain Aspect's initial experiments in 1982, and many subsequent experiments since, have definitively verified quantum entanglement.

According to the paper of J. Bell and the Copenhagen interpretation - the common interpretation of quantum mechanics by physicists since 1927 - and contrary to Einstein's ideas, quantum mechanics was **not**, at the same time:

EPR EXPERIMENT, QUANTUM STATES, QUANTUM COMPUTATION, QUANTUM ENTANGLEMENT:

The Einstein-Podolsky-Rosen paradox shows in any case that there exist experiments by which one can measure the state of one particle and instantaneously **change the** state of its entangled partner - although the two particles can be an arbitrary distance apart. However, **this effect** does **not violate** causality, since **no transfer of** information happens. Quantum entanglement forms the **basis** of quantum cryptography, which is used in high-security commercial applications in banking and government.

Gravity **is negligible** in many areas of particle physics, so that **unification between** general relativity and quantum mechanics is not an urgent issue in those particular applications. However, the lack of a correct theory of **quantum gravity** is an important issue in cosmology and the search by physicists for an elegant "Theory of Everything" (TOE). Consequently, resolving the inconsistencies between both theories has been a major goal of 20th and 21st century physics. Many prominent physicists, including Stephen Hawking, have labored for many years in the attempt to discover a theory underlying **everything**. This TOE would combine not only the different models of subatomic physics, but also derive the four fundamental forces of nature - the strong force, electromagnetism, the weak force, and gravity - from a single force or phenomenon. While Stephen Hawking was initially a believer in the Theory of Everything, after considering Gödel's Incompleteness Theorem, he has concluded that one is not obtainable, and has stated so publicly in his lecture "Gödel and the End of Physics" (2002). One of the leading authorities continuing the search for a coherent TOE is Edward Witten, a theoretical physicist who formulated the groundbreaking M-theory, which is an attempt at describing the super symmetrical based string theory. **M-theory posits** that our apparent 4-dimensional spacetime is, in reality, actually an 11-dimensional spacetime containing 10 spatial dimensions and 1 time dimension, although 7 of the spatial dimensions are - at lower energies - **completely "compactified" (or** infinitely curved) and not readily **amenable to** measurement or probing.

ATTEMPTS AT UNIFIED THEORY AND ITS IMPLICATIONS ON QUANTUM COMPUTING:

The quest **to unify the** fundamental forces through quantum mechanics is still ongoing. Quantum electrodynamics (or "quantum electromagnetism"), which is currently (in the perturbative regime at least) the most accurately tested physical theory¹ has been successfully merged with the weak nuclear force into the electroweak force and work is currently being done to merge the electroweak and strong force into the electro strong force. Current predictions state that at around 10^{14} GeV the three aforementioned forces are fused into a single unified field,^[37] Beyond this "grand unification," it is speculated that it may be possible to merge gravity with the other three gauge symmetries, expected to occur at roughly 10^{19} GeV. However — and while special relativity is parsimoniously incorporated into quantum electrodynamics — the expanded general relativity, currently the best theory describing the gravitation force, has not been fully incorporated into quantum theory.

Albert Einstein, himself one of the founders of quantum theory, disliked this **loss of determinism in measurement**. Einstein held that there should be a theory underlying quantum mechanics and, consequently, that the present theory was incomplete. He produced a series of objections to the theory, the most famous of which has become known as the Einstein-Podolsky-

Rosen paradox. John Bell showed that this "EPR" paradox led to experimentally testable differences between quantum mechanics and local realistic theories. Experiments have been performed confirming the accuracy of quantum mechanics, **thereby demonstrating that** the physical world cannot be described by any local realistic theory. The *Bohr-Einstein debates* provide a vibrant critique of the Copenhagen Interpretation from an epistemological point of view.

The *Everett many-worlds interpretation*, formulated in 1956, holds that *all* the possibilities described by quantum theory *simultaneously* occur in a multiverse composed of mostly **independent parallel universes**. This is not accomplished by introducing some "new axiom" to quantum mechanics, but on the contrary, **by removing** the axiom of the **collapse of the wave packet**. All of the possible consistent states of the measured system and the measuring apparatus (including the observer) are present in a *real* physical - not just formally mathematical, as in other interpretations - **quantum superposition**. Such a superposition of consistent state **combinations of different** systems is called an entangled state. While the multiverse is deterministic, we perceive non-deterministic behavior **governed** by probabilities, **because** we can observe only the universe (i.e., the consistent state contribution to the aforementioned superposition) that we, as observers, inhabit. Everett's interpretation is perfectly **consistent with John** Bell's experiments and makes them intuitively understandable. However, according to the theory of quantum decoherence, these "parallel universes" **will never be accessible to us**. The inaccessibility can be understood as follows: once a measurement is done, the measured system **becomes entangled** with *both* the physicist who measured it *and* a huge number of other particles, some of which are photons flying away at the speed of light towards the other end of the universe. In order to prove that the wave function **did not collapse**, one would have to bring *all* these particles back and measure them again, together with the system that was originally measured. Not only is this completely impractical, but even if one *could* theoretically do this, it would **destroy any evidence that the original measurement took place** (to include the physicist's memory).

Quantum mechanics had enormous success in explaining many of the features of our world. The **individual behaviors** of the subatomic particles that make up all forms of matter (electrons, protons, neutrons, photons, and others) can often **only be satisfactorily described** using quantum mechanics. Quantum mechanics has **strongly influenced** string theories, candidates for a *Theory of Everything* (see *reductionism*), and the **multiverse hypotheses**.

QUANTUM TUNELLING, QUANTUM COHERENCE, AND QUANTUM MACHINE

Quantum Tunneling of Magnetization and Related Phenomena in Molecular Materials (SEE Dante Gatteschi dRoberta Sessoli)

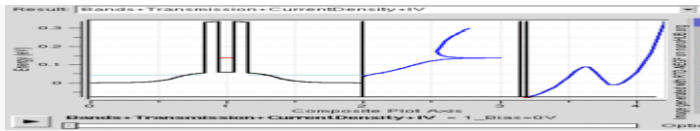
The fields in which chemistry may have a fundamental role are increasing in number, and it is becoming more and more difficult (though stimulating) for synthetic chemists to cope with requests of new compounds with highly sophisticated properties. The movement from simplicity to complexity in molecular chemistry is one which cannot be stopped, and supramolecular chemistry is just one clear example of that. The last few years have seen the opening of many new research fields in which molecular materials have been forced, through chemical ingenuity, to acquire properties which are associated with classic inorganic materials. Perhaps the most convincing evidence for this has been the development of purely organic materials, which behave as conductors and superconductors. In addition, organic materials, because of their photorefractive and nonlinear-optical properties, are now even used to make lasers. Magnetism is certainly one of the fundamental properties of matter, inextricably associated with electrical properties. One of the main difficulties in developing molecule-based magnets is that bulk magnetism is intrinsically a three-dimensional (3D) property in that only if a 3D lattice of interacting magnetic centers is assembled may the material show spontaneous magnetization below a critical temperature. The problem with molecular materials is that the design of genuine 3D connected lattices is not obvious, because the intrinsic low symmetry of the individual molecules tends to favor 1D or 2D arrangements. Here the difference between molecular magnets and conductors is striking, because for conductors exciting properties can be found even if 1D arrangements of individual molecules are obtained in the solid state. However, this has not scared the synthetic chemists and genuine room-temperature molecule based magnets are now available. The difficulties in forming 3D magnets with molecular materials have been turned into advantages when it was realized that oligonuclear compounds, comprising a large, but finite, number of magnetic centers may have unique magnetic properties which have made them almost ideal systems for observing quantum size effects in magnets.

The magnetic centers can be transition-metal or rare-earth ions, or even organic radicals. The observation of quantum phenomena in mesoscopic matter provides, in principle, confirmation to the so-called Copenhagen interpretation, which assumes that there is a continuous transition from the field of small objects, where quantum mechanics is required, to macroscopic objects, where classical physics operates well. Materials the properties of which are intermediate between classical and quantum nature, or where there is coexistence of the two, may be used for completely new types of devices. A particularly interesting field is that of **quantum computing**, where information can be handled taking advantage of quantum Tunneling. Molecules comprising a large number of coupled paramagnetic centers are attracting much interest because they may show properties which are intermediate between those of simple paramagnets and classical bulk magnets and provide unambiguous evidence of quantum size effects in magnets. To date, two cluster families usually referred to as Mn₁₂ and Fe₈, have been used to test theories. However, it is reasonable to predict that other classes of molecules will be discovered which have similar or superior properties. To do this it is necessary that synthetic chemists have a good understanding of the correlation between the structure and properties of the molecules, for this it is necessary that concepts such as **quantum tunneling, quantum coherence, quantum oscillations are understood**. In fact it gives rise to magnetic hysteresis, which is one condition for storing information in a particle. Under this respect therefore Mn₁₂ac behaves like a classical magnet. However, it is still small enough to also show large quantum effects. In fact Mn₁₂ac, and other molecules which have since

been investigated, provide the best examples to date of the observation of quantum effects, such as the tunneling of the magnetization, in magnets. These molecules are now often called TMsingle-molecule magnets]

The interactions with the environment will tend to localize the particles, because the interactions will make one well more TMattractive] than the other (that is, reduce the energy of one of the wells). In the case of strong coupling with the environment, which means that this interaction is much larger than the tunnel splitting, the particle will stay localized in one of the two wells, and will not tunnel. For intermediate coupling the particle can tunnel, but jumping incoherently from one well to the other. This means that one particle will tunnel, and localize for some time in the other well, and then tunnel again, but in an irregular way. The third case is that of weak coupling when the tunnel splitting is large compared to the interaction with the environment, and the particle oscillates coherently between the two minima. The conditions for observing coherent tunneling are severe. Evidence for coherent tunneling is the observation of energy absorption at a frequency corresponding to the tunnel splitting. In the above experiment of calyx a peak was observed in the proton-spin lattice-relaxation rate at a field corresponding to the tunneling frequency of 35 MHz

Quantum mechanics is also critically important for understanding how individual atoms combine covalently to form molecules. Relativistic quantum mechanics can, in principle, mathematically describe most of chemistry. Quantum mechanics can also provide quantitative insight into ionic and covalent bonding processes by explicitly showing which molecules are energetically favorable to which others, and the magnitudes of the energies involved. Furthermore, most of the calculations performed in modern computational chemistry rely on quantum mechanics.



A working mechanism of a resonant tunneling diode device, based on the (e)phenomenon of quantum tunneling through potential barriers

A great deal of modern technological inventions operates at a scale where quantum effects are significant. Examples include the laser, the transistor (and thus the microchip), the electron microscope, and magnetic resonance imaging (MRI). The study of semiconductors led to the invention of the diode and the transistor, which are indispensable parts of modern electronics systems and devices.\

SIMULATION OF THE REALITY-IS THIS WORLD SIMULATED BY A GIANT QUANTUM COMPUTER?

A Quantum-Digital Universe (See Giacomo Mauro D'Ariano)

Can Reality be simulated by a huge Quantum Computer? Do we believe that Reality is made of something more than interacting quantum systems? The idea that the whole Physics is ultimately quantum computation; strong quantum version of the Church-Turing hypothesis well synthesized by the Wheeler's coinage it from bit is very appealing. It is theoretically very parsimonious and curmudgeonly- an Occam razor's quality-guaranteed description of the world. But, if this is the case, then we need to understand the entire Physics as emergent(e) from the quantum computation. Universe (=) is a Quantum Field. Particles are(=) just states of the Field: they can be created and (e)&(eb)annihilated. We have indeed a beautiful Grand Unified Field Theory, and we are looking forward to see the Higg's boson at the LHC.

But what is the Quantum Field made of? Ultimately, Quantum Field is (e)made of quantum systems that are interacting,(each Quantum system located at a different position in space). Quantum field is((e)) a continuum. But is Reality actually continuous? We don't know: but it looks easier to think to Reality or Objective Reality and in fact the Subjective experience as a continuum. Now, suppose that this is not the case, namely Reality is (e&eb)ultimately discrete, and the continuum is only a mathematical fiction. Then, what else are out there more than interacting quantum systems? Is it space? No, space is "nothingness". Is it Relativity? No, that's not a "thing": Or is it? Can it not be classified based on the tensorial entities it is made of for a particle or set of particles it is meant of? That despite the fact that the 'theory' is a 'generalization' one; it is a way of looking at things. We thus come to the conclusion that Reality is made(e) only of "interacting quantum systems", and this is (=)precisely what we call a quantum computer; the interacting quantum states. David Deutsch in his seminal paper Quantum theory, the Church-Turing principle and the universal quantum computer rephrased the Church-Turing hypothesis as a truly physical principle. In short: every piece of physical reality can be perfectly 'simulated' by a quantum computer. But now: what is the difference between Reality and its simulation? Reality is indistinguishable from its simulation implies then it is its simulation. But how would you know that a situation is simulation or the Objective Reality. If you are followed by Supari Mafia, Crime Syndicates, hoodlum mugger aggregates, raucous ribaldry congregates, loutish, jeerish elements, the veritable string ray sachrochusus imperators, herrenvolk sandhurst lucubration cormorants, that cause traffic jams, create havoc in the neighborhood with the connivance and contrivance of the neighbours, or some hundred vehicles are parked at your door; somebody is keeping vigil while' casually' sitting in the park. Then? It is here consciousness comes in. Consciousness of what exactly the truth is comes from 'knowing'. How would you 'know'? From the subjective experiences of the past. That you are the victim. So it is 'consciousness' that produces 'objective reality' Next paper exactly deals with this: 'Consciousness' and 'Objective reality'; and 'consciousness' and 'Subjective experience' 'The Universe is really a huge quantum computer: the computational universe of Seth Lloyd .But we have more than that. Quantum Theory is (=)ultimately a "theory of information", an idea that has been hanging around for many years since the Wheeler's it from bit, and which has been also recently proved mathematically. Therefore, if we adopt the Deutsch's Church-Turing principle, the notion of Information becomes(e) the new big paradigm for Physics. And Physics can be classified based on the theoretical

parameters that are involved in a Theory; notwithstanding 'generalizationalness' of the theory. Take for example Heisenberg's Principle of Uncertainty. Can we not have positions and momentums that are different to different particles? That the product is always less than $h/2$ does not mean there cannot be total quantum of 'positions and momentums' of the particles or for that matter there cannot be 'total gravitational field'. The scientific approach behind the computational paradigm. The Informationalism can be ultimately regarded as a new scientific approach, very close to the spirit of Niels Bohr and the Copenhagen school. Far from being speculative, the approach is truly operational, namely everything must be defined by a precise procedure—ultimately in terms of accurate quantum measurements. The real entities are the events, facts of the world describable by the basic language obeying the rules of predicate logic (the "facts" of Wittgenstein's Tractatus). Formulating a Theory of the observed (or potentially observable) events means **building up a network** of input-output connections between them. In a causal theory these connections are causal links: Quantum Theory is exactly a theory of this kind. Translating these terms into computer-programming language, the events are the subroutines, and the **causal links** are the registers where information is written and read. Like "Transfer Scrolls" in the Bank. Total conservation and preservation of assets and liabilities does not mean that there cannot be individual debits and credits. In fact individual debits and credits are conserved; then the summary sheets of each department is conserved; then the General Ledger which gives the double entries of 'inflow' and 'outflow' are recorded gives the total quantum of energy transformed from one to another is recorded. This 'General Ledger' is the "General Theory Of Every Thing" the Quantum Mechanical Operations, Relativistic operations, or nonoperationability of accounts themselves which are taken in to consideration also but in such a case there are no inflows and out flows. Translating into physical terms: the links are the systems and the events are the transformations. There absolutely is no difference except in that there might not be (?) 'Interest' in the energy transactions or for that matter Nature might not be making any "Profit" out of each transaction. But still all these "inflow" terms are given 'Account Heads' and are 'invoked' and 'revoked' based on the concomitant and corresponding "Debits and Credits"; Whenever it is eschewed then there shall be no "transactions" under this head. It is in the light of the foregoing consideration the word or notion of "event" must be regarded as truly primordial: events **do not (e(eb)) happen** in spacetime, **they(eb) build-up** space-time. Stated in other words: space-time is **our(e&eb) way of organizing** events. The idea of deriving the geometry of space-time from apurely "causal structure"(this is the source) has been also hanging around for more than two decades after Raphael Sorkin opened the causal sets program.

A portion of a quantum circuit (left) and its causal network representation (right). The hexagon (and the corresponding circle on the right) represents a tile which allows to recover the whole circuit upon translation. This is the equivalent of a Physical Law. Physicists often identify Theory with Reality, but Theory is only our way to **connect** phenomena, **to relate** input with an output. Input and output are linked through cascades of local interactions, namely events that involve only a finite number of systems. In the quantum computer the subroutines (the potential events) are the unitary transformations of the gates, and the causal links are the quantum systems—the so-called qubits. In Fig. 1 a piece of quantum circuit is represented. The gate(box) performing the unitary transformation A reads information from two input registers (wires) which in turn are the output of two gates performing the unitary B, and so forth. What is a Physical Law in this causal-network framework? It is a piece of network—a set of events (gates) along with causal links (wires) connecting them—by translating which we can build up the whole unbounded periodic network, corresponding to our supposition that the law is true everywhere and ever. Such representation of the physical law contains only its logical essence, stripped of the "conventional" part (e. g. the conventionality of simultaneity the informational paradigm is a huge change of ontology: there is no stuff that supports the qubits, but **stuff itself is made(e) of** qubits! This is a change of perspective that is hard to swallow. Those who strongly believe in the reality of space-time with "objects" inside it in. Another objection is that, once we have the computer, we still need to provide it with the software. True: but this is the same challenge of grand unification of quantum field theory, and here at least we have a simple common "programmable" background, and we may hope to find unification in new kinds of principles, related e. g. to the topological nature of the network. The principles must be simple: the software must be simple. But the computational grand-unification, being naturally a lattice theory, would also have the great bonus of avoiding all problems due to the continuum which plague quantum field theory (ultraviolet divergences, the Feynman path integral, nonlocalizability of measurements, and many more). On the other hand, the digital theory will likely miss some of the simplicity of the continuum, whence finding easy ways to interpolate digital with analog must have top priority. Recovering the whole Physics as emergent from the quantum information processing is a large program: we need to build up a complete dictionary that translates all physical notions into information-theoretic words. And we want more than that: we want to know if the digital character of Reality is experimentally detectable at some scale. Spacetime, a physical notion, **can(e) emerge from the** quantum computation, and how the quantum-digital nature of Reality **leads to physical (eb)consequences** that are in-principle detectable. Current quantum field theory is indeed a kind of "thermodynamic" limit, valid at the Fermi scale, of a deeper theory that holds at the Planck scale, where the quantum **field is replaced** by a giant quantum computer. We'll see that the free-flow of quantum information is described by digital version of the Dirac equation and **this also provides** informational interpretations for inertial mass and Planck constant. At the same time, the notion of Hamiltonian is emerging, and, the quantum field **can be eliminated** in favor of pure qubits. Some of these ideas for the moment plainly work in one space dimension, and are only a starting point: later in the paper we will see routes to be explored for larger space dimensions. The free flow of information is the Dirac equation. One striking feature of the computational paradigm is that Lorentz covariance is a free bonus. As a matter of fact, Lorentz covariance must **emerge(e) from** the computation if this is able to simulate "Reality". And, the Dirac equation turns out to be just the freedom of quantum informations mentioned, we will restrict to one space dimension, and incorporation of larger dimensions later. In the quantum computer information can flow in a fixed direction only at the maximum speed of one-gate-per-step. In the digital world there is no physical unit: **time and space are measured by counting, and the digital-analog conversion factors**

will be given by a time τ expressed in seconds and length a expressed in meters, which can be interpreted as the minimal space distance and time-distance between events, respectively. We may think to as providing the Planck scale, namely 0.1 mm compared to an electron as huge as an entire galaxy! In analog units, the maximal speed is then given by $c = a/\tau$. Mathematically information flow in the two directions by the two field operators.

Various present and future specialized applications of magnets require monodisperse, small magnetic particles, and the discovery of molecules that can function as Nanoscale magnets was an important development in this regard. These molecules act as single-domain magnetic particles that, below their blocking temperature, **exhibit** magnetization hysteresis, a classical property of macroscopic magnets. Such 'single-molecule magnets' (SMMs)⁴ straddle the interface between classical and quantum mechanical behaviour because they also display quantum tunnelling of magnetization^{5,6} and quantum phase interference⁷. Quantum tunnelling of magnetization can be advantageous for some potential applications of SMMs, for example, in providing the quantum superposition of states required for quantum computing⁸. However, it is a disadvantage in other applications, such as information storage, where it would lead to information loss. Thus it is important to both understand **and control** the quantum properties of SMMs. Here we report a supramolecular SMM dimer in which antiferromagnetic coupling between the two components results in quantum behaviour different from that of the individual SMMs. Our experimental observations and theoretical analysis suggest a means of tuning the quantum tunnelling of magnetization in SMMs. This system may also prove useful for studying quantum tunnelling of relevance to mesoscopic antiferromagnets. Researchers are currently seeking robust methods of **directly manipulating** quantum states. Efforts are being made to more fully **develop** quantum cryptography, which will **theoretically allow** guaranteed secure transmission of information. A more distant goal is the development of quantum computers, which are expected to perform certain computational tasks exponentially faster than classical computers. Another active research topic is quantum teleportation, which deals with techniques to transmit quantum information over arbitrary distances

QUANTUM COMPUTATION AND PAULI'S EXCLUSION PRINCIPLE:

What is quantum computing? Alan Turing thought about this in 1936 with regard (implicitly) to classical mechanics, and gave the world the paradigm classical computer: the Turing machine. In a trivial sense, everything is a quantum computer. (A pebble **is a** quantum computer **for calculating** the constant-position function - you get the idea.) And of course, today's computers exploit quantum *effects* (like electrons tunneling through barriers) to help do the right thing and do it fast. For that matter, both the computer and the pebble **exploit a** quantum effect - **the "Pauli exclusion principle"**, which **holds(e) up** ordinary matter against collapse by bringing about the kind of degeneracy we call chemistry - just to remain stable solid objects. But quantum computing is much more than that.

The most exciting really new feature of quantum computing is **quantum parallelism**. A quantum system is in general not in *one* "classical state", but in a "quantum state" consisting (crudely speaking) of a **superposition of many(e&eb) classical or classical-like** states. This superposition is not just a figure of speech, covering up our ignorance of which classical-like state it's "really" in. But actually you need the whole superposition to get the time evolution right. The system *really is* in some sense in all the classical-like states at once! If the superposition can be protected from unwanted entanglement **with its** environment (known as *decoherence*), a quantum computer can **output results dependent on details** of *all* its classical-like states. This is quantum parallelism - parallelism on a serial machine. And if that wasn't enough, machines that would already, in architectural terms, qualify as parallel can benefit from quantum parallelism too -

QUANTUM TUNELLING AND QUANTUM MACHINE:.

Physicists Andrew Cleland and John Martinis from the University of California at Santa Barbara and their colleagues designed the machine -- a tiny metal paddle of semiconductor, visible to the naked eye -- and coaxed it into dancing with a quantum groove. First, they cooled the paddle until it reached its "ground state," or the lowest energy state permitted by the laws of quantum mechanics (a goal long-sought by physicists). Then they raised the widget's energy by a single quantum to produce a purely quantum-mechanical state of motion. They even managed to put the gadget in both states at once, so that it literally vibrated a little and a lot at the same time -- a bizarre phenomenon allowed by the weird rules of quantum mecha space with a complex metric permitted by quantum cosmology is given; two regions, one containing no closed causal curve and one containing closed time like curves, are separated by a complex region. Through quantum tunneling one can travel from one region to the other. The vacuum polarization stress-energy tensor converges everywhere so the space is stable. This challenges Hawking's chronology protection conjecture and highlights on building a time machine.

Superpositional quantum computation

Superpositional quantum computations **exploit the(e) fact** that a coherent quantum state is a **superposition(e&eb)** of n distinct states, α_i , each weighted by some complex scalar α_i . Under certain conditions, this quantum state decoheres, and the particle adopts one of the α_i as its determinate state, with a probability that is determined by the ratios of the α_i . The idea proposed in [Feynman, 1982] and developed in, e.g., [Deutsch, 1985], is that if such superpositional states were used to implement the states of a computer, then **various registers or memory locations** in the computer would not be conventional bits with a determinate value of 1 or 0, but would instead be quantum bits - *qubits* - which are superpositions of both the 0 and 1 values.

A key advantage to this would be that n qubits **could (e)be used** to perform 2^n computations in parallel, one computation for **each (e&eb)combination** of values of the superposed states. However, there are two principal difficulties **in (e)exploiting** this proposal. First, there is the problem of maintaining the coherence (=superpositionality) of a qubit while performing computations on it: the danger is that the kind of physical processes necessary to implement the relevant bit operations are

such that they would cause the quantum state to collapse or decohere. But even supposing one can perform such operations while maintaining the coherence of the qubit, there is still the difficulty of exploiting the superpositionality of the qubit in a way that can perform effective computational work.

The only specific idea of how this can be done was proposed by Shor [Shor, 1994]. Shor describes how to initialize a superpositional quantum state with a random number x and a number n to be factored into primes. He then describes how to transform(e&eb) that state into another which is such that the probability distribution of the measurements of the state is a simple function of a number r which is a reliable guide to the prime factors of n . A few collapses, then, of this system allows one to calculate r and thus factorize n . If this algorithm could be implemented in a real quantum computational system, one could then produce the prime factors of large (e.g., 159-digit) numbers in seconds. Since current cryptography technology relies on the fact that such numbers would take a single computer many years to factor, Shor's algorithm has generated much interest in quantum computation. However, it has proven difficult to generalize this exploitation of the qubit to other applications. The general problem of how to use a superpositional state to do computational work remains. Quantum tunneling is vital to the operation of many devices - even in the simple light switch, as otherwise the electrons in the electric current could not penetrate the potential barrier made up of a layer of oxide. Memory chips found in USB drives(e) use quantum tunneling to(e) erase their memory cells.

BLACK BODY RADIATION QUANTUM COMPUTATION

Hawking radiation is black body radiation that is predicted to be emitted by black holes, due to quantum effects near the event horizon. It is named after the physicist Stephen Hawking, who provided a theoretical argument for its existence in 1974, and sometimes also after the physicist Jacob Bekenstein who predicted that black holes should have a finite, non-zero temperature and entropy. Hawking's work followed his visit to Moscow in 1973 where Soviet scientists Yakov Zeldovich and Alexei Starobinsky showed him that according to the quantum mechanical uncertainty principle, rotating black holes should create and emit particles. Hawking radiation reduces the mass and the energy of the black hole and is therefore also known as **black hole evaporation**. Because of this, black holes that lose more mass than they gain through other means are expected to shrink and ultimately vanish. Micro black holes (MBHs) are predicted to be larger net emitters of radiation than larger black holes and should shrink and dissipate faster.

Quantum coherence and nonlocality were long regarded as primary(eb) manifestations of the counterintuitive nature of quantum theory. They are now also coming to be recognized as a potentially(e) valuable resource for information processing and communication. In contact with its environment, a quantum system can(e) lose its ability to (eb)exhibit coherence and nonlocality. The process responsible for *this transition* to effectively classical behavior is known as decoherence. While shedding new light on the origins of "the classical" decoherence makes difficult to take advantage of the full potential offered by the quantum in communication and, especially, in computation. A challenge for physics is therefore to understand more thoroughly the reasons for decoherence and to devise means to preserve(e&eb) it. The discovery by Peter Shor that quantum computers can factor large numbers much more efficiently than their classical counterparts has brought the whole field to the limelight. In quantum computers coherence must e(e&eb)be preserved throughout the calculation. The notion of quantum operations, reversible measurement and the information theoretic notions are described extensively in literature demonstrates how quantum communication can be done without (e) requiring energy extending the analogous classical result. Generalisation of the quantum factoring algorithm. Zalka demonstrates how a quantum computer can be utilized(e) for efficiently simulating quantum mechanical systems. Cleve et al., identify common pattern of quantum algorithms. Quantum information is extremely fragile. Not only there is little energy between the states $|0\rangle$ and $|1\rangle$ but any superpositions are also allowed. Superpositions with the different phase s have the same energy and therefore become exceedingly fragile. This fragility has been thought to imply the demise of quantum computers. Fortunately quantum error correction codes have been discovered thus giving hope that it may be possible to build quantum computers robust against imperfections. The third part of these proceedings deals with errors and quantum error correction. Paz and Zurek analyze the effect of errors on the factoring algorithm. Knill et al. introduce error correction and demonstrate an accuracy threshold theorem. A similar theorem is also proved and analyzed by Preskill. Finally, all these theoretical constructions would be like sand castles if it would not be possible to build quantum computers. Wineland gives a review of the ion trap quantum computer. Walther surveys single atom experiments in cavities and traps. And finally Gershenfeld et al. analyze a new system to realize a quantum computer: Nuclear Magnetic Resonance. While quantum mechanics primarily applies to the atomic regimes of matter and energy, some systems exhibit quantum on a large scale - super fluidity, the frictionless flow of a liquid at temperatures near absolute, is one well-known example. Quantum theory also provides accurate descriptions for many previously unexplained phenomena, such as black body radiation and the stability of the orbitals of electrons in atoms. It has also given insight into the workings of many different biological systems, including receptors and protein structures Recent work on photosynthesis has provided evidence that quantum correlations play an essential role in this basic fundamental process of the plant kingdom. Even so, classical physics can often provide good approximations to results otherwise obtained by quantum physics, typically in circumstances with large numbers of particles or large quantum numbers.

Examples

Topological quantum computer

A **topological quantum computer** is a theoretical quantum computer that(e) employs two-dimensional quasiparticles called anyons, whose world lines cross(e&eb) over one another to form braids in a three-dimensional spacetime (i.e., one temporal plus two spatial dimensions). These braids form(eb) the logic gates that make(eb)

up the computer. The advantage of a quantum computer based (e)on quantum braids over using (e)trapped quantum particles is that the former is much more stable. The smallest perturbations can (e)cause a quantum particle to decohere and introduce errors in the computation, but such small perturbations do (e&e)not change the topological properties of the braids. This is like the effort required to cut a string and reattach the ends to form a different braid, as opposed to a ball (representing an ordinary quantum particle in four-dimensional spacetime) simply bumping into a wall. While the elements of a topological quantum computer originate in a purely mathematical realm, experiments in 2002 by Michael H. Freedman along with Zhenghan Wang, both with Microsoft, and Michael Larsen of Indiana University indicate these elements can be(e) created in the real world using semiconductors made of gallium arsenide near absolute zero and subjected to strong magnetic fields.

Anyons are quasiparticles in a two-dimensional space. Anyons are not strictly fermions or bosons, but do share the characteristic of fermions in that they cannot occupy the same state. Thus, the world lines of two anyons cannot e(e&e)cross or merge. This allows braids to be made that make up a particular circuit. In the real world, anyons form(e) from the excitations in an electron gas in a very strong magnetic field, and carry fractional units of magnetic flux in a particle-like manner. This phenomenon is called the fractional quantum Hall effect. The electron "gas" is sandwiched between two flat plates of gallium arsenide, which (e)create the two-dimensional space required for anyons, and is cooled(e) and subjected to intense transverse magnetic fields.

When anyons are(e&e) braided, the transformation of the quantum state of the system depends only on the topological class of the anyons' trajectories (which are classified according to the braid group). Therefore, the quantum information which is stored in the state of the system is(e(e&e) impervious to small errors in the trajectories. In 2005, Sankar Das Sarma, Michael Freedman, and Chetan Nayak proposed a quantum Hall device which would realize a topological qubit. In a key development for topological quantum computers, in 2005 Vladimir J. Goldman, Fernando E. Camino, and Wei Zhou were said to have created the first experimental evidence for using fractional quantum Hall effect to (e)create actual anyons, although others have suggested their results could be the product of phenomena not involving anyons. It should also be noted that nonabelian anyons, a species required for topological quantum computers, have yet to be experimentally confirmed.

Topological quantum computers are equivalent in computational power to other standard models of quantum computation, in particular to the quantum circuit model and to the quantum Turing machine model. That is, any of these models can efficiently simulate any of the others. Nonetheless, certain algorithms may be a more natural fit to the topological quantum computer model. For example, algorithms for evaluating the Jones polynomial were first developed in the topological model, and only later converted and extended in the standard quantum circuit model.

Topological Quantum Computations

To live up to its name, a topological quantum computer must(e) provide the unique computation properties promised by a conventional quantum computer design, which uses trapped quantum particles. Fortunately in 2002, Michael H. Freedman along with Zhenghan Wang, both with Microsoft, and Michael Larsen of Indiana University proved that a topological quantum computer can, in principle, perform any computation that a conventional quantum computer can do.

They found that conventional quantum computer device, given a flawless (error-free) operation of its logic circuits, will give a solution with an absolute level of accuracy, whereas a topological quantum computing device with flawless operation will(e) give the solution with only a finite level of accuracy. However, any level of precision for the answer can be obtained by adding more braid twists (e&e) of logic circuits to the topological quantum computer, in a simple linear relationship. In other words, a reasonable(+x) increase in elements (braid twists) can(e) achieve a high degree of accuracy in the answer. Actual computation [gates] is done(e) by edge states of fractional quantum Hall effect. This makes models one dimensional anyons important. In one space dimension anyons are defined algebraically.

Error correction and control

Even though quantum braids are inherently more(e) stable than trapped quantum particles, there is still a need to control(e&e) for error inducing(e) thermal fluctuations, which(e) produce random stray pairs of anyons which(e&e) interfere with adjoining braids. Controlling these errors is simply a matter of(e&e) separating the anyons to a distance where the rate of interfering strays drops(e) to near zero. Simulating the dynamics of a topological quantum computer may be a promising method of implementing fault-tolerant quantum computation even with a standard quantum information processing scheme. Raussendorf, Harrington, and Goyal have studied one model, with promising simulation results.

Free particle

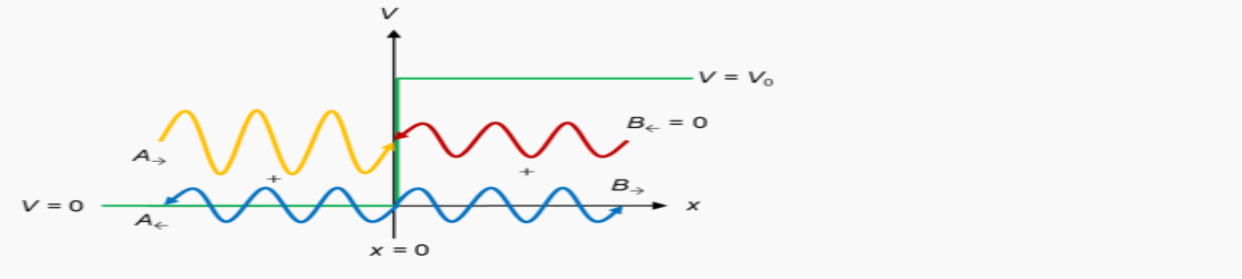
For example, consider a free particle. In quantum mechanics, there is wave-particle duality, so the properties of the particle can be described as the properties of a wave. Therefore, its quantum state can be represented as a wave of arbitrary shape and extending over space as a wave function. The position and momentum of the particle are observables. The Uncertainty Principle states that both the position and the momentum cannot simultaneously be measured with complete precision simultaneously. However, one can measure the position (alone) of a moving free particle, creating an eigenstate of position with a wavefunction that is very large (a Dirac delta) at a particular position x , and zero everywhere else. If one performs a position measurement on such a wavefunction, the resultant x will be obtained with 100% probability (i.e., with full certainty, or complete precision). This is called an

eigenstate of position - or, stated in mathematical terms, a *generalized position eigenstate (eigendistribution)*. If the particle is in an eigenstate of position, then its momentum is completely unknown. On the other hand, if the particle is in an eigenstate of momentum, then its position is completely unknown. In an eigenstate of momentum having a plane wave form, it can be shown that the wavelength is equal to h/p , where h is Planck's constant and p is the momentum of the eigenstate



3D confined electron wave functions for each eigenstate in a Quantum Dot. Here, rectangular and triangular-shaped quantum dots are shown. Energy states in rectangular dots are more 's-type' and 'p-type'. However, in a triangular dot, the wave functions are mixed due to confinement symmetry.

Step potential and Schrodinger's Equation:



Scattering at a finite potential step of height V_0 , shown in green. The amplitudes and direction of left- and right-moving waves are indicated. Yellow is the incident wave, blue are reflected and transmitted waves, red does not occur $> V_0$ for this figure.

The potential in this case is given by:

$$V(x) = \begin{cases} 0, & x < 0, \\ V_0, & x \geq 0. \end{cases}$$

The solutions are superpositions of left- and right-moving waves:

$$\psi_1(x) = \frac{1}{\sqrt{k_1}} \left(A_{\rightarrow} e^{ik_1x} + A_{\leftarrow} e^{-ik_1x} \right) \quad x < 0$$

$$\psi_2(x) = \frac{1}{\sqrt{k_2}} \left(B_{\rightarrow} e^{ik_2x} + B_{\leftarrow} e^{-ik_2x} \right) \quad x > 0$$

where the wave vectors are related to the energy via

$$k_1 = \sqrt{2mE/\hbar^2}, \text{ and}$$

$$k_2 = \sqrt{2m(E - V_0)/\hbar^2}$$

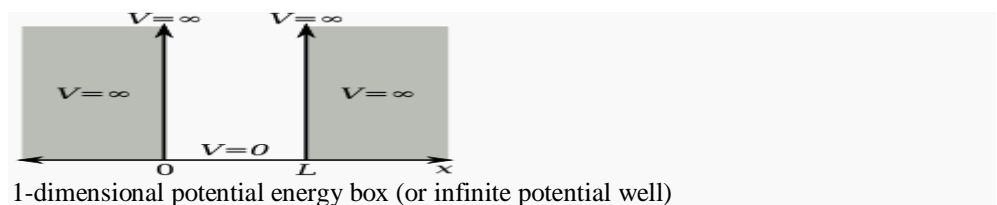
and the coefficients A and B are determined from the boundary conditions and by imposing a continuous derivative on the solution.

Each term of the solution can be interpreted as an incident, reflected, or transmitted component of the wave, allowing the calculation of transmission and reflection coefficients. In contrast to classical mechanics, incident particles with energies higher than the size of the potential step are still partially reflected.

Rectangular potential barrier

This is a model for the quantum tunneling effect, which has important applications to modern devices such as flash memory and the scanning tunneling microscope.

Particle in a box



The particle in a one-dimensional potential energy box is the most simple example where restraints lead to the quantization of energy levels. The box is defined as having zero potential energy everywhere *inside* a certain region, and infinite potential energy everywhere *outside* that region. For the one-dimensional case in the x direction, the time-independent Schrödinger equation can be written as

$$-\frac{\hbar^2}{2m} \frac{d^2\psi}{dx^2} = E\psi.$$

Writing the differential operator

$$\hat{p}_x = -i\hbar \frac{d}{dx}$$

the previous equation can be seen to be evocative of the classic kinetic energy analogue

$$\frac{1}{2m} \hat{p}_x^2 = E$$

with E as the energy for the state ψ , which in this case coincides with the kinetic energy of the particle.

The general solutions of the Schrödinger equation for the particle in a box are:

$$\psi(x) = Ae^{ikx} + Be^{-ikx} \quad E = \frac{\hbar^2 k^2}{2m}$$

or, from Euler's formula,

$$\psi(x) = C \sin kx + D \cos kx.$$

The presence of the walls of the box determines the values of C , D , and k . At each wall ($x = 0$ and $x = L$), $\psi = 0$. Thus when $x = 0$,

$$\psi(0) = 0 = C \sin 0 + D \cos 0 = D$$

and so $D = 0$. When $x = L$,

$$\psi(L) = 0 = C \sin kL.$$

C cannot be zero, since this would conflict with the Born interpretation. Therefore, $\sin kL = 0$, and so it must be that kL is an integer multiple of π . And additionally,

$$k = \frac{n\pi}{L} \quad n = 1, 2, 3, \dots$$

The quantization of energy levels follows from this constraint on k , since

$$E = \frac{\hbar^2 \pi^2 n^2}{2mL^2} = \frac{n^2 h^2}{8mL^2}.$$

Finite potential well

This is the generalization of the infinite potential well problem to potential wells of finite depth.

Harmonic oscillator

Some trajectories of a harmonic oscillator (i.e. a ball attached to a spring) in classical mechanics (A-B) and quantum mechanics (C-H). In quantum mechanics, the position of the ball is represented by a wave (called the wavefunction), with the real part shown in blue and the imaginary shown in red. Some of the trajectories (such as C, D, E, and F) are standing waves (or "stationary states"). Each standing-wave frequency is proportional to a possible energy of the oscillator. This "energy quantization" does not occur in classical physics, where the oscillator can have *any* energy.

As in the classical case, the potential for the quantum harmonic oscillator is given by:

$$V(x) = \frac{1}{2} m\omega^2 x^2$$

This problem can be solved either by solving the Schrödinger equation directly, which is not trivial, or by using the more elegant "ladder method", first proposed by Paul Dirac. The eigenstates are given by:

$$\psi_n(x) = \sqrt{\frac{1}{2^n n!}} \cdot \left(\frac{m\omega}{\pi \hbar}\right)^{1/4} \cdot e^{-\frac{m\omega x^2}{2\hbar}} \cdot H_n\left(\sqrt{\frac{m\omega}{\hbar}} x\right), \quad n = 0, 1, 2, \dots$$

where H_n are the Hermite polynomials:

$$H_n(x) = (-1)^n e^{x^2} \frac{d^n}{dx^n} (e^{-x^2})$$

and the corresponding energy levels are

$$E_n = \hbar\omega \left(n + \frac{1}{2} \right)$$

This is another example which illustrates the quantization of energy for bound states.

Quantum coherence and Quantum Computation:

In quantum mechanics, all objects have wave-like properties (see de Broglie waves). For instance, in Young's Double-slit experiment electrons can be used in the place of light waves. Each electron's wave-function goes through both slits, and hence has two separate split-beams that contribute to the intensity pattern on a screen. According to standard wave theory [Fresnel, Huygens] these two contributions give rise to an intensity pattern of bright bands due to constructive interference, interlaced with dark bands due to destructive interference, on a downstream screen. (Each split-beam, by itself, generates a diffraction pattern with less noticeable, more widely spaced dark and light bands.) This ability to interfere and diffract is related to coherence (classical or quantum) of the wave. The association of an electron with a wave is unique to quantum theory.

The effect of the inevitable coupling to external degrees of freedom of a quantum computer are extensively examined. It is found that for quantum calculations (in which the maintenance of coherence over a large number of states is important), not only must the coupling ***be small but the*** time taken in the quantum calculation ***must be less than*** the thermal time scale, \hbar/kBT . For longer times the condition on the strength of the coupling to the external world becomes much more stringent.

When the incident beam is represented by a quantum pure state, the split beams downstream of the two slits are represented as a superposition of the pure states representing each split beam. (This has nothing to do with two particles or Bell's inequalities) relevant to an entangled state: a 2-body state, a kind of coherence between two 1-body states.) The quantum description of imperfectly coherent paths is called a mixed state. A perfectly coherent state has a density matrix (also called the "statistical operator") that is a projection onto the pure coherent state, while a mixed state is described by a classical probability distribution for the pure states that make up the mixture.

Large-scale (macroscopic) quantum coherence leads to novel phenomena, the so-called macroscopic quantum phenomena. For instance, the laser, superconductivity, and superfluidity are examples of highly coherent quantum systems, whose effects are evident at the macroscopic scale. The macroscopic quantum coherence (Off-Diagonal Long-Range Order, ODLRO) [Penrose & Onsager (1957), C. N. Yang (1962)] for laser light, and super fluidity, is related to first-order (1-body) coherence/ODLRO, while superconductivity is related to second-order coherence/ODLRO. (For fermions, such as electrons, only even orders of coherence/ODLRO are possible.) Super fluidity in liquid He4 is related to a partial Bose-Einstein condensate. Here, the condensate portion is described by a multiply occupied single-particle state. [e.g., Cummings & Johnston (1966)]

On the other hand, the Schrödinger's cat thought experiment highlights the fact that quantum coherence cannot be arbitrarily applied to macroscopic situations. In order to have a quantum superposition of dead and alive cat, one needs to have pure states associated with aliveness and pure states associated with death, which are then superposed. Given the problem of defining death (absence of EEG, heartbeat,) it is hard to imagine a set of quantum parameters that could be used in constructing such superposition. In any case, this is not a good topic for a description of quantum coherence. [Ref.: Fresnel, Huygens, R. Glauber (1963)]

Regarding the occurrence of quantum coherence at a macroscopic level, it is interesting to note that the classical electromagnetic field exhibits macroscopic quantum coherence. The most obvious example is carrier signals for radio and TV. They satisfy Glauber's quantum description of coherence.

CONSERVATION LAWS AND QUANTUM COMPUTATION(INFORMATION)

The Wigner-Araki-Yanase theorem shows that conservation laws ***limit (e)*** the accuracy of measurement. Ozawa generalized the argument to show that conservation laws ***limit (e) the*** accuracy of quantum logic operations. A rigorous lower bound was obtained of the error probability of any physical realization of the controlled-NOT gate ***under the(e) constraint*** that the computational basis is represented by a component of spin and that physical implementations ***obey e(e&eb) the*** angular momentum conservation law. The lower bound ***is shown to be*** inversely proportional to the number of ancilla qubits or the strength of the external control field. Since the discovery of Shor's algorithm, physical realization of quantum computers is one of the major topics in physics. One of the formidable ***obstacles to(e) the*** realization of quantum computers is the decoherence induced by the environment. The theory of quantum error correction and the theory of fault-tolerant quantum computing have been developed to ***overcome*** this difficulty. One of the main achievements of this field is the threshold theorem: Provided the noise in individual quantum gates ***is below a certain(e) threshold*** it is possible to efficiently perform an arbitrarily large quantum computing. However, the threshold is rather demanding and the problem turns to whether there is any fundamental limit for implementing quantum gates. Recently, Lloyd and Ng have discussed how fundamental constants ***provide limits (e)on*** speed and memory of quantum computers. MASANAO OZAWA proposed another approach based on conservation laws. If we consider the ultimate performance of computing allowed by the laws of physics, elementary quantum gates should be isolated and small, so that the corresponding unitary operators should satisfy fundamental symmetries, or conservation laws. From this point of view, it is likely that the degree of conflict with a conservation law ***depends on the*** nature of its logic to be performed and that the imperfection can be ***reduced by*** increasing the size of implementation. However, no serious investigation has ever taken place. Ozawa model takes qubits as spin 1/2 objects and investigate the quantum limit ***induced by the*** angular momentum conservation law. He shows that although the

SWAP gate has no conflict with the conservation law, the controlled-NOT gate, which is one of the universal quantum logic gates, cannot be implemented by any 2-qubit rotationally invariant unitary operation within error probability $1/16$. Thus, to obtain more accuracy, we need to blow up the unitary operation to an ancilla system. Then, the size of an implementation of the quantum gate is defined as the total number of qubits in the computational basis and the ancilla.

Conservation-law-induced quantum limits for physical (e&eb)realizations of the quantum NOT gate

In recent investigations, it has been found that conservation laws generally lead(eb) to precision limits on quantum computing. Lower bounds of the error probability have been obtained for various logic operations from the commutation relation between the noise operator and the conserved quantity or from the recently developed universal uncertainty principle for the noise-disturbance trade-off in general measurements. However, the problem of obtaining the precision limit to realizing the quantum NOT gate has eluded a solution from these approaches. Tokishiro Karasawa* and Masanao Ozawa† developed a method for this problem based on analyzing the trace distance between the output state from the realization under consideration and the one from the ideal gate. Using the mathematical apparatus of orthogonal polynomials, they(eb) obtained a general lower bound on the error probability for the(eb&e) realization of the quantum NOT gate in terms of the number of qubits in the control system under conservation of the total angular momentum of the computational qubit plus the control system along the direction(e) used to encode the computational basis. The lower bound turns out to be more stringent than one might expect from previous results. Their method is expected to lead to more accurate estimates for physical realizations of various types of quantum computations under conservation laws and to contribute to related problems such as the accuracy of programmable quantum processors.

Conservation Laws, Uncertainty Relations, and Quantum Limits of Measurements

The uncertainty relation between the noise operator and the conserved quantity leads(eb) to a bound on the accuracy of general measurements. The bound extends the assertion by Wigner, Araki, and Yanase that conservation laws limit the (e)accuracy of “repeatable,” or “nondisturbing,” measurements to general measurements, and improves the one previously obtained by Yanase for spin measurements. The bound represents an obstacle to making a small quantum computer. It was found that conservation laws put a(e) limit on measurements of quantum mechanical observables. In 1960, Araki and Yanase proved the following assertion known as the Wigner-Araki-Yanase (WAY) theorem: Observables which do not commute with bounded additive conserved quantities have(e) no “exact” measurements. Subsequently, Yanase found a bound for the accuracy of measurements of the x component of spin in terms of the “size” of the apparatus, where the size is characterized by the mean square of the z component of the angular momentum. Yanase and Wigner concluded from this result that in order to increase the accuracy of spin measurement one ha(e)s to use a very large measuring apparatus. In the WAY theorem, for a measurement to be “exact” the following two conditions are(eb) required to be satisfies:

- (i) the Born statistical formula (BSF) and
- (ii) The repeatability hypothesis (RH), asserting that, if an observable is measured twice in succession in a system, then we obtain the same value each time.

Yanase’s bound does not assume the RH. Instead, a condition, to be referred to as Yanase’s condition, is assumed that the probe observable, the observable in the apparatus to be measured after the measuring interaction, commutes with the conserved quantity, to ensure the measurability of the probe observable. Elaborating the suggestions given by Stein and Shimony, Ohira and Pearle constructed a simple measuring interaction that satisfies the conservation law and the BSF, assuming the precise probe measurement, but does not satisfy the RH. Based on their model, Ohira and Pearle claimed that it is possible to have an accurate measurement of the spin component regardless of the size of the apparatus, if the RH is abandoned. However, their model does not satisfy Yanase’s condition, so that the problem remains as to the measurability of the probe observable. Yanase’s argument, however, assumes a large (but of variable size) measuring apparatus having the continuous angular momentum from the beginning for technical reasons and concludes that accurate measurement requires(e) a very large apparatus. To avoid a circular argument, a rigorous derivation without such an assumption is still demanded. Moreover, Wigner pointed out the necessity for generalizing the bound to general quantum systems other than +spin systems, as well as including all additive conservation laws. In order to accomplish the suggested generalization, a new approach to the problem is proposed by Ozawa based on uncertainty relation between the conserved quantity and the noise operator, defined as the difference between the post-measurement probe and the measured quantity. We obtain a bound for the mean-square error of general measuring interactions imposed by any additive conservation laws without assuming the RH. This bound also clarifies the trade-off between the size and the commutativity of the noise operator with the conserved quantity, unifying the suggestion by WAY and others and the one suggested by Ohira and Pearle. For spin measurements, this bound with Yanase’s condition leads to a tight bound for the error probability of spin measurement, which improves Yanase’s bound.

Quantum decoherence

Protection of Quantum Information Encoded in Decoherence Free States against Exchange Errors (See Daniel A. Lidar, David Bacon, Julia Kempe and K. Birgitta Whaley) calls for Decoherence Sub spaces The exchange interaction between identical qubits in a quantum information processor gives (eb)rise to unitary two-qubit errors. Decoherence free subspaces (DFSs) for collective decoherence undergo Pauli errors under exchange, which however do not take the decoherence Free states outside of the DFS. In order to protect DFSs against these errors it is sufficient to employ a recently proposed concatenated DFS-quantum error correcting code scheme [D.A. Lidar, D. Bacon and K.B. Whaley, Phys. Rev. Lett. 82, 4556 (1999)].

Preserving e & eb the coherence of quantum states and **controlling e & eb their** unitary evolution is one of the fundamental goals of Quantum Information Processing. When the system Hamiltonian is invariant under particle permutations, the exchange operator E_{ij} interchanging particles i and j is a constant of the motion, and definite symmetry of a state will be conserved. Models of quantum computers based on identical bosons or fermions must of course respect this elementary requirement. It was pointed out in a recent paper that active quantum error correcting codes (QECCs) designed to **correct e & eb independent** single-qubit errors, will **fail e for** identical particles in the presence of exchange errors. The reason is that exchange acts as a two-qubit error which has the same effect as a simultaneous bit flip on two different qubits. Of course, QECCs dealing explicitly with multiple-qubit errors are also available, so that exchange errors can readily be dealt with provided one accepts longer code words than are needed to deal with single-qubit errors. For example, in Ref. [2] a nine-qubit code is presented **which can e & eb correct** all single-qubit errors and all Pauli exchange errors. This is to be compared with the five-qubit "perfect" code which protects (only) against all single-qubit errors. While the nine-qubit code is longer than the "perfect" code, it is shorter than a code **required to e protect** against all two-qubit errors. A different error model which has been considered by several authors is that in which qubits undergo collective, rather than independent errors. The underlying physics of this model has a rich history: it dates back at least to Dicke's quantum optics work on super radiance of atoms **coupled e & eb to a** radiation field, **where it eb arose** in the consideration of systems confined to a region whose linear dimensions are small compared to the shortest wavelength of the field. The model was later treated extensively by Agarwal in the context of spontaneous emission. It was only recently realized, however, that in the collective decoherence model **there eb exist** large decoherence-free subspaces (DFSs), which are "quiet" Hilbert subspaces in which no environmentally-induced errors **occur** at eb all. Such subspaces offer **a passive e protection** against decoherence. Collective decoherence is an assumption **about the e manner** in which the environment couples to the system: instead of independent errors, as assumed in the active QECC approach, one assumes that errors are strongly correlated, in the sense that all qubits can be permuted without affecting the coupling between system and bath. This is clearly a very strong assumption, and it may not hold exactly in a realistic system-bath coupling scenario. To deal with this limitation, it has been shown recently how DFSs can be stabilized in the presence of errors that perturb the exact permutation symmetry, by concatenating DFSs with QECCs. Concatenation is a general technique that is useful for achieving fault tolerant quantum computation and trades stability of quantum information for the price of longer code words. Effect of exchange errors on DFSs for collective decoherence. These errors are fundamentally different from those induced by the system-bath coupling, since they originate entirely from the internal system Hamiltonian. It is shown that by use of the very same concatenation scheme (which was designed originally to deal with system-bath induced errors), a DFS can be stabilized in the presence of exchange errors as well. DFS is invariant under such errors, and conclude that concatenation with a QECC can generally stabilize DFSs against exchange.

In quantum mechanics, **quantum decoherence** is **the e loss of** coherence or ordering of the phase angles between the components of a system in a quantum superposition. **A eb consequence** of this dephasing **leads eb to** classical or probabilistically additive behavior. Quantum decoherence gives **the appearance** of wave function collapse (the **reduction e of** the physical possibilities into a single possibility as seen by an observer) and justifies the framework and intuition of classical physics as an acceptable approximation: decoherence is the mechanism by which the classical limit emerges out of a quantum starting point and **it determines** the location of the quantum-classical boundary. Decoherence **occurs eb when** a system **interacts e & eb with its environment** in a thermodynamically irreversible way. **This e prevents** different elements in the quantum superposition of the system+environment's wavefunction from interfering with each other. Decoherence has been a subject of active research since the 1980s

Decoherence can be viewed as **the e loss of** information from a system into the environment (often modeled as a heat bath) since every system is loosely coupled with the energetic state of its surroundings. Viewed in isolation, the system's dynamics are non-unitary (although the combined system plus environment evolves in a unitary fashion). Thus the dynamics of the system alone are irreversible. As with any coupling, entanglements are **generated eb between** the system and environment, which **have e & eb the effect of** sharing quantum information with—or **transferring it** to—the surroundings.

Decoherence does **not generate** actual wave function collapse. It only provides an explanation for the **appearance** of the wavefunction collapse, as the quantum nature of the system **"leaks" $-$ & $+$** into the environment. That is, components of the wavefunction **are e & eb decoupled** from a coherent system, and acquire phases from their immediate surroundings. In other words, wave function acquires phase (+) from the environment (-) A total superposition of the global or universal wavefunction still exists (and remains coherent at the global level), but its ultimate fate remains an interpretational issue. Specifically, decoherence does not attempt to explain the measurement problem. Rather, decoherence provides an explanation for the transition of the system to a mixture of states that seem to correspond to those states observers perceive. Moreover, our observation tells us that this mixture looks like a proper quantum ensemble in a measurement situation, as we observe that measurements lead to the "realization" of precisely one state in the "ensemble".

Decoherence represents a challenge for the practical realization of quantum computers, since they are expected to rely heavily on the undisturbed evolution of quantum coherences. Simply put; they require that coherent states be preserved and that decoherence is managed, in order to actually perform quantum computation.

Mechanisms

To examine how decoherence operates, an "intuitive" model is presented. The model requires some familiarity with quantum theory basics. Analogies are made between visualisable classical phase spaces and Hilbert spaces. A more rigorous

derivation in Dirac notation shows how decoherence destroys interference effects and the "quantum nature" of systems. Next, the density matrix approach is presented for perspective.

Phase space picture

An N -particle system can be represented in non-relativistic quantum mechanics by a wavefunction, $\psi(x_1, x_2, \dots, x_N)$. This has analogies with the classical phase space. A classical phase space contains a real-valued function in $6N$ dimensions (each particle contributes 3 spatial coordinates and 3 momenta). Our "quantum" phase space conversely contains a complex-valued function in a $3N$ dimensional space. The position and momenta do not commute but can still inherit much of the mathematical structure of a Hilbert space. Aside from these differences, however, the analogy holds.

Different previously-isolated, non-interacting systems occupy different phase spaces. Alternatively we can say they occupy different, lower-dimensional subspaces in the phase space of the joint system. The *effective* dimensionality of a system's phase space is the number of *degrees of freedom* present which—in non-relativistic models—is 6 times the number of a system's *free* particles. For a macroscopic system this will be a very large dimensionality. When two systems (and the environment would be a system) start to interact, though, their associated state vectors are no longer constrained to the subspaces. Instead the combined state vector time-evolves a path through the "larger volume", whose dimensionality is the sum of the dimensions of the two subspaces. A square (2-d surface) extended by just one dimension (a line) forms a cube. The cube has a greater volume, in some sense, than its component square and line axes. The extent two vectors interfere with each other is a measure of how "close" they are to each other (formally, their overlap or Hilbert space scalar product together) in the phase space. When a system couples to an external environment, the dimensionality of, and hence "volume" available to, the joint state vector increases enormously. Each environmental degree of freedom contributes an extra dimension.

Marcos Saraceno, in his paper represents both the states and the evolution of a quantum computer in phase space using the discrete Wigner function. Properties of the phase space representation of quantum algorithms are studied by many authors: apart from analyzing important examples, such as the Fourier Transform and Grover's search, the conditions for the existence of a direct correspondence between quantum and classical evolutions in phase space. Wigner function in a given phase space point could be measured by means of a tomographic method that, itself, can be interpreted as a simple quantum algorithm. Quantum mechanics can be formulated in phase space, the natural arena of classical physics. For this we can use the Wigner function, which is a distribution enabling to represent quantum states and temporal evolution in the classical phase space scenario. Generalization of the familiar Wigner representation of quantum mechanics to the case of a system with a finite, N -dimensional, Hilbert space. Phase space representation of both the states and the evolution of a quantum computer, has been investigated by various researchers..

One can ask if there are potential advantages in(e) using a phase space representation for a quantum computer. The use of this(e) approach is quite widespread in various areas of physics (such as quantum optics, and has been fruitful, for example, in analyzing issues concerning the classical limit of quantum mechanics. In answering the above question one should have in mind that a quantum algorithm can be simply thought of as a quantum map acting in a Hilbert space of finite dimensionality (a quantum map should be simply thought of as a unitary operator that is applied successively to a system. Therefore, any algorithm is clearly amenable to a phase space representation. Whether this representation will be useful or not will depend on properties of the algorithm. Specifically, algorithms become interesting in the large N limit (i.e. when operating on many qubits). For a quantum map this is the semi classical limit where regularities may arise in connection with its classical behavior. Unraveling these regularities, when they exist, becomes an important issue which can be naturally accomplished in a phase space representation. This representation may be useful to analyze some classes of algorithms. Moreover, the phase space approach may allow one to establish contact between the vast literature on quantum maps (dealing with their construction, the study of their semi classical properties, etc) and that of quantum algorithms. This, in turn, may provide hints to develop new algorithms and ideas for novel physics simulations. As a first application of these ideas several properties of quantum algorithms in phase space were studied by Marcos; Scientists analyzed under what circumstance it is possible to establish a direct classical analogue for a quantum algorithm (exhibiting interesting examples of this kind, such as the Fourier transform and other examples which naturally arise in studies of quantum maps). Marcos et al. have shown that, quite surprisingly, Grover's search algorithm can be represented in phase space and interpreted as a simple quantum map. To define Wigner functions for discrete systems various attempts can be found in the literature. Most notably, Wootters proposes a definition that has all the desired properties only when N is a prime number. His phase space is an $N \times N$ grid (if N is prime) and a Cartesian product of spaces corresponding to prime factors of N in the general case

The original system's wavefunction can be expanded arbitrarily as a sum of elements in a quantum superposition. Each expansion corresponds to a projection of the wave vector onto a basis. The bases can be chosen at will. Let us choose any expansion where the resulting elements interact with the environment in an element-specific way. Such elements will—with overwhelming probability—be rapidly separated from each other by their natural unitary time evolution along their own independent paths. After a very short interaction, there is almost no chance of any further interference. The process is effectively irreversible. The different elements effectively become "lost" from each other in the expanded phase space created by coupling with the environment; in phase space, this decoupling is monitored through the Wigner quasi-probability distribution. The original elements are said to have decohered. The environment has effectively selected out those expansions or decompositions of the original state vector that decohere (or lose phase coherence) with each other. This is called "environmentally-induced-super selection", or einselection. The decohered elements of the system no longer

exhibit quantum interference between each other, as in a double-slit experiment. Any elements that decohere from each other via environmental interactions are said to be quantum entangled with the environment. The converse is not true: not all entangled states are decohered from each other.

Any measuring device or apparatus acts as an environment since, at some stage along the measuring chain, it has to be large enough to be read by humans. It must possess a very large number of hidden degrees of freedom. In effect, the interactions may be considered to be quantum measurements. As a result of an interaction, the wave functions of the system and the measuring device become entangled with each other. Decoherence happens when different portions of the system's wavefunction become entangled in different ways with the measuring device. For two einselected elements of the entangled system's state to interfere, both the original system and the measuring in both elements device must significantly overlap, in the scalar product sense. If the measuring device has many degrees of freedom, it is *very* unlikely for this to happen.

As a consequence, the system behaves as a classical statistical ensemble of the different elements rather than as a single coherent quantum superposition of them. From the perspective of each ensemble member's measuring device, the system appears to have irreversibly collapsed onto a state with a precise value for the measured attributes, relative to that element.

Dirac notation

Using the Dirac notation, let the system initially be in the state $|\psi\rangle$ where

$$|\psi\rangle = \sum_i |i\rangle \langle i|\psi\rangle$$

where the $|i\rangle$ s form an einselected basis (environmentally induced **selected** eigen basis^[4]); and let the environment initially be in the state $|\epsilon\rangle$. The vector basis of the total combined system and environment can be formed by tensor multiplying the basis vectors of the subsystems together. Thus, before any interaction between the two subsystems, the joint state can be written as:

$$|before\rangle = \sum_i |i\rangle |\epsilon\rangle \langle i|\psi\rangle.$$

where $|i\rangle |\epsilon\rangle$ is shorthand for the tensor product: $|i\rangle \otimes |\epsilon\rangle$. There are two extremes in the way the system can interact with its environment: either (1) the system loses its distinct identity and merges with the environment (e.g. photons in a cold, dark cavity get converted into molecular excitations within the cavity walls), or (2) the system is not disturbed at all, even though the environment is disturbed (e.g. the idealized non-disturbing measurement). In general an interaction is a mixture of these two extremes, which we shall examine:

System absorbed by environment

If the environment absorbs the system, each element of the total system's basis interacts with the environment such that:

$$|i\rangle |\epsilon\rangle \text{ evolves into } |\epsilon_i\rangle$$

and so

$$|before\rangle \text{ evolves into } |after\rangle = \sum_i |\epsilon_i\rangle \langle i|\psi\rangle$$

where the unitarity of time-evolution demands that the total state basis remains orthonormal and in particular their scalar or inner products with each other vanish, since $\langle i|j\rangle = \delta_{ij}$:

$$\langle \epsilon_i | \epsilon_j \rangle = \delta_{ij}$$

This orthonormality of the environment states is the defining characteristic required for einselection.

System not disturbed by environment

This is the idealized measurement or undisturbed system case in which each element of the basis interacts with the environment such that:

$$|i\rangle |\epsilon\rangle \text{ evolves into the product } |i, \epsilon_i\rangle = |i\rangle |\epsilon_i\rangle$$

i.e. the system disturbs the environment, but is itself *undisturbed* by the environment.

and so:

$$|before\rangle \text{ evolves into } |after\rangle = \sum_i |i, \epsilon_i\rangle \langle i|\psi\rangle$$

where, again, unitarity demands that:

$$\langle i, \epsilon_i | j, \epsilon_j \rangle = \langle i|j\rangle \langle \epsilon_i | \epsilon_j \rangle = \delta_{ij} \langle \epsilon_i | \epsilon_j \rangle = \delta_{ij}$$

and *additionally* decoherence requires, by virtue of the large number of hidden degrees of freedom in the environment, that

$$\langle \epsilon_i | \epsilon_j \rangle \approx \delta_{ij}$$

As before, this is the defining characteristic for decoherence to become einselection. The approximation becomes more exact as the number of environmental degrees of freedom affected increases.

Note that if the system basis $|i\rangle$ were not an einselected basis then the last condition is trivial since the disturbed environment is not a function of i and we have the trivial disturbed environment basis $|\epsilon_j\rangle = |\epsilon'\rangle$. This would correspond to the system basis being degenerate with respect to the environmentally-defined-measurement-observable. For a complex environmental interaction (which would be expected for a typical macro scale interaction) a non-einselected basis would be hard to define.

DIRAC FORMALISM AND QUANTUM COMPUTER:

G. Benenti et al, modeled an isolated quantum computer as a two-dimensional lattice of qubits (spin halves) with fluctuations in individual qubit energies and residual short-range inter-qubit couplings. In the limit when fluctuations and couplings are small compared to the one-qubit energy spacing, the spectrum has a band structure and the quantum computer core (central band) with the highest density of states. Above a critical inter-qubit coupling strength, quantum chaos sets in, leading to quantum Ergodicity of eigenstates in an isolated quantum computer. The onset of chaos results in the interaction induced dynamical thermalization and the occupation numbers well described by the Fermi-Dirac distribution. This thermalization **destroys the** noninteracting qubit structure and sets serious requirements for the quantum computer operability.

The key ingredient of a quantum computer is that it can simultaneously follow all of the computation paths corresponding to the distinct classical inputs and **produce** a state which **depends on the** interference of these paths. **As a result**, some computational tasks can be performed much more efficiently than on a classical computer. Shor constructed a quantum algorithm **which performs large** number factorization into prime factors exponentially faster than any known classical algorithm. It was also shown by Grover that the search of an item in an unstructured list **can be done with a** square root speedup over any classical algorithm. These results motivated a great body of experimental proposals for a construction of a realistic quantum computer. At present, quantum gates were **realized with** cold ions and the Grover algorithm **was performed** for three qubits made from nuclear spins in a molecule. For proper operation ability, it is essential for the quantum computer to remain **coherent** during the computation process. Hence, a serious obstacle to its physical realization is the quantum decoherence due to the coupling with the external world. In spite of that, in certain physical proposals, for example nuclear spins in two-dimensional semiconductor structures, the decoherence time can be many orders of magnitude **larger than the time** required for the gate operations. **As a result**, one can analyze the operation of an isolated quantum computer **decoupled** from the external world. However, even if the quantum computer is isolated from the external world and the decoherence time is infinite, a proper operation ability of the computer is not guaranteed. As a matter of fact, one has to face a many-body **problem for a system** of n interacting qubits (two level systems): any computer operation { a unitary transformation in the Hilbert space of size $NH = 2^n$ } can **be decomposed** into two-qubit gates such as controlled-NOT and single qubit rotations. Due to the unavoidable **presence of imperfections**, the spacing between the two states of each qubit **fluctuates** in some detuning interval. Also, some residual **interaction** between qubits necessarily remains when the **two-qubit coupling is used** to operate the gates. In an isolated quantum computer was modeled as a qubit lattice with fluctuations in individual qubit energies and residual short-range inter-qubit couplings. Similarly to previous studies of interacting many-body systems **such as nuclei, clusters, complex atoms, quantum dots, and quantum spin glasses**, the **interaction leads to** quantum chaos characterized by Ergodicity of the eigenstates and level spacing statistics as in Random Matrix Theory. The transition to chaos takes place when strength is of the order of the energy spacing between directly coupled states. This border is exponentially larger than the energy level spacing in a quantum computer.

This means that a strong enough **interaction plays the role** of a heat bath, thus **leading to** dynamical Thermalization for an isolated system. In such a regime, a quantum computer eigenstate is composed by an exponentially large (with n) number of noninteracting multiqubit states representing the quantum register states. **As a result**, exponentially many states of the computation basis **are mixed** after a chaotic time scale and the computer operability **is destroyed**. We note that the dynamical thermalization has been discussed in other many-body interacting systems. **The dependence of the** critical coupling for the onset of dynamical thermalization on the number of qubits. Illustration of the equivalence between the chaos border and the thermalization border is also shown by Benenti.

CONDENSED MATTER AND QUANTUM COMPUTATION A BRIEF OVERLOOK OF THE WORK DONE:

•Christoph Kloeffer and Daniel Loss: Prospects for Spin-Based Quantum Computing

•Experimental and theoretical progress toward quantum computation with spins in quantum dots (QDs) is reviewed, with particular focus on QDs formed in GaAs heterostructures, on nanowire-based QDs, and on self-assembled QDs. We report on a remarkable evolution of the field where decoherence, one of the main(e) challenges for realizing quantum computers, no longer seems to be the stumbling block it had originally been considered. General concepts, relevant quantities, and basic requirements for spin-based quantum computing are explained; opportunities and challenges of spin-orbit interaction and nuclear spins are reviewed.

•Cotunneling in the 5/2 fractional quantum Hall regime: Robert Zielke, Bernd Braunecker, and Daniel Loss.

•Cotunneling in the 5/2 fractional quantum Hall regime allows to test the Moore-Read wave function, proposed for this regime, and to probe the nature of the fractional charge carriers. Cotunneling current for electrons that tunnel between two quantum Hall edge states via(e&eb) a quantum dot and for quasiparticles with fractional charges $e/4$ and $e/2$ that tunnel via

an antidot. While electron cotunneling is strongly suppressed(e), the quasiparticle tunneling shows(eb) signatures characteristic for the Moore-Read state. Cotunneling between Laughlin states, lead to the fact that electron-transport between Moore-Read states and the one between Laughlin states at filling factor 1/3 have identical voltage dependences.

•Non-abelian Majoranas and braiding in inhomogeneous spin ladders Fabio L. Pedrocchi, Suhas Gangadharaiah (Bhopal), Stefano Chesi (Montreal), and Daniel Loss.

An inhomogeneous open spin ladder, related to the Kitaev honeycomb model, which can be tuned between topological and non-topological phases. In extension of Lieb's theorem, it has been shown numerically that the ground state of the spin ladder is either vortex-free or vortex-full. At the phase-boundaries single Majorana states emerge which are proven to be robust against local perturbations and to obey non-abelian braiding statistics. It is also shown that a network of spin ladders provides a promising platform for topological quantum computing.

•Majorana qubit decoherence by quasiparticle poisoning Diego Rainis and Daniel Loss.Phys. Rev. B 85, 174533 (2012);

•Consideration is given to the problem of quasiparticle poisoning in a nanowire-based realization of a Majorana qubit, where a spin-orbit-coupled semiconducting wire is placed on top of a (bulk) superconductor. By making use of recent experimental data exhibiting evidence of a low-temperature residual nonequilibrium quasiparticle population in superconductors, it is shown by means of analytical and numerical calculations that the dephasing time due to the tunneling of quasiparticles into the nanowire may be problematically short to allow(eb) for qubit manipulation.

•Effect of strain on(e&eb) hyperfine-induced hole-spin decoherence in quantum dots Franziska Maier and Daniel Loss.Phys. Rev. B 85, 195323 (2012);

•Theoretical consideration is given prominence to the effect(e&eb) of strain on the spin dynamics of a single heavy hole (HH) confined to a self-assembled quantum dot and interacting with the surrounding nuclei via hyperfine interaction. Confinement and strain hybridize(e&eb) the HH states, which show(eb) an exponential decay for a narrowed nuclear spin bath. For different strain configurations within the dot, the dependence of the spin decoherence time T_2 on external parameters is shifted and the nonmonotonic dependence of the peak is altered. Application of external strain yields(eb) considerable shifts in the dependence of T_2 on external parameters. It is found that external strain affects (e&eb)mostly the effective hyperfine coupling strength of the conduction band (CB), indicating(eb) that the CB admixture of the hybridized HH states plays a(e&eb) crucial role in the sensitivity of T_2 on strain.

•High threshold error correction for the surface code (James R. Wootton and Daniel Loss).

•An algorithm is presented for error correction in the surface code quantum memory. This is shown to correct depolarizing noise up to a threshold error rate of 18.5%, exceeding previous results and coming close to the upper bound of 18.9%. The time complexity of the algorithm is found to be sub-exponential, offering a significant speed-up over brute force methods and allowing efficient error correction for codes of realistic sizes.

Kevin A. van Hoogdalem and Daniel Loss.Phys. Rev. B 85, 054413 (2012);

Motivated by potential applications in spintronics, the study concentrates on frequency dependent spin transport in noninteracting one-dimensional spin chains. A system is proposed that behaves as a capacitor for the spin degree of freedom. It consists of a spin chain with two impurities a distance d apart. We find that at low energy (frequency) the impurities flow to strong coupling, thereby effectively cutting (e) the chain into three parts, with the middle island containing (e) a discrete number of spin excitations. At finite frequency spin transport through the system increases. Authors find a strong dependence of the finite frequency characteristics both on the anisotropy of the spin chain and the applied magnetic field. A method is proposed to measure the finite-frequency conductance in this system.

Electric-Field Induced Majorana Fermions in Armchair Carbon Nanotubes Jelena Klinovaja, Suhas Gangadharaiah, and Daniel Loss.Phys. Rev. Lett. 108, 196804 (2012)

Authors' consider theoretically an armchair carbon nanotube (CNT) in the presence of an electric field and in contact with an s-wave superconductor. It is shown that the proximity effect (e&eb) opens (eb)up superconducting gaps in the CNT of different strengths for the exterior and interior branches of the two Dirac points. For strong proximity induced (eb) superconductivity the interior gap can be of the p-wave type, while the exterior gap can be tuned (e&eb) by the electric field to be of the s-wave type. Such a setup supports a single Majorana bound state at each end of the CNT. In the case of weak proximity induced superconductivity, the gaps in both branches are of the p-wave type. However, the temperature can be chosen in such a way that the smallest gap is effectively closed. Using renormalization group techniques authors' show that the Majorana bound states exist (eb) even after taking into (e) account electron-electron interactions.

Thin-Film Magnetization Dynamics on the Surface of a Topological Insulator Yaroslav Tserkovnyak (UCLA) and Daniel Loss.Phys. Rev. Lett. 108, 187201 (2012);

Authors theoretically study the magnetization dynamics of a thin ferromagnetic film exchange-coupled with a surface of a strong three-dimensional topological insulator. Focus is on the role of electronic zero modes associated with domain walls (DW's) and other topological textures in the magnetic film. Thermodynamically reciprocal hydrodynamic equations of motion are derived for the DW responding to electronic spin torques, on the one hand, and fictitious electromotive forces in the electronic chiral mode fomented by the DW, on the other. An experimental realization illustrating this physics is proposed based on a ferromagnetic strip, which cuts the topological insulator surface into two gapless regions. In the presence of a ferromagnetic DW, a chiral mode transverse to the magnetic strip acts as a dissipative interconnect, which is itself a dynamic object that controls (and, inversely, responds to) the magnetization dynamics.

Singlet-triplet splitting in double quantum dots due to spin orbit and hyperfine interactions Dimitrije Stepanenko, Mark Rudner (Harvard), Bertrand I. Halperin (Harvard), and Daniel Loss.Phys. Rev. B 85, 075416 (2012);

Authors' analyze the low-energy spectrum of a two-electron double quantum dot under a potential bias in the presence of an external magnetic field. Focus is on the regime of spin (e)blockade, taking into account the spin-orbit interaction (e&eb) and hyperfine coupling(e&eb) of electron and nuclear spins. Starting from a model for two interacting electrons in a double dot, authors' derive an effective two-level Hamiltonian in the vicinity of an avoided crossing between singlet and triplet levels, which are(e&eb) coupled by the spin-orbit and hyperfine interactions. Also, authors' evaluate the level splitting at the anticrossing, and show that it depends on a variety of parameters including the spin-orbit coupling strength, the orientation of the external magnetic field relative to an internal spin-orbit axis, the potential detuning of the dots, and the difference between hyperfine fields in the two dots. They provide a formula for the splitting in terms of the spin-orbit length, the hyperfine fields in the two dots, and the double dot parameters such as tunnel coupling and Coulomb energy. This formula should prove useful for extracting spin-orbit parameters from transport or charge sensing experiments in such systems. Authors identify a parameter regime where the spin-orbit and hyperfine terms can become of comparable strength, and discuss how this regime might be reached.

Incoherent dynamics in the toric code subject to disorderBeat Roethlisberger, James R. Wootton, Robert M. Heath (Leeds), Jiannis K. Pachos (Leeds), and Daniel Loss.Phys. Rev. A 85, 022313 (2012).

Authors' numerically study the *effects(e&eb) of two* forms of quenched disorder on the anyons of the toric code. Firstly, a new class of codes based on random lattices of stabilizer operators is presented, and shown to be superior to the standard square lattice toric code for certain forms of biased noise. It is further argued that these codes are close to optimal, in that they tightly reach the upper bound of error thresholds beyond which no correctable CSS codes can exist. Additionally, they study the classical motion of anyons in toric codes with randomly distributed onsite potentials. In the presence of repulsive long-range interaction between the anyons, a surprising increase with disorder strength of the lifetime of encoded states is reported and explained by an entirely incoherent mechanism. Finally, the coherent transport of the anyons in the presence of both forms of disorder is investigated, and a significant suppression of the anyon motion is found.

Rashba spin orbit interaction in a quantum wire superlattice(Gunnar Thorgilsson (Reykjavik), J. Carlos Egues (Sao Carlos), Daniel Loss, and Sigurdur I. Erlingsson (Reykjavik).Phys. Rev. B 85, 045306 (2012); Phys. Rev. B 85, 039904(E) (2012);

In this work authors' study the effects of a longitudinal periodic potential on a parabolic quantum wire defined in a two-dimensional electron gas with Rashba spin-orbit interaction. For an infinite wire superlattice we find, by direct diagonalization, that the energy gaps are shifted away from the usual Bragg planes due to the Rashba spin-orbit interaction. Interestingly, results show that the location of the band gaps in energy can be controlled via the strength of the Rashba spin-orbit interaction. Authors' have also calculated the charge conductance through a periodic potential of a finite length via the non-equilibrium Green's function method combined with the Landauer formalism. We find dips in the conductance that correspond well to the energy gaps of the infinite wire superlattice. From the infinite wire energy dispersion, is derived an equation relating the location of the conductance dips as a function of the (gate controllable) Fermi energy to the Rashba spin-orbit coupling strength. It is proposed that the strength of the Rashba spin-orbit interaction can be extracted via a charge conductance measurement.

Localized end states in density modulated quantum wires and ringsSuhas Gangadharaiah, Luka Trifunovic, and Daniel Loss.Phys. Rev. Lett. 108, 136803 (2012);

Authors' study finite quantum wires and rings in the presence of a charge-density wave gap induced by a periodic modulation of the chemical potential. We show that the Tamm-Shockley bound states emerging at the ends of the wire are stable against weak disorder and interactions, for discrete open chains and for continuum systems. The low-energy physics can be mapped onto the Jackiw-Rebbi equations *describing* massive Dirac fermions and bound end states. They treat *interactions via* the continuum model and show that they increase the charge gap and further localize the end states. The electrons placed in the two localized states on the opposite ends of the wire can interact via exchange interactions and this setup can be used as a double quantum dot hosting spin qubits. The existence of these states could be experimentally detected through the presence of an unusual 4π Aharonov-Bohm periodicity in the spectrum and persistent current as a function of the external flux.

Long-distance spin-spin coupling via floating gatesKoji Sato (UCLA), Daniel Loss, and Yaroslav Tserkovnyak (UCLA).

Authors' theoretically study tunneling of Cooper pairs from an s-wave superconductor into two semiconductor quantum wires with strong spin-orbit interaction under magnetic field, which approximate helical Luttinger liquids. The entanglement of electrons within a Cooper pair can be detected by the electric current cross correlations in the wires. By *controlling the* relative orientation of the wires, either lithographically or mechanically, on the substrate, the *current correlations* can be tuned, as dictated by the initial spin entanglement. This proposal of a spin-to-charge readout of quantum correlations is alternative to a recently proposed utilization of the quantum spin Hall insulator. Subtle Coriolis force, earth's differential heating, Poincare Kelvin Functional are some of the factors that get affected by the phenomenon.

Strong Spin-Orbit Interaction and Helical Hole States in Ge/Si NanowiresCarbon nanotubes in electric and magnetic fields.Jelena Klinovaja, Manuel J. Schmidt, Bernd Braunecker, and Daniel Loss.Phys. Rev. B 84, 085452 (2011);

Authors' derive an effective low-energy theory for metallic (armchair and nonarmchair) single-wall nanotubes in the presence of an electric field perpendicular to the nanotube axis, and in the presence of magnetic fields, taking into account spin-orbit interactions and screening effects on the basis of a microscopic tight-binding model. The *interplay* between electric field and spin-orbit interaction allows us to *tune* armchair nanotubes into a helical conductor in both Dirac valleys. Metallic nonarmchair nanotubes are gapped by the surface curvature, yet helical conduction modes can be restored in one of

the valleys by a magnetic field along the nanotube axis. Furthermore, authors' discuss electric dipole spin resonance in carbon nanotubes, and find that the Rabi frequency shows a pronounced dependence on the momentum along the nanotube.

Loss of interference and the transition from quantum to classical

The utility of decoherence lies in its application to the analysis of probabilities, before and after environmental interaction, and in particular to the vanishing of quantum interference terms after decoherence has occurred. If we ask what is the probability of observing the system making a transition or quantum leap from ψ to ϕ **before** ψ has interacted with its environment, then application of the Born probability rule states that the transition probability is the modulus squared of the scalar product of the two states:

$$prob_{before}(\psi \rightarrow \phi) = |\langle \psi | \phi \rangle|^2 = \left| \sum_i \psi_i^* \phi_i \right|^2 = \sum_i |\psi_i^* \phi_i|^2 + \sum_{ij; i \neq j} \psi_i^* \psi_j \phi_j^* \phi_i$$

where $\psi_i = \langle i | \psi \rangle$, $\psi_i^* = \langle \psi | i \rangle$ and $\phi_i = \langle i | \phi \rangle$ etc.

Terms appear in the expansion of the transition probability above which involve $i \neq j$; these can be thought of as representing *interference* between the different basis elements or quantum alternatives. This is a purely quantum effect and represents the non-additivity of the probabilities of quantum alternatives.

To calculate the probability of observing the system making a quantum leap from ψ to ϕ **after** ψ has interacted with its environment, then application of the Born probability rule states we must sum over all the relevant possible states of the environment, E_i , before squaring the modulus:

$$prob_{after}(\psi \rightarrow \phi) = \sum_j |\langle after | \phi, \epsilon_j \rangle|^2 = \sum_j \left| \sum_i \psi_i^* \langle i, \epsilon_i | \phi, \epsilon_j \rangle \right|^2 = \sum_j \left| \sum_i \psi_i^* \langle i | \phi \rangle \langle \epsilon_i | \epsilon_j \rangle \right|^2$$

The internal summation vanishes when we apply the decoherence / einselection condition $\langle \epsilon_i | \epsilon_j \rangle \approx \delta_{ij}$ and the formula simplifies to:

$$prob_{after}(\psi \rightarrow \phi) \approx \sum_j |\psi_j^* \langle j | \phi \rangle|^2 = \sum_i |\psi_i^* \phi_i|^2$$

If we compare this with the formula we derived before the environment introduced decoherence we can see that the effect of decoherence has been to move the summation sign \sum_i from inside of the modulus sign to outside. As a result all the cross-or quantum interference-terms:

$$\sum_{ij; i \neq j} \psi_i^* \psi_j \phi_j^* \phi_i$$

have vanished from the transition probability calculation. The decoherence has irreversibly converted quantum behaviour (additive probability amplitudes) to classical behaviour (additive probabilities). In terms of density matrices, the loss of interference effects corresponds to the diagonalization of the "environmentally traced over" density matrix.

Density matrix approach

The effect of decoherence on density matrices is essentially the decay or rapid vanishing of the off-diagonal elements of the partial trace of the joint system's density matrix, i.e. the trace, with respect to *any* environmental basis, of the density matrix of the combined system *and* its environment. The decoherence irreversibly converts the "averaged" or "environmentally traced over" density matrix from a pure state to a reduced mixture; it is this that gives the *appearance* of wavefunction collapse. Again this is called "environmentally-induced-super selection", or einselection. The advantage of taking the partial trace is that this procedure is indifferent to the environmental basis chosen.

The density matrix approach has been combined with the Bohmian approach to yield a *reduced trajectory approach*, taking into account the system reduced density matrix and the influence of the environment.^[7]

Operator-sum representation

Consider a system S and environment (bath) B, which are closed and can be treated quantum mechanically. Let \mathcal{H}_S and \mathcal{H}_B be the system's and bath's Hilbert spaces, respectively. Then the Hamiltonian for the combined system is

$$\hat{H} = \hat{H}_S \otimes \hat{I}_B + \hat{I}_S \otimes \hat{H}_B + \hat{H}_I$$

where \hat{H}_S , \hat{H}_B are the system and bath Hamiltonians, respectively, and \hat{H}_I is the interaction Hamiltonian between the system and bath, and \hat{I}_S , \hat{I}_B are the identity operators on the system and bath Hilbert spaces, respectively. The time-evolution of the density operator of this closed system is unitary and, as such, is given by

$$\rho_{SB}(t) = \hat{U}(t) \rho_{SB}(0) \hat{U}^\dagger(t)$$

where the unitary operator is $\hat{U} = e^{\frac{-i\hat{H}t}{\hbar}}$. If the system and bath are not entangled initially, then we can write $\rho_{SB} = \rho_S \otimes \rho_B$. Therefore, the evolution of the system becomes

$$\rho_{SB}(t) = \hat{U}(t)[\rho_S(0) \otimes \rho_B(0)]\hat{U}^\dagger(t).$$

The system-bath interaction Hamiltonian can be written in a general form as

$$\hat{H}_I = \sum_i \hat{S}_i \otimes \hat{B}_i,$$

where $\hat{S}_i \otimes \hat{B}_i$ is the operator acting on the combined system-bath Hilbert space, and \hat{S}_i, \hat{B}_i are the operators that act on the system and bath, respectively. This coupling of the system and bath is the cause of decoherence in the system alone. To see this, a partial trace is performed over the bath to give a description of the system alone:

$$\rho_S(t) = Tr_B[\hat{U}(t)[\rho_S(0) \otimes \rho_B(0)]\hat{U}^\dagger(t)].$$

$\rho_S(t)$ is called the *reduced density matrix* and gives information about the system only. If the bath is written in terms of its set of orthogonal basis kets, that is, if it has been initially diagonalized then Computing the partial trace with respect to this (computational) basis gives:

$$\rho_S(t) = \sum_l \hat{A}_l \rho_S(0) \hat{A}_l^\dagger$$

where $\hat{A}_l, \hat{A}_l^\dagger$ are defined as the **Kraus operators** and are represented as

$$\hat{A}_l = \sqrt{a_j} \langle k | \hat{U} | j \rangle.$$

This is known as the **operator-sum representation (OSR)**. A condition on the Kraus operators can be obtained by using the fact that $Tr(\rho_S(t)) = 1$; this then gives

$$\sum_l \hat{A}_l^\dagger \hat{A}_l = \hat{I}_S.$$

This restriction determines if decoherence will occur or not in the OSR. In particular, when there is more than one term present in the sum for $\rho_S(t)$ then the dynamics of the system will be non-unitary and hence decoherence will take place.

Semi group approach

A more general consideration for the existence of decoherence in a quantum system is given by the **master equation**, which determines how the density matrix of the *system alone* evolves in time. This uses the Schrödinger picture, where evolution of the *state* (represented by its density matrix) is considered. The master equation is:

$$\rho'_S(t) = \frac{-i}{\hbar} [\tilde{\mathbf{H}}_S, \rho_S(t)] + L_D [\rho_S(t)]$$

where $\tilde{\mathbf{H}}_S = \mathbf{H}_S + \Delta$ is the system Hamiltonian, \mathbf{H}_S , along with a (possible) unitary contribution from the bath, Δ and L_D is the **Lindblad decohering term**. The Lindblad decohering term is represented as

$$L_D [\rho_S(t)] = \frac{1}{2} \sum_{\alpha, \beta=1}^M b_{\alpha\beta} ([\mathbf{F}_\alpha, \rho_S(t) \mathbf{F}_\beta^\dagger] + [\mathbf{F}_\alpha \rho_S(t), \mathbf{F}_\beta^\dagger]).$$

In quantum mechanics, **quantum decoherence** is the loss of coherence or ordering of the phase angles between the components of a system in a quantum superposition. A consequence of this dephasing (eb) leads to classical or probabilistically additive behavior. Quantum decoherence gives the appearance of wave function collapse (the reduction of the physical possibilities into a single possibility as seen by an observer) and justifies the framework and intuition of classical physics as an acceptable approximation: decoherence is the mechanism by which the classical limit emerges (eb) out of a quantum starting point and it determines the location of the quantum-classical boundary. Decoherence occurs when a system interacts with its environment in a thermodynamically irreversible way. This prevents different elements in the quantum superposition of the system+environment's wavefunction from interfering with each other. Decoherence has been a subject of active research since the 1980s.

Decoherence can be viewed as the loss of information from a system into the environment (often modeled as a heat bath) since every system is loosely coupled with the energetic state of its surroundings. Viewed in isolation, the system's dynamics are non-unitary (although the combined system plus environment evolves in a unitary fashion).^[3] Thus the

dynamics of the system alone are irreversible. As with any coupling, entanglements are generated between the system and environment, which have the effect of sharing quantum information with—or transferring it to—the surroundings.

Decoherence does not generate *actual* wave function collapse. It only provides an explanation for the *appearance* of the wavefunction collapse, as the quantum nature of the system "leaks" into the environment. That is, components of the wavefunction are decoupled from a coherent system, and acquire phases from their immediate surroundings. A total superposition of the global or universal wavefunction still exists (and remains coherent at the global level), but its ultimate fate remains an interpretational issue. Specifically, decoherence does not attempt to explain the measurement problem. Rather, decoherence provides an explanation for the transition of the system to a mixture of states that seem to correspond to those states observers perceive. Moreover, our observation tells us that this mixture looks like a proper quantum ensemble in a measurement situation, as we observe that measurements lead to the "realization" of precisely one state in the "ensemble".

Decoherence represents a challenge for the practical realization of quantum computers, since they are expected to rely heavily on the undisturbed evolution of quantum coherences. Simply put; they require that coherent states be preserved and that decoherence is managed, in order to actually perform quantum computation.

Mechanisms

To examine how decoherence operates, an "intuitive" model is presented. The model requires some familiarity with quantum theory basics. Analogies are made between visualisable classical phase spaces and Hilbert spaces. A more rigorous derivation in Dirac notation shows how decoherence destroys interference effects and the "quantum nature" of systems. Next, the density matrix approach is presented for perspective.

Phase space picture

An N -particle system can be represented in non-relativistic quantum mechanics by a wavefunction, $\psi(x_1, x_2, \dots, x_N)$. This has analogies with the classical phase space. A classical phase space contains a real-valued function in $6N$ dimensions (each particle contributes 3 spatial coordinates and 3 momenta). Our "quantum" phase space conversely contains a complex-valued function in a $3N$ dimensional space. The position and momenta do not commute but can still inherit much of the mathematical structure of a Hilbert space. Aside from these differences, however, the analogy holds.

Different previously-isolated, non-interacting systems occupy different phase spaces. Alternatively we can say they occupy different, lower-dimensional subspaces in the phase space of the joint system. The *effective* dimensionality of a system's phase space is the number of *degrees of freedom* present which—in non-relativistic models—is 6 times the number of a system's *free* particles. For a macroscopic system this will be a very large dimensionality. When two systems (and the environment would be a system) start to interact, though, their associated state vectors are no longer constrained to the subspaces. Instead the combined state vector time-evolves a path through the "larger volume", whose dimensionality is the sum of the dimensions of the two subspaces. A square (2-d surface) extended by just one dimension (a line) forms a cube. The cube has a greater volume, in some sense, than its component square and line axes. The extent two vectors interfere with each other is a measure of how "close" they are to each other (formally, their overlap or Hilbert space scalar product together) in the phase space. When a system couples to an external environment, the dimensionality of, and hence "volume" available to, the joint state vector increases enormously. Each environmental degree of freedom contributes an extra dimension.

The original system's wavefunction can be expanded arbitrarily as a sum of elements in a quantum superposition. Each expansion corresponds to a projection of the wave vector onto a basis. The bases can be chosen at will. Let us choose any expansion where the resulting elements interact with the environment in an element-specific way. Such elements will—with overwhelming probability—be rapidly separated from each other by their natural unitary time evolution along their own independent paths. After a very short interaction, there is almost no chance of any further interference. The process is effectively irreversible. The different elements effectively become "lost" from each other in the expanded phase space created by coupling with the environment; in phase space, this decoupling is monitored through the Wigner quasi-probability distribution. The original elements are said to have *decohered*. The environment has effectively selected out those expansions or decompositions of the original state vector that decohere (or lose phase coherence) with each other. This is called "environmentally-induced-super selection", or einselection The decohered elements of the system no longer exhibit quantum interference between each other, as in a double-slit experiment. Any elements that decohere from each other via environmental interactions are said to be quantum entangled with the environment. The converse is not true: not all entangled states are decohered from each other.

Any measuring device or apparatus acts as an environment since, at some stage along the measuring chain, it has to be large enough to be read by humans. It must possess a very large number of hidden degrees of freedom. In effect, the interactions may be considered to be quantum measurements. As a result of an interaction, the wave functions of the system and the measuring device become entangled with each other. Decoherence happens when different portions of the system's wavefunction become entangled in different ways with the measuring device. For two einselected elements of the entangled system's state to interfere, both the original system and the measuring in both elements device must significantly overlap, in the scalar product sense. If the measuring device has many degrees of freedom, it is *very* unlikely for this to happen.

As a consequence, the system behaves as a classical statistical ensemble of the different elements rather than as a single coherent quantum superposition of them. From the perspective of each ensemble member's measuring device, the system appears to have irreversibly collapsed onto a state with a precise value for the measured attributes, relative to that element.

Dirac notation

Using the Dirac notation, let the system initially be in the state $|\psi\rangle$ where

$$|\psi\rangle = \sum_i |i\rangle \langle i|\psi\rangle$$

where the $|i\rangle$ s form an einselected basis (environmentally induced selected eigen basis); and let the environment initially be in the state $|\epsilon\rangle$. The vector basis of the total combined system and environment can be formed by tensor multiplying the basis vectors of the subsystems together. Thus, before any interaction between the two subsystems, the joint state can be written as:

$$|before\rangle = \sum_i |i\rangle |\epsilon\rangle \langle i|\psi\rangle.$$

where $|i\rangle |\epsilon\rangle$ is shorthand for the tensor product: $|i\rangle \otimes |\epsilon\rangle$. There are two extremes in the way the system can interact with its environment: either (1) the system loses its distinct identity and merges with the environment (e.g. photons in a cold, dark cavity get converted into molecular excitations within the cavity walls), or (2) the system is not disturbed at all, even though the environment is disturbed (e.g. the idealized non-disturbing measurement). In general an interaction is a mixture of these two extremes, which we shall examine:

System absorbed by environment

If the environment absorbs the system, each element of the total system's basis interacts with the environment such that:

$$|i\rangle |\epsilon\rangle \text{ evolves into } |\epsilon_i\rangle$$

and so

$$|before\rangle \text{ evolves into } |after\rangle = \sum_i |\epsilon_i\rangle \langle i|\psi\rangle$$

where the unitarity of time-evolution demands that the total state basis remains orthonormal and in particular their scalar or inner products with each other vanish, since $\langle i|j\rangle = \delta_{ij}$:

$$\langle \epsilon_i | \epsilon_j \rangle = \delta_{ij}$$

This orthonormality of the environment states is the defining characteristic required for einselection.

System not disturbed by environment

This is the idealized measurement or undisturbed system case in which each element of the basis interacts with the environment such that:

$$|i\rangle |\epsilon\rangle \text{ evolves into the product } |i, \epsilon_i\rangle = |i\rangle |\epsilon_i\rangle$$

i.e. the system disturbs the environment, but is itself *undisturbed* by the environment.

and so:

$$|before\rangle \text{ evolves into } |after\rangle = \sum_i |i, \epsilon_i\rangle \langle i|\psi\rangle$$

where, again, unitarity demands that:

$$\langle i, \epsilon_i | j, \epsilon_j \rangle = \langle i|j\rangle \langle \epsilon_i | \epsilon_j \rangle = \delta_{ij} \langle \epsilon_i | \epsilon_j \rangle = \delta_{ij}$$

and *additionally* decoherence requires, by virtue of the large number of hidden degrees of freedom in the environment, that

$$\langle \epsilon_i | \epsilon_j \rangle \approx \delta_{ij}$$

As before, this is the defining characteristic for decoherence to become einselection.¹The approximation becomes more exact as the number of environmental degrees of freedom affected increases.

Note that if the system basis $|i\rangle$ were not an einselected basis then the last condition is trivial since the disturbed environment is not a function of i and we have the trivial disturbed environment basis $|\epsilon_j\rangle = |\epsilon'\rangle$. This would correspond to the system basis being degenerate with respect to the environmentally-defined-measurement-observable. For a complex environmental interaction (which would be expected for a typical macro scale interaction) a non-einselected basis would be hard to define.

Loss of interference and the transition from quantum to classical

The utility of decoherence lies in its application to the analysis of probabilities, before and after environmental interaction, and in particular to the vanishing of interference terms after decoherence has occurred. If weak what is the probability of

observing the system making a transition or quantum leap from ψ to **before** ψ has interacted with its environment, then application of the Born probability rule states that the transition probability is the modulus squared of the scalar product of the two states:

$$prob_{before}(\psi \rightarrow \phi) = |\langle \psi | \phi \rangle|^2 = \left| \sum_i \psi_i^* \phi_i \right|^2 = \sum_i |\psi_i^* \phi_i|^2 + \sum_{ij; i \neq j} \psi_i^* \psi_j \phi_j^* \phi_i$$

where $\psi_i = \langle i | \psi \rangle$, $\psi_i^* = \langle \psi | i \rangle$ and $\phi_i = \langle i | \phi \rangle$ etc.

Terms appear in the expansion of the transition probability above which involve $i \neq j$; these can be thought of as representing *interference* between the different basis elements or quantum alternatives. This is a purely quantum effect and represents the non-additivity of the probabilities of quantum alternatives.

To calculate the probability of observing the system making a quantum leap from ψ to ϕ **after** ψ has interacted with its environment, then application of the Born probability rule states we must sum over all the relevant possible states of the environment, E_i , before squaring the modulus:

$$prob_{after}(\psi \rightarrow \phi) = \sum_j |\langle after | \phi, \epsilon_j \rangle|^2 = \sum_j \left| \sum_i \psi_i^* \langle i, \epsilon_i | \phi, \epsilon_j \rangle \right|^2 = \sum_j \left| \sum_i \psi_i^* \langle i | \phi \rangle \langle \epsilon_i | \epsilon_j \rangle \right|^2$$

The internal summation vanishes when we apply the decoherence / einselection condition $\langle \epsilon_i | \epsilon_j \rangle \approx \delta_{ij}$ and the formula simplifies to:

$$prob_{after}(\psi \rightarrow \phi) \approx \sum_j |\psi_j^* \langle j | \phi \rangle|^2 = \sum_i |\psi_i^* \phi_i|^2$$

If we compare this with the formula we derived before the environment introduced decoherence we can see that the effect of decoherence has been to move the summation sign \sum_i from inside of the modulus sign to outside. As a result all the cross-or quantum interference-terms:

$$\sum_{ij; i \neq j} \psi_i^* \psi_j \phi_j^* \phi_i$$

have vanished from the transition probability calculation. The decoherence has irreversibly converted quantum behaviour (additive probability amplitudes) to classical behaviour (additive probabilities)

In terms of density matrices, the loss of interference effects corresponds to the diagonalization of the "environmentally traced over" density matrix.

Density matrix approach

The effect of decoherence on density matrices is essentially the decay or rapid vanishing of the off-diagonal elements of the partial trace of the joint system's density matrix, i.e. the trace, with respect to *any* environmental basis, of the density matrix of the combined system *and* its environment. The decoherence irreversibly converts the "averaged" or "environmentally traced over"¹ density matrix from a pure state to a reduced mixture; it is this that gives the *appearance* of wavefunction collapse. Again this is called "environmentally-induced-super selection", or einselection. The advantage of taking the partial trace is that this procedure is indifferent to the environmental basis chosen.

The density matrix approach has been combined with the Bohmian approach to yield a *reduced trajectory approach*, taking into account the system reduced density matrix and the influence of the environment.¹

Operator-sum representation

Consider a system S and environment (bath) B, which are closed and can be treated quantum mechanically. Let \mathcal{H}_S and \mathcal{H}_B be the systems and bath's Hilbert spaces, respectively. Then the Hamiltonian for the combined system is

$$\hat{H} = \hat{H}_S \otimes \hat{I}_B + \hat{I}_S \otimes \hat{H}_B + \hat{H}_I$$

where \hat{H}_S , \hat{H}_B are the system and bath Hamiltonians, respectively, and \hat{H}_I is the interaction Hamiltonian between the system and bath, and \hat{I}_S , \hat{I}_B are the identity operators on the system and bath Hilbert spaces, respectively. The time-evolution of the density operator of this closed system is unitary and, as such, is given by

$$\rho_{SB}(t) = \hat{U}(t) \rho_{SB}(0) \hat{U}^\dagger(t)$$

where the unitary operator is $\hat{U} = e^{\frac{-i\hat{H}t}{\hbar}}$. If the system and bath are not entangled initially, then we can write $\rho_{SB} = \rho_S \otimes \rho_B$. Therefore, the evolution of the system becomes

$$\rho_{SB}(t) = \hat{U}(t)[\rho_S(0) \otimes \rho_B(0)]\hat{U}^\dagger(t).$$

The system-bath interaction Hamiltonian can be written in a general form as

$$\hat{H}_I = \sum_i \hat{S}_i \otimes \hat{B}_i,$$

where $\hat{S}_i \otimes \hat{B}_i$ is the operator acting on the combined system-bath Hilbert space, and \hat{S}_i, \hat{B}_i are the operators that act on the system and bath, respectively. This coupling of the system and bath is the cause of decoherence in the system alone. To see this, a partial trace is performed over the bath to give a description of the system alone:

$$\rho_S(t) = \text{Tr}_B[\hat{U}(t)[\rho_S(0) \otimes \rho_B(0)]\hat{U}^\dagger(t)].$$

$\rho_S(t)$ is called the *reduced density matrix* and gives information about the system only. If the bath is written in terms of its set of orthogonal basis kets, that is, if it has been

$$\rho_B(0) = \sum_j a_j |j\rangle \langle j|.$$

Semi group approach

A more general consideration for the existence of decoherence in a quantum system is given by the **master equation**, which determines how the density matrix of the *system alone* evolves in time. This uses the Schrödinger picture, where evolution of the *state* (represented by its density matrix) is considered. The master equation is:

$$\rho'_S(t) = \frac{-i}{\hbar} [\tilde{\mathbf{H}}_S, \rho_S(t)] + L_D [\rho_S(t)]$$

where $\tilde{\mathbf{H}}_S = \mathbf{H}_S + \Delta$ is the system Hamiltonian, \mathbf{H}_S , along with a (possible) unitary contribution from the bath, Δ and L_D is the **Lindblad decohering term**. They are basis operators for the M-dimensional space of bounded operators that act on the system Hilbert space \mathcal{H}_S -these are the **error generators**-and $b_{\alpha\beta}$ represent the elements of a positive semi-definite Hermitian matrix-these matrix elements characterize the decohering processes and, as such, are called the **noise parameters**.^[8] The semi group approach is particularly nice, because it distinguishes between the unitary and decohering(non-unitary) processes, which is not the case with the OSR. In particular, the non-unitary dynamics are represented by L_D , whereas the unitary dynamics of the state are represented by the usual Heisenberg commutator. Note that when $L_D[\rho_S(t)] = 0$, the dynamical evolution of the system is unitary. The conditions for the evolution of the system density matrix to be described by the master equation are:

¹Dr K N Prasanna Kumar, Post doctoral researcher, Dr KNP Kumar has three PhD's, one each in Mathematics, Economics and Political science and a D.Litt. in Political Science, Department of studies in Mathematics, Kuvempu University, Shimoga, Karnataka, India Correspondence Mail id : drknkumar@gmail.com

²Prof B S Kiranagi, UGC Emeritus Professor (Department of studies in Mathematics), Manasagangotri, University of Mysore, Karnataka, India

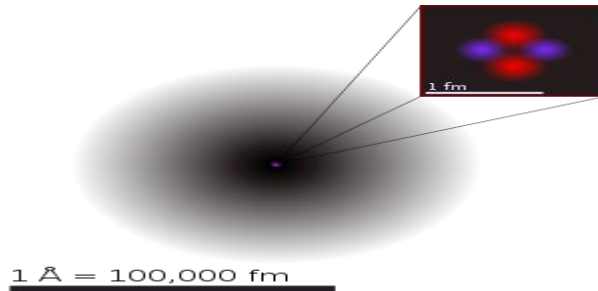
³Prof C S Bagewadi, Chairman , Department of studies in Mathematics and Computer science, Jnanasahyadri Kuvempu university, Shankarghatta, Shimoga district, Karnataka, India

QUANTUM MECHANICAL BEHAVIOUR ATOMISM (DISAMBIGUATION) AND THEORY OF CLASSIFICATION OF QUANTUM MECHANICAL BEHAVIOUR:

Dirac equation as the basic formalism of quantum mechanics, representations of Dirac matrices, covariant realization of the Dirac equation, interpretation of negative energies, Foldy-Wouthuysen transformation, Klein's paradox, spherically symmetric interactions and a treatment of the relativistic hydrogen atom, etc., and also provides excellent additional treatments of a variety of other relevant topics. The monograph contains an extensive treatment of the Lorentz and Poincare groups and their representations. The author discusses in depth Lie algebraic and projective representations, covering groups, and Mackey's theory and Wigner's realization of induced representations. A careful classification of external fields with respect to their behavior under Poincare transformations is supplemented by a basic account of self-adjointness and spectral properties of Dirac operators. A state-of-the-art treatment of relativistic scattering theory based on a time-dependent approach originally due to Enss is presented. An excellent introduction to quantum electrodynamics in external fields is provided. Various appendices containing further details, notes on each chapter commenting on the history involved and

referring to original research papers and further developments in the literature, and a bibliography covering all relevant monographs and over 500 articles on the subject, complete this text.

atom



An illustration of the helium atom, depicting the nucleus (pink) and the electron cloud distribution (black). The nucleus (upper right) in helium-4 is in reality spherically symmetric and closely resembles the electron cloud, although for more complicated nuclei this is not always the case. The black bar is one angstrom (10^{-10} m or 100 pm).

Classification

Smallest recognized division of a chemical element

Properties

Mass range: * 1.67×10^{-27} to 4.52×10^{-25} kg

Electric charge: *zero (neutral), or ion charge

Diameter range: *62 pm (He) to 520 pm (Cs) ([data page](#))

Components: *Electrons and a compact nucleus of protons and neutrons

The **atom** is a basic unit of matter that consists of a dense central nucleus surrounded by a cloud of negatively charged electrons. The atomic nucleus contains a mix of positively charged protons and electrically neutral neutrons (except in the case of hydrogen-1, which is the only stable nuclide with no neutrons). The electrons of an atom are bound to the nucleus by the electromagnetic force. Likewise, a group of atoms can remain bound to each other, forming a molecule. An atom containing an equal number of protons and electrons is electrically neutral, otherwise it has a positive charge if there are fewer electrons (electron deficiency) or negative charge if there are more electrons (electron excess). A positively or negatively charged atom is known as an ion. An atom is classified according to the number of protons and neutrons in its nucleus: the number of protons determines the chemical element, and the number of neutrons determines the isotope of the element.

The name atom comes from the Greek ἄτομος (*atomos*, "indivisible") from ἀ- (*a-*, "not") and τέμνω (*temnō*, "I cut"),^[2] which means uncuttable, or indivisible, something that cannot be divided further. The concept of an atom as an indivisible component of matter was first proposed by early Indian and Greek philosophers. In the 17th and 18th centuries, chemists provided a physical basis for this idea by showing that certain substances could not be further broken down by chemical methods. During the late 19th and early 20th centuries, physicists discovered subatomic components and structure inside the atom, thereby demonstrating that the 'atom' was divisible. The principles of quantum mechanics were used to successfully model the atom.

Atoms are minuscule objects with proportionately tiny masses. Atoms can only be observed individually using special instruments such as the scanning tunneling microscope. Over 99.94% of an atom's mass is concentrated in the nucleus,^[note 1] with protons and neutrons having roughly equal mass. Each element has at least one isotope with an unstable nucleus that can undergo radioactive decay. This can result in a transmutation that changes the number of protons or neutrons in a nucleus.^[6] Electrons that are bound to atoms possess a set of stable energy levels, or orbitals, and can undergo transitions between them by absorbing or emitting photons that match the energy differences between the levels. The electrons determine the chemical properties of an element, and strongly influence an atom's magnetic properties.

History

Atomism

The concept that matter is composed of discrete units and cannot be divided into arbitrarily tiny quantities has been around for millennia, but these ideas were founded in abstract, philosophical reasoning rather than experimentation and empirical observation. The nature of atoms in philosophy varied considerably over time and between cultures and schools, and often had spiritual elements. Nevertheless, the basic idea of the atom was adopted by scientists thousands of years later because it elegantly explained new discoveries in the field of chemistry.

References to the concept of atoms date back to ancient Greece and India. In India, the Ājīvika, Jain, and Cārvāka schools of atomism may date back to the 6th century BCE. The Nyaya and Vaisheshika schools later developed theories on how atoms combined into more complex objects. In the West, the references to atoms emerged in the 5th century BCE with Leucippus, whose student, Democritus, systematized his views. In approximately 450 BCE, Democritus coined the term *atomos* (Greek: ἄτομος), which means "uncuttable" or "the smallest indivisible particle of matter". Although

the Indian and Greek concepts of the atom were based purely on philosophy, modern science has retained the name coined by Democritus

Corpuscularianism is the postulate, expounded in the 13th-century by the alchemist Pseudo-Geber (Geber), sometimes identified with Paul of Taranto, that all physical bodies possess an inner and outer layer of minute particles or corpuscles. Corpuscularianism is similar to the theory of atomism, except that where atoms were supposed to be indivisible, corpuscles could in principle be divided. In this manner, for example, it was theorized that mercury could penetrate into metals and modify their inner structure. Corpuscularianism stayed a dominant theory over the next several hundred years.

In 1661, natural philosopher Robert Boyle published *The Sceptical Chymist* in which he argued that matter was composed of various combinations of different "corpuscles" or atoms, rather than the classical elements of air, earth, fire and water.^[13] During the 1670s Corpuscularianism was used by Isaac Newton in his development of the corpuscular theory of light. Further progress in the understanding of atoms did not occur until the science of chemistry began to develop. In 1789, French nobleman and scientific researcher Antoine Lavoisier discovered the law of conservation of mass and defined an element as a basic substance that could not be further broken down by the methods of chemistry.¹

In 1805, English instructor and natural philosopher John Dalton used the concept of atoms to explain why elements always react in ratios of small whole numbers (the law of multiple proportions) and why certain gases dissolved better in water than others. He proposed that each element consists of atoms of a single, unique type, and that these atoms can join together to form chemical compounds.^{[16][17]} Dalton is considered the originator of modern atomic theory

Dalton's atomic hypothesis did not specify the size of atoms. Common sense indicated they must be very small, but nobody knew how small. Therefore it was a major landmark when in 1865 Johann Josef Loschmidt's measured the size of the molecules that make up air.

An additional line of reasoning in support of particle theory (and by extension atomic theory) began in 1827 when botanist Robert Brown used a microscope to look at dust grains floating in water and discovered that they moved about erratically—a phenomenon that became known as "Brownian motion". J. Desaulx suggested in 1877 that the phenomenon was caused by the thermal motion of water molecules, and in 1905 Albert Einstein produced the first mathematical analysis of the motion. French physicist Jean Perrin used Einstein's work to experimentally determine the mass and dimensions of atoms, thereby conclusively verifying Dalton's atomic theory

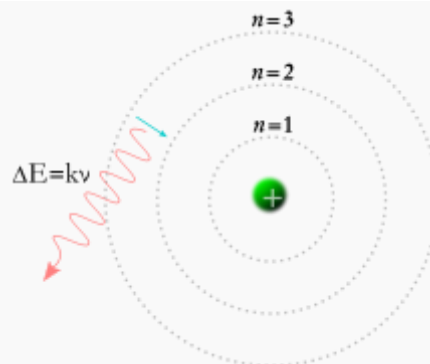
In 1869, building upon earlier discoveries by such scientists as Lavoisier, Dmitri Mendeleev published the first functional periodic table.^[23] The table itself is a visual representation of the periodic law, which states that certain chemical properties of elements repeat periodically when arranged by atomic number.

Subcomponents and quantum theory

The physicist J. J. Thomson, through his work on cathode rays in 1897, discovered the electron, and concluded that they were a component of every atom. Thus he overturned the belief that atoms are the indivisible, ultimate particles of matter. Thomson postulated that the low mass, negatively charged electrons were distributed throughout the atom, possibly rotating in rings, with their charge balanced by the presence of a uniform sea of positive charge. This later became known as the plum pudding model.

In 1909, Hans Geiger and Ernest Marsden, under the direction of physicist Ernest Rutherford, bombarded a sheet of gold foil with alpha rays—by then known to be positively charged helium atoms—and discovered that a small percentage of these particles were deflected through much larger angles than was predicted using Thomson's proposal. Rutherford interpreted the gold foil experiment as suggesting that the positive charge of a heavy gold atom and most of its mass was concentrated in a nucleus at the center of the atom—the Rutherford model

While experimenting with the products of radioactive decay, in 1913 radio chemist Frederick Soddy discovered that there appeared to be more than one type of atom at each position on the periodic table. The term isotope was coined by Margaret Todd as a suitable name for different atoms that belong to the same element. J.J. Thomson created a technique for separating atom types through his work on ionized gases, which subsequently led to the discovery of stable isotopes.



A Bohr model of the hydrogen atom, showing an electron jumping between fixed orbits and emitting a photon of energy with a specific frequency

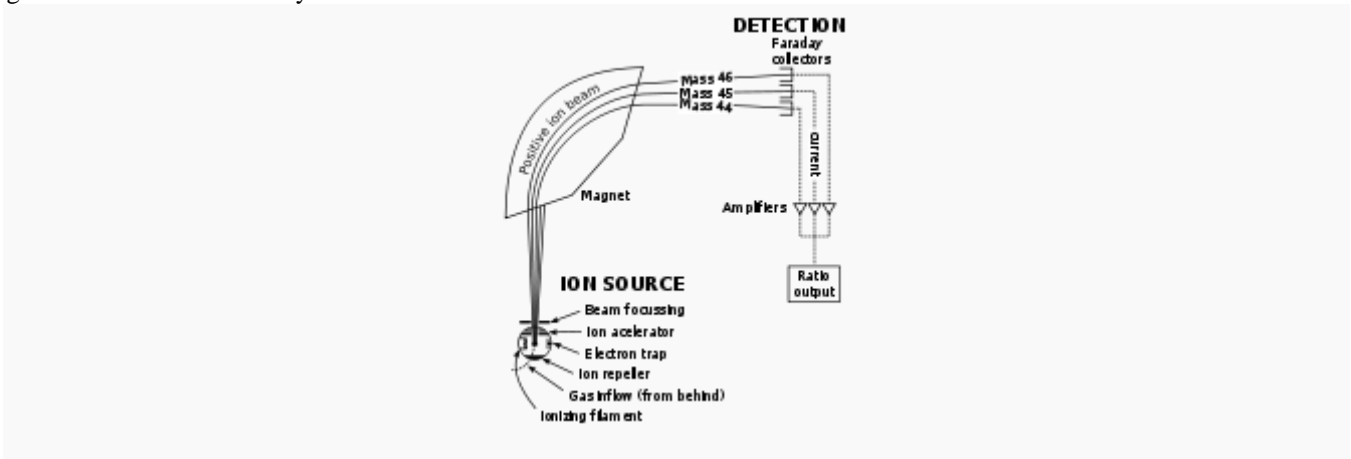
Meanwhile, in 1913, physicist Niels Bohr suggested that the electrons were confined into clearly defined, quantized orbits, and could jump between these, but could not freely spiral inward or outward in intermediate states. An electron must absorb or emit specific amounts of energy to transition between these fixed orbits. When the light from a heated material was passed through a prism, it produced a multi-colored spectrum. The appearance of fixed lines in this spectrum was successfully explained by these orbital transitions.

Later in the same year Henry Moseley provided additional experimental evidence in favor of Niels Bohr's theory. These results refined Ernest's and Antonius Van den Broek's model, which proposed that the atom contains in its nucleus a number of positive nuclear that is equal to its (atomic) number in the periodic table. Until these experiments, atomic number was not known to be a physical and experimental quantity. That it is equal to the atomic nuclear charge remains the accepted atomic model today

Chemical bonds between atoms were now explained, by Gilbert Newton Lewis in 1916, as the interactions between their constituent electrons.²¹ As the chemical properties of the elements were known to largely repeat themselves according to the periodic law, in 1919 the American chemist Irving Langmuir suggested that this could be explained if the electrons in an atom were connected or clustered in some manner. Groups of electrons were thought to occupy a set of electron shells about the nucleus

The Stern–Gerlach experiment of 1922 provided further evidence of the quantum nature of the atom. When a beam of silver atoms was passed through a specially shaped magnetic field, the beam was split based on the direction of an atom's angular momentum, or spin. As this direction is random, the beam could be expected to spread into a line. Instead, the beam was split into two parts, depending on whether the atomic spin was oriented up or down.

In 1924, Louis de Broglie proposed that all particles behave to an extent like waves. In 1926, Erwin Schrödinger used this idea to develop a mathematical model of the atom that described the electrons as three-dimensional waveforms rather than point particles. A consequence of using waveforms to describe particles is that it is mathematically impossible to obtain precise values for both the position and momentum of a particle at the same time; this became known as the uncertainty principle, formulated by Werner Heisenberg in 1926. In this concept, for a given accuracy in measuring a position one could only obtain a range of probable values for momentum, and vice versa. This model was able to explain observations of atomic behavior that previous models could not, such as certain structural and spectral patterns of atoms larger than hydrogen. Thus, the planetary model of the atom was discarded in favor of one that described atomic orbital zones around the nucleus where a given electron is most likely to be observed



The development of the mass spectrometer allowed the exact mass of atoms to be measured. The device uses a magnet to bend the trajectory of a beam of ions, and the amount of deflection is determined by the ratio of an atom's mass to its charge. The chemist Francis William Aston used this instrument to show that isotopes had different masses. The atomic mass of these isotopes varied by integer amounts, called the whole number rule. The explanation for these different isotopes awaited the discovery of the neutron, a neutral-charged particle with a mass similar to the proton, by the physicist James Chadwick in 1932. Isotopes were then explained as elements with the same number of protons, but different numbers of neutrons within the nucleus.

Fission, high-energy physics and condensed matter

NUCLEAR FISSION AND QUANTUM CHIPS:

The following dissemination of the information on the News Paper report(See references for further details):

Current technology uses ultraviolet light to (e)create the fine features in computer chips in a process called photolithography, which involves projecting the image of a mask onto a light-sensitive material, then chemically etching the resulting pattern.

New nanolithography will be needed to continue advances in computer technology and to extend Moore's law, an unofficial rule stating that the number of transistors on integrated circuits, or chips, doubles about every 18 months.

"We can't make devices much smaller using conventional lithography, so we have to find ways of creating beams having more narrow wavelengths," said Ahmed Hassanein, the Paul L. Wattelet Professor of Nuclear Engineering and head of Purdue's School of Nuclear Engineering.

The new plasma-based lithography under development generates "extreme ultraviolet" light having a wavelength of 13.5 nanometers, less than one-tenth the size of current lithography, Hassanein said.

Nuclear engineers and scientists at Purdue and the U.S. Department of Energy's Argonne National Laboratory are working to improve the efficiency of two techniques for producing the plasma: One approach uses a laser and the other "discharge-produced" method uses an electric current.

"In either case, only about 1 to 2 percent of the energy spent is converted into plasma," Hassanein said. "That conversion efficiency means you'd need greater than 100 kilowatts of power for this lithography, which poses all sorts of engineering problems. We are involved in optimizing conversion efficiency - reducing the energy requirements - and solving various design problems for the next-generation lithography."

Findings are detailed in a research paper scheduled to appear in the October-December 2009 issue of the *Journal of Micro/Nanolithography, MEMS, and MOEMS*. The paper was written by Hassanein, senior research scientist Valeryi Sizyuk, computer analyst Tatyana Sizyuk, and research assistant professor Sivanandan Harilal, all in the School of Nuclear Engineering.

Critical to the research is a computer simulation, called HEIGHTS -- for high-energy interaction with general heterogeneous target systems -- developed by Hassanein's team. Computations for a single HEIGHTS simulation using Argonne supercomputers can take several months to finish, said Hassanein, a former Argonne senior scientist who led work there to develop HEIGHTS.

The laser method creates plasma by heating xenon, tin or lithium. The plasma produces high-energy packets of light, photons, of extreme ultraviolet light.

Plasma is a partially ionized gas like material that conducts electricity. Because of this electrical conductivity, researchers are able to use magnetic fields to shape and control plasmas, forming beams, filaments and other structures. In experimental fusion reactors, magnetic fields are used to keep plasma-based nuclear fuel from touching the metal walls of the containment vessel, enabling the plasma to be heated to the extreme temperatures required to maintain fusion reactions.

HEIGHTS simulate the entire process of the plasma evolution: the laser interacting with the target, and the target evaporating, ionizing and turning into plasma. The simulation also shows what happens when the magnetic forces "pinch" the plasma cloud into a smaller diameter spot needed to generate the photons.

Findings in the paper detail the laser-produced plasma beams, showing that simulations match data from laboratory experiments recently built at Purdue, Hassanein said. One design challenge stems from the fact that lenses absorb the photons that make up light, meaning they cannot be used to focus the beam. Instead, mirrors are used in the design. However, plasma condenses on the mirrors, reducing their reflectivity and limiting the efficiency of the process.

"We are trying to help find innovative ways of producing these photons, optimizing the production and mitigating the effects of the plasma on the mirrors," Hassanein said. "So we are trying to improve the entire system."

The simulation tool combines computations in plasma physics, radiation transport, atomic physics, plasma-material interactions and magneto hydrodynamics, or what happens when a target is heated, melts and turns into a plasma.

In 1938, the German chemist Otto Hahn, a student of Rutherford, directed neutrons onto uranium atoms expecting to get transuranium elements. Instead, his chemical experiments showed barium as a product. A year later, Lise Meitner and her nephew Frisch verified that Hahn's result were the first experimental *nuclear fission*.¹ In 1944, Hahn received the Nobel prize in chemistry. Despite Hahn's efforts, the contributions of Meitner and Frisch were not recognized

In the 1950s, the development of improved particle accelerators and particle detectors allowed scientists to study the impacts of atoms moving at high energies.^[44] Neutrons and protons were found to be hadrons, or composites of smaller particles called quarks. Standard models of nuclear physics were developed that successfully explained the properties of the nucleus in terms of these sub-atomic particles and the forces that govern their interactions

Components

Subatomic particles

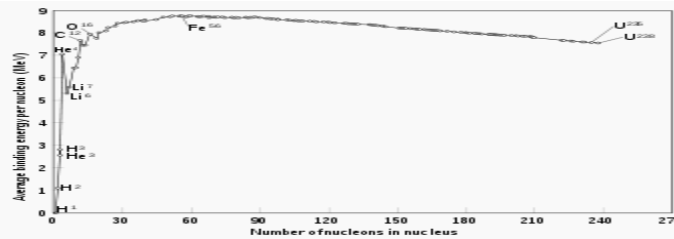
Though the word *atom* originally denoted a particle that cannot be cut into smaller particles, in modern scientific usage the atom is composed of various subatomic particles. The constituent particles of an atom are the electron, the proton and the neutron. However, the hydrogen-1 atom has no neutrons and a positive hydrogen ion has no electrons.

The electron is by far the least massive of these particles at 9.11×10^{-31} kg, with a negative electrical charge and a size that is too small to be measured using available techniques.¹ Protons have a positive charge and a mass 1,836 times that of the electron, at 1.6726×10^{-27} kg, although this can be reduced by changes to the energy binding the proton into an atom. Neutrons have no electrical charge and have a free mass of 1,839 times the mass of electrons, or 1.6929×10^{-27} kg. Neutrons and protons have comparable dimensions—on the order of 2.5×10^{-15} m—although the 'surface' of these particles is not sharply defined.

In the Standard Model of physics, both protons and neutrons are composed of elementary particles called quarks. The quark belongs to the fermion group of particles, and is one of the two basic constituents of matter—the other being the lepton, of

which the electron is an example. There are six types of quarks, each having a fractional electric charge of either $+\frac{2}{3}$ or $-\frac{1}{3}$. Protons are composed of two up quarks and one down quark, while a neutron consists of one up quark and two down quarks. This distinction accounts for the difference in mass and charge between the two particles. The quarks are held together by the strong nuclear force, which is mediated by gluons. The gluon is a member of the family of gauge bosons, which are elementary particles that mediate physical forces.

Nucleus



The binding energy needed for a nucleon to escape the nucleus, for various isotopes

All the bound protons and neutrons in an atom make up a tiny atomic nucleus, and are collectively called nucleons. The radius of a nucleus is approximately equal to $1.07 \sqrt[3]{A} \text{ fm}$, where A is the total number of nucleons¹. This is much smaller than the radius of the atom, which is on the order of 10^5 fm . The nucleons are bound together by a short-ranged attractive potential called the residual strong force. At distances smaller than 2.5 fm this force is much more powerful than the electrostatic force that causes positively charged protons to repel each other.^[52]

Atoms of the same element have the same number of protons, called the atomic number. Within a single element, the number of neutrons may vary, determining the isotope of that element. The total number of protons and neutrons determine the nuclide. The number of neutrons relative to the protons determines the stability of the nucleus, with certain isotopes undergoing radioactive decay.

The neutron and the proton are different types of fermions. The Pauli exclusion principle is a mechanical effect that prohibits identical fermions, such as multiple protons, from occupying the same quantum physical state at the same time. Thus every proton in the nucleus must occupy a different state, with its own energy level, and the same rule applies to all of the neutrons. This prohibition does not apply to a proton and neutron occupying the same quantum state

For atoms with low atomic numbers, a nucleus that has a different number of protons than neutrons can potentially drop to a lower energy state through a radioactive decay that causes the number of protons and neutrons to more closely match. As a result, atoms with roughly matching numbers of protons and neutrons are more stable against decay. However, with increasing atomic number, the mutual repulsion of the protons requires an increasing proportion of neutrons to maintain the stability of the nucleus, which modifies this trend. Thus, there are no stable nuclei with equal proton and neutron numbers above atomic number $Z = 20$ (calcium); and as Z increases toward the heaviest nuclei, the ratio of neutrons per proton required for stability increases to about 1.5.^[54]

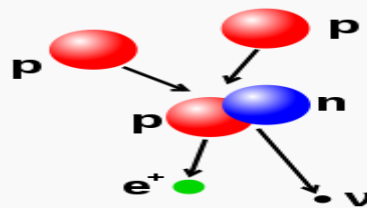


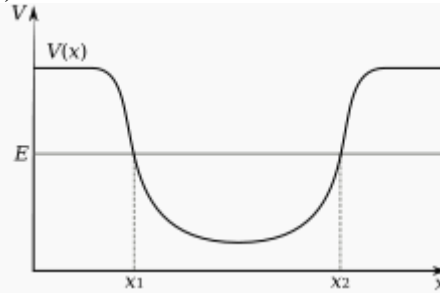
Illustration of a nuclear fusion process that forms a deuterium nucleus, consisting of a proton and a neutron, from two protons. A positron (e^+)—an antimatter electron—is emitted along with an electron neutrino.

The number of protons and neutrons in the atomic nucleus can be modified, although this can require very high energies because of the strong force. Nuclear fusion occurs when multiple atomic particles join to form a heavier nucleus, such as through the energetic collision of two nuclei. For example, at the core of the Sun protons require energies of 3–10 keV to overcome their mutual repulsion—the coulomb barrier—and fuse together into a single nucleus. Nuclear fission is the opposite process, causing a nucleus to split into two smaller nuclei—usually through radioactive decay. The nucleus can also be modified through bombardment by high energy subatomic particles or photons. If this modifies the number of protons in a nucleus, the atom changes to a different chemical element.¹ If the mass of the nucleus following a fusion reaction is less than the sum of the masses of the separate particles, then the difference between these two values can be emitted as a type of usable energy (such as a gamma ray, or the kinetic energy of a beta particle), as described by Albert Einstein's mass-energy equivalence formula, $E = mc^2$, where m is the mass loss and c is the speed of light. This deficit is part of the binding energy of the new nucleus, and it is the non-recoverable loss of the energy that causes the fused particles to remain together in a state that requires this energy to separate.^[58]

The fusion of two nuclei that create larger nuclei with lower atomic numbers than iron and nickel—a total nucleon number of about 60—is usually an exothermic process that releases more energy than is required to bring them together.^[59] It is this

energy-releasing process that makes nuclear fusion in stars a self-sustaining reaction. For heavier nuclei, the binding energy per nucleon in the nucleus begins to decrease. That means fusion processes producing nuclei that have atomic numbers higher than about 26, and atomic masses higher than about 60, is an endothermic process. These more massive nuclei can not undergo an energy-producing fusion reaction that can sustain the hydrostatic equilibrium of a star.^[54]

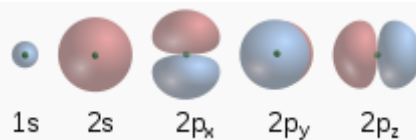
Electron cloud, Electron Configuration, Atomic Orbital:



A potential well, showing, according to classical mechanics, the minimum energy $V(x)$ needed to reach each position x . Classically, a particle with energy E is constrained to a range of positions between x_1 and x_2 .

The electrons in an atom are attracted to the protons in the nucleus by the electromagnetic force. This force binds the electrons inside an electrostatic potential well surrounding the smaller nucleus, which means that an external source of energy is needed for the electron to escape. The closer an electron is to the nucleus, the greater the attractive force. Hence electrons bound near the center of the potential well require more energy to escape than those at greater separations.

Electrons, like other particles, have properties of both a particle and a wave. The electron cloud is a region inside the potential well where each electron forms a type of three-dimensional standing wave—a wave form that does not move relative to the nucleus. This behavior is defined by an atomic orbital, a mathematical function that characterises the probability that an electron appears to be at a particular location when its position is measured.^[60] Only a discrete (or quantized) set of these orbitals exist around the nucleus, as other possible wave patterns rapidly decay into a more stable form.^[61] Orbitals can have one or more ring or node structures, and they differ from each other in size, shape and orientation.¹



Wave functions of the first five atomic orbitals. The three 2p orbitals each display a single angular node that has an orientation and a minimum at the center.

Each atomic orbital corresponds to a particular energy level of the electron. The electron can change its state to a higher energy level by absorbing a photon with sufficient energy to boost it into the new quantum state. Likewise, through spontaneous emission, an electron in a higher energy state can drop to a lower energy state while radiating the excess energy as a photon. These characteristic energy values, defined by the differences in the energies of the quantum states, are responsible for atomic spectral lines.^[61]

The amount of energy needed to remove or add an electron—the electron binding energy—is far less than the binding energy of nucleons. For example, it requires only 13.6 eV to strip a ground-state electron from a hydrogen atom,^[63] compared to 2.23 million eV for splitting a deuterium nucleus.^[64] Atoms are electrically neutral if they have an equal number of protons and electrons. Atoms that have either a deficit or a surplus of electrons are called ions. Electrons that are farthest from the nucleus may be transferred to other nearby atoms or shared between atoms. By this mechanism, atoms are able to bond into molecules and other types of chemical compounds like ionic and covalent network crystals.^[65]

Properties

Nuclear properties-Stable Isotopes, List of Nuclides and List of Elements by Isotopes:

By definition, any two atoms with an identical number of protons in their nuclei belong to the same chemical element. Atoms with equal numbers of protons but a different number of neutrons are different isotopes of the same element. For example, all hydrogen atoms admit exactly one proton, but isotopes exist with no neutrons (hydrogen-1, by far the most common form,^[66] also called protium), one neutron (deuterium), two neutrons (tritium) and more than two neutrons. The known elements form a set of atomic numbers, from the single proton element hydrogen up to the 118-proton element ununoctium.^[67] All known isotopes of elements with atomic numbers greater than 82 are radioactive.^{[68][69]}

About 339 nuclides occur naturally on Earth,^[70] of which 255 (about 75%) have not been observed to decay, and are referred to as "stable isotopes". However, only 90 of these nuclides are stable to all decay, even in theory. Another 165 (bringing the total to 255) have not been observed to decay, even though in theory it is energetically possible. These are also formally classified as "stable". An additional 33 radioactive nuclides have half-lives longer than 80 million years, and are long-lived

enough to be present from the birth of the solar system. This collection of 288 nuclides are known as primordial nuclides. Finally, an additional 51 short-lived nuclides are known to occur naturally, as daughter products of primordial nuclide decay (such as radium from uranium), or else as products of natural energetic processes on Earth, such as cosmic ray bombardment (for example, carbon-14).^{[71][note 2]}

For 80 of the chemical elements, at least one stable isotope exists. As a rule, there is only a handful of stable isotopes for each of these elements, the average being 3.2 stable isotopes per element. Twenty-six elements have only a single stable isotope, while the largest number of stable isotopes observed for any element is ten, for the element tin. Elements 43, 61, and all elements numbered 83 or higher have no stable isotopes.^{[72][page needed]}

Stability of isotopes is affected by the ratio of protons to neutrons, and also by the presence of certain "magic numbers" of neutrons or protons that represent closed and filled quantum shells. These quantum shells correspond to a set of energy levels within the shell model of the nucleus; filled shells, such as the filled shell of 50 protons for tin, confers unusual stability on the nuclide. Of the 255 known stable nuclides, only four have both an odd number of protons *and* odd number of neutrons: hydrogen-2 (deuterium), lithium-6, boron-10 and nitrogen-14. Also, only four naturally occurring, radioactive odd-odd nuclides have a half-life over a billion years: potassium-40, vanadium-50, lanthanum-138 and tantalum-180m. Most odd-odd nuclei are highly unstable with respect to beta decay, because the decay products are even-even, and are therefore more strongly bound, due to nuclear pairing effects.^{[72][page needed]}

Mass Number Of an Atom:

The large majority of an atom's mass comes from the protons and neutrons that make it up. The total number of these particles (called "nucleons") in a given atom is called the mass number. The mass number is a simple whole number, and has units of "nucleons." An example of use of a mass number is "carbon-12," which has 12 nucleons (six protons and six neutrons).

The actual mass of an atom at rest is often expressed using the unified atomic mass unit (u), which is also called a dalton (Da). This unit is defined as a twelfth of the mass of a free neutral atom of carbon-12, which is approximately 1.66×10^{-27} kg.^[73] Hydrogen-1, the lightest isotope of hydrogen and the atom with the lowest mass, has an atomic weight of 1.007825 u.^[74] The value of this number is called the atomic mass. A given atom has an atomic mass approximately equal (within 1%) to its mass number times the mass of the atomic mass unit. However, this number will not be an exact whole number except in the case of carbon-12 (see below)^[75] The heaviest stable atom is lead-208,^[68] with a mass of 207.9766521 u.^[76]

As even the most massive atoms are far too light to work with directly, chemists instead use the unit of moles. One mole of atoms of any element always has the same number of atoms (about 6.022×10^{23}). This number was chosen so that if an element has an atomic mass of 1 u, a mole of atoms of that element has a mass close to one gram. Because of the definition of the unified atomic mass unit, each carbon-12 atom has an atomic mass of exactly 12 u, and so a mole of carbon-12 atoms weighs exactly 0.012 kg.^{[73][page needed]}

Shape and size-The Atomic Radius:

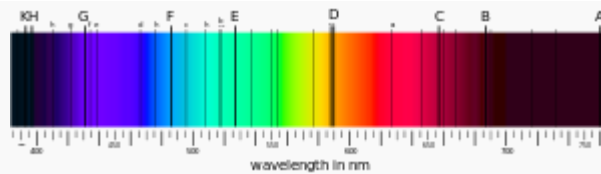
Atoms lack a well-defined outer boundary, so their dimensions are usually described in terms of an atomic radius. This is a measure of the distance out to which the electron cloud extends from the nucleus. However, this assumes the atom to exhibit a spherical shape, which is only obeyed for atoms in vacuum or free space. Atomic radii may be derived from the distances between two nuclei when the two atoms are joined in a chemical bond. The radius varies with the location of an atom on the atomic chart, the type of chemical bond, the number of neighboring atoms (coordination number) and a quantum mechanical property known as spin.^[77] On the periodic table of the elements, atom size tends to increase when moving down columns, but decrease when moving across rows (left to right).^[78] Consequently, the smallest atom is helium with a radius of 32 pm, while one of the largest is caesium at 225 pm.^[79]

When subjected to external fields, like an electrical field, the shape of an atom may deviate from that of a sphere. The deformation depends on the field magnitude and the orbital type of outer shell electrons, as shown by group-theoretical considerations. Aspherical deviations might be elicited for instance in crystals, where large crystal-electrical fields may occur at low-symmetry lattice sites. Significant ellipsoidal deformations have recently been shown to occur for sulfur ions in pyrite-type compounds.^[81]

Atomic dimensions are thousands of times smaller than the wavelengths of light (400–700 nm) so they can not be viewed using an optical microscope. However, individual atoms can be observed using a scanning tunneling microscope. To visualize the minuteness of the atom, consider that a typical human hair is about 1 million carbon atoms in width.^[82] A single drop of water contains about 2 sextillion (2×10^{21}) atoms of oxygen, and twice the number of hydrogen atoms.^[83] A single carat diamond with a mass of 2×10^{-4} kg contains about 10 sextillion (10^{22}) atoms of carbon.^[note 3] If an apple were magnified to the size of the Earth, then the atoms in the apple would be approximately the size of the original apple.^[84]

Radioactive decay

specific energy levels appear as distinct bands in the electromagnetic spectrum. Each element has a characteristic spectrum that can depend on the nuclear charge, sub shells filled by electrons, the electromagnetic interactions between the electrons and other factors



An example of absorption lines in a spectrum

When a continuous spectrum of energy is passed through a gas or plasma, some of the photons are absorbed by atoms, causing electrons to change their energy level. Those excited electrons that remain bound to their atom spontaneously emit this energy as a photon, traveling in a random direction, and so drop back to lower energy levels. Thus the atoms behave like a filter that forms a series of dark absorption bands in the energy output. (An observer viewing the atoms from a view that does not include the continuous spectrum in the background, instead sees a series of emission lines from the photons emitted by the atoms.) Spectroscopic measurements of the strength and width of spectral lines allow the composition and physical properties of a substance to be determined.

Close examination of the spectral lines reveals that some display a fine structure splitting. This occurs because of spin-orbit coupling, which is an interaction between the spin and motion of the outermost electron. When an atom is in an external magnetic field, spectral lines become split into three or more components; a phenomenon called the Zeeman effect. This is caused by the interaction of the magnetic field with the magnetic moment of the atom and its electrons. Some atoms can have multiple electron configurations with the same energy level, which thus appear as a single spectral line. The interaction of the magnetic field with the atom shifts these electron configurations to slightly different energy levels, resulting in multiple spectral lines. The presence of an external electric field can cause a comparable splitting and shifting of spectral lines by modifying the electron energy levels, a phenomenon called the Stark effect.

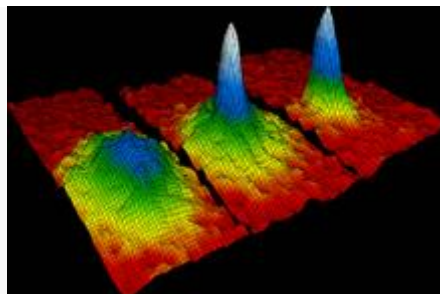
If a bound electron is in an excited state, an interacting photon with the proper energy can cause stimulated emission of a photon with a matching energy level. For this to occur, the electron must drop to a lower energy state that has an energy difference matching the energy of the interacting photon. The emitted photon and the interacting photon then move off in parallel and with matching phases. That is, the wave patterns of the two photons are synchronized. This physical property is used to make lasers, which can emit a coherent beam of light energy in a narrow frequency band

Valence and bonding behavior

The outermost electron shell of an atom in its uncombined state is known as the valence shell, and the electrons in that shell are called valence electrons. The number of valence electrons determines the bonding behavior with other atoms. Atoms tend to chemically react with each other in a manner that fills (or empties) their outer valence shells. For example, a transfer of a single electron between atoms is a useful approximation for bonds that form between atoms with one-electron more than a filled shell, and others that are one-electron short of a full shell, such as occurs in the compound sodium chloride and other chemical ionic salts. However, many elements display multiple valences, or tendencies to share differing numbers of electrons in different compounds. Thus, chemical bonding between these elements takes many forms of electron-sharing that are more than simple electron transfers. Examples include the element carbon and the organic compounds

The chemical elements are often displayed in a periodic table that is laid out to display recurring chemical properties, and elements with the same number of valence electrons form a group that is aligned in the same column of the table. (The horizontal rows correspond to the filling of a quantum shell of electrons.) The elements at the far right of the table have their outer shell completely filled with electrons, which results in chemically inert elements known as the noble gases.

STATE OF MATTER AND PHASE OF MATTER FOR CLASSIFICATION OF QUANTUM MECHANICAL BEHAVIOUR:



Snapshots illustrating the formation of a Bose–Einstein condensate

Quantities of atoms are found in different states of matter that depend on the physical conditions, such as temperature and pressure. By varying the conditions, materials can transition between solids, liquids, gases and

plasmas Within a state, a material can also exist in different phases. An example of this is solid carbon, which can exist as graphite or diamond.

At temperatures close to absolute zero, atoms can form a Bose–Einstein condensate, at which point quantum mechanical effects, which are normally only observed at the atomic scale, become apparent on a macroscopic scale This super-cooled collection of atoms then behaves as a single super atom, which may allow fundamental checks of quantum mechanical behavior.

The scanning tunneling microscope is a device for viewing surfaces at the atomic level. It uses the quantum tunneling phenomenon, which allows particles to pass through a barrier that would normally be insurmountable. Electrons tunnel through the vacuum between two planar metal electrodes, on each of which is an adsorbed atom, providing a tunneling-current density that can be measured. Scanning one atom (taken as the tip) as it moves past the other (the sample) permits plotting of tip displacement versus lateral separation for a constant current. The calculation shows the extent to which scanning-tunneling-microscope images of an individual atom are visible. It confirms that for low bias, the microscope images the space-averaged dimensions of the electron orbitals across closely packed energy levels—the Fermi level local density of states

An atom can be ionized by removing one of its electrons. The electric charge causes the trajectory of an atom to bend when it passes through a magnetic field. The radius by which the trajectory of a moving ion is turned by the magnetic field is determined by the mass of the atom. The mass spectrometer uses this principle to measure the mass-to-charge ratio of ions. If a sample contains multiple isotopes, the mass spectrometer can determine the proportion of each isotope in the sample by measuring the intensity of the different beams of ions. Techniques to vaporize atoms include inductively coupled plasma atomic emission spectroscopy and inductively coupled plasma mass spectrometry, both of which use a plasma to vaporize samples for analysis

A more area-selective method is electron energy loss spectroscopy, which measures the energy loss of an electron beam within a transmission when it interacts with a portion of a sample. The atom-probe tomograph has sub-nanometer resolution in 3-D and can chemically identify individual atoms using time-of-flight mass spectrometry

Spectra of excited states can be used to analyze the atomic composition of distant stars. Specific light wavelengths contained in the observed light from stars can be separated out and related to the quantized transitions in free gas atoms. These colors can be replicated using a gas-discharge lamp containing the same element Helium was discovered in this way in the spectrum of the Sun 23 years before it was found on Earth.

Origin and current state

Atoms form about 4% of the total energy density of the observable universe, with an average density of about 0.25 atoms/m^3 . Within a galaxy such as the Milky Way, atoms have a much higher concentration, with the density of matter in the interstellar medium (ISM) ranging from 10^5 to 10^9 atoms/m^3 . The Sun is believed to be inside the Local Bubble, a region of highly ionized gas, so the density in the solar neighborhood is only about 10^3 atoms/m^3 Stars form from dense clouds in the ISM, and the evolutionary processes of stars result in the steady enrichment of the ISM with elements more massive than hydrogen and helium. Up to 95% of the Milky Way's atoms are concentrated inside stars and the total mass of atoms forms about 10% of the mass of the galaxy. (The remainder of the mass is an unknown dark matter.)

Nucleosynthesis

Stable protons and electrons appeared one second after the Big Bang. During the following three minutes, Big Bang nucleosynthesis produced most of the helium, lithium, and deuterium in the universe, and perhaps some of the beryllium and boron. The first atoms (complete with bound electrons) were theoretically created 380,000 years after the Big Bang—an epoch called recombination, when the expanding universe cooled enough to allow electrons to become attached to nuclei. Since the Big Bang, which produced no carbon, atomic nuclei have been combined in stars through the process of nuclear fusion to produce more of the element helium, and (via the triple alpha process) the sequence of elements from carbon up to iron. Isotopes such as lithium-6, as well as some beryllium and boron are generated in space through cosmic ray spallation. This occurs when a high-energy proton strikes an atomic nucleus, causing large numbers of nucleons to be ejected. Elements heavier than iron were produced in supernovae through the r-process and in AGB stars through the s-process, both of which involve the capture of neutrons by atomic nuclei. Elements such as lead formed largely through the radioactive decay of heavier elements.¹

Earth

Most of the atoms that make up the Earth and its inhabitants were present in their current form in the nebula that collapsed out of a molecular cloud to form the Solar System. The rest are the result of radioactive decay, and their relative proportion can be used to determine the age of the Earth through radiometric dating. Most of the helium in the crust of the Earth (about 99% of the helium from gas wells, as shown by its lower abundance of helium-3) is a product of alpha decay.

There are a few trace atoms on Earth that were not present at the beginning (i.e., not "primordial"), nor are results of radioactive decay. Carbon-14 is continuously generated by cosmic rays in the atmosphere. Some atoms on Earth have been artificially generated either deliberately or as by-products of nuclear reactors or explosions Of the transuranic elements—those with atomic numbers greater than 92—only plutonium and neptunium occur naturally on Earth. Transuranic elements have radioactive lifetimes shorter than the current age of the Earth and thus identifiable quantities of these elements have

long since decayed, with the exception of traces of plutonium-244 possibly deposited by cosmic dust. Natural deposits of plutonium and neptunium are produced by neutron capture in uranium ore

The Earth contains approximately 1.33×10^{50} atoms. In the planet's atmosphere, small numbers of independent atoms of noble gases exist, such as argon and neon. The remaining 99% of the atmosphere is bound in the form of molecules, including carbon Dioxide and diatomic oxygen and nitrogen. At the surface of the Earth, atoms combine to form various compounds, including water, salt, silicates and oxides. Atoms can also combine to create materials that do not consist of discrete molecules, including crystals and liquid or solid metals. This atomic matter forms networked arrangements that lack the particular type of small-scale interrupted order associated with molecular matter

Rare and theoretical forms

While isotopes with atomic numbers higher than lead (82) are known to be radioactive, an "island of stability" has been proposed for some elements with atomic numbers above 103. These super heavy elements may have a nucleus that is relatively stable against radioactive decay. The most likely candidate for a stable super heavy atom, unbihexium, has 126 protons and 184 neutrons.

Each particle of matter has a corresponding antimatter particle with the opposite electrical charge. Thus, the positron is a positively charged antielectron and the antiproton is a negatively charged equivalent of a proton. When a matter and corresponding antimatter particle meet, they annihilate each other. Because of this, along with an imbalance between the number of matter and antimatter particles, the latter are rare in the universe. (The first causes of this imbalance are not yet fully understood, although the baryogenesis theories may offer an explanation.) As a result, no antimatter atoms have been discovered in nature. However, in 1996, antihydrogen, the antimatter counterpart of hydrogen, was synthesized at the CERN laboratory in Geneva. Other exotic atoms have been created by replacing one of the protons, neutrons or electrons with other particles that have the same charge. For example, an electron can be replaced by a more massive muon, forming a muonic atom. These types of atoms can be used to test the fundamental predictions of physics

QUANTUM MECHANICAL BEHAVIOUR: SYSTEMAL IMPLICATIONS:

ASSUMPTIONS:

- a) QUANTUM MECHANICAL BEHAVIOURS are classified into three categories;
 - 1) Category 1 **OF QUANTUM MECHANICAL BEHAVIOUR CONCOMITANT TO QUANTUM COMPUTATION CLASSIFICATION IN CATEGORY 1**
 - 2) Category 2 (second interval) **OF QUANTUM MECHANICAL BEHAVIOUR CONCOMITANT TO QUANTUM COMPUTATION CLASSIFICATION IN CATEGORY 2**
 - 3) Category 3 **OF QUANTUM MECHANICAL BEHAVIOUR CONCOMITANT TO QUANTUM COMPUTATION CLASSIFICATION IN CATEGORY 3**

In this connection, it is to be noted that there is no sacrosanct time scale as far as the above pattern of classification is concerned. Any operationally feasible scale with an eye on the classification of **QUANTUM MECHANICAL BEHAVIOUR CONCOMITANT TO QUANTUM COMPUTATION CLASSIFICATION IN Categories 1, 2, and 3** would be in the fitness of things. For category 3. "Over and above" nomenclature could be used to encompass a wider range of CATEGORICAL CONSTITUENTS. Similarly, a "less than" scale for category 1 can be used. The speed of growth of **QUANTUM MECHANICAL BEHAVIOUR CONCOMITANT TO QUANTUM COMPUTATION CLASSIFICATION IN CATEGORY 1** proportional to the total amount of **QUANTUM MECHANICAL BEHAVIOUR CONCOMITANT TO QUANTUM COMPUTATION CLASSIFICATION IN CATEGORY 2** In essence the accentuation coefficient in the model is representative of the constant of proportionality between **QUANTUM MECHANICAL BEHAVIOUR CONCOMITANT TO QUANTUM COMPUTATION CLASSIFICATION IN CATEGORY** under category 1 and category 2. This assumptions is made to foreclose the necessity of addition of one more variable, that would render the systemic equations unsolvable

DISSIPATION OF QUANTUM MECHANICAL BEHAVIOUR:

The dissipation in all the three categories is attributable to the following two phenomenon : **Aging phenomenon:** The aging process leads to transference of the **QUANTUM MECHANICAL BEHAVIOUR CONCOMITANT TO QUANTUM COMPUTATION CLASSIFICATION IN CATEGORY 1** to the next category, **Depletion phenomenon:** Complete destruction of say quantum entanglement For detailed exposition see essay at the end.*

NOTATION :

G_{36} : **QUANTUM MECHANICAL BEHAVIOUR CONCOMITANT TO QUANTUM COMPUTATION CLASSIFICATION IN CATEGORY**

G_{37} : **OF QUANTUM MECHANICAL BEHAVIOUR CONCOMITANT TO QUANTUM COMPUTATION CLASSIFICATION IN CATEGORY 2**

G_{38} : **QUANTUM MECHANICAL BEHAVIOUR CONCOMITANT TO QUANTUM COMPUTATION CLASSIFICATION IN CATEGORY 3**

$(a_{36})^{(7)}, (a_{37})^{(7)}, (a_{38})^{(7)}$: Accentuation coefficients

$(a'_{36})^{(7)}, (a'_{37})^{(7)}, (a'_{38})^{(7)}$: Dissipation coefficients*

FORMULATION OF THE SYSTEM :

In the light of the assumptions stated in the foregoing, we infer the following:-

The growth speed in category 1 is the sum of a accentuation term $(a_{36})^{(7)}G_{37}$ and a dissipation term $-(a'_{36})^{(7)}G_{36}$, the amount of dissipation taken to be proportional to the **QUANTUM MECHANICAL BEHAVIOUR CONCOMITANT TO QUANTUM COMPUTATION CLASSIFICATION IN CATEGORY**

(a) The growth speed in category 2 is the sum of two parts $(a_{37})^{(7)}G_{36}$ and $-(a'_{37})^{(7)}G_{37}$ the inflow from the category 1 dependent on the total amount standing in that category.

The growth speed in category 3 is equivalent to $(a_{38})^{(7)}G_{37}$ and $-(a'_{38})^{(7)}G_{38}$ dissipation ascribed only to depletion phenomenon.*

*
*

$$\frac{dG_{36}}{dt} = (a_{36})^{(7)}G_{37} - (a'_{36})^{(7)}G_{36} \quad *1$$

$$\frac{dG_{37}}{dt} = (a_{37})^{(7)}G_{36} - (a'_{37})^{(7)}G_{37} \quad *2$$

$$\frac{dG_{38}}{dt} = (a_{38})^{(7)}G_{37} - (a'_{38})^{(7)}G_{38} \quad *3$$

$$(a_i)^{(7)} > 0, \quad i = 36, 37, 38 \quad *4$$

$$(a'_i)^{(7)} > 0, \quad i = 36, 37, 38 \quad *5$$

$$(a_{37})^{(7)} < (a'_{36})^{(7)} \quad *6$$

$$(a_{38})^{(7)} < (a'_{37})^{(7)} \quad *7$$

We can rewrite *

$$\frac{dG_{36}}{(a_{36})^{(7)}G_{37} - (a'_{36})^{(7)}G_{36}} = dt \quad *8$$

$$\frac{dG_{37}}{(a_{37})^{(7)}G_{36} - (a'_{37})^{(7)}G_{37}} = dt \quad *9$$

Or we write a single equation as *

$$\frac{dG_{36}}{(a_{36})^{(7)}G_{37} - (a'_{36})^{(7)}G_{36}} = \frac{dG_{37}}{(a_{37})^{(7)}G_{36} - (a'_{37})^{(7)}G_{37}} = \frac{dG_{38}}{(a_{38})^{(7)}G_{37} - (a'_{38})^{(7)}G_{38}} = dt \quad *10$$

The equality of the ratios in equation (10) remains unchanged in the event of multiplication of numerator and denominator by a constant factor.*

For constant multiples α, β, γ all positive we can write equation (10) as*

$$\frac{\alpha dG_{36}}{\alpha((a_{36})^{(7)}G_{37} - (a'_{36})^{(7)}G_{36})} = \frac{\beta dG_{37}}{\beta((a_{37})^{(7)}G_{36} - (a'_{37})^{(7)}G_{37})} = \frac{\gamma dG_{38}}{\gamma((a_{38})^{(7)}G_{37} - (a'_{38})^{(7)}G_{38})} = dt \quad *14$$

The general solution of the **SYSTEM OF QUANTUM MECHANICAL BEHAVIOUR CONCOMITANT TO QUANTUM COMPUTATION CLASSIFICATION IN CATEGORY** can be written in the form *

$\alpha_i G_i + \beta_i G_i + \gamma_i G_i = C_i e_i^{\lambda_i t}$ Where $i = 36, 37, 38$ and C_{36}, C_{37}, C_{38} are arbitrary constant coefficients.*

STABILITY ANALYSIS :

STABILITY ANALYSIS OF QUANTUM MECHANICAL SYSTEMS:

THERE ARE MANY ILLUSTRATIONS AND EXAMPLES UNDER THIS HEAD THAT CAN BE DISCUSSED WHERE THE QUANTUM ENTANGLEMENT STABILITY OR INSTABILITY PERSISTS OR NOT AND ITS WIDE RANGING AMPLITUDINAL RAMIFICATIONS THEREOF:

Quantum entanglement at Nano Scale:

More often than not, issues of Quantum Entanglement theory, quantum molecular entanglement in nano-scale, quantum coherence in delocalized bond structures and quantum entanglement in Nanoscale dot- systems are interlinked to each other. One of most peculiar properties of Quantum Physics is focused on the Entanglement that get the possibility to built up special quantum shared states based on delocalized electron's field. In fact Entanglement permits **to (e&eb)change** the degree of localization of quantum/wave particles ;in fact also during a spatial separation of pair wise electrons quantum entanglement **generate(eb) a new** partial localized conjugate-systems of bonding atoms. The entanglement activity **can (eb)evolve in** strength and in coherence of simultaneity properties of mixed delocalized states and/or in the successive decay to localized single states in function of some noises (temperature and other interferences) that **dis-entangled the stability** in the time-scale of the simultaneity co-existence of entangled states . To investigate on the properties innovation of entanglement effects good experimental information **can be (eb)obtained** looking at the **spectrum of emission induced by lasers and measured in Femto-seconds** (Femto-chemistry *). In fact this fast-method of investigation can give information observed exactly what happens at the molecular level during a chemical reaction. So that ultrafast molecular dynamics in future can permit to deeply understand **the effect(e&eb) of** entangled hybridization of electron's field (in some way similar to the metallic bond) caused by the over position of electron orbitals **create(eb) the** molecular bonding in the nano-scale dimension.

FAQ General info on journals and books Site Map Contact us

Stability of atomic clocks based (e)on entangled atoms

Under this head, many authors have shown that the stability and instability of quantum evolution are analyzed in the interaction of a two-level atom with a quantized-field mode in an ideal cavity with allowance for photon recoil, which is the basic model of cavity QED. It is shown that the Jaynes-Cammings quantum dynamics **can be unstable** in the *regime of the*

random walk of the atom in the quantized field of a standing wave in the absence of any interaction with the environment. This **instability is manifested** in large fluctuations of the quantum entropy, which correlate with a classical-chaos measure, the maximum Lyapunov exponent, and in the exponential sensitivity of the fidelity of the quantum states **of the strongly coupled** atom-field system to small variations of resonance detuning. Numerical experiments reveal the **sensitivity of the atomic population inversion to the initial conditions** and to **correlation between** the quantum and classical degrees of freedom of the atom.

Stability in atomic clocks:

Effect(e&eb) of realistic noise sources for an atomic clock consisting of a local oscillator that is actively **locked to a** spin-squeezed (entangled) ensemble of N atoms. Use of entangled states **can lead (eb) to an** improvement of the long-term stability of the clock when the measurement **is(e) limited by** decoherence associated with instability of the local oscillator combined with fluctuations in the atomic ensemble's Bloch vector. Atomic states with a moderate degree of entanglement **yield (eb) the** maximal clock stability, resulting in an improvement that scales as $N^{1/6}$ compared to the atomic shot noise level. Quantum entanglement is the basis for many of the proposed applications of quantum information science. The experimental implementation of these ideas is challenging since entangled states are easily **destroyed(e) (by** decoherence. To evaluate the potential usefulness of entanglement it is therefore essential to include a realistic description of noise in experiments of interest. Although decoherence is commonly analyzed in the context of simple models, practical sources of noise often **possess(e) a** non-trivial frequency spectrum, and enter through a variety of different physical processes. **Effect(e&eb) of** realistic decoherence processes and noise sources in an atomic clock that is actively **locked(e&eb) to a** spin-squeezed (entangled) ensemble of atoms. The performance of an atomic clock can be characterized by **its frequency accuracy and stability**. Accuracy refers to the frequency offset from the ideal value, whereas stability **describes** the fluctuations around, and drift away from the average frequency. To improve the **long-term clock stability**, it has been suggested **to (e)use** entangled atomic ensembles, in the **presence of** realistic decoherence and noise. In practice, an atomic clock operates **by (e&eb)locking the** frequency of a local oscillator (L.O.) **to the** transition frequency between two levels in an atom. This locking is achieved by a spectroscopic measurement determining the L.O. frequency offset $\delta\omega$ from the atomic resonance, followed by a feedback Mechanism which steers the L.O. frequency so as to null the mean frequency offset. The problem of frequency control thus **combines** elements of **quantum parameter estimation theory** and **control of stochastic systems via feedback**. The spectroscopic measurement of the atomic transition frequency is typically **achieved** through Ramsey spectroscopy, in which the atoms are illuminated by two short, near-resonant pulses from the local oscillator, **separated by a** long period of free evolution, referred to as the Ramsey time T . During the free evolution the atomic state and the L.O. acquire a relative phase difference $\delta\phi = \delta\omega T$, which is subsequently **determined** by a projection measurement. If a long time T is used, then Ramsey spectroscopy provides a very sensitive measurement of the L.O. frequency offset $\delta\omega$. Situation IS relevant to trapped particles, such as atoms in an optical lattice or trapped ions. In this situation, the optimal value of T **is(eb) determined by** atomic decoherence (**caused by** imperfections in the experimental setup) which **therefore(eb) determines the** ultimate performance of the clock. Using a simple noise model it was shown that entanglement **provides(eb) little gain** in spectroscopic sensitivity in the presence of atomic decoherence. In essence, random fluctuations in the phase of the atomic coherence **cause(eb) a** rapid smearing of the error contour. In practice, the Stability of atomic clocks is often **limited(e) primarily by** fluctuations of the L.O. Atomic dephasing **and(e) the use of** entangled states **can (eb)lead to a** significant improvement in clocks. Pracy, Disclaimer, Terms & Conditions, and Copyright Inf

Large scale effective Theory for cosmological bounces(See for details Martin Bojowald)*

An exactly solvable bounce model in loop quantum cosmology is identified which serves as a perturbative basis for realistic bounce scenarios. Its bouncing solutions are derived analytically, demonstrating why recent numerical simulations **robustly led to** smooth bounces under the assumption **of semi classicality**. Several **effects(e&eb)**, easily **included in a** perturbative analysis, can **however(e&eb) change this** smoothness. The effective theory is not only applicable to such situations where a numerical technique become highly involved but also allows one to discuss conceptual issues. For instance, consequences of the notoriously difficult physical inner product can be implemented at the effective level. This indicates that even physical predictions from full quantum gravity **can be (e)obtained from** perturbative effective equations.

Using Lagrange–Poincare stability analysis and some catastrophe theory classification of singularities, we analyze the two-slit experiments of quantum physics. It is shown that assuming micro-spacetime to be a **Fuzzy Kähler-like manifold $K(\epsilon^{(c)})$** with an **inbuilt** wave–particle duality, **one of the two slits is always(e&eb) unstable**. Consequently, the faintest interference **with the experiment** is sufficient to **break the** symmetry of “equilibrium” and **leads (eb) to what is perceived** on the other side of the quantum-classical interface as a wave collapse.

Black strings and p-branes are (e&eb) unstable (Ruth Gregory)

Investigation is on the evolution of small perturbations around black strings and branes which are low energy solutions of string theory. For simplicity we focus attention on the zero charge case and show that there are unstable modes for a range of time frequency and wavelength in the extra $10-D$ dimensions. These perturbations can be stabilized if the extra dimensions are compactified to a scale smaller than the minimum wavelength for which instability occurs and thus will not affect large astrophysical black holes in four dimensions. We comment on the implications of this result for the cosmic censorship hypothesis.

*

Supposing $G_i(0) = G_i^0(0) > 0$, and denoting by λ_i the characteristic roots of the system, it easily results that

1. If $(a'_{36})^{(7)}(a'_{37})^{(7)} - (a_{36})^{(7)}(a_{37})^{(7)} > 0$ all the components of the solution, i.e all the three parts of the **OF QUANTUM MECHANICAL BEHAVIOUR CONCOMITANT TO QUANTUM COMPUTATION CLASSIFICATION IN CATEGORY 1** tend to zero, and the solution is stable with respect to the initial data.

2. If $(a'_{36})^{(7)}(a'_{37})^{(7)} - (a_{36})^{(7)}(a_{37})^{(7)} < 0$ and $(\lambda_{37} + (a'_{36})^{(7)})G_{36}^0 - (a_{36})^{(7)}G_{37}^0 \neq 0, (\lambda_{37} < 0)$, the first two components of the solution tend to infinity as $t \rightarrow \infty$, and $G_{38} \rightarrow 0$, i.e. The category 1 and category 2 parts grows to infinity, whereas the third part category 3 tends to zero.

3. If $(a'_{36})^{(7)}(a'_{37})^{(7)} - (a_{36})^{(7)}(a_{37})^{(7)} < 0$ and $(\lambda_{37} + (a'_{36})^{(7)})G_{36}^0 - (a_{36})^{(7)}G_{37}^0 = 0$ Then all the three parts tend to zero, but the solution is not stable i.e. at a small variation of the initial values of G_i , the corresponding solution tends to infinity.*

*

From the above stability analysis we infer the following:

1.The adjustment process is stable in the sense that the system converges to equilibrium.2.The approach to equilibrium is a steady one, and there exists progressively diminishing oscillations around the equilibrium point3.Conditions 1 and 2 are independent of the size and direction of initial disturbance7.The actual shape of the time path system is determined by efficiency parameter, the strength of the response of the portfolio in question, and the initial disturbance5.Result 3 warns us that we need to make an exhaustive study of the behavior of any case in which generalization derived from the model do not hold6.Growth studies as the one in the extant context are related to the systemic growth paths with full employment of resources that are available in question,

Traveling wave analysis of semiconductor lasers: modulation responses, mode stability and quantum mechanical treatment of noise spectra is an example of the system in which stability analysis could be conducted. A traveling wave analysis of a general class of semiconductor lasers, which includes multisession DFB/DBR lasers and gain-coupled DFB lasers. The analysis leads to new semi analytic expressions for the small-signal IM and FM modulation responses, the intensity and FM noise spectra, and the line width. The expressions are given in terms of solutions to four coupled linear homogeneous differential equations and can easily be evaluated numerically. Derivation of a stability parameter σ , for which $\sigma < 0$ indicates that the model is unstable with respect to small-scale fluctuations. The noise spectra are derived from semiclassical calculations as well as from calculations based on quantized fields, and there are limitations of the semiclassical approach. The formalism of the quantum mechanical treatment has a built-in relationship between the relative intensity noise and the noise of the injection current. This relationship is discussed and illustrated by numerical examples by various authors extensively in literature.

Carlton M. Caves and G. J. Milburn have studied Quantum-mechanical model for continuous position measurements, which is another example of the Quantum Mechanical Behaviour and Dissipation where Stability Analysis could be carried out..They present an idealized model for a sequence of position measurements, and then take an appropriate limit in which the measurements become continuous. The measurements lead to fluctuations without systematic dissipation, and they rapidly destroy off-diagonal terms in the position basis; thus the pointer basis is position. A modification of the model incorporates systematic dissipation via a feedback mechanism; in the modified model there is no decay of off-diagonal coherence in the position basis.

Igamberdiev A.U. is another author who has studied the Prigogine's dissipative structures and has analyzed the stability processes thereof. In Quantum mechanical properties of biosystems: A framework for complexity, structural stability, and transformations is provided by the author. Internal quantum non-demolition measurements are inherent for biological organization and determine the essential features of living systems. Low energy dissipation in these measurements provided by slow conformational relaxation of biomacromolecular complexes (regarded as measuring devices) is the main precondition of enzyme operation and information transfer determining the steady non-equilibrium state of biosystems. The presence of an internal formal description inside a biosystems, expressed in genetic structures (developmental program), is a consequence of its quantum properties. Incompleteness of this formal description provides the possibility of the generation of new functional relations and interconnections inside the system. This is a logical precondition of an evolutionary process. The quantum mechanical uncertainty that underlies the appearance of bifurcations is considered to be the main physical foundation of complication and irreversible transformation of biosystems. It provides a framework for temporal and spatial characteristics of the biosystems. The logic of such a framework derives from Aristotle, as in his philosophy we find the analysis of fundamental irreversibility and self determination of the living processes.

Quantum properties of biosystems structures was studied by, Pattee (1968) and Rosen (1977) concluded that its logic should reveal an internal resemblance to the logic of quantum mechanical measurement, in which a non-formal process of mapping physical events into symbols takes place. Biological molecular complexes are operational structures put in correspondence

with other molecules and processes. These considerations give a theoretical framework for a description of the complexity, **structural stability and transformations of living systems**. Quantum measurement is connected with low energy dissipation in the case where the relaxation period of a macroscopic oscillator (t^*) is many times larger than the time interval of measurement (t'). Minimal energy dissipation in quantum measurement is calculated. *

QUANTUM COMPUTER:

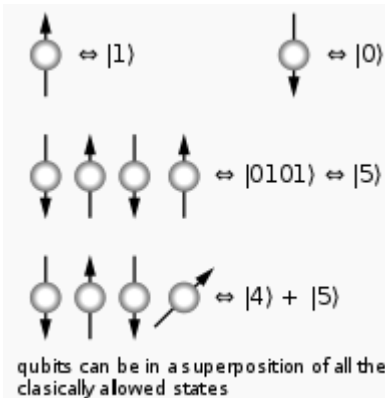
Quantum computer is a device for computation that makes **direct use of** quantum mechanical phenomena, such as **superposition and entanglement**, to perform operations on data. Quantum computers are different from digital computers based on transistors. Whereas digital computers require data to be encoded into binary digits (bits), quantum computation **utilizes** quantum properties to represent data and perform operations on these data. A theoretical model is the **Quantum Turing machine**, also known as the universal quantum computer. Quantum computers share theoretical similarities with non-deterministic and probabilistic computers, like the ability to be in more than one state simultaneously. The field of quantum computing was first introduced by Richard Feynman in 1982.

Although quantum computing is still in its infancy, experiments have been carried out in which quantum computational operations were executed on a very small number of qubits (quantum bits). Both practical and theoretical research continues, and many national government and military funding agencies support quantum computing research to develop quantum computers for both civilian and national security purposes, such as cryptanalysis.

Large-scale quantum computers could be able to solve certain problems much faster than any classical computer by using the best currently known algorithms, like integer factorization using Shor's algorithm or the simulation of quantum many-body systems. There exist quantum algorithms, such as Simon's algorithm, which run faster than any possible probabilistic classical algorithm. Given unlimited resources, a classical computer can simulate an arbitrary quantum algorithm so quantum **computation does not violate** the Church. However, in practice infinite resources are never available and the computational basis of 500 qubits, for example, would already be too large to be represented on a classical computer because it would require 2^{500} complex values to be stored. (For comparison, a terabyte of digital information stores only 2^{43} discrete on/off values) Nielsen and Chuang point out that "Trying to store all these complex numbers would not be possible on any conceivable classical computer."

Bits vs. qubits

A quantum computer with a given number of qubits is fundamentally different from a classical computer composed of the same number of classical bits. For example, to represent the state of an n -qubit system on a classical computer would require the storage of 2^n complex coefficients. Although this fact may seem to indicate that qubits **can hold** exponentially more information than their classical counterparts, care must be taken not to **overlook the fact** that the qubits are only in a probabilistic **superposition of all** of their states. This means that when the final state of the qubits is measured, they will only be found in one of the possible configurations they were in before measurement. Moreover, it is incorrect to think of the qubits as only being in one particular state before measurement since the fact that they were in **a superposition** of states before the measurement was made directly affects the possible outcomes of the computation.



Qubits are made up of controlled particles and the means of control (e.g. devices that trap particles and switch them from one state to another) For example: Consider first a classical computer that operates on a three-bit register. The state of the computer at any time is a probability distribution over the $2^3 = 8$ different three-bit strings 000, 001, 010, 011, 100, 101, 110, 111. If it is a deterministic computer, then it is in exactly one of these states with probability 1. However, if it is a probabilistic computer, then there is a possibility of it being in any *one* of a number of different states. We can **describe this** probabilistic state by eight nonnegative numbers A, B, C, D, E, F, G, H (where A = probability computer is in state 000, B = probability computer is in state 001, etc.). There is **a restriction** that these probabilities sum to 1.

The state of a three-qubit quantum computer is similarly described by an eight-dimensional vector (a, b, c, d, e, f, g, h) , called a **ket**. However, instead of adding to one, the sum of the *squares* of the coefficient magnitudes, $|a|^2 + |b|^2 + \dots + |h|^2$, must equal one. Moreover, the coefficients are complex numbers. Since the probability amplitudes of the states are represented with complex numbers, the phase between any two states is a meaningful parameter, which is a key difference between quantum computing and probabilistic classical computing.^[8]

If you measure the three qubits, you will observe a three-bit string. The probability of measuring a given string is the squared magnitude of that string's coefficient (i.e., the probability of measuring 000 = $|a|^2$, the probability of measuring 001 = $|b|^2$, etc.). Thus, measuring a quantum state described by complex coefficients (a, b, \dots, h) gives the classical probability distribution ($|a|^2, |b|^2, \dots, |h|^2$) and we say that the quantum state "**collapses**" to a classical state **as a result of making** the measurement.

Note that an eight-dimensional vector can be specified in many different ways depending on what basis is chosen for the space. The basis of bit strings (e.g., 000, 001, and 111) is known as the computational basis. Other possible bases are unit-length, orthogonal vectors and the eigenvectors of the Pauli-x operator. **Ket notation** is often used to make the choice of basis explicit. For example, the state (a, b, c, d, e, f, g, h) in the computational basis can be written as:

$$a|000\rangle + b|001\rangle + c|010\rangle + d|011\rangle + e|100\rangle + f|101\rangle + g|110\rangle + h|111\rangle$$

where, e.g., $|010\rangle = (0, 0, 1, 0, 0, 0, 0, 0)$

Assumptions:

Category 1 **QUANTUM COMPUTER(INFORMATION) CORRESPONDING TO THE QUANTUM MECHANICAL BEHAVIOUR STRATIFIED IN THE CORRESPONDING CATEGORY1**

Category 2 **QUANTUM COMPUTER(INFORMATION) CORRESPONDING TO THE QUANTUM MECHANICAL BEHAVIOUR STRATIFIED IN THE CORRESPONDING CATEGORY 2**

Category 3 **QUANTUM COMPUTER(INFORMATION) CORRESPONDING TO THE QUANTUM MECHANICAL BEHAVIOUR STRATIFIED IN THE CORRESPONDING CATEGORY 3***

The speed of growth of **QUANTUM COMPUTER (INFORMATION) CORRESPONDING TO THE QUANTUM MECHANICAL BEHAVIOUR STRATIFIED IN THE CORRESPONDING CATEGORY** is a linear function of the in category 2 at the time of reckoning. As before the accentuation coefficient that characterizes the speed of growth in category 1 is the proportionality factor between balance in category 1 and category 2. The dissipation coefficient in the growth model is attributable to two factors passage of time and DETRITION DUE TO Quantum Information (For examples please see Hawking Radiation essays and others at the end written in the form of epilogue to substantiate the factors that are used in the paper. Nevertheless, one instantaneous example that comes to mind is the following:

Quantum engineering via dissipation is an example of dissipation of Quantum Information. Due to the ongoing miniaturization of devices, one of the central challenges of the 21st century's technology will be to handle **quantum effects** at the Nanoscale. A first fundamental paradigm shift happened in the mid '90s when it was realized that quantum effects, which from the traditional point of view put fundamental limits on the possible miniaturization, could be exploited to do information theoretic tasks impossible with classical devices. The main obstacle in building such quantum devices however is the **occurrence of** decoherence, by which coherence within the quantum device gets **degraded due** to the **coupling with** the environment. In second proposal, a second paradigm shift was resorted to, by demonstrating that one can actually **take advantage of** decoherence if engineered in a smart way. The central focus will be the study of quantum processes driven by **dissipation**, and investigations whether quantum coherence and the associated applications can actually be **driven(eb) by** decoherence. The main tools that we plan to use to achieve that goal **originate from** the theory of quantum entanglement. The timing of this innovative project is actually perfect as the field of entanglement theory is just mature enough to pursue the ambitious goals stated in this proposal.

The main objectives of this proposal are:

(1)To set up a rigorous mathematical framework for studying fixed points and convergence rates of dissipative processes;(2)To investigate how highly entangled quantum states arising in strongly correlated quantum systems or in a quantum information theoretic context can be created by dissipative processes;(3)To study quantum devices powered by dissipation such as quantum memories and quantum Metropolis devices;(4)To use such devices to come up with novel ways for implementing quantum computation in the presence of decoherence(Decoherence dissipates Quantum entanglement)(5)To study non-equilibrium phase transitions driven by dissipation and associated to that new possible phases of matter.

J. Hassel, H. Seppa, P. Helisto studied the RSFQ devices with selective dissipation for quantum information processing. They study the possibility to use frequency dependent damping in RSFQ circuits as means to **reduce** dissipation and **consequent** decoherence in RSFQ/qubit circuits. They also show that stable RSFQ operation can be achieved **by shunting** the **Josephson junctions** with an $\text{\$R\$}$ circuit instead of a plain resistor. A presentation of derived criteria for the stability of such an arrangement, and discuss the **effect** on decoherence and the optimization issues. We also design a simple flux generator aimed at manipulating flux qubits.

Robust edge states and non-Abelian excitations are another example of the Dissipation of Quantum information that occurs in systems be it natural or human made ,The trademark of topological states of matter, with promising applications such as 'topologically protected' quantum memory and computing. So far, topological phases have been exclusively discussed in a Hamiltonian context. Here we show that such phases and the associated topological protection and phenomena also emerge in open quantum systems with engineered dissipation. The specific system studied here is a quantum wire of spinless atomic fermions in an optical lattice coupled to a bath. The key feature of the dissipative dynamics described by a Lindblad master equation is the existence of Majorana edge modes, representing a non-local decoherence-free subspace. The isolation of the

edge states is enforced by a dissipative gap in the p -wave paired bulk of the wire. We describe dissipative non-Abelian braiding operations within the Majorana subspace, and illustrate the insensitivity to imperfections. Topological protection is granted by a non-trivial winding number of the system density matrix

In the following we discuss some salient points and cardinal aspects of the Quantum Dissipation which is an important phenomenon in Quantum Computers:

Motivation

The goal of *dissipative quantum mechanics* or 'quantum dissipation theory' is to formulate microscopic theories of irreversible behaviour of quantum systems. Simply speaking, one would like to understand processes like, e.g., *friction* or 'damping' on a microscopic level. This requires at least two things: 'friction' means that physical objects interact with each other, i.e., we need to talk about interactions. Furthermore, this occurs as a function of time for systems which are usually out of equilibrium, i.e., we need to talk about dynamics.

A further, more ambitious goal is to better understand the relation between microscopic and macroscopic theories, e.g., the relation between mechanics (classical or quantum) and statistical mechanics (again classical or quantum).

Already in classical (Newtonian) mechanics, the description of irreversible behaviour is a non-trivial problem. One can often introduce dissipation into microscopic equations by adding phenomenological terms, such as the velocity-dependent

damping term $\gamma \dot{x}(t)$ ($\gamma > 0$) in the damped (forced) harmonic oscillator,

$$\ddot{x}(t) + \gamma \dot{x}(t) + \omega^2 x(t) = f(t).$$

1)

In this example, one of the goals would be to derive this equation and to actually calculate γ from an underlying microscopic theory.

Other examples (some of these are very tough, some not so tough problems):

- What is the spontaneous photon emission rate of an atom in vacuum?
- What is the electrical resistance of a (small or large) piece of metal at very low temperatures?
- How does a Laser work?
- What is the typical time after which a given realisation of a qubit (a quantum two-level system as realised in, e.g., a linear ion trap, the charge or magnetic flux in superconducting junctions, the electron charge or spin in semiconductor quantum dots, the nuclear spin etc.) fails to operate in the desired manner?

Origin of Dissipation, System-Bath Theories

The most successful approach to quantum dissipation has been the use of *System-Bath Theories*, which will be the main topic of this chapter. The main idea is the following:

STEP 1: we divide the 'world' into two parts: a) the part we are really interested in (for example, all the conduction band electrons in a piece of metal), and b) the part we are not so much interested in (for example, all the rest of the metal). This splitting obviously is a choice that depends on what we want to describe/calculate

STEP 2: Call these two parts 'system' and 'reservoir', identify the interaction between system and reservoir, and then derive an effective theory for the Example

Single oscillator ('system') with angular frequency ω_0 , mass M , position x , coupled to $N \gg 1$ oscillators ('reservoir') with angular frequencies ω_i , masses m_i , position x_i , coupling of the form $c_i x_i x$ via position coordinates.

The coupling leads to an effective dynamics of the system oscillator governed by the sum of many eigenmodes with eigenfrequencies. This sum is determined by the coupling constants c_i . For finite N , this is just a problem of coupled

oscillators, and the motion of the system oscillator must therefore be periodic with a (large) period T . The time T after which the entire system returns back to its initial starting point is called *Poincaré* time.

$$t \ll T \quad p$$

The key point now is: 1. For times $t \ll T$, the effective dynamics of the system (x and p of the system oscillator) very much resembles the dynamics we would expect from a *damped* system: a sum of many oscillatory terms with 'nearly

$$t \ll T$$

random' coefficients decays as a function of time t . 2. In most known cases, T is very, very large ('larger than the age of the universe'). This means that one can safely neglect the periodic 'Poincaré return' of the system.

Formal Splitting

The basic idea in microscopic theories of dissipation is a decomposition of a total system into a system S and a reservoir part R or B , 'bath'. The (Hamiltonian) dynamics of the total system is reversible, but the dynamics of the system S is

$$t \ll T$$

effectively not reversible for times $t \ll T$.

In this lecture, we formulate these ideas for quantum systems. The Hilbert space of the total system is defined by the tensor product

$$\mathcal{H}_{\text{total}} = \mathcal{H}_S \otimes \mathcal{H}_B. \quad \text{***}(2)$$

The Hamiltonian of the total system is defined as

$$H_{\text{total}} \equiv H \equiv H_S + H_{SB} + H_B \quad \text{***}(3)$$

Here and in the following, we will mostly discuss *time-independent* Hamiltonians. Time-dependent

$$H = H(t)$$

Hamiltonians can be treated

Overview

1. 'Simple' Systems with *few* degrees of freedom: typically quantum optics systems, atoms, few-level systems, cavity modes.

- Weak coupling approximation: Master Equation (Born and Markov Approximation)
- Damped harmonic oscillator.
- Solution methods: phase-space methods (P -representation etc.).
- Solution methods: quantum trajectories.
- Correlation Functions, Quantum Regression Theorem.
- Beyond weak coupling approximation: Feynman-Vernon influence functional (path integral) theories; R. P. Feynman, F. L. Vernon, Ann. Phys. (N.Y.) **24**, 118 (1963). Non-exponential decay laws at low temperatures.
- Exact solution of damped harmonic oscillator.
- Spin-Boson Problem, Two-Level System.
- Non-Markovian versus Markovian, Lindblad versus non-Lindblad.
- 'Non-standard' methods.

2. Systems with *many* degrees of freedom: typically condensed matter systems, electrons + phonons (particle statistics).

- Quasiclassical kinetic theories, Boltzmann equation.
- Quantum Many-Body Non-Equilibrium Methods. (Keldysh) Greens Function Methods, quantum Boltzmann equation.

In this chapter, we will concentrate on 1. ('Simple' Systems with *few* degrees of freedom). Also, not discussed in detail in this lecture are

- Nakajima-Zwanzig theories, Mori projection operator theories. These give a more formal approach towards system-bath theories.
- 'Early approaches' such as Wigner-Weisskopf theory of spontaneous emission.
- ...

Generally speaking, quantum dissipation can be regarded as a subfield of non-equilibrium quantum statistics/ non-equilibrium many-body theory. d as well but require additional techniques (e.g., Floquet theory for period time-dependence; adiabatic theorems for slow time-dependence).

Interaction Picture

We define an interaction picture by writing

$$H \equiv H_0 + V, \quad H_0 \equiv H_S + H_B, \quad V \equiv H_{SB} \tag{4}$$

with the Hamiltonian H_0 describing the time evolution of the uncoupled system and bath, and the perturbation V describing the interaction H_{SB} .

We define $\chi(t)$ as the total density matrix (system + bath) which obeys the Liouville-von-Neumann equation ,

$$\frac{d}{dt}\chi(t) = -i[H, \chi(t)] \rightsquigarrow \chi(t) = e^{-iHt}\chi(t=0)e^{iHt}, \tag{5}$$

where we start with the initial condition $\chi(t=0)$ at time $t=0$. In the interaction picture,

$$\tilde{\chi}(t) \equiv e^{iH_0t}\chi(t)e^{-iH_0t} \tag{6}$$

$$\tilde{A}(t) \equiv e^{iH_0t}Ae^{-iH_0t}. \tag{7}$$

The equation of motion for the density operator in the interaction picture becomes

$$\begin{aligned} \frac{d}{dt}\tilde{\chi}(t) &= i[H_0, \tilde{\chi}(t)] + e^{iH_0t}\frac{d}{dt}\chi(t)e^{-iH_0t} \\ &= i[H_0, \tilde{\chi}(t)] - ie^{iH_0t}[H, \chi(t)]e^{-iH_0t} \\ &= i[H_0, \tilde{\chi}(t)] - ie^{iH_0t}[H_0 + V, \chi(t)]e^{-iH_0t} \\ &= i[H_0, \tilde{\chi}(t)] - i[H_0 + \tilde{V}(t), \tilde{\chi}(t)] \\ &= -i[\tilde{V}(t), \tilde{\chi}(t)]. \end{aligned} \tag{8}$$

In integral form, this can be written as

$$\tilde{\chi}(t) = \chi(t=0) - i \int_0^t dt' [\tilde{V}(t'), \tilde{\chi}(t')] \tag{9}$$

which we insert into Eq. (7.8) to obtain

$$\frac{d}{dt} \tilde{\chi}(t) = -i [\tilde{V}(t), \chi(t=0)] - \int_0^t dt' [\tilde{V}(t), [\tilde{V}(t'), \tilde{\chi}(t')]] \tag{10}$$

Up t Effective Density Matrix of the System

$t > 0$

We wish to obtain an equation of motion for the *effective density matrix of the system* at time

$$\rho(t) \equiv \text{Tr}_B [\chi(t)] \tag{11}$$

This object is sufficient to calculate expectation values of *system operators* A_S :

$$\begin{aligned} \langle A_S \rangle_t &\equiv \text{Tr}_{\text{total}} [\chi(t) A_S] \\ &= \text{Tr}_S [\text{Tr}_B \chi(t)] A_S = \text{Tr}_S [\rho(t) A_S] \end{aligned} \tag{12}$$

Now use

$$\begin{aligned} \text{Tr}_B [\tilde{\chi}(t)] &= \text{Tr}_B e^{iH_0 t} \chi(t) e^{-iH_0 t} \\ &= e^{iH_S t} (\text{Tr}_B e^{iH_B t} \chi(t) e^{-iH_B t}) e^{-iH_S t} = e^{iH_S t} \rho(t) e^{-iH_S t} \\ &\equiv \tilde{\rho}(t) \end{aligned} \tag{13}$$

Note that the interaction picture $\rho(t) \leftrightarrow \tilde{\rho}(t)$ involves only the free *System Hamiltonian* H_S and not H_0 ,

$$\tilde{\rho}(t) \equiv e^{iH_S t} \rho(t) e^{-iH_S t} \tag{14}$$

Using

$$\tilde{A}_S(t) \equiv e^{iH_0 t} A_S e^{-iH_0 t} = e^{iH_S t} A_S e^{-iH_S t} \tag{15}$$

for system operators, one has

$$\langle A_S \rangle_t = \text{Tr}_S [\tilde{\rho}(t) \tilde{A}_S(t)] = \text{Tr}_S [\rho(t) A_S(t)] \tag{16}$$

Assumption (factorising initial condition):

$$\chi(t=0) = R_0 \otimes \rho(t=0) \tag{18}$$

$$R_0 \equiv \text{Tr}_S[\chi(t=0)], \quad \rho(t=0) \equiv \text{Tr}_B[\chi(t=0)].$$

This *factorisation assumption* is key to most of the results that follow. Its validity has been discussed and criticised in the past (see Weiss book for further references). Some of the issues are:

- Does the factorisation assumption only affect transient or also the long-time behaviour of the density matrix?
- Are there exactly solvable models where these issues can be clarified?

A theoretical formulation of time-evolution for arbitrary initial condition is sometimes possible: 'preparation function' (exact solution of dissipative quantum oscillator; Grabert, Ingold et al); generalisation of many-body Keldysh GF (three-by-three matrix instead of two-by-two matrix, M. Wagner).

Born Approximation

In the interaction picture,

$$\tilde{\chi}(t') = R_0 \otimes \tilde{\rho}(t=0) \text{ to zeroth order in } V. \tag{19}$$

The Born approximation in the equation of motion Eq.(7.17) consists in

$$\tilde{\chi}(t') \approx R_0 \otimes \tilde{\rho}(t') \tag{20}$$

Born approximation

This means one assumes that for all times $t' > 0$, the total density matrix remains a product of the initial bath density matrix R_0 and the system density matrix $\tilde{\rho}(t')$. Intuitively, one argues that this is justified when the bath is 'very large' and the coupling H_{SB} 'weak', so that the back-action of the system onto the bath can be neglected. In practice, one usually assumes a thermal equilibrium for the bath,

$$R_0 = \frac{e^{-\beta H_B}}{\text{Tr} e^{-\beta H_B}}, \tag{21}$$

thermal equilibrium bath,

where $\beta = 1/k_B T$ with T the bath equilibrium temperature.

Remark: A more detailed analysis of the Born approximation and alternative approximations can be done within the framework of the *Projection Operator formalism*.

Within the Born approximation, with Eq. (7.20), (7.18), and (7.17), one obtains a *closed integro-differential equation* for the reduced density operator $\tilde{\rho}(t)$ of the system in the interaction picture,

$$\frac{d}{dt} \tilde{\rho}(t) = -i \text{Tr}_B [\tilde{V}(t), R_0 \otimes \tilde{\rho}(t=0)] - \int_0^t dt' \text{Tr}_B [\tilde{V}(t), [\tilde{V}(t'), R_0 \otimes \tilde{\rho}(t')]].$$

*** (22)

Remark: Eq.(7.22) is exact up to second order in the perturbation V : set $\tilde{\rho}(t') = \rho(0)$ on the r.h.s. of Eq.(7.22).

Since $\tilde{\rho}(t')$ in the double commutator on the r.h.s. of Eq.(7.22) depends on V , Eq.(7.22) is to infinite order in V though not exact. Diagrammatically this corresponds to a summation of an infinite series of diagrams. It is non-trivial to make this statement more precise, but roughly speaking these diagrams contain certain vertex corrections as can be seen from the fact that $\rho(t)$ is a density matrix and not a wave function.

Motivation: telegraphic fluorescence (driven spontaneous emission) of single atoms

Example single V-systems: two upper levels 1 (fast spontaneous emission) and 2 (slow spontaneous emission), one lower level 0 driven by two lasers. Transition $0 \rightarrow 2$ traps the system in 2 for a long time. Resonance fluorescence intensity $I(t)$ therefore exhibits jumps: 'telegraphic fluorescence' with random switching between bright and dark periods. Aim: calculate distribution of dark periods.

Length T_D of dark period can be simply calculated from the density matrix element ρ_{22}

$$T_D^{-1} = \dot{\rho}_{22}(t=0), \quad \rho_{22} = 0, \quad \text{*(138)}$$

where the derivative is calculated from the underlying equation of motion (Master equation). However, the calculation of other, more complicated quantities related to the description of telegraphic fluorescence turns out to be technically complicated within the Master equation formalism. Example: 'exclusive probability' $P_0(t)$ that, after an emission at time $t = 0$, no other photon has been emitted in the time interval $[0, t]$.

- Some people raise 'objections' against the traditional Master equation approach: the density operator describes *ensembles* of quantum systems and is therefore inappropriate to describe *single* quantum systems such as a single ion in an ion trap. However, these objections are unjustified; as long as one sticks with the probabilistic interpretation of Quantum Mechanics, the density operator description is perfectly valid for a *single* quantum system.
- 'Single quantum systems' can not only be realised in ion traps, but also in 'artificial atoms' and 'artificial molecules' (solid state based quantum dots, superconducting charge or flux qubits). These will be discussed in a later chapter.

*
NOTATION :
 T_{36} : QUANTUM COMPUTER(INFORMATION) CORRESPONDING TO THE QUANTUM MECHANICAL BEHAVIOUR STRATIFIED IN THE CORRESPONDING CATEGORY 1
 T_{37} : QUANTUM COMPUTER(INFORMATION) CORRESPONDING TO THE QUANTUM MECHANICAL BEHAVIOUR STRATIFIED IN THE CORRESPONDING CATEGORY2
 T_{38} : QUANTUM COMPUTER (INFORMATION) CORRESPONDING TO THE QUANTUM MECHANICAL BEHAVIOUR STRATIFIED IN THE CORRESPONDING CATEGORY, namely category 3.
 $(b_{36})^{(7)}, (b_{37})^{(7)}, (b_{38})^{(7)}$: Accentuation coefficients
 $(b'_{36})^{(7)}, (b'_{37})^{(7)}, (b'_{38})^{(7)}$: Dissipation coefficients*

FORMULATION OF THE SYSTEM :FOR DETAILED EXPLANATION OF THE LOSS OF QUANTUM INFORMATION AND THE CASES AND CONDITIONALITIES UNDER WHICH IT OCCURS PLEASE SEE THE INTRODUCTORY NOTE AS WELL AS THE EPILOGUE WHEREIN IS EXPOSITION OF SUCH CASE ID GIVEN IN DETAIL

Under the above assumptions, we derive the following :

a) The growth speed in category 1 is the sum of two parts:

A term $+(b_{36})^{(7)}T_{37}$ proportional to the **QUANTUM COMPUTER(INFORMATION) CORRESPONDING TO THE QUANTUM MECHANICAL BEHAVIOUR STRATIFIED IN THE CORRESPONDING CATEGORY in category 2**

A term $-(b'_{36})^{(7)}T_{36}$ representing the quantum of balance dissipated from category 1 .

1. The growth speed in category 2 is the sum of two parts:

A term $+(b_{37})^{(7)}T_{36}$ constitutive of the amount of inflow from the category 1 of **QUANTUM COMPUTER(INFORMATION) CORRESPONDING TO THE QUANTUM MECHANICAL BEHAVIOUR STRATIFIED IN THE CORRESPONDING CATEGORY**

A term $-(b'_{37})^{(7)}T_{37}$ the dissipation factor of **QUANTUM COMPUTER(INFORMATION) CORRESPONDING TO THE QUANTUM MECHANICAL BEHAVIOUR STRATIFIED IN THE CORRESPONDING CATEGORY**

*
*

GOVERNING EQUATIONS: QUANTUM COMPUTER(INFORMATION)

Following are the differential equations that govern the growth in the terrestrial organisms portfolio*

$$\frac{dT_{36}}{dt} = (b_{36})^{(7)}T_{37} - (b'_{36})^{(7)}T_{36} \quad *12$$

$$\frac{dT_{37}}{dt} = (b_{37})^{(7)}T_{36} - (b'_{37})^{(7)}T_{37} \quad *13$$

$$\frac{dT_{38}}{dt} = (b_{38})^{(7)}T_{37} - (b'_{38})^{(7)}T_{38} \quad *14$$

$$(b_i)^{(7)} > 0, \quad i = 36, 37, 38 \quad *15$$

$$(b'_i)^{(7)} > 0, \quad i = 36, 37, 38 \quad *16$$

$$(b_{37})^{(7)} < (b'_{36})^{(7)} \quad *17$$

$$(b_{38})^{(7)} < (b'_{37})^{(7)} \quad *18$$

Following the same procedure outlined in the previous section , the general solution of the governing equations is

$\alpha'_i T_i + \beta'_i T_j + \gamma'_i T_i = C'_i e_i^{\lambda' i t}$, $i = 36, 37, 38$ where $C'_{36}, C'_{37}, C'_{38}$ are arbitrary constant coefficients and $\alpha_{36}, \alpha_{37}, \alpha_{38}, \gamma_{36}, \gamma_{37}, \gamma_{38}$ corresponding multipliers to the characteristic roots of the System

*

QUANTUM COMPUTER AND QUANTUM MECHANICAL BEHAVIOUR- A DUAL SYSTEM ANALYSIS

Various present and future specialized applications of magnets require monodisperse, small magnetic particles, and the discovery of molecules that can function as Nanoscale magnets was an important development in this regard^{1,2,3}. These molecules act as single-domain magnetic particles that, below their blocking temperature, exhibit magnetization hysteresis, a classical property of macroscopic magnets. Such 'single-molecule magnets' (SMMs)⁴ straddle the interface between classical and quantum mechanical behaviour because they also display quantum tunnelling of magnetization^{5,6} and quantum phase interference⁷. Quantum tunnelling of magnetization can be advantageous for some potential applications of SMMs, for example, in providing the quantum superposition of states required for quantum computing⁸. However, it is a disadvantage in other applications, such as information storage, where it would lead to information loss. Thus it is important to both understand and control the quantum properties of SMMs. Here we report a supramolecular SMM dimer in which antiferromagnetic coupling between the two components results in quantum behaviour different from that of the individual SMMs. Our experimental observations and theoretical analysis suggest a means of tuning the quantum tunnelling of magnetization in SMMs. This system may also prove useful for studying quantum tunnelling of relevance to mesoscopic antiferromagnets.

he Possibilities of Quantum Computing

The special properties of qubits will allow quantum computers to work on millions of computations at once, while desktop PCs can typically handle minimal simultaneous computations. For example, a single 250-qubit state contains more bits of information than there are atoms in the universe.

These properties will have wide-spread implications foremost for the field of data encryption where quantum computers could factor very large numbers like those used to decode and encode sensitive information.

"The quantum computing work we are doing shows it is no longer just a brute force physics experiment. It's time to start creating systems based on this science that will take computing to a new frontier," says IBM scientist Matthias Steffen,

manager of the IBM Research team that's focused on developing quantum computing systems to a point where it can be applied to real-world problems.

Other potential applications for quantum computing may include searching databases of unstructured information, performing a range of optimization tasks and solving previously unsolvable mathematical problems.

How Quantum Computing Works

The most basic piece of information that a typical computer understands is a bit. Much like a light that can be switched on or off, a bit can have only one of two values: "1" or "0". For qubits, they can hold a value of "1" or "0" as well as both values at the same time. Described as superposition, this is what allows quantum computers to perform millions of calculations at once.

One of the great challenges for scientists seeking to harness the power of quantum computing is controlling or removing quantum decoherence – the creation of errors in calculations caused by interference from factors such as heat, electromagnetic radiation, and materials defects. To deal with this problem, scientists have been experimenting for years to discover ways of reducing the number of errors and of lengthening the time periods over which the qubits retain their quantum mechanical properties. When this time is sufficiently long, error correction schemes become effective making it possible to perform long and complex calculations.

There are many viable systems that can potentially lead to a functional quantum computer. IBM is focusing on using superconducting qubits that will allow a more facile transition to scale up and manufacturing.

IBM has recently been experimenting with a unique "three dimensional" superconducting qubit (3D qubit), an approach that was initiated at Yale University. Among the results, the IBM team has used a 3D qubit to extend the amount of time that the qubits retain their quantum states up to 100 microseconds – an improvement of 2 to 4 times upon previously reported records. This value reaches just past the minimum threshold to enable effective error correction schemes and suggests that scientists can begin to focus on broader engineering aspects for scalability.

3D" superconducting qubit device where a qubit (about 1mm in length) is suspended in the center of the cavity on a small Sapphire chip. The cavity is formed by closing the two halves, and measurements are done by passing microwave signals to the connectors. Despite the apparent large feature size (the cavity is about 1.5 inches wide) for this single qubit demonstration, the team believes it is possible to scale such a system to hundreds or thousands of qubits.

A picture of IBM's "3D" superconducting qubit device where a qubit (about 1mm in length) is suspended in the center of the cavity on a small Sapphire chip. The cavity is formed by closing the two halves, and measurements are done by passing microwave signals to the connectors. Despite the apparent large feature size (the cavity is about 1.5 inches wide) for this single qubit demonstration, the team believes it is possible to scale such a system to hundreds or thousands of qubits.

In separate experiments, the group at IBM also demonstrated a more traditional "two-dimensional" qubit (2D qubit) device and implemented a two-qubit logic operation – a controlled-NOT (CNOT) operation, which is a fundamental building block of a larger quantum computing system. Their operation showed a 95 percent success rate, enabled in part due to the long coherence time of nearly 10 microseconds. These numbers are on the cusp of effective error correction schemes and greatly facilitate future multi-qubit experiments.

Imagine a computer whose memory is exponentially larger than its apparent physical size; a computer that can manipulate an exponential set of inputs simultaneously; a computer that computes in the twilight zone of Hilbert space. You would be thinking of a quantum computer. Relatively few and simple concepts from quantum mechanics are needed to make quantum computers a possibility. The subtlety has been in learning to manipulate these concepts. Is such a computer an inevitability or will it be too difficult to build?

Quantum Mechanics can be used to improve computation. Our challenge: solving an exponentially difficult problem for a conventional computer---that of factoring a large number. As a prelude, there are standard tools of computation, universal gates and machines. These ideas are then applied first to classical, dissipation less computers and then to quantum computers. A schematic model of a quantum computer is described as well as some of the subtleties in its programming. The Shor algorithm for efficiently factoring numbers on a quantum computer is presented in two parts: the quantum procedure within the algorithm and the classical algorithm that calls the quantum procedure. The mathematical structure in factoring which makes the Shor algorithm possible has been studied widely by many authors.. .

Let us start by describing the problem at hand: factoring a number N into its prime factors (e.g., the number **51688** may be

$$2^3 \times 7 \times 13 \times 71$$

decomposed as). A convenient way to quantify how quickly a particular algorithm may solve a problem is to ask how the number of steps to complete the algorithm scales with the size of the "input" the algorithm is fed.

$$\log N$$

For the factoring problem, this input is just the number N we wish to factor; hence the length of the input is . (The base of the logarithm is determined by our numbering system. Thus a base of **2** gives the length in binary; a base of **10** in decimal.) 'Reasonable' algorithms are ones which scale as some small-degree polynomial in the input size (with a degree of perhaps **2** or **3**).

On conventional computers the best known factoring algorithm runs

$$O(\exp[(64/9)^{1/3}(\ln N)^{1/3}(\ln \ln N)^{2/3}])$$

in $\log N$ steps. This algorithm, therefore, scales exponentially with the

input size $\log N$.

For instance, in 1994 a 129 digit number (known as RSA129) was successfully factored using this algorithm on approximately 1600 workstations scattered around the world; the entire factorization took eight months. Using this to estimate the prefactor of the above exponential scaling, we find that it would take roughly 800,000 years to factor a 250 digit number with the same computer power; similarly, a 1000 digit number would require 10^{25} years (significantly longer than the age of the universe). The difficulty of factoring large numbers is crucial for public-key cryptosystems, such as ones used by banks. There, such codes rely on the difficulty of factoring numbers with around 250 digits.

$$O((\log N)^{2+\epsilon})$$

Recently, an algorithm was developed for factoring numbers on a quantum computer which runs in steps where ϵ is small. This is roughly quadratic in the input size, so factoring a 1000 digit number with such an algorithm would require only a few million steps. The implication is that public key cryptosystems based on factoring may be breakable.

To give you an idea of how this exponential improvement might be possible, we review an elementary quantum mechanical experiment that demonstrates where such power may lie hidden. The two-slit experiment is prototypic for observing quantum mechanical behavior: A source emits photons, electrons or other particles that arrive at a pair of slits. These particles undergo unitary evolution and finally measurement. We see an interference pattern, with both slits open, which wholly vanishes if either slit is covered. In some sense, the particles pass through both slits in parallel. If such unitary evolution were to represent a calculation (or an operation within a calculation) then the quantum system would be performing computations in parallel. Quantum parallelism comes for free. The output of this system would be given by the constructive interference among the parallel computations.

The traditional management skills of planning, organizing, directing and controlling are inadequate in the fast-paced, constantly changing, highly complex world of twenty-first century organizations. Concepts from quantum mechanics and chaos theory as metaphors for a new management skill set can enable managers to actualize more of their leadership potential. The seven quantum skills are ancient and futuristic, scientific and spiritual, simple and complex. Together they form a model that balances the traditional left-brain management skills with new skills that more fully utilize both hemispheres of the brain. As managers master these skills, they transcend the limitations of mechanistic, deterministic, reductionistic thinking and become authentic change masters, changing themselves and their organizations at depth.

Quantum computing (For details see Andrew Steane A. M. Steane, Reports on Progress in Physics, vol 61, pp 117-173 (1998)).

The subject of quantum computing brings together ideas from classical information theory, computer science, and quantum physics. This review aims to summarize not just quantum computing, but the whole subject of quantum information theory. It turns out that information theory and quantum mechanics fit together very well. In order to explain their relationship, the review begins with an introduction to classical information theory and computer science, including Shannon's theorem, error correcting codes, Turing machines and computational complexity. The principles of quantum mechanics are then outlined, and the EPR experiment described. The EPR-Bell correlations and quantum entanglement in general, form the essential new ingredient which distinguishes quantum from classical information theory, and, arguably, quantum from classical physics. Basic quantum information ideas are described, including key distribution, teleportation, data compression, quantum error correction, the universal quantum computer and quantum algorithms. The common theme of all these ideas is the use of quantum entanglement as a computational resource. Experimental methods for small quantum processors are briefly sketched, concentrating on ion traps, high Q cavities, and NMR. The review concludes with an outline of the main features of quantum information physics, and avenues for future research.

The science of physics seeks to ask, and find precise answers to, basic questions about why nature is as it is. Historically, the fundamental principles of physics have been concerned with questions such as "what are things made of?" and "why do things move as they do?" In his *Principia*, Newton gave very wide-ranging answers to some of these questions. By showing that the same mathematical equations could describe the motions of everyday objects and of planets, he showed that an everyday object such as a tea pot is made of essentially the *same sort of stuff* as a planet: the motions of both can be described in terms of their mass and the forces acting on them. Nowadays we would say that both move in such a way as to conserve energy and momentum. In this way, physics allows us to abstract from nature concepts such as energy or momentum which always obey fixed equations, although the same energy might be expressed in many different ways: for example, an electron in the large electron-positron collider at CERN, Geneva, can have the same kinetic energy as a slug on a lettuce leaf.

Another thing which can be expressed in many different ways is *information*. For example, the two statements "the quantum computer is very interesting" and "l'ordinateur quantique est tres interessant" have something in common, although they share no words. The thing they have in common is their *information* content. Essentially the same information could be expressed in many other ways, for example by substituting numbers for letters in a scheme such as $a \rightarrow 97$, $b \rightarrow 98$, $c \rightarrow 99$ and so on, in which case the English version of the above statement becomes 116 104 101 32 113 117 97 110 116 117 109... . It is very significant that information can be expressed in different ways without losing its essential nature, since this leads to the possibility of the automatic manipulation of information: a machine need only be able to manipulate quite simple things like integers in order to do surprisingly powerful information processing, from document preparation to differential calculus, even to translating between human languages. We are familiar with this now, because of the ubiquitous computer, but even fifty years ago such a widespread significance of automated information processing was not foreseen.

However, there is one thing that all ways of expressing information must have in common: they all use real physical things to do the job. Spoken words are conveyed by air pressure fluctuations, written ones by arrangements of ink molecules on paper, even thoughts depend on neurons (Landauer 1991). The rallying cry of the information physicist is "no information without physical representation!" Conversely, the fact that information is insensitive to exactly how it is expressed, and can be freely translated from one form to another, makes it an obvious candidate for a fundamentally important role in physics, like energy and momentum and other such abstractions. However, until the second half of this century, the precise mathematical treatment of information, especially information processing, was undiscovered, so the significance of information in physics was only hinted at in concepts such as entropy in thermodynamics. It now appears that information may have a much deeper significance. Historically, much of fundamental physics has been concerned with discovering the fundamental particles of nature and the equations which describe their motions and interactions. It now appears that a different programme may be equally important: to discover the ways that nature allows, and prevents, information to be expressed and manipulated, rather than particles to move. For example, the best way to state exactly what can and cannot travel faster than light is to identify information as the speed-limited entity. In quantum mechanics, it is highly significant that the state vector must not contain, whether explicitly or implicitly, more information than can meaningfully be associated with a given system. Among other things this produces the wavefunction symmetry requirements which lead to Bose Einstein and Fermi Dirac statistics, the periodic structure of atoms, and so on.

Historically, the concept of information in physics does not have a clear-cut origin. An important thread can be traced if we consider the paradox of Maxwell's demon of 1871 (Fig. 1) (see also Brillouin 1956). Recall that Maxwell's demon is a creature that opens and closes a trap door between two compartments of a chamber containing gas, and pursues the subversive policy of only opening the door when fast molecules approach it from the right, or slow ones from the left. In this way the demon establishes a temperature difference between the two compartments without doing any work, in violation of the second law of thermodynamics, and consequently permitting a host of contradictions.

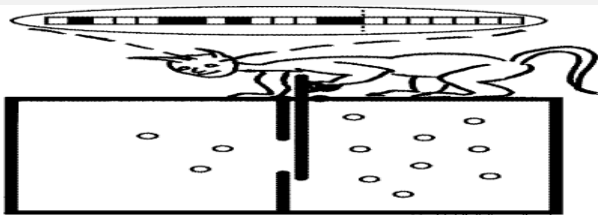


Fig. 1. Maxwell's demon. In this illustration the demon sets up a pressure difference by only raising the partition when more gas molecules approach it from the left than from the right. This can be done in a completely reversible manner, as long as the demon's memory stores the random results of its observations of the molecules. The demon's memory thus gets hotter. The irreversible step is not the acquisition of information, but the loss of information if the demon later clears its memory.

A number of attempts were made to exorcise Maxwell's demon (see Bennett 1987), such as arguments that the demon cannot gather information without doing work, or without disturbing (and thus heating) the gas, both of which are untrue. Some were tempted to propose that the 2nd law of thermodynamics could indeed be violated by the actions of an "intelligent being." It was not until 1929 that Leo Szilard made progress by reducing the problem to its essential components, in which the demon need merely identify whether a single molecule is to the right or left of a sliding partition, and its action allows a simple heat engine, called Szilard's engine, to be run. Szilard still had not solved the problem, since his analysis was unclear about whether or not the act of measurement, whereby the demon learns whether the molecule is to the left or the right, must involve an increase in entropy.

A definitive and clear answer was not forthcoming, surprisingly, until a further fifty years had passed. In the intermediate years digital computers were developed, and the physical implications of information gathering and processing were

carefully considered. The thermodynamic costs of elementary information manipulations were analyzed by Landauer and others during the 1960s (Landauer 1961, Keyes and Landauer 1970), and those of general computations by Bennett, Fredkin, Toffoli and others during the 1970s (Bennett 1973, Toffoli 1980, Fredkin and Toffoli 1982). It was found that almost anything can in principle be done in a reversible manner, i.e. with no entropy cost at all (Bennett and Landauer 1985). Bennett (1982) made explicit the relation between this work and Maxwell's paradox by proposing that the demon can indeed learn where the molecule is in Szilard's engine without doing any work or increasing any entropy in the environment, and so obtain useful work during one stroke of the engine. However, the information about the molecule's location must then be present in the demon's memory (Fig. 1). As more and more strokes are performed, more and more information gathers in the demon's memory. To complete a thermodynamic cycle, the demon must *erase* its memory, and it is during this erasure operation that we identify an increase in entropy in the environment, as required by the 2nd law. This completes the essential physics of Maxwell's demon; further subtleties are discussed by Zurek (1989), Caves (1990), and Caves, Unruh and Zurek (1990).

The thread we just followed was instructive, but to provide a complete history of ideas relevant to quantum computing is a formidable task. Our subject brings together what are arguably two of the greatest revolutions in twentieth-century science, namely quantum mechanics and information science (including computer science). The relationship between these two giants is illustrated in Figure 2.

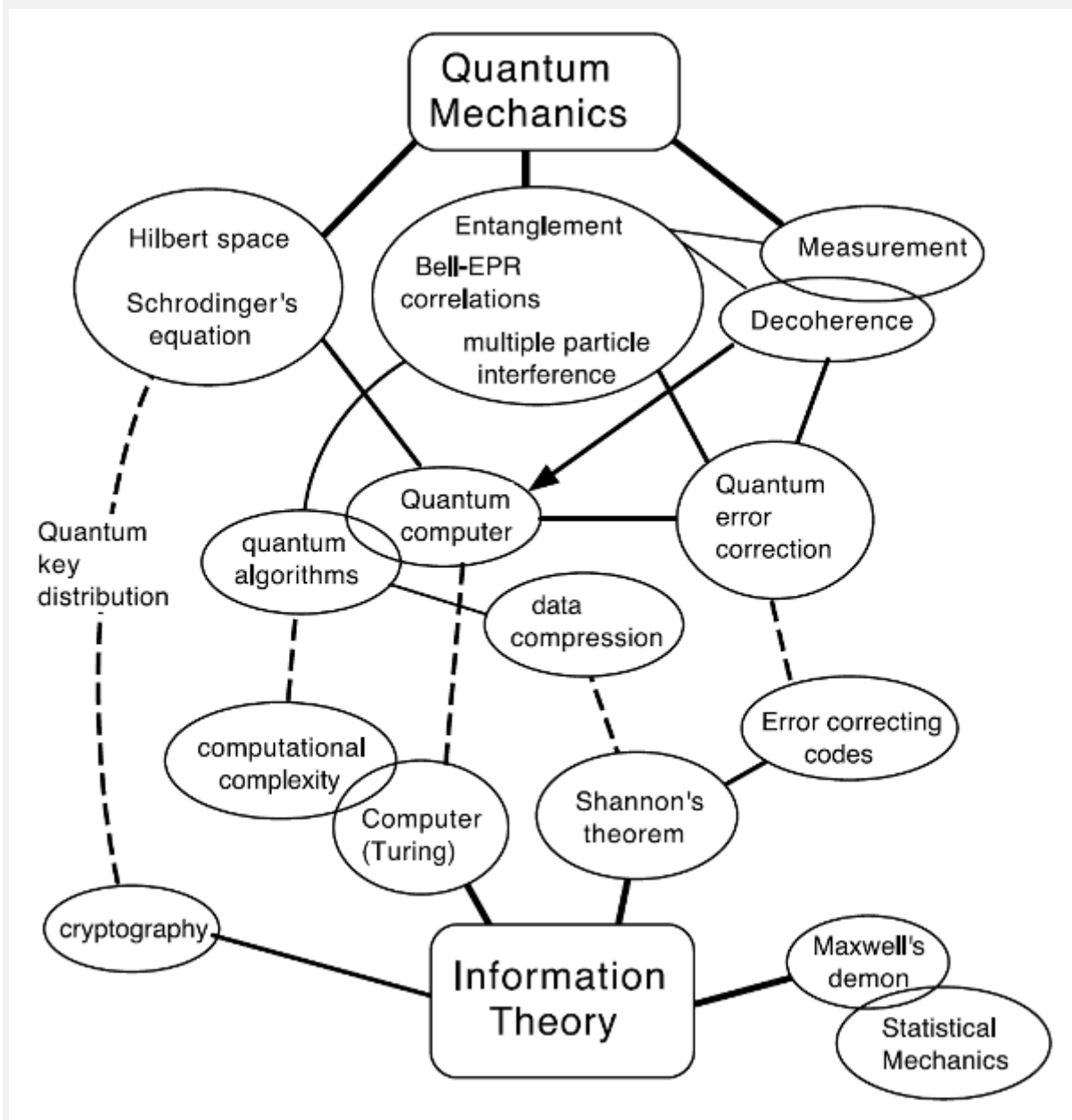


Fig. 2. Relationship between quantum mechanics and information theory. This diagram is not intended to be a definitive statement, the placing of entries being to some extent subjective, but it indicates many of the connections discussed in the article.

Classical information theory is founded on the definition of information. A warning is in order here. Whereas the theory tries to capture much of the normal meaning of the term 'information', it can no more do justice to the full richness of that term in everyday language than particle physics can encapsulate the everyday meaning of 'charm'. 'Information' for us will be an abstract term. Much of information theory dates back to seminal work of Shannon in the 1940's (Slepian 1974). The observation that information can be translated from one form to another is encapsulated and quantified in Shannon's noiseless coding theorem (1948), which quantifies the resources needed to store or transmit a given body of information. Shannon also considered the fundamentally important problem of communication in the presence of noise, and established Shannon's main theorem which is the central result of classical information theory. Error-free communication even in the presence of noise is achieved by means of 'error-correcting codes', and their study is a branch of mathematics in its own right. Indeed, the journal *IEEE Transactions on Information Theory* is almost totally taken up with the discovery and analysis of error-correction by coding. Pioneering work in this area was done by Golay (1949) and Hamming (1950).

The foundations of computer science were formulated at roughly the same time as Shannon's information theory, and this is no coincidence. The father of computer science is arguably Alan Turing (1912-1954), and its prophet is Charles Babbage (1791-1871). Babbage conceived of most of the essential elements of a modern computer, though in his day there was not the technology available to implement his ideas. A century passed before Babbage's Analytical Engine was improved upon when Turing described the Universal Turing Machine in the mid 1930s. Turing's genius (see Hodges 1983) was to clarify exactly what a calculating machine might be capable of, and to emphasise the role of programming, i.e. software, even more than Babbage had done. The giants on whose shoulders Turing stood in order to get a better view were chiefly the mathematicians David Hilbert and Kurt Gödel. Hilbert had emphasized between the 1890s and 1930s the importance of asking fundamental questions about the nature of mathematics. Instead of asking "is this mathematical proposition true?" Hilbert wanted to ask "is it the case that every mathematical proposition can in principle be proved or disproved?" This was unknown, but Hilbert's feeling, and that of most mathematicians, was that mathematics was indeed complete, so that conjectures such as Goldbach's (that every even number can be written as the sum of two primes) could be proved or disproved somehow, although the logical steps might be as yet undiscovered.

Gödel destroyed this hope by establishing the existence of mathematical propositions which were undecidable, meaning that they could be neither proved nor disproved. The next interesting question was whether it would be easy to identify such propositions. Progress in mathematics had always relied on the use of creative imagination, yet with hindsight mathematical proofs appear to be automatic, each step following inevitably from the one before. Hilbert asked whether this 'inevitable' quality could be captured by a 'mechanical' process. In other words, was there a universal mathematical method, which would establish the truth or otherwise of every mathematical assertion? After Gödel, Hilbert's problem was re-phrased into that of establishing decidability rather than truth, and this is what Turing sought to address.

In the words of Newman, Turing's bold innovation was to introduce 'paper tape' into symbolic logic. In the search for an automatic process by which mathematical questions could be decided, Turing envisaged a thoroughly mechanical device, in fact a kind of glorified typewriter (Fig. 3). The importance of the Turing machine (Turing 1936) arises from the fact that it is sufficiently complicated to address highly sophisticated mathematical questions, but sufficiently simple to be subject to detailed analysis. Turing used his machine as a theoretical construct to show that the assumed existence of a mechanical means to establish decidability leads to a contradiction. In other words, he was initially concerned with quite abstract mathematics rather than practical computation. However, by seriously establishing the idea of automating abstract mathematical proofs rather than merely arithmetic, Turing greatly stimulated the development of general purpose information processing. This was in the days when a "computer" was a person doing mathematics.

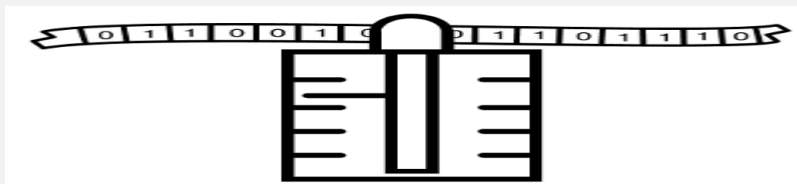


Fig. 3. The Turing Machine. This is a conceptual mechanical device which can be shown to be capable of efficiently simulating all classical computational methods. The machine has a finite set of internal states, and a fixed design. It reads one binary symbol at a time, supplied on a tape. The machine's action on reading a given symbol s depends only on that symbol and the internal state G . The action consists in overwriting a new symbol s' on the current tape location, changing state to G' , and moving the tape one place in direction d (left or right). The internal construction of the machine can therefore be specified by a finite fixed list of rules of the form $(s, G \rightarrow s', G', d)$. One special internal state is the 'halt' state: once in this state the machine ceases further activity. An input 'programme' on the tape is transformed by the machine into an output result printed on the tape.

Modern computers are neither Turing machines nor Babbage engines, though they are based on broadly similar principles, and their computational power is equivalent (in a technical sense) to that of a Turing machine. I will not trace their development here, since although this is a wonderful story, it would take too long to do justice to the many people involved.

Let us just remark that all of this development represents a great improvement in speed and size, but does not involve any change in the essential idea of what a computer is, or how it operates. Quantum mechanics raises the possibility of such a change, however.

Quantum mechanics is the mathematical structure which embraces, in principle, the whole of physics. We will not be directly concerned with gravity, high velocities, or exotic elementary particles, so the standard non-relativistic quantum mechanics will suffice. The significant feature of quantum theory for our purpose is not the precise details of the equations of motion, but the fact that they treat quantum amplitudes, or state vectors in a Hilbert space, rather than classical variables. It is this that allows new types of information and computing.

There is a parallel between Hilbert's questions about mathematics and the questions we seek to pose in quantum information theory. Before Hilbert, almost all mathematical work had been concerned with establishing or refuting particular hypotheses, but Hilbert wanted to ask what general type of hypothesis was even amenable to mathematical proof. Similarly, most research in quantum physics has been concerned with studying the evolution of specific physical systems, but we want to ask what general type of evolution is even conceivable under quantum mechanical rules.

The first deep insight into quantum information theory came with Bell's 1964 analysis of the paradoxical thought-experiment proposed by Einstein, Podolsky and Rosen (EPR) in 1935. Bell's inequality draws attention to the importance of correlations between separated quantum systems which have interacted (directly or indirectly) in the past, but which no longer influence one another. In essence his argument shows that the degree of correlation which can be present in such systems exceeds that which could be predicted on the basis of *any* law of physics which describes particles in terms of classical variables rather than quantum states. Bell's argument was clarified by Bohm (1951, also Bohm and Aharonov 1957) and by Clauser, Holt, Horne and Shimony (1969), and experimental tests were carried out in the 1970s (see Clauser and Shimony (1978) and references therein). Improvements in such experiments are largely concerned with preventing the possibility of any interaction between the separated quantum systems, and a significant step forward was made in the experiment of Aspect, Dalibard and Roger (1982), (see also Aspect 1991) since in their work any purported interaction would have either to travel faster than light, or possess other almost equally implausible qualities.

The next link between quantum mechanics and information theory came about when it was realized that simple properties of quantum systems, such as the unavoidable disturbance involved in measurement, could be put to practical use, in *quantum cryptography* (Wiesner 1983, Bennett *et al.* 1982, Bennett and Brassard 1984; for a recent review see Brassard and Crepeau 1996). Quantum cryptography covers several ideas, of which the most firmly established is quantum key distribution. This is an ingenious method in which transmitted quantum states are used to perform a very particular communication task: to establish at two separated locations a pair of identical, but otherwise random, sequences of binary digits, without allowing any third party to learn the sequence. This is very useful because such a random sequence can be used as a cryptographic key to permit secure communication. The significant feature is that the principles of quantum mechanics guarantee a type of conservation of quantum information, so that if the necessary quantum information arrives at the parties wishing to establish a random key, they can be sure it has not gone elsewhere, such as to a spy. Thus the whole problem of compromised keys, which fills the annals of espionage, is avoided by taking advantage of the structure of the natural world.

While quantum cryptography was being analyzed and demonstrated, the quantum computer was undergoing a quiet birth. Since quantum mechanics underlies the behaviour of all systems, including those we call classical ("even a screwdriver is quantum mechanical", Landauer (1995)), it was not obvious how to conceive of a distinctively quantum mechanical computer, i.e. one which did not merely reproduce the action of a classical Turing machine. Obviously it is not sufficient merely to identify a quantum mechanical system whose evolution could be interpreted as a computation; one must prove a much stronger result than this. Conversely, we know that classical computers can simulate, by their computations, the evolution of any quantum system... with one reservation: no classical process will allow one to prepare separated systems whose correlations break the Bell inequality. It appears from this that the EPR-Bell correlations are the quintessential quantum-mechanical property (Feynman 1982).

In order to think about computation from a quantum-mechanical point of view, the first ideas involved converting the action of a Turing machine into an equivalent reversible process, and then inventing a Hamiltonian which would cause a quantum system to evolve in a way which mimicked a reversible Turing machine. This depended on the work of Bennett (1973; see also Lecerf 1963) who had shown that a universal classical computing machine (such as Turing's) could be made reversible while retaining its simplicity. Benioff (1980, 1982) and others proposed such Turing-like Hamiltonians in the early 1980s. Although Benioff's ideas did not allow the full analysis of quantum computation, they showed that unitary quantum evolution is at least as powerful computationally as a classical computer.

A different approach was taken by Feynman (1982, 1986) who considered the possibility not of universal computation, but of universal *simulation* -- i.e. a purpose-built quantum system which could simulate the *physical behaviour* of any other. Clearly, such a simulator would be a universal computer too, since any computer must be a physical system. Feynman gave arguments which suggested that quantum evolution could be used to compute certain problems more efficiently than any

classical computer, but his device was not sufficiently specified to be called a computer, since he assumed that any interaction between adjacent two-state systems could be 'ordered', without saying how.

In 1985 an important step forward was taken by Deutsch. Deutsch's proposal is widely considered to represent the first blueprint for a quantum computer, in that it is sufficiently specific and simple to allow real machines to be contemplated, but sufficiently versatile to be a universal quantum simulator, though both points are debatable. Deutsch's system is essentially a line of two-state systems, and looks more like a register machine than a Turing machine (both are universal classical computing machines). Deutsch proved that if the two-state systems could be made to evolve by means of a specific small set of simple operations, then *any* unitary evolution could be produced, and therefore the evolution could be made to simulate that of any physical system. He also discussed how to produce Turing-like behaviour using the same ideas.

Deutsch's simple operations are now called quantum 'gates', since they play a role analogous to that of binary logic gates in classical computers. Various authors have investigated the minimal class of gates which are sufficient for quantum computation.

The two questionable aspects of Deutsch's proposal are its efficiency and realisability. The question of efficiency is absolutely fundamental in computer science, and on it the concept of 'universality' turns. A *universal* computer is one that not only can reproduce (i.e. simulate) the action of any other, but can do so without running too slowly. The 'too slowly' here is defined in terms of the number of computational steps required: this number must not increase exponentially with the size of the input. Deutsch's simulator is not universal in this strict sense, though it was shown to be efficient for simulating a wide class of quantum systems by Lloyd (1996). However, Deutsch's work has established the concepts of quantum networks (Deutsch 1989) and quantum logic gates, which are extremely important in that they allow us to think clearly about quantum computation.

In the early 1990's several authors (Deutsch and Jozsa 1992, Berthiaume and Brassard 1992, Bernstein and Vazirani 1993) sought computational tasks which could be solved by a quantum computer more efficiently than *any* classical computer. Such a quantum algorithm would play a conceptual role similar to that of Bell's inequality, in defining something of the essential nature of quantum mechanics. Initially only very small differences in performance were found, in which quantum mechanics permitted an answer to be found with certainty, as long as the quantum system was noise-free, where a probabilistic classical computer could achieve an answer 'only' with high probability. An important advance was made by Simon (1994), who described an efficient quantum algorithm for a (somewhat abstract) problem for which no efficient solution was possible classically, even by probabilistic methods. This inspired Shor (1994) who astonished the community by describing an algorithm which was not only efficient on a quantum computer, but also addressed a central problem in computer science: that of factorizing large integers.

Shor discussed both factorization and discrete logarithms, making use of a quantum Fourier transform method discovered by Coppersmith (1994) and Deutsch. Further important quantum algorithms were discovered by Grover (1997) and Kitaev (1995).

Just as with classical computation and information theory, once theoretical ideas about computation had got under way, an effort was made to establish the essential nature of quantum information -- the task analogous to Shannon's work. The difficulty here can be seen by considering the simplest quantum system, a two-state system such as a spin half in a magnetic field. The quantum state of a spin is a continuous quantity defined by two real numbers, so in principle it can store an infinite amount of classical information. However, a measurement of a spin will only provide a single two-valued answer (spin up/spin down) -- there is no way to gain access to the infinite information which appears to be there, therefore it is incorrect to consider the information content in those terms. This is reminiscent of the renormalization problem in quantum electrodynamics. How much information can a two-state quantum system store, then? The answer, provided by Jozsa and Schumacher (1994) and Schumacher (1995), is *one two-state system's worth!* Of course Schumacher and Jozsa did more than propose this simple answer, rather they showed that the two-state system plays the role in quantum information theory analogous to that of the bit in classical information theory, in that the quantum information content of *any* quantum system can be meaningfully measured as the minimum number of two-state systems, now called quantum bits or qubits, which would be needed to store or transmit the system's state with high accuracy.

Let us return to the question of realisability of quantum computation. It is an elementary, but fundamentally important, observation that the quantum interference effects which permit algorithms such as Shor's are extremely fragile: the quantum computer is ultra-sensitive to experimental noise and impression. It is not true that early workers were unaware of this difficulty; rather their first aim was to establish whether a quantum computer had any fundamental significance at all. Armed with Shor's algorithm, it now appears that such a fundamental significance is established, by the following argument: either nature does allow a device to be run with sufficient precision to perform Shor's algorithm for large integers (greater than, say, a googol which is 1 followed by 100 zeroes) or there are fundamental natural limits to precision in real systems. Both eventualities represent an important insight into the laws of nature.

At this point, ideas of quantum information and quantum computing come together. For, a quantum computer can be made much less sensitive to noise by means of a new idea which comes directly from the marriage of quantum mechanics with classical information theory, namely *quantum error correction*. Although the phrase 'error correction' is a natural one and was used with reference to quantum computers prior to 1996, it was only in that year that two important papers, of Calderbank and Shor, and independently Steane, established a general framework whereby quantum information processing can be used to combat a very wide class of noise processes in a properly designed quantum system. Much progress has since been made in generalizing these ideas (Knill and Laflamme 1997, Ekert and Macchiavello 1996, Bennett *et al.* 1996b, Gottesman 1996, Calderbank *et al.* 1997). An important development was the demonstration by Shor (1996) and Kitaev (1996) that correction can be achieved even when the corrective operations are themselves imperfect. Such methods lead to a general concept of 'fault tolerant' computing, of which a helpful review is provided by Preskill (1997).

If, as seems almost certain, quantum computation will only work in conjunction with quantum error correction, it appears that the relationship between quantum information theory and quantum computers is even more intimate than that between Shannon's information theory and classical computers. Error correction does not in itself guarantee accurate quantum computation, since it cannot combat all types of noise, but the fact that it is possible at all is a significant development.

A computer which only exists on paper will not actually perform any computations, and in the end the only way to resolve the issue of feasibility in quantum computer science is to build a quantum computer. To this end, a number of authors proposed computer designs based on Deutsch's idea, but with the physical details more fully worked out (Teich *et al.* 1988, Lloyd 1993, Berman *et al.* 1994, DiVincenzo 1995b). The great challenge is to find a sufficiently complex system whose evolution is nevertheless both coherent (i.e. unitary) and controllable. It is not sufficient that only some aspects of a system should be quantum mechanical, as in solid-state 'quantum dots', or that there is an implicit assumption of unfeasible precision or cooling, which is often the case for proposals using solid-state devices. Cirac and Zoller (1995) proposed the use of a linear ion trap, which was a significant improvement in feasibility, since heroic efforts in the ion trapping community had already achieved the necessary precision and low temperature in experimental work, especially the group of Wineland who demonstrated cooling to the ground state of an ion trap in the same year (Diedrich *et al.* 1989, Monroe *et al.* 1995). More recently, Gershenfeld and Chuang (1997) and Cory *et al.* (1996,1997) have shown that nuclear magnetic resonance (NMR) techniques can be adapted to fulfill the requirements of quantum computation, making this approach also very promising. Other recent proposals of Privman *et al.* (1997) and Loss and DiVincenzo (1997) may also be feasible.

As things stand, no quantum computer has been built, nor looks likely to be built in the author's lifetime, if we measure it in terms of Shor's algorithm, and ask for factoring of large numbers. However, if we ask instead for a device in which quantum information ideas can be explored, then only a few quantum bits are required, and this will certainly be achieved in the near future. Simple two-bit operations have been carried out in many physics experiments, notably magnetic resonance, and work with three to ten qubits now seems feasible. Notable recent experiments in this regard are those of Brune *et al.* (1994), Monroe *et al.* (1995b), Turchette *et al.* (1995) and Mattle *et al.* (1996).

*

We will denote

By $T_i(t)$, $i = 36,37,38$, the three parts of the **QUANTUM COMPUTER(INFORMATION) CORRESPONDING TO THE QUANTUM MECHANICAL BEHAVIOUR STRATIFIED IN THE CORRESPONDING CATEGORY**

By $(a_i'')^{(7)}(T_{37}, t)$ ($T_{37} \geq 0, t \geq 0$), the contribution of the **QUANTUM COMPUTER(INFORMATION) CORRESPONDING TO THE QUANTUM MECHANICAL BEHAVIOUR STRATIFIED IN THE CORRESPONDING CATEGORY**

1) By $(-b_i'')^{(7)}(G_{36}, G_{37}, G_{38}, t) = -(b_i'')^{(7)}((G_{39}), t)$, the contribution of the **QUANTUM COMPUTER(INFORMATION) CORRESPONDING TO THE QUANTUM MECHANICAL BEHAVIOUR STRATIFIED IN THE CORRESPONDING CATEGORY**

STABILITY AND INSTABILITY OF QUANTUM INFORMATION:

Stability Diagram of a Few-Electron Triple Dot

Individual and coupled quantum dots containing one or two electrons have been realized and are regarded as components for future quantum information circuits. Mapping out has been done several authors(see references) out experimentally the stability diagram of the few electron triple dot system, the electron configuration map as a function of the external tuning parameters, and reveal experimentally for the first time the existence of quadruple points, a signature of the three dots being in resonance. In the vicinity of these quadruple points we observe a duplication of charge transfer transitions related to charge and spin reconfigurations triggered by changes in the total electron occupation number. These(e&eb) results are relevant for future quantum mechanical engineering applications within both quantum information and quantum cellular automata (QCA) architectures. A comparison between single quantum dots and real atoms confirms both analogous and dissimilar properties. Atomic-like shell structure and Hund's rules govern both systems. The very different energy scale of the artificial atom, however, manifests itself in novel interaction phenomena which have no analogue in real atoms, such as singlet triplet transitions and spin texture arrangements of electrons. The tunability of these devices makes them promising candidates for future quantum information applications as well as for fundamental studies of quantum molecular effects, and for exploiting nanospintronic functionalities

Stability, Gain, and Robustness in Quantum Feedback Networks (For details see C. D'Helon and M.R. James)

Problem of stability for quantum feedback networks, of quantum optics how stability of quantum feedback networks can be guaranteed using only simple gain inequalities for network components and algebraic relationships determined by the network. Quantum feedback networks are shown to be stable if the loop gain is less than one—this is an extension of the famous small gain theorem of classical control theory. Authors' illustrate the simplicity and power of the small gain approach with applications to important problems of robust stability and robust stabilization. Quantum feedback networks, stability, input-output stability, robustness, stabilization, quantum optics. Are all interrelated. Stable operation is a fundamental pre-requisite for the proper functioning of any technological system. Instability can cause some system variables to grow in magnitude without bound (or at least saturate or oscillate), with detrimental effects on performance and even damage. Consequently, methods for stability analysis and design have played an important role in the development of classical technologies. A significant early example was Watt's steam engine governor in the 1780's (subsequently analyzed by Maxwell in 1868), Indeed, one of the chief applications of feedback (but by no means the only application) is to stabilize systems that would otherwise be unstable. A striking example of this is the X29 plane, which has forward swept wings and requires the use of a stabilizing feedback control system. However, feedback per se does not guarantee stability: indeed, feedback can be "degenerative or regenerative—either stabilizing or destabilizing",. In particular, when interconnections of stable components include components with active elements, instability can occur (such as when a microphone is placed too close to a loudspeaker). An additional requirement of considerable practical importance is that stable operation be maintained in the presence of uncertainty (e.g., due to model error and approximation, altered operating conditions, etc.) and noise—this is a basic robustness requirement. Feedback is increasingly being used in the design of new technologies that include quantum components, In fact, a wide range of quantum technologies can be considered as networks of quantum and classical components which include cascade and feedback interconnections. Since these networks may include components that are active, e.g. optical amplifiers or classical amplifiers, questions of network stability are of considerable importance. Quantum input-output theory started developing in the 1980's, however general methods for stability analysis and design for quantum networks still do not apply to Theory of Quantum information

SOME STABILITY AND QUINTESSENTIAL REVIEWS ON QUANTUM COMPUTATION:

Loschmidt echoes (Tomaz Prosen, Thomas H. Seligman, Marko Znidaric

In this paper authors' investigate on the theoretical approach to quantum Loschmidt echoes, i.e. various properties of the so called echo dynamics -- the composition of forward and backward time evolutions generated by two slightly different Hamiltonians, such as the state autocorrelation function (fidelity) and the purity of a reduced density matrix traced over a subsystem (purity fidelity). Our main theoretical result is linear response formalism, expressing the fidelity and purity fidelity in terms of integrated time autocorrelation function of the generator of the perturbation. Surprisingly, this relation predicts that **the decay** of fidelity is the slower the faster the decay of correlations. In particular for a static (time-independent) perturbation, and for non-ergodic and non-mixing dynamics where asymptotic decay of correlations is absent, a qualitatively different and faster decay of fidelity is predicted on a time scale $1/\delta$ as opposed to mixing dynamics where the fidelity is found to decay exponentially on a time-scale $1/\delta^2$, where δ is a strength of perturbation. A detailed discussion of a semi-classical regime of small effective values of Planck constant is given where classical correlation functions can be used to predict quantum fidelity decay. Note that the correct and intuitively expected classical stability behavior is recovered in the classical limit, as the perturbation and classical limits do not commute. The theoretical results are demonstrated numerically for two models, the quantized kicked top and the multi-level Jaynes Cummings model. Method can for example be applied to the stability analysis of quantum computation and quantum information processing.

Towards scalable quantum information processing and quantum simulation with trapped ions(See Diedrich Leibfried)

Quantum information processing and experiments towards Quantum Information Processing (QIP) and Quantum Simulation (QS) with trapped ions are discussed. Most requirements for QIP and QS have been demonstrated in this system, with two big challenges remaining: Improving operation fidelity and scaling up to larger numbers of qubits. The architecture pursued by the Ion Stage Group at NIST is based on quantum information stored in long lived internal (hyperfine) states of the ions. We investigate the use of laser beams and microwave fields to induce both single-qubit rotations and multi-qubit gates mediated by the Coulomb interaction between ions. Moving ions through a multi-zone trap architecture allows for keeping the number of ions per zone small, while sympathetic cooling with a second ion species can remove energy and entropy from the system. After an introduction to these elements, I will discuss the current status of experiments and some future perspectives for QIP and QS as well as for other applications based on trapped ions.

Quantum circuits: from concept to future applications (Armand C. R. Niederberger)

Current experimental progress in quantum optics and nanophotonics is establishing a solid base for fascinating future applications. We may soon be able to create integrated circuits of nanophotonic components for ultra-low power and ultra-high speed optical switching. My theory seminar presents the methods with which we are currently studying photonic circuit models and discusses examples of circuits for classical photonic logic. Nanophotonics in general and the advantages of using optical interconnects over electronic interconnects in particular. Second, I present our high-level quantum hardware description language which links graphical circuit design tools with recent mathematical developments to describe open quantum optical networks, thus enabling scientists and engineers to simulate quantum circuits without having to deal with

the details of quantum optics. Third, author shows how to perform design optimization on nanophotonics circuits using adjoint calculus. This method is based on the use of Lagrange multipliers and drastically **reduces** the number of computations in parameter optimization and stability analysis.

Does a closed quantum system equilibrate? (Paolo Zanardi)

Author discusses the issue of whether and how we can make sense of the notion of **equilibration("convergence" to equilibrium)** for a large but finite quantum system with only internal degrees of freedom. (i.e., closed). It is illustrated that the results on equilibration of the Loschmidt echo in nearly-critical quantum many-body systems evolving unitarily.

Quantum wavelength conversion and transmission in opto mechanical systems(Lin Tian)

Optomechanical systems with strong light-matter interaction can be explored as an interface between photon modes of distinct wavelengths, e.g. an optical mode and a microwave mode. Authors' study transient and adiabatic schemes for cavity state conversion and for photon transmission in the optomechanical system. Author states that his results can be applied to various applications in optical quantum information processing, such as photon pulse generation and state manipulation, quantum repeaters, and conversion of information between different photon modes.

Protecting quantum gates from control noise (Constantin Brif)

External controls are necessary to enact quantum logic operations, and the inevitable **control** noise will **result in** gate errors in a realistic quantum circuit. Author investigates the robustness of quantum gates to random noise in an optimal control field, by utilizing properties of the quantum control landscape that relates the physical objective (in the present case, the quantum gate fidelity) to the applied controls. An approximate result obtained for the statistical expectation value of the gate fidelity in the weak noise regime is shown to be in excellent agreement with direct Monte Carlo sampling over noise process realizations for fidelity values relevant for practical quantum information processing. Using this approximate result, they demonstrate that maximizing the robustness to additive/multiplicative white noise **is equivalent to** minimizing the total control time/fluence. Also, a genetic optimization algorithm is **used to identify controls** with improved robustness to colored noise.

Exciton-Polariton Quantum Emulators (Na Young Kim)

Microcavity exciton-polaritons are hybrid light-matter quasi-particles **arising from** the mixed states between cavity photons and quantum well excitons. The inherent light matter duality **provides** experimental advantages: the stimulated scattering among interacting particles and the small effective mass ($\sim 10e-8$ times the hydrogen atom) **form** coherent condensate states at high temperatures (e.g. 4 K in GaAs and room temperature in GaN materials). In addition, the dynamics of exciton-polaritons are accessed by capturing the leaked photons out of the cavity due to the short lifetime. **Utilizing** coherence and open-dissipative nature of exciton-polariton condensates, we engineer a two-dimensional (2D) polariton-lattice system for investigating exotic quantum phase order. Via micro-photoluminescence measurements in both real and momentum spaces, authors' have observed d-orbital condensate states, vortex-antivortex phase order, massless Dirac dispersions in 2D square, honeycomb, and triangular lattices respectively. These results **demonstrate** that the polariton-lattice systems will be promising solid-state quantum emulators in the quest for better understanding strongly correlated materials and in the development of novel optoelectronic devices.

Benchmarking and Protecting Adiabatic Quantum Computation(Daniel Lidar)

How many bits does it take to track an open quantum system?

In general if one obtains information about an open quantum system by measuring its environment, that measurement will alter the future evolution of the system. However in the Markovian case this back-action is negligible and one can "track" the system i.e. assign it a (stochastically evolving) pure state at all times **without disturbing** its (deterministic) average evolution. In general this stochastic evolution **creates a** trajectory passing through infinitely many different pure states, even for a finite dimensional quantum system. Hence an infinite classical memory would be required to track such evolution. Here author shows that, for any ergodic master equation, there should **exist a** monitoring scheme (which in general must be adaptive) on the environment that can confine the system state to jumping between finitely many states, so that only a finitely large classical memory is required

Using symmetries to understand molecular devices and magnetic ad-atoms on substrates

Realizing a quantum transistor **built of** molecules or quantum dots has been one of the most ambitious challenges in nanotechnology. Even though remarkable progress has been made, being able to gate and **control** nanometer scale objects, as well to **interconnect** them to achieve scalability remains extremely difficult. Most experiments concern a single quantum dot or molecule, and they are made at ultra low temperature **to avoid** decoherence and tunnelling. Author proposes to use canonical transformations **to design** quantum devices that are **protected** by symmetry, and therefore, may be operational at high temperatures. We illustrate the idea with an example of a quantum transistor controlled by a gate electrode in a three terminal setup. They consider the **effects of** interactions, and we find that the same principles can be applied to design a device that could operate as an electrically controlled spin qubit. Author shows that similar but more sophisticated principles can be used to improve our understanding **of the effects of magnetic ad-atoms on substrates, such as** graphene.

Quantum Annealing with Superconducting Flux Qubits(Mark Jonson)

D-Wave Systems has implemented a processor based on Quantum Annealing, an algorithm for finding the ground state of a system of interacting spins. The technology is built on a superconducting chip composed of flux qubits that enable a quantum annealing algorithm, and digital components that apply programmable on-chip flux biases. In this presentation, author reviews Quantum Annealing, and then give a brief overview of the processor architecture. He also discusses a method for observing the system dynamics during the annealing process for a sample eight spin problem instance, and describe how the temperature dependence of these **dynamics(eb)** provides a signature of Quantum Annealing.*

QUANTUM MECHANICAL BEHAVIOUR AND QUANTUM COMPUTER

GOVERNING EQUATIONS

Quantum gravity (QG) is the field of theoretical physics which attempts to develop scientific models that unify quantum mechanics (describing three of the four known fundamental interactions) with general relativity (describing the fourth, gravity). It is hoped that development of such a theory would unify into a single mathematical framework all fundamental interactions and to describe all known observable interactions in the universe, at both subatomic and cosmological scales. Such a theory of quantum gravity would yield the same experimental results as ordinary quantum mechanics in conditions of weak gravity (gravitational potentials much less than c^2) and the same results as Einsteinian general relativity in phenomena at scales much larger than individual molecules (action much larger than reduced Planck's constant), but moreover be able to predict the outcome of situations where both quantum effects and strong-field gravity are important (at the Planck scale, unless large extra dimension conjectures are correct). If the theory of quantum gravity also achieves a grand unification of the other known interactions, it is referred to as a theory of everything (TOE).

Motivation for quantizing gravity comes from the remarkable success of the quantum theories of the other three fundamental interactions, and from experimental evidence suggesting that gravity can be made to show quantum effects. Although some quantum gravity theories such as string theory and other unified field theories (or 'theories of everything') attempt to unify gravity with the other fundamental forces, others such as loop quantum gravity make no such attempt; they simply quantize the gravitational field while keeping it separate from the other forces.

Observed physical phenomena can be described well by quantum mechanics or general relativity, without needing both. This can be thought of as due to an extreme separation of mass scales at which they are important. Quantum effects are usually important only for the "very small", that is, for objects no larger than typical molecules. General relativistic effects, on the other hand, show up mainly for the "very large" bodies such as collapsed stars. (Planets' gravitational fields, as of 2011, are well-described by linearised except for Mercury's perihelion precession; so strong-field effects—any effects of gravity beyond lowest nonvanishing order in ϕ/c^2 —have not been observed even in the gravitational fields of planets and main sequence stars). There is a lack of experimental evidence relating to quantum gravity, and classical physics adequately describes the observed effects of gravity over a range of 50 orders of magnitude of mass, i.e., for masses of objects from about 10^{-23} to 10^{30} kg.

Much of the difficulty in meshing these theories at all energy scales comes from the different assumptions that these theories make on how the universe works. Quantum field theory depends on particle fields embedded in the flat space-time of special relativity. General relativity models gravity as a curvature within space-time that changes as a gravitational mass moves. Historically, the most obvious way of combining the two (such as treating gravity as simply another particle field) ran quickly into what is known as the renormalization problem. In the old-fashioned understanding of renormalization, gravity particles would attract each other and adding together all of the interactions results in many infinite values which cannot easily be cancelled out mathematically to yield sensible, finite results. This is in contrast with quantum electrodynamics where, while the series still do not converge, **the interactions** sometimes evaluate to infinite results, but those are few enough in number to **be removable via renormalization**.

Effective field theories

Quantum gravity can be treated as an effective field theory. Effective quantum field theories come with some high-energy cutoff, beyond which we do not expect that the theory provides a good description of nature. The "infinities" then become large but finite quantities proportional to this finite cutoff scale, and correspond to processes that involve very high energies near the fundamental cutoff. These quantities can then be absorbed into an infinite collection **of coupling constants**, and at energies **well below** the fundamental cutoff of the theory, to any desired precision; only a finite number of **these coupling constants** need to be measured in order to make legitimate quantum-mechanical predictions. This same logic works just as well for the highly successful theory of low-energy pions as for quantum gravity. Indeed, the first quantum-mechanical corrections to graviton-scattering and Newton's law of gravitation have been explicitly computed (although they are so astronomically small that we may never be able to measure them). In fact, gravity is in many ways a much better quantum field theory than the Standard Model, since it appears to be valid all the way up to its cutoff at the Planck scale. (By comparison, the Standard Model is expected to start to break down above its cutoff at the much smaller scale of around 1000 GeV)

While confirming that quantum mechanics and gravity are indeed consistent at reasonable energies, it is clear that near or above the fundamental cutoff of our effective quantum theory of gravity (the cutoff is generally assumed to be of the order of the Planck scale), a new model of nature will be needed. Specifically, the problem of combining quantum mechanics and gravity becomes an issue only at very high energies, and may well require a totally new kind of model.

Quantum gravity theory for the highest energy scales

The general approach to deriving a quantum gravity theory that is valid at even the highest energy scales is to assume that such a theory will be simple and elegant and, accordingly, to study symmetries and other clues offered by current theories that might suggest ways **to combine them** into a comprehensive, **unified theory**. One problem with this approach is that it is unknown whether quantum gravity will actually conform to a simple and elegant theory, as it should resolve the dual conundrums of special relativity with regard to the uniformity of acceleration and gravity, and general relativity with regard to spacetime curvature.

Such a theory is required in order to understand problems involving the combination of very high energy and very small dimensions of space, such as the behavior of black holes, and the origin of the universe.

Quantum mechanics and general relativity**Gravity Probe B (GP-B) has measured spacetime curvature near Earth to test related models in application of Einstein's general theory of relativity.****The graviton**

At present, one of the deepest problems in theoretical physics is harmonizing the theory of general relativity, which describes gravitation, and applies to large-scale structures (stars, planets, galaxies), with quantum mechanics, which describes the other three fundamental forces acting on the atomic scale. This problem must be put in the proper context, however. In particular, contrary to the popular claim that quantum mechanics and general relativity are fundamentally incompatible, one can demonstrate that the structure of general relativity essentially follows inevitably from the quantum mechanics of interacting theoretical spin-2 massless particles (called gravitons).

While there is no concrete proof of the existence of gravitons, quantized theories of matter may necessitate their existence¹ Supporting this theory is the observation that all fundamental forces except gravity have one or more known messenger particles, leading researchers to believe that at least one most likely does exist; they have dubbed these hypothetical particles *gravitons*. Many of the accepted notions of a unified theory of physics since the 1970s, including string theory, superstring theory, M-theory, loop quantum gravity, all assume, and to some degree depend upon, the existence of the graviton. Many researchers view the detection of the graviton as vital to validating their work.

The dilaton

The dilaton made its first appearance in Kaluza–Klein theory, a five-dimensional theory that combined gravitation and electromagnetism. Generally, it appears in string theory. More recently, it has appeared in the lower-dimensional many-bodied gravity problem based on the field theoretic approach of Roman Jackiw. The impetus arose from the fact that complete analytical solutions for the metric of a covariant N -body system have proven elusive in General Relativity. To simplify the problem, the number of dimensions was lowered to $(I+1)$ namely one spatial dimension and one temporal dimension. **This model problem, known as $R=T$ theory (as opposed to the general $G=T$ theory)** was amenable to exact solutions in terms of a generalization of the Lambert W function. It was also found that the field equation governing the dilaton (derived from differential geometry) was the Schrödinger equation and consequently amenable to quantization. Thus, one had a theory which combined gravity, quantization and even the electromagnetic interaction, promising ingredients of a fundamental physical theory. It is worth noting that the outcome revealed a previously unknown and already existing *natural link* between general relativity and quantum mechanics. However, this theory needs to be generalized in $(2+1)$ or $(3+1)$ dimensions although, in principle, the field equations are amenable to such generalization as shown with the inclusion of a one-graviton process and yielding the correct Newtonian limit in d dimensions if a dilaton is included. However, it is not yet clear what the full field equation will govern the dilaton in higher dimensions. This is further complicated by the fact that gravitons can propagate in $(3+1)$ dimensions and consequently that would imply gravitons and dilatons exist in the real world. Moreover, detection of the dilaton is expected to be even more elusive than the graviton. However, since this approach allows for the combination of gravitational, electromagnetic and quantum effects, their coupling could potentially lead to a means of vindicating the theory, through cosmology and perhaps even *experimentally*.

Nonrenormalizability of gravity

General relativity, like electromagnetism, is a classical field theory. One might expect that, as with electromagnetism, there should be a corresponding quantum field theory. However, gravity is perturbatively nonrenormalizable. For a quantum field theory to be well-defined according to this understanding of the subject, it must be asymptotically free or asymptotically safe. The theory must be characterized by a choice of *finitely many* parameters, which could, in principle, be set by experiment. For example, in quantum electrodynamics, these parameters are the charge and mass of the electron, as measured at a particular energy scale. On the other hand, in quantizing gravity, there are *infinitely many independent parameters* (counterterm coefficients) needed to define the theory. For a given choice of those parameters, one could make sense of the theory, but since we can never do infinitely many experiments to fix the values of every parameter, we do not have a meaningful physical theory:

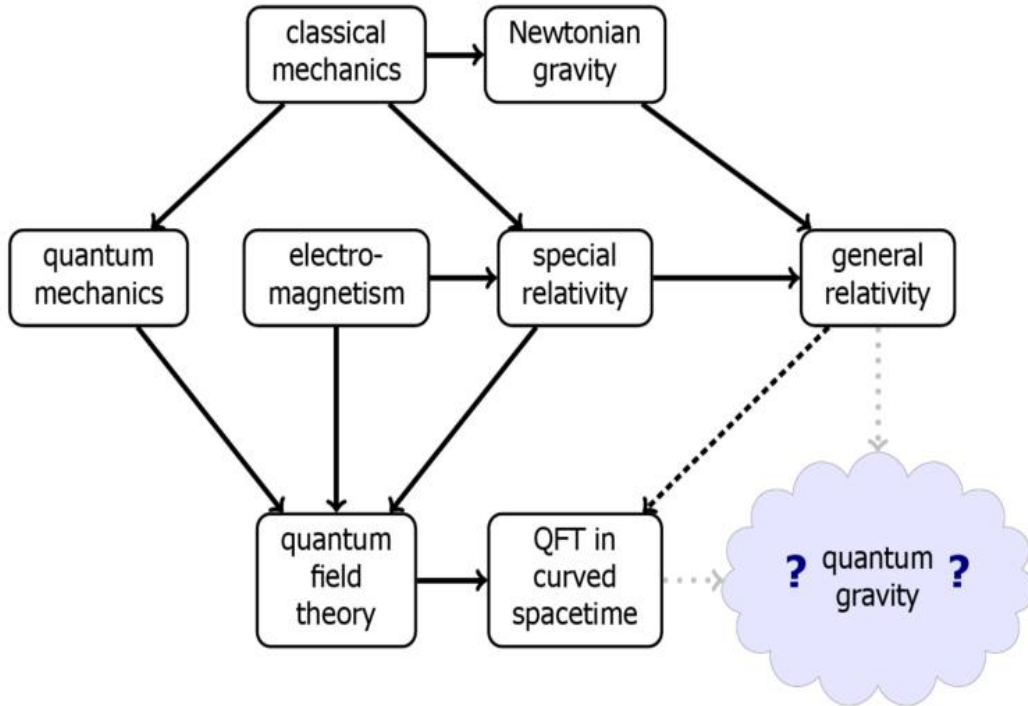
- At low energies, the logic of the renormalization group tells us that, despite the unknown choices of these infinitely many parameters, quantum gravity will reduce to the usual Einstein theory of general relativity.
- On the other hand, if we could probe very high energies where quantum effects take over, then *every one* of the infinitely many unknown parameters would begin to matter, and we could make no predictions at all.

As explained below, there is a way around this problem by treating QG as an effective field theory.

Any meaningful theory of quantum gravity that makes sense and is predictive at all energy scales must have some deep principle that reduces the infinitely many unknown parameters to a finite number that can then be measured.

- One possibility is that normal perturbation theory is not a reliable guide to the renormalizability of the theory, and that there really *is* a UV fixed point for gravity. Since this is a question of non-perturbative quantum field theory, it is difficult to find a reliable answer, but some people still pursue this option.
- Another possibility is that there are new symmetry principles that constrain the parameters and reduce them to a finite set. This is the route taken by string theory, where all of the excitations of the string essentially manifest themselves as new symmetries.

QUANTUM GRAVITY AS AN EFFECTIVE FIELD THEORY:



THE precise manner in which quantum-mechanical behaviour at the microscopic level underlies classical behaviour at the macroscopic level remains unclear, despite seventy years of theoretical investigation. Experimentally, the crossover between these regimes can be explored by looking for signatures of quantum-mechanical behaviour—such as tunneling—in macroscopic systems. Magnetic systems (such as small grains, spin glasses and thin films) are often investigated in this way because transitions between different magnetic states can be closely monitored. But transitions between states can be induced by thermal fluctuations, as well as by tunnelling, and definitive identification of macroscopic tunnelling events in these complex systems is therefore difficult. Here we report the results of low-temperature experiments on a single crystal composed of super-paramagnetic manganese clusters (Mn₁₂-ac), which clearly demonstrate the existence of quantum-mechanical tunnelling of the bulk magnetization. In an applied magnetic field, the magnetization shows hysteresis loops with a distinct 'staircase' structure: the steps occur at values of the applied field where the energies of different collective spin states of the manganese clusters coincide. At these special values of the field, relaxation from one spin state to another is enhanced above the thermally activated rate by the action of resonant quantum-mechanical tunnelling. These observations corroborate the results of similar experiments performed recently on a system of oriented crystallites made from a powdered sample.

Young's double slit experiment - Quantum mechanical behaviour

Young's double slit experiment represents the observation of an interference pattern consistent with a wave nature for objects that traverse the apparatus. This is emphasized in the figures 3 and 4

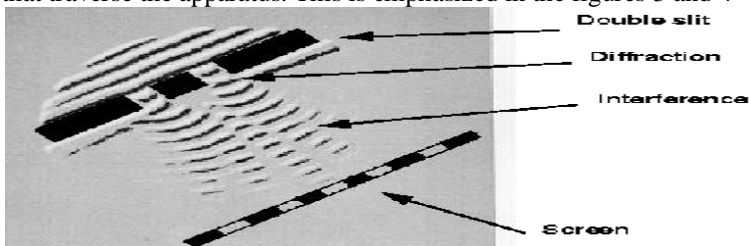


Figure 3: Young's double slit experiment with water waves.

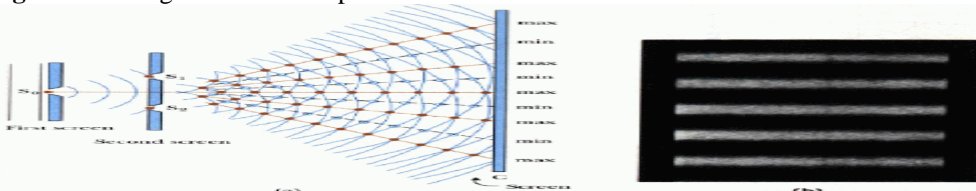


Figure 4: Young's double slit experiment, performed with either light or electrons leads to an interference pattern.

The diffraction and interference effects appear at first sight to be due to the beam of electrons, interfering with each other. However, the interference pattern still results even if only one electron traverses the apparatus at a time. In this case, the pattern is built up gradually from the statistically correlated impacts on many electrons arriving independently at the detection system. This effect is evidenced in figure 5.

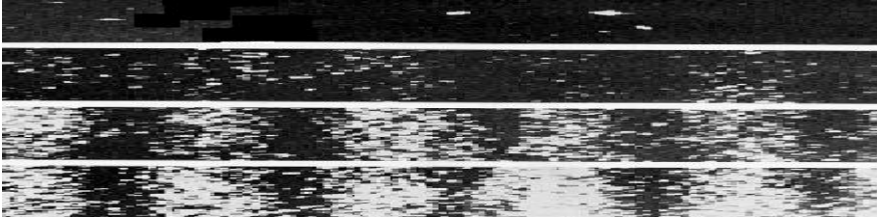


Figure 5: Young's double slit experiment, performed with electrons in such a way that only one electron is present in the apparatus at any one time.

We see that the electron must in some sense pass through both slits at once and then interfere with itself as it travels towards the detector. Young's double slit experiment has been performed many times in many different ways with electrons (and other particles). The inescapable conclusion is that each electron must be delocalized in both time and space over the apparatus.

Considering the analogies between Young's double slit experiment performed with water waves, electro-magnetic waves and with electrons, and considering the material of the foregoing section, we can now specify some properties for a new theory of mechanics, termed *wave mechanics*.

$$\Psi(\mathbf{r}, t)$$

1. There must be a wave function describing some fundamental property of matter. (We leave further physical interpretation of the wave function open to continuous debate through-out the course.)
2. As with the intensity pattern on the screen for water waves and light waves, the "observable" associated with the wave function indicating the probability of detection of the particle will be the intensity (square of the amplitude) of

$$|\Psi(\mathbf{r}, t)|^2 = \Psi(\mathbf{r}, t)\Psi^*(\mathbf{r}, t)$$

the wave. Mathematically, this is

$$\lambda = h/p$$

3. The wavelength in the wave function will be related to the de Broglie wavelength of the particle .
4. We would like to be able to proceed to develop a differential equation which would specify the time evolution of the wave function, consistent with the conservation of energy and momentum of physical systems.
5. The quantization of energy should arise in a natural way from this formalism, just as it does for other bounded systems that support oscillations.
6. Then we must develop the formalism to enable other observables than simple the probability of detection "position of the particle" to be determined. Examples would be the energy and momentum of the particle.
7. Note the judicious use of the word observable. The actual wave function itself has never yet been observed.

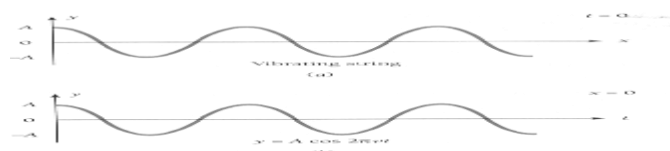
It is clear that an improved understanding of waves in physics is now necessary. To this end, some results from wave motion in physics are reviewed.

A transverse wave train, travelling on a string in the $+x$ -direction (as in figure 6) may be represented by

$$y(x, t) = A \cos 2\pi\nu \left(t - \frac{x}{v_p} \right) \tag{8}$$

where ν is the frequency of the wave and v_p is its *phase velocity*. The phase velocity is the velocity with which a point on the wave maintaining the same phase appears to be transported.

$$v_p = \lambda\nu \tag{9}$$



+x

Figure 6: A transverse wave train, travelling on a string in the +x-direction. It is more common to define the angular frequency (frequency in radians/sec rather than cycles/sec)

$$\omega = 2\pi\nu \quad (10)$$

and the wavenumber

$$k = \frac{2\pi}{\lambda} \quad (\text{by definition})$$

$$= \frac{\omega}{v_p} \quad (\text{substitution with the last two equations})$$

$$= \frac{|p|/\hbar}{\hbar} \quad (\text{using de Broglie's relation}) \quad (11)$$

$$\hbar = h/2\pi$$

where $\hbar = h/2\pi$. The wave equation for the wave moving in the +x-direction can now be written :

$$y(x, t) = A \cos(\omega t - kx) \quad (12)$$

In three dimensions, this equation would be

$$y(\mathbf{r}, t) = A \cos(\omega t - \mathbf{k} \cdot \mathbf{r}) \quad (13)$$

It turns out that in quantum mechanics, a particle will be described as a *wave packet*. By this, we mean a group of (usually infinitely many) waves which mutually interfere, creating a new wave form which exhibits some localization.

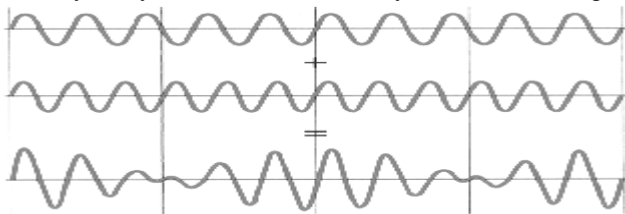


Figure 7: Two waves of nearly equal wave number combined coherently.

$$k \pm \Delta k$$

This can be illustrated by considering only two waves, of nearly equal wave number ($k \pm \Delta k$), and combining them coherently as in figure 7. Clearly, performing this process with many more waves would achieve a better localization of the wave packet, as illustrated in figure 8.



Figure 8: Localisation of a wave packet by combination of many waves.

We find that

$$y = A \cos[(\omega + \Delta\omega/2)t - (k + \Delta k/2)x] + A \cos[(\omega - \Delta\omega/2)t - (k - \Delta k/2)x]$$

... use trigonometric double angle formulae

$$= 2A \cos(\omega t - kx) \cos\left(\frac{\Delta\omega}{2}t - \frac{\Delta k}{2}x\right) \quad (14)$$

The combined wave train exhibits the phenomenon of "beats" as shown in figure 7 where an amplitude modulation envelope is superimposed on the original wave train. The amplitude modulation envelope will clearly have the frequency $\nu_g = \Delta\omega/\Delta k$, wave

number Δk and hence the velocity

$$v_g = \Delta\omega/\Delta k$$

The velocity of the localised group of waves (or beat) is known as the group velocity.

$$v_g = v \quad \text{and} \quad v_p = c^2/v \quad *(15)$$

This must be compared to the phase velocity of each wave train making up the wave packet

$$v_p = \frac{\omega}{k} \quad *(16)$$

$$v_g = v \quad \text{and} \quad v_p = c^2/v \quad *(17)$$

Thus the de Broglie wave group associated with a moving particle travels with the same velocity as the particle. The de Broglie waves in the packet have superluminal velocities, however, these do not represent the motion of the particle, and therefore the special relativity is not violated.

Finally, the form of the wave equation, yielding the above expression for a wave train is

$$y(x,t) = -iA \sin(\omega t - kx) \quad *(18)$$

We can verify that $y(x,t) = Ae^{-i(\omega t - kx)}$ is indeed a solution of the wave equation.

$$y(x,t) = -iA \sin(\omega t - kx)$$

Clearly $y(x,t) = Ae^{-i(\omega t - kx)}$ is also a solution of the wave equation. It follows that

$$y(x,t) = Ae^{-i(\omega t - kx)} \quad *(19)$$

is also a solution of the wave equation. This can be verified by direct substitution, or by exploiting the fact that any linear combination of solutions of the wave equation is itself a solution of the wave equation

$$e^{-i\theta} = \cos\theta - i \sin\theta$$

(Hint: .)

In fact a second order differential equation should have two constants of integration, which are determined by the boundary conditions of the specific problem. We can show that for the equation above, we could write

$$y(x,t) = A \cos(\omega t - kx) + B \sin(\omega t - kx) \quad *(20)$$

or

$$y(x,t) = C e^{-i(\omega t - kx)} + D e^{+i(\omega t - kx)} \quad *(21)$$

Also find the relationship between the two sets of coefficients. We will use the former set when discussing standing waves (like a guitar string), and the latter set when discussing travelling waves (like a ripple on a large pond)..

The differential system of this model is now *

$$\frac{dG_{36}}{dt} = (a_{36})^{(7)} G_{37} - [(a'_{36})^{(7)} + (a''_{36})^{(7)}(T_{37}, t)] G_{36} \quad *19$$

$$\frac{dG_{37}}{dt} = (a_{37})^{(7)} G_{36} - [(a'_{37})^{(7)} + (a''_{37})^{(7)}(T_{37}, t)] G_{37} \quad *20$$

$$\frac{dG_{38}}{dt} = (a_{38})^{(7)} G_{37} - [(a'_{38})^{(7)} + (a''_{38})^{(7)}(T_{37}, t)] G_{38} \quad *21$$

$$\frac{dT_{36}}{dt} = (b_{36})^{(7)} T_{37} - [(b'_{36})^{(7)} - (b''_{36})^{(7)}((G_{39}), t)] T_{36} \quad *22$$

$$\frac{dT_{37}}{dt} = (b_{37})^{(7)} T_{36} - [(b'_{37})^{(7)} - (b''_{37})^{(7)}((G_{39}), t)] T_{37}$$

*23

$$\frac{dT_{38}}{dt} = (b_{38})^{(7)}T_{37} - [(b'_{38})^{(7)} - (b''_{38})^{(7)}((G_{39}), t)]T_{38} \quad *24$$

$$+(a''_{36})^{(7)}(T_{37}, t) = \text{First augmentation factor}^*$$

$$-(b'_{36})^{(7)}((G_{39}), t) = \text{First detritions factor}^*$$

Where we suppose*

(A) $(a_i)^{(7)}, (a'_i)^{(7)}, (a''_i)^{(7)}, (b_i)^{(7)}, (b'_i)^{(7)}, (b''_i)^{(7)} > 0, \quad i, j = 36, 37, 38$

(B) The functions $(a''_i)^{(7)}, (b''_i)^{(7)}$ are positive continuous increasing and bounded.

Definition of $(p_i)^{(7)}, (r_i)^{(7)}$:

$$(a''_i)^{(7)}(T_{37}, t) \leq (p_i)^{(7)} \leq (\hat{A}_{36})^{(7)} \quad *25$$

$$(b''_i)^{(7)}(G, t) \leq (r_i)^{(7)} \leq (b'_i)^{(7)} \leq (\hat{B}_{36})^{(7)} \quad *26$$

(C) $\lim_{T_2 \rightarrow \infty} (a''_i)^{(7)}(T_{37}, t) = (p_i)^{(7)}$
 $\lim_{G \rightarrow \infty} (b''_i)^{(7)}((G_{39}), t) = (r_i)^{(7)}$

Definition of $(\hat{A}_{36})^{(7)}, (\hat{B}_{36})^{(7)}$: *27

Where $(\hat{A}_{36})^{(7)}, (\hat{B}_{36})^{(7)}, (p_i)^{(7)}, (r_i)^{(7)}$ are positive constants

and $i = 36, 37, 38$ *28

They satisfy Lipschitz condition:

$$|(a''_i)^{(7)}(T'_{37}, t) - (a''_i)^{(7)}(T_{37}, t)| \leq (\hat{k}_{36})^{(7)}|T'_{37} - T_{37}|e^{-(\hat{M}_{36})^{(7)}t} \quad *29$$

$$|(b''_i)^{(7)}((G_{39})', t) - (b''_i)^{(7)}((G_{39}), (T_{39}))| < (\hat{k}_{36})^{(7)}\|((G_{39}) - (G_{39})')\|e^{-(\hat{M}_{36})^{(7)}t} \quad *30$$

With the Lipschitz condition, we place a restriction on the behavior of functions $(a''_i)^{(7)}(T'_{37}, t)$ and $(a''_i)^{(7)}(T_{37}, t) \cdot (T'_{37}, t)$ and (T_{37}, t) are points belonging to the interval $[(\hat{k}_{36})^{(7)}, (\hat{M}_{36})^{(7)}]$. It is to be noted that $(a''_i)^{(7)}(T_{37}, t)$ is uniformly continuous. In the eventuality of the fact, that if $(\hat{M}_{36})^{(7)} = 7$ then the function $(a''_i)^{(7)}(T_{37}, t)$, the **first augmentation coefficient would be continuous**.*

Definition of $(\hat{M}_{36})^{(7)}, (\hat{k}_{36})^{(7)}$:

(D) $(\hat{M}_{36})^{(7)}, (\hat{k}_{36})^{(7)}$, are positive constants

$$\frac{(a_i)^{(7)}}{(\hat{M}_{36})^{(7)}}, \frac{(b_i)^{(7)}}{(\hat{M}_{36})^{(7)}} < 1 \quad *31$$

Definition of $(\hat{P}_{36})^{(7)}, (\hat{Q}_{36})^{(7)}$:

(E) There exists two constants $(\hat{P}_{36})^{(7)}$ and $(\hat{Q}_{36})^{(7)}$ which together with $(\hat{M}_{36})^{(7)}, (\hat{k}_{36})^{(7)}, (\hat{A}_{36})^{(7)}$ and $(\hat{B}_{36})^{(7)}$ and the constants $(a_i)^{(7)}, (a'_i)^{(7)}, (b_i)^{(7)}, (b'_i)^{(7)}, (p_i)^{(7)}, (r_i)^{(7)}, i = 36, 37, 38$, satisfy the inequalities

$$\frac{1}{(\hat{M}_{36})^{(7)}} [(a_i)^{(7)} + (a'_i)^{(7)} + (\hat{A}_{36})^{(7)} + (\hat{P}_{36})^{(7)} (\hat{k}_{36})^{(7)}] < 1$$

$$\frac{1}{(\hat{M}_{36})^{(7)}} [(b_i)^{(7)} + (b'_i)^{(7)} + (\hat{B}_{36})^{(7)} + (\hat{Q}_{36})^{(7)} (\hat{k}_{36})^{(7)}] < 1 \quad *32 \quad *33$$

Theorem 7: if the conditions (A)-(E) above are fulfilled, there exists a solution satisfying the conditions

Definition of $G_i(0), T_i(0)$:

$$G_i(t) \leq (\hat{P}_{36})^{(7)} e^{(\hat{M}_{36})^{(7)}t}, \quad \boxed{G_i(0) = G_i^0 > 0}$$

$$T_i(t) \leq (\hat{Q}_{36})^{(7)} e^{(\hat{M}_{36})^{(7)}t}, \quad \boxed{T_i(0) = T_i^0 > 0}$$

Proof:

Consider operator $\mathcal{A}^{(7)}$ defined on the space of sextuples of continuous functions $G_i, T_i: \mathbb{R}_+ \rightarrow \mathbb{R}_+$ which satisfy

$$G_i(0) = G_i^0, T_i(0) = T_i^0, G_i^0 \leq (\hat{P}_{36})^{(7)}, T_i^0 \leq (\hat{Q}_{36})^{(7)}, \quad *34$$

$$0 \leq G_i(t) - G_i^0 \leq (\hat{P}_{36})^{(7)} e^{(\hat{M}_{36})^{(7)}t} \quad *35$$

$$0 \leq T_i(t) - T_i^0 \leq (\hat{Q}_{36})^{(7)} e^{(\hat{M}_{36})^{(7)}t} \quad *36$$

By

$$\bar{G}_{36}(t) = G_{36}^0 + \int_0^t [(a_{36})^{(7)} G_{37}(s_{(36)}) - ((a'_{36})^{(7)} + a''_{36})^{(7)} (T_{37}(s_{(36)}), s_{(36)})] G_{36}(s_{(36)}) ds_{(36)} \quad *37$$

$$\bar{G}_{37}(t) = G_{37}^0 + \int_0^t [(a_{37})^{(7)} G_{36}(s_{(36)}) - ((a'_{37})^{(7)} + (a''_{37})^{(7)} (T_{37}(s_{(36)}), s_{(36)}))] G_{37}(s_{(36)}) ds_{(36)} \quad *38$$

$$\bar{G}_{38}(t) = G_{38}^0 + \int_0^t [(a_{38})^{(7)} G_{37}(s_{(36)}) - ((a'_{38})^{(7)} + (a''_{38})^{(7)} (T_{37}(s_{(36)}), s_{(36)}))] G_{38}(s_{(36)}) ds_{(36)} \quad *39$$

$$\bar{T}_{36}(t) = T_{36}^0 + \int_0^t [(b_{36})^{(7)} T_{37}(s_{(36)}) - ((b'_{36})^{(7)} - (b''_{36})^{(7)} (G(s_{(36)}), s_{(36)}))] T_{36}(s_{(36)}) ds_{(36)} \quad *40$$

$$\bar{T}_{37}(t) = T_{37}^0 + \int_0^t [(b_{37})^{(7)} T_{36}(s_{(36)}) - ((b'_{37})^{(7)} - (b''_{37})^{(7)} (G(s_{(36)}), s_{(36)}))] T_{37}(s_{(36)}) ds_{(36)} \quad *41$$

$$\bar{T}_{38}(t) = T_{38}^0 + \int_0^t [(b_{38})^{(7)} T_{37}(s_{(36)}) - ((b'_{38})^{(7)} - (b''_{38})^{(7)} (G(s_{(36)}), s_{(36)}))] T_{38}(s_{(36)}) ds_{(36)}$$

Where $s_{(36)}$ is the integrand that is integrated over an interval $(0, t)$ *42

(a) The operator $\mathcal{A}^{(7)}$ maps the space of functions satisfying 37,35,36 into itself. Indeed it is obvious that

$$G_{36}(t) \leq G_{36}^0 + \int_0^t [(a_{36})^{(7)} (G_{37}^0 + (\hat{P}_{36})^{(7)} e^{(\hat{M}_{36})^{(7)}s_{(36)}})] ds_{(36)} = (1 + (a_{36})^{(7)}t) G_{37}^0 + \frac{(a_{36})^{(7)} (\hat{P}_{36})^{(7)}}{(\hat{M}_{36})^{(7)}} (e^{(\hat{M}_{36})^{(7)}t} - 1) \quad *43$$

From which it follows that

$$(G_{36}(t) - G_{36}^0) e^{-(\hat{M}_{36})^{(7)}t} \leq \frac{(a_{36})^{(7)}}{(\hat{M}_{36})^{(7)}} \left[((\hat{P}_{36})^{(7)} + G_{37}^0) e^{-\left(\frac{(\hat{P}_{36})^{(7)} + G_{37}^0}{G_{37}^0}\right)} + (\hat{P}_{36})^{(7)} \right]$$

(G_i^0) is as defined in the statement of theorem 1 *44

Analogous inequalities hold also for $G_{37}, G_{38}, T_{36}, T_{37}, T_{38}$

It is now sufficient to take $\frac{(a_i)^{(7)}}{(\hat{M}_{36})^{(7)}}, \frac{(b_i)^{(7)}}{(\hat{M}_{36})^{(7)}} < 7$ and to choose

$(\hat{P}_{36})^{(7)}$ and $(\hat{Q}_{36})^{(7)}$ large to have

$$\frac{(a_i)^{(7)}}{(\hat{M}_{36})^{(7)}} \left[(\hat{P}_{36})^{(7)} + ((\hat{P}_{36})^{(7)} + G_j^0) e^{-\left(\frac{(\hat{P}_{36})^{(7)} + G_j^0}{G_j^0}\right)} \right] \leq (\hat{P}_{36})^{(7)} \quad *45$$

$$\frac{(b_i)^{(7)}}{(\hat{M}_{36})^{(7)}} \left[((\hat{Q}_{36})^{(7)} + T_j^0) e^{-\left(\frac{(\hat{Q}_{36})^{(7)} + T_j^0}{T_j^0}\right)} + (\hat{Q}_{36})^{(7)} \right] \leq (\hat{Q}_{36})^{(7)} \quad *46$$

In order that the operator $\mathcal{A}^{(7)}$ transforms the space of sextuples of functions G_i, T_i satisfying 37,35,36 into itself

The operator $\mathcal{A}^{(7)}$ is a contraction with respect to the metric

$$d\left(\left((G_{39})^{(1)}, (T_{39})^{(1)}\right), \left((G_{39})^{(2)}, (T_{39})^{(2)}\right)\right) = \sup_i \left\{ \max_{t \in \mathbb{R}_+} |G_i^{(1)}(t) - G_i^{(2)}(t)| e^{-(\hat{M}_{36})^{(7)}t}, \max_{t \in \mathbb{R}_+} |T_i^{(1)}(t) - T_i^{(2)}(t)| e^{-(\hat{M}_{36})^{(7)}t} \right\}$$

Indeed if we denote

Definition of $(\widetilde{G}_{39}), (\widetilde{T}_{39}) :$

$$((\widetilde{G}_{39}), (\widetilde{T}_{39})) = \mathcal{A}^{(7)}((G_{39}), (T_{39}))$$

It results

$$|\widetilde{G}_{36}^{(1)} - \widetilde{G}_i^{(2)}| \leq \int_0^t (a_{36})^{(7)} |G_{37}^{(1)} - G_{37}^{(2)}| e^{-(\widetilde{M}_{36})^{(7)}s_{(36)}} e^{(\widetilde{M}_{36})^{(7)}s_{(36)}} ds_{(36)} + *48$$

$$\int_0^t \{(a_{36}')^{(7)} |G_{36}^{(1)} - G_{36}^{(2)}| e^{-(\widetilde{M}_{36})^{(7)}s_{(36)}} e^{-(\widetilde{M}_{36})^{(7)}s_{(36)}} + (a_{36}'')^{(7)}(T_{37}^{(1)}, s_{(36)}) |G_{36}^{(1)} - G_{36}^{(2)}| e^{-(\widetilde{M}_{36})^{(7)}s_{(36)}} e^{(\widetilde{M}_{36})^{(7)}s_{(36)}} + *49$$

$$G_{36}^{(2)} | (a_{36}'')^{(7)}(T_{37}^{(1)}, s_{(36)}) - (a_{36}'')^{(7)}(T_{37}^{(2)}, s_{(36)}) | e^{-(\widetilde{M}_{36})^{(7)}s_{(36)}} e^{(\widetilde{M}_{36})^{(7)}s_{(36)}} ds_{(36)} *47$$

Where $s_{(36)}$ represents integrand that is integrated over the interval $[0, t]$

From the hypotheses it follows that:

$$|(G_{39})^{(1)} - (G_{39})^{(2)}| e^{-(\widetilde{M}_{36})^{(7)}t} \leq \frac{1}{(\widetilde{M}_{36})^{(7)}} ((a_{36})^{(7)} + (a_{36}')^{(7)} + (\widehat{A}_{36})^{(7)} + (\widehat{P}_{36})^{(7)} (\widehat{k}_{36})^{(7)}) d(((G_{39})^{(1)}, (T_{39})^{(1)}); (G_{39})^{(2)}, (T_{39})^{(2)}) *50$$

And analogous inequalities for G_i and T_i . Taking into account the hypothesis (37,35,36) the result follows

Remark 7: The fact that we supposed $(a_{36}'')^{(7)}$ and $(b_{36}'')^{(7)}$ depending also on t can be considered as not conformal with the reality, however we have put this hypothesis in order that we can postulate condition necessary to prove the uniqueness of the solution bounded by $(\widehat{P}_{36})^{(7)} e^{(\widetilde{M}_{36})^{(7)}t}$ and $(\widehat{Q}_{36})^{(7)} e^{(\widetilde{M}_{36})^{(7)}t}$ respectively of \mathbb{R}_+ .

If instead of proving the existence of the solution on \mathbb{R}_+ , we have to prove it only on a compact then it suffices to consider that $(a_i'')^{(7)}$ and $(b_i'')^{(7)}, i = 36,37,38$ depend only on T_{37} and respectively on (G_{39}) (and not on t) and hypothesis can be replaced by a usual Lipschitz condition.

*51

Remark 2: There does not exist any t where $G_i(t) = 0$ and $T_i(t) = 0$

$$G_i(t) \geq G_i^0 e^{-\int_0^t \{(a_i')^{(7)} - (a_i'')^{(7)}(T_{37}(s_{(36)}), s_{(36)})\} ds_{(36)}} \geq 0$$

$$T_i(t) \geq T_i^0 e^{-(b_i')^{(7)}t} > 0 \text{ for } t > 0 *52$$

Definition of $((\widetilde{M}_{36})^{(7)})_1, ((\widetilde{M}_{36})^{(7)})_2$ and $((\widetilde{M}_{36})^{(7)})_3 :$

Remark 3: if G_{36} is bounded, the same property have also G_{37} and G_{38} . indeed if

$$G_{36} < (\widetilde{M}_{36})^{(7)} \text{ it follows } \frac{dG_{37}}{dt} \leq ((\widetilde{M}_{36})^{(7)})_1 - (a_{37}')^{(7)} G_{37} \text{ and by integrating}$$

$$G_{37} \leq ((\widetilde{M}_{36})^{(7)})_2 = G_{37}^0 + 2(a_{37})^{(7)} ((\widetilde{M}_{36})^{(7)})_1 / (a_{37}')^{(7)}$$

In the same way, one can obtain

$$G_{38} \leq ((\widetilde{M}_{36})^{(7)})_3 = G_{38}^0 + 2(a_{38})^{(7)} ((\widetilde{M}_{36})^{(7)})_2 / (a_{38}')^{(7)}$$

If G_{37} or G_{38} is bounded, the same property follows for G_{36}, G_{38} and G_{36}, G_{37} respectively.

*53

Remark 7: If G_{36} is bounded, from below, the same property holds for G_{37} and G_{38} . The proof is analogous with the preceding one. An analogous property is true if G_{37} is bounded from below.

*54

Remark 5: If T_{36} is bounded from below and $\lim_{t \rightarrow \infty} ((b_i'')^{(7)}((G_{39})(t), t)) = (b_{37}')^{(7)}$ then $T_{37} \rightarrow \infty$.

Definition of $(m)^{(7)}$ and $\varepsilon_7 :$

Indeed let t_7 be so that for $t > t_7$

$$(b_{37})^{(7)} - (b'_i)^{(7)}((G_{39})(t), t) < \varepsilon_7, T_{36}(t) > (m)^{(7)}$$

*55

Then $\frac{dT_{37}}{dt} \geq (a_{37})^{(7)}(m)^{(7)} - \varepsilon_7 T_{37}$ which leads to

$$T_{37} \geq \left(\frac{(a_{37})^{(7)}(m)^{(7)}}{\varepsilon_7} \right) (1 - e^{-\varepsilon_7 t}) + T_{37}^0 e^{-\varepsilon_7 t} \text{ If we take } t \text{ such that } e^{-\varepsilon_7 t} = \frac{1}{2} \text{ it results}$$

$T_{37} \geq \left(\frac{(a_{37})^{(7)}(m)^{(7)}}{2} \right)$, $t = \log \frac{2}{\varepsilon_7}$ By taking now ε_7 sufficiently small one sees that T_{37} is unbounded. The same property holds for T_{38} if $\lim_{t \rightarrow \infty} (b''_{38})^{(7)}((G_{39})(t), t) = (b'_{38})^{(7)}$

We now state a more precise theorem about the behaviors at infinity of the solutions of equations 37 to 72

*

Behavior of the solutions of the system Quantum Information and Quantum mechanical Behaviour:

Theorem 2: If we denote and define

Definition of $(\sigma_1)^{(7)}, (\sigma_2)^{(7)}, (\tau_1)^{(7)}, (\tau_2)^{(7)}$:

(a) $(\sigma_1)^{(7)}, (\sigma_2)^{(7)}, (\tau_1)^{(7)}, (\tau_2)^{(7)}$ four constants satisfying

$$-(\sigma_2)^{(7)} \leq -(a'_{36})^{(7)} + (a'_{37})^{(7)} - (a''_{36})^{(7)}(T_{37}, t) + (a''_{37})^{(7)}(T_{37}, t) \leq -(\sigma_1)^{(7)}$$

$$-(\tau_2)^{(7)} \leq -(b'_{36})^{(7)} + (b'_{37})^{(7)} - (b''_{36})^{(7)}((G_{39}), t) - (b''_{37})^{(7)}((G_{39}), t) \leq -(\tau_1)^{(7)}$$

*56

57

58

Definition of $(v_1)^{(7)}, (v_2)^{(7)}, (u_1)^{(7)}, (u_2)^{(7)}, v^{(7)}, u^{(7)}$:

(b) By $(v_1)^{(7)} > 0, (v_2)^{(7)} < 0$ and respectively $(u_1)^{(7)} > 0, (u_2)^{(7)} < 0$ the roots of the equations $(a_{37})^{(7)}(v^{(7)})^2 + (\sigma_1)^{(7)}v^{(7)} - (a_{36})^{(7)} = 0$ and $(b_{37})^{(7)}(u^{(7)})^2 + (\tau_1)^{(7)}u^{(7)} - (b_{36})^{(7)} = 0$ and

*59

60

61

Definition of $(\bar{v}_1)^{(7)}, (\bar{v}_2)^{(7)}, (\bar{u}_1)^{(7)}, (\bar{u}_2)^{(7)}$:

By $(\bar{v}_1)^{(7)} > 0, (\bar{v}_2)^{(7)} < 0$ and respectively $(\bar{u}_1)^{(7)} > 0, (\bar{u}_2)^{(7)} < 0$ the roots of the equations $(a_{37})^{(7)}(v^{(7)})^2 + (\sigma_2)^{(7)}v^{(7)} - (a_{36})^{(7)} = 0$

and $(b_{37})^{(7)}(u^{(7)})^2 + (\tau_2)^{(7)}u^{(7)} - (b_{36})^{(7)} = 0$

Definition of $(m_1)^{(7)}, (m_2)^{(7)}, (\mu_1)^{(7)}, (\mu_2)^{(7)}, (v_0)^{(7)}$:-

(c) If we define $(m_1)^{(7)}, (m_2)^{(7)}, (\mu_1)^{(7)}, (\mu_2)^{(7)}$ by

$$(m_2)^{(7)} = (v_0)^{(7)}, (m_1)^{(7)} = (v_1)^{(7)}, \text{ if } (v_0)^{(7)} < (v_1)^{(7)}$$

$$(m_2)^{(7)} = (v_1)^{(7)}, (m_1)^{(7)} = (\bar{v}_1)^{(7)}, \text{ if } (v_1)^{(7)} < (v_0)^{(7)} < (\bar{v}_1)^{(7)},$$

$$\text{and } (v_0)^{(7)} = \frac{a_{36}^0}{a_{37}^0}$$

$$(m_2)^{(7)} = (v_1)^{(7)}, (m_1)^{(7)} = (v_0)^{(7)}, \text{ if } (\bar{v}_1)^{(7)} < (v_0)^{(7)}$$

*62

63

64

65

66

67

and analogously

$$(\mu_2)^{(7)} = (u_0)^{(7)}, (\mu_1)^{(7)} = (u_1)^{(7)}, \text{ if } (u_0)^{(7)} < (u_1)^{(7)}$$

$$(\mu_2)^{(7)} = (u_1)^{(7)}, (\mu_1)^{(7)} = (\bar{u}_1)^{(7)}, \text{ if } (u_1)^{(7)} < (u_0)^{(7)} < (\bar{u}_1)^{(7)},$$

$$\text{and } (u_0)^{(7)} = \frac{T_{36}^0}{T_{37}^0}$$

$(\mu_2)^{(7)} = (u_1)^{(7)}, (\mu_1)^{(7)} = (u_0)^{(7)}$, if $(\bar{u}_1)^{(7)} < (u_0)^{(7)}$ where $(u_1)^{(7)}, (\bar{u}_1)^{(7)}$ are defined by 59 and 67 respectively

*68

69

70

Then the solution of the system Quantum Information(machine-Computer) and Quantum Mechanical Behaviour satisfies the inequalities

$$G_{36}^0 e^{((S_1)^{(7)} - (p_{36})^{(7)})t} \leq G_{36}(t) \leq G_{36}^0 e^{(S_1)^{(7)}t}$$

where $(p_i)^{(7)}$ is defined in the foregoing

*71

$$\frac{1}{(m_7)^{(7)}} G_{36}^0 e^{((S_1)^{(7)} - (p_{36})^{(7)})t} \leq G_{37}(t) \leq \frac{1}{(m_2)^{(7)}} G_{36}^0 e^{(S_1)^{(7)}t}$$

*72

$$\left(\frac{(a_{38})^{(7)} G_{36}^0}{(m_1)^{(7)} ((S_1)^{(7)} - (p_{36})^{(7)} - (S_2)^{(7)})} \left[e^{((S_1)^{(7)} - (p_{36})^{(7)})t} - e^{-(S_2)^{(7)}t} \right] + G_{38}^0 e^{-(S_2)^{(7)}t} \right) \leq G_{38}(t) \leq \frac{(a_{38})^{(7)} G_{36}^0}{(m_2)^{(7)} ((S_1)^{(7)} - (a'_{38})^{(7)})} \left[e^{(S_1)^{(7)}t} - e^{-(a'_{38})^{(7)}t} \right] + G_{38}^0 e^{-(a'_{38})^{(7)}t}$$

*73

$$T_{36}^0 e^{(R_1)^{(7)}t} \leq T_{36}(t) \leq T_{36}^0 e^{((R_1)^{(7)} + (r_{36})^{(7)})t}$$

*74

$$\frac{1}{(\mu_1)^{(7)}} T_{36}^0 e^{(R_1)^{(7)}t} \leq T_{36}(t) \leq \frac{1}{(\mu_2)^{(7)}} T_{36}^0 e^{((R_1)^{(7)} + (r_{36})^{(7)})t}$$

*75

$$\frac{(b_{38})^{(7)} T_{36}^0}{(\mu_1)^{(7)} ((R_1)^{(7)} - (b'_{38})^{(7)})} \left[e^{(R_1)^{(7)}t} - e^{-(b'_{38})^{(7)}t} \right] + T_{38}^0 e^{-(b'_{38})^{(7)}t} \leq T_{38}(t) \leq$$

$$\frac{(a_{38})^{(7)} T_{36}^0}{(\mu_2)^{(7)} ((R_1)^{(7)} + (r_{36})^{(7)} + (R_2)^{(7)})} \left[e^{((R_1)^{(7)} + (r_{36})^{(7)})t} - e^{-(R_2)^{(7)}t} \right] + T_{38}^0 e^{-(R_2)^{(7)}t}$$

*76

Definition of $(S_1)^{(7)}, (S_2)^{(7)}, (R_1)^{(7)}, (R_2)^{(7)}$:-

$$\text{Where } (S_1)^{(7)} = (a_{36})^{(7)}(m_2)^{(7)} - (a'_{36})^{(7)}$$

$$(S_2)^{(7)} = (a_{38})^{(7)} - (p_{38})^{(7)}$$

$$(R_1)^{(7)} = (b_{36})^{(7)}(\mu_2)^{(7)} - (b'_{36})^{(7)}$$

$$(R_2)^{(7)} = (b'_{38})^{(7)} - (r_{38})^{(7)} \quad *77$$

78

79

Proof From the sytemal equations of Quantum Information and Quantum Mechanical Behaviour, and the resultant equations we get:

$$\frac{dv^{(7)}}{dt} = (a_{36})^{(7)} - \left((a'_{36})^{(7)} - (a'_{37})^{(7)} + (a''_{36})^{(7)}(T_{37}, t) \right) - (a''_{37})^{(7)}(T_{37}, t)v^{(7)} - (a_{37})^{(7)}v^{(7)}$$

Definition of $v^{(7)}$:-

$$v^{(7)} = \frac{G_{36}}{G_{37}}$$

It follows

$$- \left((a_{37})^{(7)}(v^{(7)})^2 + (\sigma_2)^{(7)}v^{(7)} - (a_{36})^{(7)} \right) \leq \frac{dv^{(7)}}{dt} \leq - \left((a_{37})^{(7)}(v^{(7)})^2 + (\sigma_1)^{(7)}v^{(7)} - (a_{36})^{(7)} \right)$$

From which one obtains

Definition of $(\bar{v}_1)^{(7)}, (v_0)^{(7)}$:-

I. For $0 < \boxed{(v_0)^{(7)} = \frac{G_{36}^0}{G_{37}^0}} < (v_1)^{(7)} < (\bar{v}_1)^{(7)}$

$$v^{(7)}(t) \geq \frac{(v_1)^{(7)} + (C)^{(7)}(v_2)^{(7)} e^{[-(a_{37})^{(7)}(v_1)^{(7)} - (v_0)^{(7)}]t}}{1 + (C)^{(7)} e^{[-(a_{37})^{(7)}(v_1)^{(7)} - (v_0)^{(7)}]t}}, \quad \boxed{(C)^{(7)} = \frac{(v_1)^{(7)} - (v_0)^{(7)}}{(v_0)^{(7)} - (v_2)^{(7)}}$$

it follows $(v_0)^{(7)} \leq v^{(7)}(t) \leq (v_1)^{(7)}$ *80

81

In the same manner, we get

$$v^{(7)}(t) \leq \frac{(\bar{v}_1)^{(7)} + (\bar{C})^{(7)}(\bar{v}_2)^{(7)} e^{[-(a_{37})^{(7)}(\bar{v}_1)^{(7)} - (\bar{v}_2)^{(7)}]t}}{1 + (\bar{C})^{(7)} e^{[-(a_{37})^{(7)}(\bar{v}_1)^{(7)} - (\bar{v}_2)^{(7)}]t}}, \quad \boxed{(\bar{C})^{(7)} = \frac{(\bar{v}_1)^{(7)} - (v_0)^{(7)}}{(v_0)^{(7)} - (\bar{v}_2)^{(7)}}$$

From which we deduce $(v_0)^{(7)} \leq v^{(7)}(t) \leq (\bar{v}_1)^{(7)}$ *82

83

II. If $0 < (v_1)^{(7)} < (v_0)^{(7)} = \frac{G_{36}^0}{G_{37}^0} < (\bar{v}_1)^{(7)}$ we find like in the previous case,

$$(v_1)^{(7)} \leq \frac{(v_1)^{(7)} + (C)^{(7)}(v_2)^{(7)} e^{[-(a_{37})^{(7)}(v_1)^{(7)} - (v_2)^{(7)}]t}}{1 + (C)^{(7)} e^{[-(a_{37})^{(7)}(v_1)^{(7)} - (v_2)^{(7)}]t}} \leq v^{(7)}(t) \leq$$

$$\frac{(\bar{v}_1)^{(7)} + (\bar{C})^{(7)}(\bar{v}_2)^{(7)} e^{[-(a_{37})^{(7)}(\bar{v}_1)^{(7)} - (\bar{v}_2)^{(7)}]t}}{1 + (\bar{C})^{(7)} e^{[-(a_{37})^{(7)}(\bar{v}_1)^{(7)} - (\bar{v}_2)^{(7)}]t}} \leq (\bar{v}_1)^{(7)} \quad *84$$

III. If $0 < (v_1)^{(7)} \leq (\bar{v}_1)^{(7)} \leq \boxed{(v_0)^{(7)} = \frac{G_{36}^0}{G_{37}^0}}$, we obtain

$$(v_1)^{(7)} \leq v^{(7)}(t) \leq \frac{(\bar{v}_1)^{(7)} + (\bar{C})^{(7)}(\bar{v}_2)^{(7)} e^{[-(a_{37})^{(7)}(\bar{v}_1)^{(7)} - (\bar{v}_2)^{(7)}]t}}{1 + (\bar{C})^{(7)} e^{[-(a_{37})^{(7)}(\bar{v}_1)^{(7)} - (\bar{v}_2)^{(7)}]t}} \leq (v_0)^{(7)}$$

And so with the notation of the first part of condition (c), we have

Definition of $v^{(7)}(t)$:-

$$(m_2)^{(7)} \leq v^{(7)}(t) \leq (m_1)^{(7)}, \quad \boxed{v^{(7)}(t) = \frac{G_{36}(t)}{G_{37}(t)}}$$

In a completely analogous way, we obtain

Definition of $u^{(7)}(t)$:-

$$(\mu_2)^{(7)} \leq u^{(7)}(t) \leq (\mu_1)^{(7)}, \quad \boxed{u^{(7)}(t) = \frac{T_{36}(t)}{T_{37}(t)}}$$

Now, using this result and replacing it in system equations for the system Quantum Information and Quantum Mechanical Behaviour we obtain:

Particular case :

If $(a_{36})^{(7)} = (a_{37})^{(7)}$, then $(\sigma_1)^{(7)} = (\sigma_2)^{(7)}$ and in this case $(v_1)^{(7)} = (\bar{v}_1)^{(7)}$ if in addition $(v_0)^{(7)} = (v_1)^{(7)}$ then $v^{(7)}(t) = (v_0)^{(7)}$ and as a consequence $G_{36}(t) = (v_0)^{(7)} G_{37}(t)$ **this also defines $(v_0)^{(7)}$ for the special case.**

Analogously if $(b_{36})^{(7)} = (b_{37})^{(7)}$, then $(\tau_1)^{(7)} = (\tau_2)^{(7)}$ and then

$(u_1)^{(7)} = (\bar{u}_1)^{(7)}$ if in addition $(u_0)^{(7)} = (u_1)^{(7)}$ then $T_{36}(t) = (u_0)^{(7)} T_{37}(t)$ This is an important consequence of the relation between $(v_1)^{(7)}$ and $(\bar{v}_1)^{(7)}$, **and definition of $(u_0)^{(7)}$.**

*85, 86, 87

IV. STATIONARY SOLUTIONS AND STABILITY

Stationary solutions and stability curve representative of the variation of the system Quantum Information and Quantum Mechanical Behaviour variation curve lies below the tangent at $(G_{39}) = G_0$ for $(G_{39}) < G_0$ and above the tangent for $(G_{39}) > G_0$. Wherever such a situation occurs the point G_0 is called the “**point of inflexion**”. In this case, the tangent has a positive slope that simply means the rate of change of Quantum Mechanical Behaviour vis a vis Quantum Information is

greater than zero. Above factor shows that it is possible, to draw a curve that has a point of inflexion at a point where the tangent (slope of the curve) is horizontal.

Stationary value :

In all the cases $(G_{39}) = G_0$, $(G_{39}) < G_0$, $(G_{39}) > G_0$ the condition that the rate of change of oxygen consumption is maximum or minimum holds. When this condition holds we have stationary value. We now infer that :

1. A necessary and sufficient condition for there to be stationary value of (G_{39}) is that the rate of change of oxygen consumption function at G_0 is zero.
2. A sufficient condition for the stationary value at G_0 , to be maximum is that the acceleration of the oxygen consumption is less than zero.
3. A sufficient condition for the stationary value at G_0 , to be minimum is that acceleration of oxygen consumption is greater than zero.
4. With the rate of change of (G_{39}) namely oxygen consumption defined as the accentuation term and the dissipation term, we are sure that the rate of change of Quantum Mechanical Behaviour-Quantum Information system is always positive.
5. Concept of stationary state is mere methodology although there might be closed system exhibiting symptoms of stationeries.

We can prove the following

Theorem 3: If $(a_i'')^{(7)}$ and $(b_i'')^{(7)}$ are independent on t , and the conditions :

$$(a'_{36})^{(7)}(a'_{37})^{(7)} - (a_{36})^{(7)}(a_{37})^{(7)} < 0$$

$$(a'_{36})^{(7)}(a'_{37})^{(7)} - (a_{36})^{(7)}(a_{37})^{(7)} + (a_{36})^{(7)}(p_{36})^{(7)} + (a'_{37})^{(7)}(p_{37})^{(7)} + (p_{36})^{(7)}(p_{37})^{(7)} > 0$$

$$(b'_{36})^{(7)}(b'_{37})^{(7)} - (b_{36})^{(7)}(b_{37})^{(7)} > 0,$$

$$(b'_{36})^{(7)}(b'_{37})^{(7)} - (b_{36})^{(7)}(b_{37})^{(7)} - (b'_{36})^{(7)}(r_{37})^{(7)} - (b'_{37})^{(7)}(r_{37})^{(7)} + (r_{36})^{(7)}(r_{37})^{(7)} < 0$$

with $(p_{36})^{(7)}, (r_{37})^{(7)}$ as defined by equation 37 are satisfied, then the system

*88

$$(a_{36})^{(7)}G_{37} - [(a'_{36})^{(7)} + (a''_{36})^{(7)}(T_{37})]G_{36} = 0 \quad *89$$

$$(a_{37})^{(7)}G_{36} - [(a'_{37})^{(7)} + (a''_{37})^{(7)}(T_{37})]G_{37} = 0 \quad *90$$

$$(a_{38})^{(7)}G_{37} - [(a'_{38})^{(7)} + (a''_{38})^{(7)}(T_{37})]G_{38} = 0 \quad *91$$

$$(b_{36})^{(7)}T_{37} - [(b'_{36})^{(7)} - (b''_{36})^{(7)}(G_{39})]T_{36} = 0 \quad *92$$

$$(b_{37})^{(7)}T_{36} - [(b'_{37})^{(7)} - (b''_{37})^{(7)}(G_{39})]T_{37} = 0 \quad *93$$

$$(b_{38})^{(7)}T_{37} - [(b'_{38})^{(7)} - (b''_{38})^{(7)}(G_{39})]T_{38} = 0$$

*94

has a unique positive solution, which is an equilibrium solution for the system Quantum Mechanical Behaviour(Quantum Entanglement, Coherence, Decoherence) and Quantum Information(Computer).

Proof:

(a) Indeed the first two equations have a nontrivial solution G_{36}, G_{37} if

$$F(T_{39}) =$$

$$(a'_{36})^{(7)}(a'_{37})^{(7)} - (a_{36})^{(7)}(a_{37})^{(7)} + (a'_{36})^{(7)}(a''_{37})^{(7)}(T_{37}) + (a'_{37})^{(7)}(a''_{36})^{(7)}(T_{37}) + (a''_{36})^{(7)}(T_{37})(a''_{37})^{(7)}(T_{37}) = 0$$

*95

Definition and uniqueness of T_{37}^* :-

After hypothesis $f(0) < 0, f(\infty) > 0$ and the functions $(a_i'')^{(7)}(T_{37})$ being increasing, it follows that there exists a unique T_{37}^* for which $f(T_{37}^*) = 0$. With this value, we obtain from the three first equations

$$G_{36} = \frac{(a_{36})^{(7)}G_{37}}{[(a'_{36})^{(7)} + (a''_{36})^{(7)}(T_{37}^*)]}, \quad G_{38} = \frac{(a_{38})^{(7)}G_{37}}{[(a'_{38})^{(7)} + (a''_{38})^{(7)}(T_{37}^*)]}$$

(b) By the same argument, the equations 92,93 admit solutions G_{36}, G_{37} if

$$\varphi(G_{39}) = (b'_{36})^{(7)}(b'_{37})^{(7)} - (b_{36})^{(7)}(b_{37})^{(7)} - [(b'_{36})^{(7)}(b''_{37})^{(7)}(G_{39}) + (b'_{37})^{(7)}(b''_{36})^{(7)}(G_{39})] + (b''_{36})^{(7)}(G_{39})(b''_{37})^{(7)}(G_{39}) = 0 \quad *96$$

97

Where in $(G_{39})(G_{36}, G_{37}, G_{38}), G_{36}, G_{38}$ must be replaced by their values from 96. It is easy to see that φ is a decreasing function in G_{37} taking into account the hypothesis $\varphi(0) > 0, \varphi(\infty) < 0$ it follows that there exists a unique G_{37}^* such that $\varphi(G^*) = 0$

Finally we obtain the unique solution of the defined system Quantum Mechanical Behaviour and Quantum Information: G_{37}^* given by $\varphi((G_{39})^*) = 0, T_{37}^*$ given by $f(T_{37}^*) = 0$ and

$$G_{36}^* = \frac{(a_{36})^{(7)} G_{37}^*}{[(a_{36})^{(7)} + (a_{36})^{(7)}(T_{37}^*)]} \quad , \quad G_{38}^* = \frac{(a_{38})^{(7)} G_{37}^*}{[(a_{38})^{(7)} + (a_{38})^{(7)}(T_{37}^*)]} \quad *98$$

$$T_{36}^* = \frac{(b_{36})^{(7)} T_{37}^*}{[(b_{36})^{(7)} - (b_{36})^{(7)}((G_{39})^*)]} \quad , \quad T_{38}^* = \frac{(b_{38})^{(7)} T_{37}^*}{[(b_{38})^{(7)} - (b_{38})^{(7)}((G_{39})^*)]} \quad *99$$

Obviously, these values represent an equilibrium solution of the system Quantum Mechanical Behaviour and Quantum mechanical System(Quantum Information)

ASYMPTOTIC STABILITY ANALYSIS

One of the studies that come to mind when one thinks of the Asymptotic Stability Analysis, is the study by Komech On asymptotic stability of solitary waves for Schrödinger equation coupled to nonlinear oscillator, The long-time asymptotics is analyzed for finite energy solutions of the 1D Schrödinger equation coupled to a nonlinear oscillator; mathematically the system under study is a Nonlinear Schrödinger equation, whose nonlinear term includes a Dirac delta. The coupled system is invariant with respect to the phase rotation group $U(1)$. The article, which extends the results of a previous one, provides a proof of asymptotic stability of solitary wave solutions in the case that the linearization contains a single discrete oscillatory mode satisfying a non-degeneracy assumption of the type known as the Fermi Golden Rule. In this article we continue the study of large time asymptotics for a model $U(1)$ -invariant nonlinear Schrödinger equation Main focus is on the role that certain solitary waves (also referred to as nonlinear bound states, or solitons) play in the description of the solution for large times.

Equilibrium: Stable or Unstable?

Equilibrium is a state of a system which does not change.

If the dynamics of a system is described by a differential equation (or a system of differential equations), then equilibria can be estimated by setting a derivative (all derivatives) to zero.

Example: Logistic model

$$\frac{dN}{dt} = r_0 N \left(1 - \frac{N}{K}\right)$$

To find equilibrium we have to solve the equation: $dN/dt = 0$:

$$r_0 N \left(1 - \frac{N}{K}\right) = 0$$

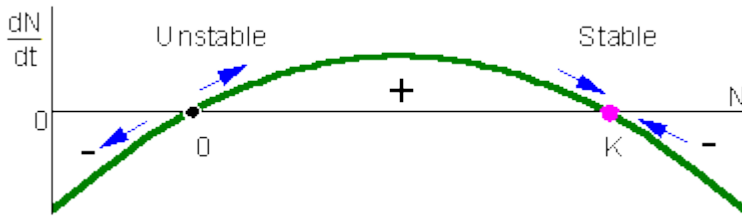
This equation has two roots: $N=0$ and $N=K$. An equilibrium may be stable or unstable. For example, the equilibrium of a pencil standing on its tip is unstable; The equilibrium of a picture on the wall is (usually) stable.



An equilibrium is considered **stable** (for simplicity we will consider asymptotic stability only) if the system always returns to it after small disturbances. If the system moves away from the equilibrium after small disturbances, then the equilibrium is **unstable**.

The notion of stability can be applied to other types of attractors (limit cycle, chaos), however, the general definition is more complex than for equilibria. Stability is probably the most important notion in science because it refers to what we call "reality". Everything should be stable to be observable. For example, in quantum mechanics, energy levels are those that are stable because unstable levels cannot be observed.

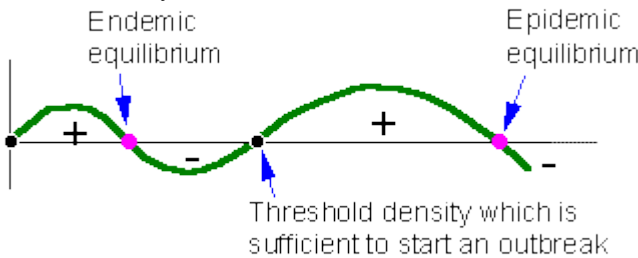
Now, let's examine stability of 2 equilibria points in the logistic model.



In this figure, population growth rate, dN/dt , is plotted versus population density, N . This is often called a **phase-plot** of population dynamics. If $0 < N < K$, then $dN/dt > 0$ and thus, population grows (the point in the graph moves to the right). If $N < 0$ or $N > K$ (of course, $N < 0$ has no biological sense), then population declines (the point in the graph moves to the left). The arrows show that the equilibrium $N=0$ is unstable, whereas the equilibrium $N=K$ is stable. From the biological point of view, this means that after small deviation of population numbers from $N=0$ (e.g., immigration of a small number of organisms), the population never returns back to this equilibrium. Instead, population numbers increase until they reach the stable equilibrium $N=K$. After any deviation from $N=K$ the population returns back to this stable equilibrium.

The difference between stable and unstable equilibria is in the slope of the line on the phase plot near the equilibrium point. Stable equilibria are characterized by a negative slope (negative feedback) whereas unstable equilibria are characterized by a positive slope (positive feedback).

The second example is the bark beetle model with two stable and two unstable equilibria. Stable equilibria correspond to endemic and epidemic populations. Endemic populations are regulated by the amount of susceptible trees in the forest. Epidemic populations are limited by the total number of trees because mass attack of beetle females may overcome the resistance of any tree.



Stability of models with several variables

Detection of stability in these models is not that simple as in one-variable models. Let's consider a predator-prey model with two variables: (1) density of prey and (2) density of predators. Dynamics of the model is described by the system of 2 differential equations:

$$\begin{cases} \frac{dH}{dt} = f(H, P) \\ \frac{dP}{dt} = g(H, P) \end{cases}$$

This is the 2-variable model in a general form. Here, H is the density of prey, and P is the density of predators. The first step is to find equilibrium densities of prey (H^*) and predator (P^*). We need to solve a system of equations:

$$\begin{cases} f(H^*, P^*) = 0 \\ g(H^*, P^*) = 0 \end{cases}$$

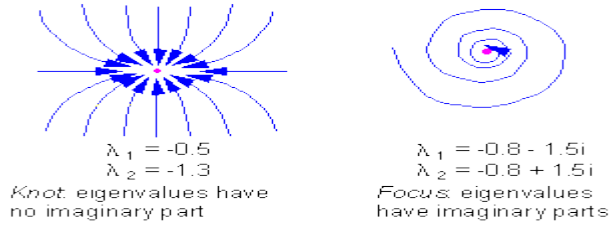
The second step is to linearize the model at the equilibrium point ($H = H^*, P = P^*$) by estimating the Jacobian matrix:

$$A = \begin{vmatrix} \frac{\partial f}{\partial H} & \frac{\partial f}{\partial P} \\ \frac{\partial g}{\partial H} & \frac{\partial g}{\partial P} \end{vmatrix}$$

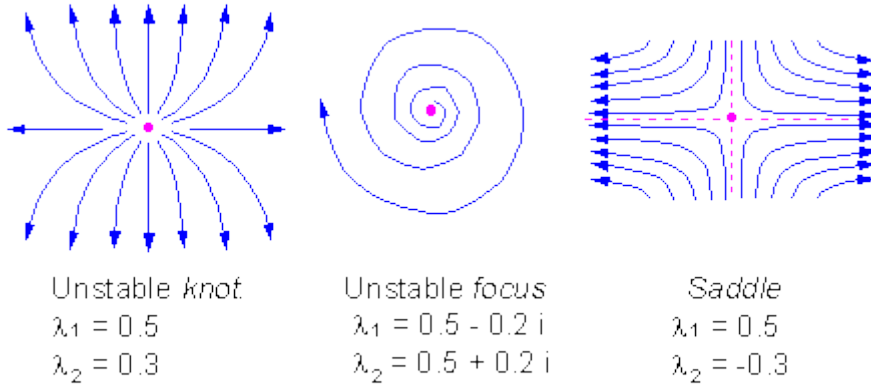
Third, eigenvalues of matrix A should be estimated. The number of eigenvalues is equal to the number of state variables. In our case there will be 2 eigenvalues. Eigenvalues are generally complex numbers. If real parts of all eigenvalues are negative, then the equilibrium is stable. If at least one eigenvalue has a positive real part, then the equilibrium is unstable.

Eigenvalues are used here to reduce a 2-dimensional problem to a couple of 1-dimensional problem problems. Eigenvalues have the same meaning as the slope of a line in phase plots. Negative real parts of eigenvalues indicate a negative feedback. It is important that ALL eigenvalues have negative real parts. If one eigenvalue has a positive real part then there is a direction in a 2-dimensional space in which the system will not tend to return back to the equilibrium point.

There are 2 types of stable equilibrium in a two-dimensional space: **knot** and **focus**



There are 3 types of unstable equilibrium in a two-dimensional space: **knot**, **focus**, and **saddle**



Stability in discrete-time models

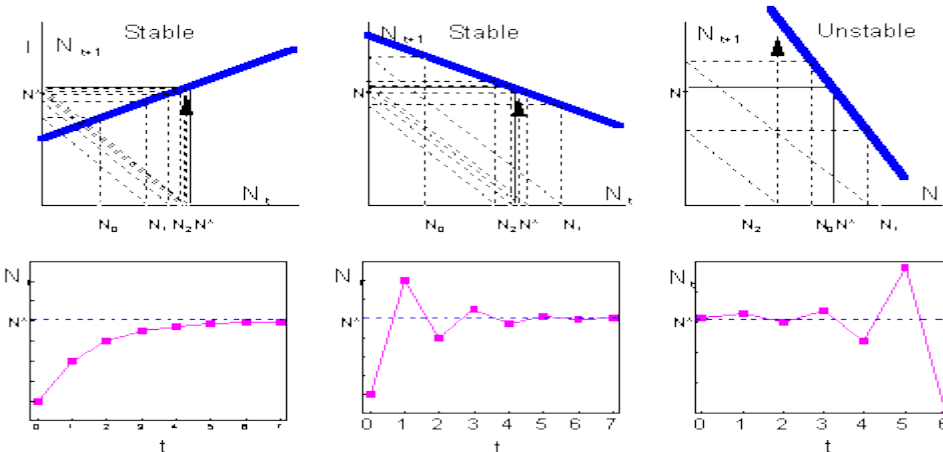
Consider a discrete-time model (a difference equation) with one state variable:

$$N_{t+1} = f(N_t)$$

This model is stable if and only if :

$$-1 < \frac{df}{dN_t} < 1$$

where $\frac{df}{dN_t}$ is the slope of a thick line in graphs below:



You can check this yourself using the following Excel spreadsheet:



Excel spreadsheet "ricker.xls"

If the slope is positive but less than 1, then the system approaches the equilibrium monotonically (left). If the slope is negative and greater than -1, then the system exhibits oscillations because of the "overcompensation" (center). Overcompensation means that the system jumps over the equilibrium point because the negative feedback is too strong. Then it returns back and again jumps over the equilibrium.

Continuous-time models with 1 variable never exhibit oscillations. In discrete-time models, oscillations are possible even with 1 variable. What causes oscillations is the delay between time steps. Overcompensation is a result of large time steps. If time steps were smaller, then the system would not jump over the equilibrium but will approach to it gradually.

Now we will analyze stability in the Ricker's model. This model is a discrete-time analog of the logistic model:

$$N_{t+1} = N_t \cdot \exp\left[r \left(1 - \frac{N_t}{K}\right)\right]$$

First, we need to find the equilibrium population density N^* by solving the equation:

$$N^* = N^* \cdot \exp\left[r \left(1 - \frac{N^*}{K}\right)\right]$$

This equation is obtained by substituting N_{t+1} and N_t with the equilibrium population density N^* in the initial equation. The roots are: $N^* = 0$ and $N^* = K$. We are not interested in the first equilibrium ($N^* = 0$) because there is no population. Let's estimate the slope df/dN at the second equilibrium point:

$$\frac{df}{dN_t} = \left(1 - \frac{r \cdot N_t}{K}\right) \cdot \exp\left[r \left(1 - \frac{N_t}{K}\right)\right] = 1 - r$$

$$N_t = N^* = K$$

Now we can apply the condition of stability:

$$-1 < 1 - r < 1$$

$$0 < r < 2$$

Thus, the Ricker's model has a stable equilibrium $N^* = K$ if $0 < r < 2$.

If a discrete time model has more than one state variable, then the analysis is similar to that in continuous-time models. The first step is to find equilibria. The second step is to linearize the model at the equilibrium state, i.e., to estimate the Jacobian matrix. The third step is to estimate eigenvalues of this matrix. The only difference from continuous models is the condition of stability. Discrete-time models are stable (asymptotically stable) if and only if all eigenvalues lie in the circle with the radius = 1 in the complex plain.

Theorem 7: If the conditions of the previous theorem are satisfied and if the functions $(a_i'')^{(7)}$ and $(b_i'')^{(7)}$ belong to $C^{(7)}(\mathbb{R}_+)$ then the above equilibrium point is asymptotically stable.

Proof: Denote

*

Definition of G_i, T_i :-

$$G_i = G_i^* + G_i \quad , \quad T_i = T_i^* + T_i$$

$$\frac{\partial (a_{37}'')^{(7)}}{\partial T_{37}}(T_{37}^*) = (q_{37})^{(7)} \quad , \quad \frac{\partial (b_i'')^{(7)}}{\partial G_j}((G_{39})^{**}) = s_{ij} \quad *100, 101$$

Then taking into account equations of the system Quantum Information and Quantum Mechanical Behaviour and neglecting the terms of power 2, we obtain*

$$\frac{dG_{36}}{dt} = -((a'_{36})^{(7)} + (p_{36})^{(7)})G_{36} + (a_{36})^{(7)}G_{37} - (q_{36})^{(7)}G_{36}^*T_{37} \quad *102$$

$$\frac{dG_{37}}{dt} = -((a'_{37})^{(7)} + (p_{37})^{(7)})G_{37} + (a_{37})^{(7)}G_{36} - (q_{37})^{(7)}G_{37}^*T_{37} \quad *103$$

$$\frac{dG_{38}}{dt} = -((a'_{38})^{(7)} + (p_{38})^{(7)})G_{38} + (a_{38})^{(7)}G_{37} - (q_{38})^{(7)}G_{38}^*T_{37} \quad *104$$

$$\frac{dT_{36}}{dt} = -((b'_{36})^{(7)} - (r_{36})^{(7)})T_{36} + (b_{36})^{(7)}T_{37} + \sum_{j=36}^{38} (s_{(36)(j)})T_{36}^*G_j \quad *105$$

$$\frac{dT_{37}}{dt} = -((b'_{37})^{(7)} - (r_{37})^{(7)})T_{37} + (b_{37})^{(7)}T_{36} + \sum_{j=36}^{38} (s_{(37)(j)})T_{37}^*G_j \quad *106$$

$$\frac{dT_{38}}{dt} = -((b'_{38})^{(7)} - (r_{38})^{(7)})T_{38} + (b_{38})^{(7)}T_{37} + \sum_{j=36}^{38} (s_{(38)(j)})T_{38}^*G_j \quad *107$$

The characteristic equation of this system is

$$\begin{aligned}
& ((\lambda)^{(7)} + (b'_{38})^{(7)} - (r_{38})^{(7)}) \{ ((\lambda)^{(7)} + (a'_{38})^{(7)} + (p_{38})^{(7)}) \\
& \left[((\lambda)^{(7)} + (a'_{36})^{(7)} + (p_{36})^{(7)}) (q_{37})^{(7)} G_{37}^* + (a_{37})^{(7)} (q_{36})^{(7)} G_{36}^* \right] \\
& \left(((\lambda)^{(7)} + (b'_{36})^{(7)} - (r_{36})^{(7)}) s_{(37),(37)} T_{37}^* + (b_{37})^{(7)} s_{(36),(37)} T_{37}^* \right) \\
& + \left(((\lambda)^{(7)} + (a'_{37})^{(7)} + (p_{37})^{(7)}) (q_{36})^{(7)} G_{36}^* + (a_{36})^{(7)} (q_{37})^{(7)} G_{37}^* \right) \\
& \left(((\lambda)^{(7)} + (b'_{36})^{(7)} - (r_{36})^{(7)}) s_{(37),(36)} T_{37}^* + (b_{37})^{(7)} s_{(36),(36)} T_{36}^* \right) \\
& \left(((\lambda)^{(7)})^2 + (a'_{36})^{(7)} + (a'_{37})^{(7)} + (p_{36})^{(7)} + (p_{37})^{(7)} \right) (\lambda)^{(7)} \\
& \left(((\lambda)^{(7)})^2 + (b'_{36})^{(7)} + (b'_{37})^{(7)} - (r_{36})^{(7)} + (r_{37})^{(7)} \right) (\lambda)^{(7)} \\
& + \left(((\lambda)^{(7)})^2 + (a'_{36})^{(7)} + (a'_{37})^{(7)} + (p_{36})^{(7)} + (p_{37})^{(7)} \right) (\lambda)^{(7)} (q_{38})^{(7)} G_{38} \\
& + ((\lambda)^{(7)} + (a'_{36})^{(7)} + (p_{36})^{(7)}) \left((a_{38})^{(7)} (q_{37})^{(7)} G_{37}^* + (a_{37})^{(7)} (a_{38})^{(7)} (q_{36})^{(7)} G_{36}^* \right) \\
& \left(((\lambda)^{(7)} + (b'_{36})^{(7)} - (r_{36})^{(7)}) s_{(37),(38)} T_{37}^* + (b_{37})^{(7)} s_{(36),(38)} T_{36}^* \right) \} = 0
\end{aligned}$$

And as one sees, all the coefficients are positive. It follows that all the roots have negative real part, and this proves the theorem.

DISSIPATION OF QUANTUM MECHANICAL EFFECTS:

The need for a quantum-mechanical formalism for systems with dissipation which is applicable to the radiation field of a cavity is discussed. Two methods that have been used in this connection are described. The first, which starts with the classical Newtonian equation of motion for a damped oscillator and applies the conventional formal quantization techniques, leads to an exact solution; but subsequent discussion shows that this method is invalid, the results being unacceptable from a quantum-mechanical viewpoint. The second method, which considers the interaction of two systems, the lossless oscillator and the loss mechanism, is adopted in the present article. No special model is used for the loss mechanism, but this mechanism is assumed to have a large number of densely-spaced energy states.

The approximations with respect to the loss mechanism that underlie the concept of dissipation are discussed. These approximations are then applied to the analysis, and a differential equation for a coordinate operator of the harmonic oscillator is obtained which has the formal appearance of the Newtonian equation of motion for a driven damped harmonic oscillator, the driving term being an operator referring to the loss mechanism. The presence of the driving term is responsible for the difference between the present theory and that of the first method mentioned above. A solution of the differential equation for the coordinate operator is given explicitly. An examination of the physical significance of the solution shows that the driving term is responsible not only for the thermal fluctuations which are due to the loss mechanism, but also for the proper commutation relationship of the conjugate coordinates of the oscillator and for its zero-point fluctuations.

A generalization of the solution to provide for a classical driving force and coupled atomic systems is given. The results are then restated in a form that refers to the loss mechanism only through the two parameters by which it is usually described—the dissipation constant and the temperature.

Some selected Examples:

A. O. Caldeira and A. J. Leggett studies the following system:

quantum system which can tunnel, at $T=0$, out of a metastable state and whose interaction with its environment is adequately described in the classically accessible region by a phenomenological friction coefficient η , is considered. By only assuming that the environment response is linear, it is found that dissipation multiplies the tunneling probability by the factor $\exp[-A\eta(\Delta q)^2/\hbar]$, where Δq is the "distance under the barrier" and A is a numerical factor which is generally of order unity

Measurements of the tunneling rate Γ out of the zero-voltage state for several Nb edge junctions with differing shunt capacitances are described. At zero temperature, increasing the shunt capacitance lowers Γ in agreement with dissipative calculations of the macroscopic-quantum-tunneling rate. As temperature increases, $\ln[\Gamma(T)/\Gamma(0)] \propto T^2$ as recently predicted.

Quantum dissipation

From Wikipedia, the free encyclopedia

Quantum Dissipation is the branch of physics that studies the quantum analogues of the process of irreversible loss of energy observed at the classical level. Its main purpose is to derive the laws of classical dissipation from the framework of quantum mechanics. It shares many features with the subjects of quantum decoherence and quantum theory of measurement.

Models of Quantum Dissipation

The main problem to address to study dissipation at the quantum level is the way to envisage the mechanism of irreversible loss of energy. Quantum mechanics usually deal with the Hamiltonian formalism, where the total energy of the system is a conserved quantity. So in principle it would not be possible to describe dissipation in this framework.

The idea to overcome this issue consists on splitting the total system in two parts: the quantum system where dissipation occurs, and a so-called environment or bath where the energy of the former will flow towards. The way both systems are coupled depends on the details of the microscopic model, and hence, the description of the bath. To include an irreversible flow of energy (i.e., to avoid Poincaré recurrences in which the energy eventually flows back to the system), requires that the

bath contain an infinite number of degrees of freedom. Notice that by virtue of the principle of universality, it is expected that the particular description of the bath will not affect the essential features of the dissipative process, as far as the model contains the minimal ingredients to provide the effect.

The simplest way to model the bath was proposed by Feynman and Vernon in a seminal paper from 1963^[1]. In this description the bath is a sum of an infinite number of harmonic oscillators, that in quantum mechanics represents a set of free bosonic particles.

[edit]The Caldeira-Leggett model

In 1981 Amir Caldeira and Anthony J. Leggett proposed a simple model to study in detail the way dissipation arises from a quantum point of view^[2]. It describes a quantum particle in one-dimension coupled to a bath. The Hamiltonian reads:

$$H = \frac{P^2}{2M} + V(X) + \sum_i \left(\frac{p_i^2}{2m_i} + \frac{1}{2} m_i \omega_i^2 q_i^2 \right) + X \sum_i C_i q_i + X^2 \sum_i \frac{C_i^2}{2m_i \omega_i^2},$$

The first two terms correspond to the Hamiltonian of a quantum particle of mass M and momentum P , in a potential V at position X . The third term describes the bath as a sum of infinite harmonic oscillators with masses m_i and momentum p_i , at positions q_i . ω_i are the frequencies of the harmonic oscillators. The next term describes the way system and bath are coupled. In the Caldeira - Leggett model the bath is coupled to the position of the particle. C_i are coefficients which depend on the details of the coupling. The last term is a counter-term which must be included to ensure that dissipation is homogeneous in all space. As the bath couples to the position, if this term is not included the model is not translationally invariant, in the sense that the coupling is different wherever the quantum particle is located. This gives rise to an unphysical renormalization of the potential, which can be shown to be suppressed by including the counter-term.

To provide a good description of the dissipation mechanism, a relevant quantity is the bath spectral function, defined as follows:

$$J(\omega) = \frac{\pi}{2} \sum_i \frac{C_i^2}{m_i \omega_i} \delta(\omega - \omega_i)$$

The bath spectral function provides a constraint in the choice of the coefficients C_i . When this function has the form $J(\omega) = \eta \omega$, the corresponding classical kind of dissipation can be shown to be Ohmic. A more generic form is $J(\omega) \propto \omega^s$. In this case, if $s > 1$ the dissipation is called "super-ohmic", while if $s < 1$ is sub-ohmic. An example of a super-ohmic bath is the electro-magnetic field under certain circumstances.

As mentioned, the main idea in the field of quantum dissipation is to explain the way classical dissipation can be described from a quantum mechanics point of view. To get the classical limit of the Caldeira - Leggett model, the bath must be integrated out (or traced out), which can be understood as taking the average over all the possible realizations of the bath and studying the effective dynamics of the quantum system. As a second step, the limit $\hbar \rightarrow 0$ must be taken to recover classical mechanics. To proceed with those technical steps mathematically, the path integral description of quantum mechanics is usually employed. The resulting classical equations of motion are:

$$M \frac{d^2}{dt^2} X(t) = -\frac{\partial V(X)}{\partial X} - \int_0^T dt' \alpha(t-t')(X(t) - X(t'))$$

where:

$$\alpha(t-t') = \frac{1}{2\pi} \int_0^\infty J(\omega) e^{-\omega|t-t'|} d\omega$$

is a kernel which characterizes the effective force that affects the motion of the particle in the presence of dissipation. For so-called Markovian baths, which do not keep memory of the interaction with the system, and for Ohmic dissipation, the equations of motion simplify to the classical equations of motion of a particle with friction:

$$M \frac{d^2}{dt^2} X(t) = -\frac{\partial V(X)}{\partial X} - \eta \frac{dX(t)}{dt}$$

Hence, one can see how Caldeira-Leggett model fulfills the goal of getting classical dissipation from the quantum mechanics framework. The Caldeira-Leggett model has been used to study **quantum dissipation** problems since its introduction in 1981, being extensively used as well in the field of quantum decoherence.

[edit]The dissipative two-level system

This particular realization of the Caldeira - Leggett model deserves special attention due to its interest in the field of Quantum Computation. The aim of the model is to study the effects of dissipation in the dynamics of a particle that can hop between two different positions. This reduced Hilbert space allows the problem to be described in terms of $1/2$ spin operators. The resulting Hamiltonian is also referred in the literature as the Spin-Boson model, reading:

$$H = \Delta S_x + \sum_i \left(\frac{p_i^2}{2m_i} + \frac{1}{2} m_i \omega_i^2 q_i^2 \right) + S_z \sum_i C_i q_i,$$

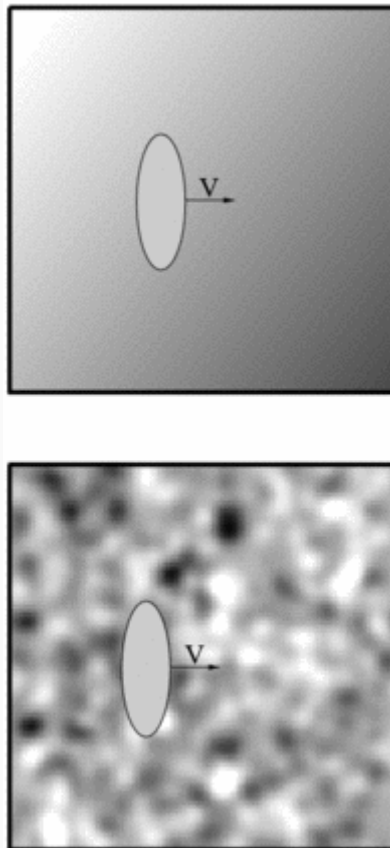
where $S_i = \frac{\sigma_i}{2}$, $i = x, y, z$ are proportional to the Pauli matrices σ_i , and Δ is the probability of hopping between the two possible positions. Notice that in this model the counter-term is no longer needed, as the coupling to S_z gives already homogeneous dissipation.

The model has many applications. In **quantum dissipation** it is used as a simple model to study the dynamics of a dissipative particle confined in a double-well potential. In the context of Quantum Computation it represents a qubit coupled to an environment, which can produce decoherence. In the study of amorphous solids it provides the basis of the standard theory to describe their thermodynamic properties.

The dissipative two-level systems represents also a paradigm in the study of quantum phase transitions. For a critical value of the coupling to the bath it shows a phase transition from a regime in which the particle is delocalized among the two positions to another in which it is localized in only one of them. The transition is of Kosterlitz-Thouless kind, as can be seen by deriving the Renormalization group flow equations for the hopping term.

Dissipation model for extended environment

From Wikipedia, the free encyclopedia



(a) The Brownian particle in the Caldeira-Leggett model experiences a fluctuating homogeneous field of force. (b) In case of the DLD model the fluctuating field is farther characterized by a finite correlation distance. The background image is a “snapshot” of the fluctuating environment. Namely, the gray levels correspond to the “height” of an instantaneous potential which is experienced by the Brownian particle.

A unified model for *Diffusion Localization and Dissipation* (DLD), optionally termed *Diffusion with Local Dissipation*, has been introduced for the study of *Quantal Brownian Motion* (QBM) in dynamical disorder^{[1], [2]}. It can be regarded as a generalization of the familiar Caldeira-Leggett model.

$$\mathcal{H} = \frac{p^2}{2m} + V(x) + \mathcal{H}_{int} + \mathcal{H}_{bath}$$

$$\mathcal{H}_{bath} = \sum_{\alpha} \left(\frac{P_{\alpha}^2}{2m_{\alpha}} + \frac{1}{2} m_{\alpha} \omega_{\alpha}^2 Q_{\alpha}^2 \right)$$

$$\mathcal{H}_{int} = - \sum_{\alpha} c_{\alpha} Q_{\alpha} u(x - x_{\alpha})$$

where Q_{α} denotes the dynamical coordinate of the α scatterer or bath mode. $u(x - x_{\alpha})$ is the interaction potential, and c_{α} are coupling constants. The spectral characterization of the bath is analogous to that of the Caldeira-Leggett model:

$$\frac{\pi}{2} \sum_{\alpha} \frac{c_{\alpha}^2}{m_{\alpha} \omega_{\alpha}} \delta(\omega - \omega_{\alpha}) \delta(x - x_{\alpha}) = J(\omega)$$

i.e. the oscillators that appear in the Hamiltonian are distributed uniformly over space, and in each location have the same spectral distribution $J(\omega)$. Optionally the environment is characterized by the power spectrum of the fluctuations $S(q, \omega)$, which is determined by $J(\omega)$ and by the assumed interaction $u(r)$. See examples.

The model can be used to describes the dynamics of a Brownian particle in an Ohmic environment whose fluctuations are uncorrelated in space This should be contrasted with the Zwanzig-Caldeira-Leggett model, where the induced fluctuating force is assumed to be uniform in space (see figure).

At high temperatures the propagator possesses a Markovian property and one can write down an equivalent Master equation. Unlike the case of the Zwanzig-Caldeira-Leggett model, genuine quantum mechanical effects manifest themselves due to the disordered nature of the environment.

Using Wigner picture of the dynamics one can distinguish between two different mechanisms for destruction of coherence: scattering mechanism and smearing mechanism. The analysis of dephasing can be extended to the low temperature regime by using a semiclassical strategy. In this context the dephasing rate SP formula can be derived. Various results can be derived for ballistic, chaotic, diffusive, both ergodic and non-ergodic motion.

In the following we give example of a recent study done in brief measure, not wholly or in full measure but very substantially as a review percussion:

Quantum Dissipation versus Classical Dissipation for Generalized Brownian motion (For details See Doron Cohen)

Authors' try to clarify what are the genuine quantal effects that **are associated with** generalized Brownian Motion (BM). All the quantal effects that are **associated with** the Zwanzig-Feynman-Vernon-Caldeira-Leggett model are (formally) a solution of the classical Langevin equation. Non-stochastic, genuine quantum mechanical effects are found for a model that takes into account either the disordered or the chaotic nature of some environment.

The role of **dissipation in** curve crossing phenomena in condensed phases is discussed. Adiabaticity criteria are found in two regimes via path integral arguments. In the high temperature regime a stochastic quantum Langevin approach is developed. In the low temperature region an instanton method is used. In both cases the curve crossing time scale competes with the time scale of molecular motion. Dissipation causes the process to be more likely to be adiabatic.

Quantum optics is one of the liveliest fields in physics at present. While it has been a dominant research field for at least two decades, with much graduated but incremental activity, in the past few years it has started **to impact the** study of Quantum Computation. There are plenty of good research monographs in this field, but it was felt that there was a genuine need for a straightforward account .This is a field which attracts the brightest students at present, in part because of the **extraordinary progress** in the field (e.g. **the implementation of teleportation, quantum cryptography, Schrödinger cat states, Bell violations of local realism and the like**).

The presentation is almost entirely concerned with the quantized electromagnetic field and its effects on atoms, and how nonclassical light behaves. One aim of presently is to connect **quantum optics** with the newly developing subject of **quantum information processing**.

Topics covered are: single-mode field quantization in a cavity, quantization of multimode fields, the issue of the quantum phase, coherent states, quasi-probability distributions in phase space, atom-field interactions, the Jaynes-Cummings model, quantum coherence theory, beam splitters and interferometers, nonclassical field states with squeezing, etc., test of local realism with entangled photons from down-conversion, experimental realizations of cavity quantum electrodynamics, trapped ions, etc., issues regarding decoherence, and some applications to quantum information processing, particularly quantum cryptography. Recent studies include involvement of computational work, some more extensively than others.

History

The ancient world already was wrestling with the nature of light as rays. By the seventeenth century the two rival concepts of waves and corpuscles were well established. Maxwell, in the second half of the nineteenth century, laid the foundations of

modern field theory, with a detailed account of light as electromagnetic waves and at that point classical physics seemed triumphant, with “minor” worries about the nature of black-body radiation and of the photoelectric effect. These of course were the seeds of the quantum revolution. Planck, an inherently conservative theorist, was led rather reluctantly, it seems, to propose that thermal radiation **was emitted and absorbed** in discrete quanta in order to explain the spectra of thermal bodies. It was Einstein who generalized this idea so that these new quanta represented the light itself rather than the processes of **absorption and emission**, and was able to describe how matter and radiation could come into **equilibrium** (introducing on the way the idea of stimulated emission), and how the photoelectric effect could be explained. By 1913, Bohr applied the basic idea of quantization to atomic dynamics and was able to predict the positions of atomic spectral lines. Gilbert Lewis, a chemist, coined the word photon well after the light quanta idea itself was introduced. In 1926 Lewis said:

It would seem appropriate to speak of one of these hypothetical entities as a particle of light, a corpuscle of light, a light quantum, or light quant, if we are to assume that it spends only a minute fraction of its existence as a carrier of radiant energy, while the rest of the time it remains as an important structural element within the atom . . . I therefore take the liberty of proposing for this hypothetical new atom, which is not light but plays an important part in every process of radiation, the name photon

Clearly Lewis’s idea and ours are rather distantly connected!

De Broglie in a remarkable leap of imagination generalized what we knew about light quanta, **exhibiting** wave and particle properties to matter itself. Heisenberg, Schrödinger and Dirac laid the foundations of quantum mechanics in an amazingly short period from 1925 to 1926. They gave us the whole machinery we still use: representations, quantum-state evolution, unitary transformations, perturbation theory and more. The intrinsic probabilistic nature of quantum mechanics was uncovered by Max Born, who proposed the idea of probability amplitudes which allowed a fully quantum treatment of interference.

Fermi and Dirac, pioneers of quantum mechanics, were also among the first to address the question of how quantized light interacts with atomic sources and propagates. Fermi’s *Reviews of Modern Physics* article in the 1930s, based on lectures he gave in Ann Arbor, summarize what was known at that time within the context of nonrelativistic quantum electrodynamics in the Coulomb gauge. His treatment of interference (especially Lipmann fringes) still repays reading today. It is useful to quote Willis Lamb in this context:

Begin by deciding how much of the universe needs to be brought into the discussion. Decide what normal modes are needed for an adequate treatment. Decide how to model the light sources and work out how they drive the system [4].

Weisskopf and Wigner applied the newly developed ideas of non-relativistic quantum mechanics to the dynamics of spontaneous emission and resonance fluorescence, predicting the exponential law for excited-state decay. This work already exhibited the self-energy problems, which were to plague quantum electrodynamics for the next 20 years until the development of the renormalization programme by Schwinger, Feynman, Tomonaga, and Dyson. The observation of the **anomalous magnetic moment** of the electron by Kusch, and of radiative level shifts of atoms by Lamb and Retherford, were the highlights of this era. The interested reader will find the history of this period very ably described by Schweber in his magisterial account of QED. This period of research demonstrated the importance of considering the vacuum as a field which had observable consequences. In a remarkable development in the late 1940s, triggered by the observation that colloids were more stable than expected from considerations of van der Waals interactions, Casimir showed that long-range intermolecular forces were intrinsically quantum electrodynamic. He **linked them to the idea** of zero-point motion of the field and showed that metal plates in vacuum attract as a consequence of such zero-point motion.

Einstein had continued his study of the basic nature of quantum mechanics and in 1935 in a remarkable paper with Podolsky and Rosen was able to show how peculiar quantum correlations were. The ideas in this paper were to explode into one of the most active parts of modern physics with the development by Bohm and Bell of concrete predictions of the nature of **these correlations**; this laid the foundations of what was to become the new subject of quantum information processing.

Optical coherence had been investigated for many years using amplitude interference: a first-order correlation. Hanbury Brown and Twiss in the 1950s worked on intensity correlations as a tool in stellar interferometry, and showed how thermal photon detection events were “bunched.” This **led to the** development of the theory of photon statistics and photon counting and to the beginnings of quantum optics as a separate subject. At the same time as ideas of photon statistics were being developed, researchers had begun to investigate coherence in **light-matter interactions**. Radio-frequency spectroscopy had already been initiated with atomic beams with the work of Rabi, Ramsey and others. Sensitive optical pumping probes of light interaction with atoms were developed in the 1950s and 1960s by Kastler, Brossel, Series, Dodd and others.

By the early 1950s, Townes and his group, and Basov and Prokhorov, had developed molecular microwave sources of radiation: the new masers, based on precise initial state preparation, population inversion and stimulated emission. Ed Jaynes in the 1950s played a major role in studies of whether quantization played a role in maser operation (and this set the stage for much later work on fully quantized atom–field coupling in what became known as the Jaynes–Cummings model). Extending the maser idea to the optical regime and the development of lasers of course revolutionized modern physics and technology.

Glauber, Wolf, Sudarshan, Mandel, Klauder and many others developed a quantum theory of coherence based on coherent states and photodetection. Coherent states allowed us to describe the behaviour of light in phase space, using the quasi-probabilities developed much earlier by Wigner and others.

For several years after the development of the laser there were no tuneable sources: researchers interested in the details of atom–light or molecule–light interactions had to rely on molecular chance resonances. Nevertheless, this led to the beginning of the study of coherent interactions and coherent transients such as photon echoes, self-induced transparency, optical notation and so on (well described in the standard monograph by Allen and Eberly). Tuneable lasers became available in the

early 1970s, and the dye laser in particular transformed precision studies in quantum optics and laser spectroscopy. Resonant interactions, coherent transients and the like became much more straightforward to study and led to the beginnings of quantum optics proper as we now understand it: for the first time we were able to study the dynamics of single atoms interacting with light in a non-perturbative manner. Stroud and his group initiated studies of resonance fluorescence with the observation of the splitting of resonance fluorescence spectral lines into component parts by the coherent driving predicted earlier by Mollow. Mandel, Kimble and others demonstrated how the resonance fluorescence light was antibunched, a feature studied by a number of theorists including Walls, Carmichael, Cohen-Tannoudji, Mandel and Kimble. The observation of antibunching and the associated (but in equivalent) sub-Poissonian photon statistics laid the foundation of the study of “non-classical light”. During the 1970s, several experiments explored the nature of photons: their indivisibility and the buildup of interference at the single photon level. Laser cooling rapidly developed in the 1980s and 1990s and allowed the preparation of states of matter under precise control. Indeed, this has become a major subject in its own right and we have taken the decision here to exclude laser cooling from this text.

Following the development of high-intensity pulses of light from lasers, a whole set of nonlinear optical phenomena were investigated, starting with the pioneering work in Ann Arbor by Franken and co-workers. Harmonic generation, parametric down-conversion and other phenomena were demonstrated. For the most part, none of this early work on nonlinear optics required field quantization and quantum optics proper for its description. But there were early signs that some could well do so: quantum nonlinear optics was really initiated by the study by Burnham and Weinberg of unusual nonclassical correlations in down-conversion. In the hands of Mandel and many others, these correlations in down-conversion became the fundamental tool used to uncover fundamental insights into quantum optics.

Until the 1980s, essentially all light fields investigated had phase-independent noise; this changed with the production of squeezed light sources with phase-sensitive noise. These squeezed light sources enabled us to investigate Heisenberg uncertainty relations for light fields. Again, parametric down-conversion proved to be the most effective tool to generate such unusual light fields.

Quantum opticians realized quite early that were atoms to be confined in resonators, then atomic radiative transition dynamics could be dramatically changed. Purcell, in a remarkable paper in 1946 within the context of magnetic resonance, had already predicted that spontaneous emission rates previously thought of as pretty immutable were in fact modified by enclosing the source atom within a cavity whose mode structure and densities are significantly different from those of free space. Putting atoms within resonators or close to mirrors became possible at the end of the 1960s. By the 1980s the theorists' dream of studying single atoms interacting with single modes of the electromagnetic field became possible. At this point the transition dynamics becomes wholly reversible, as the atom coherently exchanges excitation with the field, until coherence is eventually lost through a dissipative “decoherence” process. This dream is called the Jaynes–Cummings model after its proposers and forms a basic building block of quantum optics .

New fundamental concepts in information processing, leading to quantum cryptography and quantum computation, have been developed in recent years by Feynman, Benioff, Deutsch, Jozsa, Bennett, Ekert and others. Instead of using classical bits that can represent either the values 0 or 1, the basic unit of a quantum computer is a quantum mechanical two-level system (qubit) that can exist in coherent superpositions of the logical values 0 and 1. A set of n qubits can then be in a superposition of up to 2^n different states, each representing a binary number. Were we able to control and manipulate say 1500 qubits, we could access more states than there are particles in the visible universe. Computations are implemented by unitary transformations, which act on all states of a superposition simultaneously. Quantum gates form the basic units from which these unitary transformations are built up. In related developments, absolutely secure encryption can be guaranteed by using quantum sources of light.

The use of the quantum mechanical superpositions and entanglement results in a high degree of parallelism, which can increase the speed of computation exponentially. A number of problems which cannot feasibly be tackled on a classical computer can be solved efficiently on a quantum computer. In 1994 a quantum algorithm was discovered by Peter Shor that allows the solution of a practically important problem, namely factorization, with such an exponential increase of speed. Subsequently, possible experimental realizations of a quantum computer have been proposed, for example in linear ion traps and nuclear magnetic resonance schemes. Presently we are at a stage where quantum gates have been demonstrated in these two implementations. Quantum computation is closely related to quantum cryptography and quantum communication. Basic experiments demonstrating the in-principle possibility of these ideas have been carried out in various laboratories.

The linear ion trap is one of the most promising systems for quantum computation and is one we study in this book in detail. The quantum state preparation (laser cooling and optical pumping) in this system is a well-established technique, as is the state measurement by electron shelving and fluorescence. Singly charged ions of an atom such as calcium or beryllium are trapped and laser cooled to micro-Kelvin temperatures, where they form a string lying along the axis of a linear radio-frequency (r.f.) Paul trap. The internal state of any one ion can be exchanged with the quantum state of motion of the whole string. This can be achieved by illuminating the ion with a pulse of laser radiation at a frequency tuned below the ion's internal resonance by the vibrational frequency of one of the normal modes of oscillation of the string. This ouples single phonons into and out of the vibrational mode. The motional state can then be coupled to the internal state of another ion by directing the laser onto the second ion and applying a similar laser pulse. In this way general transformations of the quantum state of all the ions can be generated. The ion trap has several features to recommend it. It can achieve processing on quantum bits without the need for any new technological breakthroughs, such as micro-fabrication techniques or new cooling methods. The state of any ion can be measured and re-prepared many times without problem, which is an important feature for implementing quantum error correction protocols.

Trapped atoms or ions can be **strongly coupled to an** electromagnetic field mode in a cavity, which permits the powerful **combination of** quantum processing and long-distance quantum communication. This suggests ways in which we may construct quantum memories. These systems can in principle realize a quantum processor larger than any which could be thoroughly simulated by classical computing but the decoherence generated by dephasing and **spontaneous emission is a formidable obstacle.**

Entangled states are **the key ingredient** for certain forms of quantum cryptography and for quantum teleportation. Entanglement is also **responsible for** the power of quantum computing, which, under ideal conditions, **can accomplish** certain tasks exponentially faster than any classical computer. A deeper understanding of **the role of quantum** entanglement in quantum information theory **will allow us** to improve existing applications and to develop new methods of **quantum information manipulation.**

What then is the future of quantum optics? It underpins a great deal of laser science and novel atomic physics. It may even be the vehicle by which we can realize a whole new technology whereby quantum mechanics permits the processing and transmission of information in wholly novel ways. But of course, whatever we may predict now to emerge will be confounded by the unexpected: the field remains an adventure repeatedly throwing up the unexpected.

ESSENTIAL PREDICATIONS, PREDICATIONAL ANTERIORITIES, PRIMORDIAL EXACTITUDE, ONTOLOGICAL CONSONANCE OF VARIOUS VARIABLES OF QUANTUM COMPUTING SUCH AS ELECTROMAGNETIC FIELD, HARMONIC OSCILLATORS, PHASE INFORMATION, AND SPONTANEOUS DECAY; WITH SOME CONCOMITANT AND CORRESPONDING STUDIES DONE IN ABSTRACT AND SENTENTIOUS MANNER:

THE electromagnetic field can be quantized in terms of harmonic oscillators representing modes of the electromagnetic field, with states describing how many excitations (photons) are present in each normal mode.

1. Coherent states, superposition states carrying phase information are closely interrelated to each other
2. Light and matter interact.
3. Quantification of notions of coherence in terms of optical field correlation functions.
4. Optical elements such as beam splitters and interferometers, **manipulate the** states of light.
5. Nonclassical states have properties which are dictated by their fundamental quantum nature.
6. Spontaneous emission and decay in an open environment
7. How quantum optical sources of radiation can be used to provide tests of fundamental quantum mechanics, including tests of nonlocality and Bell inequalities.
8. Atoms confined in cavities and trapped laser-cooled ions **can be used to study** basic interaction phenomena.
9. Applications to the newly emerging problems of quantum information processing.

For a given 2-dimensional dissipative discrete **map generating** chaotic dynamics author presents the phenomenological construction of a quantum mechanical master equation **which reduces to the** given map in the classical limit. **Global dissipation**, caused by the non-invertibility of the map, and local dissipation, **caused by the** local contraction of the map, are both incorporated in the description. The behavior in the two opposite limits of vanishing **local dissipation and of strong local dissipation** is analyzed exactly. Using the representation of the statistical operator by the Wigner distribution, the classical and semi-classical limit has been studied. An estimate of the critical time is obtained, which determines the **crossover** between classical and quantum mechanical behavior in the chaotic state. This critical time diverges logarithmically for $\hbar \rightarrow 0$. In the main body of the text Emphasis is given to physical meaning **of dissipation** of background **fields due to** particle creation and statistical effects in **interacting** quantum field theories and in semiclassical gravitational theories. We indicate the possible existence of a **fluctuation-dissipation relation** for non-equilibrium quantum fields as occurring in cosmological particle **creation and back reaction processes**. Thus in the total, the sum and substance of the write is that it can be conjectured that all effective theories, including quantum gravity, **could manifest** dissipative behavior.

Effect of dissipation on the quantum-mechanical behavior of a macroscopic variable, in particular in situations **involving tunnelling** through a classically impenetrable barrier. Question of dissipation can be placed in the context of quantum measurement theory, and emphasize the importance of the distinction between the "adiabatic" and "dissipative" aspects **of the coupling of a macroscopic** variable to its environment. Next, there is a possible theoretical framework for the problem, with particular attention to how far the necessary input **parameters can be deduced** from the purely classical behavior of the system in question. Theoretical results obtained within this framework for the effects **of dissipation both on the decay of a metastable** state ("macroscopic quantum tunnelling") and on the coherent oscillations of a macroscopic two-state system ("macroscopic quantum coherence").

SOME RECENT DEVELOPMENTS:

The aim of recent research has been is the description of the electrical transport properties of Nanoscale systems. These properties **are influenced by** fundamental physical properties such as quantum mechanical coherence, dissipation, and **interaction among the charge carriers**. They are used to develop methods to describe the large variety of Nanoscale systems, but also work on the description of new measurable observables like current noise and **counting statistics** that provide a deeper understanding of the relevant transport processes. The following examples give an overview of the research:

Electron transport through quantum dot systems and molecules

In Nanoscale quantum dots electronic interactions play a **dominant role**, leading, e.g. to the Coulomb blockade. Electron transport and current noise using various methods like diagrammatic perturbation theory, full counting statistics, or path integral techniques are also taken in to consideration. Similar questions are relevant for charge transport through molecules. However, in long molecules (e.g. DNA) also inelastic transport processes and dissipation of energy to the molecular environment play an important role.

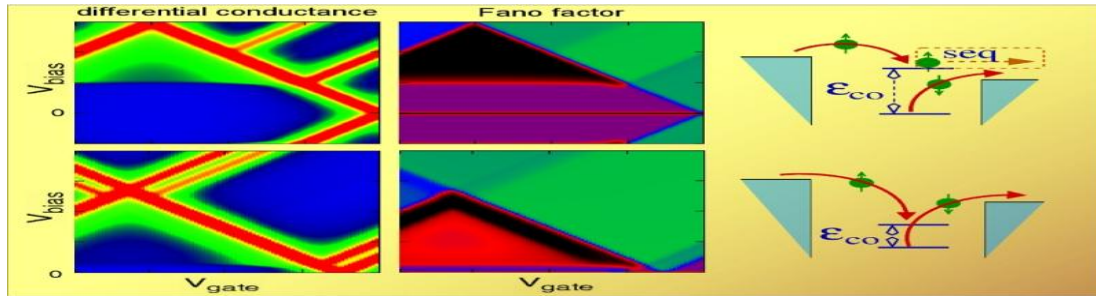


Figure 1: Differential conductance and shot **noise (Fano+ factor) of** a quantum dot with two energy levels. Within the so-called "Coulomb diamond" (area at low transport bias V_{bias} **limited by** the red lines of high differential conductance) second order processes ("**Co-tunneling**") are dominant. The sketches (right) show the dominant processes at small transport bias V_{bias} .

Electronic properties of carbon nanotubes and graphene

Carbon nanotubes and graphene are often considered as ideal examples of coherent quantum transport. In experiments, however, often effects due to disorder, in homogeneity of the environment, or phonon scattering are of importance. Some work studies observables like current noise in various experimental situations.

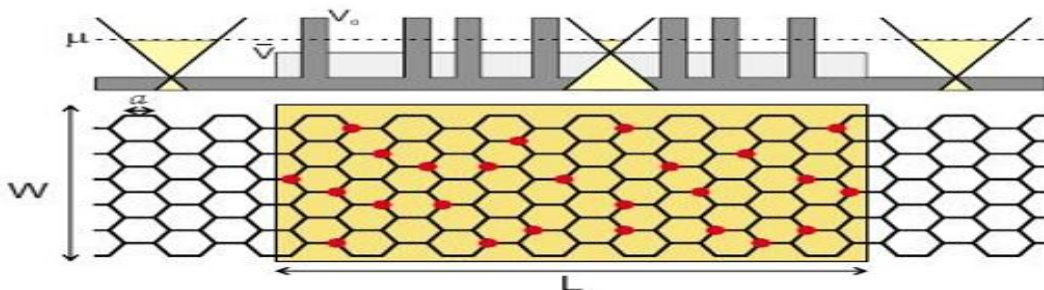


Figure 2: Sketch of the structure of a graphene ribbon with binary disorder. The disorder causes local scattering potentials V_s and a shift of the chemical potential μ away from the "Dirac points". The **conductivity depends on** the length of the graphene ribbon.

Transport through hybrid structures

In hybrid structures, materials of strongly differing (or even complementary) properties are brought together. An example is the combination of superconducting and ferromagnetic metals. Transport through such structures show phenomena that are so far poorly understood, e.g. Non-local Andreev reflections, that we describe by Green function methods. Hybrid structures are particularly interesting for applications, as their integration with established (semiconductor) technologies is feasible.

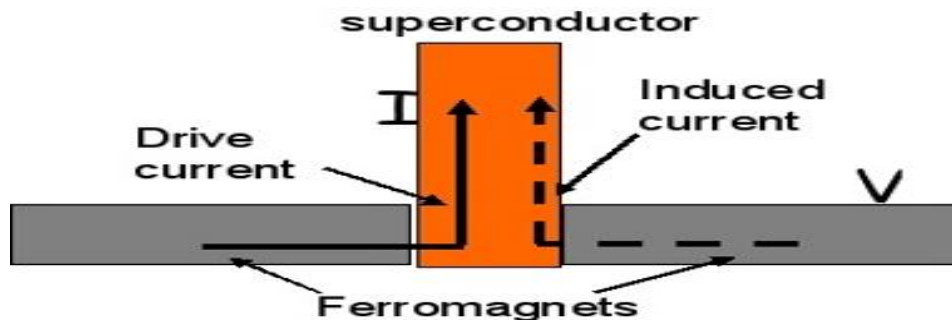


Figure 3: Sketch of a superconducting-ferromagnetic hybrid structure. The behavior of the non-local transport properties is under investigation.

Atomic contacts

The smallest possible transport system consists of single atoms. Here, the difficulty lies in the manufacturing of stable structure, with the possibility to control them via external "knobs". Our research applies a combination of Monte Carlo simulations and tight binding transport calculations, to make the bridge from a purely statistical description to possible applications of such systems with predictable transport properties.

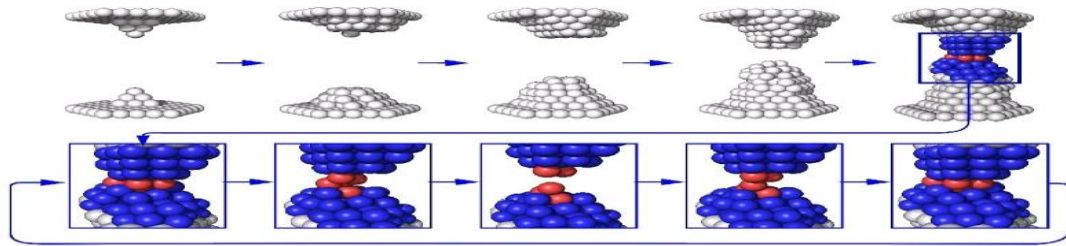


Figure 4: Monte Carlo simulation of the growth of an atomic contact of silver. In specific configurations the controlled opening and closing of the contact is possible.

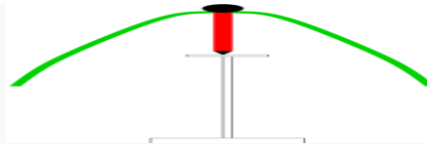
T Symmetry is the symmetry of physical laws under a **time reversal** transformation:

$$T : t \mapsto -t.$$

Although in restricted contexts one may find this symmetry, the observable universe itself does not show symmetry under time reversal, primarily due to the second law of thermodynamics. Time *asymmetries* are generally distinguished as between those intrinsic to the dynamic laws of nature, and those due to the initial conditions of our universe. The T-*asymmetry* of the weak force is of the first kind, while the T-*asymmetry* of the second law of thermodynamics is of the second kind.

Invariance

Physicists also discuss the time-reversal invariance of local and/or macroscopic descriptions of physical systems, independent of the invariance of the underlying microscopic physical laws. For example, Maxwell's equations with material absorption or Newtonian mechanics with friction are not time-reversal invariant at the macroscopic level where they are normally applied, even if they are invariant at the microscopic level when one includes the atomic motions the "lost" energy is translated into.



A toy called the teeter-totter illustrates the two aspects **of time reversal invariance**. When set into motion atop a pedestal, the figure oscillates for a very long time. The toy is engineered to minimize friction and illustrate the reversibility of Newton's laws of motion. However, the mechanically stable state of the toy is when the figure falls down from the pedestal into one of arbitrarily many positions. This is an illustration of the law of increase of entropy through Boltzmann's identification of the logarithm of the number of states with the entropy.

Macroscopic phenomena: the second law of thermodynamics

Our daily experience shows that T-symmetry does not hold for the behavior of bulk materials. Of these macroscopic laws, most notable is the second law of thermodynamics. Many other phenomena, such as the relative motion of bodies with friction, or viscous motion of fluids, **reduce to this, because the** underlying mechanism is the **dissipation of usable energy** (for example, kinetic energy) into heat.

Is this time-asymmetric **dissipation** really inevitable? This question has been considered by many physicists, often in the context of Maxwell's. The name comes from a thought experiment described by James Clerk Maxwell in which a microscopic demon guards a gate between two halves of a room. It only lets slow molecules into one half, only fast ones into the other. By eventually making one side of the room cooler than before and the other hotter, it seems **to reduce** the entropy of the room, **and reverse** the arrow of time. Many analysts have been made of this; all show that when the entropy of room and demon are taken together, this total entropy **does increase**. Modern analyses of this problem have taken into account Claude E. Shannon's relation between entropy and information. Many interesting results in modern computing are **closely related** to this problem — reversible computing, quantum computing and physical limits to computing, are examples. These seemingly metaphysical questions are today, in these ways, slowly being converted to the stuff of the physical sciences.

The current consensus hinges upon the Boltzmann-Shannon identification of the logarithm of phase space volume with the negative of Shannon, and hence to entropy. In this notion, a fixed initial state of a macroscopic system corresponds to relatively low entropy because the coordinates of the molecules of the body **are constrained**. As the system **evolves in** the presence of dissipation, the molecular coordinates can move into larger volumes of phase space, **becoming more** uncertain, and thus **leading to** increase in entropy.

One can, however equally well imagine a state of the universe in which the motions of all of the particles at one instant were the reverse (strictly, the CPT reverse). Such a state would then evolve in reverse, so presumably entropy would decrease (Loschmidt's paradox). Why is 'our' state preferred over the other?

One position is to say that the constant increase of entropy we observe **happens only because** of the initial state of our universe. Other possible states of the universe (for example, a universe at heat death equilibrium) would actually **result in** no increase of entropy. In this view, the apparent T-asymmetry of our universe is a problem in cosmology: why did the universe start with low entropy? This view, if it remains viable in the light of future cosmological observation, would connect this problem to one of the big open questions beyond the reach of today's physics — the question of initial conditions of the universe.

QUANTUM DISSIPATION AT MACROSCOPIC LEVEL- BLACK HOLES AND COSMOLOGY:

An object can cross through the event horizon of a black hole from the outside, and then fall rapidly to the central region where our understanding of physics breaks down. Since within a black hole the forward light-cone is directed towards the center and the backward light-cone is directed outward, it is not even possible to define time-reversal in the usual manner. The only way anything can escape from a black hole is as Hawking radiation.

The time reversal of a black hole would be a hypothetical object known as a white hole. From the outside they appear similar. While a black hole has a beginning and is inescapable, a white hole has an ending and cannot be entered. The forward light-cones of a white hole are directed outward; and its backward light-cones are directed towards the center.

The event horizon of a black hole may be thought of as a surface moving outward at the local speed of light and is just on the edge between escaping and falling back. The event horizon of a white hole is a surface moving inward at the local speed of light and is just on the edge between being swept outward and succeeding in reaching the center. They are two different kinds of horizons—the horizon of a white hole is like the horizon of a black hole turned inside-out.

The modern view of black hole irreversibility is to **relate it to** the second law of thermodynamics, since black holes are viewed as thermodynamic objects. Indeed, according to the Gauge-gravity duality conjecture, all microscopic processes in a black hole are **reversible**, and only the collective **behavior is irreversible**, as in any other macroscopic, thermal system.

Kinetic consequences: detailed balance and Onsager reciprocal relations

In physical and chemical kinetics, T-symmetry of the mechanical microscopic **equations implies two important** laws: the principle of detailed **balance and** the Onsager reciprocal relations. T-symmetry of the microscopic description together with its kinetic **consequences are** called microscopic reversibility.

Effect of time reversal on some variables of classical physics

Classical variables that do not change upon time reversal include:

\vec{x} , Position of a particle in three-space

\vec{a} , Acceleration of the particle

\vec{F} , Force on the particle

E , Energy of the particle

ϕ , Electric potential (voltage)

\vec{E} , Electric field

\vec{D} , Electric displacement

ρ , Density of electric charge

\vec{P} , Electric polarization

Energy density of the electromagnetic field

Maxwell stress tensor

All masses, charges, coupling constants, and other physical constants, except those associated with the weak force.

Odd

Classical variables that time reversal negates include:

t , The time when an event occurs

\vec{v} , Velocity of a particle

\vec{P} , Linear momentum of a particle

\vec{l} , Angular momentum of a particle (both orbital and spin)

\vec{A} , Electromagnetic vector potential

\vec{B} , Magnetic induction

\vec{H} , Magnetic field

\vec{j} , Density of electric current

\vec{M} , Magnetization

\vec{S} , Poynting vector

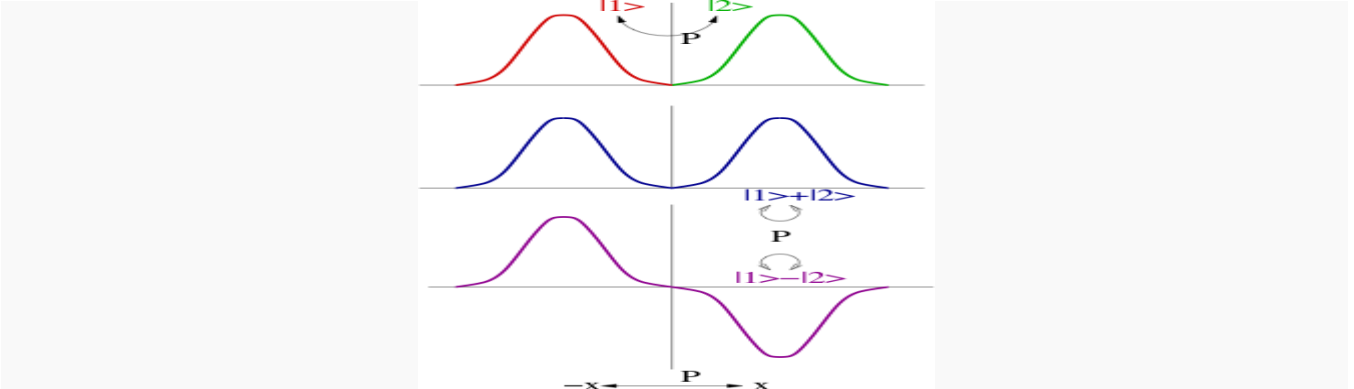
Power (rate of work done).

Microscopic phenomena: time reversal invariance

Since most systems are asymmetric under time reversal, it is interesting to ask whether there are phenomena **that do have** this symmetry. In classical mechanics, a **velocity reverses** under the operation of T , but **acceleration does not**. Therefore, one models dissipative phenomena through terms that are odd in v . However, delicate experiments in which **known sources of dissipation are removed** reveal that the laws of mechanics are time reversal invariant. **Dissipation itself is originated in the second law of thermodynamics.**

The motion of a charged body in a magnetic field, B **involves the** velocity through the Lorentz force term $v \times B$, and might seem at first to be asymmetric under T . A closer look assures us that B also changes sign under time reversal. This happens because a magnetic field **is produced** by an electric current, J , **which reverses sign** under T . Thus, the motion of classical charged particles in electromagnetic fields is also time reversal invariant. (Despite this, it is still useful to consider the time-reversal non-invariance in a *local* sense when the external field is held fixed, as when the magneto-optic effect is analyzed. This allows one to analyze the conditions under **which optical phenomena** that locally break time-reversal, such as Faraday isolators, can occur.) **The laws of gravity also** seem to be time reversal invariant in classical mechanics.

In physics one separates the laws of motion, called kinematics, from the laws of force, called dynamics. Following the classical kinematics of Newton's laws of motion, the kinematics of quantum mechanics is built in such a way that it presupposes nothing about the time reversal symmetry of the dynamics. In other words, if the **dynamics are invariant**, then the kinematics will allow it to remain invariant; if the dynamics is not, and then the kinematics will also show this. The structure of the quantum laws of motion is richer.

Time reversal in quantum mechanics

Two-dimensional representations of parity are given by a pair of quantum states that go into each other under parity. However, this representation can always be **reduced to** linear combinations of states, each of which is either even or odd under parity. One says that all irreducible representations of parity are one-dimensional. **Kramers' theorem** states that time reversal need not have this property **because it** is represented by an anti-unitary operator.

Fundamental properties of time reversal in quantum mechanics are:

1. that it must be **represented as** an anti-unitary operator,
2. that **it protects** non-degenerate quantum states from having an electric dipole moment,
3. that it has two-dimensional representations with the property $T^2 = -1$.

The strangeness of this result is clear if one compares it with parity. If parity **transforms a** pair of quantum states into each other, then the sum and difference of these two basis states are states of good parity. **Time reversal does not behave like this.** It seems **to violate the** theorem that all abelian groups be represented by one dimensional irreducible representation. **The reason it does this is that it is represented by an anti-unitary operator.** It thus opens the way to spinors in quantum mechanics.

Anti-unitary representation of time reversal

Eugene Wigner showed that a symmetry operation S of a Hamiltonian is represented, in quantum mechanics either by a **unitary operator, $S = U$, or an antiunitary one, $S = UK$ where** U is unitary, and K denotes complex conjugation. These are the only operations that act on Hilbert space so as to preserve the *length* of the projection of any one state-vector onto another state-vector.

Consider the **parity operator**. Acting on the position, it **reverses the** directions of space, so that $P^{-1}xP = -x$. Similarly, it **reverses the** direction of *momentum*, so that $PpP^{-1} = -p$, where x and p are the position and momentum operators. This preserves the canonical $[x, p] = i\hbar$, where \hbar is the reduced Planck constant, only if P is chosen to be unitary, $PiP^{-1} = i$.

On the other hand, for time reversal, the time-component of the momentum is the energy. If time reversal were implemented as a unitary operator, it **would reverse the sign of the energy** just as space-reversal **reverses the sign of the momentum**. This is not possible, because, unlike momentum, energy is always positive. Since energy in quantum mechanics is defined as **the phase factor** $\exp(-iEt)$ that one gets when one moves forward in time, the way to reverse time while preserving the sign of the energy is to reverse the sense of "i", so that the sense of phases is reversed.

Similarly, any operation that reverses the sense of phase, which changes the sign of i , will turn positive energies into negative energies unless it also changes the direction of time. So every antiunitary symmetry in a theory with positive energy must reverse the direction of time. The only antiunitary symmetry is time reversal, together with a unitary symmetry that does not reverse time.

Given the *time reversal* operator T , it does nothing to the x -operator, $TxT^{-1} = x$, but it reverses the direction of p , so that $TpT^{-1} = -p$. The canonical commutator is invariant only if T is chosen to be anti-unitary, i.e., $TiT^{-1} = -i$. For a particle with spin J , one can use the representation

$$T = e^{-i\pi J_y/\hbar} K,$$

where J_y is the y -component of the spin, and use of $TJT^{-1} = -J$ has been made.

Electric dipole moments

This has an interesting consequence on the electric dipole moment (EDM) of any particle. The EDM is defined through the shift in the energy of a state when it is put in an external electric field: $\Delta e = d \cdot E + E \cdot \delta \cdot E$, where d is called the EDM and δ , the induced dipole moment. One important property of an EDM is that the energy shift due to it changes sign under a parity transformation. However, since \mathbf{d} is a vector, its expectation value in a state $|\psi\rangle$ must be proportional to $\langle\psi|J|\psi\rangle$. Thus, under time reversal, an invariant state must have vanishing EDM. In other words, a non-vanishing EDM signals both P and T symmetry-breaking.

It is interesting to examine this argument further, since one feels that some molecules, such as water, must have EDM irrespective of whether \mathbf{T} is symmetry. This is correct: if a quantum system has degenerate ground states that transform into each other under parity, then time reversal need not be broken to give EDM.

Experimentally observed bounds on the electric dipole moment of the nucleon currently set stringent limits on the violation of time reversal symmetry in the strong interactions, and their modern theory: quantum chromodynamics. Then, using the CPT invariance of a relativistic quantum field theory, this puts strong bounds on strong CP violation. Experimental bounds on the electron electric dipole moment also place limits on theories of particle physics and their parameters.

Kramers' theorem

For T , which is an anti-unitary Z_2 symmetry generator

$$T^2 = UKUK = U U^* = U (U^T)^{-1} = \Phi,$$

where Φ is a diagonal matrix of phases. As a result, $U = \Phi U^T$ and $U^T = U\Phi$, showing that

$$U = \Phi U \Phi.$$

This means that the entries in Φ are ± 1 , as a result of which one may have either $T^2 = \pm 1$. This is specific to the anti-unitarity of T . For a unitary operator, such as the parity, any phase is allowed. Next, take a Hamiltonian invariant under T . Let $|a\rangle$ and $T|a\rangle$ be two quantum states of the same energy. Now, if $T^2 = -1$, then one finds that the states are orthogonal: a result called **Kramers' theorem**. This implies that if $T^2 = -1$, then there is a twofold degeneracy in the state. This result in non-relativistic quantum mechanics presages the spin statistics theorem of quantum field theory.

Quantum states that give unitary representations of time reversal, i.e., have $\mathbf{T}^2=1$, are characterized by a multiplicative quantum number, sometimes called the **T-parity**.

Time reversal transformation for fermions in quantum field theories can be represented by an 8-component spinor in which the above mentioned **T-parity** can be a complex number with unit radius. The CPT invariance is not a theorem but a **better to have** property in these classes of theories.

Time reversal of the known dynamical laws

Particle physics codified the basic laws of dynamics into the standard model. This is formulated as a quantum field theory that has CPT symmetry, i.e., the laws are invariant under simultaneous operation of time reversal, parity and charge conjugation. However, time reversal itself is seen not to be symmetry (this is usually called CP violation). There are two possible origins of this asymmetry, one through the mixing of different flavours of quarks in their weak decays, the second through a direct CP violation in strong interactions. The first is seen in experiments, the second is strongly constrained by the non-observation of the EDM of a neutron.

It is important to stress that this time reversal violation is unrelated to the second law of thermodynamics, because due to the conservation of the CPT symmetry, the effect of time reversal is to rename particles as antiparticles and *vice versa*. Thus the second law of thermodynamics is thought to originate in the initial conditions in the universe.

SOME RECENT DEVELOPMENTS IN THE CONTEXT OF QUANTUM INFORMATION OR QUANTUM MECHANICAL BEHAVIOUR DISSIPATION: A REVIEW STUDY THAT SUBSTANTIATES THE DISSIPATION COEFFICIENT USAGE IN THE MODEL:

Influence of dissipation on phase tunneling in Josephson-junctions (For details see. Zwerger)

The coupling between the phase and the electromagnetic field in the case of a tunnel junction is treated by Feynman's path integral method. It is shown that the elimination of the field leads to a frequency dependent mass for the motion of the

phase ψ , which is simply related to the effective dielectric constant of the junction. Considering tunneling as a motion in

imaginary time **one obtains** a polaron like mass enhancement **connected** to the dielectric function at positive imaginary frequencies, which **essentially leads to** the Caldeira-Leggett **reduction** of the elastic tunneling probability. In the weak damping limit it is shown that the emission of real excitations during tunneling is a higher order effect. At low temperatures the damping finally **is determined** by the line width of electromagnetic radiation at the Josephson plasma frequency

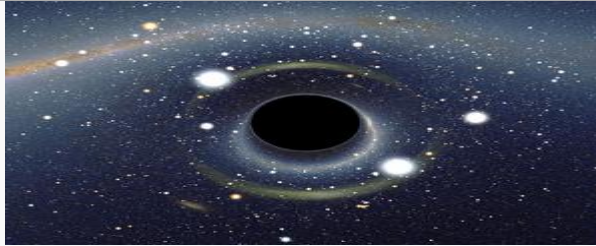
The quantum-mechanical two-level system with dissipation and feedback: multimode applied electric-field case

A two-level dissipative quantum-mechanical system subjected to a small applied multimode electric field plus a feedback term proportional to the induced dipole moment is discussed. The long-term behaviour of the induced dipole moment and of the upper level occupation probability is represented by a series expansion in terms of the applied electric-field amplitudes. First-order and third-order internal, external, and intrinsic polarizabilities **are introduced** and calculated for the model. Certain ratios of third-order to first-order polarizabilities are shown to have a common value for the internal, external, and intrinsic cases. Clausius-Mossotti relations for the linear and third-order susceptibilities **are derived**.

The quantum mechanical fluctuation-dissipation theorem:

In this paper, Kubo's spectral theorem is re-derived and developed into a fluctuation-dissipation theorem for systems which fluctuate about their equilibrium positions. This is accomplished by introducing a general link between the operator corresponding to the observable and the operator which joins the external force to the Hamiltonian. For certain systems this link takes on simple forms and the theorem then reduces to previously derived results. It is also shown how different forms of the link are related to different Langevin equations which are the basis of the corresponding classical theory.

Black hole: Quantum Information Loss:



Simulated view of a black hole (center) in front of the Large. Note the gravitational lensing effect, which **produces** two enlarged but highly distorted views of the Cloud. Across the top, the Milky Way disk appears distorted into an arc.

A **black hole** is a region of spacetime whose gravitational field is so strong that nothing which enters it, not even light, can escape. The theory of general relativity predicts that a sufficiently compact mass **will deform** spacetime to form a black hole. Around a black hole there is a mathematically defined surface called an **event horizon** that marks the point of no return. It is called "black" because it absorbs all the light that hits the horizon, reflecting nothing, just like a perfect **black body in thermodynamics**. Quantum mechanics predicts that black holes emit radiation like a black body with a finite temperature. This temperature is **inversely proportional** to the mass of the black hole, making it difficult to observe this radiation for **black holes of stellar mass** or greater.

Objects whose **gravity field** is too strong for light to escape were first considered in the 18th century by John Michell and Pierre-Simon Laplace. The first modern solution of general relativity that would characterize a black hole was found by Karl Schwarzschild in 1916, although its interpretation as a region of space from which nothing can escape was not fully appreciated for another four decades. Long considered a mathematical curiosity, it was during the 1960s that theoretical work showed black holes were a generic prediction of general relativity. The discovery of **neutron stars** sparked interest in **gravitationally compact** objects as a possible astrophysical reality.

Black holes of stellar mass are expected to form when a star of more than 5 solar masses runs out of energy fuel. **This results** in the outer layers of gas being thrown out in a supernova explosion. The core of the star **collapses** and **becomes** super dense where even the atomic nuclei are squeezed together. The energy density at the core goes to infinity. After a black hole has **formed it** can continue to grow **by absorbing mass** from its surroundings. By absorbing other stars and **merging with** other black holes, supermassive black holes of millions of solar masses may form. There is general consensus that supermassive black holes exist in the centers of most galaxies. In particular, there is strong evidence of a black hole of more than 4 million solar masses at the center of our galaxy, the Milky Way.

Despite its invisible interior, the presence of a black hole can be inferred through **its interaction** with other **matter and with light** and other electromagnetic radiation. From stellar movement, the mass and location of an invisible companion object can be calculated. A half-dozen or so binary star systems have been discovered by Astronomers where one of the stars is invisible, yet must surely exist since it pulls with enough gravitational force on the other visible star to make it orbit around their common center of gravity. Therefore these invisible stars are thought to be good **candidate black holes**. **Astronomers have identified numerous stellar black hole candidates in binary systems by studying the movement of their companion stars in this way.**

GRAVITATIONAL LENSING-PRODUCTION OF DISTORTED PICTURE:



Simulation of gravitational lensing by a black hole, **which distorts** the image of a galaxy in the background (larger animation)

The idea of a body so massive that even light could not escape was first put forward by geologist John Michell in a letter written to Henry Cavendish in 1783 of the Royal Society:

If the semi-diameter of a sphere of the same density as the Sun were to exceed that of the Sun in the proportion of 500 to 1, a body falling from an infinite height towards it would have acquired at its surface greater velocity than that of light, and consequently supposing light to be attracted by the same force in proportion to its vis inertiae, with other bodies, all light emitted from such a body would be made to return towards it by its own proper gravity.

—John Michell

In 1796, mathematician Pierre-Simon Laplace promoted the same idea in the first and second editions of his book *Exposition du système du Monde* (it was removed from later editions). Such "dark stars" were largely ignored in the nineteenth century, since it was not understood how a massless wave such as light could be influenced by gravity.

STABILITY ANALYSIS OR UNSTABILITY AT MACROSCOPIC LEVEL: A POINTER TO IMPORTANCE TO STABILITY ANALYSIS CARRIED OUT IN THE MIODEL:

In 1915, Albert Einstein developed his theory of general relativity, having earlier shown that gravity does influence light's motion. Only a few months later, Karl Schwarzschild found a solution to Einstein field equations, which describes the gravitational field of a point mass and a spherical mass. A few months after Schwarzschild, Johannes Droste, a student of Hendrik Lorentz, independently gave the same solution for the point mass and wrote more extensively about its properties. This solution had a peculiar behaviour at what is now called the Schwarzschild radius, where it became singular, meaning that some of the terms in the Einstein equations became infinite. The nature of this surface was not quite understood at the time. In 1924, Arthur Eddington showed that the singularity disappeared after a change of coordinates (see Eddington–Finkelstein coordinates), although it took until 1933 for Georges Lemaître to realize that this meant the singularity at the Schwarzschild radius was an unphysical coordinate singularity.³

In 1931, Subrahmanyan Chandrasekhar calculated, using special relativity, that a non-rotating body of electron-degenerate matter above a certain limiting mass (now called the Chandrasekhar at 1.4 solar masses) has no stable solutions. His arguments were opposed by many of his contemporaries like Eddington and Lev Landau, who argued that some yet unknown mechanism would stop the collapse. They were partly correct: a white dwarf slightly more massive than the Chandrasekhar limit will collapse into a neutron star, which is itself stable because of the Pauli exclusion principle. But in 1939, Robert Oppenheimer and others predicted that neutron stars above approximately three solar masses (the Tolman–Oppenheimer–Volkoff limit) would collapse into black holes for the reasons presented by Chandrasekhar, and concluded that no law of physics was likely to intervene and stop at least some stars from collapsing to black holes.

Oppenheimer and his co-authors interpreted the singularity at the boundary of the Schwarzschild radius as indicating that this was the boundary of a bubble in which time stopped. This is a valid point of view for external observers, but not for infalling observers. Because of this property, the collapsed stars were called "frozen stars, because an outside observer would see the surface of the star frozen in time at the instant where its collapse takes it inside the Schwarzschild radius.

BLACK HOLES: THE MACROSCOPIC LEVEL IMPECCABLE TESTIMONY FOR THE QUNTUM DISSIPATION EFFECTS (HAWKING RADIATION):

In 1958, David Finkelstein identified the Schwarzschild surface as an event horizon, "a perfect unidirectional membrane: causal influences can cross it in only one direction". This did not strictly contradict Oppenheimer's results, but extended them to include the point of view of infalling observers. Finkelstein's solution extended the Schwarzschild solution for the future of observers falling into a black hole. A complete extension had already been found by Martin Kruskal,

These results came at the beginning of the golden age of general relativity, which was marked by general relativity and black holes becoming mainstream subjects of research. This process was helped by the discovery of pulsars in 1967, which, by 1969, were shown to be rapidly rotating neutron stars. Until that time, neutron stars, like black holes, were regarded as just theoretical curiosities; but the discovery of pulsars showed their physical relevance and spurred a further interest in all types of compact objects that might be formed by gravitational collapse.

In this period more general black hole solutions were found. In 1963, Roy Kerr found the exact solution for a rotating black hole. Two years later, Ezra Newman found the axisymmetric solution for a black hole that is both rotating and electrically charged. Through the work of Werner Israel, Brandon Carter, and David Robinson, the no-hair theorem emerged, stating that a stationary black hole solution is completely described by the three parameters of the Kerr–Newman metric; mass, angular momentum, and electric charge.

For a long time, it was suspected that the strange features of the black hole solutions were pathological artifacts from the symmetry conditions imposed, and that the singularities would not appear in generic situations. This view was held in particular by Vladimir Belinsky, Isaak Khalatnikov, and Evgeny Lifshitz, who tried to prove that no singularities appear in generic solutions. However, in the late sixties Roger Penrose and Stephen Hawking used global techniques to prove those singularities are generic.

Work by James Bardeen, Jacob Bekenstein, Carter, and Hawking in the early 1970s led to the formulation of black hole thermodynamics. These laws describe the behaviour of a black hole in close analogy to the laws of thermodynamics by relating mass to energy, area to entropy, and surface gravity to temperature. The analogy was completed when Hawking, in 1974, showed that quantum field theory predicts that black holes should radiate like a black body with a temperature proportional to the surface gravity of the black hole.

The term "black hole" was first publicly used by John Wheeler during a lecture in 1967. Although he is usually credited with coining the phrase, he always insisted that it was suggested to him by somebody else..

Properties and structure

The no-hair theorem states that, once it achieves a stable condition after formation, a black hole has only three independent physical properties: mass, charge, and angular momentum. Any two black holes that share the same values for these properties, or parameters, are indistinguishable according to classical (i.e. non-quantum) mechanics. These properties are special because they are visible from outside a black hole. For example, a charged black hole repels other like charges just like any other charged object. Similarly, the total mass inside a sphere containing a black hole can be found by using the gravitational analog of Gauss's law, the ADM mass, far away from the black hole. Likewise, the angular momentum can be measured from far away using frame dragging by the gravitomagnetic field.

QUANTUM INFORMATION LOSS PARADOX IN BLACK HOLE:

When an object falls into a black hole, any information about the shape of the object or distribution of charge on it is evenly distributed along the horizon of the black hole, and is lost to outside observers. The behavior of the horizon in this situation is a dissipative system that is closely analogous to that of a conductive stretchy membrane with friction and electrical—the membrane paradigm. This is different from other field theories like electromagnetism, which do not have any friction or resistivity at the microscopic level, because they are time-reversible. Because a black hole eventually achieves a stable state with only three parameters, there is no way to avoid losing information about the initial conditions: the gravitational and electric fields of a black hole give very little information about what went in. The information that is lost includes every quantity that cannot be measured far away from the black hole horizon, including the total baryon number, lepton number, and all the other nearly conserved pseudo-charges of particle physics. This behavior is so puzzling that it has been called the black hole information loss paradox.

Physical properties

The simplest black holes have mass but neither electric charge nor angular momentum. These black holes are often referred to as Schwarzschild black holes after Karl Schwarzschild who discovered this solution in 1916.¹ According to Birkhoff's theorem, it is the only vacuum solution that is spherically symmetric. This means that there is no observable difference between the gravitational field of such a black hole and that of any other spherical object of the same mass. The popular notion of a black hole "sucking in everything" in its surroundings is therefore only correct near a black hole's horizon; far away, the external gravitational field is identical to that of any other body of the same mass.

Solutions describing more general black holes also exist. Charged black holes are described by the Reissner–Nordström metric, while the Kerr metric describes a rotating black hole. The most general stationary black hole solution known is the Kerr–Newman metric, which describes a black hole with both charge and angular momentum.

While the mass of a black hole can take any positive value, the charge and angular momentum are constrained by the mass. In Planck units, the total electric charge Q and the total angular momentum J are expected to satisfy

$$Q^2 + \left(\frac{J}{M}\right)^2 \leq M^2$$

for a black hole of mass M . Black holes saturating this inequality are called extremal. Solutions of Einstein's equations that violate this inequality exist, but they do not possess an event horizon. These solutions have so-called naked singularities that can be observed from the outside, and hence are deemed unphysical. The hypothesis rules out the formation of such singularities, when they are created through the gravitational collapse of realistic matter. This is supported by numerical simulations.

Due to the relatively large strength of the electromagnetic force, black holes forming from the collapse of stars are expected to retain the nearly neutral charge of the star. Rotation, however, is expected to be a common feature of compact

objects. The black-hole candidate binary X-ray source **GRS 1915+105^[41]** appears to have an angular momentum near the maximum allowed value.

Black hole classifications

Class*Mass*Size

Supermassive black hole* $\sim 10^5$ – $10^9 M_{\text{Sun}}$ * ~ 0.001 – 10 AU

Intermediate-mass black hole* $\sim 10^3 M_{\text{Sun}}$ * $\sim 10^3$ km = R_{Earth}

Stellar black hole* $\sim 10 M_{\text{Sun}}$ * ~ 30 km

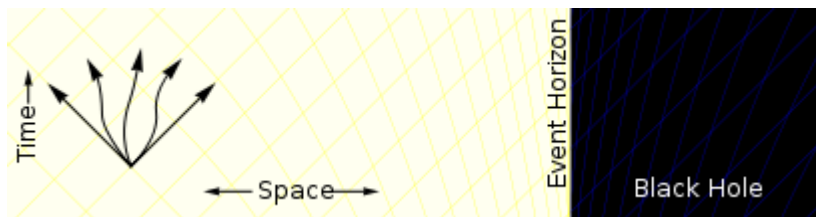
Micro black hole*up to $\sim M_{\text{Moon}}$ *up to ~ 0.1 mm

Black holes are commonly classified according to their mass, independent of angular momentum J or electric charge Q . The size of a black hole, as determined by the radius of the event horizon, or **Schwarzschild radius**, is roughly proportional to the mass M through

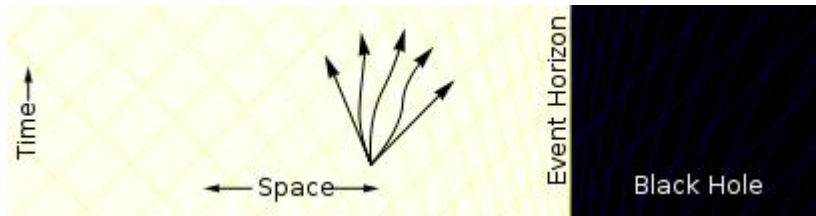
$$r_{\text{sh}} = \frac{2GM}{c^2} \approx 2.95 \frac{M}{M_{\text{Sun}}} \text{ km},$$

where r_{sh} is the Schwarzschild radius and M_{Sun} is the **mass of the Sun**. This relation is exact only for black holes with zero charge and angular momentum; for more general black holes it can differ up to a factor of 2.

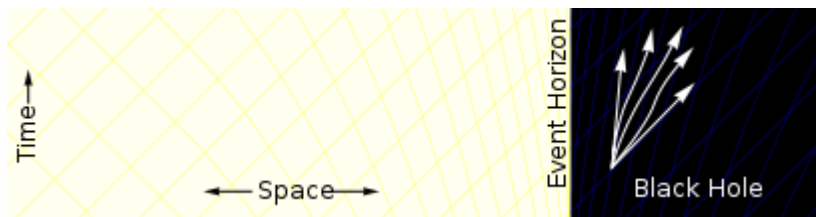
Event horizon



Far away from the black hole a particle can move in any direction, as illustrated by the set of arrows. It is only restricted by the speed of light.



Closer to the black hole spacetime *starts to deform*. There are more *paths going towards* the black hole than paths moving away



Inside of the event horizon all paths bring the particle *closer* to the center of the black hole. It is no longer possible for the particle to escape. Particle is captured

The defining feature of a black hole is the appearance of an event horizon—a boundary in spacetime through which matter and light can only pass **inward towards** the mass of the black hole. Nothing, not even light, can escape from inside the event horizon. The event horizon is referred to as such because if an event **occurs within** the boundary, **information from that event cannot reach an outside observer, making it impossible to determine if such an event occurred**

As predicted by general relativity, the presence of a mass **deforms spacetime** in such a way that the paths taken by particles bend towards the mass. At the event horizon of a black hole, this deformation becomes so strong that there are no paths that lead away from the black hole.

To a distant observer, clocks near a black hole appear to tick more slowly than those further away from the black hole. **Due to this effect**, known as **gravitational time dilation**, an object falling into a black hole appears **to slow down** as it approaches the event horizon, taking an infinite time to reach it. At the same time, all processes on this **object slow down** **causing** emitted light to appear redder and dimmer, an effect known as **gravitational redshift**. Eventually, at a point just before it reaches the event horizon, the falling object becomes so dim that it can no longer be seen.

On the other hand, an observer falling into a black hole does not notice any of these effects as he crosses the event horizon. According to his own clock, he crosses the event horizon after a finite time, although he is **unable to determine** exactly when he crosses it, as it is impossible to determine the location of the event horizon from local observations

The shape of the event horizon of a black hole is always approximately spherical. For non-rotating (static) black holes the geometry is precisely spherical, while for rotating black holes the sphere is somewhat oblate.

GRAVITATIONAL SINGULARITY-ANOTHER CARDINAL WAY OF DISSIPATION AND ENTANGLEMENT WITH QUANTUM INFORMATION:

At the center of a black hole as described by general relativity lies a **gravitational singularity**, a region where the spacetime curvature becomes infinite. For a non-rotating black hole, this region takes the shape of a single point and for a **rotating black hole**, it is **smeared out to** form a **ring singularity** lying in the plane of rotation. In both cases, the singular region has zero volume. It can also be shown that the singular region contains all the mass of the black hole solution. The singular region can thus be thought of as having **infinite density**.

Observers falling into a Schwarzschild black hole (i.e. non-rotating and no charges) cannot avoid being carried into the singularity, once they cross the event horizon. They can prolong the experience by accelerating away to slow their descent, but only up to a point; after attaining a certain ideal velocity, it is best **to free fall** the rest of the way. When they reach the singularity, they are **crushed to** infinite density and their mass is added to the **total of the** black hole. Before that happens, they will have been torn apart by the growing **tidal forces** in a process sometimes referred to as **spaghettification** or the "noodle effect".

THE ULTIMATE ELDORADO OF DESTRUCTION/OBLITERATION OF INFORMATION QUANTUM INFORMATION LOSS SYNDROME AND ARMAGEDDON OR APOCHRYPHAL ANEURISM-THE BLACK HOLE SPAGATEFICATION

In the case of a charged (Reissner–Nordström) or rotating (Kerr) black hole, it is possible to avoid the singularity. Extending these solutions as far as possible reveals the hypothetical possibility of exiting the black hole into a different spacetime with the **black hole acting as a wormhole**. The possibility of traveling to another universe is however only theoretical, since any perturbation will destroy this possibility. It also appears to be possible to follow **closed timelike curves** (going back to one's own past) around **the Kerr singularity**, which lead to problems with **causality** like the **grandfather paradox**. It is expected that none of these peculiar effects would survive in a proper quantum mechanical treatment of rotating and charged black holes

The appearance of singularities in general relativity is commonly perceived as signaling the breakdown of the theory.^[62] This breakdown, however, is expected; it occurs in a situation where **quantum mechanical effects** should describe these actions due to the extremely high density and therefore particle interactions. To date, it has not been possible to combine quantum and gravitational effects into a single theory. It is generally expected that a theory of **quantum gravity** will feature black holes without singularities.

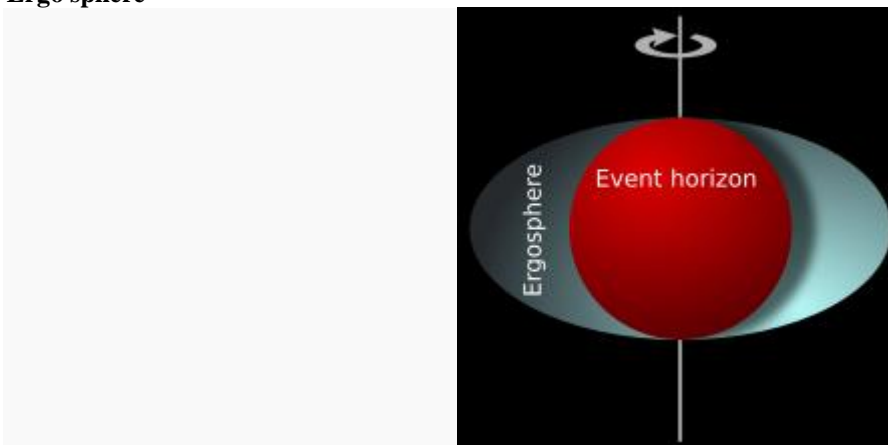
Photon sphere

The photon sphere is a spherical boundary of zero thickness such **that photons** moving **along tangents to** the sphere will be trapped in a circular orbit. For non-rotating black holes, the photon sphere has a radius 1.5 times the Schwarzschild radius. The orbits are **dynamically unstable**, hence any small perturbation (such as a particle of infalling matter) **will grow over time**, either setting it on an outward trajectory escaping the black hole or on an inward spiral eventually crossing the event horizon.

While light can still escape from inside the photon sphere, any light that crosses the photon sphere on an inbound trajectory will be captured by the black hole. Hence any light reaching an outside observer from inside the photon sphere must have been emitted by objects inside the photon sphere but still outside of the event horizon.

Other compact objects, such as **neutron stars**, can also have photon spheres. This follows from the fact that the gravitational field of an object **does not depend** on its actual size; hence any object that is smaller than 1.5 times the Schwarzschild radius corresponding to its mass will indeed have a photon sphere.

Ergo sphere



The ergo sphere is an oblate spheroid region outside of the event horizon, where objects **cannot remain** stationary.

Rotating black holes are surrounded by a region of spacetime in which it is impossible to stand still, called the ergo sphere. This is **the result of** a process known as **frame-dragging**; general relativity predicts that any rotating mass will tend to slightly "drag" along the spacetime immediately surrounding it. Any object near the rotating mass will tend to start moving in the direction of rotation. For a rotating black hole, this effect becomes so strong near the event horizon that an object would have to move faster than the speed of light in the opposite direction to just stand still.

The ergo sphere of a black hole is bounded by the (outer) event horizon on the inside and an **oblate spheroid**, which coincides with the event horizon at the poles and is noticeably wider around the equator. The outer boundary is sometimes called the **ergo surface**. Objects and radiation can escape normally from the ergo sphere. Through the **Penrose process**, objects can emerge from the ergo sphere with more energy than they entered. This energy is taken from the rotational energy of the black hole causing it to slow down.

Formation and evolution

Considering the exotic nature of black holes, it may be natural to question if such bizarre objects could exist in nature or to suggest that they are merely pathological solutions to Einstein's equations. Einstein himself wrongly thought that **black holes would not form**, because he held that the angular momentum of collapsing particles would stabilize their motion at some radius. This led the general relativity community to dismiss all results to the contrary for many years. However, a minority of relativists continued to contend that black holes were physical objects, and by the end of the 1960s, they had persuaded the majority of researchers in the field that there is no obstacle to forming an event horizon.

Once an event horizon forms, Penrose proved that a singularity will form somewhere inside it. Shortly afterwards, Hawking showed that many cosmological solutions describing **the Big Bang** have singularities without scalar fields or other exotic matter (see **Penrose-Hawking singularity theorems**). The **Kerr solution, the no-hair theorem** and the laws of **black hole thermodynamics** showed that the physical properties of black holes were simple and comprehensible, making them respectable subjects for research. The primary formation process for black holes is expected to be **the gravitational collapse** of heavy objects such as stars, but there are also more exotic processes that can lead to the production of black holes.

Gravitational collapse

Gravitational collapse **occurs when** an object's internal **pressure** is insufficient **to resist(E) the** object's own gravity. For stars this **usually occurs** either because a star has too little "fuel" left to maintain its temperature through **stellar nucleosynthesis**, or because a star that would have been stable **receives extra** matter in a way that does not raise its core temperature. In either case the star's temperature is no longer high enough to **prevent it from collapsing** under its own weight. The ideal gas law explains the **connection** between pressure, temperature, and volume.

The collapse may be stopped by the **degeneracy pressure** of the star's constituents, condensing the matter in an **exotic denser state**. The **result is** one of the various types of compact STARS. The type of compact star formed **depends on the** mass of the remnant—the matter left over after the outer layers have been blown away, such from a supernova explosion or by pulsations leading to **a planetary nebula**. Note that this mass can be substantially less than the original star—remnants exceeding 5 solar masses **are produced** by stars that were over 20 solar masses before the collapse.

If the mass of the remnant exceeds about 3–4 solar masses (the **Tolman–Oppenheimer–Volkoff limit**¹)—either because the original star was very heavy or because the remnant collected additional mass through **accretion** of matter—even the degeneracy pressure **of neutrons** is insufficient to stop the collapse. No known mechanism (except possibly quark degeneracy pressure, see **quark star**) is powerful enough to stop the implosion and the object will inevitably **collapse to form a black hole**.

The gravitational collapse of heavy stars is assumed to be responsible for the formation of **stellar mass black holes**. **Star formation** in the early universe may have resulted in very massive stars, which upon their collapse would **have produced** black holes of up to 10^3 solar masses. These black holes could be the seeds of the supermassive black holes found in the centers of most galaxies.

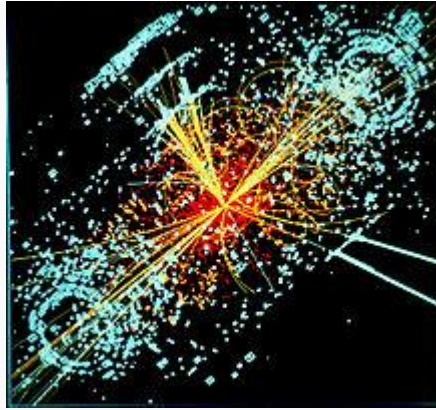
While most of the energy released during gravitational collapse is emitted very quickly, an outside observer does not actually see the end of this process. Even though the collapse takes a finite amount of time from the **reference frame** of infalling matter, a distant observer sees the infalling material slow and halts just above the event horizon, due to **gravitational time dilation**. Light from the collapsing material takes longer and longer to reach the observer, with the light emitted just before the event horizon forms is delayed an infinite amount of time. Thus the external observer never sees the formation of the event horizon; instead, the collapsing material seems to become dimmer and increasingly red-shifted, eventually fading away.

Primordial black holes in the Big Bang

Gravitational collapse requires great density. In the current epoch of the universe these high densities are only found in stars, but in the early universe shortly after the bang densities were much greater, possibly allowing for the creation of black holes. The high density alone is not enough to allow the formation of black holes since a uniform mass distribution will not allow the mass to bunch up. In order for **primordial black holes** to form in such a dense medium, there must be initial density perturbations that can then grow under their own gravity. Different models for the early universe vary widely in their predictions of the size of these perturbations. Various models predict the creation of black holes, ranging from a **Planck**

mass to hundreds of thousands of solar masses.^[25] Primordial black holes could thus account for the creation of any type of black hole.

High-energy collisions



A simulated event in the CMS detector, a collision in which a micro black hole may be created.

Gravitational collapse is not the only process that could create black holes. In principle, black holes could be formed in **high-energy collisions** that achieve sufficient density. As of 2002, no such events have been detected, either directly or indirectly as a deficiency of the mass balance in **particle accelerator** experiments. This suggests that there must be a lower limit for the mass of black holes. Theoretically, this boundary is expected to lie around the **Planck mass** ($m_P = \sqrt{\hbar c/G} \approx 1.2 \times 10^{19} \text{ GeV}/c^2 \approx 2.2 \times 10^{-8} \text{ kg}$), where quantum effects are expected to invalidate the predictions of general relativity. This would put the creation of black holes firmly out of reach of any high energy process occurring on or near the Earth. However, certain developments in quantum gravity suggest that the Planck mass could be much lower: some **braneworld** scenarios for example put the boundary as low as **1 TeV/c²**. This would make it conceivable for **micro black holes** to be created in the high energy collisions occurring when **cosmic rays** hit the Earth's atmosphere, or possibly in the new **Large Hadron Collider at CERN**. Yet these theories are very speculative, and the creation of black holes in these processes is deemed unlikely by many specialists. Even if micro black holes should be formed in these collisions, it is expected that they would **evaporate** in about 10^{-25} seconds, posing no threat to the Earth.

Growth

Once a black hole has formed, it can continue to grow by absorbing additional matter. Any black hole will continually absorb gas and interstellar from its direct surroundings and omnipresent **cosmic background radiation**. This is the primary process through which supermassive black holes seem to have grown. A similar process has been suggested for the formation of **intermediate-mass black holes in globular clusters**.

Another possibility is for a black hole to merge with other objects such as stars or even other black holes. This is thought to have been important especially for the early development of supermassive black holes, which could have formed from the coagulation of many smaller objects. The process has also been proposed as the origin of **some intermediate-mass black holes**.

Evaporation-Another Dissipatory Mode:

In 1974, Hawking showed that black holes are not entirely black but emit small amounts of thermal radiation;^[30] an effect that has become known as **Hawking radiation**. By **applying quantum** to a static black hole background, he determined that a black hole should emit particles in a perfect **black body spectrum**. Since **Hawking's publication**, many others have verified the result through various approaches.^[84] If **Hawking's theory of black hole radiation** is correct, then black holes are expected to shrink and evaporate over time because they lose mass by the emission of photons and other particles. The temperature of this thermal spectrum (**Hawking temperature**) is proportional to the **surface gravity** of the black hole, which, for a Schwarzschild black hole, is inversely proportional to the mass. Hence, large black holes emit less radiation than small black holes.

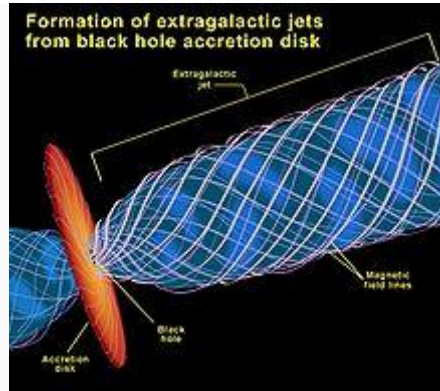
A stellar black hole of one solar mass has a Hawking temperature of about **100 nanokelvins**. This is far less than the 2.7 K temperature of the **cosmic microwave background radiation**. Stellar mass or larger black holes receive more mass from the cosmic microwave background than they emit through Hawking radiation and thus will grow instead of shrink. To have a Hawking temperature larger than 2.7 K (and be able to evaporate), a black hole needs to have less mass than **the Moon**. Such a black hole would have a diameter of less than a tenth of a millimeter.

If a black hole is very small the radiation effects are expected to become very strong. Even a black hole that is heavy compared to a human would evaporate in an instant. A black hole the weight of a car would have a diameter of about 10^{-24} m and take a nanosecond to evaporate, during which time it would briefly have luminosity more than 200 times that of the sun. Lower mass black holes are expected to evaporate even faster; for example, a black hole of mass $1 \text{ TeV}/c^2$ would take less than 10^{-88} seconds to evaporate completely. For such a small black hole, **quantum gravitation** effects are expected to play an important role and could even—although current developments in quantum gravity do not indicate so^[87]—hypothetically make such a small black hole stable.

By their very nature, black holes do not directly emit any signals other than the hypothetical Hawking radiation; since the Hawking radiation for an astrophysical black hole is predicted to be very weak, this makes it impossible to directly detect astrophysical black holes from the Earth. A possible exception to the Hawking radiation being weak is the last stage of the evaporation of light (primordial) black holes; searches for such flashes in the past has proven unsuccessful and provides stringent limits on the possibility of existence of light primordial black holes NASA's **Fermi Gamma-ray Space Telescope** launched in 2008 will continue the search for these flashes

Astrophysicists searching for black holes thus have to rely on indirect observations. A black hole's existence can sometimes be inferred by observing its gravitational interactions with its surroundings. A project run by **MIT's Haystack Observatory** is attempting to observe the event horizon of a black hole directly. Initial results are encouraging

Accretion of matter-The Accentuation Coefficient in the Model:



Formation of extragalactic jets from a black hole's accretion disk

Due to conservation of angular momentum, gas falling into the gravitational well created by a massive object will typically form a disc-like structure around the object. Friction within the disc causes angular momentum to be transported outward, allowing matter to fall further inward, releasing potential energy and increasing the temperature of the gas. In the case of compact objects such as white dwarfs, neutron, and black holes, the gas in the inner regions becomes so hot that it will emit vast amounts of radiation (mainly X-rays), which may be detected by telescopes. This process of accretion is one of the most efficient energy-producing processes known; up to 40% of the rest mass of the accreted material can be emitted in radiation (In nuclear fusion only about 0.7% of the rest mass will be emitted as energy.) In many cases, accretion discs are accompanied by relativistic jets emitted along the poles, which carry away much of the energy. The mechanism for the creation of these jets is currently not well understood.

As such many of the universe's more energetic phenomena have been attributed to the accretion of matter on black holes. In particular, active and quasars are believed to be the accretion discs of supermassive black holes.^[93] Similarly, X-ray binaries are generally accepted to be binary star systems in which one of the two stars is a compact object accreting matter from its companion.^[93] It has also been suggested that some ultra luminous X-ray sources may be the accretion discs of intermediate-mass black holes.^[94]

X-ray binaries

X-ray binaries are binary star systems that are luminous in the X-ray part of the spectrum. These X-ray emissions are generally thought to be caused by one of the component stars being a compact object accreting matter from the other (regular) star. The presence of an ordinary star in such a system provides a unique opportunity for studying the central object and determining if it might be a black hole.



Artist impression of a binary system with an accretion disk around a black hole being fed by material from the companion star.

If such a system emits signals that can be directly traced back to the compact object, it cannot be a black hole. The absence of such a signal does, however, not exclude the possibility that the compact object is a neutron star. By studying the

companion star it is often possible to obtain the orbital parameters of the system and obtain an estimate for the mass of the compact object. If this is much larger than the Tolman–Oppenheimer–Volkoff limit (that is, the maximum mass a neutron star can have before collapsing) then the object cannot be a neutron star and is generally expected to be a black hole.

The first strong candidate for a black hole, **Cygnus X-1, was discovered in this way by Charles Thomas Bolton**, Louise Webster and Paul Murdin in 1972. Some doubt, however, remained due to the uncertainties resultant from the companion star being much heavier than the candidate black hole. Currently, better candidates for black holes are found in a class of X-ray binaries called soft X-ray transients.^[93] In this class of system the companion star is relatively low mass allowing for more accurate estimates in the black hole mass. Moreover, these systems are only active in X-ray for several months once every 10–50 years. During the period of low X-ray emission (called quiescence), the accretion disc is extremely faint allowing for detailed observation of the companion star during this period. One of the best such candidates is **V404 Cyg**.

Quiescence and advection-dominated accretion flow

The faintness of the accretion disc during quiescence is suspected to be caused by the flow entering a mode called **an advection-dominated accretion flow** (ADAF). In this mode, almost all the energy generated by friction in the disc is swept along with the flow instead of radiated away. If this model is correct, then it forms strong qualitative evidence for the presence of an event horizon. Because, if the object at the center of the disc had a solid surface, it would emit large amounts of radiation as the highly energetic gas hits the surface, an effect that is observed for neutron stars in a similar state

Quasi-periodic oscillations

The X-ray emission from accretion disks sometimes flickers at certain frequencies. These signals are called quasi-periodic oscillations and are thought to be caused by material moving along the inner edge of the accretion disk (the innermost stable circular orbit). As such their frequency is linked to the mass of the compact object. They can thus be used as an alternative way to determine the mass of potential black holes.^[100]

Galactic nuclei

" to describe galaxies with unusual characteristics, such as **unusual spectral line emission** and very strong radio emission. Theoretical and observational studies have shown that the activity in these active galactic nuclei (AGN) may be explained by the presence of supermassive black holes. The models of these AGN consist of a central black hole that may be millions or billions of times more massive than the Sun; a disk of **gas and dust called an accretion disk**; and **two jets** that are perpendicular to the accretion disk.¹

Although supermassive black holes are expected to be found in most AGN, only some galaxies' nuclei have been more carefully studied in attempts to both identify and measure the actual masses of the central supermassive black hole candidates. Some of the most notable galaxies with supermassive black hole candidates include **the Andromeda Galaxy, M32, M87, NGC 3115, NGC 3377, NGC 4258, and the Sombrero Galaxy.**

It is now widely accepted that the center of (nearly) every galaxy (not just active ones) contains a supermassive black hole. The close observational correlation between the mass of this hole and the velocity dispersion of the host **galaxy's bulge, known as the M-sigma relation**, strongly suggests a connection between the formation of the black hole and the galaxy itself.

Currently, the best evidence for a supermassive black hole comes from studying **the proper motion of stars near the center of our own Milky Way. Since 1995 astronomers have tracked the motion of 90 stars in a region called Sagittarius A*. By fitting their motion to Keplerian orbits they were able to infer in 1998 that 2.6 million solar masses must be contained in a volume with a radius of 0.02 lightyears** Since then one of the stars—called S2—has completed a full orbit. From the orbital data they were able to place better constraints on the mass and size of the object causing the orbital motion of stars in the Sagittarius A* region, finding that there is a spherical mass of 4.3 million solar masses contained within a radius of less than 0.002 lightyears. While this is more than 3000 times the Schwarzschild radius corresponding to that mass, it is at least consistent with the central object being a supermassive black hole, and no "realistic cluster [of stars] is physically tenable.

Gravitational lensing

The deformation of spacetime around a massive object causes light rays to be deflected much like light passing through an **optic lens. This phenomenon is known as gravitational lensing. Observations have been made of weak gravitational lensing, in which photons are deflected by only a few arcseconds. However, it has never been directly observed for a black hole. One possibility for observing gravitational lensing by a black hole would be to observe stars in orbit around the black hole. There are several candidates for such an observation in orbit around Sagittarius A***

Alternatives

The evidence for stellar black holes strongly relies on the existence of an upper limit for the mass of a neutron star. The size of this limit heavily depends on the assumptions made about the properties of dense matter. New **exotic phases of matter could push up this bound. A phase of free quarks at high density might allow the existence of dense quark stars, and some supersymmetric models predict the existence of Q stars** Some extensions of the standard model posit **the existence of preons as fundamental building blocks of quarks and leptons, which could hypothetically form preon stars. These hypothetical models could potentially explain a number of observations** of stellar black hole candidates. However, it can be shown from general arguments in general relativity that any such object will have a maximum mass.

Since the average density of a black hole inside its Schwarzschild radius is inversely proportional to the square of its mass, supermassive black holes are much less dense than stellar black holes (the average density of a 10^8 solar mass black hole is comparable to that of water) Consequently, the physics of matter forming a supermassive black hole is much better understood and the possible alternative explanations for supermassive black hole observations are much more mundane. For example, a supermassive black hole could be modeled by a large cluster of very dark objects. However, typically such alternatives are not stable enough to explain the supermassive black hole candidates.

The evidence for stellar and supermassive black holes implies that in order for black holes not to form, general relativity must fail as a theory of gravity, perhaps due to the **onset of quantum corrections**. A much anticipated feature of a theory of quantum gravity is that it will not feature singularities or event horizons (and thus no black holes) In recent years, much attention has been drawn by the fuzz ball model in string theory. Based on calculations in specific situations in string theory, the proposal suggest that generically the individual states of a black hole solution do not have an event horizon or singularity, but that for a classical/semi-classical observer the statistical average of such states does appear just like an ordinary black hole in general relativity.

Open questions

Entropy and thermodynamics

The formula for the Bekenstein–Hawking entropy (S) of a black hole, which depends on the area of the black hole (A). The constants are the speed of light (c), the Boltzmann (k), Newton's constant (G), and the reduced Planck constant (ħ).

In 1971, Hawking showed under general conditions that the total area of the event horizons of any collection of classical black holes can never decrease, even if they collide and merge This result, now known as the second law of black hole mechanics, is remarkably similar to the second law of thermodynamics, which states that the total entropy of a system can never decrease. As with classical objects at absolute zero temperature, it was assumed that black holes had zero entropy. If this were the case, the second law of thermodynamics would be violated by entropy-laden matter entering a black hole, resulting in a decrease of the total entropy of the universe. Therefore, Bekenstein proposed that a black hole should have an entropy, and that it should be proportional to its horizon area

The link with the laws of thermodynamics was further strengthened by Hawking's discovery that quantum field theory predicts that a black hole radiates blackbody radiation at a constant temperature. This seemingly causes a violation of the second law of black hole mechanics, since the radiation will carry away energy from the black hole causing it to shrink. The radiation, however also carries away entropy, and it can be proven under general assumptions that the sum of the entropy of the matter surrounding a black hole and one quarter of the area of the horizon as measured in Planck units is in fact always increasing. This allows the formulation of the first law of black hole mechanics as an analogue of the first law of thermodynamics, with the mass acting as energy, the surface gravity as temperature and the area as entropy

One puzzling feature is that the entropy of a black hole scales with its area rather than with its volume, since entropy is normally an extensive quantity that scales linearly with the volume of the system. This odd property led Gerard 't Hooft and Leonard Susskind to propose the holographic principle, which suggests that anything that happens in a volume of spacetime can be described by data on the boundary of that volume.

Although general relativity can be used to perform a semi-classical calculation of black hole entropy, this situation is theoretically unsatisfying. In statistical mechanics, entropy is understood as counting the number of microscopic configurations of a system that have the same macroscopic qualities (such as mass, charge, pressure, etc.). Without a satisfactory theory of quantum gravity, one cannot perform such a computation for black holes. Some progress has been made in various approaches to quantum gravity. In 1995, Andrew Strominger and Cumrun Vafa showed that counting the microstates of a specific supersymmetric black hole in string theory reproduced the Bekenstein–Hawking entropy Since then, similar results have been reported for different black holes both in string theory and in other approaches to quantum gravity like loop quantum gravity

Black hole unitarity<.>

An open question in fundamental physics is the so-called information loss paradox, or black hole unitarity paradox. Classically, the laws of physics are the same run forward or in reverse (T-symmetry). Liouville's theorem dictates conservation of phase space volume, which can be thought of as "conservation of information", so there is some problem even in classical physics. In quantum mechanics, this corresponds to a vital property called unitarity, which has to do with the conservation of probability (it can also be thought of as a conservation of quantum phase space volume as expressed by the density matrix).

Open questions

Entropy and thermodynamics

, Hawking showed under general conditions that the total area of the event horizons of any collection of classical black holes can never decrease, even if they **collide and merge**. This result, now known as the second law of black hole mechanics, is remarkably similar to the second law of thermodynamics, which states that the total entropy of a system can never decrease. As with classical objects at absolute zero temperature, it was assumed that black holes had zero entropy. If this were the case, the second law of thermodynamics would be violated by entropy-laden matter entering a black hole, resulting in a decrease of the total entropy of the universe. Therefore, Bekenstein proposed that a black hole should have entropy, and that it should be proportional to its horizon area.

The link with the laws of thermodynamics was further strengthened by Hawking's discovery that quantum field theory predicts that a black hole radiates blackbody radiation at a constant temperature. This seemingly causes a violation of the second law of black hole mechanics, since the radiation will carry away energy from the black hole(-) causing it to shrink. The radiation, however also carries away (E)entropy, and it can be proven under general assumptions that the sum of the entropy of the matter surrounding a black hole and one quarter of the area of the horizon as measured in Planck units is in fact always increasing. This allows the formulation of the first law of black hole mechanics as an analogue of the first law of thermodynamics, with the mass acting as energy, the surface gravity as temperature and the area as entropy

One puzzling feature is that the entropy of a black hole scales with its area rather than with its volume, since entropy is normally an extensive quantity that scales linearly with the volume of the system. This odd property led Gerard 't Hooft and Leonard Susskind to propose the holographic principle, which suggests that anything that happens in a volume of spacetime can be described by data on the boundary of that volume.

Although general relativity can be used to perform a semi-classical calculation of black hole entropy, this situation is theoretically unsatisfying. In statistical mechanics, entropy is understood as counting the number of microscopic configurations of a system that have the same macroscopic qualities (such as mass, charge, pressure, etc.). Without a satisfactory theory of quantum gravity, one cannot perform such a computation for black holes. Some progress has been made in various approaches to quantum gravity. In 1995, Andrew Strominger and Cumrun Vafa showed that counting the microstates of a specific supersymmetric black hole in string theory reproduced the Bekenstein–Hawking entropy Since then, similar results have been reported for different black holes both in string theory and in other approaches to quantum gravity like loop quantum gravity.

Black hole unitarity Black hole information paradox

An open question in fundamental physics is the so-called information loss paradox, or black hole unitarity paradox. Classically, the laws of physics are the same run forward or in reverse (T-symmetry). Liouville's theorem dictates conservation of phase space volume, which can be thought of as "conservation of information", so there is some problem even in classical physics. In quantum mechanics, this corresponds to a vital property called unitarity, which has to do with the conservation of probability (it can also be thought of as a conservation of quantum phase space volume as expressed by the density matrix)

Some Salient Notes Relating to the relation between the Quantum Information and Quantum Mechanical Behaviour

^ The set of possible paths, or more accurately the future light cone containing all possible world line is tilted in this way in Eddington–Finkelstein coordinates, but in other coordinates the light cones are not tilted in this way, for example in Schwarzschild coordinates they simply narrow without tilting as one approaches the event horizon, and in Kruskal–Szekeres coordinates the light cones don't change shape or orientation at all.^ This is true only for 4-dimensional spacetimes. In higher dimensions more complicated horizon topologies like a black ring are possible^ In particular, he assumed that all matter satisfies the weak energy condition.

*108

REFERENCES

- (1) A HAIMOVICI: "On the growth of a two species ecological system divided on age groups". Tensor, Vol 37 (1982), Commemoration volume dedicated to Professor Akitsugu Kawaguchi on his 80th birthday FRTJOF CAPRA: "The web of life" Flamingo, Harper Collins See "Dissipative structures" pages 172-188
- (2) HEYLIGHEN F. (2001): "The Science of Self-organization and Adaptivity", in L. D. Kiel, (ed) . Knowledge Management, Organizational Intelligence and Learning, and Complexity, in: The Encyclopedia of Life Support Systems ((EOLSS), (Eolss Publishers, Oxford) [http://www.eolss.net MATSUI, T, H. Masunaga, S. M. Kreidenweis, R. A. Pielke Sr., W.-K. Tao, M. Chin, and Y. J Kaufman (2006), "Satellite-based assessment of marine low cloud variability associated with aerosol, atmospheric stability, and the diurnal cycle", J. Geophys. Res., 141, D17201, doi:10.1029/2005JD006097
- (3) STEVENS, B, G. Feingold, W.R. Cotton and R.L. Walko, "Elements of the microphysical structure of numerically simulated nonprecipitating stratocumulus" J. Atmos. Sci., 53, 980-1006
- (4) FEINGOLD, G, Koren, I; Wang, HL; Xue, HW; Brewer, WA (2010), "Precipitation-generated oscillations in open cellular cloud fields" *Nature*, 166 (7308) 819-852, doi: 10.1038/nature09314, Published 12-Aug 2010
- (5) R WOOD "The rate of loss of cloud droplets by coalescence in warm clouds" J.Geophys. Res., 141, doi: 10.1029/2006JD007553, 2006
- (6) H. RUND, "The Differential Geometry of Finsler Spaces", Grund. Math. Wiss. Springer-Verlag, Berlin, 1959
- (7) A. Dold, "Lectures on Algebraic Topology", 1972, Springer-Verlag*
- (8) ^ Wald 1984
- (9) Schutz, Bernard F. (2003). *Gravity from the ground up*. Cambridge University Press. p. 110. ISBN 0-521-45506-5.
- (10) Davies, P. C. W. (1978). "Thermodynamics of Black Holes". *Reports on Progress in Physics* **41** (8): 1313–55. Bibcode 1978RPPh...41.1313D. doi:10.1088/0034-4885/41/8/004.
- (11) Michell, J. (1784). "On the Means of Disambiguation
- (12) P. W. Shor, SIAM J. Comput. 26, 1484 (1997).
- (13) M. A. Nielsen and I. L. Chuang, Quantum Computation and quantum Information (Cambridge University Press, Cambridge, 2000).

- (14) See also, references in Ref. [2].
- (15) S. Lloyd, Nature (London), 406, 1047 (2000).
- (16) Y. J. Ng, Phys. Rev. Lett. 86, 2946 (2001).
- (17) E. P. Wigner, Z. Physik 133, 101 (1952).
- (18) H. Araki and M. M. Yanase, Phys. Rev. 120, 622 (1960).
- (19) H. Stein and A. Shimony, in Foundations of Quantum Mechanics, edited by B.
- (20) D. Aharonov, A. Kitaev, and N. Nisan, arXiv e -print quant-ph/9806029 (1998)[in Proc. 30th Annual ACM Symposium on Theory of Computing, 1997, 20-30].
- (21) H. P. Robertson, Phys. Rev. 34, 163 (1929).
- (22) S. Lloyd, Nature (London), 406, 1047 (2000).
- (23) Y. J. Ng, Phys. Rev. Lett. 86, 2946 (2001).
- (24) E. P. Wigner, Z. Physik 133, 101 (1952).
- (25) H. Araki and M. M. Yanase, Phys. Rev. 120, 622 (1960).
- (26) V. I. Paulsen, Completely bounded maps and dilations, (Longman, New York,1986).
- (27) D. Aharonov, A. Kitaev, and N. Nisan, arXiv e -print quant-ph/9806029 (1998)[in Proc. 30th Annual ACM Symposium on Theory of Computing, 1997, 20-30].
- (28) H. P. Robertson, Phys. Rev. 34
- (29) D. Aharonov, A. Kitaev, and N. Nisan, arXiv e -print quant-ph/9806029 (1998)[in Proc. 30th Annual ACM Symposium on Theory of Computing, 1997, 20-30].
- (30) H. P. Robertson, Phys. Rev. 34, 163 (1929).
- (31) S. Lloyd, Nature (London), 406, 1047 (2000).
- (32) Y. J. Ng, Phys. Rev. Lett. 86, 2946 (2001).
- (33) E. P. Wigner, Z. Physik 133, 101 (1952).
- (34) H. Araki and M. M. Yanase, Phys. Rev. 120, 622 (1960).
- (35) H. Stein and A. Shimony, in Foundations of Quantum Mechanics, edited by B.d'Espagnat (Academic, New York, 1971); T. Ohira and P. Pearle, Am. J. Phys.56, 692 (1988).
- (36) V. I. Paulsen, Completely bounded maps and dilations, (Longman, New York,1986).
- (37) D. Aharonov, A. Kitaev, and N. Nisan, arXiv e -print quant-ph/9806029 (1998)[in Proc. 30th Annual ACM Symposium on Theory of Computing, 1997, 20-30].
- (38) H. P. Robertson, Phys. Rev. 34

ACKNOWLEDGEMENTS: IT IS TO BE STATED IN UNMISTAKABLE TERMS THAT INTRODUCTORY NOTES, ACCENTUATORY, CORROBORATORY, AUGMENTATIONAL, FOMENTATIONAL, FORTIFICATIONAL, JUSTIFICATIONAL, SUBSTANTIVE NOTES ARE TAKEN FROM VARIOUS SOURCES, BOOKS, ARTICLES, JOURNALS, RESEARCH PAPERS, ABSTRACTS OF RESEARCH PAPERS, WIKIPEDIA, INTERNET, LIBRARIES OF IV LEAGUE INSTITUTIONS, DIALECTIC DELIBERATION, POLEMICAL ARUGUEMENTATION, AND CONJUGATORY CONFATALIA WITH THE COLLEAGUES. WE, AUTHORS ARE WITH ALL THE SENSE OF HUMILTY AND GRATITUDE PAY HOMAGE TO EVERY ONE WHO HAS SHARED THEIR ESTEEMED,ERUDITE AND EMINENT KNOWLEDGE WITH US WHICH HAS FORMED THE BASTIONAL,PILLAR POST,STYLOBATE,SENTINEL OF THE AUTHORATATIVE DISCUSSION OPF EVERY ASPECT OF THE PAPER. IN THE EVENTUALITY OF THE FACT THAT IF THERE ARE ANY ACTS OF OMISSIONS AND COMMISSIONS AUTHORS BEG PARDON WITH GREAT DEAL OF COMPUNCTION AND CONTRITION THE LAPSE,THE SOURCE FROM WHICH THE MODE,METHODOLOGY,OR FOR THAT MATTER SENTENCE HAS BEEN TAKEN. LIKE NEWTON SAID, GREAT SENSE OF INADEQUACY, INFERIORITY COMPLEX ENCOMPASSES WHEN ONE SEES THE ENTIRE OCEAN TO BE EXPLORED LYING IN FRONT. VERILY KNOWN IS A DROP UNKNOWN IS AN OCEAN. INFACT THE INTENTION WAS TO INCLUDE ATLEAST TEN MORE MODELS IN THE BODY FABRIC AND DIASPORA OF THE PAPER. DUE TO INSUFFICIENCY OF TIME IT HAS NOT BEEN POSSIBLE. WE ONCE AGAIN THANK EVERY ONE, STUDENT, LECTURER, PROFESSOR FOR ALL THE COOPERATION RENDERED; IT IS BECAUSE WE PIGGY RODE ON THEIR BACKS WE HAVE TRIED TO SEE WITH OUR ASTIGMAYTIC EYE SOME FURTHER. ONCE AGAIN GRATEFUL HOMAGE AND REGARDS TO EVERY ONE AND EVERY SOURCE.

Effective routing protocols for delay tolerant network

Sukhbir¹, Dr. Rishipal Singh²

¹M.Tech Student, ²Assistant Prof. CSE Deptt.

Guru jambheshwar university science & technology, hisar

Abstract: Delay-tolerant Networking (DTN) enables communication in sparse mobile ad-hoc networks and other challenged environments where traditional networking fails and new routing and application protocols are required. Past experience with DTN routing and application protocols has shown that their performance is highly dependent on the underlying mobility and node characteristics. Evaluating DTN protocols across many scenarios requires suitable simulation tools. This paper presents the existing routing protocols techniques and Comparative study of existing routing protocols of Delay-Tolerant Networks based upon the metrics like Overhead Ratio, Hop Count and Buffer Size.

I. INTRODUCTION

Delay tolerant networks are an emerging field of networks that show some different characteristics from today's internet such as intermittent connectivity, long delays etc. Delay tolerant networks arise in a variety of situation like disaster relief, military rescue operations, rural internet access etc. There are some critical situations where the ability to communicate make a significant difference for human lives. In DTN decision to drop a message is taken on several constraints like size of message, no of copies, time to live and buffer size etc.

In DTN, end to end path is very rare and unstable in nature and opportunity to establish complete route is negligible. DTN support those applications, whose time requirement is hours or even day or longer. It is necessary to deliver high priority message during "contact" phase [1]. DTN enable communication by taking advantage of Temporary connections to relay data in a fashion similar to Postal network instead of requiring an end to end network path to be available.

However communication in DTN is a very challenging task. Traditional network simply assume a complete connected graph should be there and a period of time that is long enough to allow communication. In DTN there might not even be end to end path between a pair of nodes at any moment of time as shown in the figure 1 [2]. Due to this unique feature of DTN, existing routing algorithm that are developed for Internet and MANETS do not performing well. Reason for this is that all these algorithm assume that the network is connected and end to end path exist between each pair of nodes. DTN are often resource limited and not able to deliver required performance in case of intermittent connectivity. Due to given resource limitation and uncertainty in DTN it is very difficult to deliver data.

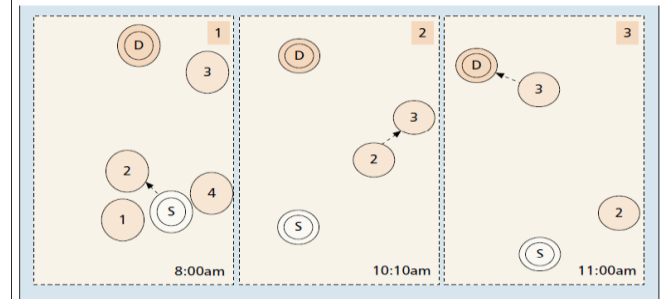


Figure 1: Time Evolving Behavior of the Network efficiently.

DTN follow store carry and forward approach. Node should carry the message until proper custodian is not found. Because of resource limitation each node in DTN has some fix size of buffer. Node store the message in its own buffer until the next custodian is found in the path towards the destination. As the buffer size is limited node should follow some policy to decide which message is dropped when the buffer size is full. Develop an algorithm and a weight function to make this decision that effectively choose message to be dropped. As a result proposed algorithm has been compare with already existing DROP FRONT policy. The approach better results in terms of delivery probability, buffer time avg and Hop count avg..

II. RELATED WORK

The major objective of routing in DTNs is to deliver packets from the source to the destination by means of the mobility of nodes. Since the end-to-end path may not be available, routing schemes have to optimize data dissemination by utilizing the connectivity information and network conditions maintained by each node. For example, in [3], the routing scheme based on the estimates of the average inter contact time between the mobile nodes in the network was proposed. This routing scheme was designed to minimize the packet delivery time. The routing properties in terms of loop-free forwarding and polynomial convergence were studied, which ensure the performance of the packet delivery in DTNs. In [4], the packet-delivery scheme based on the super node architecture and epidemic routing was introduced. With epidemic routing, the packets are forwarded to other contacted nodes (i.e., nodes with a direct connection). Unlike traditional epidemic routing, the packets are forwarded to the super nodes to improve the performance and reduce overhead. The super nodes are then responsible in carrying the packets to the destination.

III. ROUTING PROTOCOLS

(a) **First contact:** – This is simplest strategy to transmit the data from source to destination in DTN. This transmit message immediately as soon as the source and destination come in contact with each other directly. This is possible when the source and destination are one hop apart or immediately neighbor of each other.

(b) **Direct delivery:-** Scheme lets the source hold the data until it comes in contact with the destination. This simple strategy uses one message transmission. It is a degenerate case of flooding family, requiring no info about network but requires a direct path between source and destination. Hence if no contact occurs, message is not delivered.

(c) **ProPHET:-**Improve the routing performance by adopting the probabilistic scheme that reflects the contact observation of nodes. However, the single copy forwarding based on the probability may affect to the performance with limitation of the initial probability distribution and a message drop. The limited buffer space and use of an ACK message should be investigated to enhance the performance further.

Finally, although Spray and Wait can overcome the shortcomings of Epidemic routing protocol, the usability of the wait phase with an efficient single copy forwarding scheme and the optimal decision of an initial spray number are open issues.

(d) **Spray and Wait:-** The operation of Spray and Wait consists of two phases:

the spray phase and the wait phase. In the spray phase, when a node generates a message, the node makes N copies of the message to spread it to relay nodes. When the node meets the other node, the node checks N (i.e., $N > 1$). If the node has the spray message, the node hands over the message and revised N (i.e., $N/2$) to the other node. After the spray phase is finished, each of N nodes carrying a message copy performs the direct message transmission until it successfully delivered the message to the destination.

(e) **Epidemic Routing:** - Epidemic routing is an early sparse network routing protocol proposed for DTN. It assumes that each node has unlimited storage space and bandwidth. Therefore every node can store all the messages transmitted during "contact" phase. This use the concept of database replication also a relay node can exchange the entire message during "contact" phase. Each node maintains list of messages in the database called summary vector.

IV. Dynamic Spray and Wait with Quality of Node (QoN)

4.1. Delivery utility

When delivery rate stay the same, consider the relationship between network overhead and delivery utility. Delivery utility is defined as the ratio of the number of messages received by destination nodes to the number of messages forwarded by relay nodes, as shown in Equation (1).

$$delivery_utility = \frac{Messages\ of\ received}{Messages\ of\ forwarded}$$

4.2. The definition of Quality of Node (QoN)

The Epidemic and The Spray and Wait routing protocols forward messages without taking node mobile patterns into consideration, therefore the delivery utility is too low.

Now present the notion of QoN. QoN indicates the activity of a node, or the number one node meets other different nodes within a given interval. In the same period of time, the more nodes that one node meets, the greater the QoN. The variation of QoN can dynamically represents the node activity in a given period of time.

V. Drop policy algorithm

Let us assume

n = number of nodes in the network

t = number of digits in n

Bavail=buffer available at particular node

Mnew=new message

Snew=size of new incoming message

$N_i(t)$ =no copies of message i at time t

Ttl= time to live /*time duration in which message is live means message is useful only this time duration */

Rtli=remaining time to live of message for message i

5.1 Proposed Algorithm

When two nodes communicate with each other they share message to each other. It might be possible when they communicate the buffer available is not enough to accommodate a new message. At that time scheduling take place. Each node have two options at that moment of time: first it will discard a new message and second one is that it will drop some message from its buffer and make some room for the new message.

Until now all DTN routing protocol follow the DROP FRONT message approach in which they drop message from the front of nodes buffer queue.

5.2 Weight function

This function value makes the decision to drop a message from the node buffer. This weight function consider various properties of the message and node. As a result it gives a value on basis of that a node drop a particular message whose value is minimum.

Let N = no of nodes in the network

MaxTTL= maximum value of time to live of any node in the network

While($S_{new} > B_{avail}$)

```
{
Mid=call message equal (Snew); /* Search those message
in the buffer of node whose size is equal to or greater then
the size of incoming new message. This function will
return the message id of those messages who will be drop
according to SRT algo */
Bavail=Bavail+ MessageCollection.get(MID).Size();
Delete MessageCollection.get(MID);
}
```

/* Body of the function call messageEqual(Snew) */

```
Int callmessageEqual(Snew)
{
For (each message M in node buffer)
{
If (Mni>=Snew)
Add MessageCollection m; /* message id */
}
```

```
}
```

```

/* Then apply a weight function on MessageCollection m.
*/
float F,F1, $\alpha$ ;
/* initially F1 contain the function value (F) of m0
message */
int MessageId;
While (MessageCollection m)
{
F=a*(size of message)+ b/N *(no of copies) + c/MaxTTL
a=b+ $\alpha$ +1;
 $\alpha$  = 1/n
b=10n;
c =RTLi /* remaining time to live */
If (F<F1)
{
F1=F;
Messageid=MessageCollection.get(F);
}
Return MessageId;
}
    
```

VI. SIMULATION

One is an agent based discrete event simulator engine. The main functions of one simulator are the modeling of node movement, inter node contact, routing and message handling. Analysis of the result are done through visualization or reports. Movement models are used to implement the node movement. Connectivity between the nodes depends on their location and communication range. Routing modules are used to implement the routing function that decide which message to forward. Finally the message are generated through event generator. The graphical user interface(GUI) displays a visualization of the simulation.

VII. RESULTS

The results given below indicate the comparative study between DROP FRONT and SRT. The results show the comparison between DROP FRONT and SRT drop policy. These results prove that it is beneficial to use SRT drop policy as it improves the performance of any DTN.

7.1 Comparison Based on Delivery Probability

The comparative study of DROP FRONT and SRT DROP policy with respect to delivery probability has been plotted in the figure 2. The DROP FRONT policy drops the front messages from the buffer; however the SRT drops the bigger size message. But in case of FIRST CONTACT and DIRECT DELIVERY router the probability of encounter is less as a result the delivery probability is not increasing significant as compared to previous results.

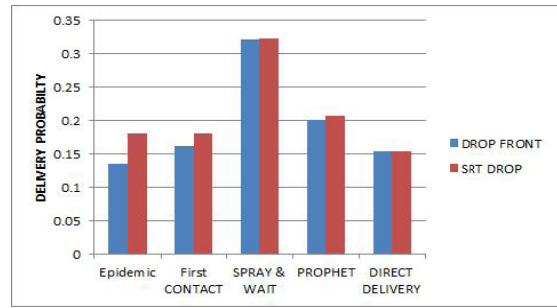


Figure 2: Drop Front, SRT Drop Delivery Probability W.R.T to Routers

7.2 Comparison Based on Buffer Time Average

Figure 3 indicates that the buffer time average for SRT DROP and DROP FRONT policy for various routers. The value of buffer time average is large in SRT drop as compared to DROP FRONT. High value of buffer time average increase the probability of message delivery in the DTN paradigm. High value of buffer time average also decreases the drop ratio. Figure 3 shows that SRT DROP increases the buffer time average as compared to DROP FRONT.

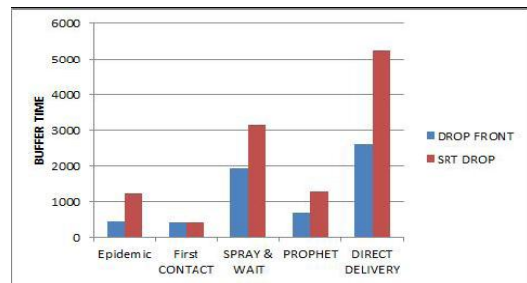


Figure 3: Drop Front, SRT Drop Buffer Time Avg. W.R.T to Routers

7.3 Comparison Based on Overhead Ratio

The overhead ratio with respect to various routers has been plotted in figure 4 for SRT DROP and DROP FRONT. The results show that the SRT DROP is less in terms of overhead ratio in all routers. Overhead ratio in DIRECT DELIVERY router is zero due to direct transmission while the overhead ratio is decreases in epidemic, prophet, fc, spray and waits up to a significant level. SRT DROP less no of messages as compare to DROP FRONT because it drop the message of nearly greater or equal size of messages.

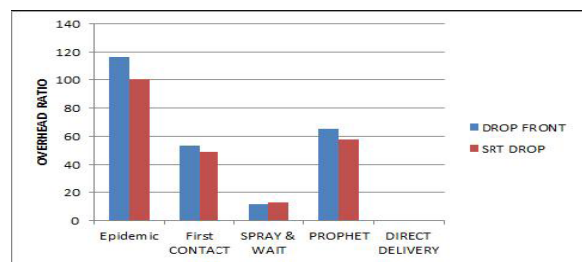


Figure 4: Drop Front, SRT Drop Overhead Ratio W.R.T to Routers

7.4 Comparison Based on Packet Dropped

The results in the figure 5 show that the SRT DROP drops less no. of messages as compared to DROP FRONT because it drops the message of nearly greater or equal size of messages. Therefore, the network overhead also decreases.

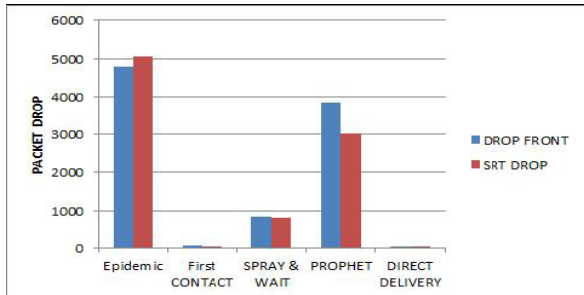


Figure 5: Drop Front,SRT Drop Packet Drop W.R.T to Routers

7.5 Comparison Based on Hop Count Avg.

Figure 6 shows the hop count for various routers for SRT DROP and DROP FRONT policy. The lower value of hop count means that message has consumed less resource to reach its destination. SRT DROP drops the messages whose size is nearly equal to the incoming message. Due to this logic it will drop less no of messages and decreases the value of hop count average.

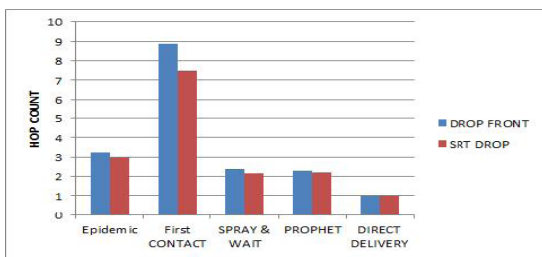


Figure 6: Drop Front,SRT Drop Hop Count W.R.T to Routers

VIII. CONCLUSION

In this paper investigated SRT DROP policy with DROP FRONT policy with respect to DTN routing protocols. Results shows that our SRT DROP policy perform well with respect to delivery probability, buffer time, overhead ratio, hop count average and packet dropped. It should motivate to examine SRT DROP policy to other existing drop policy.

Compare the SRT DROP POLICY with DROP FRONT policy. This comparison motivate to compare SRT DROP policy with DROP LARGEST POLICY because both policy gives importance to size of messages. The routing protocol other then the EPIDEMIC, FC, DIRECT DELIVERY, SPRAY ANDWAIT and PROPHET routing protocols are also an interesting direction of work.

REFERENCES

[1] Abbas Nayebi, Hamid Sarbazi-Azad, and Gunnar Karlsson Sharif University of Technology, Tehran, Iran Royal Institute of Technology(KTH) Stockholm, Sweden "Routing, Data Gathering, and Neighbor Discovery in

Delay-Tolerant Wireless Sensor Networks" IEEE 978-1-4244-3750-4-2009

[2] Z. Zhang, Routing in Intermittently Connected Mobile Ad Hoc Networks and Delay Tolerant Networks: Overview and Challenges, in IEEE Commun. Surveys , vol. 8, no.1, 1st Quarter 2006.

[3] V. Conan, J. Leguay, and T. Friedman, "Fixed point opportunistic routing in delay tolerant networks," *IEEE J. Sel. Areas Commun.*, vol. 26, no. 5, pp. 773–782, Jun. 2008.

[4] H. Samuel, W. Zhuang, and B. Preiss, "Routing over interconnected heterogeneous wireless networks with intermittent connections," in *Proc. IEEE ICC*, May 2008, pp. 2282–2286.

[5] E.P.C. Jones and P.A.S. Ward, "Routing Strategies for Delay-Tolerant Networks", Computer Communications, 2008

[6] U. Lee, S.Y. Oh, K.W. Lee, M.Gerla, "RelayCast: scalable Multicast Routing in Delay Tolerant Networks", IEEE, 2008

[7] J. Burgess, B. Gallagher, D. Jensen and B.N. Levine, "MaxProp: Routing for Vehicle-Based Disruption-tolerant Networks", Proc. Of IEEE INFOCOM, April 2006

[8] A. Lindgren, A. Doria, O. Schelen, "Probabilistic Routing in Intermittently Connected Networks", ACM SIGMOBILE Mobile Computing and Communications Review, Vol. 7, Issue 3, pp. 19-20, July, 2003

[9] A. Balasubramanian, B.N. Levine, and A.Venkataramani, "DTN Routing as a Resource Allocation Problem", Proc. of ACM SIGCOMM, Aug 2007

[10] J. Shen, S. Moh, and I. Chung, "Routing Protocols in Delay Tolerant Networks: A Comparative Survey", 23rd International Conference on Circuits/Systems, Computers and Communications, (ITC-CSCC 2008)

[11] E.P.C. Jones, L.Li, P.A.S. Ward, "Practical Routing in Delay-Tolerant Networks", IEEE Transactions on Mobile Computing, Vol. 6, No. 8, Aug 2007

[12] G. Sandulescu and S.N. Tehrani, "Opportunistic DTN Routing with Window-aware Adaptive replication" Proc. of ACM on AINTEC, Nov 2008

[13] C. Liu and J. Wu, "Scalable Routing in Delay tolerant Networks", Proc. of ACM on MobiHoc, Vol. 9, No. 14, pp. 51-60, Sep 2007

[14] M. Demmer, K. FSR: "DTLSR: Delay Tolerant routing for Developing Regions", Proc. of ACM on NDSR, 2007

[15] B. Burns, O. Brook, B.N. Levine, "MORA routing and Capacity Building in Disruption-Tolerant Networks"

[16] Y. Liao, K. Tan, Z. Zhang and L. Gao, "Estimation based Erasurecoding routing in Delay tolerant Networks" Proc. of IWCMC, July 2006

[17] L. J. Chen, C.H. Yu, T. Sun, Y.C. Chen and H.H. Chu, "A Hybrid Routing Approach for Opportunistic Networks", Proc. of ACM SIGCOMM on Challenged Networks, 2006

[18] D. Marasigan and P. Rommel, "MV routing and capacity building in disruption tolerant networks," in Proceedings of IEEE INFOCOM, vol. 1, pp. 398–408, March 2005.

[19] Q. Li and D. Rus, "Sending messages to mobile users in disconnected ad-hoc wireless networks," in Proceedings of ACM MobiCom, pp. 44–55, August 2000.

[20] W. Zhao, M. Ammar, and E. Zegura, "A message ferrying approach for data delivery in sparse mobile ad hoc networks," in Proceedings of ACM MobiHoc, (New York, NY, USA), pp. 187–198, ACM Press, May 2004.

[21] W. Zhao, M. Ammar, and E. Zegura, "Controlling the mobility of multiple data transport ferries in a delay-tolerant network," in Proceedings of IEEE INFOCOM, vol. 2, pp. 1407–1418 vol. 2, April 2005.